12th INTERNATIONAL CONFERENCE ON STRUCTURAL ANALYSIS OF HISTORICAL CONSTRUCTIONS

SAHC 2021

Online event, 29 Sep - 1 Oct, 2021

P. Roca, L. Pelà and C. Molins (Eds.)



12th INTERNATIONAL CONFERENCE ON STRUCTURAL ANALYSIS OF HISTORICAL CONSTRUCTIONS

SAHC 2021

Online event, 29 Sep - 1 Oct, 2021

A publication of:

International Centre for Numerical Methods in Engineering (CIMNE)
Barcelona, Spain

ISBN: 978-84-123222-0-0

Printed by: Artes Gráficas Torres S.L., Huelva 9, 08940 Cornellà de Llobregat, Spain

TABLE OF CONTENTS

Preface 7

Supporting Organizations 9

Organizers and Committees 11

Sponsors 15

Summary 17

Contents 19

Presented Sessions 45

Authors Index 3661

PREFACE

The International Conference on Structural Analysis of Historical Constructions (SAHC) was first celebrated in Barcelona in 1995, followed by a second edition also in Barcelona in 1998. Since then, nine subsequent editions have been organized in different countries of Europe, America and Asia. The SAHC conference series is intended to offer a forum allowing engineers, architects and all experts to share and disseminate state-of-art knowledge and novel contributions on principles, methods and technologies for the study and conservation of heritage structures. Through all its successful past editions, the SAHC conference has become one of the topmost periodical opportunities for scientific exchange, dissemination and networking in the field.

During the last decades the study and conservation of historical structures has attained high technological and scientific standards. Today's practice involves the combination of innovative non-destructive inspection technologies, sophisticated monitoring systems and advanced numerical models for structural analysis. More than ever, it is understood that the studies must be performed by interdisciplinary teams integrating wide expertise (engineering, architecture, history, archeology, geophysics, chemistry…). Moreover, the holistic nature of the studies, and the need to encompass and combine the different scales of the problem –the materials, the structures, the building aggregates, and the territory – are now increasingly acknowledged. Due to all this, the study of historical structures is still facing very strong challenges that can only be addressed through sound international scientific cooperation.

Taking these ideas in mind, the 12th edition of the SAHC conference aimed at creating a new opportunity for the exchange and discussion of novel concepts, technologies and practical experiences on the study, conservation and management of historical constructions.

The present proceedings include the papers presented to the conference, which was finally celebrated on September 29-30 and October 1, 2021, in an on-line mode due to the word sanitary emergency situation created by the Covid-19 pandemic.

The conference included the following topics: history of construction and building technology; inspection methods, non-destructive techniques and laboratory testing; numerical modeling and structural analysis; structural health monitoring; repair and strengthening strategies and techniques; conservation of 20th c. architectural heritage; seismic analysis and retrofit; vulnerability and risk analysis and interdisciplinary projects and case studies.

The SAHC 2021 conference has been possible thanks to the large contribution of the scientific committee and reviewer panel who took care of selecting and review the papers submitted. The contribution of the different sponsors and supporting organizations is also acknowledged. Above all, the conference has been possible thanks to all the authors who have contributed with very valuable papers despite the difficulties caused by the world pandemic. New editions of the conference are already planned in normal face-to-face formats which, in the upcoming years, will provide new opportunities for sharing valuable knowledge and experience on structural conservation, as well as for keeping alive and fulfilling the purpose and aims of the SAHC conference series.

The Organizing Committee

SUPPORTING ORGANIZATIONS

Universitat Politècnica de Catalunya (UPC), Barcelona, Spain

Center for Numerical Methods in Engineering (CIMNE), UPC, Spain

International Council on Monuments and Sites (ICOMOS)

International Scientific Committee for Analysis and Restoration of Structures of Architectural Heritage of ICOMOS (ICOMOS / ISCARSAH)

ORGANIZERS AND COMMITTEES

Organizing Committee



Pere Roca

Technical University of Catalonia



Climent Molins

Technical University of Catalonia



Luca Pelà

Technical University of Catalonia



Paulo Lourenço

University of Minho



Claudio Modena

University of Padova

SCIENTIFIC COMMITTEE

National Members

- Jose M. Adam, Polytechnic University of Valencia
- Ernest Bernat, Polytechnic University of Catalonia
- Pedro Calderón, Polytechnic University of Valencia
- Miguel Cervera, Polytechnic University of Catalonia
- Victor Compán, University of Seville
- Leire Garmendia, University of the Basque Country
- Lluis Gil, Polytechnic University of Catalonia
- Pilar Giráldez, University of Barcelona
- Salvador Ivorra, University of Alicante
- Miquel Llorens, University of Girona
- Ignacio Lombillo, University of Cantabria
- Camilla Mileto, Polytechnic University of Valencia
- Javier Mosteiro, Technical University of Madrid
- Belén Riveiro, University of Vigo
- Savvas Saloustros, Polytechnic University of Catalonia
- Fernando Vegas, Polytechnic University of Valencia
- Marius Vendrell, University of Barcelona

International Members

- Rafael Aguilar, Pontifical Catholic University of Peru
- Takayoshi Aoki, Nagoya City University
- Alessandra Aprile, University of Ferrara
- Oriol Arnau, National Autonomous University of Mexico
- Görün Arun, Yildiz Technical University
- Hiram Badillo, Autonomous University of Zacatecas
- Andrea Benedetti, University of Bologna
- Rita Bento, University of Lisbon
- Katrin Beyer, Swiss Federal Institute of Technology in Lausanne
- Rubén Boroschek, University of Chile
- Guido Camata, University of Chieti-Pescara
- Claudia Cancino, Getty Conservation Institute
- Eva Coïsson, University of Parma
- Dina D'Ayala, University College London
- Gianmarco de Felice, Roma Tre University
- Gianfranco de Matteis, University of Campania
- Matthew DeJong , University of California at Berkeley
- Milos Drdácký , Institute of Theoretical and Applied Mechanics
- Khalid El Harrouni, National School of Architecture
- Ahmed Elyamani, Cairo University
- Yohei Endo, Shinshu University
- Mariana Esponda, Carleton University
- Antonio Formisano, University of Naples Federico II
- Dora Foti, University of Bari
- Enrico Garbin, University of Padova
- Giorgia Giardina, University of Cambridge

- Toshikazu Hanazato, Mie University
- Mehrdad Hejazi, University of Isfahan
- Marcela Hurtado, Federico Santa María Technical University
- Jason Ingham, University of Auckland
- Wolfram Jager, Techincal University Dresden
- Stephen J. Kelley, SJK Inc.
- Debra Laefer, New York University
- Sergio Lagomarsino, University of Genova
- Alessandra Marini, University of Bergamo
- Guillermo Martínez, Michoacan University of Saint Nicholas of Hidalgo
- Arun Menon, Indian Institute of Technology Madras
- Gabriele Milani, Polytechnic University of Milan
- John Ochsendorf, Massachusetts Institute of Technology
- Daniel Oliveira, University of Minho
- Fernando Peña, National Autonomous University of Mexico
- Andrea Penna, University of Pavia
- Maurizio Piazza, University of Trento
- Mariapaola Riggio, Oregon State University
- Jan Rots, Delft University of Technology
- Antonella Saisi, Polytechnic University of Milan
- Cristián Sandoval, Pontifical Catholic University of Chile
- Vasilis Sarhosis, The University of Leeds
- Yaacov Schaffer, Israel Antiquities Authority
- Nigel Shrive, University of Calgary
- Marek Sklodowski, Institute of Fundamental Technological Research
- Pierre Smars, National Yunlin University of Science and Technology
- Luigi Sorrentino, Sapienza University of Rome
- Enrico Spacone, University of Chieti-Pescara
- Nicola Tarque, Pontifical Catholic University of Peru
- Adrienn Tomor, University of the West of England
- Daniel Torrealva, Pontifical Catholic University of Peru
- Maria Rosa Valluzzi, University of Padova
- Koenraad Van Balen, KU Leuven
- Humberto Varum, University of Porto
- Els Verstrynge, KU Leuven
- Elizabeth Vintzileou, National Technical University of Athens
- Roko Žarnić, University of Ljubljana

REVIEWER PANEL

- Daniela Addessi
- Maurizio Angelillo
- Jesus Bairán
- Elisa Bertolesi
- Maria Bostenaru
- Giuseppe Brando
- Manuel Buitrago Moreno
- Albert Cabané
- Chiara Calderini
- Ivo Caliò
- Lorenzo Cantini
- Silvia Caprili
- Giuliana Cardani
- Claudia Casapulla
- Rosario Ceravolo
- Francesca Ceroni
- Francesco Clementi
- Camilla Colla
- Cossima Cornadó
- Sara Dimovska
- Anastasios Drougkas
- Chiara Ferrero
- Virginia Flores Sasso
- Aguinaldo Fraddosio
- Donald Friedman
- Stefano Galassi
- Larisa García-Ramonda
- Lucia Garijo
- Carmelo Gentile
- Lorenzo Jurina
- Philip Karklbrenner
- David López
- Jose Machado
- Nirvan Makoond
- Nuno Mendes
- Andronki Miltiadou
- Bernt Mittnacht
- Tom Morrison
- Marius Mosoarca
- Juan Murcia
- Federica Ottoni
- Bartolomeo Pantò
- Marisa Pecce
- Chiara Pepi
- Elisa Poletti
- Bora Pulatsu
- Enrico Quagliarini
- Luisa Rovero
- Nicola Ruggieri
- Santiago Sanchez
- Mario Santana
- Michel Schuller
- Jorge Segura
- Vincenzo Sepe
- Alberto Taliercio
- Dimitris Theodossopoulos
- Filippo Ubertini
- Giuseppina Uva
- Graça Vasconcelos
- Maria Belén Jiménez

SPONSORS

PRO_SAM is a plugin which connects PRO_SAP with SAM II solver, a powerful tool for pushover analysis of new and existing structures.

SOLVER RELIABILITY

SAM II, conceived by Prof. Magenes, Eng. Manzini and Eng. Morandi, is a well-known and robust non-linear solver highly referenced in international literature.

CODES OF PRACTICE

Eurocode 8, Italian codes.

MATERIALS

Unreinforced and reinforced masonry, reinforced concrete and generic linear materials.

LOCAL FAILURE MECHANISMS

Automatic geometry interfacing with PRO_CineM for kinematic linear and non-linear analyses.

LINEAR ANALYSIS

Automatic generation of plate and shell linear model from the equivalent frame.

FREE

PRO_SAM is free for students, scholars or scientific research.

Asdea Software S.r.l. is part of the burgeoning ASDEA brand, which includes ASDEA S.r.l. and ASDEA Hardware. We are a software development company staffed with engineers, researchers, and software developers. Our goal is to provide innovative software solutions customized for clients and of original in-house design for numerical simulation and data visualization. We are the company behind the revolutionary software STKO (Scientific ToolKit for OpenSees). More than just a simple GUI, STKO features a Python scripting interface, meaning that users can customize and program the already powerful pre and postprocessors as needed, harnessing the full power of OpenSees.

CALSENS develops state-of-the-art fiber-optic sensors and designs, deploys and operates structural health monitoring (SHM) solutions to monitor bridges, buildings and vehicles (ships, airplanes, UAV), among other structures. Our services are based on constant research and innovation, creating products and services at the frontier of knowledge.

CALSENS services cover the full process of monitoring. Starting from the modelling of structural behavior and choice of control parameters, continuing with the election, design, fabrication and installation of the sensors and sensing system, until the processing, interpretation and evaluation of the data.

CALSENS has a multidisciplinary team with a high degree of expertise in the fields of civil engineering, photonic technologies, signal processing, materials engineering or computing.

Kerakoll is the international leader in the GreenBuilding sector, providing solutions that safeguard the health of both the environment and the people.

The company mission is embrace and promote GreenBuilding as the new low environmental impact approach to building and promote higher quality homes around the world through the use of eco-friendly building materials and innovative solutions.

Since 1968 – when the Group was founded in Sassuolo– Kerakoll has been pursuing a clear course of development in Italian and international markets for building materials, that has taken the company to the forefront of the GreenBuilding industry and to a level of technological supremacy famous around the globe.

S.T.A. DATA,founded in 1982 by Adriano Castagnone, civil and structural engineer since 1978, and pioneer of scientific software for structural engineering, is composed of more than 20 people, all highly qualified professionals. Our aim is to offer software for structural calculation that alallow designers to face everyday work with simplicity and effectiveness.

S.T.A. DATA offers 3Muri Project, developed specifically for masonry.

In fact, it is not a generic Finite Element software adapted for masonry structures; 3Muri Project was born from the specific research for these structures and captures all the characteristics to obtain a safe and reliable calculation of historical, exhisting and new buildings.

IRS is a smart Engineering, Research and Development company founded by a group of engineers in 1993. IRS Structural Health Monitoring division designs, develops and integrates automated systems for mechanical and structural monitoring. Thanks to technological innovation, advanced modeling and design as well as professional production and after sales service provide a complete suite of structural health monitoring solutions. Monitoring version are both portable version for laboratory tests and one shot structural assessments and long term and in situ applications like historical sites, buildings, bridges, dams and tunnels. IRS is part of a group of companies including Measureit, with whom provides consultancy and sales of precision sensor and data acquisition systems.

SUMMARY

PRESENTED SESSIONS

Conservation of 20th c. architectural heritage 47

History of construction and building technology.....200

Inspection methods, non-destructive techniques and laboratory testing.....481

Interdisciplinary projects and case studies 873

Management of heritage structures and conservation strategies 1514

Numerical modeling and structural analysis..... 1675

Repair and strengthening strategies and techniques..... 2439

Resilience of historic areas to climate change and hazard events 2746

Seismic analysis and retrofit 2846

Structural health monitoring..... 3206

Vulnerability and risk analysis 3390

Contents

PRESENTED SESSIONS

Conservation of 20th c. architectural heritage

An Innovative Shell Structure in Codogno (Italy). Evaluation of Structural and Seismic Performance 47
P. Brugnera, M.G. Costa and G. Mirabella Roberti

Anchorage of Reinforcement Bars in Hennebique R.C. Structures 59
A. Brencich and M. Nebiacolombo

Challenges in the Reuse and Upgrade of Pier Luigi Nervi's Structures 71
R. Ceravolo, G. De Lucia, E. Lenticchia, G. Miraglia, A. Quattrone, F. Tondolo, E. Matta, G. Sammartano, A. Spano and C. Chiorino

Conservation of 20th Century Concrete Heritage Structures in Cyprus: Research and Practice 82
A.V. Georgiou, M.M. Hadjimichael and I. Ioannou

Conservation of Historical Reinforced Concrete Structures 94
I. Bucur-Horváth and J. Virág

Decay Patterns and Damage Processes of Historic Concrete: A Survey in the Netherlands 105
G. Pardo Redondo, S. Naldini and B. Lubelli

Early Concrete Structures and Post-Patented Systems: Lessons to Preserve Early 20th Historical Heritage 117
I. Marcos, L. Garmendia, I. Piñero, Z. Egiluz, E. Briz and A. Gandini

Historical Buildings Made of Reinforced Concrete in Timisoara in the Beginning of the 20th Century 127
R. Oprita

Reconstruction of a Masonry Windmill Tower with a Multi-Blade Wind Turbine, Steel Reservoir and Water Supply System.....137
P.W. Sielicki

Reinforced Concrete Floors in Historic Buildings from the Beginning and the Middle of the 20th Century - Examples of Structural Strengthening in the Process of Revitalization.....144
G. Dmochowski, P. Berkowski, J. Szolomicki and M. Minch

Senate Building of Canada Case Study: Seismic Rehabilitation 156
L.M. Nicol

Structural Evaluation and Maintenance of Brooks Aqueduct Historic Site 168
A. Rouhi and N. Shrive

Structural Evaluation of the Greenhill Mine Tipple Structure Historic Site.....180
A. Rouhi and N.G. Shrive

The Safety Level of Concrete Pile Foundations under Industrial Monuments 192
S. Pasterkamp

History of construction and building technology

A study of the Historical Construction Technology of Bell Towers in Cyprus 200
M.L. Petrou and D.C. Charmpis

A User-Friendly Digital Tool for the Structural Assessment of Historic Domes: The Case Study of Saint Peter in Rome.....211
M.F. Funari, D.V. Oliveira, L.C. Silva and P.B. Lourenço

Amazonas Theater Architectural Construction and Restorations History.....221
M.S. Sampaio

An Example of Fit-for Purpose Use of Materials in Roman Architecture: P Temple, Side, Antalya/Turkey 233
G. Kaymak Heinz

First Reinforced Concrete Building in Rijeka Port - Ferenc Pfaff's Warehouse No.17 245
P. Šculac, D. Grandic and N. Palinic

Foundation Development from 1890-1942 for Long Span and High Rise Buildings at Mexico City 257
P. Santa Ana, L. Santa Ana and J. Baez

From Art to Science of Construction: the Permanence of Proportional Rules in the "Strange Case" of the 19th Century Ponte Taro Bridge (Parma, Italy).....267
F. Ottoni, V. Braglia, E. Coïsson and L. Ferrari

Gaudí, a New Architectural Concept of Maximum Structural Efficiency: Catenary Vaults, Complex Ruled Surfaces, Branched Pillars and an Endless Innovative Strategies.....279
C. Salas, C. Bedoya and J.M. Adell

Geotechnical Structures in the Ancient World. The Case of the Ziggurat of Ur in Mesopotamia.....291
E. Kapogianni

Historical and Typological Characterization of Churches in the Historical Centre of Cusco, Peru 302
K. Sovero, N. Tarque, E. Spacone, C. Mazzanti, G. Brando and C. Alfaro

Iron and Steel Construction Workshops in 19th and early 20th century Belgium: Retrieving their Oeuvre via Trade Catalogues.....313
I. Wouters and R. Wibaut

"Iron Cages". Technical Discussions after the 1906 Valparaíso Earthquake and Reconstruction with New Techniques and Materials.....325
S. Maino, K. Cabezas and M. Koch

New Lightweight Structures and Historical Heavyweight Structures in Conservation.....337
A. Mosseri

Opus Signinum - Roman Concrete without Pulvis Puteolanis: Example of the Substructures of Diocletian's Palace.....349
M.I. Šimunić Buršić

Patio as a Structural Invariant. Buildings with Patio Facing Adaptive Reuse in Barcelona.....361
P. Fuertes, R. Sauquet and N. Salvadó

Reconstructed Overhanging Battlements. Executive Techniques and their Vulnerability in the Stronghold of Arquata del Tronto (Italy).....373
E. Facchi, A. Grimoldi, A. G. Landi and E. Zamperini

Reinforced Concrete + Masonry: the 'Mixed' Structure of the Novocomum by Giuseppe Terragni.....385
A. Greppi and C. Di Biase

Safety Assessment of Existing Post-War Reinforced Concrete Bridges. The Case Study of 'Gerber Girders' Bridges in Italy.....397
I. Giannetti, S. Mornati, S. Coccia, F. Di Carlo and Z. Rinaldi

Structural Analysis as a Supporting Method for the Research of Medieval Brick Architecture.....409
P. Samol, P. Iwicki and J. Przewlocki

The "Pieve di Santa Maria" in Arezzo (Italy). From the Laser Scanner Survey to the Knowledge of the Architectural Structure.....421
P. Matracchi, C. Biagini, A. Sadocchi and M. Valieri

The Dome of the Temple of Diana in Baiae: Geometry, Mechanics and Architecture.....433
A. Sinopoli and D. Aita

The Spiral Staircase in the Fortified Tower of Nisida.....445
C. Cennamo, C. Cusano and M. Angelillo

The Structural Function of the Dutch Buttressing of the East Curtain Wall of Elmina Castle, Elmina, Ghana.....457
J. Sun, S. Tezcan and R. Perucchio

Timber Reinforcements: Local Construction Techniques in Italian Historical Buildings.....469
S. Della Torre and L. Cantini

Inspection methods, non-destructive techniques and laboratory testing

Application of Digital Close-Range Photogrammetry to Monitor Local Deformations of Architectural Monuments: A Case Study of el Mirador de Inkaraqay (Machu Picchu) 481
J. Kosciuk and M. Pakowska

Axial Compression Tests on Rubble Stone Masonry Reproducing Opus Incertum of Ancient Pompeii 492
F. Autiero, G. De Martino, M. Di Ludovico and A. Prota

Characterization of Cracks in Historical Buildings Using Image Processing Techniques 504
P. Porcel, B. Castañeda and R. Aguilar

Characterization of Historic Mortars for Compatible Restoration: Case study of South Africa 515
M. E. Loke, K. Pallav and R. Haldenwang

Comparison Between Investigation Techniques for the Evaluation of the Compressive Properties of Brick Masonry Structures 525
F. Ferretti, A. Incerti and C. Mazzotti

Compressive Behaviour of Bonded Brickwork Wallettes with Various Thicknesses: Experimental and Numerical Verification 537
J. Thamboo, M. Asad and T. Zahra

Data Acquisition, Management and Evaluation for Stone Conservation Projects with Digital Mapping 547
S. Vetter, G. Siedler and J. Kaminsky

Dynamic Identification of Damage in Brick Masonry Walls 559
S. Ivorra, D. Bru, I. Gisbert, F.J. Baeza, B. Torres and D. Camassa

Effect of Geometrical Imperfections on the Response of Dry-Joint Masonry Arches to Support Settlements 569
C. Ferrero, M. Rossi, P. Roca and C. Calderini

Evaluation of the Behaviour of Lime and Cement Based Mortars Exposed at Elevated Temperatures 581
V. Pachta and M. Stefanidou

Experimental Campaign on the Use of the Flat Jack Test in Cob Walls 593
A. Jiménez Rios, M. Grimes and D. O'Dwyer

Experimental Investigation of Scarf Joint of 'Lightning Sign' in Bending 602
A. Karolak and C. Jasieńko

Experimental Investigation on the Torsion-Shear Behaviour at the Interfaces of Interlocking Masonry Block Assemblages 614
C. Casapulla, E. Mousavian, L.U. Argiento and C. Ceraldi

Fatigue Assessment of Old Riveted Railway Bridges: Laboratory Testing of a Real Bridge 626
J.M. Adam, P.A. Calderón, M. Buitrago, E. Bertolesi, J.J. Moragues, S. Ivorra and B. Torres

Influence of Moisture Content on the Application of ND and MD Tests to Various Species of Timber Elements 639
M.R. Valluzzi, F. Casarin, L. Scancelli, M. Drdácky, M. Kloiber and J. Hrivnák

Investigation of Rubble-Masonry Wall Construction Practice in Latium, Central Italy 651
O. Al Shawa, G. De Canio, G. De Felice, S. De Santis, S. Forliti, D. Liberatore, D. Mirabile Gattia, S. Perobelli, F. Persia and L. Sorrentino

Laboratory and In-Situ Characterisation of Masonry Materials in a Large Historical Industrial Building in Barcelona 662
A. Cabané, L. Pelà and P. Roca

Mechanical Characterization of Traditional Masonry in an Homogeneous Territory: Valtellina 674
M. Sala, D. Foppoli and S. Della Torre

Methodologic Evolution Assessment of Large Deformations on Romanesque Masonry in Val d'Aran (XII-XIII centuries), Spain 685
J. Lluis i Ginovart, M. Lopez-Piquer and C. Lluis-Teruel

Modal and Structural Identification of a Multi-Span Masonry Arch Bridge 697
P. Borlenghi, A. Saisi and C. Gentile

Monitoring Deformations of a Wooden Church Tower by Laser Scanning 709
L. Truong-Hong, R. Lindenbergh, P. Woudenberg, W. Gard and J.-W. Van de Kuilen

Non-Destructive Assessment of the Adhesion at the Interface Between FRCM Reinforcements and Masonry Substrates by Non-Linear Ultrasonic Technique 722
A. Castellano, A. Fraddosio, T. Kundu and M.D. Piccioni

Non-Destructive Documentation Methods for Future Seismic and Damage Analysis of Modern Heritage Buildings using Contemporary Tools 734
S. Rajabzadeh, M. Esponda and L. Cordero Espinosa

Non-Destructive Techniques for Characterising Earthen Structures 746
E. Bernat-Maso, E. Teneva, L. Mercedes and L. Gil

Pathological and Structural Health Assessment of a Residential Building in Lota, Chile 757
M. Chávez, F. Macaya, E. Nuñez and C. Oyarzo

Point-Load Test Assesment as Study of Adobe Buildings Damaged after the 2017 Puebla Earthquake 769
A. Sánchez, E. M. Alonso and J. A. Bedolla

Quality and Strength Assessment of Butt Welds in Poland's Oldest Welded Railway Bridges 781
B. Wichtowski and J. Holowaty

Salt Contamination of Wooden Materials: the Case of Trondheim (Norway) Warehouses 791
C. Bertolin, M. Strojecki, L. De Ferri, G. Grottesi and A. M Siani

Stiffness Changes due to Static Loading of a Brick Arch 802
J. Bayer, S. Urushadze and J. Witzany

Structural Performance and Durability Issues of Vernacular Schist Masonry 809
C.E. Barroso, D.V. Oliveira and L.F. Ramos

Testing Calibration Issues in Resistance Drilling Applied to Timber Elements 821
F. Casarin, L. Scancelli, M.R. Valluzzi and E. Bozza

The NDT Investigations Carry out at the Arudj Cathedral, Armenia 830
S. Tonna, M. Cucchi and C. Tedeschi

The State and Condition of Historical Buildings Located on Partisan Hill in Wroclaw 842
A. Hola, J. Hola, L. Sadowski and J. Szymanowski

Towards a Methodology for Use of Sonic and Ultrasonic Tests in Earthen Materials 852
R. Martini, J.D. Rodriguez-Mariscal, J. Carvalho, M. Solís and H. Varum

Using the Ultrasonic Tomography Method to Study the Condition of Wooden Beams from Historical Building 863
M. Zielińska and M. Rucka

Interdisciplinary projects and case studies

A Preliminary Structural Survey of Heritage Timber Log Houses in Tonsberg, Norway 873
A. Shabani, H. Hosamo, V. Plevris and M. Kioumarsi

A Protected Landmark Monument: Reinforcement, Rehabilitation, and Restoration of the Cathedral Basilica of Manizales 885
O. D. Cardona and S. D. Prieto

Adaptation of a Mid-Nineteenth Century Representative University Building to Office Functions 897
J. Szolomicki, M. Minch, G. Dmochowski and P. Berkowski

An Interdisciplinary Approach for the Experimental Assessments of the Seismic Safety of Artworks 909
A. Di Martino, G. Cocuzza Avellino, E. Paterno, F. Cannizzaro, I. Caliò, G. Gianfriddo, R. Valenti and N. Impollonia

Application of Geophysical Prospecting Methods for Soil Structure Characterization of the Cathedral of Santo Domingo, Dominican Republic 921
J. Pérez-Cuevas, V. Flores-Sasso, E. Prieto-Vicioso, L. Ruiz-Valero and S. Sandoval

Assessment of Tunneling Induced Damage on Historical Constructions Through a Fully Coupled Structural and Geotechnical Approach 933
A. Amorosi, M. Sangirardi, G. De Felice and S. Rampello

Automated Model Updating of a Masonry Historical Church Based on Operational Modal Analysis: the Case Study of San Giovanni in Macerata 943
S. Santini, C. Baggio, E. Da Gai, V. Sabbatini and C. Sebastiani

Betang, a Traditional House of the Dayak Ngaju in Borneo Its Space Related to Structure 954
M. Guntur and K. R. Kurniawan

Claudius Aqueduct in Rome - Kinematic Analyses and Empirical Experiences for the Definition of Structural Restoration Interventions 966
F. De Cesaris

Comparison on Methodologies and Intervention for two Masonry Churches Affected after the 2017 Earthquake in Mexico 978
M. Esponda and J. Cooke

Conservation Beyond Consolidation for Prehistoric Monuments: Finding Narratives from Archaeology to Architecture for Scottish Brochs 990
C. Liu and D. Theodossopoulos

Constructive Analysis and Modelling of a Single Nave Church: a Proposal for S. Sebastiano (EN, Italy) 1002
A. Lo Faro, V. Cusmano, B. Pantò and F. Cannizzaro

Cultural Heritage Exposed to Natural Hazards: the Case Study of the Convent of San Domenico in Maiori 1014
R. Landolfo, C. Tarantino, F. Portioli and L. Cascini

Design of Protective Structures for Active Archeological Sites 1026
M. Petrović, I.D. Ilić, N.M. Džombić and N.D. Šekularac

Determining Qualities of Photogrammetric Models for the Use of Monitoring Movements in Stone Candis in Central Java 1038
D. Grandits, L. Stampfer, E. Kodzoman, A. Setyastuti and U. Herbig

Diagnosis of an Unusual Structural Instability: the Case Study of the Cathedral of San Lorenzo in Viterbo 1050
M. Candela, M. Eichberg and C. Tarantino

Documentation and Structural Appraisal of the Medieval Manor of Potamia, Cyprus: an Interdisciplinary Approach 1062
R. Illampas, D. Myrianthefs, D. Nicolaou, V. Lysandrou, M. Philokyprou, G. Papasavvas and I. Ioannou

Effect of Slow-Moving Landslides on Churches in the Liguria Region: a Geotechnical Approach 1074
L. Cambiaggi, C. Ferrero, R. Berardi, C. Calderini and R. Vecchiattini

From Reality to Point Clouds. Survey and Analysis of Sant Miquel Church of Batea (Spain) 1086
A. Costa-Jover, D. Moreno Garcia, S. Coll Pla and J. Lluis i Ginovart

Historical Analysis and In-Situ Inspections of a Cultural Heritage Masonry Building 1097
A. De Angelis, F. Santamato, G. Maddaloni, L. De Filippis and M.R. Pecce

Identification and Assessment of the Seismic Behaviour of Giotto's Bell Tower in Florence (Italy) 1109
P. Spinelli and M. Betti

Interdisciplinary Assessment, Analysis and Diagnosis of a Historic Timber Roof Structure From the 20th Century 1122
B. Isopescu, A. Keller, V. Stoian and M. Mosoarca

Non-Destructive Techniques in the Consolidation Works of the Church of S.M. of Itria in Piazza Armerina (Italy) 1133
T. Basirico, S. Campione and A. Cottone

Nonlinear Structural Analysis of the Elliptical Dome of the Church in the Universidad Laboral, Gijon, Spain 1145
J.J. Coz-Diaz, A. Lozano Martinez-Luengas, M. Alonso-Martinez, M.P. Garcia-Cuetos and F.P. Alvarez-Rabanal

Parameter Evaluation in Historical Construction: From Sensitivity Analysis to the Test Planning 1158
A. Calì, P. Dias De Moraes and A. Do Valle

Preliminary Structural Analysis of the Western Curtain Wall of Elmina Castle, Elmina, Ghana 1170
M.N. Dos Santos, S.A. Abelezele, K.A. Korslund, R.T. Cecil, S. Tezcan and R. Perucchio

Preserving Historic Bearing Structures by Prudent Integration in New Structures 1183
M. Mosoarca, V. Stoian, M. Florea, M. Niculescu and M. Palade

Reconstructing the Indoor Climate of Historic Buildings 1194
W. Stumpf

Renovation of 16th Century Salt House Roof (Lubań, Lower Silesia, Poland) - Case Study 1206
K. Alykow and M. Napiórkowska-Alykow

Research on Architectural Form and Structural Performance of the Brick-Vault Hall Heritage in China. A case study of Yongzuo Temple 1214
Q. Chun, Y. Lin and C. Zhang

Restoration Authenticity or Reality - A Case Study 1222
D. Biggs

Restoration of the Queen Victoria Market Sheds E-F and J-M, Melbourne, Australia 1232
J. Hettinga

Seismic Vulnerability Assessment of a 17th Century Colonial Adobe Church in the Central Valley of Chile 1244
N.C. Palazzi, G. Misseri, L. Rovero and J.C. De La Llera

Slow-Moving Landslide Damage Assessment of Historic Masonry Churches: some Case-Studies in Italy 1256
C. Ferrero, L. Cambiaggi, A. Fenialdi, P. Roca, R. Vecchiattini and C. Calderini

Soil Settlement and Uplift Damage to Architectural Heritage Structures in Belgium: Country-Scale Results from an InSAR-Based Analysis 1268
A. Drougkas, E. Verstrynge, K. Van Balen, M. Shimoni, T. Croonenborghs, R. Hayen, P. Y. Declercq and J. Walstra

Standard Gravity and Wind Load Analysis on 103-years old Unreinforced Masonry Building 1279
A. Kumar and K. Pallav

Static Analysis of a Masonry Arched and Buttressed Retaining Wall 1291
D.. Dogu, C. Molins and N. Makoond

Static and Dynamic Load Test of Libeň Bridge Over Vltava River in Prague and Concept of Repair 1303
P. Tej, J. Mourek and M. Blank

Structural Assessment of Cultural Heritage Buildings Using HBIM and Vibration-Based System Identification 1315
A. Cali, A. Saisi and C. Gentile

Study on Causative Agents of Damage in the Costa Rican Caribbean Architecture from a Multidisciplinary Perspective 1326
K. García-Baltodano, D. Porras-Alfaro and I. Hernández-Salazar

Studying a Masonry Sail Vault by Antonio da Sangallo the Elder in the Fortezza Vecchia in Livorno 1338
F. Barsi, D. Aita, R. Barsotti, D. Ulivieri and S. Bennati

The Bridge Over the Adda River in Brivio: History, Full-Scale Testing and FE Modelling 1346
G. Zonno and C. Gentile

The Column-Less Stair at Loretto Chapel in Santa Fe, New Mexico: Strength Analysis 1358
A. Sumali

The Dar al Consul Complex in Jerusalem: Improving the Living Conditions and the Structural Capacity 1369
F. Casarin, L. Di Marco, M. Mocellini, R. Sidawi, P. Dahabreh and A.K. Taweel

The Evangelical Church of Peace in Swidnica, Poland. Several Comments on its Wooden Construction and Building Technology in the Middle of the 17th Century 1381
U. Schaaf

The Influence of Civil Works on Heritage Architecture, El Vergel, Cuenca - Ecuador 1393
G. Barsallo, F. Cardoso, E. Sinchi, T. Rodas and M.C Achig

The Modern Impossibility of Making Art like That of the Past. Intervention Proposal for the Temple of San Juan Bautista, Tochimilico, Puebla, Mexico 1402
E. Vera

The Plaster Ceilings of Buckingham Palace and Windsor Castle: Their Construction, Condition and Conservation 1409
S. Brookes, K. Clark, R. Frostick, R. Ireland and L. Randall

The Restoration Interventions of "Forte Marghera" in Venice 1421
F. Casarin, R. Cianchetti, T. Dalla Via, M. Meggiato and M. Mocellini

The Restoration of the Medieval Walls of San Ginesio: a Dedicated Study for the Conservation, Repair and Enhancement of an Important Military Fortification 1433
M. Saracco, F. Mariano, A.A. Giuliano, L. Petetta and F. Piccinini

The Reuse of Housing Buildings in Barcelona. The Versatility of Old Constructive Structures 1445
M. Mària and X. Monteys

The Use of a Building Information Model to Support Seismic Analysis: Application to the National Palace of Sintra, Portuga 1457
M. Ponte, R. Bento, R. Machete , M. Godinho, A. B. Gonçalves and A. P. Falcão

Thermal Behavior Assessment of Two Types of Roofs of the Dominican Vernacular Housing 1470
E. Prieto-Vicioso, L. Ruiz-Valero and V. Flores-Sasso

To Reach the Light: The Monumental Byzantine Stairs of Caesarea, a Conservation and Restoration Project 1478
N. Maklada, S. Hadid, D. Abuhatsira, P. Gendelman, Y. Oz and D. Siboni

Typological Characterization of Ancient Town Walls for Disaster Prevention and Mitigation. The MO.M.U. Project 1490
A. De Falco, F. Giuliani, D. Ladiana, L. Rjolli, D. Bordo, F. Gaglio and M. Di Sivo

Vulnerability Assessment of Italian Rationalist Architecture: Two Case Studies 1502
P. Bernardi, R. Cerioni, E. Coisson and E. Michelini

Management of heritage structures and conservation strategies

British Colonial Era's Religious Built Heritage in Yorubaland, Nigeria: Key Conservation Problematics and the State of Know-How 1514
R. Sabri and O.A. Olagoke

Conservation of Architectural Complex of Manguinhos, in Rio de Janeiro, Brazil 1523
B. Oliveira

Dacian Fortresses in Orastie Mountains: Management of Heritage Structures 1535
G. Pașcu, A. Keller and C. Bocan

Design Criteria and Procedures for Archaeological Shelters: Towards Flexibility Thanks to Algorithmic Modelling 1547
L. Sbrogiò, A. Basso, P. Borin, M.R. Valluzzi and A. Giordano

Digitization of Cultural Heritage Buildings for Preventive Conservation Purposes 1559
M.G. Masciotta, L.J. Sánchez-Aparicio, S. Bishara, D.V. Oliveira, D. González-Aguilera and J. García-Alvarez

Fill-in-Glass Restoration: Exploring Issues of Compatibility for the Case of Schaesberg Castle 1571
L. Barou, F. Oikonomopoulou, T. Bristogianni, F.A. Veer and R. Nijsse

Integrated Conservation Strategies in the Netherlands 1583
S. Naldini, R. Van Hees and E. Van der Grijp

Modern Consolidation Methods for Catholic Church in Baroque Style from Arad Fortress, Romania 1594
A.C. Ion and M. Mosoarca

Preventive Conservation for Built Heritage. Analysis of Different Models Around Europe 1606
D. Stabrauskaite

Structural Typificaton of Heritage Builings Using Modern Technologies for Digital Management and Visualization: Preliminary Applications in Southern Peru 1618
S. Huaranga, P. Pórcel, C. Yaya, B. Castañeda and R. Aguilar

The Iscarsah Guidelines on the Analysis, Conservation and Structural Restoration of Architectural Heritage 1629
P. Roca

Towards a Digital Architectural Heritage Knowledge Management Platform: Producing the HBIM Model of Bait al Naboodah in Sharjah, UAE 1641
R. Sabri, S.B. Abdalla and M. Rashid

Unreinforced Masonry Structures' Seismic Improvement with F.R.C.M.: the Experience of the Vanvitellian Palazzo Murena of Perugia 1651
R. Liberotti, F. Cluni and V. Gusella

Using Information Technologies for Bridge Management in Mexico's Royal Roads Built Between XVI and XVIII Century 1663
A. Torres-Acosta, J. Bustamanta-Altamirano and A. Esparza-Carrillo

Numerical modeling and structural analysis

3D FE Modeling of Multi-Span Stone Masonry Arch Bridges for the Assessment of Load Carrying Capacity: the Case of Justinian's Bridge 1675
V. G. Mentese and O. C. Celik

A Comparison Between Traditional and Modern Approaches for the Structural Modelling of Brick Masonry Barrel Vaults 1687
E. Coïsson, D. Ferretti and F. Pagliari

A Constitutive Model for Rubble Masonry Allowing for Spread Micro-Cracks and Localized Macro-Cracks 1699
M. Scamardo, A. Franchi and P.G. Crespi

A Machine Learning Model for the Determination of Macro-Scale Masonry Properties based on a Virtual Laboratory at Micro-Scale 1712
P. Kalkbrenner, L. Pelà and R. Rossi

A Macroscale Modelling Approach for Nonlinear Analysis of Masonry Arch Bridges 1724
B. Pantò, C. Chisari, L. Macorini and B.A. Izzuddin

A Method for the Structural Analysis and Design of Arched Reinforced Masonry and/or Concrete Structures 1736
D. López López, P. Roca, A. Liew, T. Van Mele and P. Block

A Novel Non-Linear Discrete Homogenization Approach for the Analysis of Double Curvature Masonry Structures 1746
J. Scacco, G. Milani and P.B. Lourenço

A Simple and Effective Rigid Beam Model for Studying the Dynamic Behaviour of Freestanding Columns 1755
D. Baraldi, G. Milani and V. Sarhosis

A Simplified Modelling Approach for the Practical Engineering Assessment of Unreinforced Masonry Structures Using Layered Shell Elements 1766
A. Hassanieh, M. Gharib and M. King

Adaptative Pushover Analyses of a Heritage Structure: Application to a Multi-Tiered Pagoda Temple 1778
Y. Endo, Y. Kondo and G. Iwanami

Advanced Tools for Fast Micro-Modelling of Masonry Structures 1789
M. Petracca, C. Marano, G. Camata, E. Spacone and L. Pelà

Analysis and Assessment of Swedish Vaulted Masonry Structures Using Funicular Methods 1799
C. Thelin and F. Höst

Applicability of FEM and Pushover Analysis to Simulate the Shaking-Table Response of a Masonry Building Model with Timber Diaphragms 1811
M.P. Ciocci, R. Marques and P.B. Lourenço

Assemblability Constraints in the Limit Analysis of 3D Masonry Interlocking Blocks 1822
E. Mousavian and C. Casapulla

Assessment of Structural Damage and Evolution in Time in Historical Constructions Using Numerical Models: the Case of the Church of Saint Bassiano in Pizzighettone, Cremona 1834
G. Angjeliu, G. Cardani and D. Coronelli

Calibration of a FEM Model with Complex Geometry: the Case Study of Santa Maria Maddalena Church in Ischia, Italy 1846
B. Di Napoli, M.P. Ciocci, T. Celano, P.B. Lourenço and C. Casapulla

Collaborative Use of DEM and FEM for Brick Joint Splitting in Strong Earthquake Ground Motion 1859
T. Maeda, H. Tanaka, M. Shirahashi and B. Higashizawa

Combined Shear-Flexural Verification of in Plane Loaded Reinforced and Unreinforced Masonry Walls 1871
A. Benedetti, M. Tarozzi and L. Benedetti

COMPAS Masonry: A Computational Framework for Practical Assessment of Unreinforced Masonry Structures 1882
A. Iannuzzo, A. Dell'Endice, R. Maia Avelino, G.T.C. Kao, T. Van Mele and P. Block

Correlation Studies for the In-Plane Analysis of Masonry Walls Based on Macroscopic FE Models with Damage 1893
M. Nocera, L.C. Silva, D. Addessi and P.B. Lourenço

Development of a Neural Network Embedding for Quantifying Crack Pattern Similarity in Masonry Structures 1905
A. Rózsás, A. Slobbe, W. Huizinga, M. Kruithof and G. Giardina

Discrete Element Modelling of Single-Nave Churches Damaged after the 2009 Earthquake in l'Aquila, Italy 1917
F. Gobbin, R. Fugger and G. De Felice

Equivalent Frame Method Combining Flexural and Shear Responses of Masonry Buildings 1928
C. Marano, M. Petracca, G. Camata and E. Spacone

Estimation of the Clamping Force of Riveted Assemblies Through a Thermomechanical Modelling. Influence of Clearance and Thickness of the Connection 1940
P.-J. Tisserand, S. Sire and M. Ragueneau

Excess Capacity in Historic American Reinforced Concrete Floors 1947
D. Friedman

Experimental Data for the Calibration of a Non-Linear Numerical Model for Describing the Response of Masonry Constructions under Cyclic Loading 1959
A. Castellano, A. Fraddosio, M.D. Piccioni, E. Ricci and E. Sacco

Fast Seismic Vulnerability Evaluation of Historical Masonry Aggregates through Local Analyses: an Adaptive NURBS-based Limit Analysis Approach 1971
N. Grillanda, M. Valente, G. Milani, F. Formigoni, A. Chiozzi and A. Tralli

General Thrust Surface of the Masonry Domes 1984
I. Sajtos, O. Gáspár and A. Sipos

Geometric and Structural Information for the Analysis of Historical Domes: The Case of the SS. Trinità Church in Torino 1996
G. De Lucia and R. Ceravolo

In-plane Behaviour of an Iron-Framed Masonry FaÃ§ade: Comparison between Different Modelling Strategies 2007
T. Celano, L. Argiento, B. Pantò, F. Ceroni, C. Casapulla, I. Caliò and P.B. Lourenço

Influence of Settlements and Geometrical Imperfections on the Internal Stress State of Masonry Structures 2019
A. Dell'Endice, A. Iannuzzo, T. Van Mele and P. Block

Influence of Temperature on the Structural Behaviour of Masonry Buildings 2031
M. Girardi, C. Padovani and D. Pellegrini

Influence of the Spatial Variability of Joints Characteristics on the Elastic Properties of Masonry 2043
M.L. De Bellis, V. Sepe and M. Vasta

Inspection, Diagnosis and Modelling of Azurara Church in the North of Portugal 2054
E.A. Chaves Moreno, E.T. Key, A. Uplekar , O. Pino, G. Vasconcelos, J. Ortega and E. Poletti

Investigation of the Response of a Masonry Arch Railway Bridge using Membrane Equilibrium Analysis 2066
C. Olivieri, S.H. Cocking, M. Angelillo and M.J. DeJong

Investigation on the Seismic Response of a Large Monumental Complex 2076
S. Caprili, I. Puncello and P. Roca

Lower-Bound Limit Analysis of Masonry Arches with Multiple Failure Sections 2088
N.A. Nodargi and P. Bisegna

Minimum Thickness and Collapse Conditions of the Irregular Masonry Arch Subject to its Own Weigth 2100
N. Cavalagli, V. Gusella and R. Liberotti

Neomudejar Architecture and Analysis of Local Stresses of Masonry Structures: The Escuelas Aguirre Case Study 2112
J. García-Muñoz, D. Mencías-Carrizosa and F. Magdalena-Layos

New Strategies to Assess the Safety of Unreinforced Masonry Structures Using Thrust Network Analysis 2124
R. Maia Avelino, A. Iannuzzo, T. Van Mele and P. Block

Nonlinear Behaviour of Two-Whyte Stone Walls 2136
B. Dinç-Şengönül, Y.M. Hothot, B. Doran, N. Yüzer, S. Ulukaya and D. Oktay

Novel Constitutive Modelling Approach for Shape Memory Alloys Vibration Control Devices 2146
K. Wasilewski and A. Zbiciak

Numerical Analysis of Historical Reinforced Concrete Shell 2156
P. Kněž, P. Tej and J. Kolísko

Numerical Development of a Strengthened Wall-to-Diaphragm Seismic Connection: Calibration and Application on a Building Prototype 2168
F. Solarino, D.V. Oliveira and L. Giresini

Numerical Modelling of the Seismic Performance of Romanian Traditional Timber-Framed Buildings 2181
F. Parisse, E. Poletti, A. Dutu and H. Rodrigues

Numerical Simulation of Traditional Timber-Masonry Buildings Subjected to Lateral Loads 2194
B. Jimenez and L. Pelà

Numerical Study of Out-of-Plane Behaviour of Timber Retrofitted Masonry Prisms 2206
J. A. Dauda, L.C. Silva, P.B. Lourenço and O. Iuorio

Numerical Study of Pier-Wall Connections in Typical Dutch URM Buildings 2217
D. Fusco, F. Messali, J.G. Rots, D. Addessi and S. Pampanin

Safe Estimation of Minimum Thickness of Circular Masonry Arches Considering Stereotomy and Different Rotational Failure Modes 2229
O. Gáspár, I. Sajtos and A. A. Sipos

Safety Assessment of Historic Masonry Structures by Limit Analysis and Deterministic Partial Safety Factors 2240
F. Magdalena, A. Aznar, J. Antuna and J.I. Hernando

Seismic Assessment of Masonry Towers: The Case of Castellum Aquae System in Pompeii 2251
M. Salvalaggio, V. Sabbatini, F. Lorenzoni, M.R. Valluzzi and H. Wenliuhan

Seismic Behaviour Analysis of Diaphragm Arches: Case Studies from Catalan Gothic Churches 2262
D. Cacace, V. Corlito, M. Zizi, G. De Matteis and P. Roca

Sensitivity Analysis in the Rehabilitation of Historic Timber Structures on the Examples of Greek Catholic Churches in Polish Subcarpathia 2274
K. Szepietowska and I. Lubowiecka

Simplex Algorithm for 3D Limit Analysis of Roman Groin Vaults 2282
C. Baggio and S. Santini

Simulation of the Out-of-Plane Behaviour of URM Walls by Means of Discrete Macro-Element Method 2294
C. Chácara, B. Pantò, F. Cannizzaro, D. Rapicavoli, I. Caliò and P.B. Lourenço

Stochastic Micro-Modelling of Historic Masonry 2306
J. Adamek and P. Kabele

Structural Analysis of Historical Constructions by Graphic Methodologies based on Funicular and Projective Geometry 2318
J. Suárez, T. Boothby and J. A. González

Structural Assessment of the Seismic Behavior of the Dome of the Taj Mahal 2330
S. Rihal, B. Koh, A. Mehrotra and J. Edmisten

Structural Evaluation of Typical Historical Masonry Vaults of Cagliari: Sensitivity to Bricks Arrangements 2342
A. Cazzani, N. Grillanda, G. Milani, V. Pintus and E. Reccia

Structural Modelling and Numerical Analysis of the Palace of Sports of Mexico City 2354
H. Badillo-Almaraz, A. Orduña, S.G. De La Rosa, G.A. González and G.M. Roeder

Structural Performance Evaluation of Column-Nuki Connection in Traditional Japanese Wooden Buildings 2366
S. Murai and M. Miyamoto

Study on Rigid Homogenization Method and Model of Masonry under Different Bricklaying Methods Based on Regular Tessellation Theory 2378
Y. Chunxia, C. Shu, L. Chenyi and Z. Nan

Study on Seismic Performance Evaluation of Modern Wooden School Buildings in Japan 2390
M. Miyamoto

The Influence of the Passive Earth Pressure and other Factors on the Stability of the Underground Masonry Vaults of the Paris Metro 2400
O. Moreno Regan, E. Bourgeois, J. F. Douroux and A. Desbordes

The Safety of Masonry Arches Subject to Vertical and Horizontal Forces. A Numerical Method Based on the Thrust Line Closest to the Geometrical Axis 2413
S. Galassi and G. Tempesta

The Unbuilt Musmeci Parabolic Cross Vault Reinvented as a Dry-Masonry Structure 2425
C. Intrigila, N.A. Nodargi and P. Bisegna

Repair and strengthening strategies and techniques

A New Method for Assessing Compatibility of Consolidation Procedures with Conservation Principles: Intervention Quality Index (IQI) 2439
N.C. Palazzi, G. Misseri, C. Sandoval, U. Tonietti, J.C. De La Llera and L. Rovero

Characterization of FRCM- and FRP-Masonry Bond Behavior 2451
C. Gentilini, C. Carloni, R. Santoro and E. Franzoni

Cost-Effective Implementation of Nitinol to Improve the Seismic Performance of an Unreinforced Masonry Building 2458
T.F. Paret and J.M. Rautenberg

Cyclic Tests on Masonry Vaults Strengthened Through Composite Reinforced Mortar 2470
N. Gattesco and I. Boem

Evaluation of Performance of Matured Hydraulic Grouts: Strength Development, Microstructural Characteristics and Durability Issues 2480
A. Miltiadou-Fezans, M Delagrammatikas, A. Kalagri and P. Vassiliou

Experimental and Numerical Analyses on Sandstone Elements Obtained by 3D Printing 2492
C. Scuro, S. Tiberti, S. Porzio, R.S. Olivito and G. Milani

Experimental and Numerical Analysis of a FRCM Reinforced Parabolic Tuff Barrel Vault 2504
A. Castellano, J. Scacco, A. Fraddosio, G. Milani and M.D. Piccioni

Experimental Assessment of Cyclic Shear Response of Brick Masonry Walls Retrofitted with TRM 2516
L. Garcia-Ramonda, L. Pelà, P. Roca and G. Camata

Experimental Investigation of the Bond between Glass Textile Reinforced Mortar (GTRM) and Masonry Substrate: the Effect of Textile Impregnation 2528
P.D. Askouni and C.G. Papanicolaou

Experimental Study on the Shear Behavior of FRCM Strengthened Masonry Panels 2540
F. Ferretti, A. Incerti and C. Mazzotti

Experimental Tests on FRCM and FE Modelling for the Heritage Structure's Reuse 2552
R. Liberotti, N. Cavalagli and V. Gusella

Fibre Reinforced Geopolymers as Inorganic Strengthening Composites for Masonry Structures 2564
E. Garbin, M. Panizza, S. Tamburini, M. Natali and G. Artioli

Flexural Resistance of Masonry Wall Retrofitted with Timber Panels under Out-Of-Plane Loading 2576
O. Iuorio, J. A. Dauda and P.B. Lourenço

From the Cure of the Simple Structural Analysis to the Control of the Final Technological Quality - The Conservation of "Santa Maria Degli Angeli Orphanage" in Castelgrande (Potenza, Italy) 2586
F.P.R. Marino, G. Auletta, F. Baldantoni, F.C. Ponzo and F. Lembo

Historical Timber Structures in Adana-Tepebag Settlement and Consolidation Approach with Modern Timber Prefabricated Systems 2600
K. Apak

Numerical Modelling of Masonry Arches Strengthened with SFRM 2612
S. Caddemi, I. Caliò, F. Cannizzaro, D. Rapicavoli, N. Simoncello, P. Zampieri, J. Gonzalez-Libreros and C. Pellegrino

Out-of-Plane Behaviour of Tuff and Brick Masonry Walls Strengthened with FRCM Composite Materials 2620
A. Bellini, A. Incerti, A. Nanni and C. Mazzotti

Overview of the Mechanical Properties of Steel Reinforced Grout Systems for Structural Retrofitting 2632
F. Roscini, S. De Santis, P. Meriggi and G. De Felice

Performance Assessment of Basalt FRCM for the Confinement of Clay Brick Masonry Cylinders 2642
J. D'Anna, G. Amato, J.F. Chen, G. Minafò and L. La Mendola

Performance of Unreinforced Masonry Strengthened with Bed Joint Reinforced Repointing 2652
L. Licciardello, J.G. Rots and R. Esposito

Reinforcement and Consolidation of Masonry Structures. Successful Cases Implemented: From the Study to the Execution Phase 2664
J. Dobon and M.A. Soria

Repair Connection with Wooden Wedged Dowels: Preliminary Experimental Laboratory Tests and FEM Model for the Description of the Mechanical Behavior 2673
E. Perria, S. Siegert, X. Li and M. Sieder

Stabilization and Consolidation of Historical Multi-Leaf Masonry 2687
J. Witzany, J. Brožovský, T. Čejka, J. Kubát and R. Zigler

Static Test on Full Scale Rammed Earth Building with Mesh-Wrap Retrofitting Strategy 2696
K.C. Shrestha, T. Aoki, M. Miyamoto, N. Takahashi, J. Zhang, P. Wangmo, N. Yuasa, S. Shin, P. Pema and K. Tenzin

Structural Restoration and Re-Use of the Historic Coal Mine Tower 2708
D. Andic, M. Horvat and J. Pojatina

The CLT Panels in Structural Restoration: Characteristics and Technical Regulations 2718
G. Frunzio, L. Di Gennaro , L. Massaro and F. D'Angelo

Treatment for Rising Damp and Natural Hydrodynamic Equilibrium in Masonry Walls 2729
J. Dobon and M.A. Soria

TRM-Strengthened Timbrel Cross Vaults Subjected to Vertical Settlements 2737
P.A. Calderón, E. Bertolesi, M. Buitrago, J.J. Moragues and J.M. Adam

Resilience of historic areas to climate change and hazard events

A Framework for the Detailed Flood Vulnerability Modelling of Built Cultural Heritage 2746
R. Figueiredo, X. Romão and E. Paupério

Assessing the Impact of Seismic Risk Mitigation at the Urban Scale on Community Resilience and Housing Recovery 2757
A. Basaglia, A. Aprile, E. Spacone and L. Pelà

Fire Prevention in Ottoman and Habsburg Building Codes for Bosnia and their Application in Travnik 2768
C. Jaeger-Klein, A. Bajramovic and L. Stampfer

Landslide Hazard Affecting Historical Buildings: Santa Scolastica Monastery in Subiaco 2780
M. Sangirardi, A. Amorosi and G. De Felice

Post-Earthquake Reconstruction of the Historic City Center of l'Aquila: A Proposal Concerning the Rubble Transportation Problem 2790
S. Di Marco and M.A. Bragadin

Post-Quake Small Italian Historical Centres: Urban Resilience between Rhetorics and Reality. The Case Study of Nocera Umbra after the 1997 Umbria-Marche Earthquakes 2802
E. Cianci, C. Fontana, G. Occhipinti and G. Romagnoli

Preliminary Approach for a Prototype of Sustainable Antiseismic Dwelling in Nepal Based on the Historic Vernacular Tradition 2814
F. Vegas López-Manzanares, C. Mileto, W. Pisarra and F. Trizio

Resilience and Vulnerability of Historical Centres: the Case of the District of Camerino in the Marche Region 2824
E. Petrucci, L. Barchetta and D. Lapucci

Resilience of Historic Residential Areas Subjected to Natural Disasters 2836
M. Drdácký, R. Cacciotti and T. Drdácký

Seismic analysis and retrofit

An Integrated Modeling Approach that Combines Elastic Amplification and Rocking Analysis for Seismic Assessment of a Masonry Tower 2846
A. Mehrotra, A. Liew, P. Block and M.J. DeJong

Assessment of the Seismic Retrofitting of a Historical Masonry Mosque by means of Nonlinear Dynamic Analysis 2858
A. Aşikoğlu, L.C. Silva, O. Avşar and P.B. Lourenço

Comparison of Two Different Approaches for the Seismic Evaluation of the Bonet Building of the National Palace of Sintra, Portugal 2870
M. Ponte, M. Malcata and R. Bento

Damages Patterns in Historical Temples of Puebla, Morelos and Oaxaca after September 2017 Mexico Earthquakes 2882
M. Chávez, F. Peña, N. García and D. Durán

Design of Shake Table Tests of Multi-Leaf Masonry Walls Before and After Retrofitting 2894
S. De Santis, O. Al Shawa, G. De Canio, S. Forliti, D. Liberatore, P. Meriggi, I. Roselli, L. Sorrentino and G. De Felice

Effect of Historic Timber Roof Structures on the Structural Behaviour of Masonry Buildings during Seismic Events 2902
A.I. Keller and M. Mosoarca

Evolution of Lateral Design in the United States 2914
N.A. Hicks and E.P. Meade

Extrados Strengthening of Single-Leaf Vaults Against Seismic Actions 2926
S. Cominelli, C. Passoni, A. Marini, A. Belleri and E. Giuriani

Inadequate Cases of Intervention in Architectural Heritage Buildings in Mexico after the September 2017 Earthquakes 2938
F. Peña and M. Chávez

Macroelement Numerical Simulation of the Seismic Response of a Timber-Retrofitted Masonry Pier 2946
M. Miglietta, N. Damiani, S. Bracchi, G. Guerrini, F. Graziotti and A. Penna

Mechanical Characterization of Energy Dissipation Devices in Retrofit Solution of Reinforced Concrete Frames Coupled with Solid Wood Panels 2958
C. Tardo, F. Boggian, M. Hatletveit, E. Marino, G. Margani and R. Tomasi

Numerical Investigation of the Retrofitting Interventions of the San Benedetto Church Complex in Ferrara (Italy) from a Seismic Vulnerability Perspective 2970
R. Shehu

Numerical Investigations for Assessing the Seismic Performance of Multi-Tiered Nepalese Temples 2981
M. Pejatovic, V. Sarhosis and G. Milani

Numerical Simulation on Seismic Performance of Retrofitted Masonry Wall in Historical Buildings Damaged in Earthquake 2993
B. Wu, J. Dai and W. Bai

Repair and Retrofit of a Roman Bridge in Turkey 3005
H. Sesigur and M. Alaboz

Seismic Assessment and Strengthening Interventions of Atop Single-Block Rocking Elements in Monumental Buildings: the Case Study of the San Felice sul Panaro Fortress 3016
S. Degli Abbati, S. Cattari, S. Lagomarsino and D. Ottonelli

Seismic Assessment of Dutch URM Buildings According to NPR9998:2018 Code with an Equivalent-Frame Approach 3028
S. Bracchi, F. Graziotti, F. Messali and A. Penna

Seismic Assessment of Heritage Buildings in Bulgaria 3040
M.D. Traykova and A.V. Traykov

Seismic Behaviour of La Merced Temple in Morelia, Mexico 3052
L. Mejia, G. Martinez, B. Olmos and J.M. Jara

Seismic Damage Mechanisms for Churches and Damage Sequence: Considerations from a Case Study 3065
M.A. Parisi, Y. Anzilotti, G.I. Fuentes Rivera, G. Sferrazza Papa and S. Barbo

Seismic Fragility Analyses of the Cabinet Stored Artefacts with and without Damping Method 3077
W. Bai, J. Dai and Y. Yang

Seismic Performance Evaluation of Box-Shaped Wall Structures Built with Thick Earthen Walls 3087
H. Yokouchi and Y. Ohashi

Seismic Performance of Masonry Cross Vaults through Shaking Table Testing on a Scaled Model 3098
N. Bianchini, N. Mendes, P. Candeias, M. Rossi, C. Calderini, P.B. Lourenço and A. Campos Costa

Seismic Response of Hagia Sophia Church in Thessaloniki Including Soil-Foundation-Structure Interaction 3109
A. Chounta, C. Malakoudi, C. Petridis and D. Pitilakis

Seismic Retrofitting of Historical Masonry Heritage Structures: A Case Study of an Adobe Masonry Building in Lima, Peru 3121
T. Martins, J. García, A. Ferrández, N. Tarque and J. Fernández

Seismic Stability Analysis of Inca Earthen Walls 3133
A. Torres, M. Blondet and S. Santa Cruz

Simplified Method for the Lateral Strengthening of Earthen Churches ... 3145
R. Enciso, M. Noel and R. Aguilar

Structural Analysis of a Restored Byzantine Monastery: Effectiveness of the Interventions 3156
P. Condoleo and A. Taliercio

Structural Assessment of the 13th Century Great Mosque and Hospital of Divrigi: A World Heritage Listed Structure 3169
C. Demir, O.F. Halici, A.N. Sanver, M. Comert, F. Kuran, N. Berlucchi, A. Hurata and A. Ilki

The Floor Stiffness Effect on Vulnerability Assessments and Intervention Designs of Historic Buildings: the Case Study of the "Procuratie Vecchie" in Venice, Italy 3181
I. Rocca, L. Berto, S. Bellin, B.F. Dongmo, A. Saetta and R. Vitaliani

Understanding Traditional Anti-Seismic Strategies Beyond Their Disappearance and Distortions: Yazd Qajar Architecture Case Study 3193
E. Crété, S. Yadav, N. Farahza, L. Arleo, M. Hajmirbaba, Y. Sieffert and P. Garnier

Structural health monitoring

Assessment and Monitoring of Historical Timber Construction: Available Tools to Support Decision-Making Processes 3206
M. Riggio

Continuous Structural Monitoring of Adobe Buildings: Summary of a Three Years Experience in Peru 3218
G. Zonno, R. Aguilar, R. Boroschek and P.B. Lourenço

Data Analysis Using ARX Models Applied to Static Structural Health Monitoring of the Monastery of Sant Cugat 3228
N. Makoond, L. Pelà, C. Molins and P. Roca

Development of a Wireless Acceleration Measurement System 3240
T. Yamasaki, K. Ota, M. Miyamoto, Y. Amano, M. Okada and T. Kido

Dynamic Identification of the So-Called Temple of Minerva Medica: Comparison of Different Instrumentations and Methods for Mutual Validation of the Results 3252
C. Baggio, V. Sabbatini, S. Santini, C. Sebastiani, V. Fioriti, I. Roselli, A. Colucci, F. Saitta and S. Forliti

Health Monitoring Tests of Heritage Structures: Application of MEMS Accelerometers to Two Multi Tier Pagodas 3264
Y. Endo and Y. Niitsu

Long-Term Structural Health Monitoring of the Fortezza Fortress: Application of Damage Detection Techniques on Existing Cracks 3272
M. Drygiannakis, G. Vlachakis and A. Tzigounaki

Monitoring of Indoor Environmental Conditions of the Kvernes (Norway) Stave Church 3284
C. Bertolin, L. De Ferri and T.M. Olstad

Multi-Modal Analysis of Vibration and Meteorological Data for Structures on the World Heritage Site "Battleship Island" 3296
N. Kurata, K. Takai, A. Tomioka, T. Daigo, S. Saruwatari and T. Hamamoto

One-year Static Monitoring of the Milan Cathedral 3305
A. Saisi, A. Ruccolo and C. Gentile

Proposal for a Time-Dependent Dynamic Identification Algorithm for Structural Health Monitoring 3317
M.F. Hormazábal, M.G. Masciotta and D.V. Oliveira

Quantification of the Structural Response of Historical Constructions: Investigation of the Strain Variation at the Acropolis Circuit Wall 3329
E. Kapogianni, P. Psarropoulos and M. Sakellariou

Real-Time Structural Monitoring of Bibi-Khanum in Samarkand (Uzbekistan) Combined with Subsequent Laser Scans 3339
S.M. Takhirov, I. Aripov and D. Matrasulov

Structural Health Monitoring of a Historic Church: Theory and Practice of Diagnostic Approaches Used to Control Risks and Costs 3349
T. Morrison and S. Burrill

Structural Health Monitoring of the Juma Mosque in Itchan Kala in Khiva (Uzbekistan): Laser Scanning Combined with Numerical Modelling 3361
S. Takhirov and B. Rakhmanov

Structural Monitoring in the "Santa Maria de la Asunción" Cathedral of Chilpancingo, Guerrero, Mexico; through Topogeodesic-Photogrammetric Surveying and Ambient Vibration. A Methodological Proposal 3371
S. Sánchez Tizapa, R. Aurelio Felicito, R. Vázquez Jiménez, J. L. Carranza Bello and R. Arroyo Matus

The Influence of External Climate on Church Internal Microclimate 3381
L. Balik, L. Kudrnacova and K. Nedvedova

Vulnerability and risk analysis

A Comparison Between Empirical Procedures for the Definition of Vulnerability Classes of Masonry Buildings: Application to Five Historical Centres Struck by 2016 Central Italy Earthquake 3390
Y. Saretta, L. Sbrogiò and M.R. Valluzzi

A QGIS Plugin for the Seismic Vulnerability Assessment of Urban Centers: Application to the City of Popoli in Abruzzo (Italy) 3402
A. Gonzalez, A. Basaglia, E. Spacone and G. Brando

Assessment of Seismic Fragility of Historical Buildings at the Urban Scale by Typological-Mechanical Approaches: the Case Study of Foggia 3414
V. Leggieri, S. Ruggieri and G. Uva

Criteria for the Vulnerability Analysis of Structural Aggregates in Historical Centers 3426
S. Tonna, M. Boriani, M.C. Giambruno and C. Chesi

Decision Support System for Vulnerability Assessment of Masonry Churches Including Architectural and Artistic Assets 3438
V. Sangiorgio, G. Uva and J.M. Adam

Development of a Fire Damage Index for Immovable Cultural Heritage 3450
L.G. Salazar, E. Paupério and X. Romão

Evaluation of Invasive Retrofitting Interventions on an Unreinforced Masonry Heritage Building 3462
A. Scupin, R. Vacareanu and F. Pavel

Kinematic Approach for Seismic Vulnerability Assessment of Masonry Churches 3474
V. Corlito, G. De Matteis and P. Roca

Managing Natural Disasters in Historic Areas: a Novel Holistic Seismic Risk Assessment Method Applied to a Relevant Case Study 3486
E. Quagliarini, G. Bernardini and M. Lucesoli

Risk Assessment Methodologies to Safeguard Historic Urban Areas from the Effects of Climate Change 3498
L. Quesada-Ganuza, L. Garmendia, E. Rojí, I. Álvarez, E. Briz and M. Olazabal

Risk Management and Built Heritage: Towards a Systematic Approach 3510
A. Konsta and S. Della Torre

Seismic Damage Scenarios Induced by Site Effects of Masonry Clustered Buildings: a South Italy Case Study 3522
A. Formisano and N. Chieffo

Seismic Vulnerability Assessment Method for Vernacular Architecture Considering Uncertainty 3534
J. Ortega, S. Saloustros and P. Roca

Seismic Vulnerability Assessment Methodology for Historical Buildings with Cultural Value 3546
E. Onescu, I. Onescu and M. Mosoarca

Seismic Vulnerability Assessment of a Historic Brick Masonry Building by Fragility Functions 3558
K. Demirlioglu and S. Soyoz

Seismic Vulnerability Assessment of Representative Building Typologies from Barcelona's Eixample District 3569
S. Dimovska, S. Saloustros, L. Pelà and P. Roca

Seismic Vulnerability Assessment of Romanian Historical Building under Near-Source Earthquake 3581
N. Chieffo, M. Mosoarca, A. Formisano and P.B. Lourenço

Seismic Vulnerability of Heritage Churches in Québec: the Néo-Roman Typology 3593
G. Sferrazza Papa, M-J. Nollet and M.A. Parisi

Simplified Seismic Vulnerability Assessment of Medieval Masonry Churches 3605
V. Corlito, M. Zizi and G. De Matteis

The Assessment and Reduction of Seismic Risk: Towards a System of Knowledge for Archaeological Pre-Existences 3617
E. Montenegro

The Damage Survey of Cultural Built heritage Between Simplified Procedures and Needs for Implementation: the Case Study of Emilia-Romagna Cemeteries 3629
V. Vona and M. Zuppiroli

Typological Classification and Observed Damage Patterns of Masonry Churches After the 2016 Central Italy Earthquake 3641
G. Cianchino, C. De Matteis and G. Brando

Vulnerability Assessment of Dwellings in the Historic Center of Cusco (Peru) 3652
G. Brando, G. Cocco, C. Mazzanti, M. Peruch, E. Spacone, C. Alfaro, K. Sovero and N. Tarque

Vulnerability Assessment of Italian Unreinforced Masonry Churches Using Multi-Linear Regression Models 3661
A. Marotta, D. Liberatore and L. Sorrentino

PRESENTED SESSIONS

12th International Conference on Structural Analysis of Historical Constructions
SAHC 2020
P. Roca, L. Pelà and C. Molins (Eds.)

AN INNOVATIVE SHELL STRUCTURE IN CODOGNO (ITALY) EVALUATION OF STRUCTURAL AND SEISMIC PERFORMANCE

PIERANGELO BRUGNERA[1], M. GRAZIA COSTA[1], GIULIO MIRABELLA-ROBERTI[2]*

[1] SACEE s.r.l. – Dept. Structural Design (DPS)
piazza Luigi di Savoia, 22 – 20124 Milano (MI), Italy
e-mail: {pierangelo.brugnera, grazia.costa}@sacee.it – https://www.sacee.it

[2] Dept. of Engineering and Applied Sciences (DISA), University of Bergamo
viale Marconi, 5 – 24040 Dalmine (BG), Italy
e-mail: giulio.mirabella@unibg.it – https://disa.unibg.it (*corresponding author)

Keywords: Hypar, saddle shaped shell, structural assessment, prefabrication

Abstract. *The saddle-shaped shells, or hyperbolic paraboloids, often joined together to form a pitched roof or an inverted umbrella, were used by many pioneers in structural architecture, such as Félix Candela, which introduced a very innovative use of reinforced concrete in thin layers or together with some reticulated ribs.*

An innovative semi-prefabricated building system was developed in Italy in the years '30 of XX cent by a very active brick factory near Piacenza, RDB: the SAP system, that allowed building curved surfaces by prefabricating light elements. After WW2, this technique was applied also for the new structures covering wide spaces for the developing industry or also for public leisure, using prefabricated panels of the desired length. A particularly interesting application was the BISAP (double-SAP) panel that could be adapted for building large shells.

In Codogno (LO), Italy, the BISAP panels were employed to cover a large sports hall, spanning about 37 × 26 m, without intermediate supports, resting (mainly) on the four corner pillars. Border pitch beams sustain at the top two crossed beams that separate (and support) the four hypar fields. On the four sides, two rafter beams are connected by horizontal prestressed tie beams, in order to minimize displacements and assure the preservation of the original shape.

The first aim of the structural analysis was to assess the static conditions of the roof under the service loads assigned by Italian code for SLS, and then to evaluate seismic vulnerability at ULS of the whole sports hall, being a public space subjected to particular safety provisions. The FE code used (Straus7) allowed a very careful discretization of the orthotropic slab with the correct inclination and twist of the ribs, giving a reliable forecast of the behavior also in seismic conditions: the dynamic analysis of the modal shapes gives a satisfactory response of the shell, which maintains nearly unchanged his shape during free vibration modes. The seismic safety of the structure can be then increased by simply augmenting the stiffness of the four corner supports, where shear action is concentrated, by adding ribs to the L-shaped sections to form cross shaped ones. In this way also the slenderness (and weakness) of additional intermediated pillars could be overcome.

1 INTRODUCTION

In September 2018, the Municipality of Codogno charged SACEE s.r.l. to study a solution for improving the usage of the sport-hall, a public property built in 1975 as an annex to the secondary school, but over time more and more exploited as public space for sports events.

Some of the problems regarded the compliance to the codes for fire protection and for accessibility of disabled persons; moreover, a reorganization of accessory spaces was requested. A more general problem concerneded the thermal and lighting comfort improvement, both for a better energetic behaviour and economic savings. In the meantime, the safety assessment of the structure was requested, in order to forecast the impact of the needed strengthening interventions.

The main building of the Codogno Sports Hall (see Fig. 1) is about 37×26 m wide, with no intermediate supports, resting (mainly) on the four corner pillars. Border pitch beams, forming four triangular tympana, sustains at the top two crossed beams that separate (and support) the four hypar fields. On each side, the two rafter beams are connected horizontally by prestressed tie beams, in order to minimize displacements and assure the preservation of the original shape. Some low-rise buildings, used as changing and service rooms, are contiguous to the main building on two sides but supported by indipendent structural systems.



Figure 1. The Codogno sport hall: aerial view (left) and the interior (right).

2 SUCCESS AND DECLINE OF THE HYPAR SHELLS

The shape of Codogno Sports Hall roof belongs to the family of surfaces composed by hyperbolic paraboloids, which were used by many pioneers in structural architecture after WW II, such as Félix Candela in Mexico, Arata Isozaky in Tokyo, P.L. Nervi and P. Belluschi in St. Francisco [1]. Very expressive architectural forms were obtained combining simpler geometrical shapes, with a very innovative use of reinforced concrete in thin layers or with some reticulated ribs.

In a suitable coordinate system, a hyperbolic paraboloid can be represented by the equation

$$\frac{x^2}{a^2} - \frac{y^2}{b^2} = z \tag{1}$$

In this system, the traces (or cross-sections) parallel to the *xz*- and *yz*-planes are parabolas and the level curves (traces parallel to the *xy*-plane) are hyperbolas (see fig. 2). The traces open downward along the *x*-axis and upward along the *y*-axis.

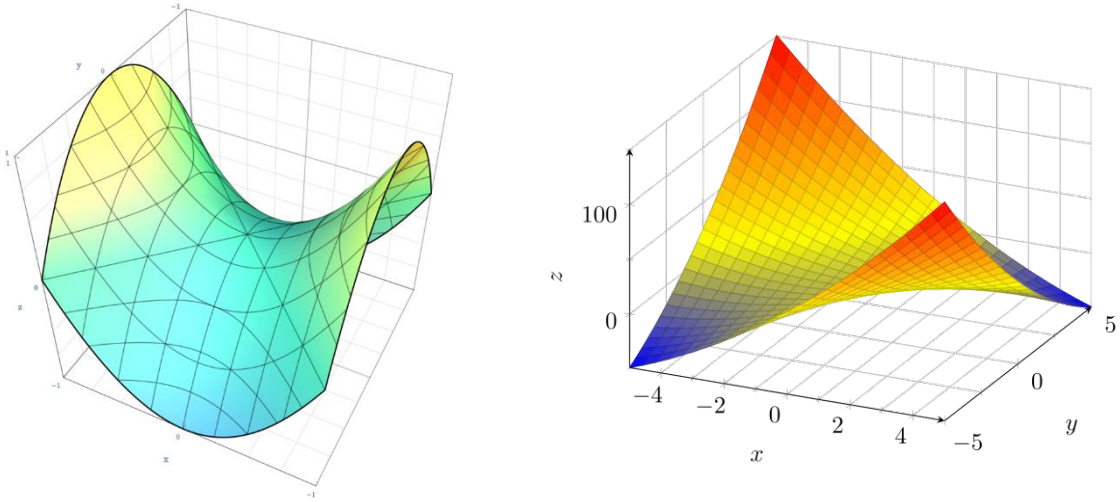


Figure 2: The surface of a hyperbolic paraboloid with $a = b = 1$ (on the left) and rotating axis's as in Eq. 2.

Rotating the reference system by 45° and putting $a = b = \sqrt{2}$ it is possible to represent the surface (1) also with the equation:

$$z = xy \tag{2}$$

Moreover, the hyperbolic paraboloid is also a doubly ruled surface: it contains two families of mutually skew lines. The lines in each family are parallel to a common plane, but not to each other. A hyperbolic paraboloid is a saddle surface, so its Gauss curvature is negative at every point. Therefore it is not developable, despite being a ruled surface. Never less, the fact that hyperbolic paraboloids are doubly ruled means that they are easy to construct using a series of straight structural members as formwork: that explain the success of this shape in the experimental development of 'structural architecture', relying on the innovative usage of cast-in-place concrete for the construction of thin shells.

The term *hypar* refers to a partial hyperbolic paraboloid, cut from the full infinite surface. It was introduced first by the architect Heinrich Engel in his 1968 book *Structure Systems* [2].

Fernand Aimond (1902-1984) can be considered as the father of the thin hypar concrete shells, who also formulated the membrane theory of the hypar. He designed and constructed several hypar roofs in France in the 1930s for aircraft hangars and workshops.

However, a master of hypars and joined hypars was a Spanish architect, engineer, structural artist and builder Felix Candela (1910-1997), who popularized the use of hypars for reinforced concrete construction [3]. Candela was influenced by Aimond but followed also the fundamentals of the Eduardo Torroja's work, a famous Spanish structural engineer renowned for his development of thin concrete shell structures.

He designed and built many innovative thin shell concrete roof structures. Most of these structures were built in Mexico in the 1950s and 60s. That was the 'golden era' for thin shell construction. Candela constructed over 300 shells during these decades. His thin concrete vaulted shells were made of reinforced concrete mixed and poured in situ, over wooden formwork. The thin shell roofs allowed the minimum thickness of concrete while having great strength and stiffness at the same time. In 1952 Candela started experimenting with the umbrella structures of four identical quadrants, called tympani. The shell geometry was created

by joining four straight-edged *hypars* whose sides rose upwards away from the central column (as if an umbrella blown upward).

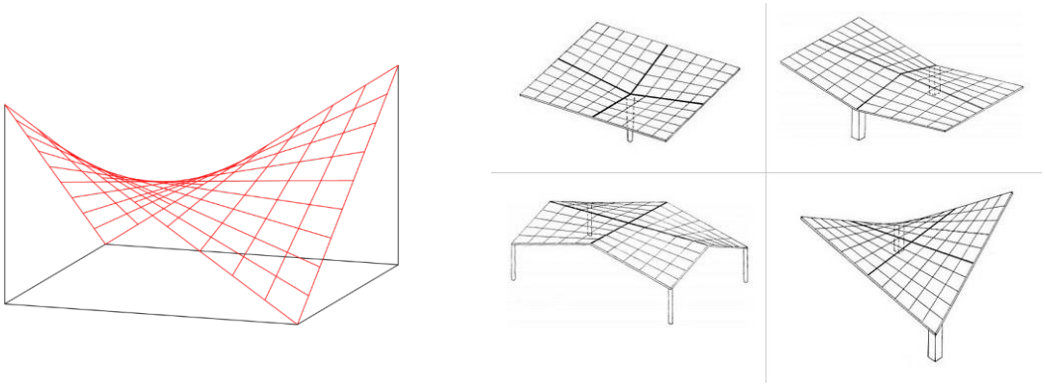


Figure 2. The *hypar* as ruled surface and four different *hypar* combinations.

One of his major works is the *Lomas de Cuernavaca* Chapel ("hills of Cuernavaca"), Mexico, built in 1958. Candela used a single hypar surface to get an open-air chapel with a pure structural form of high impact. The Cuernavaca Chapel shell is self-supporting with a span of 30 m and dramatic curvature. The open end of the chapel rise to a height of 24 m (Fig. 3).

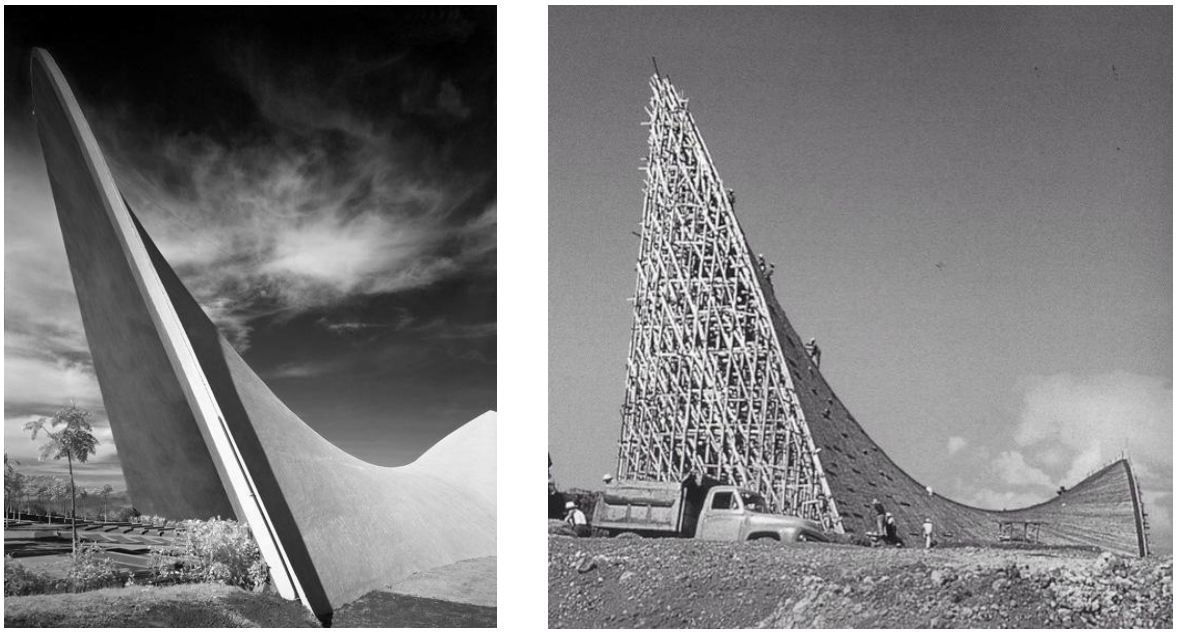


Figure 3. The Cuernavaca chapel finished and under construction.

In 1958, Candela completed also his most significant work, the *Los Manantiales* Restaurant in Xochimilco, near Mexico City. The Xochimilco shell is composed of four intersecting hypars with free curved edges [4]. The soaring shape at the edges resulted in a simple and gracefully thin shell structure. In the original drawings (Fig. 4), Candela clearly shows the form of *Manantiales* Restaurant shell. It is an eight-sided groin vault composed of four hyperbolic paraboloid saddles that intersect at the center point. The form was original and unexplored at

that time. The innovative use of V-shaped beams allows edges free of stiffening beams and produced a shell thickness of only 4 cm.

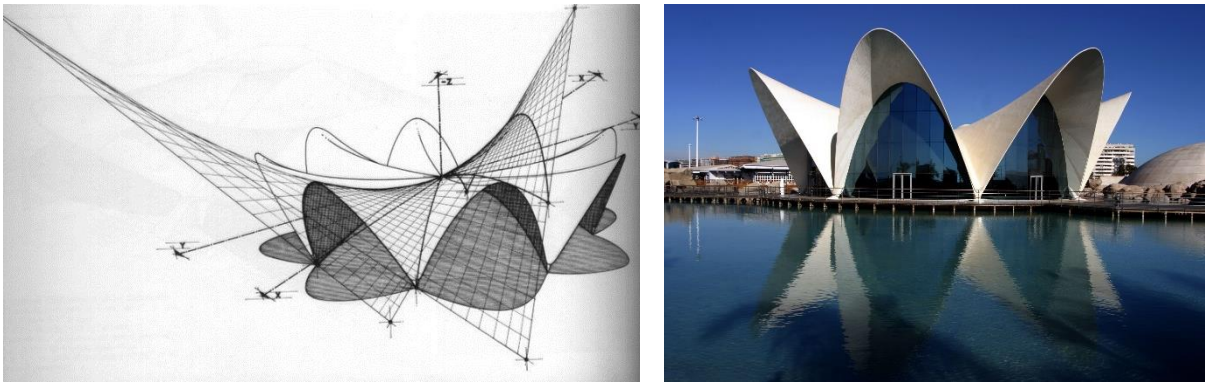


Figure 4. The sketch of *the Mantianales* (Mexico, 1958) and one of the last works of Candela, the Oceanographic park in Valencia (Spain, 1994) on the same shape.

3 THE RDB FACTORY AND THE BI-SAP SYSTEM

3.1 Starting from a brick kiln near Piacenza

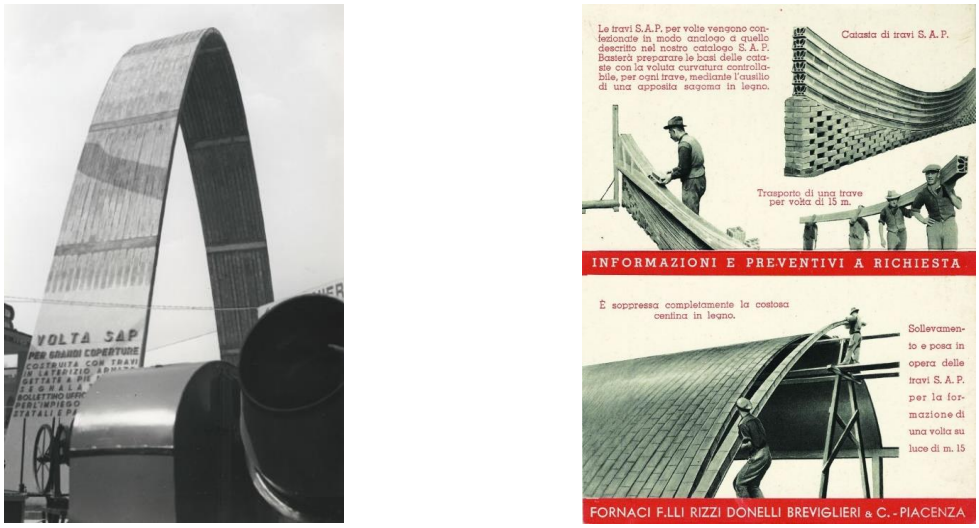


Figure 5. The vault built at Milan Fair in 1938 and a leaflet of SAP vault system.

A very innovative firm in the field of brick production developed between the two WW in the surroundings of Piacenza, in northern Italy. Starting from a brick and lime kiln acquired in 1908, the new firm was established in 1934 as *'Fornaci F.lli Rizzi, Donelli, Breviglieri & C.'* that in 1970 became simply RDB s.p.a. The firm introduced a semi-prefabricated floor system that simplified the erection of civil buildings, but also allowed the construction of large span roof for industrial and leisure settlements. In the Milano fair of 1938 a great vault in 'reinforced bricks' built by RDB shown the possibility offered by the new SAP system (the Italian acronym stands for '*Senza Armatura Provvisoria*', that is 'without provisional centring'). Other innovative product were then developed, such as prestressed floor panels, precast and prestressed concrete beams, and so on.

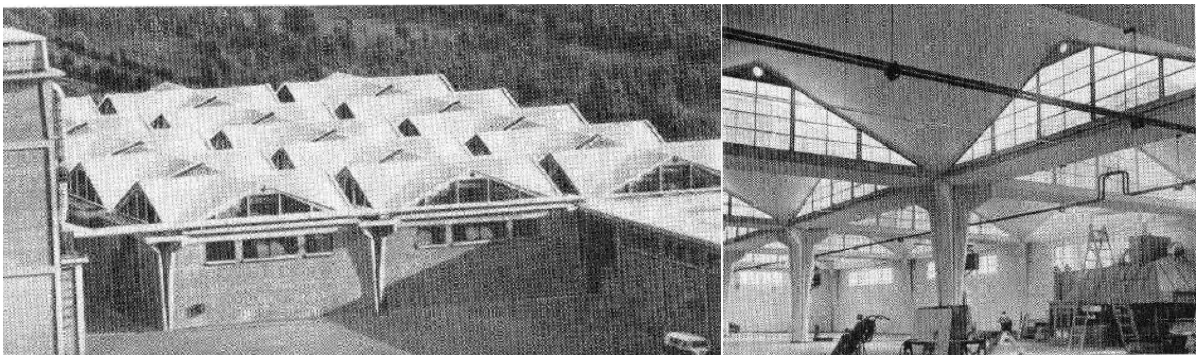


Figure 6. Italp factory, near Pisa. Arch. L. Muzio. IL 70 [6]. On the right, a view of the interior.

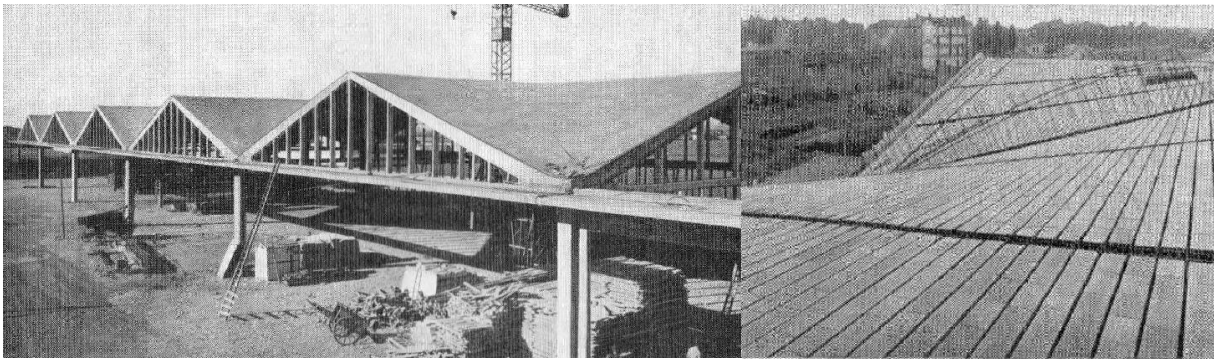


Figure 7. A shelter for car transporters near Torino, ing. S. Bizzarri. IL 71 [6]. On the right, disposition of SAP panels before the concrete casting.

3.2 The Bi-SAP system

The SAP system allowed building curved surfaces, prefabricating on-site light elements with curved shape. After second WW, this technique was applied also for building the new structures covering wide spaces for the developing industry or for public leisure spaces, with prefabricated panels of the desired length. RDB regularly published a bulletin, illustrating the recently built and under construction industrial sheds adopting patented RDB products (Fig. 7), but also giving useful suggestions for the design and verification of such structures.

A particularly interesting application of the SAP system is the BI-SAP (double-SAP) panel that could be adopted for building large shells generated from ruled surfaces. In this way, hypar shells could be built using lightly skewed panels, prefabricated on site, posed along the straight lines forming the hypar surface.

4 THE SPORTS HALL IN CODOGNO

In Codogno (LO), Italy, the BISAP panels were employed to cover a large sports hall built in 1974, about 37×26 m wide, without intermediate supports, resting (mainly) on the four corner pillars. The border pitch beams sustains at the top two crossed beams that separate (and support) the four hypar fields. On each side, the two rafter beams are connected horizontally by prestressed tie beams, in order to minimize displacements and assure the preservation of the original shape.

The prefabricated panels, disposed following the rules generating the hypar surface, form these four fields (Fig. 8). Additional reinforcement is disposed orthogonally and at 45° to the

rib direction in the concrete slab (fig. 9). Probably for lack of confidence with the structural solution adopted, beside the two big crossing beams separating the four hypar fields, some additional slender pillars supporting the border rafters are disposed on the four sides between the main corner pillars, apparently used only for windows support, but designed to collaborate to the bearing system.

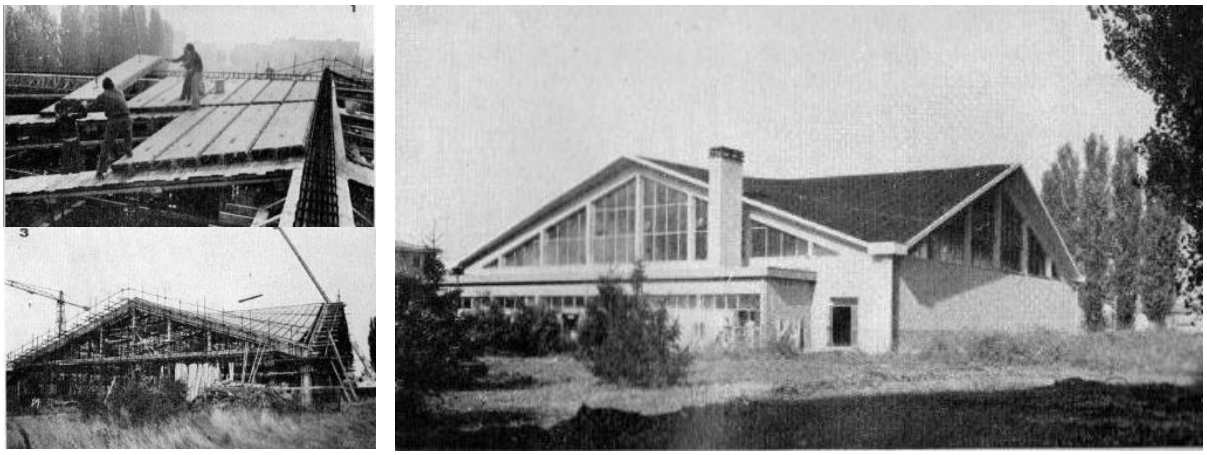


Figure 8. The construction of Codogno Sports Hall and its final appearance. IL 158-159 [7], p.1232.

4.1 Historical documents and original design

The original drawings for the entire sports hall, and the calculations certified by the RDB technical office, were found in the archive of the Municipality of Codogno, which luckily preserved and classified all the material. In this way, it was possible to reach a deeper knowledge of the construction system (concrete rib positions in the roof, reinforcement in the slab and in the beams, etc.) and to have a better definition of the 'naked' structural geometry, without claddings and waterproofing layers.

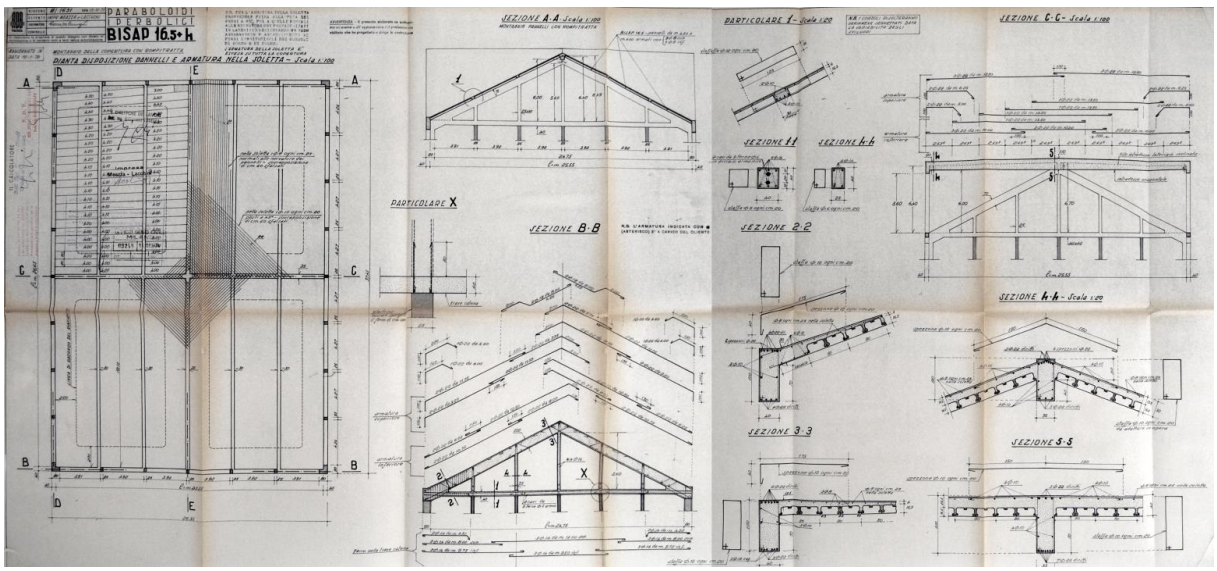


Figure 9. Example of the original drawings for the roof structure and the head gable.

5 STRUCTURAL ANALYSIS

5.1 The in-situ diagnosis campaign

A preliminary in-situ campaign was disposed to control the possible state of decay of the concrete and the reinforcement, in order to avoid an over-estimation of structure resources. In particular, n° 8 concrete cylindrical specimen (100 mm diameter) were extracted from columns and walls and tested in laboratory. The results were compared with the 16 in-situ test performed combining ultrasonic velocity and rebound index. The concrete covering of steel reinforcement was measured in 10 positions, and the concrete cylinders were used to measure the depth of carbonation. P&P Consulting Engineers, from Bergamo, made the tests.

5.2 The seismic assessment

A finite element model of the entire structure was set up, allowing to detect the overall behavior under static dead and live loads according to Italian Code (NTC18, [11]): it must be stressed that the actual loading provisions are far different from those adopted in the design in 1974. Moreover, the building structure was not at all designed for seismic loads, because only in recent years the territory of Codogno was classified in 3rd category (seismicity of moderate intensity), with a reference GPA (ground peak acceleration) of 0.092 g. That posed important questions on the possible strengthening intervention needed, because the building is open to the public and can have moderate crowding: allowing to NTC18, the building belongs to the Usage Class III, and the resulting 'reference life' is 75 years.

The model was set up using Straus7 code to simulate the complete structure by means of 4-nodes plate elements for the concrete covering and beam elements for the columns and the main beams. The concrete ribs too were modeled by beam elements, disposed at the calculated offset from the surface, with an adequate rotation of the axis in order to match with the surface of the hypar. Finally, the design pre-stress, depurated from relaxation losses, was applied to the tie beams connecting the four main corner columns. Considering also the structure sustaining the stands for the public, 8252 nodes, connected by 7729 beam and 7708 plate elements were used, producing 49180 equations. The seismic analysis has been conducted with a linear elastic approach: first of all a modal dynamic analysis was performed that allowed detecting the main aspects of structural behavior.

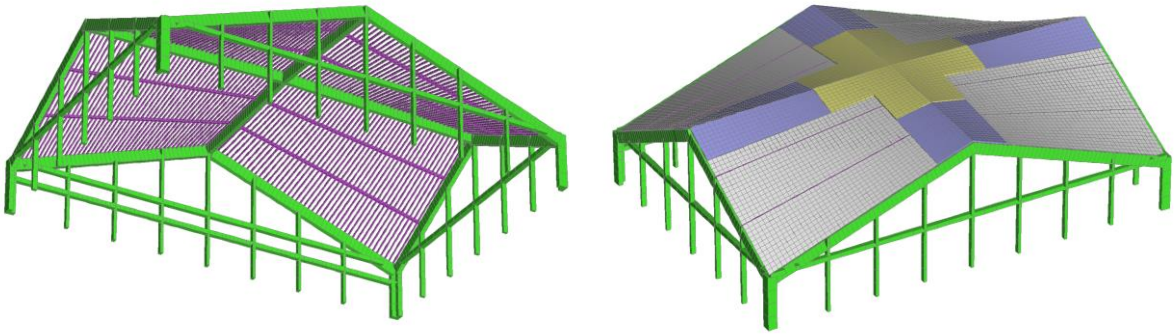


Figure 10. The Straus7 FE model: view from below (with the two cross beams) on the left, and view from the top on the right, different colors showing different shell thickness.

The first three modes excite the structure in the three principal axis's directions, the lower being 2.456 Hz in *x* (transversal) direction, and a torsional mode appear only at 6th place, for higher frequency values (5.032 Hz, see Table 1 and Figs. 11 and 12). The presence of the walls supporting the gallery increase the horizontal stiffness of one long side, altering slightly the symmetry of the response (see mode 2 in Fig. 11 and mode 6 in Fig. 12).

Table 1: Mode participation for translational/rotational excitation

Mode	*Frequency*	*Modal Mass*	*Modal Stiff*	*PF-X*	*PF-Y*	*PF-Z*	*PF-RZ*
#	(Hz)	(Eng)	(Eng)	(%)	(%)	(%)	(%)
1	**2.4561**	3.6934E+05	8.7959E+07	**70.506**	0.001	0.002	0.001
2	**3.3730**	1.4650E+05	6.5802E+07	0.001	**57.055**	0.000	3.642
3	**3.5574**	1.6221E+05	8.1043E+07	0.010	0.000	**14.511**	0.000
4	4.2796	4.2821E+04	3.0961E+07	0.005	4.941	0.000	0.851
5	4.5621	7.1018E+04	5.8352E+07	19.907	0.003	0.002	0.010
6	**5.0319**	6.8103E+04	6.8076E+07	0.011	0.794	0.000	**46.248**
7	5.4197	4.9470E+04	5.7366E+07	0.000	1.716	0.000	7.445
8	5.8253	3.1811E+04	4.2616E+07	0.001	9.851	0.000	1.553
9	6.4518	6.2159E+04	1.0215E+08	0.001	0.000	0.043	0.000
10	6.6768	5.4822E+04	9.6484E+07	2.290	0.014	10.701	0.085
11	6.7630	5.7535E+04	1.0389E+08	0.002	7.712	0.055	28.280
12	7.1368	6.5475E+04	1.3165E+08	3.284	0.010	2.669	0.014
13	7.3690	3.4617E+04	7.4212E+07	0.032	0.000	14.731	0.001

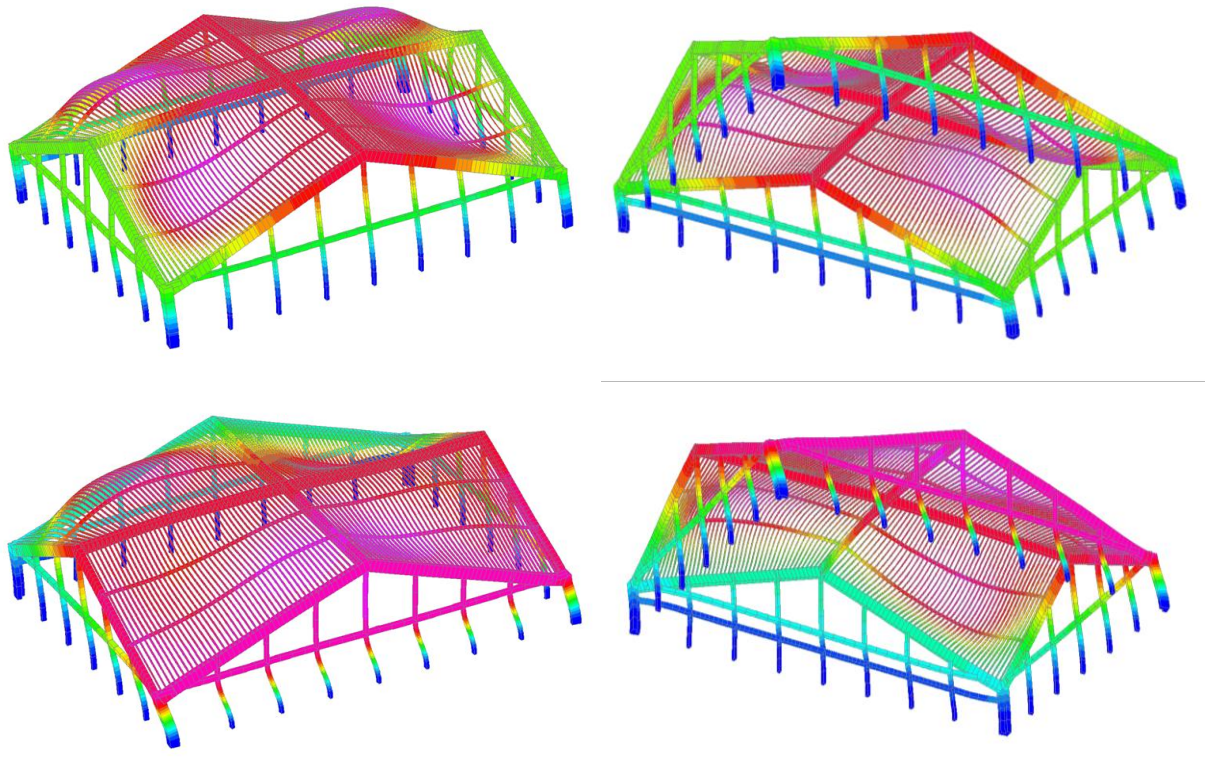


Figure 11. Mode 1 and 2 (flexural) shapes, Top: mode 1 horizontal displacement *DX*; bottom, mode 2 horizontal displacement *DY*. Colored contour levels, view from top (left) and from below (right).

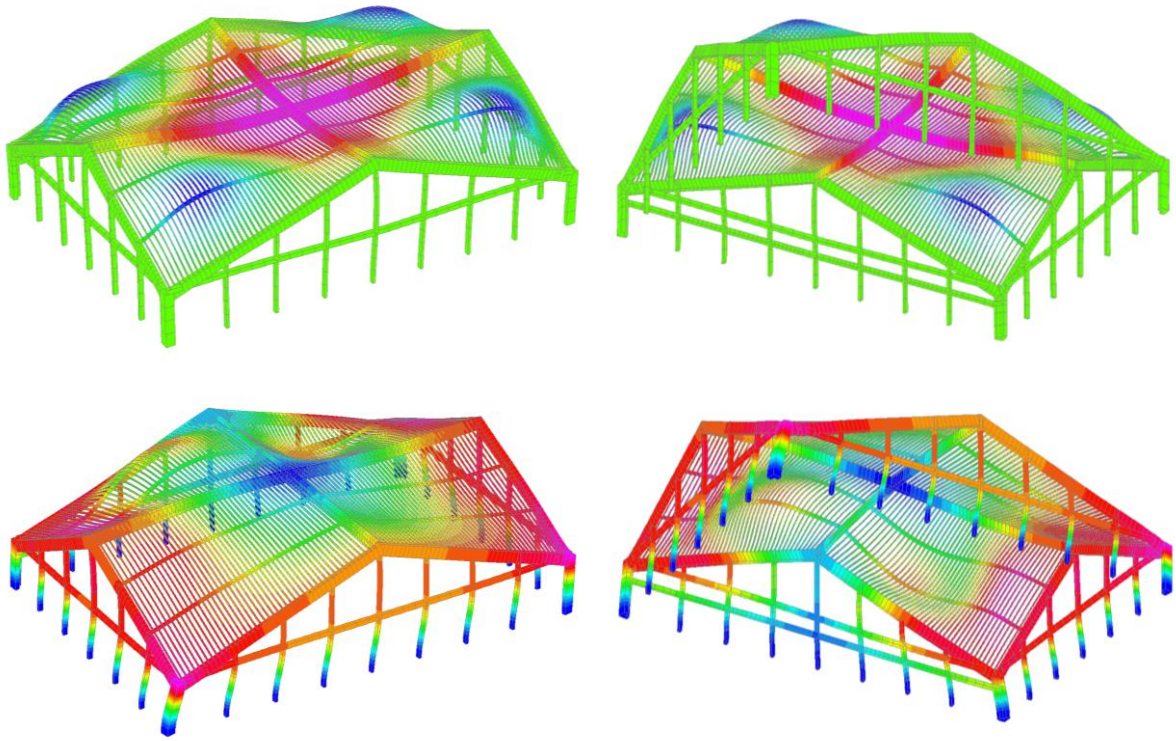


Figure 12. Top: mode 3 vertical displacement *DZ*; bottom, mode 6 (torsional) combined *DXY* displacement. Colored contour levels, view from top (left) and from below (right).

The Spectral Response solver use the mode superposition technique, applying modal excitation factors for each vibration mode; then the spectral values for all modes are calculated from the assigned spectral table by using the corresponding frequency value. The combination of maximum modal displacement values is obtained using SRSS method (Square Root of the Sum of the Squares). The design spectrum, calculated from NTC18 for Codogno, has an amplitude of $a_g S = 0.138\ g$.

The calculated stresses are then input in a verification program that check the capability of each structural member: the procedure is repeated reducing spectral amplification until the check is positive for all the members. A partial security coefficient take into account the 'level of knowledge' (LC) of materials and geometry obtained by visual and material inspections: LC2 was assumed, obtaining a factor of confidence of 1.2.

The more engaged members appeare to be the L-shaped corner columns, together with the closer slender columns that reach the gables; even the lower end of the rafters reach the limit state. The maximum capacity is attained with a spectral amplification of only $a_g S = 0.08$ g, that leads to a ratio between capacity and demand:

$$\zeta_E = 0.080 \text{ g} / 0.138 \text{ g} = 0.58$$

Nevertheless, it must be stressed that Italian Code request for existing buildings in Usage Class III a minimum value of $\zeta_E \geq 0.6$ to be reached in an 'improvement intervention' (see § 8.4.2 of NTC18, [11]).

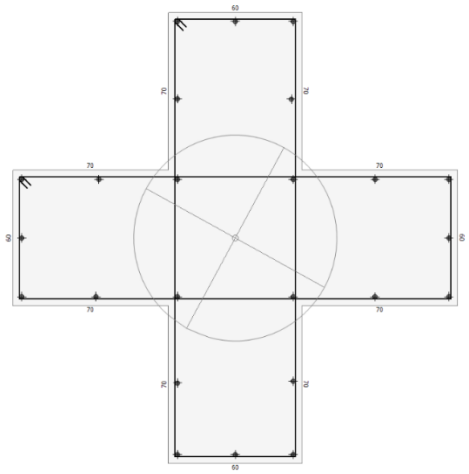


Figure 13. Enlarged cross section of corner columns

5.3 The strengthening design

In order to reach a satisfying capacity of the structure and reduce the vulnerability, the intervention chosen try to focus on the main weakness outlined by the calculations: the deformations and the shear resistance are concentrated in the corner columns.

Therefore, their section was increased changing from an L to an enlarged cross section (see Fig. 13), with an important change in stiffness. In this way, deformation amplitude was strongly reduced, and the structure results verified for the design spectrum amplitude forecast by the code, obtaining moreover a value of $\zeta_E = 1.01 \geq 1.$, that means a complete 'upgrade intervention', in the sense of § 8.4.3 of NT18 [11].

6 CONCLUSIONS

The structure of the Codogno Sports Hall demonstrated to be still very effective, and is very close to satisfying code requirements even in present conditions. Nevertheless, with a moderate upgrade only on the corner columns, it is able to reach a complete compliance to code provision for new buildings towards seismic assessment, showing the clever vision of the original design that worth some minor conservation interventions.

Acknowledgements. The administration of Codogno Municipality and the staff of historical archive is gratefully acknowledged for the cooperation in the research of original drawings; eng. Guido Campana, from Campana & Migliorin, is acknowledged for structural verifications.

REFERENCES

[1] Sprague, T.S. 'Beauty, Versatility, Practicality': the Rise of Hyperbolic Paraboloids in Post-War America (1950-1962). *Construction History*, vol. 28, no. 1, pp. 165–184, (2013). JSTOR, http://www.jstor.org/stable/43856033.

[2] Engel, H. *Structure Systems.* (1968) London: Iliffe books.

[3] Journal of the International Association for Shell and Spatial Structures n. 163, *Special Issue for the Centenary of the Birth of Félix Candela*, Vol. 51 (2010) No. 1 March

[4] Burger, N. and Billington, D.P.: Felix Candela, elegance and endurance: an examination of the Xochimilco shell, *Journal of the International Association for Shell and Spatial Structures,* Vol. 47 (2006) No. 3 December n. 152, pp. 271-278(8).

[5] Modica, M. and Santarella, F.: *Paraboloidi: un patrimonio dimenticato dell'architettura moderna.* Firenze, Edifir (2014).

[6] Paolini C. and Pugnaletto, M.: Reinforced brick lightweight vaults. *TEMA,* vol. 3, No. 1 (2017).

[7] IL, *Il Laterizio*, *bollettino tecnico RDB,* RDB, Piacenza (1961) n. 70 e 71.

[8] IL, *Il Laterizio*, *bollettino tecnico RDB,* RDB, Piacenza (1976) n. 158-159.
[9] Zienkiewicz, O.C. and Taylor, R.L. *The finite element method*. McGraw Hill, Vol. I., (1989), Vol. II, (1991).
[10] Straus7, *Theoretical Manual*. Sydney Aus.: Strand7 Pty Limited, 2005.
[11] D.M. 17.01.2018 - Norme tecniche per le costruzioni, *Supplemento ordinario alla Gazzetta Ufficiale n. 42 del 20 febbraio 2018 - Serie generale* (2018).
[12] Circolare n.7 del 21.01.2019 Istruzioni per l'applicazione dell'Aggiornamento delle «Norme tecniche per le costruzioni» di cui al D.M 17 gennaio 2018. *S.O. alla Gazzetta Ufficiale n.35 del 11 febbraio 2019 - Serie generale* (2019).

12th International Conference on Structural Analysis of Historical Constructions
SAHC 2020
P. Roca, L. Pelà and C. Molins (Eds.)

ANCHORAGE OF REINFORCEMENT BARS IN HENNEBIQUE R.C. STRUCTURES

A. BRENCICH*, M. NEBIACOLOMBO[2]

[1]Department of Civil, Chemical and Environmental Eng.ng (DICCA)
University of Genoa – Polytechnic School
viale Cambiaso 1 – 16145 Genova (Italy)
e-mail: brencich@dicca.unige.it, www.dicca.unige.it (*corresponding author)

[2] Department of Civil, Chemical and Environmental Eng.ng (DICCA)
University of Genoa – Polytechnic School
viale Cambiaso 1 – 16145 Genova (Italy)
e-mail: matteo.nebiacolombo@outlook.it

Keywords: Hennebique-type structure, Anchorage, Collapse Mechanism

Abstract. *The Hennebique system was the most successful among the patented systems in the pre-code period even though the design rules were not completely clear. Anchorage of the reinforcement is one of these unknown aspects and how it was calculated, and if it was calculated at all, is still today not clear. For this reason, the efficiency of the anchorages is one of the major issues when dealing with retrofitting a Hennebique structure or when its safety needs to be evaluated. In this paper a series of tests have been performed on the typical Hennebique an-chorages for reinforcing bars (fish-tails) and for the plate stirrups (bended ends) that were used. Different concrete types have been used so that either the collapse mechanisms of the anchor-ages and their ultimate strength may be identified.*

1 INTRODUCTION

Even though François Hennebique was not the first to deal with concrete and reinforcing bars, no doubt he was one of those who most affected the first years of reinforced concrete constructions [1-4]. His patent, although unclear in its theoretical basis and in several technological aspects, in many countries was the most exploited system in the first pioneering period of r.c. constructions [5-7] that ends approx. with WWI [8]. If the Hennebique system did not find space in Germany [9], it was used in U.K. due to the cooperation with Mouchel [5] and in Spain with Rivera [10] while in other countries, such as France [11], Belgium [4] and Italy [11-14] it remained the leading building system for a couple of decades.

Even though the first codes in Europe were issued before WWI, in 1902 for Switzerland, in 1907 for Italy and France [15] and in 1915 for Russia [16], it took more than a decade for the patent system to be substituted by a rational approach to r.c. design. This is mainly true for those countries in which the patents remained valid till their natural expiration, such as Italy and Spain. The outcome is that Hennebique structures, or Hennebique-like structures, built till approx. the '20s, remained un-engineered to a large extent.

Nowadays warehouses, industrial facilities, a large number of bridges and buildings, either residential and public, built according to the Hennebique system, are in service. For many of them retrofitting is needed due to several reasons, such as material degradation, re-functioning and, mainly for strategic buildings such as schools, hospitals and public offices, for their seismic upgrade.

The intrinsic weaknesses of the early reinforced concrete structures, among which the Hennebique system plays the major role, is well known and addressed by several authors [4, 17-22]. The two main issues need specific attention: i) concrete compressive strength, affecting the bending capacity of the beams; ii) shear capacity, which depends on the amount of shear reinforcement and on the efficiency of its anchorage.

This paper addresses a specific problem: the anchorage performance of either bending and shear reinforcing bars. Due to the reduced anchorage length, only partially compensated by the shape of the bar, it will be showed that in most cases the bending and shear capacity is limited by the sliding of the bars in the anchorage regions. This outcome is crucial when the structural performance of a Hennebique-type structure has to be estimated.

2 ANCHORAGE OF REINFORCING BARS IN THE HENNEBIQUE SYSTEM

Figures 1 to 3 show the typical reinforcement of a Hennebique beam.

- 50% of the longitudinal reinforcement (cylindrical bars from 10mm to 40mm in diameter) is bended up at 1/3 of the span, figure 1, [7] and [24], and anchored on the upper side by means of fish-tail expansions. Such a rule is simply geometric and in the archives there is no rational reason for such a choice; the upper bars, therefore, are not proportioned to the negative bending moment.

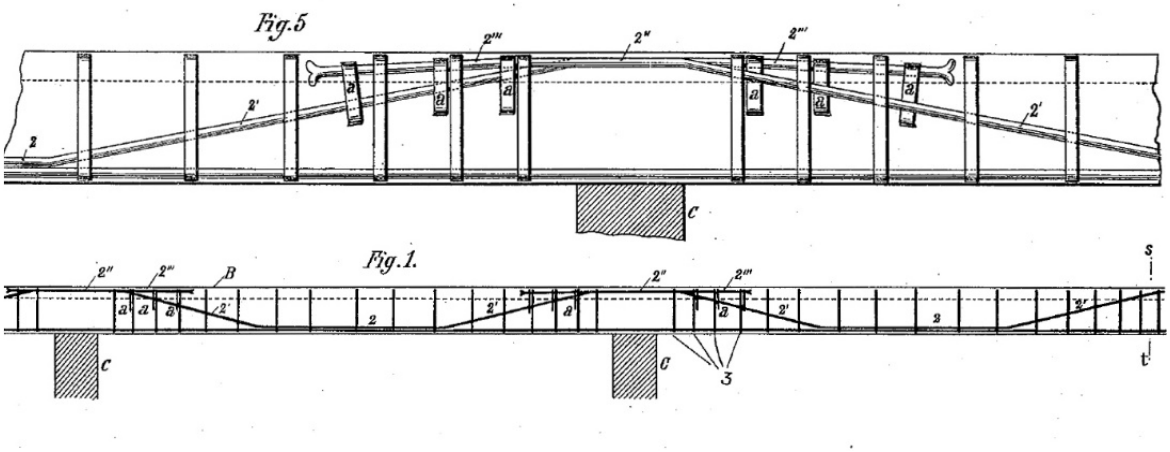


Figure 1. Longitudinal section of a beam according to the USA Hennebique patent [27]

- the anchorage of the main bars consists of fish-tail ends; hooks were used for secondary bars only, figure 2. The fish tails were open as much as to get to twice diameter of the bar. Amongst the large number of load tests to collapse performed by Hennebique and his concessionaries, some showed the collapse of the anchorage of the longitudinal bars, figure 3; there is no evidence that this outcome of the test neither lead to some change in the detailing of the bars nor raised attention on the bar anchorage.



Figure 2. Fish-tail ends and hooks of reinforcing bar of the slab of a villa inside the *Villa Gruber* park, Genoa, unknown building date, in-between 1900 to 1930.



Figure 3. Load test to collapse of a T beam performed by the Porcheddu company [24] – unpublished photo

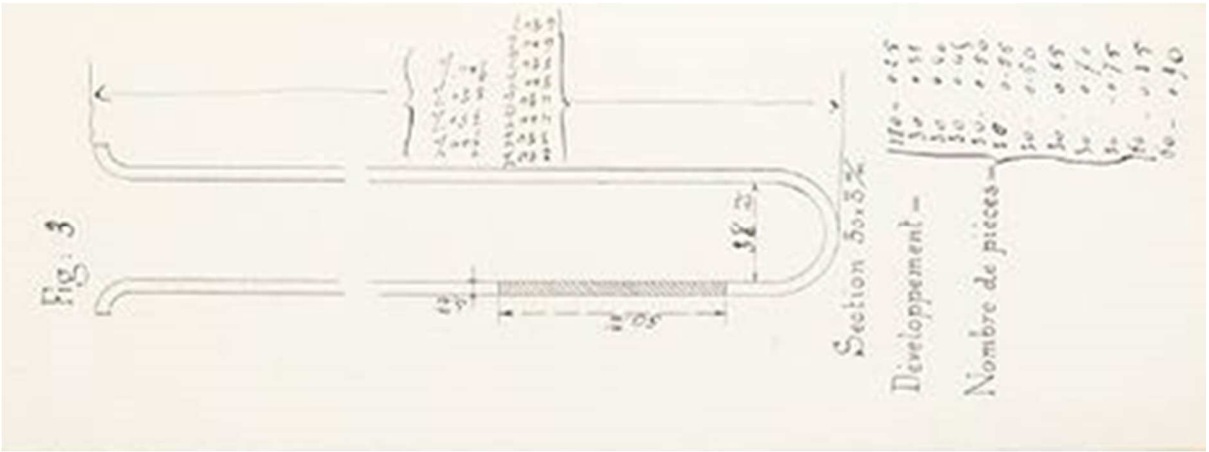


Figure 4. Typical shape of a stirrup, 1897 [28]

- The shear reinforcement consists of steel plates, 2-to-3 mm thick, 20-to-50mm wide, figure 4. The spacing of the stirrups, figure 1, was geometrical with minimum spacing close to the supports. There's no explicit origin of such a choice, that is somehow rational, that probably originates from the load tests that Hennebique in his company and his concessionaries performed up to collapse. The anchorage of the stirrups is obtained by means of a slight bend of the plate in the compressed part of the beam; also in this case the efficiency of such an anchorage system is to be discussed.

3 THE EXPERIMENTAL PROGRAM

The goals of the research are the identification of the anchorage mechanisms up to collapse, either for longitudinal bars (bending) and for stirrups (shear), taking into account different concrete compressive strength and a grading curve that resembles an ancient pre-code concrete.

3.1 Concrete mixtures

An historical concrete differs from modern concretes because of: i) improper mixture (not following any grading curve); ii) round aggregates; iii) excess in water content; iv) low strength (in general, mainly for residential buildings. Industrial facilities and bridges usually exhibit medium-to-high strength concrete).

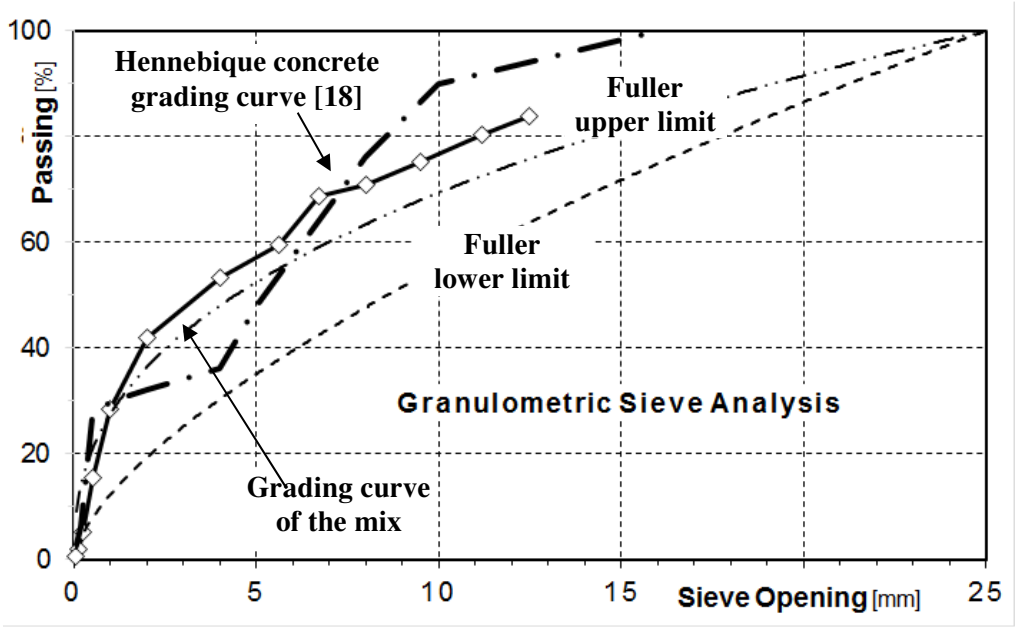


Figure 5. Granulometric sieve curve of the historical-like concrete used compared with the limit Fuller curves

The concrete mixture used for the concrete of the tests was defined according to a weight criterion, like the standard building practice in the past: 50kg of round coarse aggregate (max = 30mm) + 50kg of crashed medium aggregates (max = 15mm) + 25kg of crashed fine aggregates (max = 3mm) + 25kg of sand (max = 0.5mm).

Figure 5 shows the granulometric Fuller sieve curve [31] for the aggregates used and the grading curve deduced for a Hennebique concrete obtained in [18]; it can be seen that pre-code

concretes, and the one used in the tests, exhibit grading curves above the upper Fuller curve, nowadays used for aggregate proportioning.

Five concrete types were used, table 1, aiming at setting a mix that includes the main defects of historical concrete, such as high porosity and severe bleeding. The first four types, for which in figure 11 the maturation curves are represented (either EC2 curves [31] and the best-fitting ones, curing conditions of the specimens as in [32-33]) were used for estimating the strength of the anchorage, whilst the fifth concrete was used for estimating the effect of transversal confinement on the anchorage strength.

Table 1. Concrete strength and mixtures for the 5 ancient-type concrete

Concrete mix	**Cement** [kN/m^3]	**Cement /batch** [kg]	**Water/Cement ratio**	**Porosity [%]**	$\mathbf{R_{c,28days}}$	**C.o.V.** [%] (6 samples)
Mix_1	2.0	18.2	1.0	8.3	8.4	3.2
Mix_2	3.0	27.3	0.8	8.6	14.5	2.2
Mix_3	4.2	38.3	0.6	8.3	25.8	2.8
Mix_4	5.0	45.5	0.5	7.3	29.9	0.5
Mix_5	3.0	27.3	0.8	8.3	20.2	3.0

3.2 Specimens and loading conditions

Two steel specimens have been tested:

- fish-tailed bars, 20mm in diameter, figure 6
- plate stirrups 30 and 50mm wide, 3mm thick, shaped as the standard stirrups of the Hennebique system, figure 7.

The specimens were casted inside concrete cubes, figure 8; for both the anchorage systems the four concrete types of table 1 were used using standard curing conditions ([32] and [33]).



Figure 6: Fish-tailed anchorage of bending reinforcement. From a residential building in Genoa, *Villa Grüber* park, Genoa, *Porcheddu Building Company*, in-between 1920-to-1930. main geometric ratios.

The load test was displacement-controlled in order to get also the post-peak response of the anchorage. The load was measured by means of a CLASS 1 load cell (error less then 0.1%) and the displacement by means of digital transducers with an error less than 0.01mm. The loading rate was 3mm/minute so that the peak load was reached, on the average, after 3 minutes.

The lateral confinement was provided by means of bolts and stiff distributing steel devices, figure 8, which applied a lateral average compressive stress $_1$ and $_2$ of 0.75 N/mm^2.

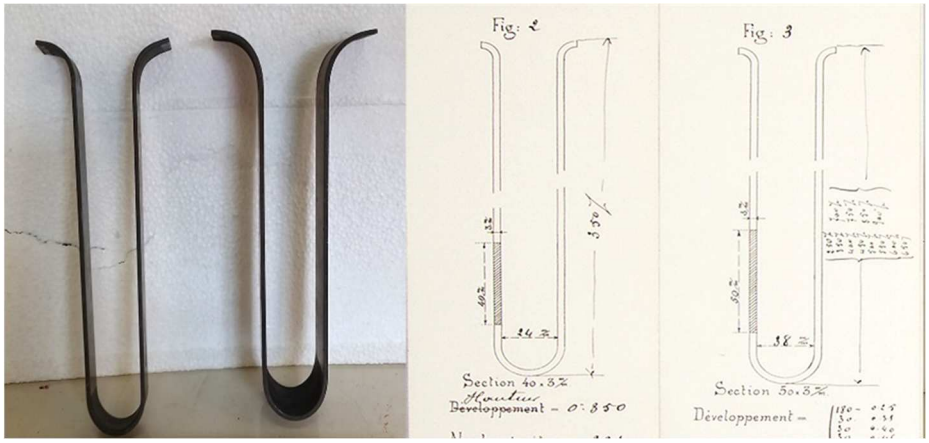


Figure 7: Plate stirrups – Porcheddu Archive, Technical University of Turin – unpublished drawings.

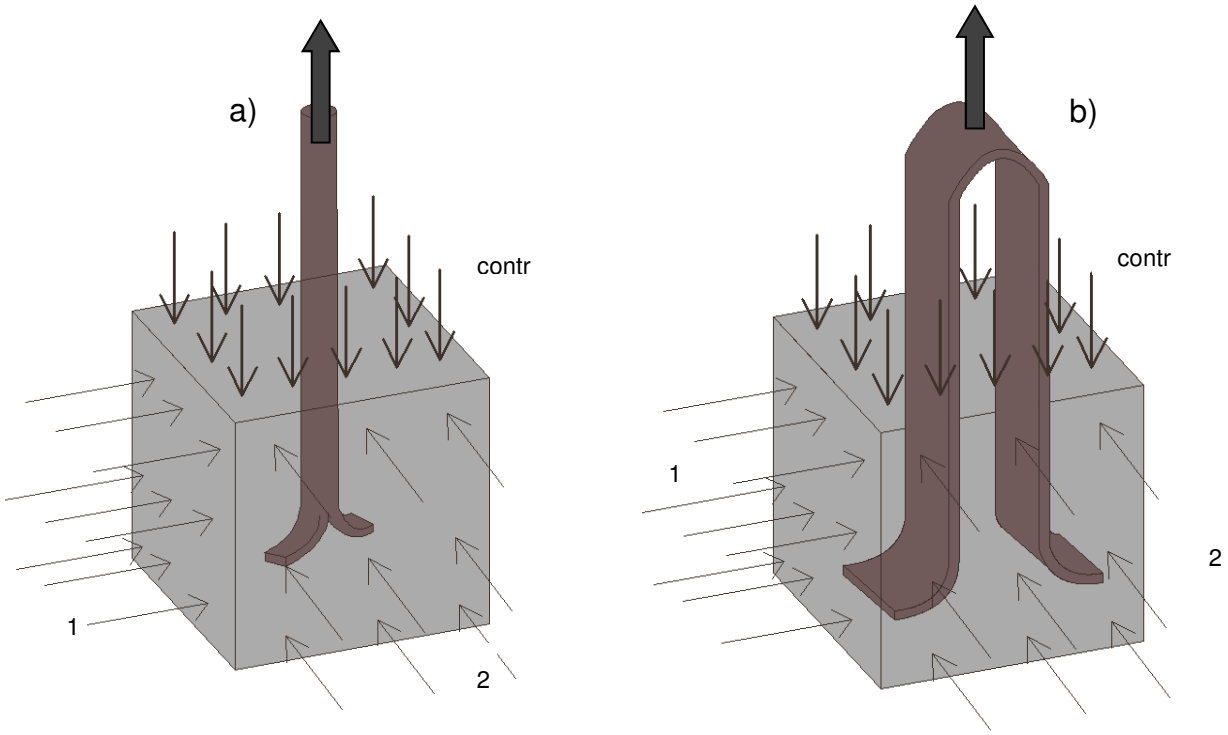


Figure 8: Tested specimens casted in the concrete cube.

4 TEST RESULTS

4.1 Test results

Figures 9-to-11 show the load-displacement response of the three different specimens for the four concrete types tested. Figure 12 shows the average load-displacement curve, i.e. plotting a curve that is the average out of the 5 diagrams of the previous figure.

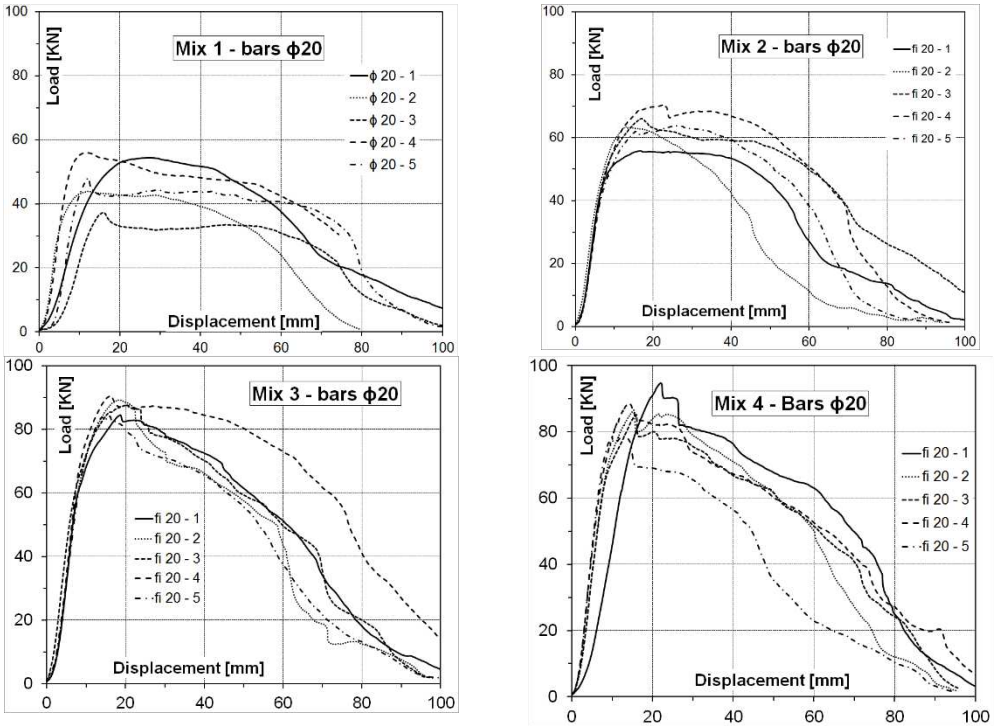


Figure 9: Load-Displacement response of fish-tailed bars (=20mm)

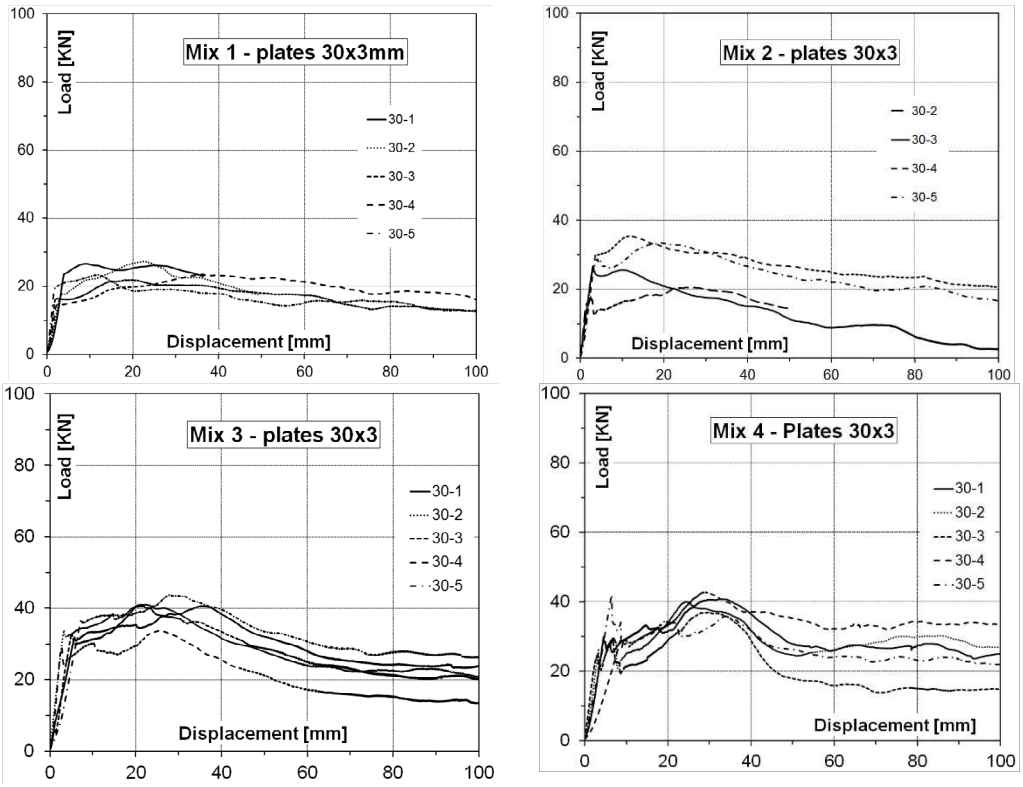


Figure 10 Load-Displacement response of 30mm wide plate stirrups

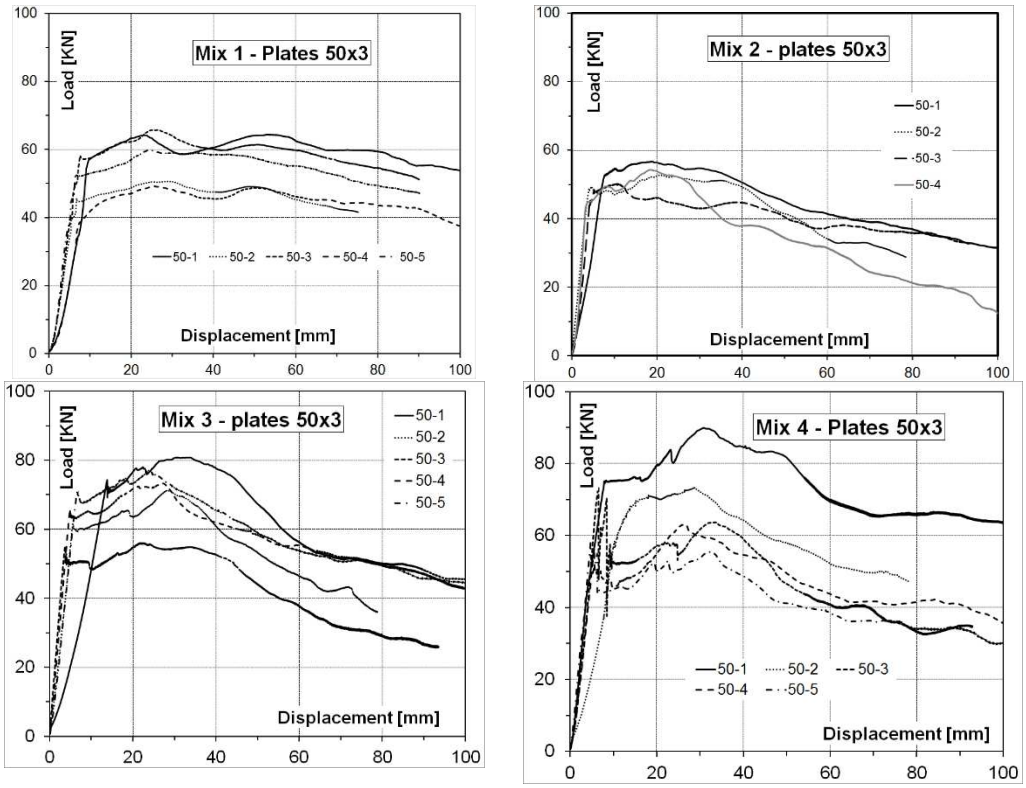


Figure 11 Load-Displacement response of 50mm wide plate stirrups.

Apart from the anchorage force, a difference is clear between the collapse of the fish-tail end and the plate stirrups: in the first case the peak load is attained at the end of a substantially linear phase and is followed by a relatively fast decrease in strength. In the case of stirrups, instead, the post peak response shows a substantially constant anchorage force also for large displacements.

We can also outline that the anchorage strength never induces in the bar a stress level close to yielding. This means that due to anchorage weakness, the steel elements used in the Hennebique System are unable of using their whole section.

4.2 Collapse mechanism of the anchorage

Figure 13 shows the fish-tail anchorage before (left) and after (right) the pull out test. It can be recognized that the fish-tail end has been shrank from twice the bar diameter to the bar dimeter for low strength concrete and to 0.75 the bar diameter for high strength concrete.

Figure 14 shows the concrete cube after the pull-out test of the bar. It is clear that the fish-tails slide inside the cube producing a rather limited crushing zone just around its original position.

Figures 15 and 16 are related to the case of plate stirrups. It can be recognized that the collapse mechanism of the stirrup anchorage system almost does not involve concrete being limited to the rectification of the bended plates.

These mechanisms explain the main features of the diagrams of figure 9: fish-tail anchorage is shrank inside the concrete but this asks come concrete crushing to take place at the beginning of the pull-out test. For this reason, the anchorage strength depends on the concrete strength

and for this same reason, concrete crushing, the post peak response shows a clearly softening branch.

For plate stirrups, instead, being the collapse of the anchorage mainly due to the plate rectification, the anchorage strength is little dependant on the concrete strength.

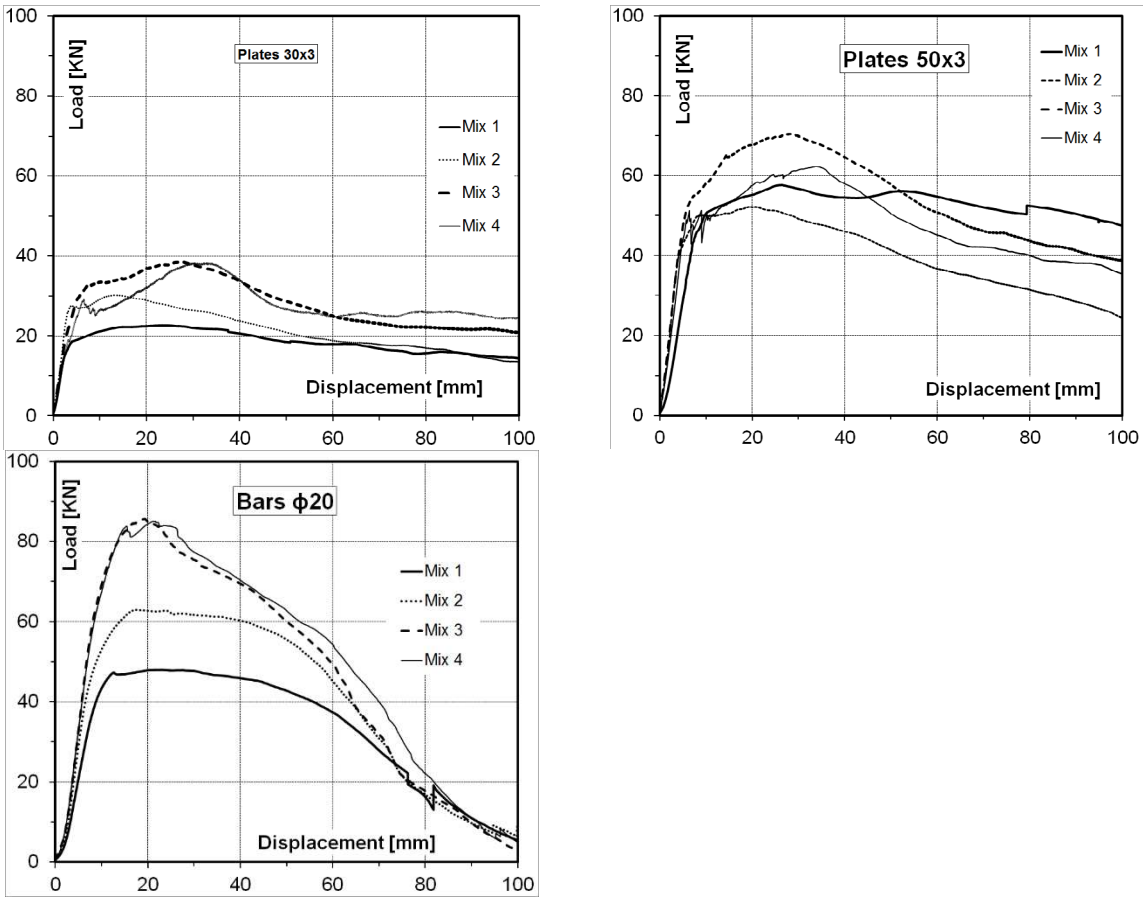


Figure 12 Load-Displacement response – average values

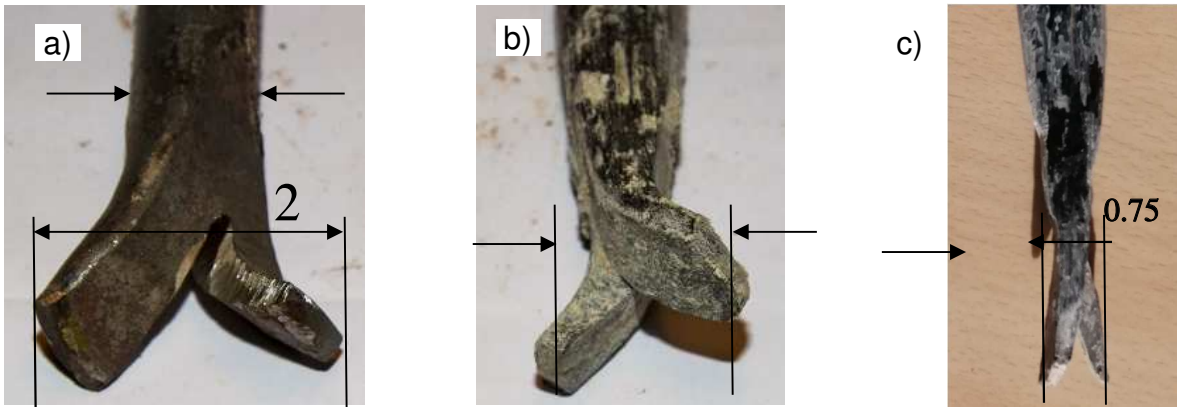


Figure 13: Fish-tail anchorage a) before and after the pull out test for b) low strength and c) high strength concrete.

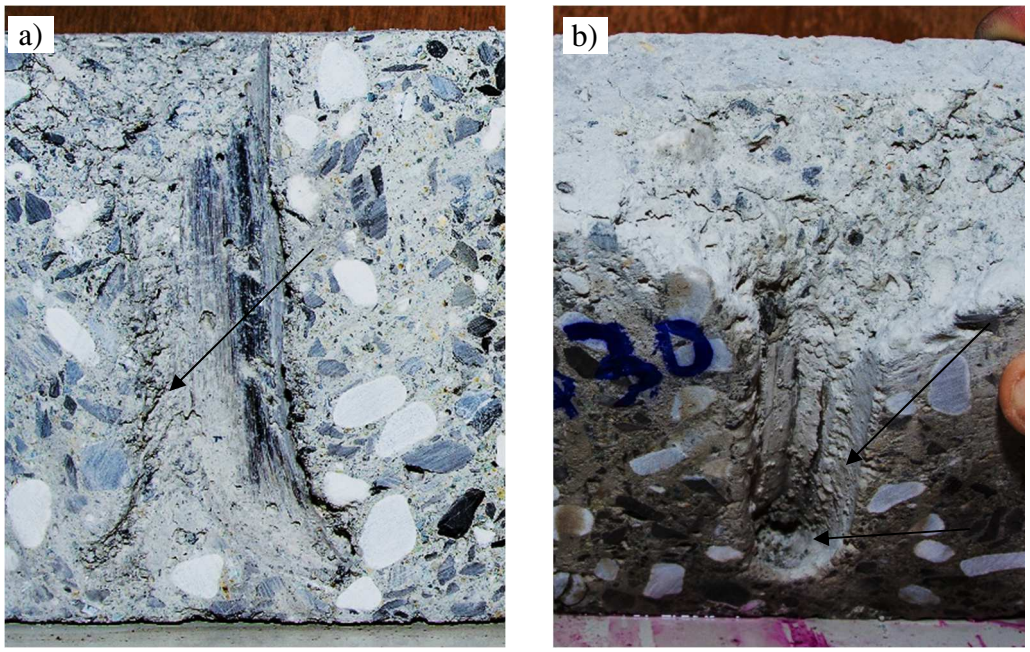


Figure 14: Track left in the concrete cube by the fish-tail anchorage. a) sliding of the bar along the steel/concrete interface; b) the central track (black arrows) show the sliding and the side crushing of the concrete due to the two tails



Figure 15: Plate stirrup: deformed stirrup after the pull-out test.

12 CONCLUSIONS

- Fish-tail ends. The strength of the anchorage never exceeds the force needed to close the fish-tails. The anchorage strength is approximately this value for medium and high strength concrete, but drops down to half this value in the rather common case of low strength concrete.
- Plate Stirrups. The collapse mechanism is that of rectification of the bended ends by sliding inside the concrete mass. It is not clear, at this point of the research, which could be a reference value for the anchorage.
- In both the test series, a biaxial confining stress state has been applied ($0.75 N/mm^2$). This transversal stress field is the best condition for this kind of anchorage. In case the lateral confinement is not biaxial and/or with lower stresses, the anchorage efficiency is expected to be lower. Further research is needed on this issue.



Figure 16: Track left in the concrete cube by the plate stirrup. It is clear that almost no concrete crushing takes place around the stirrup.

Acknowledgements. This research has been developed by means of internal resources only, which means that no funding was given by any public or private company. The authors acknowledge the contribution of the technical staff of the Civil Engineering Laboratory of the University of Genoa, among which S. Russo, G. Cassini, G. Riotto, D. Burlando and G. Tarantino.

REFERENCES

[1] Cusack P. François Hennebique: The Specialist Organisation and the Success of Ferro-Concrete: 1892–1909, *Trans. of the Newcomen Soc.*, **56**:1, 1984, 71-86.

[2] Mc Beth D.G. François Hennebique (1842–1921), reinforced concrete pioneer, *Proc. Inst. Civ. Eng.s*, **126** May, 1998, 86-95

[3] Delhumeau G. *L'invention du béton armé : Hennebique 1890-1914*, Norma, Paris, 1999

[4] Hellebois A. *Theoretical and experimental studies on early reinforced concrete structures. Contribution to the analysis of the bearing capacity of the Hennebique system*, Ph.D. Thesis, Ecole Polytechnique de Bruxelles, 2013.

[5] Cusack P. Agents of change: Hennebique, Mouchel, and ferro-concrete in Britain, 1897–1908. *Construction History* **3**, 1987, 61–74.

[6] Borden A.H. Identifying early reinforced concrete buildings in Scotland. *Proc. Inst. Civ. Eng.s – Eng. History and Heritage* **163** (3), 2010, 147–167.

[7] Hellebois A and Espion B. Domination of commercial patents in the evolution of early reinforced concrete. Case study of the region of Brussels. Proc. 7th Int. Conf. on Str. Anal. of Historic Constr.s: Strengthening and Retroffiting, 2010, Gu X & Song X ed.s. – Adv. Mat.s Res., Shanghai, China, vol. 133, pp. 119–124.

[8] de Courcy J.W. The emergence of reinforced concrete, 1750–1910. *The Str. Eng.* **65** (9), 1987, 315–322

[9] Kierdorf A. Why Hennebique failed in Germany. Strategies and obstacles in the introduction of a new construction technology, Proc. 3rd Int. Cong. On Constr. History, Cottbus, May 2009, Brandenburg University of Technology, K.H.Kurrer, Lorenz W. and Wetsk V. ed.s, NEUNPLUS1, Berlin.
[10] Marcos, I., San José, J.T., Cuadrado, J., (2014). The patents in the introduction of reinforced concrete in Spain: "Alhóndiga de Bilbao" case study (in Spanish). *Informes de la Construcción*, **66** (534), 2014,
[11] Ragot G. The Hennebique Archives: toward a new corpus for contemporary architectural history. *The American Archivist,* **59** (2), 1996, 214-220.
[12] Nelva R., Signorelli B. *Beginning and evolution of reinforced concrete in Italy: the Hennebique system* (in Italian), AITEC, Milan, 1990
[13] Sanna A., First applications of reinforced concrete in Sardinia. The "Porcheddu Company Engineering S.A." and his plan archives. *Proc. 1st Int. Congr. on Constr*. History, 2003, Huerta S., de Herrera I.J., Benvenuto E., Dragados F., 1809-1820.
[14] Iori T., *Reinforced Concrete in Italy* (in Italian), Edilstampa, Rome, 2001.
[15] Guidi C., *Constructions in Beton Armeé* (in Italian), appendix to Lessons on Structural Mechanics, Bona ed. Turin, 1907.
[16] Souponitski S.Z., Sniatkov S.V., Grigoriev S.E. Early reinforced concrete construction in Russia: specific faults and causes of failure, *Eng. Fail. Anal*., **8**, 2001, 201-212.
[17] Mueller G., Rankin G.I.B. The Hennebique system: a Renaissance? *Proc. of the Inst. of Civ. Eng.s,* **90** (1), 1991, 179–187.
[18] Hellebois A., Launoy A., Pierre C., De Lanève M., Espion B. 100-year-old Hennebique concrete, from composition to performance, *Constr. & Build. Mat.s,* **44**, 2013, 149-160.
[19] Hellebois A., Espion B. Structural weaknesses of the Hennebique early reinforced concrete system and possible retrofitting. *Str. Eng.ng Int*., **23**(**4**), 2013, 501–511
[20] Hellebois A., Espion B. Tests up to failure of a reinforced concrete Hennebique T-beam, Proc. of the Inst. of Civ. Eng.s - Structures and Buildings, 167 (2), 2014, 81-93.
[21] Foti D. Shear vulnerability of historical reinforced-concrete structures. *Int. J. of Arch. Her*., **9**(4), 2015, 453–467.
[22] Palmisano F. A preliminary study on shear capacity of historical reinforced concrete beams, Int. J. of Her. Arch., **1** (4), 2017, 608-623.
[23] Christophe P. Reinforced Concrete and its applications (in French), Paris, Beranger ed., 1902
[24] The Porcheddu Document and Photographic Archive, Technical University of Turin, Dept. of Structural, Geotechnical and Building Eng.ng.
[25] Panetti M., Swiss issues on reinforced concrete constructions (in Italian), *Civil Engineering and Industrial Arts*, XXVIII (17), Bertolero ed.s, Turin, 1902.
[26] Gotelli R. (1915) *Doubling Genova Brignole – Quarto dei Mille with deviation to Sturla,* Italian Railways, work area, special office for doubling the line Genova-Spezia, Italian Railways ed., 1915
[27] Hennebique U.S. patent n. 611907, 4th of October 1898.
[28] Porcheddu Archive, Dossier Genova, 1897, n. 38/1506, *Oriental Market*
[29] Porcheddu Archive – Dossier Genova 1896, n. 15/879, *Giant Palace*
[30] W.B. Fuller, S.E. Thompson, The laws of proportioning concrete, Trans. ASCE 59, (1907) 67–143.
[31] EN 1992-1-1:2004/A1:2014 - EuroCode 2 – Desing of Concrete Structures. General rules and rules for buildings.
[32] ASTM C192/C192M-18 Standard Practice for Making and Curing Concrete Test Specimens in the Laboratory
[33] EN 12390-2: 2019 Testing hardened concrete. Part 2: Making and curing specimens for strength tests

12th International Conference on Structural Analysis of Historical Constructions
SAHC 2020
P. Roca, L. Pelà and C. Molins (Eds.)

CHALLENGES IN THE REUSE AND UPGRADE OF PIER LUIGI NERVI'S STRUCTURES

R. CERAVOLO[1], G. DE LUCIA[1], E. LENTICCHIA[1*], G. MIRAGLIA[1], A. QUATTRONE[1], F. TONDOLO[1], E. MATTA[2], G. SAMMARTANO[2], A. SPANÒ[2], C. CHIORINO[3], G. BRUSCHI[4], P. FACCIO[4], A. NANNI[5]

[1] Department of Structural, Geotechnical and Building Engineering,
Politecnico di Torino, Turin, Italy.
e-mail: rosario.ceravolo@polito.it; giulia.delucia@polito.it; *erica.lenticchia@polito.it;
gaetano.miraglia@polito.it; antonino.quattrone@polito.it; francesco.tondolo@polito.it

[2] Department of Architecture and Design
Politecnico di Torino, Turin, Italy.
e-mail: emiliano.matta@polito.it; giulia.sammartano@polito.it; antonia.spano@polito.it

[3] Pier Luigi Nervi Project Association, Brussel, Belgium
e-mail: cristiana.chiorino@gmail.com

[4] Dipartimento di Architettura, Costruzione e Conservazione
IUAV University of Venice, Venice, Italy.
e-mail: faccio@iuav.it

[5] Civil, Architectural and Environmental Engineering Department
University of Miami, Miami, Florida, USA.
e-mail: nanni@miami.edu

Keywords: Historical Structure, 20th century architectural heritage, Conservation Plan

Abstract. *The paper presents the overall objectives of a funded research program for the development of a Conservation Plan (CP) for the two halls by Pier Luigi Nervi of the Turin Exhibition Center. The Turin Exhibition Center was conceived immediately after the Second World War to host primarily the annual Automobile Show, in connection with the presence in Turin of the FIAT motor company. The two main pavilions of the Center (Halls B and C) are outstanding examples of a pioneering use, of new advanced methods in reinforced concrete construction, combining innovative prefabrication procedures and the re-invention by Nervi of ferrocement, used to form extremely thin elements. The CP is expected to push and contribute to the preservation of the halls designed and built by Nervi, with special emphasis on structural and seismic vulnerability aspects, also due to concerns raised on the durability of concrete materials and technologies. Re-using these buildings entails the challenge to guarantee new extended service life to concrete structures built many decades ago and faces the need for a seismic assessment of these structures, in compliance to recent Italian standards.*

1 INTRODUCTION

The present work is part of a topical line regarding the analysis and structural diagnosis aimed at the conservation of 20th century architectural heritage. A heritage of great importance which is however characterized by several problems, first of all the scarce recognition of their historical-documental value. In fact, the preservation of 20th century architecture has fully entered the wider disciplinary of conservation. However, in practice, this cultural awareness clashes with the difficulties involved in adapting recent buildings to current building regulations. Moreover, many of the characteristics of modern architecture - such as the use of advanced construction methods and materials and the development of new building types and forms - challenge traditional conservation approaches and raise new methodological issues. In fact, the assessment of the twentieth century architectures poses new problems in terms of material preservation, structural analysis and reuse [1] [2]. Addressing these challenges will require convergent contributions from experts of different fields. From the point of view of their seismic improvement, 20th century buildings present specific issues, connected to the materials and techniques used for the construction, as well as to the complex and innovative spatiality; the continuous experimentations in all these areas have been among the characteristic features of architectural and engineering research of the past century [3]. For these reasons, in view of a restoration and re-functionalization of these buildings, it is a priority to carry out a careful evaluation of the structural performances, both as regards the level of safety in static conditions and from the point of view of seismic behavior. Experimental activities, including dynamic tests, are part of those operations aimed at identifying the structural characteristics, determining the state of health of the structure and predicting the response to seismic actions.
One of the reasons of the current abandonment of the Turin Exhibition Center, as well as of other Italian Nervi's buildings (e.g. Palazzo del Lavoro, Stadio Flaminio), is the lack of virtuous examples for guiding the renovation and/or reuse projects of the Modern architectural heritage in Italy. The contribution will address the issues regarding the preservation of modern heritage architecture as seen from the perspective of a country exposed to seismic risk. The paper presents the overall objectives of a funded research program for the development of a Conservation Plan (CP) for the two halls by Pier Luigi Nervi of the Turin Exhibition Center.

2 THE CASE STUDY

The monumental complex of Turin Exhibition Center represents a milestone in the history of modern engineering and architecture. The complex was designed and built between the 1948 and 1950 by Pier Luigi Nervi, one of the greatest and most inventive structural engineers of the 20th century [4] [5], as a public space to host primarily the annual Automobile Show, in connection with the presence in Turin of the FIAT motor company. In the construction of both halls of Turin Exhibition Centre, Nervi used new construction procedures that he studied for some years before this project. In fact, he had already successfully used these procedures with his engineering firm Nervi and Bartoli, though on smaller experimental buildings, such as the small storehouse in the Magliana area in Rome (1946) [6], the wharf Conte Trossi in San Michele di Pagana (1947) and the ceiling of the pavilion at the Milan Fair (1947) [7]. Reference to this celebrated and iconic masterpiece, as one of the most skillful examples of structural art, is very frequent in the literature on contemporary architecture. This combined use of two

different technologies for the construction of large concrete shells, would become one of the distinctive trait of Nervi's work.



Figure 1: Turin Exhibition Center, Pavilions by Pier Luigi Nervi: Hall B (left and center) and Hall C (right).

The roofing systems, in particular, are outstanding examples of a pioneering use, at the intersection between inspiration and technique, of new advanced methods in reinforced concrete construction, combining extensive use of innovative prefabrication procedures and reinvention by Nervi of ferrocement, as an extremely malleable building material. As in the large majority of his works, Nervi was both the designer and, through its construction company, the builder of the Exhibition Center. In the fifties Nervi will be asked to design a second pavilion (Hall C) and to enlarge the Hall B. Figure 1 shows the interiors of the two halls built by Nervi. Shaped like a fascinating modern cathedral, Hall B (1947-1948) consists of an imposing wide nave covered by a cylindrical barrel vault, and an elegant apse with ribbed hemispherical dome. For the realization of the arches of the vault, Nervi conceived wave-like prefabricated ferrocement elements joined by cast on site reinforced concrete ribs. Stylish fans connect the arches to the inclined columns. The apsidal semi-dome was built using lozenge-shaped ferrocement tiles connected by reinforced concrete cast in the lateral ribs and on their tops. Hall C (1950) is characterized by a captivating ribbed vault, constructed with the same system of ferrocement tiles and resting on four sculpturally shaped inclined arches. A clear proof on how significant the design and construction of both pavilions had been in the growth as a builder for Pier Luigi Nervi, is the fact that after the completion of both halls he immediately registered the patents of the solutions he employed during the construction site. In fact, Nervi registered various patents: patent no. 445781 in Rome on August 26th 1948, entitled "Ferrocement wave" and patent no. 465636 in on 19 May 1950, entitled "Building procedure for creating flat or curved load-resisting surfaces consisting of grids of reinforced concrete ribbing, possibly finished with connecting concrete slabs between the ribs" [8]. These patents would be adopted by Pier Luigi Nervi in the following decades until becoming a typical feature of the globally recognized Nervi's style [8] [9]. Moreover the experimentation of this new solutions was accompanied by the structural prefabrication, that Nervi already developed during the construction of a series of hangars for the Italian Air Force in the late 30s. It is important to note that Nervi's prefabrication did not concern factory-made standard construction elements. In fact, in each building he simply used prefab elements, made onsite. Nervi' s concept of

structural prefabrication meant that structures had to be broken down and each element had to be prepared on the ground (Figure 2). Every element had to be small enough and light enough to be lifted and easily assembled. Despite its misleading name (prefabrication) it is just a very old technique, in continuity with the tradition of stereometry.



Figure 2: The onsite prefabrication procedure of the undulated ferrocement elements of Hall B and their positioning.

The building is protected with a Landscape protection by the City Masterplan and since 2018 is listed in the National Heritage by the Ministry of Culture (*Codice dei beni culturali e del paesaggio,* D. Lgs. 42/2004) because it's a public building of 70 years old.
Despite its remarkable historical and architectural relevance, the Turin Exhibition Centre has been abandoned for a long time and the lack of maintenance is starting to induce serious preservation problems. In fact, after the transfer in the late 1980s of the Automobile Show to another location, the Center was used for sporadic exhibitions and events and progressive abandon followed. Even more so, these buildings were designed and built with no, or very limited, seismic provisions, due to the lack of technical standards at the time. The CP will issue guidelines to reconcile structural requirements and conservation criteria.

3 THE CONSERVATION PLAN

The conservation of the architectural heritage of the modern movement is the latest and perhaps one of the most contentious frontiers in the field of architectural preservation. Long-standing prejudices and a persistent public lethargy often overcome objective analysis when Modern buildings are faced with demolition or disfiguring renovations [2] [3].
The first act in defining approaches related to the preservation of modern architecture is aimed at recognizing the object as a monument, document, or material testimony, having the value of civilization, which implies a conservative need or a slowing down of the processes of degradation. Criteria, principles and postulates of the modern restoration critically and scientifically understood (distinctiveness, minimal intervention, potential reversibility, respect for authenticity and ancient matter, physical-chemical compatibility of additions, recognition under the double aesthetic and historical requirement of the work) correspond to those developed for the now shared actions of restoration of monuments. These statements find a first

difficulty in the specific disciplines related to the conservation project, but will be overcome thanks to a holistic approach that focuses not on individual scientific contributions but the object as a central element of research in the unity of architecture and structure.
Also the ICOMOS20 groups states that "*There is also some confusion about the basic principles of conservation that should be applied to twentieth-century sites and places*" [10]. The difficulty, or even lack, of communication between architects and engineers has always been one of the main obstacles in the analysis and conservation of the architectural heritage. In fact international guidelines states that the conservation, reinforcement and restoration of the architectural heritage require a multidisciplinary approach. A typical example of interdisciplinary approach is the interaction that has to occur between historical research and structural diagnosis: historical research can discover particular phenomena involving structural behavior whilst historical questions may be answered by considering the structural behavior.

3.1 Scope and challenges of the project

More generally, the research project may be ascribed to the structural assessment and retrofit of 20th century architectural heritage, characterized by a complex 3D structural design. The service life of civil and Cultural Heritage (CH) concrete spatial structures is typically thought to range from 10 to 200 years, but in practice, the service environment plays a pivotal role in sustained durability. We address the challenge of monitoring, conserving and rehabilitating 20th concrete CH because: concrete has become a 20th century emblem; consequently, specific studies are needed that contribute to the successful reuse of modern concrete built heritage. More specifically, large spatial concrete structures, conceived by 20th century European architects and engineers, represent a powerful common world background. Moreover, such structures are plagued by significant deterioration and most of them are in urgent need of retrofitting and/or radical refurbishment. There is a need to bring some of these buildings back to life, while respecting the spirit of their original characters, through new technologies for long-term conservation that can maintain an adequate level of structural and seismic performance. Achieving this goal would produce substantial economic impacts through activities such as tourism, restoration, maintenance, and cultural industry.
The scope of the research project is to develop a Conservation Plan for the two Halls designed and built by Pier Luigi Nervi in Turin Exhibition Center, with emphasis on structural and seismic issues. The project will be a mean to promote, support and guide the successive executive project of the building. An analytical investigation of Nervi's architecture, structures, materials and construction techniques will be supported by:

i) experimental tests on the building and its materials
ii) dynamic vibration-based tests
iii) historic and archival documents and direct observation
iv) accurate geometric survey through lidar and 3D restitution.

These activities will provide clear indications and recommendations for the conservation and restoration of the building's original characteristics, carried out by active experts of architectural heritage preservation. A special concern will be the correct modelling of the unconventional prefabricated ferrocement elements, a peculiarity of Nervi's vaulted structures which finds in these two halls a wide spectrum of constructive variants: in Hall B the wave-like elements of the undulated vault (interestingly interfering with the glass window panels); in Hall

C the diamond panels in the central portion of the vault and the undulated beams in the perimeter area. The unique features of these components make their mechanical behavior largely uncertain and their modelling a fundamental challenge to a reliable estimation of the present and future seismic safety of Turin Exhibition Center.

4. WORKPLAN

In order to overcome the difficulties in the diagnosis and the definition of a proper conservation strategy, the research propaedeutic to the Conservation Plan for the halls in Turin Exhibition Center will be centered different work streams. The various team will work together in order to carry out this main objectives:

1. Historical analysis of the building, investigating its design and construction process, with a particular focus on its technological features and characteristics.
2. Moreover a 3D dense clouds modelling derived from 3D sensing technologies (integrated and fused image and range based methods) will be produced;
3. Structural analysis of the building, considering the construction techniques and materials. Vibration-based dynamic tests will be carried out to investigate the global behavior and the health state of the two main halls and to define guidelines for possible interventions;
4. Analysis of the materials and their durability by means of experimental investigations on structural elements and laboratory mockups. These analysis will be fundamental in the definition of guidance criteria for the materials conservation and rehabilitation
5. Definition of the overall conservation and management plan for the future renovation of the halls.

Figure 3 reports a timeline of the activities of the project. A more detailed description of the activities of the various groups can be found in the following paragraphs.

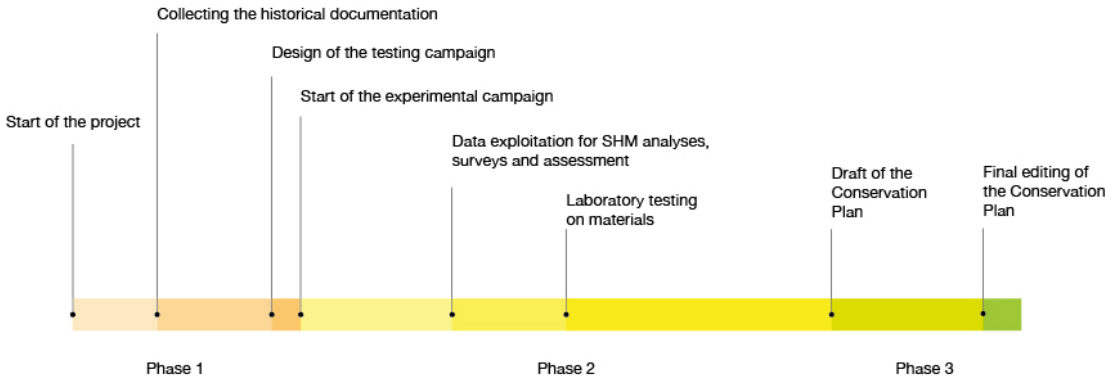


Figure 3: timeline of the project activities.

4.2 Structural Health Monitoring and Seismic assessment of the building

The first work stream is responsible for vibration-based tests and dynamic analysis in order to evaluate the response of the building to earthquakes and perform a seismic assessment of the

two Halls of the building. One of the main objective of this unit is the diagnosis of the health state of the halls. It involves a multi-scale approach based on the integration of experimental investigations carried out on-site and in the laboratory. Indeed, the conservation and rehabilitation of heritage buildings can be successfully accomplished only if a correct diagnosis has been formulated. Vibration-based structural health monitoring techniques have now become an important tool for the preservation of either antique or modern architectural heritage [11]. Dynamic tests are particularly appreciated in this field because they are a non-destructive technique and provide information about the whole-body response of the structure and its overall structural integrity. Accordingly, these techniques can in turn be undertaken for: i) understanding the structural behavior of a building; ii) assessing the response to specific events, by measuring some sensitive parameters and comparing them to typical threshold values.; iii) assessing the efficacy of structural or seismic interventions. The investigations of the structures in the dynamic and seismic domain are particularly important for this kind of structures, especially because they were designed and built to withstand only the gravity loads, accordingly to the technical standards of the time. An in-depth analysis of both hall C and B was carried out through several numerical investigations aimed at investigating the dynamic and structural response of the structures. The objective of this phase was to highlight the main criticalities of the structure and to evaluate the best strategy for the experimental campaign. An investigation of Hall C is reported in [12], while the more complex Hall B was analyzed in different steps: a preliminary model is reported in [13] and was implemented by adding the adjacent Hall A, in order to take into account the influence of an annexed structure. In the case of Hall B, the main critical aspects are connected to the large number of structural elements that govern the dynamic behavior of the structure. These macro-elements and their influence on the dynamic response of the building were described in [13]. In particular, it was pointed out that the most critical responses are those related to the undulated thin shell vault, the out-of-plane movements of the tympanums, and the presence of the apse, which cause a complex and potential vulnerable interaction with the main body of the hall. Similarly to Hall C, in Hall B bending and shear assessments were carried out on the main structural elements. Most elements, in particular the inclined pillars, are unsafe with respect to shear. Moreover, the infill walls of the tympanums are subjected to out-of-plane overturning (Figure 4).

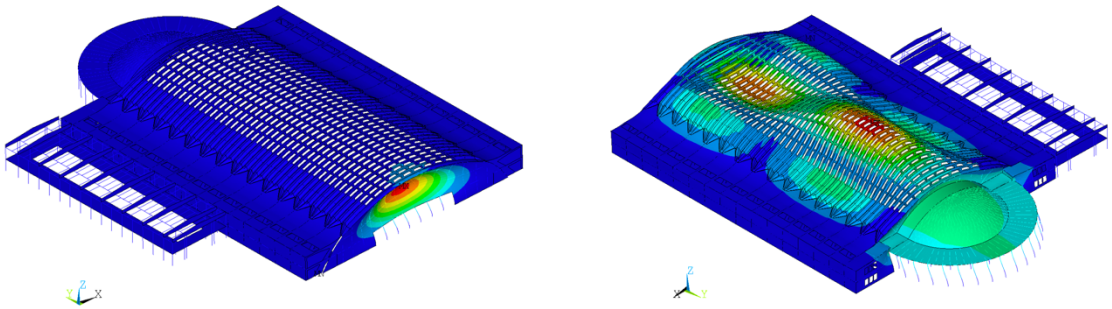


Figure 4: On the left, the out of plane movements of the front tympanum of Hall B; on the right, the interaction movements of the apse and the undulated vault.

The structure of Hall C consists of a vaulted roof supported by four inclined arches. It is completed by a perimetral slab of about 10 meters in length, sustained by a series of slim pillars and infill walls. The analysis started in [12] highlighted that the most vulnerable elements were

constituted by the dynamics of the inclined arches. These movements are amplified by their inertial mass, which is proportionally very high compared to the other elements of the hall, especially in comparison with the thin ribbed vault. Another critical aspect lies in the translation of the rigid cap of the roof with respect to the deformable contour ribs. Also due to the low ductility associated with these mechanisms, in case of moderate seismic events, the ribs may be affected by local interaction with the roof. Moreover, the main structural elements (arches, ferrocement elements, and pillars) were assessed with respect to bending and shear. In particular, results show that the arches are not verified with respect to shear loads. As a matter of fact, the shear reinforcement is weak if compared to current standards, as at the time designers were very confident about the resistance of concrete (Figure **5**). Accordingly, the standards of the time only required a shear assessment for beam elements.

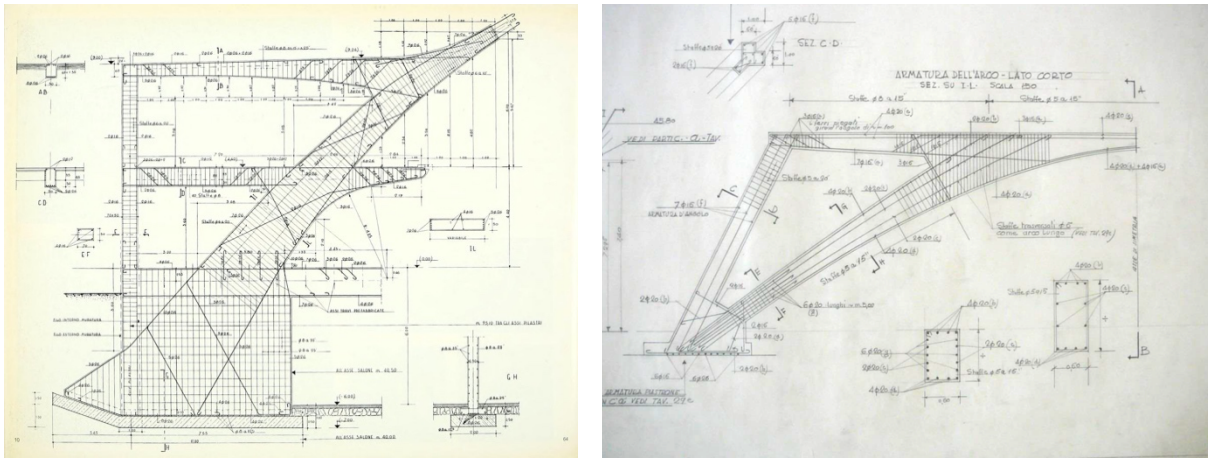


Figure 5: Original drawings reporting the details of the reinforcements of the slanted pillars of Hall B (on the left) **[14]**, and shorter inclined arch of Hall C (on the right) **[15]**.

4.3 Durability

This research stream will carry out the investigation, diagnosis and testing of the materials, by means of on-site inspections, and experimental investigations on materials and mockups on the ferrocement elements. The characterization of the structural materials employed in Hall B and C will be used to reproduce, with the help of the documentation of the construction procedures used by Pier Luigi Nervi (e.g. cement type and content, aggregate dimension, etc.), laboratory mockups to be subjected to an accelerated corrosion procedure. This phase of the experimental investigation is aimed to forecast the structural damage evolution of the main elements of the Turin Exhibition Center once the initiation period is over and the propagation period for corrosion of the reinforcing bar becomes effective. Once some reference level of corrosion will be over, mockups will be tested to compare their structures performances with undamaged reference specimens. Therefore, the evolution of the damage will be directly associated, to the loss of bearing capacity with safety reduction both in service and at ultimate conditions. Rehabilitation techniques as the use of FRCM (Fiber Reinforced Cementitious Matrix) or the use of other thin protective layers and of materials with effects on the cement mortar at the nanoscale will be also employed to explore their effectiveness with deteriorated ferrocement elements.

The experimental analyses will be crucial to define the guidance criteria for the materials conservation and rehabilitation for the CP of the halls, especially since the halls were built with newly patented construction systems and materials by Nervi himself.
The main aspects considered will concern:

- safety checks with respect to durability with a proposal of upgrade of the traditional systems from inspections methodologies to forecast formula of carbonation diffusion to corrosion structural damage for ferrocement construction improving the awareness of the residual safety level of the structures.
- guidelines for remedial actions and structural rehabilitation; a level of intervention priority will be proposed to check the actual conditions, plan the structural conservation activities and to suggest rehabilitations taking into consideration of the sustainability of interventions basically considering the most advanced and less invasive techniques; with reference also to the results of the experimentation on the effects on durability by additional materials as mentioned in the preceding section.

4.4 Historical Analysis and Conservation Recommendations

The conservation plan for the two halls built by Pier Luigi Nervi is an emblematic chance for research studies of structural concrete architectural heritage. The scientific approach implied in this kind of studies reflects the complexity of conservation, restoration and reuse policies requested for great works of modern architecture. This works stream has different objectives: it will closely collaborate with the other units in order to provide the necessary documentations for the first step of their action strategies. It will provide the historical and architectural analysis of the building, including archival researches as well as investigations on the relationship between architecture and construction. Moreover, it will also provide a complete accurate and dense 3D survey, and will define the conservation recommendations also considering the current Italian and European legislation framework. In fact, iconic structures, well known and appreciated and internationally recognized, are difficult examples on which to apply and reconcile any invasive structural retrofitting in terms of conservation.
The main challenges connected to this work stream are connected to various kind of criticalities. In fact, since the building had various owners, and since it has been abandoned for a long time, there is no unified and organized archive related. In particular, archives are located in different cities (Turin, Rome, and Parma), and some documents are in a precarious state of conservation, e.g. the original drawings were realized on tracing papers, which is a very fragile support. Moreover, a precise geometrical survey of the building has never been carried out and maintenance work, that could have caused changes in the interiors of the buildings, has not been adequately documented. The comparative analyses of different historical sources, such as archives, pictures, and videos, can be of great value when analyzing underestimated aspects, such as the use of color. For example some sequences of the film The Italian job, clearly show how the interiors of the building were painted with a cream color (Figure 6) , instead of the current bright white. The use of polychromies combined with the use of natural and artificial light sources, introduce new facets in analyzing the work of Nervi that need careful reflections. This is particularly true if we consider the impact of the interventions carried out up to now, even those that were considered not-invasive, such as the operations of ordinary maintenance and some technological updates.



Figure 6: A frame of the movie The Italian Job, 1969, Peter Collinson in which it is possible to appreciate the different polychromies between the vault (painted in grey) and both the slanted pillars and the walls (painted in dark cream color). On the right, a fragment of the plaster of the hall B showings the various layers of coloring.

5 CONCLUSIONS

After years of abandonment, the celebrated spatial structures built by Nervi in the Turin Exhibition Center will be the object of an in depth analysis in order to recover them. The grant awarded by the Getty Foundation is a remarkable occasion to establish methodological criteria and guidelines for all the steps to be undertaken for an appropriate and virtuous path of structural preservation and rehabilitation. The most challenging issues to be faced in this respect concern *a)* the evaluation of the residual service life of these dated structures and the definition of adequate remedial actions to extend it in line with the new uses foreseen, and *b)* the assessment, in compliance with current Italian standards, of the structural safety and reliability of these structures with respect to seismic actions. As far as concerns item *a)*, advanced research actions are currently being initiated with respect to the assessment and prolongation of the service life of the delicate ferrocement elements of the Pavilions by Nervi. As for item *b)* a modeling and diagnostic investigations in the dynamic and seismic domain have already been performed. These investigations show some seismic vulnerabilities typical of large span shell and spatial structures that were predominantly conceived to withstand static actions and whose behavior in the dynamic domain was not taken into account in their original conception. Appropriate remedial actions, in terms of strengthening and/or damping interventions, shall be properly defined in the final stage of the reuse project.
Finally, the guidelines will have a broad range applicability, so that it will constitute a reference for possible interventions, not only on Nervi's buildings, but also on the concrete shell architectures which at the time were experimented all over the world.

Acknowledgements. The present work is supported by the Keeping it Modern grant awarded by The Getty Foundation of Los Angeles (USA). The authors would also like to acknowledge the City of Turin, owner of the buildings and active partner of the project, and Società Committenza Piemonte (SCR).

REFERENCES

[1] K. Normandin and S. Macdonald, "A Colloquium to Advance the Practice of Conserving Modern Heritage: March 6–7, 2013: Meeting Report," The Getty Conservation Institute, Los Angeles, 2013.

[2] T. Prudon, Preservation of Modern Architecture, Hoboken, NJ: John Wiley & Sons, Inc, 2008.

[3] C. Croft, S. Macdonald and G. Ostergren, Concrete: Case Studies in Conservation Practice, Getty Publications , 2019.

[4] J. Abel, G. Arun and M. Chiorino, "Special Double Issue on Pier Luigi Nervi: Preface by the Guest Editors," *Journal of the IASS,* vol. 54, no. 176-177, pp. 79-86, April 2013.

[5] C. Chiorino and C. Olmo, Pier Luigi Nervi. Architecture as Challenge, Milano: Silvana Editoriale, 2010.

[6] C. Greco, "The "ferro-cemento" of Pier Luigi Nervi, the new material and the first experimental Building," in *Proceedings of the International Symposium of IASS*, Padova, 1995.

[7] T. Leslie, "Moving Weights: Nervi's Prefabricated 'Wave Ashlar' Roofs and the Artisanal Cantiere," in *Proceedings of the IASS-SLTE 2014 Symposium "Shells, Membranes and Spatial Structures: Footprints"*, Brasilia, 2014.

[8] C. Greco, Pier Luigi Nervi. Dai primi brevetti al Palazzo delle Esposizioni di Torino 1917-1948, Lucerna: Lucerne Quart Edizioni, 2008.

[9] T. Iori and S. Poretti, "Pier Luigi Nervi: his Construction System for Shell and Spatial Structures," *Journal of the IASS,* vol. 54, no. 176 & 177, pp. 117-126, April 2013.

[10] ISC20C, Approaches to the conservation of Twentieth-century cultural heritage Madrid – New Delhi Document, ICOMOS International Committee on Twentieth Century Heritage , 2017.

[11] R. d. L. G. L. E. M. G. Ceravolo, "Seismic structural health monitoring of cultural heritage structures," in *Seismic structural health monitoring*, Springer Tracts in Civil Engineering, 2019, pp. pp. 51-85.

[12] E. Lenticchia, R. Ceravolo and C. Chiorino, "Damage scenario-driven strategies for the seismic monitoring of XX century spatial structures with application to Pier Luigi Nervi's Turin Exhibition Centre," *Engineering Structures,* no. 137, pp. 256-267, 2017.

[13] E. Lenticchia, R. Ceravolo and P. Antonaci, "Sensor Placement Strategies for the Seismic Monitoring of Complex Vaulted Structures of the Modern Architectural Heritage," *Shock and Vibration,* no. art. no. 3739690 DOI: 10.1155/2018/3739690, 2018

[14] P. Nervi, Aesthetics and Technology in Building, The Charles Eliot Norton Lectures ed., Harvard University Press, 1965.

[15] P. L. Nervi, "Palazzo delle Esposizioni - Torino (original projects)," *Centro Studi e Archivio della Comunicazione (CSAC) , Parma,* 1948-53.

12th International Conference on Structural Analysis of Historical Constructions
SAHC 2020
P. Roca, L. Pelà and C. Molins (Eds.)

CONSERVATION OF 20TH CENTURY CONCRETE HERITAGE STRUCTURES IN CYPRUS: RESEARCH AND PRACTICE

ANTROULA V. GEORGIOU[1*], MARIA M. HADJIMICHAEL[1] AND IOANNIS IOANNOU[1]

[1]Department of Civil and Environmental Engineering
University of Cyprus
1 Panepistimiou Avenue. 2109 Aglantzia, Nicosia. P.O. Box 20537, 1678 Nicosia, Cyprus
e-mail: {ageorg44, hadjimichael.m.maria, ioannis}@ucy.ac.cy, www.ucy.ac.cy
(*corresponding author)

Keywords: Concrete Heritage, Structural Assessment, Displacement Pushover, CONSECH20

Abstract. *The conservation of 20th century concrete heritage structures poses a major challenge worldwide. Whilst these structures possess a remarkable architectural value and a rather experimental character in terms of the use of materials and technologies, at the same time there is admittedly lack of recognition of their cultural and historical value by the wide public. More often than not, such buildings are left to deteriorate and often they are even demolished. This paper follows the workings of the project "CONSErvation of 20th century concrete Cultural Heritage in urban changing environments" (CONSECH20). The aforementioned international interdisciplinary project aims to investigate concrete constructions built until 1965 in four different European countries (Cyprus, Italy, The Netherlands and the Czech Republic), in terms of their architectural, social and historical value, and to address their restoration and re-use potential. The paper initially presents the significance of 20th century concrete heritage structures in general, and describes the methodology proposed in order to ensure the protection of such buildings from demolition, and facilitate their restoration and re-use (if and where possible) for the benefit of the society. The focus is on the structural assessment and restoration of 20th century concrete heritage buildings in Cyprus, following the methodologies described by modern codes for the assessment and retrofit of existing concrete structures. A new practical analysis approach is described and compared to the force-control approach of the pushover analysis of Eurocode 8:3, which significantly overestimates the demands for seismic upgrading. The two aforementioned approaches are examined for a specific case study concrete heritage building in Nicosia, Cyprus.*

1 INTRODUCTION

Concrete has a long history of use as a construction material. However, it was not until the 20th century that it became a major building material, used in the construction of innovative and groundbreaking structures worldwide [1,2]. Whilst these structures undoubtedly possess a remarkable architectural value, and a rather experimental character in terms of the use of materials and technologies, their significance in terms of engineering technology and architectural design is not always recognized. This is also highlighted by ICOMOS, the

International Council on Monuments and Sites, in its Madrid document [3], where it is stated that '*the architectural heritage of the 20th century is at risk from a lack of appreciation and care*'. In fact, more often than not, 20th century concrete heritage structures are left to deteriorate through lack of maintenance and often they are even demolished. Hence, the conservation of 20th century concrete heritage structures poses a major challenge worldwide.

This paper follows the workings of the project "CONSErvation of 20th century concrete Cultural Heritage in urban changing environments" (CONSECH20), aiming to highlight the urgent need for the protection of 20th century concrete heritage structures. It elaborates on the structural assessment and restoration of 20th century concrete heritage buildings, following the methodologies described by modern codes for the assessment and retrofit of existing concrete structures. It also outlines existing conservation policies for such buildings in Cyprus. The paper recognizes the difficulties that arise in preserving historic Reinforced Concrete (R.C.) structures, not only because of the architectural variety of these buildings, and the experimental nature in the use of technologies and materials, but also because of the lack of regulations, good quality materials and testing procedures, or indeed knowledge of seismic design, at the time of their construction.

Regarding the latter, in the cases of R.C. historic structures in seismic prone areas, the simulation and assessment of their structural capacity is of crucial importance, since the outcome of the assessment process will also determine the requirements for retrofit and upgrading, in terms of strength and ductility, as well as the magnitude of damage, in terms of deformation, likely to develop in a future seismic event. The Codes used for structural assessment, such as EC8-Part 3 [4], use a force-controlled pushover approach to determine the target displacement of an existing structure, that is found to be problematic when applied to historic concrete structures. The problem lies in the methods and modelling technics that are adopted for assessing the existing capacities of old structures. Erroneous results yield in excessive restoration and upgrading demands. This paper focuses on three major issues that could be adjusted in the code-described procedure for the assessment of historic R.C. structures: (a) the non-linear pushover analysis must use the post-peak performance of a structure, (b) the nonlinearity introduced by hinges should take into consideration possible brittle shear, or other failures, and (c) the connection of the building's walls to the diaphragm should take into consideration possible formation of plastic hinges on the diaphragm and complete disconnection of the slab with the walls. A new practical analysis approach is hereby used and compared to the force-controlled approach of the pushover analysis of EC8-Part 3 [4], taking into account the three issues mentioned above. The two aforementioned approaches are examined for a specific case study concrete heritage building in Nicosia, Cyprus.

2 STRUCTURAL ASSESSMENT AND RESTORATION OF 20TH CENTURY CONCRETE HERITAGE BUILDINGS

Factors considered critical for the deterioration or loss of historic R.C. structures are environmental changes, changes in the surrounding landscape, natural disasters (i.e. earthquakes, floods etc.), and often demolition and replacement by skyscrapers, as many of these structures are not yet designated by the appropriate bodies as listed and their fate is thus decided by individuals who are not always sympathetic to historic structures. Moreover, even when efforts are made to restore these buildings, failure to recognize their architectural value

and blind application of the provisions of codes designed for the retrofit of ordinary structures, or indeed insufficient knowledge of the correct restoration practices, often results in architectural geometrical alterations (especially problematic in structures of the modern movement with specific geometries), or in more adverse deterioration after the repair (usually in cases of faulty repair techniques in corroded members).

2.1 Modelling of historic concrete structures

In recognition of the great likelihood of damage of existing sub-standard buildings, Codes for their structural assessment and upgrading have been developed worldwide [4–9]. In the case of listed R.C. structures in seismic prone areas, the use of elastic analysis, which is given as an option by the codes, results in high demands for structural upgrading, that usually require alteration of the architectural character of these structures. The safety of the users must nevertheless be established, while the historic form of each individual structure must be preserved. This sometimes leads to the overlooking of code provisions [10]. In the case of historic structures, correct simulation and structural assessment is of utmost importance, since the results of the structural analysis will define the displacement demand in a future seismic event.

Possible assessment analysis procedures, as described by EC8-Part 3 [4], are linear (lateral force and modal response spectrum) and non-linear (push-over and time history analysis). Linear analysis models are penalizing the structure, since by assuming linear properties of the members, the capacity in terms of loads is increased and the deformation is decreased. The linear procedure that does not take into consideration the formation of plastic hinges at the beams and columns cannot predict the actual response and the redistribution of forces in the structure, due to the failure of certain members. Especially in the case of the modal analysis, the validity of the results is disputed, since the response is a CQC or an SRSS combination of the various modes; the drifts in the lower floors are thus underestimated and the change in the stiffness of the structure due to the variation of the axial load is neglected [11].

For the nonlinear static pushover analysis, two possible variations may be used. One is the monotonically increasing lateral loads (EC8-Part 3) and the other is the monotonically increasing lateral displacements at the floor levels. The application of forces at the floor levels in programs such as SAP2000 [12] exhibits limitations when the analysis is performed for structures that include various brittle mechanisms of failures at the members of the structure. The sudden failure of a member may result in negative stiffness of the structure and the inverted matrix of stiffness cannot be used to deduct the displacements caused by the forces. This results in non-convergence issues and abrupt termination of the analysis, leading to underestimation of displacement and overestimation of the load capacity [13]. On the contrary, displacement-based procedures can overcome the non-convergence issues, redistributing the forces correctly through the structure and estimating reliably the sequence of failures of the members.

The non-linear model used for the analysis must capture the proper dynamic characteristics of the structure, as the modes of vibration and the corresponding periods define the seismic excitation of a structure. As per EC8-Part 3 (Par. 4.3.1) the proper model must use the stiffness of the elements by incorporating the effect of cracking, such that stiffness corresponds to the initiation of yielding of the reinforcement. The cross-section of each element may therefore be used to compute the Moment (M_y)-Curvature (φ_y) diagram of each cross-section and calculate

the cracked stiffness of the member as $EI_{cr}=M_y/\varphi_y$. The M-φ is used thereafter in the plastic hinges to control the load-bearing capacity after yielding, as well as the redistribution of lateral loads.

Contrary to the behaviour of new structures designed with the capacity design provisions, old structures, as indicated by previous earthquake events, suffer from brittle failures at the ends of the beams (such as shear failure), from the failure of the joint's cross-section, the punching shear in slabs without beams, while columns may exhibit shear failure, anchorage failure of the longitudinal reinforcement or failure of lap splices, even prior to the yielding of the beams [14]. The M-φ diagrams that should be used in the modelling of the structure must include all possible types of failures, even the brittle ones. This can be achieved by calculating the Moment in the beams and columns that corresponds to each type of failure, and using the weakest link to control the behavior of the hinges in the simulation.

One more subject that needs to be addressed for the correct evaluation of the structural response of old structures built without taking into consideration seismic provisions is the diaphragmatic function of the structural walls, which for new structures is considered by default. The distribution of lateral displacements and loads on the walls of the structures is achieved through their connection with the slabs. In older structures, slab reinforcement was the minimum required for vertical loads, resulting in severe cracking in the zones peripheral to the walls and eventual plastic hinge formation in the slabs and disconnection from the walls. In those cases, the disconnection of the walls leads to a sharp decrease of the stiffness and increase of the period, which in turn increases the lateral displacements that will be introduced by the seismic event on the structure and leads to its inevitable collapse.

2.2 Shear wall collectors in old R.C. structures

Diaphragms aim to support the vertical elements that carry the seismic actions, carry the seismic loads from the point of application to all the vertical elements of the load carrying system and connect the various elements in order to work as they were conceived [15]. Based on EC2 [16], diaphragms are designed for a factored combination of the vertical loads and not under seismic excitation. On the contrary, ACI 318 [17], as well as the ASCE/SEI 41-17 [10], take under consideration the dynamic influence of the seismic loads on the diaphragms, increasing stresses with appropriate factors and assigning appropriate detailing provisions for the collectors, i.e. the diaphragm's zones that transfer shear forces from the diaphragm to the elements of the lateral load resisting system. In these cases, design aims at preventing the formation of plastic hinges at the collector zones. This must be taken into consideration, especially in the cases of old structures, where appropriate detailing of those zones was not ensured. Those zones will most probably form plastic hinges when the diaphragm forces overcome the shear capacity.

The formation of plastic hinges in the diaphragms also results in the separation of the diaphragms from the lateral load bearing walls, leading to failure of the structural system, as was observed from various collapses during previous earthquakes [18,19]. The forces between a diaphragm and a shear wall can be computed either by finite element analysis, or by using free body cuts on the shear walls above and below the diaphragm with force equilibrium [20]. The diaphragms are allowed to be idealized as rigid when the span to depth ratio is less than 3 and no horizontal irregularities exist, while appropriate flexibility must be assigned in the

diaphragm in all other cases, where usual values of the stiffness modifier are between 0.15-0.5 [20].

The design of the collector for shear transfer is based on the assumption that shear stresses are uniformly distributed on the interface between the diaphragm and the wall, as per ACI 318 [17] Par. 18.12.9.1:

$$V_n = A_{cv}\left(0.17\lambda\sqrt{f_c'} + \rho_t \cdot f_y\right) < 0.66\sqrt{f_c'} \cdot A_{cv} \tag{1}$$

Where ρ_t, is the uniformly distributed slab reinforcement perpendicular to the wall's flexural reinforcement and λ=1 for normal concrete. The values are referred to structures designed as per new Code provisions and proper detailing for capacity-based design as per ACI 318 [17]. In the cases of old sub-standard structures, with low reinforcement ratios of the slabs, the ACI equation seems to overestimate the real shear transfer capacity between the diaphragms and the walls, as reported by experimental research [21]. The shear force for failure of a lightly reinforced slab, with simultaneous yielding of the reinforcement in both directions, is described by the first term of Eq. 2, while the second term of the same equation represents the yielding of the reinforcement perpendicular to the slab's main flexural reinforcement with simultaneous crushing of the diagonal compressive strut.

$$V_n = min\{\, A_{cv} \cdot f_y\sqrt{\rho_t \cdot \rho_l}\,;\; A_{cv} \cdot f_y \cdot \rho_t \sqrt{\frac{\lambda \cdot f_c}{\rho_t \cdot f_y} - 1}\} \tag{2}$$

2.3 Displacement Pushover Analysis

Recent studies [13] have shown that using a displacement based approach, instead of a lateral load pattern of increasing intensity, can increase the validity of the prediction of failure of structures, as it does not require a positive-definite stiffness matrix for convergence. The pushover analysis resistance curve in this approach is obtained by applying a drift demand pattern, based on the fundamental mode of translational vibration of the structure. The procedure of assessment proposed by Fotopoulou et al. [13] is adapted for structures with coupled translational and rotational mode shapes. In order to perform a Displacement Pushover analysis, the fundamental mode shapes of the structure must be determined. Especially in the cases where a structure has irregularities in plan and elevation, a proper 3D model must be used, including the true stiffness of the beams, columns and walls, in order to determine the torsional moments due to stiffness irregularities. The primary modal shapes of the structures in the two directions (including torsion when coupled), give the displacements in X and Y directions of each node in relation to the Center of Mass (C.M.) node on the roof of the structure. Based on the differential translation of each node to that of the C.M., incremental translations can be imported simultaneously to all the vertical elements of the structure, according to the mode shapes of vibration. For each incremental displacement of the Top C.M. node (Δ_i), the displacements of each column and wall are derived (D_{ci}) and the corresponding drifts (θ) are distributed between the beams and the columns connected on each joint, based on their relative stiffness. The drift of each column is determined as $\theta_c=\lambda/(\lambda+1)\cdot\theta_{bc}$, where $\lambda=EI_b\cdot h_c/(EI_b\cdot h_c)$, with λ being corrected in each next step, assuming the value of 1 when the column has yielded. The Shear-Drift curve of each vertical member is then used to derive the shear that is developed at each incremental step. The Shear-Drift curve of each member is determined based on both

ductile and brittle possible modes of failure. The sum of the shear forces of the vertical elements in the base floor of the structure is the Base Shear of the structure.

3 CONSERVATION OF 20TH CENTURY CONCRETE HERITAGE BUILDINGS IN CYPRUS: POLICY AND RESEARCH

In the Cypriot society, as indeed in many other societies at present, the dominant view is that only traditional masonry structures constitute part of the country's architectural heritage, due to their long span life and straightforward legal protection by the local Town Planning and Housing Department (TPH). The construction of R.C. structures in Cyprus began in the 1930s. The non-recognition of the social and historical value of these buildings by the general public, as well as the constant changes in the urban environment, are rapidly leading to their deterioration and often their demolition; thus a significant part of the history and architecture of Cyprus is lost. Some of the R.C. buildings built by 1960 are still in use, albeit in bad condition. Others have undergone interventions, which have led to the alteration of their original character. The aforementioned highlight the significance of the protection of 20th century concrete heritage structures in Cyprus and renders CONSECH20 timely.

3.1 Listing and Conserving 20th Century R.C. heritage buildings in Cyprus

The Republic of Cyprus (RoC) protects historic buildings, monuments and sites through two main legal instruments. The first instrument is 'The Antiquities Law', a law dating back to 1905, through which 'Ancient Monument' objects, buildings or sites considered to be of public interest by reason of their historic, architectural, traditional, artistic or archaeological value are listed. In 1972, the 'Town and Country Planning Law' was introduced and since then has become the foundation regarding the protection primarily of vernacular architecture. In essence, Article 37 - '*Protection Decree*' of the aforementioned Law, allows for the issuing of preservation orders by the Minister of Interior, on the recommendation of the Department of TPH. These Decrees declare as 'listed' individual buildings or structures, groups of buildings or sites of special social, architectural, historical or other interest. There are over 100 preservation orders issued until today, covering more than 5,000 buildings across the RoC. The majority of these buildings belong to the vernacular architecture, with a much smaller number of buildings belonging to the 'modern architecture' [22]. There are no restrictions regarding the age of the building to be recommended for listing through a Protection Decree, or indeed the type of construction material used. Once listed, these buildings are protected, in the sense that their demolition, as well as any alterations which could change their original character, become illegal. Legal owners of listed buildings have the responsibility and obligation to submit any planned alterations to the competent Section (i.e. the Conservation Section) of the TPH and get permission before actually implementing these changes.

3.2. Selecting 20th century concrete heritage structures for CONSECH20

Following a more global trend, there has been a rise in the interest 20th century concrete buildings have been receiving in the RoC over the past decade, in particular. In 2009 for example, the Town and Planning Department of the RoC funded the research and production of a publication titled 'Learning from the Heritage of the Modern'. Additionally, the Docomomo Cyprus list [23], including significant projects constructed roughly between 1920-

1980, was prepared by a team of architects. The goal of the list was to showcase the impact of modern architecture in modernization processes and the shaping of the built environment. It is also important to mention that there is an emerging research hub on architectural modernism in Cyprus. In this framework, the international interdisciplinary project "CONSErvation of 20th century concrete Cultural Heritage in urban changing environments" (CONSECH20) is currently in progress, aiming to investigate concrete constructions built until 1965 in Cyprus (and in three other European countries - Italy, The Netherlands and the Czech Republic), in terms of their architectural, social and historical value, and to address their restoration and re-use potential. The project is focusing on representative case studies of 20th century historic concrete buildings, the selection of which is based on certain criteria. In Cyprus, a preliminary extensive list of what could be considered as "concrete heritage buildings" has been prepared using information from relevant bibliography, as well as from various archival sources (both public and private). This list amounts to approximately 160 buildings.

In order to shortlist these buildings and perform a more in-depth analysis, a number of additional criteria were taken into account, such as representative architectural styles, materials, construction system, decorative techniques, aesthetic quality, and damage mechanisms (Table 1, Fig. 1). Starting from the period of construction, only structures built before 1965 were selected. This allowed the inclusion of key-structures built after the independence of the island in 1960. Given the social focus of CONSECH20, there was special interest on public, municipal and state-owned buildings of social and architectural significance. Both listed and non-listed buildings were included in the list. Similarly, buildings which have undergone successful interventions, which could constitute good lessons from the past, as well as buildings which are in need of restoration, have been included in the list.

Table 1: Examples of case studies selected in Cyprus in the framework of CONSECH20

Building Name	Year	Structural System	Current Use	Listed	State of the Building
Melkonian Institute	1926	Proprietary	Abandoned	Yes	Needs restoration
Pavilion at Halasultan Tekke	1960	R.C. Frame	Abandoned	No	Needs restoration
Carob Store	1960	Prefab	Industrial	Yes	Needs restoration
Ledra Palace Hotel	1947-49	R.C. Frame	Under UN occupancy	Yes	Needs restoration
Mangoian Shops and Apartments	1951-52	R.C. Frame	Education /Spectacle	Yes	Successful Past Interventions
Alexandros Demetriou Tower	1957-59	R.C. Frame	Commercial/ Residential	Yes	Successful Past Interventions
Tourist Pavilion	1960-62	Hybrid	Abandoned	No	Needs restoration
Old Municipal Market	1965	R.C. Frame	Abandoned	Yes	Needs restoration
Athienou Municipal Market	1955	R.C. Frame w/o slabs	Abandoned	Yes	Needs restoration
Technical School Nicosia	1953	R.C. Frame	School	No	Past Interventions not Successful
Kyperounta Sanatorium	1938-40	R.C. Frame	Hospital	No	Needs restoration

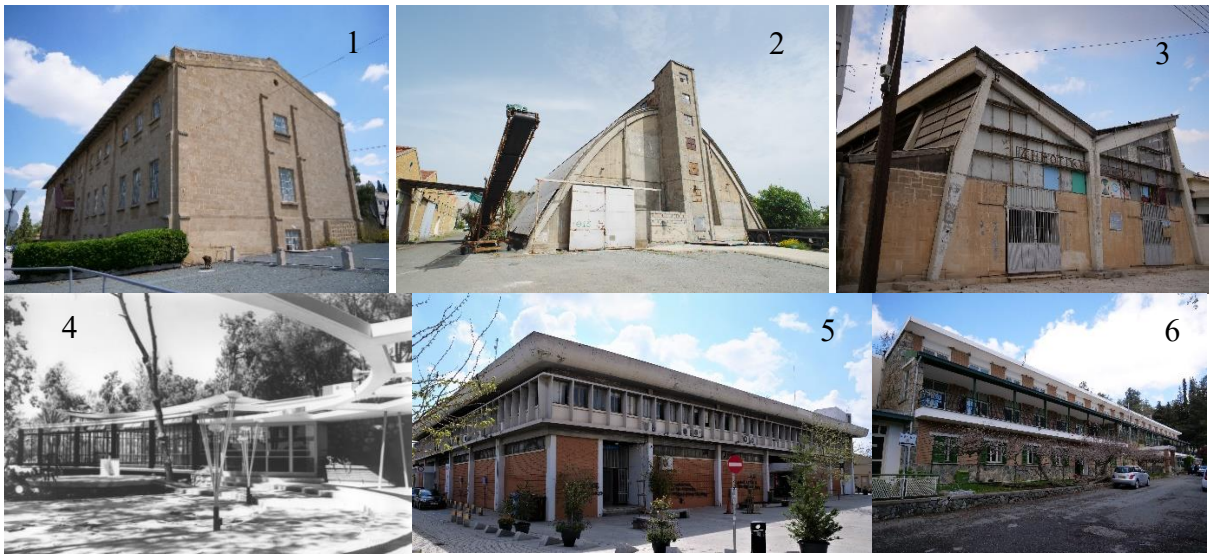


Figure 1: Buildings that will be examined in the framework of CONSECH20 project. 1. Melkonian Institute, Nicosia; 2. Carob Store, Limassol; 3. Athienou Municipal Market; 4. Tourist Pavilion, Limassol; 5. Old Municipal Market, Nicosia; 6. Kyperounta Sanatorium

For the screened case studies, the type of structural system, as well as the general state of conservation, have been noted. The type of construction was also recorded (cast in place, prefabricated). Finally, the original and the current location of the building were documented (i.e. urban, industrial, maritime, rural, etc.), alongside the original and current use (residential, industrial, offices, etc.).

3.3 Displacement pushover on selected case study

Cyprus is a seismic prone area. Up till 1979, there was no regulation in Cyprus concerning design against seismic action, while in 1979 “Short Seismic Measures” were introduced, that were not mandatory. The first “Cyprus Seismic Code” was made mandatory in 1994, while in 2012 the Eurocodes replaced local Codes.

Given that historic concrete structures in Cyprus were designed only for gravity loads, any restoration procedure must take into consideration both the safety of the public, as well as the historic fabric. In order to limit excessive restoration requirements, correct assessment of the structural capacity of existing heritage structures, especially against earthquake loading, must be adopted; therefore, the Displacement Pushover analysis is incorporated.

This section reports on an example of the Displacement Pushover analysis, performed on one of the listed buildings selected in the framework of CONSECH20. The structure in reference is the Old Municipal Market in Nicosia, Cyprus. The Market was built in 1965, following a demand from the Greek Cypriot community after the division of the old city of Nicosia in 1963, which meant that Greek Cypriot retailers lost their original retail space, located in the North of the city. In the last couple of decades, the use of the market declined and the Municipality of Nicosia has been exploring new uses for the space. Between July 2018-2019, the building was offered as a multi-use space to a group of young artists etc. It has now been decided that the market will be renovated to host RISE Centre of Excellence.

The structure consists of four parts, separated by structural joints. In this paper, only the west

part is analysed (Fig. 2). The latter comprises of a two storey R/C moment frame with 3 walls at one side of the plan, leading to eccentricity. The ground floor height is 4.45 m and the 1st floor is 3.10 m. More information on the structural system may be found in Georgiou et al. [24,25].

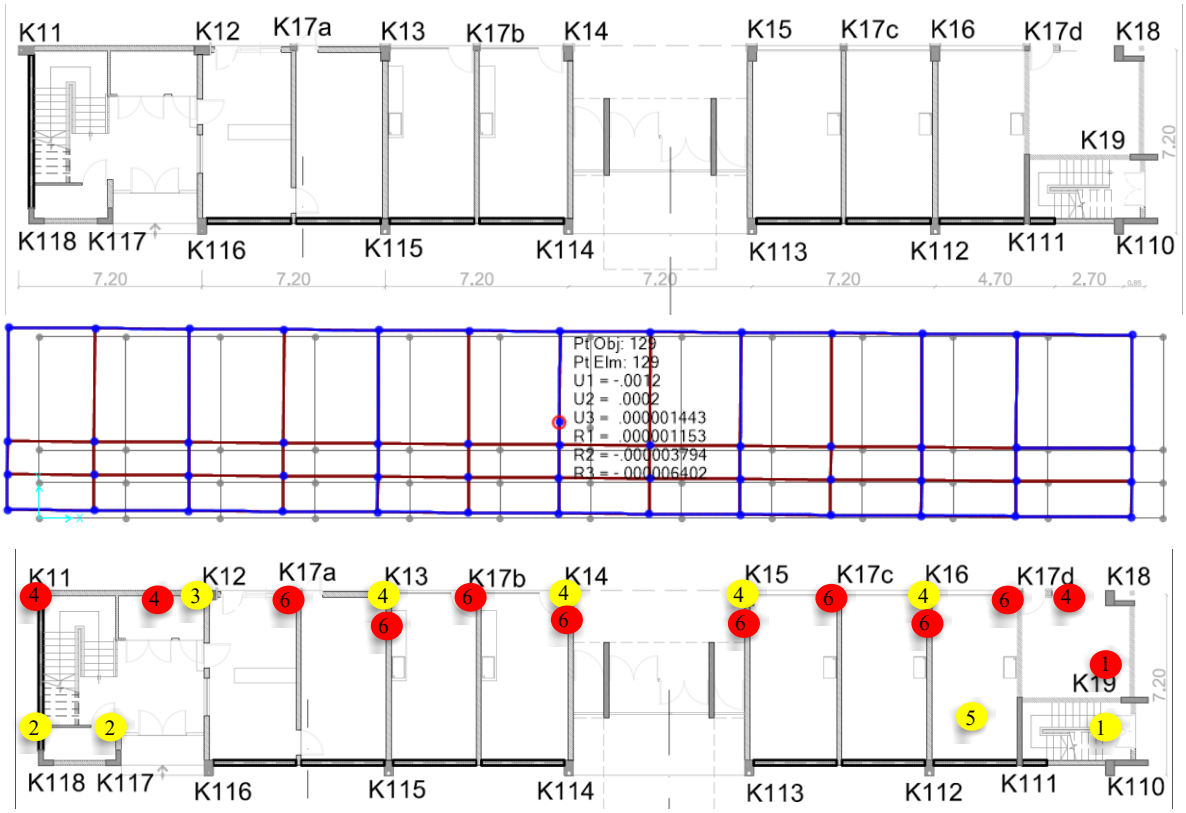


Figure 2: (Top) West part ground column denomination, (Middle) 2nd mode translational in the x-axis with a period of T_2=0.77 sec, 93% of translational mass participation and (Bottom) Displacement control pushover progressive failures in X-direction

Figure 2 also shows the 2nd mode shape of the structure, derived from a 3D model in SAP2000 [12]. Equations 1 and 2 were used to calculate the shear forces that can be transferred by the two walls acting on the X-direction of the structure, K18 and K110. In the special case of the K110 wall, which is not connected directly to the slabs, due to the adjacent staircase, but only to beams, the shear that can be transferred to the wall is the one delivered by the adjacent beam. The relation between the slab's shear and the shear at the base of the wall in the ground floor is estimated as [25]:

$$V_n = V_{wall} \cdot \left(\frac{h_{gr}^3}{h_{fl}^3} \cdot \left(\frac{1}{\Phi_{gr}} - 1 \right) - 1 \right) \tag{3}$$

Table 2 shows the capacity shear of the diaphragm connected to wall K18, as well as the wall shear forces for failure of the collector in K18 and the connecting beam in K110. The above results are used in the Displacement Pushover analysis of the structure and are compared to the same analysis, without taking into account the disconnection of the slabs from the walls.

The results are compared in Fig. 3, for imposed displacements in the X-direction, where especially for wall K110, despite its great stiffness, the shear delivered is limited by the connecting beam. Therefore, the capacity of the structure as a whole is 25% less than that estimated by assuming diaphragmatic action of the walls to the rest of the vertical elements. Furthemore, by incorporating the procedure for determining the target displacement of the structure in the two cases, as per EC8-Part 1, Annex B, the period of the SDOF in the case of the K110 connection only to the beam is higher than that of the diaphragmatic connection, as shown in Fig. 3, leading to the conclusion that the actual structure, which has lower stiffness, will be requested to exhibit greater displacements for the design seismic action.

Table 2: Shear capacity of walls due to connection with diaphragm

	$\rho_{sl}=\rho_{st}$	V_n				V_{wall}
		ACI max	ACI	double yielding	yielding ρ_t	
K18	0.00452	678.87	403.77	228.91	888.81	287.38
K110	0	-	-	-	-	115.80

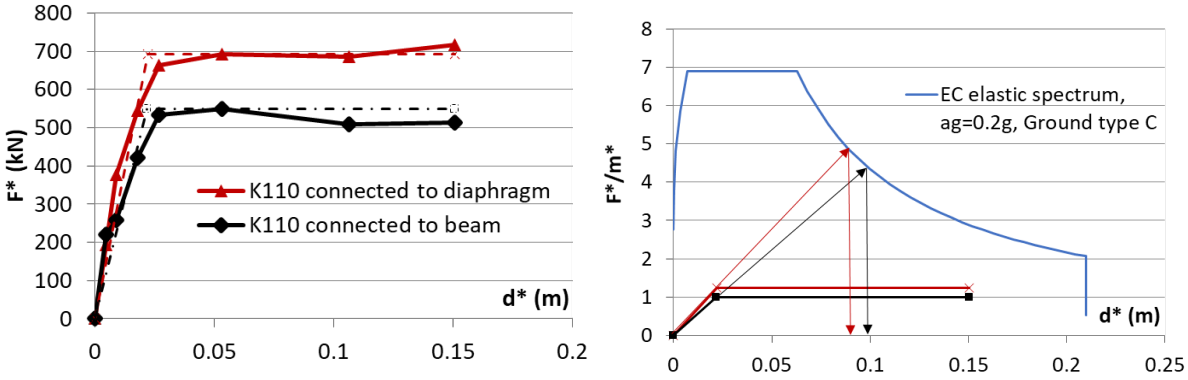


Figure 3: (Left) Base Shear-Control node X-displacement and (Right) Determination of target displacement based on EC8-Part 1, Annex B, in the cases of diaphragmatic connection of K110 and connection only with adjacent beam

4 CONCLUSIONS

- There are parallel accounts regarding the future of historic R.C. structures. On one hand, it is irrefutable that their protection has been delayed, based on a number of different rationales, starting from the uncertainty in R.C. conservation methods, and extending to cost, and of course the lack of (or the lag in) coercing political will towards their protection. On the other hand, there is a move towards the appreciation of such structures by a wider audience (from architects to engineers, as well as artists and beyond), which in turn pushes institutions to take real steps towards their protection. Time is of course of the essence.
- The social aspect of historic structures is essential and more needs to be done in order for conservation research to become really interdisciplinary. In Cyprus, many of the historic R.C. buildings have been found to have an interesting social background and importance, which can in turn be used in order to not only argue for their protection, but also to propose their restoration and rehabilitation, in combination with a use which

will enhance their social importance and appreciation by the wider society.

- Historic reinforced concrete structures present inherent challenges regarding their restoration, as possible methods of retrofit are limited by the demand to preserve the architectural concept. In order to limit excessive restoration requirements, correct assessment of their structural capacity, especially against earthquake loading, must be adopted.
- Ignoring the possibility of plastic hinge formation at the collector zones between the diaphragm and structural walls leads to overestimation of the base shear capacity and underestimation of the expected displacements.

Acknowledgements. The authors would like to acknowledge funding by the Republic of Cyprus through the Cyprus Research Promotion Foundation (Project P2P/JPICH_HCE/0917/0012). They would also like to thank Nicosia Master Plan for providing access to records and test results for the structure under study.

REFERENCES

[1] Heinemann, H.A. Why historic concrete buildings need holistic surveys. In: Proc. Int. FIB Symp. 2008 - Tailor Made Concr. Struct. New Solut. our Soc., (2008), pp. 103–8.
[2] Macdonald, S. *Concrete: Building Pathology*. John Wiley & Sons, Inc., (2008).
[3] ICOMOS ISC20C. Approaches for the conservation of twentieth-century architectural heritage. Madrid Document. (2014).
[4] EN Eurocodes. Assessment and retrofitting of buildings. EN 1998-3. Brussels: CEN/CENELEC; (2005).
[5] Japan Concrete Institute. Guidelines for Assessment of Existing Concrete Structures (2014).
[6] fib Bulletin No. 24. Seismic Assessment and retrofit of reinforced concrete buildings. Lausanne, Switzerland: International Federation for Structural Concrete (fib), (2003).
[7] NZSEE. The Seismic Assesment of Existing Buildings. 1st ed. New Zealand: Ministry of Business, Innovation and Employment and the Earthquake Commission, (2017).
[8] FEMA P154. Rapid Visual Screening of Buildings for Potential Seismic Hazards: A Handbook. 3rd ed. Washington, D.C. ATC: FEMA, (2015).
[9] ASCE/SEI 31-03. ASCE 31-03: Seismic Evaluation of Existing Buildings. American Society of Civil Engineers, (2004).
[10] ASCE/SEI 41-17. Seismic Evaluation and Retrofit of Existing Buildings. Reston, Virginia, (2017).
[11] Priestley, M.J.N. Myths and Fallacies in Earthquake Engineering, Revisited. Pavia Italy, Rose School, (2003).
[12] CSI. SAP2000: Static and Dynamic Finite Element Analysis of Structures v14.0, (2009).
[13] Fotopoulou, M., Thermou, G.E., Pantazopoulou, S.J.. Comparative evaluation of Displacement-based vs. Force-based pushover analysis of seismically deficient R.C. structures. In: Roeck, G. D., Degrande, G., Lombaert, G., Muller, G., editors. Proc. 8th Int. Conf. Struct. Dyn. EURODYN 2011, Leuven, Belgium, (2011), pp. 427–33.
[14] Syntzirma, D.V., Pantazopoulou, S.J. Deformation capacity ofR.C. members with brittle details under cyclic loads. ACI Spec Publ 236 (2007).

[15] Wyllie, L.A.J. Structural Walls and Diaphragms - How they Function. In: White, R.N., Salmon, C.G., editors. Build. Struct. Des. Handb., New York: John Wiley & Sons, Inc., (1987), pp. 188–215.
[16] EN1992-1-1. Eurocode 2. Design of Concrete Structures. . (2004).
[17] ACI Committee 318. Building Code Requirements for Reinforced Concrete and Commentary ACI 318R-08, (2008).
[18] Corley, W.G., Cluff, L., Hilmy, S., Holmes, W., Wight, J. Concrete Parking Structures. Earthq Spectra (2003), **12**:75–98.
[19] Pardalopoulos, S.J., Thermou, G.E., Pantazopoulou, S.J.. Screening Criteria to Identify Brittle R. C. Structural Failures in Earthquakes. Bull Earthq Eng (2013), **11**:607–36.
[20] Moehle, J.P., Hooper, J.D., Meyer, T.R.. Seismic design of cast-in-place concrete diaphragms, chords, and collectors: a guide for practicing engineers. NEHRP Seismic Design Technical Brief No. 3, produced by the NEHRP Consultants Joint Venture, a partnership of the Applied Technology Council and the Consortium of Universities for Research in Earthquake Engineering, for the National Institute of Standards and Technology, Gaithersburg, MD, NIST GCR 10-917-4 (2010).
[21] Pantazopoulou, S.J., Imran, I. Slab-wall connections under lateral forces. ACI Struct J (1992), **89**:515–27.
[22] Philokyprou, M. *Cyprus. In: Time Frames: Conservation Policies for Twentieth-century Architectural Heritage.* Carughi, U., & Visone, M. (Eds.). Routledge.
[23] Docomomo Cyprus. *Cyprus – 100 Most Important Building Sites and Neighbourhoods.* (2014).
[24] Georgiou, A., Ioannou, I., Pantazopoulou, S. Rehabilitation of 20th Century Concrete Heritage Buildings : the Case Study of the Municipal Market in Nicosia, Cyprus. SEDEC 2019 Conf. Earthq. Civ. Eng. Dyn., Greenwich, London, (2019).
[25] Georgiou, A., Ioannou, I., Pantazopoulou, S. Contribution of slab wall connections to the seismic resistance of structures. 4th Hell. Conf. Antiseism. Des. Eng. Seismol., Athens, (2019).

12th International Conference on Structural Analysis of Historical Constructions
SAHC 2020
P. Roca, L. Pelà and C. Molins (Eds.)

CONSERVATION OF HISTORICAL REINFORCED CONCRETE STRUCTURES

ILDIKÓ BUCUR-HORVÁTH[1], JÁCINT VIRÁG[1*]

Technical University of Cluj-Napoca
15 C-tin Daicoviciu Street, 400020 Cluj-Napoca, Romania
e-mail: ilbucurro@yahoo.com, jacint.virag@dst.utcluj.ro (*corresponding author)

Keywords: Historical Reinforced Concrete Structure, Cupola, Hollow Block Slab

Abstract. *During the 20th century, reinforced concrete brought historical structural systems back into modern times, transforming them into high-performance structures. Reflection on early reinforced concrete structures of two ancient structural systems, the dome and the girder, is presented through two Transylvanian monuments: the reinforced concrete cupola of the Hungarian Theater of Cluj, the earliest structure of this type, and the one-way hollow block slabs of Villa Tataru designed as a duet, by Gio Ponti and Elsie Lazar. Diagnosis and therapy of the hundred-year old, "new" historical structures are described. Uncovering these remarkable, but nearly unknown buildings, the paper intends to contribute to the understanding of cultural heritage and to raise public awareness towards the fundamental principle of UNESCO: "The cultural heritage of each is the cultural heritage of all".*

1 INTRODUCTION

Part of European architectural heritage is built with reinforced concrete structures. The epoch of the reinforced concrete affirmation started in the 19th century when large fields of its application opened. Due to its special qualities, there is a large competition in finding various forms of using reinforced concrete. During the 20th century, reinforced concrete brought historical structural systems back into the modern times, making them high-performance structures. At the beginning of 20th century, the state of knowledge of RC structures was far from a full understanding of the behavior of this new material and certain arbitrariness was present in the design [9].

The paper involves structural assessment for two historical reinforced concrete structures from Transylvania, to uncover their state-of-the-art. Large investigations have brought out a lot of interesting and useful structural elements. They will be extensively commented.

The spherical dome of (1909-1910) is the very first reinforced concrete cupola of large span, with basic ring, supported by masonry piles. The reinforced concrete shell is two-layered according to the antique Roman model in more ways than one.

2 THE FIRST LARGE-SPANNED REINFORCED CONCRETE CUPOLA

Bridging large spans, the dome as structural form accompanies the whole history of architecture. The roots of the cupola building can be found in the ancient dwelling constructions. Archaeological discoveries have pointed out that the inhabitants of Jericho (8th millennium BC) lived in circular houses covered with clay-brick cupolas. Curved and bound wood pieces, knitted reed, and clay were used in other cases and places. The fact that the Latin name of the cupola – *domus* – means *dwelling* cannot be a mere coincidence. Archaeological discoveries highlighted that the dome had also been used by the architects of antique Egypt and Mesopotamia. This tradition was continued by the Sassanid-Persian architecture. The cupola building was essentially improved by the Romans. Their domes were built of stone or/and "opus caementitium" (Roman concrete) cast in timber or stone shuttering. Thereupon, the cupola accompanied the entire series of architectural ages: Early Christian, Byzantine, Islamic, Roman, Gothic, Renaissance, Baroque, Neo-classical and modern architecture as well [1].

The "renaissance" of the domes is related to the discovery of the reinforced concrete. The concrete dome of St. Ursula parish church in Munich, built-in 1897, marks the beginning of concrete domes [2] and is a link between the traditional massive dome structures and modern thin shell construction.

The first modern domes mentioned by technical references were built in the first two decades of the 20th century. In chronological order, the very first ones are the little cupolas of the Anatomical Institute of München (1905-1907) placed around a central space, by Max Littman (It was demolished) and the other is the famous Jahrhunderthalle from Brest (Breslau, Wroclaw) with a span of 65 m (1910-1911) [1]. The latter is a dome (but not a shell structure) with radial arches bound by horizontal rings, built of reinforced concrete by architect Max Berg and professor Willy Gehler.



Figure 1: The original neoclassical building (postcard from 1914)

In Cluj-Napoca (Kolozsvár, Klausenburg) a similar early reinforced concrete cupola covers the central hall of the Hungarian Theatre and Opera house [3]. It is the very first large-spanned reinforced concrete cupola in the world. It features all characteristics of classic cupolas: it has

an “opeion” and “tambour” at the top and a perimeter ring at the bottom which rest on vertical masonry pillars. The original form of the building is presented in Figure 1.

Documents prove that the building was designed in 1909 as a Summer Playhouse. It was intended for operetta, comedy performances, and for social events. The original project is preserved in the National Archives of Hungary and it is signed by the architects Frigyes Spiegel and Géza Márkus, from Budapest and by the constructor Alajos Réhling from Kolozsvár (Cluj) on the 25th July 1909 (Figure 2). Reinforcement plans were approved by the engineer and professor Aladár Kovács Sebestyén. The diary news of the time confirms that the building was inaugurated on the 18th of August 1910 [1].

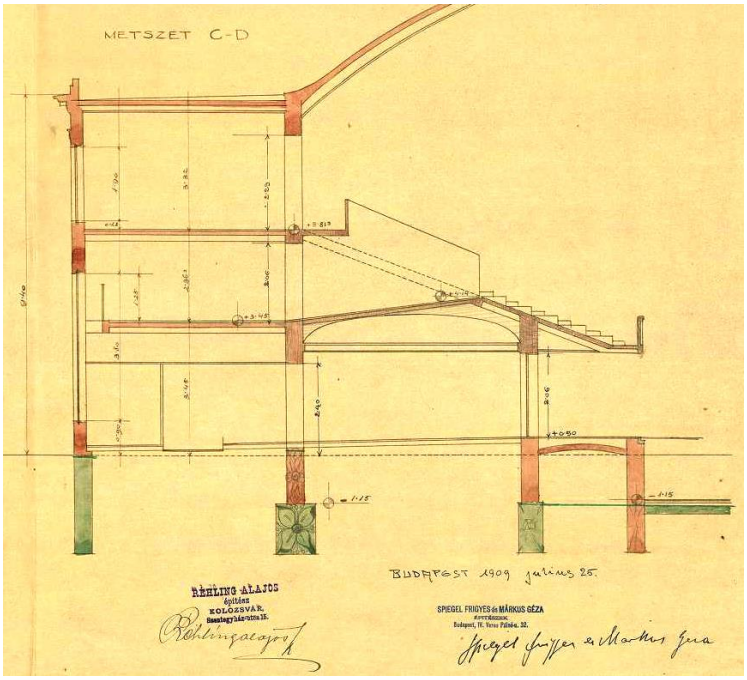


Figure 2: Section plan with the authors signatures, original project from 1909, National Archives of Hungary

The whole building is composed of several blocks corresponding to a classic organization of the space for the required function (Figure 3). The main block is that of the public hall on a circular plan, covered with a spherical cupola. More than half of its perimeter is surrounded by a circular corridor, covered with a toric shell, also unique at that time. The stage building arises behind the main hall and continues with the storage and cloakrooms.

The spherical dome was designed and built with a 21.98 m radius of curvature, 27.72 m span, and 5.00 m rise and has been preserved to this day (Figure 4). There are two superposed thin shells: a 12 cm thick upper shell with its thickness slightly increasing towards the basic ring and below – at 25 cm – another shell with a constant thickness of 8 cm, which supports the ornamental plastering of the ceiling. The two shells are connected to each other by steel wires of 2 mm in diameter placed every 40 cm apart. On the top of the cupola, there is a tambour of reinforced concrete with a wall thickness of 16 cm, 6.00 m in diameter and 1.30 m in height.

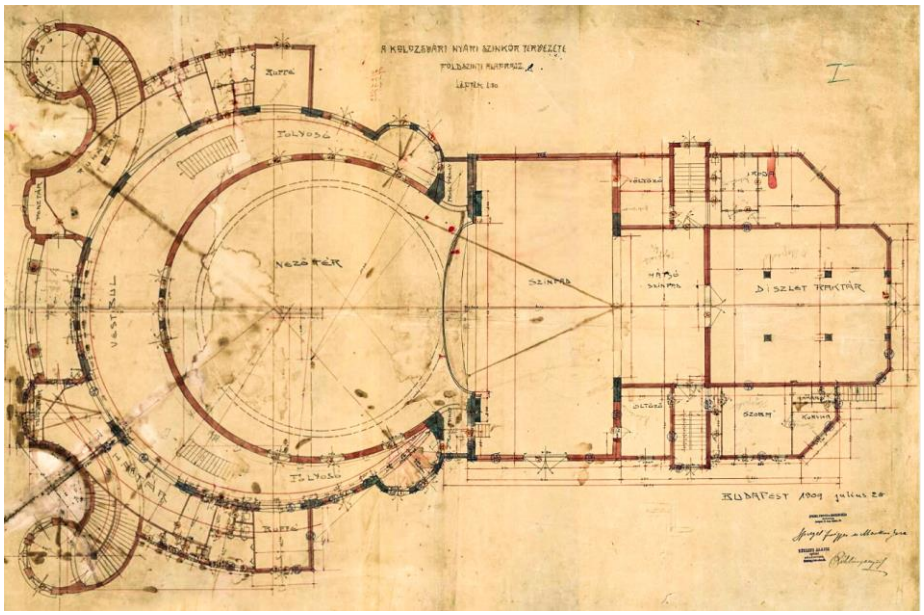


Figure 3: Ground floor plan, original project from 1909, National Archives of Hungary

The tambour is covered with a small reinforced concrete cupola of 60 cm rise. Under this small cupola, the dome has a central opening with a diameter of 2.00 m. The large candelabrum is suspended through this opening and is sustained by a special mechanism. The reinforcing of the main cupola (identified in the region of the central opening) consists of two meshes of steel bars of 8/200 mm in meridian and 8/300 mm in circular direction in the upper shell and the same mesh, as well as an additional Rabitz net, in the lower shell.

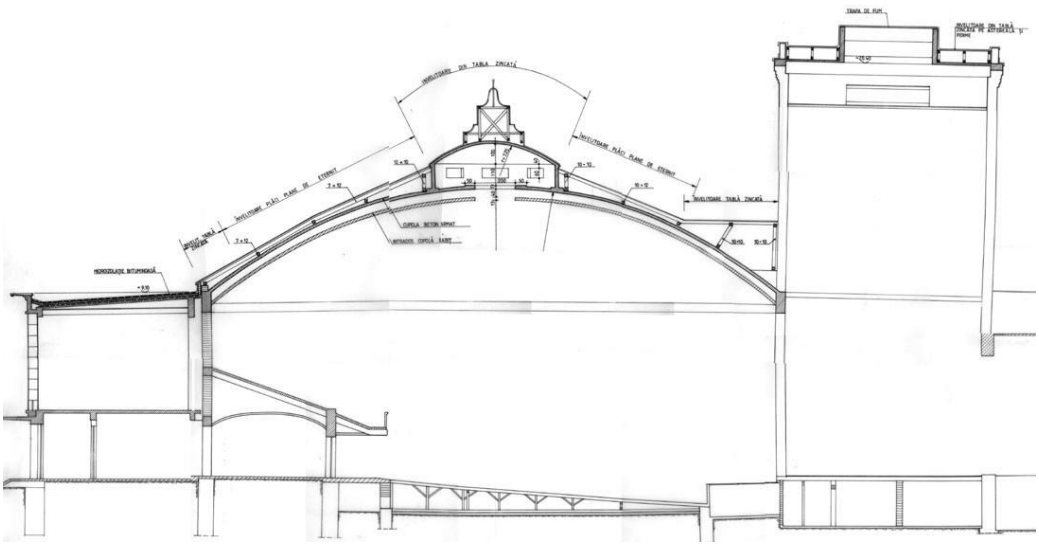


Figure 4: Cross-section: timber structure over the cupola, intervention project from 1959

The two-layered cupola lies on a basic ring with a cross-section of 50 x 110 cm along the perimeter excepting the portion neighboring the stage side (60 x 160 cm). Very ingeniously, the base ring is connected to the surrounding constructive elements, mainly slabs, at the same level, which block the lateral displacement, arising due to the action of the normal meridian forces on the edges of the shell. The cupola is supported by vertical pilasters of masonry placed under the perimeter ring. Research performed on the cupola revealed a well-balanced structure. In 1959, due to functional reasons, the old staircases were demolished and a new, larger entrance hall with large interior staircases was added. The two lateral pavilions were also demolished. Thus, the neoclassical facade disappeared. The external look of the cupola was also influenced: a timber structure supporting the covering was placed over the reinforced concrete cupola, raising the external profile line and hiding the central tambour. Due to these changes, the building, unfortunately, lost its original neoclassic personality [4] (Figure 5).



Figure 5: Street view 2020 – Hungarian Theathre Cluj, Karoly Miklos photographer

Fortunately, the main block comprising the public hall and the corridor under the dress circle, covered by reinforced concrete shells, remained unchanged. The building has been used continuously since it was built. No intervention was made on the reinforced concrete dome. No structural deficiencies were observed. However, safety reasons would require a new investigation.

The large investigation made on the building was very helpful for the two-layered cupola. It is interesting to remark that, while the upper shell surface is regular and smooth, the superior face of the lower shell is rough and unprocessed. The two shells are connected by steel wires, as mentioned above. Actually, the mesh of reinforcement of the lower shell is connected by the wires included in the upper shell. However, the inferior cupola is not suspended from the superior one. That is proved by the fact that most of the connecting wires are not straightened. All these facts make possible the assumption about the way the cupola was erected. In this

order:

(1) First, the upper shell was cast in a shuttering sustained by a general scaffolding. The connecting wires are included in this reinforced upper layer.

(2) The reinforcing mesh of the lower shell was suspended on the upper shell by the connecting wires, and a Rabitz net was fixed on its lower face. The casting of the lower shell was not possible otherwise than horizontal strip by horizontal strip beginning from the basic ring, performed by plastering (according to the antique Roman model). In this way, the lower shell became self-bearing, supporting its own weight as well as the ornaments of the ceiling.

During the investigations in several points near the central opening of the cupola, the measured compressive cylinder strength was between 26 – 30 N/mm^2. The concrete of the shell was well compacted. No damages were observed.

The characteristics of the reinforcing steel are: the grade corresponds to the characteristic yield stress of 360 N/mm^2, high ductility, and 8-10 mm size plain smooth bars. Mezzanine floors are made of reinforced concrete, of 22 cm depth by 6 cm width ribs, spaced at 27 cm and a 6 cm topping, covering spans up to 6,0 m. One-way hollow block slabs were formed by placing the blocks on a wooden formwork and concreting the reinforced ribs.

3 ONE WAY HOLLOW BLOCK SLAB

The second structural form examined was the ribbed slab. The beam, as one of the most intuitive bending structures, has been widely used from ancient times, even in the absence of beam theory and calculus. Adjoining beams, one-way slabs were formed. With the development of reinforced concrete construction, during the late 19th and early 20th century, the ribbed slab becomes a convenient structure and remains in use until today. To reduce formwork and ease the construction process, infill blocks can be introduced between the ribs. Mass fabrication of optimal shape infill blocks fostered the spread of hollow block slab construction. Voided blocks are used to reduce the weight of slab, offering easy installation with minimal formwork. Such slabs were designed in Gio Ponti's office, to be built in the villa of professor Tataru, in Cluj-Napoca.

Villa Tataru, built in 1938, is peaceful and modest: it was meant to be just a home, designed for the comfort of daily life, for a happy and fulfilled life [5].

The restoration process has recently started. Despite interventions during the lifetime of the building, the main form and structure has been preserved. Today, however, it requires rehabilitation. Aiming at minimal intervention, intensive structural research was performed under the authors' supervision. Complete documentation has been done, concerning history, geometry, materials, construction techniques, and structural works. The slab over the salon required special attention because excessive deformation has been observed at the midspan. Qualitative analysis of reinforced concrete slab was limited, because of the hollow block system, used as formwork, covers the bottom of the slab (Figure 7). In order to decide the structural intervention, the causes of damage had to be first determined [6]. Consequently, an investigation was carried out on the structure. The depth of reinforced concrete slab was found to be 24 cm, made of 8 cm width ribs at a spacing of 24 cm and 7.5 cm thick topping.

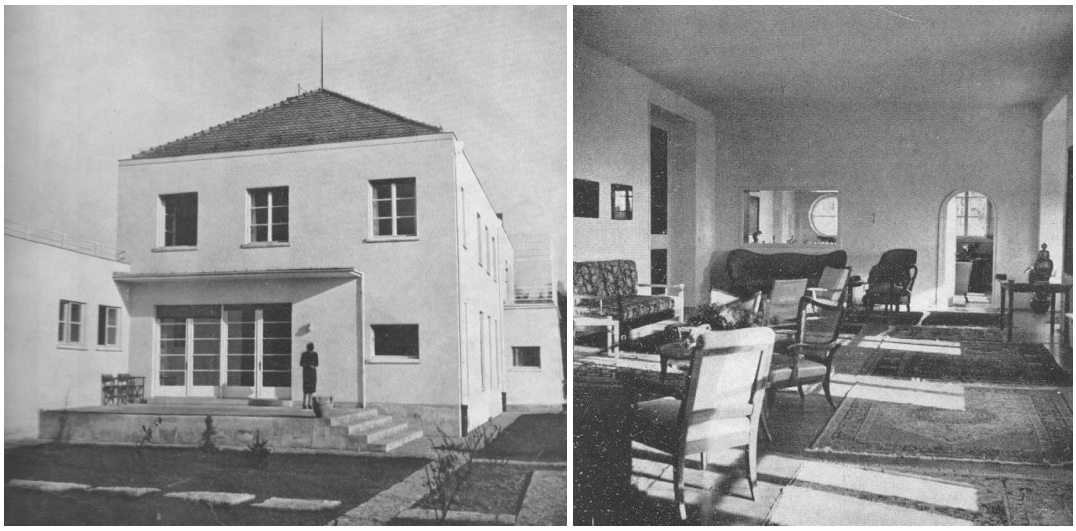


Figure 6: Original building: West side and salon [5]

The quantitative approach was based on material and structural tests, monitoring, and structural analysis. The compressive strength of the concrete was established by testing of cores and prism cut from the slab, while the modulus of elasticity was established by testing the prisms. The average cylinder strength of concrete is 28,2 N/mm^2, for the top surface and lower strength on the ribs, due to poor compaction of concrete. For serviceability assessment, the test results can be considered at points where likely minimum strength and maximum stress coincide, for deflection study of this simple supported slab, at the top surface of near midspan. The corresponding concrete class, based on EN 13791 recommendation, considering the number of samples (1) is C25/30.

$$f_{ck}=f_m - k \tag{1}$$

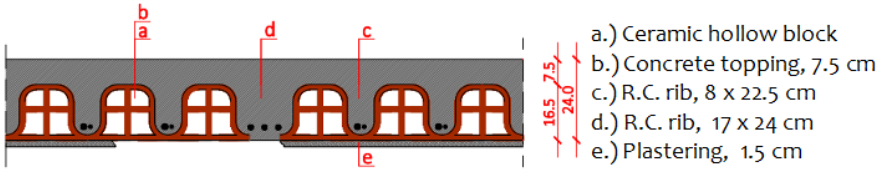


Figure 7: Cross-section of hollow block slab above salon

The value obtained for the Secant Modulus of Elasticity of slab concrete is 22.630 GPa. Rebar properties were determined on extracted samples, corresponding to a steel grade of S235C. Bottom reinforcement of thinner ribs are made of a 10- and 18-mm rebar, while the wider ribs (under partition walls) are reinforced with 3 pieces of 16 mm rebar. Concrete cover is 20 mm.

Uncertainty regarding hidden ribs and a deflection of 50 mm near the midspan of ribs indicated a need for load testing and monitoring, with the main purpose of proving structural adequacy, assuming that deflection is from the construction stage, due to a possible formwork settlement. A non-destructive static load test was carried out on the critical location, monitoring

the structural behavior, especially deflection for demonstration of serviceability.



Figure 8: Sandbags as test loads added over the slab

The maximum load of 3.5 kN/m was applied incrementally using sand bags (Figure 8). The problem of ensuring that one way spanning members under test are actually subjected to the assumed test load is often difficult, due to load sharing effects. Isolation of ribs subjected to test from the surrounding structure would be preferred but saw cutting of monument is not acceptable.

Measurement of deflection under this design load is used to demonstrate satisfactory performance. With no such precaution measure in European standards, the deflection limit, where test loads needs to be removed, was established according to ACI 318 [7] provision, as 6.5 mm (2).

$$\textit{deflection limit} = (\textit{effective span})^2 / (20\,000 \times \textit{member depth})\ [\textit{inches}] \quad (2)$$



Figure 9: Slab Deflection measurement with displacement transducers

Displacement transducers, clamped to independent support, at midspan and ¼ points (Figure 9) measured and transmitted deflections to acquisition data center. Plastering was removed from

the bottom of wider rib, for crack width monitoring. The rest of the ribs remained covered by the ceramic elements and plastering.

A structural analysis of slab strip was carried out using ATENA (Advance Tool for Engineering Nonlinear Analysis). The model contains the reinforced concrete elements, meshed with 3D FE, and non-structural elements (plastering, hollow blocks, partition wall) were considered as loads.

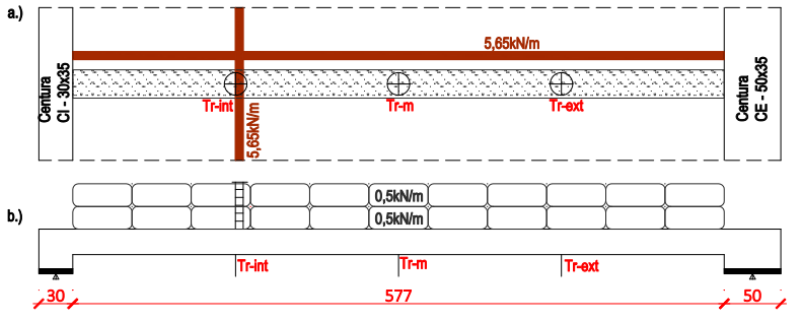


Figure 10: Slab strip scheme (a) plan and (b) section

Like the in-situ test, loads were added incrementally, considering the same step of 0.5 kN/m. The maximum deflection measured at midspan is 0.27 mm, for load step 7, corresponding to a distributed load of 3.5 kN/m (figure 11). Although test loads were applied symmetrically, due to load sharing and stiffening effect of partition walls, slab deformation is not symmetrical, having different values in quarter points.

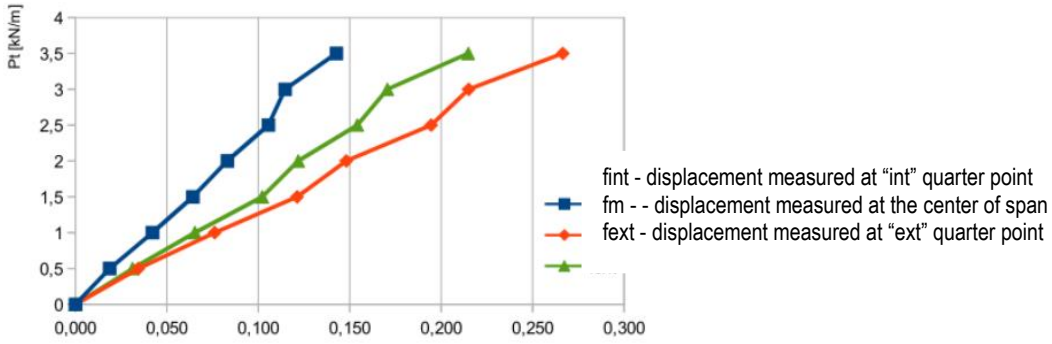


Figure 11: Measured deflection during load test [mm]

The numerical analysis results were calibrated in a conservative way, obtaining for the seven equivalent load steps almost 1 mm deflection. Dead load is not counted as a load step, but one can observe that it produces a 1.2 mm deflection (figure 12). The 27th load step corresponds to a uniform distributed load of 13.5 kN/m, which is not the ultimate load, but a satisfactory characteristic serviceability limit load, causing cracks of maximum 0.3 mm width. This demonstrates the initial assumption concerning construction stage deflection of slab.

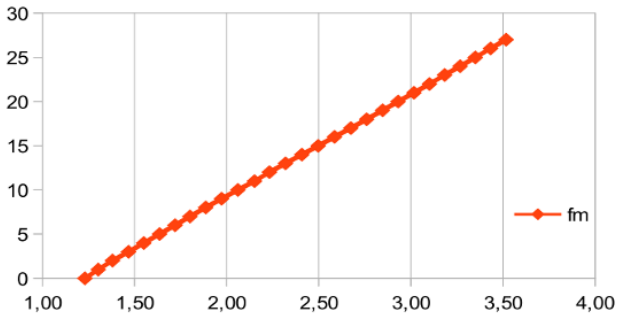


Figure 12: Calculated deflection for 27 load steps [mm]

4 CONCLUSIONS

- The Hungarian Theatre of Cluj and Villa Tataru foreground sources of cultural heritage value in the dimensions of (a) cultural resource, involving technical, artistic, and spiritual merits; (b) live document providing outstanding technical achievements, from which societies can still learn and improve by studying and using; (c) contribution to cultural diversity and global cultural wealth [8].
- The cupola of the Hungarian Theatre of Cluj, described here, is the first large-spanned reinforced concrete cupola in the world. Despite its age, the building seems to display good safety. The ensemble was initially well conceived from both, structural and architectural point of view. No intervention was made on the reinforced concrete dome. But the architectural intervention was unfortunate, like many others. Representing the very first large-spanned reinforced concrete cupola, it has an exceptional historical value. It has to be protected. Its preservation requires careful monitoring and maintenance.
- Gio Ponti's building in Cluj, Villa Tataru, reflects its creator's belief that architecture results in the harmony of form and function. The need for conservation of this heritage led us to conduct extensive investigation, including in-situ loading of deformed slab. Demonstration of the ability to sustain required loads, brings into attention the additional aspect of authenticity besides the respect for original concept, materials and construction techniques, the respect for imperfections (deformations).
- Any intervention on a historical building has to be performed with great care. Besides the general demands concerning functionality and structural reliability, the rehabilitation process must comply with specific requirements regarding authenticity. In this sense, the rehabilitation decision and technical solution should be principle-based but, in the same time, it should be aware that every case is a unique challenge. The specialist must establish the priorities in preserving authenticity, without neglecting the functional and structural reliability of the building [3].

REFERENCES

[1] Bucur-Horváth, I. and György, M. E., Cupola as a structural element and way of architectural expression. *International Symposium „Building Envelopes as Architecture's Messages"*, Universita degli Studi di Napoli Federico II, (2003), pp. 214-224.

[2] Rehm, J.: The first concrete dome in Germany? Church building using modern techniques. *Building Knowledge, Constructing Histories, Volume 1: Proceedings of the 6th International Congress on Construction History (6ICCH 2018)*, Brussels, (2018).
[3] Bucur-Horvath, I.; Popa, I.; Bulbuk, M. and Virág, J.: Historical constructions - Authenticity and adaptation to the modern demands. *Proceedings of the 6th International Conference Structural Analysis of Historical Constructions Preserving Safety and Significance,* Bath UK, (2008), DOI: 10.1201/9781439828229.ch17
[4] Bucur-Horváth, I.: Reinforced Concrete Shell Structures in Romania as the 20th Century Heritage*, Proceedings of IASS-APCS 2012 Symposium from Spatial Structures to Shell Structures,* Seoul, Korea, (2012).
[5] Lazar, E.: Una villa in Romania, *Domus (magazine) no. 136*, Milan (1939)
[6] International Scientific Committee on the Analysis and Restoration of Structures of Architectural Heritage (ISCARSAH): ICOMOS Charter - Principles for the analysis, conservation and structural restoration of architectural heritage (2003).
[7] ACI 318, Building code requirements for reinforced concrete structures. American Concrete Institute, (2014).
[8] Roca, P.; Lourenco, P.B. and Gaetani, A.: *Historic Construction and Conservation. Materials, Systems and Damage.* Routledge, (2019).
[9] Foti, D.: Shear Vulnerability of Old Historical Existing R.C. Structures. *International Journal of Architectural Heritage: Conservation, Analysis, and Restoration*, vol. 9, issue 4, 2015, pp. 453-467, DOI: 10.1080/15583058.2013.800920

12th International Conference on Structural Analysis of Historical Constructions
SAHC 2020
P. Roca, L. Pelà and C. Molins (Eds.)

DECAY PATTERNS AND DAMAGE PROCESSES OF HISTORIC CONCRETE: A SURVEY IN THE NETHERLANDS

G. PARDO REDONDO[1*], S. NALDINI[2] AND B. LUBELLI [3]

[1]Chair of Heritage & Architecture, department of Architectural Engineering + Technology
Technische Universiteit Delft
Julianalaan 134, 2628BL Delft, The Netherlands
e-mail: g.pardoredondo@tudelft.nl (*corresponding author)

[2]Chair of Heritage & Architecture, department of Architectural Engineering + Technology
Technische Universiteit Delft
Julianalaan 134, 2628BL Delft, The Netherlands
e-mail: s.naldini@tudelft.nl

[3]Chair of Heritage & Architecture, department of Architectural Engineering + Technology
Technische Universiteit Delft
Julianalaan 134, 2628BL Delft, The Netherlands
email: b.lubelli@tudelft.nl

Keywords: Historic structures, Concrete, Decay patterns, Damage processes, Assessment

ABSTRACT.

Historic concrete buildings (end of 19th century – 1960s), because of their "experimental" character, require a specific approach to both survey and conservation. Although they were built with empirical approaches, some buildings show a fair state of conservation and resilience –even though they have already exceeded the 100-year threshold– while others of comparable age are in severe need of restoration.

As part of the European project CONSECH20, aimed at contributing to the conservation of cultural-heritage concrete buildings, this paper investigates what are the most common types of damage and hypothetical causes, and what direct and non-direct parameters can lead to a faster or slower deterioration of historic concrete in the Netherlands. The research is based on an initial screening study, which will be used as a basis for a larger research among the participant countries.

The current research is divided in three phases. Firstly, a selection of 15 case studies from the Netherlands are investigated; the selection was based on criteria of age, state of conservation and type of ownership. Secondly, the history and materials of the buildings are examined. Thirdly, an on-site visual survey is performed per each building, with pre-design templates, to identify types of damage, extent and severity. The data is then analysed combining different factors with a calculated index of severity. Results are discussed and contrasted to provide further clarification of the degradation of historic concrete. A fourth phase, not discussed in this paper, will use this methodology in a broader context, with a larger number of case studies in different countries.

The results indicate that the majority of types of damage are related to corrosion, being the hypothetical cause carbonation-induced corrosion. The outcomes of the investigation point out that the factors with a higher impact on the durability are the environment, the use and maintenance of the buildings, the existence of a sacrificial plaster in exposed elements, and the type of ownership.

Considering the limited number of buildings, the conclusions presented in this paper will be further contrasted with a larger number of case studies.

1 INTRODUCTION

Reinforced concrete (RC) is a 'young' material, used from the middle of the 19th century onwards. Initially, concrete was a secondary material, used mainly for planters and small objects [1]. By the end of the 19th century, RC was used as structural construction material for not only for modest buildings but for the early skyscrapers [2,3]. By the turn of the century, RC became a primary construction system. After WWII, RC developed into the first global construction materials and thousands of buildings were built worldwide.

As in any ground-braking new technology, the first reinforced concrete buildings were experimental. There was no experience or a solid scientific knowledge behind these pioneering structures. As a result, different design flaws can be now encountered in early concrete constructions such as lack of sufficient concrete cover, use of non-suitable materials in the mix design, low concrete and steel strength, or poor compaction among others [4]. Additionally, the corrosion damage encountered in early RC structures leads to loss of rebar sections (Figure 1), bond deterioration and cover delamination (spalling), which eventually can affect the structural capacity of the building.



Figure 1. Loss of rebar section due to corrosion in exposed concrete beam from 1921

By the end of the 1970s, concrete repairs had become a major issue, but until the 1980s there was not a full understanding of some of the problems affecting RC such as the carbonation-induced corrosion [5]. However, it still took years for the conservation practice to merit cultural heritage (CH) status to concrete buildings.

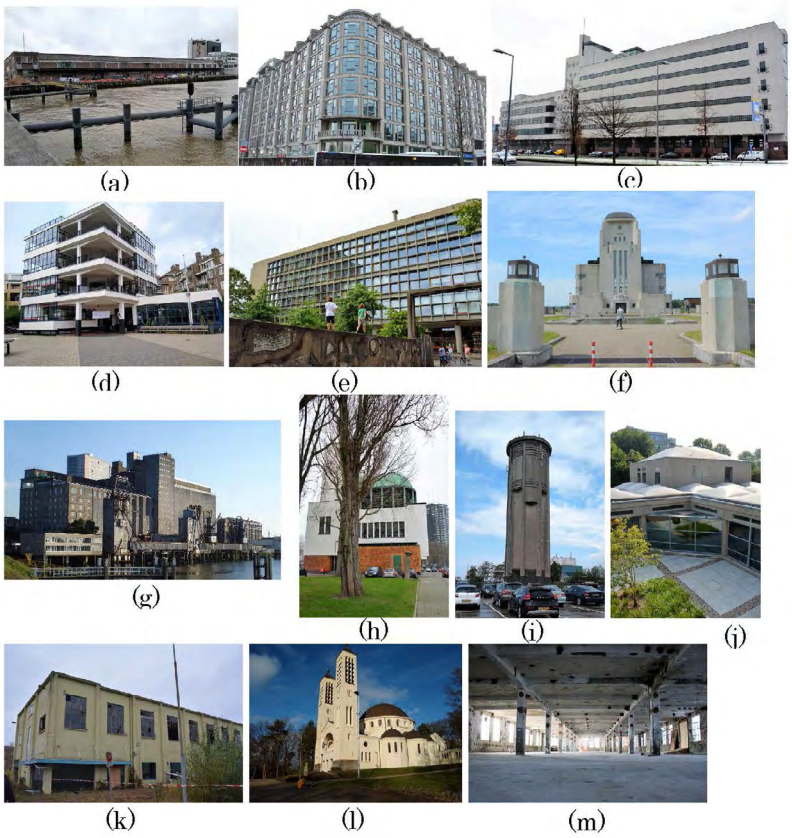


Figure 2. (a) Fenix II, Rotterdam (1922); (b) Groothandelsgebouw, Rotterdam (1953); (c) Haka buiding, Rotterdam (1932); (d) Open-air school, Amsterdam (1931); (e) Cygnus Gymnasium, Amsterdam (1956); (f) Radio Kootwijk, Kootwijk (1923); (g) Maassilo buildings, Rotterdam (1910, 1931, 1951) (source: Wikimedia: Wikifrits); (h) Maastunnel ventilation building, Rotterdam (1937); (i) Lisse water tower, Lisse (1925); (j) Burgerweeshuis, Amsterdam (1960); (k) Calve building, Delft (1908); (l) Cenakelkerk, Nijmegen (1915), and (m) Leerfabriek, Oisterwijk (1916)

One of the challenges in the (re-)use of historic concrete[1] buildings is to accurately predict the ongoing threats and how the buildings will further behave to these threats.

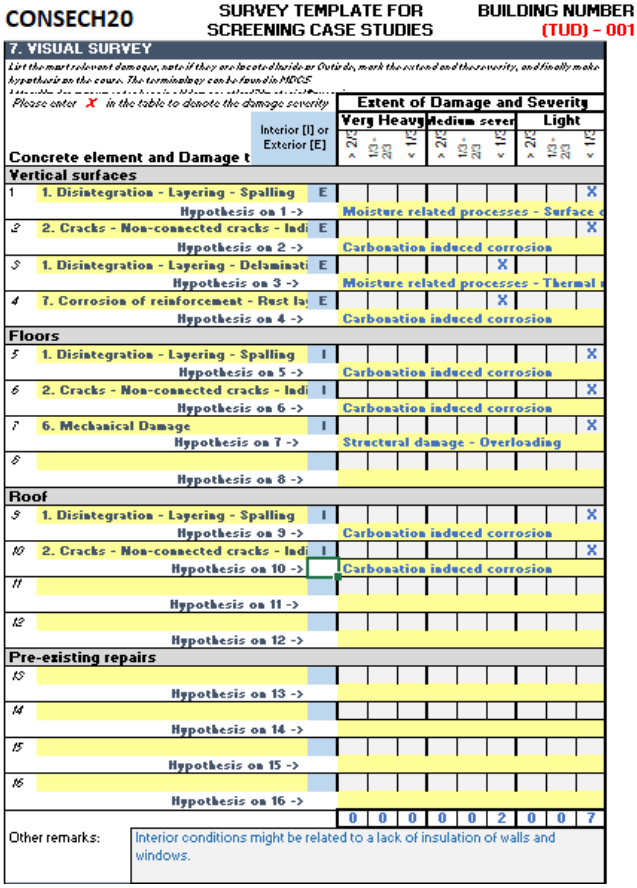
This paper is part of larger research project that aims at developing an improved methodology for the conservation of 20th century CH concrete buildings. The proposed research is fourfold. Firstly, 15 case studies in the Netherlands will be selected based on age, state of conservation and ownership. Secondly, a background research will be carried out to identify materials, uses, building characteristics, environment, and other parameters. Thirdly, on-site visual assessments will be performed at each building to record damage types, extent and severity. All the input will follow a standardized template previously designed to avoid misinterpretations, and to obtain uniform and comparable data. A severity index, related to the condition of the buildings, will be calculated based on the visual investigation, and contrasted with the different parameters in order to have an indication of the chief parameters affecting durability. Fourthly, a larger number of screening cases, from the participant countries, will be studied following the same methodology, to verify the initial results presented in here. This paper will focus on the first three of these four parts.

[1] In this article, the term “historic concrete” refers to reinforced concrete produced before the 1960s.

2 SCREENING CASES AND ON-SITE ASSESSMENT

The criteria for the selection of the case studies aimed to have a well-balanced number of buildings of different age, from the beginning of the 19th century to the 1960s; a representative number of privately and publicly owned buildings; and similar number of restored and in-need-of-restoration buildings. These two later parameters were included to have a broader context on the factors influencing the condition of the buildings. Another requirement for the selection of the buildings was that they needed to be accessible.

For each case study, a background investigation was performed about the history of the building and its characteristics (age, location, exposure, type of structure, façade, roof, exposed elements, finishes over concrete, materials, etc.). In the field, a visual assessment was performed to verify the theoretical investigation and to record types of damage and their hypothetical causes, extent and severity. The system MDCS[2] was used within the project to achieve a uniform damage identifictaon.



CONSECH20 — SURVEY TEMPLATE FOR SCREENING CASE STUDIES — BUILDING NUMBER (TUD) - 001

7. VISUAL SURVEY

List the most relevant damages, note if they are located inside or Outside, mark the extend and the severity, and finally make hypothesis on the cause. The terminology can be found in MDCS

Please enter X in the table to denote the damage severity

	Concrete element and Damage t	Interior [I] or Exterior [E]	Extent of Damage and Severity: Very Heavy (> 2/3, 1/3 - 2/3, < 1/3)	Medium sever (> 2/3, 1/3 - 2/3, < 1/3)	Light (> 2/3, 1/3 - 2/3, < 1/3)
	Vertical surfaces				
1	1. Disintegration - Layering - Spalling	E			X
	Hypothesis on 1 ->				Moisture related processes - Surface
2	2. Cracks - Non-connected cracks - Indi	E			X
	Hypothesis on 2 ->				Carbonation induced corrosion
3	1. Disintegration - Layering - Delaminati	E		X	
	Hypothesis on 3 ->				Moisture related processes - Thermal
4	7. Corrosion of reinforcement - Rust la	E		X	
	Hypothesis on 4 ->				Carbonation induced corrosion
	Floors				
5	1. Disintegration - Layering - Spalling	I			X
	Hypothesis on 5 ->				Carbonation induced corrosion
6	2. Cracks - Non-connected cracks - Indi	I			X
	Hypothesis on 6 ->				Carbonation induced corrosion
7	6. Mechanical Damage	I			X
	Hypothesis on 7 ->				Structural damage - Overloading
8					
	Hypothesis on 8 ->				
	Roof				
9	1. Disintegration - Layering - Spalling	I			X
	Hypothesis on 9 ->				Carbonation induced corrosion
10	2. Cracks - Non-connected cracks - Indi	I			X
	Hypothesis on 10 ->				Carbonation induced corrosion
11					
	Hypothesis on 11 ->				
12					
	Hypothesis on 12 ->				
	Pre-existing repairs				
13					
	Hypothesis on 13 ->				
14					
	Hypothesis on 14 ->				
15					
	Hypothesis on 15 ->				
16					
	Hypothesis on 16 ->				
			0 0 0	0 0 2	0 0 7

Other remarks: Interior conditions might be related to a lack of insulation of walls and windows.

Figure 3. Part of the standardized template designed for this research

The information was then conveyed into a standardized spreadsheet template (Figure 2), one per each building, to be used for all partner institutions. The template was based on the synthesis of different assessment forms [6–10]. To guarantee uniform and comparable data, and avoid misinterpretations, the parameters and values were previously agreed upon with the partners and programmed so that they could only be selected from a dropdown menu when entering the information in the spreadsheet.

3 RESULTS: COMMON DAMAGES AND FACTORS INFLUENCING DURABILITY OF HISTORIC CONCRETE

The investigation of the case studies in the Netherlands resulted in the following building characteristics:

- 40% of the investigated buildings were classified as “restored”, and 40% of the buildings were classified as “in need of repair”, the remaining 20% were classified as

[2] MDCS https://mdcs.monumentenkennis.nl

"Fair" and "Others".

- The original uses of the buildings were warehouses (33%), production/factories (20%) education (20%), and other uses (27%) The present uses of the buildings included business (33%), offices (20%), and not used - abandoned (20%), and other uses (27%).
- 67% of the buildings were privately owned, and 33% publicly owned.
- 87% had concrete elements exposed to the outdoors; from those, 69% were plastered, with at least 1 cm of cement mortar, and 31% were not plastered.

Regarding the types of damage and their hypothetical causes, the recorded results were:

- Spalling (26%), uniform corrosion/rust layers (19%) and non-connected cracks (17%). The rest of the damage types were scattered representing 4% or less (Figure 4).
- 85% of the damages were classified as "Light", 15% as "Medium Severe", and 0% as Very Heavy.

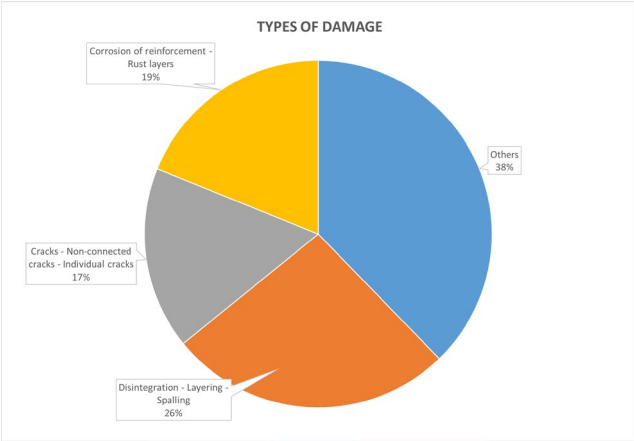


Figure 4. Common types of damage

- 90% of the damage processes were related to moisture-related issues, including corrosion, biological growth, surface condensation, and salt crystallization (Figure 5).
- It was assessed that 61% of the damage processes were related to carbonation-induced corrosion. This was supposed since the cracks and spalling observed were aligned with the reinforcement, there were no indication of chloride attack (e.g. pitting corrosion), and no structural issues were found (Figure 5).

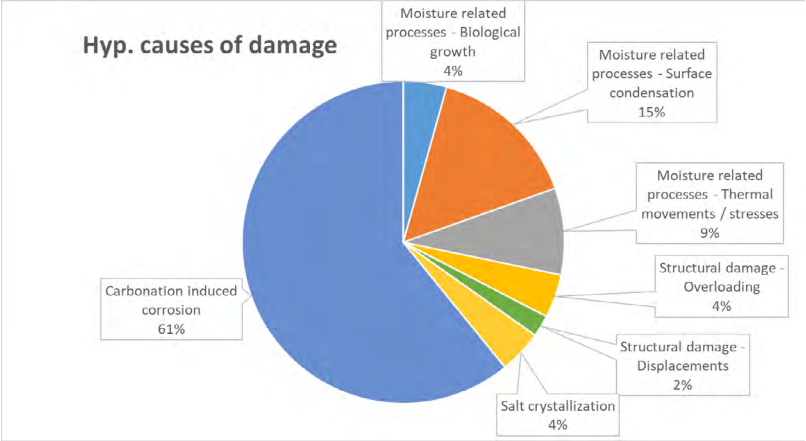


Figure 5. Common hypothetical causes of damage

To assess the state of conservation of the building, an index of "level of severity" was calculated. The different types of damage were multiplied by different coefficients depending on their extent and intensity of the damage, according to Equation 1. The resulting number provided an estimation, based on visual assessment, of the level of severity of the damage in the building, where the higher the number, the worse was the general condition.

Different parameters were then analysed against the level of severity to determine the factors affecting the degradation (Figures 6 to 11). In addition, the average age of each group of buildings and the number of the samples were analysed and shown in the graphs to better understand the relation with the age and its representativeness. The level of severity ranged from zero (very good condition) to 12 (medium-severe condition).

Equation 1

$$LI = \sum_{i=1}^{n} n_i * E_i * S_i$$

Where:

LI is the Level of severity used in Figures (6 to 11).

n_i is the number of cells marked in the same column of the template sheet, corresponding to the damages observed during the visual assessment (refer to Figure 3).

Ei is the coefficient regarding the extent of the damage as shown in Table 1.

Si is the coefficient regarding the severity of the damage as shown in Table 2.

Table 1. Coefficient regarding extent of damage

	Extent in the surface of the element		
	< 1/3	1/3 < x < 2/3	> 2/3
Coefficient **E** (Extent of damage)	1	2	3

Table 2. Coefficient regarding the severity of the damage

	Severity of the damage		
	Light	Medium severe	Very Heavy
Coefficient **S** (Severity of damage)	1	2	3

Regarding the relation between **age** and level of severity, the results showed a scattered distribution without a clear correlation (Figure 6). However, when linear trend line is plotted (Coefficient of determination R^2=9%), it is evident a weak correlation between age and level of severity, where the older the building, the worse is the condition.

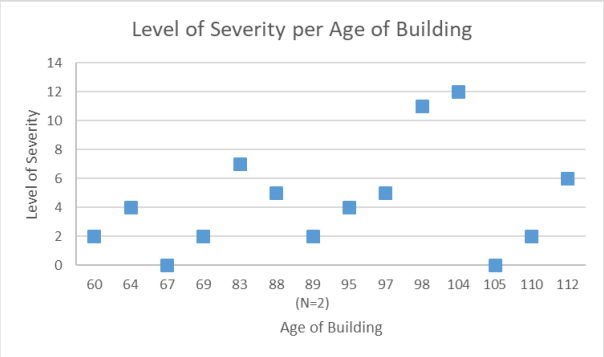


Figure 6. Graph representing level of severity with age of the buildings

Regarding the original use, position, and environment of the buildings:

- Office, religious and education buildings had the lowest level of severity. Whereas, production, warehouses and strategic services buildings (water tower, tunnel ventilation buildings, etc.) had the highest levels (Figure 7).

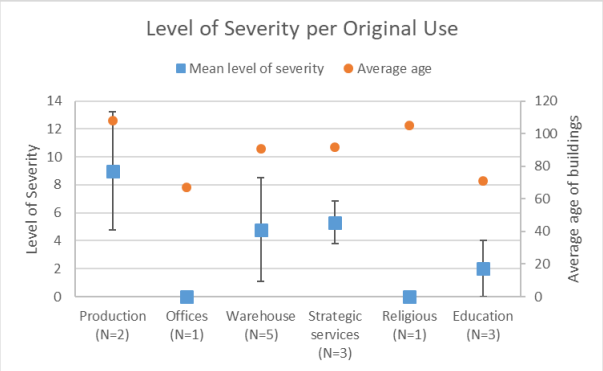


Figure 7. Graph representing level of severity per original uses of the buildings. "N" denotes number of buildings; orange dots represent mean age of buildings under the same category

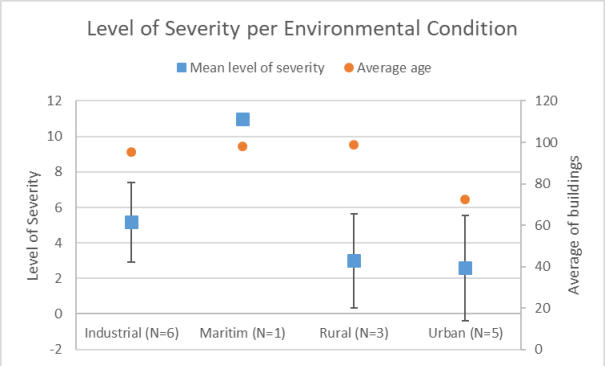


Figure 8. Graph representing level of severity per environmental condition of the buildings. "N" denotes number of buildings; orange dots represent mean age of buildings under the same category

- Damage to buildings located in maritime and industrial environment did show a higher level of severity than buildings located in urban and rural areas, all having

similar average age (Figure 8).

Regarding the monumental status (listed) and ownership of the building:

- Whether the buildings had monumental status or not did not have a noticeable impact on the level of severity.
- However, a tendency was noted regarding the ownership of the building (Figure 9). Damage in public buildings had in average a higher level of severity than private buildings, even though public buildings were on average slightly younger than private buildings.

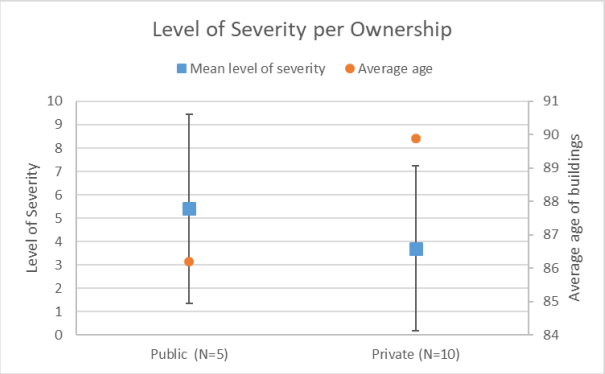


Figure 9. Graph representing level of severity per type of ownership

Regarding type of the façade (Figure 10), roof, and structure, there was not a clear influence on the level of severity of the damage found, as it followed the general tendency the higher the average age the higher the level of severity.

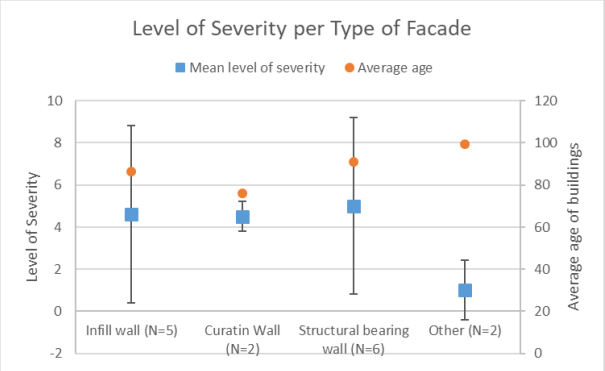


Figure 10. Level of severity per type of facade

Lastly, the reinforced concrete elements exposed to the outdoors rendered with a cement plaster had on average better performance than the exposed elements with no plaster or paint (Figure 11). It is important to note that the plastered elements had higher mean age than the non-plastered elements. On the other hand, the not-exposed elements, which are protected to weather and rain, resulted in higher level of severity. The main reason for this apparently incongruent result lays in the fact that one of the two case studies under this category was a leather fabric, where water and other chemicals were likely used inside the building.

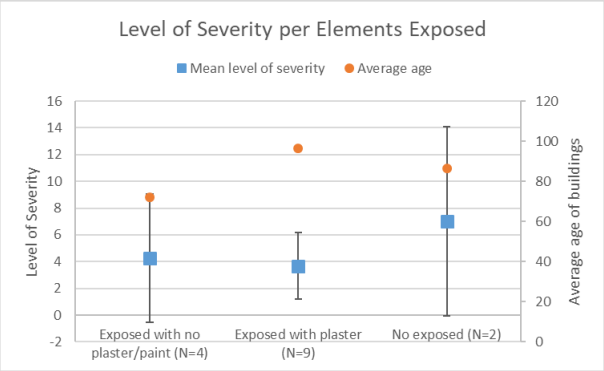


Figure 11. Level of severity per characteristics of exposed RC elements

4 DISCUSSION AND CONCLUSIONS

The current research is framed within the European project CONSECH20, which involves 5 participant countries and over 50 case studies. In this paper, a first sample of 15 RC buildings in the Netherlands built before 1960s has been studied. A background investigation of the building characteristics was carried along with a visual survey, to quantify the most common types of damage, extent and severity.

A standardized template was created to minimize misinterpretations and homogenise the data among the different countries. An indicator of level of severity was calculated and confronted with different building characteristics (e.g. original use, type of structure, type of façade, ownership, environment, etc.) to devise what parameters have a greater influence in the state of conservation of the concrete.

From the results of the 15 buildings surveyed in the Netherlands, it can be extracted that the main damage process affecting reinforced concrete buildings built before 1960 in the Netherlands is corrosion. This does not differ from other publications [11,12]; and can be attributed to a combination of thin concrete covers, higher permeability, and imperfection in the concrete such as honeycombs and cracks, which can be easily found in historic concrete buildings.

The foremost hypothetical cause of corrosion is carbonation-induced corrosion. The subsequent most common types of damage were non-connected cracks, rust layers and spalling. Other types of damage were generally not significant, almost aesthetical, and barely affected the serviceability of the buildings.

Based on this research, the following parameters seem to be relevant for the durability of the reinforced concrete:

- **Industrial and maritime environments**. Industrial areas tend to have higher concentrations of CO_2, which can increase the rate of carbonation in concrete. If the concrete cover is not thick enough, as is the case in some historic concrete buildings, the passivity layer protecting the reinforcement is destroyed due to carbonation. In addition the higher levels of pollution in these zones can increase the concentration of sulphates in the concrete [13], leading to other types of damage in the cement matrix such as the formation of ettringite [14]. In addition, high RH, as in the case of maritime zones, translates into higher moisture content (MC) in concrete. MC is the main factor influencing the electrical resistivity [15], or in other words, the higher

the MC in concrete, the lower the electrical resistivity and the higher corrosion rate [16–18]. In addition, if the building is within the splashing zone of seawater, the amount of chlorides ions in the concrete may increase, affecting the passivity layer of the reinforcement.

- **Use of the building**: Industrial and civil infrastructure buildings show more and severer damage types than the other building types. The increase of damages may be explained due to the discontinuity in the building use. In fact, the historical research revealed that 100% of the buildings constructed as warehouses or production factories were abandoned for more than 10 years in their lifetime. As any other building, the lack of the maintenance of historic concrete buildings has a great impact on the durability of concrete [19].
- **External sacrificial plaster**: Exposed RC elements with a cement-based plaster exhibited better performance against corrosion and other damage processes than RC elements without additional plaster. Rendering the exposed exterior concrete was a common practice in the Netherlands until the 1930s, apparently to hide the dull and rough aspect of raw concrete [4]. This is in line with the results of the case studies, since 100% of the buildings built before 1937 had a layer of plaster applied to the external concrete surfaces. A plaster layer can provide an additional protection against the ingress of CO_2, moisture, and other soluble substances, which may lead to corrosion and other damages in the concrete [20]. However, if the corrosion has already initiated, as it may be the case in historic concrete, the corrosion will not stop but the corrosion rate may decrease [21].
- **Ownership**: In view of the results, private buildings are in general in better condition than public buildings. Private buildings tend to have a more lucrative aim, and therefore the quality and appearance of the buildings tend to be better cared and maintained. As a new approach to tackle this issue, public-private partnerships are being used in different countries to help governments to manage the increasing costs and responsibilities typically carried by the public sector [22,23].

With a limited number of buildings, 15 cases in the Netherlands, this paper investigates different indicators to understand the chief factors affecting the degradation of historic concrete. As part of a larger project, this research aims to establish the basis for a greater understanding of the different factors affecting historic concrete buildings.

The main conclusions are:

1. Higher RH, CO_2 concentrations and levels of pollution, typically found in industrial and maritime environments, tend to decrease the durability of historic concrete.
2. A continuous use and maintenance guarantees that RC buildings, even over 100 years old, can extend their service lifespan.
3. Cement plasters in exposed elements can reduce the level of severity of the damages in the concrete.
4. Public buildings tend to be in worse condition than private ones.

ACKNOWLEDGEMENTS

This paper is framed within the JPI European project CONSECH20 Conservation of 20th century concrete Cultural Heritage in urban changing environments.

REFERENCES

[1] I. Marcos, J.T. San-José, A. Santamaría, L. Garmendia, Early Concrete Structures: Patented Systems and Construction Features, in: Struct. Anal. Hist. Constr., 2016: pp. 310–319. https://doi.org/10.1080/15583058.2017.1323241.

[2] G. Pardo Redondo, D. Friedman, B. De Miguel Alcalá, El ingeniero restaurador y los edificios de Nueva York, Loggia, Arquit. Restauración. (2017) 94. https://doi.org/10.4995/loggia.2017.6559.

[3] S.E. Wermiel, WERMIEL_Sara_CaliforniaConcrete-revised_layouted, Proc. Third Int. Congre Ss Constr. Hist. Cottbus, May 2009. (2009).

[4] H.A. Heinemann, Historic Concrete. From concrete repair to concrete conservation, TU Delft, 2013. https://doi.org/9789052694115.

[5] C.L. Page, K. Treadaway, Aspects of the electrochemistry of steel in concrete, Nature. (1982) 109–115. https://doi.org/https://doi.org/10.1038/297109a0.

[6] C. Baggio, A. Bernardini, R. Colozza, L. Corazza, M. Della Bella, G.D.I. Pasquale, M. Dolce, A. Goretti, A. Martinelli, G. Orsini, F. Papa, G. Zuccaro, Field Manual for post-earthquake damage and safety assessment and short term countermeasures (AeDES), 2007.

[7] Applied Technology Council (ATC), ATC-20 Detailed Evaluation Safety Assessment Form, (2005). https://www.atcouncil.org/atc-20.

[8] B. Taskin, K. Guler, U.M. Tugsal, M. Gencoglu, M. Celik, Z. Hasgur, M. Aydogan, A.I. Saygun, A Novel Post-Earthquake Damage Survey Sheet : Part I- RC Buildings, (2011).

[9] Applied Technology Council (ATC), Rapid Visual Screening of Buildings for Potential Seismic Hazards: A Handbook, Washington, DC, 2015. https://www.fema.gov/media-library-data/1426210695633-d9a280e72b32872161efab26a602283b/FEMAP-154_508.pdf.

[10] A.S. Arya, A. Agarwal, Rapid Visual Screening of RCC Buildings, India, 2002.

[11] C. Andrade, Propagation of reinforcement corrosion: principles, testing and modelling, Mater. Struct. 52 (2019) 2. https://doi.org/10.1617/s11527-018-1301-1.

[12] C. Van Steen, L. Koptsopoulou, E. Verstrynge, Historical and Structural Analysis of a Deteriorated Reinforced Concrete Structure: Student Residence Camilo Torres in Leuven (Belgium), RILEM Bookseries. 18 (2019) 2304–2313. https://doi.org/10.1007/978-3-319-99441-3_247.

[13] E. Marie-Victoire, M. Bouichou, T. Congar, R. Blanchard, Concrete cultural heritage in France—inventory and state of conservation, in: Concr. Repair, Rehabil. Retrofit. IV, 2015: pp. 343–350. https://doi.org/10.1201/b18972-49.

[14] M. Zhang, J. Chen, Y. Lv, D. Wang, J. Ye, Study on the expansion of concrete under attack of sulfate and sulfate – chloride ions, Constr. Build. Mater. 39 (2013) 26–32. https://doi.org/10.1016/j.conbuildmat.2012.05.003.

[15] D.A. Koleva, Corrosion and protection in reinforced concrete: Pulse cathodic

protection: an improved cost-effective alternative, (2007). https://repository.tudelft.nl/islandora/object/uuid%3A1d2af376-e92e-4864-91e4-499e53c83e75 (accessed June 15, 2019).
[16] P. Azarsa, R. Gupta, Electrical Resistivity of Concrete for Durability Evaluation: A Review, Adv. Mater. Sci. Eng. 2017 (2017) 1–30. https://doi.org/10.1155/2017/8453095.
[17] G. Markeset, R. Myrdal, Modelling of Reinforcement Corrosion in Concrete - State of the art, 2008. https://doi.org/10.1002/maco.200603899.
[18] M. Stefanoni, U.M. Angst, B. Elsener, Electrochemistry and capillary condensation theory reveal the mechanism of corrosion in dense porous media, Sci. Rep. (2018). https://doi.org/10.1038/s41598-018-25794-x.
[19] S. Macdonald, A.P. Arato Goncalves, Conservation Principles for Concrete of Cultural Significance, Los Angeles, 2020.
[20] Entreprise of the European Commission, REHABCON Manual. Strategy for maintenance and rehabilitation in concrete structures, 2004.
[21] Tekniska högskolan i Lund. Division of Building Materials., REHABCON Strategy for maintenance and rehabilitation in concrete structures. Work Package 2.3: evaluations of alternative repair and upgrading options: Final Report, Tekniska högskolan i Lund. Division of Building Materials., Lund, Sweden, 2004.
[22] S. Macdonald, C. Cheong, The Role of Public-Private Partnerships and the Third Sector in Conserving Heritage Buildings , Sites , and Historic Urban Areas, The Getty Conservation Institute, Los Angeles, 2014.
[23] N. Zahirah, M. Azizi, A. Abdul, M. Azizi, M. Din, Recurring Issues in Historic Building Conservation, Procedia - Soc. Behav. Sci. 222 (2016) 587–595. https://doi.org/10.1016/j.sbspro.2016.05.217.

12th International Conference on Structural Analysis of Historical Constructions
SAHC 2020
P. Roca, L. Pelà and C. Molins (Eds.)

EARLY CONCRETE STRUCTURES AND POST-PATENTED SYSTEMS: LESSONS TO PRESERVE EARLY 20th HISTORICAL HERITAGE

I. MARCOS[1*], L. GARMENDIA[2], I. PIÑERO[3], Z. EGILUZ[4], E. BRIZ[5] and A. GANDINI[6]

[1]Department of Mechanical Engineering, University of the Basque Country UPV/EHU
Paseo Rafael Moreno Pitxitxi 3, 48013 Bilbao, Spain
e-mail: ignacio.marcos@ehu.eus, www.ehu.eus (*corresponding author)

[2]Department of Mechanical Engineering, University of the Basque Country UPV/EHU
Plaza Torres Quevedo 1, 48013 Bilbao, Spain
E-mail: leire.garmendia@ehu.eus, www.ehu.eus

[3,6]TECNALIA, Basque Research and Technology Alliance (BRTA)
Parque Científico y Tecnológico de Bizkaia, Astondo Bidea, Edificio 700, 48160 Derio, Spain
E-mail: {ignacio.pinero, alessandra.gandini}@tecnalia.com, www.tecnalia.com

[4,5]Department of Mechanical Engineering, University of the Basque Country UPV/EHU
Paseo Rafael Moreno Pitxitxi 3, 48013 Bilbao, Spain
E-mail: {ziortza.egiluz, estibaliz.briz}@ehu.eus, www.ehu.eus

Keywords: Historical Structure, Reinforced Concrete, Pathology, Condition.

Abstract. *Reinforced concrete was introduced by patented systems into Spain towards the end of the 19th c. Early patents were effectively foreign trademarks, although Spanish engineers, architects and industrialists soon developed their own RC systems. Local builders would build structures with scarce little regard for calculated design and construction in the first decade of the 20th century. Nevertheless, as further knowledge was required, increasing research led to new RC standards in numerous countries, such as France and Germany. In the second decade of the 20th century, the use of patent systems declined. The teaching of RC started at the Spanish Civil Faculty where systems of scientific calculation were rapidly adopted, although no Spanish RC standard was drafted, unlike the situation in the leading European countries of that time. Hence, the RC structures that proliferated across Spain were mainly based on French or German standards. Spanish industrial activity began to develop in northern areas of the country where the use of new materials was pioneered over the following decades. Nowadays, some of those structures are listed heritage buildings. In this paper, some common features of 15 RC structures built between 1915 and 1936 are discussed, by focusing on their conservation problems. Preliminary structural reports from engineers, architects, municipal councils and, in some cases, the owners of the buildings are compiled with information on the pathologies affecting the buildings and analyses of*

structural morphologies, and steel and concrete strengths. The results of those studies are analysed, by connecting construction features with structural conditions, in order to gain a deeper understanding of their main characteristics and similarities. The findings will contribute to knowledge of heritage buildings, identifying key strategies for application in future rehabilitation works.

1 INTRODUCTION

In the mid-19th c., the inventive idea of Reinforced Concrete (RC) emerged when metallic elements, usually steel bars, were first used to strengthen the concrete mass. Some pioneering inventors and the dates of their patents may be mentioned, such as Lambot, in 1855, and François Coignet, in 1852, in France [1,2]; Wilkinson, in 1854, in the U.K. [1]; and Hyatt [3], in 1878, and Ransome [4], in 1884, in the U.S. In modern Europe, Joseph Monier is considered the principal inventor of RC, patenting a construction system with a wire frame covered with layers of mortar in 1867.

In the last decades of the 19th c. and the start of the 20th c., the construction of RC structures rapidly spread, as their main advantages over the separate use of masonry and steel structural materials came to be widely acknowledged: high durability (at the time and very mistakenly considered "almost eternal"), monolithism, versatility, acceptable mechanical characteristics, and very especially fireproof [5-7]. Its proliferation, based on the many patents from numerous countries, led to the launch of RC 'multinationals' such as Hennebique (France) and Wayss & Freytag (Germany). There was a proliferation of patents both in the U.S. (Goodman, Goodbridge, Jackson or Kahn) and Europe (Blanc, Coignet, Cottancin, Bordenave, Matrai, etc.).

The inventors made perhaps excessive efforts to protect their patented systems. It was assumed that the system specifications had been included the calculation of RC structures (floors, beams and columns) for the implementation of detailed reinforcements with sufficient strength for each architectural feature. Nevertheless, there were many totally experimental patents with no real scientific basis, and even the patents that had a degree of technical support were reluctant to disclose the scientific basis of their claims. At the turn of the century there were some catastrophic structural failures: a pedestrian bridge in Paris (1900), the Zum Bären Hotel in Basel (1900), the roof of a Madrid reservoir (the Third Deposit) (1905), and buildings in Berne (1906), and Milan (1908).

In the last decade of the 19th century, research into RC concrete started to expand, and design requirements and calculation methods became freely available in published form. Research was available on concrete vaults, arches, slabs, and beams, and subsequently columns. Likewise, the first courses on the subject were launched at the "École Nationale des Ponts et Chausses", Paris, in 1897. All these factors –scientific research, structural collapses, and access to academic publications- finally led to the enactment of various national regulations that greatly enhanced RC structural safety: Switzerland in 1903 and 1909, Germany in 1904 and 1907, France in 1906, Italy in 1907, Austria in 1907, the U.K. in 1907 and 1911, Russia in 1908 and 1911, Denmark in 1908, and the U.S.A. in 1908 and 1910 [8]. The combination of national standards and open access to RC knowledge ended the payment of royalties linked to patents, leading to a new panorama for RC construction. Both, patented

systems and patented free structures coexisted until WWI, although their demise after the first World War, saw the start of a new phase in its development based on knowledge and regulations.

Since the end of 19th c., RC structures have become a part of our Cultural Built Heritage. Its status as Heritage is a testimony to progress in science, economics, culture and society in its content, its technique, and its materiality. Its conservation and preservation contribute to our historical understanding of technological and social advances, as well as other events that may have occurred throughout that time [9]. This Heritage has invariably deteriorated, due to functional and typological obsolescence and irreversible modifications, inappropriate treatment, and inadequate conservation, often resulting in its abandonment and destruction. Its relevant innovative features for which it is recognized as Heritage clearly reflect the systems and materials used in its construction.

The first step for acceptable conservation, rehabilitation and maintenance is to gain knowledge of the construction techniques and the main features of the structures from that historical period. It should be focused on the targets for mechanical strength in compliance with the regulations at that time, especially in early RC structures, and durability of the concrete. Studies on structures built following patented systems are frequent [10-19], although structures built in the post-patent period are now becoming an interesting period of study too [20-26].

2 THE POST-PATENTED RC STRUCTURES OF SPAIN

In the last decades of the 20th century, the introduction of RC in Spain came later than in other European countries and was influenced by French patented systems. At the start of the 20th century, RC had become a relevant structural material, especially in civil and industrial constructions, still linked to patented systems up until around 1910. Whereas numerous Europeans countries enacted their own standards, structural safety regulations were unavailable in Spain until 1939 [27], the end of the Spanish Civil War.

From the point at which the patented systems had become obsolete at the end of 1910, up until 1939, the common references in Spain for structural concrete design and calculation were the French and the German standards [28]. Even though a Spanish Army standard was enacted in 1912, it was never applied in civil construction [29]. In fact, engineers based their RC design and calculations on foreign standards during the time between the end of the patent systems and the outbreak of the Spanish Civil War, assisted by the knowledge gained from their studies on RC, the first of which took place, in 1910, at the Faculty of Civil Engineers in Madrid.

The core industrial activity of Northern Spain, mining, ship building, and steel industries, pioneered the use of the new material, where most RC structures were built over the following decades. Numerous examples of RC constructions were built, although some have since been demolished, as a result of economic development and urban and social transformations. These lost examples of heritage were integral to the industrial and the social life of that day and age, and local government has now listed many remaining structures as heritage buildings that stand in testimony to that period of Spanish history.



Figure 1: Two examples of the buildings under analysis: a) Old Aquarium (San Sebastian), b) Villa Ducourau (Irun)

In this study, some common features of 15 RC structures built between 1915 and 1936 will be discussed: 10 from the second decade and 4 from the first decade of the 20th c., and 1 from 1936. All of them are listed heritage and none followed patented RC systems for their construction. Two examples are shown in Figure 1. A collection of 15 pathological structural studies are examined, developed by different architects and engineers as preliminary structural studies. Their common points are their construction in the period between the end of the RC patented systems and the outbreak of the Spanish Civil War, and their location in the Basque Country, north-western Spain.

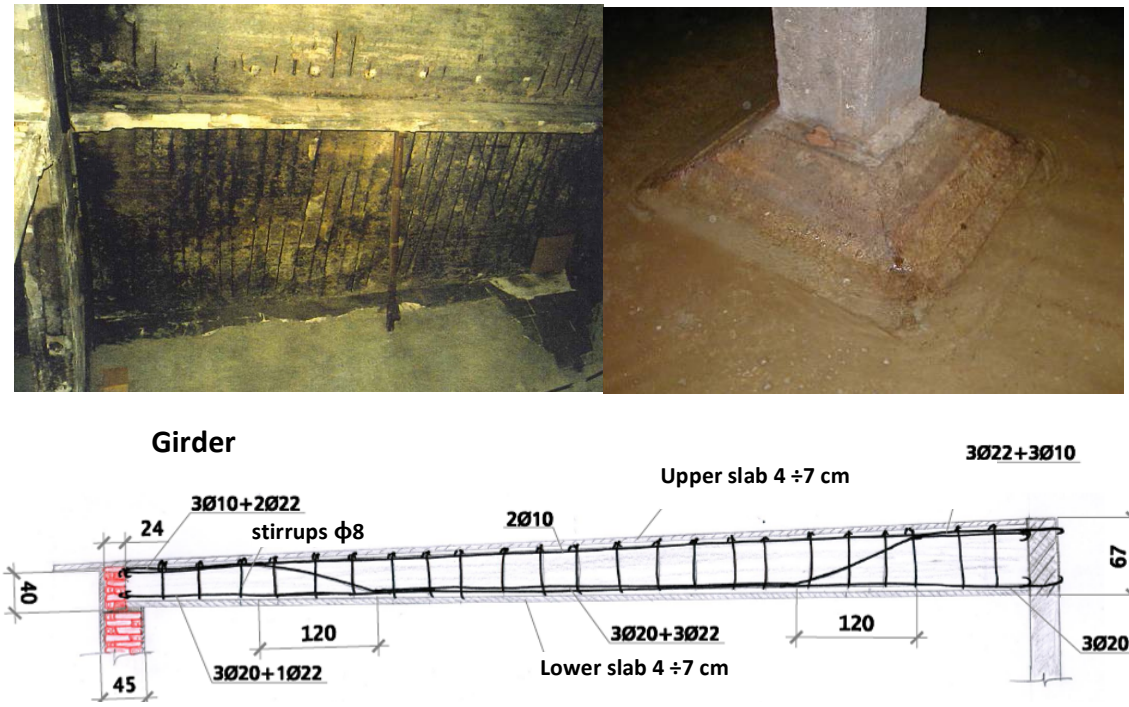


Figure 2: Usual structural layout: a) slab and narrow beams in structure Nr 3, b) trapezoidal foundation (structure Nr 2), c) beam reinforced scheme (structure Nr 6)

Also near all of then have similar structural schemes, with slabs, marrow beams, columns instead of walls and sometimes trapezoidal foundations (figure 2). The theoretical corpus for

these studies had been researched in relation to each specific construction in an appropriate way attending to location, age and owner's requirements for building use and the proposed objectives. The scope of the studies may therefore vary, but the methodology used in all of the studies was similar. However, the range of tests and the depth of analysis were conditioned by the purpose that the property served. The most common test of the concrete structure was its compressive strength, although various studies included data from steel strength, steel cover, concrete carbonation depth and chloride ions in the concrete mass.

3.1 Durability

Nearly all the studies included visual inspections for signs of pathologies. Issues related to durability were mainly observed: parallel concrete cracking in longitudinal reinforcements and the appearance of corroded reinforcements, even with cross-sectional reductions, all caused by the corrosion of steel bars. The results are summarised in Table 1; Figures 3 and 4 shows typical structural damage. This pathology was found to affect more than 80% of the structures and can be considered a widespread problem. The remaining 20% included one partial study of a building focused on well-maintained interior parts of the buildings where no corrosion would be expected due to exposure to the interior environment.

Table 1: Main pathologies detected in 15 RC structures

Concrete cracking parallel to reinforcements	87%
Appearance of corroded reinforcements	80%
Cross sectional reduction of steel rebars	67%
Pitting corrosion	53%
Dampness	60%

Environmental exposure to chlorides had affected the structures by approximately 46%, followed by seawater from tidal surges, spray and splash (33%) and by airborne salts (13%), while others had been exposed to moderate humid. It is relevant that more than 50% of structures showed pitting corrosion, connected with corrosion induced by chloride ions in the concrete. The studies concluded that nearly all of them were of internal origin, mainly due to use of coastal sand in the concrete mixture, a frequent practice in coastal areas before 1936. Only one structure was affected by environmental exposure to chloride. The use of chlorides in concrete was not prohibited in Spain until 1973 [30].



Figure 3: Typical rebar corrosion: a) lower side of a slab (structure Nr 5) b) detail of pitting (structure Nr 4)

Information on the carbonation depths of 9 structures was also ascertained. These depths were very variable, between minimum values of 9 mm and maximums of around 160 mm.

Whenever both measures, concrete cover and carbonation depth, were taken, it could be checked that the carbonation depth always exceeded the reinforcement bar depth. An exception was noted in two tests from a column in one the structures, where the depth was close to zero. The zone was in the tidal range, and the water saturating the pores prevented the penetration of air inside. Nevertheless, the columns were highly affected by pitting corrosion.



Figure 4: Cross section reduction in column (structure Nr 15)

3.2 Concrete and steel features

Although precast concrete was available in the period under analysis, it was not common, and all the structures under study were cast in situ. Nearly all the studies included an analysis of the concrete strength of extracted cores, sometimes, combined with ultrasonic velocity pulse tests. The results are summarized in table 2. They show a very variable strength with no regularity: mean strengths of between 9 and 43 MPa and characteristic strengths of between 8 and 30 MPa. The remarkable differences between the mean and the characteristic strengths in each structure were due to the usual variability in concrete strengths. These variations were caused by the methods used in dosing (usually in volume), mixing (low mechanization), on-site transport, compacting (ramming, formwork by hand hammering or a slide bar), and curing [31,33]. Poor mechanical tools for compacting frequently led to the addition of extra water to ensure workability, increasing porosity and variability and worsening the durability of the RC components [10].

Table 2: Concrete strength of extracted cores (MPa)

Structure Nr	1	2	3[a]	4[a]	5	6	7	8	9	10	12	13	14	15
Mean Strength	23	19	15	31 19	23	27	43	9	15	15	25	17	19	24
Characteristic Strength	19	13	13 8	23 13	10	21	30	7	12	10	24	10	10	17

a: two batches were considered

Although ribbed bars were standard, even in proprietary systems, in the United States, smooth bars were used for reinforcing concrete in Spain [32]. A practice that was confirmed by the observations of the structural reports. There were fewer tests on the steel rebars than on the concrete. The results shown in Table 3 showed higher strengths than the values calculated for yield strengths of 220 or 240 MPa, which were considered at the end of the 20th c. for smooth bars.

There were some difficulties obtaining rebar samples, because larger diameter rebars were not used for testing, due to the damage that could have been caused to the structure. The possible rolling effect on yield and tensile strength could not therefore be verified.

Table 3: Steel strength (MPa) of tensile tests

Structure Nr	1	3	4	7	7
Diameter (mm)	15	8	18	8,1	10
Yield strength (MPa)	298	314	311	274	311
Tensile strength (MPa)	396	398	426	383	502

3.2 Condition

Finally, an assessment of the structural condition was completed. Four categories were defined, depending on the severity of the deterioration, which yielded the following results:

- 3 structures with very low levels of damage, including incipient cracking, due to steel bar corrosion.
- 2 with a few pathologies, but with little structural damage; cracking due to corrosion was noted.
- 5 with severe damage, including structural safety risks.
- 3 with very high damage and with very high levels risk for stability and structural safety, including partial collapse, total steel cross-sectional reduction and severely damaged columns.

There was insufficient information to assess the condition of 2 structures, because their pathological analyses were only partial building studies in well maintained areas.

Over 50% of all structures had high levels of damage, mainly with problems of durability linked to steel bar corrosion. High levels of damage due to chloride-ion penetration were noted, especially caused by marine sand used in the concrete mix. This condition had dramatic consequences for the buildings under analysis: 40% had undergone total or partial demolition, while 40% needed structural repair and strengthening.

12 CONCLUSIONS

After analysing the pathological reports on all 15 structures built between 1915 and 1936, from the end of the RC patented systems until the outbreak of the Spanish Civil War, the following conclusions can be presented.

- The concrete structures under study were designed following foreign standards until

the Spanish standard was issued in 1939.

- Steel features were frequently not examined in the pathological reports, as their removal from the structure risked excessive damage. Where calculated values were needed, the features for smooth bars were taken from the literature. The test results were necessary, otherwise the mechanical features could have been underestimated.
- Concrete strength was very variable between structures and inside each structure. It was very common and was conditioned by dosage, mixing, *in situ* casting and compacting. Only two structures had characteristic strengths of under 10 MPa, even when variability reduced the characteristic strength. However, that conceptual difference was not common until the second half of the 20th century, after the period under analysis. The characteristic strengths must therefore be interpreted with caution.
- The structural condition of this group of structures had important consequences for their integrity and authenticity. Nearly 80% of them needed a complete structural intervention including total or partial demolition in 40% of cases.
- The damage was due to the combination of environmental exposure, low concrete cover and the influence of chloride ions that are the cause of steel reinforcement corrosion. An endogenous origin of chloride damage should therefore be investigated in structures near coastal areas.

The central message for the conservation of RC heritage is early and correct diagnosis for the provision of proper maintenance planning and to mitigate structural deterioration. A conservation strategy could include more specific dampness protection, and corrosion protection measures, such as cathodic protection, re-alkalinisation, and chloride removal.

Acknowledgements. The authors wish to express their gratitude to research groups: IT1314-19 (Basque Government) and GIU19/029 (UPV/EHU) and the funds from the University of The Basque Country (PPGA19/61). Furthermore, the researchers would like to thank the authors (engineers, architects, municipal councils and the owners of the buildings) of the pathological studies for their contribution to this study.

REFERENCES

[1] Collins, P. *Concrete: the vision of a new architecture*. Mc Gill-Queen's University Press, (2004).
[2] Coignet, F. *Bétons agglomérés appliqués à l'art de construire*. G. Jousset, Clet y Cia, (1861).
[3] Hyatt, T. *Improvement in composition roof, floors, pavements &c*. US patent 206112, July 16, (1878).
[4] Ransome, E.L., *Building construction*, US patent 305226, September 16, (1884).
[5] Burgos, A. *Los orígenes del Hormigón Armado en España*. Ministerio de Fomento, CEDEX-CEHOPU, (2009).
[6] Karas S. Unique Hennebique Bridges in Lublin, Poland. *Am J Civ Eng Archit* (2012) 1:47–51.
[7] Marsh, C. F. *Reinforced Concrete*. D Van Nostrad Company, (1904).
[8] Marcos I., San-José J-T., Garmendia L., Santamaría A. and Manso J.M. Central lessons

from the historical analysis of 24 reinforced-concrete structures in northern Spain. *J. Cult. Herit.* (2016) 20: 649–659.
[9] Instituto del Patrimonio Cultural de España, *Plan Nacional de Conservación del Patrimonio del siglo XX*. Ministerio de Educación, Cultura y Deporte, (2015).
[10] Hellebois A. Launoy A. Pierre C. De Lanève M. and Espion B. 100-year-old Hennebique concrete, from composition to performance. *Constr Build Mater* (2013) 44:149–60.
[11] Hellebois A. and Espion B. Tests up to failure of a reinforced concrete Hennebique T-beam. *Proc Inst Civ Eng - Struct Build* (2014) 167:81–93.
[12] Onysyk J. Biliszczuk J. Prabucki P. Sadowski K. and Toczkiewicz R. Strengthening the 100-year-old reinforced concrete dome of the Centennial Hall in Wrocław. *Struct Concr* (2014) 15:30–7.
[13] Gori R. Evaluating performance of RC beams using turn-of-the-century theories. *J Perform Constr Facil* (1999) 13:67–75.
[14] Wouters I. and Leus M. *Refurbishment of Industrial Buildings in Early Reinforced Concrete*. Third Int. Congr. Constr. Hist. Cottbus, (2009).
[15] Lewis M. *Monier and anti Monier - Early Reinforced Concrete in Australia,* Second Natl. Conf. Eng. Heritage, Melbourne, (1985).
[16] Marcos I. San José J.T. Cuadrado J. and Larrinaga P. Las patentes en la introducción del hormigón armado en España: caso de estudio de la Alhóndiga de Bilbao. *Inf La Construcción* (2014) 66:024.
[17] Grima R. Aguado A. and Gómez J. Gaudí and Reinforced Concrete in Construction. *Int J Archit Herit* (2013) 7:375–402.
[18] Marcos I. San-José J.T. Santamaría A. and Garmendia L. Early Concrete Structures: Patented Systems and Construction Features. *Int J Archit Herit* (2018) 12:310–9.
[19] Rosell J. and Cárcamo J. *Los orígenes del hormigón armado y su introducción en Bizkaia. La fábrica Ceres de Bilbao*. Bilbao: Colegio Oficial de Aparejadores y A. T. de Vizcaya, (1994)
[20] Onton H. Estimation of residual carrying capacity and restoration of the historic reinforced concrete shells and frames erected in Estonia, *WIT Transactions on The Built Environment* (2007) 407-417.
[21] Courard L. Gillard A. Darimont A. Bleus J.M.M. and Paquet P. Pathologies of concrete in Saint-Vincent Neo-Byzantine Church and Pauchot reinforced artificial stone. *Constr Build Mater* (2012) 34:201–10.
[22] Choi W-C. Picornell M. and Hamoush S. Performance of 90-year-old concrete in a historical structure. *Constr Build Mater* (2016) 105:595–602.
[23] Blanco A. Segura I. Cavalaro S.H.P. Chinchón-Payá S. and Aguado A. Sand-Cement Concrete in the Century-Old Camarasa Dam. *J Perform Constr Facil* (2016) 30:04015083.
[24] Picó Silvestre J.F. Arquitectura e ingeniería en Alcoy. 90 años del puente de San Jorge. *Inf La Construcción* (2017) 69:186.
[25] Damas L. Sagarna M. Uriarte J.A., Aranburu A. Zabaleta A. García-García F. Antigüedad A. and Morales T. Understanding the pioneering techniques in reinforced concrete: the case of Punta Begoña Galleries, Getxo, Spain. *Build Res Inf* (2019) 0:1–17.
[26] Garmendia L. Marcos I. Lasarte N. and Briz E. Damage assessment and conservation strategy for the largest covered market in Europe: the Ribera Market (Bilbao). *Int J Archit*

Herit (2018) 12:997–1018.
[27] Ministerio de Obras Públicas. *Instrucción para el proyecto y ejecución de obras de hormigón*, (1939).
[28] Taylor, P.W. and Thomson S.P. *Cálculo rápido de las construcciones de hormigón armado*, Oss, (1918).
[29] Gallego E. Estudios y tanteos. Cemento Armado: cálculo y aplicaciones, *La Construcción Moderna* (1918).
[30] Comisión Permanente del Hormigón. EH-73 *Instrucción para el proyecto y la ejecución de obras de hormigon en masa o armado*. Ministerio de Obras Públicas (1973).
[31] Espitallier, M.G. Régimbal, M. *Cours supérieur de béton armé*. Ecole Spéciale des Travaux Publics, Libre I (1931).
[32] De Zafra, J.M. *Tratado de Hormigón armado*. Voluntad (1923)
[33] Saurbrey, H. A. Plain and reinforced concrete construction. David Mckay Company, (1925).

12th International Conference on Structural Analysis of Historical Constructions
SAHC 2020
P. Roca, L. Pelà and C. Molins (Eds.)

HISTORICAL BUILDINGS MADE OF REINFORCED CONCRETE IN TIMISOARA IN THE BEGINNING OF THE 20TH CENTURY

RAZVAN A. OPRITA

Faculty of Architecture and Urban Planning (FAUT), Politehnica University of Timisoara, Traian Lalescu str. No. 2/A, 300223 Timisoara, Romania e-mail: razvan.oprita@upt.ro, web page: https://www.arh.upt.ro

Keywords: Banat Region, Reinforced Concrete, Heritage, Building types

Abstract. *At the end of the 19th and early 20th centuries, Reinforced Concrete was introduced as an innovative constructive system. Many industrial, agricultural, hydrotechnical and civil buildings have been built with structural systems incorporating reinforced concrete. The paper presents the historical context in which the Reinforced Concrete was introduced in Timisoara, the former capital of the Banat Region starting with the Habsburg Empire, the largest city in the western part of Romania. The use of reinforced concrete in constructive systems increases with the national urge, generated by the unification of the Romanian Principalities in 1918, of defining a national identity and a specific national architectural style. The paper will highlight the main architectural programs and the main historical buildings using reinforced concrete, from the beginning of twentieth century, which represents local cultural patrimony.*

1 INTRODUCTION

As well as 3D printing is a crucial technological and development moment for today's times and 21th century, so was the invention of reinforced concrete represented a defining technological evolution for the 20th century.

The history of Constructions, like the history of human civilization, is marked by technological, cultural and social evolutionary leaps. Until the 19th century, the constructive system was based predominantly on masonry (addition of finite elements, juxtaposed with each other), forming a stable and coherent assembly, having the centre of gravity in the construction design plan.

The 20th century is marked by reinforced concrete, a fluid material that takes the form of the vessel in which it is poured, and which expresses, ultimately, the malleability and fluidity of society. Architects like A. Peret, Le Corbussier, L. Khan, F.L. Wright, F. Candela or P.L. Nervi strove to define a new architectural language. The technical possibilities allowed by the new material have facilitated the construction of dynamic assemblies with the centre of gravity within the limit of the projection or even outside it.

Being only at the beginning of the 20th century and considering the amazing speed with which technology advances, we can only glimpse the changes of the digital information revolution and technological transformations of technology application or form finding. Nowadays we can already print constructions of clay, concrete or plastic.

New materials are constantly devised - materials that can be the basis for the redefinition of the future of constructions: Green Charchol or Recy-Block, Aero graphene, and in the topic of current research-Programmable Cement modified microscopic structure of cement in order to enhance its mechanical properties and in the same time minimizing the amount required. [1]

2 TO KNOW YOUR FUTURE, YOU MUST KNOW YOUR PAST-G. SANTAYANA

Reinforced concrete is today one of the most widespread building materials, having deep roots in the mist of time and in the history of construction. Concrete is a mixture of aggregates related to binders based on different types of cement. Although concrete is present in the history of human civilization from immemorial times, reinforced concrete has a short history. Reinforced concrete was invented, used and developed in the same period of time at the end of the 19th century, by several people, who for various reasons introduced reinforcement systems in their constructions.

In 1848 J.L. Lambot builds a rowboat using hydraulic concrete hull, having a skeleton of iron bars. In 1855 he patented and exhibited in Paris the rowboat. He is recognized as the first person to use reinforced concrete.

Francois Coignet, in 1852, in France builds the first structures of reinforced concrete (a four-story house) but not as improvements of the concrete property but as constructive reinforcement of the monolithic walls.

William B. Wilkinson in 1854 in England builds a two-level house using reinforced concrete slabs with iron bars. This is recognized as the first building to use reinforced concrete.

The exploratory period of reinforced concrete is completed with J. Monier, who in 1867 patented a construction method using reinforcement with iron rods in concrete. Professional gardener, J. Monier first uses reinforced concrete for making sustainable flowerpots and continues to perfect the material and system for pipes and basins (1868), reinforced concrete facade panels with iron (1869), bridges (1873), reinforced concrete beams (1878). At that time in Europe, reinforced concrete constructions were commonly referred to as the Monier System. In 1877, J. Monier developed and patented an advanced technology for reinforcing concrete in columns and beams by arranging iron bars in a "grid pattern”. In 1886 Monier sells the patent to the German company Wayss, which will spread the Monier system in Germany and Austria.

F. Hennebique's meeting with J. Monier at the 1867 World Exhibition in Paris opens for him the perspective of using the Monier system in the field of construction. In 1892, after a long period of research, Hennebique patented a complete system of constructions: pillars, beams and slabs, using reinforced concrete.

Engineer Ernest L. Ransome perfected and patented reinforced concrete with twisted steel bars, in 1894, thus opening a new era in the built environment. [2] [3] [4].

In Romania, the engineer Anghel Saligny is the one who introduced the reinforced concrete, for the first time, being a pioneer and an innovator in the field of construction. In 1884 he was ordered to build the docks and warehouses in Braila and Galati, where for the first time, in the country, in 1888, reinforced concrete was used. The cell walls were made of prefabricated elements cast into the ground and mounted in the work and for the first-time welded reinforcements were used for stiffening. In 1887 begins the design of the Fetesti-Cernavoda Railway and of the Cernavoda Danube Bridge, which was inaugurated in 1895 (Fig. 1). At that time, the largest section of it -190 m had the largest opening in continental Europe.

The bridge and viaduct system totaled 4088 m and was the third longest in the world [5].

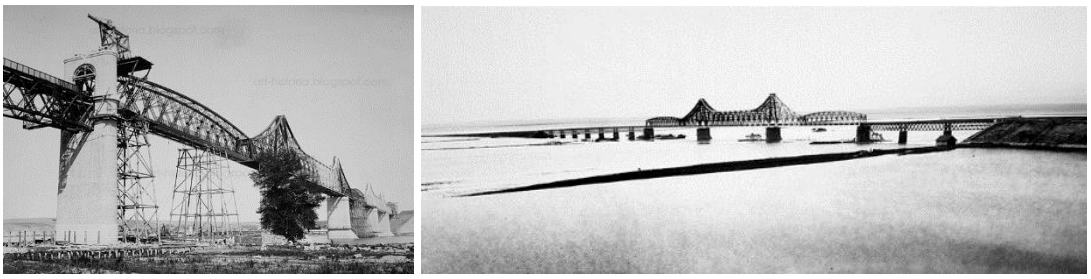


Figure 1: Cernavoda Bridge

3 HISTORICAL OUTLOOK OF BANAT REGION - ROMANIA

Banat Region is a geographical area as well as a historical regime that stands at the border between Central and Eastern Europe. Geographical is split between Romania (~ 2/3), Serbia (~ 1/3) and Hungary (~ 1%). The Banat region, since ancient, has been populated by a mix of Romanians, Serbs, Hungarians, Germans, Ukrainians, Slovaks, Jewish, French, Italian and more. It is an area of ethno-linguistic, cultural and religious interference, a state of fact that has not disappeared in time and which today represents a wealth reflected in architecture and social tolerance [6].

Banat has been part of Habsburg Monarchy and later the Austro-Hungarian Empire. Timisoara, the historic capital of Banat Region is the largest city in the Region and in the Western Part of Romania.

The Banat region, with this rich background of culture and influences materialized in the locally built fund, has become one of the main historical areas of Romania. The architectural heritage consists of a homogeneous mixture of specific styles: Viennese, Hungarian architecture, Neogothic, eclectic, secession, art nouveau, neo-Roman and neobyzantin, modernist. [7]

The end of World War II marked a crucial moment in the history of Banat and Romania. By uniting the Romanian Principalities from 1918, Banat comes back to Romania and from there, history becomes joined.

Banat, traditional has an Austro-Hungarian orientation, while Timisoara is also called Little Vienna, while Romania has a French orientation -Bucharest being called Little Paris.

In terms of education, including the technical one, we observe this similitude of influence - Timisoara is oriented towards Vienna and Budapest (L. Szekely, E. Ecker, M. Hubert, A. Suciu, V. Vlad) [8] and Bucharest towards Paris and Berlin (A. Saligny, I. Mincu, D. Germani, G. Constantinescu) [9]

The Great Union from December 1st, 1918, through which all the provinces inhabited by the Romanians were united, represents a turning point for the Romanian Modern State as well as for the national architecture. From the desire to have a common cultural identity, a strong national movement is started to create a national style rooted in Neo-Brancovenesc architecture and the vernacular and Byzantine tradition, in the popular port and in traditional way of life.

Architects like I. Mincu, N. Ghica-Budesti, G. Cerchez, P. Smarandescu or T. Socolescu lay the foundations of neo-Romanian architecture at the beginning of the 20th century, in the context of the historicism and the wave of nationalist emancipation of the times. Together with

Duiliu Marcu, I. Trajanescu and A. Suciu, the architect and engineer Victor Vlad took part in the creation of the National Style in Banat.

In the context of the economic development from the beginning of the 20th century generated by the industrial revolution - with repercussions also on the administrative structures and the consolidation of the large state structures, the new investments and programs of socio-cultural, administrative, educational, industrial architecture, commanded mainly by the state, will bears the imprint of the National Style. C. Popescu notes "Romania Great makes of the National State its architectural symbol and at the same time the emblem and means of propaganda of the state. [10].

4 REINFORCED CONCRETE HISTORIC PATRIMONY IN TIMISOARA

4.1 Beginning - Hydrotechnical Loks

As in the Romanian Principalities, the introduction of reinforced concrete in Banat begins with land improvement and technical construction works. The history of using reinforced concrete begins with sanitation and sanitation works for the regularization of the Bega river. The Danish engineer M. Fermant continues the work started in 1728 to regulate the course of the Bega river and in 1958 the construction of a hydrotechnical node upstream of Timisoara begins. Between 1900 and 1916, the 144-km range is constructed with a system of 6 locks, 4 in Serbia and 2 in Romania - at Sanmihai (Fig.2) and at Uivar, using for the first-time reinforced concrete. Figure 3 present the original design of the Sanmihai Lock and modernization works along the canal. The entire Bega River hydrotechnical system with all the locks is considered a monument. Unfortunately, like all constructions that do not have immediate financial benefits - the navigation was completely stopped in 1867, and due to a poor maintenance, they are in an advanced state of degradation.



Figure 2: Sanmihai lock

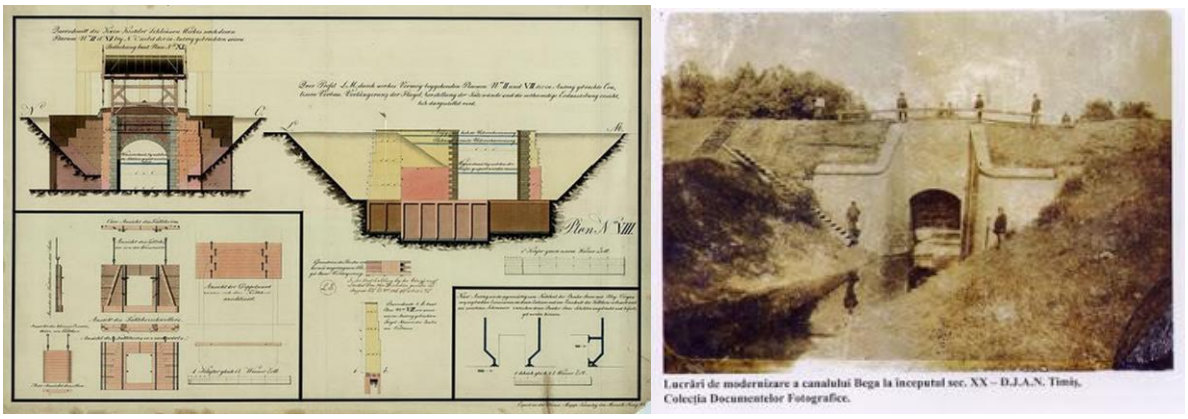


Figure 3: Original project of Sanmihai lock and modernization along the canal

4.2 Historic bridges

As a result of the construction of the Bega waterway, a series of technical buildings are becoming necessary. Thus,in Timisoara were built a series of bridges, water plant, water towers.

Decebal Bridge (Fig.4) is the most famous in Timisoara. It was built in 1909 from reinforced concrete beams and at that time was the largest span opening bridge in Europe. It has a total length of 58 m, a width of 9 m with a central arc span of 39 m. The bridge was designed by Mihailich Gyozo and was awarded at the International Exhibition, Paris 1910 [11].

The Traian Bridge, of eclectic style, built in 1913 by Elemer Wachtel (Fig. 5) is also built on a reinforced concrete beam. It was the widest bridge in Timisoara, total gauge 17 m, has a total length of 40 m, being composed of two small pedestrian openings and a main one over the river Bega with a size of 32.8 m.

Both the Decebal Bridge and the Traian Bridge are listed as historical monuments [15].



Figure 4: Decebal Bridge Timisoara



Figure 5: Traian Bridge Timisoara

4.3 Water plant

Another consequence of modernization and industrialization process I the beginning of the 20th century of the City is Timisoara Water Plant. The Timisoara hydroelectric plant was inaugurated in 1910 (Fig. 6). The project was carried out by the chief architect of the city at that time Laszlo Szekely and the engineer Emil Szilard. It is one of the first hydropower plants built in Europe. It is functional today.



Figure 6: Water Plant Timisoara

4.4 Water towers

In order to ensure the water supply of Timisoara, the city builds between 1912 -1914 two twin water towers, having a height of 52 m, at the ends of the water distribution network (Fig. 7). The two towers were intended to compensate for the maximum water consumption during the day. The project was realized in Budapest by the engineers I. Lenarduzzi and R. Sabathiel [12] according to the plans of the architect Laszlo Szekely (Fig. 8). The structural frame is made of reinforced concrete walks with perimeter circular columns. The concrete was prepared and cast in situ. Except for the water tank (500 m) which is made of stall, the entire structure is

made of reinforced concrete. The exterior and the roof which are also made of reinforced concrete are covered with ceramic elements [11]. The water towers were disabled in the 70s and poor maintenance led to overall degradation. In 2012 the Iosefin Water Tour was taken over by Timisoara City Hall, which is trying to find a proper solution for functional reconversion.



Figure 7: Water Towers Timisoara – Fabric and Iosefin

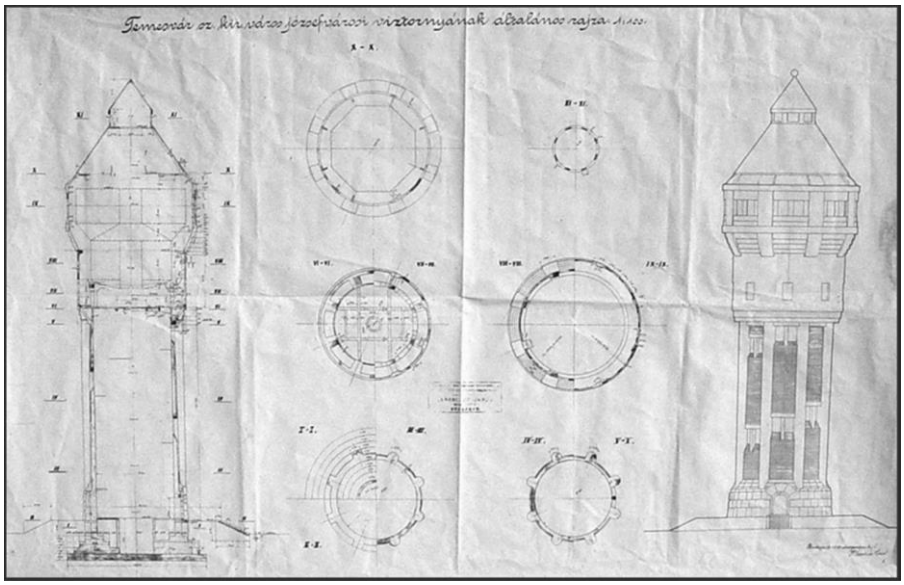


Figure 8: Water tower project in Timisoara made in Budapest in 1913

4.5 Industrial patrimony

The industrial buildings were not perceived as valuable and thus they were not introduced in the patrimony, until recently, towards the end of the 20th century. Having an economic utility, they were transformed, modified or demolished without considering the architectural values that were incorporated. Even today, important objectives of industrial heritage fall prey to financial interests at the expense of preserving the company's patrimonial values.

Being a strong economic development hub of Banat, especially focused on the light industry, Timisoara has developed a strong industry. The oldest factory was the Brewery, founded by Eugene de Savoy in 1718.

At the beginning of the 20th century there were already a series of factories - tobacco (1846), alcohol (1869), textiles (1894), hats (1894), footwear (1901). [13]

Many of these buildings have been transformed, modernized and demolished in recent years, to be replaced with modern investments and may, in a way, be ephemeral.

One such case is the "Turnul" / “Banatim” "Shoe Factory" built in 1901 and which worked, intermittently, until its complete demolition in 2016, including the administrative building. At that time, it was considered the most important shoe factory in Austro Hungary. Fig. 9).

The Slaughterhouse of Timisoara is another case, still happy, which was almost completely demolished but the central pavilion was maintained, the one with the highest patrimonial value. It was designed by Laszlo Szekely in Secession style, between 1904-1905 and at this time it is in a continuous state of degradation (Fig. 10).

In fact, most of Timisoara's industrial heritage, either as of the beginning of the century or later, has disappeared, as we have shown, due to real estate financial speculation (Guban Factory, Solvent Factory, Milk Factory).



Figure 9: Banatim Factory – Before and in the process of demolition



Figure 10: The Slaughterhouse of Timisoara - – original and present central pavilion

4.6 Residential and administrative buildings

Civil constructions: report houses, schools, administrative institutions are tributary to traditional construction systems, load-bearing structures with brick, hot mixed or brick or concrete slabs. The inertia of the introduction of new reinforced concrete construction systems is due, in large part, to the beneficiaries' habits, the low technological requirements (as opposed to the industrial and commercial ones) and the small openings and loads.

Reinforced concrete is gradually introduced into floors, floors and beams, pillars and beams.

Only in the inter-war period does it expand and become more widespread through reinforced concrete construction [14].

5 CONCLUSIONS

The buildings presented in the article are the most eloquent samples of the use of reinforced concrete in Timisoara at the beginning of the 20th century. Many of the buildings, unfortunately, are in an advanced state of degradation or are even extinct.

As shown in the study, the chronology of the introduction of reinforced concrete as a structural system, aims to meet the technical and urban needs of society which are then followed by the functional and aesthetic.

Regional differences, both in the art of building and in education and culture, with explicit references to specific parts of Europe, may represent a special chapter in the intangible heritage, which worth further study.

A process of continuous investigation and permanent cataloging of the architectural and cultural heritage is imperative necessary for the preservation and protection of human cultural values in the ultra-dynamic context of the becoming of the modern society. Anchoring in the patrimonial reality is increasingly forgotten in the virtual becoming of the present times.

In addition to the buildings already in the historical Monuments list in Romania [15], there are still many buildings that deserve and must be highlighted, protected and saved from

financial opportunism that are worth preserving for the authentic local spirit.

Although reinforced concrete is a relatively new building material in the history of construction, it should be considered and placed on the same plane of importance as masonry, stone or wood. Reinforced concrete constructions have their beauty and their historical importance and must be clarified and protected to the same extent.

Acknowledgements. The study is part of the doctoral research developed at the Politehnica University of Timisoara under the guidance of Prof. PhD. Eng. Habil. Marius Mosoarca, to whom I thank for his help and guidance.

REFERENCES

[1] Brownell, B. 5 Futuristic Materials That Could Reshape Architecture and Design. https://www.metropolismag.com
[2] Frampton, K. *Arhitetura moderna*. Editura Universitara Ion Mincu, (2016).
[3] https://en.wikipedia.org/wiki/Reinforced_concrete
[4] Antonucci, M. and Nannini, S. Through History and Technique: Pier Luigi Nervi on Architectural Resilience. *Architectural Histories*. 7. 10.5334/ah.297. (2019)
[5] ing. Nicolae St. Noica,N.S. Personalitati romanesti in constructii – Anghel SALIGNY (1854 – 1925), *Revista Constructiilor* nr. 147 (2018), pag. 56
[6] Maran, M. and Duric-Milovanovic, A. Orthodox Church and Serbo-Romania relations in Banat in the 19th and first half of 20th century. Fascicola de Stiinte Social-Umaniste, An IV, pp.42-48, (2016)
[7] Demetrescu, B., Gioncu, V. Historical structures in the Romanian Banat area. *Structural Analysis of Historical Constructions.* 1114-1118, (2012),
[8] Bratuleanu, A. Interwar Timisoara Urbanism and Architecture. *ArtPress*, (2016)
[9] https://www.revistaconstructiilor.eu/index.php/category/13-personalitati-din-constructii/
[10] Szekely, G., Arhitecti Creatori ai Stilului Neoromanesc in Zona Banatului, Patrimonium Banaticum, VI, Timisoara, (2016), pp.235-246
[11] Mosoarca, M and Gioncu, V, *Structural safety of historical buildings made of reinforced concrete, from Banat region-Romania*, Journal of Cultural Heritage, Vol. 14, Issue3, (2013), pp. 29-34,
[12] https://ro.wikipedia.org/wiki/Turnul_de_ap%C4%83_din_Iosefin
[13] Rosiu, L. and Bica, S. The reuse of industrial buildings, an emergency for the patrimony protection in the Banat Region of Romania. *Analysis of Historical Constructions.* 2769-2775, (2012)
[14] Onescu, I., Mosoarca, M. and Stoian, V. Modern Consolidation Solutions for Buildings with Historical Value. Part I: Reinforced Concrete Structures. *Modern Technologies for the 3rd Millennium.* (2017).
[15] https://patrimoniu.gov.ro/images/lmi-2015/LMI-TM.pdf

12th International Conference on Structural Analysis of Historical Constructions
SAHC 2020
P. Roca, L. Pelà and C. Molins (Eds.)

RECONSTRUCTION OF A MASONRY WINDMILL TOWER WITH A MULTI-BLADE WIND TURBINE, STEEL RESERVOIR AND WATER SUPPLY SYSTEM

PIOTR W. SIELICKI[1*]

[1]Faculty of Civil and Transport Engineering

Poznan University of Technolgy (PUT)
M. Skłodowskiej-Curie 5, 60965 Poznan, Poland
e-mail: piotr.sielicki@put.edu.pl, www.put.edu.pl (*corresponding author)

Keywords: Windmill, Turbine, Masonry, Restoration, Water supply

Abstract. *In the early 20th century, rapid industrial growth around the world enabled the development of many advanced mechanical structures. Some of these structures were successfully used to improve agricultural efficiency or increase people's comfort. Such a situation was observed in 1910 in the western part of Poland, which at the time was partitioned by Habsburg Austria, the Kingdom of Prussia, and the Russian Empire . In the city of Poznan, a Polish landlord built an advanced structure to automate his farming, using freely available wind energy. At first glance, it was a classic windmill, with a multi-blade wind turbine fixed to the top of a cylindrical masonry tower. However, some additional elements demonstrate the uniqueness of such a structure at the time. One hundred years later, the structure is located at the centre of a rapidly growing area of the city. For that reason, restoration of the tower is complex and requires the reconstruction of damaged or missing elements while observing new safety regulations. In this work, the author presents the basic assumptions necessary for the future renovation process.*

1 INTRODUCTION

Since ancient times, many unique engineering structures have been created to support human civilisations. Most of these structures supported basic existential needs, such as the extraction, supply and storage of water. These important needs were directly connected to food production. From the heritage aqueducts in ancient Rome to the thousand-year-old Nashtifan windmills of ancient Persia, the use of natural forces, such as gravity or wind power, has helped the human race to survive.

Innovative engineering ideas have also emerged in more recent centuries, including the industrialisation of the 18th century, which produced steam power, and later, wind power. As a result of such developments, there are many wind turbines around the world which, e.g., deliver water to farms in Texas or mill grain in Europe.

This study deals with one such engineering structure that was successfully used to improve agricultural efficiency and raise the quality of life of the Polish family living in the Polish city of Poznan in the early 20th century (see Fig. 1). The history of this structure is as exciting as its engineering, which will be described in a later section. Poland was in a unique position at the

end of the 18th century, wedged between three powerful empires that were supported by different local interest groups; ultimately, this resulted in the partitioning of the country. A hundred years later, Poland was still partitioned, and Poznan was under the control of the Kinngdom of Prussia. However, Poznan's residents were able to retain some parts of their original culture. In 1908, the first local industrial exhibition was approved [1].



Figure 1: Wind turbine building: structure founder (middle) with family members [1920]

The exhibition included a presentation of Poznan's industrial achievements, including the engineering machines, tools and everyday items produced by Polish companies in the region and abroad, including Great Britain. Due to this exhibition, the local Polish community was optimistic and hopeful of becoming more competitive with other countries. Some important structures were built by locals immediately after this exhibition. One of them was the structure which is the focus of this paper. In 1910, in the area which is now the city centre, a Polish landlord built an advanced structure to automate his farming. Based on evidence from his family members and letters written at the time, he was inspired by the unique ideas on display at the Industrial Poznan Exhibition 1908 (original translation from Polish) and the concept of freely available power (i.e., wind energy).

At first glance, the structure was a classic windmill with a multi-blade wind turbine fixed to the top of a cylindrical masonry tower. Some additional elements illustrate the uniqueness of

such a structure at the time. First, water was extracted from three independent inactive water points, located tens of meters away from the windmill. Second, the water was pumped to the steel reservoir located at the top of the structure, right beneath the wind turbine. Next, this efficient water source continuously supplied dozens of independent points located in the owner's fields and house, using only gravity. Finally, the most extraordinary use of this structure was the supply of electricity to the landlord's entire property.

One hundred years later, this heritage building is located in the centre of a rapidly growing area of Poznan. For this reason, restoration of the windmill is complex and requires the reconstruction of damaged or missing elements while observing new safety regulations. All these works must be performed without any of the original documentation and based only on photos from the beginning of the previous century.

In this work, the author present the basic assumptions which should underlie the future renovation process. Moreover, will propose a conceptual approach to designing elements which have disappeared due to age or damage, based on old photos and a 3D laser-scanning technique. One of the primary difficulties of the project is the existing masonry tower. The working wind turbine, together with a full water reservoir, may create a complex loading state for the mortar composite with which the original tower was constructed; therefore, author has designed a new support system for the turbine and the water tank. The design process was performed partially using numerical methods and employed the fluid-structure interaction methodology to predict displacement and stress outcomes. This methodology was applied to both the existing masonry and the newly developed support system.

2 WIND TURBINE BUILDING

2.1 Description

The paper will now turn to the engineering objective of this research, which is to reconstruct the wind turbine and modernise the supply system used to manage water in the structure. The general geometry of the structure is presented in Figure 2. The primary idea of the current owner was to upgrade the existing water supply system by developing a new system in which the water source would not be dependent on actual ground water conditions. This means that the water would be stored in the previously constructed reservoir.

According to the original builder, there were ten crucial elements for the proper functioning of this device (see Figure 2): 1- the system that extracted water from the three independent water points located outside the structure, 2 - the water pumping system powered by the vertical movement of the steel rod, 3 - the masonry supporting the tower, which was responsible for absorbing the forces of 15 tons of water, the wind turbine and all other dynamic forces caused by the wind, 4 - the steel reservoir supported directly by the tower, 5 - the steel frame supporting the turbine, 6 - the steel turbine with eighteen blades, 7 - the direction and safety wings, 8 - the gearbox responsible for the safety system and for transferring the rotational movement of the turbine to the vertical movement of the steel bar, 9 - the water overload valve, 10 - the water distribution system, with more than 2,000 m of piping located up to 300 m from the structure, and 11 - the conservation entrance to control the structure.

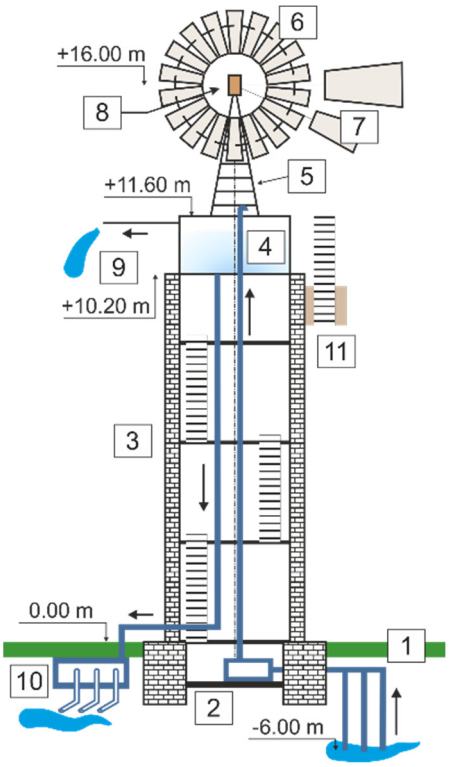


Figure 2: Wind turbine building: tower scheme [2019]

2.2 Measurements

During the collection of existing documentation on the original history of this structure the author discovered some interesting facts. One is that the steel frame and masonry were damaged by bullets during World War II. Despite these signs of damage, the structure is stable. This is because of the massive masonry wall, which is 0.4 m thick and fixed by three levels of horizontal beams. This kind of irregularity in the structure's geometry shape was easily captured using 3D laser-scanning techniques. Surphaser HXS tool was used to capture millions of points from the structure. A partial view of the laser scan is presented in Figure 3.

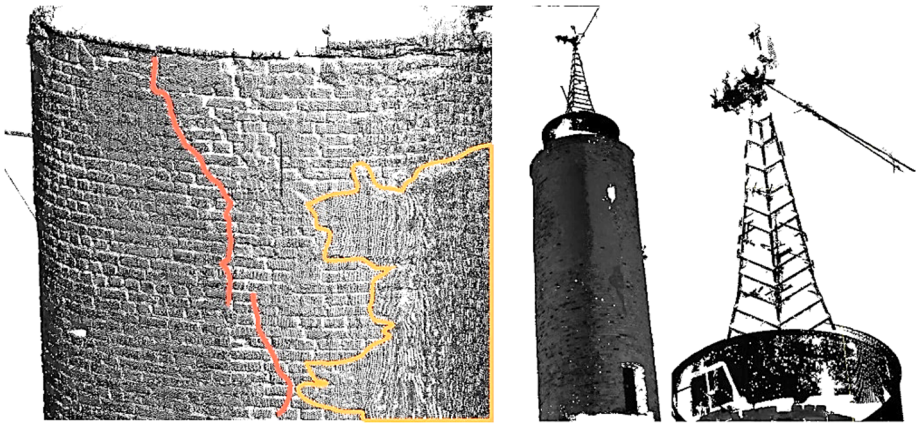


Figure 3: Wind turbine building: pre-processing 3D laser scan [2020]

A detailed analysis of the thickness and regularity of the shape of the mortar joints allowed me to confirm all locations in which the masonry had been rebuilt. The red line in Figure 3 shows the edge on the external side, which was covered by the brick units after it was damaged during the war. An additional effect in Figure 3 illustrates the geometry of the steel elements, based only on 3D modelling. The orange line shows areas with the original plaster design, which is more than 100 years old.

The next step was the collection of data to identify the geometry of the wind turbine. The pictures provided by the family members of the original builder allowed me to confirm the geometric dimensions of the primary elements of the turbine, including the blades and gearbox. This data was transferred to the 3D model to assess the stress-displacement outcomes for different loading scenarios.

3 RESTORATION PROPOSAL

3.1 Concept

Due to the rapidly growing area around the wind turbine, the need for the reconstruction is accepted by the current owner and city administration. The primary goal for the renovation includes the reconstruction of all elements to enable them to be viewed by visitors interested in such an engineering structure. The most important parts of the structure which would be incorporated into the original wind turbine concept are:

- The water supply system, including the extraction pipes, water pump, reservoir and water delivery system
  It is impossible to rebuild the original water supply system which was located beneath the ground because the area is surrounded by newly constructed buildings. Nevertheless, the reconstruction design concept presents detailed data on the proposed solution, including a retrofitted pump and water supply information presented in multimedia format.

- The masonry structures, including the foundation and cylindrical tower
  This structural element is crucial because it is located in the centre of the proposed walking path. Thus, people will be able to walk very near the structure. The simple cylindrical form includes thick walls. However, the existing mortar is damaged by age, and the structure is unstable. For that reason, the author considers that the best solution is the construction of a new supporting structure inside the masonry tower. This precast steel spatial frame should be fixed to the new foundation. Moreover, the engineering design must include a dynamic-force loading scenario caused by the rotating wind turbine and a full water reservoir.

- The blade turbine, including the supporting bar frame, turbine wheel, gearbox and control and safety mechanisms
  Multi-blade turbines are commonly used around the world. However, the geometry of this windmill is different from that of other turbines identified in the literature [2,3,4]. Rebuilding the wings and other elements connected with the capture of wind power is

relatively simple and is based on other wind turbines with similar dimensions. However, the gearbox system, including a safety mechanism for use in high wind conditions, must be designed from scratch.

3.2 Numerical support

Numerical techniques can credibly be used for structures for which default approaches and standardisation are impossible, such as heritage structures, which typically involve irregular geometry, ageing material and structural damage. Renovation processes have been supported using numerical knowledge since the first finite element codes. In this research, Abaqus code was used to assess the primary stress-displacement state under original and present-day loading scenarios. The numerical solution related to the renovation concept presented in the previous section can be separated into several independent problems. The first relates to the steel turbine and includes the dynamic response of the supporting frame structure and mechanisms inside the gearbox. The second relates to the performance of the masonry tower under static as well as dynamic loading caused by the rotating turbine wheel and wind fluctuations.

The stress-strain relation under consideration is based on the actual unit-mortar specimens. Moreover, concrete damage plasticity (CDP) behaviour has been applied numerically to estimate the potential for extraordinary cracking of the masonry under critical wind loading. The numerical design of the multi-blade wheel is another challenge. The static stress-displacement currently observed is the result of more than 1000 Pa of static wind pressure and neglect for the rotation of the wheel. Partial results are presented in Figure 4.

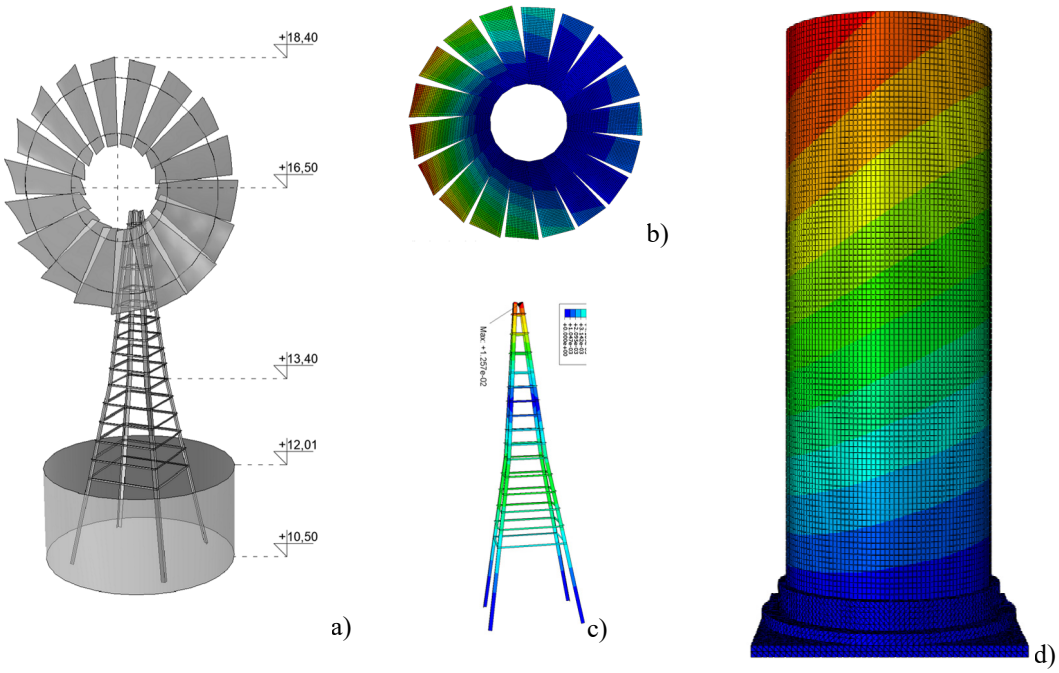


Figure 4: Numerical results of the static wind pressure modelling: a) CAD model of the wind turbine wheel, supporting bar frame and reservoir, b) displacement results for the static wind loading under a random angle of action, c) supporting frame displacement under maximum wind force transferred from the turbine wheel, and d) masonry tower displacement map during CDP material calibration process [5]

4 CONCLUSION

This paper deals with a heritage engineering structure which is currently being restored. One of the crucial steps in the restoration process has been the collection and renewal of missing documentation. The design has been solely based on an examination of existing structural elements, many of which are missing due to the structure's more than 100-year history, and a careful review of photographs supplied by family members of the original builder.

In this study, the initial data were collected, and numerical results were obtained to support the future directions of the renovation and enable the restoration of the structure to its full functionality as it was at the beginning of the previous century. The preliminary numerical static solutions have allowed me to predict the structure's likely behaviour in various scenarios and confirm the utility of the proposed renovation solutions, including, for example, a prefabricated steel frame that will lessen the load on the existing masonry walls.

Acknowledgements. The author would like to thank all family members of the structure's original owner for supporting this research by providing authenticated pictures and original family documents. The author would also like to thank the Poznan Historical Preservation Office for providing access to official heritage resources.

Furthermore, the author would like to ask anyone with data supporting the viability of the similar wind turbine building restoration (e.g., pictures or designs of similar structures around the world) to contact.

REFERENCES

[1] Gustowski A., *Pamiętnik Wystawy Przemysłowej w Poznaniu z roku 1908*, Wielkopolska Biblioteka Cyfrowa 2018 pp.102 (in Polish), www.wbc.poznan.pl/publication/12043 .
[2] Fleming P.D. and Proben S.D., *The Evolution of Wind-Turbines: An Historical Review* Applied Energy 18, 1984, pp. 163-177
[3] Neuman F., *Die Windkraftmaschinen*, Lipsk 1907, pp. 174
[4] Szowheniw J., *Silniki Wietrzne [elektrownie wiatrowe]*, Polski Komitet Energetyczny, Warszawa 1932, pp. 182 (in Polish).
[5] Dybizbanski J., Leszkiewicz J., *Projekt rekonstrukcji zabytkowej turbiny wietrznej*, Poznan University of Technology 2020, BSc thesis, pp.50 (in Polish).

12th International Conference on Structural Analysis of Historical Constructions
SAHC 2020
P. Roca, L. Pelà and C. Molins (Eds.)

REINFORCED CONCRETE FLOORS IN HISTORIC BUILDINGS FROM THE BEGINNING AND THE MIDDLE OF THE 20TH CENTURY – EXAMPLES OF STRUCTURAL STRENGTHENING IN THE PROCESS OF REVITALIZATION

G. DMOCHOWSKI[1], P. BERKOWSKI[1*], J. SZOLOMICKI[1], M. MINCH[2]

[1]Faculty of Civil Engineering
Wroclaw University of Science and Technology
Wyspianskiego Blvd. 27, PL50-370 Wroclaw, Poland
grzegorz.dmochowski@pwr.edu.pl,
piotr.berkowski@pwr.edu.pl (*corresponding author),
jerzy.szolomicki@pwr.edu.pl

[2]VEGACAD Design and Implementation Office
89, Agrestowa Str., PL53-006 Wroclaw, Poland
minch@vegacad.com.pl

Keywords: Historical Building, Concrete Slab Floor, Assessment, Strengthening

Abstract. *The paper presents a historical outline of structural solutions of reinforced concrete floors from the turn of the 19th and 20th centuries to the half of the 20th century in the Lower Silesia region of Poland. It is based on the analysis of archival documentation and expert research carried out during the design of the revitalization of historic public and industrial buildings. The structural typology of some simple RC floors slabs used in that time of introduction of concrete into construction life as well as constructional solutions of buildings erected in western Poland in those days are presented. Nowadays, while some of these buildings undergo refurbishment process to adapt them to new functional aims these RC floors have to be strengthened using different methods, depending on the assessment results. In some of the presented design study cases assessed technical state and load bearing capacity of floors ensure the possibility of their further use without the need for significant reinforcements, except for the need for surface material repairs. However, in some cases due to concrete deterioration processes and loss of its durability, despite necessity of material renovation, structural strengthening methods needed to be applied. For example, increasing the load bearing capacity of floors by making additional concrete layers cooperating with the existing reinforced concrete slab or by changing the static scheme by making new supports up to the complete replacement of floors (not only concrete ones) with modern, concrete rib-and-beam or composite ones were considered.*

1 INTRODUCTION

In many cities of the southwestern part of Poland (which geographically and historically is named Lower Silesia) there are still buildings, used for various purposes - from residential,

public and industrial, which were built in the late nineteenth or early twentieth century. Due to their former function some of those buildings required large functional areas and therefore the need to construct floor slabs having significant spans as well as sufficient bearing capacity. The best choice was then using reinforced concrete structural elements, despite the fact that that were years when concrete had its beginnings in construction.

In the recent years, in connection with the various activities carried out to adapt these facilities to new utility functions, building engineers often meet and get to know interesting structural solutions from that time, many of them made using reinforced concrete. In the course of assessment works, aimed at diagnosing the technical state of these historic structures, including their safety and the development of appropriate rehabilitation projects, there are discovered different concrete elements as, for example, different types of monolithic floor slabs in industrial or public service buildings or even complete skeletal structures of workshops or department malls. Combining construction history analysis with current diagnostic methods can give not only an understanding of the past design solutions and development of structural design and construction ideas, but also is essential for the adequate design of repair interventions. However, what is obvious, with the time pace and aging process, these historic concrete structures at least lost partially their former material properties and bearing capacity.

The paper presents a historical outline of structural solutions of reinforced concrete floors from the beginning of the 20th century (also mentioning some later design solution), based on the analysis of archival documentation and research carried out during the rehabilitation processes of historic public and industrial buildings. The structural typology of selected historic German reinforced concrete floor slabs and some typical constructional solutions used in the first half of the 20th century in buildings erected in western Poland are discussed. Nowadays, while some of these buildings undergo refurbishment processes to accommodate them to new functional goals some of these slabs have to be strengthened using classic or modern methods. Procedures of technical state assessment of old RC structures as well as selection of some applied strengthening methods are described in the paper.

2 STRUCTURAL DESCRIPTION OF HISTORIC RC FLOOR SLABS

2.1 Typical historic RC floors

A description of typical solutions of reinforced concrete floor slabs that can be found in buildings constructed at the turn of 19th and 20th centuries, also in the region of the Lower Silesia, are presented, for example, in [1,2,3]. Below, based on the aforementioned literature as well as on the conducted own expert studies and structural assessments [4,5,6,7,8,9], several selected, most commonly used and met in Poland, reinforced concrete floors are briefly presented.

Four types of many Monier floor slabs solutions are presented in Fig. 1. They were mainly in use at the turn of the 19th and 20th century. Their typical spans were between 1.00 and 2.50 m (in 1909 even to 6.0 m), a slab thicknesses was only 3 to 10 cm, and the reinforcement was made of smooth round bars with a diameter of 6 mm, laid every 10 cm. In the first versions the reinforcement was placed in the compression and tension zone.

When executing a continuous slab across several fields, the reinforcement was bent at the moment zero points and carried out above the supports. Those slabs were mainly based on double-T beams (at upper or lower flange), but also on masonry walls.

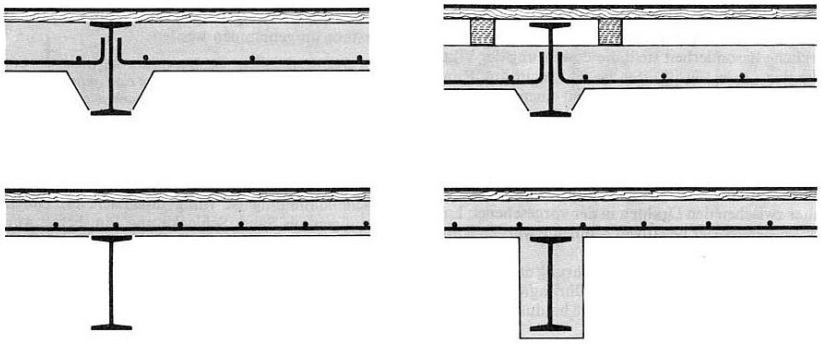


Figure 1: Examples of Monier floors (Monier decke) [1]

Another example of ingenious ideas was concrete floor with pre-tensioned reinforcement (Fig. 2). In order to achieve a higher bearing capacity of such floor and an effect of structural continuity, the iron inserts were preloaded. The round bars were pulled tight around the upper flanges of the beams or around anchor flat bars mounted in the masonry, and laterally shifted until a prestressing was reached. That floor slab was considered as a single-span one.

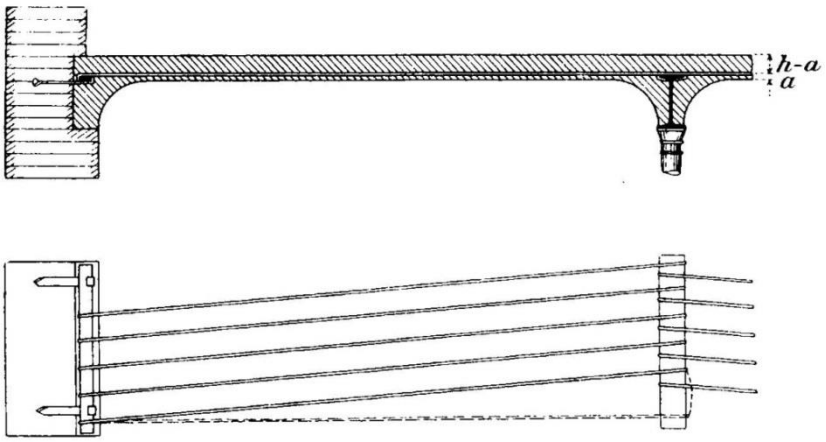


Figure 2: Tensioned concrete floor (Spanneisendecke) [1]

In 1897 the Koenen floor (Fig. 3) was built as the first version of a slab with cove-shaped supports running through several steel girders. Due to the formation of haunches at the support area, a bigger lever arm of the internal forces was achieved above the supports. The shear stresses, increasing towards the slab edge, are absorbed by the haunches. The reinforcement routes follow the moment curve and bars are bent up by the support at the moment zero points.

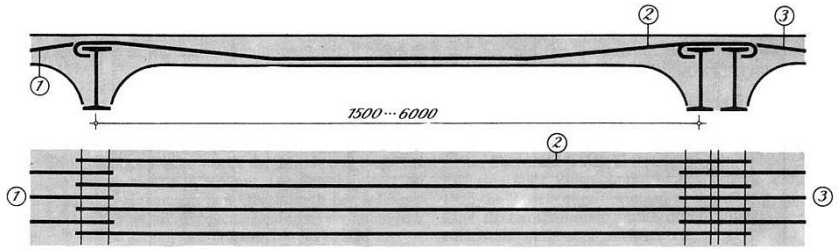


Figure 3: Koenen plate floor (Koenensche Voutenplatte) [1]

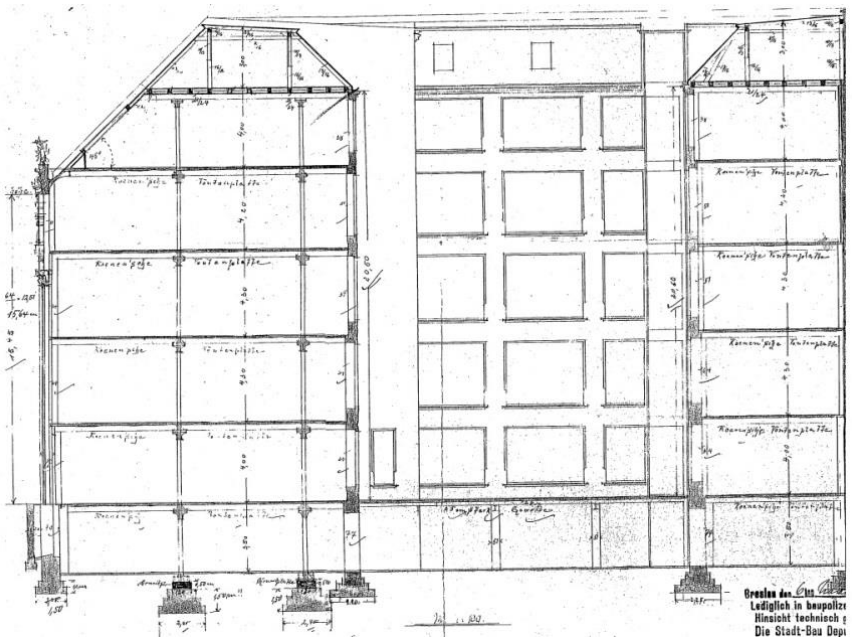


Figure 4: Cross-section of a public service building with Koenen plate floors (1899)



Figure 5: General view and rebar exposure of Koenen plate floor in a public service building

The reinforcement was anchored at the top of the slab in various ways: hooks at the upper flanges of the girders or a flat steel that was held by steel anchors mounted in masonry walls. By coupling the reinforcement with the wall clasp it was possible to achieve a high degree of clamping for the peripheral area using the wall dead load. Spans of up to 8.0 m were achieved for that floor. That type of floor can be often met in the 19th/20th century public service buildings in the Lower Silesia region (Figs 4 & 5).

The Wolles console floor (Fig. 6) is similar to the Koenen one, but there is no continuous layout of the reinforcement over supports. It is divided into bottom one in a span and upper one over supports. The characteristic element is that the upper bars were extended approximately 100 mm beyond the zero moment point.

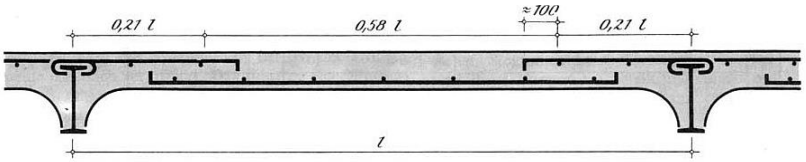


Figure 6: Wolles floor (Wollesche Konsoldecke) [1]

2.2 Examples of monolithic RC floors in historic industrial buildings

Below there are presented some examples of classic fully monolithic RC floors (being parts of 3D frame structures) that are still working without strengthening necessity in different public service and industrial buildings from the first half of the 20th century in the Lower Silesia region of Poland.

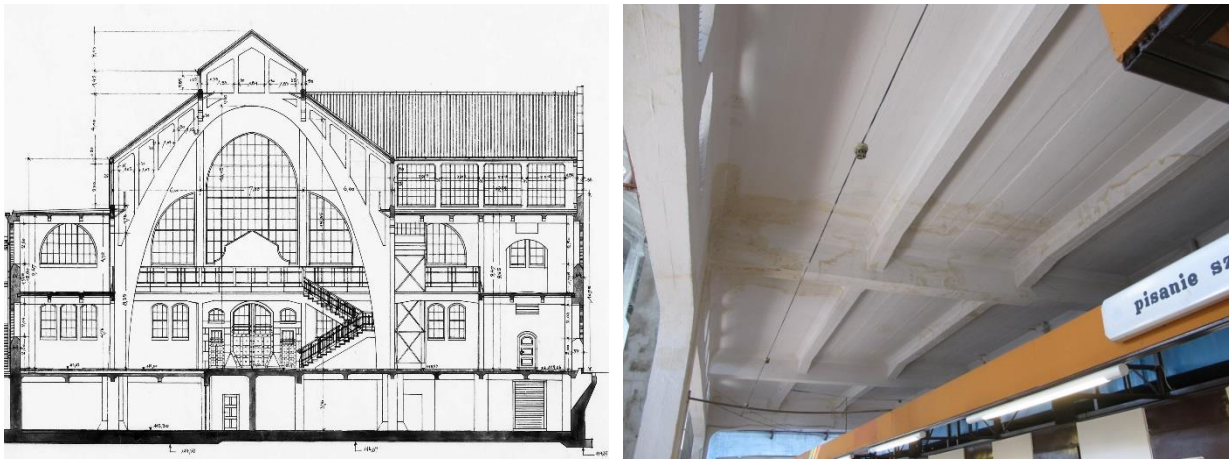


Figure 7: Archival drawing and general view of the RC rib floor in a market hall (1909)

First of them is one of the prominent monuments of RC historic structures – the market hall from 1908 (Fig. 7). The original design of the market hall building was made in the years 1901-1903 and consisted of the reinforced concrete foundation and the steel structure in the part above the ground level. However, the whole structure finally was made of concrete after performing an analysis of a variety design solutions of different market hall buildings existing

at the time as well as due to the properties of concrete material such as: durability, fire resistance and no need of intensive maintenance [6,7]. From the constructional point of view we are dealing in this building with two construction materials: concrete/reinforced concrete of foundation slabs, basement walls, floors, and arched supporting structure, and the brick masonry exterior walls. Generally, the building remains in use in a perfect technical state.

The second object is a heritage industrial building of bakery flower warehouse built about 1913 (Fig. 8). The edifice has 8 floors above the ground, but has no basement. Although the external walls of the building are made of brick masonry, the main bearing structure is made of reinforced concrete: pillars, rib-slab floors, and roof frames on two attic floors. The assessment was made with an aim to determine the possibility of reconstruction and adaptation of the warehouse building to new utility purposes, and in turn, to extend its service life. Currently, the building is under refurbishment process.



Figure 8: Archival drawing and general view of the RC rib floor in a bakery plant (1913)

The next two buildings (Figs 9 & 10) are not so spectacular examples of the historic RC structures, but present the simplicity, clarity and usefulness of the use of this material in shaping the space of industrial buildings regardless the passage of time and the development of design methods and properties of the materials used.

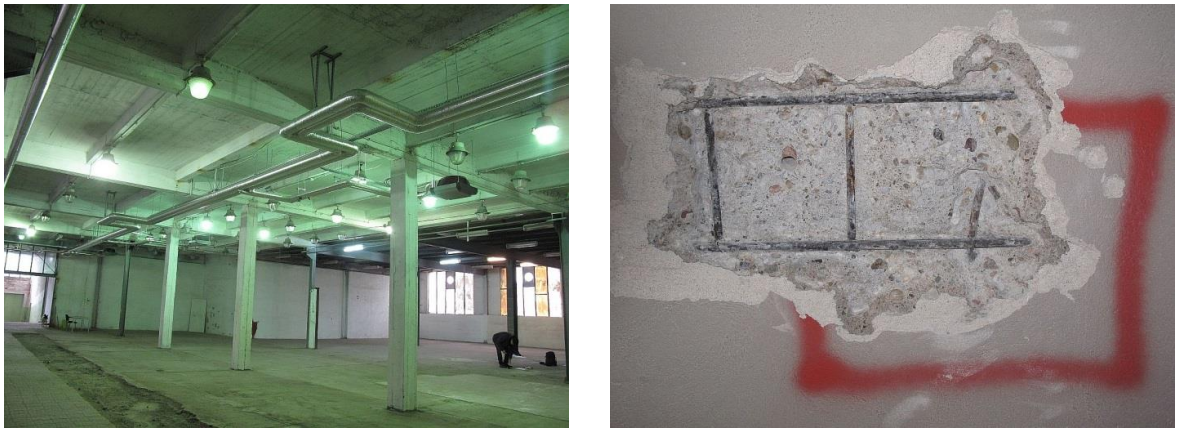


Figure 9: General view of the RC rib floor of a workshop and rebar exposure (1940)



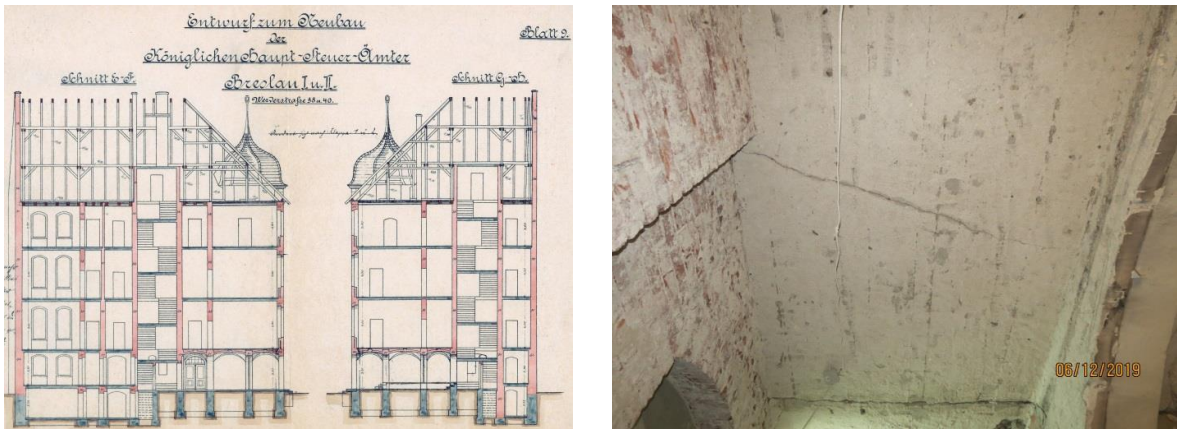

Figure 10: View of warehouse after partial demolition and the rib floor structure in a ground floor (1950)

In both cases the assessments of technical condition of buildings (including fire resistance demands) were conducted due to designed change of their future utility functions. Based on the non-destructive techniques (rebound hammer and pull-out methods) used and study of historical literature it was assumed that the concrete in the structure corresponded with concrete classes of C12/C15. According to the literature data and taking into account the age of the construction, it was determined that post-German so-called "commercial steel" with the design strength 150 MPa was used for reinforcement. Basing on the static and strength calculations it was determined that the carrying capacity of the floors in the considered buildings was sufficient to carry on new loads without necessity to strengthen their structure. The only necessary repair would be connected with improving the floors' fire resistance by creating a new spray on their lower surface which would increase the thickness of the concrete cover of the bars, by the use of nano-concrete plaster, for example.

3 STRUCTRAL STRENGTHENING OF HISTORIC RC FLOOR – A CASE STUDY

3.1 Former public service building converted into an apartment house

The analyzed building was erected about 1909. Before the 2nd world war the building was the seat of the Central Customs Office, after the war it served as militia barracks. The building has 4 floors above ground (ground floor and three floors), an unused attic and is partly a basement (Fig. 11.a). The structural system of the building is two-bay one, with corridors located along the inner courtyard. The building's structure is traditional: the foundations are brick masonry ones; the load-bearing walls are made of brick; the floors are in the form of reinforced concrete slabs, locally are made with use of the prefabricated reinforced concrete panels. The roof truss is wooden, covered with ceramic tiles. Above the ground floor slabs were found in the form of cross-reinforced concrete slabs in rooms and unidirectional reinforced slabs in corridors. The structural thickness of the floors varied from 10÷12 cm in corridors to 16÷20 cm in rooms.



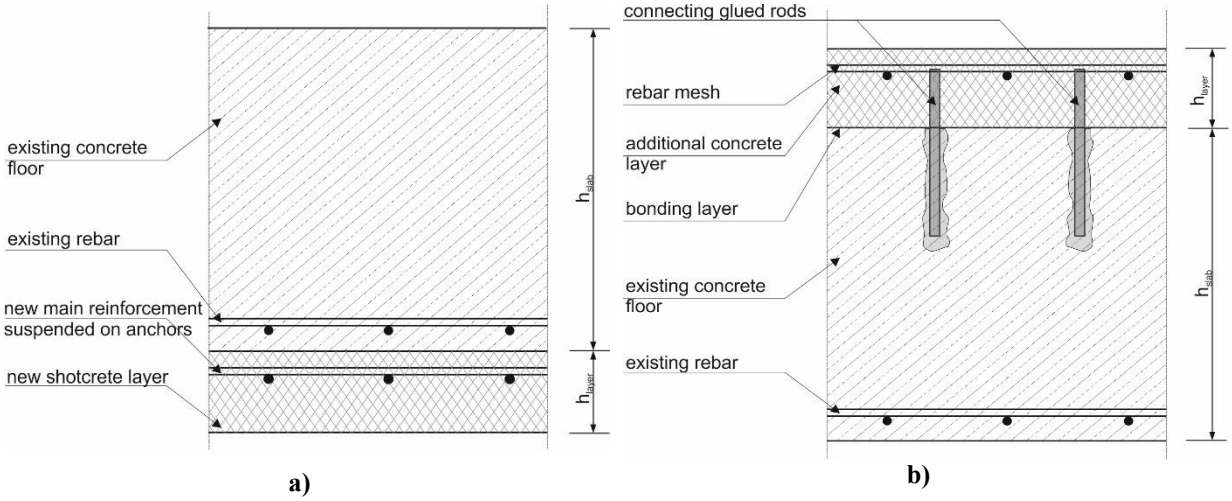
a) **b)**

Figure 11: a) Archival drawing of building cross-section; b) typical cracks in floor slabs

Numerous cracks were found in slabs over the corridors, especially at the ground and first floors. Those damages were caused by corrosion of reinforcement, poor concrete adhesion to band-iron and its torsion during concreting. In almost all the RC floors diagonal scratches of the panels were found in the slab corners (Fig. 11.b). These are typical cracks for thin reinforced concrete slabs, without upper reinforcement near supports. Such reinforcement was not found in the exposures and during rebar scanning tests.

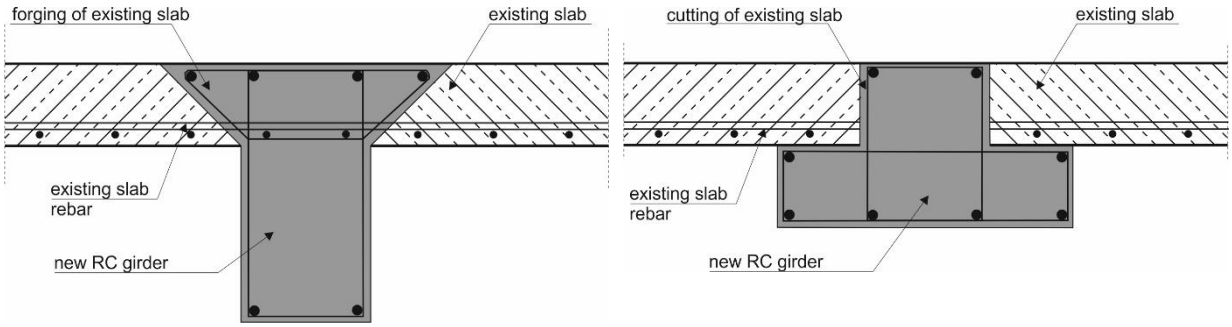
A number of rebar samples were taken out from floors projected to be demolished to determine in steel strength machine the quality of reinforcing steel used [1,10]. The test results let to assume the calculation yield stress for steel rebar as $f_{yd} = 250$ MPa.

Based on the concrete strength tests and literature analysis [1,11,12] it was assumed, due to the large variation in results, that the used concrete corresponded to the current class C12/C15 with a design strength of 8.0 MPa. Even assuming higher value of concrete strength, as 10.0 MPa, the slabs had not enough capacity for new loads. As the slabs were very thin it was impossible to state concrete strength using cores extracted from them.



a) **b)**

Figure 12: Slab strengthening ideas: a) shotcrete at bottom surface; b) additional concrete layer at upper surface



c) **d)**

Figure 12: Considered methods of floor slab strengthening: c) additional T-shape beam; d) additional inverted T-shape girder

The tensile pull-off examination of concrete surface of floors adhesion showed that it did not have enough strength to use FRP materials for strengthening and the surface repair would be too expansive.

The static and strength calculations carried out, preceded by the above mentioned material tests, showed that the reinforced concrete slabs above all the storeys did not have sufficient capacity associated with the residential, hotel or office function. This let to make a decision of strengthening all the floor slabs. Some techniques (Figs 12.a÷d) were considered, but finally construction of additional supporting inverted T-beams were applied (Figs 13.a,b).



a) **b)**

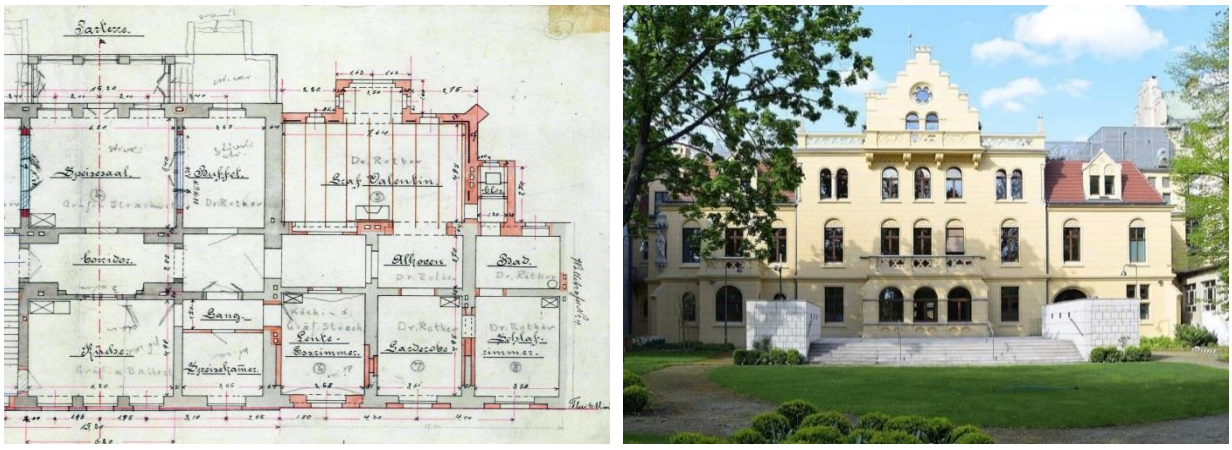
Figure 13: a) Floor slab with cuttings; b) floor with additional inverted T-shape RC girder supports

4 MODERN CONCRETE FLOORS IN HISTORIC BUILDINGS – A CASE STUDY

4.1 Former city palace converted into a public service building

According to the preserved archival documentation the revitalizing object, in its current architectural and structural form, was designed and built in 1898 as a city palace of the family of the Ballestrem counts. Buildings that had existed in this place before were completely

destroyed as a result of the explosion of the gunpowder tower in 1749, and new buildings were erected in their place. During its existence, the building was rebuilt and extended, as evidenced by the preserved historical documentation. The palace is a three-floor building with basement and attic (Fig. 15.a). The object has a central symmetry axis, a straight front elevation and a fragmented rear elevation (Fig. 15.b). The building's structure is traditional, i.e. foundations and load-bearing walls are made of solid brick, floors – vaults above basements, Klein type and wooden on the other floors, and the roof truss structure – wooden.



a) **b)**

Figure 15: a) Archival plan of old palace building; b) the palace after rehabilitation

According to the assumptions of the revitalization project, the building was to serve as a hotel, with a restaurant in a basement. In relation to these assumptions and the resulting design and functional requirements, a detailed assessment of the technical condition of the object, as well as conservatory opinion (including stratigraphic ones) was developed by specialists. The results of this assessment provided the basis for developing a construction design for the reconstruction and adaptation of the palace building to new utility functions. However, during the construction works, after full exposure or demolition of subsequent fragments of the structure, it was necessary to modify the adopted design solutions or introduce additional reinforcements. The designed new building function also enforces the introduction of correspondingly higher functional loads. All these factors had a major impact on the need to strengthen virtually all the foundations by using jet-grouting. All inter-floor floors, except for those located in rooms such as bathrooms or kitchens, were made as wooden ones. The layout of the floors was mixed, often even the neighboring rooms had a different course of bearing beams. Finally, all old wooden floors had to be replaced with new ones.

Originally, ceilings were considered to be made as traditional RC panel slabs on steel beams or modern rib-and-slab floor (RECTOR type) (Fig. 16). RECTOLIGHT floors are beam-honeycombed, prefabricated dense ribbed slabs. These floors consist of prestressed concrete beams and ceiling fillings made of pressed wood. The system is supplemented with: supporting reinforcements, welded steel mesh and monolithic concrete made on site. The biggest advantage of this system floor is its lightness and easy installation, which are of great importance when performing works in historic buildings located in the city center.



Figure 16: View of the RECTOLIGHT concrete floor

However, in the final solution, due to economic reasons, new inter-story floors were designed in the form of composite reinforced concrete slabs, made on lost formwork made of trapezoidal steel sheets, based on steel I-beams (Fig. 17).



Figure 17: View of the composite floor

5 FINAL REMARKS

Recently, many historic buildings in Poland undergo refurbishment process to adapt them to new functional aims and new loads. In case of public or industrial buildings from the end of the 19th and beginning of the 20th century there can be found ones in which concrete was used for the first time as structural material, especially for floor slabs. In most of the cases, due to concrete deterioration processes and loss of its durability, despite necessity of material renovation, strengthening methods are necessary to be applied. One of the main elements of proper definition of reinforcement method to be applied is historical analysis of design and construction of such structural elements, according to the archival and contemporary literature (what was presented in this paper), and the other indispensable action is careful assessment of their real construction and technical condition [13]. As the final resulted of such analyses

some examples of different techniques of strengthening of old reinforced concrete floor slabs in historical buildings were presented in this paper. Also, examples of application of modern concrete slabs in place of deteriorated floors (not only the RC ones) were briefly described.

REFERENCES

[1] Ahnert, R. and Krause, K.H. *Typische Baukonstruktionen von 1860 bis 1960 zur Beaurteilung der vorhandenen Baussubstanz, Band 1. Gründungen, Wände, Decken, Dachtragwerke*. Verlag für Bauwesen Gmbh Berlin (1991) (in German).

[2] Van de Vorde, S. *International References for a building manual on postwar housing in Brussels*. Innoviris retrofit: RetroCo. VUB re-use: https://www.brusselsretrofitxl.be.

[3] Voormann, F. Von der un bewehrten Hohlsteindecke zur Spannbetondecke. Massivdecken zu Beginn des 20. Jahrhunderts. Beton- und Stahlbetonbau (2005) (9)**100**: 836-846 (in German).

[4] Berkowski, P., Dmochowski, G., Barański, J., Szołomicki, K. The construction history and assessment of two heritage industrial buildings in Wrocław. In: D. Beben et al. (Eds): *3rd Scientific Conference Environmental Challenges in Civil Engineering*, MATEC Web of Conferences EDP Sciences (2018), pp. 1-10.

[5] Dmochowski, G., Berkowski, P. Analysis of adaptation of reinforced concrete structures from early 20th century to the needs of modern requirements - a case study. In: Grantham M.G. et al. (Eds): *Concrete Solutions, 6th International Conference on Concrete Repair*, CRC Press (2016), pp. 9-12.

[6] Berkowski, P., Kosior-Kazberuk, M. Historical and structural aspects of the durability and maintenance of a reinforced concrete market hall building from the early 20th century. In: Grantham M.G. et al. (Eds): *Concrete Solutions, 6th International Conference on Concrete Repair*, CRC Press (2016), pp. 335-343.

[7] Berkowski, P., Kosior-Kazberuk, M. Construction history as a part of assessment of heritage buildings. *Procedia Engineering* (2016) **161**:85-90.

[8] Berkowski, P., Dmochowski, G. Examples of concrete structural elements in early 20th century buildings in Wrocław (Poland) - case studies. In: Grantham M.G. et al. (Eds): *Concrete Solutions, 5th International Conference on Concrete Repair*, CRC Press (2014), pp. 699-706.

[9] Berkowski, P., Dmochowski, G. Strengthening and repair of damaged structural elements of revitalized apartment, public service and industrial buildings from the turn of the 19th and 20th century Poland. In: A. Strauss at al. (Eds): *3rd International Symposium on Life-Cycle Civil Engineering*, CRC Press (2012), pp. 1212-1219.

[10] Czaplinski, K. *Former iron alloy products*. DWE (2009) (in Polish).

[11] Hellebois, A., Espion, B. Material properties of reinforced concrete at the turn of the 20th century: a review of primary literature. In: R. Drochytka at al. (Eds): *2nd WTA PhD Symposium Building Materials and Building Technology to Preserve the Built Heritage*, WTA Schriftenreihe, 36 (2011), pp. 248-260.

[12] Foti, D. Shear Vulnerability of Old Historical Existing R.C. Structures. Int. J. of Architectural Heritage: Conservation, Analysis, and Restoration (2015) (9)**4**: 453-467.

[13] Roca, P., Lourenço, P.B., Gaetani, A. *Historic Construction and Conservation. Materials, Systems and Damage*. Taylor &Francis (2019).

12th International Conference on Structural Analysis of Historical Constructions
SAHC 2020
P. Roca, L. Pelà and C. Molins (Eds.)

SENATE BUILDING OF CANADA
CASE STUDY: SEISMIC REHABILITATION

LISA M. NICOL[1]

[1]Senior Structural Engineer
at John G. Cooke & Associates Ltd. (JCAL)
17 Fitzgerald Road, Suite 200
Ottawa, Ontario K2H 9G1
e-mail: lnicol@jgcooke.com, www.jgcooke.com

Keywords: Historical Structure, Seismic, Masonry, Rehabilitation

Abstract. *Ottawa's landmark Union Station was constructed between 1902 and 1912 to house Ottawa's central railway station. Located in the Ottawa downtown core, it's situated a short distance from Parliament Hill and across the street from the iconic Fairmont Chateau Laurier Hotel. In the early 1960s, the train tracks and train sheds were removed and replaced with Colonel By Drive parkway. The building sat vacant for quite some time, until it was revived when it underwent renovations in the early 1970s. A south addition was added with a unique geodetic canopy structure. The former Union Station had officially been adapted into the Government Conference Centre, which it remained until this rehabilitation project 2014-2018, which transformed the building into the temporary house of the Senate of Canada. The building was not accessible to the public when it was a Conference Centre, however since 2018 the building is again open to the public for the first time in 55 years.*

The client's objective for this rehabilitation was to increase useable floor space. A seismic upgrade of the existing heritage building was also required, along with the design of a new east addition. Existing floor plates required upgrading based on new user requirements. High heritage areas of the building had to be maintained in their original integrity and worked into the design upgrade.

Creative solutions were demanded to bring this existing heritage masonry building up to current seismic code, without the structure taking any more room within the floor spaces. Maximizing space was absolutely critical. As well as, ensuring the new building materials were compatible with the existing heritage building materials. Innovation was found in the balance between a minimal intervention approach and upgrading for current code requirements.

1 INTRODUCTION

The building was constructed with five distinct Blocks, originally there were only four blocks. In the 1970 upgrades the South Addition was added to the end of the building.

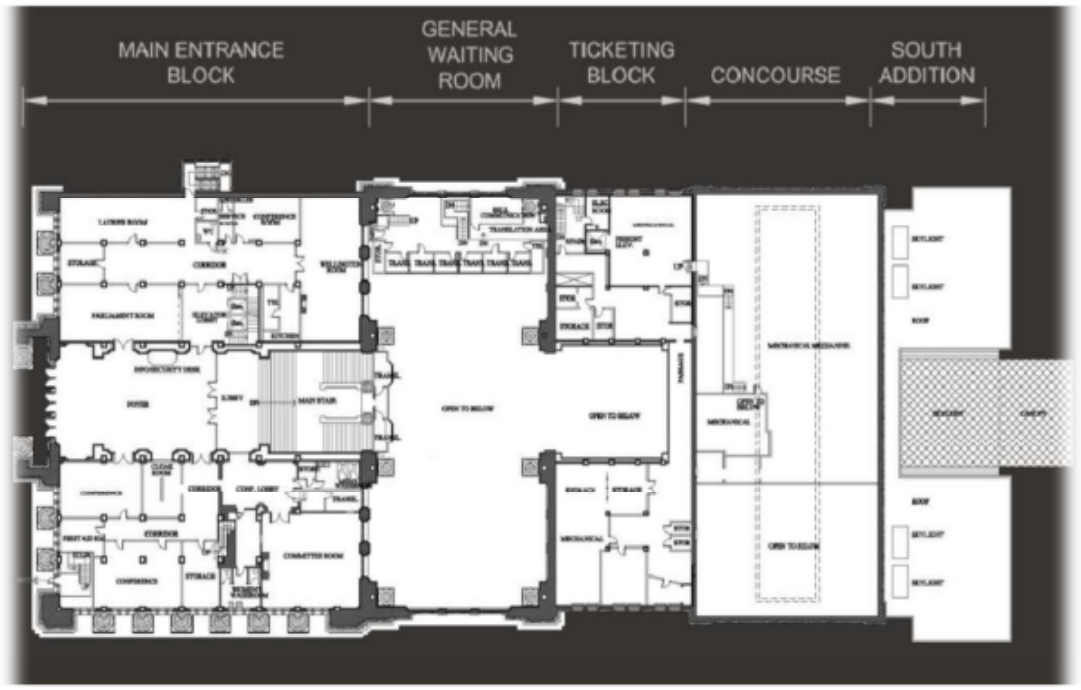


Figure 1: First floor plan (pre-2014)

The Main Entrance Block has always housed offices and washrooms, it is a five-storey structure.

The General Waiting Room is a four-storey structure and was originally where the public would wait for their trains and say their hellos/goodbyes to people coming or going. This area was a conference room and event space when the building was a Government Conference Centre.

The Ticketing Block is a three-storey structure and it was the block where one could purchase train tickets. As a Conference Centre the block was used as back of house rooms and mechanical/electrical rooms.

The Concourse was the block where the public met their trains, it is a two-storey structure. As a Conference Centre this area was used as event space and had a kitchen area as well as a mechanical mezzanine cutting the height of the area in two.

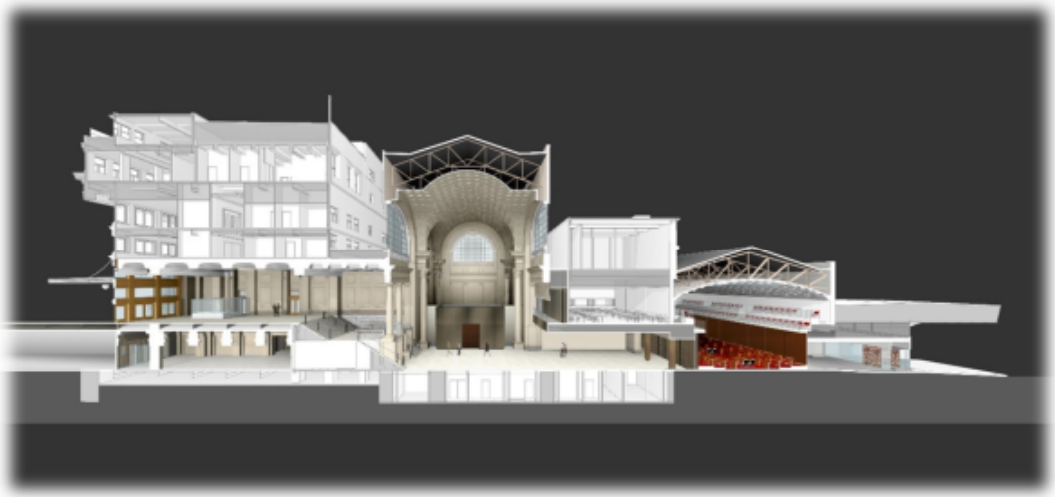


Figure 2: Section through building – New Layout (post-2014)

The building has very distinct blocks structurally as well, as shown from the section through the building. The first few storeys of the building are tied together but above the 2nd floor level the blocks are essentially independent from each other.

Solving the seismic and structural issues around the building would prove challenging because there were so many different scenarios. However, the building on whole has an abundance of multi-wythe masonry walls, and the base structure of the building was generally in good condition. There were also fully detailed original structural drawings for the building, which helped a great deal in anticipating what was found once finishes were removed.

2 PROJECT INITIATION AND CONTEXT

The driving reason for this rehabilitation project was that the Senate of Canada was looking for a temporary home while their original home, East Block on Parliament Hill in Ottawa, was undergoing its own renovations.

Secondary reasons for the rehabilitation were that incongruent upgrades were done in the 1970s, along with piecemeal additions. The bottom line was that the space was not effectively used and access between the building blocks was non-existent except at the ground floor level.

2.1 Is a seismic upgrade necessary?

When considering whether a seismic upgrade was necessary, a quick review of the proposed functional program for the Senate made it clear that there were major changes to the occupancy in some areas of the building. This brings the structural capacity into question, as the new loading would be higher/different than the historic floor loading would have been.

There was a new addition proposed, which added more weight to the building as well as more floor square footage, which would trigger a seismic upgrade of the existing structure unless the new structure was designed as a separate building.

The tipping point was that, seismic upgrade or not, the building would be under construction for several years, so there was a huge opportunity to bring the whole building up to current codes and standards.

2.2 Structural mandate

Through initial schematic designs with the Consultant team, the following became the major structural changes to the building:

- Seismic upgrade to a minimum of 60% National Building Code Canada (NBCC) loads. The project was able to upgrade to 75% of the NBCC.
- New 5 storey addition along east side of building.
- New first floor level structure with General Waiting Room (GWR) Block, at both the east and west ends of the block. These structures had to be completely independent from the existing building, to ensure the solution was completely reversible, within this high heritage space.
- New first floor level structure within the Concourse Block.
- New full basement within part of the GWR and full basement within entire Ticketing Block.
- New Ticketing Block structure. The existing structure was gutted, existing heritage masonry walls were shored, and new 3 storey structural infill was constructed.

3 EXISTING BUILDING STRUCTURES

Main Entrance Block (MEB) and Ticketing Block (TB): Structural steel roof/floor beams, supporting concrete slabs. Columns or multi-wythe brick masonry walls support these steel beams.

General Waiting Room (GWR): Structural steel roof trusses span the full width of this block. The trusses bear on structural steel columns that are embedded into huge multi-wythe brick piers along the north and south walls.

Concourse Block: Structural steel roof trusses span the full width of this block. The trusses bear on structural steel columns that are embedded into the multi-wythe brick wall along the north wall of this block. Along the south wall, the trusses bear on a huge structural steel truss that spans the full length of the block.

South Addition: Structural steel skeleton, with conventional lateral resisting system. It is presumed that the unreinforced concrete block masonry, along with the pre-cast panel façade, acted as the lateral resisting system.

3.2 Condition of existing structure

The condition of the structural steel within the building was excellent, apart from the structural steel framing the ground floor of the Ticketing Block which was rusting to various degrees. This framing was removed when the Ticketing Block structure was demolished.

The brick and stone masonry load bearing walls were generally in good condition. A masonry restoration program was completed over the course of this project to ensure the masonry was in the best condition possible, as all of the walls were used as shearwalls within the new design.

4 HERITAGE CONSERVATION VS STRUCTURAL/SEISMIC UPGRADES

Heritage Rehabilitation projects are the most challenging and most innovative because there is constant tension between two opposing objectives 1) creating a design that has minimal impact on the existing structure and 2) meeting current seismic code requirements. The structural designs for heritage buildings are endlessly being assessed based on the question – is this the least intrusive solution?

This requires an understanding of how the existing materials perform and finding compatible solutions to satisfy the two opposing objectives. When using the existing building materials to the fullest extent of their capacities, the new reinforcing required in the building naturally becomes a minimal intervention solution.

Becoming comfortable with heritage materials, and the way they perform, requires smart testing for physical properties and assessment of the existing condition of the building.

5 SEISMIC STRATEGY

To gain the seismic upgrade required, the focus was on reinforcing existing building elements, to minimize the space required for new structural elements as well as to minimize the impact of the upgrade on the existing structure.

A few examples of these structural seismic solutions used to achieve the client's main objectives are discussed below.

Excavation/underpinning was undertaken within the basement of the Ticketing Block and GWR, to increase usable floor space. This allowed the East Addition required to be much smaller and therefore have a smaller impact to the heritage façade overall. This also served to minimize the overall seismic forces acting on the existing building because extra floor space was created below grade.

A seismic upgrade of the existing building was complete, integrating the existing stone and brick masonry walls as lateral resisting elements. Using the masonry walls as shearwalls instead of modelling them as simple gravity walls, allowed for cost effective space savings.

This involved a full masonry restoration program to ensure the masonry walls were in good condition structurally.

A hybrid model was created in ETABS. Existing masonry walls were input as shearwalls with physical properties determined by on site testing. New concrete shearwalls were introduced where new stairwells or elevator shafts were created for the functional program. Concrete shearwalls were ideal for consistency of stiffness of materials. From the model, the most effective locations for new shearwalls could be established, loading on the existing masonry walls could be easily calculated and the existing capacities of existing floor structures was also determined.

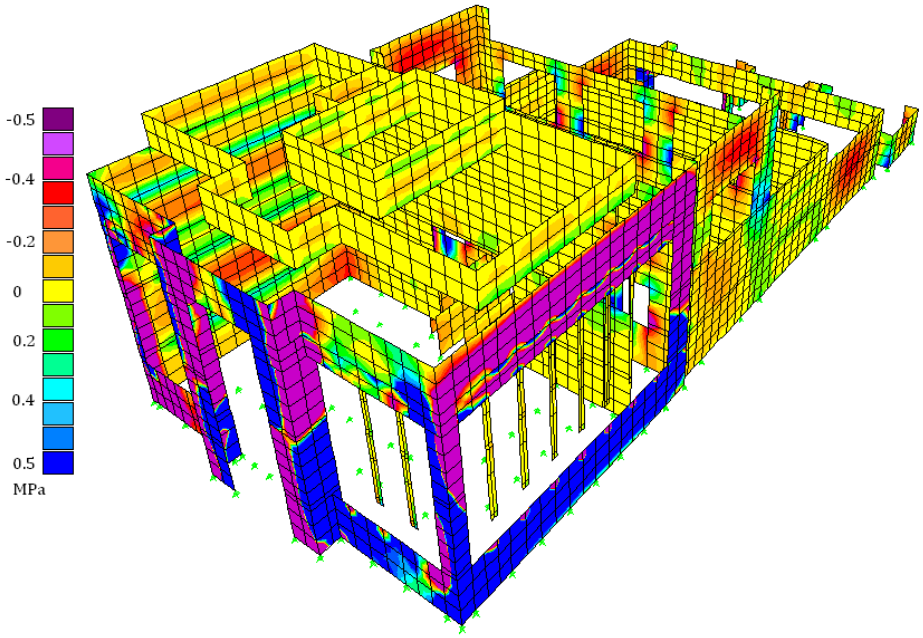


Figure 3: ETABS model of existing building

A lot of time was spent confirming that the model output was verifiable based on stresses on the building materials noted during on site assessments. The model is only as good as the level of accuracy is contains with the on-site existing conditions. For example, the existing building on site review of the masonry showed stress cracking and fractures at the North West corner of the MEB. When the model was reviewed, it also showed high levels of deflection and torsion at this same corner.

The on-site assessments also showed that there was masonry cracking at the corners of both the GWR Block and the Concourse Block, where the masonry walls had multi-storey unbraced heights. When reviewing the model, these corners were all high stress areas, due to excessive deflections and weak connections to the roof diaphragm.

The model was responding the same way the existing building had over its lifetime. This is a critical requirement of a model on any rehabilitation project, the importance of which cannot be stressed enough. Once the model is in tune with the existing building's behavior, the model becomes an extremely useful tool for seismic upgrades that meet the intent of current codes without over strengthening or stiffening the building. There is a definite point, where stronger and stiffer solutions do not provide favourable results, as it changes the way the building has generally performed over the course of its lifetime, producing an overall negative effect.

6 SEISMIC UPGRADES

6.1 Main Entrance Block (MEB)

Seismic upgrades that were complete within the MEB were as follows:

- New concrete shearwalls were introduced around existing and new stairwells. The shearwalls introduced on the west side of the block were critical to minimizing the torsional seismic effects that the original building had, as the North and west elevations of this block had a lot of curtain walls above 2nd floor level, with essentially no shear walls.
- All floor slabs were mechanically connected to masonry shear walls using Cintec grouted anchors. These anchors are designed with a weak grout, which is more compatible with masonry than most other anchors on the market.

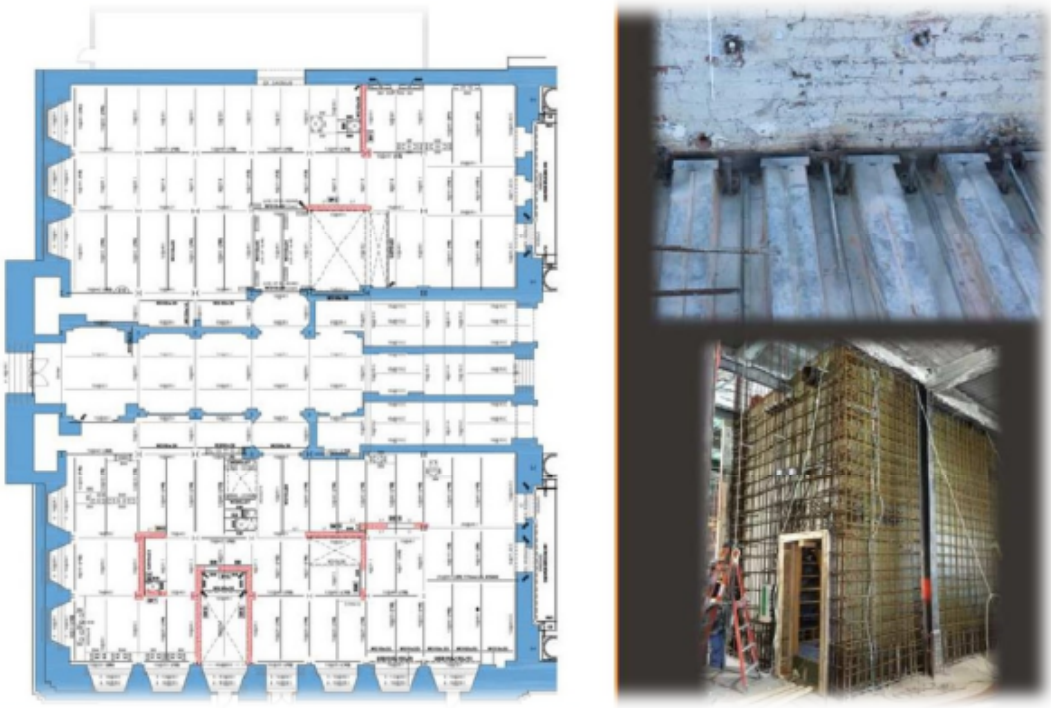


Figure 4: MEB Seismic Upgrades

6.2 General Waiting Room (GWR)

Within this space, new 1st floor level floor plates were constructed as stand alone structures. These were constructed from structural steel with x-bracing and inset from the heritage perimeter walls so that new structure could be completely removed from the building without damage to the heritage finishes. Expansion joints surround the three sides of these new floor plates.



Figure 5: GWR looking east from the new western 1st floor level

Within the attic space, steel x-bracing was introduced between the existing steel roof trusses, just under the plane of the existing timber roof diaphragm. This increased the strength of the roof, to decrease the torsional seismic effects the original building had which were causing the masonry to fracture at the corners of the building. The roof diaphragm was anchored to the top of these 4 storey walls, which also reduced deflection because the tops of these walls were no long unbraced.

6.3 Ticketing Block

As the best solution to making the functional program work within the existing building footprint, it was decided that the existing steel and concrete slab structure of the Ticketing Block would be demolished, and the exterior stone masonry facades would be shored to keep them intact. A new structure would then be built within the existing four perimeter masonry walls

of this block. Structurally, this worked well, as new concrete shear walls could be positioned around new stairwells within the corners of this block, which would lend lateral support to the 4 storey masonry walls of the GWR at the north end of this block as well as the 2 storey free standing walls of the Concourse at the south end of this block.



Figure 6: looking down at Ticketing Block from NW corner

6.4 Concourse

This block is the location of the house of the Senate of Canada, which meant that in addition to seismic concerns, a new 1st floor level was required to allow for a balcony seating area around the perimeter of the chamber. This floor level was designed for the minimum number of penetrations through the high heritage fabric of the perimeter walls.

Additional to this scope, the roof of the Concourse was reinforced with steel x-bracing, very similar to the GWR roof noted in section 6.2



Figure 7: Concourse looking west, from new 1st floor seating level

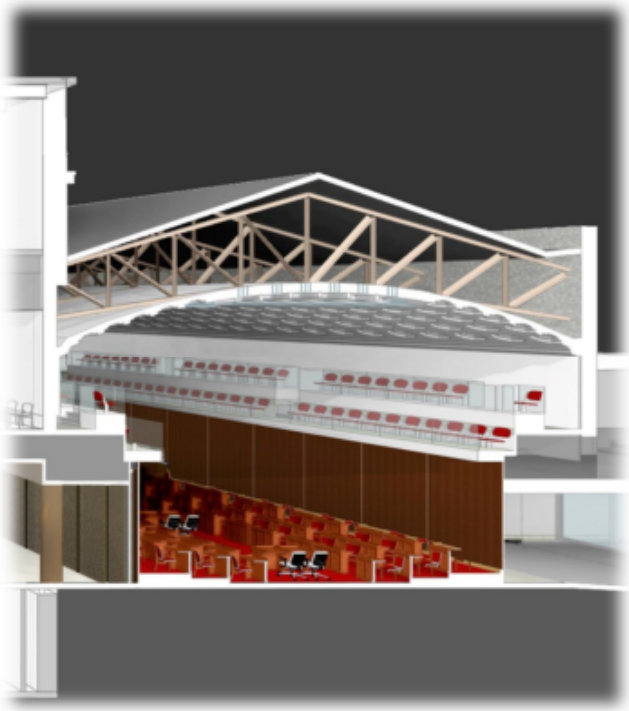


Figure 8: Perspective of new Concourse looking east

6.5 South Addition

The seismic upgrade in this area of the building consisted of adding additional reinforcing into the cells of the concrete block masonry perimeter walls and grouting the reinforced cells, to strength critical areas. The existing concrete block masonry was originally unreinforced.

7 CONCLUSIONS

The conservation and rehabilitation of this building is a fantastic example of how much character and history a heritage building can provide a city and country's narrative. It is truly a service to the downtown core to save these heritage buildings and repurpose them for current needs. Sustainable design strategies were achieved throughout the project.

The repurposing of this existing heritage building adds to the richness of the streetscape and history of the City of Ottawa. Now that the public can access the building again, the structure is a part of the community in a way that it hadn't been in 55years.

The story of this building continues to unfold for decades and centuries to come.



Figure 9: Exterior North East side of the Senate Building of Canada

Acknowledgements. Integral in making this project a reality was the engineering team at John G. Cooke & Associates Ltd., the Consultant team lead by Diamond Schmitt & KWC Architects in Joint Venture, and PCL Construction who were the Construction Managers on the project. And of course, the Government of Canada for initiating the project and seeing it through.

12th International Conference on Structural Analysis of Historical Constructions
SAHC 2020
P. Roca, L. Pelà and C. Molins (Eds.)

STRUCTURAL EVALUATION AND MAINTENANCE OF BROOKS AQUEDUCT HISTORIC SITE

ALIREZA ROUHI[1], NIGEL G. SHRIVE[2*]

[1&2]University of Calgary, Schulich School of Engineering
622 Collegiate Pl NW, Calgary, AB, CANADA T2N 4V8
e-mail: alireza.rouhi@ucalgary.ca,
email: ngshrive@ucalgary.ca, www.ucalgary.ca (*corresponding author)

Keywords: Reinforced Concrete, Aqueduct, Structural Evaluation, Durability, Numerical Modeling, Damage

Abstract. *Brooks Aqueduct in Alberta, Canada is one of the largest and most sophisticated reinforced concrete aqueducts in the world. Now a national historic site, Brooks Aqueduct was built in 1914. The structure suffers from cracking and degradation in certain locations. To find out the possible main causes of potential overstress and damage in the different areas of the structure, it was evaluated by site inspections, some laboratory tests and analyzed numerically using Abaqus finite element software. Results of the numerical analysis are compared with the inspection and testing results and conclusions are made about the causes of deterioration and ways to conserve and repair the structure.*

1 INTRODUCTION

Brooks Aqueduct is a 3.2 km long elevated flume built by the Canadian Pacific Railway (CPR) near the city of Brooks in southeast Alberta, Canada. The aqueduct was constructed to supply water to irrigate 50,000 hectares of land, and thus had a significant effect on the economy of that region for a long time.

The concrete in the aqueduct was subject to significant damage and deterioration almost from the beginning of operation. The damage was mostly because of the poor quality of the concrete with respect to durability issues, poor design and a lack of proper workmanship, all stemming from the paucity of knowledge about these issues at the time of construction.

To address the problems and issues of the aqueduct, and to maintain the structure in a safe condition for the public to view, several assessments have been performed on the structure over the last few years. We used the results of past field and laboratory tests (such as concrete cover measurements, carbonation depths, corrosion potentials, areas of delamination, concrete and rebar strength, air void analysis and petrographic analysis) to develop a 3-D finite element model of the aqueduct using Abaqus software. Both the concrete and the steel reinforcement are modelled with the software.

2 HISTORY AND SIGNIFICANCE

The aqueduct (Figure 1) had a noticeable role in the CPR's efforts to settle Western Canada and played an important role in the growth of farming establishments in southeast Alberta. The

aqueduct was commissioned in 1914 to transfer water at a volume of 25.5 cubic meters per second over a valley 3.2 km wide and 20 m deep [1]. The Eastern Irrigation District operated and maintained the aqueduct after 1935.

The flume is a shell (as seen in Figure 1) in the shape of a "hydrostatic catenary". This geometric shape is supposed to place the flume under direct axial tension with no moment or shear when the flume is filled to the design level.

The aqueduct was abandoned in 1979 after 65 years of service and was replaced with a larger earthen canal built to the south of the aqueduct. Brooks Aqueduct is a nationally significant civil engineering achievement because of its design, materials, and large size. The Canadian Society for Civil Engineering named Brooks Aqueduct as a National Historic Civil Engineering Site in 2000 [1][2]. An interpretative centre has been constructed and a part of the aqueduct has been removed to improve access for the public. More than 3 km still remains with various problems in terms of cracking and spalling of the concrete, and some sections of the flume missing patches of concrete.



Figure 1 : A view of Brooks Aqueduct

3 CONSTRUCTION

Construction of the aqueduct (Figure 2) allowed the irrigation of a region of Southern Alberta called “the Eastern Irrigation District”. It is a remarkable product of Canadian engineering and one of the largest aqueducts of its kind in the world [1]. Brooks Aqueduct would be considered a significant construction project even on today’s scales. Despite the flaws that have been observed during its century of existence, the people who built this structure deserve high respect for their innovation and work [1].

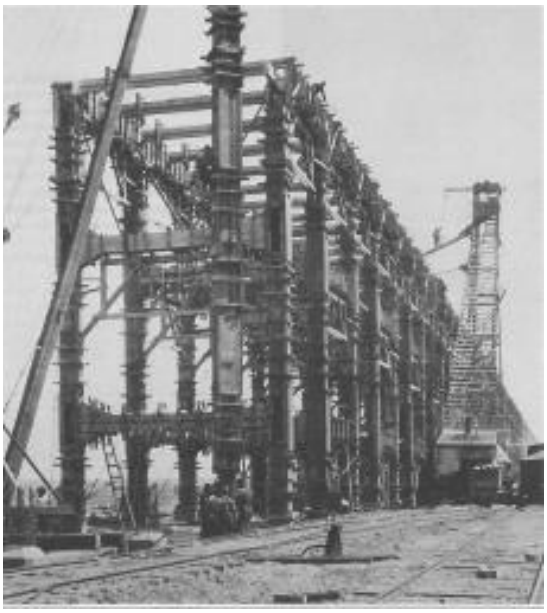


Figure 2 : Superstructure forms for Brooks Aqueduct, July 18, 1914 [1]

4 EARLY REPAIRS AND PROBLEMS

The concrete in the aqueduct has been subject to significant damage and deterioration since the early stages of operation (e.g.: Figure 3). The damage is mainly due to a lack of durability from issues unknown at the time of construction. Some of the most critical issues are a high water-cement ratio, lack of freeze-thaw resistance (air-entrainment), lack of proper cover over the steel, lack of pre-stressing of the concrete in tension areas such as the flume, inconsistency in the placement of rebars, alkali-silica reaction of the concrete in contact with the soil, lack of rebars in the footings, and poor grading of the aggregates (by today's standards) [3].

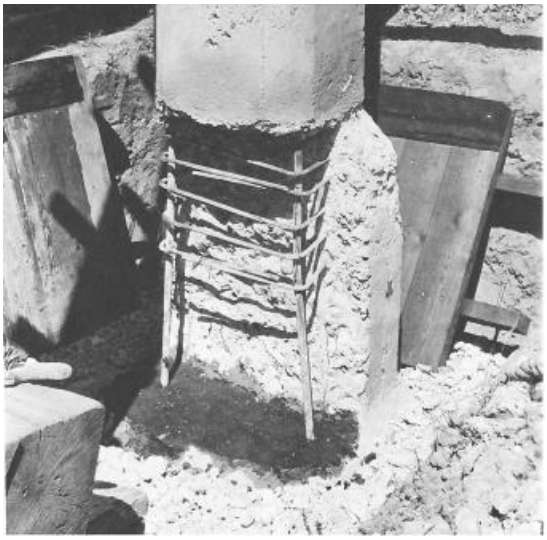


Figure 3 : Repair of footing – 1927 [3]

To address the problems being faced in the conservation and repair of the aqueduct adequately, the leading causes of damage and deterioration of the structure have to be identified. Repair and conservation options then have to be investigated. The structure was under repair pretty much constantly from the early days of operation, due to its design flaws [3]. Lots of problems occurred near the expansion joints due to water leakage. Some of these repairs are documented and branded with date stamps on-site, but unfortunately, complete registration of repair works during the long period of its service life and subsequently does not exist. Table 1 shows a summary of different damage types, the severity of the damage, and the approximate time of their first recorded repair.

Table 1 : Recorded damages and repairs of the aqueduct [3][4]

	Damage Type	**Location**	**Severity of damage (qualitative)**	**First recorded repair**
1	Pedestals	Base of frames	High	1921
2	Construction / Cold Joint	Columns	High	unknown
3	Honeycomb	Column Bases	High	1914
4	Expansion Joints	Flume every 80.’	Moderate	1915
5	Beams at expansion joints	Flume beams	Moderate	unknown
6	Spalling of Concrete Surface	Transverse Beams And Columns	Moderate	unknown
7	Column Cracking	Columns Near the Column to Beam Joints	Moderate	unknown
8	Delamination	Flume top surface	Moderate	1921
9	Column head	Column Head at expansion joints	Low	unknown
10	Exposed Embedded Reinforcement due to Construction Deficiency	Beams	Low	unknown
11	Scaling of the concrete surface	Flume top surface	Low	1921

5 PREVIOUS CONDITION ASSESSMENTS

To address the problems and issues of the aqueduct, and to maintain the structure in a safe condition, several assessments have been performed on the structure. The first available condition assessment was performed by a structural engineering company in 2006 and consists only of visual evaluation [4]. Another set of field and laboratory tests were performed on the Brooks Aqueduct in 2016, and a summary of the results of these tests is shown in Table 2 [5]. The results of these tests were used in the structural analysis of the aqueduct.

Table 2 : Concrete and steel test results of Brooks Aqueduct [5]

Average Values	**Flume**	**Bent**
Concrete Cover (mm)	33	73
Carbonation Depth (mm)	28	62
Delamination (% of Area)	34	14
Rebar Yield Strength (MPa)	N/A	293
Rebar Tensile Strength (MPa)	N/A	446
Concrete Strength (MPa)	N/A	16.4
Petrographic Analysis	N/A	Minor ASR

6 FINITE ELEMENT MODEL OF THE AQUEDUCT

A finite element model using Abaqus software [6] was made to assess the behaviour of the structure under loading and environmental effects. Given the three-dimensional nature of the concrete members, eight-node continuum elements (C3D8) were used to model the concrete. Parameters used in the concrete damage plasticity model of Abaqus were taken from the literature and are shown in Table 3 [7].

Table 3 : Parameters of concrete damage plasticity model [7]

Dilatation Angle	Eccentricity	f_{bo}/f_{co}	K	Viscosity parameter
36	0.1	1.16	0.667	0

Two-dimensional truss elements (T3D2) were used to model the steel reinforcing bars, as these elements were proved to be efficient for modelling tensile forces and stresses. The truss elements were coupled to the C3D8 concrete elements using the “embedded regions” function of Abaqus. This function is commonly used to model reinforcement of concrete in Abaqus and constrains the displacements of the nodes of the reinforcing bars (truss elements) to the displacements of the neighbouring nodes of the concrete (solid elements) in which the bars are embedded [6][8]. The steel reinforcement was modelled as elastic-perfectly plastic material, with a yield stress of 240 MPa, to be conservative, according to the results of the tension tests on actual bars and the availability of material at the time of construction of the aqueduct.

A section of the aqueduct between movement joints was analyzed under what was considered normal loading conditions and a series of different effects to determine if any environmental or time-dependent effect could cause some of the observed cracking.

7 RESULTS OF ANALYSIS UNDER NORMAL CONDITIONS

The finite element model of the aqueduct was analyzed under normal loading conditions which consisted of the self-weight of the structure and the flume full of water (or snow). The

maximum principal stresses in the concrete are shown in Figure 4. The maximum compressive stress is 4.02 MPa, while the maximum tensile stress was found to be 0.58 MPa: both of these stresses are well below the strength of the concrete. Principal stresses in the flume and column caps are shown in Figure 4.

Axial stresses in the rebars are presented in Figure 5. The maximum rebar tensile stress is 140 MPa, and the maximum compressive rebar stress is 28 MPa which are also well below the yield strength of the reinforcement.

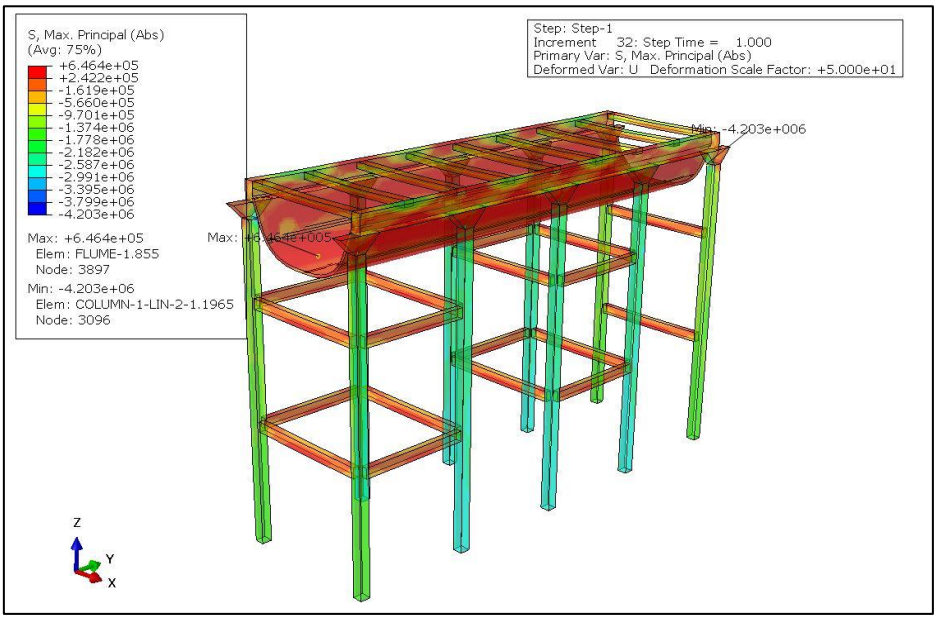


Figure 4 : Maximum principal stresses in concrete under normal loading conditions

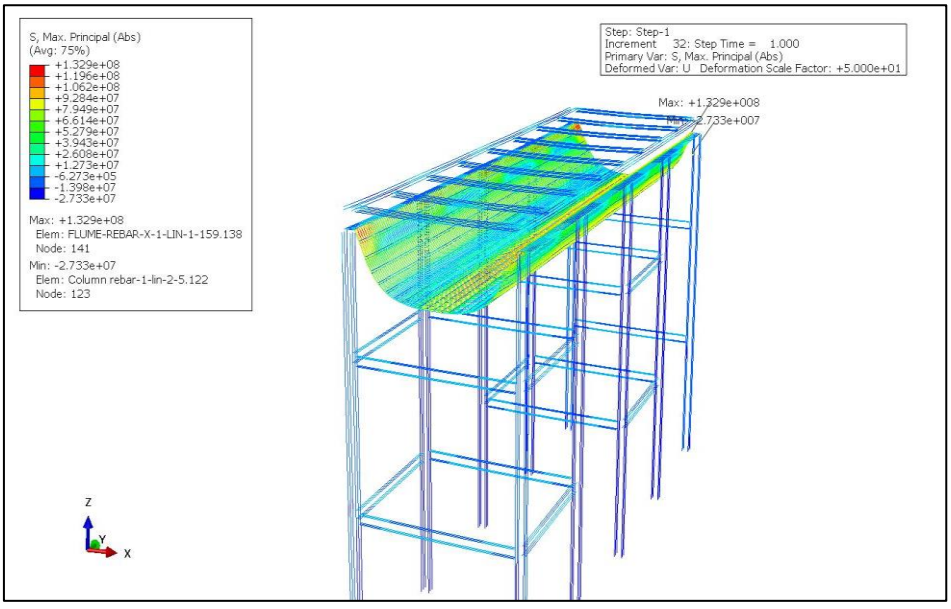


Figure 5 : Maximum principal stresses in rebars under normal loading conditions

8 EFFECT OF A POSSIBLE SETTLEMENT OF ONE COLUMN

Differential settlement under one column can happen due to local poor soil conditions. This kind of settlement would induce displacements and stresses, and possibly cause damage to the structure. To evaluate the effect of such possible settlement on the structure, a 50 mm downward displacement was applied to each of the five columns on one side of the flume in turn. Because of the symmetry of the structure along the longitudinal centerline of the flume, the effect of the settlement of the columns on the other side of the flume will be the same. Results of the analysis due to the settlement at one column are shown in Figure 6 and Figure 7. The results show that except for very local areas due to the concentration of stresses in very small elements, the compressive and tensile stresses in the structure are well below levels that would cause damage despite imposing such a big and unusual settlement.

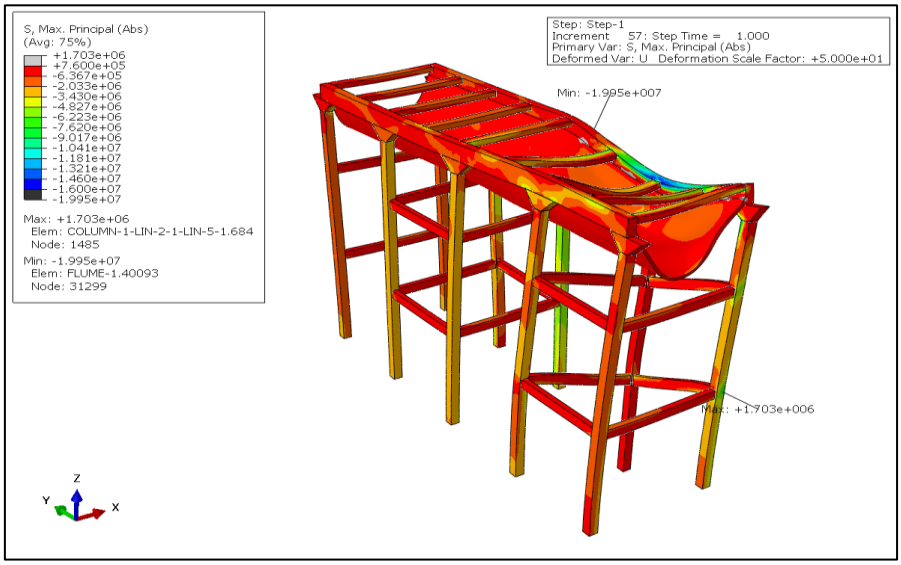


Figure 6 : Maximum principal stresses in concrete due to the 50 mm settlement at one column

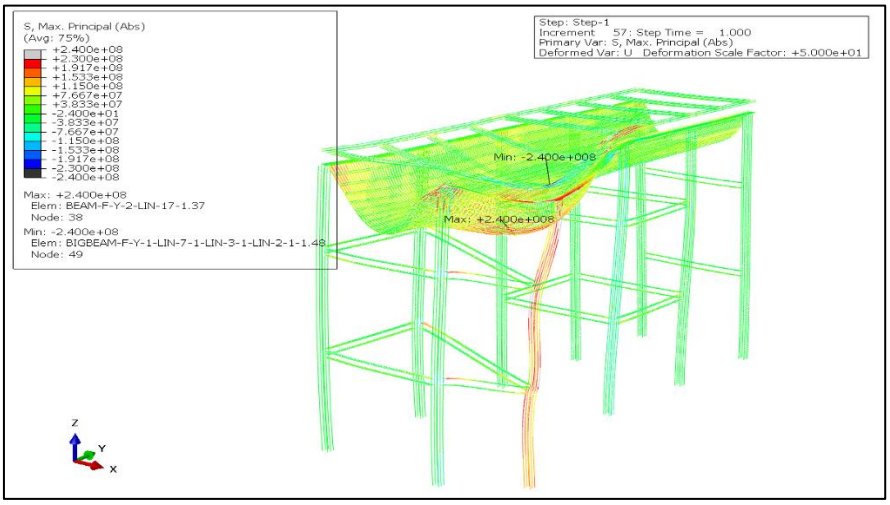


Figure 7 : Maximum principal stresses in rebars due to the 50 mm settlement at one column

9 EFFECT OF TIME-DEPENDENT RELATIVE SETTLEMENT AT ONE SIDE

Creep in concrete is defined as an increase in strain in the concrete under sustained load. The creep rate is higher at higher temperatures and is accelerated with rapid heating as well as fast cooling. In the case of Brooks Aqueduct, the aqueduct has an east-west alignment, so the south side is exposed to more sun than the north side and is therefore subject to higher temperatures and less humidity than the north side. This is obvious from the extensive amount of lichen on the north side where more moist conditions exist, and the lack of lichen on the south side of the aqueduct (Figure 8). A possible effect of this situation is differential creep between the north and south columns of the aqueduct. This case was studied by imposing a 25 mm relative movement on the south side of the structure to represent the shortening of columns due to differential creep. The results of this analysis are shown in Figure 9 and Figure **10**.



Figure 8 : Lichen on a column and beams on the north side of the aqueduct (left) due to the existence of more humidity and cooler temperatures compared the south side (right)

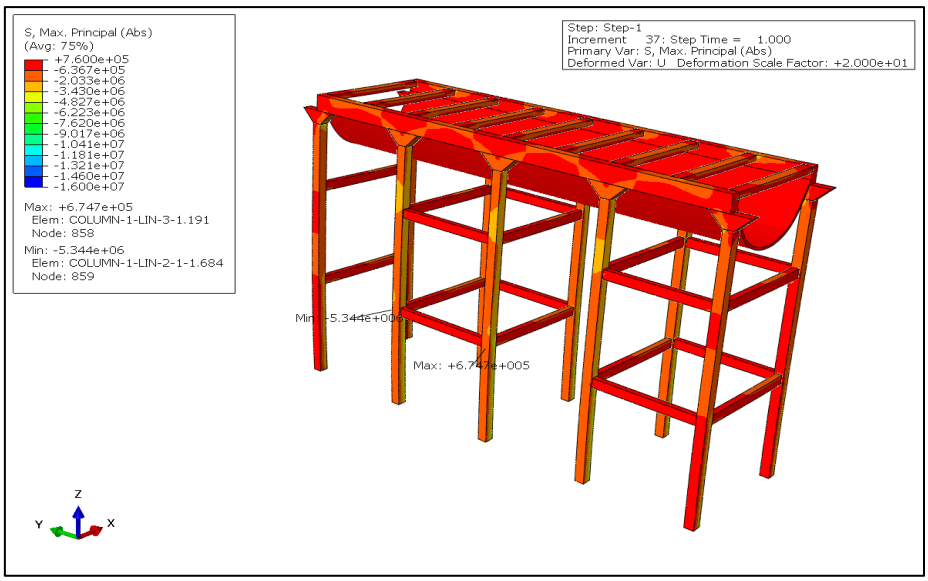


Figure 9 : Max. principal stresses in concrete due to settlement in all south columns

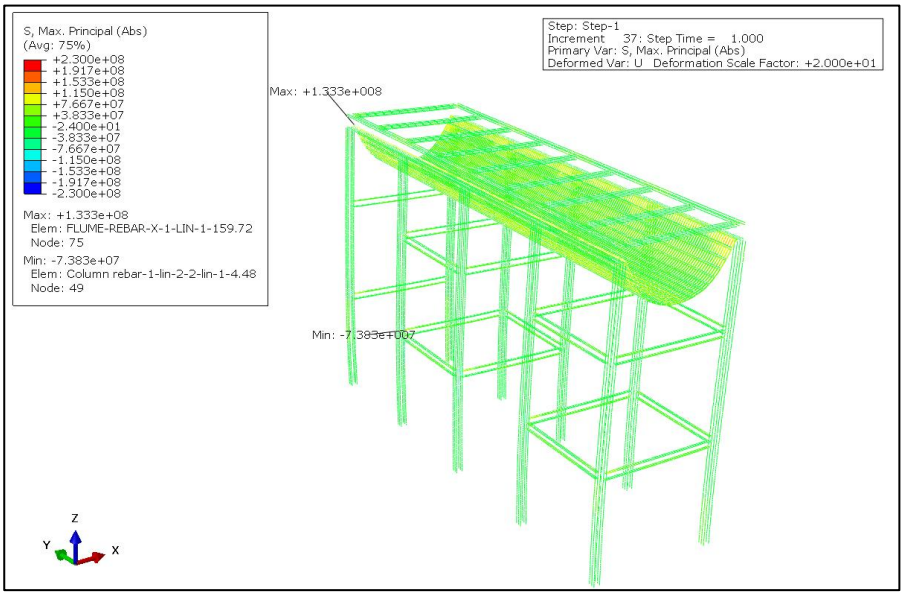


Figure 10 : Max. principal stresses in rebars due to settlement in all south columns

10 OVERALL RESULTS OF ANALYSIS

A summary of the results of the finite element analyses of the structure under different possible loading and environmental conditions are as follows:

1- The maximum stresses due to thermal loading are 15 MPa in compression and 1.1 MPa in tension which occurs in small areas due to stress concentration.

2- The location of higher stresses are not where most of the damage and deterioration exist.

Based on the results of the analyses and comparing the results with the site inspections, it can be concluded that the most probable cause of deterioration of the concrete near the expansion joints is the infiltration of water through damaged joints and the consequence of the accumulated water in these areas freezing/thawing or corrosion of steel (Figure 11).



Figure 11 : Deterioration of flume at expansion joints

Corrosion of steel could have happened due to lack of adequate concrete cover, poor quality of concrete and poor workmanship in proper placement of the rebars in the concrete according to drawings and specifications. As shown in Figure 12, in some places, the reinforcing bars were placed at the edge of the concrete formwork and thus had little or no cover which makes them very vulnerable to corrosion and deterioration. Damage and deterioration of longitudinal beams at expansion joints are also shown in Figure 13.



Figure 12 : Lack of proper cover for concrete



Figure 13 : Deterioration of longitudinal beams near expansion joints

11 SELECTION CRITERIA FOR REPAIR MATERIALS

One of the most common methods in the preservation of concrete structures is to use patch repairs in the areas that concrete is damaged or lost due to spalling or degradation. In the past, patch repairs were usually done based on the availability of material and the experience of the contractor: little attention was paid to the compatibility of the patch material with the existing materials in the structure. Unsuccessful repairs of the aqueduct in the past also highlight the

importance of selecting the proper materials and methods of restoration.

Some research has been performed on the selection criteria for the repair material, and a summary of patch repair selection criteria for structural compatibility is shown in Table 4.

Table 4 : General requirements for patch repair material [9]

Property	Repair mortar (R) vs existing concrete (C)
Compressive, tensile and flexural strength	$R \geq C$
Modulus of elasticity	$R \geq C$
The coefficient of thermal expansion	$R \approx C$
Adhesion in tension and shear	$R \geq C$
Curing and long term shrinkage	$R \geq C$
Fatigue performance	$R \geq C$
Poisson's ration	Depends on the type of repair
Creep	Depends on the desirable or undesirable effect of creep

12 CONCLUSIONS

Based on the results of numerical models, visual site assessments, historical reports and laboratory tests, the most probable causes of damage and deterioration in Brooks Aqueduct are:

1- In inland areas such as Brooks, where the winters are long and cold, the main durability issues with reinforced concrete are usually severe freeze-thaw damage of the concrete, concrete carbonation and corrosion of the steel reinforcing bars. These issues were not considered in the design of the aqueduct, because at that time, they were not known to be issues that needed to be considered.

2- Poor quality of concrete which is a result of the lack of knowledge about the effect of factors such as water-cement ratio, aggregate selection, curing, vibration, etc. on the quality and performance of the concrete at the time of construction of the aqueduct.

3- Poor workmanship in the placing of reinforcing bars, maintaining proper cover, concrete quality, etc. – again not known as issues that needed to be dealt with at the time of construction.

4- Lack of proper understanding of the behaviour of the concrete of the flume in tension and detailing of the reinforcement in different areas (adequate splice length, cover, etc.)

5- Lack of appropriate design of expansion joints to prevent water infiltration.

Given the factors mentioned above, the need to prioritize and plan for proper repair and restoration of the aqueduct is critical to prevent further damage. Because of the massive size of the aqueduct and the different areas that need to be addressed, and because of limitations in available conservation resources, it is essential that the structure be inspected and repaired frequently and that resources are allocated based on the importance and priority of the problem.

Acknowledgements. The authors gratefully acknowledge the support of Alberta Culture in providing access to the site and their archives. The University of Calgary provided substantial support through their computing resources and the Department of Civil Engineering, all of which is sincerely acknowledged.

REFERENCES

[1] Manz, D.H. and Loov, R.E. Brooks Aqueduct. *Canadian J. of Civil Engineering (1899),* pp. 684-692.
[2] Finch, D. The Brooks Aqueduct, A Technological and Engineering History 1912-79. *Environment Canada, Canadian Parks Services Report Series 360* (1988).
[3] Finch, D. Much Brain and Sinew: *The Brooks Aqueduct Story.* (1993), p. 50.
[4] Quinn Saretskey Structural Engineers Inc. *Brooks Structural Assessment Report* (2006).
[5] ISL Engineering. *Brooks Aqueduct, Quantitative Engineering Assessment* (2016).
[6] Dassault Systems. *Abaqus 6.14 Analysis User's Guide* (2014).
[7] Kmiecik, P. and Kamiński, M. Modelling of reinforced concrete structures and composite structures with concrete strength degradation taken into consideration. *Archives of Civil and Mechanical Eng.* (2011), vol. 11, no. 3, pp. 623–636.
[8] Sümer, Y. and Aktaş, M. Defining parameters for concrete damage plasticity model, *Challange J. of Structurl Mechanics* (2015), vol. 1, no. 3, pp. 149–155.
[9] Morgan, D.R. Compatibility of concrete repair materials and systems. *Construction and Building Materials (1996).* vol. 10, no. 1 SPEC. ISS., pp. 57–67.

12th International Conference on Structural Analysis of Historical Constructions
SAHC 2020
P. Roca, L. Pelà and C. Molins (Eds.)

STRUCTURAL EVALUATION AND MAINTENANCE OF GREENHILL MINE TIPPLE STRUCTURE HISTORIC SITE

ALIREZA ROUHI[1], NIGEL G. SHRIVE[2*]

[1&2]University of Calgary, Schulich School of Engineering
622 Collegiate Pl NW, Calgary, AB, CANADA T2N 4V8
e-mail: alireza.rouhi@ucalgary.ca,
email: ngshrive@ucalgary.ca, www.ucalgary.ca (*corresponding author)

Keywords: Reinforced Concrete, Mine Tipple, Structural Evaluation, Durability, Damage, Numerical Modeling,

Abstract. *The tipple building located within the Greenhill Mine complex (a Provincial historic site) in southern Alberta, Canada is a reinforced concrete frame with a steel superstructure. The structure has been analyzed to assess its current state and the extent and causes of deterioration. The analysis is performed using data obtained from field and laboratory tests and evaluations and by using SAP2000 structural analysis software. Possible ways for conservation and restoration of the building for two different future uses are explored, and recommendations are provided.*

1 INTRODUCTION

The Greenhill mine primary rotary tipple structure is a part of the mining complex located in the Crowsnest Pass area of southern Alberta, Canada and is the most important building at the site. The structure consists of a 40-metre-long, 9-metres wide concrete frame supporting a steel superstructure. This type of construction was quite innovative and was considered state-of-the-art at the time of its development in 1914 because of using new methods and materials such as steel and reinforced concrete. Various types of damage and deterioration are visible on the tipple structure. The causes and extent of these deteriorations are examined and possible methods for repair and conservation of the structure are discussed.

2 HISTORY AND SIGNIFICANCE

Coal mining was the main part of the economy of the Crowsnest Pass area of southwest Alberta during the first half of the 20th century. The historic Greenhill Mine Complex was one of a series of active coal mining operations in the Crowsnest Pass area, being a significant part of the industry. The complex is located north of Highway 3 next to the town of Blairmore. The mine began service in 1914, operated by West Canadian Collieries. Like other mining communities in the area, the mine suffered from rapid changes in coal prices during its time of operation. With the introduction of diesel engines by the Canadian Pacific Railway Company (CPR) in the early 1950s, the mining operations at Greenhill ceased in 1957, and the site was abandoned [1]. An overall view of the tipple building is shown in Figure 1.

In the 1980s, in recognition of the significance of coal mining to the surrounding communities culturally and economically in the first half of the twentieth century, the Greenhill Mine Complex was designated as a Registered Historical Resource. It is now under the care and control of the Government of the Province of Alberta.



Figure 1: Overall view of Greenhill mine tipple structure and its roof trusses

3 CONSTRUCTION

The primary tipple building consists of a concrete moment frame supporting a steel superstructure. The steel superstructure consists of Fink trusses at the roof (Figure 1) built from double angle chords, single angle web members, and channel purlins.

The columns of the steel superstructure are built-up members of channels and angles. Single angle braces located at two bays on each side of the building provide lateral load resistance in the longitudinal direction. Some parts of the braces, as well as some steel elements of the roof trusses, have been removed at some unrecorded time in the past (for example Figure 2). No lateral load supporting system exists in the short direction of the superstructure and it is not clear if any bracings existed originally in that direction, as there are no records of design, construction, alterations or maintenance. As a result, only moment frame action of the steel columns provides lateral resistance in the short direction. Thus, additional bracings have to be provided in the short direction to ensure the stability of the superstructure. This issue is discussed later.

The steel superstructure was built on a 200 mm-thick concrete slab, which is supported on an exposed concrete frame with 300 mm square concrete columns and beams. The beams and columns are each reinforced with at least four round rebars of 20 mm diameter. Bars of different dimensions and sections were used with inadequate lap splicing (for example, see Figure 3).



Figure 2: Roof truss with part of the bottom chord removed



Figure 3: A round bar overlapped with a square bar in a splice. Also note variation in aggregate size and shape

3.1. PREVIOUS CONDITION ASSESSMENTS

A visual condition assessment of the primary tipple was conducted in 2013 [1]. Based on the results of structural evaluation of the tipple building structure, the following types of deterioration and damage and their respective areas were detected and listed based on the severity of damage from most to least important [1]:

1- Section loss and spalling due to freeze-thaw in concrete columns
2- Removed members in the steel superstructure
3- Section loss and spalling due to freeze-thaw in concrete beams

Some signs of damage and deteriorations are shown in Figure 4.



Figure 4: Signs of deterioration on concrete members

3.2 CONCRETE TEST AND SAMPLING

To investigate the condition of the structure further, field sampling was performed (Figure 5). To avoid inclusion of steel reinforcement in the concrete samples as well as to identify the location of rebars in the concrete for further analysis, a ground-penetrating radar scan device called “structure scan” was used during the sampling process (Figure 6). “Structure scan” is manufactured by GSSI (a member of the OYO group) and can find the location, depth, and size of reinforcing bars as deep as 500 mm. The existence of large size aggregate particles in the concrete caused some difficulties such as the failure of several cores during the sampling process. Fourteen concrete cylinder cores were obtained. Six cores had a diameter of 95 mm (3.75 inches), and eight had a diameter of 70 mm (2.75 inches). The core samples were cut wet with diamond cutters. The sample holes were filled with a cementitious mortar.



Figure 5: Concrete sampling



Figure 6: Ground-penetrating radar scan

3.3 CONCRETE PROPERTIES

In the absence of any construction documents and drawings, visual inspection of the concrete material revealed some useful information about the properties of the material used in the concrete. The aggregates used in the concrete include a very broad range of size and shape, including some large aggregate particles more than 100 mm in the largest dimension (Figure 7 and Figure 3). One may surmise that the contractor used gravel obtained directly from the river nearby as there appears to be no grading of the aggregate.

Three core samples were tested to obtain the compressive strength of the concrete. Samples were prepared for the compressive testing by cutting the ends with a 20" masonry saw. The ends were then glycapped (Figure 7), and the samples tested according to ASTM C-39.

The compressive strengths obtained from the three core samples were 12.1, 23.4 and 17.9 MPa, so the equivalent compressive strength of the concrete for the Greenhill mine structure based on ACI standard 562-16 (Code requirements for assessment, repair, and rehabilitation of existing concrete structures) was calculated to be 15 MPa [2]. This value was used as the initial concrete compressive strength in the analysis and strengthening of the structure. The average mass density of the concrete samples was 2323 kg/m^3.



Figure 7: Preparation of samples for compressive test. Note the large aggregates in the samples

3.4 REINFORCEMENT STEEL PROPERTIES

ACI 562-16 [2] suggests using default strengths for structural steel based on their

construction time frames. Based on the time of construction of the tipple building (around 1914) and in the absence of construction documents and data from tests, the minimum yield strength of structural steel reinforcing bars is considered to be 227 MPa (33000 psi) [2].

4 STRUCTURAL MODEL OF THE BUILDING

Analytical models of the tipple structure were made in SAP2000 software version 19.0 for two future use scenarios:

1- Adaptive re-use of the building as a restaurant

2- Utilizing the structure in the current loading condition with occasional visitors

The geometry of the model was obtained from existing recently created as-built drawings and additional site measurements. The load cases and combinations were obtained from "National Building Code of Canada (NBCC–2015)" [3]. Load cases are defined as follows:

D: Dead load (including self-weight of the structure + superimposed dead load)

L: Live Load (if structure to be developed into a restaurant)

S: Snow Load

W: Wind Load

For the case of adaptive reuse as a restaurant, a live load of 4.8 kPa and superimposed dead load of 1 kPa in the main floor were considered based on NBCC 2015. The missing steel members of roof truss were replaced, and steel bracings added in both directions of the building to ensure the stability of the steel superstructure. Figure 8 shows the structure modelled.

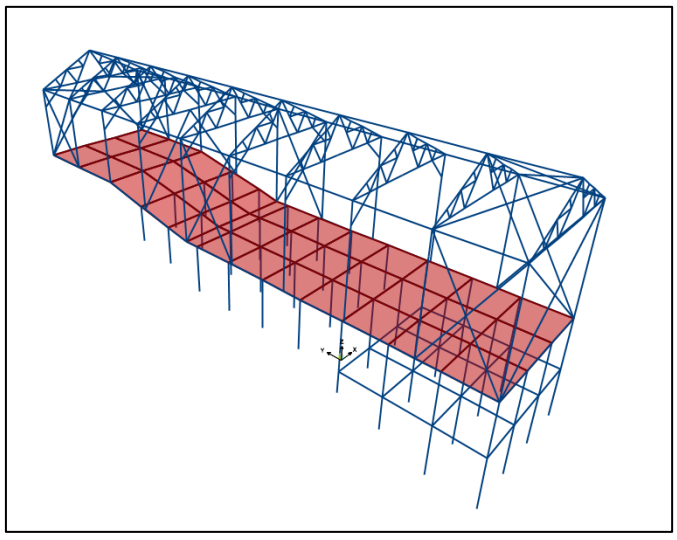


Figure 8: The structural model of Greenhill building in SAP2000

4.1 STRUCTURAL EVALUATION BASED ON ADAPTIVE REUSE AS A RESTAURANT (SCENARIO 1)

The main purpose was to evaluate the sufficiency of the existing structure if the building were to be developed as a restaurant and to identify the potential areas that may require strengthening. "Commentary L" of the NBCC [3] requires that in the evaluation of an existing structure, when public life safety is involved, the structural integrity of the building be checked

with respect to the ability of the structure to provide alternative load paths in the case of a local failure, such as losing a column due to an accident, overloading, deterioration, etc. This criterion was checked in the structural analysis of the building and effect of the most severe local failure (losing a corner column) was added to the results of other load combinations. Examples of the axial forces and bending moments due to some load combinations are shown in Figure 9.

The following conclusions can be drawn based on the results of the structural analysis:

1- Cross Beams: In general, the middle two-thirds of the concrete cross beams can resist the applied loads in their original form although the existing transverse reinforcement of the beams does not satisfy current minimum code requirements. More attention has to be paid to the joints between the beams and the columns (item 3 below).

2- Columns: The columns are slender and in a sway frame. Based on the site inspections, they do not satisfy minimum code requirements for transverse reinforcement (ties). They are subject to a maximum combined axial load of 170 kN compressive load and 21 kN-m bending moment. In some extreme cases, the column can be subjected to 120 kN tensile force (uplift) combined with 23 kN-m bending moment.

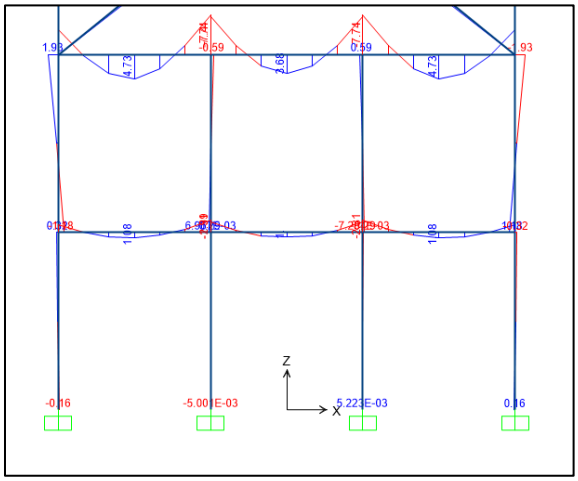


Figure 9: Bending moment in members due to applied vertical loads (Max=10 kN-m)

3- Beam-column connections: the details of the reinforcement in the beam-column joint areas are not clear, but based on visual site inspections, it is almost certain that the code requirements for beam-column joints in a moment frame are not satisfied.

Because life safety is involved if the building is re-used as a restaurant, and to make sure that the structure can resist the loads adequately, attention has to be paid to existing uncertainties such as the quality of the concrete, the existence and size of steel rebars and stirrups, and the adequacy of rebar splice lengths.

4.2 STRUCTURAL EVALUATION BASED ON CURRENT USE (SCENARIO 2)

In the case of keeping the current use of the structure, the occupancy of the building will not change from its current state, and future loads will be similar to past loads and even less than

the loads applied during operation of the building. In this case, public life safety is also not involved, and because of the lower reliability level of the building, more relaxation in the load combinations is allowed based on Commentary "L" of the NBCC [3]. In this case, the live load on the main floor is reduced to 2 kPa, with no superimposed dead load. Also due to the existence of large openings in the walls, the applied basic wind load is less than the loads in scenario 1.

Based on the results of structural analysis and the section properties of the concrete members, and due to satisfactory past performance of the building under similar or higher loads for more than 100 years, according to Commentary "L" of the NBCC [3], no further strengthening other than repairing the deteriorated members to their original shape and protecting them from further deterioration is required for this case. Thus, the damaged beams and columns should just be repaired with compatible and durable material, and a coating applied to protect them from the ingress of water and other damaging materials as well as freeze-thaw cycles. Accumulation of water has to be avoided in the top of the beams, the bottoms of columns, footings and other susceptible areas by providing proper slopes and drainage systems.

5 SELECTION OF REPAIR AND STRENGTHENING METHODS

For Scenario 1, strengthening is required. Several repair and strengthening techniques have been used to strengthen concrete moment frame structures. Some of the "traditional" techniques are steel or concrete jacketing, prestressing and the use of external steel plates. Most of the "traditional" techniques are highly intrusive, expensive and involve heavy equipment. High strength composite materials such as Fibre Reinforced Polymers (FRP) bonded externally to the concrete member provide a good alternative for the strengthening of concrete structures. These materials bond with the existing structure and perform as reinforcement. FRP materials can be used to strengthen concrete structures as follows:

1- Concrete beams and one-way slabs in flexure and shear
2- Concrete columns by wrapping and confinement which improves strength and ductility
3- Prestressed concrete beams
4- Two-way slabs and flat slabs for flexure and punching shear
5- Beam-column connections by improving ductility and shear strength

In recent years, high modulus Carbon FRP materials with a modulus of elasticity of more than 200 GPa have become available for use in the construction industry. These materials are thin, lightweight and easy to install using adhesives.

The performance of FRP strengthening of concrete structures depends on two main elements:

1- The durability and performance of the bond between the FRP laminate and the concrete substrate
2- The durability and performance of the FRP material itself.

It is well known that the interface or bond between the FRP and the substrate materials such as concrete can be the weak link when failures occur. Several standard tests have been developed over time to study the durability of the bond between FRP and concrete. Among them are pull-off tests, pull-apart/push-apart shear tests, peel tests, flexural tests, torque tests,

pull-out tests as well as non-destructive tests such as impact-echo and infrared thermography. The following factors can influence the bond between FRP and concrete [8]:

1- Exposure to moisture
2- High Temperature
3- Freeze-Thaw Conditions
4- Saline and Alkaline Environment

Error! Reference source not found. shows the main characteristics of three different fibre types used in FRP composites.

Table 1: Comparison of the three main types of FRP [9]

Criterion	Fibre Type		
	Carbon	Aramid	Glass
Tensile Strength	Very Good	Very Good	Very Good
Modulus of Elasticity	Very Good	Good	Adequate
Long Term Behaviour	Very Good	Good	Adequate
Fatigue Behaviour	**Excellent**	Good	Adequate
Bulk Density	Good	**Excellent**	Adequate
Alkaline Resistance	Very Good	Good	**Inadequate**
Price	Adequate	Adequate	Very Good

Design codes and standards provide coefficients for taking into consideration the effect of different factors such as environmental effects, type of material and their application. The Canadian Highway Bridge Design Code (CSA-S6-14 2014) [5] and CSA-S806 (CSA S806-12 2012) [4] have also provided resistance factors for the calculation of FRP composite resistance.

5.1 STRENGTHENING USING FRP COMPOSITES

In recent decades, different codes, standards and guidelines are published to regulate the use of FRP composites in design and strengthening of structures. In Canada, two codes, CSA S806 [4] and CSA S06 [5], have provisions for the use of FRP in buildings and bridges respectively.

According to CAN/CSA-S806-12[4], before using any FRP strengthening method, an assessment of the current situation of the existing structure or elements should be conducted to assess the current condition of the existing structure and find out the main causes of damage and deterioration. The effects of the applied loads and the capacity of the structure should be calculated. The possibility and feasibility of using FRP strengthening systems such as Externally Bonded or Near-Surface Mounted FRP systems can then be evaluated.

5.2 STRENGTHENING OF THE BEAMS FOR FLEXURE AND SHEAR

The cross beams are 300 x 300 mm square concrete reinforced with 2 x 20M longitudinal rebars at the top and bottom and 10 mm stirrups at every 600 mm. The size and spacing of the rebars and stirrups were obtained from inspection of exposed areas. Some beams, especially exterior beams, have suffered from extensive spalling and delamination of the concrete primarily due to freeze-thaw cycles, but section losses in the reinforcing bars of the beams are not significant and usually consist of minor surface corrosion.

If extra resistance for shear and bending moment in the beams are required, the Canadian code S806-12 has provided methods for strengthening using externally-bonded FRP. Schematic views of beam flexural and shear strengthening are shown in Figure 10 and Figure .

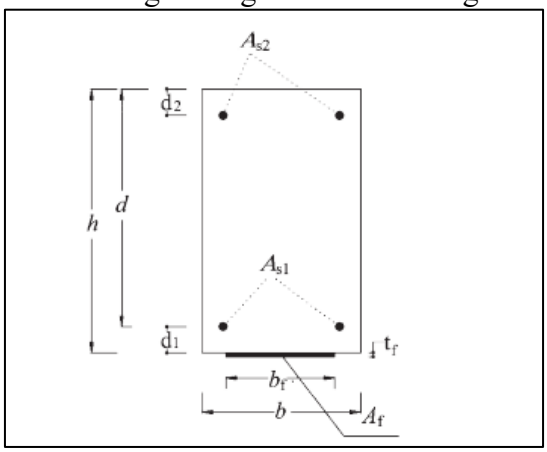


Figure 10: Flexural strengthening of concrete beams using externally-bonded FRP [6]

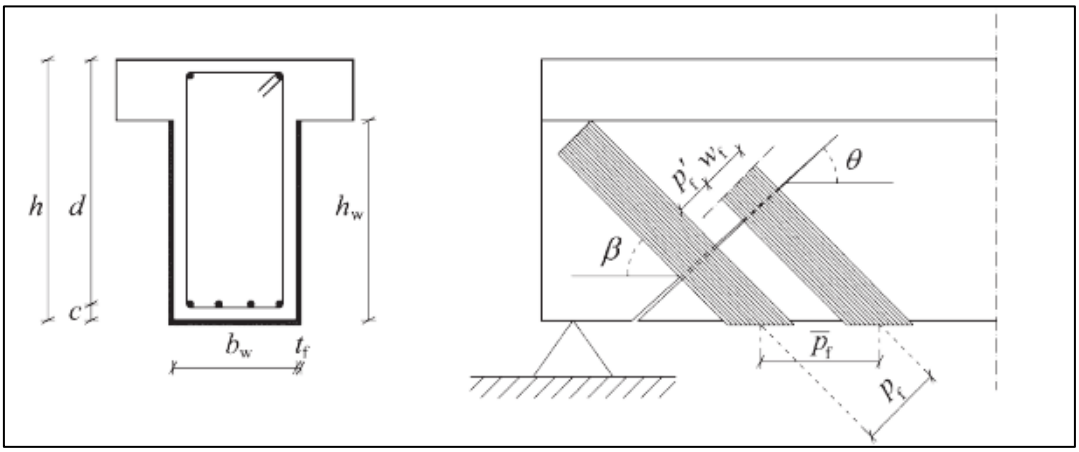


Figure 11: Shear strengthening of concrete beams using externally-bonded FRP [6]

In the FRP flexural and shear strengthening systems, stresses transfer from the FRP to the concrete through the adhesive and these systems are bond-critical applications. Therefore, it is necessary to have appropriate surface preparation and sufficient concrete strength to reach the required strengthening.

5.3 STRENGTHENING OF THE COLUMNS

Confining concrete columns with externally-bonded FRP (EB-FRP) wraps is an effective way to improve the behaviour of concrete columns in several ways such as increasing column axial load capacity, preventing buckling of reinforcement bars, reducing the lap length required for the rebars, and reducing the rate of water ingress into concrete which slows the rate of steel corrosion (Figure). FRP wrapping also improves the ductility of the member which is beneficial in the dynamic and seismic response of the structure.

Along with several national and international codes from around the world, Canadian codes ("S6-06: Canadian Highway Bridge Design Code" and "S806-12: Design and construction of building structures with fibre-reinforced polymers") have provided methods and formulas for the calculation of the compressive strength of confined members with composite materials.

Given the new occupancy and loadings and existence of uncertainties in quantity and quality of concrete and rebars in the members, and to satisfy the life safety requirement in respect of the reuse of the structure, it would be preferable to strengthen the columns and make sure about the structural stability and integrity of the tipple building. It can be observed that confinement by FRP wraps can theoretically increase the compressive strength of the concrete in the columns from 15 to 20.7 MPa. The compressive strength of the columns could be further increased by circularization of the existing rectangular-shaped columns which will increase the effectiveness of confinement by FRP wraps.

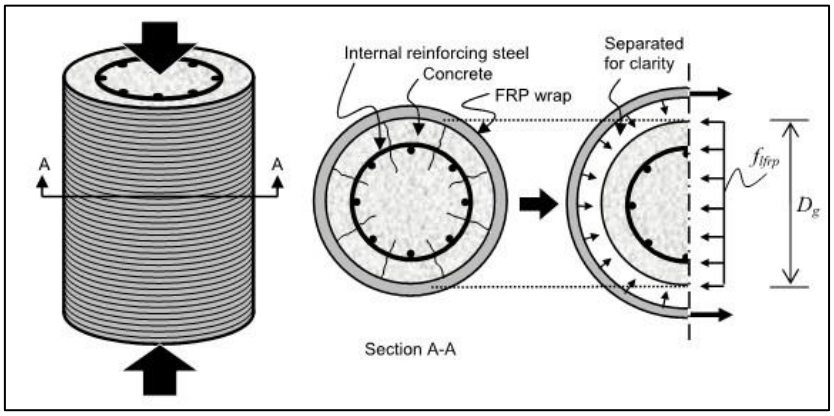


Figure 12: Confinement mechanism for the axial strengthening of circular concrete columns using externally bonded FRP wraps [7]

5.4 STRENGTHENING OF OTHER MEMBERS

Other members of the structure such as the concrete slab and the beam-column connections can also be strengthened using externally-bonded FRP wraps.

6 CONCLUSION

The Greenhill mine tipple structure is a Provincial historic site and was assessed by field and laboratory tests together with computer modelling to evaluate the current state of the structure and to recommend interventions to ensure the adequacy of the building to resist the loading

from possible adaptive reuse as a restaurant or maintained as a monument.

The structure was built before knowledge of some critical issues in the design and construction of reinforced concrete structures had been gained, such as the need for adequate concrete cover, durability requirements, freeze-thaw resistance, the need for adequate transverse rebars in beams and columns, proper design and detailing of beam-column joints in moment resisting frames, splice and development lengths of rebars, etc. As a result, damage and deterioration have happened to the structure with freeze-thaw damage being one of the most important ones.

Lack of knowledge about concrete composition and proper grading of the aggregate has resulted in the existence of very large particles in the concrete. It looks like the contractor used ungraded gravel from the nearby river as the aggregate source.

Externally bonded FRPs are recommended for strengthening of different parts of the structure because of their several advantages such as durability, ease of use, lightweight, reversibility and minimum intervention. In the design of the strengthening systems, the existence of several uncertainties about the quality of concrete and aggregates, position, size, cover and splice lengths of longitudinal reinforcing bars, amount of damage and deterioration in different areas, and life safety involvement in the new proposed use of the structure have to be considered.

Acknowledgements. The authors gratefully acknowledge the support of Alberta Culture in providing access to the site and their archives. The University of Calgary provided substantial support through their computing resources and the Department of Civil Engineering, all of which is sincerely acknowledged.

REFERENCES

[1] G. Associates. *Structural Review of Greenhill Mine* (2013).

[2] American Concrete Institute. *ACI 562-16, Code requirements for assessment, repair, and rehabilitation of existing concrete structures* (2016).

[3] CSA Group. *National Building Code of Canada* (2015).

[4] CSA Group. *CSA S806-12, Design and Construction of Building Components with Fibre-Reinforced Polymers* (2012).

[5] CAN/CSA-S6-14, *Canadian Highway Bridge Design Code* (2014), vol. 1, no. 1.

[6] ISIS Canada. *FRP Rehabilitation of Reinforced Concrete Structures FRP Rehabilitation of Reinforced Concrete Structures, Design Manual No. 4.* (2008).

[7] Banthia N. et al. *ISIS Educational Module 4: An Introduction to FRP Composites for Construction* (2010). ISIS Canada Educational Module.

[8] Bisby, L. *ISIS educational module 8: Durability of FRP Composites for Construction* (2006), p. 22.

[9] Banthia N. et al. *ISIS Educational Module 2: An Introduction to FRP Composites for Construction*. ISIS Canada Educational Module. ISIS Canada (2006), pp. 1–54.

12th International Conference on Structural Analysis of Historical Constructions
SAHC 2020
P. Roca, L. Pelà and C. Molins (Eds.)

THE SAFETY LEVEL OF CONCRETE PILE FOUNDATIONS UNDER INDUSTRIAL MONUMENTS

SANDER PASTERKAMP[1*]

[1]Delft University of Technology
Faculty of Civil Engineering
Stevinweg 1, Delft, The Netherlands
e-mail: s.pasterkamp@tudelft.nl, web page: http://www.tudelft.nl (*corresponding author)

Keywords: Pile Foundation, Pile Capacity, Adaptive Reuse, Codes

Abstract. *Prefabricated concrete piles have been used for the foundation of bigger buildings for about a century. Often a change in function, an addition (also vertically) or another type of alteration is required, resulting in different loads on the foundation. There are several complicating factors that return regularly in these assessments. The first one is a lack of data. Often drawings are missing or incomplete, e.g. showing only pile head dimensions or maximum calculated load but not the pile length, pile tip shape or material properties. Inspection is hard and only possible for the part directly under the pile head. And a third complication is that in The Netherlands there have only been official codes for piles since 1992.*

Various calculation and design methods from WWII until 1985 are discussed to see if there is any consistency that might lead to an indication of the load bearing capacity of piles in The Netherlands from that era.

It is concluded that design rules for the load bearing capacity of concrete pile foundations in The Netherlands have been inconsistent over time. If the original detailed geotechnical calculations and/or structural drawings cannot be found in archives then the given ultimate loads cannot only not be exceeded; even if the load on a pile is currently less than stated on the technical specifications designers are advised not to increase the load.

1 INTRODUCTION

Prefabricated concrete piles have been used for the foundation of bigger buildings for about a century. Some of these buildings have now become industrial monuments, which has as a consequence that their life span will go beyond their original economic life span. This often requires a change in function, an addition (also vertically) or another type of alteration in order to maintain economic viability (use it or lose it), resulting in different loads on the foundation. The question is then whether or not the old piles can carry the new load with sufficient safety.

There are several complicating factors that return regularly in these assessments. The first one is a lack of data. Often drawings are missing or incomplete, e.g. showing only pile head dimensions or maximum calculated load but not the pile length, pile tip shape or material

properties. Inspection is hard and only possible for the part directly under the pile head. And a third complication is that in The Netherlands there have only been official codes for piles since 1992. Before then pile foundations were designed using technical manuals with a much lower status.

Van Tol and De Jong[1] discuss pile foundations under monuments. They treat mainly wooden pile foundations. According to them post-WWII pile foundations are in a much better shape because of the better quality of the soil research, the introduction of the cone penetration test (CPT), the introduction of concrete piles and the improving insight in the behaviour of pile foundations and the calculation methods derived from that. No further information is given.

Scholten and Vrouwenvelder[2] discuss the backgrounds of the Dutch national standard series NEN 8700. This series is dealing with Assessment of existing structures in case of reconstruction and disapproval. It is currently under development and should finally contain eight parts as shown in Table 1.

Table 1 Overview of the contents of the NEN 8700 code series

Code number	Title	Status	Related Eurocode part
NEN 8700	Basic Rules	Final	EN 1990
NEN 8701	Actions	Final	EN 1991
NEN 8702	Concrete Structures	Draft	EN 1992
NEN 8703	Steel Structures	Draft	EN 1993
NEN 8704	Composite Steel and Concrete Structures	Draft	EN 1994
NEN 8705	Timber Structures	Draft	EN 1995
NEN 8706	Masonry Structures	Draft	EN 1996
NEN 8707	Geotechnical Constructions	Final	EN 1997

According to Scholten and Vrouwenvelder the safety assessment of an existing building structure differs from that of a new one in three essential ways: increasing the safety level for an existing building is usually more expensive than for buildings that are still in the design phase, the remaining lifetime of an existing building is often different from the standard reference period of 50 years that applies to new buildings, and in an existing building actual measurements can be made in order to gather additional data. This is reflected in the NEN 8700 series and is to some extent also true for pile foundations.

For existing concrete foundation piles the parts NEN8700, NEN 8701, NEN 8702 and NEN 8707[3] are relevant. Together they give a set of values for required safety levels, loads, material properties, safety factors et cetera that can be entered into the common Eurocode formulas. The values follow from a set of research programs into the properties of construction materials as produced through old codes and production methods. Although this is very helpful for the assessment of existing structures in general it does not solve the basic problem of the unknown properties of the foundation under the specific building at hand. This is illustrated in NEN 8707:2018 in § 3.3: “(1) The quality of concrete foundation elements must be determined with

sufficient accuracy to be able to verify it to the concrete related part of the NEN 8700 series."

F3O was the branch organization for independent foundation inspection experts. F3O has published a report titled "Guidelines Wooden Pile Foundations under Buildings"[4]. It gives alternative methods to assess the stability of pile foundations when the pile tip level is unknown, such as the measurement of deformations and cracks over time. From that it derives an expected remaining lifetime. This is an effective way to assess the stability of the current situation, however it does not give any information on possible overcapacity.

Rijkswaterstaat is part of the Dutch Ministry of Infrastructure and Water Management and responsible for the design, construction, management and maintenance of the main infrastructure facilities in the Netherlands. Rijkswaterstaat has published a report titled "Guidelines Assessment Infrastructure" or RBK[5] for the structural assessment of existing structures. The RBK give rules and methods that are additional to the Dutch NEN 8700 code series. According to the RBK foundations only have to be recalculated in case of notable structural damage to the foundation, in case of serious settlements, or in case of a significant load increase. How foundation piles should be recalculated is not mentioned.

This study presents an investigation in de developments in designing, calculating and building prefab concrete pile foundations in the Netherlands during the last 80 years, and conclusions are drawn about load bearing capacity and the reusability of historic concrete pile foundations.

2 HISTORY OF CONCRETE PILE FOUNDATIONS

2.1 Methodology

To get better insight in the expected load-bearing capacity of existing prefabricated concrete foundation piles we have to look in more detail at the way in which these piles were designed, produced, and placed. By comparing these aspects with the provisions of the Eurocode we can get an insight in possible over or undercapacity even if we have only limited information.

2.2 Historic Pile systems

Both according to Van Tol and De Jong[1], and the author's own experience with many renovation projects pile foundations from before WWII are always wooden piles. The earliest use of concrete in pile foundations was first for foundation beams and then for pilecaps, to make sure the wooden pile head remains under the groundwater table.

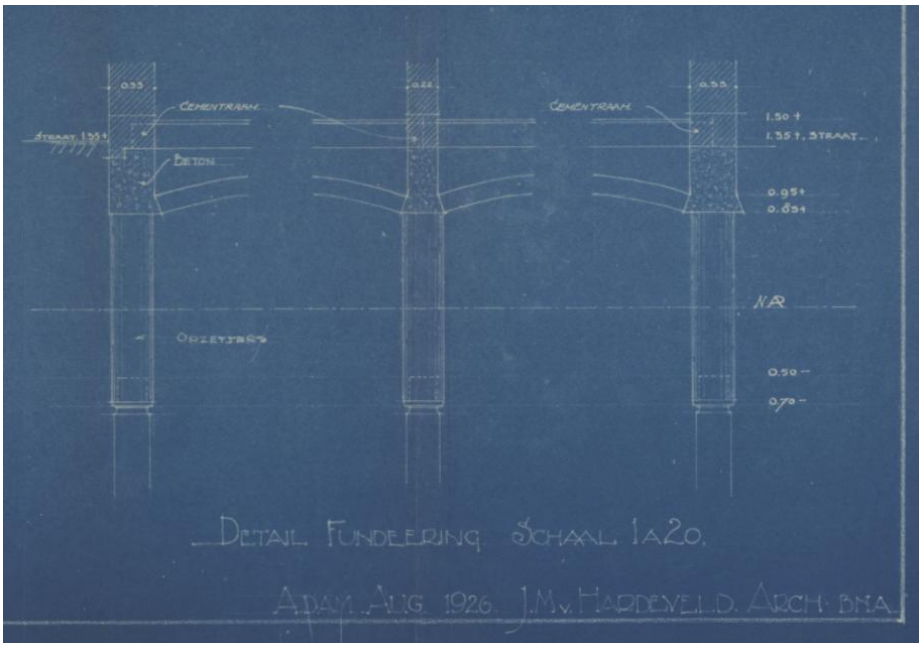


Figure 1 Concrete pilecap system "Brunwasser" on a construction drawing of a 1927 Amsterdam housing block

Van der Schrier describes in the 10th edition of his book[6] the calculation and production of precast concrete foundation piles. The length of the piles is limited to 25 m for practical reasons. Reinforcement is traditional; only one factory (N.V. Betondak) is mentioned that produces pretensioned concrete piles. Van der Schrier mentions prismatic piles with square, octagonal, massive circular, and hollow circular sections. Interestingly the pile tips for these piles seem always to be pointed or semi-pointed. Van der Schrier also mentions various alternative pile tip enlargements. According to Van der Schrier the pile capacity was supposed to be proportionate to the CPT value at the pile tip level and thus a bigger pile tip surface would directly result in a higher bearing capacity. It was also supposed to reduce negative skin friction.

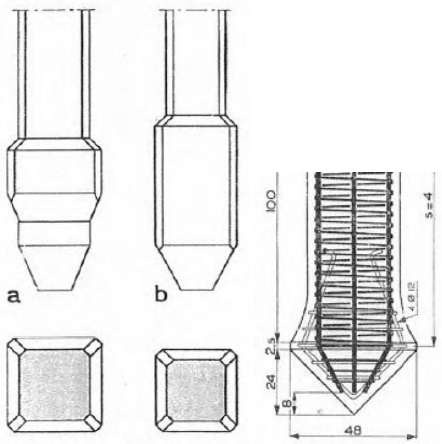


Figure 2 Pile tip shapes: a Waco point, b Sprenger point, c Condor point (Schrier, 1956)

One type of pile tip could be expanded through small explosive devices that would be set off

just before the pile was driven to its final depth.

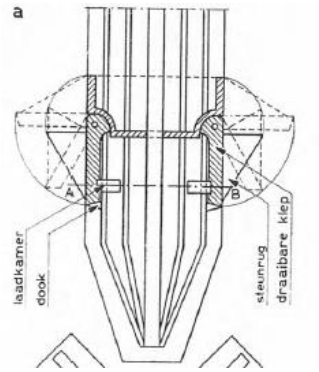


Figure 3 H.B.T. explosion piles (Schrier, 1956)

In spite of this the positive influence of shaft friction must have been known at least qualitatively. The wing pile was designed specifically to increase shaft friction and was therefore also recommended for piles loaded in tension.

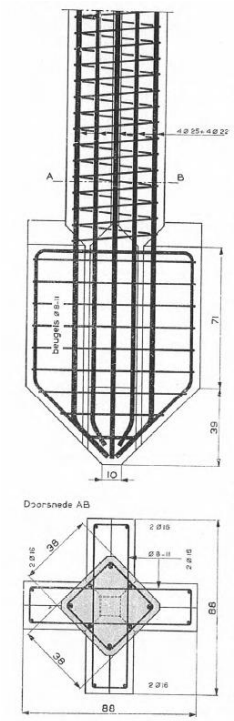


Figure 4 Pile tip of wing pile (Schrier, 1956)

17 years later Tussenbroek, Vlas, and Krikke[7] mention in their book on prefabricated concrete piles much less variation in pile tip shapes. Only wide pile tips with a width-height ratio of at least 1 are mentioned and a ratio of at least 2 is recommended. Furthermore the pile tips are mostly flat (not pointed). He also has an entire chapter on prismatic prefabricated piles,

indicating that this modern pile type is now very common.

2.3 Bearing Capacity

The bearing capacity of wooden piles before WWII was never calculated, but was assumed to be 10 tons or 100 kN based on experience. The pile length was also based on local experience, usually meaning similar to that of neighbouring buildings. For bigger projects test piles were used. Van der Schrier (Schrier, 1956) mentions a table in the building regulations of the city of Amsterdam, stating the maximum displacement of the wooden pile head given 30 blows with a specified weight dropping 2 m if the pile has to take a certain load.

The current way in which pile bearing capacity is calculated in The Netherlands is originally based on research from Plantema[8], and Van Mierlo and Koppejan[9]. It took some time for this research to seep through into building practice. Van der Schrier in 1956 still gives a simple calculation example of pile bearing capacity. The cone penetration test is basically seen here as a test pile. The influence of positive and negative skin friction is not mentioned.

> The size of the section of the pile tip enlargement follows from the result of a deep sounding. If for example at a depth of 15 m a cone resistance of 75 kg/cm^2 is found, then with a 3-fold safety margin 25 kg/cm^2 can be allowed. For a pile load of 60 tons a surface area of 60000 : 25 = 2400 cm^2 is needed, or round 50 x 50 cm. The pile shaft dimensions will be taken as 35 x 35 cm with 2% longitudinal reinforcement to take into account buckling, lifting and allowable stress in the concrete.

Figure 5 Example pile capacity calculation (Schrier, 1956)

Zeevaert[10] still mentions that “theories on point bearing capacity of piles and piers are still not satisfactory”. He then works out a method for the calculation of point bearing capacity of piles including positive skin friction based on Terzaghi’s theories on the ultimate bearing capacity for a pier or deep footing. He also gives detailed theory for the calculation of negative skin friction.

Van Tussenbroek, Vlas, and Krikke[7] mention the Koppejan method as a way to calculate the bearing capacity of piles, worked out in a way that quite closely resembles the current Dutch Eurocode practice. However according to them some organizations use different values for the influence depth of the ground layers above and below the pile tip level. The safety coefficient for a prismatic pile is 2.0. For piles with a pile tip area of more than 100 cm^2 a “somewhat bigger” coefficient is used. For piles with an enlarged pile tip “often a safety coefficient of 2.5 is used when the height of the enlargement is at least twice the pile tip width.” For pile tips with a smaller height the safety coefficient becomes partially a correction coefficient and is enlarged by 10% for pile tip enlargements with a height equal to the width.

According to Van Tussenbroek, Vlas, and Krikke the negative skin friction was usually just estimated but "recent measurements" have shown that the negative skin friction could become much greater than previously assumed. They refer to Zeevaert's book[10] for further information.

In 1985 the Commission Consultation Building Structures of the Nuisance Act and Building Department Association (an organization of municipal building specialists) published the Guidelines for foundations of Buildings[11]. In the introduction they wrote that until then different cities had different regulations. The purpose of the new guidelines was to create more uniformity and thus to create more clarity for designers and builders. They are however still not an official standard and local governments still had the freedom to make up their own rules.

2.4 Durability

Reinforced concrete always carries the risk of corrosion of the reinforcement. One possible problem is carbonatation, although the carbonatation rate of underground concrete is relatively low. Another possible attack comes from peat acids. Van der Schrier mentions that when peat acids are present the pile is covered with a bitumen emulsion.

The risk of corrosion is greatly reduced with increasing concrete cover. Therefore the concrete cover in the Dutch concrete codes are shown below.

Table 2 Required concrete cover over time

Code	Year	Concrete cover	
		Traditional	Pretensioned
G.B.V. 1940	1940	35 mm	
N 1009	1950	35 mm	
N 1009	1962	30 mm	
RVB 1962	1962		40 mm
NEN 3863	1974	30 mm	35 mm
NEN 6720	1992	35 mm	40 mm
NEN-EN 1992	2012	25 mm	30 mm

In all the historic codes the required concrete cover has been more that currently required by the Eurocode.

3 CONCLUSIONS

Design rules for the load bearing capacity of concrete pile foundations in The Netherlands have been inconsistent between WWII and the creation of the R.F.G. 1985. The exact calculation methods did not only differ over time but also geographically per city. Therefore it has to be concluded that care has to be taken when interpreting ultimate loads on foundation

piles on historic documents. If the original detailed calculations cannot be found in archives then the given ultimate loads cannot only not be exceeded; even if the load on a pile is currently less than stated on the technical specifications designers are advised not to increase the load by for instance adding additional floors. For buildings for which the building permit was given in or after 1985 is can be assumed that the R.F.G. 1985 has been applied if the local government does not indicate otherwise. Designers are advised to ask.

In all the historic codes the required concrete cover has been more that currently required by the Eurocode. Durability of the concrete structure will therefore probably not be governing.

LITERATURE

[1] Veen, J.v.d. and S. Binst, *Praktijkboek instandhouding monumenten*. 1998, Den Haag: Sdu Uitgevers.

[2] Scholten, N.P.M. and A.C.W.M. Vrouwenvelder, *Eurocodes and the structural safety of existing buildings - Considering the publication of the Dutch NEN 8700*, in *4th International Conference CIVIL ENGINEERING`13*. 2013: Jelgava.

[3] NEN, *NEN 8707 Assessment of an existing structure in case of reconstruction and disapproval – Geotechnical constructions*. 2018: Delft.

[4] F3O/SBRCURnet, *Richtlijn Houten Paalfunderingen onder gebouwen*. 2016.

[5] Rijkswaterstaat, *Richtlijnen Beoordeling Kunstwerken*. 2013, Rijkswaterstaat.

[6] Schrier, W.v.d., *Bouwen in gewapend beton : materiaal, berekening, constructie en toepassingen*. 10 ed. 1956, Amsterdam: Argus.

[7] Tussenbroek, P.J.v., G. Vlas, and J. Krikke, *Palen van gewapend beton*. 2e dr. ed. 1973, Amsterdam [etc.]: Agon Elsevier.

[8] Plantema, G., *Results of a special loading test on a reinforced concrete pile, a so-called pile sounding, interpretation of the results of deep soundings, permissible pile loads an extended settlement observations*, in *Second International Conference on Soil Mechanics and Foundation Engineering*. 1948: Rotterdam.

[9] Mierlo, W.C.v.K., A.W., *Lengte en draagvermogen van heipalen; vaststelling hiervan en enige daarbij verkregen ervaringen.* Bouw, 1952. **3**.

[10] Zeevaert, L., *Foundation engineering for difficult subsoil conditions*. 1973, New York: Van Nostrand Reinhold.

[11] bouwtoezichtvereniging, C.O.B.v.d.H.-e., *Richtlijnen voor funderingen van gebouwen - R.F.G. 1985*. 1988.

12th International Conference on Structural Analysis of Historical Constructions
SAHC 2020
P. Roca, L. Pelà and C. Molins (Eds.)

A STUDY OF THE HISTORICAL CONSTRUCTION TECHNOLOGY OF BELL TOWERS IN CYPRUS

MARGARITA L. PETROU[1*] AND DIMOS C. CHARMPIS[1]

[1]Department of Civil and Environmental Engineering, University of Cyprus
75 Kallipoleos Str., P.O. Box 20537, 1678 Nicosia, Cyprus
e-mails: mpetro03@ucy.ac.cy (*corresponding author),
charmpis@ucy.ac.cy

Keywords: Construction Technology, Stone Masonry, Earthquake Engineering, Historical Survey, Slender Structures

Abstract. *This paper aims to present the historical construction technology of churches' bell towers in Cyprus, starting with the initiation of their use and addressing the development of their distinctive morphology adapting and mixing various architectural styles. Traditional bell towers are tall and slender unreinforced masonry structures that are known to be particularly vulnerable to earthquake actions encountered in seismogenic regions, such as Cyprus. Therefore, iron and wood elements with high tensile capacities were commonly utilized in Cypriot bell towers in the form of ties. In particular, the bell tower of Saint John's church in Psevdas village was constructed using such technology and is an example case studied in more detail in the present work. This tower suffered a partial collapse during an earthquake on May 12th, 2016 and underwent restoration within the next year. Based on the knowledge gathered from the case of the damaged tower and the visual inspection of other bell towers in Cyprus, the use of timber and iron ties in these masonry structures is deemed to be essential for their protection from seismic actions.*

1 INTRODUCTION

Building seismic resistant structures has always been of major importance in seismogenic regions, such as Cyprus. Tall and slender unreinforced masonry structures, such as the bell towers of churches, have proven to be particularly vulnerable to seismic actions. Taking this fact into consideration, various specialized construction and intervention technologies have been developed throughout history to enhance the seismic resistance of such masonry structures. For this purpose, construction materials associated with high tensile capacities, such as iron and wood, were commonly utilized in the form of ties. Such technology was used for the construction of the bell tower of the Saint John's church in Psevdas village, Cyprus. The particular about 100-year-old stone masonry bell tower suffered a partial collapse on the 12th May 2016, when an earthquake of magnitude 4.5 Richter struck the southeastern part of Cyprus [1].

The present study was triggered by the restoration process of the aforementioned damaged tower and aims in providing an overall review of the historical construction technology of bell towers in Cyprus. Hence, this paper first reports an overview regarding the initial and thereafter

the regular use of bells and bell towers in Cyprus. Next, the morphology of traditional Cypriot bell towers and their susceptibility to earthquake hazard are addressed. Following a rigorous visual inspection of various bell towers in Cyprus, including the bell tower in Psevdas presented herein in more detail, it can be deduced that the use of timber and iron ties in such masonry structures is essential for their protection from seismic actions.

2 INITIAL AND REGULAR USE OF BELLS AND BELL TOWERS

2.1 Origin of bells and bell towers

Bells are idiophone instruments made of bronze. Since antiquity, various civilizations used bells for both ritual and practical purposes. It is uncertain when precisely the use of bells became part of the Christian tradition. However, the need for a means to summon the people to the church and regulate monastic life appeared since the early years of Christianity. The development of the *semantron* (metal or wooden strip knocked with a hammer) [2], which was broadly used in the monasteries – and is actually still in use in the orthodox monasteries – and generally in the eastern church, came to satisfy this need.

The first uses of bells are tracked in the West around the 6th century. The Latin name for bell '*campana*' derives from the region of Italy, Campania, where bells were first used in the church [3]. During the reign of Pope Sabinian (604-606), the use of bells was adopted by the western church. Gradually, due to the popularity of bells during the Carolingian period, the need emerged to develop specially dedicated structures to accommodate the bells. The realization that the ring sound of the bells would be traveling at a larger radius from high altitudes led to the development of the bell towers. A prominent early example of a bell tower is the one raised by Pope Stephen II (752-757) above the old Saint Peter's basilica in Rome [4].

2.2 Bells and bell towers in Byzantium

The origin of bells' use and thus the construction of bell towers in the Byzantine East is even less clear. Western sources report that bells were gifted to the byzantine emperor Michael III (842-867) by the Venetian Doge Ursus I Partecipazio (864-881) as a gesture of gratitude for assisting the Venetians to defeat the Arabic troops in Dalmatia [4] [5]. These bells were raised on a tower in the yard of Hagia Sophia, in Constantinople [2]. Though, as the use of the *semantron* was a point of differentiation between the two principal dogmas of Christianity, the use of bells popularized only during the occupation of Constantinople by the Latins (1204-1261) [4]. Bells were ringing in Constantinople until its fall (May 29th, 1453), after the siege by the Ottomans.

Ottomans looted the areas they conquered, destroying bell towers and turning churches into mosques. Thereon, the Islamic law enforced by the conquerors was not only the personal law for the Muslims, but also the state law for all inhabitants of the empire, regardless of their religion. The Christian church, as was the case also with other religious groups of the empire, was granted privileges for administrative reasons. However, various restrictions were imposed. These included the ban of bell ringing and posting of the cross on churches [5]. Alongside, the construction of new churches and bell towers was prohibited (with few exceptions), while only the preservation and renovation of the existing churches was allowed [6].

2.3 Bells and bell towers in Cyprus

In 1571, Ottomans conquered Cyprus and imposed the same restrictions for the ecclesiastical constructions. Due to the bell ringing ban, the *semantron* returned in use for summoning the people to the church. Kokkinoftas [5] reported that the first bell imported in Cyprus during the Ottoman period was most probably the bell of Holy Cross church in Omodos village (Fig. 1) situated at Limassol district. An inscription dates the bell back to 1812. In 1839, the Sultan proclaimed reforms for the reorganization of the empire with the issuance of Gülhane Hatt-ı Şerif edict. Hence, some bells, gifted by Cypriots living in Venice, were raised on churches around the island. Ottoman authorities consented for the use of the bells; still, there were opposing reactions by the Muslim population [5].



Figure 1: Bell tower of the Holy Cross's church, Omodos, Limassol district

In 1856, the Ottoman Imperial rescript Hatt-ı Hümayun eventually recognized the right of all non-Muslim communities to administer their religious affairs. The reforms stipulated by the rescript raised the nationalism of the local population, as their religious leader (the Archbishop of Cyprus) also became the national leader, concentrating both religious and civil authorities under the *millet* system applied in the Ottoman Empire [7]. The rescript also lifted the bell ringing ban, leading to several bell tower erections in numerous existing churches [8]. Thereon, all new churches constructed in Cyprus bear at least one bell tower.

3 MORPHOLOGY OF THE CYPRIOT BELL TOWERS

3.1 Architectural style

The events of the Cypriot history have influenced the ecclesiastical architecture of Cyprus. As a part of the Orthodox East, the Byzantine style and standards were always an integral part of the ecclesiastical architecture. During the Frankish period (1191-1489), however, the pointed gothic arch was adopted and embodied in the traditional architecture, leading to the

development of a combined style. This style is the so-called Franko-Byzantine style by some authors [9]. During the Ottoman period, due to the restrictions imposed, the style was simplified to single nave pointed vaulted churches with low windows and buttresses.

The liberation of the religious affairs and practices resulted in the development of a new architectural style, the Cypriot Neo-Gothic style, which appeared first on the newly constructed bell towers and later transferred to new churches. The combination of Neo-Gothic towers with churches of Byzantine or Franko-Byzantine style is a frequent phenomenon in Cyprus. A notable example of this is the church of Saint Lazarus in Larnaca. The massive multi-dome Byzantine basilica was built with the funding of the byzantine emperor Leo VI (866-912) in the 890s. In 1857, a bell tower following the Italian standards was added on the southside of the chancel [10]. The bell tower is 23 m tall and bears detailed carved ornamentation and two belfry storeys (Fig. 2).



Figure 2: Church of Saint Lazarus, Larnaca

The Cypriot Neo-Gothic style (1850s-1930s), similarly to the international Gothic revival of the mid-19th century [11], symbolizes the religious freedom and the formation of the national identity of the Cypriots. The main characteristic of the Cypriot Neo-Gothic is the elaborate carved ornamentation of the bell towers and the lintels. Often, Neo-Gothic features are mixed with Neo-Classical – such as at pediments and columns – as well as with Neo-Byzantine and Eclectic features. The use of the Neo-Byzantine style was accented in the 1930s, following the influence of architects descending from Greece. The later added towers were not consistent with the architectural style of the church they were attached to.

3.2 Form and structure

A typical bell tower has a four-part structure. First, a strong base provides support and stability to the tower. Second, the shaft is the part primarily intended for attaining the desired height of the tower and contains stairs leading to the belfry. The third part is the belfry, in which the bells are housed, and it is often the most decorated part. Finally, the tower is completed at

the top with a roof.

The tall (over 30 m in height) famous Italian *campanili* usually stand at a distance from their corresponding church [12]. Unlike these towers, Cypriot bell towers do not exceed 30 m in height, with their free-standing height often being within the range 10-15 m. As such towers were later supplements to existing churches, any newly added tower was based on and sat atop the main body of the church or it was attached to the exterior of the church, at one of the four corners of the rectangular main structure. New churches built after 1856 usually included bases for one or two bell towers as part of the church's structure.

It is unclear where the morphology of the early Cypriot bell towers derived from. Kiessel and Tozan [8], who studied the architecture of the Cypriot bell towers from the mid-19th century to 1974, noted that their typology showed significant similarity to the 16th century Italian Renaissance predecessor, as it appears in the 'Wedding at Cana' by Veronese (1560-1563). Actually, there is a general sense that monumental paintings in local churches dating back to the period of the Venetian rule might have influenced the form of Cypriot bell towers [13]. Hence, a bell tower usually consists of a solid base, up to four storeys divided by entablatures and a canopy at the top. If the tower is attached to the church's body, the solid base reaches the height of the wall cornice [8]. Each storey is formed by four pillars and arched openings at all four sides. The upper one or two storeys are the belfries of the tower. Usually, each belfry bears one bell, which hangs from an iron bar anchored into the pillars.

Between 1856 and the 1930s, the primary material used for the construction of the towers was limestone masonry. In the 1940s, the use of reinforced concrete gradually spread, replacing stone masonry. The form and structure of the bell towers follows the typical typology described firstly. The example of the bell tower of the church of 'Panagia Faneromeni' located in the historical centre of Nicosia indicates the transitional stage reflecting the change of the construction material. The current 26 m tall tower was erected in 1938 and is made of concrete and regular masonry blocks, while metal brackets are installed at the perimeter [14]. The current tower designed by the architect Theodoros Photiades, the first Cypriot architect, was built as a replacement of the original masonry tower, which sustained extensive damage and cracking [6] (Fig. 3).



Figure 3: The old masonry (left) [6] and current concrete (right) [15] bell tower of the church of 'Panagia Faneromeni', Nicosia

4 EARTHQUAKES VS. CYPRIOT BELL TOWERS

The island of Cyprus sits to the north of the boundary where the African and Eurasian tectonic plates meet. The seismic activity of the local 'Cyprean arc' has been the cause of numerous devastating earthquakes on the island. Many settlements and masonry structures, in particular, have collapsed as a result of seismic actions since antiquity [16]. According to the records of the Cyprus Geological Survey Department, an earthquake of magnitude 7.0 Richter (VIII-IX Mercalli) struck the island in 1491, causing extensive damage to Hagia Sophia cathedral, in Nicosia. Other significant seismic events (of average magnitude 6.5 Richter and V-IX Mercalli) occurred in 1577, 1735, and 1896, causing damages and casualties.

In 1906, the earthquake that struck Limassol area (magnitude 5.6 Richter/VIII Mercalli) caused damage to many buildings, among which was the cathedral of Hagia Napa and its bell towers [17]. During the last 100 years, the most significant event occurred in 1953, when the damage caused by the earthquake of magnitude 6.5 Richter (IX Mercalli) in the district of Paphos was very severe, leaving, numerous masonry and concrete structures destroyed and resulting in several casualties and homeless people [18] (Fig. 4).



Figure 4: Structures in Cyprus damaged by earthquakes [18]

The need for making masonry structures more earthquake-resistant led to the development of various relevant construction and intervention technologies. Among such technologies, the installation of iron and timber ties has been often used as an effective way to better cope with the earthquake hazard in Cyprus [19]. Hence, tie-rods were installed during the initial construction phase on the arches of bell towers, as well as on opposite walls of the churches' main body. The use of timber tie-rods in Cyprus is minimal. An outstanding example application of this technique employing timber ties is on the bell tower (built in the 1890s) of archbishopric cathedral of Saint John (built in 1662) in Nicosia [20] (Fig. 5). On the other hand, the use of iron tie-rods was more popular and many example applications can be found in various regions of the island. Moreover, iron ties (cramps) were occasionally installed between the storeys of the bell tower, in order to better fasten the entablatures.

Various previous studies focused on examining the effectiveness of tie-rods and their contribution in the seismic response of a structure [19] [21]. Kouris and Kouris [22] specifically studied the influence of tie-rods on the seismic behavior of slender towers. In all relevant studies, there appears to be a consensus regarding the effect of tie-rods on structural behavior: such ties promote integral behavior and result in increased seismic resistance for the tied up structural system [23]. In light of the above, the use of tie-rods in various constructions by Cypriot master craftsmen even more than a century ago reveals these workers' awareness and

concern regarding the high significance of the seismic hazard for the island's buildings stock.



Figure 5: Bell tower of Saint John's Cathedral with timber ties, Nicosia

5 THE CASE OF SAINT JOHN'S BELL TOWER IN PSEVDAS VILLAGE

Saint John's church was built in 1897 as a renovation and extension of an older church dating back in 1780 (date noted on the chancel's outer wall). Later, in the 1910s, a bell tower on the southside of the chancel was erected following the Cypriot form. The upper part of the bell tower collapsed due to an earthquake on May 12th, 2016 [24]. The earthquake's epicenter was 11 km west of Larnaca and its hypocenter was at a depth of 5 km. The magnitude of the mainshock was 4.5 Richter/V Mercalli, while an aftershock of magnitude 3.3 Richter followed. Thankfully, there were no casualties from the fall of tower parts, as the event occurred early in the morning. The church is located at Psevdas village, 16 km southwest of Larnaca.

5.1 The bell tower before the damaging earthquake

Before the earthquake, the bell tower of Saint John's church consisted of: (a) a solid base built on top of the church's main body at the southside, (b) four masonry pillars connected with arches – in all four sides – in two storeys divided by entablatures and (c) an arched octagonal canopy. The upper storey was used as a belfry for one bell. The height of the tower's parts was: about 1.5 m for the base, 2 m for each storey and 1.5 m for the canopy. The cumulative height was 14 m from the ground or 7 m from the cornice of the church's masonry (free-standing height). The horizontal cross-section of the base and the storeys was about 1.70×1.70 m^2, while the storeys' entablatures had a central hole of 0.60×0.60 m^2. The canopy covered the hole of the upper entablature.

Typically, the preferable way of construction in Cyprus in the past was by utilizing locally available materials. Hence, the masonry of the particular bell tower was built of natural white limestone (compact chalk), coming from the nearby Lympia village, and lime mortar. The main body of the church is of masonry made by cobbels taken from the nearby river. Limestone was a popular building material due to its softness and the ease it provided in carving upon the masonry. Another frequent practice was the use of impermeable cementitious material on the exposed upper surfaces for waterproofing purposes. The canopy's roof and the surface of the

upper entablature were covered with such material.

As regards the architectural style aspect, the decoration of the tower combined at least two distinctive styles. The carved ornamentation on the pillars, the cornice of the entablatures and four acroteria placed on the upper entablature followed the Neo-Classical style, while the decoration of the arches and the canopy followed the Neo-Gothic style. In contrast to the elaborate decoration of the tower, the church was a Neo-Gothic single-nave basilica with minor decoration.

5.2 The bell tower after the damaging earthquake

The earthquake caused the collapse of the canopy, the three out of four acroteria and a large part of the upper entablature. Only two out of eight pillars of the canopy's arches were standing after the earthquake (Fig. 6). Most of the fallen parts turned into rubble.

During the visual *in situ* inspection of the damaged bell tower of Saint John's church, it was found that iron tie-rods connect the intrados of the arches of the two storeys, while a grid of four iron camps fasten each storey at the height of each entablature (Fig. 6). The bell hangs from an iron bar anchored into the masonry pillars. There is another iron cramp just beneath the bell, which protects the masonry from the mechanical action (erosion) caused by the friction between the bell's rope and the stone. All metal elements were installed during the initial construction phase using gypsum mortar.

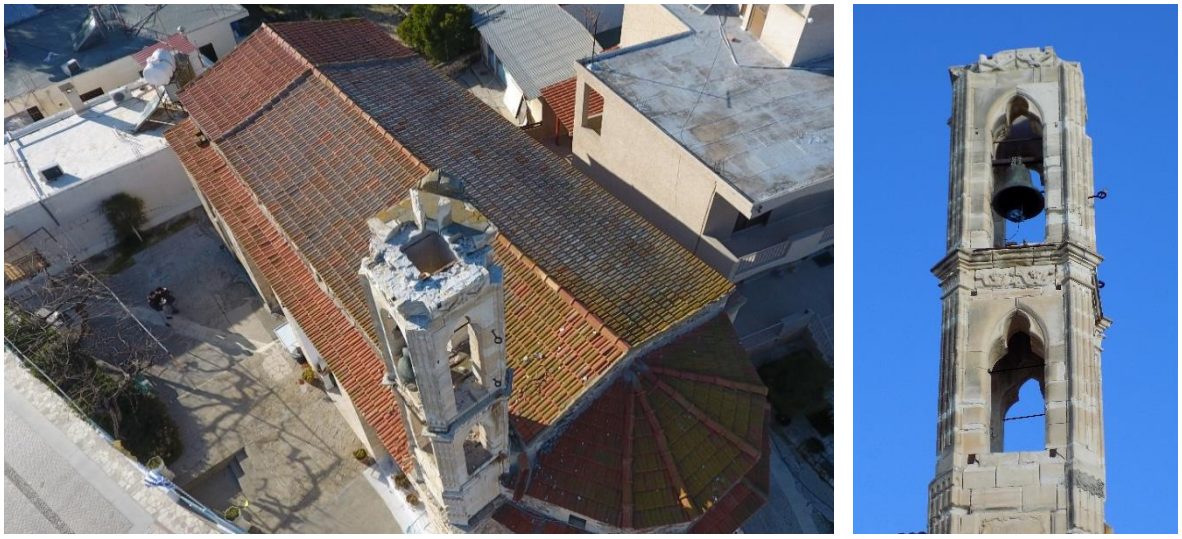


Figure 6: Bell tower of Saint John's church in Psevdas village after the earthquake (photos taken in February 2017)

The exposure of the iron elements of the bell tower to atmospheric oxygen and humidity led to corrosion. This resulted in cracked stone units and exposed anchorages of the cramps, which became visible at the exterior face of the bell tower (Fig. 6). This phenomenon was observed also in other cases, such as at the bell tower of Saint John's church in Larnaca (Fig. 7). However, cramps may not always become visible at an exterior wall face, as metal elements may have been placed in protected interior parts of the structure, which hinders the oxidation process from taking place.



Figure 7: Bell tower of Saint John's church (left), Larnaca, where the anchorage of the cramps is visible (right)

Nonetheless, except for a few weathered stone units and some cracking around the metal elements, the overall condition of the survived part of the bell tower was good. It is quite clear that the damage actually occurred at the most sensitive and the only 'untied' part of the bell tower, the canopy.

5.3 Restoration of the bell tower

During the restoration works, the canopy and the whole upper part of the bell tower were reconstructed to their original form. The corroded craps and tie-rods of the upper storey were replaced by similar stainless-steel elements. The weathered stone units were replaced with similar ones and the cracks were sealed with lime grouting. Finally, a special dedicated base for the bell was installed, in order to prevent damage to the masonry due to dynamic excitation from the bell's swing and the corrosion of its iron base (Fig. 8).



Figure 8: Restoration (left) and strengthening (right) of Saint John's bell tower in Psevdas (photos taken in December 2017)

6 CONCLUSIONS

Bell towers appeared throughout the history of Cyprus as a symbol of religious and national freedom for the people on the island and emerged to be an integral part of the local ecclesiastical architecture. Ensuring the long-term safety and functionality of such traditional structures is a matter of heritage preservation. A major hazard opposed to the purpose of preservation is the significant seismic activity resulting from the 'Cyprean arc'.

The need to mitigate the earthquake hazard has led to the use of suitable technologies improving the seismic capacity of such structures. In particular, an approach widely applied in Cyprus is the installation of timber or iron tie-rods during initial construction of a bell tower. The contribution of such elements seems to be critical for the adequate long-term seismic resistance of traditional bell towers. The imperative need for effective tying is highlighted in the characteristic example presented in more detail in this work: the unfastened canopy of the Saint John church's bell tower in Psevdas village collapsed during a recent earthquake due to the absence of iron ties.

Although installed iron tie-rods are often encountered in traditional stone masonry structures all over the island of Cyprus, their application during construction was based on the then available empirical knowledge and intuition and lacks formal engineering validation following the current codes and established scientific knowledge. This induces a need for a campaign to study the traditional anchorage setup of iron ties and their effect on the structural behavior of masonry structures. The results of such studies will facilitate the structural assessment process and, if needed, the development of compatible restoration and strengthening technologies respecting the traditional character of these structures.

Acknowledgements. The authors would like to acknowledge the contribution of Hercules Charalambides and Constantinos Christou, who took the aerial photos presented and gave concession for their use herein.

REFERENCES

[1] Damages on church due to earthquake in Larnaca (in Greek). *Kathimerini*, (2016).
[2] Kallinikou, C. *The Christian temple and its rituals* (in Greek). Grigoris Publications, (1969).
[3] Gatty, A. *The Bell: Its Origin, History, and Uses*. George Bell, 186, Fleet Street, (1848).
[4] Williams, E.V. *The Bells of Russia: History and Technology*. New Jersey: Princeton University Press, (1985).
[5] Kokkinoftas, C. The raise of bells on churhces in Cyprus during the Ottoman period (1571-1878) (in Greek). *Church of Cyprus*, (2018). [Online]. Available at: https://churchofcyprus.org.cy/41390. [Accessed: 09-Jan-2020].
[6] Myriantheus, D. The church of Panagia Phaneromeni, Nisocia. In: *The Lady of Nicosia, Phaneromeni and the relics* (in Greek), Bank of Cyprus Cultural Foundation (2012), pp. 15-25.
[7] Emilianides, A. Religion and the state in dialogue: Cyprus. In: *Religion and Law in Dialogue: Covenantal and Non-Covenantal Cooperation between State and Religion in Europe* (2006), pp. 19-32.
[8] Kiessel, M. and Tozan, A. *Orthodox Church Architecture in the Northern Districts of*

Cyprus from the mid-19th Century to 1974. Prostor, (2014).
[9] Myriantheus, D. Ecclesiastical Architecture (13th-20th century) (in Greek). In: *The Holy Bishopric of Morphou. 2000 years of Art and Holiness* (2000).
[10] Michaelides, S.G. Saint Lazarus – The history of the church in Larnaca" (in Greek). *Holy Church of Saint Lazarus*. [Online]. Available at: http://agioslazaros.org.cy/ιστορια-ναου/. [Accessed: 30-Jan-2020].
[11] Lewis, M.J. *The Gothic Revival*. Thames & Hydson, (2002).
[12] Baruffi, F., Boucher, J., Coryea, M. and Spector, D. VENICE BELLS AND BELL TOWERS A Striking Source of Knowledge. (2012).
[13] Constantinides, E. Monumental Painting in Cyprus during the Venetian Period, 1489-1571. In: C. Ševèenko et al. (Eds): *Medieval Cyprus. Studies in Art, Architecture, and History in memory of Doula Mouriki*, Princeton University Press (1999), pp. 263-300.
[14] J+A Filippou, Vitti, P. and De Vito, S. *Church of Panagia Faneromeni, Nicosia: Architectural Interventions Report*. (2016).
[15] Committee of the church of Panagia Phaneromeni. Holy Church of Panagia Phaneromeni (Nicosia): Official Memorial of the Archibishop Cyprianos and the Ethnomartyrs of 9th July 1821 (in Greek). *Church of Cyprus*, (2017). [Online]. Available at: https://churchofcyprus.org.cy/35384. [Accessed: 30-Jan-2020].
[16] Seismicity (in Greek). *Cyprus Geological Survey Department*. [Online]. Available at: http://www.moa.gov.cy/moa/gsd/gsd.nsf/page56_gr/page56_gr?OpenDocument. [Accessed: 30-Jan-2020].
[17] Strong Earthquake. Damages in Limassol (in Greek). *Cypriot*, (1906).
[18] Earthquakes (in Greek). *Cyprus Geological Survey Department*. [Online]. Available at: http://www.moa.gov.cy/moa/gsd/gsd.nsf/page40_gr/page40_gr?OpenDocument. [Accessed: 30-Jan-2020].
[19] Petrou, M. and Charmpis, D.C. Iron Ties Originally Anchored into Masonry as a Historical Construction Technology – Case Study: A Church in Cyprus. In: R. Aguilar et al. (Eds): *Structural Analysis of Historical Constructions*, RILEM Bookseries 18 (2019), pp. 153-161.
[20] Papageorgiou, A. and Committee of the Saint John's Cathedral. The Saint John's Cathedral. *Church of Cyprus*, (2019). [Online]. Available at: https://churchofcyprus.org.cy/9632. [Accessed: 30-Jan-2020].
[21] Sorrentino, L., Liberatore, L., Decanini, L.D. and Liberatore, D. The performance of churches in the 2012 Emilia earthquakes. *Bulletin of Earthquake Engineering* 12 (2014), pp. 2299-2331.
[22] Kouris, E.G. and Kouris, L.A. Investigation of the Influence of Tie-Rods on the Seismic Behaviour of Slender Towers. In: *International Conference on Computational Structures Technology* 12 (2018).
[23] Roca, P., Lourenco, P.B. and Gaetani, A. *Historic Construction and Conservation. Materials, System and Damage*. Taylor and Francis Group, (2019).
[24] Significant Earthquakes (in Greek). *Cyprus Geological Survey Department*. [Online]. Available at: http://www.moa.gov.cy/moa/gsd/gsd.nsf/All/AD24AEF6F60B0E14C22583C9004258A9?OpenDocument [Accessed: 30-Jan-2020].

12th International Conference on Structural Analysis of Historical Constructions
SAHC 2020
P. Roca, L. Pelà and C. Molins (Eds.)

A USER-FRIENDLY DIGITAL TOOL FOR THE STRUCTURAL ASSESSMENT OF HISTORIC DOMES: THE CASE STUDY OF SAINT PETER IN ROME

MARCO FRANCESCO FUNARI[1*], LUIS CARLOS SILVA[2], DANIEL V. OLIVEIRA[1] AND PAULO B. LOURENÇO [1]

[1] ISISE, Institute of Science and Innovation for Bio-Sustainability (IB-S)
University of Minho, Guimarães, Portugal
e-mail: marcofrancesco.funari@civil.uminho.pt, danvco@civil.uminho.pt, pbl@civil.uminho.pt
[2] ISISE, Faculty of Engineering, Universidade Lusófona de Humanidades e Tecnologias, Lisboa, Portugal
e-mail: luisilva.civil@gmail.com

Keywords: Limit Analysis, Visual Programming, Historic Masonry Domes, Nelder-Mead method

Abstract. *This paper presents a digital tool for the rapid structural assessment of historic masonry domes. It is especially suited for masonry domes that present long meridian cracks, ergo each partitioned element governed by a pushing failure mode. The proposed procedure considers a Heyman's no-tension mechanical model has been implemented within a commercial user-friendly visual programming environment. The numerical approach consists of a parametric modelling of the failure mechanism and, therefore, exploring the domain of possible solutions using the theorems of the limit analysis. Hence, a heuristic search method is subsequently adopted to refine the geometry of the collapse mechanism and to compute the value of the horizontal trust. The validation of the developed approach has been achieved considering the Saint Peter's dome. As reported in the literature, the behaviour of the Saint Peter's dome gradually shifted from a rigid shell-type – stiffened by hoop stresses –, towards a pushing type of dome partitioned by long meridian cracks. The study also evaluated the structural integrity of the drum. In converse with more time-consuming and advanced methods of analysis, the present procedure allows the users to perform a structural assessment of a historic masonry dome in a fast and computationally efficient manner. The developed digital tool will be freely available from a web archive hosted by the University of Minho and, therefore, easily able to reach students, researchers and structural engineers.*

1 INTRODUCTION

The structural assessment of historic masonry dome is still a challenge. Main difficulties are especially related to the intrinsic complexity of the mechanical behaviour of masonry, with the uncertainty when modelling the potential dome load paths and with the damage-induced anisotropy. Still, a significant number of studies can be found in the literature and include both numerical and analytical methods [1-4]. The majority of such studies address the structural

analysis and structural safety problem of masonry domes by using a numerical model based on the Finite Element Method (FEM) [5] or Discrete Element Method (DEM)[6, 7].

In the case of FEM models, the masonry is typically modelled following a continuum approach (designated as macro-modelling) [8, 9] or discretizing explicitly both units and joints (designated as micro-modelling) [6]. For instance, Bacigalupo et al. [10] investigated the structural assessment of the dome and drum of the Basilica of S. Maria Assunta in Carignano. The authors developed a refined FEM model and performed non-linear quasi-static analyses. Bartoli et al. [11] developed a detailed FEM-based model to perform the structural analysis of the Brunelleschi's Dome of Santa Maria del Fiore, in which both static and dynamic types of analysis were considered. Cavagli and Gudella [12] studied the dome of the Basilica of Santa Maria degli Angeli in Assisi. Static analysis was performed by means of a FE model considering whereas material nonlinearity for the masonry has been included.

In the case of DEM models, the masonry is typically modelled as the assemblage of rigid blocks inter-connected through interfaces of a given stiffness, which enables to capture large displacement and the opening and closing of joints [13]. For instance, Boni et al. [14] proposed a DEM model to study both the effects of brick pattern and infill on the stability of masonry vaults when supports are subjected to settlements.

It is worth noting that such methods require a large set of input parameters and can be both time-consuming and computationally expensive, especially when trying to model collapse. Hence, powerful analytical tools based on the theorems of the limit analysis can be an appropriate alternative. The main advantage of limit analysis approaches is that require less knowledge of the mechanical behaviour of materials and are, therefore, more practical. Anselmi et al. [15] proposed a computer program based on the static theorem of the limit analysis that demands, only, an a-priori discretization of the dome in macroblocks. Casapulla et al. [16] developed a novel digital tool to design semi-circular masonry arches composed of interlocking blocks. Recently, Funari et al. [17] proposed a new digital tool aimed to parametrize the geometrical variables that characterize the failure mechanism and compute the load multiplier based on an upper bound limit analysis coupled with a genetic algorithm.

In such a context, the main aim of this paper is to demonstrate how generative/parametric modelling is a useful tool for the structural assessment of historic masonry domes. The parametric modelling of the failure mechanism allows the user to explore the domain of possible solutions using the upper bound method of the limit analysis. Then, a heuristic solver based on the Nelder-Mead method [24] is used to refine the geometry of the failure mechanism and obtain the value of the minimum horizontal thrust of the dome. The proposed methodology has been all integrated within the commercial visual programming environment offered by Rhinoceros3D + Grasshopper. The program appears easy to understand and might be used by both students and structural engineers. Unlike more advanced methods of analysis, the proposed algorithm is integrated into a user-friendly environment and allows us to perform a quick structural assessment of masonry domes. The paper is organised as follows: section 2 included the theoretical aspects of the proposed methodology and its implementation; section 3 briefly describes the selected case study; section 4 reports the obtained results; and finally, the main conclusions are discussed in section 5.

2 METHODOLOGY: THE COMPUTATION OF THE MINIMUM THRUST OF MASONRY DOMES: THE KINEMATIC APPROACH

Masonry domes tend to crack due to the low tensile strength that masonry hoop rings typically present. Hence, a diffused type of cracking along the meridian lines is observed. As extensively reported in the literature [18], the number of these cracks is not easily detectable but only one is sufficient to change the structural behaviour of the domes, i.e. from a membrane type of behaviour to a pushing dome [19].

In this framework, the computation of the minimum thrust following a static or kinematic limit-based approach is a relevant task [18]. The static approach traces the statically admissible funicular curves of the load. In the incipient collapse state, the pressure curve passes by the extrados of the key section, whereas a rotational hinge is supposed to appear. The pressure curve continues running inside the dome's thickness skimming the intrados in a point in which the second hinge appears. Yet, due to computational convenience, the present paper adopts a kinematic approach. In particular, the formulation by Como [18] has been assumed to build the digital analysis tool.

The application of the kinematic approach is based on the proper positioning of hinges to allow horizontal sliding of the dome at its springing. According to [18], the first hinge has to be placed at the extrados of the key section. In converse, the second hinge is placed at the intrados of the dome, but its position over the latter is assumed to be a variable of the mathematical problem ((h)). The minimum value of the thrust can be computed by solving the following optimization problem arising from the Principle of the Virtual Work (PVW) [18]:

$$\begin{cases} \max \ \dfrac{[\![o,V(h)]\!]}{\Delta(h)} \end{cases} \tag{1}$$

where $[\![o,V(h)]\!]$ is the work performed by the vertical load associated to the to the vertical displacement, $\Delta(h)$ is the radial widening of the dome at its base due to the mechanism. Fig. 1 shows different positions (h) for the hinge along the intrados of the dome. When the horizontal thrust assumes the maximum value, it means that the pressure curve is inside the thickness of the dome and it is tangent to the intrados at the point (h). The parametrization of the collapse mechanism is achieved by writing a generative algorithm using Grasshopper's component. The same algorithm integrates the capability to define the horizontal thrust and the numerical algorithm to compute the safety factor of the drum/attic/buttresses system. This approach allows the user to have full control of the problem and to visualize, at the same time and in an interactive fashion, the collapse mechanism. In this work and aiming the solution of the optimization problem reported in Eq. (1), the Nelder–Mead method has been adopted [20]. The Nelder-Mead iterative method is commonly applied to find the minimum or maximum of an objective function in a multidimensional space. It is a direct search method (based on function comparison) and is often applied to nonlinear optimization problems for which derivatives may not be known. Figure 2 represents a synoptic representation of the proposed methodology that has been implemented in the visual programming environment offered by Rhinoceros3D + Grasshopper.

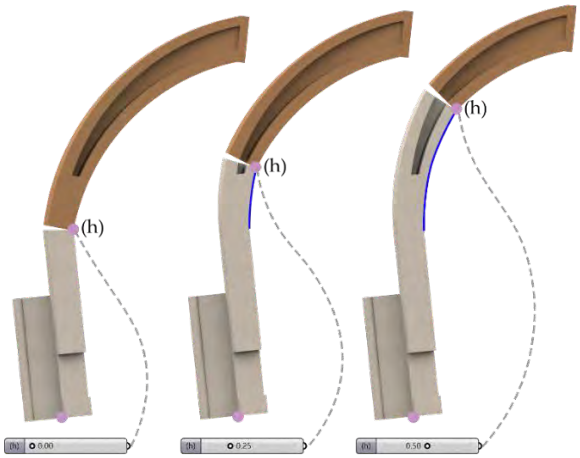


Figure 1: Parametrization of the collapse mechanism.

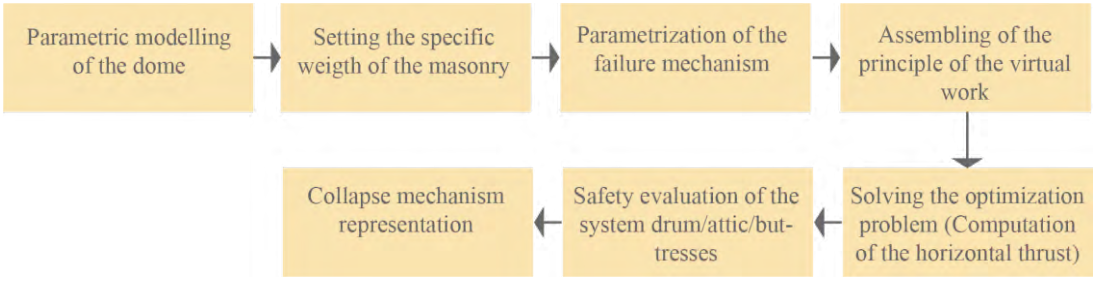


Figure 2: Flow-chart representing the proposed methodology.

3 HISTORY OF THE SAINT PETER'S DOME

Saint Peter's dome has been designed by Michelangelo and is worldwide known for its remarkable size and architectural features, see Figure 3. The dome has a diameter of 42.3 m and it is formed by two interconnected shells stiffened by 16 ribs. The thickness of the internal and external shells is 2.0 m and 1.0 m approximately, whereas the total thickness of the dome ranges from 3.00 m at the interface to 5.00 m at the crown. Concerning the original concept idealized by Michelangelo, the design of the dome was slightly modified by G. Dalla Porta. The curvature of the dome has been slightly changed to make it alike with the Florence domes designed by Brunelleschi. Two iron rings were also introduced, which revealed to be essential containing the structure after the damage occurred during the seismic event of 1703 [18]. After 50 years of its completion, some damage has been reported on the dome. By the mid-18th century, the latter damage was rather evident and, therefore, a survey was performed by L. Vanvitelli. It revealed that the drum and the attic were rotating outwards causing the onset of meridian cracks that lead to the split of the dome in several pushing arches. This is, from a structural standpoint, undesirable as these arches behave independently and the membrane effect is lost. In 1742, two reports published by three famous mathematicians [21] stated that Saint Peter's dome was seriously damaged and would require extensive straightening interventions.

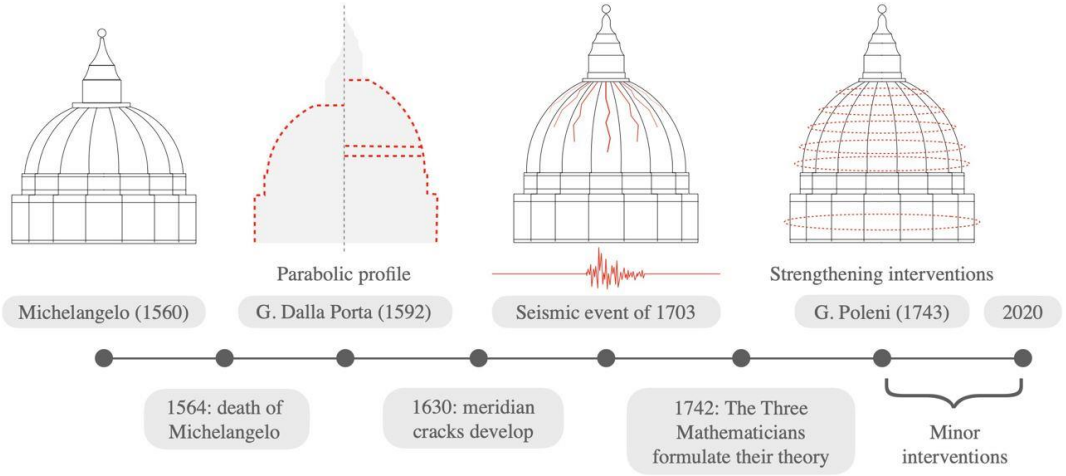


Figure 3: Timeline of the San Peter's dome.

The latter theory, the so-called "The Three Mathematicians" theory, was formulated based on a simple but ingenious model able to identify the thrust of the dome (Figure 4). While other scientists gave controversial opinions, Pope Benedict decided to follow the recommendations from another brilliant scholar, Giovanni Poleni [22]. Together with L. Vanvitelli, the researchers stated that Saint Peter's dome was adequately designed and proposed non-invasive interventions that allowed to keep the original architectural elements and concept.

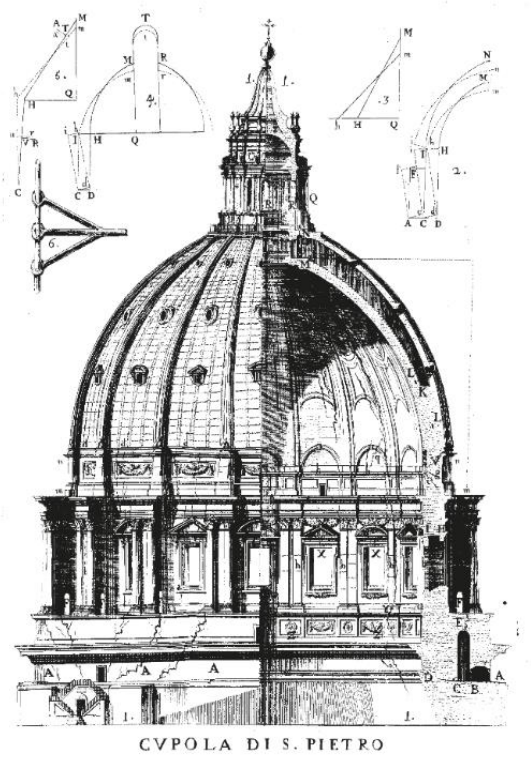


Figure 4: San Peter's dome: drawings presented by the so-called "The Three Mathematician".

The most crucial strengthening operation on the dome was encircled by six iron rings. Recently, it may be remarked that other researchers are trying to better understand the structural behaviour of Saint Peter's dome using advanced methods of diagnosis [23].

4 RESULTS

In this section, the structural safety assessment of San Peter's dome has been performed by adopting the digital tool described in Section 2. The main aim is to compute the horizontal thrust of the dome and verify the structural safety of the drum/attic/buttresses system. For that, the structural verification is performed considering the absence of the strengthening interventions designed by G. Poleni. (1743). Poleni [22] and M. Como [18] investigated the structural behaviour of the dome on a single 1/50 slice of the entire dome. Here, the parametric modelling of the dome allows us to consider a 1/16 slice of the dome (see Fig. 5). This is the most rational choice when considering the architectural geometry and its symmetry conditions (Fig. 5). After the parametric modelling of the dome, the second step consists of the evaluation of the minimum horizontal thrust of the dome and associated failure mechanism.

The failure mechanism depends of the rotational hinge (h) position and the algorithm proposed is capable to incorporate the formulation of the PVW equation given in Eq. (1). The digitalization of the geometry allows us to instantly compute distances and to perform the integral calculus to evaluate the centroids' positions of the macroblocks and corresponding weights.

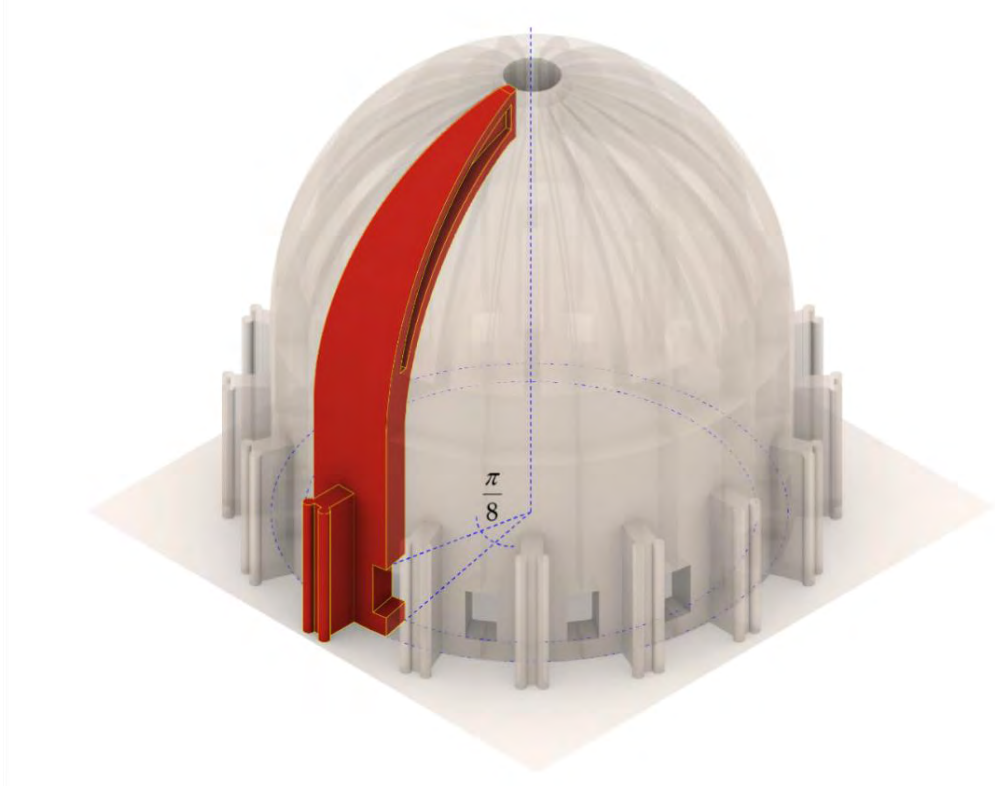


Figure 5: Representation of the 1/16th slice of the dome.

Table 1: Specific weight of the masonry and the lantern body force.

Specific weight [kN m^{-3}]	Lantern weight [kN]	Lantern weight (1/16) [kN]
18.50	14877	930

Furthermore, the program integrates the capability to consider the work performed by other loads, as the lantern's weight. Table 1 shows the specific weight assigned for the masonry, as well as the lantern self-weight (note that the lantern has been simulated using its body force).

Once the minimum horizontal thrust is computed, the tool can verify the structural safety of the drum/attic/buttresses system. The user can set the position of the rotational hinge based on engineering considerations, i.e. the crack pattern that affects the buttresses. To compare the result with the one given by Como [18], the position of the rotational hinge is assumed to be at the interface between the drum and buttresses (Fig. 6a). The obtained results are in agreement with those obtained by Como [18] and are summarized in Table 2. Figure 6b shows the capabilities of the proposed digital tool which shows the failure mechanism obtained in no time. Referring to a slice of 1/16 of the dome, the horizontal thrust computed is equal to 2287 kN, whereas the vertical weight is equal to 12676 kN. Hence the structural efficiency of the San Peter's dome, defined as the ratio between the thrust and the weight of a single slice, is equal to 0.18. The solver converges after few interactions, in 3s with an Intel® Core™ i7-6700HQ.

Furthermore, it is worthy of mentioning that the modelling of the geometry has been conducted having the available drawings as a basis. However, a more detailed geometrical survey should be performed to get more representative results.

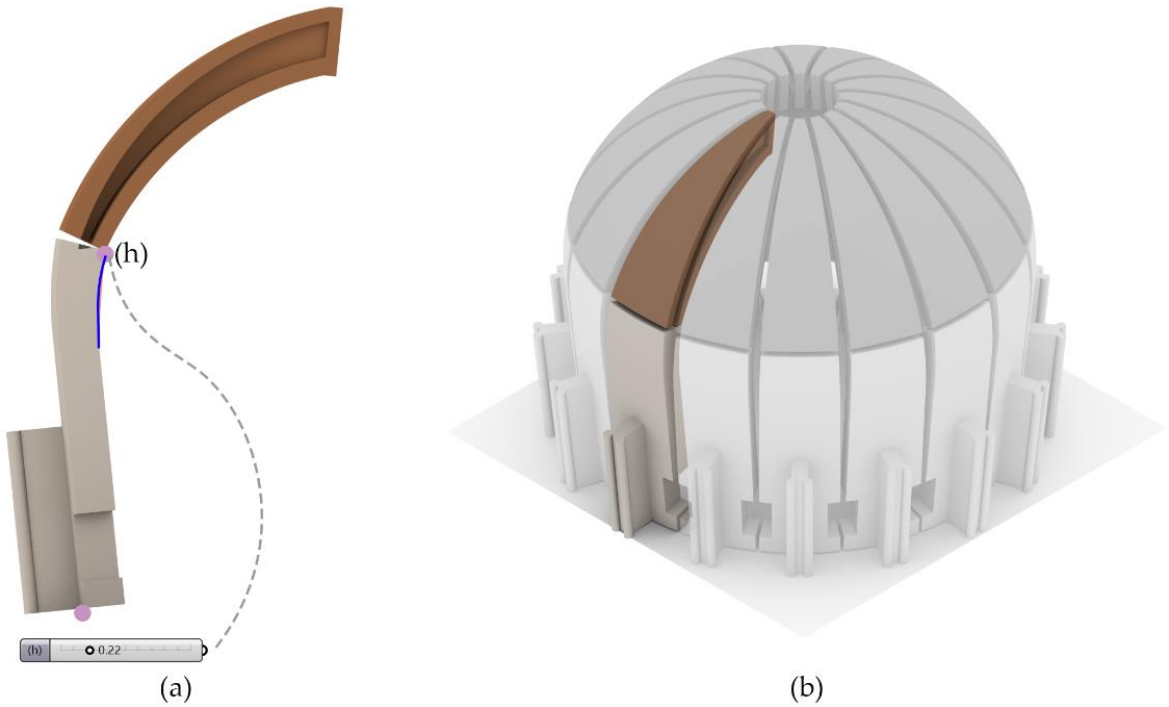


Figure 6: Obtained failure mechanism: (a) 1/16 slice of the dome; and (b) collapse mechanism of the entire dome.

Table 2: Summary of the results.

Horizontal Thrust [kN.m^{-1}]	Dome efficiency [-]	SF drum/attic/buttresses [-]	Computational Time [s]
255.0	0.18	1.08	3.00

5 CONCLUSIONS

This work presents a digital tool for the structural assessment of historic masonry domes. The method embeds an upper bound limit analysis under a no-tension capacity hypothesis for the masonry material and an optimization scheme based on the Nelder-Mead method. The workflow is integrated within a user-friendly computational tool implemented in the visual programming environment offered by Rhinoceros3D+Grasshopper.

The numerical performance of the proposed methodology has been validated on the case study of San Peter's dome. According to Como's model, the proposed methods can evaluate the minimum horizontal thrust of the dome and properly find the geometry of the prone failure mechanism. Furthermore, the structural integrity of the system drum/attic is evaluated. The numerical result is in agreement with that obtained by Como. Unlike other more time-consuming advanced methods of analysis, the proposed method allows the users to perform a structural assessment of historic masonry domes in a rapid and computationally efficient manner. Furthermore, the graphical visualizer allows us to give, in a direct way, the failure mechanism. The proposed visual script has been developed by using existing grasshopper components. However, future works will be focused on the development of a single component (ad-hoc programmed in C# language). The digital tool developed in this study will be freely available from a web archive hosted by the University of Minho. Future studies aim including the effect of the iron rings designed by G. Poleni and the investigation of the structural behaviour of the San Peter's dome through advanced methods of analysis.

REFERENCES

[1] Stepinac, M., et al., *Methods for the assessment of critical properties in existing masonry structures under seismic loads-the ARES project.* Applied Sciences (Switzerland), 2020. **10**(5).

[2] Porter, D.W., et al., *Material and seismic assessment of the great house at casa grande ruins national monument, arizona.* Journal of Architectural Engineering, 2020. **26**(1).

[3] Morici, M., et al., *Empirical predictive model for seismic damage of historical churches.* Bulletin of Earthquake Engineering, 2020. **18**(13): p. 6015-6037.

[4] Olivito, R.S., et al. *A numerical-geometrical methodology to represent out-of-plane mechanisms of unreinforced masonry structures by using pushover analysis*. in *COMPDYN Proceedings*. 2019.

[5] Fortunato, G., Funari, M.F., and Lonetti, P., *Survey and seismic vulnerability assessment of the Baptistery of San Giovanni in Tumba (Italy).* Journal of Cultural Heritage, 2017. **26**: p. 64-78.

[6] Savalle, N., Vincens, É., and Hans, S., *Experimental and numerical studies on scaled-down dry-joint retaining walls: Pseudo-static approach to quantify the resistance of a dry-*

joint brick retaining wall. Bulletin of Earthquake Engineering, 2020. **18**(2): p. 581-606.
[7] Mehrotra, A., Arede, A., and DeJong, M.J., *Discrete element modeling of a post-tensioned masonry arch.* Civil-Comp Proceedings, 2015.
[8] Cascardi, A., et al. *Structural analysis of a masonry church with variable cross-section dome*. in *Brick and Block Masonry-From Historical to Sustainable Masonry: Proceedings of the 17th International Brick/Block Masonry Conference (17thIB2MaC 2020), July 5-8, 2020, Kraków, Poland*. 2020. CRC Press.
[9] Silva, L.C., et al., *Seismic Structural Assessment of the Christchurch Catholic Basilica, New Zealand.* Structures, 2018. **15**: p. 115-130.
[10] Bacigalupo, A., Brencich, A., and Gambarotta, L., *A simplified assessment of the dome and drum of the Basilica of S. Maria Assunta in Carignano in Genoa.* Engineering Structures, 2013. **56**: p. 749-765.
[11] Bartoli, G., Betti, M., and Borri, C., *Numerical modeling of the structural behavior of Brunelleschi's Dome of Santa Maria del Fiore.* International Journal of Architectural Heritage, 2015. **9**(4): p. 408-429.
[12] Cavalagli, N. and Gusella, V., *Dome of the basilica of santa maria degli angeli in Assisi: Static and dynamic assessment.* International Journal of Architectural Heritage, 2015. **9**(2): p. 157-175.
[13] Bretas, E.M., Lemos, J.V., and Lourenço, P.B., *A DEM based tool for the safety analysis of masonry gravity dams.* Engineering structures, 2014. **59**: p. 248-260.
[14] Boni, C., et al. *DEM modelling of masonry vaults: influence of brick pattern and infill on stability during supports displacements*. in *Proceedings of IASS Annual Symposia*. 2019. International Association for Shell and Spatial Structures (IASS).
[15] Anselmi, C., Galizia, F., and Saetta, E., *3D limit analysis of masonry pavilion domes on octagonal drum subjected to vertical loads.* Frattura ed Integrita Strutturale, 2020. **14**(51): p. 486-503.
[16] Casapulla, C., Mousavian, E., and Zarghani, M., *A digital tool to design structurally feasible semi-circular masonry arches composed of interlocking blocks.* Computers and Structures, 2019. **221**: p. 111-126.
[17] Funari, M.F., et al., *Visual programming for structural assessment of out-of-plane mechanisms in historic masonry structures.* Journal of Building Engineering, 2020. **31**.
[18] Como, M., *Statics of historic masonry constructions*. Vol. 1. 2013: Springer.
[19] Feizolahbeigi, A., et al., *Discussion of the role of geometry, proportion and construction techniques in the seismic behavior of 16th to 18th century bulbous discontinuous double shell domes in central Iran.* Journal of Building Engineering, 2021. **33**.
[20] Gregson, S., *Nelder-Mead Optimisation (EOC),* https://www.eocengineers.com/en/news/digital-design-group-tackles-classic-engineering-problem 2018.
[21] Le Seur, T., Jacquier, F., and Boscovich, R., *Parere di Tre Matematici Sopra i danni, che si sono trovati nella cupola di San Pietro sul fine dell'anno MDCCXLII.* Dato per ordine di Nostro Signore Papa Benedetto XIV, Roma. **1742**.
[22] Poleni, G., *Memorie istoriche della gran cvpola [cupola] del tempio Vaticano, e de'danni di essa, e de'ristoramenti loro, divise in libri cinqve: Repr. der. Ausg. 1748*. 1982: Intemac.

[23] Baldrati, B., *LA CUPOLA DELLA BASILICA DI SAN PIETRO IN VATICANO. IL CANTIERE E IL SISTEMA COSTRUTTIVO*. 2009.

12th International Conference on Structural Analysis of Historical Constructions
SAHC 2020
P. Roca, L. Pelà and C. Molins (Eds.)

AMAZONAS THEATER ARCHITECTURAL CONSTRUCTION AND RESTORATIONS HISTORY

MARIA S. M. SAMPAIO

Escola Superior de Tecnologia (EST)
Universidade do Estado do Amazonas (UEA)
Darcy Vargas Avenue, 1.200 - Parque Dez de Novembro, 69050-020, Manaus/Amazonas - Brazil
e-mail: msampaio@uea.edu.br; socorrosampaio@hotmail.com

Keywords: Amazonas Theater, Historical Structure, Construction History, Restoration

Abstract. *Built in the artistic splendor that prevailed in the late 19th century, Amazonas Theater is considered the most significant architectural construction of the so-called golden age of rubber, both for the values applied in its construction and for the symbolic importance it assumed, that is, the man's victory over the jungle, financial prosperity and the alleged artistic-cultural effervescence. However, when compared to the millenary constructions of the Ancient World, Amazonas Theater can be considered a "baby" and therefore a source of knowledge to be explored. In this sense, this paper intends to be the first one of a series of other ones that intends to study the behaviour of this structure. The paper is focused on describe the history of the construction of the Amazonas Theater highlighting the structural solution adopted to overcome the logistical challenges faced by a construction carried out in the middle of the largest tropical forest in the world and the main interventions performed during its 123 years. To this end, the building records of the Theater, an indispensable documentary source of the building´s history, were consulted.*

1 INTRODUCTION

Located in the middle of the Amazon forest in Manaus, Amazonas capital city, Brazil, the Amazonas Theater (Figure 1) took 17 years to be built from its conception until its opening in December 31, 1896. A place that would be frequented by the elite of *belle époque*, as it was called the period in which Manaus lived the golden age of rubber, Amazonas Theater became a symbol of a period of prosperity.

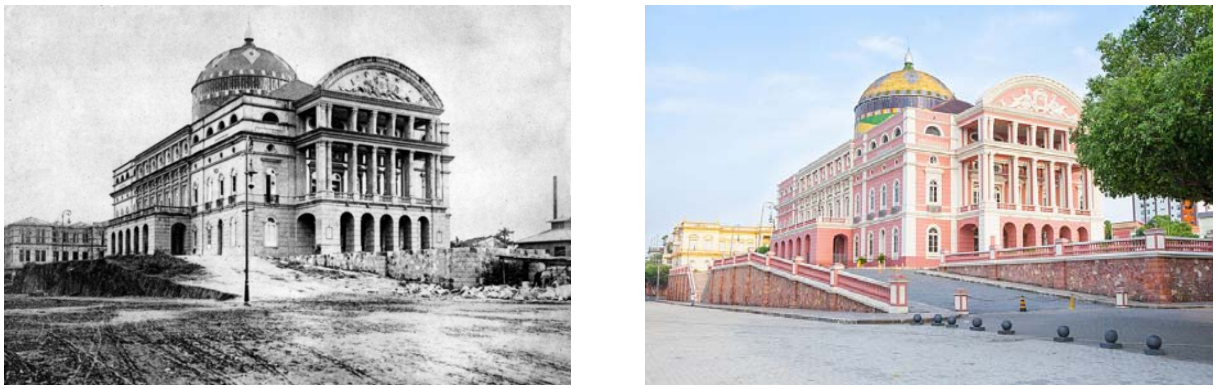


Figure 1: a) Amazonas Theater in construction [1,2]; b) Amazonas Theater in 2019.

For its construction, not only architects, builders, painters, decorator and sculptors were brought from Europe, but also various materials such as *Carrara* marbles, *Murano* chandeliers, pieces of worked iron from England and French tiles. In the internal structure, the steel dome was manufactured in Belgium by the "*Compagnie Centrale de Construction Haine-Saint-Pierre*". The dome roof is composed of 36 thousand pieces of enamelled ceramic pottery and glazed tiles, coming from Alsace. The original coloring in green, blue and yellow is an analogy to the Brazilian flag.

It is important to mention that due to the difficulty of importing noble materials, some colonnades, straighteners, glasses and balusters were made of cement, masonry and plaster, but prepared to look like marble and other noble materials. Besides that, its construction caused controversy, as the city had only one hundred thousand inhabitants.

Throughout its history, the theater underwent four major structural interventions, being the last two real restorations. The four interventions took place, respectively, from 1926 until 1929, from 1959 until 1962, from 1972 until 1974 and finally, from 1987 until 1990.

In 1966, on the occasion of its 70th birthday, the building was listed by the National Historical and Artistic Heritage Institute (IPHAN) being the first monument registered in Manaus by the Historical Patrimony.

2 A BRIEF HISTORICAL CONSTRUCTION CHRONOLOGY

On May 21, 1881, the congressional representative A. J. Fernandes Júnior presented at the Amazonas Provincial Assembly the project for the construction of a masonry theater in the Manaus city [3,4,5]. On May 31, 1881, the Provincial Assembly approved the project, but only on May 29, 1882, the Law 593 authorizing the provincial president to open competition for the presentation of plans for the construction was approved [3,4,6]. In compliance with Law 593, the provincial president José Paranaguá declared open competition for the presentation of plans, establishing the period from June 3, 1882 to November 23, 1882 for the proposals submissions. Only two projects were submitted: one presented by C. Celeste Saccardi and another one presented by the merchant Bernardo Antônio de Oliveira Braga. The project presented by Bernardo Braga and signed by the Portuguese Office of Engineering and Architecture of Lisbon (Figure 2) was chosen by the jury composed of the engineers Joaquim Leovilgido de Souza Coelho, João Carlos Antony, Charles B. Brisbin and the master builders José Pires dos Santos and Ismael Vitório Gomes [3,4,7]. On January 13, 1883, the Provincial Assembly accepted the plans chosen by the jury and ordered competition for the construction of the theater [3,4,7]. On January 17, 1883, the provincial treasury was authorized to open competition for the construction of the theater, and on May 17, 1883, four proposals were submitted. The proposal presented by the Manuel de Oliveira Palmeira de Meneses was approved and the contract was signed on August 23, 1883 [3,4,8]. Later the contract was transferred to the Italian company Rossi & Irmãos [3,4,9]. Although the construction contract was signed on August 23, 1883 until December 31, 1883, the works had not been started because the earthwork was not properly prepared. In the following year, the earthworks began and finally on February 14, 1884 the foundation stone of the building was laid [3,4,9]. In September 1885, President Ferreira Júnior reported that in that year the theater had not progressed, but announced that in April 1885, almost all the iron material needed for the construction of the building arrived on a British

steamer [3,4,10]. In February 1886, the director of the Public Works Bureau reported that in August of the previous year the president had the works suspended [3,4,11]. The construction contract with Rossi & Irmãos was terminated on January 12, 1886 [3,4,11]. Construction was only restarted in 1893 by Governor Eduardo Gonçalves Ribeiro. In May 1893, Manuel Coelho de Castro signed a contract to restart the works. Eduardo Gonçalves Ribeiro hires the Brazilian artist Crispim do Amaral for the decoration, painting, ornamentation and furniture works of the Theater. Despite all the dedication of Eduardo Gonçalves Ribeiro, it was not possible to complete the work during his administration and still unfinished, Amazonas Theater was opened on December 31, 1896 [3,4,12,13,14]. In March 1897, Governor Fileto Pires Ferreira stated in his first message that despite all efforts, it was not possible to inaugurate the theater in the desired conditions. The work was not completed. The back facade, the balconies, the platform around the building and some internal work, including the decoration of the Noble Hall, were still missing [3,4,15]. In 1897, the Governor Fileto Pires Ferreira hired the Italian painter Domenico de Angelis to decorate the Noble Hall of the Amazonas Theater, which was opened only on the probable date of June 24, 1901 [3,4].

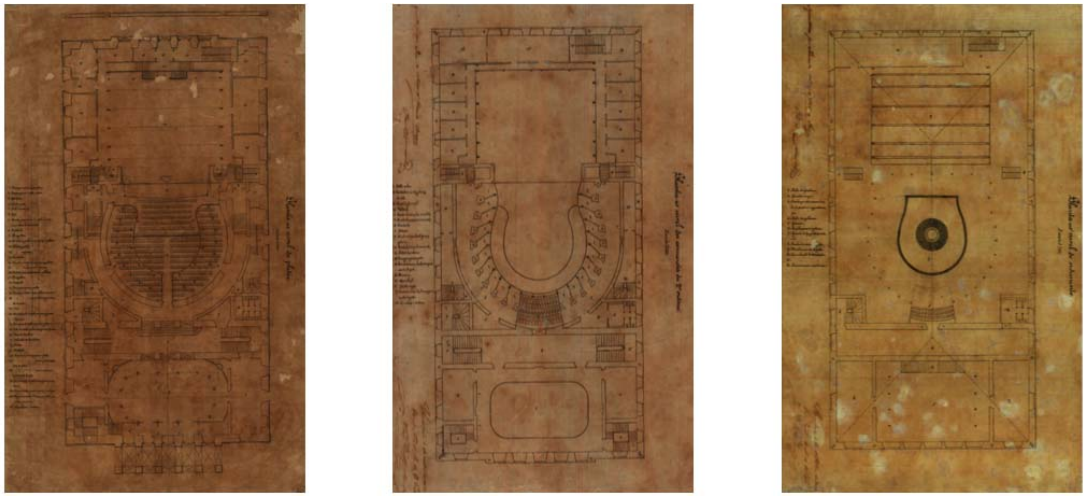


Figure 2: Original drawing of the Portuguese Office of Engineering and Architecture of Lisbon [16]: a) Ground floor plan [16]; b) 3th floor plan [16]; c) Attic plan [16].

3 STRUCTURE AND CONSTRUCTION DETAILS OF AMAZONAS THEATER

When researched about the structural solutions and construction details of the Amazonas Theater, it can be easily seen that Amazonas Theater have a very simple patterns, including a simple dome above, and a very common roof solutions. The construction structure of the theater is quite conventional, adopting the traditional four-walled box format (Figure 3a).

The monumentality of the building, with the overlapping of floors, required the use of much iron material, especially the large structures, which embrace the building and are hidden under the masonry. The presence of the iron elements in the construction of the theater is not so evident, but are revealed in the attic of the building, as well as in the roof and dome structures. The structural solution of the whole building in terms of the load transferring structure, start from the top of the dome to the end of the columns and the perimeter masonry, supported with iron bar in between columns, to the earth level.

Although, externally, the Amazonas Theater presents renaissance composures, the diversity of materials and the variation of stylistic trends applied to the building facade and the different stylistic treatments adopted in the various environments defined the Amazon Theater as an eclectic architectural building.

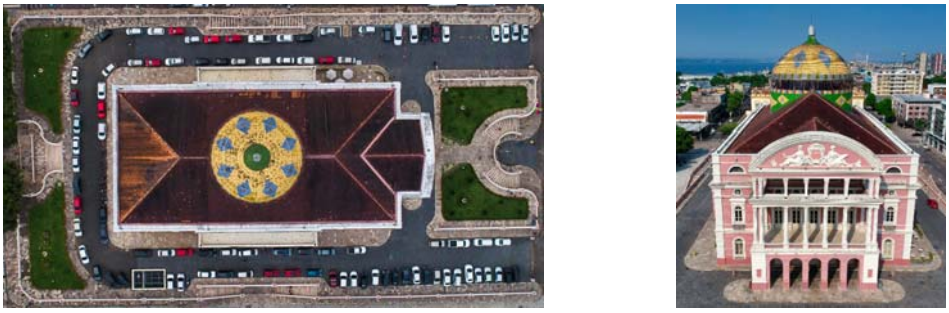


Figure 3: Amazonas Theater: a) Upper View; b) Frontal facade. Photo by Ivo Brasil Filho on June 4, 2019 [17].

3.1 The facade

The facade is divided into three bodies, the prominent central body consisting of a frame that, on the ground floor, has five arches supported by pillars. On the second floor of this frame, there is a balcony surrounded by balustrades interrupted by the bases of the eight Corinthian columns that camouflage the pillars and support the entablature; above it stands another set of pillars that support the base of the pediment, these pillars being disguised by eight small pillars with capitals decorated with feminine faces. On these elements stands the curved pediment which in its tympanum presents a relief set composed of two female figures, probably allegories to music and theater, among them a card engraved with the date 1896 (Figure 3b).

3.2 The plans

The Amazonas Theater has a ground floor, three floors and the Attic floor (Figure 4), being covered in masonry treated with continuous bossing, except for the floor corresponding to the Attic floor. The mains environments on the ground floor are the Foyer and the Concert Hall. The Noble Hall is located on the first floor. In the ground floor, the audience has 266 armchairs and 93 chairs distributed in 20 trimmings.

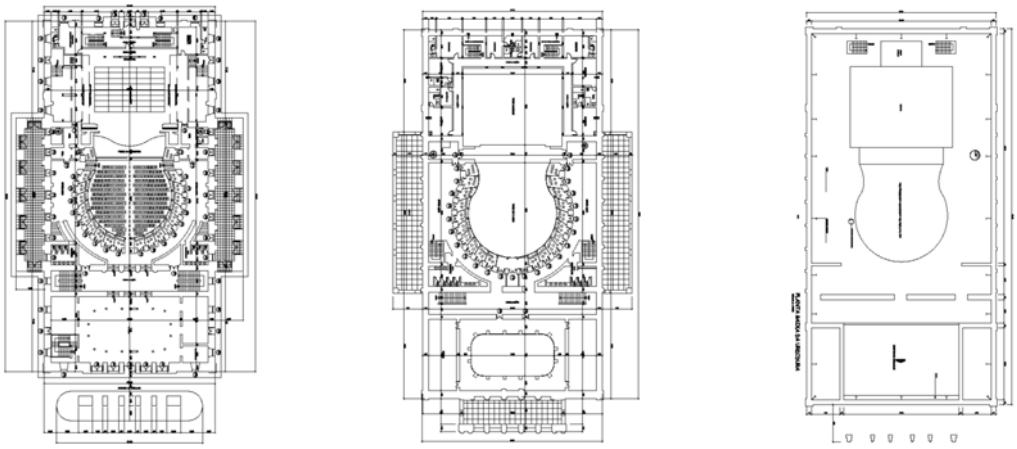


Figure 4: The plans of Amazonas Theater after renovation of 1972-1974: a) Ground floor plan; b) 3th floor plan; c) Attic plan. Filed in the Amazonas Theater Museum [18].

The 1st floor has 110 chairs distributed in 22 staterooms and the Governor's cabin. The 2nd floor has 125 chairs distributed in 25 cabins and finally, the 3rd floor has 95 chairs distributed in 19 staterooms. In according to the architectural ground plan, the Amazonas Theater has a plan with around 60.80 m x 30.80 m and a height of 35 meters considering the dome.

3.3 The Dome

In the internal structure, the steel dome (Figure 5) was manufactured in Belgium by the "*Compagnie Centrale de Construction Haine-Saint-Pierre*". The dome roof is composed of 36 thousand pieces of enamelled ceramic pottery and glazed tiles, coming from Alsace. The original coloring in green, blue and yellow is an analogy to the Brazilian flag (Figure 5f).

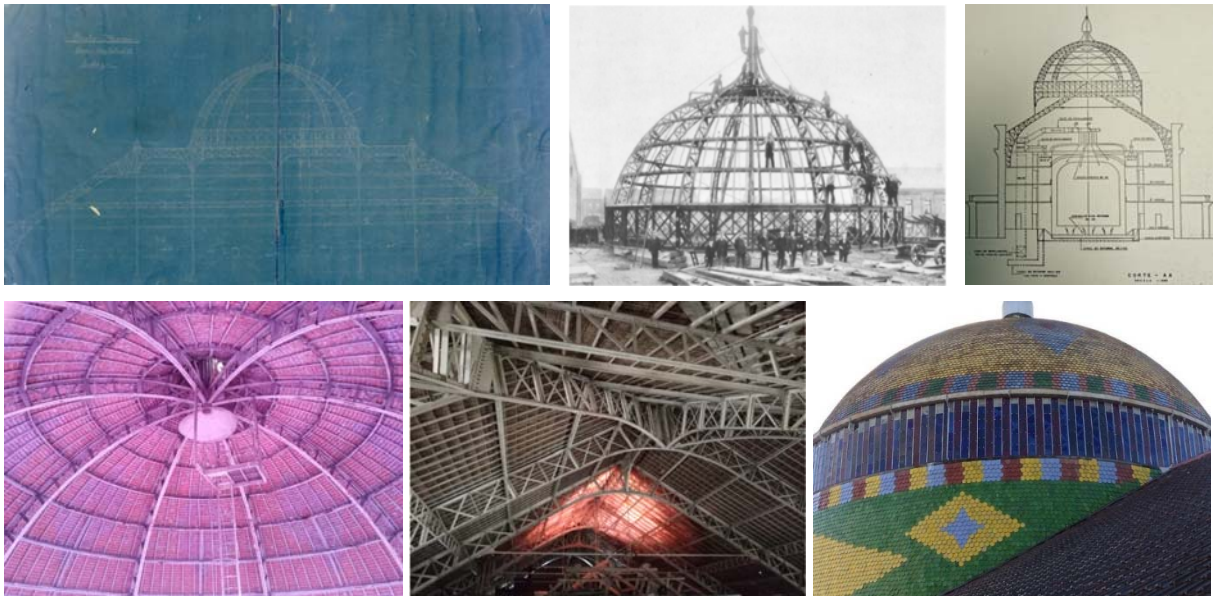


Figure 5: The Dome: a) Original Prussian Iron Dome Charpent Plant filed in the Amazonas Theater Museum [18]; b) The iron dome in 1885 [18]; c) In section dome plan [19]; d) The iron dome in 2019; e) The iron roof in 2019; f) The dome roof in 2019.

In according to the architectural plan, the dome has a diameter of around 19 meters. The iron dome is composed of 8 curved flat trusses of variable height. In according to historical records [12,13,14], the metallic structure of the roof and the dome took two years to assemble.

3.4 Foyer, Concert Hall and Noble Hall

The Foyer has 16 iron columns from Glasgow lined with concrete supported by pedestals lined in marble (Figure 6a).

The Concert Hall has a floor plan in the shape of a lyre or horseshoe. Around this hall there are three floors of cabins or friezes. Between the friezes on the ground floor there are columns of the Ionian order. These concrete-coated iron columns extend to the third floor, the capitals are of the Corinthian order. There are a total of 22 iron columns from Glasgow (Figura 6b). The decoration of the Concert Hall is by Crispim do Amaral. The ceiling of the Amazonas Theater concert hall consists of a barrel vault, an arched roof, built in wood pieces that lean into each other, in order to support their own weight and external loads. The wood used are blonde lead

wood and black wood called “envira”. The barrel vault structure, all made of interlaced wood, forming a kind of the shell which is supported by a intricate system of levers and wood beams, attached to rods, to resist efforts, forces or stress, fixed to the iron frame of the ceiling.



Figure 6: Amazonas Theater in 2019: a) Foyer; b) Concert Hall; c) Noble Hall. Filed in the Mário Ypiranga Library [19].

The Noble Hall also has 16 columns. Although supported by Carrara marble, the shaft is covered in plaster in order to imitate marble. The floor of the Noble Hall is the most original part of the Amazonas Theater, composed of 12 thousand pieces of wood placed with a technique called marquetry, which consists of not using nails or glue, making the woods stay in the perfect fit position. between the pieces. It is important to highlight that the Noble Hall decoration work, perfomed by the Italian painter Domenico de Angelis, extended for a few years after the official opening in 1896 (Figure 6c).

4 STRUCTURAL INTERVENTIONS

According to consulted building and historical records, the four major structural interventions underwent by Amazonas Theater took place, respectively, from 1926 until 1929, from 1959 until 1962, from 1972 until 1974 and finally, from 1987 until 1990.

4.1 First structural intervention (1926-1929)

In the Ephigênio Ferreira de Sales administration (1926-1929), the building underwent internal changes (Figure 7a,b). The seven front cabinets of the second order were removed and a grandstand topped by a large stylized shell was built there (Figure 7b). There was also suppression of internal walls, which separated two longitudinal and continuous corridors to the friezes of the first order. The orchestra venue was expanded and stucco and painting works were done in the hall and corridors [20,21,22]. The Foyer was decorated with *guaraná* leaves and half *pupunhas* changing the original design of the Theater (Figure 7a). No record of changes in the Noble Hall during this renovation was found (Figure 7c).



Figure 7: Amazonas Theater after renovation of 1926-1929: a) Foyer; b) Concert Hall; c) Noble Hall. Filed in the Mário Ypiranga Library [19].

Figure 8 shows the branches of *guaraná* behind the columns. The columns with capitals alluding to the Amazonian flora have half *pupunhas* and simple half flutes on the plinth [19].



Figure 8: Foyer after renovation of 1926-1929. Filed in the Mário Ypiranga Library [19].

Amazonas Theater has been open for a long time, but since the 2nd World War it has remained almost closed for about 20 years.

4.2 Second structural intervention (1959-1962)

During the government of Gilberto Mestrinho de Medeiros Raposo (1959-1962), the theater underwent the second main structural intervention. Although the consulted historical records mention this restoration, details of the modifications, interventions and changes made in the original structure of the Theater have not been found.

4.3 Third structural intervention (1972-1974)

This restoration performed in the João Walter de Andrade administration was based on the resumption of the original propositions of the theater and, at the same time, the installation of indispensable technical devices capable of giving it a compatible contemporaneity, without harming the appearance, details or character of the time when it was inaugurated (Figure 9). For this, a careful research work has been done to verify the details of its original design that have not been completed and, in addition, those that in subsequent renovations have been modified or misrepresented [23].

A thorough examination of the foundations, the structure in general, the steel structure in particular, the situation of the roof, the installations of light, power, water and sewage, the state of conservation of the frames and the ironmongery and the valuable existing paintings in theater. Some surveys were carried out to verify the foundations of the theater building and sufficient solidity and stability were found [23]

The steel structure that supports the roof was the object of special study in the face of deformations in the main element of the ridge. Structural stability analysis was performed and a report on the subject was presented suggesting corrective measures. As a result, reinforcements of steel profiled elements were added to the structure by electric welding. All steel frame paint was treated with a metallic brush and solvent, receiving new anti-oxide paint protection and two-coat finish. The wooden framework of the Noble Hall floor received, for reinforcement, a special steel structure, supported by the peristyle columns [23].

Still in terms of structural steel, it is worth mentioning that 120 tonnes of profiled steel,

constituting the imported warp from Austria, were mounted on the stage box. To support this structure, another reinforced concrete was built, after being completely demolished the old wooden for improper and obstructive. As for the wood in the theater, there was a need to replace almost ninety percent of the structural elements, floors, ceilings and frames [23].

About two thousand and one hundred linear meters of wood beams were replaced. On these rebuilt frameworks, two thousand square meters of new floor were put in place, replacing the floor damaged by time and poor conservation. One thousand eight hundred square meters of wood lining have been replaced in the same way, preserving the shape, size, quality of the wood and the original look [23].

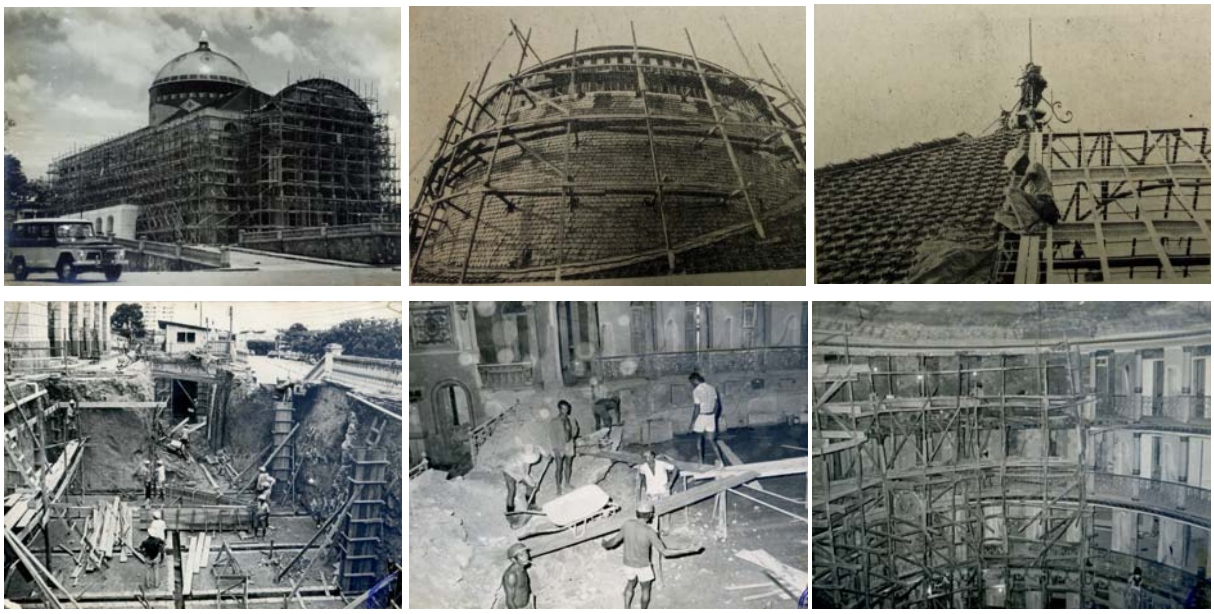


Figure 9: Amazonas Theater under renovation of 1972-1974: a) The facade [19]; b) The dome roof [19]; c) The roof [19]; d) Excavations for the construction of the air conditioning unit and generator room [18]; e) Internal works of the Concert Hall [18]; f) Renovation of the friezes of the Concert Hall [18].

The frames, doors and windows, were removed, repaired and replaced their ironmongery, some of them had to be manufactured according to model. The two main side access stairs to the staterooms and friezes were demolished and replaced by reinforced concrete stairs and covered with Liós marble [23].

The lack of sanitary facilities required the construction of new units, thirty-two sets in the dressing room area and ten sets in the audience area. Taking into consideration the type and age of the theater building, one can get an idea of the difficulties in locating, building, finishing and installing the whole system, which is indispensable for the operation of a theater house with a larger population, a thousand people, including spectators, artists, musicians and technicians [23].

The stage box has been totally reformulated. All internal constructions were demolished and removed, taking advantage only of the outer walls. Then, with reinforced concrete structure, were built twenty dressing rooms, with capacity for seventy people, besides other service facilities, walkways, access, stairs, toilets, bar, involving a built area of nine hundred square meters and more than two thousand and five hundred square meters of brick masonry. A new

wooden stage floor, including its structure, was built [23].

The original form and appearance of the concert hall has been restored and a gallery built in one of the renovations at the expense of the mutilation of the second and third cabins was demolished. This work restored the hall, restoring it to the classical, elegant conformation typical of the lyric theaters of the time. To this end, cast-iron railings and special columns were ordered to merge, completing, in the smallest detail, the boxes that had been suppressed [23].

4.4 Fourth structural intervention (1987-1990)

A decade after the last renovation, during the Amazonino Armando Mendes government (1987-1990), the theater underwent the last major restoration. The building's condition was precarious and a survey was conducted that pointed to the urgent need for further reform [18].

A long work of prospecting was carried out in all internal environments of the theater, as well as on the facades and walls. This technique was applied in places where supposedly there had been no previous interventions to observe the original. Several layers of paint and decorative elements were discovered [18].

The woods underwent several types of treatment. Thousands of liters of immunizers were consumed. Even so, about 40 m^3 of wood totally damaged by the action of termites had to be removed. The new woods that were applied strictly followed the same specifications as the previous ones (Figure 10a).



Figure 10: Amazonas Theater under renovation of 1987-1990: a) Treatment of the wooden structure of the Concert Hall plafond [18]; b) The dome roof [19]; c) Apparent surrounding wall restoration [18], d) The parallelepiped blocks restoration [18].

A reservoir with a capacity of forty thousand liters of water was built exclusively for fire fighting. The entire sewage and water installation system was replaced since the previous ones were in a high state of oxidation. In addition, a further 2,300 meters of piping were installed. To facilitate maintenance, the rainwater pipes that were embedded in the external walls gained a new direction and were connected to the network through external PVC rigid tubes [18].

For the feasibility of presenting any type of show, the theater was equipped with modern sound equipment. Over two hundred and seventy scenic projectors and other accessories have been restored. These are originally from England. The audience and the stage now have an efficient cooling system with the installation of a central. The dressing rooms also have cooling units. A new telephone installation system was developed and executed, serving the entire dressing room, bar, foyer and ticket office area. Closed circuit TV was installed covering the main space and interconnecting them through video monitors [18].

The drainage of the gardens was planned in such a way as not to allow water to seep into the apparent stone walls that delimit the external area of the Theater and was carried out in the four flowerbeds. In order to avoid infiltrations caused by the porosity of masonry and coverings, all terraces, slabs, substation, engine room, water tanks, cisterns, cornices and plateaus were waterproofed [18].

Part of the 36,000 enamelled ceramic tiles of the dome have been replaced. In previous renovations, original tiles were replaced and those that remained were given a coat of paint. The paint from thousands of original parts were removed while the non-original ones were completely replaced due to the very low quality standard (Figure 10b). The metal structure of the dome received careful repairs and the various points of oxidation were eliminated.

All the wooden ceilings in the circulation of the friezes were replaced since the ones that were there were placed without previous historical study. The other ceilings were overhauled and the damaged parts were replaced. The plaster-like ceiling of the frontal circulation to the Noble Hall was completely rebuilt after reinforcing the structures. The dressing rooms and circulations received a lowered ceiling made of easy-to-maintain aluminum material [18].

The wall surrounding the theater was completely painted and grafted with cement and sand mortar imitating stone. As the research showed the wall was originally apparent, all the suspicious material found was removed and other stones with the same characteristics were cut and placed in the necessary places (Figure 10c).

The woods on the stage floor that were previously in *Louro-Preto* and *Jacareúba* were completely replaced by *Freijó*. The other floors that bring wood such as *Pinho de Riga*, *Acapú* and *Macacaúba*, *Amarelinho* were scraped and sanded by hand. The white marble floors of the terraces, the noble balcony and the sills of the 1st floor have been replaced by *Aurora Pérola* marble. The Liós stone floors were polished and waxed [18].

The imported stones on the external sidewalks and staircases that had defects were reconstituted. The parallelepiped blocks of the external street were analyzed and 74 thousand pieces with the same characteristics and resistance as the originals were produced and laid (Figure 10d).

In the bathrooms and toilets, high-strength materials such as granite, marble and tiles were applied [18].

A total of 800 pieces of furniture including Concert Hall chairs and armchairs has been restored. Specialized restorers performed the restoration work on the theater's rich collection of 32 chandelier in *Murano* crystals, 166 bronze chandeliers equipped with 1,360 tulips, 2 curtains making a total of 308 m^2, arch of proscenium, medallions, plafond of the Concert Hall with 204 m^2, railings of the Concert Hall, fresco to the mask of the Concert Hall, plafond of the Noble

Hall with 100 m^2, parietal paintings of the Noble Hall, 6 cast iron statues, ceiling of the Noble Hall balcony, fresco to the mask of the room 37, 28 plans of the original drawing and the foyer columns

Finally, the structural wood embedded in the facades was totally attacked by termites. The classification and restoration of reusable wood was planned and a technical solution for structural recovery without causing architectural changes was studied [18].

During its renovations, the Amazon Theater had the colors imperial rose, bluish gray, and gray. Currently, Amazonas Theater is back to being imperial rose (Figure 11).



Figure 11: a) Before restoration of 1972-1974 painted in gray [19]; b) Under renovation of 1972-1974, painted in bluish gray [19]; c) Under renovation of 1987-1990, when it was painted in imperial rose, its current color [19].

Recently, during a painting's scraping a deep gold layer was discovered. Gold was applied in a small amount, more or less in the same proportion that exists in the Noble Hall. Nowadays, almost 30 years after its last major restoration, Amazonas Theater retains much of its original decoration, architecture, paintings, furniture, floors and objects used 100 years ago. Besides that, a rigorous and permanent maintenance keep the original environment solid [18].

5 CONCLUSIONS

- In this paper, a brief historical construction chronology of Amazonas Theater is presented. The structure and construction details as well as the main structural interventions performed during its 123 years are described. Considering all the challenges faced by a construction carried out in the middle of the largest tropical forest in the world, its construction presented advanced solutions for the time, highlighting the metallic structure of the roof including the dome that took two years to assemble. According to consulted building and historical records of the Theater, that took 17 years to open, its construction taking all this time mainly because of logistical issues, since practically all the materials used in its construction came from Europe.

Acknowledgements. The author would like to acknowledge the Escola Superior de Tecnologia, the Universidade do Estado do Amazonas, the Governo do Estado do Amazonas, the Secretaria de Cultura e Economia Criativa do Amazonas, the Gerência de Acervos Digitais, the Amazonas Theater, The Arquivo Público do Estado do Amazonas and the Memorial e Biblioteca Mário Ypiranga Monteiro for the support for this research.

REFERENCES

[1] D.M. Durango. *Manaus entre o passado e o presente*. 1st Edition, Mídia Ponto Comum, 2009.

[2] A. Caccavoni. *Album Descriptivo Amazonico*. Genova: F. Armanino, 1899.

[3] M.Y. Monteiro. *Teatro Amazonas*. 2ª edição revista e aumentada. Manaus: Editora Valer. Governo do Estado do Amazonas, 2003. 686p.

[4] O.M. Mesquita. *Manaus: história e arquitetura (1669-1915)*. 4th Edition revisada e ampliada – Manaus: Editora Valer, 2019. 362 p.

[5] *Annaes da Assembléia Legislativa do Amazonas*. 1880-1881. Manáos: Typ. do Amazonas, 1881.

[6] A.J.Furtado. *Exposição do presidente Alarico João Furtado, 7 de março de 1882.* Manáos: Typ. do Amazonas, 1882.

[7] J.L.C. Paranaguá. *Relatório do Presidente em 25 de março de 1883.* Manáos: Typ. do Amazonas, 1883.

[8] J.L. Paranaguá. *Relatório do Presidente em 16 de fevereiro de 1884.* Manáos: Typ. do Amazonas, 1884.

[9] J.L.S. Coelho. *Relatório do diretor da Repartição de Obras Públicas em 8 de julho de 1884*. Manáos: Typ. do Amazonas, 1884.

[10] J.J. Ferreira Júnior. *Fala do presidente da Provincia em 21 de setembro de 1885*. Manáos: Typ. Jornal do Amazonas, 1886.

[11] L.B.Bitancourt. *Relatório do diretor interino da Repartição de Obras Públicas em 10 de fevereiro de 1886*. Manáos: Typ. Jornal do Amazonas, 1886.

[12] E.G. Ribeiro. *Mensagem do governador em 10 de julho de 1893.* Manáos: Typ. do Diário Official, 1893.

[13] E.G. Ribeiro. *Mensagem do governador em 10 de julho de 1894.* Manáos: Imprensa Official, 1894.

[14] E.G. Ribeiro. *Mensagem do governador em 1 de março de 1896.* Manáos: Typ. do Diário Official, 1896.

[15] F.P. Ferreira. *Mensagem do governador em 4 de março de 1897.* Manáos: Typ. do Diário Official, 1897.

[16] *Governo do Estado do Amazonas. Secretaria de Cultura e Economia Criativa do Amazonas. Gerência de Acervos Digitais*.

[17] I.B. Filho. *Acervo pessoal*. Manaus: 4 de junho de 2019.

[18] *Governo do Estado do Amazonas. Secretaria de Cultura e Economia Criativa do Amazonas. Museu do Teatro Amazonas*.

[19] *Governo do Estado do Amazonas. Secretaria de Cultura e Economia Criativa do Amazonas. Memorial e Biblioteca Mário Ypiranga Monteiro*.

[20] E. F. Salles. *Mensagem do governador do Amazonas em 21 de dezembro de 1927*. Manáos: Typ. da Imprensa Publica. 1927.

[21] E. F. Salles. *Mensagem do governador do Amazonas*. Manáos. 1928.

[22] E. F. Salles. *Mensagem do governador do Amazonas*. Manáos. 1929.

[23] C.P. Valladares. *Restauração e recuperação do Teatro Amazonas*. Governo do Estado do Amazonas, 1974.

12th International Conference on Structural Analysis of Historical Constructions
SAHC 2020
P. Roca, L. Pelà and C. Molins (Eds.)

AN EXAMPLE OF FIT-FOR PURPOSE USE OF MATERIALS IN ROMAN ARCHITECTURE: P TEMPLE, SIDE, ANTALYA/TURKEY

GAMZE KAYMAK HEINZ

Faculty of Engineering and Architecture, Department of Architecture
Beykent University
Hadımköyyolu, 08034 Ayazağa, Sarıyer, Istanbul, Turkey
e-mail: gamzekaymak@beykent.edu.tr

Keywords: Side, Pamphylia, Temple P, Fit-for Purpose Use of Material, Historical Structure

Abstract. *The high-podium Roman Period temple, with a semi-circular plan scheme, was discovered by Lanckoroński and his team in Side, Turkey and named after 'P' in 1890 [1]. The temple was unearthed by Mansel [2] and his team in 1947 through archaeological excavations. In 2013, further studies started on the temple. The aim of the still ongoing work is to seek answers to such issues that haven't been clarified yet, as the plan scheme, to whom it was dedicated, and the date of construction.*

In this context, the construction structure of the Temple P was investigated during the present study based on in-situ and precise documentation: At least five different types of stones were classified by purpose, including conglomerate, travertine, sandstone, marble and rubble stone mixed with mortar as infilling material. It was seen that fit-to purpose use of the material was considered more important than the ideal and repeated dimensions of the building blocks. Moreover, local material was used except for the outsourced marble.

In addition to the large-sized clamps and dowels in the load-bearing core blocks of the walls, the spaces between the coatings and the load-bearing core were filled with mortar. In this construction technique, opus revinctum and opus caementitium were used together. The partition walls separating the three rooms of the lower floor and the vault cover made with mortar and formwork system belong to the construction period of the temple. However, there are indications that the outer walls, about 2,5 m thick, originated from the foundations of a precursor structure. Four construction stages of the pillar profiles of the orthostat coating blocks of the podium, each having different lengths, can be traced from the upper surface workmanship, without scalping. The podium, which is approximately 2,30 cm high, is reached by one main and two side stairs. Numerous, high quality marble blocks in front of the cella on the podium indicate the presence of a monumental entrance structure made in opus revinctum technique. Unlike the profiled orthostat blocks of the podium, which were processed in situ after assembly, the cassette and cornice blocks of the entrance structure were produced 'on the ground' previously. The restitution of the marble cassette ceiling of the monumental entrance structure has been developed by combining the 1:10 scale precision surveys of the blocks via a computer aided method. The efforts for a modular planning and production are witnessed in the construction of cassette ceilings.

1 INTRODUCTION

The temple P, with high podium and a plan scheme of slightly larger than a semi-circle, is about 100 m away from the Athena and Apollo temples dedicated to the chief gods of the city in the Ancient city of Side in Pamphylia region. The 231 cm high podium forms the lower floor of the temple with its three vaulted rooms. The semi-round cella over the podium has a linear entrance façade of 16.80 m to the west and a depth of 11.15 m measured at right angles from the middle of the façade. In front of the cella there is a filled-in platform forming the lower structure of the monumental entrance structure, bounded by orthostat coatings on both sides. The arrangement of the orthostats suggests the presence of a wide main staircase leading up to the podium to the west and a secondary staircase each from the northern and southern sides.

The lower floor, which houses three spaces connected to each other by door openings, has an outer wall thickness of 2.50 m, excluding the outer orthostat coatings. The bottom level of the lower floor is below the street level. Today it is accessed from the partly collapsed vault cover; there is no external access **(Figure 1)**.



Figure 1: Temple P aerial view (Side Excavation Archive)



Figure 2: Remains of the *cella* wall

2 TYPE AND LOCATION OF MATERIALS USED AT TEMPLE

In Roman architecture, adaptation to regional conditions was achieved by means of different construction techniques rather than by different building styles. Different construction techniques were developed as a result of the use of more economical and easily accessible local building materials [3].

Greek master builders meticulously paid attention to the harmony of stone joints in order to obtain repetitive measurements and maintained this rule for centuries. For the Roman building masters, the fit-for-purpose use of material was more important than the ideal and repetitive dimensions of the building blocks [4,5].

Wright states that the precision of the Roman craftsmen in joining face stones lacked the ability to combine them with almost no joint spacings as in the Classical Greek workmanship. He argues that the Greeks used tools for ‘forging’ where Romans for ‘cutting’, and that the Romans preferred soft, less crystallized stones due to the difference in the methods of stonework [6]. The fact that Temple P, a Roman Temple, had six different types of stones in

various sizes, distributed in accordance with the location and construction technique, confirms these claims:

Table 1: Types of stones used in Temple P

Conglomerate	Foundations
Travertine	In the carrier core of the *cella* wall
Sandstone	*Orthostat* coatings
Marble	At two-storey monumental entrance structure and *cella* gate, at the inner coating of *cella* in thin plates
Face stone	On the vault cover of the lower floor
Rubble	In the filling of the lower structure of the monumental entrance structure

There is a distinctive hierarchical structure among the building materials used in the temple, according to their functioning as bearing unit or surface layer. Also, different applications regarding the mortar use are seen, depending on the location, such as whether there is a mixture of bricks (rough and fine construction works) or not.

2.1. Conglomerate

Conglomerate (*conglomerāre*, Lat. = gathered into a ball or rounded mass), local 'natural concrete' or so-called 'sea coastal stone', which has a very high bearing capacity and durability, occurs spontaneously in the nature and formed by hardening of sea stones, pebbles, sand, and remains of sea creatures altogether by means of the dissolution of lime in sea shells. If the pebbles in the conglomerate are not rounded but angular, they are called '*breccia*'. Their color varies according to the color distribution of pebbles [7,8].

Lamprecht suggests it can be asserted that the master builders were inspired by the conglomerate in nature, in other words 'natural concrete' in development of *opus caementicium*, also called as Roman concrete [3]. Regarding its technical properties, conglomerate is generally a difficult-to-cut building material; it is difficult to obtain smooth-edged blocks because the hard gravels within it are broken in heaps during the production and processing of the blocks. Therefore, the location of their use is generally determined by the size of the gravel grains. The smaller the grain size, the better it is suitable for fine profiling. In Side, fine-grained conglomerate blocks as used in the jambs and lintels of some gates on the walls were profiled with fascia. The conglomerate used in Temple P has a coarse-grained structure (**Figure 3-4**).



Figure 3: Example of conglomerate block used in foundations



Figure 4: *Cella* wall foundation

2.1.1 Use of conglomerate in the structure: foundations

It can be observed that the master builders had more confidence in conglomerates, which was frequently used in the antique buildings of Side, compared to the travertine in static terms. They preferred conglomerate for the point foundations set for the frontal columns of the monumental entrance structure, the continuous, uninterrupted foundation of the second row of columns, and in the lowest sequence of the *cella* wall, i.e. where the structure should be 'stronger' in static terms (**Figure 4**).

The conglomerate blocks, which form the lower row of the travertine bearing core of the *cella* wall, were aligned side by side on the massive wall of the lower floor. They contained clamp slots indicating that they were connected to the sandstone blocks at the same level and in front of them. However, they do not have a clamp connection between each other or dowel slots for fixing the next row of stones onto them. This indicates the fact that the master builders were more concerned with the pull and push force than the compressive force. There are no dowel holes on the upper surfaces of the conglomerate blocks forming the basis of the columns. The singular column foundations or 'continuous conglomerate blocks' of the monumental entrance structure also function as a binder and reinforcer in static terms, preventing the sliding of small sized rubble and fill material forming the substructure.

2.2 Travertine

Travertine is a type of large perforated limestone formed by continuous addition of lime to the fossilized residues of seashells. The formation of these stones can be clearly understood from the fossilized residues of living beings or the traces they left on the stone. Travertines, which are available in quite different qualities, are generally very robust and weather resistant. It takes a long time for travertines to reach ideal properties such as having different color layers used by sculptors, being able to be polished well and weather resistant [7].



Figure 5: Travertine blocks used in the bearing core of *cella*

2.2.1 Use of travertine in the structure: the inner core of the *cella* wall

The travertine used in Temple P is of lime tuff, which had not yet completed its crystallization process. These hard-to-break, porous (thanks to the traces of the fossils), and hard travertines with fossil traces are not suitable to be used as surface layers because of several pores and are not suitable for producing blocks of standard dimensions. The cella wall of the temple was built by a three-walled construction technique. Here, the carrier core is formed by travertine blocks behind the façade coverings and on invisible surfaces (**Figure 5**). Sandstone

was used as a coating material on the outside of travertine. A 2,2 cm thick marble cladding material was used *inside the wall*, facing the *cella* space.

On the upper floor, travertine blocks were brought together side by side in longer format in the *in-situ* wall part of the linear western facade of the *cella* and in shorter format in the rounding part of the cella wall (**Figure 2-3**). This wall technique, where the 6-8 cm gap left between the inner and outer claddings is filled with mortar, did not require that the travertine blocks were very precise in size or the blocks were cut circularly. Long clamps up to 30 cm were used to cover the mortar-filled distance between travertine blocks and cladding blocks. In the northern corner of the *cella*, there is an in situ 96 cm high and 20 cm thick *orthostat*-style sandstone outer crust and 55 cm thick travertine array (**Fig. 2**). The dowel slots on the inward side of the travertine blocks and the remains of 2,2 cm thick marble slabs over the surface levelled by 5-6 cm mortar indicate that the cella was covered with marble.

2.3. Sandstone

As mentioned, the conglomerate and travertine blocks were used only in foundations and in the bearing core, on the grounds that they failed to meet the expectations as surface layer. Homogeneous, smoothly cut and processed gray, local sandstones with fine pores were used on the sides of the temple that were visible from outside. Static integrity was achieved with dowels and clamps, where sandstone met conglomerate and travertine. Mortar was used as additional support.

Sandstone is a type of sedimentary rock formed by fusing sand grains smaller than 2 mm. It has a friable structure; and it is not possible to obtain a glossy surface. It is easy to cut and process and hardens by drying in the air. The sandstone, which may have very different technical properties, is available in many colors including red, yellow, brown, greenish, and whitish [9].

The local sandstone must have been easy to acquire because of its friable characteristics; therefore, it can be considered an economic option. Such characteristics as easy formability and a homogeneous structure must have been effective in the decision to use it as cladding material at the podium and Temple P, with a circular-formed *cella*. Surface damages on this type of stone occur in the form of crumbling, wearing, and scouring. Due to the bedding property fractures generally occur in thin layers. Due to this feature, the top and bottom profiles of *orthostats*, the block of the *cella* wall after the base, and the round architrave-frieze block of *cella* were not embellished.



Figure 6: Sandstone *orthostat* blocks used for podium coating

2.3.1 Use of sandstone in the structure: *orthostat* coatings

The 2,50 m thick outer wall of the lower floor of the temple was cladded with *orthostat* blocks of various lengths made of approximately 20-30 cm thick sandstone (**Figure 6**).

Aschenheim suggests that the vertical stones (*orthostats*) placed in front of the masonry made of rubble stones were taken from Greek Architecture of the Archaic Period and that the 'tripartite base' was introduced by incorporating the foot and 'head' profiles [10]. Hueber asserts that the first use of *orthostats* was based on building physics, and that moisture, as drawn from the soil with homogeneous and upright blocks, was prevented from damaging the building. Furthermore, this principle of construction was transformed into a design and style tool over time [11].

The first connection between the 146 cm high *orthostats* of the podium and the massive circular wall was made by placing the profile blocks, which were deeper than the *orthostats* on top, onto this thick wall. After the *orthostat* was placed in its location, the 5-6 cm gap with the wall was filled in with mortar and clamped to the rearward block. Thus, in terms of structural physics, any moisture that might have occurred would be directed upwards through the filling mortar between the *orthostat* and the massive wall. This would possibly prevent the mortar from disintegration by drying out, before trying to drain out of the dense stone texture of the vertical blocks.

Orthostat blocks of various lengths and thicknesses indicate that the stones were not ordered in standard sizes but delivered in such sizes that satisfied the 'preliminary data', perhaps in the terms of lower and upper limits. The ordered stones must have been pre-treated after they were brought to the construction site, either at the crane's area of operation or in a stone workshop within easy reach. While this is done, the stones must have been worked after the visible surfaces of the blocks were placed in their location with their back surfaces roughly machined -perhaps left as they came from the quarry- and the bottom and side faces were the smoothest. It's even advantageous if the back surface was not very smooth, considering that the gap left with the existing wall would be filled in with mortar. This is because five stages can be determined until the end of the profile.

The upper surface workmanship of the foot profiles, which are 14–15 cm deep, approximately 31 cm high and of different lengths, such as the *orthostat* blocks of the podium, indicate that these blocks were roughly machined with stonemason's chisel and placed as cut at a certain angle in the direction of the profile. This type of assembly, which can only be done from the front, requires a clearance on the rear surfaces to ensure precise placement of the blocks. In a section showing the untreated stage of the profile, it is found that three dovetail-shaped 'docking slots' were drilled into the upper surface of the stone in order the *orthostat* block above could be aligned and pushed towards the neighboring stone or backwards. Thus, the *orthostat* block was placed in its position as much as it was possible, it must have been pushed to its the ideal position with the help of a lever. This lever detail in the foot profile must have been made after the *orthostat* block array was placed. From the differences in surface workmanship of the foot profile array of *orthostats*, it can be observed that the profile was brought to the desired final state in five stages. As for the section, the profile was not yet processed, the workmanship was completed, and that there were irregularities in the workmanship that continued beyond the joints: This proves that the surface layer was treated after assembly. On the front side, the marks of the stonemason's chisel are visible under the

marks left by the stonemason's dredge. This detail shows that the final process was delayed after the completion of the construction.

2.4. Marble

All material used in the construction of Temple P is the local material, except for the marble preferred in the monumental entrance structure in front of the *cella*. Ward-Perkins states that only the 'marble style' was preferred in the monumental buildings of the Roman Empire in Pamphylia in the middle of the 2nd Century [12].

İnan suggests that the absence of a marble quarry near Side shows that the marble requirement for sculpture was met from outside [13]. However, the remains of many buildings in the city, and many of the statues and sculpture fragments that have been recovered show that marble was used in abundance. It also indicates that the overseas ordering and delivery of the material was successfully implemented. The marble brought from outside must have been processed in the city workshops.

Nolle acknowledges that the people of Side have rich donors from the wealthy strata, who were willing to pay the high price of overseas transport in order to give their cities a marble appearance by covering the local building materials with marble. He considered the same as a sign that it was very popular as a way to make oneself immortal by being memorialized on the buildings. As a matter of fact, the marble used in the monumental entrance structure in temple P in front of the *cella* and oriented towards the square must have been be acquired from overseas.

Scientifically, marble is a crystallized rock stone, the grains of which can be individually discerned by naked eye [7]. They can be of various colors depending on the additive source; they are statically resistant and have good weather resistance. A gray-white veined marble was used in Temple P; the fractures are along the veins and in layers.

An important difference of marble compared to other materials used in the construction is the construction technique. The richly decorated marble blocks of the monumental entrance structure were worked out almost entirely on the ground before assembly. The one-piece cassette and cornice blocks suggest that they might have been produced at accurate and precise sizes by taking measurements in place after the assembly of the columns and architraves. Like the ceiling cassettes of the stage building of Side ancient theater and the cassettes surrounding the *cella* of Tyche Temple, the cassettes of the entrance structure of Temple P were carved from a single block with all its profiles and frames.



Figure 7: Cassette-Cornish block



Figure 8: Marble threshold block of *cella* door

2.4.1 Use of marble in the structure: Monumental entrance structure (*revinctum* construction technique)

There are many architectural blocks made of gray-white veined marble such as column body fragments, column bases, column caps, elaborately worked richly decorated cassette-cornices (**Figure 7**), architrave-frieze blocks with double-sided appearance, and *tympanons* on the platform in front of the *cella*. It is also understood from the *in-situ* threshold block (**Figure 8**) and the gate lintel that fell just in front of it that the door on the western wall of the *cella* was made of marble.

The technical connections between the blocks are limited to dowels; clamps were not considered necessary in the construction of the ceiling. There are remains proving that a lead channel was used in addition to iron dowels for the installation of columns and bases. *Anathyrosis* was not applied to the seating surfaces of cassette and toothed cornice blocks and the whole surface was smoothed to distribute the load over a larger area. It is seen in the single column cap available that the surface on which the architrave will sit was made higher by pulling back from the profiles. This, therefore, secured the profiles against compressive strength and fractures.

There are slots for two small lower dowels each on the two lower ends of the cassettes, where the clamps are not used and the frieze seats. With smooth machining of the side faces, the blocks were able to approach each other with zero clearance. Very few blocks have lifting holes. Use of deeper reliefs on visible surfaces and less deep reliefs on less visible surfaces in embellishments should be interpreted as an economic working method.

Hoepfner suggests that the oldest example known to have influenced the design of marble ceilings is Hieron in Samothrake dating to the 2nd Century. There cassettes of various sizes were brought together. He asserts that while it was previously preferred that cassettes should be as uniform as possible, combining areas of different sizes was preferred as from the Late Hellenism. According to Hoepfner, this solution shows that the high beams surrounding the cassettes were considered disturbing, because they covered the painted or relief-decorated main surfaces of the cassettes [15].

The large cassette type at both ends of Temple P occupies a large area. In the parts close to the *cella*, many smaller cassettes were brought together, extending the cassette area, and therefore the field of view, to prevent the likelihood of a beam hindering the appearance.

2.5 Face stone

Opus caementicium technique was used in the vaulting of the rooms on the lower floor of Temple P. Gruben states that the vault construction, the most important invention of the Roman Period, was not prominent in the temple buildings, because it was preferred to adhere to the Classical Greek temple construction as proposed by Vitruvius [16]. This technique, which did not require a great deal of manual dexterity, could have been done by local builders well as by unskilled workers. To that end, use of rubble stone, mortar, and mold night have been enough. In Temple P, the vault cover was used only on the ceiling of the lower floor. The fact that not only rubble stones but also stones with smoothly cut side and bottom surfaces were used indicates that the stonemasons worked in the construction of the vault.

2.5.1 Use of face stone in the structure: vault cover of the lower floor (mortar and formwork system)

The cradle vault cover in the middle of the lower floor starts at the same height on the two side walls and transfers the static load to those walls equally. On the underside of the barrel vault, from the semi-round shaped print marks left by the molds to the mortar, approx. It is still clear that logs with a diameter of 16 cm (round trunk of cut trees) have been used.

The apex of the half vaults in the triangular planned side rooms are positioned approximately 50 cm away from the wall separating the middle space in the southern room and approximately 70 cm in the northern room. They sit on this wall by reducing the height of the vault by only 6-7 cm. They sit on the thick outer wall with a fairly steep incline in the other direction. Thus, the loads of the vaults of the side rooms were transferred to the 2.50 m thick outer wall. The vaulted cover of the triangular planned side rooms was mounted on a circular thick wall at an increasing height and irregular geometry towards the top of the triangle in the plan.

The fact that the vault was placed on the thick wall in such an irregular geometry suggests a repair that was conducted subsequently on the wall rather than a designed construction. During the Roman period, if the area, where a building was located, was to be reused, the building was not demolished and destroyed. Alternatively, the old building was covered with filling and incorporated into the foundations of the new construction. In Rome, for example, some of the walls of Nero's Golden House, built in 64-68 AD, were used as the basis for the Trajan Baths built in 109 AD [17].

The wood formwork system was also used in the construction of the vaults of the side rooms. The round form of wood that made up the formwork is understood from the traces on the mortar over the vault left by the wood added end to end in short pieces in order to rotate. The clear visibility of the mold marks also suggests that the lower surfaces of the vaults were not plastered after the mold was removed. The front of these three rooms, which had the appearance of a closed cave when they were built, must have been kept open during construction. This section, which also forms the boundary of the platform in front of the podium to the temple, was closed by a wall about 70 cm thick, which was considerably less than the 2,5 m thick wall of the lower floor after dismantling and removing the mold used to build the vaults.



Figure 9: Vault cover of the lower floor



Figure 10: Infrastructure of one of the side stairs

2.6 Rubble (untreated) stone and its place of use: Infrastructure of the monumental entrance and stairs

In addition to the conglomerate foundations, a mortar mixture without rubble stone and bats were used as the filling material for raising the infrastructure of the platform in front of the *cella* up to the podium level and for the infrastructure of the stairs. It is known that mortar was especially important for the Roman construction technique [18]. In Temple P, rubble stone, bats, and a mortar mixture without bats were used for the bases of the vault covers of the lower floor that were placed on the thick outer wall. They were also used for the filling of the platform, where the monumental entrance structure was located, in front of the *cella* (**Figure 10**). In general, two types of mortars were used: one without bat addition as seen in the masonry and fillings, and another one with bat addition, where there was contact with marble. As in today's buildings, rough and fine work was differentiated in construction.

3 CONSTRUCTION TECHNIQUE AND STONEWORK

In ancient times, while architectural ideas and aesthetic creativity were tested by means of application, special requests encouraged the development of the technique and generation of new building ideas.

Opus caementicium, one of the most important “inventions" in architectural history, which Ward-Perkins described as “a turning point in the history of architecture” [19] and Deichmann as “revolution of building technique” [20] had long been known when P Temple was built. Although the foundations of the podium of the Concordia-Temple (121 B.C.) has been considered the oldest surviving example that used this technique [21], a wall-building technique, where the gaps between the bedrock and the cladding blocks were filled in with mortar was found at Belevi Mausoleum, a Hellenistic period structure dating back to 280 B.C. in Anatolia [22]. Thanks to *“opus caementicium”*, the Romans were able to build more ambitious, more durable monuments with increasingly larger domes and vaults along with bridges and aqueducts. As a matter of fact, in 118-125 AD, this technique reached to a peak with Pantheon, which has a dome of 43 meters in diameter. Especially, the fact that the density of the components of the mortar used in the Pantheon gradually decreases from the bottom to the top [23], suggests that they were very competent about statics and the said construction technique.

In his second book on building materials and construction techniques, Vitruvius compared the wall technique of the Roman and Greek structures: He criticized the way Romans used vertically positioned stones and filled in the gap with a mixture of mortar and broken stones with an aim to form the outer shell and the three-layered method with two outer shells and the filling wall between them. He stated that the Greeks made the whole wall massive, which consisted of an inner and outer shell made of carefully engineered stone blocks without using mortar and the core between them again made of smoothed stone blocks. He praised the Greek method of *emplecton* stating that the outer and inner shells were held together by clamping, stone blocks, or metals covering the entire width [24]. With its wall technique, Temple P is different from the two definitions by Vitruvius', and even that it is a combination of the two. The *opella revinctum* was used along with mortar in the construction technique of the *cella* wall of Temple P. Despite its coarse texture, the inner travertine block was prepared by cutting all the surfaces to have it function as filling in the wall. The mortar used in the space between the

bearing core and the coatings does not have a bearing function. The load bearing function is predominantly assumed by the travertine core in this wall technique. Although Lamprecht asserts that generally the core wall was responsible for load bearing in concrete structures of the Roman period, he meant the core made by *opus caementicium* [3]. In Temple P, the travertine core layer assumes that function.

4 CONCLUSIONS

- The selection and distribution of materials suitable for the purpose of Temple P is only possible with great building experience and material knowledge. Because it requires an insight into not only the bearing capacity of the material, but also the likely movement and pressure forces that may occur in the structure.
- Master builders preferred to use as little material as possible in each period. This approach had a positive effect as a working method on the acceleration of the construction process and the construction economy. We can define this as rationalization: Nowadays, the concept of rationalization means the use of modern production methods, in which better results can be achieved with the same effort or the same results with less effort. It can be said that this approach also applies to Side building masters from during Antiquity. Use of *opus caementicium* and *opus revinctum*, where it's deemed necessary, is an example of the foregoing. It must have provided a rapid construction process beyond being an economic option.
- Nowadays, while there are standardized ready-made ceiling elements produced in high numbers taking into consideration a certain tolerance in dimension, a 'same style' production mode was preferred in 'Temple P', which allowed conducting adaptation processes during assembly. As it is today, the construction elements were pre-finished elsewhere as much as possible, in order to ensure easy and quick production during construction. However, no cassette element at Temple P is exactly the same as another but used as mirrored due to symmetry at most. Nevertheless, even in this state, it is a candidate of being a pioneer of prefabricated production.

Acknowledgements. The activities at Temple P are carried out under Side Excavations. Geodetic measurements; conducted in 2015 thanks to the financial support of Suna-İnan Kıraç AKMED Research Institute. The studies were supported by TUBITAK at Beykent University within the scope of 2232 BIDEB scholarship program between 2016-2018.

REFERENCES

[1] K. G. Lanckoroński, *Städte Pamphyliens und Pisidiens I* (1890)
[2] A. M. Mansel, E. Bosch ve J. İnan, 1947 Senesi Side Kazılarına Dair Önrapor - *Vorläufiger Bericht über die Ausgrabungen in Side im Jahre 1947*, TTK (1951).
[3] H.-O. Lamprecht, *Opus Caementitium*. Bautechnik der Römer (1996). Römisch-Germanisches Museum Köln, Beton-Verlag.
[4] E. R. Fiechter, Der Ionischer Tempel am Ponte Rotto in Rom. *S. Maria Egiziaca.*

Mitteilungen des kaiserlich deutschen archäologischen Instituts. Band 21. 1906, 220-279.
[5] H. von Hesberg, *Römische Baukunst* (2005).
[6] G.R.H. Wright, *Ancient Building Technology*, Vol.1, Historical Background, (2000). Leiden-Boston-Köln: Brill.
[7] A. Kieslinger, *Gesteinskunde für Hochbau und Plastik. Fachkunde, für Steinmetz, Bildhauer, Architekten und Baumeister* (1951). Wien: österreichischer Gewerbeverlag.
[8] E. M. Winkler, *Stone in Architecture. Properties, Durability*[3] (1994). Berlin Heidelberg: Springer-Verlag.
[9] M.–H. Wanetschek, *Naturstein und Architektur. Materialkunde und Anwendung Steintechnik* (1992). München: Callwey: 16.
[10] C. Aschenheim, *Der Sockel: seine Form und Entwicklung in der griechischen und hellenistisch-römischen Architektur und Dekoration von den ältesten Zeiten bis zur Verschüttung Pompejis.* von M. Vetter (1910). VIII Bl. (Zur Kunstgeschichte des Auslandes; 75), Straßburg: Heitz
[11] F. Hueber, *Ephesos gebaute Geschichte*. Sonderheft AW (1997)
[12] J. B. Ward-Perkins, *Roman Imperial Architecture*[7] (1990). London: Penguin.
[13] J. İnan, *Roman Sculpture in Side*, TTK 5, 30a, Antalya bölgesinde araştırmalar 8. Researches in the Region of Antalya 8 (1975).
[14] J. Nollé, *Side im Altertum. Geschichte und Zeugnisse I, Inschriften griechischer Städte aus Kleinasien* 43 (Bonn 1993).
[15] W. Hoepfner, Zum Problem griechischer Holz- und Kassettendecken, in: *Bautechnik der Antike*, internationale Kolloquium in Berlin vom 15.-17. Februar 1990 veranstaltet vom Architekturreferat der DAI in Zusammenarbeit mit dem Seminar für klassische Archäologie der Freien Universität Berlin. Herausgegeben von Adolf Hoffmann, Ernst-Ludwig Shwandner, Wolfram Hoepfner und Grunnar Brands, Verlag Philipp von Zabern, Mainz am Rhein, (1991), 90-98.
[16] G. Gruben, Die Rolle der Architekten in der Geschichte, (50-58) in: *Aus der Geschichte der Bautechnik*, Fritz Scheidegger (ed.), Band 1: Grundlagen, (1990). Basel, Boston, Berlin: Birkhäuser Verlag.
[17] R. Mark (ed.), *Vom Fundament zum Deckengewölbe: Großbauten und ihre Konstruktion von der Antike bis zur Renaissance*, Basel [u.a.]: Birkhäuser 1995
[18] B. Cech, *Technik in der Antike*[2] (2011), Darmstadt: Theiss Verlag.
[19] J. B. Ward-Perkins, *Architektur der Römer* (1975). Stuttgart: Belser
[20] F. W. Deichmann, *Westliche Bautechnik im römischen und rhomäischen Osten*, Mitteilungen des Deutschen Archäologischen Instituts, Römische Abteilung, Bd. 86, 1979, S. 473 f. Mainz.
[21] G. Haegermann, Vom Caementum zum Zement, in: *Vom Caementum zum Spannbeton*, Bd. 1, (1964). Wiesbaden: Bauverlag. 3-72
[22] G. Kaymak, Kültürel mirasın yapı malzemeleri tarihine katkı boyutu: Belevi Mausoleumu Örneği, in: TMMOB yayınları, *5. Ulusal Yapı Malzemeleri ve Sergisi Kongresi,* Istanbul, 03-05 Kasım 2010, 205-218.
[23] H.-O. Lamprecht, *Verwendung von Beton bei Wasserbauten in der Antike*, Mitt.bl. BAW Nr. 65, Bundesverband der deutschen Zementindustrie, Köln 1989
[24] P. M. Vitruvius, *Mimarlık Üzerine On Kitap* (çev. S. Güven), İstanbul, 1990.

12th International Conference on Structural Analysis of Historical Constructions
SAHC 2020
P. Roca, L. Pelà and C. Molins (Eds.)

FIRST REINFORCED CONCRETE BUILDING IN RIJEKA PORT – FERENC PFAFF'S WAREHOUSE NO. 17

PAULO ŠĆULAC*, DAVOR GRANDIĆ AND NANA PALINIĆ

University of Rijeka, Faculty of Civil Engineering
Radmile Matejčić 3, 51000 Rijeka, Croatia, www.gradri.uniri.hr
e-mail: paulo.sculac@uniri.hr, davor.grandic@uniri.hr, nana.palinic@uniri.hr (*corresponding author)

Keywords: industrial heritage, reinforced concrete, frame structure, construction history, reinforcement detailing

Abstract. *This paper will explore an early reinforced concrete warehouse, constructed from 1906 till 1909, which is the most impressive warehouse in Rijeka Port – with ground floor dimensions equal to 45x100 m, consisting of a basement, high ground floor and three storeys, designed to sustain 15 kN/m^2 floor loading. This warehouse is the first building in Rijeka Port constructed entirely as a reinforced concrete structure and demonstrates significant technical achievements, which have not been sufficiently valorised so far. Besides obtaining information about the structural design of early reinforced concrete structures special attention will be given to better understanding of early 20th century construction techniques and particularly to reinforcement detailing, since original plans and construction drawings with detailed information about the reinforcement have been preserved.*

1 INTRODUCTION

As the main port of the Kingdom of Hungary the city of Rijeka experienced significant growth at the end of the 19th and in the beginning of the 20th century, when becomes the largest construction site in the Monarchy. The largest construction works took place in the port where grand extension of the coast was made, with coastline shifts up to even 200 m. The port was built mostly from 1872 till 1894 [1], and can be described as a typical Mediterranean port with wide piers in the shape of a comb, protected by a 1707 m long breakwater (Fig. 1).

By 1940 there were around 40 warehouses built in the port and in the neighbouring railway zone. These warehouses were first built as temporary timber structures but were soon replaced using more permanent materials such as brick, steel and reinforced concrete. Due to damages caused by bombing in WWII and followed by modernization of the Port, there are only nine warehouses preserved from this period [2].

This paper will explore one of this preserved warehouses - the reinforced concrete Warehouse no. 17 (former XIV) located on 120 m long and 80 m wide Visin Pier (former Marie Valerie Pier), which is the largest warehouse in Rijeka Port. Although reinforced concrete has already been used in the port from 1893, as part of the Monier's floors in several warehouses – two of which still exist [3], this is the first building in Rijeka Port constructed entirely as a reinforced concrete structure. This warehouse is protected as a heritage monument inscribed in the Croatian registry of cultural objects. It is still part of the port, but nowadays, due to changes in the way the goods are transported it is no longer in use.

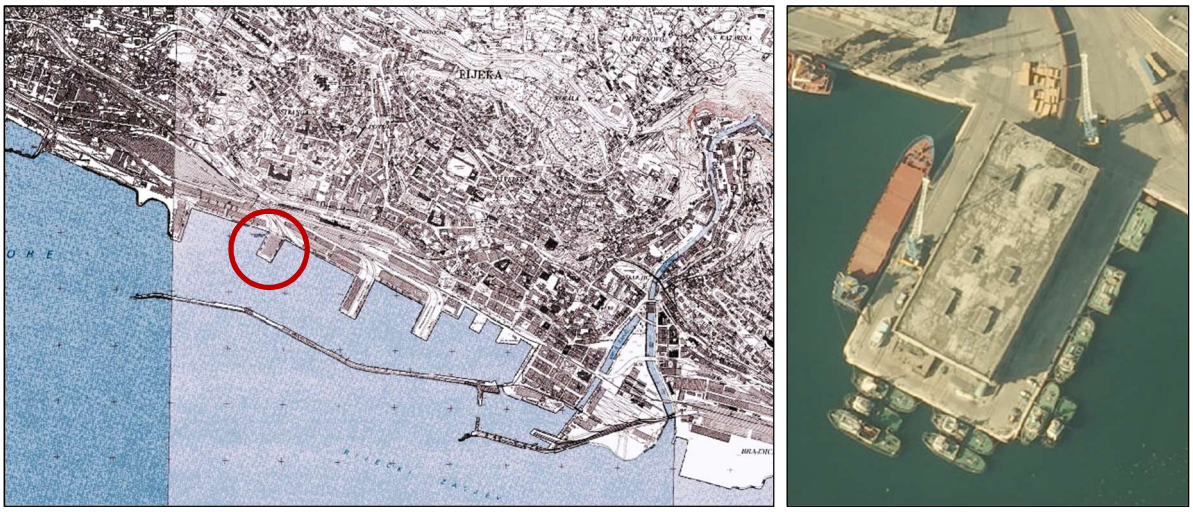


Figure 1: The Port of Rijeka with enlarged view of Warehouse no. 17 located on Visin Pier [4]

It should be emphasized that at the same time another monumental building (160 m long, 24 m wide and 17,5 m high) made completely of reinforced concrete was being constructed in Rijeka: the Emigrant Hotel, as the only purpose-built hotel to be used by emigrants travelling to America. It was designed by Szilárd Zielinski, professor of Polytechnics at the University of Budapest, as a frame structure according to Hennebique patent. These two buildings with the earliest use of reinforced concrete place Rijeka side by side with other European cities in terms of introducing new materials and construction techniques.

In this work emphasis will be given to: (I) obtaining information about the design of early reinforced concrete structures; (II) better understanding of early 20th century construction techniques and local peculiarities (reinforced concrete structures were constructed according to systems based on the original patents but were frequently adopted to the individual building as well as to the work of local builders); (III) since original plans and construction drawings are preserved with detailed information about the reinforcement provided (size and spacing of reinforcement as well as joint detailing) the next goal will be to analyse the detailing of reinforcement with an indication of the differences with respect to today's practice.

We will present results based on the research of archival materials [5], what would be the first step in condition assessment of this historic building. Warehouse no. 17 is no longer in use and there are currently no plans for future usage; on the other hand it demonstrates significant technical achievements, which have not been sufficiently valorised so far, therefore our intention is to point out the importance of this 20th century heritage building.

2 ABOUT THE STRUCTURE

Warehouse no. 17 has been designed by Hungarian architect Ferenc Pfaff, at that time in charge of the Building Construction Division of the Hungarian Royal State Railways. It is a symmetric structure 100 m long and 45 m wide, consisting of a basement (with slightly larger dimensions – 100 x 49 m), high ground floor and three storeys (Fig. 2). The basement and the ground floor are divided in the longitudinal direction into two parts, separated by two tracks for railway wagons passing throughout the middle of the ground floor. All the floors above ground

floor are divided by transversal walls into five smaller sections 20 m long, each provided with two elevator shafts (Fig. 3). Besides transportation of goods within the building, goods could also be transported from the outside by portal cranes since 1,6 m long cantilevered balconies are located on each floor along the building. A 1,7 m solid concrete slab is used as the foundation of the building (Fig. 4). Such a thick foundation base has been used due to very soft deposit under the pier. The lower edge of the foundation base is 0,3 m below the sea level. Additionally, under the columns 0,3 m deep square 1,3x1,3 m pad foundations are formed.



Figure 2: Front view of Warehouse no. 17 [6]

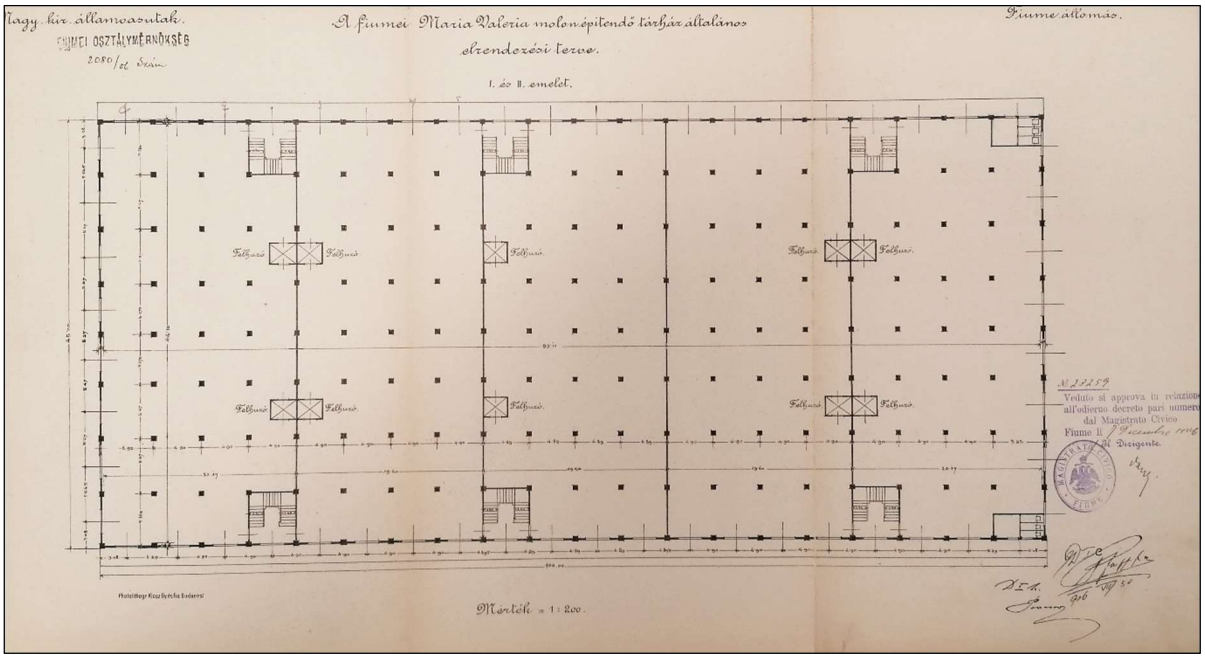


Figure 3: 1st and 2nd floor plan [5]

This warehouse is designed as a, for that time common, space frame structure. When selecting cross-sectional dimensions special attention was paid to being economical. Therefore, columns have a square cross-section variable over the building height: from 77 cm in the basement up to only 32 cm on the top floor. Peripheral columns have a rectangular cross-section. There is a total of 189 columns per floor: 9 columns in the transversal direction, spaced at 5,6 m, and 21 columns in the longitudinal direction spaced at 4,9 m (Fig. 3). Besides primary beams, intermediate beams have been added in both directions. In this way the slab span was effectively reduced from the basic grid of 5,6x4,9 m into just 2,8x2,45 m (Fig. 5).

The cross-sectional dimensions are summarized in Table 1. Near the supports (at a distance about 40 cm from the column/beam face) beams have slightly bigger dimensions: 8 cm increased width and 4 cm increased depth. All structural elements are in quite good condition: there is no spalling of concrete or visible rust from the reinforcement (Fig. 5).

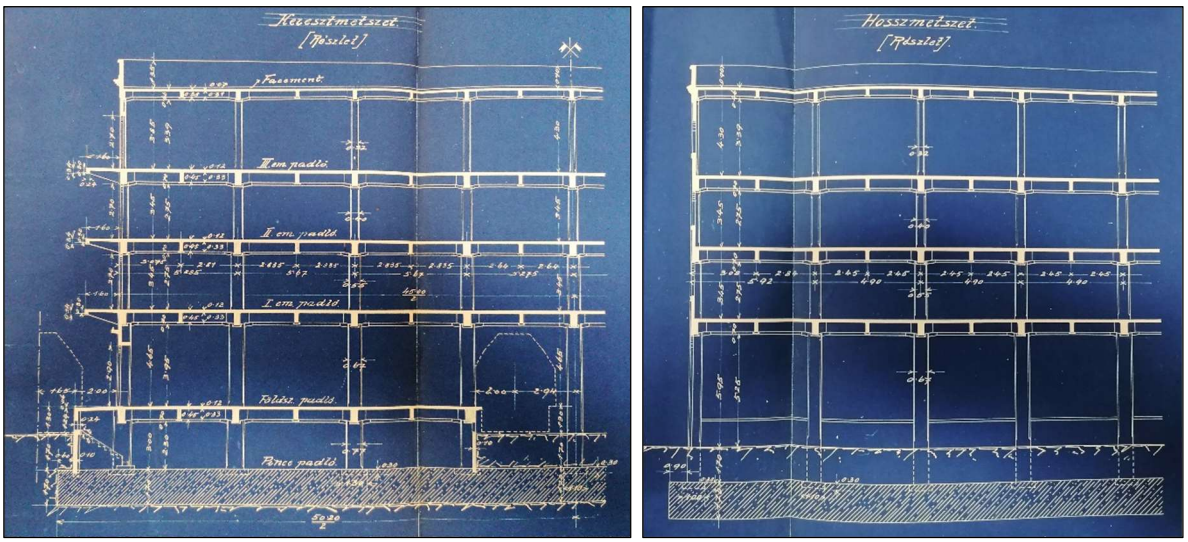


Figure 4: Transversal (left) and longitudinal cross sections (right) [5]



Figure 5: Layout of the basic column grid (5,6x4,9 m), primary and secondary beams on the 3rd floor [5]

Table 1: Cross-sectional dimensions in cm

	storey height	columns	primary beams (bxh)	secondary beams (bxh)	slab thickness
basement	2,30 m	77x77			
ground floor	3,95 m	67x67			
1st floor	2,75 m	55x55	midspan: 32x70 support: 40x75	midspan: 24x45 support: 32x49	12
2nd floor	2,75 m	40x40			
3rd floor	3,39 -3,84 m	32x32			
roof			midspan: 24x46 support: 32x50	midspan: 16x38 support: 24x42	7

3 CONSTRUCTION

Warehouse no. 17 has been constructed from December 1906 till January 1909. The building contractor was *Grünwald Testvérek* (Brothers Grünwald) from Budapest. Fig. 6 presents two photographs taken during the construction, where one may notice that first the columns, beams and slabs have been built, while the 10 cm thick façade walls have been added afterwards.

Since the construction site was rather large, there were a lot of participants involved. To be specific occasionally even more than 300 workers were present, although their number varied on a daily basis, mostly due to wageworkers. For example on 29th August 1907 (Fig. 7) there were 2 construction foremen, 3 stockmen, 5 mechanics, 57 carpenters, 18 blacksmiths, 42 concreters, 4 stonemasons, 10 women, 167 wageworkers and 6 carriers present at the construction site [5]. Also, on the same day three concrete test specimens (43-45) were cast (no record of obtained concrete strengths was so far detected).

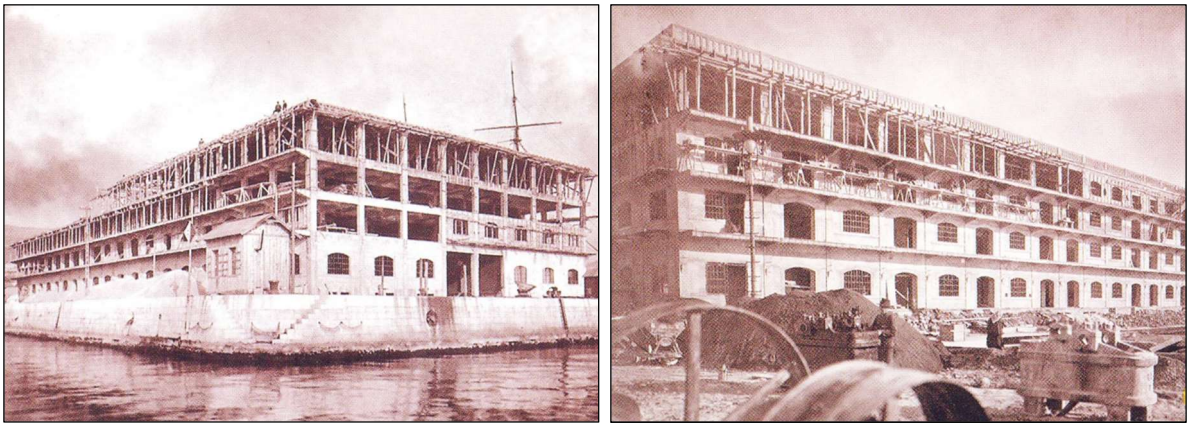


Figure 6: Warehouse no. 17 during construction [1]

4 STRUCTURAL DESIGN

Structural design and reinforcement plans were made by Kálmán Balogh, a chartered engineer from Budapest. All the floors are designed to withstand imposed storage load of 15 kN/m^2, except the (not accessible) roof which is designed for 3 kN/m^2. Exterior walls are calculated for wind load of 2 kN/m^2.

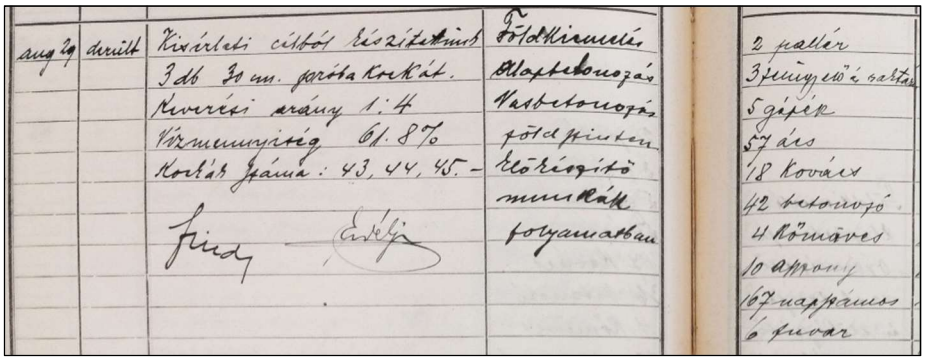


Figure 7: An extract from the Construction log book for 29th August 1907 [5]

At the end of the 19th century reinforced concrete has taken such a development that almost every day a new patented system appeared [7,8,9,10]. The theory of reinforced concrete was yet not completely understood (no generally recognized theory existed for the design [11]) and each system had different reinforcement details. At the beginning of the 20th century first standards and regulations appeared: about 1907 in England, France and Germany [10].

According to the linear theory, the stress distribution in the cross section is linear [7,9,12]. Concrete carries no tension, therefore bars are installed in the tensile region (Fig. 8). The rebars should not be subjected to loads exceeding 100 MPa. After hardening for 28 days under normal climatic conditions in 30 cm cubes concrete has to develop a compression strength of 20 MPa. The permissible stress in concrete in bending is limited to 3,5 MPa. The ratio of modulus of elasticity of steel and concrete is adopted as equal to 15 [5].

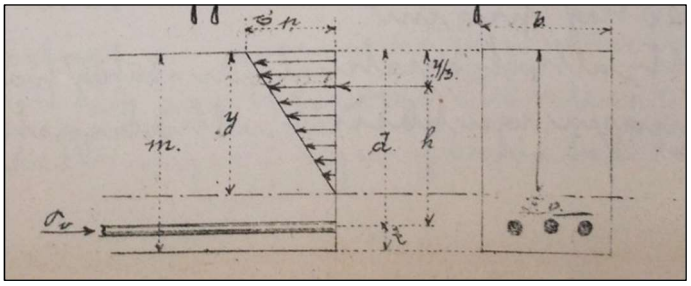


Figure 8: Distribution of stresses in reinforced concrete in case of simple bending [5]

Floor slabs are designed as two way spanning plates (Fig. 9). Continuous primary and secondary beams are designed as T-sections only for bending moments, not for shear (Fig. 10).

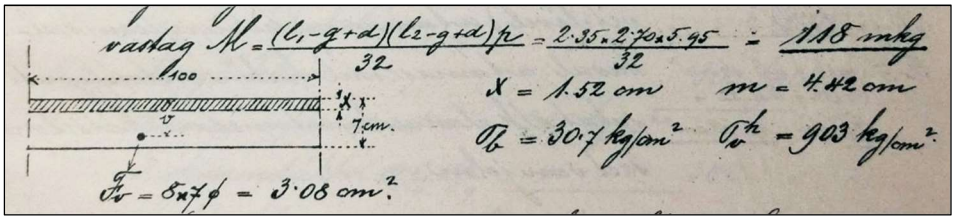


Figure 9: Structural design of the roof slab [5] (Note: old units are used in the figure 1000 kg/cm^2 = 100 MPa).

It was a common practice until 1908 when Mörsch published his book *Concrete-steel construction* [11] where he introduced the truss model for shear design based on experiments on T-shaped beams. The width of the slab acting with beam was taken as 1/3 of the span. Columns are designed only as compression members (Fig. 11).

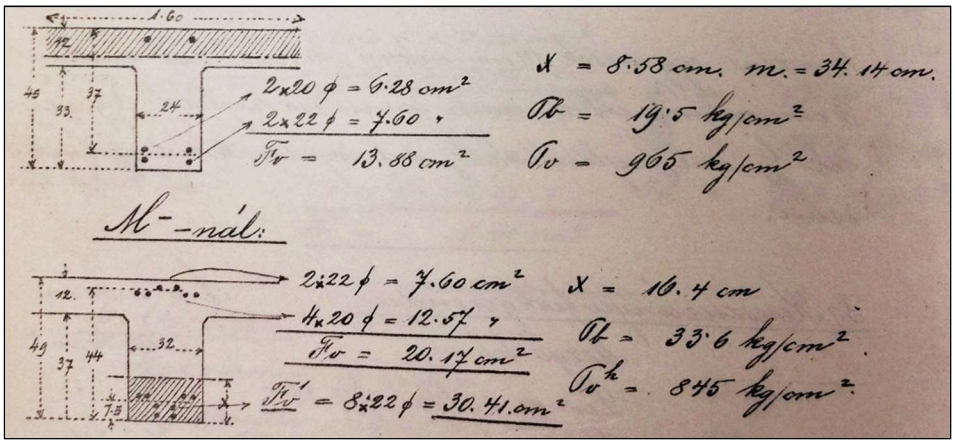


Figure 10: Structural design one of the secondary beam with 4,9 m span [5]

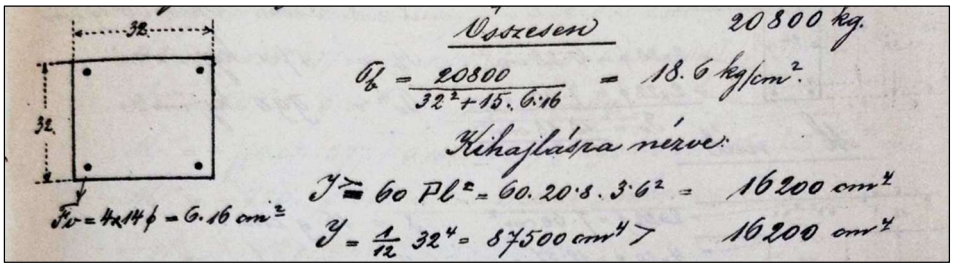


Figure 11: Structural design of the columns at the 3rd floor [5]

5 REINFORCEMENT DETAILING

Some basic features of the reinforcement detailing, with emphasis on the size, arrangement and shape of reinforcement, will be presented from the original construction drawings [5]. All the reinforcement plans were made by Kálmán Balogh, who used E. Coignet and N. de Tedesco principles for arrangement and detailing of reinforcement.

Concrete cover was not specified on the drawings. We may assume that it is thinner than what is prescribed by standards today, since at the time of construction adverse effects of chlorides infiltration and related deterioration of concrete structures was unknown. As indicative values, we may use values as reported in [11]: (I) recommendations from 1904 prescribe that the concrete cover should not be less than 1 cm, (II) in regulation from 1907 the cover should be at least 2 cm thick in beams and at least 1 cm in slabs.

5.1 Slabs

Fig. 12 reviews the reinforcement layout in the roof slab. Rebars ϕ7 are spaced at 16 cm, except in the middle third of the slab where spacing is 8 cm. In the middle third of the slab,

half of the reinforcement is bent into the upper zone at the supports, at a distance of L/8 (60 cm) from the axis of the beam, and extended by L/16 (30 cm) over the beam axis (bent bars marked as dashed lines). Fig. 13 presents the reinforcement of the slab before concreting [1].

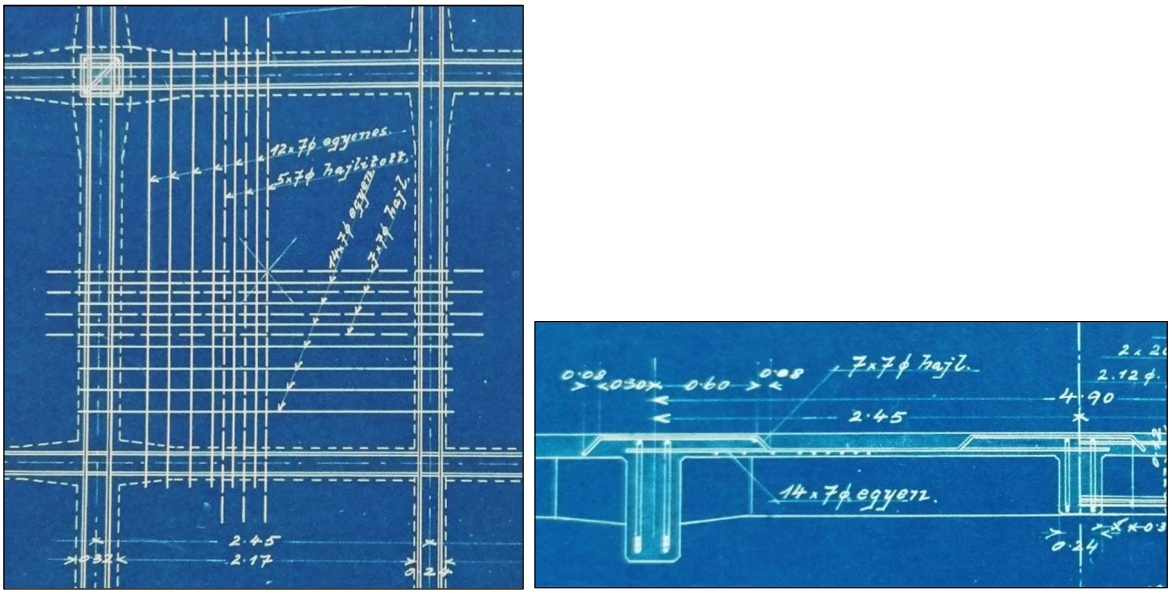


Figure 12: Reinforcement details of the roof slab (bars are labeled as: *egyeness* – straight, *hajlitott* – bent) [5]

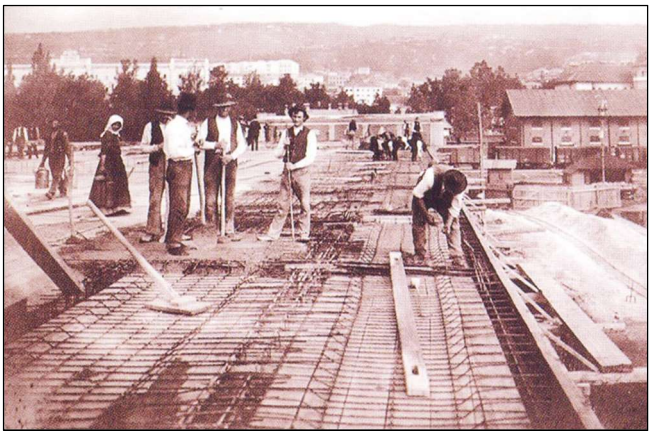


Figure 13: Warehouse no. 17 during construction - reinforcement arrangement of the slab [1]

5.2 Beams

Table 2 summarises the required reinforcement area in primary and secondary beams, while Fig. 14, 15 and 16 review the reinforcement detailing. Bottom bars (instead of being cut at the point where they are no longer required) are lifted into the upper zone at an angle of 45° and extended over the column, where they serve as main tensile reinforcement. At the same time this bent-up bars also serve as shear reinforcement. Mandrel diameter for bending was recommended as 20-40 cm [5]. The ends of reinforcing bars are not made with a hook (despite using plain round bars), meaning that bond relies only on adhesion and friction.

In addition to bent-up bars special enclosed type bars of trapezoidal shape are placed above the columns (as a "rider") and used as shear reinforcement. In the middle of the span two (or three) upper bars are of smaller diameter than the lower bars (ϕ12 in primary or ϕ10 in secondary beams). They are used for connection with lower bars via stirrups (see also Fig. 17). The branches of stirrups are twisted together over the upper bars so as to tie the bars together [8]: ϕ6 and ϕ5 are used for primary and secondary beams, respectively. Note that this shear reinforcement is spaced at 35 cm in primary beams and 30 cm in secondary beams. This spacing is decreased near supports: first and second spacing measured from the column face are reduced to 10 cm and 25 cm in primary beams, and 10 cm and 20 cm in secondary beams.

Table 2: Cross sectional area of required reinforcement in primary and secondary beams [5]

floor	position	primary beams		secondary beams	
		span 5,6 m	span 4,9 m	span 5,6 m	span 4,9 m
ground floor, 1st, 2nd and 3rd floor	midspan bottom	6ϕ24	6ϕ22	2ϕ20+ 2ϕ22	
		27,14 cm^2	22,81 cm^2	13,88 cm^2	
	support top	10ϕ24	10ϕ22	4ϕ20+ 2ϕ22	
		45,24 cm^2	38,01cm^2	20,17 cm^2	
	support bottom	8ϕ24	8ϕ22	8ϕ22	
		36,19 cm^2	30,41cm^2	30,41 cm^2	
roof	midspan bottom	6ϕ16	6ϕ15	1ϕ16+ 2ϕ12	1ϕ15+ 2ϕ12
		12,06 cm^2	10,6 cm^2	4,27 cm^2	4,02 cm^2
	support top	2ϕ18+ 8ϕ16	2ϕ20+ 8ϕ15	2ϕ16+ 2ϕ14	2ϕ15+ 2ϕ14
		21,17 cm^2	20,42 cm^2	7,10 cm^2	6,61 cm^2
	support bottom	4ϕ16+ 4ϕ18	4ϕ15+ 4ϕ20	4ϕ14+ 4ϕ12	4ϕ14+ 4ϕ12
		18,22 cm^2	19,64 cm^2	10,68 cm^2	10,68 cm^2

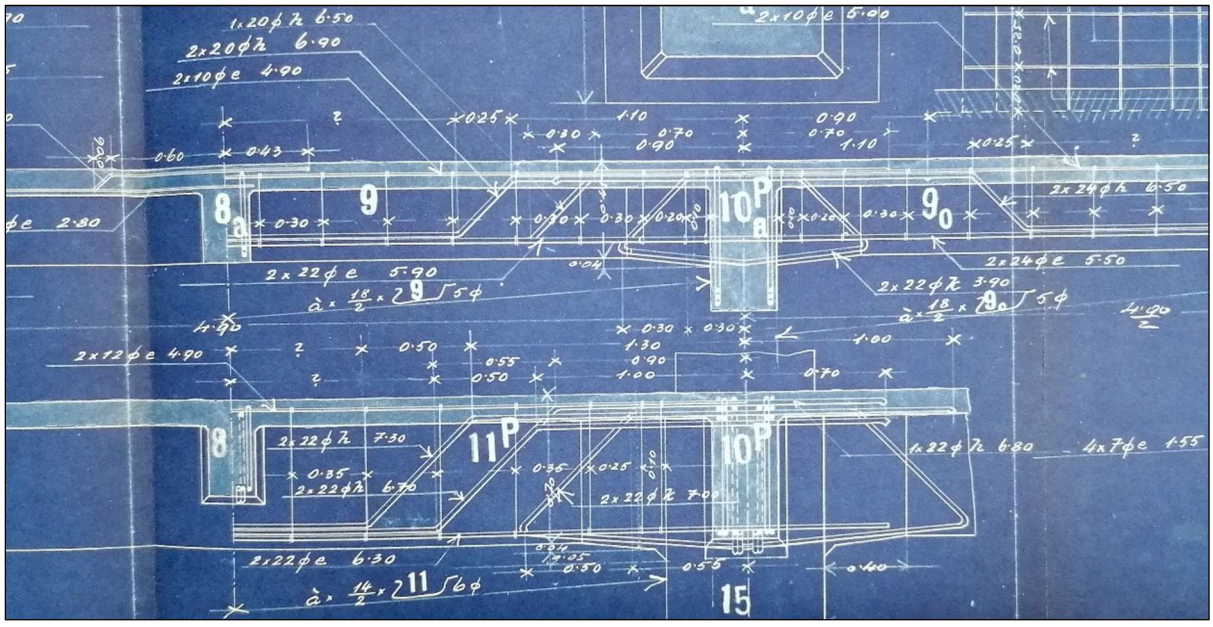


Figure 14: Reinforcement details of a secondary (above) and primary beam (below) – above the column in longitudinal direction (bars are labeled as: *e.* – straight, *h.* – bent) [5]

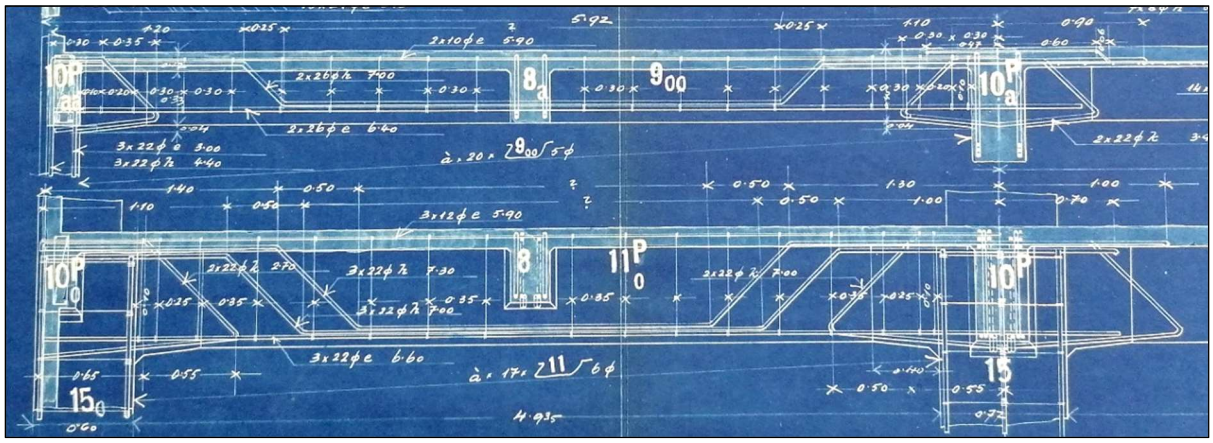


Figure 15: Reinforcement details of a secondary (above) and primary beam (below) – end span in longitudinal direction [5]

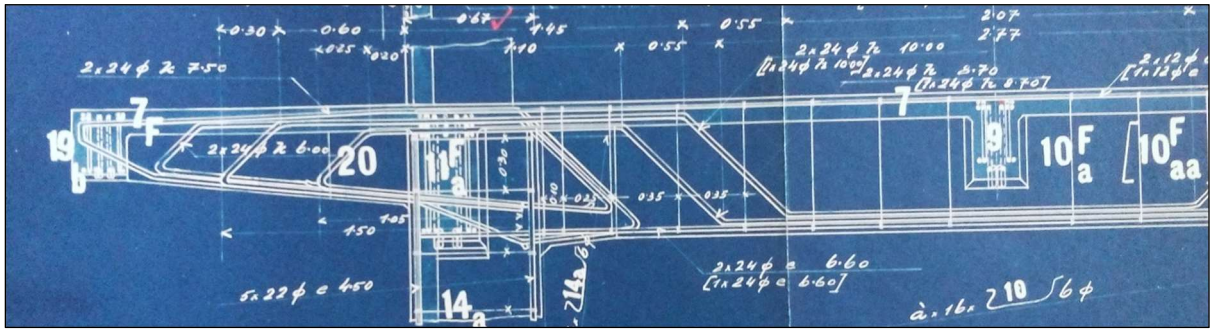


Figure 16: Reinforcement details of a primary beam – end span in transversal direction including cantilever [5]

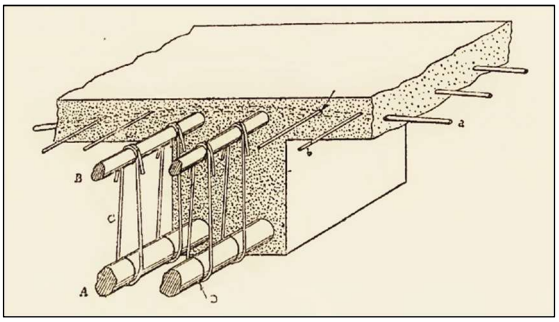


Figure 17: System *Coignet* - reinforcement details of a beam [13]

5.3 Columns

Columns are rigidly connected with the beams, whilst the haunches in beams give additional strength to the joint. They are reinforced with 8 longitudinal bars, except for columns on 3rd floor which have only 4 bars (Fig. 18). Stirrups enclosing the section of ϕ6 mm are spaced at 30 cm along the entire column length; additional inner links are also provided. Reinforcement for continuity between the floors is marked with red colour.

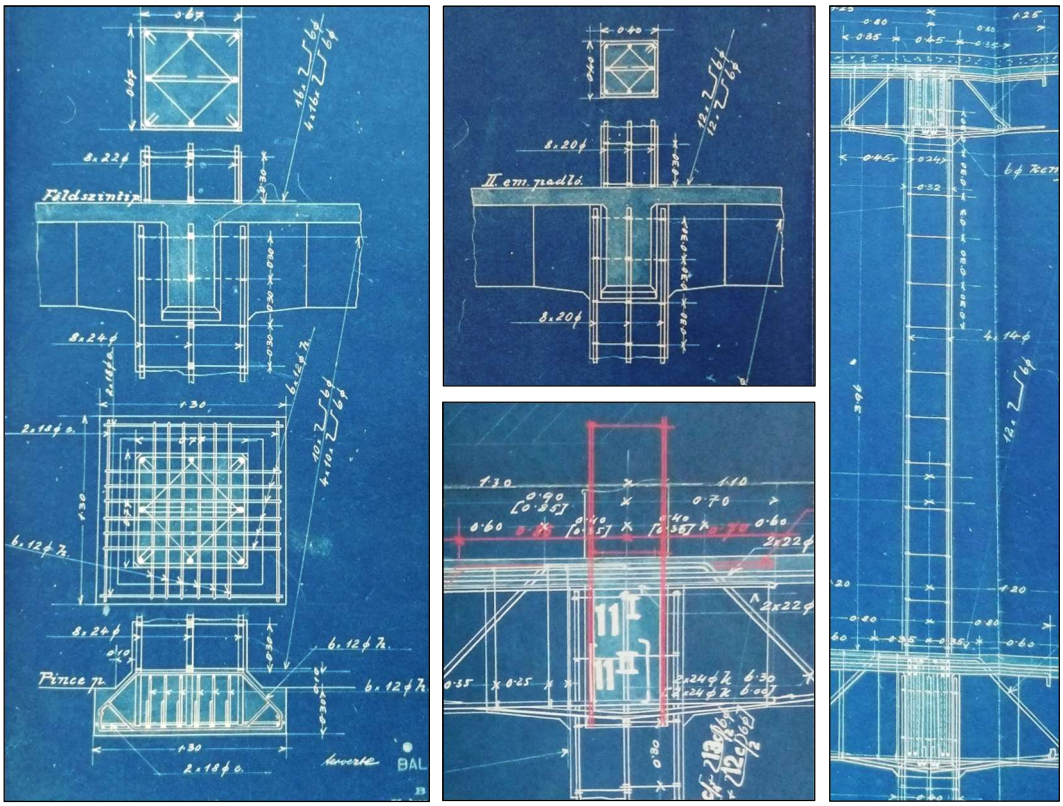


Figure 18: Reinforcement details of the columns [5]

5.4 Walls

Fig. 19 shows the reinforcement of an inner wall, only 8 cm thick. It consists of vertical and horizontal bars of ϕ7 spaced at 25 cm both in horizontal and vertical direction, on both sides of the wall. U shaped anchor bars ϕ8 of total length 80 cm are installed in bounding members (beam, column and plate) for connection with the wall.

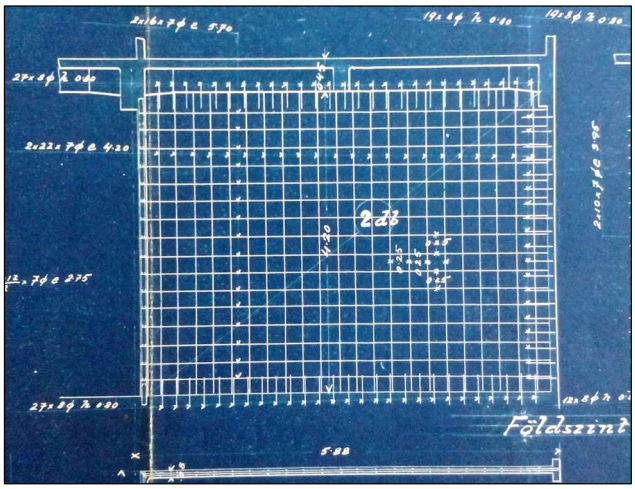


Figure 19: Reinforcement details of an inner wall [5]

6 CONCLUSIONS

- This paper presents an early reinforced concrete frame structure where special attention was given to better understanding of the early 20th century construction techniques.
- Basic features of the reinforcement detailing rules have been presented. At the time of construction, the theory of reinforced concrete was yet not completely understood and each patented system had different reinforcement details. Nevertheless, regardless of the reinforcement detailing this building is still operational, despite its long-term usage and environmental conditions (located next to the sea).
- This building demonstrates significant technical achievements, which are not sufficiently valorised. Regardless of the age of the building, it still has exceptional potential. Such a 20th century heritage industrial building should be given a new purpose and preserved for future generations.
- We presented results based on the research of archival materials. In the next step a more detailed field research should be performed in order to determine material characteristics (concrete and rebar strength, the amount of chloride ions, through visual inspection, evidences of historical repair) which would be used to assess the remaining lifespan in a more detailed analysis.

Acknowledgements. The Authors thank the University of Rijeka for supporting the publication of this paper through grant No. uniri-tehnic-18-127 and No. uniri-pr-tehnic-19-28. The Authors gratefully acknowledge Ferenc Cservenák for providing help with translation from Hungarian.

REFERENCES

[1] Dubrović, E. (Ed.) *The port of Rijeka: history, construction, transport* (in Croatian), Rijeka's City Museum, Rijeka, (2001).
[2] Palinić, N. Historical warehouses of Rijeka Port (in Croatian), *Sušačka revija*, (2014) **42**/**43**:27-42.
[3] Palinić, N. Early reinforced-concrete structures in Rijeka Port (In Croatian). *Građevinar.* (2009) **61**(5):435-444.
[4] http://gis.rijeka.hr/gis/ (retrieved 25.1.2020.)
[5] State Archives in Rijeka, Collection Technical offices of the city of Rijeka, sign. DARI, JU 51, box 30, (1906-1908).
[6] https://rijekaheritage.org/en/kj/luckoskladiste14 (retrieved 25.1.2020.)
[7] Christophe, P. *Le Béton armé et ses applications*, Ch. Béranger, Paris, (1902).
[8] Marsh, C.F., Dunn, W. *Reinforced concrete*, D. van Nostrand Company, (1909).
[9] Kurrer, K.E. *The History of the Theory of Structures: From Arch Analysis to Computational Mechanics*, Ernst & Sohn, (2008).
[10] Colby, A.L. *Reinforced concrete in Europe*, The Chemical Publishing Co., (1909).
[11] Mörsch, E. *Der Eisenbetonbau. Seine Theorie und Anwendung.* Verlag von Konrad Wittwer, Stuttgart (1908.)
[12] Coignet, E., Tedesco, N. de. *Le Calcul des ouvrages en ciment avec ossature métallique.* Mémoires de la Société des Ingénieurs civils de France, Paris, (1894), pp. 282-363.
[13] Tédesco, N. de, Forestier, V. M. *Théorique et Pratique du Constructeur en Ciment Armé*, Ch. Béranger, Paris, (1909).

12th International Conference on Structural Analysis of Historical Constructions
SAHC 2020
P. Roca, L. Pelà and C. Molins (Eds.)

FOUNDATION DEVELOPMENT FROM 1890-1942 FOR LONG SPAN AND HIGH RISE BUILDINGS AT MÉXICO CITY

PERLA SANTA ANA[1*], LUCIA SANTA ANA[1] AND JOSE I. BAEZ[2]

[1]Laboratorio de Materiales y Sistemas Estructurales,
Facultad de Arquitectura
Universidad Nacional Autónoma de México, CDMX, México
e-mail: psal@unam.mx, lsl@unam.mx, https://sites.google.com/fa.unam.mx/papiit-in404318

[2] Baez Santa Ana Ingenieros Consultores,
Research Area, CDMX, México
email: jibg@bsiconsultores.com

Keywords: Historical Structure, Foundations, High Rise Buildings, Development

Abstract. *The subsoil of Mexico City, Mexico, has had a complex behavior; filled with light flocculent structure and layers at different depths of stiff material, producing regional and local differential settlements and liquefaction being a seismic zone. Long Span and High Rise buildings in this City have been a challenge to construct, being its foundation solution, one of the essential elements for its success. This study aims to present the evolution of the long span and skyscraper in Mexico City, being the foundation solution a crucial issue for this new construction era. The foundation solution of five iconic buildings built during this period analyzed by their designers and authors of this paper is presented. Each foundation solution is evaluated considering today's advance in Mexican soil mechanics, arriving at the solution most used nowadays in the city for this kind of buildings.*

1 INTRODUCTION

Since early times the subsoil of Mexico City has been a challenge for engineers and architects to erect buildings without suffering settlements because of its stratified soil sediments of high and very high compressibility in addition to strong earthquakes and ground surface subsidence. The characterization of Mexico City subsoil started in 1948 with Engineer Nabor Carillo [1] and continue with Leonardo Zeevaert in 1952 [2] and Marsal and Mazari in 1959 [3] continuing this task until nowadays. Its complex behavior is due to its stratigraphical and hydrological conditions.

2 GEOTECHNICAL PROPERTIES OF THE VALLEY

The Valley of Mexico City is formed by volcanic and pyroclastic materials, interspersed with alluvial deposits covered with lacustrine clays. The valley remained a closed basin with several shallow lakes (like Texcoco, Chalco, Xochimilco, among others), and it became an open basin in 1789. The lakes were drained during the 20th Century, leaving the valley with lacustrine sediments. These are highly plastic soft clays interbedded with layers of silt, sand,

and sandy gravels of alluvial origin. [4]. According to Marsal and Mazari [3], there is at the top a desiccated crust of artificial fill, underneath are the upper and lower clay layer separated between by a hard layer and a sandy, clayey stratum. The composition of this volcanic clay is a mixture of a) clayey and non-clayey minerals with microorganisms, b) dissolved salts and, c) organic components (i.e., ostracodes and diatoms). [5].

This soft lacustrine soil has been suffering a consolidation process due to the exploitation of the aquifers underlying the old lake zones. [5]. Because of its composition and drainage, the subsoil of this Valley has a subsidence today around 30 to 40 cm per year, and the sinking process of the city will continue producing differential settlements on the foundations, especially from the iconic heritage buildings. Earthquake of 1985 shows that this soft soil on the surface settled after the tremor being interpreted this behavior as an instantaneous vertical displacement induced by the residual expansion as the seismic waves travel through the soil mass. [6]. The upper layer clay is highly plastic, remaining elastic with low damping, explaining that for large-amplitude cyclic strains, the clay structure degrades continuously, causing pore water pressure variations and reductions in stiffness and strength. [5].

3 FOUNDATION DEVELOPMENT AT THE CITY VALLEY

Around 1840 first general studies of the subsoil were made to get an unconfined compressive strength that avoids or diminishes structural settlements. Militar engineer Gonzalo Garita worked hypothesis from the practical engineering point of view and, as a result, established a value of 5 ton/m2 as bearing capacity of the substrate [7] and started using slab foundations for small buildings. The most effective foundation solution was the concrete slab to distribute the one or two-story building load to the substrate.

3.1 Casa Boker, 1898

The main objective of the Porfirio Diaz government was to build iconic buildings showing to the world Mexico modernity. Building materials and construction machines were imported from Europe and the United States, and so the engineering practice and knowledge arrive in Mexico too.

Living Mexico City in this modernity, Family Boker introduced to the country the new way of shopping and decided to open a department store downtown. This building was constructed by architects De Lemos y Cordes with the participation of the engineer Gonzalo Garita. It was one of the first steel department store buildings built in Mexico City with four stories high (higher than all the buildings around). The structural design, building system, and must materials (steel and concrete) were imported mainly from the United States, as the contractor hired for this job was Milliken Brothers Company around 1980, with their main offices in New York.

The spans for this new building were 5.5 m in both directions, with a floor height of 4 m. As this store was a replicate from the ones being constructed in New York, selling any engine, car, or electro domestic furniture, the live load used for its structural design was 119 MPa as it was considered as a warehouse. [7]. The structural system used for this building by Milliken Brothers was the “Skeleton Construction Plan” (a semirigid steel frame with “Z bars” columns and standard I beams). Floors were fireproof constructed with a steel rolled plate supported by secondary beams and filled the upper part with concrete.

The foundation solution used was the “continuous grillage foundation”; it consists of two-layer steel beam grillage embedded in concrete with a bed thickness of 1.96 meters and covering an area of 1700 m^2 (¾ of the total building area). The main steel beams for this grillage had a section designated “IE” with a depth between 45 and 50 cm., while the second line was steel beams of 20 cm depth. This kind of foundation solution was used around 1905 in Chicago and New York tall buildings; the only difference was that rails of cast iron were used instead of steel. [13].

Analyzing today the weight of the building, considering live loads (63 MN) and the weight of the foundation (76 MN), it can be observed that the foundation system weights 20% more than the building´s load. The weight of the foundation and structure was of 68.64 KPa, slightly higher than the 49 KPa bearing capacity established for that site. Fortunately, the building never had the live load considered in its structural design, reaching the 49 KPa of soil bearing capacity. This building still stands today, and it continues to be a store with offices in its upper levels, and it has only a small differential settlement of around 5 cm over one corner, concluding that this kind of foundation could be used for buildings of 3 to 4 levels) over soft soil.



Figure 1: Casa Boker Construction, from Milliken Brothers Catalogue 1903.

3.2 Palacio de Bellas Artes, 1904

This iconic building design by architect Adamos Boari and structural design by W. Birkmire started its construction in 1904 and ended until 1934. This building is four stories high with a structural system of steel frames for all its stories. Perimeter non-bearing walls are

of concrete wrapped with marble plaques; they make the façade of the building. In its interior, spans are variable; the small spacing between columns is 5 m, and the longest is around 25m located inside the main theater. Concrete and most of the steel structure was imported from the United States, only the steel for its foundation was produced in Mexico.

The foundation selected for this massive building was continuos grillage, made with two layers of beam grillage embedded in concrete. It was considered an underground basement of two meters for all the building except under the theater stage, which was three meters depth. During the excavation process, they found pre-hispanic ruins (consolidating clays where the ruins were) underneath the substrata, so they decided to increase the basement depth only 50 cm more. [14]

This steel building has an extraordinary deadweight (floors and walls were covered with marble, spans were 13m long, more significant than any other edifice constructed by that time). Engineer Birkmire decided to use as main steel beams for the grillage sections "IE" type of 60 cm depth. This steel section was used for making the two layers grillage embedded in a concrete slab of 2.32m of thickness. The total weight of the foundation was 381 MN, while the building weight was 395 MN, making a total weight of 778 MN. Considering today the basement as a floating raft foundation, the total weight of the building that received the substrata was 72 KPa, higher than the 51 KPa substrata capacity [8]. Differential settlement problems started since the beginning of the construction and, along with the construction progress, stopping it several times; the problem was not the weight of the building, while it was only the steel skeleton erected.

When the settlement problem started, Birkmire suggested the use of some metallic flashboards around the building to avoid hydraulic issues caused by the underneath phreatic water. Still, the settlement continued being worse while it was differential and not uniform. The problem was partially solved, pumping concrete into the clay subsoil to confined it, slowing the subsidence, and getting a uniform settlement [8]; this procedure lasted from 1910 to 1925. Analyzing today the foundation of this building, it can be concluded that the pre-consolidation of some spots under the slab foundation and the different levels of depth of the underground levels played an essential role in the differential settlements suffered during the building progress. Today this building is 2.33 m below its original construction level, being subsidence the leading cause of this effect.



Figure 2: Construction of Palacio Bellas Artes, from Milliken Brothers Catalogue 1912.

3.3 La Nacional Building, 1930

Since 1908, Mexican engineers did not consider the grillage foundation as an adequate solution for soft clay soils like the one in Mexico City. Hence, engineers of that time decided to use wood point bearing piles supported in the bearing stratum as a better foundation solution, using it for the column of independence built in Mexico City in 1900 and inaugurated in 1910 by Porfirio Diaz.

With the growth of Mexico City, there was a need to control the building process, so authorities created and published in 1920 the first Building Code. This code contained regulations about architecture solutions and spaces, but few things about the construction process. Because must of the times buildings had problems with settlements, this code just stated the bearing capacity of the soil as 49 KPa and must housing buildings should have a slab of 10 cm depth made with unreinforced concrete as the foundation. [15].

More water was extracted from the subsoil, and subsidence increased, causing failure in the city drainage system and soil surface cracking all over the city. In 1925, Roberto Gayol was the first engineer to study the properties of the subsoil from Mexico City while building the main drainage of the city.

The life insurance company called La Nacional, Compañía de Seguros para la Vida SA, (founded by W. Woodrow and L. Neergard) hired in 1901 the architects Monasterio and Calderón to design a building for their company. They proposed a 13 story building with 55 m height; it was the first skyscraper of Mexico City. The primary structural system is steel frames with reinforced concrete floors; all the steel structure was protected with reinforced concrete to make it fire resistant and giving a higher strength to the structural system without knowing. Because the Building code of 1920 did not include any section about structural design, engineers used the American 1923 AISC allowable stress design. Spans are regular of 7m in both directions; floors support the facades which are made with non-bearing concrete walls.

The building has a total weight of 89 MN with a built surface of 735m2, generating a unit pressure to the substrate in case of using a slab foundation of 142 KPa, which is a higher pressure than the substrata capacity established by the building code (49 KPa). Soil tests were

performed and analyzed; standard penetration tests were made, and the soil profiles were analyzed, finding sand with a small amount of lime and clay stratum with the thickness and resistance required for supporting piles. The depth of this resistant stratum was 36m from the surface [9].

With Dr. Karl Terzaghi working as a consultant, the foundation solution assigned for this building was a two-level box type and wood point bearing piles below the box. Because floating foundations were not known by that time, it was ignored the compensation effect of the box, and all the weight was considered to be supported by the woodpiles. A total of 373 piles of 30 cm diameter were used; piles were segmented in sections of 6 to 8 m long. The piles were fitted with cast iron points and caps to prevent damage to its bottom during the phase of operation; they were joined together in their upper part with the beams that support the concrete slab of the box. [9].

Not all the piles reached the hard stratum, but considering the compensation work of the basement box, the piles that reached the stratum were enough to support the building. After a series of 4 strong earthquakes and changes in live loads, this building remains until today open and functioning. It has a differential settlement of 7 cm over a corner, and it has emerged approximately 50 cm. This settlement produced where the piles did not reach the hard stratum; also, this stratum could have suffered changes, while the other four buildings nearby (Torre Latinoamericana among them) also stands over it.



Figure 4: La Nacional Building, courtesy of Archive Fundacion Ramos.

3.4 Loteria Nacional Building, 1933

In 1933 the National Lottery system hired architect Ortiz Monasterio and engineer José Antonio Cuevas to built its new house. With an irregular shape and three sections, this building is 66 m tall, with 20 stories in the central tower. Its structural system consists of

steel frames using beams and trusses because of the spans at the auditorium (15 m long approximately and a height of 18 m). Columns are protected with reinforced concrete, and floors are reinforced concrete slabs. This building is one of the first skyscraper built with Mexican materials (concrete and steel).

The foundation solution design and built for this building was a floating foundation; this was the first time this foundation solution is used in Mexico City. The global solution consisted of a two-level concrete box of 10 m depth, stiffened with concrete trusses; the soil is in general composed of clay stratum with a high phreatic level creating heave as the soil was removed.

Before beginning the construction, engineer Cuevas started analyzing the mechanic properties of the soil. He evaluated the soil's density, which changed as ít came from a deeper layer; the variation of its specific weight was from 12.6 kN/m^3 at the top to 10 kN/m^3, at 1.8 m depth. The phreatic level was found at -1.80 m., so the soil under this level could reach a density of 28.5 kN/m3. Phreatic water was pumped out of the field to maintained dry the construction site.

Because there were no soil mechanic laboratories, engineers could not know the soil elastic and plastic reaction; Cuevas started measuring deformations every day, discovering that the subsoil swells 1.27m in eight months. He lay a flexible wood with a waterproof membrane over it; concrete “T” inverted beams were constructed, and additional weight was placed like ballast in order to push the subsoil to its original level. The ballast was removed as the construction developed, and the weight of the box foundation restrain the soil to its original position and the loads transmitted. [10].

As the building was finished and to gain stability, it was ballast using water inside the concrete box below the auditorium, and water tanks of 80m^3 were placed on the endpoints in the basement of the main body. The total height of the building is due to restrain the soil and compensate the weight of the soil excavated. This building still stands today, functioning normally; earthquakes have cause minor affectations, and differential settlements (19 cm at the top) have been reported.

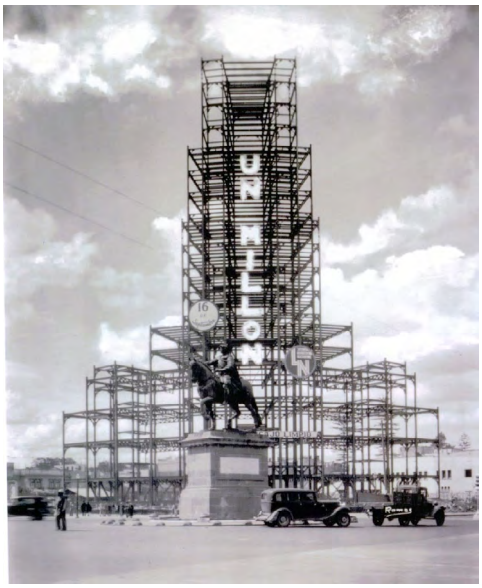


Figure 5: La Loteria Nacional, courtesy of Archive Fundacion Ramos

3.5 Introduction in Mexico City to soil mechanics and seismic effects

In 1941 an earthquake stroke Mexico City; buildings from 10 to 18 stories constructed over soft soil suffered structural damages. This earthquake forced authorities to review the building code and invited engineers to research soil properties and seismic actions.

In 1942 the new building code for Mexico City was published; this is the first code to established a substrata capacity equal to 49 kPa when the soil was pre-consolidated or 29.4 kPa if it has never been used for construction. The most popular foundation solutions were concrete slabs and isolated concrete footings; the use of grillage using reinforced concrete and iron or steel sections remained. When tall or heavy buildings were built, it was allowed to use bearing piles supported on rigid stratum; piles could be made of concrete or wood. [16].

Between 1946 to 1956, engineer Nabor Carrillo began the scientific study of soils (soil mechanics), especially of clays and soft soils. He specialized in the behavior of foundations supported by different types of soil, stablishing that difficult foundation problems were found in very fine water laid sediments of high compressibility stratified with sand layers, exhibiting high secondary compression (or intergranular viscosity, as he named it) as these silty clays or clayeye silts have high viscous behaviour induced by the relative displacement of the mineral grains. [11].

3.6 Torre Latinoamericana, 1948

The insurance company Latinoamericana Seguros gave the commission to architect Agusto Alvarez to design an iconic building at the city center of Mexico City. This tower was built between 1948 to 1956, became the first tall building constructed in a seismic zone with compressive soil. The structural system consists of rigid steel frames and concrete slab floors. The steel sections were imported from the Bethlehem Steel Company, which fabricated the steel sections for the Empire State Building in New York. This Steel Company questioned the engineer Ph.D. Leonardo Zeevaert because the steel sections of the Latinoamericana Tower were more significant and more massive than the ones from the Empire State Building. The response from Zeevaert was simple; the seismic effect needed those sections. The span length is constant of 7m in each direction.

Zeevaert was in charge of the foundation and structural design. He studied the structural system and foundation solution in order to get a safe building. The architectural design followed the recommendation of the engineer in order to obtain an excellent seismic and foundation behavior, some of the action taken was: light partition walls, regular geometry of the building, number of stories. The foundation and soil behavior was considered when the seismic design for this building was evaluated. [17].

The subsoil conditions were investigated, with the following results: the first 5.55m a fill was found of clayey silt, sand with humues and Aztec pottery remain; the content of water was 45%. The following 20 cm a layer with black volcanic ash with silt and clay was found. The next 2 m were formed with light grey silty clay with high content of calcium carbonates and a water content of 100% and pumice sand. The last layers were lacustrine volcanic clay with brown pumice sand. [12].

The foundation solution was a floating raft with a concrete box, with a unit load at the foundation of 206.9 kPa. The reinforced concrete mat foundation is located at a depth of 13 m, and it is 60 cm thick; in order to ensure no settlements, 361 concrete point piles were built

under the reinforced concrete mat. Piles were driven to a depth of 33.5m into a firm sand layer acting as point bearing piles; this layer was selected to avoid large negative friction on the piles. Both elements (box and piles) were designed to stand the total weight of the building separately. Piles were Button Bottom with 30 cm of diameter; they were poured in the site, and the concrete compression stress was equal to 73.54 MPa, having a prefabricated concrete point of 43 cm diameter.



Figure 6: Torre Latinoamericana, courtesy of Instituto Investigaciones Esteticas UNAM.

Because engineers believed that the piezometric level would push up the building, 13.3 m3 per day of water was pumped to the soil in order to assure flotation. This special hydraulic system was design also to reduce the heave of the bottom of the excavation and avoid settlements outside. The area to be excavated was surrounded by a wood sheet pile 16m depth; upon saturation this membrane did not allowed the entrance of water in the excavation; the pressure in the sand layers was maintained by injecting clean water under pressure in the subsoil using eight wells all over the building surface. The heave was avoided by producing a strong reduction in the piezometric water levels inside the wood sheet-pile to keep the same effective pressures. In order to take care of ground surface subsidence, the ground floor was was divided into panels supported on wood blocks, permitting the panels to be lowered as required. [12].

This building has emerged approximately 100 cm as predicted by Dr. Zeevaert; it has survived the most significant earthquakes of Mexico City, and it stands without any damage or settlement.

4 CONCLUSIONS

It is essential to learn about the success and failure of foundation solutions applied for compressible clay soil like the one in Mexico City. The buildings that are designed and constructed today, taller, with irregular shapes and greater span lengths, are a product of the advances in technology but mainly in the research of soil properties and behavior of

foundations over different kinds of soils.

Acknowledgments. Authors acknowledge all researchers that have made possible the development of soil mechanics in Mexico City. This work was supported by UNAM-PAPIIT IN404318.

.

REFERENCES

[1] Carrillo N. Influence of artesian wells in the sinking of Mexico City. *Second International Conference on Soil Mechanics and Foundation Engineering. Rotterdam, Nederland* (1948)

[2] Zeevaert L. Estratigrafía y Problemas de la ingeniería de los depósitos de arcilla lacustre de la ciudad de México. *Scientific Congress of the Fourth Centenary of the National University of Mexico, Proceedings, Mexico* (1952) 30: 155-176

[3] Marsal R. and Mazari M. The Subsoil of Mexico City. *Contribution to First Pan-American Conf. on Soil Mechanics and Found. Engineering, Facultad de Ingeniería, UNAM, Mexico* (1959)

[4] Marsal R. and Mazari M. The Subsoil of Mexico City. *Contribution to First Pan-American Conf. on Soil Mechanics and Found. Engineering, Facultad de Ingeniería, UNAM, Mexico* (1959)

[5] Auvinet G. y Juarez Moises. Geotechnical characterization of Mexico City Subsoil. *Pan-Am Geotechnical Conference*, (2011)

[6] Zeevaert-Wiechers L. Análisis y pronóstico del hundimiento de la superficie del suelo motivado por el sismo. (Eds.): *Ingeniería Investigación y Tecnología*, II.2, (2001), pp. 49-54.

[7] Katzman I. *La Arquitectura Contemporánea Mexicana: Predecentes y Desarrollo*. INAH, Mexico,(1993) pg 125-130

[8] Santoyo E, Ovando E. *Evolución de las cimentaciones de edificaciones de la Ciudad de México*. TGC, Mexico,(1999)

[9] Ortiz M Cimentación de pilotes en la Ciudad de México. (Eds.): *Arquitectura y decoración*, 19, (1937), pp. 22-26.

[10] Martinez R, Tamez E. *Revisión geotécnica de la cimentación del edificio de la Loteria Nacional*. TGC, Mexico,(1986)

[11] Santoyo E. *Sintesis Geotécnica de la Cuenca del Valle de México* TGC, Mexico,(2005)

[12] Zeevaert-Wiechers L. Foundation Design and Behavior of Tower Latino Americana in Mexico City. *Geotechnique*, (1957), vol.7.

[13] Böker, R. *Historia de la Casa Boker.* Casa Böker, Mexico,(2019)

[14] Birkmire,W *Contrato con Ing. Birkmire para la cimentación del Teatro Nacional.* Archivo General de la Nación, Fondo COP (1905)

[15] Gobierno Constitucional de los Estados Unidos Mexicanos. (1920).Reglamento de Construcción (D.O.Federación, Ed.)

[16] Gobierno Constitucional de los Estados Unidos Mexicanos. (1942).Reglamento de Construcción (D.O.Federación, Ed.)

[17] Zeevaert-Wiechers A. La torre Latino Americana. Mexico: División de Estudios Superiores de la Facultad de Ingeniería, UNAM.

12th International Conference on Structural Analysis of Historical Constructions
SAHC 2020
P. Roca, L. Pelà and C. Molins (Eds.)

FROM ART TO SCIENCE OF CONSTRUCTION: THE PERMANENCE OF PROPORTIONAL RULES IN THE "STRANGE CASE" OF THE 19TH CENTURY PONTE TARO BRIDGE (PARMA, ITALY)

F. OTTONI[1*], V. BRAGLIA[2], E. COÏSSON[2] AND L. FERRARI[2]

[1] Department of Engineering and Architecture (DIA)
Università di Parma
Viale Parco Area delle Scienze 181/A, 43124 Parma, Italy
e-mail: federica.ottoni@unipr.it, www.unipr.madlab.it (*corresponding author)

[2] Department of Engineering and Architecture (DIA)
Università di Parma
Viale Parco Area delle Scienze 181/A, 43124 Parma, Italy
e-mail: luca.braglia87@gmail.com, eva.coisson@unipr.it, lia.ferrari@unipr.it, www.unipr.madlab.it

Keywords: Historical masonry bridge, Proportional theory, Deformations, Crack pattern

Abstract. *The bridge commissioned by Maria Luigia to Eng. Antonio Cocconcelli and built between 1816 and 1821 over the Taro River (near Parma, Northern Italy), is a very important monument, both from a cultural and strategic point of view. This 20 arches masonry bridge reaches the length of nearly 600 meters and constitutes a very interesting case study, not only for the technical and structural issues related to its restoration and use (with increased traffic loads) but also for the role that geometry played in its history and stability. In this paper, a compared analysis on the historical 'proportional theory' and the constructive features of this ancient bridge is proposed with the final aim to show the importance of recovering "empiricism" in dealing with ancient monuments. Thanks to a high precision survey the realized structure has been compared to the original project, in order to detect the deformations suffered by the structure in time, thus applying the "historical monitoring" procedure to the monument. Hence, starting from the dimensional theory, a static analysis of the bridge is proposed by means of Mery's graphic method, in order to investigate the structural safety level of the original project, also considering the current load conditions. A comparison with the static results obtained by means of limit analysis, finally shows the validity of ancient proportional theory, which can constitute a first qualitative method for structural validation of ancient masonry structures.*

1 INTRODUCTION

It is well known that 'empiricism' has been at the base of main architectural constructions up to the 17th Century, but this geometrical method of structural design has been used, in particular for bridges, at least until the beginning of the 19th Century, despite the availability of the new theories of the newborn Building Science.

This permanence over the centuries has definitely shown that, despite the fact that the ancient master-builders didn't possess the modern mathematical instruments (proper of the modern science of construction) they have realized such complex structures, perceiving by intuition a 'static sense' which permitted them to correct the previous constructive 'errors', just by observing the past.

Not always these geometrical rules have been codified in proper architectural treatises; most of times – also etymologically – 'monuments' are 'documents' of many basic evolutions (geometrical and constructive) in the history of construction.

Each improvement or dimensional change is due to a significant technological enhancement which derives from the understanding of failures: each successful construction can be considered as the result of a 'pre-vision', adequate and complete, of what would have not worked. We can call this method 'empiricism'.

The 'error', is the vantage point for observing the evolution of masonry structures during centuries and the reconstruction of this historical route can represent an additional fundamental instrument for a deeper knowledge of these magnificent historical structures and it can help in clarifying the difficult process from 'art' to 'science' of construction [1].

This procedure can help in investigating the real present structural behavior of ancient masonry buildings and infrastructures, considering and reliably interpreting their present geometry in terms of constructive corrections or deformations occurred during time. The final aim of the work is to show the permanence of empirical analysis and proportional theory in defining reliable strategies of conservation for ancient masonry structures, thus confirming – even in structural analysis – the "Art of building" principles.

2 THE DIMENSIONAL RULES AND THE STRANGE OF BRIDGES

In the 'correct' ancient constructions (and those arrived to us, definitely are) each structural element has a proper role – from the aesthetical, static and technical point of view – matured through the observational method: by finding the solution to constructive 'mistakes'.

The ancient master-builders were certainly unaware of the theory at the base of the structural behavior of masonry, which slowly developed after centuries of construction practice; nevertheless, they could experiment the final effects of this structural mechanism through the simple observation of cracks.

Despite their massive appearance, masonry structures are essentially labile, not isostatic. Still at the beginning of the 20th century, G.B. Milani, shows their peculiarity, underlying the difference with the new 'elastic systems': a monolithic structure "*can remain in equilibrium for each value of S for which the resultant R is internal to the section*" [2].

What has to be avoided is its overturning, that, regardless of resistance values, inevitably occurs when the resultant force falls outside its thickness. Then, the geometrical ratio between the thickness of the wall and its height is the fundamental parameter, in order to state the stability condition of the wall itself in front of horizontal forces (like the thrust of arches).

It is well known that there are at least three main prescriptions provided by the various treaties for a correct construction of arches [3]: the best shape (the "more solid" one); the limit thickness (the minimum possible) for that shape (*e*), which is often provided in relation to the

span of the arch itself (e / L); and finally the thickness of the piers (p), also very often given compared to the span (p / L).

Only few ancient authors [4] explicitly solved the question of pier slenderness (h/p) for arches, while this fundamental data is, more often, derivable by the "architectural orders" theory. For these fundamental structures, until the 17th century few variations are recorded in the proportional rules, which see the best shape in the round arch, an ideal thickness equal to 1/10 of the span and an ideal ratio between span and thickness of the piers equal to 1/3, recovering the “medieval rule”, also knew as “Gothic rule n.1” [5].

In time, the thickness of piers is reduced to p=L/4, which increases in the case of the lowered arches and decreases for the acute ones, thus displaying the thrust intensity.

In this permanence, an interesting case is that of the bridges, which bring together different dimensional issues (foundations, pillar thickness, thickness and shape of the vaults, span and size of the spandrel walls), closely related to precise and particular technical-construction problems (filling, roadway materials, hydraulic and material problems).

In particular, the size of the pillars represents a central theme, having to answer both questions simultaneously: the piles of a bridge must resist the thrust of the various spans and, at the same time, must have a shape and a size which do not hinder the passage of the water between the spans, often of different sizes.

In step with this, the ‘proportional theory’ at the base of the main architectural treatises and buildings (from XV to XVII Century) have been herein analyzed, relatively to bridge constructive criteria and in the following Tab.1, the dimensional prescriptions for masonry bridges given by the most important treaties from XV to XVII century are presented.

As for the treatises, the rules formulated by Alberti coincide, with few alterations, with what will be the official doctrine for bridges until the 19th century, which still sees the span (L) of the bridge as the main reference. According to this rule, the arch thickness must be equal to one tenth of the span (e=L/10) while the pile thickness must be between L/4 and L/6 [6].

However, as often happens, it is in the technical prescriptions that the intuitions of the ancient master builders on the functioning of the masonry can be really seen.

Table 1: The dimensional prescriptions for bridges, on vaults (e) and piles (p) thickness, in comparison to their span (L).

BRIDGE RULE	e/L	p/L
Roman bridge – Rimini	1/6	1/2
Medieval bridge on Bacchiglione	1/10	1/5
Alberti’s rules	1/12	1/4 -1/6
Palladio bridge in Vicenza (on Rerone)	1/12	1/6
Palladio’s bridge (treatise)	1/12	1/5
Fra Lorenzo da San Nicolas rules	1/10	1/3
Vincenzo Scamozzi’s rules	1/12	1/4
Hubert Gautier (1716)	1/12	1/6
Cocconcelli’s bridge in Ponte Taro	1/18	1/6

As for the best shape to be assigned to the arches, indeed, we assist to a "license" - granted only to bridges - with respect to Alberti's "doctrine of the ideal arch": the possibility of using lowered arches (if necessary) is foreseen, only on condition of strengthening the spandrel walls. In particular, Alberti insists on the need - on a technical-constructive level - to reinforce

the filling of the vaults and to set them in the best way, using solid and large-sized blocks, especially when bridges are called to support large live loads. For these structures, indeed, the proportional rules are not simply reducible to dimensional parameters; conversely, in the technical/qualitative construction prescriptions the most interesting insights on the real behavior of masonry can be read. In this peculiar aspect – thus in the need to support not only their own dead load, but also additional, even large, ones – coupled with the hydraulic performance, we can fix the main difference between bridges and other historical vaulted masonry structures: these two combined aspects led, over time, to the maximum reduction of the pile thickness (for hydraulic efficiency) compensated by an extreme care in the construction technology used.

Therefore, only the occurrence of both aspects involved in the design of an ancient masonry bridge - thus the respect of the ancient dimensional rules and proportions, and the use of the correct technology in material arrangement and in vault construction - can constitute a reliable qualitative method for expeditious "stability analysis" of ancient bridges, thus anticipating the results of further limit analysis.

This is the case of the Ponte Taro bridge, below described, in which, on one side, the evidence of respect of proportional rules has anticipated the results of further static analysis (Mery's method and safe theorem application) showing a first guarantee of its stability, and, on the other side, the damage observed can be directly attributable to the inadherence to some technological prescriptions, which conversely are central to bridges.

3 THE PONTE TARO BRIDGE, BETWEEN "ART" AND "SCIENCE"



Figure 1. The Ponte Taro bridge: longitudinal prospect by Antonio Cocconcelli (below) and virtual reconstruction of the structure (above, right)

The construction of the Ponte Taro bridge, commissioned by Maria Luigia, duchess of Parma, to Eng. Antonio Cocconcelli, took place between 1816 and 1821. After several calculations and comparison with proportional rules [7], the final shape of this important infrastructure was articulated in 17 three-centered, lowered arches, with a 24 m span, supported by rectangular pillars (rounded on the two to longitudinal prospects in order to reduce the water impact) laying on 5 m long timber poles as foundations. This first project was changed in 1818, after a flood, adding three arches and deepening the foundations. Moreover, in the final 20 arches bridge, whose external brick structure unfolds an internal filling of river cobblestones mixed with mortar, Cocconcelli inserted an oculus above each pillar, thus easing the outflow of water (Fig.1).

3.1 Starting from the end: the bridge current state

The bridge nowadays is still in use, although the main heavy traffic has been diverted on a larger road, which passes over the river Taro about 1 km North. The 19th century bridge, indeed, is too narrow for the modern traffic requirements, not allowing a safe passage by cars, bicycles and pedestrians at the same time on the two directions. In the past, several accidents happened on the bridge and some ended up with vehicles breaking through the lateral walls, which are now rebuilt in about half their extension.

Most of the works carried out on the latest decades on the bridge regarded the upper “used” parts – including the roadbed layers and the lateral walls – and the bottom foundation elements – to ensure their stability with regards to the water-flow actions. Conversely, they rarely faced the conservation problems of the masonry arches, which lay now in a poor state: brick pieces have started falling from the barrel vaults on the underlying roads and paths and some deformations are detectable on the original shape.

Are these detachments only due to surface material decays or can they be related also to structural movements? Did the previous interventions on the piles foundations solve their stability problems or did they evolve in time? Is the crack pattern of the vaults intrados connected to constructive phases or is there a connection with the arch mechanisms?

In order to define a correct intervention approach on the bridge, and to correctly evaluate its present conditions, answering to these questions is crucial and a deep analysis of its current geometry, in comparison with the original shape, has constituted the first step in a progressive investigation path, which has mapped the decay phenomena and the crack pattern, looking for proofs on the building itself.

All the further analyses start from a reliable and detailed geometrical survey carried out in 2018 by Parma University – fully described in (Bruno et al., 2019) [8] – which used different integrated techniques: proximity range UAV photogrammetry, laser scanning and terrestrial photogrammetry with DSLR high resolution digital cameras. The over 50 TLS scans allowed to reach a Ground Sampling Distance (GSD) of about one centimeter and a resolution of the same order of magnitude of the UAV and terrestrial photogrammetric survey (0.7÷1.0 cm).

3.2 Decay and cracks analysis

The decay phenomena on the masonry surfaces were mapped on the photogrammetric surveys of the two façades (North and South) and of the pillars and arches, with a specific

attention to the correct representation and quantification of the affected areas on curved shapes [8]. The analysis of the uneven distribution of these decays can supply meaningful indications about their possible origins: as predictable, the North façade is clearly more affected than the South one, due to the higher level of humidity and the consequent higher diffusion of biological patinas, black crusts and erosions. The top part of the arches is also affected by percolation of rainwater out of the roadbed: nowadays the use of de-icing salts worsens the effects of these waters on the masonry and the loss of effectiveness in time of the original drainage pipes let these waters reach the inner part of the masonry, causing diffuse efflorescence in the vaults.



Figure 2: cracks caused by brickwork disposition, on the left. and structural fractures originated from differential deformations and settlements. In particular, in the center longitudinal crack on the intrados vault worsened by post-WWII reconstructions (span n.12) and, on the right, lateral cracks on the arch extrados (span n.17).

It is also interesting to notice that the position of the brick masonry areas more affected by missing parts appear related to the brickwork disposition: in particular, the edge between the vault and the arch front elevation in some cases shows the detachment of a more or less long masonry portion along the edge itself, whose boundaries seem related to the intersection between the header course masonry of the vault and of the arch, possibly also enhanced by structural stress concentrations (Fig.2, left). In some cases, the masonry portions are still in place, but already detached by a characteristic crack pattern at about 20 cm from the edges. Other cracks are clearly related to reconstructions, carried out after bombs hit the structure in World War II and after car accidents damaged the lateral walls.

Nevertheless, some other cracks in specific parts of the bridge can have a structural origin. These can be schematically divided in two typologies: cracks on the fronts, related to the arch mechanisms and cracks under the vaults, related to differential deformations. In the vaults n.2, n.5 and n.12, starting from the West end, longitudinal cracks are visible: these could be connected to different settlements of the North and South arches, possibly already during the removal of the centering in the building phase, as reported in some historical documents.

On the fronts, several arches show cracks on the extrados, laterally, in positions that are typical for depressed three-centered arches. When movements of the imposts (for settlements

or rotations) are present, the crack pattern loses its symmetry. In some cases, also the parapet shows inclined cracks, related to the settlement of the arches and of the supporting piers. Both for the piers and arches settlements, for a confirmation of these hypotheses it is important to check the actual present geometry, thanks to the precise survey, identifying deformations and loss of horizontality in the two directions.

3.3 Deformations analysis

In order to identify the deformations, the geometrical survey has been analyzed comparing the levels of the pillars and the levels of the arches crowns, in the hypothesis that they were all (respectively) at the same level and that all the arches had the same geometry. Another basic hypothesis is that no elements increased their level in time. Therefore, comparing the levels of the elements originally aligned it was possible to identify the differential settlements both longitudinally and transversally to the bridge.

Table 2: Data of longitudinally and transversally settlements of piers and arches

	PIRES SETTLEMENTS				ARCHES SETTLEMENTS			
SPAN	HNORD	HMAX-HP	HSOUTH	HMAX-HP	FNORD	FMAX-FA	FSOUTH	FMAX-FA
-	541,67	6,90	539,96	6,49	-	-	-	-
1	540,52	8,05	539,1	7,35	425,12	8,53	427,98	5,45
2	543,8	4,77	542,81	3,64	**433,65**	0	**433,43**	0
3	545,16	3,41	545,04	1,41	418,86	14,79	417,53	15,9
4	540,98	**7,59**	542,11	4,34	428,86	4,79	424,42	9,01
5	541,53	7,04	542,15	4,30	425,78	7,87	421,44	11,99
6	544,12	4,45	544,13	2,32	411,96	21,69	407,26	26,17
7	543,85	4,72	543,91	2,54	405,54	28,11	417,61	15,82
8	544,94	3,63	543,69	2,76	411,15	22,50	415,84	17,59
9	**548,57**	0	**546,45**	0	400,44	**33,21**	392,09	**41,34**
10	544,33	4,24	544,36	2,09	410,55	23,10	407,63	25,80
11	547,81	0,76	545,66	0,79	399,32	**34,34**	405,62	27,81
12	544,96	3,61	543,00	3,45	387,68	**45,97**	393,56	**39,87**
13	545,20	3,37	545,03	1,42	385,43	**48,22**	394,20	**39,23**
14	546,00	2,57	542,69	3,76	410,30	23,35	408,31	25,12
15	544,94	3,63	544,51	1,94	401,01	**32,64**	418,94	14,49
16	535,23	**13,34**	539,09	7,36	407,20	26,45	412,46	20,97
17	541,50	7,07	538,19	**8,26**	411,38	22,27	397,81	**35,62**
18	543,05	5,52	537,12	**9,33**	396,10	**37,55**	404,97	28,46
19	542,98	5,59	537,86	**8,59**	393,25	**40,40**	380,56	**52,87**
20	542,03	6,54	538,74	**7,71**	407,84	25,81	417,88	15,55

The first analysis regarded the pier top levels (Tab.2). The differential settlements turned out to be quite limited: less than 10 cm on more than 600 m of length and never more than 6 cm among two subsequent piers. These data prove the effectiveness of the underpinning interventions of the central piers foundations (from n.4 to n.14, starting from the West end): although these pillars are more directly affected by the river water flow, they show a mean settlement of 2.9 cm compared to 9 cm in the West piers (1 to 5) and 5.4 cm in the five more eastern piers. Indeed, also the geological tests had identified thicker layers of deformable silty sands on the West side while, on the East side, the stiffer gravels reach 17 m of depth.

Comparing these levels on the two fronts, the differences are quite small: the maximum inclination is 6 cm Southwards (i.e. upstream), on the Eastern piles.

As far as the shape of the arch is concerned – and particularly its rise – a comparison was made between the survey and the design shape, as inferred by the descriptions and drawings of Cocconcelli (Fig.3, left).

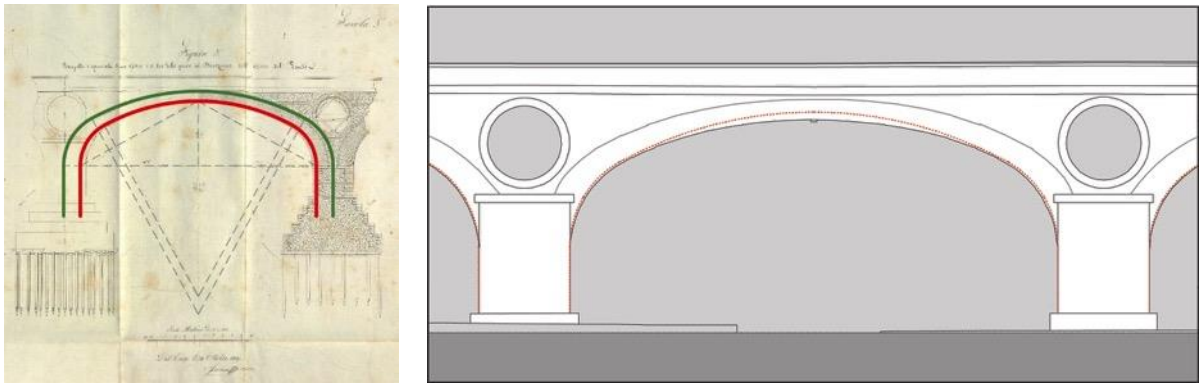


Figure 3: Differences of geometry between the original drawing by Cocconcelli (on the left) and the surveyed one (on the right, arch n.12).

7 out of 20 arches show a lowering of the keystone higher than 30 cm (Fig.3, right): this value seems to be imputable to further movements after the physiologic lowering of the arches during the centering removal in the construction phase (quantifiable from literature in a range between 16 and 30 cm [9]). Moreover, in order to evaluate if the longitudinal cracks could be connected to some torsional effects, the levels of the keystones of the North and South arch of each span were compared.

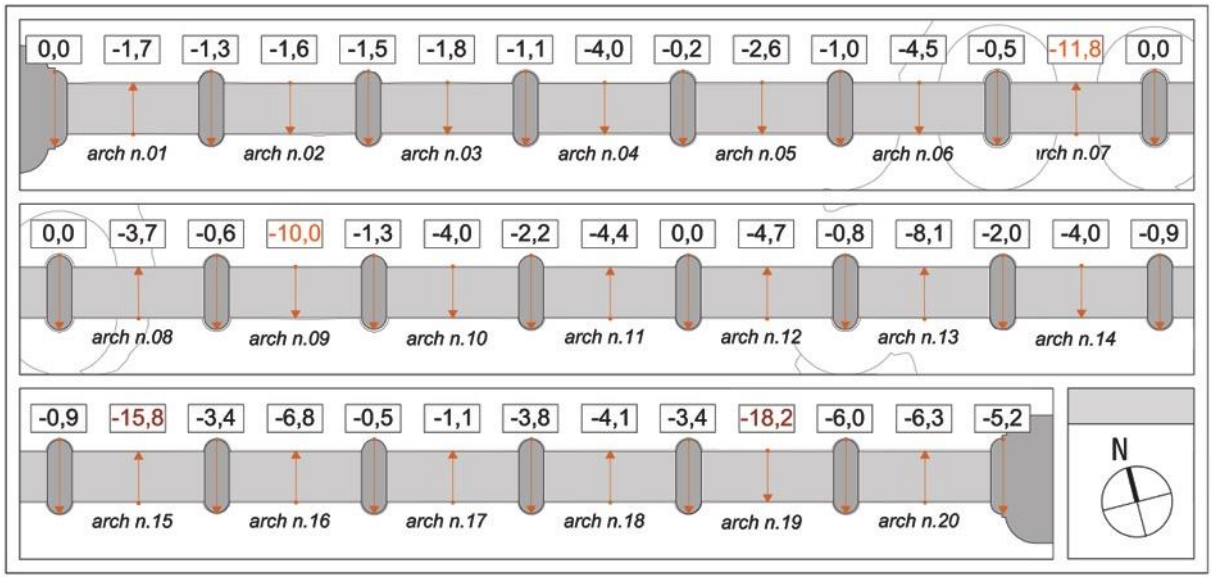


Figure 4: Comparison between the levels of keystones in the northern and southern side for each arch.

From the Figure 4 it's possible to see that the highest differences – between 15 and 20 cm - were measured in the arches n.19 (-18.2 cm) and n.15 (-15.8) while the arches n.7 and n.9 show differences between 10 and 15 cm. It is noteworthy that these level differences are not always in the same direction; anyway we can state that most of these inclinations are Southwards in the West Side of the bridge, changing Northwards in the East side (as represented by the arrows in Fig.4).

In conclusion, comparing the crack pattern with the deformation analysis, only in two arches it is possible to find correlations between the longitudinal cracks in the vault and the lowering of the keystone (n.12), as well as between the cracks in the extrados (arch n.9) and the settlement of the vault itself. This fact, together with the evidence of some loss in masonry apparatus and considering the possible mistakes during the construction phase (particularly important in the case of bridges with independent arches [10], as the case of study, Fig.5) leads to speculate that the cause of the damage is not structural but more reliably linked to local mechanisms ascribable to as many construction defects: only in these cases indeed, the question of resistance (otherwise not influential for the massive historic masonry constructions [11]) intervenes, showing local cracks.

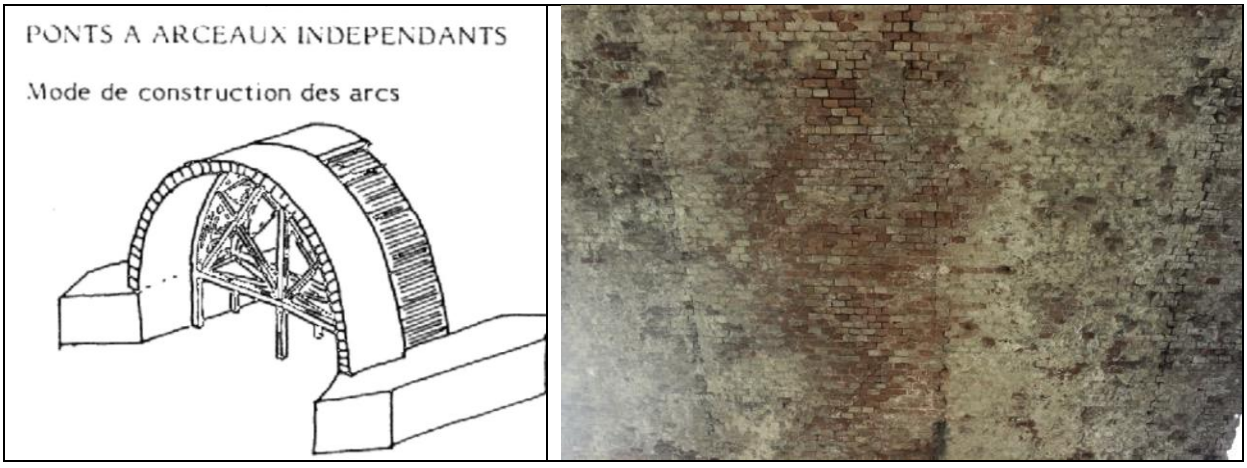


Figure 5: The longitudinal cracks below the arcades, imputable to as many mistakes in masonry apparatus during the construction phase (and the centering removal).

3.4 The simplified static analysis: back to geometry

In this geometrical route, an integrated analysis of the historical 'proportional theory' and the constructive characteristics of this peculiar masonry bridge has been carried out, in order to verify its stability, by a simplified and qualitative approach.

Many studies exist in literature on structural calculation of masonry bridges, which have included different load cases by using analytical and experimental methods [12, 13].

In this case, the first "verification" has been the adherence of the dimensions of the bridge to the prescribed proportional rules recalled in the first part of this paper (Fig.6, left).

By analyzing the main dimensions of the span and the pillars, indeed, it can be seen that the prescribed ratio of p/L equal to 1/6 is verified, thus following the proportional method, as explicitly declared by Antonio Cocconcelli himself in his project [7].

What we can notice is a slight "licence" in the thickness of the arches: Cocconcelli applied in his bridge a smaller ratio than the one prescribed by treatises, reaching – in the keystone – a thickness equal to L/18. This advancement certainly derived from the Mery's method results, used during his calculations of the bridge, whose reliability is definitely confirmed by the evidence that, despite the load over the bridge has significantly increased in time (up to the current traffic), it has demonstrated, until now, a surprisingly high load bearing capacity.

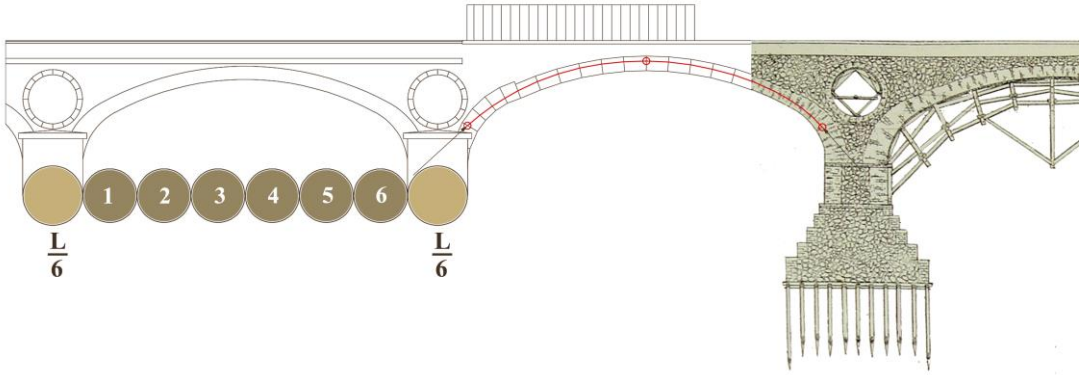


Figure 6: From the left, the analysis of the bridge: starting from the proportional theory to the "safe theorem" with the current loads.

Therefore, recovering the Mery's method, used by Coccocelli for the primeval dimensioning of its bridge, the first step has been the validation of the arch by static graphic analysis (fig.7, left), considering only the dead load of the three-centered arch and the abutments, constituted by bricks (specific weight equal to 18 kN/m3) and the internal filling of river cobblestones mixed with mortar (21 kN/m3), thus proceeding with a homogenization of the blocks. From this simple analysis, the curve of pressure was found to be all contained in the middle third of the arch thickness, thus guaranteeing the best beahviour of the masonry, within the imposed hinges at the extrados at the key and at 45° on the impost plane.

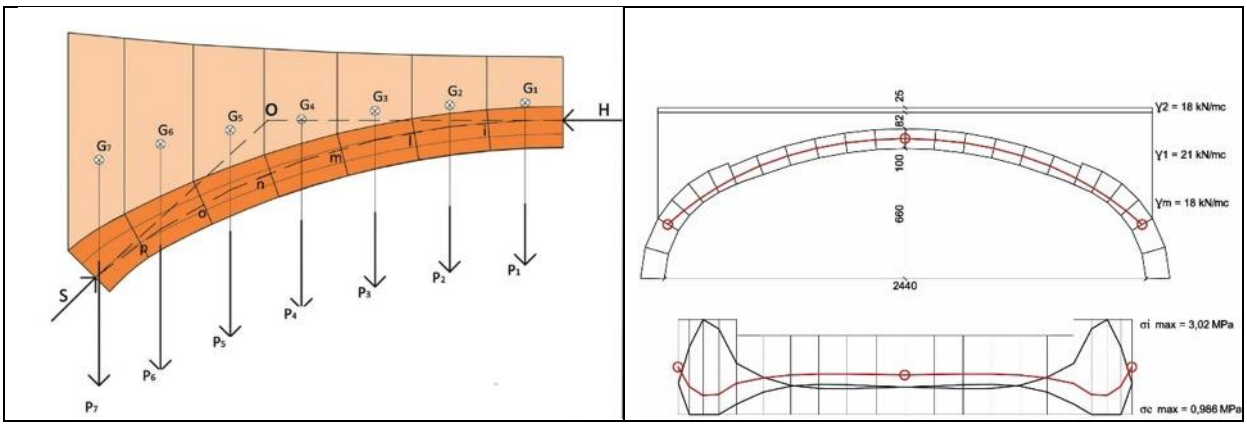


Figure 7: On the left, the result of the pressure curve with Mery's static analysis method, applied to the arch subject to dead load (with filling). On the right the same condition analyzed by limit analysis method.

The same result has been obtained by applying simplified limit analysis to the complete arch, considering the abutments and the different thickness at the imposts (1,30 m in the key and 1,6 m at the abutments).

The "safety factor" obtained in this case (intended as a ratio between the thickness of the arch and the minimum one suitable to contain the pressure curve) was 3,88, thus well above the collapse limit stated by Heyman [14].

As well known by literature and observed in the built evidences, the load on the abutments improves the stability of the structure: indeed, the same analysis carried out on the arch itself, without this additional load (Fig.8, left), restituted a sensibly lower "safety factor" (2,54), however far above the minimum required for stability.

Surprisingly, even the simulation of the current worse load combination has given good results: the third simulation saw the load of a 5-axle articulated lorry (17kN / m) in the worst, asymmetrical, configuration on the arch. Also for this extreme condition, the limit analysis of the arch, even simplified, has shown a sufficient "safety factor" (2,22).

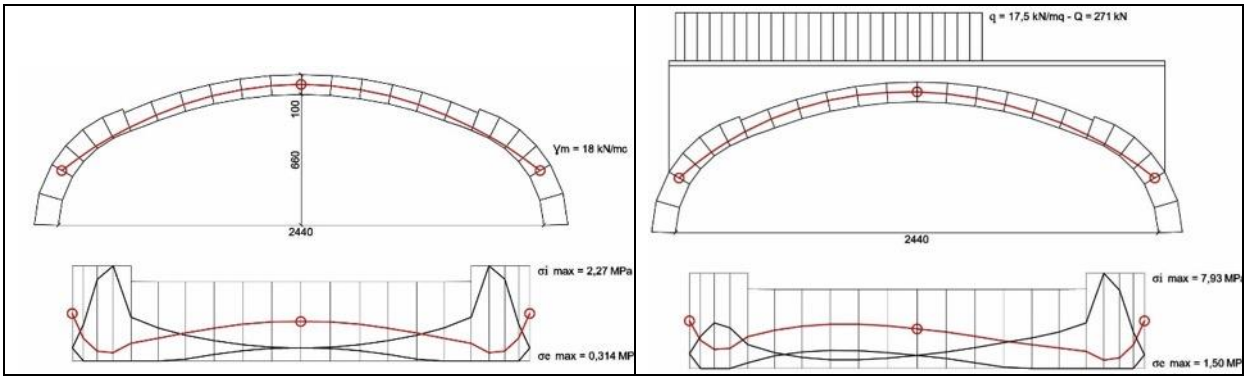


Figure 8: The results of limit analyses of the arch in the simple configuration (with the only dead load, without abutments) and in the current load conditions (on the right).

4 CONCLUSIONS

The history of construction can be ultimately seen as the translation of structure into geometry: the final shape of a construction used to be the formal result of an empiric calculation – strict and scientific: each built monument constitutes an experiment, 1:1 scale, whose positive, or even more negative outcomes (as repeated collapses) has given in time important pieces of information for the correction of the 'mistakes'.

The comparison between similar mechanisms and pathologies has allowed to trace the field of application of these theories in solving the safety problem and in guaranteeing the equilibrium of masses.

In step with this, the information obtainable through a specific interpretation of the geometrical survey data can represent powerful tools for the comprehension of the present structural conditions of an historical structure and precious elements for the validation of any further numerical model [15]. Moreover, retracing in the structure, the ancient dimensional rules prescribed for the specific building typology, can constitute a first and expeditious method of analysis which, recovering the equilibrium principles, can give a reliable base for further and more complex analyses, which are not always gobernable in the final results.

Recovering the principles (dimensional and technical) which governed the design and the construction of ancient structures, is the first step to reliably interpret, even in a very simplified way, their current damage and residual behavior, which is the first condition for setting up a correct strategy of structural strengthening.

REFERENCES

[1] J. Heyman, *Structural Analysis: an historical approach*, Cambridge University Press, Cambridge, 1998.
[2] G.B. Milani, *L'ossatura murale*, Crudo & C., Turin, Italy, 1920.
[3] S. Huerta, *Arcos, bovedas y cupolas: Geometria y equilibrio en el calculo tradicional de estructuras de fabrica*, Tapa Blanda, 2004
[4] S. Sanabria, *The mechanization of design in the 16th century: The structural formulae of Rodrigo Gil de Hontañón*, Journal of the Society of Architectural Historians, 41, 1981, pp. 281-293
[5] F. Blondel, *Cours d'architecture enseigné dans l'Académie Royale d'Architecture*, Paris, 1675, parts II-V
[6] E.M. Gauthey, *Traité de la construction des ponts*, Firmin Didot, Paris 1809
[7] A. Cocconcelli, *Descrizione dei progetti e lavori per l'innalzamento dei due ponti sul Taro e sulla Trebbia*, Parma, 1825
[8] N. Bruno, E. Coïsson, F. Diotri, L. Ferrari, S. Mikolajewska, U. Morra di Cella, R. Roncella, A. Zerbi, *History, geometry, structure: interdisciplinary analysis of a historical bridge*. ISPRS Annals of the Photogrammetry, Remote Sensing and Spatial Information Sciences, 2019, Vol XLII-2/W11, pp.317-323.
[9] F. Derand, *L'Architecture des voûtes, ou l'Art des traits et coupe des voûtes... par le R.P. François Derand,* Sebastian Cramoisy, Paris 1643
[10] J. Mesqui, *Chateaux at encentes de la France médiévale: de la défense à la résidence*, Editions A&J Picard, Paris, 2013
[11] S. Huerta, *Galileo was wrong: the Geometrical design of masonry arches,* Nexus Network Journal, 8, 2006, 2, pp. 25-52
[12] A. Brencich, D. Sabia, *Experimental identification of a multi-span masonry bridge: The Tanaro Bridge*, Constr. Build. Mater., 22, 2008, pp.2087-2099
[13] D.V. Oliveira, P.B. Lourenco and C. Lemos, *Geometric issues and ultimate load capacity of masonry arch bridges form the northwest Iberian Peninsula*, Eng. Struct., 32, 2010, pp. 381-394.
[14] J. Heyman, *The Masonry Arch*, Ellis Horwood, Chichester, 1982.
[15] S. Huerta S. *Mechanics of masonry vaults: The equilibrium approach,* Historical Constructions, PB Lourenço, P Roca (Eds.), Guimarães, 2001.

12th International Conference on Structural Analysis of Historical Constructions
SAHC 2020
P. Roca, L. Pelà and C. Molins (Eds.)

GAUDÍ, A NEW ARCHITECTURAL CONCEPT OF MAXIMUM STRUCTURAL EFFICIENCY: CATENARY VAULTS, COMPLEX RULED SURFACES, BRANCHED PILLARS AND AN ENDLESS INNOVATIVE STRATEGIES

CARLOS SALAS[1], CÉSAR BEDOYA[2], JOSÉ M. ADELL[3]

[1] PhD from the Polytechnic University of Madrid - ETS Higher School of Architecture
Department of Architectural Construction and Technology (DCTA)
Member of the Innovative and Sustainable Construction (TISE) Research Group
E-mail: carlossalasm@gmail.com

[2] Professor at the Polytechnic University of Madrid - ETS Higher School of Architecture
Department of Architectural Construction and Technology (DCTA)
Member of the Innovative and Sustainable Construction (TISE) Research Group

[3] Professor at the Polytechnic University of Madrid - ETS Higher School of Architecture
Department of Architectural Construction and Technology (DCTA)
Head of the Innovative and Sustainable Construction (TISE) Research Group

Keywords: Antonio Gaudí, structural efficiency, mechanical optimization, catenary vaults, catenary arches, ruled surfaces

Abstract. *For the first time in the history of architecture, Antonio Gaudí used structural elements based on complex ruled surfaces – beyond traditional conical or cylindrical surfaces –, catenary vaults or branched pillars, in order to increase the structural efficiency of his buildings. The catenary arch had been used only in the construction of bridges by a few engineers, starting in the 18th century. Arata Isozaki said that the "scale model and the structural analysis of the church at the Güell Colony are the most original in the history of architecture". Beyond his artistic and creative genius – which has now been widely studied and acknowledged – Gaudí was a revolutionary architect, whose experimental approaches to the design and calculation of structures implied a focus that was so far ahead of its time that later, hugely significant engineers and architects have coincided with the methods and systems used by Gaudí half a century earlier. Norman Foster said in reference to Gaudí: "his methods, a century later, are still revolutionary".*

1 INTRODUCTION

Antonio Gaudí – the architect of seven buildings on the UNESCO World Heritage List – has been acknowledged as one of the great authors of the formal renovation of architecture in the twentieth century [1]; his artistic talent, the innovation in his natural architectural style – with surprising forms and colours – his technical and constructive innovation, and even the bioclimatic progress in his architecture have all been valued. Not enough work, however, has been done on the importance of his person, the great legacy of his work in many other fields, such as sustainability and biomimetics in architecture; we could make special mention of the

mechanical optimization of structural designs and structural efficiency.

We could state that the "significant formal renovation brought about by Gaudí's architecture in the early twentieth century was not just an aesthetic or stylistic renovation, but also functional and technological, planting its roots deeply in numerous social, economic and environmental causes, the forerunners of modern ecology and sustainability" [2]. Antonio Gaudí was not just a great architect and a great artist – as is generally acknowledged – he was much more in addition; he was a great engineer and a great scientist, comparable to the great geniuses of the Renaissance, such as Leonardo Da Vinci and Michelangelo. Just like the great humanists of the Renaissance, he did not just study architecture and art, but also cultivated many other fields of knowledge; he devoted his life to study and research.

As shown in the PhD thesis entitled *Antonio Gaudí, precursor de la sostenibilidad en la arquitectura* [3], Gaudí may be seen as one of the fundamental forerunners of sustainability in architecture – 100 years ago – and at the same time, of twenty-first century biomimetic architecture too [2]; nevertheless, some of his most outstanding achievements – in the field of sustainability and biomimetics in architecture – are related to structural design, the fruit of the tireless quest for mechanical optimization and structural efficiency.

Gaudí – by means of a profound scientific study of mechanical models in nature – came up with surprising and innovative structural designs. These designs implied the first significant progress – in the field of structural architectural design – after many centuries of the cyclical repetition of the same mechanical principles: the mechanical principles of Gothic, Renaissance, Baroque, Neo-Gothic, Neo-Classical architecture and numerous other historical styles. Examples of this innovative structural design can be found in buildings as diverse as the Sagrada Familia Church, the Sagrada Familia Schools, the Crypt at the Güell Colony and Güell Park.

2 NATURE AS A MODEL: BIOMIMETIC ARCHITECTURE

We could say that there are two creative forces: nature and mankind. Nature has its own laws, which we cannot change and which we are subject to; mankind – in his creations – may respect the laws of nature or go against them – fighting against the elements – whimsically or opportunistically; this does not mean that mankind's respect for nature implies limiting his creative capacity, but rather simply bringing both creative forces together to avoid conflict between them [4]; creativity in Gaudí's architecture – and his respect for nature – is a good example of this.

Gaudí realized the importance of studying models in nature, not just aesthetically or artistically – as had been done throughout the history of architecture – but rather in a much more profound way; in a purely scientific way. Gustavo García Gabarró states that:

"Faced with architects' foolish passion for 'inventing' new forms that turn out to be a repetition or combination of previous ones (…) the great merit of Gaudí resides precisely in turning his gaze to nature, recognizing it as a generous teacher and maintaining a humble state of mind in its presence, not so much in order to invent anything but rather to discover it all" [4].

"This inspiration in nature is not approached as a romantic dream, removed from daily reality, but rather consists of working through the profound observation of the models nature has been rehearsing for millions of years, taking advantage of its experience, capable of reading wise lessons of welfare, economy and the reduction of costs, expressions so often repeated in

today's world" [5].

En 1969, Ian McHarg published the book *Design with nature* [6], a pioneer in the concept of the "ecological project". In 2000, the *Hannover Principles* explicitly expressed the importance of nature as a model of sustainability and architectural efficiency: "Those who create and plan should practice humility in the face of nature. Treat nature as a model and mentor… [7]".

There is today a new science known as "biomimetics", in which – just as Gaudí said 100 years ago – nature is taken as a model, or source of inspiration, for the development of new technologies. Nature – in its 3.8 billion years of evolution – has developed extraordinarily efficient designs, the result of a lengthy process of adaptation to endless geographical, orographic, geological, biological, climatic and environmental variables; we could say that the complex equation of these variables has been solved by nature, giving rise to "smart design" structures. This kind of functional structure can be studied and mimicked – or more precisely, reinterpreted – in order to develop more efficient and more sustainable technologies.

Janine M. Benyus, the founder of the "Biomimicry Institute", says that "the first level of biomimicry is the mimicking of natural form, but you can reach a second level, which is when you mimic the natural process". Access to this second level is the great contribution of Gaudí's architecture, a century before the beginning of what we now know as "biomimetic architecture". The first level – i.e. the mimicry of natural forms on an aesthetic level – had already been used in architecture since ancient times.



Figure 1: "One Ocean" Pavilion at EXPO 2012 (South Korea)
Source: www.youtube.com/watchv=iCAGlu4vPog

By way of example, the thematic pavilion "One Ocean" (figure 1), at EXPO 2012 in Yeosu (South Korea) – designed by the Austrian company Soma – includes a folding system known as "Flectofin", inspired by the pollination mechanism in the Bird of Paradise flower, whose petals are capable of folding up to 90°; the system has no need for hinges, and operates on changes in the temperature. Ventilation and solar radiation can thereby be controlled.

3 GAUDÍ'S GEOMETRY: BIOMIMICRY, SUSTAINABILITY AND STRUCTURAL EFFICIENCY

We could say that geometry is architecture's own language, just as sound is for music, and language for literature [4]; this is why Gaudí said that:

"The architect should not talk vaguely (…) but rather specifically; his language is geometry" [8].

From the point of view of biomimicry, we could say that architectural design and the varied geometries of nature are the best model for efficiency and sustainability, as they are the result of a process of adaptation over millions of years (figure 2); the problem resides in its formal complexity and the difficulty in transferring it to the field of architectural design.

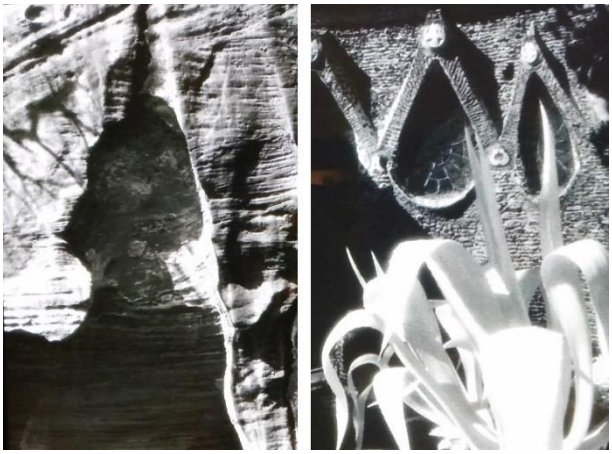


Figure 2: La Roca (Mont-Roig) and windows of the Crypt at the Güell Colony
Source: C. Salas Mirat ("Gaudí Centre" Museum in Reus)

And yet Gaudí realized that some forms of nature can be easily transferred into architecture, assimilating them to those derived from ruled geometry; in other words, those which can be generated by means of straight lines which move in space. The builders who worked with Gaudí erected them quickly and simply using no more than rulers and cord. Even though these figures are not easy to depict graphically on plans, Gaudí also overcame this problem, by working with scale models [4].

For the first time in the history of architecture, Antonio Gaudí used structural elements based on complex ruled surfaces – beyond traditional conical or cylindrical surfaces –, catenary vaults or branched pillars, in order to increase the structural efficiency of his buildings, saving huge amounts of material, improving the use of inner spaces [9], ventilation, illumination and exposure to sunlight, with the consequent savings in energy.

The vaults in the Sagrada Familia (figure 3) are formed by hyperboloids. These ruled surfaces are hollow in the middle – where the keystone was on old Gothic arches – and this means the vaults are lighter and their mechanical function is performed better, providing a great deal of natural light in the transepts. At the same time, at the intersection of the vaults – where the ribs were in the Gothic style – the hyperboloids open up small bays, achieving the effect of a starry sky.



Figure 3: Vaults in the Sagrada Familia
Source: esbocoseprojetos.wordpress.com/2017/04/02/exposicao-gaudi-barcelona-1900/

The Sagrada Familia Schools are built with just hollow brick tiles and wooden beams (figure 4). The technology employed is extremely simple. It consists of the traditional Catalonian vault, adapted to the shape of the conoid, as "this ruled surface could serve vertically to provide structural rigidity for the perimeter walls of the building, with a minimum use of materials and labour" [10]. Le Corbusier himself was impressed and publicly expressed his admiration for this little building when he visited it in 1928.



Figure 4: Sagrada Familia Schools
Source: www.gypsynester.com/gaudi.htm

Gaudí said that the "true silhouette is born of the structure itself" [11]; and later on, Eduardo Torroja also said that "the best buildings are held up by their form and not by the hidden resistance of their material" [11].

4 STRUCTURAL EFFICIENCY IN GAUDÍ

Gaudí did not search for easy solutions, but on the contrary, he studied the advantages and disadvantages of each of his innovations in great detail; some of them are the fruit of many years of research, tests and trials.

Carlos Flores says that "the experimental approaches to design and the calculation of structures used by Gaudí were such an advanced solution to the problem for their time that later engineers and architects of great prestige have all inadvertently employed the methods and

systems used by Gaudí half a century earlier" [12]; a good example of this is the double-curve ruled structure of the Olympic Park in Munich, built by Frei Otto in 1972 (figure 5).



Figure 5: Olympic Park in Munich, Frei Otto
Source: footage.framepool.com/es/shot/665113940-estadio-olimpico-pilar-puntal-frei-otto

New information technology for structural calculation has shown how accurate Gaudí's designs and calculations were. In 1986, the professors of structure at the Polytechnic University of Catalonia Juan Margarit and Carlos Buxadé calculated the structure of the Sagrada Familia Church, and saw that it coincided perfectly with Gaudí's previsions [13].

The calculation system developed by Gaudí in the stereostatic scale model of the Church at the Güell Colony – in over ten years of research before work actually started – "goes beyond what was achieved by his predecessors in experiments with (hanging) models. In accordance with what was known at the time, Gaudí built the first ever three-dimensional hanging model for the design of a building" [14].

4.1 Catenary arches, ruled surfaces and branching pillars

The catenary arch and ruled surfaces are the fruit of many years of research by Gaudí, "gathering information from studies published at the time by mathematicians, physicists, biologists, architects and other scientists" [15]. The mechanical properties of the catenary have been known since 1691; the first mathematicians confused it with the parabola, until Dutchman Christiaan Huygens showed that they were in fact two different curves. In the history of architecture, however, this kind of arch was rarely used until it was rediscovered by Gaudí [16].

In ancient times, especially in the East, stable arches were intuitively built with the curvature of inverted catenaries. In Sudan, for example, catenary adobe vaults were built. However, western culture – from Greece and Rome – designed its arches and vaults based on curvatures derived from the circle; this type is easier to build, but less stable and efficient. During the Middle Ages and the Renaissance, catenary arches and vaults were forgotten in Europe, despite the poor functioning of the semi-circular arches. Later on, even the Gothic architects were unable to find the appropriate form to transmit the horizontal forces.

From the 17th century onwards, theoretical research on inverted catenary began. In 1675, Robert Hooke wrote that "a*s hangs the flexible line, so but inverted will stand the rigid arch"* thus opening up the path for the investigation of catenary arches; in 1697, David Gregory showed that the arches are supported when they have a catenary inside; La Hire, from 1695 to 1712, studied in detail the friction between voussoirs and the stability of the arches; from 1730

to 1732, Complet and Danyzy carried out a number of mechanical experiments; in 1743, Giovanni Poleni, based on the investigation of the fissures in the Dome of Saint Peter, progressed in the study of the static model of the functioning of Gregory's catenary; in 1744, Euler carried out research on catenoid surfaces and consequently many other scientists – mathematicians, physicists, architects, engineers, etc. – devoted themselves to the investigation of catenary arches and catenary vaults during the 17th, 18th and 19th centuries. However, all these studies on the inverted catenary were only put into practice by a few engineers, starting in the 18th century, for the construction of bridges. Therefore, they did not have repercussions in the field of architectural design – nor in the different architectural trends and styles of the 19th century – until the arrival of Antonio Gaudí.

At the end of the 19th century, Antonio Gaudí devoted himself to the in-depth study of all these sources during many years until he achieved – for the first time in the history of architecture – the development and systematic application of the catenary and other anti-funicular arches in large buildings; he was the first to investigate and make use of them in his works. By way of example, as mentioned above, in the Crypt of the Colonia Güell, ten years of studies with funicular models preceded the start of the works. In these years, Gaudí developed an ingenious and practical calculation system using funicular models based on strings and small bags of shot pellets (figure 6), of which he later took photographs from different angles. By turning the photographs upside-down, he obtained the layout of the catenary arches and the vaults.



Figure 6: Funicular model of the Colonia Güell Church
Source: C. Salas Mirat ("Diocesano" Museum in Barcelona)

However, the use of arches and catenary vaults are not Gaudí's only great contribution to architecture in the field of structural design. In the Sagrada Familia, Gaudí's intention was to create architecture with new, more balanced and more resistant structures, to improve on the

structures of European Gothic cathedrals. He therefore came up with pillars with a branching tree structure – based on a complex study of cord and weights, used in the crypt in the Güell Colony – which enabled him to determine the diameter and inclination of the pillars and the load transmitted onto the central core. He thus got the greater part of the structure to work under compression – instead of by flexion – and made the distribution of load more balanced, transferred onto the inner pillars and not just the perimeter elements. He was thus able to eliminate the huge Gothic flying and other buttresses, thereby saving material and space in the layout [3].

The branched tree structure of the pillars in the Sagrada Familia – like a self-supporting wood – eliminates the flying buttresses, which Gaudí called the "crutches of the Gothic style" [14]. Gaudí liked comparing the stability and resistance of Cologne Cathedral to those of the Sagrada Familia (figure 7), taking into account that with similar spans, the pillars cross-section of the latter is three times less, and in the buttresses four times less [17]:

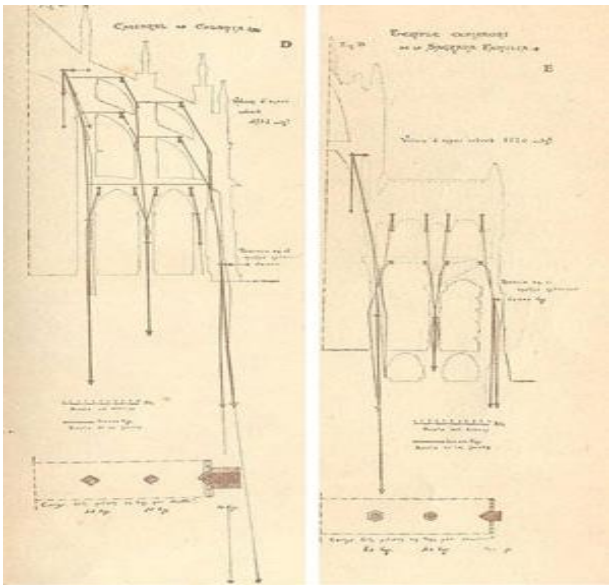


Figure 7: Pillars and buttresses in Cologne Cathedral and the Sagrada Familia
Source: www.sagradafamilia.cat/sf-cast/docs_instit/estructura1.php

"When Gaudí took charge of the Sagrada Familia, which started out in the Gothic style – at the time this was almost compulsory for religious buildings – his main concern was how to diminish the inclined force, which would have meant building buttresses, flying buttresses and spires which act as mainstays and dead weights to verticalize the force. His spirit of synthesis could not accept the complex of centrifugal force which acts in Gothic churches and favours the disintegration of the elements, compensated by parasitical superstructures of dead weights and contrary thrust which tend to compensate the disintegrational force" [18].

Furthermore, in the Sagrada Familia Church the parabolic belfries with a circular horizontal cross-section, designed by Gaudí, reduce the wind force by over half – one of the main problems when building at height – in comparison to the continuous square horizontal cross-section belfries – designed by Francisco de Paula del Villar – in the original project. The openings in

the belfries also contribute to this [17].

Gaudí thereby brings together three fundamental principles: mechanics, geometry and construction, in order to produce a logical architecture in which each element fulfils its function with the minimum effort. The "mechanical" fact is manifested "geometrically" and specified in the appropriate "constructive" element [18].

4.2 Other structural innovations by Gaudí

In the Casa Milá, Gaudí – ahead of his time – placed one of the first garages in Barcelona in the basement; in order to achieve a more open space, he designed an innovative metallic structure with radial beams – shaped like a bicycle wheel – which was later mimicked in the United States pavilion at the Universal Exhibition in 1958 (figure 8), where it was the object of great praise [19]. It is a radial structure with triangular metallic beams, joined in the middle to a metal ring and resting on metallic pillars on the outside [9].

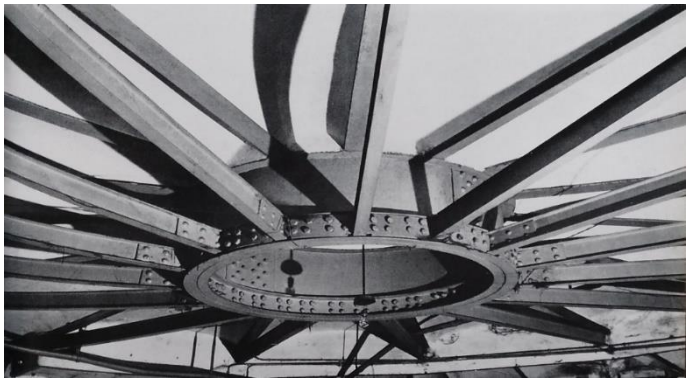


Figure 8: Metallic structure with radial beams in the basement of Casa Milá
Source: Martinell Brunet, C. (1967)

Still in Casa Milá, Gaudí designed an innovative metallic structure – lying on a base of mainstays and pillars – replacing the heavy load-bearing walls which buildings had at the time [20]. This structure enabled large spans and almost clear floors; i.e. the "Le Corbusian open floor, which Gaudí anticipated in this project" [21]. Furthermore, the elimination of the load-bearing walls meant considerable financial savings [18], and the possibility of opening up large spaces on the front for the ventilation and illumination of buildings, with the consequent savings in energy.

In the Güell Palace, the coffered ceiling in the visiting room is surprising thanks to its daring mechanics; its spatial structure boasts a greatly resistant efficacy, anticipating the future structures of reticular beams. Likewise, the ceiling in the dining room and the adjoining rooms is made up of reticular beams with Hispano-Muslim decoration [22].

In the Bellesguard Tower, we could say that Gaudí anticipates ribbed forging by an original brick design, whose solidity means that no joists were needed [23].

5 CONCLUSIONS

- The Catalonian architect Antonio Gaudí was not just a great architect and artist – extremely ingenious and creative, as is generally acknowledged – but also a great

scientist and a great engineer, who devoted many years of his life to researching the calculation of structures. He made such great progress in the concept of mechanics and the structural design of buildings that his contributions defined a before and after in the history of architecture.

- From a structural point of view, Antonio Gaudí was the author of a change which was many centuries in the coming; Gothic architecture was a significant step forward, but in the subsequent centuries – the Renaissance, Baroque, Neoclassicism, etc. – there had been no further significant progress in the field of structural design.
- Gaudí is one of the fundamental forerunners of sustainability and biomimicry in architecture; at the same time, he was the author of a new concept of organic architecture, of great mechanical perfection and innovative, never before imagined geometries: complex ruled surfaces, branching pillars, inclined pillars, catenary vaults and arches and endless geometries with the greatest possible structural efficiency.
- One might think that Gaudí's architecture was of great value in its historical moment, but that today it is a difficult model to follow, however nothing could be further from the truth. As was mentioned at the beginning, some of the world's most prestigious architects of the 21st century, such as Norman Foster, have come to affirm that: "Gaudi's methods, one century on, continue to be revolutionary" [17]. In order to fathom this, one must understand that interpreting the message of Gaudí's architecture is not about imitating his forms, textures or colours – or even his innovative construction systems – but rather it is about imitating the depth and scientific rigor with which he studied his works, focusing on nature as an example of efficiency, economy, ecology, functionality and beauty: "In this way, looking to the past, Gaudí's example and the genius of his architecture are projected into the 21st century, to help us in our search for authentic scientific progress" [2]. Hence, the architectural values of Gaudí that have been described, are not – as it might appear – a panegyric on Gaudí, but rather a rigorously scientific argument.

Acknowledgements. We are grateful for the collaboration by the TISE (Innovative and Sustainable Construction Techniques) Research Group and the Architectural Construction and Technology Department (DCTA) of the Higher School of Architecture at the Polytechnic University of Madrid (ETSAM - UPM).

Authors' contributions. The first author wrote the Paper, the second author reviewed the contents of sustainability in architecture and the third author reviewed the contents of Gaudi's construction systems. The authors declare that there is no conflict of interest.

REFERENCES

[1] González Moreno-Navarro A. *Gaudí, constructor (la materialización de una arquitectura singular)*. Informes de la Construcción. (1990);42(408 julio-agosto).

[2] Salas Mirat, C., Bedoya Frutos, C. and Adell Argilés, J.M. *Antonio Gaudí, precursor de la sostenibilidad y la biomimética en la arquitectura, con 100 años de antelación.* ACE: Arquitectura, Ciudad y Entorno. (2018);13(37 junio).

[3] Salas Mirat, C. *Antonio Gaudí, precursor de la sostenibilidad en la arquitectura* [tesis doctoral]. Universidad Politécnica de Madrid; (2018).

[4] Bassegoda Nonell, J. and García Gabarró, G. *La cátedra de Antoni Gaudí: estudio analítico de su obra*. Ediciones UPC, (1999).

[5] García Gabarró, G. *Leyes de la naturaleza y composición arquitectónica: el ejemplo de Antonio Gaudí* [tesis doctoral]. Universidad Politécnica de Cataluña; (1994).

[6] Mac Harg, I. *Design with nature.* American Museum of Natural History, (1969).

[7] McDonough, W. *The Hannover principles: design for sustainability*. William McDonough & Partners, (1992).

[8] Puig Boada, I. *El pensamiento de Gaudí*. Dux, (2015).

[9] Vila Rodríguez, R. *El uso del hierro en la Casa Milá de Barcelona.* Informes de la Construcción. (1990);42(408 julio-agosto).

[10] Bonet Armengol, J. *Las Escuelas de la Sagrada Familia*. Escudo de Oro, (2002).

[11] Andrés, O. and Ortega, N. *Extensión de la técnica funicular de Gaudí a la concepción y génesis de superficies estructurales*. Informes de la Construcción. (1993);44(424 marzo-abril).

[12] Flores López, C. *Gaudí, Jujol y el modernismo catalán, Tomo I.* Aguilar, (1982).

[13] Bassegoda Nonell, J. *El gran Gaudí.* Ausa, (1989).

[14] Tomlow, J. *El modelo colgante de Gaudí y su reconstrucción. Nuevos conocimientos para el diseño de la Iglesia de la Colonia Güell.* Informes de la Construcción. (1989);41(404 noviembre-diciembre).

[15] Cussó Anglés, J. *Disfrutar de la naturaleza con Gaudí y la Sagrada Familia.* Milenio, (2010).

[16] Bassegoda Nonell, J., Bassegoda Musté, B. and Lloveras Montserrat, J. *Aproximación a Gaudí.* Doce Calles, (1992).

[17] Bergós Massó, J. *Gaudí, el hombre y la obra.* Lunwerg, (1999).

[18] Martinell Brunet, C. *Gaudí: su vida, su teoría, su obra.* Colegio de Arquitectos de Cataluña y Baleares, (1967).

[19] Giordano, C. and Palmisano, N. *La última obra civil de Gaudí, La Pedrera, Casa Milá.* Dos de Arte Ediciones, (2011).

[20] Adell-Argilés, J. *Arquitectura sin fisuras.* Munilla-Lería, (2000).

[21] Flores López, C. *Sobre arquitecturas y arquitectos.* Colegio Oficial de Arquitectos de Madrid, (1994).

[22] González Moreno-Navarro, A. and Lacuesta Contreras, R. *Palacio Güell Gaudí, itinerario de visita*. Diputación de Barcelona, (2013).

[23] Giordano, C. and Palmisano, N. *Guía visual de la obra completa de Antoni Gaudí.* Dos de Arte Ediciones, (2011).

12th International Conference on Structural Analysis of Historical Constructions
SAHC 2020
P. Roca, L. Pelà and C. Molins (Eds.)

GEOTECHNICAL STRUCTURES IN THE ANCIENT WORLD. THE CASE OF THE ZIGGURAT OF UR IN MESOPOTAMIA

ELENA KAPOGIANNI

National Technical University of Athens 9 Heroon Polytechniou str.
Zografou, 15780 Athens, Greece
email: elkapogianni@mail.ntua.gr

Keywords: Historical Structures, Antiquity, Geotechnical Structures, Earth Retaining Structures, Numerical Modelling, Ziggurat, Cultural Heritage Preservation.

Abstract. *The current study presents several geotechnical structures which were built during the antiquity, aiming to illustrate the ancient technological achievements and to provide an insight into the geotechnical skills in the past. It is evident that ancient civilizations had awareness of the various geological and climatological / meteorological hazards (i.e. natural hazards) that affected the structures and used rather reliable techniques for that time. Furthermore, the study aims to illustrate how some of these are related to modern geotechnical structures. More specifically, the earth retaining techniques used for the construction of the massive pyramid-like structures Ziggurats are shown, highlighting their contribution to structural safety. In this framework, several numerical models have been built and analysed, using the Bishop Analysis for slope stability method and the Finite Element Stress Analysis Method. The results of the numerical simulations are presented and discussed.*

1 INTRODUCTION

Initial efforts of humans to understand the basic principles of geotechnical engineering date back to the prehistoric ages while using soil as a construction material has probably taken place well before the historical records. It is reasonable to assume that the first attempts to add materials to soil to increase its strength were made to stabilize swamps and marshy soils, using tree trunks, shrubs, and other 'reinforcement' materials. Such stabilization efforts may have continued with the development of a more systematic approach where for example tree trunks were uniform in size and length and tied together to form a uniform surface. Such an example are the corduroy roads (Figure 1), which were roads made of tree trunks in around 3000 BC [1].

Furthermore, retaining and fortification walls were often built during the antiquity, usually from stones and mud. Many archaeological sites worldwide include such walls, relatively well preserved. Foundation engineering techniques were also well known, aiming to control the water content in the soil and to distribute the loadings of the constructions uniformly. In the following section, examples of various geotechnical related constructions of the antiquity are shown.



Figure 1. Sketch of a corduroy road. (left) and excavation of a corduroy road (right).

2. ANCIENT GEOTECHNICAL STRUCTURES

Regarding ancient geotechnical structures, a well documented example consist the fortification walls of Troy [2], built during the Bronze Age (1700-1300 BC). The great walls of Troy were constructed using large hewn stones attached together, including also a layer of soil between foundation and bedrock (Figure 2). The specific structure is considered to be quite atiseismic, since the earth fill of the subfoundation acted like a seismic absorber. Another important example of ancient geotechnical structure is the polygonal wall in Delphi, Greece, where the well known ancient sancturary of Pythia was located. The walls were built from stones with curved joints that had excellent adaptation between them (Figure 3).

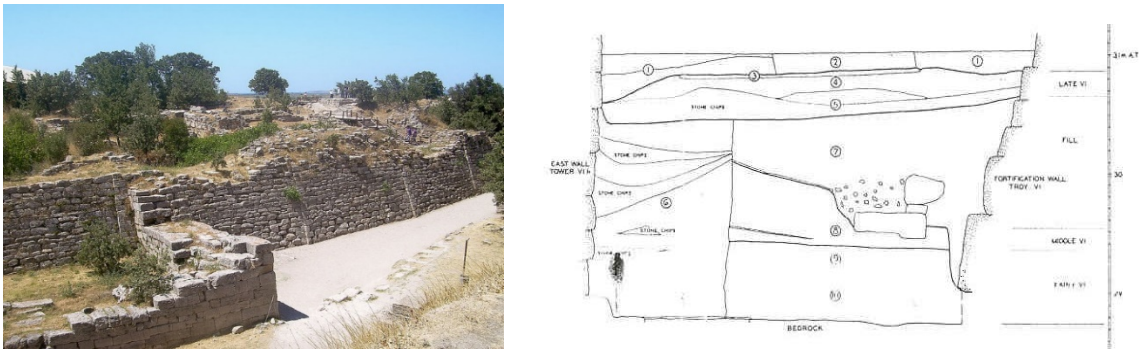


Figure 2. A view of the Troy wall (left) and a section showing the layer of earth between the foundation and the bedrock (right) (Blegen 1953).



Figure 3. The polygonal walls in Delphi, Greece (left), a wall failure in Delphi, Greece (right).

The very important archaeological site of the Acropolis of Athens, also includes extensive geotechnical works. More specifically, the Acropolis Hill was chosen due to its geomorphology by the fist inhabitants of Attica since the Neolithic period (4000 / 3500-3000 BC). Among the standing monuments of the Hill (i.e. Parthenon; Erechtheion; Propylaia; Arrephorion etc), the Circuit (Perimeter) Wall serves a pure geotechnical purpose, since it functions as a typical gravity wall, retaining the backfill that forms the plateau of the Acropolis and has total length of about 800 m and variable height areas 5-20 m [3], [4]. In Figure 4 the Acropolis Hill and the Circuit Wall are shown and a cross section of the south-east side of the Wall.

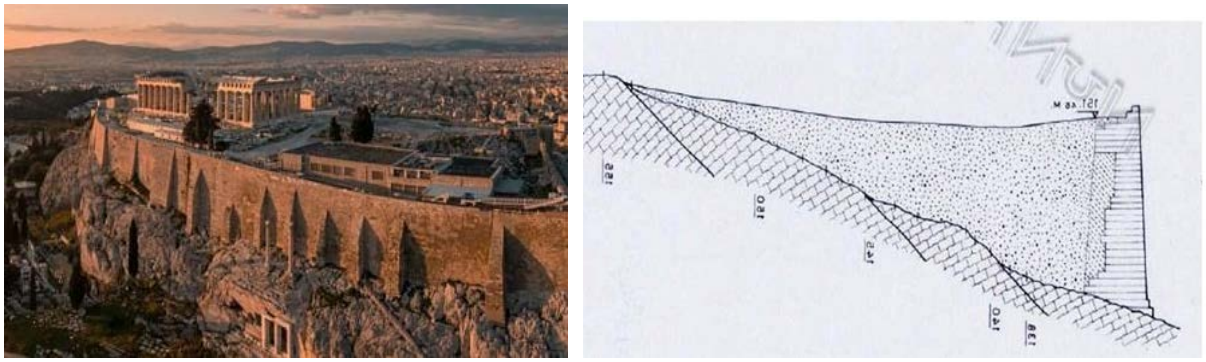


Figure 4. The Acropolis Hill and the Circuit Wall (left), and a cross section of the Wall (right).

Soil stabilization with reinforcement materials is another geotechnical engineering technique used during the antiquity. The Great Wall of China includes parts which were formed as reinforced soil. More specifically, layers of earth and gravel were reinforced with layers of desert brush branches and rammed solid (Figure 5).



Figure 5. Surviving Great Wall from the Han Dynasty.

Earth reinforced techniques also included the Ziggurats (Figure 6) which were built by the Sumerians, Babylonians, and Assyrians in ancient Mesopotamia, from the 40th to the 6th century BC. [5]. These constructions consisted of walls covered with clay bricks and layers of mats made of baskets, which were placed in the mud between the bricks as horizontal reinforcements. Additional reinforcement was included in some of the Ziggurats in the form of ropes, about 50 mm in diameter each, placed perpendicular to the wall at even intervals, in horizontal and vertical directions.



Figure 6. The reconstructed facade of the Great Ziggurat of Ur.

3 ZIGGURATS AND EARTH REINFORCEMENT

The operation of reinforced earth lies in the combination of the soil and reinforcement, in such way that a new composite material is created, combining their best characteristis. More secifically, the low cost soil has high resistance to compression and represents the largest volume of the construction material. On the other hand reinforcement materials increase the tensile strength and contribute to the development of a composite construction material with improved mechanical properties. The idealized reinforced soil mass can be seen in Figure 7 where friction between soil grains and reinforcement contributes to stabilization [6].

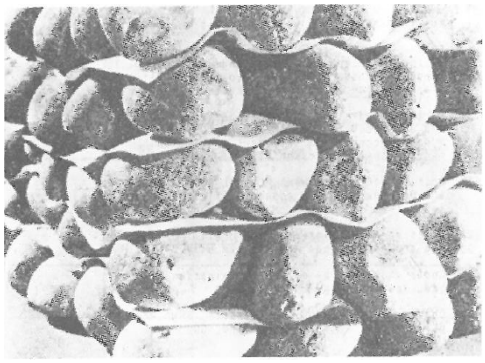


Figure 7. Idealized reinforced soil mass.

One of the oldest applications of soil reinforcement can be found at the Ziggurats in ancient Mesopotamia and western Iran. The Ziggurats were massive pyramid-like structures with the form of terraced steps of successively receding levels. They were constructed of clay bricks varying in the thickness between 13-40 cm, reinforced with woven mats of reed laid horizontally on a layer of sand and gravel at vertical spacings varying between 50 and 200 cm. A characteristic Ziggurat is the Aqar Quf structure, near Baghdad, Iraq which originally is believed to have been over 80 m high and now is 45 m tall [7]. Reeds were used to form plaited

ropes approximately 10 cm in diameter which passed through the structure and acted as reinforcement (Figure 8).

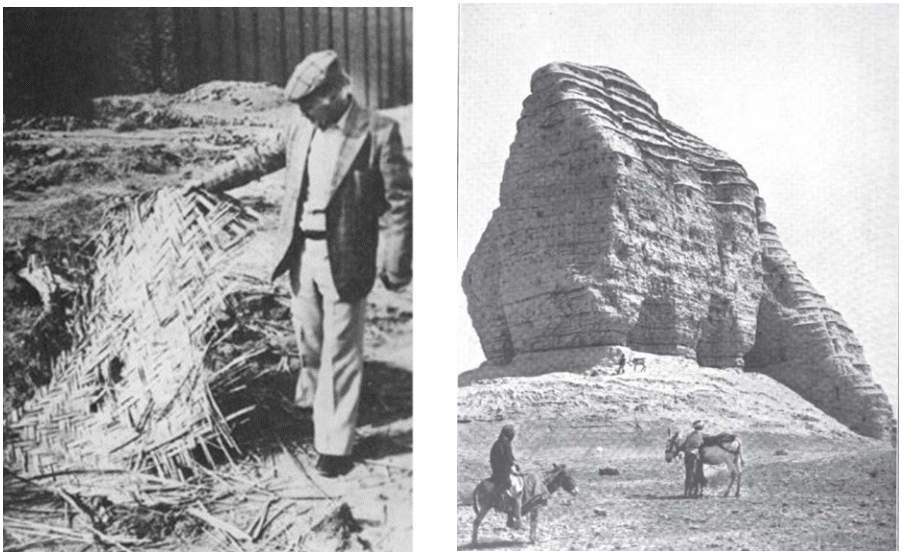


Figure 8. Stabilisation of foundations and brickworks with reet mats at Ziggurat temple at Aqar Quf (left). The Ziggurat of Aqar Quf in 1915 (right).

Another well known Ziggurat is the Great Ziggurat of Ur, which is Neo-Sumerian and was built in the Early Bronze Age (21st century BC). The famous ziggurat of Ur was constructed in three layers and the temple was built on the top layer. The structure was built from the outside with grilled wrapped bricks and woven canes in thick layers, and the inside with grill weges. The lower layer of the Ziggurat was built in a height of about 15 m and its dimensions were approximately 60 *45 m. The second layer was built with a height of about 6 m and dimensions approximately 35 * 25 m, and the third layer with a height of about 3 m, and dimensions approximately 20 * 10 m. In Figure 9 a representation of the Ziggurat of Ur can be seen (Amiet et al. 1981) and relatively recent restoration works.

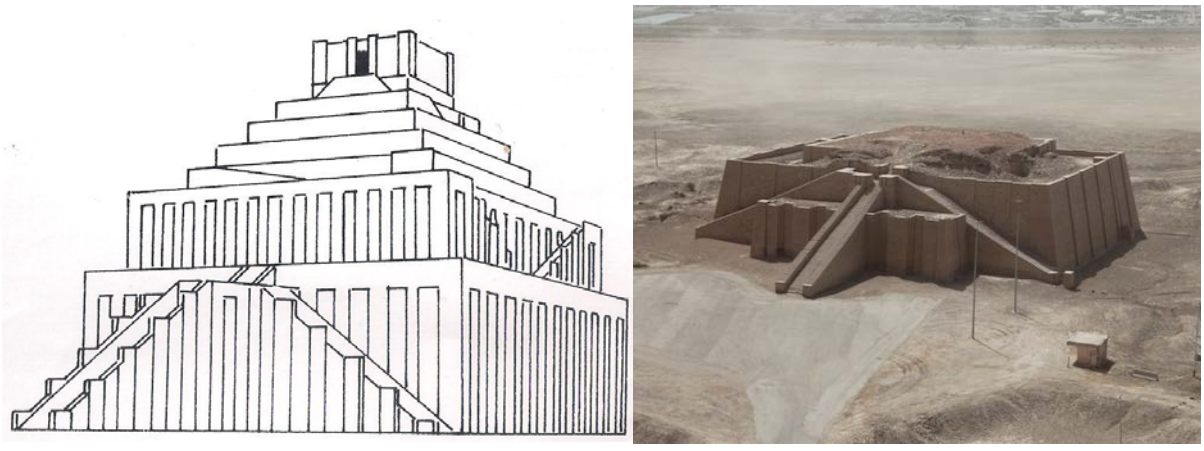


Figure 9. Representation of Ziggurat (left) and extensive reconstruction works (right).

4. NUMERICAL MODELLING

In the current section numerical simulations of constructions similar to the great Ziggurat of Ur are shown, focusing on the soil reinforcement that was included at the initial ancient construction. More specifically two dimensional, three-step numerical models have been built, with a height of 15m and length 45m for the first step, a height of 5m and length 30m for the second step, and a height of 3m and length 26m for the third step. The temple that existed at the top of the highest step has been replaced with a uniform loading, equal to 100kN/m. Sand was used for the soil material with friction angle equal to 35 degrees. Inclined walls were included at the exterior surface of every step, following their inclinations. Two different numerical methods have been used and more specifically a) numerical modelling with the Bishop Method for slope stability analysis, and b) numerical modeling with the use of the Finite Element Stress Analysis. The results are presented and discussed in the following and the importance of the horizontal reinforcement of the soil material is highlighted.

In Figure 10, the first model built can be seen, as it was analysed with the Bishop Method for slope stability analysis. This model includes inclined walls at the exterior surface of every step, without horizontal reinforcement layers at the soil mass. The Safety Factor (SF) that has been calculated is significant smaller than 1, which would be relatively acceptable SF. More specifically it has been calculated equal to 0.389 and the shape and center of the failure mechanisms are shown. The most critical failure mechanism is located at the fist step of the construction, which is expected since this step is the highest one (15m), with the steeper inclination (80 degrees). In Figure 11, the analysis at the other side of the model (right) is shown, and the results are quite similar as expected. It is therefore safe to examine only one side of the numerical model (left), with the Bishop Method for slope stability analysis. In Figure 12, the previous model with significant increased strength of the inclined walls is presented, and the results show that while the critical failure mechanisms are fewer, there is no impact to the Safety Factor of the construction.

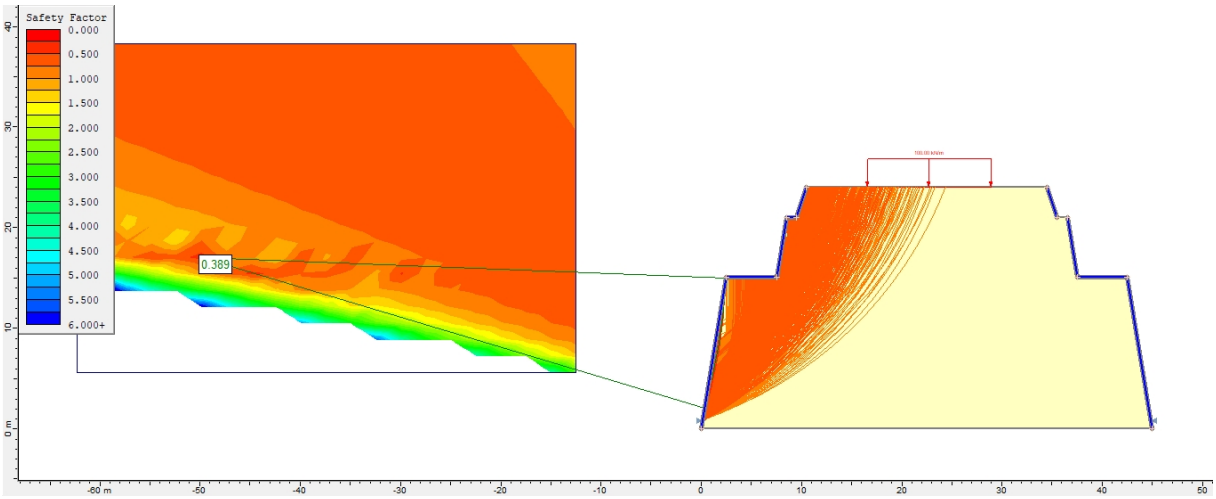


Figure 10. Numerical Model including inclined walls. Safety Factor: 0.389.

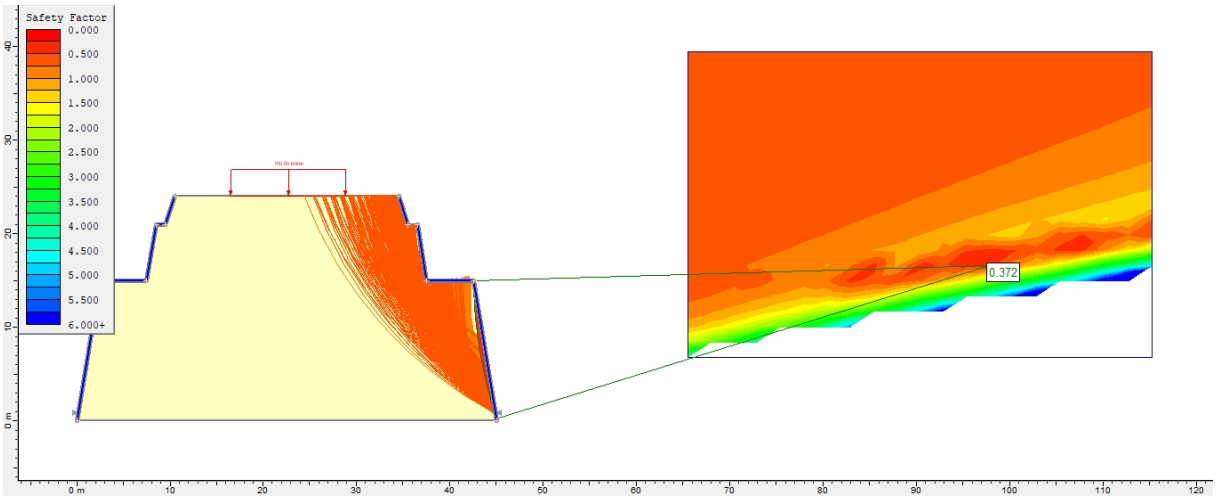


Figure 11. Numerical Model on the right side. Safety Factor: 0.372.

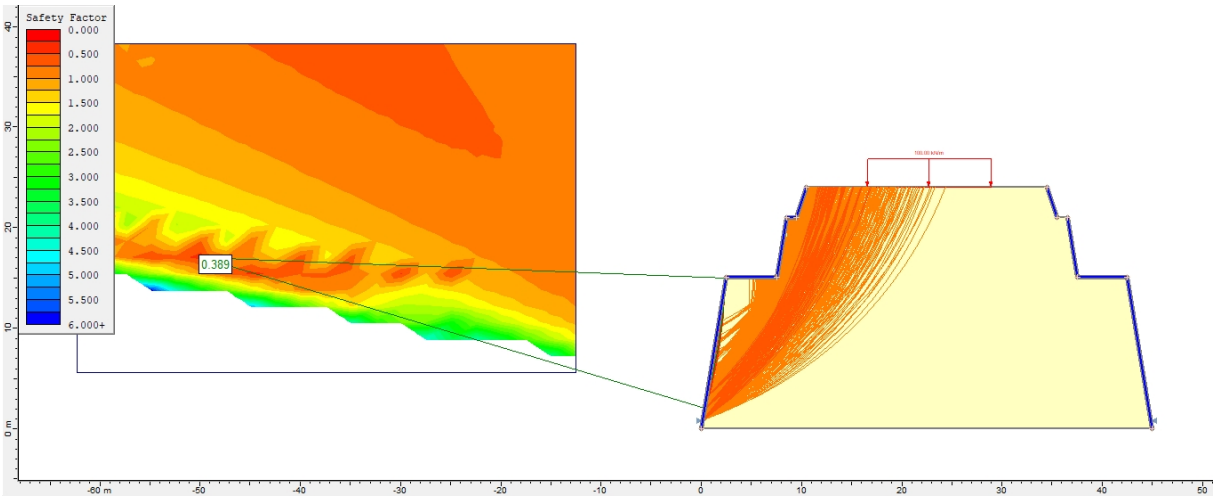


Figure 12. Numerical Model including inclined walls with increased strength. Factor of Safety: 0.389.

For the next series of analyses, horizontal reinforcement has been included in every step of the construction. More specifically, in Figure 13, horizontal reinforcement with tensile strength equal to T=40kN/m has been added with a length of 5m and spacing (i.e. distance between support) equal to 1m. The new Safety Factor is 0.780, significant higher that the Safety Factors that were calculated in Figures 10 to 12. Furthermore, the failure mechanism is now extended from the top to the bottom of the model and not exclusively to the first step. In Figure 14, the length of the reinforcement layers has been increased from 5m to 15m for the first and second step and to 10m for the third step of the construction. The tensile strength of the reinforcement layers remains equal to T=40kN/m. As can be noted, the Safety Factor increases significantly to 1.071, higher than 1, indicating that the length of the reinforcement layers plays an important, stabilizing role to the construction.

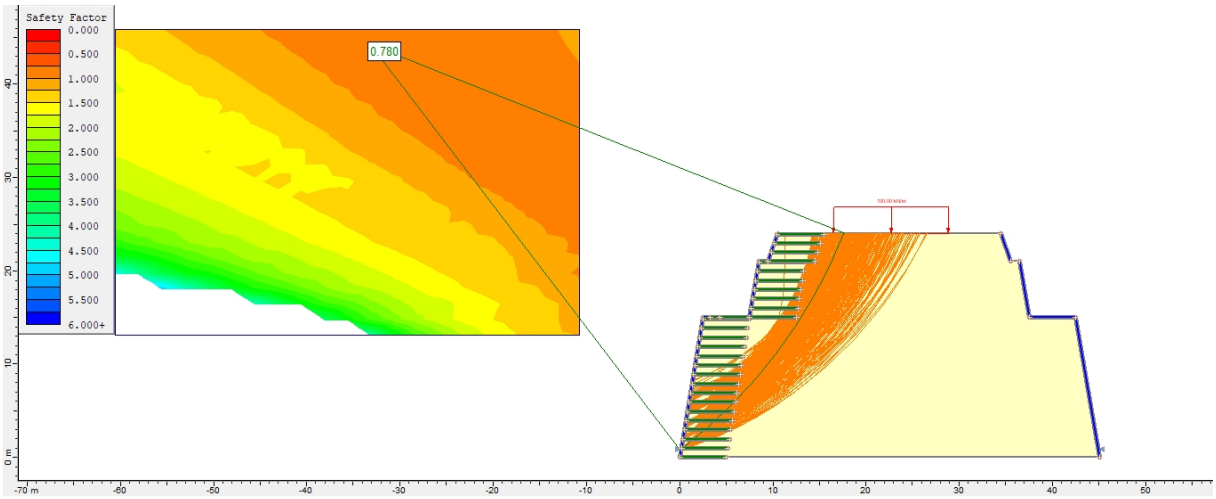


Figure 13. Numerical Model including inclined walls and horizontal reinforcement with tensile strength equal to T=40kN/m and reinforcement length equal to 5m. Safety Factor: 0.780.

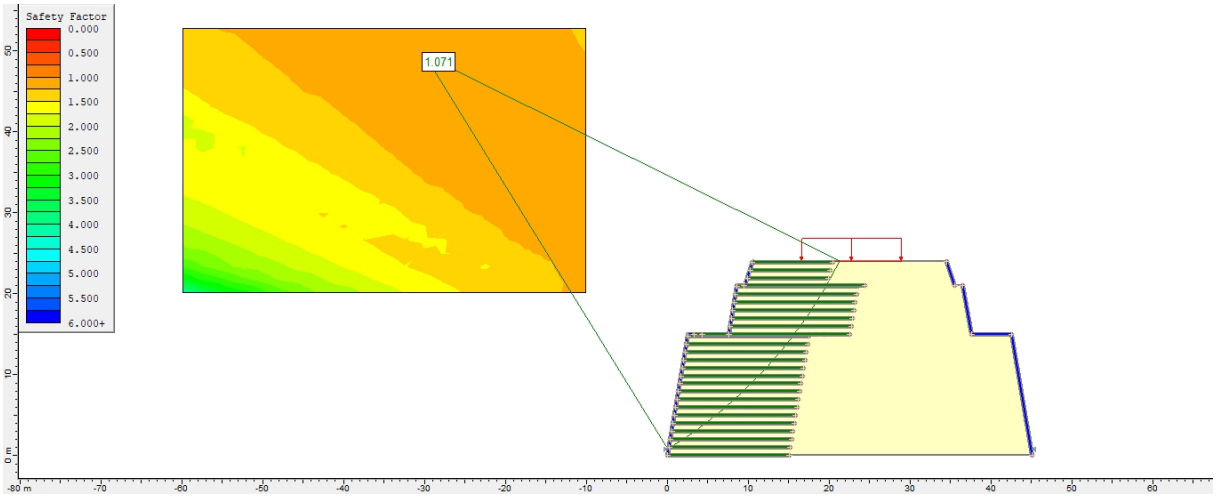


Figure 14. Numerical Model including inclined walls and horizontal reinforcement with tensile strength equal to T=40kN/m and reinforcement length equal to 15 and 10m. Safety Factor: 1.071.

The next series of analyses present results of the same previous models analysed anew with the Finite Element Stress Analysis Method. The first model can be seen in Figure 15 and more specifically a three stepped soil construction with walls at the exterior that follow the inclination of the three steps. Uniform loading of 100kN/m has been included on the top of the construction. This model is similar to the model shown in Figure 10 and was analysed with the Bishop Method for slope stability analysis. In Figure 16 the maximum shear strains developed are shown and very high deformations are noted. Additionally, the strain vectors can be seen (in red). Horizontal reinforcement materials have been included at the left side of the model as can be seen in Figure17. The reinforcement is uniform (i.e. with a spacing of 1m), with a length of 15m for the first two steps and 10m for the third step of the construction. In Figure 18 the maximum shear strains developed are shown and significant deformations are noted on the right side of the model, where no reinforcement has been included. The variation between the left

and right side of the model in terms of strains developed is significant, demonstrating the importance of the reinforcement layers on the overall safety of the construction. Furthermore, the failure mechanism on the right side can be seen. Finally, in Figure 19 the strain vectors are shown (in red) demonstrating the significant differences between the left and the right side of the model.

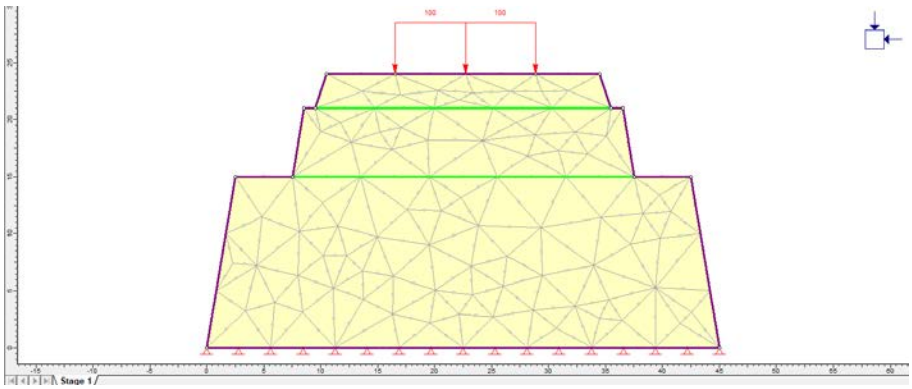


Figure 15. Numerical Model with inclined walls, utilizing the Finite Element Stress Analysis Method.

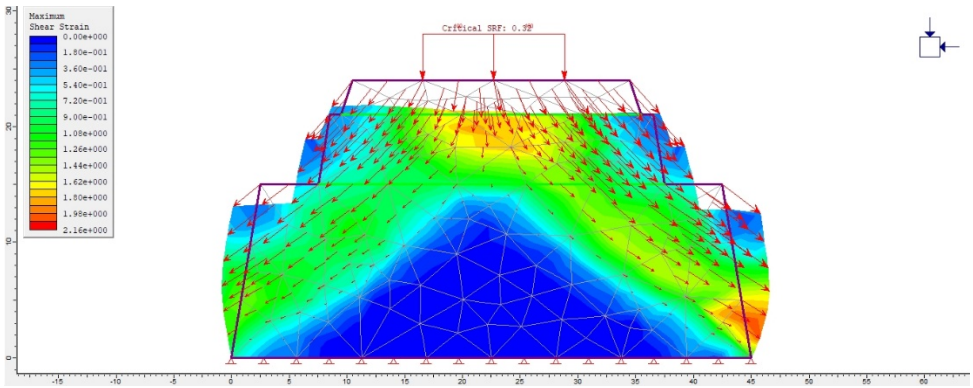


Figure 16. Maximum shear strains, failure mechanism and strain vectors developed at the Numerical Model with inclined walls.

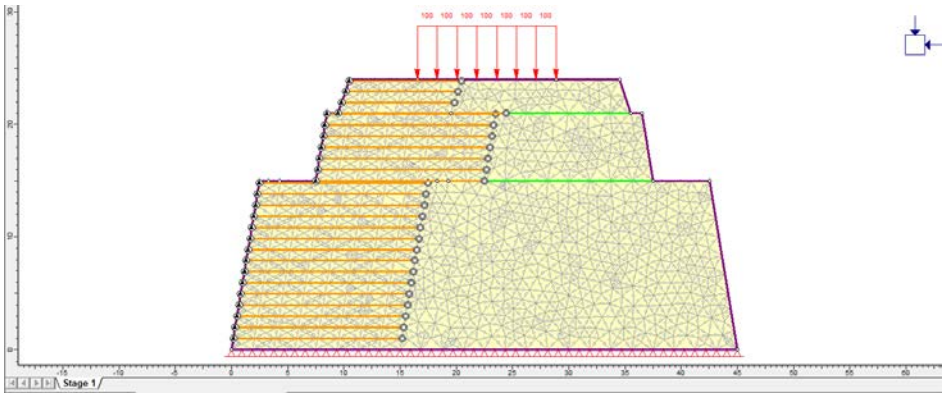


Figure 17. Numerical Model with inclined walls and horizontal reinforcement at the left side.

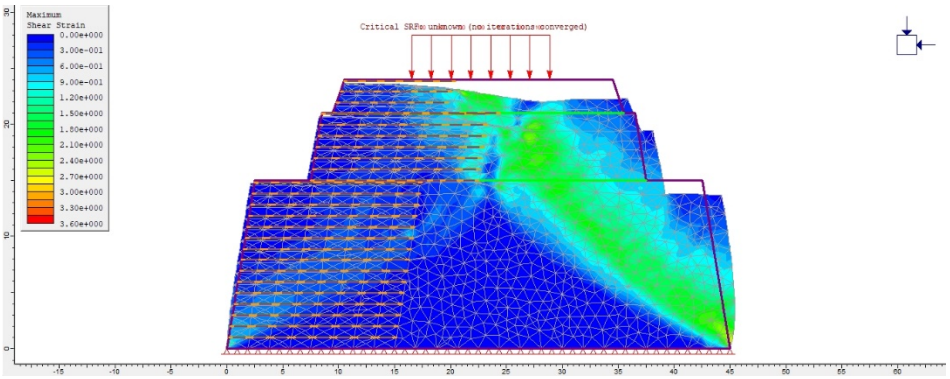


Figure 18. Maximum shear strains developed and failure mechanism at the Numerical Model with inclined walls and horizontal reinforcement at the left side.

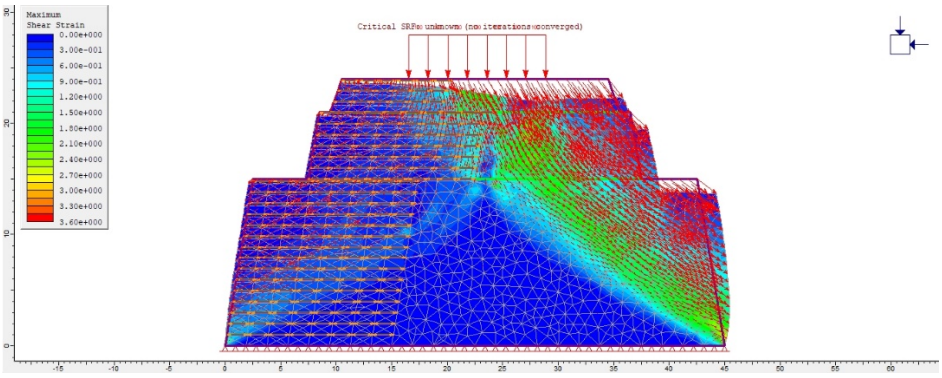


Figure 19. Flow vectors at the Numerical Model with inclined walls and horizontal reinforcement at the left side.

4 CONCLUSIONS

In the current study various geotechnical structures built in the antiquity have been presented, aiming to demonstrate that ancient civilizations had awareness of advanced construction techniques and applied reliable methods to deal with structural loadings and various natural hazards. These structures can be found in various archaeological sites worldwide. Furthermore, the earth retaining techniques used for the construction of the massive pyramid-like structures Ziggurats were examined and more specifically, the contribution of soil reinforcement to structural safety.

Several numerical models were analyzed utilizing the Bishop Analysis for slope stability method and the Finite Element Stress Analysis Method. The results of the numerical simulations were presented and discussed. The analyses showed that soil reinforcement plays an important role to structural safety, increasing significant the Safety Factor of the constructions. Furthermore, the increased length of the reinforcement is also a factor that benefits the high, inclined soil-mass structures. The numerical models utilizing the Finite Element Stress analysis method are in good coherence with Bishop Analysis numerical models and showed that the reinforcement materials decreased the strains and deformations of the

construction. It is evident that it would be rather difficult to build the Ziggurats at the specific heights and with such steep inclinations, without the reinforcement materials.

ACKNOWLEDGMENTS

The author is grateful for financial support provided by the State Scholarships Foundation of Greece (IKY). This research is co-financed by Greece and the European Union (European Social Fund- ESF) through the Operational Programme «Human Resources Development, Education and Lifelong Learning» in the context of the project "Reinforcement of Postdoctoral Researchers - 2nd Cycle" (MIS-5033021), implemented by the State Scholarships Foundation (IKY).

REFERENCES

[1] Dewar, S., 1962. The Oldest Roads in Britain, The Countryman, Vol. 59, No. 3, pp. 547-555.

[2] Blegen, C.W., 1953. Troy: Excavations Conducted by the University of Cincinnati, 1932-38, vol. 3, Princeton.

[3] Kapogianni E., Psarropoulos P.N., Kokoris, D., Kalogeras I., Michalopoulou, D., Eleftheriou, V., Sakellariou M.G. 2020. Impact of Local Site Conditions on the Seismic Response of the Athenian Acropolis Hill. Geotechnical and Geological Engineering, Springer International Publishing. https://doi.org/10.1007/s10706-020-01589-8

[4] Kapogianni, E., Kalogeras, I., Psarropoulos, P., Michalopoulou D., Eleftheriou, V., Sakellariou, M. Suitability of Optical Fibre Sensors and Accelerographs for the Multi-disciplinary Monitoring of a Historically Complex Site: The Case of the Acropolis Circuit Wall and Hill. Journal: Geotechnical and Geological Engineering, Springer International Publishing (2019). Volume 37, Number 5, p 4405

[5] Ratchet, G., 1983. Dictionnaire L' Archéologie, Ed. Robert Laffont, S.A., Paris, France.

[6] Vidal, H., La Terre Armée, 1969. Annales de L Institut Technique du Batiment et des Travaux Publics, No. 259-260, pp. 1-59.

[7] Ziegler, M., 2017. Application of Geogrid Reinforced Constructions: History, Recent and Future Developments, Procedia Engineering 172, 42 – 51

12thInternational Conference on Structural Analysis of Historical Constructions
SAHC 2020
P. Roca, L. Pelà and C. Molins (Eds.)

HISTORICAL AND TYPOLOGICAL CHARACTERIZATION OF CHURCHES IN THE HISTORICAL CENTRE OF CUSCO, PERU

K. SOVERO[1], N. TARQUE[1], E. SPACONE[2], C. MAZZANTI[2], G. BRANDO[2] AND C. ALFARO[3]

[1] Pontificia Universidad Católica del Perú
Universitaria Av. 1801, San Miguel, Lima 32, Peru
e-mail: karim.sovero@pucp.edu.pe, sntarque@pucp.edu.pe

[2] Università degli Studi "G. d'Annunzio"
Via dei Vestini,31, Chieti, Italy
e-mail: espacone@unich.it, claudio.mazzanti@unich.it, gbrando@unich.it

[3] Universidad Andina del Cusco
Ingeniería Larapa Grande Urbanization, A-7 - San Jerónimo, Cusco, Peru
email: calfaro@uandina.edu.pe

Keywords: historical structure, masonry, failure mechanism, colonial churches

Abstract. *UNESCO declared Cusco a historical site due to the importance of its constructions and traditions. However, Cusco lies on an active tectonic area with several plate faults and thus, is prone to endure seismic activity. The 1650 and 1950 earthquakes had devastating consequences on churches, with collapses of bell towers, roofs and vertical walls. After these earthquakes, the churches became more complex because of reinforcement and diverse structural changes introduced. Therefore, it is necessary to understand their current static and dynamic behaviour. In addition, it is fundamental to establish control measures to preserve churches and to guarantee safety of the hosted people, as well as to protect the artistic, architectural and cultural treasures they contain. The first step, however, is to survey the churches and to fully identify their structural features.*

This article presents a description of the architectural and structural typologies of the churches in the historic centre of Cusco and its relation to the most common failure mechanisms experienced by churches during earthquakes. To this end, this research carefully recreates typologies, geometry, materials and interventions carried on over centuries on these churches. It contributes to the seismic vulnerability knowledge of the studied churches and gives conclusions for decision-makers in future resilience plans.

1 INTRODUCTION

Nowadays, Cusco is one of the most important UNESCO World Heritage sites in Latin America. Its historical centre still shows a valuable case of superposition of various historical phases. Among its main architectural expressions are religious buildings. After the XVIth century Spaniards occupation of Cusco, the city's urban organization experienced some

adaptation to European architectural standards. The new inhabitants occupied the most important areas and replaced ancient Inca structures with their buildings. The conquerors built their residences around parish churches while natives had to move to peripheral sub-urban areas, so-called *barrios de Indios*, which also expanded around smaller churches.

In order to establish their religious beliefs, Spaniards started immediately construction of valuable sacred architecture, often atop ancient Inca structures such as temple walls. This superimposition of Spaniards building techniques over Inca ones is still visible today in churches [1].

The arrival of Spaniards to America brought construction techniques already widespread in Europe at that time, such as arches and domes. In Peru, most churches had large naves that ended at the presbytery where baptistery, choir, and altar with sacristy and other accessory places on the sides were located. The material used for churches depended on their location**.** In some areas stones were mainly used (Figure 1a) rough-hewn or in square blocks joined with lime mortar. Alternatively, the material was adobe with mud mortar and mud plastering (Figure 1b). The Spaniards also introduced terracotta roof tiles but continued to use thatched roofs for smaller or temporary churches [2]**.**



(a) (b)

Figure 1: Materials used in Cusco churches a) Stone with lime mortar in the *Basilica de la Catedral* and, b) Adobe with mud mortar in the *Templo de San Blas*.

The 1650 earthquake produced serious damage to many buildings, especially religious ones. Most of them were totally rebuilt or drastically modified until the end of the 17th century. These architectural features remained almost unchanged until 1950 when, following another major earthquake, all main churches in the city were restored. This restoration kept shapes identical but in some cases used different materials for reconstruction or consolidation [3]. A large-scale vulnerability evaluation was carried on in the centre of Cusco based on experiences learned from the L'Aquila earthquake. It took in account mainly adobe and stone masonry dwellings. The conclusion was that changes at the historical centre increased vulnerability of this important part of the city [4].

Nowadays, it is a fact that unreinforced masonry churches are more vulnerable to earthquakes. This is mainly due to their volumetric configuration and large dimensions of interior spaces. In addition, they have several potential sources of fragility problems such as inadequate connection between walls or absence of restraining elements, buttresses or similar, to help support vertical and horizontal loads from sub-horizontal structures (roof) [5]. Churches

analysis is complex due to their architectural configuration and the difficulty in material characterization because of its non-linear behavior and low tensile strength. In this type of buildings, it is possible to identify multiple macro elements as main façade, sidewalls, columns, vaults, apse, transept, dome, and bell tower. Therefore, there are multiple potential failure mechanisms as compared to common masonry buildings [6].

This research describes the main characteristics of Cusco churches and their historic, architectural and structural features, taking into account interventions made after earthquakes, with the purpose of understanding their seismic behaviour. The International Council of Monuments and Sites (ICOMOS) established a series of steps to diagnose and implement interventions in structures considered as cultural heritage. These steps are: (a) data acquisition, to obtain basic information about main characteristics of the building; (b) historical, structural and architectural research; (c) structure survey and (d) field research, laboratory tests and monitoring. Natural causes expose cultural heritage to deterioration and even to socio-economic phenomena deriving from society evolution. ICOMOS indicates that it is mandatory for governments to identify, protect, conserve, rehabilitate and transmit cultural and natural heritage to future generations. As part of this, the development of scientific and technical studies as well as research is needed to improve intervention methods on monumental heritage.

2 CHURCHES IN CUSCO CITY

In Cusco there are nineteen colonial churches from the XVIth century of relevant historical-architectural value, concentrated mainly in the historic center. Those in the main square have two symmetrical bell towers on the main front, while others have usually only one bell tower. Churches plan view have a rectangular layout with geometric regularities or a Latin cross configuration [1]. Figure 2 lists the twelve churches inside the Historical Centre of Cusco and shows their geographic localization. Four of them are around the *Plaza de Armas* (Cusco main square) and the others are at the perimeter of the area.

The construction of most churches started twenty years after the fall of the Inca Empire, in 1531. In most cases, materials came from the destruction of Inca temples. The 1650 earthquake destroyed most structures, which were rebuilt in a different style. Table 1 presents the construction year of each church, as well as some useful information such as construction material, plan view shape and number of towers or bell gables.

The former National Institute of Culture [8], now Ministry of Culture of Peru, declared all the historic buildings described in this article as Cultural Heritage on December 28, 1972.



1. *Basílica de la Catedral.*
2. *Iglesia de Santa Catalina de Sena.*
3. *Iglesia de la Compañía de Jesús.*
4. *Basílica Menor de La Merced.*
5. *Templo de Santa Clara.*
6. *Iglesia de San Francisco de Asís.*
7. *Templo de Santa Teresa.*
8. *Iglesia de San Cristóbal.*
9. *Templo de San Blas.*
10. *Iglesia de Santo Domingo.*
11. *Iglesia de San Pedro.*
12. *Iglesia de Santa Ana.*

Figure 2: Location of the basilicas, churches, and temples in the Historic Centre of Cusco [7].

Table 1: Main characteristics of Cusco churches

Church	Construction year	Plan view shape	Main material	Number of bell towers	Number of bell gables
1. *Basílica de la Catedral.*	1560, 1650-1654	Rectangular	Carved stone	02	--
2. Iglesia de Santa Catalina de Sena.	Before 1650, 1669	Rectangular	Carved stone	01	01
3. Iglesia de la Compañía de Jesús.	Before 1650 1651-1668	Latin cross	Carved stone	02	--
4. Basílica menor de La Merced	1650-1657	Latin cross	Rounded stone	01	--
5. *Templo de Santa Clara.*	1622	One-nave	Rounded and carved stone	01	--

Table 1 (continuation): Main characteristics of Cusco churches

Church	Construction year	Plan view shape	Main material	Number of bell towers	Number of bell gables
6. *Iglesia de San Francisco de Asís*.	1549-1652	Latin cross	Rounded and carved stone	01	--
7. *Templo de Santa Teresa*.	1673-1676	One-nave	Rounded stone	--	01
8. Iglesia de San Cristóbal.	1546	Latin cross	Adobe and carved stone	01	--
9. *Templo de San Blas*.	1559	One-nave	Adobe and carved stone	--	01
10. Iglesia de Santo Domingo.	1633, 1650-1680	Latin cross	Carved stone	01	--
11. *Iglesia de San Pedro*.	1556, 1650-1657, 1688	Latin cross	Rounded stone	02	--
12. Iglesia de Santa Ana.	1560	One-nave	Adobe and rounded stone	--	--

2.1 Description of the churches in Cusco

Church 1. The *Basílica de la Catedral* is the most important building for its symbolic value. Part of the reuse construction material came from destruction of Sacsayhuaman fortress, close to Cusco downtown. The Basilica rises on rests of an ancient Inca building. Its construction began in 1560 and ended in 1654 [9]. The structure consists of three main buildings: the central *Basilica* (at the center of the complex), the *Iglesia del Triunfo* (at the left) and the *Iglesia de la Sagrada Familia* (at the right). The *Basilica* has five naves, three central ones higher than the two lateral ones; the roof consists of twenty-one vaults supported by fourteen columns, twenty-one stone arches, and thirty-two semicircular arches. The façade has a Baroque style [1]. The two quadrangular stone bell towers were completed after the 1650 earthquake, with a height lower than the one of the initial project.

Church 2. The *Iglesia de Santa Catalina de Sena*, located 100 meters from the cathedral, was rebuilt after the 1650 earthquake. It was probably completed in 1669 but was already in use since 1653. The new walls rest on an embankment formed by the fall of the ancient building stonewalls [10]. The church has a single rectangular nave [1] covered with cross vaults and a dome. Around the church are two cloisters, the main one with stone and brick galleries and the other one with adobe. From there, it is possible to observe twenty-nine niches that belonged to a wall of the Hunkunkancha, an important building from the Inca era. Currently, the monastery, besides being a religious center, has become a tourist museum.

Church 3. At Cusco main square, besides the Cathedral, there is also the *Iglesia de la* Compañía *de Jesus*. Before the Spanish conquest there was an important Inca architecture where this church stands. It became property of Hernando Pizarro (one of the Spanish conquerors), and was later demolished. Later on, the land was sold to the Jesuits who built a Church and a school; both were seriously damaged by the 1650 earthquake. Reconstruction began in 1651, starting from the chapel of the *Virgen de Loreto*. The new *Iglesia de la Compañía de Jesús*, with a Latin cross plan view, was completed in 1668 [10]. The symmetrical

bell towers are the most interesting external architectural elements because of the indirect visual relationship with those analogous of the cathedral.

Church 4. Not far from the three churches already presented is the *Basílica Menor de La Merced*, facing *Plaza Espinar*. For construction of this church, Francisco Pizarro donated the land to the *Orden de La Merced* (Mercedarian Order), who began construction in 1535. In the beginning, it was a very simple church, in adobe with trusses of the type called "*par y nudillo*" (sort of reticular two-beam truss with horizontal stiffening element). The 1650 earthquake devastated the first building; that year the new construction began and lasted around seven years. In 1680, construction of a second cloister and the bell tower began [1]. This church has a Latin cross plan view with three naves; the central nave with a vaulted roof is wider and taller than the lateral ones.

Church 5. The *Templo de Santa Clara* is 500 m from the *Plaza de Armas*. Its construction began in 1599; this first building was replaced by the current one-nave building together with the monastery, both completed in 1622 [1].

Church 6. The construction of the *Iglesia de San Francisco de Asís*, located at the square of the same name, began in 1549 and ended in 1652. The delay was due to the devastation caused by the 1650 earthquake. The church has a Latin cross configuration with three naves; the central one is higher than the lateral ones.

Church 7. One block from the *Plaza de Armas* is located the *Templo de Santa Teresa*, in front of the square of the same name. Captain Don Antonio de Zea and his wife Doña María Urrutia donated the land to the *Orden de los Carmelitas* (Carmelite Order) in 1673, but its construction started in 1676. This church has only one rectangular nave with a two-sided roof. In addition, it has two bell gables with three columns each. At the façade, it is possible to observe openings with round arches, where is located the corner balcony rebuilt over Inca walls [1].

Church 8. The *Iglesia de San Cristóbal* is close to Cusco main square. Built in 1546, in 1560 it became a parish reserved for Indians. The plan view presents a Latin cross scheme with a single nave and a gable roof.

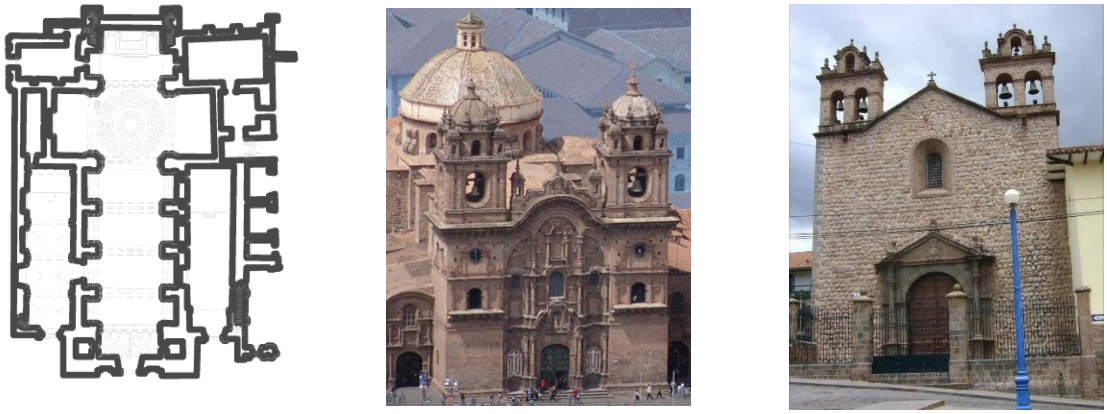
Church 9. Another building initially reserved for Indians is the *Templo de San Blas*, one of the first five temples built following a special evangelization request from Viceroy Andrés Hurtado de Mendoza in 1559. The church consists of a single nave, with two access portals, one overlooking the San Blas square and the other facing the main front. On the right side of the main façade is a bell tower built in stone masonry with semicircular arch openings.

Church 10. The *Iglesia de Santo Domingo*, located in the homonym square, was built over remains of the *Templo del Sol* (Qorikancha), area which was assigned to Pizarro´s brothers. Juan Pizarro donated the land to Fray Vicente Valverde, who belonged to the Dominican order. Transformation of the Inca temple into a Catholic church took place in 1633, but the original building suffered serious damage with the 1650 earthquake. Reconstruction of the church was completed in 1680.

Church 11. The *Iglesia de San Pedro* was built by the architect Juan Tomás Tuyrutupa. It is located six blocks from Cusco main square. This church has a Latin cross shape in plan view with two bell towers made of carved stone. This building has a main central nave with chapels at each side. The roof consists of five vaults over the main nave, two above the transepts and one over the baptistery. Its façade is baroque, three bodies in height.

Church 12. The *Iglesia de Santa Ana* was constructed as a church for town people, so its structure was very simple. The 1650 earthquake did not produce much damage to it. The structure has rectangular shape plan view, with a single nave. The roof is simple, made of wooden structure with triangular shape and colonial tile coverage.

The characteristics of most churches are a Latin cross plan view with one central dome (Figure 3a). Furthermore, almost all façades are two or three bodies in height (Figure 3b) with baroque pilasters close to the main entrance. In addition, they have at least one or two towers with round arches or bell gables (Figure 3c).



(a) (b) (c)

Figure 3: Classic architecture of Cusco churches, a) Latin cross shape plan view, b) façade with three bodies and columns and, c) façade with bell gable instead of bell tower.

2.2 Structural system of the churches

Structural system analysis of these buildings is very important for their protection, especially their seismic risk. The Cathedral is made of perimeter stone masonry walls, with 1.60 to 2 m thickness. There is no information about another material inside the walls. Columns are externally made of stones and internally have a filler material; together with arches, they support the roof system (vaults). The stone used is granite and is mainly obtained from the Sacsayhuaman fortress. Both *Iglesia de la Sagrada Familia* and *Iglesia del Triunfo* constitute buttresses to the Basilica walls. The difference in height among the three buildings could increase seismic vulnerability of the central Basilica.

Other churches have structural characteristics similar to the Cathedral, with thicker walls (about 2 m) formed by square stone blocks joined with lime mortar. The *Iglesia de Santa Catalina de Sena* has brickwork with non-rectangular blocks. The relatively regular configuration of this building would indicate that it has adequate seismic behavior. However, window openings are not aligned correctly and this makes the sidewalls areas weak.

The *Basílica Menor de La Merced* has two stone buttresses that strengthen the side façade. The second floor walls of the cloisters and the sacristy are of adobe bricks. The roof system of this church consists of vaults supported by arches and covered with light roofing bricks.

The *Templo de Santa Clara* has similar structural characteristics as the *Basílica Menor de La Merced*. Inside, arches are made of brick masonry and outside vaults are of bricks protected

with handmade tiles. The plan view of the entire complex (church and cloister) is of irregular shape. The cloister walls are of adobe masonry, with a "*par y nudillo*" type roofing system and handmade tile covering [7].

Other churches are made of adobe. The *Iglesia de San Cristóbal* has mixed masonry with carved stone at the base and adobe walls at the top. Externally, walls have stone masonry buttresses. Inside, the roof is a wooden structure supported by five semicircular carved stone arches. A baptistery deposit and the sacristy are two small adobe buildings at the back façade. At the *Templo de San Blas*, the structural system is adobe masonry with stone cladding. Inside, the choir rests on a simple stone arch. Its roof system is "*par y nudillo*" type, covered with handmade tiles. Only the bell tower is completely stone structure.

As previously explained, the churches structural system consists of stone walls, adobe walls, or a combination of both. They are bearing walls that also support earthquake lateral loads. The condition of these walls may play an important role in their seismic vulnerability analyses. Some churches also have stone buttresses. The Cathedral has stone columns to support the roof system but in other churches stone or brick arches directly support them.

3 PAST EARTHQUAKES AND IMPACT ON CUSCO CHURCHES

3.1 Earthquakes in Cusco

Cusco region is prone to several types of hazards, such as landslides, floods, earthquakes, and fires. The Peruvian code [11] classifies Cusco as an area with moderate seismicity. Soil accelerations can reach up to 0.25 g on rock soil during an earthquake event. Although Cusco is distant from subduction between South American and Nazca plates, its high seismicity is by cause of geological faults across the city.

Fifty-three geological faults go through the Cusco region [12]. Most are active faults and have been source of the main Cusco earthquakes in the past. Table 2 shows a list of the seismic events in Cusco, counted since the XVIIth century to present. This table also reports the magnitude of each earthquake expressed in Richter scale (ML), its intensity in Modified Mercalli scale and the geological fault that produced it. As shown, the major intensity in Cusco was IX (MM scale) in the 1650 seismic event produced by the Tambomachay geological failure. In addition to this event, the earthquakes of 1950 and 1986 had a macroseismic intensity of VIII in the MM scale. Table 2 also indicates that Tambomachay, Pachatusan and Qoricocha geological faults have caused the main earthquakes in Cusco. Other seismic events with epicenter in the Peruvian coast due to the subduction phenomenon were perceived in Cusco, but they caused only minor damage.

Table 2: List of earthquakes at the Cusco city since 1650 [12]

Date	Deep (km)	Magnitude (ML)	Intensity (MM)	Fault
31/03/1650*	30	7.2	IX	F.Tambomachay
19/11/1744*	----	----	VI	F. Tambomachay
21/05/1950*	15	6.0	VIII	F.Pachatusán
03/06/1980	20	5.0	VI	F. Zurite-Huaracondo
05/04/1986*	07	5.3	VIII	F. Qoricocha

10/01/1998	38	6.4	V	------
08/08/2003	32	5.1	V	F. Capacmarca
28/09/2014	06	5.1	VII	Many
2015 - 2019	07 - 30	3.2 - 4.4	II - IV	

*Sismos que han afectado el Centro Histórico de Cusco

3.2Damages in Cusco churches due to earthquakes

The 1650 earthquake was one of the most destructive in Cusco. According to Chara and Caparó [1], several churches suffered serious damage and in most cases, some structures were demolished and rebuilt with other materials. Such is the case of the *Iglesia de la Compañía de Jesús* that originally was of adobe and after the earthquake was rebuilt with stone; also the *Iglesia de Santa Catalina de Sena*, where all Spaniard made walls were destroyed and only the Inca stone base did not suffer damage. Another example is the *Iglesia de Santo Domingo* that was totally destroyed.

After the 1650 earthquake, some constructions needed a change on their architecture. For example, the *Basilica de la Catedral* originally was designed with three towers but after the event, only two towers were built. Similar case is the *Iglesia de San Francisco de Asís* that remained with only one bell tower. On the other hand, some churches did not suffer damage, like the *Templo de Santa Clara* and the *Templo de San Blas*.

After the 1950 earthquake, according to Kubler [10], four churches needed restoration and two churches needed partial intervention. In addition, five churches needed only minor repairs and one needed demolition. The *Basilica de la Catedral* needed only partial intervention due to little damage in the façade, in the arches and in the towers. The *Iglesia de Santa Catalina de Sena* presented only some cracks in the transverse arches. In the *Iglesia de la Compañía de Jesús* the central arch of the façade, the tower, and the central dome collapsed. The *Templo Santa Clara* had only separation of perpendicular adobe walls.

In addition, damage on buildings was classified. Four categories were identified: buildings that must be restored, buildings that need partial or small interventions, buildings that need some major interventions, and buildings that must be replaced.

After the 1950 Cusco earthquake, six failure mechanisms were reported as the most common in churches [7]: at the façade top, aisle vaults, domes, apse overturning, bell tower fail, and bell gable fail (Figure 4).

As seen, churches may collapse partially or totally during earthquakes. In consequence, it is necessary to study and understand their seismic behaviour, and to propose fast and minimal interventions.



a) Mechanism at the top façade.



b) Aisle vaults.



c) Dome.



d) Apse Overturning.



(e) Bell tower.



f) Bell gable

Figure 4: Common failure mechanism in churches of Cusco [7].

4 CONCLUSIONS

In the past, Cusco has undergone some earthquakes that have damaged its historical constructions. Therefore, it is urgent to understand the seismic vulnerability of these buildings in order to draw mitigation plans. This task should be done with simplified tools to cover the entire historical city and not only individual structures. Thus, large-scale methodologies could be useful for this purpose. This paper presents a historical and typological characterization of Cusco churches as a first step of a large-scale study. The main conclusions are as follows:

- In Cusco city there are nineteen colonial churches, but only twelve are inside the Historical Centre. Most of them were built before the 1650 earthquake. Nine of these churches were made with stone (carved or rounded). The other three (*Templo de San Blas, Iglesia de San Cristóbal and Iglesia de Santa Ana*) were made with adobe walls over a stone base. Furthermore, two of the colonial churches were built over Inca remains. This is the case of *Iglesia de Santo Domingo* built over the *Templo del Sol*, and *Iglesia de Santa Catalina de Sena* constructed over the Hatunkancha.
- It is possible to know the geometry of these buildings through chronicles and old paintings. The Latin cross shape with one nave and one bell tower or bell gable is common in the analyzed churches.
- Based on the same chronicles, it is possible to know the churches main material type. In most cases, masonry was made with stones (belonging to ancient Inca walls) and lime

mortar.

- Since 1650, three big earthquakes had epicenters in Cusco city: earthquakes of 1650, 1950 and 1986 with intensities of IX, VIII and VIII in the MM scale respectively. Of them, the 1650 and 1950 events have had the most important consequences in the churches structures. However, only after the 1950 earthquake was it possible to identify the six most common failure mechanisms: at the façade top, aisle vaults, domes, apse overturning, bell tower fail and bell gable fail.

Acknowledgments. The authors thank all local authorities that helped collect important information and all Italian and Peruvian students who participated during data collection in Cusco.

REFERENCES

[1] Chara Zereceda, O., Caparò Gil, V. Iglesias del Cusco: historia y arquitectura, Editorial Universitaria UNSAAC, Cusco, (1998).
[2] Mendoza, R., Arquitectura religiosa en los Andes: apogeo, crisis y restauración. Universidad Mayor de San Marcos. Lima, Perú, (2016).
[3] Brando, G., Cocco, G., Mazzanti, C., Peruch, M., Spacone, E., Alfaro, C., Sovero, K., Tarque, N. Structural Survey and Empirical Seismic Vulnerability Assessment of Dwellings in the Historical Centre of Cusco, Peru. International Journal of Architectural Heritage (2019).
[4] Villegas, A; Estrada E. Centro histórico de Cusco, rehabilitación urbana y vivienda. Editorial Universitaria UNSAAC, Cusco, (1990).
[5] Mele E., Gatto, D., and De Luca, A. Structural analysis of basilica churches: A case study. Historical Constructions, P.B. Lourenço, P. Roca (Eds.), Guimarães, (2001).
[6] De Matteis G., Brando G., Corlino V. Predictive model for seismic vulnerability assessment of churches based on the 2009 L'Aquila earthquake, (2019).
[7] Municipalidad Provincial del Cusco. Plan Maestro del Centro Histórico de Cusco, (2018).
[8] Instituto Nacional de Cultura. Templos, Conventos y Cementerios declarados Patrimonio Cultural, (2000).
[9] Arzobispado de Cusco, Tesoros de la Catedral del Cusco, Dirección Desconcentrada de Cultura de Cusco, Telefónica del Perú - Gráfica Biblos, (2013).
[10] Kubler, G. Cusco. Reconstrucción de la ciudad y restauración de sus monumentos. UNESCO, (1951).
[11] Reglamento Nacional de Edificaciones del Perú. Norma Técnica de Edificaciones, NTE E.030, (2018).
[12] Benavente, C., Delgado F., Taipe E., Audin L. y, Pari, W. Instituto Geológico Minero y Metalúrgico del Perú. Boletín N°55 Serie C. Geodinámica e Ingeniería Geológica, (2013).

12th International Conference on Structural Analysis of Historical Constructions
SAHC 2020
P. Roca, L. Pelà and C. Molins (Eds.)

IRON AND STEEL CONSTRUCTION WORKSHOPS IN 19TH AND EARLY 20TH CENTURY BELGIUM: RETRIEVING THEIR OEUVRE VIA TRADE CATALOGUES

INE WOUTERS[1*] AND ROMAIN WIBAUT[1,2]

[1]Department of Architectural Engineering (ARCH)
Vrije Universiteit Brussel (VUB)
Pleinlaan 2, 1050 Brussel, Belgium
e-mail: ine.wouters@vub.be, www.vub.be/ARCH (*corresponding author)

[2] Department of Architecture, Faculty of Engineering Science
University of Leuven (KU Leuven)
email: romain.wibaut@vub.be, www.vub.be/ARCH

Keywords: Iron and Steel, Bridges and Roof Trusses, Trade Catalogue, Construction History

Abstract. *In the 19th and 20th centuries both iron and steel were worldwide applied to construct structures such as halls, markets, stations and bridges. Belgium, an early industrialised country on the European mainland, was famous for its iron and steel production and the export of iron and steel structures. Nevertheless, most early Belgian construction workshops are under explored. Since the company archives of Belgian construction workshops are seldom preserved, trade catalogues are analysed in this paper to get insight in the structures the workshops built. These catalogues offer a broader context for the individual structures that were transported and built worldwide.*

1 INTRODUCTION

When studying historic iron and steel structures such as bridges, roof trusses, halls, markets, etc. it is not always feasible to retrieve the iron construction workshop that assembled the iron and steel structure. And if the name of a workshop can be retrieved, we often do not know much about it [1,2]. Nevertheless, it is important to position a construction within the global oeuvre of the workshop, as these workshops brought in their own expertise and insights [3]. Moreover, iron and steel structures occupy an exceptional position within the construction sector: they were often transported over long distances. Structures manufactured in Belgium have been shipped to countries all over the world.

Up until now, iron construction workshops got little attention in literature. In Belgium, too, there are only a few texts devoted to the subject [1,4]. The workshop *Baume & Marpent* is one of the few iron construction workshops that has been studied in depth in Belgium [5,6]. However, this is in great contradiction with the importance that Belgian workshops had in the 19th and early-20th centuries, both nationally and internationally [1].

In order to increase the knowledge of Belgian iron and steel workshops, this paper concentrates on trade catalogues published by Belgian iron workshops to promote their

activities. The catalogues enable to attribute a construction to a specific workshop and to position the importance of the construction of bridges and buildings in their activities.

2 TRADE CATALOGUES OF BELGIAN IRON AND STEEL WORKSHOPS

Two tracks were followed to collect historical catalogues of iron and steel companies with a workshop in Belgium. First the *Museum voor de Oudere Technieken* in Grimbergen (MOT), that contains a large collection of trade catalogues, was visited and all catalogues connected to the iron and steel industry were consulted to check if a company constructed bridges or buildings (as main or secondary activity) [7]. Second, the *Receuil Financier,* a yearly publication that lists and describes all stock-listed companies in Belgium was analysed to draft a list of companies that were involved in the construction of iron and steel bridges and buildings. By doing so, about 100 iron and steel workshops were retrieved that constructed bridges, roof trusses, frames, gasometers, etc. in Belgium in the 19th and early-20th centuries [7]. Next, national and international databases were consulted in order to trace trade catalogues of these companies. Additionally, city and company archives were consulted containing trade catalogues of their own and of competing companies.

Since companies still publish trade catalogues today, we set the end date in this paper to 1950 as from then on, the Belgian iron and steel workshops merged into larger national and international entities such as *Les Ateliers Belges Réunies* [7]. As most trade catalogues do not specify a publication date, the estimated publication date is derived, taking into account the dates indicated in the introductory texts as well as the construction date of the structures depicted in the trade catalogue. The starting date of the period studied in this paper is determined by the oldest trade catalogue found during the search, being approx. 1875. Table 1 gives an overview of the 15 trade catalogues of Belgian iron and steel workshops (c. 1875-1950) that included photographs or drawings of bridges and buildings.

It is noteworthy that the vast majority of the abovementioned trade catalogues do not focus on the construction sector, but on the railway sector. These trade catalogues mainly show wagons, tenders and railway equipment. It is also remarkable that the projects included in the trade catalogues are mainly intended for foreign markets. Yet this is not strange when we look at the broader Belgian context. In the 19th century, the Belgian state had followed a twin-track strategy with regard to the development of the railway network [8]. The state had first laid an iron cross over the country, whereby the main axes of the railway network were financed and exploited by the state (1835-1843). These main axes ensured a good connection between a large number of Belgian (harbour) cities, mining and industrial areas and the connection to the international network. Subsequently, private capital was stimulated for the construction of a secondary network. From 1843 onwards, massive private investments in the railway sector took place, in the beginning almost exclusively English capital, and after the crisis of 1847-48, Belgian capital plunged into the railway sector. Between 1843-1870, more than 2500 km of railroads were built by the private sector (and 24 km by the state). When the Belgian State started buying back the concessions from 1870 onwards, Belgian companies turned abroad to continue their investments in the construction of railway networks [8]. So, from 1870 onwards Belgian iron and steel construction workshops focused actively on foreign markets.

The trade catalogues we study all date from after 1875, corresponding to the period where Belgian companies strove to be strongly involved in building railways abroad. It is clear that

the trade catalogues target an international audience: some catalogues were printed on the occasion of a world exhibition, photographs of exhibition stands were included in the catalogue and several companies took up a description in four languages including French, English, Spanish and German or Portuguese. Business studies show that during the nineteenth century, Belgian iron and steel workshops exported between 70 to 90% of their production which corresponds with the proportion of foreign structures shown in the trade catalogues [9].

In the following paragraphs we zoom in on five trade catalogues (indicated in bold in table 1). First the oldest catalogue *S.A. des ateliers de la Dyle à Louvain* (c. 1875) is analysed. We then discuss the only catalogue that exclusively mentions bridges and buildings *Aug. Lecoq et Cie* (c. 1880). And finally, we compare the catalogues of two companies *Nicaise & Delcuve* and *La Brugeoise* before and after they merged.

Table 1: Trade catalogues of Belgian iron and steel construction workshops (1875-1950). Archives: Biblioteca National de Espana (BNE), Company archive Bombardier Transportation in Bruges (Bombardier), City Archive Bruges (CAB), Ecomusée Bois-du-Luc (EBL), Museum voor de Oudere Technieken in Grimbergen (MOT), Archive of the National Railway Company of Belgium (NMBS/SNCB)

Name of trade catalogue	Date	Archive
S.A. des Ateliers de la Dyle à Louvain	±1875	BNE
Aug. Lecoq et Cie. Constructeurs. Hal (Belgique)	±1880	MOT
S.A. des Ateliers Nicaise et Delcuve à la Louvière (Belgique)	±1895	NMBS/SNCB
S.A. des Aciéries d'Angleur. Liège	1896	MOT
S.A. de Produits Galvanisés et de Constructions Métalliques. Successeur de J.F. JOWA à Liège.	±1900	MOT
S.A. Compagnie Centrale de Construction	±1905	EBL
S.A. Compagnie Centrale de Construction. Wagons. Voitures. Ponts. Charpentes.	±1905	EBL
Société John Cockerill. Seraing	1905	MOT
Les Ateliers Métallurgiques. Bruxelles	±1910	MOT
S.A. La Brugeoise. Usines métallurgiques. Saint-Michel-Lez-Bruges	±1910	CAB
S.A. Ateliers de construction d'Hérinnes-lez-Enghien	1912	MOT
Baume et Marpent. Haine-St-Pierre (Belgique)	±1920	NMBS/SNCB
S.A. La Brugeoise et Nicaise & Delcuve. Usines métallurgiques. Ateliers de construction. St.-Michel-lez-Bruges et La Louvière	±1930	CAB
La Brugeoise et Nicaise & Delcuve	±1937	CAB
S.A. La Brugeoise et Nicaise & Delcuve	±1949	Bombardier

3 AN EARLY TRADE CATALOGUE : *SOCIETE ANONYME DES ATELIERS DE LA DYLE A LOUVAIN*

The oldest Belgian trade catalogue depicting the works of an iron workshop, traced back so far, dates from approx. 1875 and depicts the works of *Société Anonyme des Ateliers de la Dyle à Louvain (Belgique).* The subtitle *Matériel de Chemins de Fer, Sucreries, Raffineries, Distilleries, etc* already indicates that rolling stock for railways and equipment for refineries were products they produced. Another source that gives insight in the activities of the company

is the notarial act that was drafted when, in 1875, engineer Aimé Durieux changed the name of his company *Société en Commandite A. Durieux et Cie* (1866-1875) into *Société Anonyme des Ateliers de la Dyle* (1875-1879). The notarial act mentions that the main object of the company is 'the execution, sale and rental of railway equipment, all supplies for road, river and canal works, all metal construction for bridges, frames and other structures, all construction of machines for use in distilleries, breweries, refineries and others, in general, all construction of large iron and copper boiler works' [10]. Between 1879 and 1928 the company cooperated with the French naval company *Société des chantiers de Bacalan* in Bordeaux, moved its headquarter to Paris and changed its name to *Société de Travaux Dyle et Bacalan* (1879-1928). In the Belgian workshops in Louvain all activities continued and in 1928 the company split up again and pursued its activities as *SA des ateliers de la Dyle* (1928-1959). Since 1866 the company was located in Louvain in between the railway and the canal, offering excellent conditions for material supply and the presence of skilled workers [9].

The trade catalogue contains 87 photographs of which two depict the exterior and interior of the workshop, 76 illustrate wagons for railways and tramways, and only eleven photographs show bridges and roof trusses. A photograph of the stand for the World Exhibition in Vienna (1873) is included. Although the *Ateliers de la Dyle* is seen as an important actor within the construction sector, the main activities of the company are thus situated within the railway sector.

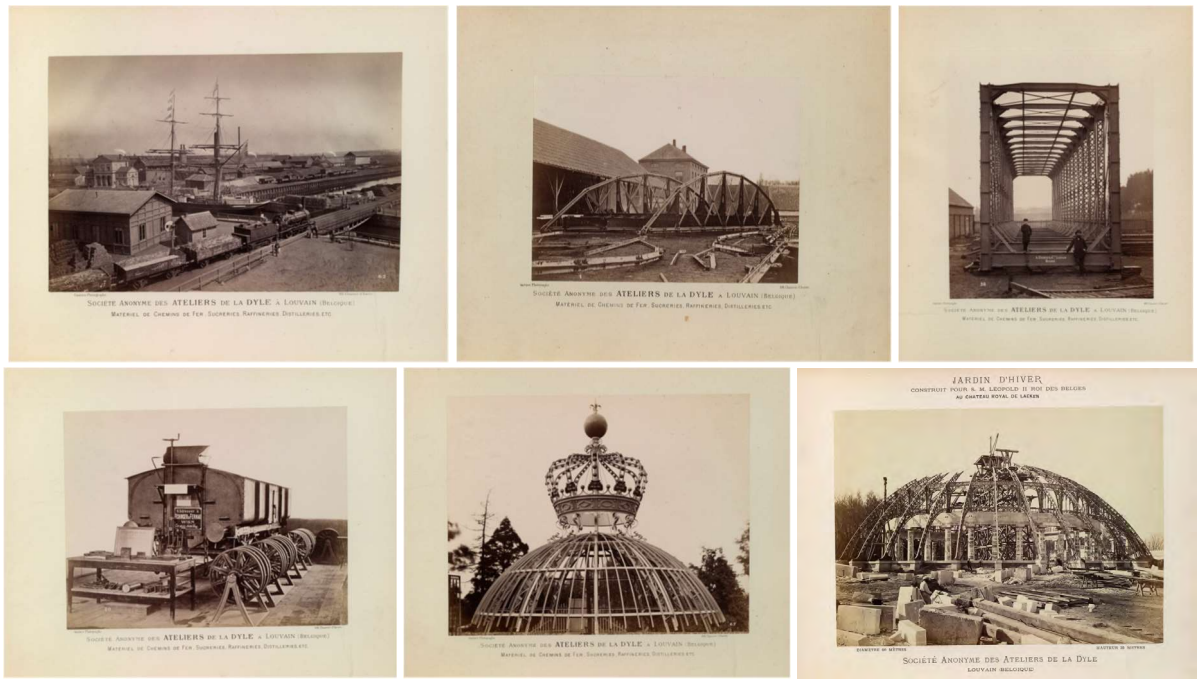


Figure 1: Album *Société Anonyme des Ateliers de la Dyle à Louvain* depicting an outside view of the factory in Louvain, two bridges assembled at the factory, the company's stand at the world exhibition in Vienna (1873), the crown of the Royal Wintergarden at the factory and the almost completed iron structure of the Royal Wintergarden at the Royal Palace in Laeken (1875) © Bibliotheca National Espana

The catalogue does not add titles to the objects depicted (see figure 1), but names mentioned on the wagons such as Lille-Valenciennes, Elsas-Lothringen, Chemnitz-aue-Adorf, Merida à Sevilla, Carlsruher Pferdebahn, Séville-Xeres-Cadix and abbreviations such as E.F.D.P.II (Estrada de Ferro Dom Pedro II) point to the export of rolling stock to France, Germany, Spain and Brazil. The catalogue depicts two bridges and four roof trusses and frames. The photographs are taken on a plot adjacent to the workshop. The geometry of the bridges and trusses, which is quite generic, does not enable to identify the structures. Yet, the shape of the cupola of Royal Wintergarden in Laeken, designed by architect Alphonse Balat is easily recognisable and is the only project that gets a caption *Jardin d'Hiver construit pour S.M. Leopold II Roi des Belges*. No less than five photographs of this construction are included in the album. They depict the pre-assembled crown at the workshop yard and several stages of the construction site until the completion of the iron structure in 1875.

The 1953 trade catalogue of the company mentions that *Ateliers de la Dyle* was the first Belgian workshop exporting rolling stock to Brasil [11]. By 1879 the workshop had supplied 39 bridges for the Baturité Railway and they constructed inter alia the Railway line Paranagua – Corytya (1880-1885) [12]. Furthermore they contributed to the Spanish railway line Palancia-Villalon and the electric lines of Nyon-Saint-Cergue (1916, Switzerland) and La Cure-Morez (1921, France) [11].

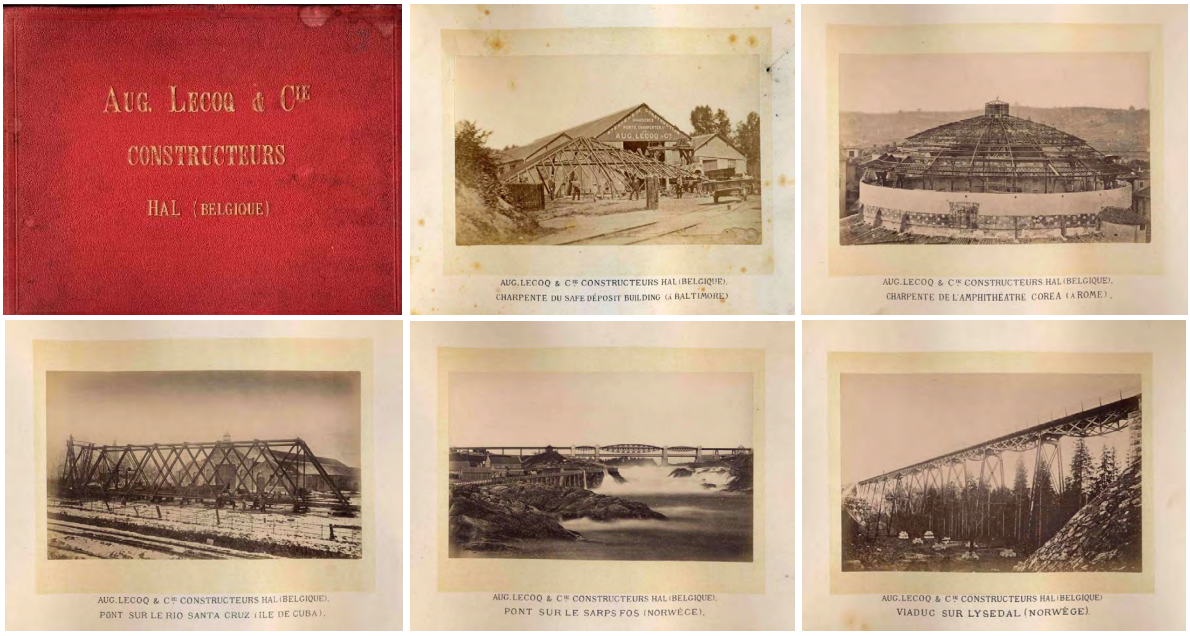


Figure 2: Trade catalogue *Aug. Lecoq & Cie. Constructeurs Hal (Belgique)* (c1880) depicting the roof truss of a safe deposit in Baltimore, the Corea Amphitheatre in Rome, a bridge over river Santa Cruz in Cuba, the Sarpsfos twin bridge and the Lysedal viaduct in Norway © het MOT, Grimbergen

3 BRIDGES AND ROOF TRUSSES BY *AUGUSTE LECOQ ET COMPAGNIE*

Although the company of Lecoq was involved in both the railway and the construction sector, the trade catalogue *Aug. Lecoq* is exceptional as it only mentions bridges and buildings.

In 1873 the industrial Auguste-Joseph Lecoq from Halle collaborated with Emile Ehlers from Antwerp, director of *Emile Ehlers et Cie*, to establish *La société commerciale en commandite "Auguste Lecoq et Compagnie, à Hal"* to make and sell iron and copper boilers and railway material [10]. After two years, in 1875 the company dissolved and Lecoq started a new cooperation with the Antwerp industrialist Charles Faider, who represented the company *Société commerciale "Bernstein et Faider"*. From august 1875 the company is called *Société commerciale en commandite "Aug. Lecoq et Cie, à Hal"*. It is unclear how the company developed during the following ten years, yet it can be expected that the production of rolling stock rose as *Bernstein et Faider* was active in the exploitation of Belgian and foreign railways and tramways since 1870. In 1875, for example, they became shareholder of the *Société des tramways d'Algers* [10].

In June 1894, after the death of Auguste Lecoq, widow Lecoq and family members erected the company *J.L. Lecoq et Cie* that went bankrupt by the end of 1895. In 1898, the production of fixed and rolling stock for railways and trams, steam engines, bridges and trusses was continued by the *Société des ateliers de construction de Hal* [9]. Although we do not have information about the activities in the period 1895-98 photographs taken during the positioning of a metallic bridge in Congo in 1898 show the partly visible painted letters *Ch. De Fer. Matadi Congo. Ateliers [de] construct[ion]. Aug. Lec[oq]. J.L. Lecoq Hal. Belg[ique]*' suggesting that bridge construction continued [13].

In the *Recueil Financier* we can follow up the yearly financial balances from 1898 onwards. The company stayed successful until the 1930s, but was loss-making in 1910 because of an incoherent contract for the construction of bridges in Bulgaria [14].

The trade catalogue that explicitly mentions *Aug. Lecoq & Cie* on the cover could have been published in the time period 1875-1894. Although the catalogue is not dated, the structures that could be identified date back from around 1877.

Although the company was also active in the railway sector, the catalogue *Aug. Lecoq & Cie. Constructeurs Hal* is the only catalogue in table 1 that solely contains bridges and roof trusses. The catalogue contains 16 photographs provided with explanatory titles. Only two structures in Belgium are depicted: the Kattendyck lock in Antwerp and a private suspension bridge in Mariemont. The other photographs show a roof truss to be shipped to England for the reading room in Liverpool, for the aquarium in Tynemouth and for a safe deposit building in Baltimore, frames for the panorama in Milan and the Corea Amphitheatre in Rome, lattice bridges for Australia (Parramatta) and Cuba (Arroyo Manso over Rio Santa Cruz) and four large bridges for Norway: the Prestebakke and Liadalen railway bridge, the Lysedal viaduct and the twin-deck bridge over river Sarps Fos (see figure 2). The export destinations of this company differ from the other workshops. Although Spain and Italy are a common destination, exporting Belgian iron structures to USA and England is rather exceptional as these countries had a flourishing iron and steel industry.

The bridges in Norway were all part of the construction of the Ostfold Railway Line and were designed by the Swedish-Norwegian structural engineer Axel Jacob Petersson. The Sarpsfos bridge was one of the first designs on this Railway Line. The English weekly magazine *Engineering* dedicated two issues to this bridge in January 1878 [15]. The bridge was built on top of an existing suspension road bridge, dating from 1854. Figure 2 shows how the lower road bridge deck is suspended to the new railway deck shaped as a lenticular truss spanning 54 meters at midspan. For this bridge the existing deck and columns of the former suspension

bridge were re-used, yet for the following bridges Petersson applied hinged columns, which was considered innovative. This design of Lysedal viaduct was praised in the English magazine *Engineering* in 1879 not only for its facility and quickness of erection, but also for the structural efficiency and economic advantages [16]. Tyrrell mentioned the Lysedal viaduct (1877) in his book *The history of bridge engineering* and explained the innovative shape of the pillars: the columns taper longitudinally, being wider at the middle than at the ends, and they are hinged at the shoes [17]. The railway line was in use from 1879 onwards. As the requirements of the railway network evolved, these bridges and viaducts were replaced over time.

4. TRADE CATALOGUES OF MERGING COMPANIES *LES ATELIERS NICAISE ET DELCUVE* AND *LA BRUGEOISE*

Today, most of the remaining Belgian iron workshops that have their roots in the 19th century are part of the international company *Bombardier Transportation* (1986-today). This company took over *B.N. Constructions Ferroviaires et Métalliques* in 1977, that is in its turn an alliance between *Les Ateliers Belges Réunis* (1956-77) and *La Brugeoise et Nivelles* (1956-77). [7] In the following, we study how companies merged between 1855 and 1956 to establish the company *La Brugeoise et Nivelles*.

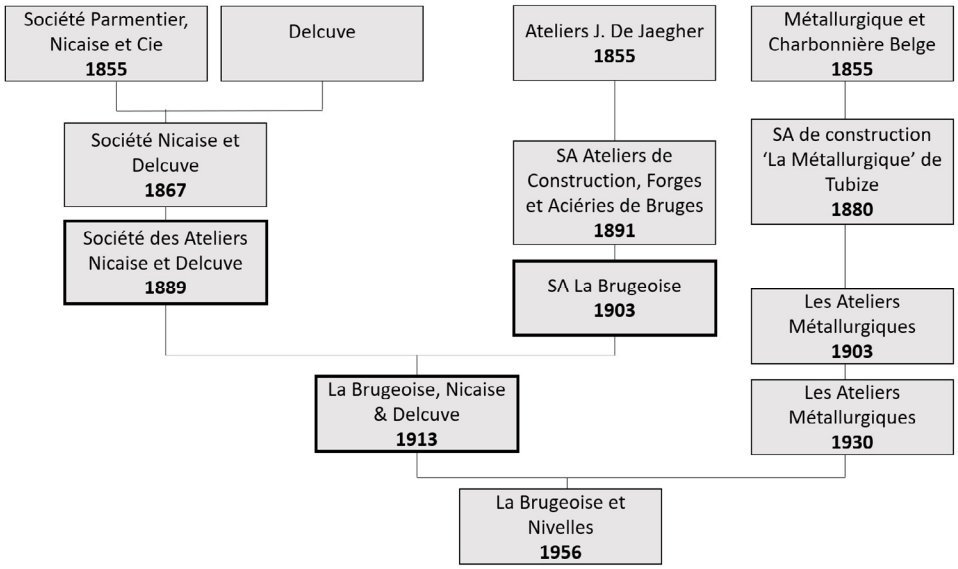


Figure 3: *La Brugeoise et Nivelles* was founded in 1956 by merging several Belgian workshops [7].

4.1. *Société des Ateliers Nicaise et Delcuve*

In 1956 the company *La Brugeoise et Nivelles* (1956-77) was founded. Figure 3 illustrates how the company brought together *La Brugeoise, Nicaise et delcuve* and *Les Ateliers Métallurgiques*. The first company in itself is an alliance between *Société des ateliers Nicaise et Delcuve* and *La Brugeoise* that merged in 1913 [7]. These different acquisitions explain why the image of a structure is sometimes repeated in various trade catalogues. In figure 3 the catalogues of the three companies we discuss in this section are marked with a bold frame.

The company *Société Nicaise et Delcuve*, founded in 1867 changed its statute in 1889 and underwent a minor name change: *Société des Ateliers Nicaise et Delcuve*. Next to rolling stock for railways and tramways they constructed bridged and metallic structures, and pieces of foundry in iron and copper. A famous employee of this company is the Belgian structural engineer and professor Arthur Vierendeel who invented the Vierendeel girder and published handbooks on iron architecture. After his graduation in 1874, Vierendeel started his career in the iron workshop *Société Nicaise et Delcuve* in La Louvière until 1885. That year he became provincial engineer in West-Flanders and combined this position with a professorship at the University in Leuven [18].

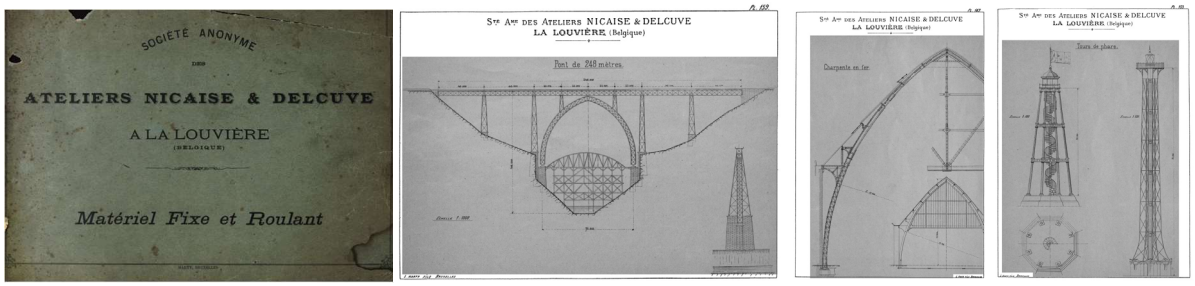


Figure 4: Trade catalogue *Société Anonyme des Ateliers Nicaise & Delcuve à La Louvière (Belgique). Matériel fixe et Roulant* (c1895) depicting a bridge spanning 248 meters, the hall calculated by Vierendeel in La Louvière, and two towers © Ecomusée du Bois-du-Luc

The catalogue *S.A. des Ateliers Nicaise et Delcuve à la Louvière (Belgique*) is not dated and does not contain any photographs but drawings. The catalogue contains 126 plates of which 43 wagons, 17 cranes and 18 plates depicting iron roof trusses for stations, halls and markets, iron towers, small and large bridges and gasometers. The title of the drawings is kept quite general (*charpente en fer, pont de 248 mètres, passerelle jardin*) and does not allow identification. It is therefore not clear whether the catalogue refers to structures that have been built or structures that could be build. However, some drawings could be identified. For example, there is a clear resemblance between plate 149 *charpente en fer* in the trade catalogue and the colour plate 65 in Vierendeel's publication *La construction architecturale en fonte, fer et acier* (1902*)*. As Vierendeel's plate is entitled *Atelier à La Louvière (Calculé et excécuté en 1881 par A. Vierendeel)* it is clear this structure had been built.

4.2. *La Brugeoise*

The trade catalogue *La brugeoise. Usines métallurgiques. Société Anonyme. Saint-Michel-lez-Bruges. Belgique* is published after the relocation of the factories to a plot in between the canal and the railway station in Saint-Michel-lez-Bruges, in the South of Bruges. This relocation might explain why so many interior pictures are included in the catalogue. One general drawing of the factory and twelve photographs depict the different workshops. A picture of the workman leaving the factory is also included. The catalogue starts off with a description and small history of the company in four languages (French, English, German, Spanish). These international ambitions are underpinned by adding two photographs of their participation in the world exhibition in Liège (1905) and Milan (1906). The main part of the catalogue shows 45 photographs of wagons and tenders shipped to all parts of the world. As the purchasers are

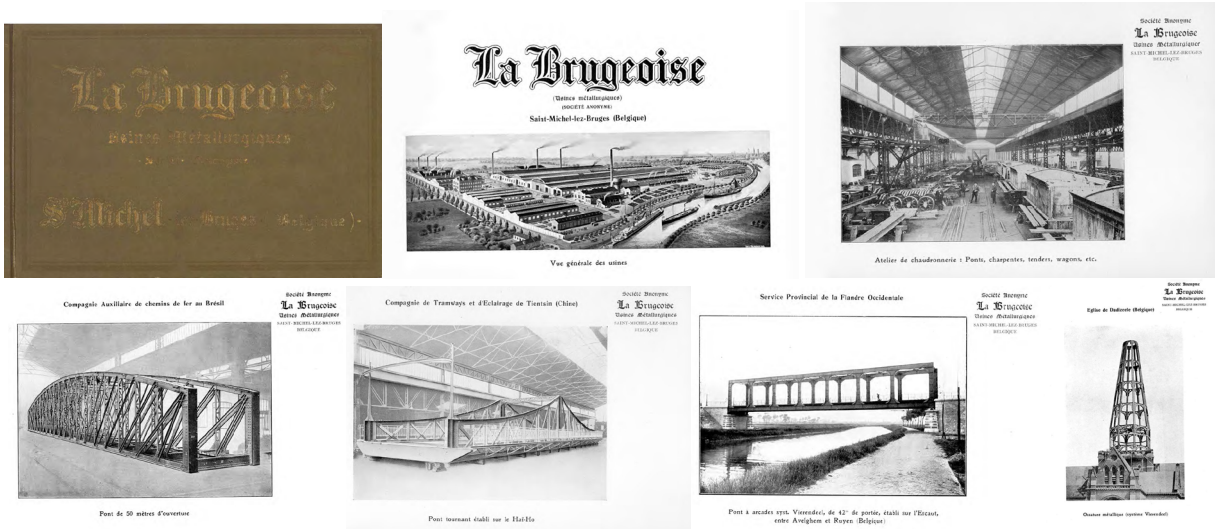


Figure 5: Trade catalogue *La brugeoise. Usines Métallurgiques. St-Michel-lez-Bruges* (c1910) depicting view of the new factory in Bruges, an interior view, a bridge spanning 50 meters for *Compagnie Auxiliaire de Chemins de fer au Brésil*, a turning bridge for *Compagnie de Tramways et d'Eclairage de Tientsien* (China), the first Vierdendeel bridge in Belgium (built 1904) and the iron tower of Dadizeele church © City Archive Bruges

clearly mentioned we get a view on their international clients : *Compagnie des chemins de fer de l'Ouest Paris*, *Chemin de fer du Nord de l'Espagne*, *Compagnie des Chemins de fer de la Tajuna* (Spain), *Chemin de fer de l'Etat Italien*, *Compagnie générale des tramways d'Athènes et du Pirée*, *Chemins de fer des Indes Anglaises*, *Chemins de fer de Rosario à Puerto-Belgrado*, *Compagnie Générale de Chemins de fer dans la province de Buenos-Ayres*, *Compagnie générale de Chemins de fer et de tramways en Chine. Chemins de fer du Pienlo*. The catalogue includes 19 photographs of bridges and structures. (see figure 5) Some of the destinations reappear: three bridges with a span of 10, 25 and 50 meters are destined for the *Compagnie auxiliaire de Chemins de fer au Brésil*, a dome for the Necroterio in Bello Horizonte (Brasil), a turning bridge over the Haï-Ho for *Compagnie de tramways et d'éclairage de Tientsin* (China) and a bridge with a span of 30 meters over the yellow river for *Chemin de fer de Pékin à Hankow (China)*. The photographs show the construction of these structures in the workshop. For the Belgian structures, iconic examples were selected: the catalogue includes two photographs of the first Vierendeel bridge, constructed in 1904 over river Sheldt, between Avelghem and Ruyen [3]. The bridge is commissioned by *Service provincial de la Flandre Occidental*, which is not a coincidence as Arthur Vierendeel was heading this department. Furthermore, there are two photographs of the iron tower of Dadizeele church (system Vierendeel), a military hall for balloons in Antwerp, bridges in Charleroi, Termonde and Marchienne-au-Pont and a gasometer. The Belgian examples are depicted in situ, during or just after construction.

4.3. *La Brugeoise et Nicaise & Delcuve*

In 1913 the two companies *Nicaise et Delcuve* and *La Brugeoise* join to become *La Brugeoise, Nicaise et Delcuve*. Table 1 includes three catalogues of this company dating from around 1930, 1937 and 1949. In the 1930 catalogue the German language has been replaced by Portuguese. The catalogue shows interior views of both factories in Bruges and La Louvière,



Figure 6: Trade catalogue *La brugeoise et Nicaise & Delcuve* (c1937) depicting the photos of the construction of the Vierendeel railway bridge Val Benoît in Liège (1935), a bridge in Argentina - a Vierendeel railway bridge for Congo (Bas-Congo au Katanga), roof trusses and the windscreen for the Alexandria station in Egypt © City Archive Bruges

followed by photographs of wagons, cranes, bridges and buildings. Many photographs are recuperated from the previous catalogues. Therefore, we go into the catalogue dating back to c1937. The lay-out of that catalogue is completely different, combining several pictures on one page (figure 6). After an introduction of the two factories in Bruges and La Louvière, bridges are the first structures that are shown. Indeed, large reconstruction and infrastructure works had taken place in inter-war Belgium. The construction and onsite pictures of Vierendeel bridges in Liège (Val Benoit), Gellick and Geel are shown. The pictures illustrate how the shape of Vierendeel bridges had been optimised: the upper part is curved as a parabola. In the 1930s also the connection techniques of steel Vierendeel bridges evolved from riveted to welded connections and Espion pointed out the leading role of the iron construction workshops in this evolution [3]. When workshops were invited to send in their offers to construct a Vierendeel bridge over the Albert canal the iron construction workshop *Société Métallurgique d'Enghien Saint-Eloi* send in a counterproposal in 1932 to weld parts of the Lanaye bridge in the workshop and hot rivet the parts on site. This method was accepted and the bridge in Lanaye became the first partly welded Vierendeel bridge in Belgium in 1933. In 1934 the first entirely welded Vierendeel bridge was constructed in Herentals, again because of an accepted counterproposal by *Société Métallurgique d'Enghien Saint-Eloi.* When a fully welded Vierendeel bridge collapsed in Hasselt in 1938, without any prior sign of failure, the optimism about this progress was tempered [3].

In the trade catalogue 'welded' is added to the description of the Vierendeel road bridge in Geel, spanning 49 meters. The other two depicted large span railway bridges are still hot riveted: Vierendeel bridge in Val Benoît (1935, spans 60m, 85m and 60m), Vierendeel bridge in Ghellick (1938, spans 113m). Next to these Belgian bridges, a Vierendeel railway bridge for Congo (chemin de fer du Bas-Congo) and several bridges for Republique Argentine are depicted: a road bridge 109m long over the Riachuelo with two movable parts, a railroad bridge for the line J.V. Gonzalez à Pichanal over Rio San Francisco and a bridge for Rio Sali. The two pages dedicated to buildings contain a roof structure mentioning *charpente coloniale* and the windscreen for the Alexandria station in Egypt (1927).

The main body of the catalogue is still dedicated to rolling stock (wagons and tenders), yet

new destinations appear which explain the link between bridge orders and rolling stock orders: Congo (*Chemin de fer Leopoldville-Katanga-Dilolo, Compagnie du chemin de fer du Bas-Congo au Katanga*), Maroc (*Chemin de fer de Maroc*), South-Africa (*Chemins de fer Sud-Africains, Johannesburg*), Peru (*The Peruvian Corporation LTD*), Egypt (*Chemins de fer de l'Etat Egyptien*), Argentina (*Chemin de fer de l'Etat Argentine*). Next to these destinations, wagons and tenders were still exported to France, Spain, China and Brazil.

5 CONCLUSIONS

In the 19th century about 100 Belgian iron and steel workshops were active in the construction of buildings and bridges. The search for trade catalogues of these workshops showed that widely-distributed catalogues were not used by companies whose main activity was in the construction sector. The 15 trade catalogues identified in this study all relate to companies with their main activity in the railway sector. For these companies it was an advantage to take up the construction of bridges and related structures when developing railway lines abroad to bridge rivers and roads when constructing a railway or tramway line. From the 1870s onwards Belgian construction workshops exported a vast amount of structures to countries where railway activities took place such as Spain, Italy, Egypt, Congo, Brazil, Argentina and China.

The trade catalogues are not comprehensive as they only cover a selection of projects and the data they provide is often too limited to identify a bridge or a building. However, these catalogues often provide new information because they contain little known pictures from the construction in the workshop or of the construction on site. The catalogue also provides insight into the company's broader oeuvre.

Acknowledgements. This research is supported by Growth Funding SRP23 Construction History granted by Vrije Universiteit Brussel. The authors are grateful to Gertjan Baesberg for tracking down and inventorying trade catalogues in the framework of his masterthesis and to the city and company archives and institutions for opening their doors.

REFERENCES

[1] Espion, B. et al. (eds). *Patrimoines de fonte, fer et acier. Architectures et ouvrages d'art*, FABI, 2018.

[2] Ortiz-Colom, J. European iron bridges in Puerto Rico: The example of the Guamaní bridge. In: I. Wouters et al. (Eds): *Building Knowledge, Constructing Histories*, CRC press, (2018), pp. 1021−1027.

[3] Espion, B. Les ponts Vierendeel, une histoire belge. In: M. Provost (Ed.): *Ponts Métalliques Belges*, ICOMOS Wallonie-Bruxelles (2016), pp. 37-43.

[4] Verswijver, K., Bertels, I., Wouters, I. and Collette, Q. The Development of Belgian Ironworks in the 19th Century: Case Studies and Reflections on Sources and Historiography. In: R. Carvais et al. (Eds): *Nuts & Bolts of Construction History.* ePicard, Vol. II (2012), pp. 81-90.

[5] Haoudy, K. *Baume et Marpent: de la Haine au Nil … Itinéraire d'un géant*, Ecomusée Régional du Centre, (2006).

[6] Piaton, C., Godoli, E., and Peyceré, D. *Construire au-delà de la Méditerranée. L'apport des archives d'entreprises européennes (1860-1970) / Building beyond the mediterranean. Studying the Archives of European Businesses (1860-1970),* Honoré Clair (2012).
[7] Baesberg, G. *Ateliers de construction: a first exploration of Belgian iron and steel workshops in the 19th and 20th centuries*, Vrije Universiteit Brussel, unpublished Master Thesis (2019).
[8] Beulens, F. and van den Broeck, J. *Financieel-institutionele analyse van de Belgische beursgenoteerde spoorwegsector 1836-1957.* Garant (2004).
[9] De Maeyer, J. and Heyrman, P. *Geuren en kleuren*, Peeters Press (2001).
[10] *Annexe au moniteur Belge. Recueil spécial des actes, extraits d'actes, procès-verbaux et documents relatifs aux sociétés.* Tome III (1875).
[11] *Société Anonyme des Ateliers de la Dyle*. Louvain (1953).
[12] Storms, M. *Société Anonyme des travaux Dyle et Bacalan.* Retrieved Jan. 2020 from http://www.belgianclub.com.br/
[13] Provost, M. Le premier chemin de fer Matadi-Kinshasa. In: M. Provost (Ed.): *Ponts Métalliques Belges*, ICOMOS Wallonie-Bruxelles (2016), pp. 120-46
[14] Société des Ateliers de construction de Hal. In: *Le Recueil Financier (Bourse de Bruxelles)*, Bruylant (1911), pp. 1066-67.
[15] Bridge over the river Sarpsfos: Norwegian State Railways, *Engineering* 25 (1878), pp. 10,16, 61-63.
[16] The Lysedal Viaduct, *Engineering* 27 (1879), pp. 1-2.
[17] Tyrrell, H. G. *History of bridge engineering.* Chicago, (1911).
[18] Verswijver, K. et al. The writings of Belgian engineer Arthur Vierendeel (1852-1940): homo universalis or contemporary propagandist? In: W. Lorenz et al. (Eds): *Proceedings of the Third International Congress on Construction History,* BTUCottbus (2009), pp. 1463-1470.

12th International Conference on Structural Analysis of Historical Constructions
SAHC 2020
P. Roca, L. Pelà and C. Molins (Eds.)

"IRON CAGES." TECHNICAL DISCUSSIONS AFTER THE 1906 VALPARAÍSO EARTHQUAKE AND RECONSTRUCTION WITH NEW TECHNIQUES AND MATERIALS

SANDRO MAINO[1]*, KATHERINE CABEZAS[2] AND MARION KOCH[2]

[1]Architecture Department
Universidad Técnica Federico Santa María
Campus Casa Central, 08034 Valparaíso, Chile
e-mail: sandro.maino@usm.cl, web page: http://www. http://arquitectura.usm.cl/

[2] Architecture Department
Universidad Técnica Federico Santa María
Campus Casa Central, 08034 Valparaíso, Chile

Keywords: earthquake-resistant construction, Steel frame, Prefabrication, Factory Building, Chile

Abstract. *A few months after the San Francisco earthquake and fire in April 1906, the prosperous and cosmopolitan city of Valparaíso (Chile) suffered a similar catastrophe, sparking the forerunner application of new materials and construction systems. After the earthquake, reports, and articles were produced analysing the characteristics of the earthquake and its effects on the built environment, emulating at a more basic level those emanating from the ad hoc commissions created to analyse the earthquakes in San Francisco and Messina (1908). At the theoretical level, solutions for reconstruction were discussed between reinforced concrete and steel structures, and the applications of these new materials, structural systems, and constructions in the world were closely observed. The solutions used for reconstruction ranged from proven inefficiencies prior to the earthquake to new techniques and materials. In this area, the use of steel with imported pre-manufactured systems as well as local solutions stands out. The need to reconstruct public and private buildings in Valparaiso with a reliable and fast system leaned the choice at the beginning towards the use of pre-manufactured metal structures. The article will expose and analyse the discussions of the time regarding construction systems and materials from a seismic-resistant point of view, complemented with the description of three emblematic cases of metal medium height construction in Valparaiso, after the earthquake: the Hucke Factory, Cardonal Market and the "Jabonería La Estrella" Factory.*

1 INTRODUCTION

On August 16, 1906, a few months after the earthquake and fire in San Francisco, the prosperous and cosmopolitan port of Valparaiso suffered a similar catastrophe, detonating the pioneering application in Chile of new construction systems and materials for the local area. The Valparaiso earthquake along with the San Francisco earthquake of the same year[1] and the Messina earthquake of 1908 was a turning point for seismology and seismic engineering, setting the end of the so-called historical earthquakes, with the transition in the approach to seismic engineering from one based on empiricism to another based on science. After the San Francisco earthquake, detailed reports made on the effects of the quake as regards the built environment and seismological aspects [1]. Lawson's work, one of them, focuses on describing earthquake effects on rural areas, buildings, drinking water, and railway networks. In Italy, Engineer Mario Baratta and a team also prepared a detailed report with injury surveys, and damage planimetry in the main cities [2] and a committee of experts analyzed, evaluated and proposed dynamic seismic calculation formulas and new regulations [3]. After the Valparaiso earthquake, some reports and articles arose, analyzing the characteristics of the quake and its effects on the built environment, quoting in one of them the reports and scientific articles of the San Francisco earthquake [4]. Chile also published a series of articles analyzing the San Francisco earthquake that had considerably more ground information than the local earthquake [5-7]. Discussions among specialists reveal the heterogeneous flow of knowledge and the freedoms given to architects, engineers, and builders in the absence of national building regulations and weak local ordinances, a weakness that has persisted for almost three decades[2].

The solutions used for reconstruction ranged from the proven inefficiencies before the earthquake, to new techniques and materials. On a theoretical level, reconstruction solutions were discussed between the use of reinforced concrete and steel structures, looking closely at the applications of these new materials in the world. The need to rebuild public and private buildings in Valparaiso with a reliable and fast system, at first favored the choice of prefabricated metal structures. Both the speed of assembly and the seismic-resistant characteristics of the steel structural systems influenced this choice, as did, to a not lesser extent, the origin of the owners and principals of the buildings. In the analysis of the material choice, it should take into account that Chile did not have local steel production until 1924, with a brief and failed attempt in 1910 at the Altos Hornos de Corral [8, 9].

2 THE ASSESSMENT OF THE EARTHQUAKE'S EFFECTS

Five days after the earthquake, in New York, 8,200 kilometers away, The New York Times interviewed Chilean engineer Juan Tonkin [10]. According to Tonkin, the destruction in Valparaíso had not been as high as indicated by different sources, affirming his belief that the earthquake damage reports were exaggerated. We are not clear who Tonkin's informants were. Yet, the information he received was incorrect, as the earthquake for Valparaiso was a catastrophe, and for a sector of the city called El Almendral, the ruin [11]. Despite this error, Tonkin's comments regarding the characteristics of the construction in Valparaíso, its possible problems, and the projections for the reconstruction are understandable. Tonkin was clear that the area most affected by the earthquake had been the land reclaimed from the sea, the sector of El Almendral, characterized by uncontrolled sand and artificial fillings. Another relevant factor was that it had been years since Valparaiso had suffered an earthquake of magnitude,

with buildings constructed without the necessary provisions, stone, and brick buildings that did not have the required flexibility to withstand an earthquake. In the interview, Tonkin declared his preference for lightweight partitions and steel structures, due to the advantages in their behavior against earthquake and fire, arguing how convenient it was to build buildings of up to 8 or 10 floors of steel, thinking how limited was the space of the city plan.

After the earthquake, the Chilean government appointed an ad hoc commission to analyze the quake, headed by geographer Hans Steffen. Steffen, aware of the importance of on-site observation used in his explorations, applied the observer method for earthquake analysis [12]. However, these methods had long since fallen into disuse. The magazine of the Chilean Institute of Engineers published the report's results [13]. Within the analysis line of the seismological phenomenon, there is also the article by Luis Zegers [14]. Although we found a series of published works on seismology, such as those mentioned above, the analysis of the earthquake effect in Valparaiso on the built environment and the rest of the affected cities is limited. It is in contrast to the series of articles published in Chile analyzing the San Francisco earthquake[3].

The first report published on the earthquake effects on the built environment was by Prussian engineer Carlos Koning [15], Director of Public Works and founder of the Materials Resistance Laboratory of the Universidad de Chile. In his article, Koning describes the effect of the earthquake on commercial construction to learn lessons for future buildings, assessing the problems in masonry and possible solutions. Undoubtedly the most interesting analysis of the earthquake is that of the young engineer Hormidas Henríquez, who published in the newspaper La Unión de Valparaíso a scientific article in six editions gathered under the title "The earthquake of Valparaíso under its constructive aspect." [16]. The article was published in a book and also in two well-known Spanish magazines[4]. They contrast the knowledge of seismic engineering of Henriquez, a newly qualified engineer, with that of Koning, an experienced engineer. Henríquez had up-to-date knowledge about seismic engineering; he knew Lawson's report on the San Francisco earthquake and the work of Milne in Japan, one of the pioneers of seismology worldwide. Koning sought to position "well-executed masonry" alongside iron and reinforced concrete masonry. On the contrary, Henríquez proposed the abandonment of masonry, judging the "detestable brick." Henríquez cites a series of articles in Engineering Record magazine about the effects of the earthquake and the suggested solutions. One of the cited articles is that of the engineer Edward Boggs [17], who postulates that "Steel Frame" is the best solution to earthquakes for high-rise buildings, as the Claus Spreckels building. Other engineers also cited shared this position[5]. Henríquez was debating himself between the reinforced concrete systems and the metallic structures. The entry of reinforced concrete into Chile was delayed after the disastrous collapse of the Casa Prá building in 1904, built with the Cottancin system [18].

3 « VALPARAISO OF THE FUTURE »

Before the earthquake, in Valparaiso, iron, and steel were used in building construction as insulated parts (i.e., columns, beams) and reinforcements (i.e., hardware, inserts), just as in the early days of iron use in Europe [19]. These pieces and reinforcements were inserted in traditional masonry models, resulting in some cases detrimental to their seismic performance. The deficiencies of mass construction systems in seismic behavior were exposed, after the catastrophic consequences of the earthquake, leading to a debate among professionals who

proposed various solutions for reconstruction. Most of them based on construction models used abroad, considering the use of steel structures among them.

A few months after the earthquake, the illustrated current affairs magazine Sucesos published a report entitled "Valparaíso of the future," with photographs of a metal structure building under construction, in a central area of the city (figure 1). The architect and director of the work Antonio Lafoglia designed the building in question, the metal structure assembled by Alejandro Beltrami, and the masonry by C. Pirazzoli, all of the Italian origin. The building, designed before the earthquake, was originally a masonry structure. Nevertheless, the experience of the catastrophe made it necessary to rethink the construction system, replacing the weighty masonry walls with an "elegant iron cage." Note the term "elegant," perhaps related to the lightness of the construction system's appearance, a symbol of modernity. Since the building construction started before the earthquake, the plinth was made of masonry, and the metal structure mounted on it. The steel and concrete building is advertised in the news report as a fire-resistant building rather than an earthquake-resistant building. In contrast to "Valparaíso of the future," the same magazine publishes in another edition the "Valparaíso of the Past," a photograph of the Valparaíso Theatre under construction, a building with masonry walls and a wooden structure on the roof that did not finish due to the earthquake. Lafoglia's work can be seen as a relevant milestone in the constructive transition from mass systems to metallic systems. This building is positioned as an example of replacement of the traditional systems, making possible the construction of more slender buildings, with a greater number of floors and free of the ornamentation that predominated in the masonry buildings.

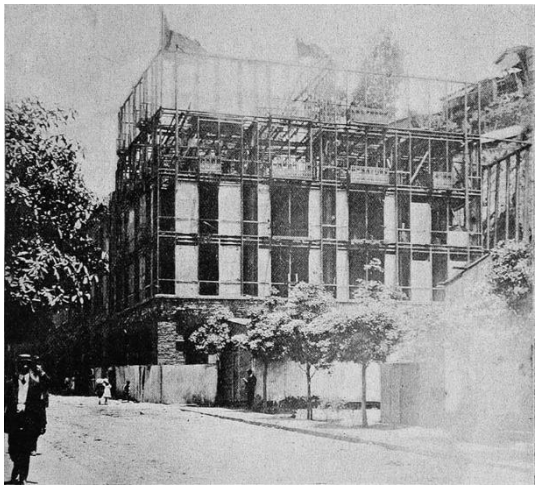


Figure 1: Construction of the metal structure building by architect Antonio Lafoglia, San Agustín slope, Valparaíso (Revista Sucesos 1907, No. 227, January 10, 1907).

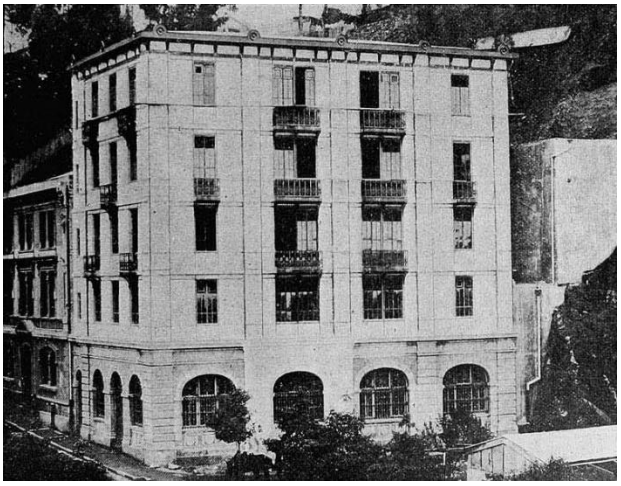


Figure 2: Building with a metal and concrete structure resistant to fire and earthquakes, San Agustín slope, Valparaíso (Revista Sucesos 1907, No. 251, June 28, 1907).

Concerning the architectural aspect, but also structural construction, there are two possibilities for integrating the metal structures and their filling: expressing the steel framing in its facade or hiding it. The latter will not be discussed in this article as they are seen as a precedent for reinforced concrete systems. Among the first we will analyze three emblematic cases of metal construction in Valparaíso after the earthquake: the Mercado El Cardonal, the

Hucke Factory, and the Jabonería La Estrella[6]. In the studied buildings, of compact geometry, walls' filling is placed between the steel profiles, keeping them visible both towards the outside and inside. The three analyzed buildings correspond to the Steel Frame system, a metal grid with infill walls, whose first exponent as a medium height building with an iron structure is the Chocolaterie Menier by Jules Saulnier built-in 1872 near Paris. However, the analyzed structures differ from the building of the chocolate factory in two significant aspects. In the studied cases, laminate steel predominates, as a construction material, and the configuration of the bracing elements are cross-linked beams and columns, not a net as in the Menier factory.

4 EL MERCADO EL CARDONAL

Mercado El Cardonal building occupies an entire block. Before occupying the land, the market was located in an adjacent block, under the name of "Recova del Cardonal," built-in 1855 by the American builder Alexander Livingstone [20]. The masonry building had two floors with a central courtyard.

As with other buildings in El Almendral, the earthquake and subsequent fire destroyed the Market. In the first instance, a temporary facility called "El Mercado de las Delicias" was built while waiting for a project for the new market. Then, there were a series of proposals, such as the one from the municipal official Abelardo Arriagada, influenced by the European markets of the 19th century. Also, the one from the well-known architect Eugenio Joannon, who finally became the architect of a project, whose authorship is still unclear. Eduardo Feureisen Harms, a Civil Engineer, graduated from the Universidad de Chile in 1903.

In 1912, the works of the new Mercado building began, a steel and concrete block structure imported by the Municipality of Valparaíso through the company based in Valparaíso, Vorwerk y Co., representative of the German company specialized in steel constructions, Aug. Klönne from Dortmund (figure 2). In mid-1914, the new Mercado de El Cardonal opened. According to a publication for the 50th anniversary of the company, El Mercado was one of the projects of Aug. Klönne abroad. The 1,000-ton building was manufactured, moved, assembled, and delivered on a turnkey basis [21]. The company had specialized departments for the integral development of steel projects.

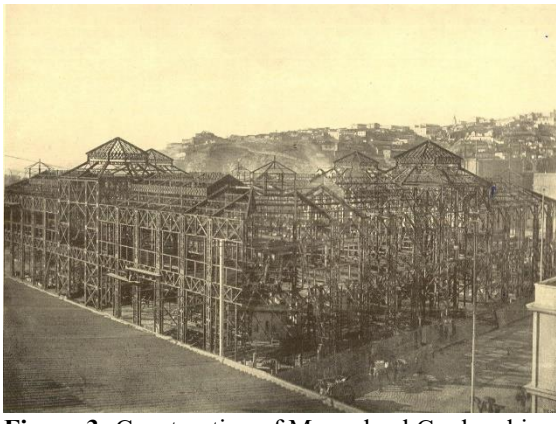


Figure 3: Construction of Mercado el Cardonal in 1913 (Source: Aug, K., Aug. Klönne Dortmund 1879-1929. 1929, Dortmund: Krüger GmbH)

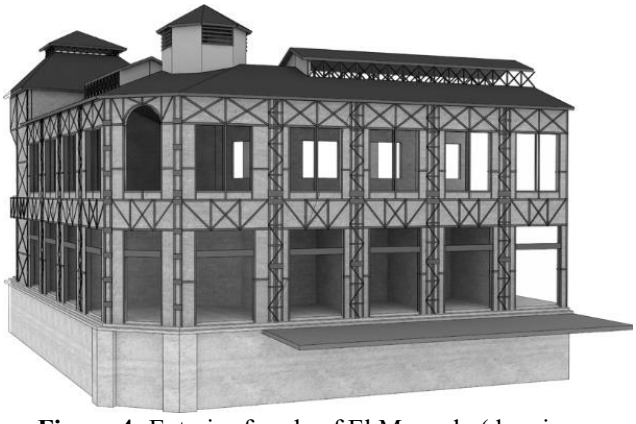


Figure 4: Exterior facade of El Mercado (drawing: Katherine Cabezas).

4.1 Building description

Mercado El Cardonal is a trapezoid-shaped building whose sides measure 67, 54, 68, and 60 meters, and its corners are octagonal. The building has a compact appearance and occupies the entire surface of the block, with two floors plus a basement (Figure 3).

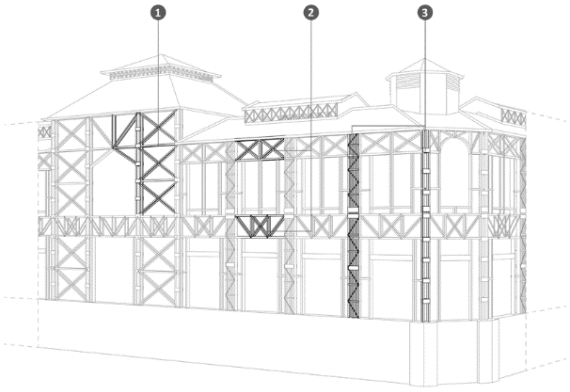


Figure 5: Components of the structure of the exterior facade of El Mercado. 1) braced walls 2) lattice beams 3) simple composite column and bracing (drawing by Katherine Cabezas)

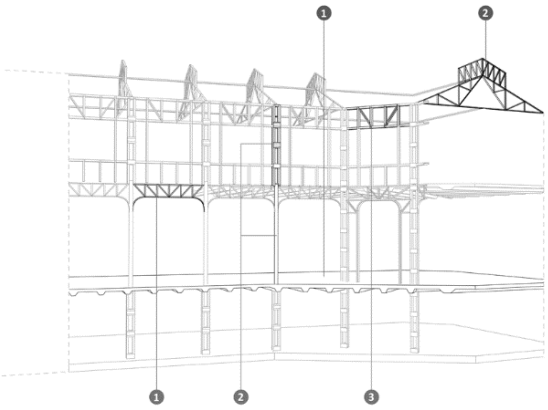


Figure 6: Components of the internal structure of El Mercado. (top) 1) rigid diaphragm 2) cross-linked truss (bottom) 1) lattice beam 2) column 3) bracing (Katherine Cabezas drawing).

A perimeter ring and a central piece shape the building, both separated by a double-height space that makes them structurally independent. Both the perimeter ring and the central piece are structured based on flexible steel frames, achieving free floors on each of their levels. As an enclosure of the building and also its interior partitions, the metal structure was filled with concrete blocks, giving the structure greater rigidity. The metal framework consists of single-section, cross-linked pillars, and beams, on the outside and part of the inside of the building (Figure 4). The cylindrical pillars inside the first floor are cast-iron pieces. In the underground, only its interior skeleton is exposed, leaving the metal structure embedded in a concrete wall on the perimeter, thus avoiding the oxidation of the metal parts. The roof structure is composed of exposed steel trusses and turnbuckles with a corrugated zinc plate covering. The latticework of its exterior facade stiffens the building. The façade made up of two lattice beams that extend along its entire length and of pillars made up of triangular and plain profiles, which make up the building's frames. The interior facade is made up of trusses with few diagonals on the upper level and a lattice beam on the first floor. The rigid diaphragm is a slab ribbed by a succession of steel beams that rest on pillars and intermediate walls of the building in a perpendicular direction to the perimeter axes (Figure 5).

5 HUCKE COOKIE FACTORY BUILDING

The Hucke factory[7] is a particular case in this selection, with a building inaugurated in 1901 with two floors, built with brick perimeter walls and a wooden interior structure. The building resisted the earthquake with minimal damage, restoring normal factory operations within a few weeks. However, three months later, a fire destroyed the entire factory[8]. First Ernst Hucke and after his death his brothers, Otto and Georg, traveled to Germany to observe on-

site the buildings and facilities of the most important factories. In Germany, they contracted at the German steelworks Burbacher Hütte in Saarbrücken a prefabricated steel structure for a five-story, 10,000 square meter building [22]. Fourteen months after the fire, and under the direction of the architect-engineer Otto Andwanter, the building was inaugurated (Figure 6). Its height and aesthetics positioned it at the time as the tallest and most modern building in Valparaiso.

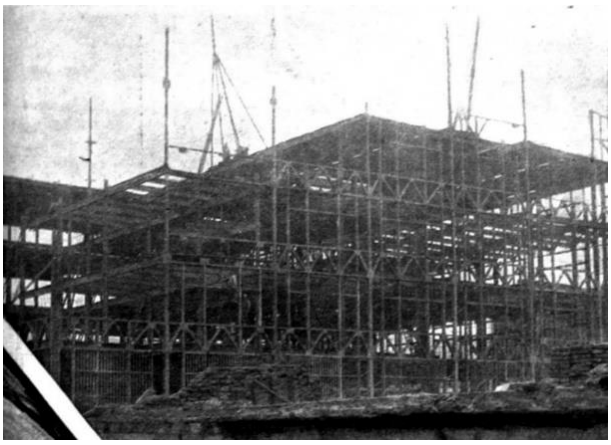


Figure 7: Construction of the new Hucke factory in 1908 (Source: Resurgence of Valparaíso, 1908, August 16, Zig-Zag Magazine No. 182).

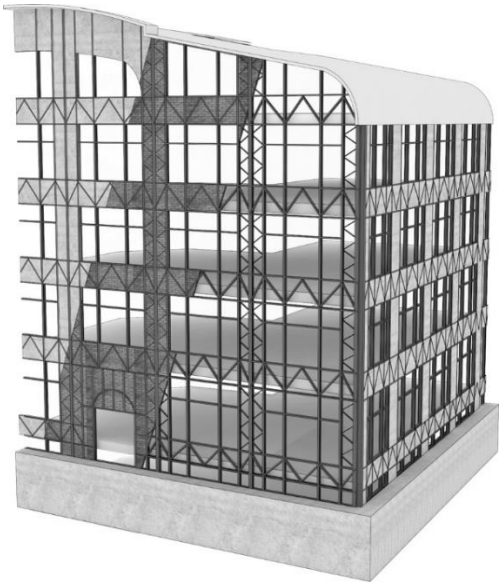


Figure 8: Structure of Hucke factory facade (drawing by Katherine Cabezas).

5.1 Building description

The Hucke factory building occupies the end of an elongated block, with three facades facing the street and a dividing wall adjacent to the reinforced concrete construction of the sugar refinery built years later, designed by architect Karl Mönch. The factory is a compact trapezoid-shaped volume with sides ranging from 38 to 40 meters and a maximum height of 30 meters, divided into a basement, five floors, and the mansard. Inside, it housed large and heavy machinery for the production of its products. The interior luminosity of the building is possible thanks to its structure, which in addition to reducing the mass, allows for larger openings in its walls compared to masonry buildings.

The first bay next to the façade absorbs the difference between the plant's perimeter irregularity and the interior structure regularity. The interior distribution in each one of its floors resolved in a free level divided into seven crossings of 5.70 meters wide by 40 meters long and six transversal to these of similar measures. The widths of the bays are variable on the facades: one goes from 5.20 meters to 1.70 meters and the other from 5.30 meters until it disappears at the other end. The height of each floor is, on average, 3.70 meters between the slab and main beam and a maximum of 4 meters between slab and vault. From the underground level, the floors are vertically connected by an inner courtyard that adapts to the frames of the primary structure, located off the central axis of the building. The metal skeleton

is mainly made up of nine uniformly spaced frames, which are transversally tied by eight main beams in each of their slabs. At the same time, the perimeter of the structure acts as support against lateral forces as it is made up of lattice beams and columns (Figure 7). In the basement, the perimeter walls in reinforced concrete and in the upper floors in brick masonry.

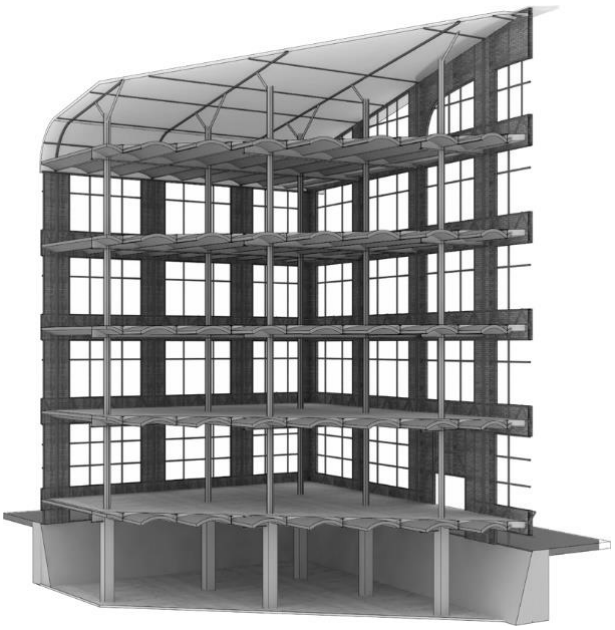


Figure 9: Interior structure of the Hucke factory (drawing by Katherine Cabezas)

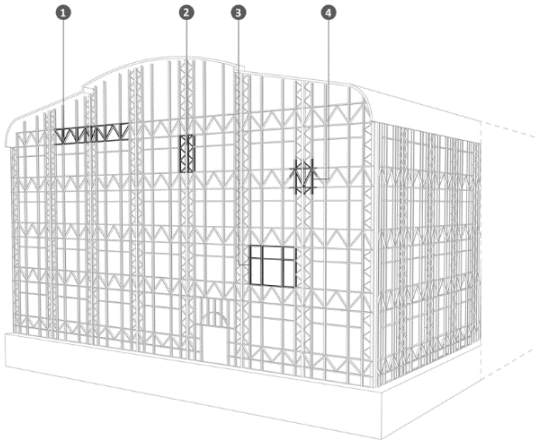


Figure 10: Structural components of the Hucke factory facade. 1) lattice beam 2) structural panel 3) span reinforcements 4) meeting of lattice beam with structural panel (drawing by Katherine Cabezas)

Inside the building, the horizontal structure is constituted from the basement to the fourth floor by a secondary steel beam that supports masonry vaults and that are arranged transversely to the main beams, transferring the loads to the vertical structure. The vaults are covered with concrete, leaving an approximate thickness of 50 centimeters. As for the internal vertical structure, it consists of pillars made of simple laminated steel profiles joined by plates, stiffeners, and rivets, obtaining vertical continuity through connecting plates. On the fifth floor, this structure changes by creating branched support for the roof structure. The joints between the vertical and horizontal structures use angle plates and bolted or riveted gussets (Figure 8). It should be noted that the general structure of the case is mainly supported by a rigid perimeter and center, which in the building can be recognized as the exterior façade and the interior façade towards the inner courtyard, concentrating in them all the bracing systems (figure 9).

6 LA ESTRELLA SOAP FACTORY

John Deichert founded the candle and soap factory in 1866, with experience in the business in his own factory in Kassel [22]. His son, John William, who studied at one of Brunswick's leading soap factories, took over the factory in 1899. The soap factory before the earthquake was located on a central street in Valparaiso in a colonial building. After the earthquake, the

building was in ruins, and the factory moved to another lot in the city where they built a shed. In September 1910, the shed was burnt down, and in October of the following year, the new building with metal and reinforced concrete structure was inaugurated, a building specially built for its functions (Figure 10). In the Municipal Archives, the current lot of the factory has the entrance of a building project of metallic structure similar to the existing one, the first semester of the year 1908; the construction of a new building was already in the horizon.



Figure 11: Interior of La Estrella soap factory (Source: German progress in America, 1924).

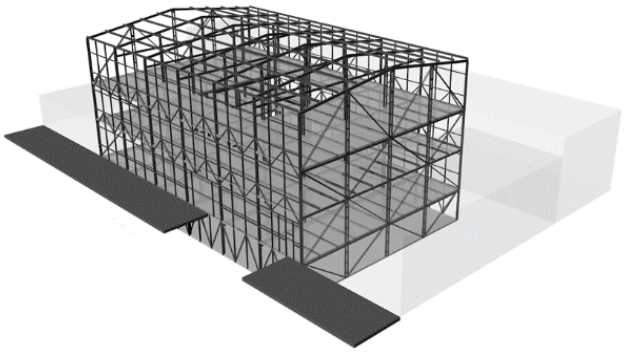


Figure 12: The steel structure of the soap factory (drawing: Katherine Cabezas)

6.1 Building description

"La Estrella" factory is a rectangular-shaped volume with three blindsides and a façade facing the street, measuring 33 by 22 meters at the base and 19 meters high from its underground level (figure 11). Structurally, the building's interior is regularly divided into six bays on its longest side and four cross bays, while its height is made up of three open-plan floors plus a basement level, with the upper levels connected by a large central void that served as ventilation and natural lighting system (figure 12). The factory is structured by steel elements from the underground level to the roof, with reinforced concrete enclosures in the whole of its perimeter walls. Additionally, brick masonry is used as a lining for the metal elements located in the underground, as a strategy for protection against moisture and to provide greater strength. The metallic skeleton is made up of seven frames that cross the smaller side of the volume, composed of five pillars each and intersected in the same direction by main beams and a transversal framework of eleven secondary beams that tie up the set of structural elements. The perimeter of the building has stiffening elements, which in its smaller walls, are made up of V-shaped braces that intercalate their orientation between floors, from the basement to the roof (Figure 13). As for the larger walls, stiffening is based on the formation

of two lattice beams at the height of the slabs and a V-shaped bracing in the basement wall, embedded in the reinforced concrete.

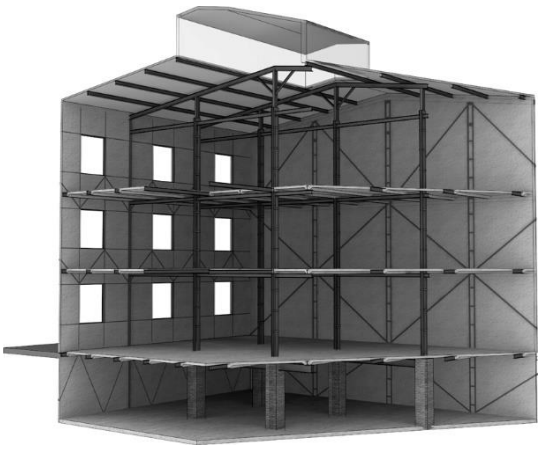


Figure 13: The internal structure of the soap factory (drawing: Katherine Cabezas).

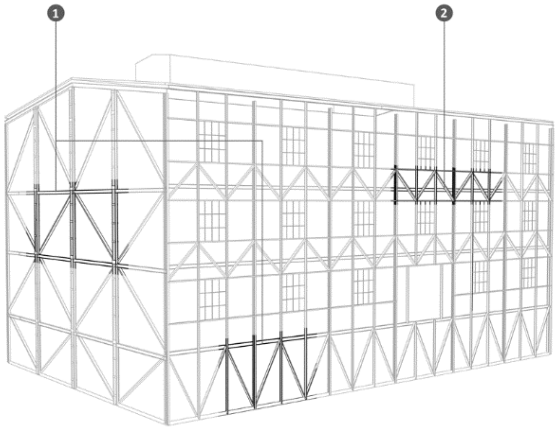


Figure 14: Structural components of the factory facade. 1) braced wall 2) lattice beam (drawing by Katherine Cabezas)

7 CONCLUSIONS

The use of metal construction systems in Valparaíso had an unprecedented application after the earthquake, an expression of its capacity for reconstruction and its booming industry, in a cosmopolitan city that was economically projected in the Pacific due to its potential as a commercial exchange port. The fact that it was a port allowed the fast-import of new technologies and construction materials from North America and Europe (e.g., cement, steel beams, pipes, wood, etc.). Thus, the origin of the structural components of at least two of the three cases is German steel companies - Mercado el Cardonal and Hucke Factory -, and the Soap factory certainly as well. It should be noted that at that time, there were no steel mills in Chile that supplied iron or steel parts; however, there were central-workshops capable of assembling a structure based on imported standard profiles.

The excellent performance of the metallic structures in the San Francisco earthquake earned it a good reputation among the engineers and architects of Valparaiso, in addition to the similar characteristics of the soil.

According to the seismic-constructive strategies, a configurable relationship is established between the traditional construction models of mass and steel frames, where both distribute a large part of the stiffening elements in the structure perimeter. For the study cases, the elements are braced columns, structural panels, lattice beams, and complete wall bracing, distributed symmetrically with respect to the main structural axes of the buildings. On the other hand, in some cases, the filling of the metal structure through a hidden reinforcement contributes to the stiffening of the steel framework avoiding deformations. About the structural elements, these are mainly U-section, double T-section, flat and angular profiles, while for the joints, riveted and bolted gussets and connecting plates are used.

Finally, as a general conclusion, it is argued that the 1906 earthquake considerably accelerated the process of architectural transformation that had begun in the mid-19th century,

positioning steel trusses as the most reliable and fastest system for reconstruction. However, the close link with international technical and technological development means that the use of reinforced concrete will soon replace this system.

Acknowledgements. FONDECYT Initiation 11190301 of the National Fund for Scientific and Technological Development (FONDECYT- Fondo Nacional de Desarrollo Científico y Tecnológico) managed by the National Agency for Research and Development (ANID-Agencia Nacional de Investigación y Desarrollo) financed this research. Acknowledgments to the Historical Heritage Archive of the Illustrious Municipality of Valparaíso and its manager Ana María Ojeda, to the administration of Mercado El Cardonal, to the Faculty of Engineering of the Universidad de Valparaíso and to the administration of the Labor Court of Valparaíso for their collaboration in the elaboration of this article.

REFERENCES

[1] Lawson, A.C. and C.S.E.I. Commission, *The California earthquake of April 18, 1906 Report of the State Earthquake Investigation Commission in two volumes and atlas*. 1908, Washington, D.C.: Carnegie Institution of Washington.

[2] Baratta, M. and i. Società geografica, ... *La catastrofe sismica Calabro messinese (28 dicembre 1908)*. 1910, Roma: Presso la Società Geografica Italiana. 2 p. ., [vii]-xv, 426, [2] p.

[3] Freeman, J.R., *Earthquake damage and earthquake insurance : studies of a rational basis for earthquake insurance, also studies of engineering data for earthquake-resisting construction*. 1932, New York: McGraw-Hill Book Co.

[4] Henríquez, H., *El terremoto de Valparaíso bajo su aspecto constructivo. Artículo dedicado a la I. Municipalidad y a los que edifican*, in *La Unión*. 1906: Valparaíso.

[5] Hoerning, C., *El Terremoto de San Francisco de California sus efectos i la reconstrucción (Continuará).* Anales del Instituto de Ingenieros de Chile, 1907. **año VII**(n° 4): p. p. 168-180.

[6] Calvo Mackenna, D. and G.H.d. Canto, *El Terremoto de San Francisco de California sus efectos i la reconstrucción (Continuación).* Anales del Instituto de Ingenieros de Chile, 1907. **año VII**(8): p. p. 391-407.

[7] Herreros, J., *Reglas de construcción que debe seguirse en vistas de los terremotos.* Anales del Instituto de Ingenieros de Chile, 1906. **Año VI**(n° 1): p. p. 523-526.

[8] Sánchez, C., *Evolución histórica de la industria siderúrgica chilena e ibero-americana*. 1952, Santiago de Chile: Nascimento.

[9] Palmer, M., *50 años de arquitectura metálica en Chile: 1863-1913*. 1970, Santiago de Chile: Instituto de Historia de la Arquitectura : Facultad de Arquitectura y Urbanismo Universidad de Chile.

[10] *Engineer says city will rise from ruins*, in *The New York Time*. 1906: New York.

[11] Rodríguez, A. and C. Gajardo, *La catástrofe del 16 de agosto de 1906 en la República de Chile*. 1906, Santiago de Chile: Barcelona.

[12] Valderrama, L., *Observando la catástrofe: terremotos y conocimiento sísmico en Chile (1868-1912)*, in *Departament de Història de la Ciència i Documentació*. 2017, Universitat de Valencia: Valencia.

[13] Steffen, H., *Contribuciones para un Estudio Científico del Terremoto del 16 de Agosto de 1906.* Anales de la Universidad de Chile, 1907: p. 633-713.
[14] Zegers, L., *El terremoto del 16 de agosto de 1906.* Anales de la Universidad de Chile, 1906. **tomo 119**: p. p. 1-33.
[15] Koning, C., *Las construcciones i el terremoto, informe pasado por la dirección de obras públicas al ministerio del ramo.* Anales del Instituto de Ingenieros de Chile, 1906. **Año VI**(n° 8-9): p. p. 405-411.
[16] Henríquez, H., *El terremoto de Valparaíso bajo su aspecto constructivo. Artículo dedicado a la I. Municipalidad y a los que edifican*, in *Diario la Unión*. 1906: Valparaiso.
[17] Boggs, E.M., *Comments of Californian Engineers on the Earthquake and Fire.* The Engineering Record, 1906. **53**(18): p. p. 558-560.
[18] Booth, R., *La irrupción del hormigón armado: circulación de conocimientos, patentes y terremotos. Chile en un contexto global, 1896-1920*. 2019, unpublished.
[19] Mark, R., ed. *Tecnología arquitectónica hasta la revolución científica: arte y estructura de las grandes construcciones*. Textos de Arquitectura. 2002, Akal: Madrid.
[20] Pereira Salas, E., *La arquitectura chilena en el siglo XIX*. 1956, Santiago, Chile: Ediciones de los Anales de la Universidad de Chile.
[21] Aug, K., *Aug. Klönne Dortmund 1879-1929*. 1929, Dortmund: Krüger GmbH.
[22] *El Progreso alemán en América*. Vol. 1: Chile. Resumen general de las actividades que ha desarrollado en Chile la colonia alemana. 1934, Santiago de Chile: Rio de La Plata.

[1] On January 31, 1906, the Esmeraldas earthquake occurred between Ecuador and Colombia, with a calculated magnitude of 8.8 Mw. Despite the magnitude, the impact of this earthquake was less than that of Valparaíso and San Francisco because it did not affect urban centers (Moncayo, M., et al., *Terremotos mayores a 6,5 en escala Richter ocurridos en Ecuador desde 1900 hasta 1970*. Ingeniería, 2017. **vol. 21**(n° 2): p. 55-64).

[2] The General Law and Ordinance on Construction and Urbanization promoted after the 1928 Talca earthquake, published in 1936. The law dedicates a section to the calculation of building stability to achieve *the assimilation of the constructions.*

[3] As an example the following articles: Hoerning, Cárlos. 1907. "El terremoto de San Francisco de California sus efectos y la reconstrucción (will continue)." *Anales del Instituto de Ingenieros de Chile* año VII (n° 4): p. 168-180; (n° 5):p. 197-284. Calvo Mackenna, Domingo, and G. H. del Canto. 1907. "El Terremoto de San Francisco de California sus efectos y la reconstrucción (Continued)." *Anales del Instituto de Ingenieros de Chile* año VII (n° 7):p. 374-375; (n° 8):p. 391-407.

[4] Henríquez, Hormidas. 1907. "El Terremoto de Valparaíso bajo su aspecto constructivo." *Arquitectura y Construcción*. Año XI (n° 177):p. 119-127; (n° 178):p. 147-156. Henríquez, Hormidas. 1907. "El terremoto de Valparaíso bajo su aspecto constructivo." *La Construcción Moderna* (n° 7): p. 116-119; (n° 8): p. 130-137; (n° 9): p. 146-151; (n° 10): p. 165-170.

[5] Phillip E. Harroun, Maurice C. Couchot, W. C. Ambrose, profesor Frank Soulé y Carl Leonardt.

[6] At present the Market building continues to fulfill the same functions, the Hucke factory houses the Faculty of Engineering of the Universidad de Valparaíso and the La Estrella soap factory the Labor Court of Valparaíso. Both factories have been subjected to reinforcement works of their structure due to their excessive flexibility.

[7] The Hucke cookie factory in this period achieved great success both locally and internationally, reaching a position as the largest factory in the entire Pacific coast (Sucesos Magazine n°s 208-225, 1906).

[8] On November 17, 1906, a fire in the biscuit ovens destroyed the factory in two hours (Sucesos Magazine n° 208-225, 1906).

12th International Conference on Structural Analysis of Historical Constructions
SAHC 2020
P. Roca, L. Pelà and C. Molins (Eds.)

NEW LIGHTWEIGHT STRUCTURES AND HISTORICAL HEAVYWEIGHT STRUCTURES IN CONSERVATION

A. MOSSERI[1*]

[1]The David Azrieli School of Architecture, The Yolanda and David Katz Faculty of the Arts.
Tel Aviv University. Israel.
e-mail: mosseriavi@bezeqint.net

Keywords: Lightweight Structures, Historical Structures, Conservation, Integration.

Abstract. *The field of lightweight structures becomes an important field of activity, not only in the built environment. The relevancy of this field to the conservation of the historical built environment is also very high. One of the most important and innovative issues is the integration between lightweight structures and historical heavyweight structures. But in in the current situation, many of the the practice and the research activities in this field are relatively specific and local. The activities are in many cases even done using different kinds of terminologies. This in addition to the fact that in general most of the research in conservation focuses mainly on historical heavyweight structures. In the current situation there is a need to create a wider and more integrated body of knowledge in order to explain and guide the existing activities as well as the future research and developments. The present research lays the foundations for a conceptual framework and a theoretical basis for the integration of new lightweight structures and historical heavyweight structures; reviews the recent theoretical and historical background; and defines an initial scheme of intervention design strategies for integrating lightweight structures with historical heavyweight structures. The basic implications of those strategies, in relation to the architectural – structural visual language, are presented and discussed, while other implications will have to be developed in future research. These efforts are part of an overall activity for developing a body of knowledge dealing with lightweight structures and conservation.*

1 INTRODUCTION

The conservation process of the built environment deals with a large gamut of structures. The richness of structures is continuously growing in the last centuries and nowadays it includes as well many structures with advanced technologies. These structures become more and more relevant to the conservation field. One important group of structures is the one of lightweight structures, in their contemporary meaning.

Lightweight structures always existed in the history of the built environment and different examples like tents, canopies, and other lightweight shelters can be brought. In parallel, designers and builders invariably aspired to lighten the weight of structures even when dealing with heavyweight structures. But in the last eras, different scientific engineering and technological developments enabled to lighten the weight of structures outstandingly, creating great challenges to the conservation field.

Despite the importance and relevancy of lightweight structures to the field of conservation, most efforts of research and practical activities focus on historical heavyweight structures, since naturally, many of the historical structures are still heavyweight structures. In the current situation, there is a great necessity to concentrate more on lightweight structures in the conservation field, in parallel to historical heavyweight structures.

This research deals with the use of new lightweight structures in a historical heavyweight conservation context, which is one of the challenges in the field of lightweight structures and conservation. The present research lays the foundations for a conceptual framework and a theoretical basis for the integration of new lightweight structures and historical heavyweight structures; reviews the recent theoretical and historical background; and defines an initial scheme of intervention design strategies for integrating lightweight structures with historical heavyweight structures. The basic implications of those strategies, in relation to the architectural – structural visual language, are presented and discussed, while other implications will have to be developed in future research.

The term "architectural-structural visual language" is used since in lightweight structures, very often, it is nearly impossible to separate between the architectural and the structural language. In addition, the focus in this research is on the intervention design strategies in which there is a clear visual distinction between the new lightweight structures and the historical heavyweight structures. The term “historical heavyweight structures” relates not only to historical structures but also to old existing structures.

2 LIGHTWEIGHT STRUCTURES AND CONSERVATION – THEORETICAL BACKGROUND

2.1 Lightweight structures – General background

The issue of lightweight structures is an interdisciplinary issue, which gets a special focus in a wide range of fields as: mechanical engineering aeronautical engineering, industrial and product design, architecture, civil engineering, materials engineering, morphology science, and other fields including art (for example, in connection to the possible relations between lightweight structures and sculptures[1]). Indeed, many objects surrounding us, such as laptops, cars, air-planes, etc., have a strong connection to the issue of lightweight structures. But "lightweight structures" is a relative and dynamic term. Accordingly, what we consider today as "lightweight" in the built environment can be considered heavyweight in the future. This relativity, beside additional reasons, makes it sometimes difficult to determine which buildings and structures have to be included in this category of lightweight structures. The borders can change with time and are not always clear. Generally, lightweight structures can be identified nowadays with the topics of minimal structures, minimum use of materials, natural structures and others. Yet, lightweight structures are connected especially with tensile structures like membrane structures, cable net structures, cable domes etc., as well as with other kinds of structures [2] like lightweight grid shells [3]

In the architectural language, lightweight structures are connected, in many cases, with transparency, and weightless appearance. Lightweight structures are special structures, not only due to their lightness, but also due to the fact that within them, little, if anything, is dividing between the configuration and the formal expressions. This topic deals with the question whether a structure can be beautiful by itself [4] and other issues dealing with the connection

between science and art in lightweight structures. There are many ways to lighten structures and different strategies can be identified to reduce the structure's weight, addressing aspects such as materials, overall geometry and other characteristics [2]. In general, all these strategies to lighten structures are continuously in a process of evolution, towards more lightness of the structures.

3.2 Lightweight structures and conservation

The field of lightweight structures can be strongly connected and relevant to conservation engineering and architecture in different facets, and is especially important since the modern era. Lightweight structures, many of which are from the recent past, contribute to the unique diversity of the modern heritage. The study of those structures, can contribute to understanding the philosophy of lighter structures along history and it is also relevant to the field of conservation engineering and architecture. Different mutual benefits can derive from connecting lightweight structures to the field of conservation.

Various examples of the challenges in the field of lightweight structure and conservation can be brought: the conservation of aging lightweight structures from different periods, the integration of new lightweight structures with historical heavyweight structures, lightweight strengthening intervention in historical heavyweight buildings, pedagogical issues of lightweight structures and conservation, etc. [2]. All these, in addition to the challenge of understanding the history and the philosophy of lightweight structures and their connection to conservation. As mentioned, this research focuses mainly on the challenge of the integration between new lightweight structures and historical heavyweight structures. It is important to stress that especially today, in the digital era that enables the application of very innovative technologies, those new lightweight structures can be designed as outstanding and unique ones. The results can be a mixture of new complex geometries, new advanced materials, in different variations together with the historical heavyweight structures. It is emphasized in this paper that researchers, engineers and architects who deal with conservation of the built heritage, should also concentrate on lightweight structures, generally and also specifically, on issues like integration of lightweight structures with historical heavyweight structures.



Figure 1: Examples of integration of lightweight structures with historical heavyweight structures (Photographs by the author)

2.3 Relations between new lightweight structures and historical heavyweight structures

The issue of the relations between new and old-historical in conservation is a complex and multi-dimensional issue, dealing with many subjects. It can have cultural, social, aesthetic, economic, environmental and other aspects. Indeed, different strategies and approaches to those relations can be developed. The focus in our research is on the cases where the new structure integrated with historic heavyweight structure is lightweight, and there are relations which create a clear visual distinction between the old and the new. In the new situation the old historical entity is not the same any more. The new and the old are now an innovative system with new specific and unique characteristics and features.

3 NEW LIGHTWEIGHT STRUCTURES INTEGRATED WITH HISTORICAL HEAVYWEIGHT STRUCTURES – HISTORIC PERSPECTIVE

3.1 General

Understanding the development of the field of the integration between new lightweight structures and historical heavyweight structures along history is an important and fundamental step in this relatively new field in conservation. Understanding its evolution and architectural and engineering expressions along time can help us to analyze the developments and the main trends in the past, but also to acquire a background for the future developments of new abilities and strategies of design in this field. Accordingly, in the next paragraphs different selected milestones along time will be introduced.

3.2 New lightweight structures and historical heavyweight structures in early days

Creation of new structures integrated with old structures always existed in the history of the built environment. From early days of history, many buildings were designed and erected on the same site, in different periods and by different people, in a process of evolution. Indeed, in this process numerous buildings were heavyweight and it is reasonable to assume that many of the integrations between new and old were done with heavyweight structures. In addition to heavyweight structures, lightweight structures were also erected from the early days of the human being, as tents, canopies etc. Between the more sophisticated lightweight structures, it is possible to find deployable lightweight structures, which were integrated in the Roman amphitheaters to provide protection against the sun. For example, In the Roman Coliseum, which is considered to be a heavyweight structure, there was a lightweight deployable fabric, which created an upper shelter [5]. In the Renaissance one can find the use of lightweight textile structures integrated with heavyweight structures for covering courtyards. This, in order to create ephemeral shelters for public events, as the covering of the courtyards in Medici Palace and Pitti Palace in Florence [6].

In parallel, also in vernacular architecture it is possible to find lightweight fabric structures. Those were used also for shading, integrated in heavyweight historic buildings or urban areas, as a cover for courtyards, streets, or other open spaces. In Sevilla, Spain, there is an old tradition called the "Seville awning" [7] and it can be seen even nowadays in Sevilla and in other places.

3.3 Lightweight structures in the industrial revolution and the modern era

In the industrial revolution, new materials and technologies, industrial production, advanced theories and other achievements facilitated significant improvements in the capacities to diminish weight and create much lighter structures. Especially, the new technologies using iron and steel allowed designers to lighten the weight of structures [4]. This process had a great impact also on the architectural language which became, in many cases, lighter, transparent, with new elements of visual lightness. The Crystal Palace, which was designed and erected with iron and glass [8], can serve as an example for this phenomenon, besides many other projects. In parallel, textile structures for tents, circuses and other purposes were created as well and can be brought as examples for lightweight temporary shelters in this era [6]. Those structures were erected in different environments, including in the historical built environment. Other developments in lightweight structures include activities of figures like Vladimir Suchov, Buckminster Fuller and other designers, who had new ideas and visions in different aspects like geometry, materials etc. [2].

3.4 Integration of new lightweight structures since Frei Otto and beyond

One of the most important contribution to the field of lightweight structures in the modern era is the work of Frei Otto. His fields of activities and projects include structures like fabric tensile structures, cable structures, pneumatic structures and other lightweight structures from different materials and with various geometries. One of the projects which deals with the integration between new lightweight structures and historical heavyweight structures is the open-air theatre roof for the Bad Hersfeld church - a retractable textile roof over the courtyard of the church, designed for a seasonal purpose [9].

As an outcome of the developments in the field of lightweight structures, more lightweight structures integrated with historical heavyweight structures were erected. For example, the retractable roof installed for the "Schubertiade" in the inner court of the Hohenems Castle. The roof consists of a white translucent inner membrane, plus a loosely tensioned outer membrane [9]. Other examples can be brought from the work of the architect Renzo Piano. The first is the Otranto urban regeneration workshop - a UNESCO-supported project aimed at the renovation of historic town centers, with the purpose of testing the feasibility of using local artisans to restore an ancient town center [10]. The project included a tent roof that sheltered a wide range of activities open to and inviting the participation of the local citizens [11]. The next example is the Schlumberger Renovation, Paris, France [10], which includes the usage of a lightweight structure – a membrane structure - in the rehabilitation process [12]. Schlumberger Renovation was the first of a series of projects aimed at reclaiming industrial sites. While extensive changes were made inside the precinct of the site, the original exteriors were conserved to keep the historical identity of this area in the outskirts of Paris [10]. This project is one of the earliest cases of using membrane architecture in the rehabilitation of a significant area of urban landscape [12]. Other examples from the work of Renzo piano are from the historical old port - Porto Antico, in Genova Italy. Here, new lightweight structures, like tensile membrane structure and others, were built in the historical context of the old port of Genova as part of the urban renewal plan [10].

In addition to the examples above, which are mainly membrane tensile structures, many other tensile structures were erected. Among them it is important to mention pneumatic

structures integrated in historic buildings. The pneumatic structure which was built to cover the historical heavyweight arena in Nimes, France [13], can serve as an example.

3.5 Advanced transparency in lightweight structures integrated with historical heavyweight structures

In parallel to all the above developments with lightweight structures, great important advances took place during the 80's of the twentieth century, in the field of lightweight-transparent structures, mainly with glass. This advancement towards more transparent architecture happened thanks to different innovative figures like Peter Rice and Jörg Schlaich [14] and others. One of the main important milestones related to the integration of those lightweight-transparent structures with heavyweight ones is the Pyramid at the Louvre in Paris, France. The structure of the glass pyramid is an early example of structural glazing stabilized with the help of cables [15]. In this case the space grid structure was innovative at the time in its large use of tensile elements [16].

In addition to this important project, examples of other new lightweight structures integrated with historical heavyweight buildings, can be brought. The covering of the courtyard of the Museum of the History of Hamburg in Germany with a glass grid shell is one of them. According to Addis, only the utilization of a sophisticated three-dimensional structural analysis software, made available in the late 1980's, enabled to build such a structure [14]. Indeed, the influence of the digital revolution was significant to lightweight structures developments.

Other important examples for transparent structures are the Louvre Sculpture Courts - courtyards in the Louvre museum, which were covered with lightweight glazed roof [17] in addition to projects like the inverted pyramid in the Louvre, Paris [18]. Later, additional significant transparent structures were erected like the glass dome for the historical heavyweight Reichstag in Berlin [19], the new lightweight glazed roof for the Great Court in the British Museum redevelopment [20] and others.

3.6 High level of Complexity – materials, geometries, design, fabrication

In addition to lightweight glass structures advancements, various developments like design technologies, fabrication, materials, and others, had a great impact on the integration of lightweight structures with historical heavyweight structures. For instance, other materials like ETFE were also used in new lightweight structures which were integrated. Some examples are: the "Kleiner Schlosshof" – the central meeting place within the castle complex in Dresden – in which the courtyard was covered with a lattice shell, filled with ETFE cushions [21]; the HM Treasuries renovation project, in which new lightweight transparent ETFE roofs were integrated to cover the large light-wells punctuating the building [22]. In addition, printing abilities on ETFE were also developed. The Aarau Bus Terminal in Switzerland, which is a lightweight structure in an urban fabric with old and heavyweight buildings, includes a large cushion wrapped by an arbitrary net of steel cables [23]. A pattern of bubbles was printed on the blue upper and the transparent lower ETFE-foil [21]. In parallel to ETFE, a great diversity of other materials relating to lightweight structures can be brought as for example composite materials [24].

Beside more advanced materials, different advanced technologies, dealing with the creation of non-standard geometries, enabled new lightweight structures with complex geometry to be

integrated. An example for this case is the "Capital C" (De Diamantbeurs) in Amsterdam. Here, a new lightweight grid shell structure with a free form, was built on the roof of a historical heavyweight building. In this case an advanced design process with parametric design tools and a unique fabrication process [25] were part of the architectural and engineering creation of new with old.

4 NEW LIGHTWEIGHT STRUCTURES INTEGRATED WITH HISTORICAL HEAVYWEIGHT STRUCTURES IN THE CURRENT SITUATION

In the current situation, in the digital era, there are many types of new lightweight structures which can be integrated, in a great richness of configurations, with historical heavyweight structures. Examples of this richness include different structural strategies, advanced design tools, simulation abilities and advanced theories, different materials, textures and colors using advanced technologies, different kinds of geometries including free form, different fabrication abilities using traditional beside advanced tools and other abilities. All these achievements create great challenges in the integration of new lightweight structures with historical heavyweight structures. These can be used in innovative and creative manners, in different intervention design strategies which have to be analyzed and identified, as shown in the next paragraphs.

5 DIFFERENT DESIGN STRATEGIES FOR NEW LIGHTWEIGHT STRUCTURES INTEGRATED WITH HISTORICAL HEAVYWEIGHT STRUCTURES

5.1 General

Dealing with the issue of new lightweight structures, integrated with historical heavyweight structures, requests defining an initial scheme of intervention design strategies in the conservation process. This act is especially important as a vital step for the development of the theoretical body of knowledge of this unique field in conservation. Knowing the possible intervention design strategies can significantly improve understanding and analyzing existing situations. It can also help in the future to achieve successful synthetic and integrative design between new and old. In the next paragraphs, the focus is on cases where there is a clear visual distinction between the new and the old. Accordingly, the new lightweight interventions in these cases have also a visual lightness which can be expressed by different means such as light appearance, transparency, immateriality etc. The basic implications of those strategies, in relation to the architectural – structural visual language, are presented and discussed, while other implications will have to be developed in future research.

5.2 Addition of new lightweight structures to historical heavyweight structures

In this case there is a need to add new parts or elements, which in our scope are also lightweight, to the historical heavyweight structure. The additions can be external or internal and they can get different configurations and possibilities. External additions can consist, for example, of an enlargement of the existing old heavyweight structure with a new lightweight structure placed aside, above or in other positions. The new lightweight additions can fulfill different functions as additional floors, entrances, lifts, stairs etc. Internal additions can be different lightweight elements, used inside the original buildings for the separation of spaces,

internal lifts, stairs, etc. The additional lightweight roofs over many courtyards in historical heavyweight buildings are one type of addition. The new lightweight roof for the courtyard in the renovated "Palacio de Comunicaciones"– a single layer glass grid shell over the courtyard [3] – is an example of this type. This intervention design strategy enables to conserve the visual identity of the historical heavyweight structure as an independent historical entity versus the new lightweight structure. This distinction is especially important when dealing with the different architectural-structural languages of each period – the historical versus the new.

5.3 Replacement of historical heavyweight structures by new lightweight structures

In the conservation process there is, in some cases, a need to replace original elements or parts, like walls, ceiling or stairs, of the historical heavyweight building. This replacement can be needed as an outcome of destruction or deterioration of the original elements or of other reasons. In such situations one of the possibilities is to replace the historical heavyweight element with a new lightweight structure. The replacement of the original elements can be internal or external. The replacement of the original dome in Reichstag Berlin by a new transparent lightweight dome can serve as an example for this case. Other examples can be the replacement of original heavyweight elements by ETFE in Corbera d' Ebre church restoration in Spain [26] and the Speicherstadt Hamburg Chimneys Boiler House, Germany. In this later project two new filigree steel grid towers were erected, which remind the chimneys destroyed during World War II, and thus re-create the historic silhouette of the boiler house [27]. This intervention design strategy allows to understand visually which parts of the original buildings were destroyed and what was the real situation before the new intervention. The story of the deterioration process along time is not erased in this case and it even becomes an undivided part of the whole story of the building.

5.4 Completion of historical heavyweight structures with lightweight structures

There are cases when different parts or elements of the original historical heavyweight structure were not completed in the original construction process. Different reasons exist for this situation but in the conservation process it may be possible to complete the unbuilt elements or parts with a new lightweight structure. An example for this case can be brought from Lille in France - The Cathedral of Notre Dame de la Treille. Here one of the original façades was not completed during the historical construction process and a new lightweight façade was erected nowadays [18]. This way a clear visual distinction is seen between the new completed façade and the uncompleted historical heavyweight structure. This strategy allows to visually understand the building's uncompleted story and the completion act in the conservation process. This intervention design strategy requires a thorough understanding of the intentions of the original designers and builders of the historical heavyweight structure and to create an appropriate solution using new lightweight technologies.

5.5 Covering historical heavyweight structures with new lightweight structures

New lightweight structures can be used not only in cases of addition, replacement or completion, but also as a shelter or covering for historical heavyweight structures. In this case the new lightweight structure acts as a kind of canopy or envelope and not as part of the original building. One of the most common usages in this category is lightweight shelters above

archeological sites. Examples for tensile membrane structures covering archeological sites can be found in different places. Another outstanding example in this category, dealing with covering an historical building, is the initial scheme for the rebuilding of the historical Reichstag, Berlin. Norman Foster's initial scheme included a large canopy to cover the existing structure [20] of the historical heavyweight Reichstag. At the end, this proposal was not built, but in spite of that this proposal had a great exposure in the literature until nowadays. In relation to the visual language aspect, this intervention design strategy allows to create wide-span covering solutions, which enables relative visual freedom under the canopy. It can release the internal space and minimize visual disturbances. This in addition to the visual lightness of such covers that in many cases have a relatively large scale.

5.6 A new independent lightweight structure in vicinity to a historical heavyweight structure

A new lightweight structure can also appear as an independent structure in vicinity to or beside a historical heavyweight structure or structures. For example, in a case of two structures - the new and the old structures are not necessarily physically connected as one continuous element and they can act as two different objects, standing near each other. This category mainly focuses on the building scale - the relations between close buildings or structures. The space between the structures can act as a mediator between them, and they can behave as separated projects or as a united one. In addition, the new lightweight structure can be temporary or permanent, according to different circumstances and needs. An example for this strategy is the project of Zaha Hadid in Serpentine Gallery, London [21]. This design strategy allows a visual duality in the composition between two objects in space, standing one near the other. This duality is inherent to old versus new but can be expressed also by opacity versus transparency, static versus dynamic and other possible visual relations, which are enabled by lightweight technologies.

5.7 New lightweight structures within historical and large-scale built areas

The conservation process relates to different levels in the built environment. One of the most important levels is the urban level, which deals with the conservation of historical urban areas or other historical built places like big archeological sites that can also be in this category. In these areas or sites there may be a need to place structures which have an urban role, such as an urban landmark, or fulfill a specific function in the historic urban space. In such cases the use of a new lightweight structure can be relevant. The new lightweight structure can be easily identified in different public spaces like Piazzas, squares and it can act as a distinctive feature in the space, either temporary or permanent. Possible examples are: entrances to Metro stations, bus stops, structures for temporary markets and others. One example is the lightweight pneumatic structure erected in the historic urban environment of Berlin, directly in front of the Brandburg Gate (for the Ecumenical Church Day in 2003) [27]. A second example is the tower including a membrane structure in Phänomenta Science Centre in Lüdenscheid, Germany [28]. This intervention strategy enables to distinguish, in the urban scale, between the historical heavweight environments and new lightweight structures in this landscape. In addition, the lightweight structure can, in some cases, act as a landmark in the urban context, that draws attention to the historical heavyweight structure.

5.8 Lightweight structures and artistic-design activities in historic environments

Historical buildings and historic urban fabrics can be in many cases a place where different artistic and design activities take place. Lightweight structures can take an important part in this unique activity. They may appear outside in historic public spaces or in internal spaces of historical buildings. The lightness, transparency, flexibility, and other properties of these structures allow them to serve in a wide span of possibilities in art and design. They can be used as sculptures, monuments, structures or for other artistic and design activities. An example of using lightweight elements for an outstanding art activity is the wrapping of the historical Reichstag building in Berlin as a temporary sculpture [29]. Another example which can be considered as a design creation with artistic values, integrated in a historic environment, is the Elytra Filament Pavilion. The pavilion was erected in the Victoria and Albert Museum in London, using advanced technologies which include a robotic fabrication process. The pavilion establishes a dynamic space and an evolving structure. The pavilion structure is also inspired by lightweight construction precepts found in nature – the fibrous structures of the forewing shells of flying beetles known as elytra. The cover forms a fibrous tectonic system that is as architecturally expressive as it is structurally efficient [30]. This intervention design with lightweight artistic structures, in historical heavyweight environments, requires in many cases a lot of scientific understanding beside visual-artistic abilities. In addition, the issue of an object or a figure and its background is especially important in many visual artistic creations, and here the historical heavyweight structures can act as a background for the new lightweight creation.

5.9 Lightweight strengthening intervention in historical heavyweight structures which create a new visual and architectural appearance

There are cases where new lightweight structures are used to strengthen historical heavyweight structures. For this purpose, one can use steel tie rods, steel ribbons and other lightweight components according to specific circumstances [2]. In cases where the new lightweight structures are visible, they can, together with the historical heavyweight structure, create a new system which has also an architectural-structural visual language. This system has its own unique visual and aesthetic properties, which were born as an outcome of the necessity to strengthen the historical ruins. Since many historical heavyweight structures are strengthened by lightweight elements and components, which are visible in many cases, it is very important for the designers to understand the integration of the new and the old also from this point of view. In this intervention design strategy, the functional aspects of the lightweight strengthening system within the historical heavyweight system are strongly connected to the architectural-structural aspects. Functional strengthening elements, which naturally are engineering oriented, can also have a visual architectural-structural contribution.

5.10 Other possible design strategies

The intervention design strategies, which were identified and analyzed above, are selected principal strategies. Each one of them can be a crucial element in the conservation process. In addition, it is also possible to search and create new different combinations between these strategies and, as a result, to have new design strategies, which can be called hybrid strategies. In parallel it is very important to continue to deepen the study and the research in each strategy and to enrich our knowledge about its main characteristics.

6 PEDAGOGICAL ASPECTS

The study and research in the field of integration between new lightweight structures and historical heavyweight structures can also bring pedagogical benefits. It can enrich the people who are involved in the conservation studies and open them to new horizons for future design. Since in many cases most of the attention is devoted to historical heavyweight structures, understanding the possibilities of using new lightweight structures within the historical conservation context can create new innovative solutions in the conservation field. This issue is especially important in this era which is characterized by richness of different advanced technologies and possibilities of design.

7 CONCLUSIONS

The field of lightweight structures in conservation is a relatively new field. The findings of this research show that there are many advanced developments in lightweight structures, such as complex geometries and new advanced materials in different variations, which can be integrated with historical heavyweight structures. It is also demonstrated that there has been a significant evolution along time in this field. The findings also indicate that, in the first stage, a wide span of intervention design strategies for integration of lightweight structures with heavyweight historical structures can be identified. In this research a discussion is started on the implications of the different strategies on the architectural-structural visual language.

In the current situation it is important to continue the development of the body of knowledge in this field. This paper is one of the efforts to enlarge and to deepen this field of activity. In the future it is important to continue the research dealing with lightweight structures and conservation. For example, it will be useful to further develop the database on different cases of intervention such as additions, replacement, completion etc., according to different criteria and to follow the performance of the new-old systems. More research in this field can focus on further understanding the implications of different strategies on the visual architectural-structural language, in addition to other performance and functional aspects like climatic, lighting, acoustic, and other aspects.

REFERENCES

[1] Neurohr, T.and Pasini, D. Principles of lightweight structures in the sculptural conceptions of Naum Ga-bo, Interdisciplinary Science Reviews, (2009) 34:4, 366-380.

[2] Mosseri, A. Lightweight Structures and Conservation - Engineering and Architectural Perspective. In: Aguilar R., Torrealva D., Moreira S., Pando M.A., Ramos L.F. (Eds.): *Structural Analysis of Historical Constructions.* RILEM Bookseries, vol 18. (2018) pp. 116-124. Springer, Cham.

[3] Schlaich, M., Burkhardt, U., Irisarri, L. and Goni, J. Palacio de Comunicaciones – a Single Layer Glass Grid Shell over the Courtyard of the Future Town Hall of Madrid. In: Domingo, A. and Lazaro, C. (eds). *Evolution and Trends in Design, Analysis and Construction of Shell and Spatial Structures.* Universidad Politecnica de Valencia, Spain (2009) pp. 1338-1348.

[4] Kawaguchi, M. 1996. Forward by Mamoru Kawaguchi. in Berger H. *Light structures structures of light*. Birkhauser Verlag. (1996).

[5] Berger H. *Light structures structures of light*. Birkhauser Verlag. (1996).

[6] Campioli, A., Mangiarotti, A. and Zanelli, A. Textile Architecture in the Italian Context.

International Journal of Space Structures. Vol. 23 No. 4 (2008).
[7] Hermeking, T. Msheireb - Heart of Doha, Qatar, retractable shade canopy. *TensiNews 2015, Newsletter of the European based network for the design and realization of tensile structures*. Nr. 29 September (2015), pp 14.
[8] Curtis, W.J.R.(1982). Modern architecture since 1900. Phaidon Press Limited.
[9] Mollaert, M. Retractable membrane roofs. *Transactions on the Built Environment* vol 21, (1996). WIT Press.
[10] RPBW Architects. Renzo Piano Building Workshop. Available in: www.rpbw.com
[11] Buchanan P. *Renzo Piano Building Workshop. Selected Projects: Part 3*. The Architectural League of New York (1992). Available in: https://archleague.org/publications/renzo-piano-building-workshop
[12] Scheuermann, R. and Boxer, K. *Tensile Architecture in the Urban Context*. Butterworth Architecture. 1996.
[13] Zanelli, A. Architectural fabric structures in the refurbishment of archaeological and cultural heritage areas. In: Ignasi de Llorence, J. (Ed.) *Fabric Structures in Architecture*. Elsevier Ltd. Chapter 15, pp. 481-527 (2015).
[14] Addis B. *Building: 3000 Years of Design Engineering and Construction*. Phaido. 2008.
[15] Bijster, J., Noteboom, C. and Eekhout, M. Glass Entrance Van Gogh Museum Amsterdam. *Glass Struct. Eng.* (2016) 1:205–231.
[16] Patterson, M. *Structural Glass Facades and Enclosures*. John Wiley & Sons Inc. (2011).
[17] Ian Ritchie Architects. Available in: https://www.ianritchiearchitects.co.uk
[18] Rice, P. and Dutton, Hugh. *Structural Glass*. E & FN Spon. (1995)
[19] Schulz, B. *The Reichstag*. Prestel. (2000).
[20] Jodidio, P. *Sir Norman Foster*. Taschen. (1997).
[21] Mollaert, M., Dimova, S. Pinto, A. and Denton, S. (2016). Prospects for European Guidance for the Structural Design of Tensile Membrane Structures. European Commission Joint Research Center, Institute for the Protection and the Security of the Citizen. (2016).
[22] Foster + Partners. Available in: https://www.fosterandpartners.com
[23] form TL. Available in: https://www.form-tl.de/home
[24] L. du Peloux, F., Tayeb, O., Baverel. and J.F. Caron. Construction of a large composite grid shell structure: A lightweight structure made with pultruded glass fiber reinforced polymer tubes. *Structural engineering international.* Nr.2/2016.
[25] Octatube. Available in: https://www.octatube.nl/en_GB
[26] Llorens J. and Zanelli A. (2016). Structural membranes for refurbishment of the architectural heritage. Procedia Engineering 155 (2016) 18 – 27.
[27] sbp, Schlaich Bergerm Partners. Available in: https://www.sbp.de/en
[28] form TL. Phanomenta. In: *TensiNews 2015, Newsletter of the European based network for the design and realization of tensile structures*. Nr. 29 September (2015), pp 10. Available in: https://www.tensinet.com
[29] Mollaert, M. Haase, J. Hollander, S. Designing Tensile Architecture TensiNet Symposium (2003).
[30] achimmegnes .net. Available in: http://www.achimmenges.net

12th International Conference on Structural Analysis of Historical Constructions
SAHC 2020
P. Roca, L. Pelà and C. Molins (Eds.)

OPUS SIGNINUM - ROMAN CONCRETE WITHOUT *PULVIS PUTEOLANUS* : EXAMPLE OF THE SUBSTRUCTURES OF DIOCLETIAN'S PALACE

MARINA I. ŠIMUNIĆ BURŠIĆ*

University of Zagreb, Faculty of Architecture
Kačićeva 26, HR-10000 Zagreb, Croatia
e-mail: marina.simunic@arhitekt.hr (*corresponding author)

Keywords: Roman Concrete, Opus Signinum, Vaults, Roman Imperial Palace, Emperor Diocletian, Substructures

Abstract. *The palace of the Roman emperor Diocletian in Dalmatia, a Mediterranean region of Croatia, is an important Late Antique complex, whose most important buildings have been excellently preserved, including their vaults: the brick dome of the Diocletian's Mausoleum, the stone barrel vault of the so-called Jupiter's temple, and the vaults of the large substructures of the imperial apartments, constructed in Roman concrete. Because in Dalmatia there was no pozzolana (pulvis Puteolanus) – a volcanic material used for making first opus caementicium structures in the Roman world, the concrete for the vaults of the substructures of the Palace was made with crushed terracotta. This type of Roman concrete was called opus signinum. The vaults of the substructures of the imperial apartments within Diocletian's palace are important for the research of Roman concrete structures because the whole complex of vaults of various types, covering the area of approx. 150 m by 35 m, has been entirely preserved. In this article, of this variety of vault types, several interesting vault solutions are analyzed.*

1 INTRODUCTION

The most prominent example of *opus signinum* structure in Croatia are the vaults of the substructures of the emperor Diocletian's palace. The Palace was built at the end of the third – beginning of the fourth century AD, in the vicinity of Salona, the capital of the Roman province of Dalmatia, and presumably the homeland of the Emperor.[1]

The Palace has been admired and researched by important European artists and scholars since the 18th century.[1,2] Although the major part of the large complex of substructures of the Emperor's apartments was filled with trash and not accessible from the Early Middle Ages to the 20th century,[3] the interest for the *Grotte*, as locals called the substructures, arose already in the mid-18th century: Scottish architect Robert Adam attempted to do excavations, but was not allowed by the local authorities.[1] Systematic excavation of the substructures began only in the mid-20th century.[3]

As the disposition of the walls of the substructures delineate and reveal the disposition of the Emperor's residential and ceremonial rooms, they have been in the focus of scientific interest;[1,4] but on the other hand, the vaults of the substructures have not been given enough interest as important examples of Roman concrete structures.

2 ROMAN CONCRETE

Roman concrete (*opus caementicium)* is one of the most important innovations in Roman *ars aedificatoria*. Made with volcanic material called by Romans *harena fossicia*[5] or *pulvis Puteolanus* (from Puteoli – Pozzuoli), it proved to have excellent mechanical properties. This enabled major innovations in building technology and development of large-span vaults.[6] There is evidence of skilful use of *opus caementicium* in important public buildings already in the first half of the first century BC. Substructures of the temple of Jupiter Anxur at Terracina and of the sanctuary of Fortuna Primigenia at Palestrina imply that the Roman builders by that time already had got impressive experience of building with *opus caementicium.*[6, 7]

Vitruvius (first century BC) describes raw materials for making mortars and concrete, mentioning different kinds of sand. He distinguishes *harena fossicia* from *harena fluviatica*, appreciating the special characteristics of *harena fossicia* for making *structurae caementiciae*.[5] *Opus caementicium,* first used for less important buildings, proved to be an excellent material, so that in the imperial period it was used even for the most prominent representative buildings, e.g. the Pantheon in Rome.[6, 7]

Construction of Roman concrete structures depended on its essential component: volcanic materials found only in volcanic regions, the deposits of which are limited. Roman builders, knowing the advantages of Roman concrete, found a substitute for *harena fossicia*: instead of volcanic material, they used broken terracotta, i.e. tiles broken up into very small pieces, to achieve characteristics similar to those of *opus caementicium* made by using *pozzolana*. Thus, they invented *opus signinum* (*'cocciopesto'*).[8]

Opus signinum is a hydraulic material, i.e. it hardens also under water, just like *opus caementicium* made with *harena fossicia. Opus signinum* is also a waterproofing material; it is even better for this purpose than concrete made with *pozzolana*. Therefore, it was used for lining aqueducts, cisterns and exterior surfaces of vaults in the entire Empire.[6]

3 PALACE OF THE ROMAN EMPEROR DIOCLETIAN IN DALMATIA

The palace of the Roman emperor Diocletian (284 AD – 305 AD) is one of the best preserved Late Antique imperial palaces and is therefore important for the research of ancient structures and their evolution from Hellenistic period to the end of Antiquity. In the 7th century, during Great Migrations, the fortified Palace provided shelter for the inhabitants of the nearby town of Salona and in the Middle Ages was transformed into the town of Split.[3] It has been inscribed on the UNESCO World Heritage List as an outstanding example of architectural ensemble, which testifies to developments in architecture and technology. [9]

3.1 Historical context

The Palace was commissioned and built by the Roman emperor Diocletian in a relatively short period, probably from 293 AD (when he instituted tetrarchy) to 305 AD, when he abdicated the throne by his own will.

The Palace was built on the Adriatic coast, near Salona, as Diocletian's home after his withdrawal. It was conceived as a combination of imperial villa and military camp,[10] with garrison buildings in its northern part and representative buildings (religious edifices and imperial apartments) in its southern part. This concept is clearly visible in the plan of the Palace,

conceived as *castra* (military camp): as a fortified complex, nearly square in plan, with *cardo* and *decumanus* and four gates at their ends; the perimetral walls of the Palace are fortified with 16 towers.[1, 4] The function of a lavish villa is materialized within the residential zone in the southern part of the Palace, overlooking the sea.

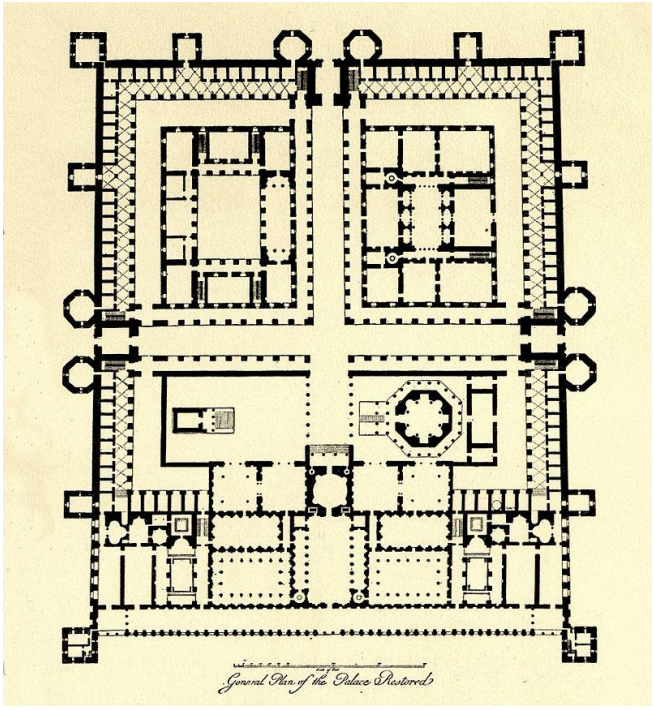


Figure 1: Diocletian's Palace (reconstruction according to R. Adam, published by G. Niemann, 1910

3.2. The Emperor's residential and representative buildings

According to historians' hypothesis, Diocletian decided to build his palace on the Adriatic coast in 293 AD when he reformed the administration of the huge Empire and decided to withdraw from the throne within a certain number of years. Thus, the palace near Salona was planned for the time when he would no longer be emperor. Still, the art-historians believe that the so-called residential area of the palace included also representative and ceremonial rooms – from the Prothyron, where the ex-emperor appeared before his prostrating subjects as *Sol Invictus* – a divine title that he retained even after his "retirement"[11] - to the series of representative rooms in the western part of the apartments. The eastern part of the apartments is believed to have been a private residential area.[3]

Imperial apartments are situated on a higher level than other parts of the Palace: indeed, they are constructed on the platform created by a large substructure consisting of a number of thick walls and pillars carrying vaults. The imperial apartments are stretched along the south façade. The centrally positioned entrance to the *palatium* divides the emperor's residence into two parts.

The large central hall, preceded by the *Prothyron* and the *Vestibule*, led to the so-called *Cryptoporticus,* southern corridor - porch opening to a beautiful sea view through a series of large arched openings. The *Cryptoporticus* was the main communication corridor of Diocletian's private and ceremonial *suites*, running the whole length of the southern façade.

Of the large central entrance hall only scarce traces exist. Its substructure, on the contrary, is well preserved. The same applies to most rooms of the imperial residential zone: from the Emperor's residential and ceremonial buildings, raised on the artificial platform, only the circular *Vestibule* and the *Prothyron* are preserved.[4]

3.3. Substructures of the imperial apartments

Unlike the major part of the structures of the imperial apartments, the substructures of these residential buildings have been excellently preserved. The huge complex of substructures occupies an area of approx. 150 m by 38 m.[12] It was constructed to form a raised base for the Emperor's apartments. In spite of their popular name "Diocletian's basements" or "Diocletian's cellars", they were built only to support the structures above.[3] As such, they also protected the apartments from rising damp – which is important, especially considering the proximity of the sea.

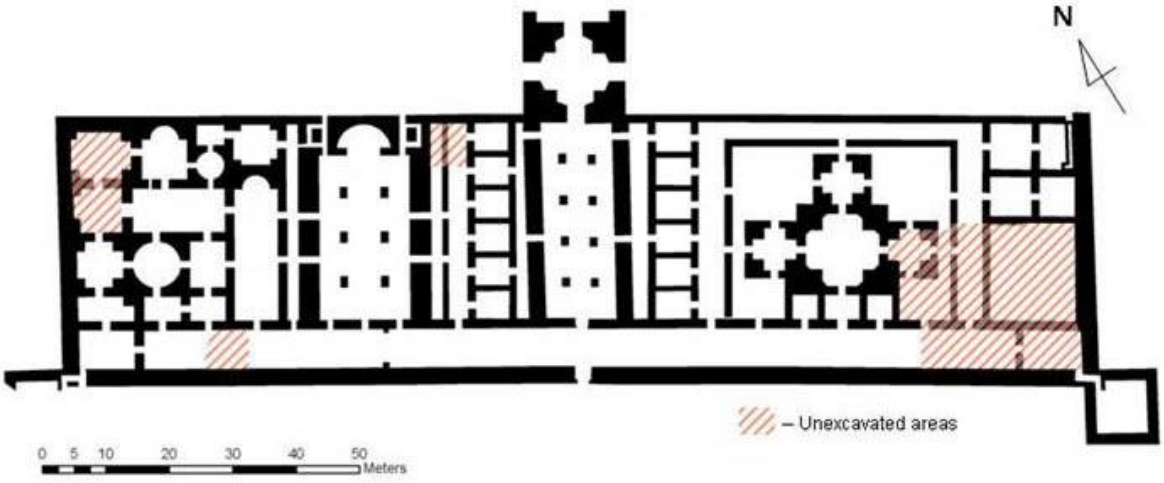


Figure 2: Substructures of the imperial apartments, plan

The substructures form a large assembly of rooms of different shapes and sizes, divided by thick bearing walls. The walls are constructed of high-quality stone masonry - *opus quadratum*. The massive pillars are also constructed of large stone blocks, perfectly cut and constructed with extreme precision.[3, 4] From historical sources it is known that the high-quality limestone for the construction of the Palace was brought primarily from the quarries on the island of Brač.[13]

Due to the high quality of the stone and excellent workmanship, vertical structural elements (walls and pillars) have resisted all the aggressive impacts for 17 centuries. Another reason for the excellent preservation of the substructures might be the fact that most of them were inaccessible for more than a millennium. Nevertheless, the inhabitants of Split were aware of the existence of the substructures, they even used parts of them as storage. In the 18th century, R. Adam describes substructures as "*half sunk or vaulted story. Part of these vaults now remain entire, and at present are used by the merchants for warehouses. They lie all along that side of the Palace next to the sea… There is also another vault which runs from South to North,*

…which appears to have been a common entry to all the under-ground offices. These have been partly destroyed, and partly filled up…".[1]

The structures of representative residential quarters were very heavy, because the imperial apartments were undoubtedly vaulted, as we can deduce from other Roman imperial palaces. Following the structural logic, the walls of the substructures were planned and built exactly on the positions of the walls of the superstructures. This has enabled the scientists to propose ideal reconstructions of the imperial quarters – from Adam and Niemann to Marasović.[1, 3, 4]

4 VAULTS OF THE SUBSTRUCTURES OF THE IMPERIAL APARTMENTS

The vaults of the substructures of the emperor's residential quarters display a multitude of Roman vault types: barrel vaults, cross vaults, domes, semi-domes and their variations.

The materials of the vaults have not yet been researched systematically: according to a few samplings that have been done to date, the structure of the vaults is made of a kind of *opus caementicium*, with *caementa* of tufa (very light sedimentary rock, locally called *sedra*), but without *harena fossicia* component in the mortar paste (G. Nikšić, personal communication, July 2015). Already Vitruvius knew that *harena fossicia* can be found only in a limited region of south-western part of Italy: *"… fossicia harenaria, trans Appenninum vero, quae pars est ad Adriaticum mare, nulla inveniuntur, item Achaia, Asia, omnino trans mare, nec nominantur quidem"*.[5] Builders in other parts of the Roman empire had to substitute *harena fossicia,* the essential component of *opus caementicium*, with brick rubble, which also gives strength and durability characteristic of the Roman concrete.[8]

4.1. Cross vaults of the central hall of the substructures

The large central hall of the substructures is the main communication hall that connects the Peristyle with the southern gate.

The vertical structures of the large hall, approx. 35 m long and 10.5 m wide,[12] carried the upper ceremonial entrance hall of the imperial apartments. The representative entrance hall was presumably covered with a large-span barrel vault, as can be concluded from the very thick longitudinal walls of its substructure; hence, the large entrance hall of the imperial apartments did not have any additional supports within the large span.

Into the substructure hall of the ceremonial entrance hall, which has approximately the same dimensions as the demolished hall above it, the constructors of the Palace inserted two rows of strong pillars which divide the central substructure hall into three "aisles". In this way they reduced the spans of the vaults, and also their height. Reducing the height of the vaults was essential in order to achieve the horizontal platform for the imperial apartments.

Unfortunately, the vault of the central hall of substructures has been damaged and considered structurally unsound. The reconstruction of the Roman vault in mid-20th century was carried out with a wrong assumption that the original Roman vault was a stone masonry structure, so it was reconstructed as a modern prestressed concrete structure with intrados faced with stone (G. Nikšić, personal communication, January 2020). The fake "stone vault" can be misleading, although it can be seen that this is not a stone masonry vault, because the stone pieces are not put together as a set of *voussoirs*.

4.2 Cross vault of the largest hall in the western part of the substructures

The original, intact (i.e. not reconstructed nor repaired) Roman concrete cross vault can be seen in the largest hall in the western part of the substructures, which is approx. 26.2 m long and 14.3 m wide.[12] The room of imperial apartments above it was undoubtedly a representative (probably ceremonial) hall: a large undivided space, with a vault spanning the whole width of the room – approx. 14.3 m.

The room below it, its substructure, is divided by two rows of strong pillars into three aisles: the central one is 5 m wide (clear span), and side aisles 3.10 m. Like in the central communication hall, the pillars were probably inserted to avoid a too high rise of a vault: all the vaults of the substructures should have had the summits at approximately the same height.

In order to achieve the same height of the summits of the vaults of the central aisle and of those of side aisles, constructors had to find a solution, which is not in accordance to the orthodox rules of the *ars aedificatoria*. The vaults of the side aisles do not have a semi-circular cross section: they have a nearly parabolic form.



Figure 3: The largest hall in the western part of the substructures:
cross vault in the central aisle (left) and in the side aisle (right)
(photograph by the author)

The spatial and structural concept of this hall is similar to that of the central communication hall of the substructure: it has mighty pillars (1.75 m * 1.17 m in cross section) made of large stone blocks; the walls are constructed in *opus quadratum* to the height of approx. 4.25 m. Above this height, the walls are constructed in *opus mixtum*, with layers of unhewn stone and bricks. *Opus mixtum* is the usual facing of Roman concrete walls: the core of the walls is made of *opus signinum*.

Brick was used for the springings of the cross vaults on pillars, because constructing this part of the structure required special care.[14] The same applies to the vault springings on the walls. Above the springings, the vaults have *opus mixtum* facing, like do the upper parts of walls. *Opus mixtum* in this substructure hall does not have a regular, neat pattern, neither on walls nor on vaults.

In the upper parts of the vaults one can discern unhewn tufa pieces within thick mortar. Tufa pieces are not shaped and set like *voussoirs* of the stone vaults: indeed, they are separated by

thick mortar. Obviously, tufa elements alone cannot create a bearing structure. They are not elements of a stone masonry, but *caementa* within *opus signinum* mortar. In this type of structure, stone pieces do not act as a masonry vault. The concrete structure, made of mortar paste with crushed tiles and tufa *caementa,* is the real bearing structure of the vault.

The longitudinal walls of this hall are very thick, and its orthogonal, "gable" walls are considerably thinner. The cross vaults concentrate forces in several points: the thrust of the cross vault acts on the structure in both directions (X and Y). The very thick longitudinal walls indicate that the hall of the imperial apartments above this substructure hall was not divided by pillars and that it had barrel vault, with continuous thrust acting only on the longitudinal walls.

4.3. Barrel vault of the smaller longitudinal hall

The third-largest longitudinal rectangle hall (approx. 20.8 m long and 7.0 m wide) has a barrel Roman concrete vault. Longitudinal walls are constructed in excellent *opus quadratum.* The „gable walls", i.e. the walls at the narrower sides of the hall, are constructed in *opus quadratum* up to the height of springings of the vault; in the upper part they are faced with *opus mixtum*, with unhewn stone pieces and thin horizontal layers of bricks; the core of the walls is undoubdetly of *opus signinum*.



Figure 4: Barrel vault of the smaller longitudinal hall of the substructures
(photograph by the author)

The barrel vault, semi-cylindrical in cross section, spanning 7.0 m, has the intrados faced in a kind of *opus mixtum*, with longitudinal rows of brick and irregular pieces of tufa (sedra). The core of the barrel vault, i.e. its structural, bearing part, is obviously made of concrete.

As the substructures did not have function (except for that of bearing the imperial apartments), the intrados of vaults did not have a protecting layer of plaster. Therefore, they were exposed to adverse impacts of rising damp and saline aerosol. Materials of the vault - *opus signinum* and tufa - are less resistant to humidity and salinity than high-quality limestone from the island of Brač; therefore, vaults are much more damaged than pillars and walls made of limestone in *opus quadratum*.

4.4 Dome of the circular room

The walls of the room with a circular plan (diameter 7.33 m) were built in excellent *opus quadratum*. The lower part of the dome is faced in *opus mixtum*, and the upper part in thin bricks. *Opus mixtum* was usually a lining of a concrete core. It is reasonable to assume that the bricks of the intrados of the dome are only a lining of a much thicker dome of *opus signinum*. In the Palace there is a dome built exclusively of bricks: the representative Mausoleum is covered with a thin brick dome, spanning approx. 13.3 m. [15] This elaborate double-shell brick structure, consisting of two layers of bricks (33 * 33 cm square)[14] with the inner layer constructed of fan-like relieving arches,[16] which were self-supporting during the construction of its lower part,[17,18] was undoubtedly constructed by specialized experts invited to the important imperial building site.[14] On the other hand, in the massive substructures, built to carry the load of a superstructure, it is reasonable to suppose that the dome, like many other vaults of the substructures, was constructed of Roman concrete, and that only the intrados of the dome was lined with bricks.



Figure 5: Dome of the circular room
(photograph by the author)

4.5 Dome of the "crypt" of the Mausoleum

The dome of the so-called crypt, or substructure of the Diocletian's Mausoleum, is interesting for the research of the vaults of the substructures of the imperial apartments, although it is not physically connected to them. The dome, spanning 8.25 m, is constructed of Roman concrete, without any covering layer; in fact, the imprints of formwork are still visible on its intrados. (G. Nikšić, personal communication, July 2015).





Figure 6: Mausoleum of the emperor Diocletian (by Niemann 1910)
Figure 7: the dome of the crypt of the Mausoleum with the imprints of formwork

5 CONCLUSIONS

5.1 Vaults of the substructures - Types and materials

The solution of vaults of the substructures of the imperial apartments of the Diocletian's palace is a logical and simple answer to the complex requirements of their superstructure. Due to the complex disposition of rooms of the imperial suite, the rooms of their substructures display a great variety in size and shapes, and so do their vaults.

For spanning rooms of various forms, spans, and proportions, the constructors of the Palace constructed various types of vaults: barrel vaults in elongated rectangular rooms, domes in circular rooms, semi-domes and cross vaults in apsidal rooms. In rooms with larger spans, rows of pillars were introduced, in order to reduce spans and, accordingly, also the height of the vaults, because the substructures, including their vaults, had to form a horizontal platform for the imperial apartments. In these rooms cross vaults were constructed, to concentrate loads and forces into the non-continuous bearings of pillars.

The material of the vaults has not been systematically analyzed. Systematic excavation of the substructures of the Diocletian's palace began only in the mid-20th century. It is easy to recognize the material of the vertical structures - walls and pillars: it is local limestone, in large precisely cut blocks. On the other hand, the material of the vaults is not so easy to recognize.

Because in the mid-20th century the vaults of the central hall of substructures were considered not to be structurally sound, they were repaired without proper research on the materials and techniques used for their construction, which resulted in inadequate reconstruction of these vaults.

The vaults of the central hall of substructures, reconstructed in a modern material (pre-stressed concrete) with a stone lining which gives the appearance of a stone vault, could be misleading: it was believed that the vaults of substructures were stone masonry structures (G. Nikšić, personal communication, January 2020). The thesis that the major part of the substructure vaults was made out of stone can be easily refuted by simply observing the intrados

of the vaults. As they were only a substructure without other function, they have never been plastered, so the texture of the vaults is clearly visible.

The intrados of the vaults is rough, with visible irregular pieces of tufa inserted into thick mortar; some of them are faced with *opus mixtum*, with rows of brick between stone layers. These vaults are not stone vaults, as interpreted by some scholars; the pieces of tufa are not constructed in a regular masonry bond: in fact, they are *caementa* of the *opus caementicium.* The vaults of the substructures are built of Roman concrete, made without *harena fossicia:* in fact, the complex of vaults of the Diocletian's palace's substructures is an important, precisely dated structure of *opus signinum,* constructed by skillful builders employed specially for an important imperial building.

The intrados of certain vaults are faced in the *opus mixtum* technique: the intrados of the upper parts of domes and semi-domes is made of bricks. According to G. Nikšić, brick was one of important materials used for building the Diocletian's palace because of the tight deadline within which all the construction work should have been completed.[14]

Whether the upper parts of domes and semi-domes were constructed of brick in their whole thickness or is the visible surface of intrados just a brick lining of a concrete dome – this cannot be asserted with certainty without further investigation. However, it is more likely that the bricks are only a lining of the intrados of the dome. The fact that the lower part of the dome is constructed of concrete faced by *opus mixtum* ascertains this claim; the concrete dome of the crypt of the Mausoleum is another argument for this hypothesis.

5.2 Hierarchical use of materials

As far as it is known from the preserved structures, the constructors of Diocletian's palace used concrete only in the complex of substructures of the Emperor's apartments and in the substructure of the Mausoleum. They were not concerned about the appearance of the vaults of substructures: in the "crypt", the imprints of the wooden formwork are still visible on its concrete dome. For the representative vaults (the ones of the Mausoleum and of the so-called temple of Jupiter), they used "traditional", "classical" materials – brick and stone.

The tradition of building with *opus caementicium* was at the end of 3rd – beginning of 4th century already well established. In Rome itself the most representative large-span vaults and domes had been erected in *opus caementicium.* We can hypothesize that, for some reasons, several centuries after the Pantheon had been built, constructors of the Diocletian's palace appreciated the "traditional", "natural" materials higher then concrete.

In a way, the attitude of the architects of the Diocletian's palace toward *opus caementicium* seems to have returned to the practice of the architects in the initial phase of construction with Roman concrete: the use of Roman concrete in the substructures of Diocletian's palace (and not in the representative parts of structures) has a direct parallel in the structural concept of the sanctuaries of Jupiter Anxur at Terracina, of Fortuna Primigenia at Praeneste (Palestrina), and of that of Hercules Victor at Tibur (Tivoli); in these complexes, built in the first century AD, the substructures were built of *opus caementicium,* and the temples upon them were constructed of stone.[6, 7]

The use of concrete spread first to utilitarian buildings like markets, *thermae* etc.[7] The first large concrete dome, still preserved, is the dome of the so-called "Temple of Mercury" at Baiae (diameter 21.6 m). The domed edifice, built in the late first century BC, was actually part of

thermae.[6] Temples, the most traditional building type in Roman architecture, were constructed in the traditional form and materials for several centuries after the early examples of concrete substructures had been built. In 118-128 AD the largest dome made of Roman concrete, the one of the Pantheon in Rome (diameter 43.3 m), was built,[7] testifying that by then *opus caementicium* was acknowledged as a "noble" material, suitable for the most representative edifices, and irreplaceable for large-span vaulting.

Analyzing the preserved structures of the palace of Diocletian, it could be concluded that the approach and taste of the investor and of his architects changed. The traditionalism in the choice of materials for different parts of the Palace, i.e. for its representative and utilitarian parts, should not be surprising in a complex of buildings constructed as a residence of an emperor.

In ancient Rome (and in other ancient civilisations) the meaning of materials and colours was defined: e.g. porphyry (used for imperial sarcophagi, for the well-known statue of Tetrarchs and for other imperial statues and decorative elements) symbolized imperial power. Maybe similar rules and traditions also determined the use of materials in the Diocletian's palace.

Acknowledgements. I wish to express my most sincere gratitude to Prof. Dr. Goran Nikšić for sharing his great knowledge on the structures of the Palace of Diocletian in Split. I would like to acknowledge and thank Mrs. Branka Brekalo, the director of the Museum of the town of Split and to the staff of the Museum, for enabling me to do research within the substructures of the Diocletian's palace, and to Mrs. Jasna Jerkov, the director of the Department for the Old City Core of Split, for giving me access to the survey plans of the substructures.

REFERENCES

[1] Adam, R. *Ruins of the Palace of the Emperor Diocletian at Spalatro in Dalmatia*. (1764).
[2] Fischer von Erlach, J. B. *Entwurff einer historischen Architektur*. (1725).
[3] Marasović, T. *Diocletian's Palace*, Sloboda, (1982).
[4] Niemann, G. *Der Palast Diokletians in Spalato*. Hölder, (1910).
[5] Vitruvius, M. P. *De architectura libri decem.*
[6] Lancaster, L. C. *Concrete Vaulted Construction in Imperial Rome*. Cambridge University Press, (2005).
[7] Ward-Perkins, J. B. *Architettura Romana*. Electa Editrice, (1979).
[8] Lamprecht, H.-O. *Opus caementitium – Bautechnik der Römer*. Beton-Verlag, (1987).
[9] Historical Complex of Split with the Palace of Diocletian. http://whc.unesco.org/en/list/97 (retrieved January 23, 2020)
[10] Nikšić, G. Dioklecijanova palača – od projekta do izvedbe (Diocletian's Palace – from Design to Construction). In: N. Cambi et al. (Eds): *Dioklecijan, tetrarhija i Dioklecijanova palača o 1700. obljetnici postojanja (Diocletian, Tetrarchy and Diocletian's Palace on the 1700th Anniversary of Existence)*, Književni krug Split (2009), pp. 117-134.
[11] Bužančić, R. Dioklecijanova palača (Diocletian's Palace). In: N. Cambi et al. (Eds): *Dioklecijan, tetrarhija i Dioklecijanova palača o 1700. obljetnici postojanja (Diocletian, Tetrarchy and Diocletian's Palace on the 1700th Anniversary of Existence)*, Književni krug Split (2009), pp. 235-278.
[12] Survey plan of the substructures of Diocletian's Palace, Department for the Old City Core of Split (unpublished)

[13] Diocletian's Palace and the Historical Nucleus of Split (extension). http://whc.unesco.org/en/tentativelists/2015/ (retrieved January 28, 2020)
[14] Nikšić, G. The use of brick in Diocletian's Palace at Split, *Archeologia dell'Architettura* (2015) 20: 206-209.
[15] Nikšić, G. Prilog o arhitekturi Dioklecijanovog mauzoleja i rekonstrukciji splitske katedrale u 13. stoljeću. *Prilozi povijesti umjetnosti u Dalmaciji* (1997) 35: 105-122.
[16] Jackson, T. G. *Dalmatia, the Quarnero and Istria, with Cettigne in Montenegro and the Island of Grado*. Clarendon Press (1887).
[17] Nikšić, G. The Influence of Building Materials on Architectural Design: Dalmatian Stone at the Cathedrals in Korčula and Šibenik. In: A. Payne (Ed.): *Dalmatia and the Mediterranean: Portable Archeology and the Poetics of Influence*. Brill (2014) pp. 382-401
[18] Lancaster, L. C. *Innovative vaulting in the architecture of the Roman Empire*. Cambridge University Press (2015).

12th International Conference on Structural Analysis of Historical Constructions
SAHC 2020
P. Roca, L. Pelà and C. Molins (Eds.)

PATIO AS A STRUCTURAL INVARIANT. BUILDINGS WITH PATIO FACING ADAPTIVE REUSE IN BARCELONA

PERE FUERTES[1], ROGER SAUQUET[2], NÚRIA SALVADÓ[3]

[1] Department of Architectural Design, Universitat Politècnica de Catalunya
Av. Diagonal, 649, pl. 5. 08028 Barcelona, Spain
e-mail: pere.fuertes@upc.edu, web page: habitar.upc.edu

[2] Department of Architectural Design, Universitat Politècnica de Catalunya
Av. Diagonal, 649, pl. 5. 08028 Barcelona, Spain
e-mail: roger-joan.sauquet@upc.edu, web page: habitar.upc.edu

[3] Department of Architectural Design, Universitat Politècnica de Catalunya
Av. Diagonal, 649, pl. 5. 08028 Barcelona, Spain
e-mail: nuria.salvado@upc.edu, web page: habitar.upc.edu

Keywords: Patios, Structuring Patios, Architectural Renewal, Adaptive Reuse, Life-Cycle, Barcelona

Abstract. *Certain architectural structures have the ability to persist over time when a building undergoes a change of use. This is the case of patios, according to the conclusions of a study focused on the reused buildings of Barcelona recently developed. The survey of this architectural element should enable us to better understand the behaviour of these buildings.*

If we define the open-air inner courtyard of a building as a patio, this study is especially interested in those who have the capacity to organize spaces, systematize circulations — along with stairs and corridors — and configure the building as a whole. This set of structuring patios particularly applies in a dense city like Barcelona because their position and size also provide liveability to interior rooms. In light of these qualities, such patios can be regarded as an essential piece of both the formal and the bearing structure of a building.

The location and attributes of these patios can be associated with the potential for adaptive reuse: they can help achieve a lower impact on the architectural and formal structure of a renovated building, when used appropriately. Hence the patio can be seen as an indicator of how a new programme adapts to the existing support. 171 out of 565 buildings documented and analysed in Barcelona — a thirty percent of the overall — have at least one patio of a kind whose characteristics have outlived one or more renovation processes. The percentage rises to 50% in Ciutat Vella and Eixample districts, where density and architectural typology make them particularly relevant.

Buildings with patios match different uses and periods from the 11th to the 20th century. In spite of the expected differences, the studio draws conclusions on the understanding of material transformations and changes of use they have undergone.

In short, with regard to buildings included in this category — both heritage and common ones — this paper helps verify the hypothesis that the very existence of a patio is responsible for the persistence of the internal arrangement and structure and must be carefully considered in future interventions when addressed to extend the life-cycle of a building.

1 INTRODUCTION

The 2013 call for proposals of the Spanish National R&D Programme Aimed at the Challenges of Society resulted in a study on the reused buildings in the city of Barcelona, which concluded with the publication of an *Atlas del aprovechamiento arquitectónico, estudio crítico de los edificios reutilizados en Barcelona* [1], hereinafter *Atlas*. This research, carried out by the Habitar UPC group, revealed the extent of the phenomenon of change of use in the city of Barcelona and, among other conclusions, brought to light the importance of the patio, not only as a structural and structuring element of the functionality and use of a building, but also in its preservation, durability, evolution and transformation over time, that is, in its adaptive capacities for reuse.

The concept of *adaptive reuse* — as a sustainable strategy to extend the life of a building considered as a resource — constitutes a consistent corpus of research that has been intensively developed in recent decades. If, the literature on this concept can be initially associated with the transformation of heritage buildings [2], the logical evolution of the term has expanded to the capacity to value any building susceptible of being adapted to a new use and to the particular conditions of the necessary transformation process [3, 4, 5, 6, 7].

In this sense, the *Atlas* considers built architecture and the urban environment as a resource that can be triggered when the life cycle of buildings is strategically addressed; a resource that allows the generation of urban habitability by taking maximum advantage of what already exists and minimizing the need to consume more territory. In the consolidated city, where the availability of space is so limited, the programmed conversion of the building stock is a feasible sustainable alternative to satisfy the needs that are generated at any time. For this purpose, it is essential to identify the room for manoeuvre in which this reprogramming can move [8], and to analyse the capacity of the patio as a fundamental piece for structuring reprogramming and change of use. Therefore, this paper aims to analyse the patio as an element that makes the pre-existing architectural support and the proposed new activity compatible, emphasizing the attributes of both the container and the new contents.

The term patio describes a variety of spatial situations in architecture directly related to a building's inner courtyard, usually in the open air or under a skylight. The patio — whose main task is to provide light and aeration to the interior areas of a building — plays various roles depending on its scale, shape, character and use. We can identify as patios cloisters, backyards, courtyards of public buildings, patios of palaces and private houses, peristyles, atriums, or air yards [9].

Beyond this wide spectrum of situations, the archetypal patio considered here is one whose purpose is not only to illuminate and aerate, but also to structure a building, linking the different parts that constitute it. Thus, the patio can be identified as the 'main room' of the house, a piece without a roof that organises space and activity around it. Its character is that of an introverted space that may recreate a small fragment of nature, a delimited and secluded space that becomes the stage for everyday life. And which, at the same time, grants the independence of the private parts of the building from the public space.

2 PERMANENCE OF THE PATIO

The persistence of the patio in Barcelona's urban architecture, despite the changes in the use of the building in which it is located, proves the significance of this first-rate element both as a space and structural configurator. This permanence occurs in buildings that correspond to a very broad time framework, ranging from the 11th century to the 20th century.

The origin of the Barcelona patios that have been preserved over time corresponds to a wide variety of typologies: detached palace houses, town houses, apartment blocks, religious buildings, barracks, schools, offices, industries and facilities. Such buildings were initially erected to meet specific functional needs, but they have evolved and modified their interior layouts to a certain extent. In contrast, the structure of the patio and its connections with the staircase and galleries or corridors, have remained unchanged and have favoured a relative preservation of the spatial organisation of the building.

3 PATIO AND URBAN FABRIC

In Barcelona, the patio has a special relevance in denser urban fabrics as it is an element of clearance that provides hygienic conditions to buildings set in narrow and deep plots whose inner rooms need this space to provide a connection with the open air. For this reason, a large number of patio buildings are preserved in Ciutat Vella district, despite the diversification of uses they have undergone over the centuries.

Statistical data can be drawn from the 571 reused buildings in Barcelona listed and documented in the *Atlas*.[1] It can be noted that there is a greater number of reused buildings that preserve the courtyard in the most compact urban fabrics. Out of the 571 registered buildings, 171 have at least one patio that has preserved its original features with the changes of use, representing a 29 percent of cases — almost a third of the total. This scenario shows the relevance of this element in maintaining the structural characteristics of a building over time, especially in high-density cities like Barcelona.

Table 1: Number of cases by District

District	*Reused buildings (with patio)*	*Average %*
Ciutat Vella	194 (88)	45.8
Eixample	83 (45)	54.2
Sants-Montjuïc	44 (7)	15.9
Les Corts	29 (4)	13.7
Sarrià-Sant Gervasi	95 (7)	7.3
Gràcia	25 (4)	16.0
Horta-Guinardó	47 (3)	6.4
Nou Barris	8 (2)	25.0
Sant Andreu	21 (1)	4.7
Sant Martí	43 (8)	18.6

However, the dissemination by district is uneven (Table I). The evidence that patios in Ciutat Vella are maintained in most cases has already been mentioned. In addition, the significant number of reused buildings with a patio in the Eixample district may be the result of the emphasis given by Ildefons Cerdà to hygiene issues in order to provide ventilation and sunlight to the dwellings. Due to the building compacity, most of the constructions in the Eixample have one or more inner patios — some of them sheltered by a skylight to house a central staircase — that tend to remain in place when the function changes. Yet the buildings located in less dense

[1] The *Atlas* gathers a total of 1,464 currently existing buildings that have changed use at least once during their lifetimes. Of these, a sound amount of documentary detail is available in 571 cases to illustrate their original structure and discuss the transformation processes they have undergone.

urban fabrics, and even those located in garden cities, seldom use the courtyard as a key element in the internal structure of rooms. And if they do, it is in unique facilities or buildings. Such is the case of districts like Sarrià-Sant Gervasi, or Horta-Guinardó.

4 SCENARIOS AND CASE STUDIES

The *Atlas* describes thirteen situations in which the plays a specific role in the change of use. These situations are determined by two factors: the typology of the patio and the modifications occurred with the new activity. On this basis, the following five basic categories can be highlighted:

1. *Noble patios* of medieval buildings and later reinterpretations of the 19th and 20th centuries, mostly located in Ciutat Vella and Eixample districts. They are part of the entrance system to noble houses or urban palaces. They maintain a structural function by means of bearing walls, although some of the patios — halfway through the cloister — have an inner section of pillars or columns on the ground floor.
2. *Cloisters* that organise the central void of a variety of buildings, from the Middle Ages to the 19th century, with a main function in the distribution of activity and which, on a structural level, are bounded by a perimeter gallery defined by an outer wall and an inner arcade supported by columns or piers.
3. *Patios of apartment buildings* involved in the access system, lighting and ventilation of multi-storey constructions basically erected in the Eixample district from the 19th century to the present day. Usually defined by brickwork bearing walls, they maintain a basic structural function, often as a shear core of the building.
4. *Industrial courtyards* conceived as empty spaces between factory buildings.
5. *Other courtyards* resulting from the gap between buildings, either in a planned way, as part of a built complex, or spontaneously, as a result of the combination of different buildings developed over time.

Out of these five categories, this paper focuses on the first three, as they are the most intimately related to the building structure. Noble patios and cloisters along with patios of apartment buildings constitute the core of their corresponding constructions, to the extent that their identity as primary structural elements and their ability to organize the activity of the building cannot be considered separately, especially when a strategic change of use is envisaged.

Regarding these categories, two basic scenarios are worth mentioning when it comes to adaptive reuse: a) Conservation of structure and function and b) Preservation of the structure, but alterations of the function. Accordingly, six combinations between the three categories considered and the two basic scenarios are possible. Each of the combinations can be illustrated with outstanding cases and by listing other examples in which a similar situation occurs.

4.1 Noble patios that preserve structure and functions

Case study 1: Casa de l'Ardiaca, 1190. Association of Lawyers of Barcelona, 1895 (Lluis Domènech i Montaner). Historical Archive of Barcelona, 1920 (Josep Goday) and 1998 (Lluís Doménch, Roser Amadó).

The patio of L'Ardiaca has special characteristics that distinguish it from the rest of the archetypal palatial patios. Firstly, it is elevated above street level and is accessed by steps that extend into the public space. At the same time, as the plot is not very deep, the main bay of the house is located adjacent to the Roman wall and there is no space left for a central patio. Its

position is shifted, it is attached directly to the enclosure's urban wall and the entrance door opens directly onto the street. This marginal situation gives it a hybrid functional and spatial character, as it acts simultaneously as a vestibule and a patio. In spite of this, it preserves the morphological characteristics of any noble patio: a perimeter deambulatory and a main staircase that, from one of its sides, leads to the first floor.

These original features have been maintained over the centuries, despite the changes in use and the successive extensions to the adjacent buildings. The various alterations have mainly affected secondary vertical communication nuclei, which have moved from a central position to the space freed up by the rooms formerly attached to the Decuman Tower. The position of the lift has also moved the axis of circulation to an area parallel to the wall, thus clearing a larger space for the archive's reading rooms.



Figure 1: Casa de l'Ardiaca, Carrer de Santa Llúcia, 1

Case study 2: Palau de la Virreina, 1772 (Josep Ausich, Manuel Amat, Carles Grau). Museum of Decorative Arts, 1949. Museum of Bobbin Lace, 1968. Art Centre and Seat of the Local Cultural Services, 1983.

The location of the main and secondary patios and staircases — as well as the hierarchy of circulation and connection elements — have been maintained over time, despite the various changes in use. Both the main patio and a second smaller one are located in the central bay of the wing adjacent to Les Rambles. As they are aligned with the axis of the main entrance, the presence of these 'wells of light' can be perceived from the street, particularly since the recent opening of a second entrance from the back alley. They thus become reference elements both from the outside and from all the internal areas of the building. The smart geometric layout of the floor plan places them in an eccentric position with respect to the rest of rooms on the plot, but in a central position with respect to their depth.

On the upper floors, the main courtyard is surrounded by a glassed-in gallery that opens up to the rooms on La Rambla, to the back rooms and to the side corridors with service rooms and secondary staircases. Recent alterations in use have placed the lift shafts in this bay. The current use of the museum, together with the relevant placement of the lifts, coexists perfectly with the original structure of the palace, with hardly any modification to the original circulation or the load-bearing elements. In addition, the large gallery is optimised as a complementary exhibition space to the displays in the other noble rooms.



Figure 2: Palau de la Virreina, Les Rambles, 99

Other documented cases:
1. Palau in Carrer de Montcada 18, 1450. Nursery School Nen Jesús, 1899 and 2009.
2. Palau Cervelló-Giudice, 1490 (circa). Maeght Art Gallery, 1974. Gaspar Art Foundation, 2015.
3. Palau Centelles, 1517. Barcelona Philharmonic Society, 1847. Advisory Council of the Generalitat of Catalonia, 1980. Headquarters of the IEA, Institute of Autonomic Studies, 2002 (Soler-Farriol).
4. Palau Bassols, 1550 (circa). Royal Artistic Circle, 1959.
5. Palau Moxó, 1770 (Francesc Mestres). Museum – Restaurant – Housing, 2015.
6. Palau Moja, 1774 (Josep Mas Dordall). Office Building, 1936 and 1959. General Directorate of Cultural Heritage, 1981.
7. Palauet Alòs, 1807-14 (Antoni Centelles). Atheneum Polytecnicum, 1925 and 1936. Cultural Association, 1940. Apartment building, 2008 (Eduard Montané Balagué).
8. Reial Acadèmia de Bones Lletres, 1907. Renovation, 1992 (Joan Bassegoda Nonell).

4.2 Cloister patios that preserve structure and functions

Case study 1: Palau del Lloctinent, 1557 (Antoni Carbonell). Seat of the Archive of the Crown of Aragon, 1836 and 2006 (Lluis Domènech, Roser Amadó).

Despite the interior changes undergone over the centuries in the four bays that structure the building, the main patio, of generous dimensions, remains the central articulator of the palace. The same applies to the adjacent staircase, located in the bay adjacent to the only party wall that connects the building with the rest of the constructions in the complex.

On the ground floor, an ambulatory open to the cloister through four bell arches connects the two entrances currently facing each other: one opens onto the Plaça del Rei and the other onto Carrer dels Comptes. On the first floor, the gallery built with Tuscan-style carved stone arches supported by balusters continues to serve as a connection and distribution of the rooms organized around it. Two elevators placed in pieces near the staircase, solve the current requirements of accessibility without interfering with the original circulations.

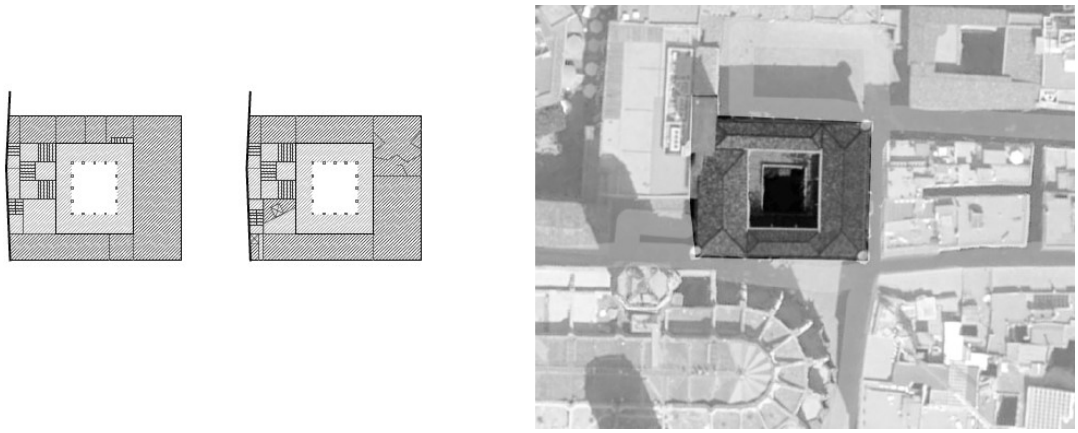


Figure 3: Palau del Lloctinent, Carrer dels Comtes, 2

Case study 2: Convent of La Mercè, 1590. Headquarters of the General Capitaincy of Barcelona, 1845 and 1920.

As a result of the Law of Confiscation, issued in 1836, the convent was converted from religious to military use. Even so, the original layout of the building remains practically intact. The convent was initially organised into two areas: a section containing a large cloister, the main entrance from Carrer de la Mercè, the most relevant rooms and the main staircase; and an equivalent section of service rooms, refectory and kitchen on the ground floor, with a secondary entrance on the same street and another secondary staircase, bedrooms, a small courtyard and other private rooms on the first floor. The upper galleries of the cloister were connected to the church by a covered bridge across the street.

With the change of use, the dichotomy between the two sections is maintained, as well as the large cloister, the secondary patio and the stairs. In 1845, three new entrances were added to the two original doors from Carrer de la Mercè, from the recently developed Passeig de Colom. Circulations extend transversally, now connecting the two façades and permeating the cloister. The 1920 reforms also added other floors and changed the interior decoration of the rooms.

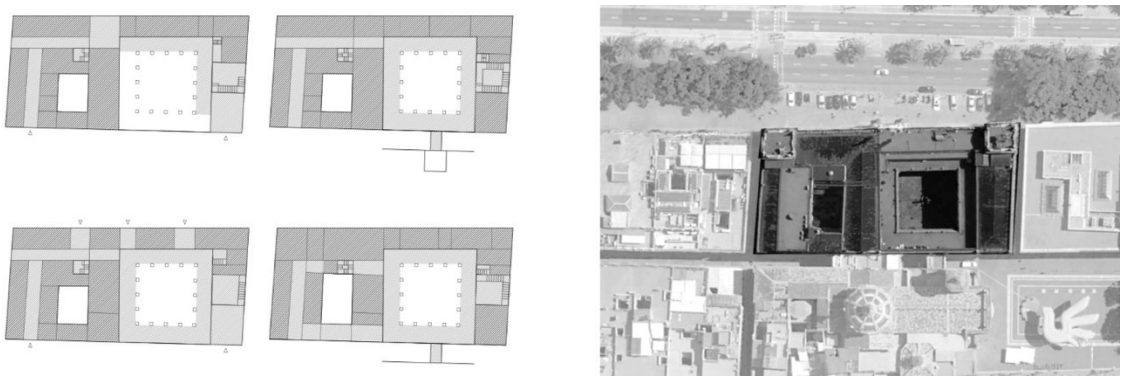


Figure 4: Convent of La Mercè, Passeig de Colom, 14

Other documented cases:

1. Casa de Convalescència (House of Convalescence), 1629. Institute of Catalan Studies, 1931. Barcelona Provincial Council, 1939. Institute of Catalan Studies, 1982.
2. Casa de la Caritat (House of Charity) – Pati Manning, 18th century. Center for Cultural

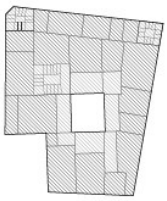
Studies and Resources CERC, 1981 and 1995.
3. Former Customs House, 1790 (Conde de Roncali). Spanish Government Delegation, 1902. End of activity, 2008.
4. Llars Mundet Llevant Pavilion, 1927 (Joan Rubió i Bellver). Concentration Camp, 1939. Old Ladies' Home, 1982 (Manuel Baldrich). Llevant Building, Mundet University Campus, 1996 (F. Labastida, M. Ribas).

4.3 Patios of apartment buildings that preserve structure and functions

Case study 1: Caixa de Barcelona Headquarters, 1899 (August Font i Carreras). Directorate General of Contentious Affairs, 1998 (TAC Architects).

The building — with facades facing four streets — has a trapezoid-shaped floor plan from which a portion has been subtracted in order to regularize the geometry of the Plaça de Sant Jaume. The central space, visually connected with the entrance axis from Carrer de la Ciutat, limits at one of its angles with the noble staircase, which is shifted from the access line to adapt to the irregularity of the plot. The building has also two secondary staircases located at the two corners of Carrer Jaume I. This central space serves as a hall on the ground floor, as it is covered at the height of the first floor by a skylight.

In one of the renovations the patio was occupied by a suspended auditorium located on the upper floor. In the last intervention, the auditorium was removed, recovering the original qualities of the central space and bringing light and ventilation back to the lower floors. The secondary stairs — situated on the two corners of Carrer Jaume I — are complemented by a core of lifts that do not affect the original structure.



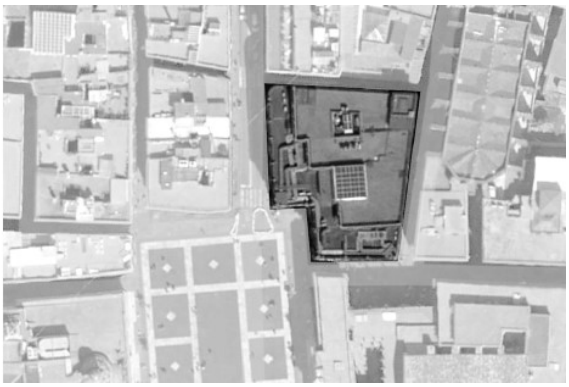


Figure 5: Caixa de Barcelona Headquarters, Plaça de Sant Jaume, 7-8

Other documented cases:
1. Community of Dominican Sisters, 1868 (Francisco de Paula Villar Lozano). Elisabets University Housing (Sergi Burgada Rodríguez).
2. Transmediterranean Ship Company, 1917 (Juli Maria Fossas). Department of Universities and Research of the Generalitat of Catalonia, 1994.
3. Provincial Savings Bank Offices, 1956 and 1962 (Robert Terradas i Via). Apartment building, 2014.

4.4 Noble patios that preserve structure but modify functions

Case study 1: Casa Macaya, 1899. Architect: Josep Puig i Cadafalch. Institute for Deaf-

Mutes, 1949. 'La Caixa' Cultural Centre, 1988. Architect: Eugeni Bach & Gabriel Mora.

The building is a former urban palace, organized in four bays around a central patio with a roofed staircase leading to the first floor. The wide façade bay contains, on the upper floors, the rooms of larger dimension and, on the ground floor, the access to the building located off the axis of the courtyard. The double back bay is formed by equivalent rooms — which ventilate and illuminate through the backyard — and by smaller rooms that accompany the secondary staircase that gives access to all the floors.

The changes in use have preserved the main access, through a side entrance hall that, after the first two bays, opens out onto the large patio. Both the noble staircase and the secondary staircase have remained intact. The main renovations affecting the circulations occur in one of the two secondary patios that originally ventilated and illuminated the side rooms. With the latest alteration, this space has been used to house a third staircase and two lifts. This has displaced the original circulation around the main patio towards the bay that connects with the new stairs and lifts.

The partition walls around the main patio have been removed, causing the disappearance of the passageway around it and modifying circulations. At the same time the patio has been covered by a skylight.



Figure 6: Casa Macaya, Passeig de Sant Joan, 108

Other documented cases:

1. Palau Mercader, 1550. Cercle Artístic de Sant Lluc, 2014 (Portal Ballber Architects).
2. Palau Mornau-Palau Nadal, 1590 (circa). Cannabis Museum.
3. Palau Gomis, 1750. European Museum of Modern Art, 2011 (Josep Infiesta, Jordi Garcés).
4. Urban House, 1770. Cercle Barcelonés de Sant Josep, 1879 (Joan Martorell). 'Antic Teatre' Space of Creation, 2003.
5. Palau Sabassona, 1796 (Josep Francesc Ferrer de Llupià). Ateneu Barcelonès, 1907 and 2011 (Manel Brullet, Mateu Barba).
6. Palau Dou, 1818 (Antoni Celles Azcona). Cervantes School and High School, 1940 (Juan Antonio Zaragoza).
7. Casa de les Altures, 1890 (Enric Figueres). Summer Camp House, 1936. Hydrological Research Institute and Headquarters of theHorta-Guinardó District, 1989 (Víctor Argentí).
8. Palau Baró de Quadras, 1904 (Josep Puig i Cadafalch). Music Museum, 1980. Asia House. Ramon Llull Institute, 2003.
9. Pérez Samanillo House, 1910 (J.J. Hervás). 'Círculo Ecuestre' Club, 1950 (Raimon Duran i Reynals).

4.5 Cloister patios that preserve structure but modify functions

Case study: Convent of Santa Monica, 1635. Santa Monica Art Centre, 1987 (Albert Viaplana, Helio Piñón).

The convent — the only one left standing in the final section of the Ramblas after the Law of Confiscation of 1836 — used to organise all its chambers around a large square cloister with a central well. On the ground floor, the galleries, with Roman arches on Doric pilasters, connected the rooms located in the four adjacent bays. On the upper floors, balconies or windows opened onto the cloister. The other rooms in the complex adapted to the unevenness of the plot, so that the geometry of the cloister was left regular. The cloister communicated laterally with a still existing church that was also accessed from Les Rambles through a narthex, while the entrance to the convent was from the Carrer del Portal de Santa Madrona.

The 1987 renovation redefines the formal and functional logic of the original cloister by erecting two parallel walls that divide its centre into three parts. This fact, together with the new roof, totally changes its open character and its perimetral circulation. On the ground floor, the cloister becomes a walkable exhibition area. In contrast, on the upper floors, the intercommunicating rooms continue to open with balconies or windows to this great central empty space, now interrupted by thick concrete walls. The original entrance to the convent is preserved but a new main access is added from Les Rambles directly to the first floor through a wide ramp that also serves as a large public balcony. The relationship with the church — which currently functions as a parish — is broken. Despite these changes, the building maintains the location of the original staircase and, in general, the original rooms of the former convent, even though internal circulation has been severely disrupted.

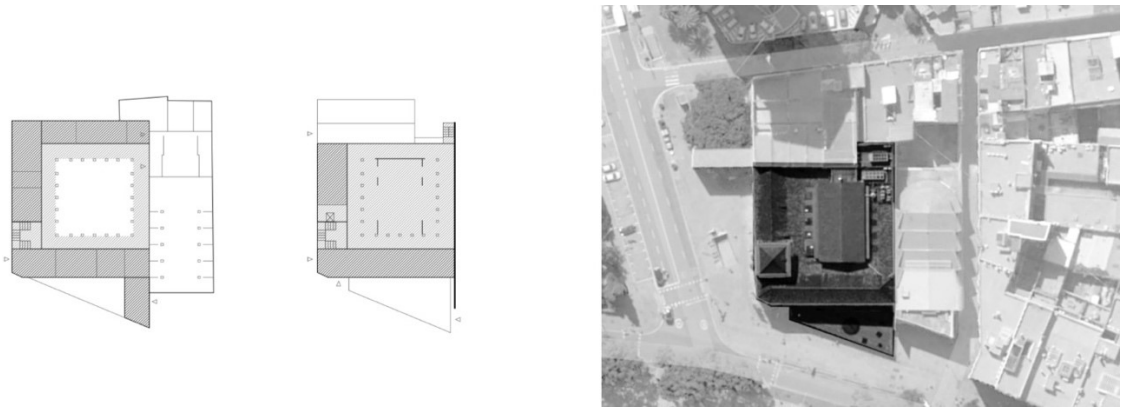


Figure 7: Convent of Santa Monica, Les Rambles, 7

Other documented cases:

1. Convent of Sant Agustí Vell, 1347. Sant Agustí Barracks, 1738. Sant Agustí Vell Civic Centre, 1994 (Antoni de Moragas). Museum and Photographic Archive, 1994.
2. Convent of the Franciscan College of Sant Bonaventura, 1652. Hotel Orient, 1881 (Eduard Fontseré) and 2001 (Robert Brufau).
3. Palace of the Governor, Ciutadella Park, 1718 (Joris Prosper van Verboom). Fire Station, 1932. Verdaguer High School, 1932.
4. Casa de la Caritat (House of Charity), 1736, 1804, 1861 (Josep Oriol Mestres), 1912 (Josep Goday). Centre of Contemporary Culture of Barcelona CCCB, 1991-1995 (A. Viaplana, H. Piñón, R. Mercadé).

4.6 Patios of apartment buildings that preserve structure but modify functions

Case study: Joan Puig House, 1872 (Pere Bassegoda Mateu). Warehouses and Offices. Hotel, 1997 (José Luis Sayos).

The late 19th century building was organised around a main patio with a noble staircase, located in the fourth bay of the building, closer to the backyard than to the façade. Four secondary patios, two of which had service staircases, completed the ventilation and lighting of the entire floor. The building's circulation was basically around the main patio, connecting the various rooms directly to each other, in an "Italian-style" layout.

With the latest conversion to a hotel, the noble patio and the staircase to the main floor have been maintained, but two lifts have been added. The rest of the secondary patios are used to ventilate and illuminate some of the new hotel rooms, covering the entire surface of the floors. The service stairs change their configuration but not their position and interlink with each other and with the lifts connected to the main patio through a new network of corridors.

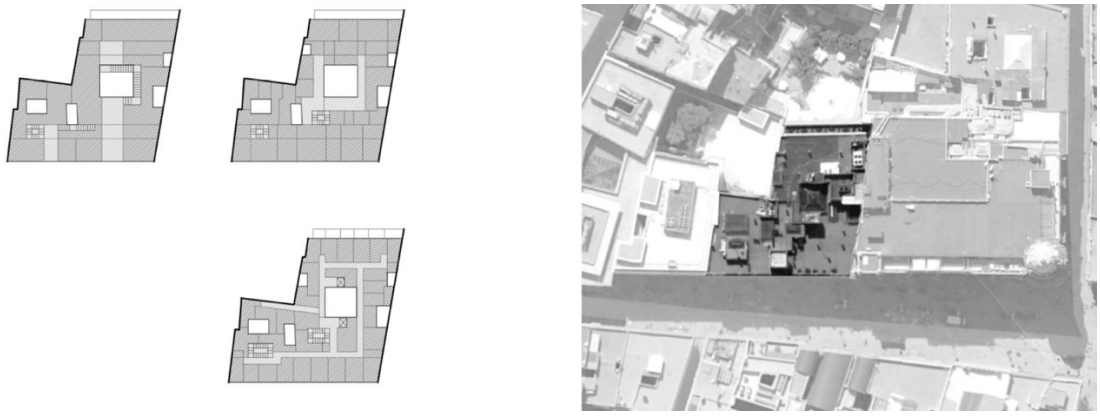


Figure 8: Joan Puig House, Portal de l'Àngel, 15-17

Other documented cases:

1. Apartment building, 1850. Fernando Hostel, 1998 (G. Amigó Buixaderas).
2. Apartment building, 1863 (Narcís Nuet). Hostel, 2010.
3. Joan Serra House, 1867 (Francisco de Paula Villar). 'Las Noticias' and 'El Correo Catalán' Newspaper's Office, 1925. Montecarlo Hotel, 2000 (Lluis Jaumandreu i Anglada).
4. Apartment building, 1870. Cocoon apartaments, 2000 (A&M arquitectes).

5 DISCUSSION AND CONCLUSIONS

The *Atlas* has been able to classify buildings with a patio according to their structural, organisational, and typological characteristics along with the changes undergone in those fields. Despite the differences initially revealed among those buildings, the research draws conclusions on the understanding of material transformations and changes of use.

On the basis of the study on the evolution of the urban patio and its capacity to adapt, transform and reconfigure when a change of use applies, it is possible to state — in the light of the documented cases — that the patio is an enduring architectural element, because of the combination of both its structural and organizational characteristics. This double potential is also largely responsible for preserving the structural characteristics of the rest of the spaces adjacent to it, even if changes in the functioning and organization of the building occur when

there is a change of use. Indeed, it could be argued that the enclosing walls of the patio — as they simultaneously belong to such a consistent bearing and functional system — define an area of influence on both sides that has the capacity to persist over time, even when the building undergoes profound transformations.

Thus, the patio — defined as the open-air inner court of a building — is an element that clearly shows the relationship between the supporting structure and its function — understood as the use or activity that takes place in a building. This clear and direct relationship, which also characterises and defines its spatial qualities, is the key to its adaptive capacity and must therefore be carefully considered in future interventions that seek to extend the lifespan of buildings, especially when environmental factors are considered, along with artistic, historical, social and heritage aspects. Public policies should address these processes, by establishing clear and useful criteria to evaluate transformations. Political support is definitely needed to facilitate this scenario [10].

Acknowledgements. This paper is made possible by the funding of the Spanish Ministry of Economy and Competitiveness, through the National R&D Programme Aimed at the Challenges of Society 2013.

REFERENCES

[1] Monteys, X., Mària, M., Fuertes, P., Sauquet, R., & Salvadó, N. (2018) *Atlas del aprovechamiento arquitectónico. Estudio crítico de los edificios reutilizados en Barcelona*. Barcelona: MINECO, Universitat Politècnica de Catalunya.

[2] Austin, R. L., Woodcock, D. G., Steward, W. C., & Forrester R. A. (1988). *Adative Reuse: Issues and Case Studies in Building Preservation*. New York: Van Nostrand Reinhold Company.

[3] Ball, R. (1999). Developers, regeneration and sustainability issues in the reuse of vacant industrial buildings. *Building Research & Information*, *27(3),* 140-148.

[4] Bon R., Hutchinson K. (2000). Sustainable construction: some economic challenges. *Building Research and Information*, 28(5/6), 310-4.

[5] Douglas, J. (2006). *Building Adaptation*, 2nd ed., Burlington: Butterworth-Heinemann.

[6] Bullen, P. A. (2007). Adaptive reuse and sustainibility of commercial buildings. *Facilities*, 25, 20-31.

[7] Langston, C. A. (2008). The sustainability implications of building adaptive reuse. In *CRIOCM 2008 International Research Symposium*. Retrieved January 21, 2019 from https://works.bepress.com/craig_langston/1/

[8] Rueda, S. (2018). Carta para el diseño de nuevos desarrollos urbanos y regeneración de los existentes. *Congreso Post-Habitat III*. Retrieved December 15, 2018 from Barcelona.http://www.cartaurbanismoecosistemico.com/

[9] Díaz Recasens, G. (1992). *Recurrencia y herencia del patio en el movimiento moderno*. Sevilla: Universidad de Sevilla.

[10] Yung, E. H., & Chan, E. H. (2012) Implementation Challenges to the Adaptive Reuse of Heritage Buildings. Towards the Goals of Sustainable, Low Carbon Cities. *Habitat international*, 36(3), 352-361.

12th International Conference on Structural Analysis of Historical Constructions
SAHC 2020
P. Roca, L. Pelà and C. Molins (Eds.)

RECONSTRUCTED OVERHANGING BATTLEMENTS. EXECUTIVE TECHNIQUES AND THEIR VULNERABILITY IN THE STRONGHOLD OF ARQUATA DEL TRONTO (ITALY)

EMANUELE FACCHI[1], ALBERTO GRIMOLDI[1], ANGELO G. LANDI[1*] AND EMANUELE ZAMPERINI[1]

[1]Dipartimento di Architettura e Studi Urbani (DAStU), Politecnico di Milano
piazza Leonardo da Vinci 26, 20133 Milano, Italy
e-mail: angelogiuseppe.landi@polimi.it, www.polimi.it (*corresponding author)

Keywords: Fortified Buildings, Overhanging Battlements, Seismic Vulnerability

Abstract. *The stronghold of Arquata del Tronto was heavily damaged by earthquakes in 2016 and it drew the attention of the experts in reinforcing historic buildings. They regarded it as a case study, a predicting model of the failure in employing specific construction elements in fortified architecture, whose geometric and material data were only approximately considered. The overhanging battlement is the most seriously damaged part of the building and has raised particular attention and interest. As often happens in other castles and fortresses, it dates back to the late 19th and even more to the 20th century. A first close examination of the building's repairs shows how the new additions, whose maintenance is difficult, ended in failure. The additions were inspired by ancient details, but nonetheless they are unreasonable from the point of view of structure and durability: they – and even more the irrational repairs of the last decades – are the principal cause of failure. Material decay – closely linked to circumstances and places – has also played a decisive role. An extensive and rigorous historical research is necessary to find the sources and to evaluate their nature and limits, as well as to relate all information to the building, thus operating in close correlation with the building archaeology, by now a so widespread and consolidated research field. . Jointly, the written documents and the building itself in its historical stratification allow a better analysis of the structural behaviour , an essential step to achieve an effective restoration planning.*

1 THE XIX CENTURY STUDIES ON MEDIEVAL FORTIFICATIONS AND THEIR RECENT USE IN THE FIELD OF STRUCTURAL STRENGTHENING

Recent technical literature on seismic prevention aimed at developing calculation models and identifying typical cases in order to take preventive action. For this purpose, the studies outline a story in broad lines, by types and periods (which only conjure the infinite number of possible variants), and in parallel develop a synthetic calculation of some concrete cases, only in broad terms corresponding to the identified types. By quantitative data, this kind of approach reiterates only some intuitive general remarks. Actually the heterogeneity of construction techniques and decay, peculiar to each building, as well as the numerous repairs carried out in areas of high seismic risk – where damage has repeatedly occurred – determine very different behaviours. So the results could be scarcely useful in few actual cases, whose

structure deeply differs from its often only formal type. The battlements of the medieval architecture offer a significant example of these contradictions.

An overhanging battlements is a *chemin de ronde* on top of the walls protected by a parapet with merlons built on the extremity of brick or stone corbels, between which machicolations are realized; they originate from the necessity of making the vertical flanking – or plunging fire – easier. Overhanging battlements characterized many Italian fortifications between the end of the 13th and the middle of the 15th century, when artillery progress made this type of defence obsolete. The construction – an overhanging wall on thin corbels – is intrinsically vulnerable. Its duration in time depends on the cohesion of mortar, porosity of bricks and compactness of stones: the decay of materials due to the ravages of weather affected structural efficiency. Horizontal surfaces were protected from water with hydraulic mortar of lime made hydrophobic with the addition of protein materials as testified by so numerous 19th century manuals in all European languages that one reference in Italian can be enough [1]. Where machicolations were not protected, they let rainwater leak on the top of the walls and even between the corbels. Especially in harshest climates, it was preferred to cover the battlement with a roof. Under the entry for *Mâchicoulis* in his *Dictionnaire* [2], Viollet-le-Duc emphatically underlined the difference between the overhanging battlement of Avignon walls – lacking a roof – and the covered one in Pierrefonds. Thanks to his surveys of the construction details in Piedmontese fortifications of the 13th-14th centuries, Alfredo d'Andrade drew up a documentation that was unparalleled in the rest of Italy [3]; he himself began to write a *Dictionnaire* and carefully covered numerous towers which he repaired or entirely rebuilt. Owing to these maintenance issues, nowadays almost all existing overhanging battlements date back to late 19th and 20th century. Where they have not been rebuilt entirely, the lack of homogeneity between ancient and added parts may determine significant behavioural differences: being often more fragile than their prototypes, over time they have required continuous maintenance and further substitutions.

The recent studies focused on the two principal failure mechanisms: either the out-of-plane overturning of merlons around a hinge at the top of the parapet or of the whole battlement around a hinge at the top of corbels; the cross-cracking of merlons that mainly occurred when they were hold – but also loaded – by a roof, widespread in the XIV-XVth century examples.

2 STRUCTURAL BEHAVIOUR OF OVERHANGING BATTLEMENTS

The copious specialist bibliography on medieval fortifications, published during the 19th century in various European languages, thoroughly illustrates the origins, evolution, and characteristics of the battlements, merlons and crenels. Printed monuments, such as the work by Otto Piper (1895) [4] for the German-speaking area, or erudite syntheses, such as the text in Italian by Enrico Rocchi (1908) [5], are only two, but reliable examples. Even the general works on medieval architecture are rich in references. Among these, the earliest ones are the most reliable: they describe still preserved, ancient examples, but the culture of their time influenced the observations. A subsequent generation of studies dates back to the post-World War II period, while parallel developments in postclassical archaeology introduced stricter truth criteria. The use of this literature requires a critical comparison of almost two centuries' publications, up to the most recent syntheses of archaeologists and medievalists.

Two different construction techniques were commonly used to build the corbels which had to support these overhanging structures (fig. 1): the former involved the insertion of several superimposed orders of large stone corbels into the masonry: the latter had to realize a brick or stone

masonry that protruded gradually from the vertical plane below. If we do not consider the friction in the contact surfaces, when stone cantilevers are used, each element is subjected to bending independently of the upper and lower ones, and there are tensile (in the upper fibres) and compression (in the lower fibres) stresses in its cross section. When we take friction into account, axial compression is generated in the lower cantilevers and traction in the upper ones. To support the weight of the parapet and merlons at their external ends, the stone cantilevers are to be considered as fixed in the masonry; they should be loaded by a weight at their internal end (for example a back wall), held downwards by a metal bracket anchored in the masonry, or balanced inwards with a significant load. In all cases it is necessary to use stones with a high tensile strength and compactness, to avoid a rapid decay caused by rainwater absorption. It was possible to create a considerable overhang with corbels of reduced height using a very resistant stone. To achieve the same overhang, masonry corbels should necessarily be higher. Given the significant height in relation to the projection, on their upper surface fewer tensile stresses are generated than in the previous case; however these stresses can hardly be balanced by the tensile strength of the masonry, which in this case is essentially given by the adhesion of mortar. It was therefore common to insert a wooden beam at the top of the corbels which adhered to the masonry thanks to friction, thus allowing to provide it with the necessary tensile strength; at the same time, owing to its bending stiffness this beam contributed to directly transfer part of the load to the masonry behind. For this reason – especially in the fortifications of the middle Adriatic area – another beam was often inserted at half height of the corbels (e.g. Gradara, Jesi, Acquaviva Picena, Canzano). Alternatively – or together with the wooden beams – a more expensive iron tie rod could be inserted, equipped with an external anchor: it could guarantee a greater tensile strength. Although initially it produced a greater resistance, later the presence of wooden elements within the masonry often became a source of vulnerability: not adequately protected from atmospheric agents, timber gradually decayed, losing contact with the adjacent masonry, therefore generating a discontinuity within it.

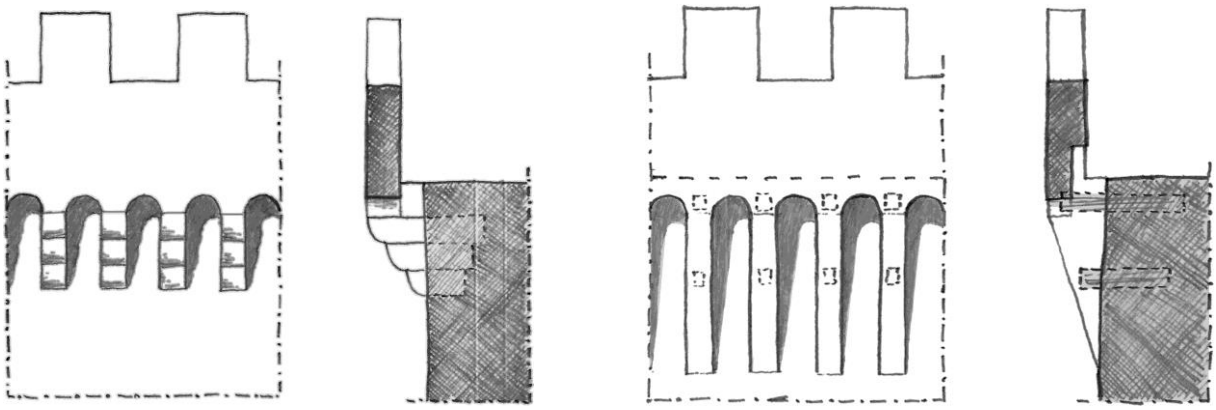


Figure 1: Overhanging battlement with corbels made of stone cantilevers (on the left) or of brick or stone masonry reinforced with timber cantilevers (on the right) (drawings by E. Zamperini).

3 *RESTAURARE EST REFICERE*: EARLY 20TH CENTURY WORKS IN THE STRONGHOLD OF ARQUATA DEL TRONTO

The stronghold of Arquata del Tronto, already subject to at least two expeditious interpretations [6, 7] of the damage following the earthquakes of August 24th and October 30th, 2016, is halfway the result of restoration works carried out during the 20th century (from

1903-06 till 1991-94). The earthquake damaged all inadequate additions, repairs and prevention systems; the only few ancient parts to be damaged were those whose maintenance was omitted and waterproofing had not been realised, seriously weakening the walls.

The quadrilateral donjon is probably the most ancient part of the fortress. It may date back to the mid-14th century, but no documents citing its existence allow us to distinctively identify the still preserved remains; there are not even ancient construction elements that can be compared with others having a firm date in the same geographic area. A curtain wall was connected to the donjon to define a protected area. By the 15th century, two minor towers were added to reinforce the wall. The first has a pentagonal plan and it's still existing; the second was approximately circular and had a triangular buttress; between 1903 and 1950, without proper consolidation it gradually collapsed and it was finally demolished. Works were documented in the seventh decade of the century, [8, pp. 135-137] [9, p. 30] and the upper part might have been in ruins in 1525 [9, p. 30, n. 63]. In 1655 the fortress – abandoned for over fifty years – laid in ruins and was not suitable for hosting the castellan [10]: the situation was acknowledged in a decree issued by Pope Alexander VII on February 9th, 1657. The earthquake of L'Aquila in 1703 [11, 12] and that of Valnerina in 1730 [11, 13] caused serious damage to the town. The fortress also needed repairs, which were contracted for the remarkable amount of four hundred *scudi* in five years [14]. Subsequently, till the end of 18th century, it's very doubtful that the Community spent other funds to maintain the building [15]. Still in 1815 [16], it's documented that a newly appointed castellan took over the stronghold, but there is no information about its conditions.

The divestment by the State coincided with the drafting of a summary restoration project by Vincenzo Pascucci of the Provincial Finance Office (*Intendenza di Finanza*) of Ascoli (May 7th, 1883) [17], which gives a summary idea of the state of the building in that moment. After the transfer to the Municipality of Arquata in 1890 [18] – following a decade of negotiations [19] – the State's commitment to the restoration involved the direct intervention of the Provincial Commission for the Protection of Monuments, and in particular of its more active member Giulio Gabrielli, an amateur gentleman; through reports and writings he offered many useful elements to document the state of the building [20]. The problematic financing of the works by the Ministry of Education directly brought into question the General Directorate of Antiquities and Fine Arts, whose fonds has preserved some preliminary material, including a first series of photographs [18] (fig. 3). In 1901 the Regional Office for the Protection of Monuments – then directed by Count Giuseppe Sacconi, the architect of the Vittoriano [21, 22] – was charged with drafting the project on which to quantify the funding. His illness and death (1905) almost coincided with the establishment of the Superintendencies (1907). The first superintendent of the Marche region was Icilio Bocci [23], who had previously worked at the Lombard Regional Office.

It may be asked whether this mobility between offices had determined conventional restoration solutions, as a result of common references. The answer is difficult, both for the intrinsic diversity of the buildings and contexts, and because – especially in places that are difficult to reach – the project gives only rough indications referred to shared rules of art, and it was managed by local people such as contractors and municipal technicians.

4 RECONSTRUCTION OF THE DONJON'S OVERHANGING BATTLEMENT

In 1901 the project was drafted by Guglielmo Giustiniani, on behalf of the Regional Office [17]: the costs envisaged by the previous appraisal of the Provincial Finance Office of Ascoli

were considered excessive. According to the project report, the donjon was reduced to the perimeter walls and even the existence of the upper vault (at the level of the battlement) is doubtful; however «traces of ancient wooden ties with anchor rods to support the overhanging merlons were still visible». The appraisal instead provided for the construction of a masonry staircase on rampant vaults to access the top, and for the "restoration" of the vault: the term is ambiguous, indeed it's used even for large reconstructions in correspondence of fragments or simple traces. As the photos [24] show, on the north wall the corbels had collapsed to a level incompatible with the existence of the vault, however the existing round barrel vault – made in large irregular sandstone ashlars – suggests that on the other sides at least the springers were still remaining. The reconstruction of the overhanging battlement needed an «Iron frame around, to support the overhang of the merlons», defining an encircling tie about 10 m long on each side. The appraisal enumerates also eight tie rods, however their position is not described. To protect the underlying vault, a square room of about 4.30 m on each side was designed; its perimeter walls were 60 cm thick built in continuity with the internal side of the tower walls: therefore a large terrace difficult to maintain was avoided. The pavilion roof was set on 3.50 m high walls, and had to protrude to protect the *chemin de ronde*. A schematic drawing shows the eaves leaving Guelph merlons (about 1.2 m high over the parapet) uncovered (on the left in fig. 2) and remaining about 40 cm above their upper face, on the contrary a dimensioned sketch suggests a bigger protrusion of the eaves to cover the entire overhanging battlement (on the right in fig. 2), as already designed by Pascucci [17]. However, the wooden eaves included «struts with iron connection to the frame of the merlons». Giustiniani recognized the function – even static – of the roof, and he suggested an essential, hardly visible version of it, based on presumptive dimensions; indeed there was no means of climbing to the top of the donjon.

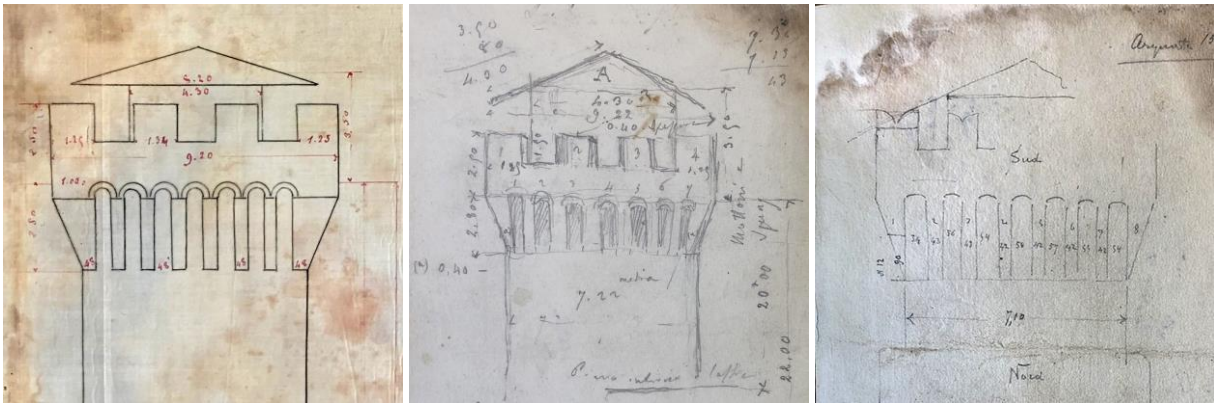


Figure 2: From the left: design drawing and dimensioned sketch of the donjon battlement by Guglielmo Giustiniani; design sketch by Dante Viviani [15].

Again this project was rejected because it was too expensive. Dante Viviani [25] – from Arezzo, but trained in Rome, later first Superintendent of the Monuments of Umbria – was commissioned to scale it down. His succinct elaborations [26] were developed by the municipal surveyor according to his indications. All the correspondence that replaced the inspections, the quoted sketches (which Viviani recommended to follow faithfully), and the construction accounting documents clarify the nature of the project and are confirmed by the

existing tower. According to ancient – or at least supposed to be so – traces, instead of the masonry stair designed by Giustiniani, Viviani designed a brick vault at one third of the internal height and two timber floors, connected by subsequent timber stair flights. Against Viviani's instructions, the mayor ordered the master masons to build a vault corresponding to the entrance floor. Thus providing an access to the top of the tower, the reconstruction of the overhanging battlement began, using a suspended scaffold. Viviani reduced the height of the central room to 2,40 m, but he increased its side, placing its perimeter walls aligned with the axis of the underlying masonry; furthermore he reduced the protrusion of the eaves to 60 cm. They therefore covered the last part of the access stair which entered the thickness of the wall and turned parallel to it. Corbels were rebuilt «from the most resistant part of the [clay brick] base», so almost completely, although photographs taken before 1903 show that they were largely preserved, except on the southern side. Arguably, due to long exposure to weather mortar became incohesive and bricks splintered, thus leaving no alternative. The scaffolding allowed accurate surveys, and Viviani's sketches provide significant indications, although it is difficult to distinguish the existing parts, its interpretation and the project.



Figure 3: Views of the stronghold of Arquata before [18] and after the restoration works.

Parapet and merlons are 40 cm thick, but rectangular niches (about 40 cm high, 50 cm wide, 13÷15 cm deep) were obtained in the thickness of the parapet itself to reduce corbelled masonry protrusion (in the middle, fig. 4); this allowed to widen machicolations without reducing the net passage within a *chemin de ronde*, that did not exceed 1.60 m in width. Therefore for about half of its length the thickness of the parapet was reduced to 25 cm, while the external face of the tower wall tilted inwards to increase the width of the machicolations. In this way the overall protrusion of corbels was no more than 60 cm, with a height of about 2.4 m. Although modified several times, the construction of the parapet and merlons is revealed by the damage they suffered: they consist of two external wythes made of brick and tuff stones and a nucleus built with less carefully, mainly in probably reused bricks; some larger tuff blocks act as headers. Above the machicolations, masonry was supported by single

tuff ashlars worked in segmental arches; each of them lays for about 10 cm on the corbels, which are 42 cm large like three brick headers. The large remains – equal to one third of the masonry according to Giustiniani – in 1901 included the two corner merlons on the west side, the two central ones on the north side and, at least in part, the two central ones on the east side; however the merlons of the northern side collapsed in December 1903 and subsequently the right corner had to be demolished. The surviving specimens allowed a substantially faithful reconstruction, at least in size and in the use of materials.



Figure 4: From the left: battlement of the donjon and one of niche above the machicolations in 2012 (user: interminatispazi - wikimedia commons); view of the stronghold of Arquata after the earthquakes of 2016 (courtesy of the Arquata del Tronto Municipality).

The bricks were either recovered or similar in size to the existing ones, measuring 26 cm x 13 cm x 5.5 cm, as Viviani had insistently requested. It's possible that the mixed masonry of the parapet and the merlons didn't reproduce the original construction, but the result of subsequent repairs in which the most versatile brick had gradually replaced the stone. Iron tie-rods had been placed inside the parapet masonry, crossing each other in the corners, thus hooping the wall that supported the merlons. Unlike the underlying sandstone masonry, the top part of the tower has a brick face; the corbels protrude from it. Ten to twelve brick courses constitute the lower part of them, while above there were limestone tuff blocks – of different heights and with horizontal laying surfaces – up to the maximum protrusion. A sketch suggests that there are wooden cantilevers inserted in the masonry. They are located at the height of the arches that support the parapet and are testified by the presence of bricks between the springs of the tuff ashlars, to allow a reduction of the thickness of the external wythe; in the south-eastern corner other two timber cantilevers can be seen at the height where tuff ashlars begin and at an intermediate level, but it is impossible to know if there are similar cantilevers in the other corbels (on the left in fig. 5). At each corbel, wrought iron tie-rods were placed 15÷20 cm above the timber cantilevers, as shown by the anchor rods still present or by the grooves in the masonry that housed them before their removal. The presence of timber cantilevers and iron tie-rods is confirmed by the booklets of measures. Merlons were 1.3 m high over the parapet; in the drawings appeared the dovetail of the ghibelline merlons (on the right in fig. 2), an interpretation of the discontinuous top plane of the remaining elements and probably of some iconographic references: probably a low relief depicting a small castle with a tower, on the Sant'Agata Gate of Arquata [27], and a painted ex voto existing in the sanctuary of the Icona Passatora about 30 km from Arquata [28]. Despite the care dedicated to the bricks, however the materials used for the additions to the donjon battlement

were the same commonly used at the time, including machine-made bricks, and the undifferentiated use of hydraulic lime, pozzolana or even cement in mortar. As the documents relating to the supply of materials testify, the works continued until the summer 1909. Owing to the changes to the design of the upper room, Viviani renounced to provide the battlement with effective weather protection. Even before the earthquakes of 2016, bricks above all, but also stones had extensive cracks and splintering, and the joints were often lacking mortar; favoured by percolation of rainwater, in the machicolations vegetation could grow. Wind is another significant pathogenic factor, since it strongly erodes mortar joints and the sandstone of the masonry below the battlement, especially in the corners of the tower.



Figure 5: From the left: the damaged battlement (courtesy of the Municipality of Arquata); the bars for reinforced concrete without anchors inserted to replace the old tie-rods; the collapsed south merlons of the donjon, in which we can see the x-crossing reinforcing bars.

4.1 One hundred years of replacements.

The construction was fragile and already in 1922 a series of partial renovations began, but they were of little use, since an appraisal of 1932 states that crenellation was «in total ruin» [29]. Following the 1943 earthquake, three of the donjon merlons collapsed and were rebuilt in 1946 [29]. After the 1979 earthquake, an extensive renovation of the battlement followed in 1982 [29]. However the most problematic intervention was the removal of the parapet hoop made in the early 20th century, replaced with bars for reinforced concrete without terminal anchor bars (in the middle in fig. 5); to put them in place, deep chases were cut in the already slender section of the parapets, then filled with a cement grout that only partially adhered to the masonry. The merlons were subject to a nominal strengthening realised by perforating them and inserting a couple of inclined reinforcement bars. These were placed in the barycentric plane of the merlon, parallel to the parapet below; at the base of the merlon they crossed exactly at the centre of gravity of the section (on the right, fig. 5). In 1992-93 the timber structure of the roof – already rebuilt in 1960-61 [30, 31] and resting on a reinforced concrete ring beam – was replaced by a reinforced concrete slab and six out of twelve merlons were rebuilt. Very little of the ancient remains existing in 1903-04 survived till the earthquakes of August 24th and October 30th 2016.

The collapse of parapets and crenellation on the two sides perpendicular to the seismic wave can be easily explained: the battlement had been weakened by the chases made at its base and the lack of anchor bars made the new tie-rods totally unable to provide any

connection with the perpendicular walls. The significant seismic force induced by the mass of the roof slab caused the collapse of the upper room on itself, further contributing to the failure of the southern side of the battlement, towards which it ruined. On the eastern side, only the central merlons remained, the corner ones collapsed with northern and southern parapets. On the western side, only the parapet is preserved; the two central merlons suffered in plane failure due to shear: the reinforcement bars were not only useless – due to their position – but also harmful, since the perforation for their insertion weakened the masonry; moreover the masonry at the base of the merlons was probably decayed by the stagnation of water in the crenel. Given their significant width compared to the height, merlons generally collapse by out-of-plane overturning if they don't have a roof loading them. However, material decay and incorrect strengthening interventions play an essential role in the activation of the out-of-plane collapse mechanism and can also cause an in-plane shear failure; nonetheless it's very difficult to translate their influence into a numerical parameter.

5 THE OVERHANGING BATTLEMENT OF THE EASTERN CURTAIN WALL

In the works of the first two decades of the 20th century two other overhanging battlements were rebuilt, using techniques very different from the one that has already been examined. On the eastern curtain, the building site was active between 1908 and 1909 [26]. The corbels of the external façade (on the left in fig. 6), towards the town, are made up of four rectangular-shaped sandstone cantilevers which – fixed in the core conglomerate – cross the external wythes and progressively protrude. The free end of each cantilever is rounded to form a quarter of an ellipse, which originates at the end of the cantilever below; the corbel has the shape of a scalene right triangle in which height is about 1 m and protrusion about 60 cm. The spacing of the corbels is about 60÷75 cm, while their width is 20 cm. To prevent stone cantilevers overturning, wrought iron straps were placed to connect them to the masonry. Parapet and merlons were never rebuilt. The cantilevers are still largely ancient as documented by the photos of the early 20th century. The additions are recognisable by workmanship and decay.



Figure 6: From the left: stone cantilevers in the corbels of eastern curtain wall; stone cantilevers supporting brick arches; I-beam with L shaped anchor bar in one of the brick masonry corbels of the polygonal tower.

The greatest damage, up to the loss of an entire corbel, is due to the sandstone decay: in some cases splintering affects also the internal parts of the material decreasing its strength. On the internal face of the same wall a simpler overhanging structure widens the *chemin de*

ronde: this has corbels about 30 cm wide, made of two layers of sandstone cantilevers, the lower one is rounded, the upper one has a simple parallelepiped shape; they support brick arches one header thick and three header deep (about 40 cm) (in the middle in fig. 6). In this case the corbel spacing is more than 1 m. Some of the stone cantilevers are ancient, the whole is a probably faithful interpretation of existing traces. Apart from some percolation, due to the cracks produced in the concrete cover that should have waterproofed the top of the wall, this system has not reported any damage.

6 THE OVERHANGING BATTLEMENT OF THE PENTAGONAL TOWER AND ITS STRUCTURAL DISORDER

The reconstruction of the battlement of the pentagonal tower started in 1908-09, but it was later abandoned. Neither the internal space of the tower was covered with the designed vault, nor the stairs were built, nor the *chemin de ronde* was finished. In some photos taken before 1990, the last was covered by a discontinuous layer of soil [29]. No traces of pre-existing structures were left. The overhanging battlement was Viviani's invention. He reinterpreted the crenellation of the donjon: the structure was entirely made of bricks on the discontinuous plane of the perimeter walls. The stepped corbels projected from the vertical masonry; the distances from each other varied – about 30÷60 cm – while their width is uniform and about 40 cm, i.e. three headers. The small arches are made of rowlocks reinforced by headers above, however their out-of-plane depth doesn't exceed half the thickness of the superior parapet: as in the donjon, to widen the machicolations, in correspondence with each of them the parapet had a niche, whose back is aligned to the arch. The top of the niches is horizontal, and the parapet is made of two external wythes between which there is a casting of broken bricks and hydraulic lime or cement. Accentuating a peculiarity of the donjon, in the machicolations the façade masonry tapers inwards with an inclination almost mirroring that of the corbels. In this way the parapet rests only on the corbels, entirely overhanging outside the walls of the tower. On this unstable base, Viviani designed heavy angular merlons loaded with a triple dovetail. This battlement is a sort of autonomous screen: on the curtain walls no battlement was built, which would have partially contributed to the stability of the extreme merlons. Thus some merlons collapsed (and were rebuilt) several times, in particular after the 1943 earthquake; finally all the merlons were reconstructed during the last restoration campaign in 1992 [29]. So it's easy to understand the failure in 2016. The rigid block of merlons and parapet crushed the internal part of the pilasters between the niches, and fell in blocks on the *chemin de ronde*, thanks to its more resistant mortar. The damage suffered by the upper part of the corbels has brought to light various metal elements inside them, in a non-systematic way: tie rods with anchors are positioned at the springs of the arches, just below the parapet; about 30 cm lower, inside the masonry of the corbels, some I-beams show a hole at the end of their web, inside which a circular L-shaped bar is inserted (on the right in fig. 6).

The deterioration of the bricks – probably from the beginning a lower quality material – not sufficiently protected from atmospheric agents gave rise to a significant decrease in the structural strength. The detachment of splinters or entire portions of bricks would have required a constant maintenance effort. Owing to the scarce economic resources and the administrative procedures of a small town, maintenance works were unsustainable and in fact they could not be realized. As on the donjon, also here a part of the damage to bricks might be due to the use of waterproofing substances, described in all the restoration specifications of

the second half of the 20th century: they ensure a very discontinuous protection, and they impede evaporation, thus causing the permanence of water in the masonry.

6 CONCLUSIONS

A research susceptible of numerous insights – both on the sources and on the building and its materials – is summarized and simplified here, rather than illustrated; it proves that in a not large construction there are five different overhanging battlements, in which the formal analogies with other buildings do not correspond to the structural ones. The failure occurred in significantly different ways owing to a specific vulnerability, construction methods, repairs and material decay. It would be more useful to investigate in-depth into individual cases, to evaluate the differences between them and to identify future situations of real or potential risk. If such a practice were widely carried out, a sort of abacus would be established, the more valid, the more numerous the cases studied. In particular, it would be possible to establish a catalogue of failure phenomena that occur – especially in seismic events – when certain inadequate ways of building or repairing are employed, facilitating prevention on a territorial scale. Building diagnostics and interventions would be better addressed.
An essential tool is the historical research, particularly referred to the last centuries, carried out in a scientific and rigorous way, on the archival sources and on a selected bibliography, avoiding all texts – principally the most recent ones – that do no mention their sources … It is necessary to start from the present state and gradually go back to all documented interventions, trying to identify their traces in the building. As for instability and decay phenomena, it is necessary to identify not only their nature, but also their duration and try to determine their remote or recent causes. A micro-history of construction, degradation and repairs prevents from falling into generalizations – only briefly above described – paying the utmost attention to every single and real feature of the building, leaving nothing for granted. On the basis of a very detailed diagnosis it is therefore possible to find solutions and respond adequately to the real and peculiar problems that engineers and architects are called to solve.

Acknowledgements. The research was carried out as part of the project "Territorial fragilities", funded by the Ministry of Education, Universities and Research and by Department of Architecture and Urban Studies (MIUR, Dipartimento d'Eccellenza, 2018-2022).

REFERENCES

[1] Pegoretti, G. Dei mastici. In: Id. *Manuale pratico per l'estimazione dei lavori architettonici* […] *Volume primo*, Angelo Monti (1843), pp. 227-231.
[2] Viollet-le-Duc, E.E., Mâchicoulis. In: *Dictionnaire raisonné de l'architecture française du XIe au XVIe siècle. Tome sixième*, Bance (1863).
[3] Cerri, M.G., Biancolini, D. and Pittarello, L. (eds.), *Alfredo d'Andrade, Tutela e restauro*. Vallecchi (1981).
[4] Piper, O., *Burgenkunde. Forschungen über gesammtes Bauwesen und Geschichte der Burgen innerhalb des deutschen Sprachgebietes.* Ackermann (1895).
[5] Rocchi, E., *Le fonti storiche dell'architettura militare*, Officina Poligrafica, 1908.
[6] D'Altri, A. M., Castellazzi, G. and de Miranda, S. Collapse investigation of the Arquata del Tronto medieval fortress after the 2016 Central Italy seismic sequence. *Journal of*

Building Engineering (2018) **18**: 245-251.
[7] Ferretti, D., Coïsson, E. and Lenticchia, E. Seismic damage on merlons in masonry fortified buildings: a parametric analysis for overturning mechanism. *Engineering Structures* (2018) **177**:117-132.
[8] Zippel, G. *Le vite di Paolo II di Gaspare da Verona e Michele Canensi.* Lapi (1904-11).
[9] Cordella, R. Arquata sotto la dominazione nursina. In: *Piceno* (1986) **1/2**:11-32.
[10] Supplication of the Arquata Community, May 9th, 1655. In: Archivio di Stato di Roma (ASRm), Congregazione del Buon Governo, Serie II, Atti per luoghi, folder no. 263.
[11] Boschi, E., Guidoboni, E., Ferrari, G. and Valensise G. L. *I terremoti dell'Appennino umbro marchigiano. Area sudorientale dal 99 a.c. al 1984*, Compositori (1998).
[12] Various supplication of the Arquata Community, 1703-1711. In: ASRm, Congregazione del Buon Governo, folder no. 263.
[13] ASR, Congregazione del Buon Governo, folder no. 264.
[14] The *Prefetto* [Governor] of Norcia, Flavio Ravizza to the Cardinal Renato Imperiali, May 24th, 1705. In: ASR, Congregazione del Buon Governo, II serie, folder no. 263.
[15] Giovanardi Bufferli, G., *Risposta per la Rev.ma Camera apostolica contro la magnifica Comunità di Arquata*, Lazzarini (1778). In: ASR, Camerale, Parte III, Comuni, Arquata, folder no. 267.
[16] Letter from the Congregazione del Buon Governo to the Delegato di Spoleto, May 9th, 1815. In: Archivio di Stato di Ascoli Piceno (ASAP), Delegazione Prov. di Spoleto.
[17] Archivio di Stato di Ancona (ASAn), Sopr. delle Marche, Tutela, folder no. 94/a.
[18] Archivio Centrale dello Stato Roma (ACSR), Ministero della Pubblica Istruzione, Direzione Generale AA.BB.AA., III versamento, II parte, folder no. 536.
[19] ACSR, Ministero della Pubblica Istruzione, Direzione Generale AA.BB.AA., II versamento, folder no. 27.
[20] Archivio Biblioteca Comunale "Giulio Gabrielli" di Ascoli Piceno, Prefettura, folder no. 5-25, fasc. E6 – Rocca d'Arquata.
[21] David, P.F. *Giuseppe Sacconi architetto restauratore (1854-1905)*. Gangemi (1990).
[22] Savorra, M. Giuseppe Sacconi. In: *Dizionario Biografico degli Italiani. Vol. 89*, Istituto della Enciclopedia Italiana (2017).
[23] Zacchilli, I. Icilio Bocci. In: *Dizionario biografico dei Soprintendenti Architetti (1904-1974)*, Bononia University Press (2011), pp. 114-117.
[24] ACSR, Ministero della Pubblica Istruzione, Direzione Generale AA.BB.AA., III versamento, II parte, folder no. 536.
[25] Lampe, M., Dante Viviani. In: *Dizionario biografico dei Soprintendenti Architetti (1904-1974)*, Bononia University Press (2011), pp. 615-618.
[26] ASAn, Archivio della Soprintendenza delle Marche, Tutela, folder no. 94/b.
[27] Gabrielli, G. *Quaderno 18*. In: Archivio Biblioteca Comunale "Giulio Gabrielli" di Ascoli Piceno, Fondo Gabrielli.
[28] D'Achille, P. I miracoli della "Cona Passatora". Affreschi votivi con scritte in volgare in un santuario dell'Amatriciano. In: *La Ricerca Folklorica* (1995) **31**:15-24.
[29] SABAP Marche, Archivio corrente, "Arquata del Tronto-Rocca".
[30] ACSR, Ministero della Pubblica Istruzione, Direzione Generale AA.BB.AA., Ufficio Conservazione Monumenti (1953-1959), folder no. 30.
[31] ASAP, Genio Civile, folder no. 2435.

12th International Conference on Structural Analysis of Historical Constructions
SAHC 2020
P. Roca, L. Pelà and C. Molins (Eds.)

REINFORCED CONCRETE + MASONRY: THE 'MIXED' STRUCTURE OF THE NOVOCOMUM BY GIUSEPPE TERRAGNI

ANNA GREPPI[1*], CAROLINA DI BIASE[1]

[1]Department of Architecture and Urban Studies (DASTU)
Politecnico di Milano
Via Bonardi 9, 20133 Milano, Italy
e-mail: {anna.greppi, carolina.dibiase}@polimi.it, www.dastu.polimi.it/ (*corresponding author)

Keywords: Novocomum, 'mixed' structure, structural components, archival research, digital imaging

Abstract. *With his design of the Novocomum building in Como (1928-29), the famous first example of Rationalist architecture in that city, Giuseppe Terragni began to experiment with a mix of different architectural languages and construction techniques. Within the space of less than a year – from January to October 1928 – Novocomum saw a shift from the traditional to the innovative. Starting out with a weight-bearing structure of brick walls, the development of the project led to the introduction of reinforced concrete, which however did not entirely substitute the former: by 1929, such 'mixed' structures were to be seen in many buildings then being created and might be taken as a hallmark of the various forms of so-called Italian modernisms. Within the enclosed building site, work on Novocomum preceded right up to the terraced roof, and would only be unveiled to the unsuspecting citizens of the city once completed (1930), giving rise to a fierce controversy. The paper here proposed draws upon wide-ranging research into the Novocomum project to offer material of great significance for our understanding of the characteristic features, methods and phases of construction work – all aspects that have received little attention in the many studies dedicated to Terragni's architecture. The research made ample use of the documents now conserved in numerous public and private archives in Lombardy, continually comparing the information therein with the building as it stands nowadays. There was a focus on documents relating to work on the building site, which record each successive phase in construction. This material included: notes, technical drawings, estimates of costs, work reports, calculations, payment records and letters, as well as the documents relating to the tense dispute with the building contractor which involved the architect's brother, the engineer Attilio Terragni. A systematic analysis of the data thus gathered made it possible to reconstruct the far from straightforward interweave between the different phases in the building's construction and the various ideas advanced in the project designs. Furthermore, study of the structural aspects themselves could draw upon a 3D graphic model, which made it possible to assembly and dismantle the various parts of the structure and thus understand the articulation of the building more fully. At the same time, study of how the various building materials were used provided a further key to understanding the different components of the weight-bearing structure. Comprising an analytic assessment of the material collected, the study aims to be an important source of knowledge for future research into issues*

related to the structural behaviour and durability of the building.

1 INTRODUCTION

The issue of housing was of central importance to modern architectural research in the 1920s and 30s. This was a period when experimentation with new types of materials and new systems of construction resulted in developments in both design and building techniques. [1] And a decisive factor here was the use of structures in reinforced concrete.

Within Italy, structural components in reinforced concrete did not entirely replace walled structures but were gradually combined with them, resulting in the 'mixed structures' adopted in the still largely traditional construction sites which existed in the period between the two world wars. [2].

A significant example of this phenomenon, the Novocomum building (Como, Lombardy, 1927-30) directly reflects developments in contemporary European architectural design – in particular, within work by the leading figures of the Modern Movement, to which Giuseppe Terragni belonged.

By the time he graduated from the Politecnico di Milano in 1926, the young Terragni (1904-43) was already challenging the historicist tendency that was so dominant in the teaching of architecture. And in his first important work in Como – a building of apartments with a ground floor partly given over to office space – he would, from the very start, set the forms of Rationalist architecture in clear contrast to the eclectic forms proposed by the architects of preceding designs for the building. As he himself put it in the presentation of his project: "Starting from the premise that, as a result of rational study of modern environments, new trends in architecture emphasize simplicity of line, lightness and rationality in the framework of construction, and highly-developed service facilities [...] this project arises not from [the design] of pointless ornamentation but from the composition of a few, finely-finished, materials, and the careful study of the combination of masses and forms." [3]

Nevertheless, his initial designs were for a traditional brick-built structure of six floors (above ground level), which ran in a straight line along Via Sinigaglia and was defined by the use of cylindrical volumes at the corners.

The whole Novocomum project was far from straightforward, and right from the very earliest stages one can see continual modifications. In part, these responded to functional needs, reflecting Le Corbusier's notion of housing as a machine-à-habiter in which each part performs to a precise purpose; in part, they reflected the "rational study of modern environments." [3] Ultimately, these modifications also included the adoption of structural components in reinforced concrete, while nevertheless maintaining part of the solid-brick structures that had been envisaged in the initial designs. Within Terragni's studio, it was his brother Attilio – in later years the podestà [the mayor, in the fascist period] of Como – who was responsible for structural planning.

Various studies of Terragni's work have offered chronologies and interpretations of the sequence of plans drawn up for the Novocomum project. [4,5,6,7,8] And in a recent research project concerning the construction of Novocomum and the alterations it has undergone over time [9], the already-published material was compared with further visual documents (studio

designs, intermediate versions) that were interpreted in the light of material that had yet to be fully explored (including the instructions drawn up at various phases in the construction work). Most of the drawings consulted in that research (the basis of the present paper) can be dated over the period from 1927 – when Giuseppe Terragni received the commission for the project – to 1929. And it is precisely the dates of these drawings and designs which, together with the dates of the different phases of building work, reveal how the changes in the project design were bound up with the development of the on-going construction; how the chronology of the solutions proposed overlaps with that of the building work. This was true right up to the completion of the project, even if it is also the case that the final versions of the designs do not correspond fully to the structure as built. The study and organization involved documents from many public and private archives – first and foremost, the archive of the Terragni studio - made it possible to reconstruct the complex history of the design and of construction work. 3D graphic reproductions were created to study the relation between the various components of the structure.

2 THE STRUCTURE OF NOVOCOMUM

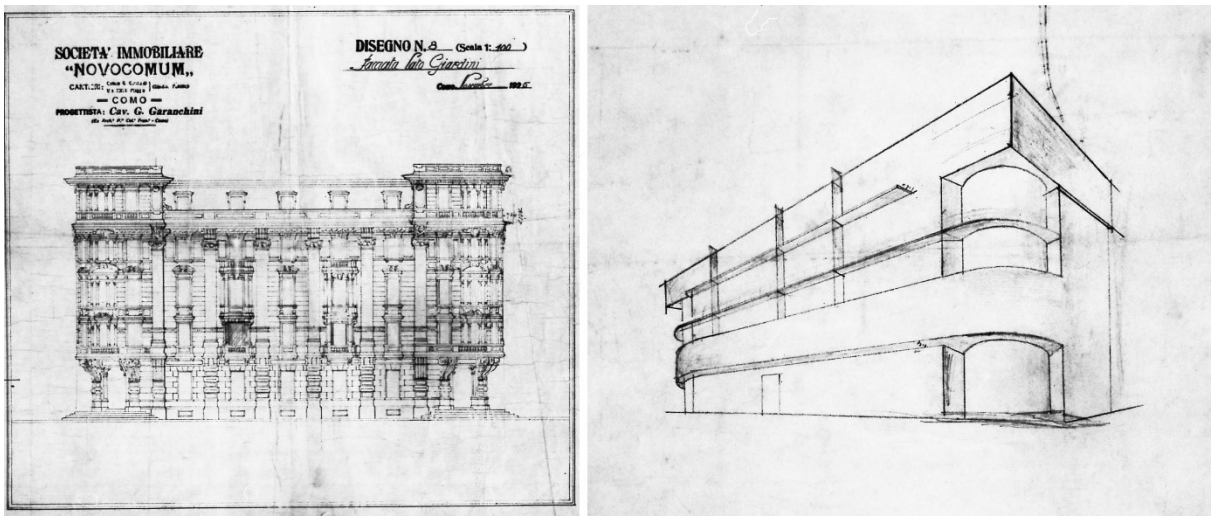


Figure 1: Project for the building in Via Sinigaglia (Como) which was intended to occupy the entire city block, elevation, G. Caranchini, November 1925, Terragni's studio Archive (ATCo), 6/016/B2/S/E, on the left; "Maison de rapport Novocomum", sketch of the elevation, signed, 1929, ATCo, 6/005/D1/S/L, on the right.

The origin of the Novocomum project is to be found in the desire to complete a trapezoidal city block after work on a residential building designed by the architect Giacomo Caranchini (fig. 1) had been interrupted. The existing structure at this point was a C-shaped building of five floors above ground, with facades "characterised by sinuous lines inspired by late Secessionism" [10], complete with oriel windows at the corners and pitched roofs. The ideas that inspired Terragni's design were entirely different, and so innovative that the completed building dumbfounded the unhappy citizens of Como and the local authorities.

By the end of 1927 Terragni was at work on the project, producing various designs that can

be grouped in four main versions (fig. 2). The first "floorplan study" [11] reveals the initial ideas for the project: the C-shaped structure develops around the slightly projecting volume of the central staircases and the two trapezoidal staircases located at the internal corners of the building, with the apartments laid out along a central corridor.

In the first version of the project, dated January 1928, the weight-bearing structure comprised brick walls of a certain thickness, whilst columns of reinforced concrete supported the two staircases giving access to the basement. There were two solutions for the distribution of access to the building: the first involved four staircases (the two in the corners and two in the central block); the second involved the creation of three staircases and is comparable with that finally adopted.

A second version of the project is dated May 1928. Luigi Zuccoli, who worked with Terragni for years, would later write that this version, presented to Como City Council on 23 May [12], was deliberately outlined using drawings different to the solution ultimately adopted in order to facilitate approval by the Council's Building Committee [13].

On 30 May authorization was requested to erect fencing around the site. [14] Work began on 8 June and ten days later the Podestà sent a letter [15] to the engineer Ezio Peduzzi of the Società Novocomum to inform him that authorisation of the beginning of work was provisional upon the elimination of the intermediate floor envisaged within the structure, and the submission of plans which had been modified accordingly to the authorities responsible for building permits.

The third version of the project (October 1928) is the closest to what was actually built. Here, the structure comprises pillars and beams in reinforced concrete, with the exception of the three main staircase wells, which are in brickwork. The use of reinforced concrete was in line with the eagerness with which the various members of "Gruppo 7" had championed that material, a stance which in turn reflected the enthusiasm voiced by many of the engineers, and of the architects and militant critics belonging to the Modern Movement. This new construction technique, it was argued, combined the properties of a composite material with high-quality structural performance and opportunities for new freedom in architectural composition [16, 17].

To return to the chronology of the project, on 10 July 1928 the Società Ghisleri, which had taken on the task of carrying out the work, had forwarded the first plan of the layout of the concrete pillars, so that the architect could then draw up definitive working designs. On 2 August the company then sent the structural project designs to the Prefecture, which would on 23 August send then back as failing to meet ministerial guidelines. Only on 10 October 1928 would authorisation be granted for the structures in reinforced concrete. At the same time, the authorities also requested the submission of definitive designs, which would be the above-mentioned drawings and plans of October 1928.

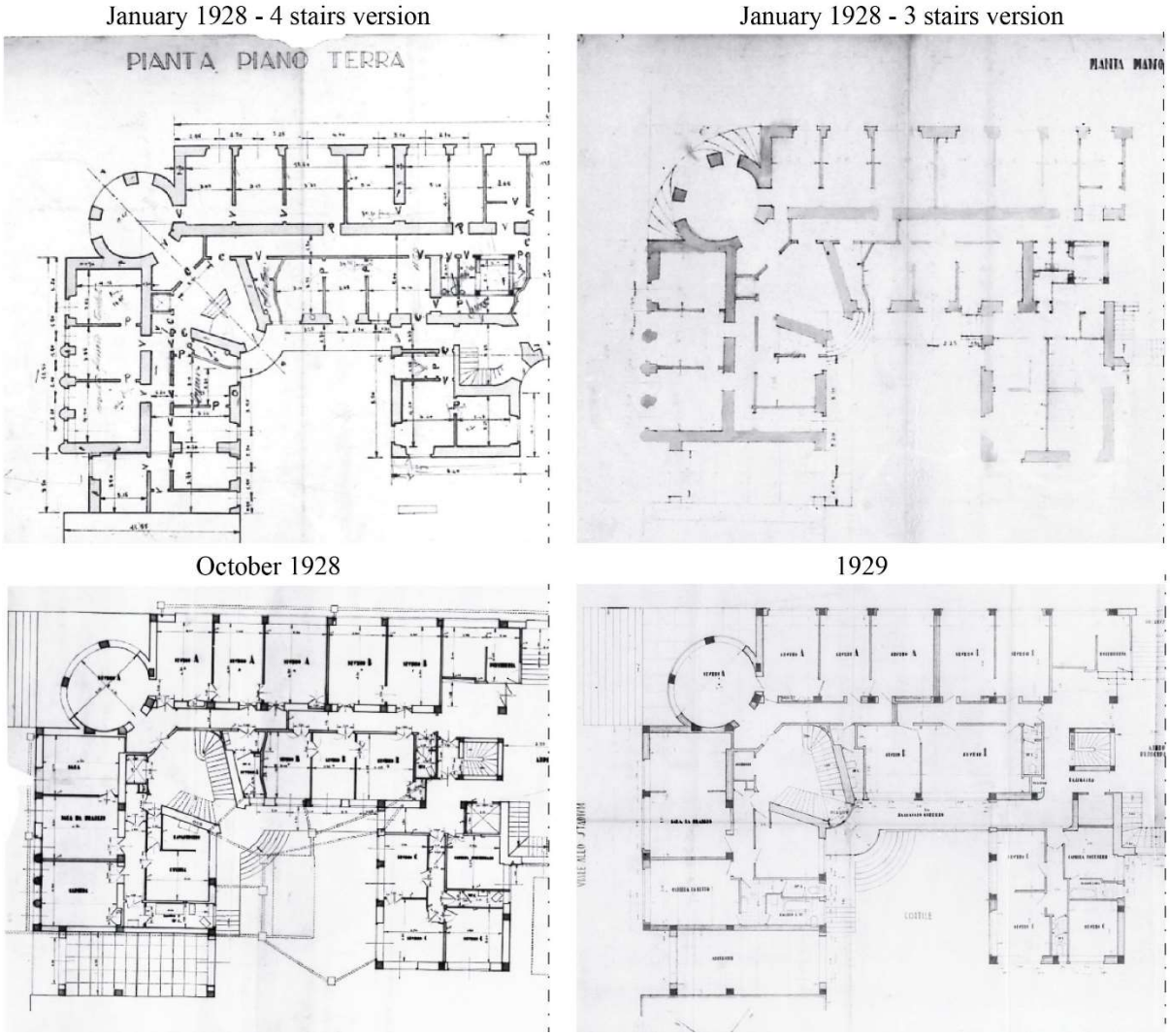


Figure 2: Project designs for Novocomum. Ground plans for the raised/ground floor in the various versions of the project (ATCo).

3 A MIXED STRUCTURE

Even before implementation of the plans for the structure had been authorised, behind the wooden fencing around the site work began on casting the cement for the building's foundations. On 12 December 1928 the structures for the basement, raised floor and first floor seem to have been completed, given that on that day work began on casting the floor between the first and second storeys [12].

Documentation from the worksite provides apparently contradictory information. It would seem that from 22 December 1928 to 28 February of the following year work on the concrete components had to be suspended due to freezing temperatures. However, the report submitted to the arbitration panel – hence a very important document – claims that the floor of the last

storey was cast at the end of March, whilst another passage in the same document attributes the delays in proceeding with work on the reinforced structures to the lack of timber for the formwork (before proceeding to one floor, they had to wait for the dismantling of the formwork from the floor below). Furthermore, delays in submitting the full project drawings and plans had an effect on the sequence of work on site and on the rate of progress.

Overall, the reports prepared by the opposing parties for the arbitration panel depict a worksite where progress was troubled by continual disagreements and clashes between the Director of Works and the building contractors. Nevertheless, even if they portray the state of affairs from very different viewpoints, these documents provide very useful information with regard to the work carried out, the materials used and the construction methods adopted.

3.1 The Components in Reinforced Concrete

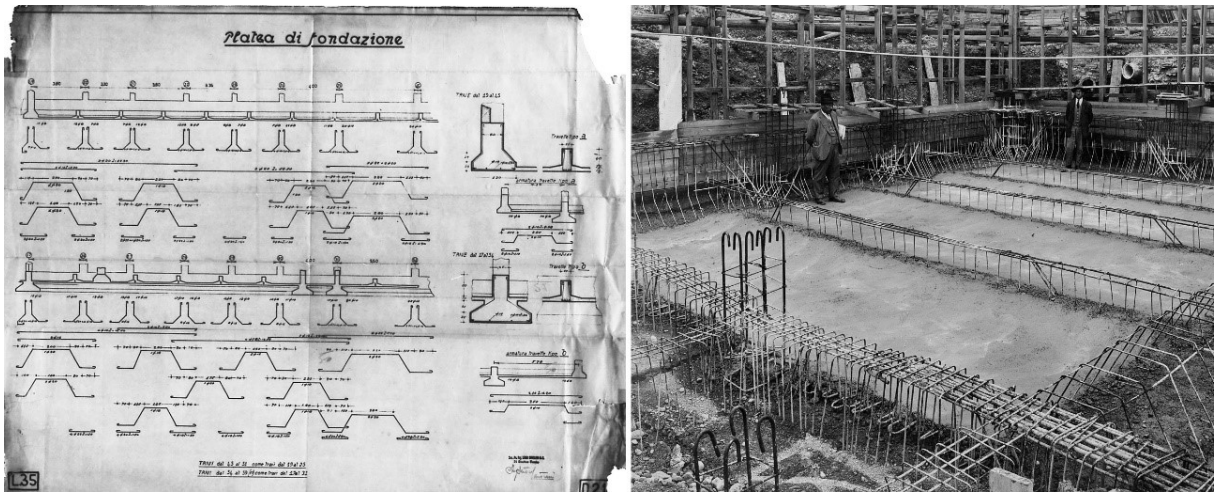


Figure 3: Project designs of the structure: foundation bed, 1:20 – 1:50, 6/009/E1/S/E (left, ATCo); photograph of the reinforcing for the foundations and the jutting rods in the pillars, 12 August 1928 (right, ATCo).

The drawings and documents relating to the execution of building work reveal that the designs of the raised structures were drawn up as work was proceeding to excavate and consolidate the site; that in the early phases of work there was as yet no design project that had been fully approved and then submitted as such to the contractors [18]. As far as the materials used were concerned, it was "first-quality man-made cement from Caluso" that was chosen, and tests were carried out on normal mortars at the Material Testing Laboratory of the Politecnico di Milano. The material chosen for the reinforcing comprised "solid round rods of homogeneous iron, without any imperfections"; these were to be smooth and of a diameter that varied from 14 to 20 mm. After a seasoning of 28 days, the resistance to compression was 595 kg/cm^2 (certificates n. 4210-4211, 9 August 1928). The sand and gravel used in the cement mix were fully in compliance with the prescriptions laid down in art. 6 and 7 of chap. II, second part of the law decree 1431 of 7 June 1928 ("Prescriptions for the approval of hydraulic agglomerates and for the execution of work in cement conglomerates"). The proportions of aggregate/cement were 0,40 m^3 of sand and 0,80 m^3 of gravel per 300 kg of cement [19].

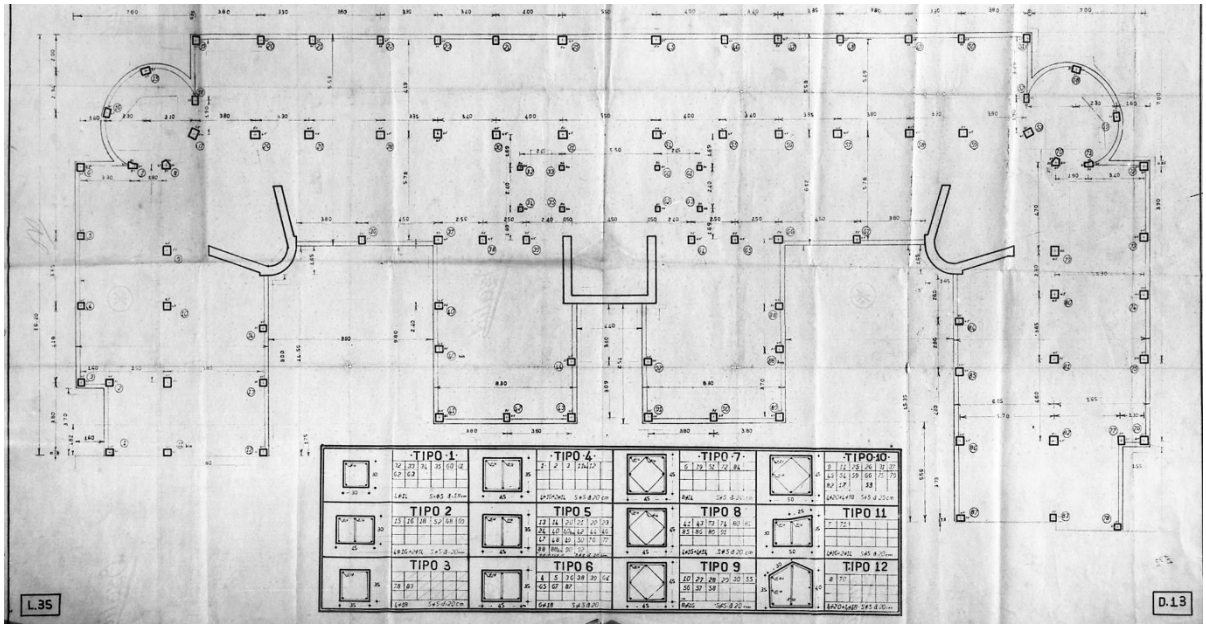


Figure 4: Groundplan of the basement with the abacus of the pillars, 1:50, 6/011/E1/D/E FTGR. 1 and 2 (ATCo).

The site of the building was near the lake, and the presence of water at foundation levels required a series of measures to prevent infiltration and provided protection for the foundation structures. Thus a "robust foundation bed" in reinforced concrete was laid; this was made up of two types of inverted beam and two types of "small beam" (components in reinforced concrete that were to serve as linking crossbeams). The lower and upper ends of the inverted beams were, respectively, 120 and 60 centimetres below the perimetral pillars, and 45 cms below the internal pillars. The small crossbeams measured 45 by 65 centimetres. Thanks to worksite photographs (fig. 3) one can see the dense weave of reinforcing rods in the inverted beams of the foundation.

Through comparison of the details regarding the execution of the foundation bed (fig. 3), the plan of the pillars in the basement (fig. 4), the structural report for the arbitration panel and on-site photographs, it was possible to develop a virtual reconstruction of the structure in reinforced concrete that was created (fig. 5). This could be done by analysing the position of each pillar and assuming the entire structure to have been symmetrical around a supposed axis running through the entrance atrium.

The floor plan of the basement (fig. 4) shows that the system of pillars, of twelve different types (varying in shape and size), was designed to be adapted to the layout and development of the walls. Also the statics calculations were carried out following the rules laid down in art. 17 and 18 of the Royal Law Decree 1431 of 7 June 1928. Armor brackets were to be placed at a distance equal to ten times the diameter of the longitudinal reinforcing rods, with the exception of some pillars where there were to be double lattice brackets. [18] The bases of the pillars were mainly square or rectangular in section, with the exception of those used in the corner cylindrical structures, which were polygonal in base section. In the structural report it is stated that the designs included no pillars of a section less than 25x35 cm, "so as to avoid problems

with column loads".

The sizing of the beams distinguishes between the perimeter beams – of base 45 cm and height 40 cm – and the rooftree beams (base: 45 cm; height: 56 cm). The beams were created with a "countersink" at the point where they met the pillars, which was then concealed within the walled structure. This detail, which can be made out in the worksite photographs now in the Terragni archives, appears to be very similar to something one sees in the Hennebique system: "a characteristic feature [of which] is the link between pillars and beams, which often involves inclined brackets near their point of support." [20].

In accordance with the final plans and designs there were three staircases to the upper floors, right up to the roof. All of these gave onto the internal courtyard and comprised projecting ramps of steps. The solid slabs in reinforced concrete were cast on site, and the bond-beam was inserted into the weight-bearing walls, which were five bricks thick (fig. 7). Between the basement and the raised floor level there were two staircases in reinforced concrete. From the basement level to street level there was a ramp (again in reinforced concrete) that opened into the internal courtyard in correspondence with the central block of the building.

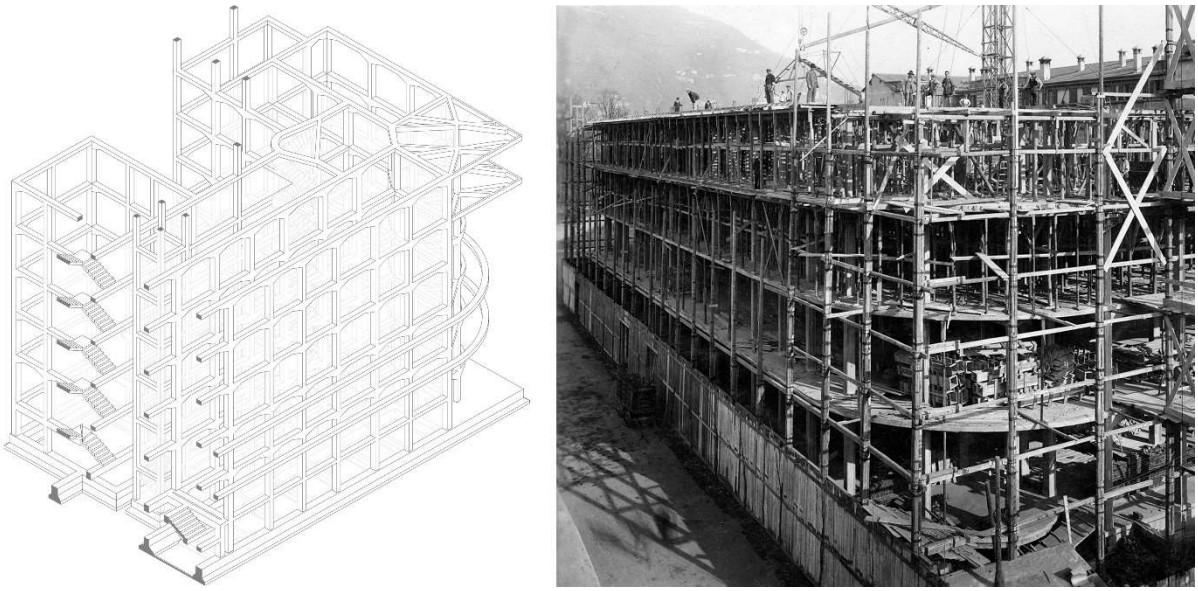


Figure 5: 3D reconstructions of the skeletal framework in reinforced concrete (left); photograph of the structures in reinforced concrete (right, ATCo).

3.2 The Walls

The documents relating to the materials used are here incomplete. We know that for the masonry veneer work and the internal partition walls, hollow bricks were used; whilst for the weight-bearing walls of the stairwells – which were pierced by windows from the ground floor up to the level of the roof – it was solid bricks that were used.



Figure 6: Novocomum under construction: one can see the outside and internal walls in perforated brick (ATCo).

As regards hollow bricks, Terragni would use Frazzi bricks in his Casa del Fascio; we can also find advertisments by the Frazzi company of Cremona, which produced bricks of similar size to those used in Novocomum in some architectural magazines such as 'Edilizia Moderna' and 'Quadrante'.

The on-site photographs (fig. 6), as well as the documents submitted to the arbitration panel between Società Ghisleri and the Novocomum, show the bricks used for the outside walls to have had four perforations in them, whilst for parts of the walls of the corner cylinders two-perforation bricks were used to face the pillars. The overall thickness of the external non-bearing walls of Novocomum is 57 cm. Further information can be gleaned from the technical notes to be found in Luigi Figini's article entitled *Una casa* (1930), where it is specified that the perimeter walls of Novocomum were made up of two layers of masonry veneer in hollow bricks separated by an air gap [21].



Figure 7: Novocomum. Worksite photographs showing the stairwells with walls of solid brick (ATCo).

Indirect confirmation of the systems described by Figini can be found in Griffini's textbook [22], and in various other structures built in the 1930s (including Terragni's own Casa del Fascio).

3.3 The Floors between Storeys and the Roofing

The floors of the building were created in hollow-core concrete, that is, hollow bricks and beams of reinforced concrete cast on site. Here, too, thanks to on-site photographs (fig.8) one can see that the reinforcing rods of the beams were fitted into brick ends. The project defined the "spans" delimited by the beams, with specific characteristics depending on the greater or lesser distance between the pillars. The graphic reconstruction of the structure brought out the similarities and differences that exist between the floors in the various parts of the building. In some "spans" the planned floor was to have an overall thickness of 20cm. This comprised a 5-cm slab of reinforced concrete with hollow-block bricks to a depth of 15 cm: these blocks were laid in pairs, whilst at the edges (near the beams) they were laid singly. In other open spans the floor was designed to be 23 cm in thickness: a 5-cm concrete slab and 18 cm of hollow-block bricks. These were either laid out in pairs, with the end bricks next to the concrete beams laid singly, or in groups of 8, with the end bricks in groups of 4 [18]. In the absence of exhaustive records, we proceeded by approximation, supposing the structure to be symmetrical – that is, that the solution proposed for the west side of the building was like that used for the east side. Similarly, it was supposed that one solution was standard for all floors, being integrated with other "spans" in the parts that did not exist on all storeys of the building.

The flooring of the last storey – in particular, the projecting corner sections – was again reconstructed by comparing executive drawings, on-site photographs and the structural report for the arbitration panel and finally found evidence in a technical description and related illustration published by engineer Candiani (Ghisleri company). [23] Novocomum's "weight-bearing structure in reinforced concrete" was declared completed on 15 May 1929, and on 15 July work began on casting the "roof slabs".

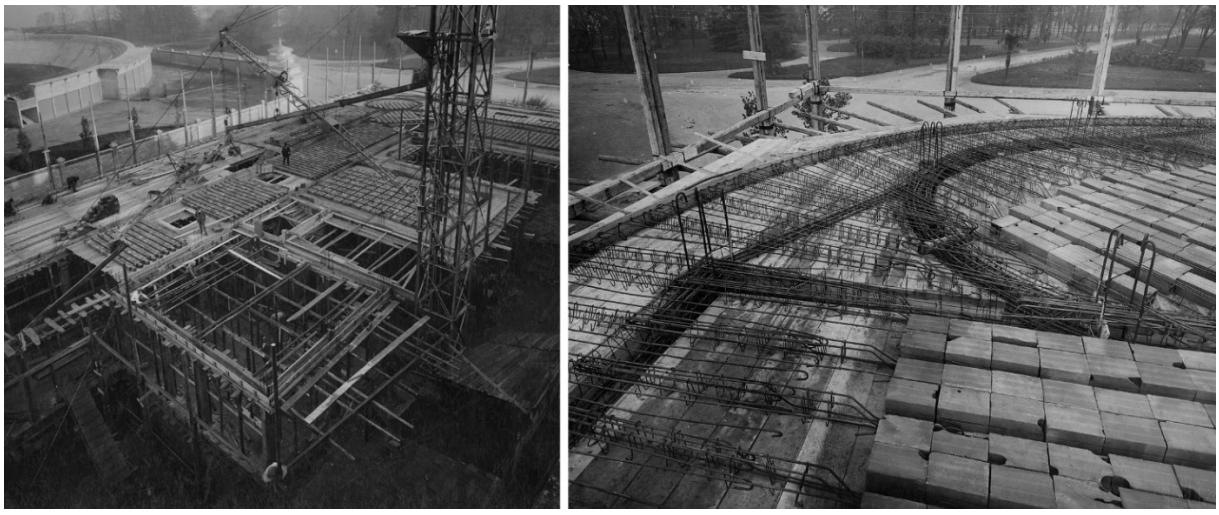


Figure 8: Novocomum. Worksite photographs showing the floors of the building in hollow-core concrete (ATCo).

4 CONCLUSIONS

In October the scaffolding and worksite fencing around Novocomum came down, and the building finally became visible. Echoing protests by numerous citizens of Como, the local newspaper «La Provincia» published an article that lambasted a structure which it nickname "the ocean liner" and described as "ugly ... and in bad taste" [24]. The city authorities declared themselves surprised, saying that the final building did not correspond to the plans that had been approved by the Building Committee, and on 9 December 1929 set up a commission to decide whether Novocomum "was a feature that disfigured the area, and, if so, what measures might be taken to make it fit in better with the surrounding environment" [25]. As is well-known, the members of that commission – Piero Portaluppi, a planner and a professor at the Politecnico di Milano; Giovanni Greppi, a Milanese architect who also worked in the Como area; Luigi Perrone, a state functionary at the Soprintendenza ai Monumenti della Lombardia [Superintendence for Preservation of Lombardy's Monuments] – ultimately decided in favour of keeping as it had been completed a building which would soon be said to mark "the birth of a new aesthetics, a new way of living; a new way of envisaging housing [...] It will, for everyone, become 'home', the 'house of tomorrow'." [26]

Nowadays, Novocomum is recognised as one of the great examples of twentieth-century architecture, even if in the 90 years since its completion the structure has undergone various alterations – both before and after it became a listed building on 17 November 1986. These changes have gradually and noticeably altered the internal appearance and layout of the building, even if the demolition, shifting and replacement of various partition walls does not seem to have compromised the weight-bearing structure.

By reconstructing the history of the construction process itself, it was possible to get a first outline of the material history of a building which is one of the various examples of a "mixed structure" created in this period; in the case of Novocomum, this was the result of an eight-month sequence of changes to the project, leading to the replacement of a brick-wall weight-bearing structure with one in pillars and beams of reinforced concrete (brick walls ultimately only figuring in the stairwells). The knowledge generated by this research provides a useful basis for studies of the structural behaviour of the building and for planning the maintenance work necessary to preserve a monument of twentieth-century architecture.

REFERENCES

[1] Griffini, E. *Costruzione razionale della casa. I nuovi materiali. Orientamenti attuali nella costruzione, la distribuzione, la organizzazione della casa*. Hoepli (1932), p.VII.
[2] Poretti, S. *Modernismi italiani. Architettura e costruzione nel '900*. Gangemi (2008), p. 11.
[3] Terragni's studio Archive, Project File for the Como City Council, *Project Report*, (13 May 1928).
[4] Zevi, B. Edificio ad appartamenti "Novocomum", Como. In: *Giuseppe Terragni*. Zanichelli, (1980), pp.24-26.
[5] Fosso, M. and Mantero, E. *Giuseppe Terragni 1904-1943*. Cesare Nani, (1982), pp.56-57, 82-85.

[6] Vitale, D. in: Cavalleri, G. and Roda, A. *Novocomum. Casa d'abitazione.* Nuove parole (1988), pp.9-46, 81-132, 165-178.
[7] Vitale, D. Edificio ad appartamenti Novocomum a Como. In: Ciucci, G. (ed.): *Giuseppe Terragni. Opera completa.* Electa (1996), pp.315-321.
[8] Schumacher, T. L. Dal Novecento al razionalismo. In: *Giuseppe Terragni. 1904-1943*, Electa Mondadori (1992), pp.71-84.
[9] Greppi, A. and Facchi, A. *Il Novocomum di Giuseppe Terragni alla prova del tempo. Costruzione, trasfromazioni, tutela, restauro*. Masters degree thesis in Architecture, academic year 2016-2017, Politecnico di Milano, supervised by Carolina Di Biase and Camilla Casonato.
[10] Longatti, A. *Tra Eclettismo e Razionalismo.* Contributo monografico di approfondimento storico al Piano delle Regole del Comune di Como (2013), p. 376.
[11] Terragni's studio Archive, 6/025/B1/S/L, *Study of the floor plan*.
[12] Terragni's studio Archive, Ghisleri file for the arbitration panel, *Report to the Arbitration Panel* (8 July 1932).
[13] Zuccoli, L. *Quindici anni di vita e di lavoro con l'amico maestro Giuseppe Terragni*. Ed. C. Nani (1981), p.14.
[14] Historical municipal Archive of Como, cart. N. 575/2, P.G.11552/28, Building permit 1928, *Authorization for the erection of the scaffolding* (20 November 1928).
[15] Terragni's studio Archive, Ghisleri file for the arbitration panel, *Letter from the Podestà of Como to the engineer Ezio Peduzzi* (18 June 1928).
[16] Gruppo 7 (Figini, L., Frette, G., Larco, S., Libera, A., Pollini, G., Rava, C.E. and Terragni G.,). Architettura IV. Una nuova epoca arcaica*, Rassegna Italiana: politica, letteraria e artistica* (May 1927), XIX-CVIII-II:467-471.
[17] Gruppo 7. Architettura IV. *Quadrante* (April 1935), **24:**22-24.
[18] Terragni's studio Archive, Ghisleri file for the arbitration panel, *Comments accompanying the list of project drawings* (25 July 1932).
[19] Terragni's studio Archive, Ghisleri file for the arbitration panel, *Structural Report* (s.d.)
[20] Nelva, R. and Signorelli, B. *Avvento ed evoluzione del calcestruzzo armato in Italia: il sistema Hennebique.* Edizioni di scienza e tecnica (1990), p.16.
[21] Figini, L. Una casa. *Natura* (January 1930) **1:**47-52.
[22] Griffini, E. *Costruzione razionale della casa.* Hoepli (1947) (1° ed. 1932), pp. 94-95.
[23] Candiani, S. Rubrica tecnica. Strutture mensolari a intradosso piano. *Rassegna di Architettura* (15 December 1931) **12:**473-476.
[24] Editorial. Edilizia pubblica e pubbliche proteste. *La Provincia di Como. Il Gagliardetto* (13 October 1929).
[25] Editorial. Una commissione per giudicare il transatlantico di Campo Garibaldi. *La Provincia di Como. Il Gagliardetto* (19 December 1929).
[26] Pagano, G. I benefici dell'architettura moderna (A proposito di una nuova costruzione a Como). *La Casa Bella* (March 1930) **27:**14.

12th International Conference on Structural Analysis of Historical Constructions
SAHC 2020
P. Roca, L. Pelà and C. Molins (Eds.)

SAFETY ASSESSMENT OF EXISTING POST-WAR REINFORCED CONCRETE BRIDGES. THE CASE STUDY OF 'GERBER GIRDERS' BRIDGES IN ITALY

I. GIANNETTI*, S. MORNATI[1], S. COCCIA[1], F. DI CARLO[1] AND Z. RINALDI[1]

[1]Department of Civil Engineering and Computer Science Engineering (DICII)
University of Rome "Tor Vergata"
1 Via del Politecnico, 00133 Rome, Italy
e-mail: {coccia, di.carlo, mornati, rinaldi}@ing.uniroma2.it

* Department of Civil Engineering and Computer Science Engineering (DICII)
University of Rome "Tor Vergata"
1 Via del Politecnico, 00133 Rome, Italy
e-mail: ilaria.giannetti@uniroma2.it (*corresponding author)

Keywords: 20th century heritage, reinforced concrete bridges, safety assessments, construction history, Italy

Abstract. *The interest in the structural maintenance design of existing bridges of the Italian road network is nowadays growing, due to the need to overcome structural inadequacies and/or degradation phenomena. In this framework, the new "Guide-lines for risk management, safety assessment and monitoring of existing bridges" outline the required procedures and tools, identifying the most critical issues of the different bridges' structural typologies, including Gerber girders in reinforced concrete bridges. A safety assessment of Gerber bridges is thus mandatory as for the presence of joints which do not comply with current design practice and codes as for the occurrence of aging-related decay phenomena, e.g. due to water infiltration. In this context, a novel cross-disciplinary procedure for the assessment of Gerber bridges is here presented, giving an insight on the so-called 'knowledge phase'. Firstly, the paper analyses the introduction and diffusion of this structural typology in Italy, giving a classification of existing Gerber bridges and focusing on their recurrent degradation phenomena. Finally, a discussion on historical sources which can be used to draw useful information, e.g. construction history surveys, archival drawings, calculation manuals and codes, is presented.*

1 INTRODUCTION

In Europe, during the 1950s and 1970s the wide development of roads and highways network led to the fast construction of a wide stock of reinforced concrete bridges. Alongside the development of the typology of the arch bridge, the diffusion of girders bridges was supported by the adaptation, from the 1930s onwards, of the Gerber scheme to reinforced concrete bridges. Concerning the half-joint design, building code and calculation methods of the time led to reinforcements arrangement solutions that today, following the calculation theory evolution, are considered improper for the actual structural task [1,2]: as a

consequence, the whole stock of existing Gerber truss bridges of the Italian road network exhibits insufficient performance in terms of structural safety, representing an urgent task for the structural maintenance design.

On May 6th, 2020 the Italian National Ministry of Infrastructures and Transports approved the new "Guide-lines for risk management, safety assessment and monitoring of existing bridges" [3]. In addition to the procedures and the tools to respond to the general purposes of this document, it identifies critical issues related to different bridge structural typologies.

In particular, a detailed classification of "critical elements" (i.e. those bridge parts that are particularly subject to degradation phenomena and whose possible malfunctions can significantly affect the overall structural behaviour of the structure) was provided. These elements include Gerber girders in reinforced concrete bridges, requiring a mandatory and urgent general safety assessment of the structure of Gerber bridges.

If, from the one hand, internal steel reinforcement layouts of the Gerber joints do not comply with current design practice and codes, from the other, Gerber joints are difficult to inspect and, due to their shape, they are particularly subject to water infiltration.

Moreover, the Guidelines highlight the importance of “an accurate investigation of the technical and administrative documentation of the existing bridges” [3], in order to acquire the knowledge necessary for any conservation project, regarding both the adopted design and construction procedures, as well as the transformations of works over the years of their functioning. From the cited document, on the one hand, the importance of the role of the historical research in the monitoring and preservation projects of existing bridges emerges and, on the other hand, the urgency to focus the analysis on reinforced concrete "Gerber bridges" that still exist in the Italian national territory.

In this code framework, the proposed paper presents a novel cross-disciplinary procedure for the performance analysis. According to the actual flowchart in the assessment analysis, composed of the two steps of the ‘knowledge phase’ and the analysis phase’, the proposed procedure gives an insight on the ‘knowledge phase’ through construction history surveys, in order to set useful data for the accurate safety assessment.

The paper is structured as follows: firstly, the analysis focuses on the introduction and diffusion of this structural typology in Italy and on the list and classification of existing Gerber bridges alongside their recurrent degradation phenomena; then, the historical sources typologies are discussed, focusing archival drawings and calculation manuals and codes.

2 THE GERBER BRIDGE

The progressive introduction of the static scheme of the cantilever beam (cantilever bridges) was developed with the intention of transforming the continuous beam on several supports into a statically determined system, through the introduction of a strictly indispensable number of hinges. In fact, this solution permitted simplification of calculations, optimisation of stresses on the structural elements, compensation of vertical failure whilst developing construction processes without falsework.

The scheme of the cantilever bridge, which had been systematically developed in the nineteenth century, with the rise of iron and steel as construction materials, dates back to ancient times [4,5]. As noted in the literature [4,6-9], the development and systematization of this bridge typology took place in the second half of the 19th century. Between the 1940s and

the 1960s several engineers (Fairbairn, Clark, Ritter, Culmann) tried their hand at the subject, obtaining substantial theoretical and design solutions. The scheme, already known as a cantilever bridge, *portes à faux* in French, took the name 'Gerber girders', from the German engineer Heinrich Gerber (1832-1912), in the 1860s. Although it was not always mentioned in the treatises of the time [9], Gerber was nonetheless recognized as the author of the first bridge built with this static scheme. It was the bridge over the Main in Hassfurt (1867), in which the central span beam was placed on the two lateral cantilevered beams, by hinge joints. The static solution was repeated the same year in the Sofia Bridge in Bamberg. The system was patented in 1866 [10] (Fig. 1).

In 1877, Charles Shaler Smith (1836-1886) built the Kentucky Viaduct, the first large span cantilever bridge in America: in this structure and, in the subsequent Niagara Viaduct, built in 1883 by Charles Conrad Schneider (1843-1916), the assembly of the beam without fixed scaffolding was adopted. The names of the two American viaducts identified the types that classify the construction procedures without false works, which were later adopted for the construction of structures of this type. In 1889, the opening of the Forth Bridge on the Firth of Forth, by John Fowler (1817-1898) and Benjamin Baker (1840-1907), marked the end of the experimental period of this structural typology and its definitive systematization for large span metal truss bridges.

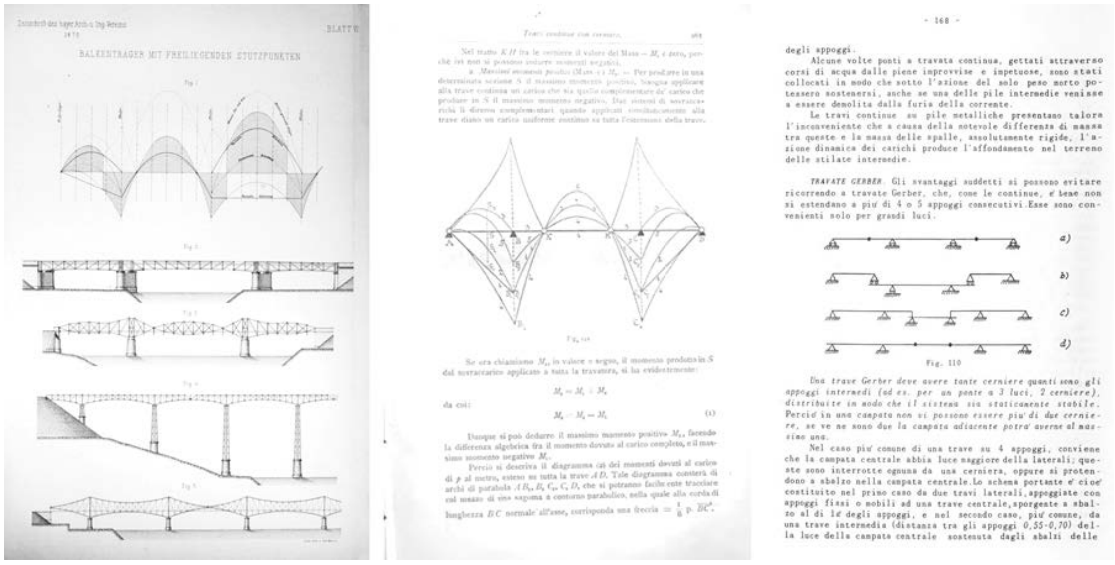


Figure 1: Gerber patent, 1866 [10] and Italian bridge design manuals [11, 19]

2.1 Introduction in Italy

In Italy the 'Gerber bridge', entered engineering practice late; this was testified by the well-known and widespread Manual of the Engineer [11] edited by engineer Giuseppe Colombo (1836-1921) from the first edition of 1877 to 1917; still, in the 1926 edition of this Manual, the Gerber beam was not included in the chapter dedicated to structural schemes.

In 1905, Antonio F. Jorini (1853-1931) dedicated chapter VI of his manual "Theory and Practice of Bridge Construction" to "continuous beams with hinges" [12]. The bibliographical references at the bottom, all foreign, suggest that this text was the first published in Italy on

the subject. In the manual, where the calculation of a three-span beam, with two hinges in the central span, was illustrated, the convenience of introducing hinges into the continuous beam schemes was defined because "with the choice of the number of hinges, and their position in the continuous beam, it is possible to obtain a statically determined structure, in which the internal stresses are independent of the vertical movements of the supports" [12].

In Italy, given the limited development of large span metal viaducts at the end of the nineteenth century when compared to other industrialized countries, the spread of Gerber-type bridges was directly due to the introduction of reinforced concrete.

In 1930, Giuseppe Albenga (1882-1957) in chapter V of his book Lessons of Bridges reported the convenience of adopting hinged patterns in continuous reinforced concrete trusses. "Introducing as many hinges as there are superabundant support conditions", with the warning "not to drop more than two hinges between two consecutive supports and not to have more than two supports between two successive hinges" [13]. In the Manual, there are no examples of "Gerber bridges" in reinforced concrete built in Italy, but the "very frequent use in reclamation areas" of cantilevered beams is mentioned, in particular for "three-span schemes characterized by two intermediate piers and small cantilevered bank spans" [13]. On the other hand, not even the two editions, published in 1924 and 1932 respectively, of the "Ponti in cemento armato Italiani" manual by G. Santarella and E. Miozzi, reported built examples of 'Gerber bridges' [14,15].

In 1933, the catalogue of the Ferrobeton firm [16], at the time one of the main Italian companies active in the sector of reinforced concrete construction, reported the construction of the following bridges known as 'Gerber-type girders': the bridge over the Amendolea river in Calabria; the bridge over the Leira torrent in Voltri and the bridge over the Volturno in Capua designed by the engineer Giulio Krall (1901-71).

Only in 1953, when Albenga published an updated edition of his book Lesson of Bridges [17] reporting the greatest diffusion of the typology also for large span bridges, examples of reinforced concrete Gerber bridges built in Italy were cited: the bridge of the Empire over the Arno in Pisa, designed by Krall (1901-71) and built by Ferrobeton himself in 1936 [18] and the Belvedere overpass in Vercelli, designed by Antonio Giberti (1883-1963). The diffusion of the typology was also testified by the updated edition of the same Albenga manual, dedicated instead to theory [19]: the third chapter was entitled "the simple beam and the Gerber beam", testifying the diffusion of the latter structural typology for reinforced concrete buildings. In 1974, Giuseppe Rinaldi in his manual “The construction of bridges” [20] reported a series of economic considerations on the use of different types of reinforced concrete bridges, in the light of the development of the freeway network (1956-73): even if "recently works of this type have been carried out with positive results", there was an overall decrease in the application of the scheme. The Gerber scheme, considered more suitable for casting, was considered ideal for spans within 65 meters and “limited for higher spans by the costs of centering” [20].

2.2 For a census of the existing reinforced concrete Gerber bridges in Italy

From a first survey on the Italian territory road bridges, the existing reinforced concrete ‘Gerber bridges’ were mostly built between the 1930s and 1970s, in particular according to

the urgency of the reconstruction after WWII and the development of the national road network between the 1950s and 1960s.

These structures feature a remarkable shape variety and can be classified according to the three static schemes represented in Figure 2. The first scheme represents an articulated girder with multiple supports: considering the general principle that a Gerber girder must have as many hinges as there are intermediate supports and that these hinges must be placed in order to ensure the stability of the system, an articulated girder is placed between the two overhangs (internal hinge - *Niagara Type*) or between the central piers and the abutments (external hinge - *Kentucky type*) (Fig. 2a). The second diagram describes a sequence of cantilevered piers and suspended span (Fig. 2b). The third scheme describes a sequence of multiple statically determinate frames (Fig. 2c).

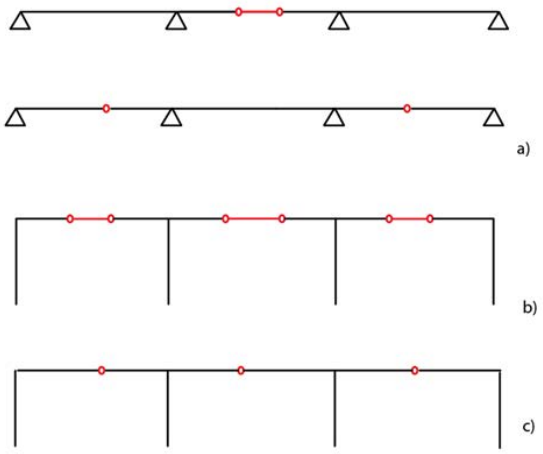


Figure 2: Sketches of the major static schemes adopted for Gerber bridges built in Italy

As showed in Figure 3, the first scheme (Fig. 2a), codified in the bridge design manuals, was widely adopted for the construction of ordinary roads and urban bridges that, built mainly between the 1930s and the 1950s, were featured by the exclusive use of cast in situ reinforced concrete. Some significant examples were among the first bridges featuring this static scheme: the aforementioned bridge over the Arno river in Pisa, rebuilt by the same construction company Ferrobeton in 1947 after the WWII; the Magliana bridge over the river Tiber in Rome (1938) and the Marconi bridge over the rives Tiber in Rome (1939).

The second scheme (Fig. 2b) was mainly used for the construction of highway bridges built in the 1950s and 1960s. Also taking advantage of the greater diffusion of industrialization in the building sector and of the pre-stressing technique in reinforced concrete construction, these bridges feature prefabricated suspended spans and cast in situ cantilevered piers. Noteworthy examples of this typology are: both the Rio Sanda bridge over the Teiro bridge on the Voltri-Albissola highway (1955) and the Settefonti viaduct of the Autostrada del Sole highway (1959); the Colle Isarco viaduct for the Brennero highway (1962), characterized, instead, by the combined use of the cantilever construction technique, pre-stressing systems and prefabricated elements [21]. On developing the same optimization goal of the execution, avoiding falsework, the third scheme (Fig. 2c) representing a sequence of multiple statically determinate frame was in the viaducts designed by engineer Silvano

Zorzi (1921-94). Between them, noteworthy examples are the Stura viaduct of the Turin-Savona highway (1968-70) [22] and the Poala viaduct at Veglio Mosso (1972-73) [23]. If, from the construction site point of view, the adoption of this static scheme brought an actual construction effectiveness, on the structural level this scheme proves to be, today, completely devoid of the recent concept of 'structural strength' [24].

In addition to the types mentioned, the Gerber girders were even adopted for special works, such as the bridges designed by the engineer Riccardo Morandi (1902-89). In his research on 'balanced structural systems' Morandi relied on this bridge typology several times. This bridge typology was used for both the project of articulated girders on multiple supports - as in the case of the Quercia-Setta viaduct on the Autostrada del Sole (1957-58) that also featured prefabrication of the elements forming the suspended span [25] - and the conception of special schemes, such as the cable-stayed bridges (i.e. the existing Carpineto viaduct (1976) on the Basentana road [26]).

	Years	Bridge name	Designer	Client	Firm	Archives	Picture	startic scheme
1	1932	Volturno bridge in Capua	G.Krall	Voltri Municipality	Ferrobeton	Voltri Municipality Archive		
4	1936	Ex Impero bridge over the river Arno in Pisa (re-built 1947)	G. Krall	Pisa municipality/ANAS	Ferrobeton	Pisa State Archive & ANAS Archive		
6	1948	Pescara bridge overe the Pescara river (reconstruction)	C. Cestelli Guidi	Pescare Municipality	Rotundi	Pescara Municipality Archive		
7	1949	Poggio Mirtetobridge over the river Tiber	C. Cestelli Guidi	ANAS, Roma	Ugo Allegri & C	ANAS Archive		
11	1954	Lerone viaduct, Voltri-Albissola motorway	A. Assereto, R. Antola	ANAS, Genova	Sugliani e Tissoni	ANAS Archive		
14	1958	Casalmaggiore bridge over the river Po	G. Borzani	Parma and Cremona Discrit	Fincosit	Parma District Archive		
17	1959	Quarcia Setta viaduct, Sole motorway	R. Morandi	Società Autostrade	Sogene	R. Morandi Found & Sogene Found, Central State Archive		
18	1959	Settefonti viaduct, Sole motorway	C. Castiglia, F. Levi	Società Autostrade	Edilstrade Ligure (brevetto BBRV)	Società Autostrade Archive		
19	1960	Eur lake bridges in Rome	E. Schmidt, G.Belloni	ANAS, Rome	Grassetto	ANAS Archive		
30	1971	Bridge over the Po river, Centro Padana motorway	B. Gentilini, L.Gentilini	Centro Padane Motorway	E. Romagnoli (BBRV)	Centro Padane Motorway Archive & Ing. Gentilini Foundation		
31	1972	Poala viaduct in Veglio Mosso	S. Zorzi, L. Lonardo, E. Faro	Ministry of Public works	CIS Compagnia Italiana Strade (Torino)	Vercelli Genio Civile Archive		

Figure 3: Table extracted from the census of Gerber bridges in Italy

2.3 Detected common aging and deterioration phenomena

The whole stock of existing Gerber bridges in Italy feature numerous aging-related decay phenomena. If, most of them are common issues for reinforced concrete structures, such as the natural aging of the materials and the phenomena of carbonation, others are, instead, specifically related to the Gerber bridge half-joint shape. In particular, in Italy, most detected phenomena [27] are leakage of water through the joint causing deterioration of the concrete and corrosion of the reinforcing steel, as it was detected in the Magliana and the Marconi

bridges in Rome (Fig. 4) and errors during execution, such as misalignment between the cantilever extremes.



Figure 4: Water leakage effects through the half-joint, Magliana and Marconi bridges in Rome, 2020



Figure 5: Metallic support device of Magliana bridges during maintenance operation [28] and reinforced concrete pendulum of Faenza Gerber bridge [29]

Furthermore, even the half-joint equipment, placed on the protruding nib of the structural element, are particularly subject to premature aging, causing dangerous discontinuities in the road surface that, due to even contained disruption, alter driving comfort. In this joint deterioration phenomena framework, it is, thus, necessary to understand how the Gerber half-joint equipment were built in Italy and whether it is possible to trace the adoption of some recurrent details or solutions. In executive practice, indeed, the use of metal devices (hinges,

pendulums, rollers) [28], derived from metallic construction practices, was combined with the extensive use of lead sheets, steel plates and the design of the special reinforced concrete pendulums devices, such the one showed in Figure 5 [29].

3 THE HISTORICAL SOURCES

Historical data for the 'knowledge phase' of an accurate safety assessment of existing heritage structures requires specific sources. Construction history discipline traditional sources, ranging from primary archival sources to the technical literature of the time period, fit this research purpose [30]. In this investigation framework, the reinforced concrete bridges in Italy, built between 1930s and 1970s feature specific archival sources, that reflected the Institutional framework of the administration charged for the road bridge construction, and specific technical literature, such as bridge design manuals [12,13,17,20] and calculation code.

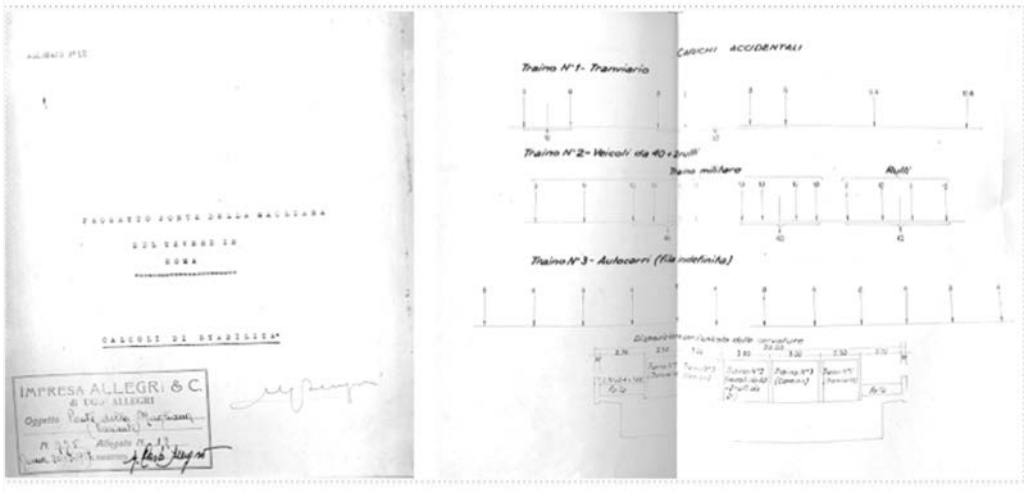


Figure 6: Load pattern considered in the calculation of the Magliana bridge in Rome, 1939 (Courtesy of Rome State Archive)

3.1 The archival documentation

Archival documentation represents the base source to acquire strong knowledge of the original design. In particular, through original design drawings is possible to find the actual geometry and dimensions of the structural elements and of the reinforcement of the half-joints. Furthermore, through original design reports it is possible to find the adopted calculation, embedding the code regulation of the time period, mechanical characteristic of the employed material and load test results. For example, for the investigated Magliana bridge in Roma (1938-50), through the archival documentation it was possible to extract data relating to the mechanical properties of materials, the load pattern embedded in the original calculations, as reported in Figure 6 and reinforcements geometry and dimensioning, as shown in Figure 7 and Figure 8. Within archival documentation, a crucial source is represented by the construction-site photography. Indeed, through construction-site photos, as

shown in Figure 8, the design drawings data can be verified, thus providing accurate information about both the built construction details, and the adopted construction processes.

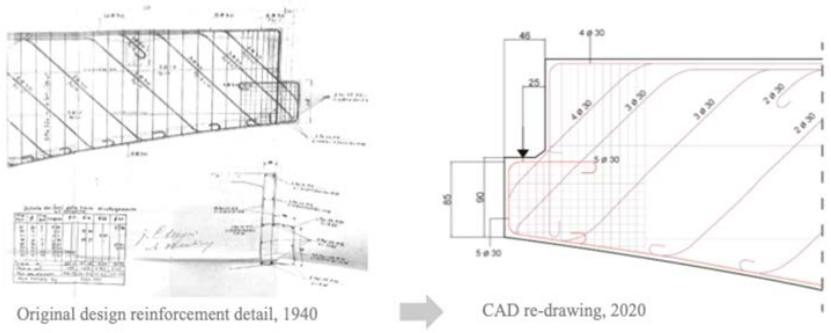


Figure 7: Reinforcement arrangement and dimensional detail of the Magliana bridge in Rome, 1940(Courtesy of the Rome State Archive) , reinforcement CAD redrawing by F. Di Stefano, 2020

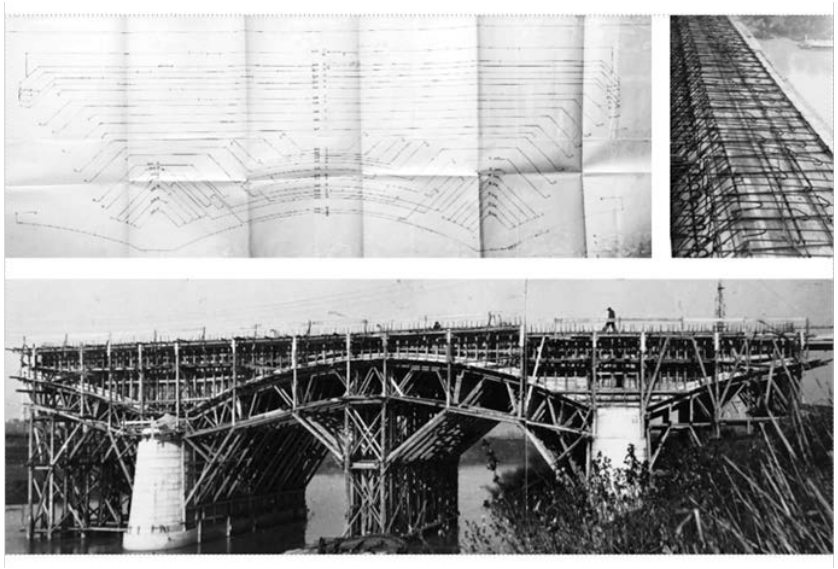


Figure 8: Reinforcement arrangement and dimensional detail of the Magliana bridge in Rome and construction site picture of the same bridge, 1940-43 (Courtesy of the Rome State Archive)

3.2 The bridge design and calculation manuals and code

Bridge design and calculation manuals represent the base documentation to understand the evolution of the calculation models of this bridge typology over the different period of their major diffusion. In particular, Albenga manual published in 1930 [12] represent the first treaty dedicated to the calculation of this bridge typology, as explained in paragraph 2.1.

For a proper safety assessment of Gerber bridges, useful information regarding load patterns considered in the original calculations can be derived by past codes. The Circolare n.8, September 15th, 1933 of the High Council of the Italian Ministry of Public Works [31], classifying the road network in three categories depending on the traffic flow, provided three elementary loading patterns: an indefinite column composed by 12 tonne trucks, a 18 tonne

road roller and a column made up vehicles up to 40 tonne (Fig. 9). These last had to be differently combined, depending on the category of the road, according to the schemes reported in Figure 10.

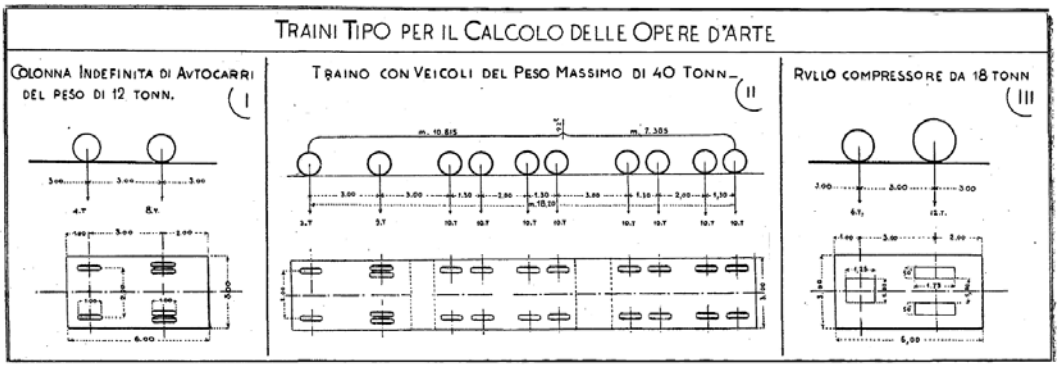


Figure 9: Load patterns from Circolare M.LL.PP. n.8, September 15th, 1933 [31]

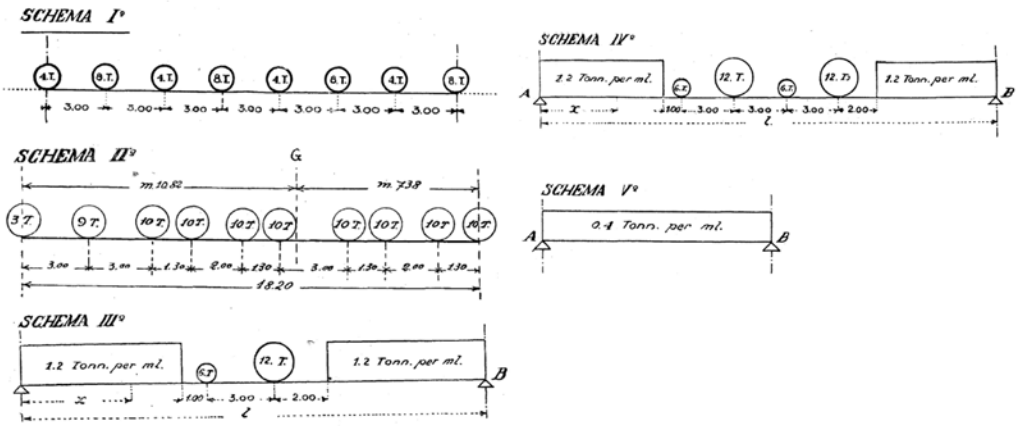


Figure 10: Load schemes from Circolare M.LL.PP. n.8, September 15th, 1933 [31]

Subsequently, with the Circolare n.6018, June 9th, 1945 of the High Council of the Italian Ministry of Public Works [32], the Italian road network was classified in the two categories of high and low/medium traffic flow roads, for which the following load patterns (Fig. 11) and schemes (Fig. 12) had to be adopted in the calculation phase.

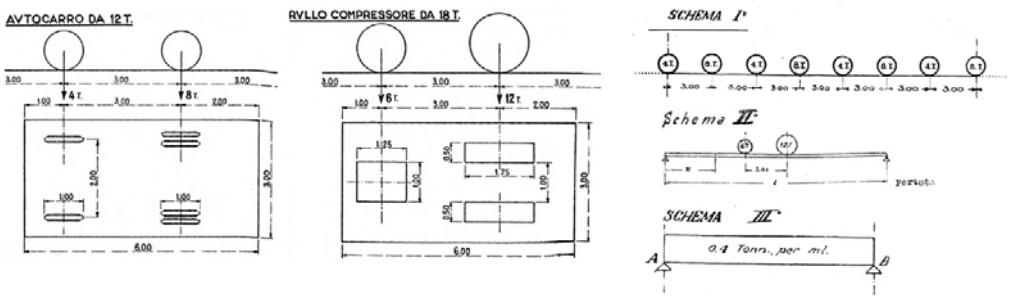


Figure 11: Load schemes and patterns from Circolare M.LL.PP. n.6018, June 9th, 1945 [32]

Finally, aiming to account for the flow of military vehicles, the Circolare n.384, February 14th, 1962 of the High Council of the Italian Ministry of Public Works [33] divided the road network in first category roads, intended for the flow of civil and military vehicles, and in second category roads, in which civil vehicles only were allowed. New load patterns were introduced to this end, including 61.5, 32 and 74.5 tonne military vehicles (Figure 13).

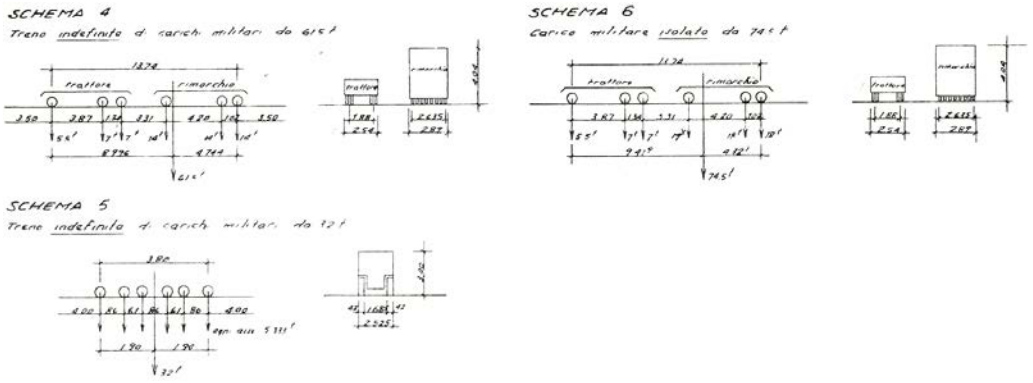


Figure 12: Load patterns from Circolare M.LL.PP. n.384, February 14th, 1962 [33]

CONCLUSIONS

Among all reinforced concrete bridges' structural typologies, it is worth to count the Gerber bridge, whose diffusion in Italy dates to the years 1930-1970, concurrently with the urgency of the reconstruction after WWII and the development of the national road network between the 1950s and 1960s. Nowadays the need for the safety assessment and structural maintenance of Gerber bridges is fundamental, due to joints which do not comply with current codes and to the occurrence of aging-related decay phenomena. In this framework, a great contribution to the 'knowledge phase' of the entire process of the assessment analysis can result from construction history investigations. In this direction, the paper outlines the history of this particular structural typology, from its introduction and diffusion along the Italian road network, together with a description of the main historical sources at the disposal of engineers called to carry out a crucial role in this context.

Acknowledgments. Researches are supported by the University of Rome "Tor Vergata" Research Grant n. E84I19002380005, project "EpoCA" (P.I. Zila Rinaldi)

REFERENCES

[1] Norme Tecniche CNR 10037/86, 1992 / EN 1992-1-2:2004
[2] Desnerck, P., Lees, J.M. and Morely, C.T. *Reinforcement Layout Implications for Reinforced Concrete Half-Joint Structures*, Proceedings of the fib Symposium 2016
[3] Linee guida per la classificazione e gestione del rischio, la valutazione della sicurezza ed il monitoraggio dei ponti esistenti. C.S.LL.PP. (2020).
[4] Steimann, D.B. *A Mathematical Study of Cantilever Bridge Design*. Vancouver: Read books (2011).
[5] Di Pasquale, S. *L'arte del Costruire – Tra conoscenza e scienza*. Venezia, Marsilio (1996).

[6] Mehrtens, L. *A hundered years of German bridge building*. Berlin, Julius Springer (1900).
[7] Panetti, M. *Le costruzioni metalliche moderne nei loro recenti progressi*. Ingegneria e Arti Industriali, 22 (1900).
[8] Timoshenko, S. *Strenght of Materials*. Toronto: D. Van Nostrand Company, (1983).
[9] Wilcox, RM. *Theory and Calcultaion on Cantilever bridges.* New York. D. Van Nostrand Company, (1898).
[10] Gerber, H. Balkenträger mit freiliegenden Stützpunkten, patent filed 6th December 1866
[11] Colombo, G. *Manuale dell'ingegnere.* Milano, Hoepli, (1877).
[12] Jorini, A.F. *Teoria e pratica della costruzione dei ponti*. Milano, Hoepli, (1905).
[13] Albenga, G. *Lezioni di Ponti*. Milano, Hoepli, (1930).
[14] Santarella, L. and Miozzi, E. Ponti Italiani in cemento armato. Milano, Hoepli (1924).
[15] Santarella, L. and Miozzi, E. Ponti Italiani in cemento armato. Milano, Hoepli (1932).
[16] Ferrobeton, Impresa Generale di Costruzioni, 1908 – 1933. Catalogo, Roma, (1933).
[17] Albenga, G. *Lezioni di ponti. La Pratica*. Milano, Hoepli, (1953).
[18] Krall, G. *Un nuovo ponte sull'Arno a Pisa*. Ind. Italiana del cemento (1937) **4**:112-123.
[19] Albenga, G. *Lezioni di ponti. La Teoria*. Milano, Hoepli (1958).
[20] Rinaldi, G. *La costruzione dei ponti*. Roma, Editrice Eredi (1974).
[21] Gentilini, B. and Gentilini, L. *Viadotto del colle Isarco nel tratto Brennero-Cave dell'Autostrada del Brennero*. In Realizzazioni italiane in cemento armato precompresso, VI congresso FIP, 180-185, Roma, AITEC (1970).
[22] Zorzi, S. *Viadotto sul torrente Stura, Autostrada Torino-Savona*. In Realizzazioni italiane in cemento armato precompresso, VI congresso FIP, 58-63, Roma, AITEC (1970).
[23] Zorzi, S. *Viadotto sul torrente Poala a Veglio Mosso*. In Realizzazioni italiane in cemento armato precompresso, VII congresso FIP, 56-59. Roma, AITEC (1974).
[24] D.M. 17 gennaio 2018, *Aggiornamento delle "Norme tecniche per le costruzioni"*.
[25] Morandi, R. *Viadotto Quercia Setta Autostrada del Sole*. In Costruzioni in Cemento Armato. Studi e Rendiconti, 176-77. Milano Politecnico, Italcementi (1967).
[26] Morandi, R. *Il viadotto Carpineto 1 per le strade di grande comunicazione Basentana*. Industria Italiana del Cemento, (1977) **10**: 817-830.
[27] Malerba, P.G. *Ponti articolati e continui: 150 anni di esperienze, seconda parte. Una approfondita analisi dell'evoluzione delle principali tipologie dei ponti Gerber e Cantilever*. Strade e autostrade, (2018) **131**: 60-63.
[28] Lavori di manutenzione straordinaria del ponte e viadotto della magliana, Relazione Descrittiva Generale, 6/12/2018 https://romacapitale.tuttogare.it/gare/id2859-dettaglio
[29] Micheloni, M., La Monica, M., Parmeggiani, D. and Barchi, P. *Sustainable structural rehabilitation and strengthening of the "Ponte delle Grazie" bridge in Faenza*. IOP Conf. Series: Materials Science and Engineering (2018) **442**:012021.
[30] Pelke, E. and Brühwiler, E. *Engineering History and Heritage Structures - Viewpoints and Approaches.* Zurich, IABSE (2017).
[31] Circ. M.LL.PP. n.8, 15 settembre 1933, *Carichi da considerare nel calcolo dei ponti per strade ordinari.*
[32] Circ. M.LL.PP. n.6018, 9 giugno 1945, *Carichi da considerare nel calcolo dei ponti per strade ordinari.*
[33] Circ. M.LL.PP. n.384, 14 febbraio 1962, *Nome relative ai carichi per i ponti stradali.*

12th International Conference on Structural Analysis of Historical Constructions
SAHC 2020
P. Roca, L. Pelà and C. Molins (Eds.)

STRUCTURAL ANALYSIS AS A SUPPORTING METHOD FOR THE RESEARCH OF MEDIEVAL BRICK ARCHITECTURE

PIOTR SAMÓL[1*], PIOTR IWICKI[2] AND JAROSŁAW PRZEWŁÓCKI[3]

[1]Gdańsk University of Technology, Faculty of Architecture,
Narutowicza St. 11/12, 80-230 Gdańsk
e-mail: piosamol@pg.edu.pl (*corresponding author)

[2] Gdańsk University of Technology, Faculty of Civil and Environmental Engineering,
Narutowicza St. 11/12, 80-288 Gdańsk
email: piotr.iwicki@pg.edu.pl

[3]Gdańsk University of Technology, Faculty of Architecture,
Narutowicza St. 11/12, 80-230 Gdańsk
e-mail: jprzew@pg.edu.pl

Keywords: Historical Structure, Masonry, Brick Architecture, Numerical Analysis, Architectural Investigation

Abstract. *Chronology of brick historical buildings might be established much more precisely than the chronology of stone ones due to the architectural and metrical analysis of bricks, mortars and brickworks. Comparison of historical sources allows to reconstruct the previous stages of constructing monuments. Causations between transformations and developments of monuments are usually interpreted as the results of artistic or ideological influence rather than pragmatic decisions. Such explanations neglect, however, the impact of structural disasters and imperfections. Experience, delivered by the previous erroneous solutions or failures, undoubtedly influenced the further development of architecture.*

In this paper the authors present how numerical modelling and structural analysis of complex historical brick buildings and different stages of their alterations might be used as a supporting method for the research of their history. Consequently, modern numerical tools for structural analysis can also be useful in investigating of the process of creating architectural solutions [1]. Because more accurate historical analyses belong to the qualitative research, it is not possible to examine very wide group of different monuments. Therefore the authors chose for that purpose the homogeneous group of the mendicant orders' medieval churches in the former State of Teutonic Order in Prussia, which have been the subject of authors' in situ research since 2009 [2]. This group is thought to be representative for the medieval techniques of the brick architecture in northern Europe and Baltic Sea Region.

The aim of this research is to find out whether structural analysis might be carried out in a historical building in which consecutive transformations partially erased its original form (reconstructed on the base of the architectural and archaeological research)? A positive answer to that question allows to put another one – about whether the numerical modelling of the structure of monument might give some additional information on its history? The results

of described research might give a new tool for conservators, architects, archaeologists and engineers in their research and other conducting works.

1 INTRODUCTION

Medieval brick structures are the subject of research in many different fields of art, humanities and science including history, archaeology, architecture and engineering. Despite the fact that such types of research have been continuously conducted and developed, the combined interdisciplinary studies on historic buildings are rare and usually limited to the most significant ones. It is caused by financial reasons as well as different state of art in particular disciplines. In most typical cases, the history of a monument was elaborated without any archaeological or architectural examines, which - in turn - did not include the structural analysis. Moreover, because of the development of no-destructive methods of the structural analysis the current state of structure might be examined without intervention in the historical substance of monument. Undoubted benefits for conservational values give, however, highly limited support in expanding the knowledge about the history of the monument. What is more, historians very rarely used the results of research in situ as a primary source although they might allow to reinterpret information gained from the written sources.

The most recent research on using advanced digital technologies (like BIM, FEM) in the heritage preservation focuses on the analyzing the current state of particular structures or the managing and fixing the data from different sources [1, 3, 4, 5]. An important element of the protection of cultural heritage related to buildings is the appropriate analysis of their structures. The reviews of methods applicable to the study of masonry historical structures have been presented in [6-9]. In general, such structures can be analysed based on limit analysis, distinct element methods or finite element methods, although it is the latter that is used most often. The FE method for masonry is based on two main modelling approaches, namely, Micro-modelling and Macro-modelling [8]. In the first case, the units and mortar are modelled as continuum elements and unit-mortar interfaces are modelled as discontinuum elements. In the latter, the masonry is considered a homogenous material with no distinguishing between units and mortar. Some interesting examples of applications of finite element methods to analyze historical masonry structures are given, among other, in [7-8, 10]. Recently, the damage model based on plastic degradation, proposed by Lubliner [11], is increasingly used in modelling historical masonry structures [12-14]. Numerical analysis of masonry should take into account not only its above-ground parts, i.e. walls, pilars, ceilings or vaults, but also foundations. Unfortunately, there are few comprehensive studies devoted to foundations of historical buildings [15, 16]. Most of the papers concern the diagnostics and maintenance of specific buildings foundations and case studies. Various aspects of the history of foundation engineering, with particular focus on its development, techniques applied, materials used and stabilization methods, are described in the latter. Numerical analysis of stone foundation by the finite element method is given in [17, 18]. In the latter, the damage model based on plastic degradation was applied.

The aim of this paper is to present how structural analysis might be used to supply the architectural investigations and give a feedback to the interdisciplinary studies of historic

monuments. This thesis is to be illustrated on the examples of mendicant churches from the former state of Teutonic Knights in Prussia.

2 METHODOLOGY

Architectural investigation was carried out with computer support - inventories were supported by photogrammetry, inventory drawings and reconstruction drawings that had been processed using AutoCAD programs. Although the historical research includes mostly traditional method of analyzing the monuments, using the numerical methods allows to verify particular reconstructions proposed on the basis of architectural research. Such a verification has not been proposed yet. Therefore, the architectural research will be supplemented in selected facilities with engineering research. The authors of this paper selected particular objects, in which state of art allowed to compare the historical, architectural and engineering research. The archival and library queries were conducted in State Archives in Gdańsk and Elbląg (Poland) and the Images Archive of Herder Institute in Marburg. In the next step, the results of historical studies were confronted with the architectural investigations which methodology is described below. Eventually, the numerical analyzes for subsequent stages of construction were performed.

Architectural research presented in this paper is based on destructive and non-destructive examines that have been conducted in situ since 2010. The aim of that research was to acknowledge the stratigraphy of the historic building. It was completed thanks to accomplishing five following tasks: 1. Performing architectural and conservation inventory, 2. Comparing the results of previous research (including historical studies as well as archaeological surveys); 3. Determining construction systems, masonry analysis, statistical measurement (about 20 per node) of bricks to distinguish the parts, sampling of bricks, mortar, 4. Relative dating based on determined construction stages, 5. Absolute dating based on historical research and other date stamps (mortar studies, dendrochronology).

Described research was possible to conduct because of the state of survived medieval brick architecture in northern Europe. Most historic objects in this area were partially destroyed during the Second World War, which caused huge wastes for cultural heritage but also gave an opportunity to recognize the structure of buildings. In case of the church in Elbląg, almost whole authentic uncovered brick walls were accessible for the research team. Therefore, it was possible to establish over 200 nodes and conduct a very precise analysis of its architectural structure. Those works bring the evidence basis for the further examines – the structural analysis of the following stages of construction. This will allow verifying the hypothetical reconstructions proposed on the basis of architectural research. Because such a study requires comparing the results of architectural investigation and structural analysis for each stage of construction, they will be described in two following parts, but the relations between them will be summarized together.

3 RESULTS OF ARCHITECTURAL INVESTIGATION

Dominican church of Our Virgin Lady in Elbląg (Elbing) is the oldest brick building within the territory of the former state of Teutonic Knights in Prussia. The lower part of the east choir was elevated after 1246, which was connected to the foundation of the first brickyard at the southern coast of Baltic Sea that was confirmed in historical written sources [2, 19]. The

current research, that was conducted in years 2010-2019, allowed to recognize the several stages of its construction which were unknown before. The stratigraphy of the church is presented at the Fig 1.

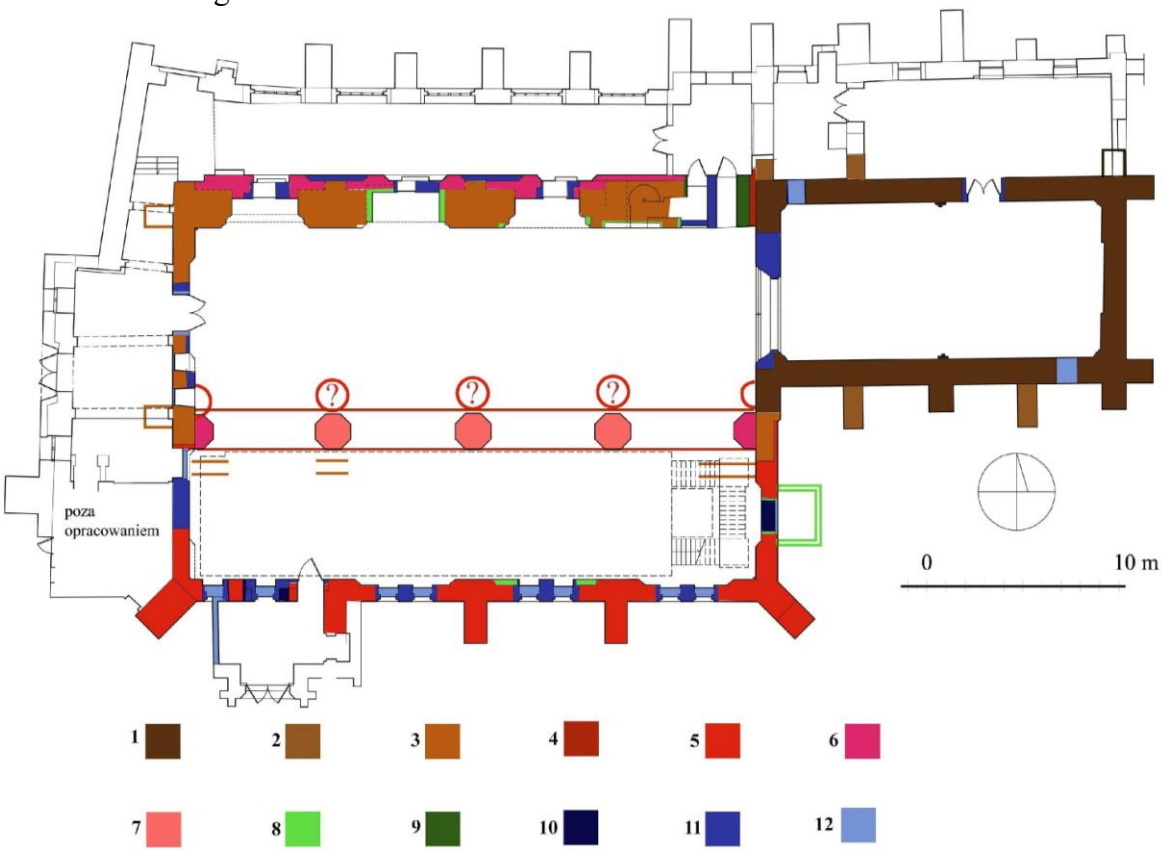


Figure 1: Plan of the church of Our Virgin Lady in Elbląg. The results of architectural research [2]: 1 - 1246-c. 1250, 2 - around 1275, 3 - 1287/1288 - end of the 13th century, 4 - hypothetical, approx. 1300, 5 - 1st quarter of the 14th century, 6 - 2nd half of the 14th century, 7 - around 1470-1504?, 8 - 2nd half of the 16th century - early 17th century, 9 - 17th - early 18th century, 10 – 1st half of the 19th c., 11 – 2nd half of the 19th c. - 1930, 12 after 1960.

Multiple spatial transformations in the Middle Ages were typical for the mendicant orders' architecture in large merchant cities like Elbląg, (as well as Gdańsk or Lübeck). The first choir was enhanced twice ca. 1275 and then, at the end of the 13th century. The archaeological surveys from 1959 and 2008 [20, 21] gave information about the construction of foundations of the church and the rests of previous versions of the rebuilt nave. Those results had not been interpreted however by the excavators because they did not conduct the parallel examines on architecture. The corpus was erected as a single nave church (around 1300) and extended later to a symmetrical two-nave hall (around 1320). The central row of circular pillars, that separated two naves, was situated then on the stone bases, which were later reused in fundaments of the octagonal pillars. The choir screen and vaults above the naves were probably set at the same time. Although, during next two centuries, the church was enhanced several times, the external plan of the building was not transformed. Therefore the analysis of the eastern wall of the nave is crucial for aknowleding the history of the monument (Fig 2.).

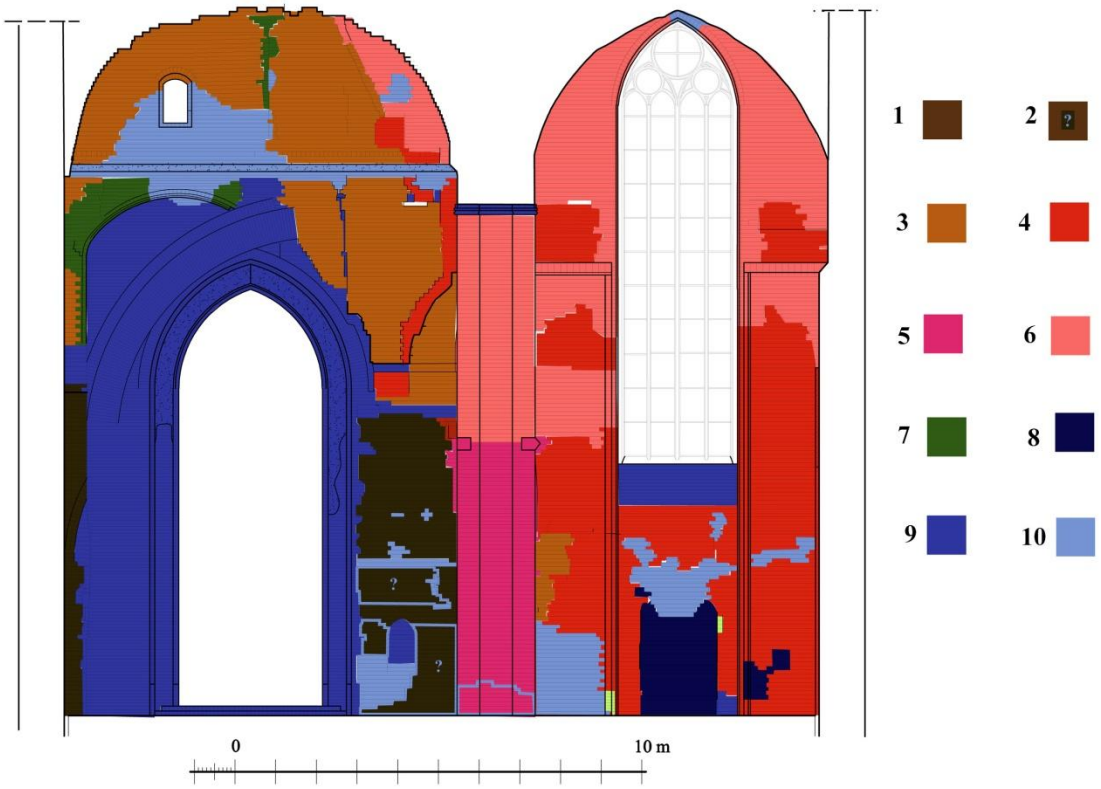


Figure 2: Inner view of the eastern wall of the church of Our Virgin Lady in Elbląg. The results of architectural research [2]: 1 - 1246-c. 1250, 2 – wall from c. 1250 repair in the 19th century, 3 - 1287/1288 - end of the 13th century, 4 - 1st quarter of the 14th century, 5 - 2nd half of the 14th century, 6 - around 1470-1504?, 7 - 17th - early 18th century, 8 - First half of the 19th century, 9 - second half of the 19th century - 1930, 10 - after 1960.

The low two-nave church from ca. 1320 was rebuilt in the second half of the 14th century (Fig. 3a). Because of changing architectural trends the friars wanted to erect the nave on the axis of the east choir. However, such decision caused demolition of the circular pillars and then replacing them by the octagonal ones. The new construction needed better foundations than the previous one, therefore the row of octagonal pillars was not situated exactly in the place of circular pillars but around 1.5 m to the south. As a consequence, the corpus lost its symmetrical plan. The two naves got then different height and width, though they were covered by the one roof. Such a construction used to be called a “pseudobasilica” [22]. Described action is proved by the evidence such as the shape of the demolished vaults, which is situated on the eastern wall, between the current pillar and the chancel arch.

After the Thirteen Years War (1454-1466) the church was enlarged once again. The southern nave was enhanced to the height of the northern one. At the end of the 15th century the western and eastern walls got a new gable (partially reconstructed after the Second World War). The new hybrid crystal-netted vaults were set before 1504. Although those alterations caused the height of the nave to arise from 14 m to 22 m, Dominicans remained the chancel arch from the middle of the 13th century which was only around 10 m in high (Fig. 3a).

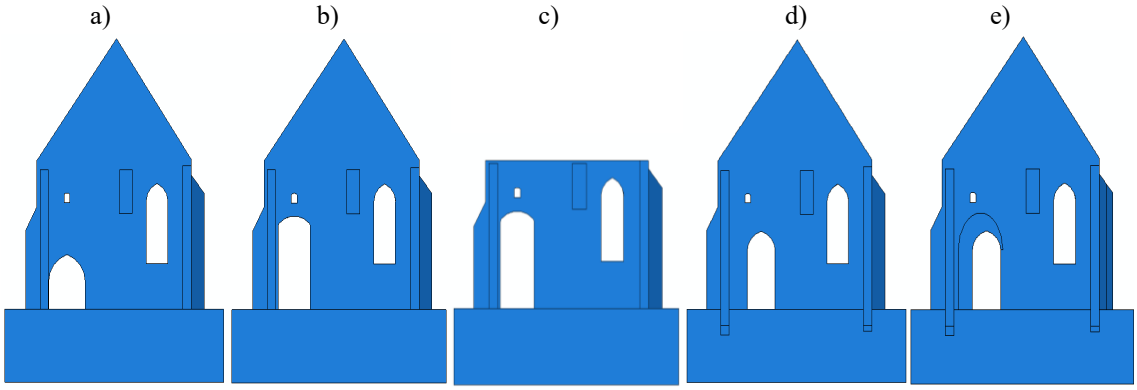


Figure 3: Church wall resting on soil foundation from: a) 1504, b) ca. 1680, c) 1827, d-e) after 1880

A decade later, the reformation gained many supporters in Elbląg (as well as in whole northern Poland) which caused the cancelation of the Dominican monastery. The church was taken by the protestants, whose aesthetical beliefs focused on the purity of architecture and its functionalism. Therefore, the new owners had not conducted any important transformations of the church for the next 150 years. In the 17th century new chancel arch was created through the demolition of 8 m of the wall above the previous one. The new arcade was topped with an elliptic arch, typical for the baroque period. The historical sources gave no information why ecclesial administration decided to rebuild this part of the church, It might have been caused by the destruction of the spire and the vaults in the east choir in 1680 [23]. However, the structural reasons of that damage remained unknown (Fig. 3b).

At the beginning of the 19th century Prussian government centralized building administration in the entire state. As an effect of that reform, the former Dominican church was controlled by some officials because of visible cracks on the vaults. Similar observations were made in other former mendicant temples in Eastern and Western Prussia [2]. In 1827 a system of supporting construction and removal of the gothic roof was designed, but its realization was delayed and later cancelled [24]. The structural analyses of potential rebuilding described above allowed to evaluate whether the proposed repairs would have been needed and reasonable (Fig. 3c).

In the 1880s the ecclesial administration decided at least to strengthen the cracked walls of the church including baroque chancel arch. In the first step a massif flying buttress across the chancel arch was built, which supported the central part of the eastern wall. Then the space above the flying buttress was filled with modern, fabric-made bricks from Kadny (Imperial brickyard in the neighbourhood of Elbląg) [25]. The last step was creating of a smaller gothic-revival chancel arch, which is preserved to the present day. The partial demolition of the church during the last war (1945) fortunately did not include the eastern wall except for the gable (Fig 3d, 3e).

4 NUMERICAL ANALYSIS

The structural analysis of the former Dominican church in Elbląg was prepared for its four stages. The aim of this investigation is to present how the modern, numerical methods of

structural analysis might be used in research of historic brick buildings, enlarging the knowledge on their past.

The FE calculations were carried out for gable wall of a height about 36.80 m and width 21.13 m. The wall thickness was 1.25 m. In the numerical model parts of other (perpendicular) walls of width 1.2 m were included. Four types of the church wall static schemes were considered (Fig.3 a-c, e). In all variants both the church masonry walls, stone foundations and the soil were included in the numerical model. There was a cut made in the soil for the masonry and stone foundations block. The structure was loaded by inertia and by self-weight.

The numerical static analysis was performed by means of non-linear explicit procedure and commercial program [26]. The method is effective for simulation of damage and degradation of masonry structures. The total number of finite elements of type C3D10M used in the analysis was equal 492983 (model 1A - Figs. 3e, 5a), 487602 (model 1B – Figs. 3d, 5a), 259731 (model 2 – Figs. 3c, 5b), 447368 (model 3 – Figs. 3b, 5c) and 454278 (model 4 – Figs. 3a, 4, 5d). The finite element size for the church masonry and stone fundament was 250 mm while for the soil 1000 mm. The damage model based on plastic degradation implemented in Abaqus software program was used for masonry wall. The following soil parameters were assumed [26]: density 2000 kg/m^3, Young modulus 40 MPa, Poisson's Ratio 0.2. The stone foundations characteristics were the following: modulus of elasticity 1200 MPa, Poisson's ratio 0.2, density 2000 kg/m^3 (Fig. 5b-d, 6a-c).

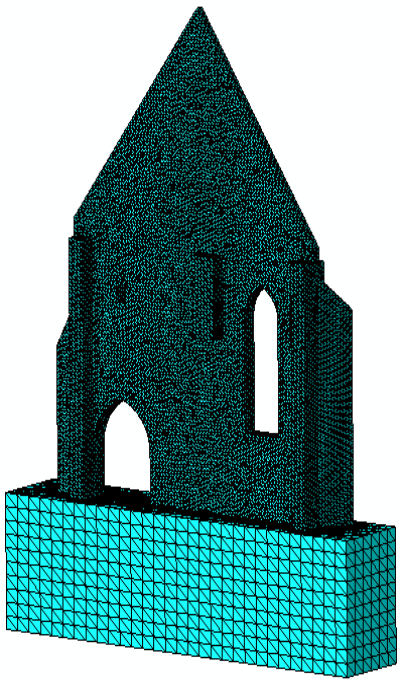


Figure 4: FE mesh of church wall resting on soil foundation from for model 4.

Modulus of elasticity for masonry from Middle Ages was 1910 MPa, Poisson's ratio was 0.166, and masonry density equal 2000 kg/m^3. The parameters of reinforced parts of the

model (1A – Figs. 3e, 6d) were assumed according to the results of research by Kujawa [14], which was conducted for a similar brick village church situated about 50 km from the examined temple: modulus of elasticity 7634 MPa Poisson's ratio 0.209, density 1800 kg/m^3. The damaged model plasticity (CDP) characteristics were: dilation angle 20, eccentricity 0.1, the ratio of biaxial compressive yield stress to uniaxial compressive yield stress 1.16, the ratio K of the second stress invariant on the tensile meridian to that on the compressive meridian for the yield function 0.667, viscosity parameter 10 $^{-6}$.

The displacements of the wall for all considered models are presented in Figs. 5a-d. The maximal displacements of the wall were 86 mm (model 4), 64 mm (model 3), 38.5 mm (model 2) and 31.5 mm (model 1B), 27.8 mm (model 1A).

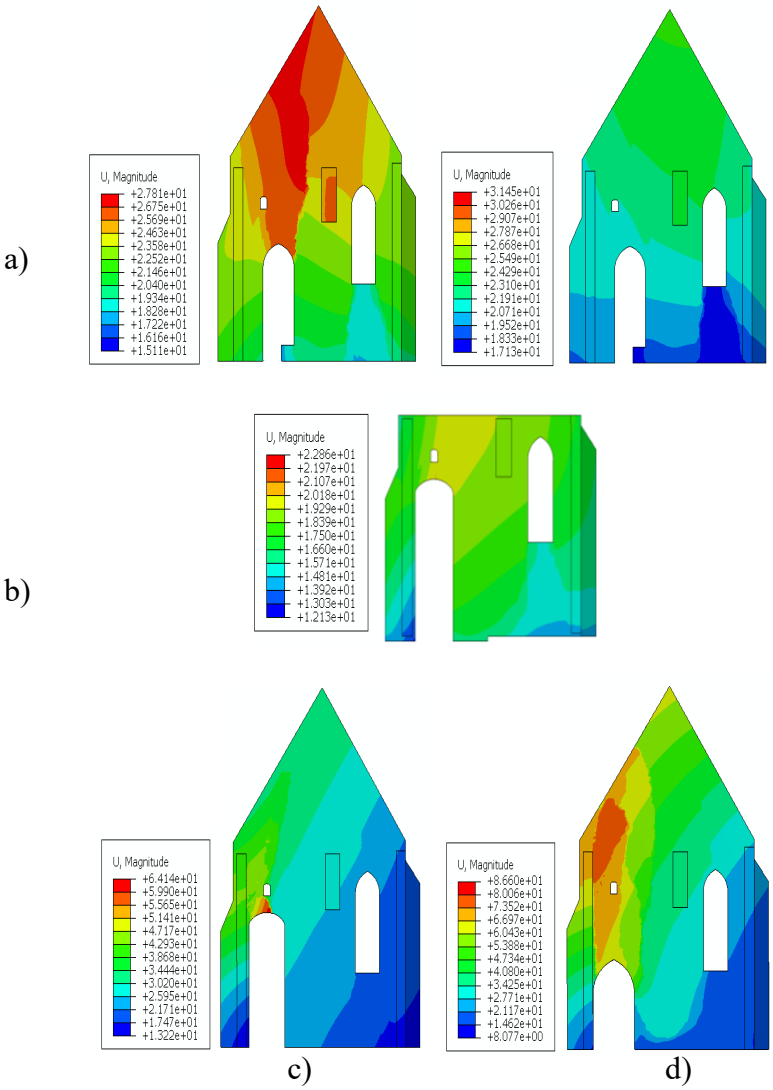


Figure 5: Displacement of church wall for model a) 1A, 1B, b) 2, c) 3, d) 4

The crack propagation for the cases considered is shown in Figs. 6a-d. The main cracks were located above the door and above and under the window and depended on the weight of the masonry. For the case with restrained wall (1B) the cracks were clearly smaller than for

the original masonry (1A). The results for the tension tests are presented as color maps of equivalent plastic strains in tension (PEEQT). Analysis of material parameters shows that cracks occur for deformations greater than $10^{-3} \times 10^{-3}$.

The first analysis is prepared for the model of the church from the end of the Middle Ages (Figs. 3a, 6a). The form of the triumph arch was created at the turn of $13^{th}/14^{th}$ century and was not transformed during the following medieval building actions, although the height of eastern wall arose from 12 up to 38 m. The structural analysis allowed to recognize the process of damaging the wall through the quadrupled pressure, which was observed in the following centuries (Fig. 6a).

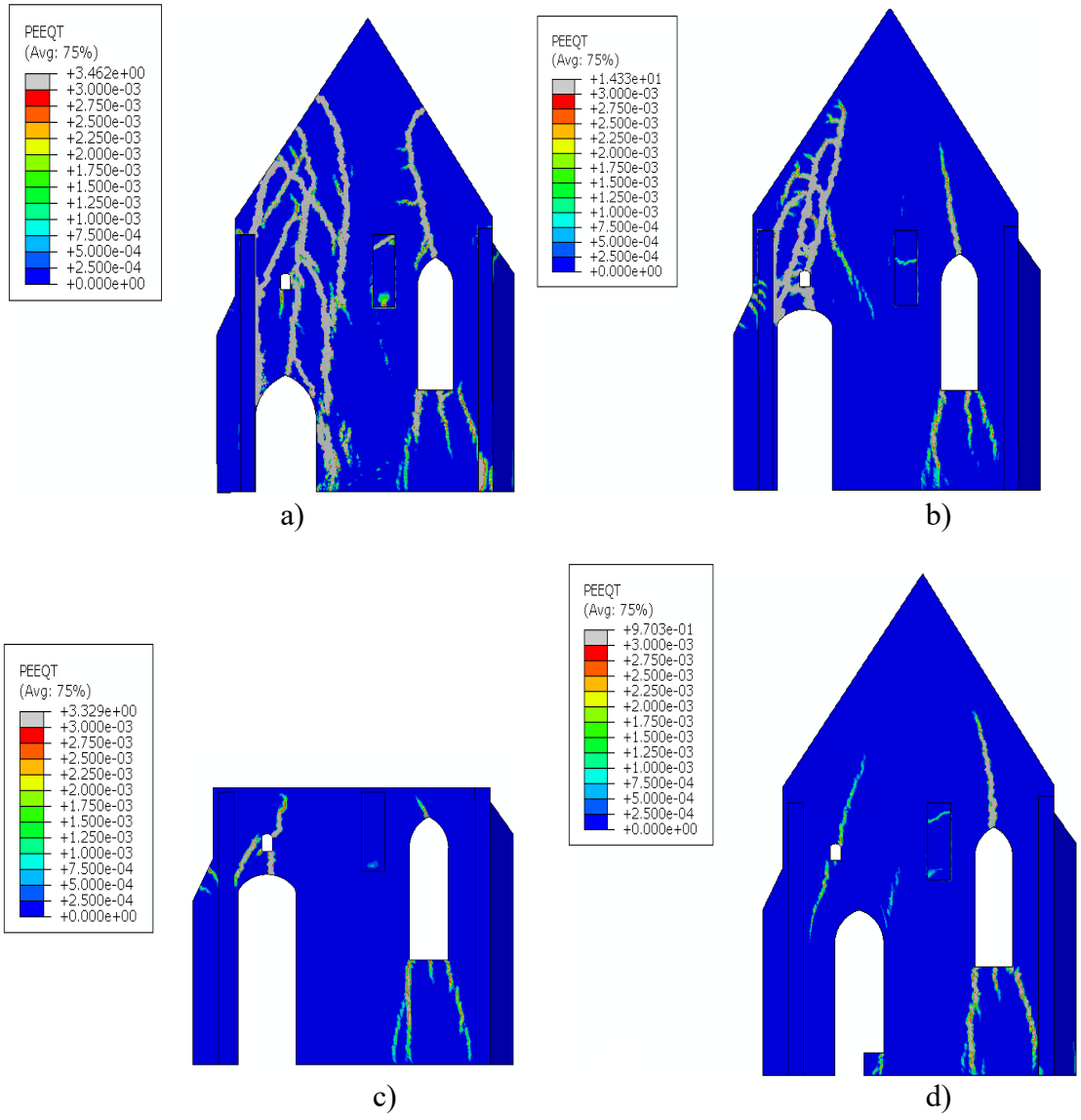


Figure 6: Eastern wall of the church (a - after 1504, b – ca. 1680, c – 1827, d – ca. 1880) with main cracks according to FEM solutions expressed by equivalent plastic strains in tension.

The second analysis allows to examine the transformation of the church after the collapsing of the spire in 1680 (Figs. 3b, 6b) The falling parts of wooden bell tower destroyed the roof and vaults above the east choir. Although there is no evidence for a coincidence between those events and the rebuilding of the chancel arch, the eastern wall was transformed undoubtedly during that period. Comparing the previous version of the chancel arch with the new one (baroque), allowed to note two issues. The shape of baroque arch is similar to the main cracks above the gothic arch. Thus, the rebuilding of the triumph arch seemed to have been an attempt of its repairing through liquidating the part of the wall directly above the archade, which had been separated from the structure above. It should be mentioned here, that at the turn of the $17^{th}/18^{th}$ century there were no professionals who could interpret the behaviour of structures like engineers in contemporary meaning of this term. Therefore, the structural analysis of the historical transformations may give some additional information on the ability of people back then to react on structural accidents and damages. Descriptions of such actions are often neglected in historical written sources.

The next issue (Figs. 3c, 6c) lets verify whether the project of removal of the eastern gable from 1827 was necessary from the engineering point of view, or whether it was rather an attempt to change the aesthetic value of the church to a more fashionable one. It was remarkable, that the design of urgent repairs was delayed before the ecclesial authorities would finance the construction works. The removing of the gable would have solved the structural problems of the eastern wall but it was also a radical move, changing not only the shape of the church but also the panorama of the whole city.

The last analysis (Figs. 3e, 6d) illustrates the repair of the chancel arch in the 1880s. As it may be observed those works solved the structural problems of eastern wall which allowed the church to survive through the war damages. What is more, the using of more durable bricks and mortar was as important for strengthening the wall as changing of the shape of the chancel arch.

5 CONCLUSION

Architectural investigations allow to reconstruct the history of the heritage monument, but they are almost always conducted separately from the structural analyses. What is more, most researchers focus on interpreting architects' decisions through the artistic and ideological aspects rather than the pragmatic issues. This scientific method may be observed well particularly in central Europe, where many historical written primary sources were lost. As a result of that, many objective reasons of building actions from the past were neglected. The presented example of Dominican church in Elbląg allows comparing the results of its architectural investigations with the structural analysis of recognized stages of construction. This research gives an opportunity to expand the evidence base and to seek the answer about, why some architectural and engineering solutions were ever adopted. It is obvious that such a research may be conducted only during the traditional architectural examines, because the representatives of different scientific disciplines give and receive a proper feedback then. This is also the reason, why structural analysis has not been used as a supporting method to historical studies on architecture yet.

The authors of this paper expand their research on other monuments (e.g. Franciscan church in Chełmno, Poland), which were created in a multi-stages process.

6 ACKNOWLEDGEMENTS

This paper partially presents results of the research project No. 2017/1/X/HS2/00626 financed by the National Science Centre, Poland.

The numerical calculations were performed using the computing resources of CI TASK at Gdańsk University of Technology.

7 REFERENCES

[1] Roca, P., Cervera, M., Gariup, G. and Pela, L. Structural Analysis of Masonry Historical Constructions. Classical and Advanced Approaches, *Arch. Comput. Methods Eng.* (2010) **17**: 299–325.

[2] Samól, P. *Architecture of the Dominican Churches in medieval Prussia*, Gdansk: [PhD Thesis] (2015).

[3] Godinho, M., Machete, R., Ponte, M., Falcao, A. P., Concalves, A. B. and Bento R BIM as a resource in heritage management: An application for the National Palace of Sintra, Portugal, *Journal of Cultural Heritage*, in print (2020).

[4] Dall'Asta, A., Leoni, G., Meschini, A., Petrucci, E. and Zona, A., Integrated approach for seismic vulnerability analysis of historic massive defensive structures, *Journal of Cultural Heritage* (2019) **35**: 86-98.

[5] Groat, L. and Wang, D. *Architectural research methods*, Wiley (2013).

[6]Lourenço, P.B. Analysis of historical constructions: From thrust-lines to advanced simulations. In: Lourenço P.B., Roca P. (Eds.): *Historical Constructions*, Guimarães, (2001): 91–116.

[7] Lourenço, P.B. Computations of historical masonry constructions. *Prog. Struct. Engng. Mater.* (2002) **4/3**: 301–319.

[8] Roca, P., Cervera, M., Gariup, G. and Pela, L. Structural Analysis of Masonry Historical Constructions. Classical and Advanced Approaches. *Archives of Computational Methods in Engineering* (2010) **17**: 299–325.

[9] Theodossopoulos, D. and Sinha, B. A review of analytical methods in the current design processes and assessment of performance of masonry structures. *Construction and Building Materials* (2013) **41**: 990–1001.

[10] Giordano, A., Mele, E. and De Luca, A. Modelling of historical masonry structures: comparison of different approaches through a case study. *Engineering Structures* (2002) **24**: 1057–1069.

[11] Lubliner, J., Oliver, J., Oller, S. and Oñate E. A plastic-damage model for concrete. *Int. J. Solids Struct.* (1989) **3**: 299–326.

[12] Resta, M., Fiore, A. and Monaco, P. Non-Linear Finite Element Analysis of Masonry Towers by Adopting the Damage Plasticity Constitutive Model. *Advances in Structural Engineering* (2013) **16(5)**: 791-803.

[13] Liberatore, D., Addessi, D. and Sangirardi, M. Nonlinear Analysis of Masonry Walls Based on a Damage-Plastic Formulation. *Structural Analysis of Historical Constructions* (2019), **18**: 1009-1017.

[14] Kujawa, M., Lubowiecka, I. and Szymczak, C. Finite element modelling of a historic church structure in the context of a masonry damage analysis. *Engineering Failure Analysis*

(2020) **107**: 104233.
[15] Kerisel, J. Old Structures in Relation to Soil Conditions. *Geotechnique* (1975) **25**: 433–483.
[16] Przewłócki, J., Dardzińska, I. and Świniański, J. Review of historical buildings' foundations. *Geotchnique* (2005) **55**: 363–372.
[17] Przewłócki, J. and Zielinska, M., Analysis of the Behavior of Foundations of Historical *Buildings. Proc. Eng.* (2016) **161**: 362-367.
[18] Przewłócki, J., Zielińska, M. and Grębowski, K. Numerical modelling of connections between stones in foundations of histrical buildings, *WMESS, IOP Conf. Series, Earth and Environmental Science* (2017), **95**.
[19] Samól, P. Pierwsze oratorium dominikanów w Elblągu z połowy XIII wieku [=First Dominican chapel in Elbląg from the half of the 13th century], In: D. Stryniak, T. Janiak [Eds.]: *Architektura skralna w średniowiecznej Polsce*, Gniezno (2016): 543-554
[20] Gajewska, M. and Kruppe, J. Badania archeologiczne na terenie kościoła NMP w Elblągu w roku 1959 [=Archaeological excavations in the area of Our Virgin Lady church in Elbląg in 1959]*, Rocznik Elbląski* (1959) **1**: 207-226.
[21] Archive of Contemporary Art Centre "Galeria EL" in Elbląg: report of Gołembnik, A. *Sprawozdanie z badań archeologicznych w obrębie podominikańskiego kościoła p.w. Najświętszej Panny Marii. Centrum Sztuki Galeria EL* [=Archaeological excavation inside the former Dominican church of Our Virgin Lady – Contemporary Art Centre "Galeria EL"] Elbląg (2008).
[22] Piwek, A. *Kościoły gotyckie o układzie pośrednim (pseudohala, pseudobazylika) w Polsce* [=Gothic churches built as pseudobasilicas in Poland], Gdańsk [PhD Thesis] (1996).
[23] Fuchs, M. G. *Ein Schulactus auf dem Elbinger Gymnasio den 14ten April 1796 zum Andenken der Gründung der Hauptkirche zu St. Marien in Elbing vor 550 Jahren gehalten,* Elbing (1796).
[24] State Archive in Gdansk, acts no. 300, 1151/192.
[25] Hauke, K. and Stobbe, H. *Die Baugeschichte und die Baudenkmäler der Stadt Elbing*, Stuttgart (1964).
[26] ABAQUS, *Theory Manual*, Version 6.8, Hibbit, Karlsson & Sorensen Inc, (2008)

12thInternational Conference on Structural Analysis of Historical Constructions
SAHC 2020
P. Roca, L. Pelà and C. Molins (Eds.)

THE "PIEVE DI SANTA MARIA" IN AREZZO (ITALY). FROM THE LASER SCANNER SURVEY TO THE KNOWLEDGE OF THE ARCHITECTURAL STRUCTURE

PIETRO MATRACCHI[1], CARLO BIAGINI[1],

ANDREA SADOCCHI[2], MATTEO VALIERI[2]

[1] Department of Architecture (DIDA)
University of Florence, Italy
e-mail: pietro.matrachi@unifi.it; carlo.biagini@unifi.it

[2]Architect
e-mail: andreasadocchi@hotmail.it; matteovalieri@hotmail.it

Keywords: Historical Structure, Non-Destructive Inspection, Laser scanner survey, Architectural diagnostics

Abstract. *The parish church of "Santa Maria" is considered one of the most important medieval buildings of Arezzo Although the church is attested from 11th century, it is between the 13th and 14th centuries that reached its current consistency, characterized by the particular façade with small columns on several levels and an imposing bell tower. Later, from the 16th to the 18th century, the church underwent profound transformations, that were almost completely erased by extensive restoration works in the second half of the 19th century.*

The architectural survey of the parish church of "Santa Maria" was carried out with a phase-shift laser scanner and a digital reflex camera (Z+F 5006h). 189 scans were performed for generating the 3D model of the church: 180 of them with high density and normal quality, lasting 5-6 minutes; the remaining ones with super high density and high quality, lasting 13-14 minutes. Vectorial drawings of plans and sections were then created from the 3D model.

Thanks to laser scanner survay of the chuch, it was possible to highlight the singularity of the structure of the basilical body and the transept. The tilt of walls and columns, the variations in the thickness of the walls, the considerable deformations of some arches, the cracks and textures of the wall facing were thus shown.

The information obtained attested an architectural structure created by complex construction events that over time have affected this building. The cnstructive singularities involve the medieval genesis of the building, the transformations during the following centuries and the following restoration works.

These composite features are specific and common to every ancient building. This peculiar epistemological condition eschews from simplifications and requires deep and complex studies closely linked to the problems of conservation of the structures.

1 INTRODUCTION

On the origin of the “Pieve” a fragmentary documentation is avaiable, such as the date of the foundation in 1009. Thus the dating of sculptural works in the church takes on particular relevance. The bas-relief of the Assumption in the central portal of the facade is dated to 1216; a further date 1221 is engraved in the lunette of the right portal. The extremely significant sculptures which represent the Months in the vault in front of the main entrance portal are dated to the thirties and forties of the XIIIth century[1]. It is believed that, except the bell tower and the presbytery completed around 1330[2], the construction of the church, including the entire external facade with the three levels of overlapping loggias, were completed around 1250.

The medieval structure, built through complex construction phases, is only a part of the history of the church, which was subsequently subject to further incisive changes. The structures today constitute a palimpsest very difficult to understand in its own varied formation.

In this article the understanding problem of the structural peculiarities is faced by integrating the historical sources with information obtained from laser scanner survey, using the 3D model to obtain useful plans and sections.

2 CHANGES TO THE BUILDING FROM XVITH CENTURY

From the XVIth century, significant transformations began with the aim of modernising the church. Among those that have had the greatest impact in the consistency of the structures, we can mention the opening of new windows and the expansion of others existing at that time. Furthermore the floor was raised, the crypt destroyed and new vaults were built[3]. Cristofano Conti's drawings, executed at the end of the XVIIIth century[4], document the naves of the Pieve covered by barrel vaults.

In the first half of the XVIIth century, a series of expert reports regarding the static instability of the Pieve began, and some interventions to the structures followed[5]. The engineer Francesco Nave in 1649 was first called. He removed the spandrel of the vaults and recommended the partial demolition of the drum to reduce the load on the arches of the crossing; he provided the crossing with a new roof and by ties made the structure reinforced. The work of Nave was not considered satisfactory, so in 1657 an opinion was asked to the engineer Francesco Valle, who carried out supports for the wall on via della Seteria and infilled the openings of three shops of the same side[6].

In the second half of XIXth century extensive restoration works of the church erased all the modifications deemed later of the medieval construction. It was a very common restoration methodologies at the time and persistent even in the following decades. In some cases it affected entire ancient towns[7]; in the Pieve extensive reconstruction of both wall facings and entire walls were involved; the crypt was built with a new design[8].

3 THE LASER SCANNER SURVEY OF THE PARISH CHURCH

Current survey methodologies of historical building heritage, exploiting massive geometric data captured by laser scanning or 3D Imaging techniques, rise many procedural questions

about the treatment of these data in the various processing stages of the historical architecture knowledge[9].

In recent years, in fact, Geomatics have developed many measuring instruments characterized by high portability, ease of use, speed and precision in capturing. The outcome of an acquisition process carried out with these tools is represented by a point cloud, which provides a digital model of the building. It essentially consists of a dataset of geospatial coordinates, corresponding to as many points on the building surface, whose number depends on the acquisition density established in the instrumental setting phase. Then dedicated management software operate automated registration procedures of the various point clouds. The reliability of the obtained datasets is very high, in relation to the geometric accuracy generally required in the subsequent multidisciplinary analyzes to be carried out on the historic building.

However, the extraction of a "significant" geometry from massive data, useful for developing knowledge deepening phases, frequently proves to be a complex challenge. The outcome in uncertain, if not adequately oriented to the purposes[10].

In fact the vector mapping procedures require a huge activity of recognition of planes, surfaces, volumes, primitive or complex geometric shapes on the 3D point cloud; despite the recent automated procedures development, it is essentially based on manual editing. So the quality of the 2D/3D implementation depends not only on the appropriate choice of approximation algorithms, but also and not secondarily on the operator's ability to interpret the captured data. Every adopted simplification in the digital building implementation processes leads to a "modeling error"[11], which is always greater than the uncertainty owned by the raw data contained in the point cloud. The control of this deviation must be managed through a specific planning by preparing appropriate validation procedures of the modeled data.

This problem assumes considerable importance in the field of Building Information Modeling (BIM) techniques, because the digital model reliability does not lie exclusively in the degree of its geometric convergence with the physical artifact. The overall information content qualifies the "level of development" (LOD) of the BIM model[12] and the geometric accuracy is only one of the many parameters to be considered.

3.1 Data capture: the 3D model of the parish church of "Santa Maria"

The knowledge project of the parish church of "Santa Maria" in Arezzo intended to test a capture and implementation process of geometric data, divided into different study stages. It was aimed at interpreting the structural singularities of the basilica body, through the identification of a management workflow of geospatial datasets collected in geometric and informative outputs consistent with the research objectives.

In particular the point cloud has generated different exploration possibilities of the digital model, from which multiple 2D/3D implementations have been derived and focused on specific aspects of the building geometric configuration.

The use of digital scanning technology for three-dimensional surveying has had a significant development in the last decade. Taking advantage of the speed of light propagation

and the reflective capacities of the materials, the laser scanner allows to capture in a very short time the spatial coordinates of millions of points[13].

Although the remote sensing technologies let us accomplish a large amount of measurements, the selection of points to be detected no longer takes place at the time of capturing, except the scanning grid; this is set more or less dense to be capable of grasping evident discontinuities and small deformations. The point cloud creates a sort of intermediate model between physical reality and graphic representation, in which building is broken down in spatial coordinates. Just later we can move selecting of the most significant points, discarding the redundant ones, and then define the 2D/3D geometric digital model. The undifferentiated set of captured points must undergo a processing procedure before extracting necessary information for the mathematical model implementation. The recognition of the primitive forms of the surveyed artifact represents one of the most critical but also interesting study phases; it is aimed to element classification, structural analysis and evolution in time of the building. In fact the point cloud conveniently processed makes available a massive data amount, which is useful to product graphics such as plants and elevations, but above all sections; these can have an accuracy and reliability much higher than those made through traditional techniques of survey.

However laser scanner technology has a series of inherent limitations, due to the way the geospatial point data are captured on the surface of the object. The laser ray must have a completely free rectilinear trajectory for reaching the point to be measured. Therefore any obstacle between the point and the laser source generates an information gap equivalent to the shadow projected by this obstacle on the object, the so called "occlusion space". The same morphological characteristics of the historic architecture (rich in details and irregular shapes) make the cited problem particularly complex in the data management phase. The need to carry out a high number of scans addressed to the same building area, for ensuring complete coverage, creates likewise a great redundancy of captured geospatial data.

A phase-shift laser scanner and a digital reflex camera were used to accomplish the survey project of the Parish Church of "Santa Maria", integrating where necessary with direct survey. The Z + F 5006h (Zoller+Fröhlich) laser scanner has a range of 79 m, a maximum speed of 1.000.000 points per second, a gripping angle of 360° horizontally and 310° vertically. The scanner is equipped with 5 acquisition presets, which correspond to as many levels of point cloud density: Preview, Middle, High, SuperHigh, UltraHigh.

One hundred and eighty nine scans were carried out over three days for generating a point cloud, which consisted of the whole geospatial data of the basilica body and the bell tower. The scans were recorded using Autodesk ReCap© software for assembling them together; they were used at least three targets located in the scene to shift and rotate the various point clouds, one on the other. Once the registration procedure was completed, the result was an only one point cloud with the complete 3D building model.

The file was saved in .rcp format to be imported for graphics production into the Autodesk Autocad© software, where it was possible to section the cloud with ideal plans at will and obtain screenshots. Then after setting the orthogonal UCS on the current section and the plan view, it was possible to outline the various profiles of interest of the building in wireframe and draw elevations, plans and sections.

The referred procedure allowed final drawings to reach the level of accuracy, decided upon the 1:50 scale at the start of the survey activities. The further detail required for representing moldings and architectural elements (1:20/10) was achieved by integrating the laser scanner survey with 3D Imaging techniques (digital photogrammetry and photo-modeling) with high resolution images from camera.

4 IDENTIFICATION OF DEFORMATIONS AND MODIFICATIONS OF THE STRUCTURES: AN APPROACH BASED ON THE 3D MODEL

The point cloud of the Pieve provides an almost unlimited possibility of extracting plans and sections. It is a very versatile tool both for studying structures and to obtain a rapid acquisition of information. In case of data processing does not require processing in autocad format, it is sufficient to perform sections by the 3D model.

The studied aspects of the church have concerned:
- the verticality and deformations of the pillars and walls;
- the conformation of the arches of the aisles;
- the configuration of the crossing structures.

4.1 The basilican body. Pillars, arches and walls

The inclination of the construction elements, walls and columns, has been verified by comparing plans carried out at different levels. The columns flanking the nave show diagonal displacements towards the outside, that have different magnitude in longitudinal and transversal directions (Figure 1).

On the side with three columns the inclinations towards the facade vary from 5 to 7 cm; starting from the facade, the external movement of the first two columns is small, 2/3 cm; it becomes about 10 in the column next to the cross, where the inclinations towards the outside have the greatest extent. The section across these columns shows a tilt under the thrust of the arches of the crossing, where not by chance the pillar is inclined about 6 cm towards them. In the opposite side of the crossing, the conspicuous wall of the facade, being an effective buttressing, has maintained the plumb position of the pillar.

It is noted that the greatest deformation have occurred in the two central arches. In the current construction, the crossing thrusts on a system of diaphragm arches that rests on the massive facade wall, and such deformation seems little justifiable.

This deformation could not even be attributed to the thrust of the barrel vaults which were added in the basilican body after the medieval period and then demolished by the restoration works. It could be hypothesised that the peculiar static conditions occuring in the construction works phases could have contributed to determine it; in many cases the static condition during and after the construction works are infact very different.

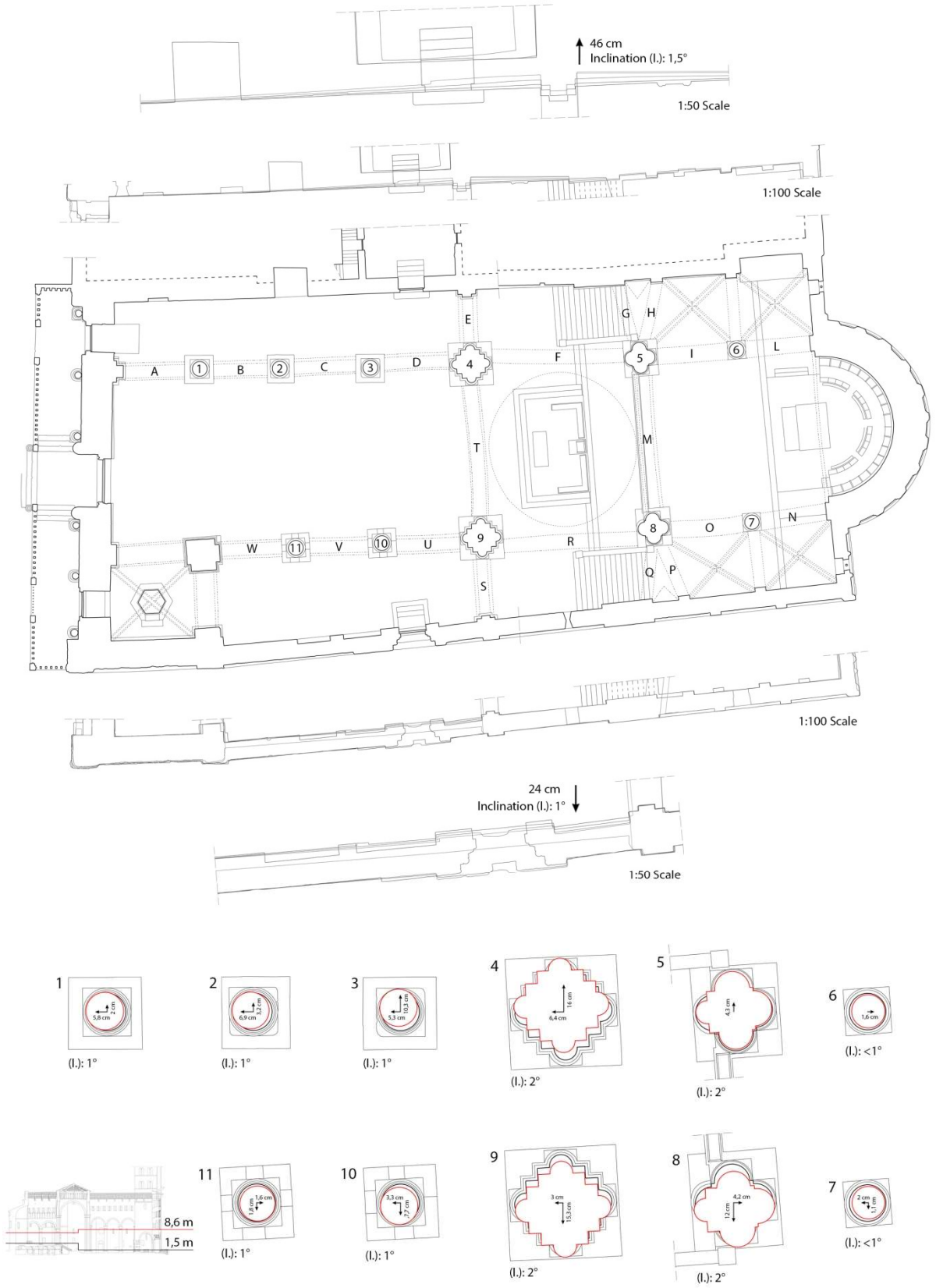


Figure 1: Plan of the church; we can see the maximun inclinations of the pillars and walls.

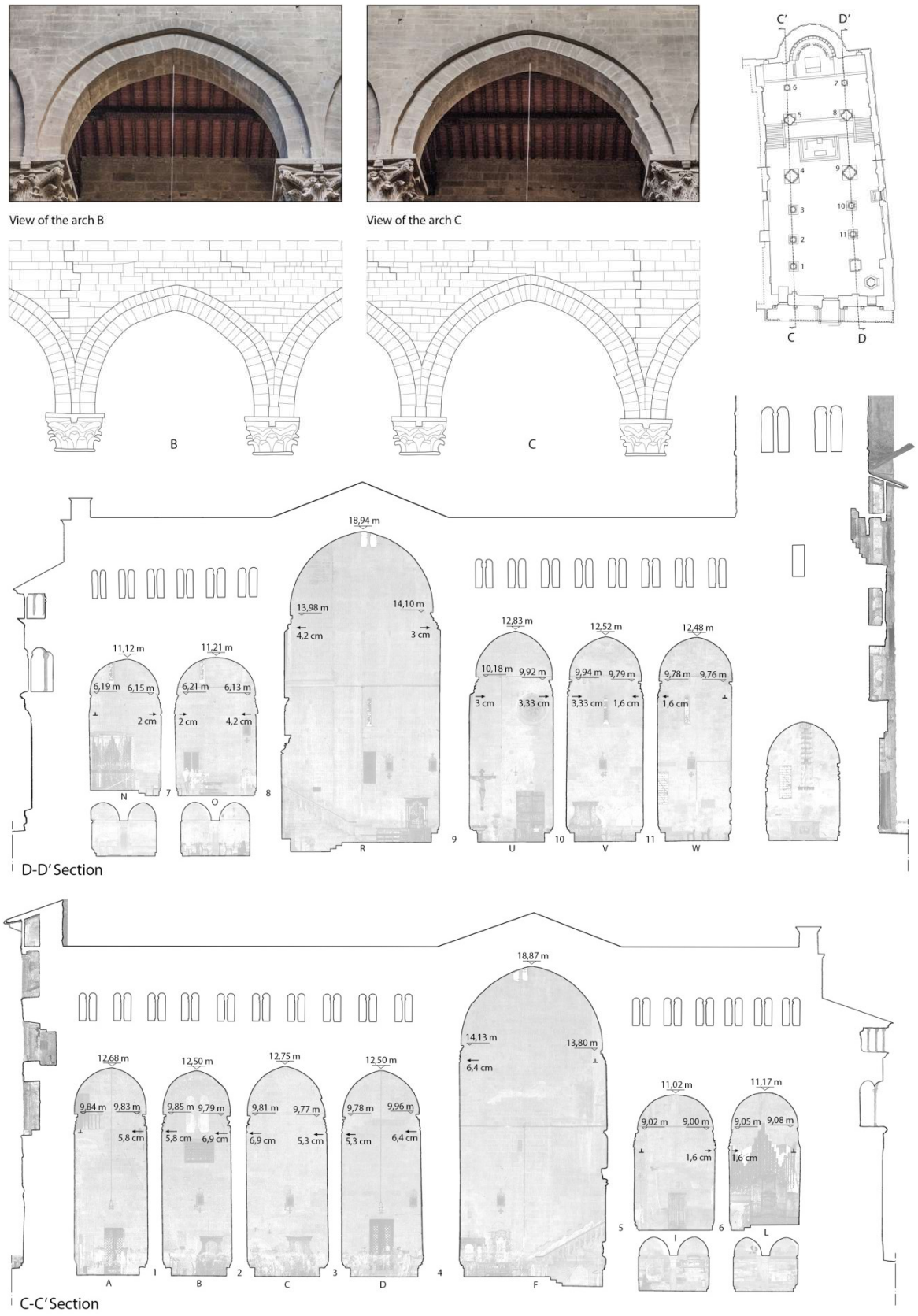


Figure 2: Longitudinal sections corresponding to the pillars which highlight the deformations of the structure.

The XIXth century restorations contributed to make the interpretation of the elements under consideration particularly complex. The barrel vaults of the naves, for example, should have necessarily left relics of the springer, of which today there is no trace in the facing wall. This is substantially homogeneous except for small vertical discontinuities.

The third arch (starting from the facade) is equally singular for the offsets on the intrados (Figure 2). It is unknown if consider them construction phases evidence, or corrections of curvature of the arches made during the restoration works.

On the opposite side of the nave the arches are three due to the presence of the bell tower; here the inclination of the columns is few accentuated, except for the one close to the crossing that has a tilt by about 8 cm on the outside.

The sides of the church have the greatest deformations where the transverse arches are aligned with the largest pillars of the crossing. Each of the pillars has an inclination of 2° towards the outside; the corresponding sides of the church have outwards tilts of 1° on via della Seteria, 1.5° on the opposite side.

However, the wall on via della Seteria has a particularity which needs to be explained. The part that flanks the aile is inclined, while the remaining stretch that extends to the presbytery area is perfectly vertical. The part between the out plomb wall to the vertical one takes place in correspondence of the pilaster aligned with the largest pillars of the crossing.

This peculiar structure makes clear that the vertical wall was definitely rebuilt and this had to be carried out during the restoration works in the years 1873-1874[14].

The characteristics of these walls have a further relevant aspect to consider. The entirely rebuilt wall should be considered homogeneous, while the out plomb one is made up of stone facing rebuilt in adherence to an original nucleus. In this case, the problem of the effectiveness of the connection between facing wall and inner core arises. In fact, for the earthquakes impact, detachment sometimes occurs between reconstructed facing and original masonry. That is due to the difficulty of creating a strong connection between these two differents parts.

This happened for example in the basilica of San Francesco in Assisi, where the earthquake of 1997 caused the collapse of a recontructed portion of masonry in the southern tympanum of the transept[15].

4.2 The crossing

The four pillars of the crossing have a first singular aspect concerning the difference, not only in features but also on resistant section, between the two adjacent to the naves and the other towards the apse. These last compared to the first ones have a reduced section by 30%. Today the pillars support a drum covered by a wooden covering, which might seem an unfinished work.

Moving on the examination of structural deformations, the pillars of the crossing show an inclination of 2° to the outside, except for the north-east one inclined by 1°; while they are on a modest tilt towards the naves.

It should be underlined that between the pillars of the crossing there are also differences in the structural connections with the sides of the church. The largest ones are connected with a

diaphragm arch, the smaller ones with two diaphragm arches that diverged into a V starting from the pillars themselves, thus distributing the thrusts on a wider area of the sides.

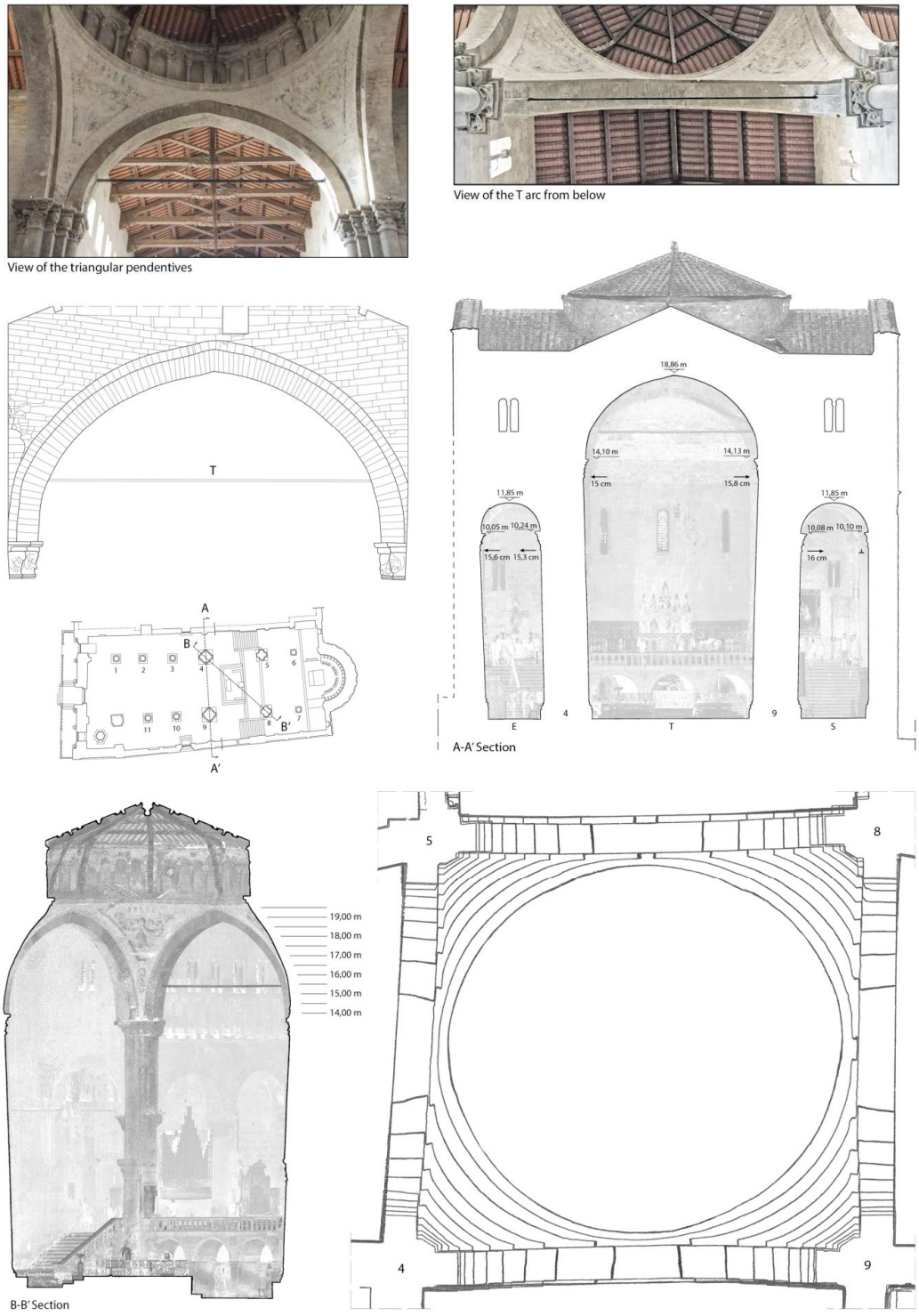


Figure 3: Crossing surveys: plan of the pendentives with horizontal level lines, the arch in front of the nave, cross and diagonal sections.

The arch of the crossing in front of the nave has a number of unique features (Figure 3). Its horizontal projection is not as straight as one would expect, but is visibly curved towards the crossing. In addition, the arch has the intrados with a marked vertical displacement in the central part; it is a deformation that must be related to the fact that, at the height of the capitals, the underlying pillars are inclined outside by a total of about 31 cm.

The structural alteration of the pillar-arch system has been confirmed by the stone facing above the arch. It shows rows with a rotation, towards the center of the arch, which varies between 7° and 9°; so the maximum vertical displacement of the rows is about 50 cm.

The pendentives of the crossing, analysed with plans at different levels, look similarly curved. The diagonal sections highlight pendentives with similar and slightly curved profiles.

We have no specific information on the facing wall of the pendetives. However, as far as visible from their facing, it can be assumed they were made by rows of progressive overhanging ashlars and they are probably part of a wall extended in depth until reaching the extrados of the adjacent arches. The pendetives are probably a type of massive masonry block which extends as far as inserting itself into the haunches of the arches. At the same time, the pendentives made stiffened the haunches and created a cantilever supporting the drum. In fact, in the arch in front of the nave, the center is the most subjected part to deformation over the level of the haunches.

The construction context of the crossing has a larger transversal vulnerability, resulting by displacements. Longitudinally, diaphragm arches stand on the massive walls of the facade and of the apse, which act as buttressing. The diaphragm arches, transversely, rest on the sides of the aisles, built up of rather thin walls.

However, it is questionable whether the displacements were produced by loads due to both the current modest drum and the wooden roof of the crossing; otherwise it should be assumed at least the beginning of the construction of a dome, which collapsed following the displacement of the underlying structures.

The investigations on the crossing and the data obtained pose therefore new questions concerning the construction phases and the interpretation of the structures. In this regard, the structural modeling of the church could be useful, to deepen the relationship between displacements and loads, such as an in-depth study of the blind loggia placed on the inner side of the drum.

5 CONCLUSIONS

The analysis of the structures of the "Pieve" highlighted the importance of understanding the history of the constructions varied over time, by relating different fields of studies, archival documents, architectural diagnostics and structural modeling.

In the current situation the building shows architectural features and types of structural alterations that reflect conditions changed over time. The time dating back to the organization of the medieval construction sites, the time of subsequent modifications, the time of the restoration works that deeply contributed to built the architecture and consequently the structure of the "Pieve di Santa Maria".

Starting from the outcomes illustrated in this work, a new research line based on Scan-to-BIM processes, was also identified for the implementation of parametric models aimed at the information management of the historical building heritage (H-BIM). Some investigation developments are already underway regarding the following areas of study: 4D modeling of the evolution phases of the monument; structural analysis and simulations; integration of heterogeneous datasets (archive data, photographs, drawings and geospatial datasets); integration of intangible information (cultural meanings and values) associated with specific components or spaces; interoperability for data sharing and their reuse by the property manager; testing of interfaces with different information management systems, such as GIS, CAFM and other databases.

Acknowledgements. We wish to thank Don Alvaro Baldelli, priest of the "Pieve di Santa Maria", for allowing us access to the church to carry out the laser scanner survey.

REFERENCES

[1] Curzi G., *Gli scultori della Pieve, in Arte in terra d'Arezzo, il Medioevo*, a cura di Collareta M. e Refice P., Firenze, (2010), pp. 127-135.

[2] Freni G., *Spazio liturgico e luoghi sacri nella cattedrale e nella pieve, in Arte in terra d'Arezzo. Il Trecento*, a cura di Galli A. e Refice P., Firenze (2005), pp. 218-220.

[3] Mercantini M., *La pieve di S. Maria ad Arezzo. Tumultuose vicende di un restauro ottocentesco*, Ed. Arezzo (1982), pp. 39-41.

[4] Freni G., *Spazio liturgico e luoghi sacri nella cattedrale e nella pieve, in Arte in terra d'Arezzo. Il Trecento*, a cura di Galli A. e Refice P., Firenze (2005), p. 220.

[5] Mercantini M., *La pieve di S. Maria ad Arezzo. Tumultuose vicende di un restauro ottocentesco*, Ed. Arezzo (1982), p. 17.

[6] Mercantini M., *La pieve di S. Maria ad Arezzo. Tumultuose vicende di un restauro ottocentesco*, Ed. Arezzo (1982), pp. 41-42.

[7] Matracchi P., *Symbol, identity, restoration, in Le torri di San Gimignano. Architettura, città restauro/The towers of San Gimignano. Architecture, town, restoration*, Firenze, (2019), pp. 33-64.

[8] Bardeschi M. D., *La storia tradita. Guida ai monumenti in fedeli d'Italia, in L'architettura cronache e storia,* ed. Fabbri, Milano, n. 330, (aprile 1983).

[9] Meschini A., Petrucci E., Rossi D., Sicuranza F., *Point cloud-based survey for cultural*

heritage. An experience of integrated use of range-based and image-based technology for the San Francesco convent in Monterubbiano, in: Int. Arch. Photogramm. Remote Sens. Spat. Inf. Sci. ISPRS Arch. (2014), pp. 413–420.
Grussenmeyer P., Landes T., Boegtle T., Ringle K., *Comparison methods of terrestrial laser scanning, photogrammetry and tacheometry data for recording of cultural heritage buildings*, in: ISPRS Congr. (2008), pp. 213–218.

[10] Manferdini A.M., Galassi M., *Assessments for 3d reconstructions of cultural heritage using digital technologies*, Int. Arch. Photogramm. Remote Sens. Spat. Inf. Sci. XL-5 W (2013) pp. 167–174.
Quattrini R., Malinverni E.S., Clini P., Nespeca R., Orlietti E., *From TLS to HBIM, high quality semantically-aware 3D modeling of complex architecture*, ISPRS Annals (2015), vol. XL-5/W4, pp. 367-74.

[11] GSA, *BIM Guide for 3D Imaging*, (2009), p. 53. Retrieved: www.gsa.gov/bim.

[12] Murphy M., Mc Govern E., Pavia S., Historic Building Information Modelling - Adding intelligence to laser and image based surveys of European classical architecture, *ISPRS Journal of Photogrammetry and remote Sensing* (2013), 76, pp. 89-102.
Brookes C., *The application of building information modelling (BIM) within a heritage science context*, Project n. 7351. Ramboll (2017), pp. 63.

[13] Historic England, *3D Laser Scanning for Heritage: Advice and Guidance on the Use of Laser Scanning in Archaeology and Architecture*. Swindon (2018), pp. 113.
Historic England, *Photogrammetric Application for Cultural Heritage. Guidance for Good Practice*. Swidon (2017), pp. 124.

[14] Mercantini M., *La pieve di S. Maria ad Arezzo. Tumultuose vicende di un restauro ottocentesco*, Ed. Arezzo (1982), p. 50.

[15] Rocchi Coopmans de Yoldy G., *La basilica di San Francesco ad Assisi. Prima, durante e dopo il 1997*, Firenze, (2002), p. 22.

[16] Bartoli M.T., Biagini C., *San Giovanni di Dio, un contributo di conoscenza dal rilievo*. In: Diana E., Ghidetti E., *Settecento anni di storia. San Giovanni di Dio, un ospedale da non dimenticare*, (2012), Polistampa, Firenze, pp. 49-77.

[17] Verdiani G., Peruzzi A., Gualandi M., *The Piacenza Cathedral, from the Digital Survey to a Complete Multimedia Documentation*. In: Toniolo L., Boriani M., Guidi G., *Research for Development Built Heritage: Monitoring Conservation Management*. Springer, (2014), pp. 313-21.

12th International Conference on Structural Analysis of Historical Constructions
SAHC 2020
P. Roca, L. Pelà and C. Molins (Eds.)

THE DOME OF THE TEMPLE OF DIANA IN *BAIAE*: GEOMETRY, MECHANICS AND ARCHITECTURE

A. SINOPOLI[1], **D. AITA**[2]

[1] Department of Structural and Geotechnical Engineering
Sapienza University, Rome, Italy
e-mail: anna.sinopoli@uniroma1.it

[2] Department Architecture and Design
University of Genoa, Italy
e-mail: danila.aita@edu.unige.it

Keywords: *Opus caementicium*, Domes, Geometry, Building techniques, Structural analysis

Abstract. *The purpose of this paper, which is part of a multi-disciplinary research project started in 2018 [1], is to investigate both the geometry and stability of the dome of the temple of Diana, which partially survived for many centuries. Important observations made by De Angelis d'Ossat [2] and results of the architectonic survey performed by Rakob [3] will be presented and discussed; they introduce the delicate issue concerning the identification of the geometric profile of the dome, on which its structural stability depends. It is the Authors' opinion that ascertaining the geometric profile of a dome is not only a matter of measuring, but also of historical context, geometric knowledge and traditions in construction. Thus, by taking all the above issues into account and making use of data from a recent architectonic survey [1], this paper searches for possible connections with consolidated traditions of the Sassanid architecture imported by the Emperor Alexander Severus, verifies the geometric knowledge presumed to have been acquired by the time of the dome's construction and identifies the most probable theoretical design: the dome's meridian profile is a unique curve – to be precise, a parabola, the best approximation of a catenary. Thus, once the profile of the dome has been identified, structural analysis confirms not only the stability of the dome, but also that the Romans were aware of the dome's behaviour in relation to the construction solutions adopted.*

1 INTRODUCTION

Roman mortar, a refinement of the most ancient building systems, common throughout the Mediterranean basin since at least the 5th century BC, was introduced into Roman building methods from at least the 3rd century BC. It consisted of slaked lime and fillers such as "*pozzolana*" sand, gravel, and "*cocciopesto"* (crushed earthenware, tiles, and/or bricks).

It was only in the 1st century AD that *opus caementicium* began to be used on a massive scale; at first, only for the interior design of buildings and then, in the 2nd and 3rd centuries AD, for various types of public buildings and territorial urbanization. Certainly, the switch from a radial arrangement of the elements used in the construction of arches and vaults to the horizontal layout typical of the *caementa* in *opus caementicium* is in line with the principle of economy and industrialization of the construction process, which determined the building technique

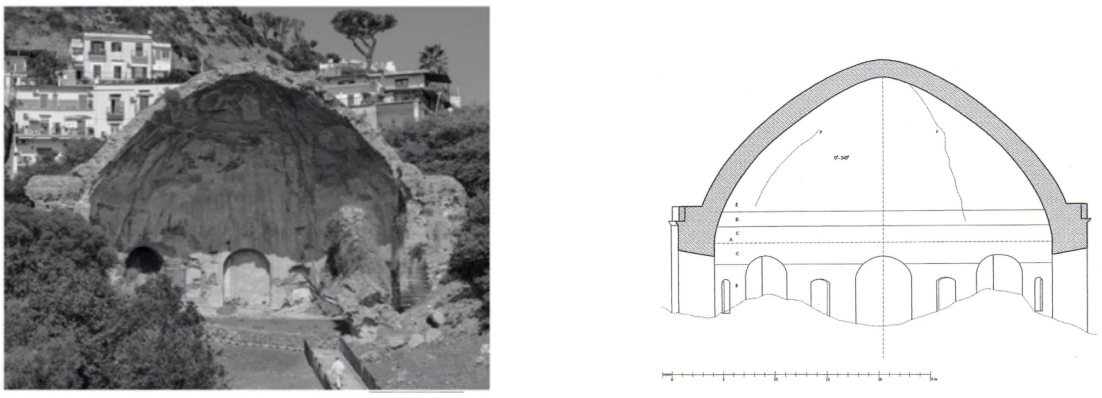
typical of Roman architecture. The Romans extended experimentation with *opus caementicium* from the 1st century AD by using it also to build domes.

In this paper the dome of the temple of Diana will be investigated with a double purpose: to ascertain the dome profile adopted by the Romans, and to verify the consequence on the dome's structural stability. In Section 2 geometrical and architectonic features of the dome will be presented. Section 3 is focused on the historical reconstruction of the events that probably induced the Roman emperor *Severus* to build this temple in *Baiae*. Section 4 analyses the debated question of the dome profile, by discussing the results of the surveys performed up to now. Section 5 tackles the problem of searching for a possible geometric profile, both theoretical and experimental, by identifying the distributions of deviations of the theoretically presumed profiles of the meridians from the corresponding experimental data.

By assuming that the most probable intrados profile of the dome meridians corresponds to an upper parabola and a lower circle arc, the Authors demonstrate in Section 6 that the geometrical knowledge to design and build the dome was adequate and well known at the time the dome was built. Finally, in Section 7, a preliminary structural analysis of the dome will be performed by means of the membrane theory.

2 THE PRIMACY OF THE DOME OF DIANA

The architectural choice of covering a spacious circular hall with a monumental dome in *opus caementicium* was first made in *Baiae* – the *pusilla Roma* – for the construction of the temple of Mercury [3]. The domed circular halls of *Baiae* date from the late Republican to the late Severian period; there is no reason to presume that they derive from pre-existing models of the capital. On the contrary, it can be assumed that the new construction technique found its first practical and architectural application at the *Campi Flegrei*. Our analysis follows on from previous investigations, such as those proposed by Maiuri [4], De Angelis D'Ossat [2] and Rakob [3]. The temple of Diana (3rd century AD) is the largest in *Baiae* and its dome, for the most part still extant, is the largest in antiquity after the Pantheon; the diameter of the dome is in fact about 29.80 metres (Fig. 1). Its construction represents the biggest challenge in building a dome in *opus caementicium* in *Baiae*: the largest rise, largest span, largest windows, and thinnest thickness of the dome. Small openings are interposed between the large, high span windows, which are surmounted by double ring splayed arches (Fig. 1).



(a) *(b)*

Figure 1: The temple of Diana. The remaining part *(a)*; Rakob's vertical section *(b)* [3].

The plan of the internal hall is circular, whereas externally it is octagonal. The tambour surrounding the dome springing is very thick, as it is the only external strengthening device in the lower part of the dome. Half of the structure has collapsed; although the causes are not completely understood, this may be due to a combination of local bradyseism and earthquakes.

3. THE RELATIONSHIP BETWEEN OCCIDENT AND ORIENT

Because of the special techniques used in building it, the temple of Diana has been attributed to the Emperor *Severus Alexander* (222-235) by De Angelis d'Ossat [2], who quotes from the detailed work *Vita Severi Alexandri* by *Aelius Lampridius*: "*Et in Baiano palatium cum stagno fecit, quod Mammeae nomine hodieque censetur. Fecit et alia in Baiano opera magnifica in honorem adfinium suorum et stagna stupenda admisso mari*", (24, 9-10). *("And in the Baiae district he created a palace with a lake, which, named after Mamaea [his mother] is still in the records today. He also did magnificent works in Baiae, in honour of his family, and formed amazing artificial lagoons by allowing water to flow in from the sea"* [translation by the Authors].

Severus Alexander (208-235 AD) was only 13 years old when he ascended to the throne: he died after about 13 years as Emperor. The leadership then passed to the women of his family, who were of Syrian origin: his grandmother *Iulia Maesa* and his mother *Iulia Avita Mamaea*. *Severus* was remembered as a good and gentle emperor, but he was probably not capable of dealing with the military problems that faced him. The most important event in his life was the military campaign against *Ardashir* – the founder of the Sassanid dynasty – who started an offensive to win the Syrian lands from the Romans. The sequence of events forced *Severus Alexander* to leave Rome in 231 and to spend a long time – at least until 233 – in the Orient, where his mother *Iulia Mamaea* had joined him.

Based on the observations made by De Angelis d'Ossat [2] and the events characterising *Severus Alexander*'s life, the Authors will try to demonstrate that the dome of Diana could be the *opus magnificum*, the *Severi* family's *Heroon* in *Baiae*, in the form of an *Îwân*.

3.1 Sassanid architecture: the Palace of Ardashir and the Temple of Diana

During the Sassanid Empire, the most essential innovation in architecture occurred with the construction of domes, which were often erected over palace reception halls (*Îwân*), such as the domes over the palace of *Sarvestan* and *Ardashir* (Fig. 2) in *Firuzabad*. These domes provide the first known examples of the use of squinches, a technique that had an enduring effect on the development of the dome in Islamic architecture [5, 6]. The palace of *Ardashir* (3rd century AD) is the most famous and imposing domical monument of the Sassanid era, which extended from 224 to 651. The building consists of three oval domes, with a span of 13.30 m., resting on squinches that are used as transition parts between the horizontal polygonal section and the upper circular calotte. By analysing the organization of the various architectonic elements in the palace of *Ardashir*, some similarities with the organisation of space in the temple of Diana can be ascertained (see Fig. 1). Bearing in mind that the lower part of the temple of Diana collapsed due to bradyseism, it is possible to observe in both structures that small recesses intersperse the high, large span windows, which are surmounted by splayed arches. The domes of both structures seem to spring just above the arches, resting on squinches located in between two adjacent arches; the domes are immersed in the tambour (see Fig. 1, *a*), whereas only the

upper cap (characterised by a small *oculus* in the case of the domes on the palace of *Ardashir*), is self-supporting with constant thickness.

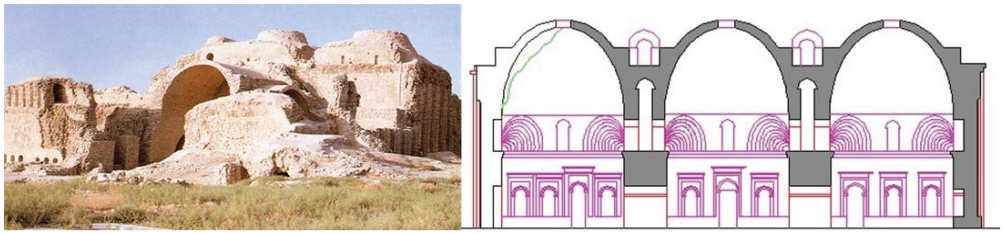


Figure 2: The palace of *Sarvestan* and *Ardashir*. Sassanid period. Firuzabad [5].

The dome's profile in both structures can be defined as gibbous. *Balneum Gimburusu* is in fact the term used by *Pietro da Eboli* (Fig. 3, left) as nickname for the temple of Diana [7]. Moreover, the oriental inspiration of the profile of the dome of Diana is proved by the *Ctesiphon* vault (Fig. 3, right), built in the palace of the Persian King *Kosrow* (591-628). The entrance hall to the palace – an *Îwân* with a span of 26 metres and a rise of 31 metres – is one of the most emblematic examples of parabolic barrel vaults**,** a sign of the faraway beginnings of vaulted roofs in the Sassanid era, built according to the ancient *Mesopotamian* technique using bricks without centring.



Figure 3: *Balneum Gimburusu*, Biblioteca Angelica, Roma, ms. 1474, end of 13th century, fol. 18 (left), (from Sinopoli *et al*. 2018); *Îwân* in *Tâq-Kisrâ* in Ctesiphon, Iraq: the vault of the *Kosrow* palace (right).

4. THE DEBATED QUESTION OF THE DOME PROFILE

With reference to the dome of Diana in *Baiae,* De Angelis d'Ossat affirms: "We do not know if the dome's profile – which has never been surveyed – corresponds to either one or more curves (catenary, parabola, circle's arcs). Nevertheless, the typical curve trend we have defined as ovoid, can usually be observed in the vaults of all the ancient Orient, starting with the rare significant Egyptian examples of barrel vaults" [2].

4.1 Rakob's photogrammetric survey

More recently, Rakob [3] tried to solve the question of the profile of the dome of Diana through a photogrammetric analysis. He thus proposed a polycentric profile composed of four

circle arcs, characterized by two different *radii* and aligned centres, in order to guarantee tangency continuity along the meridians at the parallel connection. Rakob stated that the dome is characterized by span and rise equal to 100 and 50 Roman feet, respectively.

It is the Authors' opinion that, by proposing the polycentric profile, Rakob followed the analyses performed by Choisy [8], who, observing the form of many Egyptian barrel vaults, proposed an oval form composed of circular arcs with aligned centres. As a matter of fact, the oval form appeared in Europe in Roman times for the design of amphitheatres, whereas it seems that the Romans did not build oval domes characterised by a polycentric design. Moreover, it is the Authors' opinion that ascertaining the geometric profile of a dome is not only a matter of measuring, but also of historical geometric knowledge, construction tradition and problems posed in practical building by the use of a given profile [9, 10]. These are the reasons that motivated the start of a research project in 2017, aimed at solving the controversial question of the dome profile [1].

4.2 Recent survey of the dome of Diana and preliminary interpretations

In accordance with the research project, the architectonic survey of the intrados of the dome of Diana was performed by Valenti and Romor [1] using two instrumental technologies: 3-D laser scanning and digital photogrammetry. The detailed analysis of the critical approach pursued during the measuring process, together with the preliminary interpretations of the results obtained, have been reported in [1].

In synthesis, the central symmetry of the dome with the corresponding symmetry axis was tested through the identification of nine horizontal sections, defining circle arcs as approximation for the parallels. The identification of the vertical symmetry axis also allowed the dome meridians to be drawn as well, by sectioning the experimentally obtained cloud of points through 16 vertical planes crossing the symmetry axis and spaced out from each other by 10 degrees. The preliminary interpretations of the experimental data do not seem to be either conclusive or definitive, although the polycentric profile proposed by Rakob in [3] has been considered as plausible with the results obtained.

It has indeed been assumed (presuming that Rakob made the same assumption) that the springing of the dome is located just over the extrados key of the double splayed arches (see Fig. 1, *b*), where a horizontal string of large bricks seems to outline the plane height reached. Consequently, the rise of the dome thus identified by Valenti and Romor was found to be only 47.70 Roman feet rather than 50. Neither they nor Rakob took the experimental data of the meridian points located under the assumed springing into consideration.

Moreover, the *radii* of the circle arcs of the polycentric profile turned out on the whole to be significantly lower than those proposed by Rakob.

5 SEARCHING FOR THE DOME PROFILE

To begin their investigation the Authors made use of the numerical file kindly provided by Valenti and Romor [1], which includes all the geometrical data of the 16 meridians surveyed. By performing analytical elaborations based on these data, the Authors have tried to solve the question of the meridians' profile. On her first on-site inspection in *Baiae* in 2016, the first Author certainly had the impression that the extrados profile of the dome of Diana over the tambour was parabolic; this impression needed to be analysed.

5.1 Theoretical investigation into possible profiles

Before analysing the experimental numerical data, it was necessary to investigate if, assuming Rakob's theoretical features of the dome design – namely, the dome's span and rise corresponding to 100 and 50 R.ft., respectively –, it was possible to identify a polycentric profile made up of a lower circle arc, with its centre at the same height as the dome springing, and an upper curve – either a circle or a parabolic arc – matched in tangency continuity conditions.

For the profile composed of a lower circle arc and an upper parabola, the tangency continuity requirement for the connecting point identified infinite solutions depending only on the lower circle arc *radius*. By considering a *radius* equal to 37 Roman feet for the lower circle arc, as proposed by Rakob, both the parabola curvature and the matching point *C* have been identified; the curvature is equal to –0.0153, while the connection occurs for x_C = 42.2885 Roman feet and y_C = 22.6093 R.ft., respectively, as shown in Fig. 4*a*.

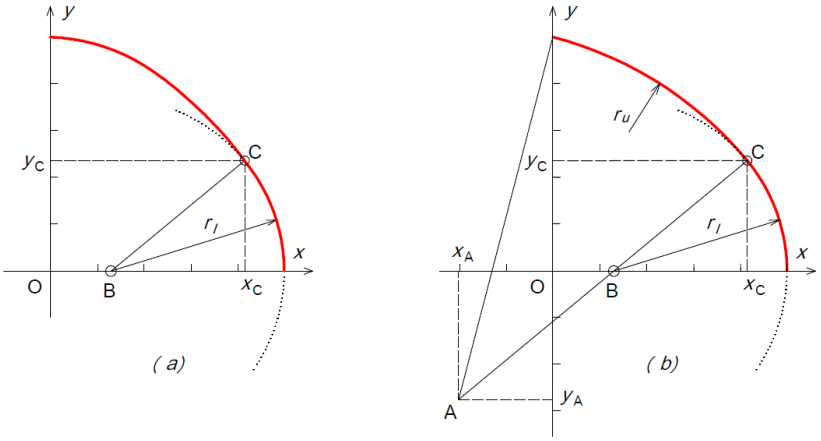


Figure 4: Theoretical dome profiles, composed of a lower circle arc, with *radius* r_l=37 Roman feet: theoretical upper parabolic arc (*a*); upper Rakob's circle arc with *radius* r_u=80 Roman feet (*b*).

The search for Rakob's theoretical polycentric curve has been simpler. If the *radii* of the two circle arcs are assumed equal to r_l=37 and r_u=80 Roman feet, respectively, as Rakob proposed, in this case (Fig. 4, *b*), the coordinates of the upper circle centre are x_A = –20.1150 R.ft. and y_A = –27.4299 R.ft., while the matching point lies at the height of y_C = 23.6024 R.ft.. Obviously, a slight modification of the value of either *radius* is sufficient to obtain different values for both the centre coordinates of the other circle and the height of the connecting point. In conclusion, if the *radii* of the two circle arcs are unknown and the dome span and rise are given, ∞^2 solutions corresponding to Rakob's polycentric profile exist; moreover, if the dome rise is changed a further indeterminacy is added to the problem.

5.2 Comparison between theoretical and experimental data

Identification of the value of the lower arc *radius* – which better approximates the experimental data distribution – has been obtained from the comparison between the experimental data with the results of the theoretical analysis of a profile made of a lower circle and an upper parabola. Moreover, it has been possible to demonstrate that the dome's springing is at the zero value of the *y* coordinate, where the tangent's slope to the profile is *90*°.

The dome starts with eight squinches located in between two adjacent arches; the squinches end just above the extrados of the double splayed arches, where the intrados parallel of the dome finally becomes a whole circle. This relevant result confirms the oriental inspiration of the temple of Diana in the use of squinches to connect the springing to the circular contour of the upper calotte.

The procedure adopted to compare theoretical results and surveyed data – a reliable approximation of the standard statistical regression – considered the analytical expression of the assumed profile and the known experimental coordinates; both y coordinates corresponding to the same experimental x coordinate were then evaluated, in order to compare theoretical and experimental y and minimise the mean absolute deviation of the corresponding distributions.

Fig. 5*a* shows the distribution of the points encompassing the sixteen theoretical meridian profiles corresponding to the upper parabola and lower circle arc, in comparison with the experimental data; the value of the lower circle *radius* is equal to 37 Roman feet, as already found by Rakob.

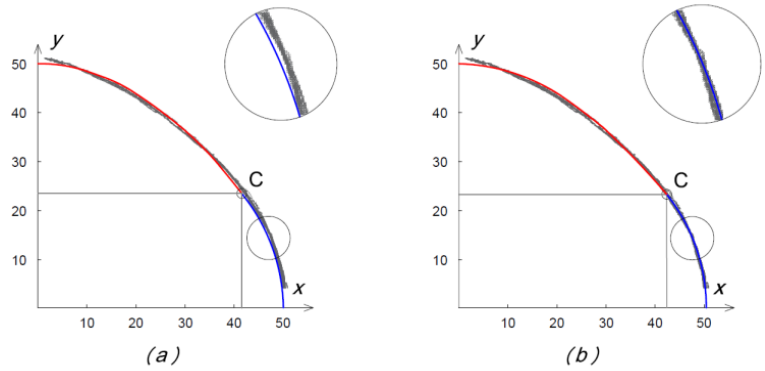


Figure 5: Theoretical parabolic-circle arc profile and experimental data (a); best-fit parabolic-circle arc profile and experimental data (b).

Figure 5*a* suggests that the theoretical parabola approximates the experimental data; however, it shows a mean deviation of the lower circle arc, as if the built dome was characterized by a span larger than 100 Roman feet. By slightly modifying the centre coordinate x of the lower circle, it has been possible to obtain the best-fit dome profile shown in Fig. 5*b*; the centre coordinate x of the lower arc is x=13.41 (rather than 13), corresponding to a dome span of 100.82 R.ft.. Obviously, the best-fit matching point coordinates are changed: they become x=42.3354 and y=23.0058, respectively.

An investigation similar to that discussed so far was also performed for Rakob's polycentric curve, made of two circle arcs of *radii* equal to 37 and 80 Roman feet, respectively. The comparison with the experimental data is shown in Fig. 6*a*; the assumed rise and span of the dome are still 50 and 100 Roman feet. As can be observed, in addition to the deviation of the lower circle arc, probably due to an actual span larger than 100 Roman feet, as in Fig. 5*a*, agreement between the upper circle arc and experimental data is lacking.

When looking for a best-fit polycentric profile the parameters on which the problem depends must be modified. For the lower circle arc, it is sufficient to increase the x coordinate of its centre; for the upper circle arc, on the contrary, the indeterminacy is doubled, since its profile

depends on both the dome rise and the upper circle *radius*. Assuming the experimental dome rise to be correct, it is clear that the possible polycentric profile admits infinite solutions, depending on the *radius* and the corresponding centre of the upper circle. Moreover, by varying both the rise and the *radius* among infinite possibilities, a very good approximation can be obtained; the comparison between experimental data and best-fit polycentric profile obtained is shown in Fig. 6*b*. The theoretical rise of the dome is, however, equal to 51.41, whereas the upper *radius* corresponds to 79.70 feet and the connection point is at a height of about 22 feet.

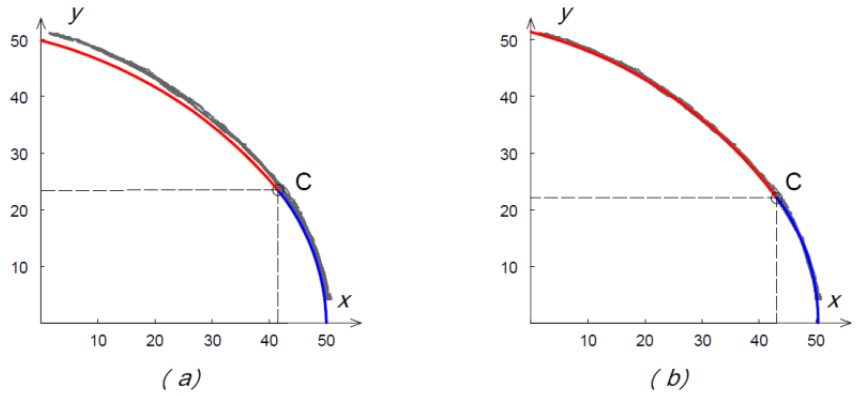


Figure 6: Theoretical Rakob's circle arcs and experimental data (a); best-fit polycentric circle arcs and experimental data (b).

In spite of the apparently good result shown in Fig. 6*b*, the Authors believe that, in investigating the profile of a dome, the most important comparison is between the built profile – inevitably badly affected by construction irregularities, tested by the experimental data – and the presumed theoretical design. In this respect, Rakob affirms that the dome rise is equal to 50 Roman feet, in agreement with a consistent theoretical design, by obtaining a fake agreement between experimental data and theoretical design, unless the dome's springing is moved from y=0 R.ft. to y=1.5 R.ft.. To confirm this, the absolute Δy deviations distributions of the two theoretical upper profiles (circular and parabolic, respectively), corresponding to a dome rise equal to 50 Roman feet, and evaluated with respect to the experimental data, are shown in Fig. 7; Rakob's deviations distribution is double that of the parabolic profile.

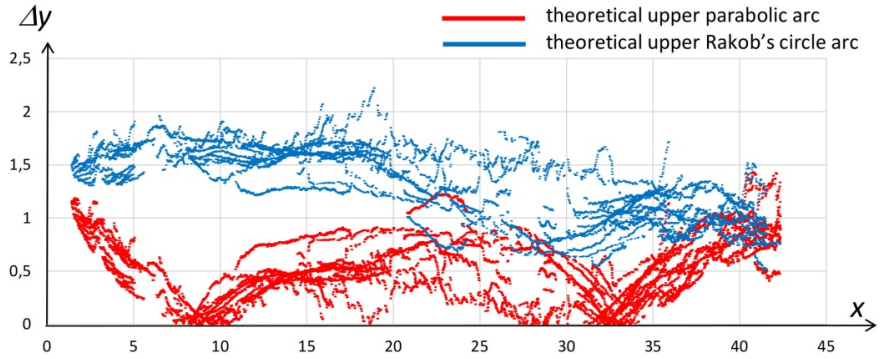


Figure 7. Absolute Δy deviations distributions between theoretical upper profiles and experimental data. Both distributions correspond to a dome rise and span equal to 50 and 100 Roman feet, respectively.

6. FROM THEORY TO PRACTICE

To support the Authors' opinion that the theoretical profile of the dome of Diana is composed of a lower circle arc and an upper parabola matched at the height of about 23 Roman feet, let us analyse the geometric knowledge assumed to have been acquired by the time of the dome's construction. The period in which the body of Greek geometric rules was formed extends from the third century BC to 550 AD, that is, from the Hellenistic civilization of the Mediterranean basin and throughout the Roman dominion, until the time of the Byzantine hegemony. Euclid (about 300 BC), Archimedes (287-212 BC) and Apollonius (262-190 BC) form the triad of the greatest Greek geometers.

6.1 Apollonius of Perga and the *Conics*

Apollonius's fame is due to his *Conics*, a fundamental work that is partly a collection of instruments deduced from preceding scientists (including Euclid), and partly an original treatise containing very profound results. Apollonius uses as reference the stereometric origin of conics only to obtain the fundamental properties of each one – these are plane properties constituting the basis for further theoretical developments. The most important of Apollonius's theorems concerning the properties of the parabola, useful for the purposes of this paper are contained in book *I* of his *Conics* [11].

His *Proposition I.11* can be detailed as follows: Let QV be any ordinate relative to the symmetry axis PM (Fig. 8). If a line is drawn, crossing P and perpendicular to PM, then: $QV^2 = PL \times PV$, where PL is a defined constant segment named as "right side" of the parabola. This proposition and the segment PL are precisely the parabola "symptom" and the "right side", respectively, which allow the construction of a parabola starting from a circle, the diameter of which represents the "right side".

In *Propositions I.33-I.35* Apollonius introduces two theorems concerning the tangent to a parabola, in this way: consider a point T (Fig. 9), along the symmetry axis of a parabola and outside the curve, so that: $TP = PV$, where V is the foot of the ordinate corresponding to a generic point Q; thus, the line TQ is tangent to the parabola at point Q (*Proposition I.33*). Conversely, if the line TQ is tangent to the parabola, thus: $TP=PV$ (*Proposition I.35*).

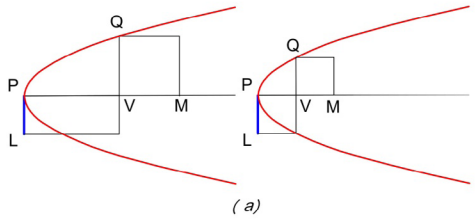


Figure 8: The parabola "symptom".

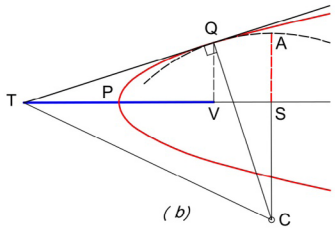


Figure 9: Drawing the tangent to a parabola.

These theorems are fundamental for defining the features of a dome design, the profile of which corresponds to an upper parabola and a lower circle arc, once the dome span and rise have been defined. In fact, having fixed only the height SV of the connection between lower circle arc and upper parabola, it is possible to identify the unique right-angled triangle TQC,

with its right-angle at point Q (Fig. 9), which intercepts the lower circle centre C at the springing height, guaranteeing the tangency continuity condition of the two curves at point Q.

7. STRUCTURAL ANALYSIS OF THE DOME OF DIANA

The static regime of an axio-symmetrical dome subject to its own weight depends on the profile of the meridians. The search for its best shape is, in fact, the extension in 3-D of that funicular principle, according to which the funicular curve of a load distribution is the best shape for plane arches and ropes of negligible thickness, by guaranteeing equilibrium in terms of pure compressive/tensile stresses.

In fact, the spatial organization of an axio-symmetrical dome is always able to resolve its static functions in terms of compressive and tensile stresses, since the hoop forces provide the missing action deriving from the deviation of the meridian profile from the funicular curve. This peculiarity allows a thin dome, built with material resistant to both tension and compression, to be characterized by membrane behaviour and configures it as a thin form resistant structure. For a hemispherical dome, compression is guaranteed along the meridians: it grows from the crown to the springing. Along the parallels, on the other hand, the stress state is characterized by a reversal of the sign at a colatitude of 51.82°: compressive stresses decrease from the crown to the critical parallel, while a state of increasing tensile stresses manifests itself as far as the springing.

Depending on the shape of the dome profile, however, the colatitude of the critical parallel could tend to approach the springing: a cap-like regime – characterized by compression along both meridians and parallels – could therefore act on most of the dome. Is this the reason why the dome of Diana is characterized by a parabolic upper profile (Fig. 1)? In the next Section some preliminary results obtained using membrane theory are presented.

7.1 Membrane theory of shells for identifying the theoretical stress state

The thickness of the dome of Diana – from the key to the maximum height of the drum – is almost constant and is roughly equal to 5 Roman feet; membrane theory can therefore be used to perform its structural analysis. The dome under examination is subjected to axial symmetrical loading, represented by its self-weight; it is characterised by intrados height and span equal to 50 and 100 feet, respectively, while the intrados profile corresponds to the theoretical upper parabolic and lower circular curves identified in Section 5 (Fig. 5a).

By adopting the same notation proposed in [12], Figure 10 shows dimensionless meridian and hoop forces $s_1(x)$ and $s_2(x)$, obtained by dividing the forces S_1 and S_2 by span, thickness and specific weight. It can be seen that meridian forces are compressive along the whole dome (Fig. 10*b*), whereas hoop forces are compressive only in the upper parabolic segment (Fig. 10*c*); tensile hoop forces, in fact, arise below the connection joint (Fig. 10*a*).

This relevant result can thus justify why the height of the drum is roughly equal to that of the connection point between lower circle and upper parabola: thus the self-supporting portion of the dome is the only part that corresponds to the upper parabolic segment, while the lower part is completely immersed in the drum, which acts as an extended buttress. In this case, the lower arc-shaped intrados profile simply has a merely aesthetic role, being only a geometric connection in tangency continuity conditions rising with the parabola and descending with the vertical drum.

A further controversial question tackled by the Authors concerns the possibility of building the dome of Diana in *opus caementicium* without the need of global supporting centring. Therefore dome-building processes, and in particular domes corresponding to different steps of construction, have been considered. These domes (Fig. 11) are characterised by an increasing rise, so that the diameter of the *oculus* – measured at the intrados – varies with the dome height from 100 R.ft. (first construction stage) to zero (last construction stage) in correspondence to the achieved rise of 50 Roman feet.

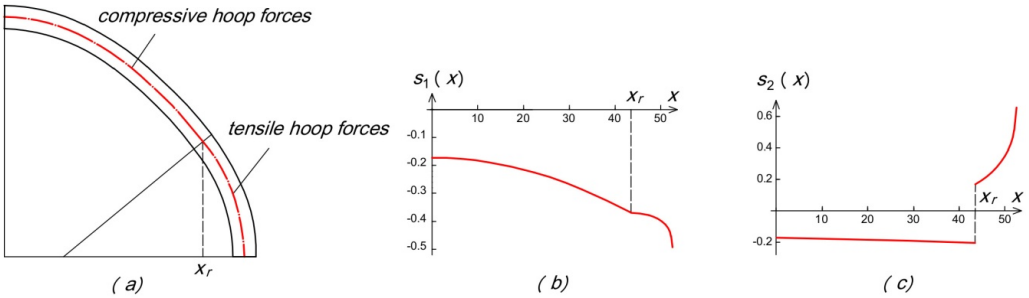


Figure 10: Profile made of an upper parabola and lower circle arc. $s_1(x)$ and $s_2(x)$, as function of abscissa x.

Making use of membrane theory, it was demonstrated that, whereas meridian forces are always compressive irrespective of the dome rise achieved, hoop forces are always characterised by a change of sign. The height y_ζ at which such a change of sign occurs is always lower than the rise reached y_ω (Fig. 11); during the simulated construction process, therefore, hoop forces are compressive in the upper part of the dome and tensile in the lower part.

The position of the change of sign varies as long as the building process in elevation, until it asymptotically converges to a stable value. It is worthwhile to observe that the height of the rise over which hoop forces are always compressive corresponds exactly to the connection between the upper parabolic and lower circle-arc intrados profile. In this case, the asymptotic height corresponding to the change of sign is identified by the value y_ζ = 24.4 Roman feet at the axis line; the corresponding *oculus* height y_ω is greater than 40.8 R.ft.

Thus, De Angelis d'Ossat's opinion [2] that the dome was built from the intrados side without global centring, as a standard masonry wall, is now decisively confirmed by the above.

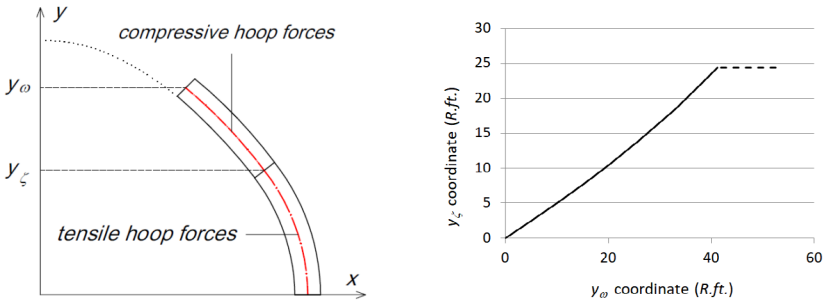


Figure 11: Varying height y_ζ at which hoop forces change sign (continuous line) and asymptotic behaviour (dotted line), as function of the *oculus* height y_ω reached.

8 CONCLUSIONS

The temple of Diana (3rd century AD) is the largest in *Baiae* and its dome, for the most part still extant, is the largest in antiquity after the Pantheon; the diameter of the dome is in fact about 29.80 metres. Its construction represents the biggest challenge in building a dome in *opus caementicium*: the largest rise, largest span, largest windows, and thinnest thickness.

De Angelis d'Ossat first recognized in the dome's profile an ovoid shape by him ascribed to an oriental tradition, that the Authors recognised as belonging to the Sassanid architecture. Moreover, since ascertaining the geometric profile of a dome is not only a matter of measuring, but also of historical context, geometric knowledge and traditions in construction, the Authors first performed a theoretical investigation on possible geometric profiles, having assumed the fundamental features of the dome's span and rise [3]. Then, the most probable dome's design has been identified by comparison with the experimental data of a recent architectonic survey [1]: the upper dome's meridian profile is a unique curve – to be precise, a parabola, the best approximation of a catenary –, which immerses itself in the tambour. Finally, the geometric knowledge presumed to be known at the time of dome's construction has been verified, and a preliminary structural analysis of a dome has been performed by using membrane theory.

It is worthwhile to outline that the Romans' primacy in dome construction was the result of their awareness (based on intuitive and experimentally verified knowledge) of the static flow generated in a dome depending on its geometric profile. In any case, the building techniques adopted were based not only on *empiricism*, but also on theoretical knowledge of a substantially geometric nature. In fact, from an early start in Greek cultural history, up to the 17th century, Mechanics was to develop as a Science of Weights governed by Geometry.

REFERENCES

[1] Sinopoli, A., Valenti, G.M., Bruno, M., Conti, C., Romor J. and Martines, G. Primato romano delle volte: Il tempio di Diana a Baia, In: S. D'Agostino et al. (Eds.), *History of Engineering*, Cuzzolin, Napoli, (2018), Vol I, pp. 57-72.

[2] De Angelis d'Ossat, G. L'architettura delle Terme di Baia, In: *I Campi Flegrei nell'archeologia e nella storia, Atti dei Convegni Lincei* (1977) **33**: 227-274.

[3] Rakob, F. *Römische Kuppelbauten in Baiae*, In: *Mitteilungen des Deutschen Archäologischen Instituts, Römische Abteilung*, (1988) **95**: 257-301.

[4] Maiuri, A. *I Campi Flegrei*, Roma (1958).

[5] Grabar, O. *Islamic art and beyond*, Variorum Press, United Kingdom (2006).

[6] Ashkan, M., and Ahmad Y. Persian Domes: History, morphology and typologies. *Archnet-IJAR, International Journal of Architectural Research* (2009) **3**(3): 98-115.

[7] Maddalo, S. *Petrus de Ebulo, Nomina et Virtutes Balneorum seu De Balneis Puteolonorum et Baiarum. Codice Angelico 1474* (1998), Istituto Poligrafico dello Stato, Roma.

[8] Choisy, A. *L'art de bâtir chez les Égyptiens*, E. Rouveyre, Paris, (1904).

[9] Huerta, S. Oval domes: History, Geometry and Mechanics, *Nexus Network Journal* (2007) **9**(2): 211-248.

[10] Migliari, R. Ellissi e ovali: epilogo di un conflitto, *Palladio* (1995) **8**(16): 93-102.

[11] Apollonius, *Apollonius of Perga Conics Books I-III*, Translated by R. Catesby Taliaferro, Santa Fe, Green Lion Press (1998).

[12] Belluzzi, O. *Scienza delle costruzioni*, Zanichelli, Vol. III, (1982), pp. 245-270.

12th International Conference on Structural Analysis of Historical Constructions
SAHC 2020
P. Roca, L. Pelà and C. Molins (Eds.)

THE SPIRAL STAIRCASE IN THE FORTIFIED TOWER OF NISIDA

CLAUDIA CENNAMO[1*], CONCETTA CUSANO[1] AND MAURIZIO ANGELILLO[2]

[1]Department of Architecture and Industrial Design, Università degli Studi della Campania 'Luigi Vanvitelli', 81031 Aversa (CE), Italy
e-mail: {claudia.cennamo, concetta.cusano}@unicampania.it, www.architettura.unicampania.it
(*corresponding author)

[2] Department of Civil Engineering, DICIV, Università degli Studi di Salerno, 84084 Fisciano (SA), Italy
e-mail: mangelillo@unisa.it, www.diciv.unisa

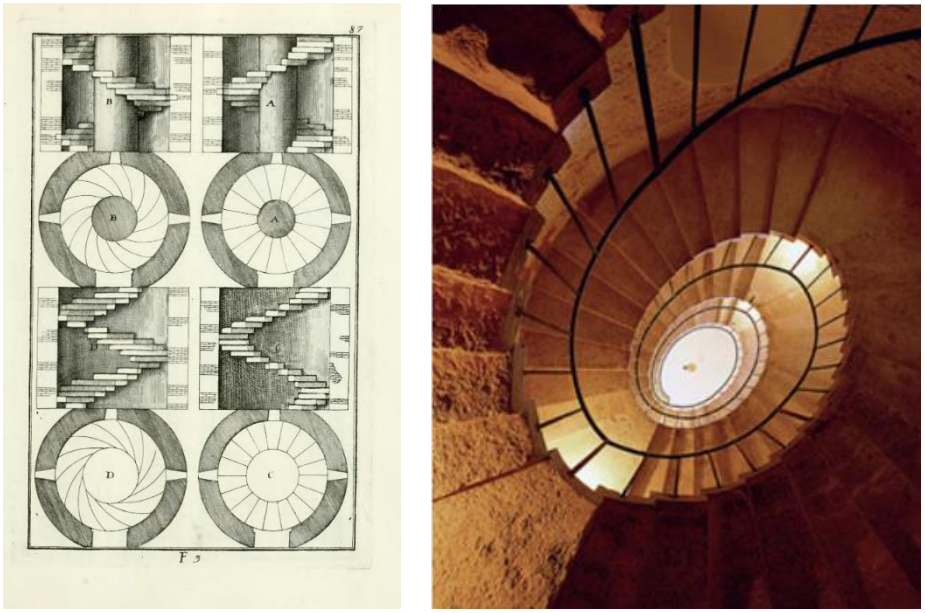
Keywords: Historical Structure, Spiral Stairs, Masonry, Unilateral Materials, Equilibrium Analysis

Abstract. *This contribution is part of a larger study on the island of Nisida (Naples) and its architectures, that has been conducted by the authors for several years now in collaboration with a research group at the Department of Architecture of University of Campania "Luigi Vanvitelli". The work previously proposed constitutes a state of progress of the current knowledge on the architectures present on the island, in particular on the cylindrical tower (with the original paths to access it) and on the buildings of the Institute for Juvenile Justice (IPM). By comparing the data taken from the historical iconographic sources with those derived from the architectural and structural surveys, it has been possible to advance a number of hypotheses on the modifications of the cylindrical tower (placed on the highest part of the island) and of the buildings that belong to IPM. The small spiral staircase found in the inner back side of the circular tower is part of this study. This spiral staircase can be seen as an unrolled ribbon of extreme proportionality and architectural accuracy despite its small size, and its helical movement shows the ability reached by masters of stonemasonry in the realization of one of the main elements in the building composition of space. The research focuses on studying the structural behavior of the spiral-shaped masonry stair of the Tower of Nisida, with a circular plan and a central circle, in the framework of Limit Analysis. García Ares (2007) demonstrates for the first time the static equilibrium of this type of constructions (helical-shaped stairs) from the point of view of Limit Analysis and, some years later, Block (2009) analyses them by using the Thrust Network Analysis. Through the equilibrium approach, which can be considered the more suitable for the study of masonry structures, one of the equilibrium solutions of this construction has been found analytically. The analysis also demonstrated that the geometry and proportion of the spiral stairs play a fundamental role in their structural behavior by deepening the conceiving process that allowed to the construction of such splendid artefacts.*

1 INTRODUCTION

Spiral staircases with a central oculus are a very widespread typology found in several buildings of the architectural heritage. It is a constructive system that has been used since ancient times adopting different materials in relation to the geographical position and time of construction.

In his treatise *I Quattro Libri dell'Architettura* (1570) Palladio introduces the theme of the spiral staircase, whom he named *"a lumaca"* (snail). In particular, in chapter XXVIII he makes a classification (figure 1a) and in chapter XVIII he highlights the constructive qualities of one of them, the helical staircases without central support, as they allow the passage of light and enhance the visual permeability between the different levels [1]. This description, as well as the stair built by Palladio in the Convento della Carità in Venice (figure 1b), can be considered as the constructive antecedent for the spiral staircases with central eye realized in England and Spain.



a b

Figure 1: a) Palladio, I Quattro Libri dell'Architettura, Book I - Chap. XXVIII - *Delle Scale e varie maniere di quelle, e del numero e grandezza de' Gradi*. Classification of spiral staircases; type C is the spiral staircase with central opening. b) Venice, Convento della Carità, spiral staircase.

In England this type of staircase is known as *cantilevered stairs* or *geometrical stairs*. It was the English architect Inigo Jones (1573-1652) who was the first to build such a spiral staircase in England (the *Tulip Staircase* in the Queen's House in Greenwich) and, after him, Robert Hooke and Christopher Wren (the spiral staircase inside the *Monument London*).

Instead in Spain, this type of staircase is known as *caracol de Mallorca* taking its name, probably, from the spiral staircase located in the *Lonja* of Palma de Mallorca. This model is collected in all the main texts dedicated to stereotomy in Spain in the sixteenth century (Rodrigo Gil de Hontañón, Vandelvira, Martínez, Gelabert) which contain drawings and rules for the realization of the cuts of the stones.

1.1 Objectives and motivations

For further information on the treatises on spiral staircases, you may refer to the extensive bibliography on the subject. This article is mainly concerned with the issue of the stability and mechanical behavior of this type of masonry staircase through a critical retrospective of the several structural analysis models adopted up to now.

Secondly, the work is completed with the analysis of the spiral staircase of the Tower of Nisida. This typological solution with an *open eye* or *central oculus*, despite being a protagonist among the different varieties present in the towers, bell towers and buildings dating back to before the eighteenth century, and, despite not appearing innovative or sensational with reference to the historical period of the case study, is part of a scenario whose study can be configured as "the missing piece" in an ongoing investigation on the fortified structures of the Neapolitan island. A project that the authors have been conducting for several years in collaboration with a research group at the Department of Architecture of the University of Campania "Luigi Vanvitelli".

2 LITERATURE REVIEW

The structural analysis of spiral staircases was a challenge for architects and engineers primarily because of the complexity of their geometry. Hence, several computational codes based on the finite element method (FEM) have been introduced in recent years. Anyway, the application of known solutions based on the elastic analysis of helical beams [2] or shells [3] is not easily applicable to the study of helical staircases in masonry, due to the significant relationship between the parameters of the material and the boundary conditions [4]. Consequently, it is more appropriate to work in the theoretical framework of limit analysis, whose principles were formulated by Heyman and applied to masonry [5].

In this section, a brief critical retrospective of approaches for the modelling of these kind of historic staircases is illustrated within Heyman's frame, namely considering that masonry structures are modeled as composed of rigid-unilateral material, that can resist compressive loads but not tensile loads. Many works in the literature have focused on this theoretical assumption, applying it to different types of historical vaulted constructions, from the simplest case of the arch (see [6,7]) to vaults and domes [8-10]. More recently, a work by some the authors on the topic of the open roman staircases in the Neapolitan area [11].

2.1 Solutions that involve torsional actions

Heyman's solution.

The first approach to the study of the mechanical behavior of spiral staircases in masonry, was the one provided by Heyman and it is based on the equilibrium of a series of rigid interlocking blocks. As Heyman remarked [12], the basic structural action for a small cantilevered staircase (quarter or half landing) is the twist of the individual steps. This action generates shear stresses in the masonry, which are low for short staircases but becoming increasingly dangerous for long flights. This solution can be defined as the superimposition of two balanced distributions of vertical forces consisting of the own weight of the single block, or of the applied load P, and of the contact force transmitted by the previous one. By combining these two equilibrium conditions, the whole stair can be studied by analyzing in sequence all

the steps from the top down. A particular feature of this solution is that a torque is produced inside each step, which increases proportionally with the height of the structure. As you can see from figure 2, in Heyman's solution each step is sustained by the step below on the free edge and, on the other edge, it is embedded into the wall: thus, he looks at each step as a simply supported beam[1]. It is evident that this simple equilibrium solution can work only for open stairs of modest flight, otherwise high values of torque can appear inside the steps close to the ground, leading them to breakage [13].

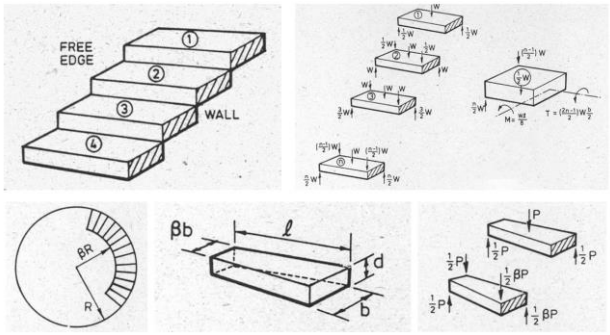


Figure 2: Equilibrium solution from Heyman [6] for a helical staircase with the tread under its own weight (or applied load P) and the contact force transmitted by the step above.

Continuum (Ring-Like) equilibrium solution.

Similar considerations can be drawn from the solution proposed by Angelillo in [13] for the analysis of helical staircases composed of monolithic steps interacting only through the internal rib. This different model combines Heyman's equilibrium solution with a sort of ring-like solution valid, by itself, only for a generic helical stair structure fixed at both ends. It is shown as the torsional Heyman's mechanism, combined with a Ring-Like regime, gives rise to large compressive forces and to moderate torsional torques, whose intensity reaches a plateau for long flights too.

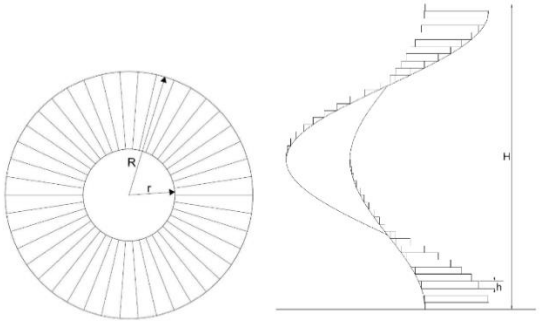


Figure 3: Plan and elevation of a typical helical stair [13].

[1] By applying the load P in the centroid of each step, the values of the reactive forces at the edges are equal to P/2. Looking at the top down, the forces applied in the four edges of the step determine the equilibrium on the second step: it means that each step is subject to a torque equal to $Mt = \frac{1}{2}Pb$. The forces acting on the second step are given by the forces on the step 1 and that of the step 2, and so on. In this way, on the generic step, the stress values are: $t = \left(\frac{2n-1}{2}\right) W \frac{b}{2}$; $Mf = \frac{Wl}{8}$ where W is the self-weight of the step [12].

In figure 3, the stair is considered as a helical surface, composed by radial segments AB (the steps) and by a helical arch (the rib), on which the steps transmit part of the load. On the outer edge of the step, inserted into the wall, a bending and torsional support is considered; the inner edge of the step is simply supported on top of the step below, and modelled as a unilateral contact. On assuming that the stair is a membrane, the stresses concentrate on a surface (as a fan of uniaxial stresses) and on a line, namely the internal rib.

According to Heyman's behavior, the loads are transferred from the upper steps to the lower steps through vertical forces applied at the contact points between them. These vertical forces, balanced with the vertical load, form a torque, representing a torsional moment acting on the step and that, increasing from the top down, produces shear stresses (that is tensile stresses) inside the step (figure 4b). Considering the Ring-Like behavior, there is an axial contact force tangent to the spiral arch. Moreover, the steps, besides the vertical load acting and defined per unit length, transfer to the spiral arch, at each point, a distributed compressive force contained inside the steps. From the equilibrium, we obtain a constant axial force N, which is tangent to the spiral arch (figure 4c).

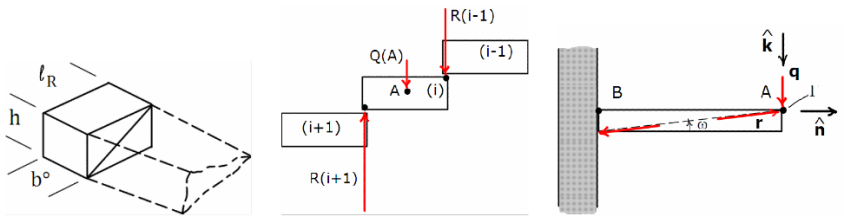


Figure 4: Equilibrium solution from Angelillo [13]: Coupling of Heyman's and Ring-Like behaviours. (a) Scheme of the connection to the wall. (b) Heyman's solution. (c) Ring solution.

Considering that Heyman's solution is valid for stairs of moderate flight and the Ring-Like solution is valid for stairs constrained at both ends, or equivalently, to stairs whose ends are subject to convenient compressive axial forces, the combination of the two models, implies to use the Heyman's equilibrium solution in a first sector springing from the top of amplitude (minimal amplitude), and the Ring-Like solution in the remaining part of the stair.

This combined solution allows obtaining limited shear and tensile stresses into the steps and also limited compressive stresses into the central rib, for any flight of the helical stair.

Despite the complexity of this model, a confirmation of the complementarity of Heyman and Ring-Like stress regimes is achieved in [14] for the case study of the triple helical stair of San Domingos de Bonaval, by employing a discrete model formed by rigid pieces, which are the steps of the stair. By applying the energy criterion, this complex multi-body model gives a razonable solution in terms of displacements and internal forces. Thus, it confirms the general validity of the proposed approach for the analysis of discrete structures, whose pieces are in unilateral contact, without sliding, among each other.

2.2 Unilateral membranes

The challenge of finding equilibrated solutions for non-tensile materials has led to the development of increasingly advanced models, based on the definition of a "unilateral membrane" entirely contained within the thickness of the masonry structure. This approach was

first adopted for the analysis of masonry vaults in [15] (also see [16,17]) and then successfully used for the analysis of helical staircases in [18,19].

By adopting the membrane theory of shells [20], the geometry of the membrane is assigned in the form $z = f(x, y)$, assuming a non-orthonormal covariant reference system to define the T of surface tensions. Its projection S on the x-y plane (figure 5) is expressed by the Airy function $F(x, y)$. The F function assumes concave to ensure that the S tensor is semi-defined negative, while the requirement of differentiability ensures the continuity of the S field [21]. Therefore, the function F may have concave folds that can be interpreted as singular tensions [22].

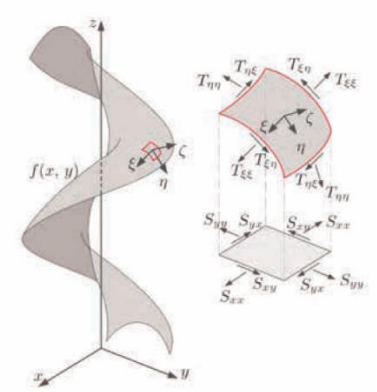


Figure 5: Image taken from [22]. Geometry of the no-tension membrane f(x,y), stresses T of the membrane and projected forces S.

2.3 Funicular polygon nets and the Thrust Network Analysis (TNA)

Another approach to the analysis of masonry helical stairs is to consider the membrane as a discrete network of interacting thrust lines. García Ares in [23] proposed a solution for spiral staircases by considering that longitudinal thrust lines interact with the transversal funicular curves that convey the vertical loads through the supporting walls. García Ares [23] presents a solution by applying the lower bound theorem (Static Theorem) and he demonstrates the static equilibrium of these helical shells.

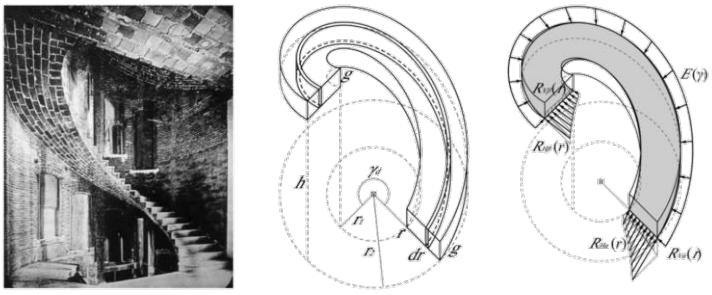
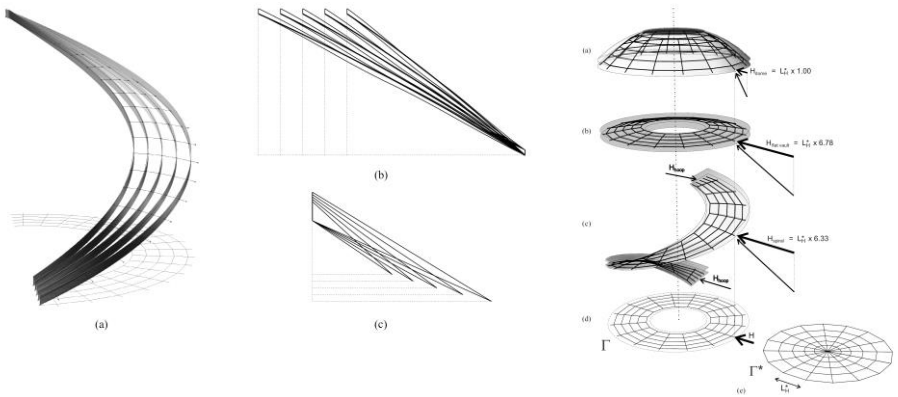


Figure 6: Parameters used by García Ares and applied to the elliptical spiral staircase by Guastavino in the National Bank of Peterson (New Jersey) [23].

Figure 6 shows the parameters used by García Ares and applied to the elliptical spiral staircase by Guastavino in the National Bank of Peterson (New Jersey). García Ares [23] finds

the minimum horizontal thrust state of a strip unrolled formed by the intersection of the spiral with a cylinder having the same central axis. An intuition out of the helical spiral property of having a constant slope, or "climb angle" [24]. The minimum thrust found (figure 7) is the deepest parabolic funicular between the parabolas[2].



a) b)

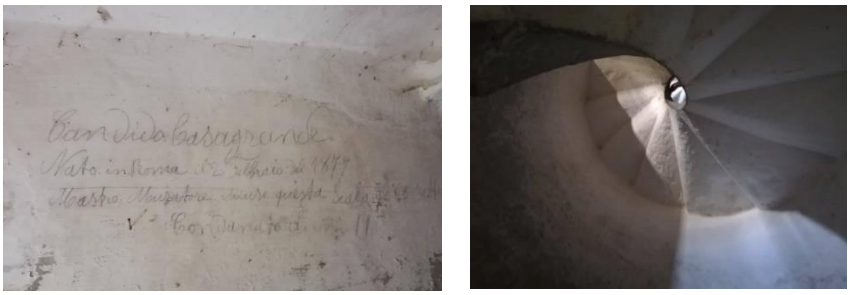
Figure 7: a) Straight strips (when unrolled) formed by the intersection of the spiral with a cylinder having the same central axis, unrolled sections and outlines of the funicular polygons of the parabolas [24]. b) Identical force pattern. From the top: dome with a circular oculus; circular at vault with an oculus; helical spiral stair with compression hoops; primal grid and dual grid. Image taken from [24].

Block introduced the TNA in [24] to study an equilibrium solution for this typology of stairs. A three-dimensional equilibrium solution in compression of vaulted structures has been found for different load cases based on the use of a network of thrusts, meaning compressive forces acting inside the structure, in equilibrium with the applied loads. He clearly explains the topological relationship between a dome spiral, a circular at vault, and a helical staircase with an oculus: in plan, the assumptions for an appropriate force network for all three structures are identical, namely a compression central ring and meridian "hoops" and radial arches [24]. For the dome with a circular oculus (figure 8a) or the circular at vault with an oculus (figure 8b), the compression ring of the oculus (and each meridian hoop) is in the same horizontal plane and in equilibrium by itself under applied vertical loads. Instead, for the helical stair (figure 8c), where the compression ring also circular in plan, becomes spirals in the z-direction: due to the fact that compression hoops are not closed, external reactions are required at the landings to keep them in equilibrium. In fact, the horizontal thrusts of all radial arches are to be equal in the circular inner compression ring, considering that a uniform loading applied radially generates a circle as funicular shape. Consequently, the force pattern assumed by Block for these helical stairs (figure 8d) needs a continuous wall and supports at the landings. In [24], a comparison between the TNA and the solution proposed by García Ares is also discussed.

[2] According to García Ares, the minimum horizontal thrust RH(r) given in kN/m per strip to be:
$\mathrm{RH(r)} = \frac{wL^2}{8h} = \frac{\rho(g\Delta r)\cdot(\gamma_d r)^2}{8g} = \frac{\rho\Delta\gamma_d^2 r^2}{8g}$ where Δr is the tributary width of the strip.
The distributed reaction forces E at the wall are equal to $E_{r_2-r_1} = \frac{\Delta\gamma_d^2\,\rho(r_2^3-r_1^3)}{16}$

3 CASE STUDY

All that remains of the coastal defense tower on the island of Nisida today is the sole scarp (integrated in the circular plan), a volume containing the spiral staircase and an annular body leaning against the scarp. The small spiral staircase with a central hole, object of this work, allows access from the outside to the original tower; it is placed inside the scarp and leads to the only surviving space of the upper floor. It is almost possible to date its construction to the year 1899 for the presence of an epigraph (figure 10a) on the wall at the entrance to the staircase that reports this inscription: *"Candido Casagrande, born in Rome on February 2, 1877, master mason completed this staircase on September 20, 1899".*[3]



a) b)

Figure 10: a) Epigraph on the wall at the entrance to the staircase. b) View of the stair from the bottom.

3.1 Geometrical and constructive configuration of the staircase

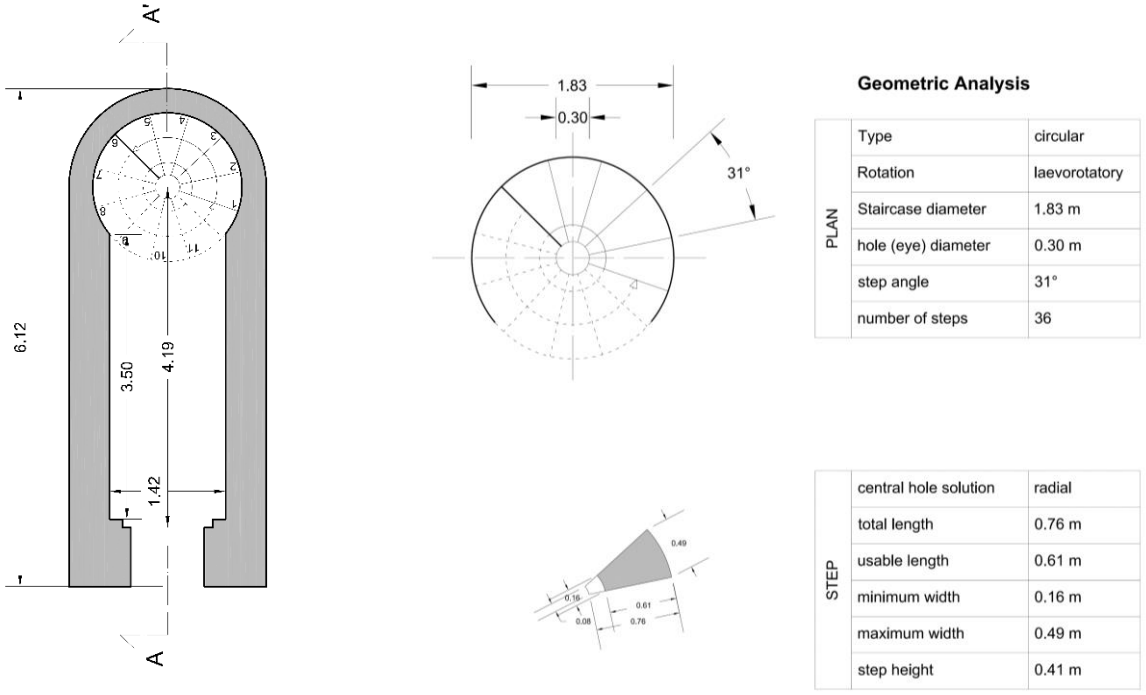
The spiral staircase of the tower of Nisida has a circular plan of 1,83m in diameter and it is located in a "well", a vertical void of 8,10m in height. Along the staircase, there are two empty windows for lighting and ventilation. The steps are made of cut stone with a rise of 21cm, 61cm wide without considering the part of the step embedded in the wall of the staircase cylinder. The perimeter wall is in tuff masonry covered with plaster. It consists of 36 steps that rest on the helical pillar and, as it rises, rotates and moves from the vertical so that the transmission of loads through the central support is somehow compromised.



Figure 11: Photographs of the spiral stair by the authors.

[3] The original text is as follows: *"Candido Casagrande, nato in Roma il 2 febbraio del 1877, mastro muratore chiuse questa scala il 20 settembre 1899".*

The tracing of each step starts from the plan drawing, carving a vertical prism with the fixed height of the step and removing excess material from the bottom face, so that each piece connected to the adjacent one generates a continuous helical surface.



Geometric Analysis

PLAN	Type	circular
	Rotation	laevorotatory
	Staircase diameter	1.83 m
	hole (eye) diameter	0.30 m
	step angle	31°
	number of steps	36
STEP	central hole solution	radial
	total length	0.76 m
	usable length	0.61 m
	minimum width	0.16 m
	maximum width	0.49 m
	step height	0.41 m

a) b)

Figure 12: The spiral staircase in Nisida: a) plan (by F. Bocchino); b) geometric analysis (by the authors).

Recent studies have shown that up to the 4th step the complex is very stable, capable of supporting itself even when materials and workers are placed on the edge. Only considering its own weight, the staircase can accumulate up to 7 cantilevered steps without the risk of tipping over. The eighth step presents clear stability problems [25]. Figure 12 shows the geometric analysis of the staircase and the identification of its main dimensional parameters.

3.2 Stability analysis

Premise. We consider the helical pillar as a space filament Γ* that can carry a compressive axial force N and to which the steps transmit an external force $\boldsymbol{q}$ per unit length of Γ*, whose vertical component is a known action, whilst its horizontal components are unknown reactive forces transmitted to the steps.

Geometry. We consider a 1d space filament Γ* and its plane projection Γ onto the planform of the stair. We parametrize both Γ and Γ* with the arc length s along Γ. We can write:

$$\Gamma = \{\boldsymbol{x} = \boldsymbol{x}(s)\,, s\epsilon[0, L]\}\,; \quad \Gamma^* = \{\boldsymbol{y} = \boldsymbol{x}(s) + f(s)\boldsymbol{e}_3\,, s\epsilon[0, L]\} \tag{1}$$

L being the length of the curve Γ, and $f(s)$ a continuous function of its argument describing the elevation of the curve Γ* with respect to the planform.

We call the tangent and normal unit vectors to Γ, and, on introducing the arc length σ along Γ*, consider the unit tangent vector along Γ*

$$\boldsymbol{t} = \frac{d\boldsymbol{x}}{ds}\ ;\ \ \boldsymbol{n} = \boldsymbol{e}_3 \times \boldsymbol{t}\ , \boldsymbol{\tau} = \frac{d\boldsymbol{y}}{d\sigma} \tag{2}$$

Define $J = \frac{d\sigma}{ds}$, as the ratio between the length along Γ* and the projected length along Γ. By calling α the angle between $\boldsymbol{\tau}$ and $\boldsymbol{t}$, one has

$$J = \frac{1}{cos\alpha}\ \ ;\ \boldsymbol{\tau} = \frac{1}{J}\frac{d\boldsymbol{y}}{ds} \tag{3}$$

Finally $\frac{d\boldsymbol{t}}{ds} = \rho\boldsymbol{n}$, ρ being the curvature of Γ. In the present notation, the curvature ρ has a sign: it is positive if the centre of curvature is on the positive side of $\boldsymbol{n}$.

Equilibrium analysis. We call $N \leq 0$ the contact axial force along the filament, and introduce the thrust

$$S = \frac{N}{J} \tag{4}$$

In terms of the thrust$S$, the three equilibrium equations of the filament reduce to the form

$$S' + p_t = 0\ ,\ \ \rho S + \ p_n = 0\ ,\ \ Sf'' + p_3 - f'p_t = 0 \tag{5}$$

$\boldsymbol{p}$ being the load per unit projected length, defined as follows:

$$\boldsymbol{p} = J\ \boldsymbol{q}\ , \boldsymbol{p} = Jq_t\,\boldsymbol{t} + Jq_n\boldsymbol{n} + Jq_3\boldsymbol{e}_3\ , p_t = Jq_t\ , p_n = Jq_n\ , p_3 = Jq_3 \tag{6}$$

Considering that $p_3 = Jq_3$ is given, we can solve this system of differential-algebraic equations for S, p_n, p_t on any given shape f.

The case study. For the case study, we can assume:

$$f = \frac{h}{2\,\pi\,r}s\ ;\ \ \ p_3 = p = const\ ;\ \ \rho = -\frac{1}{r} = const \tag{7}$$

then, by solving the system of the equilibrium equations, one obtains

$$S = \frac{1}{f'}(-ps) + S^{\circ}\ ; p_t = -S' = \frac{p}{f'} = \frac{2\,\pi\,r}{h}p\ ; p_n = \rho S = \ \frac{1}{rf'}ps - \frac{S^{\circ}}{r} = \ \frac{2\,\pi}{h}ps - \frac{S^{\circ}}{r} \tag{8}$$

On assuming $S^{\circ} = -10\ KN$, and $p = 10\ KN/m$, since for the case at hand h=5.04m, r=0.45m, we obtain

$$S = \left(-\frac{50\,\pi}{28}s - 10\right)KN;\ \ \ p_t = \frac{50\,\pi}{28}\frac{KN}{m};\ p_n = (\frac{250\,\pi}{63}s + \frac{200}{9})\frac{KN}{m} \tag{9}$$

3 CONCLUSIONS

The assessment of the stability of a remarkable structural element, such as the small staircase discovered in Nisida, represents only an aspect of a wider research program already developed [26, 27, 28]. It offered the opportunity to experiment a combined approach between graphical and analytical methods [29]. In fact, as part of the now classic Heyman's methodology for masonry structural elements, in the present work the stability is achieved based on specific graphic parameters, which end up connecting the scientific process to the geometry of the artefact in an unavoidable way.

REFERENCES

[1] Palladio, A. *Quattro Libri dell'Architettura*. Venice (1570).
[2] Busool, W. and Eisenberger, M. Exact static analysis of helicoidal structures of arbitrary shape and variable cross section. *Journal of Structural Engineering* (2001) **127**(11):1266-1275.
[3] Calladine, C.R. A preliminary structural analysis of a Guastavino spiral staircase shell. *History of Structures: Essays in the History of the Theory of Structures in Honour of Jacques Heyman*. Instituto Juan de Herrera, Escuela Tecnica Superior de Arquitectura de Madrid (2006).
[4] Huerta, S. The analysis of masonry architecture: A historical approach: To the memory of Professor Henry J. Cowan. *Architectural Science Review* (2008) **51**(4):297-328.
[5] Heyman, J. The stone skeleton. *International Journal of solids and structures* (1966) **2**(2):249-279.
[6] Cennamo, C., Cusano, C. and Guerriero, L. The slicing technique for the evaluation of the formal efficiency: a comparative study. In: *AIMETA 2017 - Proceedings of the 23rd Conference of the Italian Association of Theoretical and Applied Mechanics,* 2017*,* **2**:1543-1554, Mediglia (MI): Gechi Edizioni.
[7] Iannuzzo, A., Olivieri, C., and Fortunato, A. Displacement capacity of masonry structures under horizontal actions via PRD method. *J. Mech. Mater. Struct*. (2019) 14(5):703-718.
[8] Iannuzzo, A. Energy based fracture identification in masonry structures: the case study of the church of "Pietà dei Turchini. *J. Mech. Mater. Struct.* 14(5):683-702.
[9] Cennamo, C., Cusano, C., and Angelillo, M. A limit analysis approach for masonry domes: the basilica of San Francesco di Paola in Naples. *Int. J. Mason. Res. Innov.*, (2019), **4**:227-242.
[10] Iannuzzo, A., De Luca, A., Fortunato, A., Gesualdo, A. and Angelillo, M. Fractures detection in masonry constructions under horizontal seismic forces. *Ing Sismica-Ital*. (2018) 35(3):87-103.
[11] Cennamo, C. and Cusano, C. Roman masonry stairways. Geometry, construction and stability. In: A. Carcaterra et al. (Eds.): *AIMETA 2019, LNME*, 1–14, Springer Nature Switzerland AG 2020.
[12] Heyman, J. The mechanics of masonry stairs. In: C.A. Brebbia and B. Leftheris (Eds.): *Structural studies of Historical Buildings*, Vol. 2 (1995), pp. 259–265.
[13] Angelillo, M. The equilibrium of helical stairs made of monolithic steps. *Int. J. Archit. Herit*. (2016), 10(6):675-687.
[14] De Serio, F., Angelillo, M., Gesualdo, A., Iannuzzo, A., Zuccaro, G., and Pasquino, M.

Masonry structures made of monolithic blocks with an application to spiral stairs. *Meccanica*, (2018) **53**(8):2171-2191.

[15] Angelillo, M. and Fortunato, A. *Equilibrium of masonry vaults. Novel approaches in civil engineering* (2004). Berlin: Springer: 105-111.

[16] Cennamo, C., Cusano, C., Angelillo, M. and Fortunato, A. A study on form and seismic vulnerability of the Dome of San Francesco di Paola in Naples. *Ing Sismica-Ital*., (2018) **35**:88-108.

[17] Ferrero, C., Cusano, C., Dell'Endice, A., Yavuzer, M. N., Wu, Y. X. and Iannuzzo, A. Where cracks are (not) a structural concern: the case study of "Giovanni Vinciguerra" school in Anagni. In: *Proceedings of the SAHC Symposium*, Barcelona, (2020).

[18] Angelillo, M. Static analysis of a Guastavino helical stair as a layered masonry shell. *Composite Structures* (2015) **119**: 298-304.

[19] Gesualdo, A., Cennamo, C., Fortunato, A., Frunzio, G., Monaco, M. and Angelillo, M. Equilibrium formulation of masonry helical stairs. *Meccanica* (2017) **52**(8):1963–1974.

[20] Ventsel, E. and Krauthammer, T. *Thin plates and shells: theory, analysis and applications*. New York: CRC press, (2001).

[21] Angelillo M., Babilio E., Fortunato A. Singular stress fields for masonry-like vaults. *Continuum Mechanics and Thermodynamics* (2013) **25:**1-19.

[22] Marmo, F., Masi, D. and Rosati, L. Una retrospettiva dei metodi di analisi strutturale di scale in muratura. In: S. D'Agostino, F. R. d'Ambrosio Alfano (Eds): *Proceedings of the 3rd International Conference on History of Engineering*, Naples, 2018 April 23rd - 24th, Cuzzolin Editor.

[23] García Ares, J.A. Una nueva solución de equilibrio para el análisis límite de helicoides de fábrica con óculo central como los construidos por Guastavino. In *Actas del Séptimo Congreso Nacional de Historia de la Construcción* (2011), Institute Juan de Herrera, SEdHC, CICCP, CEHOPU.

[24] Block, P. Thrust network analysis: exploring three-dimensional equilibrium. *PhD thesis*, Massachussets Institute of Technology (2009).

[25] Fernández, C., González Uriel, A. and De Miguel, M. La triple escalera de caracole n el Convento de Santo Domingo de Bonaval (Santiago, España): hipótesis de diseño y construcción. *Informe de la construcción* (2017) 69(546).

[26] Zerlenga, Ornella; Cennamo, Claudia; Guida, Gianluca; Michele, Lettiero; Daniele, Petagna; Francesco, Vasta, Nisida and its architectures. pp.1606-1615. *In World Heritage and Degradation. Smart Design, Planning and Technologies* | Le vie dei Mercanti", XIV Forum Internazionale di Studi - vol. 61 (2016).

[27] Cennamo, Claudia; Zerlenga, Ornella, Nisida: integrated and transdisciplinary survey for interpretation of sources. pp.2379-2388. In *HERITAGE and TECHNOLOGY Mind Knowledge Experience* Le Vie dei Mercanti _ XIII Forum Internazionale di Studi - vol. 56 (2015).

[28] Cennamo, Claudia; Zerlenga, Ornella, Nisida, the memory of a myth. pp.1583-1593. In *XII International Forum Le vie dei Mercanti-From the World to Pompeii* - (2014).

[29] Angelillo, M., Fortunato, A., Gesualdo, A., Iannuzzo, A., and Zuccaro, G. Rigid block models for masonry structures. *Int. J. Mason. Res. Innov*. (2018) 3(4):349-368.

12th International Conference on Structural Analysis of Historical Constructions
SAHC 2020
P. Roca, L. Pelà and C. Molins (Eds.)

THE STRUCTURAL FUNCTION OF THE DUTCH BUTTRESSING OF THE EAST CURTAIN WALL OF ELMINA CASTLE, ELMINA, GHANA

JIACHENG SUN[1], SELMAN TEZCAN[1] AND RENATO PERUCCHIO[2*]

[1]Department of Mechanical Engineering
University of Rochester, Rochester, NY 14627, USA
e-mail: {jsun29, stezcan}@ur.rochester.edu

[*]Department of Mechanical Engineering, and
Program of Archaeology, Technology and Historical Structures
University of Rochester, Rochester, NY 14627, USA
e-mail: renato.perucchio@rochester.edu

Keywords: Elmina Castle, Masonry Wall, Lateral Capacity, Non-Linear FE Explicit Analysis, Concrete Damaged Plasticity, Abaqus/CAE.

Abstract. *Elmina Castle is the first of a series of European trading bases along Africa's west coast, and it is the oldest and best preserved early European building in Sub-Saharan Africa. The structure shows a combination of mud-mortared and lime-mortared sandstone masonry macro elements and has undergone reconstructions and modification throughout time under Portuguese and Dutch occupation. This study focuses on the structural analysis of Elmina Castle's east curtain wall, which features two massive masonry buttresses built only along selected portions of the wall. The hypothesis that these buttresses were built in correspondence of deep voids in the foundation bedrock platform is numerically evaluated using pushover analysis. The lateral capacity is determined based on energy considerations using nonlinear FE models in Abaqus/CAE Explicit and concrete damaged plasticity. Results indicate that, at a later Dutch stage of structural modification, loose soil filling might have caused rotational instability of the curtain wall, requiring the addition of the buttresses.*

1 INTRODUCTION

As the oldest and best preserved early European building in Sub-Saharan Africa, Elmina Castle is the first of a series of trading bases along Africa's West Coast. Erected in 1482 by the Portuguese Crown to protect its control of the gold trade, after the 1637 Dutch conquest the castle became a major hub of the Atlantic Slave Trade involving Europe, Africa, and the Americas. Acquired by the British in 1872, the castle came under control of Ghana with the country independence in 1957 and is currently part of a UNESCO World Heritage Site in Ghana.

The Elmina Castle has been the object of a multidisciplinary (engineering and historical archeology) field school conducted at Elmina, Ghana, by the Archaeology, Technology, and Historical Structures program of the University of Rochester in summer 2017 and 2018. At the present time, the building consists of an inner keep of three-story buildings and a large courtyard surrounded by curtain walls, with bastions at the southeast, southwest, and northeast corners (Figure 1). The structure shows a combination of mud-mortared and lime-mortared sandstone

masonry macro elements, incorporating original 1482 Portuguese elements (towers, walls) with successive Portuguese, Dutch, and British reconstructions and modifications. European built fired-clay bricks were first used sparingly by the Portuguese for windows and doors openings, and then in very large number for extensive vault construction by the Dutch.

The present paper focusses on the structural analysis of the east curtain wall which features two massive masonry buttresses which reach up to the parapet but were built only along selected portions of the wall (Figure 2). Historical documents clearly show that these buttresses are a Dutch addition, since they do not appear in the only drawing showing the castle still in Portuguese hands in 1637 (Figure 3). However, they are present in detailed - and particularly accurate – Dutch maps of the second half of the 1700's [1]. Similar to the western curtain wall, the original eastern curtain wall appears to be built with foundation resting on levelled limestone bedrock, as reported by the Portuguese chronicles describing the 1482 construction process [2]. The laser-scan and photogrammetric survey conducted during the field school and information extracted from the historical record allow us to construct a reasonably accurate building sequence beginning from late Portuguese period (before 1637) to the mid 1700's.

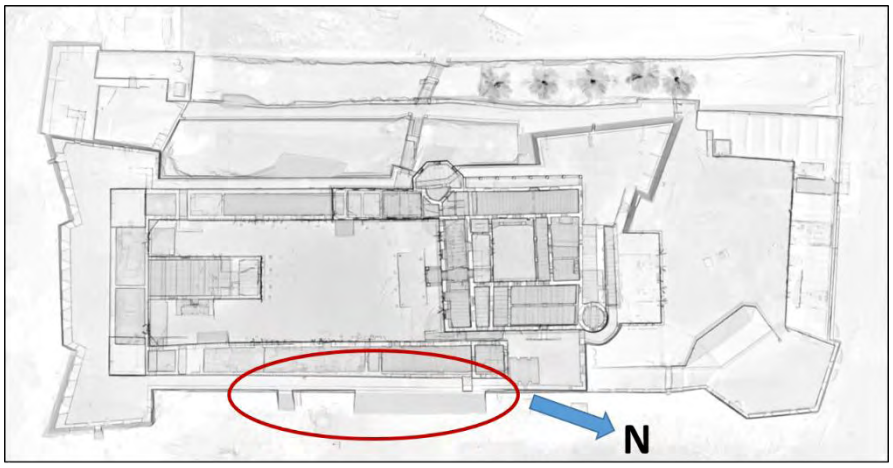


Figure 1: Elmina Castle floor plan with Dutch buttress highlighted, based on 2017-2018 FARO scans taken by Michael Jarvis – U. Rochester/ U. Ghana, Field school.

The late Portuguese east wall was extended in elevation and considerably thickened with mud-mortared masonry covered by lime plaster, and a two-story building was added along its entire length, with the inner side of the curtain wall becoming part of the new building. The first (ground) story of the building is vaulted with a 4 m-span barrel vault approximately 16 cm thick (the length of an average Dutch brick). This thin vault – excellently executed with bricks interlocking in two directions – carries a considerable dead load of loose material 1 m deep at the crown and is in undamaged structural conditions. To explain the presence of the irregular buttressing architecture noted above, we make the following hypothesis (Figure 2b). The section of the original Portuguese wall later covered by the buttress is likely not built on the bedrock but on compacted loose soil and debris used to fill a void where the bedrock dips below the level of the courtyard. Using compacted loose soil to fill such voids is largely attested in other European forts along the coast of Ghana. The wall carried by this weaker foundation could

have been damaged by the 1615 earthquake in Elmina or by the Dutch assault on the castle, or both. The dead loads introduced with the extension and thickening of the wall and the construction of the vaulted building could possibly have caused concerns in the Dutch builders, who, noticing signs of rotational instability, reinforced the wall with a buttressing system limited only to the affected areas. We test the structural conditions on which the hypothesis is based through a sequence of 2- and 3D nonlinear FE models, by first testing how the presence of a pocket of loose soil affects the structural response of the Portuguese wall under lateral accelerations, then testing the structural effect of the Dutch modifications to the wall, and finally introducing the effect of the vaulted building. In modeling the curtain wall, we test separately the case of a solid masonry wall or, as it is more likely, of a wall with an internal mass of loose material bounded by external and internal masonry curtain. The masonry physical characterization is based on published material and the nonlinear mechanical behavior is modeled through the concrete damaged plasticity formulation available in Abaqus/CAE Explicit.

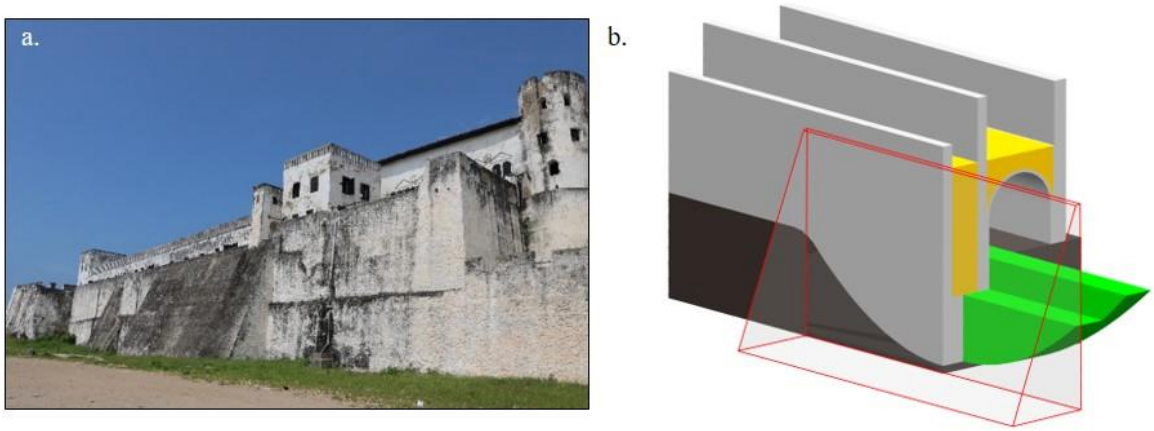


Figure 2: (a) East curtain wall and buttressing wall in current condition; (b) Hypothesized wall and foundation composition behind buttresses.



Figure 3*:* Elmina Castle in 1637, Frans Post, 1637 [3].

2 METHODOLOGY

Pushover analysis is a well-established approach for assessing the overall behavior of a structure due to seismic activity that uses an incremental-iterative solution based on static equilibrium to determine the response of the structure under monotonically growing lateral load

patterns [4] [5]. These can be implemented by lateral displacements or forces applied to one side of the structure or by subjecting the entire structure to a uniformly applied horizontal acceleration. In this study, after gravitational loading, a uniform monotonically increasing horizontal acceleration is applied to the entire model using the explicit FE formulation available in Abaqus. The desired quasi-static condition is enforced by adopting long time intervals for the application of both gravitation and lateral accelerations: for example, five seconds for gravitation to increase linearly from 0 to 1 g followed by ten seconds for lateral acceleration to go from 0 to 0.8 g.

The time-evolution of strain (SE), kinetic (KE), and dissipative energy (PD – due to plastic deformations simulating internal fractures) is used to identify the development of local damage conditions up to structural collapse (Figure 4a). As long as structural integrity is maintained under increasing lateral acceleration, KE remains negligible during the evolution of quasi–static structural response. Structural failure is associated with the sudden transition from quasi-static to a fully dynamic state and is detected by the accompanying asymptotic growth of KE. In the example shown, PD follows an identical asymptotic growth pattern, while SE immediately decreases after having reached a peak at failure. Notice also that the viscous dissipative energy (VD) produced by the fictitious viscosity parameter used in Abaqus/CAE Explicit to dampen possible oscillatory behavior remains negligible during static conditions and then goes asymptotic at failure. Figure 4b shows the concomitant time-evolution of the horizontal and vertical reactions normalized by the weight of the wall and expressed as fractions of g. As a result of the inertial forces caused by the applied lateral acceleration, an equilibrating horizontal reaction force (basal shear) develops at the constrained boundary face. In the first five seconds only gravitational load is applied and thus only a vertical reaction is developed. Thereafter, the gradual application of lateral acceleration causes almost linear increase in the basal shear versus time while the vertical reactions hold constant. At failure, both curves show a sudden decrease indicating that the structure has lost the capability of resisting the lateral load and, in this case, the mass of the wall has nearly completely separated from its base. As expected, failure occurs by outward rotation about the base of the wall. The fracture pattern at failure – represented in the concrete damaged plasticity formulation by the formation of plastic zones – is shown by the black band on the inner side at the base of the wall in the insets of Figure 4a.

The examination of the energy and reaction plots in Figure 4 suggests complementary ways to associate a specific time interval to failure. KE begins to develop at 7.3 s and becomes asymptotic at 7.9 s, reaching the 10% value of the total internal energy (i.e. SE + PD + KE) at 7.7 s. PD, which can be taken to represent the work necessary to propagate the fractures at the base of the wall, begins to appear at 6.6 s and crosses the SE at 7.85 s. Thus, purely on energy considerations, total failure can be reasonably defined to happen between t = 7.7 s (when the loading process cannot anymore be regarded as static) and t = 7.85 s (when the PD equals the SE). Hereafter we will use the 10% kinetic energy criterion to determine failure.

The explicit (dynamic) nonlinear FE formulation is preferred over the implicit one because of its capability to sustain large deformations and attendant local material failures, and to capture unequivocally the collapse condition due to lateral accelerations [6]. In fact, in most of the cases of the present study, it may be not possible to detect the actual failure condition using an implicit nonlinear FE formulation because the analysis terminates due to numerical error (e.g., the stiffness matrix becomes singular) before the actual structural failure occurs. On the negative side, dynamic explicit models are computationally costly. In order to ensure

algorithmic convergences, Abaqus Explicit requires the time increments of the order of 10^{-6} second for both gravitation and lateral acceleration [7].

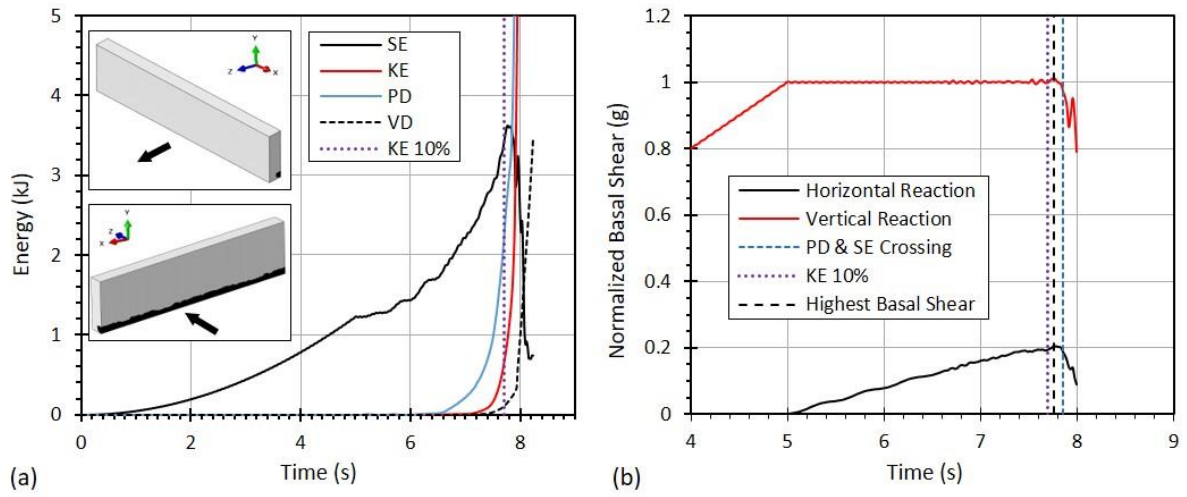


Figure 4: (a) Energy curves versus analysis time; (b) Normalized reaction force versus analysis time.

3 MODELS

The geometric models in this study follow an assumed chronological building sequence. Thus, the 3D "P" models simulate the original Portuguese curtain wall; 3D "D" models simulate curtain wall's height elevation introduced by the Dutch; 3D "T" models simulate thickening of the curtain wall and the effect of loose soil filling at foundation level. Within each of the above cases, the wall length, the length and depth of the downward extension, and the number of these extensions are varied to explore their effects on the lateral capacity of the curtain wall. Finally, we use 2D "V" models to simulate the effect of construction of a vaulted structure against the curtain wall. We vary the density (due to the uncertainty of filler density) and the height of vault filling (due to possible variation of filler thickness from historical map from 1774 [8]) to explore their effects on structural capacity of the curtain wall. The "V" models are then explored with the effect of adding the external buttressing walls. Figure 5a shows a basic "P" model. Due to symmetry, only half the length is represented. The wall thickness is taken as 1.3 m based on the measured thickness of the exterior wall at the current "door of no return" where the original Portuguese structure is still visible. The height of the original Portuguese curtain wall is taken as 2 m based on Frans Post's 1637 drawing shown in Figure 3, in which the height ratio between curtain wall and bedrock platform is 2:5. Figure 5b shows a basic "D" model with wall thickness unchanged from "P" models and the height elevated to 5 m, which is the current measured wall height. As shown in Figure 1, the two buttresses have different lengths: the southern is 4 m long while the northern is 20 m long. To explore the possible downward configurations of the curtain wall in correspondence of these two buttresses, we consider the length of the downward extension to be either 1 m or 10 m, and as for the long buttress, the possible presence of either one or two extensions. As for the depths of the extensions, we assume either 2.5 m or 5 m. Notice that the P/D0 models represent the uniform wall without downward extension. The

various subcases are summarized in Table 1. Notice also that in this table "A" indicates the curtain wall with two downward extension dips for the specific subcase.

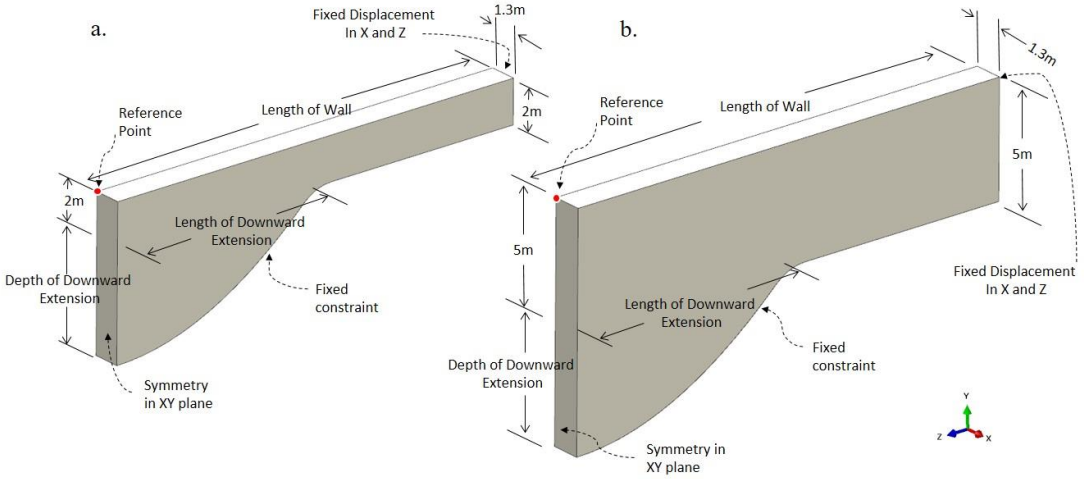


Figure 5: (a) Dimensions of basic "P" model; (b) Dimensions of basic "D" model.

For the "T" models, the thickness and the height are taken as 3 m and 5 m, respectively, based on the current wall thickness and height. In correspondences of the voids of the bedrock, the thickened wall is assumed to be partially supported on loose material as shown in Figure 6b. As stated above, similar foundation conditions are attested in other European forts along the coast of Ghana. The bedrock void is inclined by 75° following the visible average bedrock eastward inclination. As for the previous models, subcases T1, T2, T3, T3A, T4, and T4A are created to represent the variations on the wall configurations based on the voids depth, length and number (Table 1). For the T4 subcase, Figure 6b gives the cross-sectional dimensions.

The "V" models represent east curtain wall with the construction of vaulted structure. Figure 6d shows the dimensions of "V" models, in which loose material is bounded by internal and external masonry curtain walls. Only one depth (5 m) of downward wall and soil extension is explored in the "V" case, and subcases (VA and VB) are created to explore the effect of the construction of buttressing on the curtain wall with vaults in place.

Table 1: Dimensions of subcases with reference to Figure 5.

Configuration	Length of wall (m)	Depth of downward extension (m)	Length of Downward Extension (m)	Number of Dips
P/D0	10	0	0	0
P/D/T1	10	2.5	1	1
P/D/T2	10	5	1	1
P/D/T3	20	2.5	10	1
P/D/T3A	20	2.5	10	2
P/D/T4	20	5	10	1
P/D/T4A	20	5	10	2

Quadratic tetrahedral elements and quadratic triangular plane strain elements are used for 3D and 2D models, respectively. Figure 6a and 6c show the mesh and material distribution for T4 and VA. Grey indicates mud mortar (adobe in Table 2), green indicates stone masonry

(masonry in Table 2), yellow indicates loose material (lateritic soil in Table 2), and purple indicates sandstone. For all models, the base of the curtain wall is tie-constrained to the sandstone surfaces. Surface to surface contact is defined for all other surface contact interactions.

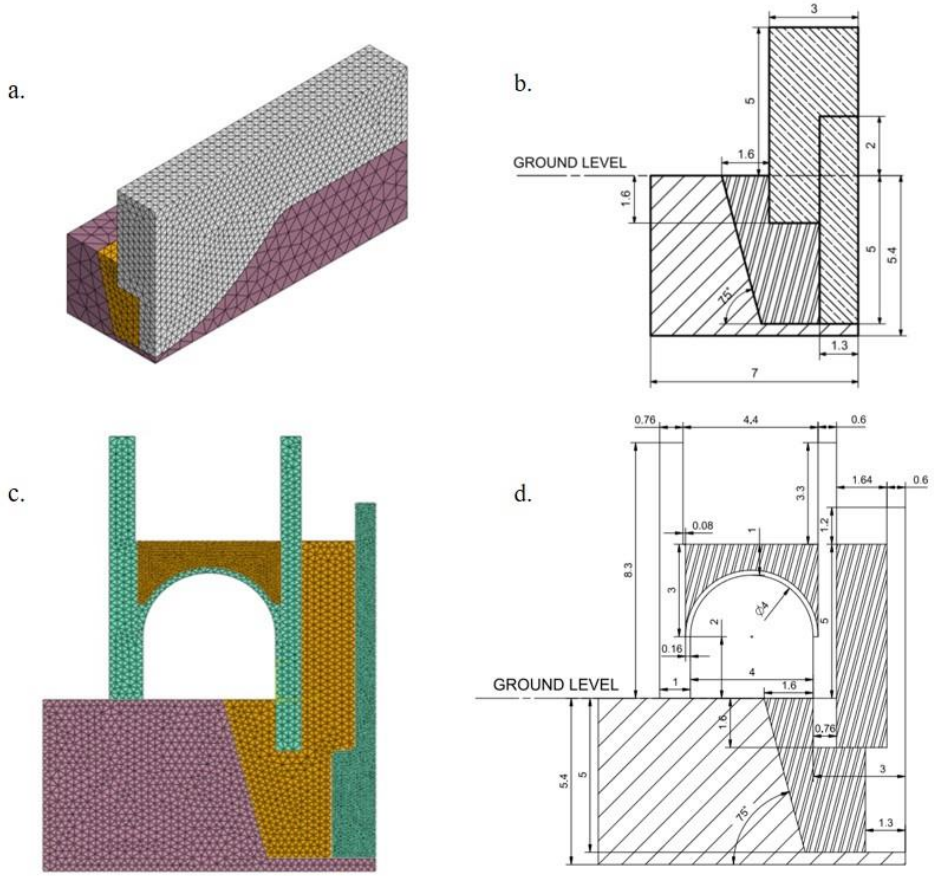


Figure 6: (a) T4 model shown with color-coded material distribution; (b) Dimensions of T4 model cross-section at deepest downward wall extension; (c) VA model shown with color-coded material distribution; (d) Dimension of "VA" model. (All units are shown in meters).

4 MATERIALS

The concrete damaged plasticity model in Abaqus/CAE is primarily intended to provide a general capability for the analysis of concrete structures under dynamic/cyclic loading. The model is also suitable for the analysis of quasi-brittle material such as mortar [9]. It is a plasticity-based model that assumes the two main failure mechanisms for the concrete material are tensile cracking and compressive crushing. The material's brittle behavior can be characterized by a stress-displacement response under tension and by a stress-strain response under compression [10]. We use concrete damaged plasticity to model post critical behavior of mud mortar (adobe in Table 2) and stone masonry (rough-hewed stone in Table 2). General concrete damaged plasticity parameters shown in Table 2 are taken from Tarque [11], and elastic material properties of stone masonry are taken as the average of the range of rough-hewed stone [12]. The post critical softening compressive behavior is represented parabolically,

and the post critical softening tensile behavior is represented by exponential decay. The tabulated values of mud mortar's post critical behaviors are taken from previous research [13]. The tabulated values for stone masonry's post critical behaviors are hypothesized to be between that of mud mortar and Roman pozzolanic concrete [14]. Therefore, both post critical behaviors are scaled down from those of pozzolanic concrete based on stone masonry's compressive and tensile strength [12]. For two subcases in "V" models, Mohr-Coulomb model is used to represent loose material filling. Mohr-Coulomb criterion assumes that yield occurs when the shear stress on any point in a material reaches a value that depends linearly on the normal stress in the same plane [15]. The parameters needed to construct Mohr-Coulomb model are obtained based on previous research and are documented in Table 2.

Table 2: Material properties used in this study.

Materials /Properties	Adobe [13]	Masonry / Rough-hewed Stone [11], [12]	Lateritic Soil [17]	Elmina Sandstone [18]
E (MPa)	123	1740	26	12100
ν	0.2	0.2	0.38	0.29
ρ (kg/m^3)	1735	2000	2200	2000
Dilation Angle (°)	1 [11]	1 [11]	0 [16]	
Friction Angle (°)			17.13 [16]	
Cohesion Yield Stress (kPa)			21.43 [16]	
Eccentricity	0.1 [11]	0.1 [11]		
fb0/fc0	1.16 [11]	1.16 [11]		
K	0.67 [11]	0.67 [11]		
Viscosity Parameter	1E-8 [11]	1E-8 [11]		
Compressive Strength (MPa)	0.41	2		
Tensile Strength (MPa)	0.04	0.07		

5 RESULTS

Capacity curves and failure mechanisms of model "P", "D" and "T" are shown in Figure 7 to Figure 9. Displacements are measured at the reference point (Figure 5), a point with the largest displacement.

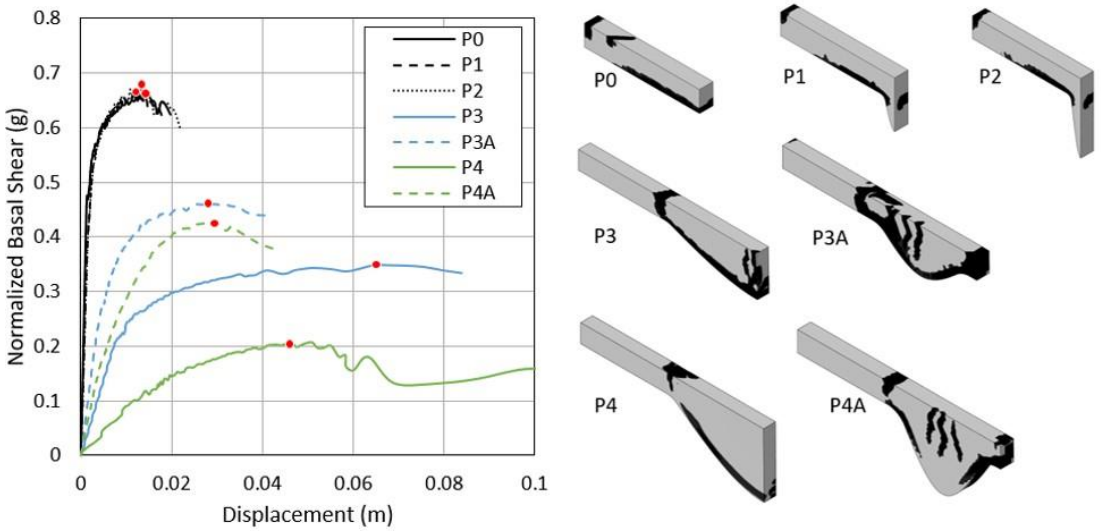


Figure 7: Capacity curves and failure mechanisms of "P" subcases.

Capacity curves and failure mechanisms of P0, P1 and P2 show that structural capacity and stiffness are not sensitive to downward wall extension when its length is small compared to wall length. They also show that structural capacity and stiffness are sensitive to the length and depth of downward wall extension. The same observations can be made for both "D" and "T" models. The worst structural condition in "P" models, P4, gives a structural capacity of 0.21 g in resisting lateral acceleration. However, due to the increase in wall height, structural capacity and stiffness in "D" models have both decreased. The worst structural condition in "D" models, D4, gives a structural capacity of 0.14 g in resisting lateral acceleration. The worst structural condition in "T" models, T4, gives an increased structural capacity of 0.23 g in resisting lateral acceleration due to thickening of the curtain wall.

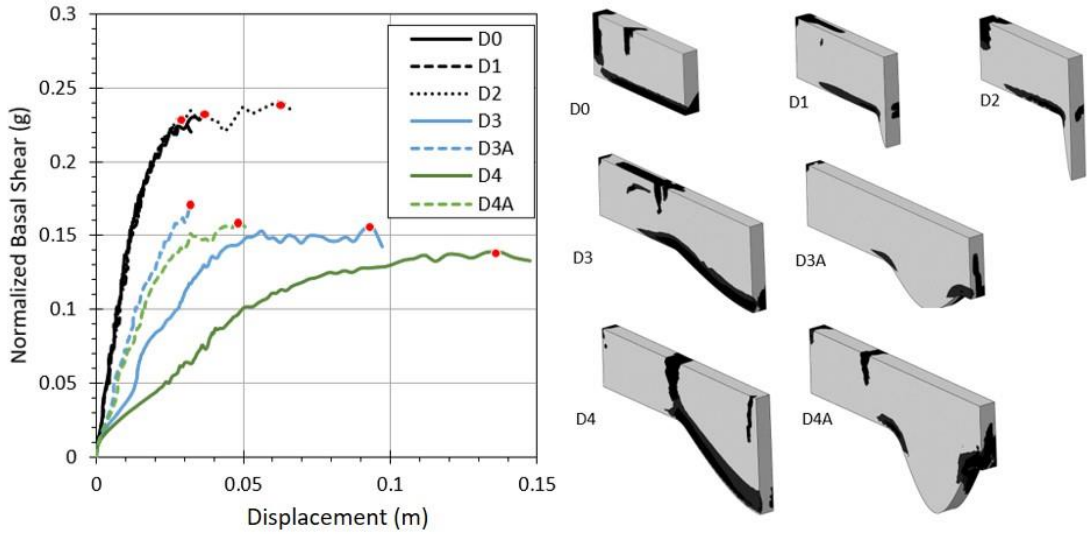


Figure 8: Capacity curves and failure mechanisms of "D" subcases.

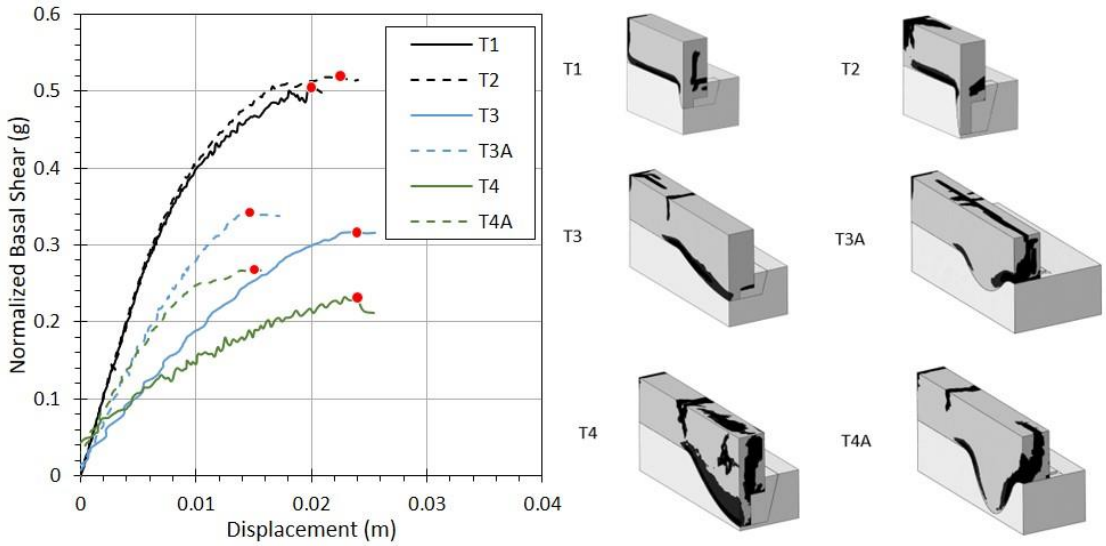


Figure 9: Capacity curves and failure mechanisms of "T" subcases.

For model VA, the density is varied (2200 kg/m3, 1600 kg/m3, and 1200 kg/m3) for the loose material filling above the vault with its other material properties unchanged, resulting in models VA1, VA2, and VA3 respectively. The three models are repeated with half the vault filler thickness (0.42 m), resulting in models VA4, VA5, and VA6 respectively. For model VB, lateral acceleration is applied toward (VB1) and away (VB2) from the external curtain wall. For VA and VB1 models, failure takes place by outward rotation of external curtain wall. For model VB2, failure takes place by outward rotation of inner wall. Therefore, the structural failures of model VA and VB1 are determined from energy curves of the external curtain wall, and the structural failure of VB2 are determined from energy curves of inner wall. The structural capacities are hence shown in Table 3, and failure mechanisms of model VA1, VB1, and VB2 are shown in Figure 10.

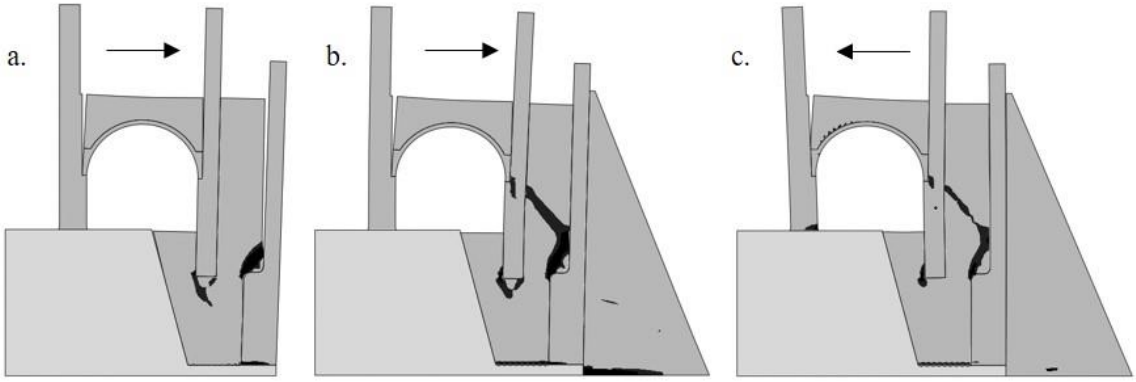


Figure 10: Failure mechanisms of (a) VA1, (b) VB1, and (c) VB2.

Table 3: Structural capacities at failure for "V" models

Models	Structural capacity at failure	Models	Structural capacity at failure
VA1	0.46 g under gravity	VA5	0.51 g under gravity
VA2	0.52 g under gravity	VA6	0.52 g under gravity
VA3	0.57 g under gravity	VB1	0.14 g under lateral acceleration
VA4	0.49 g under gravity	VB2	0.08 g under lateral acceleration

The structural capacities at failure shown in Table 3 for VA1 - VA3 and VA4 - VA6 indicate that the structural capacity of the external curtain wall is not sensitive to the density and thickness of loose material filling above the vault. However, as expected, it is altered by the addition of the supporting buttress.

6 DISCUSSION

The presence of the bedrock voids and the attendant downward extensions of the curtain wall induces localized failures that lower the lateral capacity of the external curtain wall to 0.21 g, 0.14 g, and 0.23 g for the "P", "D", and "T" configurations respectively. The peak ground acceleration (PGA) of the coastal region of Ghana ranges from 0.026 g to 0.2 g [19]. Considering the proximity to Cape Coast, we take the PGA of the Elmina area to be 0.05 g. Given this value of PGA, all the possible Portuguese and early Dutch configurations considered here are likely to have survived seismic action. This picture may have changed dramatically when the Dutch built the vaulted system along the entire curtain wall. As shown by model VA,

without the counterbalancing presence of the external buttress, the vaulted system would fail during construction in correspondence of the bedrock void by the combination of the pressure exerted on the loose soil and the effect of the lateral thrust generated by the vault itself. The addition of the buttress (model VB) stabilizes the external curtain wall under static conditions. However, the results of VB2 show that a minimal amount of lateral acceleration directed away from the curtain wall would bring structural failure to the inner wall, indicating that the structure is still prone to collapse under a very modest seismic action.

In conclusion, this initial study suggests that while a Portuguese 2 m high curtain wall would have survived local seismic action, the height elevation to 5 m due to the Dutch would have considerably weakened the structure. Noticing possible signs of rotational instability, the Dutch builders would have likely thickened the curtain wall to the current dimensions. Thus, under the conservative hypothesis that the wall was initially made entirely of mud-mortared masonry, the analysis shows that the thickened structure would again be able to sustain the same level of seismic activity as the original Portuguese curtain wall. At a later stage, before the introduction of the vaulted system, following a common procedure, the Dutch reconstructed the curtain wall as an external and internal curtain made of lime-mortared rough stones bounding a loose material filling. The construction of the vaults is likely to have caused concerns about failure conditions in correspondence of the bedrock voids, and thus would have required the addition of the present buttressing system. Finally, we note that the 2D plane strain models adopted to test the "V" configurations overestimate the effect of the soil filling. Under actual 3D conditions, portion of the vaulted structure is supported by bedrock, which would help stabilize the portion built on soil, as shown in the failure mechanisms of the "T" models. This issue will be addressed in future work.

Acknowledgements. We thank Michael Jarvis and Christopher Muir for their contributions to the surveying of Elmina Castle. Louisa Anderson helped us in establishing the early Portuguese architecture. Global engagement provided support through Global Partnership Fund travel support to Jiacheng Sun.

REFERENCES

[1] Lawrence, A.W. Trade castles and forts of West Africa. Jonathan Cape, (1963).

[2] Hair, P. E. H. The Founding of the Castelo De São Jorge Da Mina: An Analysis of the Sources. Madison: African Studies Program, University of Wisconsin-Madison, (1994).

[3] Post, F. Sao Jorge da Mina. Dutch National Archive (1637).

[4] Pinho, R. Using pushover analysis for assessment of building and bridges. Advanced earthquake engineering analysis, *International Center of Mechanical Sciences 494* (2007), pp. 91-120.

[5] Chopra, A. K. *Dynamics of Structure: Theory and Applications to Earthquake Engineering*, Pearson/Prentice Hall, Upper Saddle River, New Jersey (2007).

[6] Tezcan, S., Tambe, N., Muir, C., Perucchio, R. Nonlinear FE analysis of the response to lateral accelerations of the triumphal arch of the church of Andahuaylillas, In: R. Aguilar et al. (Eds.): *Structural Analysis of Historical Constructions*, RILEM Bookseries 18 (2019), pp. 1301-1309.

[7] Abaqus Analysis User's Manual Simulia v.6.14.6.3.3 Explicit dynamic analysis. Dassault System Corporation, Providence, RI (2018).
[8] The Hague, Collection Foreign Maps Leupe, number access 4. Vel, inventory number 779A, Dutch National Archive, (1774).
[9] Abaqus documentations, Concrete damaged plasticity, (2017). https://abaqus-docs.mit.edu/2017/English/SIMACAEMATRefMap/simamat-c-concretedamaged.htm
[10] Abaqus Theory Manual, 4.5.2 Damaged plasticity model for concrete and other quasi-brittle materials, (2009). https://classes.engineering.wustl.edu/2009/spring/mase5513/abaqus/docs/v6.6/books/stm/default.htm?startat=ch04s05ath120.html"
[11] Tarque, N. Numerical modelling of the seismic behavior of adobe building. PhD dissertation, Universitá degli Studi di Pavia, Italy, (2011).
[12] Angelillo, M., Lourenco, P.B., Milani, G. Masonry behavior and modelling. *Mechanics of Masonry Structures, CISM international center for mechanical sciences*, Vol 551, Springer, Vienna, (2014), pp. 1-26.
[13] Aguilar, R., Zavala, G, Pando, M.A., Briceno, C., Zavala, G., Castaneda, B., Perucchio, R., Uceda, S. Structural and geotechnical engineering assessment of Huaca de la Luna – A massive earthen Moche culture pyramid in Norther Peru. *Journal of Cultural Heritage 34,* Elsevier Masson SAS, (2018), pp.83-94.
[14] Brune, Philip F. The Mechanics of Imperial Roman Concrete and the Structural Design of Vaulted Monuments. Thesis: Department of Mechanical Engineering, Arts, Science and Engineering, University of Rochester, (2010).
[15] Abaqus documentations Mohr-Coulomb plasticity, (2017). https://abaqus-docs.mit.edu/2017/English/SIMACAEMATRefMap/simamat-c-mohrcoulomb.htm
[16] Chen L.J., Dai Z.H., Liu Z.W. Three-dimensional nonlinear finite element analysis of soft soil excavation engineering considering K0 consolidation. *Rock Soil Mech. 32(12)* (in Chinese), (2011), pp. 3796-3804.
[17] Fall, M., Sarr, D., Ba, M. Evolution of lateritic soils geotechnical parameters during a multi-cyclic OPM compaction and correlation with road traffic. *Geomaterials 1*, (2011), pp. 29-69.
[18]Zhu, T. Some Useful Numbers on the Engineering Properties of Materials. http://www.jsg.utexas.edu/tyzhu/files/Some-useful-numbers.pdf. University of Texas, (2014).
[19] Ahulu, S. T., Danuor, S. K., and Asiedu, D. K. Probabilistic seismic hazard assessment of southern part of Ghana. *Journal of Seismology*, 22(3), (2017), pp. 539–557.

12th International Conference on Structural Analysis of Historical Constructions
SAHC 2020
P. Roca, L. Pelà and C. Molins (Eds.)

TIMBER REINFORCEMENTS: LOCAL COSTRUCTION TECHNIQUES IN ITALIAN HISTORICAL BUILDINGS

STEFANO DELLA TORRE AND LORENZO CANTINI*

Dept. of Architecture, Built environment, Construction engineering (DABC)
Politecnico di Milano
Piazza Leonardo da Vinci 32, 20133 Milan, Italy
e-mail: stefano.dellatorre@polimi.it, www.polimi.it
email: lorenzo.cantini@polimi.it, www.polimi.it (*corresponding author)

Keywords: Historical Structure, Masonry, Monitoring, Non-Destructive Inspection

Abstract. *The role of timber connections as reinforcement for vertical masonry walls is well known but still requiring a systematic study. Considering the main sources coming from the architectonic treatises, a real identification of the use of wooden poles as binding elements between walls is not recognized. Several important authors belonging to the 15th and 16th century recommended avoiding the use of timbering elements into the section of the walls, arguing that the perishability of this material cannot provide a long durable solution. Nevertheless, since the 17th century also some indications from the so called "high knowledge" seem to identify a reliable technique in the timber reinforcements for masonry walls. This work explores the contraposition between theoretical approaches and the building site practice, focusing on the mechanical function of orthostatic timbers inserted into masonry structures. Recent contributions based on archive studies indicated that the use of wooden reinforcements was widely diffused in Italy, but rarely documented by the architectural theorists. The technical documentation discovered into archives is instead a rich source of information concerning the persistence of timbers inside walls as a solution against the vulnerability of masonry structures to shear forces. The case of the building site documentation for the realization of Volpi Palace in Como offers an important occasion for improving the studies on a building practice that did not meet official credits by the theoretical experts in architecture.*

1 INTRODUCTION

Defined as a creative process produced by the mutual influences among strictly connected entities, the idea of coevolution can be applied to the rich panorama of the historical building techniques for interpreting the realization of peculiar construction solutions. Wooden elements used for improving the common connection system among masonry elements, like vertical walls and masonry arches and vaults, are an example of an upgrade required by those structures showing forms of vulnerability interacting with the environment [1].

Referring to historical buildings, local construction solutions represent the response to technical demands appeared in different times for facing specific problems, from common state of stress distribution in masonry structures to seismic mitigation. The introduction of wooden elements into masonry walls, for instance, is a widely diffused measure for reinforcing stone or

brickworks [2]. These connections, inserted into the masonry walls, were identified by Vitruvius' treatise, as orthostatic timbers, considering the version edited by C. Cesariano. The peculiar vulnerability of masonry structures to shear stresses required such reinforcements. In Italy, after recent earthquakes (L'Aquila 2009 and Amatrice 2016), the rediscovery of such building techniques, in some cases belonging to a sort of forgotten world of knowledge, drove to design alternatives and more sustainable retrofitting interventions for historical buildings [3].

The authors, with the aim to improve the attention on these construction solutions, focused on the rich contributions contained in the historical treaties of the Italian building tradition and on some archive documents describing original design for reinforcing elements [4]. Among the various materials, the study proposes the analysis of some specific contests: Como Lake in Lombardy and the regions that in the past were under the control of the Vatican State or the Kingdom of the Two Sicilies, where this technology, based on tie beams and hut-oriented diaphragms, improved the mechanical properties of the buildings.

2 MASONRY BUILDINGS AND WOODEN REINFORCEMENTS

The vulnerability of historical masonry structures is an issue that becomes always prior especially after seismic events. The use of wooden frames as mitigation techniques against seismic actions was codified since the 18th century for local situations (as in Naples kingdom). In the rich theoretical tradition about architecture, the Italian theorists did not reserve a peculiar role for the timbering elements used as reinforcing supports for masonry structures. In some cases, authors are considering the use of wooden elements into the masonry walls as a technical mistake. This assumption contrasts with several evidences indicating a tradition in the use of timber elements into the masonry sections of the buildings. This study tries to deal with an apparent conflict between the building technical knowledge expressed by the so-called "high culture" contained in the architectonic treaties and the common practice of building that adopted the use of timber elements together with masonry walls as a reliable solution.

2.1 The "high culture" approach

The use of timber elements into the section of masonry walls was observed in several archaeological campaigns on historical buildings. Even during restoration works, the traces of wooden elements into cavities arranged in the masonry section of the walls testified the common application of wooden reinforcements into the masonry apparatus. A first important reference for this technical solution comes from the treaty De Architectura written by Vitruvius. In the edition translated in Italian by C. Cesariano in 1521 [5], the insertion of timber into the section of the walls is described as "orthostate", a technique used for improving the connection between the walls and more in general the box-like behavior of the buildings. In the 8th chapter of the second book of his illustrated edition, Cesariano offers a representation of some masonry typologies. The sketches at page 39 of the second book (see figure 1), referred to sepulchral monuments, show the transversal connections for masonry walls with large sections: the use of metal anchorage for linking the stone blocks is clear, but also vertical wooden elements are here represented along the edges of the structures. This chapter of the De Architectura treaty contains also the comments provided by Cesariano to its illustrations and, more than in the sketches, the role of metal or wooden connections is emphasized in his description. Respect to other theorists that will follow during 16th and 17th century, Cesariano did not denigrate the timber material as

a cheap alternative to the more expensive use of metal reinforcements. He recalled the building tradition of empty cavities arranged into the masonry walls in order to be used for placing transversal connectors, which could be made by wood or metal material. Both materials were able to provide the tie effect to the stones, according to the author.

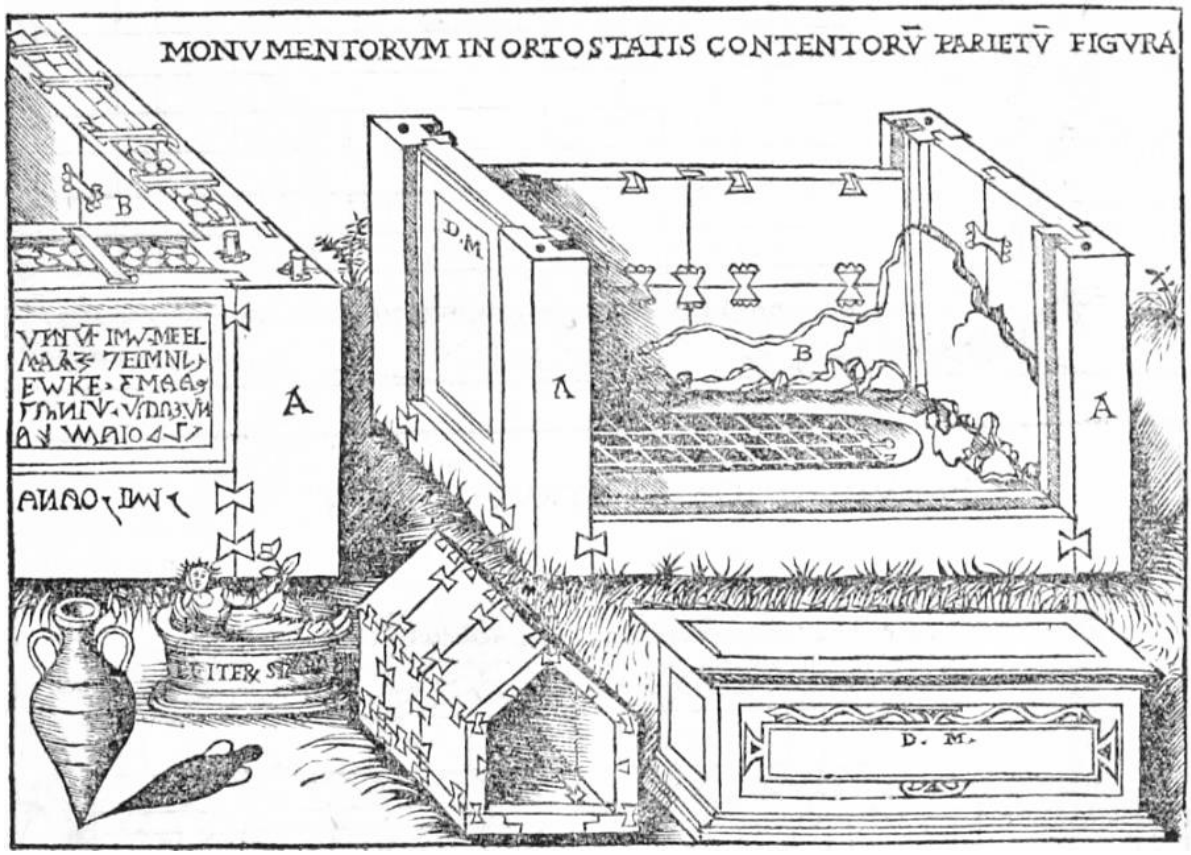


Figure 1: illustration to the Vitruvius' De Architectura issued by Cesariano (page XXXIX of the second book) in 1521. Letters A and B identify the position of wooden or metal connections inserted in the masonry structure.

The building tradition maintained the use of the tie beams into the masonry structures as documented by Viollet Le Duc for the monuments dated back to Merovingian and Carolingian era in France [6]. The linking function of the timber elements inserted in the walls is underlined by the author that in the first chapter of the Dictionnaire, about the principles of Gothic architecture, describes the mechanical logic of the masonry structures used in the Medieval cathedrals. Respect to the Romans' tradition mentioned by Vitruvius, the masonry apparatus of Gothic buildings was composed by rabble materials contained into an external layer of well-shaped stones. No cavities were here arranged for hosting timber elements, but wooden beams were inserted into the chaotic core of these structures with a fundamental role: the reinforcement of the connection between the main joints of the masonry structures, as for longitudinal walls and pillars (see figure 2a). He also stated that the long timbers inserted into the masonry at the springs of the vaults had a stabilizing and linking function in the constructive logic addressed to a reliable containment of the thrust effects generated by the masonry vaults (see figure 2b).

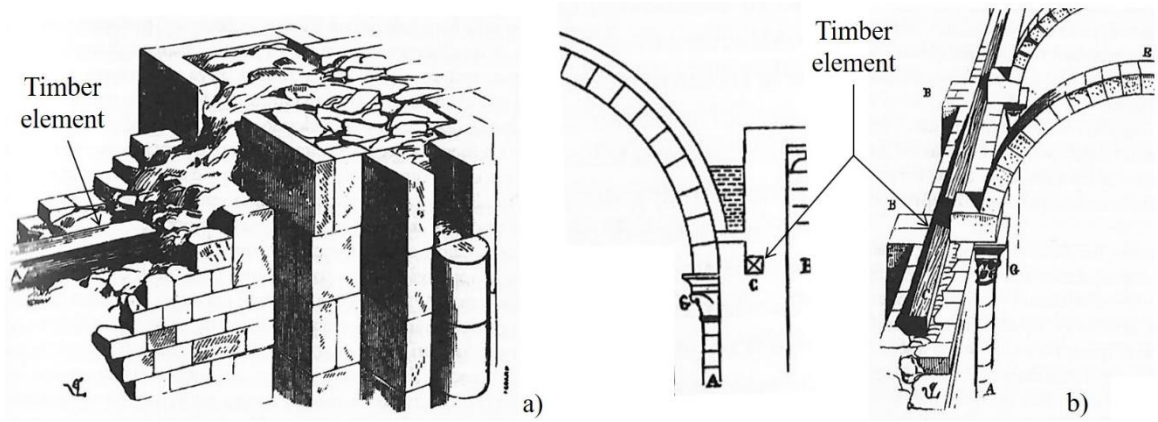


Figure 2: drawings from the *Dictionnaire raisonné de l'architecture française du XI au XVI siècle* by Viollet le Duc. Use of timber reinforcements in Mediaeval architecture: a) timber connection into a masonry section (from picture 2 of the Dicionnaire [6], elaborated by the authors); b) timber link for the masonry support of the wall (from picture 3 of the Dictionnaire [6], elaborated by the authors).

The structural role of timber elements integrated into masonry walls, described by Viollet-le-Duc in the 19th century, comes after a long period characterized by a negative opinion concerning the use of wooden materials as reinforcement material for the walls, stated by several important theorists. L. B. Alberti, S. Serlio and later Palladio, following the setting of Vitruvius' treatise, reserved detailed descriptions about wooden structures and the preparation of the material before its building use, but they recognized its application for specific construction categories: horizontal floors and roofing systems. Any structural aids for contrasting shear forces, should be realized by the introduction of metal tie rods into the masonry apparatus, being the material more durable than the wooden beams. The reinforcements realized by timber structures are here considered a cheap alternative respect to the more expensive, but more proper, technique based on metal chords crossing the section of the walls.

Among several negative opinions, V. Scamozzi, in the 9th book of his treatise on the "universal architecture" [7], offers a description of the reinforcement aids introducing the masonry vaults, indicating both metal and wooden connections as reliable solutions. He states that timber elements request more attentions, due to the nature of the material, recommending a proper displacement near masonry structures, but not inside their sections. As an example, he mentioned the case of the cupola built by Brunelleschi for S. Maria del Fiore in Florence, where e retaining ring made by timbering system is placed at the base of the structure, in the open space between the internal and the external dome. As pointed out by Di Teodoro in [8] and Ottoni in [9], since the realization of the Florentine dome, F. Brunelleschi addressed his efforts to solve the problems connected to the discontinuities created by the octagonal geometry of the cupola. The insertion of the chain in chestnut (the "catena dei castagni") at the base of the dome (Figure 3), close to the drum, anticipated the further debate on the reinforcements requested by masonry domes and prefigured the passage from the building competences based on empirical knowledge to the more scientific analytical approach that will characterize the studies of the 17th and the 18th century. The builders of the 15th century could not be supported by the studios coming from the modern solid mechanics, but the empirical experience matured on domes and vaults raised to the topic of the improvements needed by vertical masonry walls connected to

those structures. The awareness of Brunelleschi over the thrusting effects of his dome is still discussed by the experts [8, 9], but the reinforce obtained by the wooden ring inscribed into the internal and the external dome of the Florence Cathedral has two main effects:

- supporting the linkage between each masonry segment of the dome and the main angular ribs:
- contrasting the elastic deformation imposed by the increasing load of the structure during its realization and induced by the low hardening process of the mortar joints composing the brickwork.

The use of timber elements for improving the connections between perpendicular walls at the level of other thrusting structures, like the dominical cross vaults of Santa Maria Novella (dated back to 1355), testifies the attention to the mechanical problems deriving from the interaction between masonry walls and masonry vaults. Instead of using metal tie rods, in this case diagonal timbers were placed at the extrados of the vaults, between the perpendicular walls of each span containing the vaults, in order to create a sort of tension ring effect around them.

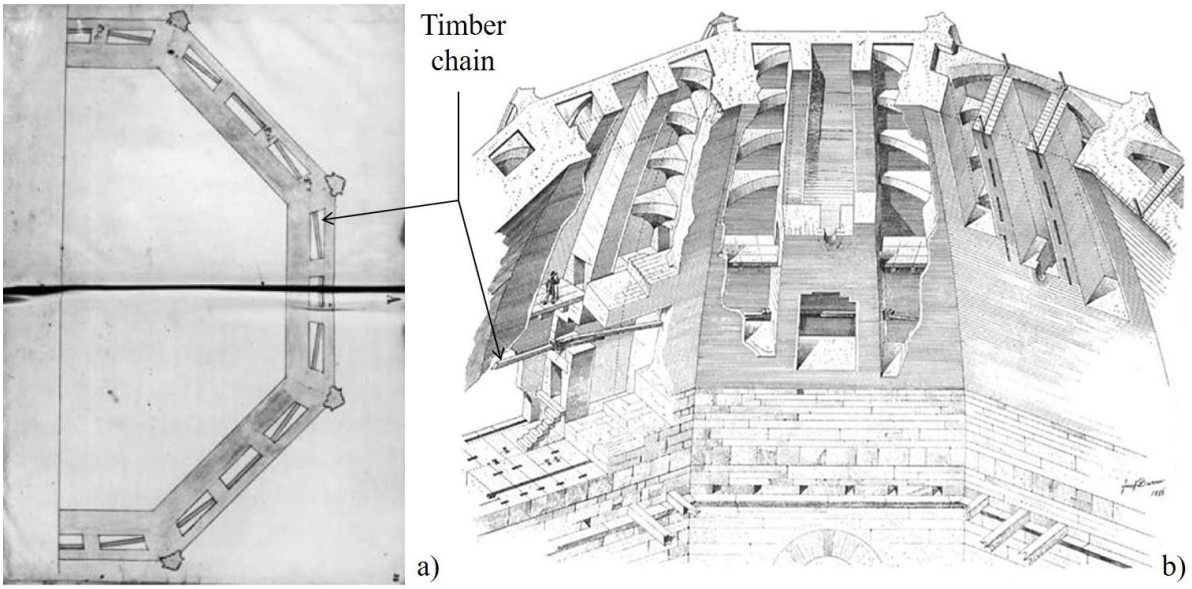


Figure 3: The wooden chain realized around 1420 at the base of the dome by Brunelleschi: a) archive drawing published in [9], p. 159 and b) the constructive system of the dome (from Margani L. *Archi e volte in muratura*, Caltanissetta: Lussografica edizioni, 2009).

Even if the use of wooden reinforcements is documented in outstanding historical buildings, the peculiar attentions requested by wood material was considered a limit for its application in civil engineering. At the beginning of the 20th century, S. Mastrodicasa, whose treatise on the mechanical behaviour of masonry buildings [10] produced an important impact on the construction field, referred to the presence of timbering systems into masonry walls as an “anomaly”. A revaluation of the role of such structures had to come from other studies matured in occasion of recent seismic events, with new analysis of wooden reinforcements observed into the masonry structures of damaged buildings.

2.2 The "on-site practice" approach

The use of timber elements into masonry structures is commonly accepted as a cheap alternative to the use of the more expensive metal tie-rods. As anticipated in the previous paragraph, theorists considered the use of reinforcements made of wood as a deviant solution from the so-called "good practice". Changing the perspective from theoretical field to the construction practice, the continuous research of strategical solutions for ensuring a global equilibrium, among the structural components of the building, required the utilization of timber elements. The constructive tradition based on timber-frames widely diffused in Central and North Europe was not largely adopted in Italy, but the presence of wooden ties and reinforcing timbering continued to be applied in masonry buildings. Several examples were recently documented by different studies developed in Central Italy, where the last seismic events renewed the attention to the use of timbers as preventive measure against the earthquake effects.

M. D'Antonio in [11] offers a detailed description of the wooden elements inserted in the masonry walls, adopted in Abruzzo Region. The so-called "radiciamenti" (literally "rooting systems") are wooden beams placed in the wall section at different levels along the vertical structure. Their function is a reinforce able to constitute a linkage for the masonry apparatus. These "radiciamenti" can be inserted transversally into the wall, in order to connect the different layers forming the masonry section, or longitudinally, for reinforcing the wall against flexural stress and for improving the connection in the corners (Figure 4a), if jointed by metal carpentry with another perpendicular timbers. By the inspections carried out after the 2009 L'Aquila earthquake, several examples of wooden reinforcements were documented in masonry buildings, like in the partially collapsed dome of Santa Maria del Suffragio (figure 4b).

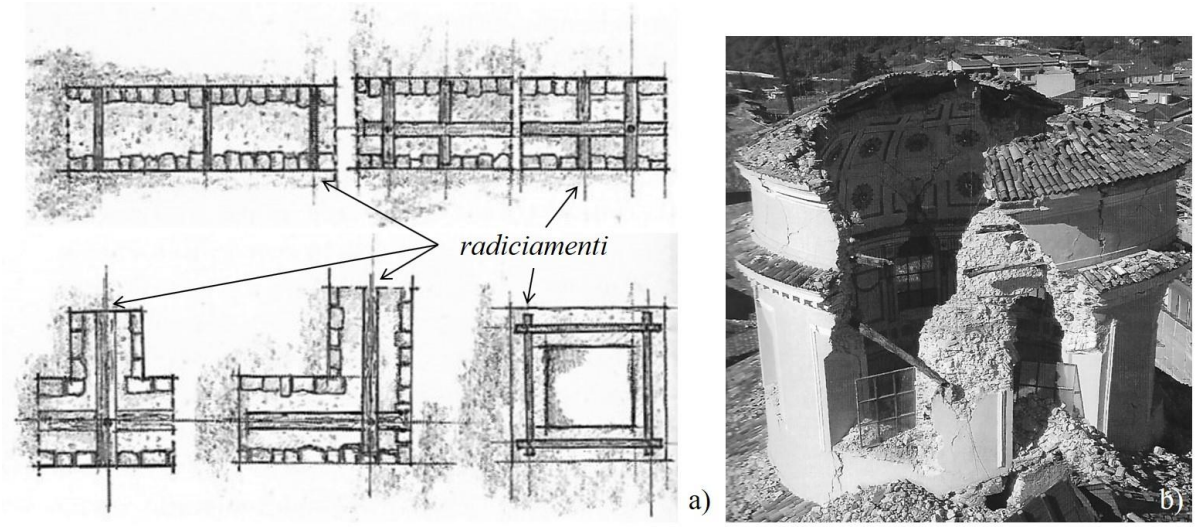


Figure 4: The wooden anti-seismic technique diffused in L'Aquila, known as "radiciamenti": a) wooden frames with different structural functions and b) the 3 orders of "radiciamenti" visible in the partially collapsed dome of Santa Maria del Suffragio hit by the 2009 L'Aquila earthquake (source from [11], pp. 27 and 52).

The frequent use of timbers into masonry walls was documented also by other studies [12, 13, 14] carried out in Central Italy. The analysis on the masonry quality of the walls, often characterized by multiple leaf sections with chaotic rubble materials in the core, underlined a

problem connected to the lack of resources that required the use of wooden beams for a general improvement of the masonry properties. Independently from the seismicity of the territory, the building technologies observed over the entire Italian territory showed this common feature: the recourse to timbering systems supporting the masonry apparatus. The wooden elements could be limited or inserted with a certain regularity along the vertical development of the walls, displaced inside the section or organized along its borders (Figure 5a and 5b), but in the various regional declinations, this technology supplied to the intrinsic vulnerability of masonry structures realized with poor materials. The same studies testify the diffusion of the wooden reinforcements also as preventive aid for contrasting the lateral thrust of masonry vaults and domes, as represented in the reconstruction of the timbering system surrounding the dome of San Giovanni Battista church in Penne (Pescara), reported in figure 5b.

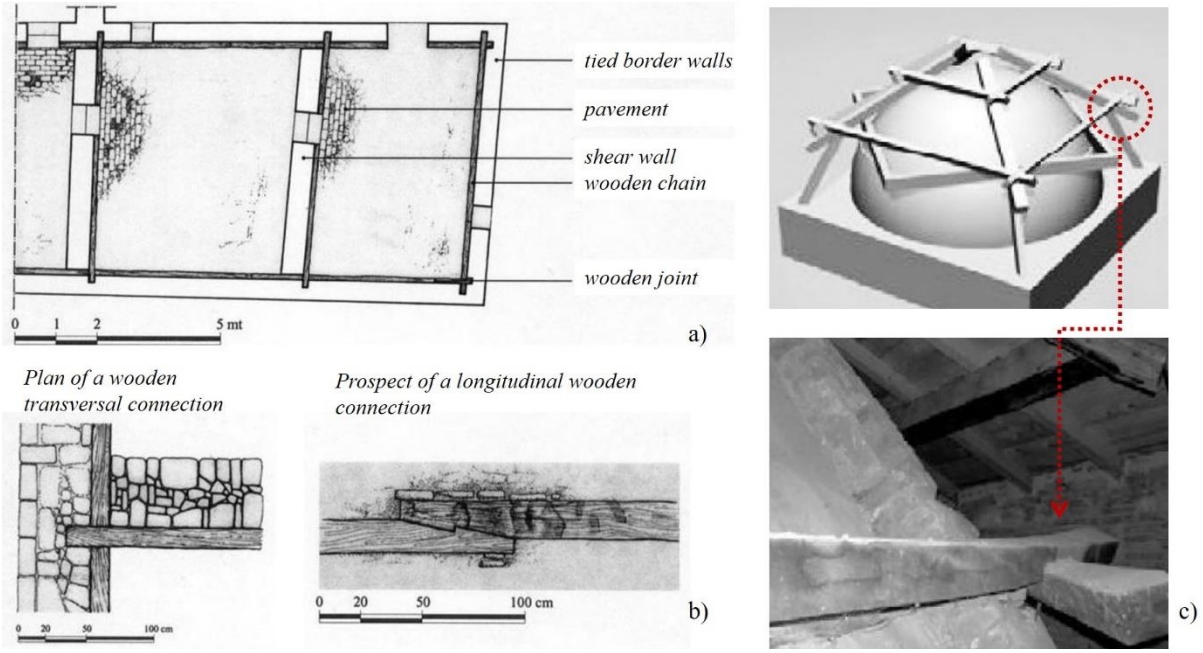


Figure 5: Tie beams: a) historical masonry building in Guardiagrele (Chieti) with improving connection between the walls (survey by E. Candigliota and published in [12], p. 16, modified by the authors); b) two details of transversal and longitudinal connections; c) the extrados of a dome in Penne with the layout of the timbering system realized for containing the lateral forces, with a picture (source in [13], p. 62, modified by the authors).

These bindings solutions are also present in Italian areas where earthquakes have a minor impact, demonstrating that the on-site practice assumed the wooden reinforcements as a reliable solution. As remarked by several authors, the building techniques based on the multiple leaf masonry typologies, belonging to the Italian constructive tradition, maintained a long-lasting relationship with timber aids. A sum of this technical knowledge about the application of reinforcements in opposition to the intrinsic vulnerability of masonry structures is provided by Pellegrino Tibaldi, one of the most influential architect of the second half of the 16th century [14], active before in Rome and later in Milan. In his treaty (*L'architettura*, remained unpublished until 1990), he pointed out that the wooden floors, although not providing lateral thrusts to the walls in normal conditions, were often connected by metal tie rods and even

integrated by timber linkages (named "ligamento", literally "tying beam") inserted into the masonry and more rarely by metal tie rods. These reinforcements had to improve the mechanical behaviour of the building that could be simplified to a box-like behaviour. Aware of the fact that wooden materials are subjected to a limited durability if confined into the wall sections, Tibaldi provided also the indications for the preliminary preparation of the material, stating that a general benefit to the stability of the building could be obtained by the use of "legno biusciato", interpretable as "burnt wood" in authors' opinion (but other experts suggested a different interpretation, translating it as "debarked wood") applied into the walls for each order of room, connected to the heads of the roofing timbers or to the springs of the vaults. This description gives a new perspective to the state of the art of the building modalities diffused in North Italy at the end of the 16th century, where a consolidated methodology seems to be based on the common use of timber structures strictly connected to the masonry elements.

3 RECENT CONTRIBUTES FROM SEISMIC AREAS

The presence of timber frames applied into masonry walls for reinforcing their ligature and for implementing their deformability is widely documented in Central and South Italy. From an historical point of view, the Kingdom of Naples produced important laws and studies for the post-seismic reconstruction on different areas of its territories hit by seismic events, like Calabria and Sicily. The active support provided by timber-frames set into the masonry walls was codified after important seismic events occurred in the 18th century in Lisbon (1756) and Calabria (1783). The large destruction left by those earthquakes led to the introduction of new constructive principles for the buildings and the organization of the rebuilt towns. The main anti-seismic typologies developed in that period are characterized by timber-frames, built into the vertical walls, organized in primary vertical and horizontal beams, connected by diagonal and horizontal joists. In the recent earthquake that stroke Ischia island, some partial collapsed in the village of Casamicciola, a village rebuilt after a previous earthquake occurred in 1883, showed the recourse of such reinforcement technique for the common buildings (figure 6). The references for this kind of wooden aid are the Pombalina technique in Portugal and the Casa Baraccata in Calabria Region.



Figure 6: A timber-frame realized in a masonry wall of a house hit by the 2018 Ischia earthquake (representation realized by the authors).

If the intensity of the damages of some seismic events created the conditions for the formation of the so-called local seismic culture, with the preparation of specific measures for improving the buildings, it is also known that the long periods from an earthquake to another, sometimes with low magnitudes, did not contribute to maintain alive these technical solutions. The large amount of damages occurring to the built heritage in seismic areas are mainly due to the discontinuous application of the reinforces introduced immediately after the earthquakes and later abandoned when the perception of the risk becomes a far memory of past times.

The sensibility to the vulnerability of masonry structures to horizontal stresses, matured in Central and South Italy, traditionally more subjected to earthquakes respect to the North, supported the use of wooden aids with the masonry structures. As shown in the recent study set by C. Bartolomucci [15], a form of resilience can be recognized in the historical set of measures applied in important architectures belonging to a city subjected by several earthquakes like L'Aquila. Here, historical palaces are the result of a complex modification of the structures, realized in origin without the proper preventive measures for facing the seismic actions, later modified with peculiar solutions, able to contrast the telluric strains. Among them, the realization of light timber vaults, the connections between flooring systems and vertical walls by metal tie rods and the use of timber-frames into the walls introduced during the realization of some additions (see figure 7).



Figure 7: Anti-seismic measures adopted in Carli Benedetti Palace in L'Aquila: a) heads of the metal tie rods connecting vertical walls to horizontal structures; b) timber (radiciamento) reinforcing a masonry wall, connected to a metal tie rods crossing a chimney flow; c) tie rods at the intrados of the arches of the porch; d) the 18th century additions composed by wooden frames, directly connected to e) the wooden reinforcements of the vaults, forming a box-like devise with f) the vertical partitions (pictures from [15] elaborated by the authors).

The same consolidated culture based on the use of wooden reinforcements for masonry load bearing walls and partitions is also characterizing the building technology of the 18th and the 19th century in the Kingdom of Naples [16, 17]. Examples coming from Naples and Palermo demonstrate the attention of the designer addressed to anti-seismic preventive measures and the problems concerning thrusting structures. The large use of vaulted ceiling in monumental palaces and churches build in Baroque age and the experiences matured with the domes from the archetypes of Santa Maria Novella in Florence and St. Peter in Rome contributed to keep attention on wooden and metal reinforcements.

4 THE ARCHIVE DOCUMENTS ABOUT VOLPI PALACE IN COMO

The long-lasting tradition of beam systems systematically applied to masonry structures is also testified by the technical drawings realized for the project of an important palace in Como, during the first half of the 17th century. Volpi Palace had to become the residence of Volpiano Volpi, an important ecclesiastic that matured relevant assignments also in Rome [18].

The project was developed by Sergio Venturi, an architect from Siena, active in Rome at the court of Pope Paolo V. The on-site activities for the building of the palace were based on an intensive epistolary exchange between the designer, in Rome with Volpi, and the local builders.

Among the various technical aspects described in the letters, some technical drawings contain important information concerning the building technique proposed for the realization of the main representative rooms set at the ground floor of the palace. All the rooms are characterized by cloister vaults (figure 8a), a typology largely diffused in Baroque age and also known for the high lateral forces transmitted to the supporting walls. The document showing the plan of the ground floor with the vaults presents interesting details: the setting of the wooden carpentry is displayed along the masonry walls, with the timbers centered in the middle of the section, and wooden joists are also arranged at the corner of each room for providing a tension ring effect around the extrados of the vaults (figure 8b).

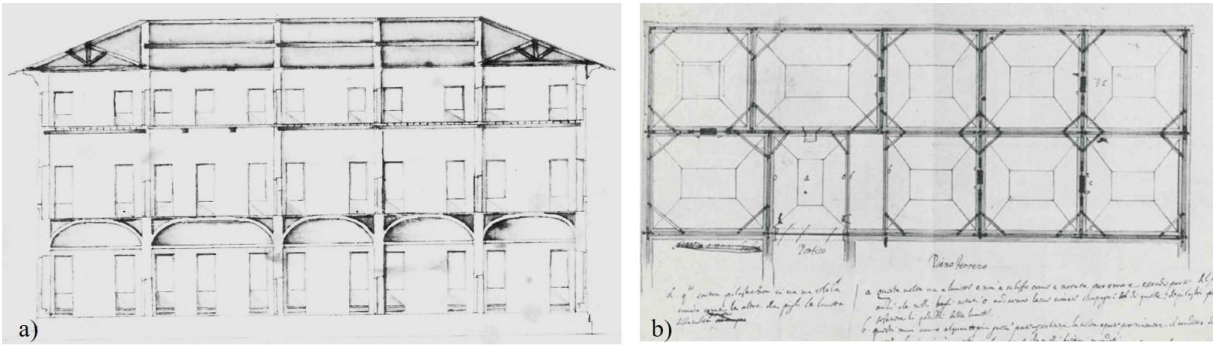


Figure 8: Archive documents of the executive project proposed for Volpi Palace in Como dated back approximately to 1623: a) vertical section and b) plan of the ground floor with the tie beam system arranged around the vaults and inserted into vertical walls (published in [18], pp. 20-21).

The case of Volpi Palace represents an experience overpassing the physical limits of the distance between the designer and the on-site builders, but also crossing over two well defined different cultural environments, where the art of building was deeply based on local traditions [19-20]. An aspect of the physical and cultural distance between the actors involved in the building of the palace is represented by the technical lexicon found in the letters, alternatively influenced by the Roman jargon and the Lombard dialect. The timbering system is described by using two terms, “ligato” and “telaro”, which seem equivalent, even if coming from slightly different semantic domains. They both mean a wooden tie-rod, or a system of tie-rods [21], used for the global firmness of the building, usually working as a passive aid. The use of timber as additional components of the masonry walls appears here as a common practice, demonstrating an advanced knowledge over the mechanical behaviour of vaulted spaces. Even if important contributes in the literature, concerning historical structures, emphasized the role

of wooden elements as anti-seismic measure, the analyzed archive documents are showing a technical solution based on strain containment, that is described as a non-written standardized methodology.

The practice of tying the masonry walls, involved in the load distribution under the actions produced by masonry vaults, is described both by graphical drawings and written documents. The role of the timbering system surrounding the vaults is more connected to the research of the congruence of the building components more than a general response to seismic actions.

12 CONCLUSIONS

The use of timber elements in historical buildings knew a limited success in the Italian literature produced by the main theorists about architecture. The present study collects several examples of the application of timbering systems to the masonry building, showing a mature knowledge of the mechanical behaviour of complex structures, like vaulted spaces, requiring special attentions. The common practice of using tying beams in wooden material, described in the archive documents concerning Volpi Palace, is a useful evidence of the state of on-site practices. The common assumption that the timbering systems applied into masonry walls, as a reinforcing grid mainly connected to the response in case of seismic actions, should consider that the diffused knowledge of the mechanical properties of masonry vaults constituted a first substrate for founding the technological solutions against the vulnerability of historical buildings to seismic events.

REFERENCES

[1] Ferrigni, F. Vernacular architecture: a paradigm of the local seismic culture. In M. Correira et al. (Eds): *Seismic Retrofitting Learning from Vernacular Architecture*, CRC Press Balkema (2015), pp. 1-13.

[2] Touliatos, P. Coopereting Timber and Stone Antiseismic Frames in Historic Structures of Greece. In H. Cruz et al. (Eds.): *Historical Earthquake-Resistant Timber Framing in the Mediterranean Area*, Springer (2015), pp. 3-15.

[3] Campisi, T., Saeli, M. Timber anti-seismic devices in historical architecture in the Mediterranean area. In K. de Proft et al. (Eds): *Timber Structures and Engineering*, Witpress (2018), pp. 149-161.

[4] Della Torre, S. Alcune osservazioni sull'uso di incatenamenti lignei in edifici lombardi dei secoli XVI e XVII. In M. Casciato et al. (Eds.): *Il modo di costruire. Atti del I Seminario Internazionale*, Roma 6-8 giugno 1988, Edilstampa (1990), pp. 135-144.

[5] Cesariano. C. *Di Lucio Vitruvio Pollione De architectura libri dece traducti de latino in vulgare, affigurati, comentati*. Como, (1521).

[6] Viollet-le-Duc, E. E. voice *Chainage* in *Dictionnaire raisonnè de l'architecture francaise du Xie au XVIe siècle*, Tome II. De Nobele. Paris, (1868), pp. 396-404.

[7] Scamozzi, V. *Dell'idea della architettura universale*. Vicenza, (1714).

[8] Di Teodoro, F. P. Giovanni Poleni, Domico Maria Manni e le catene per la cupola di Santa Maria del Fiore: per la storia delle fratture e dei previsti risarcimenti alla "grande macchina di Filippo Brunelleschi". In *Annali di architettura*. 23 (2011), pp. 152-177.

[9] Ottoni, F. *Delle cupole e del loro tranello*. Aracne, Roma, (2015).

[10] Mastrodicasa, S. *Dissesti statici delle strutture edilizie*. Milano, (1978).

[11] D'Antonio, M. *Ita terraemotus damna impedire*. Carsa Edizioni, (2013).
[12] Varagnoli, C. Abruzzo. Un ritratto edilizio. In C. Varagnoli (Ed.): *La costruzione tradizionale in Abruzzo*. *Fonti materiali e tecniche costruttive dalla fine del Medioevo all'Ottocento*. Cangemi Editore, Roma, (2008), pp. 11-34.
[13] Varagnoli, C. Tecniche e materiali nella costruzione delle volte in Abruzzo. In C. Varagnoli (Ed.): *La costruzione tradizionale in Abruzzo*. *Fonti materiali e tecniche costruttive dalla fine del Medioevo all'Ottocento*. Cangemi Editore, Roma, (2008), pp. 49-64.
[14] Panizza, G. *Pellegrino Pellegrini. L'architettura*. Milano, (1990).
[15] Bartolomucci, C. *Terremoti e resilienza nell'architettura aquilana*. Edizioni Quasar, Roma, (2018).
[16] Campisi, T., Sibilia F. The Use of Wood with an Anti-seismic Function in the Architecture of Palermo during the 18th Century. In H. Cruz et al. (Eds.): *Historical Earthquake-Resistant Timber Framing in the Mediterranean Area*. Springer, (2005), pp. 113-124.
[17] Montana, S. L'uso dei dispositivi di rinforzo ligneo nell'architettura siciliana di età moderna. In *Lexicon. Storie e architettura in Sicilia e nel Mediterraneo*. 18, (2018), pp. 32-39.
[18] Della Torre, S. Il Palazzo Volpi. In S. Della Torre (Ed.): *Il mestiere di costruire. Documenti per una storia del cantiere. Il caso di Como*. Nodo Libri, (1992), pp. 99-104.
[19] Scavizzi, C. P. *Edilizia a Roma nei secoli XVII e XVIII. Ricerca per una storia delle tecniche*. Quaderni, 6, Ministero dei Beni Culturali e Ambientali, Roma, (1983).
[20] Patetta, L. Le "catene" come scelta progettuale negli edifici tra XIII e XV secolo. In L. Patetta (Ed.): *Scritti sull'architettura del Rinascimento*, (2000), pp. 205-217.
[21] Pracchi, V. Tecnologia ed organizzazione edilizia nel territorio di Como: appunti e considerazioni. In S. Della Torre (Ed.): *Il mestiere di costruire. Documenti per una storia del cantiere. Il caso di Como*. Nodo Libri, (1992), pp. 29-48.

12th International Conference on Structural Analysis of Historical Constructions
SAHC 2020
P. Roca, L. Pelà and C. Molins (Eds.)

APPLICATION OF DIGITAL CLOSE-RANGE PHOTOGRAMMETRY TO MONITOR LOCAL DEFORMATIONS OF ARCHITECTURAL MONUMENTS: A CASE STUDY OF EL MIRADOR DE INKARAQAY (MACHU PICCHU)

J. KOŚCIUK[1*], M. PAKOWSKA[2]

[1] Laboratory of 3D Laser Scanning and Modeling (LabScan3D)
Faculty of Architecture, Wroclaw University of Science and Technology
Wyb. Wyspiańskiego 27, 50-370 Wroclaw, Poland
e-mail: jacek.kosciuk@pwr.edu.pl (*corresponding author)

[2] Doctoral student
at Faculty of Architecture, Wroclaw University of Science and Technology
Wyb. Wyspiańskiego 27, 50-370 Wroclaw, Poland
e-mail: marta.pakowska@op.pl

Keywords: Historical Structure, Deformation, Monitoring, Digital Photogrammetry

Abstract. *The monitoring of deformations on a historical construction, both over the entire building as well as on selected parts, is one of the essential elements of conservation strategies. Traditional surveying techniques require placing permanent, stable markers around the object being monitored to define a fixed reference system, and then, at specified intervals, repeating measurements of characteristic points on the construction. The situation becomes complicated when markers cannot be placed, and at the same time, the site is remote and difficult to access. This is the case for El Mirador de Inkaraqay - the Incan astronomical observatory on the northern slopes of Huayna Picchu. A method for monitoring local deformations at this particular place was sought. The research resulted in a photogrammetric method allowing the detection of local deformations greater than 2 mm despite the lack of permanent reference markers.*

1 INTRODUCTION

Since its very beginning, terrestrial laser scanning (TLS) has been seen as a useful tool for documenting cultural heritage [1÷2]. Its effectiveness in monitoring structural health [3÷7] and virtual strength test simulations of historical constructions [8] also quickly became widely recognised. The parallel development of digital close-range photogrammetry (DCRF), both in terms of digital camera performance and the constant evolution of software solutions, has also directed researchers to DCRF [9÷11]. The last decade, in particular, is abundant with publications comparing the range of application, feasibility and accuracy of TLS and DCRF in monitoring the structural health of historical constructions [12]. The theoretical foundations for the use of DCRF [13] as well as specific applications have been considered, and case studies of the most famous monuments have been presented [14÷17]. An important subject among these publications is the use of DCRF in monitoring deformations.

2 AIM OF THE RESEARCH

Monitoring possible deformations on an archaeological site or a historical building, both over the entire object as well as on selected parts, is one of the essential elements of conservation strategies. The basic monitoring method requires placing stable markers around the object in order to define a fixed reference system, and then, at specified intervals, repeating measurements of characteristic points on the structure. Usually, laser theodolites are used for this kind of analysis, and recently TLS has also begun to be applied.

The situation becomes complicated when, within the visibility range of the instrument, we cannot place stable marks around the object, and at the same time the site is remote and difficult to access, so sending a crew with special equipment is complicated and expensive. This is the case with the Incan astronomical observatory El Mirador de Inkaraqay [18÷20], a site located within the borders of the Machu Picchu Archaeological Park on the northern slopes of Wayna Picchu and covered with dense jungle (Fig.1).

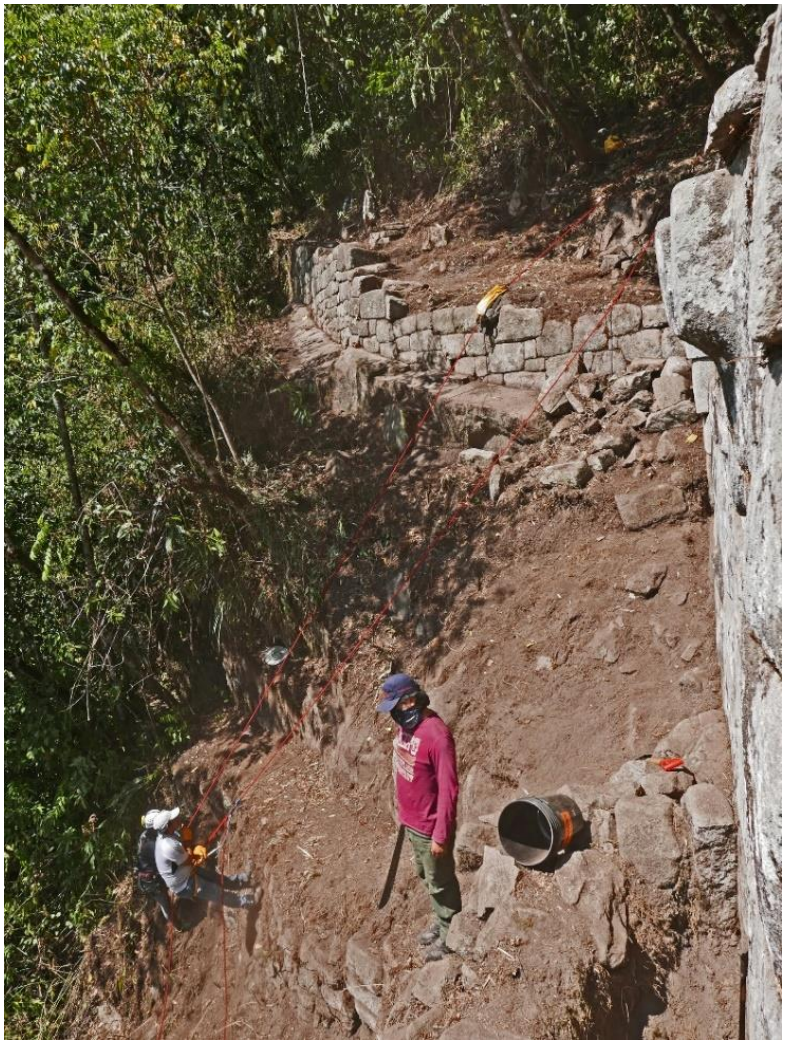


Figure 1: View of El Mirador de Inkaraqay ruins
exposed in the jungle in 2016 (courtesy of M. Ziółkowski)

The very steep and insecure hill, as well as the condition of the main walls of the observatory and the retaining walls protecting the slope, raises concerns about stability. In the case of a monument such as an ancient astronomical observatory, it is crucial to preserve its original geometry. Even slight deformations can lead to a state where astronomical phenomena observed in the past will no longer be visible. For example, such as the situation with the famous "Sun Dagger" in the Chaco Culture National Historical Park, in northwest New Mexico [21].

The essential part of the El Mirador de Inkaraqay observatory consists of two niches with two observation holes pointing towards the Yanantin peak towering above the eastern horizon. One of them was used by ancient astronomers to observe the Sun rising over Yanantin summit during the June solstice, the other to follow the path of the Pleiades during their heliacal rising along the southern slope of the Yanantin mountain [20]. Therefore, the most crucial task was to monitor possible changes in the geometry of both niches and both observation holes. The lower part of the niches on the solid masonry platform seems to be relatively stable. What could be worrying are the observation holes in higher parts of both niches that are exposed to direct erosion caused by the frequent rainfall in this area and exuberantly growing vegetation.

As already mentioned, placing stable reference markers around the observatory is not possible due to the steep and slippery slopes. Even if it were conceivable, since this site cannot be permanently guarded, there is a danger of possible vandalisation of markers. Although it is remote from the part of the Park that is accessible for tourists, it is still occasionally visited. For the same reason, it was considered not sensible to use any permanently installed devices such as inclinometers, gap gauges or MEMS sensors [22] to monitor the condition of the monument. Another essential factor to consider was that it was not feasible to repeatedly send a well-trained surveying crew equipped with a 3D laser scanner or at least a precise total station to the site. Thus a simple monitoring method that met the two following criteria was needed:

- stable reference markers near the site would not be required,
- the most straightforward equipment that did not require professional handling could be used.

It was also necessary to determine the effectiveness and accuracy of such a method, and at the same time propose an adequate workflow covering both the phase of data acquisition in the field and the subsequent processing in a specialised laboratory.

3 METHODS AND TOOLS

Under the conditions of the site, DCRF with the use of a middle-class consumer camera was the first choice. A Sony Alpha STL-A65 camera with an APS-C sensor matrix of 24 megapixels and an attached Sony 18-55mm f/3.5-5.6 standard lens was selected for collecting photos. The AgiSoft Metashape Professional package was used as the photogrammetric software [23]. A Leica P40 laser scanner (Tab. 1) was the reference measuring tool to which results of the photogrammetric approach were compared.

Table 1: Technical specification of the Leica P40 scanner [24].

Range accuracy	1.2 mm + 10 ppm over the full range
3D position accuracy	3 mm at 50 m; 6 mm at 100 m
Range noise at 78 % albedo	0.4 mm rms at 10 m; 0.5 mm rms at 50 m

Three additional applications were also used to embed measurement results into the common coordinate system: Leica Cyclone [25], open-source application CloudCompare [26], and Artec Studio Professional [27] usually sold together with an Artec 3D scanner.

4 TESTING THE METHOD

The search for an effective method for detecting local deformations was divided into two main phases (Fig. 2):

- testing the most effective methods of registering the results of photogrammetric studies into the common coordinate system,
- determining the accuracy of the DCRF method compared to the results of TLS and direct measurement with the calliper.

Additionally, the impact of camera pre-calibration on measurement accuracy was checked.

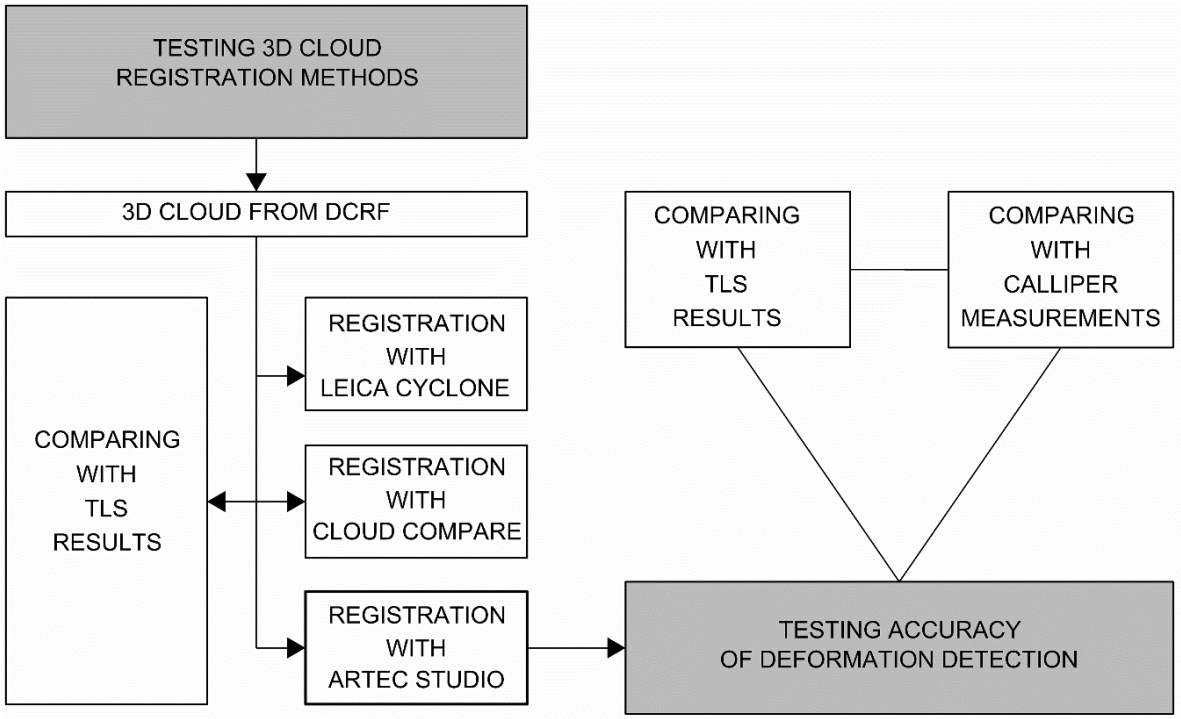


Figure 2: Two main phases of testing the method.

As testing fields, two sites (both in Poland) were chosen (Fig. 3). One was the rusticated stone socle of the building of our faculty (Fig. 3 A), the other a fragment of a wall of the medieval castle in Grodno (Fig. 3 B). Each of the selected walls has a slightly different character. In the case of the first one, the stone blocks were closely adjacent, similar to the original, undeformed fragments of the Incan walls of the El Mirador de Inkaraqay observatory. The other wall, with deep, empty joints between individual stones, was to simulate a situation when, as a result of local deformations, the joints open. A layer of modelling clay a few millimetres thick (approx. 2-8 mm) stuck to the faces of the walls simulated local deformations.



Figure 3: View of both testing fields.
A – the stone socle of the faculty building; B – the stone socle of the faculty building with modelling clay simulating deformations; C – the wall of the mediaeval castle in Grodno; D – the wall of the mediaeval castle in Grodno with modelling clay simulating deformations

4.1 Testing referencing methods

The first phase of tests aimed to indicate the most effective method of registering the results of photogrammetric projects in a common coordinate system. Two series of measurements were carried out. The first documented the original conditions, and the second documented the simulated displacements of stone blocks from the application of an approximately 2 - 8 mm thick layer of modelling clay on the axis perpendicular to the wall surface.

Two measurement methods were employed on both test fields. For the first method, the Leica P40 scanner was used. Since the scanner did not change its position between both series of measurements (for the undeformed and deformed wall), there was no need to adjust the coordinate systems of both scans. Thus, the results obtained from TLS could be considered as a reference point for further evaluation of photogrammetric projects.

The second method was the photogrammetric project, with the use of the Sony Alpha STL-A65 camera and AgiSoft Metashape Professional software. Both projects (for the undeformed and deformed wall) were scaled with meter-stakes placed alongside and perpendicularly to the wall surface. Scaling errors for individual scale bars were within the range of +/- 0.5 mm, and the average scaling error for both projects was below 1 mm. Resulting 3D point clouds were exported as *.pts files and imported into the three already mentioned applications for registering 3D point clouds into the common coordinate systems.

As expected, due to the different registration algorithms implemented in each software package, the results varied. The differences in registration became apparent after calculating the range of detected deformations. CloudCompare software was used for this purpose. It offers several ways of calculating the distance between two 3D point clouds. The most accurate (cloud to mesh) calculates the distance between the points of one cloud and the centroids of the nearest triangle of the mesh grid resulting from the other 3D point cloud. However, the process is slow and requires a lot of computing power. In our case, we used a more straightforward (cloud to cloud) method that directly calculates the distance between the points of both clouds. Because

both 3D point clouds obtained from the photogrammetric projects were filtered so that the density of each of them was within the 1 x 1 mm range, any errors caused by using the cloud to cloud method were smaller (<1 mm) than the required accuracy.

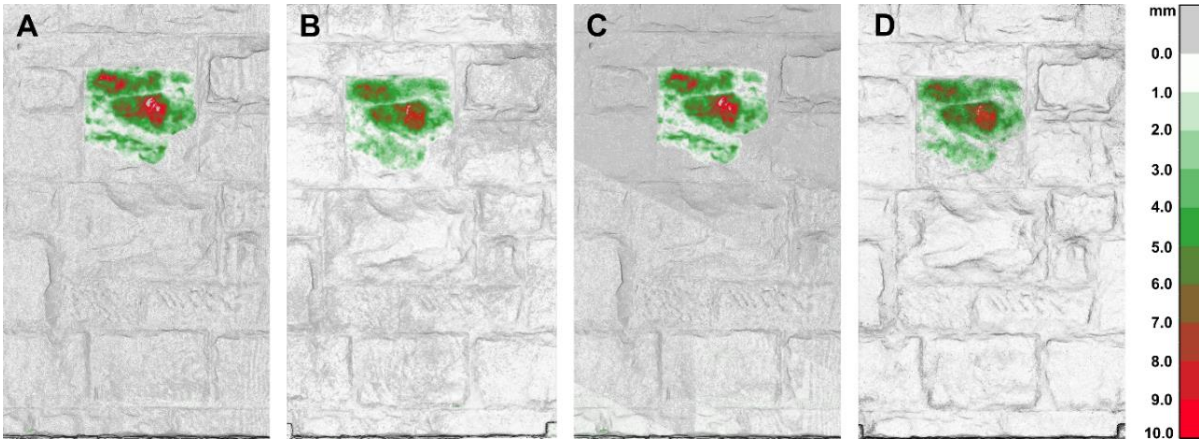


Figure 4: Testing referencing methods – the stone socle of the faculty building.
Comparison of detected deformations: A - reference results (Leica P40); B - photogrammetric project (Leica Cyclone registration); C - photogrammetric project (CloudCompare registration); D - photogrammetric project (Artec Studio registration)

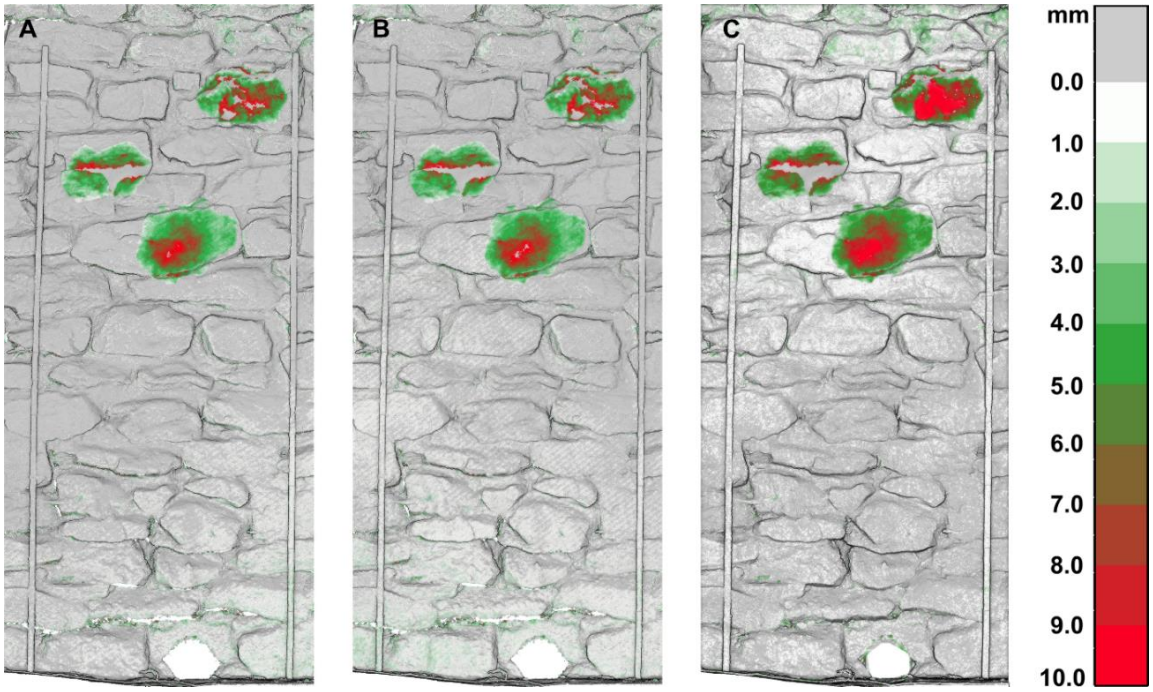


Figure 5: Testing referencing methods – the wall of the mediaeval castle in Grodno.
Comparison of detected deformations: A - photogrammetric project (Leica Cyclone registration); B - photogrammetric project (CloudCompare registration); C - photogrammetric project (Artec Studio registration

On both test fields, the best results, i.e. results closest to those acquired by TLS, were obtained with the use of Artec Studio Professional software for registration (Fig. 4 and Fig. 5).

The algorithm implemented there mainly takes into account the distinctive features of the local relief of compared 3D clouds (edges, vertices, pits), and does not rely only on minimising the root mean square error.

4.2 Testing the accuracy of the method

The second phase of testing determined the accuracy of the proposed method and was carried out on data from a fragment of the walls of the medieval castle in Grodno registered with the use of Artec Studio Professional software. Additionally, at several selected points, the thickness of the applied modelling clay was measured using a calliper. At these points, detected deformations were measured by comparing thin slices of both 3D clouds representing the deformed and undeformed wall (Fig. 6).

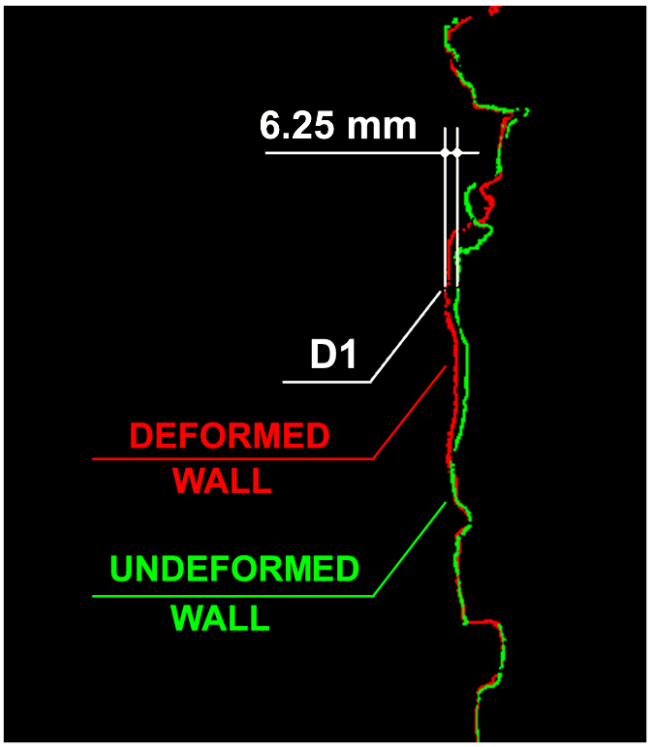


Figure 6: Wall deformations detected by the DCRF method

An analogous procedure was repeated for both TLS and DCRF measurements. The results obtained from both remote sensing methods (TLS and DCRF) were compared with direct measurements made with the calliper (Tab. 2).

The comparison of results shows that TLS measurements tended to understate the detected deformations (mean error = -0.29; median = -0.29), while the DCRF method overstated the results (mean error = +0.19; median = + 0.50). Also, comparing the root mean square (RMS) calculated for both methods indicated, as expected, that the results obtained from TLS measurements were more accurate than those collected using DCRF. The average differences oscillated around -0.5 mm.

Table 2: Comparison of detected deformations

Point	Measuring method			Differences in detected deformations (Δ=TLS–calliper) [mm]	Differences in detected deformations (Δ=DCRF–calliper) [mm]	Differences in detected deformations (Δ=TLS–DCRF) [mm]
	Detected deformations (TLS) [mm]	Detected deformations DCRF [mm]	Deformations measured with the calliper [mm]			
D1	5.68	6.25	5.31	+ 0.39	+ 0.94	- 0.57
D2	3.52	4.32	3.70	- 0.20	+ 0.62	- 0.80
D3	5.16	5.03	5.56	- 0.40	+ 0.53	+ 0.13
D4	5.51	6.50	6.02	- 0.71	+ 0.48	- 0.99
D5	4.11	4.15	5.04	-0.93	- 0.89	- 0.04
D6	3.82	4.41	3.90	- 0.08	+ 0.51	- 0.59
Mean error				**- 0.29**	**+ 0.19**	**- 0.48**
Median				**- 0.29**	**+ 0.50**	**- 0.58**
Root mean square (RMS)				**0.49**	**0.69**	**0.62**

4.3 Determination of camera pre-calibration impact on measurement accuracy

Although the primary objective was to use any middle-class consumer camera, the last test checked whether usage of pre-calibrated cameras could significantly improve the accuracy of measurements. For this purpose, the open-source application AgiSoft Lens was used [28].

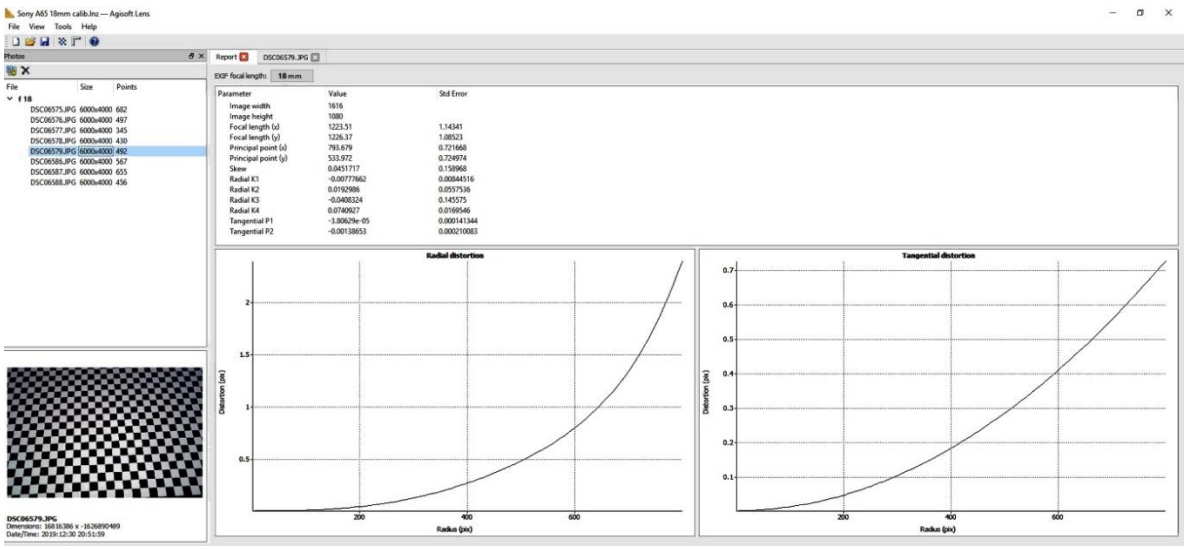


Figure 7: Sony A65 18 mm camera calibration in AgiSoft Lens application

Based on several photos of the standard checkerboard pattern, the software calculates and stores all the coefficients necessary for lens calibration (Fig. 7). Stored results can be used as pre-calibration data in every subsequent photogrammetric project based on photos taken with the same camera. In order to determine the impact of the pre-calibration process on the final result, two 3D point clouds obtained from the same set of photos were compared - first for a

not pre-calibrated, and second for a pre-calibrated camera. It turned out that because the software used in these studies had it's own built-in lens calibration algorithms, for projects based on over 50 images, pre-calibration of the camera had a negligible impact on the final results - differences in the scaling of both projects did not exceed 0.2 mm.

However, it should be clearly stated that this particular conclusion is valid only for the Sony Alpha STL-A65 camera with a Sony 18-55mm f/3.5-5.6 standard lens attached, when at least 50 images were used for the project. For other cameras and DCRF projects with a fewer number of images, the impact of camera pre-calibration could differ.

5 DISCUSSION AND CONCLUSIONS

Analysing the results (Tab. 2), in some cases (points D4 and D5) one can notice the unexpected large discrepancy between the results of direct measurements (calliper) and the results obtained from TLS. They are more significant than the +/- 0.5 mm accuracy usually mentioned in the literature when TLS is used for monitoring displacements [13]. In the case of scanning a porous surface of crystalline rocks, this can be explained by a high scanner range noise - much higher than that declared by the manufacturer (Tab. 1). The scanner's pulses not only disperse on an uneven rock surface but they also partially penetrate quartz crystals where internal, multiple reflections occur.

The results obtained (Tab. 2) allow the proposed, specific method for monitoring local deformations by DCRF to be considered adequate for detecting displacements larger than 2 mm. Moreover, the scope of application of the method should be limited only to situations where the use of other, more accurate and effective methods is not possible, as in the case of the El Mirador de Inkaraqay. Further limitations of the method relate to the proportion between the non-deformed and deformed part of the monitored object. So far, it seems that the non-deformed part should constitute at least 50% of the surveyed area. However, this issue requires further investigation.

The proposed method enables successive monitoring of the monument only with the help of photographs taken in the field by the crew of the Machu Picchu Archaeological Park that will be then sent to our laboratory for analysis. The crew necessary for collecting such data in the field can consist of only an inspector equipped with any middle-class consumer camera who is familiar with general rules for taking photos for photogrammetric projects, and one *machetero* who knows the area and can blaze a trail through the jungle. An additional factor that can be considered is the possibility of using archived sets of photos from the past.

It is also worth mentioning that the proposed method can also be used to monitor the progress of erosion of the faces of the monument or land surface.

Acknowledgements. This study is part of a Polish-Peruvian research project on the satellite sites of Machu Picchu. It was funded by the National Science Centre of Poland and granted to the Centre for Andean Studies of the University of Warsaw in Cusco led by Mariusz Ziółkowski (grant OPUS no. UMO-2015/19/B/HS3/03557). The hardware and software used in this project received additional support from the Ministry of Science and Higher Education (grant no. 1928/E-366/SPUB/2018/1) awarded to the Laboratory of 3D Scanning and Modeling at Wroclaw University of Science and Technology. The research was carried out in close cooperation and with the consent of directors of the Machu Picchu National Archaeological Park – Fernando Astete Victoria and José Bastante Abuhadba.

REFERENCES

[1] *3D Laser Scanning for Heritage: Advice and guidance to users on laser scanning in archaeology and architecture*, s.l., English Heritage (2007). Internet source: https://www.cices.org/pdf/newcastle%20uni%203d%20laser%20scanning.pdf (accessed 18.12.2019); See also for the latest 3rd edition: s.l., English Heritage (2018). Internet source: https://historicengland.org.uk/images-books/publications/3d-laser-scanning-heritage/heag 155-3d -laser-scanning/, (accessed 18.12.2019).

[2] Yastikli N., Documentation of cultural heritage using digital photogrammetry and laser scanning, *Journal of Cultural Heritage* (2007) 8(4), 423–427.

[3] Monserrat, O. and Crosetto, M., Deformation measurement using terrestrial laser scanning data and least squares 3D surface matching, *ISPRS Journal of Photogrammetry and Remote Sensing* (2008) 63, 142-154.

[4] Vatan, M., Selbesoglu, M.O. and Bayram, B.,. The use of 3D laser scanning technology in preservation of historical structures, *Wiadomości Konserwatorskie* (2009), 659-669.

[5] Moropoulou, A., Labropoulos, K.C., Delegou, E.T., Karoglou, M. and Bakolas, A., Non-destructive techniques as a tool for the protection of built cultural heritage, *Construction and Building Materials* (2013) 48, 1222-1239.

[6] Selbesoglu M. O., Bakirman T. and Gokbayrak O., Deformation measurement using terrestrial laser scanner for cultural heritage, *The International Archives of the Photogrammetry, Remote Sensing and Spatial Information Sciences* (2016), vol. XLII-2/W1, 89-93.

[7] Kościuk J., *Modern 3D scanning in modelling, documentation and conservation of architectural heritage*. In: w: J. Jasieńko (Ed.), *Structural analysis of historical constructions: Proceedings of the International Conference on Structural Analysis of Historical Constructions*, SAHC 2012, Wrocław (2012), vol. 1, 64-76.

[8] Kościuk J, Kogut J, *Numerical modeling of hypothetical quincha walls on Samaipata Roc*k. In: Aguilar R. et all [eds], *Structural analysis of historical construction: an interdisciplinary approach*, Springer, 2019, 835-843.

[9] Grussenmeyer, P., Landes, T., Voegtle, T. and Ringle, K., Comparison methods of terrestrial laser scanning, photogrammetry and tacheometry data for recording of cultural heritage buildings, *The International Archives of the Photogrammetry, Remote Sensing and Spatial Information Sciences* (2008) Vol. XXXVI, 213–218.

[10] Teza G., Arianna Pesci A. and Andrea Ninfo, Morphological Analysis for Architectural Applications: Comparison between Laser Scanning and Structure-from-Motion Photogrammetry, *Journal of Surveying Engineering* (2016), 142/3, DOI: 10.1061/(ASCE)SU.1943-5428.0000172.

[11] Murtiyoso, A. and Grussenmeyer, P., Documentation of heritage buildings using close-range UAV images: dense matching issues, comparison and case studies, *The Photogrammetric Record* (2017), 32, 206–229, DOI: 10.1111/phor.12197.

[12] Li, L. and Zhang, X., Factors influencing the accuracy of the photogrammetry-based deformation measurement method, *Acta Geotechnica* (2019), vol. 14, no. 2, 559-574. Internet source: https://doi.org/10.1007/s11440-018-0663-4 (accessed 10.09.2019).

[13] Kędzierski M., *Metodyka wykonywania ortofoto z wykorzystaniem naziemnej kamery z obiektywem rybie oko*, Warszawa 2008.

[14] Gruen A., Remondino F., Zhang L., Photogrammetric reconstruction of the Great Buddha of Bamiyan, *The Photogrammetric Record* (2004), 19, 177–199.
[15] El-Hakim S., Beraldin J., Remondino F., Picard M., Cournoyer L., Baltsavias E., Using Terrestrial Laser Scanning and Digital Images for the 3D Modelling of the Erechteion, Acropolis of Athens, in: *Proceedings of DMACH Conference on Digital Media and its Applications in Cultural Heritage, 3–6 November 2008*, Amman, 3–16.
[16] Themistocleous K., Ioannides M., Agapiou A., Hadjimitsis D.G., The methodology of documenting cultural heritage sites using photogrammetry, UAV, and 3D printing techniques: the case study of Asinou Church in Cyprus, in: *Proceedings of the Third International Conference on Remote Sensing and Geoinformation of the Environment (19 June 2015)*, internet source: https://doi.org/10.1117/12.2195626, (accessed 12.09.2019).
[17] Kościuk J., 3D scanning and modeling of the upper terrace of the Hatshepsut Temple in Deir el-Bahari as an example of architectural heritage documentation for restoration purposes, *Wiadomości Konserwatorskie*, 26 (2009), 705 - 717.
[18] Astete, Victoria, F., Ziółkowski, M., Kościuk, J., *Inca precise astronomical instruments: the observatory of Inkaraqay - El Mirador (National Archaeological Park of Machu Picchu, Peru)*. In: González, García, C., Martin-Rodilla, P. and Belmonte A., J., (eds.), *INSAP X – Oxford XI - SEAC 25 Conference: Road to the Stars*, Santiago de Compostela (2017), 15-16.
[19] Astete, Victoria, F., Ziółkowski, M., Kościuk, J., *Discovery of an Inca precise astronomical observatory at el Mirador de Inkaraqay*. In: Sánchez Choclote J. L. (ed.), *The top of great discoveries of Peru*, Lima 2017, 577-595.
[20] Astete, Victoria, F., Ziółkowski, M., Kościuk, J., On Inca astronomical instruments: the observatory at Inkaraqay - El Mirador (National Archeological Park of Machu Picchu, Peru), *Estudios Latinoamericanos* (2016/2017), vol. 36/37, 9-25.
[21] Palca J., Sun Dagger misses its mark, *Science* (1989), vol. 244, issue 4912, 1538. Internet source: https://science.sciencemag.org/content/244/4912/1538.2, (accessed 14.12.2019).
[22] Ćmielewski B., Kontny B., Ćmielewski K., Use of low-cost MEMS technology in early warning system against landslide threats, *Acta Geodynamica et Geomaterialia* (2013), vol. 10, no. 4, 485-490.
[23] Internet source: https://www.agisoft.com/features/professional-edition/, (accessed 26.01.2020).
[24] Internet source: https://w3.leica-geosystems.com/downloads123/hds/hds/general/brochures-datasheet/Leica_ScanStation_P30-P40_Plant_DS_en.pdf, (accessed 12.01.2020).
[25] Internet source: https://leica-geosystems.com/products/laser-scanners/software/leica-cyclone, (accessed 12.01.2020).
[26] Internet source: https://www.danielgm.net/cc/ (accessed 6.01.2020).
[27] Internet source: https://www.artec3d.com/3d-software/artec- studio?utm_ source=google &utm_medium=cpc&utm_campaign=1954117596&utm_term=%2Bartec%20%2Bstudio %20%2Bprofessional||kwd- 750863444384&utm_content=72277307938||&keyword=%2 Bartec%20%2Bstudio%20%2Bprofessional&gclid=EAIaIQobChMIgv-6iqup5wIVxOJ3 Ch2PVgoGEAAYASAAEgLYjPD_BwE#swview, (accessed 11.01.2020).
[28] Internet source: http://downloads.agisoft.ru/lens/doc/en/lens.pdf (accessed 3.01.2020).

12th International Conference on Structural Analysis of Historical Constructions
SAHC 2020
P. Roca, L. Pelà and C. Molins (Eds.)

AXIAL COMPRESSION TESTS ON RUBBLE STONE MASONRY REPRODUCING *OPUS INCERTUM* OF ANCIENT POMPEII

FRANCESCA AUTIERO[1*], GIUSEPPINA DE MARTINO[1], MARCO DI LUDOVICO[1], ANDREA PROTA[1]

[1]Department of Structures for Engineering and Architecture
University of Federico II
Edificio 6-7, Via Claudio 21, 80125 Naples, Italy
e-mail: francesca.autiero@unina.it

Keywords: Pompeii Archaeological Site, Masonry Panels, Rubble Stone Masonry, Axial Compression Test, Mechanical Properties

Abstract. *In order to investigate the mechanical behaviour of the typical ancient rubble stone masonry type at the archaeological Pompeii site, an experimental program was carried out on masonry panels realized with the aim of reproducing the ancient technique opus incertum. Three panels (1.20m x 1.20m x 0.45m) were realized by using original rock units from ruins emerged in the excavation works at Regio V at the site and pozzolanic lime-based mortar realized according to the traditional technique. The first phase of the experimental program involved the accurate reproduction of Pompeii-like masonry panels and the execution of sonic pulse velocity tests to be compared with those carried out on original structures at the site. Thus, three in-situ diagonal compression tests were carried out to derive masonry shear strength and relevant correlation with sonic velocities. The last phase of the experimental program focuses on laboratory axial compression tests on five specimens extracted from the three panels analyzed in the first phase and is herein described in detail. The results of axial compression tests on two of such specimens in terms of axial compression strength and elastic modulus as well as the analysis of the crack pattern and failure mode is herein presented and discussed.*

1 INTRODUCTION

The achievement of a deep knowledge of the mechanical behaviour of ancient masonry structures is a critical issue for the preservation of the built heritage, especially in the archaeological field [1]. Indeed, the main mechanical properties of the single building materials and the masonry assemblages are required for the structural assessment of the masonry structures and for the definition of proper restoration interventions. However, the need to preserve the built heritage clearly set restrictions to the collection of standard specimens for the execution of laboratory tests on materials and assemblages and also set restrictions to the execution of destructive and minor-destructive *in situ* tests. Thus, the development of new methodologies and investigation protocols for the knowledge of the built heritage is required and should include: i) the contribution of different disciplines to achieve a comprehensive knowledge and to limit the number of tests needed; ii) the application of non-destructive methodologies, to ensure the preservation of the heritage [2,3].

In the archaeological Pompeii site, a specific database on the mechanical properties of the different building materials and masonry type is still lacking. Therefore, the present study is a part of a wide experimental programme aimed to the mechanical characterization of one of the most common masonry building technique at the archaeological Pompeii site: the rubble stone masonry, traditionally known as *opus incertum*. Since the investigation of the original masonry structures at the site is restricted to the execution of Non-Destructive Tests, NDTs, this part of the experimental programme involved the realization of masonry panels reproducing the ancient technique *opus incertum*, for the execution of Destructive Tests, DTs. The design of the panels (i.e. definition of the mortar; shape, size, nature and arrangement of the rock units; arrangment of the cross-section and wall thickness) was defined based on datailed geometric and material surveys of the original structures at the site. Original rock units from the ruins emerged in the excavation works in *Regio V* started in May 2018 and pozzolanic lime-based mortars compliant with the traditional typologies were selected to built the panels. Thus, a preliminary investigation of the mechanical properties of the single building materials was carried out including the execution of both NDTs and DTs [4,5]. Therefore, three panels (1.20m x 1.20m x 0.45m) were built and sonic pulse velocity tests were performed in order to provide a useful tool for a comparison with the same tests performed on original structures at the site. Thus, three in-situ diagonal compression tests were carried out to derive the masonry shear strength and relevant correlation with sonic velocities. The last phase of the experimental program focuses on laboratory axial compression tests on five specimens extracted from the three panels analyzed in the first phase.

In this paper, the results of the first phase of the experimental programme as well as the realization of the specimens are summarized, while the axial compression tests performed on two specimens are described in detail. The results in terms of axial compression strenght and elastic modulus as well as the analysis of the crack pattern and failure mode of such specimens is herein presented and discussed.

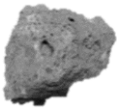
2 BUILDING MATERIALS

The definition of the building materials for the construction of the panels was based on a in-depth knowledge process on the typical rubble stone masonry type at the Pompeii site, i.e. the ancient *opus incertum*. Specifically, the definition of the shape, size, nature and arrangement of the rock units was based on datailed surveys of original structures, particulartly focusing in the area of the *Regio V* at the site, while the defintion of the mortar was mainly based on the the traditional composition and materials knowledge.

2.1 Original rock units

Three different rock types were defined to be used for the construction of the masonry panels: travertine, lava and foam lava (i.e. "*calcare del Sarno*", "*lava*" and "*cruma*"). Over the course of the archaeological excavation work started in May 2018 at the *Regio V*, it was possible to collect original units of such rock types from the newly-emerged ruins [5]. A brief description of such rock types is summarized in Table 1.

Table 1: Brief description of the rock types defined for the construction of the masonry panels

Travertine	Lava	Foam lava
		
Carbonate rock, whitish coloured, cavernous fabric	Effusive rock, dark grey coloured, scoriaceous, glass-rich	Tephrite subtype, dark red to grey coloured, air bubble fabric

Ten units (i.e. three travertine units, five lava units and two foam lava units) were used for a preliminary experimental programme that included both NDTs and DTs for the machanical characterization of these materials. As NDTs, the experimental programme involved the execution of Schmidt hammer rebound tests, SHR, and ultrasonic pulse velocity tests, UPV: the first allowed obtaining the rebound number, H_r, that was related to the surface hardness of the material; the second allowed obtaining the compression wave velocity, V, that gived information on the homogeneity of the specimen and and can be used for the estimation of physical and mechanical properties of the material [6–10]. In detail, the units were tested by SHR and UPV first, then UPV and uniaxial compression tests were performed on thirty-two cubic specimens 70mm x 70mm x 70mm obtained from the units according to [11] for the definition of the uniaxial compressive strenght and correlation with NDTs results. Table 2 reports a synthesis of the main results of the tests performed on the rock specimens [4]. In detail it reports for each investigated rock type: the number of units involved, n_{units}; the average value of rebound number obtained on the units, H_r; the number of cubic specimens tested for each rock type, n_{cubes}; the average bulk density of the cubic specimens, ρ; the average compression wave velocity evaluated along the same direction of the compression load, V; the average compressive strenght, σ.

Table 2: Main results of tests performed on the rock specimens

Rock type	n_{units}	H_r [-]	n_{cubes}	ρ [kg/m³]	V [m/s]	σ [MPa]
Travertine	3	17	11	1382 (CoV = 14%)	2315 (CoV=19%)	5.88 (CoV = 75%)
Lava	5	29	8	2300 (CoV = 4%)	1987 (CoV=26%)	38.43 (CoV = 40%)
Foam lava	2	15	13	904 (CoV = 10%)	1532 (CoV=13%)	3.90 (CoV = 35%)

The main outcomes showed a significant difference among the investigated rock types. Moreover a notable variability of the outcomes resulted for each rock type, especially as regards the compressive strenght. This is probably due to the natural heterogeneity of the investigated materials and the mechanical and physical decay of the collected units. As concerns the correlation between NDTs and DTs results, the uniaxial compressive strenght was correlated with: i) the rebound number, H_r, and ii) the parameter $V \cdot \rho$, where V is the ultrasonic pulse velocity evaluated along the direction of the compression load and ρ is the bulk density of the specimen evaluated before the execution of the DTs [4]. In the first case a linear function was

defined, while in the second case a quadratic function was defined. Both correlation showed a good matching between analytical formulation and experimental results (R^2 = 0.75 and R^2 = 0.80 respectively), as reported in Table 3.

Table 3: Empirical correlation between NDTs and DTs

Parameters	Empirical correlation	Coefficient of determination
σ, H_r	$\sigma = 1.9454\ H_r - 25.254$	$R^2 = 0.80$
σ, V, ρ	$\sigma = 3^{12}\ (V\rho)^2 - 1E\text{-}05\ V\rho + 13.507$	$R^2 = 0.75$

2.1 Pozzolanic lime-based mortar

A mortar consisting of putty lime as a binder and pozzolana as a aggregate with a ratio 1:3 by volume was defined for the construction of the panels. The constituent materials were defined to be very similar to the ones traditionally used in the ancient techniques [12,13]. In particular, the pozzolana used came from the area of the Phlegrean Fields in Campania, Italy, as the volcanic ash that the ancient builders in Roman time used and called *pulvis puteolanus.* For the mechanical characterization of such mortar six prismatic specimens 40mm x 40mm x 160mm were realized for the execution of flexural and compression tests according to [14]. In order to evaluate the strenght evolution, a set of three specimens was tested at one month and another set of three specimens was tested at two months from casting [4]. The main average otucomes obtained on each set of specimens are summarized in Table 4. In detail Table 4 reports: the age at which the tests were performed; the number of prismatic specimens, n_{prisms}; the average bulk density evaluated on the prismatic specimens, ρ; the average flexural strength evaluated on the prismatic specimens, f; the number of cubic specimens, n_{cubes}; the average compressive strength evaluated on the cubic specimens, σ. The results showed an increase of +21% of the compressive strength moving from one month to two months of curing time.

Table 4: Main average results of tests performed on the mortar specimens

Age	n_{prisms}	ρ [kg/m³]	f [MPa]	n_{cubes}	σ [MPa]
1 month	3	1181 (CoV = 3%)	0.77 (CoV = 6%)	6	2.39 (CoV = 3%)
2 month	3	1105 (CoV = 2%)	0.55 (CoV = 9%)	6	2.87 (CoV = 5%)

3 RUBBLE STONE MASONRY SPECIMENS

Three panels 1.20m x 1.20m x 0.45m were specifically designed based on in-depth survey of the original structures at the site (Figure 1 (a)). Specifically, a newly-emerged *opus incertum* masonry structure as part as the archaeological excavation at *Regio V* was selected, analysed and used as a reference for the realization of the new panels. The panels were realized with original units and putty-lime-and-pozzolana-based mortar, as described above. The wall thickness was defined to be 0.45m based on a survey of similar ancient structures at the same area at the site. The cross-section was defined to be double-leaves without connecting elements. The leaves were realized with travertine, lava and foam lava ancient units with irregular size and shape plus some fragments of other nature as in the real masonries. The units were

embedded in the putty-lime-and-pozzolana-based mortar, without any vertical or horizontal alignment. The internal part of the masonry was filled with the same mortar and rock fragments or smaller units.

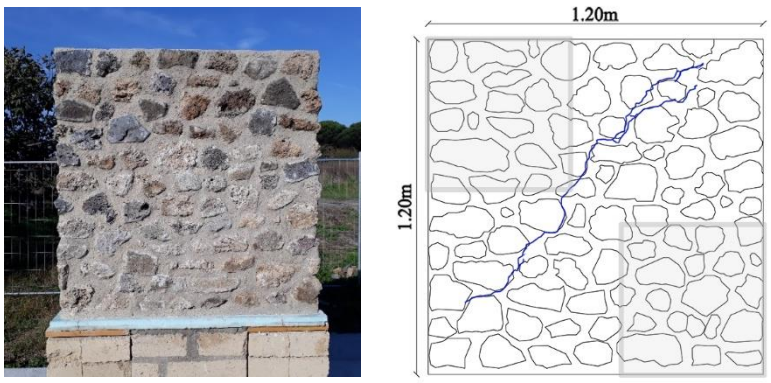
A campaign of sonic tests was performed on the panels as a preliminary phase to the execution of DTs at different ages in order to: i) evaluate the evolution of the curing of the panels; ii) compare the results with the ones of the DTs to be performed; iii) provide useful data to set up comparison with similar old structures at the site. Indeed, sonic pulse velocity tests is one of the most common NDT used for the assessment of old masonry structures and some experimentation at the Pompeii site are already present in literature [15,16].

Afterwards, the first phase of the experimental programme of DTs involved the execution of three in-situ diagonal compression to derive the masonry shear strength and relevant correlation with sonic velocities. Diagonal compression tests were performed according to [17], with a specific set-up designed for the execution of outdoor tests. The main results of the diagonal compression tests and sonic pulse velocity tests are summarized in Table 5 in terms of: average sonic pulse velocity detected before the execution of the diagonal compression tests, V; average shear strenght evaluated according to [17], τ_{max}; average shear strain corresponding to the maximum shear stress, γ_{max}; average shear modulus, G. Note that the shear modulus G was evaluated only for two specimens due to inaccurate local recordings detected on one panel.

Table 5: Main experimental outcomes of the diagonal compression tests

V [m/s]	τ_{max} [MPa]	$\gamma_{\tau max}$ [-]	G [MPa]
2767 (CoV = 11%)	0.23 (CoV = 16%)	0.16% (CoV = 3%)	520.83

Finally, after the diagonal compression tests five masonry specimens were extracted from the undamaged portion of the panels to perfom laboratory axial compression tests (Figure 1 (b)). In the following the first axial compression tests performed on two of such masonry specimens are described in detail and their results in terms of axial compression strenght and elastic modulus as well as the analysis of the crack pattern and failure mode are presented and discussed.



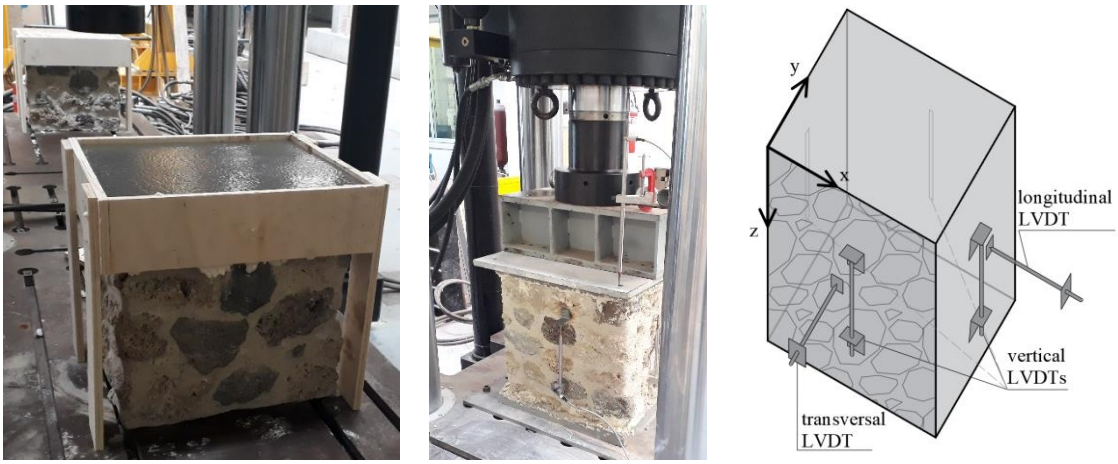
(a) (b)

Figure 1: Masonry panel 1.20m x 1.20m x 0.45m (a); scheme indicating the portion of one of the panels extracted for the execution of the axial compression tests

4 COMPRESSION TESTS

The axial compression test allows obtaining important information on the mechanical properties of masonry specimens in the vertical direction: the ultimate compressive strength; the deformation capacity; the elasticity properties (i. e. modulus of elasticity and Poisson's coefficient). The tests consist in applying monotonically or cyclically an uniform compression load to the masonry specimen. To obtain the compressive strength of the masonry and investigate the deformation capacity in compression, the load must be applied to the specimen up to the failure and the maximum load achieved and the vertical displacement must be recorded. If the modulus of elasticity, E, is to be determined, specific measuring devices must be applied to the specimen for measuring the vertical shortening. Moreover, for the definition of the modulus of elasticity the compressive load should be applied by several loading cycles until a load stage estimated to be in the elastic range with respect to the maximum load expected [18].

In the present study, the axial compression tests performed on two masonry specimens C1 and C2 are presented. In order to ensure that the load distribution faces of the specimens were flat, parallel between them and perpendicular to the direction of application of the load and als in order to prevent local brittle damages, a layer of about 30 mm-thick shrinkage-free and quick-setting mortar was applied at the top and bottom surfaces of each specimen. Between the specimens and the hydraulic cylinder of the testing apparatus, a steel beam and a steel platen were placed on the top surface of the specimens in order to ensure a uniform loading. The test on C1 was performed under displacement control with a rate of 0.02 mm/s in order to define the maximum force attained. Conversely, a cyclic testing protocol including three loading ramps until one third of the maximum expected force with the same rate was used in case of C2 specimen in order to investigate the elastic behaviour of the specimen. At the achievement of each relative maximum load, a constant ramp of 120s was defined, in order to stabilize the state of stress in the specimen. Several measuring devices, i.e. linear variable displacement transducers, LVDTs, were applied to the specimens. Given a reference system with the axes x parallel to the leaves of the masonry specimen, the axes y parallel to the cross section and the axes z in the vertical direction, the measuring devices were positioned for each specimen as follows: i) one longitudinal LVDT (i.e. positioned along the direction x and fixed to an external support; ii) one transversal LVDT (i.e. positioned along the direction y and fixed to an external support); iii) four vertical LVDTs (i.e. positioned along the direction z and directly fixed to the specimen). Figure 2 shows the preparation of the specimens, the test set up and the location of the measuring devices.



(a) (b) (c)

Figure 2: Compensating layer on the up and bottom surfaces of the specimens (a); test set up (b); location of the measuring devices for each panel (c)

4.1 Experimental outcomes

The specimens showed similar maximum compressive load, thus similar compressive strenght (i.e. F_{max}=369.12 kN and F_{max}=368.12 kN, σ_{max}=1.52 MPa and σ_{max}=1.49 MPa, for C1 and C2 respectively). For the evaluation of the vertical strain, the average measurements recorded by the four vertical LVDTs fixed on the specimens were used. Similar results were obtained in terms of vertical strain corresponding to the achievement of the maximum compressive stress also (i.e. $\varepsilon_{\sigma max}$=0.0050 mm/mm and $\varepsilon_{\sigma max}$=0.0052 mm/mm, for C1 and C2 respectively). For C2 the modulus of elasticity, E, was evaluated as the average of the slopes of the loading ramps in the stress-vertical strain curves.

The main experimental outcomes obtained for C1 and C2 are summarized in Figure 3, Figure 4 and Table 6. In detail, Figure 4 reports the compression stress-vertical strain curves for C1 and C2 and Figure 4 reports the compression load-displacement curves in the direction x, y and z for C1 and C2.

The recordings were stopped on the post-peak phase in correspondence of the attainement of the 85% of the maximum stress, except where the measurements were stopped before due to the low quality of the acquisition or the detachment of the measuring devices. From the curves it is possible to observe that the specimens showed very similar behaviour in terms of compression stress-vertical strain relationship despite the different loading protocols applied. A more relevant difference between the two specimens can be detected for the displacement in the horizontal plane. However, both specimens showed a more significant expansion in the direction x than in the direction y.

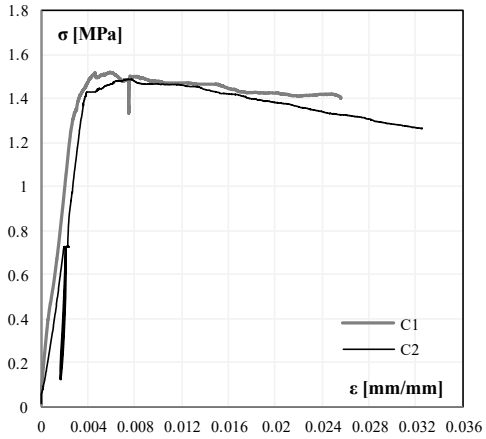


Figure 3: Compression stress-vertical strain curves for C1 and C2

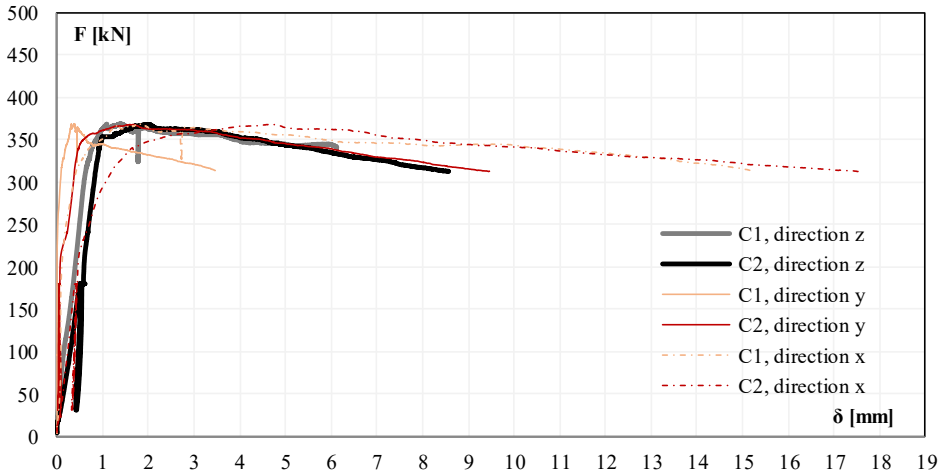


Figure 4: Compression load-displacement curves in the direction x, y and z for C1 and C2

Table 6 summarizes the main experimental outcomes in terms of: maximum compressive load attained, F_{max}; area of the cross section, A; compressive strenght, σ_{max}; vertical strain corrsponding to the achievement of the compressive strenght, $\varepsilon_{\sigma max}$; modulus of elasticity, E.

Table 6: Main experimental outcomes

F_{max}	A	σ_{max}	$\varepsilon_{\sigma max}$	E
[kN]	[mm^2]	[MPa]	[mm/mm]	[MPa]
369.12	243000	1.52	0.0050	-
368.12	247500	1.49	0.0052	1252.7

A preliminary comparison is reported with reference to the elastic modulus computed through the sonic pulse velocity test and the elastic modulus experimentally obtained. Indeed, according to [19], it is possible to evaluate the dynamic modulus of elasticity, E_d, for a concrete specimen from the pulse velocity, V, of the longitudinal stress waves according to the following equation:

$$V = \sqrt{\frac{E_d(1-\upsilon)}{\rho(1-2\upsilon)(1+\upsilon)}}$$

Where

- V is the sonic pulse velocity of the specimen;
- E_d is the dynamic modulus of elasticity;
- υ is the dynamic Poisson ratio;
- ρ is the density.

Such equation was defined on the assumption of solid, elastic, isotropic and homogeneous material. Despite masonry is not an homogeneous material, the use of such equation has been considered in some studies for a primary estimation of the mechanical properties of a masonry specimen from the results of a sonic pulse velocity test [20,21]. Thus, in order to assess a comparison between compression tests and sonic pulse velocity tests results, the dynamic modulus of elasticity E_d was calculated, by assuming:

- V equal to 2767 m/s (i.e. average sonic pulse velocity of the specimen);
- υ equal to 0.25;
- ρ equal to 1406 kg/m^3.

The density was evaluated according to a simplified homogenization procedure based on the bulk density of the single components reported in Table 2 and Table 4. According to such procedure the the dynamic modulus of elasticity E_d resulted to be 8971.3 MPa.

In the present evaluation, the calculated value of E_d was significantly higher than the one evaluated through the compression test. This confirmed the need to establish specific experimental relationship for the estimation of mechanical parameters from the sonic test results, based on the specific masonry typology.

As concerns the crack pattern, almost vertical thin cracks developed in the mortar matrix at first, then the crushing of certain units and the expulsion of material outward also occurred. In particular, the units with a lower strenght, i.e. travertine, foam lava and clay fragments were mainly invlolved in the crack pattern. The view at failure of the two specimens is showed in Figure 5.



(a) (b)

Figure 5: Collapse of the specimens: C1 (a) and C2 (b)

4 CONCLUSIONS

Three rubble stone masonry panels 1.20m x 1.20m x 0.45m were realized reproducing the ancient technique *opus incertum* at the archaeological Pompeii site. The panels were realized with original rock units collected at the site and mortar made with putty lime and pozzolana. The experimental program on the panels involved a preliminary phase for the characterization of the building materials, including the execution of both NDTs and DTs on the rock units. Therefore, sonic pulse velocity tests were performed and then three in-situ diagonal compression tests were performed on the panels. Finally, five masonry specimens were extracted from the three panels and the first laboratory axial compression tests were performed on two specimens. The first outcomes showed:

- The axial compression strength were almost the same for C1 and C2 (i.e. σ_{max}=1.52 MPa and σ_{max}=1.49 MPa respectively) despite the variability of size, shape, nature and arrangement of the units within the two specimens;
- The modulus of elasticity of the specimen C2 resulted 1252.7 MPa;
- Despite the different loading protocols applied, the specimens showed very similar behaviour in terms of compression stress-vertical strain relationship with almost the same vertical strain corresponding to the achievement of the maximum compressive stress (i.e. $\varepsilon_{\sigma max}$=0.0050 mm/mm and $\varepsilon_{\sigma max}$=0.0052 mm/mm, for C1 and C2 respectively);
- Both specimens showed higher lateral expansion in the direction perpendicular to the cross section compared to the direction perpendicular to the main surfaces;
- The crack pattern mainly developed in the mortar matrix (σ_{max}=2.87 MPa at two months of age) and the expulsion of material outward occurred;
- The units with lower compressive strenght (i.e. travertine and foam lava with σ_{max}=5.88 MPa and σ_{max}=3.90 MPa respectively) were damaged while the units with higher compressive strenght were not involved in the crack pattern (i.e. lava with σ_{max}=38.43 MPa)

Based on the design process and the building materials adopted for the realization of the masonry specimens, the experimental results showed above could be a unique and useful tool for a preliminary examination of the mechanical behaviour of one of the most common masonry building technique at the archaeological Pompeii site.

Acknowledgements. The Authors would like to acknowledge the director of *Parco Archeologico di Pompei* (*PAP*), Prof. Massimo Osanna; the Project Manager of the work at *Regio V*, Archit. Annamaria Mauro, the Managers of the *Laboratorio di Ricerche Applicate* of *PAP*, Archit. Bruno De Nigris and Dr. Alberta Martellone for the guide and the support provided to the present research project.

REFERENCES

[1] B. De Nigris, M. Previti, L'affidabilità strutturale degli interventi di messa in sicurezza del patrimonio archeologico, in: N. Augenti, L. Jurina (Eds.), Ing. Forense, CRolli, Affidabilità Strutt. Consolidamento, Dario Flaccovio Editore, Milan, 2017: pp. 493–502.

[2] Recommendations PCM, Assessment and mitigation of seismic risk of cultural heritage with reference to the Italian Building Code (NTC2008). Directive of the Prime Minister,

9/02/2011. G.U. no. 47, 26/02/2011 (suppl. ord. no. 54) (in Italian), (2011).
[3] ICOMOS, Recommendations for the analysis, conservation and structural restoration of architectural heritage, (2003) 1–37. https://ancientgeorgia.files.wordpress.com/2012/04/recommendations_icomos-principles-and-guidelines.pdf.
[4] F. Autiero, G. De Martino, M. Di Ludovico, A. Prota, Mechanical Behavior of Ancient Mortar Specimens From Pompeii Site, in: 2019: pp. 1251–1262. https://doi.org/10.7712/120119.6994.18836.
[5] F. Autiero, G. De Martino, M. Di Ludovico, A. Prota, Mechanical properties of rock units from the Pompeii archaeological site, Italy, in: P. De Wilde (Ed.), Struct. Stud. Repairs Maint. Herit. Archit. XVI, 2019: pp. 341–350. https://doi.org/10.2495/STR190291.
[6] RILEM MS.D.2, Determination of masonry rebound hardness, Mater. Struct. 31 (1998) 363–377.
[7] UNI EN 12504-2, Testing concrete in structures - Determination of rebound number, (2012).
[8] ASTM D5873, Determination of Rock Hardness by Rebound Hammer Method 1, Current. (1981) 4–7.
[9] UNI EN 14579, Natural stone test methods - Determination of sound speed propagation, (2005).
[10] ASTM D2845-08, Standard Test Method for Laboratory Determination of Pulse Velocities and Ultrasonic Elastic Constants of Rock, (2017).
[11] UNI EN 1926, UNI EN 1926:2000. Natural stone test methods - Determination of compressive strength, (2003).
[12] C.. Giuliani, L'edilizia nell'antichità, 2007.
[13] J.P. Adam, L'arte di costruire presso i romani. Materiali e tecniche., Milan, 2014.
[14] UNI EN 1015-11, UNI EN 1015-11:2007. Methods of test for mortar for masonry - Part 11: Determination of flexural and compressive strength of hardened mortar, (2007).
[15] H. Dessales, Villa de Diomède. Campagne d'étude 2015, Chronique des activités archéologiques de l'École française de Rome, 2015. http://cefr.revues.org/1293.
[16] M.R. Valluzzi, F. Lorenzoni, R. Deiana, S. Taffarel, C. Modena, Non-destructive investigations for structural qualification of the Sarno Baths, Pompeii, J. Cult. Herit. 40 (2019) 280–287. https://doi.org/10.1016/j.culher.2019.04.015.
[17] ASTM E 519-02, Standard Test Method for Diagonal Tension (Shear) in Masonry Assemblages, Am. Soc. Test. Mater. (2002) 5. https://doi.org/10.1520/E0519.
[18] EN 1052-1, Methods of test for masonry - Part 1: Determination of compressive strength, Eur. Comm. Stand. (1999) 11.
[19] ASTM C 597-02, Pulse Velocity Through Concrete, United States Am. Soc. Test. Mater. 04 (2003) 3–6. https://doi.org/10.1520/C0597-09.
[20] L. Miranda, L. Cantini, J. Guedes, L. Binda, A. Costa, Applications of sonic tests to masonry elements: Influence of joints on the propagation velocity of elastic waves, J. Mater. Civ. Eng. 25 (2013) 667–682. https://doi.org/10.1061/(ASCE)MT.1943-5533.0000547.
[21] L.F. Miranda, J. Rio, J. Miranda Guedes, A. Costa, Sonic Impact Method - A new technique for characterization of stone masonry walls, Constr. Build. Mater. 36 (2012)

27–35. https://doi.org/10.1016/j.conbuildmat.2012.04.018.

CHARACTERIZATION OF CRACKS IN HISTORICAL BUILDINGS USING IMAGE-PROCESSING TECHNIQUES

P. L. PÓRCEL[1*], B. CASTAÑEDA[1], R. AGUILAR[1]

[1] Engineering Department, Civil Engineering Division
Pontificia Universidad Católica del Perú
Av. Universitaria 1801, Lima, Perú
e-mail: {pporcel, raguilar}@pucp.pe, castaneda.b@pucp.edu.pe
(*corresponding author)

Keywords: Crack Monitoring, Image Processing, Masonry structures.

Abstract. *Cracks are structural pathologies that affect the structural integrity of historical buildings. The methodologies commonly used to detect cracks are based on visual inspections or in intrusive techniques that involve removing external wall layers. The main objective of this study is to develop and validate a semi-automatic and non-destructive tool that helps the user to analyze the position and growth of the cracks in masonry constructions based on a photogrammetry analysis. The developed tool uses image processing to plot a curve of the crack area, and, in case needed, its evolution over time. The tool was validated in laboratory using earthen samples that were subjected to uniaxial compression tests. The research also provides the results of the tool used in a case study of a 16th Century stone masonry church located in the main square of Cusco; Southern Peru. This case study validates the qualitative metrics of the present work, and indicates that the tool provided accurate results when compared to the ground truth, which could be helpful in future research studies in order to automatize crack monitoring.*

1 INTRODUCTION

When the Spanish arrived to Peru, they started the evangelization process, that was done among others, by replacing sites that were sacred to the Inca culture, with churches to impose Christianity. Therefore, destroying partially or fully the predominant stone structures and introducing an earthen mixture of materials called adobe as the main material. These structural modifications resulted in multiple constructions of adobe and mixed structures combining adobe with stone [1]. In Peru, 30% of dwellings are built with adobe because the supply materials are low-cost and comfortable. The downside of this material comes from its vulnerability to the destructive effect of telluric movements [2]. Structural Health Monitoring of heritage constructions allows researchers to have a better understanding of the current behavior of the structure and it benefits its preservation. Often this procedure requires the installation of many of sensors in order to extrapolate the global behavior of the structure and process that information about the anomalies present in the structure [3]. Machine Vision technologies have been studying procedures that could benefit Structural Health Monitoring; the most commonly used system consists of an image acquisition device, a computer and an image-processing tool. Using a system like this would allow the user to record how the structure changes through time, therefore allowing the image-processing tool to detect anomalies like cracks as they change in time [4].

2 MACHINE VISION TECHNIQUES

Machine vision techniques have come as the technological approach for crack detection and monitoring, given that the conventional methods are usually performed by experienced human inspectors who identify and manually draw the crack patterns [5]. Machine vision methodologies mostly use a configuration as shown in Figure 1. This set up consists of the tested structure and targets, the Image Acquisition Device that captures and stores the information in a computer where it is processed with an Image-Processing Tool that is tailored to the specific purpose of the study [4].

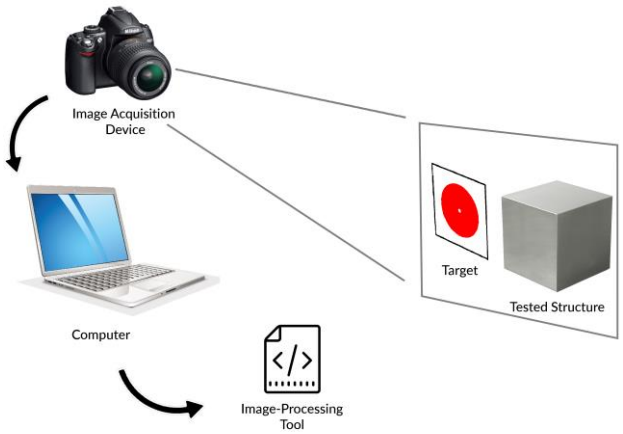


Figure 1: Machine vision methodologies most used measurement system.

In recent years, different types of technologies are being used towards the development of better tools to facilitate the work involving of monitoring structures. These techniques are of great importance due to the non-destructive approach that they provide regarding the assessment of buildings [6]. Specifically, for crack detection and monitoring, there has been a variety of approaches involving new technologies like photogrammetry, which allows a better detection of the targets in order to give more precise quantitative results [7]. In most cases, there is a specimen preparation process that involves the creation and insertion of the targets that would later be used by the image-processing tool to correlate images within the same test or to assess how much has the crack changed [8,9]. Therefore, the creation and selection of the target used is an important step that affects directly the results; however, even more important is the ability to detect and use the information that the target provides to the image-processing tool [10].

3 DEVELOPMENT OF IMAGE PROCESSING TOOL

The initial hypothesis of this work is based in the use of tensor voting in order to detect the pixels, that belong to the crack, in an image, by properly analyzing edges between these pixels and the background [11]. This tool was developed with Matlab 2019b, and its Image Processing and Computer Vision toolboxes [12]. First, the images were captured with the acquisition device, in this case a D5000 Nikon camera. Next, the images (Figure 4) were processed by isolating the part of the image where the target is located and then cropping the ROI (Region of Interest). The ROI is used as the area where all the binarization algorithms are performed.

Initially, a sparse detection of the pixels belonging to the crack is performed by analyzing the overall variation in color between the crack and the background. After that, stick voting is applied to the previously detected pixels to analyze the interaction between them. Finally, the tensor voting algorithm is applied to establish which pixels are proximate enough to others to be part of the crack. On the other hand, the region where the target is contained is processed to detect the red target and extract its measurements. The real measurements of the target are known; therefore, they were compared to the metrics extracted from the previous step. This process allows the tool to obtain a resolution in pixels/meters. Due to human error introduction, the images taken are not entirely parallel to the surface of the specimen, thus, the measure in pixels of the target will not be exactly the same horizontally and vertically, as it should be, given the shape of the target. The final step, consists of calculating the area of the crack in pixels and converting it to meters with the previously calculated resolution.

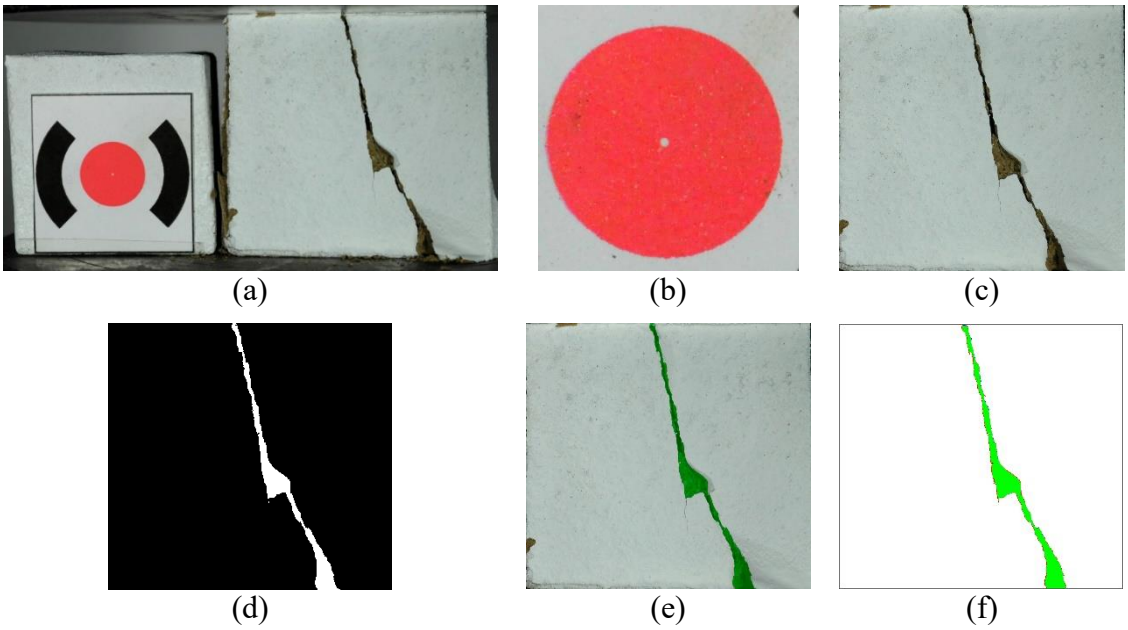


Figure 2: Process that the acquired images follows (a) image acquired (b) target region (c) ROI of the image (d) image after the binarization algorithms (e) final binarization in green over the original ROI in RGB and (f) the comparison between the ground truth and the final binarization.

All of the binarization algorithms use the resolution provided by the target in order to clean the image from little imperfections that could be mistaken by a crack pixel. The user sets the minimum and maximum thickness of the crack, this is very important because it provides the approximate scale of the crack compared to the scale of the image, all the measurements are set in meters. While creating the target the circle was selected, because it is an easy shape to detect and it fits in a rectangle, therefore the horizontal diameter and vertical diameter would be given by the size of the rectangle that wraps it. The red color for the circle was selected because in an RGB image it is easier to eliminate any of its primary colors (red-R, green-G, blue-B). The first part of the detection of the target allows the user to select where the target is, it does not have to be precise because, the algorithm detects only round objects, after that, a bounding box is stablished and later used for the calculation of the resolution in pixel/m. This part of the process

is straightforward but it is taken into account that the camera might not be directly parallel to the surface of the specimen, thus, whereas the actual measurements of the circle are the same vertically and horizontally this is not necessarily the case with the measurements of the bounding box. Therefore, this step calculates the vertical and horizontal resolution.

The algorithm starts to process only the last image in the database, in order to get the fully formed crack and goes backwards from there. This helped reduced the errors regarding sudden detachment of adobe that could introduce error in the segmentation. The first step to find crack pixels consists in a binarization where the threshold was calculated according to where did the most difference in color occurred by gray value. A Laplacian 3x3 kernel was used to do a local convolution and stablish local differences between the neighbor pixels. After that, the differences where added up according to its corresponding gray value. The first binarization is performed using the gray value with the most difference and a binary image with the initial crack pixels is obtained. After this process, Tensor Voting is applied to the binary image that shows the sparse set of pixels belonging to the crack. Tensor voting uses a proximity vote, which allows pixels close to each other to have a stronger vote, therefore, the further a way they are the weaker the vote. This allows to easy rule out the noise that could be introduced into the image for various reasons.

Lastly, the area is extracted at every stage for each specimen, obtaining the graphics that could be analyzed later to see the relation between the load and the change of area. This process consists on another vote in a 4 neighborhood, which assigns the area of 1 to a pixel that is fully surrounded by 4 crack pixels. Thus, gathering the area in pixels for all images. With the horizontal and vertical resolution obtained in the target detection process, the calculation for the actual area in meters done by multiplying both resolutions to get the pix^2/m^2. Finally, the monitoring process involves the same steps repeated through all the images acquired for each specimen.

4 VALIDATION IN LABORATORY

4.1 Data acquisition:

This research used the C109 standard by ASTM to elaborate the specimens for the data base, even though this standard is set for cement mortars [13], it is used for adobe in this case because of the lack of any international standards referring to compression tests in adobe. Therefore, the specimens used in this first stage where made in cubic molds of 50mm per side, the proportions used to get an stabilized earthen mixture were 60% of natural soil earth and 40% of sand. The added water needed to be between the 8% or 9% of the total weight of the previous mix [14]. However, the mentioned proportion of water was used to build compressed blocks in a compression machine, so for this process the water used was between 10% and 20%. For the present paper there were 10 specimens evaluated, all the samples were tested in a MTS E45 compression machine until the crack became a rupture compromising the integrity of the block.

The acquisition system used in this process is consistent with the machine vision methodologies used in recent years. In Figure 3, there is a representation of the layout configuration for the compression tests that were performed in the specimens to generate the cracks that would be evaluated later. In this layout, a set of two stereo lights was used to enhance the illumination inside the compression machine as its structure introduced shadows that would pollute the acquisition of data. The camera captures the images with a resolution of 12MP

(4288x2848), it was set at a distance of 45cm from the specimen with the lenses approximately parallel to the surface of the specimen. A separate program was created in Arduino for the acquisition of data to obtain the pictures automatically while running the compression test. Therefore, we obtained a different number of images per specimen, because the time of rupture was moderately different. The Arduino was connected to a Surface tablet in order to stop the acquisition when the compression test finished. After that, all the images where introduced in a computer where each data base went through an automatic organization process, that would help later with the image processing tool developed in this work.



Figure 3: Data acquisition system layout.

Finally, in order to scale and get an approximately measurement of the cracks area a target was introduced into the tests. The target is shown in Figure 2.a, the red circle in the middle has 12.7mm of diameter. This would be later detected and used to scale the image in order to have the resolution in pixels/m, the target was positioned parallel to the surface of the tested specimen.

4.1 Results

The qualitative results of this methodology are given by the Intersection over Union (IoU) metric which measures the intersection of the pixels detected and the pixels provided by the ground truth over the union of the same groups. Considering, that the pixels that are part of a crack do not represent more than 20% of the images, the accuracy would not be the best fit for a qualitive metric for the results given by the present tool. The IoU metric of each of the ground truths for all the specimens is given in Table 1, which shows that the IoU for the first frame in almost all the tests is 0.0%, this is because the first frame does not have any cracks, therefore, the ground truth does not have any pixels to be compared with. However, during the tests, specimen 4 did have some visible cracks that where drawn on the ground truth but since their thickness is lower that the resolution of the tool its segmentation does not show optimal results. Moreover, specimen 2 did not have any cracks shown until after the frame corresponding to the second ground truth, therefore, its IoU in the second column shows a 0.0%. Accordingly, the column corresponding to the second ground truth, mostly represent cracks that could be below the 1mm thickness required to be detected. Finally, the columns that show the ground truths 3 and 4 provide a good result given the resolution condition.

Table 1: Qualitative metric IoU percentage obtained by the comparison of the tools output and the ground truth of every specimen.

Intersection over Union (IoU)				
Ground Truths	*1*	*2*	*3*	*4*
Specimen 1	0.0%	74.0%	85.3%	92.1%
Specimen 2	0.0%	0.0%	70.9%	91.0%
Specimen 3	0.0%	67.6%	79.2%	78.4%
Specimen 4	13.9%	58.5%	65.2%	84.8%
Specimen 5	0.0%	78.6%	84.9%	85.5%
Specimen 6	0.0%	70.3%	84.1%	90.2%
Specimen 7	0.0%	51.1%	79.9%	87.4%
Specimen 8	0.0%	83.3%	79.9%	79.2%
Specimen 9	0.0%	82.4%	84.5%	90.3%
Specimen 10	0.0%	84.9%	87.3%	90.1%

In Figure 5, it is shown the result of the comparison between the Ground Truth segmentation to the one realized by the tool in two specimens. The color green represents the accurate segmentation of the crack, the color red provides information about the false negative pixels and lastly the color blue displays the false positive pixels. For each test, four ground truth images were created in order to validate the monitoring of the cracks through time, this manual segmentation was performed with the Image Labeler belonging to the Computer Vision toolbox and was done pixel by pixel



(a) (b)

Figure 4: (a) Comparison of the proposed segmentation with the ground truth in the last frame of specimen 3 and (b) Comparison of the proposed segmentation with the ground truth in the last frame of specimen 5.

The quantitative results of the tool are provided by the change in the crack's area produced through time. Thus, each row in Figure 5, represent different frames in time while the crack in each specimen starts to grow. The first column represents the first frame where no crack was previously formed. The next column corresponds to the 150^{th} image for each specimen in this part both adobe cubes where still on the elastic deformation region. Specimen 2 shows cracks but little segmentation, this is because the cracks in that image are thinner than 1mm which is the minimum thickness that the tool perceives. The third column shows the image in the elastic limit point where the adobe cubes enter the plastic deformation region and the crack starts growing faster. The last column the last frames of each test.

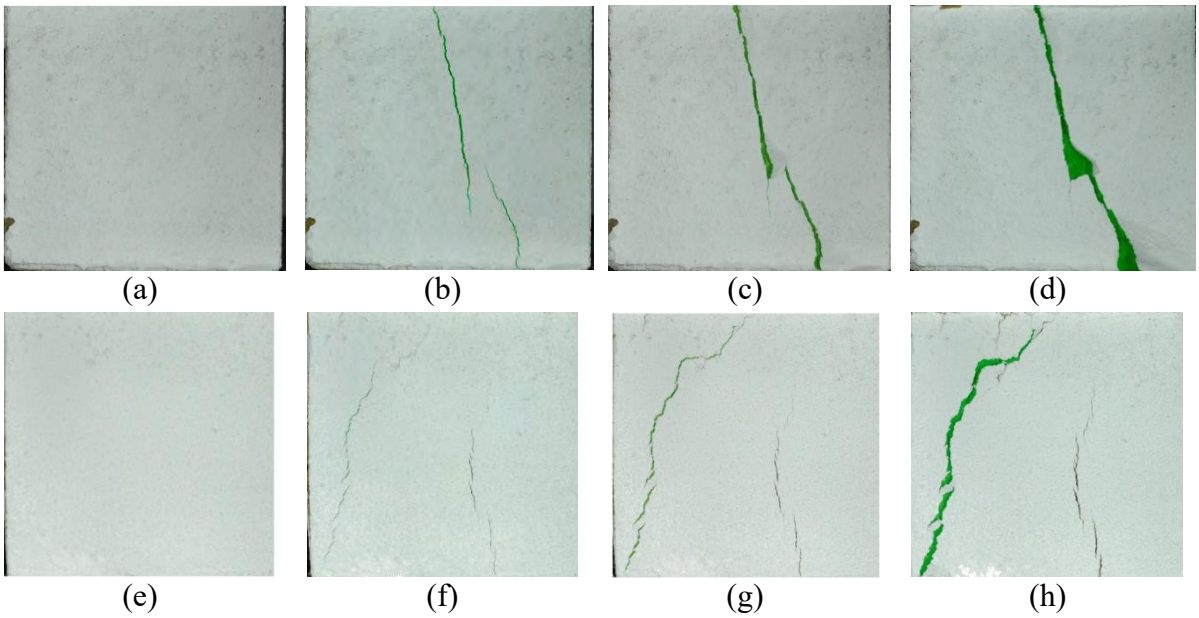


Figure 5: Images that represent how does the crack changes (a) first image of specimen 1, (b) image 150 of specimen 1, (c) image 293 of specimen 1, (d) last image of specimen 1,(e) first image of specimen 2, (f) image 150 of specimen 2, (g) image 273 of specimen2 and (h) last image of specimen 2.

The results of the first 5 specimens are shown in Figure 6, which is a graphic corresponding to the change of the area versus the time of duration in each test. It is correlated to Figure 5, the letter indices correspond to the frame the belong to. Thus, Figure 5a and 5e are the first frames of the tests for Specimen 1 and 2, and so on. The graphic shows that two specimens where more resistant and the growth in their cracks area is moderately constant, it also compares how in some specimens the area of the crack is substantially bigger. The points "c" and "g" correspond to the limit where the behavior of the adobe cubes stops representing a constant growth, the crack's area starts to change rapidly and reaching faster the rupture point.

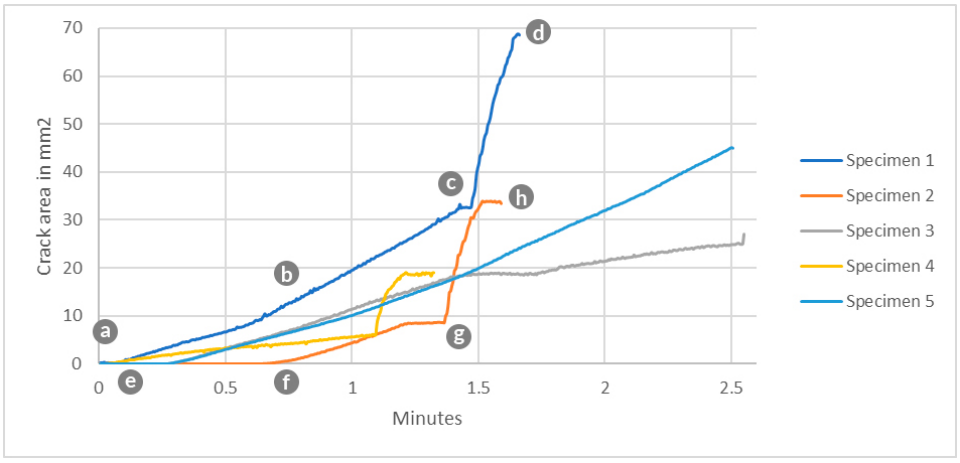


Figure 6: Graphic of the change in area of the cracks in the first 5 specimens through the duration of the tests.

5 VALIDATION IN A HISTORICAL STONE MASONRY CHURCH

The case study evaluated in this paper is focused on an important heritage building, which is part of the Andean Baroque Route, composed of four representative churches of Cusco, Peru. The Church of the Society of Jesus, was built in 1576 over the Inca temple called Amaru Cancha, however, it suffered the consequences of the 1650 earthquake and had to be re-built in 1651. In this occasion, it was contemplated with three doors facing the main square; the main vault was finished and closed in august of 1653. In 1950, another earthquake caused damage mainly in the structures of the façade and choir. The structure was rebuilt in a Latin cross shape, its façade, shown in Figure 7.a, is made of profusely decorated stone and it has two bell towers and two external chapels.

This research was part of a project for the Structural Health Assessment of the church. In order to know the current state of the building image registration was performed. Consequently, cracks and humidity spots on the inside and outside of the church were registered. A great number of cracks was found in the façade, therefore, a large number of images was collected. The pictures shown in Figure 7.a and 7.b, were some of the most representatives within the research. In order to assess the cracks in this structure these pictures were evaluated with the tool provided by the research on this paper. Particularly, for this evaluation it was not possible to use the target. However, the results obtained validate the accuracy of the test using the IoU metric.



(a) (b) (c)

Figure 7: (a) The church of the Society of Jesus, (b) right bell tower and (c) left side of the façade.

5.1 Results

The qualitative results are shown in Table 1, which confirm that the great variations in contrast that the façade has play against the capabilities of the presented tool. However, the results do not correspond to a poor segmentation, it is also seen in Figure 8 how some junctions are not detected as cracks.

Table 2: Qualitative results for two pictures from Figure 9.

	1	2	3
IoU	56.3%	61.1%	55.5%

In Figure 8, the results of the tool being used are shown in the images obtained of the representing cracks of the façade of the church. Due to, the large variation in color in the façade

the use of the tool was performed in parts as its shown in Figure 8, the first two columns represent parts of the same image, in this case the full image is presented in Figure 9.b. The third column of Figure 8 represents another part of the façade, in this case only one section had visible cracks, the full image is presented in Figure 9.b. In the second column belonging to Figure 8, it is shown how some parts of the borders and shadows introduced become false positives for the tool being represented in blue. Moreover, in Figure 8.f, some cracks that were not detected represent cracks of a thickness below the proportional minimum, given that these images represent a bigger surface than the adobe cubes previously tested.

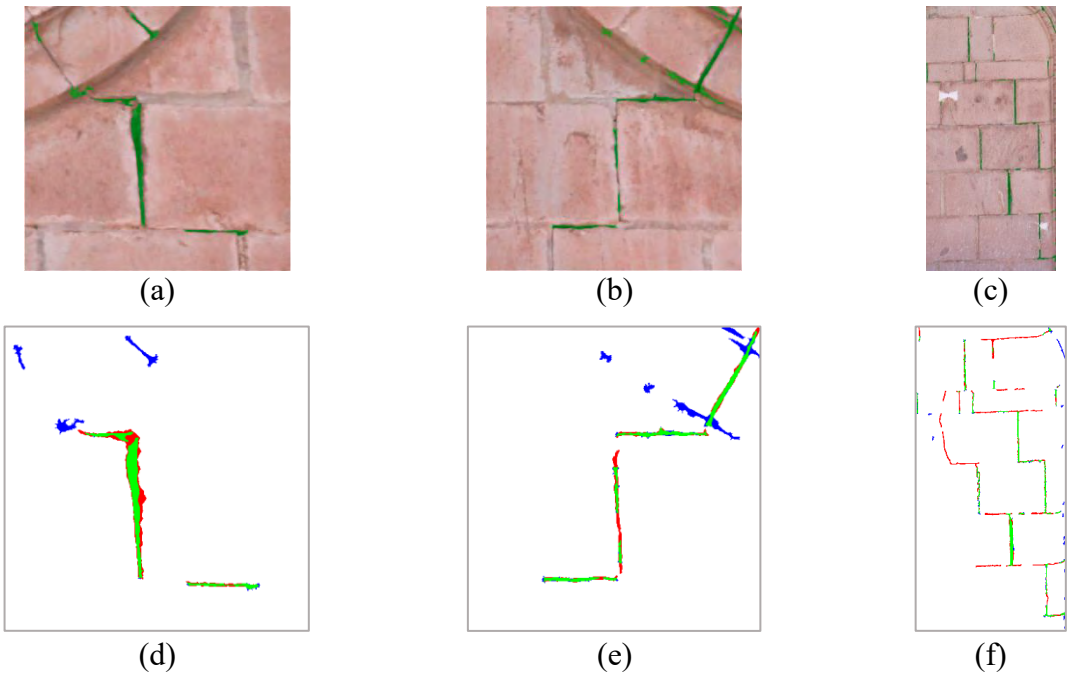


Figure 8: (a),(c) and (e) are the segmentation in green over the ROI, (b),(d) and (f) are the qualitative result of the tool from different cracks on the façade of the Society of Jesus.

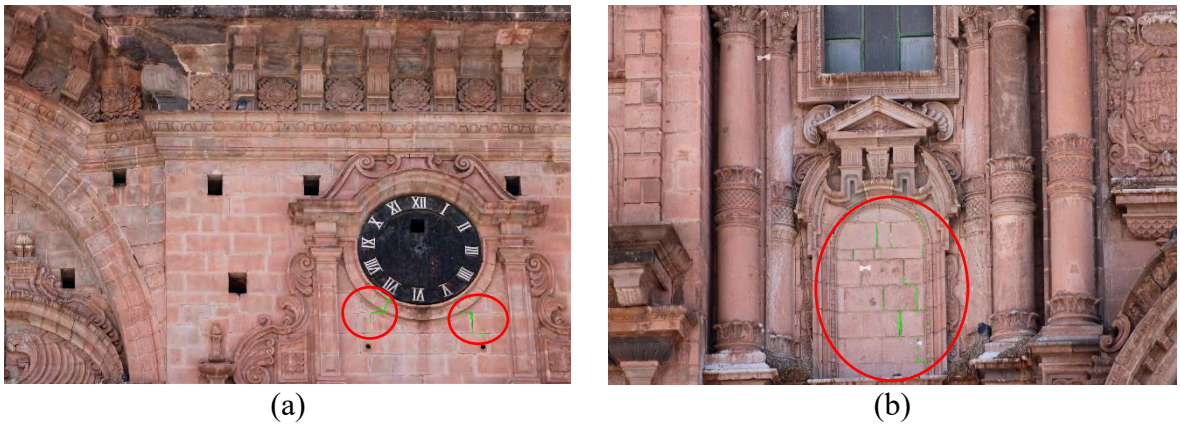


Figure 9: (a) Image 1 of the top part of the façade, (b) Image 2 of the middle part of the façade.

6 CONCLUSIONS

The results in this research show that the tool developed has high accuracy in segmenting the crack selected in order to perform a geometric characterization to get the crack's area and see how it changes trough time. This feature is the key contribution of this research, because it provides a tangible measurement of the change the crack suffers in time. For the field of civil engineering and real estate business, it is of upmost importance to control cracks as they start to form in order to assess if the crack will become a danger to the integrity of the studied building.

Therefore, it can be used in studies regarding cracks that could potentially become a great danger, the change in the area could become a red flag if it starts to increase rapidly compared to the rest of the monitored time.

Acknowledgements. Engineering and Heritage Laboratory at PUCP performed this research. The authors acknowledge the funding provided by STIC Amsud in the framework of the project entitled "Development of STIC tools for the structural diagnosis of heritage constructions", that has been a collaborative project of the University of Orleans, the University of Chile and PUCP. The authors also acknowledge the funding provided by DGI-PUCP in the framework of the project No 2019-0- 0004.

REFERENCES

[1] R. Segre, *America Latina en su arquitectura*, Ciudad de Mexico, (1983).

[2] M. Blondet, M. Serrano, A. Rubiños y E. Mattson, *La Experiencia de Capacitación de una Comunidad Andina en Construcción Sismorresistente con Adobe*» de Seminario Iberoamericano de Arquitectura y Construccion con Tierra, Cuenca, 2015.

[3] D. Inaudi, A. Rufenacht, B. von Arx, H. P. Noher, S. Vurpillot y B. Glisic, «Monitoring of a concrete arch bridge during construction,» Smart Structures and Materials, 2002

[4] X. W. Ye, C. Z. Dong y T. Liu, «A review of Machine Vision-Based Structural Health Monitoring: Methogologies and Applications,» Journal of Sensors, 2016.

[5] T. Yamaguchi y S. Hashimoto, «Fast crack detection method for large-size concrete surface images using percolation-based image processing,» Machine Vision and Applications, pp. 797-809, 2010.

[6] Z. Chen y T. C. Hutchinson, «Image-Based Framework for Concrete Surface Crack Monitoring and Quantification,» de Advances in Civil Engineering, Hindawi Publishing Corporation, 2010.

[7] J. Valenca, D. Dias-da-Costa, E. Julio, H. Araujo y H. Costa, «Automatic crack monitoring using photogrammetry and image processing,» de Measurement, 2013, pp. 433-441.

[8] W. Benning, J. Lange, R. Schwermann, C. Effkemann y S. Gortz, «MONITORING CRACK ORIGIN AND EVOLUTION AT CONCRETE ELEMENTS USING PHOTOGRAMMETRY,» de TS COMM V: Metrology and Industrial Applications, 2004.

[9] U. Hampel y H.-G. Maas, «Cascaded image analysis for dynamic crack detection in material testing,» ISPRS Journal of Photogrammetry and Remote Sensing, vol. 64, pp. 345-350, 2009.

[10] S. Nishiyama, N. Minakata, T. Kikuchi y T. Yano, «Improved digital photogrammetry technique for crack monitoring,» de Advanced Engineering Informatics, 2015.

[11] G. Medioni, C.-K. Tang y M.-S. Lee, «Tensor Voting: Theory and Applications».
[12] The Mathworks, «MATLAB, Image Processing Toolbox and Vision Computer Toolbox,» Natick, 2019.
[13] A. International, Standard Test Method for Compressive Strength of Hydraulic Cement Mortars (Using 2-in. or [50-mm] Cube Specimens), Philadelphia, 2019.
[14] S. Y. Alvarez Ordoñez, «COMPARACIÓN DE LAS PROPIEDADES MECÁNICAS DE UNIDADES Y PRISMAS DE BLOQUES DE TIERRA COMPRIMIDA ESTABILIZADA CON CEMENTO Y GEOPOLÍMERO DE PUZOLANA,» PUCP, Lima, 2018.
[15] L. E. Yamin Lacouture, C. Philips Bernal, J. C. Reyes Ortiz y D. Ruiz Valencia, «Estudios de vulnerabilidad sismica, rehabilitacion y refuerzo de casas en adobe y tapia pisada,» de APUNTES, 2007, pp. 286-303.
[16] G. K. Velarde Abugattas, «ANÁLISIS DE VULNERABILIDAD SÍSMICA DE VIVIENDAS DE DOS PISOS DE ADOBE EXISTENTE EN LIMA,» Lima, 2014.

12th International Conference on Structural Analysis of Historical Constructions
SAHC 2020
P. Roca, L. Pelà and C. Molins (Eds.)

CHARACTERIZATION OF HISTORIC MORTARS FOR COMPATIBLE RESTORATION: CASE STUDY OF SOUTH AFRICA

Maphole E. Loke[1*], Kumar Pallav[2] and Rainer Haldenwang[3]

[1] Department of Civil Engineering & Surveying, Cape Peninsula University of Technology
Bellville main campus, 7535 Cape Town, South Africa
e-mail: lokemaphole@gmail.com, www.cput.ac.za (*corresponding author)

[2] Department of Civil Engineering & Surveying, Cape Peninsula University of Technology
Bellville main campus, 7535 Cape Town, South Africa
e-mail: {kumarp@cput.ac.za, haldenwangr@cput.ac.za} www.cput.ac.za

Keywords: Historical Structures, Mortar characterization, Compatibility, Restoration

Abstract: *The history of the South African construction industry dates as far back as the Castle of Good Hope (1666), Slave Lodge (1679), Robben Island (1700), Union Buildings (1913), memorials and cathedrals, among many others. These structures represent the political, slavery, liberation and religious history of South Africa and its development throughout the years, while also contributing towards economic growth through tourism. Historical buildings stand out from the rest of the modern constructions as they portray marvellous architectural designs and unique materials used for their construction. However, due to ageing and environmental conditions, they often show critical signs of deterioration, which threaten the existence of some. In attempts to rescue these national treasures, the use of Portland cement, which is considered incompatible with the original materials, has become a common practice, not only in South Africa but abroad. To avoid disparity in materials during repair of historic structures, original material characterization is therefore recommended. This paper investigates the effects of Portland cement used on the repairs of historical masonries of the Castle of Good Hope, Cape Town and buildings on Robben Island, in South Africa. The mortar samples were collected from the Castle and analyzed using the techniques such as the visual investigation, cohesion test, microscopic and titration test. It is observed that the original lime-based mortars are not compatible with the Portland cement produced mortars. It was evident on the masonry, as the repairs are repelling from the original surfaces on these two structures.*

1 INTRODUCTION

Historical buildings deteriorate with apparent signs of material failure which is caused by several factors that include the following: Ageing of the structure, human negligence and ignorance, high humidity and rainfall, temperature changes due to seasonal changes and drastic fluctuations in day and night temperatures, atmospheric moisture, exposure to soluble salts, air pollution, chemical processes and biological attack by plants and animals [1]. Despite the factors outlined above, the durability of historic buildings depends on their regular maintenance. It is of obvious benefit that defects are prevented beforehand. However, regular maintenance with incompatible materials is equally discouraged. If these heritage legacies are not properly maintained, the economy suffers because of repeated repairs and loss of authenticity during restoration, which causes a reduction in tourist traffic. Hence, their protection with proper maintenance and use of compatible materials needs to be prioritized to ensure their continued existence and functionality.

The repair and restoration of heritage structures is a major challenge, as most of these buildings were built using materials that have been superseded by modern construction materials. The overall challenge is incorporating the old mortars (of unknown properties) with new materials, to solve the problem of decay. The challenge is a result of the availability of many new materials caused by growth in the construction industry in recent years. As a result, the construction industry opts for modern construction materials to solve the decay problems associated with historical structures. The typical procedure for restoration of ancient lime-based mortars is through the application of Portland cement, but the approach often fails to remedy the problem [2]. The use of Portland cement binders that are different from the original has negative repercussions on repaired surfaces, and therefore, more damage than benefit is usually the case [3].

The properties of Portland cement differ significantly from the original materials, thus causing reactions and acceleration of defects [2]. The application of Portland cement-based materials on historic masonries is common in South Africa. This was mentioned in an interview with the manager of the Built Environment Unit of the South African Heritage Resources Agency (SAHRA). He stated that during the most heritage building maintenance projects in South Africa, the common practice is the replacement of the original material with Portland cement [4].

The failure of Portland cement-based mortar when repairing structures where historic lime-based mortars were used is due to the difference in properties of Portland cement when compared with most of the ancient materials (lime in particular). Therefore, the substitution of original materials with Portland cement intensifies damage to the original fibers in the mortar, hence, causing deterioration of the masonry.

The current lack of understanding of the original material behavior has seen several restoration projects result in disaster. Most researchers fail to understand the concept of compatibility when it comes to restoration of historic mortars [5]. For developing countries such as South Africa, this approach has undoubtedly impacted negatively on the economy, as repeated repairs have been necessary in the case of the re-pointing and re-plastering of Robben Island, where incompatible cement materials were used [6]. The Conditional Assessment Report indicates that some of the oldest buildings on the island appeared to have lost their historic

features due to previous maintenance, which did not consider air circulation within the wall structures. The conclusion made was that most buildings' plaster and raised pointing needed to be removed, as they were suspected to be silicone and Portland cement, which are detrimental to the overall fabric. It was therefore recommended to replace the plaster and the pointing material with lime-based material which matches the original material. This is a compatibility criterion, according to the International Charters and Balkesten (2010). It is emphasized that newly introduced materials in conservation and restoration of historic structures need to match the properties of the old materials; otherwise, failure is guaranteed[7].

Compatibility can be achieved through characterization of the original materials before searching for new repair materials [8]. A study on the charaterization of historic mortars is a requirement prior to restoration, and it includes information on aesthetic and material property compatibility (*physical, chemical and mechanical*) [5]. The compatibility of heritage materials is entirely dependent on the characterization of the original materials prior to restoration. Mortars and grouts used for repair of historic buildings must have properties that are compatible with the original: equal in strength, adhesion, flexibility and porosity.

2 USE OF PORTLAND CEMENT ON LIME MORTARS

The use of Portland cement for the repair of historical monuments as mentioned by SAHRA Bult Environment Manager is visible on the Robben Island and Castle of Good Hope, in South Africa. The island has undergone maintenance and repair works in recent years (1999 onwards) [6]. In the Island's assessment report, it was stated that the repairs on the wall pointing did not consider how air circulates through wall sections and how condensation and dampness were to be treated. It has been concluded that the repair work caused further damages to wall sections. SAHRA has proposed maintenance work to rectify the previous restoration mistakes on the island. The deterioration seen on some of the oldest buildings on the island is shown in Figure 1. Regrettably, the material used for repair proved to be incompatible with both the original mortar and the masonry surface itself, and thus are seen to be detaching from the original surface on both the maximum-security prison (1700s) and the pre-primary school building (1800s).

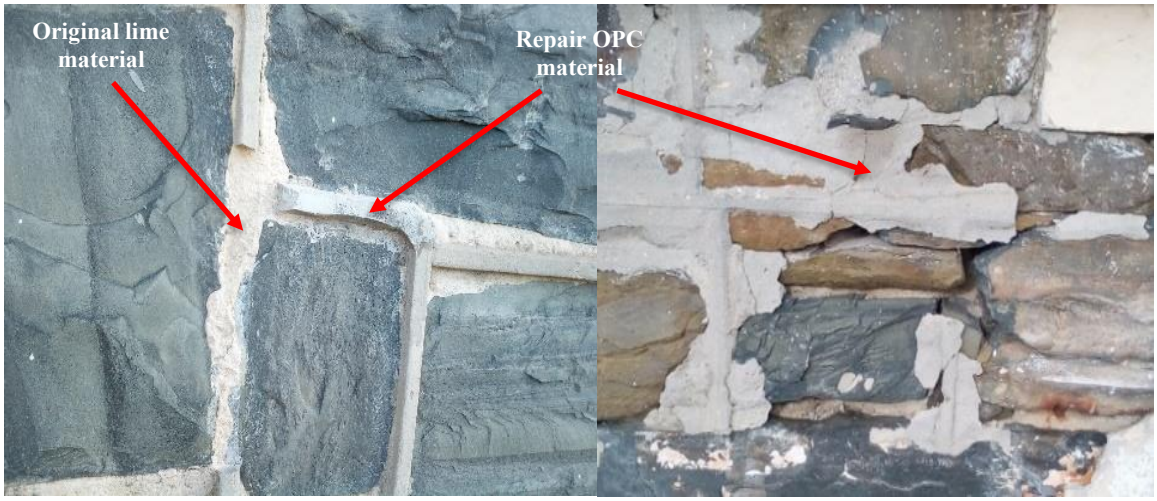


Figure 1: Deterioration and use of Portland cement on Robben Island masonry

The disparity in materials (Figure 1) is due to the difference in properties of the lime materials that have a low modulus of elasticity and high permeability to water and water vapour [9]. The Portland cement, on the other hand, has a high soluble salts content which results in salt crystallization, large thermal expansion coefficient and low porosity [2].

3 CHARACTERIZATION FOR COMPATIBILITY

Compatibility is "*utilizing materials that do not have negative consequences on the original materials*" [10] and is a significant factor to assess before selection of a mortar to be used alongside suitable procedures for restoration of heritage mortars [11]. The definition is based on the properties of the original mortars, which are compared to the repair mortars and should match the original in terms of physical, mechanical and chemical properties [12]. This is to guarantee the long-term durability and strength of historical structures. It is therefore essential to conduct a detailed assessment of the material properties before carrying out repair works. Finding a compatible material to duplicate the original is an ever-greater challenge globally [13]. However, original material analysis assists in the production of a good repair mortar that matches the original [14]. The knowledge of original material properties makes it possible to foresee and predict how the historic structure will react with restoration materials applied to it.

4 STUDY LOCATION

The Castle of Good Hope is located in Cape Town, South Africa. It is the second fort at the Cape, dating from 1666 to 1679, and is the oldest existing colonial building in South Africa [15]. It was originally located on the coastline of Table Bay, but, after land reclamation activities, it is now some distance from the coast [15]. It has a pentagonal shape (Figure 2a) and is made of stone and block masonry, as shown in Figures 2(b) and (c). The castle, like any other old building, experienced deterioration, threatening its continued use and even existence. A complete restoration was executed around the mid to late 1960s [16]. Some of the most recent repairs on the Castle are visible from a distance, as depicted in Figure (2c).



Figure 2: (a) Sky view of the Castle[17] (b) Entrance (c) Masonry

5 MATERIALS AND METHODS

5.1 Materials

In terms of the South African National Heritage Resources Act (Act No. 25 of 1999), Section 34, a permit was granted by SAHRA before collecting the hardened mortar samples from the old kitchen wall at the Castle. An experimental approach following an on-site assessment was used for characterization of the sampled mortars. The sections that are in poor condition were identified, and their condition carefully assessed. The representative mortar samples were collected in accordance with the procedure by Ngoma [18], using a small hammer and chisel. The description of colour, texture, sample type and location were recorded on a data sheet [18]. After collection of the in-situ materials, the samples were gently crushed using a mortar and pestle then, further physical, mineralogical and chemical analyses were carried out.

5.2 Methods for material analyses

The proposed tests were performed based on non-destructive and minor destructive testing. A series of aesthetic (visual investigation and microscopic analysis), mineralogical and chemical tests (titration) were carried out. A limited quantity of samples was used due to the limitations associated with the removal of materials from historical structures. The aesthetic characterisation was undertaken to avoid harm to the original material and to preserve the aesthetic effect created by a specific colour or texture. From this survey, it was possible to distinguish between the original and the repair material. The colour difference helped to track down the possible application of the modern material on the structure. This can clearly be seen on the Castle's wall section in Figure 2 (c). The difference seen is a clue for the investigator in terms of the possible difference in materials, though this hypothesis, needs to be tested with further analysis of the materials in the laboratory. The detailed procedure for physical analysis is presented in [19].

Additionally, mineralogical and chemical characterization (complexometric titration test using ethylenediaminetetraacetic acid) was carried out to determine the minerals present in the mortars and the type of binder and aggregates used[20,21]. For mineralogical analysis, the filtrate was investigated using reagents and indicators to determine salts present in a sample. The chemical analysis was carried out using a method that analyzes the filtrate containing oxides of elements present in a sample [20]; from that, the cementation index (CI) was calculated. The cementation of historic mortars is one of the essential aspects to investigate during the characterization process [22]. The procedure identifies the element oxides such as silica (Si), aluminium (Al), iron (Fe) and magnesium (Mg) to be used for calculation of CI as shown in Equation (1) [22].

$$\mathrm{CI} = \frac{(2.8 \text{ x } \%\mathrm{SiO_2} + 1.1 \text{ x } \%\mathrm{Al_2O_3} + 0.7 \text{ x } \%\mathrm{Fe_2O_3})}{(\%\mathrm{CaO} + 1.4 \text{ x } \%\mathrm{MgO})} \quad (1)$$

6 RESULTS

The aesthetic and physical results indicated whitish lime mortars made of sand aggregates, incorporating seashell fragments having diameters between 0.5 and 25 mm, and grey repair mortars as shown in Table 1. Part of the physical characterization results have been presented in [23]. Looking at the structure as a whole, the grey material occupies only a minor area, making it the repair material. It was evident from the masonry that the applied repair materials did not match well with the original materials. This was concluded based on the time frame of the repairs and the condition of the recently repaired areas.

Table 1: Mortar characterization

Sample ID	Color	Cohesion	CI	Binder	Aggregates
SK1	Whitish	Tough	0,30	Sub-hydraulic lime	Fine sand
SK2	Whitish grey	Tough	0,38	Slightly hydraulic lime	Coarse sea sand
SK3	Whitish yellow	Tough	0,20	Sub-hydraulic lime	Fine sand
SK4	Whitish grey	Very tough	0,63	Moderately hydraulic lime	Fine sand
SK5	Whitish	Tough	0,46	Slightly hydraulic lime	Fine sand
SK6	Cream white	Tough	0,24	Sub-hydraulic lime	Fine sand
SK7	Light yellowish	Friable	1,18	Natural or Portland cement	Very fine clayey sand
SK8	Reddish brown	Friable	1,08	Eminently hydraulic lime	Clayey soil
SK9	Yellowish orange	Friable	2,41	Natural or Portland cement	Clayey soil

The mineralogical characterization was carried out using the precipitation method, which analyzes the colour change, denoting the presence of the salt minerals in a filtrate of mortar sample, as shown in Figure 3.



Figure 3: Precipitation of salts infiltrates of mortar

A majority of the Castle materials were high in chlorides and carbonates, while the nitrates were present in limited quantities for both the binder enriched materials (Particles < 0.063 mm) and the aggregates (Particles > 0.063 mm) as indicated in Tables 2 and 3.

Table 2: Salt content in mortar (Particles < 0.063 mm)

Sample ID	Sulfates	Chlorides	Nitrites	Nitrates	Carbonates
SK1	+++	++	±	-	+
SK2	+++	+++	+	-	+++
SK3	++	+++	+++	+	+++
SK4	++	++	+	-	+++
SK5	±	+++	+	±	+++
SK6	+	+++	-	-	+++
SK7	+++	++	-	-	++
SK8	±	++	-	+	±
SK9	±	++	±	-	+

Table 3: Salt content in mortar (Particles > 0.063 mm)

Sample ID	Sulfates	Chlorides	Nitrites	Nitrates	Carbonates
SK1	+	++	±	-	++
SK2	-	++	+	-	++
SK3	+	++	±	-	+++
SK4	-	+	±	-	+++
SK5	-	+	-	-	+++
SK6	-	+	±	-	+++
SK7	±	+	-	-	+++
SK8	±	++	±	-	-
SK9	±	±	+	±	+

Where:
- Indicates the absence of an ion
± Indicates the presence of an ion at the limit of perceptibility
+ Indicates the presence of an ion
++ Indicates the presence of an ion in notable quantity
+++ Indicates the presence of an ion as a principal component [27].

7 CONCLUSIONS

- Even though characterization of heritage mortars for compatible and sustainable restoration is proven to yield repairs which would last for decades, it has received less attention in Africa. Thus, restoration of historic masonries is carried out using the materials that do not match the original.

- A further study to analyze the mechanical properties would be a worthwhile investment. The study addressing general material analysis other than mortars could yield a detailed recommendation on the repair of heritage buildings that will better suit the original materials.
- As is evident on the surfaces of the Castle and Robben Island, Portland cement fails on the restoration of historic lime mortars. Therefore, further investigation into the alternative repair materials that would match the original is underway. Such materials need to have similar or better properties than the original.

Acknowledgements: The authors wish to acknowledge the financial support from the government of Lesotho and the Cape Peninsula University of Technology for this project. The permission to sample materials from the Castle of Good Hope and Robben Island by the South African Heritage Resources Agency and the Sites' management is appreciated. A special thanks to the laboratory assistance by Ms Dlanjwa and Ms Mathobela from the Department of Chemistry at the Cape Peninsula University of Technology. I am also thankful to the reviewer for improving the quality of the paper.

REFERENCES

[1] Feilden, B. M. Conservation of Historic Buildings. 3rd edition, Architectural press, Elsevier (2003).

[2] Marini, A., Cominelli, S., Zanotti, C. and Giuriani, E. Improved natural hydraulic lime mortar slab for compatible retrofit of wooden floors in historical buildings. *Construction and Building Materials* (2018) 158: 801 – 813.

[3] Gleize, P. J. P., Motta, E. V., Silva, D. A. and Roman, H. R. Characterization of historical mortars from Santa Catarina (Brazil). *Cement and Concrete Composites* (2009) 31: 342–346.

[4] Mwasinga, B. Interview with SAHRA Built Environment Manager on 26 July 2018, Cape Town; South Africa (2018).

[5] Apostolopoulou, M., Aggelakopoulou, E., Siouta, L., Bakolas, A., Douvika, M., Asteris, P. G. and Moropoulou, A. A methodological approach for the selection of compatible and performable restoration mortars in seismic hazard areas. *Construction and Building Materials* (2017) 155: 1–14.

[6] Conditional Assessment of Buildings on Robben Island: Outline Description of Material Testing Required. 2018. Cape Town, South Africa. Available at: https://sahris.sahra.org.za (accessed in March 2019).

[7] Balksten, K. Understanding Historic Mortars and their Variations – a Condition for Performing Restorations with Traditional Materials. *2nd Historic Mortars Conference HMC2010 and RILEM TC 203-RHM Final Workshop* 22-24 September 2010, Prague, Czech Republic (2010).

[8] Hormes, J., Diekamp, A., Klysubund, W., Bovenkamp, G. L. and Börste, N. The characterization of historic mortars: A comparison between powder diffraction and synchrotron radiation-based X-ray absorption and X-ray fluorescence spectroscopy. *Microchemical Journal* (2016) 125: 190–195.

[9] Palomo, A., Blanco-Varela, M. T., Martinez-Ramirez, S., Puertas F. and Fortes, C. Historic Mortars: Characterization and Durability. New Tendencies for Research (2014).
[10] Isebaert, A., Van Parys, L. and Cnudde, V. Composition and compatibility requirements of mineral repair mortars for stone – A review. *Construction and Building Materials*, (2014) 59: 39–50.
[11] Bertolini, L., Carsana, M., Gastaldi, M., Lollini, F. and Redaelli, E. Binder characterisation of mortars used at different ages in the San Lorenzo church in Milan. *Material Characterization* (2013) 80: 9-20.
[12] Cizer, Ö., Schueremans, L., Serre, G., Janssens, E. and Van Balen, K. Assessment of the Compatibility of Repair Mortars in Restoration Projects. *Advanced Materials Research*, (2010) 133-134: 1071-1076.
[13] Deshpande, U. L. Repair, restoration and strengthening of building. *International Journal of I Innovations in Engineering Research and Technology* (2017) 4(3): 121 - 124.
[14] Gulzar, S., Chaudhry, M. N., Burg J. P. and Saeed S. A. Characteristics of Ancient Mortars and Plasters from the Archaeological Site of Akbari-Serai (Pakistan). *Journal of Chemistry* (2013) 25(15): 8484-8488.
[15] Castle of Good Hope. 2018. Available at https://castleofgoodhope.co.za (accessed in September 2018).
[16] Gilbert, C. The Castle of Good Hope: An Examination of Controversies and Conflicting Perceptions – A Case Study in Public History. An Honours degree thesis, University of Cape Town, South Africa (1994).
[17] Sky view of the Castle of Good Hope. 2019. Available at: https://blog.parkinn.com (accessed in January 2020)
[18] Ngoma, A. M. K. Characterisation and Consolidation of Historical Lime Mortars in Cultural Heritage Buildings and Associated Structures in East Africa. PhD thesis, University of Dar-es-Salaam, Tanzania (2009).
[19] Groot, C.J.W.P, Ashall, G.J., Hughes, J.J. and Bartos, P.J.M. Characterisation of old mortars with respect to their repair. *RILEM TC 167-COM: State of the art Report* (2004).
[20] Middendorf, B., Hughes, H., Callebaut, K., Baronio, G. and Papayianni, I. Investigation Methods for the Characterisation of Historic Mortars, Part 2: Chemical Characterisation. *Materials and Structures* (2005) 38: 771-780.
[21] Teutonico, J. M. ICCROM Arc laboratory manual for architectural conservators. Rome, Italy, 1988.
[22] Brosnan, D. A. Characterization and Degradation of Masonry Mortar in Historic Brick Structures. Hindawi Publishing Corporation, *Journal of Structures*, volume 2014, Article ID: 85987 (2014), pp. 1-7.
[23] Loke, M.E., Kumar, P. and Haldenwang, R. Physical characterization of heritage mortars for restoration interventions. *IEEE 10th International Conference on Mechanical and Intelligent Manufacturing Technologies (ICMIMT 2019)*, Cape Town: South Africa, 20-22 January 2020 (Presented).

12th International Conference on Structural Analysis of Historical Constructions
SAHC 2020
P. Roca, L. Pelà and C. Molins (Eds.)

COMPARISON BETWEEN INVESTIGATION TECHNIQUES FOR THE EVALUATION OF THE COMPRESSIVE PROPERTIES OF BRICK MASONRY STRUCTURES

FRANCESCA FERRETTI[1*], ANDREA INCERTI[2] AND CLAUDIO MAZZOTTI[1]

[1] Department of Civil, Chemical, Environmental and Materials Engineering (DICAM)
University of Bologna, Italy
Viale Risorgimento 2, 40136 Bologna, Italy
e-mail: {francesca.ferretti10, claudio.mazzotti}@unibo.it, www.dicam.unibo.it
(*corresponding author)

[2] CIRI Buildings & Construction (CIRI-EC)
University of Bologna, Italy
Via del Lazzaretto 15/5, 40131 Bologna, Italy
email: a.incerti@unibo.it, www.edilizia-costruzioni.unibo.it

Keywords: Brick Masonry, Compressive Behavior, Slightly-Destructive Testing, Double Flatjack Test, Core Testing

Abstract. *Existing masonry buildings, representing a large portion of the building stock in the Mediterranean area, are usually characterized by the presence of different constituent materials. The modifications experienced over time could have modified the static configuration of the structures and could trigger local damages and crises. Therefore, it is of fundamental importance to assess the safety of these constructions and to determine if retrofitting interventions are needed. In this framework, one of the crucial aspects is the mechanical characterization of masonry. Concerning brick masonries, several testing methodologies exist for the determination of the compressive strength, the elastic modulus and the Poisson's ratio. In particular, slightly-destructive tests, such as double flatjack tests and compressive tests on masonry cores, can be performed in place of destructive tests due to their limited invasiveness. However, they could be less representative of the overall behavior of masonry structural elements. The objective of the research is to evaluate the reliability of slightly-destructive tests in evaluating the compressive properties of masonry. An experimental campaign is presented, in which masonry specimens were built to reproduce a poor-quality brick masonry typology. Standard compression tests on wallets and double flatjack tests, both monotonic and cyclic, were performed. Moreover, masonry cores were extracted from the masonry specimens and tested in compression. Compressive strength, elastic modulus and Poisson's ratio were evaluated from each testing methodology. The results obtained from the double flatjack tests and the tests on cores, in terms of strength and deformability properties, were compared with the results of the standard compression tests, taken as reference. Correlations between the results of the slightly-destructive tests and the standard compression tests were established, obtaining a good agreement and confirming that the experimental techniques can be reliably adopted for the evaluation of the compressive properties of brick masonry.*

1 INTRODUCTION

Existing masonry buildings, which represent a large portion of the building stock in the Mediterranean area, are usually characterized by the presence of different constituent materials, whose quality often depended on the final use of the constructions [1]. The variations that existing buildings experienced over time, such as changes regarding the acting loads or the environmental conditions, could have modified the static configuration of the structures and could trigger local damages and crises. Therefore, it is of fundamental importance to assess the safety of these constructions and to determine if some retrofitting intervention is needed.

In the framework of the vulnerability assessment procedures, one of the most important aspects is the mechanical characterization of the materials. For what concerns the compressive behavior of brick masonry structural elements, the masonry can be characterized as a composite or starting from the mechanical properties of the constituents, i.e. bricks and mortar. Moreover, different testing methodologies can be adopted and, in general, it is possible to distinguish between non-destructive, slightly-destructive and destructive procedures [2]. When dealing with existing masonries, the level of invasiveness of the experimental investigations on the construction should be possibly limited. Therefore, usually the execution of slightly-destructive tests is preferred to the execution of destructive tests.

For the determination of the compressive properties of masonry, in terms of compressive strength, elastic modulus and Poisson's ratio, some slightly-destructive tests can be performed, such as double flatjack tests [3,4] and compression tests on masonry cores [5]. Even if these tests are characterized by a limited invasiveness, they are local tests and could be less representative of the overall behavior of the masonry structural elements. Several researches investigated the reliability of these techniques in evaluating the compressive properties of masonry [6-8]. More in detail, concerning the compression tests on masonry cores, which is a non-standard technique, different testing procedures were proposed, mainly varying the geometry of the mortar capping and the dimensions of the cores, studying the influence of different bond patterns, i.e. presence of both vertical and horizontal joints. The research here presented is aimed at evaluating the compressive properties of brick masonry through the cited slightly-destructive tests and, eventually, at establishing correlations between the results of these tests and the standard compression tests.

2 MATERIALS AND METHODS

In the present experimental campaign, slightly-destructive tests were performed for the determination of the compressive properties of brick masonry, i.e. compressive strength, elastic modulus, Poisson's ratio. More in detail, double flatjack tests and compressive tests on cores were performed and the results were compared with the ones from standard compression tests on wallets, taken as reference. The tests were conducted in laboratory on replicated clay brick masonry samples whose properties are described in the following.

2.1 Brick Masonry

The replicated samples were built using fired clay bricks, with dimensions 250×120×55 mm^3, and natural hydraulic lime-based mortar; specimens were cured in a laboratory-controlled environment [9]. The mortar mix was designed to obtain a poor-quality mortar with the objective of reproducing an existing historical masonry. Standard laboratory tests [10-13] were

performed on the constituent materials for their mechanical characterization. The results are reported in Table 1, in terms of compressive strength (f_c), flexural strength (f_{fl}), elastic modulus (E).

Table 1: Mechanical properties of the constituent materials

Material	f_c (MPa)	f_{fl} (MPa)	E (MPa)
Brick	18.7	4.6	6846
Mortar	1.4	0.4	2549

2.2 Standard Compression Test on Wallets

For the execution of the compression tests on wallets, according to the Standard EN 1052-1 [14], four double-wythe masonry panels were built. They were characterized by dimensions equal to 710×790×250 mm^3 and by a Flemish bond pattern. A universal testing machine, having a maximum capacity of 6000 kN, was used to apply the compression load to the panels. Two monotonic and two cyclic tests were performed. More in detail, the loading protocol of the cyclic tests was defined to progressively apply the 20%, 40%, 60%, 80% and 100% of the maximum load, as evaluated from the monotonic tests. A further load cycle was performed after the reaching of the peak load. The wall panels were equipped with vertical and horizontal linear potentiometers to monitor their shortening and elongation. On one sample, Digital Image Correlation was also used on one side. The test setup is presented in Figure 1.

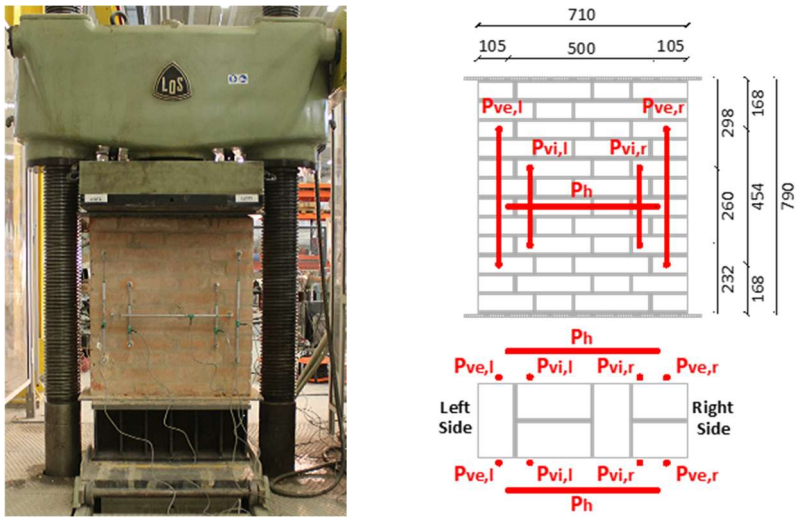


Figure 1: Compression test on wallets: test setup

2.3 Double Flatjack Test

The double flatjack tests were conducted on two masonry panels, having dimensions 1290×1115×250 mm^3, according to the Standard ASTM C1197 [3]. The purpose was to reproduce the execution of a double flatjack test in an existing masonry building. For this reason, the universal testing machine used for the standard compression tests on wallets was

adopted to apply a uniform compression on the masonry panels, reproducing the acting dead loads, and to provide the contrast needed for the correct execution of the double flatjack test. Indeed, it is well known that one of the possible issues of the test is not to have a sufficient contrast over the superior flatjack, thus producing the uplift of the masonry portion above the superior cut.

The testing phases can be summarized as follows: (i) execution of two semicircular cuts in correspondence of two masonry joints of the wall panels; (ii) seating of the flatjacks; (iii) application of a uniform compressive stress equal to 0.2 MPa; (iv) application of the flatjack pressure. During the last phase, the displacements of the plates of the testing machine were fixed, so to provide the contrast to the pressure applied by the flatjacks. Of course, having an increasing contrast pressure, equilibrating the flatjack pressure, is not a real condition when the test is performed on an existing masonry building. However, it is here considered so to allow to reach the compressive failure of the masonry portion between the flatjack and to compare the results with the standard compression tests. Moreover, the redistribution capacity of the masonry beyond the flatjacks, i.e. outside the tested portion, can be much lower if compared to an existing masonry pier, due to the smaller dimensions of the masonry panels in the present experimental campaign. This could determine even a more probable occurrence of the failure of masonry outside the tested area. For these reasons, it was decided to fix the displacements of the loading plates to provide an adequate contrast pressure for the entire duration of the tests.

At the beginning of the tests, one initial cycle was conducted to seat the flatjacks up to a pressure equal to half of the estimated compressive strength of masonry. Subsequently, the pressure was applied monotonically or cyclically up to the compressive failure of the masonry portion between the flatjacks. For the cyclic test, the loading protocol adopted for the standard compression tests was used.

For the measurements of the vertical and horizontal displacements within the tested masonry portion, linear potentiometers were applied over the surface of the samples, on both sides, as shown in Figure 2. Moreover, two linear potentiometers were also installed laterally to monitor the diffusion of stresses outside the investigated masonry portion. Linear Variable Differential Transducers (LVDT) were used to control the displacements of the loading plates.

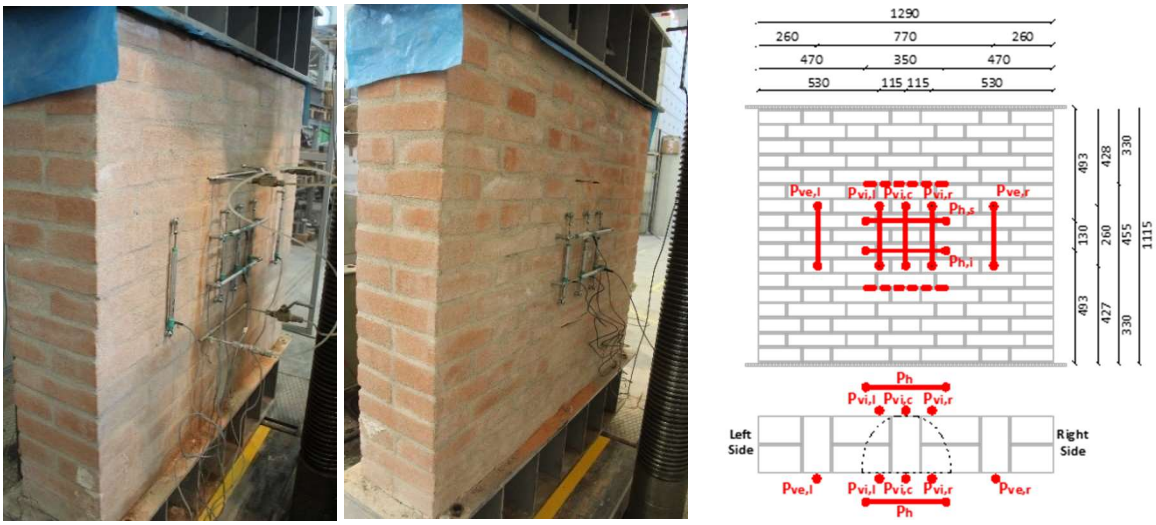


Figure 2: Double flatjack tests: test setup

2.4 Compression Test on Cores

Masonry cores were extracted from one of the masonry panels on which the double flatjack test was performed through a wet coring procedure. The samples were taken from the masonry portions resulted undamaged after the tests. Two different types of cores, having a diameter equal to 100 mm, were chosen: (i) 6 samples including one horizontal joint only (*HJ* samples, Figure 3*a*); (ii) 5 samples including both one horizontal and one vertical joint (*VJ* samples, Figure 3*b*). After the extraction procedure, the cores were cut to obtain single-wythe samples. To apply a compressive load and provide an adequate confinement to the samples, the masonry cores were capped with a good-strength mortar, characterized by a compressive strength equal to 22 MPa. The geometry of the cap, with a width equal to 80 mm and a height of 30 mm, was chosen according to previous studies [5,6].

The compression tests were performed in displacement control, using a hydraulic actuator having a maximum capacity of 100 kN. The displacement rate was equal to 0.02 mm/s. During the tests, vertical displacements were monitored using LVDTs, positioned on both sides of the masonry cores, as shown in Figure 4.

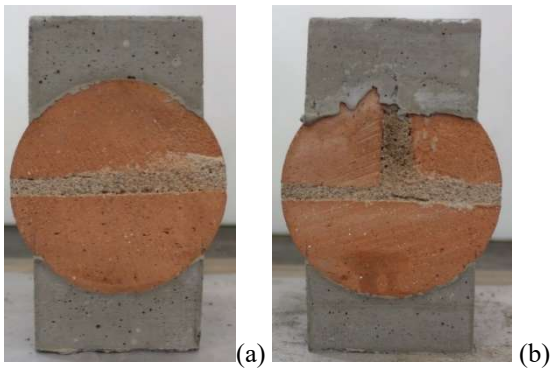
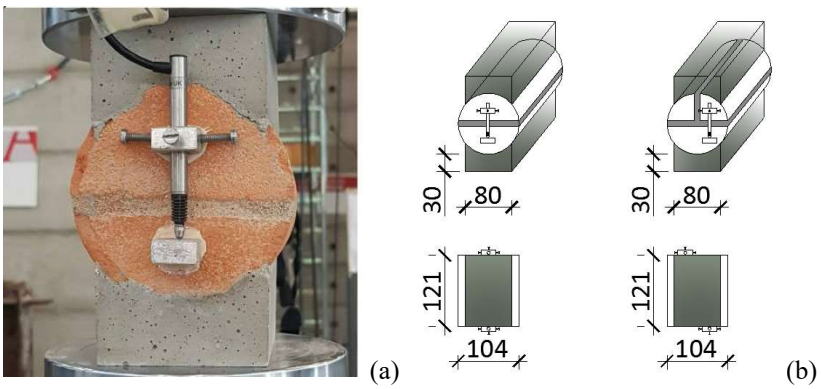

(a) (b)

Figure 3: Core samples: (a) type *HJ*; (b) type *VJ*



(a) (b)

Figure 4: Compression tests on cores: (a) experimental setup; (b) geometry and instrumentation

3 EXPERIMENTAL RESULTS

3.1 Standard Compression Tests on Wallets

The results of the standard compression tests are reported in Table 2 in terms of compressive

stress at first cracking f_{cr}, compressive strength f_M, elastic modulus E_M and Poisson's ratio ν. The elastic modulus E_M was determined between 1/10 and 1/3 of the maximum stress registered. Inside this range, the behavior of masonry can be reasonably assumed to be linear elastic. The Poisson's ratio ν was evaluated in the initial linear elastic stage as well, in which a constant value was identified. For cyclic tests, the elastic properties were evaluated in each load cycle, showing a stiffness degradation as expected. The values reported in Table 2 represent the average values determined by considering the reloading branch of each cycle with the exception of the last cycles, in which the nonlinear behavior was evident. It can be observed that the experimental results are quite homogeneous, with no significant differences between monotonic and cyclic tests.

In general, a similar behavior was observed for the masonry panels tested. It was characterized by a first vertical cracking, located at the center of the samples, visible on both sides. Subsequently, further vertical cracks appeared, quite distributed over the panels. At the end of the tests, a vertical crack across the wall thickness occurred (Figure 5).

The stress *vs* strain curves obtained for the samples SCT_M1 and SCT_M3, representative of a monotonic and a cyclic test, respectively, are reported in Figure 6 and Figure 7. As expected (Figure 6*a*), the displacements measured by the external potentiometers (P_{ve}) were lower than the ones registered by internal potentiometers (P_{vi}). The external instruments were positioned to better monitor the behavior of the samples, but they were not considered for the determination of the mechanical properties, e.g. E_M, ν. Moreover, the behavior of the panel SCT_M1 was investigated by means of the Digital Image Correlation (DIC), obtaining the horizontal strain maps reported in Figure 8, where the most significant phases of the tests were considered, corresponding to the appearance of macroscopic cracks.

Table 2: Results of the compression tests on wallets

Sample Code	Test Type	f_{cr} (MPa)	f_M (MPa)	E_M (MPa)	ν (-)
SCT_M1	Monotonic	2.4	6.4	3381	0.14
SCT_M2	Monotonic	1.7	6.3	2974	0.19
SCT_M3	Cyclic	1.1	6.7	3656	0.15
SCT_M4	Cyclic	2.1	6.1	2832	0.20



Figure 5: Compression test on wallets: failure mode of the sample SCT_M1.

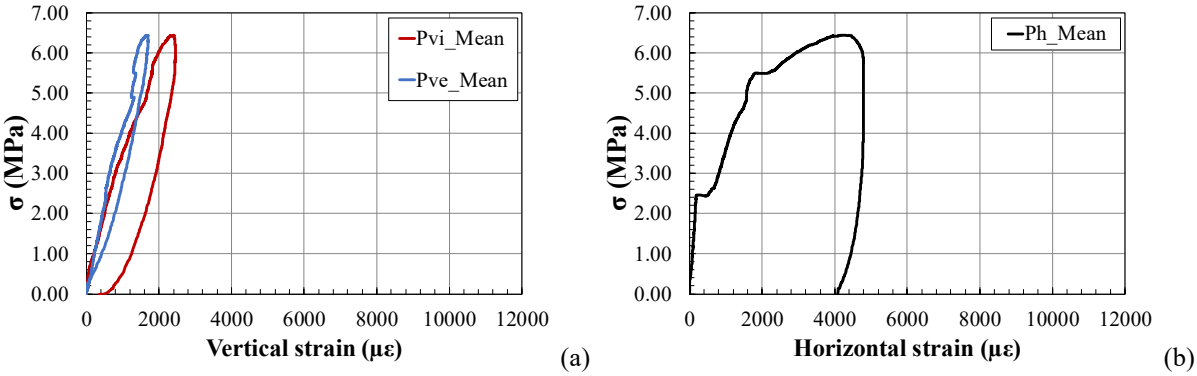


Figure 6: Stress *vs* vertical (a) and horizontal (b) strain diagrams of the sample SCT_M1

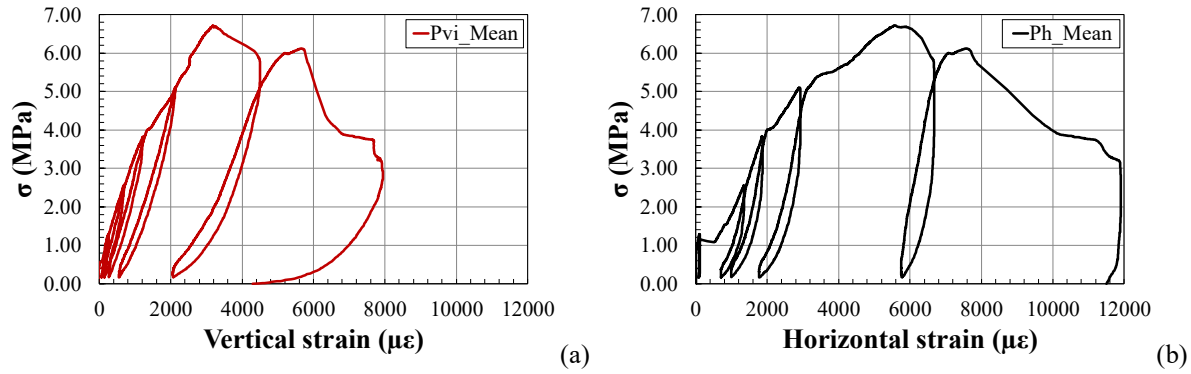


Figure 7: Stress *vs* vertical (a) and horizontal (b) strain diagrams of the sample SCT_M3

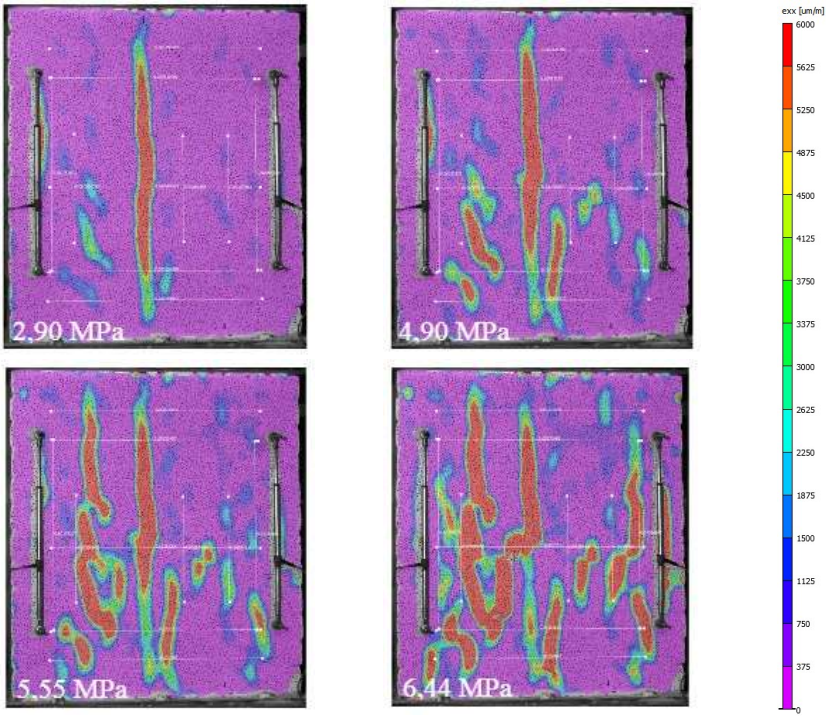


Figure 8: Compression test on wallets: horizontal strain maps of the sample SCT_M1.

3.2 Double Flatjack Test

The results of the double flatjack tests are reported in Table 3 in terms of compressive stress at first cracking f_{cr}, compressive strength f_M, elastic modulus E_M and Poisson's ratio ν. The elastic properties of the masonry were determined as described for the standard compression tests on wallets, considering the instruments positioned on the front side of the panel, i.e. the side from which the cuts were executed, within the tested masonry portion. In Table 3, the calibration constant k_m of the flatjack and the constant k_a, determined as the ratio of measured area of the flatjack to the average measured area of the slot, are also reported. According to the Standard [3], by multiplying the pressure of the flatjack and these constant, the stress on the tested portion can be evaluated at each instant of the test.

The failure mode of the two samples was similar (Figure 9), with vertical cracks located in the masonry portion between the flatjacks and inclined cracks outside this region, e.g. following a diagonal path from the edges of the flatjacks to the loading plates of the machine. This was, indeed, able to provide a sufficient contrast, even if at the end of the test, with quite high values of the flatjack pressure, horizontal cracks appeared in correspondence of the cuts.

The stress *vs* strain diagrams are reported in Figure 10 for both samples. In particular, it is possible to recognize the stress associated to the first cracking (f_{cr}). From this point on, the horizontal deformations progressively increased. In the cyclic test (DFJ_M2), a lower compressive strength was obtained, while a stiffness degradation was not recognizable, except from the last load cycle.

Table 3: Results of the double flatjack tests

Sample Code	Test Type	k_m	k_a	f_{cr} (MPa)	f_M (MPa)	E_M (MPa)	ν (-)
DFJ_M1	Monotonic	0.95	0.94	4.3	6.8	4350	0.09
DFJ_M2	Cyclic	0.95	0.92	3.8	5.8	3900	0.10



Figure 9: Double flatjack test: failure mode of the sample DFJ_M2

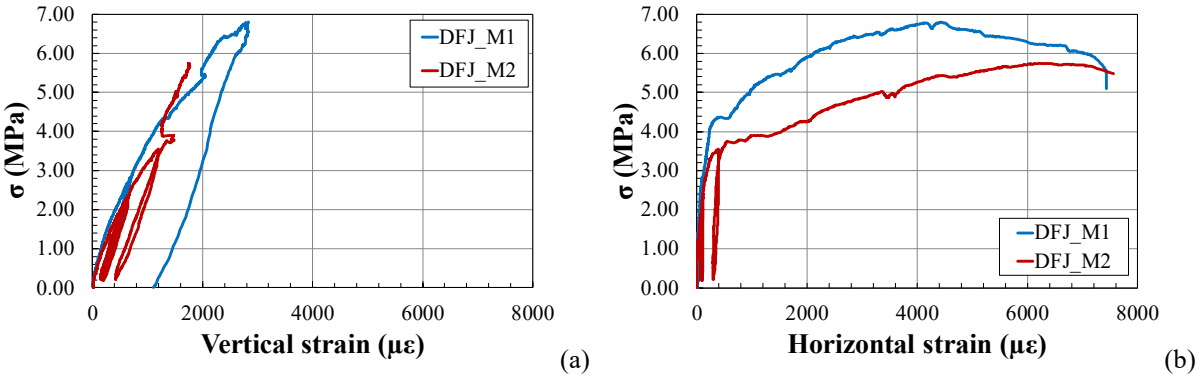


Figure 10: Stress *vs* vertical (a) and horizontal (b) strain diagrams of the double flatjack tests

3.3 Compression Test on Cores

The results of the compression tests on cores are presented in Table 4, in terms of compressive stress at first cracking f_{cr}, compressive strength f_M and elastic modulus E_M. The Poisson's ratio ν was not determined since only vertical potentiometers were applied to the samples.

Table 4: Results of the compression tests on cores

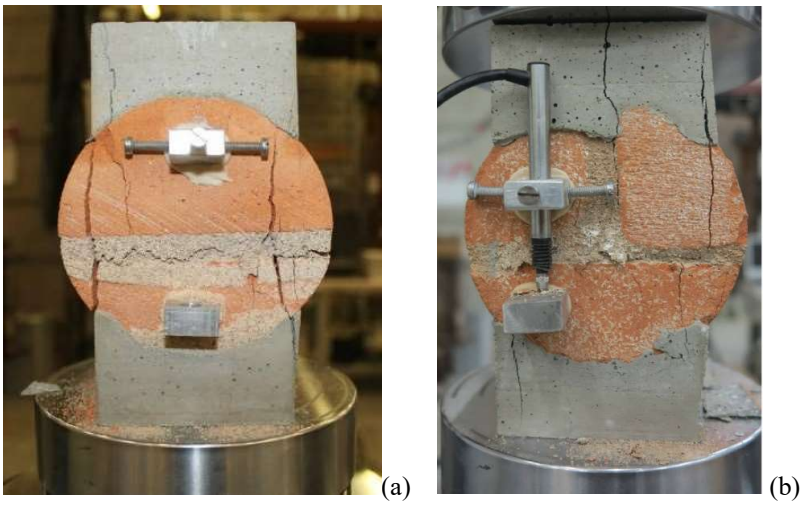
Sample Code	f_{cr} (MPa)	f_M (MPa)	E_M (MPa)
CTC_HJ1	6.4	11.1	2746
CTC_HJ2	-	11.2	3774
CTC_HJ3	6.1	10.7	3591
CTC_HJ4	8.5	11.3	2326
CTC_HJ5	4.4	9.1	1932
CTC_HJ6	7.7	10.7	2858
CTC_VJ1	5.8	9.9	1907
CTC_VJ2	7.9	11.1	2668
CTC_VJ3	2.6	7.5	1173
CTC_VJ4	6.8	8.1	1130
CTC_VJ5	6.7	8.5	-

With reference to the failure mode of the cores, a distinction should be made between the *HJ* samples and the *VJ* samples. Indeed, the presence of a vertical joint did influence the onset and the propagation of the failure. In general, the mortar capping was able to provide an adequate confinement to the samples, leading to the desired failure mode. More in detail:

- For *HJ* samples (Figure 11*a*) the first vertical crack was located in the center of the samples, starting close to the mortar bed joint and propagating vertically; subsequently, several cracks appeared and, at the end of test, vertical cracks were visible also in correspondence of the edges of the mortar capping, where the confinement was lower.
- For *VJ* samples (Figure 11*b*) the cracking process started in correspondence of the vertical joint, at the mortar-to-brick interface; it then propagated towards the extremities of the cores. At the end of the tests, multiple cracks were visible, spread over the entire

surface of the samples, even in correspondence of the edges of the mortar capping.

The stress *vs* vertical strain diagrams reported in Figure 12 are representative of the compressive behavior of the *HJ* and *VJ* samples. In general, it can be stated that lower compressive strength and elastic modulus were obtained for the cores characterized by the presence of the vertical mortar joint (*VJ* samples).



(a) (b)

Figure 11: Compression test on cores: failure mode of (a) *HJ* samples, (b) *VJ* samples

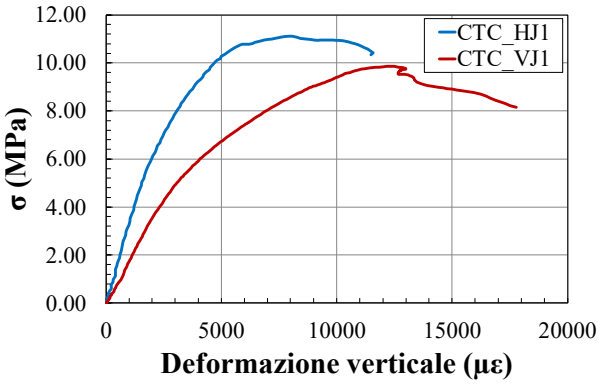


Figure 12: Stress *vs* vertical strain diagrams from the compression tests on cores

4 DISCUSSION

In this Section, the comparisons between the results of the different experimental tests are presented. In Table 5, the average values of the mechanical properties obtained with each testing methodology are reported.

A good agreement was obtained by comparing the results from the double flatjack tests and the results of the standard compression tests, taken as reference, especially for what concerns the masonry compressive strength f_M. A stiffer behavior was observed during the double flatjack tests, associated to higher E_M and lower ν values, which can be probably related to the smaller dimensions of the tested masonry portion and to the fact that the masonry within the flatjacks was more confined laterally with respect to the masonry wallets.

With reference to the compression tests on masonry cores, higher strength values were obtained, as expected, given that this test is a local test and that the mortar capping provides a strong confinement to the samples [5]. The results obtained by testing cores, overestimated the compressive strength of masonry by 67% and 43% for *HJ* samples and *VJ* samples, respectively. The values of the elastic modulus from the compression tests on cores are significantly lower than the ones obtained from standard compression tests. This can be explained by considering that the gage length of the vertical potentiometers is short and include small brick portions and one mortar joint, the latter significantly influencing the deformability of the samples.

The obtained results were also compared with the formula provided by the Eurocode 6 (EC6) for the evaluation of the masonry compressive strength. For this purpose, besides the standard compression tests described in Section 2.1, mortar samples extracted from the bed joints of the tested wall panels were subject to double punch test [15], obtaining an average compressive strength equal to 6.8 MPa. This value is significantly higher than the one obtained from the standard laboratory tests reported in Table 1. Such a difference can be attributed to the very different curing conditions of the mortar in the bed joints of the wall panels compared to the mortar standard prismatic specimens used for the mechanical characterization, as also confirmed by other researches on this topic [7]. By evaluating the masonry compressive strength through the EC6 formula, the following values were obtained: 4.7 MPa, considering the result reported in Table 1, and 7.6 MPa, considering the double punch test result.

Table 5: Comparison of the results

Test	f_{cr} (MPa)	f_M (MPa)	E_M (MPa)	ν (-)
SCT	1.8	6.4	3211	0.17
DFJ	4.1	6.3	4125	0.09
CTC_HJ	6.6	10.7	2871	-
CTC_VJ	6.0	9.0	1720	-

5 CONCLUSIONS

In the present work, different slightly-destructive tests were performed to evaluate the compressive properties of clay brick masonry samples. Standard compression tests, double flatjack tests and compression tests on cores were conducted. The results obtained from the double flatjack tests and the tests on cores, in terms of strength and deformability properties, were compared with the results of the standard compression tests, taken as reference. Correlations between the results of the slightly-destructive tests and the standard compression tests were established, obtaining a good agreement and confirming that the experimental techniques can be reliably adopted for the evaluation of the compressive properties of brick masonry.

Acknowledgements. This paper was supported by the PRIN 2017 research program of the Italian Ministry of Education, University and Research, project DETECT-AGING, grant N. 201747Y73L. Mr. Diiterihs Erra (Technical staff at CIRI Buildings & Construction) and the master student Valeria Rocco are gratefully acknowledged for their work during the setup of the tests.

REFERENCES

[1] Ferretti, F., Ferracuti, B., Mazzotti, C. and Savoia M. Destructive and minor destructive tests on masonry buildings: Experimental results and comparison between shear failure criteria. *Constr. Build. Mater.* (2019) **199**:12–29. https://doi.org/10.1016/j.conbuildmat.2018.11.246.

[2] Binda, L., Saisi, A. and Tiraboschi, C. Investigation procedures for the diagnosis of historic masonries, *Constr. Build. Mater.* (2000) **14:**199–233. https://doi.org/10.1016/S0950-0618(00)00018-0.

[3] ASTM C1197-14. Standard Test Method for In Situ Measurement of Masonry Deformability Properties Using the Flatjack Method. *American Society of Testing Material* (2014).

[4] Binda, L. and Tiraboschi, C. Flatjack test as a slightly destructive technique for the diagnosis of brick and stone masonry structures. *Int. Journal for Restoration of Buildings and Monuments* (1999):449-472.

[5] Sassoni, E., Mazzotti, C. and Pagliai, G. Comparison between experimental methods for evaluating the compressive strength of existing masonry buildings. *Constr. Build. Mater.* (2014) **68**:206–219.

[6] Sassoni, E. and Mazzotti, C. The use of small diameter cores for assessing the compressive strength of clay brick masonries. *J. Cult. Herit.* (2013) **14S**:e95-e101.6.

[7] Pelà, L., Canella, E., Aprile, A. and Roca, P. Compression test of masonry core samples extracted from existing brickwork. *Constr. Build. Mater.* (2016) **119**:230–240.

[8] Jafari, S., Rots, J.G. and Esposito, R. Core testing method to assess nonlinear behavior of brick masonry under compression: A comparative experimental study. *Constr. Build. Mater.* (2019) **218**:193–205.

[9] Incerti, A., Rinaldini, V. and Mazzotti, C. The evaluation of masonry shear strength by means of different experimental techniques: a comparison between full-scale and laboratory tests. *International Brick & Block Masonry Conference (IBMAC)*, CRC Press (2016), pp. 1645–1652.

[10] EN 772-1. Methods of test for masonry units - Part 1: Determination of compressive strength, *European Committee for Standardization* (2011).

[11] EN 12390-5:2009. Testing hardened concrete - Part 5: Flexural strength of test specimens, *European Committee for Standardization* (2009).

[12] EN 12390-13. Testing hardened concrete - Determination of secant modulus of elasticity in compression, *European Committee for Standardization* (2013).

[13] EN 1015-11:1999/A1:2006. Methods of test for mortar for masonry - Part 11: Determination of flexural and compressive strength of hardened mortar, *European Committee for Standardization* (2006).

[14] EN 1052-1:1998. Methods of test for masonry - Part 1: Determination of compressive strength, *European Committee for Standardization* (1998).

[15] Henzel, J. and Karl, S. Determination of strength of mortar in the joints of masonry by compression tests on small specimens. *Darmstadt Concrete* (1987) **2**:123-136.

12th International Conference on Structural Analysis of Historical Constructions
SAHC 2020
P. Roca, L. Pelà and C. Molins (Eds.)

COMPRESSIVE BEHAVIOUR OF BONDED BRICKWORK WALLETTES WITH VARIOUS THICKNESSES: EXPERIMENTAL AND NUMERICAL VERIFICATION

JULIAN THAMBOO*, MOHAMMAD ASAD†, AND TATHEER ZAHRA†

*Department of Civil Engineering, South Eastern University of Sri Lanka, 32360 Oluvil, Sri Lanka,
e-mail: jathamboo@seu.ac.lk, (*corresponding author)

†School of Civil and Environmental Engineering, Queensland University of Technology, 4000, Brisbane, Australia
e-mail: m.asad@qut.edu.au, t.zahra@qut.edu.au

Keywords: Brickwork, Compressive Strength; Stress-strain response, Micro Modelling, Slenderness.

Abstract. *Bonded brickwork loadbearing walls are commonly seen in many colonial period structures around the world; however, most research studies in the past and the current design provisions are primarily based on single leaf brickwork. Due to the anisotropic nature of brickwork, the strength and deformation characteristics would be different for bonded brickwork walls and their design using the provisions of single leaf bonded brickworks may be un-conservative. Therefore, to understand the compressive behaviour of differently bonded brickworks, an experimental programme followed by a numerical investigation were carried out in this research. The experimental programme comprised of testing nine wallettes under uniaxial compression. Three different types of bonded thicknesses (single, double and triple) were used to construct the wallettes. The experimental results are presented and discussed in terms of failure modes, compressive strengths and stress-strain responses obtained. Further a numerical investigation based on the micro modelling approach was employed to verify the experimental findings. The experimental and numerical modelling results indicate that the change in brickwork thicknesses does not significantly increase the compressive strength of the masonry. The increased number of weak perpend joints in the bonded brickwork wallettes, could be a reason of lower strength and thus, a general notion of increment in compressive resistance due to the reduction in slenderness is not applicable for bonded brickwork. Parametric analyses were also carried out and reported for different slenderness ratios to extend the understanding on the behaviour of bonded brickworks under compression.*

1 INTRODUCTION

Brickwork is widely used as loadbearing element in many historical and modern structures around the world. Consequently, the compressive resistance and deformation characteristics of brickwork were extensively researched in the past at material and structural scales. Primarily the strengths of the constitutive materials (unit and mortar) play a major role in determining the compressive strength of brickwork [1-5]. The current design standards

provide either expression or tabulated values to verify the compressive strength and Young's modulus of brickwork using the designated unit and mortar strengths/classes.

Generally, loadbearing brickworks are designed and built with many architectural bonding patterns resulting in different thicknesses depending on the design requirements. Particularly walls consisting of two or more brick thicknesses are generally found in historical structures. Despite various types of brickworks being constructed with different thicknesses, the compressive strength assessment is generally derived by testing single leaf brickwork prisms/wallettes and subsequently the design expressions/tables were developed from these test data. However it can be hypothesised, that the compressive strength characteristics of brickworks with various bonded thicknesses could be different to the brickwork with single leaf thickness as more weak joints exists [6-8], thus it demands systematic investigation.

Most of the research works carried out in this regard was on stone masonry, which constitutes quite complex morphology, where inner and outer leaves are made of different masonry types [9-11]. However, the bonded brickworks are also very common elements in the many clay brick masonry structures around the world. These buildings are often of historic importance and require intervention, thus understanding of their fundamental loadbearing behaviour is highly necessary. Subsequently an attempt has been made to investigate the compressive strength characteristics of bonded brickworks through experimental and numerical studies. The experimental programme comprised of testing nine bonded brickwork wallettes under uniaxial compression with three different thicknesses. Further, a simplified Finite element (FE) based micro modelling approach was used to numerically verify the experimental findings and the verified modelling technique was later extended to parametrically investigate the influence of slenderness to the compression behaviour of bonded brickwork.

2 EXPERIMENTAL PROGRAMME

The wallettes in this experimental programme were constructed using a locally sourced low strength clay brick (CB), whose dimensional and mechanical properties resembles the brick types found in the colonial masonry structures in the Sri Lanka. A locally available Natural Hydraulic Lime (NHL) was used as the binder in this research similar to the NHL mortars found in the colonial masonry structures. The lime mortar mix was prepared using a binder to filler ratio of 1:3 by volume proportion. The measured compressive strengths and elastic moduli of the brick and mortar are given in Table 1 with the coefficient of variation in the parentheses. In total, nine masonry wallettes were constructed and tested as shown in Fig 1. For each unit-mortar-masonry thickness combination, three wallettes were built as per BS EN 1052-1 [12] provisions. The dimensions and notation of constructed wallette specimens are listed in Table 2. The dimensions of the triple thick brick wallettes slightly violated the outlined BS EN 1052-1 provisions, where the height of the wallettes was not more than three times the thickness. As the intention of the research was to compare the performance of masonry wallettes of different thickness and bonding pattern under compression, height of the wallettes were kept same for all cases and only the thickness was varied. The single brick thick wallettes were constructed with running bond and the double and triple thick wallettes

were constructed with English bond which are the common bond patterns found in new and historical masonry structures.

Table 1: Mechanical properties of bricks and mortar.

Specimen	Compressive Strength (MPa)	Elastic modulus (MPa)
B1	5.1 (9.5)	4123 (6.4)
NHL	2.4 (5.6)	1402 (3.6)

Table 2: Test scheme and dimension of wallette specimens.

Notation	Brick Type	Thickness	Dimensions (mm)
B1-S	B1	Single (S)	410 (L) × 740 (H) × 95 (T)
B1-D		Double (D)	410 (L) × 740 (H) × 200 (T)
B1-T		Triple (T)	410 (L) × 740 (H) × 305 (T)

The compression testing was carried out using a 1000 kN capacity servo-controlled universal testing machine. The wallettes were placed carefully centred between the platens of the UTM to avoid any accidental eccentricity in loading. A 5 mm plywood capping was inserted between the contact steel plates and brickwork to reduce platen restraint. A displacement-controlled compression with the loading rate of 0.25 mm/min was used. In total, six displacement transducers were attached on the wallettes to capture the vertical and lateral deformations of the wallettes under compression. Four displacement transducers (two per face) were attached to capture the axial deformation. Another two displacement transducers were attached on the face (one per face) of the wallette to capture the lateral dilation. The testing arrangements of single, double and triple brick thick wallettes are shown in Figure 1. More details of the experimental programme can be referred in Thamboo and Dhanasekar [13].



(a) (b) (c)

Figure 1: Compression testing of (a) single, (b) double and (c) triple brick thick wallettes.

3 EXPERIMENTAL RESULTS

The failure modes were approximately similar across different thicknesses of wallettes tested under compression and shown in Figure 2. The failure of the wallettes were largely characterised by parallel vertical cracks originated at brick- mortar interface and propagated through the middle of the bricks. It must be highlighted that the double and triple thick brick wallettes showed predominantly single splitting cracks on the short sides along with the tensile parallel cracks on the long sides.

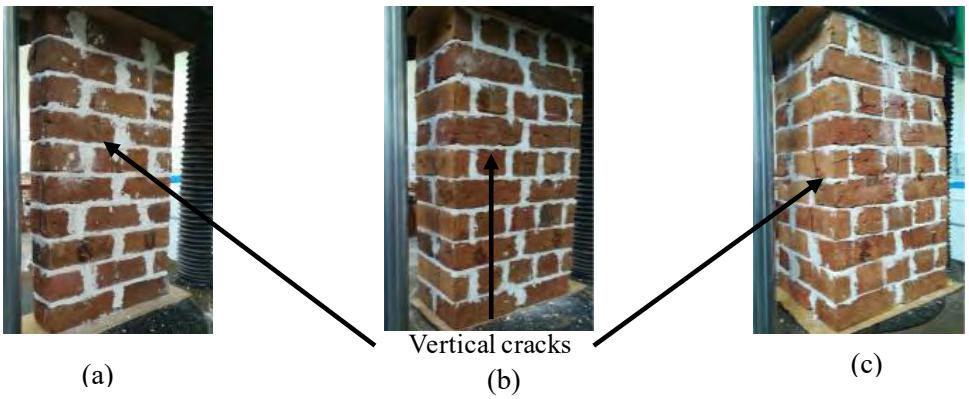


Figure 2: Failure modes of (a) single (b) double and (c) triple thick wallettes.

Table 3 presents the mean compressive strengths of tested wallettes and their COVs are given in parenthesis. It can be noted that there is nearly 10% increase in compressive strength between single and double brick thick wallettes. However, no prominent differences in the compressive strengths are noted between double to triple brick thick brickworks. This marginal increase in compressive strength with the increase in the thickness of wallettes could be attributed to the reduction in their slenderness ratio. However, the increase of compressive strength with the increase in thickness was not significant, due to the presence of weaker joints (i.e. more perpend joints) in the brickwork. Therefore it means the inhomogeneity of the masonry increased with the increase of thickness; hence the strength increment was not witnessed. This idea can be drawn from recent studies of compressive strength correlation between single brick thick masonry prisms and wallettes, where the corresponding wallette strength is nearly 25 % less than the prism strength, where the introduction of the perpend joints in the masonry reduced the compressive strength than that of prism [8].

Table 3: Compressive strength and elastic properties of the tested wallettes.

Notation	Compressive Strength (MPa)	Elastic modulus (MPa)	Poisson's ratio
B1-S	2.1 (6.4)	175 (12.6)	0.2 (6.0)
B1-D	2.3 (9.3)	219 (10.4)	0.19 (9.8)
B1-T	2.4 (9.6)	224 (3.0)	0.2 (9.0)

The compressive stress-strain curves of the monotonically loaded wallettes have displayed approximately linear stress-strain behaviour up to 60 to 70% of the peak strength and afterward nonlinear behaviour was observed up to the failure. Moreover, the elastic, peak and ultimate strain measurements indicated a slight increase in the ultimate strain at failure in the triple brick thick wallettes than of single and double brick thick wallettes. The increase in inhomogeneity, thereby increase in weaker planes in the triple leaf masonry wallettes could have contributed to the increased deformation characteristics.

4 NUMERICAL MODEL

The experimental results of the wallettes were verified through a simplified FE based micro-modelling technique. This micro-model of bonded brickwork considers that the bricks are joined through equivalent contact interfaces to replicate the masonry behaviour without specifically modelling the mortar layers [14-15]. Therefore, the bricks are expanded to take the combined effect of brick and mortar and equivalent interfaces with zero thickness are modelled to simulate the combined mortar and mortar-brick contact behaviour as described in Figure 3. Subsequently, a three-dimensional (3D) FE model with plastically damaging nonlinear solid brick elements and zero thickness interface elements with cohesive and damaging properties was developed for each wallette. The ABAQUS finite element software [16] was used for the numerical simulations. The bricks were modelled using eight-nodded 3D elements (C3D8R). Top and bottom loading plates (similar to experiments) were also modelled as rigid body to apply a uniform compressive displacement on top of wallettes, whilst the vertical transition bottom surface was restrained as shown in Figure 4.

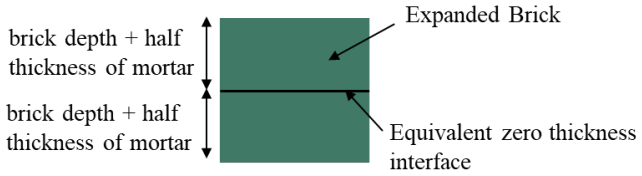


Figure 3: Meso-modelling concept of masonry.

A mesh size of 20 mm × 20 mm × 20 mm was employed for the brick elements after carrying out the mesh convergence studies. Material behaviour of the expanded clay bricks was simulated using 'Concrete Damage Plasticity Model' that includes the failure mechanism of tensile cracking and compressive crushing. The stress-strain properties taken for the bricks were calibrated based on the experimental test results of single brick wallettes as given in Thamboo and Dhanasekar [13]. Hence, the same material model was then employed to validate the results of double and triple wallette compression tests. The zero-thickness interaction was simulated using a constitutive law accounting for the traction-separation of the interface from the ABAQUS library. This model considers initially a linear elastic behaviour of the interface, which is followed by the initiation and evolution of interface damage. With the increase in compressive load, the stresses increase until the limiting stresses are assigned, after which friction model is activated which contributes to the shear stresses. Mohr-Coulomb failure criterion was used to model the friction behaviour. The interface parameters used for

the contact modelling were taken from [17]. A uniform monotonic displacement of 10 mm was applied on the top of the loading plate with boundary constraints to simulate the compression tests as shown in Figure 4.

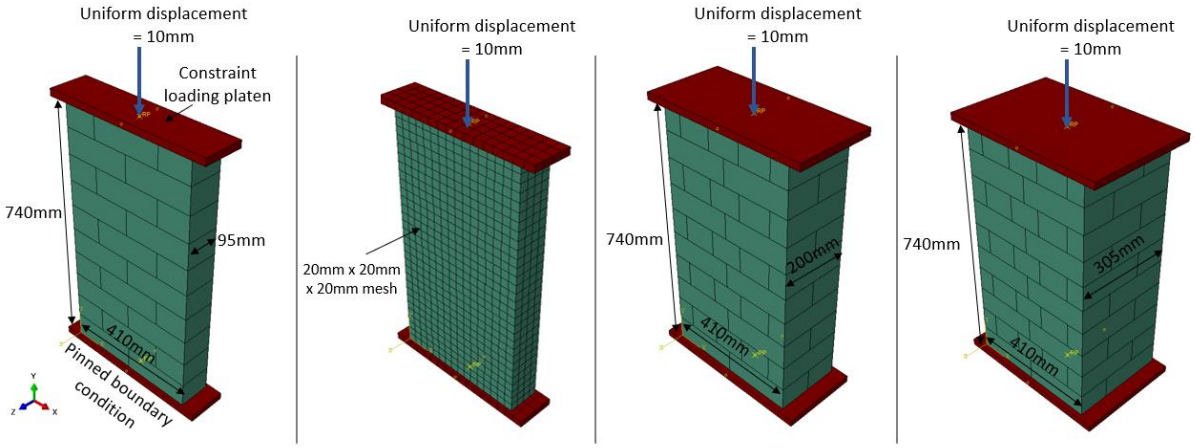


Figure 4: Wallettes model details (a) Single brick (b) Typical meshing (c) Double brick and (d) Triple brick wallette.

4.1 Numerical Validation

The outcome of the FE model results were validated with the experimental findings in terms of failure patterns observed and comparing the stress-strain curves. The failure modes of FE modelling of single, double and triple brick thick wallettes are shown in Figure 5. Similar to experimental results, splitting cracks in thickness, and cracks on the face of wallette samples were observed. The failure strain levels are also same as that were observed in the experimental results.

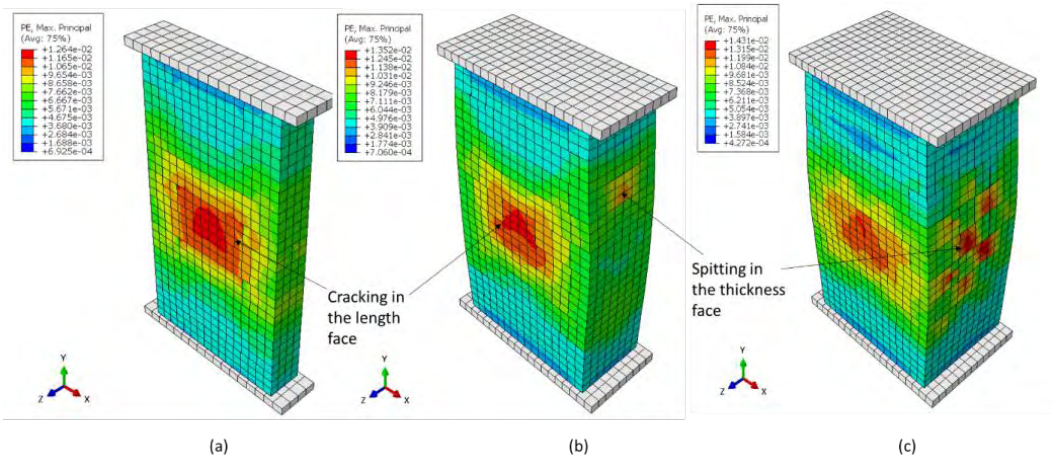


Figure 5: Failure modes of wallettes (a) Single brick (b) Double brick and (c) Triple brick.

The stress-strain response validation for single, double and triple wallettes is presented in Figure 6. The overall stress-strain curves matched well with the experimental data. The pre-peak and post peak behaviour of all wallettes was found similar to the experimental measurements. As discussed in the experimental results, not a significant difference in the strength due to change in bonded thicknesses was observed. This verifies that the increase in perpend joints in the thickness of double and triple walls affect the compressive behaviour of masonry.

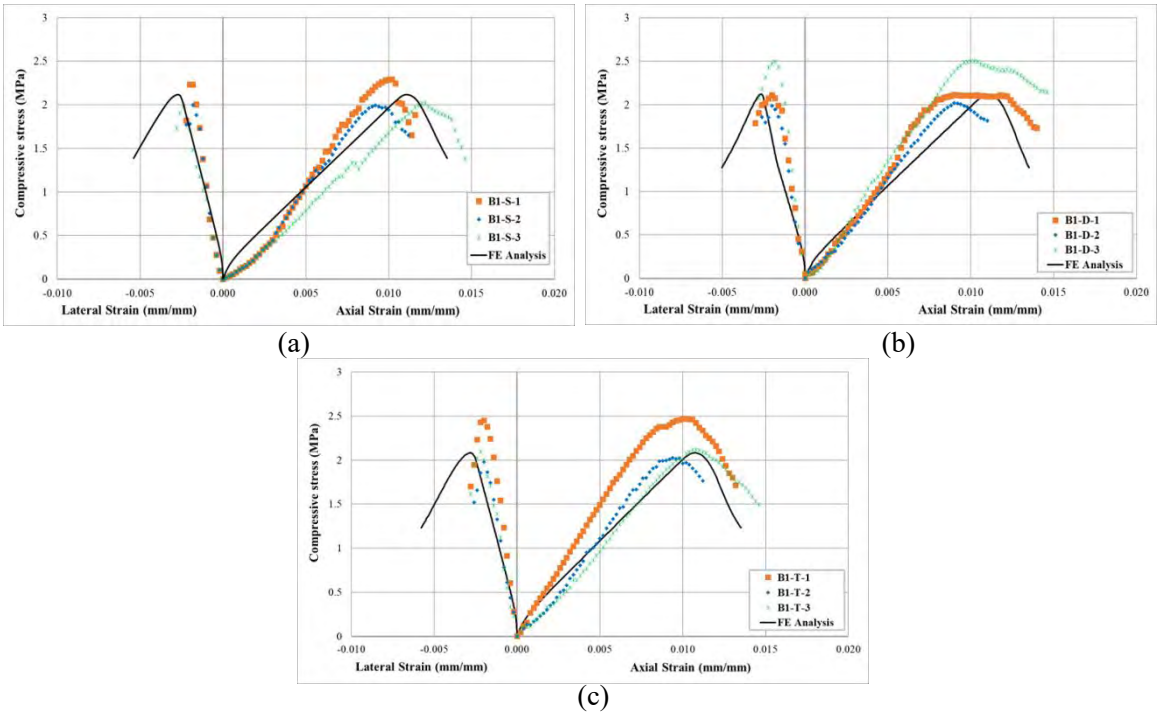


Figure 6: Stress-strain validation of wallettes (a) Single brick (b) Double brick (c) Triple brick

5 PARAMETRIC STUDY

The validated models of single, double and triple bonded brickwork wallettes were then employed to investigate the effect of the slenderness on the compressive behaviour of bonded brickworks. In the parametric study of bonded brickwork wallettes, the height of the wallettes was changed to 1040 mm to simulate different slenderness, in addition to the validated models. The 1040 mm height of the wallettes corresponds to the fifteen courses of brick layers. Subsequently, the corresponding slenderness ratio (height to thickness ratio, h/t) of the analysed single, double and triple bonded brickwork wallettes were 10.9, 5.2 and 3.4, respectively. The same constitutive material (i.e. brick and mortar) and interface properties that were considered for the model validation were used in the parametric study.

Figure 7 shows the failure pattern of the single, double and triple bonded brickwork wallettes with relatively higher slenderness than the previously analysed cases in section 4. It could be said that the failure modes of the wallettes did not significantly change as the

slendernesses, of the wallettes were increased by about 1.5 times from the previously analysed cases, where predominant tensile dilation of the masonry wallettes was noted regardless of the considered bonded thicknesses. However, the compressive strengths of the bonded brickworks have dropped about 5-10%, when the slenderness was increased by 1.5 times. The compressive strengths obtained in the parametric study are given in Table 4. In order to verify the strength variation in the bonded brickworks with different slenderness values, the compressive strength obtained were normalised with respect to the strength of single brick thickness wallette of 740 mm height. It can be seen that the change in bonded thickness (single, double and triple) in the 1040 high wallettes did not change the compressive strength of the masonry, thus it confirms that the general notion of increase in compressive strength with the reduction in slenderness of the masonry is not applicable for bonded brickworks.

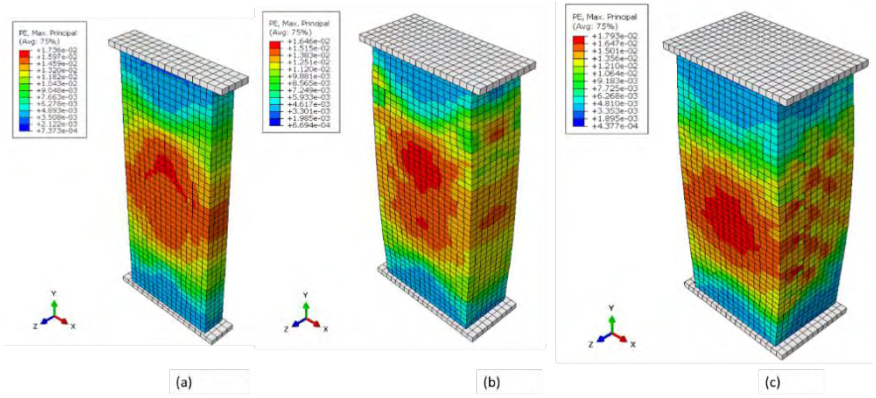


Figure 7: Failure modes of 1040mm high walls (a) Single brick (b) Double brick (c) Triple brick.

Table 4: Slenderness (H/t) ratio effect.

Wallette dimensions (W×H×T)	H/t	Compressive Strength (MPa)	Normalised Strength
410 × 740 × 95	7.8	2.12	1
410 × 1040× 95	10.9	2.01	0.92
410 × 740 × 200	3.7	2.19	0.98
410 × 1040 × 200	5.2	2.04	0.96
410 × 740 × 305	2.4	2.18	0.96
410 × 1040 × 305	3.4	2.02	0.95

However, changing the slenderness by changing the height of the wallettes have reduce the compressive strength in all the thicknesses analysed, which is in agreement with the common understand of the behaviour of masonry under axial compression. Therefore, it could be stated, that for the bonded brickworks, the slenderness increment due to increase in thickness should be carefully assessed to verify the compressive resistance. Further experimental and numerical studies have to be carried out to develop correction factors to adjust the compressive strengths of the bonded brickworks with various masonry assemblies and slenderness ratios in the future, similar to the correction factors for masonry prism test [18].

6 CONCLUSIONS

The compressive strength characteristics of bonded brickworks were assessed through experimental and numerical studies. Subsequently, single, double and triple thickness bonded brickwork wallettes were assembled with lime mortar to replicate the historical masonry buildings, and tested to ascertain the strength, failure and complete stress-strain response. The limited experimental testing results have shown that the change in thickness of the brickwork did not significantly change the failure pattern and as well as the strength characteristics, which is against the common notion of that as the reduction in slenderness would increases the compressive strength of masonry, however this phenomenon in bonded brickwork is due to anisotropic nature of masonry, where with increase in thicknesses, increases the inhomogeneity with the presence of more joints in the masonry, subsequently no substantial strength increment could be achieved.

Subsequently in order to verify the experimental findings, a FE based micro-modelling technique was developed to model bonded brickwork tested in this research and the established modelling technique was validated with the experimental results in terms of failure patterns and compressive stress-strain curves. Later the validated FE modelling method was extended to parametrically analyse the effects of different heights of the bonded brickwork wallettes, and the results indicate that with the increase height (thereby slenderness) reduce the compressive resistance with in the same thickness of the wallettes. Therefore, the influence of bonded thickness of the brickwork should be cautiously verified to determine the compressive resistance of bonded brickwork walls. Hence the experimental and numerical studies have to be extended to develop correction factors to adjust the compressive strength of bonded brickwork with various brickwork assembly properties and slendernesses, similar to the correction factors for masonry prism test [18].

Acknowledgements. The technical assistance provided by Mr Mohamed Jiffry, Mr Mohamed Farhan and Mr Mohamed Imthyas are greatly appreciated. The support of Professor Manicka Dhanasekar is acknowledged. This research was funded by the South Eastern University of Sri Lanka under the grant number SEU/ASA/RG/2019/02.

REFERENCES

[1] Bennett, R.M., Boyd, K.A., and Flanagan, R.D. Compressive properties of structural clay tile prisms. *J. Struct. Eng* (1997) **123(7):** 920–926.

[2] Thamboo, J.A. and Dhanasekar, M. Behaviour of thin layer mortared concrete masonry under combined shear and compression. *Aust. J. Struct. Eng* (2016) **17(1):** 39–52.

[3] Zahra, T. and Dhanasekar, M. Prediction of masonry compressive behaviour using a damage mechanics inspired modelling method. *Constr. Build. Mater* (2016) **109**: 128–138.

[4] Pelà, L., Canella, E., Aprile, A., and Roca, P. Compression test of masonry core samples extracted from existing brickwork. *Constr. Build. Mater* (2016) **119**: 230–240.

[5] Segura, J., Pela, L. and Roca, P. Monotonic and cyclic testing of clay brick and lime mortar masonry in compression. *Constr. Build. Mater* (2018) **193**: 453–466.

[6] Gumeste, K.S. and Venkatarama Reddy, B.V. Strength and elasticity of brick masonry prisms and wallettes under compression. *Mater. Struct* (2007) **29**: 241–253
[7] Zahra, T. and Dhanasekar, M. A generalised damage model for masonry under compression. *Int. J. Damage Mech*. (2016) **25(5):** 629–660.
[8] Thamboo, J.A. and Dhanasekar, M. Correlation between the performance of solid masonry prisms and wallettes under compression. *J. Build. Eng* (2019) **22**: 429–438.
[9] Valluzzi, M.R., Da Porto, F. and Modena, C. Behavior and modeling of strengthened three-leaf stone masonry walls. *Mater. Struct* (2004) **37(3):** 184–192.
[10] Binda, L., Pina-Henriques, J., Anzani, A., Fontana, A. and Lourenco, P.B. A contribution for the understanding of load-transfer mechanisms in multileaf masonry walls: Testing and modelling. *Eng. Struct* (2006) **28:** 1132–1148.
[11] Oliveira, D.V. and Lourenço, P.B. Experimental behaviour of three-leaf stone masonry walls The construction aspects of built heritage protection, Dubrovnik, Croatia 2006 (2006) 356–362.
[12] BS EN 1052-1:1999 Methods of test for masonry. Determination of compressive strength, BSI.
[13] Thamboo, J.A. and Dhanasekar, M. Assessment of the characteristics of lime mortar bonded brickwork wallettes under monotonic and cyclic compression. *Const. Build. Mater* (2020) **261**: 120003.
[14] Nazir, S. and Dhanasekar, M. Modelling the failure of thin layered mortar joints in masonry. *Eng. Struct* (2013) **49:** 615–627.
[15] Bolhassani, M., Hamid, A. A., Lau, A.C.W. and Moon, F. Simplified micro modelling of partially grouted masonry assemblages. *Constr. Build. Mater* (2015) **83:**159–173.
[16] ABAQUS, Finite element software documentation, Dassault Systèmes, Simulia RI, USA, 2018.
[17] Zahra, T. and Dhanasekar, M. Characterisation and strategies for mitigation of the contact surface unevenness in dry-stack masonry. *Constr. Build. Mater* (2018) **169:** 612–628.
[18] ASTM C1314 – 14 Standard Test Method for Compressive Strength of Masonry Prisms, ASTM International, USA.

DATA ACQUISITION, MANAGEMENT AND EVALUATION FOR STONE CONSERVATION PROJECTS WITH DIGITAL MAPPING

DIPL.-ING. GUNNAR SIEDLER[1], DIPL.-INF. (FH) SEBASTIAN VETTER[1], JENS KAMINSKY[2]

[1]fokus GmbH Leipzig
Lauchstädter Straße 20, 04229 Leipzig, Germany
e-mail: Siedler@fokus-GmbH-Leipzig.de, web: www.fokus-GmbH-Leipzig.de

[2] Restauratorische Bauplanung Jens Kaminsky
Wartburgstr. 11, 08525 Plauen, Germany
e-Mail: mail@jenskaminsky.de, web: www.restaurierungsplanung.de/

Keywords: Documentation, Conservation, Mapping, Object hierarchy, Photogrammetry, Laserscanning

Abstract. *Several years of experience in heritage documentation have given a background to develop methods of digital photogrammetry and mapping. The outcome is the development of a mapping software over a period of 20 years.Main features of the software are image rectification, vector based mapping, quantity survey and data analysis. In Germany, it is mainly used in the field of stone conservation. Small projects can be processed as a single mapping project, whilst complex projects like a cathedral can be organised as a hierarchical project, with several mapping projects for individual object parts. Each mapped element can be connected with additional attributes. This allows visual analysis of mapping activities, quantities and attributes – like in a geographical information system (GIS) for conservators. Tools and procedures for efficient mapping are developed in close cooperation with conservators from different fields. It is shown how large stone objects can be managed efficiently with an example project from the field of natural stone. This applies to the overall data acquisition and data evaluation for condition analysis, conservation planning, accounting documentation and monitoring. Due to the advances in the fields 3D laser scanning and digital photogrammetry within the past 5 years the R&D project „PROQUATO“ (2016 – 2018) was initiated by fokus GmbH Leipzig with the institute for photogrammetry and remote sensing of TU Dresden and Scan 3D GmbH, Berlin. Project results for efficient data processing and functions for 3D mapping will be presented. Current developments deal with the fast processing of point clouds scanned by laser scanner for the use as reference for image rectification, deformation analysis and creation of section lines.*

1 DOCUMENTATION – TRUE TO SCALE IMAGE RECTIFICATION AND ORTHOGONAL PROJECTION

1.1 Definition of quality parameters - image scale / image resolution

The required detail resolution (pixel size at the object) is reliant on the image scale / resolution as well as the metric accuracy and has to be specified depending on the task on the object. So the subsequent user (architect, planner, conservator) can process their own

graphical / metrical evaluation and content interpretation in CAD or mapping software.



Fig. 1: Detail resolution depending on image scale 1:20, 1:50, 1:100 for 400 dpi image resolution

The required detail resolution is traditionally defined by image scale and resolution. For an image resolution of 400 dpi (400 points per inch = 25.4mm) the point size is 0.06mm. Multiplying the point size with the image scale provides the metric size of the pixel at the object, which means 0.06mm for scale 1:1, 1.3mm for 1:20, and 3.2mm for 1:50 (Fig. 1).

Sector Pixel size 400dpi Pixel size 200dpi Accuracy	**1:1** 0.06mm 0.13mm 0.5mm	**1:2** 0.13mm 0.25mm 1.0mm	**1:5** 0.32mm 0.64mm 2.5mm	**1:10** 0.64mm 1.3mm 5.0mm	**1:20** 1.3mm 2.6mm 1.0cm	**1:50** 3.2mm 6.4mm 2.5cm	**1:100** 6.4mm 12.7mm 5.0cm
architects/ consultant				x	x	x	x
building archaeology			detail	stone by stone detail	stone by stone	general overviews	
field archaeology			graves, other details	sections, elevations graves	plans		
Conservation	**1:1**	**1:2**	**1:5**	**1:10**	**1:20**	**1:50**	**1:100**
stone				x	x	x	
wall painting / stucco			x	x	x		
wood / objects archaeology		x	x	x			
wall painting / textile / paper	x	x	x	x			

Fig. 2: Overview for required detail resolution depending on application examples; Detail resolution (pixel size at the object) for 400dpi and 200 dpi; Evaluation accuracy depending on image scale (0,5mm x image scale); mural painting highlighted in red boxes [4]

The table shown in Fig. 2 displays evaluation scales, two quality levels (200 and 400 dpi) and the requirements for evaluation accuracy resulting from the image scale for different application examples. In general natural stone objects are processed for a scale 1:25 and 400dpi (1.6mm point size) or 1:50 and 400dpi (3.2mm point size), if lower quality is enough. For objects with higher levels of details or for sculptures a scale of 1:10 and 400dpi (0.6mm point size) is used.

1.2 Evaluation methods

Not every evaluation method is suited for each project. Dependent on the object surface (flat walls, vaults, ornaments) the suited method must be chosen.

2D image rectification allows mathematical transformation of 2D plane within the bundle of rays of one camera (central projection). The result is a true to scale image plan that allows measuring on one object plane.

An image can be rectified simply by geometry like rectangle, parallel lines (Fig. 3) or distance net. For complex objects, it is recommended to rectify images on the base of imported ground control points measured with totalstation.

In addition measuring of coordinates in the project based on CAD-drawing, image plan, ortho-projection is possible as well as the automatic image rectification of partial detail images by image matching.

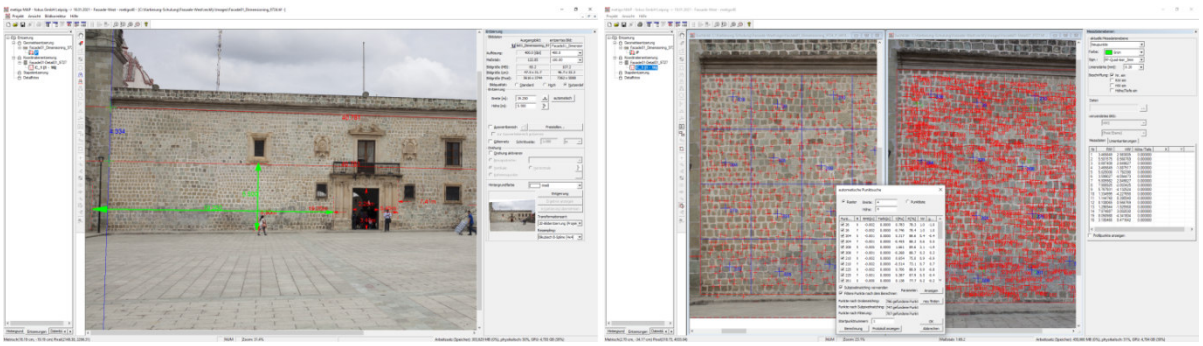


Fig. 3: Training course; left: image rectification by parallel line; right: automatic image rectification of detail with higher resolution by image matching; Palacio Municipal de Oaxaca de Juarez, Mexico

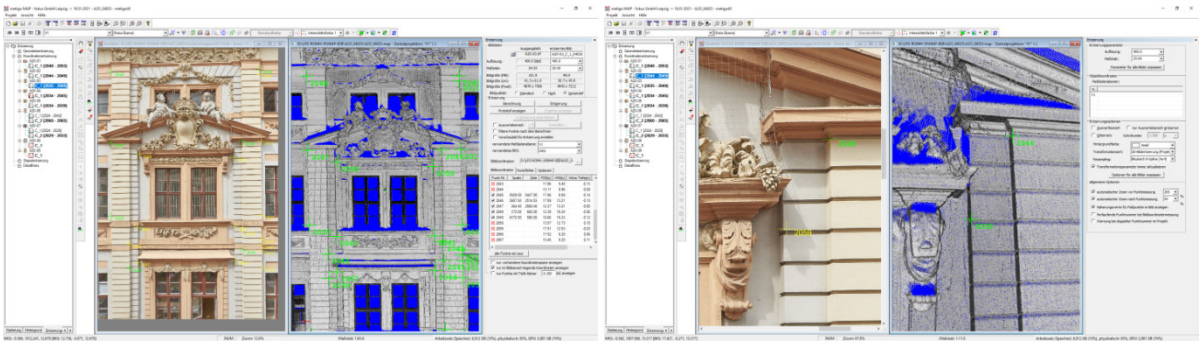


Fig. 4: rectification based on point cloud in two views; left: total image; right; detail from the image; Romanushaus, Leipzig, Germany

The **3D orthogonal projection** always assumes the 3D recording of the object surface. The 3D data (point-cloud, textured surface model) are projected orthogonally onto a reference geometry (plane, cylinder, cone) [2]. The creation of 3D data can be done by digital photogrammetry (Structure from Motion - SfM) or terrestrial laser scanning (TLS). The result is a true to scale image plan (orthophoto), which allows measuring on all planes PARALLEL regarding the reference geometry. The orthophoto can be calculated by a textured surface model or by the combination of an orientated image and an untextured surface model (Fig. 5).

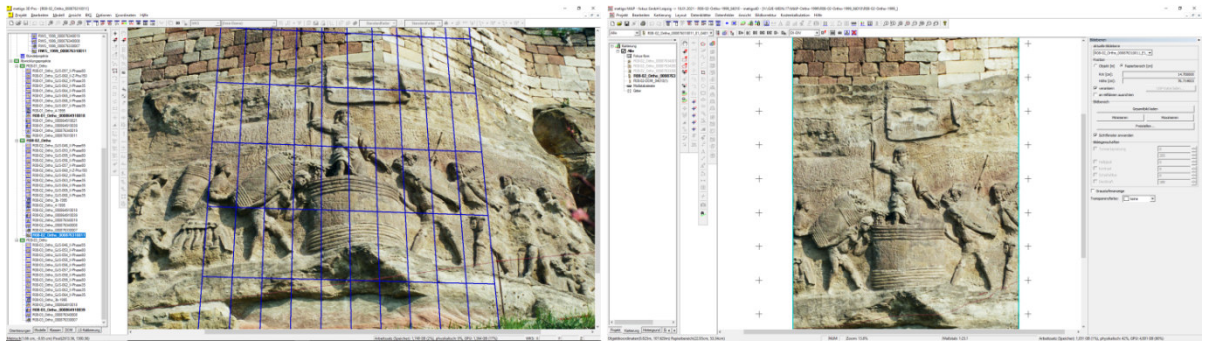


Fig. 5: orthogonal projection of an orientated image supported by a surface model; left: orientated image with projected plane; right: true to scale image plan in metigo® MAP; Stone Album, Großjena, Germany

3D object documentation is based on 3D recording of the object surface by point-cloud using TLS or SfM. In a second step the points are connected by triangulation to create a digital surface model (DSM). If necessary, the DSM is textured using orientated images. The result is a true to scale textured DSM that allows three dimensional measurements, creation of section and deformation analyses as well as creation of orthogonal projection onto several geometries.

For all these methods applies: A lack of good photography means a good result cannot be created. In our opinion, 2D-rectification is the cheapest method, which provides the highest image quality. 3D orthogonal projection is the most time expensive method, because images need to be orientated photogrammetrically and DSM need to be scanned or created by SfM.

2 PROJECT STRUCTURE – MAPPING PROJECT AND OBJECT HIERARCHY

The mapping software metigo® MAP has been developed since the year 2000 to create digital, vector-based mappings including mass calculation. The mapping software metigo® MAP offers functions for creation of true to scale documentation, digital mapping, analyses and quantity surveys.

2.1 Mapping project

The base for digital mapping are rectified images, CAD-drawings (DWG) or 3D-surface models (ortho-projection). For every topic (condition, material, measurement), a mapping class with a special type for area and line mapping, image and vector symbols or annotation and dimensioning have to be defined. Different mapping classes can be grouped within a mapping project to turn several mapping themes (e.g. conditions and damages, planning of measurements and invoicing) on or off.

For the final layout of the plans, there are several documentation classes like grids, scale bars, auxiliary lines and legends with integration of quantity surveys and analysis. (Fig. 6).

The extended group management is useful for the repeated use of class sets (loan, excavation layers, project phases). This structure of a mapping project (classes, groups, attributes, legends, title blocks etc.) can be reused in subsequent projects (import/export).

Areas and lines can be drawn with different vector based mapping tools like polygons and free hand lines, beziér lines (splines) and arcs, rectangles and circles, circle arc, as well as dimensioning functions for lengths and heights. Areas can be filled transparently.

For editing lines, there are different CAD-commands such as extend, trim, align, mirroring and different modes for object snap. For editing outlines of adjacent areas and the integration of inclusions, there are several intersection functions. A large library with hatchings, line types, image and vector symbols as well as colour tables enables the user to define layouts of mapping classes. The user interface can be set up easily for work in office as well as for work on mobile mapping with tablet PC on site.

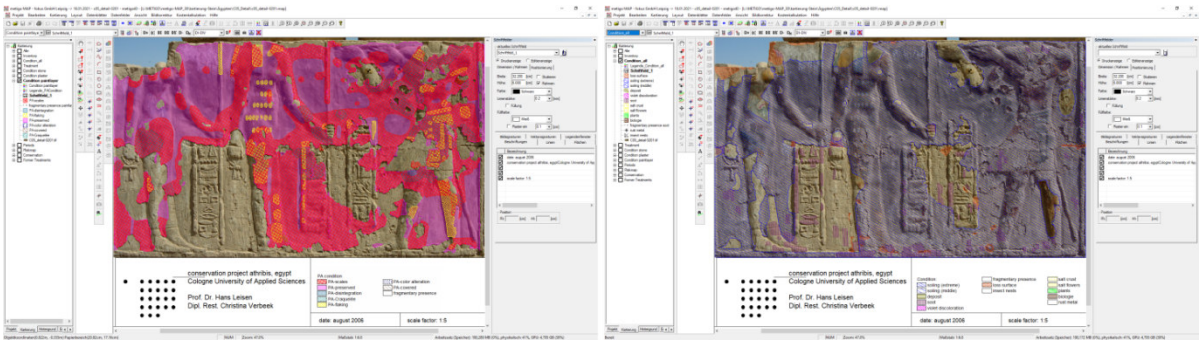


Fig. 6: Different groups of the same mapping project with legend; temple of Athribis at Sohag, Egypt;Mapping: Sabine Krause, Cologne.

Every element can be sorted according to size ranges within a mapping class. Mapping activities, quantities and attributes within a class can be analysed visually or related to another class (stone, material ranges, scaffolding layers, project phases).

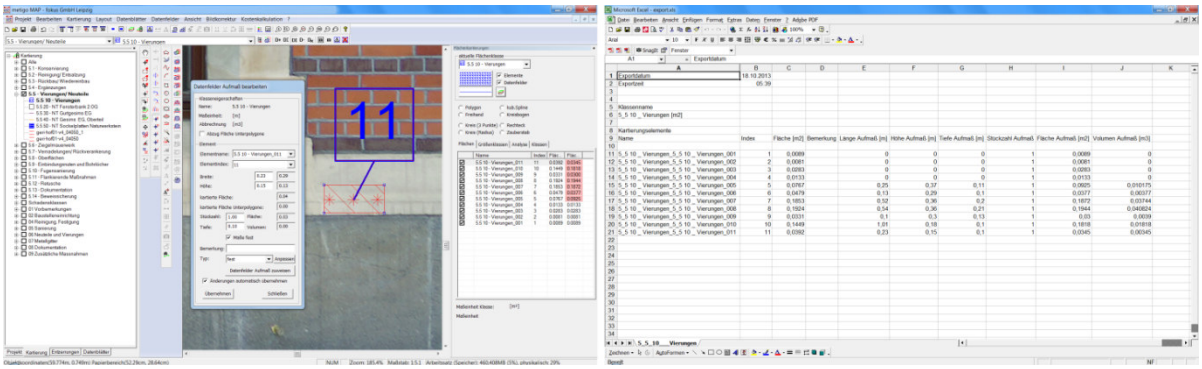


Fig. 7: left: Mapping with manual measurement; right: Quantity export to spreadsheets; District Court, Zwickau, Germany; Mapping: Jens Kaminsky, Plauen.

metigo® MAP allows a user management for analysing the mapping history (querying users, creation and modification dates) as well as a rights management to protect mapping elements of third parties (e. g. loan systems, project phases).

Several approaches for computing areas (mapped polygon, bounding box, manual measurement) are available and individual attributes for recording of object properties (measurements, findings, technological information of the measure) can be used.

Quantity tables can be exported sorted by classes or groups (CSV, MS Excel, Open Office) (Fig. 7). The mapping can be exported in a true-to-scale image (TIFF, multi-layer-TIFF) or CAD-file (DWG) as well as print-out and PDF-file (external PDF-printer).

2.2 Object hierarchy

The object hierarchy offers the management and adjusting of several mapping projects in one object. Therefore a central mapping project with mapping classes, groups, attributes, legends and title blocks is used as mapping template. Each mapping project within an object hierarchy is connected to that template. A later modification, e.g. of colours or names, can be transferred automated on the involved mapping projects.

The hierachy allows the output of quantity tables across projects (CSV, MS Excel, Open Office). The project comprehensive usage of title blocks with variable entries reduces time for creation of title blocks. The user can navigate in object hierarchies via project tree or navigation maps. Using navigation maps, he can execute visual quantity analysis of mapping contents and project attributes (Fig. 8).

The class analysis via complete object hierarchies (mapping contents, class and group structure) allows also the resolving of similar class names, wrong class types or duplicates.

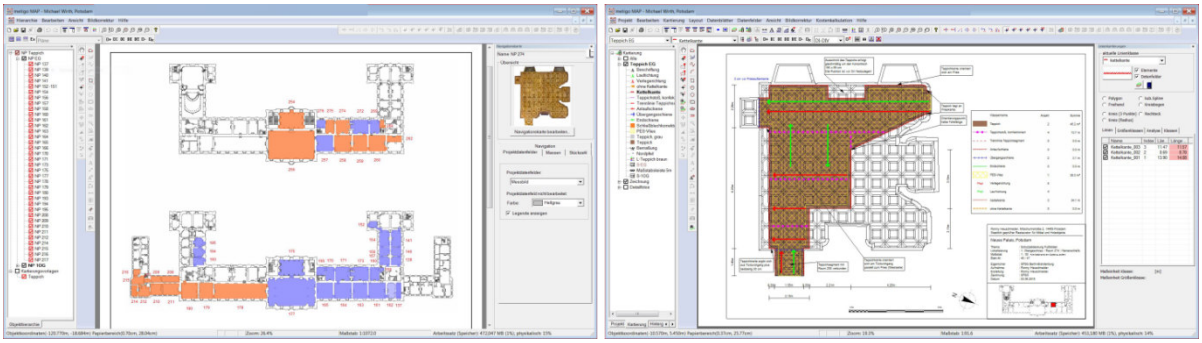


Fig. 8: left: Navigation map coloured by project attribute; right: Mapping of measures for floor of room 274; New Palace, Potsdam, Germany; Mapping: Michael Wirth, Potsdam, SPSG.

3 CURRENT RESULTS FROM THE R&D PROJECT „PROQUATO“

The main usage of the mapping software is currently mapping on the base of two dimensional mapping bases. Current development tasks for 3D evaluation are described in the chapters 3 and 4. In the R&D project PROQUATO (“process optimization, quality enlargement and evaluation tools for multi textured surface models”) requirements for 3D mapping were analysed and developed in cooperation with the clients from 2016 to 2018.

3.1 Data import

metigo® MAP allows the import of textured surface models in VRML- and OBJ-format or without texture (STL). For mapping, a mesh made of triangles is always required. The import window (Fig. 9, left) allows the insertion of a scaling factor for true to scale import of surface models. Later scaling inside the mapping project is not possible.

Free navigation is possible within the 3D display. Within 2D display of model views (orthogonal projections), the image data is reduced to the set project scale and resolution.
If the textured surface model was created within a defined coordinate system, the congruent combination of orthogonal projection with existing CAD plans is possible (Fig. 10).

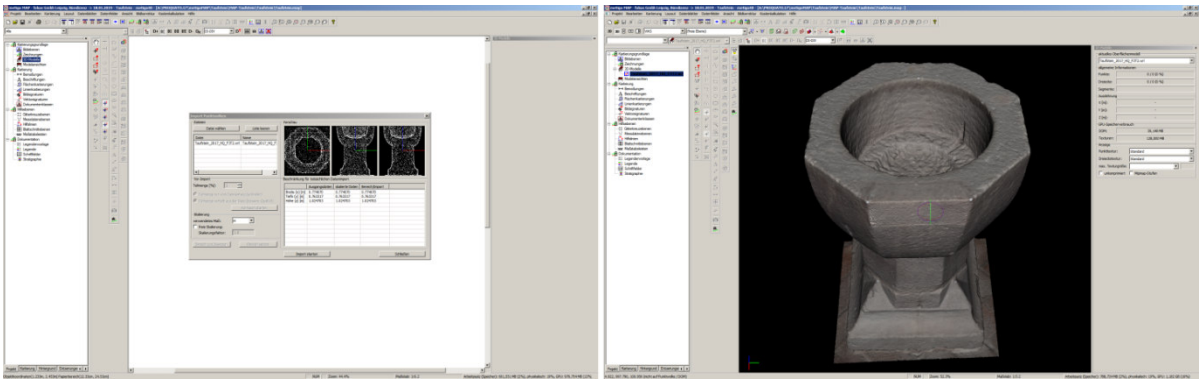


Fig. 9: left: Import window for surface model in STL-, VRML- and OBJ- files with insertion of scaling factor and unit; right: 3D display of textured surface model; Baptismal font, church Kuehren, Germany

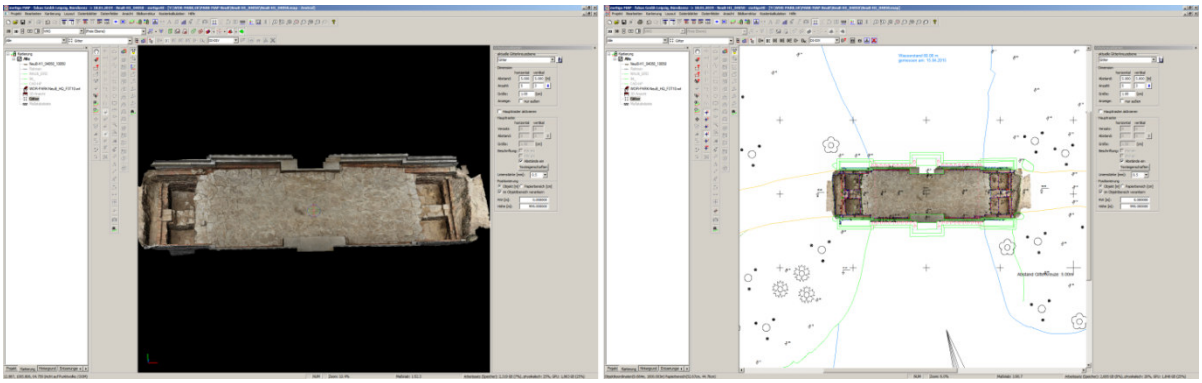


Fig. 10: left: 3D display of textured surface model of an exposed bridge construction; right: combination of drawing with ortho projection; New Bridge, Woerlitzer Park, Dessau-Wörlitz Cultural Foundation, Germany

3.2 Combination of several surface models into one coordinate system

In general, the 3D data is displayed through OpenGL via the graphic card. That means the performance of the 3D display predominantly relies on the characteristics of the graphic card. If the hardware is powerful enough, several models within one coordinate system can be evaluated together.

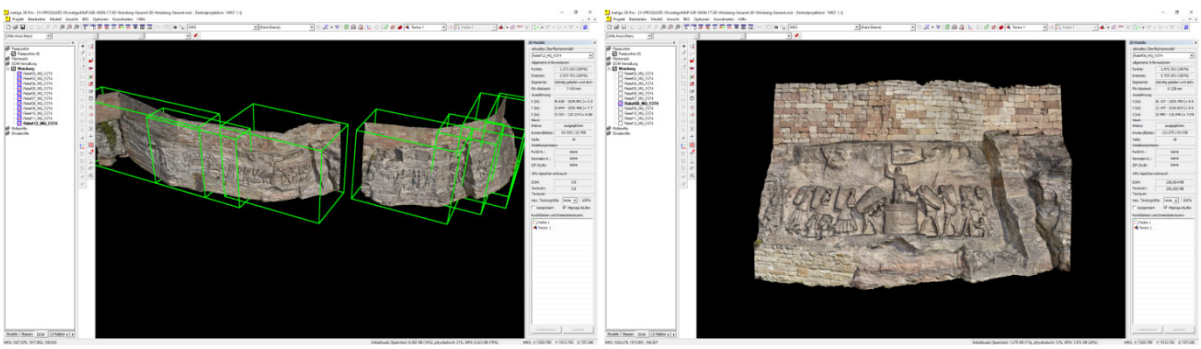


Fig. 11: Mosaic of several textured surface models of one object within one coordinate system, left: Every surface model is displayed with its bounding box (green); right: Single textured surface model; Stone Album, Großjena, Germany

3.3 Evaluation of complex surface models by model segmentation

If the surface model is too big for the used hardware, it is possible to evaluate only segments of the complete surface model. Segmentation allows partial loading of the surface model (Fig. 12). At the start the user can load the surface model in reduced resolution as complete point cloud to define segments, e.g. single parts of a façade. Later, only the required segments need to be loaded.

For complex objects such as sculpture, it is useful to create individual segments e.g. for arms, legs, hands, because it is easier for navigation and makes evaluating obstructed areas (e.g. between an arm and the torso) much easier.

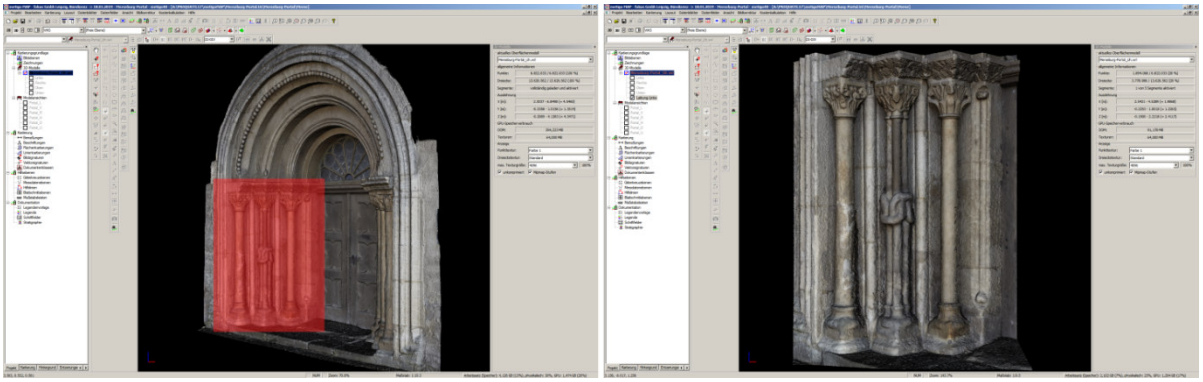


Fig. 12: left: 3D display with selection of a new segment; right: 3D display of the new segment;Portal, Neumarktkirche St. Thomae, Merseburg, Germany

3.4 Drawing modes for 3D mapping

Using the 3D polygon mode, 3D lines can be mapped as well as 3D areas. Therefore, the drawn polygon is intersected with the surface model and the result stored as individual 3D object (Fig. 13). Cutting tools for area mapping are available like in 2D mapping. They enable a later extension or reduction of mapped areas as well as the custom-fit cutting of adjoining areas. Additionally vector symbols or text elements can be used. Border lines and transparent area fillings can be shown in the 3D display. Hatching is visible in 2D / 3D views (Fig. 14).

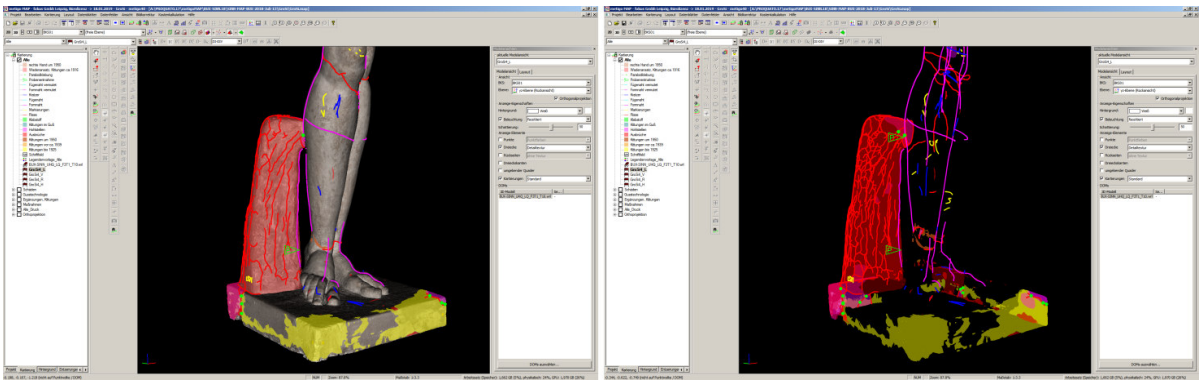


Fig. 13: 3D display; left: textured surface model and mapped elements; right: 3D mapped elements without surface model; Große Sinnende, Wilhelm Lehmbruck, Staatsgalerie Stuttgart; Mapping Peter Bux, Leipzig

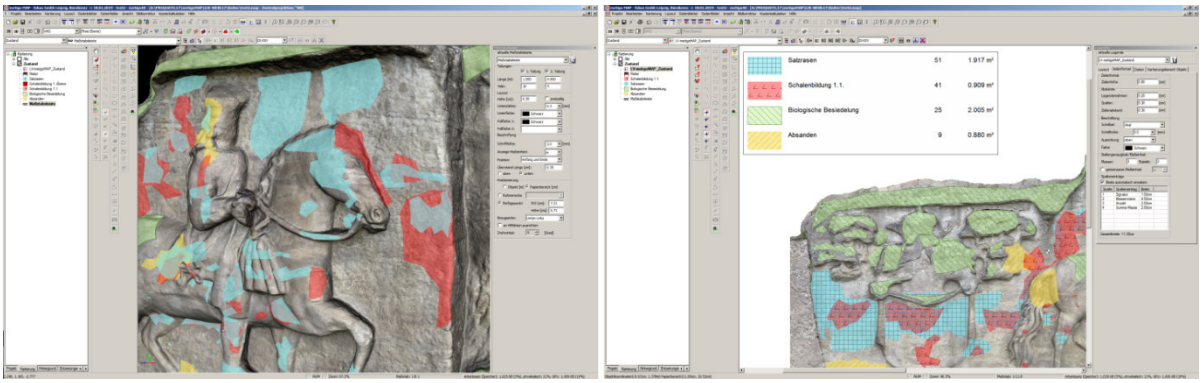


Fig. 14: left: 3D display of area mapping with transparent filling; right: Hatching on 2D model view with orthogonal projection and legend; Stone Album, Großjena, Germany; Mapping: Benjamin Huebner, Potsdam

3.5 Printing with the help of 2D model views

A true to scale 2D model view of the chosen 3D display can be created to be used for 2D printouts (Fig. 15). Display options like texture quality, shading, scale and position as well as projection mode (orthogonal/perspective) can be set up.

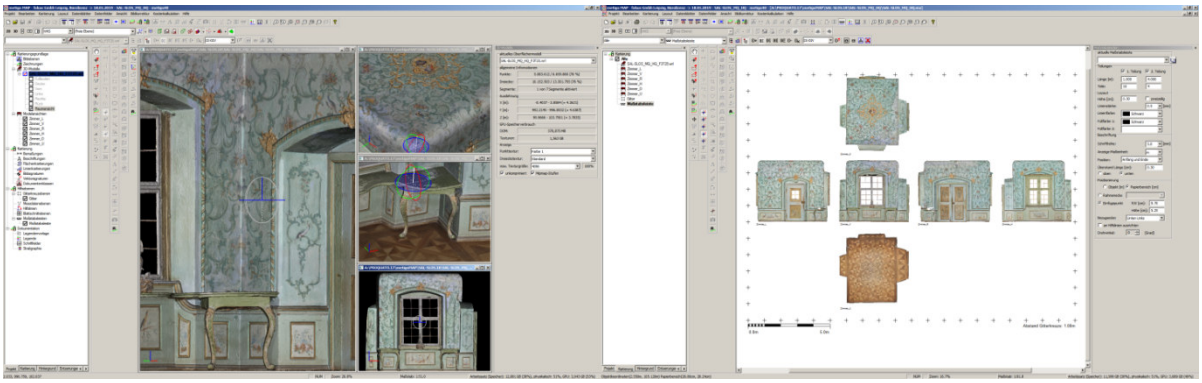


Fig. 15: left: 3D display of textured surface model of the room; right: true to scale inside unwrapping of 6 model views with orthogonal projection; Abbot's quarters, Castle Salem, Salem, Germany

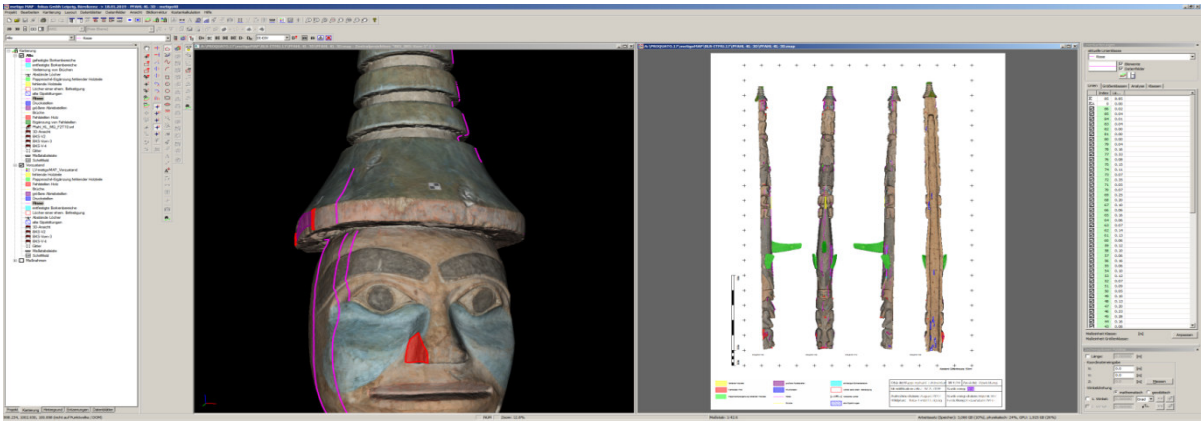


Fig. 16: left: textured DSM of the totem pole with mapping; right: True to scale unwrapping of 4 model views with orthogonal projection; Totem Tshimshian, Ethnological Museum, Berlin; Mapping: restauratum ArGe

Automated creation of "model view unwrapping" (inside/outside; 4 or 6 orthogonal views) allows a complete display of the object (Fig. 15, 16). The plan can be completed by inserting grid crosses, scale bar and title block. The 3D display can be controlled like the 2D model views, using mapping groups and group legend (Fig. 16). The true to scale printing or image output is carried out in the same way as 2D mapping. Currently the 3D mapping can only be passed on as complete mapping project with a free viewer.

Quantity measurement is determined automatically based on the true to scale surface model. So the amount, length and areas of mapped elements are calculated immediately and the sum can be shown within the legend for each class. If the total amount of the object is mapped, the mass fraction for each area mapping class can be shown in the legend (Fig. 17)

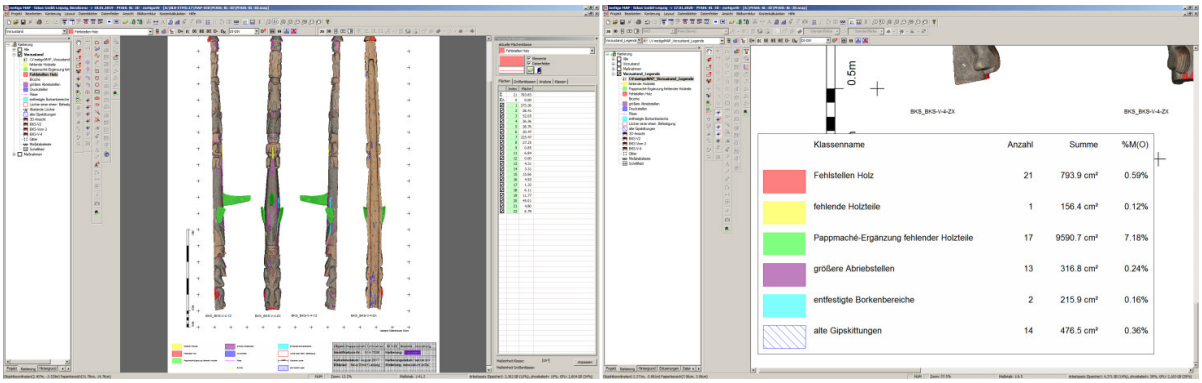


Fig. 17: left: 3D display of textured surface model of the totem pole with mapping; right: legend of the mapping including the quantity survey; Totem Tshimshian, Ethnological Museum, Berlin, Germany

4 LASERSCANNING – 3D DATA EVALUATION

Laser scanning is the line-scanning of object surfaces with a laser beam in order to measure it three-dimensionally. The result is a three-dimensional point cloud grey scaled depending on reflection intensity. With additional camera shots, the dots can also be coloured with real object colour. With a suitable orientation software, the individual point clouds are automatically oriented in a uniform coordinate system. The so oriented point clouds can be used as base for CAD-evaluation of floor plans, sections and elevations.

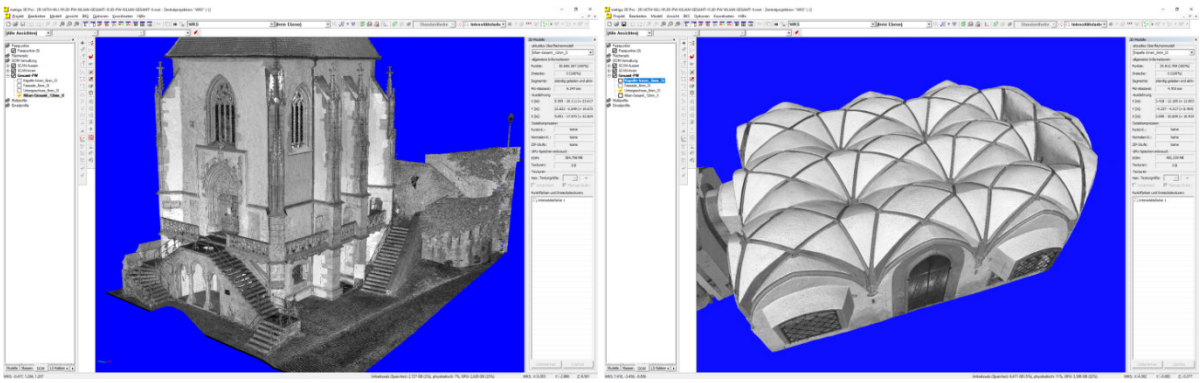


Fig. 18: left: 3D view of the complete point cloud; right: 3D view of the basement; St. Killian's Chapel, Wertheim upon Main,

4.1 3D data processing

In metigo® 3D software, the oriented point clouds of the individual scanner positions can be merged to an object point cloud / complete point cloud with a defined point distance. The quality of the resulting point cloud can be controlled by using functions to filter noise depending on intensity, position or recording angle (Fig. 18).

4.2 3D data evaluation

To evaluate 3D data the complete point cloud is needed within metigo® MAP. Point clouds can be imported in a metigo® internal format (*.SHP) or standard formats like E57, PTS, PTB. Selection polygons can be used to create partial point clouds as base for creation of orthogonal projections. Settings for shading, lighting and closing of holes in the orthogonal projection allow the quality enhancement of the final result (Fig. 19).

Defining user coordinate systems section lines with a tolerance distance can be extracted from the point cloud automatically. These section lines can be used for the creation of CAD drawing in 2D or 3D (Fig. 20).

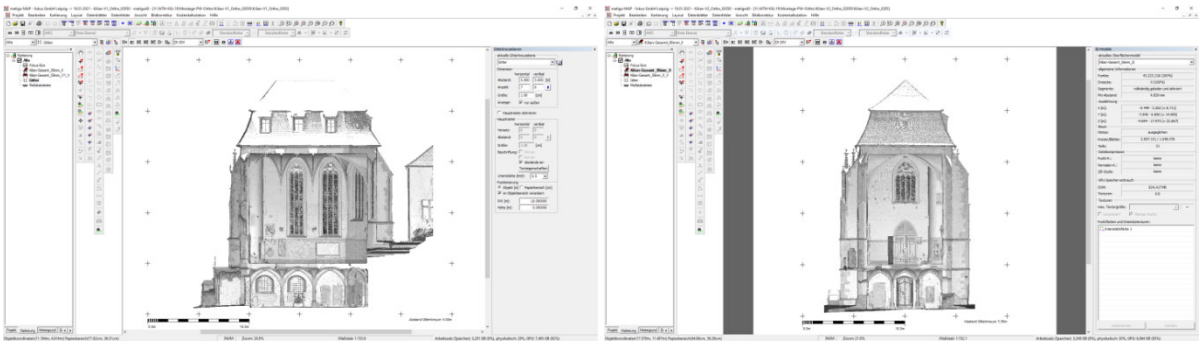


Fig. 19: Different Ortho-projected sections of the point cloud (left: longitudinal; right: latitudinal); St. Killian‘s Chapel, Wertheim upon Main,

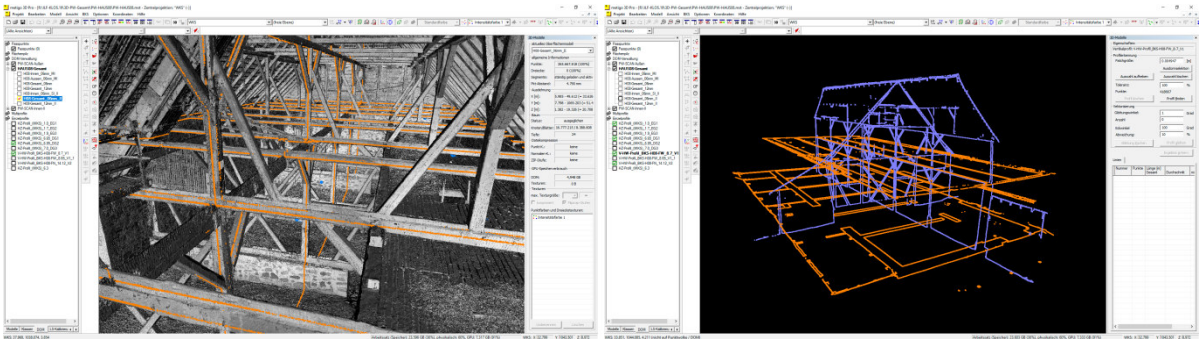


Fig. 20: Ilfeld, Priory Manor.3D laser scanning, detailed survey of plans and sections. left: 3D view of the complete point cloud with coloured section planes (longitudinal and horizontal section); right: 3D view only of the coloured section planes; monastery estate, Ilfeld, Germany

5 SUMMARY

The procedures described allow the true to scale documentation on the base of 2D or 3D data, assuming the quality of the 3D data is sufficient to the object requirements. In this way several 3D documentation projects have been processed. But in our experiences there is often a lack of accuracy and detail resolution – image texture or the point cloud – especially if the 3D data is used as working base in conservation documentation. Many 3D documentation results are created currently by third parties, that have no information or knowledge about the needed requirements.

The software metigo® MAP is developed in the past 20 years in close cooperation with our customers to their special needs – at the beginning in the field of digital 2D mapping and later in quantity survey and data analyses. In future there will be additional developments in the field of 3D evaluation, depending on the needs of our users. So the step from two dimensional to three dimensional evaluation is now possible, depending on the quality of the 3D data, the requirements of the project and the existing hardware.

REFERENCES

[1] Siedler, G. and Sacher, G.: Photogrammetrische Auswertung historischer Fotografien und Messbilder. In: Führerauftrag Monumentalmalerei, Veröffentlichungen des ZIKG, Band XVIII, 2006, Böhlau Verlag GmbH & Cie, S.189-198.

[2] Vetter, S. and Siedler, G., Automated 3D-object documentation on the base of an image set. 13. International CIPA Symposium, Prag (Tschechische Republik), 2011

[3] Siedler, G. and Vetter S., Modern Methods of documentation – Photogrammetric evaluation of historic images. ICOM CC - Interim Meeting of the Wood, Furniture, and Lacquer & the Sculpture, Polychromy, and Architectural Decorations Working Groups in Potsdam, Germany, 2016

[4] Siedler, G. and Vetter S., Qualitätskriterien bei der Ausschreibung von photogrammetrischen Leistungen. Natursteinsanierung Stuttgart 2018 – Neue Natursteinrestaurierungsergebnisse und messtechnische Erfassungen sowie Sanierungsbeispiele, Stuttgart, Germany, 2018

[5] Luhmann, T., Nahbereichsphotogrammetrie – Grundlagen, Methoden und Anwendungen. Verlag für Bauwesen, Berlin, Germany, 1978

[6] W. Pietschner, J. Regensburger, K. Rüger, Photogrammetrie. Verfahren und Geräte. Herbert Wichmann Verlag, Heidelberg, Germany, 2003

[7] Brumana R. and Galeazzo, G.; St. Marcus' Basilica in Venice. An apply of image projection on a dome. XVII ISPRS Congress Technical Commission V: Close-Range Photogrammetry and Machine Vision, page 786-793, Washington, D.C., USA, 1992

[8] Stephani, M.; Object Modelling and Visualization in Architecture. XVII ISPRS Congress Technical Commission V: Close-Range Photogrammetry and Machine Vision, page 821-824, Washington, D.C., USA, 1992

All shown examples are documentation projects processed by fokus GmbH Leipzig, otherwise the author is named in the belonging caption.

12th International Conference on Structural Analysis of Historical Constructions
SAHC 2020
P. Roca, L. Pelà and C. Molins (Eds.)

DYNAMIC IDENTIFICATION OF DAMAGE IN BRICK MASONRY WALLS

S. IVORRA[1], D. BRU[2], I. GISBERT[3], FJ.. BAEZA[4], B.TORRES[5] D. CAMASSA[6]

[1]Department of Civil Engineering. Universidad de Alicante
Carretera San Vicente, S/N, 03690 San Vicente del Raspeig (Alicante), Spain
e-mail: sivorra@ua.es, web page: http://www.ua.es

[2] Department of Civil Engineering. Universidad de Alicante
Carretera San Vicente, S/N, 03690 San Vicente del Raspeig (Alicante), Spain
e-mail: david.bru@ua.es, web page: http://www.ua.es

[3] Department of Civil Engineering. Universidad de Alicante
Carretera San Vicente, S/N, 03690 San Vicente del Raspeig (Alicante), Spain
e-mail: ignacio.gisbert@ua.es, web page: http://www.ua.es

[4] Department of Civil Engineering. Universidad de Alicante
Carretera San Vicente, S/N, 03690 San Vicente del Raspeig (Alicante), Spain
e-mail: fj.baeza@ua.es, web page: http://www.ua.es

[5] Department of Civil Engineering. Universidad de Alicante
Carretera San Vicente, S/N, 03690 San Vicente del Raspeig (Alicante), Spain
e-mail: Benjamin.torres@ua.es, web page: http://www.ua.es

[5] Department of Civil Engineering Sciences and Architecture. Politecnico di Bari
Via Re David, 70125 Bari, Italy
e-mail: domenico.camassa@poliba.it, web page: http://www.poliba.it

Keywords: OMA, Masonry, Monitoring, Non-Destructive Inspection

Abstract. *This paper shows the experimental and numerical analysis developed on a brick masonry wall of 3x2.5x0.2 m to understand the changes on its dynamic behaviour with different stiffness situations: (i) original, (ii) loaded with different load levels, (iii) damaged by horizontal in plane loads, (iv) retrofitted with Textile Reinforced Mortars (TRM) and (v) retrofitted and damaged by horizontal in plane loads. This analysis has been developed at the Civil Engineering Lab at the University of Alicante. On this masonry wall a matrix of 8 seismic accelerometers have been installed to evaluate, in plane and out of plane, changes in the main frequencies, modal damping ratios and modal shapes. By the use of Operational Modal Analysis techniques the results shows that the changes on the stiffness have important influence on the main frequencies and in the modal damping ratios. Very low influence have been detected on the modal shapes due to the low level of external vibrations generated during the tests. Due to the low level of vibrations inside the lab,the classical*

application of ambient vibrations for OMA has been not possible and an external white noise force has been introduced on the top the wall by the use of a shaker to generate a general level of vibrations on the specimen.

1 INTRODUCTION

Masonry walls are a traditional structural system used in many buildings, and it can be found today as the constructive solution for new buildings. However, these elements show a brittle behavior for in plane and out plane loads, especially for seismic or dynamic loads [1]. In particular, the more usual failure modes for in plane loads are toe crushing, rocking, diagonal cracking or sliding [2]. In case of out of plane loads, these elements shows a very slow bending strength. Different reinforcement techniques can be used to improve the in plane and out plane behavior of the masonry walls. Fiber reinforced polymers (FRP) has been used for different authors such as [3]. However, these solutions show problems related with the contact between them and the masonry. Other solution is the textile reinforced mortar (TRM) [4]. These materials show a better compatibility with masonry and avoid problems related to debonding or permeability issues.

The main objective of this research is the evaluation of the TRM reinforcement for dynamic loads. In particular, changes in the vibration frequencies, modal shapes, and damping factor [5] have been evaluated by means of OMA (Operational modal analysis), before and after the reinforcement process.

2 MASONRY WALLSAND REINFORCEMENT MATERIAL

A scaled masonry wall, was built at the Civil Engineering Laboratory in the University of Alicante (Alicante, Spain) with the aim of assessing the general structural behavior for shear forces and dynamic loadas. In particular, the cracking pattern and the changes in modal parameters as damping, frequencies and modal shapes has been evaluated. Figure 1 shows the general view of the building.

The masonry walls were constructed using clay bricks laid by means of 10 mm thick lime mortar joints adopting an English bond disposition. Table 1 shows the dimensions and compression strength of bricks and the mean compression strength of lime mortar at 28 days and 100 days (days in which tests, described later, were performed). The total dimensions of each wall is 3x2.5x0.2 m.

Table 1. Geometric characteristics and compression strength of bricks and lime mortar.

Bricks		Lime mortar	
Dimensions [mm]	230 x 110 x 50	Compression strength at 28 days [MPa]	4.25
Compression strength [MPa]	13.99	Compression strength at 100 days [MPa]	5.98

Foundations were prepared for constrain displacements with the use of steel plates and anchors to the main concrete slab of the laboratory, Figure 1. In addition, the building might have connected at the top of the lateral walls to a servo-hydraulic jack by means of a steel beam supported by props. Dimensions of the walls, its disposition and experimental set-up are shown in Figure 1. By the use of some steel elements the wall was preloaded with a compression load of 300 kN to simulate the weight of the structural elements in a real situation. With this preload, to generate damage on the wall, a cyclic incremental pushover load the top of the wall to achieve the complete cross crack pattern due to shear forces.

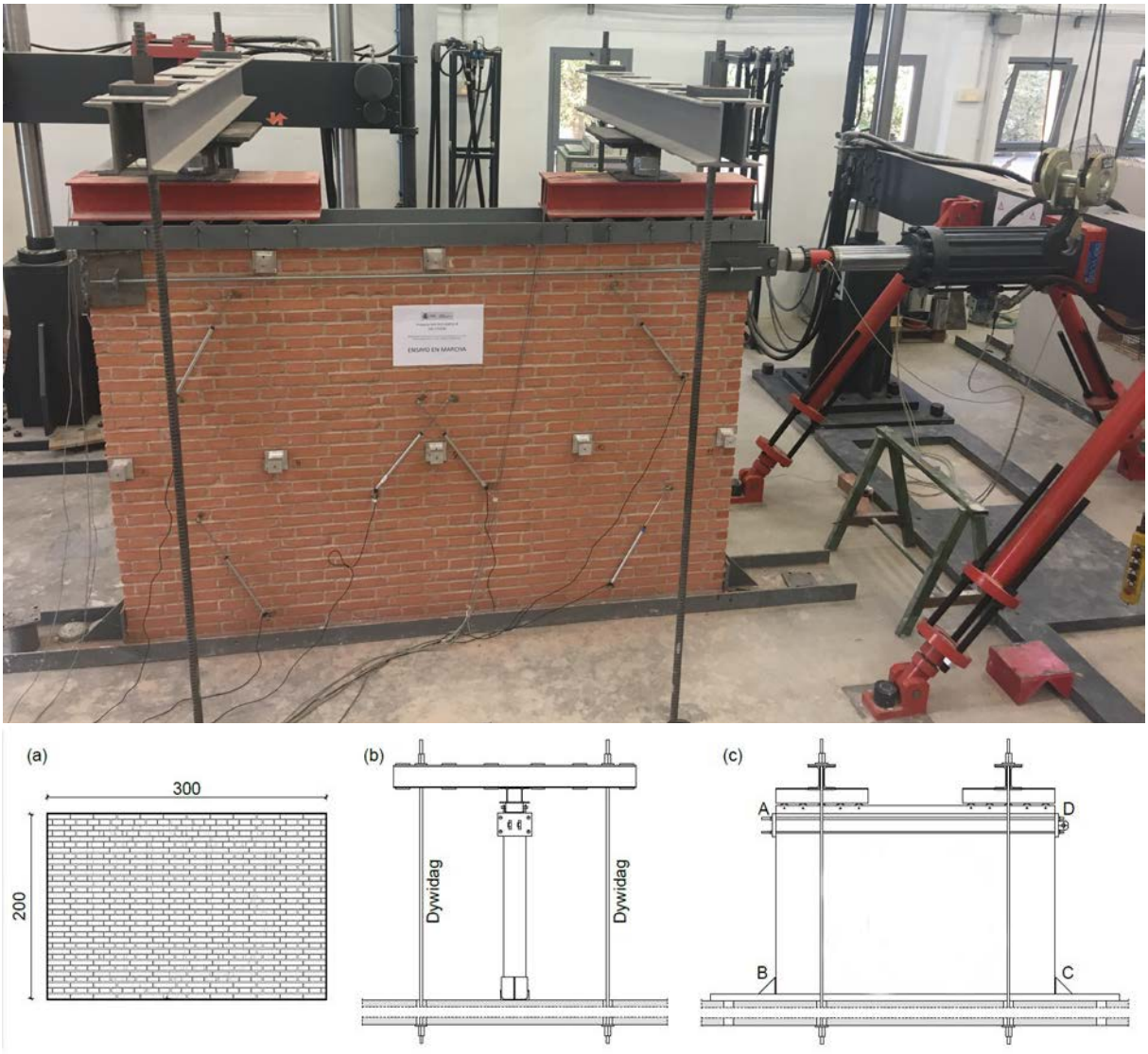


Figure 1. General view of sensors location, anchorage system, preload device and jack for the horizontal loads

Once the tests were performed, specimens have been reinforced with Textile Reinforced Mortar (TRM) materials. On the one hand, the cracks have been sealed with semiliquid mortars. On the other hand, the wall was reinforced with TRM with the aim of evaluating the efficacy of

cementitious-based strengthening to: (i) improve the seismic behavior of masonry structures, and (ii) avoid a seismic-induced premature failure of poor-quality masonries. The adopted TRM retrofitting technique comprised a 25x25 mm glass textile grid embedded into a 10 mm thick cementitious layer applied along the outer face of the overall building (Figure 2). Table 2 shows the mechanical properties of the reinforced material used in this research.

Table 2. Mechanical properties or reinforced materials.

Mortar		Textile mesh	
Compression strength at 28 days [MPa]	15	Tensile strength [kN/m]	45
Elastic modulus [MPa]	8000	Elastic modulus [MPa]	72000

When this kind of reinforcement is applied on damaged structures, it comprises different steps. Indeed, the masonry support was preliminarily treated injecting the wider cracks (Figure 2.a) to restore the original load bearing capacity of the damaged masonries. Then, a 5 mm thick cementitious layer was applied on the outer face of the walls (Figure 2.b). This layer is necessary to allow the bond between the masonry support and the glass textile grid (Figura 2.c). It is worth mentioning that, conversely to FRP composites, TRM materials allow to comply with the current requirements of compatibility and reversibility of the retrofitting with respect to brittle supports due to the presence of a mortar matrix instead of an epoxy one [6]. Finally, the glass grid was covered with a second 5 mm thick layer of the cementitious binder (Figure 2.d). The layers composing the TRM composite adopted in the present investigation are showed in Figure 2.



(a)



(b)



(c)



(d)

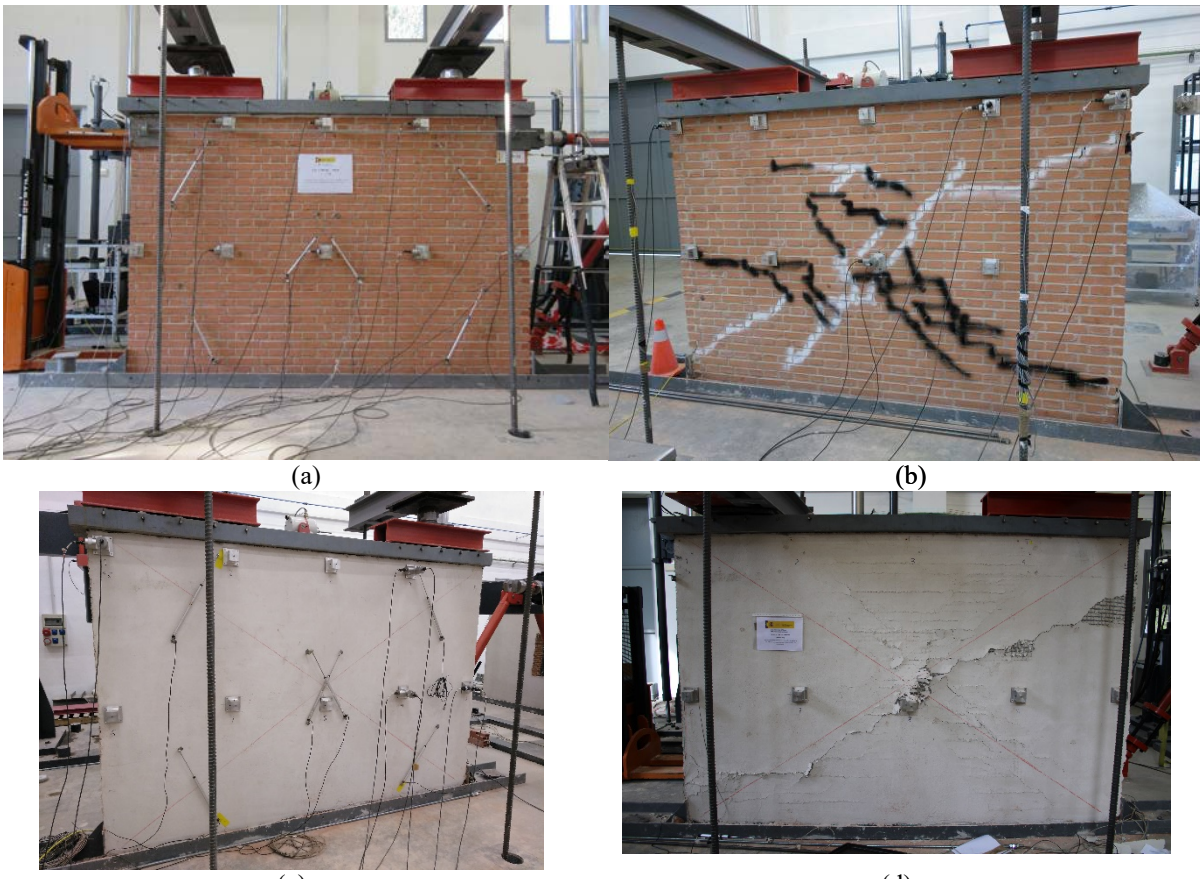
Figure 2. (a)- Injection the wider cracks. (b)- 5 mm thick cementitious laye applied on the outer face. (c)- Application of the glass fiber mesh. (d)- Reinforced masonry wall.

3 MONITORING AND DESCRIPTION OF THE MODAL ANALYSIS

The methodology for dynamic identification has been divided in four phases: (i) Unreinforced pre-damage; (ii) Unreinforced post-damage; (iii) Reinforced pre-damage; (iv) Reinforced post-damaged. White noise vibrations has been registered during all phases with a sampling frequency of 2000 Hz. Three records of 300 s have been done in each phase, and the mean values have been used. For data acquisition, 8 piezoelectric accelerometers of sensitivity equal to 10 V/g have been employed. They were located according to Figure 2. Signals have been registered using a data acquisition device model Kyowa PCD-320 and signal conditioner model PCB 482A22.

With the aim to introduce a general damage distribution, similar to the seismic loads, a cyclic load with increasing amplitude of the displacement from 0.2 mm to 12 mm has been used, like a cyclic pushover tests. The horizontal load has been applied by means of a hydraulic jack with a displacement load control. In this paper the results showed are related with the initial phases previously to the damage and the final phases after the full damage procedure. It is important to note that the reinforced building is the unreinforced building repaired after all the damage phases.

Finally, Operational Modal Analysis (OMA) was used to analyze the vibration frequencies and the damping factor. The technique used is the Enhanced Frequency Domain Decomposition (EFDD), according to the Artemis software.



(a) (b)

(c) (d)

Figure 2. General view of sensors location; (a) Undamaged (b) Damaged (c) Retrofitted with TRM (d) Retrofitted with TRM – Damaged.

4 RESULTS

In case of the unreinforced wall, a classical crack pattern (Figure 2) arose with increasing damage. In particular, a well-defined diagonal crack (white crack) and some diffused cracks (black cracks) appeared. As it can be seen in Figure 2, the cracks mainly follow mortar joints, except in some points where it cross one or more bricks.

Regarding operational modal analysis, the first three vibration modes have been identified. The Figure 3 shows a typical Singular Value Plot, in a value range from 0 to 50 Hz, obtained through the EFDD technique. The estimated natural frequencies and damping ratios are shown in Table 3 and the mode shapes are represented in Figure 4. The first two vibration modes are out-of-plane modes, the third is an in-plane mode. For each identified vibration mode, the natural frequency decrease and the damping ratio increase due to damage. In particular, a reduction of natural frequency equal to 21.14%, 22.04% and 57.15% and an increase of damping ratio equal to 10.11%, 69.94% and 12.04% have been evaluated respectively for the first, the second and the third mode. Finally, in order to evaluate the changes in mode shapes due to damage, the Modal Assurance Criterion (MAC) has been used.

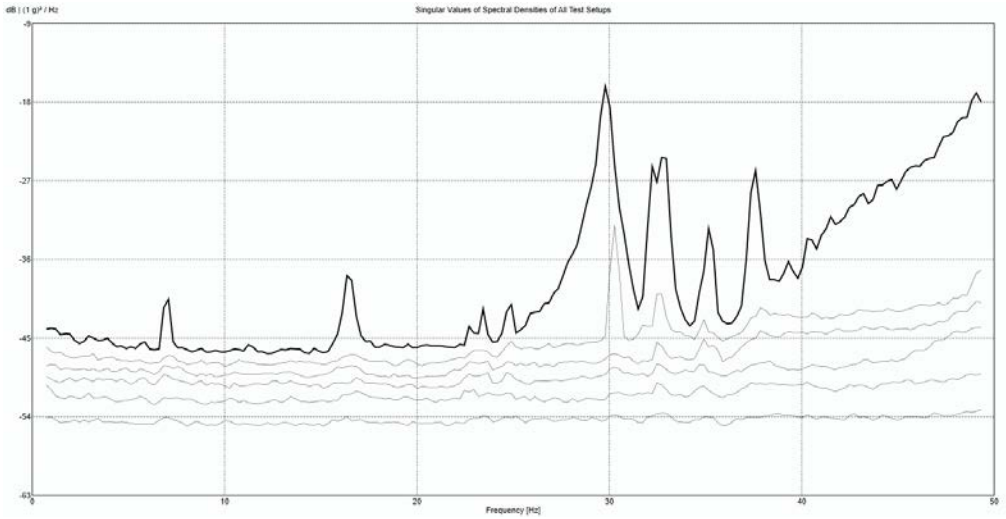


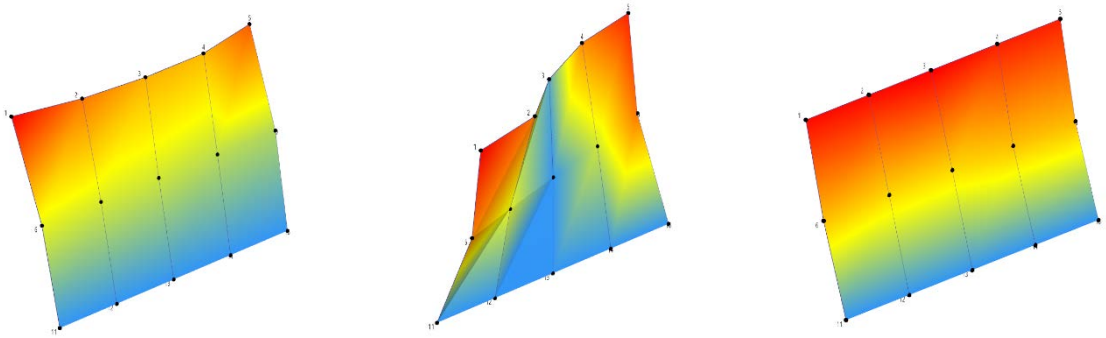
Figure 3. Typical Singular Value Plot obtained by processing acceleration data of the wall through the EFDD technique.

The reduction of natural frequency due to damage indicates a reduction of wall stiffness. Moreover, the increase of damping ratio suggests an increase of energy dissipation due to material friction along the cracks. It is worth noting that, since the greatest frequency reduction corresponds to the third mode, the damage has mainly affected the in-plane stiffness. Moreover, the MAC values reported in Table 4 suggest that the damage mainly affects the mode shape of the second vibration mode.

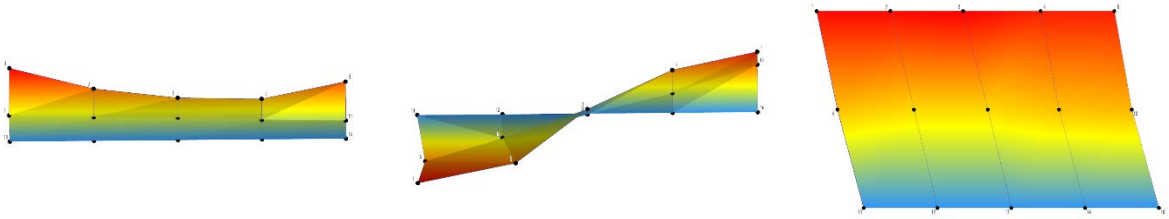
Table 3: Estimated natural frequencies and damping ratio for unreinforced pre/post-damage wall.

Pre-damage		Post-damage	
Frequency (Hz)	Damping (%)	Frequency (Hz)	Damping (%)
4.953	2.957	3.906	3.256
12.394	1.221	9.662	2.075
22.357	1.570	9.580	1.759

4.953 Hz **12.394 Hz** **22.357 Hz**



(a) **(b)** **(c)**



(d) **(e)** **(f)**

Figure 4. Frequencies and mode shapes for the unreinforced pre-damage wall. General view: (a), (b), (c), (d). Plan view: (e), (f), (g). Front view: (h).

Table 4: MAC values between unreinforced pre and post damage wall.

Frequency (Hz)	**4.953**	**12.394**	**22.357**
3.906	0.891	0.022	0.039
9.662	0.044	0.728	0.010
9.580	0.000	0.016	0.929

Figure 2 shows the crack distribution for the reinforced wall. The damage configuration appears very similar with the unreinforced case, but less severe.

Regarding operational modal analysis, the first three vibration modes have been identified. The estimated natural frequencies and damping ratios are shown in Table 5 and the mode shapes are represented in Figure 5 The first two vibration modes are out-of-plane modes, the third is an in-plane mode. As in the unreinforced case, for each vibration mode, the natural frequency decrease and the damping ratio increase due to damage. In particular, a reduction of natural frequency equal to 25.47%, 31.84% and 52.22% and an increase of damping ratio equal to 22.10%, 34.62% and 82.75% has been evaluated respectively for the first, the second and the third mode. The MAC values are reported in Table 6.

As in the unreinforced case, the results suggest that the mode shape of the second vibration mode was the most affected by the damage and that the third mode (in-plane mode) shows the greatest reduction of modal stiffness.

Table 5: Estimated natural frequencies and damping ratio for reinforced pre/post-damage wall.

Pre-damage		Post-damage	
Frequency (Hz)	Damping (%)	Frequency (Hz)	Damping (%)
6.992	2.339	5.211	2.856
16.475	1.473	11.230	1.983
29.823	0.684	14.250	1.250

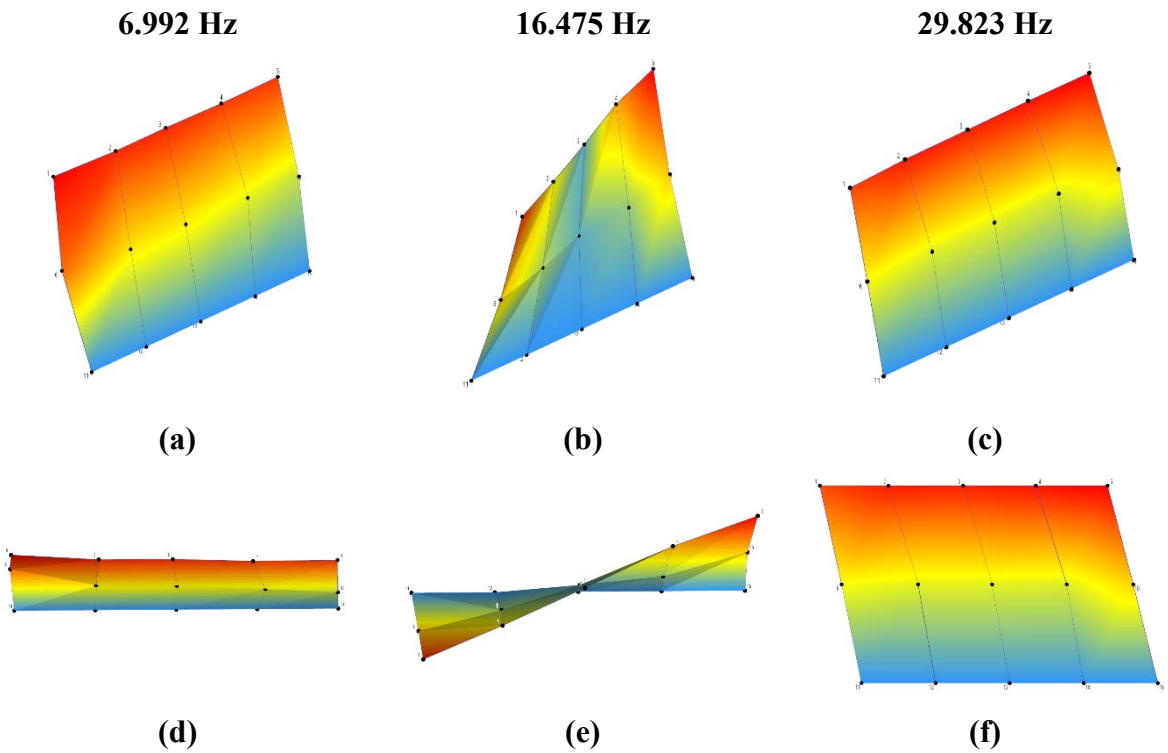


Figure 5. Frequencies and mode shapes for the reinforced pre-damage wall. General view: (a), (b), (c), (d). Plan view: (e), (f), (g). Front view: (h).

Table 6: MAC values between reinforced pre and post damage wall.

Frequency (Hz)	6.992	16.475	29.823
5.211	0.845	0.009	0.001
11.230	0.097	0.401	0.121
14.250	0.004	0.100	0.861

5 CONCLUSIONS

The dynamic behavior of a brick masonry wall before and after reinforcing with TRM was assessed. After the cyclic loads, the damping factor, the modal shapes and the vibration frequency have been evaluated. The following conclusions may be drawn for unreinforced and reinforced masonry building due to the cracking process: Reduction of vibration frequencies by 20-30%, increase of the damping factor by more than 100%. However no significant changes in the modal shapes have been evaluated for the first vibration modes. Regarding the effect of the TRM, the most important conclusions are related with the possibility of recovering the pre-damage stiffness of the building, and the negative effect in the damping factor due to the elastic behavior of these materials.

Acknowledgements. The authors want to acknowledge Spanish Ministry of Universities for the funding provided through Projects RTI2018-101148-B-100 and BIA2015-69952-R, and also the Grupo Mapei and the Grupo Puma for their invaluable assistance.

REFERENCES

[1] Magenes, G., Calvi, G.M. In-plane seismic response of brick masonry walls, Earthq. Eng. Struct. Dyn. 26 (1996) 1091–1112.

[2] Bhattacharya, S., Nayak, S., Dutta, S.C. A critical review of retrofitting methods for unreinforced masonry structures, Int. J. Disaster Risk Reduct. 7 (2014) 51–67. doi:10.1016/j.ijdrr.2013.12.004.

[3] Triantafillou, T.C., Strengthening of masonry structures using epoxy-bonded FRP laminates, J. Compos. Constr. 2 (1998) 96–104. doi:10.1061/(ASCE)1090-0268(1998)2:2(96).

[4] Bilotta, A., Ceroni, F., Lignola, G.P., Prota, A., Use of DIC technique for investigating the behavior of FRCM materials for strengthening masonry elements, Compos. Part B Eng. 129 (2017) 251–270. doi:10.1016/j.compositesb.2017.05.075.

[5] Bru, D., Baeza, F. J., Varona, B., Garcia-Barba, J., Ivorra, S., Static and dynamic properties of retrofitted timber beams using glass fiber reinforced polymers, Materials and Structures 49(1-2) 181-191. doi: 10.1617/s11527-014-0487-0.

[6] Kouris L.A.S., Triantafillou T.C. (2018). State-of-the-art on strengthening of masonry structures with textile reinforced mortar (TRM). Construction and Building Materials 188:1221-1233. doi: 10.1016/j.conbuildmat.2018.08.039.Idelsohn, S.R. and Oñate, E. Finite element and finite volumes. Two good friends. Int. J. Num. Meth. Engng (1994) **37**:3323-3341.

[7] Salvador Ivorra, David Bru, Javier Baeza, Benjamín Torres, Dora Foti. Numerical model of TRM reinforced masonry walls under lateral in plane loads. 12th International Conference on Earthquake Resistant Engineering Structures ERES 2019. 5th June 2019, Seville, Spain.

[8] Juan I. Gisbert, David Bru, Antonio González, Salvador Ivorra. Masonry Micromodels Using high order 3D elements CINPAR 2018. XIV International Conference on Building Pathology and Constructions Repair. Florencia (Italy), 2018.

[9] David Bru, Salvador Ivorra, Manuel Buitrago, Elisa Bertolesi, OMA identification on a scaled masonry building pre and post reinforced with TRM. 8th International Operational Modal Analysis Conference. Copenhagen May 2019

12th International Conference on Structural Analysis of Historical Constructions
SAHC 2020
P. Roca, L. Pelà and C. Molins (Eds.)

EFFECT OF GEOMETRICAL IMPERFECTIONS ON THE RESPONSE OF DRY-JOINT MASONRY ARCHES TO SUPPORT SETTLEMENTS

CHIARA FERRERO[1,2]*, MICHELA ROSSI[1], PERE ROCA[2] AND CHIARA CALDERINI[1]

[1] Department of Civil, Chemical and Environmental Engineering
University of Genoa
Via Montallegro 1, 16154 Genoa, Italy
email: chiara.ferrero@edu.unige.it, michela.rossi@dicca.unige.it, chiara.calderini@unige.it
(* corresponding author)

[2] Department of Civil and Environmental Engineering
Technical University of Catalonia (UPC-BarcelonaTech)
Jordi Girona 1-3, 08034 Barcelona, Spain
e-mail: pere.roca.fabregat@upc.edu

Keywords: Masonry arches, Experimental tests, FE micro-modelling, Support displacements, Collapse mechanisms, Geometrical imperfections.

Abstract. *This paper aims to investigate the effects of geometrical imperfections on the response of a scaled dry-joint arch to the vertical displacement of one support. The arch behaviour was analysed in the large displacement regime using both physical and numerical modelling. The experimental tests were performed on 1:10 small-scale models made of bi-component composite blocks with dry joints. In order to evaluate the geometrical accuracy of the blocks, two different sets of voussoirs were produced. The numerical simulations were carried out using a finite element (FE) micro-modelling approach, where the arch was modelled as an assembly of very stiff voussoirs connected by nonlinear interfaces. Particular attention was paid to the interface stiffness, which was set so as to tune the numerical model with the experimental evidence. Experimental and numerical results were then compared in terms of collapse mechanism, hinge configuration and ultimate displacement capacity. The imperfections of the physical models were found to significantly affect the arch response.*

1 INTRODUCTION

The safety assessment of masonry arches is a crucial issue for the conservation of cultural heritage, as arches have been often used as structural elements in historic masonry constructions. Masonry arches are sensitive to any change in the external environment and thus crack when the abutments move. Support movements can be produced by a wide range of different causes, including differential settlements, subsidence, landslides, soil heterogeneity, instability of the supporting walls/pillars, construction defects and many others. Although small

movements do not represent a threat to stability since they can be easily accommodated by arches through the opening of some cracks (idealized as hinges [1]), large movements involving progressive changes in the geometry may lead to serious damage and collapse.

Over the years, considerable research effort has been devoted to finding new methods and computational tools to investigate the response of masonry arches to large support displacements. Several analytical methodologies were developed to evaluate the collapse mechanisms and ultimate displacement capacity of masonry arches with different geometries subjected to spreading supports (e.g. [2-4]) or generic support displacements (e.g. [5-7]). In the framework of numerical methods, different computational approaches were proposed to investigate the response of arches and, more in general, masonry structures to support displacements, such as finite element (FE) modelling (e.g. [8-10]), discrete element (DE) modelling (e.g. [11]) and rigid block modelling (e.g. [12,13]), among others. Nevertheless, both analytical and numerical methods require to be validated against experimental tests to prove their capability of accurately simulate the collapse of masonry structures. For this reason, the analytical and numerical predictions were often validated by comparison with the results from small-scale model testing (for arches on moving supports, the reader is referred to [2,5-10]). Compared to full-scale models, small-scale models offer several advantages, such as short set-up times, reduced cost, and possibility to repeat the experiments several times. Furthermore, as first demonstrated by Heyman [1], they are effective to predict the collapse of masonry structures, which depends mainly on geometry rather than material strength and thus can be studied independently on scale. This also explains why physical scale-models have been widely used to investigate the stability of masonry arches and vaults not only under support displacements, but also under seismic actions (e.g. [14-18]) or point loads (e.g. [18,19]).

In the case of arches and vaults on moving support, the comparison between analytical and numerical predictions on one side and experimental evidence on the other side showed that both analytical and numerical models are generally able to capture accurately the collapse mechanisms of the physical models. However, they tend to overestimate the displacement capacity obtained experimentally (see [2,5,20,21]). As described in [5,20,21], this behaviour can be attributed to the imperfections and assembly inaccuracies that characterize the physical models compared to the "perfect" numerical ones. More in detail, the imperfections in the dimension of the individual blocks as well as the manual assembly of the physical models, which cannot be perfect, can lead to an inaccurate interlocking between the blocks. Furthermore, the edges of the blocks can become rounded if tests are repeated several times. The combination of these factors result in a reduction of the effective thickness of the physical models, causing collapse to occur for smaller ultimate displacements than the ones predicted by analytical or numerical simulations. A similar effect was also observed when testing small-scale arches under seismic actions. In this case, in order to take into account the imperfections of the physical models and tune the numerical results with the experimental evidence, several authors (e.g. [15-17,22]) proposed to consider a reduced thickness in the numerical models.

In this work, the effect of geometrical imperfections on the response of scaled dry-joint masonry arches to the settlement of one support was investigated through experimental tests and numerical simulations. The experimental tests were performed on 1:10 small-scale models built as dry-joint assemblages of bi-component composite voussoirs. Two sets of voussoirs with

different geometrical accuracies were produced by using different manufacturing techniques. The numerical simulations of the experimental tests were carried out by adopting a FE micro-modelling approach, according to which the arch was modelled as an assembly of very stiff voussoirs connected by no-tension friction interfaces. Differently from what proposed in the literature for small-scale arches subjected to seismic actions, the numerical results were here tuned with the experimental evidence by properly setting the stiffness of the interface elements. This approach was already adopted by the authors in [10] for the simulation of the experimental tests performed using one of the two sets of voussoirs.

The aims of this work were (i) to evaluate to what extent the imperfections of the physical models can affect the arch behaviour in terms of collapse mechanism, hinge position and displacement capacity, and (ii) to assess the capability of the proposed FE micro-modelling approach to simulate the experimental response.

2 EXPERIMENTAL TESTS

The experimental tests were performed on a 1:10 small-scale model of a segmental dry-joint arch supported by two piers (Figure 1, Figure 2). The arch geometry was determined taking as a reference the cross-section of the barrel vaults that are generally used as ceiling in the main nave of historic masonry churches. More specifically, a two-course brick barrel vault with a radial thickness of 0.24 m and a net span of 6 m was considered. It is worth noting that, when this type of vaults is used as a ceiling and not as a load-bearing floor, it does not typically include any backfill. Instead, it is structurally merged with the supporting walls at the abutments. For this reason, the springings of the physical model were considered at about 27° from the horizontal plane.

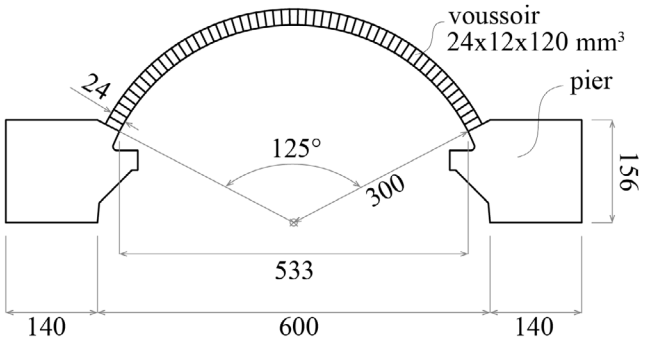
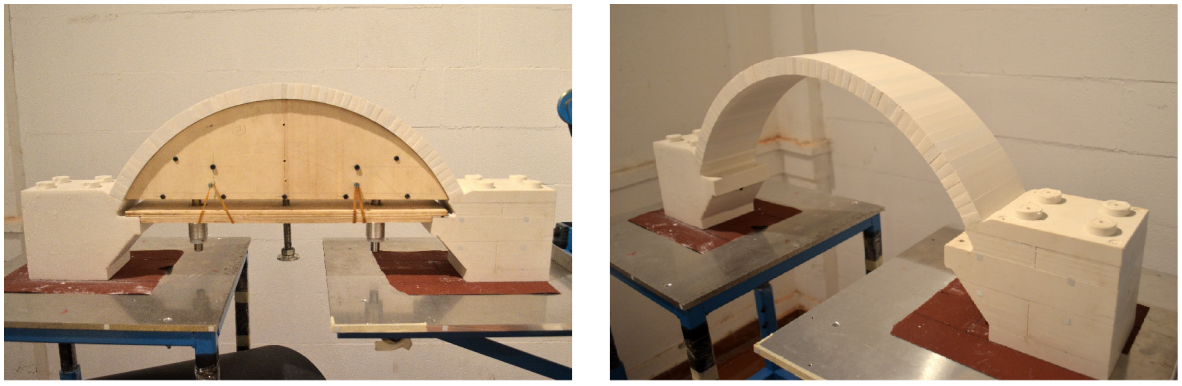


Figure 1: Geometry of the arch mock-up (in mm).

Figure 1 shows the geometry of the mock-up. The arch has an angle of embrace of 125°, an internal radius of 300 mm, a net span of 533 mm, a radial thickness of 24 mm and a depth of 120 mm. It is composed of 55 voussoirs with a height of 24 mm and a width of about 12 mm. Each voussoir represents the scaled dimensions of two adjacent bricks of standard size (60x120x240 mm^3) positioned with their longest side along the radial plane. The voussoirs are slightly trapezoidal in shape in order to compensate for the lack of mortar between them. The piers are shaped in such a way that they can sustain the plywood scaffolding needed to build

the arch (Figure 2a).

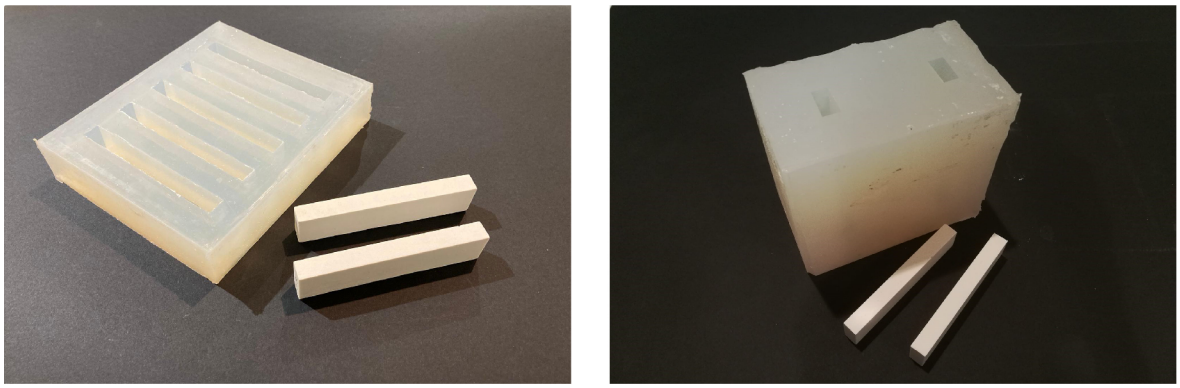


a) b)

Figure 2: Physical model: a) plywood scaffolding, b) view after the removal of the scaffolding.

All the blocks (voussoirs and piers) are made of a bi-component composite material, obtained by mixing a mineral powder with an acrylic polymer in aqueous solution. The mixture was poured, let it harden and then removed from special silicone moulds (Figure 3), which were created using aluminium matrices shaped as the blocks. The density of the blocks was measured to be 1.64 g/cm^3 and the friction angle 41.2°. The Young's modulus, determined by compressive tests (see [10]), was equal to 941 MPa.

Since this manufacturing technique is innovative in the framework of small-scale model testing, the dimensional accuracy of the blocks was evaluated by producing two different sets of voussoirs (Figure 3).



a) b)

Figure 3: Silicone moulds used to produce the voussoirs: a) 1st set, b) 2nd set.

For the 1st set of voussoir, the aluminium matrices were manufactured using a manual milling machine; the mould was made of a deformable silicone and was created by positioning the aluminium matrices with their longest side horizontal (Figure 3a); the mixture was not vibrated; no admixtures were added to the bi-component composite material. For the 2nd set of voussoirs,

the aluminium matrices were produced through a CNC machine (precision ±0.05mm); the mould was made of a stiffer silicone and was manufactured placing vertically the longest side of the aluminium matrices (Figure 3b); the mould was vibrated mechanically in order to eliminate the air bubbles from the freshly poured mixture; the mixture was fluidified by adding a plasticizer (1% of the total weight).

The two sets of voussoirs are significantly different. The voussoirs of the 1st set (Figure 4a) have more imperfections and less sharp corners compared to the voussoirs of the 2nd set (Figure 4b). Furthermore, when they are placed side by side, their lateral faces are not perfectly coplanar (Figure 4a). The use of a manual milling machine to produce the voussoirs of the 1st set did not allow an accurate reproduction of the trapezoidal shape of the individual blocks. This resulted in a not perfect interlocking between voussoirs, causing gaps and hinges to occur (Figure 4c). Conversely, when a CNC machine was used to manufacture the blocks of the 2nd set, the assembly was very accurate and no gaps between adjacent voussoirs were observed (Figure 4d).

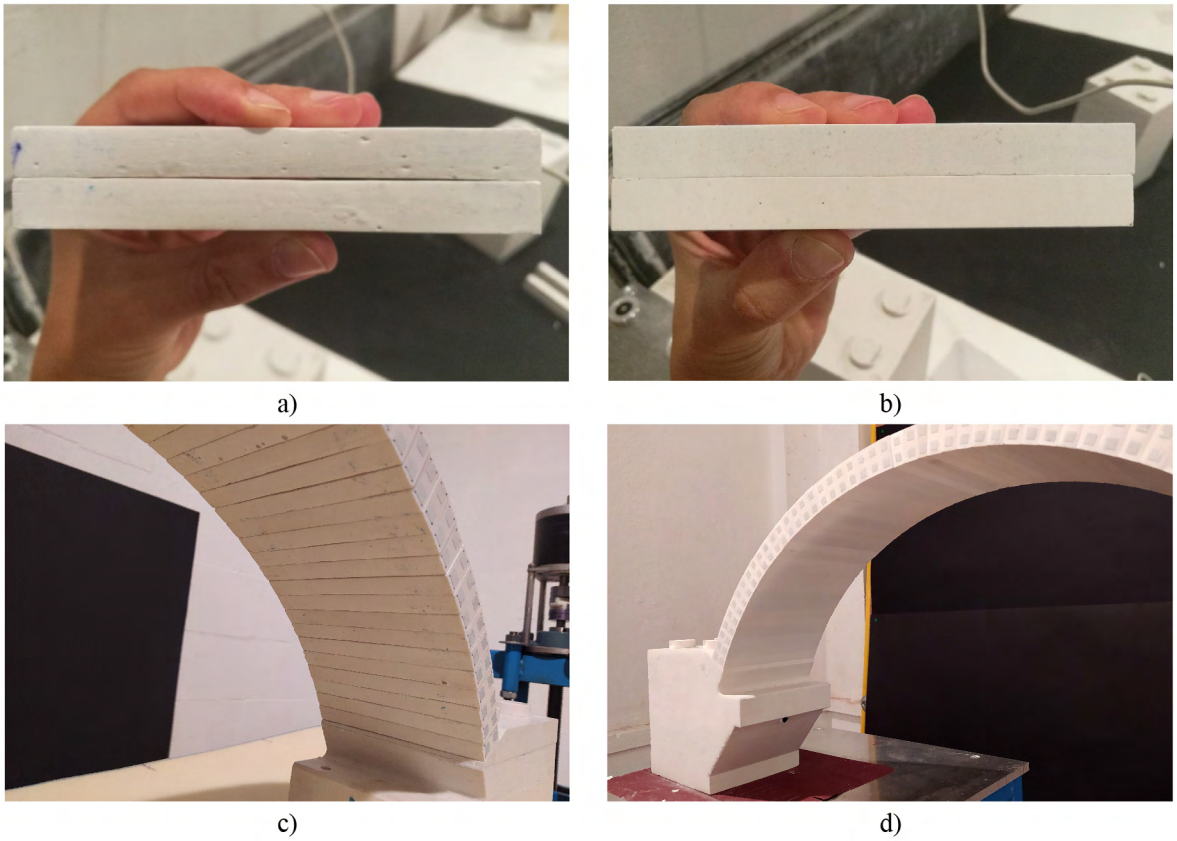
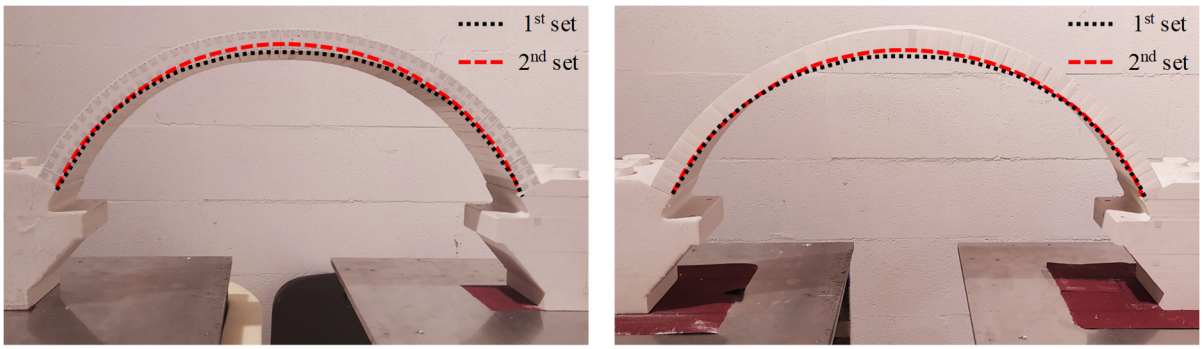


Figure 4: Different sets of voussoirs produced: a-c) 1st set, b-d) 2nd set.

Figure 5 depicts the initial geometry of the physical models created using either set of voussoirs. The shape of the two models is slightly different since the keystone of the arch built with the 1st set of voussoirs descended by few millimetres as soon as the scaffolding was removed (Figure 5a), while no significant movement was noticed for the arch built using the

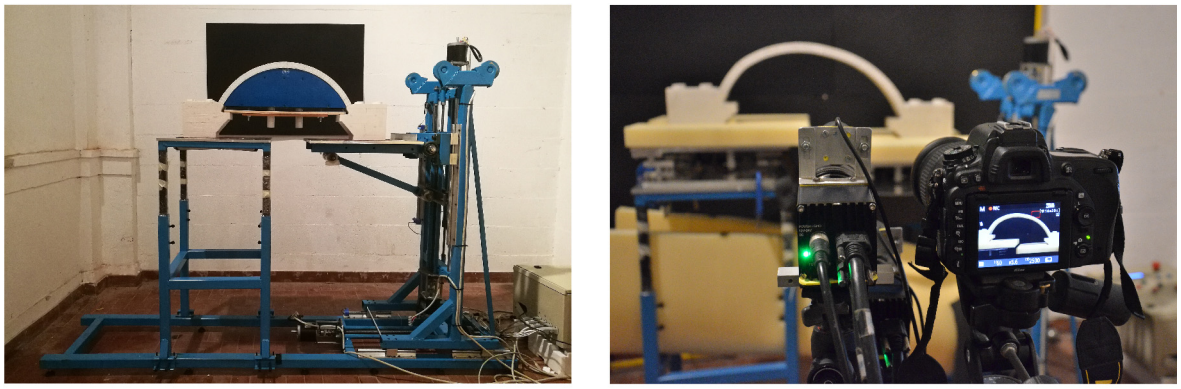
2nd set of voussoirs (Figure 5b). It is worth noting that the downward displacement of the keystone observed for 1st set of voussoirs produced a slightly change in the geometry of the free-standing arch with respect to the "perfect" one shown in Figure 1.



a) b)

Figure 5: Initial geometry of the arch after the removal of the scaffolding: a) 1st set of voussoirs, b) 2nd set of voussoirs.

The arch was tested under an increasing downward quasi-static vertical displacement δ applied at the right support through an external stepper motor linear actuator controlled via software (Figure 6a). Two high-resolution, high-frame rate (60 Hz) cameras were used to record the development of the damage up to collapse (Figure 6b).



a) b)

Figure 6: a) Testing machine, b) high-resolution, high-frame rate cameras.

3 FINITE ELEMENT MICRO-MODELLING

The numerical simulations of the experimental tests were performed through the FEM software DIANA [23]. A two-dimensional FE model of the arch was created in Midas FX+ Version 3.3.0 (Customized Pre/Post-processor for DIANA software [24]) adopting a micro-modelling approach, where each voussoir was modelled as a distinct (very stiff) block and dry joints were represented as no-tension frictional interfaces placed in between the voussoirs.

Further interface elements were placed at the springing of the arch to allow for hinge opening at the supports. The piers were not included in the FE model, as they only provided support to the arch.

Four-node quadrilateral isoparametric plane stress elements (Q8MEM) were used to model the voussoirs, while 2D four-node line interface elements (L8IF) were employed for the interfaces. A mesh size of 2 mm (i.e. 12 FEs elements along the arch radial thickness) was adopted based on a sensitivity analysis on the ultimate vertical displacement δ_u obtained at collapse. For further details about the mesh sensitivity analysis, the reader is referred to [10].

The mesh of FE micro-model of the arch, composed of 5031 nodes and 4632 elements, is presented in Figure 7. Note that the outer edges of the interface elements placed at the supports were pinned to provide boundary conditions.

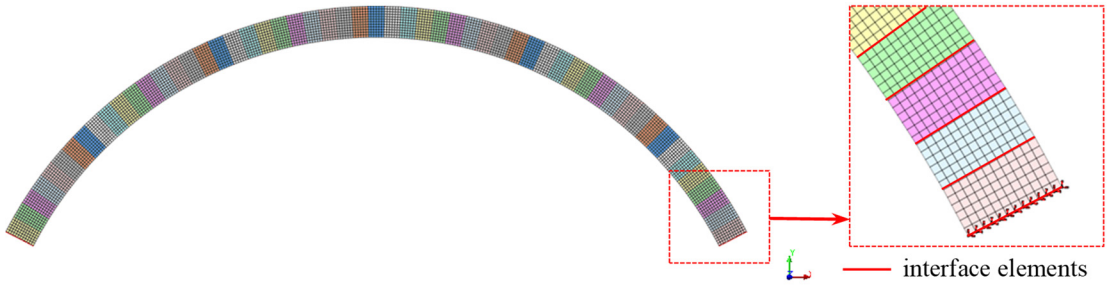


Figure 7: FE micro-model of the arch.

The voussoirs were modelled as linear elastic elements with infinite compressive strength. Young's modulus and mass density were set equal to 941 MPa and 1.64 gr/cm^3, respectively, in accordance with the values measured experimentally (see section 2). A Poisson's ratio of 0.2 was assumed. For the interface elements, a Coulomb friction model was used. Cohesion and dilatancy angle were set equal to zero, while a friction angle of 41.2° was adopted, as measured for the voussoirs of the physical model. In order to simulate hinge opening, the friction criterion was extended with a gap criterion [23] with zero tensile strength. For further details about the Coulomb friction model, the reader is referred to [23].

The stiffness of the interface elements was evaluated through a sensitivity analysis (Figure 8), where the collapse displacement δ_u was determined for different values of k_n in the range 0.1÷100 N/mm^3 (this latter was defined according to the values proposed in [16]). The interface tangential stiffness k_s was set equal to $0.5k_n$ for any considered value of k_n. This choice was made only to optimize numerical convergence, since the ratio between the two stiffnesses did not influence the arch structural response. As described by the authors in [10], very large stiffness values simulate rigid contact surfaces, allowing to treat the arch as a rigid-no tension structure, but they lead to significantly overestimate the displacement capacity obtained from experimental methods. Conversely, reduced stiffness values enable to consider the imperfections (and resulting deformability) that characterize the contact surfaces of the physical models. With the aim of simulating the experimental tests, the interface normal stiffness was chosen so that the numerical collapse displacement matched closely the experimental result for

each of the two sets of voussoirs considered. Consequently, k_n was set equal to 0.25 N/mm^3 and 5.2 N/mm^3 for the 1st and 2nd sets of voussoirs, respectively.

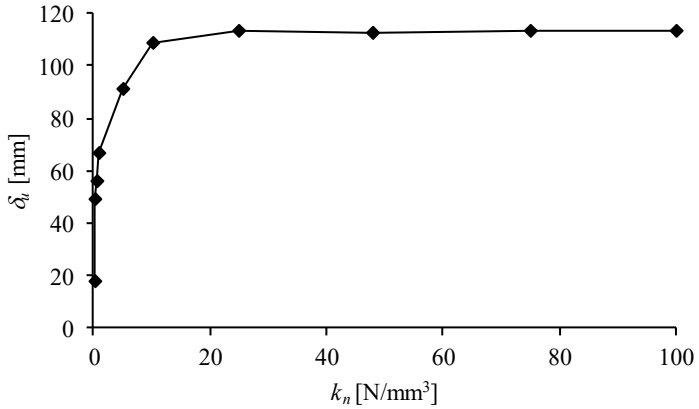


Figure 8: Collapse displacement δ_u vs. interface normal stiffness k_n.

The response of the arch to large support displacements was evaluated through non-linear static analyses. After the application of the self-weight, the imposed vertical displacement δ was increased monotonically until collapse was reached. A regular Newton-Raphson iteration method combined with a line search algorithm was employed. An energy-based convergence criterion with a tolerance value of 0.001 was assumed. Geometrical non-linearities were taken into account by adopting the Total Lagrange formulation available in DIANA [23].

4 EXPERIMENTAL VS. NUMERICAL RESULTS

This section presents and compares the experimental and numerical results obtained from both sets of voussoirs in terms of collapse mechanisms (Figure 9) as well as hinge position and ultimate displacement at collapse δ_u (Table 1). In Table 1, the interfaces where hinges appear are numbered from left to right, being interface no. 1 the interface at the left support.

The collapse mechanisms obtained from the experimental test and relevant numerical simulation for the 1st of voussoirs are illustrated in Figure 9a-c. In the experimental test (Figure 9a), three hinges, A, B and C, initially occurred in the sequence I-E-E (from left to right, where E = extrados; I = intrados). Hinge A was located at the haunches between 11th and 12th voussoirs (interface no. 12), hinge B appeared close to midspan between 31st and 32nd voussoirs (interface no. 32), and hinge C opened at the right support (interface no. 56). Hinges B and C remained in their initial position and did not move as the imposed vertical displacement increased. Conversely, hinge A moved towards the crown by one voussoir just before collapse. The arch collapsed by an asymmetrical four-hinge mechanism when a fourth hinge (D) occurred at the left support at the extrados for a vertical displacement of 48.9 mm (Figure 9a).

Figure 9c illustrates the collapse mechanism predicted by FE analyses when adopting a value of k_n equal to 0.25 N/mm^3. For the latter, the numerical collapse displacement δ_u (48.8 mm) matched very closely the experimental one. Collapse occurred again by an asymmetrical four-hinge mechanism with hinges located according to the sequence E-I-E-E. The predicted final

hinge position agreed well with the experimental results since hinges B, C and D appeared at the same location of the physical model, and hinge A was shifted by one voussoir only. Differently, hinge A did not move with increasing support displacements. Despite the good agreement in terms of displacement capacity and hinge position, the FE analysis did not perfectly capture the actual behaviour of the physical model, since hinges A and B, which concentrated in one single interface in the test, appeared to be distributed over adjacent interfaces in the numerical simulation. Nevertheless, this discrepancy could be attributed to the not perfect geometry of the physical model, which was slightly different from the numerical one since the keystone descended by few millimetres after the scaffolding was removed (as already shown in Figure 5).

Figure 9b and Figure 9d show the collapse mechanisms obtained for the 2nd set of voussoirs from the experimental test and numerical simulation, respectively. In the test, the three initial hinges A, B and C appeared in the sequence I-E-E and did not move as the support displacements increased. The position of hinges B and C was very similar to that obtained for the 1st set, since hinge C occurred again at the left support and the location of hinge B differed by only one block, opening between 30th and 31st voussoirs (interface no. 31). However, a significant difference was found in the final position of hinge A, which appeared four blocks closer to the left support (interface no. 9) in the 2nd set compared to the 1st set. The failure mode was the same as that obtained for the 1st set of voussoirs, since collapse occurred when the fourth hinge D appeared at the left support. Nevertheless, the collapse displacement δ_u was significantly larger, being equal to 91.5 mm. As can be observed from Figure 9d, the numerical results obtained for k_n equal to 5.2 N/mm^3 (δ_u = 91.8 mm) were in very good agreement with the experimental results in terms of both collapse mechanisms and hinge position. As for the latter, the predicted position of hinges A, C and D was in full accordance with the experimental tests, while hinge B was shifted by only one voussoir. As already observed in the test, also in the numerical simulation all hinges remained in their initial position and did not move with increasing support displacements.

Table 1: Comparison of numerical and experimental results in terms of hinge position (indicated with the interface where hinges appear, numbered from left to right) and collapse displacement δ_u.

	1st set of voussoirs		2nd set of voussoirs	
	Experimental	Numerical	Experimental	Numerical
Position of hinge A at collapse	13	11-12	9	9
Position of hinge B at collapse	32	29-30-31-32	31	30
Position of hinge C at collapse	56	56	56	56
Collapse displacement δ_u [mm]	48.9	48.8	91.5	91.8

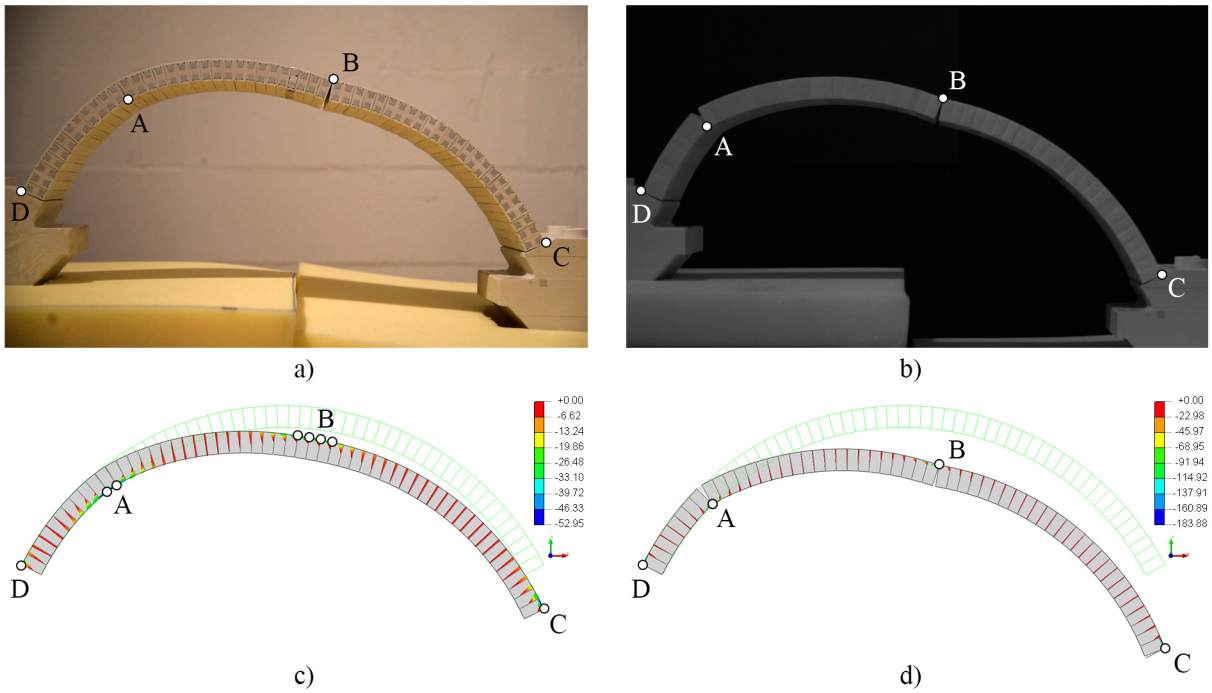


Figure 9: Collapse mechanism obtained using the 1st set (left) and 2nd set (right) of voussoirs: a-b) experimental tests, c-d) numerical simulations.

5 CONCLUSIONS

In this paper, the response of a segmental dry-joint masonry arch to the vertical displacement of one support was investigated using both physical and numerical modelling. With the aim of evaluating the effect of geometrical imperfections on the arch response, two different sets of voussoirs with different geometrical accuracies were employed to build the small-scale models. The experimental tests were then simulated through FE micro-modelling. The stiffness of the interface elements used to model the dry joints was calibrated so that the ultimate displacement capacity obtained numerically matched closely the experimental one.

The results of the experimental tests proved that the imperfections and assembly inaccuracies of the physical models significantly affect the arch response, especially in terms of displacement capacity. Indeed, although the same collapse mechanism occurred for either set of voussoirs, the collapse displacement obtained using the 1st set, which was characterized by more imperfections, was significantly lower than that obtained with the 2nd set.

For both sets of voussoirs, the numerical predictions were in good agreement with the experimental results in terms of collapse mechanism, hinge position and displacement capacity. This demonstrated that calibrating the interface stiffness based on the experimental evidence is an effective strategy to accurately capture the experimental response of dry-joint masonry arches to large support displacements. The difference in the hinge distribution obtained when simulating the test performed using the 1st set of voussoirs can be explained considering that the geometry of the physical model was slightly different from the perfect numerical one.

In conclusion, this work provides a contribution for a better understanding of the effect of geometrical imperfections on the response of scaled dry-joint masonry arches. Future works will include the application of different configurations of support displacements as well as the measurement of the reactions at the arch supports in the experimental tests. This will allow to evaluate the effect of geometrical imperfections on the arch response in terms of support reaction-displacement curves.

Acknowledgements. The financial support of PRIN 2015 Program by the Italian Ministry of Education, University and Research (MIUR) is gratefully acknowledged for funding the research project "Protecting the Cultural Heritage from water-soil interaction related threats" (Prot. No. 2015EAM9S5), which is the main framework of the study presented in this article.

REFERENCES

[1] Heyman, J. *The stone skeleton. Structural engineering of masonry architecture*. Cambridge University Press, Cambridge (1995).
[2] Ochsendorf, J. A. The masonry arch on spreading supports. *Struct. Eng.* (2006) **84**(2):29-35.
[3] Coccia, S., Di Carlo, F. and Rinaldi, Z. Collapse displacements for a mechanism of spreading-induced supports in a masonry arch. *Int. J. Adv. Struct. Eng.* (2015) **7**(3):307-320.
[4] Di Carlo, F. and Coccia, S. Collapse state of elliptical masonry arches after finite displacements of the supports. *Eng. Fail. Anal.* (2020) **114**.
[5] Galassi, S., Misseri, G., Rovero, L. and Tempesta, G. Failure modes prediction of masonry voussoir arches on moving supports. *Eng. Struct.* (2018) **173**:706-717.
[6] Zampieri, P., Simoncello, N. and Pellegrino, C. Structural behaviour of masonry arch with no-horizontal springing settlement. *Frat. ed Integrità Strutt.* (2018) **12**(43):182-190.
[7] Smars, P. Kinematic Stability of Masonry Arches. *Adv. Mater. Res.* (2010) **133-134**:429-434.
[8] Alforno, M., Monaco, A., Venuti, F. and Calderini, C. Validation of Simplified Micro-models for the Static Analysis of Masonry Arches and Vaults, *Int. J. Archit. Herit.* (2020).
[9] Masciotta, M-G., Pellegrini, D., Girardi, M., Padovani, C., Barontini, A, Lourenço, PB, Brigante, D. and Fabbrocino, G. Dynamic characterization of progressively damaged segmental masonry arches with one settled support: experimental and numerical. *Frat. ed Integrità Strutt. (*2020) **51**:423-441.
[10] Ferrero, C., Rossi, M., Roca, P. and Calderini, C. Experimental and numerical analysis of a scaled dry-joint arch on moving supports. *Int. J. Mason. Res. Innov.* (2020).
[11] McInerney, J. and DeJong, M. J. Discrete Element Modeling of Groin Vault Displacement Capacity. *Int. J. Archit. Herit.* (2015) **9**(8):1037–1049.
[12] Gilbert, M. and Melbourne, C. Rigid-block analysis of masonry structures. *Struct. Eng.* (1994) **72**(21).
[13] Portioli, F. and Cascini, L. Large displacement analysis of dry-jointed masonry structures subjected to settlements using rigid block modelling. *Eng. Struct.* (2017) **148**:485-496.

[14] Calderini, C., Lagomarsino, S., Rossi, M., De Canio, G., Mongelli, M.L. and Roselli, I. Shaking table tests of an arch-pillars system and design of strengthening by the use of tie-rods. *Bull. Earthq. Eng* (2015) **13**(1):279–297.
[15] DeJong, M., De Lorenzis L., Adams, S. and Ochsendorf J.A. Rocking stability of masonry arches in seismic regions. Earthq. Spectra (2008) **2**:847–865.
[16] Gaetani, A., Lourenço P. B., Monti, G. and Moroni, M. Shaking table tests and numerical analyses on a scaled dry-joint arch undergoing windowed sine pulses. *Bull. Earthq. Eng.* (2017) **15**:4939-4961.
[17] Misseri, G., DeJong, M.J. and Rovero, L. Experimental and numerical investigation of the collapse of pointed masonry arches under quasi-static horizontal loading. *Eng. Struct.* (2018) **173**:180-190.
[18] Shapiro E.E. *Collapse mechanism of small-scale unreinforced masonry vaults*. M.S. thesis in Building Technology, Massachusetts Institute of Technology (2012).
[19] Pippard A.J.S. and Ashby, R. An experimental study of the voussoir arch. *J. Inst. Civ. Eng Journal of the Institution of Civil Engineers* (1939) **10**(3):383-404.
[20] Van Mele, T., McInerney, J., DeJong, M. and Block P. Physical and Computational Discrete Modelling of Masonry Vault Collapse,' In: *Proceedings of 8th International Conference on Structural Analysis of Historical Constructions,* (2012), pp. 2552–2560.
[21] Quinonez, A., Zessin, J., Nutzel, A. and Ochsendorf J.A. Small-Scale Models for Testing Masonry Structures. *Adv. Mater. Res.* (2010) **133–134**:497–502.
[22] Albuerne, A, Williams, M and Lawson V. Prediction of the failure mechanism of arches under base motion using DEM based on the NSCD method. Wiadomości Konserw (2013) **34**:41–47.
[23] TNO DIANA BV. DIANA Finite Element Analysis User's Manual Release 9.6, Delft, The Netherlands (2014).
[24] Midas FX+ for DIANA, Customized Pre/Post-processor for DIANA (2013).

12th International Conference on Structural Analysis of Historical Constructions
SAHC 2020
P. Roca, L. Pelà and C. Molins (Eds.)

EVALUATION OF THE BEHAVIOUR OF LIME AND CEMENT BASED MORTARS EXPOSED AT ELEVATED TEMPERATURES

VASILIKI PACHTA[1*] AND MARIA STEFANIDOU [1]

[1] Laboratory of Building Materials, School of Civil Engineering
Aristotle University of Thessaloniki, 54124, Thessaloniki, Greece
e-mail: vpachta@civil.auth.gr, stefan@civil.auth.gr

Keywords: Mortars, Elevated temperature, Fire, Lime, Cement

Abstract. *Exposure to fire and elevated temperatures is diachronically a significant decay factor, influencing the stability of structures. Cement and lime-based mortars have a different behavior when exposed at elevated temperatures, usually testified by the post-fire preservation state of historic and contemporary constructions. In this paper, the correlation of their properties is envisaged, in order to identify the key elements of their performance. To this direction, five compositions of cement and lime based mortars were manufactured and tested, after their exposure at 200°C, 400°C, 600°C, 800°C and 1000°C. The binders used concerned CEM I42.5N (C), hydrated lime (L) and natural pozzolan (P), while the systems applied regarded C, C:L (1:1), L, L:P (1:1) and L:P:C (1:0.8:0.2) (parts per weight). The aggregates used were natural of siliceous origin and their gradation varied from 0-4mm to 0-8mm. The B/A ratio was 1/2 by weight and the W/B ratio was adjusted in order to maintain workability around 15±1cm. The physico-mechanical properties of the specimens, were recorded before and after their exposure at the selected temperatures. From the evaluation of the results, it was concluded that the mortars' behavior was different at the early temperature rate (up to 600°C) according to their type, whereas the results were more comparable at the extreme temperature level. Generally it was observed that although the initial strength of the lime-based mortars was low (1-4MPa), they presented a more stable and efficient performance at the elevated temperatures, rendering them probably more resistant at the first stages of fire actions. Cement-based mortars seemed to present a better performance at the highest temperatures of 800°C and 1000°C.*

1 INTRODUCTION

Fire has been diachronically a significant decay factor of historic and modern structures, leading to extreme damages and loss of their stability. The post-fire state of constructions maybe related to several factors, such as the fire characteristics (i.e. heating rate, fire duration, maximum temperature), the ground plan of the building, as well as the type and properties of building materials.

The influence of fire on concrete has been studied from the beginning of the 20th century (1922) [1], while during the last decades research has been induced [2-6]. Researchers focus on various assets, such as the analysis of fire scenarios (heating rate, exposure temperature and time), the performance of building materials at elevated temperatures, the design and testing of

fire-resistant materials, as well as the development and application of post-fire assessment and repair strategies [4-10]. Relevant Standards and Recommendations exist, providing accumulated data (RILEM TC 129-MHT, RILEM TC 200-HTC, EN 1991-1-2 Eurocode 1, EN 1992 Eurocode 2, ISO 834-11:2014, BS 476-3:2004) [10-15].

The temperature/time development curves, as given by the Standards (Fig. 1), show that the maximum temperature attained during a fire, is around 1100-1200ºC, while the temperature rate may vary [16]. During the first 30 minutes of the action, temperature is rapidly increased up to 822ºC. Due to the difficulty of simulating such an extreme temperature rate at laboratory level and in order to study the performance of building materials at elevated temperatures, researchers propose a development rate ranging from 5 to 10ºC/min [1-9].

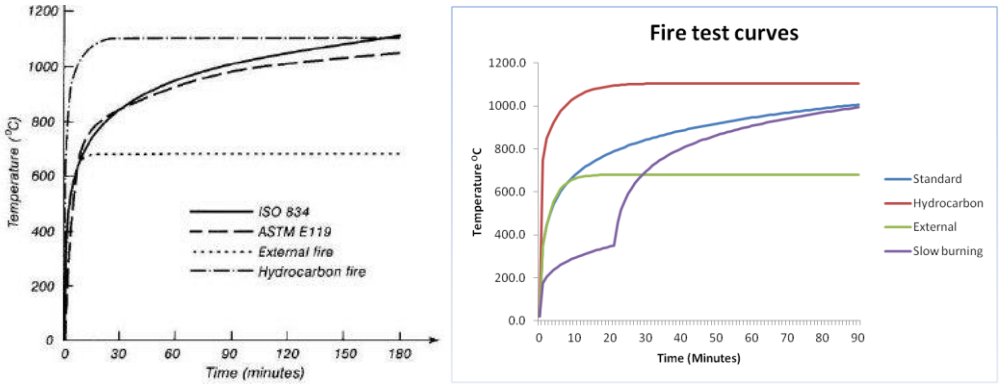


Figure 1: Temperature / time development standard curves during fire action [16]

When subjected to fire, specific properties of materials are influenced, regarding both physico-mechanical and chemical characteristics [1-6]. Since mortars are heterogeneous materials, elevated temperatures influence both their paste and aggregates in different ways and according to their constituents and thermal strains (expansion of aggregates, shrinkage deformations of the paste) [1-6]. Their post-fire pathology symptoms, usually concern colour change, spalling, cracking, delamination, and deformation [7-9].

According to literature, between 100-200°C, the free moisture of the materials evaporates, while above 250°C the dehydration or loss of the bonded water begins [1-6]. Above 300°C the silicate hydrates of the cement paste (C–S–H gel) decompose and above 500°C portlandite, influencing the stability of the matrix [4]. Aggregates function according to their origin, whereas siliceous aggregates seem to be more resistant than calcareous ones [4].

In the case of cement-based mortars, the residual strength is maintained for temperatures up to 300°C, while between 300°C and 500°C it is decreased around 15-40% [1-6]. Above 550-600°C, it is minimized and secondary chemical reactions occur (decarbonisation of carbonates in both the cement paste and the aggregates) [4]. Usually above 800°C, complete disintegration of the constituents begins.

In the case of lime-based mortars [7, 17], compressive strength is significantly increased up to 600ºC (almost doubled). It is reduced at 800ºC (around 50% of the initial value) and minimized at 1000ºC. Generally, lime-based mortars exhibit a good performance throughout the tested temperatures, maintaining their mass and volume until 1000ºC.

In the present paper, an effort has been made to comparatively study the performance of cement and lime-based mortars at elevated temperatures. To this direction, five compositions were manufactured and exposed at 200ºC, 400ºC, 600ºC, 800ºC and 1000ºC. The binders used concerned CEM I42.5N (C), hydrated lime (L) and natural pozzolan (P), while the systems applied regarded C, C:L, L, L:P and L:P:C.

The purpose of the study was to envisage the behaviour of contemporary and traditional binding systems, found in mortars of modern or historic structures. Repaired historic constructions are also related, where traditional and cement based materials coexist, due to improper restoration works or specific demands.

2 MATERIALS AND METHODS

During the experimental work, five compositions of cement and lime-based mortars were manufactured and tested. The binding agents used concerned CEM I42.5N, hydrated lime (L) and natural pozzolan (P), while the systems applied regarded C, C:L (1:1), L, L:P (1:1) and L:P:C (1:0.8:0.2). The aggregates were natural of siliceous origin and their gradation varied from 0-4mm to 0-8mm.

In order to reduce the water demand, a sulphate free, polycarboxylate superplasticizer was added in a proportion of 1% w/w of binders. The Water/Binder (W/B) ratio was adjusted for achieving workability of 15±1cm, according to EN1015-3. The manufacture and curing of the mortar specimens was according to EN1015-11, while totally 16 specimens (dimensions 4x4x16cm) of each composition were manufactured and tested. In Table 1 the constituents and proportions of the mortar series are presented.

Table 2: Constituents and proportions of the mortar series

Raw materials	Mortar series / Parts of weight				
	C	CL	L	LP	LPC
Cement I42.5	1	0.5	-	-	0.5
Hydrated lime	-	0.5	1	0.5	0.4
Natural pozzolan	-	-	-	0.5	0.1
Sand of siliceous origin, pale colour (0-4mm)	2	2	1.4	1.4	1.4
Gravel of siliceous origin (4-8mm)	-	-	0.6	0.6	0.6
Super plasticizer (1% w/w of binders)	√	√	√	√	√
W/B ratio	0.36	0.44	0.85	0.57	0.54
Workability (cm) (EN1015-3:1999)	15.5	15.0	14.8	15.5	14.7

Twenty-eight days after their manufacture, the physico-mechanical properties of the mortar compositions were recorded, regarding porosity and apparent specific gravity (RILEM CPC 11.3), water absorption coefficient due to capillary action (EN 1015-18:2002), dynamic modulus of elasticity (BS 1881-203:1986), flexural and compressive strength (EN1015-11:1999).

Two specimens of each mortar composition were subjected to elevated temperatures (200ºC, 400ºC, 600ºC, 800ºC and 1000ºC), according to former research work [7, 9, 17]. For the experiment, an electric furnace was used, where the temperature rate and duration time could be manually set (Fig. 2). The heating scheme followed (maximum temperature, heating rate, exposure time and cooling rate) was based on former research work [7, 9, 17] and was aligned

with relevant research [1-6]. The methodology concerned heating rate 5ºC/min, exposure duration to the maximum temperature 2h and cooling rate 2ºC/min (Fig.2).

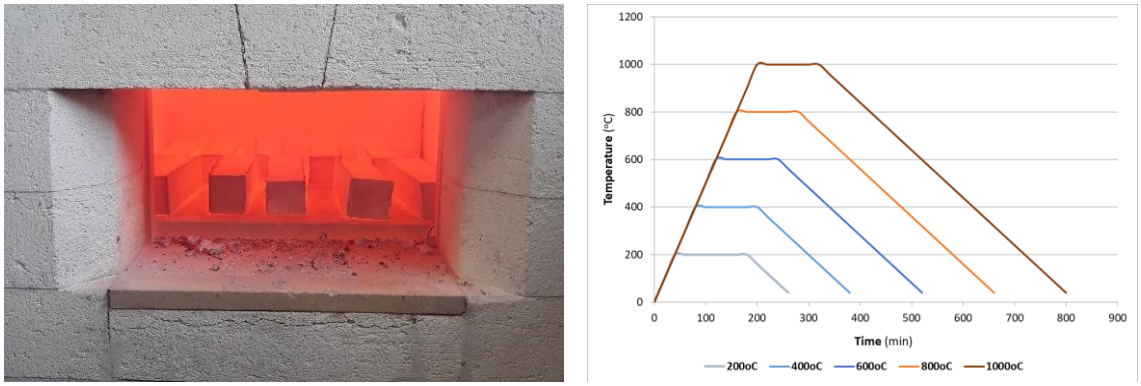


Figure 2: Electric furnace (left) and heating scheme (rate, exposure time, cooling rate) (right)

After the exposure to each temperature, the specimens maintained for 24h at laboratory conditions and their weight and dimensions were recorded, in order to estimate their mass and volume changes. Their physico-mechanical characteristics were tested, regarding porosity, apparent specific gravity, dynamic modulus of elasticity, flexural and compressive strength. Macroscopic observation of the specimens and colour determination (according to the Munsell chart) were also attained. All the results were comparatively evaluated in order to record their performance at elevated temperatures.

3 RESULTS AND DISCUSSION

3.1 Physico-mechanical characteristics

The physico-mechanical properties of the mortar specimens at the age of 28 days are presented in Table 2. The characteristics concern porosity, apparent specific gravity, dynamic modulus of elasticity, flexural and compressive strength, while the water absorption coefficient due to capillary action is presented in Figure 3.

Table 2: Physico-mechanical properties of the mortar compositions at the age of 28 days

Mortar series	Porosity (%)	Ap. Spec. Gravity	Dyn. Mod. of Elasticity (GPa)	Flexural strength (MPa)	Compressive strength (MPa)
C	8.68	2.15	37.55	9.93	60.79
CL	18.8	1.93	25.11	6.01	17.46
L	30.86	1.65	1.36	0.12	0.87
LP	16.66	1.84	13.32	1.12	3.15
LPC	16.15	1.90	16.22	1.70	4.20

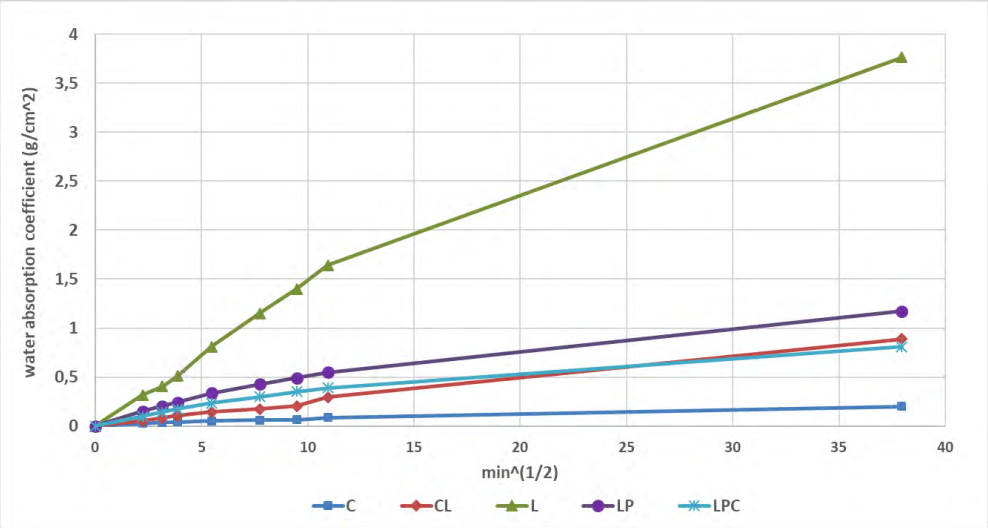


Figure 3: Water absorption coefficient of the mortar compositions (28d)

From the evaluation of the results (Table 2) it was asserted that with the substitution of 50% of cement with lime (CL), the porosity was doubled (18.8%), while the mechanical characteristics, especially compressive strength, were significantly decreased. Flexural strength dropped from 9.93MPa (C) to 6.01MPa (CL) and compressive strength from 60.79MPa (C) to 17.46MPa (CL). In the case of lime-based mortars, the substitution of 50% of lime with natural pozzolan (LP) resulted in a significant decrease of porosity (16.66%) and increase of strength. Flexural strength was increased from 0.12MPa (L) to 1.12MPa (LP) and compressive strength from 0.87MPa (L) to 3.15MPa (LP). The substitution of 20% of natural pozzolan with cement (LPC), slightly decreased porosity and increased mechanical properties around 30%.

As expected, water absorption coefficient was significantly high in the case of the lime mortar (L) and low in the cement one (C) (Fig.3). CL and LPC compositions presented almost the same behavior, while LP showed slightly higher values.

3.2 Performance at elevated temperatures

The performance of the mortar compositions was recorded after their exposure at the elevated temperatures (200ºC, 400ºC, 600ºC, 800ºC and 1000ºC). Their physico-mechanical properties, regarding volume and mass change, color alterations, porosity, apparent specific gravity, dynamic modulus of elasticity, flexural and compressive strength, were comparatively evaluated.

The volume change of the specimens presented the same trend in all compositions (Fig. 4). At 200ºC, a short expansion was observed, which was more intense for composition L (3.6%), while at 400ºC a volume decrease was recorded ranging from 0.5 to 5%. The lowest values were recorded for C and CL compositions. At 600ºC and 800ºC a slight volume increase was observed for L, LP and LPC, while C and CL showed volume reduction. At 1000ºC all volume change was minimized. Compared to all compositions, C presented the more extreme volume loss above 400ºC, ranging from 1.5-4.5%.

Regarding mass change (Fig.5), all compositions, except C, presented the same trend, with decreasing values from 200 to 1000ºC (7-21%). The highest decrease was observed for L.

Composition C presented a different behavior with a slight mass increase at 200ºC and further reduction. The highest mass loss was recorded at 400ºC (4.6%).

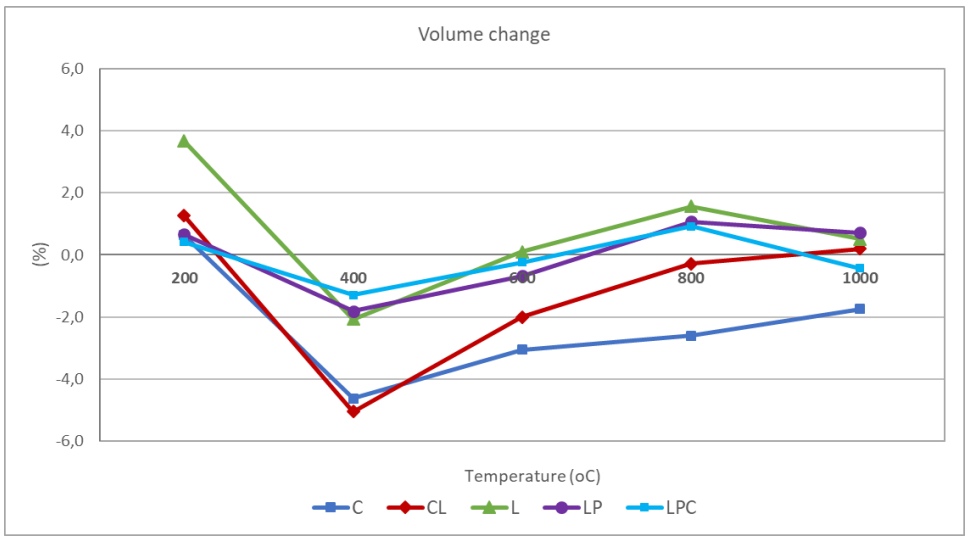


Figure 4: Volume change of the mortar specimens, exposed at elevated temperatures

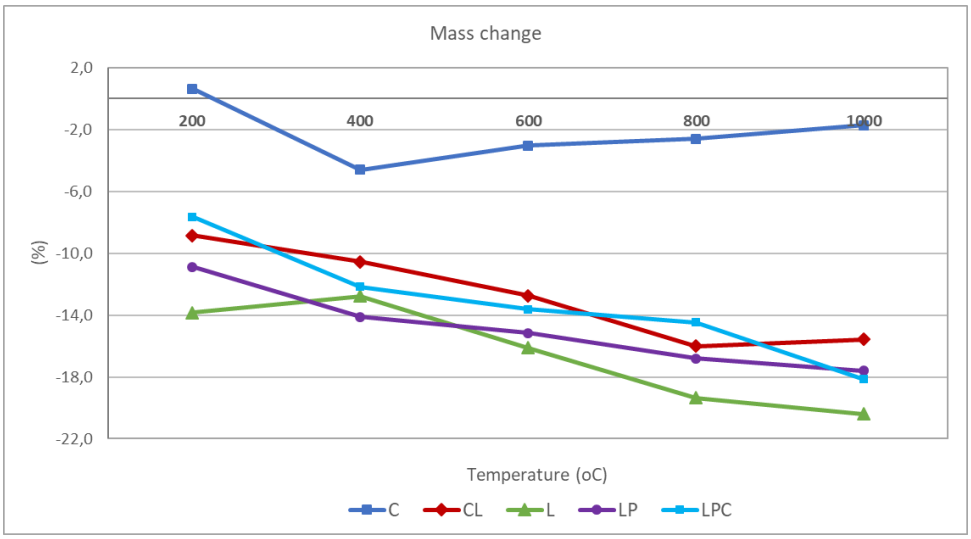


Figure 5: Mass change of the mortar specimens, exposed at elevated temperatures

Regarding porosity and apparent specific gravity (Fig.6), the performance of the specimens presented some similarities. Porosity was generally increased up to 600ºC (except of L) in all cases. C had the highest increase up to 800ºC with values ranging from 8 to 25% (at 1000ºC there was a decrease to 20%). CL presented a lower increase up to 600ºC from 20 to 30%. LP and LPC had the same behavior with an increase from 18 to 34% up to 600ºC and a further decrease. Composition L presented the lower fluctuations at all temperatures, with a short decrease of values (31-28%). Apparent specific gravity was reduced throughout the elevated temperatures (10-15%). The greatest fluctuations were recorded in compositions C and L.

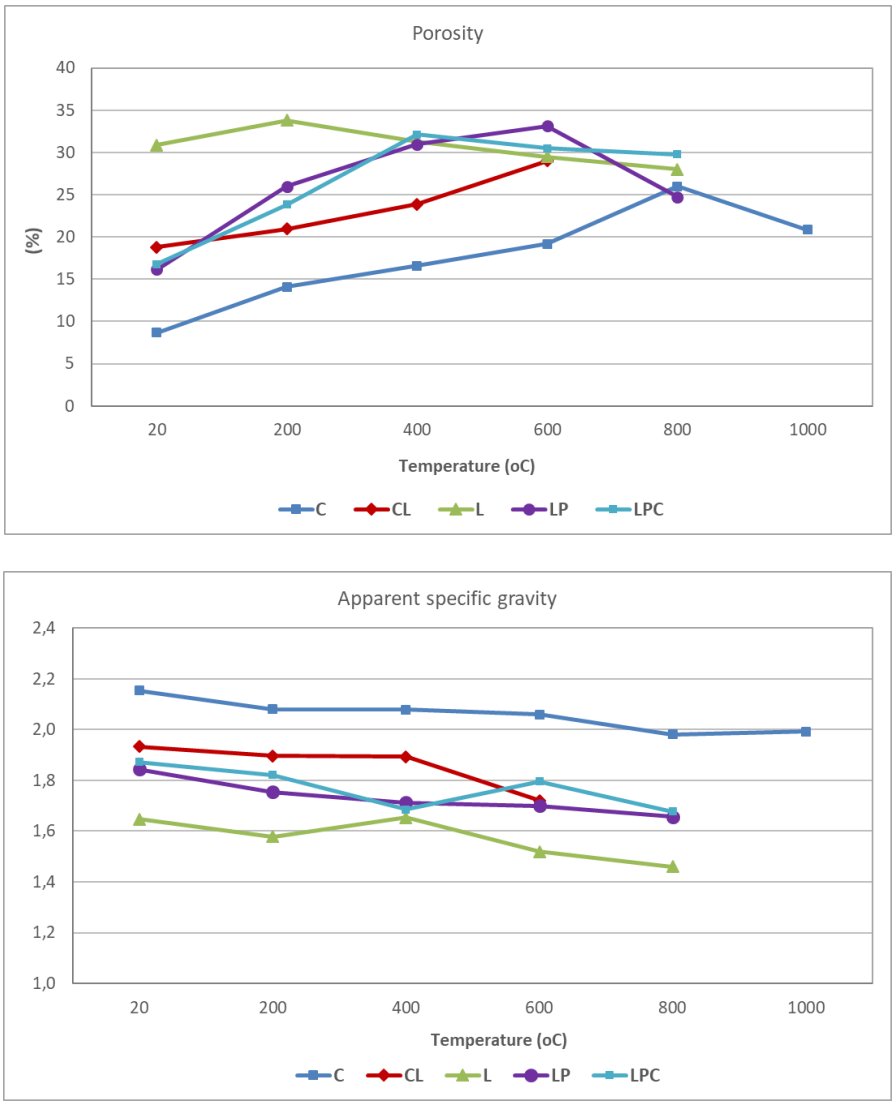


Figure 6: Porosity and Ap. Specific gravity of the mortar specimens, exposed at elevated temperatures

Concerning the mechanical properties of the mortar specimens, it was generally observed that dynamic modulus of elasticity was decreased throughout the temperature increase (Fig.7). At 200ºC, compositions C and CL presented a decrease of the initial values around 25-30%, while LP and LPC showed a reduction of 10-15%. At 400ºC there was a further decrease around 45% for C and CL and 70% for LP and LPC, while at 600ºC and further all values where minimized. Composition L, presented a different behavior, maintaining the initial value up to 600ºC.

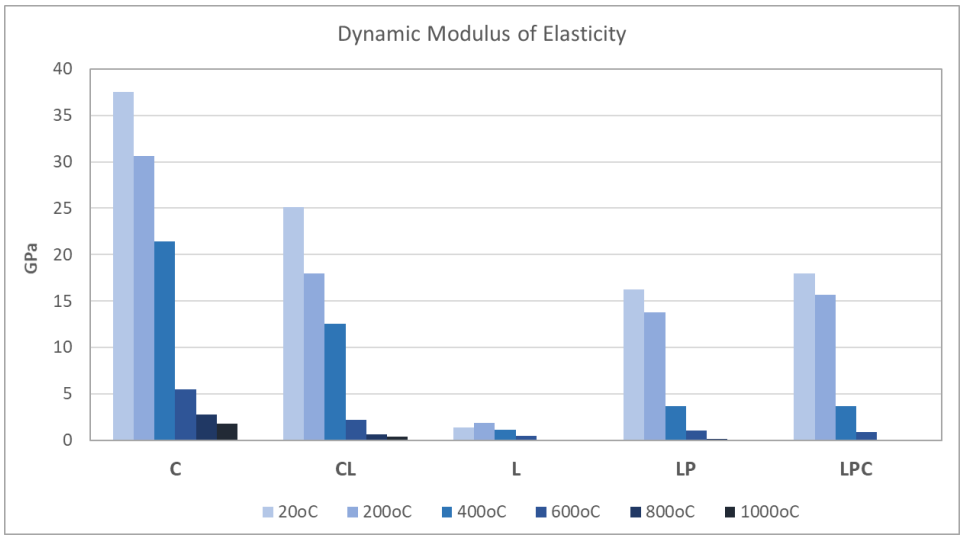


Figure 7: Dynamic Modulus of Elasticity of the mortar specimens, exposed at elevated temperatures

In flexural strength (Fig.8), compositions had a different behavior, according to their type. Although the values were decreased throughout the elevated temperatures for C, in the rest compositions there was a strength increase at 200ºC (mainly in CL). The values were further decreased, especially above 600ºC. In composition L, values maintained at a low level (~0.3MPa) throughout all temperatures.

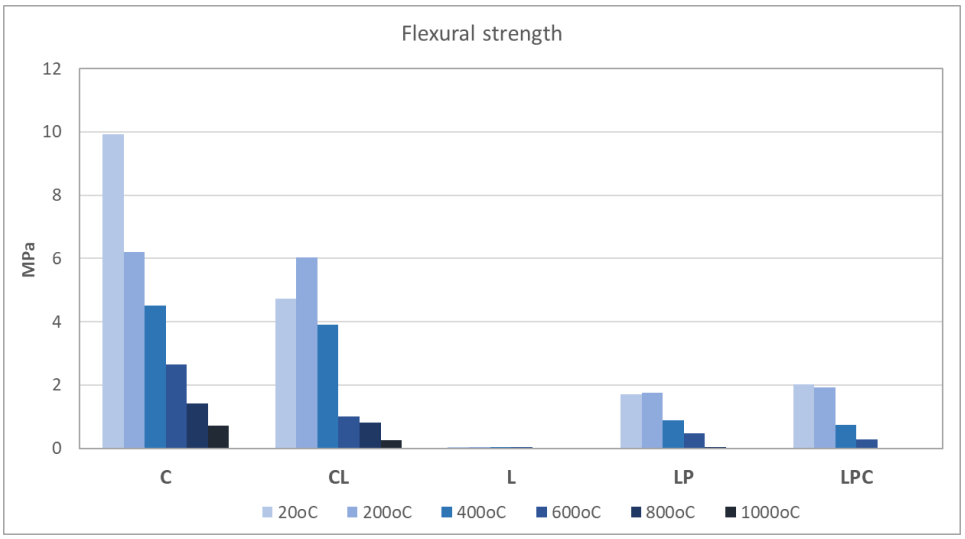


Figure 8: Flexural strength of the mortar specimens, exposed at elevated temperatures

Compressive strength values (Fig.9), also presented fluctuations among the compositions. As it is presented in Figure 10, C showed a gradual (almost linear) strength loss throughout all temperatures (30% at 400ºC and 45% at 600ºC) leading to a final loss of 85% (61→10MPa). Composition CL had a strength increase at 200 and 400ºC (30-40%), while it was significantly reduced at 600ºC (~50%) and minimized at 1000ºC (17.5→4.5MPa). Compositions L, LP and LPC showed a strength increase up to 600ºC (around 20-100%) and a further strength decrease

at 800 and 1000ºC. The highest strength increase was observed for LP at 400ºC (100%), while the lowest loss was shown for L at 800 and 1000ºC (20-30%).

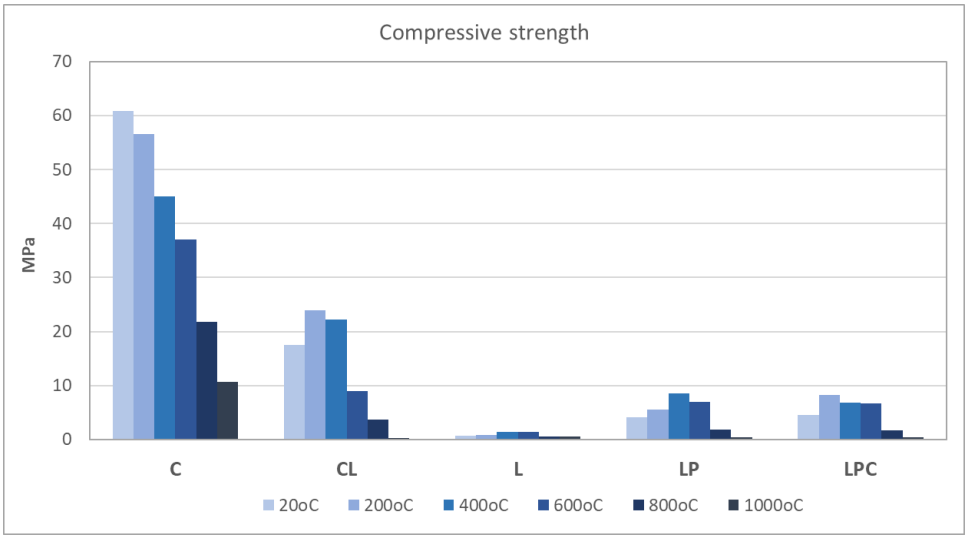


Figure 9: Compressive strength of the mortar specimens, exposed at elevated temperatures

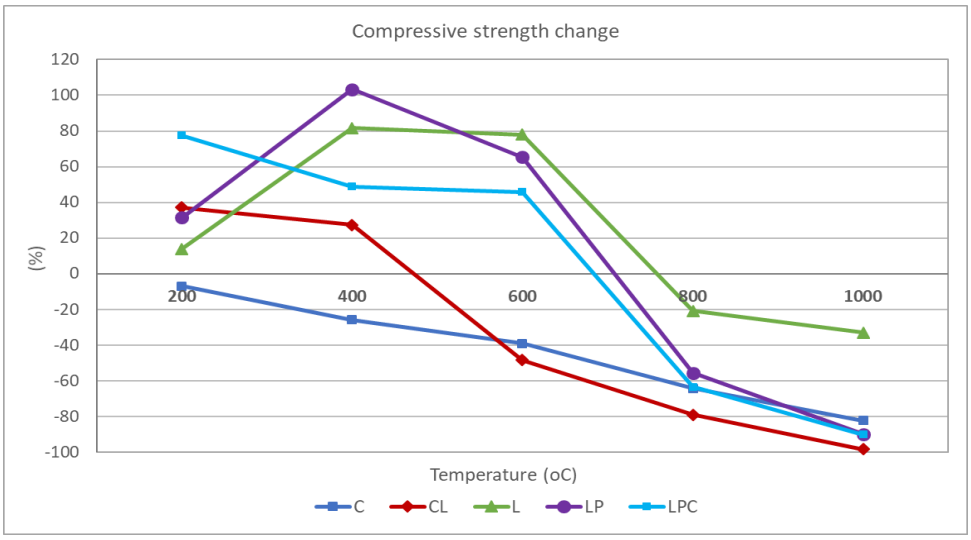


Figure 10: Compressive strength changes of the mortar specimens, exposed at elevated temperatures

The structure of the specimens, after their exposure at the elevated temperatures was generally maintained, as presented in Figure 11. At 600ºC limited spalling and color alterations were observed, which were more intense at 800 and 1000ºC. Composition L was cracked at 800 and severely damaged at 1000ºC, while LPC also presented extreme damages at 1000ºC. Regarding the more extreme color changes (according to the Munsel scale), compositions C and CL were converted from GLEY 2, 7/1 light bluish gray and GLEY 2, 8/1 light bluish gray respectively to GLEY 2, 8/1 light greenish gray.

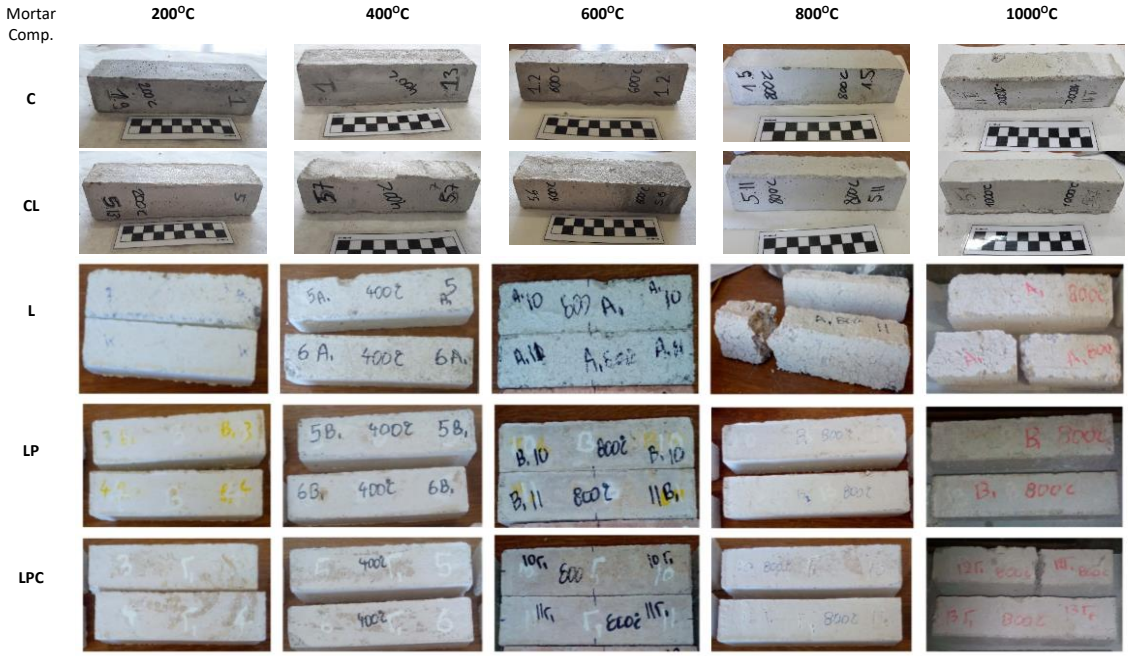


Figure 11: Macroscopic photographs of the mortar specimens, exposed at elevated temperatures

4 CONCLUSIONS

The performance of building materials at elevated temperatures, is a significant factor influencing their maintenance and preservation state. In the present study, an effort was made to assess the resistance of mortars made by contemporary and traditional binders, showing that the initial strength level of materials may not be the key element of their performance.

According to the research results, cement-based mortars (composition C) presented significant decay when exposed at elevated temperatures. High volume reduction was recorded (2-4%), extreme increase of porosity (values are tripled, 8→24%), while mechanical properties were significantly influenced. At 600ºC strength loss was around 45-75%, with the flexural strength to be severely affected (flexural strength: 10→2.5MPa, compressive strength: 60→38MPa). At 1000ºC flexural and compressive strength was reduced around 85-90%.

When lime was added in the mixture (CL), the physical properties were enhanced throughout the elevated temperatures. Mechanical characteristics were maintained (with a slight increase) up to 400ºC and were further reduced at 600ºC (50% for compressive and 80% for flexural strength). At 1000ºC they were minimized.

In the case of lime-based mortars, a slight volume change was recorded, whereas the mass change was extreme (8-20%). Porosity values were almost doubled (16→30%) except for the pure lime mortar (L), which presented the lowest fluctuations (29-34%). Mechanical properties and especially compressive strength was enhanced up to 600ºC (around 80% in the case of LP) and were minimized at 1000ºC. The pure lime mortar (L) was the one to present the lowest strength loss at 800 and 1000ºC (20-30%).

It is therefore asserted that, contradictory to the cement-based mortars, lime-based binding systems (C:L, L:P, L:P:C) presented a generally good behavior, up to the limit of 600ºC, maintaining both their physical and mechanical properties. However, at the highest temperatures of 800 and 1000ºC cement-based mortars seemed to present a better performance.

Concluding, it is noticed that the binding system significantly influences the overall behavior of the mortars at elevated temperatures. The addition of lime in traditional or contemporary mortar systems seem to be benefited in the case of extreme temperatures. However, more oriented research should be made in order to further document the physico-chemical reactions taking place in the mortar matrix.

REFERENCES

[1] Lea F. and Stradling R. The resistance to fire of concrete and reinforced concrete. *Engineering* (1922) **114**:395R-396R.

[2] Georgali B. and Tsakiridis P.E. Microstructure of fire-damaged concrete. A case study. *Cement Concrete Comp* (2005) **27**:255-59.

[3] Chan Y.N., Peng G.F. and Anson M. Residual strength and pore structure of high-strength concrete and normal strength concrete after expose to high temperature. *Cement Concrete Comp* (1999) **21**:23-27.

[4] Ingham J.P. Application of petrographic examination techniques to the assessment of fire-damaged concrete and masonry structures. *Mater Charact* (2009) **60**:700-9.

[5] Khoury G.A. Effect of fire on concrete and concrete structures. *Prog Struct Eng Mat* (2000) **2**:429-47.

[6] Chung H.W. and Law K.S. Assessing fire damage of concrete by the ultrasonic pulse technique. *Cement Concrete Aggr* (1985) **7**:84-8.
[7] Pachta V., Triantafyllaki S. and Stefanidou M. Performance of lime-based mortars at elevated temperatures. *Constr and Build Mat* (2018) **189**:576-84.
[8] Krzemien K. and Hager I. Post-fire assessment of mechanical properties of concrete with the use of the impact-echo method. *Constr Build Mater* (2015) **96**:155-63.
[9] Stefanidou M. and Pachta V. Influence of perlite and aerogel addition on the performance of cement-based mortars at elevated temperatures. In: Int. Conf. *SBE19, Sustainability in the built environment for climate change mitigation* (2019).
[10] RILEM TC 129 MHT. Test methods for mechanical properties of concrete at high temperatures and RILEM TC HTC. Mechanical concrete properties at high temperature-modelling and applications; Part 1: Introduction. *Mater Struct* (2007) **40**:841-53
[11] RILEM TC 200-HTC. Recommendation of RILEM TC 200-HTC: mechanical concrete properties at high temperatures - modeling and applications Part 1: Introduction - General presentation. *Materials and Structures* (2007) **40**:841-53.
[12] EN 1991-1-2 2002. *Eurocode 1: Actions on structures - Part 1-2: General actions - Actions on structures exposed to fire*. European Committee for Standardization (Brussels).
[13] EN 1992 2004. Eurocode 2: Design of concrete structures - Part 1-2: General rules - Structural fire design European Committee for Standardization (Brussels).
[14] ISO 834-11 2014. *Fire resistance tests - Elements of building construction - Part 11: Specific requirements for the assessment of fire protection to structural steel elements*. International Standards Organization.
[15] BS 476-3 2004. *Fire tests on building materials and structures. Classification and method of test for external fire exposure to roofs*. British Standards Institute (London).
[16] Russo S. and Sciarretta F. Masonry exposed to high temperatures: Mechanical behaviour and properties - An overview. *Fire Safety Journal* (2013) **55**:69-86.
[17] Pachta V., Triantafyllaki S. and Stefanidou M., The impact of elevated temperatures at the properties of lime-based mortars. In: J.I. Alvarez et al. (Eds): *5th Historic Mortars Conference, HMC 2019*, RILEM Proceedings, PRO 130 (2019), pp. 1156-1165.

12th International Conference on Structural Analysis of Historical Constructions
SAHC 2020
P. Roca, L. Pelà and C. Molins (Eds.)

EXPERIMENTAL CAMPAIGN ON THE USE OF THE FLAT JACK TEST IN COB WALLS

ALEJANDRO JIMÉNEZ RIOS[1*], MICHAEL GRIMES[1] AND DERMOT O'DWYER[1]

[1]Department of Civil, Structural and Environmental Engineering
Trinity College Dublin (TCD)
College Green, D02 Dublin, Ireland
e-mail: jimnezra@tcd.ie, https://www.tcd.ie/civileng/people/doctoral-students/alejandro-jimenez-rios.php (*corresponding author)

Keywords: Conservation, Minor Destructive Tests (MDT), Earthen Architecture, Mechanical Properties

Abstract. *The flat jack test is one of the most used investigation techniques in the area of architectural heritage conservation. Unfortunately, there are no results available in the literature reporting the use of the flat jack technique in cob walls. This paper presents the firs experimental campaign performed to validate the use of this Minor Destructive Technique (MDT) to determine the levels of stress in cob walls and their mechanical properties. Furthermore, three workshops organized and facilitated with the aim of increasing public engagement and awareness towards the conservation of earthen vernacular architecture are also presented.*

1 INTRODUCTION

The flat jack test was first developed and applied in the study of rock mechanics [1]. After its adoption in the years 1980s by Rossi for its use in masonry walls, the method has been used by several researchers to determine the level of stresses and the mechanical properties of ashlar, brick and stone masonry, as well as of, adobe and rammed earth walls [2].

Cob is an earthen construction technique that was traditionally used in at least 18 European countries [3], and many others around the world [4], to build, mainly, dwellings and farming buildings. Cob elements are as well present in 29 UNESCO World Heritage Sites as highlighted by the World Heritage Inventory of Earthen Architecture [5].

Despite the widespread presence of cob buildings and the popularity of the flat jack test among conservation engineers, no results have ever been reported on the application of this Minor Destructive Technique (MDT) on such kind of wall typology.

This paper presents the description of the first laboratory experimental campaign to assess the feasibility of the application of the flat jack test to determine the stress levels and the mechanical properties of cob walls.

2 EXPERIMENTAL CAMPAIGN

The experimental campaign started in the spring of 2018 with the literature review of the topic (see Figure 1 where the followed methodology is presented in a diagram form).

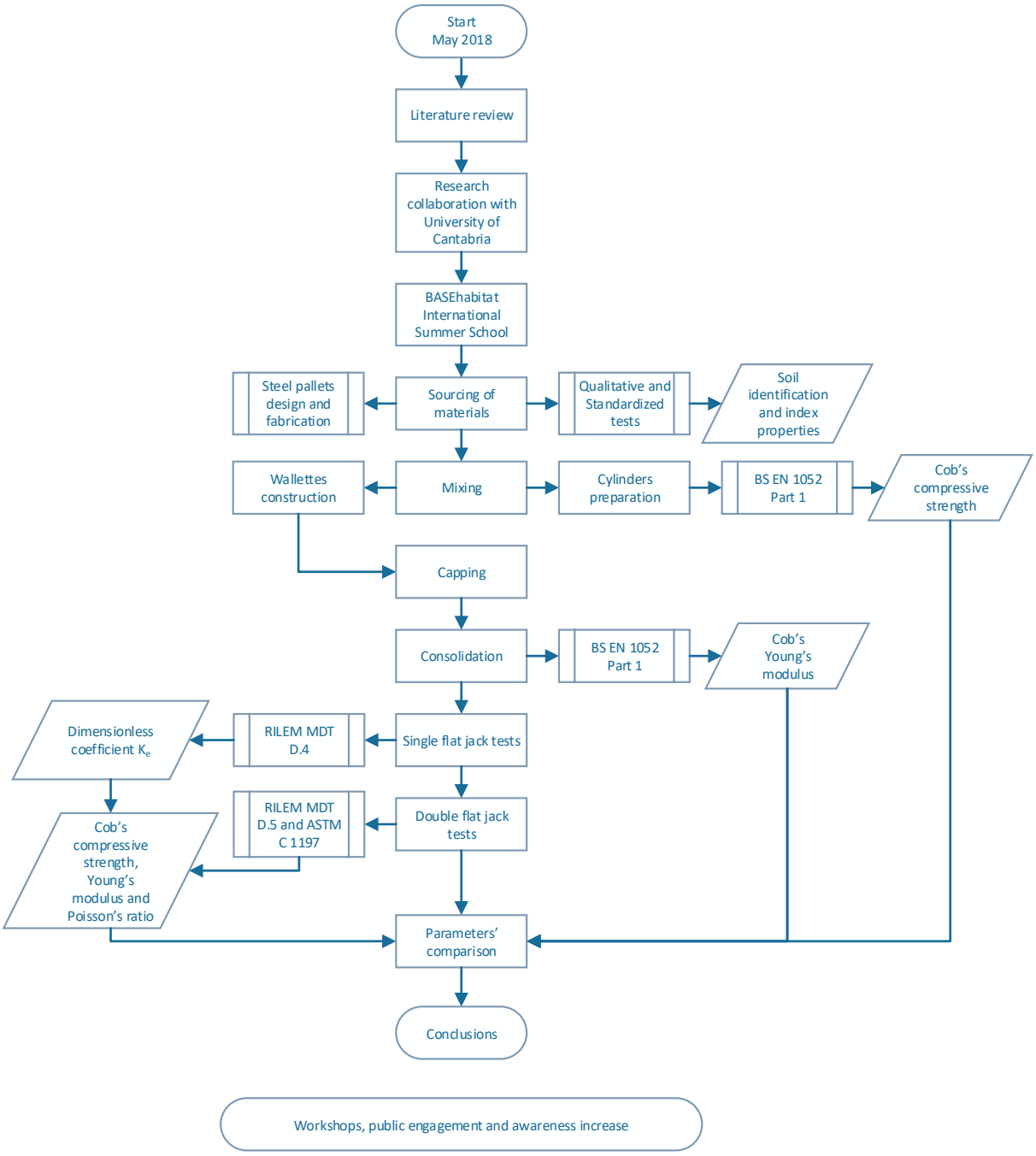


Figure 1: Methodology's steps implemented during the experimental campaign.

The necessary technical knowledge to implement the flat jack test technique was acquired thanks to a research collaboration carried out at the University of Cantabria (UC) in Santader, Spain, during the months of June and July 2018. The expertise and know-how acquired during this period proved to be invaluable for the success of the flat jack tests performed in this experimental campaign.

The traditional cob construction technique was learned by the first author during his

participation at the International BASEhabitat Summer School organized by the University of Linz, Austria. In this event, experienced earthen builders and researchers, taught the traditional skills used in France, UK and Ireland to build vernacular cob walls and these skills were used to build the wallettes at the laboratory of Civil Structural and Environmental Engineering (CSEE) in Trinity College Dublin (TCD).

The basic raw materials needed to build a cob wall are: straw, water and soil. It was intended to build the wallettes of this experimental campaign in a sustainable way and to try to reproduce the characteristics of a historical cob wall as closely as possible. Thus, materials were sourced locally, and traditional construction methods were used. The selection of the raw materials was based on recommendations provided by several authors [6–12]. Those recommendations are mainly concerned with the water quality, the type and the length of the straw, the clay content and the Particle Size Distribution (PSD) of the soil.

Qualitative soil tests have been traditionally used by vernacular builders, who had no access to complex equipment and laboratory facilities, to assess the suitability of the material for earthen construction purposes. These tests are highly related to the human senses and provide basic information about the constitution of the soil and of its behavior. The advantages of qualitative tests are their simplicity, easiness, low-cost and their relatively fast data obtainment. On the other hand, the interpretation of qualitative tests is subjective and depends on the experience and personal judgement of the test performer. Qualitative tests were performed on a sample of soil collected directly from the soil supplier yard. Those tests are shown in Figure 2.

To classify and determine the basic properties of the soil the standards followed in this experimental campaign were the BS 1377: Methods of test for soils for civil engineering purposes Part 1: General requirements and sample preparation [13], Part 2: Classification tests [14] and Part 3: Chemical and electrochemical tests [15]. Based on the data obtained from these standardized tests, the soil was identified and classified in accordance with BS EN ISO 14688 Geotechnical investigation and testing – Identification and classification of soil Part 1: Identification and description [16] and Part 2: Principles for a classification [17], respectively. Standardized tests were performed on a sample of soil obtained from the 1 m^3 bags delivered by the soil supplier.

The components' mixing proportions were based on recommendations given by several authors [11–12–18–19] and adopted to the physical constrains of the laboratory of CSEE in TCD. Thus, mixes of 80 kg of soil with 1.2 kg of straw and 12 kg of water were adopted. Each one of the mixes provided enough material to build a layer of approximately 10 cm height. Thus, in average, 10 mixes were necessary to build each one of the wallettes with approximate dimensions of 100 cm length by 100 cm height by 40 cm thickness.

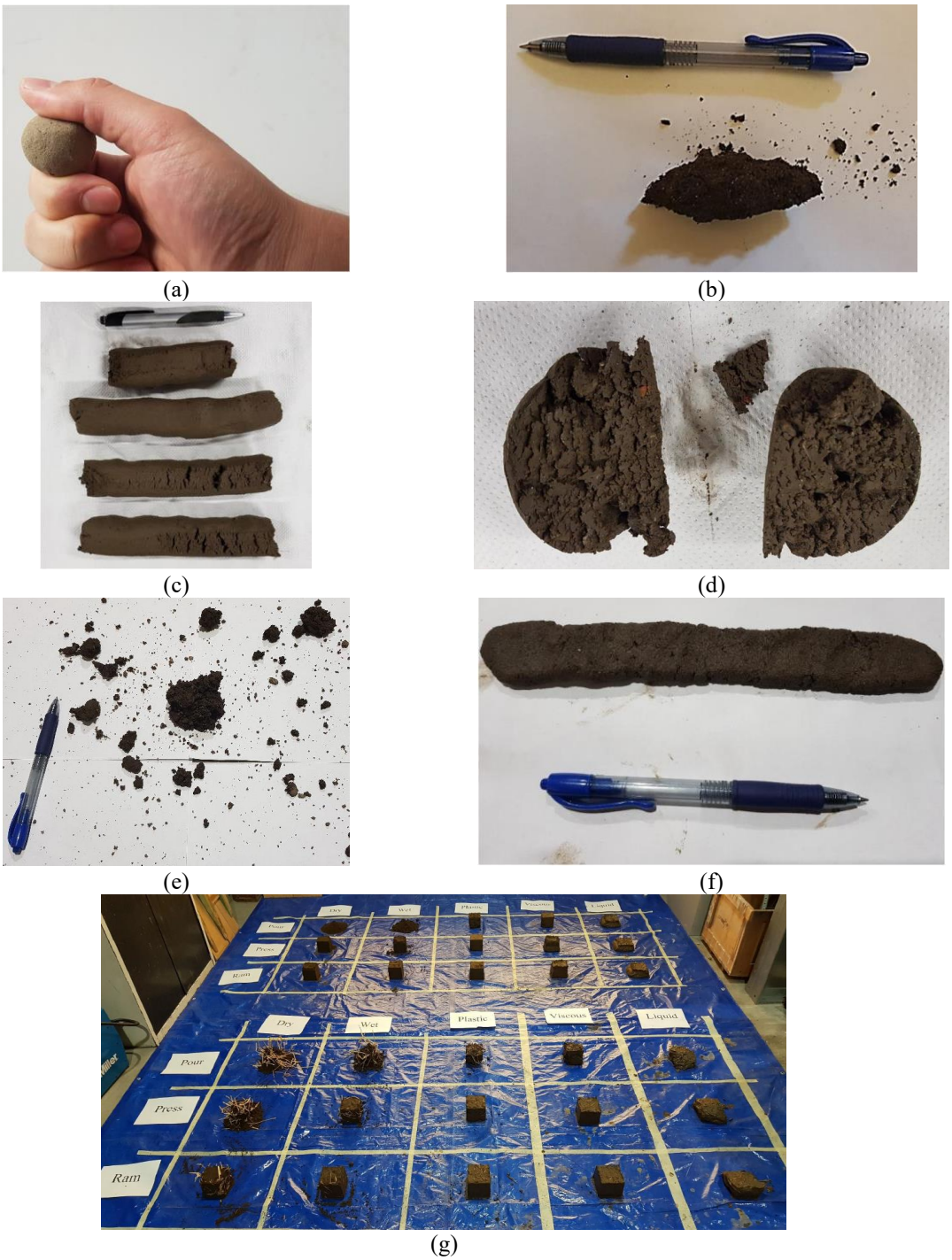
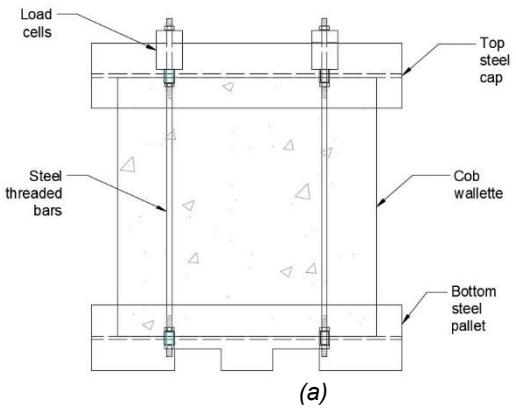


Figure 2: Qualitative tests performed, namely, (a) pressing ball, (b) touching, (c) cigar, (d) ball cutting, (e) ball dropping, (f) ribbon and (g) Carazas.

The cob wallettes were built on top of steel pallets to facilitate their transportation around the laboratory. Moreover, a top cap was also fabricated with the idea of connecting it with the

bottom pallet through threated steel bars and applying low compression force during transportation of the wallettes in order to avoid damaging the wallette due to vibrations that might have led to tensile stresses and therefore the opening of cracks. The steel bottom pallets and top cap were designed using a universal beam (UB) 533x210x82 section (this section was selected to accommodate the dimensions of the cob wallettes and of the pallet jack used in the laboratory). The bottom pallets were perforated at four locations of their flanges to allow the pallet jack to go beneath them. On the other hand, four C-channel section segments were welded to the web of the top cap to act as points of attachment and provide symmetric points of attachment for the crane's chains, thus allowing the lifting of the wallettes. Finally, four pieces of hollow steel tube were welded to both bottom and top UB flanges to provide the points of connection of the threaded bars.

Once the loam was readily mixed, it was divided into balls of approximately 20 to 30 cm in diameter. The balls were thrown to the steel pallet to build the first 10 cm layer of the first 30 cm lift of each one of the wallettes. Balls were thrown being careful to assure overlapping with previous balls and moulded with the fingers to try to fill all voids. The lifts were built a couple of cm bigger than the marked area of 0.4 by 1.0 m on the steel pallets with the aim of avoiding having any holes or cavities at the faces after the pairing of the surfaces. Once the bottom lifts achieved the desired height their top surface was marked with the fingers in order to create holes that would improve the interlocking with upper lifts. The pairing of each one of the wallettes' lifts was done four or five days after their construction and before adding the next lift on top of them. A timber saw was used to remove the extra material protruding from the faces and a bubble level was used as guidance to achieve verticality of the wallettes' faces. After the first lift was paired the second lift was added ensuring that extra material would protrude over the sawn faces. Furthermore, the top surface of the second lift was also finger-marked to ease the interlocking of the last lift. Again, after a short drying period (4 or 5 days) the second lift was paired using the timber saw and the bubble level. Next, the last lift was added and subsequently paired. They wallettes were built in three lifts, 30 cm, 30 cm and 40 cm height respectively. All dimensions varied by +/- 2 cm due to the inherent variability traditional construction process adopted. The wallettes were stored indoors for a drying period of 4 months under uncontrolled environmental conditions. A diagram of the built specimens is presented in Figure 3.



(a)

Figure 3. Diagram of the built cob wallettes.

To ensure a horizontal top surface and consequently an even distribution of the compressive load the wallettes were capped with a layer of cement mortar. Timber formwork was clamped to the wallettes and levelled with the help of a bubble level. The cement mortar was placed on top of the wallette and levelled with a straight piece of timber. The finished surface was completely flattened and cured for several days with the application of a wet hessian cloth.

In a parallel process, six cylinders were prepared, using randomly sampled material from the cob wallettes' mixes, with the objective of performing compressive tests on them to estimate cob's compressive strength. This data would give a point of reference to establish the consolidation and test loads to be applied to the wallettes. The cylinders were prepared using 15 cm diameter by 30 cm length steel molds. The mold was filled with six or seven layers of cob. Every layer was tamped by hand, pressing with the fingers to try to fill all the voids. This preparation procedure is similar to the one implemented by Pullen and Scholz [20].

After a four-months drying period the pre-consolidation of the wallettes began. The pre-consolidation load applied to the wallettes was fixed taking as reference the mechanical properties obtained from the cob cylinders tested in this experimental campaign. It was decided not to exceed the apparent yield point of cob which corresponded approximately to 30 % of the computed average compressive strength of the cylinders (0.7 MPa). Therefore, the wallettes were subjected to a consolidation force of 84 kN +/- 1 kN.

The loading set-up consisted in 4 treaded bars fixed at the bottom and top steel pallets which were tensioned by tightening the nuts at the top. The tightening of the nuts was performed manually, in increments of approximately 2 kN per bar, and the initial loading process, going from 0 up to 85 kN took approximately 15 to 20 min for each wallette. The tension forces thus applied caused the shortening of the bars, deformation that subsequently translated into a compressive force applied to the cob wallettes. Therefore, loads were applied slightly eccentrically but in a symmetric way as the points of anchorage of the bars were located at the external faces of the steel pallets flanges. A load cell was installed between each point of support at the top steel pallet and the nut to measure the load transferred for each one of the bars to the wallette. The total load transferred to the wallette was calculated as the sum of the four bars' forces.

Four linear variable differential transformers (LVDT) were attached to the wallettes' faces, two in the front and two in the back, to measure the deformation caused by the compressive forces. The LVDT's were pinned through the material using stainless-steel pins of roughly 5 to 6 cm length by 2 mm diameter. The points of support were held in place at an initial distance of roughly 30 cm at the middle third of the specimens. This arrangement was in agreement with BS EN 1052 Part 1 [21].

The procedures described in ASTM C 1196 Standard test method for in-situ compressive stress within solid unit masonry estimated using flat jack measurements [22] and in RILEM LUM D2/MDT D4 In-situ stress tests on masonry based on the flat jack [23–24], specialized in masonry walls, were adopted and adapted to perform the single flat jack test in the cob wallettes of this experimental campaign. Similarly, the procedures described in ASTM C 1197 Standard test method for in situ measurement of masonry deformability properties using the flat jack method [25] and in RILEM LUM D3/MDT D5 In-situ stress/strain behavior tests based on the flat jack [26–27], were adopted and adapted to perform the double flat jack test.

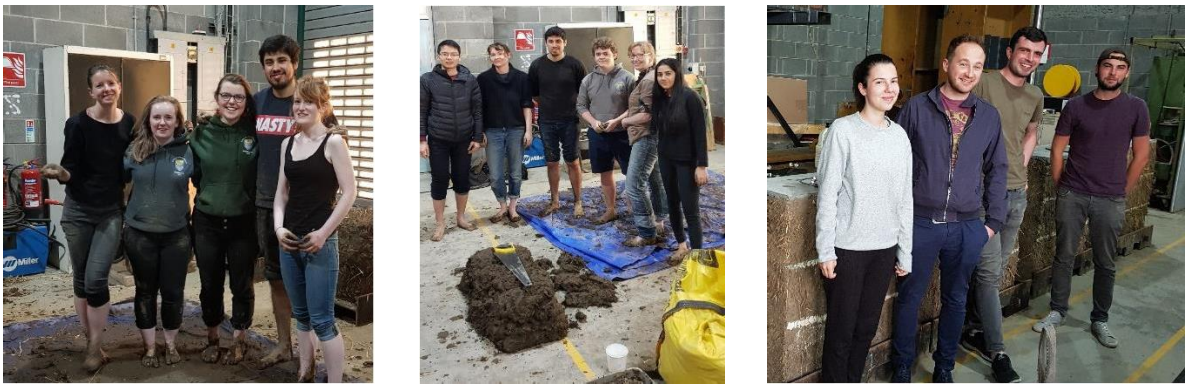
The data obtained during the experimental campaign can be consulted elsewhere [28].

3 WORKSHOPS

As this experimental campaign aimed at increasing awareness regarding the importance of conservation of vernacular architecture, the experimental campaign was used to involve a great number of people and disseminate the acquired knowledge about the subject. Academics, technical staff, researchers, as well as undergraduate students and the general public participated in the different activities developed during this experimental campaign related to the conservation of earthen vernacular buildings and the use of natural materials for sustainable construction purposes.

Two one-day workshops were run. In the first one, undergraduate students were invited to attend a morning presentation on the conservation of earthen vernacular buildings in Ireland and to participate in the construction of the wallettes of the experimental campaign. The second workshop was organized within the framework of the Trinity Green Week 2019. The Trinity Green Week is an annual environmentally themed event with a multitude of events to simulate the mind and engage the soul in creating better world citizens. Both students and the general public were invited to participate in this second workshop. Participants to both workshops are shown in Figure 4 (a) and Figure 4 (b), respectively.

Finally, students of architecture from University College Dublin (UCD) and from the Dublin Technical University (DTU) were invited to the laboratory of TCD. The students were given a presentation on the main aspects of the experimental campaign performed. After this, a tour around the laboratory facilities was conducted where they could see the specimens that were built and tested along with the flat jack tests' equipment that was used in the experimental campaign (Figure 4 (c)).



(a) (b) (c)

Figure 4: Cob workshops' participants.

4 CONCLUSIONS

The flat jack test is one of the most applied investigation techniques in the area of cultural heritage conservation, where the information obtained with this method is used, to assist in the structural safety evaluation of existent structures. The experimental campaign carried out and presented in this paper provided the first results of a flat jack test ever performed in a cob wall.

Another important part of this research comprised the series of public engagement and awareness increase activities performed around the experimental campaign presented in this work. The discussions that took place during and after the workshops proved to be extremely

rich, especially due to their multidisciplinary character and the different backgrounds and previous experiences of the participants of the events.

Acknowledgements. This work was supported by the Department of CSEE at TCD. The authors would like to thank all the technical staff of this Department for their invaluable help and support. The authors would also like to thank Professors Luis Villegas and Ignacio Lombillo for hosting the first author at University of Cantabria, Spain, and for sharing with him their experience and know-how with the at jack technique.

REFERENCES

1. P. B. Gregorczyk Pawełand Lourenço, A review on flat-jack testing. *Engenharia Civil*, (2000).
2. I. Lombillo Vozmediano, Investigación teórico-experimental sobre ensayos ligeramente destructivos (MDT) utilizados para la caracterización mecánica in situ de estructuras de fábrica del patrimonio construido, Universidad de Cantabria, 2010.
3. M. Correia, L. Dipasquale, S. Mecca, & K. Akermann, Terra Europae: earthen architecture in the European Union. *Pisa: ETS*, (2011).
4. S. Piesik, *Habitat: vernacular architecture for a changing planet* (Thames & Hudson, 2017).
5. D. Gandreau & L. Delboy, World heritage inventory of earthen architecture. *CRATerre-ENSAG, Grenoble (France)*, (2012).
6. P. Doat, A. Hays, H. Houben, S. Matuk, & F. Vitoux, *Construire en terre* (CRAterre, 1979).
7. L. Keefe, *Earth building: methods and materials, repair and conservation* (Routledge, 2012).
8. P. Jaquin & C. Augarde, *de la source Earth building: history, science and conservation* (distributeur IHS BRE Press, 2017).
9. G. Minke, *Building with earth: design and technology of a sustainable architecture* (Walter de Gruyter, 2012).
10. L. Miccoli, U. Müller, & P. Fontana, Mechanical behaviour of earthen materials: a comparison between earth block masonry, rammed earth and cob. *Construction and building materials*, **61** (2014) 327–339.
11. E. Hamard, B. Cazacliu, A. Razakamanantsoa, & J.-C. Morel, Cob, a vernacular earth construction process in the context of modern sustainable building. *Building and environment*, **106** (2016) 103–119.
12. T. Teixeira, C. Konig, & U. Schwantner, *BASEhabitat Summer School 2018 Handbook* (BASEhabitat, 2018).
13. *BS 1377-1:2016 Methods of test for soils for civil engineering purposes - Part 1: General requirements and sample preparation* (London, United Kingdom: British Standards Institution, 2016).
14. *BS 1377-2: 1990 Methods of test for soils for civil engineering purposes - Part 2: Classification tests* (London, United Kingdom: British Standards Institution, 1990).
15. *BS 1377-3: 2018 Methods of Test for Soils for Civil Engineering Purposes - Part 3: Chemical and electro-chemical tests* (London, United Kingdom: Brisith Standards Institution, 2018).

16. *BS EN ISO 14688-1:2018 Geotechnical investigation and testing. Identification and classification of soil. Identification and description* (London, England: British Standards Institution, 2018).
17. *BS EN ISO 14688-2:2018 Geotechnical investigation and testing. Identification and classification of soil. Principles for a classification* (London, England: British Standards Institution, 2018).
18. F. McDonald & P. Doyle, *Ireland's earthen houses* (A. & A. Farmar, 1997).
19. L. Watson & K. McCabe, The cob building technique. Past, present and future. *Informes de la Construccion-Revista*, **63** (2011) 59.
20. Q. M. Pullen & T. V Scholz, Index and engineering properties of Oregon cob. *Journal of Green Building*, **6** (2011) 88–106.
21. *BS EN 1052-1:1999 Methods of test for masonry. Determination of compressive strength* (London, England: British Standards Institution, 1999).
22. *ASTM C1196-09 Standard test method for in situ compressive stress within solid unit masonry estimated using flatjack measurements* (West Conshohocken, PA: ASTM International, 2009). https://doi.org/10.1520/C1196-09.
23. *RILEM LUM D2 In-situ stress tests on masonry based on the flat jack* (RILEM TC, 1994). https://doi.org/10.1617/2351580117.157.
24. *RILEM MDT. D.4 In-situ stress tests based on the flat jack* (RILEM, 2004). https://doi.org/10.1007/BF02481588.
25. *ASTM C1197-14a Standard test method for in situ measurement of masonry deformability properties using the flatjack method* (West Conshohocken, PA: ASTM International, 2014). https://doi.org/10.1520/C1197-14A.
26. *RILEM LUM D3 In-situ strength/elasticity tests on masonry based on the flat jack* (RILEM TC, 1994). https://doi.org/10.1617/2351580117.158.
27. *RILEM MDT. D.5 In-situ stress-strain behaviour tests based on the flat jack* (RILEM, 2004). https://doi.org/10.1007/BF02481589.
28. A. R. Jimenez & D. O'Dwyer, Experimental validation for the application of the flat jack test in cob walls. *Construction and Building Materials*, (n.d.).

12th International Conference on Structural Analysis of Historical Constructions
SAHC 2020
P. Roca, L. Pelà and C. Molins (Eds.)

EXPERIMENTAL INVESTIGATION OF SCARF JOINT OF 'LIGHTNING SIGN' IN BENDING

ANNA KAROLAK[1*], JERZY JASIEŃKO[1]

[1]Faculty of Civil Engineering
Wroclaw University of Science and Technology
Wybrzeze Wyspianskiego 27, 50-370 Wroclaw, Poland
e-mail: anna.karolak@pwr.edu.pl (*corresponding author)

Keywords: Carpentry joints, Scarf joints, Joint of 'lightning sign'/ 'Bolt of lightning'/ 'Trait-de-Jupiter', Experimental research, Bending tests

Abstract. *The paper presents a description and results of the research concerning one of the scarf joints, so-called 'lightning sign' (also described as 'Bolt of lightning' or 'Trait-de-Jupiter'). This joint has been used and can be commonly found in wooden historical structures and is considered to be an interesting example of carpentry longitudinal joints. In the experimental part timber beams with this type of joint shaped in the different planes, horizontal and vertical, reinforced with spindle fasteners (metal bolts), were subjected to four-point bending tests. As a result, the static equilibrium paths and the bending capacities of individual beams were obtained. They were compared to the load-bearing capacity of the continuous reference beam. Moreover, a simplified numerical analysis based on FEM was carried out for comparison the rigidity of individual beams. A comparison of the results for series of beams is discussed and some conclusions and possible directions of the future actions in the subject are presented.*

1 INTRODUCTION

For centuries, wood has been a commonly used building material for different types of buildings: simple houses, residential buildings, sacral architecture, defensive structures, and sophisticated engineered structures like bridges, etc. Some of the timber structures have survived since that time and nowadays require interventions to maintain or improve their technical condition. One of the most important factors in this work is the issue of joints, which enable building elements to be connected into a single whole and for loading to be transferred between elements. Sometimes carpentry joints, that can be found in historical buildings, had sophisticated forms, which indicates the highly developed techniques and craftsmanship of builders of that time [1].

There are many types of carpentry joints in historical buildings distinguished by researchers, depending, for example, on their function and form (i.a. in [2]). One group includes scarf joints and splice joints. They were used to create a connection along the length of the two elements, when the available material could not cover the whole beam length. It was preferably to perform them in the least stressed sections, as the connecting elements at the point of contact could not bear a load greater than that in continuous sections [3]. They were applied to extend foundation beams and capping beams in building frames of historical structures as well as roof frame

elements, such as purlins or rafter beams. Until the development of glue-laminated wood techniques, this was a commonly used method for extending wood elements [4]. Nowadays, scarf and splice carpentry joints are used i.a. to restore historical joints or to replenish the material in historical elements. Some examples of scarf and splice joints found in historical structures, from simple to refined forms, are presented in Figure 1.

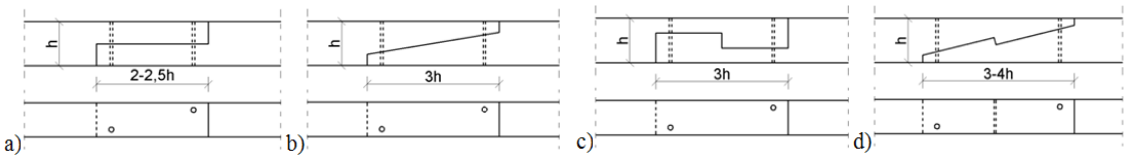


Figure 1: Different forms of scarf and splice joints: a) splice joint, b) nibbed scarf joint, c) tabled splice joint, d) stop-splayed scarf joint ('Bolt of lightning')

Scarf joints of lightning sing or stop-splayed scarf joints, also described as 'Bolts of lightning' or 'Trait-de-Jupiter' were presented i.a. in [5-8]. They are sophisticated forms of connections along the length of elements. Other examples of these forms are built-up beams or composite beams with a teethed joint – elements connected along their whole length with the scarf joints of the lightning sign, described i.a. in [9-11]. These types of joints are common for historical buildings. They have been used since ancient times (e.g., Roman bridge constructions). A great development of these forms was the time of the Italian Renaissance (e.g., Leon Battista Alberti – Figure 2a [12] or Leonardo da Vinci – Figure 2b [9]). Typically, the joints were wedged, which ensured a tight fitting joint and helped in load transferring.

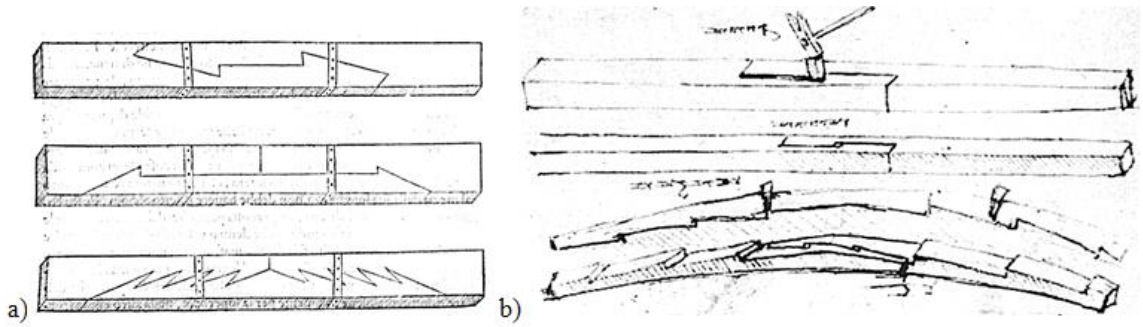


Figure 2: Drawings of scarf and splice carpentry joints according to a) L.B. Alberti [12], b) L. da Vinci [9]

A few available descriptions of research concerning typical scarf joints of lightning sign are presented, among others, in the following: [9-11,13-15]. Nevertheless, it has been observed that most of the research concerning the static behaviour of carpentry joints presented in the literature focused mainly on tenon joints and notched joints. There is definitely less research on joints subjected to bending loads as well as bending and tension or bending and compression. What is more, the vast majority of researchers, who have been dealing with this topic (among others, Rug et al. in [10,11], Hirst et al. in [14], and Fajman et al. in [16-21] as well as Kunecky et al. in [22-28]) claim that there is still a shortage of research for a full description of static behaviour of such joints and hence designing the most beneficial methods for repairing or

strengthening them. Therefore, as a part of a research project (financed by Polish National Science Centre), some tests on the static behaviour of scarf joints of lightning sign subjected to bending and a simplified numerical analysis were carried out.

2 MATERIALS AND METHODS

2.1 Models for experimental tests

For the part of the experimental testing, beam models in technical scale from pine wood (*Pinus sylvestris L.*) of the minimum C24 class were prepared. The dimensions were 360 cm length and a cross-section measuring 12 cm x 18 cm. Testing involved 3 series with 3 beam models each. Series A included continuous beams as references. Other series included beams with scarf joints of lightning sign (stop-splayed scarf joints) created in the horizontal (series E) and vertical (series H) planes. The geometry of the joints was based on data obtained from real structures and the literature. Joints were strengthened with metal bolts (M12) and double-sided tooth plate connectors type C10 (Geka). The drawings of views, sections, and axonometric schemes of the beam models with joints used for the tests are shown in Figures 3 and 4.

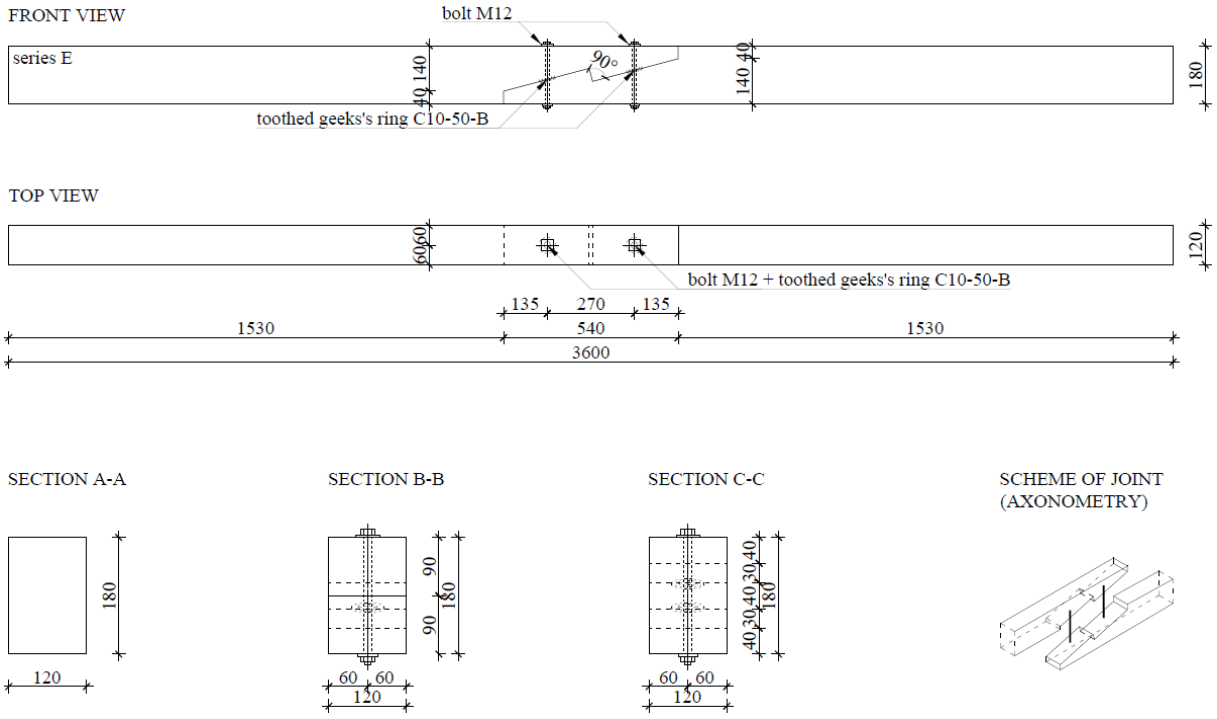


Figure 3: Beam model with scarf joint of lightning sign in the horizontal plane (series E)

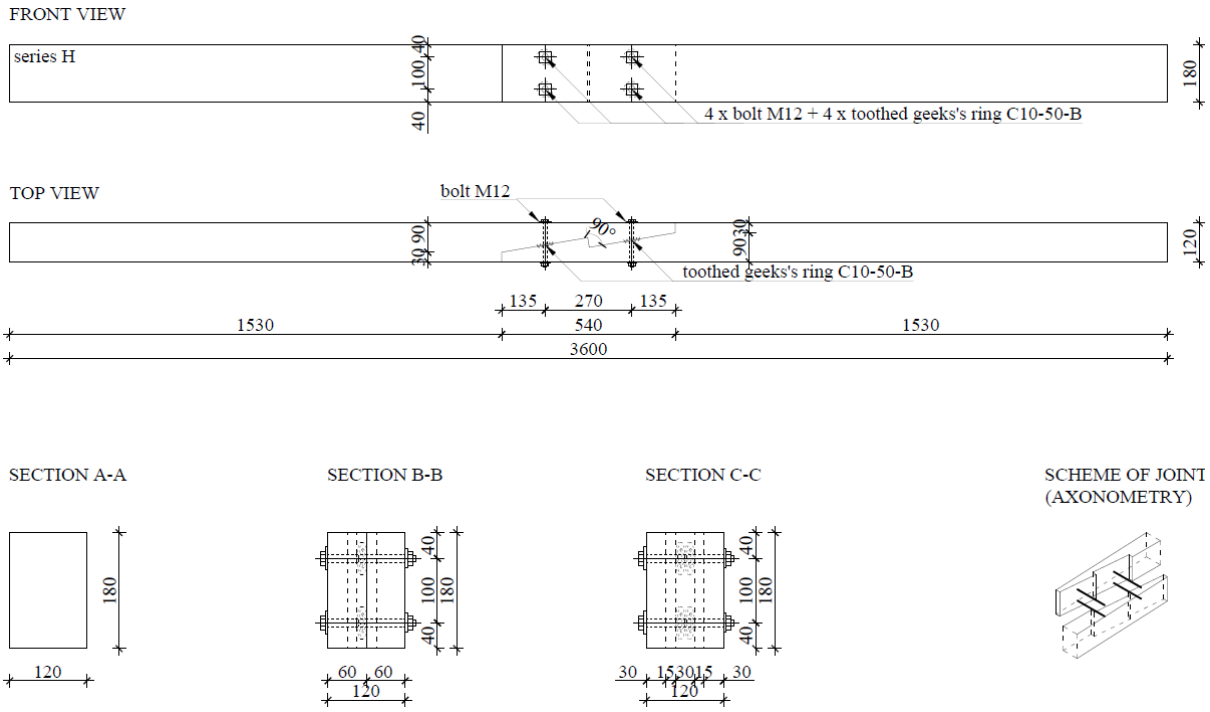
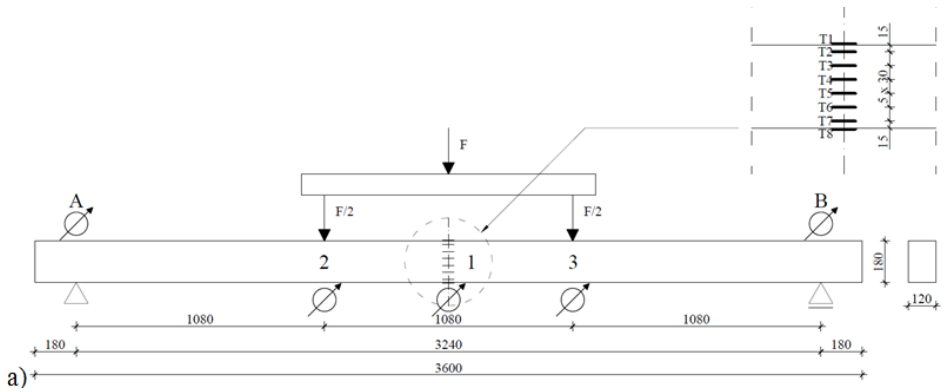


Figure 4: Beam model with scarf joint of lightning sign in the vertical plane (series H)

2.2 Experimental work – 4-point bending tests and material tests

The experimental testing was carried out at the Building Construction Laboratory of the Faculty of Civil Engineering at Wroclaw University of Science and Technology. To determine the load-bearing capacity and the static equilibrium paths (force – displacement paths), the beams were subjected to 4-point bending tests according to the standard procedure [29].

The beams were freely supported (with a fork support – no lateral buckling) at both ends. The span between the axes of the supports was 3.24 m. The beams were loaded symmetrically with a loading force applied at 2 points that allowed to obtain pure bending in the central part of the element. Load was applied with the speed of 5 mm/min. Registration of the deformations observed in the material was carried out by means of a series of strain gauges. A schematic model and view of the testing set are presented in Figure 5.



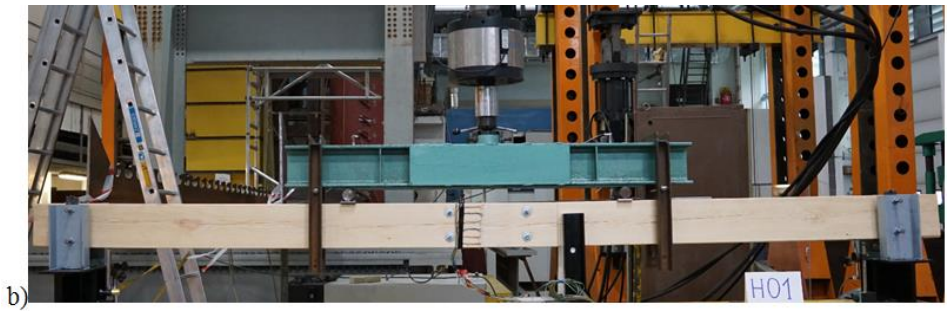


Figure 5: a) Schematic drawing of the testing set with the location of strain gauges, b) view of the testing set

Additionally, during the tests, the wood moisture content was determined using a resistance hygrometer (FMW moisture meter) in several locations on each tested beam. The moisture content of the elements was kept close to the required standard of 12% [29].

Moreover, based on the obtained force – displacement paths, the value of modulus of elasticity in bending was estimated according to the standard procedure [30]. Regression trend lines of three equilibrium paths of the tested reference beams (series A) for the load range from 0.1 F_{max} to 0.4 F_{max} were applied. The coefficient of correlation of these range lines was at least 0.998.

2.3 Finite element analysis

A simplified FEM numerical analysis was performed using ANSYS Workbench 16.0 computational programme. Wood was modelled as an elastic orthotropic material. The modulus of elasticity parallel to the grain on the basis of calculation was assumed to be 9800 MPa. Values of other material parameters needed for analysis: moduli Ey, Ez, Gxy, Gxz, Gyz and Poisson's ratios νxy, νxz, νyz (where x, y, z axes are axes respectively along the wood fibres, i.e. parallel to the grain and across the grain in the radial direction and across the grain in tangential directions, i.e. perpendicular to the grain) were estimated on the basis of relation from the literature [31,32]. Formulas and values of the material parameters used for FEM numerical analysis are presented in Table 1. The boundary conditions corresponded to the tests in the laboratory (load and support of the beam). The numerical model of the reference beam consisted of approx. 23000 hexahedral quad/tri elements (approx. 90000 nodes) with a size of 0.02 m (in the part of the beam outside the joint) and 0.01 m (in the area of the joint). An example is shown in Figure 6. Contact between the surfaces of individual elements was added as a standard contact with friction (with friction coefficients as follows: wood - wood $\mu = 0.2$ and wood - steel $\mu = 0.5$). The model was verified and then analysis was performed.

Table 1: Values of the material parameters used for FEM numerical analysis

E_x	$E_y = E_x/20$	$E_z = E_x/20$
9800 MPa	490 MPa	490 MPa
$G_{xy} = E_x/14$	**$G_{xz} = E_x/14$**	**$G_{yz} = G_{xy}/10$**
700 MPa	700 MPa	70 MPa
ν_{xy}	**ν_{xz}**	**ν_{yz}**
0.37	0.42	0.47

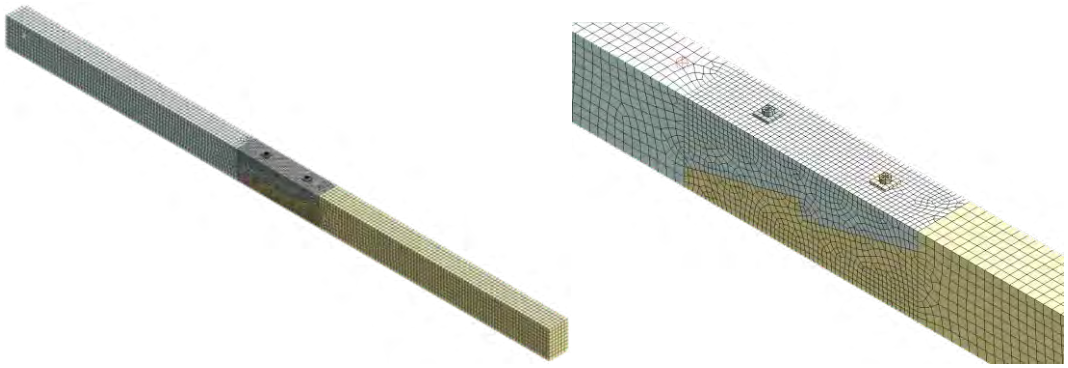


Figure 6: FEM numerical model of an example beam

3 RESULTS AND DISCUSSION

3.1 Experimental work and FEM analysis results

In the experimental testing, the beam models were loaded up to the failure. Ultimate force values were noted, load-bearing capacities for bending for each series were calculated. Deflections (displacements) in the middle span of the beam were measured by test equipment and estimated by numerical analysis. The results of experimental testing for all series of beams are presented in Table 2.

Table 2: Presentation of results for the tested beams

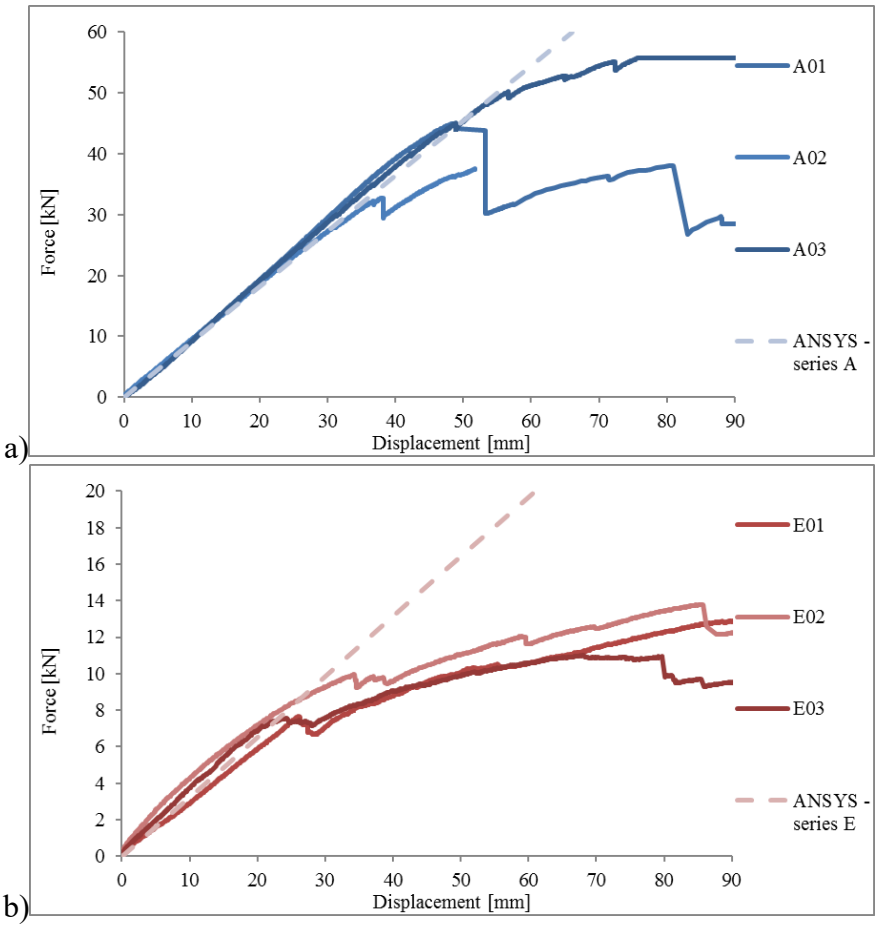
	Reference beam (series A)	Beam with joint in the horizontal plane (series E)	Beam with joint in the vertical plane (series H)
Ultimate force values [kN]	44.95 37.52 55.74	13.21 13.79 11.00	16.16 16.91 16.03
Mean ultimate force value [kN]	**46.07**	**12.67**	**16.37**
Mean load-bearing capacity for bending [kNm]	24.88	6.84	8.84
Mean deflection in the middle span by 10 kN from tests/ numerical analysis [mm]	12.40/ 11.00	37.50/ 30.50	15.00/ 17.00
Mean deflection in the middle of the span by maximum load [mm]	63.80	82.49	43.89

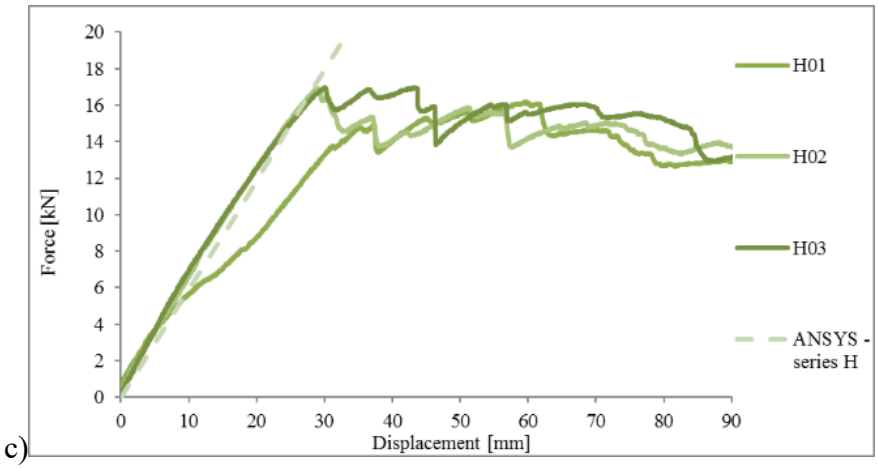
The failure of the tested beams for continuous beams (series A) resulted from shearing of fibers in the bottom part of the central area of the beam. For the beams with joints (series E and H), the failure involved a loosening of the joint in the lower zone of the central part of the beam and the appearance of cracks and fractures on the edges of the joint and in areas which had been weakened by metal fasteners or earlier material flaws, such as knots or primary cracks of the beam. The failure views of the selected models are presented in Figure 7.



Figure 7: Views of the failure of exemplary beams with joints: a) beam E02, b) beam H03

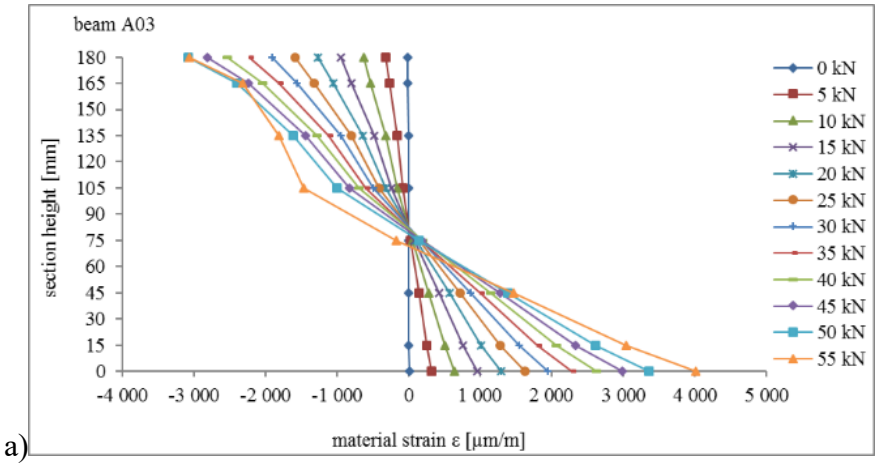
The equilibrium paths for each beam obtained from the tests and from FEM numerical analysis are presented in Figure 8. Material deformations registered by the strain gauges set for the selected beams are shown in Figure 9. For the continuous beam, it is a typical image of material strain in bending, whereas for the beam in series E it is a typical curve shape for the composite cross-section in bending (see, i.a. in [10]).



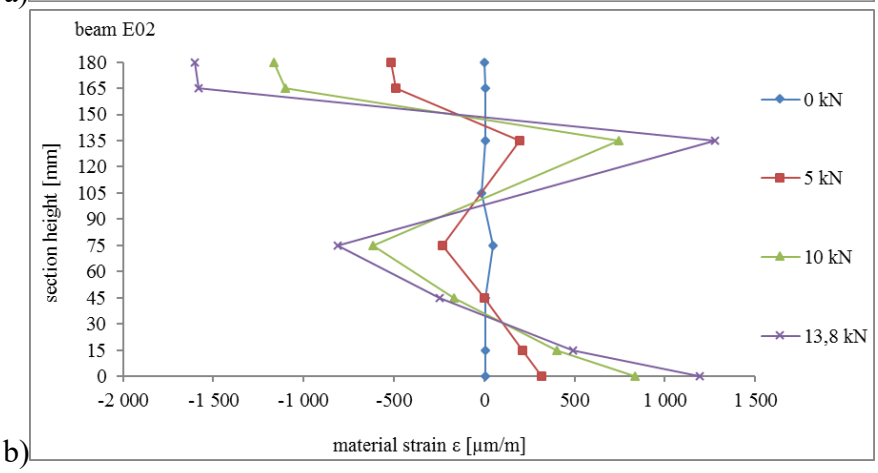


c)

Figure 8: Force – displacement paths for beams a) continuous (series A), b) with scarf joint of lightning sign in the horizontal plane (series E), c) with scarf joint of lightning sign in the vertical plane (series H)



a)



b)

Figure 9: Deformation of material in the central cross-section for selected beams: a) continuous (beam A03), b) with scarf joint of lightning sign in the horizontal plane (beam E02)

3.2 Comparison of results and discussion

The mean load bearing capacity in bending for continuous beams (series A) is 24.88 kNm, whereas beams with joints present capacities of 6.48 kNm (series E) and 8.84 kNm (series H), which constitutes respectively 27.5% and 35.5% of load-bearing capacity of reference beam. Beams with scarf joints in the vertical plane (series H) have higher values of load bearing capacity in comparison with beams with scarf joints in the horizontal plane (series E).

Regarding the stiffness of the tested beams, defined as the ratio of loading force to deflection (displacement), estimated on the basis of force – displacement paths, the highest value is noticed for the continuous beams (series A), what is an expected result. Based on the tests and numerical analysis, it was observed that beams with scarf joints have lower stiffness in relation to the continuous beams. When comparing beams with scarf joints to each other, it must be said that beams with joints in the vertical plane (series H) have higher stiffness than beams with joints in the horizontal plane (series E).

Comparison of static equilibrium paths from the tests and numerical analysis are shown in Figure 10. Comparison of load-bearing capacity and stiffness for jointed beams and reference beam is presented in Table 3.

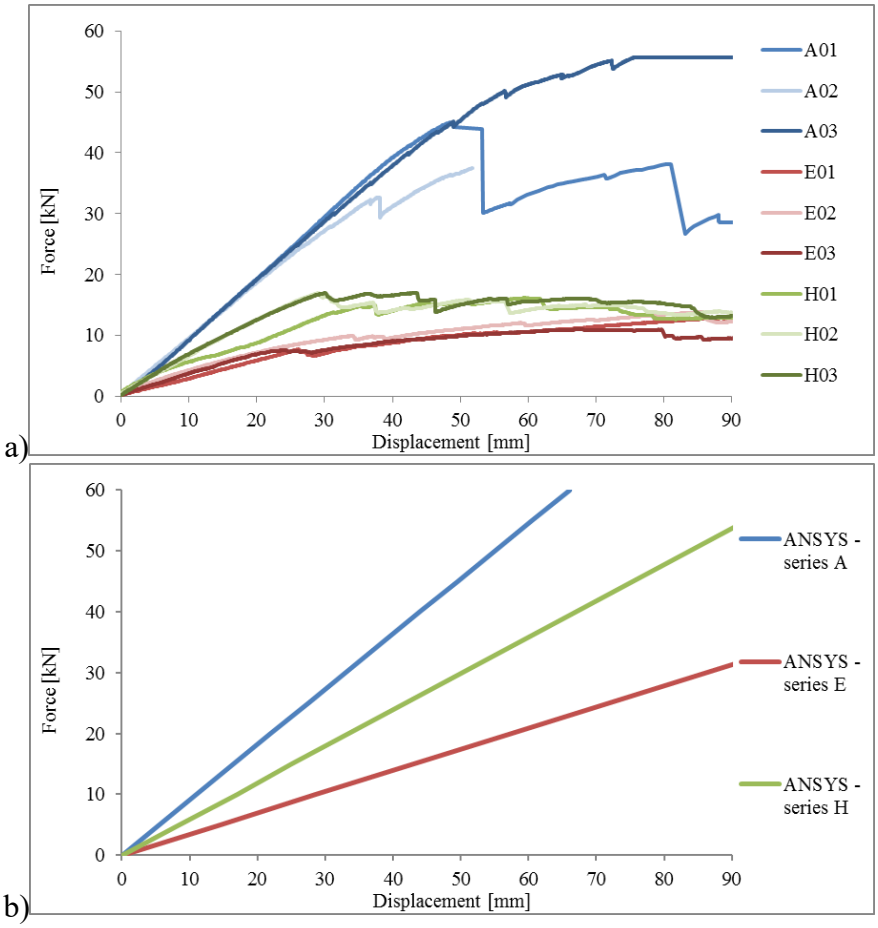


Figure 10: Force – displacement paths for tested beams a) from experimental tests, b) from numerical analysis

Table 3: Experimental tests results comparison

	Reference beam (series A)	Beam with joint in the horizontal plane (series E)	Beam with joint in the vertical plane (series H)
Ratio of load-bearing capacity in comparison to reference beam	100%	27.5%	35.5%
Ratio of stiffness in comparison to reference beam from tests/ numerical analysis	100%	33.0%/ 36.0%	83.0%/ 65.0%

4 CONCLUSIONS

What should be highlighted is the fact that the laboratory testing involved only three beam models in each series, what resulted in quite high variations of results. It can be concluded that it is due to some primary material flaws. Wood itself is a natural material and therefore it can be characterized by large variation, which is related to some initial cracks, knots, etc.

Experimental tests carried out in the laboratory on technical-scale models and simplified numerical analysis present the static behavior of the described joints under bending load in comparison to the behavior of a continuous reference beam. Regardless of the joint plane, horizontal or vertical, the failure modes of the beams were similar (loosening of the joint in the lower central zone and appearance of cracks and fractures near the edges or fasteners). The levels of load-bearing capacity in bending obtained in laboratory experimental tests for beams with joints compared to the reference beam amounted up to one-third (27.5% for joints created in the horizontal plane and 35.5% for joints created in the vertical plane). The stiffness levels obtained in the tests and numerical analysis amounted from one-third up to two-thirds or even more (33.0%/ 36.0% for joints created in the horizontal plane and 83.0%/ 65.0% for joints created in the vertical plane) in comparison to the reference beam. Beams with joints in the horizontal plane (series E) obtained significantly lower levels of load-bearing capacity and stiffness in comparison with beams with joints in the vertical plane (series H). This may indicate that the creation of scarf joints of lightning sign in the vertical plane is a more favorable solution.

The carried out research and analysis delivered a description of the static behavior of scarf joints subjected to bending. For more precise information, further laboratory tests and more detailed and accurate numerical analysis are recommended.

Acknowledgements. The research was carried out as part of the research project no. 2015/19/N/ST8/00787 funded by the National Science Centre.

REFERENCES

[1] Jasieńko J., Nowak T., Karolak A. (2014). Historical carpentry joints. *Wiadomości Konserwatorskie – Journal of Heritage Conservation*, 40, 58-82.

[2] Šobra K., Fonseca Ferreira C., Riggio M., D'Ayala D., Arriaga F., Aira J. R. (2015). A new tool for the structural assessment of historic carpentry joints. In: *Proceedings of the 3rd International Conference on Structural Health Assessment of Timber Structures – SHATIS'15*, Wrocław, Poland, 9-11 September 2015.

[3] Ross P. (2002). *Appraisal and repair of timber structures*. Thomas Telford Ltd, London.
[4] Thelandersson S., Larsen H. J. (2003). *Timber Engineering*. John Wiley & Sons Ltd, Chichester, Chapter 16.
[5] Parisi M. A., Piazza M. (2008). Seismic strengthening of traditional carpentry joints. In: *Proceedings of the 14th World Conference on Earthquake Engineering*, Beijing, China, 12-17 October 2008.
[6] Perria E. (2017). Characterization of halved undersquinted scarf joint and stop-splayed undersquinted & tabled scarf joint with key (Jupiter joint). *PhD dissertation*. University of Braunschweig – Institute of Technology, Department of Architecture and University of Florence, Department of Civil and Enviromental Engineering.
[7] Perez L. P. (2003). Design and construction of timber roof structures, built over different structural systems. Cases studium at the Valencia Community. In: *Proceedings of the First International Congress on Construction History*, Madrid, Spain, 20-24 January, 2003.
[8] Tampone G., Semplici M. (2006). *Rescuing the Hidden European Wooden Churches Heritage*, An International Methodology for Implementing a Data Base for Restoration Projects. In cooperation with Fly Events and Alter Ego Ing Arch S.r.l. (a Subsidiary Company of the Collegio degli Ingegneri della Toscana), Città di Castello.
[9] Mirabella-Roberti G., Bondanelli M. (2013). Study and analysis of XIV century timber built-up beams in Verona. *Advanced Materials Research*, 778, 511-516.
[10] Rug W., Linke G. (2015). Study on the load bearing capacity and the load- deferral behavior of wooden composite beams with a teethed joint. In: *Proceedings of the 3rd International Conference on Structural Health Assessment of Timber Structures – SHATIS'15*, Wrocław, Poland, 9-11 September 2015.
[11] Rug W., Thoms F., Grimm U., Eichbaum G., Abel S. (2012). Untersuchungen zur Biegetragfähigkeit von verzahnten Balken. *Bautechnik* 89, 26-36.
[12] Alberti L. B. (1965). L'Architettura di Leon Batista Alberti, Tradotta in lingua Fiorentina da Cosimo Bartoli. Con la aggiunta de disegni. Et altri diuersi Trattati del medesimo Auttore. Appresso Lionardo Torrentino.
[13] Ceraldi C., Costa A., Lippiello M. (2019). Stop-Splayed Scarf-Joint Reinforcement with Timber Pegs Behaviour. In: Aguilar R., Torrealva D., Moreira S., Pando M., Ramos L.F. (Eds.). *Structural Analysis of Historical Constructions*. Springer, Cham., 360-369.
[14] Hirst E., Brett A., Thomson A., Walker P., Harris R. (2008). The structural performance of traditional oak tension & scarf joints. In: *Proceedings of the 10th World Conference on Timber Engineering*, Miyazaki, Japan, 2-5 June 2008.
[15] Sangree R. H., Schafer B. W. (2009). Experimental and numerical analysis of a stop-splayed traditional scarf joint with key. *Construction and Building Materials*, 23, 376-385.
[16] Fajman P., Máca J. (2018). The effect of inclination of scarf joints with four pins. *International Journal of Architectural Heritage*, 12(4), 599-606.
[17] Fajman P. (2015). A scarf joint for reconstructions of historical structures. *Advanced Materials Research*, 969, 9-15.
[18] Fajman P., Máca J. (2015). Scarf joints with pins or keys and dovetails. In: *Proceedings of the 3rd International Conference on Structural Health Assessment of Timber Structures – SHATIS'15*, Wrocław, Poland, 9-11 September 2015.
[19] Fajman P., Máca J. (2014). The effect of key stiffness on forces in a scarf joint. In *Proceedings of the 9th International Conference on Engineering Computational*

Technology, vol. 40. Civil-Comp Press, Stirlingshire, United Kingdom.
[20] Fajman P., Máca J. (2014). The effect of key stiffness on forces in a scarf joint. In *Proceedings of the 9th International Conference on Engineering Computational Technology*, vol. 40. Civil-Comp Press, Stirlingshire, United Kingdom.
[21] Šobra K., Fajman P. (2013). Utilization of splice skew joint with a key in the reconstruction of historical trusses. *Advanced Materials Research*, 668, 207-212.
[22] Arciszewska-Kędzior A., Kunecký J., Hasníková H. (2016). Mechanical response of a lap scarf joint with inclined faces and wooden dowels under combined loading. *Wiadomości Konserwatorskie – Journal of Heritage Conservation*, 46, 80-88.
[23] Arciszewska-Kędzior A., Kunecký J., Hasníková H., Sebera V. (2015). Lapped scarf joint with inclined faces and wooden dowels: Experimental and numerical analysis. *Engineering Structures*, 94, 1-8.
[24] Arciszewska- Kędzior A., Kunecký J., Hasníková H. (2015). Mechanical response of a lap scarf joint with inclined faces and wooden dowels under combined loading. In: *Proceedings of the 3rd International Conference on Structural Health Assessment of Timber Structures – SHATIS'15*, Wrocław, Poland, 9-11 September 2015.
[25] Kunecký J., Hasníková H., Kloiber M., Milch J., Sebera V., Tippner J. (2018). Structural assessment of a lapped scarf joint applied to historical timber constructions in central Europe. *International Journal of Architectural Heritage*, 12.4, 666-682.
[26] Kunecký J., Sebera V., Hasníková H., Arciszewska-Kędzior A., Tippner J., Kloiber M. (2015). Experimental assessment of full-scale lap scarf timber joint accompanied by a finite element analysis and digital correlation. *Construction and Building Materials*, 76, 24-33.
[27] Kunecký J., Sebera V., Tippner J., Hasníková H., Kloiber M., Arciszewska- Kędzior A., Milch J. (2015). Mechanical performance and contact zone of timber joint with oblique faces. *Acta Universitatis Agriculturae et Silviculturae Mendelianae Brunensis*, 63, 1153-1159.
[28] Kunecký J., Sebera V., Tippner J., Kloiber M. (2014). Numerical assessment of behavior of a historical central European wooden joint with a dowel subjected to bending. In: *Proceedings of the 9th International Conference on Structural Analysis of Historical Constructions*, Mexico City, Mexico, 15-17 October 2014.
[29] Structural Timber—Determination of Characteristic Values of Mechanical Properties and Density; PN-EN 384: 2016-10. PKN: Polish Committee for Standardization, Warsaw, Poland, 2016.
[30] Timber Structures. Structural Timber and Glued Laminated Timber. Determination of Some Physical and Mechanical Properties. PN-EN 408+A1: 2012; PKN: Polish Committee for Standardization, Warsaw, Poland, 2012.
[31] Bodig J., Jayne B. A. (1982). *Mechanics of Wood and Wood Composites*. Van Nostrad Reinhold, New York.
[32] Nowak T. (2007). Analysis of the static work of bent wooden beams reinforced with CFRP [In Polish]. *PhD dissertation*. Wroclaw University of Science and Technology, Faculty of Civil Engineering, Wrocław.

12th International Conference on Structural Analysis of Historical Constructions
SAHC 2020
P. Roca, L. Pelà and C. Molins (Eds.)

EXPERIMENTAL INVESTIGATION ON THE TORSION-SHEAR BEHAVIOUR AT THE INTERFACES OF INTERLOCKING MASONRY BLOCK ASSEMBLAGES

CLAUDIA CASAPULLA[1*], ELHAM MOUSAVIAN[1], LUCA U. ARGIENTO[1] AND CARLA CERALDI[1]

[1]Department of Structures for Engineering and Architecture (DiSt)
University of Napoli Federico II
Via Forno vecchio, 36 – 80134 Napoli, Italy
e-mail: casacla@unina.it (*corresponding author)
email: {elham.mousavian, lucaumberto.argiento, ceraldi}@unina.it

Keywords: Masonry, Interlocking Blocks, Initial Shear Strength, Torsion-Shear Resistance

Abstract. *This paper presents an experimental investigation on the initial shear (cohesion) and torsion-shear strengths at the interface of an interlocking masonry block. An interlocking block is a rigid unit with locks avoiding the block to slide. This improves the seismic response of dry jointed assemblages of masonry structures subjected to in-plane and out-of-plane loading. The experimental investigation is designed and carried out for the corrugated interface having one lock with rectangular cross section, i.e. the specimen is an interlocking unit composed of a main body and a lock located on the upper face of the main body. Cement-based mortars are selected to reproduce the specimen, casted using a mould provided by a 3D printer, and both the lock and the main body are kept rigid during the tests. The initial shear and torsion-shear capacities of the interface at which the lock is connected to the main body are assessed together with its quasi-brittle fracture and registered in terms of load-displacement curves. In the designed setup, the horizontal force is applied to the rigid lock until it is disjointed from the rigid main body of the block, while the effect of rocking during the shear test is avoided. The force and the displacements are measured using a load cell and Linear Variable Displacement Transducers (LVDTs), respectively. The experimental programme includes four different sets with different load application points and different load directions, each set repeated on a number of similar specimens. Empirical formulations between the initial shear and compressive strengths of the lock interface are also evaluated.*

1 INTRODUCTION

Under seismic loading, unreinforced masonry walls can fail due to in-plane or out-of-plane loading. In traditional masonry block structures subjected to seismic loading, the joints between the masonry units act as planes of weakness due to their low tensile and shear bond strength. The mechanical behaviour at the joint interfaces has widely been studied within different methods of analysis, e.g. discrete or finite element analysis [1-3] and limit analysis with infinitive [4], or finite isotropic associative [5] and non-associative [6] frictional resistances. In particular, experimental investigation was carried out on 3D dry-stacked units

to evaluate yield domains in shear, torsion-shear and torsion-shear-bending moment interactions [7] and on the validation of frictional resistances of shear block walls [8].

Increasing interest has recently been devoted to interlocking blocks/interfaces capable to enhance the sliding resistance of masonry joints to external forces. The interlocking blocks are rigid block units which, on their faces, have locks keeping the blocks together and preventing blocks from sliding. Experimental and numerical tests [9,10] investigated the in-plane and out-of-plane capacity of masonry walls composed of blocks with corrugated interfaces. Out-of-plane behaviour of osteomorphic blocks and interfaces with cross shaped locks were also experimentally investigated by Dyskin et al. [11] and Ali et al. [12], respectively. Similarly, experimental and numerical investigations were carried out on the different behaviour of wooden joinery connections with different geometric properties [13-16]. A digital tool to design structurally feasible masonry structures composed of interlocking blocks is being developed by some of the presenting authors [17-19].

One of the key factors that influence the behaviour and capacity of the conventional mortared block masonry is the bond strength between the mortar and the units. Similarly, the shear strength between the lock and the main body of the interlocking block is of utmost importance for dry masonry with interlocking interfaces. This means that, if the interlocking blocks are composed of cohesive material at their interfaces, the Mohr–Coulomb criterion can be adopted for both systems, for which the bond strength itself depends on the initial shear strength (cohesion) and the coefficient of friction as well as the level of normal stresses.

In order to determine the initial shear strength and the coefficient of friction, only European Standard EN 1052-3 [20] test method is available yet. However, the scientific literature shows that generally researchers have developed and conducted their own domestic test method, indicating the difficulty of finding a general consensus [21].

In this paper, a novel and alternative test method is proposed to evaluate the initial shear and torsion-shear capacity of a single lock belonging to an interlocking block, while the coefficient of friction and shear in presence of normal forces are beyond its scope. The test setup is similar to that used for dry-stacked tuff blocks [7], but with a different application of the load and different constraints, in order to allow the absence of normal force on the cohesive interface between the two parts of the block (lock and main body) kept rigid during the tests. The block was specifically designed to reproduce a particular interlocking block shape. The material properties of two selected cement-based mortars were also experimentally evaluated in order to define or confirm empirical relationships between their compressive and initial shear strengths.

2 EXPERIMENTAL INVESTIGATION

Representing the simplest interlocking model, a main body with a lock located on its upper face was designed as the specimen for this test. An ad hoc test setup was realized to estimate the pure shear and torsion-shear resistance of the interface at which the lock is connected to the main body, while keeping rigid the lock and the main body of the interlocking block.

A first phase of the research focused on finding the proper shape and dimensions for the block. A number of specimens were made by casting mortars with different mixtures in a mould, provided in the desired shape and dimension by a 3D printer. Then, four different test configurations were set up to simulate shear and torsion-shear failures, herein named sets S1,

S2, S3 and S4. Besides, calibrating the mechanical properties of the appropriate mortar to be prepared was a crucial issue, both because of the limitations of the involved instrumentation, in particular the maximum capacity of the load cells, and of the necessity of obtaining a clear shear failure mode of the lock interface (cohesive crack). Therefore, trial samples composed of several specimens were casted with different cohesive materials and were tested under pure shear [22]. Finally, two mortars, namely M1 and M2, were chosen and their density, flexural and compressive strengths were experimentally determined.

In sum, eight samples, combining the four sets and the two mortars, were tested. Each of the two samples tested in pure shear, namely S1M1 and S1M2, involved four specimens, while the six samples for torsion-shear tests, comprised three specimens each, in total providing twenty-six experimental results.

The experimental investigation was carried out with standard and non-standard equipment at Laboratory of the Department of Structures for Engineering and Architecture (DiSt) of the University of Napoli Federico II (Italy).

2.1 Characterization of mortars

Two different mortars, M1 and M2, were chosen to make the specimens, whose composition and curing time are quoted in Table 1. Pozzolana, so named from the Pozzuoli town, is fine sand or loose blocks that can be easily found, in colours ranging from grey to red [23,24]; lime, supplied by Cimmino Calce s.r.l. (Naples), is a calcium-containing inorganic mineral still used in large quantities as building and engineering material. The mixtures were prepared using the amount of water required to ensure enough workability and normal consistency. According to the European Standard UNI EN 1015-2 [25], the pastes were compacted during the casting to remove any air bubbles and voids. Curing was performed in ambient laboratory conditions (relative humidity 60 ± 10% and 20 ± 5°C) until the test day.

Table 1: Composition of the tested mortars

Mortar	Pozzolana	Sand	Cement	Lime	Curing Time
M1	50%	24%	2%	24%	28 days
M2	47%	38%	15%	-	28 days

These non-standard mixtures were chosen to prepare specimens in the first phase of the experimental program, aimed to obtain: 1) failure load values compatible with the designed setup and within the valid range of the employed instrumentation; 2) failure modes corresponding to instantaneous and clear cutting of the lock from the main block. So, before defining M1 and M2, the traditional pozzolana based mortar [24], obtained with three parts of pozzolana and one of lime, was first employed to cast five specimens, cured in water for 28 days, and tested with pure shear setup. As the limit load (500N) of the load cell was reached before any failure on the lock, a new attempt was made by reproducing the same experimental phase in which only the curing time was reduced to 14 days. Applying this change, collapse was achieved in all the specimens, but a relatively concave shape was observed at the failure interface. Then, other mixtures were tested, adding cement with different ratios of components, with sets of five specimens cured in air for different curing times, and finally M1

and M2 mortars were chosen.

Standard specimens, i.e. rectangular parallelepipeds of 40x40x160mm were also prepared to characterize the mechanical properties of the M1 and M2 mortars, i.e. four for each mortar. Those specimens were measured with a digital calliper and weighted with an electronic weighting machine, to obtain the density of the mortars.

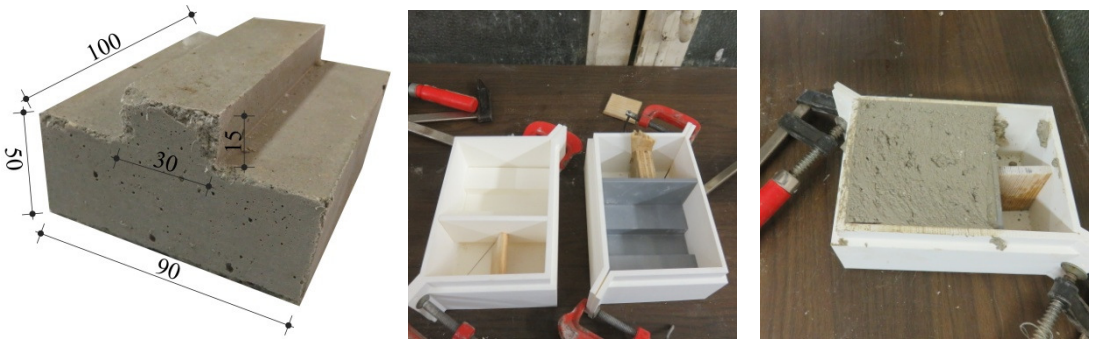
Then, flexural and compressive tests were carried out with standard equipment, following the UNI EN 1015-11 [26]. The mean values of the measured density and strengths are summarized in Table 2.

Table 2: Experimental mechanical properties of the tested mortars

Mortar	Flexural strength [MPa]	Compressive strength [MPa]	Density [kN/mc]
M1	1.05	2.69	12.7
M2	0.37	0.75	14.0

2.2 Specimen shape and test setup for shear and torsion-shear strengths evaluation

The designed specimen is composed of a main body, which is a 100x90x50mm cuboid, with a 100x30x15mm cubic lock located on its upper face (Figure 1a). It was made of the mortars described in the previous section, casted by using an ad hoc formwork to make the customized lock dimensions. The formwork was composed of pieces made by a 3D printer (Figure 1b).



(a) (b) (c)

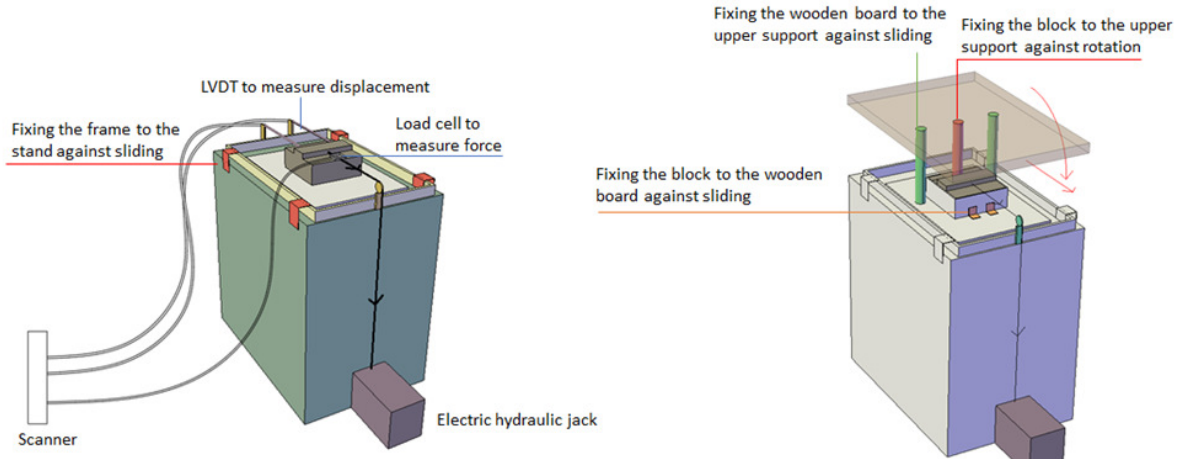
Figure 1: (a) Designed specimen; (b) printed moulds; (c) curing phase

The test setup was specifically designed to pursue pure shear and torsion-shear resistances of the lock interface, overcoming some related issues. In fact, with the aim of minimizing the effect of bending usually experienced during shear tests [21] and of avoiding the pre-compression force, which are the main challenges of the traditional experimental setup [20], a new setup was developed for the experimental tests.

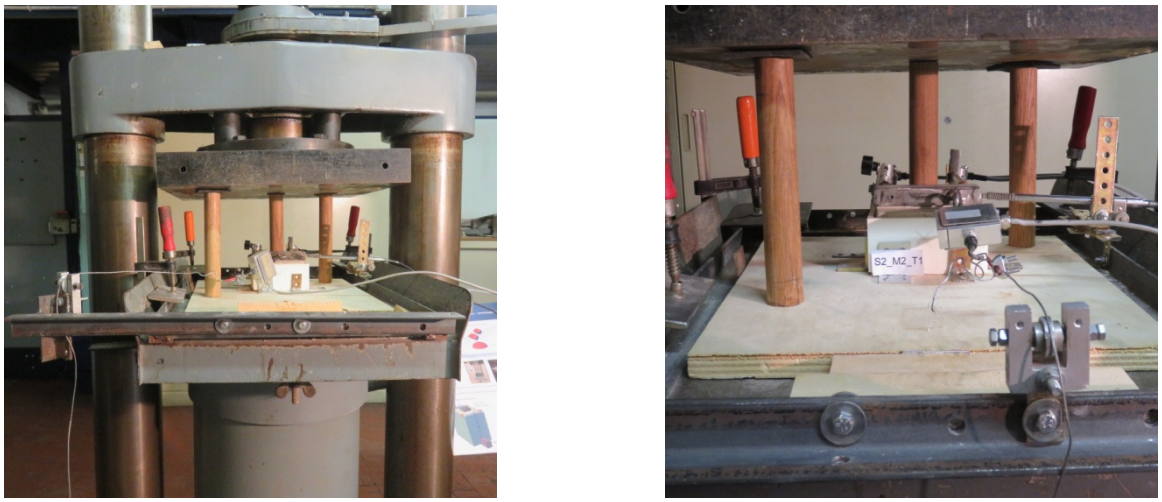
Actually, a horizontal load was applied directly on the front face of the lock by the static gravity load via a pulley system, while its main body was held fixed, until the collapse of the

lock occurred. Meanwhile, the test setup, other than measuring pure shear resistance, ought to be efficient in evaluating also torsion-shear failure, by simply changing the load eccentricity. This task was accomplished by changing the position and direction of the designed pulley system.

The test setup is schematically shown in Figure 2a: the horizontal point-load was applied to the side face of the specimen lock by means of an electric hydraulic jack, monotonically increasing until the failure mechanisms. As shown in Figure 2b, the block was fixed to a wooden board to avoid sliding and to the upper support to avoid rotation, while the board was fixed to the upper support against sliding as well.



(a) (b)



(c) (d)

Figure 2: Test setup. (a) Displacement and load measurement; (b) constraints; (c,d) realized torsion-shear setup

The application of an iron cup on the lock allowed both the simulation of this part as a rigid block and the distribution of the applied shear force along the whole lock face (Figure

3a). On the other hand, the main body of the interlocking block was kept rigid during the tests by using a rigid cup-shaped container, still provided by a 3D printer. The load was applied under displacement control at a constant rate of 3mm/min.

Forces were measured using a load cell with a maximum capacity of 500N and an acquisition frequency of 10 Hz, while displacements were measured using Linear Variable Displacement Transducers (LVDTs) with a displacement range of ± 50mm. A digital scanner, distributed by Vishay Measurements Group, was employed to acquire transducers data.

With the aim of capturing both pure shear and torsion-shear failures, three LVDTs, supported by a steel frame, were positioned to the lateral and back sides of the lock and numbered as shown in Figure 3b.

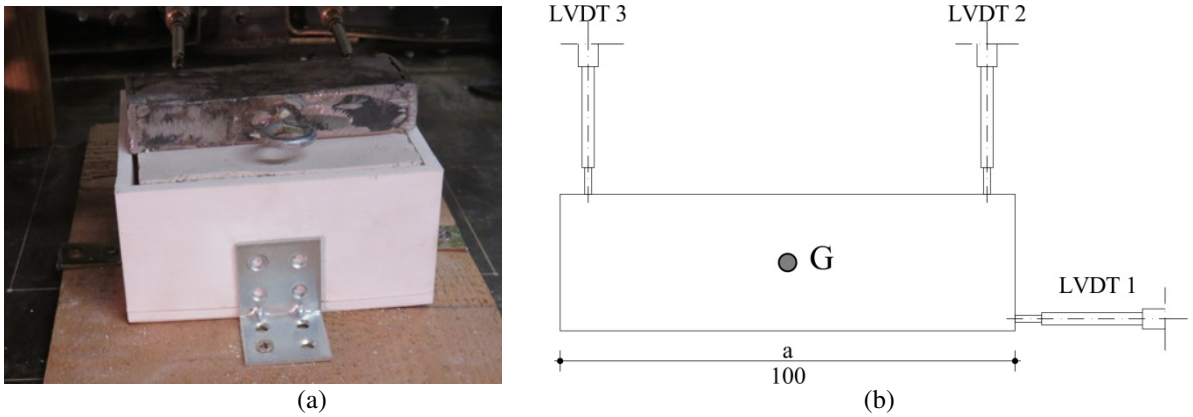


Figure 3: (a) Interlocking block with steel cup; (b) LVDT's position in the plan view

2.3 Testing program

The experimental program was planned in order to analyze the shear resistance of the lock interface in case of pure shear (S1) and torsion-shear (S2-3-4). The horizontal force, representing the shear force *V*, was applied at variable eccentricity and direction in the midplane of the lock.

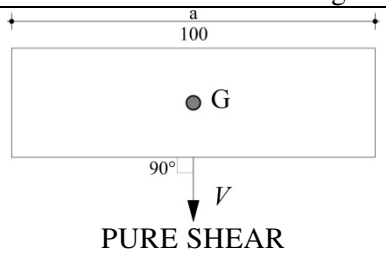
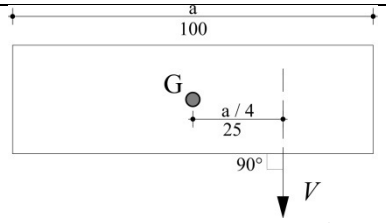
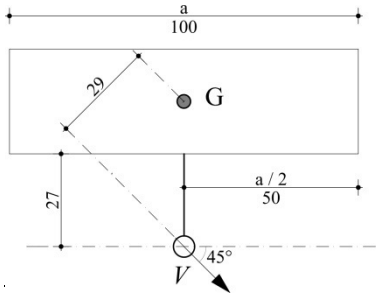
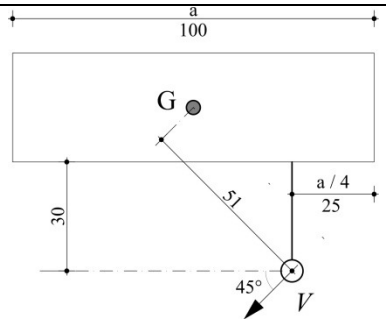
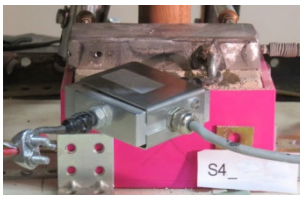
As introduced above, the specimens made of two chosen mortars, M1 and M2, were tested with four setups, resulting in eight samples (Table 3), i.e.:

- S1M1 and S1M2 for pure shear strength evaluation, each comprising four specimens;
- S2M1, S2M2, S3M1, S3M2, S4M1, S4M2 for torsion-shear strength evaluation, each comprising three specimens.

As shown in Table 3, the shear setup (S1) was modified to allow torsion-shear behaviour, in different ways:

- for S2, the force application point was moved on the lock, with *V* still orthogonal to the lock front side, applying the eccentricity e = 25mm from point G;
- for S3, the force application point was only spaced from the lock with reference to S1, with *V* rotated 45° counterclockwise, applying the eccentricity e = 29mm;
- for S4, the force application point was moved on and spaced form the lock, with *V* rotated 45° clockwise, applying the eccentricity e = 51mm.

Table 3: Experimental set configurations (the distances are in mm)

Set	Configuration	
S1M1 S1M2	 PURE SHEAR	
S2M1 S2M2	 TORSION-SHEAR (e = 25mm)	
S3M1 S3M2	 TORSION-SHEAR (e = 29mm)	
S4M1 S4M2	 TORSION-SHEAR (e = 51mm)	

3 EXPERIMENTAL RESULTS

3.1 Pure shear strength of the two mortars

In order to determine the pure shear strength (cohesion) of the two mortars, a total of 8 tests were made out for M1 and M2 mortar samples. Using the S1 shear test setup described in the previous section, it was possible to define the force causing the shear collapse of the specimens. The values of this force for the two M1 and M2 mortars are collected in Table 4.

The coefficients of variation (CV) show a low dispersion of the frequency distributions and therefore a good reliability of the test setup. The average values of the limiting forces related to pure shear failure are equal to 431N and 240N for the M1 and M2 mortar, respectively. The greater shear resistance of the M1 mortar compared to M2 is in good agreement with similar trends for the compressive and flexural strength results shown in Table 2.

Table 4: Pure shear resistance of the two M1 and M2 mortars for S1 tests

Mortar	Shear resistance V [N]				CV [%]	Average V [N]
	T1	T2	T3	T4		
M1	399	472	408	445	6.8	431
M2	250	242	226	243	3.7	240

For this setup (pure shear), two LVDTs were used to verify the effective displacements of the lock in the absence of torsion. Figure 4 shows the load-displacement curves referred to some of the four tests performed on each of the M1 and M2 mortars, i.e. T2 Test in Figure 4a, and T1 and T3 Tests in Figure 4b. From these figures it is first evident the quasi-brittle behaviour of the material for both mortars. It is then worth emphasizing that the displacements of the two LVDTs, registered as channels Ch.2 and Ch.3 in the figure, substantially tend to overlap for each test. This result confirms once again the reliability of the setup realized ad hoc in the laboratory; in fact, the specimens collapsed in pure shear as there was no torsion effect. The maximum capacity values shown in the graphs correspond to the limiting forces collected for the corresponding tests in Table 4.

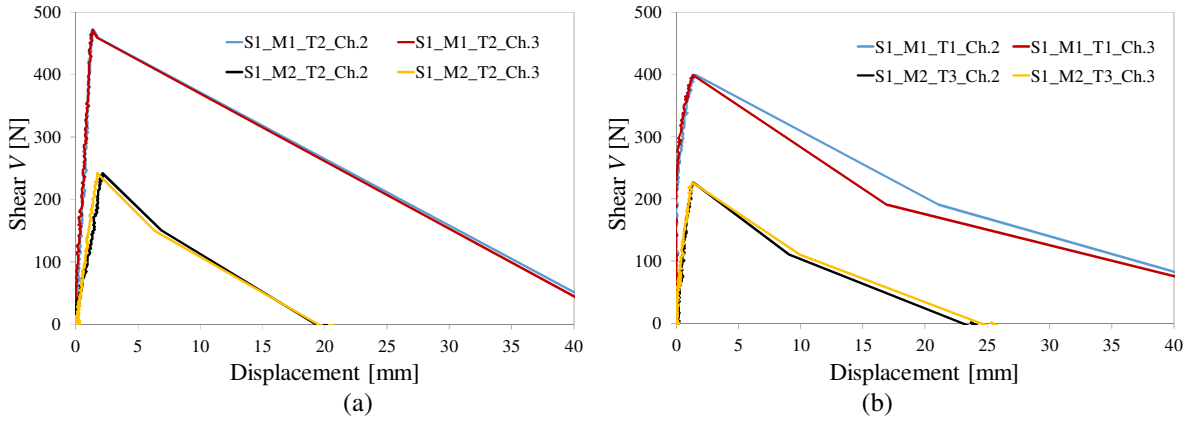


Figure 4: Load-displacement curves for S1 tests: (a) M1_T2 – M2_T2 and (b) M1_T1– M2_T3

Assuming a uniform distribution of the limiting shear force along the interface (100x30mm) between the lock and the main body of the specimens, the mean shear strength f_v can easily be derived for each tested mortar. The relationship between the experimental shear and compressive strengths are reported in Table 5, taking into account the values in Table 2. These results seem to confirm the reliability of the empirical formulation developed by Ali et al. [27], which fits experimental results on standard triplets of masonry and mortar and provides a relation between the mean bond shear strength in absence of normal stresses

(cohesion), and the compressive strength of mortar. The formulation is:

$$f_v = 0.06\, f_m^{0.8389} \quad (1)$$

where f_m is the compressive strength of mortar.
In fact, although this formulation was tested for mortars with compressive strengths greater than those of M1 and M2, the pure shear strengths obtained with this formulation for M1 and M2 are very close to the experimental results, as reported in Table 5.

Table 5: Relation between pure shear and compressive strengths of the two M1 and M2 mortars for S1 test

Mortar	Shear strength [MPa]	Compressive strength [MPa]	Shear strength/compressive strength ratio	Shear strength according to Eq. (1) [27] [MPa]
M1	0.15	2.69	5.6%	0.14
M2	0.08	0.75	10.7%	0.05

3.2 Torsion-shear strength of the two mortars

The S2-3-4 setups were developed to analyze the torsion-shear resistance of the lock. These setups differ from each other in the eccentricity of the applied force. To determine the torsion-shear strength of the two mortars, a total of 18 specimens, three per each set and mortar, were made out on the M1 and M2 mortar samples, as reported in Table 6. The first interesting remark is that the values of the forces V related to torsion-shear failure of each mortar decrease with increasing eccentricity, as expected. The small coefficients of variation CV, except one, still show quite a good reliability of the setup adopted.

Table 6: Torsion-shear resistance of the two M1 and M2 mortars for S2-3-4 tests

Set	ecc. [mm]	Mortar	Shear force V [N]			CV [%]	Average V [N]
			T1	T2	T3		
2	25	M1	314	300	330	3.9	315
		M2	213	203	181	6.7	199
3	29	M1	243	260	276	5.2	260
		M2	181	193	192	2.9	189
4	51	M1	79	177	195	33.9	150
		M2	118	133	106	9.3	119

On the other hand, through the load-displacement curves in Figure 5, it is possible to confirm the quasi-brittle behaviour of the involved materials and to analyze the rotation of the lock until collapse and its consistency with the eccentric load applied. Unlike the curves for pure shear in Figure 4, where the displacements of LVDT 2 and 3 tend to coincide, for the torsion-shear condition the displacements are very different from each other. Specifically, the displacement of the LVDT Ch.3 is generally between ± 0.5 mm, while the displacements recorded by the LVDT Ch.2 are even six times higher. Using three LVDTs allows to record three final displacements at the moment of the lock failure and therefore to build the final

deformation. Further investigation will be carried out to define the pure torsion strength as well, so that analytical yield domains in torsion-shear interaction can be experimentally validated, similarly to what developed by Casapulla and Portioli [7] for dry-stacked tuff blocks.

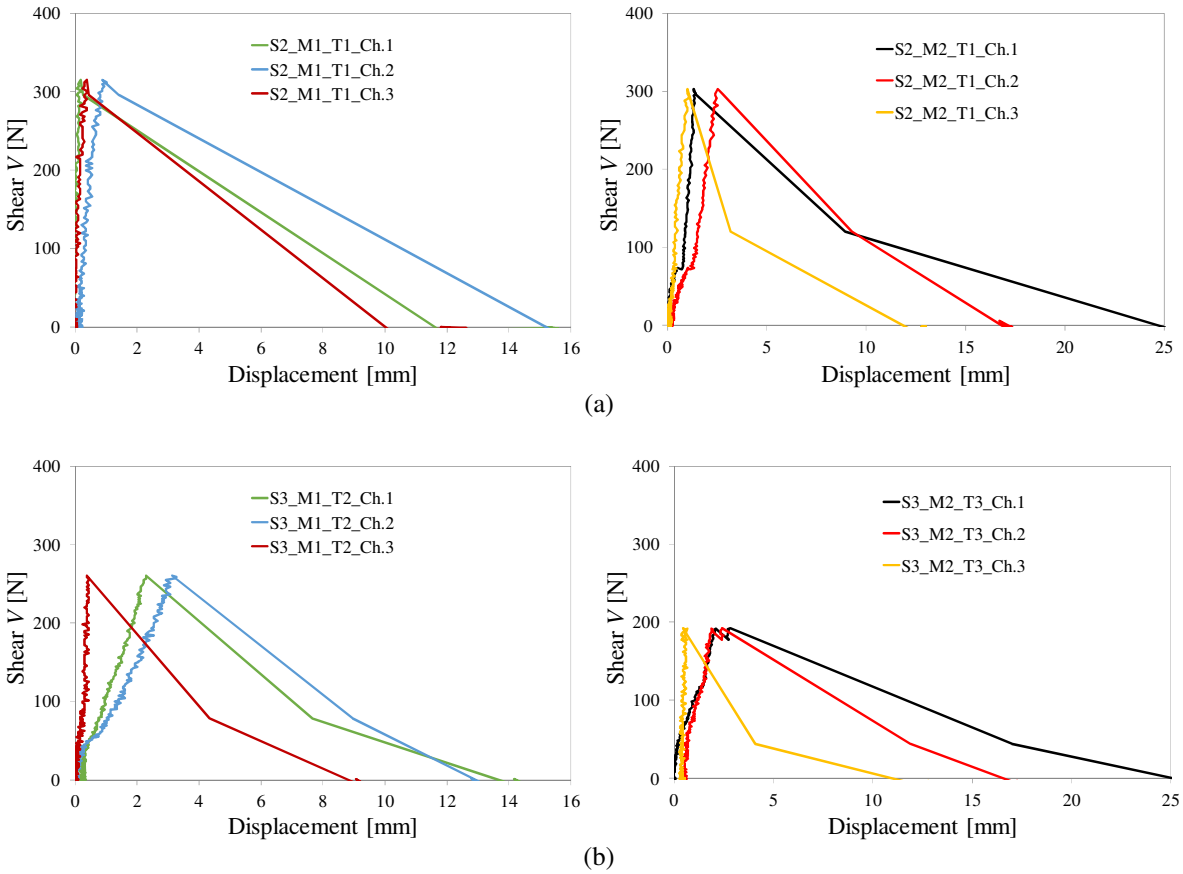


Figure 5: Load-displacement curves for S2 and S3 tests and: (a) M1 and (b) M2 mortars

12 CONCLUSIONS

Interlocking blocks/interfaces are capable to enhance the shear resistance of masonry joints to external forces, including seismic loading. If the interlocking blocks are composed of cohesive material at their interfaces, the mechanical behaviour is governed by the Mohr-Coulomb criterion for which the bond strength at these interfaces depends on initial shear strength (cohesion) and the coefficient of friction as well as the level of normal stresses.

This paper describes the experimental investigation carried out on the simplest interlocking block, composed of a main body with a prismatic lock located on its upper face and subjected to lateral loading in absence of normal force. An ad hoc test setup was realized to estimate the initial shear and torsion-shear strengths at the lock interface, with results reported in terms of load-displacement curves. Two cement-based mortars were used for specimens, casted using moulds provided by a 3D printer.

The first interesting experimental outcome is that the proposed domestic test method is reliable enough compared to others existing in the literature to assess the shear and torsion-

shear strength of cement-based mortars with low compressive and flexural strengths. In fact, using three LVDTs in key positions, pure translation of the lock was registered in the case of pure shear failure and twisting deformation was possible to be captured in the case of torsion-shear condition. Another interesting remark is that the relation between the experimental initial shear and compressive strengths of the lock interface is very close to the empirical formulation developed by Ali et al. [27], which fits experimental results on standard triplets of masonry and mortar. This result can be very useful when analysing limit conditions of assemblages of masonry interlocking blocks composed of material of known compressive strength. Further work is under development to evaluate the torsion-shear yield domain for the single lock interface and to extend the test method to interlocking blocks composed by a number of locks.

Acknowledgements.  This project has received funding from the European Union's Horizon 2020 research and innovation programme, under the Marie Skłodowska-Curie Grant Agreement No. 791235, and from the Italian Civil Protection, through the RELUIS Project - WP4: MAppe di Rischio e Scenari di danno sismico (MARS) (2020). The authors wish to express their gratitude to Mr. Domenico Imperatrice from the Laboratory of DiSt in Napoli, for his helpful assistance and support in the execution of the experimental investigations.

REFERENCES

[1] Lourenço, P.B., Rots, J.G. and Blaauwendraad, J. Two approaches for the analysis of masonry structures: micro and macro-modeling. *Heron* (1995) **40**(4):1-28.

[2] Li, T. and Atamturktur, S. Fidelity and robustness of detailed micromodeling, simplified micromodeling, and macromodeling techniques for a masonry dome. *J. Perform. Constr. Fac.* (2013) **28**(3):480-490.

[3] Cannizzaro, F., Pantò, B., Caddemi, S. and Caliò, I. A Discrete Macro-Element Method (DMEM) for the nonlinear structural assessment of masonry arches. *Eng. Struct.* (2018) **168**:243-256.

[4] Heyman, J. *The stone skeleton: structural engineering of masonry architecture*. Cambridge University Press (1995).

[5] Livesley, R.K. A computational model for the limit analysis of three-dimensional masonry structures. *Meccanica* (1992) **27**(3):161-172.

[6] Casapulla, C., Giresini, L., Argiento, L.U. and Maione, A. Nonlinear static and dynamic analysis of rocking masonry corners using rigid macro-block modelling. *Int. J. Struct. Stab. Dy.* (2019) **19**(11): art. no. 1950137, 1-32.

[7] Casapulla, C. and Portioli, F. Experimental tests on the limit states of dry-jointed tuff blocks. *Mater. Struct.* (2016) **49**(3):751-767.

[8] Casapulla, C., Argiento, L.U. and Ceraldi, C. Experimental validation of in-plane frictional resistances in dry block masonry walls. In: M. Papadrakakis and M. Fragiadakis (Eds.): *Computational Methods in Structural Dynamics and Earthquake Engineering (COMPDYN 2017)*, ECCOMAS Bookseries 1 (2017), pp. 2607-2618.

[9] Liu, H., Liu, P., Lin, K. and Zhao, S. Cyclic behavior of mortarless brick joints with different interlocking shapes. *Materials* (2016) **9**(3): art. no. 166.

[10] Hossain, M.A., Totoev, Y. and Masia, M.J. Friction on mortar-less joints in semi

interlocking masonry. In: C. Modena et al. (Eds.): *Brick and Block Masonry*, CRC Press (2016), pp. 1635-1643.
[11] Dyskin, A.V., Estrin, Y. and Pasternak, E. Topological Interlocking Materials, In: Y. Estrin et al. (Eds.): *Architectured Materials in Nature and Engineering, Berlin*, Springer (2019), pp. 23-49.
[12] Ali, M., Gultom, R.J. and Chouw, N. Capacity of innovative interlocking blocks under monotonic loading. *Constr. Build. Mater.* (2012) **37**:812-821.
[13] Ceraldi, C., D'Ambra, C., Lippiello, M. and Prota, A. Restoring of timber structures: connections with timber pegs. *Eur. J. Wood Wood Prod.* (2017) **75**(6):957-971.
[14] Ceraldi, C., Lippiello, M., D'ambra, C. and Prota, A. The influence of dowel-bearing strength in designing timber pegged timber joints. *Int. J. of Archit. Herit.* (2018) **12**(3):362-375.
[15] Fang, D. and Mueller, C.T. Joinery connections in timber frames: analytical and experimental explorations of structural behavior. In: *Annual IASS Symposium 2018*, IASS (2018), pp. 1-8.
[16] Sassu, M., De Falco, A., Giresini, L. and Puppio, M. Structural solutions for low-cost bamboo frames: Experimental tests and constructive assessments. *Materials* (2016) **9**(5): art. no. 346.
[17] Casapulla, C., Mousavian, E. and Zarghani, M. A digital tool to design structurally feasible semi-circular masonry arches composed of interlocking blocks. *Comput. Struct.* (2019) **221**:111-126.
[18] Mousavian, E. and Casapulla, C. The role of different sliding resistances in limit analysis of hemispherical masonry domes. *Frattura ed Integrità Strutturale* (2020) **51**:336-355.
[19] Mousavian, E. and Casapulla, C. Structurally informed design of interlocking block assemblages using limit analysis. *J. Comput Des. Eng.*, in press.
[20] UNI EN 1052-3 (2007). *Methods of test for masonry - Part 3: Determination of initial shear strength.*
[21] Montazerolghaem, M. and Jäger, W. A Comparative Numerical Evaluation of Masonry Initial Shear Test Methods and Modifications Proposed for EN 1052-3. In: *9th International Masonry Conference (9IMC)*, Guimarães, Portugal, 2014, pp. 1-10.
[22] Sassu, M., Giresini, L., Bonannini, E. and Puppio, M.L. On the use of vibro-compressed units with bio-natural aggregate. *Buildings* (2016) **6**(3): art. no. 40.
[23] Lippiello, M., Ceraldi, C., D'Ambra, C. and Lignola, G.P. Mechanical characterization of ancient pozzolanic mortars with additions of brick and tuff dust: a comparative investigation. In: K. Van Balen and E. Verstrynge (Eds.): *Structural Analysis of Historical Constructions*, Taylor & Francis Group (2016), pp. 558-564.
[24] Lippiello, M. Pozzolanic cementum of the ancient constructions in Campi Flegrei area. *Int. J. of Archit. Herit.* (2011) **5**(1):84-100.
[25] UNI EN 1015-2 (2007). *Methods of Test for Mortar for Masonry - Part 2: Bulk sampling of mortars and preparation of test mortars*.
[26] UNI EN 1015-11 (2007). *Methods of Test for Mortar for Masonry - Part 11: Determination of flexural and compressive strength of hardened mortar.*
[27] Ali, N., Ashraf, M., Alam, H. and Ahmed Khan, F. Effect of precompression and mortar ratios on the in-plane shear strength of unreinforced brick masonry. *Int. J. Advanced Structures and Geotechnical Engineering* (2016) **5**(3):78-82.

FATIGUE ASSESSMENT OF OLD RIVETED RAILWAY BRIDGES: LABORATORY TESTING OF A REAL BRIDGE

JOSÉ M. ADAM*, PEDRO A. CALDERÓN[1], MANUEL BUITRAGO[1], ELISA BERTOLESI[1], JUAN J. MORAGUES[1], SALVADOR IVORRA[2], BENJAMÍN TORRES[2]

*[1]ICITECH, Universitat Politècnica de València
Camino de Vera s/n, 46022, Valencia, Spain
E-mail: joadmar@upv.es (J.M. Adam*), pcaldero@upv.es (P.A. Calderón), mabuimo1@upv.es (M. Buitrago), elber4@upv.es (E. Bertolesi), jmorague@upv.es (J.J. Moragues)
Web page: http://www.upv.es

[2]Department of Civil Engineering, Universidad de Alicante
03690, Alicante, Spain
Email: sivorra@ua.es (S. Ivorra), benjamin.torres@ua.es (B. Torres)
Web page: http://www.ua.es

Keywords: Historical Structure, Fatigue, Monitoring, Riveted steel structure, Bridges.

Abstract. *The bridge over the Quisi Ravine in Alicante Province (Spain), built between 1913 and 1915, consists of six 22-22-42-42-22-22 m long steel Pratt truss spans, the lateral spans being isostatic and the central spans continuous. All the joints between the steel elements are riveted. As the bridge has been carrying railway traffic for more than 100 years, its condition needed to be assessed before carrying out the necessary repairs-reinforcement to extend its service life. One of the most interesting tasks on the bridge involved a study of its fatigue behaviour to estimate its remaining useful life. Only a few kilometres away there happened to be another bridge with identical geometry over the Ferrandet Ravine, which had recently been dismantled and taken out of service and had carried the same railway traffic as the one over the Quisi Ravine. Advantage was therefore taken of this unique opportunity to test one of its isostatic spans in order to extrapolate the results to the Quisi Bridge. These tests were carried out at the ICITECH laboratories at the Universitat Politècnica de València in two different scenarios: 1) one test on a 22 m span, and 2) another on one of its girders, in both of which simulated railway traffic cyclical loads were applied. The results allowed us to estimate the number of trains that could pass over the bridge and its remaining service life, and also to define a monitoring method to help in decision making in case of possible failures of its component parts. The study also included an analysis of the bridge's robustness in local failures of some of its elements, which led to a further bridge cyclical loading test with a deliberately damaged component. Even though other researchers had previously carried out fatigue tests on full-scale riveted bridge elements, the ICITECH study is unique in that it is the first time a full-scale bridge has been subjected to fatigue tests. This work was accompanied by advanced numerical modelling studies considering the fracture mechanics theory.*

1 INTRODUCTION

Structural maintenance and conservation received a lot of attention from the press and the media after events such as the collapse of the IW-35 bridge over the Mississippi in 2007 in Minneapolis, or the more recent case of the Polcevera Viaduct in Genoa in 2018. Special attention has been given to the older infrastructures nearing the end of their service life in which the effect of long-term continuous loads can have serious effects due to accumulated damage in their structural elements and can lead to fatigue failures. This is similar to the well-known case of the damage caused by bending of aircraft wings or the effect of waves on ships' hulls. The case studied in the present work was an example of a steel railway bridge with riveted joints that had suffered wear and tear from the continual passage of trains over many years, which could have compromised the structure's fatigue safety without ever having reached the material's yield stress. Some researchers have already studied this phenomenon in this type of structure, for example the outstanding work by Pipinato et al [1].

The present work on estimating fatigue and the remaining service life of a steel railway bridge was part of the renovation of the Alicante-Denia line belonging to the Valencia Railway Company (FGV). This line was built between 1912 and 1915 and, besides its value as transport, forms part of the civil engineering heritage of Alicante and the Valencia Community. The work was also included in the EU's Horizon 2020 social challenges and in the UN's Sustainable Development Objectives.

After this Introduction, the paper includes: a) a description of the bridge, b) the research method followed, c) a summary of the tasks carried out in the different phases, including: a preliminary, detailed and in-depth analysis, d) the remedial measures adopted, and e) the conclusions drawn from the study.

2 DESCRIPTION OF THE BRIDGE

Structurally, the bridge consists of six 22-22-42-42-22-22m spans built with Pratt trusses, and includes a pedestrian walkway and metal handrail on the upper deck. The metal piers reach a maximum height of 23.6m over the foundations. The four lateral spans are isostatic, with two continuous central spans on fixed supports but able to move in the direction of the bridge's axis. The piers consist of steel latticework between four girders that rest on masonry elements. Figure 1 gives the main dimensions and a view of a train passing over the bridge.

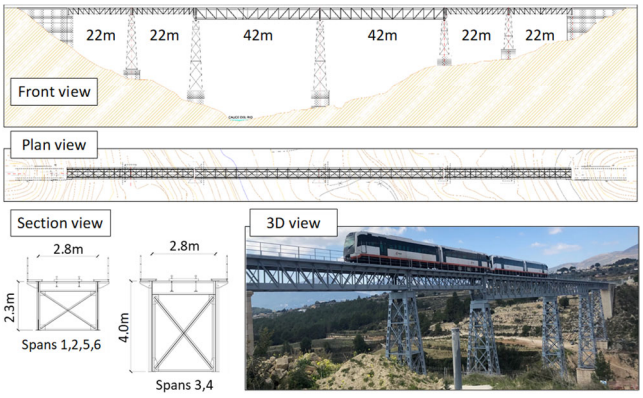


Figure 1: Geometry of the bridge and a general view

This historically interesting bridge is an example of early 20th century engineering in the province of Alicante. It was built between 1912-15 and is now more than 100 years old and has carried many different types of passenger and goods trains. However, as it was designed in accordance with the standards of the time and was unlikely to meet the present requirements [2], it was given a structural assessment in 2015 which led to its renovation and real time monitoring to ensure it can safely continue to carry trains for another few years. The tasks and studies carried out are described in detail in the following pages, with a special focus on evaluating the bridge's safety as regards its fatigue limits.

3 METHODOLOGY

This section describes the method used to assess the Quisi bridge fatigue life and the subsequent proposal of appropriate measures to ensure a safe limit state, for which the Report of the European Convention for Constructional Steelwork (ECCS) and the EC's "Assessment of existing steel structures: *Recommendations for Estimation of Remaining Fatigue Life*" [4] were followed. This document proposes a method of assessing a structure's fatigue behaviour and its remaining life based on four analytical phases. Advantage was taken of the unique opportunity of using the Ferrandet bridge, which was only a few miles away, with identical spans, built during the same period and carrying the same railway traffic, for this purpose. As this bridge had recently been replaced by a new one, the original structure had been dismantled and was available for testing and so we decided to subject it to a complete set of tests to obtain valid conclusions that could be applied to the Quisi Viaduct, including the following:

- Phase I, preliminary evaluation:
  - Inspections.
  - Static and Dynamic loading tests.
- Phase II, detailed investigation:
  - Tests on steel specimens.
  - Loading effects on the structure. Differences in the local and overall structural response.
  - Definition of the fatigue strength curve. Test until failure on a local element of the structure.
  - Test on a full-scale bridge span.
  - Remaining life based on experimental evidence.
- Phase III, in depth analysis:
  - Fracture mechanics. Failure patterns.
  - Robustness: Experimental and numerical approach.
- Phase IV, remedial measures.

4 PRELIMINARY EVALUATION

The bridge's structural behaviour was analysed in depth by means of: a) a thorough preliminary inspection in accordance with the recommendations in ITPF-05 [3], and b) a loading test to measure strains in the bottom and top chord and deflections at the centre of the

spans. Shear demand and response of the structure was assessed with strain measurements in diagonal and vertical elements near the supports. The load test considered 4 different load hypotheses (see Figure 2). The dynamic response of the structure was also analysed with trains passing over at 20km/h and 50km/h while monitoring accelerations. The results obtained showed that the bridge was still structurally sound, although the accumulated fatigue in 100 years of service life could compromise its safety and possible produce an accident. The method followed then entered the second step of the study.

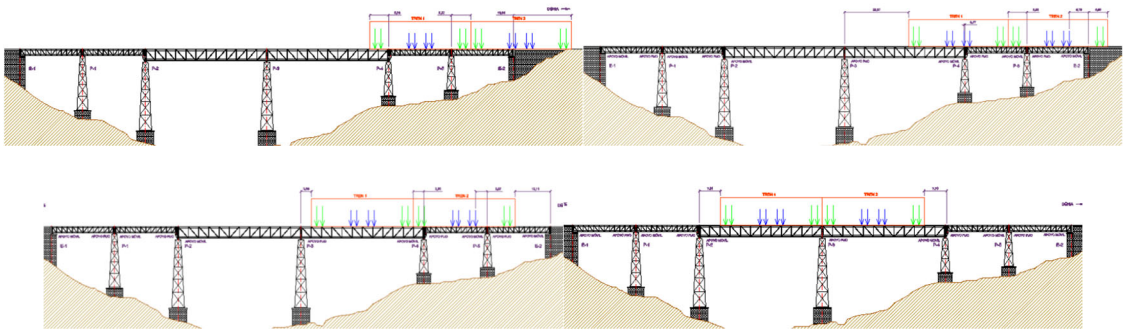


Figure 2: Load hypothesis.

5 DETAILED INVESTIGATION

This research phase consisted of the following tasks: a) tests on steel specimens and joints, b) study of the structural response, c) definition of the fatigue strength curve, d) test on a full-scale bridge span, and e) estimating the remaining life based on experimental evidence.

5.1 Tests on steel specimens and joints

Specimens extracted from different profiles and plates were analysed. Parameters such as yield stress, ultimate stress, elongation, absorbed energy or the chemical composition were determined. A total of 160 gamma ray scans were carried out on different elements, following EN ISO 5579. Although in general the joints were found to be in good condition, a number of small cracks were found in different components. Figure 3 shows some examples of flaws in scanned rivets.

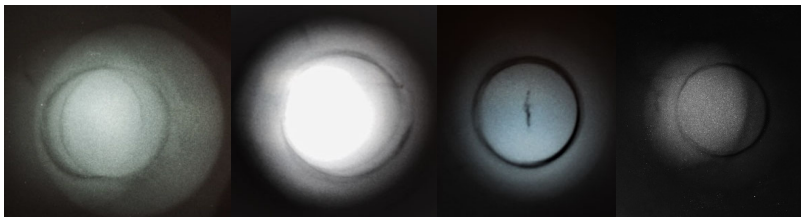


Figure 3. Gamma scans of rivets.

5.2 Loading effects on the structure. Differences in the local and global structural response

This section deals with the numerical study on the effects of passing trains on the structure, considering different loading hypotheses and the predominant stresses on different elements.

5.2.1 Loads and loading hypotheses considered

The loads selected were those of the trains that normally passed over the Quisi bridge, a Series 2500 type diesel-powered train with two fully loaded carriages. A sketch can be seen in Figure 4 with the maximum loads on the fully loaded axles.

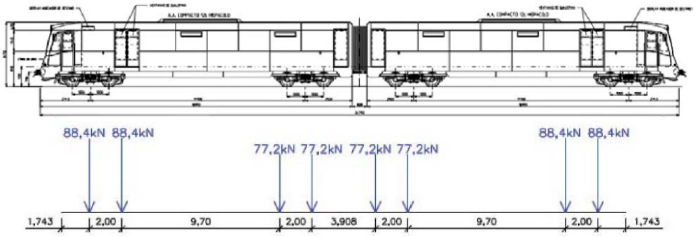


Figure 4. Sketch of train with maximum axle loads.

The maximum stresses on different elements were obtained by a simplified method for the loading hypotheses considered in Section 4 (see Figure 2).

5.2.2 Results of numerical simulation

Results were obtained for the geometry of the different bridge elements and a linear-static analysis. For example, Figure 5 gives the axial stress structural response and the vertical displacements of the structure for a specific load hypothesis. As can be extracted from the structural response and as expected, the bridge behaviour consisted of a series of isostatic and continuous high-depth beams (trusses) mainly loaded with axial forces. However, certain components had a highly local behaviour and transmitted the train loads to the main trusses by means of a series of elements working with bending stresses. Figure 6 shows the stress values of one of these elements with local behaviour working under bending stresses.

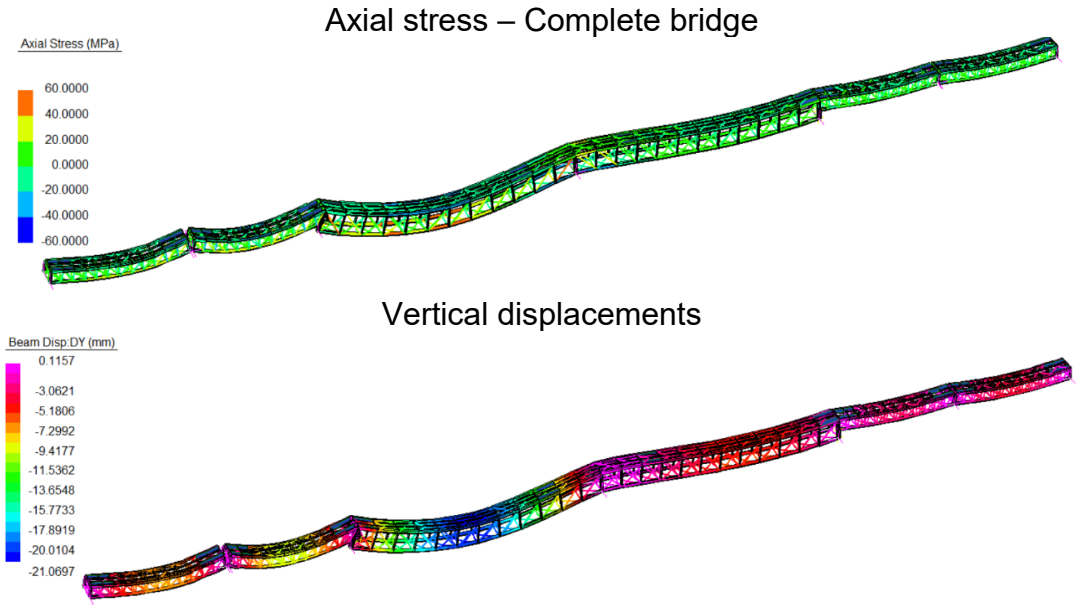


Figure 5. Axial stress and vertical displacements of the structure.

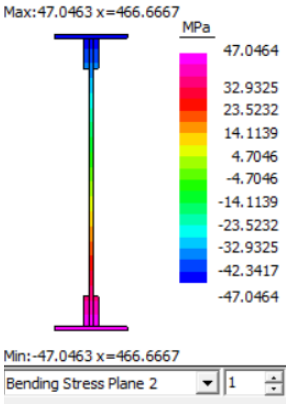


Figure 6. Stresses on an element with local behaviour.

It can be seen that train loads had different effects on the structure: a) a truss behaviour defined as the main general structural response of the structure, and b) a local behaviour of some elements under bending stresses. The study of the bridge's fatigue capacity and remaining service life was thus in two directions to evaluate both its local and general behaviour.

5.3 Definition of the fatigue strength curve. Test until failure on a local element of the structure.

To assess local behaviour a fatigue test was carried out on critical elements, which were subjected to cyclic bending stress increments until failure, including a historical analysis of stress increments throughout the bridge's history.

This section contains: a) a definition of the test, b) test results, and c) a historical analysis of the stresses on the elements to define the fatigue strength curve.

5.3.1. Definition of the test

The test was on a lateral joint element with the top chord of the main truss of the bridge as shown in Figure 7, which shows the test setup.

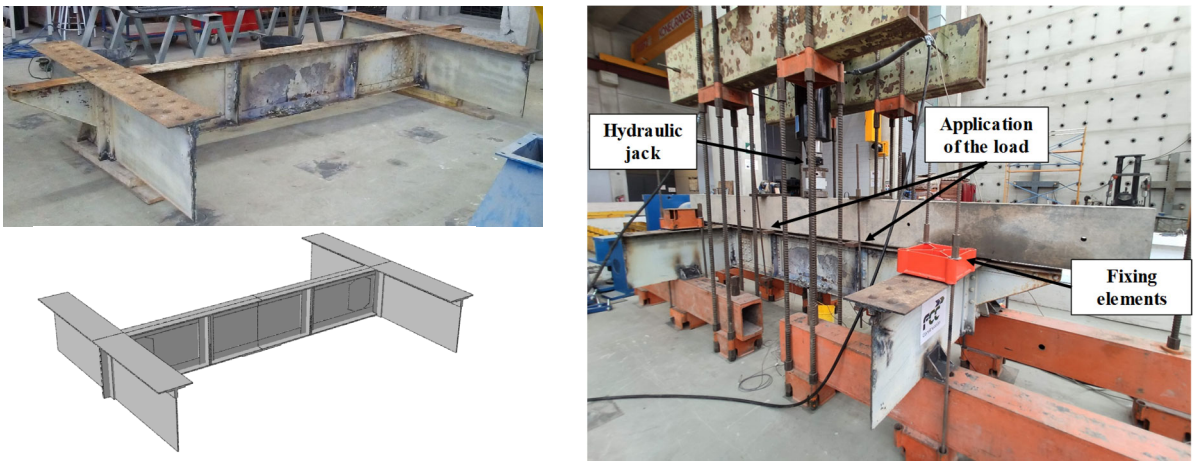


Figure 7. Element selected for testing (left) and test setup (right).

In these conditions the element was subjected to local loads that reproduced similar bending and shear stresses to those in the bridge. The applied load was defined with the aid of computer models (see also Figure 7). Diverse situations were modelled under different loads. The highest stresses and lowest number of cycles before failure were obtained at the highest load levels. The load increment finally selected was 600kN. The Von Mises stresses in the constant bending moment zone at the centre of the element were expected to reach maximum values of 212.6 MPa, at which the number of estimated cycles before failure was 74,472, adopting a category detail of 71 [4] without considering a previous history of accumulated repetitive loads.

The test was continually monitored by four strain gauges (SG) to measure deformations and two LVDTs to measure deflections and any slippage between the rivets and plates subjected to the highest shear stresses. The positions of the sensors can be seen in Figure 8.

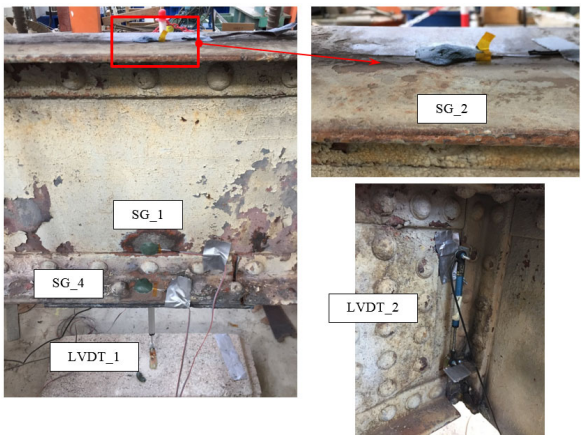


Figure 8. Position of the sensors.

5.3.2 Test results

Figure 9 gives an example of the readings from a strain gauge in a short period of time and Figure 10 shows the evolution of the deformation increment measured in each cycle from the start until failure (cycle 31377). The element failed at normal stresses in cycle 31377. Figure 10 shows the fatigue crack that started at the bottom of the element (zone in tension) and propagated to the top of the beam element.

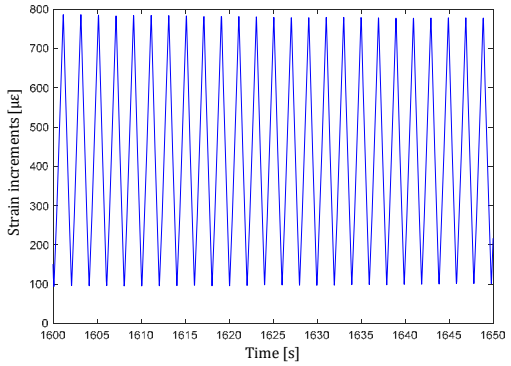


Figure 9. Example of strain measurements.

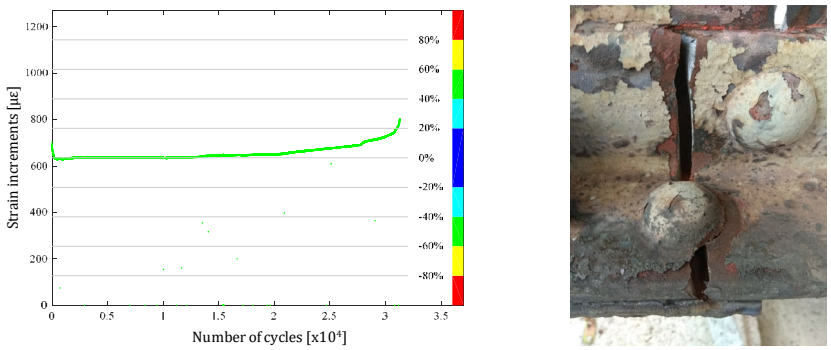


Figure 10. Strain increment evolution of SG_2 (left) and fatigue crack at the end of the test (right).

5.3.3 Historical analysis of stresses on the element. Definition of fatigue strength curve

After the girder had failed it became possible to determine the detail category of this type of element with riveted joints, which belongs to detail category 71 according to EU recommendations [4]. To determine the exact category an analysis of the historical loads was carried out to accompany the test data.

The historical data provided by the railway company on the traffic over the bridge during its lifetime after 1915 showed that 11 different types of train had been used. The only uncertainty in the data was on the weight of the trains since, there was no information available on their load factors and these ranged from completely empty to completely full.

Adopting the damage accumulation method laid down in different codes, (e.g. EC-3 Part 1-9 [5] or EAE [6]), the detail category to which the failed element belonged could be obtained by considering 100% total accumulated damage at the end of the test as follows:

- Fully loaded trains: detail category 71.
- Empty trains: detail category 63.

Figure 11 gives a summary of these calculations. It can be seen that the accumulated damage was 100% in both cases.

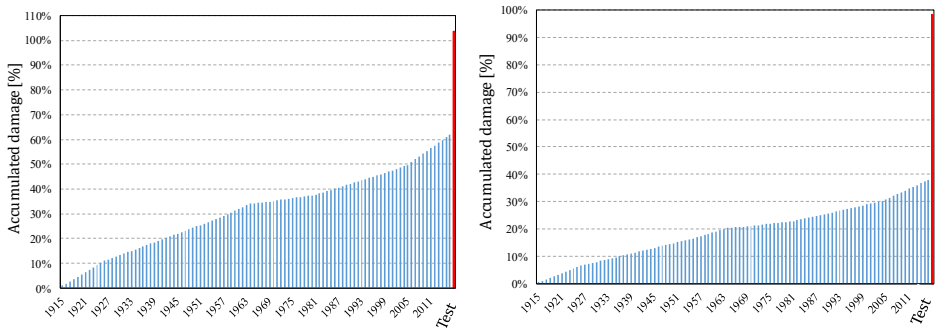


Figure 11. Hypothesis of fully loaded trains (left) and empty trains (right).

5.4 Test on a full-scale bridge span

An isostatic span of the Ferrandet bridge was transported from the railway company's premises in Campello (Alicante) to the *ICITECH* laboratories at the *UPV*. Photographs of the span during its journey can be seen in Figure12.



Figure12. Transporting the span from Campello (Alicante) to the UPV (Valencia).

The system used to support the span in its original location was used in the lab tests: hinges that allowed rotation around an axis at each end and metal boxes containing steel ball bearings that allowed longitudinal movement at one end only. Figure 13 shows the supports used in the test setup, while Figure14 contains a view of the span at the *ICITECH* laboratories.

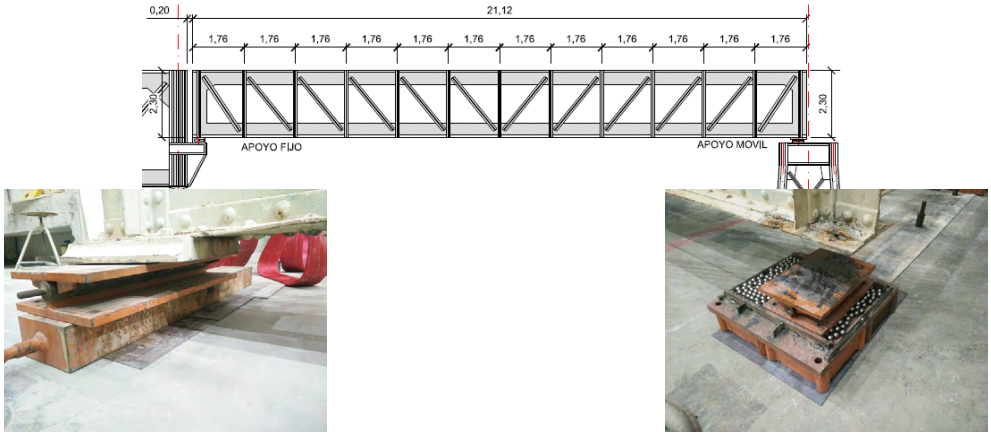


Figure 13. Support system used in the tests.

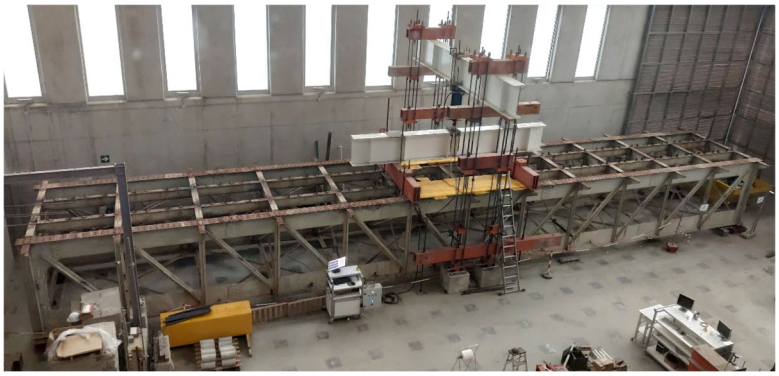


Figure14. General view of the bridge span at the *ICITECH* laboratories.

5.4.1 Definition of the test

The test was defined with the help of computational models with identical geometry and behaviour as the span under study. Figure15 shows the displacement and stress fields after subjecting the span to a central load of 1250kN.

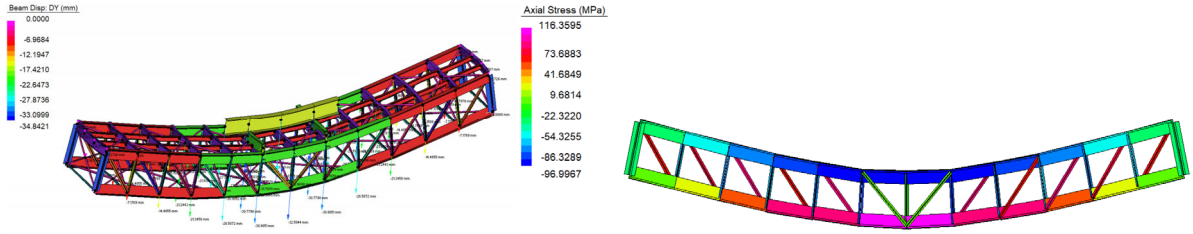


Figure15. Vertical displacements (left) and axial stresses (right) under a load of 1250kN.

LVDTs and strain gauges were used to continually monitor the span during the test, including dynamic tests at the start and finish to determine possible changes of the first mode of vibration due to damage. Figure 16 shows the 40 elements (in red) with strain gauges and the 8 points with displacement sensors. The dynamic tests were performed with accelerometers at the centre of the span and an impact was applied to the centre of the load sharing system.

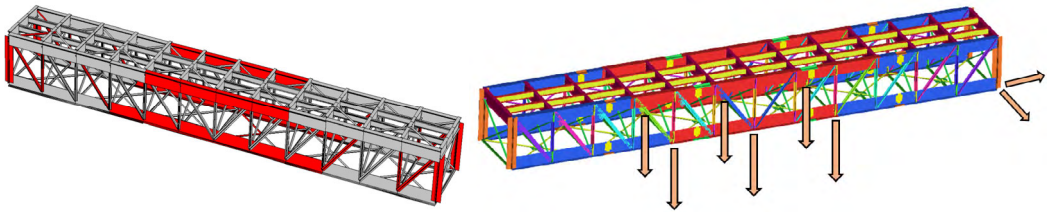


Figure 16. Elements with strain measurements (left) and position of LVDTs (right).

The defined test conditions assumed that 16517 cycles were equal to 10 years of service, so that after the 45,000 cycles reached in the test the damage to the span was equivalent to the damage expected in the next 27. 2 years.

5.4.2 Test results

Figure 17 shows an example of the strain increments in four strain gauges in the last cycle of the test. It can be seen that the structural behaviour at the beginning and end is almost identical.

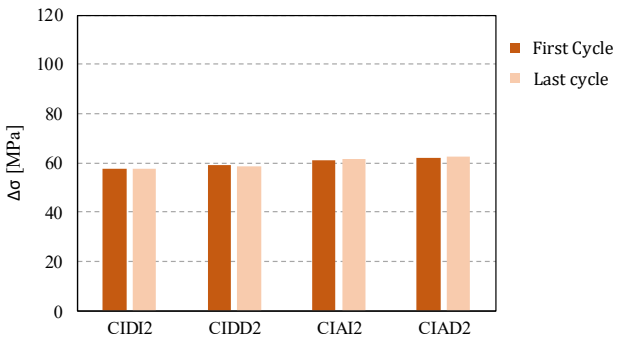


Figure 17. Example of stress increment measurements in 4 strain gauges in the first and last cycle.

The tests revealed clearly elastic linear behaviour with no apparent damage, based on:

- Stresses clearly lower than the yield stress in the different elements.
- Similar deformation and stress patterns were found in the first and last cycle. Variations were less than 5% in all cases and below 2.5% in 85% of cases.
- Similar deflections and horizontal displacements were found during the entire test and all were below 3%.

The dynamic test gave a variation of 8.40Hz at the start and 8.05Hz in the first mode of vibration in the structure at the end of the cycle, which implies a frequency reduction of 4.2% and shows a slight increase in the bridge flexibility. Together with the variations obtained by the deformation and displacement sensors, this value shows the minimum variation in the general bridge behaviour after the intense fatigue test it had been subjected to. There were no signs of failure or weakness in any of the elements.

5.5 Remaining life based on experimental evidence

The tests showed that the most critical elements were those in the load sharing structure (see Section 5.3), which reached fatigue failure in the test. The damage accumulation method was used to estimate these elements' remaining useful life, which was around 10.7 years. The remainder of the elements of the main structure (trusses) had a longer remaining life and did not reach failure with damage equivalent to 27.2 years of service.

6 IN-DEPTH ANALYSIS

Apart from the lab tests, other deeper tests were carried out by means of fracture mechanics techniques and the bridge's structural robustness was tested against possible local failures in some elements.

6.1 Fracture mechanics. Failure patterns

Computational simulations and analytical studies were used to evaluate and reinforce the conclusions reached up to this point. The analytical studies were by means of fracture mechanics and confirmed that the fracture of the elements in the local load sharing system would occur at the same or even slightly higher number of cycles than in the experimental tests and those calculated by applying the expressions in EC-3[5]. This confirmed that the bridge would have a remaining service life of 10.7 years, the same as that calculated from the experimental tests.

Similar results were also obtained from the computational models. For example, the numerical prediction found that cracks would begin to appear after 7530 cycles (experimentally, between 10,000 and 15,000) with similar propagation patterns to those obtained experimentally (see Figure 18).

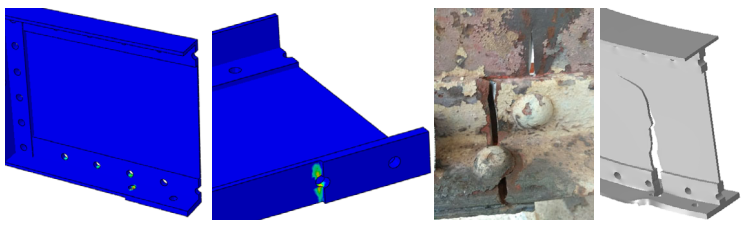


Figure 18. Computational models for triggering cracks (left) and predicting the cracking pattern (right).

6.2 Robustness: Experimental and numerical approach

Robustness against possible failure of elements in the bridge's main latticework was also studied by recreating artificially failures in the main trusses. The aim was thus, not to determine the causes of possible crack initiation and propagation, but to determine the consequences of a local element failure, known as the *scenario-independent approach* [7–10], widely used to study progressive or disproportionate structural collapse after a local failure. This method can evaluate structural robustness understood as insensitivity to or propagation of a local failure.

The study was in two parts: experimental and numerical (see Figure 19). In the first, two of the most critical diagonals were cut at different damage levels, while the second simulated the failure of a critical element under tensile loads. Both methods were aimed at studying the alternative load paths and robustness of the structure.

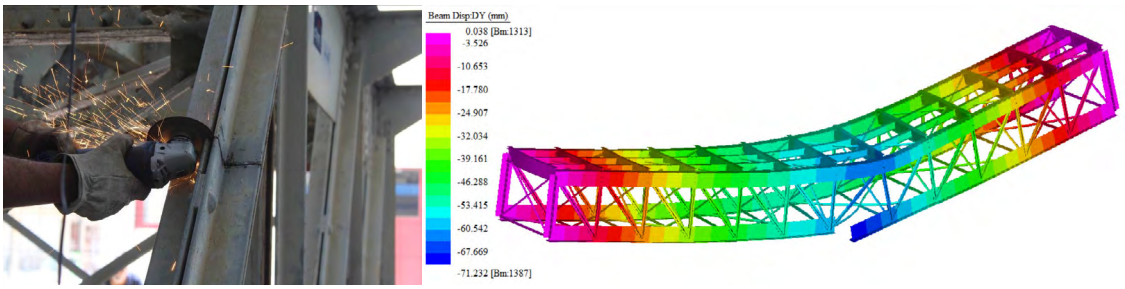


Figure 19. Experimental (left) and numerical (right) study of the influence of different levels of damage on the behaviour of the structure.

The results showed that the structure, normally considered as an isostatic structure working solely under axial stresses, had a certain redundancy and was able to withstand this type of failure, activating for this purpose some of the alternative load paths with high bending stresses at the joints.

7 REMEDIAL MEASURES

The bridge under study was planned to continue in service for three additional years. After the study it was decided to keep it in operation with a series of remedial measures.

- Real time monitoring, considering the crucial elements that could trigger a failure of the structure and develop a fatigue crack.
- Periodical inspections.
- Limitation to a lighter type of train than others.
- Limited number of trains per day.

8 CONCLUSIONS

This paper describes the evaluation of the fatigue limit state of the Quisi Viaduct in Alicante (Spain) carried out by the *Calsens Company*, a spin-off of the *Universitat Politècnica de València*, in collaboration with the *ICITECH*. The study included all the stages recommended by [4], from a preliminary assessment to an in-depth analysis and took advantage of the unique opportunity of having an identical bridge available for the study,

including ambitious experimental tests and subjecting an entire bridge span to fatigue tests at the *ICITECH* laboratories.

The results obtained showed that the Quisi Viaduct has a local load sharing system with a high amount of accumulated damage. However, the structure's overall behaviour presents a greater margin of safety and redundancy. Apart from the fact that the bridge will be out of service in three years, the tests carried out led to a series of strict remedial measures to ensure it can safely remain in service for this time.

ACKOWLEDGEMENTS

The authors wish to acknowledge their gratitude to the companies that confided this work to *Calsens*: *FCC*, *CHM* and *CONVENSA*, and special thanks to *FGV* and Juan Antonio García Cerezo for all the facilities they gave us to successfully carry out the tests.

REFERENCES

[1] Pipinato A, Pellegrino C, Bursi OS, Modena C. High-cycle fatigue behavior of riveted connections for railway metal bridges. *J Constr Steel Res* 2009;65:2167–75. doi:10.1016/j.jcsr.2009.06.019.

[2] Ministerio de Fomento. Instrucción de acciones a considerar en puentes de ferrocarril (IAPF) 2010:134.

[3] Ministerio de Fomento. Instrucción sobre las inspecciones técnicas en los puentes de ferrocarril (ITPF-05) 2005:8.

[4] Kühn B, Lukic M, Nussbaumer A, Günther HP, Helmerich R, Herion S, et al. Assessment of existing steel structures: Recommendations for estimation of the remaining fatigue life. vol. EUR 23252. Luxembourg: 2008. doi:10.1016/j.proeng.2013.12.057.

[5] EN 1993-1-9. Eurocode 3: Design of steel structures. Part 1-9: Fatigue 2009.

[6] EAE. Instrucción de Acero Estructural 2011.

[7] Lin S-C, Yang B, Kang S-B, Xu S-Q. A new method for progressive collapse analysis of steel frames. *J Constr Steel Res* 2019;153:71–84. doi:10.1016/j.jcsr.2018.09.029.

[8] Buitrago M, Sagaseta J, Adam JM. Effects of sudden failure of shoring elements in concrete building structures under construction. *Eng Struct* 2018;172:508–22. doi:10.1016/j.engstruct.2018.06.052.

[9] Adam JM, Buitrago M, Bertolesi E, Sagaseta J, Moragues JJ. Dynamic performance of a real-scale reinforced concrete building test under corner-column failure scenario. *Eng Struct* 2020.

[10] Buitrago M, Sagaseta J, Adam JM. Avoiding failures during building construction using structural fuses as load limiters on temporary shoring structures. *Eng Struct* 2020;204:1–16.

12th International Conference on Structural Analysis of Historical Constructions
SAHC 2020
P. Roca, L. Pelà and C. Molins (Eds.)

INFLUENCE OF MOISTURE CONTENT ON THE APPLICATION OF ND AND MD TESTS TO VARIOUS SPECIES OF TIMBER ELEMENTS

M.R. VALLUZZI[1*], F. CASARIN[2], L. SCANCELLI[2], M. DRDÁCKÝ[3], M. KLOIBER[3] AND J. HRIVNÁK[3]

[1] Department of Cultural Heritage
University of Padova
Piazza Capitaniato 7, 35139 Padova, Italy
e-mail: mariarosa.valluzzi@unipd.it (*corresponding author)

[2] Expin s.r.l.
Via Panà 56ter, 35027 Noventa Padovana (PD), Italy
e-mail: casarin@expin.it, scancelli@expin.it, www.expin.it

[3] Institute of Theoretical and Applied Mechanics (ITAM) of the Czech Academy of Sciences
Prosecká 809/76, 190 00 Prague 9, Czech Republic
e-mail: drdacky@itam.cas.cz, kloiber@itam.cas.cz, hrivnak@itam.cas.cz

Keywords: Timber species, moisture content, resistance drilling, ultrasonic tests, pin-pushing test, correlation

Abstract. *Variations in environmental conditions can affect the structural performance of timber components and constructions. Especially in case of historic masonry buildings, where timber elements can be found either in roof or floor structures, intrinsic defects (e.g., knots, cracks, degradation), as well as the surrounding environmental conditions (e.g., temperature and moisture) can play an important role in the assessment of the mechanical response of the elements. In this connection, non-destructive (ND) and minor-destructive (MD) procedures are used to investigate the onsite conditions of wood, which are commonly based on either tool penetration resistance or wave transmission devices. In the paper, the influence of moisture content (MC) measured with various devices on a series of both old and new timber elements was compared. The elements made of various wood species (mainly red fir, but also white fir, pine and larch) were subjected to laboratory ND and MD testing by three research groups. Results showed the low influence of the MC on MD tests (i.e., resistance drilling and pin penetration) in comparison to the ND (i.e., sonic/ultrasonic) ones. Correlation relationships are provided, which illustrate and approximatively quantify the effect of MC for the experimentally investigated conditions and test equipment.*

1 INTRODUCTION

Investigation of timber structures relies on both visual and instrumental inspections, the latter based on both non-destructive (ND) and minor-destructive (MD) test procedures [1] [2]. ND and MD tests are basically local tests which can qualify a parameter in a small portion of the

material but whose results are not representative over an overall element. Moreover, as well known, outcomes are affected by many aspects, among which moisture content (MC) is one of the most sensitive for wood [3] from the site condition viewpoint. The 'oven dry' procedure [1] is recognized as the most effective way to measure the MC in wood. Nevertheless, being it a destructive method, usually moisture meters are used onsite to manually check that parameter.

The paper compares the results obtained by the application of various ND and MD methods to a series of deteriorated timber beam elements retrieved from existing structures (19 components over 21, made of fir, oak, elm, and pine) and 12 new ones (made of fir and larch).

Experimental tests were performed by research groups of the University of Padova (UNIPD), Italy and the UNIPD's spin-off Expin srl, and the Institute of Theoretical and Applied Mechanics of Prague, Czech Republic (ITAM).

Results were compared by grouping similar methods, i.e.: resistance drilling (two types of Resistograph®, one for each group), pin penetration (Novatester device for UNIPD and the pin pushing device for ITAM), wave velocity-based methods (ultrasonic for UNIPD and stress wave for ITAM) [4]. Pin pushing is an in-house new MD device provided patented by ITAM, which is able to gradually apply, monitor and record the force occurring for the pin penetration into the wood [5]. Three types of moisture measurement devices were used (two electric and one electromagnetic).

The research aims are: i) to contribute on the quantification of the influence of MC according to different devices applied to various species in different conditions, and ii) to evaluate the possible MC effect on the results provided by the application of common ND/MD testing methods for the onsite investigation in existing/historical structures.

The problem has already been partially studied in laboratory conditions typically on clear wood specimens – spruce boards. Thus using well defined moisture content conditions the pin pushing [6] and the mini-jack [7] behavior has been investigated. Experimental measurements were carried out using 30 spruce boards at moisture contents of 12, 18 and 24%. The effect of the wood moisture on the measurement by means of the both devices was confirmed. In the case of the mini-jack the assessed relationship was linear while for the pin pushing non-linear. The impact of the MC on ultrasonic measurements was studied in [8] mostly at high MC in artificial climate chamber environment. It has been found that velocity decreases sharply as the moisture content increases from 0% to the fiber saturation point of 30%, and then decreases at a much slower rate as the MC increases further.

However, the effect of the moisture content at ND/MD measurements has not been so frequently studied because these methods are mostly applied for investigation of built-in timber in buildings where the MC does not vary significantly and the other wood parameters (e.g. species, structure, defects etc.) influence much more the measurement results.

2 EXPERIMENTAL CAMPAIGN

Several experimental procedures were applied to either new or old timber elements. The former all had rectangular cross-section of 160x160 mm^2, length of about 5 m and were equally distributed between larch and red fir woods (six elements for each wood type), whereas the latter were retrieved from a roof dismantled from an existing masonry buildings and were therefore suffering decay conditions. These old elements had not homogeneous dimensions for cross-sections (mostly larger than the new elements) and lengths (from about 3 to 5 m) and

belonged to various species (mainly red fir, but also few elements were made of pine, white fir, oak and elm).

The new elements were already classified as C24, according to UNI EN 338 (2016) [9]. The retrieved beams were affected by the presence of cracks (e.g., R-RF_4 and R-RF_10 beams) and quite diffused single and groups of knots, and presented a slope (of about 10%) of grain in tangential sections. Therefore, they resulted in categories I, II or III (or non-classifiable, in few cases, due to high deteriorated conditions), according to the onsite increasing grades (form I to III) provided by UNI 11119 (2004) [10]. Just to compare the two sets of components (new and old) for the fir specie, a new element would have a bending strength of 24 MPa and a parallel bending modulus of elasticity of 11000 MPa (according to [9]), whereas an old one would refer to decreasing values for I-II-II grades of 11,5-10,0-7,5 MPa and 13000-12000-11000 MPa for the bending strength and modulus of elasticity, respectively (according to [10]).

Figure 1 shows some examples of the types of beams considered in the study.



Figure 1: Example of some typical features of tested elements

After visual inspection, the beams were examined according to the following procedures:

- Moisture content (MC) measurement, applied with three types of devices: two electric, i.e., LogicaH&S LG43 type for UNIPD and WHT 860 for ITAM, and one electromagnetic, i.e., Wagner L620 Digital Lumber Moisture Meter for ITAM as well;
- Resistance drilling (RD) tests, applied with two types of Resistograph®: IML RESI PD400 for UNIPD and Rinntech Resistograph 4453-P for ITAM;
- Pin penetration (PP) tests, applied with two types of devices: Novatest Woodtester for UNIPD (2.21 Nm of impact energy) and pin-pushing device patented by ITAM;
- Wave velocity-based methods (WV), applied either in direct (D) (crossing section) and

indirect (I) (longitudinal on the surface) configurations, i.e., ultrasonic wave for UNIPD (Proceq Pundit Lab+ device) and sonic stress wave for ITAM (Fakopp Microsecond Timer tool).

Moisture meters are based on the correlation of electric resistance and water content on the wood: the higher is the electric resistance the lower is the MC. Moisture meters can be either pin meter (electric) or pinless meter (electromagnetic). The measurements with pin meters are carried out on two points of about 20 mm spaced. Pinless moisture meters are completely ND: they use electrical waves at a certain electromagnetic frequency, which are transmitted through the base pad in contact with the wood. Moisture meters can give reliable results in a range of humidity of 7-30%, i.e. below the saturation point of the wood [11]. They are calibrated for non-damaged wood structures, therefore, they provide more precise and coherent data for the sound wood than for the wood with deteriorated structure of cells by fungi or worms.

Resistance drilling devices measure the energy consumption to allow a thin needle (about 1.5-3 mm in diameter and over 400 mm long) to be driven in the wood [3]. The test outcomes are the density profiles of the penetrated section of wood, which can indicate the condition of the material and identify possible inner defects or voids.

Pin penetration tests apply a needle impact from the surface of wood and can investigate the wood up to few cm in depth [3]. The device used by UNIPD had a needle of 5 mm in diameter; five consecutive strikes were applied to the element and a displacement transducer measured the reached depth, which can be correlated to variations of density along the element. Instead, the pin-pushing tests results were the average forces that allow the pin (about 25 mm in diameter and 120 mm long) to penetrate into the wood [5].

Test methods based on either sonic or ultrasonic wave velocities measure the time occurring the wave to be transferred from two points of an element, those points being either on opposite sides (direct tests) or on the same side (indirect tests) [12]. The former configuration investigates the cross-section of an element, the latter mainly the surface of it. The higher is the density of the material the higher is the wave velocity. Usually, due to the cellular structure of wood, direct tests are characterized by lower velocity then indirect ones [12]. Indirect (longitudinal) ultrasound tests are more representative of the possible onsite applications in buildings due to possible problems of accessibility to some sides of the structural elements.

Table 1 shows the characteristics of all the timber elements and the number of tests (i.e., measurement points on the beams) carried out for each procedure applied by the research groups (numbers are shown as UNIPD+ITAM measurement points). Notations for labels: R stands for ‘recovered’, N for ‘new’; RF stands for ‘red fir’, WF for ‘white fir’, L for ‘larch’, P for ‘pine’.

Station points were distributed along two faces of the elements, as in the examples showed in Figure 2. MC was measured along with the other ND/MD tests. All the various tests (MC, RD, PP, SW) were performed on the same points along the elements (see Figure 2). As for SW, direct tests were carried out from one of the points mentioned above to the corresponding one on the opposite side (three measures for each pair); indirect tests were performed on three sides of the elements, i.e., two pairs starting from 1 m from the two ends and one pair from the center of the element (three measures for each pair spaced of 100, 150, 200, 300, 450 and 600 mm).

Table 1: Experimental program and description of specimens

Element label	Cross-section		Length [mm]	Classification	MC	RD	PP	WV	
	Dimensions [mm^2]	Type						D	I
R-RF_1	221x185	quite regular	4030	II grade	17+2	17+2	17+2	0+2	0+2
R-RF_2	175x160	quite circular	4600	II grade	9+2	9+2	9+2	9+2	18+2
R-RF_3	220x152	regular	4500	I grade	10+2	10+2	10+2	7+2	18+2
R-RF_4	224x171	regular	4810	n.c.	12+2	12+2	12+2	0+2	0+2
R-RF_5	250x220	regular	4980	I grade	11+2	11+2	11+2	8+2	10+2
R-RF_6	223x183	regular	2980	I grade	11+2	11+2	11+2	0+2	0+2
R-RF_7	258x214	regular	4230	I grade	6+2	6+2	6+2	0+2	10+2
R-RF_8	207x162	regular	4625	I grade	6+2	10+2	10+2	3+2	0+2
R-RF_9	234x215	quite circular	4030	I grade	7+2	7+2	7+2	0+2	0+2
R-RF_10	199x158	regular	4680	n.c.	18+2	18+2	18+2	18+2	18+2
R-RF_11	194x125	trapezoidal	4530	I grade	17+2	17+2	17+2	7+2	18+2
R-RF_12	214x175	regular	4670	II grade	17+2	17+2	17+2	0+2	0+2
R-RF_13	201x135	regular	4660	I grade	18+2	18+2	18+2	16+2	18+2
R-RF_14	220x178	regular	4510	II grade	17+2	17+2	17+2	9+2	18+2
R-RF_15	218x165	quite regular	4565	I grade	18+2	18+2	18+2	0+2	0+2
R-WF_1	203x178	regular	4715	I grade	18+2	18+2	18+2	9+2	18+2
R-WF_2	209x193	regular	4090	I grade	16+2	16+2	16+2	12+2	18+2
R-P_1	248x225	regular	5030	I grade	6+2	6+2	6+2	10+2	18+2
R-P_2	225x248	regular	4570	I grade	17+4	17+4	17+4	0+4	18+4
N-RF_1	160x160	regular	5075	C24	20+2	20+2	20+2	20+2	18+2
N-RF_2	160x160	regular	5090	C24	2+2	20+2	20+2	20+2	18+2
N-RF_3	160x160	regular	5085	C24	2+2	20+2	20+2	20+2	18+2
N-RF_4	160x160	regular	5085	C24	20+2	20+2	20+2	20+2	18+2
N-RF_5	160x160	regular	5085	C24	2+2	20+2	20+2	20+2	18+2
N-RF_6	160x160	regular	5085	C24	2+2	20+2	20+2	20+2	18+2
N-L_1	160x160	regular	5090	C24	2+3	20+2	20+2	20+2	18+2
N-L_2	160x160	regular	5090	C24	2+2	20+2	20+2	20+2	18+2
N-L_3	160x160	regular	5085	C24	20+3	20+2	20+2	20+2	18+2
N-L_4	160x160	regular	5100	C24	20+3	20+2	20+2	20+2	18+2
N-L_5	160x160	regular	5080	C24	2+3	20+2	20+2	20+2	18+2
N-L_6	160x160	regular	5085	C24	2+3	20+2	20+2	20+2	18+2

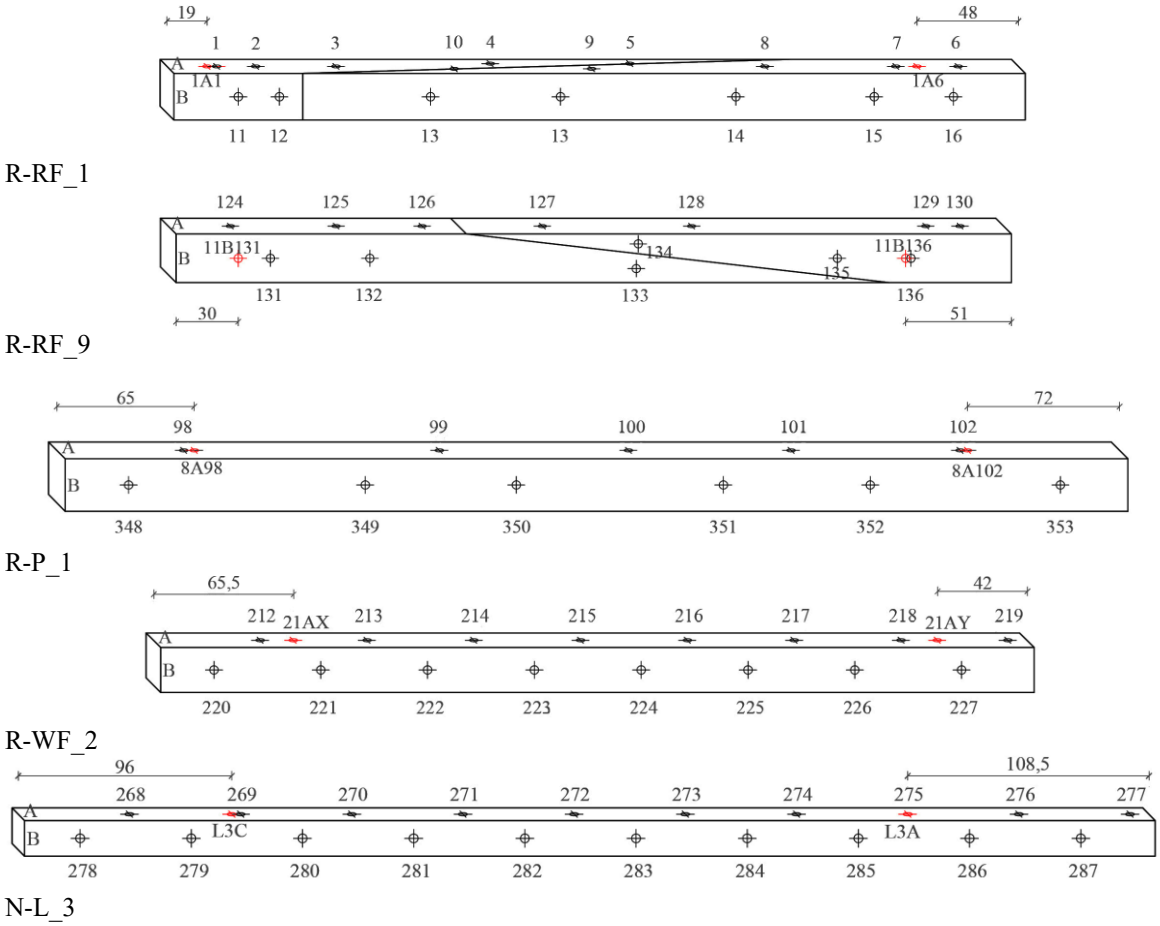


Figure 2: Example of tested elements showing measurement stations (black and red points are stations used by UNIPD and ITAM, respectively) (dimensions are in cm)

3 RESULTS

Figure 3 and Figure 4 show the distribution of MC values according to tests performed on the old and new timber elements, respectively. Values vary from 8.5% to 22.2% (ITAM) and from 16.8% to 68.5% (UNIPD), thus denoting high moisture content conditions in the elements. Many RF old elements were stored outside and were therefore exposed to some rain before storing them in the laboratory; this affected their integrity and, consequently, the experimental results. Highest values of MC concerned retrieved elements (68% detected in R-RF_5 from UNIPD and 22.2% detected in R-P_2 from ITAM), whereas in new elements ranges of 17%-28% (UNIPD) and 11.2%-18% (ITAM) were detected (highest values refer to N-L_6 for both research groups). The differences between results obtained by UNIPD and ITAM were probably due to the different type of moisture meters. The device used by UNIPD was a pin meter able to measure MC values up to 3 cm in depth from the surface, while both the devices used by ITAM measured the MC values on the surface of the elements. In fact, the comparison of the average values (Table 2 and Figure 5) showed a good agreement between the electric and electromagnetic methods used by ITAM (see also Figure 6). Results also showed MC measurements in new elements more stable than for the old ones.

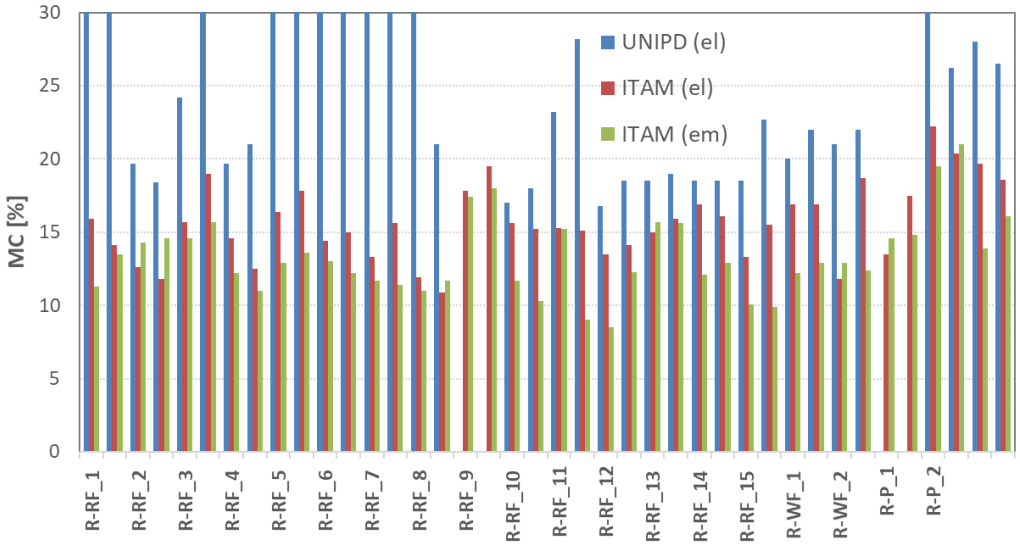


Figure 3: Moisture content measured on old timber elements (values higher than 30% are cut from graph)

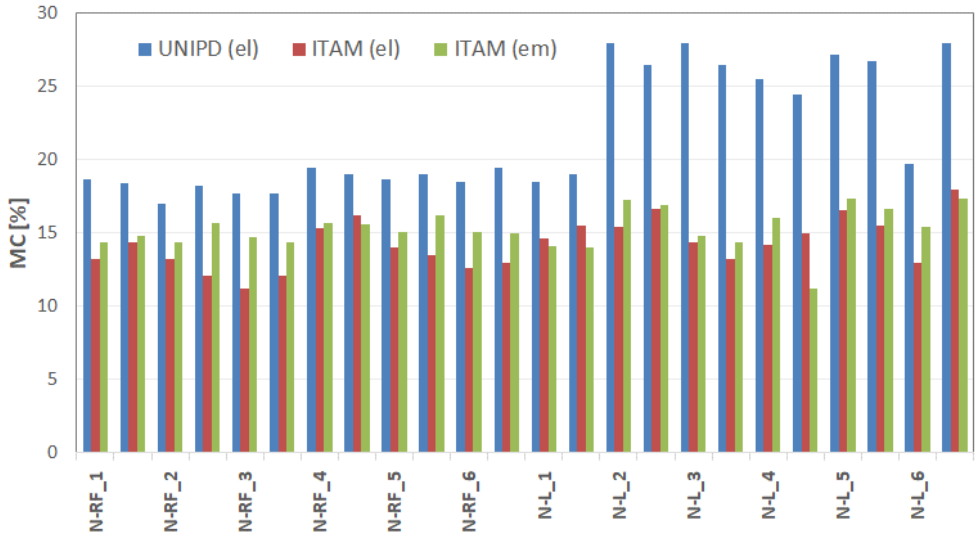


Figure 4: Moisture content measured on new timber elements

Table 2: Moisture content on elements measured with electrical (el) and electromagnetic (em) devices: average values and CoV (in brackets)

	UNIPD (el)	ITAM (el)	ITAM (em)	Average (all)
R-RF	22.17 (0.24)	15.01 (0.14)	12.78 (0.18)	16.65 (0.29)
R-WF	21.25 (0.05)	16.08 (0.18)	12.60 (0.03)	16.64 (0.26)
R-P	28.35 (0.11)	18.65 (0.16)	16.65 (0.18)	21.22 (0.29)
N-RF	18.49 (0.04)	13.94 (0.10)	15.21 (0.04)	15.88 (0.15)
N-L	24.84 (0.15)	15.18 (0.10)	15.41 (0.12)	18.48 (0.30)

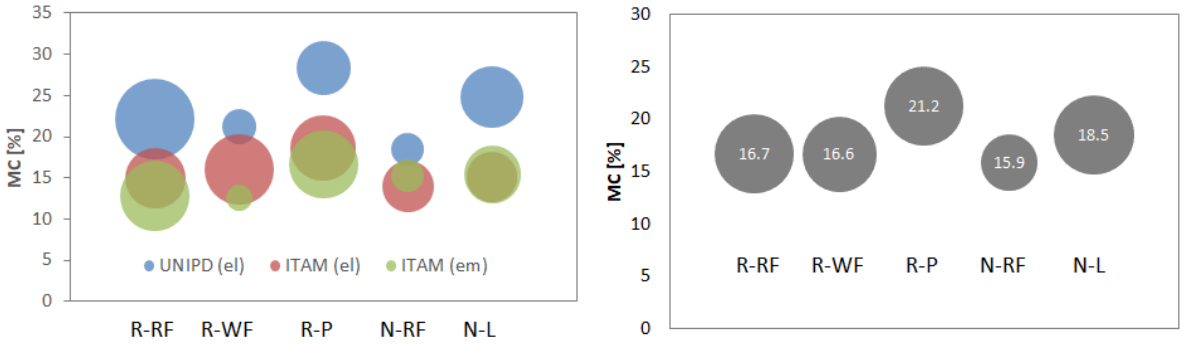


Figure 5: Average values of MC measured on all timber elements

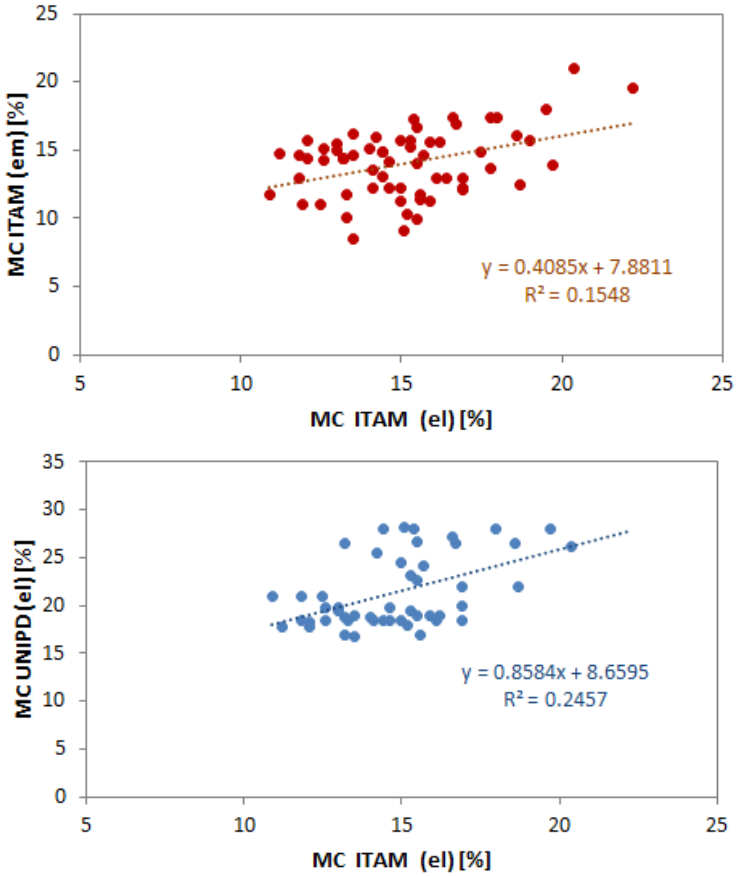


Figure 6: Correlation of MC values measured with different devices on timber elements (values higher than 30% are not included in graph)

Results were also compared by taking into consideration the station points (mostly positioned close to the ends of elements, see Figure 2) used by UNIPD and ITAM according to the ND/MD test procedures (see Table 1). The high-deteriorated conditions of most of the old beams also affected the pin penetration tests: when less than five strikes were possible, a proportion was made to compare the values among the tested elements, taking into consideration the energy transmitted by the device at each strike. In general, no significant

influence of MC was detected for both RD and PP test results (Figure 7 and Figure 8). WV tests were more affected by MC variations, especially in the case of superficial (indirect) tests (Figure 9 and Figure 10), where a general decreasing trend (for increasing MC) was detected. Correlation coefficients were negligible for RD and PP tests; for WV, although not high coefficients were achieved, their values denoted a mutual influence between the transmitted wave velocities and the humidity rate measured in the elements.

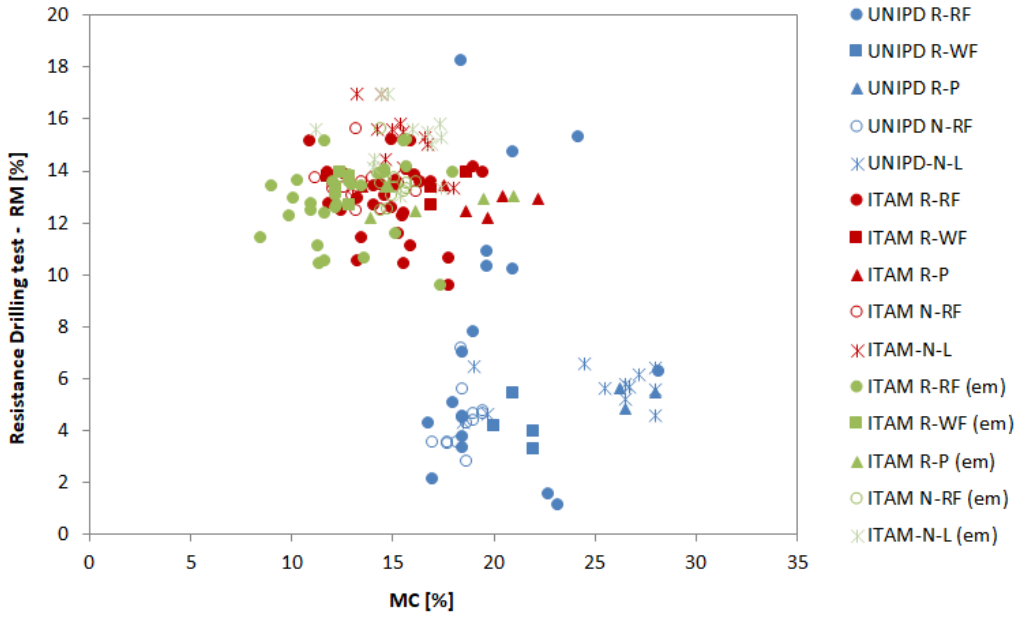


Figure 7: Comparison of RD results and MC on corresponding pairs of UNIPD and ITAM measurements

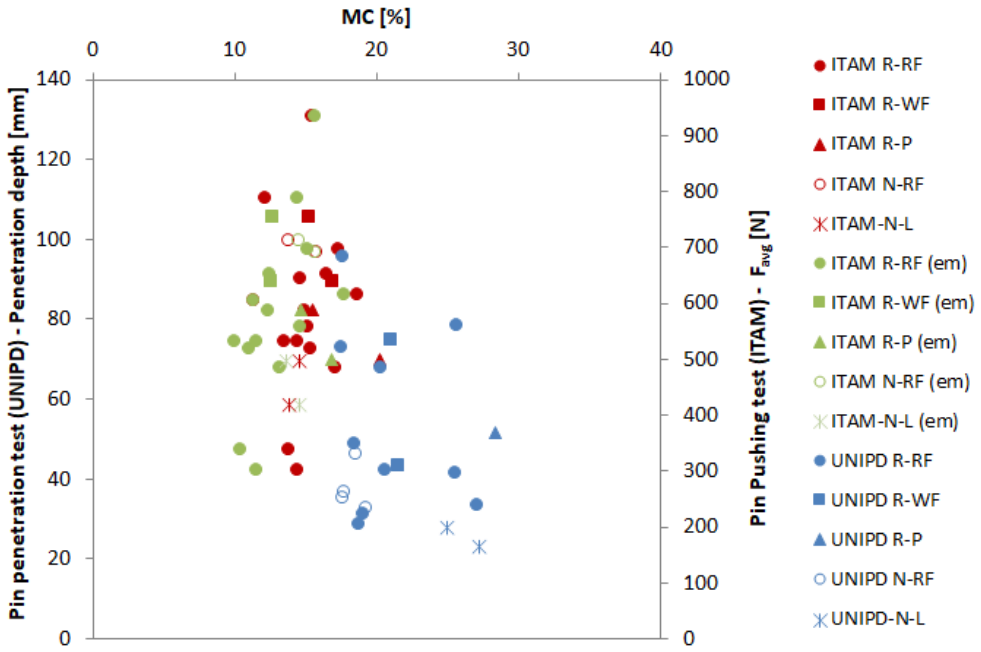


Figure 8: Comparison of PP results and MC on corresponding pairs of UNIPD and ITAM measurements

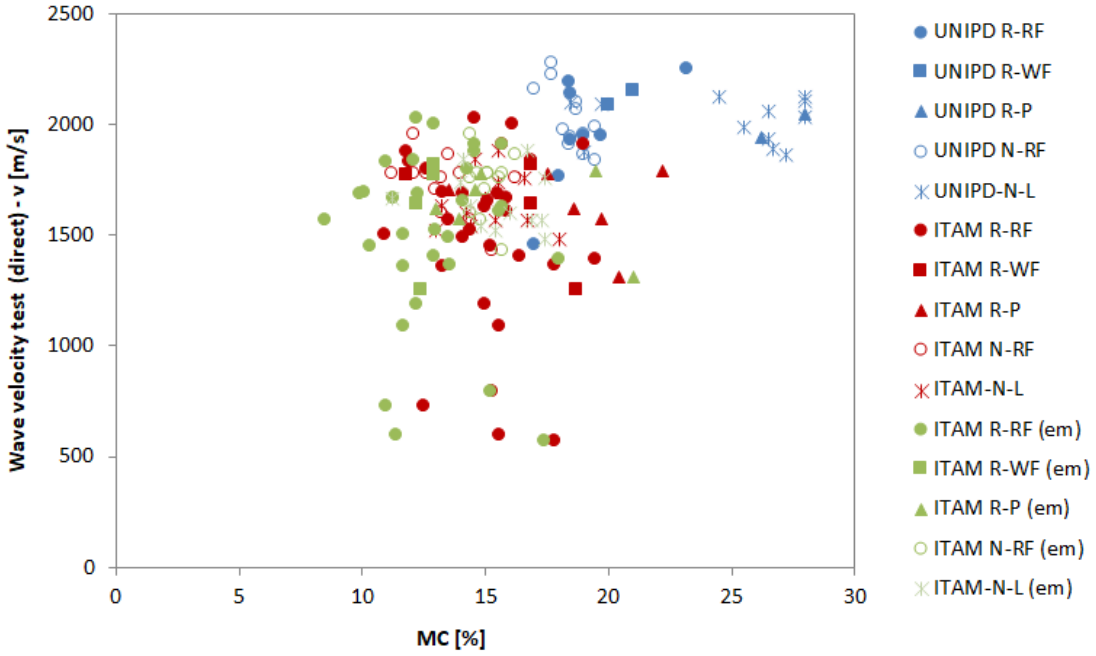


Figure 9: Comparison of WV (direct tests) results and MC on corresponding pairs of UNIPD and ITAM measurements

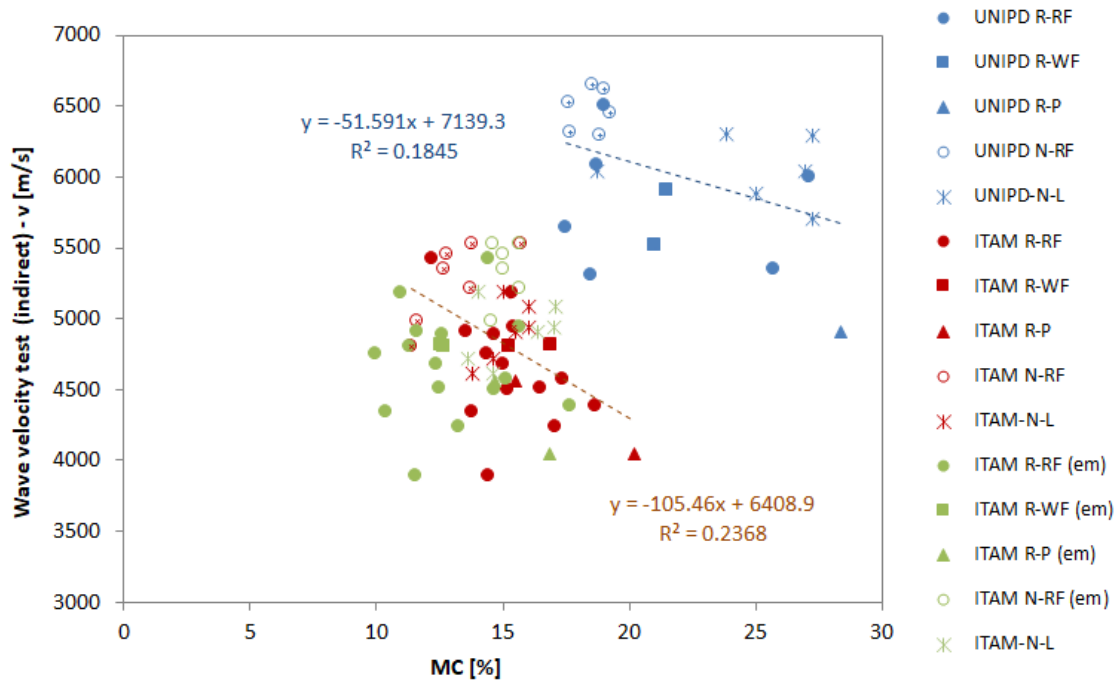


Figure 10: Comparison of WV (indirect tests) results and MC on corresponding pairs of UNIPD and ITAM measurements

CONCLUSIONS

An experimental research was carried out in collaboration among three research groups to investigate the effect of different devices for the measurements of moisture content on various species of timber elements in either new or old conditions. Especially retrieved elements had high MC to take into consideration worse onsite conditions in existing buildings.

Results showed that:

- Electrical and electromagnetic devices for surface MC measurements used by ITAM are comparable methods. Pin meters going more deep from the surface (e.g. device used by UNIPD) showed an increase of MC ranging from 32% (R-WF elements) to 64% (N-L elements).
- Although the large variation of MC values, resistance drilling methods were not affected by the MC of the tested wood. However, preventive conditioning of wood is always suggested, when possible, in order to even the current state out.
- Pin penetration tests applied in timber elements (UNIPD) with high MC was problematic (no application following the protocol of five blows was possible in most cases) and no significant correlations were found.
- Pin pushing (ITAM) as well as all other penetration resistance methods are strongly influenced by the density and the structure of the wood, i.e. by the species and the condition or the degradation state of wood. This fact suppresses the influence of the moisture content on the measurements. The results confirm the MC effect discovered in [6], i.e. a slight increase of the resistance against pushing the needle through the cross-section with an increase of the MC between the values of 10% to 20%.
- The lowest dispersion of data was detected for the combination of MC and the results of wave velocity-based tests. A decreasing trend of velocity according to increases of MC was confirmed. especially in the case of indirect wave transmission configuration.

Future developments of the research will extend the dataset to improve relationships among the variables under study and will be aimed at investigating the possible correlation among ND/MD and destructive tests on real-scale timber elements to calibrate mechanical parameters.

Acknowledgements. The authors wish to thank Bozza s.r.l. for the availability of timber elements and space for the experimental tests. The research was partially funded by the Italian project Corewood POR FESR Veneto 2014-2020.

REFERENCES

[1] Riggio, M., Anthony, R.W., Augelli, F., Kasal, B., Lechner T., Muller, W. and Tannert, T. In situ assessment of structural timber using non-destructive techniques. *Materials an Structures*, 47(5) (2013), pp 749–766.

[2] Piazza, M. and Riggio, M. Visual strength-grading and NDT of timber in traditional structures. *Journal of Building Appraisal*, 3 (2008), pp. 267-296.

[3] Tannert, T., Anthony, R.W., Kasal, B., Kloiber, M., Piazza, M., Riggio, M., Rinn, F., Widmann, R., Yamaguchi, N. In situ assessment of structural timber using semi-destructive techniques. *Materials and Structures*, 47(5) (2013), pp 767–785.

[4] Drdácký, M. and Kloiber, M. In-situ compression stress-deformation measurements along the timber depth profile. *Advanced Materials Research*, 778 (2013), pp. 209-216,

[5] Kloiber, M., Drdácký, M., Tippner, J. and Hrivnák, J. Conventional compressive strength parallel to the grain and mechanical resistance of wood against pin penetration and microdrilling established by in-situ semidestructive devices. *Materials and Structures*, 48 (2015), pp. 3217-3229.

[6] Tippner, J., Kloiber, M., Sebera, V., Kunecký, J.: Health diagnostics of timber by continual pushing-through method. In: 17th International Conference on Experimental Mechanics (ICEM 17), 7/2016, Rhodes, Greece.

[7] Kloiber, M., Drdácký, M., Kunecký, J., Sebera, V., Tippner, J.: Mini-jack based direct determination of wood mechanical characteristics in situ. In: 17th International Conference on Experimental Mechanics (ICEM 17), 7/2016, Rhodes, Greece.

[8] Knag, H., Booker, R.E.: Variation of stress wave velocity with MC and temperature. Wood Science and Technology 36 (2002) 41–54 Springer-Verlag 2002, DOI 10.1007/s00226-001-0129-x

[9] UNI EN 338:2016 Structural timber - Strength classes.

[10] UNI 11119:2004 Cultural Heritage. Wooden artefacts. Load-bearing structures - On site inspections for the diagnosis of timber members.

[11] Uzielli, L. *Il manuale del legno strutturale. Ispezione e diagnosi in opera*. Mancosu, Vol. 1 (2006).

[12] Dackermann, U., Elsener, R., Li, J. and Crews, K. A comparative study of using static and ultrasonic material testing methods to determine the anisotropic material properties of wood. *Construction and Building Materials*, 102 (2016), pp. 963-976.

12th International Conference on Structural Analysis of Historical Constructions
SAHC 2020
P. Roca, L. Pelà and C. Molins (Eds.)

INVESTIGATION OF RUBBLE-MASONRY WALL CONSTRUCTION PRACTICE IN LATIUM, CENTRAL ITALY

O. ALSHAWA[1], G. DE CANIO[2], G. DE FELICE[3], S. DE SANTIS[3], S. FORLITI[2], D. LIBERATORE[1,*], D. MIRABILE GATTIA[4], S. PEROBELLI[1], F. PERSIA[4], G. ROSELLI[5] AND L. SORRENTINO[1]

[1] Department of Structural and Geotechnical Engineering, Sapienza University of Rome
Via Antonio Gramsci 53, 00197 Rome, Italy
e-mail: {omar.alshawa, domenico.liberatore, luigi.sorrentino} @uniroma1.it
perobelli.1816032@studenti.uniroma1.it, Web page: www.disg.uniroma1.it

[2] Department for sustainability, Laboratorio Tecnologie per la Dinamica delle Strutture e la Prevenzione del rischio sismico e idrogeologico, ENEA Centro Ricerche Casaccia
Via Anguillarese 301, 00123 Santa Maria di Galeria (Rome), Italy
Email: {gerardo.decanio, sara.forliti} @enea.it
Web page: www.enea.it

[3] Department of Engineering, Roma Tre University
Via Vito Volterra 62, 00146 Rome, Italy
Email: {gianmarco.defelice, stefano.desantis} @uniroma3.it
Web page: www.romatrestrutture.eu

[4] Department for sustainability, Chemical and physical technologies Laboratory in the Division Sustainable Materials, ENEA Centro Ricerche Casaccia
Via Anguillarese 301, 00123 Santa Maria di Galeria (Rome), Italy
Email: {daniele.mirabile, franca.persia} @enea.it
Web page: www.enea.it

[5] School of Architecture and Design, University of Camerino
Colle dell'Annunziata, Via della Rimembranza, 63100 Ascoli Piceno, Italy
Email: graziella.roselli@unicam.it, Web page: www.unicam.it

Keywords: 2016-2017 Central Italy seismic sequence, Amatrice, Masonry wall section, Masonry geometry, Mortar recipe, Finite-discrete elements

Abstract. *The 2016-2017 Central Italy seismic sequence severely affected existing unreinforced-masonry constructions in four regions. Those in Latium region proved the most prone to fragmentation because of an unfortunate combination of undressed natural stone units and very low lime content in mortar. Within the framework of a research project funded by the regional government, shake table tests are planned to investigate masonry disintegration as well as possible intervention techniques, as described in a companion paper. All specimens will have natural stone units retrieved from the debris in Collespada, a settlement of the municipality of Accumoli, one of the most affected by the seismic sequence. To push further the representativeness of the specimens with respect to field conditions, wall geometry, masonry*

fabric and mortar recipe are carefully designed. The wall thickness will be approximately equal to 0.5 m, close to average thickness surveyed in the area. Following the survey of several vertical sections of actual masonry walls, the specimens will present unconnected external leaves with a limited nucleus. Based on tests on mortar sampled from collapsed buildings, mortars will be prepared by a part of natural lime every nine parts of sand. Shear tests on sampled mortar delivered apparent cohesion and friction coefficient that are used as preliminary values of a finite-discrete element model, which can account for masonry fragmentation in dynamic non-linear analyses. The numerical model was tested under the envisioned sequence of records, belonging to the Amatrice station and related to the East component, approximately fault normal, of the two main seismic events, 24 August and 30 October, 2016.

1 INTRODUCTION

On 24 August 2016 a severe seismic sequence started in Central Italy with a M_w 6.0 event originated in the municipality of Accumoli (Figure 1). The sequence counted nine events having $M_w \geq 5.0$ until 18 January 2017, and a M_w 6.5 event on 30 October, the largest earthquake in Italy since 1980, and in Central Italy since 1915. The sequence affected four administrative regions: Abruzzi, Latium, Marches, and Umbria, but the most catastrophic collapses occurred in Latium, in the municipalities of Accumoli and Amatrice [1,2]. The response of historical constructions belonging to this area was particularly unsatisfactory [3], in comparison to other areas such as that of Norcia [4] or to previous earthquakes [5,6]. Already the first event of the 2016 sequence caused very frequently masonry fragmentation (Figure 2), leading to a dramatic failure of the whole construction. When masonry disintegration occurs [7], other response modes such as out-of-plane local mechanisms [8] and a box-like behaviour governed by walls in-plane performance [9] cannot develop [10,11].

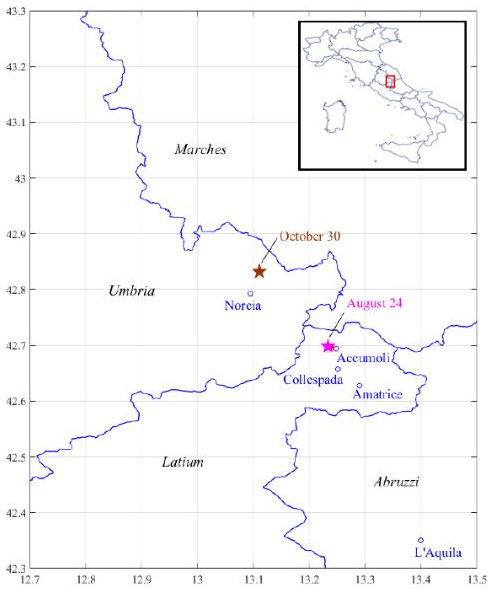


Figure 1: Map of the area affected by the 2016-2017 Central Italy seismic sequence



Figure 2: Amatrice historical centre, after the 24 August event in a snapshot from a movie released by the Firefighters Corps (www.vigilfuoco.tv)

Seismic demand in and around Amatrice was certainly severe, but not more than in Norcia [12], highlighting a higher vulnerability of the buildings in the portion of Latium closest to the epicentral area. In order to deepen the understanding of this poor performance and to design appropriately the characteristics of laboratory wall specimens to investigate possible strengthening interventions [13], an investigation was launched in the area and is briefly reported hereinafter.

2 SURVEY OF MASONRY WALL PRACTICE

Given the large number of collapses occurred in the area, it was possible to survey several rubble masonry walls cross sections. An example is given in Figure 3, wherein it is evident the lack of bond stones and the presence of a nucleus, largely constituted by small-size units. Additionally, horizontal mortar joints are frequently discontinuous and vertical joints are not properly staggered. Despite the use of compact limestone as unit material, because of the poor mortar's properties described in the following, the overall characteristics of the walls were extremely inadequate, as can be shown computing the masonry quality index proposed by Borri et al. [14] or by comparison with wall sections in L'Aquila [15]. The specimens of the envisioned laboratory investigation [13] will reflect these characteristics.

Additionally, wall geometries have been investigated in terms of ground floor thickness, wall height, transverse wall spacing, building number of stories (Figure 4). Average wall thickness was about 0.6 m and height/thickness ratio about 11. These values are smaller and larger, respectively, of those reported for L'Aquila [16], thus contributing to explain the higher vulnerability of the buildings of Accumoli and Amatrice. An approximate thickness of 0.5 m will be used for the wall specimens to be tested on the shake table [13].

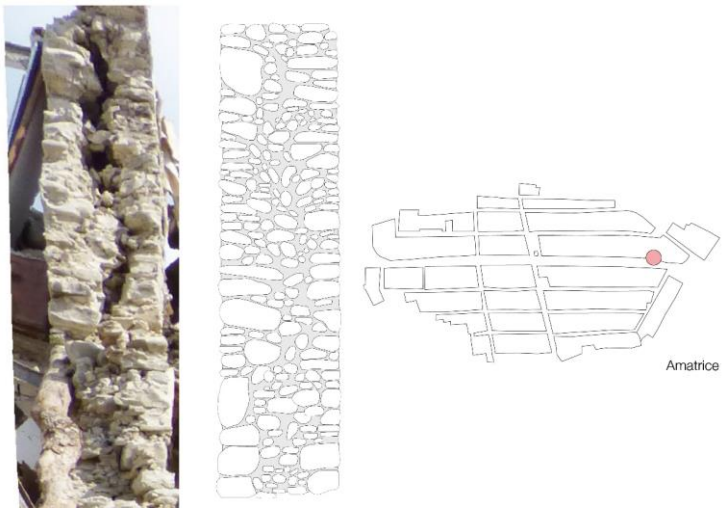


Figure 3: Survey of vertical section of a masonry wall in Amatrice

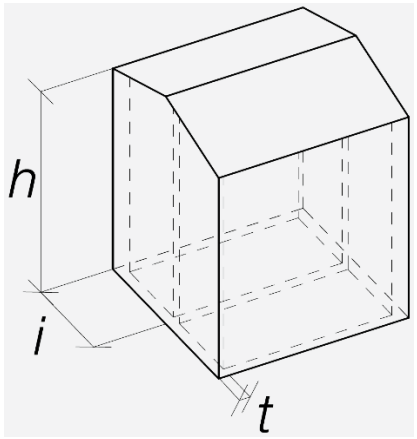


Figure 4: Survey of walls geometry

The walls to be tested will be manufactured with natural stone units retrieved from the debris of the buildings in the settlement of Collespada, within the municipality of Accumoli (Figure 1). However, mortar cannot be retrieved in the same way, and will be manufactured for this laboratory campaign. Therefore, it is necessary to properly design the mortar recipe in order to make it representative of local construction practice. The mortar sampled from buildings severely damaged by the 2016-2017 seismic sequence was investigated within a larger endeavour [17,18], involving also Marches and Umbria regions. On mortar samples, mechanical, physical and chemical experimentations were performed.

Mechanical investigations involved direct shear tests (Figure 5a), performed cyclically for different normal-stress levels. Values for the Latium samples are reported in Table 1, highlighting an average friction coefficient of about 0.9 and cohesion of about 25 kPa. These values will be used in the numerical model presented in the following. Cyclic behaviour resulted remarkably stable (Figure 5b).

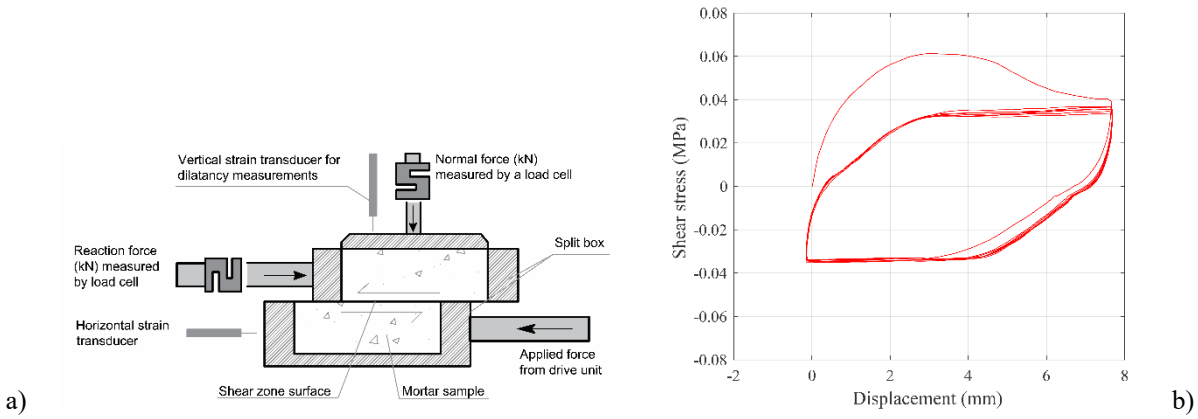


Figure 5: a) Direct shear test, b) Example of shear force vs. displacement curve

Table 1: Synthesis of direct shear test (maximum shear stress, Latium)

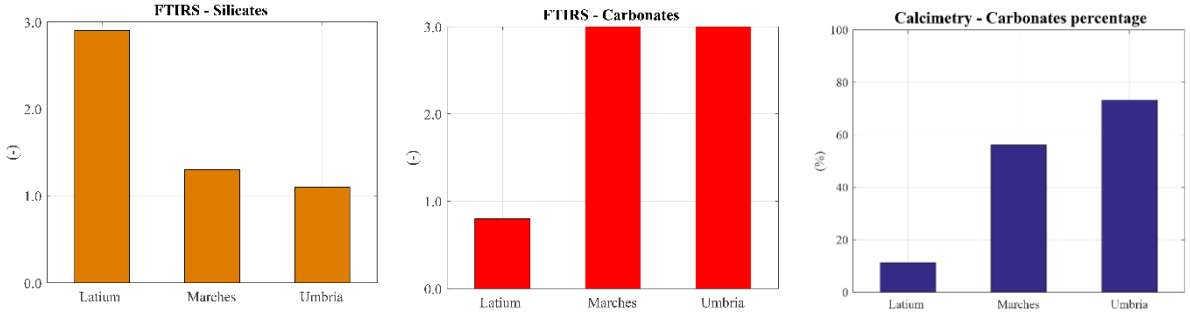
	μ [-]	c [kPa]
max	1.01	44.2
min	0.77	10.8
mean	0.89	26.4
std dev	0.07	8.2
CoV	0.08	0.31

Physical and chemical investigations have been used to determine the recipe of the mortar mix, such as infrared spectroscopy, calcimetry and X-ray diffraction. Infrared spectroscopy identifies chemical substances by exploiting their interaction with infrared radiation. Molecules absorb radiations matching their resonant frequencies, thus allowing their detection. A qualitative analysis of the associated Fourier-transform spectra, confirmed by crystalline phase analysis performed by X-Ray diffraction, allows recognising the very large presence of silicates in Latium mortars in comparison with those in the other investigated regions corresponding to a lower content of carbonates (Figure 6a,b).

Since carbonates can be present in mortar both as binder and as aggregate, the identified proportion represents an upper bound for actual lime proportion. Nonetheless, it is interesting to observe that even such an upper bound is very low in Accumoli and Amatrice. This qualitative observation is confirmed by quantitative tests performed with a calcimeter. In this instrument the carbonate is exposed to hydrocloridic acid and the pressure increase related to the released carbon dioxide is measured, hence estimating the mortar carbonate percentage at about 11% (Figure 6c). Such low presence is an indicator of a seismic risk awareness lower than in other areas such as that of Norcia [19]. Based on previous results, a proportion of 1 lime part by 9 sand parts will be intentionally used when manufacturing the unretrofitted and retrofitted walls to be tested on the shake table [13].

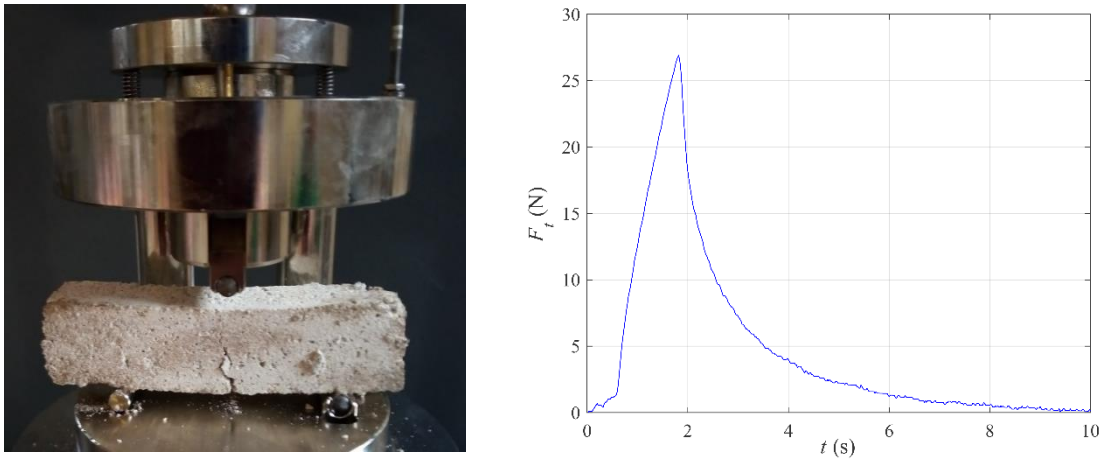
Having determined a tentative composition of the mortar, standardised 40 mm × 40 mm ×

160 mm specimens were manufactured to perform bending (Figure 7) and compression (Figure 8) tests according to EN 1015-11 [20]. As expected, flexural response is rather brittle, while compressive one is remarkably ductile. Average strength values in bending and compression at 28 days are 0.13 MPa and 0.40 MPa, respectively. Tests were performed also at a reduced number of days in order to preliminarily investigate the possibility of constructing natural-scale walls with such poor mortars.



(a) (b) (c)

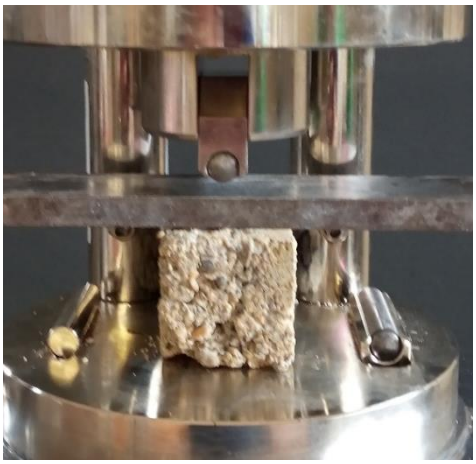
Figure 6: Mortar analysis: a) Fourier-transform infrared spectroscopy, silicates; b) Fourier-transform infrared spectroscopy, carbonates; c) Calcimetry, carbonates percentage by weights

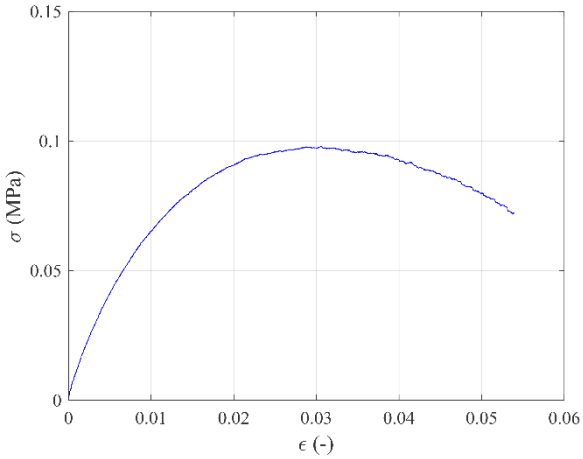


a) b)

Figure 7: a) Bending test on mortar prism, b) Force time history

a)





b)

Figure 8: a) Compression test on mortar, b) Stress-deformation plot

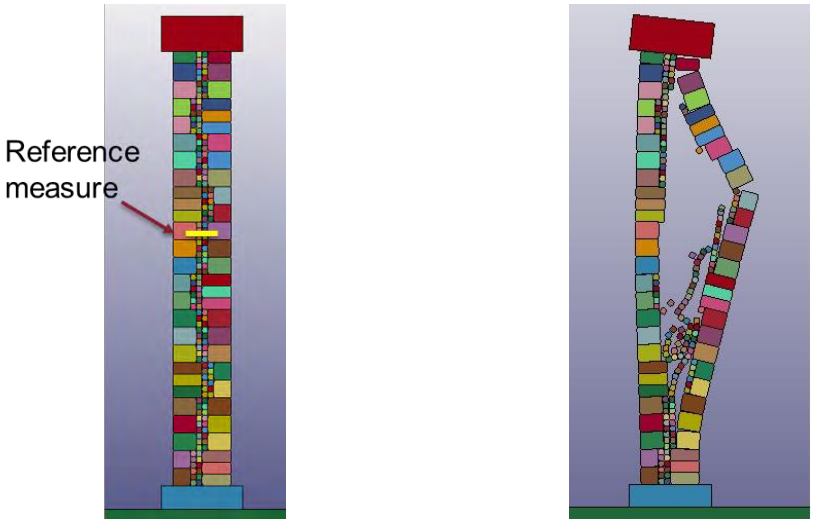
3 NATURAL ACCELEROGRAMS SELECTION FOR THE SHAKE TABLE TESTS

Shake table tests will investigate the propensity of masonry to fragmentation and possible strengthening techniques. Walls will have a natural scale and will be loaded along the out-of-plane direction. The walls will rest on a reinforced-concrete foundation and horizontal displacement at the top will be restrained, while the vertical one can develop freely [21]. Additional information are given in [13]. A set of numerical analyses was performed to select the appropriate accelerograms, and their scale factors.

The model was implemented in LS-DYNA, a code capable of simulating dynamic problems [22]. The wall was modelled within a combined finite-discrete element framework, as done elsewhere [23], in order to represent the actual morphology of the wall cross-section, which is a crucial element in case of out-of-plane seismic loads [24]. The model accounts for the elastic response, the formation of cracks and their closing down, the finite displacement of blocks as well as the formation of new contacts. All materials are linear elastic, the interfaces between blocks initially in contact react to both compressive and tensile forces, and a standard penalty method governs the contact behaviour through linear springs. Springs fail in tension when the normal stress on the contact surface is greater than the normal failure limit stress. Similarly, springs fail in shear when the shear stress is greater than the shear failure limit stress. After that, a frictional sliding is possible and is governed by static and dynamic friction coefficients.

The physical walls will have two external leaves and a central nucleus made of smaller units. Such arrangement is reproduced in the numerical wall, although with a simplified geometry (Figure 9a). Contact parameters have been preliminarily calibrated based on previously described mortar tests. Given that the experimental program was motivated by the 2016-2017 seismic sequence, the numerical model was tested using the records of the Amatrice station, already in place at the time of the first event. The East component, approximately fault normal and more severe, was selected and the two main events of the sequence, 24 August and 30 October, were chosen as representative of possible damage accumulation [12]. However, in order to study the incremental response of each wall, the amplitude of the records, both horizontal and vertical, will be scaled according to a non-dimensional factor S_f increased by

0.25 steps. In Figure 10 it is possible to observe the sequence of records preceded by the initial slow application of gravity, necessary to avoid unrealistic vibrations. The response and the damage accumulation can be monitored by means of the variation of the distance between the two external leaves at a specific height (Figure 9a). The corresponding time history is given in Figure 11, and it highlights that failure (Figure 9b) occurs for $S_f = 0.50$ of the 30 October 2016 event.



a) b)

Figure 9: a) Finite-discrete element model, b) Damage mechanism. Colours used only to emphasize unit discretisation

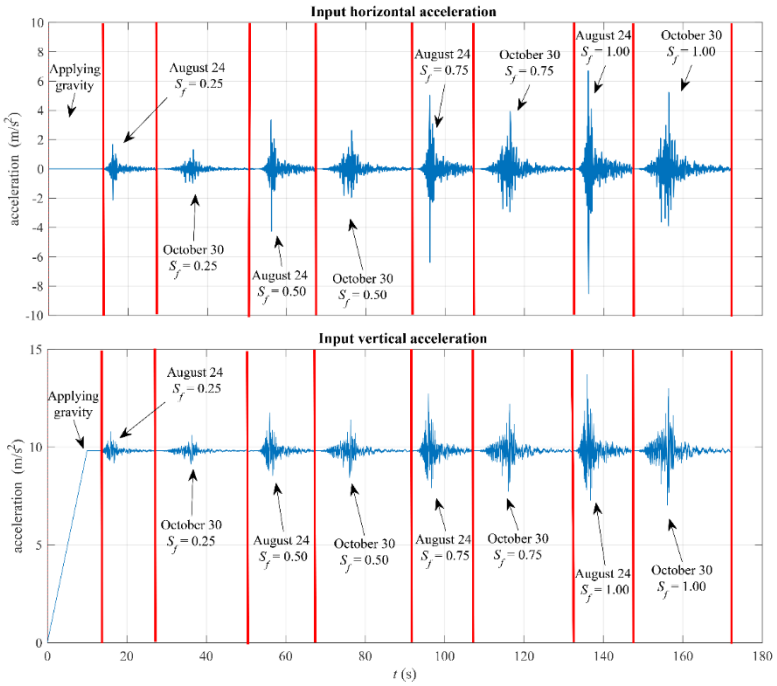


Figure 10: Input horizontal and vertical acceleration time histories (time lapse between two events 2 s)

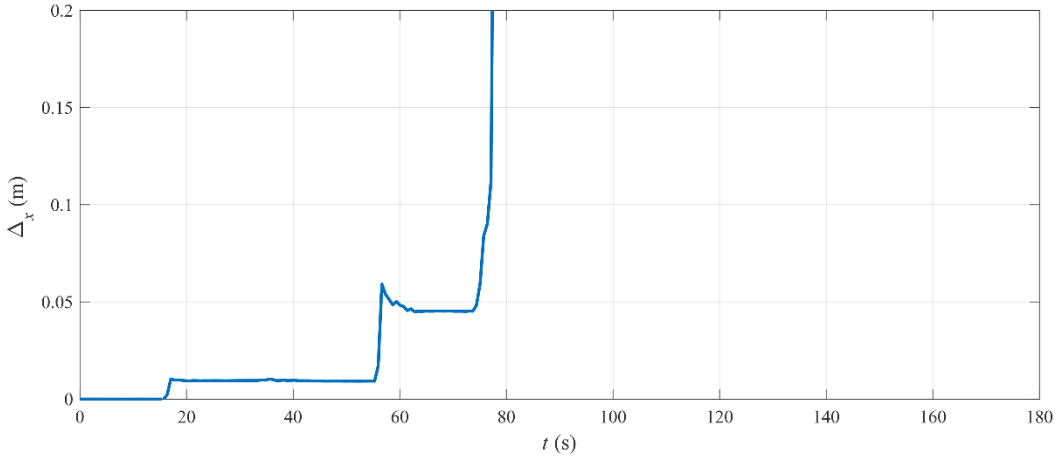


Figure 11: Variation of the distance between the external leaves (Figure 9a) time history

4 CONCLUSIONS

The 2016-2017 Central Italy seismic sequence has determined a dramatic performance in historical masonry constructions in the portion of Latium region affected by severe ground shaking. To contribute explaining this behaviour, construction practice was investigated. Rubble masonry wall sections were surveyed, highlighting the lack of bond stones, the use of small-size and undressed units with an inadequate arrangement of mortar joints, evidencing a poorer quality compared to those in L'Aquila. Geometrical features such as wall thickness and height/thickness ratio show higher vulnerability compared to values surveyed again around L'Aquila. Infrared spectroscopy, calcimetry and X-Ray diffraction measurements showed a very low lime percentage in the mortar, a possible indicator of a lower seismic risk awareness compared to Norcia.

All these characteristics will be considered in the design of wall specimens to be tested in unstrengthened and strengthened conditions on a shake table. Moreover, in order to select the proper sequence of records to be used as excitation, a finite-discrete element model was implemented. The model is tested with a sequence of accelerograms obtained by scaling those recorded in the Amatrice station during the two main events of the seismic sequence, accounting for both the east-west and up-down components. The tentative scale factor adopted will allow for about four tests before the unstrengthened wall reaches failure.

Acknowledgements. This work was partially carried out within the Research Project "SISMI Technologies for the improvement of the seismic safety and the restoration of historical centres" (2018-2020) funded by Latium Region. GdF and SDS acknowledge funding also by Lazio Region within the Research Project "SICURA Sustainable technologies for the seismic protection of the cultural heritage" (2018-2020) and by the Italian Ministry of Education, University and Research (MIUR), attributed to the Department of Engineering of Roma Tre University, within the framework of the Departments of Excellence Initiative (2018-2022).

REFERENCES

[1] Azzaro, R., Tertulliani, A., Bernardini, F., Camassi, R., Del Mese, S., Ercolani, E., Graziani, L., Locati, M., Maramai, A., Pessina, V., Rossi, A., Rovida, A., Albini, P., Arcoraci, L., Berardi, M., Bignami, C., Brizuela, B., Castellano, C., Castelli, V., D'Amico, S., D'Amico, V., Fodarella, A., Leschiutta, I., Piscini, A., Sbarra, M., The 24 august 2016 Amatrice earthquake: Macroseismic survey in the damage area and EMS intensity assessment. *Ann Geophys* (2016), **59**, 1–10.

[2] Tertulliani, A., Azzaro, R., QUEST - Rilievo Macrosismico per i Terremoti Nell'Italia Centrale. Aggiornamento Dopo Le Scosse Del 26 e 30 Ottobre 2016. Roma (2016).

[3] Fiorentino, G., Forte, A., Pagano, E., Sabetta, F., Baggio, C., Lavorato, D., Nuti, C., Santini, S., Damage patterns in the town of Amatrice after August 24th 2016 Central Italy earthquakes. *Bull Earthq Eng* (2018), **16**, 1399–1423.

[4] Sisti, R., Di Ludovico, M., Borri, A., Prota, A., Damage assessment and the effectiveness of prevention: the response of ordinary unreinforced masonry buildings in Norcia during the Central Italy 2016–2017 seismic sequence. *Bull Earthq Eng* (2019), **17**, 5609–5629.

[5] Penna, A., Morandi, P., Rota, M., Manzini, C. F., da Porto, F., Magenes, G., Performance of masonry buildings during the Emilia 2012 earthquake. *Bull Earthq Eng* (2014), **12**, 2255–2273.

[6] Augenti, N., Parisi, F., Learning from Construction Failures due to the 2009 L'Aquila, Italy, Earthquake. *J Perform Constr Facil* (2010), **24**, 536–555.

[7] De Felice, G., Out-of-plane seismic capacity of masonry depending on wall section morphology. *Int J Archit Herit* (2011), **5**, 466–482.

[8] Doherty, K., Griffith, M. C., Lam, N., Wilson, J., Displacement-based seismic analysis for out-of-plane bending of unreinforced masonry walls. *Earthq Eng Struct Dyn* (2002), **31**, 833–850.

[9] Lourenço, P. B., Mendes, N., Ramos, L. F., Oliveira, D. V., Analysis of masonry structures without box behavior. *Int J Archit Herit* (2011), **5**, 369–382.

[10] Giuffrè, A., A Mechanical Model for Statics and Dynamics of Historical Masonry Buildings. Springer, Wien (1996).

[11] de Felice, G., De Santis, S., Lourenço, P. B., Mendes, N., Methods and Challenges for the Seismic Assessment of Historic Masonry Structures. *Int J Archit Herit* (2017), **11**, 143–160.

[12] Mollaioli, F., AlShawa, O., Liberatore, L., Liberatore, D., Sorrentino, L., Seismic demand of the 2016-2017 Central Italy Earthquakes. *Bull Earthq Eng* (2019), **17**, 5399–5427.

[13] De Santis, S., AlShawa, O., De Canio, G., Forliti, S., Liberatore, D., Meriggi, P., Roselli, I., Sorrentino, L., de Felice, G., Design of Shake Table Tests of Multi-Leaf Masonry Walls before and after Retrofitting. 12th International Conference on Structural Analysis of Historical Constructions. (2020).

[14] Borri, A., Corradi, M., Castori, G., De Maria, A., A method for the analysis and classification of historic masonry. *Bull Earthq Eng* (2015), **13**, 2647–2665.

[15] Rovero, L., Alecci, V., Mechelli, J., Tonietti, U., De Stefano, M., Masonry walls with irregular texture of L'Aquila (Italy) seismic area: validation of a method for the evaluation of masonry quality. *Mater Struct Constr* (2016), **49**, 2297–2314.

[16] Sorrentino, L., Reconstruction Plans After the 2009 L'Aquila Earthquake. From Building Performance to Historical Centre Performance. 9th International Conference on Structural Analysis of Historical Constructions, Mexico City, 14–17 October. (2014).

[17] Roselli, G., Mirabile Gattia, D., AlShawa, O., Cinaglia, P., Di Girolami, G., Francola, C., Persia, F., Petrucci, E., Piloni, R., Scognamiglio, F., Sorrentino, L., Zamponi, S., Liberatore, D., Mortar analysis of historic buildings damaged by recent earthquakes in Italy. *Eur Phys J Plus* (2019), **134**, 540.

[18] Mirabile Gattia, D., Roselli, G., Alshawa, O., Cinaglia, P., Di Girolami, G., Francola, C., Persia, F., Petrucci, E., Piloni, R., Scognamiglio, F., Sorrentino, L., Zamponi, S., Liberatore, D., Characterization of historical masonry mortar from sites damaged during the central italy 2016-2017 seismic sequence: the case study of arquata del tronto. *Ann Geophys* (2019), **62**, SE341.1–11.

[19] Marotta, A., Liberatore, D., Sorrentino, L., Historical Building Codes issued after the strong Italian earthquakes of Norcia (1859) and Ischia (1883). *Ann Geophys Geophys* (2019), **62**, SE337.1-13.

[20] EN 1015-11, Methods of Test for Mortar for Masonry. Part 11: Determination of Flexural and Compressive Strength of Hardened Mortar. European Committee for Standardization, Brussels (2006).

[21] De Santis, S., De Canio, G., de Felice, G., Meriggi, P., Roselli, I., Out-of-plane seismic retrofitting of masonry walls with Textile Reinforced Mortar composites. *Bull Earthq Eng* (2019), **17**, 6265–6300.

[22] Hallquist, J., LS-DYNA Theory Manual. Livermore Software Technology Corporation, Livermore (2006).

[23] AlShawa, O., Sorrentino, L., Liberatore, D., Simulation Of Shake Table Tests on Out-of-Plane Masonry Buildings. Part (II): Combined Finite-Discrete Elements. *Int J Archit Herit* (2017), **11**, 79–93.

[24] Meriggi, P., de Felice, G., De Santis, S., Gobbin, F., Mordanova, A., Pantò, B., Distinct Element Modelling of Masonry Walls under Out-Of-Plane Seismic Loading. *Int J Archit Herit* (2019), **13**, 1110–1123.

12thInternational Conference on Structural Analysis of Historical Constructions
SAHC 2020
P. Roca, L. Pelà and C. Molins (Eds.)

LABORATORY AND IN-SITU CHARACTERISATION OF MASONRY MATERIALS IN A LARGE HISTORICAL INDUSTRIAL BUILDING IN BARCELONA

ALBERT CABANÉ[1*], LUCA PELÀ[1] AND PERE ROCA[1]

[1]Department of Civil and Environmental Engineering
Universitat Politécnica de Catalunya (UPC-BarcelonaTech)
Jordi Girona 1-3, 08034 Barcelona, Spain
e-mail: albert.cabane@ upc.edu, luca.pela@upc.edu, pere.roca.fabregat@upc.edu

Keywords: Masonry, MDT, Brick, Lime mortar, Core drilling, Compressive strength.

Abstract. *This paper presents an experimental campaign carried out in an historical industrial building of Barcelona from the 19th century, considering in-situ and laboratory minor destructive testing (MDT) techniques. The results obtained showed a good relationship between the in-situ MDT techniques and the tests carried out in the laboratory. The experimental results from different portions of the large-scale building allowed the discovery of different material typologies deriving from different construction phases.*

1 INTRODUCTION

The determination of the mechanical properties of existing masonry structures faces significant difficulties due to the intrinsic complexity of this composite material. However, acquiring a full knowledge of the main parameters is necessary to design adequate conservation actions for the built cultural heritage [1]. The mechanical characterisation of existing masonry structures usually requires an optimum combination of laboratory and in-situ techniques, especially in large constructions. This research presents the experimental methodology applied to an extensive campaign carried out in an historical industrial building of Barcelona built in the 19th century.

The experimental campaign resorted to minor destructive testing (MDT) techniques, both based on in-situ testing of masonry components and extraction of small samples for laboratory testing. The in-situ MDT allowed a preliminary evaluation of the variability of the properties over the large building in order to optimize the sampling and the execution of the laboratory tests. The results from different MDT techniques allowed useful cross-checking in order to keep a continuous control throughout the entire experimental program. The tests were developed on the units and mortar joints of both masonry walls and timbrel vaults, as well as on the plasters.

The main objectives were to obtain a careful characterisation of the material components in order to evaluate their strength capacity and to choose compatible restoration materials of similar properties.

The in-situ experimental characterisation was carried out by means of the Pin Penetration Test (PPT) and the Helix Screw Pull-off Test (HPT) [2] on the mortar joints and bricks, as well as the PPT and Pull-off Test (POT) [3] on the mortar plasters. The experimental characterisation in the laboratory consisted in: compressive testing of small samples of bricks extracted from walls [4]; double punch testing (DPT) of mortar joints from the walls and the timbrel vaults; DPT of plaster specimens [5]; compressive testing of core drilled masonry (CDM) samples [6], [7]; and compressive testing of ceramic tile samples from the timbrel vaults by means of a novel nonstandard setup.

2 EXPERIMENTAL PROGRAM IN-SITU

2.1 Windsor pin penetration test on mortar joints, bricks and plasters

The pin penetration test (PPT) is a MDT method developed to evaluate in-situ the compressive strength of the concrete, mortars and bricks. A previous research [3] investigated how to adapt the test to historical lime mortar joints with a low compressive strength, as well as to historical fired clay bricks.

The PPT was executed on six zones of masonry walls and four zones of mortar plasters. Figure 1 illustrates the operations. A 3 mm diameter pin, with a conical end, is inserted into the device. The retraction nut is tightened until the trigger mechanism closes to hold the spring in place and is then it completely loosened. The device is positioned perpendicularly to the surface to be tested (Figure 1a). The trigger is pulled while holding the device against the surface. After the pin is taken out, a bulb air blower is used to remove the residual material inside the hole. Then, a micrometer is inserted to the bottom of the hole using the knurled thimble on the head of the micrometer (Figure 1b). The micrometer reading is noted. The penetration is obtained by subtracting the reading from one inch (25.4 mm).



Figure 1: Pin Penetration Test operation: (A) the device is positioned perpendicularly to the surface to be tested, and, after firing the pin, (B) a micrometer is inserted to the bottom of the produced hole.

2.2 Screw (helix) pull-out test on mortar joints and bricks

The helix pull-out test (HPT) was carried out on the mortar joints and on the bricks. According to a previous research focusing on HPT in low strength mortars [3], a 3 mm diameter pilot hole was executed and preferred to the 4 mm diameter pilot one suggested by the provider.

In the same way, a 4 mm diameter pilot hole was preferred for bricks instead of the 5 mm one suggested by the provider [8].

The procedure for HPT is executed as follows. A pilot hole of 3 mm diameter is made in the mortar joints with a drill working at the minimum speed and with the tightening power adjusted at the weakest position. A pilot hole of 4 mm diameter is made in the bricks using a rotary-hammer drill with a masonry bit (Figure 2a). A high-strength steel helical tie with a diameter of ¼ in. (6.3 mm) is mounted into a supplementary tool. While holding it horizontally, the tool is hammered carefully until the helical tie is introduced into the pilot hole to a depth of 30 mm and results embedded in the masonry component (Figure 2b). This process allows the helical tie to rotate and cut a thread in the mortar or the unit during insertion. After insertion, a Load Test Key (LTK) is screwed onto the remaining outer part of the tie. The LTK restrains from rotating the helical tie during the test, assuring a shear failure in the tested material. The Load Test Unit (LTU) is connected to the LTK and the mechanism is rotated to screw down the tie and take up any slack. The LTU provides the contact with the material's surface by means of a steel circle. The load is applied by turning a grip lever to increase progressively the load until failure (Figure 2c). The maximum load reached during the test is recorded as the pull-out force. Figure 2 shows the test layout, as well as the sequence of the operations during the HPT.



Figure 2: Helix Pull-out Test operation: (A) drilling the pilot hole, (B) hammering the tool until the helical tie is introduced in the pilot hole, (C) loading by turning the grip lever until failure, (D) failure in the brick.

2.3 Pull-off test on mortar plasters

The pull-off test (POT) is a test developed to evaluate the adhesion strength of gypsum and lime mortar plasters [9]. The POT was executed on lime mortar plasters in the investigated building. Figure 3 shows the sequence of operations of the experimental in-situ tests. The first operation consists in removing the surface paint layer with a mechanical sanding that does not alter the physical and chemical characteristics of the lime mortar and ensures proper adhesion (Figure 3a). The plaster is cut until reaching the masonry substrate by using a core bit with 50 mm diameter (Figure 3b). After notching a number of circles, 50 mm diameter metal discs are stuck to the coating with a two components adhesive consisting of methylmetacrylate (Figure 3c). Once the adhesive has hardened, the disc is pulled off with a dynamometer by applying a perpendicular force to the surface. Two different dynamometers were used. A manual reaction dynamometer with a capacity of 500 N and a digital accuracy of 0.1 N was used in the position ZA. This position was characterised by lower adhesion strength (Figure 3d). In zones with higher adhesion strength, a different device with a mechanical dynamometer support, capacity of 5000 N and manual reading was used (Figure 3e). The pull-off load applied to the metal disc

is increased steadily until failure (Figure 3f). The peak load reached during each test is recorded as the pull-off strength.



Figure 3: Pull-off test operation: (A) removing the surface paint layer with a mechanical sanding, (B) drilling the plaster until reaching the masonry substrate using a 50 mm diameter core bit, (C) sticking the metal discs, (D) manual dynamometer, (E) mechanical dynamometer support, and (F) failure of plaster substrate.

2.4 Extractions of the specimens

The masonry walls investigated were 450 mm thick, built with fired handmade clay brick units with nominal size 295.7 × 146.2 × 42.9 mm^3, and lime mortar joints with thickness variable between 12 mm and 18 mm.

The extractions of the CDM samples were done by horizontal drilling using the dry technology proposed in [6]. Figure 4 shows the sequence of operations of the in-situ extractions. Before drilling, 152.5 mm diameter core samples were marked to guarantee the correct drilling, including one vertical and two horizontal mortar joints and four bricks (Figure 4a). Twenty-one specimens were drilled in five extraction zones (Figure 4b and c). Only three out of twenty-one specimens were discarded after the extraction operations due to irregularities inside the wall. All the CDM samples had an approximate depth of 300 mm and were cut in the laboratory using a dry radial saw in order to obtain an approximate depth of 145 mm (Figure 4d). After drilling, some courses of the wall were disassembled using a chisel and a hammer to extract whole bricks and mortar joints. The selected specimens were stored and labelled carefully to preserve their integrity until taken to the laboratory.

The timbrel vaults of the industrial building were composed of two layers of fired handmade clay tiles. Their bond was staggered through the thickness of the vault in order to prevent the alignment of the tile joints. The components used in the vaults were tiles with nominal size of 294.3 × 145.3 × 20.8 mm^3. The lime mortar joints had thickness of 17 mm in the 1st timbrel vault and of 10 mm in the 2nd timbrel vault.

Figure 5 shows the sequence of operations of the in-situ extractions, executed from the top of the timbrel vaults by removing first the pavements and then the vault filling (Figure 5a). The

mortar joints between tiles were marked with a radial saw (Figure 5b) and then extracted carefully with a chisel and a gauging trowel (Figure 5c and d).

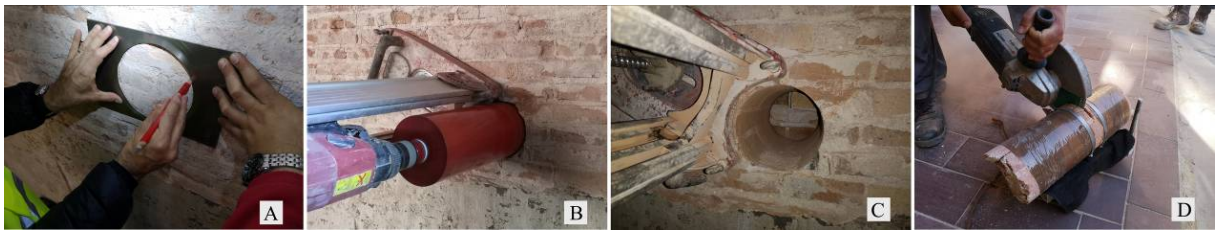


Figure 4: The sequence of operations of the cylinder extractions: (A) marking the core perimeter before extraction, (B) drilling, (C) hole in the wall after extraction, (D) cutting the specimen with a dry radial saw until obtaining an approximate depth of 145 mm.



Figure 5: The sequence of operations of the extractions of samples from the timbrel vaults: (A) removing the pavements and the vault filling, (B) removing the mortar between tiles by using a radial saw, (C) extracting the tiles with a chisel, (D) extracting the tiles with a gauging trowel.

3 EXPERIMENTAL PROGRAM IN THE LABORATORY

3.1 Compressive tests on brick specimens

The specimens considered for the experimental programme were prepared according to the procedures specified in standard EN 772-1:2011+A1 [4]. The use of a grinder fitted with a diamond-impregnated head could guarantee the flatness and parallelism of the faces. The specimens were cut from the bricks using a table saw equipped with a water jet, and air conditioned in a dry mode at a constant temperature of 105°C. Two types of specimens were obtained from every extraction zone, i.e. a specimen measuring 100 × 100 × 40 mm^3 (identified as "CB_10") fulfilling the standard requirements, and 40 × 40 × 40 mm^3 cubes (identified as "CB_C4") as a nonstandard size that allows a considerable increase of the number of available samples.

The specimens were tested under uniaxial compression by using two hydraulic testing machines, with a capacity of 3000 kN for CB_10 specimens, and a capacity of 200 kN for CB_C4 samples. The tests were executed under load control with a rate of 0.15 MPa/s with duration of the test higher than 60 seconds.

3.2 Compressive tests on tile specimens

The characterization of the clay tiles from the timbrel vaults is not possible according to the European standard EN 772-1:2011+A1 [4] or American ASTM C67 [10] due the reduced thickness of the units. To overcome this problem, the proposed solution consisted in assembling two specimens with a cement mortar layer allowing the connection between the samples. This strategy allowed the reduction of the slenderness of the specimen (Figure 6a).

The specimens were cut from the clay tile using a table saw. Two specimens were obtained for every clay tile measuring 100 × 100 × t mm^3, were t is the thickness of the specimen (identified as "CB-F"). These two specimens were assembled using a mould designed and built specifically for this research. The cement mortar was kept 10 mm away from the contact with the testing machine plates. The specimens were grinded on loaded faces to ensure a uniform distribution of compression forces (Figure 6b). The specimens were tested under uniaxial compression using a hydraulic testing machine with a capacity of 200 kN. The loading rate under displacement control was 0.025 mm/s to ensure a duration of the test higher than 60 seconds (Figure 6d).

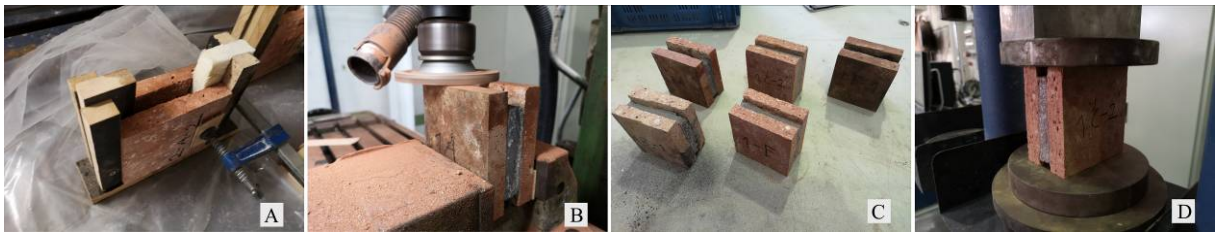


Figure 6: The sequence of operations of compressive tests on tiles: (A) two specimens assembled with an intermediate cement mortar layer, (B) grinding on the side surfaces, (C) tile specimens in test position, (D) execution of the test.

3.3 Double punch tests on mortar joints and plasters samples

The mortar bed joints extracted between the units, as well as the plaster samples, had low consistency and cohesion. This fact, usual in historical structures, made the preparation of regular specimens difficult. For this reason, it was not possible to test mortar slabs with exact dimensions of 50 × 50 mm^2 as recommended by the German standard DIN 18555-9 [5]. A gypsum powder layer with a thickness of 1 mm was interposed between the specimen and the loading punches, which had a diameter of 20 mm.

The specimens were tested under uniaxial compression using a hydraulic testing machine with a capacity of 10 kN. The loading rate under load control ensured that the test would last approximately 60 seconds. After the DPT, the specimens showed a crushed central part shaped like a sandglass between the loading punches and radial cracks toward the outer perimeter.

3.4 Compressive strength of core drilled specimens

Once brought to the laboratory, two high strength mortar caps were casted on top and bottom of the CDM cores by using a special mould. The mortar caps created two flat surfaces allowing a distributed load, as proposed in [6] and [7] and unlike the UIC leaflet [11] recommendation

on the use of steel concave plates and lead sheets in contact with the sample. The sizes of the caps were about 110 mm width and 150 mm length.

The specimens were tested under uniaxial compression using a hydraulic testing machine with a capacity of 3000 kN. The force was applied perpendicularly to the horizontal joints. The tests were carried out in two stages. The first stage was oriented to the study of the elastic behaviour of the masonry and consisted in the application of three loading/unloading cycles under load control ranging from 5% to 20% of the estimated maximum load. Its value was determined by using the expression proposed by the Eurocode 6 (EC6) [12] to obtain the characteristic compressive strength of masonry, f_c, using the normalised compressive strength of the units, f_b, and the mortar, f_m. The Young's modulus was calculated for the loading branch of the third cycle. The second stage of the test was aimed to characterize the compressive strength of masonry. The cylinders were tested under displacement control, at a rate of 0.004 mm/s. The compressive strength was calculated as the ratio between the maximum load and the cross-section of the mortar caps [13].

4 DISCUSSION OF THE RESULTS

4.1 Summary of in-situ and laboratory experimental results

Table 1 reports a summary of the in-situ experimental results on mortar joints (MJ), bricks (B) and plasters (P) for the PPT and HPT, as well as the POT results in lime mortar plasters (P) on masonry wall (zone A and B) and at the bottom of the timbrel vaults (zone D).

Table 2 reports a summary of the experimental compressive strength, f_b', of 49 CB_10 and 98 CB_C4 brick specimens, as well as of 22 clay tile specimens obtained from two zones (F1 and F2). It also reports a summary of the experimental compressive strength results, $f_{m,DPT}$, of 193 DPTs on mortar joint (MJ) specimens, and 94 DPT of plaster (P) specimens obtained from the different zones. Finally, Table 2 presents the values of the experimental compressive strength, f_{c150}, and the experimental Young's Modulus, E_{c150}, of 18 CDM specimens.

Table 1: Experimental results on mortar joints (MJ), bricks (B) and plasters (P) from the PPT, HPT and POT tests, in terms of the average values (Av) and coefficients of variation (CV), for six zones of masonry walls (Z1, Z2, Z2bis, Z3, Z4 and Z5) and four zones of plasters (ZA, ZB, ZC and ZD).

		Z1	**Z2**	**Z2bis**	**Z3**	**Z4**	**Z5**	**ZA**	**ZB**	**ZC**	**ZD**
		Lime Mortar Joints (MJ) / Plasters (P)									
PPT	Av	10.4	10.6	10.4	11.3	10.4	9.8	9.9	7.4	5.6	7.0
[mm]	CV	4.5%	4.8%	4.3%	7.7%	8.3%	5.9%	8.4%	15.2%	8.2%	9.5%
HPT	Av	415	405	455	531	435	765	-	-	-	-
[N]	CV	35.5%	34.3%	24.0%	33.3%	18.0%	20.0%	-	-	-	-
POT	Av	-	-	-	-	-	-	77	295	-	350
[N]	CV	-	-	-	-	-	-	38.6%	94.4%	-	49.5%
		Fired Handmade Clay Brick (B)									
PPT	Av	6.6	6.2	5.9	5.8	5.9	6.0	-	-	-	-
[mm]	CV	23.6%	13.3%	16.7%	11.3%	11.6%	15.2%	-	-	-	-
HPT	Av	1700	2005	1665	1625	1795	1670	-	-	-	-
[N]	CV	14.1%	13.7%	9.2%	16.5%	20.2%	10.3%	-	-	-	-

Table 2: Experimental compressive strength averages values (Av) and coefficients of variation (CV) on brick specimens (CB_10, CB_C4), tile specimens (CB_F1, CB_F2), mortar joint specimens (MJ), plaster specimens (P) and Core Drilled Masonry (CDM) samples obtained on six extraction zones of masonry wall (Z1, Z2, Z2bis, Z3, Z4 and Z5), on two extraction zones of timbrel vaults (F1 and F2) and on t five extraction zones of plasters, three from wall (ZA, ZB and ZC) and two from the bottom of the timbrel vaults (ZD and ZE).

			Z1	Z2	Z2bis	Z3	Z4	Z5	F1	F2
Brick f_b'	**CB_10**	Av [MPa]	26.2	46.0	33.7	32.7	25.0	30.5	-	-
		CV	21.3%	21.3%	13.6%	13.4%	16.8%	22.7%	-	-
	CB_C4	Av [MPa]	15.0	25.3	14.8	16.4	13.6	17.8	-	-
		CV	16.5%	29.5%	21.0%	26.4%	25.2%	24.0%	-	-
Tile f_b'	**CB_F**	Av [MPa]	-	-	-	-	-	-	22.8	22.2
		CV	-	-	-	-	-	-	21.8%	19.7%
DPT $f_{m,DPT}$	**MJ**	Av [MPa]	1.1	0.4	0.5	0.4	1.4	1.8	0.7	4.0
		CV	30.8%	33.7%	32.5%	25.0%	33.3%	33.4%	31.4%	45.2%
CDM f_{c150}		Av [MPa]	6.4	-	7.0	6.4	5.3	7.8	-	-
		CV	4.0%	-	9.8%	9.5%	21.1%	9.4%	-	-
		E [MPa]	2,673	-	4,378	2,804	2,297	3,523	-	-
		CV	18.0%	-	1,5%	10.4%	21.9%	18.2%	-	-

			ZA	ZB	ZC	ZD	ZE
DPT $f_{m\ DPT}$	**P**	Av [MPa]	1.6	3.9	3.0	7.1	7.5
		CV	17.6%	33.1%	56.8%	29.6%	27.9%

4.2 Compressive strength from in-situ MDT and laboratory results

Table 3 presents the comparison between the in-situ and the laboratory tests results for lime mortar joints and bricks. The laboratory strength values for bricks were normalized with the application of the shape coefficient of 0.7, as proposed by EN 772-1:2011+A1, to the CB_10 specimens, f_b'. The reduction factor of 0.7 given by the standard UIC 1995 was applied to the laboratory strength of the mortar specimens, $f_{m,DPT}$. The HPT results were expressed in terms of the tangential stress, τ_H, corresponding to the pull-out force, F, and derived from the embedment length and the external diameter of the helix, D_e, as given by Equation 1 [14].

$$\tau_H = F / (\pi \cdot D_e \cdot L) \quad (1)$$

The variation trends of HPT results in terms of pull-out forces are fairly consistent with ranges of variations of the depth measurements obtained with PPT, as well as strengths derived from DPT for lime mortars. The HPT allowed the identification of significant in mortar performance except in the Z5 zone. The PPT showed the same result, with Z5 exhibiting a higher resistance to penetration. The variation trends of the PPT also showed good agreement with the DPT in plasters (ZA, ZB and ZC).

It is worth to mention that HPT and PPT on tested mortars provided a better agreement between them than with the DPT values. This disagreement is attributed to the fact that the specimens were dried and better conditioned when brought to the laboratory and therefore had a different moisture contents compared to the mortars in their original location. As for the bricks, the HPT and PPT values were very close to each other in spite of the variations of the

laboratory compressive strengths, not allowing to identified a clear relationship between on site and laboratory results.

Figure 7a shows the comparison between the HPT results and the laboratory results for this campaign, together with those reported in previous research studies by Pelà et al. [2] and de Vekey et al. [8]. Figure 7b shows the same results for bricks tested in this campaign, together with literature values of units of compressive strength over 10 MPa according to Ferguson [15]. The HPT on mortars provides a good relationship with the laboratory values for this campaign, as well as with the values reported in the previous researches, especially for low strengths. However, the case of bricks no clear relationship is obtained between HPT and compressive strength test as already observed by Ferguson [15]. As explained by de Vekey et al. [8], the stress could exceed the elastic limit of the tie when the material tested had a compressive strength over 10 MPa. Actually, reliable relationships for historical masonry constituents are still under investigation.

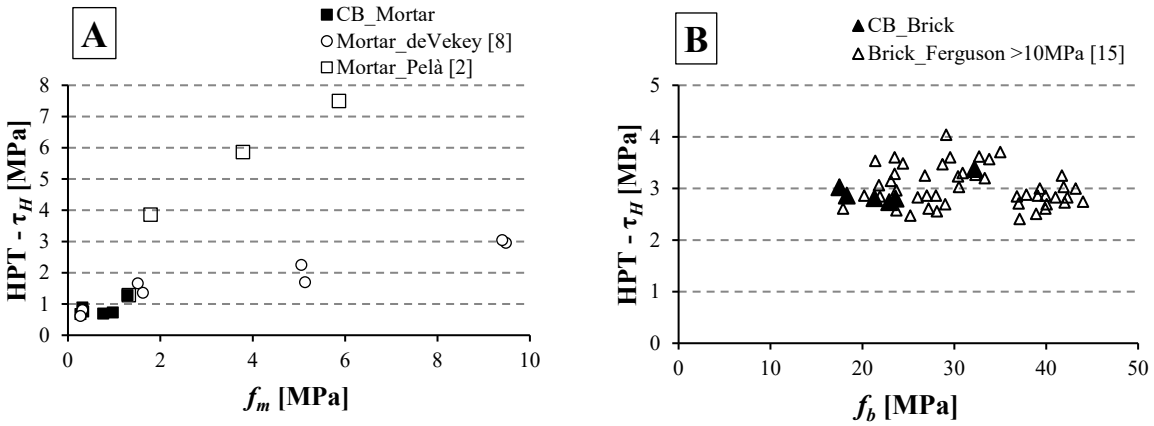


Figure 7: (A) Tangential stress of HPT on mortar joints compared with Pelà et al. [2] and de Vekey et al. [8] values. (B) Tangential stress of HPT on bricks compared with Ferguson values [15].

Table 3: Comparison among in-situ MDT and laboratory results on lime mortar joints, bricks and lime plasters.

		Z1	Z2	Z2bis	Z3	Z4	Z5	ZA	ZB	ZD
		Lime Mortar Joints (MJ) / Plasters (P)								
DPT f_m	Av [MPa]	0.76	0.27	0.33	0.31	0.97	1.29	1.12	2.73	4.97
PPT	Av [mm]	10.4	10.6	10.4	11.3	10.4	9.8	9.9	7.4	7.0
HPT τ_H	Av [MPa]	0.70	0.68	0.77	0.89	0.73	1.29	-	-	-
		Fired Handmade Clay Brick (B)								
Brick f_b	Av [MPa]	18.3	32.2	23.6	22.9	17.5	21.3	-	-	-
PPT	Av [mm]	6.6	6.2	5.9	5.8	5.9	6.0	-	-	-
HPT τ_H	Av [MPa]	2.86	3.38	2.80	2.73	3.02	2.81	-	-	-

4.2 Relationship between CB_10 and CB_C4 brick specimens

Another stage of the experimental campaign considered compression tests on nonstandard specimens measuring 40 × 40 × 40 mm^3, CB_C4. The average values of experimental

compressive strengths of the CB_C4 samples ($f_{b\,C4}$) have been related with the standard CB_10 ones ($f_{b\,10}$). Table 4 reports the ratio between the uniaxial compressive strengths (f_{b_C10} / f_{b_C4}). The given ratios resulted between 1.71 and 2.28. In average, the f_{b_10} strength was equal to 1.90 $f_{b\,C4}$ with CV equal to 11%.

Table 4: The relationship between the experimental compressive strength of the nonstandard specimen CB_C4 and the standard specimen CB_10.

			Z1	Z2	Z2bis	Z3	Z4	Z5	
Brick	CB_10	Av [MPa]	26.2	46.0	33.7	32.7	25.0	30.5	
	CB_C4	Av [MPa]	15.0	25.3	14.8	16.4	13.6	17.8	**Average**
	$f_{b\,CB_10} / f_{b\,CB_C4}$		1.74	1.82	2.28	1.99	1.84	1.71	**1.90 [CV 11%]**

4.3 Evaluation of masonry compressive strength from available analytical equations

The characteristic compressive strengths of masonry, f_c, has been evaluated from the experimental average compressive strengths, f_{c_exp}, and the empirical equation provided by Eurocode 6 [12], f_{c_EC6}, and American Requirements for Masonry Structures (ACI 530.1-05) [16], f_{c_ACI}. The characteristic f_{c_exp} values were calculated according to the procedures described in EN 1052-1 [17] using the CDM experimental values, f_{c150}. Accordingly, the f_{c150} values have been divided by 1.2 for inspection zones with less than five specimens. The f_{c_exp} corresponded to the 5% fractile value based on a confidence level of 95% if there were five or more specimens. The f_{c_EC6} and f_{c_ACI} were obtained through the Equations 2 and 3 respectively. Eurocode 6 relates the characteristic compressive strength of masonry with the characteristic compressive strength of brick, f_b, and mortar, f_m, using as a constant K the value 0.55, and ACI equation relates it to the compressive strength of the unit, f_b.

$$f_{c_EC6} = \mathrm{K} \cdot f_b^{\,0.7} \cdot f_m^{\,0.3} \text{ [in } MPa\text{]} \tag{2}$$

$$f_{c_ACI} = \mathrm{A} \cdot (400 + \mathrm{B} \cdot f_b) \text{ [in } psi\text{]} \tag{3}$$

The Young's modulus of masonry, E_c, has been also analysed. The Eurocode 6 suggests that E_{c_EC6} is 1000 times the compressive strength, while ACI 530.1-05, E_{c_ACI} suggests that is 700 times the compressive strength. The experimental values of Young's modulus, E_{c_exp}, were obtained as explained in Section 3.4 testing the CDM specimens.

Table 5 reports a summary of the experimental and empirical evaluations of the masonry compressive strength and Young's modulus. The Eurocode 6 provides values lower than the experimental ones, while the ACI 530.1-05 results are higher than the experimental ones. The only good agreement between laboratory and analytical evaluations has been found for specimens of zone Z4 for EC6 equation, and of zone Z5 for the ACI equation. Previous research [18] provided good relationships between the empirical and experimental strengths for lime mortars with 2 MPa strength. Table 5 also presents that the Young's modulus estimated from the standards is overestimated compared with the experimental ratios E_c/f_c ranging between 475 and 759.

Table 5: Experimental and empirical compressive strengths, f_c (MPa) and Young's moduli, E_c (GPa).

		Z1	Z2bis	Z3	Z4	Z5
Masonry f_c [MPa]	f_{c_exp}	5.4	5.9	5.9	4.4	7.2
	f_{c_EC6}	3.9	3.6	3.4	4.0	5.0
	f_{c_ACI}	6.4	7.5	7.3	6.2	7.0
Masonry E_c [GPa]	E_{c_exp}	2.7	4.4	2.8	2.3	3.5
	E_{c_EC6}	3.9	3.6	3.4	4.0	5.0
	E_{c_ACI}	4.5	5.2	5.1	4.4	4.9
E_{c_exp} / f_{c_exp}		**500**	**759**	**475**	**523**	**486**

5 CONCLUSIONS

This paper has presented the experimental results from in-situ and laboratory minor destructive testing (MDT) of the masonry materials of an industrial 19th c. building of Barcelona. Tests on samples made possible to determine the compressive strengths of bricks, tiles, mortars and masonry.

The following conclusions can be drawn from the research:

- The laboratory testing on novel types of specimen shows consistent results. In particular, the research proposes a novel methodology for the characterisation of the thin-tile of timbrel vaults.
- Tests on the nonstandard 40 × 40 × 40 mm^3 brick specimens showed similar scattering than the standard 100 × 100 × 40 mm^3 ones. Moreover, a clear correlation could be found between the compressive strength obtained with the two specimens. However, further investigation should be done to analyse the influence of the specimen size and shape on the compressive strength.
- The empirical equations provided by the building codes yielded values that overestimated or underestimated the compressive strength obtained from the extracted cylindrical cores.
- The in-situ MDTs have provided clear correlation trends in the evaluation of the mortar strength. In particular, and for the case of mortars, the sufficient sensitivity of HPT and PPT test allow the possibility of relating their results with experimental laboratory values.
- The in-situ MDT results for the evaluation of the clay bricks still do not show sufficient sensitivity to the variation of the material strength. More research is necessary in order to improve the application of HPT and PPT for a more reliable in-situ characterization of bricks.

Acknowledgements. The authors gratefully acknowledge the financial support from the Ministry of Science, Innovation and Universities of the Spanish Government (MCIU), the State Agency of Research (AEI) as well as that of the ERDF (European Regional Development Fund) through the project SEVERUS (Multilevel evaluation of seismic vulnerability and risk mitigation of masonry buildings in resilient historical urban centres, ref. Num. RTI2018-099589-B-I00). Support from MCIU through a predoctoral grant awarded to the first author is also gratefully acknowledged.

REFERENCES

[1] A. W. Hendry, *Structural Masonry*. London: Macmillan Education UK, (1998).

[2] L. Pelà, P. Roca, and A. Aprile, "Combined In-Situ and Laboratory Minor Destructive Testing of Historical Mortars," *Int. J. Archit. Herit.*, vol. 12, no. 3, (2018), pp. 334–349.

[3] European Committee for Standardization (CEN), "EN 1015-12 Methods of test for mortar for masonry - Part 12: Determination of adhesive strength of hardened rendering and plastering mortars on substrates." (2016).

[4] European Committee for Standardization (CEN), "EN 772-1+A1 Methods of test for Masonry Units - Part 1: Determination of Compressive Strength." (2016).

[5] Deutsche Norm, "DIN 18555-9 Testing of mortar containing mineral binders - Part 9: Determining the compressive strength of hardened mortar." (1999).

[6] L. Pelà, E. Canella, A. Aprile, and P. Roca, "Compression test of masonry core samples extracted from existing brickwork," *Constr. Build. Mater.*, vol. 119, (2016), pp. 230–240.

[7] J. Segura, L. Pelà, P. Roca, and A. Cabané, "Experimental analysis of the size effect on the compressive behaviour of cylindrical samples core-drilled from existing brick masonry," *Constr. Build. Mater.*, vol. 228, (2019), p. 116759.

[8] R. C. de Vekey and M. Sassu, "Comparison of non-destructive in-situ mechanical test on masonry mortars: The PNT-G method and the helix method," in *Proceedings of the 11th international brick and block masonry conference (IB2MC)*, (1997), pp. 376–384.

[9] M. L. Tavares, M. R. Veiga, and A. Fragata, "Grouting mortars for consolidation of historical renders showing loss of adhesion," in *2nd Conference on Historic Mortars - HMC 2010 and RILEM TC 203-RHM final workshop*, (2010), pp. 743–752.

[10] American Society for Testing and Materials (ASTM), "C67-18 Standard Test Methods for Sampling and Testing Brick and Structural Clay Tile." (2005).

[11] UIC, "Leaflet 778-3R: Recommendations for the inspection, assessment and maintainance of masonry arch bridges." UIC – International Union of Railways, Paris, France, (1995).

[12] European Committee for Standardization (CEN), "EN 1996-1-1 Design of masonry structures - Part 1-1: General rules for reinforced and unreinforced masonry structures." (2005).

[13] L. Pelà, S. Saloustros, and P. Roca, "Cylindrical samples of brick masonry with aerial lime mortar under compression: Experimental and numerical study," *Constr. Build. Mater.*, vol. 227, no. September, (2019), p. 116782.

[14] A. Benedetti and M. Tarozzi, "Interpretation formulas for in situ characterization of mortar strength," *Constr. Build. Mater.*, vol. 242, (2020), p. 118093.

[15] W. A. Ferguson and J. Skandamoorthy, "The screw pull-out test for the in-situ measurement of the strength of masonry materials," in *Proceedings of the 10th international brick and block masonry conference*, (1994), pp. 1257–66.

[16] Masonry Standards Joint Committee (MSJC), "Specification for Masonry Structures (ACI 530.1-05/ASCE 6-05/TMS 602-05)." (2004).

[17] European Committee for Standardization (CEN), "EN 1052-1 Methods of test for masonry - Part 1 : Determination of compressive strength." (1999).

[18] J. Segura, L. Pelà, and P. Roca, "Monotonic and cyclic testing of clay brick and lime mortar masonry in compression," *Constr. Build. Mater.*, vol. 193, (2018), pp. 453–466.

MECHANICAL CHARACTERIZATION OF TRADITIONAL MASONRY IN AN HOMOGENEOUS TERRITORY: VALTELLINA

MATTIA SALA*, DARIO FOPPOLI†, STEFANO DELLA TORRE‡

* Graduated in Building Engineering at Politecnico di Milano
e-mail:mattia5.sala@mail.polimi.it - Web page: http://www.polimi.it

† Technical director of Foppoli Moretta e Associati s.r.l.
Via G.F. Damiani 2, 23037 Tirano (SO)
e-mail: posta@foppolimoretta.it - Web page: http://www.foppolimoretta.it

‡ ABC department, Politecnico di Milano
(Department of Architecture, Built environment and Construction engineering)
Piazza Leonardo da Vinci, 32, 20133 Milano (MI)
e-mail: stefano.dellatorre@polimi.it - Web page: http://www.abc.polimi.it

Keywords : Valtellina, masonry, drystones, stones, lime mortar, Non Destructive Testing.

Abstract. *The current Italian Building Code provides tables with standard values of the mechanical characteristics of existing masonry. These tables refer to specific typologies, as described, according to masonry texture. As experience suggests, the way in which the masonry is built up could really affect its structural behaviour, both in terms of mechanical properties and failure mechanisms. Furthermore, the code entrusts each Region to improve and better define these mechanical characteristics, specifically in areas where they could be regarded as homogeneous, in order to improve definitions of the quality, the behaviour and the mechanical properties with a higher degree of precision and knowledge.*

Valtellina, located in the north of the Lombardy region and in the middle of the Alps, can be regarded as a homogeneous area because of its specific masonry, built up with hard rock stones and weak lime mortar. The available in–situ experimental data about this masonry typology, achieved through MDTs and NDTs, was collected, implemented and improved with additional tests to identify the relevant mechanical properties. This was aimed to classify and structurally identify this specific regional masonry typology, never analysed before.

1 INTRODUCTION

The assessment of historic building vulnerability is a big issue in Italy, mainly due to the fragility of the area which is often subject to devastating events, such as floods and landslides, but above all earthquakes that, in recent years, have severely affected the national territory. Natural events, although not always of high intensity, often have a devastating impact on the historical buildings, in particular from the cultural point of view, since the repairs of the damages, whenever possible, always result in an effective loss of the cultural value of the artefacts.

In Italy the attention to the structural vulnerability under the effects of natural events was drawn from the earthquake that affected the Friuli region in 1976 and further increased with the subsequent seismic events (Irpinia 1980, Umbria-Marche 1997, L'Aquila 2009, Emilia 2012 up

to the last Amatrice-Norcia 2016 earthquake and aftershocks). These experiences highlighted two crucial area of lacking knowledge that need to be improved:

- the damage and vulnerability of masonry and buildings subjected to seismic action;
- the predictive models, mechanical interpretations and effectiveness of the interventions.

The failure of a structural system focuses on the weakest link of the structural chain: while on the one hand the design of new buildings makes this evaluation simple, on the other hand for existing structures it is difficult to properly identify the relevant mechanism.

The current Italian Building Code [1] defines the properties of the masonry through numeric tables, which classify the stone and mortar masonries on the basis of six typologies, identified by the observation of the elevation texture, and the solid brick masonries on a single category. The mechanical characteristics of the walls can also be identified on a case-by-case base by carrying out MDTs (Minor Destructive Tests) and NDTs (Non-Destructive Tests). Furthermore, the code entrusts each region to improve and better define the mechanical characteristics of the masonries, specifically in areas that can be regarded as homogeneous in order to define their quality, behaviour and mechanical properties with a higher degree of precision and knowledge.

The aim of this research is a first collection of the available in–situ experimental data referred to the area of the Valtellina region, gained through MDTs (e.g. flat-jack tests, both single and parallel) and NDTs (e.g. sonic tests). Moreover, the analyses were implemented with other methods: further sonic tests to define the masonry quality and penetrometric tests to define the mortar properties. Data were finally processed in order to classify and mathematically determine the masonry typology and its relevant mechanical characteristics.

2 CONSTRUCTION MATERIALS

Valtellina, the study area, is a valley located in Lombardy, in the North of Italy, in the middle of the Alpine arc, close to the border with Switzerland. The geographical location of the valley has strongly influenced its historical and civil events: due to its key position between the South and the North of the Alps, the lordship of the valley has long been disputed between Milan in Italy and Chur in Switzerland, with alternate upheavals that have moved northward and southward the administrative and economic axis. For this reasons, this territory is a significant object of study, as it is peculiar and at the same time exemplary of the development of an area placed in "*the Alps, a unique region in the centre of Europe*"[2].

From a geological point of view, Valtellina is located in the western area of the Alps, characterized by silicate rocks, rather than the dolomitic and limestone ones which are present in the eastern area. The valley is located exactly along the Tonale fault, an imposing tectonic dislocation that runs from East to West in the central part of the Italian Alps, which means that most of the rocks placed along the territory are of metamorphic origin. The intrinsic characteristics of the metamorphic rocks (first of all their stratification) strongly influence the masonry construction techniques in the area. On the other hand, the relative difficulty in finding limestone rocks affects (in a negative way) the availability of lime mortars.

The historical buildings are usually made with the rock materials that were easily available (close to the construction site), which required minimal processing and allowed a fast use. Only for the buildings with iconic importance, as churches or noble palaces, the stones were sometimes taken at a greater distance and often selected and processed with a greater care in

order to underline the prominence of these building. Anyway, in the Valtellina context this was mainly limited to the production of decorative elements such as mouldings, columns and pilasters. As for the type of stones used, Valtellina masonries can be classified according to three types:

- Rough-stone masonries *(Fig. 1)*: shapeless pieces of stone material, obtained exclusively by splitting the rock mass or collecting the rock pieces lying on the ground; their shape, often multifaceted irregular with sharp edges, allows for stable positioning of the components to be obtained even without the use of mortar to build drystone walls;
- Rough-hewn stone masonries *(Fig. 1)*: also called *"drafts"*, they have dimensions which are generally similar to the rough ones; they have a defined shape with a tolerance due to the surfaces processing;
- Cut-stone masonries *(Fig.1):* generally coming from compact rocks characterized by a good processing capability to be regularized with the squaring and finishing processes.

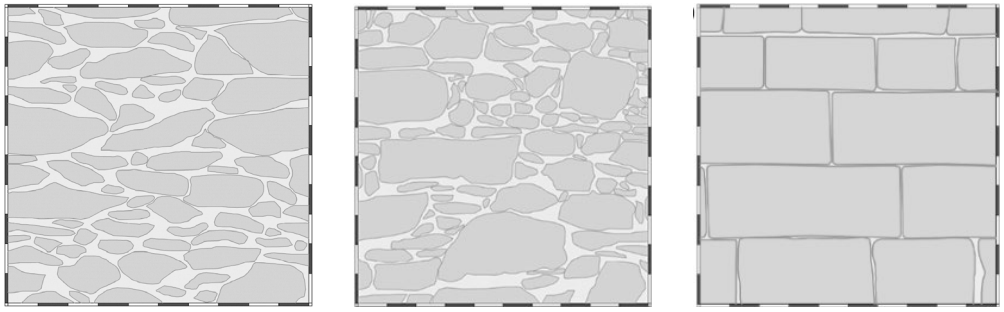


Figure 1: Rough stone masonry – *"Piatti-Reghenzani" Manor,* Teglio (TC1); Rough-hewn masonry – City hall, Ponte in Valtellina (PM1); Cut stone masonry - *Ganda Bridge,* Morbegno

The masonry walls built with rough stones represent the most common case in Valtellina. On the one side, as already stated, the scarce availability of easily workable stones limited the use of cut or carved stones to elements of particular value. The already mentioned predominant presence of metamorphic rocks naturally provided stones suitable for the construction. Indeed, because of their elongated shape and easiness of splitting according to the stratification plans, the lithic elements taken from metamorphic rocks are definitely suitable for the construction of the traditional wall texture.

The production of mortar is conditioned by the availability of suitable binders, to be used individually or in a mixture with each other. For this purpose, in the Valtellina area there are only very localized limestone outcrops. Extensive limestone outcrops, belonging to the group of the main Dolomia, can be found only in upper Valtellina, around Bormio.

The prevalent use of rough stones would lead to suppose the need of high mortar quantities inside the walls; however, the elongated conformation of the metamorphic stones implies that the rocks can be laid in rather horizontal courses, thus obtaining internal contact points and limiting the use of binding: this construction technique also derives from the tradition of the Valtellina walling method. To evaluate this circumstance, the front elevation of the walls was scanned in order to define the mortar quantity, which average percentage, referred to the whole

masonry, was found to be around 25%. It should be noted that this is only a qualitative estimation: due to wall texture the actual mortar quantity in the section can be different from the quantity calculated on the basis of the front elevation.

3 CONSTRUCTION TECHNIQUES

The construction techniques used in Valtellina are of course conditioned by the type and quality of the rocks and by the poorness of mortar used. Techniques that use rough or rough-hewn stones are defined "complex", as the arrangement has to follow precise rules and a careful selection of the stones to be used [3]. Techniques that use cut stones, called "ashlars", are defined "simple", as the parallelepiped shape deriving from shaping processes allows a simpler placement, with a lower quantity of mortar. Following the scarce use of cut-stones elements, the masonries detected on the territory of study are mainly made with “complex” techniques. It is worth noting that cut stones are often used only in the external fronts, giving a good look but no warranty that in the interior of the wall stones are laid in a correct way.

3.1 Drystone walls

Valtellina has a very peculiar “cultural” landscape, the most evident expression of which is the extensive terracing that characterizes the Rhaetian slope at the lowest altitudes, approximately up to 1000 m above sea level. The available information reports an historical overall terraced surface of around 60 km^2; the part currently cultivated (with vineyards) is less than 1/6 of its maximum historical extension. This landscape is mainly characterized by the use of retaining walls made with drystone technique [4].



Figure 2: Typical facing of a drystone wall of the Valtellina terraces

In the territorial context of this study the characteristics of drystone masonry (*Fig. 2*) have strongly permeated even the techniques of stone and mortar ones: that’s why useful information for the ordinary buildings can also came from the study of the construction techniques of the drystone masonry. On the basis of the technical literature the stability of a drystone wall is strongly related to the experience and to the skill of the mason, who has to respect six specific “rules of art” [5]: proper setting of the foundation (generally with low depth), vertical offset of the joints to obtain the optimal distribution of the weights; horizontality of the stone courses;

balancing of the stones; transversal connections to ensure a correct interlocking of the wall-layers and finally particular attention to the connection of the orthogonal walls (cornerstones).

3.2 Masonry walls

The main part of Valtellina buildings, even those that can be classified as cultural heritage (churches, palaces and rural nuclei) are characterized by a lithological variety and by the use of construction techniques almost indistinguishable from the drystone walls, although generally encompassing the use of mortar (*Fig. 3*).



Figure 3: Similarities among the drystone rural construction (left), stone and mortar rural construction (middle) and stone and mortar wall of the church of S. Ignazio in Ponte in Valtellina (right)

This results in a complication of the construction phases due to the need of lime and mortar production, but at the same time it simplifies the placement of the stones as it allows masons to pay less attention to the selection of the lithic elements, as mortar regularizes the areas of non-contact between the stones. However, the "rules of art" mentioned above for drystone masonry are systematically respected nonetheless.

Due to the scarcity of documentary and bibliographic sources, it was not possible to trace back a proper description of construction techniques in Valtellina: for this reason, a detailed analysis of the characteristic of two buildings historically representative of the local context was carried out: S. Ignazio Church at Ponte in Valtellina and Masegra Castle at Sondrio.

For the castle, the lithological variety of the stones shows a close relevance to the territorial context of the nearby Valmalenco, upstream of the Mallero river that flows in the nearby of the building; some blocks are also presumably attributable to the glacial deposits present on the Rhaetian slope. For this reason, the materials are of a crystalline nature, metamorphic or intrusive. The foundation masonry walls are laid out with sub-horizontal courses consisting in stone of various lithology and size (mainly gneiss and serpentine) and lime mortar of varying colour and grain size. The elevation walls are also characterized by sub-horizontal layers in stone blocks and mortar courses with large thickness.

The systematic observation of the wall facing masonries of the castle and of the other cases of study highlights that, regardless of the building periods, the masonries can be sorted into two types (*Fig. 4*):

- masonries made with stones laid with disordered texture,
- masonries made with stones laid with rather horizontal courses (good-texture).

These masonries can be built both with rough or rough – hewn stones, with the latter being predominant in the second type.

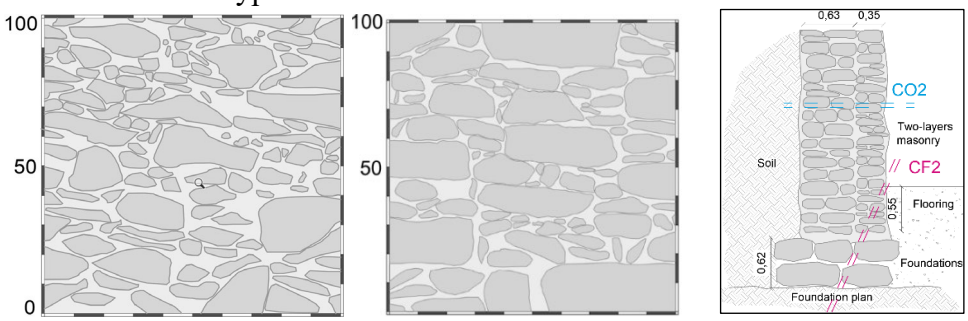


Figure 4: Masonry wall facing and section of the Masegra Castle masonries

4 DATA COLLECTION

The analysis of the masonry mechanical characteristics is a fundamental basis for the correct modelling of the structural behaviour of the building. Both for existing buildings [1] and for cultural heritage ones [7] Non-Destructive (NDTs) and Minor Destructive (MDTs) tests allow the quantitative determination of these characteristics. It is important to underline, how the Guidelines [7] explicitly state, that "*Non Destructive diagnostic Techniques of indirect type, such as sonic and ultrasonic tests, assess the homogeneity of the mechanical parameters ... but they do not provide a reliable quantitative estimation of their values ... Therefore, the direct measurement of the mechanical parameters ... in particular those relating to resistance, can be performed only through Minor Destructive or Destructive Tests, even if applied to limited portions. Calibrations of Non Destructive Tests with (Minor) Destructive Tests can be used to reduce the invasiveness of the investigation campaign.*"

The numerical analysis performed in the present research was developed from the wide database made available by the company Foppoli Moretta & Associati consulting engineers and coming from their professional activity. Both NDTs and MDTs were performed in compliance with the standards listed in Table 1.

Table 1: Reference standards for the tests performed

TEST		CODE
FJs	Single flat jack	*ASTM C 1196-14 (2014). Standard test method for in situ compressive stress within solid unit masonry estimated using the flatjack method.*
FJp	Parallel flat jacks	*ASTM C 1197-14 (2014). Standard test method for in situ measurement of masonry deformability properties using the flatjack method.*
SO	Sonic test	*UNI EN 12504-4 (2005), Prove sul calcestruzzo nelle strutture - Parte 4: Determinazione della velocità di propagazione degli impulsi ultrasonici.*
PT	Penetrometric test	Jurina, L. (2007), *La caratterizzazione meccanica delle murature parte prima: prove penetrometriche*. Politecnico di Milano – DIS
CO	Corings	*UNI EN 12504-2 (2019), Prove sul calcestruzzo nelle strutture - Parte 1: Carote - Prelievo, esame e prova di compressione.*

The available dataset has been integrated with experimental tests, specifically carried out for this work, which have been marked in bold in the following Table 2.

Table 2: Tests performed

Nr.	Location	Code	Construct. Year	FJs	FJd	SO	PT	CO
1	Vervio	SA1	1664	3	3	-	-	2
2	Sondrio	SS1	1885	4	4	-	-	4
3	Teglio	BT1	1433	-	-	**5**	**8**	-
4	Bianzone	BB1	1600	2	1	**5**	**2**	2
5	Ponte in Valtellina	SI1	1640	-	-	**3**	**10**	3
6	Sondrio	ST1	1826	6	6	-	-	-
7	Gravedona	GS1	-	3	3	-	-	-
8	Ponte in Valtellina	PM1	1942	3	3	-	-	-
9	Teglio	TC1	1700	3	3	-	-	3
10	Livigno	LS1	1954	3	3	-	-	-
11	Sondrio	CM1	1041	9	9	6	**10**	10
12	Bormio	BS1	1965	-	3	-	-	-
13	Tirano	TB1	-	2	3	9	-	2
14	Villa di Chiavenna	VC1	1800	**2**	**2**	**3**	**2**	-
15	Madesimo	MC1	-	-	-	**4**	-	-
16	Livigno	FC1	1912	-	-	**8**	**4**	-
17	Germasino	GM1	-	-	3	-	-	-
	TOTAL nr.			40	46	43	36	26

Table 3: Resume of the (average) results

Building	$E_{d\ (0.4\text{-}0.8)}$ [N/mm^2]	$G_{(0.4\text{-}0.8)}$ [N/mm^2]	ν	$E_{e\ (0.4\text{-}0..8)}$ [N/mm^2]	σ_v [N/mm^2]	σ_{max} [N/mm^2]	v_p [m/s]	f_m [N/mm^2]
SA1	3030	2702	0.10	3967	1.20	2.10	-	-
SS1	5314	-	-	4973	0.50	2.80	-	-
BT1	-	-	-	-	-	-	1590	1.80
BB1	5263	-	-	7562	0.60	2.40	1534	1.80
SI1	-	-	-	-	-	-	1603	1.70
ST1	4076	1069	0.10	5262	0.40	2.50	-	-
GS1	3724	710	0.20	5433	0.50	2.90	-	-
PM1	2119	963	0.10	3095	0.50	2.30	-	-
TC1	1095	415	0.50	2564	0.50	1.50	-	-
LS1	1340	629	0.10	2698	0.40	2.00	-	-
CM1	2744	1059	0.30	5582	0.60	3.10	2277	1.70
BS1	11142	-	-	14213	-	4.00	-	-
TB1	2256	1064	0.10	3651	0.30	2.70	1655	-
VC1	4444	1893	0.20	4829	0.60	4.00	2786	1.10
MC1	-	-	-	-	-	-	1917	1.50
FC1	-	-	-	-	-	-	2493	1.60
GM1	721	313	0.20	1802	-	1.40	-	-

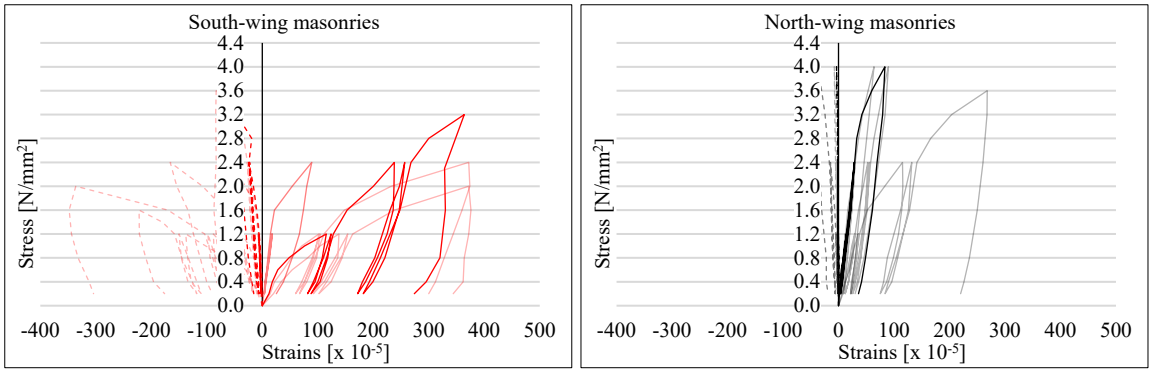
Numerical data taken from these tests have been processed to obtain the most significant mechanical characteristics of the masonries, as follow:

- Single flat jack [9], [10]: masonry compressive stress state (σ_v);
- Double flat jack [9], [10]:
  - deformability module (E_d), calculated at the first loading stage;
  - tangential deformability module (G), calculated at the first loading stage;
  - Poisson coefficient (ν), calculated at the first loading stage;
  - elastic module (E_e), calculated at the first unloading stage;
  - maximum compression strength reached for the masonry (σ_{max});
- Sonic test [10], [11]: elastic sonic wave propagation velocity (v_p) inside the masonry;
- Penetrometric test on mortar [12]: compression strength of the mortar (f_m).

The values of the average mechanical properties, determined for each of the buildings analysed, are summarized in the previous Table 3.

5 DATA ANALYSIS

The collected data is a significant statistic base that allows a relevant analysis both with reference to the single test and by matching the results of different methods in order to identify the significant characteristics. By way of example, in Graph 1 the stress vs. strain curve obtained from the double flat jacks tests performed at Masegra Castle (CM1) are plotted: the mechanical characterization suggests grouping the samples into two typologies.

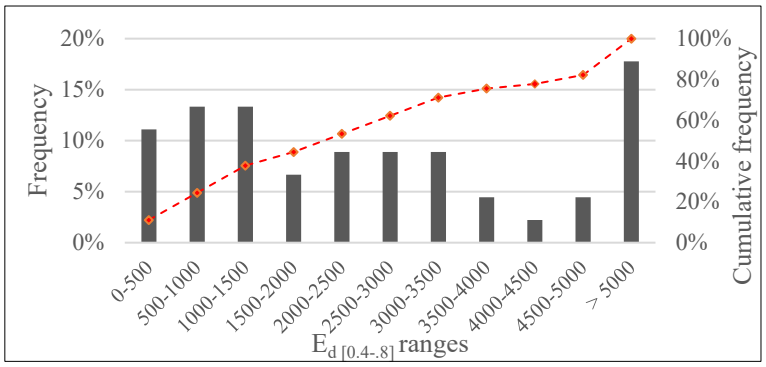


Graph 1: Stress-strain relationship of the castle masonries – South-wing (red) & North-wing (black)

Further analyses highlighted a linear correlation between the deformability modules $E_{d[0.4-.8]}$ calculated at the first load stage and the elastic modulus E_e calculated at the first unloading stage. The draft data provides a correlation with $R^2 \cong 77\%$, by purging them from some values with little reliability allow to give up to $R^2 \cong 92\%$, indicating a very good correlation.

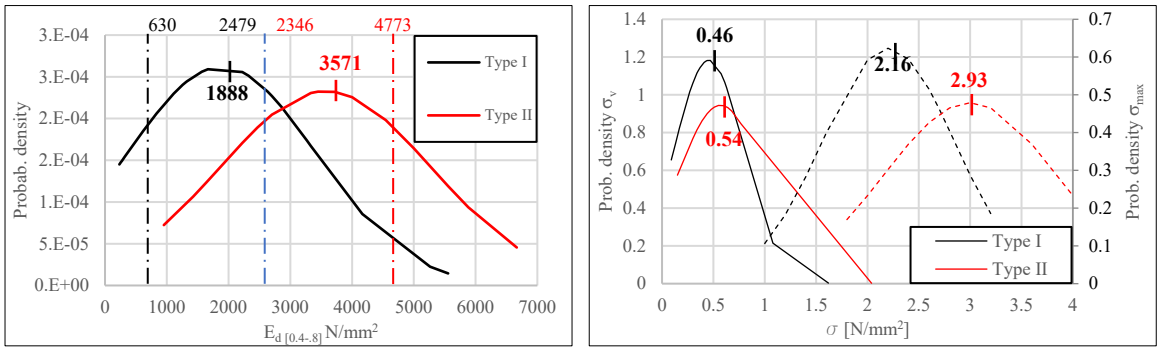
Based on the above considerations, the frequency of the deformability modules of the single tests were plotted in Graph 2. It is a matter of fact that the Valtellina masonries have a very high variance of modules, therefore it is difficult to make considerations on this draft data. Following the previous typological and mechanical observations, the walls were divided in compliance with the description of the elevation texture between "masonry with disordered texture" (type I, n. 25 reference tests) and "masonry with rather horizontal courses" (type II, n. 15 reference

test). The higher module values $E_{d\,[0.4\text{-}0.8]} > 5000$ were identified as anomalous and excluded from the analysis.



Graph 2: Deformability module frequency distribution - percentage and cumulative frequency

This way it was possible (Graph 3 left) to draft two normal distribution curves referred to type I and type II and to calculate the respective 25% and 75% percentiles. It can be noted that the disordered masonries have an average value $E_{d\,[0.4\text{-}0.8]} = 1888$ N/mm^2, while the good-texture masonries have an average value $E_{d\,[0.4\text{-}0.8]} = 3571$ N/mm^2. The values calculated according to the different typology are summarized in Table 4. It has to be noted that the average $E_{d\,[0.4\text{-}0.8]}$ values found are not very different from the values that can be calculated for the two masonry typologies identified at Masegra Castle, as previously described.



Graph 3: Normal distribution curve of deformability modulus and of σ_v and σ_{max}

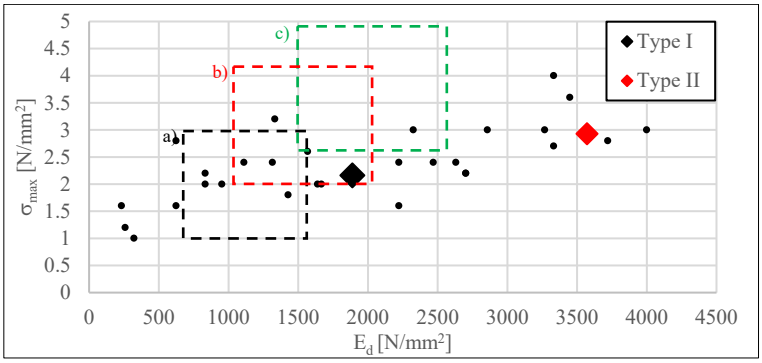
The two distribution curves (type I and type II) intersect for a good part of their development, focusing not only on the type of stone used, but also on the masonry construction technique: walls with good texture, which have a high contact among the stones (little mortar quantity) have a higher elastic modulus. Conversely the strength of the mortar is not a discriminating factor because it presents no relevant variations.

Analysing the overall masonry stress state it is possible also to note that in any case the current compression stress does not exceed the maximum detected one (Graph 3 right): thus, the average value of the safety coefficient $\gamma = \frac{\sigma_{max}}{\sigma_v}$ can be calculated, which turns out to be quite satisfactory in the test load conditions (means static with only own-weights).

Table 4: Resume of the mechanical characteristics of the masonry, according to the type

Masonry type	$E_{d\ (0.4\text{-}0.8)}$ [N/mm^2]	$G_{(0.4\text{-}0.8)}$ [N/mm^2]	ν [-]	$E_{e\ (0.4\text{-}0..8)}$ [N/mm^2]	σ_v [N/mm^2]	σ_{max} [N/mm^2]	v_p [m/s]	f_m [N/mm^2]
I	1888	750	0.18	3578	0.46	2.16	1332	1.45
II	3571	1344	0.09	5360	0.54	2.93	2443	1.41

A further attempt was made to divide the masonry characteristics by type of construction (civil, ecclesiastical and noble buildings), by location (higher, middle and lower Valtellina) and by construction period, but no significant result was obtained, proving that there was no real difference in the construction techniques among the mentioned classes. The only qualitative observation was that the noble buildings are mainly made with disordered stone masonry and that the buildings, from the 20th century onwards, are mainly built with rough-hewn ashlars.



Graph 4: $E_{d[0.4\text{-}0.8]}$ - σ_{max} correlation with the limits proposed by the Italian guidelines

Finally, the values of $E_{d[0.4\text{-}0.8]}$ were plotted versus the maximum detected compression stress σ_{max}. This graph doesn't have a very good correlation, but it allows an interesting graphic comparation with the ranges (dashed box) provided from the Italian Code [1] table C8.1.5. These ranges were be compared to the values provided from the current anaylsis (clash-dot lines): for the masonries classified as type II, the identified Valtellina masonry proved to be stiffer than the values provided by the code. The available data are of course limited to the walls that were brought to compression failure during the tests.

6 CONCLUSIONS

The masonry construction techniques in Valtellina are strictly connected to the historical, cultural and geological features of this territory. On the basis of more than 190 NDTs and MDTs, this paper proposes a preliminary classification of the typical local masonry walls (made with stone and mortar) into two typologies: "*masonry with disordered texture*", "*masonry with rather horizontal courses*". The data analysis allows the estimation of the typical mechanical characteristics and their variation. The type of construction, the location and the construction period do not seem to be influential parameters in this analysis. This work can be regarded as a first effort, as suggested the Italian Building Code, for the definition of the mechanical characteristics of the typical masonry that can be regarded as homogeneous in a specific area of Lombardy region.

ACKNOWLEDGMENTS

The research described in the present paper was carried out within a master thesis work and under the R&D plan "In Situ Testing of Masonry Characteristics" developed by the Italian company "*Foppoli Moretta e Associati consulting engineers*" with their own resources and without any public grant.

Thanks to prof. Maria Adelaide Parisi for her advice, and to all the clients who requested and allowed the tests necessary for the data collection, particularly the municipalities of Sondrio and Bianzone and the Polo Museale of Lombardy.

REFERENCES

[1] Ministero Infrastrutture e Trasporti. (2019). *Istruzioni per l'applicazione dell'«Aggiornamento delle "Norme tecniche per le costruzioni"»* (Guidelines for the Application of Italian Building Code for Constructions)

[2] Bätzing Werner (2003). *Die Alpen – Geschichte und Zukunft einer europäischen Kulturlandschaft*. Verlag C.H. Beck, München 2003

[3] Mannoni, T. (1997). *Il problema complesso delle murature storiche in pietra, in Archeologia dell'architettura, numero II*, Firenze: All'insegna del giglio.

[4] Foppoli, D. (2019). *Le Costruzioni in Pietra a Secco nel Paesaggio Culturale Valtellinese.* Tirano, Notiziario Istituto Archeologico Valtellinese n. 17, Sondrio 2019.

[5] Bretto, G. (2018). L'esperienza Ossolana ed il contesto internazionale. Tecnologia e lessico della pietra a secco. In *Paesaggi Terrazzati: Scelte per il Futuro* (pp. 317-326). Regione del Veneto.

[6] Armanasco A., Foppoli, D. (2016). Diagnostic tests vs structural models: the utility of the comparision. *Proceedings of 11th International Conference on non-destructive investigation for the diagnostic and conservation of cultural heritage (Art'14) Madrid*

[7] Ministero Infrastrutture e Trasporti. (2011). *Linee Guida per la valutazione e riduzione del rischio sismico del patrimonio culturale con riferimento alle norme tecniche* (Guidelines for the Evaluation and Reduction of seismic Hazard for Cultural Heritage Buildings)

[8] Armanasco A., Foppoli D. (2014), Diagnostic tests vs structural models: the utility of the comparison, *Proceedings of 11th International conference on non-destructive investigations and microanalysis for the diagnostics and conservation of cultural and environmental heritage (Art'14)*. Madrid

[9] Avila L., Vasconcelos G., Lourenço P. B. (2018), *Experimental seismic performance assessment of asymmetric masonry buildings,* Engineering Structures, Volume 155, pp. 298-314

[10] Binda L., Cantini L., Cardani G., Saisi A., Tiraboschi C. (2007) *Use of Flat-Jack and sonic tests for the qualification of historic masonry*. In: 10th North American masonry conference. St. Luis, Missouri, USA

[11] Podestà s., Scandolo L., Brignola A. (2013). Prove soniche per la caratterizzazione della monoliticità trasversale di pannelli murari. *ReLUIS-DPC 2010 2013. ReLUIS*

[12] Jurina, L. (2007). *La caratterizzazione meccanica delle murature parte prima: prove penetrometriche*. Politecnico di Milano – Dipartimento di Ingegneria Strutturale.

12th International Conference on Structural Analysis of Historical Constructions
SAHC 2020
P. Roca, L. Pelà and C. Molins (Eds.)

METHODOLOGIC EVOLUTION ASSESSMENT OF LARGE DEFORMATIONS ON ROMANESQUE MASONRY IN THE VAL D'ARAN (XII-XIII), SPAIN

JOSEP LLUIS I GINOVART[1], MÓNICA LÓPEZ-PIQUER[1], CINTA LLUIS-TERUEL[1]

[1]School of Architecture UIC
Universitat Internacional de Catalunya
Immaculada, 22, 08017 Barcelona, Spain
e-mail: jlluis@uic.es; m.lopezpiquer@gmail.com; cintalluis@uic.es

Keywords: Romanesque, barrel vaults, masonry pillars, great deformations, Val d'Aran

Abstract. *There is a set of Romanesque churches at Val d'Aran that were built between the eleventh and thirteenth centuries. One of the main features of these buildings is the presence of large deformations and geometrical displacements in their masonry. One of the most deformed buildings is the church of Santa Maria de Arties (XII), which arches' and vaults' have anti-funicular shapes. The assessment is based on a three-dimensional model obtained with a terrestrial laser scanner (TLS). The scanner used is a Leica ScanStation P20. In the study of built heritage, the use of direct measurement techniques for architectural surveying requires a large number of resources. These deformations have caused, in some cases, turn centerlines of the vaults into convex shapes, which have the inverted shape of an arch. Joints appeared because of active and passive thrusts that were performed to keep the structures in equilibrium. Geometrical assessment of the least rigid elements, the pillars, makes it possible to analyze the displacements, which have been the cause of anti-funicular shapes on some vaults. It is possible to deduce the regression plane of the displacements of the pillars of the central nave and to define the deformation vectors over it. Thus, these data all for the directions of the deformations of the vaults to be determined.*

The methodology of this study focuses on the assessment of the geometrical characteristics of the pillars, with the objective of studying the displacements that they have suffered. The point cloud is processed with the software; Cyclone, and the program 3DReshaper (2016), and Google SketchUp (2019). The study allows to analyze the evolution of the treatment of points, concluding that deformations of the pillars are not perpendicular to the axis of the central vault. The methodology used and its results let to understand the nature of the displacements in order to preserve these masonry structures.

1 THE STUDY OF THE GREAT DEFORMATIONS OF THE VAL D'ARAN ROMANESQUE ARCHITECTURE

The churches of Val d'Aran are located at the Spanish Pyrenees and were built between the twelfth and thirteenth centuries. Large deformations have been found on these Romanesque buildings masonry and are one of the main characteristics of them. In the church of Santa Maria Arties (XII-XIII), the most deformed building, some anti-funicular shapes have been found at their arches and vaults. This anti-funicular shape is the inverse of the natural shape of an arch since it is convex in relation to its centerline. One of the causes of these deformations is the displacement of the pillars since these are the least rigid elements of the structure.

Owing to large deformations, these Romanesque constructions were assessed by several authors, such as Emmanuel Viollet-le-Duc (1814-1879), who visited Bossost (1883) [1], and later by Lluís Domènech i Montaner (1850-1923), who was Dean of the Escuela de Arquitectura de Barcelona (1905) [2]. Subsequently, the Institut d'Estudis Catalans organized an expedition with the combined historical and archaeological purpose of visiting the Val d'Aran and La Ribagorça (1907). Two of the participants were the architects Josep Puig i Cadafalch (1867-1956) and Josep Goday i Casals (1881-1936) [3], who suggested that these churches were initially covered with timber structures and later replaced by masonry barrel vaults [4].

Juan Bassegoda i Nonell (1930-2012) stated that formal anomalies are a defining characteristic of the Catalan Romanesque architecture [5]. The case study presented in this paper focuses on the church of Santa Maria Arties, which is the most assessed building of this group. Its huge deformations were identified during the restoration work of the 70s' [6]. Afterwards, José Luis i Villanueva noted the existence of the funicular shapes [7], and in 2009, the structure was assessed by means of finite elements (FEM) by the team of Joan Polo i Berroy [8].

The structure presents a typical deformation pattern: leaning of vertical elements towards the outside because of vaults thrust, and settlement of vaults, which have caused the apparition of funicular shapes, that is the inverse of the natural shape of an arch since it is convex in relation to its axis. One of the causes of these deformations is the displacement of the pillars since these are the least rigid elements of the structure. The investigation focuses on the geometrical parametrization and evaluation of these movements. Previous investigations focused on the assessment of the overall structure, in order to understand the stability conditions, which revealed that masonry is working to the limit through the deformations suffered, while the origin of the movements can be explained by rigidity issues. The assessment is based on a three-dimensional model obtained with a terrestrial laser scanner (TLS). In the assessment of built heritage, the use of direct measurement techniques for architectural surveying requires a large number of resources. The use of massive data capture techniques, such as Terrestrial Laser Scanner (TLS), has recently become prominent in surveying architectural heritage.

Otherwise, the architectural heritage topographic documentation is a key tool for its preservation. Current techniques of Massive Data Capture (MDC), such as digital photogrammetry and terrestrial laser scanner, have become widespread in the assessment of built heritage [9], [10]. Numerous investigations have tested the technique's reliability [11],

[12], and has proven their effectiveness to survey the building's geometry with high precision. The point clouds make it possible to detect and monitor degradation processes and formal anomalies. Other applications go from heritage documentation [13], [14] to deepen in the history and buildings constructions [15], [16] between many others.

The specific issue of deformation assessment is essential for architectural heritage conservation, and many studies have developed simple procedures to address that issue from the 3D topographical information of the point clouds, i.e. the Cathedral of St. Johannis in Meldorf [17] the churches of Santa Maria in Portonovo [18] and Cantalovo [19] or the Palazzo d'Accursio, in the cathedral of Tortosa [20], and Val d'Aran in Spain [21] [22]. Those investigation focuses on the assessment of vertical elements deformations, except the Portonovo's case, where a simple assessment of the cylindrical barrel vaults is performed from standard primitives.

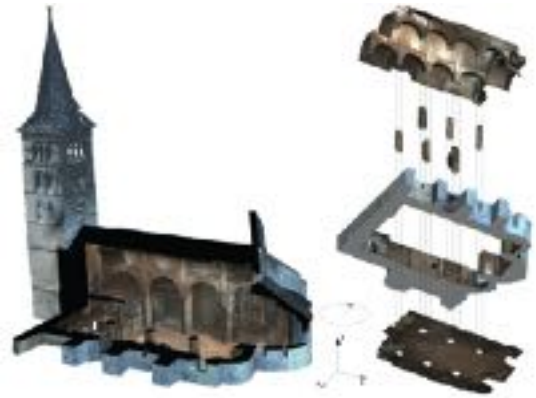


Figure 1. Santa Maria Arties (XII-XIII) [35]

In order to analyse the deformations of the church of Santa Maria Arties (XII-XIII), we used the point cloud extract from the scanner Leica ScanStation P20, with a bandwidth of 808/658, class 1. The scanning ratio is 1,000,000 points, and the noise at 100 is 9.0 mm for black surfaces, 4.30 mm for grey surfaces, and 1.5 mm for white surfaces. The field of view is 360º horizontal and 270º vertical. (Figure 1).

2 METHODOLOGY OF THE GEOMETRICAL ASSESSMENT OF ARTIES PILLARS'

The methodology of this study focuses on the assessment of the geometrical characteristics of the 6 pillars [$P_1 \ldots P_6$] of Santa Maria Arties with the objective of studying the displacements that they have suffered [23]. The pillars of the central nave have deformed in a specific way, namely, through the masonry joints (n_s). These joints are perfectly visible on pillars P_3, P_4, P_5 and P_6, while they are more difficult to see on P_1 and P_2 since these pillars are partially covered by mural paintings. The displacements can be assessed according to the coordinates of the centroid of each row (x_{ci}, y_{ci}, z_{ci}), and the point of reference is taken from the row of the floor plan, which is considered to be undeformable. This establishes the coordinates as (x_{ci}, 0, z_{ci}). These points allow one to define a regression plane P_{ri} for each pillar. Thus, it is possible to define a vector of deformation contained on each plane [$P_{r1} \ldots P_{r6}$]. Finally, these data allow one to determine the general tendency of the deformation of the vaults (Figure 2).

The assessment of shapes can only be understood in three dimensions through an interval (*a, b*), which has to impose the condition of equilibrium according to the elastic theory with the summation of the active thrusts (E_{ba}) of the vaults and the passive thrusts of the walls (E_{mp}) and buttresses (E_{mc}).

$$\sum_{b}^{a} F_{(x,y,z)}\left(E_{ba} + E_{mp} + E_{mc}\right) = 0$$

$$\sum_{b}^{a} M_{(x,y,z)}\left(E_{ba} + E_{mp} + E_{mc}\right) = 0.$$

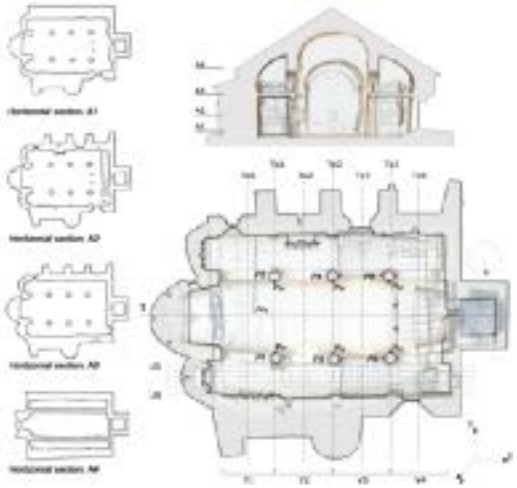


Figure 2. Methodology of the geometrical assessment of Santa Maria Arties pillars'[35]

The assessment of the deformations of the elements under its own weight, especially the central and lateral vaults, makes it possible to deduce that external actions, such as snow or seism. These external actions, together with the loss of lime mortar, inasmuch as humidity or vibrations, cause the primitive function $f_{i(x,y,z)}$ of the vaults. This function tends to deform into the function $f_{f(x,y,z)}$, which is obtained through the topographical survey.

From a historiographical point of view, the definition of vaults geometry should be overhaul through the observational technique. Robert Willis (1800-1875) was the first author that studied that fact in its architectural treatise *Remarks on the Architecture of the Middle Ages* (1835), where he makes some references to the Romanesque vaults [24]. He will explain it in more detail in the introductory part of the cylindrical vaults mechanics in 1842 in his book *On the Construction of the Vaults of the Middle Ages* **Error! Reference source not found.**. Other authors that done similar studies are: Emmanuel Viollet-le-Duc (1814-1879), who assessed the barrel vaults and the abutment with timber beams with more precision August Choisy (1841-1909) [26], who did not describe the Romanesque vaults, but he explained the barrel vaults since its Roman construction origins, with brick and concrete [27]. He also referred to the byzantine influence on construction with or without centring [28]. Otherwise, in the work *Historia General del Arte* (1901), Josep Puig i Cadafalch described the great difference between the Romanesque vaults, where elasticity is replaced by stability, which is a concept inherited from roman vaults, those that were significantly more monolithic [29].

Likewise, Puig i Cadafalch determines the characterization of the most important elements in *L'Arquitectura Romànica a Catalunya* (1918-1920), and he also explains the structural and artistic analysis of the masonry, vaults and pillars [30]. In this way, he stablishes vaults' and pillars' evolution and the introduction of the column in the Catalan Romanesque Architecture as one of its main characteristics [31]. From the typological point of view of the canon vaults, it will be Leopoldo Torres Balbás (1888-1960) who tries to explain, in *Bóvedas romanas sobre arcos de resalto* (1946), the transmission of this constructive way from the Roman world, passing through the South of France to The Iberian Peninsula [32]. At the same time, Bonaventura Bassegoda i Musté (1896-1987) will propose, from the mathematical point of view, the elastic theory through the third central part of vaults and domes [33]. Finally, Juan Bassegoda Nonell (1930-2012) explains how the traditional Roman models gave constructive form to medieval vaults in Catalonia [34].

When the geometry of these vaults is regular and the construction is monolithic because of the masonry disposition, the thrust is perpendicular to its centerline. Thus, the thrust of a vault is determined through the following function:

$$E_b\ (E_{bx},\ E_{by},\ E_{bz})$$

If we consider homogeneous vaults with a constant centerline, the vector of this thrust would be, according to Choisy (1873) [27], as follows:

$$E_b\ (E_{bx},\ 0,\ 0)$$

Conversely, barrel vaults of Vall d'Aran churches have specific features. These are conic vaults, as was theorised by Joan Bassegoda (1974) [5], and the stone-cutting is not regular, as stated by Josep Puig i Cadafalch (1901) [29]. Finally, the supports of the vaults, external walls and arches, have a different stiffness, as noted by Luis Villanueva (1974) [7]. Those three conditions are far from the general theory of the thrust of homogeneous vaults with cylindrical axis. In addition, the assessment of the pillar deformations and their stiffness is influenced by the contributions of Josep Puig i Cadafalch (1908) [4].

In any or in a combination of the precedent hypotheses, thrusts work in two directions (x, z) as long as the supports stand still. Thus, the resultant force is not perpendicular to the axis of the vault. The general vectorization in those cases can be defined as the thrust of the vault $E_b\ (E_{bx},\ E_{by},\ E_{bz})$, and deformations can occur in two directions:

$$f\ (df_x,\ 0,\ df_z)$$

The forces caused by the vaults are transmitted to vertical structural elements. The vaults of the central nave are supported by the walls over former arches, which at the same time are supported by the pillars of the central nave. Thus, the elements can deform over the three planes, pillars $df_p(df_{px},\ df_{py},\ df_{pz})$, and perimeter walls $df_m(df_{mx},\ df_{my},\ df_{mz})$.
On the other hand, the deformations of the pillars are a function of their monolithic nature. Thus, the deformations are directly related to the stone cutting of the pillar and the thrust *Ep* ($E_{px},\ E_{py},\ E_{pz}$). According to the internal distribution of forces, the masonry stone cutting and mortar (E_{pz1}), and the irregular geometry of the vault (E_{pz2}), the structure tends towards a state of equilibrium (E_{pz1}- E_{pz2}) or to the opposite state (E_{pz1}+E_{pz2}).

A monolithic, infinitely rigid pillar tends to rotate on its base. The upper part moves over the axis (x) towards the exterior since the main horizontal thrust (E_x) with the consequence that there is also movement in the axis (y) since their extreme upper part declines. Finally, there is also movement over axis (z) due to E_{bz}, which defines the deformations df_p (df_{px}, df_{py}, df_{pz}). If pillars are not monolithic and are built with numerous joints, they tend to deform in the upper part so that there is not Δdf_{py}. If we suppose that the extremes of the vaults have not suffered differential settlements and that the movement of these extremes is thus ($\Delta y=0$), then the deformations are df_p (df_{px}, 0, df_{pz}), which is the hypothesis of the present case study. There can be a combination of rotations and translations as a function of the stone cutting, so the general characterization of the displacements should be made through intervals I_1; df_p (df_{px}, df_{py}, df_{pz}). Then, in I_2; df_p (df_{px},0, df_{pz}) displacements ($\Delta y>0$) can occur because of the contact between mortar and stones or the friction between stones where there is no more mortar.

The displacement of the pillar can be deduced through analysis of the displacement of the centroid of n sections (n_s) of the pillar. Thus, coordinates (x_{ci}, y_{ci}, z_{ci}) are set for each section (n_s). The centroid of reference (x_{c0}, y_{c0}, z_{c0}) is set in the section of the floor plan since it would have not suffered any displacement. The final section is located at the impost of the pillar (x_{cs}, y_{cs}, z_{cs}). The obtained points define a function f (c_i), which makes it possible to deduce the regression plane P_{ri}. It characterizes the tendency of the displacement vectors of the structural section supported by the pillar.

The assessment of this displacement vector determines the clearance angle (ω) of the regression plane P_{ri} of the plane over the centerline of the vault (τ). Thus, this angle can be understood as:

(ω φ) = 90º, perpendicular to the centerline φ1,
(ω φ) < 90º, displacement towards the apse,
(ω φ) > 90º, displacement towards the façade.

The reparation and containment of these deformations are the cause of the reinforcement of the perimeter walls by means of the construction of buttresses or strategical placement of bell towers, which are usually built in the façade opposite to the apse. The active thrusts (E_{ba}) of the vaults over pillars and walls have been determined, but to understand the equilibrium of these constructions, it is essential to understand the passive thrusts of the buttressing elements: walls (E_{mp}) and buttresses (E_{mc}). Owing to these thrusts, some vaults have deformed towards anti-funicular shapes.

In the year 2016, the point cloud was processed with the software Cyclone, and the program 3DReshaper, which is used to obtain the three-dimensional mesh with an average distance of points of 0.05 m as well as a measure of the triangle for detecting 0.1 m holes. The model of the interior of the building has 80,582 points and 156,449 triangles, and the exterior has 314,650 points and 609,472 triangles.

Otherwise, in 2019, the point cloud has been processed with the plug-in Undet of the software Google SketchUp (2019). In this occasion, the point cloud has not been converted to a mesh, because this plug-in works with points, not with meshes. The models that we are working with have a grid of points in coordinates (x, y, z) ranging from [0.06 to 0.09 m].

3 DATA TREATMENT WITH THE SOFTWARE CYCLONE (2016)

The use of the specific software Cyclone to process the data enable to visualize the point cloud obtained and to process and join all the scanners done and convert the point clouds to a mesh. This processing occurs through an automatic process with slight manual adjustments, and a complete, depurated point cloud and triangular mesh is obtained. The morphological features assessment of the pillars is made through the visible elements, such as the masonry joints. Non-visible elements are not considered. Thus, data are obtained according to the centroids of each visible row. Thus, pillars have following rows: (P_1=26), (P_2=26), (P_3=27), (P_4= 25), (P_5= 23) and (P_6= 23). Rows are numbered from bottom to top [35]. The identification of pillars' joints was made by means of a manual measurement system, for the reason that the graphical capacity of the software Cyclone, and the program 3DResheaper, does not allow to specify pillar's joints because it constructs it three-dimensionally (Figure 3).

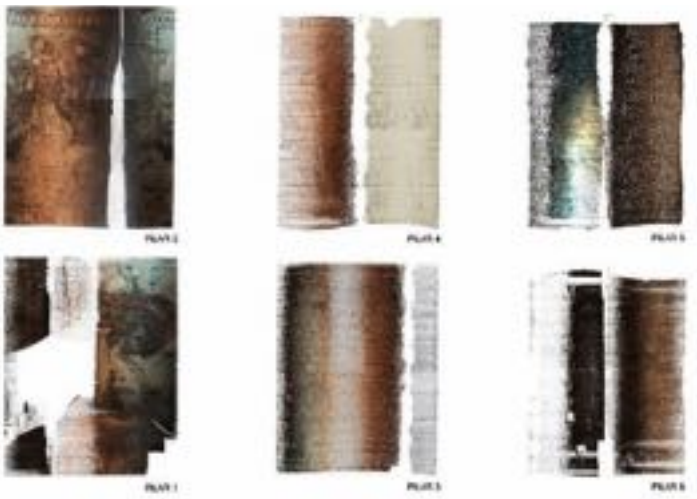


Figure 3. Visualization of pillars' joints with software Cyclone

The greatest displacement is found in pillar P_1, with a range of displacement on each row of [0.270, 0.001]. That displacement is followed by that in pillar P_3, with a range of [0.190, 0.001]. The range of displacements of the rest of the pillars is as follows: P_2 [0.108; 0.002], P_4 [0.109; 0.002], P_5 [0.101; 0.001], and finally, the least deformed pillar, P_6 [0.065; 0.001]. Thus, pillars P_1, P_3 and P_5 have greater deformations than the others. None of the regression planes P_{ri} is perpendicular to the axis of the central vault. Each one is gently sloped. The angle in P_1 is 85.466º, so (ω_{φ}) < 90º (Figure 4). It is also the most inclined pillar (0.270 m) and is the highest (4.170 m). The rest of the pillars have angles (ω_{φ}) > 90º, with a range [103.893º - 126.169º]: P_2 [103,893º], P_3 [108.665º], P_4 [117.245º], P_5 [112.066º] and P_6 [126.169º].

4 DATA TREATMENT WITH THE PLUG-IN UNDET FOR GOOGLE SKETCHUP

With the plug-in Undet for Google SketchUp (2019) the identification of pillar's joints was made directly with the image of the software. Undet is a plug-in that combine individual scan stations into groups and point clouds from a wide range of scanners, in this case, we have

used the data that we extract from the Massive Data Capture (MDC) of the Leica ScanStation P20 scanners. What we have experienced with this plug-in is that the management of the point clouds is more efficient and quicker than with the software Cyclone.

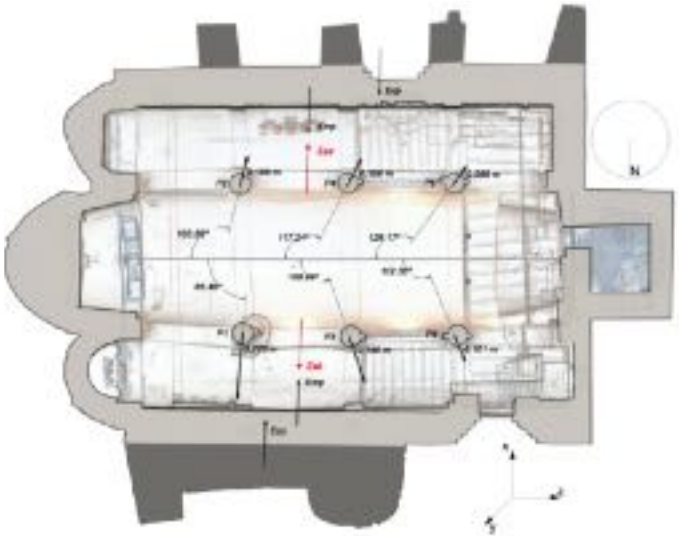


Figure 4. Characterization of the regression planes Pri from the software Cyclone (2016) [35]

Undet for SketchUp (2019) has an interactive colouring and density management, so it let us to adjust transparency, change point cloud and point size and, the most important thing for our research, it we are able to see the point cloud coloured by planes or heights. This function let us to see pillar's joints in detail, so, from now on we will be able to check the manual measurement that we previously have done and to say that the joints measured with Undet range from [0.007 m] to [0.015 m] of width. (Figure 5).

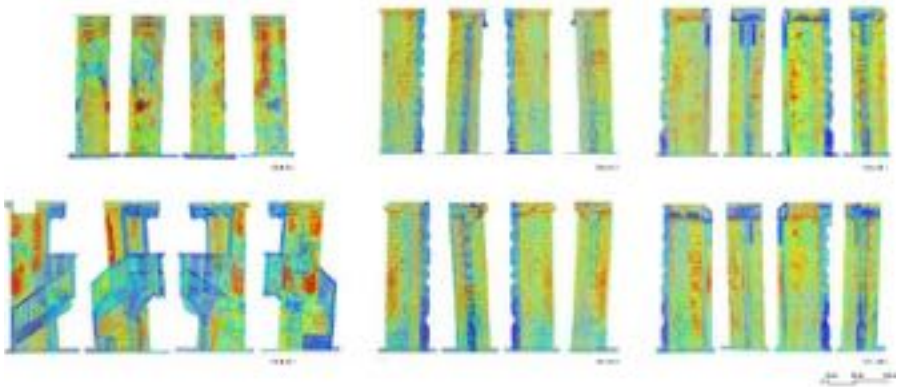


Figure 5. Visualization of pillars' joints with plug-in Undet SketchUp (2019)

We have also analysed the regression planes P_{ri} from the pillars, which, like the previous results obtained from the software Cyclone, they are also not perpendicular to the axis of the central vault. We have observed that there are little differences between the other results and these, being the deformation of P_2 the biggest difference [2.599º] less and the one of P_3 the smallest

[0.003º] less. The angle in P_1 is 85.474º, so (ω_{φ}) < 90º (Figure 6). It is also the most inclined pillar [0.206 m]. The rest of the pillars have angles (ω_{φ}) > 90º, as we have previously seen, with a range [101.291º - 124.756º]: P_2 [103,893º], P_3 [108.657º], P_4 [119.417º], [P_5 124.756º] and P_6 [110.553º]. We have also seen that the deformations of P_4 and P_5 are biggest in the middle of pillars' height than in the top of it. With Cyclone we didn't found that deformations.

5 DISCUSSION

The obtained results from both methods used are very similar to determine deformations in Romanesque masonry buildings, where the interest of the displacements is more qualitative than the quantitative order magnitude. The graphic precision of the plug-in Undet for Google SketchUp (2019) should be noticed, due to it is much higher and it allows to identify the points that each point that composes the point cloud extract from the Terrestrial Laser Scanner (TLS). To work with this plug-in there is no need to have a computer with a lot of graphic capacity, seeing that you can section the point cloud in few seconds. As for its precision, in a section of [0.005 m] the error is about [0.006 m] (0.030%), unlike the one obtained from the software Cyclone (2016), which was of [0.03 m].

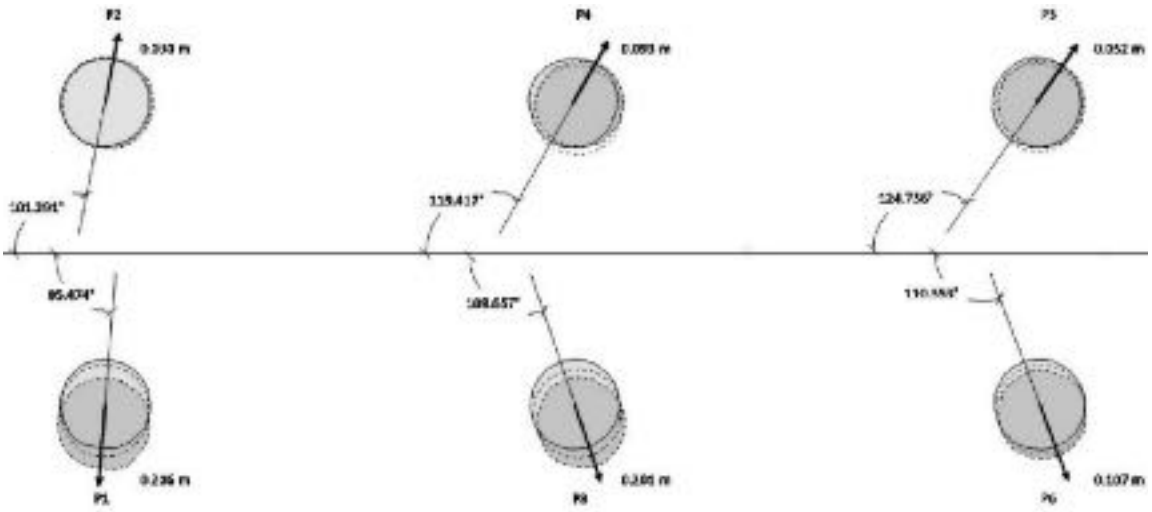


Figure 6. Characterization of the regression planes Pri from the plugin Undet (2019)

6 CONCLUSIONS

The obtained regression planes P_{ri}, which contain the deformations df_p (df_{px}, df_{py}, df_{pz}) for each pillar, tend to have the direction of the thrust over the pillar P_i. These displacements are the result of the active thrusts of vaults (E_{ba}) and the passive thrusts of the buttressing system, walls (E_{mp}) and buttresses (E_{mc}). This study revealed that the direction of the displacements of the six pillars P_i is not perpendicular to the central axis of the church φ_1 since (ω_{φ}) ≠ 90º. This results proves the hypothesis that the thrusts of the vaults are not perpendicular to the axis of the church, as was the case in Roman vaults, which Choisy (1873) [27] defined with regular geometry and stone cutting. The direction of displacements is caused by the

irregular geometry of the vaults of Santa Maria de Arties as well as the masonry stone cutting and the above mentioned passive thrusts of the walls and buttresses. The last ones were placed to maintain equilibrium during the last millennium.

The displacement of the five pillars ($P_2 \ldots P_5$), where (ω_{φ}) > 90º, tends to the opposite façade of the apse. In addition, pillars P_5 and P_6, built during twelfth century on that façade, are the least deformed pillars because of two subsequent transformations: the construction of the bell tower over the centre of the façade (XIII-XIV) and the wood choir (XVIII). These elements have a stiffening function.

Pillar P_1 is the most deformed pillar of Santa Maria de Arties and has (ω_{φ}) < 90º over the main axis. The displacement tends to the apse. This pillar, together with pillar P_3, where (ω_{φ}) > 90º, have achieved a great balancing through the passive thrust of the walls (E_{mp}) and buttresses (E_{mc}). For a specific weight of more than 24 kN/m^3, the buttressing system weighs 3,144.96 kN. Here is where anti-funicular shapes, inverted, arches, have appeared, so: ff''(x) > 0.

Pillars deformations' df_p (df_{px}, df_{py}, df_{pz}) tend to have the same direction of the thrust over pillars P_i, so, regression planes P_{ri}, which contain these deformations, are essential to define any intervention over these masonry buildings, because they show the direction of possible preventive actions.

Otherwise, the vectorization of the displacements of each row, deduced from the regression plane, makes it possible to parametrize the leaning of each pillar. Second, three deformation modes were identified, so the displacements of the pillars are not uniform. Moreover, on pillars (P_2, P_3, P_5), the displacements are variable and appear to be negative displacements on (x) in relation to the vertical, and the deformation of pillars (P_4, P_5) is biggest in the middle of their height tan in the extremes of pillars.

The ranges of heights where great deformations occur have also been identified, which are: P_1: [1.50 – 2.00 m], P_2 [3.00 – 3.50 m], P_3 [2.00 – 3.00 m], P_4 [1.50 – 2.50 m], P_5 [2.00 – 3.00 m] and P_6 [1.00 – 2.50 m]. There is a difference between the height of the base pillars too, since the inclination of the church floor, being P_1 and P_2 at the same height from their base centre, P_3 is at the same height of P_4, but they begin [0.047 m] upper than P_1 and P_2 and, finally, P_5 is [0.0577 m] upper than P_1 and [0.019 m] lower than P_6. These points are extremely important in order to determine the appropriate actions that needs to be taken for intervention on these buildings and preserve this Romanesque architectural heritage.

REFERENCES

[1] Español, F. (2011). El Pirineu desvetllat: Viatges i descoberta del patrimoni medieval. Annals Del Centre d'Estudis Comarcals Del Ripollès, 7, 13–36.
[2] Granell, E., & Ramon, A. (2006). Lluís Domènech i Montaner. Viatges per l'arquitectura romànica catalana. Barcelona: Colegio de Arquitectos de Cataluña, España.
[3] Alcolea Blanch, S. (2008). La missió arqueológica del 1907 als Pirineus. Exhibition catalog. Barcelona.

[4] Puig i Cadafalch, J. (1908). Les iglesies romàniques amb cobertes de fusta de les Valls De Bohí y d'Aran. Anuari de l'Institut d'Estudis Catalans, MCMVII, 119–136.
[5] Bassegoda, Nonell, J. (1974). Estética expresionista de la arquitectura románica lombarda en Catalunya como consecuencia de las deformaciones formales y estructurales de las iglesias. In De Re Restauratoria (Vol. Vol II, pp. 33–64). Barcelona: Catedra Gaudi UPB.
[6] Saez. (1976). Primera fase del proyecto de restauración de la Iglesia de Santa María de Artíes en el Valle de Arán (Lérida). Cuadernos de Arquitectura Y Urbanismo, 116, 63–71.
[7] Villanueva, J. L. (1974). "Las bóvedas de cañón." In De Re Restauratoria Vol. II, 145–158). Barcelona : UPB.
[8] Polo, C. (2009). Santa Maria d'Arties (Naut Aran, Val d'Aran): Un exemple integrau a nivèu de restauracion d'un monument a compdar des entresenhes arqueologiques. Cicle de Conferències Patrimoni Arqueològic I Arquitectònic a Les Terres de Lleida 2009, Departament de Cultura I Mitjans de Comunicacó.p. 75–103.
[9] Kadobayashi, R., Kochi, N., Otani, H., & Furukawa, R. (2004). Comparison and evaluation of laser scanning and photogrammetry and their combined use for digital recording of cultural heritage. Congress of ISPRS, Istanbul 12-23 July. International Archives of Photogrammetry and Remote Sensign, vol. XXXV, part B5, p. 401-406.
[10] Yilmaz, H. M., Yakar, M., Gulec, S. a., & Dulgerler, O. N. (2007). Importance of digital close-range photogrammetry in documentation of cultural heritage. Journal of Cultural Heritage, 8(4), 428–433. http://doi.org/10.1016/j.culher.2007.07.004
[11] Grussenmeyer, P., Landes, T., Voegtle, T., & Ringle, K. (2008). Comparison methods of terrestrial laser scanning, photogrammetry and tacheometry data for recording of cultural heritage buildings. International Archives of Photogrammetry, Remote Sensing and Spatial Information Sciences, 37 (B5), 213–218.
[12] Vendrell, M., Giráldez, P., González, R., Cavallé, F., & Roca, P. (2008). Santa Maria del Mar. Estudi històric-constructiu, materials de construcció i estabilitat estructural. Barcelona: UB-Patrimoni, Veclus, UPC.
[13] Dhonju, H., Xiao, W., Shakya, B., Mills, J., & Sarhosis, V. (2017). Documentation of Heritage Structures Through Geo-Crowdsourcing and Web-Mapping. ISPRS Geospatial Week 2017.
[14] Dhonju, H., Xiao, W., V. Sarhosis, V., Mills, J. P., Wilkinson, S.; Wang, L. Thapa, U. S. P. (2017). Feasibility study of low-cost image-based heritage documentation in Nepal. Int. Arch. Photogramm. Remote Sens. Spatial Inf. Sci., XLII-2/W3, XLII-2, 237–242. http://doi.org/https://doi.org/10.5194/isprs-archives-XLII-2-W3-237-2017, 2017.
[15] Benito, M. A. (2011). La Catedral de Ávila: Evolución constructiva y análisis estructural. PhD thesis. Escuela Técnica Superior de Arquitectura de Madrid. Universidad Politécnica de Madrid.
[16] Sternberg, H. (2006). Deformation measurements at historical buildings with terrestrial laserscanners. IAPRS Volume XXXVI, Part 5, Dresden 25-27 September. p. 303–308.
[17] Quagliarini, E., Clini, P., & Ripanti, M. (2016). Fast, low cost and safe methodology for the assessment of the state of conservation of historical buildings from 3D laser scanning: The case study of Santa Maria in Portonovo (Italy). Journal of Cultural Heritage. https://doi.org/10.1016/j.culher.2016.10.006
[18] Bonali, E., Pesci, A., Casula, G., & Boschi, E. (2014). Deformation of Ancient Buildings inferred by Terrestrial Laser Scanning methodology: The Cantalovo church case study

(Northern Italy). Archaeometry, 56(4), 703–716. http://doi.org/10.1111/arcm.12028
[19] Pesci, A., Bonali, E., Galli, C., & Boschi, E. (2012). Laser scanning and digital imaging for the investigation of an ancient building: Palazzo d'Accursio study case (Bologna, Italy). Journal of Cultural Heritage, 13(2), 215–220. http://doi.org/10.1016/j.culher.2011.09.004.
[20] Lluis i Ginovart, J., Costa-Jover, A., Coll-Pla S., & Puche Fontanilles, J. M. (2016). Techniques of massive data capture: A comparative approach for the assessment of complex spaces in architectural heritatge. Revista de la Contrucción, 15(1), 42–50.
[21] Costa-Jover, A., Lluis i Ginovart, J., Fortuny-Anguera, G., & Coll-Pla, S. (2014). Large deformations on a XII Century Romanic church at Val d'Aran (Spain). 9th International Masonry Conference 2014 in Guimarães. Book of Abstracts, 221.
[22] Costa Jover, A., & Coll Pla, S. (2017). Mecánica de bóvedas de obra de fábrica en las Iglesias del Valle de Arán. Actas Del Décimo Congreso Nacional y Segundo Congreso Internacional Hispanoamericano de Historia de La Construcción, 1.
[23] Lluis i Ginovart, J., Costa-Jover A., Coll-Pla, S. (2016). La determinación del concepto de homogeneidad versus resistencia en los pilares de una catedral gótica mediante técnicas no invasivas. Informes de la Construcción. Julio-septiembre 2016. Vol. 68, 543, 155. doi: http://dx.doi.org/10.3989/ic.15.119.
[24] Willis, R. (1835). Remarks on the Architecture of the Middle Ages, especially of Italy., Cambridge: Pitt Press.
[25] Willis, R. (1842). On the Construction of the Vaults of the Middle Ages. Transactions of the Royal Institute British Architects, 1: 3-13.
[26] Viollet-le-Duc, E. E. (1868). Dictionaire raisonné de l'architecture française du XIe au XVIe siècle (Vol. III). Paris: B. Bance (A. Morel).
[27] Choisy, A. (1873). L'Art de batir chez les Romains. Paris : Ducher et Cie. Retrieved from http://www.academia.edu/9953727/AugusteChoisy
[28] Choisy, A. (1883). L'art de batir chez les Byzantins. Paris : Librairies de la Sociètè Anonyme de Publications Périodiques.
[29] Puig i Cadafalch, J. (1901). HIstoria General del Arte. Escrita y editada en vista de los monumentos y de las mejores obras publicadas hasta el día, bajo la dirección dels arquitecto Don José Puig i Cadafach. Barcelona: Montaner y Simón Editores.
[30] Puig i Cadafalch, J., et alt. (1918). L'Arquitectura Romànica a Catalunya. Vol III. Barcelona: Institut d'Estudis Catalans.
[31] Puig i Cadafalch, J. (1920). L'Arquitectura Romànica a Catalunya. Barcelona: Ricard Durant i Alsina.
[32] Torres Balbás, L. (1946). Bóvedas romanas sobre arcos de resalto. Archivo Español de Arqueología, 64: 217-262.
[33] Bassegoda Musté, B. (1944). Racionalismo a ultranza en la arquitectura ojival. Separata Memorias de la Real Academia de Ciencias y Artes de Barcelona. Tercera época, núm. 504, vol. XXVII, núm. 4. Barcelona: Real Academia de Ciencias y Artes de Barcelona.
[34] Bassegoda Nonell, J. (1977). Bóvedas medievales a la romana. Separata Memorias de la Real Academia de Ciencias y Artes de Barcelona. Tercera época núm. 782. Vol. XLIII Núm. 8: 287-382. Barcelona: Real Academia de Ciencias y Artes de Barcelona.
[35] Lluis i Ginovart, J. Coll-Pla, S., Costa-Jover, A., López-Piquer (2017). Evaluation of large deformations on Romanesque masonry pillars: The case of Santa María de Arties http://dx.doi.org/10.7764/rdlc.16.3.468.

12th International Conference on Structural Analysis of Historical Constructions
SAHC 2020
P. Roca, L. Pelà and C. Molins (Eds.)

MODAL AND STRUCTURAL IDENTIFICATION OF A MULTI-SPAN MASONRY ARCH BRIDGE

PAOLO BORLENGHI[1*], ANTONELLA SAISI[1] AND CARMELO GENTILE[1]

[1] Department of Architecture, Built environment and Construction engineering (DABC)
Politecnico di Milano, Milan, Italy
Piazza Leonardo da Vinci, 32 - 20133 Milan, Italy
e-mail: {paolo.borlenghi, antonella.saisi, carmelo.gentile}@polimi.it (*corresponding author)

Keywords: Masonry bridges, Ambient vibration tests, FE model updating, Non-Destructive Inspections

Abstract. *The Olla bridge is a multi-span masonry arch bridge dating back to the second half of the 19th century. The bridge is 117 m long and includes five arches of different spans. Since no original drawings or blueprints of the bridge were found in the archives, the missing information on the geometry of the structure were retrieved through a geomatic survey, whereas the unknown structural details were assumed according to historical handbooks and similar projects. In addition, limited material samples were taken to solve typical uncertainties such as the effective thickness of arches. Subsequently, ambient vibration tests were performed, and different output-only techniques were applied to the acquired time series with the two-fold objective of identifying the dynamic characteristics of the bridge and roughly verifying the invariance of the modal parameters. Finally, all the available information were summarised in a Finite Element model, that – after the updating of uncertain parameters – turned out to be capable of reproducing the identified dynamic characteristics of the structure with a high level of accuracy.*

1 INTRODUCTION

The development of the rail transport in the 19th century involved the construction of a large number of masonry arch bridges giving impulse to the improvement of this structural typology. Consequently, masonry arch bridges were the dominant technology in bridge design until the first half of the 20th century, when reinforced concrete progressively replaced brick and stone masonry. Nevertheless, many masonry bridges are still in use today and they represent essential infrastructures for the European road and railway networks. In recent years, due to their key role and uncertain state of preservation, masonry bridges have received increasing attention from the scientific community, resulting in a series of experimental investigations and numerical studies (see e.g. [1-3]). Furthermore, as all historical constructions, masonry bridges are affected by numerous uncertainties related to material properties and construction details: when neither the original blueprints nor the documentations on repairs and interventions are available, extensive experimental surveys are needed to retrieve the actual internal morphology of the bridge (i.e. backing arrangement or effective thickness of arches).

In this context, documentary research and limited material tests, together with Operational Modal Analysis (OMA) and Finite Element Model Updating (FEMU), can be applied to reduce uncertainties and contribute in establishing a reliable numerical model. The paper summarises the investigations carried out on the Olla bridge, involving the following steps: (i) documentary research, (ii) geomatic survey, (iii) minor destructive and ambient vibration tests and (iv) FE modelling and updating.

2 THE OLLA BRIDGE

The Olla bridge (*Ponte dell'Olla* in Italian, Fig. 1a) is a multi-span masonry arch bridge built in the second half of the 19th century over the Stura river. It carries the State Route no. 21 (SS21, i.e. the roadway connecting the city of Cuneo with the French border) between the municipalities of Gaiola and Borgo San Dalmazzo in the northwest part of Piedmont, Italy. Due to its localisation, the bridge has a strategic role for the economy of the area since it is the only entry to the *Stura di Demonte* Valley for trucks and commercial vehicles.

The structure is approximately 117 m long and has a maximum height over the river of about 42 m. It is composed of five masonry arches, symmetrically distributed, with spans of 10, 20, and 25 m, respectively. Piers and abutments are in a good quality ashlar stone masonry while arches and spandrel walls are in brick masonry. The documentary research started in the archive of the local Authority that was responsible for the design (the *Genio Civile*) but the original drawings were not found. Therefore, various construction details on the internal morphology of the structure were initially assumed according to historical construction handbooks and then eventually modified in establishing the FE model.

2.1 Geometry survey

In order to obtain a complete representation of the existing structure, a topographic survey was performed in September 2018 [4] using a total station (Leica TCRA 1203) and a laser scanner (Leica C10). Hence, the survey relied on different techniques, integrating local and global measurements, ensuring a 360° coverage of the bridge complexity. The 3D model resulting from point clouds (Fig. 1b) was used to extract a series of 2D drawings from which the FE model was developed. It is worth noting that once a point cloud is available, it is possible to extract an unlimited number of 2D sections for future applications.



Figure 1: The Olla bridge: (a) View from the Stura river; (b) 3D model from the geomatic survey [4].

2.2 Historical background

Firstly, the historical analysis focused on the research of the original blueprint of the Olla bridge at the State Archive of Cuneo: unlikely, this first phase did not bring to any result. Consequently, the focus moved to the general history of the roadway to which the bridge belongs, examining the maintenance reports of the Ministry of Public Works [5] and the history of a tramway that was passing on the bridge in the first half of the 20th century [6].

The first record regarding the existence of a bridge called "Olla", between the small towns of Gaiola and Borgo San Dalmazzo, dates back to the 18th century. In that period and for one more century, the main route from the valley to the city of Cuneo was not crossing the river, so that the bridge served just as a secondary connection. In 1857 [5] – a few years before the proclamation of the Italian Kingdom – the road between Borgo San Dalmazzo and the French border was declared of national importance and a large project of renovation started, involving the construction of a new Olla bridge. The new structure was completed in 1887 [5] shortening the road and removing the difference in altitude caused by the older single-span masonry bridge (Fig. 2a). The design was carried out by the local chief engineer of the Italian Royal Corps of *Genio Civile* (public works office), Giovanni Delfino [6].

In 1912 the construction of a steam tramway between Borgo San Dalmazzo and the Stura valley was approved by the National Authority, completing the existing part that was starting from Cuneo [6]. The rails were installed in the downstream side of the bridge deck, and the tramline worked until 1948 [6], with some interruptions during the war periods.

During the Second World War, the old and the new Olla bridge were heavily damaged (Figs. 2b and 3): according to Taricco [6], both structures were detonated by the partisans on July 13th, 1944 to isolate the valley from the German army. The most recent bridge was repaired starting from September 1945 [6] but no specific records were found on the execution of the intervention. Regarding the older Olla bridge, it was abandoned, and the remains of the abutments are still visible nowadays (Fig. 1a).

In conclusion, the documentary research revealed the construction period and the Authority that was responsible for the design, as well as the collapse of the central arch with numerous historical pictures. Nevertheless, a large number of missing information regarding the structural details remain unsolved.

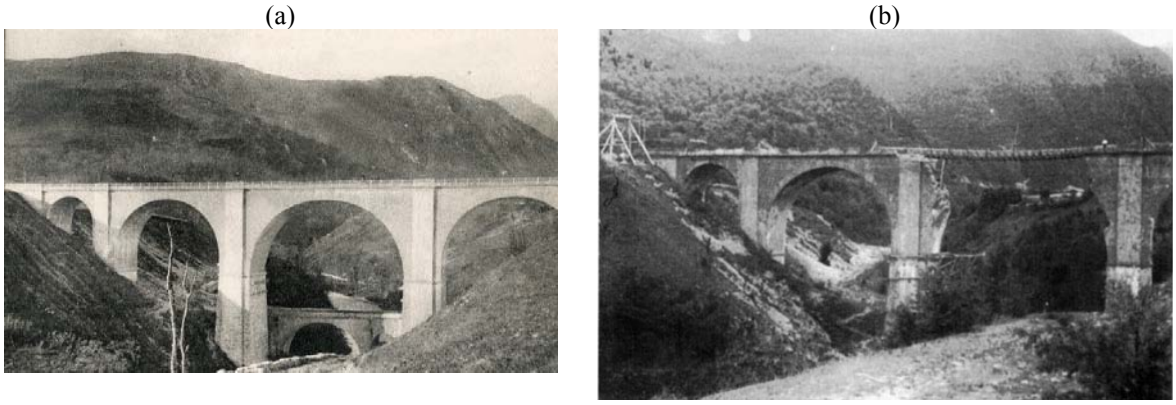


Figure 2: Historical views of the investigated structure before (a) and after (b) the damages of 1944 [6].

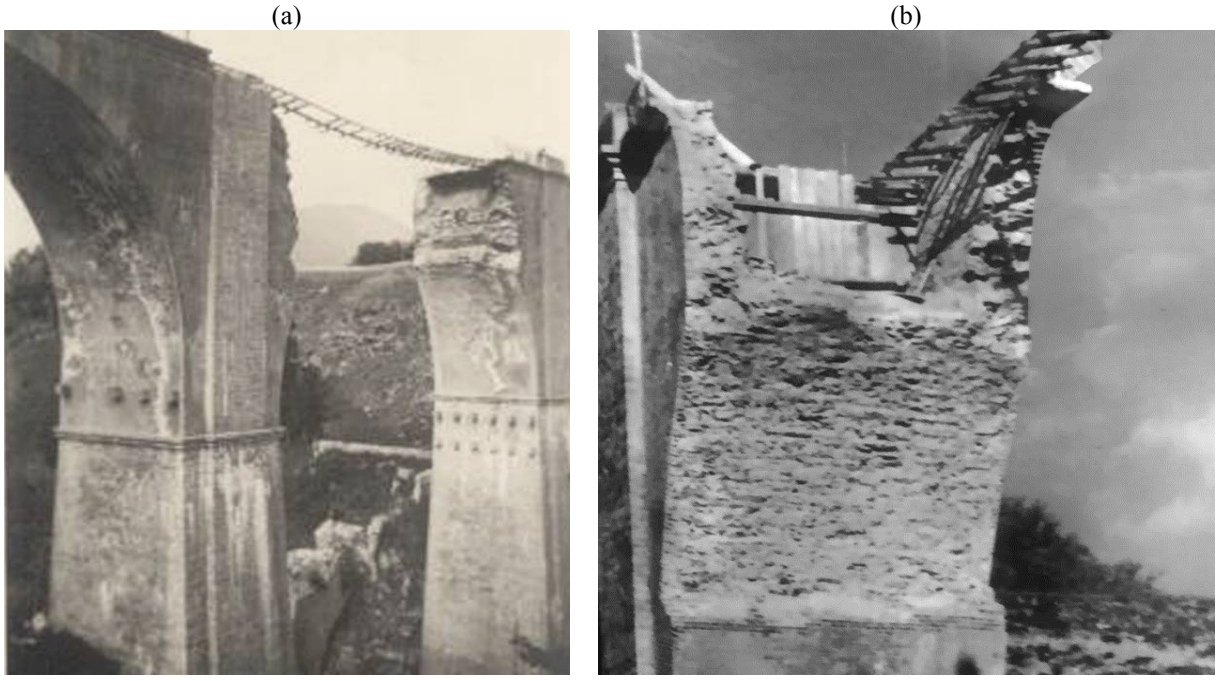


Figure 3: Views of the damages occurred in 1944, before (a) and after (b) the complete detachment of the collapsed arch.

2.3 Structural details and internal morphology

Evaluating the contribution of backing and spandrel walls to the load-bearing capacity of a masonry bridge is often a complex task. The structural role of these elements can vary substantially according to their geometric arrangement and material characteristics.

To overcome the missing knowledge on structural details and internal morphology, the following steps were taken: (i) assuming a geometrical configuration (height and inclination of the backing and thickness of the spandrel walls) according to contemporary construction handbooks and similar projects, (ii) verifying some of those assumptions with a limited number of coring tests, and (iii) including the material property of the backing among the updating parameters in the FEMU procedure.

In the case of Olla bridge, the well-known construction handbook of Curioni [7], published in 1873, and the projects of masonry viaducts published on the Journal of Public Works (*Giornale del Genio Civile* [8]) were adopted as reference. This choice was motivated by both the time of publication and the geographical proximity, suggesting a remarkable affinity with the investigated bridge. Generally, when the distance between the arch and the deck was quite high, the thickness of the spandrels had a variable section, wider near the arch [7]. In addition, the height of the backing – in the pier axis – was equal to 2/3 of the arch radius [7] but it can variate considerably according to the designer. Fig. 4 shows two examples of masonry viaducts published in [8] with a backing height almost equal to arch radius.

Furthermore, from the historical pictures taken after the collapse of the central arch (Fig. 3) it is possible to verify the presence of a solid backing that prevented the overturning of the central piers from the unbalanced trusts coming from the lateral arches (both with spans equal to 20 m). Regarding the collapse mechanism, it is worth noting that: (i) at first the arch did not

collapse in the ideal skewback at the end of the pier (Fig. 3a), while (ii) subsequently the remaining part of the arch on the Gaiola side collapsed separately in respect to the backing (Fig. 3b). These observations underline the importance of better understanding the role of backing and spandrels in the structural response of the Olla bridge.

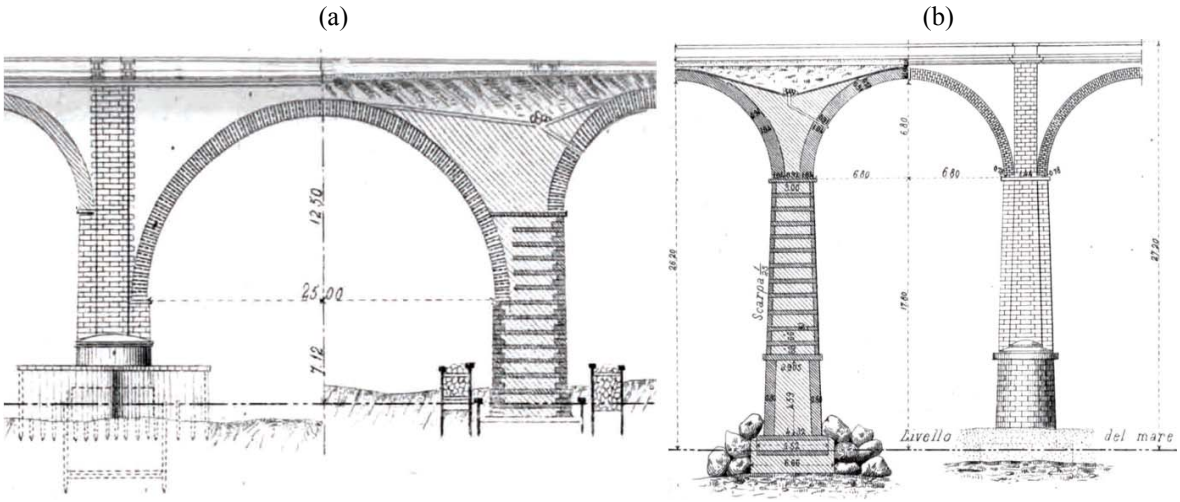


Figure 4: Historical drawings (1879) of the railway viaducts of Zoagli (a) and Sori (b) [8].

3 EXPERIMENTAL SURVEY

The experimental survey conducted on the Olla bridge included Ambient Vibration Tests (AVTs) and Minor Destructive Tests (MDTs). Particularly, the AVT was performed with the objective of identifying the modal parameters of the structure (i.e. natural frequencies and mode shapes) and verifying their time invariance. Subsequently, the identified frequencies were used to correct the numerical model of the bridge within a FEMU procedure. The MDTs consisted in a limited number of coring tests with the aim to obtain information on the effective thickness of arches and spandrels and material type for the fill. Due to the limited extension of the core drill machine, no information on the backing was obtained.

3.1 Ambient vibration tests and modal identification

The AVT was conducted on July 31st, 2018 with one lane open to traffic; the acceleration responses of the bridge were measured in 11 selected points belonging to the downstream side of the deck. As represented in Fig. 5a, the sensor layout was designed to guarantee a complete representation of the lateral mode shapes (11 transversal sensors), and a partial reconstruction of vertical and longitudinal ones, deploying 3 vertical sensors placed in the centre of the major arches, where the maximum modal displacements were expected.

During the test the following devices were used: (a) an acquisition laptop; (b) a multi-channel acquisition system with 4 NI9234 modules (24-bit resolution, 102 dB dynamic range and anti-aliasing filters); (c) 14 WR731A piezoelectric accelerometers (10 V/g sensitivity and ±0.50g of peak acceleration); (d) 14 power unit amplifiers (WR P31). The amplifiers were aimed at enhancing the performance of the acquisition chain, providing a constant current to power the internal amplifier, signal amplification and selective filtering. The sampling

frequency adopted was equal to 200 Hz, which is more than enough for the considered structure whose dominant frequencies are below 10 Hz. Therefore, low pass filtering and decimation were applied to down-sample the data to 40 Hz, obtaining a Nyquist frequency of 20 Hz. The acquired data were then divided in 4 dataset of 2400 s to verity the invariance of the identified modal parameters over the testing time.

The extraction of the modal parameters was performed by applying three well-known algorithms: the Frequency Domain Decomposition (FDD [9]), the data-driven Stochastic Subspace Identification (SSI-data [10]) and the Covariance-based Stochastic Subspace Identification (SSI-Cov [10]). The first two techniques are available in the commercial software ARTeMIS [11] whereas the third one was developed in a previous research [12].

Overall, 5 lateral and 3 vertical vibration modes are identified in the frequency range of 0-10 Hz. Figure 5b shows the first singular value (SV_1) lines obtained by applying the FDD technique to the vertical (blue curve, V) and lateral (red curve, L) signals collected in one dataset (dataset 1). The first three peaks in the $SV_{1\ lat.}$ curve – corresponding to lateral modes L_1, L_2 and L_3 – are associated with smaller peaks in the $SV_{1\ vert.}$ curve, that refers to the vertical direction. Conversely, the other local maxima (corresponding to modes V_1, V_2, L_4, L_5 and V_3) are associated with a unique dominant component of motion.

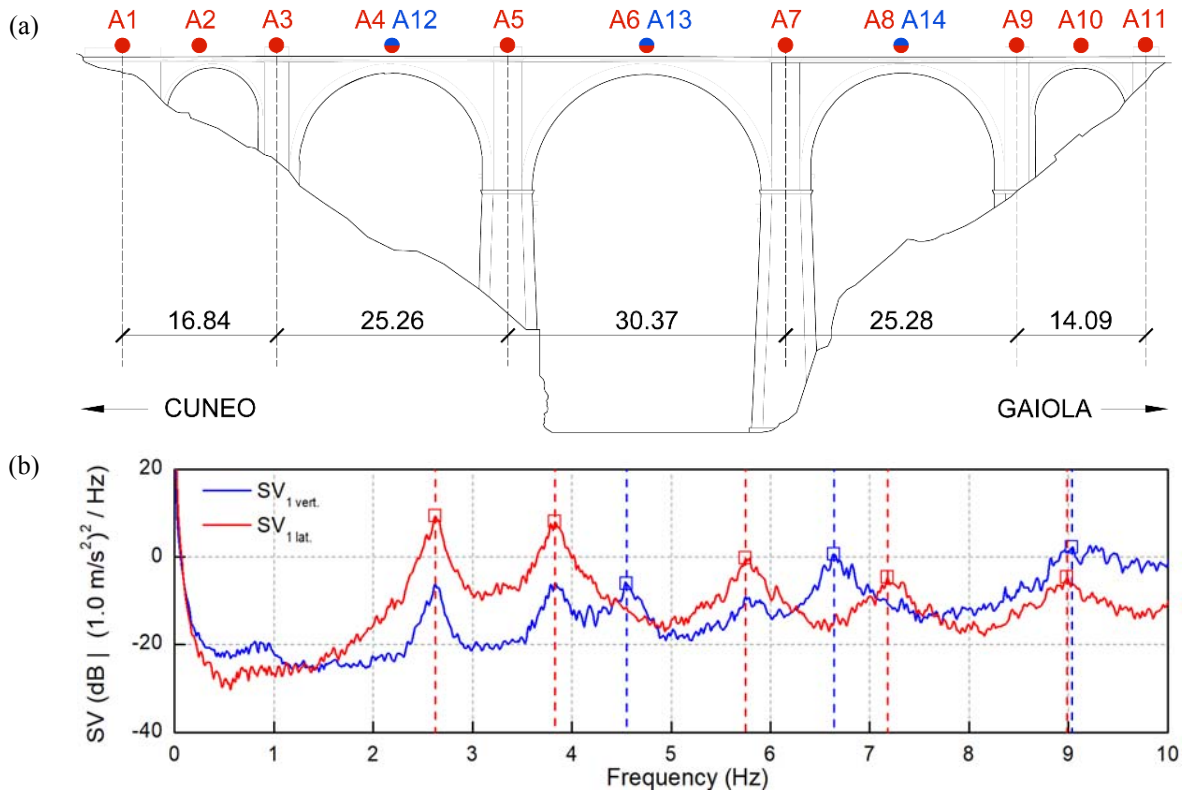


Figure 5: (a) Sensors layout during the AVT (dimensions in m): the red and blue dots refer to transverse and vertical sensors, respectively; (b) Comparison between the first singular value lines of lateral ($SV_{1\ lat.}$) and vertical ($SV_{1\ vert.}$) responses and identification of modal frequencies (dataset 1).

The application of different output-only techniques (i.e. FDD, SSI-data and SSI-Cov) to the different datasets resulted in remarkably consistent natural frequencies and mode shapes, suggesting the invariance of the dynamic behaviour of the structure over the testing time. It is worth mentioning that during the test, the traffic on the open lane was quite intense. To exemplify the low variations of natural frequencies, the identification of lateral modes (SSI-Cov) in four different datasets are reported in Tab. 1 and Fig. 6. Furthermore, the identified mode shapes are shown in Fig.7.

Table 1: Natural frequencies identified (SSI-Cov) in 4 different datasets (lateral modes).

Mode		$f_{SSI\text{-}Cov}$ (Hz)					
No.	Type	Dataset 1	Dataset 2	Dataset 3	Dataset 4	Mean (Hz)	St. dev. (Hz)
1	L_1	2.613	2.604	2.619	2.641	2.619	0.013
2	L_2	3.832	3.835	3.839	3.836	3.835	0.003
4	L_3	5.777	5.802	5.780	5.808	5.792	0.013
6	L_4	7.213	7.223	7.239	7.224	7.225	0.009
7	L_5	8.971	-	8.993	9.012	8.992	0.017

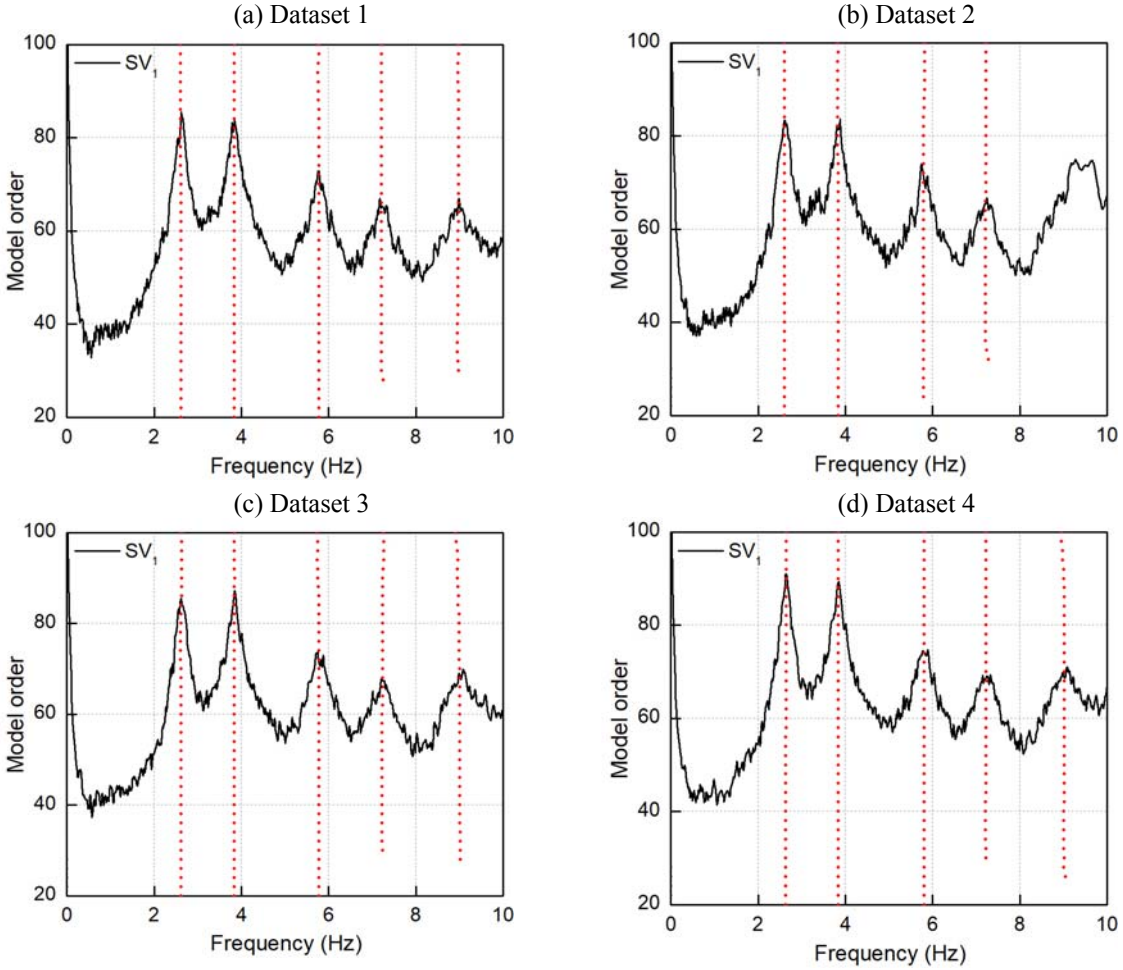


Figure 6: First singular values line (FDD) and alignments of stable poles (SSI-Cov) of different datasets: (a) dataset 1; (b) dataset 2; (c) dataset 3; (d) dataset 4.

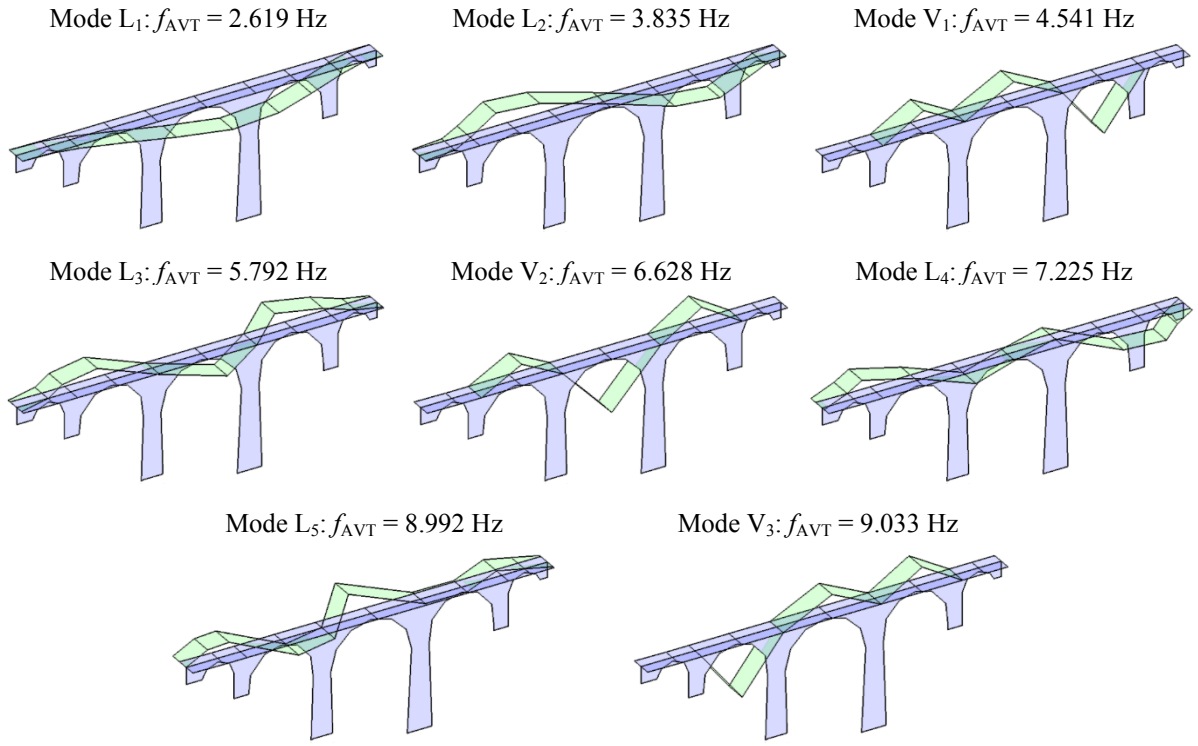


Figure 7: Identified vibration modes (L = dominant lateral, V = dominant vertical).

3.2 Coring tests

The coring tests on the Olla bridge were executed in Autumn 2018. Six coring samples were taken from the following elements: 2 on the arches, 2 on the spandrels and 2 on the deck. The tests revealed that the arches are constituted only by brick masonry while the spandrels are a mixed of stone and brick masonry. The thickness of the asphalt, over the fill, is equal to 20 cm.

4 FINITE ELEMENT MODELLING AND UPDATING

The structural contribution of spandrels and backing is often not clear and hard to determine. Therefore, the standard approach in modelling masonry bridges considers the arches as the main load-bearing structure [1], neglecting the role of the other parts that form the deck (spandrels, backing and fill).

In a previous study [13], a simplified model was developed for the Olla bridge to clarify the contribution of non-structural components in the bridge dynamic response under operational conditions. The simplified model emphasised the importance of considering the stiffening effect given by the elements above the arch. Nevertheless, due to the simplified nature of the model it was impossible to match both lateral and vertical response. Consequently, the three-dimensional FE model herein presented reproduces as closely as possible the actual geometry of the bridge. Therefore, the spandrel walls, backing and fill have been modelled along with arches, abutments and piers; the material properties of each structural element are updated according to the adopted system identification procedure and a perfect connection between the different components is assumed.

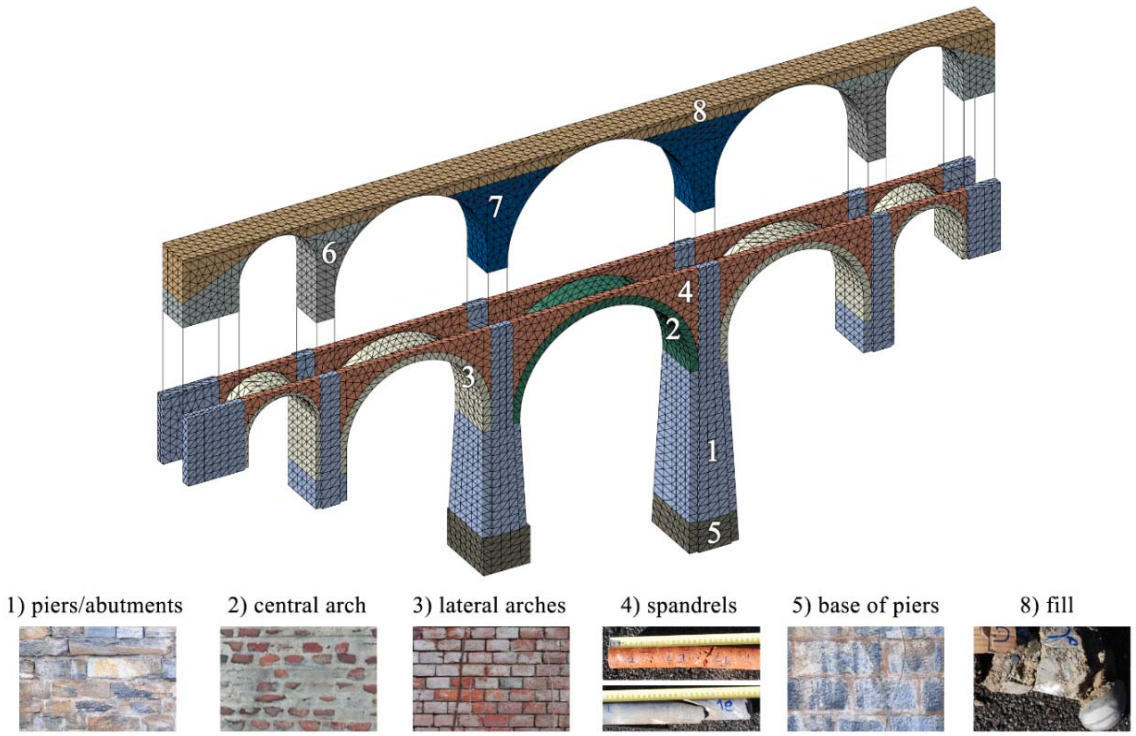


Figure 8: FE model of the Olla bridge with the indication of different materials.

The 3D model was developed with the FE code ABAQUS using the ten-node tetrahedral elements (C3D10). A relatively large number of elements were employed to obtain a regular distribution of masses, a good description of geometrical details, and to avoid frequency sensitivity to mesh size. Overall, the numerical model consists of 45604 tetrahedral elements with 211818 degrees of freedom and an average mesh size of 1.15m (Fig. 8).

Once the geometry of the numerical model is established, the selection of the structural parameters to be updated is the next key issue. To prevent the ill-conditioning of the inverse problem and to improve the robustness of the updated parameter estimates, the following aspects were considered: (i) the number of updating variables was kept smaller than the experimental parameters used as targets; (ii) only the uncertain structural parameters were updated; (iii) the sensitivity of natural frequencies to the different parameters was checked and low-sensitivity structural parameters were not updated.

Overall, 8 regions with constant material properties were identified based on visual inspections and coring tests (Fig. 8): (1) piers and abutments; (2) the central arch (reconstructed in 1945); (3) lateral arches; (4) spandrels; (5) base of central piers; (6) backing over the abutments and the lateral piers; (7) backing over the central piers (partially reconstructed in 1945); (8) fill.

In addition, the following assumption were adopted: (a) the effect of soil-structure interaction was neglected, (b) all the materials were considered isotropic with constant mass density and Poisson's ratio (see Tab. 2), (c) the spandrels were assumed 1.0 m thick, and (d) the Young's modulus of fill material was not adjusted due to its low sensitivity. In view of the clear presence of superficial rocks at the river level, the base nodes of piers and abutments were assumed pinned. Similarly, the longitudinal translation of the abutments was restrained.

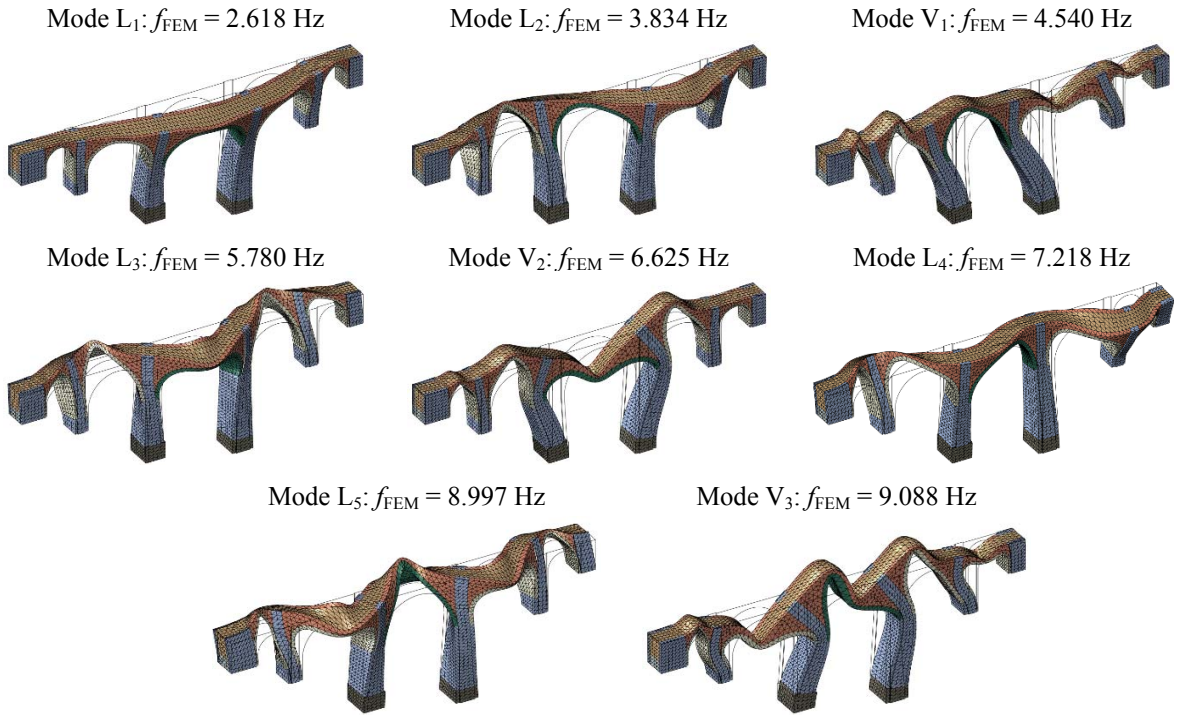


Figure 9: Lateral (L) and vertical (V) vibration modes of the optimal (updated) FE model.

Table 2: Summary of the identified structural parameters (* indicates the non-updated parameters)

		Assumed properties		Base model	Refined model
No.	Structural elements	ν (-)	γ (kN/m^3)	E (GPa)	E (GPa)
1	Piers / abutments	0.15	20	16.50	16.10
2	Central arch	0.15	17	4.50	7.73
3	Lateral arches	0.15	17		3.23
4	Spandrels	0.15	19	15.00	16.85
5	Base of central piers	0.15	21	22.00	27.49
6	Backing lateral piers / abut.	0.15	18	2.00	1.38
7	Backing central piers	0.15	18		4.56
8	Fill *	0.3	16	0.30	0.30

Table 3: Comparison between experimental (SSI-Cov) and numerical frequencies.

Mode		Exp. (SSI-Cov)	Base model		Updated model	
No.	Type	f_{AVT} (Hz)	f_{FEM} (Hz)	DF (%)	f_{FEM} (Hz)	DF (%)
1	L_1	2.619	2.56	2.2	2.621	-0.07
2	L_2	3.835	3.83	0.3	3.828	0.18
3	V_1	4.541	4.53	0.2	4.541	-0.01
4	L_3	5.792	5.80	-0.2	5.793	-0.02
5	V_2	6.628	6.14	7.4	6.629	-0.02
6	L_4	7.225	7.45	-3.2	7.225	-0.01
7	L_5	8.992	9.17	-2.0	9.044	-0.57
8	V_3	9.033	8.64	4.3	9.062	-0.32
	DF_{ave} (%)	-	-	2.46	-	0.15
	DF_{max} (%)	-	-	7.35	-	0.57

An initial FE model (Base model) was developed to check the similarity between experimental and numerical modal parameters. As shown in Tab. 2, the Young's modulus of arches and backing was assumed equal to 4.5 GPa and 2.0 GPa respectively. Tab. 3 illustrates the imperfect correlation with the experimental results, showing a maximum frequency discrepancy (*DF*) of 7.4%. However, the one-to-one correspondence of the experimental-numerical modes seems to provide a sufficient verification to the main model assumptions.

The adopted FEMU procedure was implemented in MATLAB environment and it is based on the Douglas-Reid method [14] with the Particle Swarm Optimisation (PSO) algorithm: the updating parameters are iteratively corrected in a constrained range until a stable minimum solution for an objective function is found. Particularly, the following objective function was adopted:

$$J(\boldsymbol{x}) = \frac{100}{n}\sum_{i=1}^{n}\left|\frac{f_i^{AVT} - \widehat{f}_i(\boldsymbol{x})}{f_i^{AVT}}\right| \tag{1}$$

where f_i^{AVT} are the i-th experimentally identified natural frequency and $f_i(\boldsymbol{x})$ are the *i*-th polynomial approximations [14] of the numerical natural frequencies, expressed as functions of the $\boldsymbol{x}$ updating parameters.

Tab. 2 lists the optimal estimates of the uncertain parameters of the model. The differences between the elastic moduli of the central and lateral arches, as well as the one of the backing, are motivated by the different years of construction: as shown by the historical analysis, the central arch was rebuilt in 1945. As demonstrated by the coring tests, the spandrels are made of bricks externally and stone internally, justifying the high values elastic modulus obtained. Finally, the base of the central piers is built in a better-quality stone masonry in respect to the rest of the piers and, moreover, the optimal elastic modulus conceivably accounts for the stiffening effect provided by the compacted soils surrounding the piers.

5 CONCLUSIONS

The paper focuses on the OMA-based structural identification based of the Olla bridge of Gaiola, Piedmont region, northwest Italy. The occasional brick fall from one of the arches had caused concerns on the state of preservation of the structure by the local Authorities, motivating the following research programme. The investigations included documentary research, geometric survey, minor destructive and ambient vibration testing, and FE modelling and updating. The following conclusions can be drawn:

1) The documentary research revealed the construction period and designer, along with a series of historical pictures of the collapsed central arch in 1944;
2) During the AVT, performed with one line open to traffic, 5 lateral and 3 vertical vibration modes were identified in the frequency range of 0-10 Hz;
3) Notwithstanding the initial model represented accurately the geometry retrieved from geomatic survey, a relatively poor correlation with the actual structural response was obtained (DF_{ave} = 2.46%, DF_{max} = 7.35%);
4) On the contrary, as shown in Fig. 9, applying the developed FEMU procedure and considering the effects of the reconstruction of 1945, an excellent correlation with the experimental results was obtained (DF_{ave} = 0.15%, DF_{max} = 0.57%), highlighting the importance of backing and spandrels in the dynamic response of masonry bridges.

To complete the structural assessment of the Olla bridge, a full-scale load tests and additional minor-destructive and non-destructive tests on materials should be performed in near future.

Acknowledgements. The support of ANAS (Struttura territoriale Piemonte e Valle d'Aosta) is gratefully acknowledge. Sincere thanks are due to M. Cucchi and M. Iscandri (LPMSC, Politecnico di Milano) who assisted the authors in conducting the field tests.

REFERENCES

[1] Brencich, A. and Morbiducci, R. Masonry arches: Historical rules and modern mechanics. *Int. J. Archit. Herit.* (2007) **1**(2):165-189.

[2] Costa, C., Ribeiro, D., Jorge, P., Silva, R., Arêde, A. and Calçada, R. Calibration of the numerical model of a stone masonry railway bridge based on experimentally identified modal parameters. *Eng. Struct.* (2016) **123**:354-371.

[3] Scozzese, F., Ragni, L., Tubaldi, E. and Gara, F. Modal properties variation and collapse assessment of masonry arch bridges under scour action. *Eng. Struct.* (2019) **119**:109665.

[4] Fassi, F. and Achille, C. *Relazione delle attività di rilievo topografico e laser-scanner: Ponte dell'Olla località Gaiola (CN)* (in Italian). Technical report, Politecnico di Milano (2018).

[5] Ministero dei lavori pubblici. *Relazione sul mantenimento delle Strade Nazionali durante il periodo dal 1° Luglio 1887 al 30 Giugno 1888* (in Italian). Tipografia Eredi Botta, Rome (1889).

[6] Taricco, S. *Il tramvai di Demonte: ricordi di una storia passata* (in Italian). Mauro Fantino Editore, Borgo San Dalmazzo (2001).

[7] Curioni, G. *L'arte del costruire: costruzioni civili, stradali ed idrauliche* (in Italian). Augusto Federico Negro Editore, Turin (1873).

[8] *Giornale del Genio Civile. Tavole* (in Italian). Istituto Poligrafico dello Stato, Roma (1879).

[9] Brincker, R., Zhang, L. and Andersen, P. Modal identification of output-only systems using frequency domain decomposition. *Smart Mater. Struct.* (2001) **10**(3):441-445.

[10] Peeters, B. *System identification and damage detection in civil engineering*. Ph.D. Thesis, Katholieke Universiteit Leuven, Belgium (2000).

[11] Structural Vibration Solutions (SVS). ARTeMIS Extractor 2010. Aalborg, Denmark (2010).

[12] Cabboi, A., Magalhães, F., Gentile, C. and Cunha, A. Automated modal identification and tracking: Application to an iron arch bridge. *Struct. Control Health Monit.* (2017) **24**(1): e1854.

[13] Borlenghi, P., Saisi, A. and Gentile, C. Preliminary Structural Assessment of a Multi-span Masonry Arch Bridge. In: *Arêde A. and Costa C. (Eds.)*: Proceedings of ARCH 2019, Structural Integrity 11 (2020). Springer, Cham.

[14] Douglas, B. M. and Reid, W. H. Dynamic tests and system identification of bridges. *J. Struct. Div. ASCE* (1982) 108(10):2295-2312.

12th International Conference on Structural Analysis of Historical Constructions
SAHC 2020
P. Roca, L. Pelà and C. Molins (Eds.)

MONITORING DEFORMATIONS OF A WOODEN CHURCH TOWER BY LASER SCANNING

LINH TRUONG-HONG[1*], RODERIK LINDENBERGH[1], PIETER WOUDENBERG[2], WOLFGANG GARD[2], JAN-WILLEM VAN DE KUILEN[2,3]

[1]Department of Geoscience and Remote Sensing, Faculty of Civil Engineering and Geosciences
[2]Department of Engineering Structures, Faculty of Civil Engineering and Geosciences
Delft University of Technology
Stevinweg 1, 2628 CN Delft, The Netherlands
[3]Chair of Wood Technology, Technical University of Munich
Arcisstraße 21, 80333 München, Germany
e-mail: l.truong@tudelft.nl (*corresponding author)
email: {r.c.lindenbergh,w.f.gard, j.w.g.vandekuilen} -@tudelft.nl
email: pieter.woudenberg@hotmail.com

Keywords: Point Cloud, Deformation, Monitoring, Ransac, Segmentation, Heritage Structure, Wooden church tower

Abstract. *Churches are part of heritage structures that take an important role in Europe´s cultural identity. As such, these structures must be protected to prevent catastrophic collapse and any damage must be reported timely to establish planning to maintenance and restoration. This can be achievable when the churches are monitored periodically with regular intervals. However, this monitoring strategy has not been available in most of the Europe's churches for a number of reasons, complexity of the structures and limited budget are just two of them. Laser scanning has been widely used in capturing rich three-dimensional (3D) topographic data of visible surfaces of a structure with high accuracy. This paper presents a methodology to determine the shape and possible deviation from verticality of the church's tower for monitoring deformation using a terrestrial laser scanner. The 500-year old wooden tower of St. Bavo Church in Haarlem, Netherlands is selected as a case study. First, point clouds of the tower captured from different views are registered into the same coordinate system. Second, a RANSAC method is employed to extract point clouds of a whole façades of the tower. Next, a point and surface-based method is proposed to compute the deformation of the surface from its data points. The results indicate that there is slightly different deformation between the tower facades in the same story and in neighbour stories. Moreover, the maximum total relative deformation at Story 7 of the tower by 0.63m.*

1 INTRODUCTION

Monitoring of structures is becoming an important task allowing to discover deficiencies, movements, rotations and any time related effects, allowing to better protect the structures and to predict and prevent possible adverse events. Common methods are based on measured signals from sensors (e.g. accelerometers, deformometers) or on measured discrete points by using

digital levelling and total stations. However, for heritage structures, non-contact methods are preferable because of cultural value restrictions, that prohibit any structural alterations. By using traditional surveying equipment (e.g. digital levelling, total station), resulting deformations of structures are based on a point-wise approach. This requires high accuracy of the measuring devices. However, with such methods, as often only a few points on the structure can be measured, the deformation may not fully reflect the actual condition of the structure. As such, assessment results must only be interpreted by experienced inspectors.
Laser scanning has appeared as one of the best available technologies to capture details of structures' surfaces quickly, efficiently and accurately. The accuracy of a single point that can be achieved is about a millimetre, whereas it can be up to a centimetre for registered points coming from multiple scanning stations. Laser scanning has been widely used in various applications, e.g. finite element mesh generation [1], structural assessment [2, 3] and deformations [4]. In terms of using laser scanning for deformation measurements, the accuracy of registered points may not fully satisfy the requirements, but surface-wise methods are often used to determine the surface deformation based on a point cloud of the surface. Such approaches can compensate the accuracy of the point cloud by exploring correlations between the points, which allows to define an extent of a (surface) deformation or a surface anomaly in an accurate and reliable way [5]. In this paper, a methodology is presented to measure deformations of the wooden tower of St. Bavo Church in Haarlem, the Netherlands, by using terrestrial laser scanning data. Main challenge of this study is that the long-term behaviour of the wooden tower has resulted in non-uniform deformations in the entire structure, which requires to determine deformations of individual surfaces. Moreover, as complexity of the tower's geometry is high, exterior planar surfaces of the tower are difficult to extract from massive point clouds.

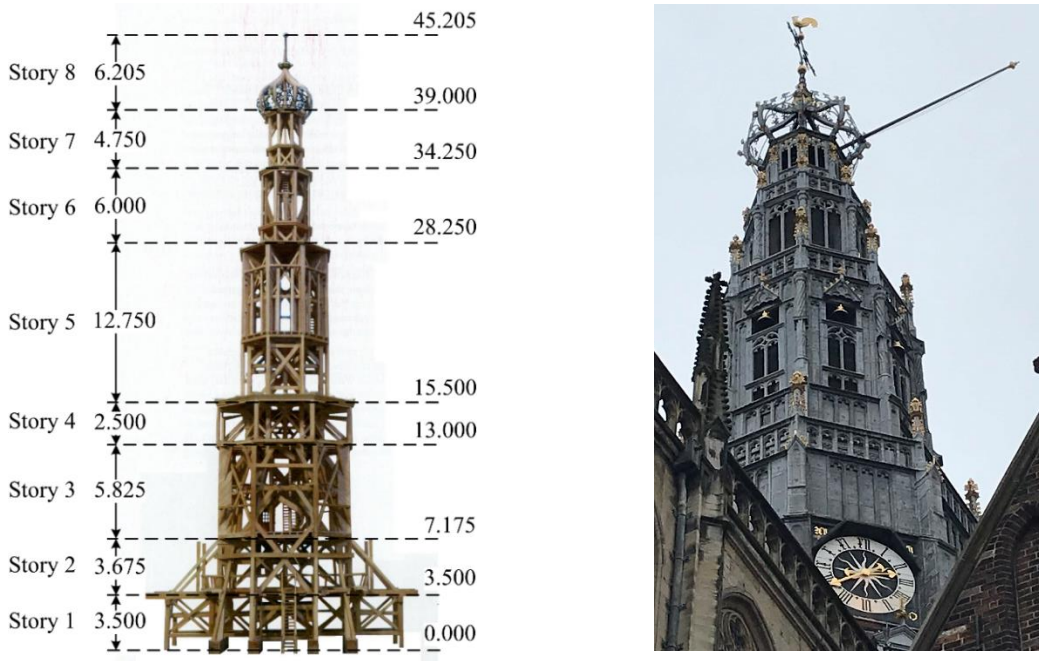
2 RELATED WORKS

Laser scanning has been commonly used to capture surfaces of structural components for structural engineering's purpose, e.g. deformation measurement, surface damage detection and finite element generation. A systematic overview of a wide range of applications of laser scanning in heritage and civil structures was recently published at [6]. This survey is restricted to deformation measurements of the heritage structures.

González-Aguilera el at. [7] measure deformation of the Mediaeval Wall of Avila (Spain) by analysing a point cloud of the wall acquired by a Trimble GX200 laser scanner. Surfaces of the wall are extracted by using a planar surface fitting and then multiple vertical and horizontal cross-sections of the fitted surfaces are used to determine wall deformation between different epochs. Also using a surface-based method, in measuring deformation of the Garisenda and Asinelli towers in Bologna (Italy), Pesci et al. [8] propose two reference surfaces, which are (i) the vertical surface through the base of the towers, and (ii) the best fitting plane of a point cloud of a surface. Deformation is herein the distance from the points to the reference points. Additionally, Bonali et al. [9] determine deformation of the Cantalovo church (Italy) as distances from point clouds to surfaces to its fitting primitive.

In measuring deformations of the Asinelli tower in Bologna, Bertacchini et al. [10] slices the point cloud of the tower in the elevation direction at an interval 10cm and computes the centroid of each horizontal slice, which is considered as the point of a barycentre axis for determining deviation from verticality (out-of-plumb) of the tower [10]. Similarly, Bhadrakom and Chaiyasarn [11] reconstruct the central line of a tower of the Ayutthaya temples (Thailand) by measuring a tilt angle. A point cloud of the tower is separated in multiple horizontal slices along elevation. As the tower shape is a cylinder, the center points of the horizontal slice are determined as the centre of a fitting cylinder. The strategy using a central line to determine a deformation is also applied by Muszynski and Milczarek [12] when they measure the inclination of chimney's axis.

Although those methods can determine deformations of historic structures, they still have some drawbacks. First, methods-based fitting surface through all points of the façade may not be applicable for structures subjected to non-linear or multi-linear deformations along the elevation of the façade. Moreover, using the best fitting surface as the reference surface may include an error of data acquisition and registration, and existing damage in the surface, which lead to relative low accuracy of the reference. Second, using a point cloud of horizontal slices to determine the central line is applicable only when the data points cover major surfaces of the section. In addition, when a small damage is available on the cross-section, a change of the centre point compared to one from an undamaged cross-section may not be detected because the centre point determination is dominated by a large amount of the points on an undamaged area. Moreover, when the structure is subjected to a large deformation, the horizontal slice is not perpendicular to the central line of the structure, which means the centre points of the horizontal slice is slightly offset the centre line. Therefore, this paper proposes a point and surface-based method to analyse a point cloud of a wooden tower of a heritage church to monitor its deformation.



a) A 1:25 scale of the timber frame b) A photo of the tower

Figure 1. The wooden tower of St. Bravo church in Haarlem, The Netherlands

3 CASE STUDY

The St. Bavo church in Haarlem, Netherlands was built in 1370 and completed in 1520, with a total height of 49m excluding the tower [13]. The church was made from stone while the European Oakwood was used to build the current tower, which exterior surfaces of the tower were covered by the lead cladding. Figure 1 shows a skeleton and exterior texturing surfaces of the wooden tower. The skeleton model was made based on hand measurements.

4 PROPOSED METHODS

A goal of this study is to determine the shape and possible deviation from verticality of the wooden tower of the St. Bavo Church, which is then used for monitoring its deformation. The proposed method consists of 3 steps as shown in Fig. 2. Step 1 and 2 extract point clouds of surfaces representing octagon facades of the tower, which are done using as-built tools in software, while the proposed automatic algorithm is developed to compute deformation of each surface of the tower (Step 3).

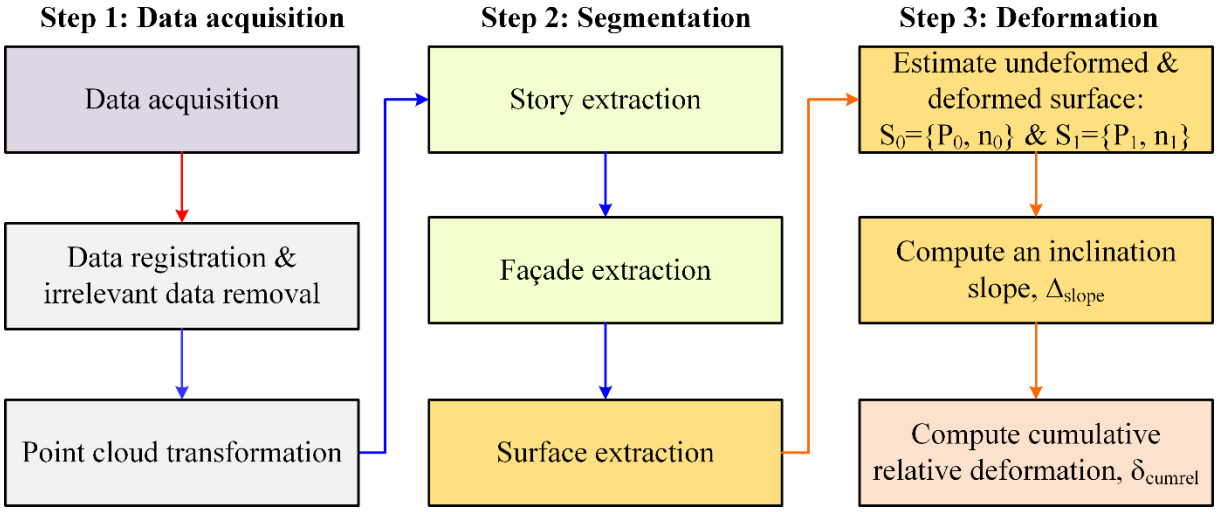
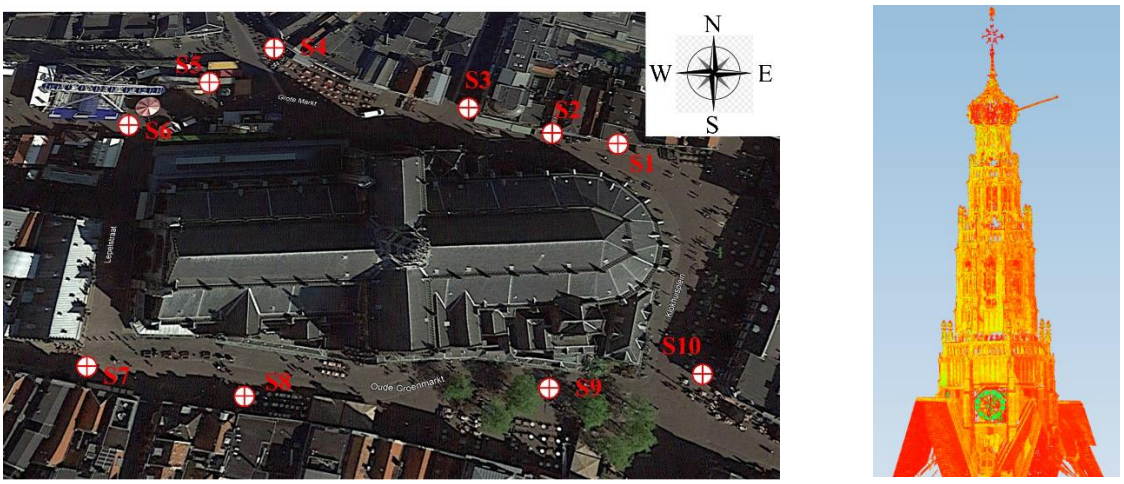


Figure 2. Proposed workflow for deformation measurement

4.1 Data acquisition

Geometric data of exterior surfaces of the tower are acquired by a Leica ScanStation P40 on Feb. 2019. This scanner was selected because it can capture visible surfaces at high details quickly and accurately from a long distance. A Leica ScanStation P40 has a maximum scanning range at 270m and an angular accuracy of 8 seconds of arc in both vertical and horizontal [14]. However, due to the complexity of the church itself and a limited budget, only parts of the exterior surfaces of the tower could be captured from the ground level. During data acquisition, a sampling step of 0.8mm at a range of 10m was used, which translates to an average sampling step of 6.2mm on the surface for an average scanning distance of 55.5m from the ground level. A total of 10 scanning stations was established to maximize data coverage (Fig. 3a). A total of 57.64 million acquired points represent the tower.

To register point clouds from 10 scanning stations, 4.5inches circular black-white artificial targets were used as mutual references between 2 scanning stations. The registration process was done within the Leica Cyclone software [15] with the registration error about 5mm. However, during data acquisition, although only parts of the tower was selected to capture, the overlap between scans from different stations and irrelevant surfaces are often available. As such, irrelevant surfaces were manually cleaned within the Leica Cyclone software [15]. Moreover, point density is linear proportional to the scanning range, which can cause a negative impact on surface extraction because of un-even point distribution. In addition, as dense data points in overlap areas may not be necessary in determining deformations, the point cloud is down-sampled with the distance between two adjacent points of no more than 5mm, which also reduces intensive computation in data processing. This reduced the initial scanning data set from 57.64 million points to 22.44 million points. Finally, the point cloud in the scanning coordinate system (Fig. 3b) is translated to a tower coordinate system (Fig. 1a), which means the elevation of the story-based point cloud matches the elevation on the sketched skeleton model (Fig. 1a).



a) Locations of the scanning stations b) A point cloud of the tower

Figure 3. Data acquisition for the tower of the St. Bravo Church

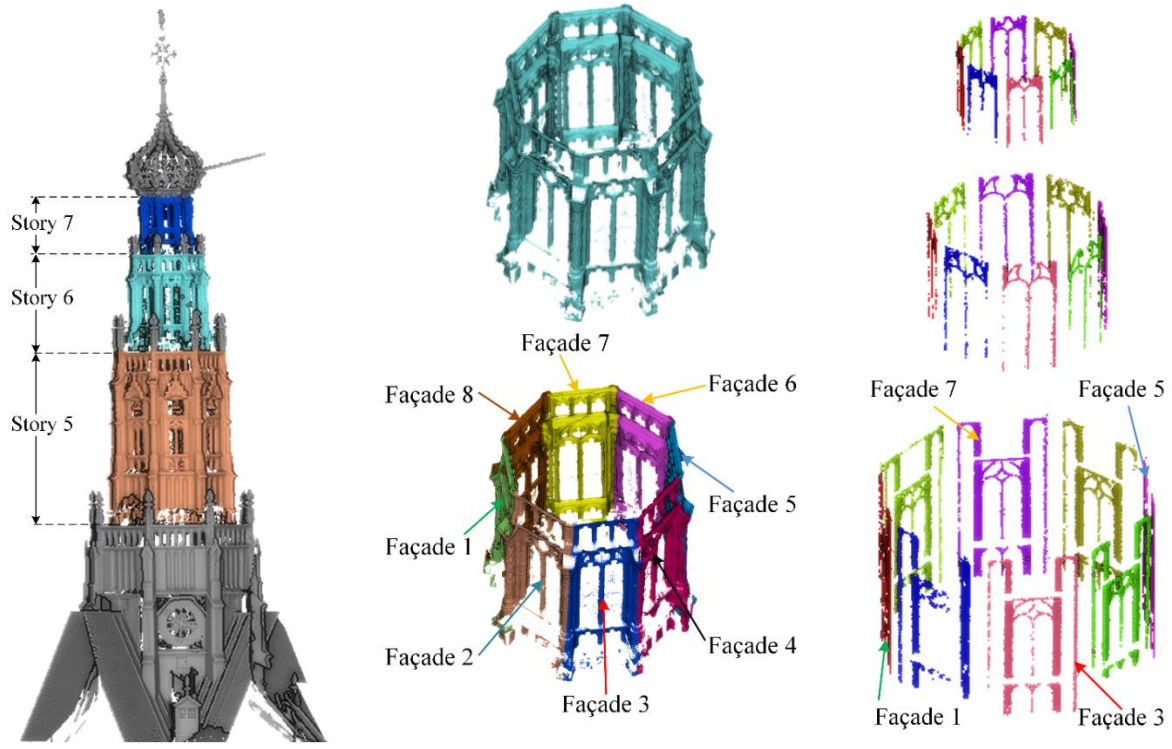
4.2 Segmentation

Well-known segmentation methods for point clouds are region growing-based methods [16, 17] and Random Sample Consensus (RANSAC) methods [18]. However, as region growing based methods are time consuming and difficulty to select appropriate parameters to segment surfaces of the complex structures like this tower, the RANSAC method efficient in extracting planar surfaces is selected in this study. The RANSAC method starts randomly to select a number of points to generate a hypothesis close to a truth geometric model, and the hypothesis is then evaluated based on the number of inlier points, which are the points having an error, which is commonly Euclidian distance, less than a threshold. The final estimation model is the model having the largest number of the inlier points.

As the tower is made from wood, its behaviour may not be fully rigid. That implies a deformation of each surface/facade in each story and of each story are different. As such, surfaces on the octagon façades of each story are needed to extract. However, if the RANSAC method is applied on the data set of the tower, the desired results may not be obtained because the point clouds of different stories may impact to evaluate a local surface of a façade. Moreover, using the point cloud of the tower as a whole input data for segmentation is unnecessary since in this case the RANSAC method must process a large data set to extract the façade surfaces.

As such, the point cloud of each story is first manually extracted based on the elevations of the bottom and top of the story (Fig. 4a), and then the point cloud of each façade for each story was manually separated through the columns between the facades (Fig. 4a and b). This work was done within CloudCompare software [19]. Notably, although this work is manually, it does not affect the façade surface extraction. Finally, the RANSAC method proposed by Schnabel et al. [18], which is implemented in CloudCompare [19], is selected to extract planar surfaces. The segmentation is required to define three important input parameters: (1) the minimum number of points to define the final model - *min_ptc*, (2) the maximum distance from the point to the model ε_{max}, and (3) the deviation of points' normal vectors to the model normal at the points -

α. These values are respectively pre-defined as 300 points, 0.01m and 5 degrees. Although the RANSAC method can extract planar surfaces efficiently, a resulting segment may contain several objects' surfaces, so-called spurious surfaces. This issue can be eliminated by implementing a connected component labelling [20] to cluster the points of the segment, in which the distance between the points in the cluster is no larger than 0.2m. The final resulted segments for each façade for deformation measurement are shown in Fig. 4c.



a) Point clouds after registration and cleaning

b) Point cloud of Story 6 (top) and its façades after separation (bottom)

c) Resulting segmentation from RANSAC method

Figure 4. Extracting a point cloud of facades' surfaces

4.3 Deformation measurement

As the tower is made from wood, a deformation of each surface/facade in each story and of each story can be different because connections between elements are not rigid. In this study, the deformation of the tower computed from the point cloud is based on following assumptions: (1) an un-deformed or initial surface is the perfectly vertical surface, (2) a segmented surface represents the façade surface, (3) the deformation of the tower is herein defined as the out-of-plumb of the vertical surface and (4) the deformation is a relative deformation respecting to the bottom story or the bottom of Story 5. The schematic diagram for computing relative deformation of the surface at each story is shown in Fig. 5.

From the point cloud of the segmented planar surface, a fitting surface is estimated using a principal component analysis [21], in which the normal vector of the surface is the eigen-vector ($n_1 = (n_1.x, n_1.y, n_1.z)$) corresponding to the smallest eigen-value determined from a covariance

matrix (Eq. 1).

$$C = \sum_{i=1}^{N}(p_i - p_0)(p_i - p_0)^T \quad (1)$$

where p_0 is the centroid point computed from the points $\mathbf{P} = \{\mathbf{p}_i \in \mathbf{R}^3 \mid i = [1,N]\}$

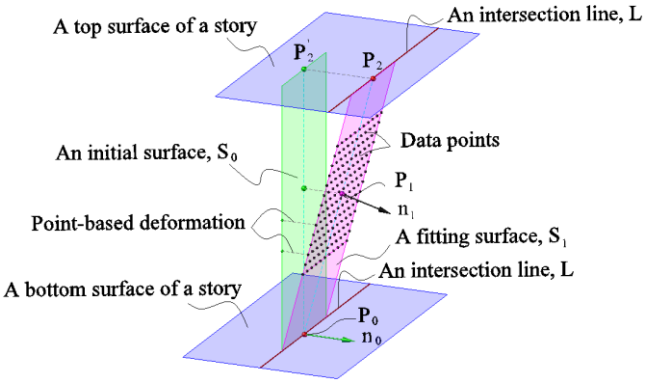


Figure 5. Schematic diagram for estimating deformation

The fitting plane S_1 can describe as the point $P_1 = (x_1, y_1, z_1)$ and the normal vector n_1. Based on the assumptions above, an initial or undeformed surface S_0 of the façade is the vertical surface through an intersection between the fitting surface and the horizontal bottom surface (S_{bottom}) of the story (Fig. 5). The process starts to determine the intersection line (L) between $S_1(P_1, n_1)$ and S_{bottom} (P'_0, n_z), where $P'_0 = (x_1, y_1, z_0)$, $n_z = (0,0,1)$, and z_0 is the elevation of the bottom story. Next, the initial or undeformed surface S_0 is defined by the point P_0 and the normal vector n_0, where P_0 and n_1 are the projection of P_1 and n_1 onto L and S_{bottom}, respectively.
To estimate the deformation, a vertical slope of each surface is calculated as given in Eq. 2.

$$\Delta_{slope} = \frac{d(P_2, P'_2)}{H} \quad (2)$$

where $d(P_2, P'_2)$ is the distance from the point P_2 to S_0, P_2 is the projection of P_1 onto the intersection line between S_1 and the horizontal top surface of the story, H is the height of the story.
Next, point and surface-based methods for computing a relative deformation of the surface is given as expressed in Eq. 3, which are distances from the data points of the segmented surface to the undeformed surface $S_0(P_0, n_0)$.

$$\delta_{rel} = d(\boldsymbol{p}_i, S_0) = \frac{n_0.x * x_i + n_0.y * y_i + n_0.z * z_i + d_0}{\sqrt{n_0^2.\mathrm{x} + n_0^2.\mathrm{y} + n_0^2.\mathrm{z}}} \quad (3)$$

where $\mathbf{P} = \{\mathbf{p}_i \in \mathbf{R}^3 \mid i = [1,N]\}$ are the point cloud of the façade surface and $d_0 = n_0.x * x_0 + n_0.y * y_0 + n_0.z * z_0$. For the surface-based method, p_i is the point on the fitting surface S_1.

Finally, cumulative relative deformation ($\delta_{cumrel,i}$) of Story i is calculated according to Eq. 4.

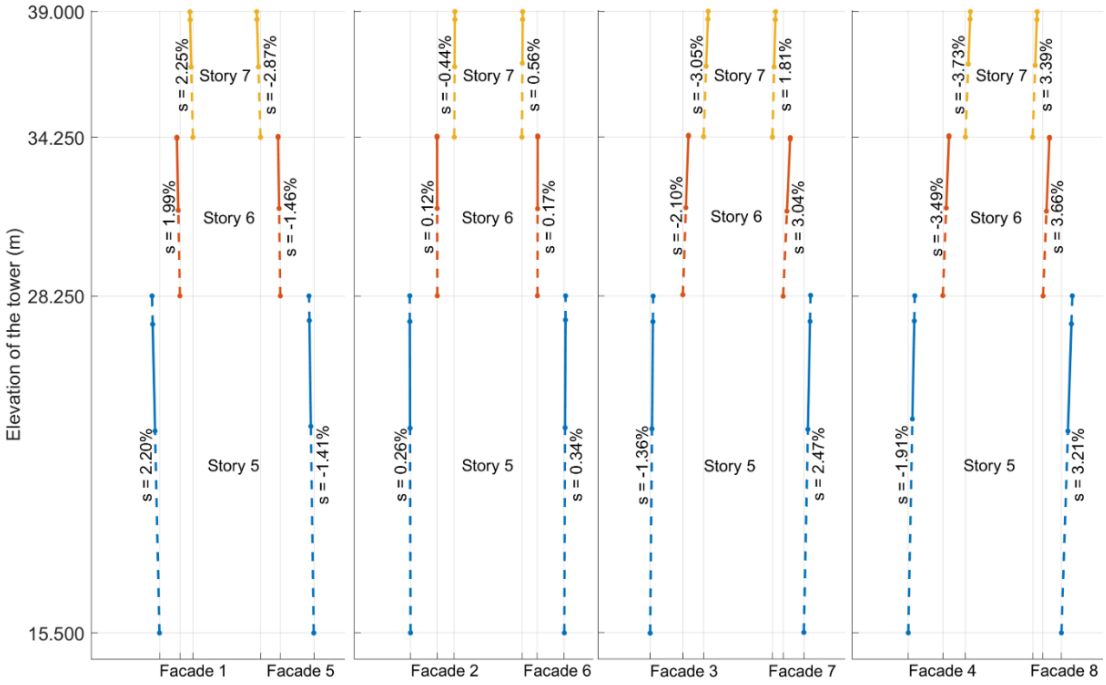
$$\delta_{cumrel,i} = \delta_{cumrel,i-1} + \delta_{rel,i} \quad (4)$$

where $\delta_{cumrel,i-1}$ is the cumulate relative deformation-based surface at Story i-1, and $\delta_{rel,i}$ is the relative deformation from the point- or surface-based methods of Story i.

4.4 Results and Discussions

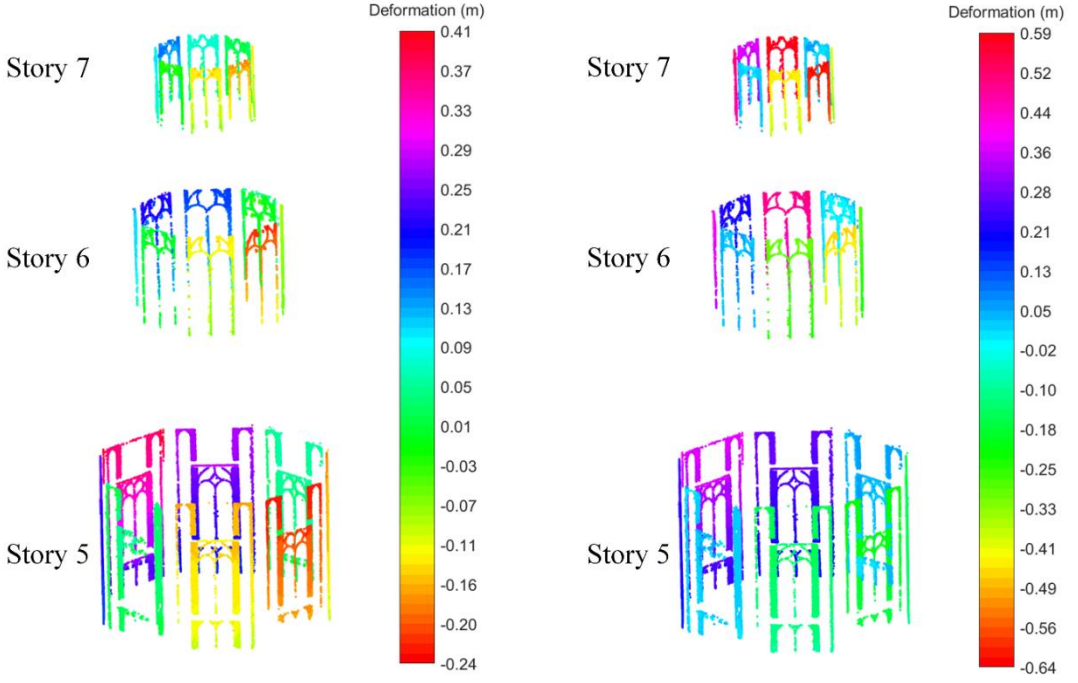
As exterior surfaces of the tower are captured by laser scanning, geometric data of the tower skeleton is not available. Based on dimensions from the skeleton models and point clouds of exterior facades of the tower, in this data acquisition, only data points representing the exterior surfaces of Story 5 to Story 7 are available. Vertical slopes of facades are illustrated in Fig. 6, in which the absolute vertical slopes vary from 0.26% (Façade 2) to 3.21% (Façade 8) for Story 5, from 0.12% (Façade 2) to 3.66% (Façade 8) for Story 6, and 0.44% (Façade 2) to 3.73% (Façade 8) for Story 7. Even though in the same story, the vertical slopes of two opposite facades are different. For example, in Story 5, the vertical slopes of Façade 3 and 7 are respectively -1.36% and 2.47%. Moreover, the slopes of the same facades in different stories are also different, which can be seen when comparing the vertical slopes of Façade 7 are 2.47%, 3.04% and 1.81% for Story 5, 6 and 7. From resulting vertical slopes, it can conclude that the shape of the stories are not in line and each story is slightly tilted compared to the neighbour stories.

Relative deformation from the point-based method is illustrated in Fig. 7a. Large relative deformation is found in Story 5, with values varying from -0.24m to 0.41m outward and inward to the towers´ central line, respectively. For other stories, the relative deformation is not more than -0.22m outward and 0.25m inward. Additionally, cumulate relative deformation shows that the largest deformation of the tower is up to 0.59m and -0.64m inward and outward the tower central line, respectively (Fig. 7b). As the deformation from the point-based method computed from the points of the fitting surface S_1, it does not reflect overall deformation of the facades or the tower. Therefore, the deformation of the facades can be seen through the cumulate relative deformation from the surface-based method (Fig. 8). Except for Façade 2 and 6, other façades are subjected to a large deformation. The maximum cumulate relative deformation is 0.51m inward and -0.63m outward of the tower central line. Moreover, the cumulate relative deformation also illustrate that deformation of the tower is not following a linear relationship, for example, in Façade 8, the cumulative relative deformation from the bottom of Story 5 and the top of Story 7 is respectively 0.0m, -0.41m, -0.22m, and -0.38m.



(*) Note: (i) Negative slopes mean facades deformed inward to the tower central line and vice-versa; (ii) Continuous lines represent the fitting surface while dashed lines are extrapolation surfaces

Figure 6. Vertical slopes of Facades



a) Relative deformation-based point b) Accumulate relative deformation-based point

(*) Note: Negative values represent a relative deformation inward to the tower central line and vice-versa

Figure 7. Point-based relative deformation of the tower (*)

A visualization check shows that the tower is clearly inclined in North-West direction, which is completely in agreement with the resulted deformation estimated from the 3D point cloud. Moreover, the last measurement in 2011 reported that the total displacement of the tower from 1898 to 2011 is about 32 cm. That implies the tower deformation is more than 2 times larger than that of the last record. As the tower deformation is increased significantly in the last 8 years, it would recommend to monitor the tower's deformation with higher frequency and additional technique should be implemented to measure deformations of the entire tower. However, the deformation of St. Bavo church's tower is still smaller than that of Walfridus church (Bedum, Netherlands) and San Bendetto Church (Ferrare, Germany), which total deformations are of 2610mm [22] and 2530mm [23], respectively.

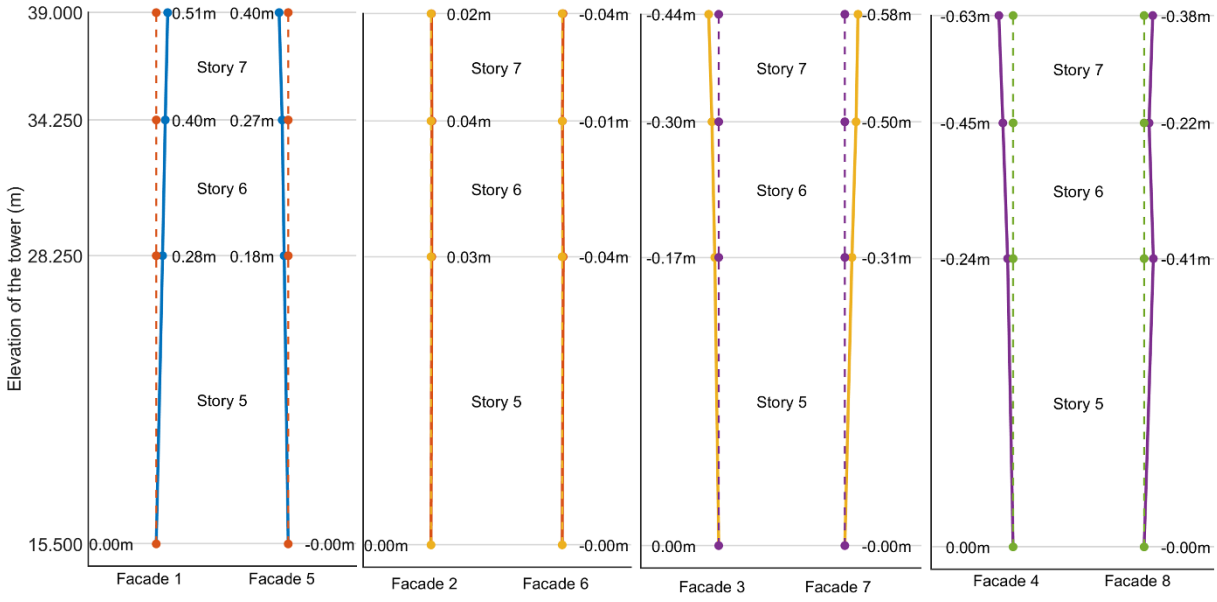


Figure 8. Cumulate relative deformation of the tower from a surface-based method

5. CONCLUSIONS

Heritage structures are delicate with environmental impact, which must be monitored with high frequency and accuracy, but limited budget does not always allow to implement this strategy. Using 3D Laser scanning to monitor cultural heritage structures could allow for a better understanding of the state of the structure with respect to its shape and dimensions. This is a fast and efficient technology and allows for extraction of data that can be used in structural analysis. This paper presents a methodology to measure relative deformation of a wooden tower of the St. Bavo Church in Haarlem, Netherlands. Surfaces describing the tower are extracted from point clouds of octagon facades in each story by using a RANSAC method. Next, a deformation of each surface is computed from point- and surface-based methods with the assumption that an initial or undeformed surface is perfectly vertical. The results show that the deformation of each façade in the same story and in different story are different and the large deformation is found in Story 5 with a relative deformation about 0.41m outward the tower central line. Moreover, a total relative deformation at the top of Story 6 is up to 0.63m outward the tower central line, which is about 2 times larger than the last record in 2011 with a total

deformation of 0.32m comparing to that in 1898. As a cost to measure deformation of an entire tower is relatively low, a monitoring campaign can easily increase a measurement frequency to identify anomaly response of the tower. Moreover, the permanent scanning can capture a change of the tower in a specific interval time, which allows to report the deformation in nearly continuously. However, in this case, only parts of the structure within the effective range of the scanner can be measured.

Acknowledgements

This work was funded by the generous support of the European Commission through H2020 MSCA-IF, "*BridgeScan: Laser Scanning for Automatic Bridge Assessment*", Grant 799149. The first author is graceful for this support. The Association Friends of the Grote Kerk in Haarlem is gratefully acknowledged for their support during the Master thesis work of the 3rd Author.

REFERENCES

[1] Truong-Hong, L., Laefer, D.F., Hinks, T., Carr, H. Combining an angle criterion with voxelization and the flying voxel method in reconstructing building models from LiDAR data. *Computer-Aided Civil and Infrastructure Engineering*, 28 (2012) 112-129.
[2] Teza, G., Galgaro, A., Moro, F. Contactless recognition of concrete surface damage from laser scanning and curvature computation. *NDT & E International*, 42 (2009) 240-249.
[3] Gyetvai, N., Truong-Hong, L., Laefer, D.F. Laser scan-based structural assessment of wrought iron bridges: Guinness Bridge, Ireland. *Proceedings of the Institution of Civil Engineers - Engineering History and Heritage*, 171 (2018) 76-89.
[4] Arias, P., Riveiro, B., Armesto, J., Solla, M. *Terrestrial laser scanning and non parametric methods in masonry arches inspection*. in: Comission V Symposium. *ISPRS*, Newscalte upon Tyne, UK 2010 pp 39-44.
[5] Cabaleiro, M., Lindenbergh, R., Gard, W.F., Arias, P., van de Kuilen, J.W.G. Algorithm for automatic detection and analysis of cracks in timber beams from LiDAR data. *Construction and Building Materials*, 130 (2017) 41-53.
[6] Haddad, N.A. From ground surveying to 3D laser scanner: A review of techniques used for spatial documentation of historic sites. *Journal of King Saud University - Engineering Sciences*, 23 (2011) 109-118.
[7] González-Aguilera, D., Gómez-Lahoz, J., Muñoz-Nieto, Á., Herrero-Pascual, J. Monitoring the health of an emblematic monument from terrestrial laser scanner. *Nondestructive Testing and Evaluation*, 23 (2008) 301-315.
[8] Pesci, A., Casula, G., Boschi, E. Laser scanning the Garisenda and Asinelli towers in Bologna (Italy): Detailed deformation patterns of two ancient leaning buildings. *Journal of Cultural Heritage*, 12 (2011) 117-127.
[9] Bonali, E., Pesci, A., Casula, G., Boschi, E. Deformation of Ancient Buildings inferred by Terrestrial Laser Scanning methodology: the Cantalovo church case study (Northern Italy)*. *Archaeometry*, 56 (2014) 703-716.
[10] Bertacchini, E., Boni, E., Capra, A., Castagnetti, C., Dubbini, M. *Terrestrial Laser Scanner for Surveying and Monitoring Middle Age T owers*. in: XXIV FIG International Congress 2010-

Facing the Challenges-Building the Capacity. *FIG Federation International des Geometres*, 2010 pp 1-13.
[11] Bhadrakom, B., Chaiyasarn, K. As-built 3D modeling based on structure from motion for deformation assessment of historical buildings. *Int. J. Geomate*, 11 (2016) 2378-2384.
[12] Muszynski, Z., Milczarek, W. Application of Terrestrial Laser Scanning to Study the Geometry of Slender Objects. *IOP Conference Series: Earth and Environmental Science*, 95 (2017) 042069.
[13] Dunk, T.H.v.d. *Haarlem als Hollands Jeruzalem: De oorsprong van de toren van de Grote of St.-Bavokerk. Hilversum Verloren*, (2016).
[14] Leica Geosystems. *Leica ScanStation P40*. in., 2020 pp.
[15] Leica Geosystems. *Leica Cyclone 3D Point Cloud Processing Software*. in., 2020 pp.
[16] Rabbani, T., Van Den Heuvel, F. Efficient hough transform for automatic detection of cylinders in point clouds. *Isprs Wg Iii/3, Iii/4*, 3 (2005) 60-65.
[17] Truong-Hong, L., Laefer, D.F. Octree-based, automatic building façade generation from LiDAR data. *Computer-Aided Design*, 53 (2014) 46-61.
[18] Schnabel, R., Wahl, R., Klein, R. *Efficient RANSAC for point-cloud shape detection*. in. *Wiley Online Library*, pp 214-226.
[19] CloudCompare. *CloudCompare*. in., 2020 pp.
[20] Dillencourt, M.B., Samet, H., Tamminen, M. A general approach to connected-component labeling for arbitrary image representations. *J. ACM*, 39 (1992) 253–280.
[21] Laefer, D.F., Truong-Hong, L. Toward automatic generation of 3D steel structures for building information modelling. *Automation in Construction*, 74 (2017) 66-77.
[22] Thijssen, W. *Who has the crookedest?* in: de Volkshrant. Netherlands 2011 pp.
[23] Pellegrinelli, A., Furini, A., Russo, P. Earthquakes and ancient leaning towers: Geodetic monitoring of the bell tower of San Benedetto Church in Ferrara (Italy). *Journal of cultural heritage*, 15 (2014) 687-691.

12th International Conference on Structural Analysis of Historical Constructions
SAHC 2020
P. Roca, L. Pelà and C. Molins (Eds.)

NON-DESTRUCTIVE ASSESSMENT OF THE ADHESION AT THE INTERFACE BETWEEN FRCM REINFORCEMENTS AND MASONRY SUBSTRATES BY NON-LINEAR ULTRASONIC TECHNIQUE

ANNA CASTELLANO[1*], AGUINALDO FRADDOSIO[2], TRIBIKRAM KUNDU[3] AND MARIO DANIELE PICCIONI[2]

[1]Department of Mechanics, Mathematics and Management (DMMM)
Polytechnic University of Bari
via Re David, 70125 Bari, Italy
e-mail: anna.castellano@poliba.it (*corresponding author)

[2]Department of Civil Engineering Sciences and Architecture (DICAR)
Polytechnic University of Bari
via Re David, 70125 Bari, Italy
e-mail: aguinaldo.fraddosio@poliba.it, mariodaniele.piccioni@poliba.it

[3]Department of Civil & Architectural Engineering & Mechanics
The University of Arizona
1209 E. Second St., Tucson, AZ 85721, USA
Email: tkundu@email.arizona.edu

Keywords: Masonry, FRCM Reinforcements, Non-Destructive Tests, Nonlinear Ultrasonic, SPC Technique.

Abstract. *The strong diffusion of Fiber Reinforced Cementitious Matrix (FRCM) composites for the reinforcement of historic masonry constructions requires suitable experimental techniques for assessing possible defects in the adhesion between FRCM and masonry, and between FRCM layers. To this aim, in this paper, an innovative nonlinear ultrasonic approach based on the Side-band Peak Count (SPC) technique is proposed. This approach is discussed and validated through experimental tests made on tuff substrates reinforced with FRCM mortars embedding a basalt fibers grid and having known artificial defects at the adhesion between tuff and FRCM as well as in the fiber grid.*

1 INTRODUCTION

In recent years, the development of suitable strengthening techniques for historic masonry constructions has received increasing attention from research community. One of the main motivations is the pronounced seismic vulnerability of the built heritage made of masonry. Among possible strengthening materials, Fiber Reinforced Cementitious Matrix (FRCM) composites have gained interest over the classical Fiber Reinforced Polymer (FRP) composites since FRCM composites appear to be more compatible with historical masonries, both from the technological and the structural point of view [1]. This is mainly due to the fact that FRCM composites are based on a mortar matrix embedding high-strength long fiber grids (Glass, Carbon, Basalt, etc.); as well as matrix containing short reinforcement fibers. It should

be noted that the relatively low cost of FRCM reinforcements makes it possible to build distributed reinforcements, that reveal to be much more effective than the localized ones (like those built by FRP strips) in view of improving the overall structural performances of masonry constructions.

A number of studies concern the interactions between FRCM composites and masonry, the adhesion and the delamination of FRCM reinforcement from masonry supports, investigating possible collapse modes and the overall structural capacity of the strengthened constructions, both from the theoretical and the experimental point of view [2-3]. Anyway, the problem of the detection of possible defects in the adhesion between FRCM and masonry and of the fiber grids, formed during the application of the reinforcement or during the service life of the construction, for example due to exceptional loads like earthquake actions, fire, etc., needs to be further investigated. Indeed, these defects may strongly undermine the strength of the reinforced construction. Thus, suitable experimental techniques must be developed.

On this issue the literature is rather limited, even if the field of application is widened to include also the FRP reinforcements [4]. Here, an innovative non-linear ultrasonic technique is proposed for detecting defects in the adhesion between FRCM composite layers and masonry substrates.

Non-linear ultrasonic techniques may be very effective for detection of defects and damage [5]. Here the principle that is exploited for experimental evaluations is that defects act like an active non-linear radiation source of new frequency components rather than passive scatters as in the case of classical linear ultrasonic techniques [6]. Based on this, the Side-band Peak Count (SPC) technique reprocesses results of ultrasonic guided wave tests by relating the level of the non-linearity of the ultrasonic response, i.e., the damage, to the appearance of additional minor components in the spectrum of the received signal [7].

Experiments performed on specimens made of masonry tuff substrates reinforced with FRCM mortars embedding a basalt fiber grid and having known artificial defects allows for discussing the proposed approach. In particular, those defects represent a small and a large discontinuity in the adhesion between tuff and FRCM, and a small and a large discontinuity in the fiber net. Experimental results show the effectiveness of SPC technique in detecting the defects and allows for highlighting the influence of the defect dimensions on the variation in SPC.

2 NON-LINEAR ULTRASONICS AND SPC TECHNIQUE

Acoustic (sonic and ultrasonic) Non-Destructive Testing techniques represent one of the most important NDT approach for testing material and structures. The difference between sonic and ultrasonic tests relies on the frequency of the acoustic waves employed in the experiments, below 20 kHz for sonic tests, and above that frequency threshold for ultrasonic tests. Sonic tests are suitable for very dispersive and/or very thick specimens but are characterized by poor accuracy in the detection and localization of defects. On the other hand, ultrasonic tests allow for a definitely better resolution and accuracy, but generally their application to masonry constructions is strongly obstructed by the high attenuation of ultrasonic waves [8].

Here the attention is given on ultrasonic tests, since the propagation material is represented by FRCM layers, where the attenuation is not such that it would prevent the acquisition of

signals with enough energy.

The traditional approach for ultrasonic tests, i.e., the classical linear ultrasonic approach, is based on the analysis of so-called linear acoustic parameters like flight time (and, consequently, wave speed), resonance frequency and attenuation of acoustic waves. Ultrasonic waves are reflected and scattered by internal cracks; these phenomena can be analyzed from the linear analysis of the interaction between the material defects and the propagating elastic waves. Indeed, internal damage can be detected and characterized based on the study of velocity and attenuation of elastic waves in the material.

However, the wave propagation-based linear ultrasonic techniques fail to detect small defects, much smaller than the wavelength of the interrogating ultrasonic signals, or particular kind of defects like those represented by localized discontinuities in the adhesion between layers of multilayer materials.

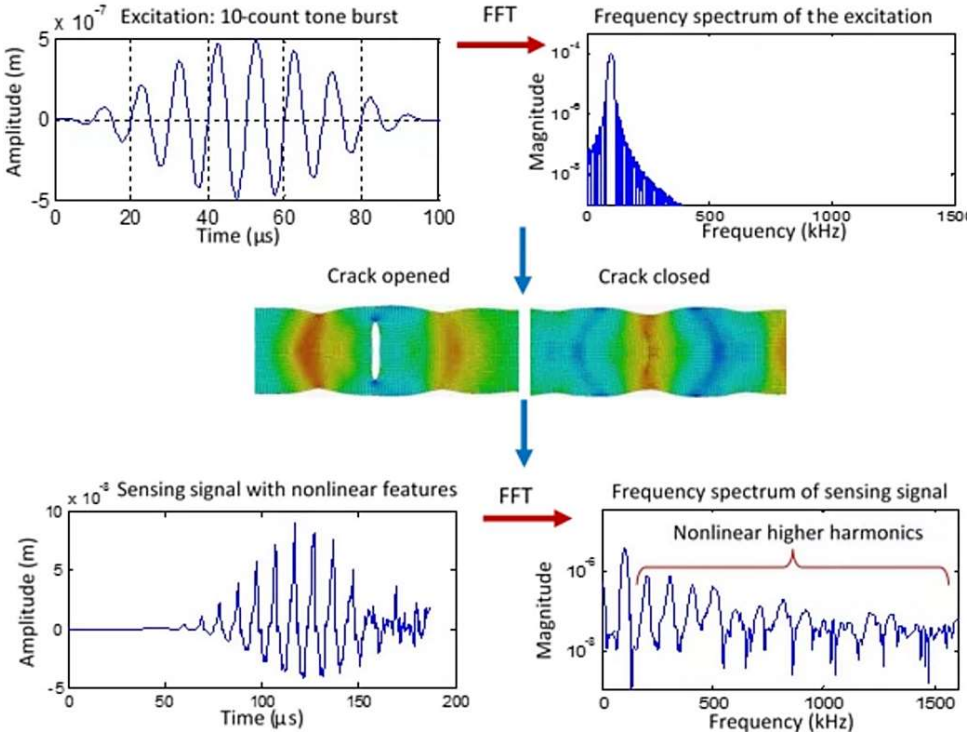


Figure 1: Generation of higher harmonics due to the damage [9]

In order to overcome the above limitations, in recent years a lot of research works appeared in the literature about non-linear acoustical/ultrasonic techniques. Nonlinear acoustical techniques are based on nonlinear stress–strain relationship assumptions. A very important aspect is that when two waves of different frequencies propagate through a linear material their frequencies do not change. But, if the material is non-linear, then the interaction between these two waves produces secondary waves having frequencies that are linear combinations of the frequencies of the primary waves. Even when a wave of single frequency propagates through a non-linear material new waves of higher frequency (higher harmonics) and lower frequency (subharmonics) can be generated in the material. Figure 1 shows that if a signal is

sent through a nonlinear material (in particular, due to an internal crack defect), in addition to the fundamental frequency the higher frequencies (higher harmonics) - multiples of the fundamental frequency - appear in the spectrum of the received signal.

Moreover, in a nonlinear system both resonance frequency and attenuation coefficient change with the vibration amplitude.

Higher harmonic, subharmonic, and modulated waves can be effectively used for detecting defects. Various non-linear ultrasonic techniques have been developed for internal defect detection by efficiently using higher harmonic, subharmonic, and modulated waves. Indeed, even tiny discontinuities or defects can produce detectable acoustic nonlinearity; the detectability comes from the fact that defect-related nonlinearity is orders of magnitude higher than the intrinsic nonlinearity of the intact material. Thus, nonlinear ultrasonics is very sensitive to small defects like fatigue cracks, fiber debonding and delamination, and is very interesting because the onset of the damage can be assessed in a very early stage.

Here, an advanced nonlinear ultrasonic technique is studied with reference to the analysis of adhesion defects and delamination of FRCM reinforcements of masonry structures: the Sideband Peak Count (SPC) technique which was proposed first in [10] for the analysis of prismatic bars. SPC is based on the nonlinear interaction between different Lamb wave modes: if the Lamb wave is generated by a broadband excitation then multiple Lamb modes are generated and, if the plate material is nonlinear (this can be, for example, due to the damage), then the interaction between these various Lamb modes can generate multiple sidebands (see Fig. 2).

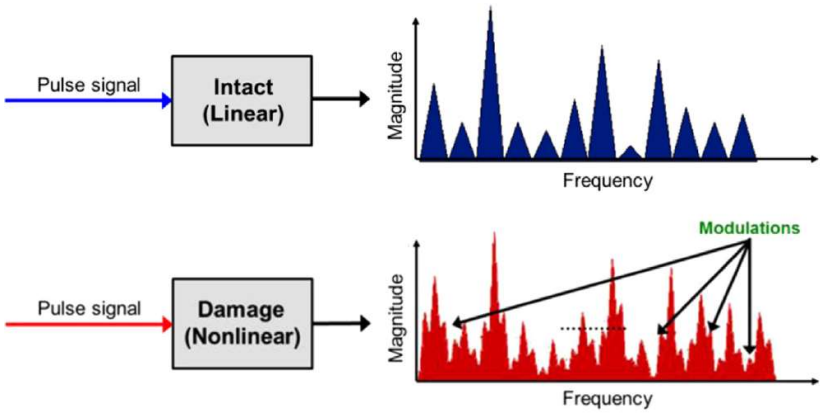


Figure 2: Generation of sideband peak due to the wave propagation through a damaged (nonlinear) medium [11]

In particular, the SPC technique is a feature extraction technique aimed at quantifying the degree of nonlinearity in a damaged structure from its response to broadband pulse excitations. The level of nonlinearity, related to the damage, is associated with the number of peaks of the sidebands; in particular, the number of peaks above a suitably taken threshold value is counted (see Fig. 3-a). It is also possible to gather information on the damage by comparing the number of peaks of the sidebands above a threshold value for the initial (undamaged) state and the current (damaged, nonlinear) state, i.e., by studying the SPC difference: Figure 3-b highlights that the damaged specimen shows a significantly higher number of frequency-domain peaks especially for low values of the threshold.

For the representation of SPC results, usually diagrams of the SPC parameter (1), defined as the ratio of the number of sideband (modulation) peaks N_{peak} over a moving threshold (th) to the total peak number N_{tot} in the considered frequency domain, versus the amplitude of the threshold are employed.

$$SPC(th) = \frac{N_{peak}(th)}{N_{tot}} \tag{1}$$

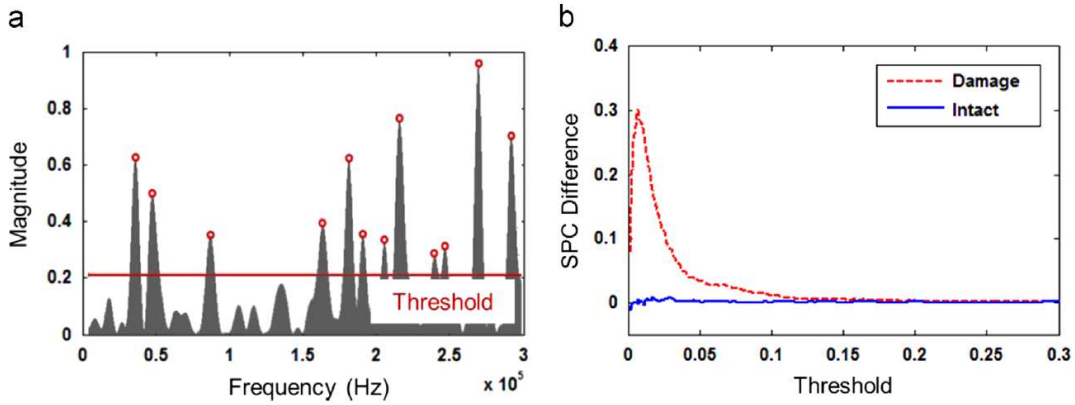


Figure 3: Illustration of the Sideband Peak Count (SPC) technique [11]

The example in Fig. 4, concerning the SPC response for a cracked material, shows that a thin crack involves a much higher number of sideband peaks with respect to the undamaged material. A thick crack might also be detected by the SPC technique, although the nonlinear effect is less prominent in this case.

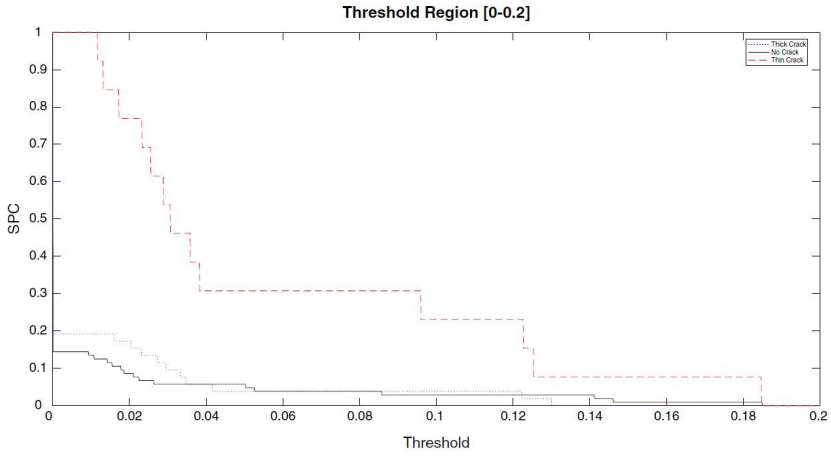


Figure 4: SPC response in case of thin or thick cracks [12]

SPC has been successfully applied in fields like inspection of concrete ageing, monitoring of heat treatments of metals, detection of fatigue damage in metals, etc. [13]. It should be emphasized that, although the data processing needed for SPC is different from that of classical linear ultrasonic methods, the experiments can be performed by standard ultrasonic

devices. Thus, SPC appears to be very interesting in view of practical applications, especially in fields where only the use of simple instruments is allowed such as for monitoring the strengthening of masonry constructions.

3 EXPERIMENTAL TESTS

The purpose of the experimental tests performed at "Laboratorio Ufficiale Prove Materiali M. Salvati" of Polytechnic University of Bari is to study the capability of SPC nonlinear ultrasonic technique for characterizing defects in FRCM reinforcements of masonry constructions.

To this aim, 5 pairs of specimens consisting in a tuff support with a FRCM reinforcement embedding a basalt fiber grid have been analyzed: 2 of them (labeled S1 and S2) are undamaged; 2 specimens (labeled SDIA1 and SDIA2) present a discontinuity in the adhesion of the FRCM layer obtained by interposing between tuff and FRCM a 20 mm wide scotch tape (Fig. 5-a, above); 2 specimens (labeled SDIB1 and SDIB2) are similar to the previous pair, except for the width of the discontinuity in the adhesion, obtained by a 30 mm wide scotch tape (Fig. 5-a, below); for 2 specimens (labeled SDFA1 and SDFA2) a defect in the fiber-mortar matrix interface is simulated by a small cut about 15 mm wide in the basalt fiber grid (Fig. 5-b, above); finally, for 2 specimens (labeled SDFB1 and SDFB2) a defect in the fiber-mortar matrix interface is simulated by a large cut about 30 mm wide in the basalt fiber grid (Fig. 5-b, below).

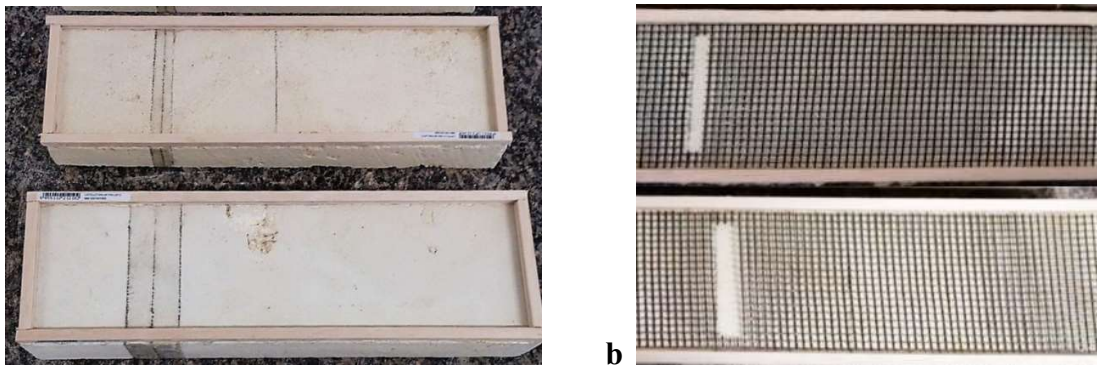


Figure 5: Artificial damage in the specimens: a) small (20 mm) and large (30 mm) defect of FRCM-tuff adhesion; b) small (15 mm) and large (30 mm) defect in the grid.

All specimens are prismatic, with dimension of the face to be reinforced by the FRCM layer about 485 mm x 150 mm; the overall thickness of the FRCM layer is 10 mm. The defects are located about 110 ÷ 125 mm from one of the short edges of the face. FRCM reinforcement is made by a two-component, pre-blended, fiber-reinforced mortar embedding a basalt fiber grid (6 mm x 6 mm, 250 g/m^2).

The ultrasonic setup is composed of an Olympus 5072PR ultrasonic pulser with two probes for longitudinal waves having a central frequency of 50 KHz; the emitting probe is inclined at 65 degree for generating surface waves in the FRCM layer. The signals are managed by an Agilent MSO–X-4954 oscilloscope.

For determining the ultrasonic response in the damaged area, the emitting probe has been

kept fixed left to the defect, whereas the receiving probe has been placed on the defect (position 1) or on the right of the defect (position 2). For determining the reference ultrasonic response in the undamaged area, the two transducers have been placed on the right end of the specimen at the same distances of position 1 and position 2 (Fig. 6).

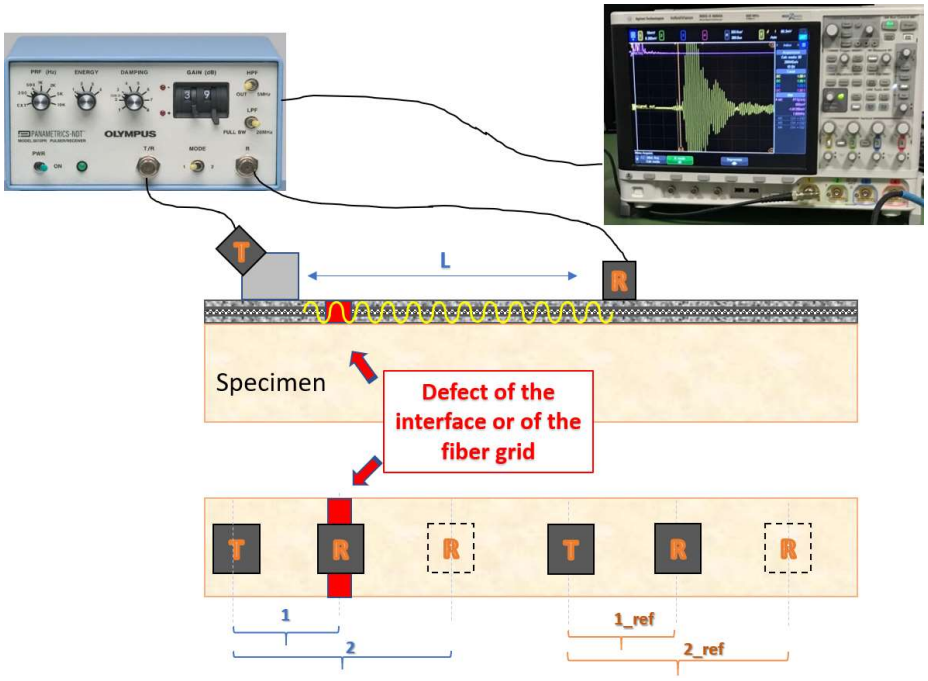


Figure 6: Experimental setup.

For reprocessing the signals, an ad hoc Labview software has been developed; this software compares the acquired signals, current (that is, in presence of the damage) and reference (that is, in the undamaged area). The signals are compared in terms of the waveform, of normalized frequency response function and of frequency spectra. Finally, the software performs the SPC evaluation of the acquired signals.

4 RESULTS AND DISCUSSION

In what follows, the diagrams of SPC results for the 8 artificially damaged specimens are shown and discussed. For the sake of brevity, all diagrams refer only to the case of receiving probe located in "position 2", i.e., on the right of the defect (receiving probe far from the defect). Moreover, only the results of one of the two specimens for each kind of defect is shown (the results for the specimens labeled "1", SDIA1, SDIB1, and so on). The influence of the defect on the SPC response can be inferred from the comparison between the SPC diagram obtained for signals acquired in the undamaged area (reference line, in orange) and the SPC diagram obtained for signals acquired in the damaged area (in light blue).

In Figure 7, the SPC response of the specimen with small adhesion defect SDIA1 is presented. In this case, the light blue curve, representing the SPC parameter for the damaged area is distinctly lower than the reference orange curve, representing the SPC parameter for signals acquired with the same distances between probes in the undamaged area, for threshold

values above 0.01. The different behavior below the very small threshold value of 0.01 is likely ascribable to noise in the signals and therefore it is not to be considered representative of difference due to the damage.

Figure 8 is analogues to Figure 7, but for the specimen with large adhesion defect SDIB1. Here, the curves are inverted with respect to those in Figure 7, with the light blue curve, representing the SPC parameter for the damaged area higher than the reference orange curve referring to the undamaged area.

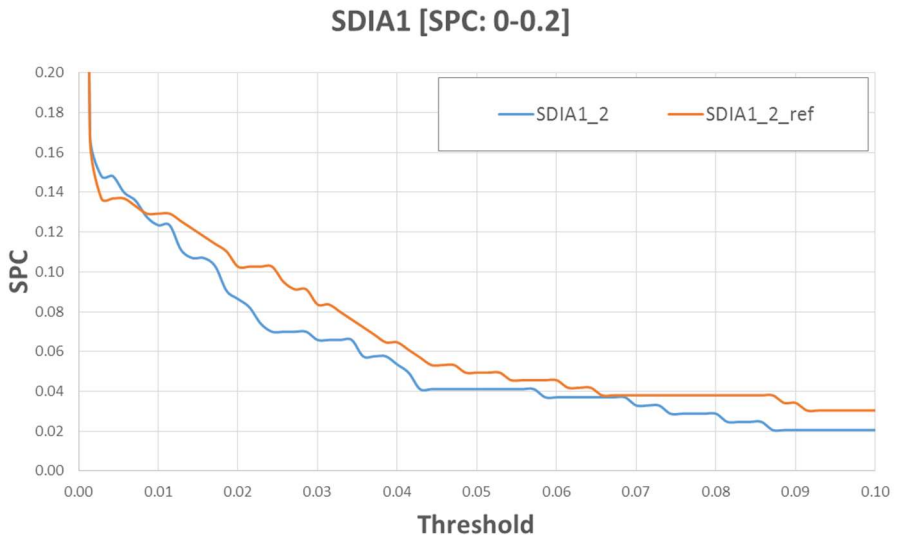


Figure 7: SPC response of the specimen with small (20 mm) adhesion defect SDIA1: damaged area (light blue) vs reference undamaged area (orange).

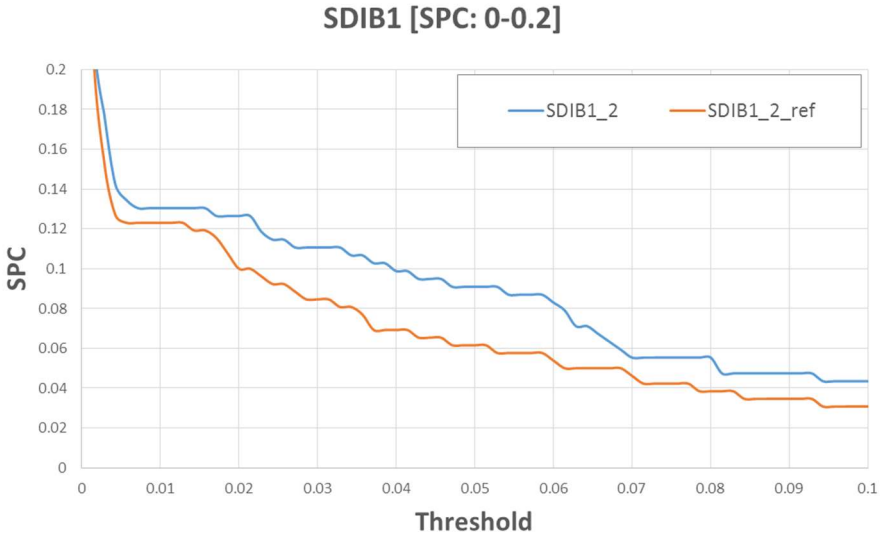


Figure 8: SPC response of the specimen with large (30 mm) adhesion defect SDIB1: damaged area (light blue) vs reference undamaged area (orange).

In Figure 9, the SPC response of the specimen with small grid defect SDFA1 is presented. Also in this case, like for the case of the specimen with small adhesion defect SDIA1, the light blue curve, representing the SPC parameter for the damaged area is considerably lower than the reference orange curve, representing the SPC parameter for signals acquired for the same distances between probes, but in the undamaged area.

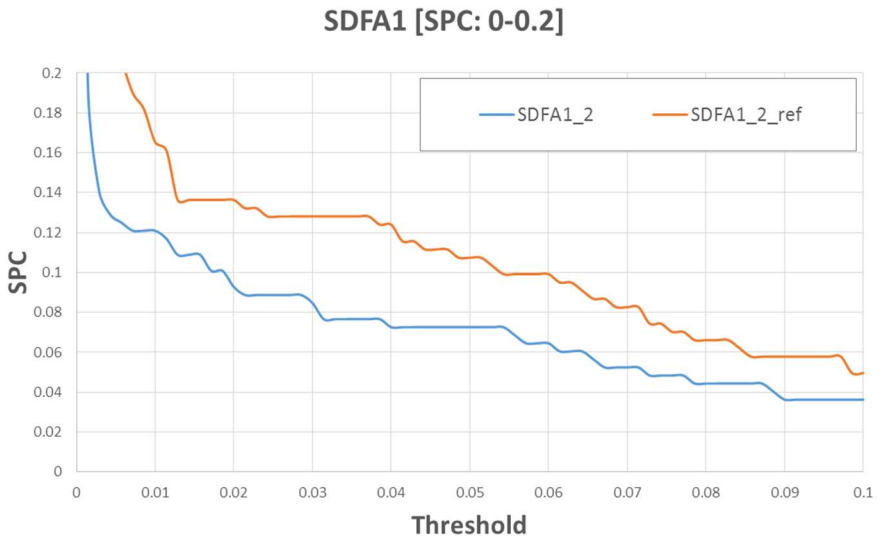


Figure 9: SPC response of the specimen with small (15 mm) grid defect SDFA1: damaged area (light blue) vs reference undamaged area (orange).

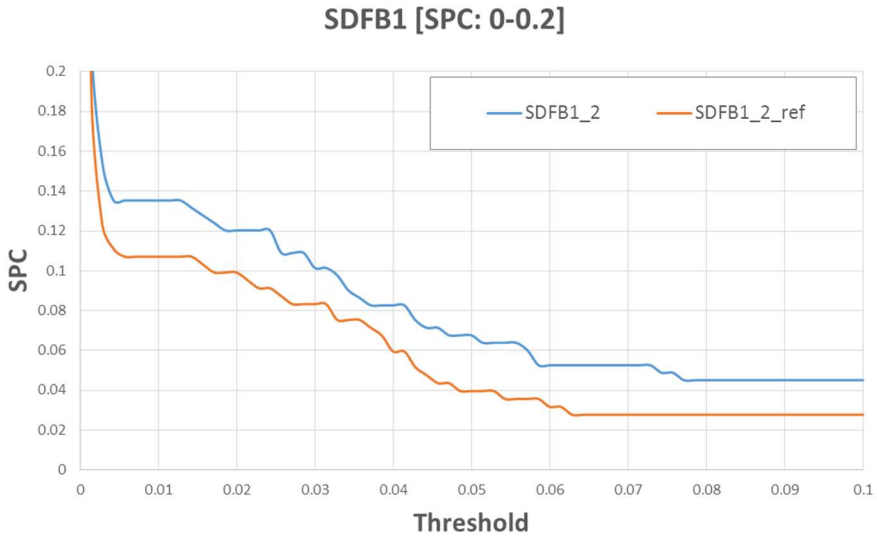


Figure 10: SPC response of the specimen with large (30 mm) grid defect SDFB1: damaged area (light blue) vs reference undamaged area (orange).

Finally, Figure 10 is analogues to Figure 9, but for the specimen with large grid defect

SDFB1. Also in this case, like the specimen with large grid defect SDIB1, an opposite behavior with respect to those in Figure 9 is observed: the damage results show much higher values of the SPC (light blue curve) in comparison to the undamaged area (orange curve).

From the above results it is clear that SPC technique can identify even small defects of FRCM reinforcement. Indeed, for each examined specimen, embedding different kinds of artificial defects, a very different behavior between the damaged and the undamaged area in terms of SPC parameter values has been observed. Note that this conclusion holds also for the specimens labeled "2" (SDIA2, SDIB2 and so on), and for different positions of the receiving probe (the position called "position 1" in the above).

The SPC response of the specimens with large defects (adhesion defects, SDIB1 and SDIB2, and grid discontinuity, SDFB1 and SDFB2) is what is expected based on the literature: the defect involves a higher level of nonlinearity, and thus an increase of the SPC parameter values for all the threshold values considered. On the contrary, the SPC response of the specimens with small defects (adhesion defects, SDIA1 and SDIA2, and grid discontinuity, SDFA1 and SDFA2) is to some extent unexpected: the SPC curves of the undamaged area are systematically above the SPC curves of the damaged area. Notice that the experimental tests have been repeated multiple times in order of ascertain that the latter unexpected behavior was not caused by experimental errors.

Maybe a possible reason of this peculiar behavior relies on the wavelength of the employed ultrasonic waves and on the features of the examined media, composed by a relatively thin FRCM layer in adhesion on a tuff masonry substrate. Moreover, the FRCM layer itself can be subdivided in three sublayers, that is two mortar layers separated by a thinner mortar layer embedding the fiber grid.

Indeed, the reference literature is mostly related to Lamb wave tests on thin specimens, whereas in the present case the tests involve the propagation of Rayleigh waves in the three-layer FRCM reinforcement. The examined artificial defects can be considered as localized discontinuity conditions between layers in adhesion, that is, imperfection of the boundary conditions for the layer subjected to the wave propagation [14,15]. Moreover, it turns out that by considering the frequency of the employed ultrasonic signals and the mechanical parameters of the FRCM mortar, the ultrasonic wavelength have the same order of magnitude of the dimensions of the defects. Finally, a fact not irrelevant should be that the material being investigated is markedly nonlinear also in the undamaged state.

The above considerations open an intriguing and challenging research perspective in order to establish the reasons of the observed SPC behavior: to this aim suitable theoretical and numerical investigations have to be developed.

5 CONCLUSIONS

- The reported experiments on tuff samples reinforced by FRCM embedding basalt grids show that SPC nonlinear ultrasonic technique is capable of detecting defects in adhesion and in the fiber net, with quite different values of the SPC parameter in the damaged area with respect to those related to the undamaged area.
- This result appears interesting in view of applications mainly for three reasons. First, the proposed technique is simple to be applied, since standard ultrasonic equipment can be used: moreover, the developed Labview software is very fast in giving final

results in terms of SPC curves. Second, nonlinear ultrasonic techniques like SPC technique allows for detecting defects also quite far from the application areas of the probes; sometimes nonlinear effects increase with the distance, whereas linear effects quickly decay. Third, SPC technique is capable of detecting small defects, out of reach of conventional linear ultrasonic techniques, and assessing the onset of the damage in its early stage.

- Finally, the obtained results encourage further theoretical and numerical analysis aimed at justifying the very different behavior observed for small and large defects.

REFERENCES

[1] Carozzi, F.G., Milani, G. and Poggi, C. Mechanical properties and numerical modeling of Fabric Reinforced Cementitious Matrix (FRCM) systems for strengthening of masonry structures. *Compos. Struct.* (2014) **107**:711-725.

[2] Bove, M., Castellano, A., Fraddosio, A., Scacco, J., Milani, G. and Piccioni, M.D. Experimental and numerical analysis of FRCM strengthened parabolic tuff barrel vault. *Key Eng. Mater.* (2019) **817 KEM**:213-220.

[3] Olivito, R.S., Codispoti, R. and Cevallos, O.A. Bond behavior of Flax-FRCM and PBO-FRCM composites applied on clay bricks: Experimental and theoretical study. *Compos. Struct.* (2016) **146**:221–31.

[4] Büyüköztürk, O., Haupt, R., Tuakta, C. and Chen, J. Remote Detection of Debonding in FRP-strengthened Concrete Structures Using Acoustic-Laser Technique. In: O. Büyüköztürk et al. (Eds.): *Nondestructive Testing of Materials and Structures*, RILEM Bookseries 6 (2013), pp. 19-24.

[5] Kundu, T. *Ultrasonic nondestructive evaluation: Engineering and biological material characterization*. CRC Press, (2003).

[6] Yan, D., Drinkwater, B.W., Neild, S.A. Measurement of the ultrasonic nonlinearity of kissing bonds in adhesive joints". *NDT E Int.* (2009) **42**(5):459-466.

[7] Liu, P., Sohn, H., Kundu, T., Yang, S. Noncontact detection of fatigue cracks by laser nonlinear wave modulation spectroscopy (LNWMS)". *NDT E Int.* (2014) **66**:106-116.

[8] Camassa, D., Castellano, A., Fraddosio, A., Piccioni, M.D. Improvements of the Ultrasonic Tomography for Applications to Historical Masonry Constructions. In: R. Aguilar et al. (Eds.): *Structural Analysis of Historical Constructions*, RILEM Bookseries 18 (2019), pp. 447-455.

[9] Shen, Y. and Cesnik, C.E.S. Nonlinear scattering and mode conversion of Lamb waves at breathing cracks: An efficient numerical approach. *Ultrasonics* (2019) **94**:202-217.

[10] Eiras, J.N., Kundu, T., Bonilla, M. and Payá, J. Nondestructive monitoring of ageing of alkali resistant glass fiber reinforced cement (GRC). *J. Nondestruct. Eval.* (2013) **32**(3):300-314.

[11] Liu, P., Sohn, H., Kundu, T. and Yang, S. Noncontact detection of fatigue cracks by laser nonlinear wave modulation spectroscopy (LNWMS). *NDT E Int.* (2014) **66**:106-116.

[12] Hafezi, M.H., Alebrahim R. and Kundu T. Peri-ultrasound for modeling linear and nonlinear ultrasonic response". *Ultrasonics* (2017) **80**:47-57.

[13] Kundu, T., Eiras, J.N., Li, W., Liu, P., Sohn, H. and Payá J. Fundamentals of Nonlinear

Acoustical Techniques and Sideband Peak Count. In: T. Kundu (Ed.): *Nonlinear Ultrasonic and Vibro-Acoustical Techniques for Nondestructive Evaluation*, Springer, Cham (2019), pp. 1-88.

[14] Castellano, A., Foti, P., Fraddosio, A., Marzano, S. and Piccioni, M.D. Ultrasonic immersion tests for mechanical characterization of multilayered anisotropic materials. In EESMS 2014 - 2014 IEEE Workshop on Environmental, Energy and Structural Monitoring Systems, Proceedings (2014), pp. 63-68.

[15] Castellano, A., Fraddosio, A. and Piccioni, M.D. Quantitative analysis of QSI and LVI damage in GFRP unidirectional composite laminates by a new ultrasonic approach. Compos. B. Eng. (2018) **151**: 106-117.

NON-DESTRUCTIVE DOCUMENTATION METHODS FOR FUTURE SEISMIC AND DAMAGE ANALYSIS OF MODERN HERITAGE BUILDINGS USING CONTEMPORARY TOOLS

S. RAJABZADEH[1*], M. ESPONDA[2] , L. CORDERO ESPINOSA[3]

[1*]Carleton Immersive Media Studio (CIMS), Bachelor of Architecture - Carleton University, Ottawa, ON, Canada
sepidehrajabzadeh@cmail.carleton.ca

[2] Associate Professor at the Azrieli School of Architecture - Carleton University, Ottawa, ON, Canada - 1125 Colonel By Dr, Ottawa, ON K1S 5B6
mariana_esponda@carleton.ca

[3] Bachelor of Architecture - National Autonomous University of Mexico (UNAM)
lailacorderoespinosa@gmail.com

Keywords: Felix Candela, Pabellón de Rayos Cósmicos, Hyperbolic Paraboloid, National Autonomous University of Mexico (UNAM), Photogrammetry, Digital Documentation, HBIM.

Abstract. *This paper presents a comparative approach between a digital documentation workflow of a hyperbolic paraboloid heritage building using contemporary tools versus a traditional documentation technique. This documentation was undertaken to better understand the building's structure, its evolution, and to assess the performance of this modern concrete structure for future seismic and damage analysis. Furthermore, this paper discusses the challenges related to producing a Heritage Building Information Model (HBIM) of this building using point cloud data in Autodesk's Revit BIM-authoring software. This project states the importance of a parallel study between the traditional and the contemporary documentation methods; which led to discoveries about the current state of the extrados in the hyperbolic parabola after several earthquakes. Upon analyzing the HBIM and comparing it to the historical drawings, we discovered a gap between the moisture barrier membrane and the concrete shell. Visualizing the building in 3D provides a deeper and more accurate understanding of the current state of this pavilion and is one of many advantages of using digital technologies. The insights provided by digital documentation techniques and analyzing the historical images of the pavilion showed that the curvature of the pavilion had changed over time. The results that we found imply two hypotheses. First, the profile of the curvature had been modified due to earthquakes, and second that the modification was due to improper maintenance of the pavilion, namely, multiple additions of the membrane layers. This could not have been detected by solely relying on traditional documentation techniques.*

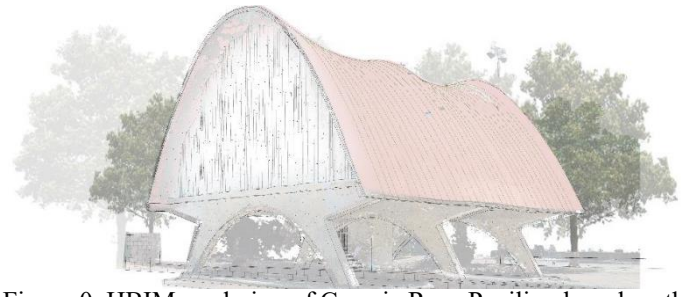


Figure 0. HBIM rendering of Cosmic Rays Pavilion based on the point cloud data

1 INTRODUCTION

Felix Candela was born in Spain and emigrated to Mexico in 1939. He experimented with the hyperbolic paraboloid form for most of his career. His first project using this innovative construction was the Cosmic Rays Pavilion completed in 1951 in Mexico City, located on the campus of the National Autonomous University of Mexico (UNAM) [1], with a 5/8" (16 mm) thin reinforced concrete shell at their crown, increasing to 1 ½" (37mm) at the base [2]. The structure still stands after 70 years; despite undergoing 3 major earthquakes in 1985, 1999, and 2017 with magnitudes over 7.1. The pavilion was the thinnest highly durable shell membrane [3]. The strength of the pavilion is derived from its hyperbolic paraboloid geometry and craftsmanship [4]. It was important for the structure to be as thin as possible since its original purpose as a physics laboratory required cosmic rays to pass through the roof and to a device inside for measuring neutrons [3]. The pavilion now serves as a storage space for board games and sports equipment.

The preliminary objectives for the project were to produce two sets of drawings from the existing pavilion using two methods: traditional and digital. The two sets of drawings were then overlaid and compared with the original construction drawings of the pavilion done by Candela. The comparison between the digital models and the original construction drawings revealed the extent of decay a building can go through without proper maintenance, and the importance of consistent conservation and maintenance efforts for this modern structure.

The traditional documentation was done by Laila Cordero over a period of 64 days in the Fall of 2018. Laila, a recent graduate from UNAM, applied a technique using ropes and measuring devices to document and produce a new set of 2D drawings of the current state of the building. The digital approach was done by Carleton University Students and Carleton's Immersive Media Studio (CIMS) from Canada over 49 days in May and June 2019. A team of four students spent six days in Mexico City recording the pavilion and one of them, Sepideh Rajabzadeh, continued working on the project until completion in Canada. This team used digital equipment such as DSLR cameras, a drone, and computer software to capture the existing geometry on site. The other 43 days were spent at CIMS in Canada processing the photogrammetry and 3D point cloud data, producing HBIM and 2D drawings.

This report aims to highlight the lack of research for the conservation of 20th century concrete shells in Mexico, thus generating a field of interest to encourage more professionals from diverse fields to address the issue of proper interventions for modern architecture.

1.1 Design

Colin Faber describes the original intent of this pavilion in his book *Candela: the shell builder* as a barrel shape. Candela changed it into a hyperbolic paraboloid because he stated "the extreme thinness would require the extra stiffening offered by this form" [4]. (Figure 1)

"Candela was able to achieve a solution endowed with compelling three-dimensional force. On the ground level, three paraboloid-shaped arches rise up with protruding support. The upper portion of the arches serves as the structural framework of the laboratory, and the encompassing concrete membrane seems to rest in place above it without being anchored to the ground. The

beauty of the design's three-dimensionality emerges directly from its clever devised proportion. As thin discs with well-balanced pressure and stress points, the arches do not seem to dominate the design: in light of the lateral bearing areas, the former seem to function like supports on the one hand and, because of their parabolic shape, convey a sense of elasticity on the other." [3]



Figure 1. **Left:** Cosmic Rays Pavilion, Mexico City, 1951 [5]. **Right**: Cosmic Rays Pavilion in Construction, Mexico City [6]

1.2 Construction

Colin Faber reveals that a few days before the construction started, the officials at UNAM approached Candela to see his calculations for the shape of the pavilion, but he had none. Instead, he wrote a few pages explaining why the shape would support itself. It was easier done than said, because the hyperbolic paraboloids can be achieved by straight boards crossing at 60-degree angles. After building Cosmic Rays, Candela went on to build and to explore more hyperbolic paraboloid structures. Later on in his career he realized that he did not need to add the three stiffening arches to add to the strength of the pavilion, Candela recognized that the shape was strong enough without the arches [4].

2 THE DOCUMENTATION WORKFLOW

Two methods were used to document the pavilion:

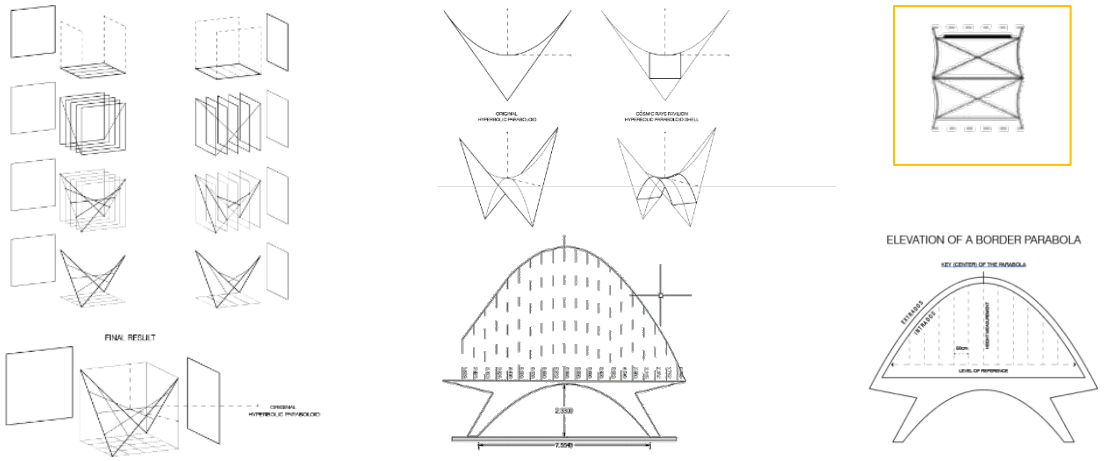
- Laila Cordero's traditional method: ropes and measuring tools by hand, and 2D drawings [7]
- CIMS' digital method: DSLR cameras and a drone to capture, photogrammetry, an HBIM produced from point cloud data, and 2D drawings.

2. 1 Laila Cordero's workflow

Laila, one of the authors, used an architectural surveying method that was a technique specifically applied to measure the geometry of the hyperbolic paraboloid shell. Laila created a complete analysis of the geometry of the pavilion shown in Figure 2.

To start the measurements, two essential elements were located: an axis and a reference level to identify the guide plane perpendicular to the parabola. Ropes were then installed across the interior connecting two legs of the parabolic columns at the bottom where they reached the floor. The rope was divided into 50 cm segments, and the height was measured by firing the distance meter twice which was positioned on a tripod. In the end, an average of the two measurements obtained at each point was calculated.

In this type of structure, it is possible to find an eccentricity between the center of the shell and the center of the floor. The eccentricity study was double checked by measuring the



a) b) Exterior Measurements b) Interior Measurements

Figure 2. a) Laila's analysis of the shell's geometry (formation of hyperbolic paraboloid shape using straight lines). b) Laila's drawings illustrating ropes that she used (the plan drawing in the yellow box) [7]

distance between the intersection of the diagonal ropes with respect to the ends of the supports and the center of the surface.

Laila Cordero's thesis suggests the hypothesis that Félix Candela's constructional drawings for Cosmic Rays Pavilion do not match the documented work she produced. The plans and elevations that were published in the books and magazines were of a preliminary nature, since they were drastically modified during construction [7]. This discrepancy between the constructional drawings and the as-built structure exists because hyperbolic paraboloid structures had not been constructed before in Mexico, and there was a learning curve for the construction process which did not allow for a perfect recreation of the design. Also, throughout studies of the archival information, it was noted that this building had been modified multiple times during the construction because of its experimental nature. These are just a few of the reasons why this building needs to be preserved and properly maintained [7].

2. 2 CIMS workflow while in Mexico (NPNT internship)

Part of the research for this project was supported by The *New Paradigm New Tools for Architectural Heritage in Canada* (NPNT) research program supported by the Social Sciences and Humanities Research Council of Canada (SSHRC). The internship program focuses on using emerging digital technologies including the digitization of existing buildings using tools such as Photogrammetry with DSLR cameras and computer software. Some of the benefits of this documentation method explored through the NPNT program are efficiency of labour and ease of gathering data, while providing great accuracy.

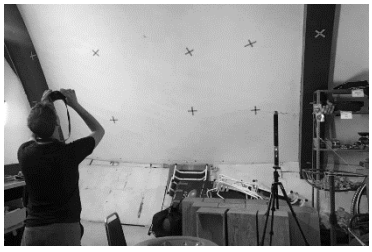


Figure 3. One of the Canadian students collecting interior photogrammetry data of the pavilion using a hand held DSLR camera.

The project started with an introduction to the site and a tour of the University and Mexico City. Then, the documentation of the Cosmic Rays Pavilion began. Techniques used during this time included the use of an Unmanned Aerial Vehicle (UAV) to capture aerial photography of the roof and its curvature, as well as the site. Also, handheld cameras including the Nikon D5200, 24.1 MP (APS-C), and Nikon 40mm Macro Lens were used for terrestrial photogrammetry. Furthermore, an interior material catalogue using a gray chart was recorded.

Throughout the week, more interior and exterior photogrammetric images were taken as well as context elevation photos. Then, the exterior material catalogue was documented as well as an exterior condition assessment. The quality of photogrammetric models and data were tested while on site as well as the quality of elevation photos using Bentley ContextCapture and Adobe Photoshop. This was important to ensure all documentation was collected prior to leaving the site.



Figure 4. **Left**: Two separate interior and exterior Point cloud data of the pavilion in CloudCompare software. **Central**: Shows interior point cloud data in Agisoft Photosca Software. **Right**: Shows exterior point cloud data in Agisoft Photosca Software - the blue squares show the location of the cameras [9].

2. 3 CIMS workflow after documentation (NPNT internship)

While students were getting to know the "contemporary tools" such as the photogrammetry software Agisoft Photoscan, it was decided to create the interior and exterior point cloud models separately and merge them together to create one unified point cloud model. (Figure 4)

2.3.1 Workflow in Agisoft Photoscan Software

The diagram in Figure 5 shows the complete digital workflow that was performed to produce a point cloud model from photogrammetric data. The team created target points on the interior wall of the pavilion. These targets were located in the software to stitch the images together. After importing all of the images into the Agisoft Photoscan software, target points, which had been attached to the roof during data acquisition, were used to align the images together. The previously measured distance between the targets was used to accurately scale the model in Agisoft Photoscan (Figure 6) [9].

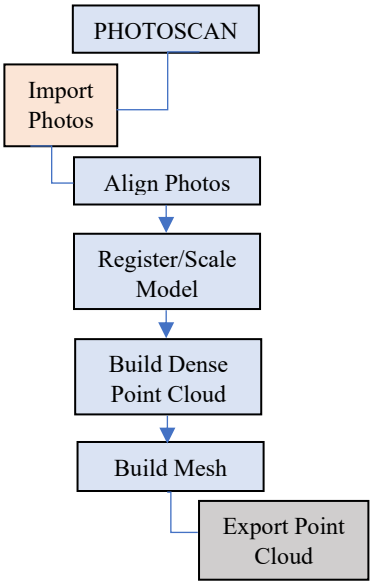


Figure 5. Photogrammetry workflow in Agisoft Photoscan [9].

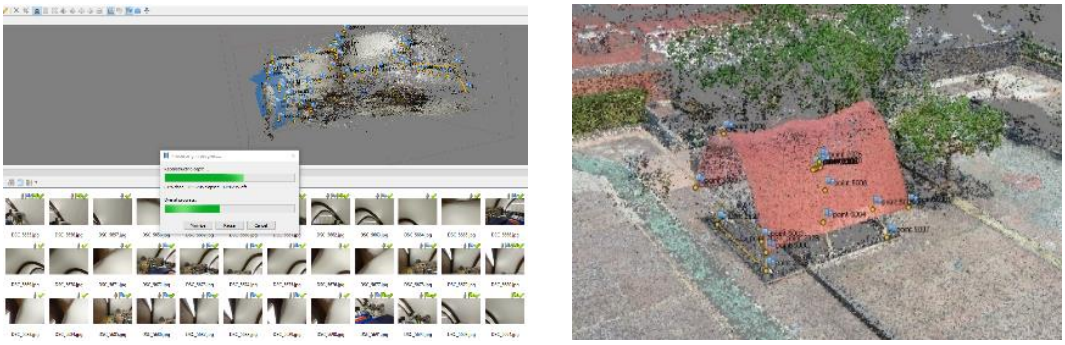


Figure 6. **Left**: Photo aligning process in Aigsoft Photoscan Software using the target points. **Right**: Dense cloud of the whole site created in Agisoft Photoscan Software [9].

Furthermore, a dense cloud was built to create the 3D point cloud model. Then, it was exported out of this software and imported into Revit to create an HBIM of the pavilion.

Once the point cloud data was imported to Revit, different strategies and protocols were applied to find the best methodology in order to create the double curved roof accurately. These different methods and their challenges are briefly mentioned in the challenge section of this paper. The method that proved to be most accurate is explained in the following section:

2.3.2 Workflow in Revit Software

Both interior and exterior point cloud data were imported into Revit. First, it was important to identify different elements of the building in order to understand how to model the pavilion efficiently. The roof membrane was considered an exterior element which was captured best via the exterior point cloud data; while the concrete shell itself was considered an interior element, which was captured best via the interior point cloud data. This increased the ease by which the membrane and the concrete shell could be modelled, since the different point clouds can be turned on and off in Revit using visibility and view settings. The strategy to capture the shape of the hyperbolic paraboloid is described in Figure 7. Through the roof, thin sections were taken by introducing vertical reference planes in close proximity to one another. Using the section box tool, the curvature of each section on the roof was carefully traced with model lines. Then, while selecting all the model lines, the "Create Form" tool was used to create a surface that followed the curvature, deformations, and deviations of the documented roof membrane.

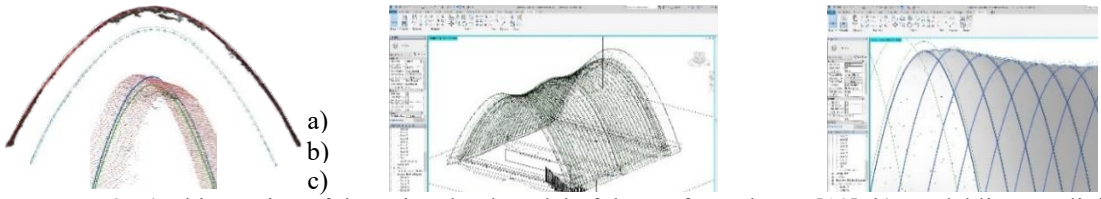


Figure 7. **Left**: a) Thin section of the point cloud model of the roof membrane [10], b) Model lines outlining the roof membrane and the concrete shell [11, 12], c) Thin section of the roof membrane with model lines [10]. **Central**: Roof membrane and the concrete shell model lines. **Right**: Green: The roof membrane model lines. Blue: The concrete shell model lines.

This process was repeated to model the concrete shell, using interior point cloud data. Lastly, both surfaces were given proper thicknesses based on their point cloud data (Figure 8). The HBIM includes structural and mass elements together, and is developed accurately based on the existing conditions and geometry of the pavilion because of the original objectives of the project. However, this model could further be studied for seismic load analysis by converting it into a model for structural analysis.

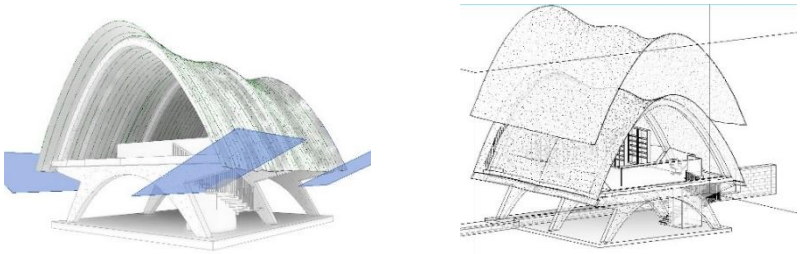


Figure 8. The surfaces of the roof membrane and the concrete shell are given thickness. Modeling them separately allows for exploded axo. diagrams and further studies of each component separately.

3 CHALLENGES

Since the objectives of this project were to introduce a new method of documentation, compare digital method with traditional method, and provide the local staff with the capacity to perform the digital documentation, there were many lessons learned for the students involved which are mentioned below.

3.1 Receiving drone data from Mexico

Although the drone was used while the team was still in Mexico, the drone data was only received in Canada while two weeks of the project was remaining. It was delayed due to security reasons prior to leaving Mexico. The Canadian team recorded the exterior data from ground level by handheld cameras and the point cloud model was missing data from the top of the roof. Once the drone info was received, the exterior photogrammetry was reprocessed to include the data from the top of the roof, aligned with the interior point cloud data, and then imported into Revit to be modelled (Figure 9).



Figure 9. **Left**: Drone movement (Left: First round, red dots are the shots taken and Right: Second round). **Central**: Exterior point cloud model before receiving drone information, the top part is missing. **Right**: Exterior point cloud model after receiving drone data.

3.2 Merging interior and exterior point cloud data manually

One of the main lessons learned in this project arose from the fact that the main strategy was to rely on point-to-point correspondences for the software to merge the interior and the exterior point clouds. Later on, it was understood that there was a lack of redundancy in the process. Although there were thorough hand measurements taken by the team, no ground control points were collected in case of the software failure to stitch the pictures together.

The one common area between the interior and exterior is the railing on the stairs. Although there are many images of this part, the software could not reconcile the two point cloud data fully buy itself. We surmised that this did not work because the exposure levels in the images of the railings from inside of the pavilion were very different from those of outside. Therefore, the software could not recognize matching features between the sets of photographs and failed to merge them (Figure 10).

Consequently, the two point clouds had to be merged manually, by matching all the measurements as closely as possible in order to reduce the errors.

Having encountered such challenges played an essential role in helping the team understand the limits of the software. Moving forward, it is recommended to have at least three common targets that are captured by both the interior and exterior photographs.



Figure 10. **Left**: Software not being able to merge the two point clouds properly – CloudCompare [13]. **Central**: Standing on the outside looking toward the railings which is the entrance to the pavilion. **Right**: Standing on the inside looking at the railings.

3.3 Location of the Building

Beyond the technical challenges of this work, there were other difficulties in the recording process. One of which was the location of the building: Cosmic Rays Pavilion is located on the busiest part of the campus of UNAM. The campus could not restrict access for the documentation work, so there were frequently many students near the pavilion. The team had to take a lot of images at different times of the day and different days of the week, with different weather and lighting conditions in order to record high quality images for the production of high quality point cloud data without people and other obstructions in the photos.

4. NEW DISCOVERIES

Once the HBIM was developed, more in-depth studies were done to understand how the building was constructed and evolved throughout time. One of the more interesting discoveries was that there is a gap between the red roof membrane and the hyperbolic paraboloid concrete shell. Further studies on the model revealed that this gap varies throughout the entirety of the pavilion and it is at its greatest in the middle of the roof (Figure 11).

Once this new piece of information was shared with Laila, she provided us with thermal images which strengthened our finding about the poor maintenance and vulnerable state of the concrete roof (Figure 12).

In Figure 12 the picture on the left shows an even distribution of heat on the roof membrane taken from outside, but the picture on the right shows uneven heat distribution on the concrete shell itself taken from the inside. The extent of the membrane failure was apparent in the concrete shell through the thermal images. The image reinforces the discovery of the gap between the roof membrane and the concrete shell, and the non-uniformity of the gap. This new piece of information shows the roof membrane has not been maintained properly over the years. It was speculated that the poor maintenance of the membrane may have led to cracks and openings in the membrane, which allowed water and moisture into the concrete shell resulting in its gradual deterioration.

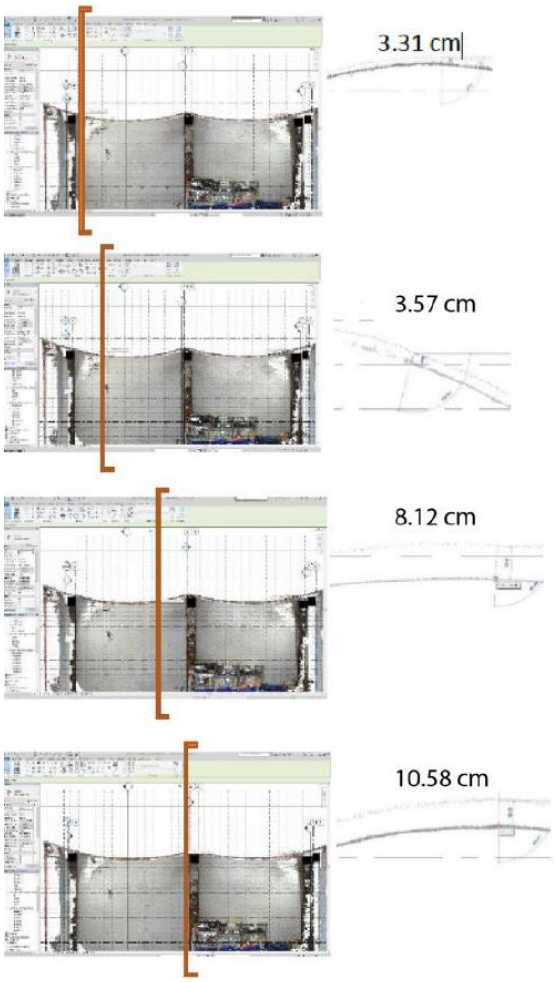


Figure 11. Series of sections showing the gap size between the roof membrane and the concrete shell – East Section

5 DELIVERABLES

At the start of the project, the team sought out to compare the different recording approaches, traditional and digital, but eventually realized that there were differences between the current state of the building and the original drawings.

When the two elevation drawings from each documentation method were overlaid, they aligned very well with negligible differences (Figure 13). However, once the new drawings were overlaid with the original construction drawings, they did not correlate (Figure 13).

Since Cosmic Rays Pavilion was Felix Candela's first hyperbolic paraboloid, he learned how to solve constructional challenges with this geometry along the way during construction. The lack of accurate construction, or as-built drawings of this pavilion means that if the building is not properly taken care of and gets damaged over time, it cannot be rebuilt as it looks now. The original construction drawings were only done as a guideline for how to approach the construction process of the hyperbolic paraboloid using reinforced concrete, however the execution and final product showed a different result.

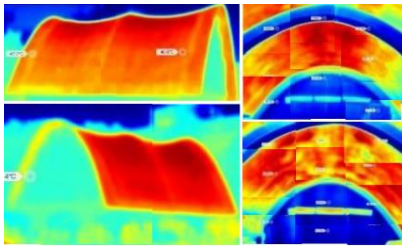


Figure 12. Thermal images [7]

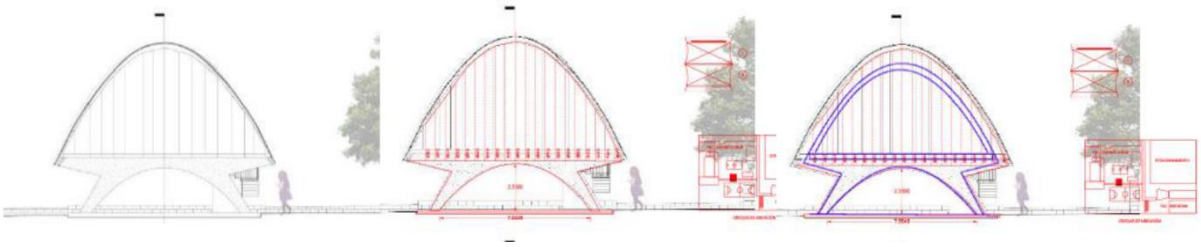


Figure 13. **Left**: 2D drawing done by CIMS using Revit software and point cloud data. **Central**: 2D drawing done by CIMS using Revit software and point cloud data (In red: Laila Cordero's drawing) [7]. **Right**: 2D drawing done by CIMS using Revit software and point cloud data (In red: Laila Cordero's drawing, in blue: Original construction drawing) [7,14]

6 CONCLUSION

After the HBIM creation of the pavilion, collaboration with Laila Cordero's traditional measurements, and a thorough study of the archival documents; the results show that the traditional and contemporary techniques produced the same results. However, using new digital techniques led to more in-depth discoveries of the state of the building. Also, our hypothesis, which speculated that there is a gap between the concrete shell and the roof membrane, which was a result of poor maintenance, was proven to be true. One of the stakeholders, Julio Valencia Navarro (Dirección General de Obras y Conservación) from UNAM, has since confirmed that there is a gap between the roof membrane and the concrete shell. Over the years, there has been moisture damage on the concrete shell due to the improper removal of the waterproofing roof membrane and this long-term damage is changing the curvature, and probably the capacity of the pavilion.

Although the project was missing control points, the relatively small scale of the project allowed for the interior and exterior point cloud data sets to be compiled manually. The target points were accurate to allow for a comprehensive point cloud data sets of the pavilion to be created using photogrammetry. While laser scanners can quickly produce a point cloud, they are less accessible and more expensive than DSLR cameras and drones. Using photogrammetry technique helped facilitate a maintenance approach to visually show which part of the building required immediate attention.

The collaborative and comparative approach developed for recording the as-found conditions of the Cosmic Rays Pavilion provided an opportunity for the local staff to have a meaningful learning experience about the value of this building and proper conservation techniques. Moreover, the HBIM can be studied further for seismic analysis on the concrete shell, damage scenarios, and risk management purposes in the future.

Finally, it was crucial to continually reference the archival images and to understand the traditional technique that was used in order to better understand the building, and to make sure the analyses provided by the contemporary tools were accurate.

7 ACKNOWLEDGEMENT

This research was supported by the Social Sciences and Humanities Research Council of Canada (SSHRC). Special thanks go to Professor Stephen Fai (principal Investigator of the New Paradigm/New Tools internship program and Director at CIMS), Lara Chow (Associate Director at CIMS), Mariana Esponda for leading the project, Carleton Immersive Media Studio (CIMS), Carleton University. Thanks to Adrian Soble, Khadija Waheed and Luis Panchi for helping gather the data for the project. Laila Cordero Espinosa for sharing her undergraduate thesis. Special thanks to Dr. Xavier Cortes Rocha, Dr. Juan Ignacio del Cueto Ruiz-Funes, Mtro. Julio Valencia Navarro (Dirección General de Obras y Conservación), Arq. Alberto Hernández, EPY CIG Company: Ing. Alejandro Rodriguez Garcia, Ing. Miguel Eduardo Chavez Huerta, and Alejandro Minero Huerta for exchanging their knowledge. National Autonomous University of Mexico (UNAM) for allowing the team to work on the site for data collection.

8 REFERENCES

[1] Interview with Dr. Juan Ignacio del Cueto (May 2019).
[2] Moreyra Garlock, M.E. Billington, D.P. *Félix Candela: Engineer, Builder, Structural Artist*. New Haven, Conn: Yale University Press (2008, p. 91).
[3] De Anda Alanis, E. X. *Candela.* Mexio: Taschen (2008).
[4] Faber, C. *Candela: The Shell Builder*. New York: Reinhold Pub. Corp., (1963).
[5] Cosmic Ray Pavilion. Architectuul.com. Available at: http://architectuul.com/architecture/cosmic-ray-pavilion
[6] Del Cueto Ruiz-Funes, J.I. CANDELA ACE. Acción Cultural Española (AC/E), TF Graphic Arts, (2011). Available at: https://www.accioncultural.es/media/Default%20Files/files/publicaciones/files/catalogo_candela.pdf
[7] Cordero Espinosa, L. G. Undergraduate tesis. *Pavellón de Rayos Cósmicos: pasado, presente y futuro.* National Autonomous University of Mexico, Mexico. (2019).
[8] Aimond, F. *F. Etude statique des voiles minces en paraboloide hiperbolique, travaillant sans flexion.* memories de la ASCC. INT. DESPONTS ET CHARPENTES. VOL. IV.
[9] Carleton Immersive Media Studio (CIMS). *Processing in Photoscan, pre-training workshop*. Carleton University, Ottawa, Canada. (2018).
[10] Godin A.A. *Algonquin BIM workshop tutorials.* Carleton Immersive Media Studio (CIMS) Carleton University, Ottawa, Canada. (2018).
[11] BIM - Revit 3D Organic Form 03 Tensile Structure. Non-Stop Learning101 Youtube. (2017). Available at: https://www.youtube.com/watch?v=9_jJBtKGLyc&fbclid=IwAR1PrpN6Gw7iNQWyo5KlQyPlef_1NJasWfYVf7_qX5ed8uDcop-rY9AcSVE
[12] Learn revit in 5 Minutes- Mass forme Felix Candela. Niko G. Youtube. (2016). Available at: https://www.youtube.com/watch?v=mxwGfNWwM-I&fbclid=IwAR1Bjmc4i23eThRigbOeo7rCvh1jpNtyn2_tn_-rbRe7XpEFTWDTEGq1tUk
[13] Aligning & Merging .DP Data in CloudCompare. DotProduct Youtube. (2016). Available at: https://www.youtube.com/watch?v=48xILOe9d7I&fbclid=IwAR0PieUuwsVVbM1--l764xM2HvTufFd-XLQuAvqML0BEfMjEu_nj-zfbzgM
[14] Mendoza Morfín, G. Campus Central C.U. Lecturas de un Patrimonio Vivo. Facultad de Arquitectura UNAM. (2019).

[15] Flelix Candela, Major Works. The Princeton University Art Museum, (2008). Available at: https://artmuseum.princeton.edu/legacy-projects/Candela/cosmicrays.html
[16] Morganti C., Bartolomei C. *Digital Survey and Documentation of La Habana Vieja in Cuba.* In: Ioannides M., Martins J., Žarnić R., Lim V. (eds) Advances in Digital Cultural Heritage. Lecture Notes in Computer Science, vol 10754. Springer, Cham. (2018).
[17] Ace D., Marrs J., Santana Quintero M., Barazzetti L., Demas M., Friedman L., Roby T., Chamberlain M., Duong M., Awad R. *Documenting Nea Paphos for Conservation and Management.* Carleton Immersive Media Studio (CIMS) Carleton University Canada, Politecnico di Milano, Department of Architecture, Built Environment and Construction Engineering Italy, Getty Conservation Institute U.S., Department of Antiquities of Cyprus., (2019).

12th International Conference on Structural Analysis of Historical Constructions
SAHC 2020
P. Roca, L. Pelà and C. Molins (Eds.)

NON-DESTRUCTIVE TECHNIQUES FOR CHARACTERISING EARTHEN STRUCTURES

ERNEST BERNAT-MASO[1*], ELITSA I. TENEVA[2], LUIS E. MERCEDES[2] AND LLUIS GIL[2]

[1]Department of Strength of Materials and Engineering Structures (RMEE). Serra Húnter Fellow
Universitat Politècnica de Catalunya (UPC-BarcelonaTech)
Building TR45, Campus Terrassa UPC. Colom 11, 08222 Barcelona, Spain
e-mail: ernest.bernat@upc.edu, litem.upc.edu (*corresponding author)

[2] Department of Strength of Materials and Engineering Structures (RMEE)
Universitat Politècnica de Catalunya (UPC-BarcelonaTech)
Building TR45, Campus Terrassa UPC. Colom 11, 08222 Barcelona, Spain
email: elitsa.ivanova@upc.edu; luis.enrique.mercedes@upc.edu; lluis.gil@upc.edu, litem.upc.edu

Keywords: Ultrasound transmission method; Rammed earth; Young's modulus; Modal analysis. Non-Destructive Inspection

Abstract. *Earthen architecture is one of the most relevant building technologies among heritage structures. However, mechanical properties are commonly obtained from destructive tests. To contribute at changing this trend, two non-destructive mechanical techniques (ultrasound and modal analysis) are studied to determine their ability at characterizing earthen materials and their possible correlation.*

To achieve these purposes, twenty cubic-shaped earthen specimens were produced for testing the capability of ultrasound transmission method to control moisture content and its evolution during drying process at different environments. Additionally, a real-scale rammed earth wall was built to assess the feasibility of using ultrasound technique to determine elastic dynamic Young modulus. This analysis was validated by indirect comparison with experimental modal analysis test results.

The most important findings are that the relationship between moisture content and ultrasound transmission speed is linear. This information is useful to control the drying process of earthen materials and to control the moisture content distribution on larger in-service structures. Finally, numerical simulation using ultrasound transmission data as input information allow to predict the vibrational response of the tested wall with an error around 3%.

1 INTRODUCTION

Earthen architecture has been traditionally analysed under the eye of the cultural heritage and preservation specialists. The corresponding building techniques and their performance have been extensively documented by several authors, like Miccoli et al. [1]. In addition, a recent

survey [2] points out that this technology is gaining attention again because of the increasing interest in sustainable building techniques.

In this context, scientific research on earthen building materials is experiencing a remarkable diversification. There are studies aimed to discuss the optimum particle size distribution and the suitable moisture content at production to achieve the best mechanical performance [3–5]. Other researches deal with the mechanical characterisation of earthen materials [6–11] and there is also a significant trend to research about the thermal inertia of earthen materials [12], which is one of their physical main advantages.

However, the moisture content is always highlighted as the most important parameter. In fact, in-situ measured mechanical properties depend on the water content and matric suction. Schroeder et al. [13], Bui et al. [14], Gerard et al. [15] and Champire et al. [16] presented interesting results on how moisture content affects different mechanical properties. Although the importance of moisture content, there is little research about how to determine this parameter using non-destructive techniques. In this line, it is worth highlighting the works by Chabirac et al. [17] and Aubert et al. [18], who used Time-Domain Reflectometry (TDR) and ultrasound transmission tests respectively to assess the moisture content.

Despite the evident relationship between moisture content and ultrasound transmission speed in earthen materials, there is not known research which uses this effect to control the evolution of the moisture content during the production process of earthen materials using ultrasonic non-destructive methods.

In another research line, modal analysis has been used on earthen structures to characterise their mechanical response. Two main research branches are observed: obtaining natural frequencies and damping ratios of existing buildings, like Bui et al. [19] did, or indirectly determine mechanical properties from experimental-numerical vibrational response fitting, as Bui et al. [20] and Aguilar et al. [21] did. In this second research trend, results are always compared with destructive compression tests. There are no studies which used another non-destructive method, e.g. ultrasound transmission technique, to validate the Young's modulus numerically adjusted from the experimental dynamic response from modal analysis.

Thus, the literature review reveals two main applications for ultrasound transmission method on earthen elements which require further research: (i) to control the drying process during the construction stage and (ii) to obtain the dynamic Young's modulus in a reliable way. This second application requires proving that the values measured with ultrasound transmission method are coherent with the values obtained with other dynamic tests like modal analysis. The aim of this paper is to provide knowledge on these two particular topics for the specific case of rammed earth.

2 MATERIALS AND METHODS

Cubic samples were produced to perform the study of the drying process using ultrasound measurements. A rammed earth scale wall was used to correlate ultrasound transmission method and modal analysis method through numerical simulations.

2.1 Materials and specimens

The particle distribution of the clayey-sand soil used to produce specimens is shown in Figure 1. Twenty rectangular prisms specimens (100mm x 100mm x 90mm), called cubic

specimens from now on, and a wall (900mm x 160mm x 1200mm) were built. The moisture content of the soil at the production time was 12.6% according previous researches [30].

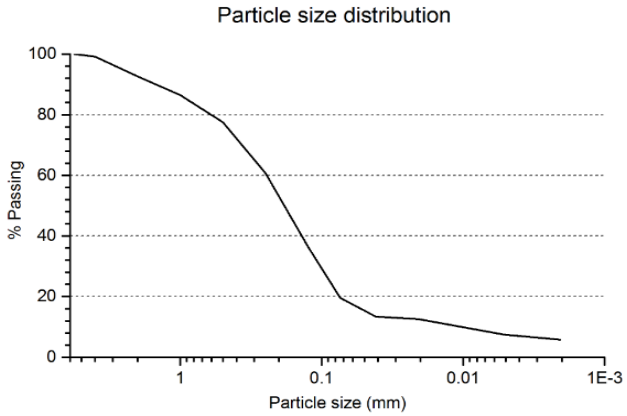


Figure 1: Particle size distribution of earthen material used to produce specimens

For the production of cubic specimens, the soil filling the mold was subjected to a compressive pressure of 200kPa applied at a constant rate of 2.5kPa/s. The apparent density of the specimens was determined just after unmolding them. The drying process of these specimens was controlled with ultrasound transmission technique after five different curing times, four in high humidity environment (RH>95%): 3days, 7 days, 14 days, 21 days and no curing in high humidity environment. Four specimens were subjected to each curing time. The list of the cubic specimens and their initial density are summarized in Table 1.

The wall was produced into a modular wood framework. Each earth layer was 13cm thick before any compression and approximately 10cm thick after applying a compressive stress of 200kPa. The bottom of the wall was built into a steel tool (see Figure 2a) which was 140mm width and 80mm depth. Analogously, the top layers of the wall (corresponding to the top 80mm) were manufactured with a reduced width of 140mm to place an identical steel tool on the top of the wall. These two steel tools were used later on to hold and move the rammed earth wall. The wall was unmolded 42 days after completing its construction and left drying at indoor environmental conditions.

2.2 Ultrasound transmission test method

Ultrasound transmission tests on cubic specimens started 3 days after their production in the case of specimens C0 and 3 days after removing them from the high humidity environment for the rest of the specimens. These were repeated daily while specimens were drying at indoor conditions until measurements became stable. Specimens were measured and weighed before and after every ultrasound test in order to take into account the effect of the contact paste (petroleum jelly).

Ultrasound transmission test method was also applied on the wall to control its drying process and to obtain the dynamic Young's modulus of the used rammed earth. The ultrasound transmission speed (V) was measured in three points (see Figure 2a) at five ages. In addition, a single measurement at mid-height was performed before carrying on the modal analysis. This last measurement was used to obtain the dynamic Young's modulus (E_{us}) applying equations (1) and (2).

$$E_{us} = \frac{\rho V^2}{K} \tag{1}$$

$$K = \frac{1-\upsilon}{(1+\upsilon)(1-2\upsilon)} \tag{2}$$

where υ is Poisson's ratio, ρ the density of rammed earth and V the ultrasound transmission speed.

Table 1: Cubic specimens

Curing time (d)	*Specimen*	*Density fabrication (kg/m³)*	*Density after curing (kg/m³)*
0	C0_1	1.89	---
	C0_2	1.83	---
	C0_3	1.81	---
	C0_4	1.84	---
3	C3_1	1.88	1.90
	C3_2	1.85	1.85
	C3_3	1.85	1.85
	C3_4	1.86	1.87
7	C7_1	1.90	1.82
	C7_2	1.86	1.88
	C7_3	1.86	1.99
	C7_4	1.87	1.98
14	C14_1	1.87	1.94
	C14_2	1.83	1.86
	C14_3	1.84	1.87
	C14_4	1.87	1.88
21	C21_1	1.85	1.89
	C21_2	1.84	1.96
	C21_3	1.83	1.84
	C21_4	1.86	1.98

2.3 Modal analysis test method

The wall was subjected to a modal analysis six months after its construction. 90 points, where wall was impacted afterwards, were defined. A unidirectional accelerometer was placed in the point number 71 (see Figure 2a) oriented in the out-of-plane direction. An impact hammer was used to excite the wall impacting on those 90 points. The cross-spectrum of the Fast Fourier Transformed (FFT) hammer and accelerometer signals was calculated using PULSE™ software analysis platform software. Data was post processed using ME'scopeVES™ software to obtain modal shapes and their corresponding oscillation frequency and damping.

During the experimental data acquisition, the wall was hanged so the boundary conditions were clear to compare with simulation results.

2.4 Numerical simulation

The numerical modal analysis of the wall was implemented using ANSYS® Workbench platform to compare with modal experimental data. The idea was to use the dynamic Young's

modulus obtained using ultrasound transmission technique (E_{us}) as an input of the model. Then, the simulated vibrational response (modal shapes and frequencies) was compared with the experimental response obtained from modal analysis.

A three-dimensional geometric model of the wall was defined using its real dimensions. The geometry of the steel tools was simplified but maintaining its volume and position of the center of gravity (see Figure 2b). Rammed earth was defined as an isotropic linear elastic material. The Young's modulus, determined using ultrasound transmission technique (1418MPa according with results in section 3), was introduced. The density of the rammed earth was experimentally determined obtaining a value of 1780 kg/m^3 and the Poisson's ratio was set to 0.35 according with literature [27].

The wall was discretised using hexahedral elements whereas the complex geometry of the steel tools recommended using tetrahedral elements for these parts. The model had 5289 elements in total. In addition, the contact between the parts representing the steel tools and the wall were defined as perfectly bonded. Finally, no boundary conditions were introduced. This approach allows neglecting the rigid-solid movements from the numerical analysis.

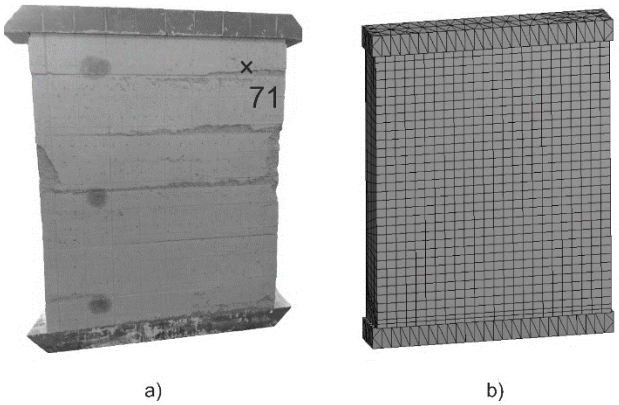


Figure 2: a) Rammed earth wall with impact grid lines for modal analysis, position of accelerometer and positions for ultrasonic tests b) Geometric model and discretisation mesh for the numerical simulation.

3 RESULTS

After performing experimental tests and numerical simulations, the following results are obtained:

Figure 3 summarizes the values of the moisture content and ultrasound transmission speed relationships and evolution along curing time for the tested cubes. It is noticed that the drying process finished with a constant moisture content around 1%. Ultrasound transmission speed is between 1400 m/s and 1500 m/s for all specimens in the "dry" state (constant moisture content). Finally, a linear relationship between the moisture content and ultrasound transmission speed is envisaged when the moisture content is below 2%.

Similarly, the evolution of the ultrasound transmission speed along time was also determined for the compressed earth wall at three different heights. Different drying rate is observed depending on the position of the material, being the top part the drier one and the bottom part the one with more moisture content (lower transmission speed), according with the data presented in Figure 4.

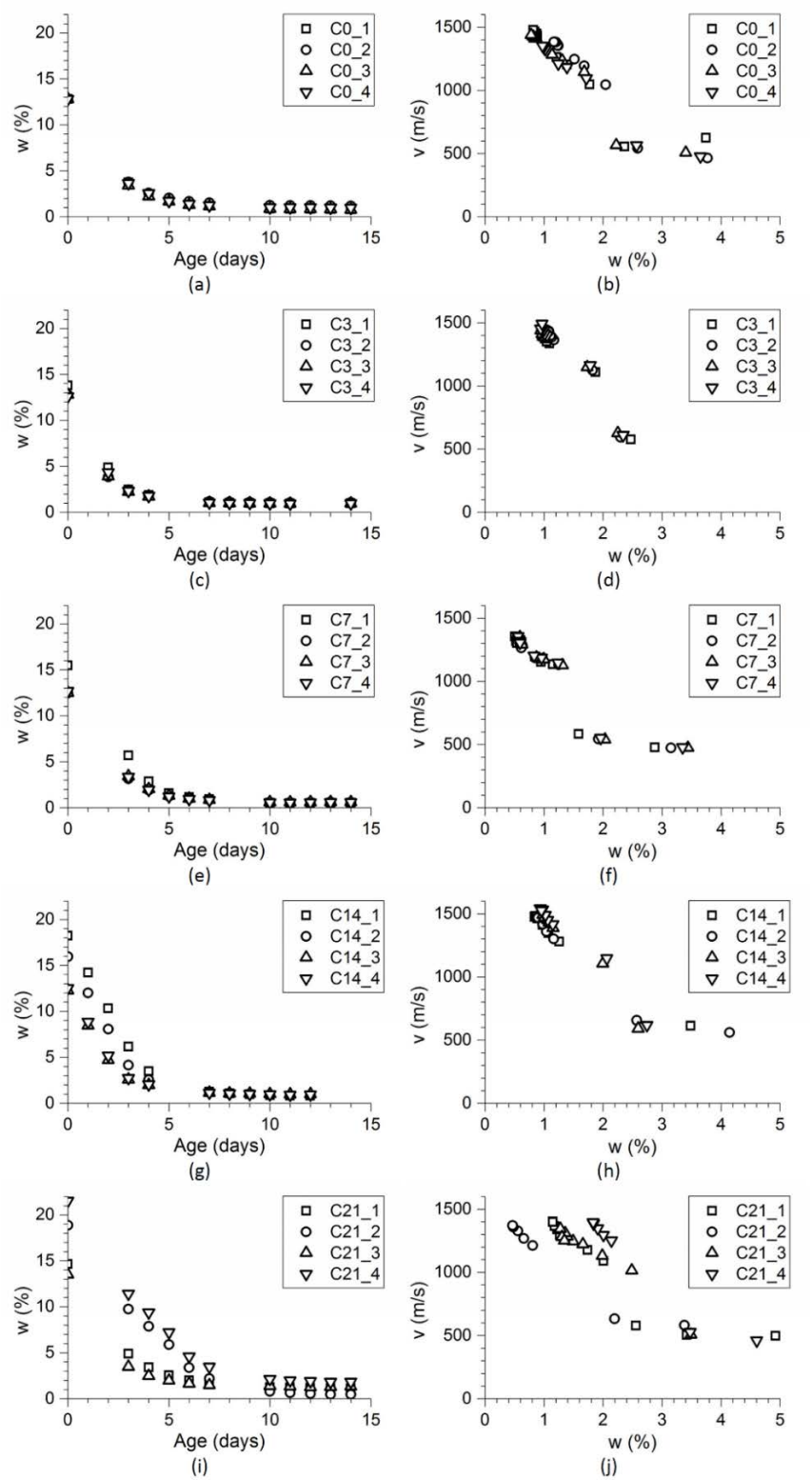


Figure 3: Moisture content evolution during the drying process (left) and relationship between the moisture content and the ultrasound transmission speed (right).

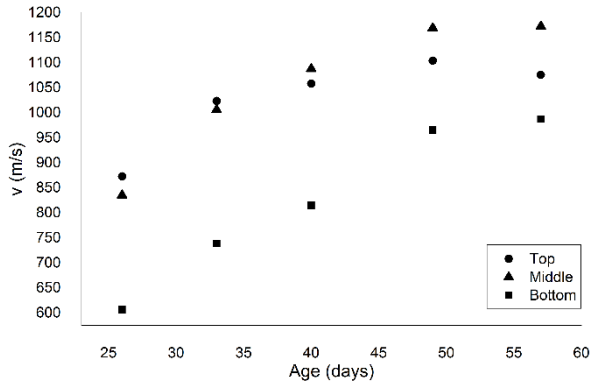


Figure 4: Ultrasound transmission speed at different heights of the compressed earth wall along the drying process.

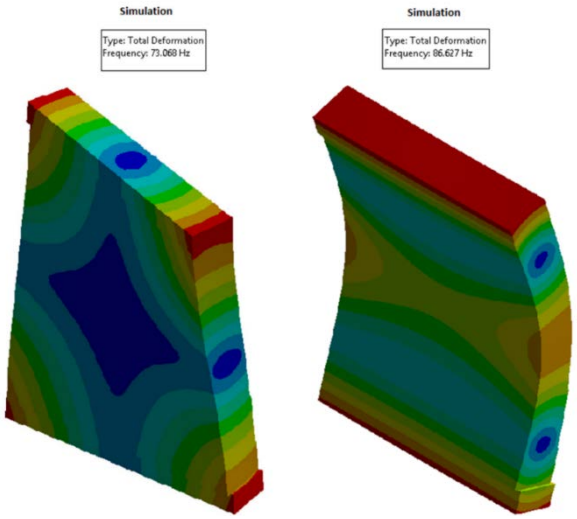


Figure 5: Simulated modal shape of the first mode (left) and the second mode (right)drying

Finally, before modal analysis, the ultrasound transmission speed measured at mid-height of the wall was 1130 m/s. That corresponded to a dynamic Young's modulus of 1418 MPa, which was calculated with equations (1) and (2) and considering a Poisson's coefficient of 0.35 and the measured density of 1780 kg/m^3.

Figure 5 summarizes the results (modal shapes and frequencies) of numerical simulations and experimental modal analysis. Numerical simulation was carried out using the Young's modulus determined by ultrasound transmission technique. Only the first two vibration modes were experimentally determined. Comparing numerical and experimental results shows good agreement: $f_{EXP_mode_1}$ = 69.4Hz vs. $f_{SIM_mode_1}$ = 73.1Hz (5.3% error) and $f_{EXP_mode_2}$ = 87.2Hz vs. $f_{SIM_mode_2}$ = 86.6Hz (0.7% error). According with experimental results, the damping for the first mode (4.1%) was greater than for the second mode (2.4%). This particular result would indicate that the second modal shape might define the vibrational response of the wall at long-term because the amplitude of the first mode decreases faster

4 DISCUSSION

4.1 Ultrasound transmission method to control the drying process

As mentioned before (see Figure 3), there is a linear (V = Sw +b) relationship between ultrasound transmission speed (V) and moisture content (w) of earthen cubes for moisture content values below 2%. It was experimentally observed that ultrasound transmission speed increased when the moisture content decreased during the drying process of the specimens. In addition, there is a qualitative change in the state of the soil when the moisture content is around 2%. At this moisture level, the V-w curves showed a sudden increase of speed transmission, which may be explained because the soil turns from a malleable matter, which barely transmits ultrasound waves, to a stiff, fragile solid material. In addition, this change indicates that the nature of the water dissipated at moisture content over 2% is free water which occupies the largest voids in the soil structure whereas the water dissipated at moisture content below 2% is interstitial water placed between particles. Matric suction is significantly increased when this second type of water dissipates until reaching the hygrometric equilibrium with the environment, causing the ultrasound transmission speed increase.

Regarding the coefficients of the linear fitting (S and b), it is observed that the independent term (b) can be considered constant with an average value of 1837.5 m/s (COV = 10%). In contrast, it is observed that the slope of the V-w linear fitting (S) linearly depends on the time the specimens were cured into a high humidity environment (t). Fitting these data (S and t) without considering specimens not exposed to high humidity environment, led to the following relationship (R^2=0.98):

$$S = 10.6t - 602 \tag{3}$$

$$V = 1837.5 - Sw \tag{4}$$

So the final V-w relationship is presented in (4).

The initial distribution of the water content between voids and interstitial spaces may be influenced by the fact of curing or not curing the specimens. It seems that curing specimens for a short period of time contributes to increase their interstitial amount of water, whereas long curing periods in a high humidity environment contribute to reduce the interstitial water but increasing the proportion of free water in the voids. In addition, at the end of the drying process all specimens showed similar moisture content independently of their initial curing period. Thus, if all specimens reached a similar final state in an analogous time but departing from different moisture contents, the rate of water dissipation had to be different, being faster in those specimens subjected to longest curing times. This statement supports the idea that specimens subjected to long periods of curing in high humidity environment had larger ratio of free water out of interstitial water. These cases showed faster initial drying because free water is easier to dissipate than interstitial water.

Experimental evidences showed that drying process of an earthen structure depends on its geometry, the earthen mixture composition, its production moisture content and the environmental conditions. Thus, ultrasound transmission method needs to be calibrated for every particular application. For example, the threshold value of the ultrasound transmission speed, over which the drying process has finished and hygrometric equilibrium is attained, is set at 1100m/s for the tested compressed earth specimens.

However, it is feasible to directly apply ultrasound transmission method to control the drying process and check that the hygrometric equilibrium has been reached by means of the stabilization of ultrasound transmission speed. This approach would not require particular calibration.

4.2 Ultrasound transmission method to obtain dynamic Young's modulus

The dynamic Young's modulus of the compressed earth used in the wall was correctly predicted by using the results of ultrasound transmission technique to compare numerical simulations with the experimental modal analysis. The simulation carried out considering a Poisson's ratio of 0.35 and calculating the Young's modulus from the ultrasound transmission speed correctly met the experimental results obtained with modal analysis. The average error on the eigenfrequencies was around 3%, supporting the idea that combining ultrasound transmission method with modal analysis is an easy non-destructive technique to evaluate the dynamic Young modulus of massive earthen materials and their corresponding Poisson's ratio by sensitivity analysis on this second parameter once the Young's modulus is set from ultrasound transmission technique. In the particular study case presented, Poisson's ratio of 0.35 showed lower error than other tested values in simulation.

Finally, the shape and order of the first and the second vibrational modes are the same in simulation than in modal analysis, supporting the idea that choosing clear boundary conditions is essential to obtain experimental results to be compared with a numerical simulation.

5 CONCLUSIONS

The following conclusions arise from the conducted research:

- Ultrasound transmission method is useful to identify the hygrometric equilibrium of earthen materials but requires a specific calibration process to correlate ultrasound transmission speed with moisture content.
- A methodology combining ultrasound transmission method and modal analysis is suitable for determining the dynamic Young's modulus of earthen materials and their corresponding Poisson's coefficient.

In addition, the results of the study pointed a future research topic:

- Studying the source of the water being dissipated and its relationship with the sudden change in V-w curve at a moisture content around 2%.

Finally, it is worth remarking that ultrasound transmission method has proved to be efficient at determining mechanical properties of raw earthen materials and controlling the drying process that characterize their production.

Acknowledgements. First author is a Serra Húnter fellow and acknowledges the support of Serra Húnter Programme.

REFERENCES

1. Miccoli L, Müller U, Fontana P. Mechanical behaviour of earthen materials: A comparison between earth block masonry, rammed earth and cob. *Constr Build Mater*. 2014;61:327-339. doi:10.1016/j.conbuildmat.2014.03.009

2. Niroumand H, Zain MFM, Jamil M. A guideline for assessing of critical parameters on Earth architecture and Earth buildings as a sustainable architecture in various countries. *Renew Sustain Energy Rev*. 2013;28:130-165. doi:10.1016/j.rser.2013.07.020
3. Ciancio D, Jaquin P, Walker P. Advances on the assessment of soil suitability for rammed earth. *Constr Build Mater*. 2013;42:40-47. doi:10.1016/j.conbuildmat.2012.12.049
4. Jiménez Delgado MC, Guerrero IC. The selection of soils for unstabilised earth building: A normative review. *Constr Build Mater*. 2007;21(2):237-251. doi:10.1016/j.conbuildmat.2005.08.006
5. da Rocha CG, Consoli NC, Dalla Rosa Johann A. Greening stabilized rammed earth: devising more sustainable dosages based on strength controlling equations. *J Clean Prod*. 2014;66:19-26. doi:10.1016/j.jclepro.2013.11.041
6. Maniatidis V, Walker P. Structural Capacity of Rammed Earth in Compression. *J Mater Civ Eng*. 2008;20(3):230-239. doi:10.1061/(ASCE)0899-1561(2008)20:3(230)
7. Ciancio D, Gibbings J. Experimental investigation on the compressive strength of cored and molded cement-stabilized rammed earth samples. *Constr Build Mater*. 2012;28(1):294-304. doi:10.1016/j.conbuildmat.2011.08.070
8. Morel JC, Pkla A. A model to measure compressive strength of compressed earth blocks with the "3 points bending test." *Constr Build Mater*. 2002;16(5):303-310. doi:10.1016/S0950-0618(02)00023-5
9. Khadka B, Shakya M. Comparative compressive strength of stabilized and un-stabilized rammed earth. *Mater Struct*. 2015;49(9):1-11. doi:10.1617/s11527-015-0765-5
10. Aubert JE, Maillard P, Morel JC, Al Rafii M. Towards a simple compressive strength test for earth bricks ? *Mater Struct*. 2015;(APRIL):1641-1654. doi:10.13140/RG.2.1.4641.4242
11. Jayasinghe C, Kamaladasa N. Compressive strength characteristics of cement stabilized rammed earth walls. *Constr Build Mater*. 2007;21(11):1971-1976. doi:10.1016/j.conbuildmat.2006.05.049
12. Heathcote K. El comportamiento térmico de los edificios de tierra. *Inf la Construcción*. 2011;63(523):117-126. doi:10.3989/ic.10.024
13. Schroeder H. La transferencia de humedad y el cambio en la resistencia durante la construcción de edificios de tierra. *Inf la Construcción*. 2011;63(523):107-116. doi:10.3989/ic.10.023
14. Bui QB, Morel JC, Hans S, Walker P. Effect of moisture content on the mechanical characteristics of rammed earth. *Constr Build Mater*. 2014;54:163-169. doi:10.1016/j.conbuildmat.2013.12.067
15. Gerard P, Mahdad M, Robert McCormack A, François B. A unified failure criterion for unstabilized rammed earth materials upon varying relative humidity conditions. *Constr Build Mater*. 2015;95:437-447. doi:10.1016/j.conbuildmat.2015.07.100
16. Champiré F, Fabbri A, Morel JC, Wong H, McGregor F. Impact of relative humidity on the mechanical behavior of compacted earth as a building material. *Constr Build Mater*. 2016;110:70-78. doi:10.1016/j.conbuildmat.2016.01.027
17. Chabriac PA, Fabbri A, Morel JC, Laurent JP, Blanc-Gonnet J. A procedure to measure the in-situ hygrothermal behavior of earth walls. *Materials (Basel)*. 2014;7(4):3002-

3020. doi:10.3390/ma7043002
18. Aubert JE, Gasc-Barbier M. Hardening of clayey soil blocks during freezing and thawing cycles. *Appl Clay Sci*. 2012;65-66:1-5. doi:10.1016/j.clay.2012.04.014
19. Bui QB, Hans S, Morel JC, Do AP. First exploratory study on dynamic characteristics of rammed earth buildings. *Eng Struct*. 2011;33(12):3690-3695. doi:10.1016/j.engstruct.2011.08.004
20. Bui Q-B, Morel J-C. First Exploratory Study on the Ageing of Rammed Earth Material. *Materials (Basel)*. 2015;8(1):1-15. doi:10.3390/ma8010001
21. Aguilar R, Marques R, Sovero K, Martel C, Trujillano F, Boroschek R. Investigations on the structural behaviour of archaeological heritage in Peru: From survey to seismic assessment. *Eng Struct*. 2015;95:94-111. doi:10.1016/j.engstruct.2015.03.058

12th International Conference on Structural Analysis of Historical Constructions
SAHC 2020
P. Roca, L. Pelà and C. Molins (Eds.)

PATHOLOGICAL AND STRUCTURAL ASSESSMENT OF A RESIDENTIAL BUILDING IN LOTA, CHILE

M. CHÁVEZ[1*], F. MACAYA[2], E. NÚÑEZ[3] AND C. OYARZO[4]

[1]Department of Civil Engineering, Universidad Andres Bello, 4300866 Concepción, Chile; manuel.chavez@unab.cl(*corresponding author)

[2]Civil Engineer, Universidad Andres Bello, 4300866 Concepción, Chile; f.macayapalma@uandresbello.edu

[3]Department of Civil Engineering, Universidad Católica de la Santísima Concepción, 4090541 Concepción, Chile; enunez@ucsc.cl

[4]Department of Civil Engineering, Universidad Católica de la Santísima Concepción, 4090541 Concepción, Chile; coyarzov@ucsc.cl

Keywords: Concrete Pathologies, Structural Assessment.

Abstract.

The urban development of Lota city (Chile) was strongly influenced by the coal-mining industry during 19th and 20th century. Virtually, the entire city was built, initially, by Matias Cousiño's Coal Company and, later, by the National Coal Company of Chile (ENACAR). At the beginning of the 21st century, the city began to experience a decline because of the closure of coal mines. This situation affected not only the economy and employment of the city, but also the maintenance of its infrastructure and the conservation of historical buildings.

The "Anibal Pinto Building" is a 5 stories reinforced concrete and masonry structure, built in 1966. Besides of an aggressive coastal environment and poor maintenance, this building has experienced one major earthquake (Mw 8.8 in 2010). As a consequence, cracks, concrete spalding and reinforcement corrosion is observed in several structural elements.

To evaluate the current state of the building and determine it remaining operation life, a structural assessment procedure was implemented based on field explorations, laboratory analysis and numerical modeling. Field explorations considered tests to identify carbonation, humidity, porosity, concrete hardness. While, laboratory analysis included compression test of concrete cores extracted from the building. These investigations were developed with the aim of determine the mechanical properties of buildings materials and for identifying pathologies that affects reinforced concrete.

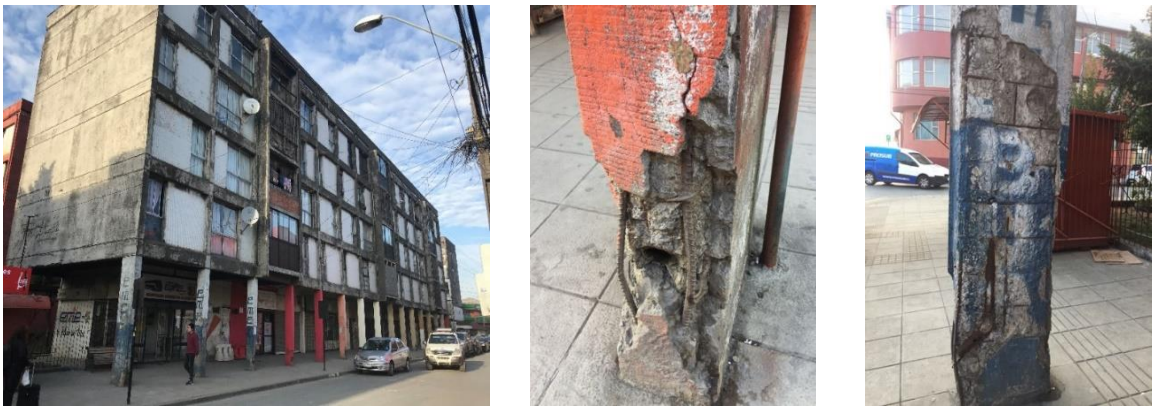
The experimental data was used to elaborate a finite element model in SAP 2000 to estimate building performance compared to the current seismic regulation in Chile.

1 INTRODUCTION

Natural events, such as earthquakes, floods, fires and climate conditions, affect the structural performance of buildings. The accumulated effect of these events may progressively deteriorate the structure, becoming a pathology that needs to be treated to restore structural safety and serviceability to buildings [1-4]. The analysis of pathologies on reinforced concrete structures aims to detect and quantify accumulated damage to provide information to make decision regarding to repairing, retrofitting or demolishing the structure [5-7]. The most common pathologies on reinforced concrete structures are oxidation and corrosion of rebars, concrete spalding and carbonation, cracking, settlement and creep, in addition to problem related to design and construction errors or geometry alterations [8-10].

The research presented here corresponds to a pathological and structural assessment of the "Anibal Pinto Block", located in Lota, Chile. Lota´s urban development was strongly influenced by the coal-mining industry during 19th and 20th century. Virtually, the entire city was built, initially, by Matias Cousiño's Coal Company and, later, by the National Coal Company of Chile (ENACAR). At the beginning of the 21st century, the city began to experience a decline because of the closure of coal mines. This situation affected not only the economy and employment of the city, but also the maintenance of its infrastructure and the conservation of historical buildings.

The "Anibal Pinto Block" is a five stories residential building structured on reinforced concrete frames and shear walls, with masonry partition walls. All connected by a reinforced concrete slab that provides rigid diaphragm conditions. The building has 47.5 m x 8.8 m in plan and a total height of 13,5 m. The ground level has a commercial use, while the upper levels have 8 apartments per floor. This building was constructed in 1966 and at that moment no seismic regulation was mandatory in Chile, but engineering designs were already strongly influenced by the traumatic experience of the Mw 9.5 Valdivia earthquake (1960). Considering its age, the Anibal Pinto Block has been exposed for more than 50 years to an aggressive costal environment and has experienced the Mw 8.8 Maule earthquake in 2010 [11]. Currently, this structure presents extensive damage that may imply a potential risk to community (Figure 1). Hence, a structural assessment was required to decide what action needs to be taken.



(a) (b) (c)

Figure 1: Anibal Pinto Block.
(a) General view, (b) damage on internal columns, and (c) damage on lateral column

2 METHODOLOGY

The study presented here considers a complete damage survey, and field and laboratory tests consisting of sclerometric, carbonation, humidity and porosity measurements, in addition to concrete core extraction for compression tests. This information was used to elaborate numerical models to evaluate the seismic performance of the building under undamaged and damaged conditions.

3 EXPERIMENTAL PROGRAM

3.1 Damage survey

A survey was conducted to identify damage on reinforced concrete elements, such as, cracks, spalding, carbonation, corrosion and rebars buckling or failure [12]. This information was presented as a color diagram (Figure 2) representing damage severity according to Table 1. It can be observed in Figure 1 that the base columns suffered moderate to severe damage, being at least seven columns on a condition near to collapse. Hence, this level was considered as the critical zone.

One particular condition observed in some columns (1-3-4-6-8-9-11-13-14-16) was the inclusion of a steel pipe inside of the column core to be used a rainwater drainage (Figure 3). In most cases, these pipes have suffered severe corrosion affecting the surrounding concrete and rebars.

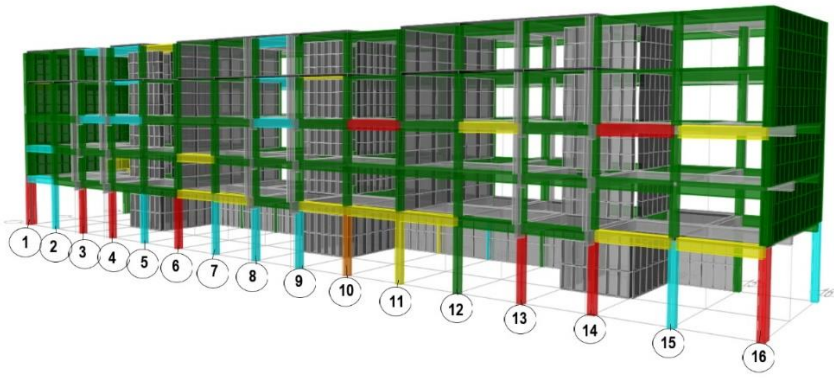


Figure 2: Damage diagram of the building



Figure 3: Steel pipe

Table 1: Damage classification

Damage severity	Damage description
None	No damage
Moderate	Cracks and fissures
Strong	Exposed rebars
Severe	Rebars buckling and/or corrosion
Near Collapse	Reduction of concrete effective area
No information	No information

3.2 Concrete carbonation

Carbonation is the process in which the atmospheric carbon dioxide (CO_2) reacts with alkaline components of the aqueous phase of concrete, resulting in a neutralization of the entire material. Because of this, the pH of the concrete (pH≈13) decreases to below 10 [13]. The advance speed of the carbonation is mainly a function of the dosing, compacity, homogeneity, moisture and porosity of concrete, being the last two the most important factors [14, 15].

In the case of moisture, if the pores are completely dry, the CO_2 will not be able to react and, if they are completely saturated, their penetration will be slow, due to the low solubility of the CO_2 in the water. Only when the pores are partially filled with water (between 50% and 80% of the relative humidity) do the optimum conditions for carbonation occur [16].

In relation to porosity, the smaller capillary pores are generally always saturated with moisture, therefore, CO_2 is inaccessible. On the contrary, porous concretes carbonate at higher speed.

The concrete gives protection to steel rebars by two mechanisms. On the one hand, it is a physical barrier that separates it from the environment and, on the other, the liquid enclosed in the pores of concrete is an electrolyte that can form a protective oxide in a lasting way. When the concrete is in the process of carbonation, a breakage of this protective film towards the steel occurs, giving rise to the corrosion of the reinforcements and loss of the strength of the concrete [17, 18]. This triggers a triple consequence: (i) steel decreases its section because of corrosion, (ii) the concrete cracks due to the pressure exerted by the expansive oxide, and (iii) reinforcement-concrete adherence decreases or disappears.

The most common method for detecting concrete carbonation is spreading the concrete surface with an acid-base indicator solution. Usually, phenolphthalein diluted in ethyl alcohol and distilled water was used [19]. After applying the solution, the surface turns into a violet color when it is not carbonated. On the contrary, it remains colorless when the surface is carbonated [20, 21]. In our study, this test was carried out in concrete coating of columns of the ground floor (critical area).

Together with the above, 27 concrete core samples were extracted and tested to determine the depth of the carbonation. Figure 4 shows the results of a carbonation test performed on columns in the front of the building. All the coating mortar samples extracted from the columns have carbonation, and penetration into concrete was also observed.



Figure 4: Test results of carbonation with phenolphthalein solution.
(a) Partially carbonated sample, and (b) Fully carbonated sample

3.3 Concrete porosity and humidity

Relative humidity (RH) and porosity accessible to water (η) were determined for the critical zone. Relative humidity was measured by an infrared digital double laser thermometer (EXTECH Model 42570), while porosity was determined from the extracted samples by equation (1) according to ASTM C642-13 [22]:

$$\eta = \frac{m_{sat} - m_{dry}}{m_{sat} - m_{sub}} \quad (1)$$

where m_{sat} is the water-saturated mass of the test specimens, m_{sub} is the water-submerged mass of the test specimens, and m_{dry} is the oven-dried mass of the test specimens.

The representative porosities and humidity of the concrete in the critical zone were defined as the average value of 27 specimens (Table 2).

Table 2: Results of Porosity and Relative Humidity

Representative Humidity	64 %
Representative Porosity	15 %

3.4 Steel corrosion

Reinforcement steel bar samples were extracted from the ground level columns. Steel quality was classified as A440-280 H [23] (f_y = 280 MPa and f_u = 440 MPa) for longitudinal rebars and stirrups.

Table 3 shows data of steel rebars in columns of the ground floor. It can be observed significant loss of cross section of longitudinal rebars due to corrosion (diameter 18 and 22), while in the case of stirrups, they retain their initial 6 mm cross section. However, some stirrups have failed at the base of the columns, inducing buckling in the longitudinal steel rebars. The spacing between stirrups corresponded to 200 mm. It should be noted that the deterioration of the steel coincides with the type of damage classified as Near Collapse on Table 1.

Table 3: Steels in columns

Column	Original rebar diameter (mm)	Corroed rebar diameter (mm)	cross section loss
Front Columns	18	15	17%
	25	25	0%
Rear Columns	18	15	17%
	22	21	5%

3.5 Concrete characterization

Along with the damage survey, information was collected in order to mechanically characterize the concrete. A total of 64 trials were conducted with Schmidt´s hammer. (4 trials for each column of the critical area). Each of these tests consisted of 10 horizontal measurements performed following the procedure described in the NCh. 1998 Of.89 [24] and ASTM C805 [25]. On the other hand, 4 compression tests were carried out in concrete cores

extracted from 4 columns of the critical zone. The results obtained from both tests are presented in Table 4.

Figure 5 shows a good level of linear correlation between Schmidt´s hammer measurements and compression tests [26]. From these results, it was determined that the lowest resistance (20 MPa) was observed in the critical zone (ground level columns), while the upper levels have resistances around 35 MPa.

Table 4: Results of concrete characterization tests

Column	Location	Schmidt´s hammer (MPa)	Compressive Strength (MPa)
5	Front	34	37,6
5	Rear	23	24,6
12	Front	39	41,7
12	Rear	34	34

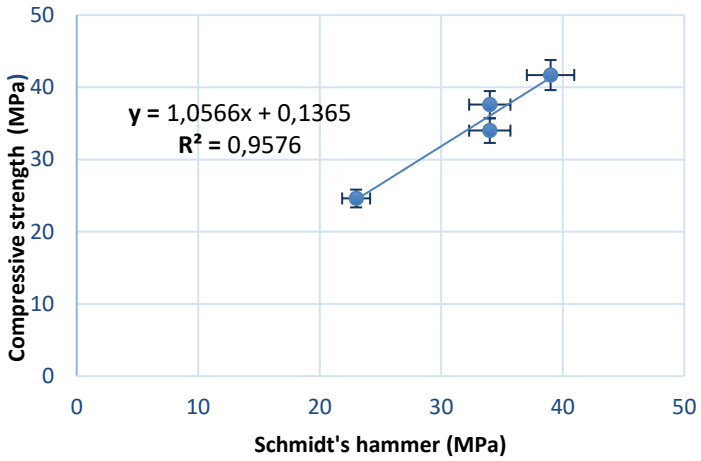


Figure 5: Correlation of results obtained from concrete strength

4 NUMERICAL MODELS

The information collected from original architectural drawings, on-site surveys, soil mechanics studies in the nearby area and the determination of the mechanical properties of concrete make it possible to elaborate numerical models of the building in SAP2000 (Figure 6).

Three models were considered in the analysis. One model represents the structure on its undamaged original state and the other two consider damaged conditions based on the observations made on the actual building. All models were analyzed considering the seismic loads defined by NCh433 [27] and DS61 [28] for the building site in Lota. The most relevant seismic parameters are displayed in Table 5.

In the case of the undamaged building (Model 1) a G35 concrete quality (f'_c=35 MPa), A440-280H steel quality (f_y=280 MPa) and handmade solid brick (mnM according to [29]) were considered. The second model (Model 2) represents general concrete degradation due to age and environmental conditions by reduction in ground floor concrete quality to G20

(f'_c=20 MPa). In the third model (Model 3), localized damage was included by eliminating the most severely damage columns.

These models were used to assess the effect of damage in the modal response of the building, but also non-linear time-history analyses were conducted to identify potential zones of damage. The time history analysis was performed applying the Concepción record of the Mw 8.8 2010 Maule earthquake (Figure 7), considering concentrated plasticity on beams and columns. Walls and slabs were modeled as elastic elements, because damage was not observed in those elements on the actual building. Global P-Δ effect was included in the analysis. Each analysis was conducted considering simultaneously two perpendicular components of the earthquake along the E-W and N-S directions. The plastic hinges were defined according to established in [30] and the Takeda´s hysteresis model was considered.

Table 5: Seismic Parameters.

Building category	II (resindential)
Response Modification Factor (Ro)	11
Seismic zone	3
Soil type	E

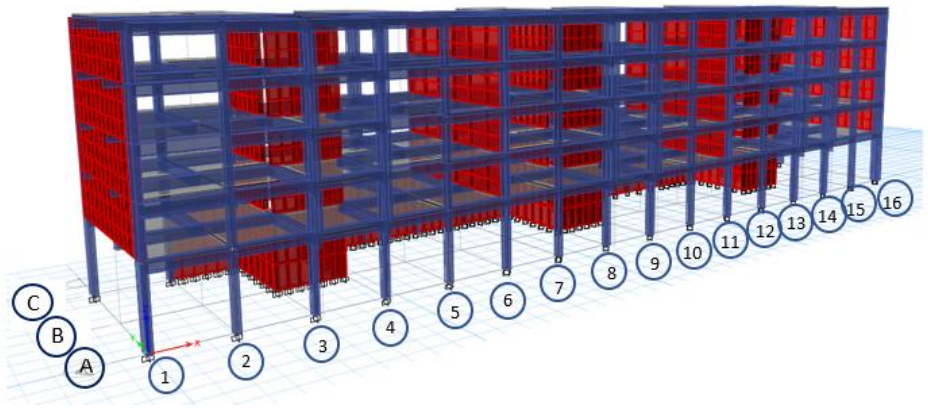
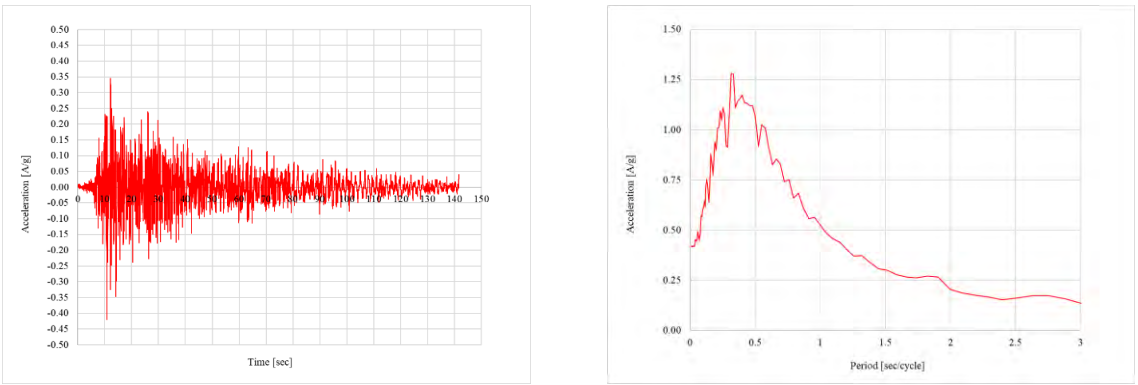


Figure 6: Building model in SAP2000



(a) (b)

Figure 7: Concepción record of the Mw 8.8 2010 Maule earthquake.
(a) Accelerogram, and (b) Acceleration spectrum

5. RESULTS AND DIAGNOSIS

5.1 Pathologies analysis

Figure 8 shows the relation between carbonation, porosity and percentage of cross-sectional loss of steel rebars. It becomes evident that the greater is the concrete porosity, a deeper carbonation is generated. This situation facilitates corrosion in the reinforcements, with the subsequent increment in the loss of steel rebars cross section. On the other hand, Figure 9 illustrates how concrete porosity affects the material strength. Therefore, carbonation not only produced rebars corrosion, but also generates a loss of strength in the elements of the critical zone.

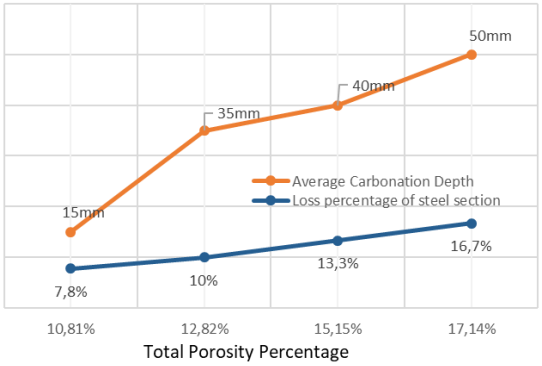


Figure 8: Carbonation, Porosity and Steel Corrosion Loss Ratio

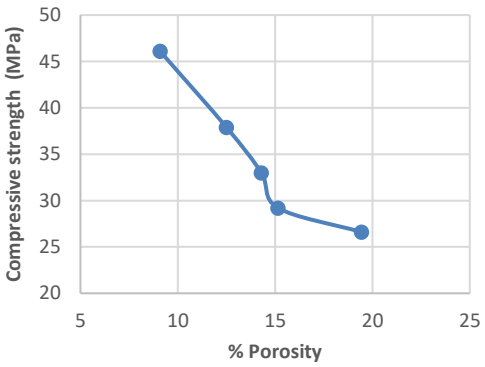


Figure 9: Strength – porosity relation

5.2 Numerical model

The results of the modal analysis are presented in Table 6. It can be seen that both the natural periods and the mass participation do not change significantly between Model 1 and Model 2. However, the change is more significant in Model 3, because of the elimination of ground level columns. This change was not only observed in terms of natural periods, but also in terms of mass participation and modal order. While in Model 1 and 2 the first two mode corresponded to translational modes, and the third mode was associated to rotation; in Model 3, the rotational mode is activated earlier as a second mode.

Table 6: Modal analysis results

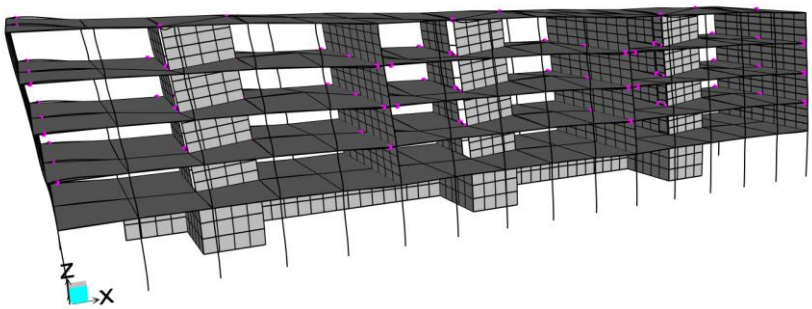
	Model 1		Model 2		Model 3	
	T [s]	Mass participation	T [s]	Mass participation	T [s]	Mass participation
Mode 1	0.22	73% (displ. X)	0.22	73% (displ. X)	0.23	69% (displ. X)
Mode 2	0.12	74% (displ. Y)	0.12	73% (displ. Y)	0.18	52% (torsion)
Mode 3	0.11	79% (torsion)	0.12	79% (torsion)	0.15	57% (displ. Y)

The results of the Time-History analysis are presented in Table 7 and Figure 10, where the magenta dots represent plastic hinges. It is observed that the seismic event of 2010 do not affect significantly the vertical elements (columns and walls) and most of the damage was

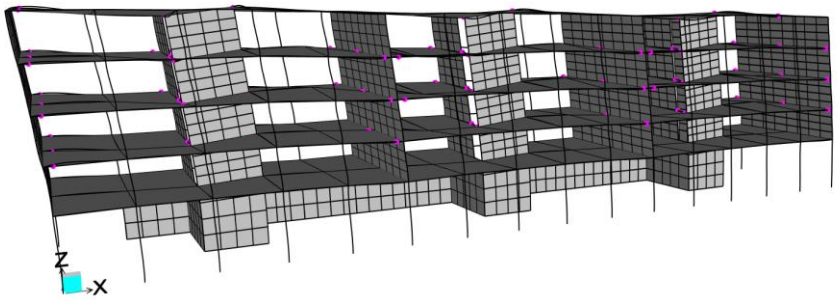
concentrated in the beams. Roof displacements and interstory drift are small and within the range accepted by current Standards [27, 28], even in the case of the severely damage building (Model 3). This is explained by the secondary importance of columns to control lateral displacements, which is mostly resisted by shear walls. These stiff elements (shear walls) not only imposed strong restrictions to lateral displacements, but also produce low natural periods. These periods are below the range where most of the earthquake's energy is concentrated (only 5% of the energy affects structures with periods below 0.15s), which explains why this kind of structures were able to withstand the 2010 Maule earthquake. However, the elimination of columns in Model 3 produced an increment in the number of plastic joints in beams, because of the building rotation generated by the early activation of rotational modes. This condition sets an alert and reveals the need of retrofitting columns to prevent further damage in the structure, not only in vertical elements, but mainly in beams and slabs.

Table 7: Time-History analysis results

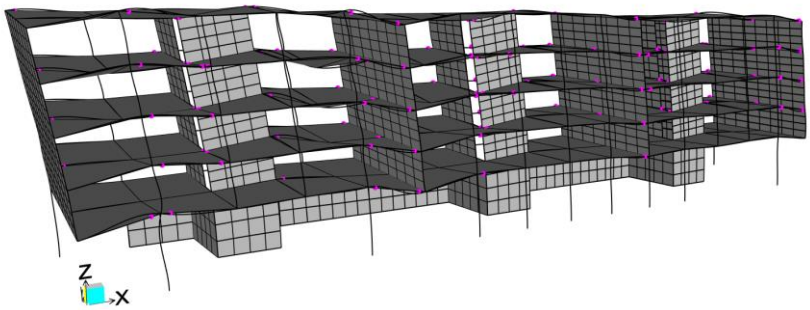
	Model 1	Model 2	Model 3
Max. roof displacement [mm]	15	15	14
Max. drift	0.0016	0.0016	0.0016



(a)



(b)



(c)

Figure 10: Plastic hinges generated on the structure.
(a) Model 1, (b) Model 2, and (c) Model 3

6. CONCLUSIONS

- Reinforced concrete structures with significant percentages of porosity and relative humidity benefit the carbonation process. This process is even more severe when these structures are in aggressive environments, such as, coastal zones. This carbonation may produce cracks, steel rebars corrosion and a reduction in concrete strength that may compromise the structural capacity of the element.
- The drain pipe longitudinally embedded in the column considerably reduced its structural capacity in compression, flexocompression and shear, but more critically it promotes internal process of carbonation and corrosion.
- The seismic behavior of the building was mainly controlled by the shear walls, with few variations in the overall results, when the undamaged and the damaged model are compared.
- The structure under study presented local failures that did not compromise global stability, especially due to the amount of shear walls of the building, which have not presented significant damage. Even tough, repairing is needed to comply serviceability requirements and control further structural deterioration due to rotational effects.

Acknowledgements.
The authors want to recognize the valuable contribution of Prof. Felipe Zavala and the students of the course “Concrete Technology” (2018-2) of Universidad Andres Bello that assisted in the building´s damage survey. As well as the company VANROM for their collaboration during the development of the work.

REFERENCES

[1] Mark G. Stewart, Xiaoming Wang, Minh N. Nguyen. Climate change adaptation for corrosion control of concrete infrastructure. Structural Safety 35 (2012) 29–39
[2] Seung-Jun Kwon, Ha-Won Song. Analysis of carbonation behavior in concrete using neural network algorithm and carbonation modeling. Cement and Concrete Research 40 (2010)

119–127
[3] I. Monteiro, F.A. Branco, J. de Brito, R. Neves. Statistical analysis of the carbonation coefficient in open air concrete structures. Construction and Building Materials 29 (2012) 263–269
[4] P.F. Marques, A. Costa. Service life of RC structures: Carbonation induced corrosion. Prescriptive vs. performance-based methodologies. Construction and Building Materials 24 (2010) 258–265
[5] Sang-Hun Han, Woo-Sun Park, Eun-Ik Yang. Evaluation of concrete durability due to carbonation in harbor concrete structures. Construction and Building Materials 48 (2013) 1045–1049
[6] Anna V. Saetta, Renato V. Vitaliani. Experimental investigation and numerical modeling of carbonation process in reinforced concrete structures Part I: Theoretical formulation. Cement and Concrete Research 34 (2004) 571–579
[7] H. Kuosa, R.M. Ferreira, E. Holt, M. Leivo, E. Vesikari. Effect of coupled deterioration by freeze–thaw, carbonation and chlorides on concrete service life. Cement & Concrete Composites 47 (2014) 32–40
[8]Dodge Woodson, R. (2009). Concrete Structures: Protection, Repair and Rehabilitation.Burlington, USA: Butterworth-Heinemann imprint of Elsevier.
[9] Talakokula, S. Bhalla, R.J. Ball, C.R. Bowen, G.L. Pesce, R. Kurchania, B. Bhattacharjee, A. Gupta, K. Paine. Diagnosis of carbonation induced corrosion initiation and progressionin reinforced concrete structures using piezo-impedance transducers. Sensors and Actuators A 242 (2016) 79–91
[10] Alexander Steffens, Dieter Dinkler, Hermann Ahrens. Modeling carbonation for corrosion risk prediction of concrete structures. Cement and Concrete Research 32 (2002) 935–941
[11] Astroza M., S. Ruiz and R. Astroza, 2012, Damage Assessment and Seismic Intensity Analysis of the 2010 (Mw8.8) Maule Earthquake, Submitted to Earthquake Spectra.
[12] CYTED. (2006). "4ta Edición del Manual de inspección, evaluación y diagnóstico de corrosión en estructuras de hormigón armado". Programa Iberoamericano de ciencia y tecnología para el desarrollo.
[13] Ha-Won Song, Seung-Jun Kwon. Permeability characteristics of carbonated concrete considering capillary pore structure. Cement and Concrete Research 37 (2007) 909–915
[14] M.A. Peter, A. Muntean, S.A. Meier, M. Böhm. Competition of several carbonation reactions in concrete: A parametric study. Cement and Concrete Research 38 (2008) 1385–1393
[15] J. Khunthongkeaw , S. Tangtermsirikul , T. Leelawat. A study on carbonation depth prediction for fly ash concrete. Construction and Building Materials 20 (2006) 744–753.
[16] W. Aperador, R. Mejía de Gutiérrez, D.M. Bastidas. Steel corrosion behaviour in carbonated alkali-activated slag concrete. Corrosion Science 51 (2009) 2027–2033
[17] In-Seok Yoon, Oguzhan C- opuroglu, Ki-Bong Park. Effect of global climatic change on carbonation progress of concrete. Atmospheric Environment 41 (2007) 7274–7285
[18] B.G. Salvoldi, H. Beushausen, M.G. Alexander. Oxygen permeability of concrete and its relation to carbonation. Construction and Building Materials 85 (2015) 30–37
[19] Cheng-Feng Chang, Jing-Wen Chen. The experimental investigation of concrete carbonation depth. Cement and Concrete Research 36 (2006) 1760– 1767
[20] UNE-EN 14630 (2007)." Determinación de la profundidad de carbonatación en un

hormigón endurecido por el método de la fenolftaleína". AEONOR-España.
[21] UNE 112011 (2011). "Determinación de la profundidad de carbonatación en hormigones endurecido y puestos en servicio". AEONOR-España.
[22] ASTM C642-13, 2013. Standard Test Method for Density, Absorption, and Voids in Hardened Concrete. ASTM International, West Conshohocken, PA.
[23] NCh 204 Of 2006. Aceros – Barras laminadas en caliente para hormigón armado. IIN-Chile.
[24] NCh 1565. Of 2009: "Determinación del índice esclerometrico". INN-Chile.
[25] ASTM C805. (s.f.). Standard Test Method for Rebound Number of Hardened Concrete.
[26] NCh 1171/1. Of 2001. Hormigón – Testigos de hormigón endurecidos – Parte 1: Extracción y ensayos. IIN- Chile.
[27] NCh 433-1996 Modificada 2009. Diseño sísmico de edificios. INN Chile
[28] Ministerio de Vivienda y Urbanismo – MINVU (Chile). 2011. Reglamento que fija el diseño sísmico de edificios y deroga D.S. N°117 MINVU of 2010.
[29] NCh. 2123-1997 Mod2003. Albañilería confinada - Requisitos de diseño y cálculo. INN Chile.
[30] ASCE/SEI. Seismic rehabilitation of existing buildings (ASCE/SEI 41-13). Reston, VA: American Society of Civil Engineers; 2013.

12th International Conference on Structural Analysis of Historical Constructions
SAHC 2020
P. Roca, L. Pelà and C. Molins (Eds.)

POINT-LOAD TEST ASSESMENT AS STUDY OF ADOBE BUILDINGS DAMAGED AFTER THE 2017 PUEBLA EARTHQUAKE

A SANCHEZ[1*], E. M. ALONSO[1,2] AND J. A. BEDOLLA[3]

[1] Programa Interinstitucional de Doctorado en Arquitectura
Faculty of Architecture, Universidad Michoacana San Nicolás de Hidalgo
Gral. Francisco J. Múgica S/N, 58040 Morelia, Michoacán, México
e-mail: adria.sanchez.9@hotmail.com

[2] Materials Department, Faculty of Civil Engineering, Universidad Michoacana San Nicolás de Hidalgo,Gral. Francisco J. Múgica S/N, 58040 Morelia, Michoacán, México
email: eliamercedesalonso@gmail.com

[3] Faculty of Architecture, Universidad Michoacana San Nicolás de Hidalgo
Gral. Francisco J. Múgica S/N, 58040 Morelia, Michoacán, México
email: bedollaalberto@gmail.com

Keywords: Adobe Masonry, Point-load test, Vernacular architecture, Seismic affectation

Abstract. *The 2017 Puebla Earthquake on September 19 struck a big part of Mexico causing the loss of historic buildings in several states, being the state of Morelos one of the most damaged in the whole country. Jojutla de Juarez was the most affected locality of Morelos presenting important structural damages or total collapse in the built heritage, being the traditional earthen buildings, made of adobe bricks, the most vulnerable buildings to seismic efforts.*

Some of the causes which contributed to the poor behaviour of the buildings were the improper handling of the constructive systems and materials, the insufficient resistance of the structures and the problems derivate by the foundations. The adobe houses of Jojutla presented a mixture between the traditional building techniques and industrial materials like concrete, bricks, blocks and steel; also with irregular heights and plant layouts and inadequate connections between the walls and foundations and roofs, resulting into a higher seismic vulnerability when the earthquake impacted. Also the adobe bricks presented irregularities in its composition and use of additives which resulted in completely different typologies and the loss of the traditional construction techniques.

There was conducted a study to determine the earthquake resistance of the adobe bricks of the houses in Jojutla, considering that the remaining structures were severely damaged and a whole study of the seismic vulnerability would not be possible due the loss of the physical buildings. The granulometry and composition of the adobe samples of the buildings were determined as well as the natural aggregates like straw and its proportion. Also the compressive strength of the pieces was tested by two methods: the compression test and the point-load test, in order to obtain the indicative values which could be compared with other patrimonial and vernacular study cases.

It was observed that the construction materials and therefore the adobe bricks of Jojutla presented different compositions which caused an unpredictable behaviour during the earthquake of September 19th. Loss of the traditional earthen construction techniques has provoked a poor manufacture of the adobe houses, creating new scenarios where people do not trust in the material and substitutes the earthen architecture by modern materials. The conduction of point-load tests in situ could be an alternative to study the mechanical properties of patrimonial samples before its disappearance.

1 INTRODUCTION

México is a country with an important seismic history, experiencing recurrently huge earthquakes of great magnitude which have big impact in its population. The nearest states to the Trans-Mexican Volcanic Belt, the Cocos Plate, the Rivera Plate and Pacific Plate, present high seismic hazards, being prone to experiment earthquakes which cause acute damages in the cultural heritage. In the month of September of 2017 the country suffered two big seismic events which had an enormous impact on the affected regions.

The first earthquake struck on September 7th of 2017 in the Gulf of Tehuantepec, near the Mexican state of Chiapas, with a magnitude of 8.2 Richter magnitude scale, being originated in the Cocos Plate. This natural disaster was marked by the multiple aftershocks which were detected on the following days, causing damages mainly in Chiapas and Oaxaca [1]. On the other hand, the second earthquake was reported by the Servicio Sismológico Nacional of México on September 19th with a magnitude of 7.1 and the detected epicentre was in the boundaries between the states of Puebla and Morelos, located 12 Km southeast Axochiapan, Morelos [2]. In this case, the most affected states were Puebla, Mexico State, Morelos, Tlaxcala, Guerrero and Mexico City.

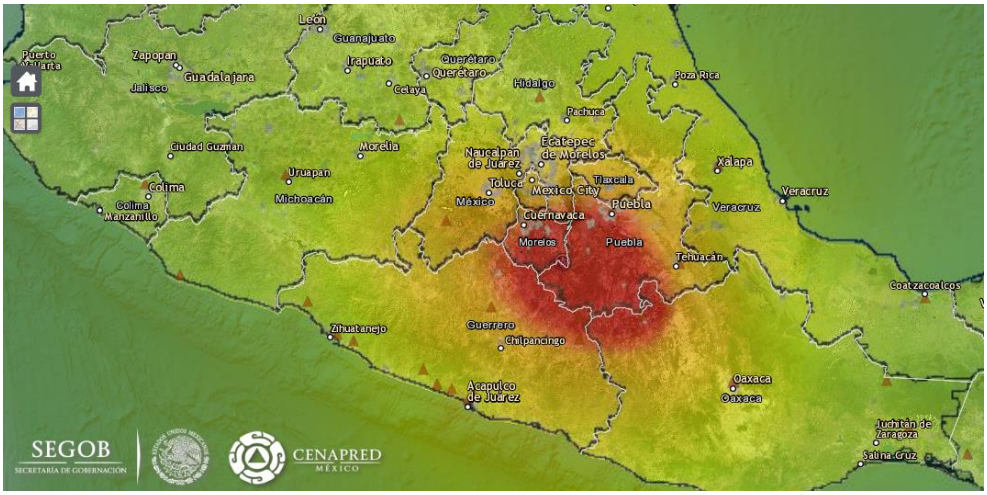


Figure 1: Seismic intensity map of the 2017 Puebla Earquake. Source: Atlas Nacional de Riesgos, map generated by Earthquake Institute of the National Autonomous University of México (UNAM)

The impact of the 2017 Puebla Earthquake on the region was especially destructive for the colonial buildings which are part of the Mexican cultural heritage, resulting in severe damages mainly in the states of Puebla and Morelos. In Morelos, the National Institute of Anthropology

and History (INAH)[1] reported a total number of 259 buildings affected, suffering damages classified as severe in the 47% of the whole ensemble [3]. The study case of Jojutla de Juarez, was the most affected locality of Morelos presenting important structural damages or total collapse in the built heritage, being the traditional earthen buildings, made of adobe bricks, the most vulnerable buildings to seismic efforts (See Fig. 2).

1.1 Background

Despite the great impact of these events, the seismic memory of the population is short, the state of alert only remains for a short period of time following the earthquake, disappearing gradually, as the disaster ceases to seem an immediate danger [4]. In the study case of the State of Morelos, the closest seismic events which had a deep impact in the society were the 1985 Mexico City earthquake and the 1999 Tehuacan or Central Mexico earthquake, with meaningful consequences on the architectonic and cultural heritage of the region; however these two remained distant in the collective memory of the population [5].

The destructive effect in the architectonic and cultural heritage was translated into the physical destruction of the buildings and monuments, being especially remarkable the damages in the Mexican colonial churches, which are very significant elements for the local culture and the identity of the communities [5]. Due to the importance of these constructions, the damages were analysed, full-filling appropriate research jobs to understand the seismic response of these structures [6].



Figure 2: Municipality of Jojutla de Juárez after the 2017 Puebla Earthquake

Nonetheless, despite the reconstruction and restoration work done by the authorities and responsible entities, the traditional housing, in particular the typologies with adobe walls, were ignored. The resources were invested in the restoration of the ancient churches and monuments and the rehabilitation of homes and public structures as well as the building of new housing with modern materials. Notwithstanding the great consequences for the vernacular architecture, the organisations in charge decided not to support this local culture, appraising adobe bricks as an unsafe material [7]. The result of these disputed resolutions turned into the abandonment of the traditional techniques and the reconstruction of the localities of the region with prefabricated concrete blocks and ceramic brick walls and roof structures of metal casing.

[1] The INAH, Instituto Nacional de Antropología e Historia, is the Mexican federal government bureau established in 1939 to guarantee the research, preservation, protection, and promotion of the prehistoric, archaeological, anthropological, historical and paleontological heritage of México.

1.2 Case study

The state of Morelos has a strong adobe building tradition which can be observed from tis vernacular architecture, being the adobe housing one of the most representative typologies found. This architecture has resisted over time, withstanding important natural disasters. Most of these traditional structures present earthquake-resistant features through several properties in the materials, form, dimensions and functionality of the buildings [8]. These earthen constructions have suffered over time the struck of historic earthquakes which had a big impact on the built heritage, withstanding thanks to the qualities of the local architecture.

In the study case of Jojutla de Juarez, the traditional adobe houses of the locality were fairly modified over the years, changing the ancient materials and construction systems for modern ones; the vast majority of the buildings had important alterations to its morphology too. Besides, the conservation and maintenance of the constructions were precarious, as a result of the lack of knowledge and interest of the vernacular technologies, which always responded to the natural environment [9]. On the other hand, the traditional houses which conserved their morphology, dimensions, materials and techniques; had a better performance agains the 2017 Puebla earthquake, suffering non significant damages, as it has been demonstrated in posterior research works [7] [10].

Jojutla de Juarez shown a micro-seismic-regionalisation, especially in some of its colonies or neighborhoods. The historic centre of the town was widely damaged, suffering important losses in the built heritage, like the churches and main institutions, as well as public housing. The large majority of the adobe houses were located in the downtown colony, which was the most affected zone with the Emiliano Zapata colony, this one re-built more recently. Both zones experienced severe damages, including the collapse of many buildings and structures [11].



Figure 3: Damaged adobe building with mixed construction techniques

2. METHODOLOGY

In order to study the seismic disaster affectation on the adobe buildings of Jojutla de Juárez, several samples were collected to work with them. Considering that the remaining structures were severely damaged and a whole study of the seismic vulnerability would not be convenient due the loss of the traditional buildings, it was decided to apply compressive strength and point-load tests in order to obtain the indicative values of mechanical resistance, which could be compared to other patrimonial and vernacular study cases.

2.1 Sampling adobe and soil

There were collected 11 representative shards of adobe bricks from 11 different traditional houses in the downtown of Jojutla. These samples were collected before the demolition of the buildings, which was shortly after the field trip in May 2018. There also were taken samples of quarry soils of the region, concretely in the extraction area for the manufacture of adobe bricks and ceramic bricks. The region is recognized by their rice production, even the Morelos rice is a trade mark, and of course they have plenty of water. Taking into account the emergency state of Jojutla de Juarez and the situation between the inhabitants and their damaged buildings, the sample collection responded to the criteria of taking the maximum permissible amount possible of material before the demolition of the remaining houses and the consequently disappearing of the earthen architecture. All the samples were classified by the Unified Soil Classification System (USCS) to obtain the composition of the adobe bricks and the type of soils used for construction materials in the region. There was also obtained the fibre percentage, straw in the case of study, in each one of the adobes.

2.2 Compressive strength test

In order to performance the compressive strength of the samples, these had to be prepared. Due to their precarious state, most of them were found between the building remains of Jojutla de Juarez, not all the original samples qualified for the compression strength test, as they didn't accomplish the minimum dimensions or were extremely inconsistent. From the 11 patrimonial samples only 6 could be eligible for the mechanical characterisation trials, needing a previous preparation. For being able to perform the analysis the samples were carved till obtain appropriate dimensions, and later capped with melted sulphur, due to the irregularities presented in their surface. Once prepared, they were introduced in the Tinius Olsen Universal Test Machine to obtain their ultimate resistance to compressive strength.



Figure 4: Preparation and compressive testing of the adobe samples

2.3. Point-load test

Point-load test allows determining mechanical resistance of non-carved samples of several types of masonries and rocks, both: natural or artificial, being especially designated for the study of rocks [12]. The first research works which utilised the test achieved to associate the uniaxial compressive resistance with the point-load index (Is), creating the basis to apply the analysis to rock fragments [13]. Nevertheless, the materials researched in this work are adobe bricks, being a first approximation to the characterisation of solid clay fragments with this technique.

The equipment used for the point-load test was Digital rock strength index apparatus 100 kN cap of Controls Group, which has the advantage of being a portable equipment which allows to test samples both in the laboratory or in field research, with the only preparation of the measurement of each one of the fragments before performing the test.

The samples were tested under Compression strength, after cracking; the fragments were also submitted to point-load test applying an incremental load leading to the failure of the fragments, to compare the data. The equipment gave a rupture load value which needed to be transformed by an equation system to the ultimate unconfined uniaxial compression resistance. The methodology followed was according the ASTM standards and previous research works performed in the materials laboratory [12, 14-15].



Figure 5: Adobe sample in the point-load equipment

The point-load index without correction factor is calculated with the following equation:

$$I_s = \frac{P * 1000}{D_e^2}$$

Where:

I^s = Point-load index, MPa.

P = Maximum load, kN.

De = Equivalent core diameter, mm.

The resistance index value (I_s) is a non-corrected value which varies depending on the thickness of the fragments tested. To obtain the corrected resistance index ($I_{s(50)}$) it is necessary to multiply the first index by the correction factor:

$$I_{s(50)} = F * I_s$$

Depending on the size of the fragments, there will be used two different correction factors. The election between one or other will be the proximity of each sample to the standard value of 50 mm [12]. For the specimens near to this 50 mm thickness (D), the correction factor is calculated with the following equation:

$$F = \sqrt{\left(\frac{D_e}{50}\right)}$$

Instead, when calculating fragments with thickness distant of 50 mm, the following formula will be used:

$$F = \left(\frac{D_e}{50}\right)^{0.45}$$

The estimation to the compressive strength σ or UCS (Uniaxial Compressive Strength) is obtained with the following equation:

$$\sigma = (C)\, I_{s(50)} = 24\, I_{s(50)}$$

The value σ is the main purpose which the point-load test follows and it is going to be compared with other values of mechanical resistance obtained by other tests. Other interesting aspect of the test is to observe the rupture mode of the fragments, finding relations between the composition of adobes, their morphology, size, fibres distribution or aggregates (See Figure 6).



Figure 6. Fracture in adobe fragments with point-load equipment

3. RESULTS

Figure 7 shows the classification of all the samples, including the adobes and the soils of the region, by the Unified Soil Classification System (USCS); while Table 1 shows the results of the soil classification and the grading of each one of the specimens which were subdued to the mechanical analysis. M1 and M13, the two soil samples from the clay material quarry were classified as high plasticity clays, while the adobes vary from clays of low plasticity to mods. The low plasticity was probably due to the stabilization with other materials, for example, lime was found by RXD in some specimens.

Table 1: USCS Classification of the specimens

Material	USCS Classification	
M2	CL	Clay of low plasticity
M4	CL	Clay of low plasticity
M5	ML/OL	Silt / Organic silt
M9	ML/OL	Silt / Organic silt
M11	ML/OL	Silt / Organic silt
M12	ML/OL	Silt / Organic silt

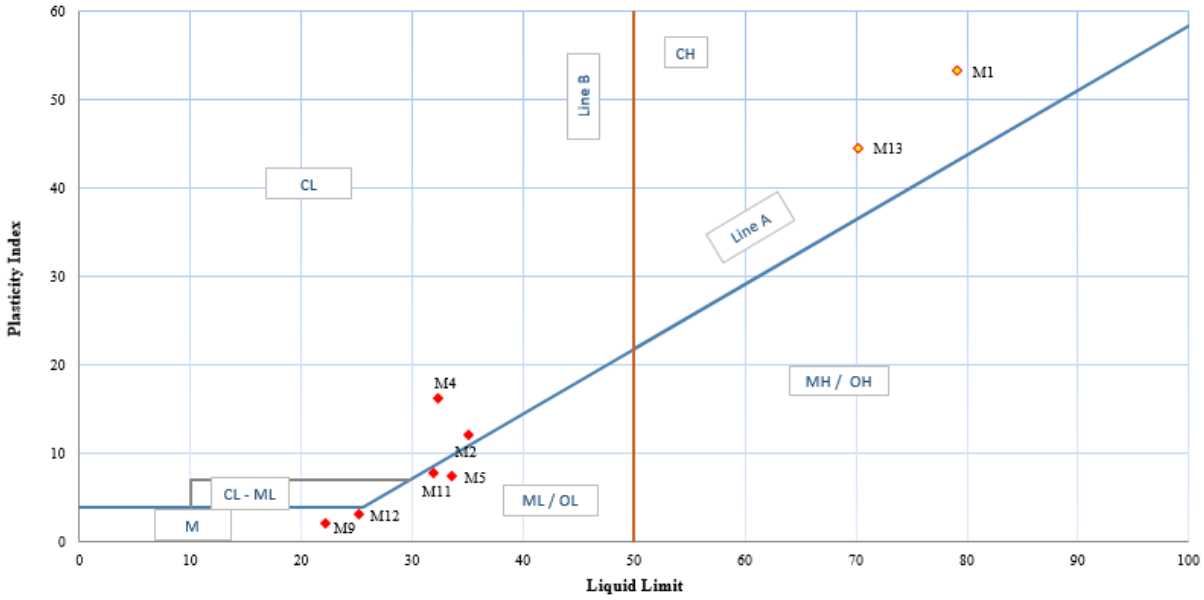


Figure 7: Plasticity graphic and position of the adobes and soil samples

The sieve analyses also permitted to separate and classify the mineral grains and vegetal fibres in the adobes. It was calculated the percentage of straw, the only fibre used in this case, from the weight (See Table 2). Some of the adobes did not have any amount of straw (sample 5) or an insignificant percentage (sample 9) or other fibres as reinforcement or strategy to diminish shrinkage, situation which contributes to expect the lower mechanical values obtained.

Table 3: Fibre percentage results

Sample	Fibre percentage (% Weight)
M2	0.38
M4	0.68
M5	-
M9	0.06
M11	0.27
M12	0.23

From the destructive tests, specifically the compressive strength, the mechanical resistance varies between 5-13 Kg/cm2, being the average of the adobe bricks 8.16 Kg/cm2. These values obtained with the compression strength test and the point-load tests are lower than values from other researches which similar characteristic cases in México [7, 16-18]. The adobe blocks of Jojutla presented low performance perhaps because of inefficient manufacture and the absence of fibre material or other stabilisers. Nevertheless, the proportion of the fibres does not seem to have a direct relation with the compressive mechanical resistance, as samples M5 and M9 had the lowest amount of straw, otherwise reached some of the highest values during the test.

The point-load test allowed to quantify some of the samples, after the compressive strength test. Because of that fragments of lower dimensions can be tested again with the equipment, it

resulted in more number of specimens and results. The values obtained were more variable with an extended range being the average of all the adobes 3.95 Kg/cm2, lower than the compression strength results. The ratio between compressive strength and point-load values was 2.13:1, something comprehensible considering that the point-load test is designed for the analysis of different types of rocks.

Table 3: Comparative of compressive strength and point-load values results

Sample	Compressive strength (Kg/cm^2)	Point-load σ (kg/cm2)^2	cs/pl
M2	5.97	3.24	1.84
M4	9.35	3.64	2.57
M5	12.33	5.78	2.13
M9	5.08	4.62	1.10
M11	9.13	3.91	2.33
M12	7.09	2.52	2.81
Mean	**8.16**	**3.95**	**2.13**

The compressive strength and point-load values were compared (See Figure 8) in a graphic to observe the correlation between the two tests. Considering the compressive strength values slightly higher, most of the samples shown a lineal reciprocity, while some shown deviation, near the 2:1 ratio calculated for the tests.

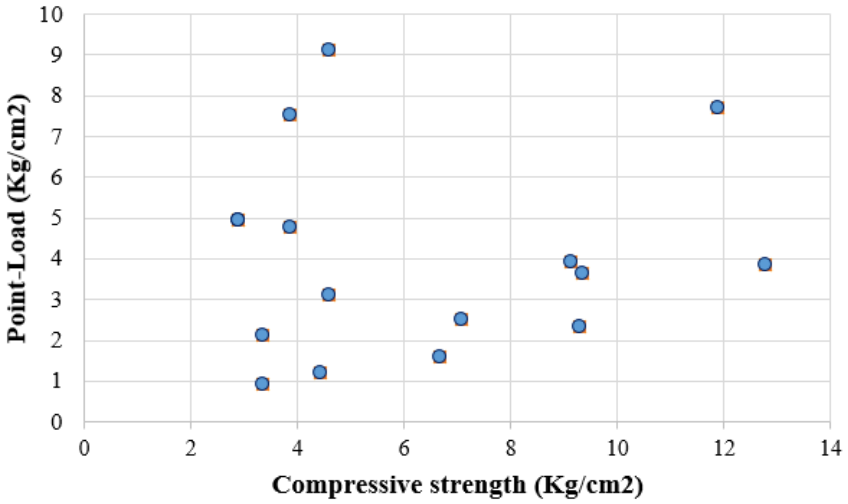


Figure 8: Correlation between the Compressive strength and the point-load tests

[2] The final value of the uniaxial compression resistance has been converted to kilogram per square centimetre. The original value was found in megapascals.

4. CONCLUSIONS

While seismic affectations in monumental and vernacular architecture has been widely researched, it is very complicated to analyse study cases where the materials and buildings have been lost or demolished. Point-load test could be a useful analytic tool for measuring the mechanical resistance of patrimonial samples found in emergency situations like earthquakes or other natural hazards. The test can be performed in situ, being suitable for these cases, where the specimens are corrupted.

Point-load allows the characterisation of non-complete fragments, like the ones found in Jojutla de Juarez, Morelos. It could be a support for research works where it is impossible to access to the original constructive system. The samples could be tested in situ, which is a great benefit, nevertheless it is recommended to compare the values obtained with other mechanical resistance studies to achieve a more complete research.

The test has not been yet assessed for adobes or other earthen masonry, the standards are determined for sandstone. Nevertheless, it has been proved useful for other rocks like ignimbrites [14-15]. The comparison between compressive strength and point-load for the adobes tested shows a relation ratio compressive strength/point-load very near to 2:1, comprehensible considering that the point-load index (I_s) was designed for sandstones [12]. More research is required as these earthen structures have not been analysed by this method and it can be useful for in-situ works.

The percentage of fine grained soils of the adobes was comprised around 15-40%, corresponding to indicative values of the traditional earthen architecture. It also was observed that half of the adobes had not any visible fibre proportion, it could be possible the clays was used before and re-use for new adobes so the straws almost disappeared, one of the basic features of the traditional architecture of the region, being a symbol of the loss of this cultural heritage, and a detrimental factor for the adobes, as fibres reduce the shrinkage and improve the mechanical resistance [19]. The soil and grain size classification of the adobes show insufficient or absent amount of fibres, however there weren't found significant proportions of gravel or lithic in the pieces. The Figure 7 shows how the healthy clays of the soil samples are in very different zone of the graphic than the adobe samples. To diminish the plasticity of the adobes from high to light there could have been some type of stabilization with local materials, for the age of the adobes it could be lime.

Nevertheless, this low values didn't justify for itself the bad seismic behaviour of the dwellings, which were very vulnerable due to multiple factors like the lack of reinforcements and confinement of the structures, the incompatibility between the construction materials or the poor maintenance of the buildings among others, the social-economic necessity of divide the land into minor spaces to inherit descendants and so the impossibility to continue using the traditional thickness of adobe. In the study case, all these conditions converged, resulting into the loss of most of its architectural heritage and infrastructure. The adobe walls did not have any reinforcement, being this method unknown by the local population, which prefer to substitute the traditional materials for modern ones representing for them a better social status.

ACKNOWLEDGEMENTS

The authors acknowledge the Materials Laboratory "Ing. Luis Silva Ruelas" of the Faculty of Civil Engineering of the UMSNH for the equipment support, the Postgraduation coordination

of the Faculty of Architecture of the UMSNH, the economic support given by CONACYT and CIC-UMSNH, and the technical support of B.C.E.: D. Preciado Villicaña and M. Ruiz Mendoza.

REFERENCES

[1] Servicio Sismológico Nacional. *Reporte especial. Sismo de Tehuantepec (2017-09-07 23:49 Mw 8.2).* UNAM, Grupo de trabajo del Servicio Sismológico Nacional. México: Universidad Nacional Autónoma de México, (2017).

[2] Servicio Sismológico Nacional. *Reporte especial. Sismo del día 19 de Septiembre de 2017, Puebla-Morelos (M 7.1).* UNAM, Grupo de trabajo del Servicio Sismológico Nacional. México: Universidad Nacional Autónoma de México, (2017).

[3] Meli Piralla, R. La ingeniería civil ante los efectos de los sismos de 2017 en los edificios patrimoniales (el equilibrio entre la autenticidad y la seguridad). In S. d. Cultura, *Sismos y patrimonio cultural. Testimonios, enseñanza y desafios, 2017 y 2018* (pp. 62-81). Ciudad de México: Dirección General de Publicaciones de la Secretaría de Cultura, (2018).

[4] Blondet, M. Mitigation of Seismic Risk on Earthen Buildings. In H. Gökçekus, U. Türker, & J. W. LaMoreaux, *Survival and Sustainability. Environmental Concerns in the 2st Century* (pp. 391-400). Berlín: Springer, (2011).

[5] Campos Goenaga, M. I. Las dimensiones del sismo, un año después. *El Tlacuache. Órgano de difusión de la comunidad del INAH Morelos*(847), 31-34, (2018).

[6] Díaz Fuentes, D., Baquedano Julià, P. A., D'Amato, M., & Laterza, M. Preliminary Seismic Damage Assessment of Mexican Churches after. *International Journal of Architectural Heritage*, (2019).

[7] Guerrero Baca, L. F. Comportamiento sísmico de viviendas tradicionales de adobe, situadas en las faldas del volcán Popocatépetl, México. *Gremium, 6*(11), 105-118, (2019).

[8] Guerrero Baca, L. F., Meraz Quintana, L., & Soria López, F. J. Cualidades sismorresistentes de la vivienda de adobe en las faldas del volcán Popocatépetl. In L. F. Guerrero Baca, *Reutilización del patrimonio edificado en adobe* (pp. 194-215). México D.F.: Casa Abierta al Tiempo: Universidad Autónoma Metropolitana, (2014).

[9] Jorquera, N. Culturas sísmicas: Estrategias vernaculares de sismorresistencia del patrimonio arquitectónico chileno. *Arqutiecturas del Sur, XXXII*(46), 18-29, (2014).

[10] Ríos Ramírez, G., & Porcayo Victoriano, C. Vivienda vernácula: la transformación a través de sistemas constructivos y tipología, Hueyapan, México. In C. Neves, Z. Salcedo Gutierrez, & O. Borges Faria (Ed.), *19º Seminario iberoamericano de arquitectura y construcción con tierra : conservación sostenible del paisaje, tierra y agua* (pp. 516-521). San Salvador, El Salvador: FUNDASAL/PROTERRA, (2019).

[11] del Campo Alatorre, R. M., Ochoa González, G. H., & Álvarez Partida, F. *Estudio Geotécnico de la Colonia Emiliano Zapata, Jojutla, Morelos, tras los daños de los Sismos del 19 de septiembre de 2017.* ITESO, Universidad Jesuita de Guadalajara, Departamento de Hábitat y Desarrollo Urbano, (2018).

[12] ASTM Standards. *ASTM D5731 - 05 Standard Test Method for Determination of the Point Load Strength Index of Rock*, (2007).

[13] Broch, E., & Franklin, J. A. The point-load strenght test. *International Journal of Rock Mechanics and Mining Sciences & Geomechanics Abstracts*, 9 (Issue 6), 669-676, (1972).

[14] Navarrete Seras, M., Mártinez Molina, W., Alonso Guzmán, E. M., Arteaga Arcos, J., Chávez García, H. L., Lara Gómez, C., . . . Díaz González, N. Mathematical models applied to the physical mechanical characterization of stone materials bank Huiramba, México. In K. Esquivel Escalante, E. Elizalde Peña , & J. A. Rodríguez Morales (Ed.), *X Congreso Internacional de Ingeniería. Engineering and its applications Vol. 1*. Querétaro: Universidad Autónoma de Querétaro, 252-256, (2014).

[15] Navarrete Seras, M., Martínez Molina, W., Alonso Guzmán, E., Lara Gómez, C., Artega Arcos, J., Bedolla Arroyo, J. A., & Delgado Hernández, D. J. Rocas ígneas extrusivas e intrusivas para mampostería, método de carga puntual. *XII Congreso Latinoamericano de Patología de la Construcción y XIV Congreso de Control de Calidad en la Construcción CONPAT* (págs. 493-502). Cartagena de Indias, (2013)

[16] Arroyo Matus, R., Sánchez Tizapa, S., & Catalán Quiroz, P. Caracterización experimental de las propiedades mecánicas de la mampostería de adobe del sur de México. *Ingeniería, 17*(3), 167-177, (2013).

[17] Cruz Farrera, F. J. *Propuesta de uso de tecnologías sismorresistente de adobe para una vivienda progresiva en Cuauhtémoc, municipio de Villaflores, Chiapas.* Tuxtla Gutiérrez, Chiapas, México: Universidad Autónoma de Chiapas. Facultad de Arquitectura, (2018).

[18] Ordaz Zapata, F. A. *Estudio de las características mecánicas y térmicas del adobe, para su revalorización en la construcción de vivienda, en la ciudad de Torreón Coahuila, México*. Torreón, Coahuila, México: Universidad Autónoma de Coahuila, Escuela de Arquitectura, Unidad Torreón, (2019).

[19] Yetgin, Ş., Çavdar, Ö., & Çavdar, A. The effects of the fiber contents on the mechanic properties of the adobes. *Construction and Building Materials* (22), 222-227, (2008).

12th International Conference on Structural Analysis of Historical Constructions
SAHC 2020
P. Roca, L. Pelà and C. Molins (Eds.)

QUALITY AND STRENGTH ASSESSMENT OF BUTT WELDS IN POLAND'S OLDEST WELDED RAILWAY BRIDGES

BERNARD WICHTOWSKI[1] AND JANUSZ HOŁOWATY[1*]

[1]West Pomeranian University of Technology Szczecin

al. Piastów 50, 70-311 Szczecin, Poland
e-mail: janusz.holowaty@zut.edu.pl, www.zut.edu.pl (*corresponding author)

Keywords: Welded Structure, Historical Bridge, Non-Destructive Inspection, Imperfection

Abstract. *Fitness-for-purpose (FFP) assessment is used for estimation the durability of welded plate girders in Poland's four oldest welded railway bridges. For the girders, the 20.2 m span length was designed. The bridges were constructed over the years 1937-1939 and now being readied for refurbishment. The first radiographic tests on the butt welds in 18 bridge plate girders were conducted in 1958 during which 101 internal cracks in 49 butt weld splices were found, and which were subsequently riveted. The usefulness of such a strengthening is assessed upon structural calculations for design and service loadings, fatigue tests on specimens with internal cracks in the welds, literature service strength of welds with cracks and design fatigue strength of welds with cracks using FFP assessment. The results provide a unique experimental database on the behavior of welds with inadmissible imperfections. They also allow to assess the likely length of their further service life.*

1 HISTORICAL OUTLINE

The transition to welding facilitated some aspects of steel construction and allowed steel weight savings by eliminating the connecting angles used in riveted structures. However, early welding technologies created new problems, both in terms of ensuring weld quality and also the qualifications of welding workers. The first welded bridge structures were of a test character, trying to solve the many problems which appeared during the design, manufacture and construction, and ensuring the proper quality as well as the strength of welded joints. The problems caused some skepticism among the engineers and scientists involved in welded bridge projects. Early attempts were quite modest, such as a railway bridge with a little over 5 m span constructed in 1921 by English structural engineers for the Newcastle and Carlisle railway line, GB [1]. Nevertheless, welding technology was moving forward in many countries. The introduction of high strength steels in bridge construction proved the worth of welding technology, and new problems associated with notch toughness and ductility appeared to be solved.

The world's first recognized welded plate girder bridge was a railway bridge over the Turtle Creek in East Pittsburgh, Pennsylvania, USA [2, 3]. The bridge was constructed in 1928 with a length of 16 m and a width of 4.67 m. The plate girders utilized web sections of 1460×10 mm and three flange plates of depths 10 and 25 mm with widths of 380 and 400 mm. Cross girders and stringers were from rolled beam sections of depths 640 mm and 457 mm. The bridge was

constructed at a 60° skew with non-parallel abutments, which resulted in different girder span lengths of 15.97 and 16.29 m. Around 520 m of welds were executed, using 200 kg electrodes. The bridge was used to transport large generators by rail to the rest of the country.

The first all-welded plate girder railway bridge was constructed in Germany in 1930 with a span of 10 m [4, 5]. The construction was preceded by broad research, tests and theoretical studies. The bridge was initially installed on a track subjected to the movement of heavy locomotives, even at high speed. The bridge was also tested dynamically by a vibrating machine. Following positive results from the tests, the bridge was installed on a trunk railway line.

2 THE FIRST WELDED RAILWAY BRIDGES IN POLAND

The first welded railway bridge in Poland, designed by F.K. Szelągowski, later a professor at the Warsaw Technical University, became operational in July 1936 [6]. Two external spans of the bridge crossing over the Drwęca river on the Nasielsk and Toruń railway line were constructed as a welded plate girder structure of span length 13.0 m (Figs. 1 and 2). The main truss span of the bridge still utilized a riveted construction as it was estimated to be cheaper. The welded plate girders had a web section of 1600×11 mm and the flanges were from a single plate of 230×30 mm in the span middle sections, lowering into the supports to 210×20 mm and 190×10 mm plates.

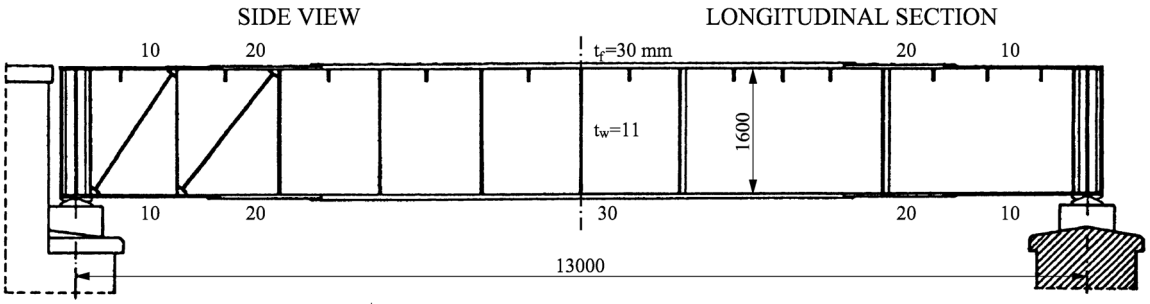


Figure 1: Plate girder for the external spans of the Drwęca river bridge

The web was connected with flanges by continuous fillet welds of leg length 6 mm. The flange joints were executed in a non-typical way according to Fig. 2. The ends of the thicker plates were whittled down at 160 mm length to the thickness of the thinner plate and then welded with a single v butt and around the fillet weld. All the welding works were executed in the workshop using a variable current and heavy coated Jotem type A electrodes for the vertical welds and Jotem type B-extra electrodes for the horizontal welds.

The successful construction of the first welded bridge encouraged the Ministry of Transport to construct a further four welded bridges on the same railway line [7, 8, 9]. The bridges were erected in the years 1937-1938 according to a design by F.K. Szelągowski and M. Witordowa (MoT). The welded structures were made by the L. Zieleniewski & Fitzner-Gamper company in Cracow. All the welding works were carried out in the factory shop, with only the riveted connections executed on site. For welding, direct current and *Baildon* domestic electrodes were used.

The bridges of semi-through plate girder construction have a span length of 20.2 m (Figs. 3 and 4). The main girders, along with the cross beams, were manufactured in the shop as fully welded components and transported, ready to use, to the construction sites. The welded plate girders have web plates of 2400×12 mm with two shop butt splices covered by two-sided vertical plates of thickness 8 mm. The flange plates are of constant width 240 mm with variable thickness from 10 to 40 mm. The flange plate sections are connected by double v-butts which were covered by two one-sided rhomboidal horizontal plates (Fig. 4 – flange splice).

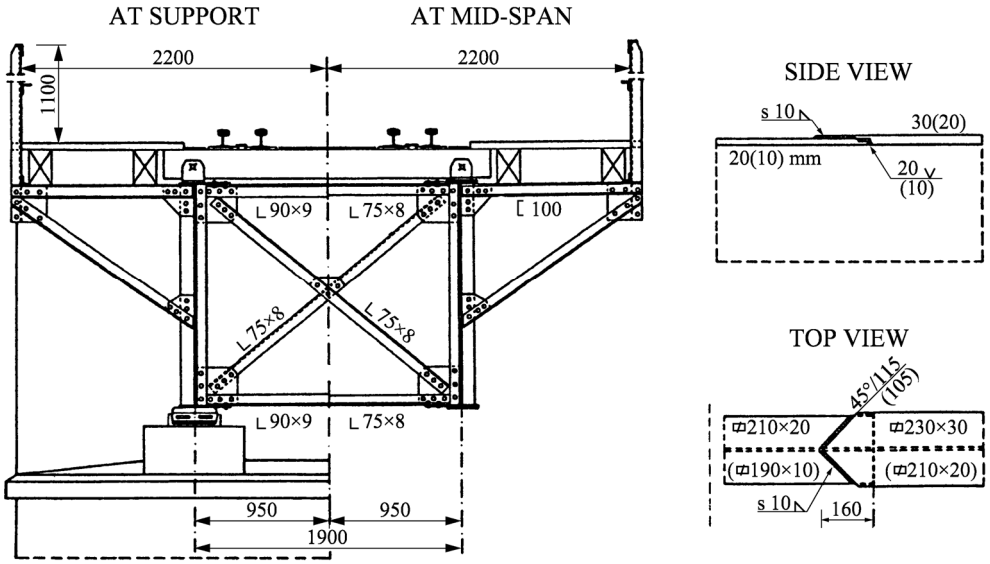


Figure 2: Bridge cross section and the welded flange splice

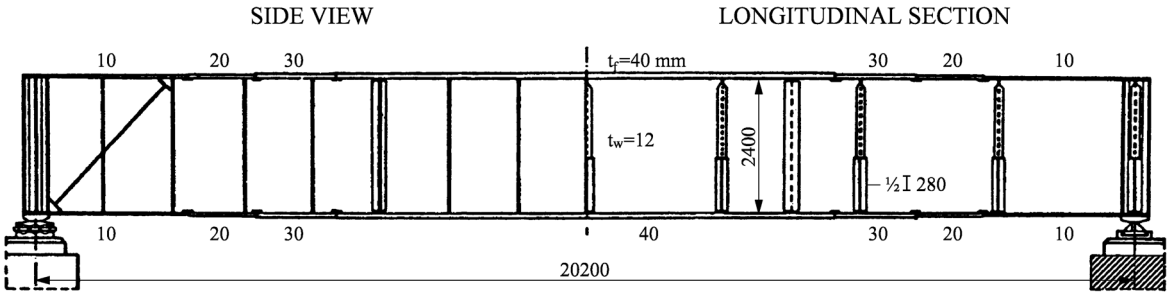


Figure 3: Plate girder for the four bridges constructed in the years 1937-1939

There are K-type wind bracings from single angles of 100×100×8 mm in the girder planes of the lower flanges. These were connected by riveted joints using 22 mm rivets. The joints were executed on site along with the riveted joints of the crossbeams, stringers and other deck members. The first bridge of this group was constructed over the Sierpienica river and became operational in October 1937 (No. I). The condition of the bridge during a butt splice radiographic examination is shown in Fig. 5.

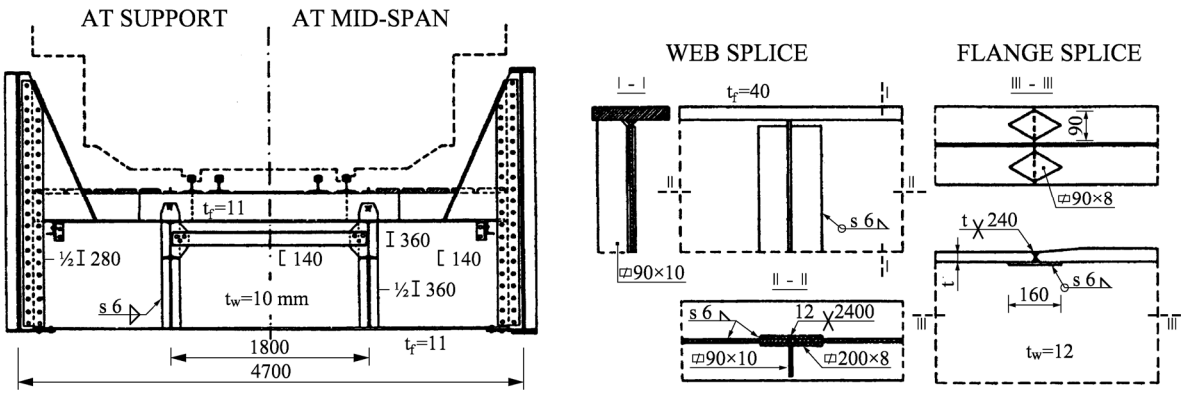


Figure 4: Bridge cross section and welded butt splices



Figure 5: View of the two-span bridge over the Sierpienica river in 1958 during radiographic examination

Over their eighty years of operational life, the bridges suffered partial structural and material degradation. In 2018 the second of the authors drew up a technical design for retrofitting one of the bridges, the two-span bridge (No. III) over the Płonka river in Płońsk (Fig. 6). While preparing the retrofit design it was necessary to estimate the grade and quality of the structural steel used for the bridge construction as well as its design strength value. The bridge steelwork was planned to be refurbished via welding so the weldability of the steel required estimating. The properties were calculated by the authors along with the methodology used for determining them. The procedure undertaken may be used for the retrofitting and repair of similar bridge structures.



Figure 6: Actual views of the two-span bridge over the Płonka river in Płońsk before retrofitting (2019)

The full range of material testing, together with notch toughness and static tensile tests, is expected to be conducted on the material from the members dismantled from the bridge during the retrofitting works.

3 RADIOGRAPHIC TESTS AND THEIR ANALYSIS

The Steel Structure Chair at the Technical University of Szczecin carried out the radiological examination on the flange butt joints in the main girders of the four bridges with the construction shown in Fig. 4 (web splice). The technical data for the bridges are given in Table 1 in chronological order of construction. Radiological examinations were carried out twice, in 1958 and in 1971. The tests were limited to the flange splices, as vertical stiffeners were welded directly in the axis of the welded web splices, thus preventing inspection (see Fig. 4 - web splice).

Table 1: General data for the bridges and their radiological examination

Bridge No. and river	Building year	Test year	Number of girders (joints)	Number of rtg.		Number of cracks		
				Σ	With cracks	Upper flange	Bottom flange	Σ
1	2	3	4	5	6	7	8	9
I Sierpienica	1937	1958 1971	4 (44)*	88	7	3	5	8
II Karsówka	1938	1958 1971	2 (24)	48	6	4	2	6
III Płonka	1938	1958 1971	4 (48)	96	46	21	27	48
IV Wkra	1938	1971	8 (72)	144	31	22	17	39
Total			18 (188)	376	90	50	51	101

* during the post-war repeairs 4 flange splices had been riveted

Table 2: Butt weld specification according to their quality levels

Bridge No.	Type of splices	Number of rtg.	Number of rtg. for the quality level					Total rtg.	
			B+	B	C	D	>D	B+ ÷ C	D and >D*
1	2	3	4	5	6	7	8	9	10
I	Upper flanges	44	2	1	2	1	38	5	39 (3)
	Bottom flanges	44	-	2	-	3	39	2	42 (4)
II	Upper flanges	24	1	3	3	4	13	7	17 (4)
	Bottom flanges	24	3	4	5	1	11	12	12 (2)
III	Upper flanges	48	1	7	3	2	35	11	37 (21)
	Bottom flanges	48	4	-	5	5	34	9	39 (25)
IV	Upper flanges	72	11	11	7	2	41	29	43 (18)
	Bottom flanges	72	11	9	9	7	36	29	43 (13)
	Total	376	33	37	34	25	247	104	272 (90)

* the values in brackes are the number of rengenographs with cracked welds

In total, 188 welded butt splices were X-rayed: 94 in the top flanges and 94 in bottom tensile flanges, taking 376 weld X-rays – col. 5÷9 in Tab. 1. 101 cracks were ascertained on 90 radiographs. The length of the cracks was from 8 mm to 240 mm, so at the extreme a breakage appeared over the total length of the splice – the flange width (Fig. 7)

Table 2 shows a summary of the quantity of radiographs with a division into imperfection classes. At the time of the tests, the imperfection classes were marked as R1 ÷ R5 according to PN-87/M-69772 Polish standards. Now the classes may be compared with the quality levels the of welds: B+, B, C, D and >D, as determined by EN ISO 5917:2014, and in Table 2 the welds are qualified according to these quality levels. In the total summary (cols. 9 and 10), the welds are divided into two groups: a group with quality levels B+, B and C which complies with the requirements of the standard EN 1090-2:2018, and a group of welds which are not allowed for new bridge constructions, D and >D. The latter is up to 72.3% of the rested sections and for the bridge over the Sierpienica river (No. I) this value is 95.5% for the lower tensile flanges. Generally, the condition of the butt splices in all bridges was ascertained to be poor: 101 cracks on 90 radiographs (23.9%) were discovered. These cracks could lead to fatigue cracks developing (Tab. 1 col. 6 and 9).

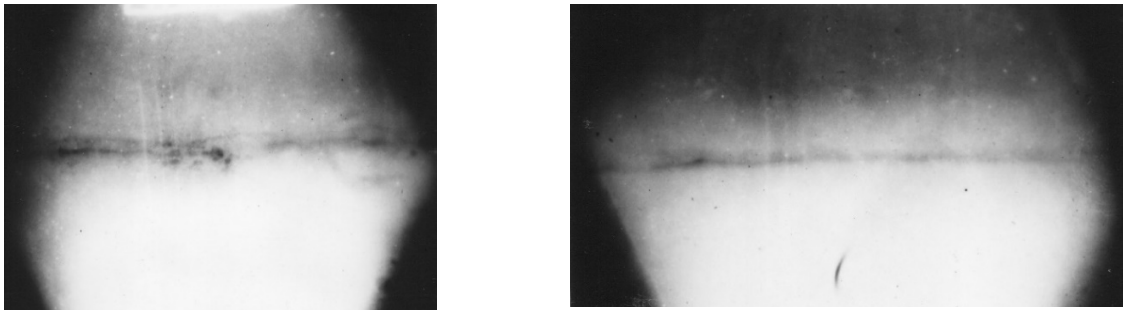


Figure 7: Two radiograms with cracks from the bridge over the Sierpienica river (No. I) - 1958 and 1971

The negative results of the tests were a surprise for bridge engineers and required the splices with cracks to be riveted for bridge Nos III and IV (Płonka river and Drwęca river). The decision to reinforce the crack flange splices was undertaken based on static standard loadings, which had never been taken into account in experimental and theoretical analysis [7-12]. The Paris equation, recognized as the first to take into account the parameters from fracture mechanic $dl/dN = C(\Delta K)^m$, was published in 1957. In 1959, 26 flange splices were riveted onto bridge No. III (13 in the upper flanges and 13 in the lower flanges). For bridge No. IV, 23 splices with cracks were riveted (12 in upper flanges and 11 in lower flanges).

4 CHEMICAL AND MECHANICAL PROPERTIES OF BRIDGE NO. III STEEL

Spectrometric chemical analysis of the steel on bridge No. III was carried out in 2018 on the basis of three samples cut out from an upper flange (U), a stringer (S) and a bracing diagonal (B). The results are given in Table 3. The analysis was carried out using a Leco GDS500A emission spectrometer. For comparison, the chemical composition of old mild steels, former Polish bridge steel (St3M) and a contemporary non-alloy structural steel S235 are given.

The comparison of the results for particular samples shows the bridge structure was manufactured from one steel type. It is a low-carbon mild steel with limited carbon, manganese

and silicon content. Of note are the small differences in content of the individual elements in the samples analyzed.

Using the chemical composition content, the metallurgic and structural weldability were assessed. For this purpose, the following ratios were established [15]:

- the equivalent carbon content (for steel with C < 0.18%)

$$CEV = C + \frac{Si}{30} + \frac{Mn+Cu+Cr}{20} + \frac{Ni}{60} + \frac{Mo}{15} + \frac{V}{10} + 5B = 0.12\% < 0.41\% \quad (1)$$

- the material resistant ratio for hot cracking

$$HCS = 1000(S + P + \frac{Si}{25} + \frac{Ni}{100}) \frac{C}{3Mn+Cr+Mo+V} = 3.10\% < 4\% \quad (2)$$

- the material resistant ratio for cold cracking

$$CEV' = C + \frac{Mn}{6} + \frac{P}{2} + \frac{Mo}{4} + \frac{Ni}{15} + \frac{Cu}{13} + \frac{Cv+V}{5} + 0.0024\text{t} = 0.24\% < 0.41\% \quad (3)$$

- the hardness of the heat effected zone

$$HVmax = 90 + 1050C + 47Si + 75Mn + 30Ni + 31Cr = 219 \text{ HV} < 350 \text{ HV} \quad (4)$$

The plate girder structural steel is weldable without limitations, as all the ratios are lower than the limit values. At the same time, the phosphorus and sulfur contents are lower than 0.05% in each case and the manganese content is lower than 1%, along with a vestigial content of silicon (rimmed steel).

Table 3: Comparative chemical composition for the bridge steel

Type of steel	Chemical composition, %							
	C	Mn	Si	P	S	Cu	Cr	Ni
U - t_f = 10 mm	0.083	0.479	3.6 ppm	0.030	0.027	0.151	0.111	0.089
S – I360	0.086	0.539	4.4 ppm	0.026	0.015	0.162	0.131	0.062
B – L100×10	0.078	0.417	7.5 ppm	0.021	0.013	0.121	0.158	0.108
Mild steel	0.03÷0.35	0.04÷0.75	< 0.18	< 0.16	< 0.11	0.11÷0.14	< 0.014	0.03÷0.04
St3M	max 0.20	min 0.40	0.12÷0.30	max 0.05	max 0.05	–	max 0.30	max 0.30
S235J0	max 0.17	max 1.40	–	max 0.03	max 0.03	max 0.55	–	–

Table 4: Brinell hardness measurement

Type of sample	Thickness of sample, mm	Diameter of imprint, mm			Brinell hardness			
					HBW	R_{mB}, MPa	α	R_{eB}, MPa
U - flange	10	2.7	2.7	2.7	121	404	0.7	282
S – I360	18	2.8	2.8	2.8	111	375	0.7	262
B – L100×10	10	2.8	2.8	2.8	111	375	0.7	262

The mechanical properties of the bridge steel were assessed on the basis of Brinell hardness measurements. The hardness was measured under standard conditions using a steel ball of 5 mm

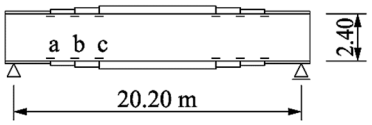
in diameter. The measurements were carried out on samples for chemical analysis. The measurement results are given in Table 4. After determining the value of R_{mB} taking into consideration that $\alpha = R_{eB} / R_{mB} = 0.70$, $R_{eB} = 260$ MPa. Taking according to Polish bridge standard the partial coefficient $\gamma_s = 1.15$ with a 5% increase when $R_{eB} < 355$ MPa we obtain:

- characteristic strength $f_y = R_{eB} = 260$ MPa,
- design strength $f_{yd} = 260/1.2 = 215$ MPa.

5 FLANGE WELD STRESS ANALYSIS AND FATIGUE DURABILITY

Strength analysis was undertaken for a global analysis of the weld behavior (Table 5). The characteristic values of stresses in the butt welds were established (in the axes of the cover plates) and beyond the cover plates in the flange plates. The calculations were made according to Polish bridge standards – as for fatigue verification, the standard vertical traffic loads (LM71) were taken with a dynamic factor. Nominal values of stresses for permanent actions are given in col. 2 and for permanent and rail traffic model actions in col. 3. The stresses are calculated for the persistent design situation using the classified vertical loads with factor $\alpha = 1.21$. The stresses for service loads are also calculated for permanent actions and a heavy locomotive with dynamic effects; the results are shown in col. 4. Column 6 gives the number of load cycles on the bridge up to 1959 (the riveting of the butt splices), until the present day (2019) and after a further 50 years in service in 2069.

Table 5: Normal stresses in butt welds (value in numerators), in flange plates (value in denominaters) and number of load cycles

Girder scheme	Stresses, MPa			Number of load cycles $N \cdot 10^6$
	Permanent loads	Persistent situation		
		LM71	Locomotive ET - 21	
1	2	3	4	5
	$\sigma_a = \frac{14.3}{16.8}$	$\frac{116.1}{136.5}$	$\frac{68.4}{80.4}$	$N_1 = 0.31^{1)}$
	$\sigma_b = \frac{15.1}{17.1}$	$\frac{122.1}{138.1}$	$\frac{74.4}{84.2}$	$N_2 = 1.18^{2)}$
	$\sigma_c = \frac{15.4}{17.0}$	$\frac{123.7}{136.6}$	$\frac{72.4}{79.9}$	$N_3 = 1.91^{3)}$

[1)] Number of load cycles up to 1959 (splice riveting)
[2)] Number of load cycles up to now (40 passages per day)
[3)] Number of load cycles in 2069 (after further 50 years)

The values of the service stresses σ_{ser} obtained constitute about 60% of the stresses from standard loading. The service stresses are compared with the fatigue stresses obtained during laboratory tests, given in Fig. 8 [16, 17]. The regression lines given there are concerned with:

- tests on specimens marked “a” – butt welds of quality level B+, B and C, for which the infinitive life fatigue strength (endurance limit) is 125 MPa,
- tests on specimens marked “b” – butt welds with internal cracks, for which the obtained

infinitive life fatigue strength is 90 MPa,

- tests on specimens marked "c" – butt welds with one-sided rhomboidal cover plates, for which the obtained infinitive life fatigue strength is 79 MPa.

The fatigue stress values are marked as red lines in Fig. 8 (logarithmic scale) according to the regression lines for the number of load cycles N_1 and N_2. The minimal values of these stresses are σ = 120.1 and 95.6 MPa. At each case these values are larger than the calculated service stresses $\sigma_{ser,\,max}$ = 74.4 MPa (Table 5).

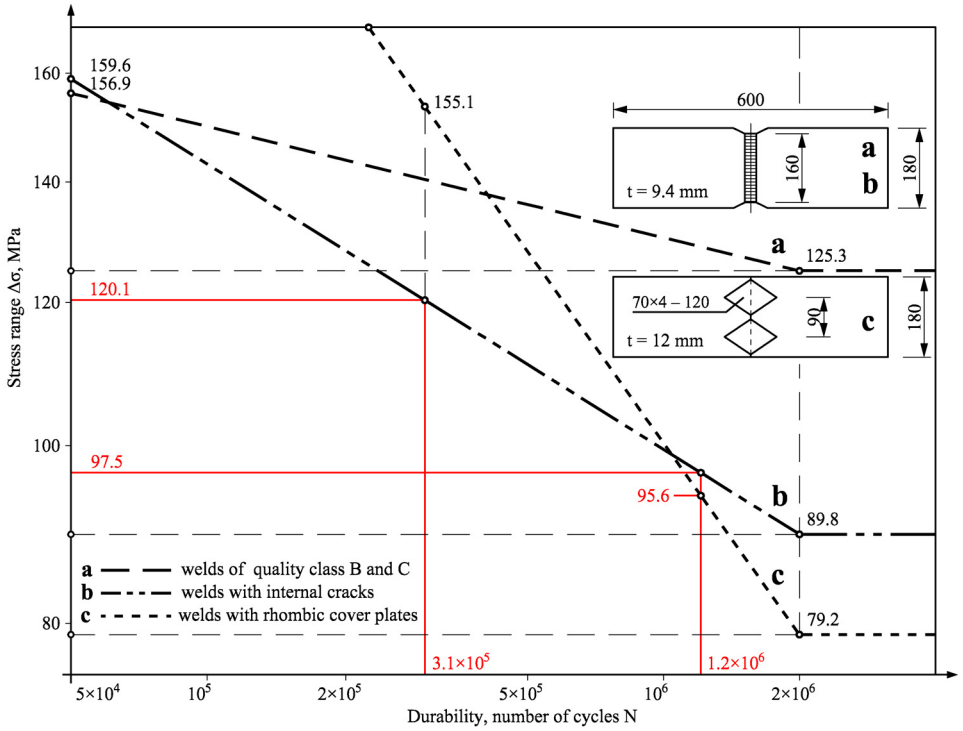


Figure 8: Regression lines and service load data

This is evidence for the safe operation of bridges Nos I and II, whose cracked welded splices were not strengthened in 1959. For a further 50 years of bridge service, in 2069, at the number of load cycles $N_3 = 1.9 \cdot 10^6$, the stress according to the regression line "c" will be σ = 80.5 MPa, so the stress will also be larger than the maximum value of the service stress $\sigma_{ser,\,max}$.

6 SUMMARY

The radiographic testing of welded butt splices in the first welded railway bridges in Poland revealed their very low quality. The considerable number of cracks in the flange splices on bridges Nos III and IV (48 and 39 cracks) and the stress values calculated for standard loadings led to the decision to undertake strengthening work. In total, 49 splices were retrofitted by additional cover plates and riveting. The rest of the splices were X-rayed after 13 years of further service life. These additional examinations showed no growth in the existing cracks nor the formation of new cracks. It is rightly noted in EN-19931--9: 2005 that "cracks … do not necessarily mean the end of the service life". The pulse tension from the service loading is Δ_e

= 74.4 – 15.1 = 59.3 MPa and is 25.1% lower than the infinitive life fatigue strength Δ_c = 79.2 MPa (Fig. 8).

The bridges on the railway line were constructed from low-carbon mild steel with actual characteristic values of ultimate strength R_m = 375 MPa and yield strength R_e = 260 MPa. Global tests on the structural steel of bridge No. III will be carried out during its nearest planned retrofit.

These steel bridges constitute an unique experimental base on the behavior of welds with non-tolerated welding imperfections – internal cracks.

REFERENCES

[1] Wittfoht, H. *Building bridges. History, technology, construction*. Beton-Verlag, Düsseldorf (1984).

[2] A History of Welding (weldinghistory.org)

[3] Bryła, S. Welded iron bridges. *Road News* (1931) **51**: 542-594 (in Polish).

[4] Schaper, G. Die erste geschweiβte eisenbahnbrücke für vollbahnbetrieb. Die Bautechnik (1930) **8**, Heft 32: 323-325.

[5] Schaper, G. *Recent achievements and developments in German bridge construction*, American Institute of Steel Construction (1938).

[6] Szelągowski, F.K. The first railway bridge in Poland with welded girders. *Railway Engineer* (1936) **11**: 388-390 (in Polish).

[7] Szelągowski, F.K. The railway bridge over the Sierpienica river on the Nasielsk – Toruń railway line. *Railway Engineer* (1937) **12**: 478-480 (in Polish).

[8] Wichtowski, B. The behavior of the oldest welded bridges in Poland. *II International Scientific Conference, Durability and Service Life of of Bridge Structures*, Poznań (1994): 351-356.

[9] Wichtowski, B. Service durability of the first welded bridges in Poland in the light of their butt joints investigation. *Archive of of Civil Engineering* (2003) **XLIX**, No. 2: 165-190.

[10] Warren, W.G. Fatigue tests on defective burr welds. *Welding Research* (1952) **6**, No. 2: 112-117.

[11] Stüssi, F. *Entwurf und Berechnung von Stahlbauten*. Springer-Verlag, Berlin - Heidelberg (1958).

[12] Newman, R.P. Effect on fatigue strength of internal defects in welded joints. *British Welding Journal* (1959) **6**, No. 2: 59-64.

[13] Newman, R.P. and Gurney, T.R. Fatigue tests on a thick transverse butt welds containing slag intrusions – first interim report. *British Welding Journal* (1964) **11**, No. 11: 341-351.

[14] Fischer, J.W. and Mertz, D.R. Hundreds of bridges – thousands of cracks. *Civil Engineering* (1985) **4**: 64-67.

[15] Hołowaty, J. and Wichtowski, B. Properties of structural steel in early railway bridges. *Structural Engineering International* (2013) **23**, No. 4: 512-518.

[16] Wichtowski, B. *Fatigue strength of welded butt splices in steel railway bridges*. Research Works PS No. 572, Szczecin (2002) (in Polish).

[17] Wichtowski, B. Assessment of fatigue and selection of steel on constructions of steel bridges welding according to Eurocode 3. *Welding International* (2013) **27**, No. 5: 345-352.

12th International Conference on Structural Analysis of Historical Constructions
SAHC 2020
P. Roca, L. Pelà and C. Molins (Eds.)

SALT CONTAMINATION OF WOODEN MATERIALS: THE CASE OF TRONDHEIM (NORWAY) WAREHOUSES

CHIARA BERTOLIN[1]*, MARCIN STROJECKI[2], LAVINIA DE FERRI[1], GIULIA GROTTESI[3] AND ANNA MARIA SIANI[3]
Department of Mechanical and Industrial Engineering, Norwegian University of Science and Technology, Trondheim, Norway.
e-mail: chiara.bertolin@ntnu.no, https://www.ntnu.edu/employees/chiara.bertolin (*corresponding author); lavinia.de.ferri@ntnu.no
[2] Jerzy Haber Institute of Catalysis and Surface Chemistry, Polish Academy of Sciences, Krakow, Poland
ncstroje@cyf-kr.edu.pl, http://www.ik-pan.krakow.pl/Szczegoly-profilu.293+M5f6db5c33ab.0.html
[3]Physics Department, La Sapienza University, Rome
1655269@studenti.uniroma1.it annamaria.siani@uniroma1.it.

Keywords: wood, acoustic emission, vacuum microbalance, salts; moisture meters.

Abstract. *Warehouses are big architectonical structures mostly made of spruce wood and utilized as storage buildings principally by food traders in Northern Countries. Trondheim's warehouses currently observable along the river Nidelva, date back between the 17th and half of the 19th century were mostly used to stock and process fish. Therefore, where the food goods were stored, residuals are expected to be still present and/or to be responsible for the formation of alteration products on the wooden surfaces as well as inside the wooden structure.*

Here we propose a characterization of residual and neo-formed compounds inside and on the surface of wooden logs by means of vacuum microbalance that allowed both to individuate the type of salts, as well as, to estimate the maximum water film thickness adsorbed on the wooden samples at 93% of RH. These data have been related to variations in the acoustic emission (AE) intensity detected at the log surface and to the wood moisture content measured with capacitive and resistance operating moisture meters. The application of three independent techniques have allowed obtaining interestingly information indicating their potentiality as decay assessment techniques in the field of historical materials and specifically in the study of salts weathering on wood. The methodology allowed identifying a clear relationship between the amount of water in logs as a function of their distance from the ground and variations in the amplitude of the acoustic emission signals.

1 INTRODUCTION

Wood based warehouses represent unique historical coastal buildings with peculiar construction features ascribable to the Norwegian construction tradition [1]. The main problem for these buildings were both to resist local weather conditions (strong winds, rain, high humidity, low temperature) and being functional for the specific needs of fishing/trading societies. Nowadays these structures are still present in cities developed starting from the Middle Age on the coasts and whose economy was based on the export of stockfish (dried cod) [2]. Trondheim has always been one of the most important Norwegian ports even if warehouses were constantly destroyed by fires and re-built always on the same sites and following the same construction rules established in the 12th century [2]. The quite big structures along the river

(Nidelva), mostly made of spruce wood, date back to between the 17th and ~1950 and were generally created as a combination of wood frames and log structures permitting the formation of many different space distributions. They were used as storage buildings mainly by food traders and merchants trading in other goods such as lumber, copper (from the Røros mines), flour, grain, sugar and precious textiles [2].

Food storage is supposed to leave residuals, that could also be responsible for the neoformed products (salts) on the wooden surfaces as well as inside the wooden structure. Wood alteration phenomena driven by salts have almost never been studied in the field of cultural heritage, basically because wood was usually employed for mobile artworks and only in few specific geographical regions such as Norway it was used as building material. Additionally, very few areas with historical wooden buildings are in a marine environment and this is the case of Scandinavia or other Antarctica regions. Consequently, the few studies regarding wood salt degradation of heritage buildings have been dealt with phenomena strictly associated with these peculiar environmental conditions [3-7]. Salts efflorescence and sub-efflorescence on wood were only rarely studied [3-6,7, 8-10] and in many cases researches are related to the influence of chemicals used for preservations purposes (pesticides, flame retardants, consolidants, etc.) As reported [7], such phenomena could be related to chemicals solubility by free water leakage and to the following crystallization into the porous microstructure of wood and on the surface in form of salts.

The final step in the alteration of wood when affected by salt crystallization is the so-called *fuzzy wood*, that manifests itself as a defibration of structures persistently exposed to salt, induced and intensified by freeze-thaw cycles or by drying of salty water raised into the internal structures of wood. Such vessels, in fact, are continuously stressed by forces deriving from the growing of salt crystals that tend to separate the fibres from each other [3] within quite short periods of time (up to 5 years). Furthermore, when water evaporates salts concentrate leading to chemical reactions corroding the middle lamella region of the cells walls. The progress of reactions brings to the separation of cells and the development of detached and eroded fibres, strongly affecting the stability of structures in ca. 30 years [3,5].

At the opposite, the detrimental effects of salts on stone-based structures have been widely investigated, also by means of Acoustic Emission (AE) [e.g. 11], a technique widely exploited in many fields but still representing a quite innovative diagnostic tool in the field of cultural heritage. Only few studies, in fact, are currently available on this topic when compared with the total amount of publications related to the use of other diagnostic tools in artworks, and they are mostly related to wooden based artworks [11-15] or to architectural heritage sites [16-18]. Being a non-destructive technique (NDT), AE has been mostly utilized during monitoring campaigns in order to obtain a fast detection of newly formed cracks or older crack propagation within the frame of preventive conservation projects, structural health monitoring of restored elements [19], evaluation of seismic risks [20,21], and detection of infestation of xylophagous insects [13]. This is because dimensional changes of wooden objects are related with changes in temperature and relative humidity, and with seismic or biological activities. AE lets the very fast recognition of these events even when occurring at a very low intensity level (e.g. due to microcracks appearance)

Here, acoustic emission, sorption isotherm and three different moisture content measurements (i.e. 2 capacitive and 1 resistance operating) techniques are proposed to investigate the state of one of the last almost original and never studied warehouses of Trondheim (Norway). The proposed research reports about residual and neo-formed salts, whose chemistry and concentration in four different structural elements or logs has been related to differences registered in terms of acoustic emission amplitude and moisture content in order to obtain information about their state of conservation.

2 MATERIALS AND METHODS

Three logs (Norwegian spruce - *Picea abies*) at different heights (Figure 1a) of the internal wall indicated in Figure 1b (ground floor) were tested, as well as a spruce trunk in the warehouse (Figure 1c) basement.

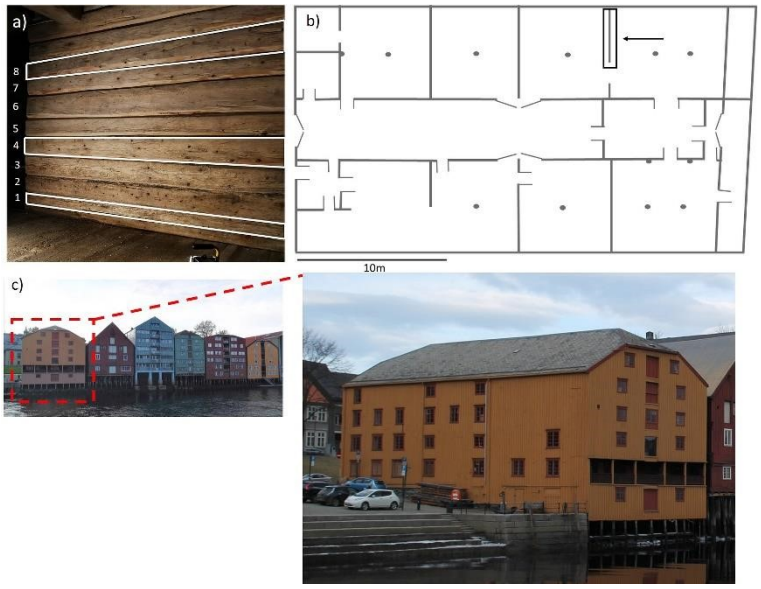


Figure1: a) Selected logs; b) Plan of the ground floor. The studied wall is circled, and the arrow indicates the tested side; c) The warehouse studied in Trondheim.

Samples to perform the water vapor sorption experiments were collected from every log and from the trunk using a drill bit (Ø = 2 cm). Measurements were taken gravimetrically by means of a vacuum microbalance from CI Electronics Ltd, following the methodology described in Bratasz et al. 2012. Adsorption branches of the water vapor isotherms were determined later in the laboratory at room conditions (T=24°C) and for a full range of water vapor relative pressures. Typically, a 0.1 g wood fragment was weighted and outgassed prior to the measurement under a vacuum of a residual pressure of less than 0.1 Pa in order to move the air out of the wood and to eliminate most of the species physisorpted during the storage of the sample, especially adsorbed water. The process was fully automated and measuring of 10 adsorption points took on average several hours.

Acoustic emission measurements were carried out by means of an AMSY-6 AE system (Vallen System GmbH, Icking, Germany). Each AE channel was equipped with a VS900-M sensor (frequency operating range = 100-900 kHz) in line with an AEP5 signal preamplifier (2.5 kHz to 2.4 MHz). Each channel, sensor and preamplifier combination was kept fixed during the monitoring of the logs. The rearm time and duration discrimination time were set to 3.2 and 1.6 ms, respectively, while pre- and post-trigger times were maintained equal to 0.2 and 0.4 ms, respectively. The signal sampling rate used to calculate the primary AE parameters was 10 MHz, whereas a value of 1 MHz was used to record the transient signal. Signals were acquired after applying a low-pass filter of 500 kHz, then the first peak amplitudes (i.e. maximum value of the first amplitude peak) were integrated to obtain the amplitude values to be verified in the attenuation models presented here. The disturbance caused by environmental noise was filtered using the system-predetermined threshold level set to 40 dB. All the monitoring campaign was conducted under environmental condition: relative humidity (RH) = 75%, and temperature (T) = 6-10 °C.

During the monitoring, at the surface of each selected logs, an acoustic emission events was simulated using the pencil lead break (PLB) method, first proposed by Nelson N. Hsu [22]. Each PLB was performed following the requirements given by the standards (Ø= 0.3 mm and 2H lead) ASTM E2374-16 2016 and ASTM E976-15 2015 [23,24]and executed five times to test the homogeneous sensors response. On every log, a linear series or array of 6 points, spaced 25 cm from each other, was created to locate the AE sensors (i.e. AE sources, Figure 2). Every sensor was fixed to the wood surface by means of hot glue [25], and the PLB test was performed 4 cm above every sensor location. The same sensor array was created on a trunk in the warehouse basement but using a spacing of 35 cm to avoid intercepting defects present on wood. During the data analysis, collected data have been filtered following the constrains reported in Table 1 ensuring the exclusion of signals linked to noise. Successively, a polynomial fitting of the amplitude attenuation curve was used to obtain comparable distance values [25].

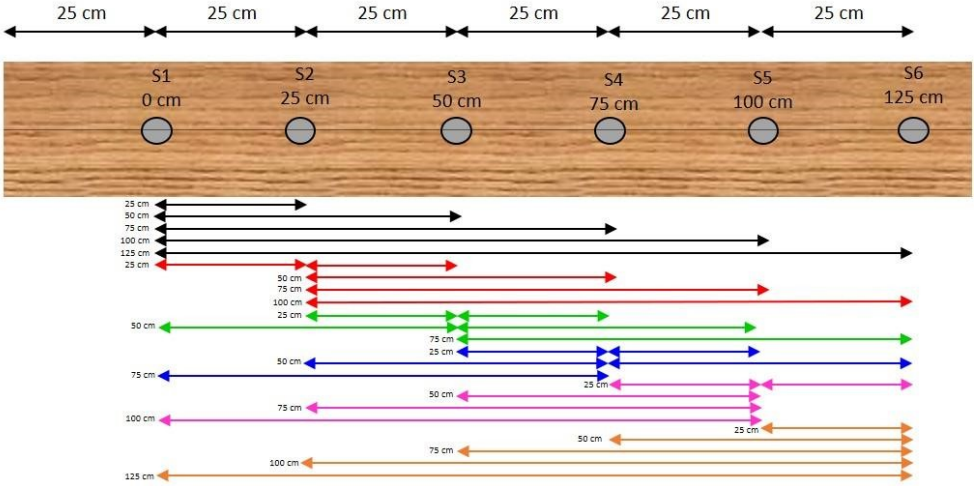


Figure 2: Scheme of sensors array and of distances between AE source (PLB) and sensors.

Table 1: Required level of accuracy during an AE event obtained by the PLB test procedure

Parameter	Required level of accuracy
Amplitude	40 < dB < 95
COUNTS	> 3
Rise Time	> 3 µs
Duration	> 3 µs
Root Mean Square	< 10 µV

Moisture content (MC) measurements on logs and trunk were taken by means of a Trotec T660 capacitive moisture meter (Trotec, Wels, Austria). The capacitive measurement method is non-destructive since the dielectric constant □ of the wood is determined via the highfrequency field of the capacitor. When wood is altered by moisture content, □ increases. In the T660 the generated electric field by the sensor (i.e. the measurement field) forms between the active spherical head and the substrate that is to be assessed up to a depth of about 0.5-4.0 cm (see Figure 3, left), keeping the probe sphere (Ø= 1.2 cm) perpendicular to the structure surfaces. Being the radius of a Log of about 15 cm, this means the measurement field is representative of the MC within ca 13% depth of the whole Log. With the T660, three measurements were taken in the same points where the PLB tests were performed on every investigated structural element (three Logs and the Trunk). The second utilized moisture meter i.e. Trotec T610 microwave method, belonged to the category of dielectric MC measurement method too. Being water a polar molecule, when subjected to an external applied altermatic electromagnetic field it can be polarized, at macroscopic level this is evident by change in □

values, which increase of more than one order of magnitude in presence of water (i.e. $\varepsilon_{H2O} \approx 80$ while $\varepsilon_{Dry\ spruce} \approx 1\text{-}3$). In the microwave range, beside the high dielectric constant of water (i.e. real part of ε), the dielectric losses (i.e. imagery part of ε) can also be used as measurement parameter. An advantage of this second NDT is, in fact, that the influence on the resistive losses caused by ionic conductivities due to the salts presence/weathering is reduced within the operating frequency of the instrument i.e. 2.43 GHz. At such frequency these losses are virtually negligible compared with dielectric ones, indicating that the microwave method is theoretically independent by the presence of salts. In reality, as reported by experimental tests conducted by Camuffo and Bertolin in 2012 [26], the efflorescence is almost not noticeable when RH is below the salt deliquescence level very because the water layer adsorbed in the superficial salt efflorescence is a very small fraction of the whole MC into the bulk material. However, when RH exceeds the deliquescence level, the thin aqueous film that forms on the surface reflects the signal giving the appearance of a damp material (e.g. approaching the Fiber Saturation Point (FSP) conditions). T610 microwave sensor contains an antennae assembly that enable a measurement field up to a penetration depth of ca. 30 cm i.e. the whole dimensions of the monitored Logs (see Figure 3, right). Finally, the third and last moisture meter used was the Trotec T3000 which uses the resistance or conductivity measurement principle i.e. an electrical current generated in the device and conducted in the wood thanks to the insertion of 2 electrodes or pins (length =2,0 cm, see Figure 3, central). With higher water content in wood the conductivity increases and the resistance reduces (i.e. water is inversely proportional to measured resistance). The resistance curve was corrected for the tested wooden material i.e. spruce and automatically adjusted as a function of the surface wood temperature that was in equilibrium with the air T. Surface and air T were detected using a thermistor NTC sensor.

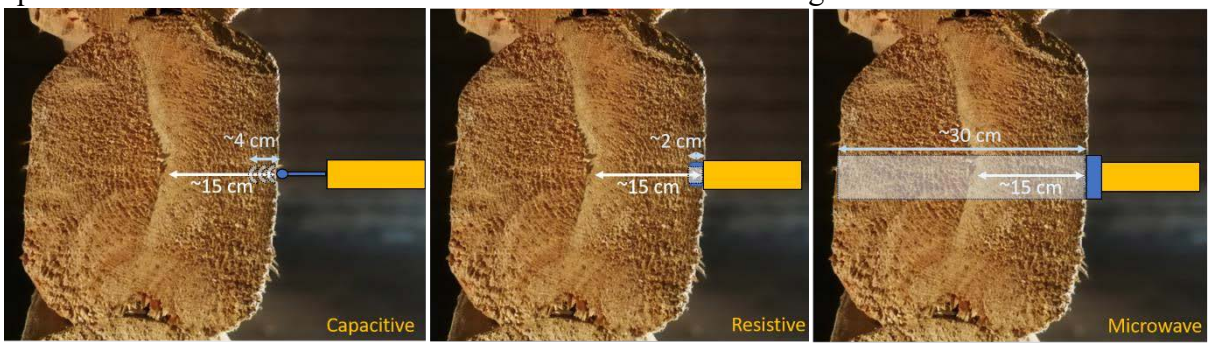


Figure 3: Scheme of the penetration depth of the three moisture meters into the wooden Log.

3 DISCUSSION OF THE RESULTS

Two alteration forms have been observed on the investigated wooden elements: salts efflorescence and what was interpreted as starting of *fuzzy wood*, being the log surfaces covered by a quite soft and easily detaching fibrous layer.

The adsorption isotherms obtained by vacuum microbalance permit the identification of salts crystallized inside the structures, that are: Sodium Chloride (NaCl), Sodium Nitrate ($NaNO_3$); Ammonium Nitrate (NH_4NO_3) and Magnesium Nitrate hexahydrate ($Mg(NO_3)_2 \cdot 6H_2O$) [25]. Table 2 resumes trends for the 4 analyzed samples reporting the statistical thickness of the water layer (nm), the volume of adsorbed water (V_{ads}= M_{ads}/100, being M_{ads} the % mass of water vapor) and the percentage deviation from theoretical linearity. Our standard reference was the trunk element as it was a clear wood sample with no salts presence.

Table 2: Statistical thickness of the water layer (nm), volume of adsorbed water (%) and percentage deviation from theoretical linearity obtained for the four analyzed logs. Red circles indicate values of deviation form theoretical linearity corresponding to the salts critical RH levels allowing determining the presence of $Mg(NO_3)_2$ (53%), NH_4NO_3

(64%), $NaNO_3$ (64%) and NaCl (75%)

Log1			Log4			Log8			Trunk		
t (nm)	V_{ads} (%)	%	t (nm)	V_{ads} (%)	%	t (nm)	V_{ads} (%)	%	t (nm)	V_{ads} (%)	%
0.11	3.58	10	0.11	4.53		0.11	4.07		0.11	2.80	
0.19	5.65	20	0.19	6.95		0.19	6.35		0.19	4.40	
0.25	7.24	30	0.25	9.00		0.25	8.25		0.25	5.78	
0.31	8.64	40	0.31	10.95		0.31	10.10		0.31	7.17	
0.37	10.51	50	0.37	12.79		0.37			0.37	8.78	
0.44	13.78					0.44	13.57		0.44	10.62	
0.53	19.53					0.53	16.75	70	0.53	12.74	70
						0.65	21.48	80	0.65	15.24	80
0.65	28.63								11.61		
0.81	44.94	90	0.81	32.68	90	0.81			28.30	90	
0.92	66.048	93	0.88	34.91	93	0.88			30.72	93	
1.00	90.81	98							0.81	19.19	90
									0.88	20.72	93

The t_{max} value i.e. the maximum thickness of water film adsorbed at 93% of RH on the surface of the sample collected by each log was calculated according to Bratasz et al. [27] and then referred to the trunk element. Values of 2.3, 1.5,1.3 and 0,8 nm were found for Log1, Log4, Log8 and the Trunk, respectively. This calculation was based on two preliminary assumptions: i) the mass of adsorbed water changes linearly when the sample representative of a Log is not affected by salts presence; ii) the effective diameter of water molecule is equal to 0.26 nm. Parallel, also the number of water monolayers adsorbed by each sample could be calculated, being 9, 4,3 and2 for Log1, Log4, Log8 and the Trunk, respectively. These assumptions are reliable because plotting data reported in Table 2, a straight-line graph is expected if the water layer can grow freely on the entire surface of the sample since water volume adsorbed is a product of surface area and water layer thickness [25]. Deviations from linearity occur in presence of condensation phenomena generally due to deliquescent salts responsible for an extra amount of water. During our laboratory measurements, the point where the trend line deviates from the linearity specifies the type of the dominant salt in the sample. Results shows the most affected elements are respectively Log1 and 4, while Log8 remains quite safe from salts crystallization. Summing up, the identified phases well match with both the environmental conditions and the historical use of the warehouse. The presence of NaCl, in fact, can be imputed to the marine setting as well as to its utilization for conservation and dehydration of fish, in turn accountable for the presence of nitrates [25, 28, 29].

Attenuation curves obtained by AE measurements [25] show a strong amplitude decrease with distance from the PLB event. As stated in literature, the alteration degree (including the presence of rot) and the material moisture content can be detected using AE data [30]. Also in this study, in fact, differences were observed for the studied logs, containing different amounts of salts and moisture [25]. For the most affected one, Log1, the strongest signal lowering was found if compared to the other wooden elements [25]. Considering that AE waves propagate as plane waves with a 1D front of the simple harmonic wave travelling through the absorptive medium without diffusion attenuation [31], an exponential absorption- scattering equation can be extracted [25]:

$$|A_x - A_{THR}| = A_0 e^{-kx} \quad (1)$$

being A_x the amplitude at distance x from the PLB point (dB), A_0 the maximum amplitude at the source (i.e. source distance = 0) (dB), A_{THR} a constant background amplitude, k the amplitude attenuation factor (cm^{-1}) and x the source-sensor distance (cm). The proposed equation resembles the hydration model already proposed in literature [32] to explain the wave propagation on materials surfaces at different hydration degrees.

Salts only barely affected the detection capability of sensors, since signals were registered for almost all the distances [25]. Notwithstanding the very high relative humidity and low temperature (85% and 2°C) conditions of the basement, the highest values were registered on the trunk, while the highest amplitude attenuation was found for Log1. Consequently, differences between the acoustic wave attenuation behavior in the three decayed Logs can be related to their decay condition.

Analogues results on the type and level of decay of the monitored wooden elements, as well as some limits of the applied techniques can be underlined looking at the data obtained by the three used moisture meters (Figure 4). Here, original readings were analyzed in comparison to the reference Log demonstrated to be safe and dry i.e. the Trunk. An equation (i.e. eq.2), that resemble the definition of MC was used to conduct such analysis: $\frac{(MC_{Log,i} - MCTrunk)}{MCLog,i} * 100$ (2).

In the plot, values of ca. 28-30 becomes therefore proxy for assessing the Fiber saturation Point (FSP) within wood. Lower values proxy representative of adsorbed moisture which can modify bound water (BW) embedded in the cell wall through adsorption and desorption; Higher values proxy representative of free water (FW) that fills the wood cavities, once having filled the wooden cells. Within each Log (i.e. Log1=L1; Log4=L4; Log8=L8), differences in the average values of MC are representative of optimal conditions for specific type of decay within the sensitive measurements field of the three instruments (i.e. areas highlighted in Figure 3). In the case of the Capacitive moisture meter (red dataset in Figure 4), it demonstrates a low accuracy in discriminating between different MC level among Log1, 4 and 8 as they result almost at the same MC range between 76 and 79 (Unit: 100 * MC (%)). Notwithstanding a weak linear increase among them exists; Log1 being the wooden element where a higher content of water is detected which resembles values of FW i.e. liquid water embedded in wooden cavities. In a similar way, the resistive moisture meter (black dataset in Figure 4) shows similar results with values resembling MC in a range between 76 and 81. This means that the detected resistance values are lower than 0.02 MOhm in a low accuracy range, strongly influences by wooden species (although the calibration done automatically by the instrument) and the surface temperature. In addition, although the physical principles of detection differ, both the 2 moisture meters are strongly affected by the presence of salts, especially in deliquescence form. In the first case they cause reflection of the signal with an output which can increase up to the full range dampness [26]; in the second case they cause higher conductivity resulting in an overestimation of the MC (i.e. resistive losses caused by ionic conductivities due to the salts presence). Finally, in the case of the capacitive moisture meter, physical heterogeneities or micro blistering (as in the presence of fuzzy wood appearance in Log1 and 4) can additionally cause misleading high dampness values. For this reason, results from both the two methods have low significance in this case study, although they demonstrate presence of salts in deliquescence forms within the first 2 cm pf the superficial level of the Logs. At the opposite the microwave moisture meter (blue dataset in Figure 4), provides more detailed information about the level of decay in the Logs. Such method can detect that the whole Log8 is not affected by high value of MC. This means that -in average - the bulk material is not damaged by salt weathering and still in good condition, while is only the superficial layer that is affected by the presence of a thin

layer of salts in deliquescence form (output provided by the 2 other moisture meters). This is confirmed by the measurements done with the vacuum microbalance that detected 1.3 nm of maximum thickness of water film adsorbed at 93% of RH corresponding to 3 water monolayers. Different is the situation for Log4 and 1 which equally demonstrates the probability of having average value of bulk material at the FSP, or a thick superficial layer contaminated by deliquescent salts which reflects the penetrating electromagnetic field thus overestimating the output and the MC values. Although we know, from the measurements conducted with the microbalance, that such hypothesis if the most likely, however with the measurements from the microwave moisture meter only such discrimination is not possible. The comparison with the microbalance results demonstrates that already 4 monolayers of water (i.e. a maximum thickness of 2.3 nm) at the surface of the material are sufficient to eventually overestimated MC values at the level of FSP thus invalidating the capability of the instrument to penetrate deeper layer of the material.

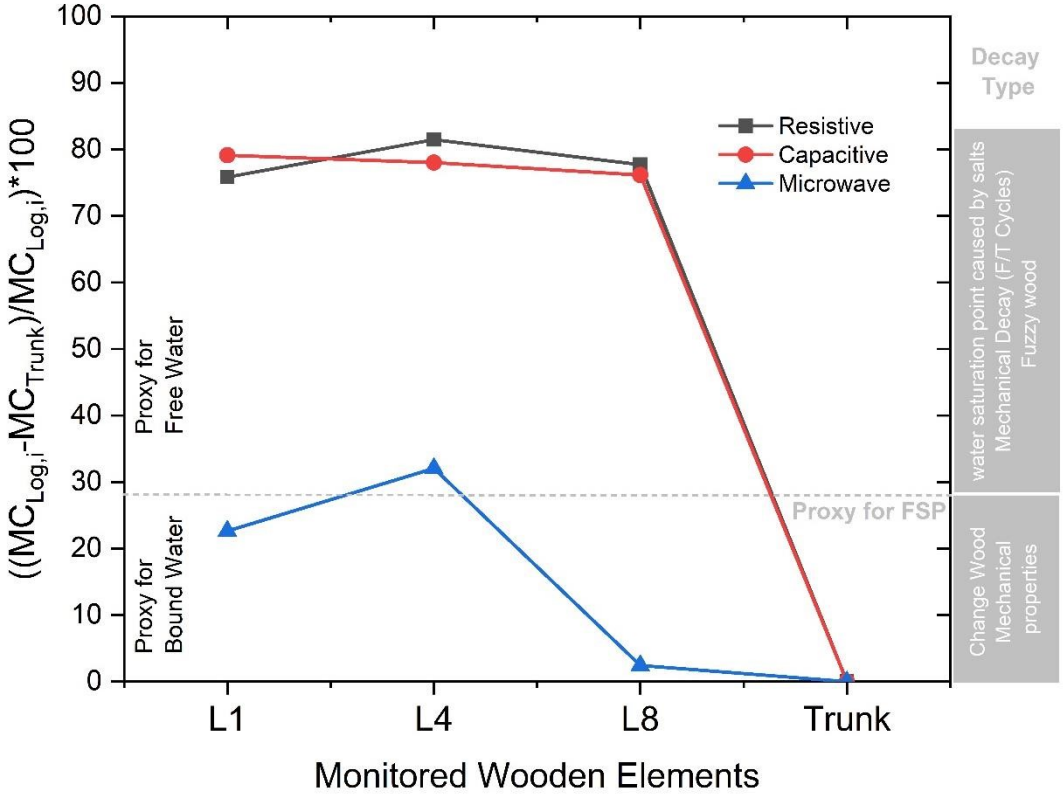


Figure 4: Analysis of moisture meters readings (i.e. black square and line: resistive moisture meter; red circle and line: capacitive moisture meter and blue triangle and line: microwave moisture meter), elaborated to resemble the definition of MC in reference to the Trunk as dried wooden element. Values of ca. 28-30 are a proxy for the Fiber saturation Point (FSP). Lower values are proxy representative of adsorbed moisture which modifies bound water embedded in the cell wall; Higher values are proxy representative of free water that fills the wood cavities. On the right, the effects of such MC modifications are described as type of visible decay.

4 CONCLUSIONS

The proposed study of four spruce logs form a 20th century warehouse in Trondheim (Norway) involved a multi-technique approach allowing obtaining complementary information concerning the state of conservation of such structural elements.

The contamination degree of wood by salts has been evaluated performing water absorption-desorption measurements by means of a vacuum microbalance that permitted the identification of the main phases crystallizing inside the wooden structures and on the surfaces, as well as the maximum thickness of the water film adsorbed on the samples surface. Outcomes

indicated how the most contaminated and hydrated elements were Log1 and 4, while Log8 and the Trunk resulted quite safe. Parallel, AE measurements evidenced differences in the attenuation curves get on the four elements as a function of the alteration degree. Particularly a direct connection between the wood hydration degree and how acoustic waves propagates into the material, or more precisely on the material surface. These findings are also confirmed by the measurements conducted with different moisture meters that, in the area of sensitiveness i.e. their measurement fields, have demonstrated to be effective in (i) detecting the presence of salts in deliquescence form already after the appearance of very few monolayers of water as the case of the resistance and capacitive methods and (ii) in assessing an average level of MC in the bulk material that remains representative of the overall conditions of material also under extreme environmental conditions as the case of the microwave moisture meter working on Log8 during this monitoring campaign (i.e. environmental conditions with high RH, low T conditions; material with high contents of salts in deliquescent form and decayed by salt weathering and fuzzy appearance). However, also this last method has demonstrated its limitation because already 4 monolayers of water (i.e. 2.3 nm) at the wooden surface cause signal reflections which overestimate the MC thus invalidating the capability of the instrument to penetrate deeper layer of the material.

Acknowledgements. The authors are grateful to Prof. Eileen Garmann Johnsen for her kind support during the monitoring campaign. The activity has been possible thanks to the Norwegian Research Council funded "SyMBoL—Sustainable Management of Heritage Building in a Long-term Perspective" Project (Project No. 274749). This research was funded in part by the statutory research fund of ICSC PAS.

REFERENCES

[1] http://stiftelsenbryggen.no/verdensarven-bryggen/byggemate/ (accessed on 09/01/2020)
[2] Grytli, E. A journey along the norwegian coast: warehouses and historical wooden structures. *Int. Holzbau Forum* (2013) **19**:1-11.
[3] Kirker, G., Glaeser, J. Salt damage to wood "fuzzy wood" often confused with fungal decay. Techline, Forest Products Laboratory (2011) Madison.
[4] Blanchette, R.A. (2003) Deterioration in historic and archaeological woods from terrestrial sites. In: R.J. Koestler et al. (Eds): *Art, biology, and conservation: biodeterioration of works of art.* The Metropolitan Museum of Art, New York, pp. 328-347.
[5] Blanchette, R.A., Held, B.W., Farrell, R.L. Defibration of wood in the expedition huts of Antarctica: an unusual deterioration process occurring in the polar environment. *Polar Rec* (2002) **38**:313-322.
[6] Kim, D.W., Kim, C.W., Han, S.H., Chung, Y.J., Han, G.S. Flame retardant treatment's effects and detection method on wooden buildings' pigment layer. *J. Korean Wood Sci. Technol.* (2014) **42**:393-406.
[7] Catelli, E., Bănică, F.G., Bănică, A. Salt efflorescence in historic wooden buildings. *Herit Sci.* (2016) **4**:31-44.
[8] Madhoushi, M., Eimanian, J., Ansell, M.P. Non destructive and laboratory evaluation of strength of decayed wood members in a historic construction located in Gorgan (North of Iran). In: *Structural analysis of historic construction: preserving safety and significance—proceedings of the 6th international conference on structural analysis of historic construction*, SAHC08, Vol 1 (2008) pp. 469-472.
[9] Campos, .AF., de Macedo, L.B., de Castro, E., Silva Bortolucci, M.A.P., Lahr, F.A.R.

Evaluation of health conditions of wooden structures of the former slave quarters of farm Santa Maria do Monjolinho, located in the state of São Paulo, Brazil. *Adv. Mater. Res.* (2013) **778**:1096-1101.

[10] Piotrowska, M., Otlewska, A., Rajkowska, K., Koziróg, A., Hachułka, M., NowickaKrawczyk, P., Wolski, G.J., Gutarowska, B., Kunicka-Styczyńska, A., Zydzik-Białek, A.
Abiotic determinants of the historical buildings biodeterioration in the former Auschwitz II—Birkenau concentration and extermination camp. *PLoS ONE* (2014) **9**: e109402-1-12.

[11] Jakiela, S., Bratasz, L., Kozlowski, R. Acoustic emission for tracing the evolution of damage in wooden objects. *Stud. Conserv.* (2007) **52**:101-109.

[12] Strojecki, M., Łukomski, M., Krzemień, L., Sobczyk, J., Bratasz, Ł. Acoustic emission monitoring of an eighteenth-century wardrobe to support a strategy for indoor climate management. *Stud. Conserv*. (2014) **59**:225-232.

[13] Le Conte, S., Vaiedelich, S., Thomas, J.H., Muliava, V., de Reyer, D., Maurin, E. Acoustic emission to detect xylophagous insects in wooden musical instrument. *J. Cult. Herit.* (2015) **16**:338-343.

[14] Łukomski, M., Strojecki, M., Pretzel, B., Blades, N., Beltran, V.L., Freeman, A. Acoustic emission monitoring of micro-damage in wooden art objects to assess climate management strategies. Insight (2017) **59**:256-265.

[15] Łukomski, M., Beltran, V., Boersma, F., Druzik, J., Freeman, A., Strojecki, M., Learner, T., Taylor, J. Monitoring acoustic emission in an epidemiological pilot study of a collection of wooden objects. *Stud Conserv*. (2018) **63**:181-186.

[16] Carpinteri, A., Lacidogna, G. Damage evaluation of three masonry towers by acoustic emission. *Eng. Struct*. (2007) **29**:1569–1579.

[17] Niccolini, G., Carpinteri, A., Lacidogna, G., Manuello, A. Acoustic emission monitoring of the syracuse athena temple: scale invariance in the timing of ruptures. *Phys. Rev. Lett.* (2011) *106*:108503-1–108503-4.

[18] Niccolini, G., Manuello, A., Marchis, E., Carpinteri, A. Signal frequency distribution and natural-time analyses from acoustic emission monitoring of an arched structure in the Castle of Racconigi. *Nat. Hazards Earth. Syst. Sci.* (2017) **17**:1025–1032.

[19] Kourkoulis, S.K. Recent advances in structural health monitoring of restored elements of marble monuments. *Procedia Struct. Integr.* (2018) **10**:3-10.

[20] Carpinteri, A., Lacidogna, G., Niccolini, G. Acoustic emission monitoring of medieval towers considered as sensitive earthquake receptors. *Nat. Hazards Earth Syst. Sci.* (2007) **7**:251-261.

[21] Carpinteri, A., Lacidogna, G., Invernizzi, S., Accornero, F. The sacred mountain of Varallo in Italy: seismic risk assessment by acoustic emission and structural numerical models. *Sci. World. J.* (2013) 170291-1–17029111

[22] Hsu, N., Simmons, J.A., Hardy, S. An approach to acoustic emission signal analysis—theory and experiment. *Matls. Eval.* (1977) **35**:100-106-

[23] ASTM E976-15: 2015. Standard guide for determining the reproducibility of acoustic emission sensor response

[24] ASTM E2374-16: 2016. Standard guide for acoustic emission system performance verification

[25] Bertolin, C., de Ferri, L., Grottesi, G., Strojecki, M. Study on the conservation state of wooden historical structures by means of acoustic attenuation and vacuum microbalance. *Wood Sci. Technol*. (2020) **54**: 203-226.

[26] Camuffo, D., Bertolin C. Towards standardisation of Moisture Content measurement in Cultural Heritage Materials. *e-Preservation Science* (2012) **9**:23-35.

[27] Bratasz, Ł., Kozlowski, R., Kozlowska, A., Rachwal, B. Analysis of water adsorption by wood using the Guggenheim–Anderson–de Boer equation. *Eur. J. Wood Prod.* (2012) **70**: 445–451
[28] Arthur, M.A., Siccama, T.G., Yanai, R.D. Calcium and magnesium in wood of northern hardwood forest species: relation to site characteristics. *Can. J. For. Res.* (1999) **29**:339346.
[29] Li, D., Ou, J., Lan, C., Li, H. Monitoring and failure analysis of corroded bridge cables under fatigue loading using acoustic emission sensors. *Sensors* (2012) **12**:3901-3915.
[30] Zhang, J., Yang, S., Hao, R., Gu, X. Amplitude attenuation laws of acoustic emission waves in plate structures. *Tecnol, Ing. Mec.* (2019) **94**:67-74.
[31] Nadelman, E.I. Hydration and microstructural development of Portland limestone cementbased materials. Doctoral dissertation, Institute of Technology, (2016) Georgia
[32] Schindler, A.K., Folliard. K.J. Heat of hydration models for cementitious materials. *ACI Mater. J.* (2005) **102**:24-33.

12th International Conference on Structural Analysis of Historical Constructions
SAHC 2020
P. Roca, L. Pelà and C. Molins (Eds.)

STIFFNESS CHANGES DUE TO STATIC LOADING OF A BRICK ARCH

JAN BAYER[1], SHOTA URUSHADZE[1*] AND JIŘÍ WITZANY[2]

[1]Institute of Theoretical and Applied Mechanics of the Czech Academy of Sciences
Prosecká 809/76, 190 00 Praha 9, Czech Republic
e-mail: {bayer@itam.cas.cz, urushadze@itam.cas.cz}, www.itam.cas.cz (*corresponding author)

[2] Czech Technical University Prague, Faculty of Civil Engineering
Thakurova 7, 166 29 Prague 6 – Dejvice, Czech Republic
email: witzany@fsv.cvut.cz, www.fsv.cvut.cz

Keywords: Masonry arch, impact testing, static loading, stiffness evaluation, flexibility change

Abstract. *A brick arch was loaded under laboratory conditions in three successive loading steps. No cracks were observed but reduction of natural frequencies and stiffness of the arch was experimentally documented. The stiffness was evaluated in a non-destructive test using an impact hammer and only two accelerometers. The proposed identification technique based on known experimental modal analysis theory is tailored to stiffness evaluation of masonry vaults. The results and the applied method are extensively discussed.*

1 INTRODUCTION

Modal parameters reflect stiffness changes in building structures and are therefore applied in the framework of health monitoring, estimated in order to detect possible damage in structures or just to check the integrity of finite element models [1,2,3].

Application of experimental modal analysis to masonry structures (overview [4]) is less common than to bridges, but there are numerous tests of churches [5,6,7] and publications dedicated to the dynamic behaviour of masonry arches. The presented article follows up on investigations performed in the nighties in England [8,9,10] and applies similar approach as [11]. A good example of laboratory research appeared recently in [12].

Brittle materials that form cracks under static loading are more suitable to vibration based damage detection than steel structures or pre-stressed concrete. On the other hand, they are likely to behave in a non-linear way which makes the application of experimental modal analysis questionable. Experience with similar structures shows that the influence of non-linear effects (probably mainly due to damping) increases with distance from the excitation (loading) point, and the dynamic response of the structure depends on loading location [13].

The proposed experimental procedure therefore only uses measured driving point frequency response functions (FRF) for the evaluation of the condition of the investigated brick arch. It does not extract the modal properties but instead estimates the static flexibility from the FRFs directly. The experimentally obtained flexibility increases with applied static load as the measured response to the hammer impact confirmed.

The proposed method is therefore possibly applicable in the health monitoring of brick vaults as well as in the experimental assessment of the collapse mechanism of masonry arches.

2 STATIC FLEXIBILITY ESTIMATION

Flexibility (which is the inverse of stiffness) has been successfully applied for damage detection in the past [14]. The main advantage is that it converges early with the few first modes when derived from measured results.

Static flexibility can be estimated as the frequency response function (receptance) at zero frequency [8,15]. The FRF at each driving point can be approximated as the sum of as many single degrees of freedom (SDOF) systems as there are distinct frequency peaks in the particular FRF for each driving point independently.

The FRFs were obtained from hammer impacts, and the driving (hitting) points were selected at regular distances along the vault (see Fig.1) – 16 points along the arch. As it is impossible to measure the vibrations at the excitation point, two points to the left and right of it were selected. It was measured only in the direction perpendicular to the vault surface, and the two accelerometers were moved along with the hammer.

In order to estimate the FRFs at the zero frequency it is necessary to perform a curve fit and transfer the measured inertances into receptances. A good curve fit around the peaks is essential for the success of the method, however, a simple SDOF fitting worked fairly well here. The dominant peak frequencies were estimated from the summarized FRF, and then a simple amplitude fitting was performed. Application of more sophisticated fitting methods is planned next.

3 ANALYSIS

In order to check the credibility of the experimental results a linear finite element (FE) model was created in ANSYS 17.2 using Solid185 elements. First comparisons of the measured and computed results confirmed that the boundary conditions were close to the clamped state. After adjustment of the elasticity modulus to 3 GPa and the density to 1700 kg/m3 the natural frequencies roughly corresponded to the measured ones (see Tab.1). This model was used to compute the static deformations due to unitary static load at measured locations which correspond to the experimentally evaluated flexibilities (see Fig.3). Only the intact condition was simulated.

Table 1: Comparison of computed and measured natural frequencies for the intact condition

Mode No.	Analytical Frequencies [Hz]	Experimental Frequencies [Hz]
1	28,52	30,7
2	35,32	32,4
3	55,75	52,0

4 EXPERIMENT

The experimental site is shown in Figure 1. The radius of the arch was 1.625 m, its span was 3m and width 0.75m. Accelerations were measured with the transducers SKF CMSS 793L in two rows of measured points perpendicularly to the surface at equal distances of approximately 255 mm. The 8202 Brüel&Kjaer impact hammer was used to hit the surface of the arch between the measured points with a peak force of approximately 400 N. The sampling rate of 1 kHz was used and the time for each measurement point took cca 120 s including five impacts for averaging.

After the dynamic experiments on the intact arch the static force of 24, 36, 48 kN (x2) was applied in three successive steps at the 1/3 points. After each loading step dynamic impact measurements were repeated in the unloaded condition. Finally, the arch was destroyed by 2x129 kN total force (it was reinforced by CFR plates).



Figure 1: Experimental site (note the two moving accelerometers at the vault´s heel)

In spite of the fact that no cracks could be observed on the arches after the stage where 48 kN was applied, the shifts in frequency spectra (see Fig.2) and the evaluated flexibilities (see Fig.3) revealed a gradual loss of stiffness. This drop in stiffness was not confirmed however by the deformations measured during the static loading. The hypothetical explanation for this phenomenon may be a possible development of micro cracks.

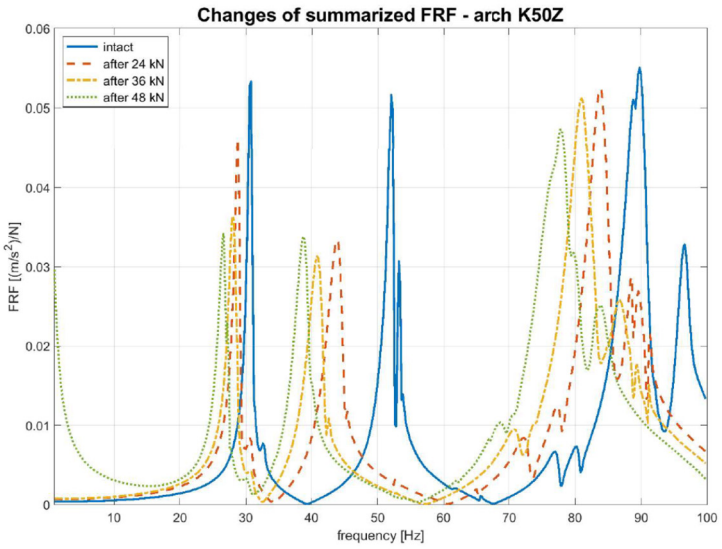


Figure 2: Summarized measured Frequency Response Functions

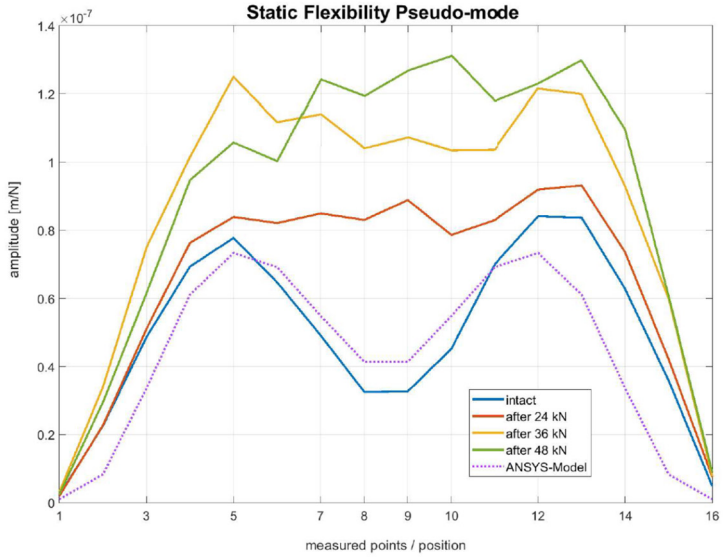


Figure 3: Experimentally estimated calculated flexibility

The increase in flexibility (or loss of stiffness) can be plotted relatively to the intact condition (see Fig.4) showing that the major damage occurred in the middle of the arch. This indicates that the experimentally estimated flexibilities could potentially be used to predict the failure mode which is sometimes a problem with ageing masonry structures, as mentioned in [10].

5 CONCLUSIONS AND DISCUSSION

The completed experiments showed that the dynamic properties of the tested masonry arch were influenced by the applied static load. The estimated flexibilities and the drop in natural frequencies indicate a gradual loss of arch stiffness due to the static loading. However, no significant drop in stiffness was observed during the static loading. A possible explanation may be that the behaviour of the arch at very low vibration levels (induced by the impact hammer) is influenced by micro cracking and is therefore of a different character than static behaviour under substantial static load.

The experimentally estimated flexibilities will therefore not be reliable in predicting static deformations of masonry structures – unlike steel structures [16] – but they could possibly be applied to predict failure modes after further research.

The tested arch was a bare structure without infill or permanent static loads, which made the dynamic testing easier. However, further application of the proposed procedure to test its applicability to the condition assessment of ageing masonry structures seems reasonable.

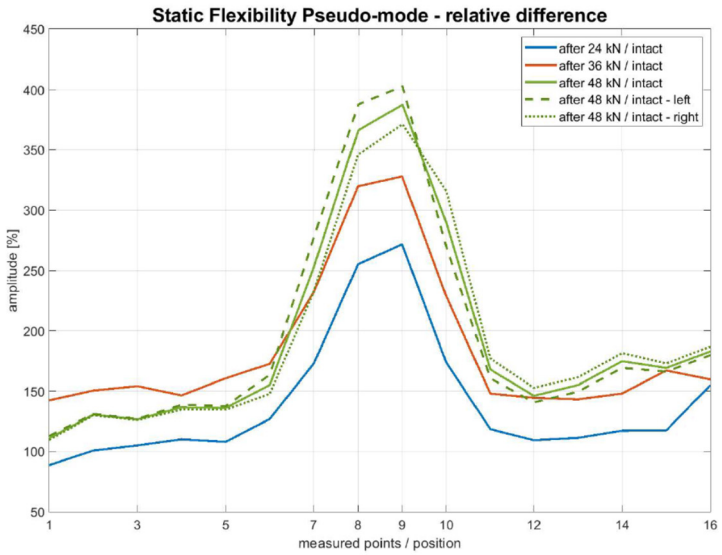


Figure 4: Relative Increase of Flexibility

Acknowledgements. The tested structure and the static part of the tests were completed thanks to the funding provided by NAKI DG16P02M055 “Development and Research of Materials, Methods and Technologies for the Restoration, Preservation and Strengthening of Historic

Masonry Constructions and Surfaces and Systems of Preventive Conservation of Cultural Heritage Buildings Threatened by Anthropogenic and Natural Hazards" and the dynamic tests and their evaluation was done in the framework of the grant project DG18P02OVV040 "Monuments in motion"; NAKI programs provided by the Ministry of Culture of the Czech Republic.

REFERENCES

[1] Rücker W., Hille F. Rohrmann R., Guideline for Structural Health Monitoring, BAM, SAMCO, F08a, Berlin 2006

[2] Maeck J., De Roeck G., Dynamic bending and torsion stiffness derivation from modal curvatures and torsion rates, JSV 225(1), 1999, p.153-170 (cracks)

[3] Sinou J-J., A review of damage detection and health monitoring of mechanical systems from changes in the measurement of linear and non-linear vibrations, Robert C. Sapri. Mechanical Vibrations: Measurement, Effects and Control, Nova Science Publishers, Inc., pp.643-702, 2009, 978-1-60692-037-4. <hal-00779322>, https://hal.archives-ouvertes.fr/hal-00779322

[4] Cescatti E., Combined experimental and numerical approaches to the assessment of historical masonry structures, Dissertation, PHD, University of Trento, 2016

[5] Ramos L., Marques L., Lourenço P., De Roeck G., Campos-Costa A., Roque J., Monotoring of historical masonry structures with operational modal analysis: two case studies, July 2010, Mechanical Systems and Signal Processing 24(5):1291-1305, DOI: 10.1016/j.ymssp.2010.01.011

[6] Atamturktur S., Hemez F., Unal C., Calibration Under Uncertainty for Finite Element Models of Masonry Monuments, Los Alamos report. LA-14414, February 2010

[7] Atamturktur S., Fanning P., Boothby T. E., Traditional and operational modal testing of masonry vaults, Engineering and Computational Mechanics 163, September 2010 Issue EM3, Pages 213–223, doi: 10.1680/eacm.2010.163.3.213

[8] Armstrong D.M., Sibbald A., Forde M.C., Integrity assessment of masonry arch bridges using the dynamic stiffness technique, NDT&E International, vol. 28, No.6, pp. 367-375, 1995

[9] Brown G., Pretlove A.J., Ellick J.C.A., Hogg V, Choo B.S., Changes in the dynamic characteristic of a masonry arch bridge subjected to monotonic loading to failure, Proc. of the First International Conference on Arch Bridges held at Bolton, UK on 3-6 September 1995, p.375-383

[10] Hughes T.H., The testing, analysis and assessment of masonry bridges, Structural Analysis of Historical Constructions, P. Roca, J.L. González, A.R. Marí and E. Onate (Eds.) © CIMNE, Barcelona 1996

[11] Heiland D., Mistler M., Investigation of dynamic performance of LASER building, report Nr. 40-10252-01-D1 for ELI Beamlines, Prag, 12/2015, Baudynamik Heiland & Mistler GmbH, Bergstraße 174, 44807 Bochum, internet: www.baudynamik.de

[12] Masciotta M-G. at al., Dynamic characterization of progressively damaged segmental masonry arches with one settled support: experimental and numerical analyses, Frattura ed Integrità Strutturale, 51 (2020) 423-441; DOI: 10.3221/IGF-ESIS.51.31

[13] Sortis, A. D., Antonacci, E., and Vestroni, F. 2005, "Dynamic Identification of a Masonry Building Using Forced Vibration Tests," Engineering Structures, Vol. 27, pp. 155–165.

[14] Reynders E., De Roeck G., A local flexibility method for vibration-based damage localization and quantification, Journal of Sound and Vibration 329 (2010) 2367–2383, https://doi.org/10.1016/j.jsv.2009.04.026

[15] Ewins D.J., "Modal Testing, Theory, Practice, and Application" ISBN-10: 0863802184, Mechanical Engineering Research Studies: Engineering Dynamics Series, 1984, 2nd Edition

[16] Pasha H., Allemang R. J., Phillips A. W., Young A., Poland J., Estimation of Bending Compliance (Stiffness) from Free-Free FRF Measurements: eBCF Theory Experimental Techniques, Rotating Machinery, and Acoustics, Volume 8, DOI: 10.1007/978-3-319-15236-3_14, January 2015

12th International Conference on Structural Analysis of Historical Constructions
SAHC 2020
P. Roca, L. Pelà and C. Molins (Eds.)

STRUCTURAL PERFORMANCE AND DURABILITY ISSUES OF VERNACULAR SCHIST MASONRY

CARLOS E. BARROSO[1*], DANIEL V. OLIVEIRA[2] AND LUÍS F. RAMOS[2]

[1] Center for Studies in Architecture and Urbanism (CEAU)
University of Porto, Faculty of Architecture (FAUP)
Via Panorâmica s/n, 4150-564 Porto, Portugal
e-mail: cbarroso@arq.up.pt, www.ceau.arq.up.pt (*corresponding author)

[2] Institute for Sustainability and Innovation in Structural Engineering &
Institute of Science and Innovation for Bio-Sustainability (ISISE & IB-S)
University of Minho, School of Engineering
Campus de Azurém, 4804-533 Guimarães, Portugal
email: danvco@civil.uminho.pt, lramos@civil.uminho.pt, www.isise.net

Keywords: Vernacular Masonry, Schist, Axial Compression, Retrofitting, Durability

Abstract. *Stone masonry is recognized as one of the most used vernacular construction techniques around the world. Although centuries of proven resilience and high adaptability to context, stone masonry has been progressively replaced in construction industry in the last decades, namely in countries as Portugal, by industrial and concrete-based materials and building systems. Nowadays, with the lack of traditional masons, an important part of traditional stone masonry constructive know-how is endangered. In face of growing concerns regarding heritage preservation, researchers are aware of the need to scientifically know such structures. Being less studied, vernacular schist rubble masonry was selected as case study and tested to characterize its mechanical behaviour and durability parameters. The potential of retrofitting of such structures was also assessed [1].*

Eighteen double-leave wallets were built following local building traditions [2] and prepared according to 3 different setups of 6 specimens each: i) non-coated; ii) coated with commercial lime coating; iii) coated with commercial lime coating and injected with lime-based grout. The experimental campaign was designed and implemented in stages for a period of three years: i) experimental characterization of stones and mortars; ii) axial compression testing of reference specimens; iii) salt-based accelerated aging following wet-dry procedures [3]; iv) axial compression testing. Damage progression was monitored by visual inspection, mass variation and sonic testing [4].

1. INTRODUCTION

Stone masonry has been for centuries a main tool used all around the world, helping mankind to shape its territory, and thus answer community's survival needs. Built using almost all kind of available natural materials, a wide diversity of types of masonry can be found, being most examples developed for specific uses. In Western Europe, the long stone masonry building tradition lost its leading role around the mid-20th century due to strong industrialization of

construction, mostly based on cement products. As a result, much of the empirical knowledge associated to vernacular stone masonry is endangered. Such risk is much higher in rural contexts, due to the loss of traditional ways of life, but also due to rural abandonment that leaves stone masonry structures without any kind of maintenance. Resulting from centuries of trial error experience-based knowledge, stone vernacular masonry heritage has been used as active farming and territory management tools until recent decades [5]. Such heritage is a vital element of the rural landscape and part of its priceless cultural value due to its high authenticity (tangible value) [6, 7]. For being a testimony of past ways of life, vernacular stone masonry is an inseparable dimension of European rural identity (intangible value) [8]. However, vernacular masonry preservation faces severe challenges, mostly related with insufficient knowledge. Although academia's recent investment, scientific and technical knowledge on the topic of preserving vernacular heritage is still scarce.

Taking into consideration the risks, but also the social-economic potential of such endeavour, a research was undertaken to understand the structural behaviour of vernacular masonry. Aligned with ongoing research on the topic [2], Northwestern Portuguese vernacular schist rubble stone masonry was selected as case study for this paper.

2. METHODOLOGY

To achieve the research objectives, schist rubble masonry was tested for axial compression to determine its main mechanical parameters. Also, to understand the influence of durability over masonry structural performance, axial compression tests were performed on accelerated-aged masonry. The topic of masonry preservation was also addressed, by testing retrofitted masonry under both test conditions.

Eighteen schist rubble masonry wallets (600 x 600 x 300 mm^3) were built in a controlled laboratory environment at University of Minho, using traditional building methods [2]. Wallets (W) were prepared according to specific setups and divided into 3 sets of 6 wallets each, being: *i*) non-coated masonry (N); *ii*) coated masonry using commercial lime mortar similar to traditional coating (C); *iii*) coated masonry with the same commercial lime mortar and injected with a lime-based grout (I). Wallets were then tested under two different test conditions (3 wallets of each set and test condition) to obtain reference and durability mechanical parameters, namely wallets tested after the curing period (WU) and wallets tested after being aged (WA).

The experimental campaign was designed and carried out in three different stages (three years period) as follows: *i)* wallets were built and left to cure for a period of 120 days; *ii)* WU wallets were tested under axial compression; *iii)* WA wallets were aged using a specifically designed salt-based accelerated aging test, divided into a salt loading stage of 9 wet-dry cycles during 2 months, followed by an aging stage at natural conditions, for 12 months; *iv)* WA wallets were tested under axial compression. During this time period, complementary tests were performed to collect additional data (results under elaboration), namely: *i)* main physical and mechanical parameters of stones and mortars [9]; *ii)* sonic testing of walls at the beginning and throughout the accelerated aging period to assess the potential of applying such technique to determine rubble masonry parameters [4]; *iii)* regular visual inspection of walls and mass variation analysis.

2.1. Wallets construction

Wallets were built by a professional stonemason using local schist stone blocks (average compressive strength f_c of 35 MPa on both anisotropic directions), collected from demolished buildings, being their final shape given on-site. Local granitic soil, locally named *"saibro"*, was used as bedding and joint mortar. Soil was sifted and mixed with water until reaching the required workability (between 160 mm and 180 mm checked by flow table test), resulting in a very poor mortar (f_c < 0.1 MPa), known for regaining workability if wet. As shown in Figure 1, double-leaf cross-sections (30 cm wide) were built by overlapping header and stretcher proportioned parallelepiped stone blocks of different sizes (< 250 mm x < 60 mm x < 400 mm). Stones were bedded parallel to foliation orientation, using small size schist wedges and soil mortar. Wallets' wythes were connected by using bond stones and by overlapping stone blocks at the inner core. The inner core was filled with soil mortar and small stones. Joints were pointed with soil mortar.

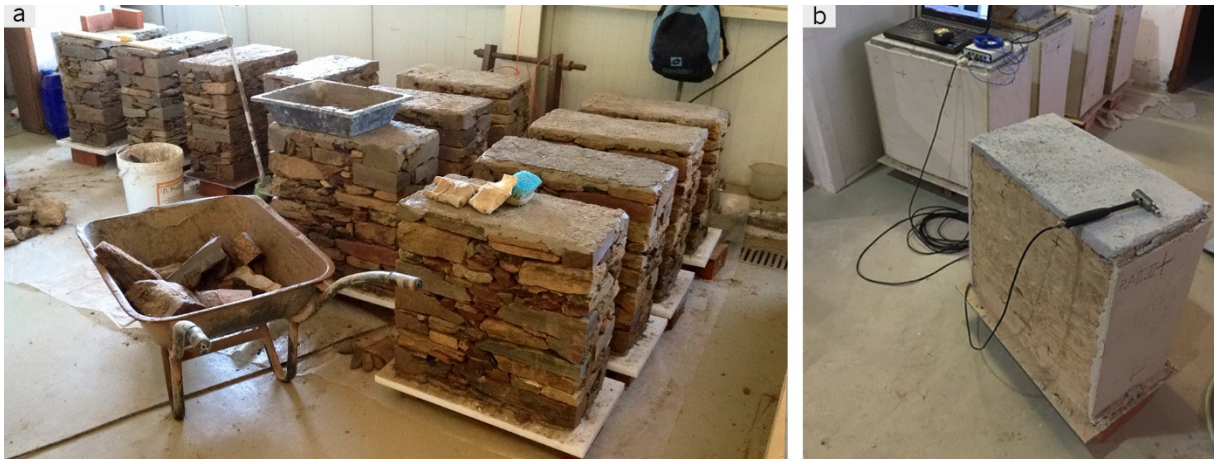


Figure 1: Wallets: (a) construction stage; (b) sonic testing.

As illustrated in Figure 2, wallets were built over either a 50 mm thick iron plate (WU) or a 300 mm thick nylon plate (WA). The latter was selected for its resistance to salt damage. As shown in Figure 3a and Figure 3b, cross-section was built over a 20 mm layer of cement mortar.

At the top, a cap of cement mortar was also built to stabilize the masonry. Afterwards, see Figure 3c, the main faces of wallets were coated with a commercial lime mortar exhibiting a performance similar to traditional lime mortars, and it was applied in two layers with an average thickness of 20 mm. Lateral faces were coated with a another lime-based mortar with 15 mm thick, reinforced with a commercial acrylic mesh. The purpose of the later was to improve walls resistance during transport and water immersion operations. To allow transporting and injecting wallets, a second 50 mm thick iron plate was placed over the cap, with styrofoam absorber in between, and attached with rods to the base plate.

Grout injection was applied to I wallets after repointing the joints with soil and before applying the coatings (see Figure 3d). Injection hoses were inserted into the masonry fabric forming a grid

pattern. Water was injected to moisten the masonry. After a period of 24h, a commercial lime-based grout was injected at low pressure from the bottom towards the top of the wall.

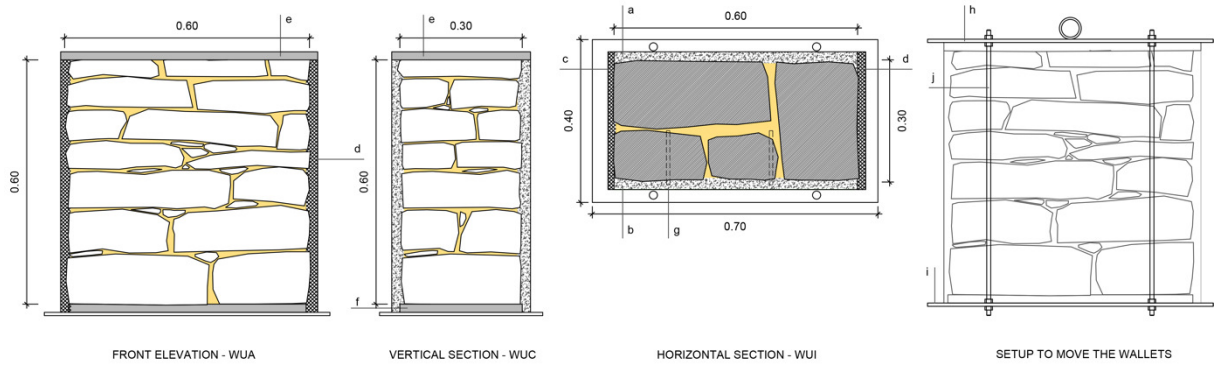


Figure 2: Schist masonry wallets schematics (dimensions in meters): (a) and (b) main faces coated with commercial lime mortar similar to traditional mortar; (c) and (d) lateral covers coated with commercial lime mortar; (e) top cement cover (stabilizing layer + levelling layer); (f) cement base layer; (g) grout injection hoses; (h) top transport and injection iron plate; (i) base plate in iron (WU) or Nylon (WA); (j) iron rods.



Figure 3: Wallets construction stages: (a) bottom cement mortar layer; (b) construction procedure; (c) application of the main faces coating; (d) grout injection.

2.2. Compression tests

Axial compression tests were performed to determine masonry wallets strength (f_c) and elastic parameters (E) [10], using a servo-controlled actuator under axial displacement control at a rate of 20 μm/s. As shown in Figure 4, LVDTs were used to monitor displacements between plates (P1-P2), and to monitor deformations on the walls faces (main faces: V1-V2; H1-H2; lateral faces: H3-H4). Preliminary testing showed that due to schist well-defined foliation, thus with high risks of lamellar disaggregation, the use of bolts to attach LVDTs to masonry was unfeasible. Therefore, glue was used to attach LVDTs. All coatings were prepared in order to avoid its direct contact with the loading plates, so the axial load was applied to the masonry wall only.

Observations during the WU compression tests showed an early detachment of the coatings, making the attached LVDTs data unusable. Moreover, attaching LVDTs to WA wallets was unfeasible due to salt presence. Therefore, the setup was adjusted for the second stage of compression tests, reducing the number of LVDTs to the P1-P2 (see Figure 4c). If required, the top of wallets was levelled with a very thin layer of fast hardening mortar. A spherical seat was used under the top loading plate to ensure specimens a proper alignment and adjustment to the loading plates. For each set, a first wallet was tested under axial monotonic compression to determine the peak load. Based in this value, parameters for the cyclic tests were set: *i)* until peak load, unloading procedure was controlled by load, and started at every 30 kN of additional load for N and C wallets, and 150 kN for I wallets; *ii)* after peak load, unloading was controlled by displacement, and started at every 12 mm for N and C wallets, and 20 mm for I wallets; *iii)* reloading was started when unloading force reached 10 kN.

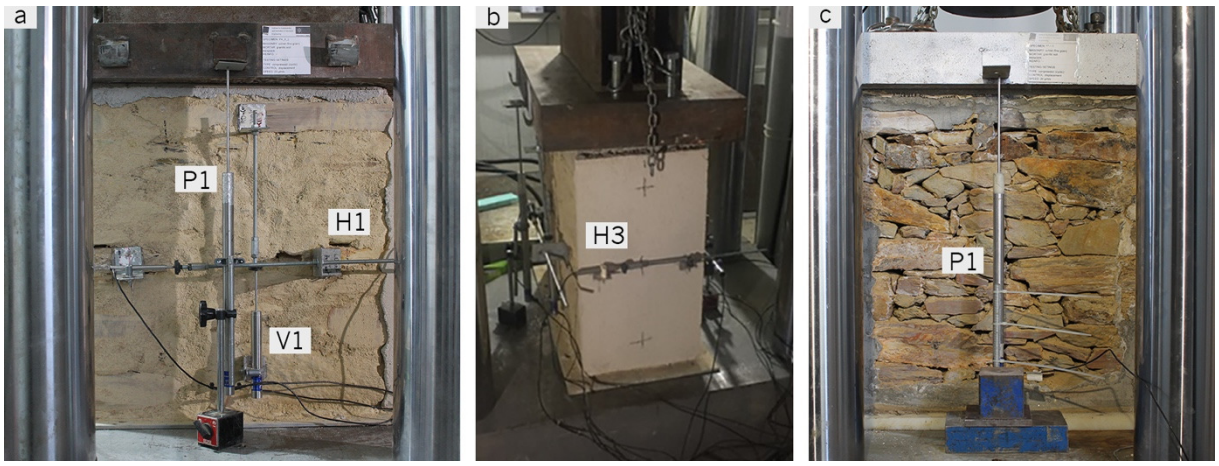


Figure 4: Axial compression test setup: (a, b) WU wallets; (c) WA wallets.

2.3. Accelerated aging tests

For its known damaging effects over masonry, salt was selected as weathering agent [11,12]. Masonry wallets were subjected to wet-dry cycles with full immersion into a 20% sodium chloride (NaCl) solution by weight. The selection of the salt was carried out using preliminary salt weathering tests on cubic specimens [13]. Sodium sulphate decahydrate ($Na_2So_4.10H_2O$) was ruled out for its excessive destructive effect over schist, as shown elsewhere [9]. NaCl is a hygroscopic and deliquescence salt, meaning that it absorbs atmospheric moisture and can form a solution, if environmental RH is above salt's equilibrium RH at a given temperature (30 ºC, 75.1% RH) [12,14].

By varying temperature and RH conditions during the WA testing, the number of dissolution-crystallization cycles increased, inducing a higher level of damage to wallets [3]. Taking into consideration the unfeasibility of oven-drying the wallets, a 20% concentration by weight was selected as suitable for such required effect. Wallets were previously weighted, and to ensure water absorption only through the main faces, a waterproofing coating was applied over the top and lateral covers, see Figure 5a.

The WA test was implemented in two stages: *i)* an initial wet-dry cyclic stage to load wallets with salt (WA1), see Figure 5b; *ii)* a subsequent natural drying stage under laboratory conditions (WA2), see Figure 5c. WA1 was implemented into 9 cycles (168 hours of duration each), being each cycle started with an initial full immersion stage (72 hours), during which the solution was kept in continuous motion to avoid areas of salt crystallization (walls and edges of the tank), followed by a monitored and controlled drying period inside the enclosed tank (96 hours). In turn, each drying period was subdivided into a period of drying with heated ventilation (7 hours with an average of 40 ºC and 25% RH), followed by natural drying (17 hours with an average of 23 ºC and 78% RH). WA2 drying lasted for a continuous period of 365 days, in which wallets were kept at room temperature and RH, inside the opened tanks. Environmental conditions variations along this period where monitored but not controlled. To monitor damage progression, wallets were again weighted at the end of the test, and visually inspected, photographed and analysed with sonic testing at each cycle and test stage. To monitor the effectiveness of the salt solution, 5 cubic stone specimens were placed inside the tank. These were weighted, visually inspected and analysed by UPV at each cycle and test stage. The solution temperature was on average 25 ºC, being samples collected to check concentration by weight variation. If needed, salt or water were added.

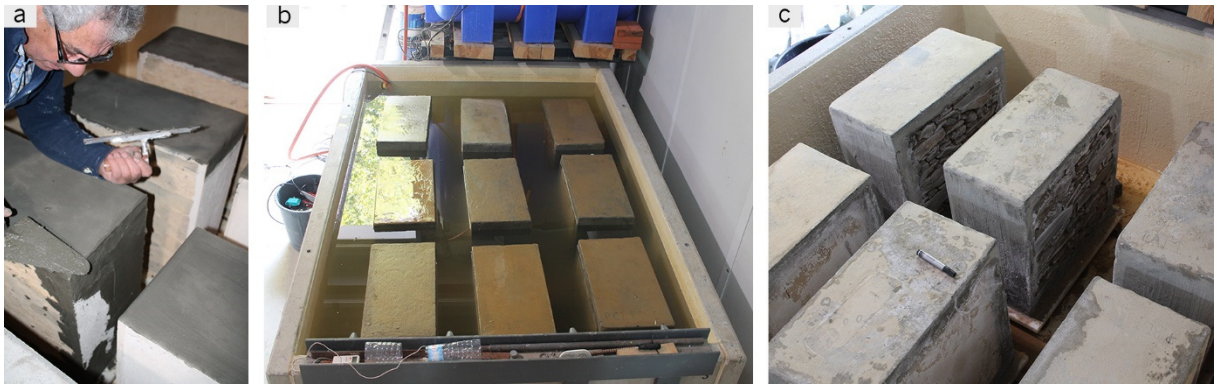


Figure 5: WA test: (a) application of the final waterproofing coating (b) filling of the tank with salt solution for immersion of wallets (WA1); (c) wallets during the natural drying stage (WA2).

3. RESULTS

WU test results are presented in Table 1, which reveal a lower compressive strength (f_c) in comparison with other common types of Portuguese stone masonry presented in Table 2. Non-injected N and C wallets were only stronger than adobe masonry. Analysing results for the elastic modulus (E), both present low values. Analysing results for inject I wallets, average values for f_c are similar to the reference schists, although with a higher average value for E. These results demonstrate the positive effect of grout injection over rubble schist masonry strength and stiffness. A detailed analysis to N and C wallets mechanical parameters, show similar f_c values, thus revealing no significant influence of traditional coating over strength. However, and although higher values for CoVs and E values for C wallets may indicate some influence of traditional coating over masonry elastic behaviour. The obtained results for strength and stiffness may be explained by schist stone initial weathering, taking into

consideration the origin of the stones, the very low strength of its soil mortars, and the high percentage of voids of the tested rubble masonry. Using I wallets specific weight (average of 19.30 kN/m^3) and the known volume of injected grout (27 *l* on average), the masonry voids index was calculated revealing high average percentage of voids of about 24%.

Analysing in detail results for I wallets, obtained values show an undeniable performance improvement, being 5 times stronger (on average) than non-injected walls, 2 times stiffer (on average) than N and 5.5 times (on average) than C. The compressive strength increase of injected wallets in comparison with non-inject wallets is similar to the gain values obtained elsewhere [15] for compressive strength, but higher regarding *E* gains (injected schist wallets tested in [15] were 3 times stronger and stiffer than non-injected ones).

Analysing Table 1 regarding WA wallets results, the loss of strength and stiffness is visible for all tested walls. Being on average 1.3 and 1.4 times weaker and on average 2 and 5 less stiff, results show non-injected wallets higher susceptibility to the WA test. On the other hand, being in average 1.1 times weaker and 1.4 times less stiff, injected I wallets showed higher resilience to the WA test. Explanation of such results may be related to the high percentage of internal voids of non-inject N and C wallets, which acted as moisture penetration and accumulation points, decisively contributing to the higher levels of observed damage. In the same way, lower losses of mechanical performance for I wallets may be pointed to the lower percentage of internal voids, thus being less exposed to water penetration and resulting in lower level of observed damage. Preliminary tests showed schists strong water absorption (average A_b of 7.5%, see [9]), thus higher susceptibility to salt damage [11,12].

Analysing damage resulting from the WA test, Figure 6a to c, WAN wallets stone blocks presented severe superficial salt damage with efflorescence and the formation of crust and patina. As observed, stone blocks show also powdering and disaggregation of faces and edges, and some level of lamellar disaggregation [17]. With undeniable influence over masonry structural performance, non-coated joints mortar was washed away during immersion, resulting in cases of loose wedges. As observed, soil mortars settled at wallets lower half, changed the internal dispersion of voids (increasing at the top and decreasing at the bottom). Additional internal stress caused by the activation of clays inside schists and soil mortar should also be taken into consideration [14,18].

Table 1: Strength (f_c) and elastic modulus (E) results (in MPa).

Test conditions	N				C				I			
	f_c (MPa)		E (MPa)		f_c (MPa)		E (MPa)		f_c (MPa)		E (MPa)	
U	0.69		54.50		0.63		299.74		3.41		318.8	
	0.67	**0.72**	58.97	**59.76**	0.65	**0.62**	144.58	**165.09**	3.07	**3.30**	234.8	**332.07**
	0.81	[0,06] (9%)	65.82	[4.65] (8%)	0.59	[0,06] (9%)	50.94	[102.6] (62%)	3.41	[0,16] (5%)	442.59	[85,35] (26%)
A	0.55		-		0.42		26.05		3.03		256.5	
	0.68	**0.57**	27.39	**28.78**	0.40	**0.44**	42.41	**32.70**	3.22	**2.91**	210.4	**231.89**
	0.48	[0,08] (15%)	30.17	[1.39] (5%)	0.49	[0,08] (15%)	29.64	[7.02] (21%)	2.47	[0,32] (11%)	228.71	[18.95] (8%)

Note: Compression (f_c) and elastic modulus (E) average results are indicated in bold; Standard deviation (SD) is indicated inside rectangular brackets; Coefficient of variation (CoV) is indicated in percentage inside rounded brackets.

Water penetrated through the coating applied to C wallets main faces and accumulated inside, causing the same type of damage above-described. It is noteworthy that all coatings showed severe effloresce and salt accumulation, with WAC and WAI wallets main faces coating presenting areas of granular disaggregation. The loss of lime coating stiffness was confirmed during the sonic tests. As observed, such type of coating became successively less stiff after each wet-dry cycle, being this damage severe in the case of WAC wallets, due to the strong presence of internal moisture. The loss of performance of main faces coatings can explain the WAC strong drop in *E* parameter. As shown in Figure 6d and f, internal stress combined with salts accumulation at the stone/coating interface led to lime coatings early detachment in WAC. Such damage was not detected in WAI wallets.

Table 2: Results from common types of Portuguese stone masonry [16].

type of masonry	f_c (MPa)	E (MPa)
granite	48.9	7490.6
limestone	8.0	1640.0
schist	3.8	164.6
adobe	0.3	113.0
rammed earth	1.3	1034.0



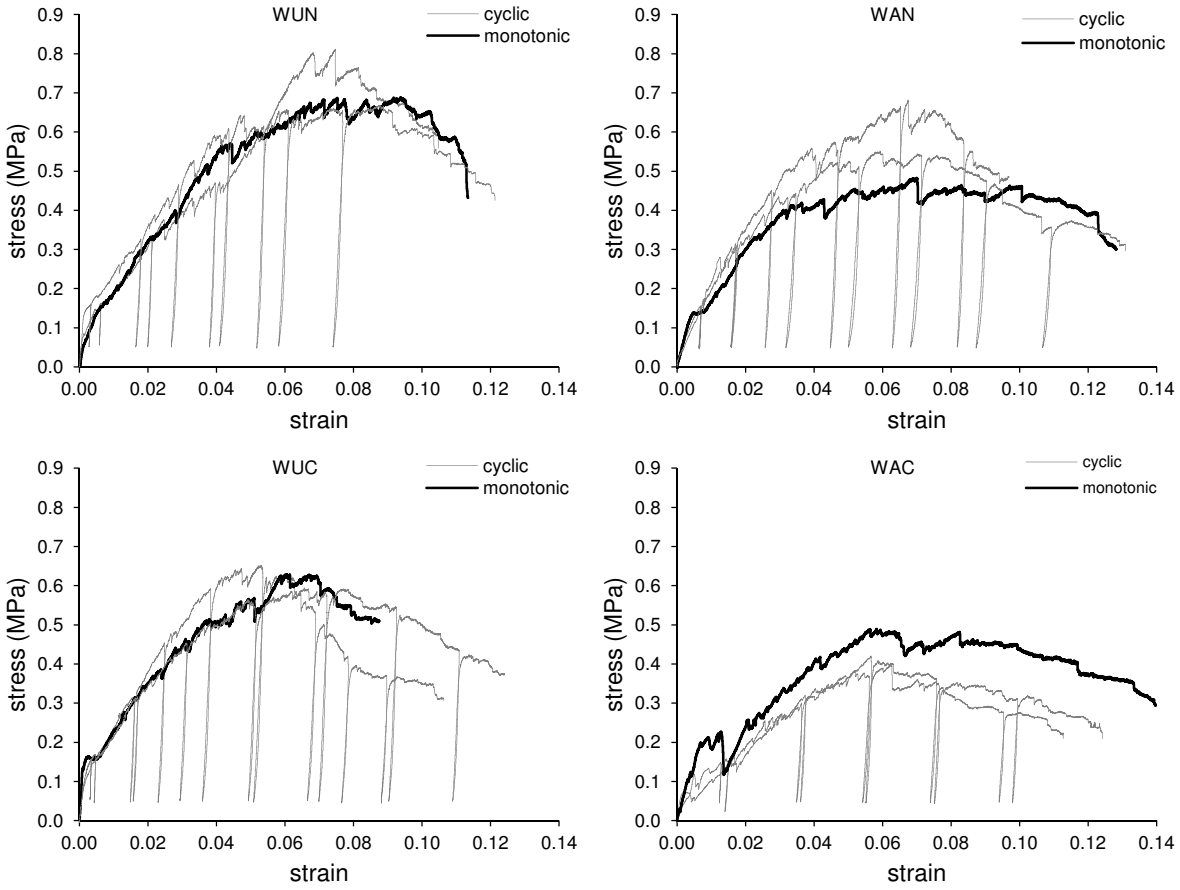
Figure 6: Damage observed during the WA test: (a) and (b) examples of different salt deposits on schist stone; (c) efflorescence; (d) efflorescence located at the coating/masonry interface; (f) example of WAC with superficial salt deposits, ruptured lime coating and detached lateral covers.

Damage in WAC main faces coatings was always severe in one side of the wallet (typically face A), with full coating thickness fractures and even ruptures. On the opposite side, only superficial crack patterns were detected, and were similar to the ones observed for the WAI wallets. On one hand, these results show that higher amounts of water inside wallets resulted in higher levels of damage on coatings. On the other, it became clear that water follows out through the easier way, in this case through the damaged coating, thus avoiding blockades and causing less damage over the remaining coatings. The observed preferential penetration

direction (face A) seems to be related to unforeseen effects related to the solution for water circulation inside the tank.

Without coatings, such behaviour was not clear on WAN wallets, and was not observed in WAI wallets. A lower percentage of internal voids restricted water movements inside WAI wallets, and it seems the injection hose's tips provided a stronger stone/coating connection, preventing coating detachment or severe mechanical damage. By the end of the natural drying stage, due to salt accumulation at the interface, lateral covers detached from masonry in WAN and WAC wallets. In all WA wallets, salt accumulation at the interface between the coatings and the final waterproofing coating, caused the latter to rupture. By the end of WA test, control specimens showed lamellar rupture, and severe powdering faces and edges [17].

Analysing stress-strain diagrams in Figure 7, the similar brittle behaviour for all tested wallets and for both testing conditions is clear. N and C wallets showed a trilinear behaviour for all tested wallets, characterized by a very short initial linear stiff branch until the cracking of the first large stone block, followed by a longer deformation branch (non-linear) up to peak. As shown in the cyclic behaviour diagrams, N and C wallets linear hysteretic cycles reveal inability to dissipate energy, but almost no strength degradation was observed. Figure 7 shows stronger and stiffer I wallets when compared with the non-injected wallets.



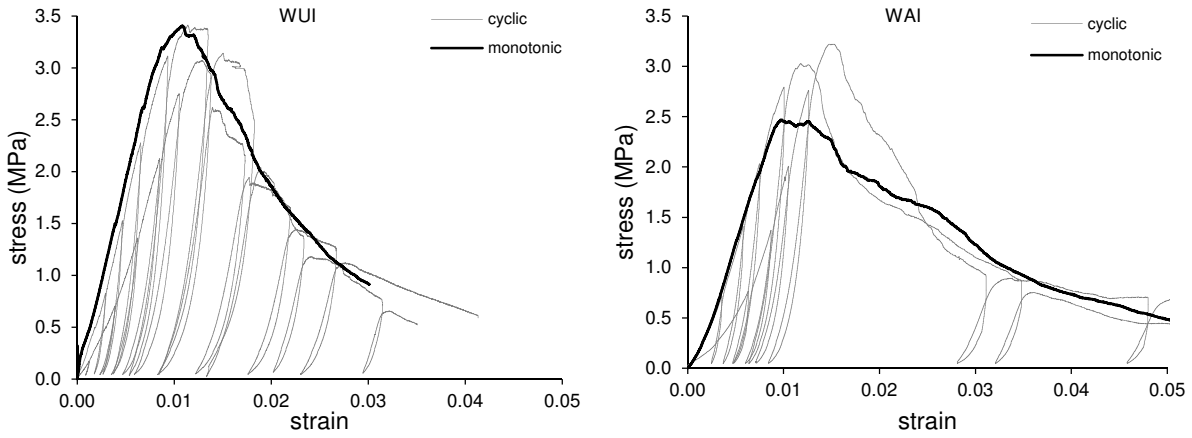


Figure 7: Stress-strain diagrams for WU (left) and WA (right) wallets.

The observed bilinear behaviour is characterized by a long stiff branch almost up to peak. The hysteretic curves confirm the injected masonry higher stiffness, with undeniable recovery capability in unloading-loading cycles. However, I wallets diagrams also show an initial accommodation stage that may be related to the use of soil as mortar.

Figure 8 and Figure 9 illustrate typical failure patterns, which may be described in 4 levels: (1) damage started with the expulsion of mortar joints due to compression, with slight opening of joints and cracking of smaller stones and wedges; (2) the fracture of larger stone blocks, generally located at the lower half of the wallet, led to the formation of diagonal cracks, which propagate through joints, causing the detachment and rupture of the coating; (3) external leaves start to deform and to detach, and large and deep cracks propagate with large opened joints exposing the inner-core; (4) external leaves start to disintegrate by losing loose and crushed stone blocks. Due to very poor bond in N and C masonry, wallets show higher deformability and were more exposed to disaggregation. Due to a stronger stone/mortar bond provided by the grout, I wallets disaggregate into large blocks of masonry.

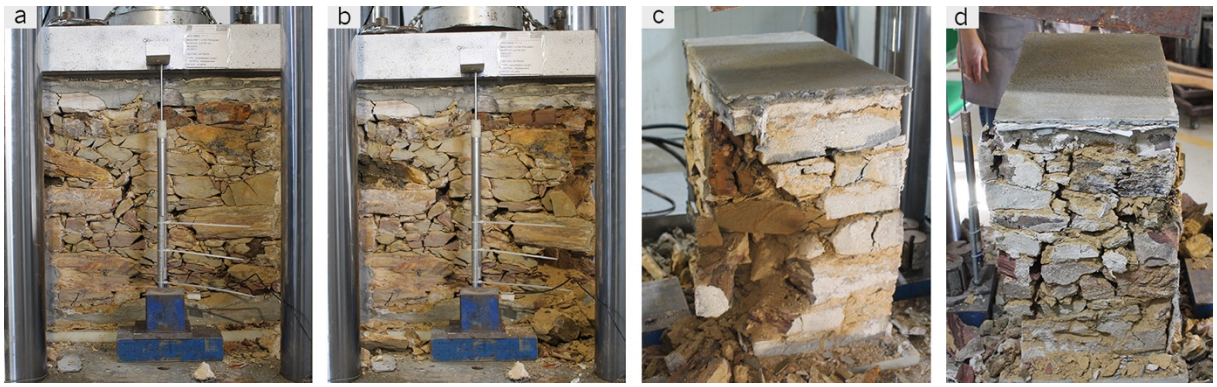


Figure 8: Example of WUN wallet: (a) initial damage with opening of joints and cracking of smaller stones and wedges; (b), (c) and (d) final damage with deep cracks, loss of stone blocks and leaves detachment.

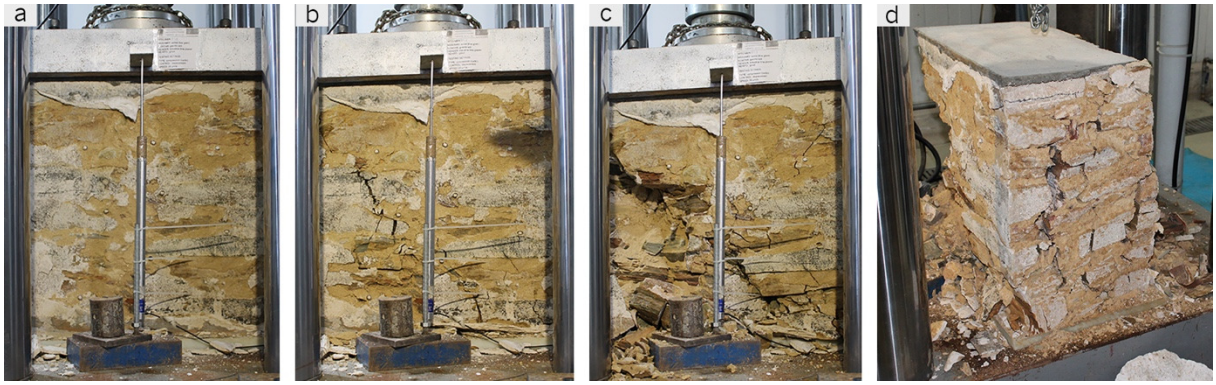


Figure 9: Example of tested WAI: (a) initial damage (visible after the rupture of the coating) with opening of joints and cracking of smaller stones and wedges; (b) formation of large diagonal cracks and fractures in stone blocks; (c) and (d) extensive damage with disaggregation of leaves and formation of different blocks.

4. CONCLUSIONS

From the research presented in this paper, it became clear the low strength and stiffness of vernacular rubble schist masonry from Northwest Portugal. The use of lime coatings, similar to traditional ones, does not affect the masonry strength, but it seems to have a positive influence over stiffness.

Results show that grout injection increases is effective in filling the voids, thus it improves vernacular schist rubble masonry mechanical performance. Simultaneously, results show that this retrofitting technique reduces water penetration and accumulation inside walls, thus improving its durability.

Regarding failure, the cracking of larger stone blocks decisively affects rubble masonry stiffness. The opening of joints, the detachment of leaves and disaggregation of leaves, caused by deformation, were the most common types of mechanical damage.

The accelerated aging tests, with full immersion in salted water and drying cycles, to cause aging, as proven its validity to analyse stone masonry durability.

Without the grout protection, aged schist masonry presented severe damage and mechanical performance losses due to the washing and settlement of mortars. Damage also resulted from the cracking and rupture of coatings, due to salt damage at the coating/masonry interface. Although the overwhelming salt damage observed in the surfaces of the stone blocks posed no immediate structural threat, preliminary tests revealed that it inevitably evolves to the complete disintegration of stone blocks (lamellar and granular).

Acknowledgements. This work was partially financed by FEDER funds through the Competitivity Factors Operational Programme (COMPETE) and by national funds through the Foundation for Science and Technology (FCT) within the scope of project POCI-01-0145-FEDER-007633. Authors wish to express their gratitude to S. Pedro de Rates Civil Parish for its support with the wallets' preparation. The first author expresses his gratitude to the Portuguese Science and Technology Foundation for the scholarships granted (SFRH/BD/ 86704/2012).

REFERENCES

[1] D. V. Oliveira, R.A. Silva, E. Garbin, P.B. Lourenço, Strengthening of three-leaf stone masonry walls: an experimental research, Mater. Struct. 45 (2012) 1259–1276.

[2] C.E. Barroso, D. V. Oliveira, L.F. Ramos, Vernacular schist farm walls: materials, construction techniques and sustainable rebuilding solutions, J. Build. Eng. 15 (2018).

[3] T. Wijffels, B. Lubelli, Development of a new accelerated salt crystallization test, Heron. 51 (2006) 63–75.

[4] H. Van Eldere, F. Ramos, E. Verstrynge, N. Shetty, K. Van Balen, C.E. Barroso, The Application of Sonic Testing on Double-LEaf Historical Portuguese Madonry to Obtains Morphology and Mechanical Properties, in: R. Aguilar, D. Torrealva, S. Moreira, M.A. Pando, L.F. Ramos (Eds.), Struct. Anal. Hist. Constr. (RILEM Bookseries), 1st ed., Springer International Publishing, 2019.

[5] C.E. Barroso, D. V. Oliveira, L.F. Ramos, Preservation of vernacular schist masonry farm walls, in: C. Mileto, F. Vegas, J.G. Soriano, V. Cristini (Eds.), VERSUS2014 - Vernac. Archit. - Towar. a Sustain. Futur., CRC Press/Balkema, Valencia, 2015: pp. 117–122.

[6] ICOMOS, Charter on the built Vernacular Heritage (1999), Mexico, 1999.

[7] ICOMOS-IFLA, ICOMOS-IFLA principles concerning rural landscape as heritage, New Delhi, 2017.

[8] ICOMOS, The Nara document on autenticity, Nara, 1994.

[9] C.E. Barroso, The rural vernacular construction of the Entre-Douro-e-Minho, PhD Thesis, University of Minho, 2018.

[10] BS EN 1052-1:1999, Methods of test for masonry - Part 1: Determination of compressive strength, (1999).

[11] C. Rodriguez-Navarro, E. Doehne, Salt weathering: influence of evaporation rate, supersaturation and crystallization pattern, Earth Surf. Process. Landforms. 24 (1999).

[12] A. Goudie, H. Viles, Salt Weathering Hazards, John Wiley & Sons, Oxford, 1997.

[13] NP EN 12370, Natural stone test methods - Determination of resistance to salt crystallisation (in Portuguese), (2001).

[14] A.E. Charola, Salts in the Deterioration of Porous Materials : An Overview., J. Am. Inst. Conserv. 39:3 (2000) 327–343.

[15] E.C.P. Luso, Experimental analysis of lime-based grouts for the injection of ancient masonry (in Portuguese), PhD Thesis, University of Minho, 2012.

[16] R.S. Barros, Material and structural behaviour assessment of buildings in schist (in Portuguese), PhD Thesis, University of Minho, 2013.

[17] V. Verges-Belmin, Illustrated glossary on stone deterioration patterns, 2008.

[18] I. Jiménez-González, C. Rodríguez-Navarro, G.W. Scherer, Role of clay minerals in the physicomechanical deterioration of sandstone, J. Geophys. Res. 113 (2008).

12th International Conference on Structural Analysis of Historical Constructions
SAHC 2020
P. Roca, L. Pelà and C. Molins (Eds.)

TESTING CALIBRATION ISSUES IN RESISTANCE DRILLING APPLIED TO TIMBER ELEMENTS

F. CASARIN[1*], L. SCANCELLI[1], M.R. VALLUZZI[2] AND E. BOZZA[3]

[1] Expin s.r.l.
Via Pisacane 34, 35138 Padova, Italy
e-mail: casarin@expin.it (*corresponding author), www.expin.it

[2] Department of Cultural Heritage
University of Padova
Piazza Capitaniato 7, 35139 Padova, Italy
e-mail: mariarosa.valluzzi@unipd.it

[3] Bozza Legnami s.r.l
Via Regia, 70, 35100 Busa di Vigonza (PD), Italy
e-mail: info@bozzalegnami.it, www.bozzalegnami.it

Keywords: Timber, resistance drilling, needle consumption, densiometric profile, NDT visual inspection, wood classification

Abstract.
Resistance drilling devices are commonly used for the onsite inspection of wood and timber structural components in existing buildings. Although they provide a measure related to the density variation along a section of an element, results are used mainly qualitatively, due to several parameters that affect the computed values.
In this paper, several new and old timber elements, taken from the dismantling of original roofs from a large existing historical building in northern Italy, are tested through a series of ND (non-destructive), SD (semi-destructive) and destructive testing procedures. Various wood species (spruce, fir, larch, oak, elm, pine) are taken into consideration.
Among the applied testing methods (visual inspection, resistance drill, ultrasonic, needle penetration, radar, lab tests bending/compression), not all reported here, a focus on the resistance drill tests results is addressed, to evaluate the influence of consumption of the needle tip on the amplitude output. This was done by correlating the drillings to a reference sample on each test position to obtain data with an enhanced quantitative content. From the visual old timber elements grading, SD tests execution and successive element strength characterization through laboratory tests, it finally emerged the need for proper calibration of assessment methodologies through the application of a combined approach, in order to achieve more reliable results.

1 INTRODUCTION

Diagnosis of current state of timber components in existing buildings is supported by investigation tools applied onsite as non-destructive (ND) and semi-destructive (SD) test

procedures [1][2]. Among them, resistance drilling devices [3] are commonly used to check the conservation condition of wood and detecting possible inner flaws, joints, etc. This device provides a densiometric profile along the investigated section, based on the drilling power consumption of a thin long needle driven into the wood at speed rates kept constant by electronic control [4]. Being a local test method, timber components in existing buildings often require multiple measures, depending on specific problems to investigate (e.g., beam ends threatened by moisture due to masonry contact, presence of decay, cracks).
The need of defining the state of conservation of existing timber elements, related to local material consistency, is often coupled with the request of element classification according to the reference standards for safety evaluations [5][6], which is related to the overall features of the timber element (mechanical damage, wood fibers angle, presence of knots).
The paper investigates some issues arising from the application of the resistance drilling method proposing test procedures aimed at minimizing the data inherent qualitative aspects, with the final goal to improve the existing timber elements classification methodology as proposed by the Italian reference technical standard [6].

2 EXPERIMENTAL ACTIVITY LAYOUT

The experimental program included a series of ND/SD tests on new and old structural timber elements, followed by destructive tests aimed at determining some mechanical properties of the elements. The non-invasive testing campaign took place at the Bozza srl timber company (located in Vigonza, Italy), while the mechanical tests were carried out in the laboratory for tests on building materials, in the Department of Civil, Architectural and Environmental Engineering of the University of Padua.
The timber beams investigated in the context of the work carried out were:
- 21 “old” beams of different species, recovered from the dismantling of the roof of the Moncucco farmhouse in Milan (now a student house of IULM University of Milan), having different dimensions and cross sections (Figure 1).
- 12 new beams (6 spruce and 6 larch beams), having a cross section of 160x160 mm and different lengths. The new beams are classified as C24 (spruce) and C22 (larch) according to the resistance classes of UNI EN 338 [5].



Figure 1: Timber beams ready to be tested at Bozza Legnami premises

2.1 Resistance drill distributed testing

Rather than obtain densiometric profiles of the timber elements in few or singular points, it was chosen a *distributed* test procedure, still considered feasible during onsite professional activity, to obtain an overall (averaged) drill resistance amplitude value. This attempt was done in order to take into consideration the presence of material inconsistency (cracks, decayed wood, etc.) with its balanced influence on the entire element. As acquisition pattern, a line of points with a regular spacing of 50 cm on orthogonal faces was chosen (Figure 2). Each beam was then investigated on two adjacent sides with about 4 to 10 measurement stations per side.

In all the tested points the equipment was not directly placed in contact with the timber: between the tip of the drill and the beam a C24 spruce timber sample of known height was placed. Such samples were parts of spruce boards classified C24, having a height of 27 mm and a moisture content of around 12% at the time of testing. To standardize the results and thus make them as homogeneous as possible, an attempt was made to cross perpendicularly the growth rings of the spruce sample elements with the tip of the drill.

The purpose of this procedure was to have a direct comparison between the density of the known wood with what was going to be tested, obtaining a first estimate of the relative density between the two materials; moreover, in this way it was possible to compare the various densiometric measurements with each other even if different settings of the instrument were used (i.e. velocity of penetration or rotation), as the outputs were normalized always referring to the initial portion of 27 mm of spruce (Figure 3).

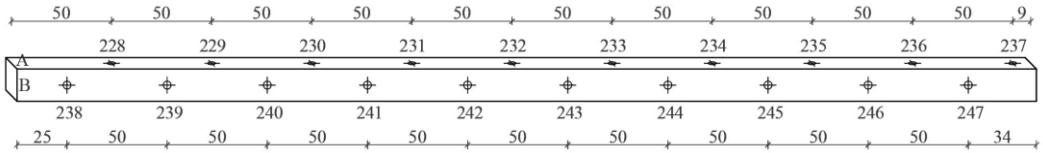


Figure 2: Test layout for beam L1 (larch): regular 50 cm spacing was selected on two orthogonal faces of beam

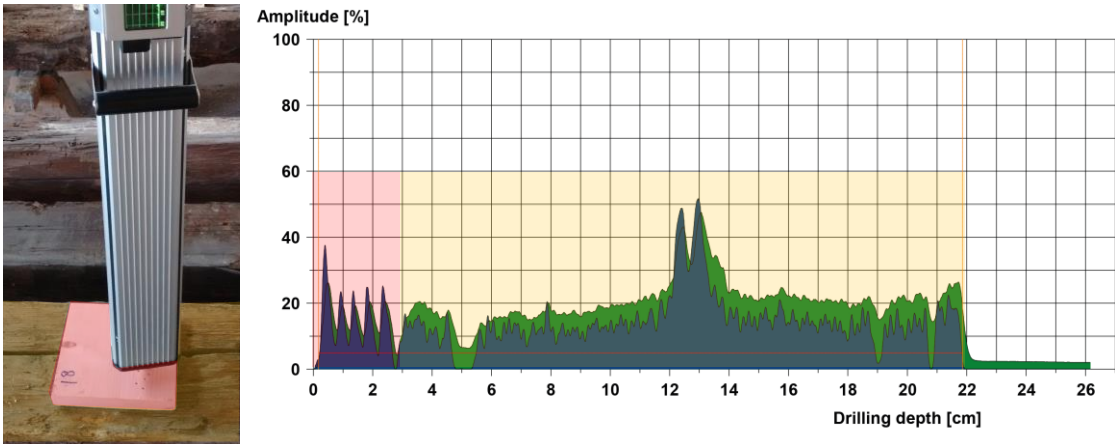


Figure 3: Element of known characteristics (spruce C24, height 27 mm) positioned between wood to be investigated and instrument, and corresponding densiometric profile (red: sample; yellow: tested element)

A quantitative parameter was chosen that could identify a summary value for each measurement made with the instrument:

$$RM = \frac{\int_0^l R(x)dx}{l}\% \quad (1)$$

where:
RM = averaged test amplitude value [%]
R(x) = instantaneous test amplitude value [%];
l = depth of needle penetration [mm].

The reference parameter was then RM_{norm}, intended as the ratio between RM calculated from a test position on the timber element and RM_{C24}, i.e. the RM value calculated only for the first 27 mm of known spruce; in both cases, the parameters were determined considering the "feed curve" of the used device [7]. The aggregate RM_{norm} values for all tests per each beam are shown in Figure 4. The C24 sample element applied on the timber surface of the investigated beams to compute normalized values of RM proposes indeed more informative data on the evaluation of the actual state of wood, for allowing immediate test results comparison among different cases and conditions. The use of the C24 spruce element allowed also to evaluate the trend of the RM value over time, observing how this increase with the number of the measurements. The use of a normalization element is therefore necessary as measurements performed on the same element at different times lead to different (increased) RM values (Figure 5).

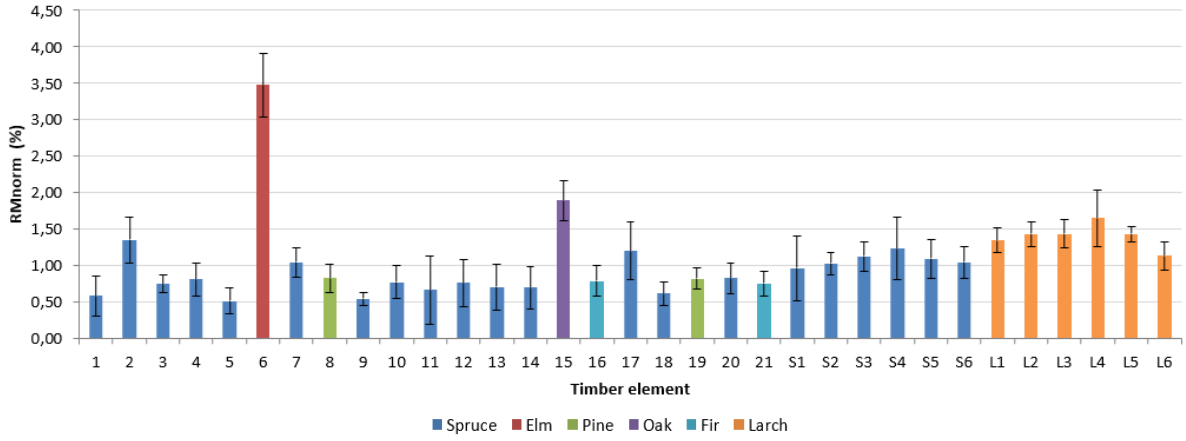


Figure 4: RM_{norm} values for all the tested timber elements, corresponding nr. 1-21 to old elements and acronyms S1-S6 / L1-L6 to spruce C24 and larch C22 new elements

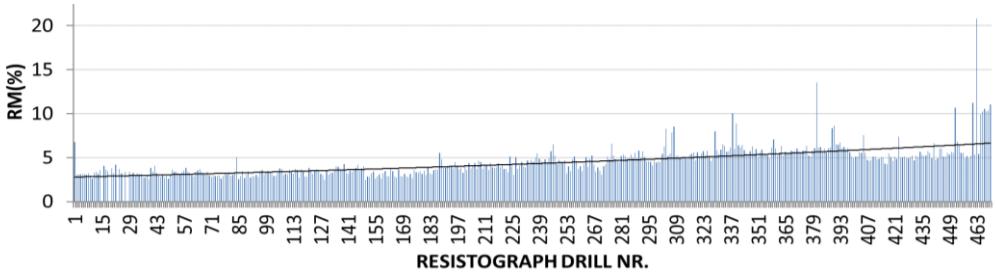


Figure 5: Influence of pin consumption on resistance drill amplitude chart on timber sample elements, which remarkably increases with the use of device

This phenomenon, likely due to the consumption of the tip of the resistance drill (tip sharpness progressively reduced), is not the only factor influencing the instrument outputs: it has been noticed that as the instrument settings vary (feed and rotation speed) the RM value is remarkably different. The influence of the drill settings in the amplitude response chart was quantified on the spruce sample element (27 mm thick at 12% MC, classified as C24 according to UNI EN 338 [5] by using various speed/rotation rates (keeping one parameter constant when varying the other and vice versa), thus obtaining relevant data for test output interpretation. For the same feed speed, RM will increase as the rotation speed decreases, while on the contrary it decreases with the penetration speed, with the same rotation speed (Figure 6).

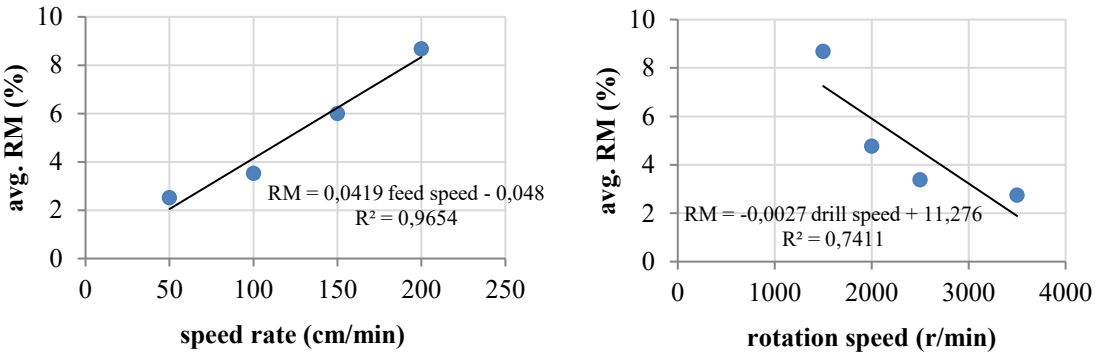


Figure 6: Drill resistance amplitude by varying feed speed and drill rotation speed (rpm)

3 MECHANICAL CHARACTERIZATION AND MD/D TESTS COMPARISON

Experimental laboratory tests were carried out with the aim of obtaining the mechanical parameters that can be correlated with the results of the non-destructive and semi-destructive tests carried out on the same timber elements. The tests carried out were bending and compression tests on real-scale elements (Figure 7).

Both types of test refer to the requirements indicated in UNI EN 408 [8], which specify the test methods and the dimensions of the samples. Tests involved 9 reused and 6 new timber elements.



Figure 7: Execution of mechanical tests at DICEA laboratory, according to EN 408 (compression/bending)

A comparison between the resistance drill averaged values RM and the mechanical characteristics emerged from the laboratory tests are given in Figure 8. As it can be seen, the correlation coefficient between $f_m/f_{c,0}$ vs. RM (charts above) is very low and almost no relationship can be established between the laboratory and onsite results. On the contrary, very interesting results emerge when plotting the mechanical results versus the parameter RM_{norm}, i.e., normalizing the average value on the sample element of known characteristics. This allowed to balance the overall densiometric profiles on a well characterized sample, depending from parameters (i.e., pin consumption) which are uncontrollable on site.

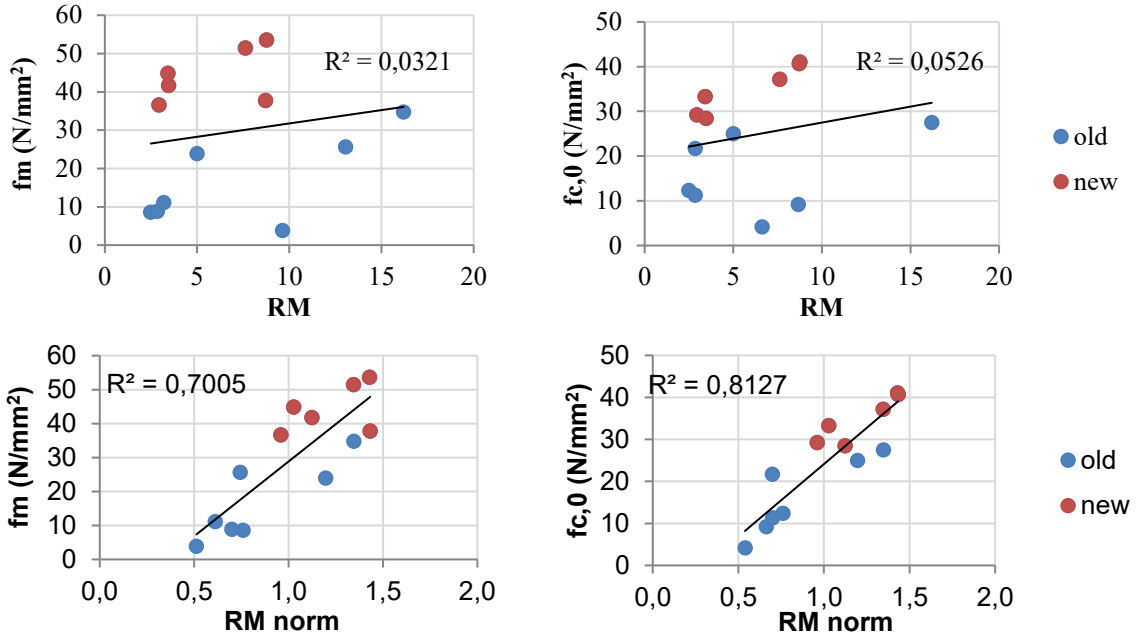


Figure 8: Correlation of mechanical characteristics of old and new timber elements in terms of compressive and flexural strength, versus the parameter RM (above) and RM_{norm} (below)

4 VISUAL INSPECTION AND ELEMENTS GRADING

The UNI 11119:2004 standard [6] (Cultural heritage, Wooden artefacts, Load-bearing structures of buildings - In situ inspection for the diagnosis of existing timber elements), indicates the classification rules and the methods for measuring the quantifiable characteristics on the structural existing timber elements. For assignment to a category, all characteristics and/or defects must fall within the specified limits (Table 1).

Starting from these indications it therefore reports, for wooden elements of different wood species and categories: (i) the maximum stresses, which can be adopted for the application of the allowable stress method; (ii) the average values of flexural modulus of elasticity, which can be used for the calculation of deformations of the structure in operating limit states.

All of the old timber elements of this experimental work were classified according to the UNI 11119 standard.

Table 1: Values for allowable stress extracted from table 1 and 3 of UNI 11119:2004 standard

Feature	Grade			Specie	Cat.	Compression // - ⊥ (N/mm²)		Flexural (N/mm²)
	I	II	III					
Edge chamfer	≤1/8	≤1/5	≤1/3	fir	I	11	2	11,5
Shakes (star, ring,.)	absent	absent	limited		II	9	2	10
Single knots	≤1/5 ≤50 mm	≤1/3 ≤70 mm	≤1/2	spruce	III	7	2	7,5
					I	10	2	11
					II	8	2	9
Grouped knots	≤2/5	≤2/3	≤3/4		III	6	2	7
Fiber angle radial	7%	12%	20%	larch	I	12	2	13
Fiber angle tangent	10%	20%	33%		II	10	2	11
splits	allowed if not passing				III	7,5	2	8,5

Visual grading is the basics of the new timber elements classification, and its counterpart for the existing elements on-site evaluation [6] represents a valid and viable assessment method. However, a single investigation method may not be totally adequate – especially in case of historical wood - for a correct assessment of the timber element under observation [1]. Results of the present experimental work showed remarkable discrepancies, even if on a reduced samples number, between the classification according to UNI 11119 and the mechanical characterization through laboratory tests, for some of the tested elements. Beams nr. 2, 5 and 9 were indeed classified in 1st (5, 9) or 2nd class (2), with reference values proposed by the standard – transposed to EN338 classes and related to the wood specie – respectively referable to C24 and C18. On the contrary, beams 5 and 9 (only tested in bending and compression, respectively), demonstrated a very weak response, with f_m and $f_{c,0}$ equal to 3.91 and 3,76 N/mm^2 respectively, which is far below any suggested value. Beam nr.2, a II class element, performed similarly to the new C24 spruce elements, with flexural and compression strength equal respectively to 34,76 N/mm^2 and 25,73 N/mm^2.

Comparing however the visual classification of the above mentioned elements with the distributed normalized Resitograph® amplitude RM_{norm} (Table 2), it can be seen that even if in class II, element nr. 2 had a remarkable RM_{norm} value (1,35), higher than the reference C24 sample element. At last, elements 5 and 9 had a very poor performance in terms of RM_{norm} values, equal respectively to 0,51 and 0,54.

Table 2: Mechanical tests results related with UNI 11119 elements classification

Sample	Specie	f_m (N/mm²)	$f_{c,0}$ (N/mm²)	RM_{norm} (%)	Cat. UNI 11119:2004
2B / 2C	spruce	34.76	25.73	1,35	II
3B	spruce	25.65	---	0,74	I
5B	spruce	3.91	---	0,51	I
9C	spruce	---	3.76	0,54	I
11C	spruce	---	6.88	0,66	I
12B / 12C	spruce	8.6	11.42	0,76	NC
13B / 13C	spruce	8.91	9.78	0,70	I
14C	spruce	---	19.05	0,70	II
17B / 17C	spruce	23.94	22.08	1,20	I

5 CONCLUSIONS

An experimental work concerning combination of methodologies for the on-site assessment of structural timber elements was carried out at the University of Padua by using available ND, SD and destructive investigation procedures. Results showed that:

- As part of the non-invasive methodologies for investigating wooden structural elements, it has been noted that the visual classification is not always sufficient to determine the mechanical characteristics in favor of safety, although it is the first step in the investigation procedure.
- Resistance drill tests propose quantitative results however limited to a single investigation point/investigated element, since it was noted that several parameters influence the test output, some of them basically uncontrollable (tip consumption).
- An attempt procedure for results generalization was employed, corresponding to a distributed resistance drill test application on the length of the element, employing per each test position a sample reference element of known mechanical characteristics.
- Satisfactory correlations in terms of determination coefficients were obtained plotting the normalized amplitude proposed parameter RM_{norm} with the mechanical characteristics of the elements derived from laboratory tests.
- The consideration of such parameter – substantially proposing distributed information on the inner sections (non-visible from outside) - seems promising to complement the strength class visual grading as prescribed by reference standards, possibly calibrating the given strength parameters today only related to the visual classification.

The authors will continue the investigations since it is noted a strong need for further relevant amount of data to be treated on a statistical basis.

Acknowledgements. The research was made possible by the availability of new and old timber elements, as well as spaces and kind advice of E. Bozza of Bozza Legnami, Vigonza, Italy. The research was partially funded by the Italian project Corewood POR FESR Veneto 2014-2020.

REFERENCES

[1] Riggio M., Anthony R.W., Augelli F., Kasal B., Lechner T., Muller W., Tannert T., "In situ assessment of structural timber using non-destructive techniques", *Materials and Structures*, Vol **47**(5), pp 749–766, (2013).

[2] Tannert T., Anthony R.W., Kasal B., Kloiber M., Piazza M., Riggio M., Rinn F., Widmann R., Yamaguchi N., "In situ assessment of structural timber using semi-destructive techniques", *Materials and Structures*, p Vol **47**(5), pp 767–785 (2013).

[3] Rinn F., Schweingruber F.-H., Schär E. "RESISTOGRAPH and X-Ray Density Charts of Wood. Comparative Evaluation of Drill Resistance Profiles and X-ray Density Charts of Different Wood Species", *Holzforschung - International Journal of the Biology, Chemistry, Physics and Technology of Wood*, Vol. **50**(4), pp. 303-311, (1996).

[4] Piazza M., Riggio M., "Visual strength-grading and NDT of timber in traditional structures, *Journal of Building Appraisal* 4, Vol. **3**, pp. 267-296, (2008).

[5] EN 338:2016 - structural timber – strength classes.

[6] UNI 11119:2004 (Beni culturali, Manufatti lignei, Strutture portanti degli edifici – Ispezione in situ per la diagnosi degli elementi in opera). In Italian

[7] User manual, IML RESI PD400

[8] EN 408:2010+A1 – Timber structures - Structural timber and glued laminated timber - Determination of some physical and mechanical properties

12th International Conference on Structural Analysis of Historical Constructions
SAHC 2020
P. Roca, L. Pelà and C. Molins (Eds.)

THE NDT INVESTIGATIONS CARRY OUT AT THE ARUDJ CATHEDRAL, ARMENIA

S. TONNA[1*], M. CUCCHI[2] AND C. TEDESCHI[3]

[1] Politecnico di Milano – DAStU Department
Piazza Leonardo da Vinci, 32 – 20133 Milano, Italy
e-mail: sandra.tonna@polimi.it (*corresponding author)

[2] Politecnico di Milano – LPMsc Laboratory
Piazza Leonardo da Vinci, 32 – 20133 Milano, Italy
e-mail: marco.cucchi@polimi.it

[3] Politecnico di Milano – D.I.C.A. Department
Piazza Leonardo da Vinci, 32 – 20133 Milano, Italy
e-mail: cristina.tedeschi@polimi.it

Keywords: Historical Structure, Masonry, Monitoring, Non-Destructive Inspection

Abstract. *Arudj Cathedral, Armenia, is an example of early-Christian domed-hall that dates 671-672. A deep structural analysis of the building was developed by Politecnico di Milano, during the II° Level Master for Architects and Archaeologists named "Restoration Training and Support to Local Institutions for the Preservation and Conservation of Armenian Heritage". The preservation project mainly focuses on deepen the knowledge level of the building in relation to the architectonical and structural aspects in order to offer a working method with the aim to propose and teach alternative solutions for static and seismic consolidation.*

This paper reports the NDT investigations of the surveys carried out at the Cathedral of Arudj and the results obtained at the laboratory of the Politecnico di Milano.

The NDT investigations were carried out by the Authors and here following are briefly described. Sonic investigations on masonry structures were applied for a qualitative comparison of the walls, based on the variation of the sonic velocity values in the presence of areas with lower density, voids or cavities. The passive thermographic technique was applied to identify the distribution of capillary ascent in masonry structures. In order to offer a long-term verification of the evolution of the crack pattern, after having identify the cracks present on the masonry structures some displacement transducers have been fixed to state their evolution hourly.

Finally, a series of laboratory tests were carried out to determine the main mechanical characteristics of the constituent stone.

1 INTRODUCTION

This report describes the results obtained with an extensive experimental investigation applying NDTs, in order to evaluate the structural damage, their extension and their causes. As known, a proper preservation project for existing structure starts only after an accurate diagnosis of the state of the art based on: on site survey and laboratory investigation. These operations will deepen the knowledge of the building and held respecting its authenticity through an appropriate choice of intervention techniques. The lack of knowledge on the original materials and structures was frequently the main cause of unsuccessful interventions. Furthermore, as happened in this case study, a further problem was found in those buildings that have already been repaired with unsuccessful techniques. From this state of the art a series of questions arise: What actually caused the failures? How did they develop? How serious were their consequences on the overall response of the building?

In particular this is a common condition in seismic areas where masonry structures are characterized by partial or full reconstruction due the earthquake damage.

In order to fulfil these needs by overcoming the gap between our poor knowledge and the complexity of these structure an experimental on site investigation is required and recommended also by Codes and Standards in several Countries. Non destructive techniques (NDTs) and/or Minor destructive Techniques (MDTs) can be helpful in detecting hidden features (wall texture, internal voids and flaws and characteristics of the wall section) which are so much important to define the structural behaviours under dead loads and environmental action [1]. It is then important before choosing the appropriate NDTs to know which type of problem has to be solved, i.e. what it is necessary to find by NDT. In the case of ND tests, a correlation between the measured parameters and the mechanical ones is usually difficult, but they can give an overall qualitative response of the masonry. At present the most diffused ND techniques are represented by the sonic (or ultrasonic), radar and thermography tests [2]. It must be clear that the responsible of the on site diagnosis must: (i) set up the in-situ and laboratory survey project, (ii) constantly follow the survey, (iii) understand and verify the results, (iv) make technically acceptable use of the results including their use as input data for structural analyses, (v) choose appropriate models for the structural analysis, (vi) arrive at a diagnosis at the end of the study [3].

2 CASE STUDY FRAMEWORK

The Aruch settlement is located to the west of the Aghbri, a small stream at the southern foot of the Mount Aragats. The urbanization of Aruch dates from a pre-Christian age when a water basin was dug in the bedrock surface, probably with reference to the cult of the spring water. Always belonging to this age, archeological excavations have discovered a large burial ground with approximately 8-12 thousand sepulchres located close to this holy area. After the advent of Christianity the area maintains its religious importance and Aruch became one of the first important Church attested since the early 7th century A.D.

By the second half of the 7th Century the historical complex took a new more detailed and monumental form, due to the fact that Prince Grigor Mamikonian selected Aruch as the admistrative seat of his government [4]. From this period belong: the costruction of the Catedral and the building located at the south side, as well as the trasforamtion of the previous Church into

a civil building. The kingdom of Grigor Mamikonian, which coincides with the presence of the Cathilicos Anastas, is described as particulary prosperous for the Aruch site and the city played and maintained an important economic role until the the second half of the 9th century A.D. Nowadays the Cathedral is the only surviving edifice to that golden age.

3 INVESTIGATIONS CONDUCTED ON MASONRY STRUCTURES

This report shows the results of the on-site investigations carried out at the Arudj Cathedral and of the laboratory tests conducted at the Politecnico di Milano. On site, non-destructive surveys were conducted on the entire monumental complex, investigating all the structural components: from the foundations to the masonry and roofing structure and for each investigation, the methodology and purposes will be described here following [5].

For the purposes of this article, the results of the tests conducted on a single portion are reported, in order to facilitate the comparative reading of the investigations. The portion under consideration (Fig. 1) was chosen as characteristic of the complex in terms of materials and construction technique, but at the same time, representative of the borderline case as it was seriously damaged by important instability phenomena.

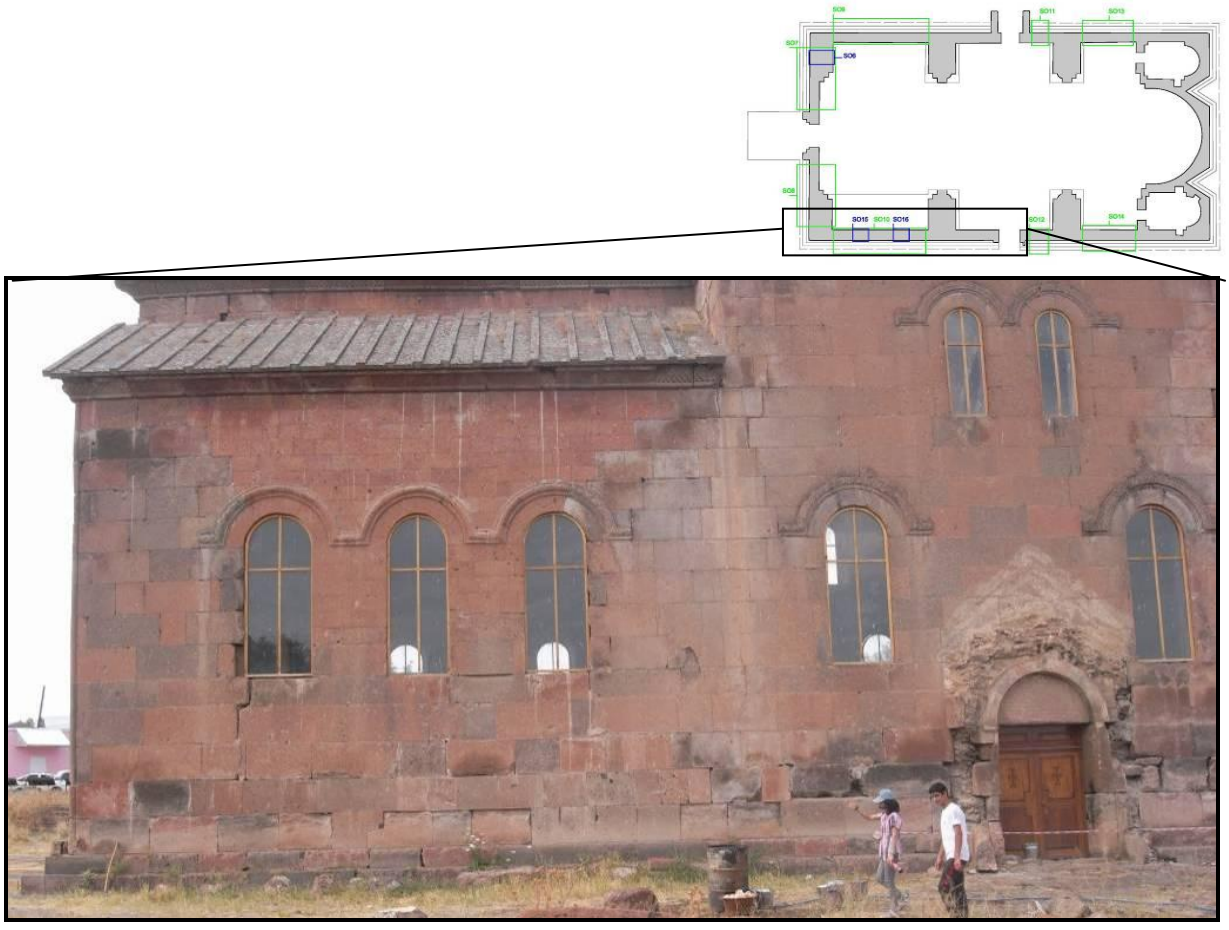


Figure 1: The selected structural portion belonging to the North front

3.1 Geometrical and crack pattern survey

As it known, a well detailed in-situ survey is fundamental to provide informations on the structural geometry and the architeconical elements, in addition, to put the base to identify the points where more accurate observations have to be concentrate. As consequance a more refined investigation has to be carried out, identifying irregularities (vertical deviations, rotations, etc.) and transformations in order to be able to learn them in comparison the historical evolution of the structure. Only throuhg this reading will be possible to explain the signs of damage detected on the building. Following this basic principle an important role has been assumed by the crack patterns survey and drawing (Fig. 2). The interpretation of the crack pattern can be of great help in understanding kinematic mechanism the state of damage of the structure, its possible causes and the type of survey to be performed, provided that the development history of the building is already known [6].

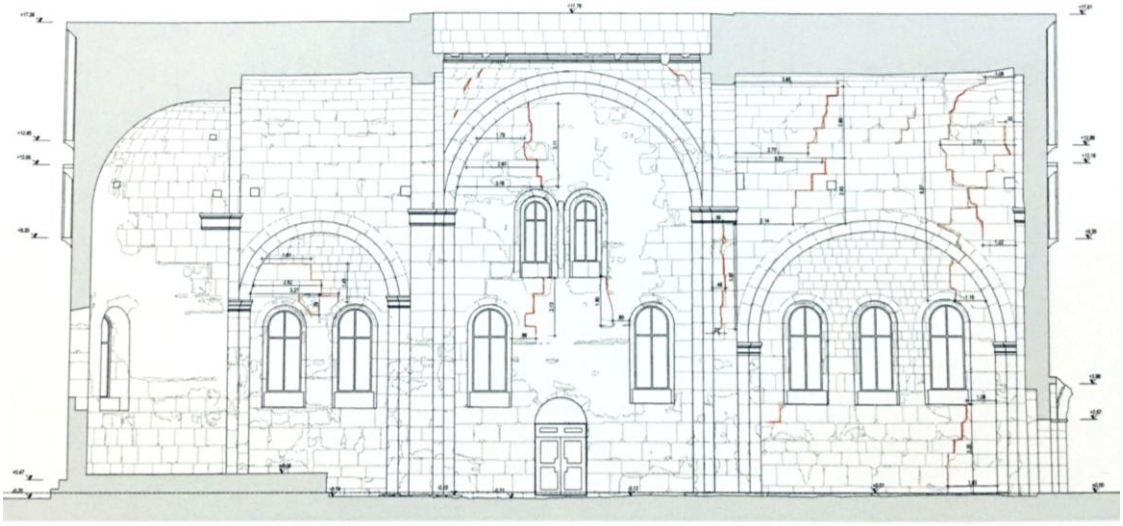


Figure 2: The internal side of the South front, the main cracks are underlined by circles.

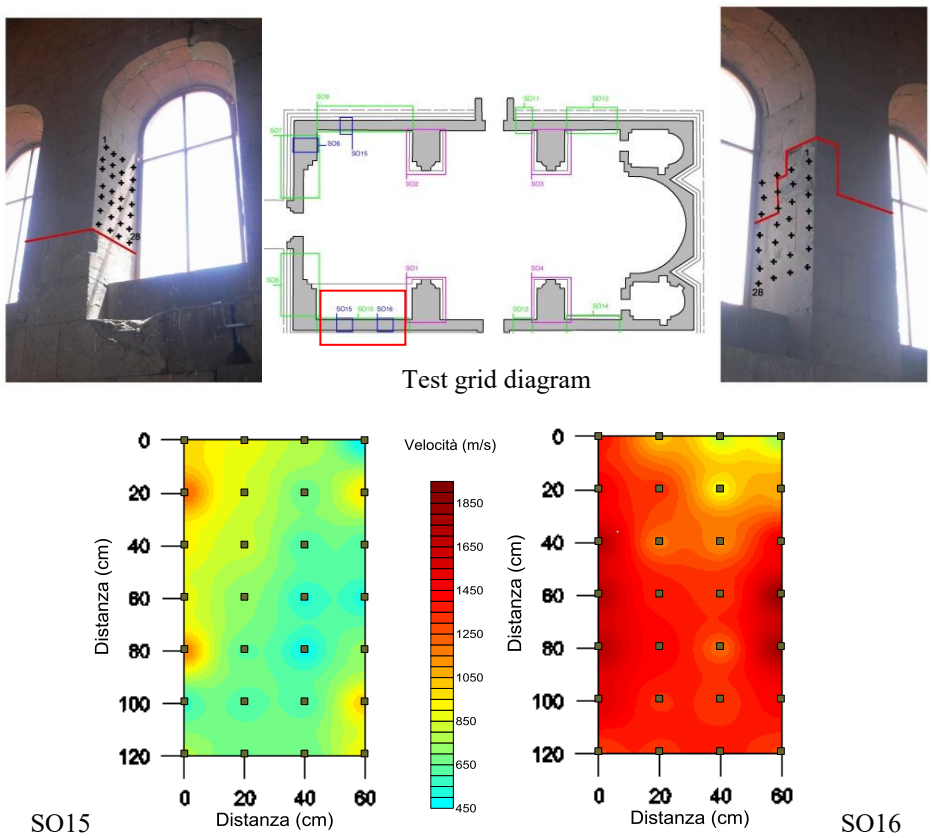
3.2 Sonic tests

Among the ND investigation methods, the sonic methods are with no doubt, the most widely used [7]. The testing technique is based on the generation of sonic or ultrasonic impulses at a point of the structure. A signal is generated by a percussion (transmitter) and collected through a receiver which can be placed in various positions. The elaboration of the data consists in measuring the time the impulse takes to cover the distance between the transmitter and the receiver. The use of sonic tests for the evaluation of masonry structures has the following aims: (i) to qualify masonry through the morphology of the wall section, to detect the presence of voids and flaws and to find crack and damage patterns; (ii) to control the effectiveness of repair by injection technique in others which can change the physical characteristics of materials [8]. In agreement with the NDT survey plan, sonic tests have been carried out on the most damaged part of the walls, sixteen areas were detected to analize all the pillars and a large part of the masonry. As requested, the equipment used for the survey is composed by an impact hammer as transmitter, an accelerometer as receiver and by an d a DAQ board to acquire data. In figure 3, the velocity average recorded in few wall portions is

visible. In table 1 it is possible to observe the speed differences between the original pillars and those subject to the restoration intervention made with new stones.

Table 1: Example of a sonic test result, here has been selected a survey conducted on a window pillar composed by two different bricks (the original and another type used during a restoration intervention).

Prova S15: - Speeds Bar charts	Date: 20-07-2013



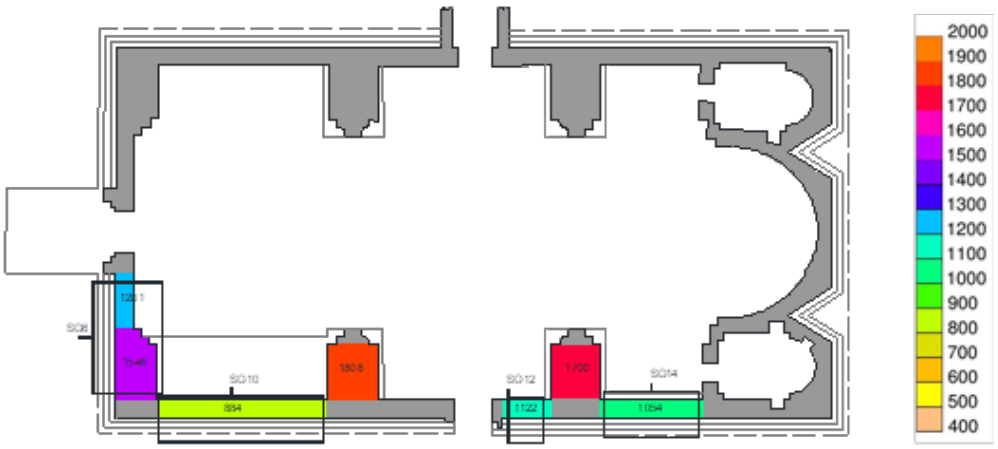


Figure 3: The sonic test investigations, marked in according with the proper color of the corresponding velocity class. At the top right the reference plan with the wall thicknesses

3.3 Thermography

Thermovision is a NDT which has been applied since several years to works of art and monumental buildings. The thermographic survey has the advantage of being applicable to wide surfaces of walls; it is a telemetric method and has high thermal and spatial resolution. Thermovision can be very useful in diagnostic; in fact it is used to identify areas under renderings and plasters that can hide construction anomalies. Other applications can be: (i) survey of cavities, (ii) detection of inclusions of different materials, (iii) detection of water and heating systems, (iv) moisture presence.

Figure 4 shows the presence of moisture and the capillary rise, thanks to the camera which identify the coldest surface areas, where there is continuous evaporation. The evaporation is due to the difference in R.H. between the inside of the masonry and the environment outside and to natural air movements [9].

a) 

Figure 4a: The thermography test investigations, conducted on the North front external side.

b) 

Figure 4b: The thermography test investigations, conducted on the South front external side.

3.4 Laboratory tests

Samples of the materials are needed for caracterization tests. The technique of sampling is very important, since samples must be as undamaged as possible in order to be representative of the material in situ. The aims of these tests are the followings: (i) to characterise the material from a chemical, physical and mechanical point of view, (ii) to detect its origin in order to use similar materials for the repair, (iii) to know its composition and content, and (iv) to measure its decay and the durability to aggressive agents from new materials used for restoration. Since it is very difficult to sample prisms representative of the walls, only single components or small assemblages are removed [10].

The materials sampled from the walls of the Cathedral were tested in laboratory to be characterized (Figs. 5, 6). Prisms of about 50x50x50 mm and 50x50x150 have been obtained from the stone and have been subjected to two series of uniaxial compression tests, dry (Tab. 2) and wet (Tab. 3) after being characterised through ultrasonic tests (Tabs. 4-5).

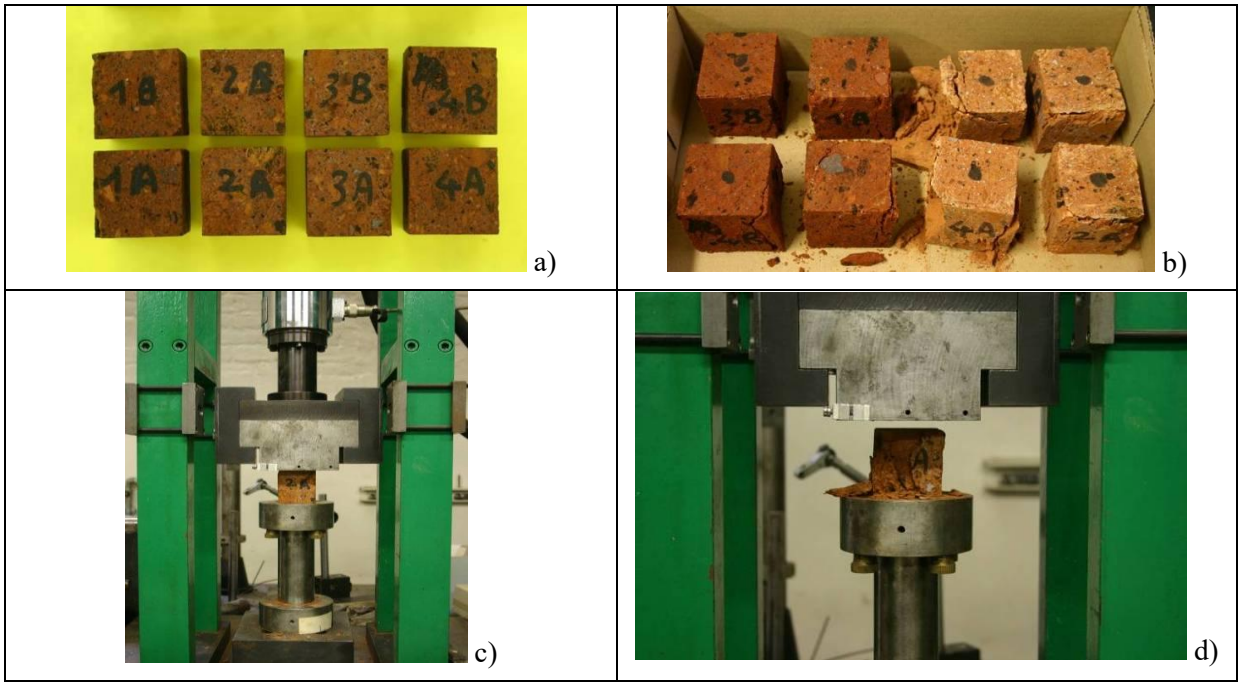


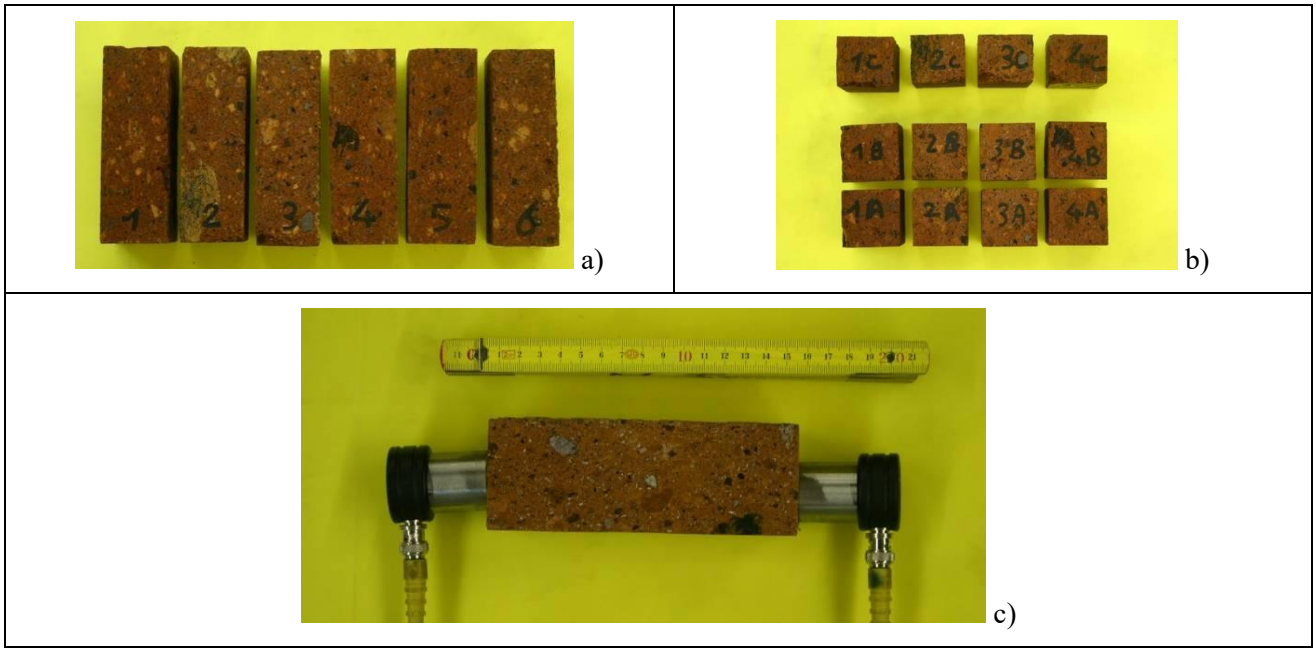
Figure 5: a) Prisms befor test; b) Prisms after test; c) and d) Prism during compressive test.

Table 2: Compression test results on specimens dried at 70°C

Name	Length (mm)	Width (mm)	Height (mm)	Dry weight (g)	Area (mm^2)	Load (N)	σr (N/mm^2)
1-A	51.4	50.7	50.4	217	2606	43772	16.8
2-A	48.4	51.8	50.8	206	2507	38259	15.3
3-A	48.2	52.1	50.7	206	2511	45940	18.3
4-A	51.2	49.5	50	207	2534	41496	16.4
Average							**16.7**
Standard deviation							**1.3**

Table 3: Compression test results on specimens saturated with water

Name	Length (mm)	Width (mm)	Height (mm)	Dry weight (g)	Area (mm^2)	Load (N)	σr (N/mm^2)
1-B	51	50.4	50.7	240	2570	31588	12.3
2-B	48.3	51.6	50.9	229	2492	33158	13.3
3-B	48.1	51.2	50.6	230	2463	42968	17.4
4-B	51.7	49.5	50.9	240	2559	34826	13.6
Average							**14.2**
Standard deviation							0.7



a) b) c)

Figure 6: a) Prisms cut and rectified; b) Cubes cut and rectified; c) Prism during measurement

Table 4: Measurement of the ultrasonic velocity – UR 0% and UR 100%

Abb.	Length (mm)	UR 0% Velocity (m/sec)	Abb.	Length (mm)	UR 100% Velocity (m/sec)
1-A	50	2994	**1-B**	50	2632
2-A	50	2809	**2-B**	50	2747
3-A	50	2941	**3-B**	50	2674
4-A	50	2924	**4-B**	50	2703
5	150	2804	**6**	150	2688
Average		**2894**	**Average**		**2663**
Standard deviation		**84.4**	**Standard deviation**		**25.4**

4 A FEW CONSIDERATIONS

Due these investigations, both on site and in the laboratory, to some punctual inspections and to the comparison with similar cases located nearby, it has been possible to characterize the masonry by providing a hypothetical schematization of the wall section and its connection to the foundation structure. From what emerges from a preliminary analysis of the masonry, it can be assumed that the section can be defined as a three layers: two masonry facings (internal and external) and, the third one, composed by a filling in mortar and medium / large sized stones (Fig. 7). The longitudinal section of a type ashlar has an almost conical extrusion towards the inside and, thanks to this alternation, the middle layer is reduced, the internal and external facing are partially damped and the masonry acquires greater homogeneity and compactness. The masonry has a section of 90 cm and, at a height of about 60 cm from the walking surface, it progressively increases by 30 cm at a time until doubling thanks to a system of external steps adhered to the masonry through the filling that composes them. From a static point of view, this system recalls the structural benefits of a scarp wall (Fig. 7).

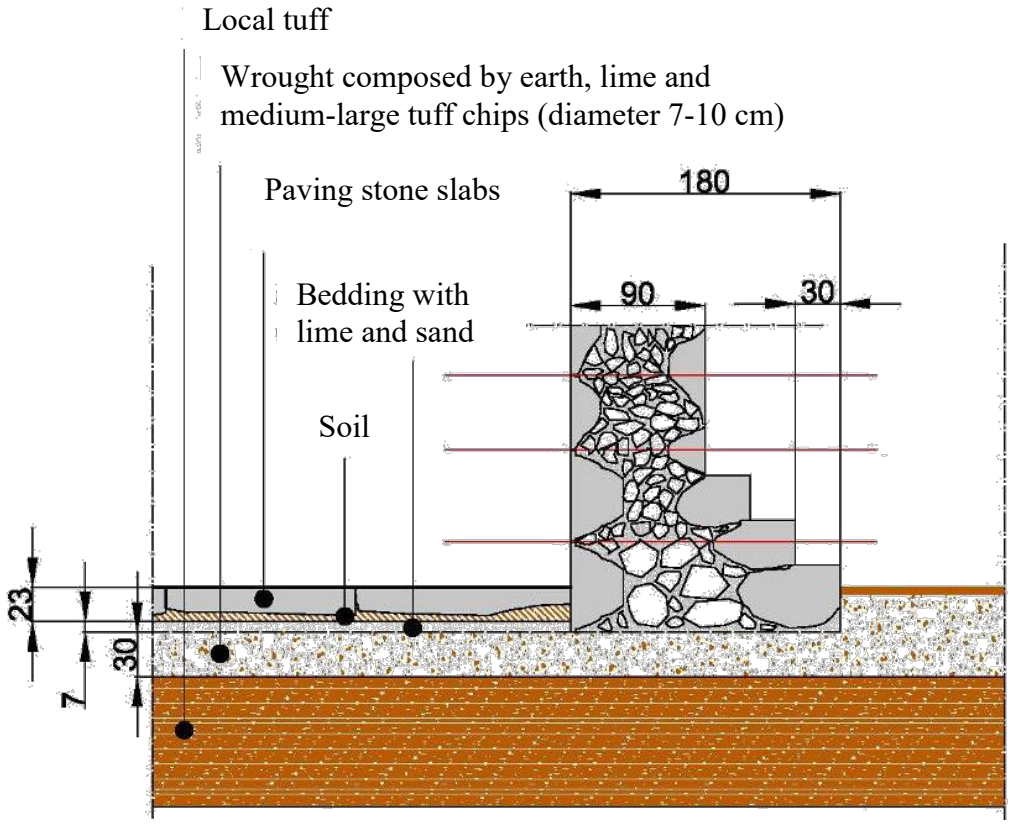


Figure 7: Hypothesis of the wall and foundation

In the case of Aruch, the stone is a tuff with chromatic variations from earth red to black, characterized by a very high porosity. The external fronts are obtained through large, well-squared ashlars, generally arranged with alternating joints between inside and outside. From a first critical reworking of the results obtained from the sonic investigations, it was found that

the joints of the external face are in correspondence with the center line of the internal one. This arrangement may have been specifically designed to give the masonry greater compactness in the absence of diatons (Fig. 8).

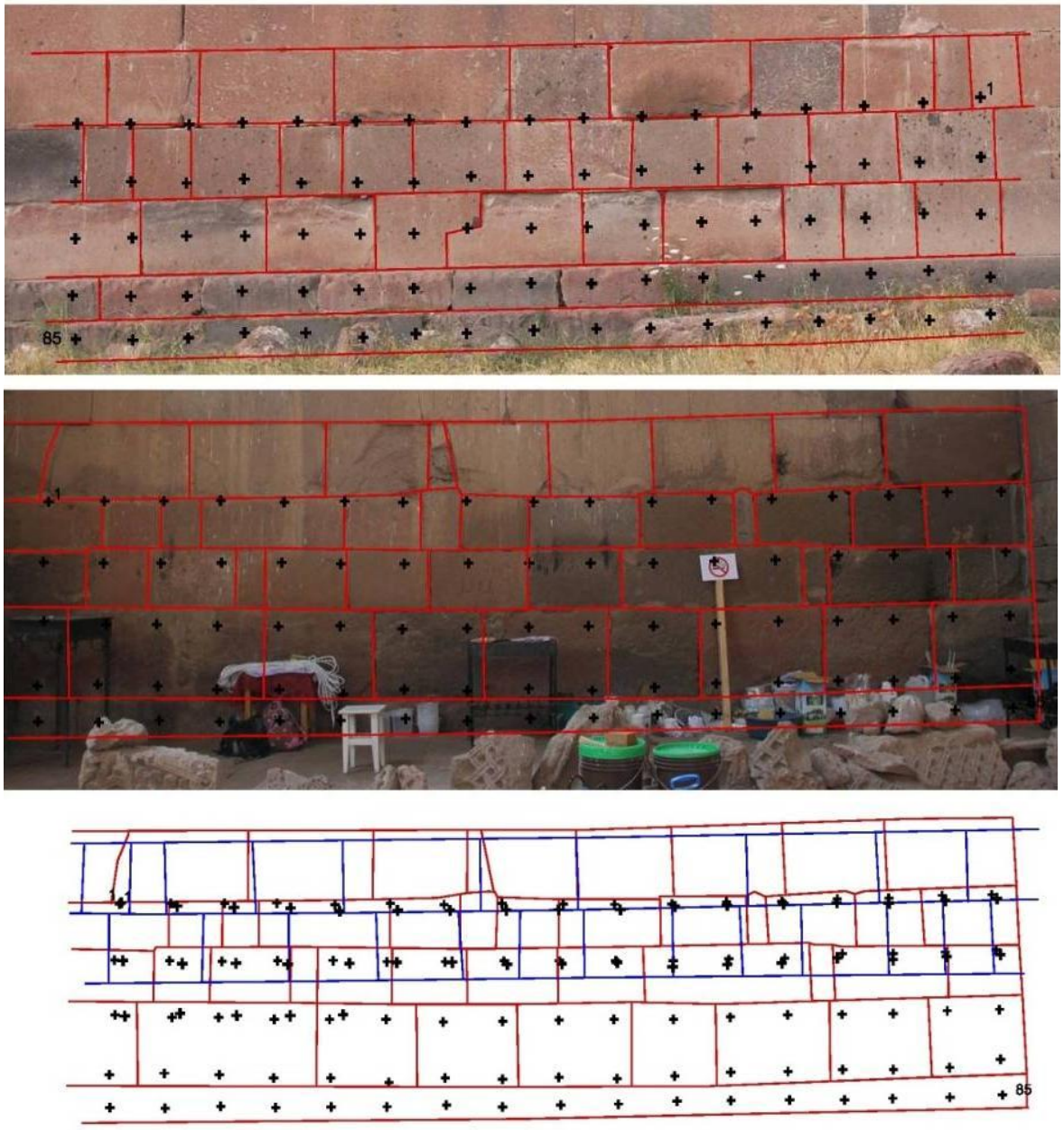


Figure 8: a) External front; b) Internal front; c) overlapping joints

CONCLUSIONS

This brief description of available techniques and procedures illustrates the difficulty faced by the designer who must select the technically and economically correct method to define the state of preservation or damage of the structure to be restored.

The visual inspection and non-destructive techniques performed on the Cathedral of Aruch allowed to highlight the critical issues especially regarding the structural aspect. The crack pattern survey highlighted the main active kinematic mechanisms such as the rotation of the facade, the overturning of the tympanum, the thrust of the arches and vaults on the lateral structural elements and the weak connection of the main facade. The damages are due both to some original geometric imperfections and to seismic events, which have occurred in the past. In fact, Aruch is located in an area characterized by a very high seismicity.

The thermographic investigations carried out both on the south and north fronts have highlighted the presence of capillary rise and, especially in the southern prospect, a very high temperature during the recovery, this identifies an ongoing evaporative process and a wide temperature ranges, one of the main deterioration causes surveyed on these walls.

The sonic investigations carried out on the south front masonry and pillars have shown the difference density between the original materials and the new one (always stones) used for the restoration. Furthermore, the recorded data show that the pillars have a slightly dispersed sonic velocity values, this is indicative of a good state of conservation; in the masonry the results are different: the velocities are particularly low and dispersed. The lowest speeds are recorded in the south-facing walls which present the greatest deterioration on the masonry, in fact important crack patterns have been highlighted too.

The results relating to laboratory tests have shown the different compression behavior of saturated stones and dry ones. The ultrasonic speeds of the stone elements tested in the laboratory and the data recorded in situ, demonstrate the good state of conservation especially of the pillars building materials.

The test campaign extended to the whole church and the accurate crack survey allowed to design a structural monitoring [11]. In fact, a series of transducers have been installed that will allow to give a complete picture of the kinematic mechanisms in progress, as well as the possibility of evaluating a consolidation and restoration intervention [12].

REFERENCES

[1] Binda, L., *The importance of investigation for the diagnosis of historic buildings: application at different scales (centers and single buildings*). In: IV International seminar structural analysis of historical constructions, 10–12 November, Padova, Italy, Keynote lectures, vol 1, pp 29–42. (2004)

[2] Michael, P., Schuller, P.E., *Non destructive testing and damage assessment of masonry*

structures, in NSF/ RILEM workshop*:* In-Situ Evaluationof Historic Wood and Masonry Structures, July 10-14, 2006 – Prague, Czech Repubblic) (2006).

[3] Binda, L., Saisi, A., Tiraboschi, C., Investigation procedures for the diagnosis of historic masonries. *Constr. Build. Mater.* (2000). **14**(4):199–233. https://doi.org/10.1016/S0950-0618(00)00018-0.

[4] Casnati, G. (a cura di), *The Politecnico di Milano in Armenia. An Italian Ministry of Foreign Affairs project for Restoration Training and Support to Local Institutions for the Preservation and Conservation of Ar-menian Heritage*, OEMME, Venezia (2014).

[5] Cucchi, M., Tedeschi, C., Structural diagnostic, in G. Casnati (a cura di) *The Politecnico di Milano in Armenia. An Italian Ministry of Foreign Affairs project for Restoration Training and Support to Local Institutions for the Preservation and Conservation of Armenian Heritage,* OEMME, Venezia (2014), pp. 144-157.

[6] Binda, L., Cantini, L., Tedeschi, C., *Diagnosis of Historic Masonry Structures using Non-De-scruttive Techniques*. In: O. Gunes, Y. Akkaya (a cura di) Nondestructive Testing of Materials and Structures, *Springe*r Netherlands, Dordrecht (2013), ISBN: 9789400707238, doi: 10.1007/978-94-007-0723-8_152 pp. 1089-1102 .

[7] Cantini, L., Condoleo, P., Munda, S., Tedeschi, C., Tiraboschi, C., Casarin, F., Simonato, E., Binda L. , *Investigation Methodology Applied to the Structure of the Church of St. Biagio in L'Aquila*. In: Nondestructive Testing of Materials and Structures. p. 1195-1201, Springer Netherlands, (2013) ISBN: 9789400707238, doi: 10.1007/978-94-007-0723-8_166

[8] Binda, L. Saisi, A. Tiraboschi, C., Application of Sonic Tests to the Diagnosis of Damaged and Repaired Structures. *NDT&E International* (2001) 34(2):123-138. https://doi.org/10.1016/S0963-8695(00)00037-2

[9] Binda, L., Cantini, L., Cucchi, M. Thermovision: *Applications in Conservation Field to Detect Hidden Characteristics of Building Structures*, in: Conference Proceedings Eleventh North American Masonry Conference (eleventh NAMC), DVD, pp. 1-11, Ed. The University of Minnesota - Twin Cities, 5-8 June 2011, Minneapolis, USA, (2011), ISBN:1-929081-39-1.

[10] Baronio, G., Binda, L., Tedeschi, C. Tiraboschi, C., Characterisation of the materials used in the construction of the Noto Cathedral. *Construction and Building Materials*, (2003) 17:557-571. doi:10.1016/j.conbuildmat.2003.08.007.

[11] Casarin, F., Lorenzoni, F., Islami, K., Modena, C. *Dynamic identification and monitoring of the churches of St. Biagio and St. Giuseppe in L'Aquila*. In Proceedings of EVACES (2011), October 3-5. Varenna, Italy.

[12] Silva, B. Pigouni, E. Valluzzi, MR. Da Porto, F., Modena, C., *Assessment of the effectiveness of grout injection on the consolidation of 3-leaf stone masonry walls through the use of NDT and DT*. In: Proceedings of SACH2012 structural analysis of historical constructions, Wroclaw (Poland), 15–17 October (2012), pp 1931–1939

12th International Conference on Structural Analysis of Historical Constructions
SAHC 2020
P. Roca, L. Pelà and C. Molins (Eds.)

THE STATE AND CONDITION OF HISTORICAL BUILDINGS LOCATED ON PARTISAN HILL IN WROCLAW

ANNA HOŁA[1], JERZY HOŁA[2], ŁUKASZ SADOWSKI[3] AND JACEK SZYMANOWSKI[4*]

[1] Faculty of Civil Engineering
Wroclaw University of Science and Technology
Wybrzeże Wyspiańskiego 27, 50-370 Wroclaw, Poland
e-mail: anna.hola@pwr.edu.pl

[2] Faculty of Civil Engineering
Wroclaw University of Science and Technology
Wybrzeże Wyspiańskiego 27, 50-370 Wrocław, Poland
e-mail: jerzy.hola@pwr.edu.pl

[3] Faculty of Civil Engineering
Wroclaw University of Science and Technology
Wybrzeże Wyspiańskiego 27, 50-370 Wroclaw, Poland
e-mail: lukasz.sadowski@pwr.edu.pl

[4] Faculty of Civil Engineering
Wroclaw University of Science and Technology
Wybrzeże Wyspiańskiego 27, 50-370 Wroclaw, Poland
e-mail: jacek.szymanowski@pwr.edu.pl (*corresponding author)

Keywords: Partisan Hill, historical buildings, state of preservation, non-destructive testing, semi-non-destructive testing

Abstract. *The paper presents fragments of original archival documentation, which are used to identify the historical outline of the colonnade building and the peristyle pavilion located on Partisan Hill in an old part of Wroclaw. Traces of these buildings date back to the Middle Ages. The state of preservation of these objects was presented on the basis of conducted assessments, drilling cores, and non-destructive and semi-non-destructive tests. Much attention was devoted to the brick walls, brick and reinforced concrete ceilings in flat roofs, as well as to the elements of architectural detail. The presented results include tests of the moisture content and salinity of walls, tests of the compressive strength of concrete and distribution of reinforcement in ceilings. They constitute the first stage of activities that aim to restore the buildings to their former glory.*

1 INTRODUCTION

The purpose of the paper, apart from presenting a brief historical outline, is to present the current picture and condition of buildings erected in the 1860s and preserved to this day on Partisan Hill, which is located in an old part of Wroclaw, namely the colonnade building and

the peristyle pavilion. The assessment was based on extensive research and analysis, which aimed to clarify conclusions and recommendations for the purpose of restoring the former splendour, not only of the buildings in question, but of the entire concept of Partisan Hill. So far, no renovation works have been carried out on Partisan Hill. The research described in the manuscript was first of a series of actions that are taken to restore the objects to their former glory.

It should be noted that Partisan Hill is a complex of great historical value. In 1967, it was included in the area of the urban complex of the Old Town of Wroclaw, which is in the register of monuments under the number: A/1580/212. The object itself, due to a decision of a conservation officer, was included in the register of monuments in 1970 under the number: A/2714/211. In turn, in 1994, by order of the President of the Republic of Poland, Partisan Hill was recognized as an historical monument (Fig. 1).

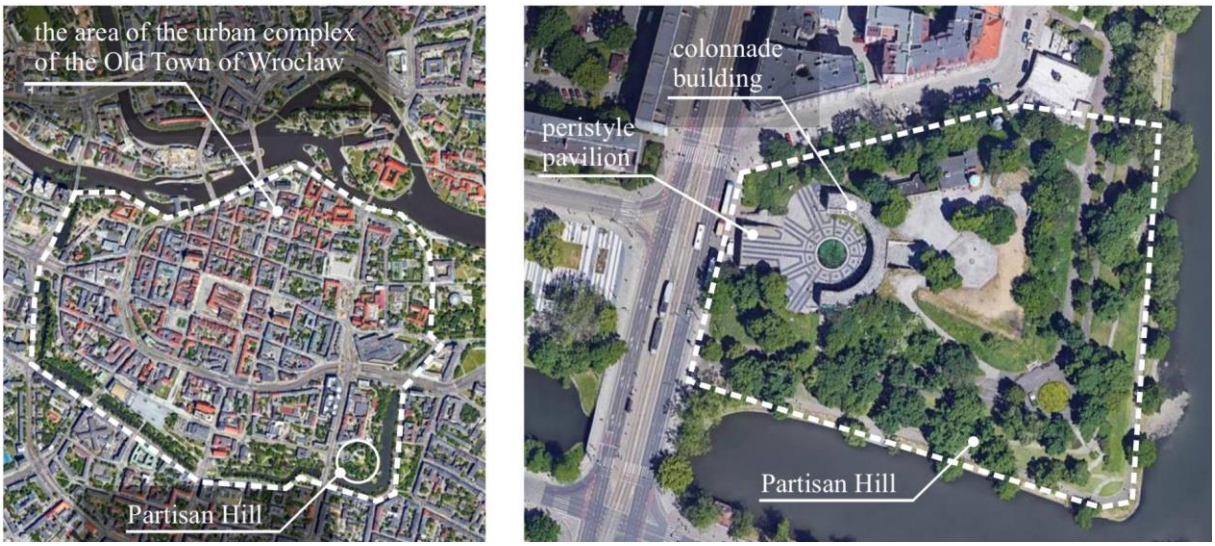


Figure 1: Aerial photos of the urban complex of the Old Town of Wroclaw and Partisan Hill

2 HISTORICAL OUTLINE

The first traces of the buildings of today's Partisan Hill date back to the Middle Ages, when in the area of the hill, then called Sakwowy Hill, a city gate was created that was called Sakwowa gate. In 1591, along with the extension and strengthening of the Wroclaw fortifications, a bastion designed by Hans Schneider was built on the hill.

During the liquidation of the city fortification system in the first decade of the 19th century, the bastion, as one of only a few buildings, was not demolished. Only military equipment was removed and the bastion was transformed into a viewing hill in a park complex that was called the Old Town Promenade, which was created in the area of former fortifications.

In the 1860s, the hill was developed with a complex of entertainment and recreation buildings that were founded by Adolf Liebich and designed by the architect Carl Schmidt. The complex included a belvedere standing on a plateau with a lookout tower, and also a colonnade building (Fig. 2a) and a peristyle pavilion (Fig. 2b), which were integrated into a terrace on the western slope of the hill. The peristyle pavilion was located at the foot of the

hill, and it served as a mineral water pump room. On both sides of the pavilion, a wide staircase leading to the terrace was designed. In turn, a circular pool with a fountain was located in the centre of this terrace. From the east, the terrace was limited by a semi-circular loggia with stairs leading to the Belvedere palace, which was a central tower-like building designed on an octagonal plan and topped with a dome in which a confectionery was located. All the listed objects were in the style that correlates to the Italian Renaissance [1], and their mutual arrangement and location on the hill can be seen in digitized and generally available archival plans and maps [2].

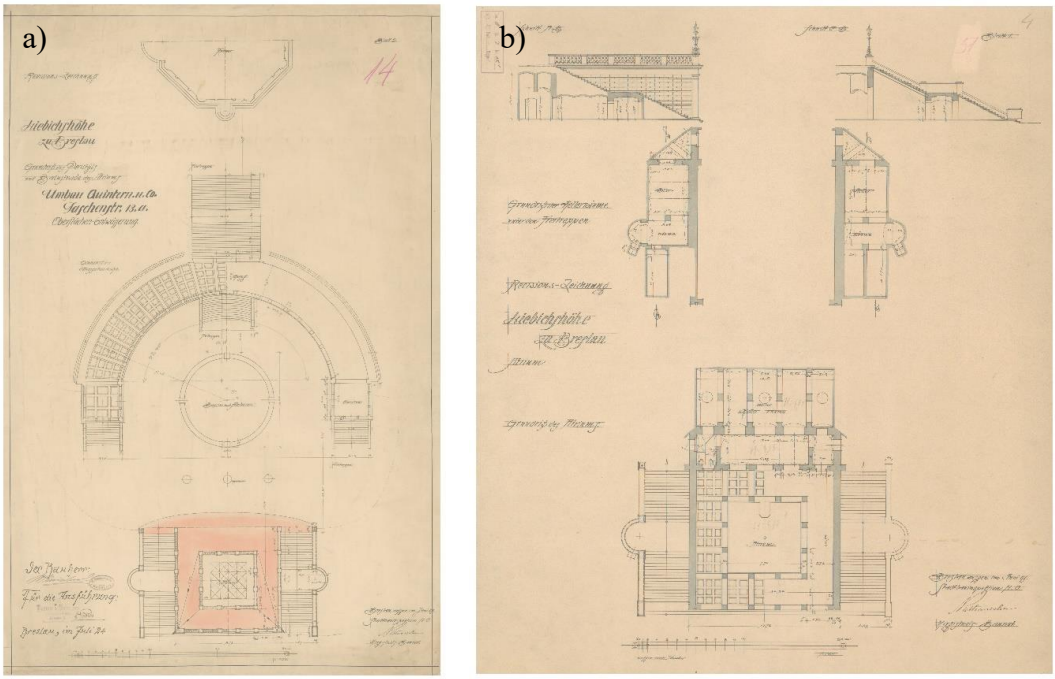


Figure 2: A fragment of the original documentation of the buildings that exist to this day: a) colonnades; b) the peristyle pavilion (source: archive of the Museum of Architecture in Wroclaw)

Major changes that refer to the architectural appearance and the way the buildings were used occurred in the 20th century. In the 1920s, the peristyle pavilion was rebuilt and commercial premises were set up there. In the 1940s, due to the warfare conducted during World War II, anti-aircraft shelters were organized in the former casemates of the bastion, which later became the main defence headquarters of the city. The belvedere building was completely destroyed at that time.

In 1952, after the end of World War II, the municipal authorities of Wroclaw adopted the official name for the area in question - Partisan Hill - which has been operating to this day. In the period from the 1950s to the 1990s, there were several unsuccessful attempts to revalorize the entire complex and restore its former glory. At that time, access to the buildings, i.e. the colonnade building and the peristyle pavilion, was temporarily suspended, and is now completely suspended due to their poor technical condition that threatens the health and life of people.

3 THE STATE OF PRESERVATION

As mentioned in the introduction, the subject of the manuscript are all the buildings erected on Partisan Hill in the 1960s, which have survived to this day. Those are colonnade building and peristyle pavilion whose state of preservation has been described below.

3.1 Colonnade building

The colonnade building, which is shown in Figure 3, has two floors, one of which is mostly recessed in the ground. Its building area is about 460 m^2. The walls of the lower floor are made of brick, and their thickness is in the range from 50 to 90 cm. The flat roof based on them has a brick ceiling in the form of arched vaults with ribs (Fig. 3c). In turn, the ceiling of the above-ground floor is slab-ribbed and partly based on walls and partly on brick columns with a diameter of 50 cm (Fig. 3b). Both flat roofs were made in around 1870 and they are accessible directly from the area adjacent to the building.

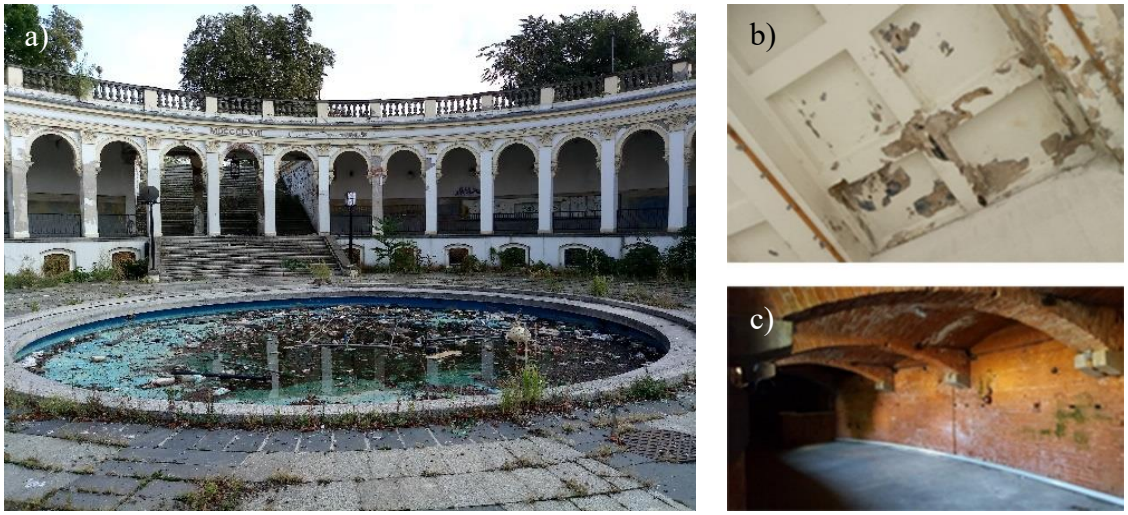


Figure 3: General view: a) the colonnade building (in the foreground is a swimming pool with a fountain); b) the slab-ribbed reinforced concrete ceiling; c) the basements and the brick ceiling

The brick construction elements of the basement, both the walls and the ceiling, are preserved in relatively good condition. They are free from significant damage in the form of wall cracks and deformations of arched vaults and ribs. However, they are very moist and covered with salt efflorescence and mold fungi. This is the result of a lack of vertical and horizontal damp-proof insulation, which was proved by the executed exposure works of the walls. In addition, due to excessive moisture, these elements have local losses of brick fragments and numerous places with crumbling of the mortar between the bricks.

The brick elements of the above-ground structure, in particular its columns, are in a similar condition. They are also damp and show mortar crumbling between bricks on surfaces that are partially free of plaster. The reinforced concrete ceiling of the roof is also very damp. Its bottom surface shows numerous patches of corrosion in its reinforcement (Fig. 4b).

Elements of architectural detail, such as e.g. posts, balusters, the stucco decorations of arches and column heads, plasters, and also granite flooring are incomplete, damaged, or completely damaged, as illustrated in Figure 4.



Figure 4: View: a) damage to stucco and plasters in the colonnade building; b) incomplete elements of the balustrade and granite floor

In both flat roofs of the colonnade building, semi-non-destructive testing was performed by taking core samples with a diameter of 100 mm in order to determine the layout of layers and their thicknesses. The places of taking samples, as well as the obtained core specimens, are shown in Figures 5 and 6. In the layout of the layers in the flat roofs above the floor embedded in the ground, which is shown in Figure 5, the lack of damp-proof insulation is noteworthy. In the layout of the layers of the flat roof above the ground (Figure 6) it can be seen several layers of concrete with different thickness, a layer of bituminous insulation, a layer of mortar and granite slab all laid on reinforced concrete ceiling slab.

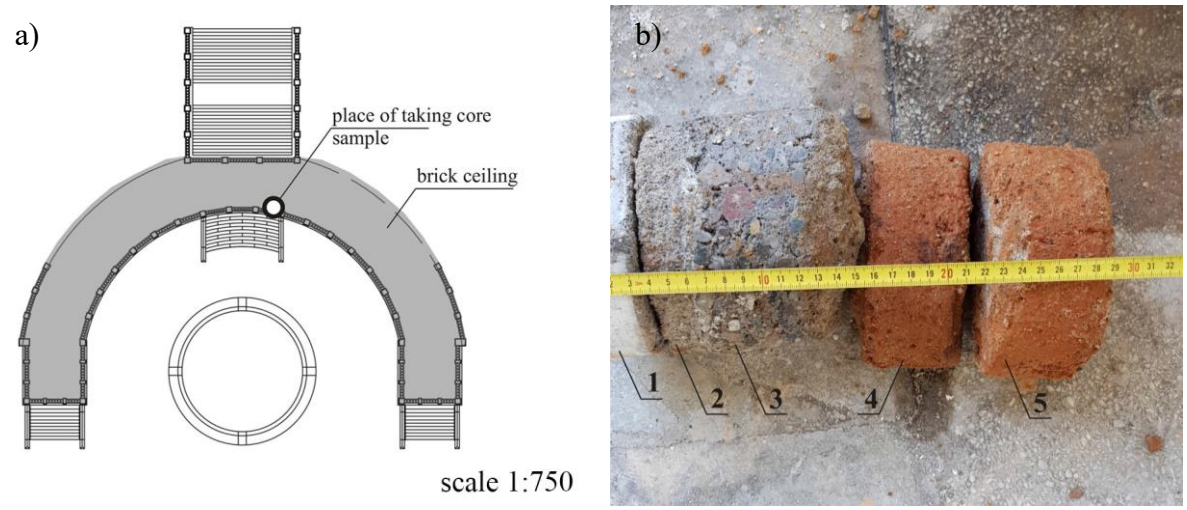


Figure 5: Colonnade building: a) place of taking core samples in the flat roof above the floor embedded in the ground; b) flat roof system: 1- granite slab with a thickness of 30 mm, 2 - cement mortar with a thickness of 40 mm, 3 - concrete with a thickness of 100 mm, 4- brick vault with a thickness of 120 mm

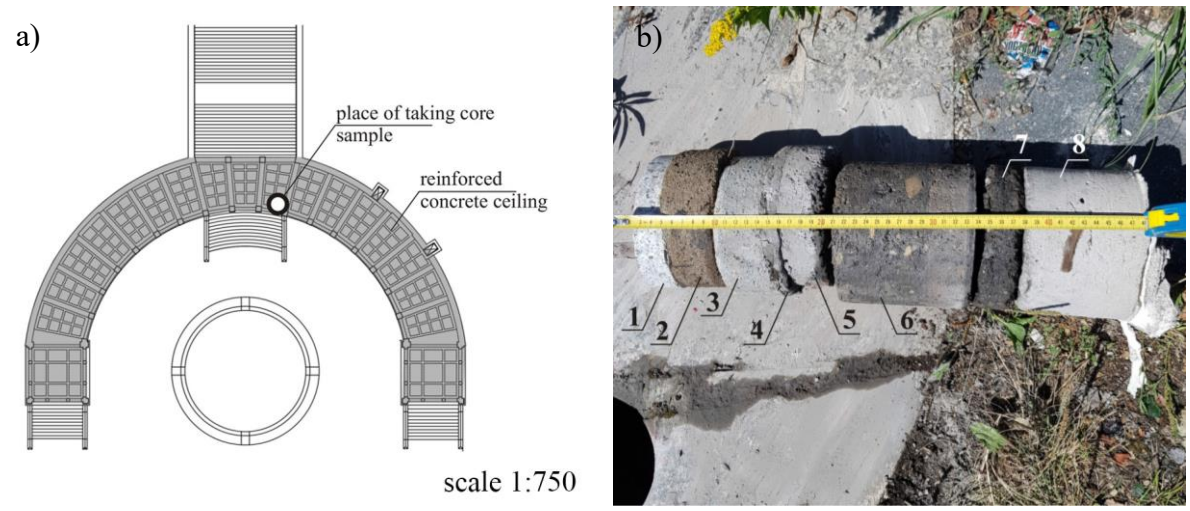


Figure 6: Colonnade building: a) place of taking core samples in the flat roof above the ground floor; b) flat roof system: 1- granite slab with a thickness of 30 mm, 2 - cement mortar with a thickness of 45 mm, 3 - concrete with a thickness of 55 mm, 4- bituminous insulation with a thickness of 5 mm, 5 - concrete with a thickness of 40 mm, 6 - concrete with a thickness of 120 mm, 7 - concrete with a thickness of 30 mm, 8 - reinforced concrete ceiling slab with a thickness of 100 mm

3.2 Peristyle pavilion

The peristyle pavilion is a one-story building with a building area of about 610 m^2. It is on one side completely, and on two sides partially recessed in the ground. It is shown in Figure 7a. Its external and internal walls are made of brick with a thickness in the range of 50 to 70 cm. Inside the pavilion, there are brick pillars with a thickness similar to the thickness of the walls, as well as brick columns with a diameter of 50 cm.

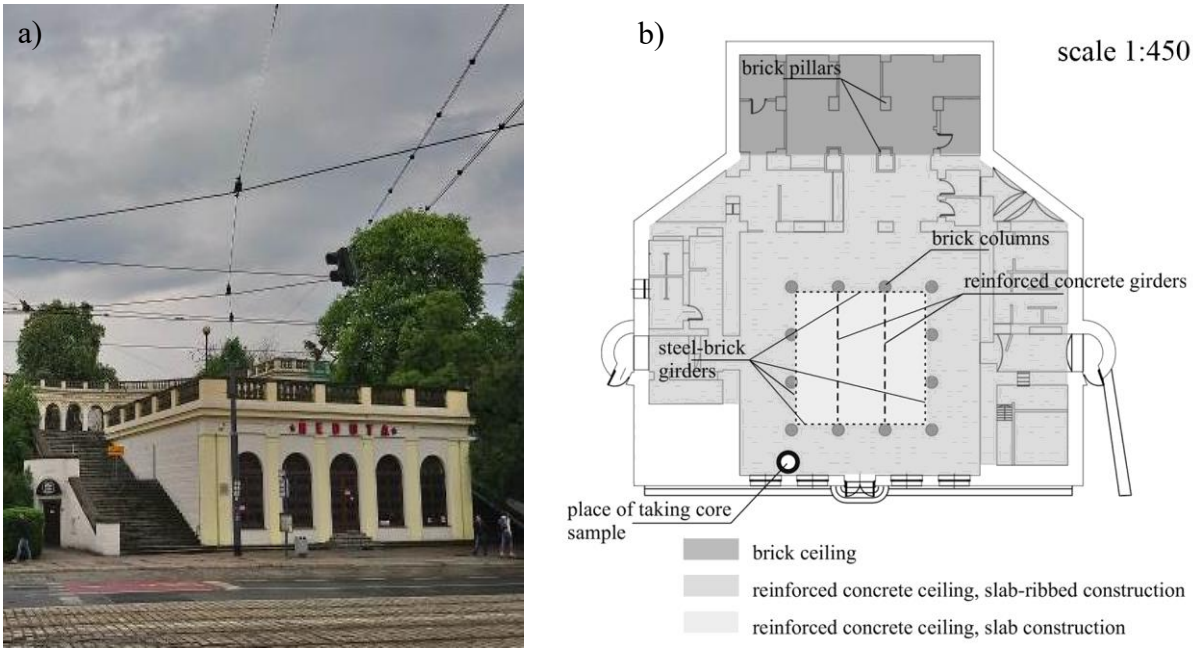


Figure 7: Peristyle pavilion: a) view of the building; b) scheme of the projection with marked structural elements

The pavilion's ceiling is directly accessible from the adjacent area. It has a reinforced concrete, partly slab-ribbed, and partly slab construction, while the girders are reinforced concrete or steel-brick. On a small fragment there is also a brick ceiling. The layout of the specified structural elements is shown in Figure 7b.

The brick constructional elements of the pavilion, as is the case with the colonnade building, are preserved in relatively good condition. However, they are very damp and covered with salt efflorescence and mold fungi (Fig. 8). The execution of the exposures showed that neither vertical nor horizontal damp proof insulation was executed in this building. The mortar in the joints between the bricks is crumbing, and in some places reaches a depth of up to several centimetres.



Figure 8: View of a fragment of a brick wall that is very wet and covered with mold fungi

The reinforced concrete ceiling of the flat roof, despite the existence of bituminous waterproof insulation, is very damp in the support zones. In addition, in the area of masonry walls, the corrosion patches of the reinforcement are visible on its lower surface, as illustrated in Figure 9. In this flat roof, semi-non-destructive testing was performed in order to take a core sample. The layout and layer thicknesses were found to be the same as those in the flat roof above the ground floor in the colonnade building.



Figure 9: Sample view of moisture and patches of corrosion of a reinforced concrete ceiling

4 RESULTS OF CONDUCTED TESTS AND ANALYZES

Due to the limited volume of the paper, it is not possible to present full descriptions of the conducted tests and their detailed results, as well as computational analyzes that were based on them. For this reason, only the most important conclusions are presented in the further part of the paper.

4.1 Results of the tests of the moisture content and salinity of the brick walls

The moisture content tests were performed using the weighing method and the non-destructive dielectric method (Fig. 10). It was found that in both buildings, the brick walls that are covered with soil from the outside are wet, because according to the classification adopted in literature [3,4,5], their mass moisture content along the entire height exceeds 12%. In the case of the internal walls, pillars, and columns, a similar situation occurs up to a height of about 50 cm above the floor level. Above 50cm to a height of almost 100 cm, the brick walls are very and moderately damp, with their moisture content being in the range of 12% to 5%.



Figure 10: Examination of the moisture content in a brick wall using the dielectric method

The salinity tests of the brick walls were carried out using the semi-quantitative method, and it showed that the limit concentration of sulphate salts, which according to the classification adopted in literature is 0.5% [3,4,5], is exceeded more than two times.

4.2 Test results of the ceilings in the flat roofs

Concrete compression strength tests in the reinforced concrete ceilings were carried out using the non-destructive sclerometric method. The regression curve was assumed based on [6]. The minimum compressive strength evaluated based on this method was 22 MPa and this concrete was classified as being C20 / 25 class.

Tests on the distribution of steel in the reinforced concrete ceiling elements, slabs, ribs and girders were carried out using the non-destructive electromagnetic method and then verified by executing the exposure works. It was found that the reinforced concrete slabs are reinforced with 12 mm smooth bars with a spacing of 150 mm, whereas the reinforced

concrete girders are reinforced with ribbed bars ø 22 mm that are spaced every 60 mm. In turn, the reinforcement of the steel and brick girders consists of a flat bottom rail with a height of 149 mm [7].



Figure 11: Exemplary view of: a) reinforcement in a reinforced concrete girder; b) flat bottom rail's foot

5 SUMMARY

The paper presents the current state and condition of the historic buildings located on Partisan Hill in Wroclaw, namely the colonnade buildings and the peristyle pavilion that have survived to this day. Selected results of extensive research work were presented, which involved the use of non-destructive and semi-non-destructive methods, as well as the execution of control exposure works.

The above works were carried out within the first stage of activities that aim to restore the former splendor of the buildings in question. The conclusions and recommendations resulting from the conducted research and analyzes will be used to make the right decisions, in consultation with the conservator, regarding the scope and method of renovation and reconstruction works, as well as the selection of the method of executing the necessary reinforcements of the structural elements.

REFERENCES

[1] Tomaszewicz A., Żurek A. Partisan Hill. In: R. Eysymontt et al. (Eds.): *Leksykon architektury Wrocławia*, Wydawnictwo Via Nova, Wroclaw (2011), pp.331–332.

[2] www.fotopolska.eu/Wzgorze_Partyzantow_Bastion_Sakwowy_Wroclaw (dostęp 02.01.2020).

[3] Rokiel M. *Hydroinsulations in the construction industry* (in Polish). Grupa MEDIUM, Warsaw (2006).

[4] Hoła A. Measuring of the moisture content in brick walls of historical buildings the overview of methods. In: *3rd International Conference on Innovative Materials, Structures and Technologies (IMST 2017)*, Riga, Latvia. [Bristol]: IOP Publishing (2017).

[5] Hoła J. *Degradation of historic buildings due to excessive moisture* (in Polish). In: *Budownictwo i Architektura* (2018) vol. 17(1), pp.133–148.

[6] Runkiewicz, L. Testing of Concrete Structures (in Polish); Biuro Gamma: Warszawa (2002).

[7] Czapliński K. *Old iron alloy products* (in Polish). Dolnośląskie Wydawnictwo Edukacyjne, Wroclaw (2009).

12th International Conference on Structural Analysis of Historical Constructions
SAHC 2020
P. Roca, L. Pelà and C. Molins (Eds.)

TOWARDS A METHODOLOGY FOR USE OF SONIC AND ULTRASONIC TESTS IN EARTHEN MATERIALS

RACHEL MARTINI[1*], JOSÉ DANIEL RODRÍGUEZ MARISCAL[2], JORGE CARVALHO[3], MARIO SOLÍS[4], AND HUMBERTO VARUM[5]

[1]CONSTRUCT-LESE – Faculty of Engineering (FEUP)
University of Porto, Portugal
e-mail: martini.rachel@fe.up.pt (*corresponding author)

[2]Escuela Técnica Superior de Ingeniería
University of Seville, Spain
e-mail: josedrm@us.es

[3]DEM/CERENA – Faculty of Engineering (FEUP)
University of Porto, Portugal
e-mail: jorcarv@fe.up.pt

[4]Escuela Técnica Superior de Ingeniería
University of Seville, Spain
e-mail: msolis@us.es

[5]CONSTRUCT-LESE – Faculty of Engineering (FEUP)
University of Porto, Portugal
e-mail: hvarum@fe.up.pt

Keywords: wave velocity, nondestructive test, mechanical characterization and earthen materials

Abstract. *In many regions around the world, earth has been used through history as a traditional building material. Nowadays, there is a significant revival of its use due to its ecological value and architectural performance. However, there is still a significant lack of knowledge about its actual mechanical properties and behavior. This work aims at the development of consistent methodologies for the characterization of this building material based on non-destructive tests, NDT's. Ultrasonic and sonic tests on prismatic rammed earth specimens and adobe bricks were carried out. The paper presents an optimized method for estimating S-waves and P-waves based on direct and indirect non-conventional sonic testing methods. Finally, the paper discusses methodological issues for estimating the earthen material properties through the propagation velocity of sonic waves.*

1 INTRODUCTION

The careful evaluation of earthen constructions in order to make the most of the existing building is imperative prior to restoration and rehabilitation. A good approach is to use non-destructive testing methods, NDT's, providing the necessary characteristics of the materials without causing damage. This paper presents a new methodology based on the use of sonic tests (ST) and ultrasonic tests (UST) for prismatic rammed earth specimens and adobe bricks.

The discussion allowed having a better perception of the test limitations and potentialities, as well as on the difficulties and peculiarities of these techniques. The application of non-destructive tests on earthen materials can be frustrating in that the interpretation of results is often not straightforward and may be potentially misleading. This is partly because it is a heterogeneous composite material and it presents non-linear and non-isotropic behavior under mechanical destructive tests [1, 2]. It should also be noted that these techniques come mostly from other fields of research, namely geophysical exploration, so proper calibration is required [3–6].

The wave propagation time in ST and UST is the time lapse between the generation of a wave and the respective arrival time at the receiver location. The arrival time and traveling distances of the waves are often not accurately recognizable even when it does correspond to a first arrival as well as the corresponding type of wave. The study involving determining the velocity of waves has been much discussed in the last 50 years, because it allows deriving several properties of the materials namely the elastic moduli [7]. In the present research work, ST and UST are being applied conventionally and non-conventionally on laboratory assembled prismatic rammed earth specimens and adobe bricks elements and the respective results are analyzed and compared.

The results provide qualitative information to develop a predictive methodology of failure and mechanical behavior. The tested rammed earth samples contains the same composition and particle size distribution of a construction recently built within the framework of the Eramus+ Project "LearnBION - Learn Building Impact Zero Network (2015-2028) 2015-1-PT01-KA204-013132" in Valverde del Burguillos, Spain (Figure 1).



Figure 1: Rammed earth building in Valverde del Burguillos, Spain.

2 SONIC AND ULTRASONIC TEST THEORY

Using direct and indirect sonic tests, it is possible to obtain propagation velocities of P, R and S waves and then estimate values of Poisson's ratio, Young's modulus and shear modulus.

The ST may operate using the direct, refraction or reflection propagation paths of the emitted signals, the receiver(s) being positioned in different configurations in relation to the shot-point, SP. The energy may propagate from the point where it is generated namely as compressive P-waves, surface R-waves and shear S-waves. P-waves being the fastest are often more easily and accurately identified using the ST direct configuration, Figure 2, a).

The waves are generated by the impact of a hammer instrumented with a piezoelectric sensor that records the force of the impact. The generated signal is received by piezoelectric accelerometer transducers used as sensors (receivers) in preset positions and orientations. The acquisition of the readings was performed using a data acquisition board, connected via USB to a laptop computer with software specifically developed in LabVIEW. The analysis of the hammer and accelerometers recorded signals, to identify the initial point of the impact of the hammer and the point of arrival of the waves [8–11].

The frequency and amount of energy of the thrust force are governed by the characteristics of the hammer, the impacted material as well as the impact force. The hammer mass, tip hardness and impact force determine the amplitude and duration of the pulse, where harder tips generate shorter duration signals and broader frequency bandwidths. The material vibrations related to the propagation of the sonic waves are measured as varying voltages by means of transducers such as accelerometers fixed to the surface of the masonry. In the tests carried out, the aluminum tip was chosen as this guarantees shorter contact times and consequently broader frequency bandwidths.

To carry out ST, three different conventional configurations are considered regarding the relative position between the emitter and the receiver and depending on the type of waves to be studied (P, S or R): direct, semi-direct and indirect test configurations (Figure 2).

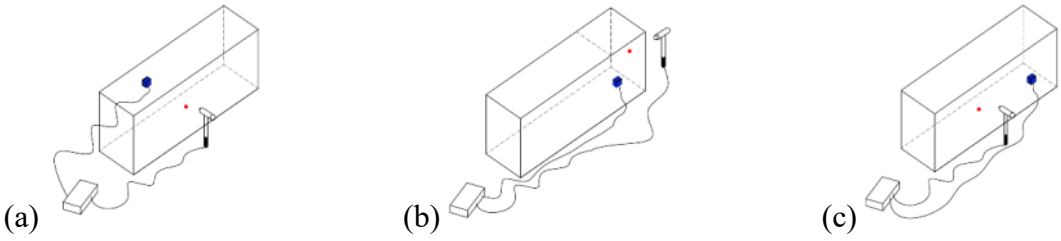


Figure 2: Sonic test (a) direct, (b) semi-direct and (c) indirect.

The direct test assumes a linear wave direct transmission through the thickness of the element to be tested, being the shot-point and receiver in opposite sides of the element, which aims to determine P-waves velocity. The velocity of the P-waves is dependent on the quality and consistency/density of the section tested, i.e. it is directly related to the mechanical properties of the material.

In the semi-direct test, the shot-point and receiver are in adjacent faces of the element.

In the indirect test, the shot-point and receiver are on the same face of the element and it is conventionally assumed a linear wave direct transmission, along the surface of the tested

element. The waves obtained by this configuration are conventionally assumed to be those that cross mainly the outermost part of the element, so the quality and consistency of the most superficial layer of the material are considered to mainly govern the acquired wave velocities.

The identification of the waves depends on the intrinsic characteristics of each type and the type of configuration test to be performed. In indirect configurations, P-waves are not always clearly identified despite being the fastest (first arrival) waves, having comparatively with R-waves lower energy content. Note that despite their higher energy content, R-waves are not always readily detectable, being the acquired signal the result of different contributes, namely P-waves and S-waves.

According to the literature, [12–16], UST is more accurate than ST to calculate wave propagation velocities when using the direct configuration. According to [17], this method is widely used and consolidated for concrete samples.

3 METHODOLOGY

3.1 Materials and geometry

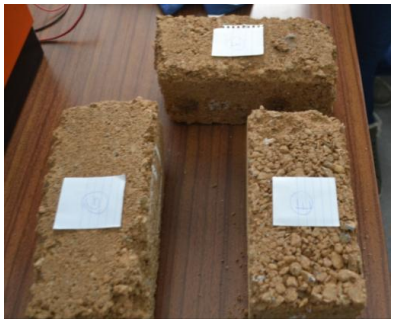
An adobe specimen (Figure 3) is a brick made of earth, sand and fiber molded and sun-dried. The earth composition determines the physical behavior, cohesion and mechanical properties being influenced by the proportion of sand, silty clay and clay presented in the earth. Generally, the content of silty clay is between 20% and 40%, the content of clay is between 10% and 25% [18]. Furthermore, size and length of fiber are determinant parameters, their modification affects mechanical properties [19]. The adobe tested is composed of natural fibers (straw) of 5-10 cm length. The adobe bricks presented the following nominal dimensions: [320x160x80] mm in order to comply with the Peruvian recommendations of NTE0.80 [20]. The selected soil was collected from the riverbank of the Guadalquivir River in Seville (Spain).

The rammed earth is a clayey soil (earth) compacted into a formwork. That soil has suitable proportions of sand, gravel, clay. The earth composition varies greatly but contains no organic component. Compaction is carried out using an optimum water content; this value can be obtained by Proctor compaction test. The rammed earth is made of layers of earth. After compaction, the thickness of each layer should be comprised of between 8 and 10 cm [1].



Figure 3: Adobe specimens.

Two size specimens of rammed earth (Figure 4) were produced with the following nominal dimensions: [200x175x220] mm^3 (1^{st} Group) and [100x100x220] mm^3 (2^{nd} Group). The specimens were produced by molding the soil mixture preparation into a wood framework. The manufacturing process was carried out following two different compaction methodologies: manual compaction for specimens of the 1^{st} Group and automatic compaction for 2^{nd} Group. The selected soil was collected from the local quarry of Valverde del Burguillos in Badajoz (Spain). The specimens were stored in a stable laboratory environment for approximately 100 days (approximately 24 ºC and 50% relative humidity) until the hygrometric equilibrium was reached. The moisture content of specimens was not measured at NDT, therefore the eventual influence of this parameter in the propagation velocities was not evaluated.



(a)



(b)

Figure 4: (a) Rammed earth specimens – samples E, F and G; (b) Adobe samples – A and Rammed earth specimens – samples B and C.

The list of specimens tested and their dimensions are summarized in Table 1.

Table 1: Specimens tested

Code	Samples	Dimensions (mm)	Direct ST	Indirect ST	Direct US
Adobe brick	Adobe brick - A	322x170x80	X	X	X
1^{st} Group	Rammed earth - B	200x175x245	X	X	X
	Rammed earth - C	200x175x235			X
	Rammed earth - D	200x175x218	X	X	X
2^{nd} Group	Rammed earth - E	105x95x222			X
	Rammed earth - F	105x105x222			X
	Rammed earth - G	100x105x222	X		X

3.2 Test set-up and equipment

Two ST sequences were performed, using direct and indirect configurations. The indirect configuration was developed using the conventional and a non-conventional approach, so-called 'key methodology' (Figure 5), aiming at improving the generation and estimation of S-waves velocity. An ordinary key was used to provide a different impact direction that

paralleled the reception axis of the accelerometer. The rammed earth specimens were tested in two different directions: the compaction (hereafter C) and non-compaction (hereafter NC) directions during the manufacturing process.



Figure 5: "Key" methodology.

The tests were conducted following some recommendations of international standards, which were developed for other materials (rocks and concrete) [21–23]. An instrumented hammer and two accelerometers were used for the sonic tests. The signal conditioning has carried out by a National Instrument device; the data acquisition and analysis were performed by software LabView designed, from LESE (FEUP), for this proposal.

The UST were also developed using indirect and direct configurations (Figure 6). The ultrasonic equipment used was Proceq brand, PUNDIT device, with an 82 kHz emitter. The value of transmitter pulse amplitude is 500 V and the receiver probe gain is 10x. The Geotechnical Laboratory of FEUP provided this equipment.

The procedure steps are the following: calibrate the equipment and perform a new calibration whenever atmospheric conditions change, select the location of the transducers, keep the surfaces clean and smooth, mark and measure the distance between these points, apply the gel conductor, compress the transducers against the surface until it stabilizes and perform the reading following signal generation.

The eventual gel conductor effects in the ultrasound velocities have not been included in the present experimental campaign. The application of the gel conductor can affect the contact surface quality between transducers and specimen. The gel application repeatedly on earthen materials can produce softening on the external surface and loose sand and gravel, worsening the transducer coupling.

This equipment consists of a central unit, which includes a pulse generator with frequencies between 20 and 150 kHz, an emitter transducer, a receiver transducer, an amplifier and a device for measuring the time between sending and receiving the pulse. Some of these tests were performed for comparison with the ST results.

The indirect configuration for UST was applied in the specimens (Figure 6a). However, it has not been possible to detect, confidently enough, R-waves. The close proximity between emitter-receiver and the used frequencies may be the cause. So, R-waves travel-times have not been included in the investigation.


(a)

(b)

Figure 6: (a) indirect UST and (b) direct UST.

4 RESULTS AND ANALYSIS

This section summarizes the results obtained with the ST and UST on all samples described above. These results are presented by box-plot graphs, being separated according to the identified wave type (P or S). On each graph, the central mark indicates the median, and the bottom and top edges of the box indicate the 25th and 75th percentiles, respectively. The whiskers extend to the most extreme data points not considered outliers, and the outliers are plotted individually using the '+' symbol.

In these preliminary results, the P-wave velocities are showed based on mixing two test methodologies to obtain qualitative information depending on compaction rate. The graph of Figure 7 shows all P-wave propagation velocity values for both ST and UST.

Variations of the compaction methodologies of samples influence the results. Sample A (adobe) presented a different value from the other samples, this was expected due to its differentiated composition. Samples B, C, D, E, F and G are composed of the same material (rammed earth) but have different dimensions and compaction methodologies. First group with samples B, C and D had approximated median velocity values to each other. The second group of samples E, F and G presents different median velocity values. This was expected since they have different compaction methodologies between these two groups, therefore the internal structure and particle distribution can be affected by compaction process.

The graph in Figure 8 presents the results of S-wave propagation velocity. These are samples B and D, both are of rammed earth and with the same dimensions. These samples present approximated median velocity values. There are no difference between UST or ST, and Compaction (C) or Non-Compaction (NC) direction as shown in Figure 7 and Figure 8.

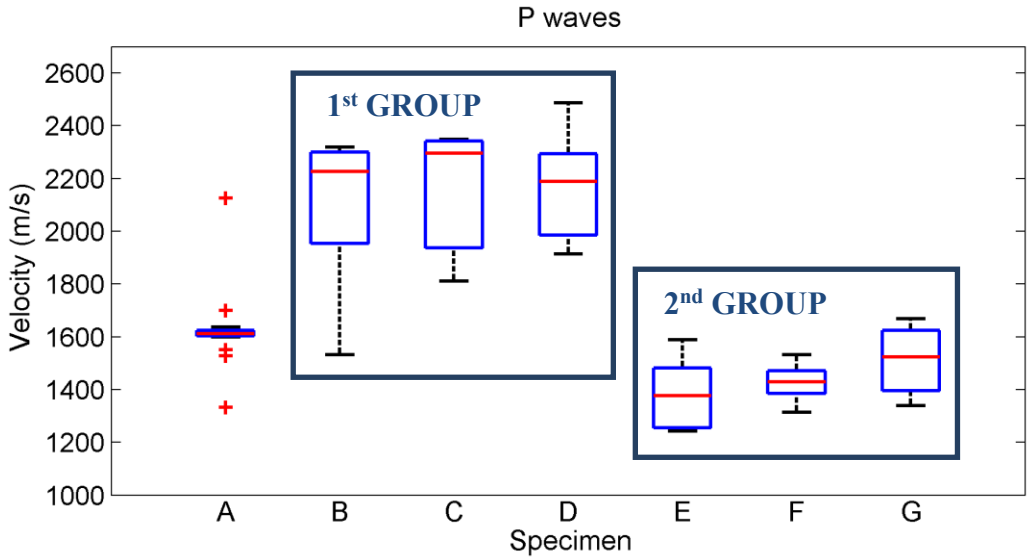


Figure 7: P-waves velocity with UST and ST, direct configuration.

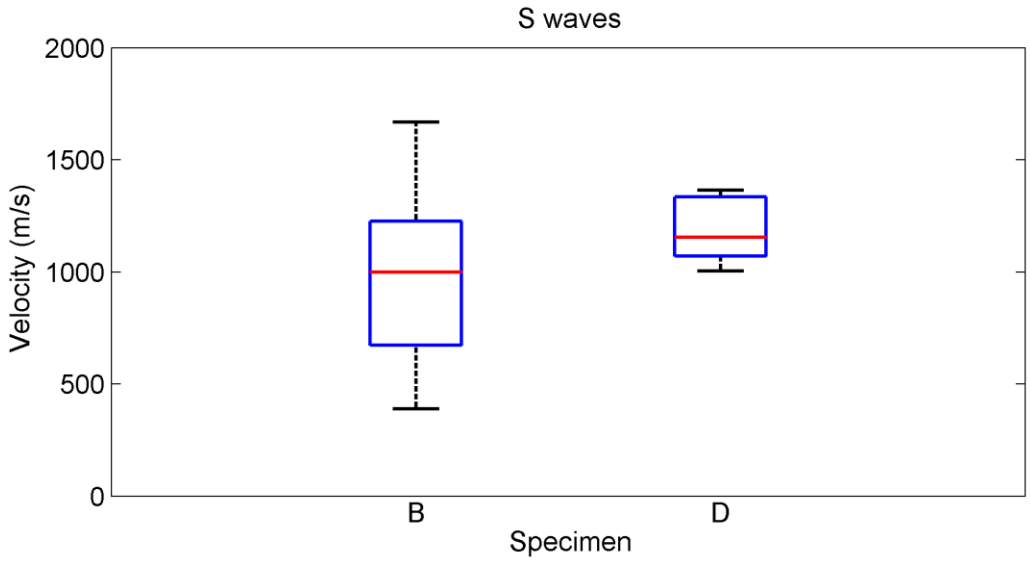


Figure 8: S-waves velocity, ST – "key" methodology.

The graph in Figure 9 shows all P-wave propagation velocity values for UST only. As in Figure 7, variations in compaction process influence the results. Sample A (adobe) presented a different value from the other samples. The first group with samples B, C and D had approximate average velocity values. The second group of samples E, F and G have different but also approximate median velocity values, which was expected due to the different compaction methodologies between these two groups. There is no difference between C and NC directions.

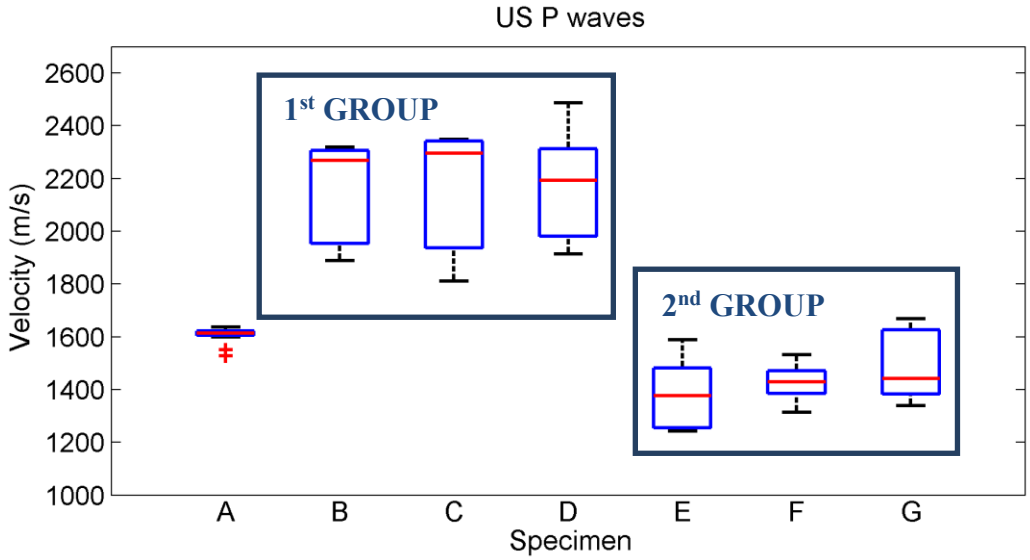


Figure 9: P-waves velocity, UST, direct configuration.

The graph in Figure 10 presents the P-wave propagation velocity results obtained by the UST, as well as indicating the C and NC variations. As in the previous results, the samples were divided into two groups according to their geometric characteristics. The second group has lower P-wave propagation velocity values than the first group, due to its compaction method. In this graph it is also possible to see, in the first group, the influence of the effect that the compaction samples have, since they have lower velocity values.

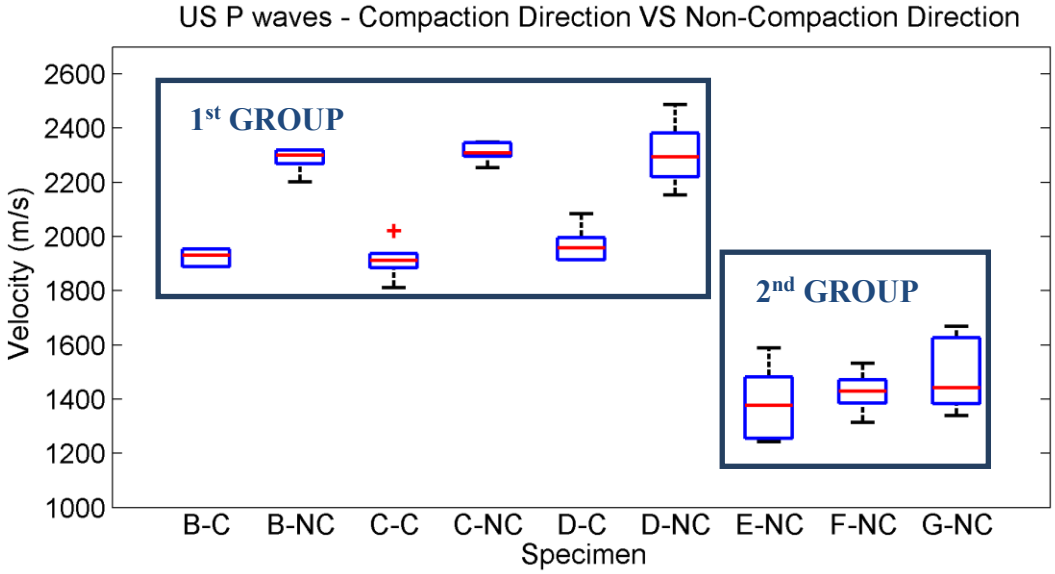


Figure 10: P-waves velocity, UST.

5 CONCLUSIONS

This paper presents an exploratory study that used the well-known ST and UST in earthen materials. The results show a high degree of scattering due to the heterogeneity and anisotropy of the tested material.

These methodologies allowed to obtain some preliminary reference P and S-waves velocity values for this material used in a rammed earth building (Valverde del Burguillos, Spain).

Currently, several non-destructive tests on specimens of different size are being carried out to estimate mechanical properties and obtain correlations with those obtained from compression tests.

Ongoing work is also focused on in-situ investigating the wave propagation velocities of the building walls recently constructed (Valverde del Burguillos, Spain).

Acknowledgements. This work was supported by Junta de Andalucia (Consejería de Economía y Conocimiento) through research project US-126491, the Spanish Ministry of Science, Innovation and Universities (Ministerio de Ciencia, Innovación y Universidades) through research project PID2019-109622RB-C21 and European Commission UE through Eramus+ Programme - Student Mobility for Traineeships. This work reports research partially financed by the UID/ECI/04708/2019- CONSTRUCT - Instituto de I&D em Estruturas e Construções funded by national funds through the FCT/MCTES (PIDDAC). The authors would like to thank CEFET-MG (Centro Federal de Educação Tecnológica de Minas Gerais - Brasil), CAPES (Coordenação de Aperfeiçoamento de Pessoal de Nível Superior - Brasil) for financial support.

REFERENCES

1. Bui Q-B, Morel J-C (2009) Assessing the anisotropy of rammed earth. Constr Build Mater 23:3005–3011. https://doi.org/10.1016/j.conbuildmat.2009.04.011
2. Bui T-T, Bui Q-B, Limam A, Maximilien S (2014) Failure of rammed earth walls: From observations to quantifications. Constr Build Mater 51:295–302. https://doi.org/10.1016/j.conbuildmat.2013.10.053
3. Binda L, Lenzi G, Saisi A (1998) NDE of masonry structures: use of radar tests for the characterisation of stone masonries. NDT E Int 31:411–419. https://doi.org/10.1016/S0963-8695(98)00039-5
4. Binda L, Saisi A (2002) State of the art of research on historic structures in Italy. Dep Struct Eng Politec Milan, Italy
5. Anzani A, Binda L, Lualdi M, et al (2006) Use of Sonic and GPR Tests to Control the Effectiveness of Grout Injections of Stone Masonry. ECNDT 3:1–7
6. Miranda L, Cantini L, Guedes J, et al (2013) Applications of Sonic Tests to Masonry Elements: Influence of Joints on the Propagation Velocity of Elastic Waves. J Mater Civ Eng 25:667–682. https://doi.org/10.1061/(ASCE)MT.1943-5533.0000547
7. Mishina H, Asakura T (1975) Zero-crossing probability density of Doppler beat signals

in the wave-period measuring system. Appl Phys 8:179–182. https://doi.org/10.1007/BF00896035
8. Guimarães M (2009) Caracterização de paredes de alvenaria de pedra por técnica sònica. Faculdade de Engenharia da Universidade do Porto
9. Miranda LFB (2011) Ensaios acústicos e de macacos planos em alvenarias resistentes. Faculdade de Engenharia da Universidade do Porto
10. Maia I da S (2016) Caracterização de alvenaria de granito com recurso a ensaios de propagação sónica e de macacos planos. Faculdade de Engenharia da Universidade do Porto
11. Matos SRPR (2016) Caracterização de estruturas de alvenaria de pedra por recurso aos métodos do georadar, resistividade eléctrica e ensaios sónicos - Tese de mestrado. Instituto Superior de Engenharia do Porto
12. Finas M, Ali H, Cascante G, Vanheeghe P (2016) Automatic shear wave velocity estimation in bender element testing. Geotech Test J 39:557–567. https://doi.org/10.1520/GTJ20140197
13. Wu Y, Cascante G, West JS, Pandey MD (2015) Ultrasonic Testing of a Grouted Steel Tank for Debonding Conditions. J Environ Eng Geophys 20:31–46. https://doi.org/10.2113/JEEG20.1.31
14. Wu YC, Cascante G, Pandey MD (2014) Condition assessment of longitudinal pavement joints using ultrasonic surface waves. Can J Civ Eng 41:1019–1028. https://doi.org/10.1139/cjce-2013-0301
15. Tallavó F, Cascante G, Pandey MD (2009) New methodology for source characterization in pulse velocity testing. Geotech Test J 32:16. https://doi.org/10.1520/GTJ101689
16. Cascante G, Najjaran H, Crespi P (2008) Novel Methodology for Nondestructive Evaluation of Brick Walls: Fuzzy Logic Analysis of MASW Tests. J Infrastruct Syst 14:117–128. https://doi.org/10.1061/(ASCE)1076-0342(2008)14:2(117)
17. Júlio ES (2005) Avaliação in situ da resistência à compressão do betão. In: 2º Seminário - A intervenção no patrimônio. Práticas de conservação e reabilitação. pp 41–52
18. Wu F, Li G, Li H-N, Jia J-Q (2012) Strength and stress–strain characteristics of traditional adobe block and masonry. Mater Struct 46:1449–1457. https://doi.org/10.1617/s11527-012-9987-y
19. Parisi F, Asprone D, Fenu L, Prota A (2015) Experimental characterization of Italian composite adobe bricks reinforced with straw fibers. Compos Struct. https://doi.org/http://dx.doi.org/10.1016/j.compstruct.2014.11.060
20. SENSICO (2017) Reglamento Nacional de Edificaciones. Norma Técnica de Edificación NTE 0.80 Diseño y construcción con tierra reforzada. Servicio Nacional de Capacitación para la Industrial de la Construcción, Lima, Peru
21. ASTM (2017) D2845-08 - Standard Test Method for Laboratory Determination of Pulse Velocities and Ultrasonic Elastic Constants of Rock. United States
22. AENOR (2005) UNE-EN 14579:2005 - Métodos de ensayo para piedra natural. Determinación de la velocidad de propagación del sónido. Madrid, Spain
23. AENOR (2006) UNE-EN 12504-4:2006 - Ensayos de hormigón en estructuras. Parte 4: Determinación de la velocidad de los impulsos ultrasónicos. Madrid, Spain

12thInternational Conference on Structural Analysis of Historical Constructions
SAHC 2020
P. Roca, L. Pelà and C. Molins (Eds.)

USING THE ULTRASONIC TOMOGRAPHY METHOD TO STUDY THE CONDITION OF WOODEN BEAMS FROM HISTORICAL BUILDINGS

M. ZIELIŃSKA[1*], M. RUCKA[2]

[1]Department of Technical Fundamentals of Architectural Design, Faculty of Architecture
Gdansk University of Technology
Narutowicza 11/12, 80-233 Gdansk, Poland
e-mail: monika.zielinska@pg.edu.pl (*corresponding author)

[2]Department Mechanics of Materials and Structures, Faculty of Civil Environmental Engineering
Gdansk University of Technology
Narutowicza 11/12, 80-233 Gdansk, Poland
e-mail: magdalena.rucka@pg.edu.pl

Keywords: Historical Structure, Wood, Monitoring, Non-Destructive Inspection

Abstract.*The need to evaluate the integrity of wooden structural elements is constantly increasing. Non-destructive methods are becoming more popular in this field of research. One type of non-destructive testing is the ultrasonic imaging method, which allows the analysis of internal wood structures without disturbing their state and integrity. In this study, we are interested in assessing the effect of wood condition on the ultrasound time of flight (TOF). The research was carried out on wooden beams, which were obtained from a historical building. The images obtained from ultrasound tomography were compared with results of a visual inspection.Places of discontinuities, voids and cracks in wood caused a much lower velocity of wave propagation.The location of the wood core was illustrated by the places with the highest velocity. The article proved the validity of using ultrasonic tomography to assess the technical condition of historic wooden beams.*

1 INTRODUCTION

In historical objects, it is essential to preserve as many elements in the original character as possible. It is particularly difficult in the case of wood, which is one of the most susceptible construction materials. Over the years, the wooden structure elements undergo destructive processes. Their development and progress depend on various factors amongst which an important role is played by the historical events that took place while the structure existed. Mechanical wear and long-term mechanical stress together with its consequences are the elements resulting in the destruction of wooden elements of the cultural heritage. Wood is subject to degradation also under the influence of stresses from the humidity changes and insect effect. The fungi decay emerging when the humidity is above 20%, is an important issue in case of wooden objects in civil engineering [1].

Examining the condition of wooden elements is crucial from the perspective of the correct structure performance. Detecting the internal wood condition deterioration without any

symptoms visible from the outside allows preventing the further spread of the decay. Research conclusions frequently result in the necessity to conduct repairs, renovations, replacement of the wooden beams structure, or even the substitution of a significant part of the structure. Apart from simple tests, such as a visual inspection or tapping to determine the near-surface defects, non-destructive testing (NDT) play an important role in the process. The non-destructive testing on wooden elements are conducted with ground penetrating radar (GPR) [2, 3], thermal techniques [4], microwaves [5], acoustic emission [6], ultrasonic tomography [7] and X-ray tomography [8–11].The use of the ground penetrating radar may be problematic in case of elements of small size. This is when the acoustic test methods are more advantageous, as they allow identifying the heterogeneous or damaged areas based on the time-of-flight value. A map presenting the distribution of a specific parameter, for example, the wave propagation velocity, is created on the basis of the aforesaid values, which facilitates the interpretation of the information on the examined area.

The evaluation of the ultrasonic tomography implementation in wooden elements was first described by Tomikawa et al. [12] in 1986. The measurements taken on the wooden columns provided satisfactory effects; nevertheless, the image was of poor resolution. From that time onwards, the implementation of the ultrasonic tomography for wooden elements is in constant development. Comino et al. [13], Deflorio et al. [14], Brazee et al. [15] used the ultrasonic tomography to evaluate the condition of alive trees. Yan et al. [16] detect discontinuities of non-metallic elements by applying the proposed algorithm on a wooden element. The internal discontinuities were also detected by Alves et al. [17]. Colla [18] described the ultrasonic tomography results and juxtaposed them with destructive tests. Niemz and Mannes [1] compared the results obtained from the ultrasonic tomography of the wood with other non-destructive methods. Perlin et al. [19] proposed a method to locate the pith of timber (unprocessed wood), as well as lumbers (processed wood), while Qin et al. [20]showed how to detect knots in wooden beams. In spite of numerous tests, the ultrasonic tomography in wooden elements can still be a difficult task. The reason for that lies in wood anisotropy, long-lasting measurements taking, high ultrasonic signal damping, or noise in a signal. The anisotropy results in bending of paths of ultrasonic waves. The wavefront propagating in wood has a deformed shape in comparison to spherical waves obtained for isotropic media. The traditional tomographic imaging takes into account the straight radius transfer. In this particular case, however, the actual waveform shall be taken into account, which is taken up by Espinosa et al. [21, 22].

The paper evaluates the possibility to implement the ultrasonic tomography for wooden beams. Both healthy and defective wood was taken for the purpose of the experimental test. The beams were acquired from the historical object and their degradation was significant. Additionally, in order to compare the results, the measurements were taken also for a new beam with the cross-section corresponding to the historic beams. The paper is focused on the influence of anisotropy condition on the wood ultrasonic wave propagation, by estimating the transfer time. The transfer time measurements were obtained for various transmission and reception points configuration. Their influence on the tomographic image reconstruction was described.

2 THEORY OF ULTRASONIC TOMOGRAPHY

Ultrasound tomography allows determining the internal structure of an element in the examined cross-section (Figure 1). At first, the object should be divided into finite area elements. These elements are called pixels. The resolution of the final image depends on the number of pixels. Then, the information from the ultrasonic signals passing through the element is collected. This information is usually the time of flight (TOF), which can be described by the equation:

$$t_i = \sum_{j=1}^{n} w_{ij} s_j \,, \quad i = 1,2,3,\ldots,m \,, \quad j = 1,2,3,\ldots,n \,, \tag{1}$$

$$s_j = \frac{1}{v_j}, \tag{2}$$

where t_i is the total time from the transmitter to the receiver for i-th path, s_j is the ultrasonic pulse slowness in pixel j, v_j is the ultrasonic pulse velocity in pixel j, w_{ij} is the length of the i-th path passing through the j-th pixel.

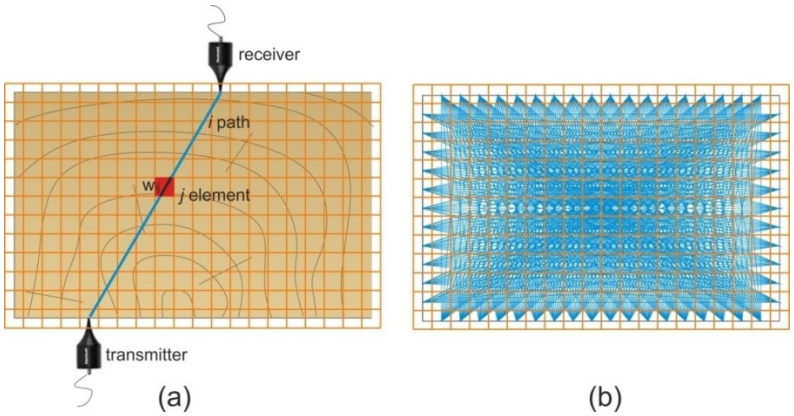


Figure 1: Scheme of passing: (a) i path through j element, (b) several paths through the object.

Based on known cross-sectional geometry, it is possible to determine the ultrasonic pulse velocity in each pixel. In ultrasound tomography, equation (1) is usually overdetermined or underdetermined. Therefore, usual methods of resolution such as simple inversion or Gaussian elimination cannot be used. The equation can be solved by iterative methods. The calculations presented in this paper are based on the algebraic reconstruction technique (ART) [23], which is described by the following equation:

$$s_j^{(k)} = s_j^{(k-1)} + \frac{w_{ij} \Delta t_i}{\sum_{j=1}^{n} w_{ij}^2}, \tag{3}$$

where Δt_i is the difference between the measured and the reconstructed time of flight, and the k index symbolizes the step of the iteration.

3 MATERIALS AND METHODS

3.1 Description of specimens

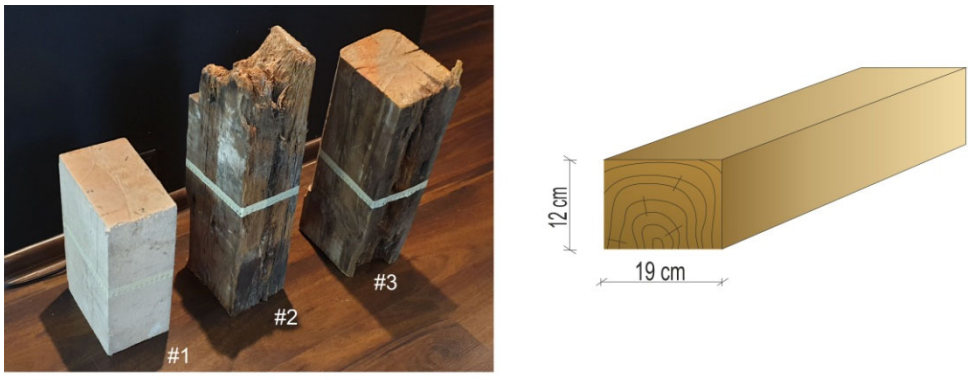
The tests were conducted on wooden beams taken from the historical Monastery of Congregation of the Sisters of St. Catherine located in Orneta, in the northern part of Poland (Figure 2). The beams were the elements of a roof framework, which due to its poor technical condition underwent the restoration works.



(a) (b)

Figure 2: Photographs of the roof framework from the Monastery of Congregation of the Sisters of St. Catherine in Orneta (Poland).

The ultrasonic tomography was conducted on three beams (Figure 3a). The beam cross-section had the dimensions equal to 19 cm x 12 cm (Figure 3b). For the purpose of the study, the beams of significant (#3) and partial destruction (#2) were implemented. Both beams were waste materials from a roof framework (they were replaced due to their bad technical condition by the new wooden beams). The measurements were also taken for a new beam (#1) in order to compare the results. This material replaced the deteriorated wood or wood damaged by the insects.



(a) (b)

Figure 3: Laboratory models of wooden beams.

3.2 Experimental setup

Ultrasonic tomography was performed based on measured times of flight for waves passing through the element. Wave signals were measured by the PUNDIT PL-200 instrument (Proceq SA, Schwerzenbach, Switzerland). Two exponential transducers of 54 kHz were used in the through transmission mode. The experimental setup and scheme of image reconstruction are shown in Figure 4.

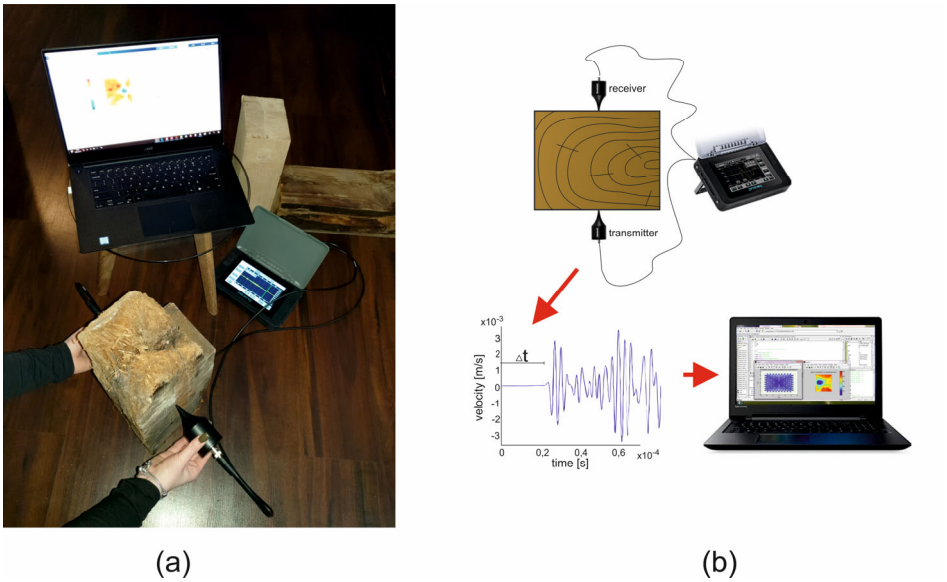


Figure 4: Experimental setup: (a) testing in through transmission mode; (b) scheme of image reconstruction by ultrasonic tomography.

Measurements were carried out in the cross-section located in the middle height of each beam. The configuration of transmitters (t_1-t_{29}) and sensors (s_1-s_{29}) is shown in the Figure5. The transmitters and receivers were placed to the edge, with an interval of 1 cm between each other. The signal for each transmitter was recorded at the receiver points lying on the opposite wall. For each of the beams 445 measurement signals were obtained.

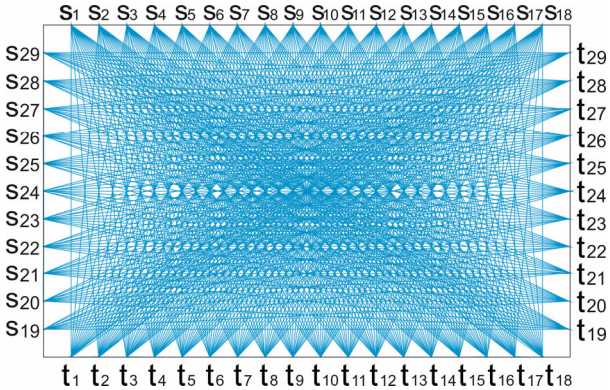


Figure 5: Configuration of the wave paths from transmitters (t) to sensors (s).

4 RESULTS AND DISCUSSION

The first laboratory model (#1) was a new beam. This material was used to replace the wood damaged by insects. The edges were straight and the beam did not have any significant damages or cracks. The internal structure was recreated based on the collected transfer time signals (Figure 6a). A significantly higher velocity was observed in the upper part of the map. This place indicates the location of the cross section's core. The signals collected from the transmitters t_1 – t_{18} showed major differences between the waveforms' velocities. They ranged from 650 to 1550 m/s. For each of the transmitters t_1 – t_{18} a waveform with the highest wave propagation velocity was chosen. The waveforms were marked in red in Figure 6b. It was observed that the intersection of the waveforms indicates the exact location of the wooden element's core. (Figure 6c). The wave propagation velocities from the transmitters t_{19} – t_{29} did not indicate equally high differences between each other (900 – 1150 m/s).

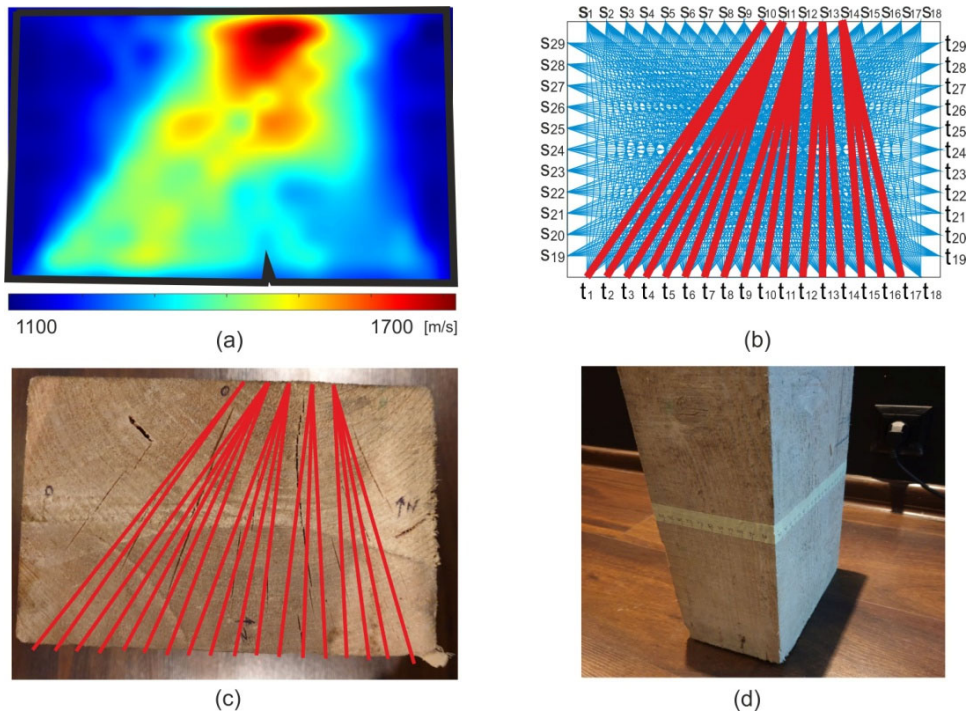


Figure 6: Results obtained for beam #1: (a) ultrasound tomography image, (b) ray paths with the fastest paths marked for t_1-t_{18} transmitters, (c) top view of the beam, (d) side view of the beam.

Beam #2 was taken from the historical roof framework. One of its sides included a major wood fibrosis (Figure 7c). The remaining three contained cracks. The ultrasonic tomography image clearly shows the places where the beam is damaged (Figure 7a). The edge with the wood fibrosis showed the reduced wave transfer velocity. A similar effect was observed in places where the cracks were located. Furthermore, an increased velocity may be spotted at the location of the cross-sections core, similarly to the reference beam (#1).

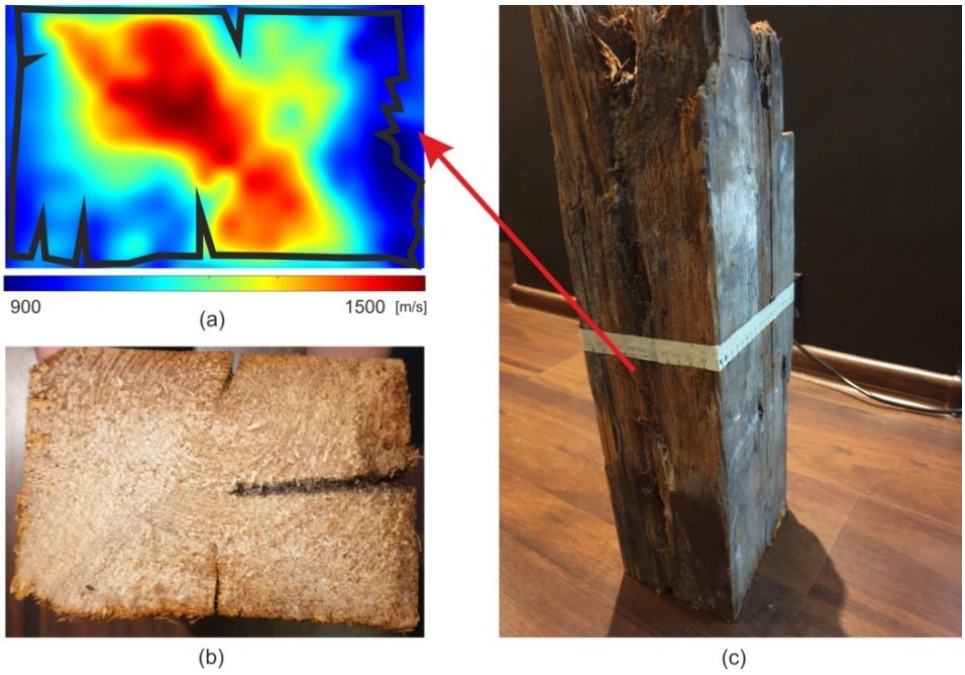


Figure 7: Results obtained for beam #2: (a) ultrasound tomography image, (b) top view of the beam, (c) side view of the beam.

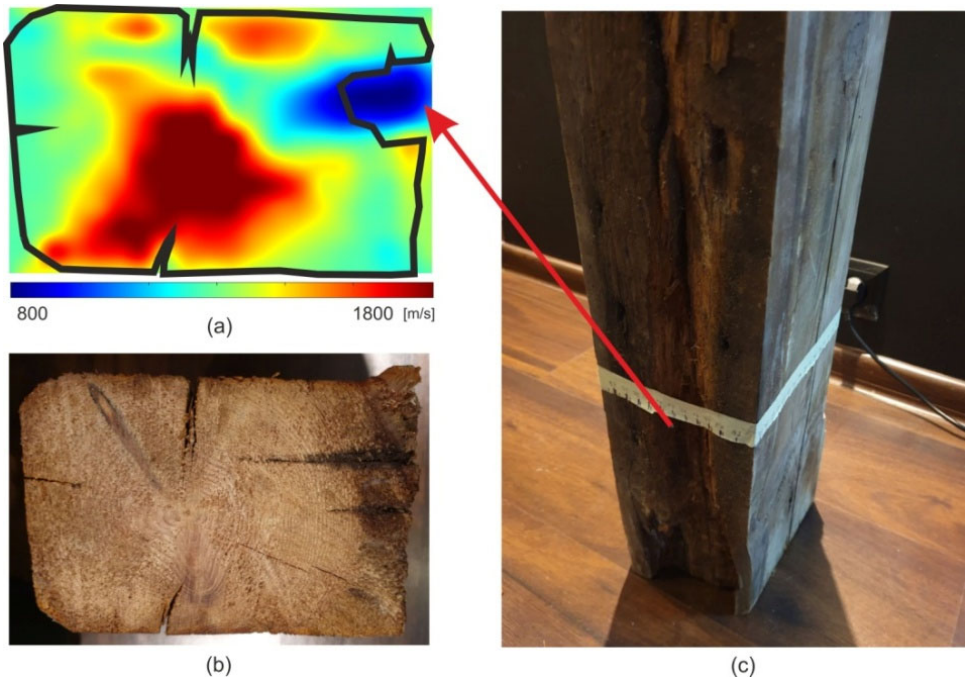


Figure 8: Results obtained for beam #3: (a) ultrasound tomography image, (b) top view of the beam, (c) side view of the beam.

The beam #3 had the highest level of degradation. One of the sides included a significant cavity caused by insects (Figure 8c). This place is marked in blue on the ultrasonic tomography map (Figure 8a). The remaining sides included cracks. The biggest crack was marked on the tomographic image. Similarly to beam #1 and #2 the greatest concentration of the wave propagation velocity determined the location of the wood cross section's core.

5 CONCLUSIONS

The article describes experimental research conducted on wooden beams from a historical object. Two damaged beams were used for the research, and their technical condition was determined employing the ultrasonic tomography. The obtained results were compared with the tomography performed for a new, undamaged beam with equal cross-section dimensions.

The conducted research aimed at evaluating the possibility to use the ultrasonic waves for imaging the internal structure of historical wood. It was focused on the reconstruction of tomographic velocity in chosen cross-sections that enabled the development of the method allowing to identify the location of the wood cross-section core. For the correct interpretation of the obtained tomographic image, it is essential. The areas with wood fibrosis and damages caused by insect activity indicate the significant reduction in the tomographic velocity. A similar effect is visible in places where the cracks in wood occur.

The ultrasonic tomography is an effective tool enabling the reconstruction of the internal cross-section of the examined wooden element. The presented approach may be used to evaluate the quality of the wooden beams, which damages are not always in plain sight. Owing to this, a more effective plan of wooden structure repair and renovation works can be prepared and used for such elements as roof framework or ceiling, which often appear in historical objects. Further research shall consider the possibility to apply the in situ method, without the necessity to remove the wooden elements.

Acknowledgements. The research work was carried out within the project No. 2017/27/N/ST8/02399, financed by the National Science Centre, Poland.

REFERENCES

[1] P. Niemz and D. Mannes, "Non-destructive testing of wood and wood-based materials," *J. Cult. Herit.*, vol. 13, no. 3, pp. S26–S34, 2012.

[2] T. C. Mai, S. Razafindratsima, Z. M. Sbartaï, F. Demontoux, and F. Bos, "Non-destructive evaluation of moisture content of wood material at GPR frequency," *Constr. Build. Mater.*, vol. 77, pp. 213–217, 2015.

[3] R. Martínez-Sala, I. Rodríguez-Abad, R. Diez Barra, and R. Capuz-Lladró, "Assessment of the dielectric anisotropy in timber using the nondestructive GPR technique," *Constr. Build. Mater.*, vol. 38, pp. 903–911, 2013.

[4] V. Bucur, "Techniques for high resolution imaging of wood structure: A review," *Meas. Sci. Technol.*, vol. 14, no. 12, 2003.

[5] M. Pastorino *et al.*, "A microwave tomographic system for wood characterization in the forest products industry," *Wood Mater. Sci. Eng.*, vol. 10, no. 1, pp. 75–85, 2015.

[6] F. C. Beall, "Overview of the use of ultrasonic technologies in research on wood properties," *Wood Sci. Technol.*, vol. 36, no. 3, pp. 197–212, 2002.
[7] A. Arciniegas, F. Prieto, L. Brancheriau, and P. Lasaygues, "Literature review of acoustic and ultrasonic tomography in standing trees," *Trees - Struct. Funct.*, vol. 28, no. 6, pp. 1559–1567, 2014.
[8] P. Nilakantan, "X-ray studies of wood, lignin and wood-cellulose," *Proc. Indian Acad. Sci. - Sect. A*, vol. 5, no. 2, pp. 166–174, 1937.
[9] Q. Wei, B. Leblon, and A. la Rocque, "On the use of X-ray computed tomography for determining wood properties: A review 1," *Can. J. For. Res.*, vol. 41, no. 11, pp. 2120–2140, 2011.
[10] K. Kobayashi, S. W. Hwang, T. Okochi, W. H. Lee, and J. Sugiyama, "Non-destructive method for wood identification using conventional X-ray computed tomography data," *J. Cult. Herit.*, vol. 38, pp. 88–93, 2019.
[11] J. L. Paris and F. A. Kamke, "Quantitative wood-adhesive penetration with X-ray computed tomography," *Int. J. Adhes. Adhes.*, vol. 61, pp. 71–80, 2015.
[12] Y. Tomikawa, "Non destructive Inspection of wooden Poles using Ultrasonic Tomogrphy," *IEEE Trans. UFFC*, vol. 33, pp. 354–358, 1986.
[13] E. Comino, V. Socco, R. Martinis, G. Nicolotti, and L. Sambuelli, "Ultrasonic tomography for wood decay diagnosis.," in *International Symposium on Plant Health in Urban Horticulture, Braunschweig*, 2000, p. 279.
[14] G. Deflorio, S. Fink, and F. W. M. R. Schwarze, "Detection of incipient decay in tree stems with sonic tomography after wounding and fungal inoculation," *Wood Sci. Technol.*, vol. 42, no. 2, pp. 117–132, 2008.
[15] N. J. Brazee, R. E. Marra, L. Göcke, and P. Van Wassenaer, "Non-destructive assessment of internal decay in three hardwood species of northeastern North America using sonic and electrical impedance tomography," *Forestry*, vol. 84, no. 1, pp. 33–39, 2011.
[16] B. Yan, C. Wu, and H. Ma, "Study on the method of nonmetallic defects based on ultrasonic tomography and morphology," *Proc. 2017 12th IEEE Conf. Ind. Electron. Appl. ICIEA 2017*, vol. 2018-Febru, pp. 1287–1292, 2018.
[17] R. C. Alves, J. N. R. Mantilla, C. F. Bremer, and E. V. M. Carrasco, "Application of Acoustic Tomography and Ultrasonic Waves to Estimate Stiffness Constants of Muiracatiara Brazilian Wood," vol. 10, no. 2010, pp. 1845–1856, 2015.
[18] C. Colla, "Verification of sonic tomography outcome through local testing of mechanical properties in historic timber beam," *J. Herit. Conserv.*, vol. 47, pp. 71–79, 2016.
[19] L. P. Perlin, Â. Valle, R. Caldas, and D. A. Pinto, "New method to locate the pith position in a wood cross-section based on ultrasonic measurements," vol. 169, pp. 733–739, 2018.
[20] J. Qin, X. Liu, K. Van Den Abeele, and G. Cui, "The study of wood knots using acoustic nondestructive testing methods," *Ultrasonics*, vol. 88, pp. 43–50, 2018.
[21] L. Espinosa, F. Prieto, L. Brancheriau, and P. Lasaygues, "Effect of wood anisotropy in ultrasonic wave propagation : A ray-tracing approach," vol. 91, no. April 2018, pp. 242–251, 2019.
[22] L. Espinosa, F. Prieto, L. Brancheriau, and P. Lasaygues, "Quantitative parametric

imaging by ultrasound computed tomography of trees under anisotropic conditions : Numerical case study," *Ultrasonics*, no. 26, p. 106060, 2019.

[23] A. C. Kak and M. Slaney, *Principles of Computerized Tomographic Imaging*. New York: The Instituite of Electrical and Electronics Engineers, Inc., 1988.

12th International Conference on Structural Analysis of Historical Constructions
SAHC 2020
P. Roca, L. Pelà and C. Molins (Eds.)

A PRELIMINARY STRUCTURAL SURVEY OF HERITAGE TIMBER LOG HOUSES IN TØNSBERG, NORWAY

AMIRHOSEIN SHABANI[1*], HAIDAR HOSAMO[1], VAGELIS PLEVRIS[2,1] AND MAHDI KIOUMARSI[1]

[1]Department of Civil Engineering and Energy Technology
OsloMet–Oslo Metropolitan University
Pilestredet 35, 0166 Oslo, Norway
email: {amirhose, haidarho, mahdik}@oslomet.no, www.oslomet.no
(*corresponding author)

[2]Department of Civil and Architectural Engineering
Qatar University
P.O. Box: 2713, Doha, Qatar
email: vplevris@qu.edu.qa, web page: www.qu.edu.qa

Keywords: Preliminary Survey, Heritage Timber Structures, Log House, 3D Laser Scanner, Visual Inspection, Environmental Attack, Vulnerability Assessment

Abstract. *The formulation of a multi-hazard loss model for a given structure is not only of interest for predicting the economic impact of future damage but it can also be of importance for risk mitigation. A methodology that can assess the vulnerability of the built environment is a significant component of a loss model. The multi-risk vulnerability of heritage buildings necessitates greater knowledge about the history of their construction, including aspects relating to preserving them as assets. Timber as an organic material is more susceptible to decay and the structural assessment of timber buildings is essential for their preservation. A preliminary survey as a basis for multi-risk vulnerability assessment of such buildings is essential. In this step of the process, the history of the building is investigated, as well as any intervention to it during its lifetime. A damage inspection of structural elements conducted by experts is an essential part of the second step. After this, the configuration of the building, including height, plan view and connection details should be documented. After the preliminary survey of the building, detailed methods are employed to gather further information about the structure's behaviour under different risk scenarios. In this paper, heritage timber buildings in Tønsberg, Norway have been selected as case studies for multi-risk vulnerability assessments. The preliminary survey has been conducted by a team of experts and useful data have been recorded and explained. 3D laser scanners have been used in the survey in place of traditional 2D methods to obtain a more detailed and accurate 3D representation of the buildings.*

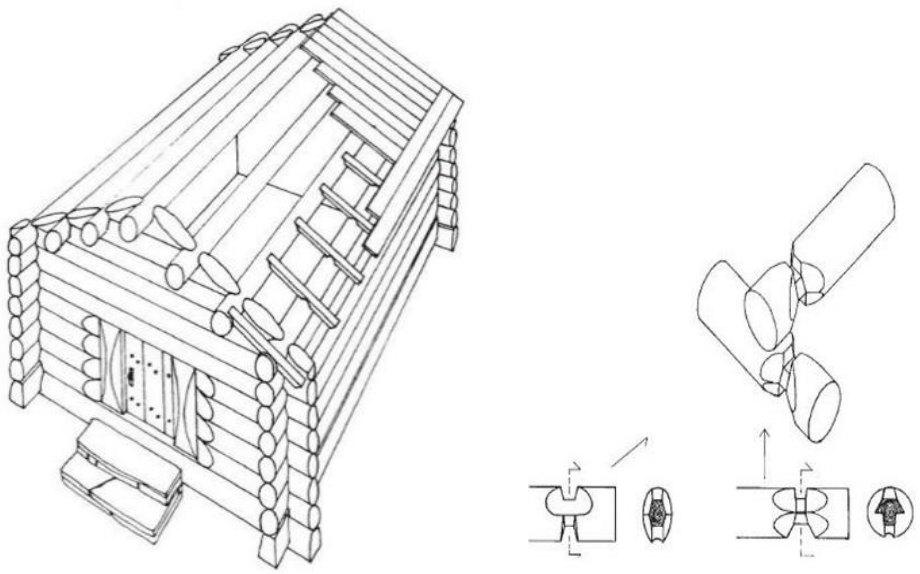
1 INTRODUCTION

Heritage structures are culturally, economically and socially important to preserve for the nations around the world. Timber as the oldest organic construction material is widely used in

heritage structures. Timber is more susceptible to environmental risks than masonry bricks or stone, and its behaviour is quite complex. The preservation of heritage structures and the preservation of craftsmanship techniques represent two sides of the same coin [1]. For other types of materials, modern preservation techniques can potentially be used, but in the case of timber, traditional techniques are recommended because of the susceptibility of timber to decay and the necessity of replacing members at given intervals [2, 3].

A methodology for the structural vulnerability assessment of heritage timber buildings is proposed by Shabani et al. (2020) [4] in the context of HYPERION project and as the first and principal step of the methodology, a preliminary survey should be conducted by experts. In this step, risk effects that can be seen by the human eye are documented and the structural system, including connections or roof structure systems, is evaluated. Moreover, a geometric survey should be carried out to document the configuration of the building, either in the form of traditional 2D drawings or modern 3D BIM files. Potential risks based on the codes, previous disaster records or visual inspections must be estimated during this stage [4, 5].

Log houses are one of the ancient timber structural systems. In a log house structural system, the horizontal timber logs are laid on top of each other and the stability of the structure is provided by the corner joints where the wall planes interlock, as illustrated in Figure 1. The log house system is used in northern European countries and in the central Alpine region, which also extends into several eastern European countries. The technique can also be seen in Japan, China and North America. The low heat conductivity of wood is taken advantage of in this structural technique for high insulation of the building, which is very important for countries with harsh winters [2].



(a) (b)

Figure 1: (a) Typical Log house schematic view, (b) Typical log house corner connection detail [2]

Laser scanners are machines that use a controlled deflection of laser beams for distance measurements. By taking a distance measurement in every direction, the scanner rapidly

captures the surface shape of objects, buildings and landscapes without representing any risk of damaging the structure. Terrestrial laser scanning has been utilised to perform stability analyses of masonry arches by transforming point clouds into metric images [6] of masonry arches in a heritage masonry Bridge. This was done by combining a set of point clouds with static methods [6-8]. Bethlehem's Nativity church has also been scanned using a laser scanner, and a 3D model was prepared for use in studies under several types of loads [9]. In addition, a new method was developed to simulate the timber roofs of the Vienna Imperial Palace using a laser scanner [10]. 3D documentation is therefore a good tool for informing risk management processes relating to heritage structures [11].

The case studies in this paper are from Tønsberg, which is a Norwegian town and municipality in the Vestfold Region. It is located south-southwest of Oslo on the western coast of the Oslo fjord. According to the sagas, Tønsberg was founded in the Viking period at the end of the 9th century, yet no archaeological discoveries have confirmed these sources. Today it is believed that the town was founded in the 10th century, which still makes Tønsberg among the oldest cities in Norway [12].

Natural conditions such as good available farmland, a safe port and possibilities for fortifications and defence laid the foundations for the city's development. Tønsberg is dominated by a steep-sided cliff (Slottsfjellet). Urban structures comprising long, narrow estates divided by streets and narrow alleys were established in the 12th century at the foot of the cliff and along the harbour. The settlement consisted mainly of one or two storey wooden log houses. The locations of the two log houses that were selected for the preliminary survey are shown in Figure 2(b) (image obtained from Google Earth).



(a) (b)

Figure 2: (a) The location of Tønsberg in southern Norway, (b) The location of the two case studies

The preliminary survey of the two historical log houses was carried out from a structural perspective by evaluating the structural system, history of the buildings including interventions, damage documentation, potential future risks and 3D architectural documentation of the buildings. Based on the possible future risks, 3D laser scanners were employed to provide accurate architectural documentation for two of the case studies which 3D BIM drawings have been provided. 3D drawing can be converted to finite element models for future numerical analysis. Compared with conventional geodetic methods (traditional single-point measurements), the 3D laser scanning technology exhibits strong advantages. Its data acquisition has the advantages of high efficiency, high precision, non-contact measurement, high data resolution and fast speed.

2 CASE STUDIES

A preliminary survey is an essential part of conducting a vulnerability assessment of heritage structures. The two selected log houses in Tønsberg were investigated from a structural perspective, as presented in the following sections.

2.1 Heierstad Loft

The Heierstad Loft is a store house originally located on the farm Heierstad, 50 km north of Tønsberg. The whole house was moved to the Slottsfjell Museum in Tønsberg, where it was restored in 1957. The lower floor is in its original state and has been dated to 1407 by dendrochronology, while the attic floor has been partly reconstructed [13].
The building has a rectangular plan measuring about 8 × 9 metres, and a total height of about 9 metres. It is built (logged) of large softwood pine or spruce logs, with a simple gable roof construction. The roofing material is traditional, consisting of coarse wooden boards, a layer of birch bark and turf. The exterior surface has been treated with tar. Two views of the building and details of the roof and connections are shown in Figure 4.



Figure 3: Heierstad Loft case study from two different views

As it is illustrated in Figure 4(b), two supporting beams are employed, and the main beams are laid orthogonally on them. All the roof system's timber logs of the second floor are laid orthogonally on the main beams. However, due to the lower dead and live loads on the second roof compared to the first roof, the supporting beams have not been utilised and the roof system's logs are laid on the main beams as it is shown in Figure 4(c).

The area of the second floor is more than the first floor. As it is illustrated in Figure 4(d), this issue can lead to overturning of the building and in order to tackle with this risk, the main beams of the first floor are continued and as it is shown in Figure 4(e), upper logs are longer in the corner joints.

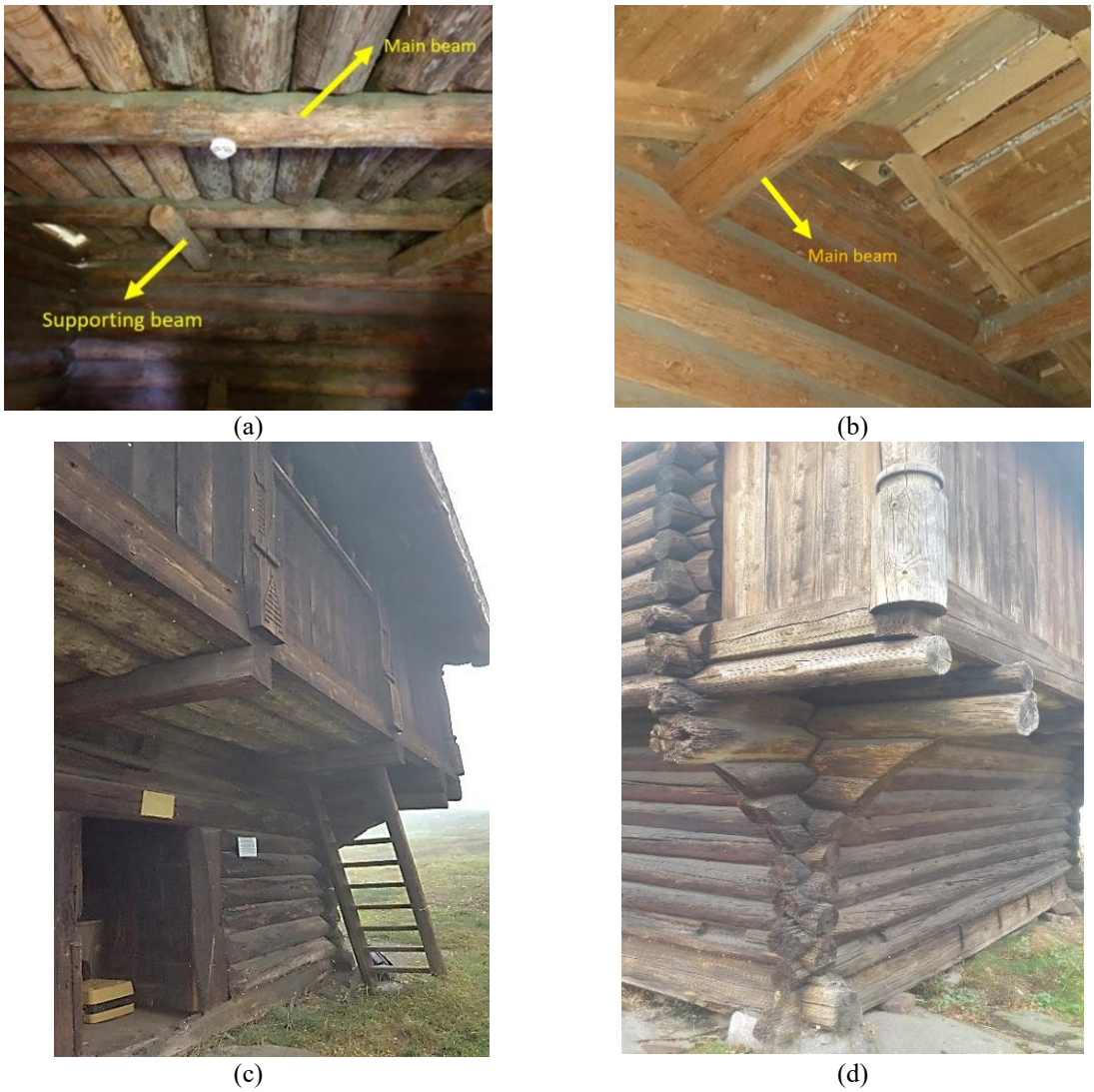


Figure 4: (a) Connection details inside the building for the 1st and (b) 2nd storey roof, (c) structural details of the 2nd floor system, (d) connection detail of the corner joint

The building is in good condition in general, but it requires continuous maintenance. The most relevant degradation factors are general weathering, high humidity levels, biological decay (see Figure 5) and foundation settlement.



(a) (b)

Figure 5: Biological defects in Heierstad Loft

2.2 Fadum Storehouse

The Fadum Storehouse is a log house covered by a coat of insulation because of its original use as a storehouse. The structure dates back as far as the 1750s, and it is constructed with small timber columns on a stone foundation. The structure has two stories with dimensions of 6.40*5.30 for each of them. The material properties and the risks are the same as those of the previous building [14].

The building and its structural details are shown in Figure 6. As it is illustrated in Figure 6(d), the floor system is laid on the short timber columns which are on stone foundations. The main surrounding beams of the floor are simply connected to the columns without any constraints for rotation.



(a) (b)



(c)



(d)

Figure 6: (a) Fadum Storehouse view, (b) Structural detail inside the coating, (c) Timber short columns under the building, (d) detail of the simply connected timber column

This building is generally in good condition but some deflection in main surrounding beams can be seen as well as biological damages Figure 7 shows some of the biological damages in logs and on the coating.



(a)



(b)

Figure 7: (a) Lichen attack to the coating, (b) Insect attack on the timber logs

3 3D DOCUMENTATION

Analysing 2D images can be very useful in many machine vision applications, but it is sometimes more helpful or even necessary to create a 3D image or representation of an object, such as in robotics, logistics applications or autonomous vehicles applications. Today, various imaging techniques can provide 3D information for machine vision purposes. Scanning techniques use a projected line of light onto a surface. [15].

Fadum Storehouse and Heirestad Loft structures are chosen for performing 3D laser scanning which can be easily converted to finite element models for further studies. A total of eighteen scans, twelve exterior and six interiors, were carried out for the Fadum Storehouse and

Heierstad Loft structures investigated in the present study. The structures have an easily accessible indoor environment and design characteristics including diversity and a number of different building components.

The equipment used was a Topcon 2000 3D laser scanner, which is able to scan the entire building. The laser scanner automatically scans and measures the area and then records the coordinates of each scanned point. In order to obtain complete and clear point cloud data of the building's surface, a multi-station scanning was required.

Because of the fact that the point cloud data collected by the 3D laser scanner contains essentially all the objects within the scanning range, including trees, persons, etc. that are not related to the structure, post-processing needs to be performed to remove such elements that are not relevant to the study. Autodesk ReCap Pro 2020 was used for de-noising, editing, measurement and visualisation of the raw point cloud data. The field tests were designed in such a way to obtain the full details of the two structures, such as connection details, log dimensions etc.

The result of the scanning was a complex set of points called point clouds. These points show information about the field environment in grey, or in a red, green and blue (RGB) colour scale, corresponding to the intensity of the return pulse. During the scanning, the team used special labelling that reflected the location (inside or outside the structure) in order to make the post-processing more manageable.

When utilising ReCap to perform the registration process, it was not possible to achieve fully automatic merging, and a manual approach was therefore chosen to complete the process. Based on this, at least three common points in two sequential scans were picked up to execute the registration and to obtain good merging results. Throughout this process, all the labelling rules and notes used in the field were taken into consideration in order to select the right scans to be merged together. The result is shown in Figure 8 for the two case studies.

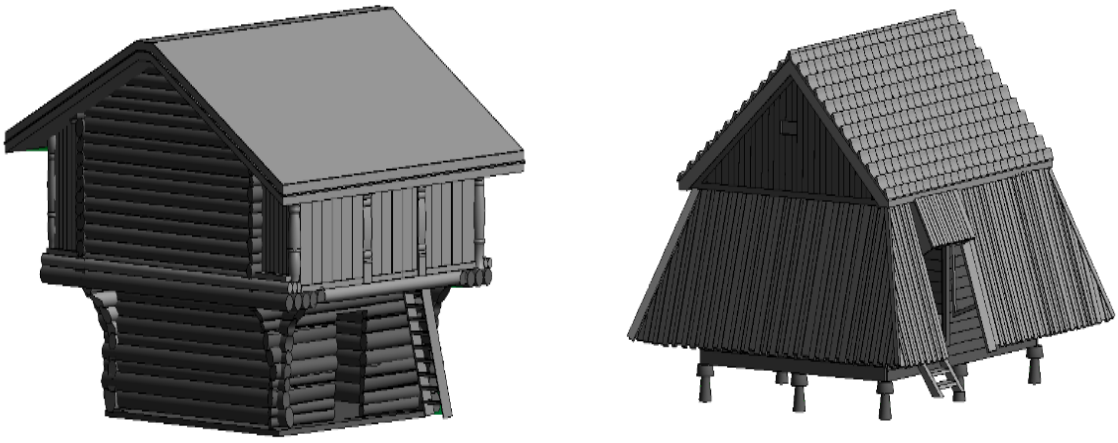


(a) (b)

Figure 8: Raw point cloud data for (a) Heierstad Loft, (b) Fadum Storehouse

After obtaining the point clouds, the Revit building information modelling (BIM) software package was utilised to visualise the clouds based on colour intensity and elevation, and to interact within the point clouds to create an accurate building information model. As can be

seen in Figure 9, the number of logs and their thickness have been identified and precisely depicted in the BIM file.



(a) (b)

Figure 9: BIM drawing files of (a) Heierstad Loft, (b) Fadum Storehouse

For more investigation at the component scale, some parts of the buildings have been chosen in order to convert the point clouds to the surface using Geomagic design X software package. This feature of the software will be so time consuming in order to achieve the precise model of the structures at the component scale. Figure 10(a) and (b) show some samples of the surfaces of the components and the deviation of some points from the reference surface which is produced from the mass point clouds. In order to investigate any deflection in beams on short timber columns in Fadum storehouse, precise models have been produced. Figure 10(c) shows one of the beams models as a sample. Two reference horizontal lines are added to the figure to show any deflection in the beam and settlement in short columns. No settlement in columns can be detected in this beam's supports but insignificant deflection in the beam can be detected in the right part of the beam.

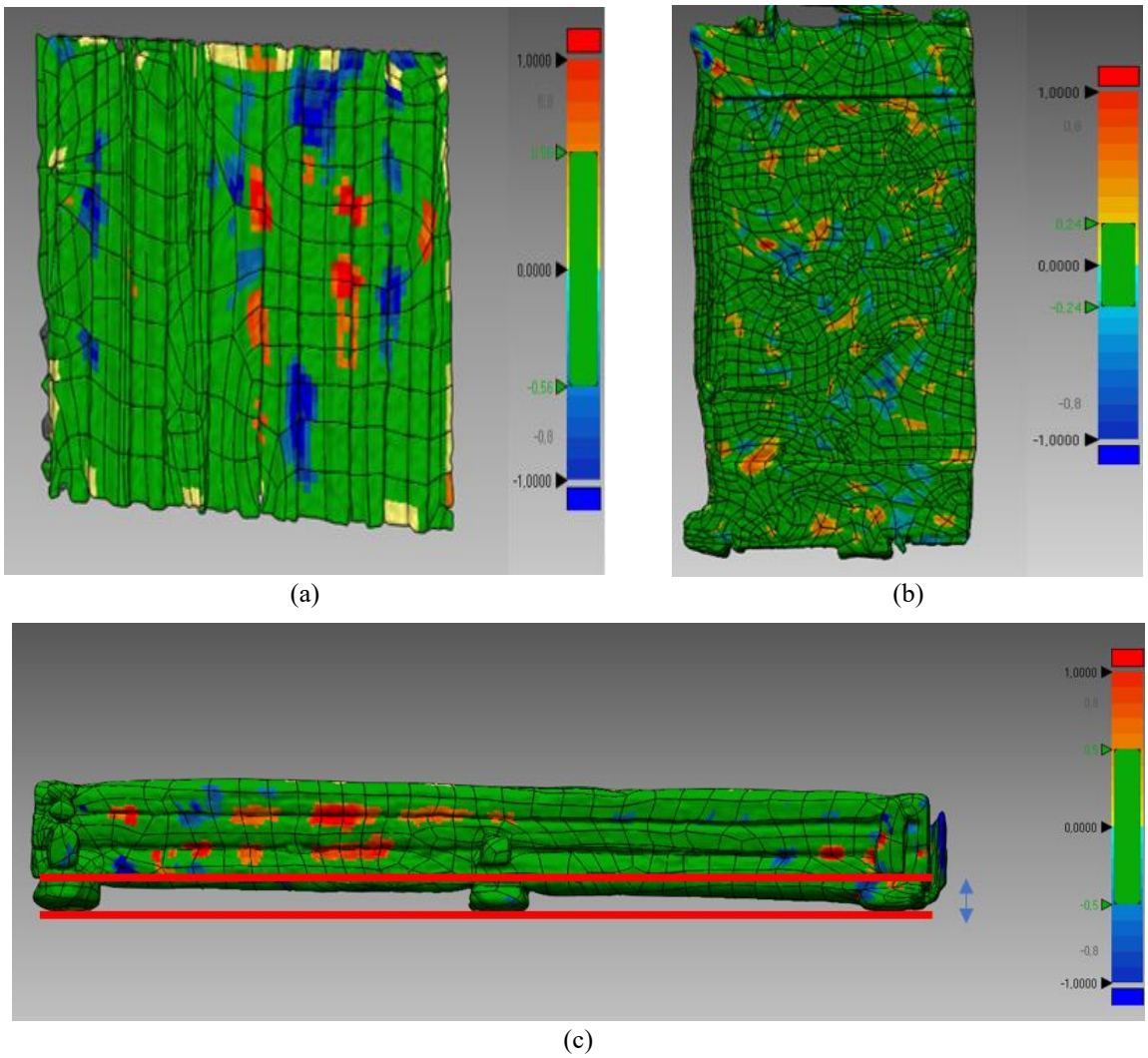


Figure 10: (a) Surface of the coating of Fadum storehouse (see Figure 5(a)),(b) Surface of the coating of Heierstad Loft as it was highlighted in yellow box in Figure 3(a), (c) Precise model of the beam in Fadum storehouse (see Figure 5(c)) (units in mm).

In order to investigate the flatness of timber coating, Geomagic Control X software is utilized. Point clouds are as an input for this inspection which gives precise images of the elements and the deviation of the different parts of the element to a set of reference points. Figure 11 shows the output image of the software for one covering timber panel of the Heiersted Loft building. As it is illustrated no significant protrusion can be detected in the covering and the deviations just show the differences of the vertical timber panels' flatness. This method can be used for detecting the large cracks or delamination in timber elements' surfaces.

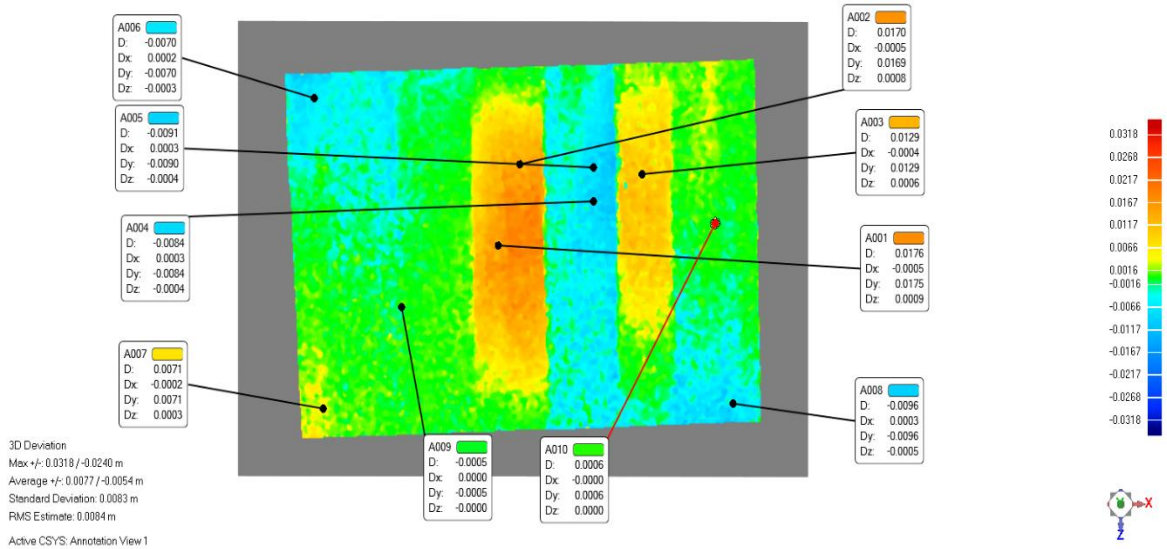


Figure 11: Covering surface of the wall of the Heierstad Loft (see Figure 3(a)) for showing any protrusion in the element (units in mm).

4 CONCLUSIONS

- A preliminary structural survey as a fundamental step in the vulnerability assessment of heritage buildings has been performed of two log houses in Tønsberg in order to investigate their structural system, damage and future potential risks.
- The buildings were selected for a further geometrical survey using 3D laser scanning. 3D documentation of Heierstad Loft and Fadum Storehouse have been produced and BIM drawing files have been derived for further investigations. 3D laser scanning is much more precise than traditional 2D geometrical surveys, especially for structures with more complicated 3D geometry. The method can be effectively used for the conservation of heritage structures against potential risks.
- Three features of 3D laser scanners have been highlighted. Point clouds not only can be used as an input for 3D documentation of the case studies but also can be utilized in order to model precise automatically models of the components to detect any deflection or settlements in structural elements or foundations. Moreover, as the third feature of the point clouds, they can be utilized in order to find any protrusion in surfaces of the timber components which can be beneficial for detecting any cracks or delamination in surfaces.

Acknowledgements. This work is a part of the HYPERION project. HYPERION has received funding from the European Union's Framework Programme for Research and Innovation (Horizon 2020) under grant agreement no. 821054. The contents of this publication are the sole responsibility of Oslo Metropolitan University (Work Package 5, Task 2) and do not necessarily reflect the opinion of the European Union.

REFERENCES

[1] Shabani A, Kioumarsi M and Zucconi M. State of the art of simplified analytical methods for seismic vulnerability assessment of unreinforced masonry buildings. *Eng Struct* (2021); 239: 112280. DOI: https://doi.org/10.1016/j.engstruct.2021.112280.

[2] Larsen KE and Marstein N. *Conservation of historic timber structures. An ecological approach*. Riksantikvaren, (2016).

[3] Riggio M, D'Ayala D, Parisi MA, et al. Assessment of heritage timber structures: Review of standards, guidelines and procedures. *Journal of Cultural Heritage* (2018); 31: 220-235.

[4] Shabani A, Kioumarsi M, Plevris V, et al. Structural Vulnerability Assessment of Heritage Timber Buildings: A Methodological Proposal. *Forests* (2020); 11: 881. DOI: https://doi.org/10.3390/f11080881.

[5] Cruz H, Yeomans D, Tsakanika E, et al. Guidelines for on-site assessment of historic timber structures. *International Journal of Architectural Heritage* (2015); 9: 277-289.

[6] Riveiro B, Morer P, Arias P, et al. Terrestrial laser scanning and limit analysis of masonry arch bridges. *Construction & Building Materials* (2011a); 25: 1726–1735. DOI: https://doi.org/10.1016/j.conbuildmat.2010.11.094.

[7] Jung R-K, Koo B-S and Yu Y-S. Using Drone and Laser Scanners for As-built Building Information Model Creation of a Cultural Heritage Building. *Journal of KIBIM* (2019); 9: 11-20.

[8] Milani G, Esquivel YW, Lourenço PB, et al. Characterization of the response of quasi-periodic masonry: Geometrical investigation, homogenization and application to the Guimarães castle, Portugal. *Eng Struct* (2013); 56: 621-641. DOI: 10.1016/j.engstruct.2013.05.040.

[9] Macchioni N, Brunetti M, Pizzo B, et al. The timber structures in the Church of the Nativity in Bethlehem: typologies and diagnosis. *Journal of Cultural Heritage* (2013); 13: 42-53. DOI: https://doi.org/10.1016/j.culher.2012.10.004.

[10] Pöchtrager M, Styhler-Aydın G, Döring-Williams M, et al. Digital reconstruction of historic roof structures: developing a workflow for a highly automated analysis. *Virtual Archaeology Review* (2018); 9: 21-33. DOI: https://doi.org/10.4995/var.2018.8855.

[11] Wilson L, Rawlinson A, Frost A, et al. 3D digital documentation for disaster management in historic buildings: Applications following fire damage at the Mackintosh building, The Glasgow School of Art. *Journal of Cultural Heritage* (2018); 31: 24-32. DOI: 10.1016/j.culher.2017.11.012.

[12] Degnbol H. *A Dictionary of old norse prose:@ Ordbog over det norrųne prosasprog*. Den arnamagnęanske kommission, (1989).

[13] Berg A. *Norske tømmerhus frå mellomalderen, bd. II: hus for hus i Buskerud, Vestfold og Oppland*. Landbruksforlaget, Oslo, (1990).

[14] Hovland JM. Kåpebur – fortidens kjøleskap eller motepåfunn? , https://www.notteroyhistorielag.no/john-m-hovland-kapebur-fortidens-kjoleskap-eller-motepafunn/ (2016, Access (2016)).

[15] Hrasnica M, Cauševic A and Rustempašić N. Laser scanning for the evaluation of historic structures. *Handbook of Research on Seismic Assessment and Rehabilitation of Historic Structures*. (2015), pp.734-764.

12th International Conference on Structural Analysis of Historical Constructions
SAHC 2020
P. Roca, L. Pelà and C. Molins (Eds.)

A PROTECTED LANDMARK MONUMENT: REINFORCEMENT, REHABILITATION, AND RESTORATION OF THE CATHEDRAL BASILICA OF MANIZALES

OMAR D. CARDONA[1*] AND SAMUEL D. PRIETO (1949-2016)[2]

[1] Instituto de Estudios Ambientales (IDEA)
Universidad Nacional de Colombia
Sede Manizales, Colombia
e-mail: odcardonaa@unal.edu.co, http://idea.manizales.unal.edu.co, (*corresponding author)

[2] INGENIAR: Risk Intelligence
CAD/CAE Ltda.
Carrera 19A 84-14, Bogotá, D.C, Colombia
web page: http://www.ingeniar-risk.com

Keywords: Historical Building, Vulnerability Assessment, Seismic Retrofitting.

Abstract. *The Cathedral Basilica of Manizales is one of the most representative buildings of the so-called "republican architecture", boosted in a remarkable and singular way after the fires of the 1920s in the city of Manizales, Colombia. Its "eclectic neo-gothic" design was made in Paris, after the fire that destroyed the city's previous cathedral in 1926. This masterpiece of Colombian architecture turned ninety years old in 2018 after the first stone was laid in 1928. Its construction was carried out in "reinforced cement"; few decades after the appearance of reinforced concrete. During its ninety years, the cathedral suffered earthquakes of high intensity, in 1938, 1962 and 1979, which have significantly compromised its structure. Earthquake-resistant rehabilitation studies to preserve the temple, declared a National Monument in 1984, were promoted at the end of the 1990s. They were the diagnosis of the structural conditions of seismic vulnerability and how it could be provided a greater capacity of response in terms of stiffness, resistance and dissipation of energy, as well as the diagnosis of the state and pathology of the materials. This included geotechnical studies of seismic amplification, dynamic behavior using environmental vibrations, 3D virtual modeling, and structural analysis, even with finite elements. For the reinforcement, the intervention of the base of the central spire was proposed, the control of the stability of the four corner spires, the construction of new structural walls joined in strategic points; founded in caissons and connected to each other in the upper level to guarantee the action of the diaphragm and a better seismic behavior of the structure. The interventions to improve the seismic resistance of the cathedral were carried out between 2002 and 2004. The treatment and protection of the concrete and other necessary interventions of its sculptures and images were carried out between 2016 and 2017. The objective of this document is to describe how a new generation of local specialists have studied and proposed, for this temple of 113 meters high, its seismic reinforcement, the treatment of its materials and other necessary protection interventions, in accordance with the state of the art of earthquake engineering, design, and construction of RC structures and the protection of historical heritage.*

1 INTRODUCTION

The Cathedral Basilica of Manizales has endured earthquakes of significant intensity, in 1938, 1961, 1962 and 1979 that they have seriously compromised their structure. The earthquake of 1962 produced partial destruction and the collapse of the northwest tower. In 1979, although the cathedral had been repaired, it suffered serious damage to its main structural walls. The temple originally thought as invulnerable was not and demanded to make new structural reinforcements and interventions that were projected twenty years later (1999) and that have been carried out during the two following decades of the new millennium. The departmental government, with the support of the national government, promoted the accomplishing of these earthquake-resistant rehabilitation studies to preserve the monument. Taking into account similar works carried out in other Latin American countries, such as the intervention of the Cathedral of Mexico City or the experience with churches from Antigua, Guatemala, the objective of this work is to illustrate in synthesis the studies and interventions carried out in the Cathedral Basilica of Manizales, Colombia, between 1979 and 2019.

2 AN EMBLEM OF LOCAL SEISMIC CULTURE

The Cathedral Basilica of Our Lady of the Rosary of Manizales, a temple declared a National Monument in 1984, today of national public interest, is the symbol of a culture: that of the coffee landscape. Its history represents the evolution and innovation of a technique, of science and a culture, immersed in a context characterized by disasters and risk in the face of intense events. Although the roundwood and the bamboo, *guadua*, had been used by the Quimbaya people and since the Neolithic period in the pre-Columbian period, the possibility of molding earth walls, using *tapia* and adobe, the result of the colonization process following the European canon from Spain, entered to be part of the constructive options. The flexible gave way to the rigid and fragile in the search for status with the increase in the thickness of the walls. Thus, between 1854 and 1869 a temple of trodden *tapia* was built that replaced the first straw chapel. After the foundation of Manizales in the middle of the 20th century, this church built with the splendor of this rigid material, with two lateral towers and a central bell tower, meant the advent of a new but fragile constructive paradigm in the face of earthquakes. In 1875 the strong earthquake that destroyed Cucuta, another city in the Northeast, also had effects in the coffee region of Colombia. The church cracked importantly, as did other tapia and adobe houses that had been built with the same technique. Subsequently, these damages were increased because of the earthquakes that occurred in 1878, 1884 and 1885. The temple of *tapia* and adobe was repaired several times, but these last earthquakes severely affected its façade. As a result of the observation and awareness of the inhabitants of the region of the possible consequences due to the earthquakes on the *tapia* and adobe buildings, the community not only made the decision to demolish the temple but to explore new combinations and constructive techniques more appropriate for the city which they called the “tremors architectural style”.

The demolition of the temple of trodden *tapia* was not an isolated solution to the problem of seismic vulnerability. Noting the rediscovery of the earthquake-resistant empirical techniques of the "tremors architectural style" of the houses from the coffee farms and from the urban center, Mariano Santamaría, Bogota architect, proposed a new design for the church that would take advantage of the “bahareque” from the region. Wood and *guadua* would adopt the forms of a

temple that would adapt to the natural peculiarities of this new landscape and its construction was carried out between 1888 and 1897. In the 1920s the novel but precarious electrical network was the cause of they will present short circuits and fires. The fire of 1925 meant the destruction of the city center; tens of blocks were destroyed. The flexible bahareque fell into disrepute because of its vulnerability to fire. In 1926, the wooden Cathedral and two more blocks, which had not been previously affected, suffered the action of a new fire, thus completing a disaster scenario no longer caused by the force of nature. This situation made it necessary to rethink the risk and its different causes and the possibility of exploring new alternatives based on the introduction into the world of the recent Portland cement at that time. In the midst of the controversy about the level of protection against earthquakes and fire, finally, the cemented bahareque replaced the old bahareque and definitively banished the *tapia* and adobe of the city. The cultural landscape of the rural bahareque evolved into a unique and modern urban bahareque, the result of adaptation and a peculiar awareness of risk in Manizales. Under the name of reinforced cement at that time, concrete technology also became an attractive innovation and an apparent and legitimate alternative for the construction of the new Manizales Cathedral, which should be in principle immune to fires and earthquakes. Angelo Papio & Jean Carlo Bonarda, Italian engineers resident of Manizales at that time, who would be the builders of the new temple, described the construction system proposed by the French architect Julien Auguste Polti, who won the international competition in Paris for the new Cathedral of Manizales, as follows: “The type of construction we use is the monolithic of reinforced cement throughout its structure and the one that offers absolute guarantees of resistance and fire. This system is adopted in countries where earthquakes are frequent, not only by the structure but also the walls come into play in the resistance against the stresses and movements due to the earthquake. This type of construction suits Manizales's floor perfectly. Moreover, it is the most suitable.” The new Cathedral of Manizales, in “reinforced cement”, became the emblem of local seismic culture, which developed with the curious evolution of the “tremors architectural style”; predominant technique with which the city would develop its “Republican” Architecture. The new Cathedral, by itself, meant a peculiar innovation in that unique process, being the first massive building of reinforced concrete that was built in the country and in the region of the coffee cultural landscape; declared as World Heritage by UNESCO in 2011.

3 DIAGNOSIS AND DESIGN OF INTERVENTIONS

The new Cathedral of Manizales, of “neo-Gothic eclectic style” in reinforced concrete, was completed in 1939. It suffered its first earthquake in 1938 when its central spire had not yet been built. Subsequently, during the following decades until the end of the 20th century, its structure suffered the action of several earthquakes that significantly affected it. Although reinforcements, repairs were made and the tower that had collapsed in 1962 was rebuilt, it was early concluded that its conservation depended on the degree of earthquake-resistant protection that could be provided, as a result of a study and a preventive and careful intervention that preserved the monument to the future. The earthquakes of 1962 and 1979 had caused serious damage, his condition was critical, and his permanence depended on the correct interventions being carried out in the shortest possible time. Even a moderate earthquake, such as those that occur with some frequency in the region, was known to compromise the partial or total stability of the monument. For this reason, at the request of the Government of Caldas in the mid-1990s

and with the support of the Subdirectorate of Monuments of the National Road Institute, today the Directorate of Heritage of the Ministry of Culture, between 1997 and 1999 were carried out studies for the earthquake-resistant rehabilitation of the Cathedral, in order to protect this National Monument. These studies were conducted by a large group of experts [1], according to the state of the art, with the aim of make a detailed diagnosis of the conditions of structural seismic vulnerability and the way in which the monument could be given greater capacity in terms of rigidity, resistance and dissipation of energy to face the seismic demand.

For this purpose, it was based on the realization of a detailed survey and virtual construction of the model of the Cathedral, in order to verify the original plans of Polti, several of which had been restored by the Coffee Cultural Fund (see Figure 1). The plans offered invaluable information for the geometric survey stage, although the information included there did not correspond exactly with the real dimensions of the building. The virtual model was the basis for a three-dimensional discretizing of the temple and analyzing its structural behavior using finite element-based computer programs (e.g. ANSYS, SAP, PDCOMP) (see Figure 2).

The ANSYS program was used to define the structure geometry. In the finite element model, two types of elements were used: Type Beam 4- (elastic beam) and Type Shell 63- (elastic shell). For the construction of the model, it was necessary to use 6437 nodes, 8738 shell-type elements, and 108 beam type elements. For the dynamic analysis, an Eigenvectors analysis was used for the first 10 modes of vibration of the structure. The period of vibration for the fundamental mode was 0.90 sec. and for the second and third mode 0.54 sec. and 0.36 sec respectively. Using the SAP2000 NL Push, a pushover analysis was carried out, which allowed verifying the capacity of the structure. After analyzing the stratigraphic profile, it was established that the soil that controls the local seismic response is silt of high plasticity. Therefore, cyclic triaxial tests were performed, one for each of the samples recovered at different depths. The cyclic properties of the other strata were estimated based on correlations taking into account their index properties. The cyclic triaxial tests were performed for confinement pressures of $\sigma 3 = 0.5$ kg / cm², $\sigma 3 = 1.0$ kg / cm² and $\sigma 3 = 1.5$ kg/cm². The observed behavior of the soil corresponds to that of relatively rigid clays that begin to degrade from deformations of the order of 0.1%. For values of the order of 0.5% they have already lost up to 50% of their stiffness. The values of Go varied between 60 and 130 kg/cm² depending on the confinement pressure which, in this case, varied between 0.5 and 1.5 kg/cm². The damping coefficient with respect to the critic remained at small values until deformations of the order of 0.1% and only from this value were considerable values achieved until reaching values between 12% and 23% for deformations close to 1%.

Taking into account the dynamic properties of the soils, feasible accelerograms and the seismic response spectra for different periods of vibration at the site, the dynamic response of the structure was modeled and evaluated, considering the characteristics and condition of the materials in terms of its resistance and pathology, for which it was necessary to take a large number of samples. This allowed evaluating the structural seismic vulnerability and to design the seismic-resistant reinforcement in such a way that the benefit that these reinforcements would have on the structure could be verified and without generating excessive invasive interventions and preserving the authenticity of the temple.

Initially, with the use of a model of elastic behavior and the definition of a pattern of cracking and fissures simulated by previous earthquakes, obtained from the analysis with environmental vibrations, the inelastic behavior of the structure was assessed. This type of study allowed determining the main deficiencies and weaknesses of the temple to face earthquakes.

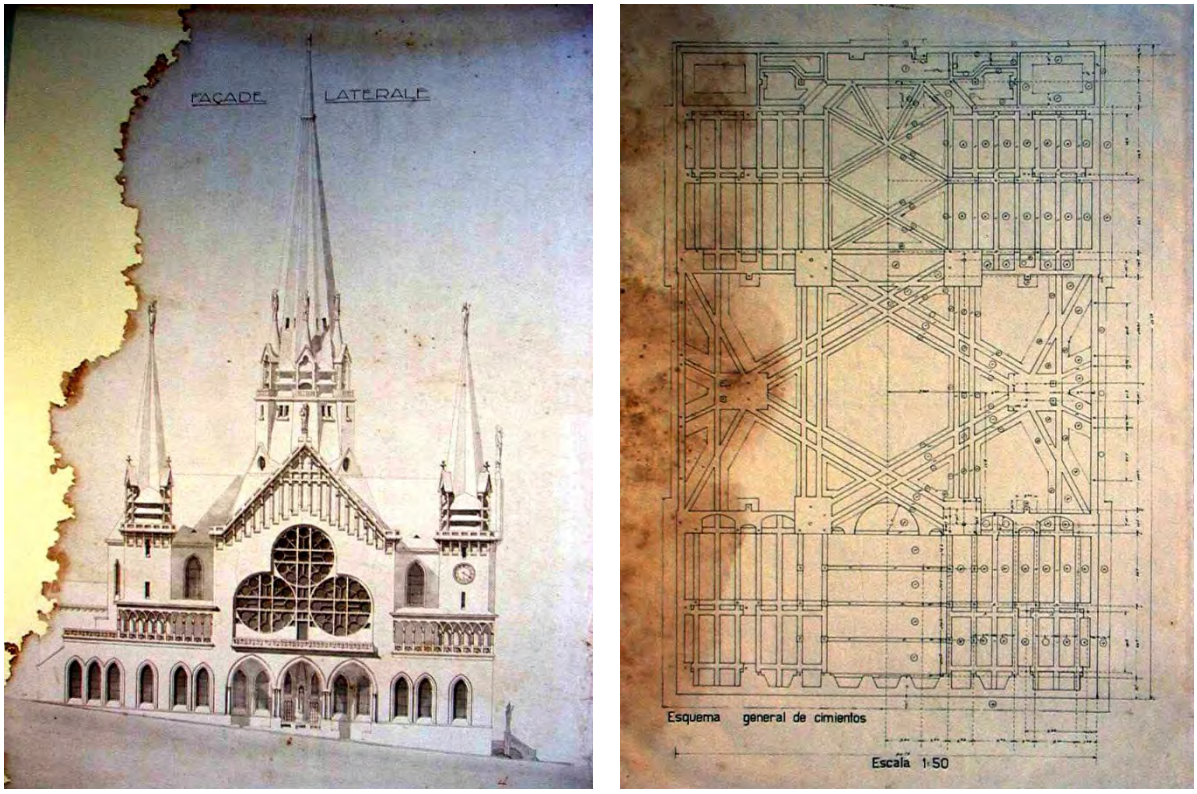


Figure 1: Example of original plans of the Cathedral restored and used for structural modeling

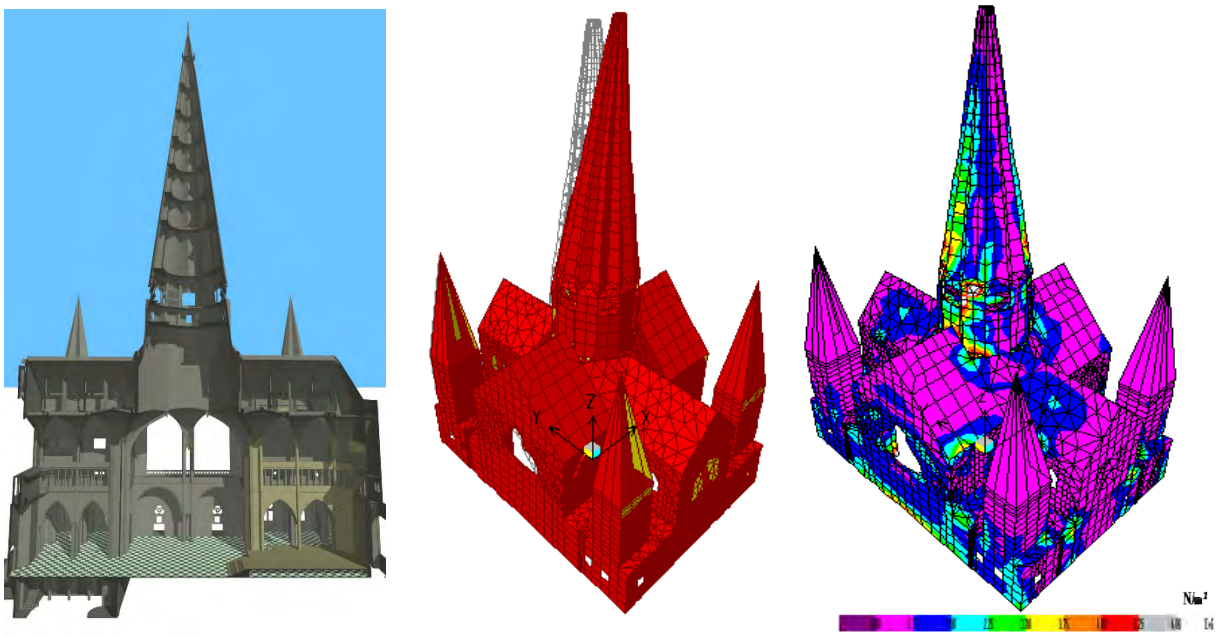


Figure 2: The virtual model was the basis for a three-dimensional fine-element discretizing of the structure

Efforts could be determined throughout the structure and therefore at critical sites or that could be insufficient to address the most severe seismic actions, a soil-structure interaction analysis was carried out to estimate how the period of vibration of the building and how its structural behavior could relax. The results of these studies indicated that the walls of the Cathedral had cracked in previous earthquakes because they acted in practice in an uncoupled manner. The cracks had arisen precisely because there was no capacity in the walls of the structure to move monolithically in a single set. Most of the cracks and fissures had occurred because of their insufficiency to withstand shear force. On the other hand, since the foundation was a system of joists, some of which are not very rigid due to their height reduction, this would allow, in addition to the seismic action, that the walls would rotate due to lack of embedment. This kind of situation, very unfavorable, explained the decoupling of the walls and their cracks and would have to be corrected. For this reason, it was concluded that it was essential to strengthen the capacity of the existing walls with competent structural elements that would improve the strength and the energy dissipation capacity of the structure and that a new foundation would be carried out that would guarantee its proper embedding in the base.

It was also detected that the central spire induced remarkable efforts at its base when it vibrated at the action of an earthquake. Since near its base where the folded plate that forms the tower was supported in a group of pillars whose reinforcement was insufficient to absorb tension stresses, it was considered that this area was critical and would have to be reinforced. Finally, it could be ratified that the towers or corner spires that had been reinforced after the 1962 earthquake with an internal steel structure were not properly anchored, offering a high possibility of instability in case of a severe earthquake. For this reason, it was considered pertinent to carry out an intervention that could guarantee greater stability and foundation anchorage.

4 EARTHQUAKE RESISTANT STRUCTURAL REINFORCEMENT

In summary, the diagnostic and design studies had proposed the realization of several new and attached structural walls at strategic points to improve the seismic response and the overall behavior of the structure, the intervention of the central spire base and the control of the stability of the four corner spires. At the beginning of the 2000s, the Foundation “Amor por la Catedral Basílica de Manizales” was established, resources were obtained from citizens, the municipality, and the national territorial finance agency, FINDETER. With unique technical coordination, between June 2002 and August 2004, the proposed earthquake-resistant reinforcement works were carried out by direct administration of said Foundation and through several contractors [2].

For a better behavior before the lateral loads it had been established that it was necessary to reinforce the structure by means of eight new orthogonal structural walls located in the periphery; in the places considered of greater efficiency for structural effects and where they will not cause major changes in the original architecture of the building. These walls could replace existing walls, however, due to the difficulties that this meant for the construction, it was established that said walls should be built attached by means of anchors to the existing walls (see Figure 3). This situation, although minorly modifying the façade, was preferable since the vertical loads were still transferred to the foundation by the existing walls. On the other hand, great difficulties and risks were avoided in the construction process, otherwise it would have been necessary to temporarily

hold large vertical loads as well as the thrusts of the arches that converge there. These new walls had to have edge elements capable of supporting the moments that would be generated in case of an earthquake and that must reach the foundation based on a new high foundation beam, located below the existing foundation, which in turn should be built supported by caissons that will guarantee the embedding or non-rotation of the new walls; issue that was very difficult to carry out but that was necessary (see Figure 4). These new structural walls had beams at different levels and at the top to ensure that they could be connected by a network of new beams that formed a ring at the level of the diaphragm between levels 24 and 27 meters and with the purpose to provide an ideal system to absorb tension stresses when the structure would be moved by an earthquake. These beams were built using steel plates attached and bolted to the high ribs of the vaults that reach the heads of the walls and that connect to the dome under the central spire, achieving the connection and transmission of forces and the effect of diaphragm with the new structural walls in the form of L and that finally they were built internally and externally attached to the walls of the structure (see Figure 5).

The central spire was intervened at its base by means of six reinforcing walls attached to the folded plate that forms the tower. In this way, the capacity of the structure at the base of the spire to withstand tension stresses when it becomes subject to lateral forces caused by earthquakes was improved. These walls were built internally so that from the outside it is not possible to see them and because of a recent earthquake they have already presented cracks, which illustrates that they have already been working (see Figure 6). In addition, this internal work was used in the central spire to make a new internal metallic helical staircase that allows people to climb up to the tip of the central spire where is placed the so-called “Polish Corridor”.

Finally, in order to improve the stability of the corner spires, a connection was made using eight special rods of 7.5 cm in diameter that connect the base of the internal steel reinforcement structure of each tower at the 11.20 meter level with a new beam located in the foundation to which they must be anchored (see Figure 7). In this way these rods act as tensioners that prevent the turn of the towers in case of a strong earthquake.

4 TREATMENT AND PROTECTION OF CONCRETE

The treatment of the concrete’s state of the Cathedral has been, together with other general maintenance activities, the last interventions that have been made to the monument. The treatment and protection of concrete was one of the interventions that, with special emphasis, should be carried out accordingly with the recommendations of the comprehensive diagnostic and structural reinforcement project in 2000 [1]. At that time when the evaluation of the state of the materials and the pathology of the concrete was made, it was concluded that there was already a significant advance in the carbonation of the concrete and that it would surely be aggravated if it was allowed to pass a long time without intervening. This was ratified in a more detailed study that was carried out in 2013 [3] and that resulted in the urgent need to intervene “the skin” of the Cathedral and also carry out another series of relevant interventions related to the repair of decorative elements and cornices, the construction of a new and adequate system of downspouts, the reconstruction of the sewer system and the intervention of the sculptural works and images of the facades and towers [4]. This maintenance, which must actually be a periodic activity, was carried out in 2018, following the technical and protection recommendations of the Heritage Directorate of the Ministry of Culture.

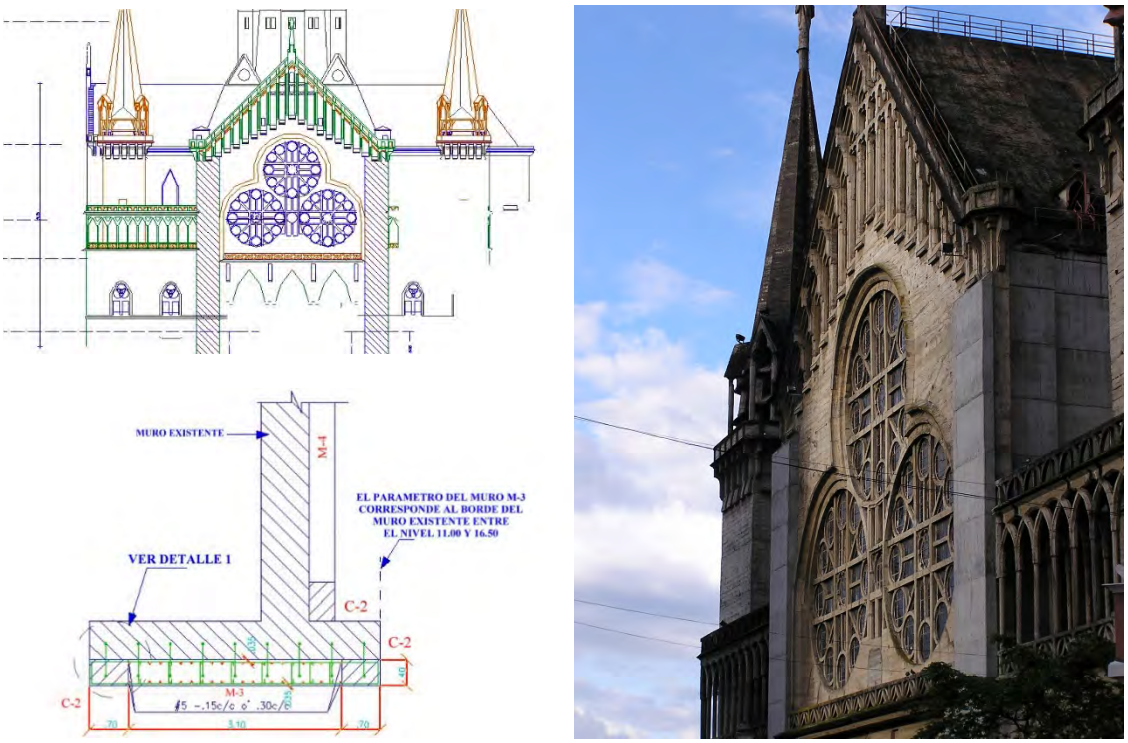


Figure 3: Attached walls were built to provide greater stiffness, resistance and energy dissipation



Figure 4: Foundation with caissons to prevent rotation at the base of the structural walls

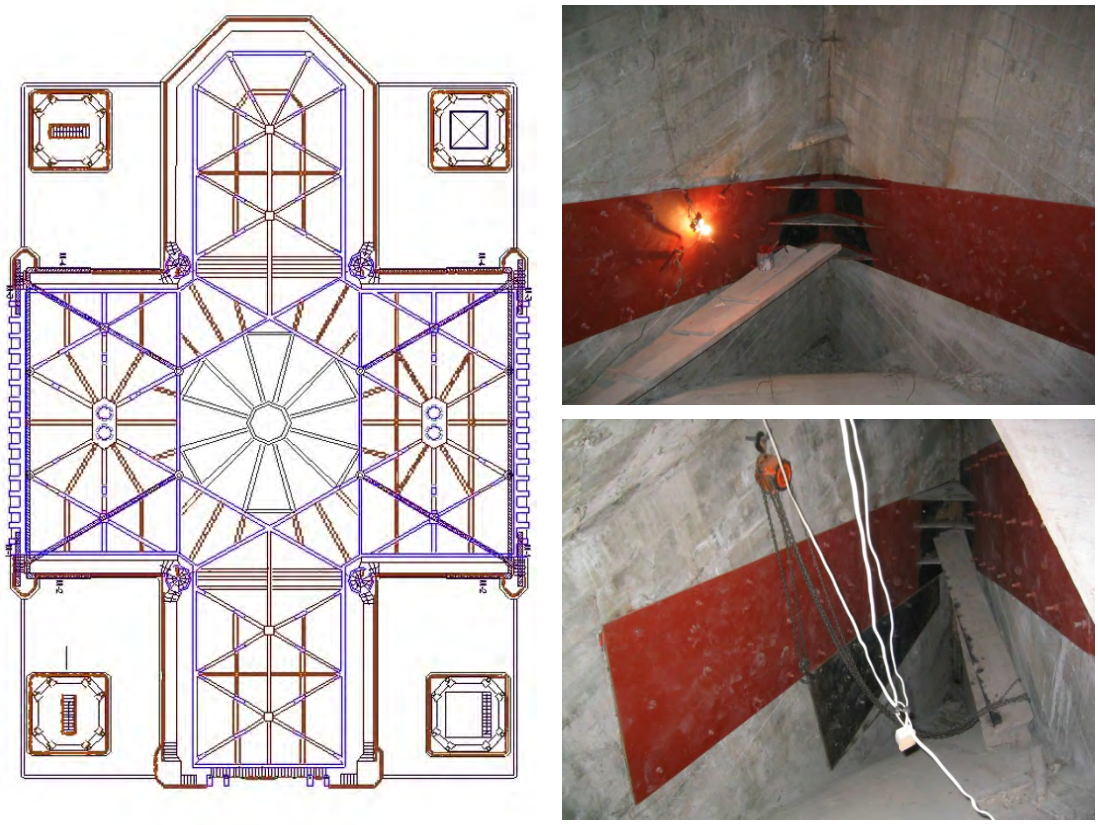


Figure 5: Steel beams make up a diaphragm and connect the heads of the structural walls

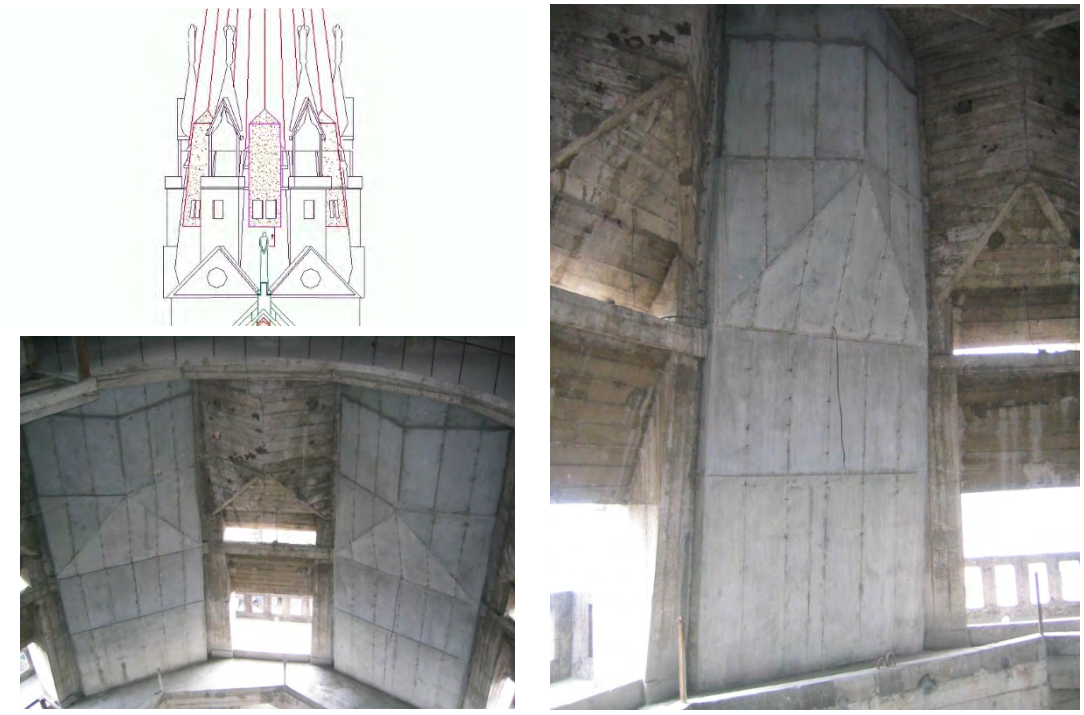


Figure 6: Internally attached reinforcing walls were constructed at the base of the central spire

Two phases of this maintenance were planned. In its first phase, the most urgent activities were included. On the one hand, the removal of mortars from terraces, canals, and walkways, which were replaced with sloping cement to improve adhesion, waterproofing and mechanical resistance to traction and bending. This process was complemented by the application of a product that minimized cracking and where necessary additional reinforcements were made with welded mesh. The slopes were oriented towards the grilles that were projected according to the new hydraulic installations that were projected and made. Also, the washing and disinfection of the façade were carried out by applying a corrosion inhibitor and a water repellent was applied. A type of biocide with properly diluted benzalkonium chloride was applied and for the minimum recommended time, which was also facilitated with the use of plastic bristle brushes to improve the action of this product in the different layers of the dirt layers, particles pollutants, and biofilm that had formed over the years. Then the cleaning was carried out with a pressure washer with a pressure less than 750 psi, with a fan jet and more than 30 cm away between the nozzle and the concrete to avoid damage to the concrete. Once the surface dried, for which at least three sunny days were required, the corrosion inhibitor or passivator was applied to the reinforced concrete at the sites of greatest relevance of the bases and towers. This process had setbacks due to changes in color in the concrete that had to be corrected with abundant rinses and due to the need for the surface to dry, which was not facilitated due to persistent rains. Additionally, due to the lack of water pressure in the highest parts of the temple, a system that kept the pressure constant had to be developed. The final stage was the application of the water repellent in order to repel water, prevent corrosion and achieve a coating that prevents the new appearance of moss. To the extent that this product was applied, gaps and fissures were intervened with another product suitable for this type of repairs, on façades and towers from top to bottom to the 11.20 m level, pending completion of this work in a new phase that allows continuing until this treatment to the base of the temple. Figure 8 illustrates the new clean and clear appearance of the concrete surface of the Cathedral. The dark appearance that it had due to the dirt and carbonation that the concrete had suffered for many years was eliminated.

On the other hand, this was also the opportunity to repair the cornices and decorative elements of the façade, as well as the covering of the downspouts using a mixture of mortars or concrete using proportions of dyes. Multiple trial and error tests were performed in order to simulate the original color of the concrete of the Cathedral. Sixty-five samples and cores were taken to verify the carbonation state of the concrete and dust extraction tests to verify from a chemical point of view in the laboratory the condition of the concrete paste. Cleaning the interior vaults of bird droppings, garbage, fragments and even wood that were from the construction was carried out, and synthetic meshes were also placed to prevent birds from entering these sites as they did before. To improve water management that was very precarious, an appropriate system of siphons, grilles, and downspouts was constructed, and the sewer of the surrounding streets was replaced due to its very poor condition when its respective revision was made. Finally, as a result of the strong deterioration, twenty-two sculptures of the five spires of the temple were changed, replacing them with new ones or repairing them, which allowed preserving the original icons of the Cathedral. These images were made using weather-resistant epoxy resin and the existing cross in the central spire was replaced by the one called the Levitating Christ, which required not only careful technical work on materials, construction processes, platforms and scaffolding in height, but the skill and artistic ability of a renowned sculptor of the city. The concrete sculptures that are located on the roofs were also maintained, as well as the sculptures of the guardian angels located at the base of the central spire. The concrete of these images was washed, disinfected and hydrofuge was applied like in the structure.



Figure 7: Eight rods or tensioners provide stability to corner spires in case of an earthquake



Figure 8: The current appearance of the Cathedral after washing and concrete treatment and protection

5 CONCLUSIONS

A summary description of the interventions of the structure, the conditions of the concrete, the decorative elements and the sculptures, which have been made to the Cathedral of Manizales, have been presented. These interventions were the result of the Integral Project of Diagnosis and Design of the Structural Reinforcement, which was disclosed in 2000 [5]. The reports indicated the works of structural reinforcement and protection of the monument that should be carried out to protect this masterpiece of Colombian architecture, after the study that was carried out on the state of the materials, modeling, and evaluation of the response seismic, vulnerability diagnosis and structural reinforcement design. The earthquake-resistant intervention was carried out between 2002 and 2004 and the treatment of concrete and other necessary interventions were carried out between 2016 and 2017 [6]. This illustrates the effort that is necessary in these cases to obtain the necessary economic and professional resources to carry out the protection works of a heritage monument. Although the second phase of maintenance is still needed, which must actually be permanent in such a structure, it can be concluded that the decision of a number of people committed to these efforts, with their expertise and management, have been the ingredient fundamental to ensure that this monument has been protected and that it is preserved for posterity, with the aim of continuing to be an emblematic masterpiece of the local seismic culture of the city of Manizales.

Acknowledgements. These works were supported by Departamento de Caldas, Subdirección de Monumentos INVIAS, Fundación Amor por la Catedral Basílica de Manizales, Municipio de Manizales, Findeter, Arquidiócesis de Manizales, Ministerio de Cultura, Dirección de Patrimonio.

REFERENCES

[1] Cardona O.D., García-Reyes, L.E., Aycardi, L.G., and Esguerra, J.E., Ocampo, J.G., Zambrano, J., Arcila, C.A., Correal, J.F., Jaramillo, J.D., Estrata, W., Sarmiento, J.M., Prieto, S.D. *Proyecto Integral de Diagnóstico y Diseño del Reforzamiento Estructural, 1997-1999,* Departamento de Caldas, Subdirección de Monumentos, INVIAS, (1999). Manizales.

[2] Prieto, S.D., Estrada, J., Botero, J.B. *Construcción del Reforzamiento Estructural Sismorresistente, 2002-2004,* Aquaterra, S.A., Caseven, Ltda., Fundación Amor por la Catedral Basílica de Manizales, Municipio de Manizales, Findeter. (2004). Manizales.

[3] Arcila, C.A. *Evaluación detallada de la patología del concreto*. (2013). Manizales.

[4] Londoño, J.I., Muñoz, J.F., Vallejo, L.G., Estrada, H., Mejía, E., Bermúdez, J.M., Cardenas, D.C., Flórez J.F., Serpa, E., Parra, C.R., *Reparación y Mantenimiento, Conservación y Restitución de Esculturas, 2016-2017.* Arquidiócesis de Manizales, Diprecón, Ministerio de Cultura - Dirección de Patrimonio, (2017). Manizales.

[5] Cardona, O.D. Protegiendo nuestro patrimonio. Estudios de vulnerabilidad y reforzamiento estructural: Catedral Basílica de Manizales *Noticreto* (2000) **55**:59-65.

[6] Cardona, O.D. and Prieto. S.D. Protección de un monumento emblemático. Refuerzo, rehabilitación y restauración de la Catedral de Manizales *Noticreto* (2019) **154**:10-15.

12th International Conference on Structural Analysis of Historical Constructions
SAHC 2020
P. Roca, L. Pelà and C. Molins (Eds.)

ADAPTATION OF A MID-NINETEETH CENTURY REPRESENTATIVE UNIVERSITY BUILDING TO OFFICE FUNCTIONS

J. SZOLOMICKI[1], M. MINCH[2], G. DMOCHOWSKI[1] AND P. BERKOWSKI[1*]

[1]Faculty of Civil Engineering
Wroclaw University of Science and Technology
Wyspianskiego Blvd. 27, PL50-370 Wroclaw, Poland
grzegorz.dmochowski@pwr.edu.pl,
piotr.berkowski@pwr.edu.pl (*corresponding author),
jerzy.szolomicki@pwr.edu.pl

[2] VEGACAD Design and Implementation Office
89, Agrestowa Str., PL53-006 Wroclaw, Poland
minch@vegacad.com.pl

Keywords: Historical Building, Masonry, Revitalization, Structural Solutions, Construction

Abstract
The rehabilitation of historical buildings plays an important role in enhancing the sustainable built environment of a city. Re-use of old buildings when adapting them to new functions has become a common way to protect the significance of historical buildings and keep them for future generations as examples of the achievements of former architects and construction masters. Issues connected with the adaptation of an old university three-story building from 1866 that has exceptional artistic qualities is the subject of the analysis presented in this paper. Originally, the building was multifunctional, and intended for the activities of various university units. During the II World War, the main body of the building was seriously damaged. After the war, the building was reconstructed using the current building materials and construction solutions, and was handed over to the Medical Department of Wroclaw University. The building is now undergoing renovation, the purpose of which is to change its function into an office building. The greatest value of the building is its façade - with excellent proportions - which perfectly fits into the spatial context and the development of this part of the city. For this reason, the preservation of the building's main structure was the most important aspect of the renovation design process. The paper presents the results of the assessment of the building's technical state, analysis of the planned functional changes and renovation ideas, and finally, a description of the structural and constructional solutions adopted to solve the problems occurring during the renovation works.

1 HISTORICAL OUTLINE OF THE FORMER UNIVERSITY BUILDING

The building, with its exceptional artistic value (Fig. 1), was designed by the outstanding Wroclaw architect Theodor Milczewski and put into use in 1866 [1].

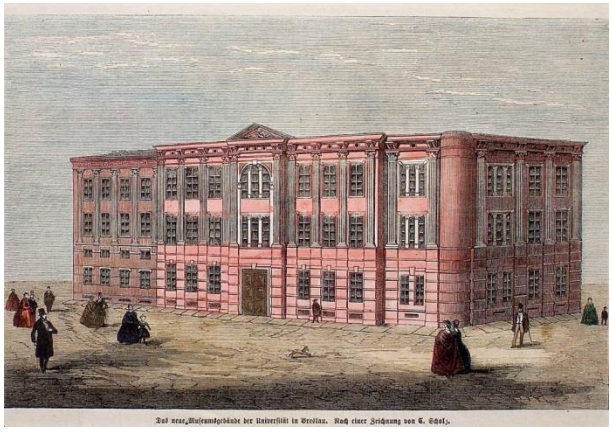


Figure 1: General design view (from north) of the building presented in a newspaper from 1866 [2]

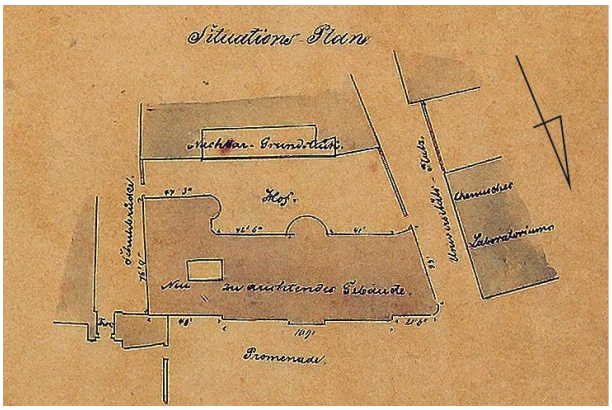


Figure 2: Location of the considered building within the city environment (1864) [3]

The three-story building was located on Grodzka Street (Burg Str.), which ran along the promenade by the Odra river (Fig. 2). The building filled the entire northern part of the area between Szewska Street (Schuchbrücke Str.) and Uniwersytecki Square (Universität Platz). From the east it was adjacent to the middle school of St. Maciej that was located in the baroque Monastery of Crusaders of the Red Star, and from the west it was adjacent to the Institute of Chemistry that was erected 10 years earlier.

The main entrance to the building (Fig. 3) was located from Grodzka Street and led through a representative vestibule and staircase to a museum and lecture halls. In addition, a short side wing was erected on Szewska Street, which had residential and auxiliary functions (Fig. 4). The Pharmacy Institute was located on the ground floor of the newly erected building. It continued the traditions of the university pharmacy, which was founded by the Leopoldina authorities and later leased by Wilhelmin University.

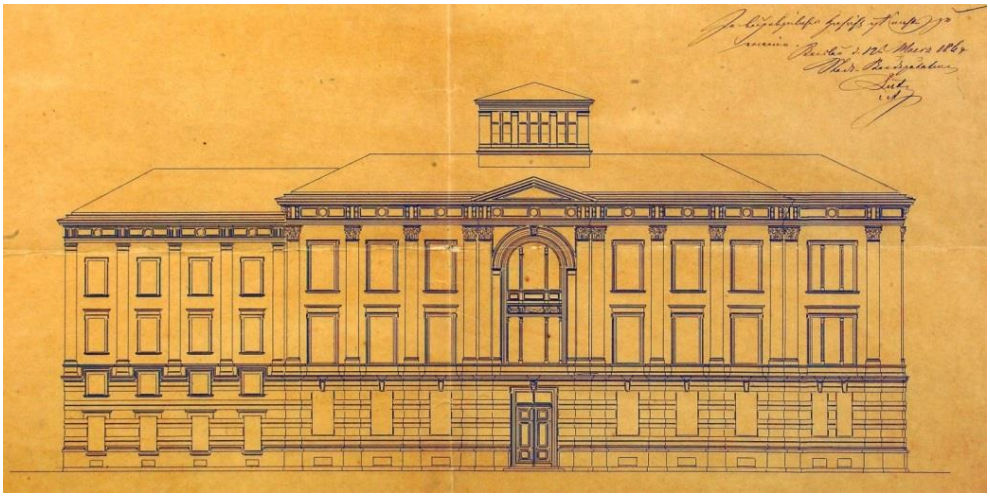


Figure 3: Archival view of the front (northern) building elevation (1864) [3]

The museum that was located on the upper floors of the building collected and presented mineralogical, petrographic and paleontological collections. The lower wing along Szewska Street initially had mainly residential functions: on the full floors there were flats with several rooms for researchers, while in the mezzanine above the ground floor there were three smaller flats for servants and watchmen. Over time, the residential function gradually gave way to the need to arrange an increasing number of offices for researchers.

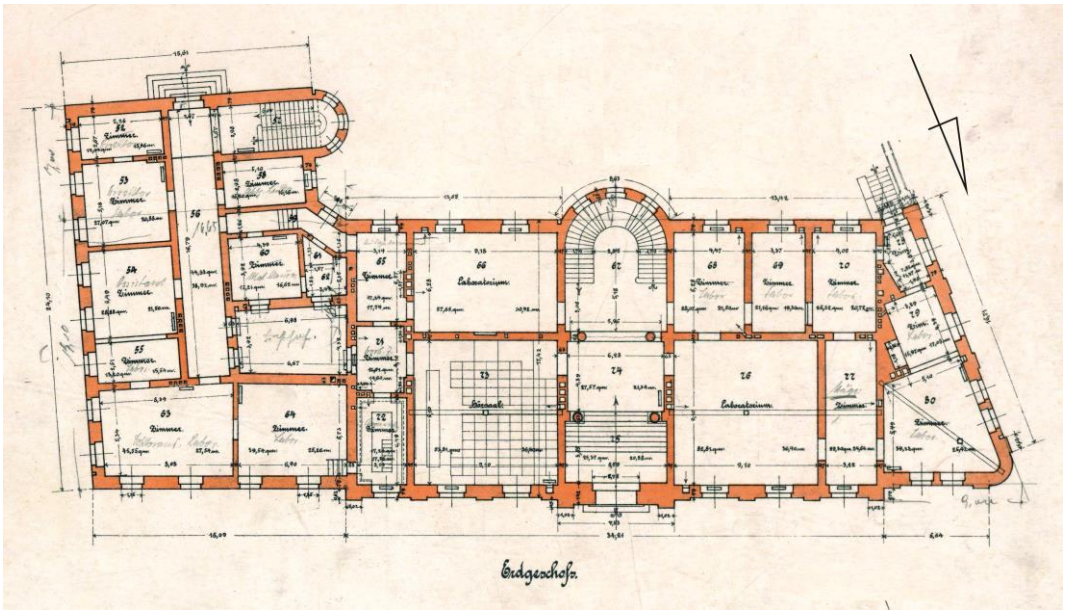


Figure 4: Archival drawing of the first floor (1930) [3]



Figure 5: View of the destroyed building in 1945 (southern side) [4]

During the war in 1945, the main body of the building was seriously damaged (Fig. 5). The eastern part of the building, which included the entire lower wing along Szewska Street that was originally residential, survived without any major damage to its body and slate roof. In turn, the main body of the building was completely burned out, and the part located on the west of the vestibule and the main staircase was demolished to ground level. The ruined building was handed over to the Faculty of Medicine of Wroclaw University and to Wroclaw University of Science and Technology. It was meant to be the location for the Pharmaceutical Department.

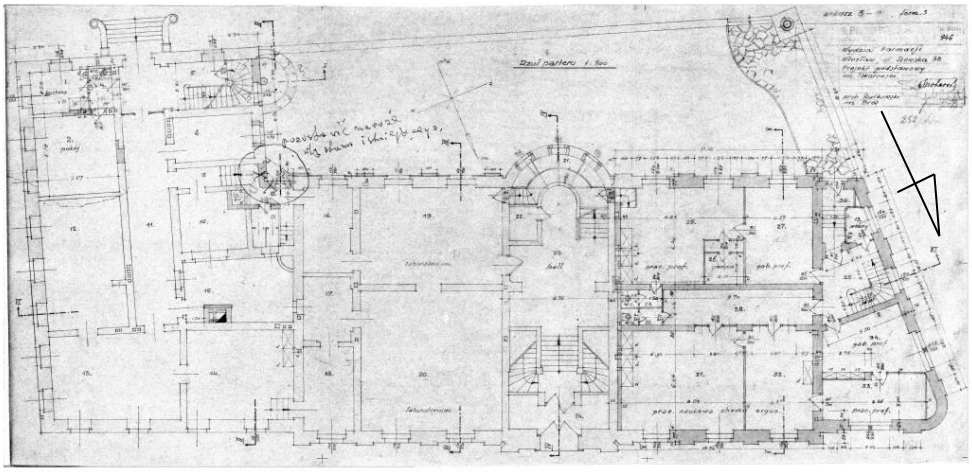


Figure 6: First floor plan – 1955 reconstruction design [3]
(darkened walls at the right side – existing ones; walls at the left side – reconstructed)

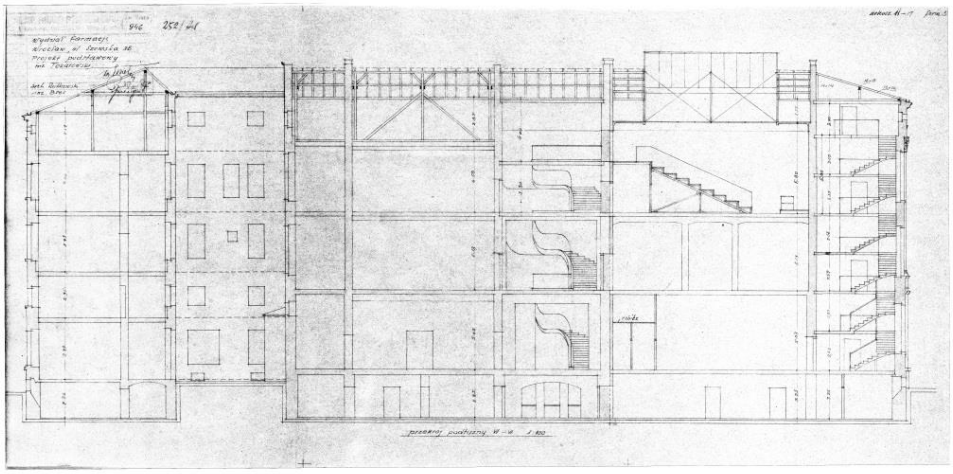


Figure 7: Cross-section VI-VI (east-west direction) of the building – 1955 reconstruction design [3]

The renovation of the eastern part of the building, with the main staircase and vestibule, was completed in 1948. A provisory lecture room on the first floor, and a workshop for inorganic and analytical chemistry on the second floor, were opened at that time. The

reconstruction of the west wing began in 1955 (Figs. 6, 7). Renovation work included the construction of new floors. A reinforced concrete slab was made above the basement where the bunker was planned, while in the rest of the basements and on the upper floors there were massive dense ribbed floors. In addition, steel roof trusses with a skylight were made above the auditorium room.

2 THE STRUCTURAL LAYOUT AND DIAGNOSIS OF THE TECHNICAL STATE OF THE BUILDING

2.1 The building's current architectural and structural elements

The analyzed building is a freestanding object, situated on a plan that is similar to the letter L, and consisted of two parts: the west and east wings (Fig. 4). The building has three floors above ground (a ground floor and two upper floors), an unused attic, and a basement. In the east wing there is an additional floor between the ground floor and the first floor - the mezzanine (Fig. 8).



Figure 8: Current view (from north) of the front façade of the building

The greatest value of the building can be seen to be its historic front (northern) façade, and its body with excellent proportions, which perfectly fits into the spatial context of the estate. The façade from the Grodzka Street side is distinguished by a seven-axis avant-corps. The entrance portal is located on the axis of the apparent avant-corps. Above the portal, there is a two-storey triple window, which is finished with a full arch, enclosed by an arcade that is supported on Tuscan pillars, and topped with a keystone with a carved head.

The in between window pillars and small pilasters that support the cordon cornice, which are placed on the line of pediments of the other windows of the first floor, have decorative details in the form of the Doric order. Above the façade axis there is a tall, three-axle belvedere. The four-axis façade of the lower side wing is expressed similarly to the facade of the body. The eight-axis eastern (side) façade is also preserved in a similar style, however, the Tuscan pilasters only decorate the corners of the building.

The foundation of the building is in the form of brick continuous footings, with or without offsets. Under part of the continuous footings there is a foundation made of stone boulders, which may indicate that the previously existing foundations were locally used as a foundation of this building. The width of the continuous footings is from 0.75 to 1.00 m, and the height is about 1.90 m. The depth of the foundation of the continuous footings is 3.35 m below the existing terrain, and 1.85 m below the existing floors in the basement. The main structural system of the building consists of walls made of solid brick with varying thicknesses (Figs 4, 6 & 7). The basement walls are made of solid brick, and have the following thicknesses: external walls from 0.38 to 1.00 m, and internal structural walls from 0.38 to 0.80 m. Horizontal wall insulation was found, but there is no vertical insulation. The upper wall thicknesses amount to approx. 1.02 to 0.64 m for the external walls, and from 1.02 to 0.38 m for the internal structural walls.

The completed structural inventory showed a very large variety of types and systems of floors. In the eastern wing, segmental vaults and the Klein floor on steel beams were found above the basement. The upper storeys have wooden floors and locally Klein slabs. The west wing is even more diverse in terms of its floor structures. Above the basement there are segmental vaults, prefabricated ribbed floors, and also reinforced concrete slabs. On the upper floors there are prefabricated floors, Ackermann slabs, and reinforced concrete slab floors. The roof structure is also not a homogeneous solution for the entire building. There are classic wooden purlin-rafter and suspension systems in the east and west wings, and a completely different arrangement of steel trusses above the auditorium in the west wing (Fig. 7).

2.2 The diagnosis of the technical state of the building

As a result of the detailed analysis of the technical condition of the building, which was carried out before the renovation design works started, it was found that the entire facility is in a poor technical condition. This forces the necessity of a wide range of renovation works to be carried out. The reason for the building's condition was primarily due to its long-term operation without conducting appropriate renovation and modernization works, the natural wear of the used materials, and also environmental impacts.



Figure 9: Exposure of the foundation walls



Figure 10: High dampness of the basement walls

With regards to the condition of the foundations, and based on the conducted exposure works (Fig. 9), it was found that they were probably made at a variable level of the load-bearing soil layers. In addition, the level of groundwater in the vicinity of the building is above the level of the native load-bearing soils, and a quick water flow into the executed excavations was observed. It was also found that all the basement walls have a very strong moisture content – the existing horizontal insulation no longer fulfills its function (Fig. 10). It was necessary to dry the walls and to at least make horizontal insulation using the injection technique.

Static calculations showed that the foundations of the left internal walls do not have a sufficient load-bearing capacity to transfer the designed loads. These foundations must be reinforced by e.g. jet-grouting. In addition, due to increased vibrations that are generated by trams passing on the neighboring Szewska Street, it was also recommended to jet-grout the wall of the building along this street. However, the analysis of the working conditions of the entire facility after strengthening the foundations showed that jet-grouting of only part of the walls will change the rigidity of the entire building and may contribute to the cracking of walls in different places. Therefore, for the implementation of the modernization project, it was recommended to strengthen the foundations of all the load-bearing walls of the building.

In the external walls, nearly all the brick window lintels and the under-sill walls located underneath them have been scratched or cracked. However, the largest extent of damage occurs in the wall that is located by the street that is loaded with tram traffic (Figures 11, 12, 13). Consequently, it was recommended that all repair work on the brick lintels and windowsill walls should be carried out before the demolition of ceilings.

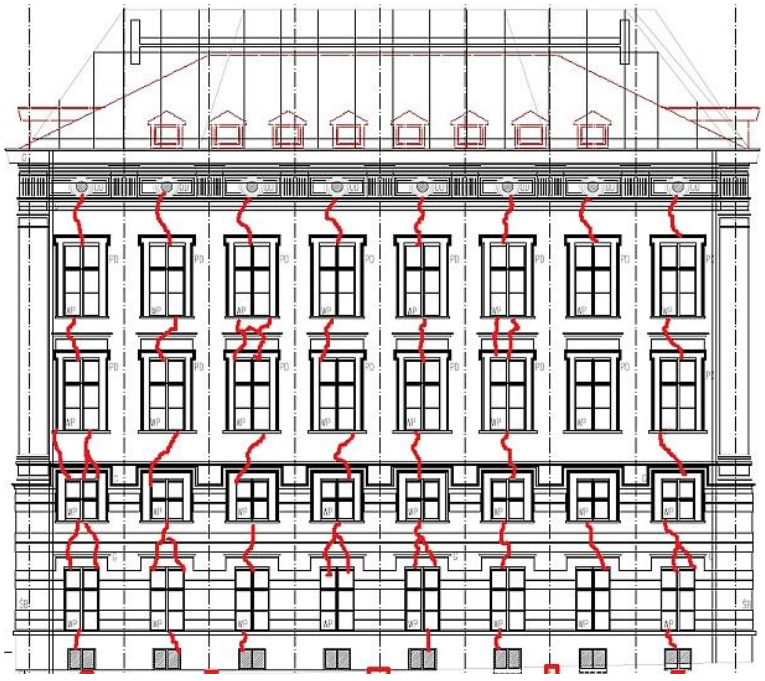


Figure 11: The location of cracks in the side (eastern) façade lintels and wall



Figure 12: Example of cracks in lintels and walls



Figure 13: Exemplary cracks in lintels

In the case of the internal walls of the building, which will remain in accordance with the architectural concepts, are currently, despite damage that locally occurs in them, in a sufficient technical condition. However, the structure of most of these walls is very heterogeneous: there are numerous traces of reconstruction, holes, and masonry works. Most of the transverse walls have a large number of ventilation, exhaust and other technical ducts, which were used by the laboratories that previously existed in the building. The course of these ducts is practically impossible to determine. Static calculations, which were preceded by tests of masonry samples and by NDT methods, showed that the majority of the walls and internal pillars do not have a sufficient load-bearing capacity to transfer designed loads, and therefore they require reinforcement with e.g. reinforced concrete sleeves.

3 CONCEPT OF THE BUILDING'S RENOVATION - SOLUTIONS OF STRUCTURAL PROBLEMS

The adaptation project of the historic building includes the renovation, reconstruction and change of its operation function into a public service one. The planned adaptation program for the facility also involves the use of basement floors as technical rooms. The ground floor and higher floors will be allocated for office spaces.

The design of the reconstruction of the facility for new utility purposes forces the implementation of a very wide range of demolitions (Figs 14, 15). From the existing building, only the external walls, part of the internal walls, a fragment of brick vaults above the basement in the south-east part, and a staircase located in the corner of the building will remain.

Wooden floors, Klein type slabs, ribbed Ackermann and concrete hollow brick floors are planned to be replaced with monolithic reinforced concrete floors supported on reinforced concrete ribs, as well as with a RECTOR ribbed ceiling. Because the replacement of floors and the execution of works related to the perforation of existing walls can cause secondary scratches and cracks, it is proposed to strengthen the surfaces of the walls in the FRCM (Fiber Reinforced Cementitious Matrix) system, which is based on a matrix made of mineral mortar and PBO (Polyphenylene Benzobisoxazole) fibers.

Regarding the roof structure, it was considered to construct a reinforced concrete flat ceiling with a roof in the spatial form with a glazed aluminium structure, which would be supported on large-size reinforced concrete perimeter beams and anchored in the perimeter tie beam of the knee walls. An innovative roof construction solution also involves the use of a recessed tub for air conditioning devices in order for the roof to maintain a regular outline and for these devices to not be visible (Figs 14, 15).

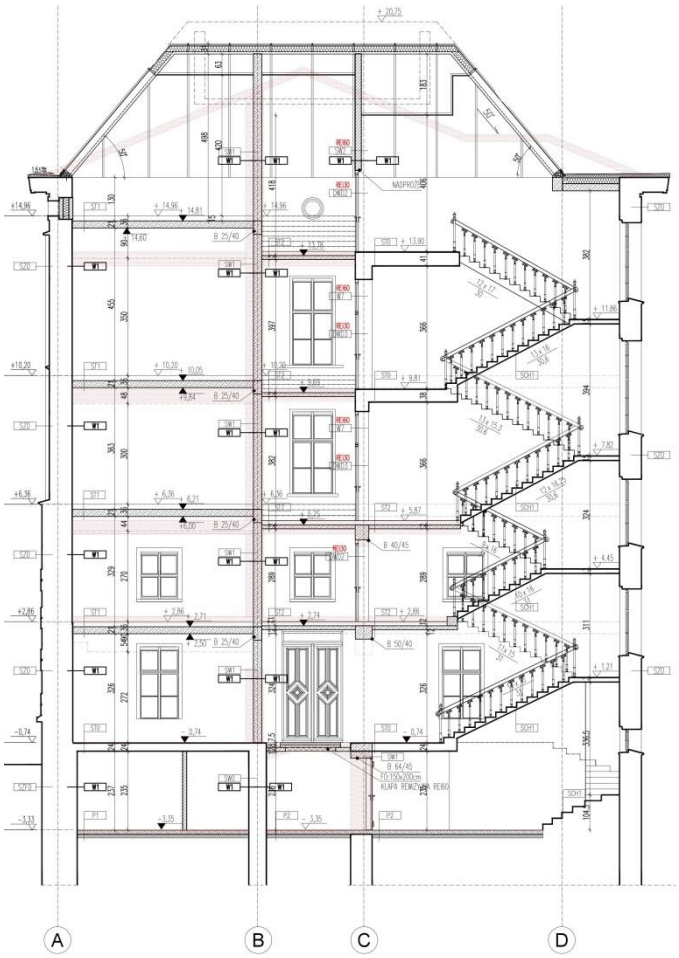


Figure 14: The cross-section (eastern wing) of the building showing the demolition plan (darkened walls) [5]

During the implementation of such a wide range of demolitions, it is very important to stage the demolition and reconstruction works. In order to adapt the building to its new form, a one-stage method of building renovation was proposed. It consists of performing demolition and reconstruction works using a combined method – partially using the "chimney" (bottom-up) method, which involves demolishing the ceilings and restoring their structure from the bottom to the top, and partially using successive dismantling of the ceilings with their reconstruction being conducted from the top to the bottom of the building (Fig. 16).



Figure 15: The cross-section (east-west direction) of the building with the demolition plan (darkened lines) [5]

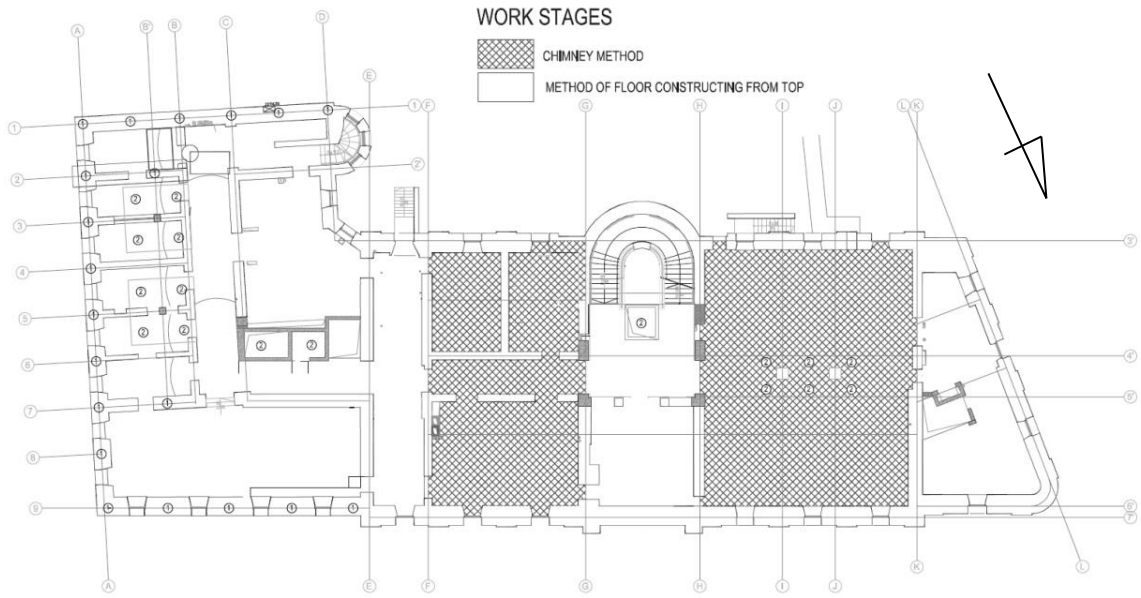


Figure 16: The plan of the combined method of renovating the building [6]

Such a solution will ensure the stability of the walls without the need to mount additional temporary steel safety elements. The proposed combined way of performing the demolition and reconstruction works will also enable the renovation time to be significantly reduced and the commissioning of the building to be faster, which will in turn translate into an economic profit of the investment and a reduction in the costs of protections.

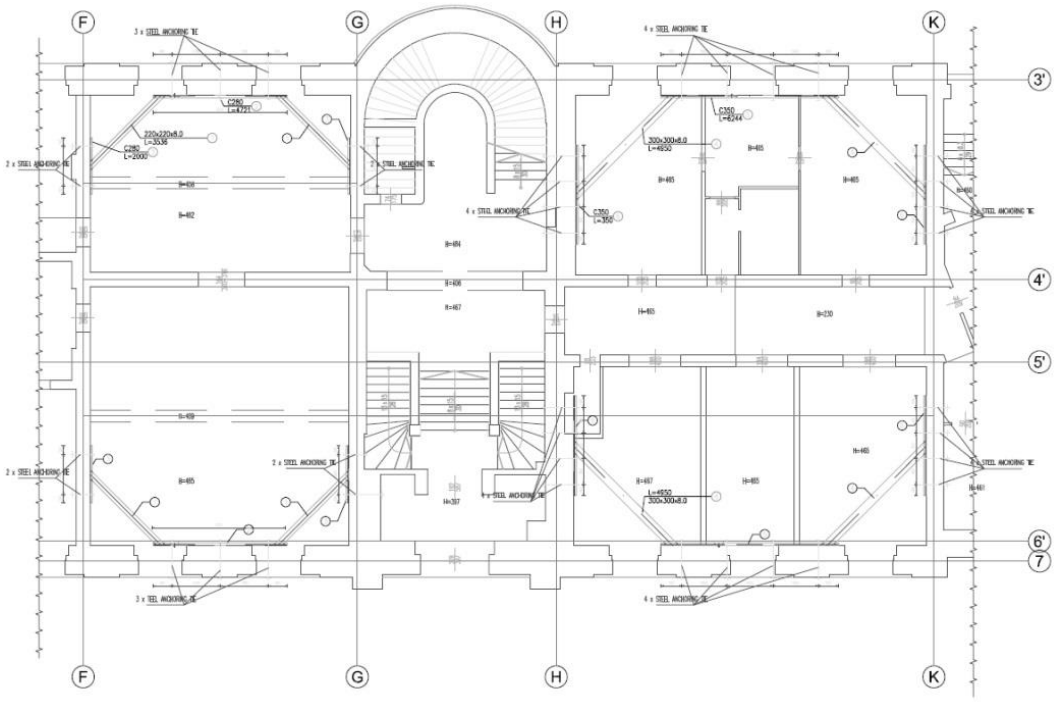


Figure 17: Scheme of wall stability protection that involves a steel structure for the “chimney” method [6]

The proposed combined building renovation technique will be carried out in one stage, and will cover a period of 1.5 years, whereas the originally planned reconstruction of individual parts was planned for 2 years and was meant to be conducted in stages.

In the part of the building where the ceilings will be demolished up to the basement ceiling, the protection of the walls’ stability will involve the use of a temporary steel structure. Moreover, it is planned to reconstruct all the ceilings from the bottom to the top - the hatched surface in Figure 16. Other parts of the building will be made using the method of successive demolition of ceilings and by reconstructing them from the top to the bottom of the building (Fig. 16).

The use of temporary steel protections for the walls’ stability when using the "chimney" method is shown in Figure 17. The angle brace protections will be installed successively, along with the demolition of the ceilings from the top to the bottom on each floor. The angle brace protection will be installed above the demolished ceiling at a height that is equal to half of the distance between the top of the ceiling and the windowsill in the wall. Such an assembly technique will allow for a collision-free reconstruction of monolithic ceilings from the bottom to the top of the building.

4. FINAL REMARKS

The article presents in a general way selected aspects of the architectural and structural modernization of an old university building that was built in the first half of the 19th century. One of the requirements of the proposed adaptation was to preserve the historical context of

the building at the same time strengthening and supplementing the value of the cultural heritage of the city of Wroclaw. All the methods of changing the building structure and adapting it to new functions were developed and applied after reaching a compromise with conservation services regarding the possibility of interference in the historical character of the building [7].

Due to the technical condition of the building, the construction design and the plan of the execution of works had to include complex works, such as:

- performing jet-grouting under all the foundations of the building;
- securing the stability of the building's walls along their entire height due to the very wide range of necessary demolitions;
- use of modern floors;
- preserving the form and shape of the roof, which was designed to contain all the technical equipment (incl. HVAC and fire protection systems).

The most challenging works connected to the building refurbishment are demolitions of some of its structural elements (walls and floors) with parallel construction of the necessary temporal stability structural strengthening. These works are planned to be performed at the same time in two ways, depending on the range of demolition: bottom-up method in which demolishing of the ceilings and restoring their structure is done from the bottom to the top, and up-down method in which dismantling of the ceilings with their reconstruction are to be conducted from the top to the bottom of the building. The proposed combined building renovation technique will cover a period of 1.5 years, whereas the originally planned reconstruction of individual parts was planned for 2 years.

REFERENCES

[1] Kodzis, E. *Wrocławskie Kamienice. Grodzka 9.* Available online: http://wroclawskie-kamienice.blogspot.com/2015/09/ul-grodzka-9.html, Accessed: 9 January 2020 (in Polish).

[2] https://fotopolska.eu/Wroclaw/b9533,Grodzka_9_-_Szewska_38-39.html?f=105513-foto.

[3] Building Archive of City of Wroclaw.

[4] https://fotopolska.eu/Wroclaw/b9533,Grodzka_9_-_Szewska_38-39.html?f=704451-foto.

[5] Architectural design of reconstruction, renovation and change of use of a public building at ul. Grodzka 9 in Wroclaw, Maćków Design Office, (2016).

[6] Technical expertise of a public building at ul. Grodzka 9 in Wroclaw, VEGACAD Design and Implementation Office, (2019).

[7] Roca, P., Lourenco, P.B. and Gaetani, A. *Historic Construction and Conservation. Materials, Systems and Damage*. Routledge, (2019).

12th International Conference on Structural Analysis of Historical Constructions
SAHC 2020
P. Roca, L. Pelà and C. Molins (Eds.)

AN INTERDISCIPLINARY APPROACH FOR THE EXPERIMENTAL ASSESSMENT OF THE SEISMIC SAFETY OF ARTWORKS

ALESSIA DI MARTINO[1], GIUSEPPE COCUZZA AVELLINO[1], EMANUELA PATERNÒ[1], FRANCESCO CANNIZZARO[1*], IVO CALIÒ[1], GIANFRANCO GIANFRIDDO[1], RITA VALENTI[1] AND NICOLA IMPOLLONIA[1]

[1]Department of Civil Engineering and Architecture (DICAR)
University of Catania
Viale Andrea Doria 64, 95125 Catania, Italy
e-mail: alessiadimartino@alice.it, giuseppe.cocuzzaavellino@unict.it, patermanu@hotmail.it, francesco.cannizzaro@ unict.it, ivo.calio@unict.it, ggianfrid@unict.it, rvalenti@unict.it, nicola.impollonia@unict.it www.dicar.unict.it (*corresponding author)

Keywords: Rigid block, Seismic vulnerability, Shaking table, Scale effect, Nonlinear dynamics, Digital model

Abstract. *Recent seismic events occurred in areas rich of ancient remains and full of cultural and artistic heritage in terms of artworks. Earthquakes may damage buildings, but the vibrations may also induce the uplift and overturning of their content, implying irreparable loss of cultural values. The seismic assessment of objects is usually tackled modelling them as rigid blocks. This paper focuses on statues, which generally present a very complicated geometry, and proposes a general methodology involving different disciplines, for their experimental seismic assessment. The methodology is here applied to the masterpiece of "Paolo Orsi" museum in Syracuse (Italy), that is the "Venere Landolina". Due to the complexity of statues, traditional techniques cannot be considered reliable for a proper geometry reconstruction; therefore, Terrestrial Laser Scanner (TLS) and Unmanned Aerial System (UAS) technologies are here employed to obtain a highly detailed and complete digital model. Aiming at providing a low-cost scaled physical model of the statue, a wooden specimen has been arranged employing a Computer Numerical Control (CNC) milling machine, cutting off disks from flat panels which are then superimposed and glued, progressively reconstructing the actual geometry of the statue. The specimen, able to approximately reproduce the scaled actual geometry, was then tested on a shaking table with ground motions compatible with those expected for the site where the statue is located. The obtained results are finally correlated with those expected for the real scale statue.*

1 INTRODUCTION

The seismic assessment and protection of the content of buildings represents a challenge of modern engineering; it is relevant in two main cases, that is machinery located inside strategic buildings (e.g. hospitals, control towers) which have to keep their operability in the earthquake aftermath, and artworks whose damage would imply a significant cultural economic and social loss. It is reasonable to consider such objects as lightweight bodies.

In the context of the seismic protection of artworks, the crisis of the material is encountered only in few cases, for which FE models are usually employed, mainly to study and interpret the presence of cracks in statues in static [1] and dynamic [2] conditions. Such objects mostly tend to get damaged not so much for material crisis as for their uplift and the subsequent overturning. For this reason, there is a broad literature aiming at a proper modelling of such systems in seismic conditions; most of these models are based on the rigid body motion [3]-[10], which is governed by nonlinear differential equation. Even in the case of simplified geometry the rigid body motion is difficult to be modelled because of the impairments in the contacts with the base [11] and due to the chaotic character of the rigid body motion [12]. Analogous studies on geometrically complex objects are rarely considered [13] since the governing equations are further complicated; moreover, experimental studies in such cases are prohibitive due to the difficulty to faithfully reproduce specimens consistent with the original model in the laboratory. The interest towards the seismic protection of artworks has been growing in the last decades. Some masterpieces, such as Michelangelo's David [1], the "Juno's fountain" [2] and the "Bronzi di Riace", underwent detailed studies, and in the latter case their seismic protection is assured by a ball system isolation [14]. Other studies concerning the seismic isolation of lightweight objects can be found in [15],[16].

The study presented in this paper is focused on statues, and presents a novel interdisciplinary approach for the experimental assessment of statues involving survey, technology and structural skills. The proposed methodology is applied to the "Venere Landolina", the masterpiece of "Paolo Orsi" museum in Syracuse (Italy). The proposed approach includes three main phases: a) the 3D digital modelling of the statue by means of UAS and TLS technologies, b) the reconstruction of a scaled wooden model created with a CNC milling machine based on the digital model, c) the experimental campaign conducted with the application of ground motions compatible with the design spectrum by means of a shaking table, the interpretation of the results, and the correlation with the actual geometry of the statue. The three phases of the proposed methodology are briefly elucidated and then applied to the chosen case study, showing its applicability to other meaningful artworks.

2 SEISMIC PROTECTION OF ARTWORKS: THE CASE OF THE "VENERE LANDOLINA" IN "PAOLO ORSI" MUSEUM

The proposed methodology aims at the assessment of the seismic safety of lightweight objects. In the context of artworks, former studies were conducted oriented to their seismic protection. Some of them are oriented to describe the main mitigation strategies [17], some others are detailed studies of statues. In the case of the "Bronzi di Riace" a low invasive semi-passive isolation system (based on a ball system with dissipative wires) on a marble base was devised [14]. In the case of Michelangelo's David, a detailed FEM study was conducted to verify the riskiness associated to cracks observed on one of the legs [1].

In the following sections a novel methodology for the seismic assessment of statues involving an experimental campaign on a scaled specimen, reconstructed with a faithful geometry, is proposed. The proposed methodology includes three phases which are summarized in Figure 1. All the considered phases require the adoption of advanced hardware and software tools. The stages of the proposed strategy can be summarized in a *knowledge phase*, a *prototyping phase* and the *seismic assessment*. The knowledge phase consists in a non-invasive geometric scanning of the statue (see section 3 for details) and the manipulation of the output of the survey providing a photorealistic digital model of the statue. In the prototyping phase the solid model is further processed, and a 3D digital prototype is elaborated; the obtained simplified model represents the input to create a scaled physical counterpart, by superimposing of wooden disks shaped with a Computer Numerical Control machine (see section 4 for details). Finally, the physical prototype is tested on a shaking table considering ground motions compatible with the design spectrum and duly modified to account for the scale factor of the specimen; the results obtained by experimental campaign are elaborated with a tracking motion software and interpreted with the aim of rating the safety of the statue (see section 5 for details).

The conceived methodology is here applied to a meaningful case study selected in the archeological museum "Paolo Orsi" in Syracuse (Italy). Specifically, the "Venere Landolina", that is the masterpiece of the museum, is considered, Figure 2. The marble structure goes back to the II century A.D. and is probably a copy of a former greek statue; its name is related to Saverio Landolina, the archeologist who discovered the Venere in 1804. This artefact was selected for its artistic relevance, but also for some geometric features which make this case study particularly meaningful. The statue is quite slender, which makes it keen to the uplift, and is also irregular since the position of the center of gravity is not centered with respect to the base. In the first column of Figure 1 the main steps of the proposed methodology applied to the Venere Landolina are depicted where the physical model and the intermediated stages of the digital models are easily identifiable. The statue, which is placed on a 80 cm high pedestal, with a hexagonal base inscribed in a circle of radius 160 cm, is 165 cm tall, has the base of support inscribed in a rectangle of 55,6x50,6 cm. The mass of the marble object, approximatively equal to 430 kg, is estimated considering a volume of 162098.79 cm^3 and a specific weight equal to $\rho = 0.00265$ kg/cm^3.

3 3D DIGITAL MODELLING OF THE STATUE

The present study establishes a synergy between the teaching and research methodologies and between technological innovation and operational technologies of the specific subject areas, in particular, surveying and data processing and communication.

It is important to develop digital integrated strategies in order to obtain an efficient performance of all the research indicators. In general, the study wants to provide the scientific community with an operational protocol for the virtual rendering of artistic and museum objects [18]. In particular, 3D modelling aims to the development of a physical model for the seismic evaluation of sculptures. In this regard, 3D computer graphics gives an immediate perception of reality less affected by discretization modalities than traditional drawing.

The implementation of software which can transform data coming from TLS, UAS technologies and photogrammetry into 3D models allows the visualization and 3D printing

concretisation of artistic objects characterised by sinuous geometric shapes. The present experimental work on "Venere Landolina" has been conducted with the innovative technological instruments of the Laboratory of Representation, SDS of Architecture, University of Catania.

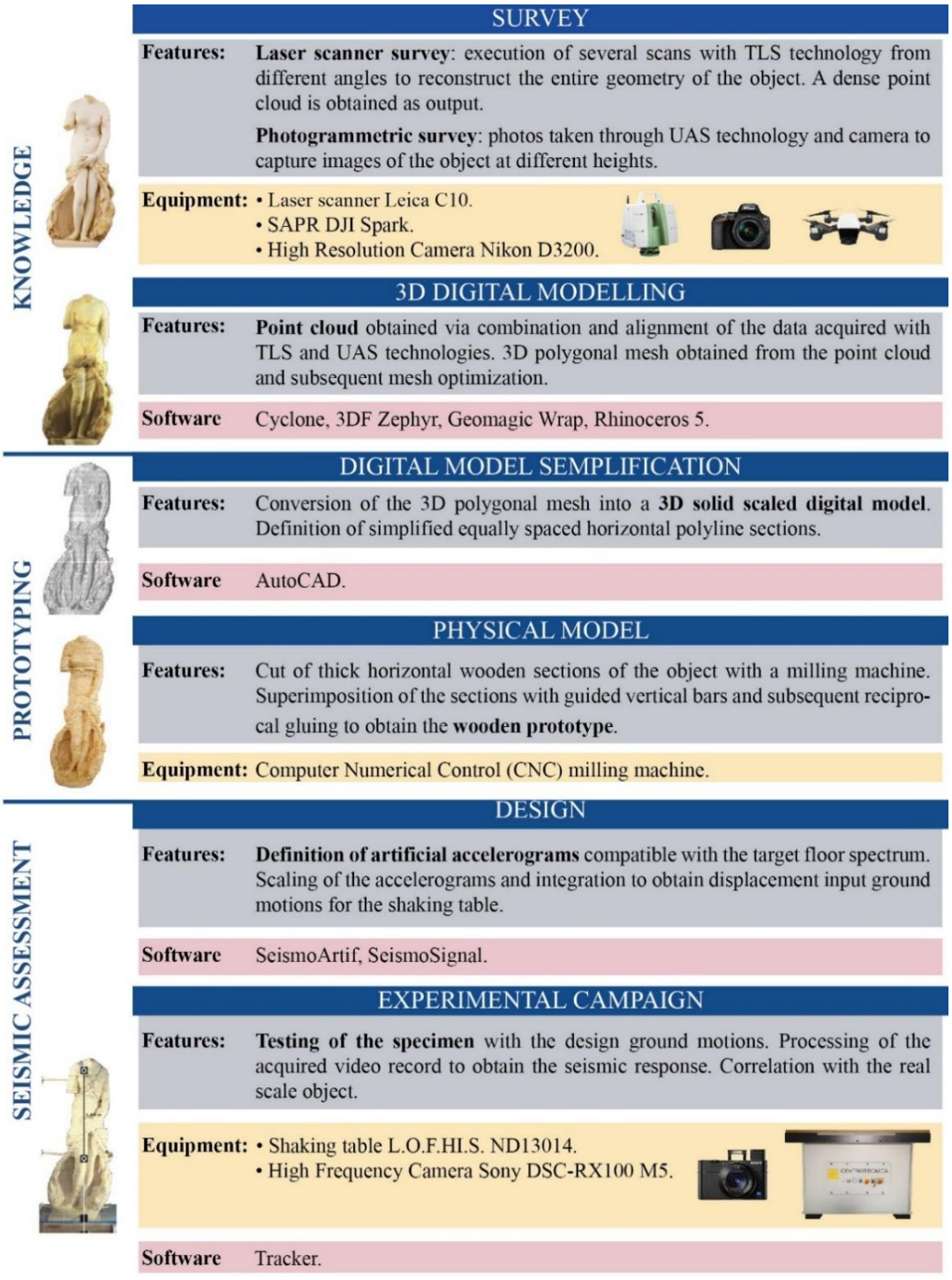


Figure 1: The proposed methodology.



Figure 2: Venere Landolina

The methodological process of the 3D model production through a high precision mathematical representation of the object surface, provided the virtual development of the real artistic object.

The formal complexity of the examined sculpture suggested, as previous research [19], an integrated survey analysis obtained through the combination of range-based and image-based techniques. More specifically, starting from data acquired with TLS, Terrestrial Laser Scanner, and SfM, Structure from Motion, the research produced a 3D model able to provide complex information, to visualize formal material and colour data and to analyse and interpret architectural data.

From the operational point of view, two survey campaigns have been conducted: the first instrumental survey campaign was conducted with Leica Scan Station C10, Figure 3; the second photogrammetric survey was performed with digital camera and UAS technology, Figure 3.

In the first campaign, in particular, four targeted scans were obtained in order to accurately align the various digital images in the post processing phase through Cyclone Software.

In the second campaign various shots were taken at different heights turning around the sculpture.

SfM technique can produce a texturized 3D model starting from a set of digital shots. 3DF Zephyr Aerial can automatically process image features, all the visible key-points on different shots, creating correspondences for the image matching. The detected features were then computed in a 3D sparse point cloud and all the coordinates to the key-points of the surrounding items were optimized to generate a dense point cloud.

In order to acquire a greater amount of data, UAS technology has been introduced. It can produce high-resolution imagery which is almost impossible to obtain with traditional systems. In the specific case, a quadcopter DJI Spark weighing just 300 grams captured aerial imagery of the upper surface of the Venus.

This technology has aroused considerable interest in the scientific community and UAV, Unmanned Aerial Vehicles, are used in different fields of engineering, architecture and archaeology [20]-[23].

It generates, rapidly and at low cost, the necessary data for the production of precise models with the integration of vertical and oblique imagery.

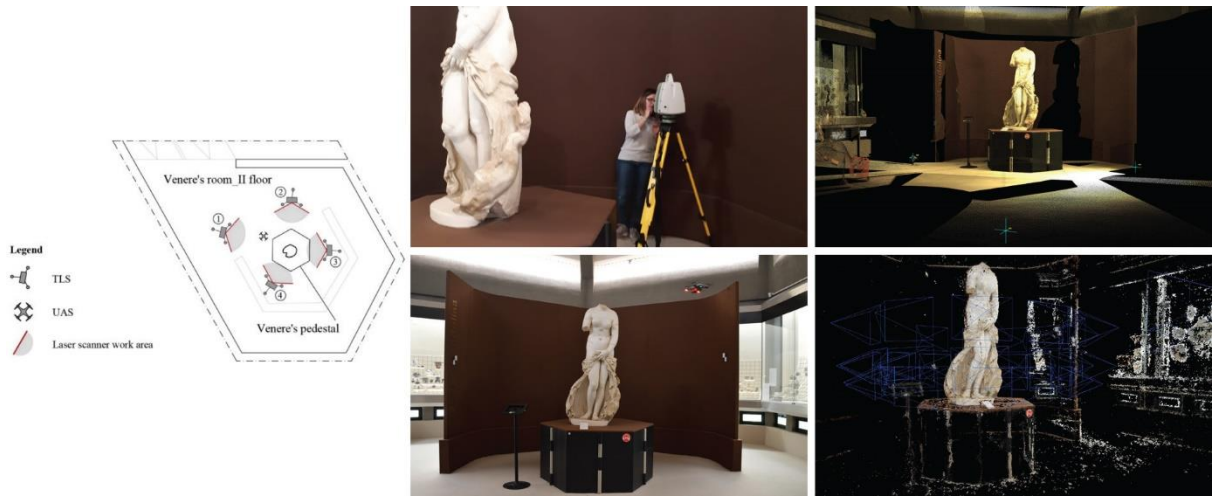


Figure 3: TLS and UAS technology

The point cloud obtained with instrumental survey was imported to 3DF Zephyr Aerial and the dense point cloud obtained from digital automatic photogrammetry was aligned to it. Such a model was then exploited to start the mesh generation and texture mesh generation in order to obtain a photorealistic 3D model.

Finally, Geomagic Wrap performed a long and patient retopology procedure in order to optimise the polygonal model generated through the integration of the different applied techniques, Figure 4.

The last phase was extremely important to create the final printing of the model. The use of quick prototypization generated a single copy of the physical model exclusively designed for the study and the proposed research. For the correct interaction between the survey product and the printing instrument, it was necessary to convert the model to .dxf format in order to ensure system compatibility.

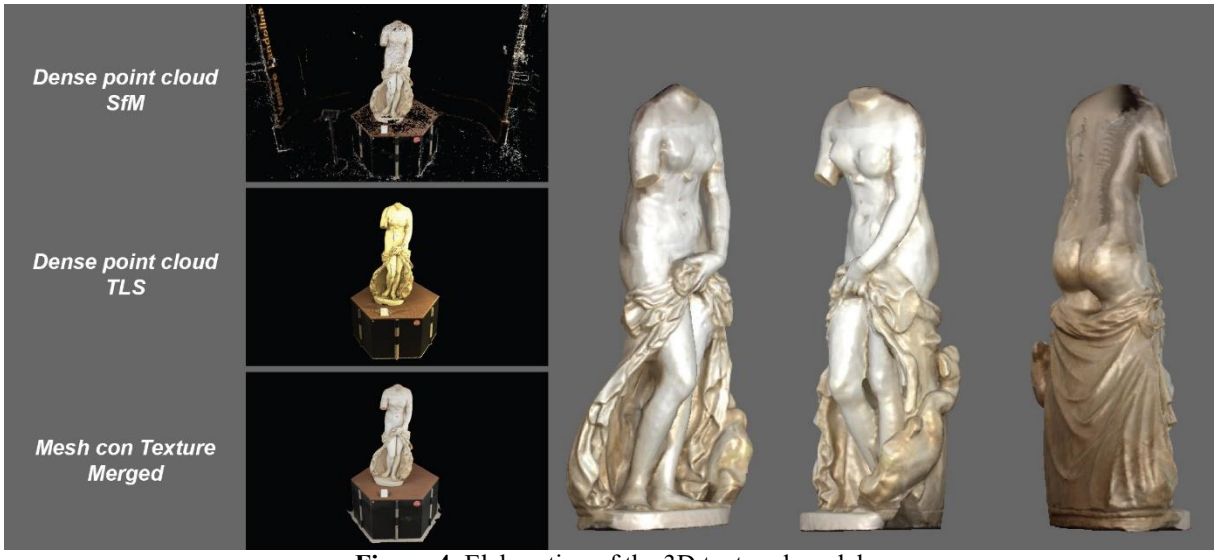


Figure 4: Elaboration of the 3D textured model

4 RECONSTRUCTION OF A WOODEN SCALED PHYSICAL MODEL

The digital model arranged in the previous section has to be manipulated to generate proper input files to reconstruct a scaled and simplified physical model of the statue. In particular, a wooden specimen (with scale factor 1:2) is created by superimposing thick sections to each other obtained by flat OSB (Oriented Strand Board, a product made of glued wood shavings layers) 9 mm panels. To this purpose, the solid model is cut with equally spaced horizontal planes (with spacing equal to the thickness of the OSB panels), identifying the contour of each section; each of the considered horizontal section is approximatively considered representative of a certain thickness (9 mm), Figure 5a. It is worth to mention that the main difficulty in reproducing the actual behaviour of the statue results not from the complex geometry but to the complex interface between the statue and its support on which it can rock, wobble and slide. The real marble statue might have different properties from those associated to the woodden specimen; for this reason, additional tests will have to be performed considering different contact materials.

91 sections are considered in this case taking into account the additional thickness of the glue, and the corresponding contours represent the input for the CNC milling machine. The cuts were performed adopting a cutter with a diameter of 3 mm and 2 blades, considering a depth increment equal to 4,7 mm, a cut velocity equal to 800 m/min and a safety vertical distance equal to 12 mm. The shaping of the 91 sections took 48 hours of worktime for the CNC machine, Figure 5b. In addition, each section is endowed with 2 (to 4) 10 mm holes intended to allow the insertion of vertical wooden bars to guide their superimposition, Figure 5c. Each section is then refined sanding their border. The assembly of the specimen and the subsequent glue hardening took 15 days. The final physical specimen has a height of 87,5 mm, a volume of about 20257,897 cm^3 and a weight of 12,073 kg and a footprint of about 28x28 cm. The position of the center of gravity is in relation to the left base edge at 19,7 cm (dir. x), 33,7 (dir. y), -14,0 cm (dir. z), Figure 6. Such edges have been chosen considering the smallest base of the statue; however, for a comprehensive study additional experimental tests considering different input direction should have been performed.

The simplified scaled digital model of the statue depicted in Figure 5a-d allowed to easily identify some geometric features of the specimen, as shown in Figure 6 where the adopted reference system is also identified. As better shown in the next section, the specimen will be subjected to ground motions through a single degree of freedom shaking table. The two edges around which the specimen can rotate are identified as 1 and 2, and the relevant geometrical moments of inertia around the edges are equal to I_1 = 4,2808 x 10^7 cm^5 and I_2 = 3,6318 x 10^7 cm^5, respectively. The critical angles which may lead the statue to the overturning are δ_1 = 30,31° and δ_2 = 13,84° in the negative and positive directions, respectively.

5 THE EXPERIMENTAL CAMPAIGN

Aiming to a proper seismic assessment of the statue, the scaled wooden specimen was subjected to shaking table tests considering different ground motions. The experimental setup includes a single degree of freedom shaking table (from the LO.F.HI.S. series ND13014 (Low Frequency High Stroke and Velocity Shaker) and a high frequency acquisition camera (DS-RX100 M5) for contactless displacement data acquisition. To this purpose, the video records are processed using the Tracker Video Analysis and Modeling Tool software ver. 5.0.7" [24].

Details on the experimental setup, on the contactless data acquisition and the subsequent data processing can be found in [11].

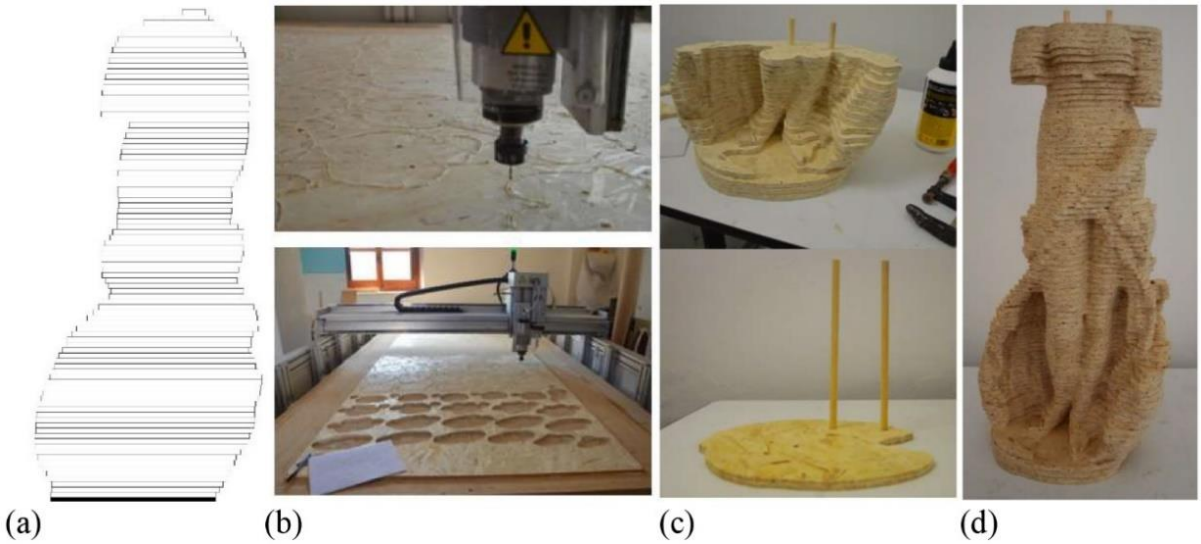


Figure 5: Wooden scaled specimen: (a) simplified digital model, (b) CNC machine, (c) superimposition of the sections, and (d) near-final result.

The design of the experimental campaign was performed considering the design spectrum for the location where the Venere Landolina is located (Syracuse, Italy) according to the Italian code [25], considering a soil type C and the SLA limit state according to the Italian guidelines for artistic heritage [26]. A floor spectrum is duly considered which allows accounting for the location of the statue inside the museum (second of three levels with equal interstorey).

Since no specific data of the building were available the fundamental period T_s of the structure was estimated according to the following approximated formula $T_s = C\,H^{3/4} = 0.32\ s$

In Figure 7 the adopted design spectrum is depicted, together with the main data for its definition.

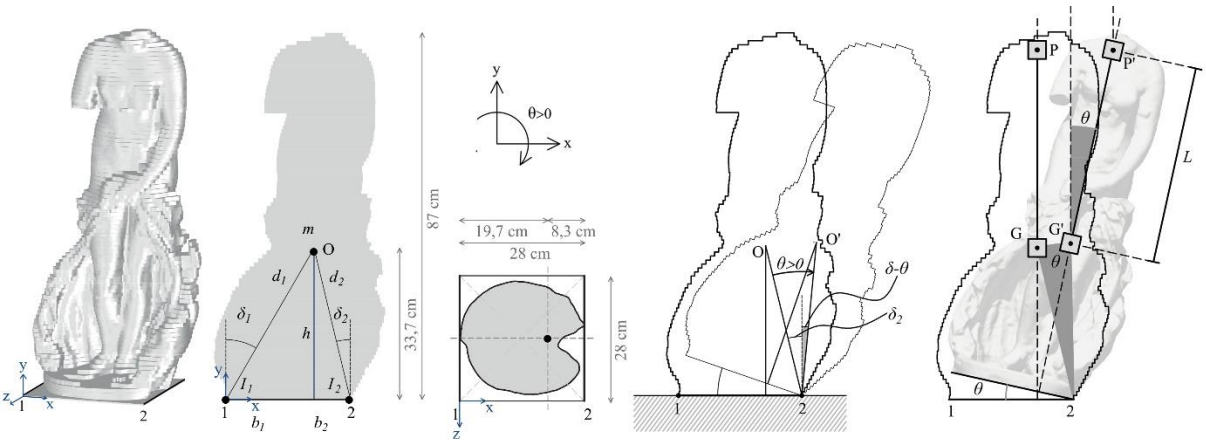


Figure 6: Main geometric features of the wooden specimen and adopted kinematic model and markers layout

Seven artificial spectrum-compatible accelerograms were then generated through the software SeismArtif [27]. Since the scale factor λ of the specimen with respect to the actual statue is equal to 2, in order to obtain the ground motion to be applied to the shaking table, the time axis was scaled by a factor $\lambda^{0.5}$, according to the Froude analogy [28]. One of the generated accelerograms is reported in Figure 8 (light grey) together with the corresponding scaled one (black); in the same Figure the theoretical (dashed lines) and experimental (dashdot lines) uplift accelerations (for both side) are also reported. The spectrum compatibility of the generated accelerograms is duly verified, Figure 7; then, the scaled accelerograms are integrated twice thus defining the input ground motions to be applied to the specimen with the shaking table.

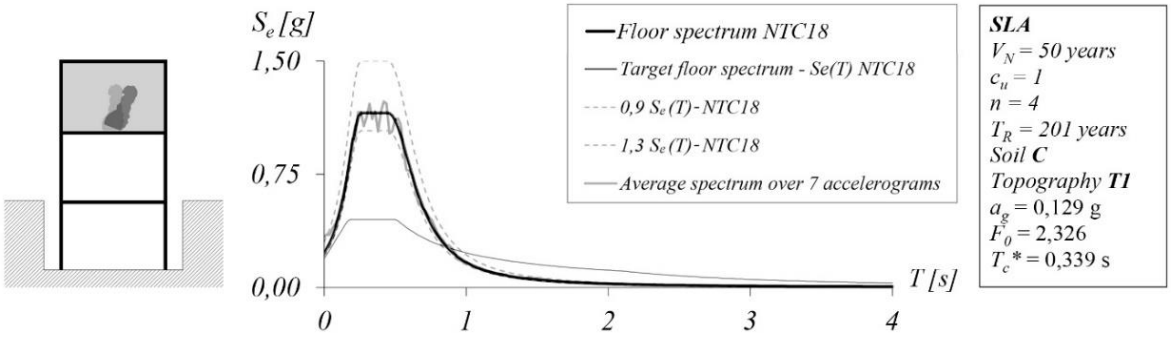


Figure 7: Design spectrum adopted to generate the ground motions and spectrum compatibility

Each of the accelerograms was then applied twice to the specimen considering both sides. The results obtained for all the considered tests, after being duly processed considering the markers layout identified in Figure 6, are collected and reported in Figure 10 for all the considered tests.

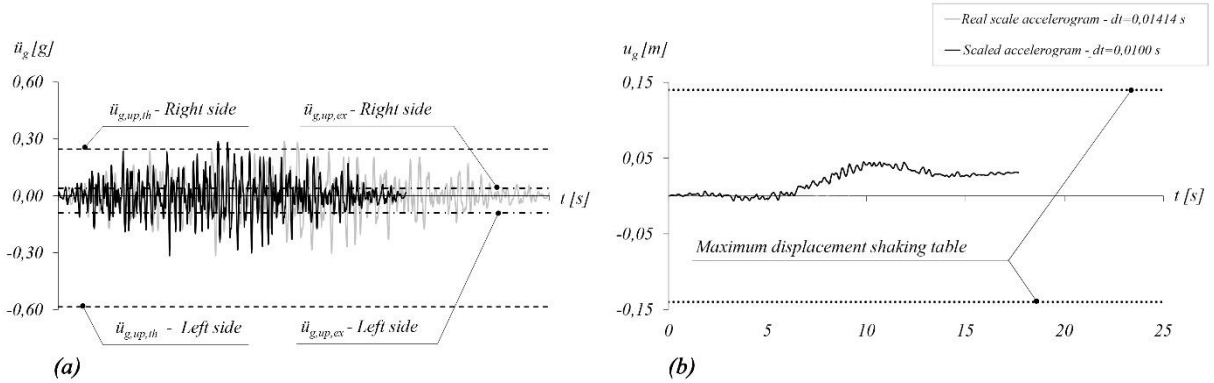


Figure 8: Design of the experimental campaign: (a) artificial accelerogram and corresponding scaled one, (b) input ground motion for the shaking table.

The obtained results show that, as expected, the specimen uplifts for all the considered ground motions (the normalized Peak Ground Acceleration is greater than the ratio b_i/h, i=1,…,4); however, no overturning is observed. The obtained responses in terms of rotation angle θ, normalized by the minimum critical angle δ_2, show that the specimen tends to a more pronounced rocking around the edge 2. The average maximum angle over the seven ground

motions for the positive and negative directions are $\theta_{av_max,1}$ = 8,26° and $\theta_{av_max,2}$ = 24,82°, respectively; the corresponding absolute values are $\theta_{ab_max,1}$ = 12,30° (observed for the 5th accelerogram^{+}) and $\theta_{ab_max,2}$ = 47,26° (observed for the 1st accelerogram^{-}), respectively, which are those reported in Figure 9.

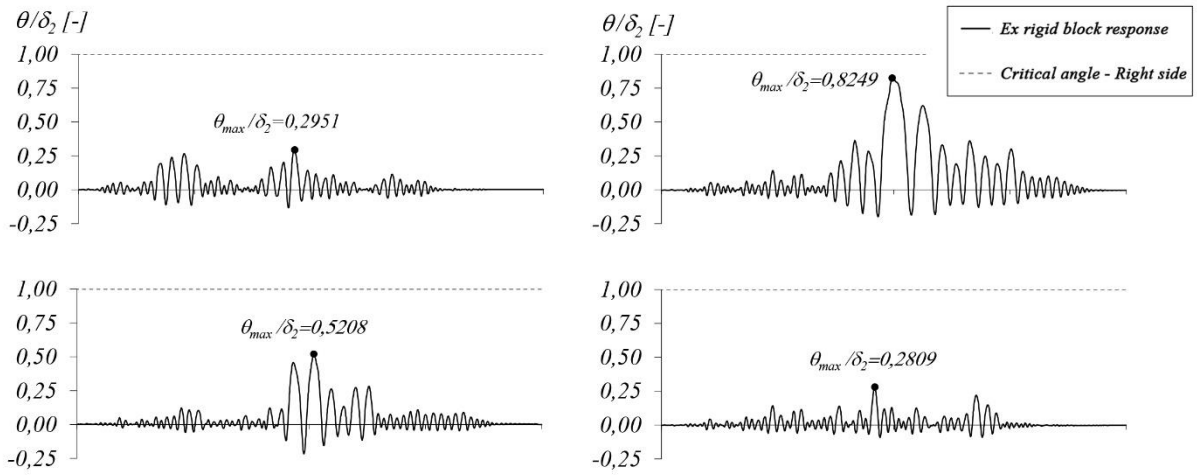


Figure 9: Normalized angle response vs time: (a) positive and (b) negative ground motions

The specimen and the real scale statue, according to the Buckingham theorem, should provide comparable response in terms of angles, therefore, the safety rating obtained for the wooden specimen should apply for the real statue as well.

CONCLUSIONS

- In this paper a novel interdisciplinary methodology to experimentally assess the seismic safety of lightweight artefacts is proposed. The procedure is here applied to the Venere Landolina statue, preserved in Paolo Orsi museum in Siracusa (Italy).
- The proposed strategy involves the construction of a scaled wooden specimen based on a digital model obtained by means of a laser scanner non-invasive relief and photogrammetry survey using UAS and TLS technologies.
- After processing and scaling the 3D digital model, the physical model is obtained through superimposition of wooden thick sections, properly shaped by means of a Computer Numerical Control machine.
- The specimen is then tested on a single degree of freedom shaking table, considering seven artificial spectrum-compatible ground motion, duly modified to account for the scale factor of the specimen with respect to the real statue. Specific guidelines for artistic heritage are employed to generate the accelerograms.
- The obtained results show a limited variability of the specimen response to the different inputs, and a substantial safety of the statue with respect to the design earthquake. As expected, the different properties of the specimen with respect to the load directions imply a strong asymmetry with respect to the uplift side.
- The proposed methodology, which involves several disciplines, has the great advantage to allow conducting experimental tests (through the construction of a

faithful physical model) on objects of priceless value. The original artefact does not undergo any direct contact and does not need to be moved to capture its geometry. Objects with complex geometry can be handled without loss of generality. The obtained results show the applicability of the proposed geometry on a larger scale.

Acknowledgements. The authors gratefully thank the management of the "Paolo Orsi" museum, in particular Dr. Maria Musumeci, for her sensitivity toward the seismic protection of the museum content and for the authorization to carry out the survey of the "Venere Landolina". This research was partially supported by the research project "eWAS – A nearly warning system for cultural heritage".

REFERENCES

[1] Borri, A. and Grazini, A. Diagnostic analysis of the lesions and stability of Michelangelo's David. *Journal of Cultural Heritage* (2006) **7**:273-285.

[2] Cerri, G., Pirazzoli, G., Tanganelli, M., Verdiani, G., Rotunno, T., Pintucchi, B. and Viti, S. Seismic Assessment of Artefacts: The Case of Juno's Fountain of the National Museum of Bargello. *IOP Conference Series: Materials Science and Engineering* (2018) **364**, 012057.

[3] Housner, G.W. The behavior of inverted pendulum structures during earthquakes. *Bull. Seismo. Soc. Am.* (1963) **53**:404-417.

[4] Aslam, M., Godden, W. G. and Scalise, D. T. Earthquake Rocking Response of Rigid Bodies (1978) Lawrence Berkley Laboratory.

[5] Giannini, R., Giuffre, A. and Masiani, R. La dinamica delle strutture composte di blocchi sovrapposti: studi in corso sulla colonna Antoniana, VIII Congresso nazionale dell'Associazione Italiana di meccanica Teorica ed Applicata, 1986, Turin, Italy 29-September – 3 October, **1**:299-304.

[6] Spanos, P.D., Di Matteo, A., Pirrotta, A. and Di Paola, M. Nonlinear rocking of rigid blocks on flexible foundation: analysis and experiments. *Procedia Engineering* (2017) **199**:284–289.

[7] Ioannis, N., Psycharis, N. and Jennings, P.C. Upthrow of objects due to horizontal impulse excitation, *Bulletin of the Seismological Society of America* (1985) **75**(2):543-561.

[8] Chatzis, M.N., and Smyth, A.W. Robust Modeling of the Rocking Problem. *Journal of Engineering Mechanics* (2012) **138**(3) 247-262.

[9] Spanos, P.D. and Koh, A.S. Rocking of rigid blocks due to harmonic shaking. *Journal of Engineering Mechanics* (1984) **110**(11):1627-1642.

[10] Shenton III, H.W. and Jones, N.P. Base excitation of rigid bodies. I: formulation. *Journal of Engineering Mechanics* (1991) **117**(10):2286-2306.

[11] Cocuzza Avellino, G., Caliò, I., Cannizzaro, F., Caddemi, S. and Impollonia, N. Response spectra of rigid blocks with uncertain behaviour. COMPDYN 2019 7th ECCOMAS Thematic Conference on Computational Methods in Structural Dynamics and Earthquake Engineering M. Papadrakakis, M. Fragiadakis (eds.) Crete, Greece, 24–26 June 2019.

[12] Jeong, M.Y., Lee, H., Kim, J.H. and Yang, I.Y. Chaotic behavior on rocking vibration of rig-id body block structure under two-dimensional sinusoidal excitation (in the case of no sliding). *KSME International Journal* (2003) **17**(9):1249-1260.

[13] Di Egidio, A., and Contento, A. Seismic response of a non-symmetric rigid block on a constrained oscillating base. *Engineering Structures* (2010) **32**:3028–3039.
[14] De Canio G. Basi antisismiche in marmo per i Bronzi di Riace. *Archeomatica* (2011) **2**(1).
[15] Caliò, I. and Marletta, M. Passive control of the seismic rocking response of art objects, *Engineering Structures* (2003) **25**:1009–1018.
[16] Donà, M., Hugh Muhr, A., Tecchio, G. and da Porto, F. Experimental characterization, design and modelling of the RBRLseismic-isolation system for lightweight structures. *Earthquake Engng Struct. Dyn* (2017) **46**:831–853.
[17] Podany, J. An Overview of Seismic Damage Mitigation for Museums. International Symposium on Advances of Protection Devices for Museum Exhibits, April 13-17, 2015 Beijing and Shanghai China.
[18] Valenti, R., Paternò E., 2017. The Itineraries of Drawing: from museum works to art places. In: Territories and frontiers of representation, p. 1307-1314, Roma:Gangemi Editore, ISBN: 978-88-492-3507-4
[19] Valenti, R., Paternò E., 2020. Imagined spaces in church architectural furnishings: Solomon's temple in small scale architectural language. In: *Advances in Utopian Studies and Sacred Architecture*, Cham: Springer, in press.
[20] Remondino, F., Barazzetti, L., Nex, F., Scaioni, M., Sarazzi, D., 2011. UAV photogrammetry for mapping and 3d modeling -current status and future perspectives -. In: ISPRS International Archives of the Photogrammetry, Remote Sensing and Spatial Information Sciences, Volume XXXVIII-1, pp. 25-31 https://doi.org/10.5194/isprsarchives-XXXVIII-1-C22-25-2011
[21] Bolognesi, M., Furini, A., Russo, V., Pellegrinelli, A., Russo, P., 2014. Accuracy of cultural heritage 3D models by RPAS and terrestrial photogrammetry. In: ISPRS International Archives of the Photogrammetry, Remote Sensing and Spatial Information Sciences, Volume XL-5, pp. 113-119
[22] Aicardi, I., Chiabrando, F., Grasso, N., Lingua, A. M., Noardo, F., Spanò, A. T., 2016. UAV photogrammetry with oblique images: First analysis on data acquisition and processing. In: ISPRS-International Archives of the Photogrammetry, Remote Sensing and Spatial Information Sciences, Volume XLI, pp. 835-842
[23] Carnevali, L., Ippoliti, E., Lanfranchi, F., Menconero, S., Russo, M., Russo, V., 2018. Close-range mini-UAVs photogrammetry for architecture survey. In: ISPRS International Archives of the Photogrammetry, Remote Sensing and Spatial Information Sciences, Volume XLII-2, pp. 217-224
[24] D. Brown, C. Wolfgang, Simulating what you see: combining computer modeling with video analysis, MPTL 16 – HSCI 2011, Ljubljana 15 -17 September 2011.
[25] Ministero delle infrastrutture e dei trasporti, Decreto 17 gennaio 2018, Aggiornamento delle "Norme tecniche per le costruzioni" – NTC18
[26] Linee guida per la valutazione e la riduzione del rischio sismico del patrimonio culturale con riferimento alle Norme tecniche per le costruzioni di cui al decreto del Ministero delle Infrastrutture e dei trasporti del 14 gennaio 2008
[27] Seismosoft 2020 "SeismoArtif - A computer program for generation of artificial accelerograms". Available from URL: www.seismosoft.com.
[28] Sandro Longo, Analisi dimensionale e modellistica fisica. Principi e applicazioni alle scienze ingegneristiche, Springer-Verlag, Italia 2011

APPLICATION OF GEOPHYSICAL PROSPECTING METHODS FOR SOIL STRUCTURE CHARACTERIZATION OF THE CATHEDRAL OF SANTO DOMINGO, DOMINICAN REPUBLIC

PÉREZ-CUEVAS. JARUSELSKY[1*], FLORES-SASSO. VIRGINIA[1], PRIETO-VICIOSO. ESTEBAN[2], RUIZ-VALERO. LETZAI[1] AND SANDOVAL. SENÉN[3]

[1]Pontificia Universidad Católica Madre y Maestra, PUCMM
Av. Abraham Lincoln esq. Simón Bolívar
Santo Domingo, Distrito Nacional, Dominican Republic
e-mail: jaruselskyperez@pucmm.edu.do, www.pucmm.edu.do (*corresponding author)
email:{virginiaflores@pucmm.edu.do, letzairuiz@pucmm.edu.do}

[2] Universidad Nacional Pedro Henríquez Ureña, UNPHU
Av. John F. Kennedy Km 7 ½
Santo Domingo, Distrito Nacional, Dominican Republic
email: {eprieto@unphu.edu.do} http://www.unphu.edu.do

[3] Everest Geophysics
Cosme Gamella 23, 28270 Colmenarejo Spain
email: {senen@everestgeophysics.com} https://www.everestgeophysics.com

Keywords: Geophysical methods, MASW, H/V spectral ratio, Georadar, Cathedral of Santo Domingo

Abstract. *Hispaniola is in the edge of interaction between the North American and Caribbean plates. In this zone, the occurrence of earthquakes greater than 5.0, Mw is frequent, characterizing it as a seismically active zone. These earthquakes cause considerable material damage and can provoke loss of human lives. The Cathedral of Santo Domingo, Primate of the Americas, is in the Colonial City of Santo Domingo. It is the most important colonial building in Dominican Republic, was built between 1521-1541, and is a masonry building made with stone ashlars and covered with stone ribbed vault. However, it is essential to know about the possible seismic behavior that the ground could have in case of a relevant earthquake to try to avoid possible damage to this heritage. For this reason, the aim of this research is to apply geophysical prospecting methods for the seismic site characterization of the Cathedral of Santo Domingo. For this study, the geophysical methods applied were: MASW (Multichannel Analysis of Surface Wave), H/V Spectral Ratio and Georadar. The characterization of site conditions was determined with the values of the average shear wave velocity for the top 30 m of soil (Vs30) obtained with the MASW method. As a main result it was found that the site seismic class determined with the MASW method was type C-very dense soil and soft rock (360-760 m/s), according to the NEHRP classification. In addition, the Georadar tests allowed confirming that there are no unknown caverns in the basement of the Cathedral in the first 5 m, thus it is accepted as valid the seismic classification of the soil obtained by the MASW method.*

1 INTRODUCTION

Commonly, conventional seismic approaches to near-surface evaluation have been either high-resolution reflection studies or refraction studies dealing with a depth range of a few tens to hundreds of meters. In addition, geophysical surveys are useful tools to characterize the buildings making up the cultural heritage and to monitor the subsoil features on which they are constructed. The information obtained is necessary for planning future restoration work [1]. Therefore, the aim of this research is to apply geophysical prospecting methods for the seismic site characterization of the Cathedral of Santo Domingo.

In 2004, a seismic modeling to simulate a monostatic survey with a single simulation used a ground-penetrating radar (GPR) modeling by using the analogy between acoustic and electromagnetic waves. The exploding-reflector method provides the correct travel times of diffraction and reflection events, whereas the plane-wave method yields more realistic amplitudes and multiple reflections [2]. While in 2007, Barilaro et al., carried out the identification of natural or anthropic buried cavities under the church of St. Sebastiano in Catania, Sicily, Italy, where they used GPR surveys on the pavement of the church and three in situ drillings outside. Through this investigation, the existence of hidden structures was revealed; the results obtained by in situ drillings allowed a detailed characterization of the most superficial layers of the ground [3].

Georadar prospections and three mechanical drillings were carried out in 2008 in a Roman Amphitheatre of Catania, Sicily, Italy, by Castellaro et al., where they studied the lithological features of the foundation subsoil of the Amphitheatre and identified possible underground voids, buried crypts and other heterogeneities. In addition, they used a passive seismic method, which allows to retrieve information on subsoil stratigraphy and on possible seismic site effects [4]. In 2016, Leucci et al., carried out a case study that involves a geophysical survey employing the surface three-dimensional (3D) GPR techniques, to characterize the ancient Messapian Necropolis in Lecce, south Italy, characterized by different types of graves (pits dug in the bedrock or built with slabs, sarcophagi and hypogea) that lay also inside the settlement surrounded by city walls [5].

An integrated geophysical survey was carried out in 2018, to confirm the potential occurrence of archaeological remains of the Roman temple dedicated to the Emperor Augustus, at the Tarragona's Cathedral in Spain. The project included electrical resistivity tomography (ERT) and GPR [6]. Also, in 2018, Di Giacomo et al., studied the Medieval cave village of Casalrotto, Mottola, Apulia, Italy [7].

In 2019, Sabrina et al., carried out geophysical surveys for the dynamic characterization of a cultural heritage building and its subsoil: The S. Michele Arcangelo Church, Acireale, eastern Sicily, Italy [1]. These authors argued that the extensive use of geophysical techniques in the last decades, especially for surveys on the cultural heritage, is linked to their low or zero invasiveness, compared to other survey techniques.

On the other hand, the Multichannel Analysis of Surface Waves (MASW) technique was introduced in the late 1990's by the Kansas Geological Survey [8]. The method exploits proven multichannel recording and processing techniques that are similar to those used in conventional seismic reflection surveys. The MASW technique deals with surface waves in the lower frequencies (e.g., 1-30 Hz) and uses a much shallower depth range of research (e.g., a few to a

few tens of meters). The main advantage of MASW is its ability to take into full account the complicated nature of seismic waves that always contain noise waves, such as unwanted higher modes of surface waves, body waves, scattered waves, traffic waves, etc., as well as fundamental-mode surface waves [8].

Anukwu et al., used the MASW method to identify the cause of fractures/cracks observed on the walls and ceilings of a heritage building located in Georgetown, Malaysia. The S-wave velocity revealed that the site is composed of materials with a low shear wave velocity which varies across the site and with depth, thus determining a phenomenon that might be the possible cause of the observed fractures/cracks on the building [9].

In 2013, Tarque et al., carried out a soil seismic profile below the San Felice Martire church, at Poggio Picenze (L'Aquila area, Abruzzo, Central Italy). They studied field geologic observations and drilling and geophysical tests retrieved from previous investigation campaigns. These authors said that the dynamic soil properties were obtained by literature and by the test results. Amplification effects at the site under investigation have been estimated using fully 1D stochastic site response analyses and for the object motion seven (7) real records compatible to the Italian code-based spectrum referred to 475-year return period [10].

Cercato et al., in 2019, applied several geophysical techniques (ambient noise recordings, surface wave methods, electrical resistivity tomography and seismic downhole) to assess the geometry and the low-strain stiffness properties of the different geological units and to provide continuous subsurface imaging throughout the hill of Civita di Bagnoregio (Viterbo, Central Italy). The authors complemented the research with borehole seismic and geotechnical laboratory testing to provide a detailed dynamic/cyclic characterization of the lithotypes, which were used for investigating seismic site effects [11].

2 CATHEDRAL OF SANTO DOMINGO

The Cathedral of Santo Domingo is the most important colonial building of the Dominican Republic. It is the first cathedral in the new world (built between 1521 and 1540). Its construction begins with the arrival of Bishop Alexander Geraldini, who had the support of King Charles V. The church is oriented east-west, with the entrance to the west and the altar and polygonal Apse to the east. In the Cathedral the space is based on a canonical study of proportions. It has the ratio of 1:2 (Double Square), where the length of the church is almost double the width and it is adjusted to the golden proportion, characteristic of the late Gothic [12]. The geometrical-proportional layout of the plant and elevations of the church is based on mathematical relationships established on the golden ratio. The height from the floor to the keystone of the central nave is identical to the width of the central nave plus the side nave, giving the golden ratio.

The Cathedral is a saloon plant, with three naves, seven sections with an octagonal presbytery with five faces, fourteen chapels between buttresses and a sacristy on the south side. The floor plan is almost a perfect rectangle that has 45.80 m long by 23.40 m wide, covered with Gothic ribbed vaults and tercelets. The vaults are supported by circular pillars and columns. The church is made of coralline and marly limestone blocks. From the bottom of the presbytery to the entrance it is 54.60 m long. The central nave is 9.63 m wide from column to column and the lateral naves are 4.80 m each.

The Cathedral is delimited by to the north, the Colón Park. To the south, the Plaza of the

Priests and the Caribbean Sea. To the east, the Ozama river and to the west the main entrance of the Cathedral (Fig.1).

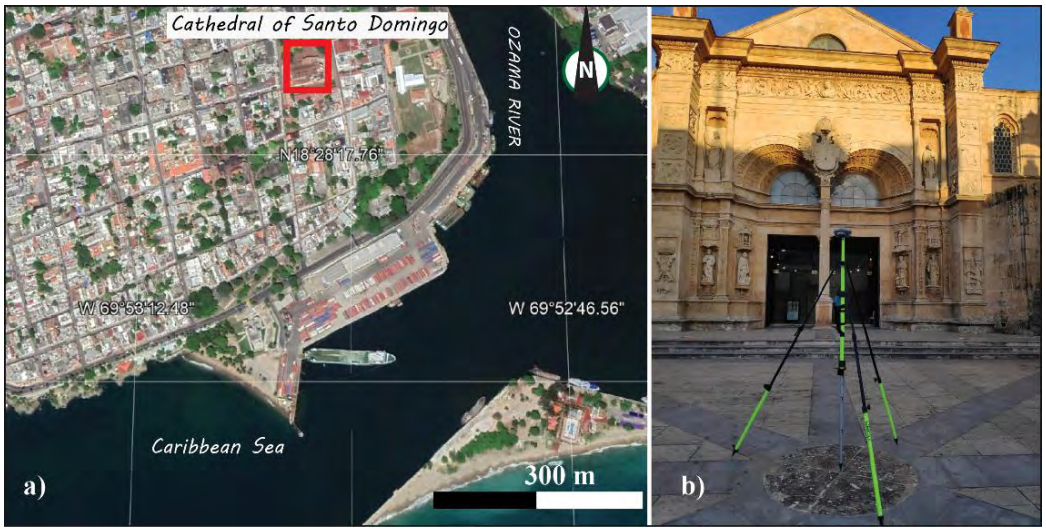


Figure 1: a) Location of the Cathedral of Santo Domingo; b) Photo of the entrance of the Cathedral of Santo Domingo

3 MATERIALS AND METHODS

In this study, the seismic site characteristics of the ground of the Cathedral were analyzed using seismic methods (MASW and HVSR) and an electromagnetic method (GPR). A topographical survey using RTK and a Trimble Total Station were also carried out during the GPR survey in order to aid in the preparation of the planimetry.

3.1 MASW method

Park et al., describe the MASW method as follows: the Rayleigh wave fundamental mode dispersion curve is extracted from a shot record. If present, higher modes can also be used and finally the extracted dispersion curves are inverted to generate a 1D shear-velocity model [13]. The shear wave velocity (Vs) depends on the geotechnical parameters of the terrain such as the shear module (G) and the density (ρ) according to equation 1:

$$Vs = \left[\frac{G}{\rho}\right]^{\frac{1}{2}} \tag{1}$$

The MASW method was chosen due to the ability to analyze the fundamental and higher modes simultaneously [14]; this advantage enabled us to obtain more accurate shear-wave velocity models. The recording array was composed of 23 vertical component geophones with a geophone spacing of 2 meters (Fig. 2). The separation between the source impact point and first geophone (offset) was 4 m to minimize near-source effects. The data recording system was a 24-channel "DOREMI" manufactured by Sara Instruments in Italy.

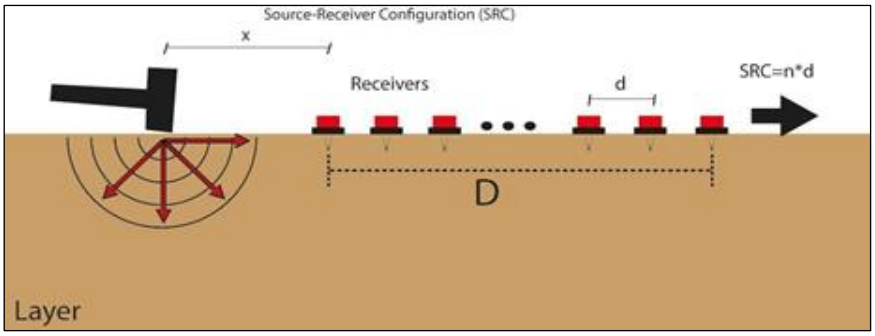


Figure 2: A schematic showing field configuration of instruments used during a seismic survey

The data analysis was carried out with "SurfSeis", software developed by Kansas Geological Survey (KGS), USA [13]. As a source to generate the Rayleigh waves was needed to derive the Vs models, we used a 20 lb. hammer.

Data processing consisted basically in geometry edition, data filtering, muting (if needed), generation of overtones (frequency-time energy diagrams), and finally fundamental and higher mode (when they appeared) identification. Once dispersion curves were determined, they were subjected individually to a mathematical inversion process to obtain a 2D-Vs profile

Four longitudinal profiles were performed for data collection (Fig. 3). A profile in the north of the Cathedral (Line No.1) with a length of 44.25 m, specifically close to Colon Park. The geophones were arranged at 2 m between them and 4 m from the source. Two longitudinal profiles in the eastern part of the study site, (Lines No. 2 and No. 3) these with a length of 15.50 m and 33.70 m respectively. For Line No. 2, 12 geophones were used and the separation between them was 1 m; Line No. 3 consisted of 15 geophones separated at 2 m each. After the completion of these, three more profiles were carried out in the Plaza of the Priests (Line No. 4), in the South, with a length of 70 m, using 23 geophones at 2 m between them and 4 m from the source.

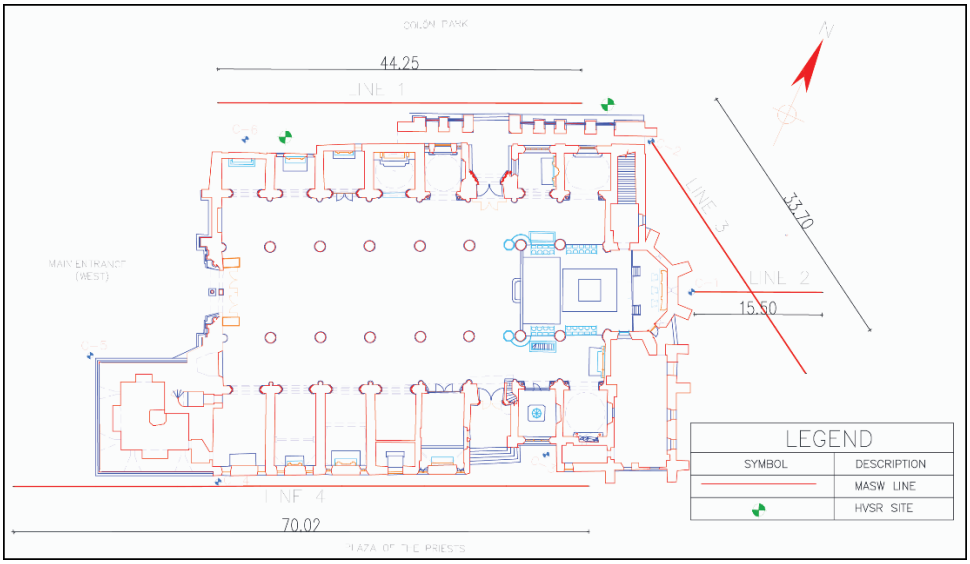


Figure 3: Location of the MASW and HVSR profiles made in the Cathedral

3.2 H/V spectral ratio

A SARA SS45PACK (integrated 4.5 Hz sensors) triaxial broadband accelerometer was used for recording the seismic data (environmental seismic noise) (Fig. 4).



Figure 4: SARA Instruments Triaxial Accelerometer of 4.5 Hz natural frequency

The implemented technique is considered a "passive" technique because it does not require an artificial seismic source, such as explosives or hammer blows. The HVSR ratio measures the vertical and horizontal components of seismic noise induced by wind, waves, and anthropogenic activities. The type of signals obtained, from the use of this equipment, are three signals in the three directions of the movement (Fig.5).

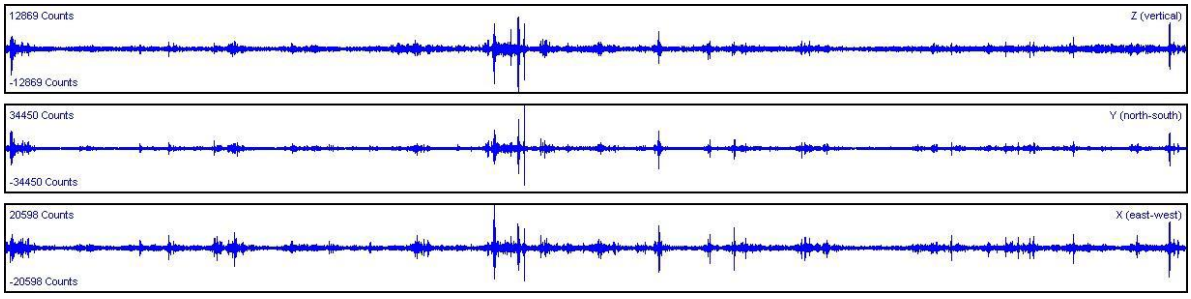


Figure 5: Seismic signals obtained from the triaxial accelerometer

The signals in the plane (Horizontal) are averaged, then the Fourier spectra are obtained and by the application of the Nakamura Modified Transfer Function [15]:

$$TF_{HW} = \frac{S_{HS}}{S_{VS}} \tag{2}$$

3.3 Georadar

The Georadar survey is an advanced geophysical technique that uses short pulses of high-frequency electromagnetic waves into the subsurface and analyzes the reflected waves [16].

The field of general applications of the Georadar is very wide, being used in construction projects, audits, site evaluations, environmental impact studies and geological and archaeological studies. In cultural heritage sites as the study area, the GPR is most useful in mapping the dimensions of crypts and ground structures.

The GPR survey (Fig. 6) was carried out using a Georadar device equipped with a 500 MHz antenna (Model DX2125 by 3D-Radar) to obtain adequate resolutions up to an investigation depth of 5 m.



Figure 6: GPR survey inside the Cathedral

The data acquisition phase was done by making lines and meshes (Fig.7). Inside the cathedral, 17 lines were made in the longitudinal direction, distributed as follows: 3 in the central span of the altar and 7 in the extreme span.

In each span, the lines were approximately 0.58 m apart. After data collection in the openings, data was taken in the chapels and the sacristy where a total of 47 lines were made, considering that the study area has 14 chapels.

Within the collection of data inside the area of interest, the study was continued in the crypt of the Trascoro, where a total of 12 lines were made, both horizontally and vertically, to check if this crypt housed some burial.

After the data collection inside the building, lines were carried out outside, specifically in the garden east of the study area, the Plaza of the Priests, the main entrance to the West and the corridors in the North part; having a total of 39 lines in these zones.

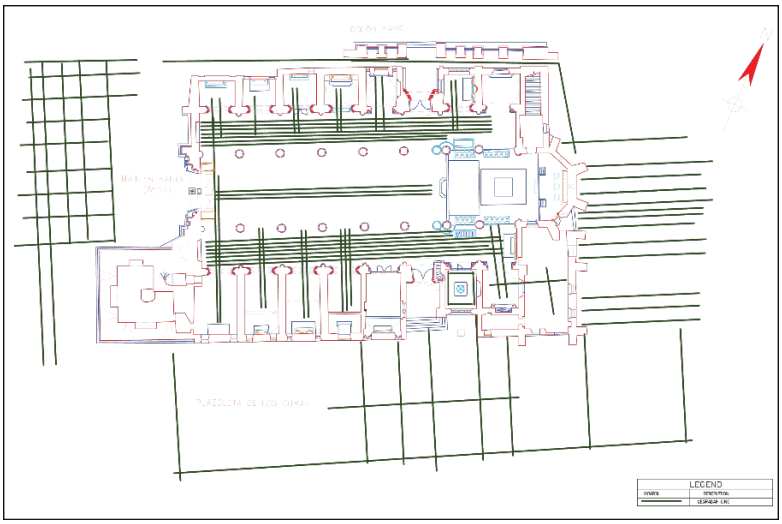


Figure 7: Plan view of the GPR lines made throughout the Cathedral

4 RESULTS AND DISCUSSIONS

4.1 Seismic Methods

Figure 8 shows the shear-wave velocity model of Line No. 4, which is labelled as profile L4 (Fig.3), obtained from the MASW method. This profile is in the southern part of the Cathedral and shows Vs values between 250 m/s right below the surface and above 1200 m/s at a depth of 30 m. From this Vs model we obtained the Vs30 values along the profile, which in this case is 70 meters long.

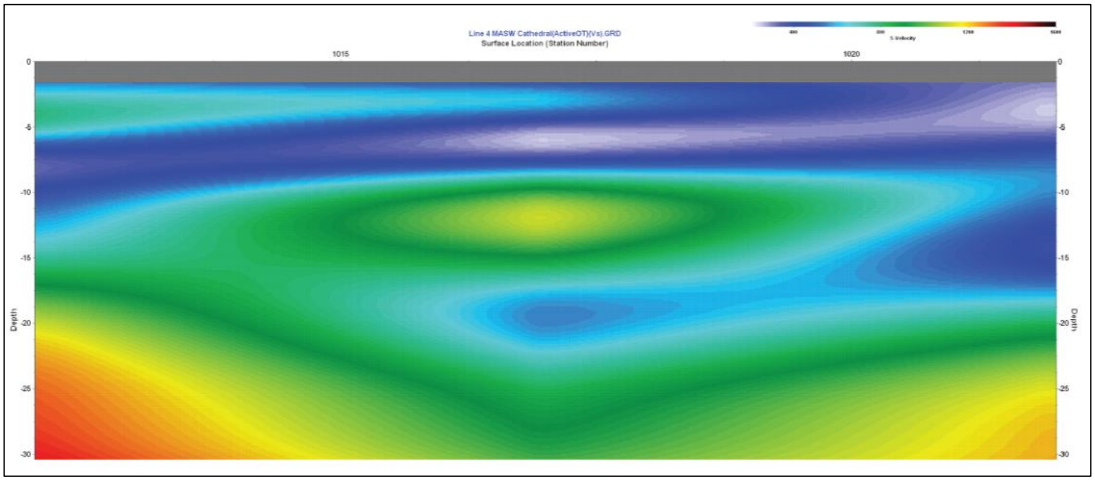


Figure 8: 2-D shear-wave velocity section from the MASW survey conducted in the southern part of the Cathedral

As it can be noted in Fig. 9, the range of Vs30 values obtained from the MASW method is between 530 m/s and 738 m/s, thereby qualifying the soils of that area as NEHRP class C-type.

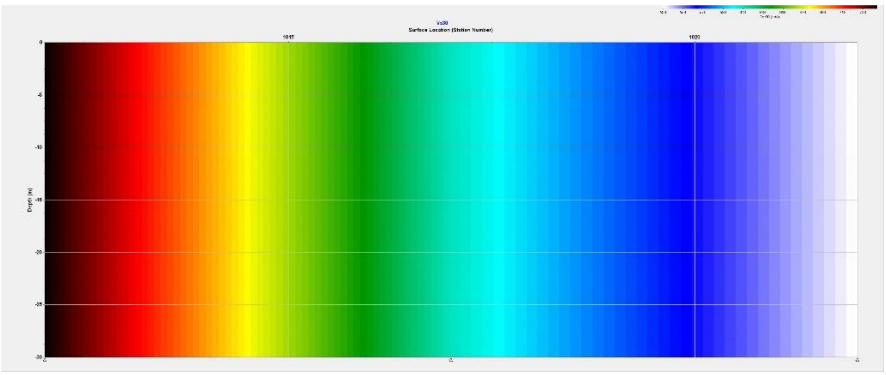


Figure 9: Vs30 MASW profile obtained in the Plaza of the Priests located in the southern part of the Cathedral

On the other hand, the results obtained by measuring the accelerations of the soil for each of the points defined above in Figure 3 are shown. After applying the filters and the smoothing proposed by Konno-Ohmachi [17], the value for the fundamental frequency of the North part of the Cathedral obtained was 0.682 Hz (Fig. 10).

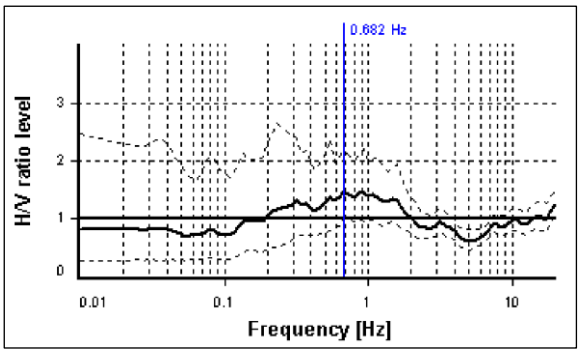


Figure 10: Fundamental frequency of the soil based on the SESAME criteria

4.2 Georadar Survey

In general, no previously unknown caverns or other cavities were found in the first 5 m of soil. The GPR003 radargram (Fig. 11) shows some vertical anomalies, but these pass through the crypt of the Trascoro and a tombstone located in the center of the aisle of the altar, which are already mapped. Therefore, the classification of the soil surface structure obtained by the MASW method is accepted as valid.

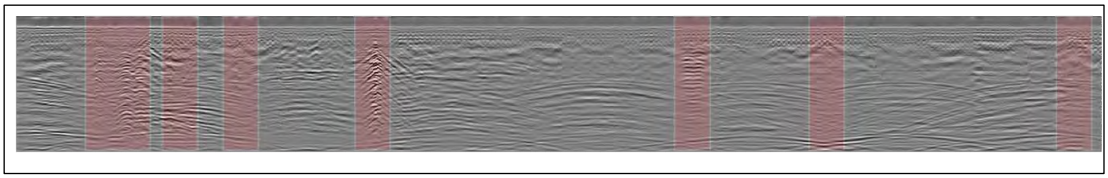


Figure 11: Radargram of a longitudinal E-W line that passes through the center vane of the cathedral.

Another detail that can be observed in radargrams is the presence of parabolas. These parabolas are the product of the influence exerted by lamps located at 5 m above ground level, in addition to the reflection of the electromagnetic wave at the end of the line. This makes it clear that the test is delicate, and that special care must be taken during the processing to correctly interpret the results.

5 CONCLUSIONS

- The GPR surveys confirmed that there are no unknown caverns or other cavities in the subsoil of the Cathedral in the first 5 m, so the classification of the surface structure of the soil obtained by the MASW method is accepted as valid.
- The Vs30 values obtained with the MASW test showed a variation that coincides with the topography of the land. The highest values of Vs30 were obtained in profile 3 and 4, which were tested in the lower part of the Cathedral, that is, in the southern part closest to the sea.
- The frequency determined by the HVSR method further confirms the site class obtained with the MASW survey.
- The site class determined with the Vs30 results found in this investigation for all models was type C (360-760 m/s), according to NEHRP soil seismic classification.
- The results of this study are consistent with other soil studies conducted in the area. The values of Vs30 in the first 3 to 4 meters of each model correspond to rigid clay and sandy soils, while from 5 m onwards values corresponding to rock are reached.

Acknowledgements. This research is part of the project “Evaluation of the dynamic soil-structure behavior of historic factory buildings using non-destructive and pseudo-destructive tests. Case: Primate Cathedral of America", Contract No. 019-2018, Code: 2016-2017-158 funded by FONDOCyT 2016-2017, MESCyT (Ministry of Higher Education Science and Technology). The authors also thanks Oficina de la Obra y Museos de la Catedral de Santo Domingo. Special thanks to Jose Caraballo in the process of editing and data acquisition of this research.

REFERENCES

[1] Sabrina, G., Sebastiano, I., Graziano, P., Domenico, B., Giuseppe, L. and Francesco, P. Geophysical surveys for the dynamic characterization of a cultural heritage building and its subsoil: The S. Michele Arcangelo Church (Acireale, eastern Sicily). *Journal of Cultural Heritage*, **36** (2019) 72-84. https://doi.org/10.1016/j.culher.2018.09.015

[2] Baradello, L., Carcione, J.M. and Gei, D. Fast monostatic GPR modeling. *Geophysics*. **69** (2004), pp.466–471. Doi: 10.1190/1.1707066.

[3] Barilaro, D., Branca, C., Gresta, S., Imposa, S., Leone, A. and Majolino, D. Ground penetrating radar (G.P.R.) surveys applied to the research of crypts in San Sebastiano’s church in Catania (Sicily). *Journal of Cultural Heritage*. 8, 73-76. doi:10.1016/j.culher.2006.10.003

[4] Castellaro, S., Imposa, S., Barone, F., Chiavetta. F., Gresta. S. and Mulargia, F. Georadar and passive seismic survey in the Roman Amphitheatre of Catania (Sicily). *Journal of Cultural Heritage*, 9 (2008) 357-366. doi:10.1016/j.culher.2008.03.004

[5] Leucci, G., De Giorgi, L., Di Giacomo, G., Ditaranto, I., Miccoli, I. and Scardozzi, G. 3D GPR survey for the archaeological characterization of the ancient Messapian necropolis in Lecce, South Italy, *Journal of Archaeological Science: Reports*, Reports 7 (2016) 290-302. http://dx.doi.org/10.1016/j.jasrep.2016.05.027

[6] Casas, A., Cosentino, P. L., Fiandaca, G., Himi, M., Macias Solé, J.M., Martorana, R., Muñoz, A., Rivero Rivero, L., Sala, R. and Teixell, I. Non-invasive Geophysical Surveys in Search of the Roman Temple of Augustus Under the Cathedral of Tarragona (Catalonia, Spain): A Case Study, *Surveys in Geophysics*, April 2018. doi.org/10.1007/s10712-018-9470-6

[7] Di Giacomo, G., De Giorgi, L., Ditaranto, I., Leucci, G., Miccoli, I. and Scardozzi, G. The Medieval cave village of Casalrotto (Mottola, Apulia): New data on the settlement and its necropolis from archaeological and geophysical measurements, *Measurement*, **128** (2018) 96-103. https://doi.org/10.1016/j.measurement.2018.06.038

[8] Park, C.B., Miller, R.D., Xia, J. and Ivanov, J. Multichannel analysis of surface waves (MASW) active and passive methods", in *Kansas Geological Survey,* Lawrence, USA, January 2007.

[9] Anukwu, G.C., Khalil, A.E., Nawawi, M., Abdullah, K. and Abdullah, F.M. Multi-channel analysis of surface waves (MASW) using CMP analysis to identify soil problems threat on the heritage site at Georgetown, Malaysia, *International Geophysical Conference*, Beijing, China, 24-27 April 2018. doi.org/10.1190/IGC2018-404

[10] Tarque, N., Lai, C.G., Bozzoni, F., Miccadei, E., Piacentini, T., Camata, G. and Spacone, E. Expected ground motion at the historical site of Poggio Picenze, Central Italy, with reference to current Italian building code, *Engineering Geology*, 166 (2013) 100-115. http://dx.doi.org/10.1016/j.enggeo.2013.09.003.

[11] Cercato, M., De Donno, G., di Giulio, A., Lanzo, G. y Tommasi, P. Dynamic Characterization of the hill of Civita di Bagnoregio (Viterbo, Central Italy) for seismic response analysis. *Engineering Geology* (2019), https://doi.org/10.1016/j.enggeo.2019.105463

[12] Flores Sasso, V. and Prieto Vicioso, E. El modelo Hallemkirche o iglesia salón en el reino de Castilla de Ultramar. La Catedral de Santo Domingo, in "Obra Congrua, 1416. 500 aniversario de la Consulta de la Catedral de Girona, Universidad de Girona, Departamento de Arquitectura e Ingeniería de la Construcción, Colegio de Aparejadores, Arquitectos Técnicos e Ingenieros de la Edificación de Girona. 2017. pp. 183-1992.

[13] Park, C. B., Miller, R. D., and Xia, J. (1999). Multichannel analysis of surface waves. *Geophysics*, 64, 800–808.

[14] Xia, J., Park, C. B., Hunter, J. A., Harris, J. B., and Ivanov, J. (2002). Comparing shear-velocity profiles from multichannel analysis of surface wave with borehole measurement. *Soild Dynamics and Earthquake Engineering* (SDEE), 22(3), 181–190.

[15] Nakamura, Y. (1989). A method for dynamic characteristics estimation of subsurface using microtremors on the ground surface. *Quarterly Report of Railway Technical Research Institute (RTRI)*: 3, 25-33.

[16] Byeong-Jin P., Jeongguk K., Jaesun L., Man-Sung K. and Yun-Kyu A. Underground Object Classification for Urban Roads Using Instantaneous Phase Analysis of Ground-Penetrating Radar (GPR) Data. Remote Sensing 10(9): 1417 (2018)

[17] Konno, K., and Ohmachi, T. (1998). "Ground-motion characteristic estimated from Spectral Radio between Horizontal and Vertical Components of Microtremors". *Bulletin of the Seismological Society of America*: 88, 228-241.

12th International Conference on Structural Analysis of Historical Constructions
SAHC 2020
P. Roca, L. Pelà and C. Molins (Eds.)

ASSESSMENT OF TUNNELING INDUCED DAMAGE ON HISTORICAL CONSTRUCTIONS THROUGH A FULLY COUPLED STRUCTURAL AND GEOTECHNICAL APPROACH

ANGELO AMOROSI[1*], MARIALUIGIA SANGIRARDI[2], GIANMARCO de FELICE[2] AND SEBASTIANO RAMPELLO[1]

[1] Department of Structural and Geotechnical Engineering, Sapienza University of Rome
Via Eudossiana 18, 00184, Rome, Italy.
e-mail: {angelo.amorosi,sebastiano.rampello}@uniroma1.it, https://web.uniroma1.it/disg/
(*corresponding author)

[2] Department of Engineering, Roma Tre University
Via Vito Volterra 62, 00146, Rome, Italy.
e-mail: {marialuigia.sangirardi,defelice}@uniroma3.it, https://www.romatrestrutture.eu/

Keywords: Tunnel construction, Masonry, Soil-Structure interaction, Nonlinearity

Abstract. *The development of urban mobility implies the construction of tunnels, often interacting with valuable historical structures. It is thus necessary to develop rational and reliable procedures to estimate the potential excavation-induced damage, dealing with complex soil-structure interaction problems. Classical approaches are often characterised by relatively simple schematisations for either one or both components of the problem, as, for example, springs for the soil or equivalent plates for the structure. Such simplified assumptions prove to be appropriate for simple soil-foundation cases, while show several limitations when tackling more complex problems, as those involving the excavation in the vicinity or beneath historical masonry structure. In such cases, the need for reliable prediction of the potential damage on surface structures induced by construction activities justifies the adoption of advanced numerical approaches. These need to be based on realistic constitutive assumptions for both soils and masonry elements and require the definition of the three-dimensional geometry as well as an accurate modelling schematisation of the excavation process. In this paper a 3D Finite Element approach is proposed to model in detail the excavation of twin tunnels, accounting for the strongly non-linear soil behaviour, interacting with monumental masonry structures, carefully modelling their geometry and non-linear anisotropic mechanical behaviour. The work focuses on a specific case-study related to the ongoing construction of the line C of Rome underground.*

1 INTRODUCTION

Urban densification requires the construction of new infrastructures to support mobility. This often implies the excavation of underground tunnels, which can interact with valuable surface buildings causing damage. The assessment of tunnelling-induced damage has traditionally been tackled by the decoupled approach, i.e. applying to the structure the displacement profiles

previously evaluated by free-field analyses of the excavation, thus neglecting all the tunnel-soil-structure interaction effects. Nowadays, more advanced coupled numerical approaches can be used resulting in more accurate description of existing structures, via equivalent embedded solids (e.g. [1]) or through an accurate simulation of their geometry (e.g. [2]), which seem to be particularly necessary when dealing with sensitive historical masonry structures.

This can only be attained with advanced three-dimensional (3D) numerical models, in which a realistic simulation of the excavation process can be performed. Moreover, the non-linearity of soil behaviour, the damaging processes involving masonry structures and the consequent evolution of the interaction process can be effectively taken into account. In the following, the 3D numerical coupled approach adopted to study an interaction problem for the Metro C line in Rome is described. The case study is first presented and the numerical model with the constitutive assumptions of both the soil and masonry are then described. Finally, the results of free-field and interaction three-dimensional analyses are presented.

2 CASE STUDY

The line C of Rome underground runs, with a total length of 25.6 km, from South-East to North-West of the city. It is characterised by twin tunnels with a single track, excavated using an earth pressure balance (EPB) tunnel boring machine (TBM) with an outer diameter D = 6.7 m, at depths of 27 to 55m and average distances of 20 to 40m. Contract T3 of the line, which runs for 3.6 km between the *Amba Aradam/Ipponio* and the *Fori Imperiali/Colosseo* stations is currently under construction and this paper focuses on the portion of the line which under-passes the ancient *Aurelian walls* at *Porta Metronia*, about 250 m West of the *Amba Aradam/Ipponio* station (Fig. 1).

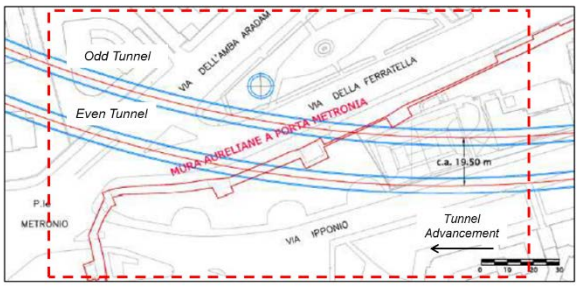


Figure 1: Plan view of the model (dashed red line marked the analysed portion).

The odd and even tunnels under-cross the *Aurelian Walls* at depths of 27.5m and 28m, respectively, with a cover to tunnel diameter ratio C/D = 3.60 and 3.68: both tunnels form an angle of about 30° with the wall axis, in plan, and deepen below the wall with a slope of about 3%.

The ground conditions at the site are shown in Fig. 2, which refers to the longitudinal section through the odd tunnel. It is characterised by an upper layer of coarse-grained made ground (MG), about 13 m thick, overlying the alluvial deposits of Pleistocene age. These consist of a layer of sandy silt and silty sand (LSO), underlain by a layer of sandy gravel (SG). A thick

deposit of stiff and overconsolidated clay from the Pliocene is found underneath the gravel, at about 3m below the sea level.

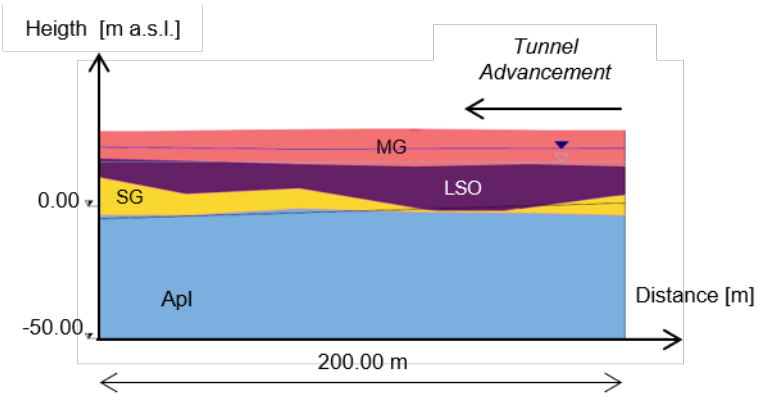


Figure 2: Detail of the ground stratigraphy along the odd tunnel.

The *Aurelian Walls* are large defensive walls built by Emperor Aurelian between 270 and 275 A.C. Most of their length (12.5 km over 19 km) has survived past centuries in a fairly good preservation state. *Porta Metronia* is in the Southeastern part of the town wall. Both in-situ and laboratory tests have been performed to detect masonry characteristics and identify its mechanical properties.

The geometry of the wall section has been determined through endoscopic surveys, while stiffness and strength properties were evaluated via ultrasonic tests, flat-jacks and compressive tests on mortar and core drill specimens. The analysed portion of the walls is characterised by a complex geometry that has been evaluated referring to five different branches (Fig. 3). The first branch (*b6-b7*) is made by a single leaf structure, 2.3 m high and 1 m thick; the second one (*b7-b8*), similar to the former, is characterised by the presence of a defensive tower 9 m high, of 5.2×9 m^2 in plan; the third branch (*b8-b9*) ends with another tower of 8.3×10.15 m^2 in plan, and a total height of 12 m. In the *b9-b10* branch, the original configuration of the walls is clearly visible, with the two facings connected by a series of arches and barrel vaults. The last section (*b10-b11*) is characterised by the presence of another tower, followed by a double facing portion of the walls very similar to the previous one (Fig 4 b,c).

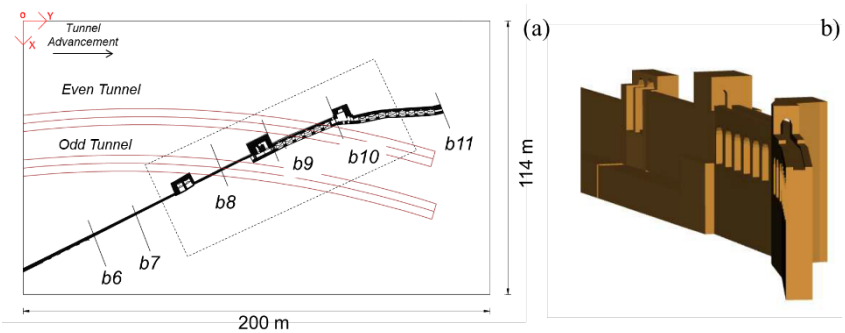


Figure 3: Plan identification of *Walls* sections (a) and 3D view of the structural model (dashed box) (b).

The considered portion of the walls features the typical roman building technique of the *opus latericium* (Fig. 4a) consisting of a brick-faced concrete core. The two external masonry leaves of the ancient wall have been schematised as a periodic assembly of bricks interacting through mortar joints.

3 NUMERICAL MODELLING

The numerical study was performed using the FE code Plaxis 3D [3]. The model was set up to simulate the twin tunnel excavation under free-field conditions and in presence of the *Aurelian Walls*.

Vertical boundaries of the model were restrained horizontally, normal to the mesh sides, while the base of the mesh was restrained both horizontally and vertically. The analysis was performed as follows: model initialisation; walls construction (only in the coupled analysis); odd tunnel excavation; even tunnel excavation. The excavation of each tunnel is simulated by a step-by-step procedure consisting of a series of progressive advancements, each having the length of one concrete lining ring according to the procedure reported in [4, 5].

All the analyses here discussed were carried out before the actual construction of the infrastructure, imposing the design volume loss V_L = 0.5 % and neglecting the activation of possible mitigation measures to prevent tunnelling-induced damage, such as compensation grouting, included in the final design. It is worth remarking that the volume loss is defined as the ratio of the volume of the surface settlement trough, per metre, to the excavated face area: it is a key scalar indicator controlling the expected (at the design stage) or observed (at the construction one) effects of the tunnelling activity on the surface settlement intensity and distribution. The value of 0.5 % is typical for EPB-TBM tunnelling technique.

The soil profile was described according to the in-situ one (Fig. 2) for both the free-field and the interaction model. The mechanical behaviour of the soils was described using the Hardening Soil model with small-strain stiffness (*HSsmall*, [6]) for the sandy silt and the Hardening soil model (*HS*, [7]) for the other layers. All the model parameters, summarised in Table 1, were calibrated based on the extensive geotechnical investigation, consisting of several in situ and laboratory tests, discussed in detail in [8].

The structure has been accurately reproduced, though some necessary modelling simplifications have been introduced. The complex geometry of the walls has been replicated between sections *b6* and *b11*, but single leaf masonry has been assumed for the wall portion between section *b6* and the left boundary of the model. Despite the presence of some discontinuities between the towers and the walls, in this model they have been considered as perfectly connected. The depth of the foundations has been considered constant according to the information available from previous surveys on the structure, and the ground surface on both sides of the wall is here assumed having the same elevation.



Figure 4: Detail of the *opus latericium* (a), portion of the walls close one of the towers in the *b8-b9* branch (a) and transversal arches in the *b9-b10* branch (b).

The constitutive model adopted for masonry is a three-dimensional anisotropic elastic-perfectly plastic one (Jointed Masonry Model, *JMM* [9]), in which block aspect ratio and staggering joints effects are considered.

Table 1: Soil model parameters (γ: unit weight; c' and ϕ': effetive cohesion and friction angle; G_0^{ref}: reference shear modulus at very small strains; $\gamma_{0.7}$: shear strain at which the secant shear stiffness equals 0.7 G_0; ν': effective Poisson's ratio; $E'_{ur}{}^{ref}$: reference unloading/reloading stiffness at engineering strains; $E'_{50}{}^{ref}$: reference secant stiffness in standard drained trisxial tests; $E'_{oed}{}^{ref}$: reference tangent stiffness for primary oedometer loading; m: power of the stress-level dependency of stiffness).

Soil	Model	γ kN/m^3	c' kPa	ϕ' °	G_0^{ref} MPa	$\gamma_{0.7}$ %	ν'	$E'_{ur}{}^{ref}$ MPa	$E'_{50}{}^{ref}$ MPa	$E'_{oed}{}^{ref}$ MPa	m
R	*HS*	17	5	34	-	-	0.2	240	24	24	1
LSO	*HSsmall*	19.5	28	27	125	0.04	0.2	150	8.2	5.52	0.8
SG	*HS*	20	0.1	40	-	-	0.2	900	90	90	0.4
Apl	*HS*	20.9	41.3	25.7	-	-	0.2	960	48	48	1

Macroscopic elastic properties are derived in the framework of homogenisation theory of periodic media, while yielding is characterized by the intrinsic material anisotropy. A set of (maximum) three sliding directions, on which failure is meant to occur, is defined in the *xyz* space and described by means of dip and strike angles, representing, for each plane, the positive rotation along the *x*-axis and the negative rotation along the *z*-axis, respectively [10]. In the analyses only two planes (head and bed joints) are activated. Yield functions are defined, for each orientation, in terms of local stress components according to Coulomb's and tensile criterion as follows:

$$f_i^c = |\tau_i| + \sigma_{n,i} \tan\phi_i - c_i \tag{1}$$

$$f_i^t = \sigma_{n,i} - \sigma_{t,i} \tag{2}$$

where i = 1,2,3 stands for the plane, $\sigma_{n,i}$ and τ_i are the normal and the shear stress along each orientation, ϕ_i is the friction angle, c_i is the cohesion and $\sigma_{t,i}$ is the tensile strength along the joints. The interlocking effect is accounted for by modifying the strength parameters on the head-joints plane, stemming from equilibrium conditions and considering the aspect ratio of the blocks through the parameter β, which depends on the friction angle of the bed joints:

$$\beta = \tan\phi_2 \frac{b}{2a} \tag{3}$$

Tensile strength and cohesion on the head joints are hence calculated according to the following expressions:

$$\sigma_{t,1} = \sigma_{t0,1} - \beta\,\sigma_{n,2} + c_{0,2}\frac{\beta}{\tan\phi_2} \tag{4}$$

$$c_1 = c_{0,1} - \left(\beta\,\sigma_{n,2} - c_{0,2}\frac{\beta}{\tan\phi_2}\right)\tan\phi_1 \tag{5}$$

The constitutive parameters adopted in the analysis are summarised in Table 2. Bed joints plane is characterised by both *dip* and *strike* angle equal to 0°, while head joints plane angles α_1 and α_2 need to be defined in every branch according to its relative rotation around the *z* axis.

Table 2: Jointed Masonry Model (*JMM*) constitutive parameters.

G	ν	γ	ϕ_i	$c_{0,i}$	$\sigma_{t0,i}$	β
MPa	-	kN/m^3	°	kPa	kPa	-
1000	0.15	10	30	50	25	1.8

3.1 Free-Field conditions

A free field (FF) analysis was first performed, comparing the numerical results with available semi-empirical estimates of ground settlements. Fig. 5 refers to the section sketched in the right bottom corner. The subsidence curves are computed at the foundations level of the wall (19.0 m a.s.l.): the comparisons refer to settlement troughs as obtained at the end of the excavation of the odd tunnel (black lines) and at the end of the even tunnel (red lines).

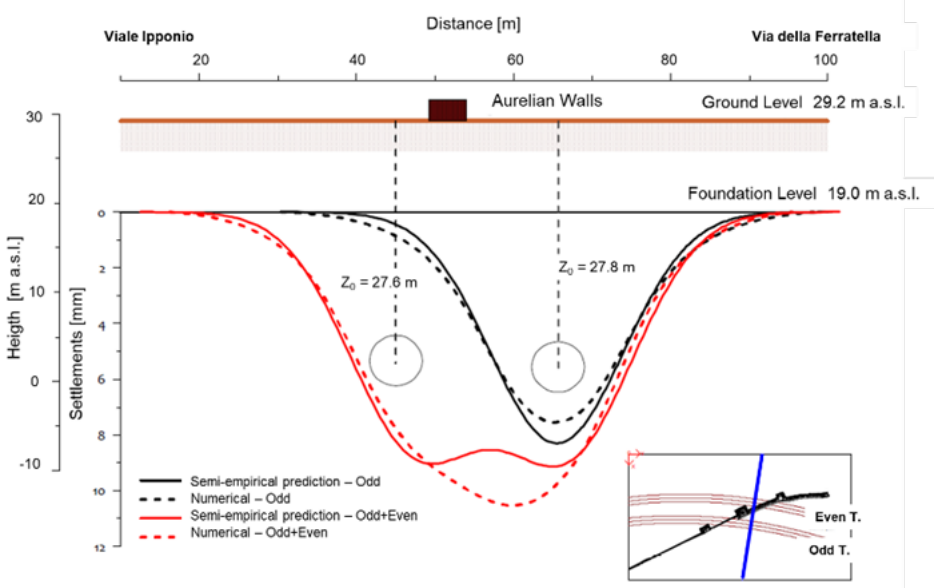


Figure 5: Settlement troughs at the walls foundation level according to semi-empirical predictions and numerical results (free-field conditions).

For the first odd tunnel, the numerical and semi-empirical predictions are in a reasonable agreement; instead, they exhibit different patterns when referring to the excavation of both tunnels, as a consequence of the plasticity-related non-linear interaction effects, realistically accounted for by the numerical model while disregarded in the empirical approach.

3.2 Interaction with the Aurelian Walls

Fig. 6 compares the results of the above free field analysis with those obtained by the coupled analysis, in which the 3D tunnel excavations are simulated considering the presence of the *Aurelian Walls*.

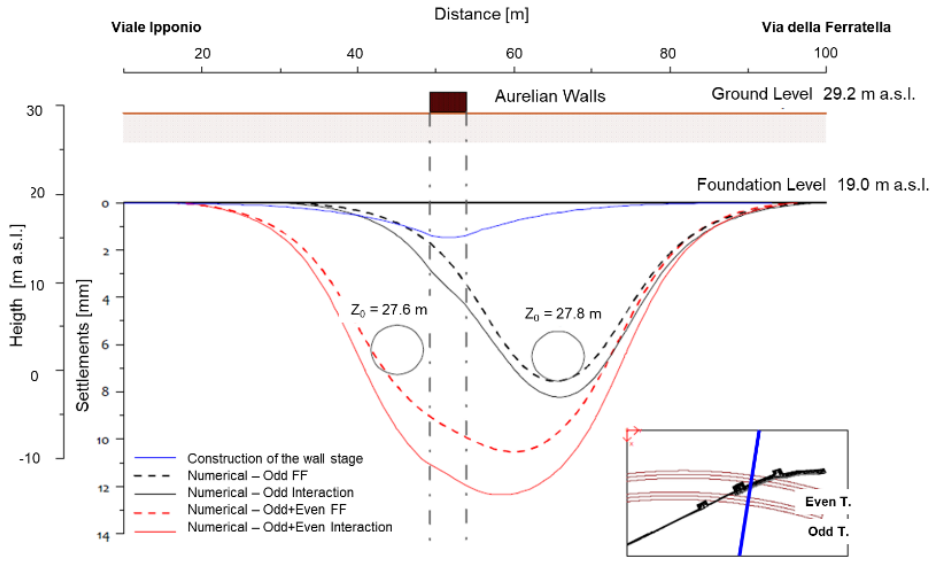


Figure 6: Settlement troughs at the walls foundation level according to semi-empirical predictions and numerical results (interaction conditions).

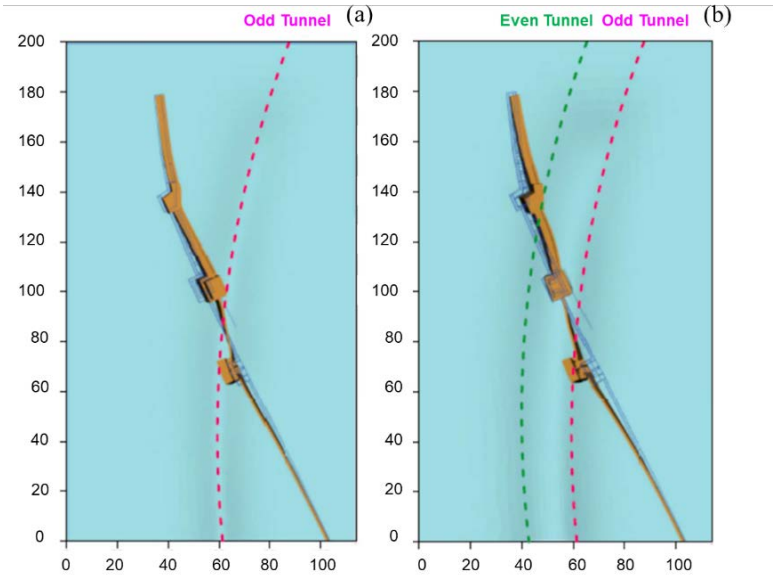


Figure 7: Magnified deformed mesh at the end of the excavation of the odd tunnel (a) and of the even tunnel (b).

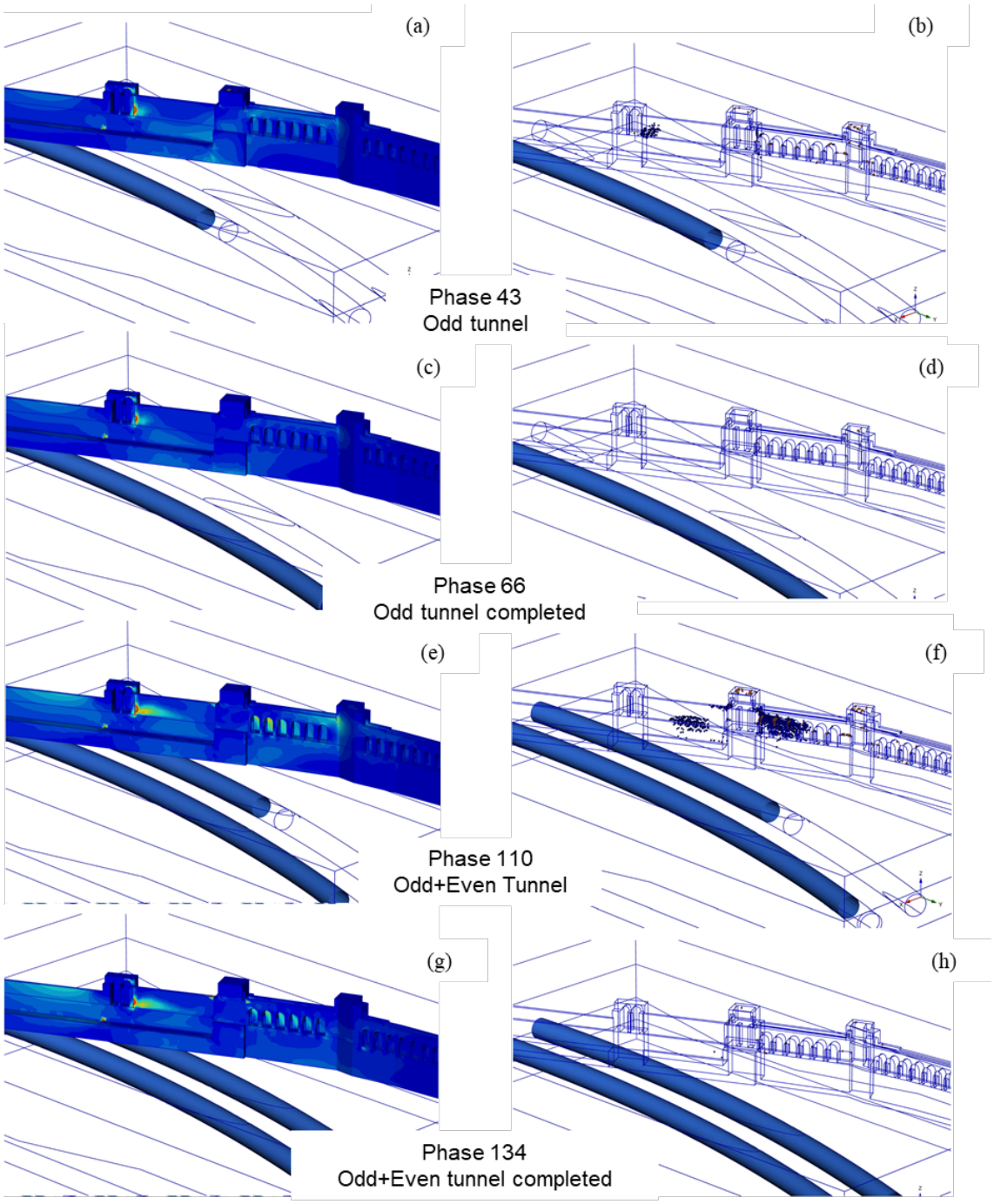


Figure 8: Tensile strain (a, c, e, g) and plastic points distribution (b, d, f, h) at different stages of the excavations.

It reports the subsidence profile at the same location considered in the FF case, at the end of each of the stages defined in the previous paragraph.

The interaction with the surface structure leads to larger settlements, while substantially preserving the shape of the settlement troughs, apart from their portions located directly below the walls, where the stiffness of these latter results in a lower inflection of the curves.

To better understand the kinematic developing during the entire process, a top view of the magnified deformed mesh of the walls is reported in Fig. 7. It shows the trace of the undeformed walls and the deformed one at the end of the excavation of the first tunnel (a) and of both tunnels (b), highlighting the out-of-plane rotation induced by tunnelling. Torsional effects are evident and contribute to the development of the tensile strain patterns during the excavation process, which are reported in Fig. 8. These are traditionally adopted to interpret damage intensity and distribution [11,12].

In this case, tensile strain patterns (results refer to four different stages of the analysis) are reported together with the plastic points distribution (i.e. points in which the tensile or shear failure has been reached). The observation of these indicators suggests that the excavation of the even tunnel (Phase 110) is responsible for most of the damage detected on the structure and that these effects are mainly located at the wall-tower connection. It is worth noting that the amount of predicted damage is very low, confirming the correctness of the design solutions adopted for this important infrastructure.

4 CONCLUSIONS

In this paper, a complex soil-structure interaction case involving a portion of the *Aurelian Wall*s affected by the excavation of the T3 contract of the line C of Rome underground has been studied.

The analyses have been performed under both free-field conditions and accounting for the presence of the walls, whose geometry has been described in detail. Soil and masonry mechanical behaviour were modelled through advanced constitutive assumptions: the calibration of the mechanical parameters was based on an extensive characterisation campaign previously performed on both materials. The results of the analyses shed some light on the evolution of the low damaging process occurring within the masonry structure, thanks to both the accurate description of the geometrical features of the *Aurelian Walls* and the adopted non-linear masonry constitutive model. In particular, not all the excavation phases seem to equally affect the structure and, possibly more interestingly, the greater damaging condition does not necessarily correspond to the final stage of tunnel excavation, when both tunnels are completed. Indeed, modelling the staged construction and the real three-dimensional conditions permitted to detect torsional effects that would be otherwise lost in any conventional 2D approach.

REFERENCES

[1] Rampello S., Callisto L., Viggiani G., Soccodato F.M. Evaluating the effects of tunnelling on historical buildings: the example of a new subway in Rome. *Geomechanics and tunnelling* (2012) **5**(3): 275-299.

[2] Amorosi, A., Boldini, D., de Felice, G., Malena, M. and Sebastianelli, M. Tunnelling-induced deformation and damage on historical masonry structures. *Géotechnique* (2014) **64**(2):118-130.

[3] Brinkgreve, R. B. J., et al. "PLAXIS 2016." *PLAXIS bv, the Netherlands* (2016).

[4] Fargnoli, V., Gragnano, C.G., Boldini, D. and Amorosi, A. 3D numerical modelling of soil–

structure interaction during EPB tunnelling. *Géotechnique* (2015) **65**(1):23-37.
[5] Burghignoli A., Callisto L., Rampello S., Soccodato F.M., Viggiani G.M.B. The crossing of the historical centre of Rome by the new underground Line C: a study of soil structure-interaction for historical buildings. In *Geotechnics and Heritage: Case Histories*, CRC Press, London (2013), pp. 97-136
[6] Benz, T. *Small-strain stiffness of soils and its numerical consequences*. Ph.D. thesis, Universität Stuttgart (2007).
[7] Schanz, T., Vermeer, P.A. and Bonnier. P. G. The hardening soil model: formulation and verification. *Beyond 2000 in computational geotechnics* (1999): 281-296.
[8] Rampello S., Fantera L. and Masini L. Efficiency of embedded barriers to mitigate tunnelling effects. *Tunnelling and Underground Space Technology* (2019) **89**:109-124.
[9] Lasciarrea, W.G., Amorosi, A., Boldini, D., de Felice, G. and Malena, M. Jointed Masonry Model: A constitutive law for 3D soil-structure interaction analysis. *Engineering Structures* (2019) **201**.
[10] Sangirardi, M., Malena, M. and de Felice, G. Settlement Induced Crack Pattern Prediction Through the Jointed Masonry Model. In *Proceedings of XXIV AIMETA Conference 2019,* Springer International Publishing 24 (2020), pp. 1971-1980.
[11] Boscardin, M. D., and Cording, E. J. Building response to excavation-induced settlement. *Journal of Geotechnical Engineering* (1989) **115**(1): 1-21.
[12] Sangirardi, M., Amorosi, A. and de Felice, G. A coupled structural and geotechnical assessment of the effects of a landslide on an ancient monastery in Central Italy. *Engineering Structures* (2020) **225**.

12th International Conference on Structural Analysis of Historical Constructions
SAHC 2020
P. Roca, L. Pelà and C. Molins (Eds.)

AUTOMATED MODEL UPDATING OF A MASONRY HISTORICAL CHURCH BASED ON OPERATIONAL MODAL ANALYSIS: THE CASE STUDY OF SAN GIOVANNI IN MACERATA

SILVIA SANTINI[1], CARLO BAGGIO[1], ENRICO DA GAI[2],

VALERIO SABBATINI[1]*AND CLAUDIO SEBASTIANI[1]

[1]Roma Tre University, Department of Architecture
Largo Giovanni Battista Marzi 10, 00153, Rome, Italy
Email: valerio.sabbatini@uniroma3.it (*corresponding author)

[2]Studio Da Gai Architetti Roma
Via Padre Raffaele Melis, 17, 00176, Rome, Italy
E-mail: info@enricodagai.it

Keywords: Historical Masonry, Ambient Vibration Test, Operational Modal Analysis, Automated Model Updating, Douglas-Reid Method

Abstract. *Over the past few decades, the conservation and seismic assessment of historical buildings has gained great importance. In particular, the prediction of the dynamic response of masonry constructions plays a central role in retrofitting and conservation interventions. Finite element modelling has become the most common and accessible approach to study the behavior of complex masonry structures, however, the gap between numerical and experimental analysis may lead to erroneous results.*
This work describes the model updating procedure applied to the finite element model of San Giovanni's church in Macerata, condemned in October 2016 after the Central Italy Earthquake. The laboratory of Proof and Research on Structures and Materials of Roma Tre University carried out an extensive in-situ testing campaign including geometric survey, video endoscopy, flat-jack test, sonic tomography and ambient vibrations test in order to investigate the state of the building. The work involved both numerical and experimental analysis: the results of the testing campaign were interpreted and correlated with an accurate finite element model developed with the software Midas Gen. Operational modal analysis was performed in order to extract the modal parameters of the building (modal frequencies, shape vectors and modal damping). Material characteristics and boundary conditions were updated according to the Douglas-Reid method. In the end, the final model was compared to the initial model to evaluate and discuss the process.

1 INTRODUCTION

The field of structural analysis has developed sophisticated numerical models able to predict the response of complex constructions. Typically, conservation and restoration practices rely on Finite Element Models (FEM) to perform structural analysis of non-linear composite materials (such as masonry) which are otherwise hard to predict. However, the results obtained from the numerical analysis occasionally differ significantly from the real response of the structure. For this reason, it is fundamental to implement multiple strategies able to describe the structural behavior of these constructions.

Model Updating is a widely used technique used for the calibration and improvement of FEM based on reference values, therefore it is possible to link this tool with Ambient Vibration Test (AVT) and Operational Modal Analysis (OMA). AVT is a powerful dynamic monitoring technique that returns information on the overall behavior of the structure through the use of environmental excitations. The results of the AVT are usually processed with the Operational Modal Analysis (OMA) in order to estimate the modal parameters of the construction. This strategy, integrated with ordinary on-site testing, allows a global and detailed characterization of the structure. This paper describes the model updating procedure applied to the Church of San Giovanni in Macerata through the Douglas-Reid method.

2 SAN GIOVANNI IN MACERATA

The church of San Giovanni is an aggregate of historical buildings, placed in the south-west area of the historic center of Macerata, between “Piazza Vittorio Veneto” and the beginning of “Corso della Repubblica”.

San Giovanni was designed by the Architect Rosato Rosati, who conceived the building based on the Church of San Carlo ai Catinari in Rome [1]. The architecture respects the typical style of the Jesuit’s order: Latin cross plan, single wide nave, several deep side chapels, impressive dome with a tall lantern and the bell tower [2]. San Giovanni was founded in 1600 on the ruins of an ancient Roman building, the church was opened in 1625 when the façade was finally concluded [3]. In 1682, the surrounding land was acquired and then the right side of the transept and the bell tower were erected. The construction of the dome suffered numerous delays but finally in 1762 the entire construction was completed [4].

3 ONSITE INVESTIGATION AND PRELIMINARY MODEL

3.1 Onsite test

From November 2018 to July 2019, the PRiSMa Lab. (Laboratory of Proof and Research on Structures and Materials) from the Architecture Department of Roma Tre University, carried out an extensive experimental campaign on San Giovanni.

During the onsite campaign different tests were performed: 4 double flat jack tests, 5 Ambient Vibration Tests, 47 video endoscopy inspections, 2 sonic topographies and 20 dynamic penetrometer tests of the mortar joints.

In the present work, only the five AVT and the double flat jack tests were considered. Figure 1 illustrates the ground floor and the basement plans of the church with the locations of the double flat jack tests, in Table 1 are shown the results obtained from these tests.

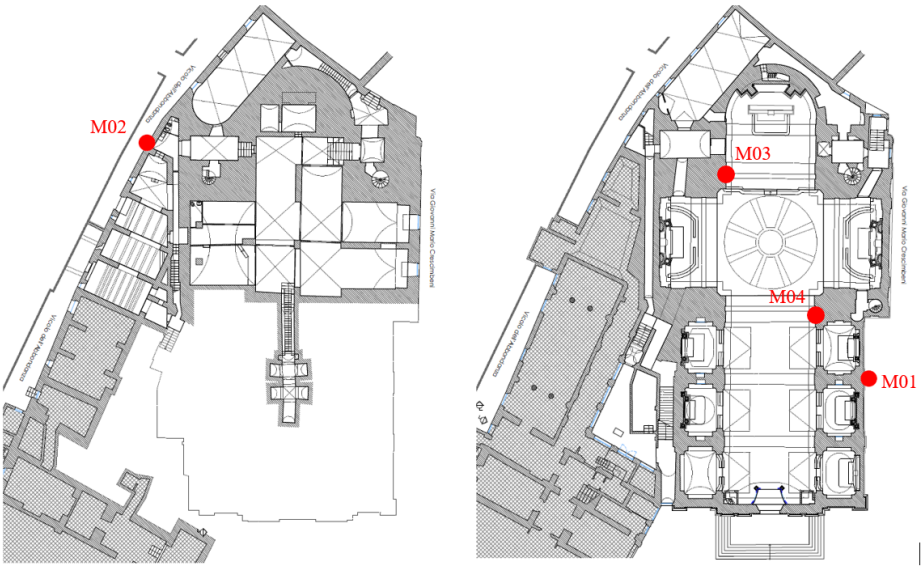


Figure 1 Double flat jacks test plan

Table 1 Results of the double flat jack tests

Test	Location	E [MPa]	ν	σ_{max} [MPa]
M01	External wall of the ground floor	4700	0,29	2,67
M02	External wall in the basement	1800	-	1,37
M03	Transept pillar	2460	0,19	2,71
M04	Nave pillar	1300	0,11	2,90

3.2 FINITE ELEMENT MODEL

A preliminary FEM of the entire church of San Giovanni was implemented with the software Midas Gen [5]. The construction was modeled with 13416 nodes and 6281 three-dimensional brick elements (Figure 2). In order to properly model the soil-structure interaction, the FEM was constrained with elastic spring elements in the x, y and z directions. The construction was divided into nine different volumes, each one with isotropic homogeneous elastic material with different characteristics. The Young modules and the Poisson's ratio were evaluated according to the results of the four double flat jack tests as reported in Table 2.

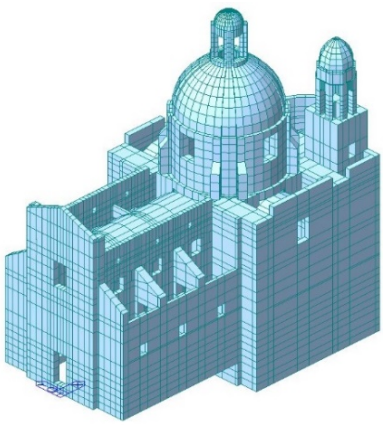


Figure 2 Finite Element Model of San Giovanni in Macerata

Table 2 Double flat jacks result implementation

Test implementation	Element	E [MPa]	ν
M01	Nave	4700	0,29
M03	Pillar 3	2460	0,19
M04	Pillar 4	1300	0,11
Average of M03, M04	Pillar 1 and 2	1880	0,15
Average of M01, M02, M03, M04	Dome, tower, façade and apse	2565	0,20

4 AMBIENT VIBRATION TEST

The response in acceleration of the construction was recorded in 5 different runs, each run was recorded with 12 uniaxial ICP piezoelectric accelerometers (n°10 PCB 393B12 with 8μg rms resolution and n°2 PCB 393B31 with 1μg rms resolution, all of them with 10 V/g sensitivity and range ±0,5g) for about 45 minutes. In the end, there were measured a total of 16 different points located at four different heights: nave level (14m), drum level (22m), dome level (29m) and lantern level (36m). The sensors were connected to a 24-bit acquisition system which recorded with a sample frequency of 441 Hz.

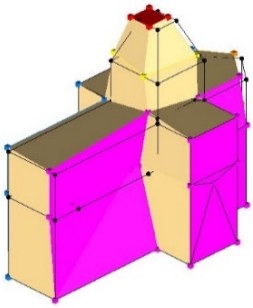
4.1 Multi Run Operational Modal Analysis

OMA is a technique used to process the results from output-only measurements (AVT), the hypothesis of white noise conditions allows to neglect the recording of the input, in this circumstances all the natural frequencies of the structure are assumed to be excited [6] [7].

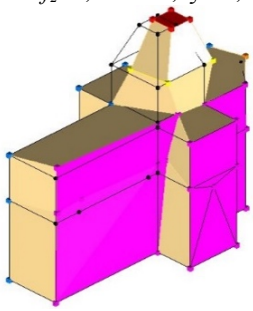
The modal parameters are extracted with specific algorithms [8], in this work the processing was carried out using the Polyreference Least-Squares Complex Frequency-Domain method implemented in the software Simcenter Testlab [9]. In order to optimize the number and the position of the accelerometers, it was adopted the Multi-Run Operational Modal Analysis, this technique allows to scale the modes based on the most appropriate and complete run, finally the results are merged to return the global behavior of the construction. In this work five different runs were recorded: one for each side of the nave, one for the transept, one for the drum and one on the extrados of the dome and lantern maintaining three common reference sensors during all the acquisitions [10].

The results are reported in Figure 3, the analysis was limited to the first three modes of vibration because the most reliable since the complex structure is part of a large irregular building aggregate that requires a relevant amount of energy to excite the higher modes thus it makes them difficult to identify and validate [11].

Mode 1: f_1=1,8785 Hz, ζ = 1,13%



Mode 2: f_2=2,3051 Hz, ζ = 1,60%



Mode 3: f_3=3,8223 Hz, ζ = 1,99%

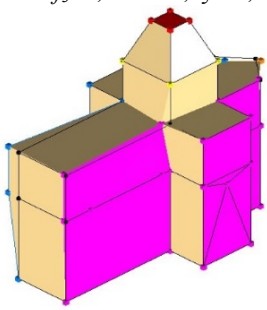


Figure 3 Experimental results from Multi run Operational Modal Analysis

5 MODEL UPDATING

The relevant parameters of the FEM were tuned in order to improve the correspondence with the experimental results. This process requires a set of preparatory phases. Initially, it is necessary to improve the preliminary model through the Manual Tuning (par. 5.1) of the parameters. Subsequently, Sensitivity Analysis (par. 5.2) is suggested to identify the relevant factors that strongly influence the behaviour of the structure. Based on the previous results, the automated Model Updating can be finally performed according to the Douglas-Reid method (par. 5.3) [12] [13].

5.1 Manual Tuning

In a dynamic system, the modal quantities are dependent on the mass, the stiffness, the damping and the boundary conditions of the model. During the Manual Tuning, these parameters are varied intuitively in order to approximate the experimental results [14].

Often the elastic constrains (boundary conditions) have more influence than the other parameters on the dynamic behavior of the construction [7]. Several numerical eigenvalue analyses were carried out with different stiffnesses of the springs in foundation. The relative frequency error with the variation of the elasticity was evaluated according to (1) and plotted in Figure 4. The minimum error corresponded to a value of stiffness equal to 10^6 N/mm.

$$Error = \frac{|f_{exp} - f_{FEM}|}{f_{exp}} * 100 \quad (1)$$

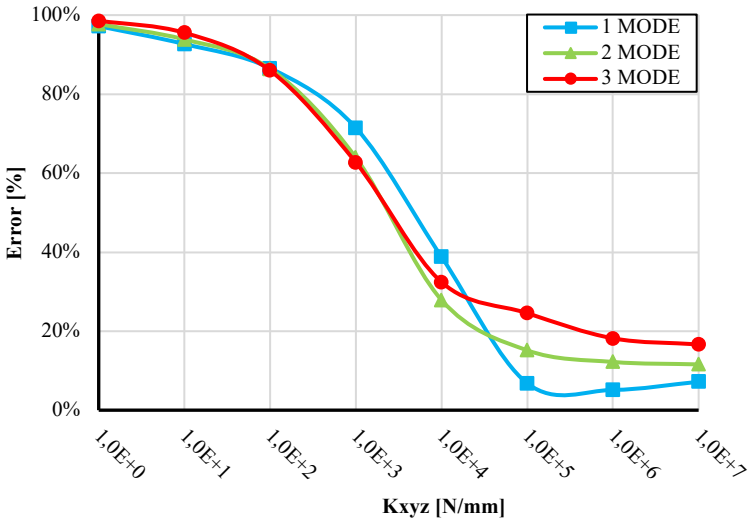


Figure 4 Relative frequency error with the variation of the soil stiffness

5.2 The Sensitivity Analysis

Every parameter of a FEM has a different influence on the global behavior depending on the geometry, the heterogeneity of the materials and the interaction between the elements. The Sensitivity Analysis identifies the parameters that mostly affect the response of the model [15] and it quantifies their influence with the sensitivity coefficient defined in (2) [16].

$$S_{i,j} = 100 \cdot \frac{X_j}{R_i^{FEM}} \cdot \frac{\Delta R_i^{FEM}}{\Delta X_j} \qquad \begin{matrix} i = 1, \dots M \\ j = 1, \dots N \end{matrix} \qquad \begin{matrix} M = Frequencies \\ N = Parameters \end{matrix} \tag{2}$$

- X_j represents the *j-th* model parameter;
- R_i^{FEM} represents the *i-th* output of the analysis (in this case the natural frequencies);
- ΔX_j represents the range of variation of the model parameter;
- ΔR_i^{FEM} represents the variation of the output of the analysis;

The Sensitivity Analysis was performed starting from the values obtained from the four double flat jack tests (par. 3.2) [17], the parameters were varied with an increment of 5%.
The parameters with the highest sensitivity coefficients resulted the most influential; based on the results of Table 3, the parameters E3, E4, E5, E6, E7 were selected in addition to the previously analyzed stiffness of the spring elements in foundation K_x, K_y and K_z (par. 5.1).

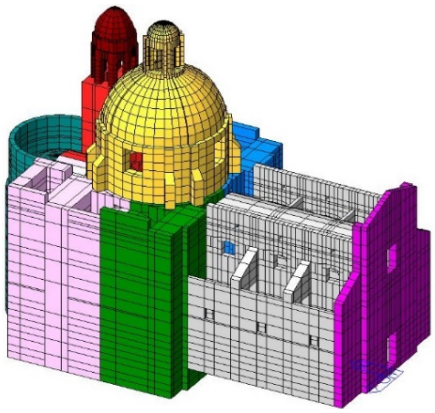


Table 3 Sensitivity Analysis

			$S_{i,j}$			
			X_j	R_i^{FEM}		
Element	**Legend**	**E [MPa]**	**Parameter**	f_1	f_2	f_3
Nave		4700	E1	1,52	2,77	0,77
Pillar 3		2460	E3	5,27	2,77	2,75
Pillar 4		1300	E4	4,66	2,57	1,22
Pillar 1		1880	E5	3,04	3,56	0,83
Pillar 2		1880	E6	3,65	4,64	27,18
Dome		2565	E7	4,25	4,64	1,53
Bell Tower		2565	E8	0,00	0,00	6,97
Façade		2565	E9	0,00	0,10	0,32
Apse		2565	E10	0,41	0,69	1,22

5.3 The Douglas-Reid method

The Douglas-Reid method [18] is a simplified procedure introduced in 1982 to minimize the error between two sets of data considering different combinations of parameters. In this work, the Douglas-Reid method was applied to minimize the error between the numerical natural frequencies of the FEM and the experimental frequencies of the OMA.

The experimental observations resulted from the OMA, indicated as R_i^{EXP} with $1 \leq i \leq M$ (M represents the total number of experimental observations), are compared with the related R_i^{FEM} values obtained from the analysis of the FEM, function of N significant structural parameter indicated with X_k (3).

$$R_i^{FEM} = R_i^{FEM}(X_1, X_2, X_3, \dots, X_k, \dots, X_N) \tag{3}$$

In order to reduce the error between R_i^{FEM} and R_i^{EXP}, the proper structural parameters X_k are selected from the set range of values using a batch analysis procedure.

The Douglas–Reid method uses an approximated model to interpolate with a quadratic function (4) the proper structural parameters within a range of coordinate points $(X_1, X_2, X_3, \dots, X_k, \dots, X_N)$ [19].

$$R_i^{DR} = C_i + \sum_{K=1}^{N} (A_{iK} X_K + B_{iK} X_K^2) \qquad \begin{matrix} i = 1, \dots M \\ K = 1, \dots N \end{matrix} \qquad \begin{matrix} M = Frequencies \\ N = Parameters \end{matrix} \tag{4}$$

- i represents the *i-th* structural parameter;
- K represents the *k-th* significant variable in the model;
- R_i^{DR} represents the structural response of the approximated model;
- C_i, A_{Ki}, B_{Ki} are 2N+1 coefficient to be determined;

The analysis was carried out according to the following steps:
1) Definition of the lower and upper bound of variation for each parameter (5), in this case a variation of ±75% was adopted on the selected parameters (par. 5.2):

$$X_K^L \le X_K^B \le X_K^U \tag{5}$$

2) Each variable was normalized over its nominal value (6):

$$\frac{X_K^L}{X_K^B} \le \frac{X_K^B}{X_K^B} \le \frac{X_K^U}{X_K^B} \tag{6}$$

3) The identification of the 2N+1 coefficients C_i , $A_{K,i}$, $B_{K,i}$ of the approximated model was carried out by equaling the modal parameters of the Douglas-Reid approach (R_i^{DR}) and those obtained from the FEM (R_i^{FEM}). The system of equations is generated considering the output frequencies from the FEM, where the X_K variables assume the basic values X_K^B, and the output from the 2N models considering once the lower bound value X_K^L and then the upper bound value X_K^U. The procedure is represented by equations (7) [12]:

$$\begin{matrix} R_i^{DR}(X_1^B, X_2^B, \dots, X_N^B) = R_i^{FEM}(X_1^B, X_2^B, \dots, X_N^B) \\ R_i^{DR}(X_1^U, X_2^B, \dots, X_N^B) = R_i^{FEM}(X_1^U, X_2^B, \dots, X_N^B) \\ R_i^{DR}(X_1^L, X_2^B, \dots, X_N^B) = R_i^{FEM}(X_1^L, X_2^B, \dots, X_N^B) \\ \vdots \\ R_i^{DR}(X_1^B, X_2^B, \dots, X_N^U) = R_i^{FEM}(X_1^B, X_2^B, \dots, X_N^U) \\ R_i^{DR}(X_1^B, X_2^B, \dots, X_N^L) = R_i^{FEM}(X_1^B, X_2^B, \dots, X_N^L) \end{matrix} \tag{7}$$

4) The system of equations is also written as (8), with the matrices expressed in (9):

$$\{R_i^{DR}\} = [C] \cdot \{K_i\} \tag{8}$$

- $\{K_i\}$ is the vector containing the unknown coefficients C_i , $A_{K,i}$, $B_{K,i}$;
- $[C]$ is the matrix containing the combinations of the variables;

$$[C] = \begin{bmatrix} 1 & X_1^B & X_1^{B^2} & & X_N^B & X_N^{B^2} \\ 1 & X_1^U & X_1^{U^2} & \cdots & X_N^B & X_1^{B^2} \\ 1 & X_1^L & X_1^{L^2} & & X_N^B & X_1^{B^2} \\ & \vdots & & \ddots & \vdots & \\ 1 & X_1^B & X_1^{B^2} & & X_N^U & X_1^{U^2} \\ 1 & X_1^B & X_1^{B^2} & \cdots & X_N^L & X_1^{L^2} \end{bmatrix} \quad ; \{K_i\} = \begin{Bmatrix} C_{i,1} \\ A_{i,1} \\ B_{i,1} \\ \vdots \\ A_{i,N} \\ B_{i,N} \end{Bmatrix} \tag{9}$$

5) The system of equations is solved according to (10). Therefore, it is defined a matrix of the constants $[K]$ containing all the vectors $\{K_i\}$ as shown in (11):

$$\{K_i\} = [C]^{-1}\{R_i^{DR}\} \tag{10}$$

$$[K] = \begin{bmatrix} \{K_1\} \\ \{K_2\} \\ \vdots \\ \{K_M\} \end{bmatrix} \tag{11}$$

Finally, it is defined R^{DR} as shown in (12) and (13):

$$\{R^{DR}\} = [K] \cdot \{x\} \tag{12}$$

$$[K] = \begin{bmatrix} C_{1,1} & A_{1,1} & B_{1,1} & \cdots & A_{1,N} & B_{1,N} \\ C_{2,1} & A_{2,1} & B_{2,1} & & A_{2,N} & B_{2,N} \\ & \vdots & & \ddots & \vdots & \\ C_{M,1} & A_{M,1} & B_{M,1} & \cdots & A_{M,N} & B_{M,N} \end{bmatrix} \quad ; \{x\} = \begin{Bmatrix} 1 \\ X_1 \\ X_1^2 \\ \vdots \\ X_N \\ X_N^2 \end{Bmatrix} \tag{13}$$

6) The objective function is defined in (14) [12]:

$$f(x) = \sum W \cdot (R^{DR} - R^{EXP})^2 \qquad ; W = \left(\frac{1}{R^{EXP^2}}\right) \tag{14}$$

W is a diagonal matrix necessary to normalize $R^{DR} - R^{EXP}$ since R^{EXP} can reach different orders of magnitude. In this work, it was used the algorithm *"fmincon"* (find minimum of constrained nonlinear multivariable function) present in the software MATLAB [20] in order to minimize the objective function (14).
The optimized parameters result in the vector $\{x\}$ previously defined in (13).

5.5 Results

The Automated Model Updating of the FEM of San Giovanni's Church in Macerata was implemented with the Douglas-Reid method considering E3, E4, E5, E6, E7 and K_x, K_y, K_z as the significant parameters. The optimized parameters are reported in Table 4.

Table 4 Optimized parameters

	Parameters		
	Initial	**Updated**	**Variation**
E3 [MPa]	2460	4305	75%
E4 [MPa]	1300	325	-75%
E5 [MPa]	1880	3290	75%
E6 [MPa]	1880	3290	75%
E7 [MPa]	2565	3073	20%
K_x [N/mm]	1000000	1520033	52%
K_y [N/mm]	1000000	1562838	56%
K_z [N/mm]	1000000	1749302	75%

The results from the updated FEM are compared to the experimental results and the initial FEM as shown in Figure 5.

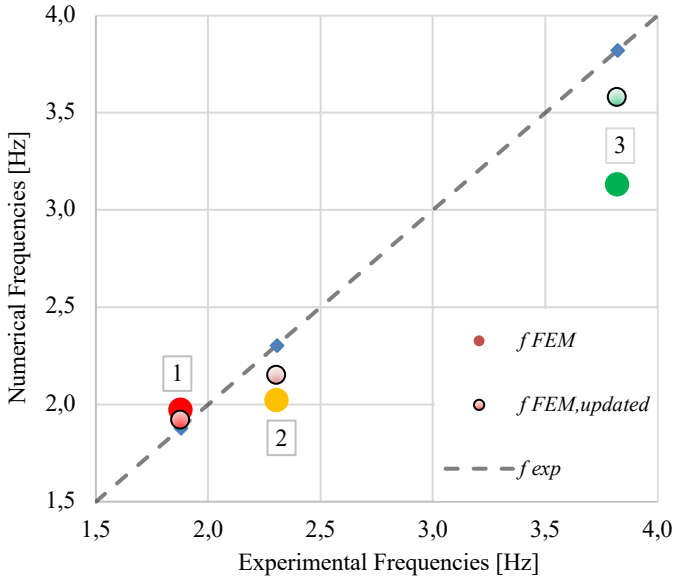


Figure 5 Frequency comparison

The frequencies from the OMA, the initial FEM and the updated FEM are reported together with their relative frequency errors (1) in Table 5 while in Figure 6 are reported the modal deflections of the updated numerical model.

Table 5 Frequency values and relative frequency error

Mode	f_{exp} [Hz]	f_{FEM} [Hz]	$f_{FEM,updated}$ [Hz]	$Error_{exp\text{-}FEM}$ [%]	$Error_{exp\text{-}FEM,updated}$ [%]
1	1,88	1,97	1,92	4,87%	2,21%
2	2,31	2,02	2,15	12,37%	6,73%
3	3,82	3,13	3,58	18,11%	6,34%
		Average error		11,78%	5,09%

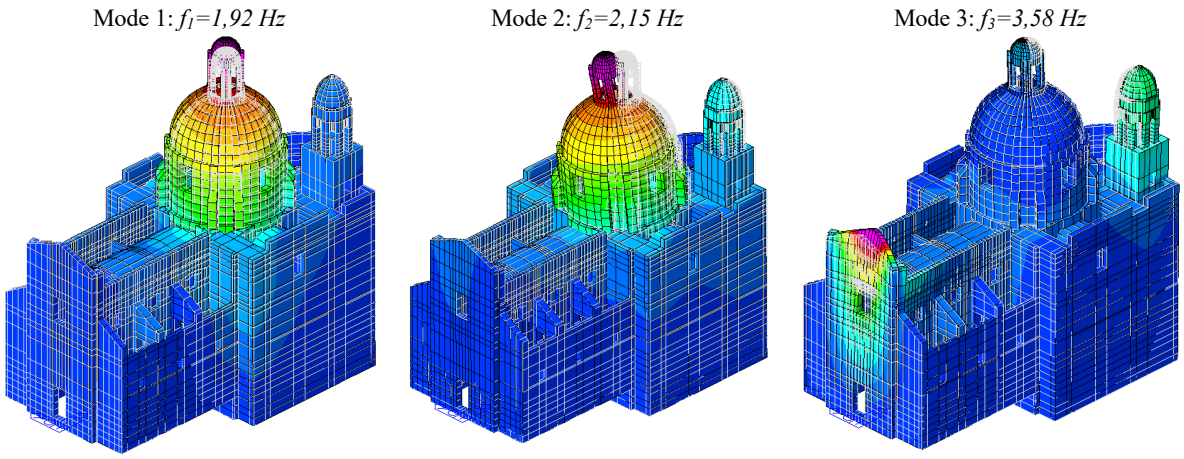


Figure 6 Numerical Modal Deformation of the Updated Model

6 CONCLUSIONS

The present work aims to create a finite element model that describes, in a sufficiently reliable way, the behaviour of an historical masonry structure. In particular, an optimized model of the Church of San Giovanni in Macerata was generated through the optimization process carried out with the Douglas-Reid method. For the proper realization of the Model Updating of the finite element model there were followed different steps.

Initially, a series of investigations were carried out in order to identify the mechanical characteristics of the materials and the current state of the construction. Once the on-site testing was completed, it was elaborated a preliminary FEM to provide an indication on the behaviour of the structure. Subsequently, the dynamic characterization of the church was carried out through the Multi Run Operational Modal Analysis. This technique identified, using the Polymax algorithm, the modes of vibration and the modal properties of the building (frequencies and damping). In order to achieve an adequate accuracy before the model updating, it was essential to calibrate the stiffness of the ground through the Manual Tuning procedure. A Sensitivity Analysis of the structural parameters investigated was subsequently carried out in order to understand the influence of the main parameters on the dynamics of the church. After the preparatory steps were completed, the Automated Model Updating according to the Douglas-Reid method was performed.

The updating of the parameters highlights a consistent variation of the modulus of elasticity of the pillars that sustain the dome and the stiffness of the foundations in the vertical direction. Disregarding the updated quantities, the variation of the parameters is indicating the necessity to increase the stiffness of certain elements rather than others. The result emphasizes the necessity to refine certain elements of the model and the behaviour of the identified parts moreover the need to cross correlate further inspection, testing and possible local damage of the building.

Despite the values obtained from the analysis, the approach shows successful results with an overall improvement of the updated numerical frequencies of 6,7% from the initial FEM.

BIBLIOGRAPHY

[1] O. Gentili, "Memorie storiche raccolte," in *Macerata sacra*, Recanati, Simboli, 1947, p. 167.

[2] Archivio Priorale di Macerata, Instrumentorum, n. 858, Macerata: Archivio di Stato di Macerata (ASM), 1606-1609.

[3] P. Pirri, "Giovanni Tristano e i primordi dell'architettura gesuitica," Roma, 1955, p. 39.

[4] G. Cruciani-Fabozzi, "Rosato Rosati e l'architettura maceratese del Seicento," in *"Vita e cultura del Seicento nella Marca"*, Macerata, 1977.

[5] MIDAS Information Technology Co., "Midas Gen v1.1," 2015.

[6] R. Brincker and C. Ventura, Introduction to Operational Modal Analysis, Wiley, 2015.

[7] C. Gentile and A. Saisi, "Ambient vibration testing of historic masonry towers for structural identification and damage assessment," *Construction and Building Materials,* pp. 1311-1321, 2006.

[8] M. G. Masciotta and L. F. Ramos, "Dynamic Identification of Historica Masonry Structures," in *Long-term performance and durability of masonry structures*, Woodhead Publishing Series in Civil and Structural Engineering, 2019, pp. 241-264.

[9] S. I. S. NV, "Simcenter Testlab Version 18.0," 2018.

[10] C. Baggio, V. Sabbatini, S. Santini and C. Sebastiani, ""Multi-Run Operational Modal Analysis of a masonry historical church: the case study of San Giovanni in Macerata," in *Rehabend 8th Euro-American COngress*, Granada, 2020.

[11] A. De Stefano, E. Matta and P. Clemente, "Structural health monitoring of historical heritage in Italy: some relevant experiences," *Journal of Civil Structural Health Monitoring,* pp. 83-106, 2016.

[12] T. Zordan, B. Briseghella and T. Liu, "Finite element model updating of a tied-arch bridge using Douglas-Reid method and Rosenbrock optimization algorithm," *Journal of Traffic and Transportation Engineering,* pp. 280-292, 2014.

[13] C. Costa, A. Arede, A. Costa, E. Caetano, A. Cunha and F. Magalhaes, "Updating Numerical Models of Masonry Arch Bridges by Operational Modal Analysis," *International Journal of Architectural Heritage,* pp. 760-774, 2015.

[14] C. Baggio, V. Sabbatini and S. Santini, "Model Updating of a Masonry Historical Church based on Operational Modal Analysis: the case study of San Filippo Neri in Macerata," in *7th International Conference on Computational Methods in Structural Dynamics and Earthquake Engineering*, Crete, Greece, 24–26 June 2019.

[15] M. Acito, C. Chesi, C. Lazzarin and E. Richermo, "Historical reinforced concrete arch bridges: Dynamic identification and seismic vulnerability assessment," *Insights and Innovations in Structural Engineering, Mechanics and Computation,* 2016.

[16] A. De Stefano, R. Ceravolo, E. Matta, A. Quattrone and L. Zanotti, "Identificazione dinamica sperimentale di edifici strategici sotto sisma," *Ingenio. Informazione tecnica e progettuale,* 12 Aprile 2012.

[17] C. Gentile, "Modal and structural identification of a R.C. arch bridge," *Structural Engineering and Mechanics,* pp. 53-70, 2006.

[18] B. M. Douglas and W. H. Reid, "Dynamic Tests and System Identification of Bridges," *Journal of the Structural Division,* pp. 2295-2312, 1982.

[19] A. Cabbai, C. Gentile and A. Saisi, "Frequency tracking and F.E. model identification of a masonry tower," in *5th International Operational Modal Analysis Conference*, Guimaraes, Portugal, 2013.

[20] Simulink, "MATLAB R2019a".

BETANG, A TRADITIONAL HOUSE OF THE DAYAK NGAJU IN BORNEO ITS SPACE RELATED TO STRUCTURE

MANDARIN GUNTUR[1]*, KEMAS RIDWAN KURNIAWAN[2], YUNITHA[3]

[1]*Department of Architecture
University of Indonesia.
Campus Depok. Jawa Barat. Indonesia
email: mandarin.guntur@gmail.com, URL: https://architecture.ui.ac.id

[2]Department of Architecture
University of Indonesia.
Campus Depok. Jawa Barat. Indonesia
email: kemas.ridwan@gmail.com, URL: https://architecture.ui.ac.id

[3]Department of Architecture
University of Palangka Raya, Indonesia
Campus UPR, 73111 Palangka Raya, Indonesia
e-mail: ynitha@yahoo.com, web page: https:// www.upr.ac.id

Keywords: Borneo, Dayak-Ngaju, Betang, Space, and Structure

Abstract. *The ancient structures of the tribes in the globe yearn to conserve. It marks their races as natives of those places. Nowadays, some of those buildings have lost through natures and cultures. This study aims to get the pieces of knowledge of the Dayak Ngaju tribe. In a structure that calls as Betang. It formed of bases, cavities, floors, walls, and roofs. As known, some of these buildings have ruined, only a few of them still stand. The methods of research led to qualitative and descriptive. It is the way to get the results. At first, Betang reviewed through the critical comparisons of the elements and space backgrounds. Then, took some points in the hypotheses, once it structures analyzed. With the processed amongst functions, ties, measures, forms, and its parts fit the old. Hence, the appraisal gave the rest of the structures formed in percentages. These sums use as conservation values. The reviews were on the profer Dayak villages sort of Tumbang Gagu, Anoi, Malahoi, and Korik. It gave samples through sketches, pictures, and some interviews. It helped to finish the research. Study proves that Betang has left 42% off its old structured elements. It is a form that shaped the spaces.*

1. INTRODUCTION

Betang is a big traditional house of the Dayak Ngaju tribe in Borneo. In many years, Betang promoted a wooden architectural characteristic. Due to cultural distillation, technology and builders whom fully unknown on how to build betang alike its original structure, then this house became slowly disappeared [6, 16, 17]. Betang in Dayak Ngaju comes in two phases of design. First, as a structure designed by approaching the belief and experience of their leader. The second based on material availability, technology, and transportation [17]. Commonly, Betang construction involved many people to build. It was

also as a symbol and as a pride to their ancestors [6, 17]. People of Dayak believe that the ancestor has done to the deity is a trajectory vision including how to build the Betang [4].

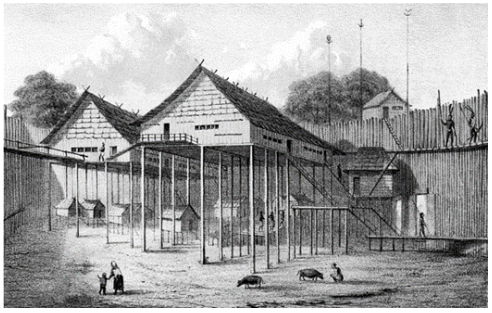


Figure 1. Betang Bakota (fortified) in Central Borneo [23]



Figure 2. Betangs in Tumbang Anoi in 1894 (*source: Tropenmuseum*)



Figure 3. Betang Tumbang Malahoi in Central Borneo (*source: 2006*)



Figure 4. Betang Tumbang Gagu in Central Borneo (*source: 2016*)

Dayak tribe's belief that the ground is the world of hades when death comes. People will go to hades as the temporary place before getting into solemn in the death rituals that famous as Tiwah [12]. Within this, they belief that man comes from the darkness. So that, the ritual to begin in the middle of the night, when the clock touches 00.00 or 12.00 am. It means that the dead man must already stay with their ancestry. At the same time, the priest will state that someone who had carried to heaven, ready arrived at its destination. Thus, the priest lay down the bones of the dead man inside the coffin and put it on the highest place. In this case, it was on the stair of the Betang. Hereafter, the bones transfers to the Sandung (heaven alike a Betang but mini) [12, 14]. Some people who belief in the Kaharingan religion still making this [17, 6]. Hence, to accommodate this structure still sustain, the conservation of Betang is necessary to avoid them from loss through natures and cultures.

2. STRUCTURE AND CONSTRUCTION IN BETANG

Before Dayak conciliation in 1894, forests in Borneo provided many resources such as ironwood and other materials for construction. Using pickaxe and knife, people of Dayak construct Betang (see **figure 10**). According to its construction ages, Betang in Tumbang Gagu that constructed in 1873, younger than in Tumbang Malahoi (in 1869) and Tumbang

Anoi (in 1868) [3]. Betang comes in rectangular with a gable roof. Its length about 63 *depe* and wide about 10 *depe* (one *depe* equal to 1.70 meters). It was high about three (3) meters or more above the ground.

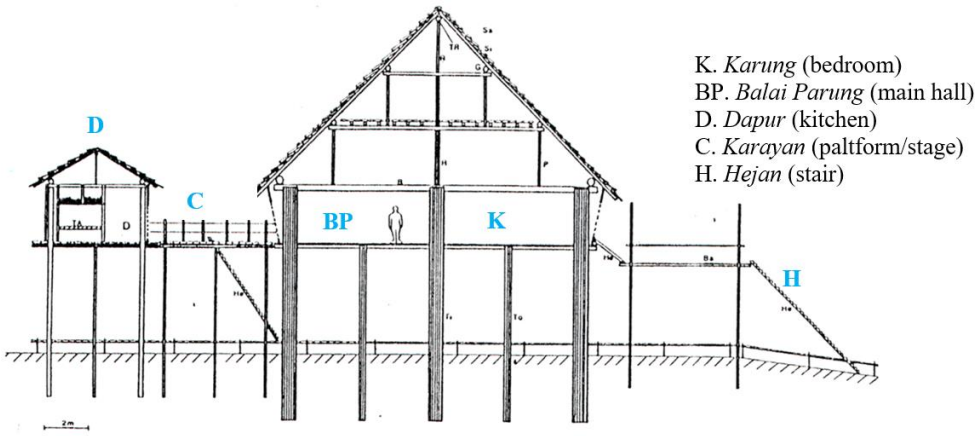


Figure 5. Section of Betang Tumbang Gagu structured in 1873 [3]

Betang consists of components as follows: *Batang-Huma* is the main room that functions as a living room (hall) and bedroom (*karung*). *Dapur* is a kitchen room and *Karayan* is a space that connects the living room and kitchen. Sometimes, it was an elevated field in front of the house that functions as a place for drying rice, saving forest products, and for drying fish about 1 – 1.5 meters above the ground.

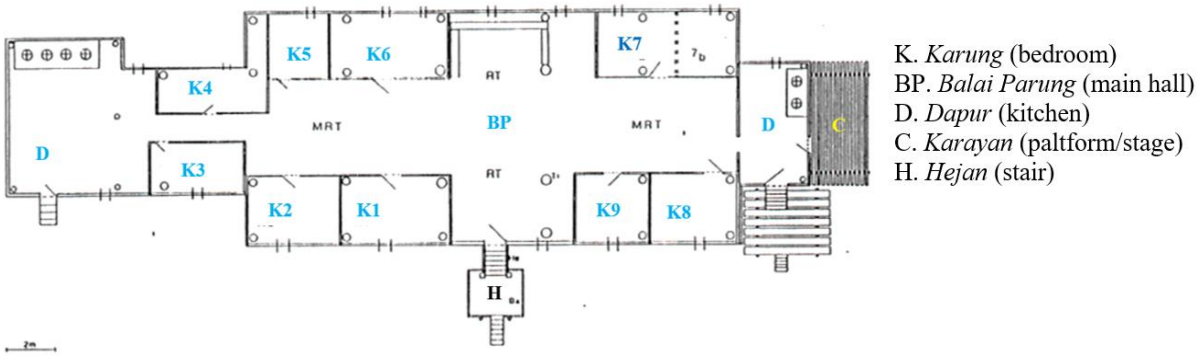


Figure 6. Plan of Betang in Tumbang Malahoi (source: Sakoh 1920) [3]

The pillars of Betang as the first element of Betang designed following *the tarah* system to count its diameters. This system was following the measurement of pickaxe incision on the pillar. One (1) *tarah* is equal to 4 – 5 centimeters. *Jihi* (as the main pillars) should come from the ironwood that shouldering the entire construction load from the rooftop until the foundation then delivers it to the ground. *Tungket* (pillars/stick) is a supporting pillar to shoulder the floor. Commonly, the height of supporting pillars is around 2.29 meters. The main pillars composed *tiang bakas* (the first pillar/32 *tarah*) until *tiang busu* (the youngest pillar/ 22 *tarah*) with the height around 5.58 meters above the ground. The second element is on the floor. It consists of ironwood board that incisions use pickaxe (*tarah*) along the 4-5 meters. The wide of the board is around 30-40 centimeters.

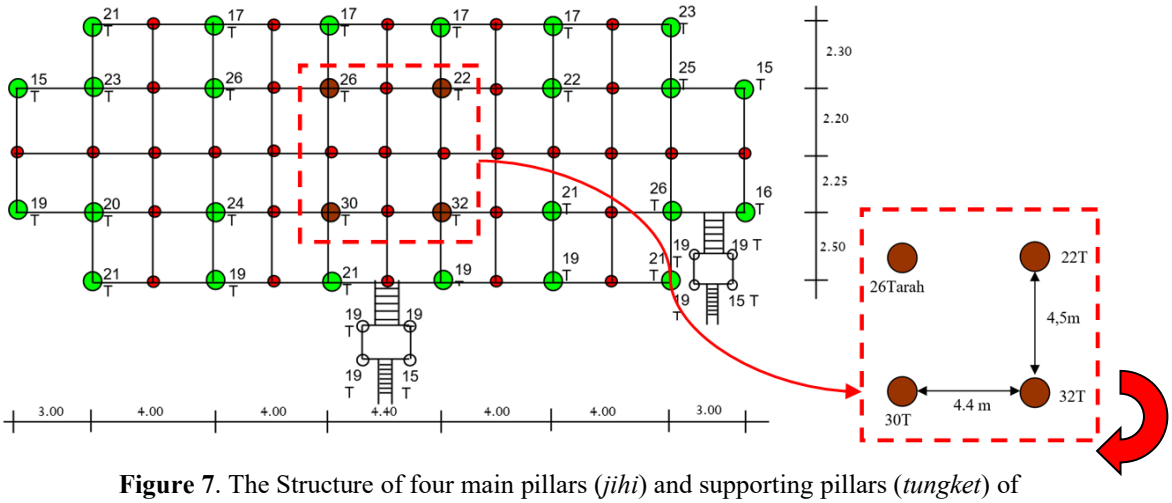


Figure 7. The Structure of four main pillars (*jihi*) and supporting pillars (*tungket*) of Betang Tumbang Malahoi (source: investigation 2006)

The pillars of Betang as the first element of Betang that laid upon *handaran* (the floor balk that used to be a log laid upon the supporting pillars or connected to the main pillars) and the joint on this construction use a wooden pin or rattan tied. The third element is the wall. It comes from the skin of trees (wooden *pendu*) that tied, neatly arranged, and already cleaned. The last element of construction is the rooftop that composed using *sirap* (thin and smooth wooden board), its wide 40 centimeters and 80-100 centimeters length. The order of sirap composes ashlar patterns. How to people of Dayak constructs the main pillar of Betang? The first step, chosen the location of the pillar or they called it as the oldest one (*tiang bakas*). The second, they dug the ground around 1 - 2 meters deep. Then inserted the pillar into the hole. How to erect those pillars? The pillar that around 300 kg should lift by many person-using traditional caterpillars and on the tip of the pillar tied by special rattan, and then people altogether pull it. The number of pillars and supporting pillars that used as the building stage are arranged in a regular pattern, with the hierarchy from the old to the youngest (see **fig. 6, 7** and **11**).



Figure 8. People of Dayak erected a pillar (*jihi*) of Betang (Source: Tropen museum, the Netherlands.)



Figure 9. People of Dayak moved the material of Betang from river (Source: Tropen museum.



Figure 10. Dayak people carved the oldest pillar (*jihi bakas*), using knife (*langgei*) and pickaxe (*beliung*) (Source: Tropen museum, the Netherlands

Betang for people of Dayak Ngaju are togetherness, unity and strengths. It means all of their descendances should come in conception of one Betang. Therefore, Betang design come in rigid, straight, and equilibrium.

3. SPACE IN BETANG

In Betang, besides the **interior**, **exterior** and **transition space**, there is heavenly space that drawn on the *sandung* (a place of dry bones) [14]. This kind of space calls as **subjective space**, a space that signified as vertical symbols, of the upper and lower realms [10,15]. Meanwhile, the daily spaces are a space from dawn to twilight, changing seasons, past and future history, depicted in the *jihi bakas*, as a symbol of orientation that determines the right hand *kan-ngawa* (downstream), *kan-ngaju* (upstream), *kan-ngambu* (top), and *kan-ngiwa* (ground) (see **fig. 11**). This kind of space called as an **objective space** [15].

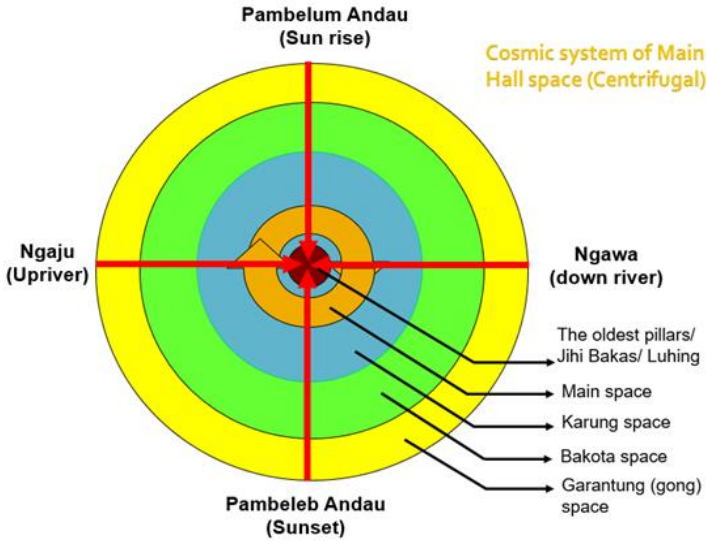


Figure 11. Cosmic system of Dayak Ngaju Modified from Scharer [12]

Betang also centre of Dayak Ngaju orientation, which means a spot where all people come back, as the first and the end [6, 12]. Therefore, Betang become a system of cosmos that determined a spot meeting between the East and the West (see **fig. 11**).

4. STRUCTURE ANALYSES FOR CONSERVATION

Conserving Betang as a historical building is always interconnection between preservation and modernization. The historic monument conservation should manage the processes of renovation and revitalization like memorialized the past and as eloquently as represented the past [7]. According to Matero [9], the prominent objective of traditional building conservation is protecting cultural heritage from loss and damage. Conservators should accomplish this via both deterrent and curative types of intervention. Meanwhile, Reyden, D [2] cites that material care and materials science are both essential elements in any entire conservation program, incorporated within key functions of preservation administration, replication, environmental control, collections upkeep, preservation treatment, investigation and school.

Therefore, through these meaning, Betang reveals its structure as a building element separated its construction technology into based, floor, wall, door, stair and roof, [11]

4.1. Based (foundation)

Generally, foundation of Betangs using many pillars and nearly having the same techniques for each Betang suited to their location where those materials to be found.

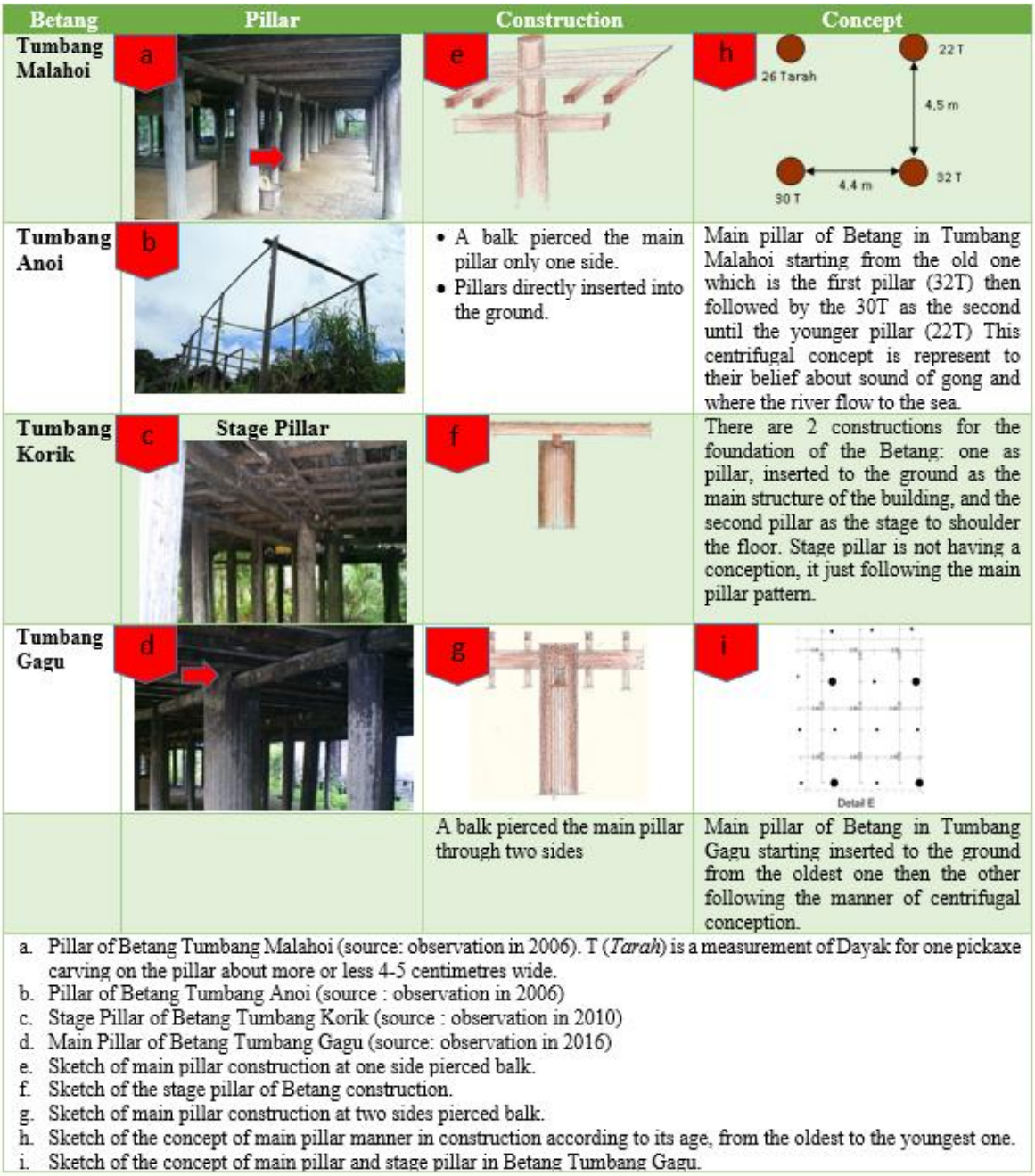


Figure 12. Pillars of Betang in Conception and Construction

The only pillar of Betang in Tumbang Anoi has rotten dan ruin because it lay down in open area and did not preserved properly. Meanwhile, other pillars of Betang in Tumbang Korik, Tumbang Malahoi and Tumbang Gagu are still standing because it still occupied in and secured by other construction.

4.2. Wall, Cavity and Stair

Wall of Betang commonly using tree skin. When Schwaner came to Tumbang Malahoi in Dec 27, 1848, temperature in his thermometer was 25.6ºC. According to level of comfort, those temperatures are still between 16º C – 26º C. With this concept, there is split cavity between the skins of trees that given the breeze easily come in and out [5]. So that, Betang is not a solid Building. In there, people felt the breeze both at night and day. The wall of Betang, commonly about 2.50 - 2.75 meters height.

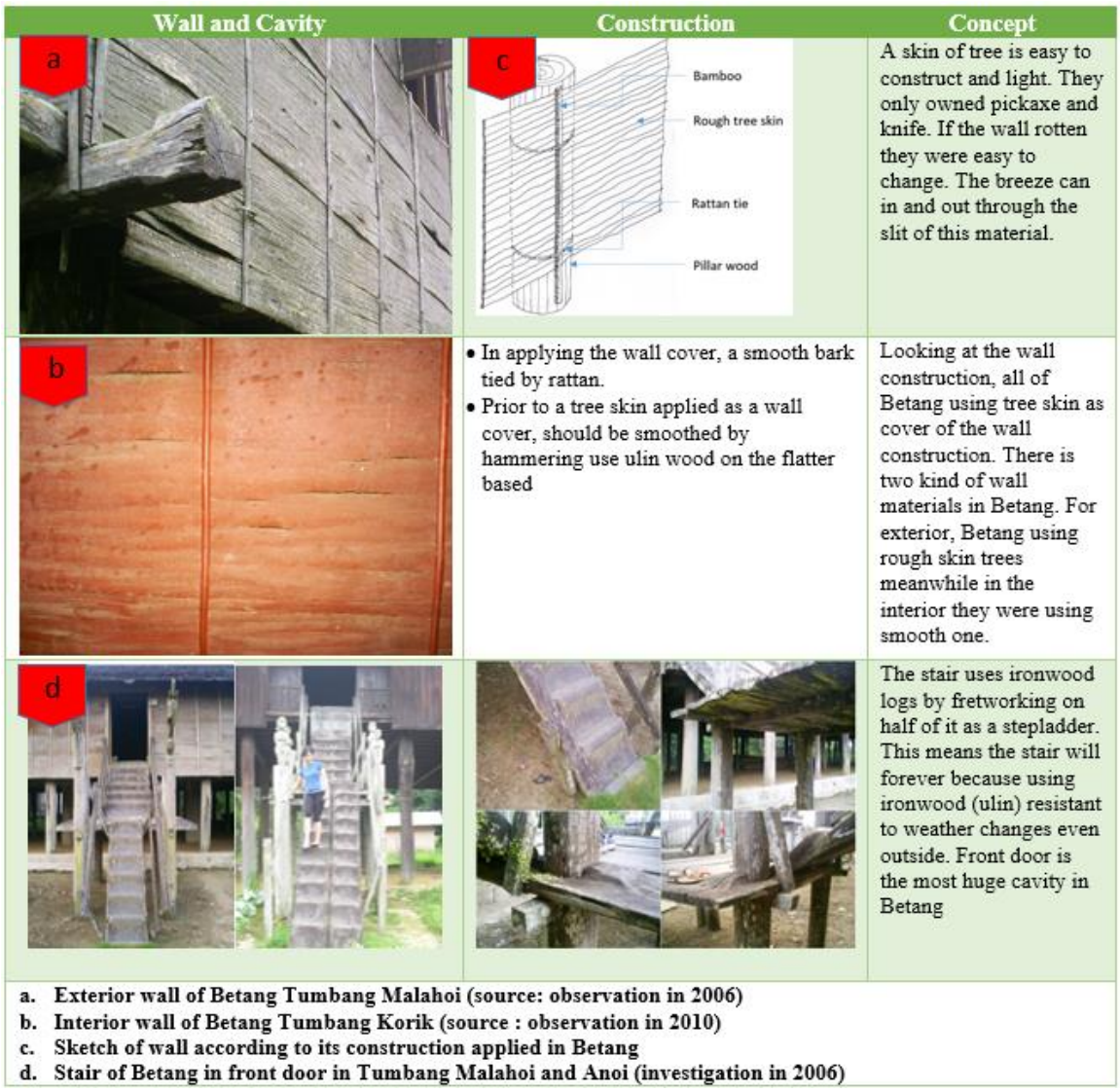


Figure 13. Walls, Cavity and Stair of Betang in Conception and Construction

Of all Betang that still exist until now, is only Betang in Tumbang Malahoi the exterior wall still using rough tree skin.

4.3. Floor

The early Betang that ever recorded was Betang Tumbang Anoi in 1868. The construction of Betang floor originally using a small timber or bamboo [12]. The floor of Betang placed on the stage poles pillars around 3-4 meters above the ground. At that time, all construction using rattan tied and origin wood materials.

Betang	Floor	Construction	Concept
Tumbang Gagu	a 		There are three layers of wooden balk to perform the floor of Betang. 1) The main balk is the first balk constructed upon the pillar that they called it as *bahat* 2) Upon the *bahat* the second layer balk that they called it as *gahagan* 3) Then the last one is floor that they called as *laseh*
Tumbang Malahoi	b 	Wooden board placed upon the second layer balk	Before they were able to make wooden board, people of Dayak commonly using a small diameter trees as a floor material that arranging in a row and tied by rattan.
Tumbang Anoi	c  	*Bahat* tied by rattan directly upon the tip of pillar that already halved. After all of *Bahat* have already tied upon pillars then they tied *Gahagan* one by one to close each other. Then the last construction is the floor, using small diameter trees that arranging in a row	• The small diameter tree that commonly chosen was a special wooden that having high durability material such as *bawang* wood or *balau* wood (light wood). • Amazingly, the rattan to tie those materials was a special rattan that weathered. Even this rattan used to be a pint on the traditional vessel of Dayak (Jukung) to cover small holes.
Betang Bahau	d 		
	Source : a. Bahat and Gahagan in Betang Tumbang Gagu observation in 2016. b. Laseh in Betang Tumbang Malahoi observation in 2006 c. Laseh of Betang Tumbang Anoi 1894 taken from Troppen Museum. d. Laseh of Betang Bahau House 1894 taken from KITLV Leiden e. Skecth of Betang floor construction		

Figure 14. Floors of Betang in Conception and Construction

Looking at Betang house of Bahau in East Borneo at the same age[d], they were using rattan tied as one of their main floor constructions. This happen equal to the Betang in Tumbang Anoi in 1894 when the first Dayak conciliation occurred [c]. Nevertheless, Betang in Tumbang Gagu [observation in 2016] and Tumbang Malahoi [observation in 2006] the floors of Betang have been transformed to the solid wood material (ironwood).

4.4. Roof.

Betang roof construction comes with difference types because of many reasons. It was depending on the condition of its Betangs. Actually, Betang in Tumbang Anoi as one of the oldest Betangs in Dayak Ngaju, so that its construction still using original material.

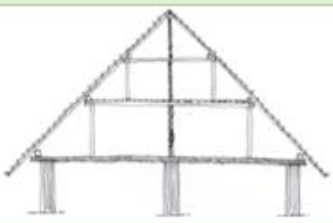
Betang	Roof	Construction	Concept
Tumbang Malahoi	a  Figure 4a.		There are three layers of wooden balk to perform the roof of Betang. • The main balk is the first balk constructed upon the pillar that they called it as *Bapahan* • Upon the *Bapahan* the second layer balk that they called it as *Habantang* • Then the last one is roof cover that they called as *Kasau*
Tumbang Korik	b  Figure 4b		Roof as a part of attic that divided into two section first and second. The first function for some valuable good and the second for deities offering.
Tumbang Anoi	c  Figure 4c.		There is no attic level. It is a simple construction, where the house does not made expansion idea.
Tumbang Gagu	d  Figure 4d		In this construction conceptually, the attic comes in three level, the first for heaving goods, the second for their valuables goods and the third is for offering to deities.
	Source : a. Bapahan and Habantang in Betang Tumbang Malahoi observation in 2006 (figure 4a) b. Roof Construction in Betang Tumbang Korik observation in 2010(figure.4b) c. Roof of renewed Betang in Tumbang Anoi Observation in 2006 (figure.4c) d. Roof in Tumbang Gagu observation in 2016 (figure.4d)		

Figure 15. Roofs of Betang in Conception and Construction

4.5. Betang Assesment for Conservation

In order to assess the change of Betang composition the value using percentage of the transformation structure of construction from its origin until today. These values can be changed according to its actual transformation or modification today.

Table 1. Conservation Assessment to Traditional House of Dayak Ngaju.

Building Composition	Origin					Transformation/Modification				
	Form	Function	Materials	Measured	Fastened	Form	Function	Material	Measures	Fastening
Foundation [a]	Pillar circle	Based	Iron wood	3-5 m height 30-70 ⌀ cm	Wood pen and rattan tied	Pillar circle	Based	Iron wood	2.2 m height 30-70 ⌀ cm	Nail and pen
Floor [b]	1st Log and 2nd Log	Floor based	Light log	8-10 ⌀ cm	Rattan tied	1st balk and 2nd balk	Floor based	Iron wood	5/10 cm 5/7 cm	Nail and pen
	3rd Log	Floor	Light log	4-5 ⌀ cm	Rattan tied	Board	Floor cover	Iron wood	3/30 cm 2/20 cm	nail
	square	Floor cover	Weaving rattan	2/3 m	Rattan tied	square	Floor cover	Plastic	1.2/2.1 m	Rattan tied
Stair [c]	Log	stair	Iron wood	40-60 ⌀ cm	Pen and Rattan tied	Log	stair	Iron wood	40-60 ⌀ cm	Pen and Nail
Wall [d]	light plat	wall	Wood skin	0.4/3 m	Rattan tied	Board	wall	Iron wood	0.2/3.75m	nail
	cavities	wind catch slit from floor and wall	Wood skin	0.3-0.5 mm	Bamboo and rattan tied	square	Window	Iron/ light wood	60/80cm	nail
	rectangular	Main entrance (door)	Skin wood	1.2/1.9 m	Rattan tied	rectangular	Main and side entrance	Iron wood	1.0/2.0m	nail
Attic [e]	rectangular	Deities offering, talisman	bamboo	free	Rattan tied	rectangular	Second floor and third	wood	free	nail
Roof [f]	Gable roof	Protection from rain	foliage	free	Rattan tied	Gable roof	Protection from rain	Iron wood	free	nail

Source: Analyses, 2019

a. Betang in Tumbang Malahoi, its floor used to be 3-5 meters in height when Schwaner came to Tumbang Malahoi in 1846-1847, then the investigation in 2006 found the height of those pillars decreased to 2.2 meters from the ground. In the Traditional Architecture seminar at the University of Palangka Raya in 2002, head officer of Education and Culture Central Borneo province Drs. Kiwok Rampai said that he was made restoration the Betang at Tumbang Malahoi after fire disaster in 1988.
b. Of all betang floor in Borneo before 1894 using light log tied by rattan but now it has modified being an ironwood board fastened by nail and pin [12].
c. One of the oldest stairs of Betangs that still exist until now is in Betang at Tumbang Anoi (the first International Dayak conciliation in 1894 organized by West Kalimantan East Indische afdelling and Damang Batoe (Dayak leader of Ot-Danum tribe).
d. None of those Betangs that still using wood skin as its wall material, it is only Betang in Tumbang Malahoi that still using it as it happens today.

e. Two of Betangs in Dayak Ngaju that still using attic as its function is in Betang Tumbang Gagu and Betang Tumbang Korik.
f. Betang roof comes in various styles concurrent to its function but most of all come in gable roof and 100% have changes its material using ironwood.

Table 2. Betang Dayak Ngaju appraisal on Building structure elements

Compositions	Form	Function	Material	Measure	Fastening	Total
Foundation	100%	100%	100%	80%	50%	86%
Floor	10%	100%	10%	5%	10%	27%
Stair	100%	100%	100%	100%	90%	98%
Wall	40%	100%	5%	10%	5%	32%
Attic	100%	10%	5%	100%	5%	44%
Roof	85%	100%	5%	100%	5%	59%
						58%

Following the result within the **table 2** depicted the foundation of Betangs that used to be using ironwood have changed its measuring and its fastening to 86%. Betang floor shows the value 27%, means the floor modified far away from its origin. Originally, Betang floor using logs that tied by rattan (see fig. 5c, 5d on Betang Bahau and Betang Tumbang Anoi in 1894) then transformed using wooden beam (fig.5a, 5b and 5c in 2016). Meanwhile, stair is the element of Betang that still exist and does not much transformed just 98% from its origin. The other compositions are wall, at first design using wooden skin but have transformed to 32%, only left its function that still using as the wall. The attic of Betang left its composition to 44% and now it merely used for talisman place and offerings for deities. The last element is the roof. Maybe function and measures still at the same of its origin but its form, material and its fastening have so much changed to 59%. Which mean that this transformation values have modified its roof construction. Overall, Betangs in Dayak Ngaju have transformed its building element that affected to all of its space composition and structure to **58%.** It will test of time as Munoz [8] said, whether the building still exist or will pass and gone.

5. CONCLUSION

Betang is a big communal house that needs many people to construct. Betang in Dayak Ngaju is having the same method to construct as well as in Borneo. Wood is the most important material in betang construction and structure. Betang come in separated between the grounds and above. Betang always using pillar for its stage construction. The stair of betang designed using the ironwood log that halves of its trunk carved for the steps. Betang at first, does not use window, they were using cavities between the wall and the floor. Gable system is the style of Betang roof construction. In applying wall, using tree skin, was one of habits of Dayak Ngaju, when those walls become rotten, they were easily replaced it by cutting off the rattan tied. A house should face the East orientation to absorb the first life and lucky in they daily life. West is the sorrow of life and the death. Betang **space** consist of the interior space, exterior, transition, subjective space and objective space. Betangs will extinct if government and other stakeholders do not involve to protect and to conserve these structures within its planning programs. Paying attention to the existence of Betangs Dayak Ngaju have transformed its building element that affected to all of its space composition and structure to

58%. Picturing to the Betang Dayak Ngaju in Borneo that will loss his valuable heritage architecture. Conservation to all of betangs in Central Borneo as well as the entire island of Borneo is an inevitably. This method also suites to assess other wood traditional building.

Acknowledgements. I owe grateful for head of tourism culture agency Central Kalimantan province who had given me a tour to Betang Tumbang Anoi and Malahoi. LPPM University of Palangka Raya, which is funding this research. The last, thank to all of colleagues who have contributed so much to help this paper present in this conference.

REFERENCES:

[1] Beccari, O. "Wanderings in the Great Forests of Borneo", New York: Oxford University Press. 1904.
[2] Dianne van der Reyden, Materials Research Society Symposium Proceedings, Pittsburgh, PA, 1995, vol. 352, pp. 63- 71)
[3] Kampffmeyer, Hanno. Die Langhauser Von Zentral Kalimantan.Anacon-Verlag, Schellingstasse 23, 8000 Munchen 40. 1991
[4] Lang, Jon. "Creating Architectural Theory, the role of the behavioral sciences in Environmental Design". VNR Company, New York. USA. 1987.
[5] Mandarin Guntur, Tari Budayanti, Yunitha, "Design of Traditional Housing" Collaboration Research UPR-Queensland University, repository LPPM University of Palangka Raya. 2018.
[6] Mandarin Guntur, Makna Ruang pada Rumah Betang Suku Dayak Ngaju di Kalimantan Tengah: Menapak Hidup ke Nirwana Tanpa Neraka. Proceeding PESAT Vol 2 | vol: | issue: | 2007
[7] Murphy, Kevin D, Change Over Time University of Pennsylvania Press Volume 4, Number 1, spring 2014, pp. 40-56
[8] Munoz V, Contemporary Theory of Conservation, Universitat Politècnica de València https://www.researchgate.net/publication/ 283234670. 2012.
[9] Frank G. Matero, Heritage, Conservation, and Archaeology, AIA Site Preservation Program. 2015.
[10] Needham, Rodney. Symbolic Classification, Goodyear publishing company, Santa Monica, California, USA. 1979.
[11] Rem, Koolhaas. "Elements of Architecture". Taschen. USA. 2018.
[12] Scharer, Hans. The conception of God among a South Borneo People. The Hague-Martinus Nijhoff. 1963.
[13] Schwaner, CALM, (1852–1854) Borneo: Beschrijving van het stroomgebied van den Barito, Amsterdam: P.N. Van Kampen, 1853.
[14] Stohr, Waldemar, Das Toten Ritual der Dajak, Kommissions-verlag, E.J. Brill, 1959.
[15] Tuan, Y. "Space and Place the perspective of experience", University of Minnesota Press. Minneapolis. 1977
[16] Winzeler, "The Architecture of Life and Death in Borneo", University of Hawai'i Press, 2004.
[17] Yunitha, "Architectural Expression of Tiwah Ceremony Case Study of Dayak Ngaju Tribes Betang House in Central Kalimantan". digilib.its.ac.id. 2007.

12th International Conference on Structural Analysis of Historical Constructions
SAHC 2020
P. Roca, L. Pelà and C. Molins (Eds.)

CLAUDIUS AQUEDUCT IN ROME - KINEMATIC ANALYSES AND EMPIRICAL EXPERIENCES FOR THE DEFINITION OF STRUCTURAL RESTORATION INTERVENTIONS

FABRIZIO DE CESARIS[1]

[1] Sapienza, Università di Roma,
Piazza Borghese 9, 00186 Rome, Italy
e-mail: fabrizio.decesaris@uniroma1.it, www.uniroma1.it

Keywords: Historical Structure, Masonry, Structural restoration, Consolidation, Empirical study, Reinforcement minimization.

Abstract. *Present work summarizes a study on the stability of some parts of the Claudius Aqueduct in Rome (1st century AD). The project provides empirical applications linked to the definition of minimal interventions for the structural restoration of a section of the structure near Capannelle. Results of the kinematic analyzes conducted and of experiment with a physical model representing the structure of the upper hydraulic conduit (speco) are reported. Ultimately, hypothetical minimal interventions are outlined for the protection of the structure and at the same time of the image and usability of the Aqueduct.*

1 INTRODUCTION

1.1 Historical outline

The Claudius Aqueduct (Caligola, 37-41 AD, Claudio, 41-54 AD) has been operating since 47 AD. C. It crosses the hills and the plain of the Roman countryside, with an artificial route 45 miles long (over 66 km) which joins the natural one of the Aniene Valley. The hilly upper section has many examples of hydraulic and structural engineering, which are necessary to divert water through the hills. The lower section - about a quarter of the structure – is instead completely emerging from the countryside plan that becomes almost flat approaching to Rome and the Tiber Valley. From Capannelle towards Rome, the height of the conduit quickly arises from the countryside ground-level, quickly reaching a height around 20 m above the elevation profile of the soil. The hydraulic canal was kept at a remarkably high altitude over the city to facilitate the subsequent parceling and branching towards buildings and baths. In fact, nowadays in the countryside it constitutes a primary presence for several kilometers, up to the Roman Aurelian Walls (270 - 275), which incorporate the Aqueduct for substantial stretches (fig. 1, left).

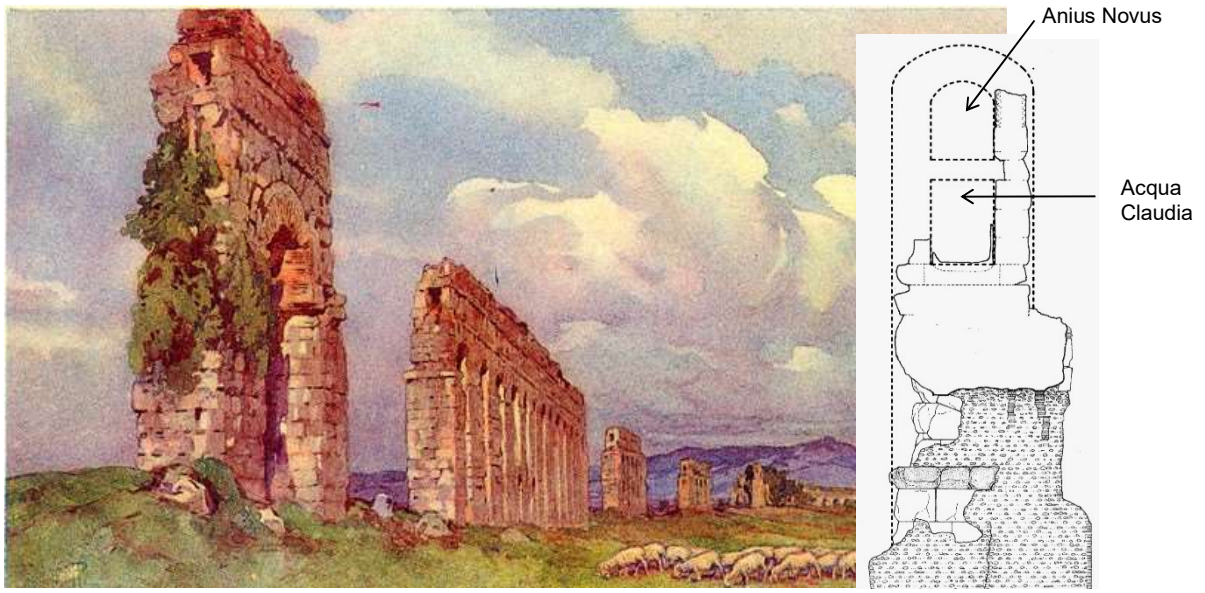


Figure 1: Historical image of the Aqueduct in a late 19th century watercolor. The typical cross section of the upper part of the Aqueduct is re-represented (archway, Claudius and Anius Novus water hydraulic conduit).

The masonries of the Claudio aqueduct were built exclusively in blocks, mostly of peperino, which is a volcanic sedimentary stone. Even though the architectural design of the arches has a rational rhythm, the size and quality of the blocks is completely heterogeneous in shape, size and quality. Modification, consolidation and reinforcement works already started in the 1st century. The constructive phases of the structure are characterized by the almost immediate overlap of the Anius Novus conduct. The use of the existing supporting structure for a double channeling follows other previous examples, but the Anius Novus is made of rubble masonry with sides in *opus mixtum* and is conserved only in minimal residual portions (fig. 1, right).

However, the second hydraulic line does not appear to be the cause of the reinforcement works. In fact, these works were carried out in sections and entailed huge funding already in 71 and 81. After that, the consolidations continued in the 2nd century, during Hadrian and Severian Ages, with the

reinforcement of other segments made with well executed *opus testaceum* and in 4th century the works were continued with the characteristic inhomogeneity of building materials. The maintenance continued until the 10th century when the structure was substantially abandoned. Subsequently, the construction was also systematically attacked to obtain material with a consequent strong reduction in discontinuous sections. Especially for the construction of the Felice Aqueduct in 16th century, which runs parallel to the Claudius aqueduct [1, 2, 5, 6].

1.2 Context and purpose of the study

The starting point for this study was a consultation requested by the Archaeological Superintendence. Emergency intervention was needed for a portion of the Aqueduct located in the Appia Antica park near Capannelle. In this section, problems occurred both for the safety of the population and for the loss of original materials.[1] The works were aimed at the direct elimination of structural problems by avoiding the incipient collapse of unstable portions as the supports for fractured roof lintels and the local repair of unstable parts. Work has also been planned to mitigate the conditions that accelerate the degradation of materials, such as infiltrations and aggressive vegetation that would have caused new and serious damage to the structures.



Figure 2: View of the hydraulic conduit in the end part of this section of the Claudius Aqueduct. The broken lintel is prop up by a metal support and in the upper part there is a residue of the Anius Novus upper structure. On the left, a recent anti-seismic intervention on an adjacent section.

During the consultancy, some particular aspects were investigated, concerning the conduit and the relative lytic covering architraves. These investigations did not lead to direct operational conclusions.

[1] The restoration was guided by Arch. Giacomo Restante (W.D.), by Arch. Stefano Antonetti (P.M.) and by Dr. Antonella Bonini (archaeologist) and performed by DucaleRestauro S.r.l. from Venice (specialized company). Thanks to Prof. Cesare Tocci (Politecnico di Torino) for adding value to this project through his inspiring suggestions and his great availability.

Indeed, the funding just covered the disposing of temporary interventions, but we hope that our studies will be useful for a future conservative maintenance works.

The attention has been focused on the critical conditions of the duct related to the state of the lytic roof lintels that have many fractures. On this occasion, the cracks of the arches corresponding to the pillars from 1st to 31st were documented and shoring-up devices present were also reported.

The different elements of deterioration can hardly be interpreted in a sufficiently simple systematic framework that adequately reflects the overall behavior of the structure.

The vibrations induced by the earthquakes that occurred in the two millennia of existence of the monument or the settlements of the grounds and walls have caused damage. However, the respective influence of the numerous parameters interfering in the behavior of the monument can hardly be defined. The most important parameters are: heights of springer of the ducts covering, which are different from in every part; the lack of homogeneity of the material and the degradation; the conditions of the soil; the structural responses, altered locally by the degradation.

The study aimed rather to identify possible methods of intervention on the stone roofs of the hydraulic conduits, using a symptomatic treatment logic. Starting from the critical conditions of the building, the negative effects brought about by degradation and discontinuities were identified to locally mitigate the consequences and to improve the original reactive capacities of the monument. This section's degradation conditions reflect those generally found in other surviving portions of the ancient infrastructure and the considerations carried out - exceeding the specific features of the section under investigation - can also be considered extensible to other portions of the Aqueduct.

To complete the study, some operational possibilities are proposed, which are aimed at improving the structural capacity of the monument, awaiting subsequent possibilities for intervention. In fact, it is also suggested, in order to standardize future interventions to aim also at the objective of a characterization that constitutes a unique and identifiable trace for the work to be carried out in the coming years.

2. MONUMENT DETERIORATION CONSISTENCE AND STATUS

From the consistency point of view, the hydraulic conduit can be described as a tunnel with two vertical and parallel walls made of stone blocks laid in semi-horizontal layers, surmounted by a lithic plate formed by lintels made up of squared, irregular blocks, placed side by side. On both sides of the lintels there are small protrusions on external facing, as a continuous frame that defines the front. Stone elements of this frame are not always whole; probably in most cases, on one or both ends, the portions that make up the projection of the architraves that cover the span and rest only on a part of the thickness of the longitudinal partitions have been added.

Almost all the wall elements were made with uneven quality peperino. To build the horizontal lintels were chosen materials of greater consistency, well cemented; whereas in the vertical masonries there are also blocks obtained from less cohesive peppers, tending to degrade with greater ease. All the elements that make up the two walls show signs of erosion on externals sides caused by atmospheric agents and stresses. These masonries were initially prepared with a sort of *anathyrosis* (i.e. with the well-worked ashlars on the edges and with a less finish accurate on the central surface of the face in view), currently have edges often worn, sometimes chipped. A less advanced deterioration is observed on the more protected internal face. The elements that make up the section of the duct are affected by cracking phenomena characterized essentially by a pseudo-longitudinal

orientation of the water conduit and the roof lintels. The longitudinal discontinuities of the arches are visible from the outside from below, while inside they are often hidden by the stratification of the limestone collected at the base of the duct, but are revealed by the detachment of the horizontal layer of limestone and the original screed related to the internal facing of the walls, due to the relative location.

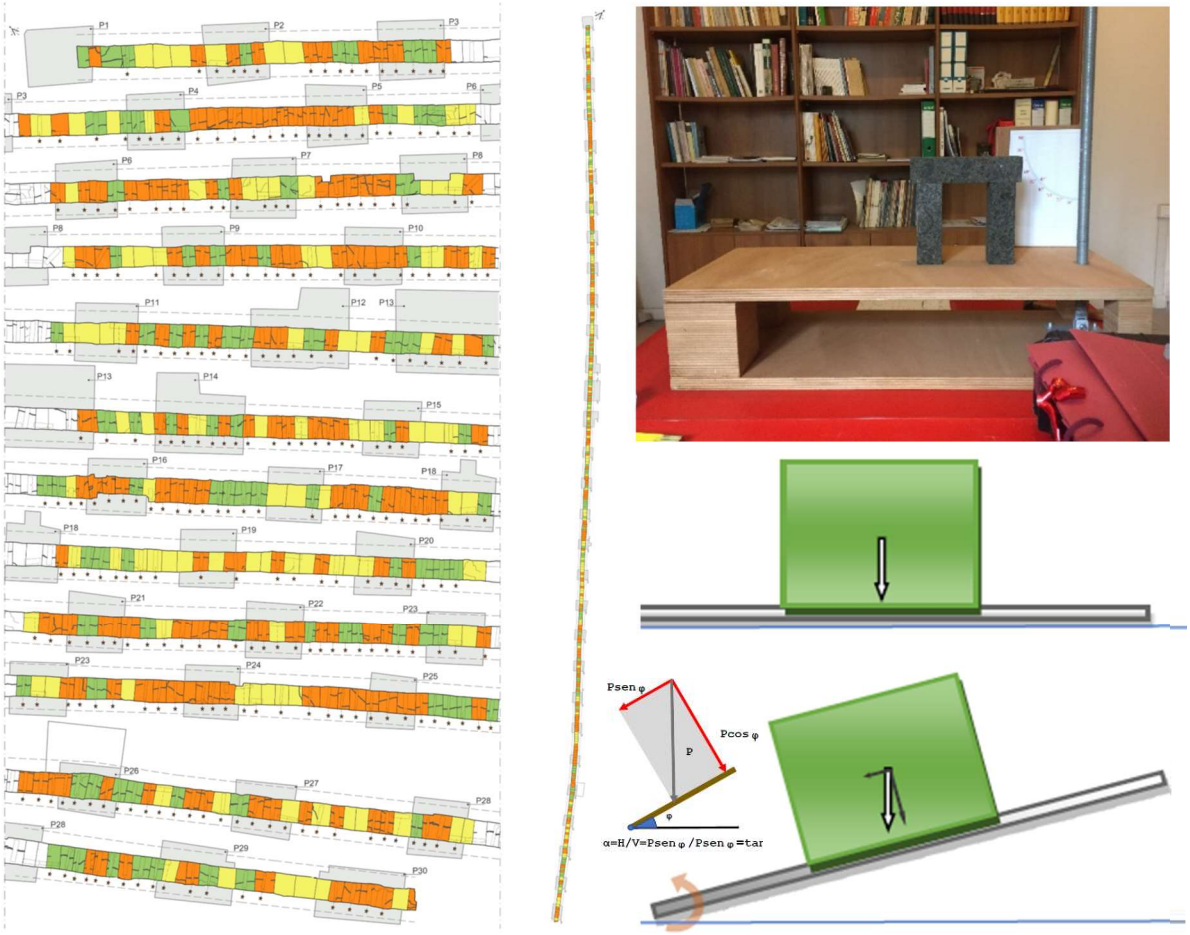


Figure 3: Survey of the state of cracking degradation in the different sections of the portion of Aqueduct analyzed, edited by Arch. P. Agrimi and re-elaborate by the author (left); inclinable plane used in the experimentation (kindly provided by DucaleRestauro S.r.l.) with the scheme adopted (right).

On this occasion, taking advantage of the special condition of accessibility to the tunnel, the survey focused above all on the cracked condition of the ceiling, considered the most critical issue. The mapping of the cracking of the lithic elements covering the roof have been extended to the entire section - arches from 1st to 31st), also localizing the presence of the support devices already adopted or introduced on this occasion. In addition, was detected the final section, where it is possible to appreciate the thicknesses of the elements constituting the span.

The fractures of the lintels caused structural failures with relative displacements due to the reduction of the continuity constraint and to the assumption of a different equilibrium condition, often characterized by relative sliding and lower degrees of safety. The effects of these stability adjustments

have induced the justified apprehension that recommended the immediate insertion of the internal support props to avoid the feared collapse of the lintels, taking advantage on the unused tunnel and its poor visibility from outside (fig. 2).

These supports are temporary and replicate a type of device already used in the last century, which is made of vertical metal supports, T-shaped with wooden planks that mediate the contrast of the architraves towards the intrados and under the support of the central upright on *cocciopesto* of the duct or on secular sediments limestone.

As can be seen in fig. 3, the fracturing of the lintels is widespread, but not homogeneous. Some elements appear intact (yellow) and others interrupted by the discontinuity that is sometimes positioned in the center (green) and often near one of the edges (orange). The presence of multiple fractures is rarely observed and sporadic is the case of an actual partial collapse; this temporary balance has recommended and allowed, in the past and at present, the insertion of the metallic supports to prevent a progression of deformation phenomena and possible collapses.

3. DEFINITION OF THE STUDY MODEL

The models studied have been defined based on the survey, with the approximations necessary to make the section as representative as possible. Only transverse vulnerability is considered, assuming as certain an adequate capacity in the longitudinal direction.

The side walls show critical issues related to aging and the lack of homogeneity of the material, which appear more relevant outside where the masonries are not protected by coatings and by the condition of a closed environment. To consider this generalized reduction of the resistant section, a retraction of the hinges on all the joints was introduced in the analyses.

On the other hand, the deterioration of roof lintels is mainly constituted by fractures that generally passing through the whole wall section. The material is overall well preserved because it is protected by the remains of the Anius Novus structure and by the reduced exposure of the confined environment of the duct. The fractures that cross the thickness of the lintels on pseudo-vertical planes appear to be the most incident element of static degradation. The roof of the hydraulic conduit can be assimilated to a series of simply-supported beams and the observed fractures transform the lintel into a sort of natural straight arch, which is supported as an arch set on the side walls and with mounts almost equal to the thickness itself.

In summary: some lintels have preserved monolithic shapes, but largely show fractures passing through the entire thickness, with regular orientation or levels with different configurations. The scheme in fig. 5 shows fractures represented simultaneously but, in general, only one is present on the same element and the scheme must also be considered in the symmetrical version. The lesions are of type A, B, or C: in case B, a portion of the lintel takes on a larger size than the other - the center of gravity is within the gap between the walls), and normally give in D before finding an adequate contrast in the natural arch. Type C is the fracture with the greatest risks due to the very reduced support section and because the lesion is not visible. Therefore, the possible presence of these discontinuities is not appreciable in the performed survey, but it is only hypothesized during the study comparing other portions of the Aqueduct. The T cuts are sometimes original, but are not always present and symmetrical on both ends of the same slab; it is possible to observe them only in the sections in which the building has lost its continuity and, consequently, they do not appear in the survey carried out as they cannot be identified.

Overall, there is a rather varied set of situations that has forced us to consider different schemes to

represent the current state of the structure, made uneven by the different degradation conditions induced by the fractures. A basic scheme was taken from the longitudinal section, which is traced back to a typical section (fig. 5, above left). On this scheme different models of structural behavior have been hypothesized. In fact, two types of structural problems are highlighted by examining the conditions of the water conduit: the first one is related to the stability of the lintels fractured in ordinary conditions and the second depends on the ability of the structure to resist seismic stresses.

In the first case, vertical supports have been introduced, to ensure the stability of the architraves subject to their weight and to that of the masses above. In the second case, only recently, in another section of the Aqueduct, have been inserted frame devices which are, however, particularly invasive, even if not visible from the outside (fig. 1. right).

In a broader analysis, other critical issues presented by the Aqueduct structure must be taken into consideration, such as the tendency to longitudinal segregation of the arches with divergence into two portions, the general deterioration of the pylons, the unevenness of the state of degradation of the blocks, etc.

These types of deterioration are already studied in other previous interventions [4] and there are forthcoming contributions. Within the limits of this analysis, only the portion of the hydraulic conduit was considered; downstream of the local checks, the specific conditions influenced by the tax quota were considered, variable in relation to the elevation of the soil, since the level of the duct set at an almost constant altitude. In order to simplify, other specific conditions, varying from section to section, have not been considered. For example, the portions related to the remains of the above structures of the Anius Novus.

The following figures show the most significant and therefore considered schemes (fig. 4). The kinematic mechanisms analyzed are essentially based on the hypothesis of the formation of hinges in the absence of sliding, prevented by friction. Only in case study 11 it was possible to consider the sliding between bodies 3 and 4.

In figure 6, the same mechanisms have been reconsidered with a retraction of all the hinges, activated simulating both the classic local subsidence on the axis of the hinge and the general state of degradation of the blocks that is widespread even if not homogeneous.

The values determined for the two cases can be considered as limits: an upper one - which is difficult to consider as a realistic result - and a lower one, more useful because it is precautionary, but sometimes more congruent with the state of degradation of the blocks.

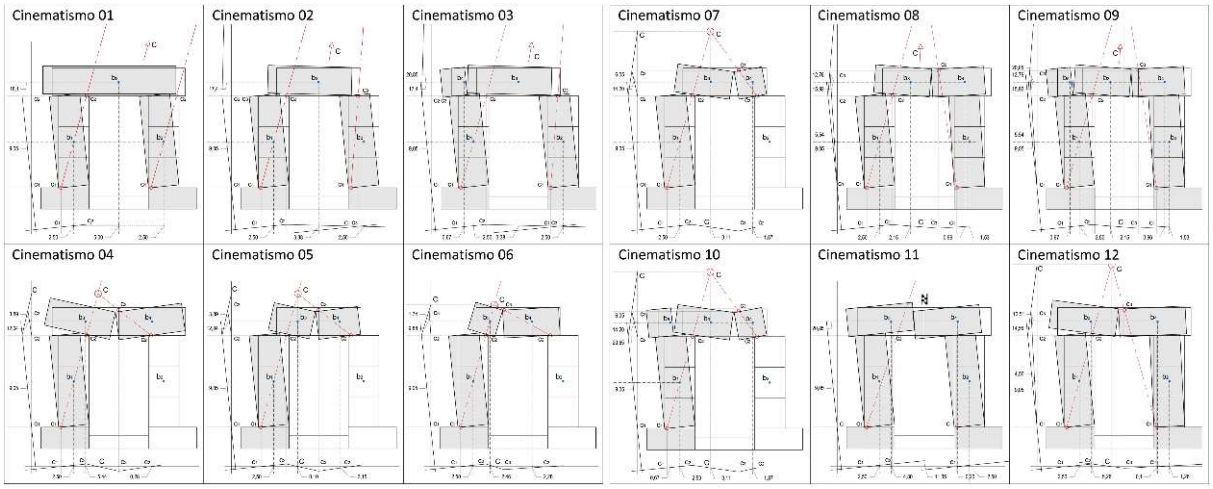


Figure 4: Synoptic framework of the kinematic mechanisms examined.

According to the studies performed during Nineties by Antonino Giuffrè and Vittorio Ceradini [3], the work on these models was conducted with kinematic and empirical analysis. So, it was possible to make an immediate comparison with a real modeling in 1:10 scale, with elements of 5 cm thick, corresponding to 50 cm. The models were subjected to static stresses, equivalent to the seismic stress condition, simulated by rotating the support surface of the models. That determines an inclination of the system whereby the vertical weight can ideally be broken down into two components similar to those induced - in real conditions - simultaneously by gravity and seismic actions (one normal to the plane and one parallel to it). The relationship between the two components is like that between the force of gravity and the seismic thrust (fig. 3, right).

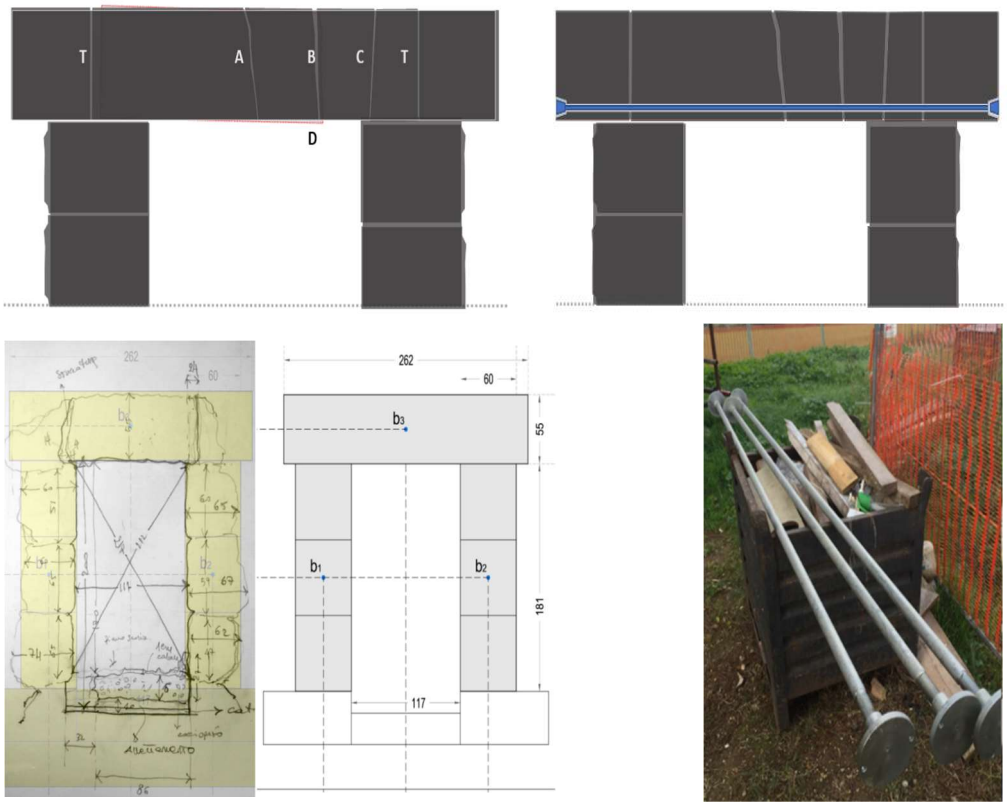


Figure 5: Representative scheme of the lintel and of the typologically repeated fractures (above, left); indication for the tie bars location (above, right); the survey and the used scheme (bottom, left); the tie bars proposed and already used in other sections of the aqueduct (right).

4. RESULTS OF THE KINEMATIC STUDY AND OF THE EXPERIMENTATION

The results of the graphical-numerical modeling and of the direct experimentation have been summarized in the following tables.

Figure 6 reports some of the results obtained with the study of the mechanisms in terms of load multiplier necessary for the activation of the mechanism; the values are obtained considering the activated hinges set back by 5 cm to give a general account of both the effects of the load concentrations and the degradation of the material. In the study, the homologous values were also calculated considering intact hinges, but for brevity they were not reported.

Figure 7 lists the results obtained empirically in the different cases already examined with numerical analysis. The photographs show the mechanism that occurred in the experiment.

All the data obtained for a possible comparison have been reported in Figure 8. Moreover, the data in terms of acceleration - calculated according to the Italian standard - have been added, with a different level of knowledge and relative Fc, at different altitudes in correspondence with the altimetry of the different ground levels crossed by the aqueduct. In many cases the mechanism is implemented in the theoretically foreseen manner; sometimes there is a discrepancy with respect to the starting hypotheses which highlights the possibility of sliding which, as mentioned, have not been taken into consideration in the numerical analysis - with the exception of case 11.

Generally, the results in terms of multiplier - determined in relation to the inclination reached at the time of priming - follow the numerical forecasts, however assuming a magnitude between the two limit values, with intact or backward hinges.

Study case 4 does not have a corresponding application. The mechanism that actually occurs is the same considered successively as case 11: the central hinge does not be formed because the sliding occurs between the two segments, which remain integral to the respective abutments and the projection of the center of gravity does not come out from the support of the slab. This process does not produce a natural arch effect by anticipating the activation of the kinematic chain. In the case study 11, the activation occurs with a multiplier equivalent to the one determined without considering the gripping work, as if the force exchanged by the two parts that remain united does not actually exchange at the time of the activation. The two portions - abutment and straight arch - separately tested, have two different multipliers (upper left, and lower right). They can be activated together with a multiplier that averages the portion values, highlighting the reciprocal exchange of forces.

Also in study cases 6, 8 and 9 the mechanism presents sliding that anticipates the trigger: in case 6 by horizontal sliding of the small block 5; in cases 8 and 9 the weight conditions cause the slumping of the major block of lintel, which slides in order to be supported in the key section, thereby producing a slightly higher thrust than expected; subsequently the vertical sliding occurs again and the natural arch takes on an even lower mount and therefore contributes to the early activation of the mechanism. In the first moment the collapse concerns the projecting block and does not produce the collapse of the wall, which, however, initially caves in, but then - at the end of the thrust in correspondence with the collapse of the horizontal block - maintains the position reached.

In case 12 an artifice was attempted to verify the response of the whole structure if the sliding had been delayed. Thanks to the sliding preventing of the sections in contact in the centerline, a mechanism similar to case 4 occurs. This mechanism brings back values of greater capacity even if not comparable with those the mechanism initially provided, but are not feasible

Generally, there is a discreet natural capacity of the original hydraulic conduit which, however, decreases with the fracturing of the roofing slab. This justifies the persistence of the structure over time. However, the lintels today appear fractured probably for causes not related to seismic stresses. In most cases, the stability situation with ordinary conditions do not cause collapse of the coverage. The necessity to find more stable configurations - especially where the fracture is close to the supports - produces those small slips deeply observed. The structures vulnerability towards the seismic event is quite evident in case of partial losses and fractured elements. It follows the requirement to intervene especially in the case of fractures that are not central and when the phenomenon affects contiguous lintels.



Figure 6: Summary of the expected results with activated retracted hinges.



Figure 7: Synthesis of experimental results with physical model.

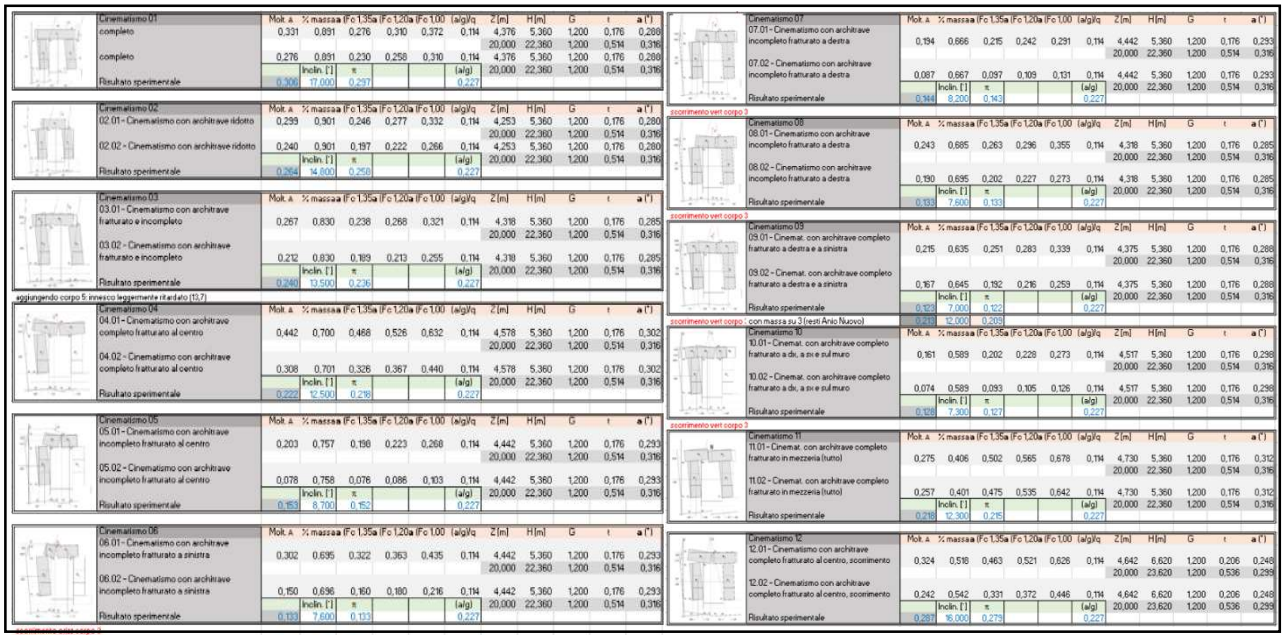


Figure 8: Summary and comparison of the results obtained with the kinematic analyzes and with the direct experimentation, related to the seismic accelerations of collapse assessed according to the Italian legislation.

5. CONCLUSIONS ON THE PRACTICAL ASPECTS OF THE INTERVENTION

In conclusion, to obtain an improvement in capacity, can be inserted devices capable of supporting the roofing slab tracing the architrave back to its original monolithic nature. The measure can be implemented by inserting titanium bars - or stainless steel - which should exert a modest compressive force, sufficient to avoid rotations and also vertical translations in the fractured sections (fig. 5, above right). The failure due to shear force near the supports is, in fact, one of the most penalizing consequences of the structural deterioration for the wood. The proposed intervention could be a substitute for the internal supports and allow full suitability of the duct. The insertion of titanium bars would not be burdensome for the lithic material as it requires the execution of small diameter holes, which can be made without difficulties. This intervention certainly appears suggestive since it allows to find a structural stability close to the original one, because it doesn't introduce invasive elements in the cavity.

The safety margin would probably be lower than those obtainable with the insertion of metal frames (fig. 2, right). However, the intervention would result minimal formal and functional invasiveness, not obstructing visibility and accessibility of the conduit. The bar - constituting a sort of tie rod - would allow the arched behavior with limited thrust of the lintel, whether it is intact (precautionary intent) or fractured (improvement intent). The presence of intact lintels allows a containing effect, even on fractured ones, provided that the latter are suitably interspersed with healthy ones. Consideration that introduces various intervention management possibilities by grading the number of bars to be inserted. End-plate anchors, as already verified in previous interventions, can easily be disguised. Once inserted, the bar can be activated with forcing, producing an axial force of minimum intensity. The same force can be transferred to the lithic straight arch by anchoring with mortar or resin injection; otherwise it can be possible to operate with dry techniques to obtain maximum reversibility. The bar can be activated by forcing the small end-plate anchors, one of which is fixed and the other can be screwed using a threaded sleeve.

REFERENCES

[1] Arizza, M. and Santolini Giordani, R. L'acquedotto Claudio: restauri antichi e moderni. In: S. Francocci (Ed.): *Materiali e Tecniche. Esperienze di restauro a confronto*, Conference proceedings (Nepi, novembre 29th 2008), Davide Ghaleb Editore (2011), pp. 11-15.

[2] Ashby, T. *Gli acquedotti dell'antica Roma*. Trasl. by A. Aiosa Gambardella [Ashby, T. *The Aqueducts of Ancient Rome*. Richmond I. A. (Ed.), Clarendon Press (1935)], Quasar (1991).

[3] Ceradini, V. Indagini sperimentali su modelli di opera muraria. In: A. Giuffrè (Ed.): *Sicurezza e Conservazione dei centri storici - Il caso Ortigia*, Editori Laterza (1993).

[4] De Cesaris F. and Vergantini L. Acquedotto Claudio: interventi di rinforzo statico e di restauro di alcune arcate nel Parco degli Acquedotti. In: S. Francocci (Ed.): *Materiali e Tecniche. Esperienze di restauro a confronto*, Conference proceedings (Nepi, novembre 29th, 2008), Davide Ghaleb Editore (2011), pp. 16-31.

[5] Orsini, B. *Comentario di Sesto Giulio Frontino degli acquedotti della citta' di Roma con note e figure illustrato da Baldassarre Orsini professore delle belle arti e direttore dell'accademia del disegno di Perugia*, Stamperia camerale di Carlo Baduel (1805).

[6] van Deman, E. B. *The building of the Roman aqueducts*. McGrath Pub. (1973; reprinted in its original form by Carnegie Institution 1934).

12th International Conference on Structural Analysis of Historical Constructions
SAHC 2020
P. Roca, L. Pelà and C. Molins (Eds.)

COMPARISON ON METHODOLOGIES AND INTERVENTIONS FOR TWO MASONRY CHURCHES AFFECTED AFTER THE 2017 EARTHQUAKE IN MEXICO

M. ESPONDA[1*], AND J. COOKE[2]

[1] Associate Professor and Coordinator of the Conservation Program
at the Azrieli School of Architecture
Carleton University, Ottawa, ON, Canada
e-mail: mariana_esponda@carleton.ca

[2] Senior Structural/Conservation Engineer at John G. Cooke & Associates Ltd. and Adjunct Professor
at the Azrieli School of Architecture
Carleton University, Ottawa, ON, Canada
email: jcooke@jgcooke.com

Keywords: Historical Structure with Unreinforced Masonry, Earthquakes in Mexico, Traditional vs Contemporary Intervention, Material Compatibility, Vapour Transmission.

Abstract. *The current state of two 16th century masonry churches were studied after being damaged during the 2017 earthquake in Mexico. The two complexes being analyzed are part of the World Heritage Site "Ruta de los Conventos": the Convento de San Guillermo Totolapan, in the state of Morelos south-east of Mexico City, and the Huaquechula Monastery, in the state of Puebla south of Mexico City. These buildings are representative of the architectural model adopted by the first missionaries who evangelized the indigenous populations in the 16th century. The churches were constructed circa 1535 and 1548, respectively. The history and cultural significance for each project is researched in coordination with the stakeholders, along with the contrasting structural systems and any known previous interventions, historic and contemporary.*

The damage inflicted to the two churches due to the most recent earthquake (2017) is critically analyzed, specifically focusing on inherent defects of the existing materials, the variation in construction methodologies and the impact of contemporary interventions such as the use of reinforced concrete and structural steel following previous earthquakes. Potential repair methodologies are discussed in order to mitigate future damage to the structures. Discussions include the importance of using compatible materials along with appropriate repair procedures and the need for ongoing maintenance of these important heritage structures.

1 INTRODUCTION

The deterioration of heritage sites resulting from natural disasters is a loss to humanity's culture. However, most existing studies on earthquakes focus on the effects on building materials from a technical standpoint. There is a need for further studies which balance the technical requirements with the significance of built heritage, focusing on risk management and the implementation of interventions which embrace appropriate technologies. There is also a general lack of understanding among the Architectural/Engineering community as to how Unreinforced Masonry (URM) structures function, how to preserve them and, where necessary, how to rehabilitate these structures. There is a misunderstanding that URM reacts poorly to seismic forces, producing extensive structural damage and loss of life. Yet, in many countries, there is evidence of masonry structures that have endured for centuries in areas of high seismic activity, simply by performing regular maintenance on the masonry with compatible materials. This prevents long term neglect and deterioration, which is the ultimate cause of structural failure. In the authors experience, it is the inability to manage moisture in masonry and resulting moisture damage that the single greatest cause of structural damage to masonry. Using contemporary materials such as Portland cement blocks vapour transmission and results in a significant proportion of the damage seen to heritage sites.

Being one of the world's most earthquake-prone countries, Mexico has been a victim of many seismic events of moderate to high intensity. Intersecting tectonic plates create subduction zones that generate high-intensity earthquakes, which can be very destructive. In the 20th century alone, 183 earthquakes with a magnitude greater than 6.5 have occurred in the area, with most of them having epicentres located on the Pacific Coast [1]. The magnitude of three of these earthquakes exceeded of 8.

More recently, September 2017 had a pair of massive earthquakes. A magnitude 8.2 on September 8 just offshore from the state of Chiapas was followed by a magnitude 7.1 on September 19, this time much closer to Mexico City, and caused heavy destruction in 11 states [1]. There were more than 2000 heritage buildings damaged, most of which were in the states of Puebla, Morelos and the Greater Mexico City. Two historic convents that were damaged in 2017 and are considered the most endangered were visited and analysed by the authors several times during 2019 (January, May and December) and are the current study: Convento de San Guillermo Totolapan, in the state of Morelos south of Mexico City, built circa 1535, and the Huaquechula Monastery, in the state of Puebla south-east of Mexico City, built circa 1548.

The damage from the 2017 earthquake is in the process of being repaired for both of these sites. It is important to assess the damage to understand how the structure behaved in the recent earthquake, and use this information to perform appropriate repairs in order to mitigate future destruction. Much of the damage which occurred during these most recent earthquakes was related to the existing conditions, contemporary changes made to the structures, and lack of maintenance. The term "appropriate repairs" refers to using compatible materials, understanding the evolution and changes through many centuries, designing interventions that work with the existing structural system, and focussing on the need for ongoing maintenance. These recent events prove that it is critical to evaluate the current state of built heritage in order to be better prepared for future earthquake disasters.

2 HISTORY

The early monasteries were not established in the style of ancient European monasteries, as places to live in isolation or divine contemplation. Instead, these convents functioned as dynamic cultural centres for religious dissemination, with schools where they transmitted the cultural elements brought from Europe, including basic beliefs of native cultures. The monasteries were founded with only a few mendicant friars who arrived in Mexico between 1523 and 1533. They were the alchemists, blending the two cultures into a new identity.

The main characteristic of these monuments is the "monastic fortress"; the impressive sobriety typical of the first attempts in which the friars had to explain to the indigenous builders the necessary criteria for these buildings [2]. The simplicity in the massing, crenellation and massive walls, small high windows and square buttresses, the integration of indigenous reliefs, and the reuse of stones from other ceremony sites are some of the main attributes.

In 1994, 14 monasteries called "Ruta de los Conventos", on the slopes of Popocatepetl, were designated a UNESCO World Heritage Site [3]. The Totolapan monastery is included in the designation. The Huaquechula monastery, despite having the same characteristics as the others, was not inscribed. These buildings are representative of the architectural model adopted by the first missionaries who evangelized the indigenous populations in the 16th century. The monasteries were founded in areas of dense indigenous settlement, with the object of providing focal points for urban settlements, a role which has survived to the present day. The fusion of the two cultures is on display in the wall murals, in the craft and skill of stonemasons, and through stories about the spiritual conquest. They are examples of a new vision of architecture, in which open spaces take on added importance as worshipping activity. The atrium, the open air chapels and the processional were an interpretation of Mesoamerican ceremonies.

2.1 San Guillermo, Totolapan, Morelos

The Convent of San Guillermo is a very good example of "primitive convent architecture". Totolapan is the second Augustinian Convent in the area. Construction at Totolapan began in 1536 after the Augustinians were expelled from neighbouring Ocuituco, Morelos. The first stage was completed in 1545 under the direction of the head master Jorge de Avila [4]. The complex of Totolapan is more modest in dimensions and decoration than the other convents in Morelos that were built later for the same religious order - Tlayacapan and Yecapixtla.

Totolapan contains certain basic elements common to this new type of monastery: a collection of buildings surrounding a great rectangular atrium, well demarcated by an atrium wall. In the atrium's internal perimeters there are two Processional Chapels. The church is located to the south of the monastic buildings, positioned around a small courtyard patio. There is also the open chapel in front of the atrium, highlighting the importance of open spaces to evangelize the indigenous people.

The church, with a single nave, is simple in plan and has less imposing proportions than other monasteries. The roof of the nave is a longitudinal barrel vault with lunette windows, without ribs, and is subdivided into four bays reinforced by transverse arches. The exterior is delineated by masonry buttresses at the arches. The nave is 28 meters long and 11 meters wide. The apse is covered by a large pendentive dome, much thinner than the walls with the thickness decreasing linearly up from the walls. It is possible, as Roberto Meli stated, that the roof was likely originally a wooden gable roof with ceramic tiles, and the barrel vault could be a 17th

century modification [4]. In the adjacent buildings, the roofs consist of smaller barrel vaults. The mortar to stone ratio is much greater in the vaults than in the walls.

The Totolapan convent was constructed of a mix of adobe mortar, volcanic stone and pebble stone. The thickness of the walls varies up to 2 meters. The quality of the masonry walls is poorer than the Huaquechula monastery. Much smaller round river stone was used, with less evidence of the larger angular masonry, and an overall lack of keying stones. Since the Totolapan was completed earlier, this suggests that the quality of these complexes improved with experience.

The known interventions are listed below, but the age of the structure and high seismicity of the region guarantees that work had been done previously on both monasteries (due to previous seismic events, wars, alterations or changes of use). In 1949, the first recorded intervention, the main wooden altar was replaced with concrete due to insect damage. In 1964, the roof was refinished with a waterproof coating using traditional, pre-hispanic methods. The coating consisted of lime, sand, laundry detergent, water and alum to create a waterproofing substance which they sampled on certain mural paintings on the walls.

The convent was damaged by a 6.7 magnitude earthquake on August 17, 1969. The barrel vaults experienced significant cracking, and were repaired using the galette technique. This technique uses small pieces of tezontle (a local volcanic stone that is extremely porous) in a mortar mix consisting of lime, Portland cement, and sand in a 1:1:3 ratio. They used this material to replace all of the existing vault material that was deemed to be in poor condition. The vaults were re-surfaced with the above-mentioned waterproofing. The main façade of the church was repaired without following good conservation practices. A layer of wire mesh was added and was subsequently painted to imitate ashlar blocks [5].

A condition assessment from 1978 stated that in many locations the mortar was in extremely poor condition due to long term exposure to moisture, humidity and poor maintenance. The mortar on the exterior of the cloister had failed and was falling off. This report recommended the intervention of reinforcing the barrel vault by injecting cement into the slab.

The final major maintenance works took place in 1995. Another waterproofing coating was added to the roof, some of the mortar was repointed, the main facade was painted, and some of the walls and buttresses were reconsolidated. The existing cracks on the east/west walls of the convent were repaired with injected cement grout [5].

2.2 The Huaquechula Monastery “Ex-Convento de San Martin”

The Huaquechula monastery was constructed between 1531 and 1569 by the Franciscan order under the direction of Juan de Alameda as the head Master Builder. It was constructed with unreinforced massive stone masonry of a higher quality than Totolapan. The use ashlar stones larger and more angular in shape demonstrates a knowledge of stereotomy [6]. The facade is Plateresque with a richly adorned main portal in sandstone and decorated with two Franciscan coat of arms and two angels. The church is a longitudinal nave with four stone ribbed vaults consisting of volcanic stone, pebble stone and adobe mortar. These stone ribs are carved ashlar finished stones constructed as intersecting arches. The church measures 48 x 14 meters and is braced by massive buttresses on the north side and a two storey convent structure with integrated buttresses on the south side. The main altarpiece from 17th century is over ten meters high and five meters wide and has paintings by Cristobal de Villalpando. The former cloister

area was rehabilitated, years ago, as a local museum. The walls still contain remnants of the monastery's rich mural work, and the rooms contain archaeological pieces and copies of various codices. Following the damages from the 2017 earthquake the museum was closed.

The Huaquechula Monastery was previously damaged during the major earthquake of 1999. At that time, the upper portion of the bell tower was reinforced with concrete and steel angles, which were anchored into the stone pillars with rebar. Based on evidence noted on site, it is assumed that the repair works at that time did not include repointing of the masonry piers. Also, the roof of the two storey convent, which consisted of heavy timber structure, with plank decking, was replaced by a concrete roof slab.

From 2012 until 2016 some conservation works continued in Huaquechula. The Conservators performing some patching in the walls and ribbed vault, with cementitious materials. Some maintenance work in the cloister was also in progress.

3 CONSTRUCTION TECHNIQUES

The construction of buildings by using the local subsoil is one of the oldest construction techniques [7]. In North America, the most prominent use of earthen construction was by the Indigenous People of Mexico and the southern United States. Before the arrival of Europeans to the area, pyramids and vernacular buildings were typically constructed of adobe which had proven over time to be a durable construction assembly.

The construction of these 16th century monasteries is generally consistent with European churches built in the same time period, except they were built using local materials: adobe mortar and volcanic stones from Popocatepetl. There have been studies on archaeological sites of early Spanish missions, where the earlier buildings were constructed of adobe mortar and the later portions were of lime mortar, which needed to be refined [8]. At these other archaeological sites, large underground kilns that were used for the production of lime mortar were discovered.

Adobe mortar is a mixture of local subsoil, sand and water, and then applied to the structure while wet. A series of tests was conducted and guidelines on the preservation and seismic stabilization of adobe structures were published in 2000 by the Getty Conservation Institute [9]. Typical strength values for adobe mortar has a significant range, but is approximately 1 MPa.

It should also be noted that the Spaniards were not familiar with earthquakes, while recent studies have shown that the Indigenous people knew how to construct adobe buildings to resist seismic forces. A study in the same region showed that well-maintained traditional adobe buildings performed significantly better than those with modern interventions such as concrete roofs, large windows, or additions [10]. These monasteries were built with indigenous labour that provided wisdom in the preparation and selection of raw materials.

However, the monasteries were constructed largely in the European style. The tall, vaulted masonry roofs with thick, buttressed walls were imported architectural features that had been refined by trial and error overseas. Historic designers and Master Builders had a knowledge and understanding of mass masonry buildings, passed down over centuries, that does not have a place in modern engineering. Prior to any rehabilitation project it is important for the engineer to understand the principles behind mass masonry. Arches or vaults, for example, are abundant and simple in form yet not immediately logical to analyse according to modern engineering principles [11]. There are many resources available which describe the principles of masonry which is outside the scope of this current report.

4 BUILDING CONDITION

4.1 The Convent San Guillermo Totolapan

The Totolapan monastery suffered significant damage during the 2017 earthquake. The barrel vaults of the church experienced significant cracking and fracturing. Part of the bell tower collapsed. The pendentive dome completely failed during the earthquake, shearing where the vault is the thinnest. The damage to the cloister includes significant fracturing of the barrel vault roofs, cracking of the walls and failure of many of the buttresses in the courtyard. At the east and west side of the courtyard, the barrel vault roofs had collapsed.



Figure 1: Left, before earthquake, Dec 2016 [12]. Right, after earthquake, roof plan showing damages. Red denotes severe damage and fractures. Pink shows missing bell tower. Blue denotes partial collapse of vaults and in green is the detachment and presence of microflora. May 2019 [5].

These vaulted roofs surrounding the courtyard were constructed using poor quality adobe mortar and small rounded river stone. The vaults had sustained fractures during previous earthquakes and had been repaired using a cementitious grout, which appears to have magnified the current failures. The vaults were coated in a plaster which has cracked, but there was no evidence of any waterproof coatings over the plaster. From this, it can be concluded that the mortar in the vault had deteriorated prior to the earthquake from continuous exposure to moisture. The presence of moisture results in activation of soluble salts, which then recrystallize, expanding and damaging the existing adobe mortar.



Figure 2: Photographed damage 4 weeks after the earthquake, Oct. 2017. **Left:** Fractures and partial collapse of nave vault. **Center:** Complete failure of the apse dome. **Right:** Collapse of vault and buttresses of the cloister.

The walls of the nave had also experienced large fractures, and many of the large buttresses were damaged, some completely collapsed and others fractured full height at the face of the walls. Some of the buttresses at the cloister failed due to bending perpendicular to the wall. There was a general lack of large tie stones to hold the masonry together. The major fractures to the walls were noted mainly where they intersected the exterior walls, or through wall openings. Several infill walls in original arches had also displaced.

The large bell tower, the stone arch above the entrance that supports the open bells, and some of the crenellations around the roof, fell outwards. The bell tower was constructed such that it was only attached to the main structure at one corner. Once it separated from the nave, it became a tall slender structure, with a different mode of vibration to the main structure.

At the other corner of the monastery there is a smaller masonry bell tower which was also damaged. It appears that the rocking of the tower resulted in hinges forming at the base of the four corner pillars, and in the apex of the arches between the pillars. It was observed that at each of the hinge locations, where the plaster had spalled, dislodged and debonded loose rubble masonry was observed. The staining indicates mould and long-term moisture saturation.

Work is proceeding on smaller areas before the more extensive interventions. Most fractured walls of the church are being consolidated, by drilling ports and inserting small copper pipes in the walls. A mix of lime, sand and pozolime grout is injected. The collapsed buttresses are also being rebuilt, using metallic ties to anchor to the walls.



Figure 3: Left: Reconstruction and consolidation of walls and buttresses in the courtyard, Dec 2019. **Two central images**: Bell tower with damages, May 2019, and after repair by integrating horizontal large volcanic stones, Dec 2019. R**ight:** Rehabilition of the roof vault by adding carbon fibres in a cross pattern, Dec 2019.

The large fractures in the apse walls are being repaired by first dismantling the masonry on each side of the fracture and removing all debonded material. The wall then is rebuilt across the crack, with compatible mortars and large volcanic stones –basalto- of high density and strength. This is an excellent solution as compatible materials are used to reinforce the masonry at known weak points. Provided that the mortars are compatible with the original adobe mortars, with similar strength and porosity, this will permit vapour transmission from the original to the new masonry and allow the assembly to function as originally intended. This construction also bonds well with the existing masonry, so that they can function as a single unit in future earthquakes. It is critical, as part of the rebuilding, that all dust is removed at the interface between the old and new mortar, otherwise the bond between these two materials will not occur.

They are also introducing tensile strength to the top of the nave barrel vaults by applying carbon fibre to better resist the formation of hinges and therefore seismic forces. The methodology applied in the barrel vault followed the cleaning of the whole area, drilling ports and injecting traditional mortar into the fractures, and applying the carbon fibre in a cross "X" pattern which is anchored to the barrel vault slab. This is a new methodology that has just been initiated in rehabilitation projects in L'Aquila, Italy after the 2009 earthquake. It will be important to monitor this new intervention for its compatibility with the 500-year-old structure.

During the site visit in May of 2019, a sample was taken of the Totolapan buff mortar. Ken Trischuk from the National Research Council of Canada performed tests for composition and strength. The strength of the single mortar sample was 8.29 MPa, and composed predominantly of calcium, carbon and oxygen; the typical signature for lime mortar. However, the main point highlighted by this sample is that more need to be taken from various locations around the complex to identify the existing conditions and mortar composition.

4.2 The Huaquechula Monastery

The Huaquechula Monastery experienced significant damage during the 2017 earthquake. The upper portion of the bell tower collapsed and fell through the first ribbed vault roof of the nave. The main facade has a large central entrance door under an ornate rose window. These openings substantially weakened the wall, resulting in a large vertical shear fracture. The masonry arch that supports the bells above the entrance collapsed. The adjacent convent experienced minor damage to the barrel vaults, and to some of the interior dividing walls.



Figure 4: **Left:** Before the earthquake, May 2017 [13]. **Center:** After the earthquake, Oct 2017. **Right:** Damage sustained by the ribbed vault caused by the collapse of the top part of the bell tower, Oct 2017.

The bell tower failed at mid-height, collapsing into the nave during the earthquake. It is important to highlight the entire section which had been reinforced with concrete and steel in 1999 had collapsed. The steel angles were still on site in May 2019, and except for minor bending, the entire structure was intact. This indicates that the tower failed under rocking motion, with hinges forming below the steel frame. Damage from the formation of hinges was evident at the base of the lower portion of the tower. The joints in the masonry at the location of the hinges were in poor condition, indicating that they had not been recently repointed.

The extents of the large hole through which the tower had fallen, clearly show the effectiveness of the ribs at reinforcing the roof structure. Only the ribs immediately impacted

by the tower failed. Adjacent ribs confined the collapse to the area of the impact only. It can be observed that this rib pattern increased the depth of the vault, giving it a greater capacity than the Totolapan Monastery, and also introduced more redundancy into the design, allowing part of the vault to remain intact despite the collapse of the tower.

The remaining roof vaults which were not damaged by the tower still exhibited recurring cracking and spalling. The side walls of the nave were subjected to out of plane forces and would have displaced in out of plane bending. The cracking is more significant at the apse which, due to the semi-circular floor plan and large number of exterior buttresses, had created a stiff point resisting the movement of the rest of the roof. The wall on the north side of the nave is stiffened by large buttresses, but the south wall is connected to the two-storey cloister that increases the stiffness of this wall, with additional cross walls/buttresses. The two walls of the nave have different fundamental periods and resonance frequencies, resulting in differential movement. At some time during the earthquake, the tops of the walls moved apart, creating a geometric imbalance and caused cracking in the vaulted roof parallel to the side walls.



Figure 5: Left: Damage caused by reinforced concrete roof in the cloister, Oct. 2017. **Central**: Proposed intervention to the nave. Blue indicates reconstruction with similar material. Yellow indicates consolidation at the crack locations. Red only requires a waterproof coating using traditional methods. [14] **Right**: Main fractures to ribbed vault, May 2019.

The roof of the adjacent convent was originally of heavy timber construction, with plank decking. This type of construction is flexible, and absorbs energy. After the 1999 earthquake the wood was removed and replaced with reinforced concrete slabs. This is an inappropriate intervention since it is now an extremely stiff element which distributes the energy to the adjacent walls. The impact of the added stiffness during the earthquake was immediately apparent. First, where the slab abutted the wall of the church, the slab pounded into the masonry, resulting in localized masonry failure. Second, these slabs have a significant impact on the natural frequency of the adjacent monastery and therefore the south wall of the nave, likely causing greater damage to the roof of the nave. The reinforced concrete slabs remained intact, with no cracking noted. In some areas the large arched openings of the convent were infilled with stone masonry. The infill masonry had separated during the earthquake. This damage is due to a poor construction detail, where the interior wall was constructed after the exterior wall, with no key stones installed across the construction joint.

In areas where the plaster was removed from the walls, it can be seen that the walls are well

constructed. The masons used large angular stones set in adobe mortar. It is probable that the stones are of variable depth, creating a keying action with the wall core. Very little cracking on the longitudinal walls of the nave was observed even though, on the upper parts of the walls, many voids and weathered mortar joints were noted. The large buttresses supporting these walls were also undamaged. It is likely the better maintenance and construction practices using larger stones and keystones ensured that these walls had adequate seismic resistance, in comparison to the buttresses at Totolapan.

The ribbed vault roof of the Open Chapel appears to have a number of fractures with a similar pattern as the fractures following the 1999 earthquake. There is evidence of previous repairs at these hinges, by filling the cracks with, possibly, cementitious grout. The repair failed during this earthquake, causing the cracks to reopen. This highlights the need to rebuild across cracks with solid material, as simple infilling leaves the previous failure as a weak point, and does not allow the assembly to act as a singular unit.

5 CONCLUSIONS

It can be clearly seen from the study of these two historic monasteries, that the ability to perform maintenance is difficult and expensive. Such lack of maintenance directly contributes to failure during seismic events. Huaquechula, the better maintained of the two, sustained less damage than Totolapan which suffered substantial loss to the bell tower, barrel vaults, buttresses and upper regions of the walls. Poor bonding of the stone masonry due to deteriorated mortar results in a greater chance of collapse, while well maintained walls may crack but are more resilient and less likely to fail. In addition, the act of forming cracks during a seismic event dissipates energy, and lowers the shear demand at the base of the structure.

The study on the performance of adobe structures following the 2017 earthquake supports the conclusion that structures conserved using compatible materials and respecting the original construction methodology will perform better than buildings upgraded using contemporary materials such as Portland mortars, concrete and steel [10].

Insufficient maintenance combined with poor construction practices such as lack of keystones contributed to the observed failures at both monasteries. The introduction of contemporary materials to repair damage resulting from repeated seismic activity over the centuries has compounded the deterioration. In the case of Totolapan, there is extensive use of Portland cements and at Huaquechula the use of steel reinforcement in the bell tower, the addition of concrete slabs at the cloister, along with lack of masonry conservation resulted in collapse of the tower. The addition of inflexible materials provided stiffness to the walls and roofs, resulting in differing return periods for the buttresses on opposite sides of the nave, supplying tension in the roof dome, and the ensuing fracturing of the roof structure.

Evidence has shown that the introduction of non-compatible materials to a historic masonry structure will accelerate decline, primarily by impeding vapour transmission, regardless of the geographical location and climatic conditions. Moisture is a natural component of a masonry wall; the amount will be dependent on how well the masonry is protected. Historically, soft, low strength, flexible lime and clay mortars acted like blotting paper to draw moisture to the surface of the masonry through capillary action and evaporate [15]. This provides resistance to freeze-thaw in colder climates. Natural salts activated by moisture trapped in the masonry can also be detrimental to the masonry components, such is the case with the use of Portland cement

based mortars, grouts and plasters where the pore size of the cement is too small to permit capillary action and vapour transmission. The outcome results in the confined moisture attacking the existing lime mortar, reducing it to sand and within a relatively short period of time the interface of the contemporary and existing material will debond. This becomes a major component in the extent of masonry failure due to seismic forces. Another factor which leads to deterioration of the masonry is the strength of the contemporary mortar. If the mortar is more than 25% to 30% stronger than the surrounding masonry, the integrity of the wall will suffer.

It is a vital part of the Conservation process to replace all deteriorated mortar and fill all voids to consolidate the masonry, so that in the event of an earthquake, the masonry will act as a single unit. Use of soft, flexible mortars will act as "shock absorbers" during a seismic event and improve longevity by allowing vapour transmission to occur. Properly maintained masonry coupled with the use of compatible materials and repair methodologies will ensure acceptable building performance in a seismic event [16].

It is clear that if we are to conserve our heritage fabric for future generations to enjoy and respect, we must reach a gentler understanding of the need to repair like with like and avoid the mistakes of past generations. It will be necessary to perform extensive testing to develop compatibility with existing materials, revive the old construction methodologies and train the tradespeople in the crafts and techniques required to achieve this.

ACKNOWLEDGEMENTS

Part of this research was supported by the International Research Seed Grant by Carleton University. Our gratitude goes to the different stakeholders from Mexico, including Instituto Nacional de Antropologia e Historia (INAH), Teresita Miravete from INAH Puebla and Fernando Duarte from INAH Morelos. As well as the Grupo Farla for allowing several site visits. Special thanks to Dr. Xavier Cortes Rocha, Ing. Roberto Heatley, Arq. Salvador Avila, Lic. Ricardo Esponda, Arq. Elisa Vera, Mary Cooke, and Jamie Marrs. The images from October 2017 were taken by Ing. Roberto Heatly.

REFERENCES

[1] Meli, R. *La ingenieria civil ante los efectos de los sismos de 2017 en edificios patrimoniales. Sismos y Patrimonio Cultural.* Secretaria de la Cultura, Mexico. (2018)
[2] Conventos Moralenses. Lunwerg, S.L. Espana. (2012)
[3] Earliest 16th-Century Monasteries on the Slopes of Popocatepetl. *UNESCO World Heritage Centre*. Available: https://whc.unesco.org/en/list/702
[4] Meli, R. Los Conventos Mexicanos del Siglo XVI. Construccion, Ingenieria Estructural y Conservacion. Instituto de Ingenieria UNAM, Porrua, Mexico (2011).
[5] Grupo Farla. *Reporte Templo Ex-Convento de San Guillermo Totolapan*, 2do Simposio Internacional entre especialistas de Mexico y Union Europea. (2019)
[6] Gonzalez Leyva, A. Construccion y Destruccion de Conventos del siglo XVI. Cultura FONCA, Mexico (2019).
[7] Hall, M.R., Lindsay, R., and Krayenhoff, M. *Modern Earth Buildings - Materials, Engineering, Construction and Applications*. Woodhead Publishing, (2012).
[8] Walter, T.L. Espiritu Santo de Zúñiga. *A Frontier Mission in South Texas*. University of Texas Press, (2007). ProQuest Ebook Central.

[9] Tolles, E.L., Kimbro, E.E., Webster, F.A., and Ginell, W.S. *Seismic Stabilization of Historic Adobe Structures: Final Report of the Getty Seismic Adobe Project*, Getty Conservation Institute, Los Angeles: Calif, (2000).
[10] Fernando, L. and Baca, G. *Comportamiento sísmico de viviendas tradicionales de adobe, situadas en las faldas del volcán Popocatépetl, México*. Gremium (2019). Vol. 6, no. 11.
[11] Heyman, J. *The Safety of Masonry Arches*. International Journal of Mechanical Science, (1969). Vol 11, pp. 363-385.
[12] Mendoza, T.C. *Ex Convento de San Guillermo.* Photo – Dec 2016 (Google).
[13] Kalalo, E. Convento de San Martin Caballero. Photo – May 2017 (Google).
[14] Grupo Escoda. Propuesta de Restauracion y Consolidacion Estructural *del Templo de San Martin Huaquechula* / *Levantamiento y Digitalizacion*. Mexico. February 2019.
[15] Wiggins, D. *Traditional lime mortars and masonry preservation.* The Journal of the Building Limes Forum. (2017) Vol 24, Pp. 28-37.
[16] Esponda, M. Ph.D thesis *"Assessment of the Reinforced Concrete in the Restoration of Buildings in Mexico & Spain"* Universidad Politécnica de Cataluña, Spain. (2004).
[17] Ledesma Gallegos, L., Gonzalez Leyva, A. *Y hasta ahora todo ha sido hacer y deshacer edificios*. Mexico, D.F. INAH. (2005) p. 44
[18] Memoria Fonden 2000. *Rehabilitacion de inmuebles historicos danados por los sismos de junio y septiembre de 1999*. CONACULTA. INAH. Mexico. (2000)
[19] Kubler, G. *Arquitectura Mexicana del Siglo XVI*. Fondo de Cultura Econ. Mexico (1984)
[20] Perales Piqueres R., Benites de Unanue M. P. *Los Conventos del siglo XVI de Puebla y Morelos.* UPAEP. (2018)
[21] Kostoglodov, V. and Pacheco, J.F. *Cien años de sismicidad en México*. UNAM, (1999).

12th International Conference on Structural Analysis of Historical Constructions
SAHC 2020
P. Roca, L. Pelà and C. Molins (Eds.)

CONSERVATION BEYOND CONSOLIDATION FOR PREHISTORIC MONUMENTS: FINDING NARRATIVES FROM ARCHAEOLOGY TO ARCHITECTURE FOR SCOTTISH BROCHS

CHANG LIU[1*], DIMITRIS THEODOSSOPOULOS[2]

[1]The Edinburgh School of Architecture and Landscape Architecture (ESALA)
The University of Edinburgh
20-22 Chambers St, EH1 1JZ Edinburgh, UK
e-mail: Chang.liu@ed.ac.uk, www.chomliu.com (*corresponding author)

[2] The Edinburgh School of Architecture and Landscape Architecture (ESALA)
The University of Edinburgh
20-22 Chambers St, EH1 1JZ Edinburgh, UK
email: d.theodossopoulos@ed.ac.uk
www.eca.ed.ac.uk/architecture-landscape-architecture/dimitris-theodossopoulos

Keywords: Brochs, Prehistoric, Conservation, Consolidation, Narratives

Abstract. *The sophisticated drystone Iron-Age brochs of Northern Scotland, called Complex Atlantic Roundhouses by archaeologists, have shown a relatively high technological culture. Their architectural conservation should strike a balance in presenting their key features (structure, materials, building use and architectural elements) in a concept of wholeness that integrates its major phases rather than design unity of a hypothetical original form. However, currently there is uncertainty due to the lack of agreement for a standard broch scheme and the need for more archaeological research. As most brochs in Scotland are fragile ruins and only a few of them have been scientifically explored, they have been conserved through basic consolidation for safety reasons in very localized methods, primarily by archaeologists. All of them are open to the public but only a few are developed as tourist sites. In both situations, none has shown the complete features of anything close to a standard typology as a narrative of their origin and a few have interpreted correctly the changes after Iron Age as narratives for modification. Significant conservation was conducted often before full archaeological excavations and did not lead to a satisfying architectural experience, so people still have a inconclusive image of brochs after a visit. This paper studies the brochs through their collective concept as a building typology rather than separate images of different sites. Conservation for brochs in Scotland could argue for modern holistic projects that go beyond consolidation, exporting narratives from archaeology to architecture.*

1 BROCH INTRODUCTION

1.1 Broch background

A broch is an Iron Age drystone hollow-walled structural type built from 800 BC to 250 AD and found only in Scotland. However, due to the huge complexity of the building structure as well as the long un-evidenced history, their conservation encounters much difficulty as their archaeology can be very sporadic and controversial. Brochs are special monuments in Scotland for three main characteristics.

- Brochs are double-circular-wall complex round houses. This characteristic is outstanding because other Iron Age roundhouses in Europe do not have double-walls with walking passage inside and they are quite smaller. The broch not only demonstrated the understanding of circular space by those prehistoric communities, but also left much mystery for our society with further discoveries through archaeological excavations, dealing the sophistication of the Iron Age characteristics.
- Brochs are house types which are typically important to Scotland. Brochs are called 'Complex Atlantic Roundhouses' [1] which means complexity both in plans and elevation, always in drystone masonry. The structure has typically demonstrated the ability to survive in the Scottish climate and geographic conditions.
- Brochs as significant Iron Age drystone structures. The Iron Age is the final epoch of the three-age system, preceded by the Stone Age (Neolithic) and the Bronze Age, in the prehistory of Europe. The British Iron Age lasted in theory from the first significant use of iron for tools and weapons in Britain to the Romanisation of the island. Also, drystone is typically local building material even for now in the North of Scotland.

The Royal Commission on the Ancient and Historical Monuments of Scotland (RCAHMS) identified a total of 571 candidate broch sites throughout the country [2]. Officially, there are 317 scheduled monument sites by Historic Environment Scotland (HES), which are designated as brochs. Besides, on Canmore, a Scottish national online database of ancient monuments, there are 860 records of archaeological sites which are brochs or possible brochs. MacKie, the foremost Scottish scholar who had much academic contribution to the recording of brochs, has said that 'brochs are among the most striking of all the prehistoric monuments of Europe' [3]. In general, brochs are important ancient monuments to both Scotland and Europe.

Based on these records, this paper studies brochs broadly as a building typology rather than separate sites and, after reviewing the current range of their conservation approaches, argues for modern holistic conservation projects that go beyond the current practice of consolidation, exporting narratives from archaeology to architecture.

1.2 The definition of broch

Mackie [4] defined five main features across all brochs like 1) round plans, 2) thick walls, 3) size, 4) a ledge or scarcement on the inside wall face and 5) at least one of certain hollow-walled architectural features- classification of a site as a broch needs at least two of characteristics 1 -4 above and in addition No.5. Based on this, hundreds of brochs could be identified. However, due to the limited excavations or recordings, only the brochs with properly

surveyed architectural plans are used for the statistical analysis in this paper. Based on the information provided by Tanja Romankiewicz [5] for around 120 surveyed monuments, there are no sites that look the same to another. Even the orientations of their entrance have no demonstration of any preferences on any directions. However, there are some similar features, like the staircases that are always going clockwise from ground floor to the upper floor.

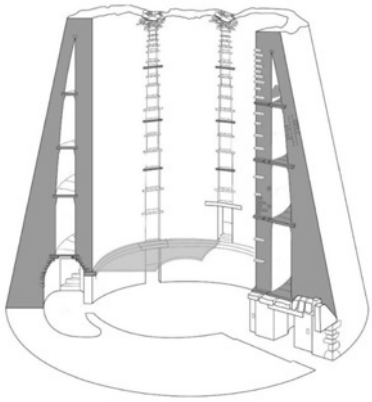


Figure 1: The configuration of Revised Standard Model for Brochs [6]

These remarkable stone-built roundhouses contain some elaborate architectural features. Their dry-stone walls were about 3m to 6m thick and internal diameters range between 5m and 20m. These dimensions could easily have supported tall structures and five out of more than 500 still survive to 9m or higher [5]. Presently, some diagrams of the original image of brochs are widely known among the public, but they are conjecture due to the lack of supporting evidence. Barber [6] studied several cases and suggested a revised model of a standard broch, aiming to show they were all built to a standard canonical plan and their apparent diversity is a product of modifications and natural decay (Figure 1).

2 BROCH CONSERVATION

2.1 Broch conservation situations

Brochs are ‘scheduled monuments’ in Scotland which offer strict conditions for investigation, preservation, and recording of matters of archaeological or historical interest. A scheduled monument in Scotland is a nationally important archaeological site or monument which is given legal protection by being placed on a list (or "schedule") maintained by Historic Environment Scotland and is governed by the Ancient Monuments and Archaeological Areas Act 1979 [7].

Brochs are open to public visitors in Scotland. A few of them are well preserved like Mousa in Shetland, Midhowe in Orkney, and Dun Telve in Glenelg, which means usually surviving of clear shapes or certain heights, aspects that determine the public’s view. The majority of brochs however are ruins of stones, very difficult to interpret by an untrained eye.

The most prominent conservation projects were done by unprofessional antiquarians who removed significant evidence to exhibit their own ideas of understanding a broch. For example, one of the first brochs explored with the intention of obtaining and publishing useful

information seems to have been the Howe of Hoxa on South Ronaldsay, Orkney, investigated by George Petrie in 1848. The clearing out of Backies broch near Golspie in Sutherland is equally memorable, and after visited by J. J. Worsaae in 1848 sketches were made that are the earlier known records of those works [4]. From 1890 to 1901, Sir Francis Tress Barry, an English businessman and antiquarian, excavated more than 10 brochs. However, Barry's excavation was limited by techniques and some of brochs were not fully excavated, which led to artefacts removal and an absence of evidence recorded [6]. Therefore, a long process of defining the origin for each roundhouse is apparently inevitable.

Even earlier changes in brochs are evident but these can be identified as essential modifications of the original design during the archaeological study. For example, Mousa, known as the tallest and most complete broch in Scotland, is assumed to have been modified by a Norseman who completed the staircase up to the parapet [8]. This created a slightly overhanging upper part of the tower, which does not appear in the other four tall brochs as Dun Telve, Dun Troddan, Dun Carloway, and Dun Dornaigil (Fig. 2). Since Mousa is the most complete surviving monument, it set a stereotype for the general public

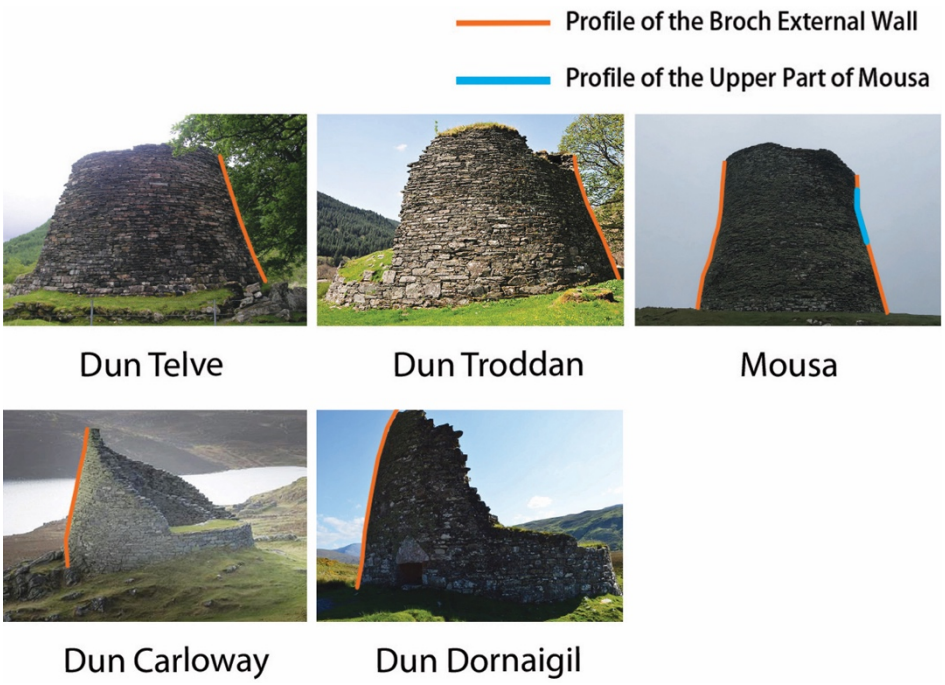


Figure 2: The profile study of Dun Telve, Dun Troddan, Dun Carloway and Dun Dornaigil.

At present, due to extensive legislation by HES protecting ancient monuments, much less external damage is expected. But brochs, as monuments with complex architectural features and controversy in dating, deserve deeper considerations for their conservation compared to other, historic monuments where the origin of buildings were documented, to make their restoration meaningful. At present any restoration attempt is conservative primarily repairs and consolidation for safety reasons in very localized areas, primarily by archaeologists, as most of them are fragile ruins and only a few have been scientifically explored.

As seen in Figure 3, an example of the recent practice is Clachtoll, where the entrance was consolidated firstly and after archaeological excavation in 2018 the staircase was dismantled and reassembled and all rubble at the interior was removed. The best-preserved tall brochs, like dun Telve, though have been strengthened in undocumented campaigns so the extent of repairs is difficult to ascertain. Gurness is a case where dating was misinterpreted or ignored (phases that never co-existed were presented together) while Midhowe restoration actually brought back features that the earlier clearing of the ruins had cancelled (edge-set slabs applied as external buttresses against the N face of the broch wall) [6].



View of broch entrance from inner side in Dun Telve (Photo taken in October 2018)

Reassembled South gallery stairs of Clachtoll (Photo taken by AOC Archaeology Group)

Falsely added lintel in Gurness (photo taken by John Barber)

Figure 3: The consolidation in broch Dun Telve, Clachtoll and Gurness

Generally, the brochs conservation should work with the archaeology. The archaeological research would offer an understanding of the building and architectural conservation should inform future archaeological excavations. What happened to brochs, damage, or repair, if identified with a date, has already become a historic event that needs to be considered in conservation planning.

This is not in general too different to practice elsewhere in prehistoric towers in Europe. The earlier nuraghe in Sardinia, for example, has invariably undergone interventions of fallen debris clearance, wellhead consolidation, and protection, rehabilitation of the staircase, removal of harmful past repairs, general re-integration of the fabric through partial reconstructions, etc (see the cases of Palmavera, Majore, Ola, and Funtana). Temporary shoring and interior clearance have also been the usual practice in the talaiots as Bronze Age megaliths on the islands of Menorca and Majorca.

Broadly speaking, the monuments at present convey two meanings: their original design idea and later modifications by people from different times. Being architectural structures, the need for narratives is also investigated, in an attempt to enhance the sense of wholeness through architectural experience.

2.2 The need for narratives

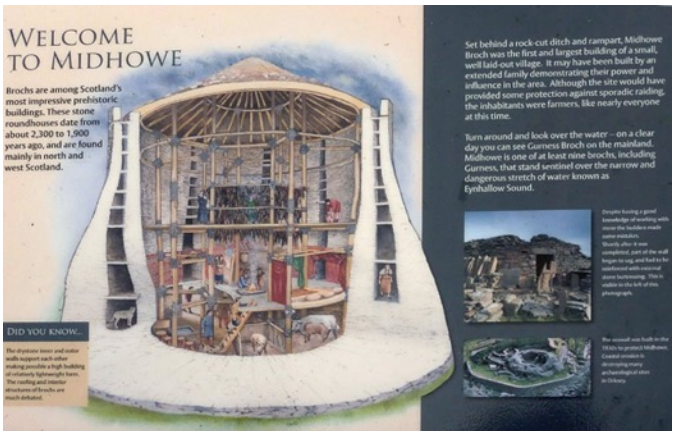


Figure 4. The schematic board for Midhowe broch in Orkney.

The image of how a broch looks like has been spread to social media nowadays, but it cannot represent all the brochs. For example, Figure 4 is one of the general images found on websites or TV programs speculating on human life in brochs. Most of the images like this are based on basic concepts like perfectly circular brochs built on even ground with constant galleries at several levels which enabled cohabitation [1] where the animals live on the ground floor and people in the upper floors. An immediate observation is that in reality there is a huge amount of them built on a slope where the galleries are not perfectly horizontal. Moreover, the roof form is only a conjecture as there is no evidence for shapes and materials.

Besides the five taller brochs mentioned in Figure 2, other brochs with lower height are obviously different in the original form they convey. There have been some proper surveys on brochs done by professional archaeologists and this research is looking at a collection of such broch plans as collected on Canmore, the book 'The complex roundhouses of the Scottish Iron Age: an architectural analysis of complex Atlantic roundhouses (brochs and galleried duns), with reference to wheelhouses and timber roundhouses' written by Tanja Romankiewicz [5] and the survey "The roundhouses, brochs, and wheelhouses of Atlantic Scotland c.700 BC-AD 500: architecture and material culture" written by Euan W. MacKie [4]. Also, archaeological reports published in the recent 10 years offered surveys of Thrumster and Nybster which are included in the data pool.

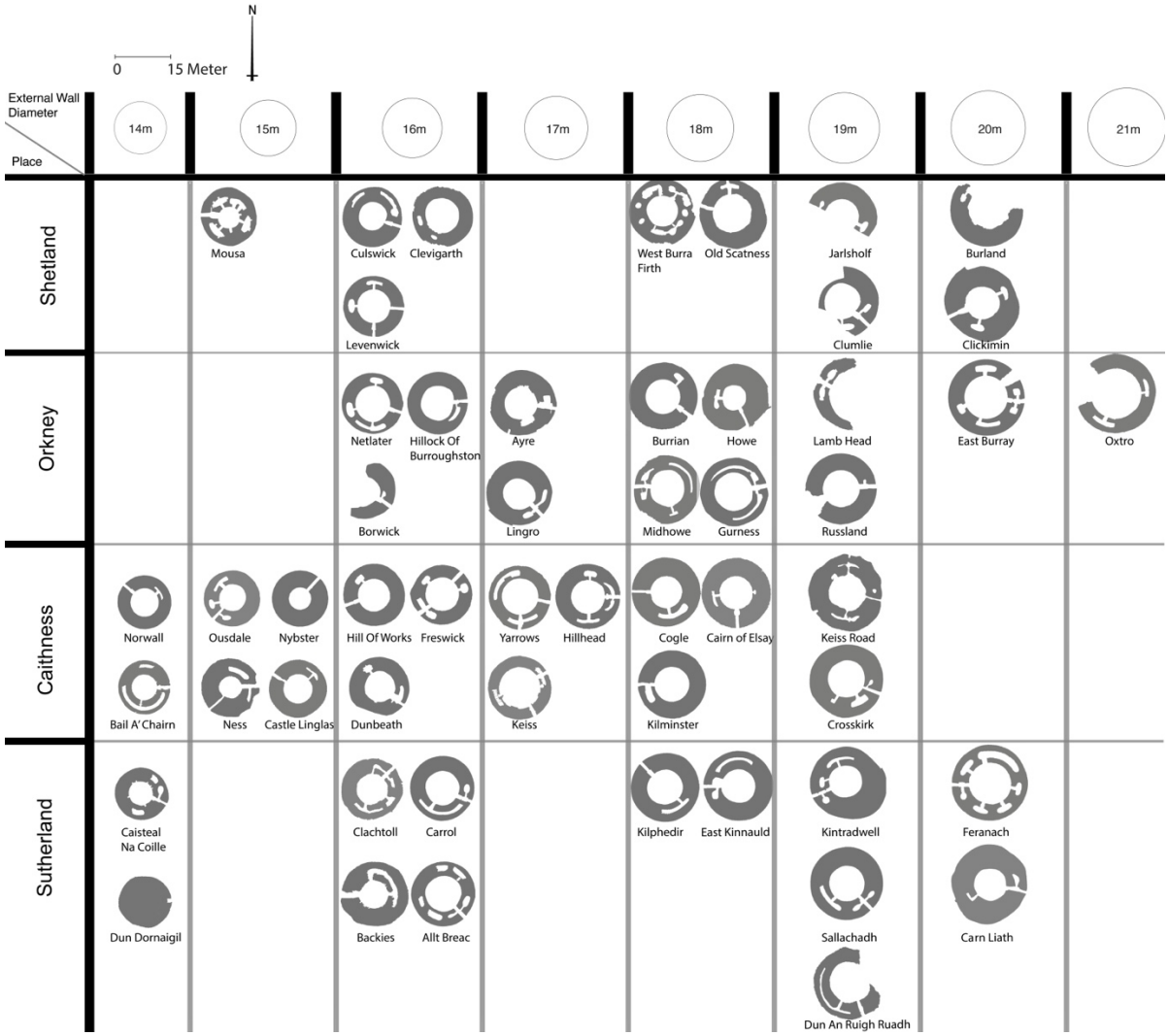


Figure 5: The broch plan study of 51 brochs in Shetland, Orkney, Caithness and Sutherland

The plans of 51 brochs, which were professionally surveyed, are selected and divided into groups based on their locations to study their design concept in multiple manifestations and adaptations as seen in Figure 5. The building parameters are mainly overall sizes, the external wall diameters of these brochs vary from 13m to 22m. The largest one, as Thrumster in Caithness, is almost double the size of the smallest one (Norwall). The other important parameter is circularity. The brochs in Caithness are much more circular-shaped except Keiss Road and Thrumster due to their incomplete survived shapes, while there are ellipse-shaped brochs like Backies and Carn Liath. Also, in terms of broch entrance, unlike other Iron age monuments which would normally face the East, the point of the day where sun is rising from, or south for the most sunlight, brochs' entrances are quite diverse. Even in some location group, brochs do not share a dominant direction. It indicates the ancient builders did not respond to the four cardinal directions, representing sunlight and shadows. Also, some brochs had two entrances, possible due to reuse in later times (like Yarrows),

There are more variations in features like stacked voids, shape of lintels, the stone type of course and bond type, and so on. The monuments are not some reproduced models of a typical building but some works following a precise idea, a way of arranging living space and a combination of feasible construction skills. Considering the different level of collapse and damage on sites, each of them is so unique being in the collection of this complex house types. Each broch does not offer much about the concepts to be understood easily, while a combination of brochs would express the idea. This paper suggests the idea of seeing the monument concepts and strategies for designs through a collection and a spectrum of different sites, rather than a precise looking of one building object.

As the recent consolidation taking dominant places, the study of ancient building concepts moderates this conservative situation and stimulate the sites to express ideas rather than just the presence.

3 CONSERVATION OF BROCH RUINS

3.1 Theory: the 'wholeness' of 'ruins'

Firstly, the broch remains should be treated as a whole building. Cesare Brandi [9] has much emphasized the aesthetic value of the work saying 'once that artistic nature is lost, nothing but a relic remains'. Hence, the restoration should aim to re-establish the potential oneness of the work of art, as long as this is possible without committing artistic or historical forgery, and without erasing every trace of the passage through time in the work of art. The importance to attribute the character of oneness to a work is very high— and specifically the oneness that refers to the whole, and not the unity that is reached by the sum of its parts. The ruins, as have been parts of the original work, should definitely not be taken separately into museum or an archaeological park as the atmosphere, including light, is as material as the broch stones itself. Brochs are impressive, which is much about the composition of the elements, the scale and location of the buildings. Dry sandstones, or parts of the broch, can exhibit the culture of the Iron Age and the "mystery" of the prehistoric building skills even if there is no mortar binder, which often indicates a certain industrialisation of the building trades. The architectural values of prehistoric houses require the wholeness of building, which provides the architectural experience to the human beings.

At the present, the wholeness of the brochs Scotland is ruined in most cases. The 'wholeness' of the original is missing while the later modification become a new part of the whole. A.M. Oteri [10] mentioned the ruins as "what remains" (of a construction, in our case) things become more complicated and our interest in ruins is not only an aesthetic interest, like the beauty of massive stones in Angkor Wat. Ruins are usually not as appreciated by people as restored historic monuments. If the ruins cannot be visited by people, at least for sightseeing, the ruins would normally have no other function and become so called 'dead monuments'

However, the consolidation of broch ruins is actually expecting to turn an old stone ruin into a newly repaired ruin, where conserved ones are still weak in demonstrating an architectural work. A readable ruined site should be better for people to understand. Thus, the conservation should go beyond the consolidation to find narratives for brochs to interpret the builders' ideas.

3.2 Consolidation dealing with structural problems

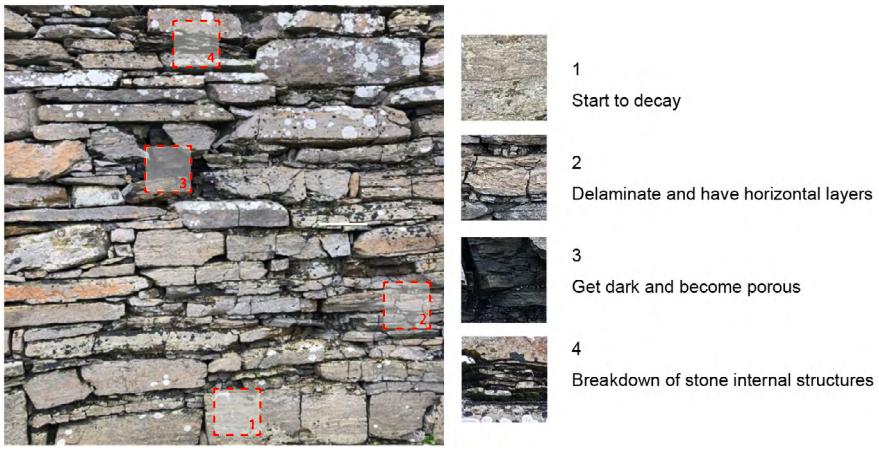


Figure 6: The dry-stone analysis of broch Midhowe.

Consolidation is definitely needed for long-existing monuments as the structures would become quite fragile to collapse due to its material decay. As Figure 6 displays, the Orkney flagstone used in Midhowe in Rousay is sandstone, which is a sedimentary rock. Based on the observation of the broch, different levels of decay conditions appear on facade. In some brochs which survived to a certain height, porous stones could be replaced especially in places like inner galleries and chambers. However, if this building plans to be open to the public for visiting or future archaeological excavations, it has to be consolidated for safety reasons. In the case of Mousa, the interior and exterior wall faces were repined, and the corbelled walls of internal passages were fixed even with steel structures so that people could climb up the stairs safely.



Figure 7: The consolidation of broch Ousdale

In broch Ousdale which is an unusual broch embedded in the ground that has been heavily damaged (Figure 7), the tree growing at the wellhead collapse was removed to clear the entrance and the stones on the ground were reused to rebuild a part of the inner wall. The consolidation work is definitely needed, where partial collapse happens and causes structural problems. Even steel structures could be used to stabilize tilted walls after the stones repined.

3.3 Interpretive conservation

The conservation of an ancient monument like a broch is to protect its architectural, historic, and archaeological values. However, the conservation of brochs could be more than that and can stress the concept of their design to make them readable and offer an architectural experience both for public and researchers. Completing architectural features can offer a precise delimitation of space, like the low and narrow galleries showing there were possibly not many people using them at the same time. These features, if existing in a whole broch, could be highlighted to archaeologists to imagine the possible activities and frame the use of the artefact found on sites. This would require the conservation of broch to be interpretive. The interpretive conservation and it has two levels of meaning:

1) Correct past conservation errors if later scientific research proved them wrong.
2) Clarify features if they are confusing.

Correcting the errors mainly aims to keep pace with the present archaeology research which may disprove the previous statements which have already influenced the finished conservation project, like the case of Gurness as discussed above. The clarification of important features is quite important for people's recognition of the monuments. For example, we could see the difference through a case study of the scarcements in brochs.

The scarcement in a broch means the stones jut out from the inner wall of brochs, to probably support a raised annular floor and perhaps also a low roof [11]. Broch could have two scarcements judging from the five tall brochs, where the lower scarcement is around 1.2 meters above ground and higher scarcement is near the wall head (Figure 8). A scarcement is usually constant on the same plane, and this might not be fully horizontal. It could stay parallel to the sloping ground, like in the case of Caisteal Grugaig. The low scarcement would make floor area at least double, which is much related to the need to build stairs going up, and the high scarcement would make the roof possible.

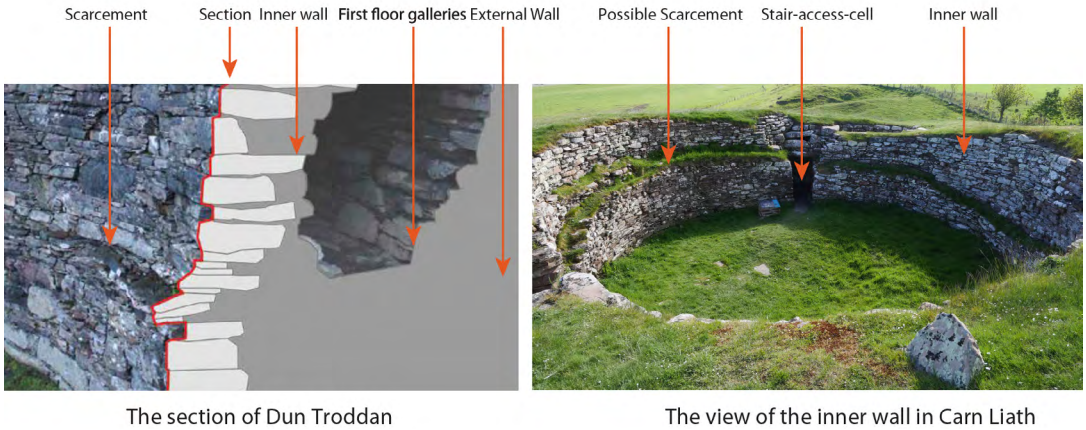


Figure 8. The section of Dun Troddan and the view of inner wall in Carn Liath

Compared to Figure 1, the curved 'possible scarcement' in Figure 8 in the inner wall circle in Carn Liath is sort of misleading. which is different from brochs nearby, like Ousdale and Dunbeath. The site was proved to be occupied in the Bronze Age before a broch was built [12]. As it was suggested as scarcement by Mackie [13], however, John Barber [6] found the scale errors in drawings which failed to find the proper position of the inner wall face. He proved that the curved scarcement was either caused by the structural failure, or by the reconstruction of the tower at and above that level which was returned. Therefore, the origin of scarcement is either lost or covered in the 'possible scarcement' which is actually an inner lining wall face built attached to the real inner wall face. Therefore, the dimensions and scarcement features of the conserved broch Carn Liath offer wrong images of this type.

If the additional inner lining wall face could be removed which accepts this result of scarcements missing, people might still agree that a broch without clear scarcement is still a broch, as the existing building is original. Like in the broch of Jarlshof, only half of the broch has survived due to the coastal erosion, while it has shown the clear and proper broch features



Figure 9. Steel bars highlight the original inner wall face in Carn Liath

If more evidence or findings are needed to confirm the changes in the conserved sits, a mark on the wrong parts of brochs should be possible. Removable structures, like steel bars as seen in Figure 9, could be used to make up the collapsed parts and the original wall head of inner wall, which could offer the impression of the function of the building elements and the sense of building scale without damaging the archaeological site. However, under the concept of being interpretive, there would be a question about what level of impact should this approach reach. In Article 9 of the Venice Charter, it stated that 'any extra work which is indispensable must be distinct from the architectural composition and must bear a contemporary stamp' [14], which stressed the importance of respect for original material and authentic documents. For brochs here, the authenticity lies in the ruins and the archaeological values should have priority to be considered. The interpretive conservation for brochs should not repair them with the same sandstones as being confusing or fake. Importantly, the added materials should always be removable to get rid of damages caused by improper conservation decisions.

Generally, the architectural features could be seen as the choices the original builders made when they were designing. Some features are quite subtle showing their thoughts or attitudes towards the environment. The brochs could not be understood properly if the integrity of the features among all the brochs were not well studied and thus lead to a loss of richness in design. The interpretive conservation would focus much on the origin of brochs, therefore, the correction of mistakes in unprofessional excavations or consolidation and clarification of

important features have become necessary. This would allow possible misjudgments in archaeology research at present and in the future as the reversible changes on prehistoric sites would mainly eliminate misunderstandings caused by modification and conservation.

4 CONCLUSIONS

The architectural features could be seen as the choices the original builders made when they were designing. The origin of brochs as rich designs and architectural spaces would ask for more interpretive works on ruined sites. The current range of conservation for brochs in Scotland could argue for modern holistic conservation projects that go beyond consolidation to find narratives for the building concepts from archaeology to architecture for Scottish brochs.

Acknowledgements. We thank our colleagues in Prokalo event from Edinburgh School of Architecture and Landscape Architecture for their comments

REFERENCES

[1] Harding, D. W. *The Iron Age in Northern Britain Celts and Romans*, Natives and Invaders. London: Routledge (2004). pp.161.
[2] Armit, I. Towers in the North: The brochs of Scotland. Stroud, Tempus (2003). ISBN 0-7524-1932-3. pp.16.
[3] Hedges, J. & Bell, B. That tower of Scottish prehistory-the broch. *Antiquity* (1980), 54(211), pp.87–94.
[4] MacKie, E.W. The roundhouses, brochs and wheelhouses of Atlantic Scotland c.700 BC-AD 500 : architecture and material culture, Oxford: Archaeopress (2002). pp 9, 31.
[5] Romankiewicz, T. The complex roundhouses of the Scottish Iron Age : an architectural analysis of complex Atlantic roundhouses (brochs and galleried duns), with reference to wheelhouses and timber roundhouses, Oxford: Archaeopress (2011).
[6] Barber, J. *Approaching the mind of the builder: analysis of the physical, structural and social constraints on the construction of the broch towers of iron age Scotland (*2017*)*, PhD thesis, University of Edinburgh.
[7] "The Ancient Monuments and Archaeological Areas Act 1979." *Antiquity* 53, no. 209 (1979): 219-22..
[8] Fojut, N "Is Mousa a broch?" *Proc Soc Antiq Scot 111.* (1981) pp.220-228.
[9] Brandi, C, 1965. *Theory of restoration*. (2005). Roma: Firenze: Istituto centrale per il restauro; Nardini.
[10] Oteri A., Ruins and Design: dialogues over Times, *Conservation/Transformation , Essegraph, Genova (ITA)*, (2011), pp. 361-374, ISBN: 978-2-930301-50-1.
[11] MacKie, E.W. The Leckie broch, Stirlingshire: an interim report. *Glasgow Archaeological Journal* (1982), 9(9), pp.60–72
[12] MacSween, Ann; Sharp, Mick. *Prehistoric Scotland. New Amsterdam.* (1989) p. 57. ISBN 071346173X.
[13] MacKie, E. W. *The Roundhouses, Brochs and Wheelhouses of Atlantic Scotland c. 700 BC - AD 500* Vol 2 Part 1. Oxford, British Archaeological Reports. (2007).
[14] International Council of Monuments Sites. *The Venice Charter: 1964-1994 = La Charte de Venise.,* Paris: International Council of Monuments and Sites. (1994).

12th International Conference on Structural Analysis of Historical Constructions
SAHC 2020
P. Roca, L. Pelà and C. Molins (Eds.)

CONSTRUCTIVE ANALYSIS AND MODELLING OF A SINGLE NAVE CHURCHES: A PROPOSAL FOR S. SEBASTIANO (EN, ITALY)

ALESSANDRO LO FARO[1*], VALERIA CUSMANO[1], BARTOLOMEO PANTÒ[2] AND FRANCESCO CANNIZZARO[1]

[1]Department of Civil Engineering and Architecture (DICAR)
University of Catania
Via Santa Sofia 64, 95123 Catania, Italy
e-mail: alessandro.lofaro@darc.unict.it, valeria.cusmano@phd.unict.it, francesco.cannizzaro@unict.it,
www.dicar.unict.it (*corresponding author)

[2] Department of Civil and Environmental Engineering
Imperial College London
South Kensington Campus, London SW7 2AZ, United Kingdom
email: b.panto@imperial.ac.uk, www.imperial.ac.uk/civil-engineering

Keywords: Historical Structure, Masonry church, Discrete Macro-element, Conservative restoration, Nonlinear analysis, Strengthening techniques

Abstract. *The seismic events occurred in Italy in the last decay (L'Aquila 2009, Emilia 2012, Central Italy Earthquakes 2016/2017) have caused the collapse of numerous historical buildings and monuments with loss of life and irreversible damages to the cultural heritage. An effective seismic prevention would avoid, or delay, the most frequent collapse mechanisms. However, it requires a correct interpretation of the structural mechanical behavior. With regard to the traditional masonry buildings, this issue presents a high level of complexity due to the uncertainties related to the materials and the constructive techniques. Furthermore, historic buildings are often the result of several modifications that induce significant structural irregularities. A possible analysis strategy is provided by a discrete macro-element modelling (DMEM) approach which is able to simulate the global behavior of traditional fabrics, if supported by an adequate level of historic, geometrical, constructive and structural knowledge. In this paper a multidisciplinary procedure is applied to the church of S. Sebastiano in Regalbuto (Italy), considered as case study. This procedure is composed of three steps: the knowledge phase in which the constructive apparatus and the static schemes are identified, the modelling phase and the assessment phase in which the current safety level of the building and possible interventions that would be compatible with its cultural instance, are individuated. According to the followed procedure, different scenarios of intervention, characterized by increasing levels of benefit and invasiveness, are considered. For each scenario, non-linear static push-over analyses are performed, to evaluate the benefits and identify the structural critical issues, useful to individuate the next scenario. The obtained results are presented and discussed both in terms of capacity curves and failure mechanisms.*

1 INTRODUCTION

The seismic protection of a historical masonry building is usually pursued not only aiming at the safety of the structure, at minimizing the human losses and at limiting the damage to its content, but also adopting techniques respectful of the original constructive concepts and employing reversible strategies which are aspects commonly included in the retrofitting design process.

When it comes to churches the choices are even more difficult and strategic for several additional reasons; the relevance of the building with respect to the loss of human lives is very high, but the structure also assumes an additional importance because of its historical, social and artistic value. A further aspect to be considered is that churches do not behave as ordinary buildings from a structural point of view; indeed, they usually present tall walls as well as lack of slabs and spinal walls which prevent to attribute to such structures a box behaviour, typical of ordinary buildings. For the mentioned reasons, the walls of masonry churches and their façades exhibit a keen tendency to overturn, and the out-of-plane mechanisms are usually limited by the presence of tie rods and buttresses. However, traditional seismic protection devices cannot be considered as general and thorough retrofitting strategies, also in the light of the stringent standards introduced with the recent codes [1,2]. In particular, in some cases the adoption of reinforcements based on steel members and the application of fiber-reinforced textiles are strategies commonly adopted by practitioners. Such approaches imply an increasing level of invasiveness of the strengthening interventions, which have to be carefully calibrated and weighed in order to obtain the desired compromise between safety and conservation of the original constructive apparatus.

In this paper, a single nave church exhibiting recurring features, is studied. The S. Sebastiano church in Regalbuto (Italy) is carefully investigated from the constructive point of view, through a detailed survey made also with photogrammetric methodology, and identifying the principal building elements. The constructive analysis allows estimating the mechanical properties adopted in the structural model by means of the rules proposed in [3]. In addition, the achieved level of knowledge of the building turned out to be crucial for a more conscious choice of the retrofitting strategy.

Then, a global numerical model aiming at the assessment of the seismic vulnerability of the church is implemented. The adopted discrete macro-element modelling (DMEM) strategy [4,5] is able to perform reliable nonlinear static analyses with a limited computational burden and has already been applied to masonry churches [6,7]. Nonlinear pushover analyses have been conducted on the model in order to evaluate the current seismic safety of the church.

Then, three different retrofitting scenarios have been considered and modelled, with increasing levels of safety and invasiveness. The considered techniques include traditional and innovative strategies, which are duly modelled, and their effectiveness is properly estimated. The three different possible strengthening approaches are intended to be a contribution towards a reasoned design process, which should be an enlightened compromise among safety, conservation and cost of the intervention, as better clarified in the comparative analysis reported at the end of the paper and in the conclusive section.

2 TOWARDS A REASONED CHOICE OF RETROFITTING STRATEGIES OF HISTORICAL MASONRY BUILDINGS

The choice of the best possible strengthening strategy for masonry buildings represents a topic with a high practical interest for which no general rule can be employed. This difficulty becomes even harder for historical masonry buildings, since additional aspects, such as the preservation of the cultural value of the building and the possible high loss of human lives in case of seismic events, have to be accounted for.

Usually the strengthening techniques to be applied are selected according to basic principles of the restoration of buildings. The adopted techniques must respect the criteria of reversibility, low invasiveness, minimum intervention, recognizability of the original structural scheme, chemical, physical and mechanical compatibility, durability [8]. Such principles are nowadays universally accepted and followed. Nevertheless, there are some additional aspects which are also accounted for when conceiving a strengthening intervention, that is the economic cost and the achieved level of safety.

To this purpose, in this paper a methodology to get to a reasoned choice of the retrofitting strategy for historical masonry building, is proposed. In particular, three stages are identified.

The first stage includes the constructive assessment of the building in the current conditions and the seismic assessment through a global numerical model on which nonlinear static analyses are performed. This stage aims at identifying the original structural scheme of the building, at evaluating the mechanical properties of the masonry and at assessing the main vulnerabilities of the structure through the interpretation of the results obtained by the numerical analyses.

The second stage consists in designing several retrofitting strategies with increasing invasiveness and effectiveness to apply on the structure in order to progressively reduce the vulnerabilities of the building. For each level of intervention, a complete seismic assessment is needed, aiming at removing the weaknesses with the highest vulnerability observed at the previous level. In such a way, increasing levels of safety factor will be obtained.

Finally, the last stage consists in the interpretation of the results and in the better decision for the strengthening strategy to be adopted. In particular, safety factor, economic cost and invasiveness of the intervention have to be weighted evaluating pros and cons of each level of considered strengthening contribution. The proposed methodology aims at more aware choices of the intervention, able to account for the main aspects which should guide a retrofitting design of historical masonry building.

In the following section the briefly described methodology is applied to a meaningful case study, that is the S. Sebastiano church in Regalbuto (Italy).

3 THE CASE STUDY: S. SEBASTIANO CHURCH

The study of traditional buildings must be framed in the context of an analysis and design process that is very different from the usual ones followed, for example, in the field of new construction. Firstly, when built heritage is considered, an in-depth knowledge of the building is required. Moreover, since in the case of historic masonry buildings are usually of complex nature, it is necessary to get all the possible information according to different points of view in order to read and understand all signs that time has left on them. Therefore, for each

building, its own story (regarding its construction and every transformation occurred on it) has to be reconstructed; in addition, a geometric-spatial investigation of the current state of the building and a technical-constructive analysis must be carried out aimed at identifying material, processes and constructive technologies. Only after having collected all the mentioned data, it will be possible to define compatible strategies to ensure the conservation of the building.

3.1 The constructive assessment of the church

San Sebastiano church is located in the homonymous district in Regalbuto, a small town in the province of Enna (Sicily, southern Italy) of about six thousand inhabitants. There is inadequate information regard its construction. It was probably built between the end of 14th century and the beginning of 15th century and it was a confraternity church strongly desired by the faithful. The homonymous neighbourhood developed around it after its construction, Figure 1.

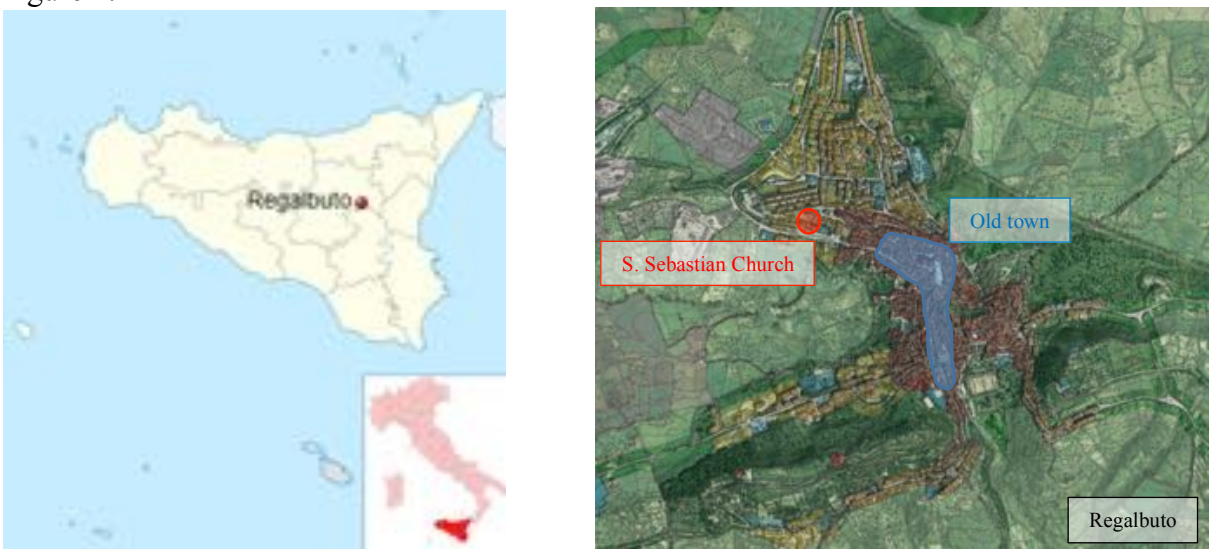
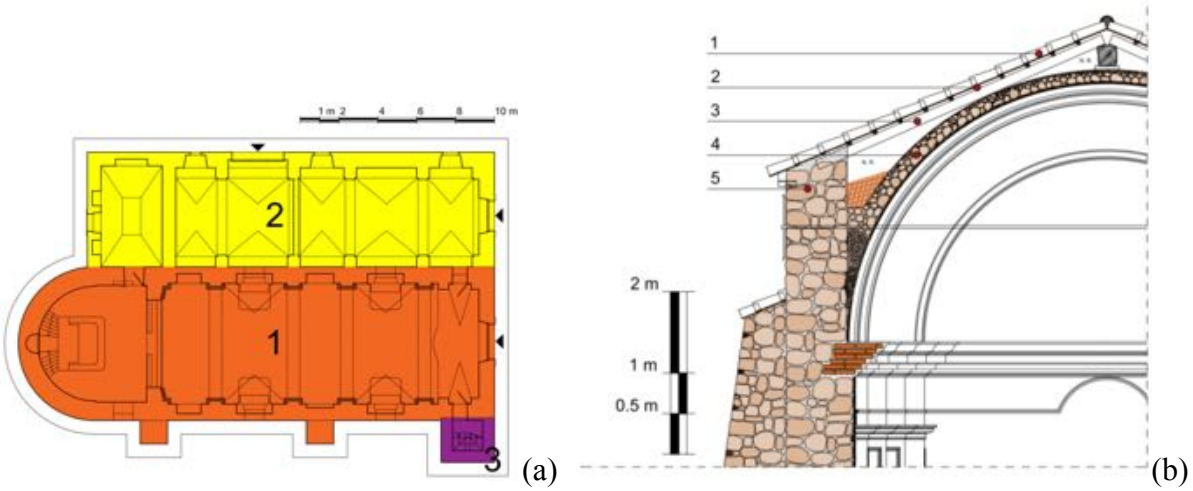


Figure 1: Territorial context

The church is structurally isolated and has a spatial organization that can be divided into three parts: single nave church having a longitudinal development (1), a lower adjacent volume which houses the former oratorio (2) and the bell tower (3), Figure 2a. The size of the nave is 24.50x8.00 m. The horizontal closure is made by a masonry barrel vault whose minimum and average thicknesses are equal to 15 cm and 18 cm, respectively. Above the masonry vault there is a pitched roof. The church is entirely built with sandstone ashlars units with lime mortar, often used in the nearby area for similar historic buildings, Figure 2b. The thickness of the walls is variable: nave's walls have a thickness of 90 cm; lower volume's walls are 80 cm-thick and the bell tower's walls have a thickness of 60 cm.

No documents have been found attesting next interventions on the building. However, it is conceivable to believe that some static aids, such as tie rods in the main vault and buttress on one of the longitudinal walls, have been inserted after the construction of the building, Figure 3. The spatiality of the church was determined by direct survey, Figure 4a, and by the use of *structure from motion methodology*, Figure 4b.

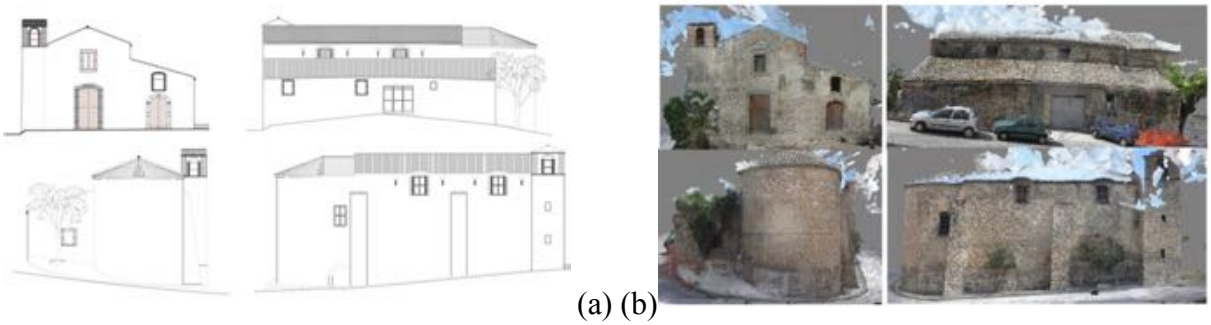


(a) (b)

Figure 2: (a) Spatial organitazion of the building: 1 Church; 2 Former oratorio; 3 Bell tower. (b) Constructive section: 1 Sicilian tiles; 2 Wooden trestles; 3 Wooden beam; 4 Masonry barrel Vault; 5 Masonry with badly connected buttress: irregular sanstone ashlars and lime



Figure 3: Internal views



(a) (b)

Figure 4: (a) External façades and (b) church model obtained with *structure from motion* methodology

3.2 The assessment of the mechanical properties through the quality of the masonry media

For the identification of masonry's mechanical characteristics, it was carried out an analysis of masonry quality, based on visual examination, that allowed us to express a qualitative overall judgment regarding compliance with the "rules of art". The judgment was expressed in terms of "Respected" ("R"), "Not respected" ("NR"), "Partially respected" ("PR") as proposed by Borri et al. (2015) [3]. This evaluation was carried out through the so-called "scoring method". This method involves the characterization of a wall panel subject to

different load conditions. In fact, the parameters that define the "rules of art" influence in a different way the response of the wall according to its load condition. The result is an index called IQM (Index of Quality of Masonry) for each applied load. Through this index a category is assigned to the masonry. There are three categories: category "A" (good behavior of masonry), category "B" (medium behavior of masonry), category "C" (insufficient behavior of masonry). The assigned score for each load condition is highlighted in Table 1. The IQM evaluation is aimed at obtaining an estimation of the mechanical parameters when there is no data available from in situ tests. A range of plausible values for three mechanical parameters, Young's modulus (E), compressive strength (f_m) and shear strength (τ_0), is associated, through an empiric relationship, to each value of IQM is associated, Figure 5; the considered upper and lower bounds of the mechanical properties are identified in blue and red, respectively. The analytical functions of the empiric correlations, previously recalled, are reported in [3]. The grid of scores for the vertical actions (suitable to determine the compressive strength and the Young's modulus) and for the in-plane actions (employed to estimate the shear strength) are summarized in the following Table 1, where the scores given to masonry media of the case study are highlighted. The value of IQM is computed as $\mathrm{IQM} = \mathrm{RE.EL} \times (\mathrm{OR.} + \mathrm{P.D.} + \mathrm{F.EL.} + \mathrm{S.G.} + \mathrm{D.EL.} + \mathrm{MA.})$ for each load condition and the obtained ranges of the mechanical properties result: $f_m = 1.38 - 2.39\ N/mm^2$; $\tau_0 = 0.028 - 0.043\ N/mm^2$; $E = 743.22 - 1093.09\ N/mm^2$.

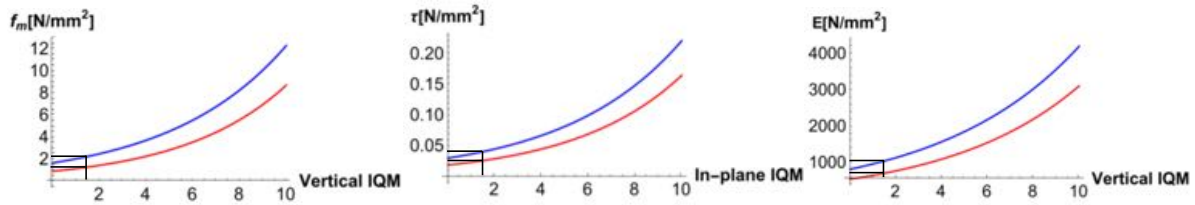


Figure 5: Relationship between IQM and f_m (to the left), τ_0 (in the center) e E (to the right)

Table 1: Scoring Method [3].

Parameter	Vertical action			In-plane action		
	NR	PR	R	NR	PR	R
O.R. (Horizontality of the rows)	**0**	1	2	**0**	0.5	1
P.D. (Presence of diatons)	**0**	1	1	**0**	1	2
F.EL. (Resistant elements shape)	0	**1.5**	3	0	**1**	2
S.G. (Vertical joints offset)	**0**	0.5	1	**0**	1	2
D.EL. (Resistant elements size)	0	**0.5**	1	0	**0.5**	1
MA. (Mortar quality)	0	**0.5**	2	0	**1**	2
RE.EL. (Resistance of stone elements)	0.3	**0.7**	1	0.3	**0.7**	1
IQM		1.75			1.75	

4 SEISMIC ASSESSMENT OF THE CHURCH

In this section a numerical assessment of the seismic safety of the church is performed. In particular, in the first subsection the adopted numerical model based on a DMEM approach is briefly recalled. Then, after evaluating the safety of structure in its current state, three possible strengthening scenarios are described and their effectiveness is numerically assessed and compared to each other.

4.1 The adopted numerical model

In this work a numerical strategy based on a discrete macro-model, already available in the literature, is employed for the nonlinear numerical simulations of both unreinforced and FRP reinforced masonry structures. According to this approach, the masonry is modeled through an equivalent mechanical scheme constituted by a hinged quadrilateral endowed with one or two diagonal links to rule the diagonal shear cracking, and interacting with contiguous elements along its four edges by means of nonlinear discrete interfaces which govern the flexional and the sliding behavior. Each discrete interface is made of a single or multiple (according to the model) rows of transversal links for the flexional behavior and single or multiple (according to the model) sliding links. The different stages of this discrete element are reported in Figure 6. This approach was originally introduced for modeling the in-plane behavior of Unreinforced Masonry Structures [9], Figure 6a. This plane element possesses four degrees of freedom, a single row of transversal links and a single in-plane sliding link, and is able to model the main failure mechanisms of the masonry in its own plane, as long as a proper calibration procedure of the links is adopted. Two subsequent upgrades were achieved to expand the potentialities of the approach. First, the out of plane (spatial) behavior, typical of historical constructions, was added [10] by considering additional rows of transversal links and two additional out-of-plane sliding links (able to govern the out of plane shear behavior and the torsion), thus enabling the out of plane degrees of freedom, Figure 5b. Subsequently, a further upgrade was introduced considering a shell macro-element characterized by an irregular geometry, variable thickness along the element and skew interfaces [11] in order to deal with structures with a curved geometry, such as vaults and domes, Figure 6c. The calibration procedures, concerning the mechanical properties of the links, were properly extended in order to account for the more complicated geometry of the element, but keeping the same general philosophy. Numerical and experimental validations of the proposed approach, with reference to full scale structures can be found in [5].

Finally, in order to model the interaction with FRP strips a textile, the model was further upgraded with the introduction of a flat element (to model the composite strips), able to interact with the masonry substrate by means of discrete interfaces, Figure 7, for which specific calibration procedures were duly introduced and validated [12].

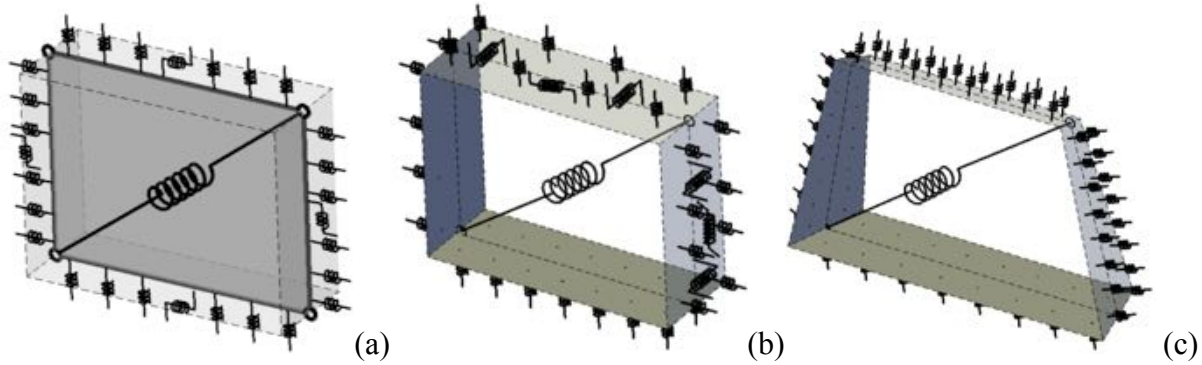


Figure 6: Layout of the macro-element adopted for masonry at its three stages: (a) plane element, (b) spatial regular element and (c) three-dimensional element for curved structures.

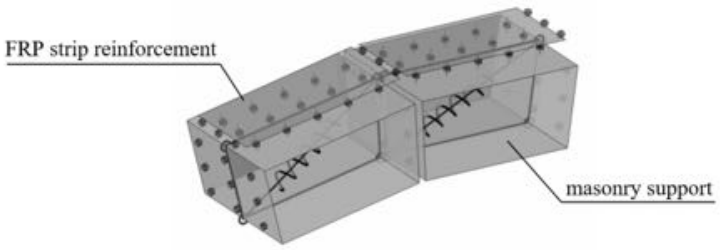


Figure 7: Layout of the interaction between flat FRP discrete element and masonry substrate [12].

4.2 Numerical results and comparative analysis of different strengthening scenarios

The entire church was modelled by a discrete 3d model developed by using an average mesh size of about 100 cm. This mesh of elements has been refined when it was necessary (for example for arched openings). The numerical model is made of 1159 quadrilateral shear deformable elements, 32 triangular shear rigid elements and 2388 interfaces, which are associated to a total amount of 8305 degrees of freedom. The model discretization has been chosen with the aim of combining reliable results with a limited computational burden. In Figure 8 two significant views of the model implemented in the software HiStrA [13] are depicted, and the adopted reference system is identified.

In addition to the self-weight of the elements, overloads associated to non-structural elements are applied as line loads, according to the characteristic values reported in Tables 2.

The diagonal shear mechanism is calibrated according to the Turnsek-Cacovic dominium while the sliding mechanism is managed by the Mohr-Coulomb criteria (enabled in correspondence of the connection between the buttresses and longitudinal walls only). The complete set of the mechanical parameters adopted in the analyses, estimated according the masonry characterization reported in the previous section, are reported in Table 3, where average values with respect to the identified ranges are selected.

Table 2: Applied loads

Central nave	Former oratorio	Bell tower	Barrel vault
2.49 kN/m	3.88 kN/m	1.17 kN/m	22.64 kN/m

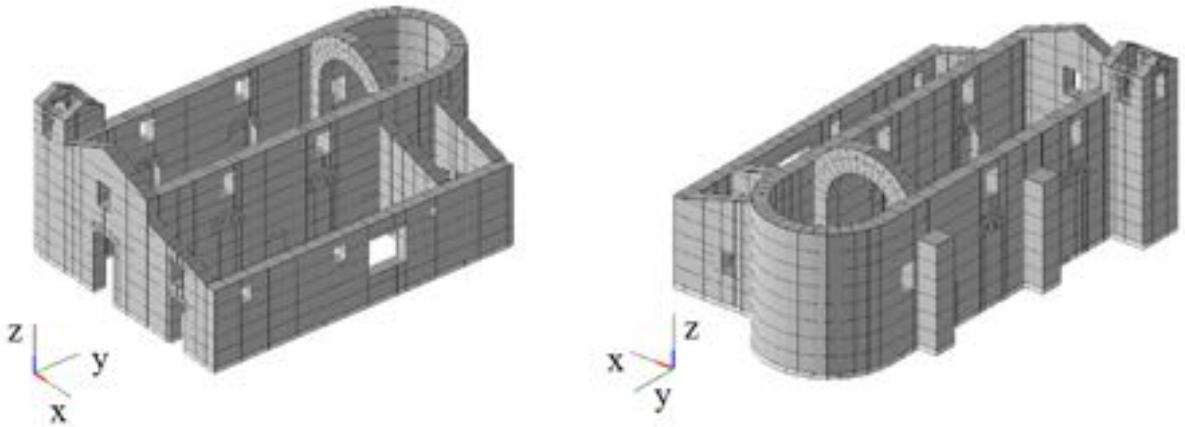


Figure 8: Numerical model and adopted reference system.

Table 2: Mechanical parameters adopted in the numerical model

	Rocking mechanism				Shear mechanism		Sliding mechanism	
	Tensile		Compression					
E [N/mm^2]	f_t [N/mm^2]	G_t [N/mm]	f_m [N/mm^2]	G_c [N/mm]	G [N/mm^2]	τ_0 [N/mm^2]	c	M
950	0.035	0.01	1.88	1	500	0.035	0.15	0.7

The first 8 fundamental periods with the effective mass ratios and the cumulated participating masses along the transversal (x) and the longitudinal directions (y) are listed in the following Table 4. In Figure 9 the modes with highest participating mass are reported, showing the absence of global modes and how the longitudinal walls are keen to the out-of-plane response. Nonlinear static analyses were performed considering mass proportional load distributions along the four main directions of the building. The results are reported in terms of capacity curves, Figure 10, and failure mechanisms, Table 5 (first row). The capacity curves are reported in terms of top displacement of the façade (point 1) and longitudinal walls (point 2) versus the base shear coefficient (base shear normalized by the total weight). The collapse mechanisms show that the longitudinal walls and the façade are keen to overturn due to the lack of horizontal elements and the inefficacy of the buttresses; the base shear coefficients range between 0.25 in the transversal direction to approximately 0.37 in the longitudinal direction (pushing the façade).

Table 3: Vibration modes

Mode	Period [s]	M_x [%]	M_y [%]	$\sum M_x$ [%]	$\sum M_y$ [%]
1	0.341	10.02	0.01	10.02	0.01
2	0.2442	13.7	0	23.72	0.01
3	0.2094	4.8	0	28.52	0.01
4	0.1736	0.05	0.29	28.57	0.3
5	0.1665	0.01	0.61	28.58	0.91
6	0.1372	11.92	0.94	40.5	1.85
7	0.1318	1.83	8.89	42.33	10.74
8	0.1264	0.03	5.2	42.36	15.94

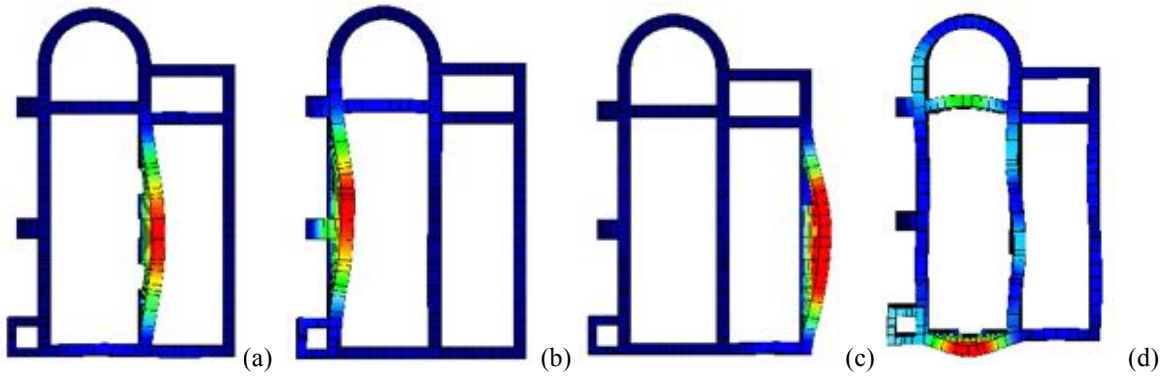


Figure 9: Vibration modes: (a) first, (b) second, (c) third and (d) seventh

In order to increase the seismic global behaviour of the structure, three different retrofitting scenarios have been considered and modelled. The first scenario, Figure 10a, consists in restoring and effective connection of the buttresses with the longitudinal walls (no sliding can occur in the numerical model) and in the re-tensioning of already existing tie rods; the second scenario, Figure 10b, includes the complete replacement of the roof with a steel and wooden roof connected to the masonry with a reinforced masonry ring beam; the last strengthening scenario, Figure 10c, consists in the use of fiber-reinforced composite material with a lime mortar matrix on the main façade of the building. This scenario is compatible with the cultural instance of the building because the fiber strips would be hidden by a new lime plaster over the facade. The three scenarios have been conceived as 'additional' in that the second scenario includes the intervention of the first one, and the third scenario also includes those associated to the first two strengthening scenarios.

The capacity curves of the reinforcing scenario are reported in Figure 11 whereas the collapse mechanisms are reported in Table 5 (second to fourth rows). The second retrofitting scenario, ensuring an effective horizontal constraint at the roof level, provides an evident contribution to the global behaviour of the structure. Consequently, both the global lateral strength and ductility capacity of the structure increased when compared to the unreinforced configuration. Moreover, the second scenario avoids the global out-of-plane failure of the façade, predicted in the unreinforced state. The first and the third scenarios do not provide a significant contribution to the global response. However, the third scenario reduces the out-of-plane displacements of the façade when compared to the scenario 2 (see Table 5).

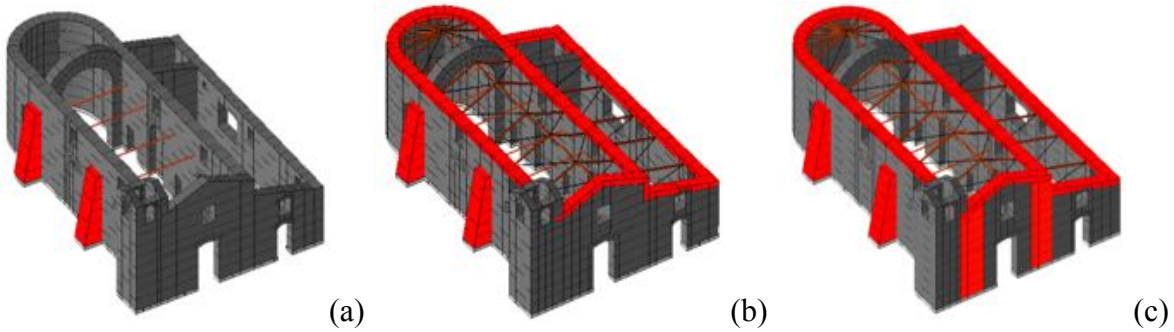


Figure 10: Retrofitting scenarios: (a) Scenario 1, (b) Scenario 2 and (c) Scenario 3

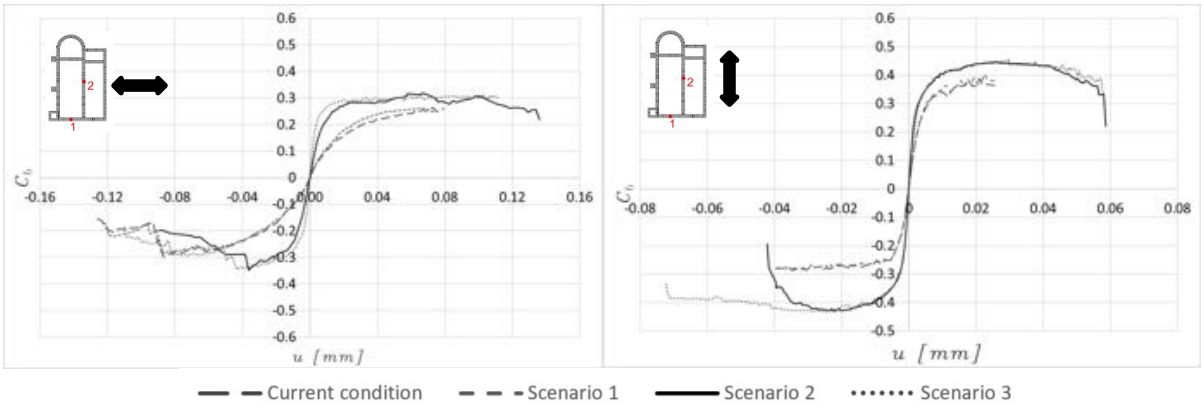
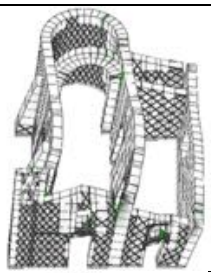
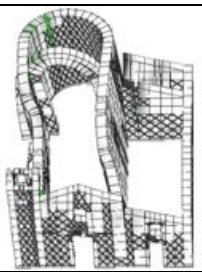
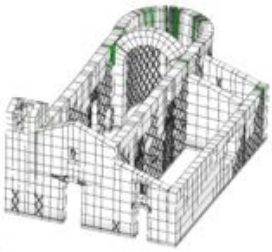
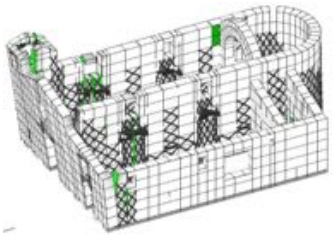
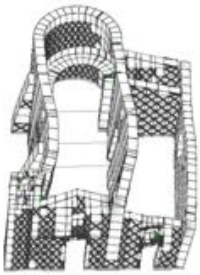
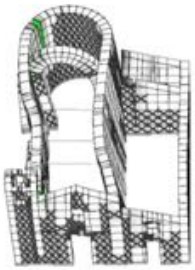
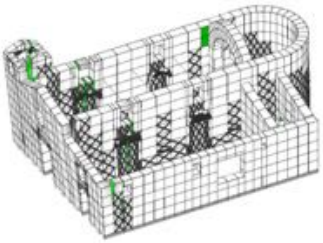
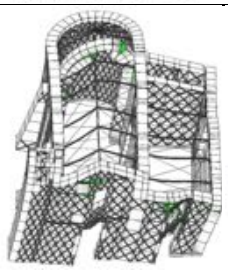
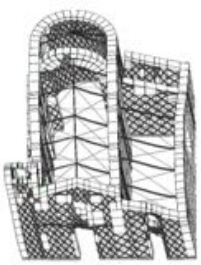
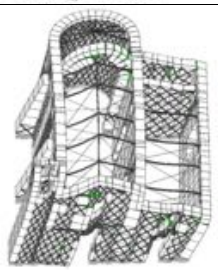
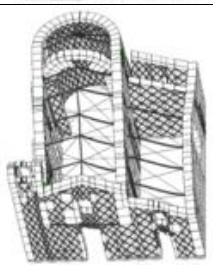
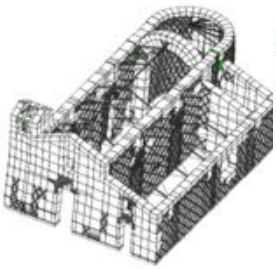
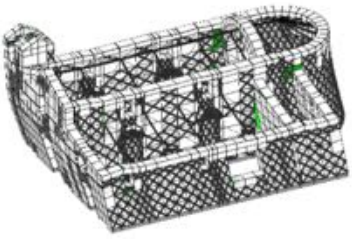


Figure 11: Capacity curves

Table 5: Failure mechanism

	+x	-x	+y	-y
CURRENT CONDITION				
SCENARIO 1				
SCENARIO 2				
SCENARIO 3				

6 CONCLUSIONS

In this study a comprehensive analysis of a monumental structure is presented. The chosen case study is analyzed from the constructive point of view, identifying the main features of the building. Then, a numerical model is implemented in the framework of a DMEM environment to assess its safety with respect to seismic conditions, and nonlinear analyses are performed considering the current configuration. Based on the obtained results, three different strengthening scenarios are modelled and analyzed. The three scenarios are conceived as additive strategies, with the aim of identifying the progressive benefits and invasiveness. In particular, the first and the second interventions are selected considering traditional techniques (restoring the original connection between orthogonal walls, re-tensioning the existing tie rods, inserting a masonry ring beam). Although the traditional techniques, whose

application was found inside the church, showed their capability to limit some of the vulnerabilities of the church, in the last considered scenario, the application of fiber-reinforced strips in the main façade has been included in the overall retrofitting strategy. This progressive strengthening design was proposed as a reasoned methodology able to identify the impact to the global safety of the building of each of the considered measures both in terms of structural improvements, economic cost and invasiveness, and might be applied to other historical buildings. Their weaknesses can be rarely removed with a single measure, but rather require a comprehensive design, starting with a deep preliminary knowledge, and including several, but always compatible, strengthening methodologies [14].

REFERENCES

[1] Eurocode 8: Design of structures for earthquake resistance – Part 3: General rules, seismic actions and rules for buildings, Design Code EN 1998-3, 2005.

[2] NTC 2008, Decreto Ministeriale 14/1/2008: Norme tecniche per le costruzioni., Ministry of Infrastructures and Transportations, 2008.

[3] Borri A., *Manuale delle murature storiche*, Vol. I., D.E.I. Editrice, (2011).

[4] Cannizzaro, F., Pantò, B., Caddemi, S. and Caliò. I., A Discrete Macro-Element Method (DMEM) for the nonlinear structural assessment of masonry arches. *Eng. Struct.* (2018) 168:243–56.

[5] Caddemi, S., Caliò, I., Cannizzaro, F. and Pantò, B., New frontiers on seismic modeling of masonry structures. Frontiers in Built Environment (2017) 3, art. no. 39.

[6] Pantò, B., Cannizzaro, F., Caddemi, S. and Caliò, I., 3D macro-element modelling approach for seismic assessment of historical masonry churches. *Advances in Engineering Software* (2016) 97:40-59.

[7] Pantò, B., Giresini, L., Sassu, M. and Caliò, I., Non-linear modeling of masonry churches through a discrete macro-element approach. *Earthquake and Structures* (2017) **12** (2):223-236.

[8] Sanpaolesi P., *Discorso sulla metodologia generale del restauro dei monumenti*, Edam, (1973), pp. 111-118.

[9] Caliò, I., Marletta M., Pantò, B., A new discrete element model for the evaluation of the seismic behaviour of unreinforced masonry buildings. *Eng Struct* (2012) **40**:237–338.

[10] Pantò, B., Cannizzaro, F., Caliò, I. and Lourenço PB. Numerical and experimental validation of a 3D macro-model for the in-plane and out-of-plane behaviour of unreinforced masonry walls. *Int J Architect Heritage* (2017).

[11] Calió, I., Cannizzaro, F., and Marletta, M., A discrete element for modeling masonry vaults. *Adv. Mater. Res.* (2010)**133-134**:447–452.

[12] Pantò, B., Cannizzaro, F., Caddemi, S., Caliò, I., Chácara, C. and Lourenço, PB., Nonlinear modelling of curved masonry structures after seismic retrofit through FRP reinforcing. *Buildings* (2017) **7**:79.

[13] HiStrA (Historical Structure Analysis) Release 17.2.3," ed. Catania, (2015).

[14] Lo Faro A., Contrafatto L., Di Stefano A. L'Aquila's single nave churches and 2009's earthquake: knowledge, modeling, intervention. In: Di Giuseppe E. et al. (Eds.): *ColloquiA.Te 2017. Demolition or Recostruction?*, EdicomEdizioni, (2017), pp. 263-274.

12th International Conference on Structural Analysis of Historical Constructions
SAHC 2020
P. Roca, L. Pelà and C. Molins (Eds.)

CULTURAL HERITAGE EXPOSED TO NATURAL HAZARDS: THE CASE STUDY OF THE CONVENT OF SAN DOMENICO IN MAIORI

R. LANDOLFO, C. TARANTINO*, F. PORTIOLI, L. CASCINI

[1]Department of Structures for Engineering and Architecture
University of Naples "Federico II",
via Forno Vecchio 36, 80134, Naples, Italy
e-mail: landolfo@unina.it, arch.cristarantino@gmail.com, fportiol@unina.it, lucrezia.cascini@unina.it

Keywords: Cultural Heritage, Masonry structures, Limit Analysis, Rigid block models, Lateral loads, Settlements.

Abstract. *Nowadays it is widely recognized that structural interventions on cultural heritage buildings shall comply with the minimum intervention principle. The main goal is to enhance the structural capacity respecting, at the same time, the authenticity of the monument. As such, the correct interpretation of the current damage is a first fundamental step in the design of an efficient structural intervention. Within this framework, the paper presents the results of an in depth investigation carried out to assess the structural capacity of a complex monument affected by several deficiencies. The case study is the convent of Saint Domenico, a seventeenth century's masonry structure, belonging to the traditional architectural typology of the court building. The building is located in Maiori, a small town in the Amalfi Coast (Italy), included in the UNESCO World Heritage List since 1997 for its great cultural and naturalistic interest. The structure was abandoned during the 80s, and currently presents an extensive and diffuse crack pattern that is the consequence of several causes such as: the natural aging of material, the lack of maintenance, the modifications occurred during the centuries, the seismic events occurred in the past and the poor quality of the foundation soil. In this paper, starting from the knowledge acquisition path of the whole Convent, a special focus on the structural behavior of the East wing is provided. A numerical model of a cross section of the wing has been developed and analyzed considering the effects of lateral loads and settlements. The numerical analyses are carried out using LiaBlock_3D, an in-house software tool for the limit equilibrium analysis of rigid block assemblages. Results of the analyses are discussed in details and a comparison with the actual crack pattern of the structure is provided as well.*

1 INTRODUCTION

The Convent of Saint Domenico (fig.1) is a seventeenth century's masonry building located in Maiori, a small town of the Amalfi Coast (Salerno, Italy), which is inscribed in the UNESCO World Heritage List since 1997, as it was recognized an "*outstanding example of the Mediterranean landscape, with exceptional cultural and natural scenic values resulting from its dramatic topography and historical evolution*"[1].

The importance of the building is related to its uniqueness features. Indeed, it contains interesting details of baroque architecture and remarkable artistic works, such as a fresco by the local painter Gaetano Capone.

Very few buildings along the Coast can compete with its dimensions, whereby it represents an important spatial resource for the city and the entire coastal area. Furthermore, it is one of the few surviving elements of the historical urban fabric of Maiori.

From a structural assessment point of view, the analysis of the current performances of the building is very challenging. First of all, the actual structural configuration is really complex, because several manipulations were carried out over the centuries to adapt the original layout to new uses. Besides, the state of conservation of materials and structural components is very poor: the building shows a severe deterioration, as it was abandoned since the '80, when a strong earthquake produced severe damages, and it has never been restored. Finally, the Convent is also threatened by several natural hazards, being exposed to high landslides risk, to floods, and to earthquakes, which already hit the building in the recent past.



Figure 1. Aerial view of the Convent of Saint Domenico in Maiori town. (Salerno, Italy).

As a matter of fact, a proper interpretation of the actual performances of the Convent of Saint Domenico requires an interdisciplinary and multidisciplinary approach, where experts coming from different fields of expertise, provide their contributions to proper characterize the hazards that threaten the building and quantify its vulnerability. Indeed, this case study is under investigation within the framework of the research project PERICLES- funded by the Italian Ministry of Education, Universities and Research in 2017- and aimed to develop sustainable strategies for the protection of the Cultural Heritage threatened by natural hazards[2].

Within the framework of the present study, a detailed analysis of a portion of the Convent is presented and a set of numerical analyses are carried out to evaluate the structural capacity of the selected part against lateral loads and settlement. The structural analyses were carried out using LiABlock_3D, an in-house software tool for the limit equilibrium analysis of masonry structures modelled as an assemblage of three-dimensional blocky structures, which provides as output the most vulnerable collapse mechanism for a given loading condition [3][4]. The software is based on a 'point-contact' formulation and implements the lower bound problem of limit analysis. The numerical model is an assemblage of rigid bodies interacting one another

through no tension-friction contacts characterized by infinite compressive strength. Static variables are the unknown shear forces and the normal force acting at each contact point. The external forces are the known dead loads and the live loads acting at the centroid of each block, the last ones being expressed as a function of the other unknown of the static limit analysis problem, that is the collapse load multiplier. The failure mechanism associated to the solution of the lower bound problem is derived from the kinematic variables which can be obtained from the dual limit analysis problem, corresponding to the upper bound - or displacement based - formulation. Further details of the formulation can be found in [3][4].

It should be noted that similar modelling approaches based on thrust line analysis or variational formulation for limit analysis of failure mechanisms induced by settlements have been also developed in the literature [5]. Incremental solution procedures based on rigid blocks interacting at unilateral contact interfaces for the analysis of the response in the large displacement regime were presented in [6][7]. Applications of alternative numerical formulations can be also found in the literature such as the distinct element method [8], homogenized, discontinuous or block-based finite element models [9][10][11][12] and rigid-body spring models [13]. The non-smooth contact dynamic method was also applied for the analysis of masonry panels subjected to settlements [14].

The paper is structured as followings: section 2 introduces the case study, providing the most relevant historical information useful for the structural characterization of the building. In Section 3 a damage analysis is introduced and details of the surveyed crack patter are reported. The numerical model developed for this study is presented in Section 4, while Section 5 deals with the analysis carried out for lateral loads and settlement. Finally, within the same section, a comparison with the observed damage is provided.

2 THE CONVENT OF SAINT DOMENICO

2.1 Brief history of the building

The Convent of S. Domenico in Maiori is a porticoed courtyard building (Fig.2), characterized by a complex plan configuration, which is the consequence of several manipulations and adaptation carried out during the centuries, to solve unexpected problems and adapt the construction to new functions[15]. The construction process, which started in 1650th, was long and complicated, due to several structural instabilities caused by the poor quality of foundation soils. In the 1809, after the suppression of the religious Orders, the Convent was abandoned and left without any use for about 50 years. In 1865, the local Authorities acquired the whole building and settled inside three different functions: the north-side of the ground floor of the Convent became a courthouse, the south-west a jail and the whole first floor became a school. Consequently, very invasive restoration works were carried out to adapt the old construction to the new functions: lofts were created at the ground floors and new windows were opened in the bearing walls. At the first floor, large arched openings were created in the transverse walls to define the classrooms, enlarging the old monks' cells. In 1980, a strong earthquake heavy damaged the structures and subsequently the building was definitively closed and abandoned. In 1985, a new project of restoration was launched but only partially completed, due to the lack of funds. Nowadays, the building is still closed, abandoned and in critical condition and used by the administration as a warehouse.

2.2 Description of the building

The Convent of San Domenico is composed by four bodies of different width and height, placed around a square courtyard of 32 side length meters. Two of them (the east and the north blocks) develop for two levels, while the last two (the South and the West blocks) feature a single above-ground level and only consist of a portico covered by a panoramic terrace facing the sea (fig 2).

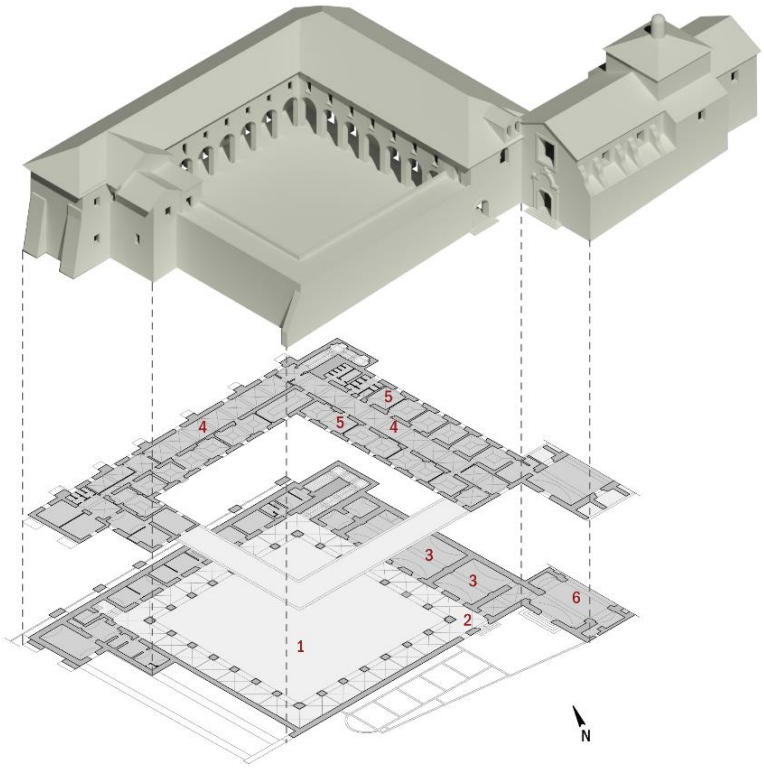


Figure 2.: The architectural asset of the Convent of Saint Domenico: 1) the courtyard; 2) the portico; 3) the big ground floor halls; 4) the first floor corridor; 5) the monks' cells; 6) the Church.

The Church is located on the south east corner, connected to the cloister along the edge, and sharing with it a bearing wall. At the ground floor, along the north and the east sides big barrel vaulted halls open off, while the south and west porticos have blind back walls. On the first floor a long corridor runs the whole building and serves all the rooms once being the monks' cells. The vertical connection was once granted by two stairways. The one on the east side is a three ramps stairway, covered with flying barrel vaults. That on the west side was cut after the first ramp by the nineteenth century's transformations, thus it is no longer serviceable.

The thickness of the masonry walls ranges between 1,2 meters (at the ground floor) and 0,6 meters (on the last level). The horizontal structures consist of a great variety of vaulted structures made of yellow tuff: big barrel vaults cover the rooms at the ground floor, while cloister vaults roof the sequence of monastery cells; groin vaults span along the portico and the corridor at the first floor. The roof is made by double slopes timber structures, covered by clay

romanstyle tiles. The foundation structures are disomogeneous and placed on different laying surfaces: superficial continuous masonry foundations, in calcareous stone; deep masonry foundations of pillars connected by arches, in calcareous stone; deep masonry foundations of pillars connected by walls, in calcareous stone.

The east wing, which is the focus of the present paper, is characterized by a modular scheme of large square rooms at the ground floor, 8.00 m large and 9.00 width, covered by barrel vaults, 7.00 meters high at the ceilings. Smaller rooms are located on the first floor, with an average area of 16 m^2 each, and covered by square cloister vaults, 4.00 m large. The masonry walls at ground floor are made of roughly cut stones of variable dimensions and presents and average thickness of 1.00 m. At the first floor, masonry walls are made of grey tuff blocks with an average thickness of 0.80 m. Special conditions can be observed in the building elevation, where it is possible to find a relevant number of masonry walls that lean against the top of the barrel vault of the lower floor.

Details of the damage status of the whole building and of the selected wing are provided hereafter.

3 THE DAMAGE SURVEY

The building currently exhibits an extensive and diffuse crack pattern that, generally speaking, presents recurrent elements and increases in intensity and thickness from the ground upwards (Fig. 3).

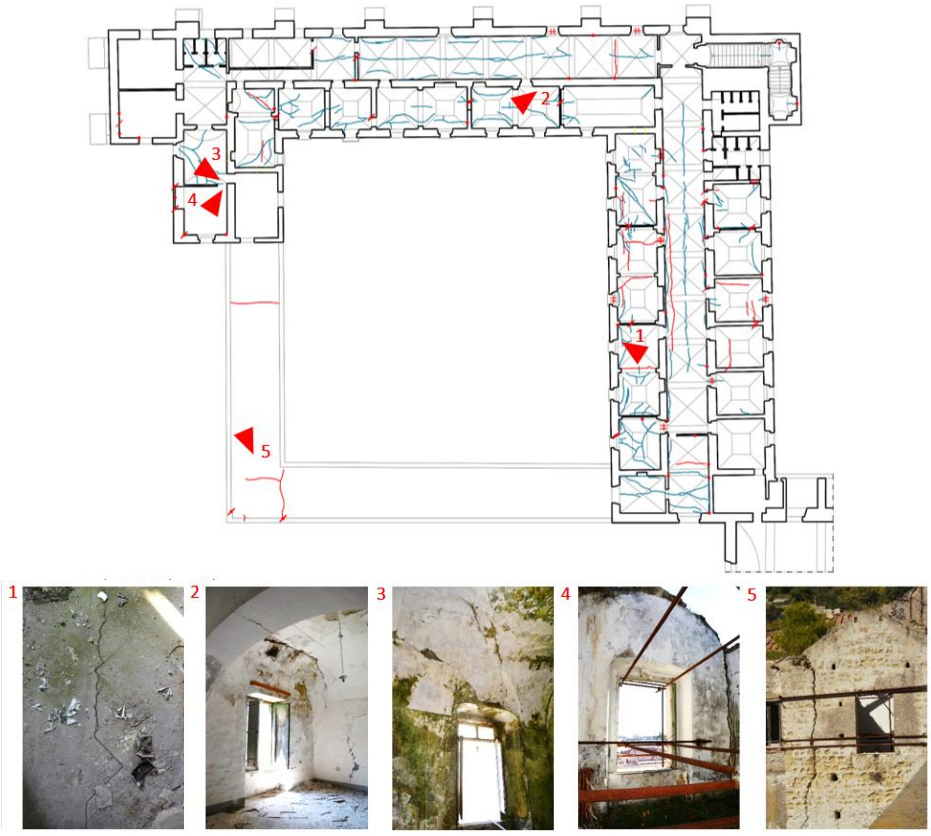


Figure 3. Damage pattern at the first floor

The groin vaults of the portico and of the corridor at the first floor show cracks in the centerline and at the attachment to the walls, corresponding to the typical three-hinged mechanism; the trough vaults of the monks' cells exhibit diagonal cracks and multiple dense cracks parallel to the courtside wall.

As for the East wing (Fig. 4), a different crack pattern is observed, which differs from the one observed in the rest of the building. Indeed, the big barrel vaults of the ground floor halls are completely detached from the head wall separating them from the court. At the first floor, the trough vaults of the monks' cells on the courtside show a more complex and braided crack pattern. Parabolic fissures develop on the shear/transverse walls and some cracks open out on the floors.

A partial collapse of the roof can be observed at the middle length of the block, not referable to a break of the timber structure, which still appears in good conditions. Moreover, the presence of sub vertical cracks on the foundation arches in the south-east corner is reported by the geognostic study associated to the 1987 restoration project.

The interpretation of the crack pattern in this area of the building is not straightforward, as it seems to be the result of different phenomena that acted on the building. As such, a numerical model of a recurrent section type of the east wing was developed and analyzed for different loading conditions, as discussed in the following sections.

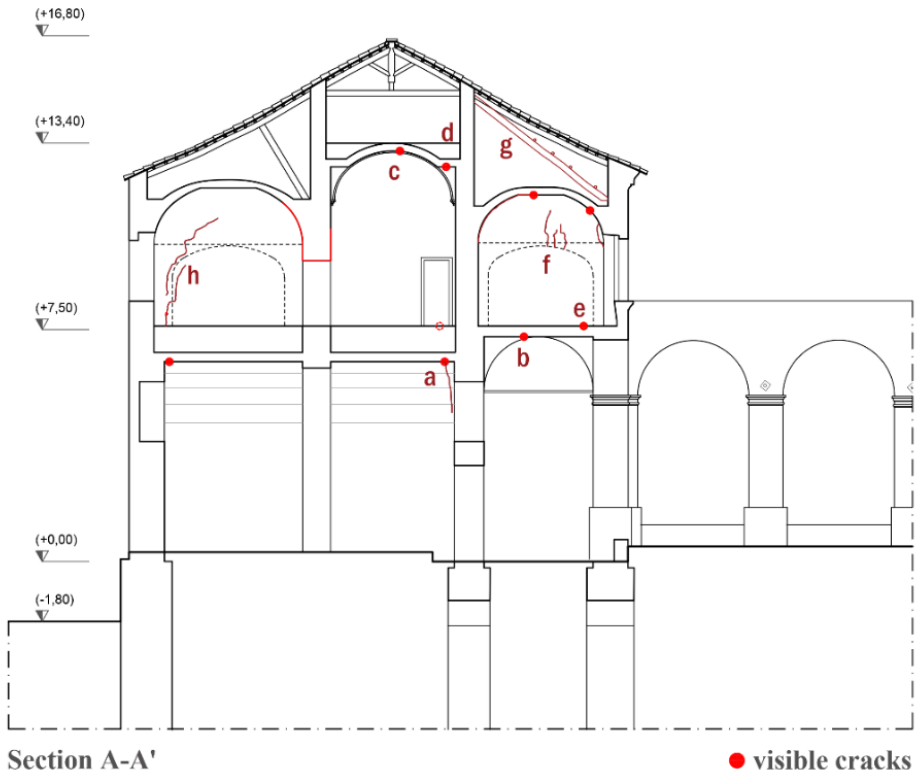


Figure 4.: Crack pattern in the East wing

4 NUMERICAL MODEL OF THE EAST WING

The numerical model of the east wing (Fig. 5) was developed for a characteristic transverse section, which is representative of the whole wing, considering the modularity of this part of the Convent. The section is obtained in correspondence of the symmetry plane between two consecutive spans of the portico and includes the most relevant structural elements of the wing. These are: at the ground floor, the arch separating the crossing vaults of the portico, and the barrel vault of the big hall on the back, in its centerline; at the first floor, the transverse walls between the monks' cells, with their low arch inner openings, and the arch between the crossing vaults of the central corridor. Also the timber roof was included in the model.

To solve some modelling issues deriving from the gap between the two dimensional model and the three dimensional conception of the construction, special components were created.

It is the case of the sub arch of the ground floor barrel vault, which develops in the orthogonal direction of the plane considered in the analysis. A support block has been introduced in its place to sustain the left wall of the first floor corridor. A similar condition is that of the barrel vault, which appears in its axial section. In order to consider the low grade of interlocking of this structure to the head walls and their possible detachment in a collapse mechanism, as it can be usually observed in historical constructions, the blocks representing the vault thickness are provided with a very short support.

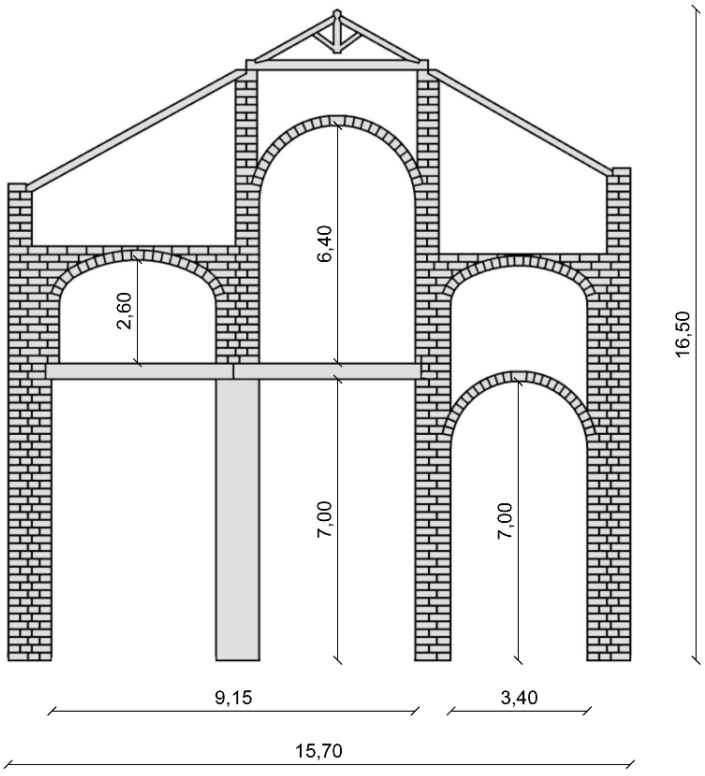


Figure 5.: The numerical model of the east wing (dimensions in meters)

The numerical model is composed by an assemblage of 685 rigid blocks. discretization of the structure in rigid blocks does not reproduce exactly the real masonry texture but was defined so as reproduce the average size of the real stones. A refined discretization was adopted along the imposts of the arches to enable the freest formation, along the whole structure, of the hinges required by the collapse mechanisms associated to the imposed actions.

The masonry walls and pillars are built with parallelepiped shape blocks. The block maximum dimensions are 50x20x40 cm. Blocks with different shape have been employed in the arches thickness and at the arches springing, to better reproduce the shape of the voussoirs and the interlocking at the attachment sections.

Additional rigid blocks have been used to model the timber structure of the roof. Apart from the geometry of the structural configuration, the additional data required as input by LiaBlock_3D for the analysis are related to the material properties. The weight per unit volume ρ of the masonry was assumed equal to 21 kN/m^3 and the value of the friction coefficient μ was set equal to 0.6.

5 NUMERICAL ANALYSES

5.1 Lateral load analysis

The numerical analyses for lateral loads have been carried out by applying a set of lateral forces, applied to the centroid of each rigid block, acting along the x-direction in two opposite directions.

An Intel® Core™ i7-7700HQ CPU 2,80 GHz Processor with 16,00 GB of RAM was used for numerical analyses. The LiABlock_3D output is summarized in Table 1.

Table 1. Numerical load factors and CPU Time for the later loads analyses

Loading axis	Associative		Non Associative	
	Load factor α	CPU Time (s)	Load factor α	CPU Time (s)
+x	0.026	0.5489	0.025	5.7854
-x	0.084	0.5679	0.084	3.8537

Figures 6a and 6b show the collapse mechanisms corresponding to the non-associative solution of the two in-plane seismic analyses, in the positive and negative x directions respectively. When the load acts in the x positive direction, the collapse condition occurs for a low value of the load factor. The overturning of the courtyard facade is activated and, as a consequence, a typical three hinges mechanism develops in both the round and low arches of the right span of the section. The mechanism also causes the sliding of the timber beam and, thus, the roof collapse. When the load acts in the x negative direction, the load factor needed for the collapse is higher. The left and the middle spans of the section almost behave as a unique block, overturning and causing the serious damage visible in the right span of the section. Here the collapse occurs again with the three hinges mechanism of the arches and the sliding of the roof's beam.

The global damage of the seismic in-plane analysis is partly compatible with the surveyed crack pattern, as it was expected, since no restoration works have been done after the 80's earthquakes. Nevertheless, it contemplates a slight damage of the innermost structures of the section and doesn't detect the floor cracks at the first level.

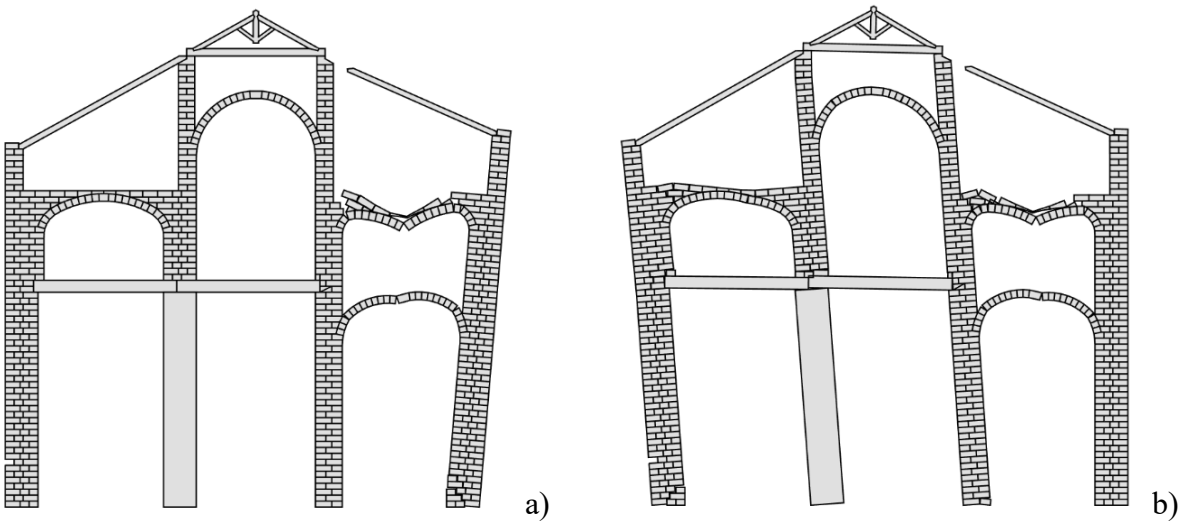


Figure 6: Plots of the collapse mechanisms provided by LiaBlock_3D for the non associative solutions. Lateral loads acting along the: a) x positive axis; b) x-negative axis

5.2 Settlement analysis

The analysis for imposed settlement has been carried out considering that, as highlighted in the previous paragraphs, the geomorphology of the site and the nearness of the river constitute a significant hazard indicator for phenomena of viscous deformations of the soil, capable of resulting in differential settlements of the foundations.

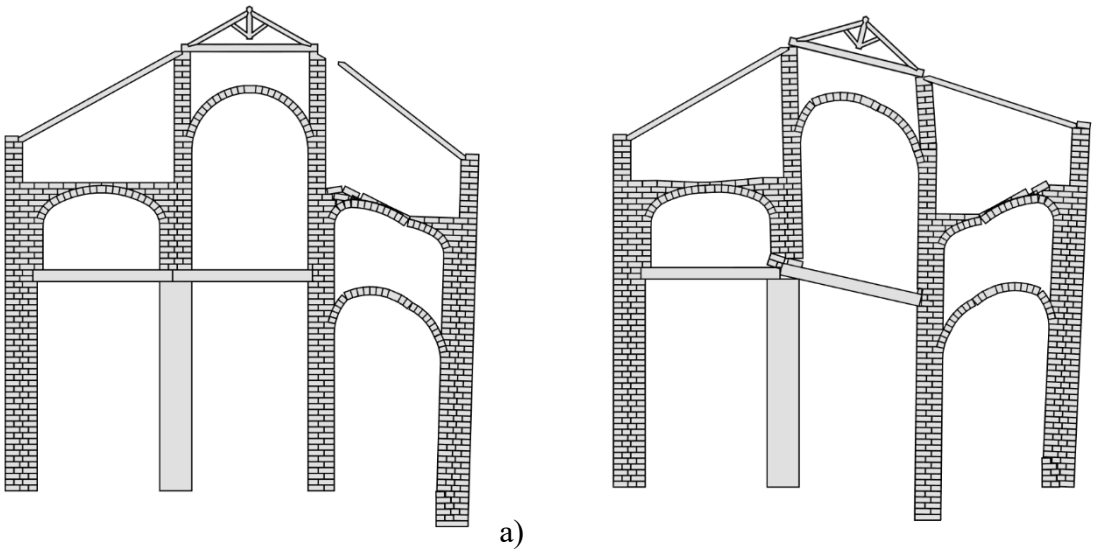
Indeed, available studies revealed the poor quality of the foundation soil, which is composed by different granular deposits - varying from the gravels to the silt - and presents a high water content. This last feature determines a high compressibility of the soil, as expressed by low value of the weight per unit and by the oedometric modulus.

On the base of the localization of the cracks and the damages traceable to a potential soil failure, two different schemes of ground vertical displacement were implemented. The first one considers a uniform vertical displacement imposed at the base of the portico's pillar (Fig7a); the second, examines the case of the same movement imposed at the base of the portico's back wall (Fig7b).

The LiABlock_3D output is summarized in Table 2. For each imposed settlement, the table reports the base reaction at collapse, calculated for the associative and non-associative solution, and the CPU Time. In such a case, considering that the collapse mechanisms do not imply significant sliding, the difference between the associative and non-associative solutions are negligible.

Table 2: Base reaction values at collapse and CPU Time for the settlement analysis

displacement axis	Associative		Non Associative	
	Base reaction	CPU Time (s)	Base reaction	CPU Time (s)
- z (A)	124.358 kN	0.4582	123.7757	1.2774
- z (B)	121.481 kN	0.5053	121.296	1.3056



a) b)

Figure 7: Non associative solutions for the downward displacement of the portico's pillar (a), and the portico's back wall(b).

For the first settlement's scheme, the failure involves only the first span of the section, corresponding to the portico side. The collapse occurs with a three hinges mechanism in the ground floor arch and a two hinges mechanism in the low arches at the first floor. The different failure mode is related to the different geometry of the arches. The overturning of the portico's pillar and the sliding of the roof's beam are also consequently triggered.

For the second settlement's scheme, the damage affects the whole structure. The collapse still occurs with a three hinges mechanism in the round arches of the portico and of the upper floor corridor, while a two hinges failure mode develops in the low arch of the transverse wall. This, again, results in the overturning of the portico's pillar and the sliding of the roof's beam on to the first span of the section. The mechanism slightly affects also the last span of the section, due to the possible little movement provoked in the barrel vault.

Between the two collapse mechanism predicted by the numerical model, the second one, corresponding to the B settlement scheme, is in good agreement with the surveyed crack pattern.

The mechanism catches almost all the existing cracks reported in the section of fig 4: at the ground floor, the barrel vault detachment from the head wall on the portico side (lesion a) and the cracks in the covering structures of the portico (lesion b); at the first floor, the cracks in the vaults and arches of the corridor (lesion c and d), at the floor (lesion e) and in the transverse wall (lesion f) of the right room, and the failure of the roof (lesion g).

Also the parabolic fissures in the upper left room (lesion h) can be traced to this failure mode.

It should be noted that the correspondence of the numerical result to the crack pattern is valid with reference to the analyzed section. Out from this plane of symmetry, the cracks follow a path determined by the complex three dimensional development of the vaulted structures and the characteristic and variable constructive texture.

6 CONCLUSIONS

In this paper, the damage analysis of the east wing of the Convent of Saint Domenico has been presented. A rigid block limit analysis has been carried out with the software LiABlock_3D to investigate the structural response of the numerical model against two different loading conditions, which are lateral loads and settlements. The main goal was to analyze the current crack pattern and to better understand the origin of the damages produced by the two phenomena. The results of the analysis confirmed that the current crack pattern can be ascribed to the concurrent action of the lateral loads and settlement. As such, further development of the study will address more in details the interaction between the structure and the soil and will also extend the analysis to a full 3D model, to better analyze the behavior of the vaults in the spatial model.

Acknowledgements. The financial support of PRIN 2015 Program by the Italian Ministry of Education, University and Research (MIUR) is gratefully acknowledged for funding the research project "Protecting the Cultural Heritage from water-soil interaction related threats" (Prot. No. 2015EAM9S5), which is the main framework of the study presented in this article.

REFERENCES

[1] UNESCO, «Decision report: Inscription: The Costiera Amalfitana (Italy). CONF 208 VIII.C.», 1997.

[2] R. Landolfo *et al.*, «PERICLES Case studies: the Convent of S. Domenico in Maiori», 2020.

[3] F. P. A. Portioli, «Rigid block modelling of historic masonry structures using mathematical programming: a unified formulation for non-linear time history, static pushover and limit equilibrium analysis», *Bulletin of Earthquake Engineering*, vol. 18, n. 1, pagg. 211–239, 2020, doi: 10.1007/s10518-019-00722-0.

[4] L. Cascini, R. Gagliardo, e F. Portioli, «LiABlock_3D: A Software Tool for Collapse Mechanism Analysis of Historic Masonry Structures», *International Journal of Architectural Heritage*, 2018, doi: 10.1080/15583058.2018.1509155.

[5] P. Zampieri, M. Amoroso, e C. Pellegrino, «The masonry buttressed arch on spreading support», *Structures*, vol. 20, pagg. 226–236, 2019, doi: https://doi.org/10.1016/j.istruc.2019.03.008.

[6] A. Tralli, A. Chiozzi, N. Grillanda, e G. Milani, «Masonry structures in the presence of foundation settlements and unilateral contact problems», *International Journal of Solids and Structures*, vol. 191–192, pagg. 187–201, 2020, doi: https://doi.org/10.1016/j.ijsolstr.2019.12.005.

[7] F. Portioli e C. Lucrezia, «Assessment of masonry structures subjected to foundation settlements using rigid block limit analysis», *Engineering Structures*, vol. 113, pagg. 347–361, 2016, doi: 10.1016/j.engstruct.2016.02.002.

[8] T. T. Bui, A. Limam, V. Sarhosis, e M. Hjiaj, «Discrete element modelling of the in-plane and out-of-plane behaviour of dry-joint masonry wall constructions», *Engineering Structures*, vol. 136, pagg. 277–294, 2017, doi: https://doi.org/10.1016/j.engstruct.2017.01.020.

[9] R. Landolfo *et al.*, «Rigid block and finite element analysis of settlement-induced failure mechanisms in historic masonry wall panels», *Frattura ed Integrità Strutturale*, vol. 14, pagg. 517–533, 2020, doi: 10.3221/IGF-ESIS.51.39.
[10] G. De Felice e M. Malena, «Failure pattern prediction in masonry», *Journal of Mechanics of Materials and Structures*, vol. 14, n. 5, pagg. 663–682, dic. 2019, doi: 10.2140/jomms.2019.14.663.
[11] A. M. D'Altri, S. D. Miranda, G. Castellazzi, V. Sarhosis, J. Hudson, e D. Theodossopoulos, «Historic Barrel Vaults Undergoing Differential Settlements», *International Journal of Architectural Heritage*, vol. 0, n. 0, pagg. 1–14, 2019, doi: 10.1080/15583058.2019.1596332.
[12] C. Alessandri, M. Garutti, V. Mallardo, e G. Milani, «Crack Patterns Induced by Foundation Settlements: Integrated Analysis on a Renaissance Masonry Palace in Italy», *International Journal of Architectural Heritage*, vol. 9, n. 2, pagg. 111–129, 2015, doi: 10.1080/15583058.2014.951795.
[13] S. Galassi, G. Misseri, L. Rovero, e G. Tempesta, «Failure modes prediction of masonry voussoir arches on moving supports», *Engineering Structures*, vol. 173, pagg. 706–717, 2018, doi: https://doi.org/10.1016/j.engstruct.2018.07.015.
[14] V. Acary e M. Jean, «Numerical modeling of three dimensional divided structures by the Non Smooth Contact dynamics method: Application to masonry structures», presentato al The Fifth international Conference on Computational Structures Technology 2000, set. 2000, pagg. 211–221, Consultato: apr. 30, 2020. [In linea]. Available at: https://hal.inria.fr/inria-00425357.
[15] C. Tarantino, «Beni culturali espsoti ai pericoli naturali. Il caso studio dell'ex Convento di San Domenico a Maiori», University of Naples Federico II, 2018.

DESIGN OF PROTECTIVE STRUCTURES FOR ACTIVE ARCHEOLOGICAL SITES

MILICA D. PETROVIĆ*, ISIDORA D. ILIĆ†, NEDA M. DŽOMBIĆ†, NENAD D. ŠEKULARAC†

[1] Faculty of Architecture
University of Belgrade
Bulevar kralja Aleksandra 73/II, 11000 Belgrade, Serbia
email: milica.petrovic@arh.bg.ac.rs

[2] Faculty of Architecture
University of Belgrade
Bulevar kralja Aleksandra 73/II, 11000 Belgrade, Serbia
email: isidora@arh.bg.ac.rs
email: neda.dzombic@arh.bg.ac.rs
email: nenad.sekularac@arh.bg.ac.rs
www.arh.bg.ac.rs

Key words: structural analysis, design methodology, protective structures, single layer structures

Abstract. *This paper presents a structural design methodology in order to find the best possible solution of protective structures for active archeological sites. Besides the typical demands for construction on these sites which arise from the typology and the level of protection of cultural heritage, active archeological sites require a structural solution with regard to time and direction of further excavation. The hypothesis is that modular spatial structures which are easily assembled or disassembled, and have the ability to be extended in one or more directions, are the most functional solution for these sites.*

This paper shows the analysis of several types of spatial structures based on the requirements of active archeological sites. It explores the possibilities of structural systems derived from multiplication of one primary element of structure, their material and joints between elements. The most adequate assembly of the entire structure is supposed to be found in the interdependency of the load and the dimension of the element's cross-section, in a suitable geometric configuration. The focus of the analysis is on structures made of short-bearing elements which have the advantage of the efficiency of transport and assembling.

One of the design criteria for this methodology is that the structural system itself looks simple and elegant in order to complement the archeological site. This is shown in the paper through the analysis of patterns in which these structures are assembled. The aim is to correlate the position of the elements in the structural system, the dimensions of cross-section, and the lengths of the straight beams which form the spatial structure in order to find a simple, functional and economical solution for protective structures at active archeological sites.

The conclusion shows the advantages and disadvantages of the design methodology presented in the paper, as well as the discussion about the analyzed spatial structures. This type of methodology that systematizes various design criteria from different fields of research

engages the problem of design of protective structures for archeological sites and opens up new questions for further research.

INTRODUCTION

Structures and structural systems formed by multiplication of one primary element of structure are analyzed in this paper. The design of these structures is based on the idea to use short-bearing elements to achieve large spans. By the term long span we assume spans longer than 35 meters, and by short elements we assume beams shorter than 12 meters.

Types of structures presented in this paper were chosen because of their ability to be expanded in multiple directions based on the criteria for design of protective structures in active archeological sites. This paper aims to show the methodology for finding the best possible solution for protective structure that would "grow" together with the archeological site, since the exact time and space span for further excavations is unknown.

It is important to analyze how the joints between elements are made, and the way the elements are positioned within a structure, regardless of scale. Therefore, it is necessary to understand their geometry in order for the design configuration to be favorable to the structural elements. Single layer lattice structures in architecture are the subject of this research, while the theoretical framework is the geometric configuration of structural elements and its effect on structural capacity. The structure is supposed to be easy to assemble and disassemble, without the need for heavy mechanization.

The exploration of the relation among geometry and structural capacity is based on literature review, followed by a comparative analysis to evaluate the possible solutions. Evaluation is conducted using a finite element analysis (FEA) software. Research will show what are the primary structural elements, types of joints and ways of forming a given structure. After the analysis, the advantages of certain structural systems would be presented to help find the solution.

The aim of this research is to find the most efficient configuration of short-bearing structural elements, that could overcome large spans in order to achieve a simple, proportional and functional structure. The hypothesis is that mathematically consistent pattern would give the adequate geometric configuration of beams that helps in establishing higher efficiency of structure. By designing the minimum dimensions of structural elements, placed in an appropriate pattern, the structure could be perceived as a non-dominant spatial structure, thereby making the archeological site the primary focus of the observer.

ACTIVE ARCHEOLOGICAL SITES

Archeological sites are places that, by their physical structure, bear witness to the past, or characteristics of the culture that was there.[1] Active archeological sites are characterized by an unknown direction and time course of the research. In this paper, the term active archeological sites will relate to those sites whose research is still ongoing, which is why it is necessary to enable the protection of already explored parts, as well as those whose research is ongoing. Most often, these archeological sites are large areas, and therefore require major interventions that involve phase development. In the localities explored so far, the emphasis is usually on the most attractive parts, whereby the view of the site as a whole is marginalized.

Due to its characteristics, it is necessary to find the right type of construction such that it meets all the set requirements. The protective structure should provide a minimum area of reliance, which means that the ideal case would be to have point supports, as well as the unobstructed movement of archeologists - researchers and visitors and the possibility of expansion in accordance with the dynamics of the research. Due to the phase research, and therefore the phase construction of the protective structure, the design of the structure should be conceptually modular, from individual segments that will form a single unique structure. This paper will outline possible types of modular structures for the design of protective structures, their advantages and disadvantages.

Active archeological sites usually cover large areas, entire complexes of objects, often cities or settlements. This implies another criteria for the design of the protective structure - the architectural expression is conditioned by the environment and must not be visually dominant in comparison with archaeological remains.

For a better understanding of the term active archeological sites, an example from Serbia - Viminacium, is presented.[2] The archeological site of the Roman city and military camp occupies an area of 670 ha with a large number of buildings, squares and necropolises. The parts explored so far are the amphitheater, the spa and the northern gate, which form an assembly in the immediate vicinity where the street network of the former city has been identified. This site, as such, has the potential to be protected precisely according to the criteria for the protection of the active site, that is - in phases, with modular structure, in accordance with the dynamics of the research. On the other hand, the protective structure could be designed so that it is large-spaced and dotted, as well as fitting in with the context - both of the formerly built mid-Roman city and of the contemporary appearance of the site.

SINGLE LAYER LATTICE STRUCTURES IN ARCHITECTURE

These structures are gridshells, geodesic domes, free form grid structures, with emphasis on self-supporting structures, such as reciprocal frame structures.

For single-layered structures of a large span, it is assumed that the configuration of the rods is spatial, the load is uniformly transmitted in all planes of space. This configuration of the rods can be designed such that all structural members are axially stressed, analogous to the shell state. On the other hand, we can design the structure so that the rods are interdependent, and that by creating a hinged or moment connection, they work as a single structural system.

This type of construction is defined as an assembly of short rods that, when connented, can overcome large spans. Also, these structures can be considered lightweight structures, which were among the first to be investigated by Frei Otto and whose experiments gave the basic postulates according to which the above mentioned structures should be designed3:

- Avoidance of the dominant bending effect,
- Transmission of tensile force, low-weight elements, for long spans,
- Transmitting force to short elements, in order to avoid stability problems and large dimensions of supporting structure,
- If it is necessary for pressure to be transmitted over long spans, then they must be integrated as a self-stabilising system,
- Use of adequate cross-sections of the elements in compression in order to avoid static problems.

Triangulated surfaces

The triangle, as the basic geometric unit of these structures, is a stable system of articulated rods. The successive extension of two rods and one hinge gives a stable system in a plane or space, thus allowing the formation of a wide variety of geometries that are based on a triangle.

A special type of these structures are geodesic domes, first designed by the architect Buckminster Fuller since 1954. In order to maximize the potential of steel and its ability to accept tension forces well, Fuller formed a dome from a series of rods that follow geodesic lines. Geodesic line is the shortest distance between two points on a curved surface, which can be approximated to a straight line. When he patented his first geodesic dome, he pointed out that his dome was as wide as the Pantheon, but a hundred times lighter.[4] This architect saw the geometric characteristics of a triangle, as a stable system, and applied them to form the surface of a sphere. In this way, a stable structural system was realized, with the stress state being analogous to reinforced concrete shells, therefore, axial forces occur in all the rods.[5] The postulate on which Fuller's geodesic domes are based is: "continuous tension - discontinuous pressure".[6] It can be clearly seen from this that each rod, which is approximately horizontal, is in tension. These rods form irregular rings of geodesic polyhedron and as such form the discontinuity of the compressive forces in the rest of the rods.

Buckminster Fuller reduced the sphere to a system of triangles and thus formed a stable structural system. On the other hand, the sphere has the largest volume relative to the surface of the envelope. From an architectural design point of view, this means that a maximum range can be achieved with minimal material consumption. Related to that, the problem of tracing the geometry of the sphere to form structural elements arises. Architect reduces the geometry of the sphere to polyhedron, and the curved meridians and parallels to short rectilinear elements. In this way it was possible to retain all the advantages arising from the geometric characteristics of the sphere as a geometric body, but also of the triangle as a stable plane structure.

The modular elements that make up the geodesic domes - the joints and rods of the same dimensions represent their greatest advantage. Due to the even distribution of forces in the structure, the dimensions of the rods are small, reducing the weight of the structure significantly. The advantages of these domes are reflected in their widespread use in practice. Most often they are made of steel or wooden rods connected by steel ties. Point supports, along the perimeter of the dome, fulfill one of the criteria for the design of structures in active archeological sites, however, very few sites have circular shaped objects in floor plan.

Mesh surfaces are evolving in simultaneously with technological progress. These surfaces emerged as a continuation of exploration of shells of non-Euclidean geometries. By extending the Gaussian curves to form complex curves in two or more directions, a free-form emerges which is much more complex for structural design and analysis.

They are often designed in a way that each element of the structure is continuous, or superimposed, which further implies that the organization of the structure must be very well composed, without improvisation, due to the fact that every element corresponds to only one position within the structure.

Also, we can consider these surfaces as a continuation of the study of triangulated surfaces, as the curvature of any structure is based on a triangle.

Through generative software, designing and looking at these structures has become simpler and more efficient. The key advantages of these structures are reflected in the placement of the

supporting points so that they correspond as closely as possible to the remains of an active archaeological site, without restriction. Free forms can be constructed in any material, which is an added advantage.

Reciprocal frame structures

The principle of reciprocal structures, mostly formed of wooden rods, dates back to the Early Stone Age, and is based on the mutual carrying rods in order to bridge a span. The lengths of the rods vary with the dimensions of the base and the pattern of the reciprocal structure itself.

The principle underlying these structures is based on the temporarily supported first element of the structure, with each subsequent beam relying on the previous one, while the last beam placed will carry the first one. In this way, a closed cyclic movement of the force in the structure is formed, which enables each element of the structure to be both load bearing and carried. Therefore, each element accepts the load equally, so it has the same structural forces. Patterns in which these structures can be formed are based on the rotation of the structural elements. Such patterns are formed over the basics of various polygons, with the number of sides of the polygon depending on the number of rods in the structure, that is, the angle of rotation of each element.[7]

Due to the possibility of combining several different configurations (e.g. triangle - hexagonal), the floor plan on which this construction is designed today does not have to be the basic geometry. Namely, the greatest advantage of these constructions is the prefabrication, that is, no matter how much the construction volume is changed, all the beams are of the same length, with a possible change in the dimensions of cross-section. These structures can be designed in a large number of patterns, with almost no restrictions. The joints between the elements of these structures nowadays are usually made of steel, however, it was initially done as a notch joint, i.e., the groove of the two elements by sealing them for the sixth of the cross-section's height. Using the notch joint, the assembly process is considerably faster. However, due to the necessity of reducing static height of the cross-section by the use of a notch joint, a connection is often accomplished with a steel element. Depending on the applied pattern, in reciprocal frame structures, the length of each element varies, as well as the way in which the connection between two or more elements is achieved. The dimensions of the cross-section can vary with the span, as well as the load capacity of the structure.[8]

Architect Friedrich Zollinger patented Zollinger's first construction in 1910. The construction consists of segments of solid wooden carriers, about 2 meters long, of uniform geometry. In the literature, Zollinger's construction is called Lamella roof, according to author Martin Tamke.[9] By the term lamella, one repetitive segment is considered, which makes this construction, so this term can be translated as a construction of the same segments. The principle by which this construction functions is such that at the endpoints of two beams of one direction there are joints to the centre of the beam from the other direction. In this way, the interlocking of the elements was achieved, resulting in a span of up to 40 meters. The pattern by which the elements are arranged, although not listed in the analyzed set of patterns, is the projection of rhombus on the roof surface. The original Zollinger construction implies the geometry of the pointed arc, which for the first time appears as a stylistic feature of Gothic architecture.[10]

The connections of wooden carriers were articulated, which was the reason for further research and improvement of these structures. Hugo Junkers, a mechanical engineer and aircraft designer, patented in 1924 a similar construction that consisted only of steel elements among which moment connections were formed. He found inspiration in the design of the aircraft itself.[11]

The Zollinger construction is very similar to reciprocal constructions according to the load transfer principle. The advantages of this construction are the simplicity and the efficiency of assembling, as well as the prefabrication of elements. A disadvantage of this construction is a geometry of floor plan on which these structures are projected, which is predominantly rectangular. In case it is necessary to use the principle of this structure for more complex geometry, each connection of the two elements should be specifically designed due to differences in the spatial orientation of the connections themselves. Therefore, each rod should have been separately designed, which would result in neglected prefabrication benefits.

Comparison of structural systems

Although geodesic domes, as representatives of regular triangulated surfaces, have the same elements as well as typical connection details, with the goal to achieve the largest possible span with the least material used, their design constraints are counteracted by the criteria that the design of structure over an active archeological site must have as flexible positions of support points as possible.

On the other hand, the flexibility of free-form shaping, and hence the position of the supporting points, is a considerable convenience when it comes to the application of these structures in the function of protective structures. Too complex structures would certainly have a strong architectural expression that would be too dominant in the context of archeological sites. Also, these structures, unlike the typical elements of geodesic domes, have complex elements and a complex assembly process.

However, reciprocal structures, as an example of free-form modular structures, are the most effective solution for covering active archeological sites. First of all, the fact that they are most often constructed in wood as an applied material, which equally accepts pressure and tension and it is also the lightest structural material. Therefore, these constructions are of high load-bearing capacity and of low weight compared to other structural materials.

With the use of wood, these structures easily fit into surrounding context, especially due to the fact that active archeological sites are often located outside the built environment, and the newly designed structure should be integrated with the landscape in which it is located. The load-bearing capacity of reciprocal structures is of the utmost importance because each element of the structure is equally loaded or the load is gradually increased, without extreme changes in load transfer. Also, the assembling of reciprocal structures, as a structure consisting of short rods, is one of the key advantages of why the reciprocal structures are suitable for covering part of the archaeological site or for the phased development of the archaeological site, and therefore the protective structure.

Reciprocal structures can also be seen as modular structures, point-supported, simply interconnected (groove joinery or by screw), or as a combination of identical elements of geodesic domes and flexibility of free forms.

INTERDEPENDENCE OF PATTERNS, LOAD-BEARING AND DIMENSIONS OF CROSS-SECTIONS OF RECIPROCAL FRAME STRUCTURES

Patterns shown in the first iteration represent two-dimensional configuration made of short rods. The structural forces of the first five patterns, which were derived from basic geometric figures, or a combination of various regular polygons, were analyzed. In the first iteration, precisely because it was a two-dimensional configuration, it was necessary to evaluate the patterns through the deflection they cause. The first check was made using a program in order to obtain the expected value of the deflection. The assumed cross-section of the beam is 20/60 cm, the input load is 2.92 kN/m' (derived from the analysis of the load of the roof cover and the own weight of the beam), and the span of this girder is 20 meters. This deflection which will be compared to the deflection of other patterns is obtained from calculation of this beam, and its value is 5.63 cm.

The patterns were formed from a system of short rods, which are rigidly connected, and then analyzed in software. Two sets of patterns were evaluated simultaneously, which differ in the way they are supported. The first set of patterns (in the table labelled T) is supported only in the vertices of the square (point supports) while the second set (in the table labelled with L) is supported by the edge of the square field, that is, in a linear assembly of point supports. It can be assumed that the second set will give better results. Each constructive field is formed over a square base that is 20x20 meters.

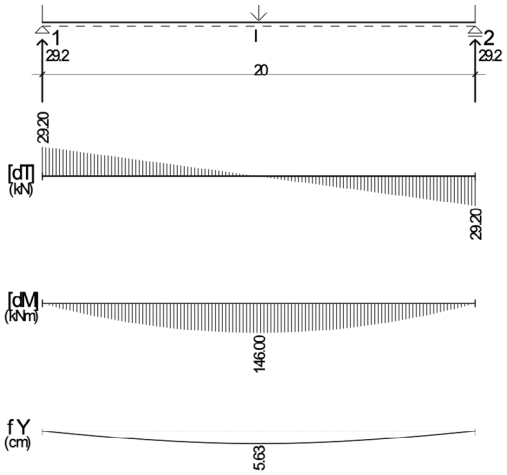
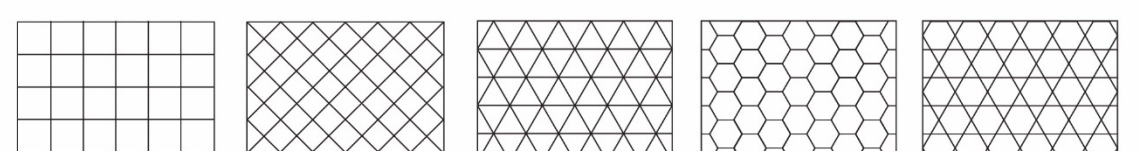
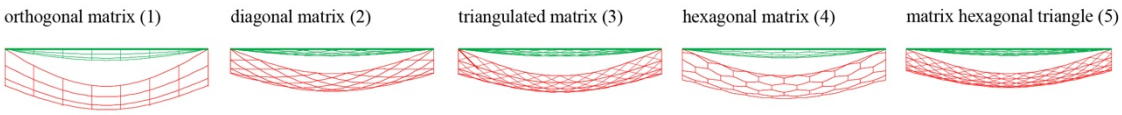


Figure 1: Static analysis of a simply supported beam of 20m span

Patterns are named according to the geometry from which they were derived, but now they will be given numerical labels: orthogonal matrix (1), diagonal matrix (2), triangulated matrix (3), hexagonal matrix (4) and matrix hexagonal triangle (5). As it was already mentioned, the

matrices are formed so that each geometry forms a field of approximately same surface, so that the linear load applied to each girder is approximately of the same intensity.





Zp	deformation in m/1000	rank	deformation in m/1000	rank	deformation in m/1000	rank	deformation in m/1000	rank	deformation in m/1000	rank
T	748	5	511	3	417	1	597	4	465	2
L	137	5	80	3	78	2	109	4	75	1
Σ		4		2		1		3		1

value 5 - worst rated, value 1 - best rated

Table 1: Deflection comparison with evaluation – basic patterns

The first comparative analysis of both sets was done through the animation of a deformed model, where it was evident that the set of matrices with support in vertices of a square base had significantly larger deflections than the linear set.

At first point, it seemed that the diagonal matrix (hereinafter: matrix 2) had the smallest deflections. However, when observing an isolated graphic attachment in which the deflections of the first and second set are seen, on the basis of the more drastic differences in the deflections in the set of point-oriented structure, one can observe which configurations have the most favourable behaviour in the plane.

Table 1 shows the deflections of analyzed patterns in two sets. Set 1, marked with the letter T, represents a support in the vertices of the square, while the set 2, marked with the letter L, represents a linear support along the sides of the square base. All the analyzed patterns were shown in the table, whereupon the maximum deflections for each were drawn. Of the five analyzed, the three patterns, according to the estimation are of the same rank, regardless of the type of reliance, however, two patterns are best rated, so the triangulated matrix has less than the matrices of the hexagonal triangle when leaning point in the square of the square. On the other hand, despite small differences, matrix no. 5 has smaller deflections than matrix no. 3, if it relies on a liner support.

Although these two matrices proved to be the best in numerical value analysis, the diagonal matrix is very close to results. Another similarity, when analyzing two of the best patterns, is their relevant angle when forming the pattern itself. Both matrices in their configurations have a triangle, or an angle of 60°. Which leads to the question of whether the diagonal matrix is

reduced if it is formed using the same angle of 60° instead of the 45°, angle at which it is currently. However, regardless of this assumption, the diagonal matrix deflections, if formed using an angle of 60°, is 10.3 cm, which is more than the first configuration with an angle of 45°.

Due to the obtained results, through the following analysis, or analysis of the geometry of the patterns that form reciprocal frame structures, these two configurations will be evaluated again as the best in the plane. It is extremely advantageous that these two matrices have proved to be the best, due to the various possibilities of combining the triangular and hexagonal configuration of reciprocal structures. Also, these configurations of reciprocal modules of the construction give the possibility of creating spatial single layer structures.

However, the biggest problem due to this analysis is the assumption that all the beams are connected using a moment connection. This can be a problem for any applied material, the detail of the connection will have to be formed in such a way that it transmits the bending moments from one structural element to the next. When the steel is the assumed structural material, this connection can be achieved by welding the girders one to another, but due to the application of short elements the assembling of the construction would take too long. However, in the case of short wooden elements, a special type of connection needs to be applied, achieved by a steel element that could transfer the bending moments.

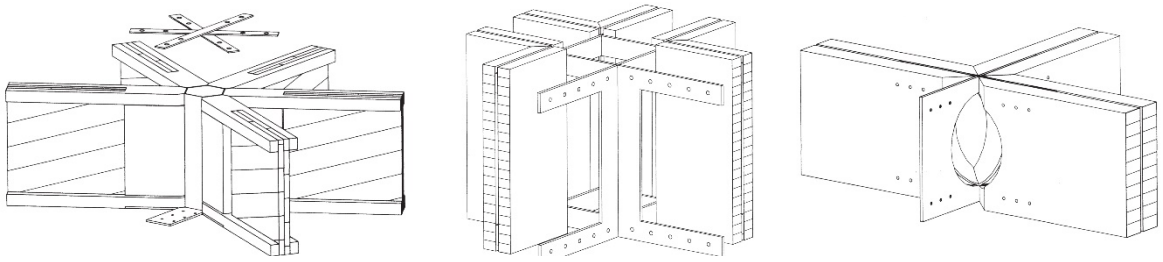
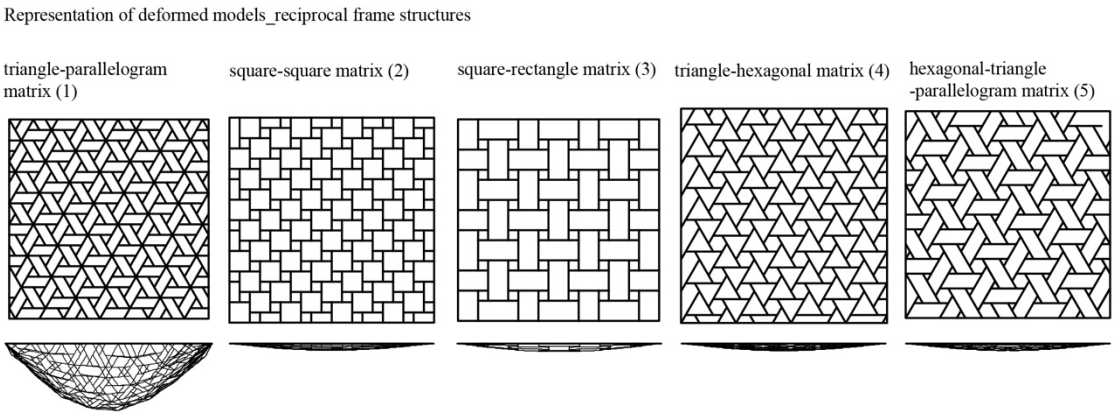


Figure 2: Types of moment joints

By analyzing the matrices of reciprocal frame structures, as expected, bigger deflections were obtained, due to the hinged connections between the elements. However, when talking about the detail of the connection in wooden structures, it can be done as a notch joint, or with a reinforcement of the steel elements. The possibility of making a notch connection would only be valid for spans up to 12 meters, while the reinforcement of the connection would apply for spans larger than 12 meters. This feature of reciprocal frame structures enables easy and efficient assembling on site. That is, the mounting process would be considerably faster, and therefore cheaper, compared to achieving a rigid connection. Software analysis of patterns that

form reciprocal structures in the plane, where the joints of the girders were done as hinged connections, gave the following results when it comes to deflection of the model.



Zp	deformation in m/1000	rank	deformation in m/1000	rank	deformation in m/1000	rank	deformation in m/1000	rank	deformation in m/1000	rank
L	1290	5	144	1	198	4	168	3	165	2
∑		5		1		4		3		2

value 5 - worst rated, value 1 - best rated

Table 2: Deflection comparison with evaluation – reciprocal frame patterns

As a result of this analyses, it is found that the best configuration of the matrix rods is no. 2, or the geometric square-square configuration. However, in the case of reciprocal structures, it can easily be seen that all deflections are of approximate values, i.e., one configuration cannot be derived as the best.

Bearing in mind the efficiency of connecting and easy assembling of reciprocal structures, or considering the economic viability of these constructions, it can be concluded that they would be significantly more applicable than patterns with rigid connections. Namely, using wood, as a natural material, as well as reducing the use of steel in the construction, can affect the reduction of carbon dioxide in the atmosphere precisely because of the reduction of CO2 emissions from the exploitation of steel. In this way, a green, economically profitable construction is obtained, which as such can be applied in different locations of specific construction conditions, such as archaeological sites.

It is necessary to note that in this chapter only two-dimensional configurations of the girders were analyzed, i.e. that considerably better static characteristics are expected by using single or double curvature.

CONCLUSION

This design approach for choosing the appropriate structural system is based on criteria set by the characteristics for active archeological sites. The analysis of interdependency between structural pattern and the dimensions of beam cross-section are in direct correlation to the structural form of the protective structure and its overall appearance in the archeological

landscape. “The good building is not the one that hurts the landscape, but one which makes the landscape more beautiful than it was before the building was built.”[12]

Other criteria in this methodology is guided by the position of the observer, because the human eye searches for natural shapes and structures in its environment that hold a sense in itself.[13] Therefore, the chosen bearing structure has to be simple and logical to a careful eye, embracing the surrounding landscape.

Reciprocal frame structures are modular, usually made of short wooden beams, connected with simple joints, making them simple for construction, with no need for heavy mechanization to and on site, thus fulfilling the criteria for active archeological sites. These structures are ecological, fitting perfectly in the natural surroundings. The most appropriate pattern for this structure is the one made of larger and smaller squares, which can be easily modified in order to be expanded. This light structure has small scale point supports that would not damage the remains on site. They are also very elegant, so they do not turn away the attention of the observer from the site.

The presented methodology is based on specific criteria for design of protective structures for active archeological sites in order to find the best possible solution, but it could be improved with case studies oriented towards specific sites. Model analysis on different types of structures could complete this methodology, so it can be used in practice, as well as in theoretical approach.

REFERENCES

[1] Cambridge University Press. *Cambrigde Dictionary*. Retrieved from Meaning of archaeology in English, (2020, January 31): https://dictionary.cambridge.org/dictionary/english/archaeology

[2] Nikolić, E. *Evaluation of the protection and presentation of historic buildings in the Viminacium Archaeological Park in relation to their spatial context*. Spatium, (2018), pp. 26-37.

[3] Nerdinger, W., Meissner, I., Möller, E., & Grđanski, M. *Frei Otto Complete Works: Lightweight construction - natural design.* Basel: Birkhäuser, (2005)

[4] Fuller, R. B., *Inventions - The patented works of R. Buckminster Fuller*. New York: St. Martin’s press, (1983), pp. 129.

[5] United States of America Patent No. 2,682,235, 1954

[6] Fuller, R. B., & Applewhite, E. *Synergetics.* Sebastopol: Macmillan Publishing Co. Inc, (1975, 1979)

[7] Popovic Larsen, O. *Reciprocal Frame Architecture*. Oxford: Elsevier Ltd, (2003)

[8] *Song, P., Fu, C.-W., Goswami, P., Zheng, J., Mitra, N. J., & Cohen-Or, D. An Interactive Computational Design Tool for Large. Nexus Network Journal, (2014) pp. 109-118.*

[9] Tamke, M., Rüber, J., & Jungjohanne, H. Lamella Flock. In C. Ceccato, L. Hesselgren, M. Pauly, H. Pottmann, & J. Wallner, *Advances in Architectural Geometry 2010,* Vienna: Springer. (2010), pp. 37-48

[10] Ceccato, C., Hesselgren, L., Pauly, M., Pottmann, H., & Wallner, J. *Advances in Architectural Geometry 2010.* Vienna: Springer. (2010)

[11] Weller, B. Lamella Roof Constructions by Hugo Junkers. *Evolution and Trends in Design, Analysis and Construction of Shell and Spatial Structures,* Valencia: Universidad Politecnica de Valencia. (2009), pp. 1611-1621
[12] Hertzberg, M., & Lloyd Wright, F. *Wright in Racine: The Architect's Vision for One American City.* San Francisco: Pomegranate, (2004)
[13] Balz, M. Phantasy in space. *An Anthology of Structural Morfology*, (2009), pp. 112.

12th International Conference on Structural Analysis of Historical Constructions
SAHC 2020
P. Roca, L. Pelà and C. Molins (Eds.)

DETERMINING QUALITIES OF PHOTOGRAMMETRIC MODELS FOR THE USE OF MONITORING MOVEMENTS IN STONE CANDIS IN CENTRAL JAVA

D. GRANDITS[1], L. STAMPFER[2], E. KODŽOMAN[2] AND U. HERBIG[2]

[1]TU Wien, Inst. of History of Art, Building Archaeology and Restoration, Research Unit of Monument Preservation (doris.grandits@tuwien.ac.at)
denkmalpflege.tuwien.ac.at

[2] TU Wien, Inst. of History of Art, Building Archaeology and Restoration, Research Unit Building History and Building Archaeology (lukas.stampfer, eva.kodzoman, herbig@tuwien.ac.at)
baugeschichte.tuwien.ac.at

Keywords: Photogrammetry, Recording, TLS, Monitoring, hybrid methods in photogrammetry, Indonesian Temples

Abstract. *The Candis (temples) of Java represent sophisticated ancient building heritage and are key features for Javanese people to identify with their own culture. Candis occupy a significant position in the cultural history of Southeast Asia and rank among the most outstanding examples of Buddhist and Hindu architecture. Well-known Candis such as Borobudur or Prambanan are also top-ranked tourist destinations.*

This ancient heritage is threatened by Indonesia's geographical location within the Pacific Ring of Fire, a tectonic subduction zone prone to environmental catastrophes such as earthquakes, volcanic eruptions and the resulting tsunamis. Previous work presented a monitoring workflow for analysing variations in the geometry of these temples to gain an understanding of structural changes produced by seismic events. As part of that workflow, we proposed a combined laser scanning and UAV-supported image match point cloud model which can be compared to a photogrammetric data set in order to provide a quick, inexpensive, and easily accessible monitoring technique. While methodology has already proved useful, some aspects still need to be refined. Also, further understanding about the structural composition of the objects being examined and what changes of geometry can be expected within the analysis after earthquakes needs to be collected.

An analysis is presented of changes that have happened within the structure over a period of several years and numerous seismic events to facilitate an understanding of geometric changes that can occur. Furthermore, this re-evaluation by laser scanning will be compared to a set of image-match models to investigate factors that have an impact on the reliability and accuracy of such models. Manuals drafted by the project team and introduced in previous work explain how to capture image data to be processed into photogrammetric models. Amendments and revisions will be made to these manuals based on new data and experiences collected during the ongoing Candi Sari case study presented in this paper.

1 INTRODUCTION

1.1 Indonesia and its cultural heritage

Indonesia is the largest island state in the world, comprising more than 17,000 islands, and inhabited by about 240 million people. The island of Java, on which the capital Jakarta is located, is Indonesia's most densely-populated island, where more than 60% of all its inhabitants live. Indonesian culture is as diverse as the archipelago itself. In addition to its geographical characteristics, reasons for the diversity and richness of Indonesian culture are the variety of traditions and different religions that have always existed side by side.[1] Numerous temples and temple ruins also bear witness to this cultural wealth and to the island's history. These temples, known as *Candis,* occupy an eminent position in the cultural history of Southeast Asia and are among the most outstanding examples of Buddhist and Hindu architecture.

1.2 The *Candis* of Java

The term *Candi* is used to describe all Buddhist and Hindu temples in Indonesia. The highest concentration of temples is in the centre of Java. In the administrative districts of Yogyakarta Special Region and Central Java, there are some 280 of these monumental relics. Complexes on the *Dieng plateau* and at *Gedong Songo* are considered to be the oldest surviving permanent structures in Indonesia.[2] Well-known *Candis* such as *Borobudur*, one of the largest Buddhist temples, and the Hindu temples of *Prambanan* are also among the highest-ranking tourist destinations in Java. Both are listed UNESCO World Heritage Sites for their outstanding universal values (OUVs).

Most *Candis* have a square floor plan and are simple dry-stone constructions, although material composition can vary. Stone sizes also often differ, with side lengths usually ranging between 30 cm and 50 cm. Interior spaces, where they exist, are not intended to accommodate large groups of worshippers.[3] In terms of elevation, there is usually an architecturally accentuated tripartite division, consisting of a substructure which forms the basis, the wall zone, and the temple roof. The interior space is covered by a corbel vault, visible both on the inside and in the shape of a pyramid roof on the outside. *Candis* occur in different variations, often as a group of buildings with surrounding walls, gates and accompanying smaller temples. Their position within the landscape and their architectural design is determined by a series of socio-cultural, religious, and economic factors.

1.3 Earthquakes

The Pacific Ring of Fire, a tectonic subduction zone, is well-known for its tendency towards environmental catastrophes such as earthquakes, volcanic eruptions and the resulting tsunamis. In Indonesia, earthquakes scoring 5 to 6 on the Richter scale are an almost daily occurrence. In the past 100 years, 175 earthquakes with a strength of at least 7 have been measured in the Indonesian area.[4] A devastating earthquake of 6.2 Richter scale hit the region around

Yogyakarta in 2006, killing almost 5,700 people and completely destroying over 156,000 houses and other structures.[5] The large number of buildings destroyed reflects the high seismic vulnerability of existing structures. Several temple complexes were also damaged. There has been partial documentation of the damage to some of the more well-known temples such as *Prambanan*, which suffered severe damage.[6]

The preservation of the cultural heritage of such problematic regions is challenging and deserves a carefully-considered approach. Digital data recordings can help to virtually capture the current state of the monuments. In case of a natural disaster, this information can be consulted to assess the potential danger of collapse, or form the basis for reconstruction work.

1.4 Monitoring workflow

The high number of earthquakes means that especially the numerous smaller, lesser-known temples are at risk. Many of the sites have to be temporarily closed to visitors after an earthquake for safety reasons, which often results in large financial losses being incurred by many small local communities. In order to provide a simple and economical solution to enable continuous monitoring, a method for rapid, reliable and cost-effective monitoring and evaluation of the situation has been developed.

As part of a contribution to the *International Archives of the Photogrammetry, Remote Sensing and Spatial Information Sciences* (ISPRS-archives), a workflow for monitoring changes in the building structure of *Candis* after earthquakes was set up, with the aim of relaxing the prevailing situation and relieving the responsible authorities.[7] The workflow stipulates that a laser scan model is to be taken of each temple as a reference model which can be compared with further data sets, generated by photogrammetry, if necessary. Models are matched using iterative closest point algorithm (ICP) and compared for cloud to cloud distance. While adopting these algorithms is not in itself a novelty, this approach was chosen as it is a quick, simple and well-established technique which delivers sufficient accuracy. This also replaced the use of points measured using a total station, as the reliability of any physical reference on-site might no longer be guaranteed after an earthquake. Although matching datasets with cloud to cloud has its limitations, the inability to apply this algorithm properly due to clouds that are significantly different would in itself be an indicator for the necessity for more extensive investigations.

The laser scans and the preliminary work will initially be carried out as a joint effort by the *Vienna University of Technology* (TU Wien) and the *Universitas Gadjah Mada* (UGM), but as the project and knowledge transfer progresses, UGM will gradually take over the work. All further on-site applications should in any case be immediately feasible if necessary and therefore require simple explanation and handling. The implementation of local monitoring should then be within the competence of the responsible authorities in cooperation with UGM.

Whereas the above-mentioned ISPRS-contribution focused on describing operational and technical details about the workflow, the aim of this work is to elaborate steps taken to increase feasibility.

2 MATERIALS AND METHODS

2.1 Literature

There is some literature available concerning the *Candis* of Java. Numerous publications and case studies have been written about the great temples like *Borobudur* or *Prambanan*. In addition, there are some diploma theses and dissertation projects concerning *Candis*. Many of the studies focus on religious, cultic, and cultural structures in the context of the different temples.

2.2 Existing plans and documentation

Except for the well-documented temple complexes such as *Borobudur* or *Prambanan*, plans for *Candis* are scarce. Several building surveys were commissioned by *Balai Pelestarian Cagar Budaya Daerah Istimewa Yogyakarta* (BPCB DIY – Cultural Heritage Conservation Centre, Special Region Yogyakarta) in the second half of the 20th century. The results show ground plans and sections which show the outlines of the objects to a relatively high degree of accuracy, but information on the construction itself is either incomplete or missing. Furthermore, no detailed plans of reconstruction work or replacement of elements are available. Occasionally, there are abstract plans showing old and new elements. Also, since little is known about the construction of the temples, it is crucial to learn about their composition and the use of dry-stone construction methods to determine if the suggested monitoring process is applicable.

2.3 Case study

Candi Sari was chosen for the case study because its compact and almost completely intact structure can be considered an ideal example of a study object. For the purpose of verification of principles, *Candi Sari* represents an ideal object because it is free standing and accessible from all sides. It has an interior space with multiple rooms, limited vegetation in the surrounding area, and several openings interlinking interior and exterior data through visual connection between inside and outside. Point cloud data from the case study object is available from a terrestrial laser scan (TLS) made by the authors in 2016. In 2018, this was supplemented with a structure-from-motion (SFM) point cloud processing images captured with a drone. Both data sets are presented in the ISPRS-archives contribution. To further test the data, additional point clouds were collected in the summer of 2019, one again using a TLS, and the other with a model from images taken with a hand-held camera. This should help to check the previous models for mistakes and changes, and allow a detailed study of the monitoring process within one object.

2.4 Other *Candis*

In order to develop a comprehensive monitoring system for the Special Region of Yogyakarta, the data set needs to be expanded. During a workshop in 2017, participants from

the TU Wien and UGM worked in mixed teams on the documentation of *Candis*. In total, twelve temples were surveyed using a terrestrial laser scanner and photogrammetry. The number of *Candis* surveyed is sufficient for the first application tests but should increase further along in the project.

2.4 Guidelines for photogrammetry

The correct way of taking photos for SFM models requires a number of basic rules to be followed, which have been summarized in a manual proposed as part of the ISPRS paper. This should enable non-experts to take appropriate photos for processing sufficient data. The comprehensibility and practicability of the instructions should be tested on several volunteers for evaluation. The goal is to translate it into several languages to increase accessibility.

3 RESULTS

3.1 Building structure and seismic resistance of *Candis*

There is as yet no consistent documentation giving information about the material composition of the individual *Candis* and in any case, this can also differ between erection and restoration phases. Contrary to some of their counterparts in Indian stone architecture, which are carved entirely from solid rock, *Candis* are constructed using dry-stone walling without binding agents, with a number of different techniques for interlocking or binding the stone blocks to shape the temple[8].

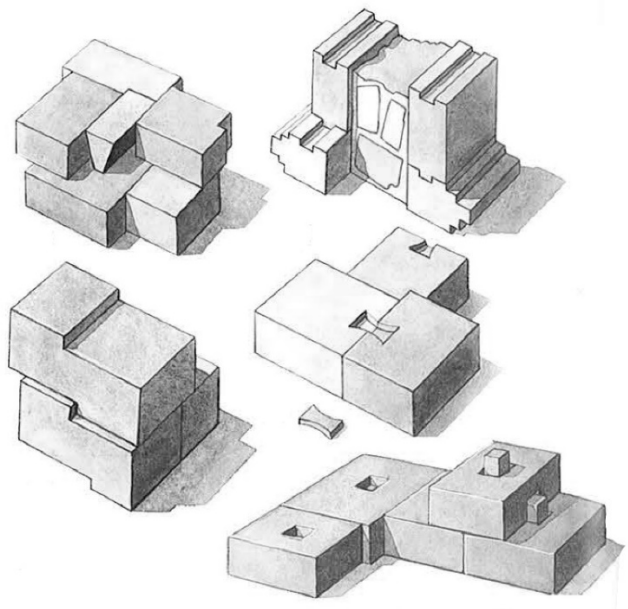


Figure 1: Different examples of interlocking stone blocks (John Miksic, 'Sources of Early Indonesian Stone Architecture', in Gunawan Tjahjono, ed., Indonesian Heritage (Singapore, 1998), p. 54.)

Later examples show the application of a shell and core principle, with stone blocks forming wall cheeks that are filled with rubble and/or unhewn stones held together by mud or sometimes lesser amounts of lime.[9] Without knowledge about a construction, it is difficult to predict how it would respond to an outside force such as an earthquake. In general, estimating seismic resistance for masonry constructions is a complex process. The inhomogeneous distribution of materials and irregular order of joints exceed the capabilities of a detailed calculation. As a result, conventional methods of determining earthquake resistance simplify the process to a great extent, thereby largely underestimating the structures' potential.[10] The amount of horizontal forces (as they occur during an earthquake) that can be absorbed in a masonry wall is directly impacted by the quantity of vertical forces such as weight, creating friction within joints. Depending on these vertical forces, scenarios can include either a failure of stones or failure of joints.[11] Methods to bind or interlink building elements with each other, as found in some *Candis*, would be advantageous, but make calculations even more complex. The undocumented extent of applying these constructional features appear to make a realistic or even acceptably simplified calculation of earthquake resistance for *Candis* impossible today.

In addition to the detail-specific observation of earthquake resistance, as described above, the geometry of a building has a strong impact on its behaviour during a seismic event. The ideal shape in terms of earthquake resistance would be to have a certain symmetry of shape. This criterion can be achieved by a structure having as many axes of symmetry as possible, ideally an infinite number. Therefore, in areas of increased seismic activity, a square or circular floor plan and a compact elevation that does not exceed a maximum height of less than 4-5 times the length of the sides can be beneficial (ideally, the ratio should be lower than three).[12] (E.g.: *Candi Banyunibo* 1.5; *Candi Gebang* 2.0; *Candi Kalasan* 1.5; *Candi Sari* 1.7) With their compact and symmetrical shape, a large, almost square base and not very extensive height, the general appearance of Javanese *Candis* appears positive in terms of earthquake resistance.

3.2 Reference model

As part of the contribution to the ISPRS-archives, as mentioned in the introduction, the process for acquiring a reference model for monitoring structural changes through seismic events was introduced. A base model with extensive coverage of the surfaces was collated for the case study object *Candi Sari*: this consists of a dataset of TLS point clouds supplemented by image-matching data from drone photography.

The results presented in the above-mentioned ISPRS paper allow an informed judgement regarding the usability of collected data as reference for a monitoring program for Javanese *Candis*. As shown within the analysis, the use of a combined laser scanning and UAV supported image-matching model should deliver proper accuracy and coverage which can be used as a reference model. The paper also presented the use of iterative closest point algorithm matching as a valuable tool for data combining, even in the absence of the possibility of measuring fixed target points that appear in both laser scanning and image matching data. Applying this workflow, a point cloud density with 50 to 70 neighbours within a range of 0.02m around a point in most areas, a suitable representation of the as-is state of the object was suggested.

3.3 Control models

As a second element to monitoring changes in Javanese *Candis*, procedures were discussed that would allow investigations to be conducted within a relatively short time-frame. These included the proposal to introduce and familiarize local temple staff and guards to the workflow and provide them with the necessary guidelines for effectively taking images that can be further processed into a 3D point cloud, using SFM. Observations from *Candi Sari* show that the quality of the images and choice of angles are essential to be able to achieve sufficient accuracy in the control model, to allow an assessment of the current state of the monument.

To determine the required quality for a model, several campaigns focused on the same case study object. As a result, the initial reference model, which used TLS from 2016 and UAV-supported SFM covering the roof structures from 2018, was supplemented by an SFM-model from a student workshop in 2017. In addition to the data presented in the ISPRS contribution, it was possible to include *Candi Sari* in another campaign in the area in 2019, thus delivering a second TLS-model and a high accuracy SFM-model.

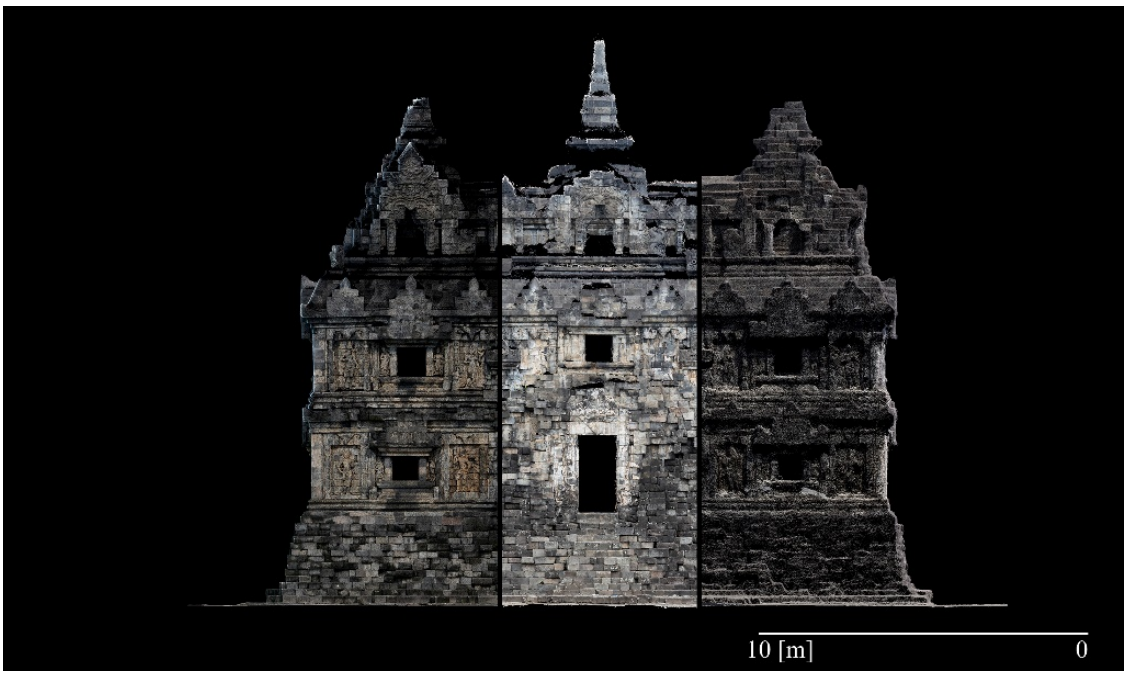


Figure 2: Point clouds from terrestrial laser scan, image-matching and drone image-matching

Using this data, we can now not only see the capabilities and limitations of image-matching for monitoring purposes, but also test for any shortcomings in the laser scanning process. Further, given that time has passed between capturing the different models, numerous earthquakes have impacted the structure.. This should allow the visualization of any changes that might have occurred by comparing two laser scanning models and check if image-matching would deliver sufficient information to pinpoint such changes.

3.4 Shifts and changes

A comparison of the 2016 TLS model and the 2019 SFM model showed some minor changes within the structure. Furthermore, using the 2019 TLS model, it was clear that these changes were not the result of shortcomings in the image-taking or image-matching process leading to the control model, but rather are actual structural changes in the monument. Although these are not considered to be the result of any seismic activity, but of human interaction with the object, they are at this point still seen as exemplary in determining the scale on which shifts within the structure could be discovered using the techniques proposed.

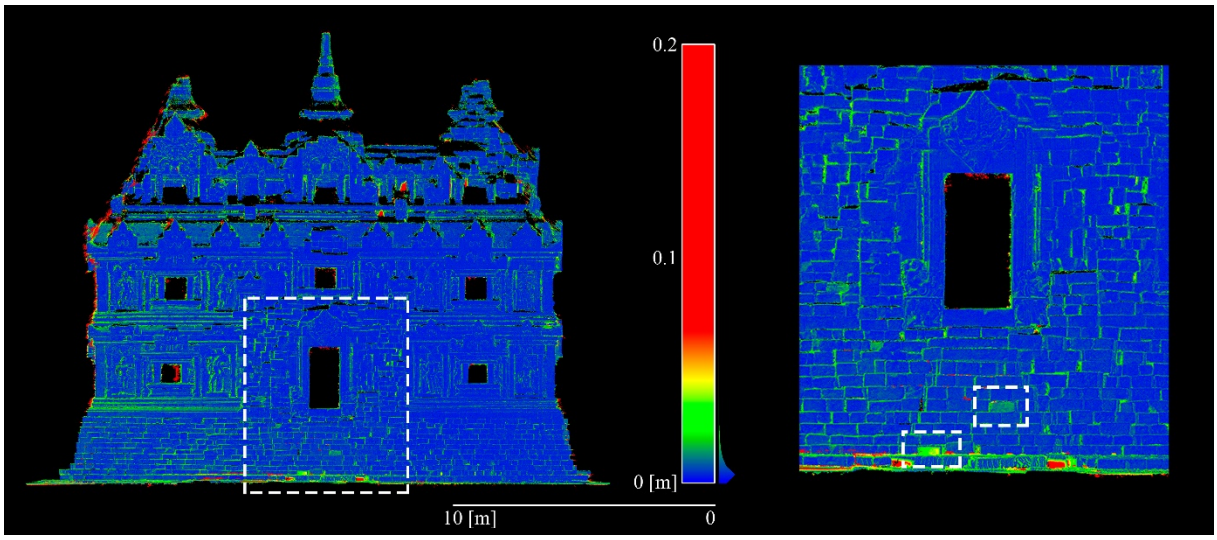


Figure 3: Shifts that become visible when calculating cloud to cloud distance between TLS 2016 and SFM 2019

The first of the shifts is rather extensive and easy to spot, as it is one loose stone block in the entrance area that has undergone some rotation on the ground (Fig. 3 & Fig. 4, lower left). The second movement that could be observed from comparing the 2019 SFM model with the 2016 TLS model was much smaller, but still visible in the false-colour elevation showing the cloud to cloud distances between the two point cloud data sets (Fig. 3 & Fig. 4, top right). Observing the same block in a horizontal section, the extent of the movement becomes apparent. In this case, the stone has moved about two centimetres and allows a rough estimation of what changes could be recognized using the proposed technique. Again, a comparison of the old and the new TLS dataset was used to prove that the observed shift was not the result of a procedural inaccuracy, but an actual movement of one element in the structural composition.

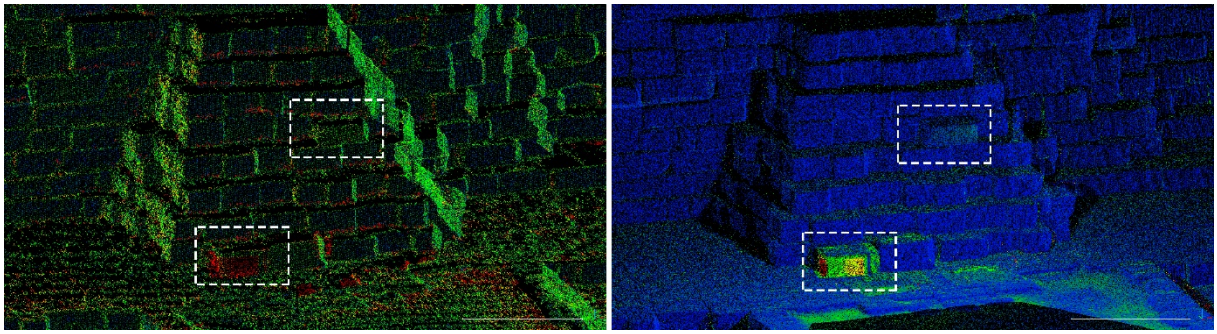


Figure 4: Three-dimensional point cloud representations of shifts and changes - SFM 2019 and TLS 2016 (left); TLS 2019 and TLS 2016 (right)

3.5 Data from student workshop

Data collected during the above-mentioned student workshop was further analysed to determine a specific workflow and key factors during post-processing that could facilitate the generation of digital models of *Candis*. In order to comply with the proposed methodology, reference models using drone SFM and TLS were connected using targets (measured points for connecting different data sets), while procedures investigated for application in collating control models had to rely solely on ICP point cloud matching. In several of the examples which were analysed, the reflective laser scanning targets (5cm diameter) were used to link photogrammetric UAV and TLS data for reference models. As a result, it was difficult to determine the centre, and thus this form of photo registration proved unfavourable. In these examples, the reflectors were ignored after all and registration was done without them.

In some of the examples analysed, drone photography was performed using only ground targets that were not included in terrestrial photos, and for this reason it was impossible to register the roof and wall data of the temple using targets. In these cases, again, ICP matching needed to be applied. Some examples even failed cloud to cloud matching, as TLS point cloud density was insufficient in overlapping areas (e.g., *Candi Ijo*).

The photogrammetric connection between indoor and outdoor areas proved to be particularly difficult during capturing control models. In some cases, it was not possible to accurately merge the parts into one model. To avoid this situation, it would be necessary to position a minimum of four targets that are visible from both perspectives. Since the proposed workflow does not include the measuring of points, but focuses solely on the use of SFM, an alternative needs to be sought. While it would be possible to use ICP matching to link interior and exterior areas to the reference model separately, this could prove a disadvantage for recognizing structural changes. Further problems occurring during photogrammetric capturing included an insufficient number of pictures, the mixture of landscape- and portrait format or different cameras, as well as pictures taken in unfavourable lighting conditions (e.g., at sunset).

While the insufficient data quality of some *Candis* led to difficulties during post-processing, data from other *Candis* proved that by using adequate capturing procedures, the suggested workflows can successfully generate the expected results. With *Candi Banyunibo*, all point clouds were successfully matched, and the required plan data was generated.

3.6 "Easy handle manual"

As was demonstrated, the usability of images for creating SFM models depends largely on the quality of the pictures as well as the proper choice of angles from which those images are taken. Therefore, it was clear that instructions for the capturing process needed to be developed. A so-called "Easy handle manual" was drafted to graphically explain the process. Based on existing work as promoted by the *International Committee for Documentation of Cultural Heritage* (CIPA),[13] instructions given for common SFM software, and personal experience, the manual is intended to introduce the procedure to non-experts step by step. To overcome cultural and language barriers, the manual provides illustrations for each of these steps and was made available in German, English and Indonesian.

Originally, the aim was to test this manual on volunteers, and to present the results as part of this paper. Unfortunately, this was not possible due to environmental conditions on site.

4 DISCUSSION

4.1 Surface comparison for monitoring

Calculation methods alone seem to be insufficient to provide an adequate representation of the flow of forces through the construction. In addition, data regarding the building elements used to assemble a *Candi* is often unavailable or has not been documented for the specific monument. Therefore, it is clear that other methods to track structural changes need to be found, as the different means of erecting a *Candi* and the different methods of linking and interlocking blocks are too complex. We therefore propose the monitoring of movement within the structure and observation of material failure within the stonework as appropriate methods for monitoring the impact of earthquakes on Javanese *Candis*. One example, discussed in the previous section, demonstrates that the new workflow enables the displacement of a stone by not more than 2 cm to be recorded (compared to a SFM-based control model with a TLS reference model (Figure 3 & Figure 4)). The question is whether this is sufficient to assess the structural stability of a *Candi* after a seismic event. It is believed that, given the common constructional techniques (despite variations) and average size of building elements, the workflow would prove to be a valuable tool for a preliminary assessment.

4.2 Limitations

Although, as mentioned, models from images taken in ideal conditions have shown good capabilities for capturing structural shifts, they are still largely dependent on two factors, one being the ability and level of skill of the person acquiring the images. Despite providing a manual, or even instructing on-site personnel on how to collect such images in case this is necessary, it is uncertain whether the resulting data will be usable. Therefore, this component of the proposed workflow should be the one given the greatest attention during the next steps of the project – as is currently the case. Image-quality remains a factor difficult to control, as it is uncertain what kind of devices might be available at the time an assessment is needed.

Another area that remains under-investigated in this work in its current state is the monitoring of interior spaces in *Candis*. Since most of them are small, with few or no windows or artificial light sources, the possibilities to use photogrammetry for monitoring the interior spaces certainly needs closer investigation and maybe even amendment of the monitoring procedure.

5 CONCLUSION

Although the proposed monitoring workflow is in theory already fit for purpose, there are still steps to be taken to assure the quality of assessment and enable correct implementation. Primarily, the process of capturing control models needs to be explored further and the manual critically tested and amended to ensure photogrammetric data can be captured as and when needed. Moreover, a more extensive network of reference models for *Candis* must be built up. A priority list should be compiled according to the policy and judgement of those in charge. It is the intention of the authors of this paper to provide and improve the workflow, as necessary, but not to be the monitoring instance. Therefore, it is crucial to explore how the local authorities (who are already involved) can best take over the main tasks of continuously capturing and managing reference models, with the TU Wien taking a step back and limiting itself to a supporting and advising role.

All investigations done so far to challenge the applicability of the proposed workflow indicate that a usage for tracing changes in Javanese *Candis* should be possible. We aim to continue and expand our research until we can provide a comprehensive workflow that reliably helps to monitor the state of Javanese *Candis* and allows a rapid assessment of these economic drivers when they have been impacted by seismic events.

REFERENCES

[1] Risda Asfina and Ririn Ovilia, 'Be proud of Indonesian cultural heritage richness and be alert of its preservation efforts in the global world', Humanus, 15 (February 2017), p. 198.
[2] John Miksic, 'Sources of Early Indonesian Stone Architecture', in Gunawan Tjahjono, ed., Indonesian Heritage (Singapore, 1998), p. 54.
[3] John Miksic, 'Sources of Early Indonesian Stone Architecture', in Gunawan Tjahjono, ed., Indonesian Heritag (Singapore, 1998), p. 54.
[4] U.S. Geological Survey, 'USGS Earthquake Hazards Program', USGS Earthquake Hazards Program (January 2020),.
[5] Amr S. Elnashai, 'The Yogyakarta earthquake of May 27, 2006' (2007), p. 7.
[6] Amr S. Elnashai, 'The Yogyakarta earthquake of May 27, 2006' (2007), p. 42.
[7] U. Herbig, L. Stampfer, D. Grandits, I. Mayer, M. Pöchtrager, Ikaputra, and A. Setyastuti, 'Developing a monitoring workflow for the temples of Java', Int. Arch. Photogramm. Remote Sens. Spatial Inf. Sci., XLII-2/W15 (August 2019), pp. 555–562.
[8] Jacques Dumarcay, 'Buddhist Architecture of Central Java', in Gunawan Tjahjono, ed., Indonesian Heritage (Singapore, 1998), p. 56.
[9] Jacques Dumarcay, 'Indonesian Methods of building with stone', in Gunawan Tjahjono, ed., *Indonesian Heritage* (Singapore, 1998), p. 57.
[10] Konstantin Meskouris, ed., Bauwerke und Erdbeben: Grundlagen - Anwendung - Beispiele (Wiesbaden, 2011), p. 469.
[11] Meskouris, ed., Bauwerke und Erdbeben, p. 470.
[12] Adrian Pocanschi, Kräfte in Bewegung : die Techniken des erdbebensicheren Bauens (2013), p. 344 f.
[13] P. Waldhäusl, C. Ogleby, J.L. Lerma, and A. Georgopoulos, '3 x 3 rules for simple photogrammetric documentation of architecture' (2013); P. Waldhäusl and C. Ogleby, '3 x 3 rules for simple photogrammetric documentation of architecture', ISPRS - International Archives of Photogrammetry and Remote Sensing, 30 (1994), pp. 426–429; Peter Waldhaeusl, 'Photogrammetric Heritage Recording: Standard and Emergency Approaches', APT Bulletin, 26 (1994), p. 20.

12th International Conference on Structural Analysis of Historical Constructions
SAHC 2020
P. Roca, L. Pelà and C. Molins (Eds.)

DIAGNOSIS OF AN UNUSUAL STRUCTURAL INSTABILITY: THE CASE STUDY OF THE CATHEDRAL OF SAN LORENZO IN VITERBO

M.CANDELA[1*], M.EICHBERG[2], C.TARANTINO[1]

[1]Studio di Ingegneria Michele Candela,
via Circumvallazione 76, 83100, Avellino, Italy
e-mail: ing.mcandela@libero.it; arch.cristarantino@gmail.com

[2]Soprintendenza archeologia, belle arti e paesaggio per l'area metropolitana di Roma, la provincia di Viterbo e l'Etruria meridionale
via Cavalletti 2, 00186, Rome, Italy
e-mail: sabap-rm-met@beniculturali.it, web page: http://www.sabap-rm-met.beniculturali.it/

Keywords: Historical Building, Masonry, Tensile Crack, Thermal Variations, FE Analysis

Abstract. *The cathedral of San Lorenzo is a Romanesque church sited in Viterbo (Lazio, Italy), founded in the XII century on a site characterized by a complex archaeological stratification. The building is a fine example of religious monumental architecture, built upon well-laid masonry walls, made of squared blocks of piperine stone and very thin layers of mortar.*
Its basilica-shaped plant is divided into three aisles by two rows of marble columns connected by arches. The structure, that has undergone many transformations during the centuries, was severely damaged during the II world war and a restoration executed in 1947 has brought it back to its romanesque appearance.
Currently, a peculiar crack pattern can be observed in the structures, which is mainly characterized by recurring sub-vertical fissures appearing on the keystones of the arches that run along the central nave.
The purpose of this paper is to illustrate the diagnostic path which enabled to rule out the most common damage mechanisms, as a main cause of the damages, and led to the identification of the most probable cause for the instabilities.
A critical reading of the geometry of the cracks, supported by several static verifications, resulted in the exclusion of mechanisms associated with the arches thrust actions or with the compressive stresses in the walls. The hypothesis of soil settlement is rejected by the mechanical characteristics of the foundation soil, provided from a previous study.
An original diagnostic hypothesis of tensile stresses induced by thermal variations is formulated and a fully coupled temperature-displacement analysis is carried out, with the FE software Abaqus, to investigate the effects of the thermal gradient on structures behavior.

1 INTRODUCTION

The history of structural damages in historical constructions went hand in hand with the evolution of constructive systems. The rise of new structural conceptions has been constantly followed by the occurence of new unknown instabilities, which highlighted the lacks of its design [1].

Based on this experience, a specific technical discipline developed, which provides advanced analytical methods for the diagnosis of the structural instabilities and new systems for classifying the recurrent damages [2]. In this regard, the damage schemes referable to masonry splitting, to foundation settlements and other phenomena affecting the masonry structures are well known [3]. Not infrequently, it is possible to find these damage schemes combined together in the same building. Yet, a keen eye is still able to distinguish them and assess their prominence.Nevertheless, there are cases, as that of the Cathedral of Saint Lorenzo, where the well known patterns are not identifiable and hence the diagnostic methodology has to proceed by steps, through studies and investigations that progressively lead to the exclusion of the main damage mechanisms.

Based on these considerations, this study presents the diagnosis path that led to the identification of the probable, and unusual, cause of the buiding instability.

The object of study is the cathedral of Viterbo (fig.1), a fine example of monumental religious' architecture. The building is affected by a peculiar crack pattern which develops along the main nave walls. On the base of the correspondence between damage intensity variations and temperature distribution along the walls, the hypothesis of thermal variations inducing tensile stresses is formulated. A fully coupled temperature-displacement analysis is carried out with the FE Abaqus software to investigate the behavior of the walls under thermal variations.

In section 2 a building description is provided, together with historical and context information; Section 3 illustrates the crack pattern and the in site inspections; The FE model and the results of the analyses are presented in Section 4.



Figure 1: The Cathedral of Saint Lorenzo. View from the square outside.

2 THE CATHEDRAL OF SAINT LORENZO

2.1 Description of the monument

The Cathedral of Saint Lorenzo lies on the highest hill of the city of Viterbo (Lazio,Italy), known as the "City of Popes", since it hosted the papal seat between 1257 to 1281.
The building was founded in the XII century on the remains of an ancient roman temple.
The original core, in romanesque style, had a limited extension. The current layout is the result of numerous transformations and enlargements related to the increase in importance of the site over the centuries.
A transept was added in 1192. The romanesque facade was demolished in the 1570 and replaced with a new one in renaissance style[4]. During the XVII century, a new baroque skin was given to the inside of the building and vaulted structures were built on the aisles spans to hide the timber structures of the roofs.
Severe damages were caused by the bombing of the II world war and significant restoration interventions were carried out which canceled the stratifications and brought the building back to its romanstyle shape [5].
The current layout of the building shows a typical basilica scheme with three aisles, a transept contained in the building width and three ending apses (fig.2).
The three aisles develops for eleven spans, scanned by monolitic columns in piperine stone and marked by double ring round arches, which separates the central aisle from the lateral ones.
Over the arches, two walls elevate themselves beyond the lateral aisles roofs, defining the central nave space. A protruding cornice, supported by corbels, runs along these walls, dividing the nave arcade from the clerestory.
The cathedral has a total lenght of 60 meters and covers a 20 meters width. The nave is 35 meters long and 22 meters high at the top of the truss roof, while the aisles reach the height of 11 meters. The masonry walls, with an average thickness of 1,00 m, are made of squared blocks, in piperine stone and thin layers of mortar. The central nave has a truss roof, while the aisles are covered by a single pitch timber roof. The foundation structures are of the shallow typology.

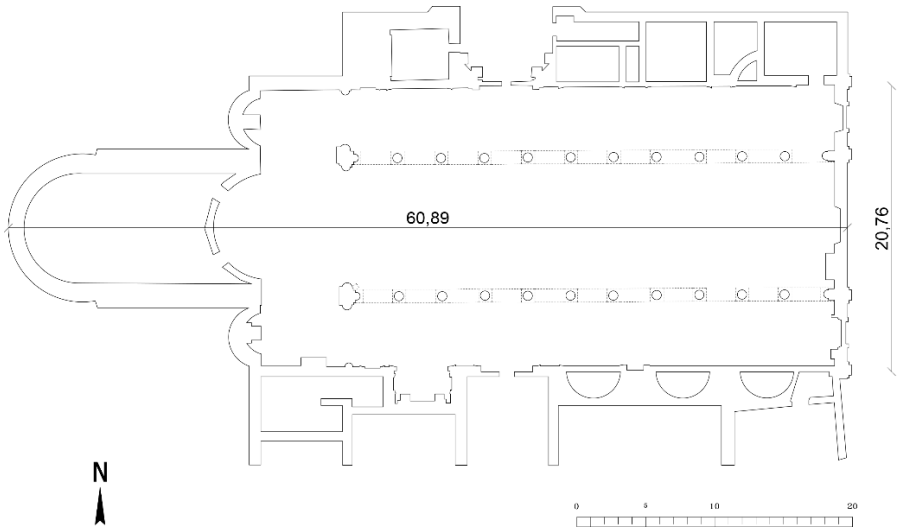


Figure 2: The Cathedral plan (dimensions in meters).

2.2 The foundation soil

The geomorphology of the site where the Cathedral is settled is characterized by the presence of volcanic formations from the Vicano district.
In particular, the formation named “Unità del tufo rosso a scorie nere del Vicano”is detectable, with thickness vary between 5 and 30 meters. Anthropic caves are detectable.
The formation is a reddish coloured tuff, with black slags made of lapillus, light plinian pumice and pyroclastic flow deposits.
The bedrock shows the following Geotechnical characteristics: 1,9 g/cm3 weight in the unit; 1,9 – 2,0 N/mm2 compressive strength; 1,7 kg/cm2 tensile strength. The values are compatible with the load conditions. Differing from the loose soils, which are susceptible to compaction under load also in the long term, this bedrock is not prone to sagging phenomena. Small displacements can only occur contextually to the application of the load. Thus, considering the long time passed since the cathedral construction, there are low probabilities of the occurance of absolute or differential settlements in the recent time.

3 THE DAMAGE SURVEY AND DIAGNOSTIC TESTING

3.1 Description of the crack pattern

The building exhibits a peculiar crack pattern which exclusively affects the high walls bounding the central nave. The damage occurs at half height of the walls and, specifically, at the level of the arches separating the aisles, where sub-vertical fissures recurrently appear in the proximity of the keystones (fig.3). The cracks start at the intrados of the arches and rise up for few meters, disappearing immediately after the cornice adorning the walls. The damage doesn't involve any fracture of the stones and the cracking path follows the arrangement of the mortar lines.



Figure 3: Lesions on the arches keystones along the nave wall.

To a close observation, the fissures'edges appear coplanar and aligned. This configuration corresponds to a horizontal displacement between the two portions of the wall the crack separates, and it can be possibly caused by a tensile stress, developing into the plane of the wall and acting parallel to its longitudinal axis.
As acknowledged by scientific literature and professional experience, this mechanism is characteristic of some recurrent phenomena: crushing, combined bending and axial loading, foundation settlements with a horizontal component [6].
The first two conditions can be excluded, considering the magnitude of the loads, the stress paths in the walls and the mechanical characteristics of the masonry structures investigated through in-site inspections.
The hypothesis of a foundation settlement is incompatible with the extension of the damage, limited to a confined area of the wall, and with the cracks' constant amplitude. Moreover, it would be inconsistent with the geomorphology of the site and the characteristics of the soil analysed by previous geognostic studies.
A correspondence between the variation of damage's intensity and that of the walls thermal conditions can be observed. The crack pattern shows a symmetry in its localization but is prominent in the south wall with respect to the north wall. The damage concentrates in a border region beween two areas characterized by different thermal conditions: the upper clerestory, highly exposed to the solar radiation, and the arcade below, protected by the aisles' roofs.
Based on these considerations, it appeared appropriate to make the assumption of the presence of tensile stresses, induced by a thermal gradient developing in the plane of the nave walls (fig.4).

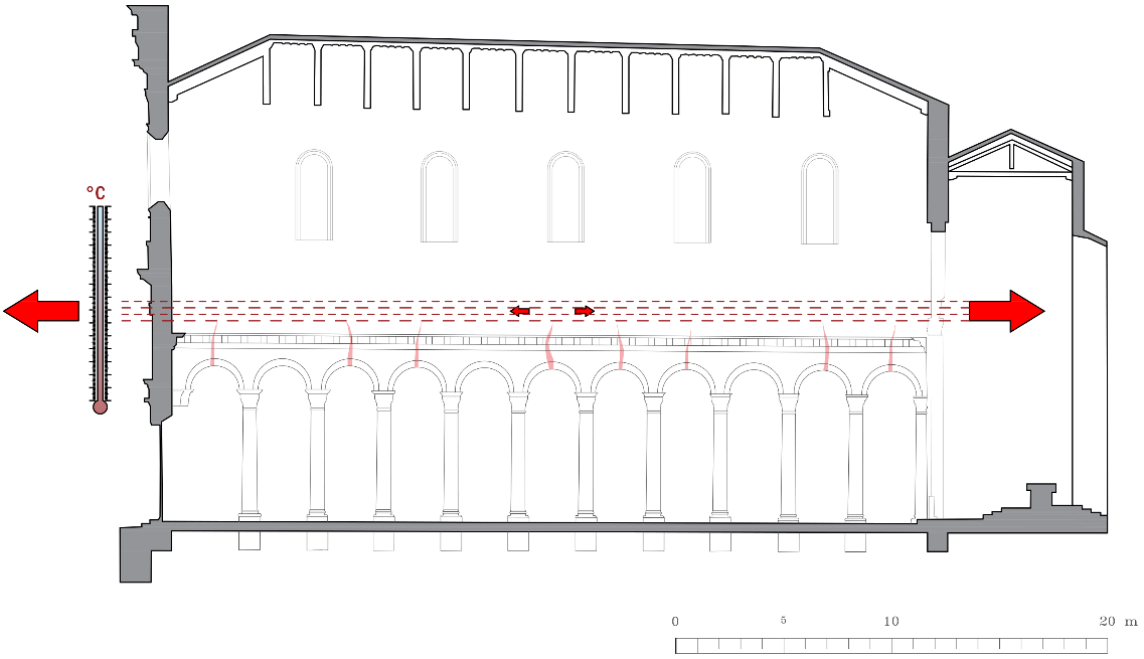


Figure 4: Longitudinal Section of the cathedral. Scheme of the effect produced by the thermal gradient inside the nave wall.

3.2 In-site inspections and material characterization

Based on the hypothesis of damages induced by thermal variations, a diagnostic campaign of non destructive tests has been planned.
Ultrasonic tests were performed to estimate elastic and mechanical characteristics of the masonry. As it is known from scientific literature, the recurring values of ultrasonic pulse velocity, referred to masonry, range between 1000 and 2000 m/s. Velocity values lower than 1000 m/s reveal the presence of fractures or voids in the thickness. Values higher than 2000 m/s are attributed to well constructed masonry, endowed with high compressive strenght values.The average value of velocity measured on the two walls is 3100 m/s.
Estensimetric tests were executed to assess the stress conditions in the walls affected by the damage. Eight tests were performed in the proximity of the arches keystones, selecting the most damaged spans of both the walls. Each test has consisted in the measurement of the stresses value in the horizontal direction in two points vertically aligned: the first at the arch intrados, the second close to the cornice. The two walls are characterized by different stress conditions. Except for the damaged areas, in the north wall the horizontal compressive stresses values vary but are constantly detected. On the south wall the values of the compressive stresses are significantly low near the cornice and frequently vanish at the arches' intrados. This result highlights that there are tensile stresses acting in the region between the arches and the cornice, where the thermal variation is greater.
Temperature measurements were carried out to estimate the thermal gradient along the wall's height and between the external and the internal face. The measurements were taken on the south wall, which is the most exposed to solar radiation (fig.5), in the month of August, during the warmer hours.The results are reported in Table 1.



Figure 5: Satellite view of the cathedral and schematization of the sun path.

Table 1: Inside and Outside temperature values (°C) on the south wall, at different heights.

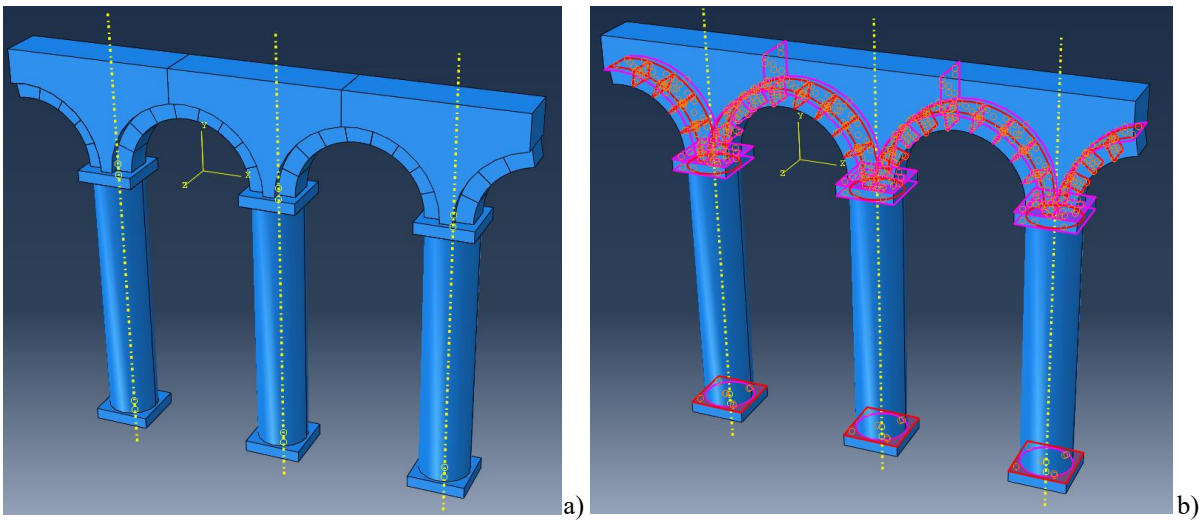
Height (m)	TEMPERATURE (°C)			
	12.00 am		1.15 pm	
	Indoor	outdoor	Indoor	outdoor
18.00	26,6	32,0	27,5	39,0
16.00	26,8	32,4	27,3	39,0
13.00	26,6	32,5	27,2	38,8
11.80	26,7	32,2	27,2	38,8
8.00	26,5	-	27,1	-

4 FULLY COUPLED TEMPERATURE-DISPLACEMENT ANALYSIS

The analytical study of the Duomo of Viterbo colonnade behavior under thermal excursion is carried out using the Abaqus v.6.14 Finite Element software. A numerical model is implemented on the basis of the real geometric dimensions of the columns, arches and walls of the colonnade, as well as on their constitutive materials, represented by *piperino of Viterbo* stones for columns, walls and arches. Mechanical characteristics of materials are derived from the Italian Standard [Circular no. 7 of 21/01/2019] using a LC2 confidence factor. Table 2 summarizes the mechanical characteristics used.

Table 2: Mechanical characteristic: w specific weight; E elastic modulus; α thermal expansion coefficient; υ Poisson's ratio; λ thermal conductivity; c specific heat.

Masonry type	w [kN/m^3]	E [N/mm^2]	υ [-]	α [1/°C]	λ [W/m·°C]	c [kJ/Kg·K]
Piperino	21,0	5500	0,5	0,6x10^{-5}	0,4	1,3



a) b)

Figure 6: The FEM model of the colonnade portion considered (a) and constraints among masonry parts (b)

In the modelling phase, a significant portion of the colonnade, consisting of three columns inferiorly and superiorly supported by masonry bases, two arches and a part of masonry wall above arches, is considered. All the FE model parts are modelled with C3D8R brick elements. The masonry arches are modelled as individual ashlars, while columns and masonry bases and wall are considered as unique finite elements (Figure 6a). Columns are superiorly and inferiorly constrained to the masonry bases by a "tie" contact; the arches are connected to the walls by a surface-surface contact (Figure 6b), where "hard" contact in case of axial loads is considered and friction and thermal coefficients of 0.5 and 1, respectively, is used. Also, ashlars are connected to each other by means of the surface-surface contact above described.

The structure is fixed to the ground through fixed supports; in order to simulate the colonnade continuity, also the two end parts of the colonnade are fully restrained (Figure 7).

A distributed load is applied at the top of the masonry wall above arches aiming at considering the actions deriving from unmodelled elements, such as the upper masonry wall and the above roof (Figure 8). A further boundary condition is considered, namely the temperature of the external and internal faces of the wall.

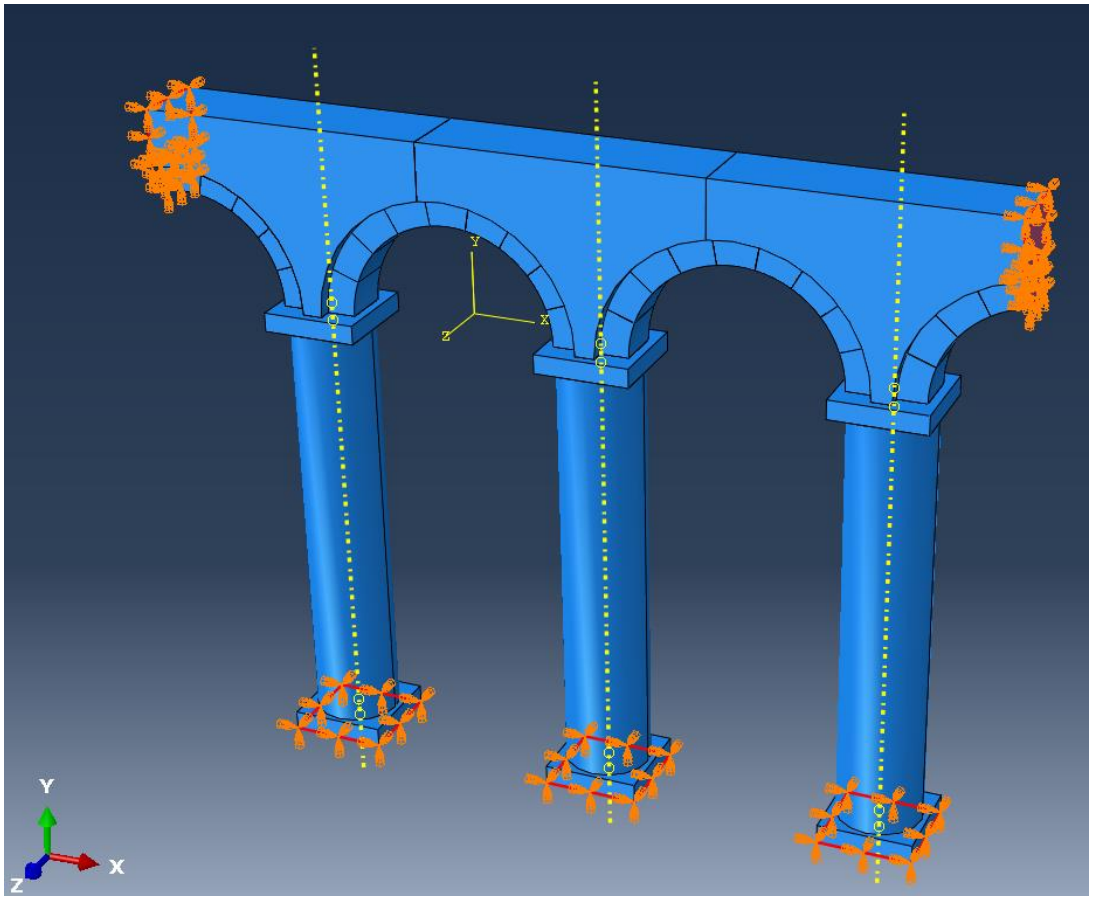


Figure 7: Restraint conditions of the FEM model.

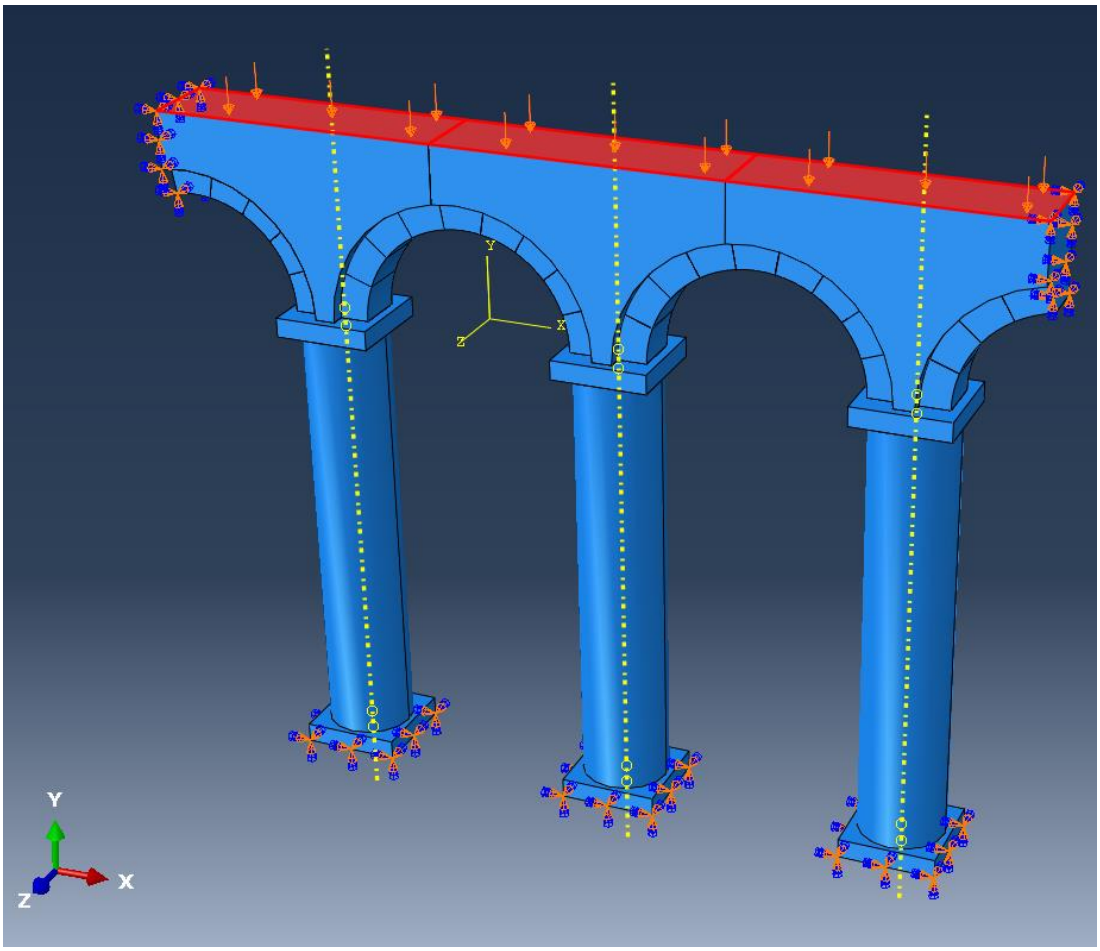
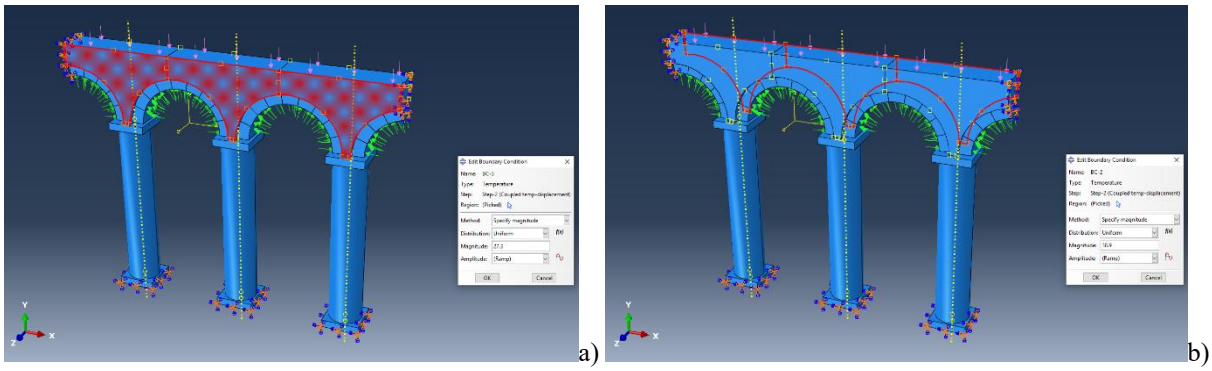


Figure 8: Loads applied on the top surface of the colonnade to simulate the presence of the above wall and roof.

Temperature values on these faces, namely 38.9°C on the external face and 27.3°C on the internal one (Figure 9), refer to the experimental data recorded inside and outside the church in the summer season. These values have a subsequent digression up to the winter conditions, where internal and external temperatures are approximately assumed as equal to 11°C and 0°C, respectively. In addition, a heat flux of 10 °C from the bottom to the top, which propagates between arches and the above wall, is considered. The colonnade parts are discretized with a mesh having side length of 10 cm (Figure 10), which guarantees the best accuracy of results with the minimum analysis time.

The numerical analysis takes place through two consecutive steps. The first step concerns a "static general" analysis, where the colonnade behavior subjected to the self-weight and the distributed loads coming from the above wall and roof structures is studied. The second step deals with a "fully coupled temperature-displacement" linear analysis. This type of analysis is chosen because stress analysis is dependent on the temperature distribution in the structure and the temperature allocation depends on the stress solution. The numerical analyses are developed by Newton's partial derivative resolving technique and direct iterative method, dividing the analysis time into amplitude increments equal to 0.1 s.



a) b)

Figure 9: Temperature fields applied on the internal (a) and external (b) sides of the structure.

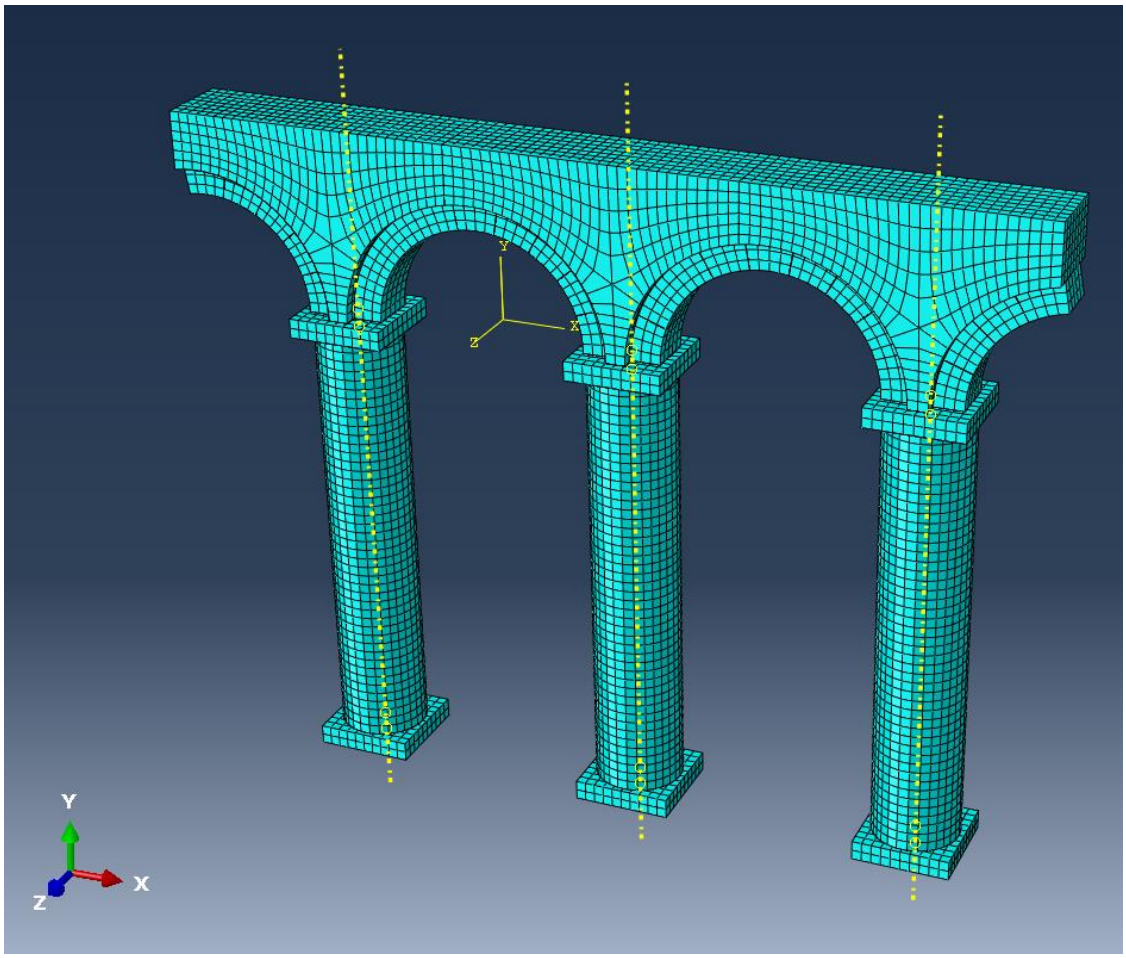
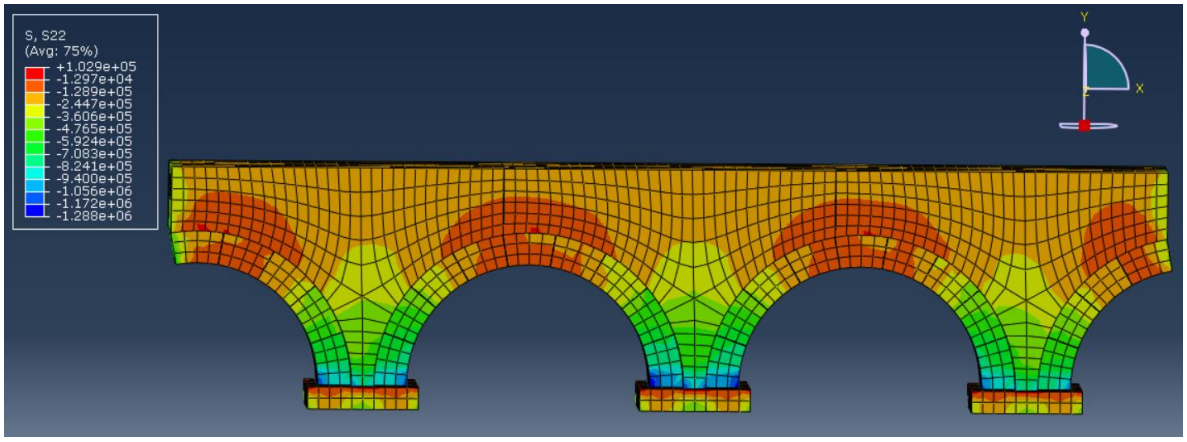


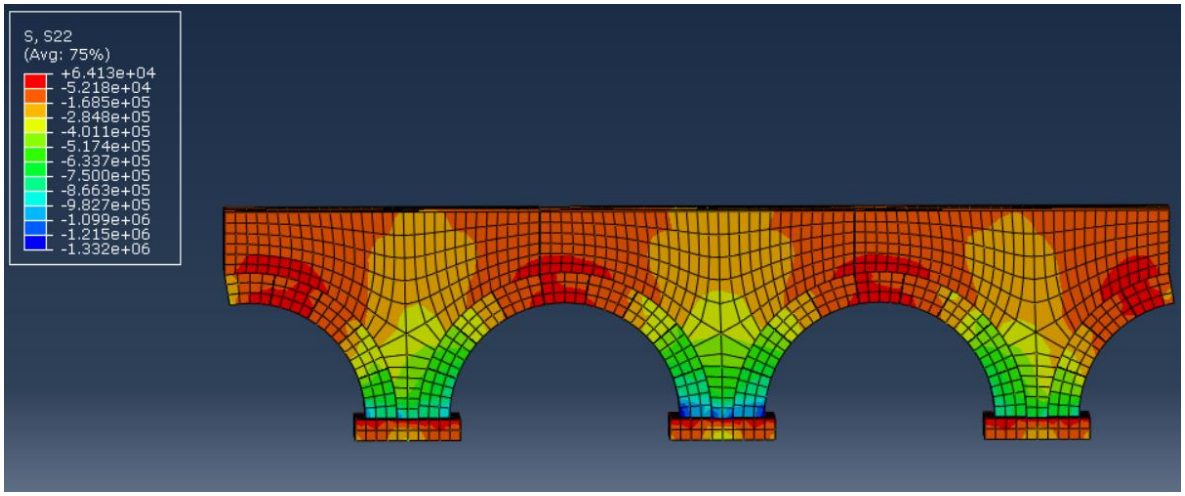
Figure 10: The discretization of the colonnade FEM model.

The results of the numerical analyses on the colonnade FEM model with reference to the summer and winter conditions are depicted in Figure 11, where a focus on the stress distribution in the model part represented by arches and upper wall only is made.

Results of Figure 11a show that in the hot season a concentration of tensile stress with more or less the same magnitude of 1,297 x 10^4 N/m^2 (0,01297 MPa) occurs in the central part of arches and in the above wall. Such a result is very close to the one attained under experimental way in the church, where in the arch internal side a tensile stress of 0,01 MPa activating the cracks in the mortar joints is detected. This means that the orange area observed in Figure 11a represents a potential damage zone where a crack pattern could develop. Contrary, in winter condition (Figure 11b), it is noted that, as temperatures decreases, tensile stresses values increase in intensity, but the extension of the masonry zone subjected to tensile actions is reduced. As a result, in the cold season, the cracks tend to diminish their size with respect to those developed in the summer period.



a)



b)

Figure 11: Stress distribution in the structure in summer (a) and winter (b) conditions.

4 CONCLUSIONS

In this paper the damage analysis of the cathedral of Saint Lorenzo in Viterbo is presented. The building is a religious monumental architecture from the XII century, built upon well-laid masonry walls, made of squared blocks of piperine stone and very thin layers of mortar.
The structures exhibit an unusual crack pattern, concentrated along the nave walls, not referable to classic and most common damage mechanisms.
Based on the correspondence between damage intensity variations and temperature distribution along the walls, an original hypothesis of tensile actions induced by thermal variations has been advanced. A Finite Element analysis was carried out with the FE software Abaqus v.6.14 to investigate the behavior of the masonry walls under thermal variations, in both cases of the summer and winter radiation.The results of the analyses are in good agreement with the stresses values measured in the experimental tests and the existent damage scenario.
The reason of the occurrence of this damage in Saint Lorenzo Cathedral, and not in other buildings with same orientation and similarly exposed to solar radiations, lies in the quality of the masonry and the stones composing it. Due to the high strength of the piperine stone and the poor presence of mortar, the masonry shows a low ductility, needed to dissipate the thermal actions, and behaves as a wall of rigid blocks. This mechanical behavior, extended to the whole length of the walls produces the observed damage.
The reason of the recent occurrence of the cracks, although the building has been always exposed to solar radiation, is to be found in the increase of the average stagional temperatures, traceable to the recent climate changes.

Acknowledgements. The Authors acknowledge: Eng. Antonio Formisano, Eng. Generoso Vaiano and Nicola Junior Petrucci, who contributed to develop the numerical analyses; Roberto Delgado, Gerardo Antoniello, Giuseppe Cicala and Eng. Alfredo Galasso, who worked on the in-site inspections and surveys; Arch. Federica Cerroni from the Archeologic, Fine Arts and Landscape Superintendence of Rome municipality, for the technical support in the study of the cathedral.

REFERENCES

[1] Benvenuto, E., *La scienza delle costruzioni: e il suo sviluppo storico*. Firenze: Sansoni (1981).

[2] Sparacio, R., *La scienza ed i tempi del costruire*, UTET Università (2012).

[3] Heyman, J., *The Stone Skeleton: Structural Engineering of Masonry Architecture*, Cambridge: Cambridge University Press (1995).

[4] Valtieri, S., Bentivoglio, E., *Viterbo nel Rinascimento*, (2012).

[5] Egidi P., L'Archivio della cattedrale di Viterbo. In: *Bollettino dell'Istituto Storico Italiano e Archivio Muratoriano*, Roma: Sede dell'Istituto Palazzo dei Lincei 28 (1906), pp 7-381.

[6] Mastrodicasa, S., *Dissesti statici delle Strutture Edilizie*. Milano: Hoepli, (2006).

12th International Conference on Structural Analysis of Historical Constructions
SAHC 2020
P. Roca, L. Pelà and C. Molins (Eds.)

DOCUMENTATION AND STRUCTURAL APPRAISAL OF THE MEDIEVAL MANOR OF POTAMIA, CYPRUS: AN INTERDISCIPLINARY APPROACH

ROGIROS ILLAMPAS[1*], DIOMEDES MYRIANTHEFS [2], DORIA NICOLAOU[3], VASILIKI LYSANDROU[3], MARIA PHILOKYPROU[2], GEORGE PAPASAVVAS[3] AND IOANNIS IOANNOU[1]

Departments of [1]Civil and Environmental Engineering, [2]Architecture and [3]History and Archaeology
University of Cyprus
University of Cyprus, 75 Kallipoleos Street, P.O. Box 20537, 1678 Nicosia, Cyprus
e-mail: rilamp01; myrianthefs.diomedes; nicolaou.doria; lysandrou.vasiliki; mphiloky; georgep; ioannis @ucy.ac.cy,
www.ucy.ac.cy

Keywords: Historical Structure, Masonry, Monitoring, Non-Destructive Inspection

Abstract. *This paper aims to present, via a case study, an interdisciplinary approach towards the comprehensive analysis of historic constructions. The case study monument examined is the Medieval Manor of Potamia in Cyprus. The work hereby presented was based on a collaboration between scientists from the fields of archeology, architecture, materials science/ conservation and structural engineering. A thorough review of historical sources was initially carried out in order to obtain data concerning the history and construction development of the Manor. Extensive field work was undertaken to study the architectural typology and construction detailing of the structures and to explicitly map the various agents of pathology. For the characterization of the historic fabric, masonry materials were sampled and studied at the laboratory. The accumulated data facilitated the development of a Finite Element (FE) model, which was used to numerically assess the structure's seismic response.*

1 INTRODUCTION

The paper reflects on practical applications of interdisciplinary collaboration in the context of historic building preservation. An operational procedure for the analysis of such heritage constructions is hereby presented through the case study of the Medieval Manor of Potamia in Cyprus. The Manor is a composite building complex that incorporates stone and adobe masonry structures dating from the 14th to the 20th century. Although the west part of the building complex has rather recently been restored, the east part remains in a ruinous condition. Detailed investigations for the documentation and structural appraisal of the Manor's east part were undertaken in the framework of this study. In this context, based on archaeological and literature sources, the major events which took place during the lifetime of the monument were examined, in order to identify the evolution of the structure. An

architectural survey was also conducted for the geometrical description of the monument and the documentation of construction detailing. A condition assessment was performed to detect any inherent deficiencies or degradation phenomena that affect the structural behavior. Furthermore, investigations necessary to achieve an adequate knowledge level regarding the mechanical properties of the historic fabric were carried out. These were based on the laboratory testing of materials sampled from the monument. The collected data facilitated the development of a numerical model, which was used for examining the seismic vulnerability of the structure. The main outputs derived at each step of the study are hereby discussed, illustrating aspects connected with the correct understanding, interpretation and analysis of heritage constructions.

2 HISTORIC ANALYSIS OF THE MONUMENT

Historic study, carried out in the framework of this project, revealed important information regarding the erection and later development of the Manor. According to some sources [1], the construction of the Manor is dated between 1369-82 AD, during the reign of King Peter II, while according to other researchers [2] [3] it was built by King James I (1382-98 AD). Narratives from the visit of Marquis Niccolò III d' Este to Cyprus (1412 AD) describe the Manor as a place with beautiful view, gardens, fountains and stables [4]. The Manor was used as a royal lodging place until 1426 [3], when it was burned down by Mameluke invaders [1].

In 1521-70 AD, the site possibly came to the possession of the Venetian noble Zegno Singlitico, who repaired the Manor, along with the area's irrigation system and mills [5]. After the Ottoman conquest of the island in 1570 AD, the Manor became a private land holding (i.e. a Chiflik) of Ibrahim Menteschologhlou [5]. It is reported that in the 17th and 18th centuries, building material removed from the Manor was used for the construction of hamam baths at the site, and of the Panagia Faneromeni church in Nicosia [6].

By the late 19th century, the Manor complex had been divided into separate family-owned properties. All title deeds were eventually sold to the Demetriou family in the early 20th century. In the 1960s, the Manor was abandoned by its residents due to intercommunal unrest and was used as a stable and a warehouse by the people of the nearby village. In 1974, the site was converted into a military camp by the Cyprus National Guard. In 1988, the Demetriou family donated part of the Manor to the Department of Antiquities of Cyprus and a study [7] for the documentation of the monument was carried out. Sections of the structures collapsed during an earthquake in 1996. Archeological surveys and excavations by the Department of Antiquities, the University of Cyprus and the University of Provence (Aix-Marseille I) were conducted in 2000-04 [8] and 2009-10 [9], and in 2005 further architectural documentation studies were commissioned. In 2019, a rehabilitation scheme that was subsidized by the Department of Antiquities of Cyprus addressed the restoration of the west part of the Manor.

3 ARCHITECTURE AND CONSTRUCTION TYPOLOGY

Following the historic study of the monument, field investigations and topographic surveys were conducted to identify the various elements composing the structure and to study their construction detailing. The load-bearing system consists of stone and adobe masonry walls, upon which timber floors and roofs rest. The thickness of the masonry sections varies from 45 to 80 cm, depending on the type and age of the construction. Three main building phases

(Figure 1) have been identified:

- Phase I (1380-1426): Medieval structures built before the destruction of the Manor by the Mamelukes. These include masonry sections composed of coursed ashlar stones.
- Phase II (1426-1570): Elements added/reconstructed during the Frankish and Venetian periods. These are stone masonry sections incorporating reused ashlar blocks.
- Phase III (1571-20th century): Additions/modifications made during the Ottoman period and up to the 20th century. Such structures are generally constructed of adobe masonry.

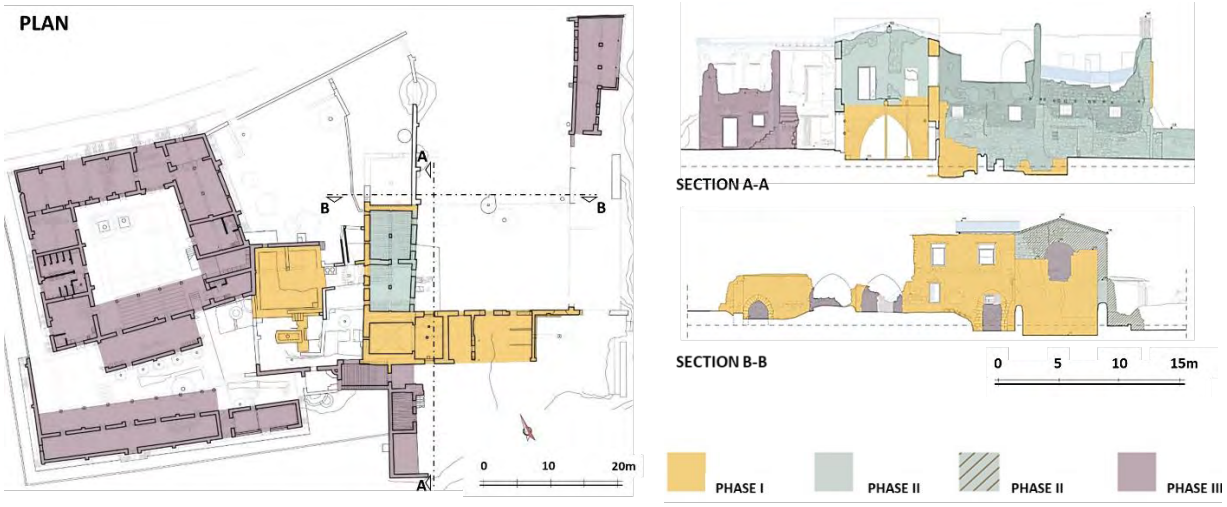


Figure 1: Plan drawing of the Potamia Manor complex and section drawings of the east part of the monument indicating the different building phases identified.



Figure 2: Photographs of the east part of the Potamia Manor showing stone masonry structures facing towards the north (left) and adobe constructions attached to stone structures at the south (right).

The Manor building complex occupies a plan area > 5500 m^2. The east and west parts of the complex are separated by a courtyard that includes the remnants of a large water tank and a well. The east part mainly consists of one-storey high stone masonry constructions dated to the 14th - 16th century, with several later modifications/additions of stone and adobes (Figure 2). Building spaces are rectangular in layout. Pointed arches that originally supported the floor structures are encountered at the interior of some rooms. A number of walls feature arched openings, some of which have been blocked. At the ground floor of this building part, a

vaulted room of unknown use exists. This is considered to be the only medieval structure surviving to its original height. Towards the south, adobe constructions were attached to the pre-existing stone structures. Many sections of the east part, including most of the roof and floor structures, and large segments of the walls at the upper floor, have collapsed.

The west part of the building complex was added during the Ottoman era. It comprises of a series of rooms, a longitudinal semi-open space (iliakos) and a portico (semi-open pass-through entrance) arranged around a central courtyard. A longitudinal building (with an iliakos on the north), which presumably served as a stable, is placed along the south boundary. All structures of the west part have nowadays been restored.

4 INVESTIGATION OF THE PATHOLOGY OF THE MONUMENT

A meticulous diagnostic survey was performed to examine the existing building pathology. The work included site inspections and detailed photographic documentation. Field measurements of (i) the moisture content of masonry walls, (ii) the crack mouth opening and (iii) the depth to which surface erosion has affected the building materials were carried out. These were conducted using dual electrode pin moisture meters, metric scales and pit gauges. The accumulated data were utilized for the preparation of drawings mapping the recorded pathologies.

It was noted that the main agents of pathology are associated with the action of water, and especially salt crystallization. The absence of waterproofing courses at the foundation level has resulted to capillary rise of ground water. The high moisture contents recorded 70-200 cm from the ground indicate the presence of a capillary rise front at this level, which is in line with the sharp front theory [10] and field observations reported elsewhere [11] [12]. The loss of roofing protection in large parts of the complex has left many building components exposed to the climatic conditions. Unobstructed water runoff and penetration of moisture at the top of the walls have contributed to material deterioration. In many areas, moisture infiltration, combined with thermal distress, have caused the detachment of render and plaster materials from the substrate, leaving the masonry surfaces exposed to the weather.

Adobe materials exhibit severe weathering due to the susceptibly of unfired earth to moisture-driven disintegration [13] [14]. Surface erosion characterized by lose of cohesion of the soil matrix was recorded on most earthen walls. Deterioration of adobes induced by rising damp has led to the formation of continuous horizontal fissures along the boundary between the walls' stone base and the adobe masonry, where the evaporation front is located (Figure 3a). Moisture-driven damage on stone walls is more noticeable at the sections affected by rising damp. At these areas, the jointing mortar has weathered away to a depth of 5-15 cm from the face of the masonry, while many stone blocks have suffered spalling and have become rather friable (Figure 3b). Biodegradation of masonry materials by lichens/mosses, as well as mechanical damage caused by vegetation growing next to or within the mass of the walls occur. Many of the remaining timber members were found to be in rather poor state, showing signs of insect infestation and/or fungal decay.

In terms of structural damage, the major issues identified are partial collapse of masonry sections, cracking (Figure 3c), loss of interaction among interconnected members and deformation of wall elements (i.e. bulging, loss of verticality). Measured crack widths were in many cases $\geq$ 10 mm, while the presence of through-cracks indicating separation among

orthogonal walls was recorded. Structural damage has been caused by the joint action of several factors, including seismic loading, climatic conditions, defects associated with original construction methods/materials, incompatible/ineffective interventions and application of excessive loads on the structure due to changes in building use. The lack of adequate connection between parts of the monument constructed at different building phases and the inherent absence of stiff floor and roof diaphragms have also affected the structural response.

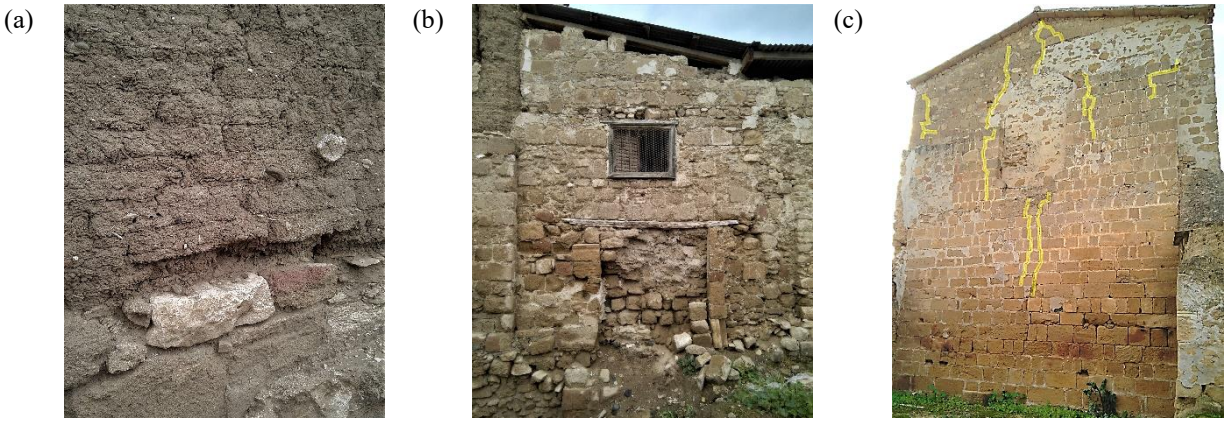


Figure 3: (a) Undercutting and surface erosion of adobe masonry. (b) Deterioration of stone masonry materials due to rising dump. (c) Marking of crack locations on the stone masonry wall of the north elevation.

5 LABORATORY TESTING FOR THE CHARACTERIZATION OF THE HISTORIC FABRIC

5.1 Sampling and testing methods

In order to assess the characteristics of the historic materials, building stones, adobe bricks, jointing mortars and render/plaster coatings were sampled from the monument and tested at the laboratory. Core drilling was used to extract stone samples (S1-4) from four different masonry blocks. Portions of adobe bricks were cut from exposed parts of the walls. Fragments of mortar (M1-3) were sampled from the joints of the stonework. Mortar samples were also obtained from earth-based coatings covering the surfaces of the adobe masonry walls.

For the implementation of tests on building stones, cylindrical specimens with nominal dimensions diameter = height = 55 mm were formed from the core samples via wet diamond sawing. Prior to testing, all stone specimens were oven-dried to constant mass at 70 ^{o}C. The apparent density and open porosity of the stone materials were measured through vacuum assisted saturation and submerged weighting, as per EN 1936 [15]. For the determination of the capillary absorption coefficient, water absorption tests were carried out in accordance with EN 1925 [16]. The compressive strength was assessed via uniaxial loading tests based on EN 1926 [17]. Loading was imposed under a displacement-controlled rate of 0.2 mm/min using a 300 kN capacity mechanical press. In all types of tests, three specimens from each stone block sampled were examined. The mineralogy of the stones was investigated through qualitative and semi-quantitative XRD analyses on powder samples. Locked-coupled continuous scans at 2θ angles from 2° to 100° were performed. XRD analyses were carried out on two of the four stone samples hereby examined.

Cubic specimens with a nominal side length of 50 mm were dry cut from the adobe brick portions sampled and were subjected to uniaxial compression tests. The bearing surfaces of the specimens were capped with gypsum mortar in order to achieve a uniform distribution of stresses during the tests. Loading was again applied under displacement control, at a rate of 1 mm/min, using a 10 kN capacity load cell. Tests were performed on three adobe specimens.

In order to obtain information regarding the mix components of the jointing mortars incorporated in stone walls, fractionation of the sampled materials was performed. Three samples originating from different parts of the monument were examined. The mortars were initially crushed to roughly segregate the aggregates from the binder. The processed material was then immersed in acetone. Repeated cycles of sonication and sieving through a 0.063 mm sieve were conducted to separate the binder and aggregate fractions. The dry weights of the fragments passing through (m_b) and retained on (m_a) the sieve were measured. Based on the hypothesis that the material with particle size < 0.063 mm consists mostly of the binder, the binder:aggregate (b:a) ratio of the sample was computed as m_b:m_a. Semi-quantitative XRD analyses were conducted on the fractionated binder and aggregate constituents of the samples. In all cases locked-coupled continuous scans at 2θ angles from 2° to 70° were undertaken.

The characterization of the earth coatings involved evaluation of the samples' contents in fines (silt and clay, $d < 0.063$ mm), sand ($0.063 \text{ mm} \leq d < 2.36$ mm) and fibers. Two samples were examined. Separation of the fibers from the soil matrix was achieved by submerging the samples into water and allowing the soil to settle and the fibers to float on the surface. The segregated fibers were dried and weighted. The soil portions were also dried and sieved through 5, 2.36, 1.18, 0.600, 0.250, 0.150 mm and 0.063 mm apertures.

5.2 Experimental results and discussion

The experimental results obtained from the testing of building stone samples are summarized in Table 1. The stones were found to possess rather low density and significant porosity. The apparent density and open porosity of samples S2-4 were found to be in the region of 1700 kg/m^3 and 35%, respectively. Corresponding results for sample S1 were somehow different, the average apparent density being 1940 kg/m^3 and the percentage of open pores approaching 26%. The porous structure of the materials explains the high rates of water absorption recorded. Capillary absorption coefficients for samples S2-4 lied between 1000 and 1400 g/m^{2}s$^{1/2}$, while specimens originating from sample S1 produced variable results in the range of 40-325 g/m^{2}s$^{1/2}$. A load-bearing capacity near 4.5 MPa was assessed for samples S2 and S3. Sample S2 also exhibited low compressive strength (< 2.5 MPa). As expected, the load-bearing capacity of the relatively less porous S1 sample was superior to those of the other stones; 15 MPa. XRD analysis of samples S1 and S4 verified that the materials under study are sedimentary stones rich in calcite (> 70%). Sample S4 is composed of 72% calcite, containing considerable amounts (9-14%) of plagioclases (i.e. albite and anorthite) and quartz. The monocrystalline mineral structure of stone S1 (~100% calcite) may explain to some extent the lower porosity and higher strength of this sample.

The test results for stone masonry jointing mortars are reported in Table 2. The high percentage content (≥ 80%) of gypsum identified in the binder fraction of samples M1 and M3 points towards the use of gypsum-based mortars. The aggregate fraction of these two samples was also found to be rich in gypsum (> 80%), indicating that gypsiferous aggregates

may have been used. The presence of gypsum-based jointing mortars in local historic constructions dating well before the construction of the Manor (i.e. 500 BC) is reported by Wright [18]. Sample M2 has been identified as a lime mortar, since its binder fraction is almost entirely composed of calcite. Considering that calcite, quartz and plagioclases are the predominant minerals in the aggregate fraction of this mortar, it can be presumed that local calcareous sand was used in its mix design. The ~1:3 b:a ratio assessed for M9 is totally in line with traditional construction practices in Cyprus.

The two earth-based coating samples examined were found to be rich in fines. The ratios between the particles < 0.063 mm and those belonging to the sand fraction were 1:0.03 and 1:0.10, respectively. The estimated fiber contents expressed as a percentage of the soil weight were 21% and 7%. These well exceed the amount of fibers traditionally used in Cyprus for the fabrication of adobe bricks [19]. Since earth renders were intended to be exposed to climatic conditions, it is reasonable to expect that high fibrous content had to be used in order to account for shrinkage effects induced by frequent wetting and drying.

Table 1: Average properties (coefficient of variation) and mineralogical composition of stone samples.

Stone sample	Apparent density (kg/m^3)	Open porosity (%)	Capillary absorption coefficient ($g/m^2s^{1/2}$)	Compressive strength (MPa)	Mineralogical composition
S1	1940 (3%)	26.1 (10%)	155 (96%)	15.2 (33%)	Calcite: 98% Albite, Dolomite traces
S2	1731 (1%)	34.7 (1%)	1253 (14%)	4.4 (27%)	-
S3	1734 (2%)	34.8 (1%)	1393 (7%)	4.6 (24%)	-
S4	1712 (1%)	35.3 (1%)	1077 (6%)	2.3 (39%)	Calcite: 72% Plagioclases: 14% Quartz: 9% Dolomite, Chlorite traces

Table 2: Binder:Aggergate ratios and mineralogy of the constituent fractions of jointing mortars.

Mortar sample	Binder: Aggregate ratio (w/w)	Mineralogical composition	
		Binder fraction	Aggregate fraction
M1	1: 0.3	Gypsum: 90% Calcite: 4% Quartz, Plagioclases traces	Gypsum: 94% Calcite: 4% Plagioclases traces
M2	1: 2.8	Calcite: 90% Quartz, Plagioclases, Gypsum, Chlorite traces	Calcite: 60% Quartz: 10% Plagioclases: 27% Gypsum, Chlorite traces
M3	1: 0.5	Gypsum: 80% Calcite: 17% Plagioclases traces	Gypsum: 83% Calcite: 15% Plagioclases traces

6 APPRAISAL OF SEISMIC RESPONSE

6.1 FE modelling

In order to assess the seismic vulnerability of the monument, a FE model was developed in Abaqus/CAE (Figure 4). The stone-mortar and adobe-mortar masonry composites were treated as homogenous continua and were modelled using an isotropic elasticity constitutive law. Plane stress failure measures were specified for identifying damage. The FE mesh consisted 3-noded shell elements with five integration points through the thickness and an average side length of 0.4 m. Pinned supports were defined along the walls' base.

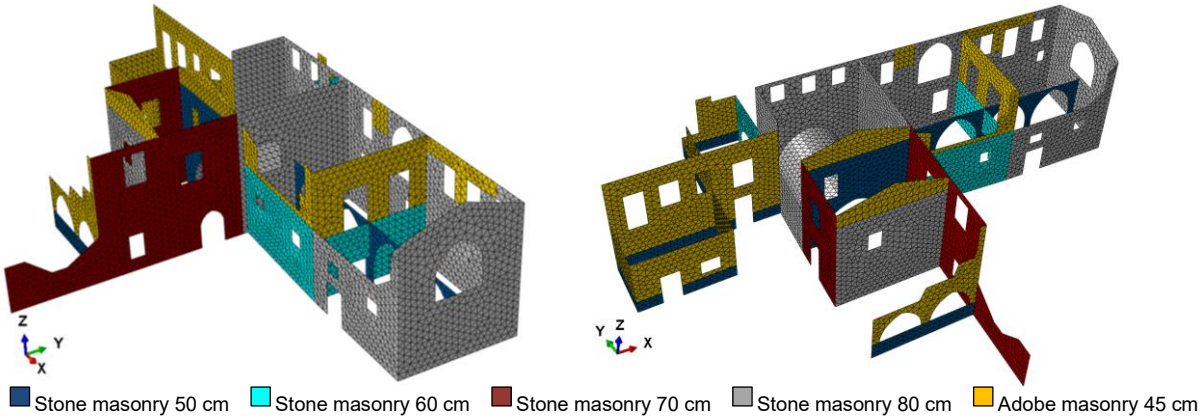


Figure 4: FE model of the east part of the Potamia Mansion.

Table 3: Numerical input parameters adopted for stone and adobe masonry.

Property	Stone masonry	Adobe masonry
Weight density – ρ (kg/m^3)	1800	1500
Elastic modulus – E (MPa)	1200	300
Poisson's ratio – ν	0.25	0.25
Compressive strength – f_c (MPa)	1.2	0.3
Allowable shear stress – f_v (MPa)	0.08	0.02
Tensile strength – f_t (MPa)	0.12	0.03

Numerical input parameters (Table 3) were based on the experimental data derived in this study. The weight density of stone masonry was defined as 1800 kg/m^3, in accordance with the properties of the stone materials. The respective value assumed for adobe masonry is 1500 kg/m^3. Compressive strength (f_c) was estimated as $f_c = K f_b^{0.7} f_m^{0.3}$ [20]. In this relation f_b and f_m are the compressive strengths of the masonry units and jointing mortar and K is a parameter accounting for the construction pattern. With reference to the results of loading tests, $f_{b,s}$ = 4 MPa and $f_{b,a}$ = 0.6 MPa were taken for the strengths of the stone blocks and adobe bricks, respectively. A value of $f_{m,s}$ = 1 MPa was assumed for the gypsum and lime mortars incorporated in the stonework [21]. For earth mortar $f_{m,a}$= $f_{b,a}$ = 0.6 MPa was adopted, as the composition of this material is typically the same as that of the adobe bricks. A value of K = 0.45 [20] was taken for stone masonry. In the absence of code prescribed clauses for adobe

masonry, K = 0.55 was adopted. The aforementioned material properties yielded $f_{c,s}$ = 1.2 MPa for stone masonry and $f_{c,a}$ = 0.3 MPa for adobe masonry. Maximum allowable stress under shear (f_v) was estimated as $f_v = 0.065 f_c$ [20]. Tensile cracking strength (f_t) was empirically taken as $f_t = 0.1 f_c$. Elastic moduli (E) were approximated by $E = 1000 f_c$ [20]. A value of v = 0.25 was assumed for the Poisson's ratio of both masonry typologies.

To assess whether imposed actions result to load-carrying demands which exceed the capacity of masonry sections, a stress-based failure criterion [22] was implemented. According to this criterion, the failure surface in the stress space $\{\sigma_x, \sigma_y, \tau\}$ is given by:

$$f(\sigma_x, \sigma_y, \tau) = F_1\sigma_x + F_2\sigma_y + F_{11}\sigma_x^2 + F_{22}\sigma_y^2 + F_{66}\tau^2 + F_{12}\sigma_x\sigma_y \quad (1)$$

The parameters of this polynomial are (strength) tensors estimated as:
$F_1 = 1/f_{c,x} + 1/f_{t,x}$; $F_2 = 1/f_{c,y} + 1/f_{t,y}$; $F_{11} = -1/f_{c,x}f_{t,x}$; $F_{22} = -1/f_{c,y}f_{t,y}$; $F_{66} = 1/f_v^2$ and $F_{12} = k(F_{11}F_{22})^{1/2}$ for k = -0.3. Although the failure surface can account for orthotropic strength measures, in this study it was assumed that masonry has the same compressive and tensile strengths along the two principal directions ($f_{c,x} = f_{c,y} = f_c$; $f_{t,x} = f_{t,y} = f_t$). The assessment criterion provides indications of material failure based on the post-processing of numerically computed elastic stresses and does not introduce material degradation properties into the analysis process. The outcome is expressed by means of a failure index (R) which indicates whether damage due to exceedance of the permissible stress state is predicted to occur ($R \geq 1$) or not ($0 \leq R < 1$).

6.2 Numerical analysis and results

Analysis of the monument's seismic response was carried out using the response spectrum method and adopting the relevant nationally determined assessment parameters. The Cyprus National Annex to EN 1998-1 [23] prescribes a 0.20g reference value of peak ground acceleration for the Potamia region. Geological data for the area indicate the presence of sand, silt, clay and gravel; the ground may be classified as Type B [23]. This corresponds to a horizontal elastic response spectrum defined by periods T_B= 0.15 s, T_C= 0.50 s, T_D= 2.0 s and a ground amplification factor of S = 1.20. Constant damping with ξ = 5% was assumed.

The FE model was initially analyzed considering only static dead loads. The first 150 eigenvectors of the system were then extracted using the Lanczos eigensolver. Complete quadratic combination of modal maxima was subsequently applied for computing unidirectional response along the X and Y axes with respect to the code prescribed spectrum. The results from the static and multimodal superimposition steps were superimposed in order to estimate the response of the structure for various load cases deduced by the combinations of quasi-permanent (G) and seismic (E_X and E_Y) actions $G \pm E_X \pm 0.3E_Y$ and $G \pm 0.3E_X \pm E_Y$.

Modal analysis yielded a multitude of modes having low mass participation. Inevitably, a structurally meaningful predominant mode of vibration could not be defined. The first 150 eigenvectors engaged 80% and 77% of the total structural mass in the X and Y directions, respectively. The predicted mode shapes indicate that dynamic behavior is governed by out-of-plane motion of individual wall elements. This was pretty much expected due to the absence of diaphragms at the floor and roof levels and the partial collapse of masonry sections, which resulted to lack of adequate restrain along the edges of many surviving walls.

Figure 5 presents contour diagrams of damage variable R over deformed FE meshes for load combinations corresponding to different directions of the principal seismic component. Good correlation between numerically predicted damage and recorded cracking is observed at

many of the stone walls (e.g. compare the crack pattern of the north elevation wall shown in Figure 3c with the corresponding areas exhibiting $R > 5$ in Figure 5). This provides a useful indication regarding the validity of the computational model. Analyses show widespread damage due to exceedance of allowable stress state. For all load combinations examined > 60% of the total surface area of the shell elements develop stresses outside the failure envelopes defined. According to Asteris [24], this can be interpreted as the structure reaching the near collapse limit state.

The computed deformation distribution indicates that the walls which sustain out-of-plane seismic loading are susceptible to overturning. This failure mode appears to be critical for the walls and parapets of the upper floor and for certain free-standing wall sections at the ground floor level. It is evident that adobe constructions are the most vulnerable parts of the monument. The low modulus of earth masonry results to the development of high deformations at these sections. In addition, the poor mechanical properties of adobe are not adequate for resisting the significant demands imposed by seismic action, particularly at wall sections which are not effectively restrained against lateral motion. Overall, spatial discontinuity of the load-bearing system due to partial collapse of sections and variation of the stiffness and mass distribution within the walls negatively affect global seismic response.

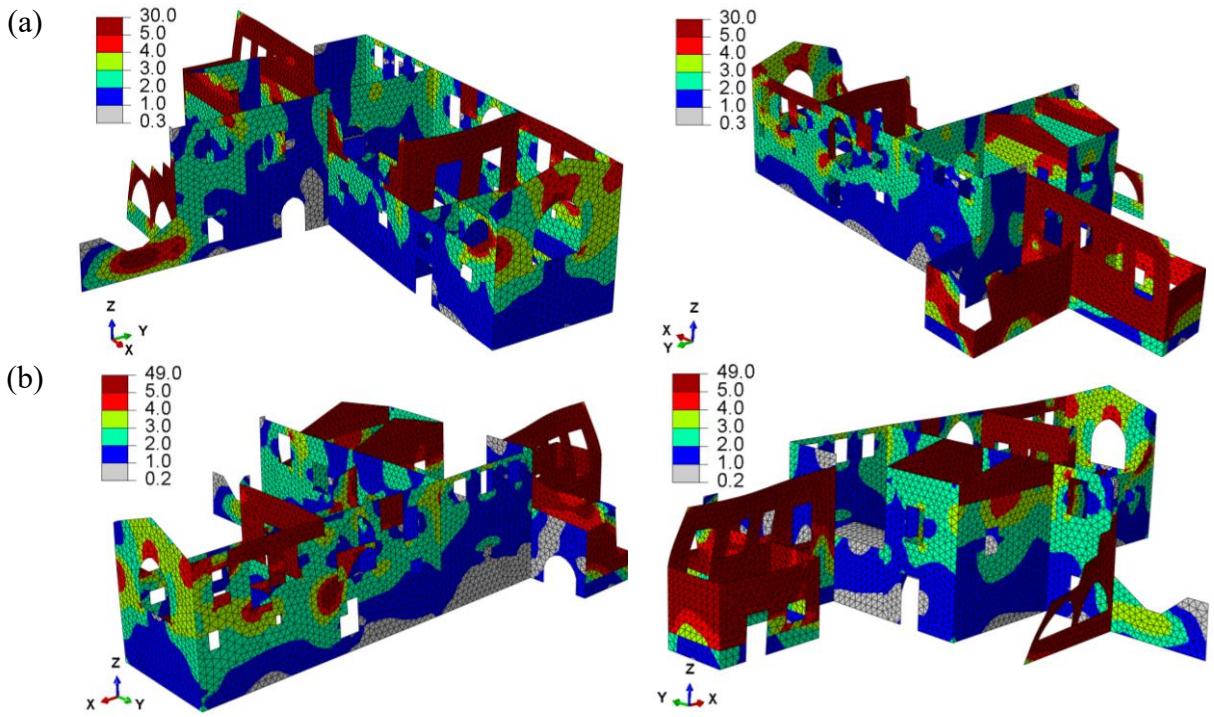


Figure 5: Isoparametric views of the structure under study showing deformed FE meshes (deformation scale x 20) with contour diagrams of damage variable R for load combinations (a) $G+E_X+0.3E_Y$ and (b) $G-0.3E_X-E_Y$.

7 CONCLUSIONS

An integrated methodology linking historic, architectural and structural analysis was adopted for the documentation and appraisal of the Medieval Manor of Potamia, Cyprus. The research included review of existing sources, field investigations, sampling and testing

campaigns and numerical assessment studies. The monument examined was found to consist of several building phases dating from the 14th to the 20th century. Its load-bearing system is composed of stone and adobe masonry walls. Significant structural damage was detected, including partial collapses, separation among orthogonal walls and extensive cracking. Furthermore, it was noted that the building materials suffer from moisture-driven decay due to inadequate protection against ground and rainwater infiltration. Tests for the characterization of the building fabric revealed that a porous sedimentary stone of relatively low compressive strength (< 10 MPa) was used for the construction of the stonework, along with lime- and gypsum-based jointing mortars. Poor mechanical properties were determined in the case of adobe materials, owing to the susceptibility of raw earth to water-mediated damage. Seismic analysis conducted using the response spectrum method showed that the monument is particularly vulnerable to earthquake action. Out-of-plane failure of poorly restrained masonry sections was found to be the critical mechanism governing seismic response. It was concluded that the structural behavior is adversely affected by inherent deficiencies, such as the lack of monolithic connections and the absence of stiff diaphragms, as well as by the pathology of the monument. Regarding the latter, degradation of mechanical properties and loss of the load-bearing system's spatial continuity due partial collapse have been identified as the factors with the most severe impact. The multifaceted approach hereby presented clearly shows that interdisciplinary collaboration is a key aspect for the comprehensive appraisal of historic constructions and hence a prerequisite for the design of appropriate intervention schemes.

Acknowledgements. The work was carried out at the University of Cyprus in the framework of the interdepartmental postgraduate program 'Conservation and Restoration of Historic Buildings and Sites'. The authors gratefully acknowledge the valuable input of postgraduate students Elina Varnava, Marios Georgiou, Malvina Yiapa, Constantinos Gavalis, Ioanna Elia, Natasa Kotsoni, Mikaella Kounnapi, Ioanna Petrou, Maria Solomou, Theodora Hadjipetrou and Stelios Hadjisoteriou.

REFERENCES

[1] Léonce Machéras, Chronique de Chypre, (french translation by E. Miller and C. Sathas), Paris: Ernest Leroux Editeur, 1882.

[2] E. de Lusignan, Description de toute l'isle de Cypre, Paris: G. Chaudière, 1580 (reprint Nicosia 2004).

[3] Archimandrite Kyprianos, Chronological history of Cyprus, Venice, 1778 (Nicosia 1902).

[4] G. Grivaud, Excerpta Cypria nova. Voyageurs occidentaux à Chypre au xvème siècle, (Sources et études de l'histoire de Chypre, XV.) Nicosia: Centre de Recherches Scientifiques, 1990.

[5] N. Lécuyer, "Marqueurs identitaires médiévaux et modernes sur le territoire de Potamia-Agios Sozomenos," in *Identités croisées en un milieu méditerranéen: le cas de Chypre*, S. Fourrier & G. Grivaud (eds), Rouen, France, pp. 241-256, 2006.

[6] N. Lécuyer, "Le territoire de Potamia aux époques médiévale et moderne: acquis récents," *Cahiers du Centre d'Études Chypriotes ,* vol. 34, pp. 11-30, 2004.

[7] S.F. Zesimou, Inventory and documentation for preservation of the royal manor of Potamia, Final Report[s.l.]: Groupement européen des campus, 1996.

[8] N. Lécuyer and D. Michaelides, "Archaeological survey at Potamia-Ayios Sozomenos," In *Archaeological Field Survey in Cyprus. Past History, Future Potentials*. Proceedings of a Conference held by the Archaeological Research Unit of the University of Cyprus, 1-2 December 2000, M. Iacovou (ed.), London: British School at Athens Studies, vol. 11, pp. 139-149, 2004.
[9] Department of Antiquities, Annual Report of the Department of Antiquities for the year 2010, Nicosia: Printing Office of the Pepublic of Cyprus, 2016.
[10] C. Hall and W. Hoff, "Rising damp: capillary rise dynamics in walls," *Proceedings of The Royal Society A,* vol. 463, pp. 1871-1884, 2007.
[11] G. Massari and I. Massari, "Damp Buildings, Old and New," *Bulletin of the Association for Preservation Technology,* vol. 17, no. 1, pp. 2-30, 1985.
[12] M. Müller, Handbuch ausgewählter Klimastationen der Erde, Trier: University of Trier, Forschungsstelle Bodenerosion, 1983.
[13] R. Illampas, I. Ioannou and D. Charmpis, "Overview of the pathology, repair and strengthening of adobe structures," *International Journal of Architectural Heritage,* vol. 7, no. 2, pp. 165-188, 2013.
[14] I. Ioannou and R. Illampas, "Durability of earth masonry," in *Long-term performance and durability of masonry and historical structures*, Ghiassi B. and Lourenco P.B., Eds., Woodhead Publishing, pp. 89-127, 2018.
[15] EN 1936, Natural stone test methods. Determination of real density and apparent density, and of total and open porosity, Brussels: CEN, 2006.
[16] EN 1925, Natural stone test methods. Determination of water absorption coefficient by capillarity, Brussels: CEN, 1999.
[17] EN 1926, Natural stone test methods. Determination of uniaxial compressive strength, Brussels: CEN, 2006.
[18] G. Wright, Ancient building in Cyprus Vol. 1, Leiden: E.J. Brill, 1992.
[19] R. Illampas, I. Ioannou and D. Charmpis, "Adobe bricks under compression: Experimental investigation and derivation of stress–strain equation," *Construction and Building Materials,* vol. 53, no. 1, pp. 83-90, 2014.
[20] EN 1996-1-1, Eurocode 6: Design of masonry structures - Part 1-1: General rules for reinforced and unreinforced masonry, Brussels: CEN, 2005.
[21] A. Marques, J. Morais, P. Morais, M. Veiga, C. Santos, P. Candeias and J. Ferreira, "Modulus of elasticity of mortars: Static and dynamic analyses," *Construction and Building Materials,* vol. 232, pp. 1-9, 2020.
[22] C. Syrmakezis and P. Asteris, "Masonry failure criterion under biaxial stress state," *Journal of Materials in Civil Engineering,* vol. 13, no. 1, pp. 58-64, 2001.
[23] EN 1998-1 , Eurocode 8: Design of structures for earthquake resistance - Part 1: General rules, seismic actions and rules for buildings, Brussels: CEN, 2004.
[24] P. Asteris, "On the Structural Analysis and Seismic Protection of Historical Masonry Structures," *The Open Construction and Building Technology Journal,* vol. 2, pp. 124-133, 2008.

12th International Conference on Structural Analysis of Historical Constructions
SAHC 2020
P. Roca, L. Pelà and C. Molins (Eds.)

EFFECT OF SLOW-MOVING LANDSLIDES ON CHURCHES IN THE LIGURIA REGION: A GEOTECHNICAL APPROACH

LUDOVICA CAMBIAGGI[1]*, CHIARA FERRERO[1], RICCARDO BERARDI[1], CHIARA CALDERINI[1] AND RITA VECCHIATTINI[2]

[1] Department of Civil, Chemical and Environmental Engineering
University of Genoa
Via Montallegro 1, 16154 Genoa, Italy
email: ludovica.cambiaggi@edu.unige.it, chiara.ferrero@edu.unige.it, riccardo.berardi@unige.it, chiara.calderini@unige.it (* corresponding author)

[2] Department of Architecture and Design
University of Genoa
Stradone S. Agostino 37, 16123 Genoa, Italy
email: rvecchiattini@unige.it

Keywords: Slow-moving landslide, Historic masonry churches, Damage assessment.

Abstract. *Protecting cultural heritage from water-soil interaction related threats is a current issue and the prediction of the effects induced on buildings by landslides is very challenging. The main difficulties lie in the lack of detailed information about landside movements as well as in the modeling of soil-structure interaction. This paper study the effects of a particular category of slow-moving landslides, namely active rotational and translational slides with movement rates of the order of some mm/year, on buildings of historical and cultural interest such as churches. Three case studies located in the Liguria region (Italy) were analyzed by performing FEM and LEM numerical analyses on sections representative of the slope.*

1 INTRODUCTION

Slow-moving landslides may cause different damage to facilities such as break of underground utilities (e.g. water and gas distribution pipelines), interruption of transport infrastructures (e.g. roads and railways) with consequent high cost of maintenances, but also cracking and tilting of buildings. Generally, their occurrence does not cause injuries or fatalities; however, relevant economic losses and damage to both cultural heritage and environmental assets can be recorded.

With respect to cultural heritage, a significant number of sites and remains are not in equilibrium with the environment. Among natural phenomena, earthquakes, flooding and landslides are the main causes of disruption of cultural heritage sites. Although it is difficult to evaluate the percentage of losses caused by each single phenomenon, it can be easily observed that earthquakes and flooding affect a very large area and a significant number of monuments

at the same time, while landslides act more locally, at the scale of the site, thus making statistical analysis rather complicated. In this respect, it is important to point out that literature is rich of methods for the prediction of seismic damage of several types of structures, while there is a lack of studies dealing with the evaluation of landslide effects on cultural heritage.

This paper investigates the effects of slow-moving landslides on historic masonry churches by means of the analysis of three case studies. Some of the authors carried out an extensive damage survey campaign in 33 listed churches located in the Liguria region (Italy) in areas affected by slow-moving landslides [1]. For each church, detailed information about the crack pattern was obtained by means of on-site inspections [1].

The case studies analyzed in this paper were selected among the buildings investigated in [1]. Firstly, for each church information regarding both the landslide-affected area and the geotechnical soil configuration was collected and analyzed. Landslide type, state of activity and direction were derived from the landslide maps of the basins plans of the Liguria region [2,3] as well as from the *Atlante dei Centri Abitati Instabili della Liguria* (hereafter called Atlante) [4]. Geotechnical data for each area were also obtained from boreholes, inclinometers, in situ tests and piezometers, when available. Secondly, by means of a GIS software and the acquisition of DTM (Digital Terrain Model) data of the area, it was possible to obtain a sufficiently precise topographic survey, in order to trace representative sections along the slope, particularly along the direction of the landslide. Finally, geotechnical numerical analyses (Finite Element Method - FEM and Limit Equilibrium Method - LEM) were performed with the aim of obtaining horizontal and vertical patterns of displacement and slope safety factors, respectively. In order to reduce the safety factor of the slope and trigger slope movements, different sets of water table were also implemented. The results of the numerical analyses, in terms of soil displacements, were correlated with the damage pattern observed in the churches in order to evaluate the effects induced by slope movements.

2 SLOW-MOVING LANDSLIDES IN THE LIGURIA REGION

The authors focused their research on Liguria, a region of northern Italy that covers an area of 5418 km^2 and is confined within a narrow strip of land bounded to the north by the Alps and Apennines mountain ranges and to the south by the Ligurian sea. Due to its geographical location, orography and morphological and geological setting, Liguria is frequently affected by landslides and floods. It is known that such phenomena are usually triggered by rain infiltration in the soil, leading to an increase in the pore water pressure and therefore in the deterioration of slope stability [5]. In Liguria, this deterioration is facilitated by the presence of numerous rivers that flow into the sea and make the territory very sensitive in rainy periods.

According to the Italian archive of historical information on landslides and floods [6], 1806 landslide events damaged 1233 localities during the period 1800–2001 in the four Provinces of the Liguria Region. The IFFI project (Italian Landslide Inventory), developed by the ISPRA's department for the Geological Survey of Italy and aimed to survey landslides in Italy [7], shows that in the Liguria region 13.475 landslides occurred between 1164 and 2017. In particular, in 2017 an area of 536 km^2, equal to 10.1% of the regional territory, was affected by landslides [8].

In a territory with such a high number of landslides, the assessment of the effects of landslides on the regional cultural heritage is a current and social issue to which scientific research must offer a contribution. For the purpose of this work, only landslides characterized by slow movements (i.e. with a speed of the order of some mm/year) were considered.

3 CASE STUDIES

This section presents the analysis of the three case studies under consideration: (i) San Nicolò di Capodimonte church in Camogli, (ii) Sant'Olcese church in Sant'Olcese, and (iii) San Carlo church in Cassingheno.

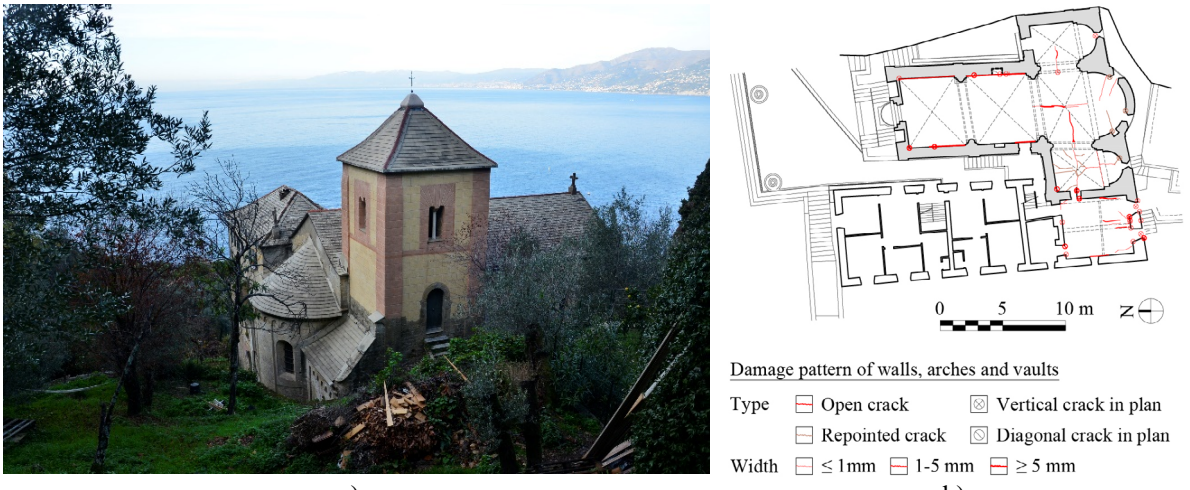
3.1 San Nicolò di Capodimonte church in Camogli

3.1.1 Description of the building and damage survey

San Nicolò di Capodimonte church (municipality Camogli, province Genoa) is located in a hilly area on the western side of the Promontory of Monte di Portofino (Figure 1a).

The church, whose construction probably dates back to the eleventh century [9,10], is a construction of limited dimensions (7 m wide, 15 m long) and has a single nave with a transept and three apses (Figure 1b). The nave and the transept are covered by cross vaults, while the apses are covered by semi-circular domes. On the upstream side there is the bell tower, while on the sea side, in the transept area, the church is connected to the rectory and to a small building called "Casa dei Pescatori" (hereafter named Fishermen's House), which was a shelter for local fishermen in the past. A ditch where water is canalized during rainy periods runs along the external perimeter of the apse. The church has been monitored since 2006 by using electrical crack gauges, which allow to follow the evolution of the cracks in different areas of the church.

The crack pattern surveyed in San Nicolò church and the Fishermen's house during on-site inspections is reported in Figure 1b.



a) b)

Figure 1: San Nicolò di Capodimonte church: a) exterior view, b) damage pattern.

The church presents slight to moderate damage. Few thin (width up to 1 mm) and medium (width between 1 mm and 5 mm) vertical cracks can be observed in the longitudinal walls as well as in apse wall above the windows. The vaults of the transept present cracks oriented parallel and perpendicular to the longitudinal axis of the church. Regarding the Fishermen's house, the authors were given access only to the building portion adjacent to the church. Extensive and severe damage was found in this area. In particular, large (width equal or larger than 5 mm) vertical cracks developing from the level of the ground were observed in the external wall continuous with the wall of the church apse.

3.1.2 Geotechnical analysis and damage assessment

The area in which the complex is located is limited by two natural streams along which water flows and groundwater is canalized. According to the landslide classification of the Liguria region [2,3], S. Nicolò di Capodimonte church is located in an area not affected by active landslides but characterized by a medium level of landslide susceptibility and high acclivity.

Geological and geotechnical investigations were carried out in 2002, with the aim of defining the stratigraphic sequence of the site, and soil analyses were performed as well. In particular, the results of seven electric tomographic sequences, five refraction seismic tests and four dynamic penetration tests with medium-light penetrometer are available.

A typical sequence of the Ligurian slopes was recognized and assumed: under a superficial heterogeneous clastic blanket, about 3-4m thick, a 2-3 m thick layer of highly fractured/weathered rock is encountered; the bedrock is a marly limestone belonging to the formation of the Flysch of Monte Antola.

In winter 2017 a laser scanner survey of both the church and the surrounding area, including other buildings and the natural slope, was performed through the acquisition of the 3D point cloud. Through its processing in CAD, it was possible to obtain the plano-altimetric profile of the area in an accurate way, improving the plano-altimetric profile obtained by processing technical charts and the available land survey.

In 2019 the authors took samples of soil in the surroundings of the church in order to perform laboratory tests. The latter allowed to estimate the soil parameters that were used for the Van Genuchten hydraulic model [11] in order to simulate partial saturation condition of soil.

Once the geotechnical and structural data were collected, several FEM analyses were carried out using PLAXIS 2D software. Figure 2 shows the different sections analyzed and the position of the available investigations for section E. The groundwater level was varied in different positions (according to piezometric monitoring) to evaluate its influence on slope stability, under both free-field conditions and introducing the presence of superstructures. In [12], the different soil types were modelled firstly with the elastic-perfectly plastic Mohr-Coulomb model; then, more accurate FEM analyses were performed by adopting the HSM (Hardening Soil Model), a non-linear isotropic hardening model used to better simulate the real behavior of soils [12]. In this paper, the HSM model was further refined using the Van Genuchten model to simulate the variation of the degree of soil saturation due to groundwater level oscillation as well as rain simulation.

Figure 3 shows the trend of vertical and horizontal displacements for section E under the

Fishermen's House and under the church. It can be noticed that, while vertical displacements exhibit a uniform distribution under the entire complex, horizontal displacements are larger under the Fishermen's House than under the church. These results can explain the crack pattern observed in both buildings. Firstly, the vertical cracks observed in the apse wall as well as in the external wall of the Fishermen's house can be attributed to the occurrence of horizontal displacements. The latter may have caused also the cracks in the vaults oriented parallel to the longitudinal axis of the church (Figure 1b). Secondly, the more severe damage observed in the Fishermen's house can be explained by the larger horizontal displacements obtained under this building. Regarding the cracks in the vaults oriented perpendicular to the longitudinal axis of the church, they may be associated to a local subsidence occurring under the apse of the church. This phenomenon may have been triggered by the significant concentration of rainwater in the area of the apse due to the presence of the ditch mentioned above.

The displacement patterns obtained from numerical analyses were also correlated with the damage levels proposed by [13]. It is important to underline that, while the analyses performed using the HSM model indicated a moderate damage level [12], the more refined analyses carried out with the Van Genuchten model classified the damage as slight, in good agreement with the real damage level of the structure (Figure 4). These results demonstrate that a refined geotechnical modeling, possible only in the presence of soil tests, is necessary in order to predict realistically the damage induced on churches by slow-moving landslides.

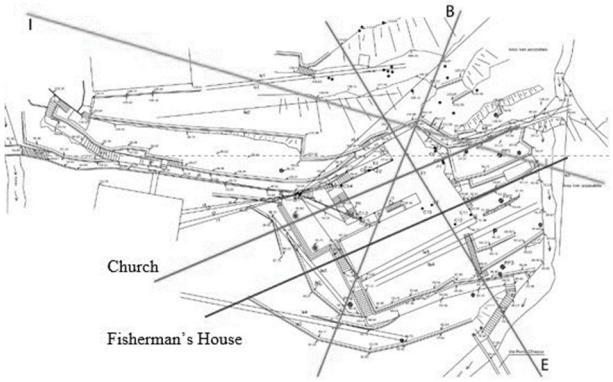


Figure 2: Slope sections analysed.

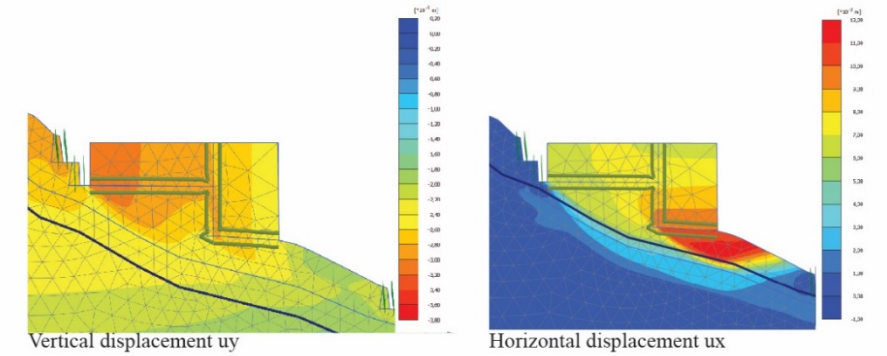


Figure 3: Vertical and horizontal displacements obtained in section E.

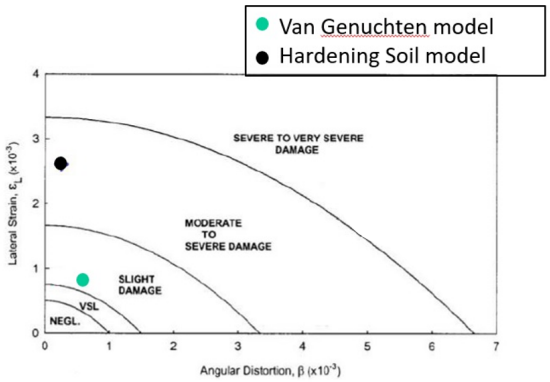


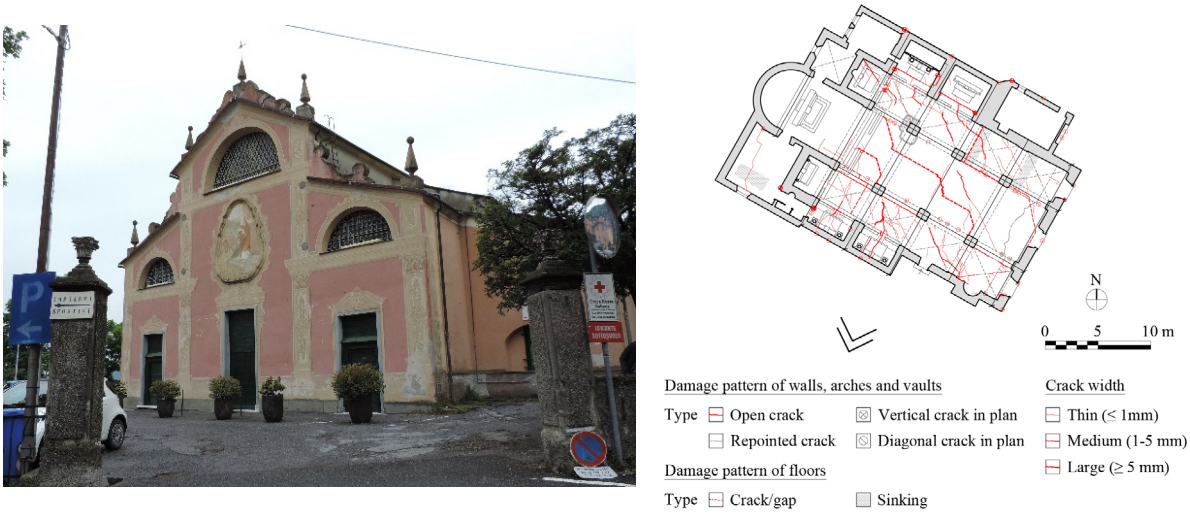
Figure 4: Correlation between angular distorsion and lateral strain (obtained from vertical and horizontal displacement, respectively) and damage level, from [15].

3.2 Sant'Olcese church in Sant'Olcese

3.2.1 Description of the building and damage survey

Sant'Olcese church is located in the municipality of Sant'Olcese, in the province of Genoa. The church, dating back to the first half of the seventeenth century, has three naves and is about 29m long and 14m wide (Figure 5a). The central nave is covered by a barrel vault made of brick masonry, while cross vaults are present in the lateral naves. The bell tower, which is now separated from to the church, was rebuilt in the 1930s after the demolition of the original one (adjacent to the church).

The crack pattern observed in Sant'Olcese church during on-site inspections performed by [1] is reported in Figure 5b.



a) b)

Figure 5 – Sant'Olcese church: a) exterior view, b) damage pattern (the direction of the landslide acting in the area is indicated with an arrow).

The church presents extensive and heavy damage, in particular in floors and vaults. Damage in the floor appears in the form of parallel gaps among tiles (ranging from 2 to 5 mm in width) and localized sinking. Extensive damage can be observed in the vaults with diagonal shear cracks widespread throughout the building. It can be observed that these cracks, which exhibit the same orientation in all the vaults, reflect the gaps observed in the floor, both being oriented almost perpendicular to the landslide direction (indicated with an arrow in Figure 5b). Finally, walls are affected by few minor vertical cracks.

3.2.2 Geotechnical analysis and damage assessment

The church is situated on a slope characterized by a slope angle of 15° (low inclined slope). The area of interest belongs to a large complex active landslide of about 1.09 km^2. From Figure 6, it can be observed that two inclinometers, installed in the framework of the REMOVER monitoring project of the Liguria Region, are present in the landslide area in the slope adjacent to the one where the church is located (Figure 6). They report a horizontal displacement of 175mm in 9 years, over 15mm/yr. However, no inclinometers can be found on the slope on which the church is situated.

It is important to point out that the area surrounding Sant'Olcese church is not actually well monitored. Only few boreholes, which allowed to define the stratigraphic sequence as well as to model soil stratigraphy, are available in the area uphill of the church. Conversely, no boreholes are present in the downhill area, as shown in Figure 6. Furthermore, no geotechnical tests for the characterization of the soil were performed.

By mean of PLAXIS 2D software, a section along the direction of the landslide was developed. The different soil types identified by the boreholes were modelled with Mohr-Coulomb constitutive law, as the absence of soil characterization tests did not allow for a more refined modeling (i.e. HSM). Several parametric analyses were developed in order to investigate the range of variability of geotechnical parameters. The groundwater level was varied in different positions in order to trigger the slope movement.

Both horizontal and vertical patterns of displacement were evaluated. The results show only very small displacements (less than 1mm) in the section under the church while an area of instability downhill of the church was identified (Figure 7). However, the latter is too far away from the building to influence its behavior.

The results of numerical analyses do not appear to be in good agreement with the crack pattern observed in the church. In fact, the heavy damage exhibited by the building as well as the occurrence of parallel cracks in vaults and floors oriented perpendicular to the landslide direction clearly indicates that the church has been subjected to slope movements. The absence of significant soil displacements obtained from numerical analyses can be attributed to the fact that the lack of detailed geotechnical data did not allow for an accurate modeling of the soil. The latter could be achieved by performing new in-situ tests and boreholes, especially in the area downhill of the church, in order to obtain a detailed stratigraphy and fully characterize soil parameters.

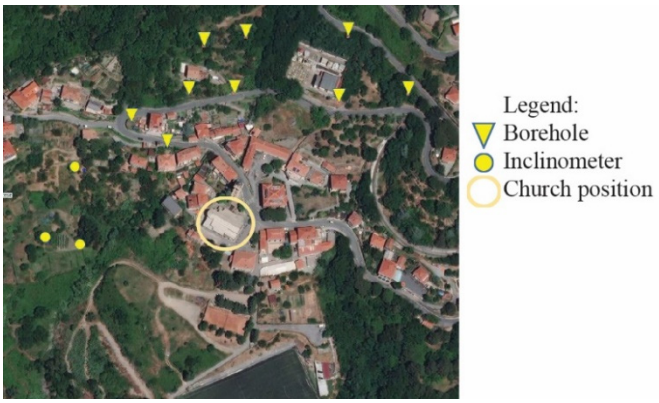


Figure 6: Localization of boreholes and inclinometers in the area of interest.

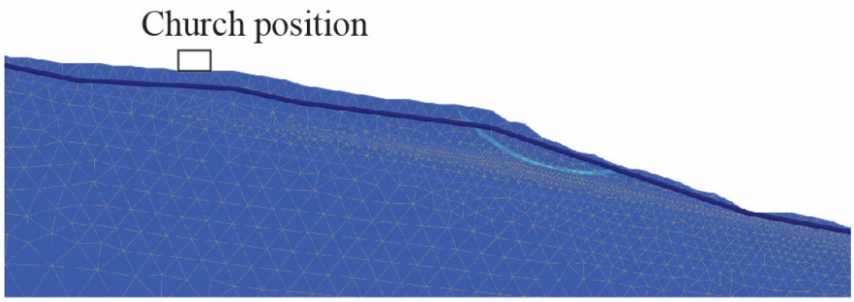


Figure 7: Shear strain concentration in area downhill of the church.

3.3 San Carlo church in Cassingheno

3.3.1 Description of the building and damage survey

San Carlo church is located in the village of Cassingheno (municipality Fascia, province of Genoa). Built at the end of the XVI century [14], the church consists of a single nave, a short transept and a semicircular apse. A bell-tower is present on the left side. Considering also the apse, the building is about 20 m long and 6 m wide. The nave is covered by a barrel vault made of stone masonry.

Figure 8a-b presents the crack pattern of San Carlo church in plan and elevation. The building exhibits extensive and severe cracking as well as large deformations. The floor presents two large parallel gaps (the largest one with a width of 18 mm) crossing the entire floor and propagating between longitudinal walls (Figure 8a). These gaps continue up into the walls with a diagonal orientation. Regarding cracking of walls, the most important damage is observed in the second bay behind the façade where series of severe diagonal cracks propagating from the level of the ground and developing upwards towards the apse are observed in both the longitudinal walls (Figure 8b). As for arches and vaults, they exhibit only few and

slight damage. In particular, a thin longitudinal crack is present in the barrel vault at mid-span. Thanks to the deformation survey performed in [15], the presence of large deformations can be observed (Figure 8b). In particular, a significant rotation of the apse towards the interior of the church can be detected. Furthermore, it can be observed that the left part of the church, where the bell-tower is located, experienced a larger settlement with respect to the right one [15].

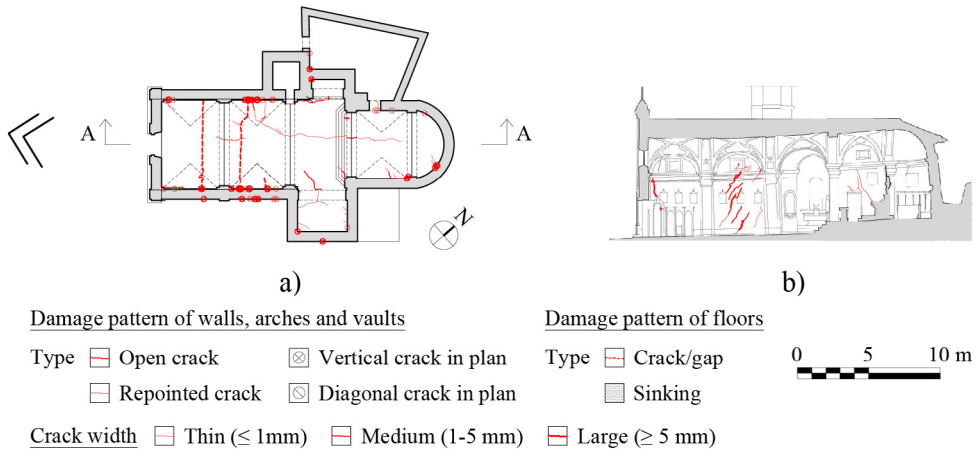


Figure 8: Damage survey of San Carlo church in Cassingheno: a) plan, b) section AA. (The direction of the landslide acting in the area is indicated with an arrow).

3.3.2 Geotechnical analysis and damage assessment

The church and the village of Cassingheno are located on a medium-low inclined slope (about 20°), probably being the accumulation zone of a relict deep slide. The area of interest lies on an active landslide of about 1.77 km^2 categorized as complex. Thanks to the REMOVER monitoring project of the Liguria Region, three inclinometers were installed in the landslide area in order to monitor slope movements. They show small displacements of the blanket at variable depths along the slope; all the instruments indicate a possible failure surface located at depth 9-12 m from ground surface.

Some boreholes performed in previous investigations [16] allowed to define the stratigraphic sequence of the soil, which indicates a thick layer (10-15 m) of very heterogeneous blanket (sand with clasts, clayey silts) separated from the bedrock (shales) by a transition zone (1-3 m) of weathered rock. The ground water table, whose oscillations follow mainly the seasonality, is located inside the blanket. The results of in-situ tests performed in the past in the area [16] were used to assess geotechnical mechanical properties. These latter were also fully characterized by means of parametric analyses in order to evaluate their range of variability.

Thanks to the GIS software and the acquisition of DTM data of the area, it was possible to obtain a sufficiently precise topographic survey, in order to trace representative sections along the slope, particularly in the direction of the landslide. Figure 9 shows a section of the slope created in SLIDE along the landslide direction. The position of boreholes and inclinometers as well as of the adopted stratigraphic sequence are also indicated.

Both LEM and FEM analyses were performed by some of the authors in [17] in order to

associate slope displacements with slope safety factors. In the FEM analyses, carried out using PLAXIS 2D, a simple linear elastic perfectly plastic model with Mohr-Coulomb failure criterion was adopted for all the soil layers. In order to reduce the safety factor and trigger slope movements, different sets of water table were considered. Twelve phreatic levels surfaces were modelled, simulating different hydrologic conditions that could actually occur.

The results show that the church is located in an area of potential instability (Figure 10) and is subjected to horizontal and vertical displacements of the same order of magnitude.

Regarding horizontal displacement, a maximum value of about 20 mm is obtained under the church when analyzing the slope section along landslide direction. This displacement value is in good agreement with the horizontal displacement recorded by the inclinometers and reflects the width of the gaps of the floors. These latter can be, indeed, attributed to the significant horizontal movement experienced by the church in the direction of the landslide. As for vertical displacements, they may explain the rotation of the apse towards the interior of the church.

The presence of severe cracks localized in the second bay of the church as well the settlement experienced by the left part of the church with respect to the right one can be attributed to the occurrence of differential settlement in this area. These displacements could have been responsible for the structural instability of the bell tower, which was strengthened in 1988. It is evident that such local phenomena cannot be captured when modeling the behavior of the entire slope.

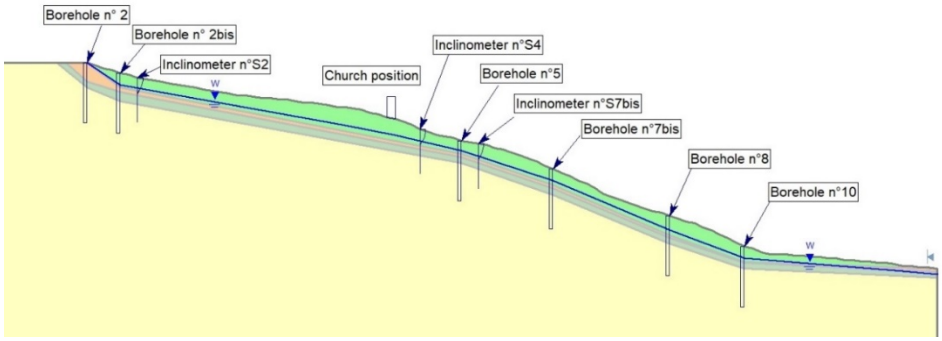


Figure 9: Boreholes and inclinometers localization along the section analysed.

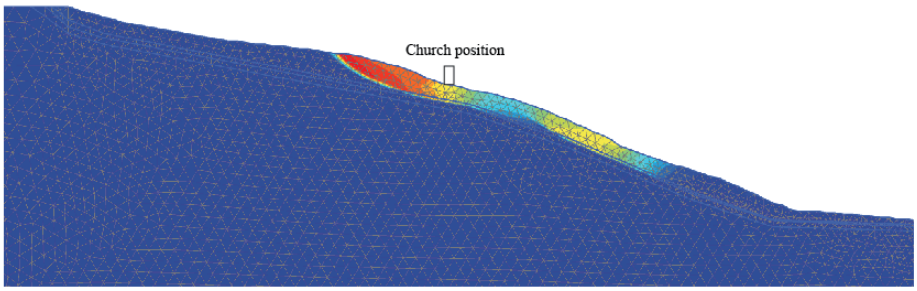


Figure 10: Total displacements |u|.

4 CONCLUSION

This work is part of a research program aimed at protecting cultural heritage from water-soil interaction related threats. In particular, the effects of slope movements on historic masonry churches were investigated by means of the study of three case studies, located in the Liguria region in areas affected by slow-moving landslides. Geotechnical numerical analyses were performed, leading to the following conclusions:

- The main difficulty encountered in the analysis of soil-structure interaction is related to the lack of exhaustive information regarding soil properties, site stratigraphy and landslide movements. In two of the three case studies under consideration, the absence of detailed geotechnical data impeded a refined geotechnical modeling, making it necessary to introduce some simplifications in numerical investigations. Furthermore, several parametric analyses were required for the definition of soil properties and groundwater level. In the case of Sant'Olcese church, the lack of geotechnical data did not allow to develop a numerical model able to catch the ground movements to which the structure was subjected. Conversely, the case of San Nicolò church underlines that a correct prediction of the damage induced by slow-moving landslide is possible only when detailed geotechnical information is available. Indeed, a more refined modeling of the slope, developed thanks to exhaustive geotechnical data as well as in-situ and laboratory test results, allowed to obtain numerical results that are in good agreement with the damage level observed in the structure.

- Geotechnical numerical analysis showed that the identification of the displacement patterns induced by slow-moving landslide is essential to interpret correctly the crack pattern of the church. Indeed, vertical and horizontal soil displacements can be correlated with the damage pattern observed in the churches.

- This work represents a good starting point to draw general conclusions about the structural response of historic masonry churches exposed to slow-moving landslide threats, as the numerical analyses performed so far allowed to associate the damage patterns observed on-site with the displacements induced by landslides.

Acknowledgements. The activity presented in the paper is part of the Research Pro-gram PRIN 2015 "PERICLES - *Protecting the Cultural Heritage from water-soil inter-action related threats*" – grant n. 2015EAM9S5.

REFERENCES

[1] Ferrero, C., Cambiaggi, L., Calderini, C., Vecchiattini, R. *Damage assessment of historic masonry churches exposed to slow-moving landslides*. Submitted in December 2019. International Journal of Architectural Heritage.

[2] Piano di Bacino Stralcio per l'Assetto Idrogeologico, Regione Liguria, 2017. *Carte della Suscettività al Dissesto (Landslide Susceptibility Maps*). Accessed October 25, 2018. http://www.pianidibacino.ambienteinliguria.it/.

[3] Piano Stralcio per l'Assetto Idrogeologico, Autorità di bacino distrettuale del fiume Po, 2017. *Atlante dei Rischi Idraulici e Idrogeologici (Atlas of Hydraulic and Hydrogeological Risks)*. Accessed October 25, 2018. http://www.pai.adbpo.it/.

[4] Federici, P.R., M. Capitani, A. Chelli, N. Del Seppia, and A. Serani. *Atlante dei Centri Abitati Instabili della Liguria. II. Provincia di Genova (Atlas of the Unstable Inhabited Centres of Liguria. II. Genova province).* Regione Liguria. (2004)

[5] Wang G., Sassa, K. *Post-failure mobility of saturated sands in undrained load-controlled ring shear tests.* Canadian Geotechnical Journal, **39** (2002), pp. 821-837

[6] Guzzetti, F., M. Cardinali, P. Reichenbach, F. Cipolla, C. Sebastiani, M. Galli, and P. Salvati. *Landslides triggered by the 23 November 2000 rainfall event in the Imperia Province, Western Liguria, Italy.* Engineering Geology (2004) 73 (2): 229–245.

[7] ISPRA: Italian Landslide Inventory Project (IFFI) 2007. Accessed June 26, 2019. http://www.progettoiffi.isprambiente.it

[8] Trigila, A., Iadanza C., Bussettini M., and Lastoria B. *Dissesto idrogeologico in Italia: pericolosità e indicatori di rischio. Rapporti 287/2018*. Istituto Superiore per la Protezione e la Ricerca Ambientale – ISPRA (in Italian). (2018)

[9] Cavaciocchi,P., Lastrico C., Molinari A., Pesce G., Soppa S. *Studi sull'antica Chiesa di San Nicolò di Capodimonte a Camogli*. Publication for public use. (2009)

[10] Pesce, G., Cavaciocchi, P., Guastella, R. and Vecchiattini, R. *La chiesa di S. Nicolò di Capodimonte (Camogli - GE): dal cantiere di diagnosi al progetto di restauro*. In: 7th IGIIC National conference - Lo stato dell'arte 7, 8-10 October 2009, Naples. (2009)

[11] Van Genuchten, M. *A closed-form equation for predicting the hydraulic conductivity of unsaturated soils*. Soil science society of America journal, **44**(5), 892–898. (1980).

[12] Cambiaggi L., Berardi R. *Investigation on the damages induced by slope movements on historic buildings: the case of San Nicolò di Capodimonte church in Liguria*. XVII European Conference on Soil Mechanics and Geotechnical Engineering ECSMGE, Reykjavik Iceland 2019 ISBN 978-9935-9436-1-3.

[13] Son, M., Cording, E. J., *Estimation of building damage due to excavation-induced ground movements*. J. Geotech. Geoenviron. Eng., (2005) **131** (2), 162–177

[14] CEI – *Chiese e Parrocchie italiane. Chiesa di San Carlo Borromeo (Cassingheno, Fascia)*. Scheda sintetica(2011) (in Italian). Accessed January 29, 2020 http://www.chieseitaliane.chiesacattolica.it/chieseitaliane

[15] Memme, C. *Studio di un borgo ligure in zona di frana attiva: il caso del paese e della chiesa di Cassingheno (Genova)*. Master thesis, Università degli Studi Genova (2017).

[16] Geoportale Regione Liguria. Visualizzatore Cartografico. Accessed January 20, 2020. https://geoportal.regione.liguria.it

[17] Berardi R., Cambiaggi L. *Prediction of slope movement effects on churches for the development of a fragility curve approach*. In: Calvetti F., Cotecchia F., Galli A., Jommi C. (eds) Geotechnical Research for Land Protection and Development. CNRIG 2019. Lecture Notes in Civil Engineering, vol 40. Springer, Cham, First Online23 June 2019 (2020) pp. 82-91.

12th International Conference on Structural Analysis of Historical Constructions
SAHC 2020
P. Roca, L. Pelà and C. Molins (Eds.)

FROM REALITY TO POINT CLOUDS. SURVEY AND ANALYSIS OF SANT MIQUEL CHURCH OF BATEA (SPAIN).

A. COSTA-JOVER*, D. MORENO GARCÍA*, S. COLL-PLA* AND J. LLUIS I GINOVART†

* Escola Tècnica Superior d'Arquitectura
Universitat Rovira i Virgili
Campus Bellissens, 43204 Reus, Spain
e-mail: agusti.costa@urv.cat; david.moreno@urv.cat; sergio.coll@urv.cat

† School of Architecture
Universitat Internacional de Catalunya
C/ Immaculada, 22, 08017 Barcelona, Spain
e-mail: jlluis@uic.es

Keywords: Historical Structure, Masonry, Terrestrial Laser Scanner, Non-Destructive Inspection, St. Miquel of Batea Church

Abstract. *Current massive data capture techniques (MDCT), such as terrestrial laser scanning and digital photogrammetry, have become widespread during the last decade, and raises the possibility of developing new assessment methodologies based on the 3D documentation. The paper exposes de results of using simple, non-invasive procedures for the assessment of the shape of a masonry building from a point clouds registered with a terrestrial laser scanner. The case study selected is the church of Sant Miquel of Batea (eighteenth century), located in the province of Tarragona (Spain). The methodology used combines 2D and 3D processes for assessment of the geometry. The results of the investigation have confirmed the good condition of the building. It presents dimensional variations, most of which can be related to the construction process, while some displacements identified provide information about the accommodation process of the masonry structure.*

1 INTRODUCTION

Current architectural heritage documentation procedures are very varied, and the use of massive data capture techniques (MDCT), such as terrestrial laser scanning and digital photogrammetry, have become widespread during the last two decades. These raises the possibility of developing new assessment methodologies based on the 3D documentation [1] [2]. Numerous investigations have tested the techniques' reliability [3], [4] and proved their effectiveness and compatibility to obtain high precision topographical documentation in architectural heritage [5], [6].

The paper exposes de results of using simple, non-invasive procedures for the assessment of the shape of a masonry building from a point cloud registered with a terrestrial laser scanner. The case study selected is the church of Sant Miquel of Batea (eighteenth century) (Figure 1),

which is located in the province of Tarragona (Spain) [7]. It is one of the most relevant Baroque constructions in Catalunya, due both for their architectural features and decorative elements. The building mainly consists on a basilica ground plan with a transept with a central dome over a ciborium, and a presbytery, where the altar is located. The main body has square columns and three naves, located at almost the same height defining an interior space of hall church (*hallenkirchen)*. In addition, it is remarkable its great measures, of 48.20 m x 26.11 m in the ground plan, and 19.95 m in height, measured in the top of the roof of the central nave.

The methodology used combines 2D a 3D processes for the assessment of the geometry, and takes as reference previous works such as [8], [9], [10]. 2D analysis is mainly based on cross sections, which allows to quantify main measures of all structural elements in detail. 3D analysis is based on the comparison with reference shapes, which allows a quantitative and qualitative comparative analysis of spatial elements such as the vaults and the dome.



Figure 1. Main façade (exterior) and nave (interior) of the church of Sant Miquel of Batea

2 METHODOOGY

The study was based on the topographic data obtained from the building in a single day (Campaign: J. Lluis i Ginovart, A. Costa-Jover, S. Coll-Pla) with a Leica laser device, as other methods were considered not cost-effective, in terms of time and resources, in obtaining the needed accuracy. Despite the survey involved all the building, the assessment was focused on the naves and the central dome.

The device used was a Leica ScanStation C10, with a position accuracy of 6 mm at 50 m. The architectural layout complexity required a large number of stations to avoid occlusions in the model. The spatial resolution of the scans was set to 1 cm at 10 m and the maximum length of the measurements were below 50 m. The coordinates (x, y, z) of each point were complemented with RGB information through the photographs taken with the incorporated camera of the device, with a resolution of 1920 x 1920 pixels (4 mp).

The software Cyclone was used to register the point clouds in the same local coordinate system with a standard deviation of 3 mm. The error considered was the result of the target based registration and the accuracy of the device. No resampling of the final point cloud was performed. Thus, the maximum error of the registration process was 9 mm, which was considered to be adequate for the assessment. The density of the obtained point cloud was more than 169 million points.

After, 3DReshaper was used to generate the 3D mesh of the model from the selected points. The mesh density was adjusted at an average triangle size of 2.5 cm, which was later refined using the same program to avoid aberrations due to point cloud noise.

Once the complete point cloud was obtained, the proposed methodology for the assessment of the building combined 2D and 3D processes. This allowed to adapt the processes according to the construction elements, optimizing the study. The analysis focused on the inside of the construction.

Prior to the assessment, all the fundamental construction elements were discretized. These are: pillars and pilasters (Pi) arches (Ai), vaults (Vi) and finally the central dome. Following, the main parameters to be registered are established, and the corresponding 2D or 3D process to obtain them. Despite being a Baroque building, the decoration is not very ornate, so there are no excessive areas where registration of measures is difficult.

The 2D study was based on the thorough sectioning of the construction elements. Figure 2 summarizes de nomenclature used for every element and section. Cross sections were made for each element, according to the main axes (i.e. cross sections from the longitudinal and transversal axes of the nave) that define the main points of the geometry of the elements assessed. Following, the study compared the differences between equal points between elements to identify possible movements.

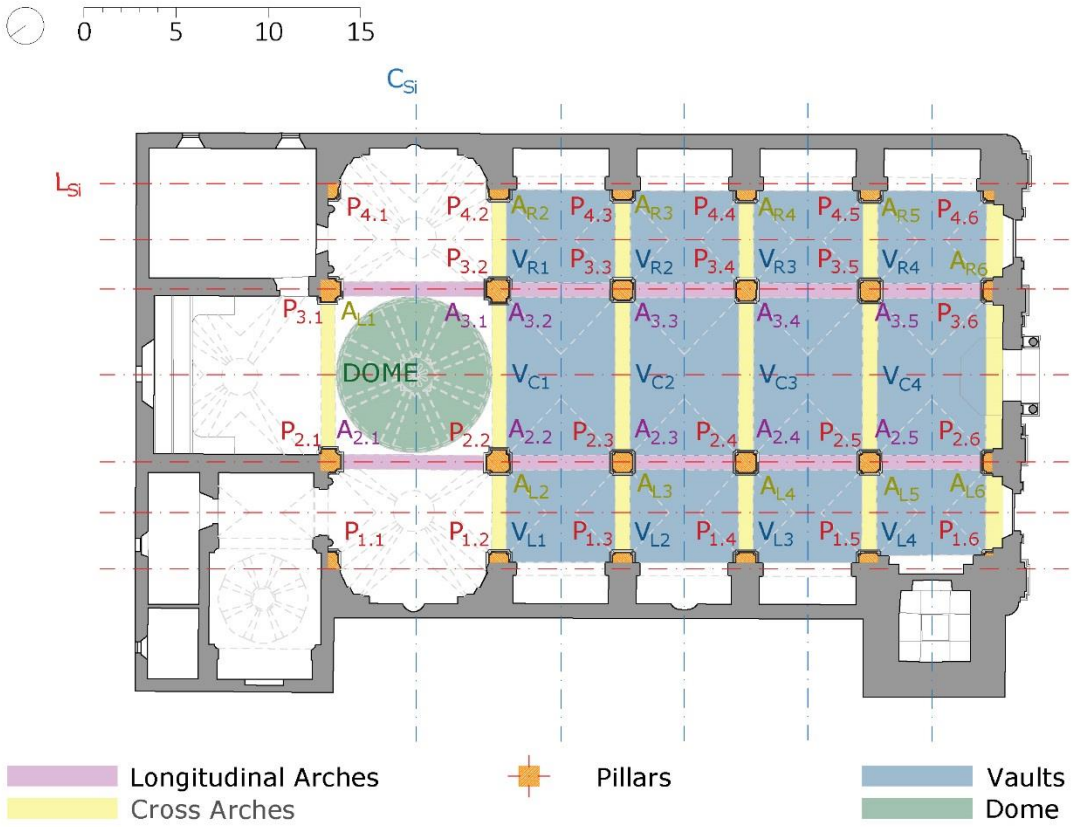


Figure 2. Elements assessed and nomenclature.

The 3D assessment was performed with the program 3DReshaper. This software allowed to

obtain the range of distances (point to surface) between a point cloud and a shape of reference. The study in that case focused on the vaults and the dome, which shape can only be fully understood in 3D. Two variants of the assessment were performed. First, the shape of the vaults was analysed compared to a horizontal reference plane. A different height from the reference plane was established for the side aisles and the central vault. This approach allowed to identify differences between the vaults simply and quickly. Complementarily, contour lines spaced every 10 cm were defined from the vaults mesh, to define a topography of the elements. Second, the central nave and the dome were assessed according to a primitive shape of comparison, a cylinder and a sphere correspondingly. These two analysis allowed to identify differences between equal elements, which at first glance may not be appreciated. The formal anomalies can be related to deviations during construction, or to movements of the structure after construction.

3 RESULTS

3.1 2D Assessment

The exhaustive sectioning allows a first and easy approximation of the formal alterations that the structural elements may have suffered. In this case, pillars and pilasters (Pi) arches (Ai) and vaults (Vi).

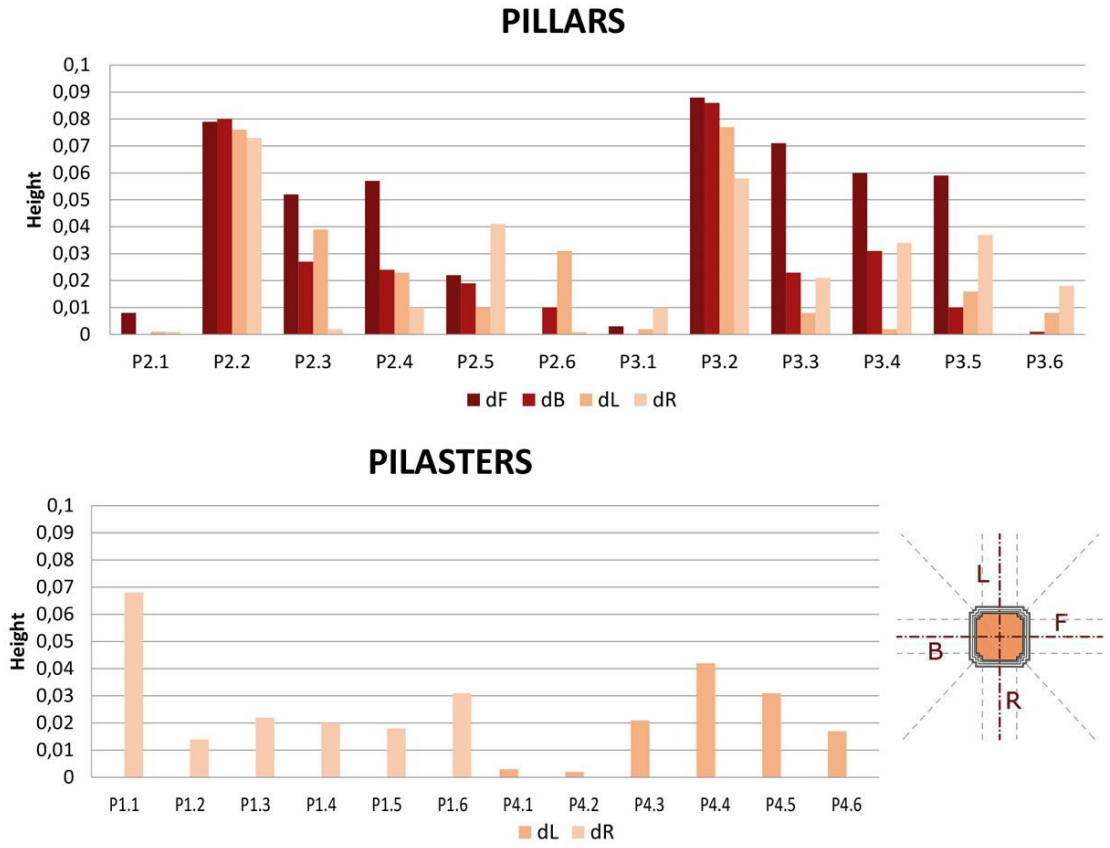


Figure 3. Values obtained in central pillars and pilasters (up) and lateral pilasters (bottom).

For the study of the pillars and pilasters the possible out of plumb points have been analysed, based on the displacements on the axis (x), measured in the upper end of the capital moulding and the lower end of the base of each column. The column shaft line was projected to the base and capital mouldings ends so as not to distort the measurement. Each pillar was measured on both sides of each axis, obtaining the measurements ($_{dF}$, $_{dB}$) through longitudinal sections (L_S), and ($_{dL}$, $_{dR}$) in the cross sections (C_S). In the case of pilasters, it was not possible to register all the coordinates, given the existence of mouldings that distorted an accurate reading at some points.

Figure 3 summarizes the measures obtained, according to the elements located in the central nave (pillars and pilasters) and in lateral walls (pilasters). It can be observed that in general terms, the values of the displacements are low. In the case of pillars, the range of displacements (x) in the longitudinal direction (L_S) is [P3.2$_{dF}$: 0.088 m - P3.6dB: 0.001 m]. In the transverse direction (C_S), the range of values is [P3.2$_{dL}$: 0.077 m - P2.1d_L-d_R: 0.001 m]. On the other hand, the values in lateral pilasters tend to be lower. The range of values in C_S is [P1.1$_{dR}$: 0.068 m - P4.2$_{dL}$: 0.002 m]. These values are very low, and can be considered invaluable on an architectural scale.

As for the rounded arches between the vaults, the spring line is measured to be over 1.35 m from the impost of each column. The arches located in the longitudinal direction have a radius of about 2.80 m, and the transverse ones 2.10 m. The measurement of the springing line presents difficulties due to the mouldings, so that only the height of the key was registered. The arches of the collateral chapels were not studied, since they present many irregularities that prevent a correct reading due to mouldings. Figure 4 summarizes the values obtained. In the longitudinal direction (L_S), the range of heights is [$A_{2.1}$: 0.016 m – $A_{2.3:}$ 0.015 m], and in the transverse direction (C_S) of heights is [C_{S5} 14.73 m – C_{S5} 14.61 m] for side arches and [C_{S6} 16.63 m –C_{S2} 16.25 m] for central arches. On the other hand, qualitatively no relevant deformations have been observed.

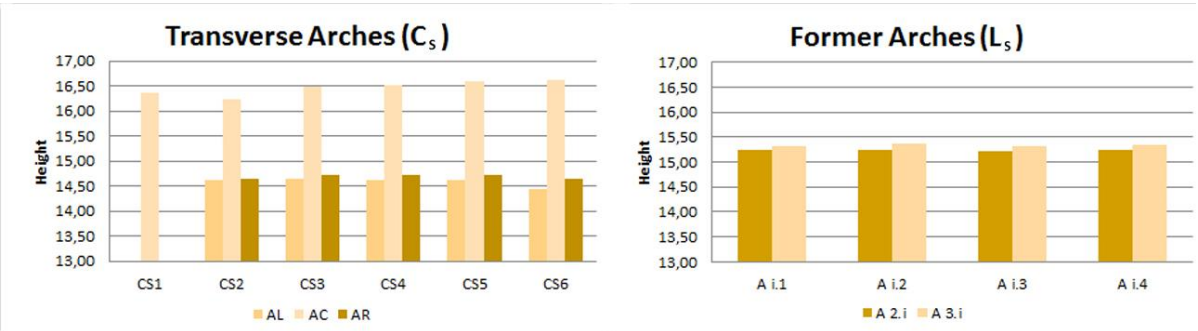


Figure 4. Values obtained in the arches keystones. Transverse arches (C_S), Former arches (L_S)

Finally, the 2D study of the vaults is made from the registration of the points located on the axial axes (longitudinal LS, transverse C_S) that determine their geometry. The (y) of selected points are registered, based on a common horizontal reference plane, which is located at the average height of the pavement of all the sections. Figure 5 shows the values obtained in the vaults located on the left (V_L) and on the right (V_R) of the central nave, and the vaults of the latter (V_C). The extreme values in the collateral vaults are (V_{R2}: 15,542 m - V_{R4}: 14,616m), and

in the central vault (V_{C4}: 16,741 m - V_{C2}: 15,309 m). The maximum difference between comparable points (i.e., same point in analogous vaults) is 0.268 m between points of V_{L4} and V_{R4} of collateral vaults, and 0.165 m between points V_{C1} and V_{C4} of central vaults.

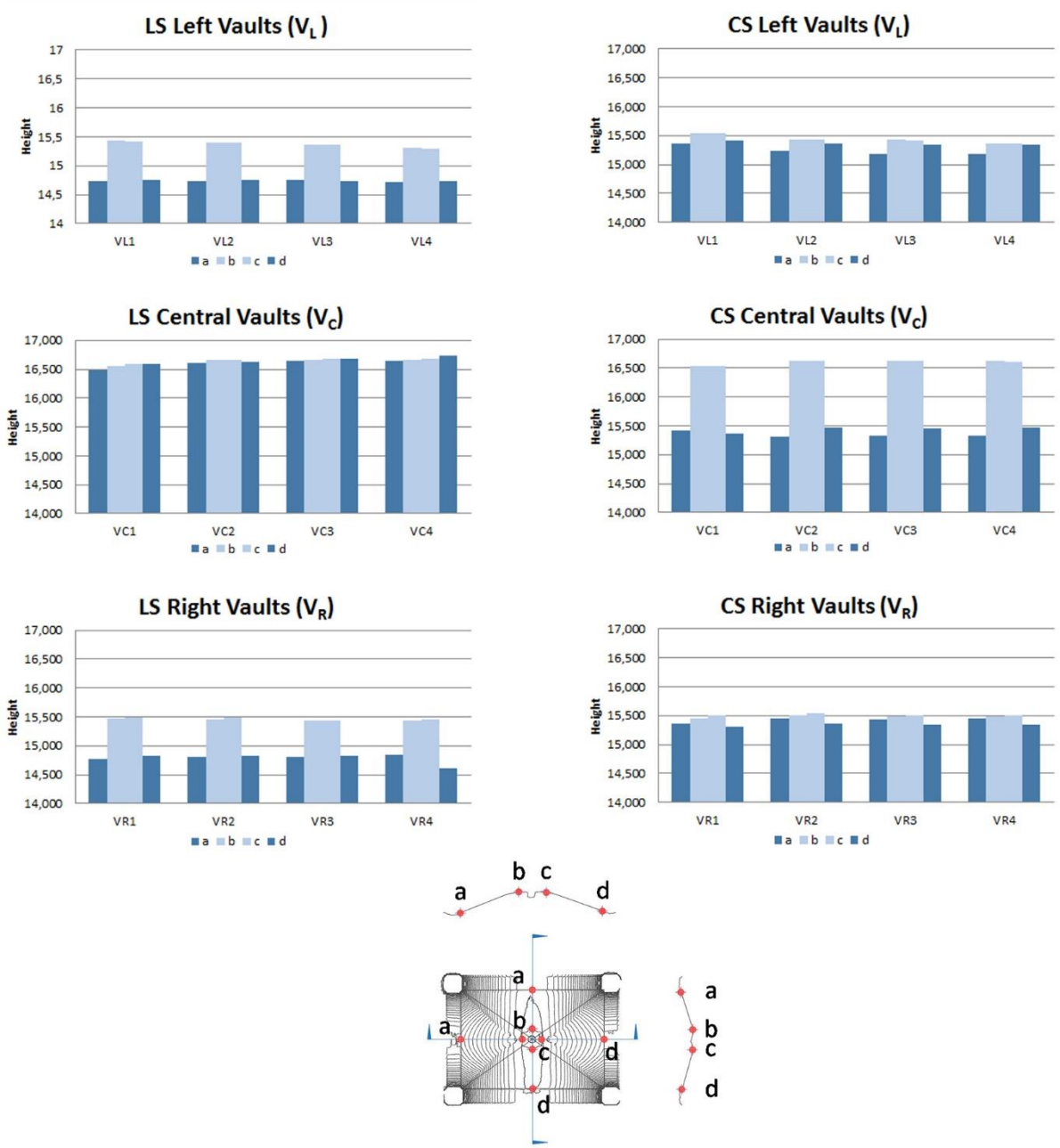


Figure 5. Values obtained in vaults for Left side aisle (V_L), Right side aisle (V_R) and the central nave (V_C), according to axial axis (LS_i) and (CS_i).

3.2 3D Assessment

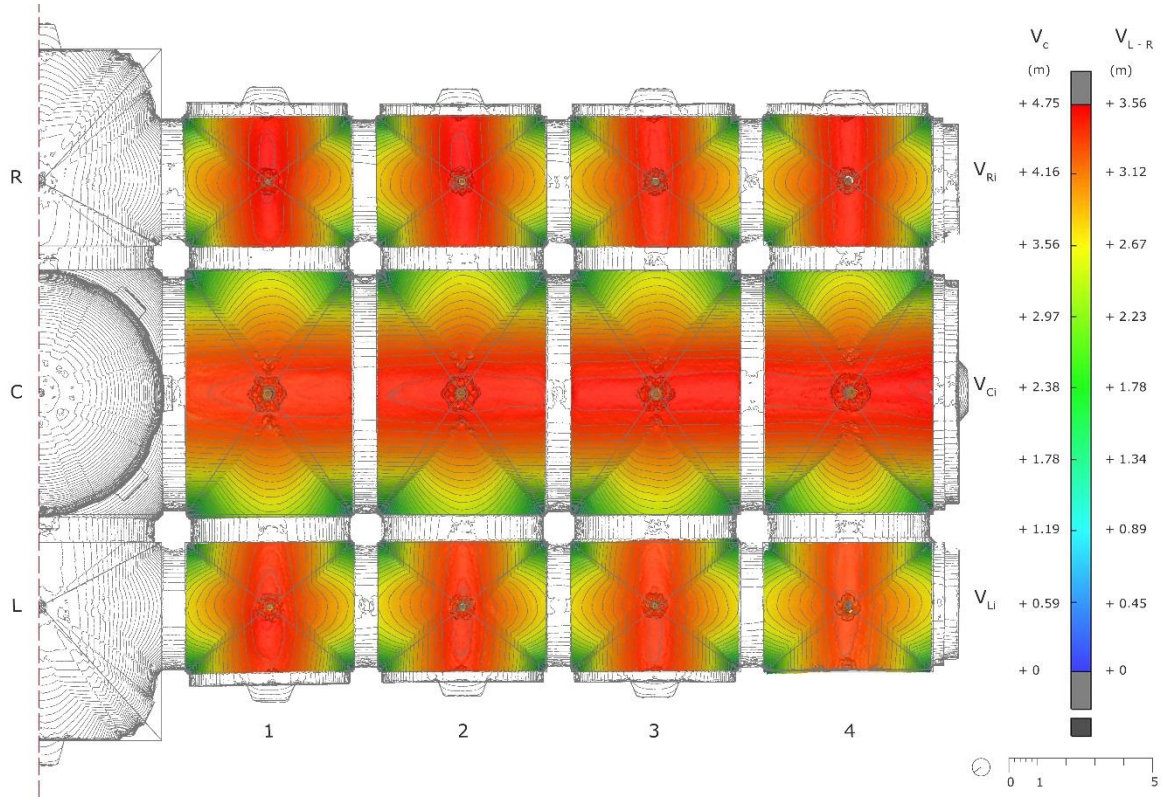


Figure 6. 3D Assessment of the vaults. Comparison with horizontal planes.

The topographical representation of the vaults revealed that most of the elements are very similar, since no relevant differences can be seen. The visualization includes the maps of the vaults' relative heights and contour lines spaced every 10 cm (Figure 6). These data allowed a very intuitive interpretation of the vaults' shape. In the case of the church of Batea, vault V_{L4} has the most relevant differential gradient with respect to the rest of the rest of vaults. This is consistent with the results obtained in the 2D study. On the other hand, Figure 7 compares the distance distributions for each vault showed in Figure 6 (V_C, V_L & V_R). The ranges measured are mainly at a distance from the reference plane between 3.56 m - 3.12 m, and 2.67 m - 3.12 m, which represent the 69.6% of the points.

Regarding the assessment from primitives, the data of the elements of comparison are summarized in Table 1. The central nave has been analysed in comparison with the cylinder that best suits the geometry of the barrel vault part (Figure 8). The results show how central sections are which best fits the ideal cylinder, while the vault section near the dome is the least. As for the dome, it is compared with a sphere. A differentiation is made between the fundamental parts, nerves and shell, and a sphere is defined for each one (Figure 9). The study reveals a certain settlement of the upper part of the dome, due to the weight of the lantern. This deformation is not uniform, and the most settled area can be related with a deformation at medium height in the opposite quarter of the dome. It is remarkable that ribs did not reproduce the same differences regarding the shell.

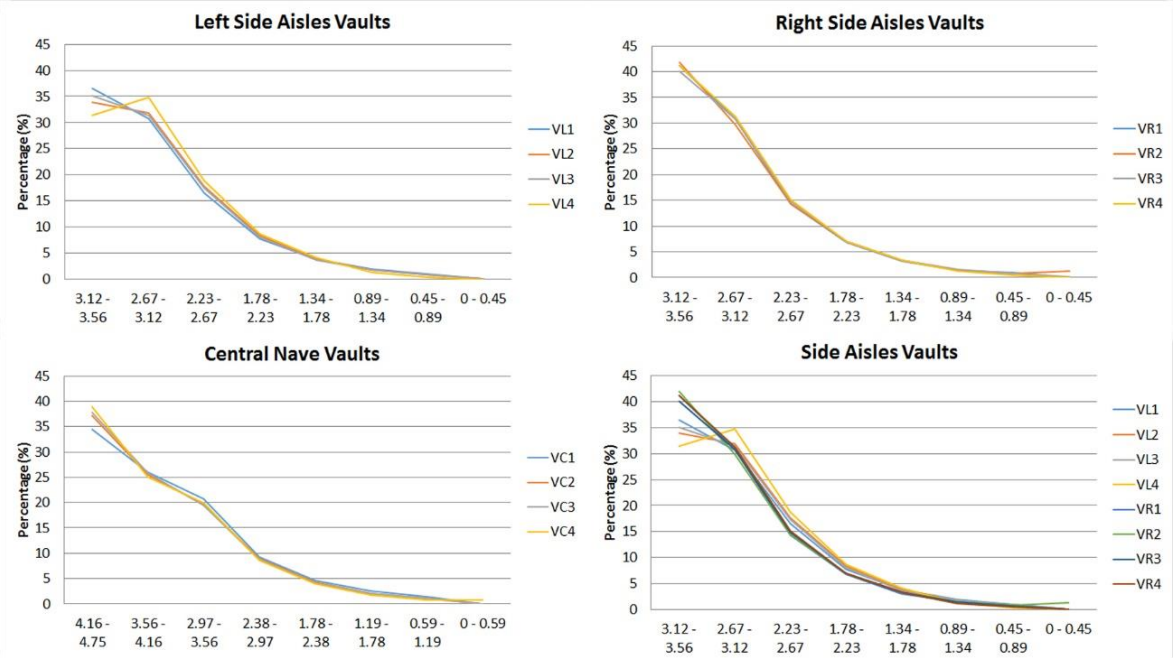


Figure 7. 3D vaults assessment. Graphics of ranges comparison.

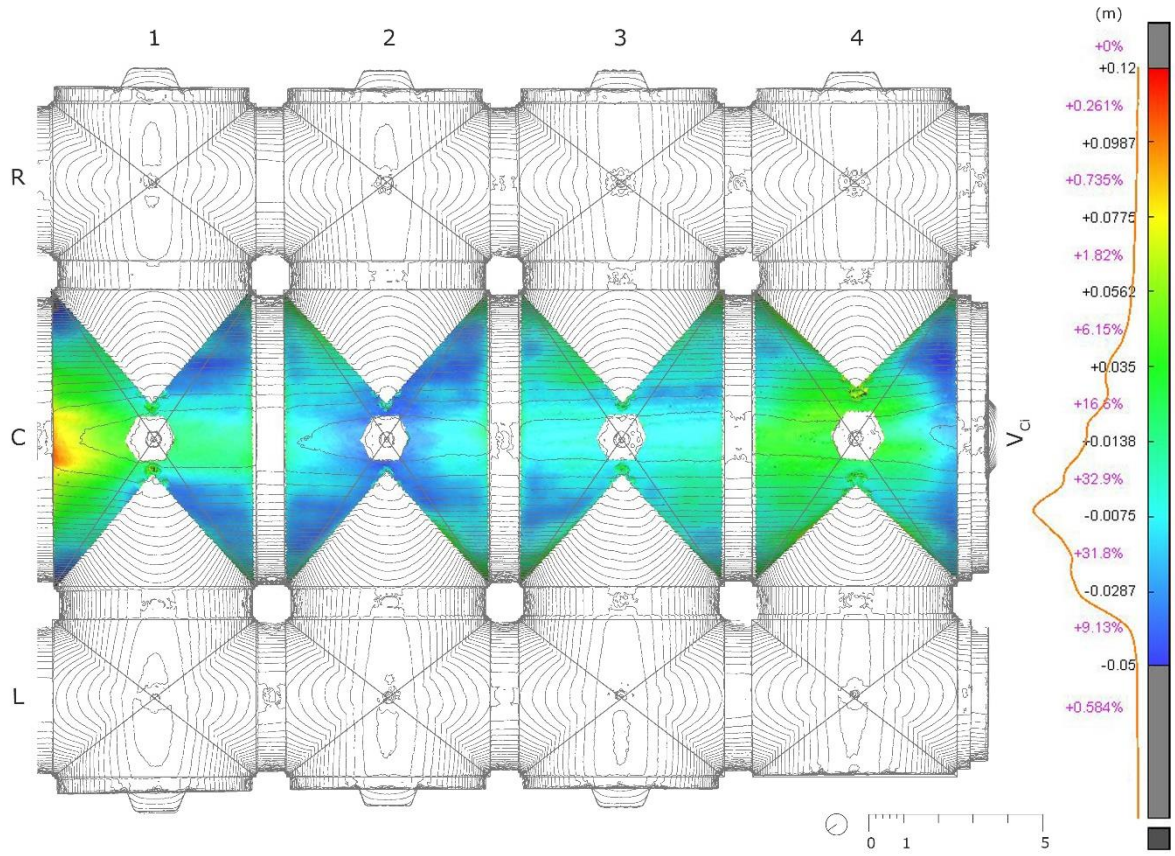


Figure 8. 3D assessment of the central vault from standard primitives.

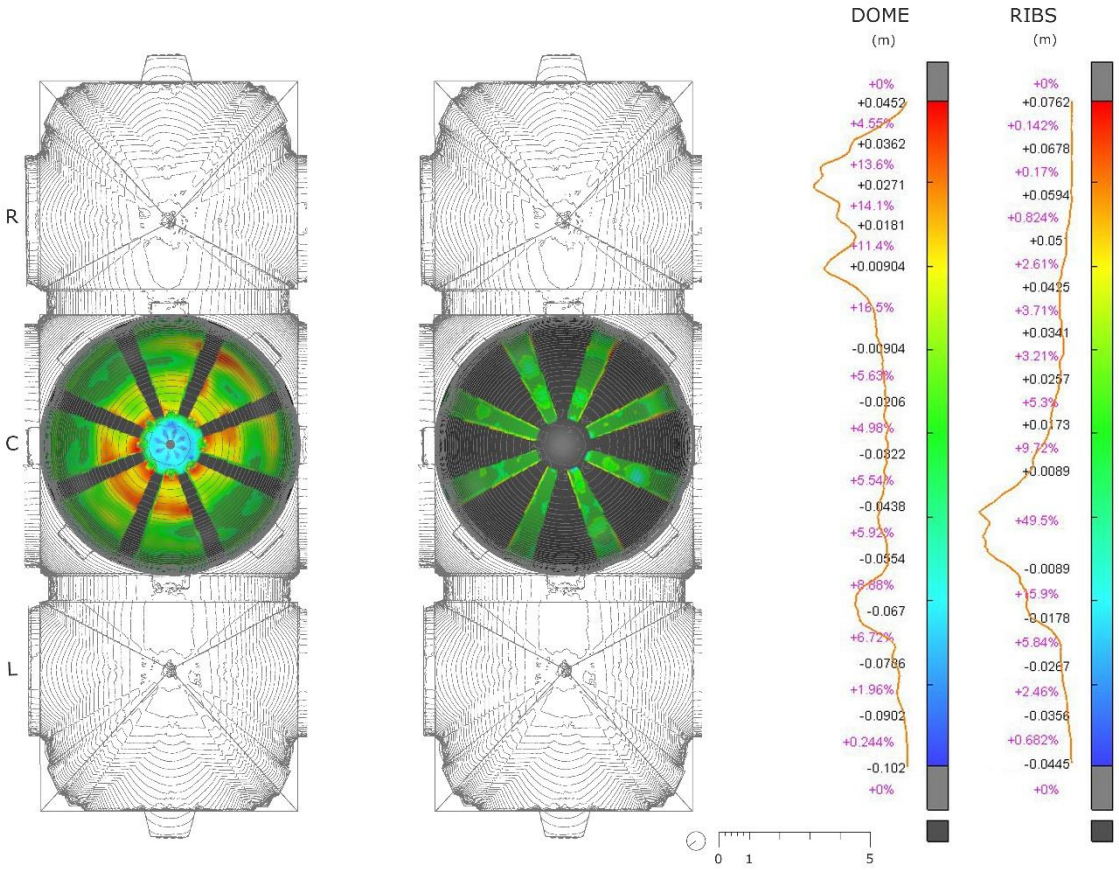


Figure 9. 3D assessment of the dome from standard primitives.

	Sphere (shell)	Sphere (ribs)	Cylinder
Height of Origin	21.949 m	22.024	12.251 m
Radius	4.680 m	4.270 m	4.243 m
Area	239.796 m^2	229.511 m^2	692.616 m^2
Volume	349.169 m^3	326.180 m^3	-
Length	-	-	25.962 m

Table 1. Main data of primitive forms of comparison.

4 DISCUSSION

The methodology used has allowed to parameterize the formal differences between the construction elements of the church of San Miquel of Batea. In general terms, no relevant discrepancies were identified, so the structure has hardly suffered formal alterations. The identified deviations usually have small values, with some exceptions, as in the case of some points of the vaults. Nevertheless, taking into account the size of the building, most of them have no impact on its state of conservation, although there are some trends that should be noted.

Cutting planes has revealed that the leaning of the pillars does not have the same value in parallel faces. There may be a certain execution error, but it is striking that systematically the highest values in the longitudinal sections (L_S) are produced towards the main facade, while in

the cross sections they tend to be higher on the face closest to the perimeter walls No differential movements have been observed in (y) between parallel faces. The average value of the displacements in (x) is 0.034 m, finding those of greater magnitude in $P2.2_{dB}$: 0,08 m) and ($P3.2_{dF}$: 0,088 m), which are caused by the action of the dome.

It is also noteworthy that the displacements of the pillars in the longitudinal direction (L_S) tend to decrease from the dome to the main facade, while in the transverse direction (C_S) they tend to increase, although with much smaller magnitudes. These values have no correspondence in the lateral pilasters, which have an average value of 0.025 m.

Regarding the arches, it can be seen that those located on the east side (A_L) are significantly lower than the analogs on the opposite side (A_R), with an average difference of 0.110 m. On the other hand, the height difference between the arches (A_L) is 0.030 m, with the exception of AL6, which is 0.190 m lower than the others. In the case of arches (A_R), all maintain a maximum difference of 0.080 m. Finally, the central arches (A_C) tend to increase their height from the dome to the main facade, with a maximum height difference of 0.380 m between them.

As for the vaults, the graphs show that in the side aisles, the transverse axis of the vaults tends to be horizontal, while the longitudinal one is pointed towards the key. This situation is reversed in the case of the central vaults. Thus the inclination of the axial axes of the vaults is related to the dimensions of the rectangle of the ground plane, and the inclined axis is the largest. The 3D study has shown a great similarity between analogous elements, although some alterations have also been identified, such as the vault V_{L4} and V_{C1}, which have a height significantly lower than their peers. In addition, it can be seen that the Lef Vaults (V_L) are noticeably lower than Right ones (V_R). Finally, it is observed that central vault (V_C) tends to be progressively higher from the dome to the façade.

Moreover, the study of the dome reveals a certain settlement of the upper part, due to the weight of the lantern. This deformation is not uniform, and the most settled area can be related with a deformation at medium height in the opposite quarter of the dome. It is remarkable that ribs did not reproduce the same differences regarding the shell. In any case, the values remain small, with a maximum distance of 0.045 m.

5 CONCLUSIONS

The use of massive data capture techniques such as Terrestrial Laser Scanner not only provides accurate geometrical information, but also valuable data about its structural state. The study has proposed a systematization of 2D and 3D operations to analyse a case study, based on a point cloud. Thus, it is possible to identify formal alterations that would otherwise be impossible to determine, and which can have an impact on the conservation of the building.

In the case of the church of San Miquel of Batea, the study has given quantitative and qualitative data about the formal anomalies of the construction elements. Most of that anomalies are no related with degradation processes, since there are no cracks or other related movements. For example, the lower height of the Left Aisle (V_{Li}) regarding the opposites (V_{Ri}) may be related to errors during the construction process, since no relevant movements in the supporting system have been identified, nor settlements in the pavement that can be related with that fact. Otherwise, other movements, such as the ones identified in pillars and pilasters, can be related with the settlement of the building, either during or after construction.

The methodology used can be easily exported to other buildings, and in fact it is easy to find

many examples of formal studies based on point clouds. Otherwise, it is always necessary to adapt to each specific case, since the characteristics of the buildings, such as size, decoration or complexity among others, conditions the data that can be analysed.

Further research should add the analysis of the exterior of the building and the extrados of the vaults. In addition, the numerical analysis of the structure should reach some light over the displacements identified. Finally, the study of the architectonic rules and possible influences, together with the historiography of the building and its context, would complete the understanding of the construction features.

Acknowledgements. The authors kindly want to thank Mn. Josep Alanyà, who facilitated access to the building under study and shared his wide knowledge. To Ana Maria Solís and Anna Saballs, who collaborated in the initial treatment of the study data.

REFERENCES

[1] M. Korumaz *et al.*, "An integrated Terrestrial Laser Scanner (TLS), Deviation Analysis (DA) and Finite Element (FE) approach for health assessment of historical structures. A minaret case study," *Eng. Struct.*, vol. 153, no. October, pp. 224–238, 2017.

[2] L. J. Sánchez-Aparicio, A. Villarino, J. García-Gago, and D. González-Aguilera, "Non-contact photogrammetric methodology to evaluate the structural health of historical constructions," *Int. Arch. Photogramm. Remote Sens. andSpatial Inf. Sci.*, vol. 40, no. 5W4, pp. 331–338, 2015.

[3] R. Kadobayashi, N. Kochi, H. Otani, and R. Furukawa, "Comparison and evaluation of laser scanning and photogrammetry and their combined use for digital recording of cultural heritage," *Int. Arch. Photogramm.*, 2004.

[4] P. Grussenmeyer, T. Landes, T. Voegtle, and K. Ringle, "Comparison methods of terrestrial laser scanning , photogrammetry and tacheometry data for recording of cultural heritage buildings," *Int. Arch. Photogramm. Remote Sens. Spat. Inf. Sci.*, vol. 37 (B5), pp. 213–218, 2008.

[5] S. Martínez, J. Ortiz, M. L. Gil, and M. T. Rego, "Recording Complex Structures Using Close Range Photogrammetry: The Cathedral of Santiago De Compostela," *Photogramm. Rec.*, vol. 28, no. 144, pp. 375–395, Dec. 2013, doi: 10.1111/phor.12040.

[6] F. Fassi, C. Achille, and L. Fregonese, "Surveying and modelling the main spire of Milan Cathedral using multiple data sources," *Photogramm. Rec.*, vol. 26, no. 136, pp. 462–487, Dec. 2011.

[7] J. Alanyà, *Sant Miquel de Batea. La catedral de Terra Alta*. Tortosa: Imprenta Querol, SL, 2019.

[8] A. Costa-Jover, J. Lluis i Ginovart, S. Coll-Pla, and M. López Piquer, "Using the terrestrial laser scanner and simple methodologies for geometrically assessing complex masonry vaults," *J. Cult. Herit.*, 2018.

[9] E. Quagliarini, P. Clini, and M. Ripanti, "Fast, low cost and safe methodology for the assessment of the state of conservation of historical buildings from 3D laser scanning: The case study of Santa Maria in Portonovo (Italy)," *J. Cult. Herit.*, 2016

[10] E. Bonali, A. Pesci, G. Casula, and E. Boschi, "Deformation of Ancient Buildings inferred by Terrestrial Laser Scanning methodology: the Cantalovo church case study (Northern Italy)*," *Archaeometry*, vol. 56, no. 4, pp. 703–716, Aug. 2014.

12th International Conference on Structural Analysis of Historical Constructions
SAHC 2020
P. Roca, L. Pelà and C. Molins (Eds.)

HISTORICAL ANALYSIS AND IN-SITU INSPECTIONS OF A CULTURAL HERITAGE MASONRY BUILDING

A. DE ANGELIS[1*], F. SANTAMATO[1], G. MADDALONI[1], L. DE FILIPPIS[2] AND M.R. PECCE[1]

[1]Department of Engineering, University of Sannio
Piazza Roma, 21, 82100 Benevento, Italy
e-mail: {adeangelis; francesco.santamato; giuseppe.maddaloni; pecce}@unisannio.it

[2] INAF – National Institute of Astrophysics
Salita Moiariello, 16 -80131 - Napoli
email: ldefilip@na.astro.it

Keywords: Historical Structure, Masonry, Historical notes, Non-Destructive Inspection

Abstract. *Recent seismic events that hit the Centre Italy have highlighted the high vulnerability of the historical and architectonical heritage that is the richness of the country, pointing out once again the difficulty of the assessment of monumental buildings such as churches or historical palaces, due to their uniqueness, the absence of a design, the limitation of invasive in situ tests, but the importance of the knowledge to understand the seismic behavior more than the static analysis under the gravitational loads. In the present paper the knowledge procedure is framed considering the case study of an important nineteenth century astronomical observatory, constructed in 1816-1819. The building, located in Naples, in the southern of Italy, classified by the Italian code as an area of medium seismic hazard, is analyzed by the use of integrated investigation activities such as coring, flat jack tests, georadar to obtain all the information due to the variability of the materials and the influence of previous alterations and repairs, that are data all necessary to develop a reliable model.*

1 INTRODUCTION

Historic and monumental constructions are the most important part of the cultural heritage of a Country and it is very important to protect those structures since they have an inestimable artistic value but also because they are open to the large assemble of people. In Italy the protection of the historical heritage against seismic hazard is paramount and requires the definition of reliable models able to represent the actual architectural, constructional and structural configuration. Thus, a preliminary diagnostic phase through geometrical surveys, photographic documentation, mapping of materials and construction techniques, decay pattern surveys play an important role for the collection of all data as extensively documented by scientific literature [1,2,3,4]. This phase of knowledge is particularly difficult because the historical constructions are always quite singular cases for which the same investigation plan cannot be applied, therefore the first step is to tailor it.

It is also worth to underline that during their life historic structures have experienced many

actions and earthquake loads that contributed to cause a non-stopping, gradual transformation of the structure [5]. Another challenging task, closely linked to the history is the understanding of the design concepts and construction technique. Their knowledge could provide precious empirical information for the analysis and the possibility of applying conventional methods of modelling.

Therefore in order to well proceed in the assessment of an historical building, the first step is the attainment of a sound knowledge of the erection history to individuate the technique and materials used. With this perspective and aiming at the seismic protection of the building, this paper deals with the knowledge and investigation phases of an important nineteenth century astronomical observatory, constructed in the period 1816-1819, that is "the Astronomical Observatory of Capodimonte", located on a hill in Naples. The diagnosis phase was carried out through survey practices and not destructive tests such as geometrical and architectonical survey, cracking outline survey and analysis, semi-destructive tests, including essays and in situ single and double jacks tests for the mechanical characterization of materials. Actually, this diagnostic phase was preceded by a historical research in libraries and archives of documents related to the building's design and construction phases; the main aim is to interpret the historical notices in order to confirm the hypothesis on the masonry morphological and structural features of the monumental building set up based on the in situ investigation. In particular the importance of historical study and non-destructive investigations emerged clearly for the identification of the structure.

2 DESCRIPTION OF THE BUILDING

The "Astronomical Observatory of Capodimonte", one of the twelve Italian observatories, which together constitute the National Institute of Astro-Physics (INAF), the main Italian company for astronomical and astrophysical research from land and space, is located on top of the hill "Miradoris" in the city of Naples (Figure 1). The construction works of the original structure were promoted by Gioacchino Murat in 1812 but the structure was inaugurated thank to Ferdinando I of Borbone in 1819. Figure 1 shows the general view of the building.



Figure 1: General view of the Astronomical Observatory of Capodimonte in Naples.

As a preliminary step, the complexity of the building required to get hold of a detailed knowledge of its geometry. Therefore, a complete in-situ inspection was carried out for understanding the organization of the structure. The plan layout of the ground floor of the astronomical observatory is reported in Figure 2. The building was realized using tuff (natural

volcanic stone) masonry typical of the Italian region where is located. The plan has an elongated rectangular shape and approximately its dimensions are 65 m × 20 m. The construction has two stories; both the underground floor and the ground floor are approximately 4.0 m high. The thickness of the walls varies between 1.00-1.55 m at the underground floor, where it was not always possible to do the measure, and 0.50-1.00 at the ground floor. A particular feature of this building is due to the presence of a heavy stone cladding whose thickness equal to 25 cm was measured by means of a hole. This aspect is particularly important in a seismic analysis as it behaves as an additional mass.

The main entrance to the building is preceded by a pronaos surmounted by an architrave, the tympanum and other classical elements of the Greek temple architecture. In the building it is possible to recognize three main blocks: a central square block and two rectangular lateral blocks. The main rectangular room (central atrium) is characterized by two lines of marble columns and it is covered by a barrel vault with a glass skylight. Also, the lateral zones adjacent to the central atrium, are covered by barrel vaults or hemispherical dome, except the last rooms at the two ends that were added in 1935 using the same stone for masonry while the floor was realized by iron beams and clay tiles.

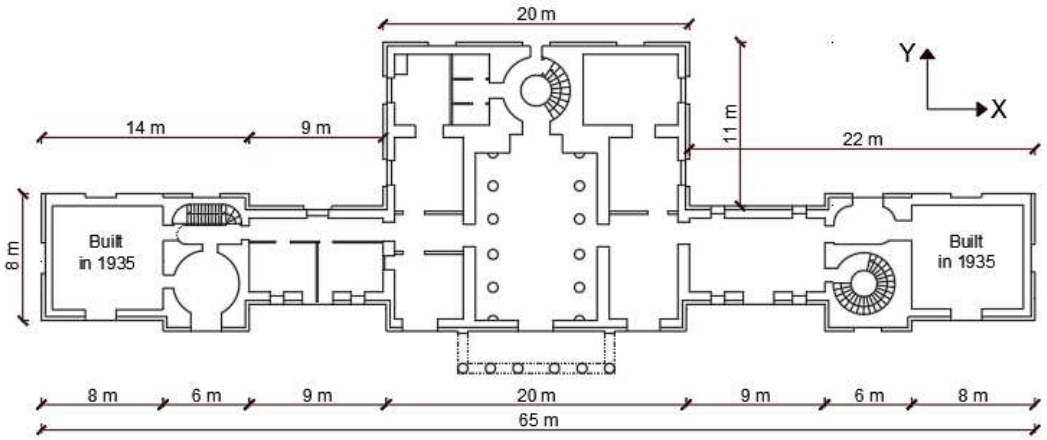


Figure 2: Plan layout of the ground floor.

3 HISTORICAL NOTES

The historical reconstruction is necessary to understand the phases and techniques of erections. Referring to an historical document found in the building archive named “Ragguaglio del reale Osservatorio di Napoli eretto sulla Collina di Capodimonte”, it is clear how the first design ideas were different and the construction of the entire building was troubled changing also during the works.

A conceptual design by Stefano Gasse, dated June 1812, included a facade similar to a classical temple with a monumental entrance formed by a tetrastyle pronaos which was reached by a staircase. Consulting other historical documents, it seems valid the hypothesis that the works corresponding to this project, reported in Figure 3 a, together with the coin celebrating the start of the work, were partially realized. In particular, the external and internal circles and the lateral wings may have been completed (the western one also completed with travertine cladding).

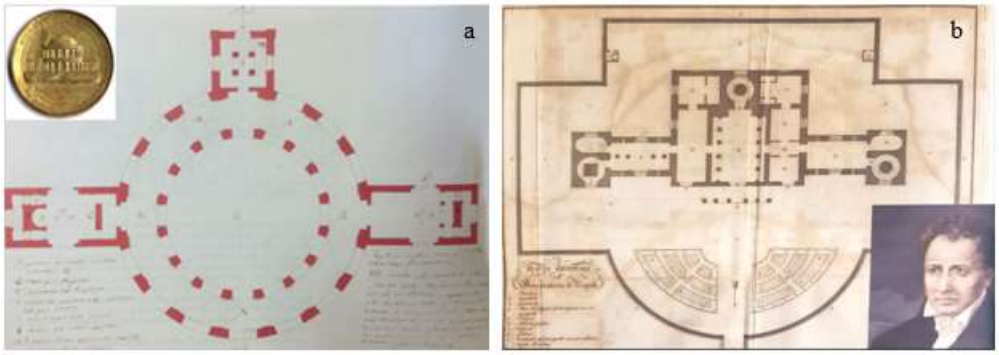


Figure 3: a) First project designed by Stefano Gasse in June 1812; b) Design of the built building.

However, the work was not completed for political and artistic reasons which led to a substantial change in the shape of the central part. The final design for the central part is that shown in Figure 3b. Therefore, it could be assumed that the plan of the ground floor of the historical building was founded on the plan envisaged by the project shown in Figure 3, but with the execution of "demolitions and excavations", as written in the historical documents, to support the walls and columns on appropriate underground walls. Unfortunately, the underground plan is not completely accessible, especially the central room, that was completely changed during the work, is closed along the perimeter. However, the considerations above introduced find partial comfort from the observation of some photos (Figure 4) of the works for the realization of an Auditorium in 1982 at the underground level adjacent to the front of the central part of the building, as better explained in the following.



Figure 4: Works for the realization of the Auditorium in 1982.

In fact, from the photos it is clear that the external circumference and the radial corridors surmounted by main and secondary arches, in accordance with the project of Figure 3a, had actually been constructed at the level currently buried in the square in front of it. Figure 5 shows the overlap of the current plan of building and the project designed by Stefano Gasse, suitably scaled considering the palm-meter conversion. This hypothesis is not surely confirmed underlining the great difficulties related to the identification of the structure of the underground

level, that is of paramount importance for the structural analysis especially under seismic actions.

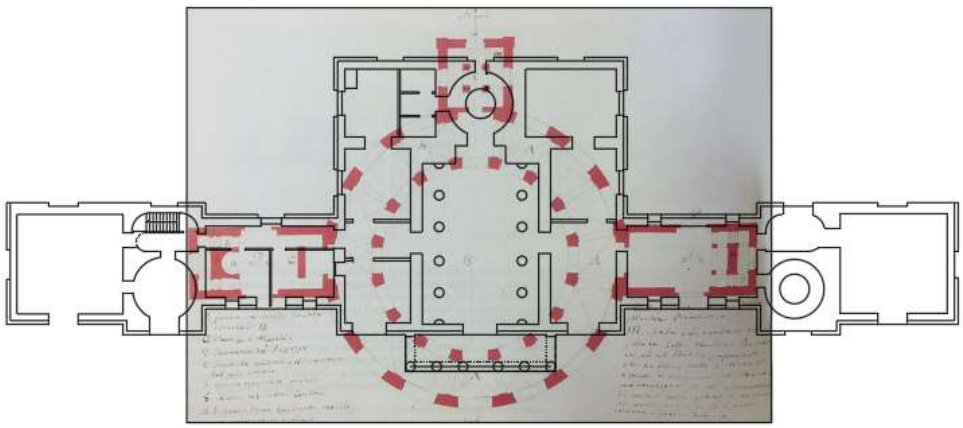


Figure 5: Overlap of the currently plan of the historical building and the project designed by Stefano Gasse.

The building was completed in 1819 but it has undergone some changes during the time especially when two rooms on two extreme sides in the longitudinal direction were realized in 1935 (Figure 3a and Figure 6), as written in other documents. Albeit the new parts were designed to be integrated in the same style of the original building they can be distinguished by the presence of a coating and a cornice in mortar and not in natural stone as for the ancient construction. Furthermore, the connection of the two new end rooms required a reorganization of the original end rooms changing the door positions and removing a large masonry column visible in the original plan in Figure 3b, that supported a telescope.

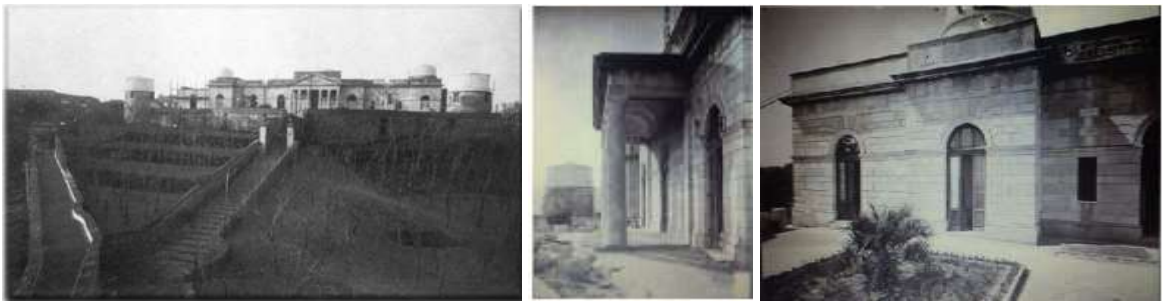


Figure 6: Enlargement work of the building in 1935.

Further interventions were realized over the time along the perimeter with the construction of two buildings separated by a joint which were built by emptying the soil contained in the boundary wall of the courtyard in front and behind the observatory. Figure 7 show a complete layout of the underground level of the building including the boundary wall, the auditorium built in 1982 and the library built in 1990.
Probably the soil contained between the basement of the building and the surrounding boundary wall was a carryover soil in 1819 after the conclusions of the original works, since the first

design of the monumental building elaborated by Stefano Gasse provided that the entrance was at the level of the currently underground floor (see the coin in Figure 3a).
Nevertheless the real configuration of the basement, where the rooms with filling in the plan of Figure 7 are not accessible is still uncertain; in fact some zones as the central atrium, visible from the photo in Figure 8 taken during the construction of the auditorium, probably are empty while others as the side areas of the atrium are presumed to be full of soil because after the realization of some structural elements in shaped excavation the soil wasn't removed.

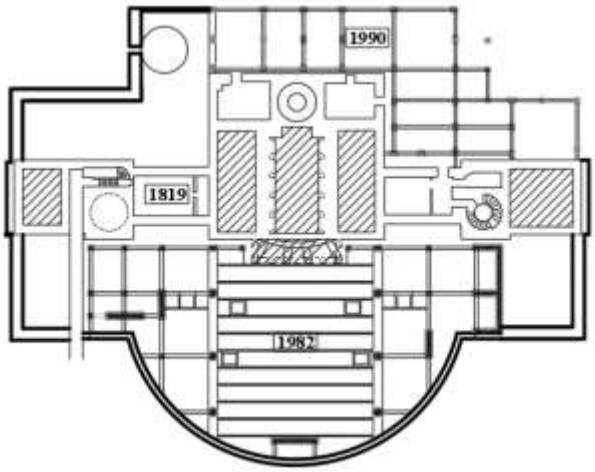


Figure 7: Complete layout of the basement.



Figure 8: Photos of the working construction of Auditorium in 1982.

3.1 Geo-radar investigation

Since the distribution of the underground layout is still uncertain, a survey was carried out by means of a georadar, to obtain further information on the inaccessible internal environments with the aim of validating the hypotheses bases on documents and photos. The RADAR

technique was developed in geophysical field for the study of the soil but it is currently employed successfully in archaeological investigations and new applications are even available for investigation on the foundations of buildings. The technique seems from one hand to be most promising, from the other it still needs of further studies and researches [6]. The method is based on the propagation of short electromagnetic impulses, which are transmitted into the building material using a dipole antenna, composed by an emitter and an acquisition unit. The impulses are reflected at interfaces between materials with different dielectric properties, i.e. at the surface and backside of walls, at detachments, voids, etc. The possibility to assess in depth the investigated structure depends on the frequency of the equipment: antenna with high frequency (2 or 5 GHz) is recommended for detailed analysis of the external layers of the composite structures, ensuring the propagation of electromagnetic impulses with short wavelength. On the contrary, antenna with low frequency (i.e. 600 MHz) generates long wavelength, indicated for characterizing large structures, but not always able to guarantee an appreciable resolution [7].

In this case the onsite investigation of the building was supported by high frequency radar scanning. The sections investigated, concentrated mainly in the central atrium area are shown in Figure 9.

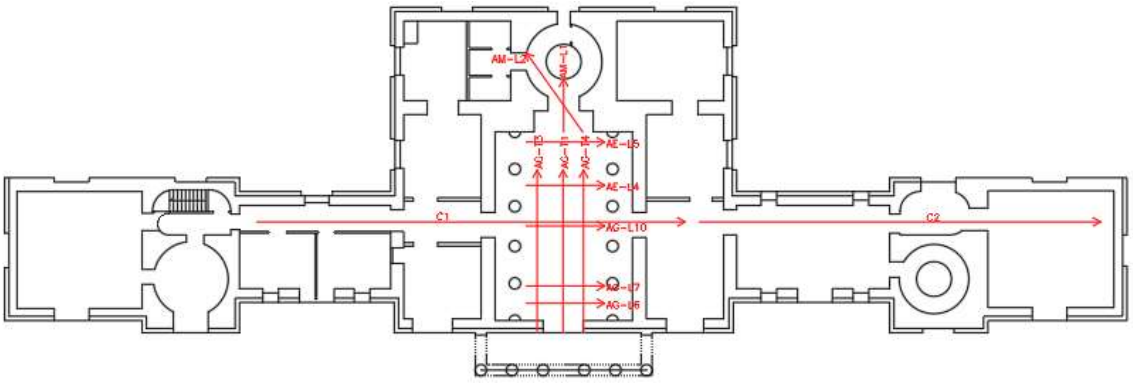


Figure 9: Section investigated by georadar.

Only the most important results produced as radargrams, i.e. grey scale intensity charts giving the position of the antenna against the travel time, are reported. The radargram acquired along the corridor (Figure 10 and Figure 11) in the longitudinal direction gives a lot of information about the presence of walls, vaults and the detection of the fully and empty zones of the underground level. For the analysis of the results it should be considered that the small waves continuous along the depth with a hyperbolic shape correspond to a presence of a wall instead small hyperbolic waves at variable depths should correspond to the presence of a vault. The areas where the response is characterized by the absence of reflections can be considered fully of soil, while all areas where there is a very dense set of points can be considered empty.

The interpretation of the radargrams in the transversal direction is more challenging as the profiles are much shorter. In detail, for example, the radar profile AG-T1 (Figure 12) shows an initial area with quite regular hyperbolical reflections at variable depths, probably due to presence of a vault. Right after, from the middle to the end of the radargram reflections due to

voids can be observed. Instead in the middle part of the radargram AM-L1, hyperbolic waves continuous in height are shown suggesting the presence of walls while the reflections at the end of the radargram are indicative of the continuation of the circular column at the stairwell up to the basement. It should be noted that despite the analysis of historical documents, the execution of the surveys and investigations also by means of georadar was important.

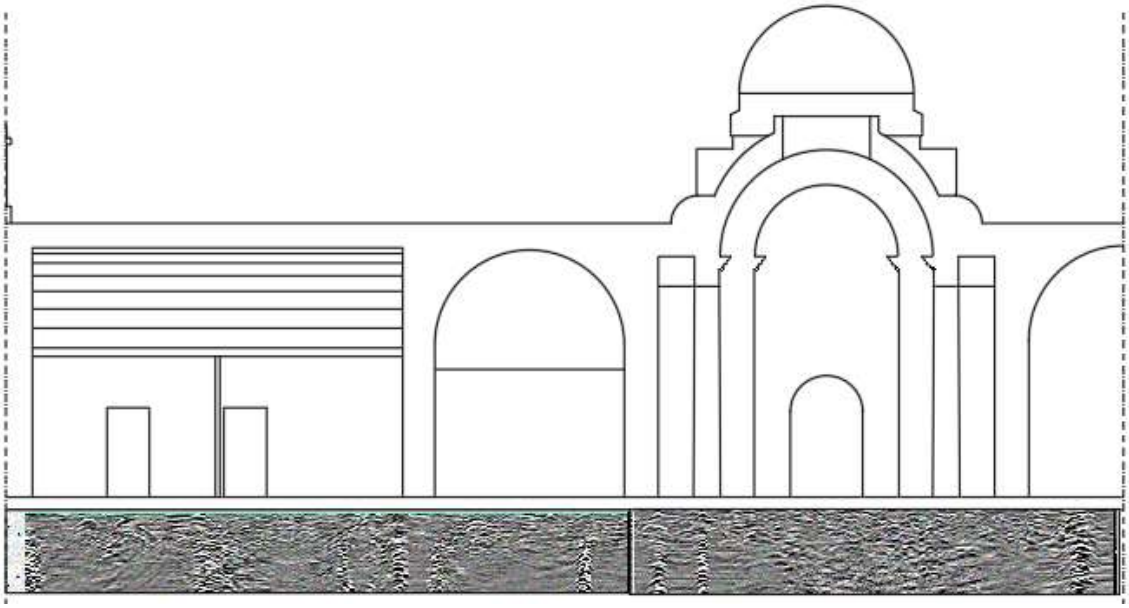


Figure 10: Radargram along the corridor C1 in longitudinal direction.

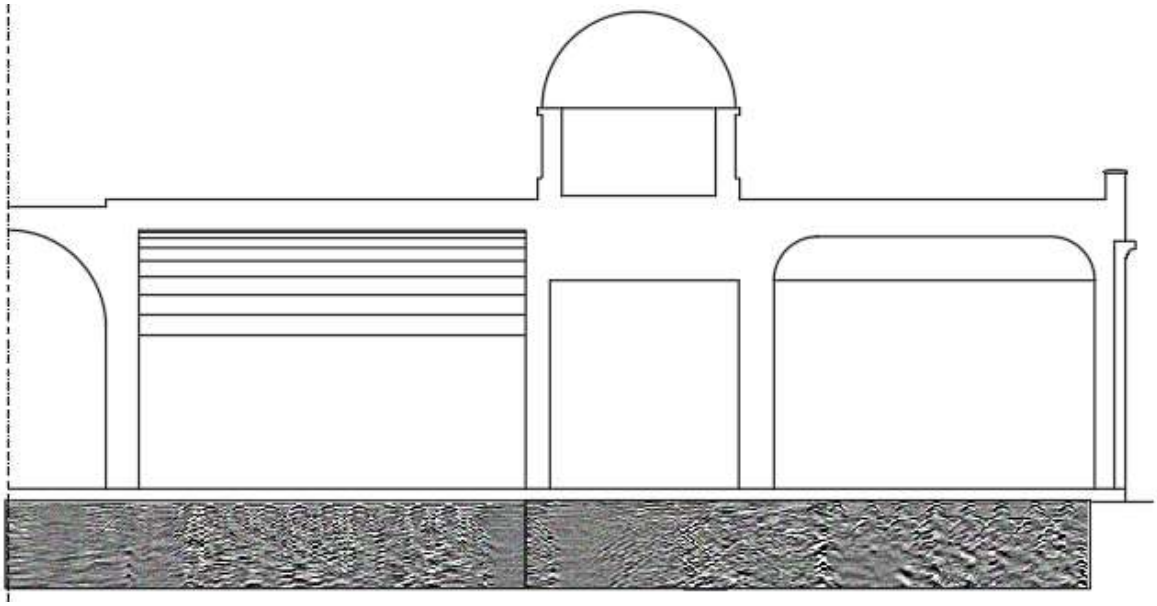


Figure 11: Radargram along the corridor C2 in longitudinal direction.

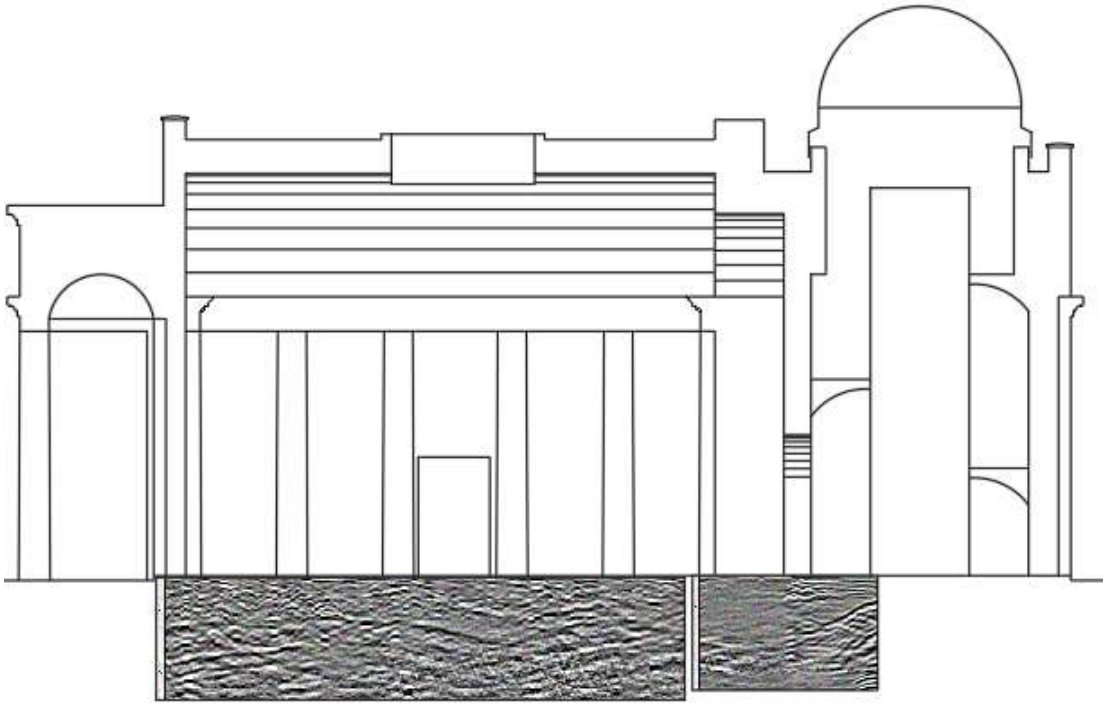


Figure 12: Radargram AG-T1, AM-L1.

4 CRACK PATTERN SURVEY

By direct visual inspection (July, 2019) it was possible to notice the current damage level of the historical building in terms of cracks and material decay. The majority of cracks are visible in the central atrium, on the lintels of the doors and windows and the vaults of the ground and underground floor. In particular a crack (Figure 13) was found at the stone frame of the arched entrance door on the outside but some slight cracks also branch off on the inside. An essay was carried out by creating a pocket of 50 cm x35 cm, seeing that the crack affects the tuff blocks that make up the vault and affects the entire thickness of the wall. The crack is probably a local phenomenon due to the tension stresses at the intrados of arch key.

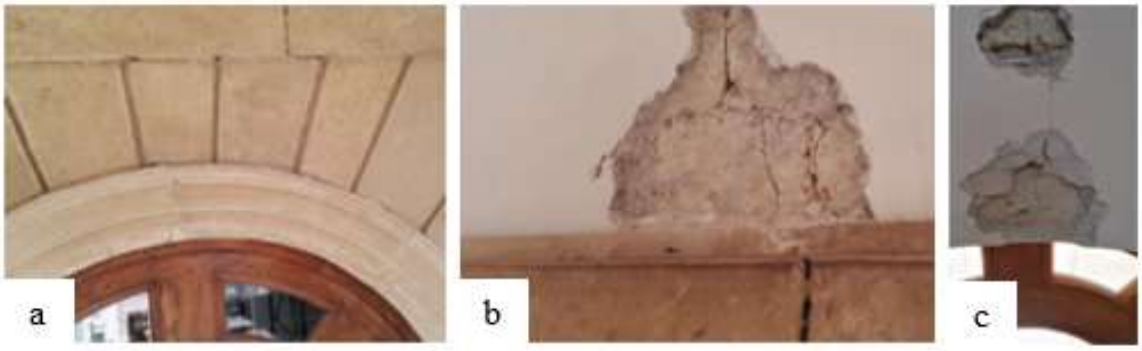


Figure 13: a) Crack at the stone arch of the entrance door; b) external essay; c) internal essay.

Another area affected by widespread cracks is that in the back side of the building where there is a spiral staircase with a central circular column that allows access to the roof.

The upper part of the spiral staircase is closed by a vault which has a lot of cracks (Figure 14 a), typically visible along the key of the vault where the maximum tension stress occurs. In fact, when the plaster was removed for an area of about 30 cm x 30 cm and a hole was realized through the thickness of the vault, it resulted made by one red brick 4 cm thick, that is a very thin structure sensible to bending effects. Another crack was visible in the middle of the entrance to the spiral staircase, therefore it was investigated removing the plaster (Figure 14b). It was observed that the entrance was realized without a stone or wood lintel even it is approximatively plane and not really an arch, thus the crack is due to bending effects.

Other widespread cracks due to the absence of lintels were found at all the openings (doors and windows) of the rooms of the building (Figure 14 c) while slight cracks were found at the barrel vaults covering some rooms (Figure 14 d). All the cracks appear as local phenomena due to the low strength of the masonry in tension and degradation of the mortar but they don't indicate a local or global failure mechanism.

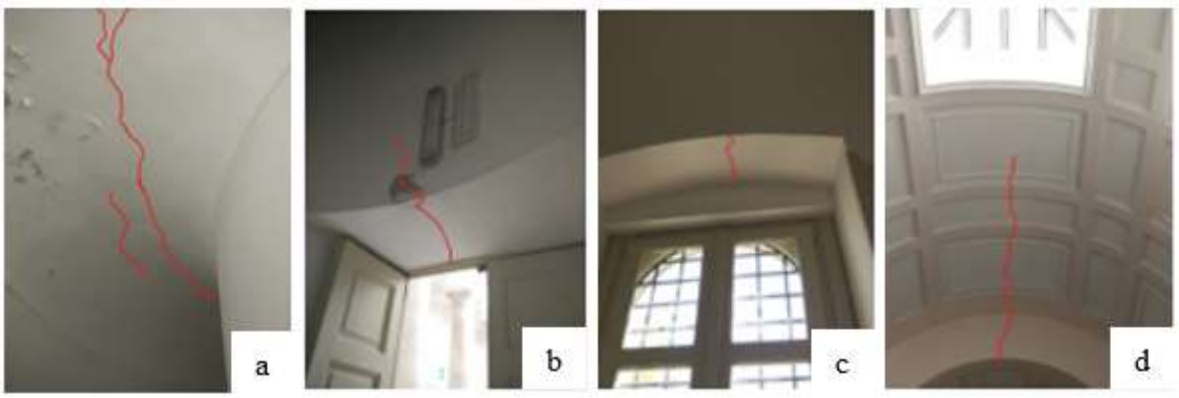


Figure 14: Crack at the vault (a) and the entrance (b) of the staircase; c) crack due to the absence of lintels; d) barrel vaults crack.

Finally, a vertical crack is located at the midspan of the stone lintel of the pronaos (Figure 15 a) that is actually shored up. An assay was performed at the crack on the internal side of the pronaos to check the stones of the vault that is supported by the stone lintel (Figure 15 b). The tuff block 28 cm thick used to realize the vault resulted not cracked confirming that the damage regards only the stone lintel and it is caused by the tensile stresses in bending together with the stone degradation (Figure 15 c) due to uncorrect raining water disposal.



Figure 15: Crack at the midspan of the stone lintel (a-b); c) essay at the internal side.

5 IN SITU SEMI-DESTRUCTIVE EXPERIMENTAL TESTS

The diagnostic tests are usually divided in two categories: qualitative and quantitative tests. Qualitative tests, as the non destructive ones [8] previously introduced, provide generic information and cannot be directly related to the physical and mechanical parameters of the materials forming the structures. On the contrary, quantitative results can be obtained by minor destructive or destructive diagnostic tests ensuring a deeper level of knowledge of the structure characteristics. In this case three tests with flat jacks were carried out; in particular a single flat jack test was performed to ensure the determination of the actual compression stresses in the masonry walls, useful for validating a numerical model.

The test was carried out by introducing a thin flat-jack into the mortar layer. A compression stress of approximately 0.25 MPa was obtained. Instead, two double flat jacks were performed to identify the mechanical characteristics, one in the more ancient part of the building and one at the extreme side rooms constructed in 1935. For the main original part of the building, the Young modulus E and the Poisson ratio υ resulted equal to 905 MPa and 0.2 respectively whereas the volumetric weight is ρ=14 kN/m^3 and the masonry average compressive strength is f_m=2 MPa. Instead for the newer zones, the Young modulus E and the average compressive strength f_m resulted equal to 450 MPa and 1.5 MPa, respectively.

It worth to note the values related to the old part of the building are in good agreement with the results from laboratory tests on Neapolitan yellow tuff masonry [9] showing a mean compressive strength equal to 2.78 MP and an experimental Young's modulus varied between 630 MPa and 2943 MPa. Instead, the values related to the new part of the building are at least 50% lower than the previous ones. The results evidenced the higher quality of the material and hand-making of the more ancient construction conversely to the idea that new structure could have better performances.

6 CONCLUSIONS

The procedure of knowledge of the case study of the "Astronomical Observatory of Capodimonte", located in Naples, is useful to underline the importance of an accurate historical investigation for the structural identification of monumental constructions also to guide the in-situ test campaign. In fact, the hypothesis on the masonry morphological and structural features of the monumental building were necessary to plan the type of tests and their location.

The geometrical survey together with a georadar investigation allowed to better assess the organization of the underground floor not completely accessible. However, the mechanical properties of the materials have to be necessarily recognized through in situ semi-destructive tests like flat jacks, because some types of stone realized in various periods can give different resistance as in the case study. The visual inspection with the survey of the crack distribution in masonry can give a reliable framework of local or global mechanisms due to the low strength of the material in tension.

The investigation described in this paper was the first necessary step for the reliable structural analysis of the building that is in progress confirming the importance of the detailed identification of the underground floor.

Acknowledgements. The work was carried out within the framework of the PON Research and Innovation 2014-2020, Axis I-Investments in Human Capital, MIUR notice AIM-"International Attraction and Mobility"-Line 1, Project: AIM 1823125-3 – Cultural Heritage. The authors are also grateful to Dr. Raffaele Zollo for his help with the georadar test.

REFERENCES

[1] Binda, L., Saisi, A., Tiraboschi, C. *Investigation procedures for the diagnosis of historic masonries*, Construction and Building Materials, (2000) **14(4)**, pp. 199-233.

[2] Roca, P., González, J. L., 2001. *Morphology, Structure and History. The case study of the upper flying arches of Mallorca Cathedral*. International Millenium Congresso More than two thousand years in the history of architecture, Ib 22, Paris: ICOMOS 2001

[3] Ramos, L., Casarin, F., Algeri, C., Lourenco, P.B., Modena C. *Investigation techniques carried out on the Qutb Minar, New Delhi, India*. In Proceedings of the 5th international seminar on structural analysis of historical constructions. New Delhi, India, November 6–8, 2006.

[4] Bosiljkov, V., Uranjek, M., Žarnić, R., Bokan-Bosiljkov, V. *An integrated diagnostic approach for the assessment of historic masonry structures*. J Cultural Herit (2010) **11(3)**:239–249.

[5] Roca P. Considerations on the significance of history for the structural analysis of ancient constructions, Structural Analysis of Historical Constructions IV, Padova: University of Padova (2004).

[6] Binda, L., Saisi, A., Zanzi, L. *Radar Investigation and Diagnosis of Historic Masonry*, 12th International Conference Structural Faults and Repair (2008), Edinburgh 10–12/06/08, CD-ROM.

[7] Maierhofer, C., Leipold, S. *Radar investigation of masonry structures*. NDT&E Int (2001), **34 (2)**:139–147.

[8] McCann, D.M., Forde, M.C. *Review of NDT methods in the assessment of concrete and masonry structures*. NDT&E Int (2001), **34(2)**:71–84

[9] Marcari, G., Fabbrocino, G., Lourenço, P.B. *Mechanical properties of tuff and calcarenite stone masonry panels under compression*. In: Proceedings of the eight international masonry conference (2010). International Masonry Society; Technische Univesität Dresden., Dresden, Germany

12th International Conference on Structural Analysis of Historical Constructions
SAHC 2020
P. Roca, L. Pelà and C. Molins (Eds.)

IDENTIFICATION AND ASSESSMENT OF THE SEISMIC BEHAVIOUR OF GIOTTO'S BELL TOWER IN FLORENCE (ITALY)

PAOLO SPINELLI[1] AND MICHELE BETTI[1*]

[1]Department of Civil and Environmental Engineering (DICEA)
University of Florence
Via di Santa Marta, 3, I-50139, Florence, Italy
e-mail: {paolo.spinelli, michele.betti}@unifi.it

Keywords: Historical Structure, Masonry, Bell tower, FE Model, Seismic behaviour

Abstract. *Among the different typologies of historic buildings, masonry towers represent a hallmark of many European town centres which embody an important heritage to be preserved and passing on to future generations. Giotto's Bell Tower in Florence together with the Leaning Tower of Pisa and the San Marco Tower in Venice (which collapsed in 1902) is one of the iconic masonry towers ever built in Italy. The assessment of the structural behaviour of these structures, together with the development of proper preservation strategies, has attracted in recent decades the interest of a plethora of scholars. Most of the studies on towers vulnerability focuses on the assessment of their seismic behaviour, since their slenderness exposes them to the dynamic effects induced by medium-to-severe earthquakes. This paper, given this background, discusses the identification and the seismic behaviour of Giotto's Bell Tower in Florence. In a first part of this paper a refined numerical model, built through the finite element technique based on a recent laser scanning survey, is reported together with the procedure adopted for its modal identification. The finite element model accounts for the soil-structure-interaction. In a second part of this paper the numerical model is employed to perform linear time-history analyses, by using natural accelerograms. The results of the analyses allow to assess the seismic behaviour of the Bell Tower of Giotto and suggest preservation strategies*.

1 INTRODUCTION

Bell and masonry towers represent a structural typology characteristic of many Italian and European cities. Usually, as for the Florentine case, they are close to churches in the form of tall and slender structures that symbolically characterize and define the image of the historic city. Giotto's Bell Tower in Florence, together with the Leaning Tower of Pisa and the San Marco Tower in Venice (collapsed in 1902), represents one of the most famous bell towers in Italy.

The assessment of the vulnerability and the seismic risk of this particular typology of structures has seen a rapid growth in recent decades, as a result of the interest aroused by them within the scientific community. Recent examples of these studies are: the masonry bell tower of Sant'Andrea in Venice (Italy) [1], the bell tower of the Monza Cathedral (Italy) [2], the Sineo tower (Alba, Italy) [3], a masonry tower of the 8th century, the bell tower of Our

Lady of Mercy (Valencia, Spain) [4], the bell tower of the Church of Santa Justa and Rufina in Orihuela (Alicante, Spain) [5], and the Ghirlandina Tower in Modena [6].

Research range from experimental works [7] [8] [9] to dynamic identifications [2] [4] [10] [11]. Generally, starting from a field test survey of the current configuration by means of non-destructive and/or weakly destructive experimental tests (e.g. tests with flat jacks, dynamic tests, sonic tests, etc.), numerical models of the structure are built by using the finite element (FE) technique. The numerical models thus created are subsequently employed to analyse the response of the structure due to exceptional load conditions (e.g. earthquake). The purpose of the experimental tests is to estimate the unknown parameters of the numerical models whose calibration is carried out by comparing numerical and experimental results. The type of analysis for which the model is used differs for the analysis methodology used: linear or non-linear (pushover) static analysis and linear or non-linear time-history analysis [12] [13] [14] [15] [16] [17] [18]. Pushover approaches include both standard methodologies in which the load profile remains constant during the development of the analysis ([15] [17]), and multimodal and/or adaptive approaches, although Peña et al. [14] have shown that the multimodal approach cannot satisfactorily reproduce the collapse phenomena that are activated in masonry towers during the seismic loading). As for the modelling technique, the finite element technique is the most frequently used, allowing an accurate reproduction of the physical geometry of the tower, and the various models differ according to the level of complexity and geometric discretization (from 1D models to 3D models [3] [13]).

This paper, which is part of a multidisciplinary research activity about Giotto's Bell Tower promoted by the "Opera di Santa Maria del Fiore", analyses the dynamic and seismic response of the this heritage masonry tower. The analysis and the assessment of the structural behaviour of Giotto's Bell Tower is carried out by using a numerical model build using the finite element (FE) technique. The numerical model is first identified on the basis of the available experimental results (dynamic tests and geotechnical results) and then it is used to perform time-history analysis on the basis of a series of seismic histories compatible, by spectral shape and by seismic zone, with the site where the Bell Tower of Giotto is located.

2 GIOTTO'S BELL TOWER

During the research activities, different three-dimensional geometric models of Giotto's Bell Tower were built, based on the data gradually recovered during the research. The different geometries have been used to build different numerical models as described below.

A first three-dimensional reconstruction of the geometry was made on the basis of the tables published by Bernardo Sansone Sgrilli in 1733; this geometry was used for the preliminary simulations of the dynamic behaviour of the Bell Tower. Even with the inherent approximations, the numerical model built on the basis of this geometric information allowed to confirm the experimental results obtained by the Pieraccini et al. [20] and Lacanna et al. [21] by providing mode shapes characterized by the first mode shape oriented according to the directions of the main diagonals of the base section.

Subsequently, based on the results of a laser scanner survey, a second three-dimensional reconstruction of the geometry was performed. The geometry allowed the construction of a geometric detailed numerical model that includes: *i*) the largest openings in the wall thicknesses; *ii*) the stairwell inside the masonry walls; *iii*) the niches and other geometric

irregularities. The geometric reference model obtained from the laser scanner survey is shown in three-dimensional form in Figure 1a.

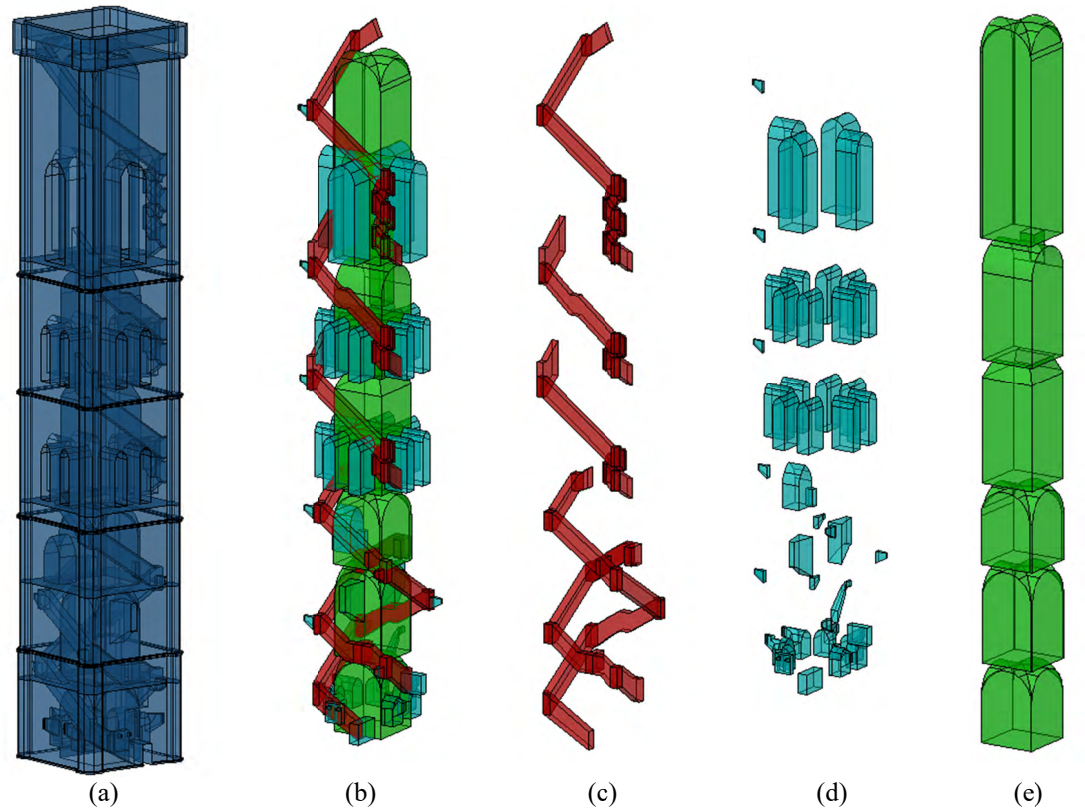


Figure 1: Perspective view of: (a) the geometry of Giotto's Bell Tower; (b) geometry of the empty spaces inside the tower; (c) stairs (detail); (d) windows and niches (detail); internal spaces (detail).

Focusing on the basement of Giotto's Bell Tower, the base section is approximately a square one with a side of about 13 m and a total thickness of the wall of about 3.3 m. The area of the resistant section at the base is 128 m^2, which corresponds to a moment of inertia of 2240 m^4 and a radius of inertia R = 4.18 m. The central core of inertia has a radius r = 2.70 m. The volume of Giotto's Bell Tower, if the openings inside the walls are not taken into account, is 10800 m^3, taking into account the opening and the stairwell it reduces to 9300 m^3. The openings (niches, staircases, single and double lancet windows, etc.) have a volume of about 1600 m^3, corresponding to 15% of the total volume.

The geometric representation of these elements is shown in Figure 1b-c.

With respect to the material properties, the walls of Giotto's Bell Tower were built with the multi-leaf technique. The inner face, the only visible, is built with a stone well dressed with regular and squared blocks (of variable dimensions between a minimum of 24 cm and a maximum of 38 cm); the mortar joints are very thin. The inner core, according to the results of the core drilling tests carried out in 2006, is composed of stone aggregates (with dimensions ranging from centimetres to decimetres) and compact lime mortar. The external face, covered by polychrome marbles, does not allow the visual investigation of the wall

texture. However, it was possible, thanks to the historic photographic documentation of past maintenance/replacement of some of the tiles, to observe the presence of a well-organised and well-preserved brick masonry apparatus.

In the absence, however, of specific tests on the materials, for the elastic and resistance parameters, reference can be made to the values suggested by the Italian standard [22] [23]. Focusing on the following classes: a) "Irregular stone masonry (pebbles, erratic and irregular stone)", b) "Dressed rectangular stone masonry" and c) "Full brick masonry with lime mortar" it can be reasonably assumed a variability of the own weight between 1800 and 2000 kg/m^3. The value of the average compressive strength is more uncertain. The strength of the stone, which forms the internal layer of the walls, can be estimated at about 140 MPa. The "Irregular stone masonry" has a compressive strength between 1.0 and 1.8 MPa, the "Dressed rectangular stone masonry" has a compressive strength in the range 2.0 3.0 MPa, while "Full brick masonry with lime mortar" has a compressive strength between 6.0 and 8.0 MPa. These values are, overall, low strength values and which are proposed Italian standard for ordinary constructions.

Assuming an average own weight of the masonry of the Bell Tower of Giotto between 1800 and 2000 kg/m^3, depending on the area of the different sections of the bell tower (i.e. different levels), it is possible to estimate the average vertical stress at the various heights. It is possible to observe how the section reductions in correspondence of the windows, in addition to the various anomalies (niches, staircases, compartments, etc.), induce localized alterations in the average value of the vertical stresses. These increases are more visible in the window areas of the upper levels. A similar increase is anyway observed at the basement due to the section reduction caused by the niches and the splayed windows. The average vertical stress at the basement is variable between 1.30 and 1.45 MPa.

The reference strength values proposed by the Italian standard (which are mainly proposed for ordinary constructions) may be are overly precautionary, if not untrue, for a historic structure with exceptional characteristics and a careful construction technique such as Giotto's Bell Tower. Given the non-standard nature of the construction, as far as the average values of the elastic and resistance parameters of the material are concerned, it is possible to make an expeditious estimate by taking as reference the value of the frequency experimentally obtained. Assuming the tower as a cantilever beam fixed at the basement having prismatic section A, height H, moment of inertia J and specific weight ρ, the frequency of the first mode can be evaluated with the following expression:

$$f_1 = \frac{1.875^2}{2\pi} \cdot \frac{1}{H^2} \sqrt{\frac{\boldsymbol{E}}{\rho} \frac{\mathrm{J}}{\mathrm{A}}} = f_{\exp} \tag{1}$$

By inverting Eq. (1), and considering that f_{exp}=0.62 Hz [20] [21], it is possible to estimate the value of modulus of elasticity (E), which results to be equal to 7.2 GPa. From this value, the compressive strength can be estimated using the literature ratios between elastic modulus E and compressive strength f_c. These ratios vary from about 400 in the case of "Dressed rectangular stone masonry" to about 1000 in the case of new brick masonry. Considering therefore the variability of E and that of the E/fc ratio, the following estimation is obtained:

$$\mathrm{f_c} = \frac{\boldsymbol{E}}{400 \div 1000} = 7.2 \div 18 \text{ MPa} \tag{2}$$

The interpretation of the results of the dynamic tests therefore indicates mechanical parameters of deformability (E) and resistance (f_c) that are much better than the reference values proposed by the Italian standard [23]. These values are compatible with both the excellent state of conservation of Giotto's Bell Tower and the good masonry quality of the structure.

3 NUMERICAL MODEL AND MODEL UPDATING

The numerical model built according the laser scanner survey was first employed to perform modal analysis. The results of the experimental dynamic campaign, both frequencies and mode shape [21], were assumed as reference to calibrate the elastic properties of the model, and the identification of the numerical model was performed according two phases, as summarized below.

In a first phase the numerical model (Figure 2a) was assumed to be fixed at the base (fixed base model). The calibration operations led to estimate, as macro-parameters, a total average specific weight of the material of 2000 kg/m^3 and a modulus of elasticity of 7.5 GPa in line, by order of magnitude, with what estimated in the previous paragraph. The results of the identification are summarized in Table 1 where it is possible to observe a good agreement between experimental and numerical results both in terms of frequencies and in terms of identified modes. The percentage differences between experimental and numerical frequencies are around 1% for the first two modes, with values however lower, or slightly higher, for the higher modes. The comparison between experimental and numerical mode shape is made in terms of MAC (Modal Assurance Criterion), and in this case a substantially adherence is observed for the first 3 modes, less for the last two forms (the higher flexural forms) which are however affected by greater experimental uncertainty.

Table 1: Comparison between experimental (Exp) and numerical (Num) results (fixed base model).

Mode #	Exp (Hz)	Num (Hz)	Δ (%)	MAC
1	0.623	0.62	0.16	0.99
2	0.647	0.64	1.20	0.99
3	2.543	2.65	4.40	0.95
4	3.081	3.17	3.10	0.72
5	3.156	3.19	1.20	0.77

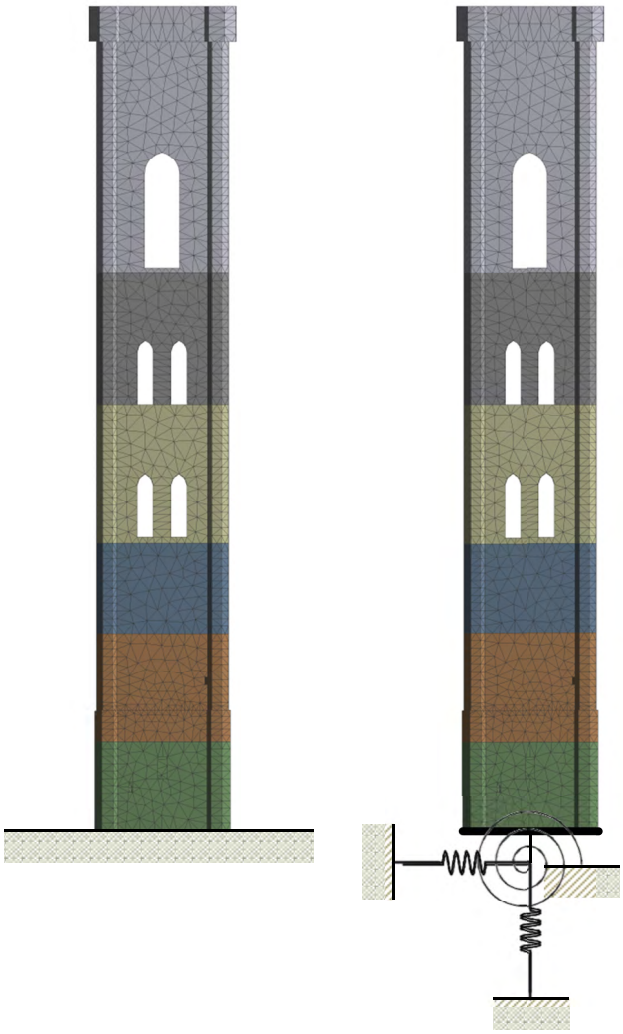
Table 2: Comparison between experimental (Exp) and numerical (Num) results (SSI).

Mode #	Exp (Hz)	Num (Hz)	Δ (%)	MAC
1	0.623	0.62	0.16	0.99
2	0.647	0.63	1.90	0.97
3	2.543	3.06	17.0	0.82
4	3.081	3.35	8.20	0.76
5	3.156	3.38	6.70	0.83

In a second phase the soil-structure interaction (SSI) has been taken into account, removing the hypothesis of rigid soil (Figure 2b). The soil was modelled with a series of elastic springs

whose impedances were estimated during the studies conducted on the geotechnical aspects. The impedances assigned to the elastic springs, simulating the interaction of the soil with the structure, were the following: K_X=21.20 GN/m; K_Z=50.90 GN/m and K_R=2278 GNm/rad. The results of the identification of the SSI model are summarized in Table 2. It is possible to observe that to account for the soil-structure interaction leads, in terms of elastic parameters of the identified model, to the following results: *i*) a reduction of the estimated own weight that, while remaining within the estimated physical parameters, decreases from 2000 kg/m^3 to 1800 kg/m^3 and *ii*) an increase of the value of the modulus of elasticity that moves from 7.5 GPa to 9.0 GPa.

Globally this corresponds to an increase in the E/ρ ratio, i.e. an increase of the velocity of the velocity of propagation of the elastic compression waves (P-waves) as expected.



a- fixed base model b- SSI model

Figure 2: FE model.

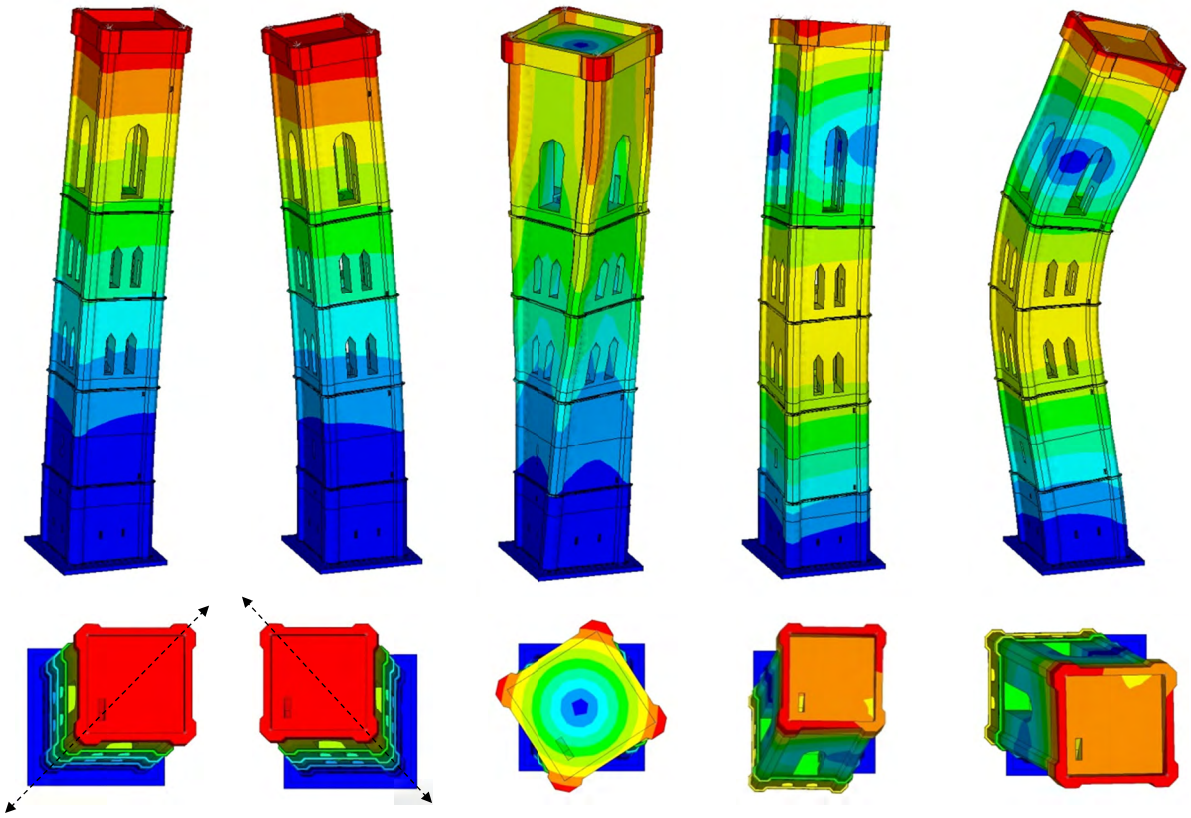


Figure 3: Mode shapes and frequencies of the numerical model with soil-structure-interaction.

The mode shapes obtained with the FE model which account for the soil-structure interaction are illustrated in Figure 3. The first two mode shapes are bending mode whose direction is oriented according to the main diagonals of the base section (and represented with a dashed line in Figure 3).

4 SEISMIC BEHAVIOUR

The FE model, identified in order to reproduce the experimental dynamic measurements, and inclusive of the soil-structure interaction (SSI, Figure 3), was used to perform time-history analysis by using a series of natural records selected during the research. Given the spatial variability of the mechanical parameters, the uncertainties still existing on the characterization of the material strength domains and the local effects that can be due to the multi-leaf nature of the masonry walls, the numerical model was here used to perform linear elastic analyses.

The 7 natural accelerograms selected for this study are reported in Figure 4; all the accelerograms were scaled to the maximum peak ground acceleration representative of the site hazard (0.16g). It is interesting to observe that if the frequency content of the natural records is calculated it almost never affects the first two natural frequencies of Giotto's Bell

Tower. On the contrary, contributions can be found on the upper mode shapes which interest the higher bending modes (modes #4 and #5).

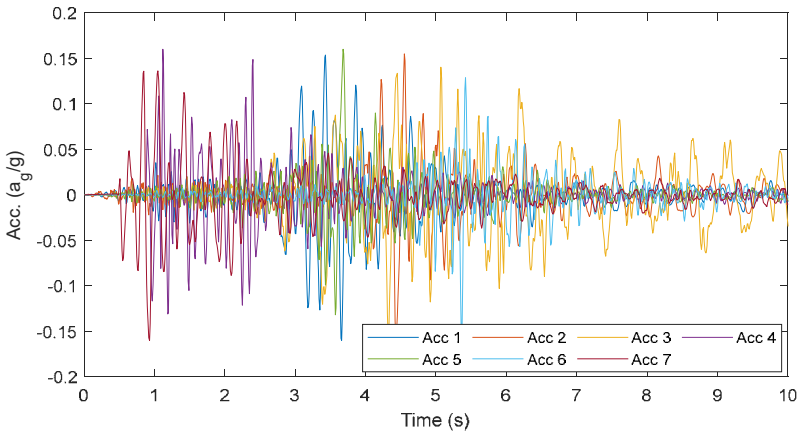


Figure 4: Time-history of the 7 natural accelerograms.

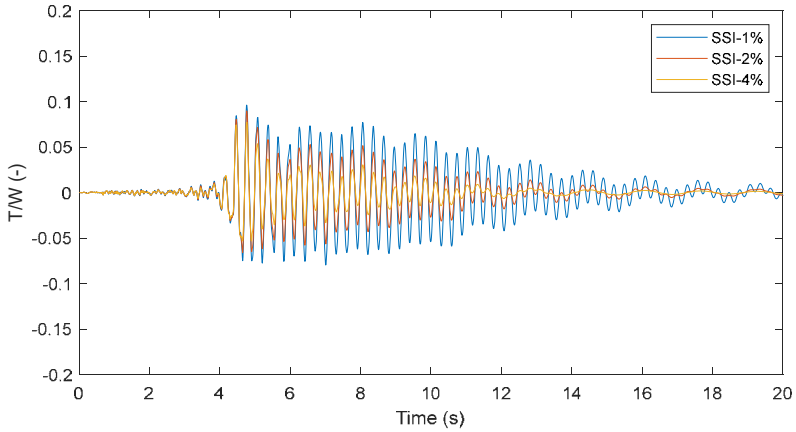


Figure 5: Base shear for three cases of damping: 4%, 2% and 1%.

The 7 natural accelerograms have thus been applied both in the two main directions of the base section of Giotto's Bell Tower, and in the two directions of the main diagonals. As an example, Figure 5 shows, when the natural record "Acc 2" is considered and applied along with one of the main directions, the evolution over time of the base shear (divided by the weight of the Bell Tower) for different values of structural damping. Three cases of damping were investigated (4%, 2% and 1%) since, given the isostatic nature of the tower, this is a relevant parameter in its seismic response. The time-history of the accelerations (for a damping equal to 2%.) as obtained at the different height of the Bell Tower of Giotto is reported in Figure 6, where it is possible to appreciate the amplification over the height of the base accelerations. The analysis of all the results shows a differentiated dynamic response between the first levels of Giotto's Bell Tower and the last one (the bell cell) and it is interesting to observe that time-history response of the tower is dominated by superior modes.

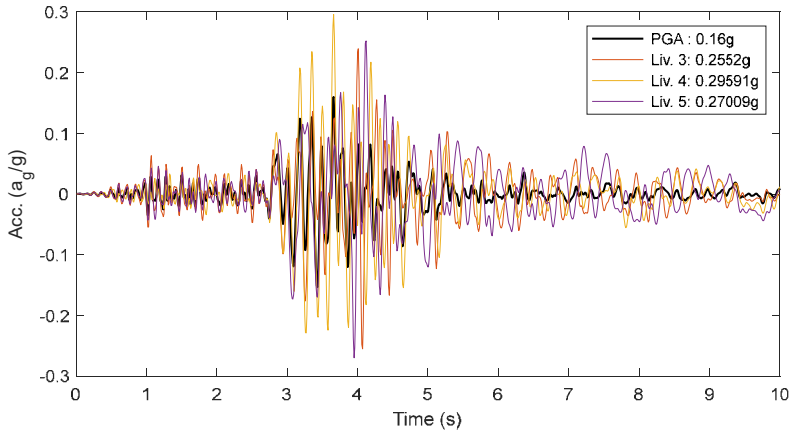


Figure 6: Base shear for three cases of damping: 4%, 2% and 1%.

Table 3: Time-history: synthesis of the results.

	Acc 1		Acc 2		Acc 3		Acc 4	
	4%	2%	4%	2%	4%	2%	4%	2%
W (kN)	164194	164194	164194	164194	164194	164194	164194	164194
T (kN)	8722	10431	12686	14738	22163	31514	6560	8279
M (kNm)	133250	156570	194610	221180	322840	475280	96131	104060
e = M/W (cm)	80.62	94.73	117.75	133.82	195.33	287.56	58.16	62.96
σ_{max} (MPa)	1.68	1.75	1.86	1.93	2.23	2.77	1.57	1.59
u_{max} (mm)	15.6	18.3	14.1	14.5	20.8	26.1	4.30	4.90

Table 4: Simplified approach: synthesis of the results.

	CR.A3062	IT.FHC	IT.SPT1	IT.MUGew	NTC2008
W (kN)	164194	164194	164194	164194	164194
T (kN)	319	1104	1057	2497	19834
M_d (kNm)	17850	61815	59170	139827	396672
M_c (kNm)	1005649	1005649	1005649	1005649	1005649
M_d/M_c	0.02	0.06	0.06	0.14	0.39
e=M/W (cm)	11	37	36	85	240
σ_{max} (MPa)	1.34	1.47	1.46	1.70	2.44
u_{max} (mm)	1.7	5.9	5.7	13.5	38.2

Overall, the results obtained with the time-history analyses are summarized in Table 3 for the first 4 natural accelerograms for two different damping values (4 and 2 %). The cases not included in the table offer similar results to the case 4 and therefore have not been reported.

From the results reported in the table, which offer a synthesis of the results obtained with all the (linear) time-history analyses, it can be observed that in almost all cases during the development of the seismic load the pressure centre at the base of Giotto's Bell Tower always

remains inside the central core of inertia (r = 270 cm). Only in the case of accelerogram #3, for a damping of 2 % a value of e=287 cm slightly greater than the core radius is observed. The corresponding maximum normal stress, evaluated with the no-tension material scheme, is 2.77 MPa lower, however, than the estimated resistance values (which has been estimated between 7.2 and 18 MPa).

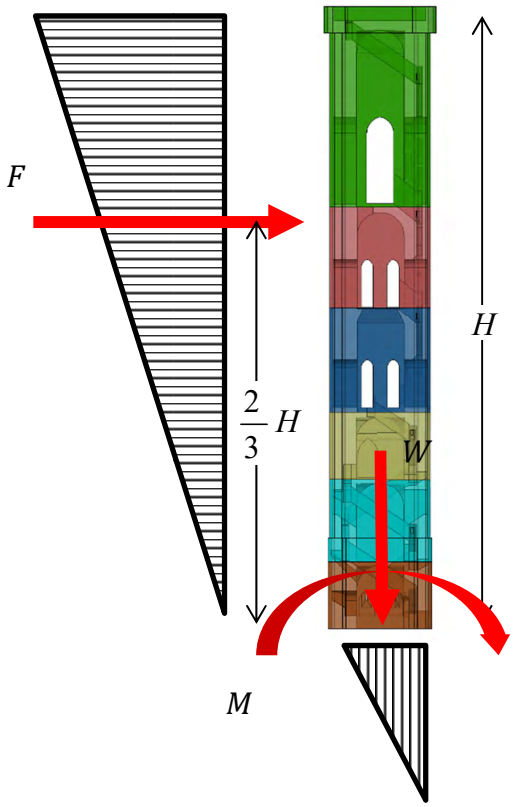


Figure 7: Static distribution of equivalent seismic actions.

As an example, and in a simplified way, the provisions of the Italian standard (valid for ordinary buildings) have been examined, and the actions induced by an earthquake have been evaluated according to the scheme of cantilever masonry beam shown in Figure 7. According to this simple scheme, starting from the spectral ordinate of the elastic response spectrum in correspondence of the fundamental mode of the structure, it is possible to determine, expeditiously, the loads (base shear T and bending moment M) induced by the expected earthquake (the Life Safety limit state with a return period of the seismic action equal to 712 years was considered) on Giotto's Bell Tower by the following:

$$F = \mathrm{S}_a(T_1) \cdot \frac{W}{qg};\ \mathrm{M} = F \cdot \frac{2}{3}H \tag{3}$$

The results obtained with this simplified approach are summarised in Table 4 where the results obtained considering the seismic hazard provided by the Italian standard are also compared with the one provided assuming the spectra derived by some of the natural records employed for the time-history analyses.

Since the spectra derived from the natural accelerograms have modest spectral ordinates (and in any case well below the ordinates of elastic response spectrum which is derived from conservative choices, based on the envelope criterion of deterministic spectra) they provide the lowers values. In general it is possible to observe that: *i*) the fundamental period of Giotto's Bell Tower is in the tail of the spectra; *ii*) the spectral ordinate of the spectra obtained from the natural accelerograms, measured in correspondence to the fundamental period of the Bell Tower of Giotto, is about one order of magnitude lower than the one of the standard. These elements justify the summary values of the results reported in Table 4.

The analyses here summarized represent a first contribution to the understanding of the seismic behaviour of the Giotto Bell Tower; the assessment of the structural behaviour of the monument under exceptional or long-lasting loads will in any case require the refinement of further modelling strategies, including modelling techniques with appropriate non-linear constituent laws and, possibly, the development of a long-term continuous monitoring necessary for the updating and validation of future numerical models. The analytical approach to be used to assess the structural behaviour of complex monumental buildings can in fact only proceed step-by-step, where possible additional research and analysis are identified based on the results of previous numerical and experimental analyses.

5 CONCLUSIONS

This paper summarized some of the results that have emerged regarding the dynamic identification and the seismic assessment of Giottos' Bell Tower. The numerical models developed during the research made possible, thanks to the results of an articulated analysis and survey campaign promoted by the "Opera di Santa Maria del Fiore", to reproduce and interpret the static and dynamic behaviour of Giotto's Bell Tower. The availability of a detailed geometric survey has allowed an accurate reproduction of the geometry of the tower with its main irregularities; the availability of a series of dynamic tests has allowed, together with the results of the geotechnical investigations, to identify and estimate some of the unknown parameters of the numerical model. The analyses carried out with the numerical model, and validated by means of a simple scheme, although carried out in a linear elastic field due to the uncertainties still existing, did not reveal any specific critical configuration in the structure.

In the static field, considering the effects of self-weight, the numerical model provides average values of the vertical stresses at the different levels well below the strength values of the materials (estimated on the basis of the results of the dynamic tests). With respect to the effects of the seismic loads both linear time-history analyses (by assuming natural ground accelerograms) and simplified static analyses were performed. On the whole, the analyses did not show critical configurations. In fact, the frequencies of the Bell Tower of Giotto are on the tail of the elastic spectrum, and the spectral ordinates of the selected natural accelerograms are much lower than the one of the standard.

Although the analyses carried out have not revealed any critical configuration, they suggest: *i*) the implementation of a long-term monitoring system with accelerometers in order to better characterize the dynamics behaviour of the structure (with particular interest for the higher modes of Giotto's Bell Tower given their relevance in the global seismic response); ii) additional experimental and numerical investigations aimed to assess the effect induced by the

swinging of the bells; *iii*) the investigation, given the sensitivity of the dynamic response to structural damping, of a tuned mass damping system (TMD) built by using the bell masses in the bell cell.

Acknowledgements. This research was financially supported by the "Opera di Santa Maria del Fiore" (which promoted a campaign of studies about Giotto's Bell Tower in 2017), that is gratefully acknowledged.

REFERENCES

[1] Russo, G., Bergamo, O., Damiani, L. and Lugato, D. Experimental analysis of the Saint Andrea Masonry Bell Tower in Venice. A new method for the determination of Tower Global Young's Modulus E. *Engineering Structures* (2010) **32**(2):353-360.

[2] Gentile, C. and Saisi, A. Ambient vibration testing of historic masonry towers for structural identification and damage assessment. *Construction and Building Materials* (2007) **21**(6):1311-1321.

[3] Carpinteri, A., Invernizzi, S. and Lacidogna, G. Numerical assessment of three medieval masonry towers subjected to different loading conditions. *Masonry International* (2006) **19**:65-76.

[4] Ivorra, S. and Pallares, F.J. Dynamic investigations on a masonry bell tower. *Engineering Structures* (2006) **28**(5):660-667.

[5] Ivorra, S., Pallarés, F.J. and Adam, J.M. Experimental and numerical results from the seismic study of a masonry bell tower. *Advances in Structural Engineering* (2009) **12**(2):287-293.

[6] Sabia, D., Aoki, T., Cosentini, R.M. and Lancellotta, R. Model updating to forecast the dynamic behavior of the Ghirlandina tower in Modena, Italy. *Journal of Earthquake Engineering* (2015) **19**(1):1-24.

[7] Binda, L., Zanzi, L., Lualdi, M. and Condoleo, P. The use of georadar to assess damage to a masonry bell tower in Cremona, Italy. *NDT & E International* (2005) **38**(3):171–179.

[8] Anzani, A., Binda, L., Carpinteri, A., Invernizzi, S. and Lacidogna, G. A multilevel approach for the damage assessment of historic masonry towers. *Journal of Cultural Heritage* (2010) **11**(4):459-470.

[9] Bartoli, G., Betti, M. and Giordano, S. In situ static and dynamic investigations on the "Torre Grossa" masonry tower. *Engineering Structures* (2013) **52**:718-733.

[10] Ramos, L.F., Marques, L., Lourenço, P.B., De Roeck, G., Campos-Costa, A. and Roque, J. Monitoring historical masonry structures with operational modal analysis: Two case studies. *Mechanical Systems and Signal Processing* (2010) **24**(5):1291-1305.

[11] Pieraccini, M., Dei, D., Betti, M., Bartoli, G., Tucci, G. and Guardini, N. Dynamic identification of historic masonry towers through an expeditious and no-contact approach: application to the "Torre del Mangia" in Siena (Italy). *Journal of Cultural Heritage* (2014) (2014) **15**(3):275–282.

[12] Casolo, S. A three dimensional model for vulnerability analyses of slender masonry Medieval towers. *Journal of Earthquake Engineering* (1998) **2**(4):487-512.

[13] Bernardeschi, K., Padovani, C. and Pasquinelli, G. Numerical modelling of the structural behaviour of Buti's bell tower. *Journal Cultural Heritage* (2004) **5**:371-378.

[14] Peña, F., Lourenço, P.B., Mendez, N. and Oliveira, D. Numerical models for the seismic assessment of an old masonry tower. *Engineering Structures* (2010) **32**:1466-1478.
[15] Milani, G., Casolo, S., Naliato, A. and Tralli, A. Seismic assessment of a medieval masonry tower in Northern Italy by limit, non-linear static and full dynamic analyses. *International Journal Architectural Heritage* (2012) **6**(5):489-524.
[16] D'Ambrisi, A., Mariani, V. and Mezzi, M. Seismic assessment of a historical masonry tower with nonlinear static and dynamic analyses tuned on ambient vibration tests. *Engineering Structures* (2012) **36**:210–219.
[17] Casolo, S., Milani, G., Uva, G. and Alessandri, C. Comparative seismic vulnerability analysis on ten masonry towers in the coastal Po Valley in Italy. *Engineering Structures* (2013) **49**:465–90.
[18] Ferrante, A., Clementi, F., Milani, G. Advanced numerical analyses by the Non-Smooth Contact Dynamics method of an ancient masonry bell tower. Mathematical Methods in the Applied Sciences (2020) 1-20.
[19] Bru, D., Ivorra, S., Betti, M., Adam, J.M., and Bartoli, G. Parametric dynamic interaction assessment between bells and supporting slender masonry tower. *Mechanical Systems and Signal Processing* (2019) **129**: 235-249.
[20] Pieraccini, M., Fratini, M., Dei, D., and Atzeni, C. Structural testing of Historical Heritage Site Towers by microwave remote sensing. *Journal of Cultural Heritage* (2009) **10**: 174–182.
[21] Lacanna, G., Ripepe, M., Coli, M., Genco, R., and Marchetti, E. Full structural dynamic response from ambient vibration of Giotto's bell tower in Firenze (Italy), using modal analysis and seismic interferometry. *NDT and E International* (2019) **102**: 9–15.
[22] NTC 2008, Nuove Norme Tecniche per le Costruzioni, G.U. n. 29, 4 Febbraio 2008, S.O. n. 30. D.M. del Ministero delle Infrastrutture e dei Trasporti 14 Gennaio 2008 (in Italian).
[23] MIT 2009, Circolare n. 617 del 2 febbraio 2009. Istruzioni per l'Applicazione Nuove Norme Tecniche Costruzioni di cui al Decreto Ministeriale 14 gennaio 2008 (in Italian).

12th International Conference on Structural Analysis of Historical Constructions
SAHC 2020
P. Roca, L. Pelà and C. Molins (Eds.)

INTERDISCIPLINARY ASSESSMENT, ANALYSIS AND DIAGNOSIS OF A HISTORIC TIMBER ROOF STRUCTURE FROM THE 20TH CENTURY

BOGDAN ISOPESCU[1*], ALEXANDRA KELLER[1], VALERIU STOIAN[2] AND MARIUS MOSOARCA[1]

[1]Politehnica University of Timisoara, Faculty of Architecture and Urban Planning
2/A Traian Lalescu, Zip code 300223, Timișoara, Romania
e-mail: bogdan.isopescu@upt.ro (*corresponding author)

[2] Faculty of Civil Engineering, Politehnica University of Timișoara (UPT)
Traian Lalescu street, nr. 2, 300223, Timisoara, Romania
e-mail: valeriu.stoian@upt.ro

Keywords: Historical Structure, Timber Truss, Assessment

Abstract. *Historic roof structures are complex systems which cannot be assessed individually but need a more holistic approach, in order to understand them as a whole. The great variety of contexts in which the building and its roof were placed, of architectural styles which ultimately influence the shape of the roof but also the diversity of technical solutions used by the craftsman to respond to these needs and its state of conservation, make a multidisciplinary approach necessary.*

While 18th and 19th century roof structures from Timisoara, a city from the western part of Romania, proved out to be complex structures which a high value from urban planning, architectural, symbolical and structural point of view, the 20th century is a period of transition with a wide array of influences, mix of styles and technological improvement of the structures.

Therefore, based on the roof structure of the Löffler Palace, built between 1912-1913, placed in the historic centre of the city, the paper tries to highlight that roof structures from this period are also far more than structural systems. Based on a thorough historical analysis and visual inspection of the structure, by using a multidisciplinary assessment procedure [1], the paper shows that 20th century roof structures are closely related to the building they belong, to their context and have a significant philosophical/symbolic and aesthetical value.

At the same time, the procedure also addresses the role of assessment, diagnosis, conservation and maintenance, the structural integrity of the roof, its influence on the seismic behaviour of the historic building, highlighting the connection between the roof, the building and its environment.

1 INTRODUCTION

Due to the complexity of heritage structures the ICOMOS principles are highly recommending a multidisciplinary approach when assessing their value and state of conservation in order to be able to properly develop intervention strategies which could preserve the integrity of the structures without affecting their historical, cultural and aesthetical value [1].

Considering this in recent years various assessment methodologies and procedures have been developed, suitable for the evaluation of historic timber roof structures which are trying to approach them for from various points of view. These methodologies, developed by different research group during COST actions, rather focus on the structural value without also considering the complex way of thinking in which these structures were built and their connection to everything that surrounds them. These methodologies mainly focus on the on-site evaluation of the roof structure and the timber elements [2,3] and their state of conservation, while also addressing the mechanical properties of the timber [4,5] and the static behaviour of the structure [6–8]. The same research groups also focus on monitoring techniques which could lead to a proper understanding of the structural behaviour of the roof structure and therefore ensure the development of coherent maintenance strategies. Only a few studies, try to look further and also include a historical analysis of the building and the roof, or also consider the effect of various environmental factors on the state of conservation of the timber [9–11] or even a geometrical analysis of the structure [12–14].

Studies performed on different roof structures from Timisoara brought forward that in the 18th and 19th century, roof structures were highly connected from an urban, architectural and philosophical point of view to their surroundings and to the building they belong to [15–18]. Since the city significantly developed at the beginning of the 20th century and roofs had an important role in defining the aesthetics and monumentality of the new buildings, an multi and inter-disciplinary analysis was also performed on the Löffler Palace, an imposing 20th century palace which could highlight the importance of also consider urban planning principles, architectural and philosophical principles during the assessment of historic timber roof structures.

At the same time, the study is also trying to highlight the importance of a thorough preliminary geometric analysis of the roof structures before performing numerical simulations. Therefore it also presents a comparison between the structural behaviour of a truss of the roof structure which is ignoring the cross-section reduction of the timber elements and is considering the joints as hinges, with a model developed considering the on-site observations concerning the decay of the timber elements and their cross-section loss and the semi-rigid behaviour of the timber joints.

2 INTERDISCIPLINARY ASSESSMENT OF THE ROOF STRUCTURE

2.1 Historic context

Timisoara is the biggest city located in the western region of Romania. Its current built fabric was defined under the Habsburg Empire's rule, most of the previous traces left after Hungarian and Ottoman occupation were removed.

The general guiding principles for the development of the city, by tearing down the

fortification and connecting the existing districts, were drawn by architect Ludwig von Ybl and engineer Aladar Sebestyen in 1895. A radial scheme was adopted, following the Viennese model, creating a green corridor alongside the Bega Canal, expanding or building new boulevards and creating new public squares. The idea of creating a large new square in front of the Opera, connecting the existing two squares in the north, reflects emphatically the spirit of the bourgeoisie of that time [19]. Several iterations were developed from this initial plan, scaling down and adapting its ambitious and idealistic proposals to the cities economic power.

As seen in Figure 1a, Ludwig von Ybl proposed a long square without obstructing the Huniade Castle, the oldest monument in the city built between 1443-1447. The first side of the square to be developed was the NW starting with the Lloyd building finished in 1912 [20]. The south-eastern side of the square was later developed but never finished in that time, but later on in the 1960's.

The Loffler Palace was built in 1912-1913, the project is assumed to be signed by the architect Henrik Telkes for the grain merchant Leopold Löffler. The building was set in front of the Huniade Castle, thus continuing the square front (Figure 1b,c). The layout and the façades of the building are atypical because of the emphasis put on the northern and southern facades and not the main one towards the square (Figure 2). Also, the back façade towards the castle is treated in a technical fashion, absent of ornaments, with recesses for lighting and ventilation. It somehow suggests that another building should be attached to form a compact block and ignores the proximity to the Castle which makes this unlikely.

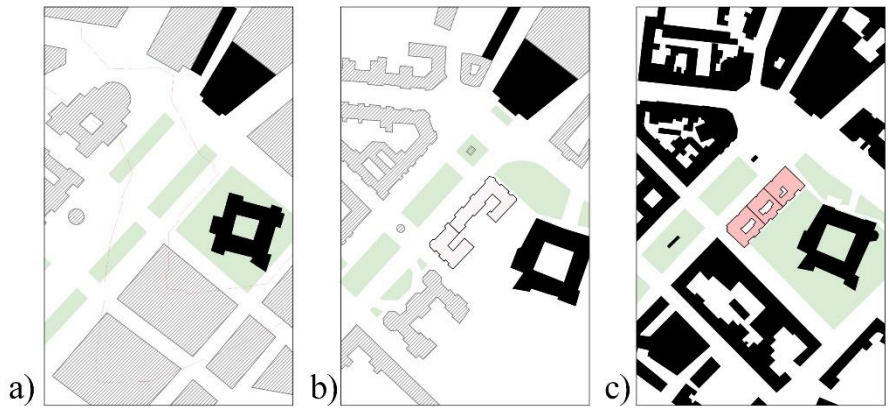


Figure 1: Page layout Evolution diagram of the urban fabric (a) 1895; b) 1913; c)2020)

The building is comprised of an underground floor for storage, a commercial ground floor, three stories of apartments for tenants and loft rooms for technical facilities and storage. The general dimensions of the building are 88 x 29 m. It consists of three distinct parts which function independently each with an interior courtyard. The structural system is quite innovative for the period. The massive brick masonry is mixed with concrete such as beams and columns to obtain larger openings at the ground floor. The slabs above the basement and the ground floor are made of concrete while the others are made of timber.



Figure 2: Loffler Palace overview

2.2 The roof structure

Architecture also plays a significant role in shaping the roof and the roof structure. The secession style of the building and the adopted urban principles led towards the definition of the tall roof above the gable (Figure 2).

The roof structure has three distinct structural typologies. The first towards the square presents a king and queen post roof structure was used and adapted according to the shape of the roof. The average span is 10.3m and height 6.9m. The part of the roof towards the Castle presents a simplified version of the previous one, a king post roof structure with a smaller span of 6.4m and a height of 4.1m. The unique and sole valuable parts of the roof are the symmetrical areas towering at the extremities. The roof structure above the masonry gables is made of a king and queen post with double compound rafters (Figure 3).



Figure 3: Roof structure above the gables

The towering roof structure consists of five trusses spanning 10.4m and having a height of 12.3m (Figure 4). The main trusses are connected through a secondary truss to the gable wall. On each of the lateral parts, there is a half truss positioned perpendicular to the main trusses and one in each corner composing the hips and adding to the overall stiffness of the structure. The half trusses are connected through the king and queen posts and fastened with double collars at the three purlin levels.

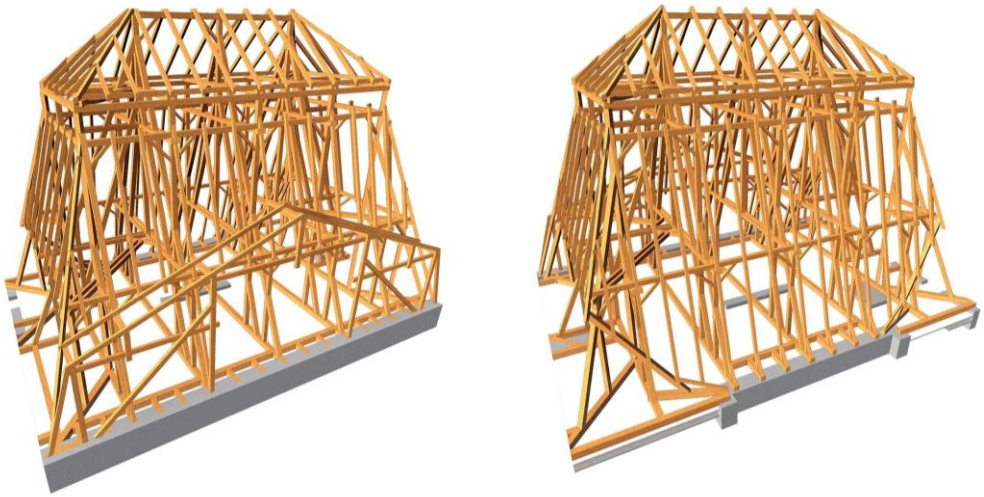


Figure 4: Studied roof model

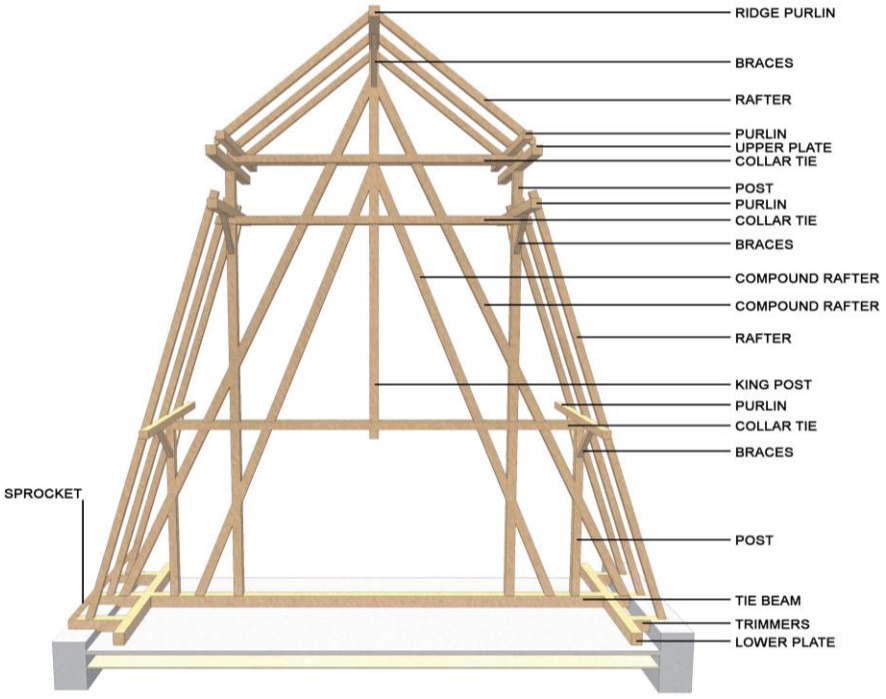


Figure 5: Truss components

The general dimensions for the timber elements are as follows: tie beams, lower plates and trimmers 250x200mm; king posts, queen tall posts and ridge purlin 180x180mm; queen short posts and purlins 160x160mm; collars 160x100mm; rafters 140x100mm; braces and sprockets 100x100mm.

The stiffness perpendicular to the trusses is minimally ensured by bracing each of the posts to the corresponding purlins and through the lower plates. The whole tower structure is stiffened at the short ends by half-trusses braced with diagonal lower plates and collar ties. Additionally, in order to increase the rigidity of the structure, all the trusses are connected by eaves and intermediate purlins and an additional system of timber elements, composed of headers and trimmers, placed over the walls. The presence of the gable wall A-frame stiffens and connects the five main central trusses.

There are two types of joints used for the connection of the various wood elements of the truss. The most common is the mortise and tenon joint, used in all post to beam, beam to beam or trimmer, compound rafter to king post or tie beam, bracket to post, rafter or sprocket to the trimmer. The second type is the half-lapped joint found in the compound rafter to queen-post connections. All the purlins and collars are notched. The rafters are bird's mouth cut and set on the purlins. There are no wooden pegs or wedges used for any of the joints while threaded rods are used in all post to collar or post to compound rafter, or compound rafter to collar connections. Iron straps are used for all the timber elements connected to the tie beam and posts to purlins. Three iron strips are used as brackets to connect the gable to the trusses.

The roof structure highlights the way urban planning principles and architectural styles are influencing the choice of roof geometries and structural systems. Their position in the urban context is increasing the cultural value of those roof structures and making their preservation an important cultural factor.

2.3 State of conservation

All visual examined pieces presented easily distinguishable growth-rings, the vessels are particularly big and have a ring porous distortion. All the elements composing the trusses are made from oak (*Quercus sp.p.*).

The timber roof is in an overall good state of conservation. No fungi or extent insect attack was spotted. Sparse decay of the trimmers was seen in the valley areas where they are in contact with the masonry. Traces of moisture induced damage are present, mainly in the area of the rafters and purlins but the leaking roof was constantly repaired. Additional damage caused by water infiltration in the ridge area led to the decay of the ridge purlins and the decorative exterior elements of the ridge.

No mechanical failures or big deflections of the timber elements have been detected.

2.3 Symbolic analysis

Previous studies performed on 18th and 19th century roof structures from Timisoara brought forward that craftsman used to define the position of main structural elements and joints based on various geometric principles and symbolic ratios. The studies brought forward that 18th century and beginning of the 19th century roof structure, build in the most active period of the craft-guilds were mainly defined by sacred ratios and dynamic ones ($\sqrt{2}$,$\sqrt{3}$ or $\sqrt{5}$) (Figure Ya) while end of the 19th century, towards the fall of the guilds, roof structures were defined by

dynamic and static ratios (1/1, 1/2, 2/3). Ultimately, 20th century roof structures tend to present a mix of various types of ratios, without clearly defining a geometrical pattern.

A geometrical analysis of the roof structure of the Löffler Palace was also performed in order to observe if this type of imposing roofs would also present any interest in complex geometries. The analysis showed that in the inferior part of the roof structure, dynamic ratios are predominantly used while the upper part is mainly defined by static ratios (Figure 6). Therefore, a √5 rectangle was used to define the distance the lower queen posts, compared to their height, while the position of the main queen posts is defined by a √2 rectangle. The same √2 rectangle was also observed in defining the distance between the inferior and intermediate collar ties compared to the distance between the main queen posts and the king post. Ultimately, the distance between the main queen posts is equal to the distance between the inferior and superior collar ties also highlighting the use of static ratios. Also, static and dynamic ratios were used to define the position of various joints, like the lower queen post and compound rafter or the compound rafter to upper collar ties joint. Still, no sacred ratios were identified.

The study revealed, as previously also observed during the geometrical analysis of the nearby placed Lloyd palace, a mix of different ratios. Still, compared to other 20th century, less imposing roof structures, this case is still presenting a more coherent geometrical approach and a clear use of dynamic and static ratios to define the position of almost all the composing structural elements.

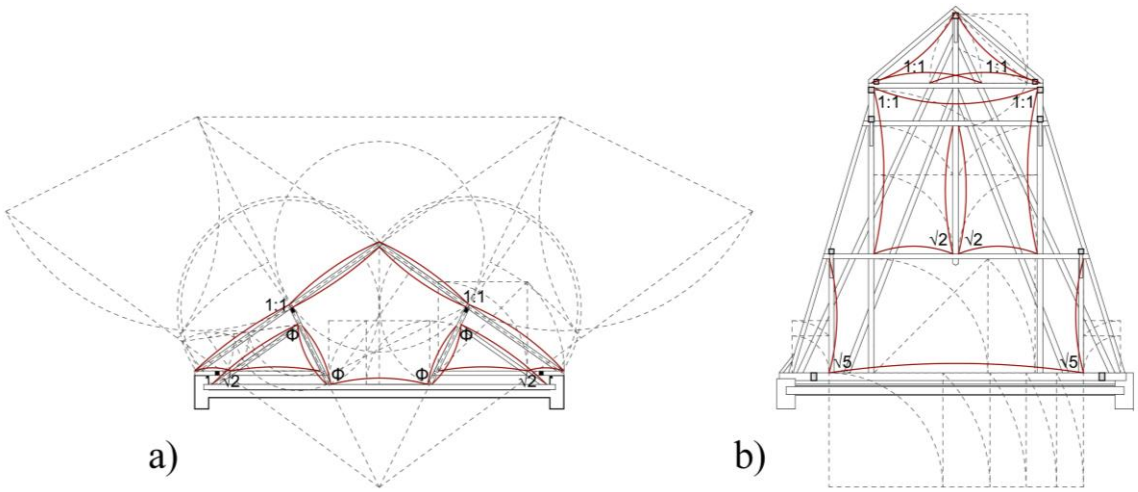


Figure 6: Analysed parameters (a) points where the displacements were measured; b) elements where the internal forces were analysed)

2.4 Structural analysis

Numerical simulations have been performed in the finite element simulation software SCIA engineer and were meant to highlight the importance of a proper investigation of a 20th century historical roof structure when addressing its structural behaviour. Therefore, two different scenarios were considered based on common practices in the structural assessment of historic roof structures. The first approach considered a more conservative approach but more time-efficient which ignored the possible cross-section loss of the timber elements and the traditionally crafted joints were modelled as hinged. The second approach was more related to the observations made on site, which led to a reduction of the cross-section of the timber

element of 10%, due to the rounded corners and the slight decay of the timber elements, while the semi-rigid behaviour of the timber joints was also considered. In this case, the axial stiffness of the joints was determined, based on their type, geometry and mechanical properties of the timber using the component method [21–23].

In order to be able to compare the results, the same loads were applied to the roof structure in both cases. The truss was loaded according to national standards with dead load, representing the self-weight of the timber elements and the weight of the roof envelope, life load and wind load. Since the roof pitch in the inferior part is of 74 degrees, the snow load was not considered in the load combination.

In order to identify the differences between the structural behaviour of the two cases, the horizontal (U_x), vertical (U_z) and total displacement (U_{total}) of a selection of six points were analysed. The points are placed in the middle of the structural elements which would suffer the most significant displacement caused by the applied loads: inferior rafters, superior rafters, tie-beam and the base of the king-post (Figure 7a). At the same time, the axial forces and bending moments recorded in the rafters, tie-beams and queen posts were analysed (Figure 7b).

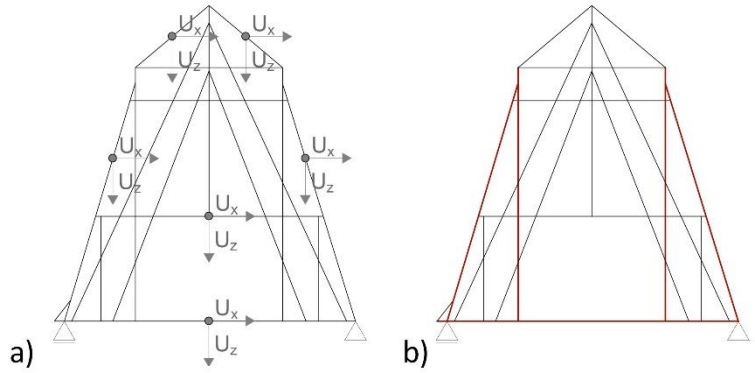


Figure 7: Analysed parameters (a) points where the displacements were measured; b) elements where the internal forces were analysed)

The displacement analysis is highlighting that the rafters are suffering the most significant displacement in both cases, up to about 10 cm, considering the total displacement, while the tie-beam and base of the kingpost are only presenting a slight vertical and horizontal displacement of up to 6 mm (Table 1).

Table 1: Displacement comparison of the two considered cases

	Conservative approach			After investigation			Comparative results		
	U_x [mm]	U_z [mm]	U_{total} [mm]	U_x [mm]	U_z [mm]	U_{total} [mm]	U_x [%]	U_z [%]	U_{total} [%]
1	81.3	-26.4	85.4	121.9	-40.4	128.4	35	35	35
2	-12.3	-5.6	13.5	-17.9	-8.3	19.8	30	30	30
3	65	-79.2	102.5	98.7	-120.4	155.7	35	35	35
4	-63.1	-78	100.3	-95.5	-118.3	152	35	35	35
5	5.7	-2.5	6.2	9	-4.1	9.9	35	40	35
6	0.3	-3.4	3.4	0.4	-5	5	25	30	30

Still in all the cases when comparing the obtained results it becomes clear that the model with reduced cross-section elements and semi-rigid joints is presenting an up to 35% increase of the horizontal and total displacement, and an up to 40% increased of the vertical displacements. However, no significant variations of comparative results were observed for the considered analysis points.

The tie-beam is also presenting a slight change in the recorded internal forces. The axial forces increase with only up to 5%, except for the tie-beam to second compound rafter, where an increase of 10% of the axial forces was recorded. Even for this element, the bending moments only vary slightly.

Ultimately, the internal forces on the queen posts were analysed. In this case, a clear difference between the obtained axial forces could be observed. Therefore, in the inferior part of the posts, up until the first collar ties, the axial forces increase with up to 5% for the second approach. Right above the first collar ties the axil forces increase with up to 25% and decrease with also 25% towards the second line of collar ties. Ultimately, at the top, the variations are insignificant. Compared to the previously analysed elements, in this case, the bending moments also present clear changes, with a 10% decrease at the base of the queen post and a 10% increase at the top.

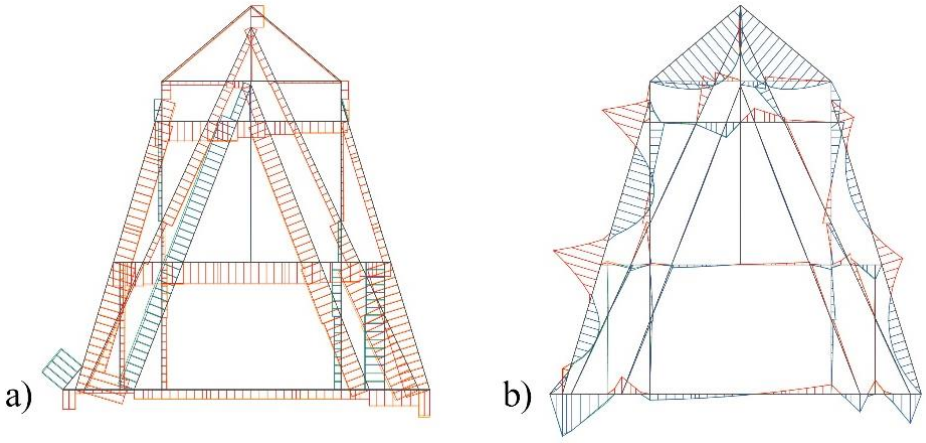


Figure 8: Internal forces a) axial forces (N); b) bending moments (M_y)

3 CONCLUSIONS

As already observed in previous studies the multidisciplinary analysis of the chosen 20th century roof structure of the Löffler Palace brought forward that the preliminary assessment of a roof structure is a complex topic and that a series of context-related features also have to be taken into consideration.

The study shows that 20th century roof structures, placed in representative places of the city are no longer simply meant to protect the building from meteorological factors but are also enhancing the importance of the building in its urban context. At the same time it can be observed that, despite being residential, the Löffler Palace is presenting an impressive roof which is not connected to its main function but rather to the urban context, the roof becoming one of the main aesthetical features of the building.

The surrounding urban area, the position of the building, related to public space and other

neighbouring buildings and shape of the roof prove, therefore, to be features which connect a roof to its urban context and ultimately influence the choice of roof structure type and its structural complexity.

The study is also highlighting that even at the beginning of the 20th century geometric principles were still used to link the height of the roof to the total height of the building, the position of main structural elements and joint, although, compared to 18th and 19th century roofs they were more simple.

Ultimately, the study is also highlighting the importance of a proper investigation of the geometry of the roof structure, the cross-section of the timber elements and their state of conservation on the structural behaviour of the roof. By using the on-site cross-section loss of the timber elements and the semi-rigid behaviour of the joints, results show a clear increase of the recorded displacements, slight changes of the axial forces and only little increase of the bending moments. Despite being more time consuming, this approach can prevent the misunderstanding of the historic timber roof structure which could lead to its partial or complete unnecessary replacement.

The study is therefore presenting a series of features which are important to be considered in order to be able to obtain a holistic and in-depth analysis of a historic timber roof structures. The proper understanding of the state of conservation and structural behaviour of the roof, is not only related to its immediate safety but also the buildings aesthetics, its role in the urban fabric and the way it is perceived from its surroundings.

The study represents a first step in the development of current roof structure assessment methodologies by highlighting additional factors which should also be considered. The next step would the confirmation of the obtained results of the numerical simulations by performing a comprehensive monitoring of the behaviour of the structural elements.

REFERENCES

[1] ICOMOS. Principles for the Analysis, Conservation and Structural Restoration of Architectural Heritage. Victoria Falls, Zimbabwe, (2003).

[2] Cruz, H., Yeomans, D., Tsakanika, E., Macchioni, N., Jorissen, A., Touza, M., Mannucci, M., Lourenço, P., Guidelines for On-Site Assessment of Historic Timber Structures. *Int J Archit Herit* (2015) **9**(3):277–289.

[3] Riggio, M., D'Ayala, D., Parisi, M.A. and Tardini, C., Assessment of heritage timber structures: Review of standards, guidelines and procedures. *J Cult Herit* (2018) **31**:220–235.

[4] Sousa, H.S., Machado, J.S., Branco, J.M. and Lourenço, P.B., Onsite assessment of structural timber members by means of hierarchical models and probabilistic methods. *Constr Build Mater* (2015) **101**:1188–1196.

[5] Sousa, H.S., Branco, J.M., and Lourenço, P.B., A Holistic Methodology for Probabilistic Safety Assessment of Timber Elements Combining Onsite and Laboratory Data. *Int J Archit Herit* (2016) **10**(5):526–538.

[6] Gocál, J., Krušinský, P., Capková, E. and Kekeliak, M., Geometric and static analysis of the historical truss in village Belá Dulice. (2014).

[7] Krušinský, P., Capková, E., Gocál, J. and Holešová, M., Geometric and static analysis of

the historical trusses in roman catholic church of the Holy Kozma and Damian in the Abramová village. *Civ Environ Eng* (2015) **11**(2):136–141.
[8] Krušinský, P., Gocál, J. and Capková, E., Static analysis of historical trusses. *Wiadomości Konserw* (2016) **47**:120–127.
[9] Tannert, T., Dietsch, P., Bertolini-Cestari, C. and Kasal, B., COST Action FP1101 - Assessment, Reinforcement and Monitoring of Timber Structures. In: Quenneville P (eds.). *World Conference on Timber Engineering (WCTE)*.Curran Associates, Inc., Auckland, New Zealand, (2012), pp. 515–519.
[10] Kasal, B., Assessment, reinforcement and monitoring of timber structures-COST FP1101. *Adv Mater Res* (2013) **778**:1037–1040.
[11] D'Ayala, D., Branco, J.M., Riggio, M., Harte, A., Kurz, J. and Descamps, T., Assessment, reinforcement and monitoring of timber structures: FPS Cost Action FP1101. In: Peña F (eds.). *9th International Conference on Structural Analysis of Historical Constructions (SAHC 2014)*.Springer, Mexico City, Mexico, (2014).
[12] Krušinský, P., Gocál, J. and Capková, E., Geometric and static analysis of the historical truss above presbytery of the Saint Peter of Alcantara monastery church in Okolicne. *Procedia Eng* (2015) **111**:485–490.
[13] Krušinský, P., Capková, E. and Gocál, J., Comparison of Two Medieval Trusses from the Viewpoint of Geometric and Static Analysis. *Adv Mater Res* (2015) **1122**:243–248.
[14] Gocál, J., Krušinský, P., Capková, E. and Kekeliak, M., Analysis of the historical truss in village Belá Dulice. *Acta Sci Pol Form Circumiectus* (2015) **14**(1):57–73.
[15] Keller, A. and Mosoarca, M., A complex assessment of historic roof structures. In: Arun G (eds.). *4th International Conference on Structural Health Assessment of Timber Structures (SHATIS'17)*.(2017), pp. 157–168.
[16] Andreescu, I. and Keller, A., Complex features in assessing historic roof structures. In: Mazzolani F (eds.). *3rd International Conference on Protection Of Historical Constructions, PROHITECH'17*. (2017).
[17] Mosoarca, M. and Keller, A., A complex assessment methodology and procedure for historic roof structures. *Int J Archit Herit* (2018) **12**(4):578–598.
[18] Keller, A., Parisi, M.A., Tsakanika, E. and Mosoarca, M., Influence of historic roof structures on the seismic behaviour of masonry structures. *Proc Inst Civ Eng - Struct Build* (2019):1–27.
[19] Opris, M., *Timisoara: small urban monography (in Romanian)*. Editura Tehnica, Bucarest, (1987).
[20] Geml, J., *Old Timisoara (in Romanian)*. Editura Cosmopolitanart, Timisoara, Romania, (2016).
[21] Drdacky, M.F., Wald, F. and Mareš, J., Modelling Of Real Historic Timber Joints. *Trans Built Environ* (1999) **39**:169–178.
[22] Descamps, T. and Lemlyn, P., Effects of the rotational, axial and transversal stiffness of the joints on the static response of old timber framings. In: Mazzolani F (eds.). *Protection of Historical Buildings, PROHITECH 09*. CRC Press, Taylor & Francis Group, Rome, Itlay, (2009), pp. 291–286.
[23] Branco, J.M. and Descamps, T., Analysis and strengthening of carpentry joints. *Constr Build Mater* (2015) **97**:34–47.

12th International Conference on Structural Analysis of Historical Constructions
SAHC 2020
P. Roca, L. Pelà and C. Molins (Eds.)

NON-DESTRUCTIVE TECHNIQUES IN THE CONSOLIDATION WORKS OF THE CHURCH OF S.M. OF ITRIA IN PIAZZA ARMERINA (ITALY)

TIZIANA BASIRICO'[1*], SAMANTHA CAMPIONE[1] AND ANTONIO COTTONE[2]

[1] Faculty of Engineering and Architecture
University of Enna Kore (UKE)
Via delle Olimpiadi, 94100 Enna, Italy
e-mail: tiziana.basirico@unikore.it, www.unikore.it (*corresponding author)

[2] Department of Architecture (DARC)
University of Palermo (UNIPA)
Viale delle Scienze, 90128 Palermo, Italy
e-mail: antonio.cottone@unipa.it, www.unipa.it

Keywords: Historical structure, masonry, foundation, non-destructive inspection

Abstract. *A real case of consolidation works is presented in which only field testing methods can reveal the causes of instability. This paper is an update of the one presented at the SAHC 2018 conference, concerning the study of the partial collapse of the Church of Itria in Piazza Armerina (Sicily, Italy). The previous paper beared hypotheses and design solutions based only on indirect investigations, theoretical formulations and checks with software. The consolidation works, started in November 2018 and still in progress, have made it possible to formulate new and documented hypotheses on the collapse and to integrate and partly modify the solutions hypothesized previously. In particular, the reconstruction techniques of the wall and chains have been confirmed. The new interventions have, instead, concerned the consolidation of the foundation soil which was found to be insubstantial, following electrical tomographic investigations, due to the presence of voids. At the same time, inspections were carried out on an old masonry sewage pipe which revealed several points of discontinuity through which large quantities of water entered under the walls of the church causing the removal of inconsistent elements from the ground. At first, the reconstruction of the collapsed wall was done and the restoration of the existing wall structures, to eliminate the causes of the collapse through the intervention on the sewage pipe and filling the voids under the foundations. The most important intervention, which required the use of innovative materials, forefront equipment and skilled labor, involved the filling the voids under the foundations through perforations every 50 cm, both on the inner and outer wire of the collapsed wall. Clamped canes were set in order to intercept the voids highlighted by the tomography. A 100% expansive mortar was injected at low pressure through the canes, filling one cane at a time and progressively raising the point of exit of the mortar until the higher far end. After this consolidation, the foundation and the wall were rebuilt with local limestone ashlars to have fair faced aspect as the original masonry. At the end of the work, further tomographic tests are planned to verify the validity of the interventions carried out.*

1 INTRODUCTION

Preliminary investigations for the knowledge of the building and its site play a fundamental role in restoration and recovery.

The definition of an investigation program often requires an interdisciplinary approach, which goes far beyond simple technical aspects; historical research can be directed to discover phenomena that have involved structural behaviour and, conversely, the analysis of structural behaviour can provide elements that help the recovery designer to find answers to his hypotheses.

A preliminary inspection of site and construction must guide the definition of the investigation plan as these can be carried out at different levels of extension and depth, with consequent different economic and time commitments. The investigation plan must, therefore, be adequate to the complexity, the architectural value of the building, the structural problems to be solved and the possibility to have real benefits from the relative deepening of knowledge.

It is sometimes convenient to start with a minimum investigation plan and then, when and where necessary, to deepen it in later stages.

It is important and this case proves it, not to limit to the analyses necessary to draw up a correct executive project, but to foresee an integration of the investigations during the construction site and continuous monitoring [1].

This methodological approach is simple to apply when it is used in the recovery of a single monument and the restoration operation is, therefore, facilitated as it is limited to a specific object, whose use is known.

2 THE CASE STUDY

In the previous SAHC 2018, we presented the case of the Church of S.M. of the Itria in Piazza Armerina (EN) affected by the collapse of the West wall of the apse and a part of the adjacent wall of the lateral nave, which happened during the 29 December 2007 night [2]. In that paper, hypotheses on the collapse were formulated and congruent solutions were proposed.

The causes of the collapse (fig. 1) were initially attributed to foundations' failure, but geological and geotechnical tests, carried out by the municipality and the Curia of Piazza Armerina, stated the substantial geological stability of the site and the absence of slipping surfaces along which a landslide could occur. It was, therefore, excluded that it was foundations' failure of the wall which did not show, in the visible part, lowering.

From the historical investigation [3], by means of documents, drawings and photographs, important information was obtained on the state of the church, before the collapse, and on previous maintenance and restoration interventions, thus being able to define the historical evolution, including any transformations of the monument.

Analysing the drawings of the previous projects, it was evident the collapse occurred in correspondence to a discontinuity of the wall, due to the construction of a niche; the photographs highlighted the masonry, consisting of irregular stone, had a reduced interlocking between the orthogonal walls. Furthermore two vertical cracks were detected. This led to the hypothesis that the most probable cause of the collapse could be attributed to the higher load on the wall, due to the replacement, occurred in the 1980s, of the existing wooden roof with an iron and brick floor. The new roof was connected to reinforced concrete curbs, placed over the longitudinal load-bearing walls and on the walls above the transverse arches.



Figure 1: Pictures of the collapse from the outside and inside the church

This new static scheme changed the load distribution on the walls, making it become eccentric due to the reduced thickness of the curb, compared to that of the wall.

With the knowledge hitherto acquired, a kinematic mechanism was, therefore, hypothesized that had produced a deformation of the wall, with a consequent partialisation of the resistant section and breaking due to peak load. By comparing historical and tests' data, the result was the intervention carried out in the 1980s had accelerated the degradation process and had been a contributing cause of the collapse.

Aware that the removal of the current roof structures would have caused incalculable damages to the monument, it was decided not to intervene on them and rebuild the wall by eliminating the previous discontinuities and consolidating the existing walls.

3 THE CONSTRUCTION SITE AND THE NEW INVESTIGATIONS

Once the construction site was set up, on 8 November 2018, the cracking situation was significantly worsened compared to the survey carried out in the design phase, mainly concerning cracks on the floor with relative failure of the pillar, near the apse, due to heavy rains that occurred at the end of October.

This situation led to investigate, through punctual excavations, the conditions of the foundations of the collapsed wall to identify the plan from which to begin the reconstruction.

The excavation work, begun under the collapsed wall at the apse, showed an evident rotation of the lower part of the wall collapsed (fig. 2) and traces of an underground compartment, which led to the need to integrate previous punctual investigations with tests on the entire subsoil of the church. This was necessary in order to have an updated situation after 12 years from the collapse and check the presence of potential underground masonry structures and cavities.

A geophysical investigation was, therefore, commissioned highlighting a completely different picture of the causes of the collapse and led to the drafting of a variation report.

Following the results of the new investigations, it was decided to carry out inspections inside the underground masonry conduct, in parallel to the wall of the church on Itria St., which conveys the white-water from the mountain and collects dispersed water.



Figure 2: Crack on the floor in proximity of the pillar and the rotation of the wall under the collapsed one

3.1 Application of electric tomography to the case study

3D electrical tomography was chosen to investigate the soil and foundation structures allowing to assess the resistivity of the subsoil [4, 5]. Three linear tomographies were performed (1, 2 and 3) to define the geoelectric situation of the site, with the aim of acquiring with 3D resolution all the elements attributable to highlighting areas of potential instability and/or anomalies of the stratigraphy, positioning a remote pole 20 meters from the investigated areas.

In particular, the electrodes were positioned externally, along via Itria, the area affected by the collapse of the wall, in adherence to the Church, setting the electrodes at 1.30 m (tomography No. 1); along the internal perimeter of the church, also paying attention to the colonnade foundations of the right nave of the church, due to the lowering of the column near the apse, setting the electrodes at 1 m (tomography No. 2); inside and outside the wall of the church adjacent to the sacristy, setting the electrodes at 1.30 m (tomography No. 3) (fig. 3).

The electrodes, consisting of metal pegs, and the energizer producing electricity to be set into the ground, were connected to a data acquisition center. The investigated area was thus ideally divided into a finite number of meshes and cells (the so-called "finite elements"), each of homogeneous and unknown resistivity. In tomographic reconstruction, the unknown is the distribution of the resistivity in the ground, while the electrical measurements carried out on the ground represent the known terms. From an operational point of view, the method consists of transmitting electricity into the ground through an energizing dipole, and measuring the potential difference induced by the electric field created in the ground, by means of a reading dipole. The measurements were recorded by alternately moving (with automatic method) the electricity dipole and the voltage dipole, in order to obtain a mesh of reading points arranged along the three cross-sections. Knowing the potential difference and the electricity intensity in the various points, the apparent resistivity was obtained at each point by applying, by means of special software, the theory of infinitesimal dipoles [6].

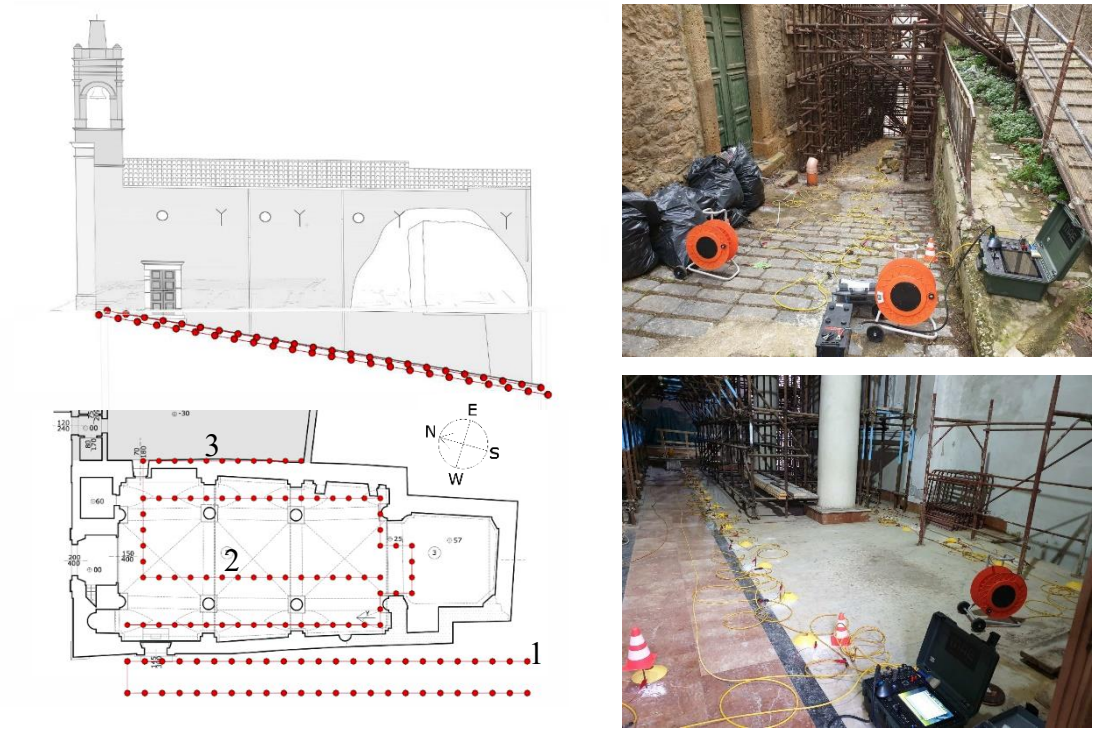


Figure 3: Setting of the pegs regularly spaced along the three determined alignments

3.2 Results of tests

Most rocks exhibit electrolytic conductivity characteristics since almost all minerals are insulating. Conductivity is, therefore, essentially due to interstitial water and is largely a function of the porosity, the water content and the amount of salts dissolved in water. The presence of fluids in the subsoil causes rocks and soils, crossed by electricity, to behave relatively like good conductors; on the contrary, structures with low fluid content such as dry, unfracted rocks and natural or man-made cavities behave like bad conductors, if not actually insulators. Therefore, the underground structures respond to the electricity flow, introduced in different ways, according to the physical parameter that regulates this behaviour: the electrical resistivity ρ.

Once the apparent resistivity values for the points of the mesh in the established cross-section were obtained, by means of the ERT LAB software, a 3D model of resistivity was obtained allowing giving a qualitative interpretation about the presence of anomalies in the ground thickness divided, as previously exposed, into three-dimensional elements [7].

The elaboration of the electrical tomographies performed allowed acquiring information on the ground the Church of Itria rests on, about the potential presence of voids and/or decompressed material, as well as information on the consistency of ground materials.

In particular, the results show that:

Tomography No. 1: the portion of ground investigated consists almost entirely of medium saturated sands, with resistivity values between 10 Ω·m and 100 Ω·m. Some areas have been identified along the electrical spreading line with significant deformations of the induced electric field, such as to define areas corresponding to decompressed material and/or the

presence of potential voids, with resistivity between 160 Ω·m and 300 Ω·m, affecting thicknesses up to 2 m deep from the road surface. The volume of these degraded thicknesses was defined by the evaluation of the ZY cross-section. In particular, from the documents referring to tomographic cross-section 1, we highlighted the critical points of the areas presenting significant deformation of the electric field and having probably triggered the failure at the base of the building, due to potential reflux phenomena at the base, with the consequent collapse of the wall along Itria Street

Tomography No. 2: the ground inside the church consists almost entirely of dry filling material, with resistivity between 10 and 100 Ω·m. In particular, it is clear that this filling material is located in the central nave of the church up to 3 m deep (fig. 4). This result led to the hypothesis of the presence of a pre-existing structure subsequently filled, a crypt or a passage, part of the XIVth century church, some news had been found by means of preliminary historical research. This hypothesis was subsequently confirmed by the discovery, following the excavations, of an underground room below the apse (an area not affected by the tomographic survey) connected through a door to the part below the central nave.

The analysis of the XY sections (fig. 5), at depths varying from 2 m to 6 m, shows areas of the ground with significant deformations of the induced electric field. Such areas correspond to decompressed material and/or partial presence of voids, already starting from the depth of about 1 m of the portion of the southeast corner building. These areas are increasing in depth and breadth at the collapsed wall between 150 Ω·m and 200 Ω·m, with deformations superimposable with those already detected in tomography No. 1. With the investigation carried out, it was also possible to identify areas with even higher resistivity, between 250 Ω·m and 300 Ω·m, at the pillar near the apse affected by the collapse.

Tomography No. 3: the area investigated with this tomography consists almost entirely of filling material, except for some areas of the ground with significant deformations of the induced electric field. Such areas correspond to buried wall structures with resistivity between 160 Ω·m and 300 Ω·m, present up to a depth of approximately 1.6 m from the floor.

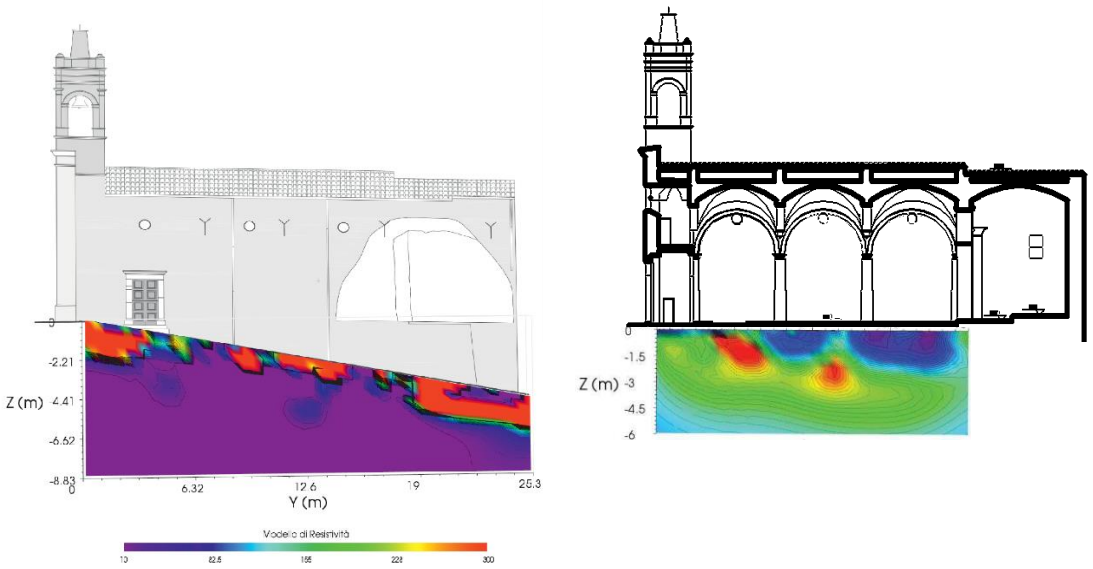


Figure 4: Results of tomography No. 1 and No. 2

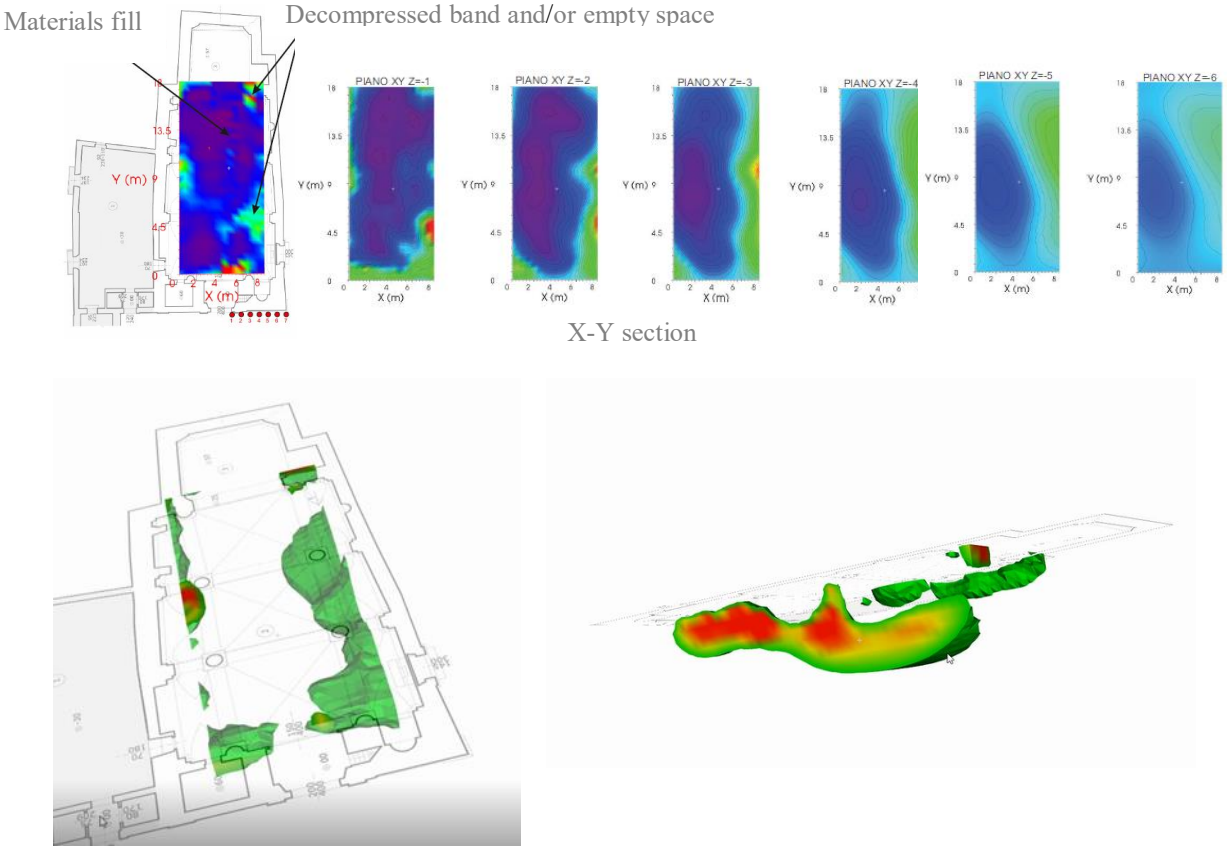


Figure 5: Results of tomography No. 2 (XY sections and 3D model)

To complete the investigation, a visual inspection of the conduct adjacent to the church along Itria Street, was also carried out. This investigation made it possible to detect the geometric and material-construction characteristics of the conduct and above all any deterioration. The rectangular-shaped conduct with a pseudo-rectilinear course, 0.75 m width and approximately 1 m height, shows a concrete base, walls with ashlars regularly arranged with bedding mortar joints and a roof made of stone slabs placed side by side and regularly arranged.

From the visual inspection inside the conduct, several water infiltrations were noticed, coming from the side of the church, with low, but still continuous influxes at the base of the conduct. The water that flows into the conduct from the mountain side disappears, significantly, to infiltrate below the concrete base without knowing the path that follows in depth, being the concrete slab damaged in several points, with some portions removed by runoff water within the same conduct.

From the overall picture of the results of the preliminary investigations, it was possible to define the main cause of the collapse in a failure of the foundations of the wall near Itria Street, due to the inconsistency of the underlying ground, presumably due to the runoff and slow removal of material, following water infiltrations from the conduct. The narrowing of the section of the collapsed wall and the excess load of the roof built in the 1980s are, at this point, to be considered secondary causes.

4 INTERVENTION METHODOLOGY

The works completed on 13 September 2019 represented the 1st stage of consolidation and restoration works of the church of Itria, aimed at consolidating the ground below the church, reconstructing the collapsed wall, consolidating the walls and highlighting an underground room, identified as the primitive XIVth century church. In the 2nd stage of consolidation, the interventions on horizontal structures, arches and damaged vaults, the plaster, the floors and the waterproofing and water disposal system will take place.

4.1 Interventions on the ground

The results of the investigations made it possible to deepen the knowledge of the building with respect to its current state of conservation and formulate a proposal for intervention assessed based on the historical information and the material data collection.

Consequently, the works management suspended the works and drew up a variation report that took into account the results and at the same time agreed with the conduct managers (Municipality of Piazza Armerina and Acquaenna Ltd) the suitable interventions to prevent water dispersion from the conduct to the ground under the church.

The intervention on the conduct was preparatory to the ground consolidation interventions. In particular, a compensation chamber has been created, upstream of the conduct, to avoid excessive flow in the conduct itself. The concrete at the base of the conduct was restored and the walls and the base were covered with three layers with different performances: polyolefins (TPO), non-woven fabric (TNT) and draining sheet (Enkadrain type) to allow the drainage of dispersed water and prevent the flow of water from the conduct towards the church.

For the consolidation of the ground, an intervention method was developed aimed at re-aggregating the incoherent elements and filling the potential voids under the foundations.

After a careful market investigation, a premixed expansive mortar composed of cement and particular additives and expansive agents was chosen, having the main characteristic of combining 100% average expansive capacities and mechanical capacities suitable for holding loads in foundations between 7.3 MPa and 11 MPa (Betonfix Espando type by Kimia). It is a material normally used for ground consolidation, filling voids and cavities and tunnel applications for anchoring nails. To ensure its reliability, two tests were carried out on site, one in a 0.30x0.30x0.60 m metal specimen, with confined expansion, and the other in a 0.50x0.50x0.40 m excavation inside the Church flooring, with free expansion. Both tests have shown within half an hour an increase in the volume of the mortar cast in situ in the confined case by 100% and 70% in the free one (fig. 6).

Once the material was identified, a set of mortar injections was realized through perforations to the external and internal side of the wall on Itria Street and Itria Square, between 0.50 m and 1 m distant and between 2 m and 6 m depth. The rotation perforations, performed vertically or slightly inclined towards the wall, allowed the insertion of drilled rigid PVC canes with an external diameter of 34 mm and an internal diameter of 27 mm; the canes equipped with tip caps were equipped with valves not more than 1 m distant each other.

In order to consolidate even the ground furthest from the holes, it was important to choose the injection pressure. Based on previous experience of the contractor, in similar works, the pressure was chosen varying between 2 atm and 4 atm, depending on the ground resistance.




Figure 6: Confined and free expansion test of the expansion mortar

The injections were carried out with staggered perforations and by injecting the material under pressure regulated by a pressure gauge, from the deeper valve, and advancing along the path. Once this stage was completed, the operation was repeated to make the material exit the upper valve, until it was rejected. Once the external injections were completed, the internal injections were placed at higher distance and consuming less mortar, as the ground was already partially consolidated by the material injected through the external perforations (fig. 7).

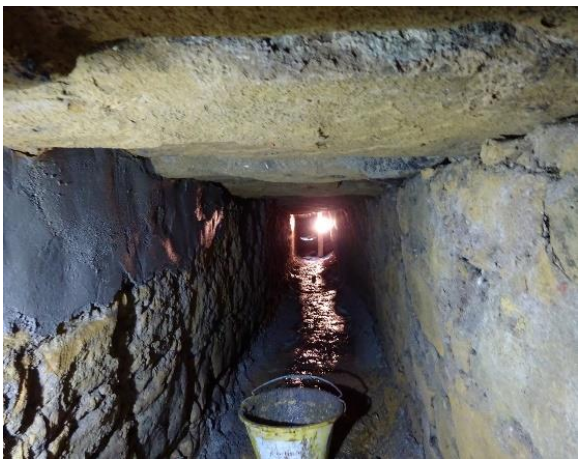



Figure 7: Perforation in the ground and interior view of the conduct

4.2 Interventions on the building

Once the foundation ground was consolidated, the enlargement of the wall was dismantled, which over the years had been built to reinforce the base of the wall downstream of Itria Street and which concealed the entrance to the underground compartment discovered by the excavations carried out during the works.

This was part of the primitive XIVth century church with access to the lower part of the current Itria Street and which justifies the characteristic shape of the current church built in the XVIIth century over this first settlement.

From direct observation of the structure, it was found that the failure had not yet stabilized.

To avoid immediate risks, it was however necessary to take urgent ground consolidation measures below the pillar adjacent to the apse.

Once the rotation of the remaining wall below the collapsed one was verified and the relative deformation, the demolition and the reconstruction of this wall was carried out, by means of stone ashlars of the quarries of Aidone, for almost the entire thickness, and with fair-faced external layer, using the ashlars recovered after the collapse and kept in the Curia spaces. The new wall has a variable thickness, in correspondence with the existing niche, which was no longer built, reaches 2 m.

The works also involved the consolidation of the existing walls of the church and the underground room with injections of fluid cement mortar (BETONFIX 200) and the anchoring of the pillar near the apse to the wall rebuilt with carbon bars and special mortar.

The rebuilt wall was also connected with the opposite wall through new chains in order to improve the box-like behaviour of the entire load-bearing wall structure. In particular, a series of perforations reinforced with carbon rods were made and 3 chains at 3 heights were placed to create the interlocking at the corner of the new wall with the existing orthogonal one: at the foot level of the church, at the roof level and at the intermediate level (fig. 8, 9). Two other chains were built on the sides of the closing arch of the apse.

During the whole-time span of the works, a monitoring system was developed in order to measure any in-progress phenomena or to ascertain the results obtained with the injections of expansive mortar. In particular, crack-gauges and pendulums were applied and left at the end of the works, at the most critical points (e.g. in the cracks of the arches converging in the pillar adjacent to the apse) to measure any structural movements during the suspension of the works.

Considering the importance of ground consolidation for the intervention carried out on the church, a new electric tomography campaign has been planned for the resumption of the works of the 2nd lot in order to verify the filling of the voids and proceed with any additions.

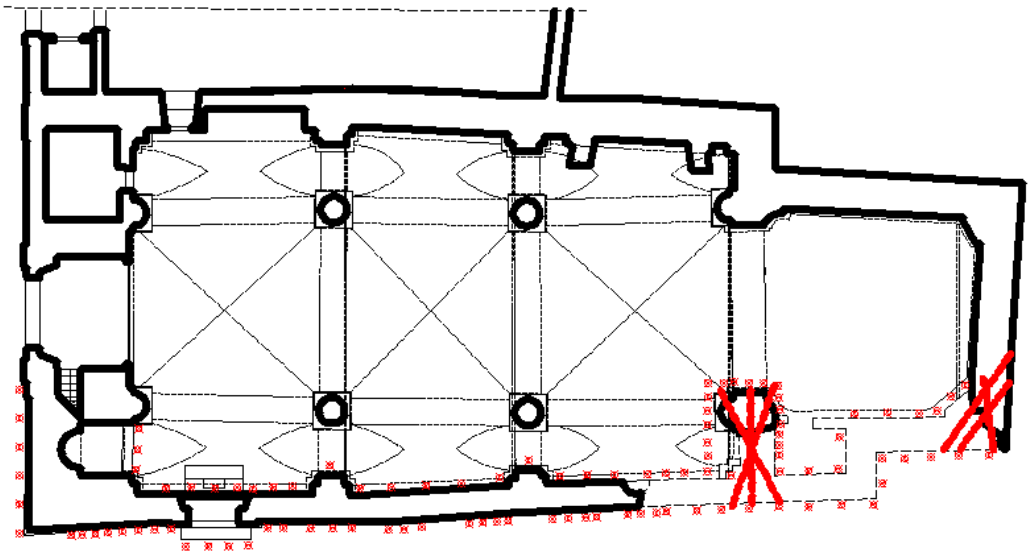


Figure 8: Plan of the church with points of perforation in the ground and with the perforations reinforced with carbon rods placed to create interlocking at the corner of the new wall with the existing one

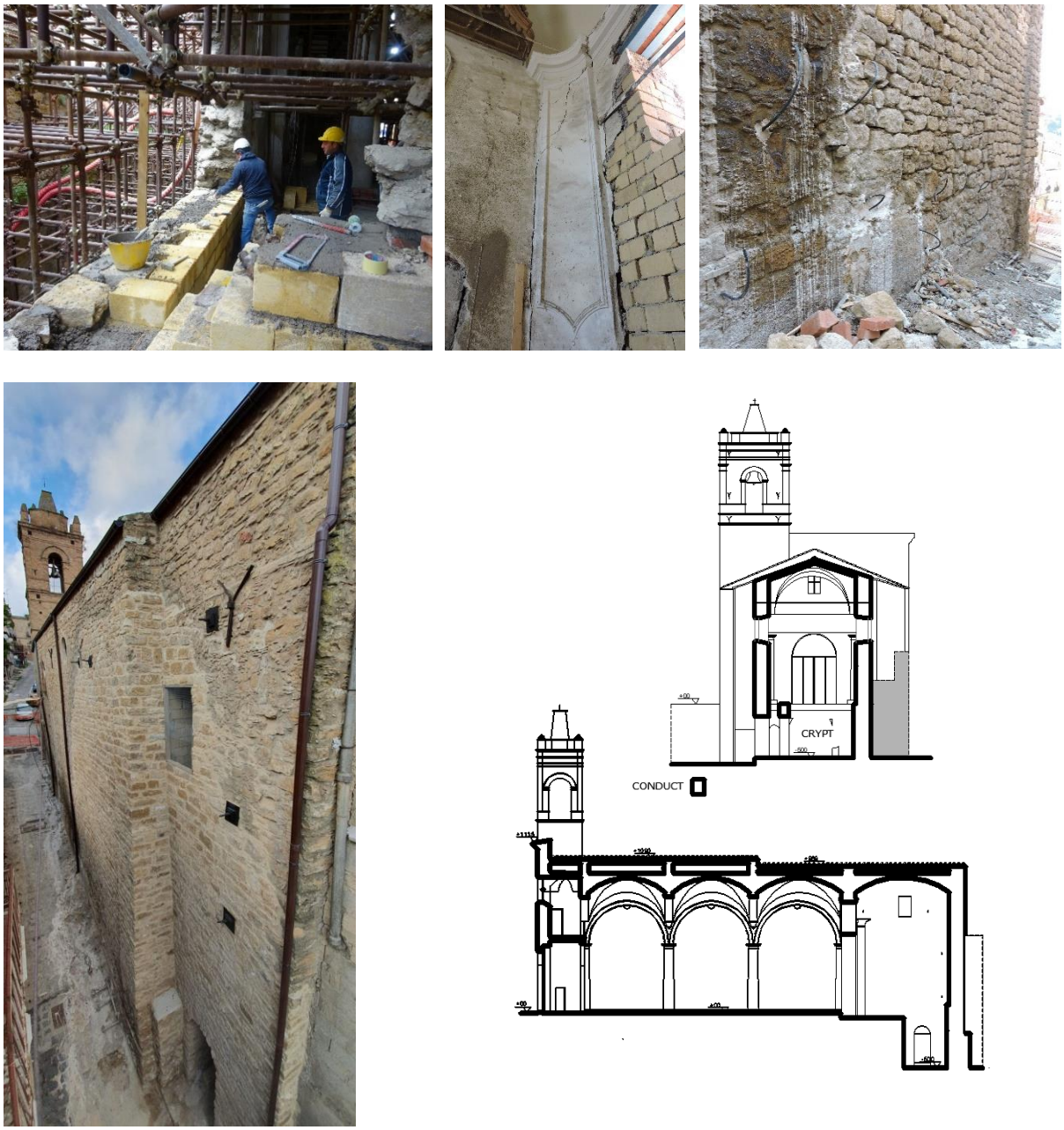


Figure 9: Photographs of the reconstructed wall and drawings of the church with the found underground room

5 CONCLUSIONS

The geometric irregularities of the church, due to original imperfections and the joints made during the construction phase of the church at the end of the XVIIth century above the pre-existing XIVth century church, as well as the subsequent modifications, have generated a very complex framework that led to errors in the design phase.

In addition, the urban evolution surrounding the church have created a complex situation. With the passage of time, the sacristy and other buildings were joined to the side facade of the church, not in all its length, and on the southern head. But above all, the location of the conduct

adjacent to the church have led to a disastrous situation.

It is important to highlight how in the case study, as in many restoration projects [8], the complexity of the monument negatively influenced the choice of preliminary investigations and how this negative influence was accentuated by an originally project lacking, by the use of unsuitable materials and subsequent inadequate interventions.

The experience of this case study demonstrates the importance in choosing the types of preliminary investigations and how these can positively or negatively influence the identification of the causes of failure.

In conclusion, it is possible to affirm that with the appropriate preliminary investigations of the ground, it would have been possible to intervene immediately in the conduct and prevent the phenomenon from continuing in the 12 years between the collapse and the start of the works, causing further damage, such as the lowering of the pillar in proximity of the apse and consequently greater interventions and expenses.

Acknowledgements. The restoration works were realized thanks to the C.E.I. (Conferenza Episcopale Italiana) cofounding, together with the Diocese of Piazza Armerina, the 70% amount of the works. Many thanks to Don Giuseppe Paci, director of the Sacred Art and Cultural Heritage Office of the Diocese of Piazza Armerina and his assistant dott. arch. Tiziana Crocco, surveyor Giovanni Di Manno, technical director of ESSE I Ltd, Regalbuto (EN), executor of the works and geologists Ranieri Santarosa and Nunzio Santarosa, owners of Geotecnhibla Ltd of Avola (SR), carrying out geophysical survey.

REFERENCES

[1] Gil E., Mas A., Lerma C., Torner M.E., Vercher J., Non-destructive Techniques Methodologies for the Detection of Ancient Structures under Heritage Buildings. *International Journal of Architectural Heritage* (Published online: 17 Dec 2019).

[2] Basiricò T., Campione S., Cottone A., The collapse and restoration of the Church of Saint Mary of Itria in Piazza Armerina (Sicily, Italy). In: R. Aguilar et al. (Eds.): *Structural Analysis of Historical Constructions*, RILEM Bookseries 18 (2019), pp. 2016-2024.

[3] Villari L., Storia ecclesiastica della città di Piazza Armerina, Società messinese di Storia Patria, Messina (1988).

[4] Trogu A., Ranieri G., Fischanger F., 3D Electrical Resistivity Tomography to Improve the Knowledge of the Subsoil below Existing Buildings. *Environmental Semeiotics* (2011) **4** (4):63-70.

[5] Torner M. E., Mas A., Lerma C., Herráez J., Analysis Method for Studying Groundwater under a Church. *Applied Mechanics and Materials* (2016) **861**:263-270.

[6] Comina C., Giordano N., Ghidone G., Fischanger, Time-Lapse 3D Electric Tomography for Short-time Monitoring of an Experimental Heat Storage System, *Geosciences* (2019) **9** (4):167.

[7] Cardarelli E., Fischanger F., 2D data modelling by electrical resistivity tomography for complex subsurface geology. *Geophysical Prospecting* (2006) **54** (2):121-133.

[8] Torner M. E., Mas A., Lerma C., Gil E., Vercher J., Embedding of the Church of the Asunción of Llíria (Spain). Origin and Consequences. *Estoa* (2019) **16** (8):111-119.

12th International Conference on Structural Analysis of Historical Constructions
SAHC 2020
P. Roca, L. Pelà and C. Molins (Eds.)

NONLINEAR STRUCTURAL ANALYSIS OF THE ELLIPTICAL DOME OF THE CHURCH IN THE UNIVERSIDAD LABORAL, GIJON, SPAIN

JUAN JOSÉ DEL COZ-DIAZ[1*], ALFONSO LOZANO MARTINEZ-LUENGAS[2], MAR ALONSO-MARTINEZ[2], PILAR GARCIA-CUETOS[3] AND FELIPE PEDRO ALVAREZ-RABANAL[2]

[1]GICONSIME Research Team – University of Oviedo
Viesques Departmental Building, 7 – Office 7.1.02. 33204 Gijon, Asturias (Spain)
e-mail: delcoz@uniovi.es, giconsime.grupos.uniovi.es

[2] Department of Construction and Manufacturing, EPI Gijón, University of Oviedo
Viesques Departmental Building, 7 – Office 7.1.04. 33204 Gijon, Asturias (Spain)

[3] Department of Art History and Musicology, Faculty of Philosophy
University of Oviedo
Teniente Alfonso Martínez s/n 33011 Oviedo, Asturias (Spain)
email: alozano@uniovi.es, mar@constru.uniovi.es, gcuetos@uniovi.es, felipe@constru.uniovi.es, giconsime.grupos.uniovi.es

Keywords: Historical Structure, Masonry, Monitoring, Non-Destructive Inspection

Abstract. *The Church of the Laboral University of Gijón has the world's largest elliptical masonry roof with 40.8 meters of mayor axis. This big structure is vertically supported with no columns using twenty pairs of masonry ribs crossing each other, and horizontally supported by means of two elliptical ring beams located at the top of the Church. In order to study this historical building, this paper presents the overall three-dimensional structural numerical analysis of the Church, taking into account different material nonlinearities - including masonry and reinforced concrete - as well as geometrical nonlinearities, such as contact effects among the different structural components of the building. Furthermore, a coupled thermal-structural analysis was carried out considering the summer temperature distribution and the Spanish standard rule dead and live loads. The most relevant results, in terms of maximum displacement, stress and, cracking and crushing phenomena are presented. Finally, valuable information from the interaction among the structural elements of the Church are discussed and the most critical points of the building are located, giving place to the most important conclusions of the nonlinear numerical analysis of this interesting structure.*

1 INTRODUCTION

The Universidad Laboral of Gijón was built between 1946 and 1956. With 270,000 m^2, it was the most important architectural work in the twentieth century and is still the largest building in Spain [1]. The church building (see Figure 1) is undoubtedly the most spectacular

architectural ensemble of the Universidad Laboral in Gijón. With an overall inside surface of 807 m², the church has the world's largest elliptical roof: with a major axis of 40.8 m and a minor axis of 25.2 m. The church is twenty-five meters high from the floor to the springing line, and thirty-three meters high to the crown. The dome has an estimated weight of 2,300 tons. For its construction, 450,000 annealed bricks from the province of León (Spain) were used. The whole structure is self-supported with twenty pairs of interlaced masonry ribs. In the crown, there is an oculus to light the interior of the Church naturally. Currently however, there is no natural lighting due to a slight sag in the dome.

The structural analysis of masonry structures, and in particular of domes, has several difficulties: nonlinearities due to the material properties, with almost no tensile strength; the lack of experimental characterisation of the mechanical properties of masonry structural elements; and in this particular case, the complexity of the geometry [2].

To solve this complex structural problem, refined mechanical models, which accurately predict the behaviour of masonry material and elements, are proposed in the literature [3-6]. These models use different strategies to consider the highly nonlinear behaviour of the material both in tension where low tensile capacity and consequent cracking phenomena are taken into account, and in compression. Some of those models are also able to provide the structural response to large displacements. Unfortunately, current models are difficult to apply to a 3D analysis of complex structural systems. This is due to the great number of parameters involved in the definition, and the large number of degrees of freedom required for structural meshing, leading to unmanageable data. In this work, a nonlinear structural static analysis of the elliptical dome of the church is developed. The most relevant results: maximum displacement, stress, and cracking and crushing phenomena are presented.

Finally, valuable information from the structural behaviour and the interaction among the elements of the structure are discussed. Furthermore, the most important conclusions of the structural analysis are drawn, and a plan for the conservation of the building is proposed.



Figure 1. Current state of the church of Universidad Laboral in Gijón

2 DESCRIPTION OF THE CHURCH IN THE UNIVERSIDAD LABORAL

Traditional church buildings are often in the shape of a cross, and frequently have a tower or dome. However, the Church of the Laboral is completely different, since the roof has an elliptical shape [7] (see Fig.2).

The main parts of the system are described as follows:

- Masonry ribs: There are 20 interlaced pairs of brick ribs, stretching from the columns to the central skylight. They are rectangular in cross section, 0.9 m wide and from 1.8 to 2 m high, with variable lengths up to 16.8 m. The main function of these elements is to transmit forces from the dome to the columns.
- Ring beams: There are two elliptical ring beams located at the top of the columns: upper and lower. Both of them are made of reinforced concrete.

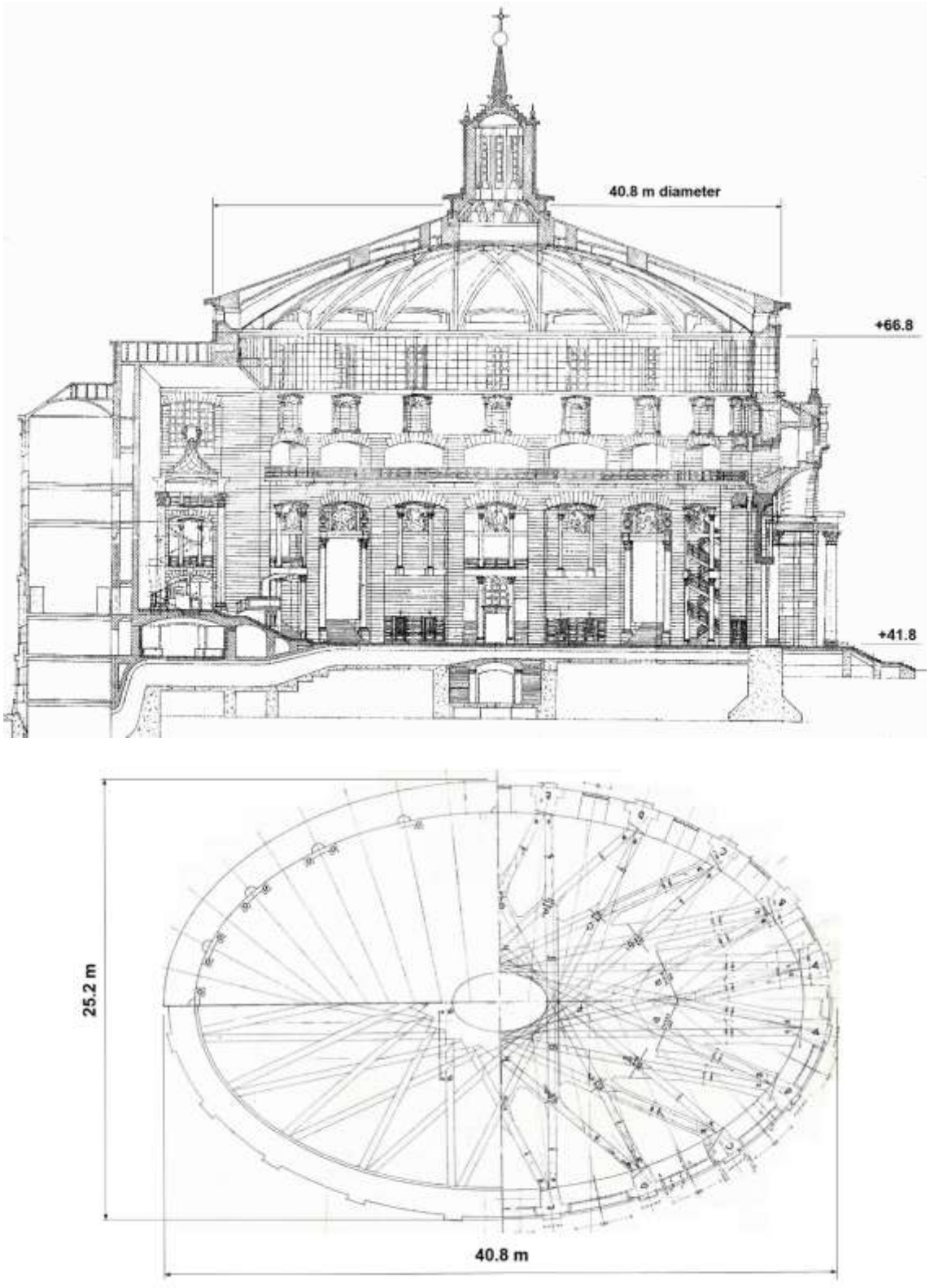


Figure 2. Church of the Laboral with main dimension: elevation view (upper) and plan of the dome (lower)

3 STRUCTURAL ANALYSIS

Analysis of the structural response of masonry structures, and in particular of domes, is complex. The nonlinear material properties of masonry, with almost no tensile strength, must be considered in the numerical model. In addition, there is a lack experimental data of the mechanical properties of the masonry. Finally, this case is particularly complex due to geometry of the dome which is elliptical in shape and has double curvature on three axes [7].

Previous numerical models [2, 5-6] are able to provide the structural response to large cyclic deformations, which occur under seismic actions. However, there are no 3D numerical models able to analyze complex geometries like the case studied in this work.

The numerical simulation carried out in this work uses the ANSYS Workbench 2019 R2 academic software. The numerical simulation developed gives great insight into the structural response of the dome, saving costs and time in relation to experimental tests [8-9].

3.1 Geometrical model

The 3D geometrical model of the dome was based on the project of the building (see Fig. 2). It was done using a parametric CAD software. The main elements considered are the following:

- Masonry ribs: elliptical arches of the dome made of masonry and concrete.
- Ring beams: there are two ring beams made of reinforced concrete to support the masonry ribs, the upper ring and the lower ring.
- Roof: the conical auxiliary structure over the ribs, including the small tower at the central skylight.

- Columns: there are twenty main building supports made of reinforced concrete.

The explode view of the geometrical model and the main components are shown in Fig.3.

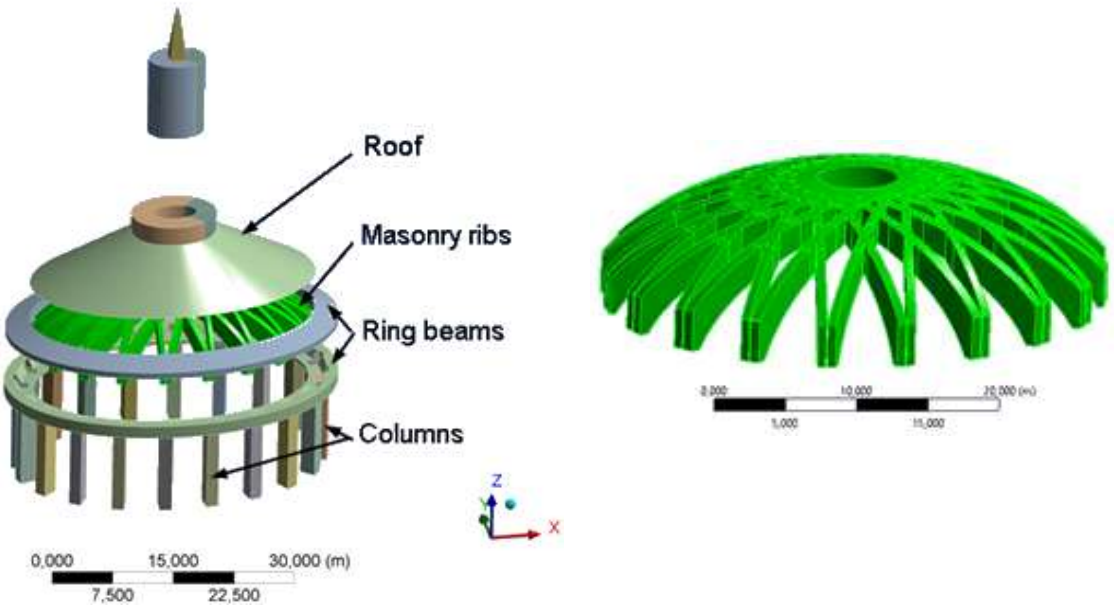


Figure 3. Geometrical model of the Church of the Laboral main parts: explode view (left) and masonry ribs (right)

3.2 Finite element model

Numerical model uses several finite elements to simulate the structural behaviour of the dome. The concrete and masonry components were modelled using the element SOLID65 and SOLID185 from ANSYS®. Both are an eight-node solid element, with three degrees of freedom at each node (translations in nodal x, y, and z directions). They are suitable numerical elements to simulate masonry and concrete components. SOLID65 supports plastic deformation, cracking in three orthogonal directions, and crushing. SOLID185 supports plasticity, stress stiffening, large deflection and large strain [8-10].

Furthermore, elements type SOLID186 and SOLID187 were used to mesh the conical roof and the smallest parts of the Church. They are three-dimensional higher order solid elements that exhibits quadratic displacement behavior. SOLID186 is a twenty-node solid element with three degrees of freedom per node. SOLID187 is a ten-node solid element and tetrahedral in shape [8-12].

Contact between structural components, masonry ribs, conical roof, upper and the small tower at central skylight, lower rings and pillars, were simulated using pairs of contact elements, CONTA174 and TARGET170 [8-12].

The MultiZone mesh method was used to solve the complex meshing of the structure. This method divides automatically the geometry in mapped regions and free regions. Then, it generates a pure hexahedral mesh where possible and fills the more difficult regions with unstructured mesh. This meshing method is suitable to mesh complex geometries.

The mesh sizing parameter ranges between 0.1 m for the masonry ribs and 0.2 m for the ring beams. The finite element model has more than 1,500,000 nodes and 1,200,000 elements (see Fig.4).

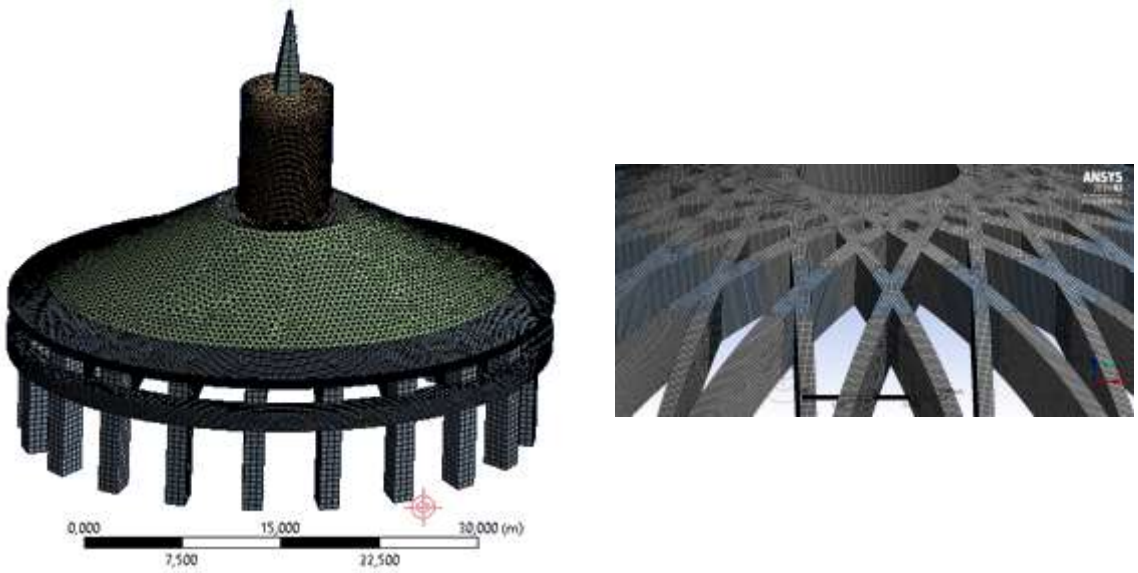


Figure 4. Mesh of the church in the Universidad Laboral: overall view (left) and masonry ribs detail (right)

3.3 Material properties

The structural behavior of the masonry dome was analyzed using a macro-modelling strategy, based on previous research works [4-6]. In this sense, mortar and unit-mortar interface are smeared out in the complex geometrical model of the roof, due to a necessary compromise between accuracy and efficiency in this specific case.

Nonlinear material models were used to simulate masonry and concrete material behavior. Two material models were combined to study both material failure modes, cracking and crushing: Drucker–Praguer material model for compression stresses, and Willam-Warnke material model for tension stresses, in order to predict both material failure modes: cracking and crushing [13-14].

In order to obtain the main masonry properties, other minor structure located near the building was tested. The brick is 0.24 m long, 0.11 m wide and 0.06 m thick. The mortar thickness is 0.01 m in all directions. [14-15].

The main material properties considered in the FEM model are shown in Table 1.

Table 1: Material properties

Material	E (Mpa)	σ_t (Mpa)	σ_c (Mpa)	μ	δ (kg/m^3)	α (°C^{-1})	λ (W/m°C)
Sandstone	10,000	14.5	95	0.30	2,250	1.16E-5	1.7
Limestone	35,000	15	140	0.25	2,750	0.8E-5	1.3
Sponge (roof)	5	-	-	0.20	10	1.4e-5	2.0
Reinforced concrete	23,000	2,9	30	0.18	2,300	1.2E-5	1.63
Masonry	870	0.5	9.5	0.25	2,000	0.5E-5	0.8

3.4 Load cases

In this work, a thermal analysis was carried out to determine the temperature distribution in the model due to the solar radiation. A thermal flux of 200 W/m^2 was applied considering the worst climatic condition in the summer [16]. Convection film coefficients were obtained from the Standard UNE-EN ISO 6946, as it is shown in Table 2 below, ranging from 25 to 5.88 W/m^{2}K [17-18].

Table 2: Convection film coefficients

Film coefficient	Thermal flux direction		
	Upper	Horizontal	Lower
Inner surfaces	10.0	7.7	5.88
Outer surfaces	25.0	25.0	25.0

Furthermore, a coupled thermal-structural analysis was carried out considering the temperature distribution obtained in the previous thermal analysis.

Dead load and snow load were considered, taking into account the following parameters:

- Dead load: density of the main materials, including a specific study to the conical roof.
- Snow load: a constant pressure of 450 Pa were applied in the exterior surface of the roof [16].

To solve the couple thermal-structural analysis the temperature distribution previously obtained was applied to nodes and transferred to the model. The nonlinear problem was solved using a Newton-Raphson method with adaptive descent including plastic material properties. The maximum number of equilibrium iterations was 100, with an initial step of 0.01 over 1. As convergence control, the displacement was considered with a minimum tolerance of 0.01 [10-12].

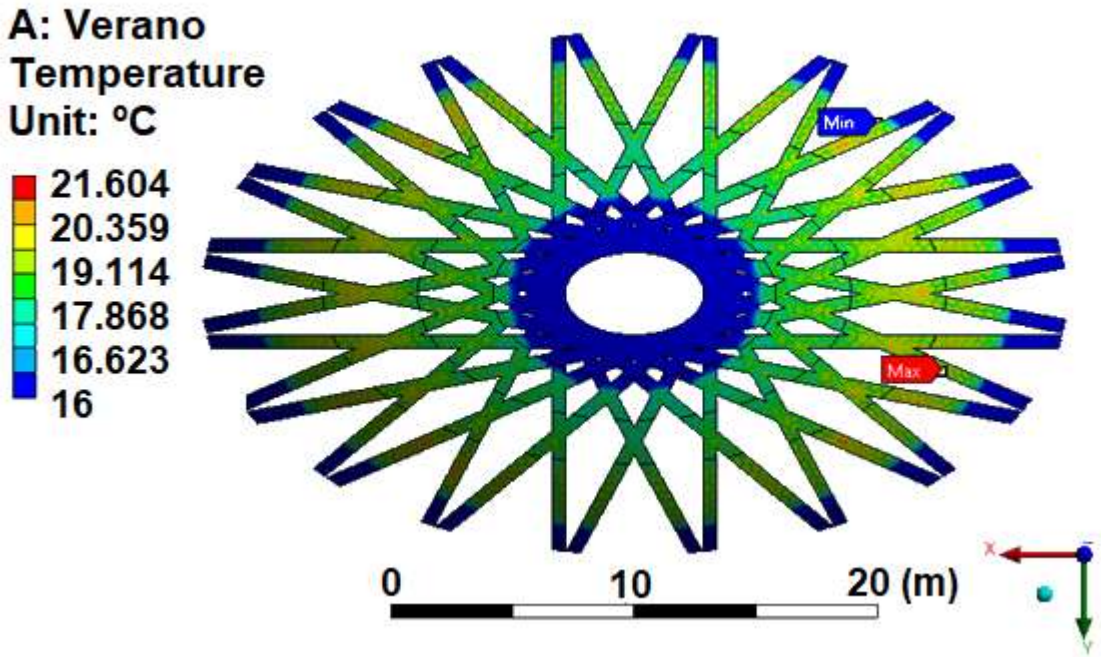
The coupled thermal-structural problem was solved in a four Intel ® Xeon ® Gold 6230 CPU @ 2.1 GHz machine, with 256 GB memory and 4 TB Raid0 NvMe SSD disks, distributed among 80 cores. Total CPU time was about 10,000 seconds, with 14 load steps and 300 iterations.

4 NUMERICAL RESULTS AND DISCUSSION

4.1 Main results

In this section, the main numerical results from the thermal and structural analyses are presented. Results include a detailed cracking and crushing analyses.

Figure 5 shows the temperature distribution obtained in the thermal analysis where summer climatic conditions were applied. Temperature values ranges between 16 ºC and 21.6 ºC at the upper part of the masonry ribs. These variations could cause thermal stresses in the dome



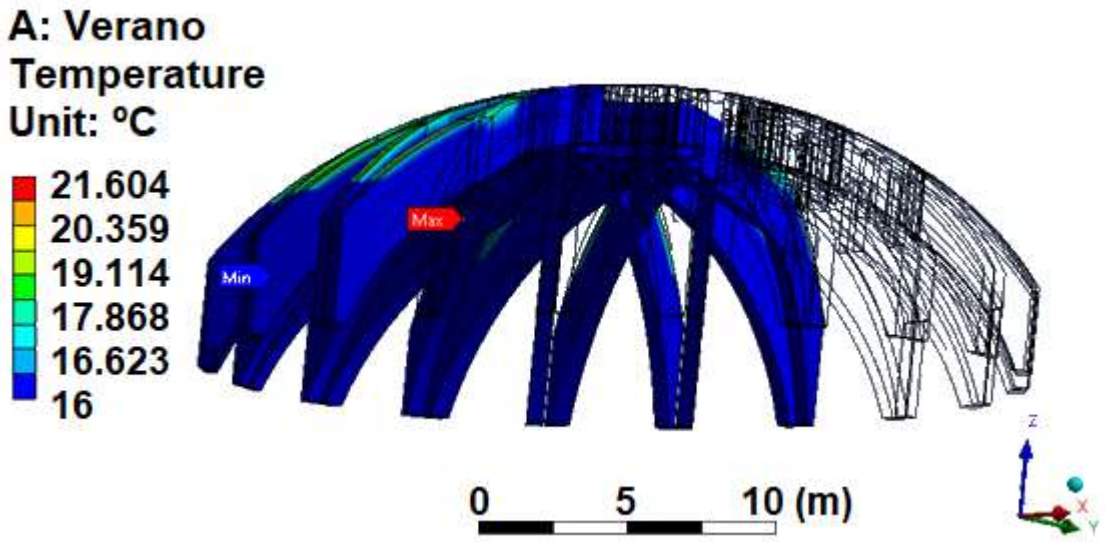
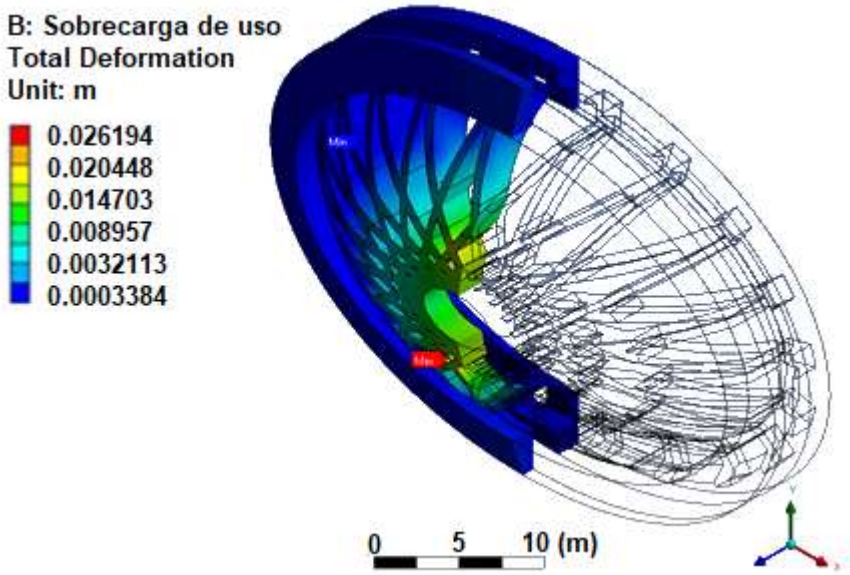


Figure 5. Temperature distribution in masonry ribs: zenithal view (upper) and isometric view detail (lower)

Figure 6 shows the main results of the coupled thermal-structural nonlinear analysis. Figure 6 upper shows the maximum displacements of the dome and Figure 6 lower, the crack patterns obtained when the total load is applied on the dome.



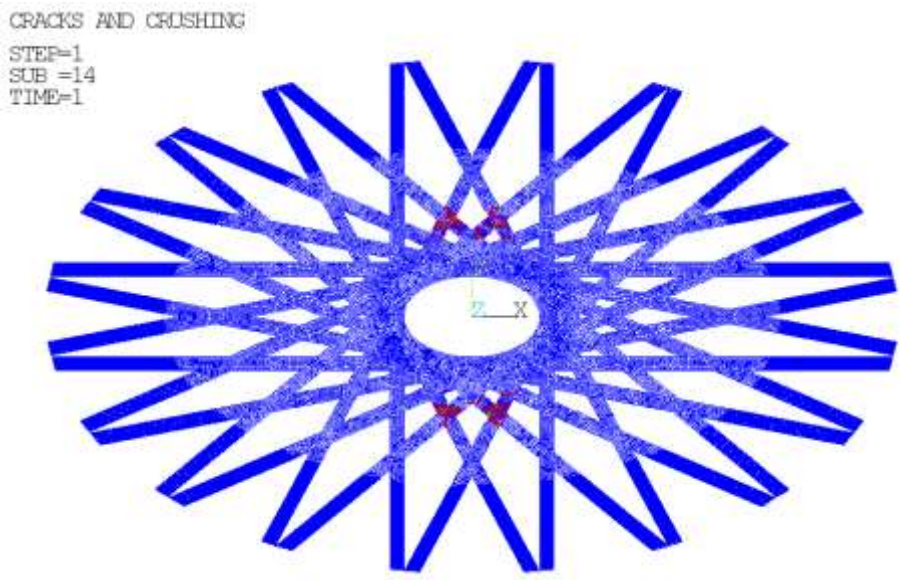
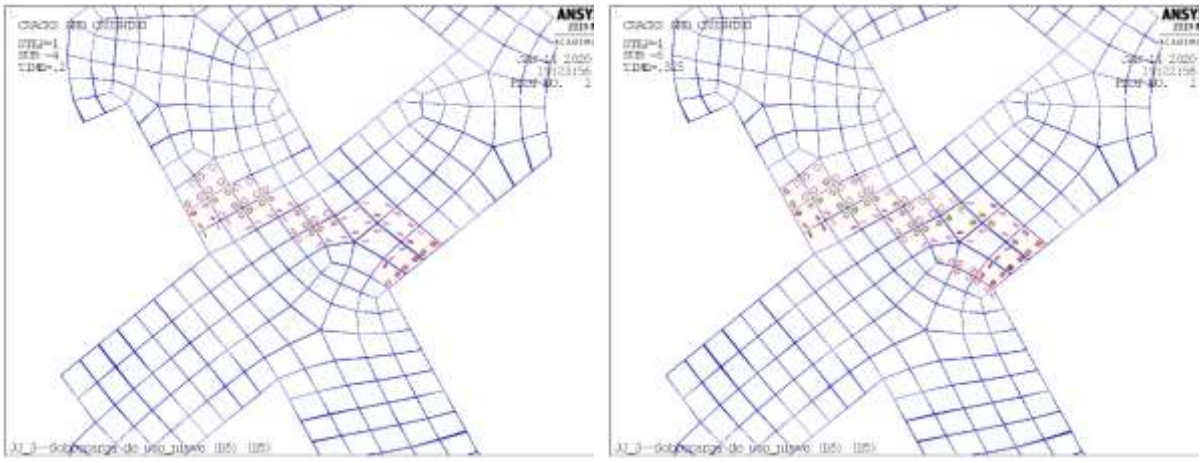


Figure 6. Maximum masonry ribs displacement (upper) and crack pattern (lower)

Maximum displacement value is about 0.026 m, which lead a ratio of 962 between short dome length and vertical displacement. With respect to the crack patterns, short masonry ribs present crushing under compression stresses in the upper zones, and cracking failures at the lower part of the short ribs.

In the non-linear region of the response, subsequent cracking occurs as more load is applied to the dome. Cracks grow in the constant region, located at the short ribs, and the masonry ribs starts cracking out towards the supports at a 20% of the maximum load (see Figure 6). Figure 6 shows the details of the crack evolution at 6 different points of the analysis (0.2 s, 0.325 s, 0.55 s, 0.75 s, 0.85 s, 1 s). Symbols in red represent the cracks and blue lines the finite elements of the numerical model.



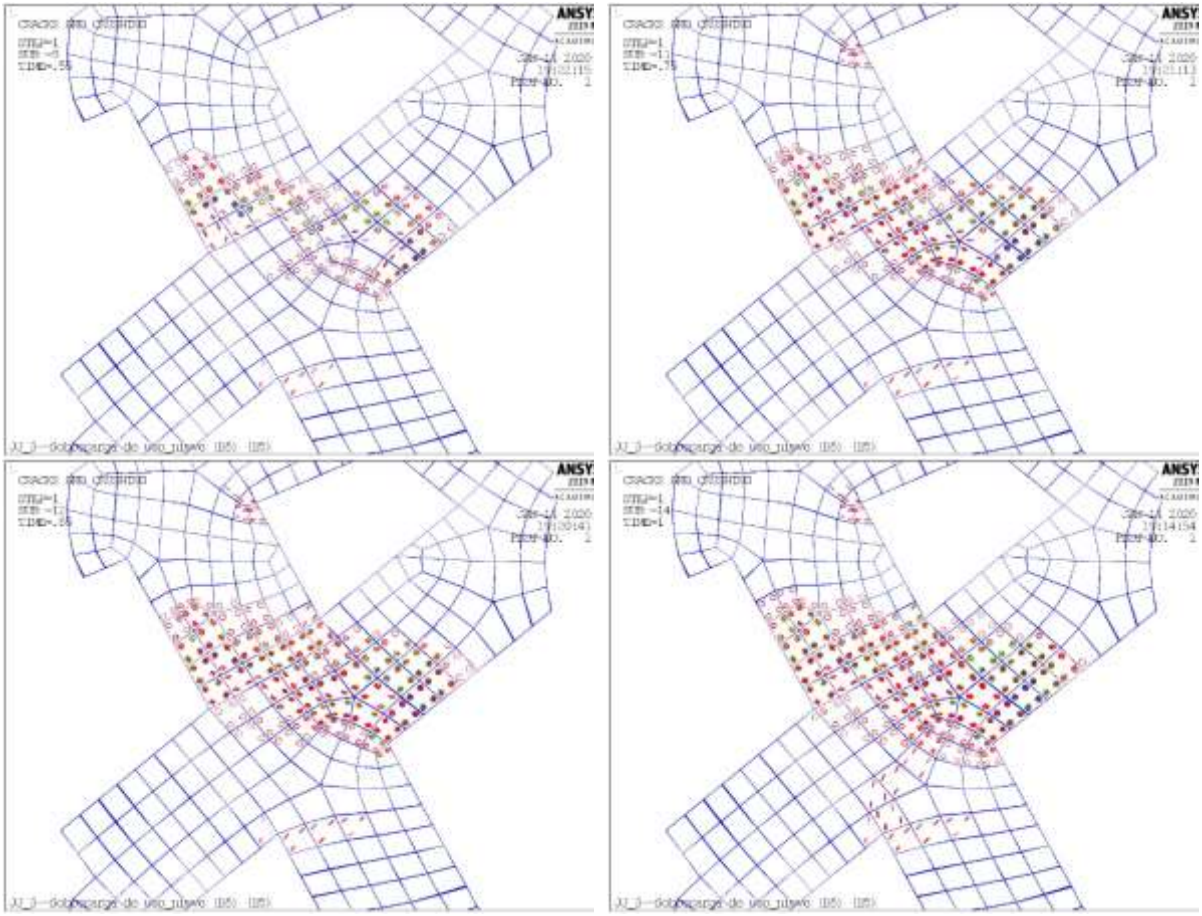


Figure 7. Crack patterns in the central part of the masonry ribs at different load steps

5 CONCLUSIONS

This paper has proved that the use of advanced numerical methods helps to obtain the structural response of a complex nonlinear model, such as the case studied in this work. The most important findings are the following:

- To define the complex geometry of the Church in the Universidad Laboral it is necessary to use a three-dimensional parametric design program.
- In order to obtain a regular tetrahedral mesh, it is necessary to use a MultiZone mesh method. In this study, suitable element size ranges between 0.1 and 0.2.
- The thermal gradient in the masonry ribs causes significantly less stresses and deformation than the expected. The low stress levels are due to the conductivity properties of the material and the air chamber in the interior of the Church.
- The use of nonlinear numerical models including contacts are suitable to study the thermal and structural behavior of complex geometries and assembles of different structural elements, such as ribs, columns and annular rings.

- A constitutive material model to simulate concrete and masonry models is very efficient to simulate the behavior of bricks. In this case, William-Warnke and Drucker-Prager models were combined to obtained accurate results.

- The numerical results of the coupled thermal-structural model show cracking patterns in the short masonry ribs. These cracks caused some deterioration in the elliptical dome.

In this work, our experience in numerical simulation provided an important contribution to know the structural conditions of an important cultural heritage. The structural behavior of the elliptical dome of the Church in the Universidad Laboral was analyzed using advanced numerical models and the most critical points were located. This study is very important to prevent and assist the conservation, or retrofitting of this building.

Acknowledgements. The authors greatly appreciate the collaboration of the GICONSIME Research Group at the University of Oviedo, and also to Ignacio Rojo Blanco, a Master industrial engineering student at the University of Oviedo. We would also like to thank Swanson Analysis Inc. for the use of the ANSYS University program and Workbench simulation environment. Furthermore, authors must acknowledge the financial support provided by regional funds from the Gobierno del Principado de Asturias and FICYT through the Research Project GRUPIN-IDI/2018/000221 also co-financed with FEDER funds. Finally, authors must acknowledge the alumni association of La Laboral and, particularly, to Victor Camblor Prieto to provide real photographs and some useful information to prepare this research work.

REFERENCES

[1] A.M. Rodríguez, J.J. del Coz-Diaz, et.al., *Los talleres de la Universidad Laboral de Gijón* 2th Edition, Ed. Cicees, 2007.

[2] Gianni Bartoli, Michele Betti,Claudio Borri. *Numerical Modeling of the Structural Behavior of Brunelleschi's Dome of Santa Maria del Fiore*. International Journal of Architectural Heritage 2014; 9(4): 408-429.

[3] J.J. del Coz-Diaz, A. Lozano Martinez-Luengas, J.M. Adam, A. Martin Rodriguez., *Non-linear hygrothermal failure analysis of an external clay brick wall by FEM – A case study*. Construction and Building Materials 25 (2011) 4454-4464.

[4] J.J. del Coz-Diaz, P.J. Garcia Nieto, F.P. Alvarez Rabanal, A. Lozano Martinez-Luengas. *Design and shape optimization of a new type of hollow concrete masonry block using the finite element method.* Engineering Structures 33 (2011) 1–9.

[5] P.B. Lourenco. Computational strategies for Masonry Structures. Ph. Thesis. Delft University Press. ISBN 90-407-1221-2, (1996)

[6] Saloustros, S., Pelà, L., Cervera, M. and Roca, P. Tracking of Localized Cracks in the Finite Element Analysis of Masonry Walls. In: R. Aguilar et al. (Eds.): *Structural Analysis of Historical Constructions*, RILEM Bookseries 18 (2019), pp. 919–928.

[7] Wikipedia. https://en.wikipedia.org/wiki/Universidad_Laboral_de_Gij%C3%B3n. Accesed January 15th , 2020.

[8] Moaveni S. Finite element analysis. Theory and application with ANSYS. New York: Prentice Hall; 2007.
[9] Madenci E, Guven I. The finite element method and applications in engineering using ANSYS. Berlin: Springer-Verlag; 2007.
[10] ANSYS® Academic Research Mechanical, Release 19.2, Help System, Analysis Guide, ANSYS, Inc.
[11] Zienkiewicz, O.C. and Taylor, R.L. *The finite element method*. McGraw Hill, Vol. I., (1989), Vol. II, (1991).
[12] Idelsohn, S.R. and Oñate, E. Finite element and finite volumes. Two good friends. *Int. J. Num. Meth. Engng* (1994) **37**:3323-3341.
[13] Fuschi P, Dutko M, Peric D, Owen DRJ. On numerical integration of the five parameter model for concrete. Computer & Structures 1994; 53(4):825–38.
[14] Willam KJ, Warnke ED. Constitutive model for the triaxial behaviour of concrete. Proceedings of the international association for bridge and structural engineering, vol. 19. Bergamo (Italy): ISMES; 1975. p. 174–8.
[15] Calderini C, Cattari S, Lagomarsino S. The use of the diagonal compression test to identify the shear mechanical parameters of masonry. Constr Build Mater 2010;24(5):677–85.
[16] CTE Spanish rule – DB-SE-AE: Structural Security, Ministry of Buildings, March 2006.
[17] UNE-EN-1745, Masonry and Masonry Products. Methods for Determining Design Thermal Values, AENOR, Madrid, 2002.
[18] UNE-EN ISO 6946, Elements and Construction Components. Resistance and Thermal Transmittance: Calculation Method, AENOR, Madrid, 1997.

12th International Conference on Structural Analysis of Historical Constructions
SAHC 2020
P. Roca, L. Pelà and C. Molins (Eds.)

PARAMETER EVALUATION IN HISTORICAL CONSTRUCTION: FROM SENSITIVITY ANALYSIS TO THE TEST PLANNING

ALFREDO CALÌ[1*], POLIANA DIAS DE MORAES[2] AND ÂNGELA DO VALLE[2]

[1]Ph.D. Student in Civil Engineering - Department of Civil Engineering Federal University of Santa Catarina (UFSC)
Rua João Pio Duarte Silva, Florianópolis (SC), Brazil
e-mail: alfredo.cali@posgrad.ufsc.br, https://orcid.org/0000-0001-8974-5866 (*corresponding author)

[2]Associate Professor - Department of Civil Engineering Federal University of Santa Catarina (UFSC)
Rua João Pio Duarte Silva, Florianópolis (SC), Brazil
e-mail: poliana.moraes@ufsc.br
e-mail: angela.valle@ufsc.br

Keywords: H-BIM, Historical Buildings, Masonry Structures, Sensitivity Analysis.

Abstract. *Uncertainties play a key role in the structural assessment in the existing buildings. They are mainly associated with materials, geometries and loads. The reduction of these uncertainties is one of the main challenges for researchers who approach this type of project. The aim of this work is the reduction of uncertainties through a sensitivity analysis. These analyses allow understanding the structural overall behaviour and they are useful to the in-situ test planning. The proposed sensitivity analysis is used as cognitive evaluation, analyzing the influences of each parameter on the structural behaviour, and as improvement assessment, evaluating the effectiveness of the intervention proposals. Furthermore, such approach reduces the impact of the experimental campaign and the intervention proposals, in terms of invasiveness, time and cost. The research is carried out through the selection of a case study, the "Quartel da Tropa" (SC), Brazil. It is used to show how the proposed approach can be applied for the structural assessment of historical buildings. The information collected was elaborated with Historical Building Information Modeling (H-BIM) and analyzed through finite element method software. The proposed research allows increasing the level of knowledge of the historical construction of the Quartel da Tropa, through the sensitivity analysis and the experimental test design of the structure. Such an approach suggests how not only the longitudinal Young's Modulus (E) and the specific weight (w) of the masonry are the main parameters to avoid significant errors in the results in terms of structural assessment. Indeed, type of wooden species, type of structural connection, different types of masonry characteristic in different structural elements must be considered.*

1 INTRODUCTION

Uncertainty analysis [1] – mostly known as Sensitivity Analysis (SA) - is a method that deals in quantifying the uncertainty in the model output [2]. SA may be also used for other purposes [2], such as increasing the robustness of a model [3], design optimization [4], identification of

parameters that requires further research [5] and its influence on the cracking pattern and extent, model simplification by eliminating variables [3], understanding of the model and variable interaction [6], etc. For these reasons, sensitivity analysis is a widespread method used to investigate the influence of parameters within the structural response assessment [4]. The knowledge elements - necessary for this analysis - concern the geometry of the structure, the construction details and the mechanical properties of materials [7]. As resumed by the Italian National Research Council (CNR) [7], those elements are usually obtained from (1) historical-critical analysis aimed at reconstructing the constructive process and the subsequent modifications and events suffered over time by the building; (2) documental projects relating to the implementation and subsequent modifications; (3) geometric-structural survey referring to the overall geometry of the construction as well as that of the constructive elements, including their associated structures, quality and state of preservation of materials and building parts; (4) experimental investigations aimed at completing the information framework related to the mechanical properties of materials. In this work, the sensitivity analysis is used as a methodological step to the test planning aimed to increase the knowledge level of the historical construction through-out the use of Non-Destructive test (NDT) investigation.

This paper aims to propose an approach that allows reducing the construction uncertainties trough the understanding of the structural overall behaviour and the *in-situ* test planning. The combination of two methodologies - (H-BIM) [8] and the path to knowledge of historical constructions [9] - offers useful tools to the proposed goal. Through those methodologies, to carry out a sensitivity analysis is possible. It allows finding out which mechanical parameters influence the global structural behaviour of historical buildings. The results of such analysis allow reducing invasiveness impacts, costs and time on an experimental testing campaign aimed to know the most relevant characteristics of the structure and its further intervention proposals. The case study is the *Quartel da Tropa* that belongs to the fortress of Anhatomirim Island (SC), Brazil. Its analysis shows how the proposed approach can be adapted to heritage constructions.

2 MATERIALS AND METHODS THROUGH THE SENSITIVITY ANALYSIS

In the proposed case study, the historical-critical analysis - made by analyzing the available documental researches and the geometric-structural surveys [10, 11] – was useful to describe the constructive phases and to obtain a qualitative interpretation of the structural performance evolution [12]. The results of previous experimental local investigations - sonic tests, physic, and biological damages assessment, etc. - on the wooden structural elements [11] suggested their complexity - in terms of assessment of mechanical characteristics – due to the presence of several wooden species.

The knowledge factors of the structure can be distinguished between [7]: (1) factors that can be considered known in deterministic terms, i.e. with a low value of uncertainty, in absolute terms or terms of the relative sensitivity of the response; (2) factors affected by the uncertainty of aleatory type, generally associated with the intrinsic variability of characteristics of the structure; (3) factors affected by epistemic uncertainty, associated with a lack of knowledge of the structure or the mechanical behaviour of its components. As proposed in the research of CNR (2014), the epistemic uncertainties cannot be modeled as continuous variables, but they can be modeled as discrete epistemic variables [7]. For this reason, a parameter that allows describing both aleatory and epistemic uncertainties was analyzed through the sensitivity of the

considered structural response [7]. In the proposed research, the response variation coefficient Δ'_k was chosen (Equation 1). This parameter was introduced by the Italian National Research Center (CNR) for the sensitivity analysis of the structural response – in terms of peak ground acceleration values that lead to the considered limit state - according to the aleatory and epistemic parameters variation [7]. In the proposed research, the authors extend the use of this parameter to evaluate structural responses in terms of static and dynamic parameters. For the static behaviour, displacements and compressive stresses were selected. For the dynamic behaviour, the first modes in each direction were chosen [6]. The parameter *Δ'* was modified to show how results in the structural response differ from the average model for the aleatory (1) and epistemic (2) parameters [7]:

$$\Delta'_k = \frac{R_{k,max} - R_{k,min}}{\bar{R}}, \quad (1)$$

$$\Delta'_j = 2\frac{max(R_p) - min(R_p)}{max(R_p) + min(R_p)}, \quad (2)$$

where $R_{k,max}$ and $R_{k,min}$ represent the values - in terms of structural response - associated with the parameter *k,* varying from its maximum to its minimum values; $\bar{R}$ is the structural response associated with the main average model, R_p is the structural response associated with the epistemic parameter *p*, which is the number of options of the discrete variable, p=1,m_j.

3 APPLICATION OF SENSITIVITY ANALYSIS TO HISTORICAL CONSTRUCTION UNDERSTANDING AND TEST PLANNING

In the case of existing buildings, the sensitivity analysis is mainly used as cognitive evaluation or as an improvement assessment [4]. In the first case, the objective is to understand how each parameter influences the structural response; in the second one, the aim is to assess where interventions have significant improvement in the overall structural behaviour [13]. The first approach can avoid performing tests in non-significant points and extending them in the greatest impact knowledge areas instead [13]. The second one allows optimizing the overall work cost, revealing itself a powerful aid for designers by finding a more effective structure's reinforcing interventions, thus improving the intervention planning and maximizing the return in terms of structural improvements [13]. Furthermore, due to the lack of knowledge about the characteristic parameters of the masonry structures, the proposed research focuses on the cognitive evaluation of the parameters aiming at elaborating a comprehensive on-site analysis planning.

3.1 The *Quartel da Tropa*: from H-BIM to FEM

The proposed methodology was applied to the case study of the *Quartel da Tropa*, located in the Anhatomirim Island - Florianópolis (SC), Brazil. This 18th-century building is characterized by masonry vertical walls and wooden horizontal elements, *i.e.* slab and roof. It is the largest quarter among Brazilian fortifications (Fig. 1). The construction is one of the main buildings of the Fortress of Santa Cruz, located on Anhatomirim Island in the municipality of Governador Celso Ramos, State of Santa Catarina, Brazil. Designed by the Portuguese military engineer Brigadier José da Silva Paes, the building was one of the vertexes of the triangular defense system, formed together with the Fortresses of São José da Ponta Grossa and Santo Antônio de Ratones.



Fig. 1. *Quartel da Tropa* (a) in the as-current configuration after the 1970s restorations (b, c, d, e) where the simple trussed roof structure (b) were replaced with collar tie beam (e) and concrete beams (d) were introduced on the masonry arches (c); 3 sides of the structure are partially buried (f, g) [10].

Both main directions are characterized by masonry arches, at the lower levels, bearing the second level of masonry walls (Fig. 1). The structure is characterized by a central slope-shaped masonry element and buttresses (Fig. 1.e). Those interventions were probably developed to counteract horizontal loads, such as the horizontal forces caused by the soil acting on three buried lower sides of the construction (Fig. 1.f and g). The wooden horizontal structural elements have undergone modifications in the 1970s restoration interventions [10], according to a trend also found in other architectural heritage sites in Brazil [14]. The roof structure was simple trussed, with king posts and struts (Fig. 1.b). It was replaced with trusses with a collar tie beam (Fig. 1.e). In the same restoration of 1970, the wooden slabs, which were fixed in the

masonry walls (Fig. 1.b), were substituted by simply supported beams resting on new reinforced concrete beams, applied on the masonry arches (Fig. 1.b) [10-12].

The geometrical surveys [10, 11] and the historical-critical analysis [12] allow defining the main characteristics of this heritage building and resuming them in a Heritage Building Information Model (H-BIM) [12]. Once previous data were implemented in a digital 3D model, the sensitivity analysis was carried out by exporting the H-BIM structural model - here created in Autodesk Revit® - in Finite Elements Method (FEM) software - Robot Structural Analysis®. In the structural model, the beam elements are simplified as linear elements and the walls are simplified and represented by their middle planes. Each node of the plane and beam elements has 6 degree of freedom. The planes are meshed with thick-shell elements, which are defined by 4-nodes quadrilaterals [15]. Discrete Kirchhoff-Mindlin quadrilaterals are used with four-point Gaussian quadrature [16]. These elements include shear strain fields, but contrary to Mindlin elements, they prevent the problem with shear locking for thin plates [16]. Coons element with size 0.3 meter was selected as meshing methods [17], subdividing the FEM model in 158070 degrees of freedom. Furthermore, the type of connections between concrete, wooden and masonry structures was assumed as pinned, according to the visual inspection.

3.2 Parameter modeling

Material properties were chosen according to experimental results [11], the suggested values of the National Standards [18–20] and proved scientific researches [9, 21, 22]. Geometrical characteristics of the construction and soil parameters - obtained from the *in-situ* test - are assumed as deterministic (Table 1). According to the results of the investigation [11], the wooden element beams were modeled as dicotyledons C20, which parameters are selected according to the Brazilian standard ABNT NBR 7190:1997 [19]. Due to the objective of the proposed research, the masonry parameters are defined as aleatory (Table 1), while concrete and wooden parameters are assumed as epistemic (Table 1). As consequence of the equation (2) the minimum number of cases to evaluate the sensitivity coefficient for epistemic parameters is two, and for this reason two type of concrete and wood are evaluated.

Table 1. Deterministic and aleatory parameters of the proposed Sensitivity Analysis

	Deterministic parameters	Epistemic parameters				Aleatory parameters of masonry structures		
	Soil	Concrete 1	Concrete 2	Wood C20	Wood C30	min	average	max
E (MPa)	-	18435	23250	9500	14500	1035	1305	1575
G (MPa)	-	7681	9964	475	725	345	435	525
v	-	0.20	0.17	0.27	0.27	0.10	0.25	0.5
w (kN/m³)	15.50	25	23	6.5	8	17	19	21
C (kPa)	14.70	-	-	-	-	-	-	-
ϕ [°]	18.40	-	-	-	-	-	-	-

Regarding the evaluation of the epistemic parameters, 9 cases are investigated. In the average model, the connections are supposed as pinned, meaning that the rotations R_y and R_z are allowed. For the type of connection assessment, in case 1, all the connections are supposed as fixed, while, in case 2, only rotations R_y are allowed. Since, case 2 shown no significant modification in terms of structural response in cases 3, 4 and 5, fixed connections are supposed in the roof, slab, and reinforced concrete (RC) beams, respectively. In case 6, wooden elements

are defined as C30, according to the Brazilian standard ABNT NBR 7190:1997 [19]. Similarly, in case 7, RC beams are assumed with different material characteristics according to the Brazilian standard ABNT NBR 6118:2007 [20] (Table 1). In cases 8 and 9, the hypotheses of different masonry characteristics are investigated, where the properties of buttresses and arches are defined according to the Italian standard *Circolare* 617/09 suggestions for brick masonry type, E = 1500 MPa, G=500 MPa and w=18 kN/m³ [18].

3.3 Analysis definition

In this work, two types of linear analysis are proposed: static and modal analysis. In the modal analysis, the contribution of the static loads – including the soil actions. Hence, the evaluation of the first modal frequencies in each direction offers an initial approach to the understanding of the global stiffness (Fig. 2.a and b). The linear static analyses allow a first understanding of distributions of loads and structural responses, in terms of stresses and displacement [21] (Fig. 2.c and .d). The structural analyses are carried out in Robot Structural Analysis® (Equations 3 and 4) for the solution of linear equation systems:

$$[K]\{U\}=\{F\}, \tag{3}$$

$$([K]-\omega_i^2[M])\{\varphi_i\}=0, \tag{4}$$

where *[K]* is the stiffness matrix, *{U}* and *{F}* are displacement and force vectors, *[M]* is the mass matrix of the structure, ω_i is the natural frequency referred to the eigenvector $\{\varphi_i\}$.

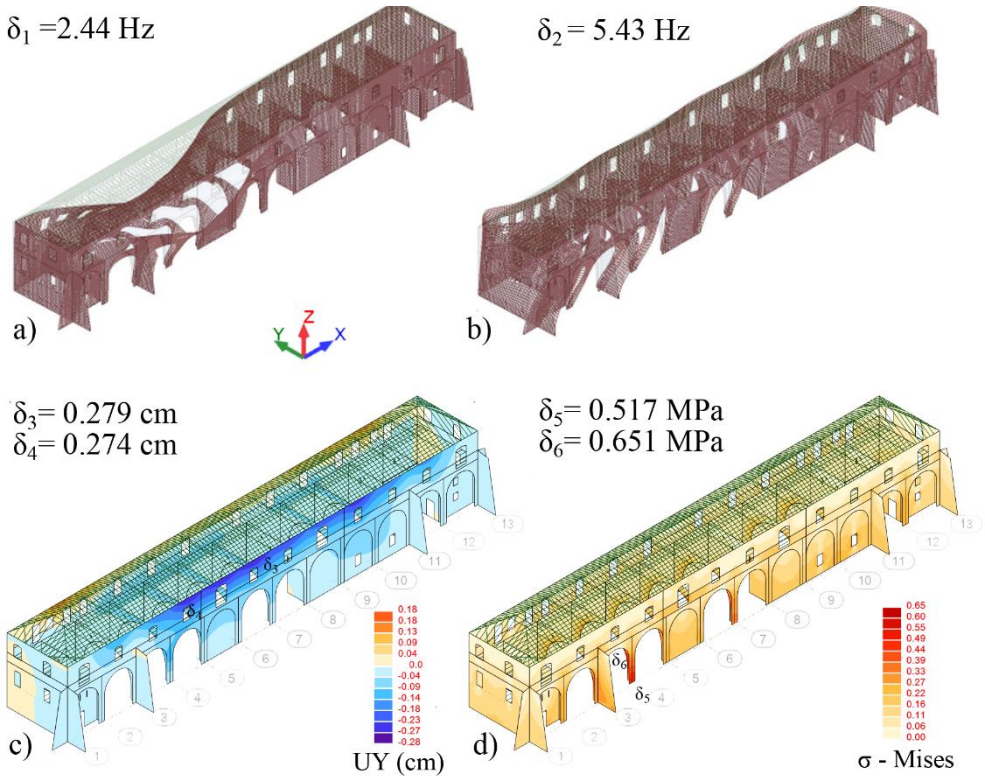


Fig. 2. First vibrational modes in transversal (δ_1) (a) and longitudinal (δ_2) (b) directions. Top out-of-plane displacements δ_3 between axes 6th and 7th and δ_4 between axes 4th and 5th (c). Mises stresses at the base of the column δ_5 and the springing line of arch δ_6 in the 4th axis (d).

4 RESULTS AND DISCUSSION

The interpretation of the proposed analyses suggests the control point selection where the results of the sensitivity analysis will be recorded. In terms of total displacements, the introduction of the central masonry element reduced the strains in the structure, concentrating the stresses on the side parts of the façade [12]. Indeed, stress peak values are reached in the column base and the springing line the 4th axis arch (Fig. 2.d). Instead, out-of-plane displacement peak values are reached on top of walls of the left part of the northeast façades (Fig. 2.c). For those reasons, the variations of the parameters in the sensitivity analysis were recorded in such control points, as defined in Fig. 2.

4.2 Sensitivity analysis

The sensitivity analysis was carried out to assess how the characterization of each one of the selected parameters affect the global structural behaviour [18]. Parameters δ_1 and δ_2 are obtained as a preliminary evaluation of the overall stiffness in each direction, in terms of first vibrational modal frequencies, while parameters from δ_3 and δ_6 describe the static behaviour of the structure, in terms of displacements and stresses (Fig. 2).

Table 2. Response variations δ_i according the sensitivity analysis of the aleatory and epistemic parameters

Aleatory parameters	δ_1 [Hz]	δ_2 [Hz]	δ_3 [cm]	δ_4 [cm]	δ_5 [MPa]	δ_6 [MPa]
Base	2.4420	5.4334	0.2791	0.2740	0.5168	0.6505
E_{min}	2.2158	4.9735	0.3123	0.3076	0.5143	0.6456
E_{max}	2.6347	5.8379	0.2564	0.2513	0.5189	0.6548
G_{min}	2.4224	5.4011	0.2858	0.2805	0.5193	0.6585
G_{max}	2.4562	5.4566	0.2743	0.2693	0.5152	0.6450
ν_{min}	2.4271	5.4828	0.2787	0.2738	0.5052	0.6535
ν_{max}	2.5385	5.4200	0.2746	0.2693	0.5129	0.6449
w_{min}	2.5194	5.6092	0.2725	0.2765	0.4509	0.5942
w_{max}	2.3702	5.2707	0.2817	0.2754	0.5564	0.6927
Epistemic parameters	δ_1	δ_2	δ_3	δ_4	δ_5	δ_6
Case 1	2.4461	5.6863	0.2347	0.2294	0.5162	0.6527
Case 2	2.4357	5.6540	0.2776	0.2712	0.5165	0.6502
Case 3	2.4572	5.5383	0.2346	0.2293	0.5173	0.6539
Case 4	2.4274	5.5383	0.2788	0.2736	0.5156	0.6493
Case 5	2.4461	5.4603	0.2794	0.2746	0.5169	0.6506
Case 6	2.4466	5.6388	0.2433	0.2393	0.5199	0.6620
Case 7	2.4536	5.4502	0.2784	0.2737	0.5163	0.6482
Case 8	2.4439	5.4403	0.2790	0.2709	0.4868	0.6129
Case 9	2.4676	5.5502	0.2742	0.2708	0.4984	0.6957

The improvement assessment of the possible intervention was evaluated according to the sensitivity analysis of the epistemic factors. It was obtained considering the quality of the connections between different structural elements. This evaluation (Table 3 and Fig. 3) shows how the main differences - in terms of out-of-plane displacements (Table 3 and Fig. 3) - are obtained considering the structure connections as fixed, mainly in roof structure Δ'_3=0.20, Δ'_4=0.15. In other terms, interventions developed to create stiffer connections in the roof

elements could improve the structural overall box-behaviour. As expected, the main variations were obtained due to the uncertainty of Young's Modulus (E) (Table 3 and Fig. 3), related to the structure stiffness. The variation of the Shear Modulus (G) the Poisson's ratio (v) does not affect considerably the overall structure stiffness. Instead, the assessment of the specific weight of the masonry (w) influences the results of the structural model global behaviour.

The type of wooden beam also affects the static behaviour of the construction – in terms of displacements - and a further investigation on the wooden physic and mechanical parameters should be done. The RC beam type and connections, instead, seems to have a very low influence on the global behaviour of the structures, meaning also that their introduction in the restoration intervention is questionable. Furthermore, since the constructive evolution of the Quartel shows that material stratification, two assumptions were investigated. Case 8 and 9 were developed considering that different material properties were used in the buttresses and the arches, respectively.

Table 3. Response variation coefficients Δ'_k according to the sensitivity analysis of the aleatory parameters

Aleatory parameters	Δ'_1	Δ'_2	Δ'_3	Δ'_4	Δ'_5	Δ'_6
E	0.17	0.16	0.20	0.21	0.01	0.01
G	0.01	0.01	0.04	0.04	0.01	0.02
v	0.05	0.01	0.01	0.02	0.01	0.01
w	0.06	0.06	0.03	0.00	0.20	0.15
Epistemic parameters	Δ'_1	Δ'_2	Δ'_3	Δ'_4	Δ'_5	Δ'_6
Timber beams	0.00	0.04	0.14	0.14	0.01	0.02
RC beams	0.00	0.00	0.00	0.00	0.00	0.00
Type of Connections	0.00	0.05	0.17	0.18	0.00	0.00
Roof Connection	0.01	0.02	0.17	0.18	0.00	0.01
Slab Connection	0.01	0.02	0.00	0.00	0.00	0.00
RC Beam Connection	0.00	0.00	0.00	0.00	0.00	0.00
Masonry buttresses	0.00	0.00	0.00	0.01	0.06	0.06
Masonry arches	0.01	0.02	0.02	0.01	0.04	0.07

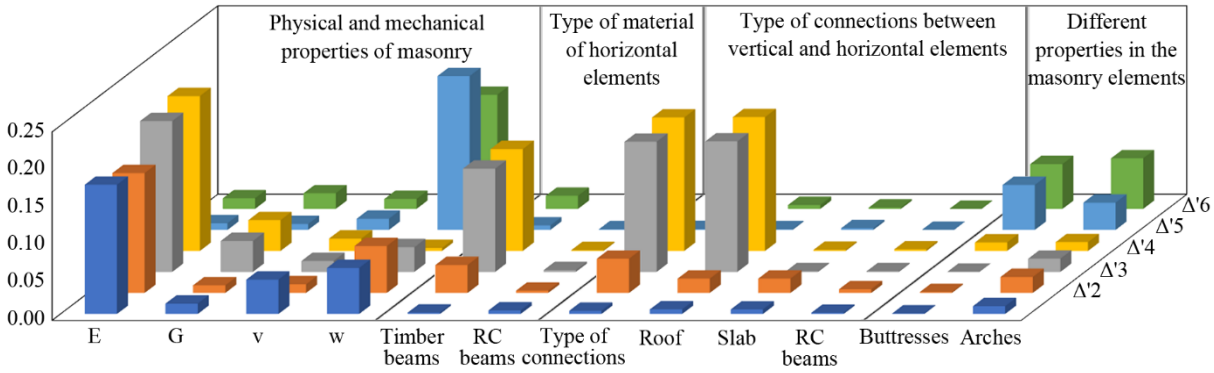


Fig. 3. Sensitivity coefficients of structural responses according to the aleatory parameters Young's Modulus (E, G), Poisson's ratio (v), average specific weight of masonry (w); Sensitivity coefficients of structural responses according to the epistemic parameters: timber and RC type of beams, quality of the connections, the types of materials in the different masonry elements

4.3 *In-situ* test planning design

An experimental investigation planning focused on these main characteristics allows reducing costs and time [23]. As shown in the analysis of the wooden structures [11], visual inspection has a key role in the preliminary assessment of the structural characteristic of the construction. This tool has allowed observing some damages in the structure of the Quartel *da Tropa*. The base of the column of the 4th axis shows an extended crack pattern in the external part of the masonry (Fig. 4.a and Fig. 4.b). The structural element of the column - situated in the 4th axis - has a high value of out-of-plane displacements and stresses (Fig. 2), confirming the asymmetrical character of the structure. Furthermore, describing the damage patterns by geometrical surveys is useful to collect such information for further analysis. The use of orthophotos improves the damage pattern surveys recording the current state of the construction, simplifying the process of data collection in the knowledge path of the heritage building. The H-BIM offers the possibility to improve the previous tools through the implementation of laser scanning, which permits a better geometrical description and representation of the historical construction. A laser scanning campaign should be done to describe the displacement pattern of the structural elements [8]. Such an approach is also available to be used for the calibration of the parameters of the structural model, comparing the laser scanning recorded displacements with the structural analysis results [8]. In the case of *Quartel da Tropa*, the laser scanning could confirm – or deny - the results of the developed structural and sensitivity analysis.



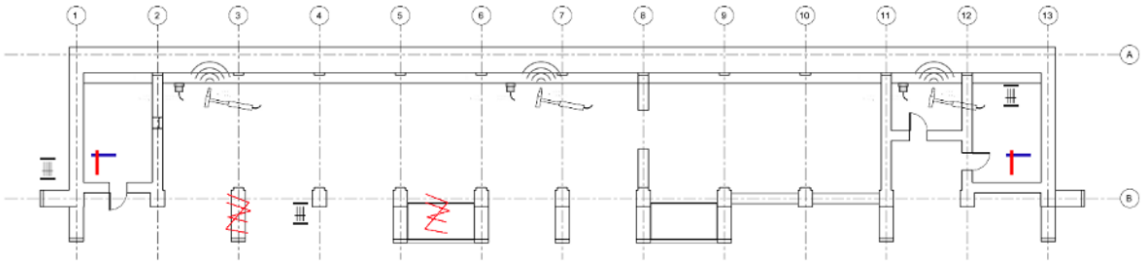
Fig. 4. Damages in the column of the 4th axis of the structure (a, b), connection between column and buttresses (c) and connection of the central slope-shaped masonry with the main façade (d)

Furthermore, the identification of vibration modes should be carried out through Ambient vibration tests [3]. It will improve the process of calibration of the structural model, also through the aleatory and epistemic parameter evaluation. In the case of historical buildings, this type of experimental tests is adequate for its non-destructive characteristic and because it describes the global behaviour of the structure [23]. The set-up of the accelerometers should be done according to the results obtained from the modal analysis (Fig. 5). Two biaxial accelerometers should be installed in the lateral parts of the ground floor – near the northeast façade - to measure the longitudinal and transversal displacements at the ground level. Similarly, two biaxial accelerometers should be set in the upper floor to measure the displacement variations in the two main directions. In the middle point – 7th axis – another biaxial accelerometer could be installed – with one uniaxial accelerometer on the opposite façade - to detect any differential

displacement by the façades in the two directions. It should record even some possible torsional effect due to the asymmetry of the structure. In the 4th and 10th axes, unidirectional accelerometers could be set to assess the behaviour of the building in the points where structural analysis showed higher values of out-of-plane displacements. Such a set-up could be used to develop a structural health monitoring system to assess the structural behaviour modifications according to the particular environment of the *Quartel*, considering winds, humidity and temperature variations (Fig. 5). Once the vibration modes are obtained from the experimental results, the sensitivity analysis proposed in this research could be compared and improved according to the experimental vibration modes and the out-of-plane displacement survey obtained from the laser scanning. A process of manual tuning of the main parameters could be adopted to assess the aleatory and the epistemic parameters of the structure proposed in the further research [3, 4].

Since the geometrical depth of the retaining wall of the considered structure is unknown, indirect sonic tests could assess the geometry of such a structural element (Fig. 5) [23]. Sonic tomography tests [23] could evaluate the consistency of the masonry elements and the effectiveness of the connections of the structural element added in the different constructive phases, e.g. the connection between the buttresses and the masonry column (Fig. 4.c) or the central slope-shape masonry element (Fig. 4.d). In the case that previous NDT test results need further analysis, another uncertainty could be introduced and investigated. Carrying out single and double flat-jack tests [23] - considered as minor destructive tests - allows understanding if the mechanical parameters of the different masonry elements can be simplified in a single type of masonry, as was chosen in the proposed research (Fig. 5) [23]. At the same time, flat-jack tests define locally the state of stress and strain, from which can be evaluated the Young Modulus *E*, which was one of the main parameters affecting the structural behaviour.

a) Non-destructive *in-situ* test, ground floor



b) Non-destructive *in-situ* test, first floor

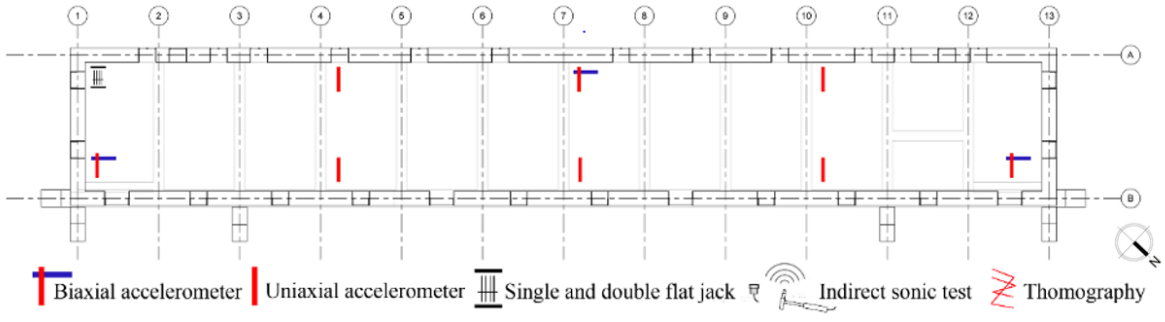


Fig. 5. Experimental test set-up: accelerometer configuration for the modal parameter assessment and the health monitoring, and other non-destructive or minor destructive tests

CONCLUSION

This research confirms how the structural behaviour of historical buildings depends on the level of knowledge of the material parameters and structural behaviour in terms of stress, deformations, and stiffness. The results of the proposed research allow concluding:

- the methodology proposed in this research allows increasing the level of knowledge of the historical construction of the *Quartel da Tropa*, through the sensitivity analysis and the experimental test campaign of the structure;
- the cognitive evaluation allows improving the test planning, focusing on the assessment of the main parameters localizing the impact of the experimental test on the relevant structural elements. In the proposed case study, the sensitivity analysis shows how not only the longitudinal Young's Modulus (E) and the specific weight (w) of the masonry are the main parameters to avoid significant errors in the results in terms of structural assessment. Indeed, type of wooden species, type of structural connection, different types of masonry characteristic in different structural elements must be considered;
- the analyses show that current construction configuration has an asymmetrical structural behaviour. In terms of stress and displacement, the left part of the building suffers the higher stresses and out-of-plane displacements. In those points, some pathology manifestations were observed;
- regarding the improvement assessment, the quality of the connections of wooden elements of the roof structure influences the out-plane displacements, meaning that interventions on such connections could be necessary to increase the box-behaviour.

Acknowledgements. This project has been funded with the support of the European Commission. This publication reflects the view only of the author, and the Commission cannot be held responsible for any use which may be made of the information contained therein - ELARCH program (Project Ref. number 552129-EM-1-2014-1-IT-ERA MUNDUSEMA21). This work was also supported by the *Coordenação de Aperfeiçoamento de Pessoal de Nível Superior* - Brazil (CAPES) - Finance Code 001.

REFERENCES

[1] Saltelli, A., Tarantola, S., Campolongo, F., and Ratto, M. Sensitivity analysis in practice: a guide to assessing scientific models, Vol. I (2004). New York: Wiley.

[2] Boscato, G., Russo, S., Ceravolo, R., and Fragonara, L. Z. Global sensitivity-based model updating for heritage structures. Comp. *Aid. Civ. Infr. Eng.* (2015) **30**(8): 620-635.

[3] Gentile, C., Saisi, A., and Cabboi, A. Structural identification of a masonry tower based on operational modal analysis. *Int. J. Archit. Herit.* (2015) **9**(2): 98-110.

[4] Asgari, B., Osman, S. A., and Adnan, A. Sensitivity analysis of the influence of structural parameters on dynamic behaviour of highly redundant cable-stayed bridges. *Adv. Civ. Eng.* (2013).

[5] Cattari, S., Lagomarsino, S., Bosiljkov, V., and D'Ayala, D. Sensitivity analysis for setting up the investigation protocol and defining proper confidence factors for masonry buildings. *Bull. Earthq. Eng.* (2015) **13**(1): 129-151.

[6] Carvalho, J., Ortega, J., Lourenço, P. B., Ramos, L. F., and Roman, H. Safety analysis of modern heritage masonry buildings: Box-buildings in Recife, Brazil. *Eng. Struct.* (2014)

80: 222-240.
[7] CNR, DT. 212 2013. Istruzioni per la Valutazione Affidabilistica della Sicurezza Sismica di Edifici Esistenti. *Consiglio nazionale delle ricerche*, 14 (2014).
[8] Antonopoulou, S., and Bryan, P. Historic England BIM for Heritage: Developing a Historic Building Information Model. Swindon: Historic England (2017). Retrieved March 10, 2019.
[9] Directive of the Prime Minister, Italian Guidelines for evaluation and mitigation of seismic risk to Cultural Heritage, Directive. Rome, Italy, 2007.
[10] Tonera R., *Fortalezas de Santa Catarina a Caminho de tornarem-se Patrimônio Mundial*. Florianópolis, Brazil (2010). Information available at http://fortalezas.org/
[11] Terezo, R. F. Avaliação das estruturas de madeira do quartel da tropa da fortaleza da ilha de Anhatomirim. (2005). GIEM, Grupo Interdisciplinar de Estudos da Madeira. Florianópolis: UFSC.
[12] Calì, A., do Valle, Â., and de Moraes, P. D. Building Information Modeling and Structural Analysis in the Knowledge Path of a Historical Construction. In: R. Aguilar et al. (Eds.): Structural Analysis of Historical Constructions, RILEM Bookseries 18 (2019), pp. 2071–2079.
[13] Lagomarsino, S., Penna, A., Galasco, A., and Cattari, S. TREMURI program: an equivalent frame model for the nonlinear seismic analysis of masonry buildings. *Eng. Struct.* (2013). **56**: 1787-1799.
[14] Pereira, R. L. Estruturas de coberta da Arquitetura religiosa em Pernambuco tipologia, patologia e intervenções. *Rev. Bras. Arquem., Rest. Cons*. (2007) **1**(6): 332 – 337. AERPA Editor, 2007.
[15] Ho-Le, K. Finite element mesh generation methods: a review and classification. *Comput. Des.* (1988) **20**(1): 27-38.
[16] Katili, I. A new discrete Kirchhoff-Mindlin element based on Mindlin-Reissner plate theory and assumed shear strain fields - Part I : An extended DKT element for thick-plate bending analysis. *Int. J. Numer. methods Eng*., (1993) **36**(11): 1859–1883.
[17] S. A. Coons, Surfaces for computer aided desing of space form. USA (1967) (No. MAC-TR-41). Massachusetts Inst. of Tech. Cambridge Project MAC.
[18] Circolare, 617/09. Istruzioni per l'applicazione delle Norme Tecniche per le Costruzioni di cui al DM 14 gennaio 2008. *Gazzetta Ufficiale Della Repubblica Italiana*.
[19] Associação Brasileira de Normas Técnicas. ABNT NBR 7190: Projeto de estruturas de madeira (1997).
[20] Associação Brasileira de Normas Técnicas. ABNT NBR 6118: Projeto de estruturas de concreto-procedimento. ABNT. (2007).
[21] Roca, P., Cervera, M., and Gariup, G. Structural analysis of masonry historical constructions. Classical and advanced approaches. *Arch Comput Meth Eng.* (2010) **17**(3): 299-325.
[22] Rocco Lahr, F. A., Christoforo, A. L., Chahud, E., Branco, L. A. M. N., Battistelle, R. A., and Valarelli, I. D. Poisson's ratios for wood species for structural purposes. *Adv. Mater. Res.* (2015) **1088**: 690-693. Trans Tech Publications Ltd.
[23] Binda, L., and Saisi, A. Non destructive testing applied to historic buildings: The case of some Sicilian Churches. *Hist. Constr.* (2001): 29-46.

12th International Conference on Structural Analysis of Historical Constructions
SAHC 2020
P. Roca, L. Pelà and C. Molins (Eds.)

PRELIMINARY STRUCTURAL ANALYSIS OF THE WESTERN CURTAIN WALL OF ELMINA CASTLE, ELMINA, GHANA

MARCOS N. DOS SANTOS[1], SABASTIAN A. ABELEZELE[1], KATHERINE A. KORSLUND[1*], ROBERT T. CECIL[2], SELMAN TEZCAN[1], AND RENATO PERUCCHIO[3]

[1]Department of Mechanical Engineering
University of Rochester
Rochester, NY 14627, USA
e-mail: {mnascim2, sabeleze, kkorslun, stezcan}@u.rochester.edu

[2]Program of Archaeology, Technology and Historical Structures
University of Rochester
Rochester, NY 14627, USA
e-mail: rcecil@u.rochester.edu

[3]Department of Mechanical Engineering and
Program of Archaeology, Technology and Historical Structures
University of Rochester
Rochester, NY 14627, USA
e-mail: renato.perucchio@rochester.edu

Keywords: Elmina Castle, Masonry Wall, Lateral Capacity, Non-Linear FE Explicit Analysis, Concrete Damaged Plasticity, Abaqus/CAE.

Abstract. *Elmina Castle, built in 1482 by the Portuguese, was the first of a series of European trading bases along the west coast of Africa and served as a commercial outpost for over four centuries of trade. The structure was captured by the Dutch in 1637 and became a major hub for the Atlantic Slave Trade. The castle is currently a UNESCO World Heritage Site and a Ghanaian national museum. The building is constructed from a combination of mud- and lime-mortared rough-hewed sandstone masonry. The primary focus of the analysis is the western curtain wall, which faces the only side of the castle accessible by land. A flaring at the base of the curtain wall points to the likely presence of an additional tower located approximately midway along the length of the wall in early Portuguese times. Using a pushover analysis with nonlinear 3D FE under Abaqus/CAE explicit formulation, we assess the stability of the tower-wall system to determine if a historical earthquake could have caused the tower to collapse. During the Dutch occupation, a two-story building, brick vaulted at the ground level, was added along the entire curtain wall. Using 2D plane strain nonlinear models, we evaluate the structural capacity of this vaulted system, considering its sensitivity to the density and the thickness of the loose material above the vault as well as the compressive strength of the rough-hewed sandstone masonry in the walls.*

1 INTRODUCTION

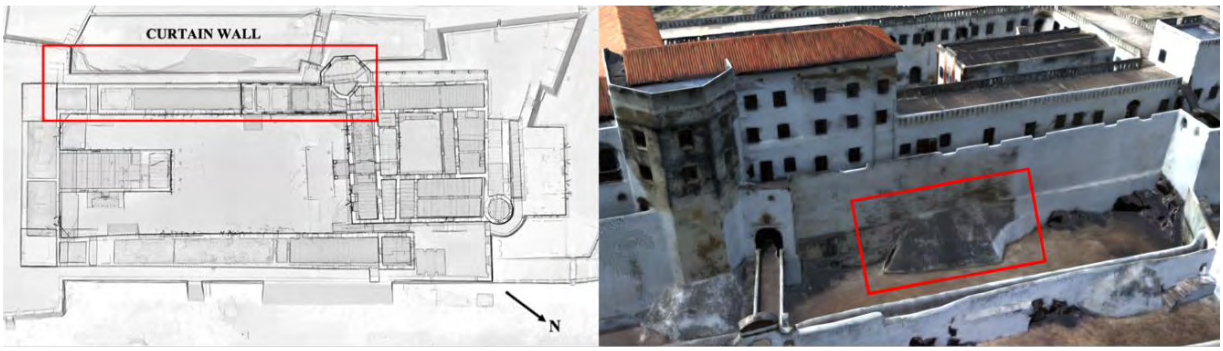
Elmina Castle is the oldest permanent European structure in Sub-Saharan Africa, the first of a series of trading bases along Africa's West Coast. Built in 1482 as São Jorge da Mina by order of the Portuguese Crown, the castle served as an imposing commercial outpost for over four centuries of international trade. After the 1637 Dutch conquest, the castle became a major hub of the Atlantic Slave Trade involving Europe, Africa, and the Americas.

The castle is a UNESCO World Heritage Site and a national Ghanaian museum. The building, built on a rock mass projecting into the Atlantic Ocean, is the best-preserved example of early European masonry construction in Sub-Saharan Africa. Elmina Castle has been the object of a multidisciplinary field school conducted in Elmina, by the Archaeology, Technology, and Historical Structures Program of the University of Rochester in conjunction with the University of Ghana during the summers of 2017-2019.

2 OBJECTIVES

The goal of the paper is to provide a preliminary evaluation of possible changes in structural stability and lateral capacity of the western wall resulting from the various architectural changes introduced during the Portuguese and the Dutch occupation periods (1482 to 1872).

The primary focus of the analysis is the western curtain wall (shown in Figure 1a), which faces the only side of the castle accessible by land. Observation of this wall as currently standing shows that it was constructed using rough-hewed stones (RHS) held by a combination of mud and lime mortars. The wall extends from an octagonal tower next to the castle's gate to the southwest bastion. As suggested by Lawrence [1], a flaring at the base of the curtain wall, marked in Figure 1b, points to the likely presence of an additional defensive tower located approximately midway along the length of the wall in early Portuguese times. This tower may have collapsed during late Portuguese occupation due to seismic activity.



(a) (b)

Figure 1: a) Plan view of Elmina Castle (western curtain wall highlighted), and b) aerial view facing the western curtain wall, with base flaring highlighted [2].

Our goal is to assess the stability of the wall-tower complex with a pushover analysis to determine if earthquakes could have been responsible for the collapse of this defensive tower. Models for these analyses were tested using nonlinear 3D finite element analysis (FEA) under

the Abaqus/CAE Explicit formulation. During the Dutch occupation (1637-1872), the height and thickness of the curtain wall were increased, and a two-story building, brick vaulted at the ground level, was added along the entire curtain wall [1]. In this portion of the study, the objective is to perform a sensitivity analysis of 2D plane strain nonlinear models to evaluate the structural response based on assumed values for the density and thickness of the filler material as well as the compressive strength of RHS.

3 METHODOLOGY

Pushover analysis uses an incremental-iterative solution based on static equilibrium to solve for the response of the structure subjected to a monotonically increasing lateral load pattern [3,4]. In this study, all models are analyzed to find their collapse condition and related failure mechanism using gravitational loads based on the pushover analysis approach in Abaqus/CAE Explicit. During the pushover step, a uniform monotonically increasing horizontal acceleration is applied to the entire model until collapse conditions are reached.

3.1 Evaluation of Collapse Conditions

The time-evolution of strain energy (SE), kinetic energy (KE), and plastic dissipative energy (PD – due to plastic deformations simulating internal fractures) are used in order to identify the onset of local damage and its development into structural collapse (Figure 2a). Conditions of collapse can be reasonably characterized by three different collapse evaluation parameters: KE reaches 10% of the total internal energy (i.e., SE + PD + KE), the crossing of strain and plastic dissipation energy curves, and the highest normalized base shear. For all explicit FE analyses, a quasi-static behavior is carefully enforced as explained below. KE is constantly monitored to ensure that the analysis remains static and thus negligible inertial forces are created up to collapse. Hereafter, we assume that failure conditions have been reached when KE reaches 10% of the total internal energy (IE) of the system.

As indicated earlier, there is historical evidence from Portuguese chronicles that an earthquake took place in Elmina in 1615 [5, 6]. Along the coast of Ghana, the Peak Ground Acceleration (PGA) has been evaluated to be 0.026 – 0.2 g in 475 years [7]. We hypothesize that such an earthquake could have caused the collapse of the defense tower during the late Portuguese period. We also use the same seismic range to provide a preliminary assessment of the Dutch architectural changes introduced along the western wall since 1637 and which are still present in today's Castle.

The example of a single wall will be used to discuss the characterization of collapse conditions [8]. While gravity is applied during the first five seconds, only a vertical reaction is developed, as shown in Figure 2b. Thereafter, as a result of the inertial forces caused by the applied lateral acceleration, an equilibrating horizontal reaction force (basal shear) develops at the constrained boundary face. The linear ramp of lateral acceleration causes a nearly linear increase in the basal shear versus time while the vertical reaction holds constant (Figure 2b). At failure, both curves show a sudden decrease, indicating that the structure has lost the capability of resisting the lateral load. In this case, the mass of the wall has nearly completely separated from its base. Failure conditions are also determined from the curves shown in Figure 2c. Structural failure corresponds to the asymptotic growth of KE and PD and to the sudden drop in SE. Finally, for each analysis, results are shown in the form of capacity curves, such as the

one shown in Figure 2c, which consist of base shear versus the displacement of a reference point. The normalized base shear is the ratio of the horizontal reaction forces to the weight of the model, expressed in terms of g. Further discussion is included in the paper by Sun et al. [8].

As for the collapse mechanism shown in Figure 2a, the black bands at the base of the wall represent areas where the plastic strain exceeds a threshold of 0.01. Hereafter, the black bands shown in figures are interpreted as fractures that propagate through the quasi-brittle material.

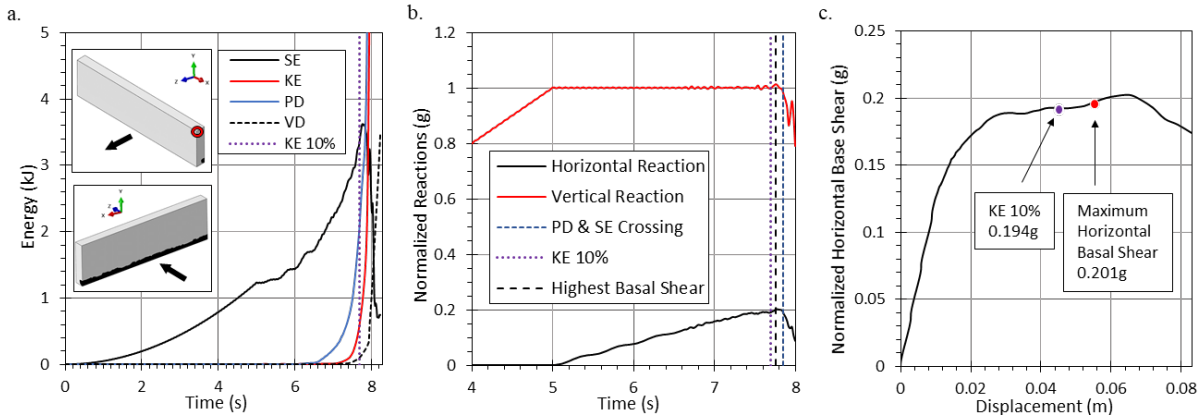


Figure 2: Single wall example: (a) energy curves versus time, (b) reaction forces versus time, and (c) capacity curve for reference point highlighted in (a). In the (a) insets, the black band indicates the fractured area.

3.2 Material properties

In all the analyses, the Abaqus Concrete Damaged Plasticity (CDP) formulation for quasi-brittle materials [9] is utilized. Currently, the nonlinear mechanical properties of RHS held together by mud and lime mortar (as observed at Elmina) are not available from the literature nor were we able to conduct any tests to evaluate them. Based on published experimental material properties for historical constructions [10, 11, 12], we hypothesize that the mechanical behavior of RHS falls in between that of adobe masonry and Roman pozzolanic concrete (PC). PC serves as an upper bound while adobe provides a lower bound for the mechanical strength of RHS. For the analyses of the Portuguese architecture, the structural responses of both RHS and adobe were analyzed. To approximate the post-critical mechanical behavior of RHS, we scale down the nonlinear postcritical PC curves in tension and compression using the ratios of the tensile and compressive strength of RHS [12] to those of PC [10]. Thus, for compression, a ratio of 2/5 MPa was used while a ratio of 0.07/0.5 MPa was used for the tensile behavior.

Based on observations conducted in Elmina Castle and other European fortifications on the coast of Ghana, we use lateritic soil, here modeled as linear elastic, as filling material for the Dutch configurations. The general material properties adopted for the present study are shown in Table 1.

Materials/Properties	E (MPa)	γ	ρ (kg/m^3)	Com Str (MPa)	Tens Str (MPa)
Adobe [13]	123	0.2	1735	0.41	0.04
Rough-hewed Stone Masonry [10]	1740	0.2	2000	2	0.07

Lateritic Soil [16],[17]	26	0.38	2200	

Table 1: Mechanical properties of the materials.

General CDP parameters are shown in Table 2, where fb0/fc0 is the ratio of initial equibiaxial compressive yield stress to initial uniaxial compressive yield stress, and k is a parameter related to the yield surface [13].

Table 2: General concrete damaged plasticity parameters.

Materials/Properties	Dilation Angle (°)	Eccentricity	fb0/fc0	k	Viscosity Param.
Adobe and RHS Masonry [13]	1	0.1	1.16	0.67	1E-8

3.3 Models of the Portuguese architecture

Figure 3a shows the earliest reliable representation of the Castle as drawn at the end of the Portuguese occupation (1637) by Frans Post [14]. This drawing serves as the basis for constructing the Portuguese architecture models. The view suggests the possible height of the eastern curtain wall, which we assume to be the same as the western curtain wall. This height was estimated to be 2 m based on features observable in the drawing and in today's Castle. The drawing also shows a circular tower next to the entrance of the castle, whose features are currently present and can also be found in the core of the current octagonal tower in the same location. This circular tower is used to estimate the dimensions of the tower in the models.

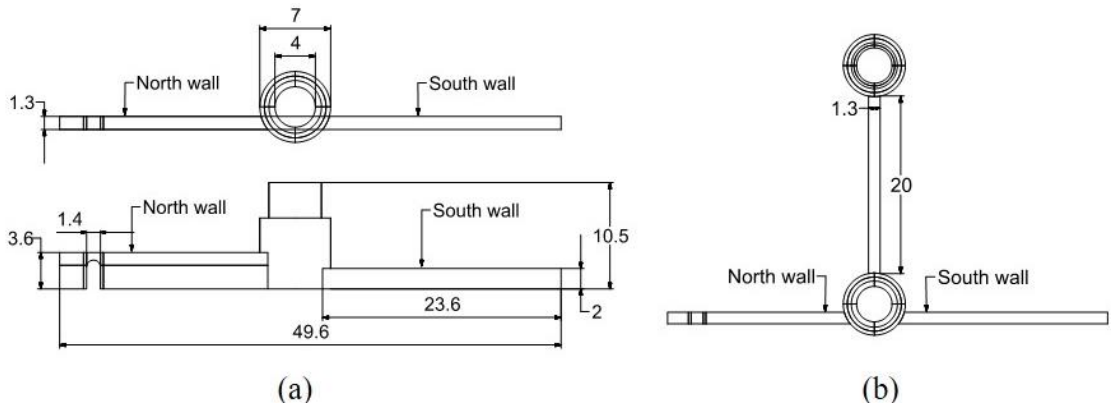
The Castle gate's dimensions would require a taller wall, which is confirmed by the trace of a 3.6 m wall (Figure 3b), north of the hypothetical tower. A total of three geometries were considered to assess the sensitivity of the structural capacity of the wall-tower complex to the geometry and the materials. The first 3D configuration, in Figure 4a, called Portuguese 1, consists of a 49.6 m long wall with a 1.3 m thickness. The wall is divided into two segments, north and south, by a circular tower. The position of the tower is based on the location of the flaring at the base approximately midway the length of the wall (Figure 1b), assumed to have been the tower's base [1]. The second architecture, Portuguese 2, only differs from Portuguese 1 in that the north and south walls are both 3.6 m tall. Furthermore, the mesh for all Portuguese models consists of linear hexahedral elements (Figure 6a) fully constrained at the base and supported by rollers on the vertical end faces of the north and south walls to prevent motion of the faces along the x axis.



(a) (b)

Figure 3: a) Drawing of Elmina Castle in 1637 by Frans Post [14] and b) aerial view of the entrance of Elmina Castle created with a point cloud [2]. The trace, boxed in red, points to a 3.6 m wall height.

Considering that in typical 16th-century Portuguese military architecture the towers are supported by at least two perpendicular walls, e.g., the fort at Calicut in India [15], a third geometry is included to evaluate how the structural capacity would be affected by a wall abutting on the tower, perpendicular to the present curtain wall. The Portuguese 3 model consists of the same geometry as Portuguese 1 but with the addition of a perpendicular wall and



a tower at the end (Figure 4b). This third configuration was adopted purely for comparative reasons since there is no available archaeological evidence to support it.

Figure 4: (a) Planar and frontal views of Portuguese 1 and (b) plane view of Portuguese 3.

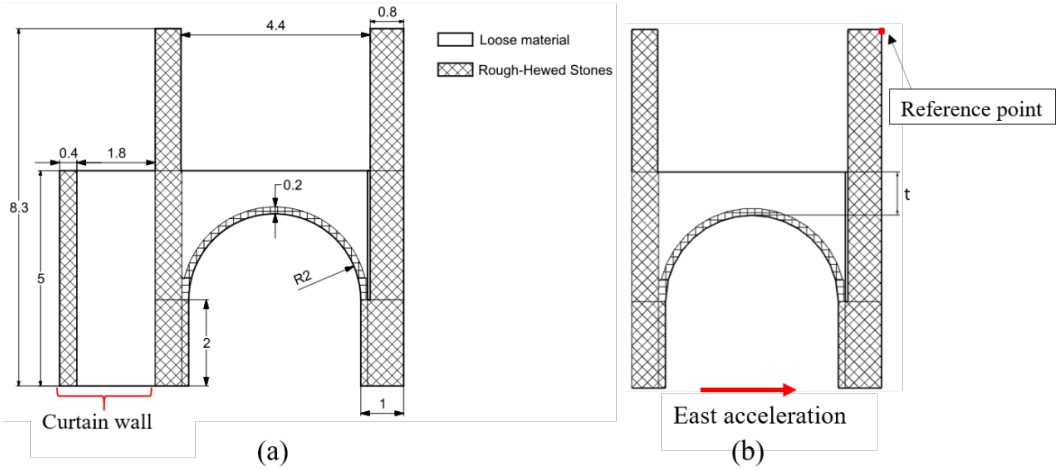
3.4 Models of the Dutch architecture

The dimensions of the vault-wall models constructed for the preliminary analysis of the Dutch architecture were derived from our survey of the current vaulted rooms adjacent to the western curtain wall (Figure 5a). Since there is no historical evidence of a middle tower along the western curtain wall after 1637, the structural capacity of the Dutch architecture was analyzed using nonlinear 2D plane strain models with a mesh of linear quadrilateral elements in Abaqus/CAE Explicit. The nature of the filler material present in between the outer and inner wall of the Dutch curtain wall and on top of the inner brick vault is currently unknown. Based on archeological evidence from other European forts along the coast of Ghana, we hypothesize that the filler material is either sand, with a density of 1200 kg/m^3 or 1600 kg/m^3, or lateritic soil, with a density of 2200 kg/m^3. In all models, the filler material was modeled as linear elastic.

There is evidence that the original floor above the vault was lower than the present one. A map from 1774 shows a stairway on the interior western wall that corresponds to the location of several filled-in openings still present in the wall under consideration. The position of the stairway and the height of the openings from the ground suggest that the original floor was 40 cm lower than the present one. Thus, to evaluate the sensitivity of the lateral capacity of the vaulted system to the height of the loose material above the vault, we consider the following values of the t parameter shown in Figure 5b: 100 cm, 60 cm, and 20 cm. Moreover, considering a sensitivity study of the structural capacity to the compressive strength (CS) of RHS, we test seventeen models (Table 3) in which the three parameters (filler density, t, CS) are varied.

Due to the lack of data on the dimensions and composition of the curtain wall, a simpler model of the actual geometry with no curtain wall is used in this preliminary analysis (Figure

5b) before running a full analysis of the vaulted building and curtain wall. The simpler geometry chosen for the analysis allows for a detailed study of the sensitivity of the structural capacity to the unknown parameters. Considering that structural damage associated with the Dutch



geometry has not been observed, the lateral capacity of the structure is tested against the local seismic demand with a PGA range of 0.026 – 0.2 g [7] to verify whether the numerical results are plausible. For the analysis of a similar Dutch vaulted architecture along the east curtain wall of Elmina castle see Sun et al. [8].

Figure 5: a) Dutch architecture with dimensions and material distribution and b) reduced architecture used for the analysis, with the variable t, reference point, and acceleration direction.

3.5 Analysis procedure

In all cases, the pushover analysis is conducted in quasi-static conditions until collapse. In order to avoid generating inertial forces during the Explicit FE analysis, relatively long time intervals are used for the gradual application of gravitational loads followed by lateral accelerations. For the Portuguese configurations, gravity is applied over two seconds as a vertical acceleration increasing linearly over time from 0 to 1g. This is followed by a uniformly distributed lateral acceleration applied to the model over twenty seconds for the Portuguese 1 model and eight seconds for the Portuguese 2 and 3 models, increasing linearly until collapse conditions are reached (shown in Figure 6b, the moment at which KE reaches 10% of IE for a Portuguese 1 model).

All Portuguese models were tested with lateral acceleration perpendicular to the wall in both east and west directions, where west points towards the exterior of the curtain wall. For all models, acceleration in the west direction resulted in the lowest lateral capacity. Therefore, only the results of the models with acceleration in the west direction will be discussed. For the construction of the capacity curves, displacements for each model are measured at the reference point shown in Figure 6a.

For the Dutch architecture, the reference point from which all horizontal displacements are measured as well as the direction of the applied lateral acceleration are shown in Figure 5b. The acceleration in this direction resulted in the lowest lateral capacity. Gravity here also is applied

over two seconds as a vertical acceleration increasing linearly over time from 0 to 1g. Application of gravity is then followed by a uniformly distributed lateral acceleration applied to the model over ten seconds for all Dutch models, increasing linearly until collapse conditions are reached.

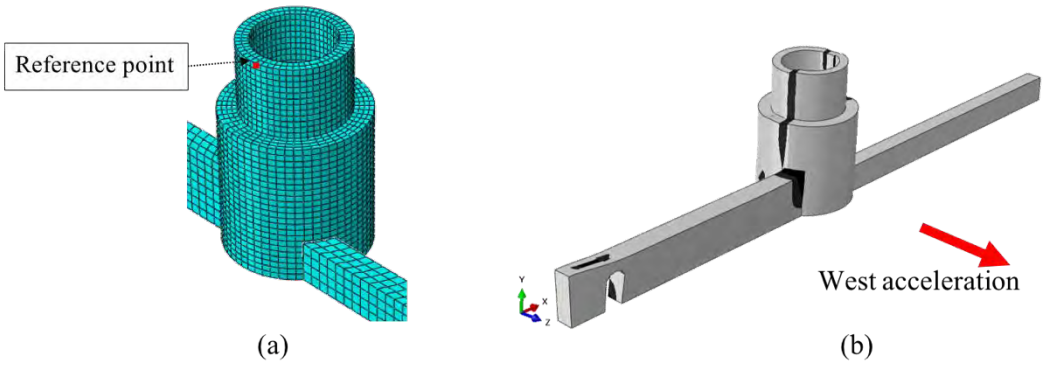


Figure 6: (a) Mesh of Portuguese 1 with reference point and (b) damage status and deformation of Portuguese 1 (RHS, 15 per) at failure (KE at 10% of IE). Black bands indicate fractures.

4 RESULTS AND DISCUSSION

4.1 Analysis of the Portuguese architecture

This section focuses on the discussion of the sensitivity of the structural response with respect to basic architectural configuration (single wall, single tower and wall-tower complex), material properties (adobe and RHS), and model configuration (Portuguese 1 – 3).

To understand the effect of a tower supported only by two side walls, we conduct a comparative test involving a single wall, a single tower, and the combination of the two (corresponding to Portuguese 2) all built with adobe. Results in Figure 7 show that a single wall has a higher lateral capacity than a single tower. When the two are combined, the lateral capacity of the structure decreases to a third of that of the single wall. For the combined model, the tower reaches collapse conditions after its upper part splits vertically into two (Figure 7).

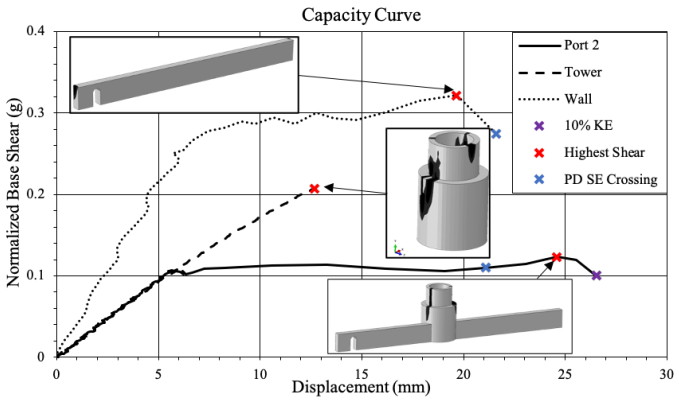


Figure 7: Curve for lone tower, single wall, and combination of tower and wall (adobe). Black bands indicate fractures.

For the sensitivity due to changes in material properties, models built with RHS have a higher lateral capacity as compared to those built with adobe. The lateral capacities of the Portuguese 1 and 3 models with RHS are about five times the lateral capacities of the same configurations built with adobe (Figures 8 and 9). The collapse of the Portuguese 1 and 2 adobe models involves the vertical splitting of the tower (Figures 8-2 and 7, respectively). The failure mechanism of the RHS model is characterized by the separation at the juncture of the intact tower and the walls (Figure 8-1) as the tower rotates as a solid body. The vertical fractures developed at the upper part of the adobe towers, directly above the walls (Figure 8-2), are due to the relatively lower tensile strength of adobe.

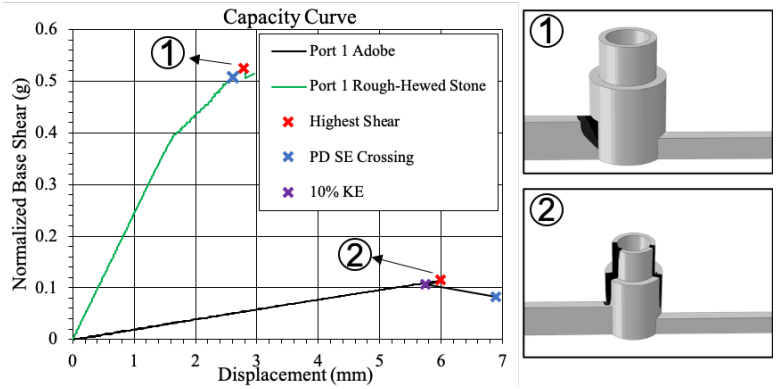


Figure 8: Capacity curve for Portuguese 1 using adobe and RHS and damage status of the models. Black bands indicate fractures.

For the results of the sensitivity due to changes in configuration, the structural capacities of Portuguese 1 and 2 models do not vary significantly for either adobe or RHS material. The lateral capacity of Portuguese 3 built with RHS (Figure 9-1), is about 20 % less than that of Portuguese 1 built with RHS (Figure 8-1). In this case, the additional tower and perpendicular wall weaken the system due to the change in the failure mechanism between the models. For the RHS model, the outward rotation of the massive tower causes an earlier separation between the tower and the perpendicular wall (Figure 9-1). For the adobe model (Figure 9-2), the perpendicular wall further constrains the tower, and rotations are minimized. However, the additional tower splits vertically, developing fractures above the perpendicular wall as it rotates.

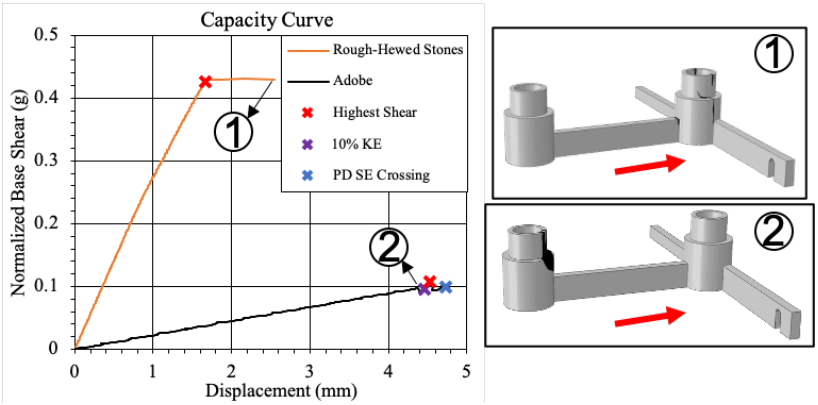


Figure 9: Capacity curve for Portuguese 3 built with adobe and RHS and damage status of the models (in black).

4.2 Preliminary analysis of the Dutch architecture

Figure 10a (1 and 2) shows the damage patterns observed for one of the seventeen models built for this study. This model, which corresponds to Model 5 in Table 3, was chosen as it exhibits the general mechanical behavior observed for all models. The model has a thickness t = 100 cm, a compressive strength of RHS of 3MPa and filler density of 1600 kg/m^3. The capacity curve from the analysis suggests a structural response to lateral acceleration that barely satisfies the seismic demand reported for the region (0.026 – 0.2 g) [7]. Since the upper part of the walls does not show signs of plasticity, they have been omitted to simplify the illustration of the damage status sequence of the model as shown in Figure 10a. Towards the end of the application of gravity, the filler material in combination with the lateral thrust of the vault imposes sufficient lateral pressure onto the left wall to cause fractures at the base (Figure 10a-1). As damage progresses to stage 2, vertical fractures develop on the left wall, indicating the crushing of the material. Horizontal damage also develops at the base of the right wall due to the bending condition imposed by the increased lateral acceleration.

As shown in the damage status sequence in Figure 10a, the outward rotation of the walls increases as a result of the increased lateral acceleration. As the horizontal fracture propagates, a hinge develops at the base of the right wall, causing a concentration of compressive stresses on the far-right side. At this point of the analysis, in addition to a vertical fracture due to crushing of RHS, rotational hinges also form on the vault. Stage 2 captures the instant at which KE reaches 10 % of IE – corresponding to the total collapse of the structure.

The results from the sensitivity analysis of the Dutch architecture, shown in Table 3, demonstrate that structural capacity increases as the compressive strength increases. Considering that models 1, 2, and 3 collapse under the application of gravity, we postulate that lateritic soil with a density of 2200 kg/m^3 may not represent the actual filler material over the vaults since the structure is still standing. Thus, we hypothesize that the density of the filler material should range between 1200 and 1600 kg/m^3. As for the sensitivity of the thickness to the structural capacity, models with t = 20 cm produce the highest capacity. For these models, the density and compressive strength do not significantly affect the results. Additionally, there is a marginal difference in capacity between the models with t = 60 cm and t = 20 cm.

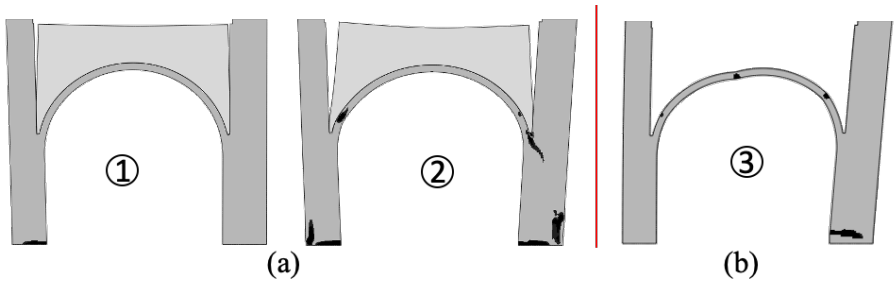


Figure 10: (a) Damage evolution of one of the Dutch architecture models and (b) analysis without filler material. The upper part of the walls has been truncated to show only the structural elements where damage occurs. Black bands indicate fractures.

An additional analysis of the Dutch architecture without filler material on the extrados of the vault is performed. The final stage of the damage evolution is shown in Figure 10b. Considering 10 % KE, maximum base shear, and PE and SE crossing, the critical λ was found to be 0.095.

This marks a 20 % increase in capacity from the models with the same filler material (λ=0.08). Clearly, further work is necessary to properly characterize the behavior and mechanical properties of this filler material due to its significant impact on the behavior of the system.

Table 3: Setup and results of the Dutch architecture sensitivity analysis.

Model	t (cm)	ρ (kg/m^3)	σ_C (MPa)	λ (g)
1 | 2 | 3	100	2200	2.0 | 3.0 | 5.0	Fails under gravity
4 | 5 | 6		1600	2.0 | 3.0 | 5.0	0.00 | 0.08 | 0.09
7 | 8 | 9		1200	2.0 | 3.0 | 5.0	0.08 | 0.07 | 0.07
10 |11	60	1600	2.0 | 3.0	0.07 | 0.08
12 | 13		1200	2.0 | 3.0	0.08 | 0.09
14 | 15	20	1600	2.0 | 3.0	0.09 | 0.10
16 | 17		1200	2.0 | 3.0	0.10

5 CONCLUSIONS AND FURTHER WORK

The results from the analysis of the Portuguese architecture demonstrate the destabilizing effect under seismic conditions of a tower sitting astride the western curtain wall. Under the assumption of a structure built with adobe-like material in early Portuguese times, the tower and the walls are likely to have collapsed under the lateral acceleration of the earthquake historically documented in the early 1600s [5, 6]. Under those conditions, it is logical to expect that the entire western curtain wall would have been rebuilt by the Portuguese without the tower, a solution maintained by the Dutch and subsequently by the British until present time.

All analyses of the Dutch architecture have critical capacities below 0.10 g. These are relatively low values, for which a seismic input with the range 0.026 - 0.2 g could be critical to the stability of the structure. Thus, the results of the Dutch modifications in terms of the introduction of the vaulted structure and substantial filler material thickening are problematic, since they appear to indicate a marginally stable structural configuration, already approaching a highly damaged condition under relatively minimal lateral acceleration. Considering that this new configuration has been around for more than two hundred and fifty years and appears to be in a good state of conservation, these unstable configurations are questionable and suggest the presence of either a less dense filler material or of a stone masonry of higher compressive strength or both.

Looking at the data on which the present model is based, the following issues can be identified: (a) The actual composition of the walls used in the Dutch models is unknown, and (b) the actual composition of the filler material resting on the extrados of the vault is also unknown. Its composition and density adopted in this preliminary work are based on observations made in another sector of Elmina Castle.

Future work should address the above issues experimentally, through in-situ study of the materials and the wall composition, and numerically, through a systematic sensitivity analysis.

Acknowledgements. We thank Michael Jarvis and Christopher Muir for their contributions to the surveying of Elmina Castle. Louisa Anderson helped us in establishing the early Portuguese architecture. Selman Tezcan provided guidance with the nonlinear numerical modeling. The

David T. Kearns Center of University of Rochester provided support through summer research scholarships to Kate Korslund and Marcos dos Santos. Jiacheng Sun helped translate a source from Chinese to English.

REFERENCES

[1] Lawrence, A.W. *Trade Castles and Forts of West Africa*. London: Jonathan Cape, (1963).
[2] Jarvis, M. Personal communication. Elmina Castle, FARO Laser Scans and UAV Aerial Image Capture. University of Rochester, Department of History, (2019).
[3] Kunnath, S. K. Identification of Modal Combination for Nonlinear Static Analysis of Building Structures. *Computer-Aided Civil and Infrastruc. Eng.* (2004), 19, pp. 246-259.
[4] Pinho, R. Using Pushover Analysis for Assessment of Buildings and Bridges. In: Pecker A. (Eds.): *Advanced Earthquake Engineering Analysis*. CISM International Centre for Mechanical Sciences, vol 494. Springer, Vienna, (2007).
[5] Ambraseys, N. N., and Adams, R. D. Seismicity of West Africa. *Annales Geophysicae*, Vol. 4B, No. 6, (1986), pp. 679-702.
[6] Vogt, J. *Portuguese Rule on the Gold Coast: 1469-1682*. Athens: GA, (1979).
[7] Ahulu, S. T., Danuor, S. K., and Asiedu, D. K. Probabilistic seismic hazard assessment of southern part of Ghana. *Journal of Seismology*, Vol. 22, (2017), pp. 539–557.
[8] Sun, J., Tezcan S., Perucchio, R. The Structural Function of the East Curtain Wall of Elmina Castle, Elmina, Ghana. *12th International Conference on Structural Analysis of Historical Constructions*, (2020).
[9] *Abaqus Analysis User's Manual Simulia, v.6.6, Damaged plasticity model for concrete and other quasi-brittle materials*, Dassault System Corporation, available online, (2006).
[10] Brune, P.F. *The Mechanics of Imperial Roman Concrete and the Structural Design of Vaulted Monuments*. Doctoral Thesis: Department of Mechanical Engineering, Arts, Sciences and Engineering, University of Rochester, (2010).
[11] Aguilar, R. et Al. Structural and geotechnical engineering assessment of Huaca de la Luna – A massive earthen Moche culture pyramid in Norther Peru. *Journal of Cultural Heritage*, Vol. 34, November–December (2018), pp. 83-94.
[12] Angelillo, M., Lourenco, P.B., Milani, G. Masonry behavior and modelling. In: M. Angelillo (Ed.): *Mechanics of Masonry Structures*. CISM International Center for Mechanical Sciences, Vol 551. Springer (2014) pp 1-26.
[13] Tarque, N. *Numerical Modelling of the Seismic Behavior of Adobe Buildings*. PhD dissertation, Universitá degli Studi di Pavia, Italy (2011), pp. 136.
[14] Post, F. São Jorge da Mina. *Dutch National Archive* (1637).
[15] Correia, G. *Portuguese outpost, Calicut, 16th century, Lendas da India*. Royal Academy of Sciences of Lisbon, (1858-1866).
[16] Chen L.J., Dai Z.H., Liu Z.W. Three-dimensional nonlinear finite element analysis of soft soil excavation engineering considering K0 consolidation. *Rock Soil Mech* (2011) 32(12): 3796–3804 (in Chinese).
[17] Fall, M., Sarr, D., Ba, M. Evolution of lateritic soils geotechnical parameters during a multi-cyclic OPM compaction and correlation with road traffic. *Geomaterials 1* (2011), pp. 29-69.
[18] *Abaqus Analysis User's Manual Simulia v.6.14.6.3.3 Explicit dynamic analysis*. Dassault System Corporation, Providence, RI (2018).

[19] The Hague, Collection Foreign Maps Leupe, number access 4.VEL, inventory number 779A, *Dutch National Archive* (1774).

12th International Conference on Structural Analysis of Historical Constructions
SAHC 2020
P. Roca, L. Pelà and C. Molins (Eds.)

PRESERVING HISTORIC BEARING STRUCTURES BY PRUDENT INTEGRATION IN NEW STRUCTURES

MARIUS MOSOARCA[1*], VALERIU STOIAN[2], MARGARETA FLOREA[3], MARIUS NICULESCU[3]AND MARIUS PALADE[3]

[1]H.I. STRUCT SRL
Ciocarliei Street, nr 86, 300600, Timisoara, Romania
e-mail: mmosoarca@histruct.ro, web page: http://www. histruct.ro (*corresponding author)

[2] Faculty of Civil Engineering, Politehnica University of Timișoara (UPT)
Traian Lalescu street, nr. 2, 300223, Timisoara, Romania
e-mail: valeriu.stoian@upt.ro

[3]H.I. STRUCT SRL
Ciocarliei Street, nr 86, 300600, Timisoara, Romania
e-mail: office@histruct.ro, web page: http://www. histruct.ro

Keywords: Historical Structure, Preservation, Re-use, Consolidation

Abstract. *For the effective consolidation of damaged historic load-bearing structures, it is necessary for the designer to understand the causes of the damage but also to know and apply the most effective consolidation methods, in order not to affect the cultural value of the building. The problem becomes even more complex for the designer when it is desired only to keep a damaged area of a historic building, which was part of an aggregate of historic buildings. Keeping this area is needed because buildings have been seismically interacting over the past 150 years, and it is necessary to maintain the static equilibrium of the building aggregate.*

In most cases, in order to safeguard a damaged historic building, is achieved by consolidating the structural elements composing the building, resulting in extensive consolidation areas, long construction periods and expensive and hard to implement solutions. Additionally, it is challenging to predict the response of the building over time to various actions without continuous monitoring, which is difficult to achieve, because of the disturbance on building occupants.

The paper presents an alternative solution of safeguarding interventions on a historic building, damaged by settlement and earthquakes, through its prudent connection to the load-bearing structure of a new building. The building is located in the St. Gheorghe Square in Timisoara, Romania, located in the Banat seismic area with a peak ground acceleration of 0,20g [1]. This alternative solution saves the historic building from the total demolition, has the advantage of minimal consolidation interventions, but also preserves the historical balance between the buildings of the aggregate. The efficiency of the alternative solution is highlighted by a comparative presentation of the internal forces and deformations recorded in different areas

of the historic building, first for the singular building and secondly of the building integrated into the new bearing structure. Internal forces and displacements were obtained following a spatial seismic analysis, performed with the ETABS program. In the same time, photographs of the execution, that present the connection between the buildings and the chosen consolidation solutions used to reduce the seismic vulnerability of the building, are presented throughout the paper.

1 INTRODUCTION

In general, the load-bearing structure of a historical building is strengthened based on a set of analyses and calculations that are applied only on the studied building, without also considering the load transfer between the buildings of an aggregate. This is difficult to do since execution details and the state of conservation in the contact area of the two buildings are hard to assess. In addition, some owners do not accept on-site investigations. This interaction between the buildings forming an aggregate is highlighted when the analysis performed on an individual building indicates the occurrence of significant damage for a given PGA, but in reality, the historical building is not presenting significant structural damages after several earthquakes.

Of course, an explanation for this can be the mechanical properties used in the numerical simulations, which are strongly reduced according to the standards, certain details which were not included into the simulations or the forces taken into account, higher compared to the real ones. In these cases, the numerical simulations highlight the need for massive, extensive and long-term consolidation interventions, which would contradict the prudent conservation recommendations regarding historical bearing structures [2]. In addition, a total demolition and reconstruction of the building could destroy the static equilibrium between the historical buildings composing the aggregate.

Generally, for an individually analysed building, there are two intervention techniques which have to be considered: the local consolidation of the load-bearing elements or the preservation of the façade and subsequent demolition and reconstruction of the building behind the historic facade. Unfortunately, these solutions cannot be used if the neighbouring buildings have different foundations, are in a bad state of conservation, the walls are presenting significant out-of-plane deformation, or the mechanical properties of the materials of the historic building are strongly reduced.

Considering these, the paper is presenting a complex consolidation solution, which maintains a static equilibrium between the neighbouring buildings by saving the facade and a significant area of the historic building.

2 THE STRUCTURE AND ITS STATE OF CONSERVATION

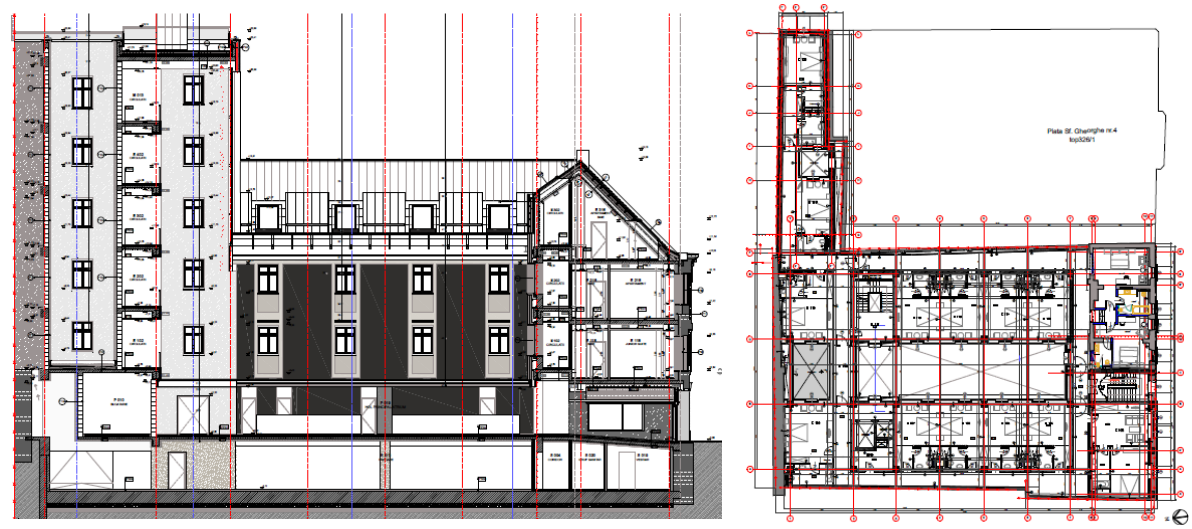
The historic buildings are located on 3 different plots (Figure 1) [1]. Located close to the St. George square, two of the buildings (no. 2 and 3), used to have a C-shaped plan while the neighbouring building (St. George square no. 4) is presenting an O-shape with an inner courtyard.

The investor bought the St. George square no. 2 and 3 buildings and leased the St. George square no. 4 one. Following a thorough technical and economic analysis, it turned out that it would be the most efficient to build a hotel on the considered plots [3] (Figure 2).



a) b) c)

Figure 1: a) St. George square no. 2 and 3 buildings facades; b) proposed building – 3D model; c) St. George square no. 4 building facade



a) b)

Figure 2: a) Transversal section of the building; b) plan of the proposed building

The buildings are located in an aggregate of historical buildings inside the former fortress area of the city of Timisoara. The buildings were made of brick masonry and lime mortar. The basement and upper floor walls had thicknesses between 75-85 cm while the façade walls had a thickness of 75cm on the ground floor decreasing down to 45 cm on the second floor. The interior walls had a thickness of 45 cm. The height of the floors is also changing. Therefore, the underground floor had a height of 2.30 m, the ground floor, 3.10 m, and the upper floors 3.47 m, respectively 2.40 m. The underground and ground floor had vaulted brick floors supported by arches. The first and second floor, on the other hand, presented wooden floors without brick arches.

The roof structures, placed on the buildings facing the street were very rigid, being composed of two layers of structural elements in the transversal direction (interior strutting device and exterior rafters connected by a collar beam) and diagonal elements placed between the rafters in the longitudinal direction [4,5]. The buildings also had steel straps in the transversal direction connecting the exterior walls.

The buildings were built during the Habsburg administration, which demolished almost all the buildings of the old city from the Ottoman period. The reuse of the old Ottoman foundations, after 1716, and the weak foundation ground produced numerous structural damages caused mainly by differential settlements. At the same time, the earthquakes recorded in the Banat seismic area are characterized by a PGA of 0.20g [6], which is amplifying these damages. However, no historical brick masonry building has suffered failure after an earthquake or after the settlements [7–10]

The onsite assessments carried out for these buildings highlighted that all the buildings of the aggregate were working together in transferring the seismic loads and the settlements and were in a state of equilibrium in 2012, the year the project was started. At that time, significant parts of the St. Gheorghe no. 2 and 3 buildings were in a bad state of conservation and in a pre-collapse condition, due to poor maintenance. The northern part of the St. Gheorghe no. 4 building suddenly collapsed in July 1988 after wrong construction work was done at a neighbouring building.

Therefore, due to the differential settlements, vertical cracks and significant damages of the walls, the doors and windows sills, arches and brick vaults were visible. Still, there were no cracks or fissures identified which could have been caused earthquakes, although some earthquakes had the epicentre about 10km from Timisoara [11,12].

3 THE SOLUTION

Initially, the hotel was composed of three dynamic independent structures: a reinforced concrete structure on the St. George square no. 4 plot, a new wing in the courtyards of the former St. George square no. 2 and 3 buildings, which also included part of the historical bearing structure from of the St. George square no. 2 building and a wing made only from the historical bricks recovered from the St. George square no. 4 building.

In this first phase, based on the recommendation of prof. Gioncu, as an expert, the preservation of the entire basement and ground floor of the historic brick masonry load-bearing structure of St. George square no. 2 and 3 buildings were considered. Considering this, steel columns had been embedded in the masonry walls of the remaining load-bearing structures, which were transformed, above the ground-floor into composite columns. For this purpose, the brick walls from the underground and the ground floor had to be strengthened.

The new construction made in the courtyard of the buildings was designed using reinforced concrete, having a rigid central perforated core, two rigid concrete tubes in the access path area and columns near to the neighbouring buildings. These columns were placed at a minimum distance of 1.50 from the neighbouring buildings, in order not to transmit loads to the foundation ground of these buildings. From the perimeter columns, cantilevers were placed towards the neighbouring buildings and a gap between the old and new of 5 cm considered [13] (Figure 3).

The load-bearing structure solution was developed after several types of structural systems were analysed. The spatial response of all considered solutions to various loads was studied with the help of the ETABS software. Finally, the most rigid solution, with a perforated inner tube was chosen, because according to the numerical simulations, the risk of collision between the neighbouring buildings and the new building during an earthquake could be avoided.

Ultimately, the historical facade was only preserved for the St. George square no. 3 building.

For this, the facade was consolidated and supported with a steel structure. Unfortunately, it was not possible to also preserve the façade of the St. George square no. 2 building since according to the project, three additional upper floors were designed over the original two.



a) b)

Figure 3: a) Perimetral columns withdrawn from the neighbouring buildings; b) 5 cm gap between the cantilevers and the neighbouring buildings

The load-bearing structure of the St. George square no. 4 building was made out of concrete walls and reinforced concrete slabs (Figure 4a).

Because it was also necessary to include an underground parking lot, in the underground level area outside the historical buildings that were kept, a raft slab was designed (Figure 4b). In order to prevent the new construction from transmitting loads to the neighbouring buildings, it was considered to build piles towards the St. George square no. 4 building and partially towards the Mercy no. 1 building in the north (Figure 4c,d). The piles were designed by Soletanche Bachy Romania.



a) b) c) d)

Figure 4: a) Reinforced concrete wall and floor of the new St. George square no. 4 building; b) raft slab in the area outside the St. George square no. 2 and 3 buildings; c) special foundations towards the old St. George square no. 4 building; d) special foundations of the St. George square no. 2 and 3 buildings.

Before the demolition works began, visual inspections were carried out in the neighbouring buildings where the access was allowed. All the cracks in these buildings were photographed, and devices for measuring the cracks were mounted, in order to be able to record their evolution during the construction works.

However, the initial project had to be adapted and modified due to unforeseen situations

discovered on-site during the works. The modifications made, were meant to ensure the structural safety of the historical buildings on site (St. George square no. 2 and 3) as well as of the neighbouring buildings during the construction works, thus managing to maintain the balance of the entire aggregate of buildings. For each change which was made to the load-bearing structure, a spatial analysis of the buildings was made, thereby verifying the effectiveness of the proposed changes.

The following measures were taken:

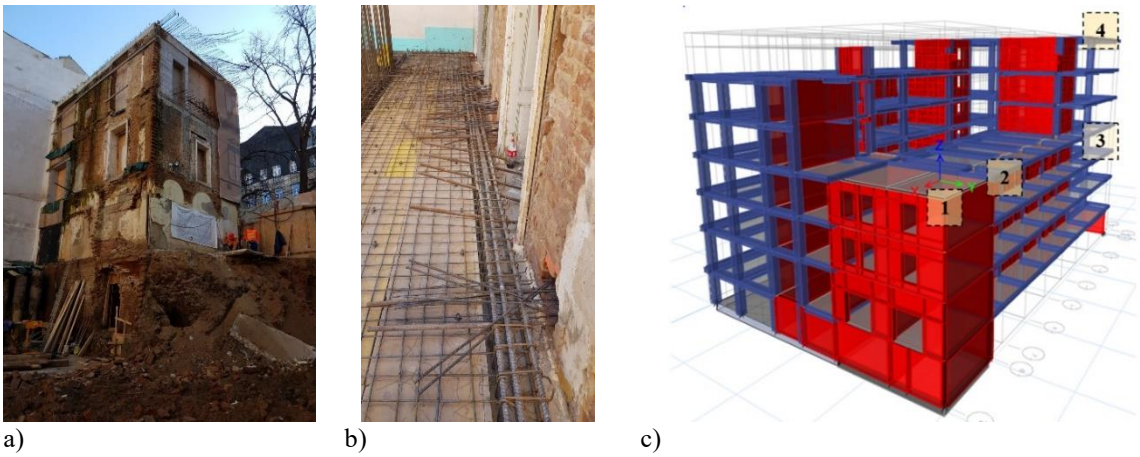
1. Four rooms were kept from the St. George square no. 3 historical building in order to take over the loads from the St. George square no. 4 building (Figure 5a).

2. The historical building was connected to the very rigid reinforced concrete structure in the floors area (Figure 5b). This structural solution allowed the reduction of the internal forces and deformations of the historical structure and implicitly the reduction of the expenses.

Figure 5c shows the contact wall between the historic building and the neighbouring building. The wall is delimited at the top by points 1 and 2. The vibration modes and periods of the connected buildings are shown in Figure 6. In figure 7 and in table 1, it can be observed that the inter-story drift values do not exceed the allowed limits. On the last floor, these values increase because this level was designed as future meeting rooms of the hotel and therefore made using a steel structure.

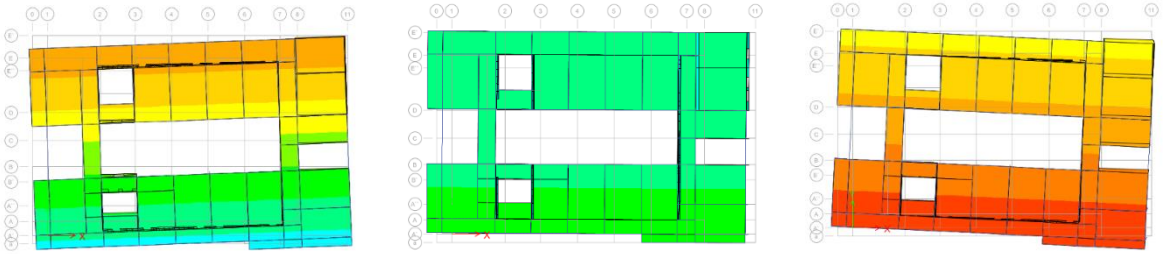
Table 2 presents comparative values of the horizontal out-of-plane and in-plane displacements of the wall in the contact area between the St. George square no. 3 and 4 buildings. The horizontal displacements were calculated for a q factor of 2, for the new building, since according to the simulations, the buildings proved out to have a sensibility to torsion and 1.65 for the original historical building. The displacements were determined in the corner of the building at the level of each floor, beneath point 1 (Figure 5c). It can be observed that out-of-plane displacements are almost unchanged for the two cases, while the in-plane displacements are reduced with approximately 50% in the case of the proposed building.

By increasing the stiffness, consolidating the historic floors and connecting the historic building to the new reinforced concrete one, the bending moments in the wall in the contact area between the buildings were reduced. The values of the bending moments at the top of each wall at every level, on the corner of the building (Figure 5c – point 1) are presented in table 3.



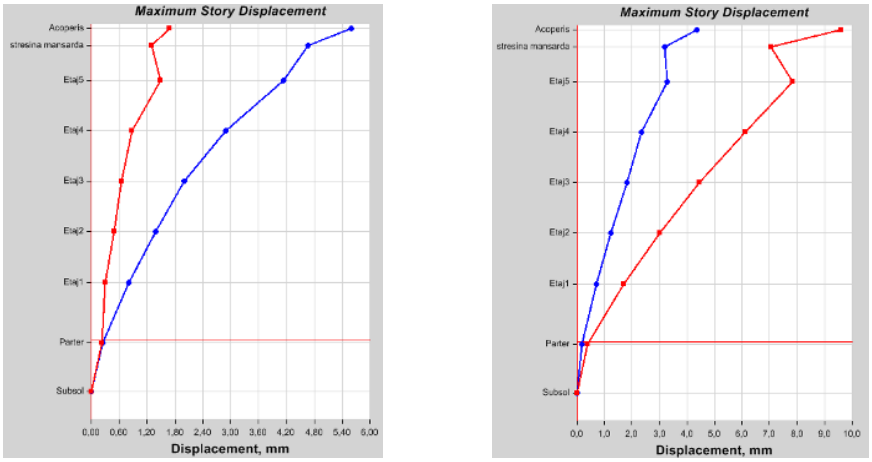
a) b) c)

Figure 5: a) Preserved section of the historic masonry building; b) connection between the historic and new building; c) contact area between St. George square no. 3 and 4



a) b) c)

Figure 6: Vibration modes a) Vibration mode 1 – T1=0.309 sec; b) Vibration mode 2 – T2=0.202 sec; c) Vibration mode 3 – T3=0.159 sec



a) b)

Figure 7: Inter-story drift

Table 1: In-plane and out-of-plane inter-story drift ratio (in point 1)

Level	Story drift	
m	OX‰	OY‰
3.60	0.147	0.347
7.30	0.182	0.413
10.05	0.193	0.444
13.25	0.360	0.527
16.45	0.393	0.533
18.65	0.471	0.177
19.75	0.419	0.513

Table 2: In-plane and out-of-plane displacement (in point 1)

Level	Out-of-plane horizontal displacement [mm]		In-plane horizontal displacement [mm]	
m	before	after	before	after
3.60	1.71	2	4.64	2.38
7.30	3.18	3.28	8.12	3.54
10.05	4.43	4.68	10.18	4.64

Table 3: Bending moments before and after consolidation interventions (in point 1)

Level	Bending moment [kNm]	
m	before	after
0	39	16
3.60	53	20
7.30	14	8
10.05	0	-4.60

3. A raft slab was made in the underground of all the buildings. This foundation solution reduced the values of the internal forces and the settlements of the foundations. In the contact area between the hotel's foundation and the St. George square no. 4 historical building, the maximum vertical deformation according to the numerical simulations is rather small, of 4.60 mm (Figure 8).

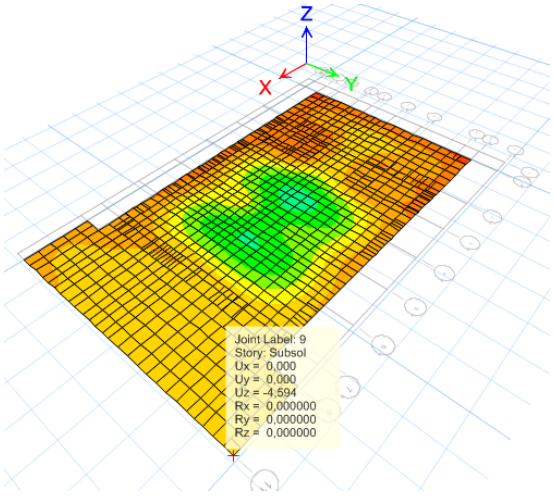


Figure 8: Deformation of the raft slab

4. The original wall was kept the entire length of the St. George square no. 4 building. This wall was reinforced with FRP and is in contact with the reinforced concrete beams from the new building (Figure 9). On the upper floors, between the beams and the walls of the neighbouring buildings, a 5 cm gap was left. In this way, in the case of an earthquake, the new building could take over but not transmit the seismic loads to the St. George square no. 4 building.



Figure 9: Consolidation of the St. George square no. 4 building wall which was not demolished using Kerakoll products

5. In order to prevent the earth discharge from beneath the foundations of the St. George square no. 4 building, reinforced concrete support walls were made, along its entire length (Figure 10).



Figure 10: Reinforced concrete support walls made near the foundations of the St. George square no. 4 building

6. Due to the significant damage caused by settlements, the underground floor area of the St. George square no. 2 building was demolished. The vaults were rebuilt with the original bricks (Figure 11).



Figure 11: Reconstruction of the underground floor vaults of the St. George square no. 2 building

4 CONCLUSIONS

The paper presents an intervention method which allows the construction of a new building in an aggregate of historical buildings in Timisoara. The proposed solution did not produce damage to the neighbouring buildings, allowed the preservation of a larger area of the historical buildings, reduced the execution time and the volume of material that had to be disposed of during the demolitions, without affecting the safety of the neighbouring buildings during the works and after their completion. This was made possible by efficiently combining the advantages offered separately by each structure, being a project in which the new and the old combine perfectly.

REFERENCES

[1] Mosoarca, M., Stoian, V., Florea, M. and Niculescu, M. Structural Balance of Historical Aggregates. In: Aguilar R (eds.). *Structural Analysis of Historical Constructions, SAHC2018*.Springer, Cham, Cusco, Peru, (2018), pp. 2448–2456.

[2] ICOMOS. International Charter for the Conservation and Restoration of Monuments and Sites (The Venice Charter 1964). Venice, Italy, (1964) https://www.icomos.org/charters/venice_e.pdf (accessed 5 May 2017).

[3] S.C. D Proiect S.R.L. *Architectural design project no. 61/2012*. (2012).

[4] Keller, A., Chieffo, N. and Mosoarca, M. Influence of roof structures on seismic behavior of historic buildings. In: Mazzolani F (eds.). *3rd International Conference on Protection Of Historical Constructions, PROHITECH'17*. (2017).

[5] Keller, A., Parisi, M.A., Tsakanika, E. and Mosoarca, M. Influence of historic roof structures on the seismic behaviour of masonry structures. *Proc Inst Civ Eng - Struct Build* (2019):1–27.

[6] MDRAP. Romanian Seismic Design Code P 100-1/2013. (2013) http://www.mdrap.ro/userfiles/reglementari/Domeniul_I/I_22_P100_1_2013.pdf (accessed 18 Apr 2019).

[7] Narita, A., Mosoarca, M., Modena, C., da Porto, F., Munari, M. and Taffarel, S. Behavior of Historic Buildings in Zones with Moderate Seismic Activity. Case Study: Banat Region, Romania. *Procedia Eng* (2016) **161**:729–737.

[8] Taffarel, S. Marson, C. Valotto, C. Roverato, M. Munari, M. da Porto, F., Modena, C. and Mosoarca, M. Seismic vulnerability maps of Timisoara historical center based on fragility curves. In: Van Balen K (eds.). *10th International Conference on Structural Analysis of Historical Constructions, SAHC 2016*.CRC Press, Taylor & Francis Group, Leuven, Belgium, (2016), pp. 1605–1612.

[9] Chieffo, N., Mosoarca, M., Formisano, A. and Apostol, I. Seismic Vulnerability Assessment and Loss Estimation of an Urban District of Timisoara. *IOP Conf Ser Mater Sci Eng* (2019) **471**(6).

[10] Apostol, I., Mosoarca, M., Chieffo, N. and Onescu, E. Seismic vulnerability scenarios for Timisoara, Romania. In: Aguilar R., Torrealva D., Moreira S., Pando M.A. RLF (eds.). *Structural Analysis of Historical Constructions*. Springer International Publishing, Cham, (2019), pp. 1191–1200.

[11] Oros, E. *Earthquakes in the Banat plain (in Romanian)*. Graffiti, Timisoara, Romania, (1991) doi:10.13140/2.1.2740.5126.

[12] Oros, E. and Diaconescu, M. Recent vs. historical seismicity analysis for Banat seismic region (western part of Romania). In: Vacareanu R (eds.). *Proceedings of the 5th National Conference on Earthquake Engineering and 1st National Conference on Earthquake Engineering and Seismology*. CONSPRESS, (2014) doi:10.13140/2.1.3497.7601.
[13] SC H.I. Struct. *Structural design project - St George square buildings*. (2012).

12th International Conference on Structural Analysis of Historical Constructions
SAHC 2020
P. Roca, L. Pelà and C. Molins (Eds.)

RECONSTRUCTING THE INDOOR CLIMATE OF HISTORIC BUILDINGS

WOLFGANG STUMPF[1*]

[1]Department for Building and Environment
Donau-Universität Krems
Dr.-Karl-Dorrek-Strasse 30, 3500 Krems, Austria
e-mail: wolfgang.stumpf@donau-uni.ac.at, www.donau-uni.ac.at/dbu (*corresponding author)

Keywords: reconstruction, usage, thermal comfort, hygrothermal simulation

Abstract. *In general, a building survey includes geometry, structure, construction, material and history. In historical buildings over the time the building structure and usage can vary greatly. If a room offers good conditions, it will be used accordingly. The usage criteria are not limited to geometric and visual design features but also include thermal comfort. When determining the use of historical rooms and buildings, it makes sense to combine the results of the construction survey and literature research with a reconstruction of the indoor climate. Constructive adjustments, spatial extensions and social developments lead to a deviation from the originally planned and implemented situation over time.*

Which parameters have to be known in order to reconstruct the indoor climate of a historic building? This paper uses three examples to describe the requirements and procedure for determining the use of rooms that are no longer in their original state. The reconstructed spaces are an office in a former tobacco factory in Krems (Austria) [1], an art gallery in Yogyakarta (Indonesia) [2] and a traditional residential building is in Jeddah (Saudi Arabia) [3]. Dynamic thermal and hygrothermal simulations of building elements show the ability of materials to influence the indoor climate and the interaction between construction and indoor climate. By monitoring or defining the user's presence and activities in a room the thermal interaction between construction and indoor climate is calculated. The detection of the airflow around and through the building provides important parameters for the assessment of thermal indoor comfort. The results were compared with the use of space as described in the literature or expected from the building survey.

The method of reconstructing the indoor climate in historical buildings works. The results provide information for evaluating the original situation. With these findings, the potential inherent in a building can be better exploited for the adaptation of historical buildings to changing user requirements or climatic conditions.

1 INTRODUCTION

The thermal conditions of a room have a great influence on its practical use. The choice for material, construction, geometry, orientation and size of the building and its openings is determined in the design process. The quality of construction is limited to the availability of resources and to the state of building techniques. Over the time, parts of the historic construction were adapted to the change of usage or technologies. Such modifications may or may not

improve the quality of the building and user comfort. During the life cycle of a building, there are periods, in which the interaction between construction, user comfort and environment are in a good balance. The circumstances in which such precious phases occur are of particular interest for the reconstruction and adaptation of historic buildings. The results provide inspiration or individual solutions for adapting a room or building to another purpose without the need to add new construction technologies or equipment.

This paper describes a method of reconstructing a user's thermal comfort in a room or building, which is no longer available in its original state.

2 MATERIALS AND METHOD

In addition to a conventional building survey specific material characteristic and the air flow around and through the building need to be determined. Temperature, humidity, air velocity in a room, activity and clothing of the user are the main parameters to assess the thermal comfort at a specific usage scenario as it can be expected from the architectural design, the description in literature or explanation from former user. A high thermal comfort confirms the supposed use of space.

Steps to reconstruct the indoor climate to proof a room's usage:

1. use information provided by a regular building survey: plans with detailed measurements of rooms, construction, openings, materials, history, its purpose and way of use, description of the surrounding neighborhood, environment, landscape,
2. find the way of air streaming through the building,
3. determine key values of air velocity in the room or its air change rate,
4. get the outdoor climate data from a database or by monitoring the microclimate on site,
5. determine specific characteristics of construction and surface materials,
6. calculate the indoor temperature and humidity,
7. assess the thermal comfort,
8. discuss and compare the results with its assumed purpose of use.

2.1 Three buildings

The method to reconstruct the indoor climate of a historic building was developed and proved on three buildings. They differ in shape, size, usage, materials, location, respectively climate zone and the data available. All testimonials use natural ventilation for the reduction of overheating. In the current situation, only Gallery 1 in Yogyakarta operates a chiller, but only during the museum's opening hours.

2.1.1. Meeting room at Danube University Krems, Austria

Krems is located in the Austrian province Lower Austria, north of the Eastern Alps at the River Danube. Hot summer and cold winter are significant for the prevailing continental climate. The former tobacco factory in Krems was designed by architect Paul Hoppe (1869-1933) and built in 1918-1922. Since 1994, it has become the main building of Danube University Krems Campus, housing office rooms and lecture halls. The building with its typical facades is a listed monument (figure 1, left).

Between June and September, indoor temperature in the examined meeting room rise up to 32 degrees Celsius. Due to the development of cooling strategies, a system of numerous sensors

has been monitoring the thermal behavior of one exemplary room without inner heat gains and its adjacent spaces since May 2018. The dataset includes the outdoor air temperature, indoor air temperatures and surface temperatures of the meeting room and all adjacent rooms, the use of the room, door, window wings and shading system (figure 1, right).

The façade construction consists of a reinforced concrete skeleton with massive brick in between, covered with whitewashed cement plaster with structural façade elements and whitewashed lime cement plaster on the inner wall side. Two layers of eight slim wooden wing frames with single glass form one big box window. A textile roller blind between the two window layers protects the room from solar radiation. A metal stud wall planked with gypsum boards detaches the room from the northern office, other walls are made of massive brick, covered with whitewashed lime cement plaster. The reinforced concrete ceiling construction is based on the Hennebique System. Mineral wool, screed and a wooden floor form the floor construction. The bottom view of the ceiling shows suspended gypsum boards. The originally dedicated use of this room was an office using night ventilation. Due to fire restrictions and for the protection from wind, rain and uninvited guests it is not possible respectively not allowed to keep windows open at night.



Figure 1: Danube University Krems, former tobacco factory (2019, [4]). The examined meeting room in the second floor, left of the risalit (2019, [4]).

2.1.2. Gallery 1 in Museum Affandi, Yogyakarta, Indonesia

The city of Yogyakarta is located on the Indonesian island Java. The climate is hot and humid with a permanent smooth wind breeze.

The Gallery building was designed by the painter and sculptor Affandi (1907-1990, figure 2, left), built in 1962 and officially opened in the year 1974. The lenticular gallery is defined by two curved massive brick walls covered with cement plaster. In the west wall, a bend of slide windows provides fresh air for the gallery. Air enters the building through large doors at the ends of the east wall. Ceramic tiles cover the floor slab made of reinforced concrete. Banana leaves gave inspiration for the shape and construction of the roof. Teak shingles on wooden roof battens are the original roof materials. Due to leakages, the roof was insulated with an additional layer of bituminous shingles. Natural light enters the building through a small glass slit among the longitudinal axes in the middle of the ceiling. A canvas underneath the transparent roof area protects the paintings from direct light (figure 2, right).

After an earthquake in 2010 and due to significant changes in the surrounding area (more

traffic, noise, dust, insects, neighboring buildings, reduced airflow, change of microclimate) ventilation openings in the upper area of the east facade were closed [2]. This measure led to uncomfortable room climate for art and visitors. Therefore, two chillers were installed in 2016 to support ventilative cooling. Every morning wardens open doors and windows to exchange the humid, warm air with fresh air from outside. Chillers operate during opening hours only. During night, doors and windows are closed, cooler, but more humid outdoor air enters the gallery through gaps between windows and roof and through gaps in the door fillings.

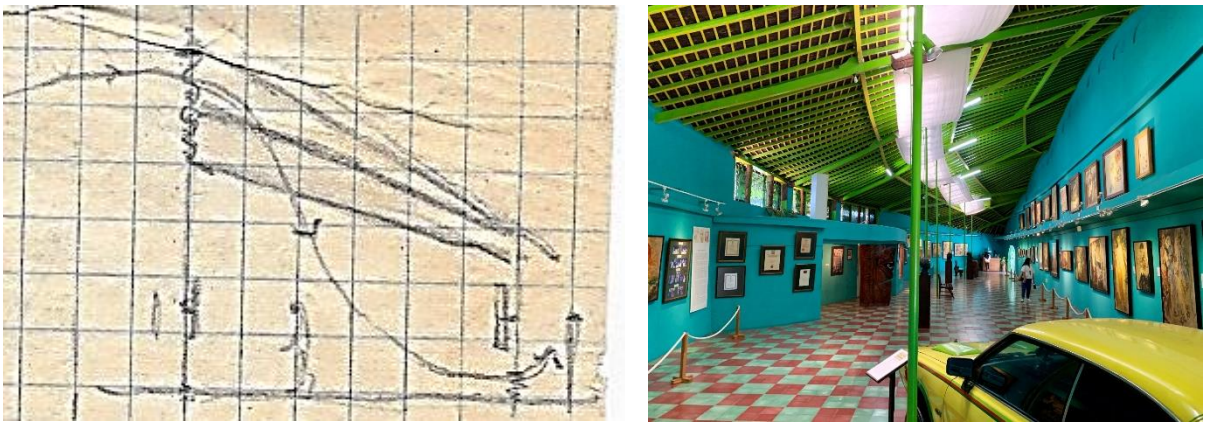


Figure 2: The design sketch for Gallery 1 with an implied ventilation concept (right, sketch 65 in Sketchbook of Affandi, 1950). Gallery 1 in Yogyakarta (W. Stumpf, 2019).

2.1.3. Al Nawar House in Jeddah, Saudi Arabia

Al Nawar House is a traditional residential building in Al Ballad, the old town of Jeddah, Saudi Arabia. The climate in the port city on the Red Sea is very hot and humid all year round. A smooth breeze permanently blows alternately from the Red Sea or from the desert of Arabian Peninsula. Outdoor temperatures are between 32 and 49 degrees Celsius, at night about 15 degrees lower. Coral stone was the only construction material for historic buildings in this area. Wooden window boxes, so called roshan or rawasheen, are the typical elements on these lime-plastered, mostly whitewashed façades. They protect the rooms from direct sunlight and unwanted glances. Their main function is the control of airflow in the building.

In 2012, a team of scientists from University of Technology Vienna and King Abdulaziz University Jeddah performed a comprehensive building survey of the about 350-year old Al Nawar House in Al Ballad [3]. As a result, there are detailed plans, a description of building, construction, material and its history (figure 3).

The people in such buildings knew how to create a tolerable indoor climate by opening and closing the shutters at certain times. The room function could change over a day. Depending on the air temperature, humidity and air velocity the indoor climate was suitable for sleeping, sitting down for a chat or doing manual work. There was no support from mechanical air conditioning systems.

Nowadays, most of such historic buildings are abandoned, or only the ground floor is used as a department store or as storage space. Since 2014 the old town of Jeddah has been listed as UNESCO World Heritage. The municipality plans to revitalize this historic urban area.

2.2 Building survey

The three chosen examples differ in the data availability of its initial situation and in the access to the building.

Which information was available, what was needed?

The meeting room at Danube University Krems, Austria, provides all necessary information. Geometry of the actual situation, construction and material characteristics are given. The author has personal access to the room at all times. Microclimate (outdoor air temperature, wind, precipitation), air and surface temperature in the examined and adjacent rooms have been monitored under several usage scenarios since 2018 [4].

The author visited Gallery 1 in Yogyakarta, Indonesia, in August 2018 and August 2019. Documents and plans about the current state of the building, geometry of the actual and historic situation, construction and material characteristics are given [2]. The original state of the building has changed in some parts, but the usage is still as it has been from the beginning. Microclimate (outdoor air temperature, humidity, wind and precipitation), indoor air temperature, humidity and even CO_2-concentration have been monitored since January 2019. Data are permanently accessible via WLAN connected sensors and internet cloud. Surface temperatures, operation hours of chillers, air velocity at different areas in and around the building, thermal comfort were measured and experienced personally on site over two periods of two weeks. Air velocity in the initial situation with numerous small openings in the façade and no buildings around Gallery 1 have to be determined.

Information about Al Nawar House in Jeddah obtain from several sources like construction plans, literature and interviews. The author had no direct contact to this building nor to the region. The state of geometry and construction in the year 2012 when the building already was abandoned, construction and the material characteristics are given [3] (figure 3). A meteonorm climate data set [5] describes the outdoor climate in the area of Jeddah. The microclimate around the building site has to be derived from meteonorm data. The building owner and scientists performing the building survey described the indoor climate and the former use of the building. Literature and material database MASEA [6] provided further information.



Figure 3: Floor plan of Al Nawar House in Jeddah, second floor (left), north direction points to the right. The examined room 101 (right) is situated on the top right of the floor plan (building survey in 2012, TU Wien [7]).

2.3 Airflow around and in the building

The determination of air velocity is based on calculations with characteristic values and the consideration of influencing factors. In addition to classic results of a building survey, this step provides further information.

The interaction between indoor and outdoor climate is influenced by heat transmission through the building envelope, by solar radiation entering a room through openings or transparent areas and by convection from air streaming into or out of a building. This paper focuses on buildings with small or well-shaded openings, so that the indoor climate is only slightly affected by sunlight. The described method of reconstructing the indoor climate is aimed at buildings such as Affandi Gallery 1 and Al Nawar House, where convection has the greatest influence on the heat and moisture transport. For the reconstruction of indoor climate, it is necessary to determine the hourly air change rate (ACH) of a room. In a qualitative building and site analysis the way of airflow around, into and through a building can be identified with curved lines and arrows on the plans. Alternatively, a CFD simulation (Computational Fluid Dynamics) based on Navier-Stokes equations offers more specific information [3].

Air movement is stimulated by wind (air flows from areas with high pressure to areas with low pressure) and buoyancy (vertical differences in air temperature respectively density). Numerous circumstances reduce the flow of ambient air into a building. Main parameters are vegetation and constructions in the surrounding, building shape, position of the building to the wind direction, size of an opening and the resistance of fillings like lattice are. The airstream in a room depends on the number, size and position of openings, size and proportion of the room, surface finish and temperatures, objects and heat sources in the room, and especially on the spatial distribution of temperature and pressure differences. Flow reduction also can be calculated by an exact analysis of each influence parameter according the established laws of aerodynamics in a quite complex way. If the examined space is still in its original structure and surrounding a tracer gas measurement delivers realistic numbers for ACH. For an early stage analysis as described in this paper, the reduction factor is estimated from the effects of the parameters written above.

The number of air changes per hour (ACH) is calculated using equation 1 and 2. Direction-dependent values for the wind velocity come from a climate database or a microclimate monitoring system on site.

$$v = S \cdot s \cdot R \tag{1}$$

$$ACH = v / V \tag{2}$$

v [m3/h] stands for air volume per hour, S [m2] is the value for open cross-sectional area of a room or an opening, s [m/h] stands for the average wind or air velocity over an investigated period, R [-] is an estimated reduction factor in the range from 1 to 0, V [m3] describes the room volume, ACH [1/h] is the air change rate per hour.

Realistic key values for air velocity in a room range from 0.05 to 2.0 m/s. The air change rate per hour during operation (person in the room) ranges from 0.1 (windows or shutters closed, but just for a few hours) to 3.0 and is usually controlled by the user. ACH values between 1.5 and 10 per hour can be assumed during night ventilation (no person in the room, all windows opened).

The envelope of the three examined buildings is not particularly airtight or even fully closed.

The box windows in Krems comply with the current technical standard for existing buildings. In Gallery 1 the air gap between the wall and roof above the windows in the eastern façade is eight centimeter wide. The windows in Al Nawar House have no glass panes, but wooden shutters and wooden lattice, so called Mashrabiya. Leakages in the building envelope are taken in account in ACH with 0.1 to 0.3 per hour.

2.4 Calculation of indoor climate

Why calculating the indoor climate? A building survey gives us the opportunity to reconstruct the geometry, construction, material, use and history of buildings in their previous and original state. Similar, still existing constructions or material samples offer a comparison option for creating virtual models. We can agree that no thermometer or hygrometer was normally installed in historic buildings and that no profiles from measured indoor temperature and humidity were documented. Historical scenes on paintings, traditional clothing, typical widespread diseases etc. indirectly provide hints about temperatures, humidity, air drafts in buildings.

The indoor climate is mainly perceived by temperature, humidity and movement of air. Chapter 2.3 describes the determination of airflow and ACH. Equation (3) and (4) give indoor air temperature and humidity [7].

$$(c_wall \cdot A_wall + c_ceiling \cdot A_ceiling + c_floor \cdot A_floor + c_air \cdot V \cdot \rho) \cdot \Delta T_i / \delta t = (c_air \cdot ACH \cdot V \cdot \rho + U_wall \cdot A_wall + U_win \cdot A_win) \cdot (T_e(t) - T_i(t)) \quad (3)$$

$$C_hyg \cdot \Delta u_i / \delta t = ACH \cdot V \cdot (u_e(t) - u_i(t)) \quad (4)$$

c is the effective specific heat capacity of a building component reacting with the room air, ISO DIN 13786 [8] describes the calculation method using thickness, bulk density, specific heat capacity and thermal conductivity of a material layer. A denotes the room-side surface of a component. V is the volume of ventilated space, ρ the air density. T_i and T_e are indoor and outdoor air temperature over time step t. T_e comes from a climate database or a microclimate monitoring on site. The examples described in chapter 3 did not consider any differences in the climate data between the current time and the time before climate change. ACH describes the air change per hour, see equation (2). The U-value or heat transfer coefficient of a building component depends on the thickness and thermal conductivity of material layers. u is the absolute air humidity, converted from the relative humidity, air pressure, saturation pressure and the gas constant. The calculations of U and u follow common building physical procedures. Values for equation (3) and (4) come from building survey, material databases or equation (1) and (2).

The results show temperature and humidity profiles over time (figures 4 to 7). For the validation of the indoor climate model, compare the calculations with the monitoring data (chapter 3.1, figures 4 and 5). Mean values over a time period in which the room is occupied are input data for the assessment of thermal comfort.

2.5 Assessment of thermal comfort

Usage criteria of a room are not limited to constructive, geometric and visual design features but also include thermal comfort. A room is used according its purpose, if comfortable climate conditions correspond to the activities and requirements of the user. If this premise is not met,

the assumptions from building survey cannot be confirmed or the user satisfaction was quite low.

The thermal comfort was assessed with the "CBE Thermal Comfort Tool" [9], an online tool, in which one of the standardized assessment methods as described in EN ISO 7730 [10], EN 16798-1 [11] and ASHRAE 55 [12] can be chosen. Building history, calculations or assumptions provide the input data for this tool. Air temperature and relative humidity result from equation (3) and (4). Operative temperature is the average of air and surface temperature. To do this, the area-weighted value of all surface temperatures must be defined, which were calculated using dynamic simulation software like WUFI pro [13]. In climate zones where outdoor air temperature lies in the range of indoor air temperature you may specify the surface temperature plus/minus three degree Celsius of the indoor air temperature. Classify a person's activities and clothing as described in the building's history. For the evaluation of air velocity follow the procedure in chapter 2.3.

The adaptive method is based on an approach in which the acceptance of higher indoor temperatures increases with higher outdoor temperatures.

The result of thermal assessment is indicated by the position of a point in a diagram and the values for PMV and PPD (Predicted Mean Vote and Percentage of Person Dissatisfied [10], figure 8). If results do not meet the standardized requirements, it should be taken into account that the assessment methods were developed in accordance to the lifestyle of the so-called western world in the second half of the 20th century. In this case, individual results are evaluated based on their relative relationship to comparable situations.

3 RESULTS

One room of each described building was examined under different usage scenarios and different climate conditions. The results show the quality of the thermal comfort and the congruence of reconstructed and described or expected situations.

3.1 Meeting room in Krems, Austria

This building was used to test and calibrate the method. In 2019, several scenarios using different control strategies for window and shading positions, could be investigated in real-time and under personal appearance. These experiments were the base for checking the congruence between monitored and calculated indoor climate.

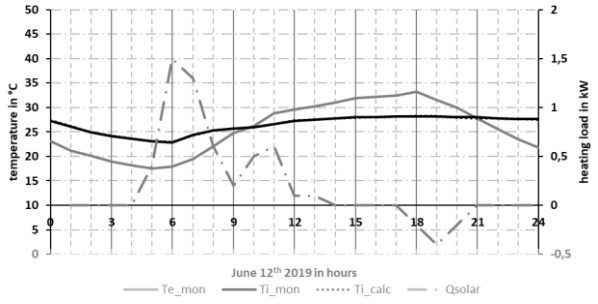


Figure 4: Monitored (Ti_mon) and calculated (Ti_calc) indoor temperature profiles over one day in the meeting room in Krems, Austria. The calculated temperature profile overlaps the measured values.

The calculations proof that the indoor air temperature can be predicted if specific data about

the outdoor air temperature and the room usage profile (window, shading and door position, occupancy) are known.

Textile roller blinds and windows are always drawn. The curve indicating the calculated indoor temperature overlaps the monitored temperature profile. The air change rate and heat flow from solar radiation (Qsolar) through the shaded window had to be adjusted in the hourly calculations according the usage and time profile (figure 4).

3.2 Gallery 1 of Museum Affandi in Yogyakarta, Indonesia

Museum Affandi gives an example for how to reconstruct the initial design concept's indoor climate.

In a first step, the calculated temperature and humidity profiles were adjusted to the monitored data in an iterative way. The air change rates were determined taking into account the reduction parameters described in chapter 2.3. The load profile "Qsolar - Qchiller" (solar radiation through the roof glass minus cooling capacity of the chiller) results from the remaining difference between monitored and calculated temperature profile (figure 5, left diagram). The dehumidification performance of the chiller also results from the difference between monitored and calculated humidity profiles (figure 5, right diagram).

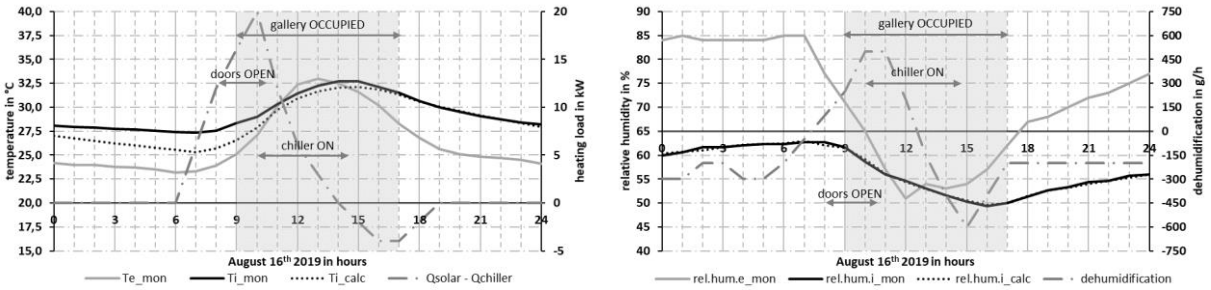


Figure 5: Indoor climate in Gallery 1 on August 16, 2019. The diagram on the left shows the approximation of the calculated (Ti_calc) to the monitored (Ti_mon) indoor temperature, taking into account the influence of solar radiation through the glass opening in the roof and the cooling capacity of the chiller. The right diagram shows the humidity profiles under the influence of the chiller's dehumidification capacity.

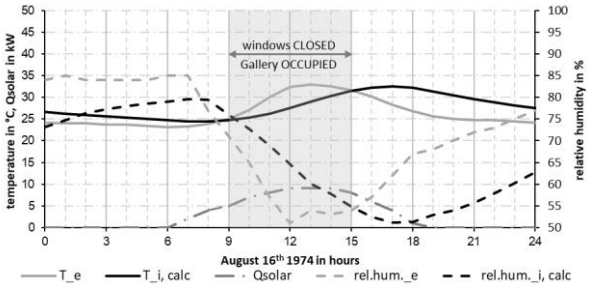


Figure 6: Reconstructed indoor climate of Gallery 1 in its original state in 1974, when there were numerous small ventilation openings in the east façade and no chillers were in operation.

In a second step, the indoor climate of Gallery 1 was reconstructed in its initial state in 1974 (figure 6). The main differences to the current state are additional small ventilation openings in the east wall construction, door wings with a wide-meshed, open metal grille, no neighboring

buildings around the museum site and therefore stronger wind, no chillers in the gallery. These features are reflected in higher air change rates. The windows in the west façade were kept closed during the day when outdoor temperature was higher than the temperature in the gallery. Due to open windows and wind pressure, a slightly higher air exchange rate was assumed at night. The same microclimate data as in 2019 was used for the calculations.

During opening hours in 2019 temperature is higher than in 1974, relative humidity is quite the same. The chiller offers the advantage of its ability to dehumidify the air, increase the air velocity in its streaming area and lower the airflow temperature well below the temperature of surrounding areas. This provides cool areas for the visitors, but is not a healthy environment for the art on display.

3.3 Al Nawar House in Jeddah, Saudi Arabia

The third example only usess information from a building survey in the year 2012, when it already has been abandoned for many years. Literature and an interview with the owner and former inhabitant of Al Nawar House were the sources to reconstruct the way of living under extreme climatic circumstances. The author never had the opportunity to see the building in reality. By organizing a climate data set and additional information about the construction, the indoor climate was calculated according chapter 2.

The result shows that the thermal comfort in room 101 on a hot and humid day in October the 8th between 9 and 14 hours is in an acceptable range (figures 7 and 8). The construction in its original state fits to its use.

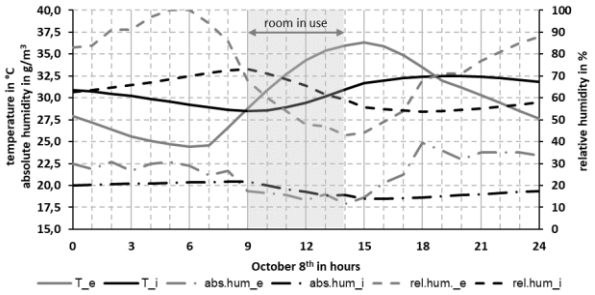


Figure 7: Reconstructed indoor climate of room 101 in the originally inhabited Al Nawar House on a hot and humid day.

During these hours the air temperature in the room is lower than the outdoor temperature, outdoor absolute and relative humidity are lower than in the room. A smooth breeze streams around and above the building. When the user enters the room, he opens the shutters of the roshan, warm air enters the room from outside and flows through the building. Smooth wind over the rooftop tries to suck air out of the building. The breeze in the lanes pushes warm air through the opened roshan into the cooler room. Due to an open connection from room 101 to the rooftop through adjacent rooms and the staircase warm air is driven by buoyancy and wind pressure. For the calculation an air change rate ACH of 5 times per hour was determined. Considering the rotating movement of air in the room the air velocity next to the floor of 0.25 meters per second was calculated by equation (2). Under the circumstances of 29 °C, 68% relative humidity, air velocity of 0.25 m/s, seated activity, summer clothes the Berkeley Thermal Comfort Tool assesses the situation as a second-class comfort (figure 8). This means,

that this room in its construction, materials, shape, position of openings provides quite good conditions for the users even on a very warm and humid day.

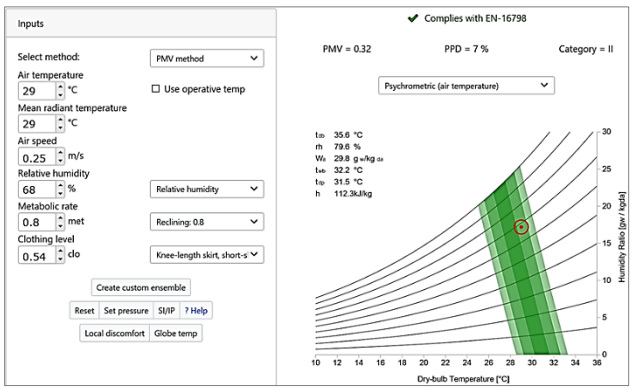


Figure 8: The Berkeley Thermal Comfort Tool [9] confirms a proper indoor climate in room 101 between 9 and 14 hours on a very hot and humid day in October.

4 CONCLUSIONS

The described method of reconstructing the indoor climate in historical buildings works. The application of this method requires a little extra effort to collect and document additional data for dynamic thermal simulations of construction components and buildings.

A closer cooperation between archaeologists, architects, historians and building physicists provides new perspectives on the results of a conventional building survey and supports the proof of concepts based on the investigations of individual groups. With these findings, the potential inherent in a building can be better exploited for the adaptation of historical buildings to changing user requirements or climatic conditions.

The results of this paper describe a first step in the holistic reconstruction of the thermal behavior of buildings that are no longer in their original state. Additional parameters for the determination of airflow around, into, in and through building, parameters for the reconstruction of solar impact through building envelope's transparent openings shall be the motive for further research.

New technologies enable a more in depth building analysis but such approaches require interdisciplinary collaboration between different branches of science.

Acknowledgements. Research reported in this publication about Gallery 1 in Yogyakarta, Indonesia, was jointly supported by the ASEAN-European Academic University Network (ASEA-UNINET), the Austrian Federal Ministry of Education, Science and Research and the Austrian Agency for International Cooperation in Education and Research (OeAD-GmbH). Research reported in this publication about meeting room in Krems, Austria, was part of the research project CoolAIR [4], which was supported by the Austrian Research Promotion Agency FFG, Austria.

REFERENCES

[1] Stumpf, W.; Winkler, M.; Trauninger, D.; Treytl, A.; Bratukhin, A.: CoolAIR – Automatisierung von Kastenfenstern zur Raumkühlung. Fachhochschule Burgenland, Tagungsband e-nova "Gebäude der Zukunft?", Band 22: p. 59-66, Leykam Buchverlagsgesellschaft, Graz, Austria 2018.

[2] Herbig, U.; Styhler-Aydın, G.; Grandits, D.; Stampfer, L.; Pont, U.: The Architecture of the Affandi Museum – Approaches to a Piece of Art. 3rd Biennale ICIAP - International Conference on Indonesian Architecture and Planning, Yogyakarta, Indonesia 2016.

[3] Jaeger-Klein, C.; Stumpf, W.; Styhler-Aydin, G.; Radinger, G.: Analysis of Building Structures and Valorization of Cultural Heritage in Jeddah (KSA). In: Proceedings of the 10th International Conference on Structural Analysis on Historical Constructions, SAHC 2016, Leuven, Belgium: p. 77, Taylor and Francis Group, London 2016.

[4] CoolAIR – Prädiktiv geregelte passive Gebäudekühlung mittels natürlicher Nachtlüftung und tageslichtoptimierter Verschattung, research project at Danube University Krems, www.donau-uni.ac.at/de/universitaet/fakultaeten/bildung-kunst-architektur/departments/bauen-umwelt/forschung/projekte/coolair.html, accessed January 15, 2020.

[5] meteonorm – Irradiation data for every place on Earth. Meteotest, Bern, Switzerland, www.meteonorm.com, accessed January 15, 2020.

[6] MASEA – Materialdatensammlung für die energetische Altbausanierung. Fraunhofer-Institut für Bauphysik, Valley, Germany, www.masea-ensan.de. Accessed January 15, 2020.

[7] Stumpf, W.; Bednar, T.: Hygrothermal Behaviour of Building Components in Context with the Room Usage of a Historic Residential Building in Jeddah, KSA. TU Delft, WTA 4th International PhD Symposium, Proceedings, Delft, Netherlands 2017.

[8] ISO DIN 13786 Wärmetechnisches Verhalten von Bauteilen – Dynamisch-thermische Kenngrößen – Berechnungsverfahren (ISO 13786:2017), Beuth Verlag GmbH, Berlin, Germany, 2018.

[9] CBE Thermal Comfort Tool, Center for the Built Environment, University of California Berkeley, https://comfort.cbe.berkeley.edu, accessed January 15, 2020.

[10] ÖNORM EN ISO 7730:2006 Ergonomie der thermischen Umgebung – Analytische Bestimmung und Interpretation der thermischen Behaglichkeit durch Berechnung des PMV- und des PPD-Indexes und Kriterien der lokalen thermischen Behaglichkeit (ISO 7730:2005). Austrian Standards, Vienna Austria, 2006.

[11] ÖNORM EN 16798:2019 Energetische Bewertung von Gebäuden – Teil 1: Eingangsparameter für das Innenraumklima zur Auslegung und Bewertung der Energieeffizienz von Gebäuden bezüglich Raumluftqualität, Temperatur, Licht und Akustik – Module M1-6, Austrian Standards, Vienna, Austria, 2019.

[12] ASHRAE 55-2017 Thermal Environmental Conditions for Human Occupancy. American Standard by ASHRAE, 2017.

[13] WUFI pro – Wärme und Feuchte instationär. Standard program for evaluating moisture conditions in building envelopes, Fraunhofer Institute for Building Physics, Stuttgart, Germany, www.wufi.de, accessed January 15, 2020

12th International Conference on Structural Analysis of Historical Constructions
SAHC 2020
P. Roca, L. Pelà and C. Molins (Eds.)

RENOVATION OF 16TH CENTURY SALT HOUSE ROOF (LUBAŃ, LOWER SILESIA, POLAND) – CASE STUDY

KRZYSZTOF AŁYKOW[1*], MAGDALENA NAPIÓRKOWSKA-AŁYKOW[2]

[1] Team of Civil Engineers AŁYKOW
Kościuszki 1/ 4
59-800 Lubań, Poland
e-mail: biuro@alykow.com, www.alykow.com (*corresponding author)

[2] Team of Civil Engineers AŁYKOW
Kościuszki 1/ 4
59-800 Lubań, Poland
e-mail: audyty@alykow.com, www.alykow.com

Keywords: Historical Structure, Carpenter Construction, Masonry

Abstract. *This article presents next step of the restoration works in the Salt House in Lubań, Lower Silesia, Poland. The first stage of technical and conservatory problems which appeared during the restoration process was described in the article "Between conservators theory and modern construction's codes. Renovation of roof of 16th century Salt House in Lubań, Lower Silesia, Poland", which was presented on 5th International Conference on Structural Health Assessment of Timber Structures, 25-27 September 2019, Guimarães, Portugal [1].*

The Salt House in Lubań, Lower Silesia, Poland was erected between 1537 and 1539. This historic building is located between medieval defense walls, and it was used as a storage house for salt and grain until the end of the 18th century.

The technical documentation was prepared in 2016, which included 3-D scans of roof truss repair, as well as technical codes and restoration works. During the first phase of the works, the author of this article, who is also a Supervising Engineer, and an expert of the Ministry of Culture and National Heritage Republic of Poland, discovered a lot of discrepancies between the technical documentation and reality. The differences as well as the attempts to adjust restoration works and the technology of works were widely presented in an article at the SHATiS'19, Portugal.

The authors of this article want to show the problems that appeared during the continuation of renovation works and their solutions with reference to historic timber and masonry structures.

1 INTRODUCTION

The Salt House was built in the years 1537 to 1539, between two rows of defense walls which had been erected in the period before the Town of Lubań received the Magdeburg rights in 1220. It was used mainly as a storehouse for salt and grains [2]. The roof was

initially thought to have been built at a later date; however, the discovery made by the authors of this article, supported by later studies, including a dendrochronological examination [3], proved that, except for the 25% of filler materials from the 19th century, the building had the original roofing from the time when it was erected.

2 PHASE 1 AND 2 OF THE PROJECT

The work, originally planned in accordance with the 2016 construction documentation, involved replacement of the entire roof covering, which was made from ceramic double lapped plain tiles, with new roof tiles, the reinforcement of the timber roof truss elements, and bracing the exterior walls at the points where cracks appeared [4].

However, in 2017, after launching the project, the Supervising Engineer found that there were large discrepancies between the way the listed building was described in the documentation and its actual condition. The scope of roofing work was changed after consulting the Jelenia Góra Provincial Historic Buildings Conservation Office, because it was discovered that the roof tiles and other roof covering components were ca. 75% original, so it was decided that they would need to be preserved and restored.

The details of the first two stages of the project implementation, including conservation of the original roof covering with roof tiles (ca. 50% of the roof surface in situ), and the rehabilitation of the timber roof truss components, were described in detail in section [1]. Some non-typical solutions were adopted, with the objective to reconcile the theory of building conservation with technical requirements set by the current standards for the construction products that were manufactured 500 years ago.

The decision to save the existing and original roof covering changed the method in which the structure of the original timber roof truss was revitalized (Fig 1.).



Figure 1: Temporary security after phase 1 and 2

3 PHASE 3 OF THE PROJECT

Because of the fact that, prior to launching the project, the historical timber roof truss and wall structure were wrongly identified by construction designers during the preparation stage of the construction documentation, some of the technical solutions for the rehabilitation of those elements were erroneously adopted [5].

As a result of the examination carried out by the Supervising Engineer, who pointed out the right way to technically protect and revitalize the historical timber roof truss and wall structure, which happened during the work carried out in the years 2017 to 2019, both the erroneous identification and the conclusions that followed had to be modified.

3.1 Timber Roof Truss Structure

When it comes to the analysis of the timber roof truss, what was not considered in the construction documentation was the fact that it interacted with the trusses of three wooden beam floors located below the attic, including their earlier alterations and reinforcement.

The alterations, which were made while the building was in use, resulted from the need to provide stability of the roof trusses which rested against the upper part of the exterior walls and the end points of the tie beams, placed in the wall pockets, rotted and became partially truncated. They involved building in, at various points of time, at all floor levels, three or five rows of posts spaced in such a way as to match the tie beams, including plates and caps, which ran parallel to the central axis of the building (Fig.2, Fig. 3). This caused a significant increase in the rigidity of the structure and transferred the load from the exterior walls to the interior posts.

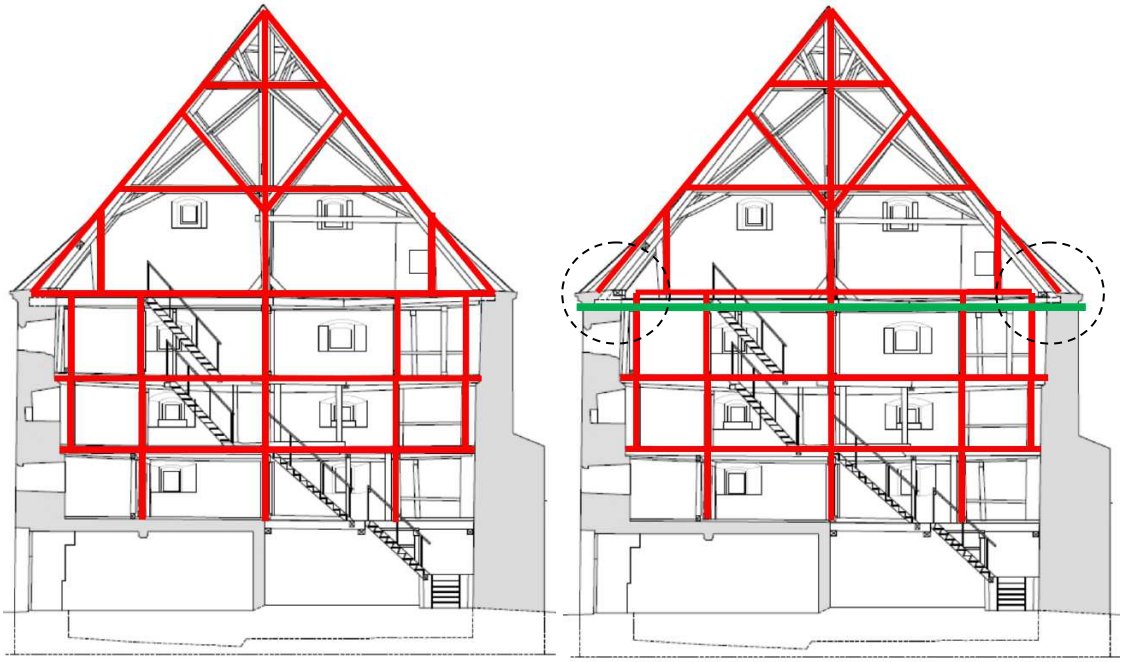


Figure 2: Cross section – original static scheme (left) and after change of its work (right); carpenter construction scheme – red, added steel tie rods – green, dashed circle – separation area



Figure 3: Longitudinal section; added steel tie rods - green

What was originally a king post truss, including two collar beams with every fourth main coupe with sloping rafters and struts, did no longer work as it was originally designed to do. Consequently, the tie beams acted as ordinary ceiling joists, and the unbalanced horizontal loads were transferred by rafters directly to the upper part of the exterior walls. This, in turn, caused damage to the walls in the way which, paradoxically, made it easier to examine their structure and changes that had taken place. Contrary to what was assumed in the construction documentation, it proved impossible to retain the original, traditional way of joining tie beams with rafters because the tie beams' endpoints became shortened by more than 30 centimeters as compared to their original length. That is why the Supervising Engineer made a decision to change the way in which the structure would work, and in order to do so, it would need to be completely separated from the upper part of the exterior walls and the endpoints of rafters (Fig. 2 – red line, dashed circle – separation area) and false rafters would have to be supported in such a way as to enable their horizontal susceptibility (Fig. 4).



Figure 4: False rafters and reinforced timber roof truss components

This made it possible to preserve the structure of the building – both with regards to timber roof truss components and, first and foremost, in terms of the original roof covering elements, including roof tiles, battens, shingles and lime mortar used for the installation of roof tiles, as well as clay mortar used as a sealant on the underside between the battens (Fig. 5) [6].



Figure 5: Roof covering components

3.2 Masonry structure

The changes that occurred within the original timber roof truss over 500 years damaged the exterior walls structure. The unbalanced longitudinal forces exerted by the damaged roof truss lead to the untypical, vertical delamination of the exterior walls. The damage revealed the original exterior and interior face of the wall and showed its original geometry when it was functioning as a defense wall. It also confirmed what was thought to be the line of the defense walls dating back to 1220, and contradicted the common belief, supported by the historiography, that the walls had been reconstructed at the time when the Salt House was built.

The Salt House was erected by building in its end walls between the existing defense walls, without traditional masonry bonding in the corners of the building.

By having determined the way in which the walls got damaged and by learning about the cause of the damage, the Supervising Engineer was forced to change the stabilization method – contrary to what was shown in the construction documentation.

The global stability of the structure was achieved due to a considerable thickness of the defense walls – up to 3-meter thick, and the presence of the unbalanced horizontal reactions resulting from the compromised structural integrity of the timber roof truss also revealed the technique in which they were erected (Fig. 6).

Because of the lack of possibility to neutralize the horizontal reactions which were transferred onto the upper part of the walls, a set of tie rods was used in order to stabilize the upper part of the walls (Fig. 7, Fig. 2 right – green line) .



Figure 6: Exterior of the end walls with cracks along the external face of the defense wall



Figure 7: A set of tie rods and the anchor plate under the cornice

The reduction of the originally planned interference in the area where the roof trusses rested against the upper part of the walls also allowed to preserve the original layers of pugging which served as a protection of the upper part of the walls against the damaging impact of precipitation (Fig. 8).



Figure 8: Pugging on the top part of the walls

4 CONCLUSIONS

The history of preparations and implementation of construction and conservation works involving the rehabilitation of the structure of the roof and walls of the Salt House in Lubań strongly indicates that even though the current measurement methods are a great tool which can help examine a historical structure, they cannot substitute knowledge and experience of an individual who performs such type of works [7, 8].

In this case, the technical solutions proposed in the construction documentation of the building could have substantially contributed to losing its historic features which gave the structure its historic character.

The case described here also proves that in order to prevent the implementation of erroneous solutions, which would have threatened the existence of the historic structure, it is important to provide technical assistance at every stage of project implementation, and the assistance must be provided by those with relevant knowledge and experience.

The solutions adopted during the implementation of the project between 2017 and 2019 enabled the structural stability of the building while preserving and protecting its original elements, contributing, at the same time, to its historic and scientific value which, in this case, is of an outstanding significance as compared to other such objects in Poland.

Apart from its technical aspects, the case of the Salt House has contributed to changing the way the Historic Preservation Officers have perceived particular elements of the building, such as roof tiles, battens or even mortar used for sealing specific roofing components, which have until now been treated as lacking their historical importance.

REFERENCES

[1] Ałykow K. and Napiórkowska-Ałykow M., Between Conservators Theory And Modern Construction's Codes. Renovation Of Roof Of 16th Century Salt House In Lubań, Lower Silesia, Poland, In: Branco J.M., Poletti E. and Sousa H.S., (Eds) *SHATIS'19 - Structural Health Assessment of Timber Structures*, Guimarães (2019), pp. 119-128

[2] Fokt K., Tekiela Ł., Bena W. and Koreś D., *Vademecum of the history of Upper Lusatia*. http://www.luzyce-wid.pl/?page_id=237 (2019)

[3] Ważny T., Ufnalski K., *Dendrochronological analysis of the Salt House in Lubań (Lower Silesia Province)* (2018)

[4] Krzywka Ł., *Historical and architectural analysis and conservation proposals for the Salt House in Lubań* (2017)
[5] Ałykow K., Napiórkowska-Ałykow M., 2008. "The renovation of historic buildings – problems and hazards of the investment process", *Renovations and Monuments* 4(28)/2008, 20-23
[6] Gąsior M., *A program of conservation and restoration works for the building of the Salt House in Lubań* (2018)
[7] Ałykow K. and Napiórkowska-Ałykow M., *On the inadequate modeling of the structure of architectural heritage. Journal of Heritage Conservation* (2015) 41/2015, pp. 59-64
[8] Murzyn-Kupisz M., 2016. "Values of cultural heritage In the context of socio-ecomomics". *In Heritage value assessment systems – the problems and the state of research*. Edited by B. Szmygin. Warszawa, 147-164

12th International Conference on Structural Analysis of Historical Constructions
SAHC 2020
P. Roca, L. Pelà and C. Molins (Eds.)

RESEARCH ON ARCHITECTURAL FORM AND STRUCTURAL PERFORMANCE OF THE BRICK-VAULT HALL HERITAGE IN CHINA—A CASE STUDY OF YONGZUO TEMPLE

QING CHUN [1*], YIJIE LIN[2] AND CHENGWEN ZHANG[3]

[1] School of Architecture, Southeast University (SEU), 210096 Nanjing, China
e-mail: cqnj1979@163.com, (*corresponding author)
[2] School of Architecture, Southeast University (SEU), 210096 Nanjing, China
e-mail: yijielin1223@foxmail.com
[3] School of Architecture, Southeast University (SEU), 210096 Nanjing, China
e-mail: zhang1chengwen@163.com

Keywords: Brick-vault hall, Yongzuo Temple, Architectural form, Structural performance, Finite element method

Abstract. *The brick-vault hall building is a special type of architectural heritage in China, which is significantly different from the western masonry arch heritages in terms of architectural form, structure, construction technology and mechanical performance. After hundred years of natural disasters and human factors, these brick-vault hall buildings mostly have a lot of damages in different degrees. In order to understand the architectural form and the structural performance of this typical type of architectural heritage, the brick-vault hall of Yongzuo Temple was taken as an example to study. Based on the survey of three-dimensional laser scanner, the accurate geometrical dimension of the brick-vault hall of Yongzuo Temple was collected, the architectural form of this building and the relationship between the brick-vault hall building and the official-type timber structure were analyzed and illustrated. The material properties were observed with the on-site non-destructive testing method. Based on the above researches, the finite element model of the brick-vault hall of Yongzuo Temple was established with ANSYS, the structural performance of the brick-vault hall structure under the vertical load and the earthquake load were studied, respectively. Thus, the weak positions of the brick-vault hall of Yongzuo Temple were found out. The results can provide the basis for the conservation of this type of architectural heritage.*

1 INTRODUCTION

The brick-vault hall buildings built in the Ming Dynasty (AD 1368-1644) is a unique type of Chinese architectural heritages. The architectural forms of these brick-vault hall buildings are very similar with those of the traditional timber building at that time, but they were usually built with grey bricks and lime mortar. For this type of architectural heritages, the brick-arch structures were mainly adopted to bear the floor load and the roof load. This type of architectural heritages has significant historical, artistic, and scientific value. In order to scientifically conserve these architectural heritages, their architectural forms and structural performance need to be studied first.

At present, some researches on brick vaults have been put forward. Gong [1] studied the architectural form and structural technology of the brick-vault hall buildings of the Ming Dynasty. Guo [2] presented the architectural characteristics and classification of the brick-vault hall buildings by investigating and mapping some brick-vault hall buildings in Beijing area. Zhu [3] and Wang [4] discussed the decorative arts and crafts of the brick-vault hall of the Longchang Temple. Chang [5] studied the historical evolution of the brick-vault buildings in China. Jin [6] presented the architectural arts of the brick-vault hall of Yongzuo Temple. Ma [7] studied the properties of tube-shaped arches, T-shaped arches, cross arches and buttress shaped arches in residential houses on the Loess Plateau. Madalena Ponte [8] built up an architectural model of the National Palace of Sintra in Portugal by BIM software. Gunes Baris [9-10] rehabilitated the particular masonry structure of a vaulted ruin located on the historical peninsula of Istanbul. Valente Marco [11] investigated the architectural forms and structural details of the two churches which were severely damaged in northern Italy.

To sum up, the research objects of foreign researchers are obviously different from the brick-vault hall buildings in China. Meanwhile, the domestic scholars' research on the brick-vault hall buildings mainly focus on the architectural history, architectural arts and crafts. There are very few researches on the technical and structural aspects of this type of architectural heritages. In this study, the brick-vault hall building of Yongzuo Temple was taken as a typical case, and the architectural form and structural performance of this building was studied in detail.

2 ARCHITECTURAL FORM

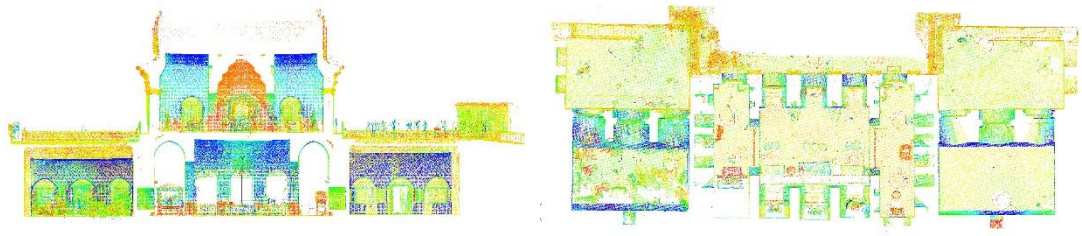
2.1 The on-site investigation of this building

The brick-vault hall of Yongzuo Temple in Taiyuan is a very typical brick-vault hall building built in the Ming Dynasty, its roof style is Chinese traditional Xieshan type, it has two floors, a width of five bays in the first floor, and a width of three bays in the second floor. The current state of the brick-vault hall of Yongzuo Temple was shown in Figure.1. The accurate geometrical information of this building was obtained through the on-site survey with 3D laser scanner. The scanning cloud points of this building were shown in Figure.2.



(a) The outdoor appearance (b) The indoor appearance

Figure 1: The brick-vault hall of Yongzuo Temple



(a) Longitudinal section （b）The first plan

Figure 2: Scanning cloud points of the brick-vault hall of Yongzuo Temple

2.2 The architectural form of this building

According to the accurate geometrical information from the scanning cloud points, the length of the first floor is 19.6 m and the width is 11.9 m, the ratio of length to width is 19.6/11.9=1.65:1. The length of the second floor is 16.8 m and the width is 10.0 m, the ratio of length to width is 16.8/10.0=1.68:1. According to the on-site surveys, the Jugao (the total height of roof) of this building is 3.820 m, the span between the front eave purlin and the back eave purlin is 10.870 m, the ratio of height to span is 3.820/10.870=1:2.85. The building roof is curve, the one side of the roof can be divided into five parts as shown in Figure.3, the height, the span and the ratio of height to span of each part is shown in Table.1.

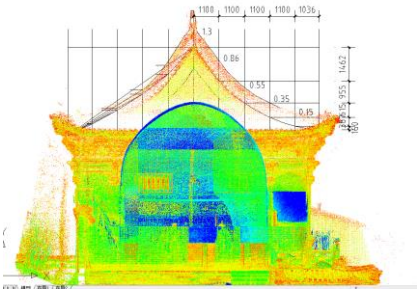


Figure 3: Roof form analysis of the brick-vault hall of Yongzuo Temple

Table 1: Roof height and roof span of the brick-vault hall of Yongzuo Temple

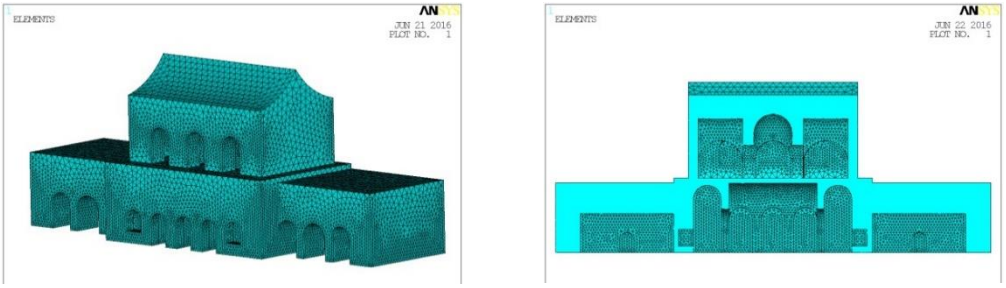
Location	Part 1	Part 2	Part 3	Part 4	Part 5
Span	1.036m	1.100m	1.100m	1.100m	1.100m
Height	0.160m	0.387m	0.615m	0.955m	1.462m
Height/Span	0.154	0.352	0.560	0.868	1.329

According to the analysis of Fig.3 and Tab.1, the roof height of this building is 3.820 m, the roof span between the front eave purlin and the back eave purlin is 10.870 m, the ratio of height to span is 3.820/10.870=1:2.85, which is within the range of 1/3.2 ~ 1/2.7 of the traditional official-type timber buildings of the Ming Dynasty, the result shows that the architectural form of this type of brick-vault hall building is very similar with that of the traditional timber building at that time.

3 STRUCTURAL PERFORMANCE

The Introduction must begin immediately below, following the format of this template. In order to find out the structural performance of the brick-vault hall of Yongzuo Temple, the software of ANSYS was used to build up the finite element model of this building (Figure.4), the structural performance of the building under the vertical load and the earthquake load were analyzed, respectively.

This building is a masonry structure, based on the test data of the brick compressive strength, the mortar compressive strength and the code for design of masonry structures (GB50003-2011), the parameter values of the finite model were obtained as follows: the elastic modulus is 3.024 GPa, the density is 1990 kg / m3, the Poisson's ratio is 0.15, the compressive strength is 1.35 MPa and the tensile strength is 0.17 MPa. The live load on the roof of the building is 0.7 kN / m2, and the live load on the floor is 3.5 kN / m2. In the finite model, there are 426,000 SOLID45 elements.



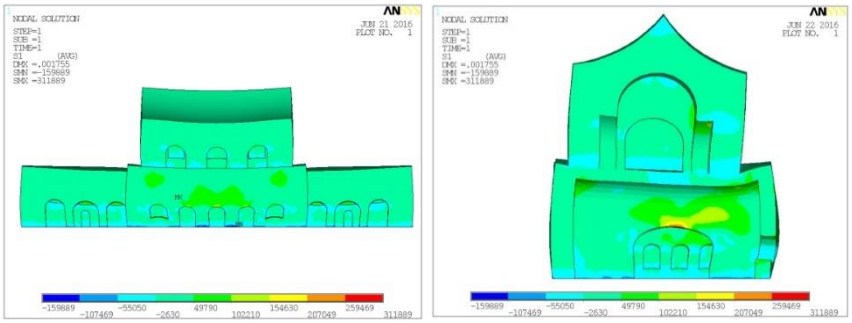
(a) The whole model (b) The longitudinal section model

Figure 4: Finite element model of the brick-vault hall of Yongzuo Temple

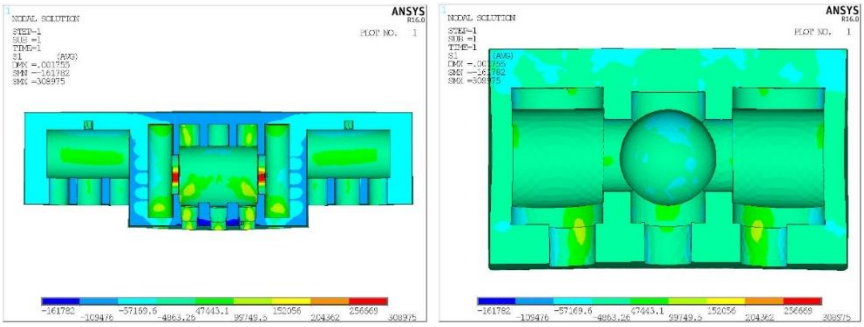
3.1 Structural performance of this building under the vertical load

The calculation results of the first principal stresses of the brick-vault hall of Yongzuo Temple under the vertical load is shown in Figure.5. The maximum value of the first principal stress is 0.312 MPa, and the tensile strength is 0.17 MPa, the position where the first principal stress exceeds the tensile strength is easy to crack. According to the analysis results, under the

limited vertical load, the top of the partition vault between the intermediate arch and the side arch is most prone to crack.



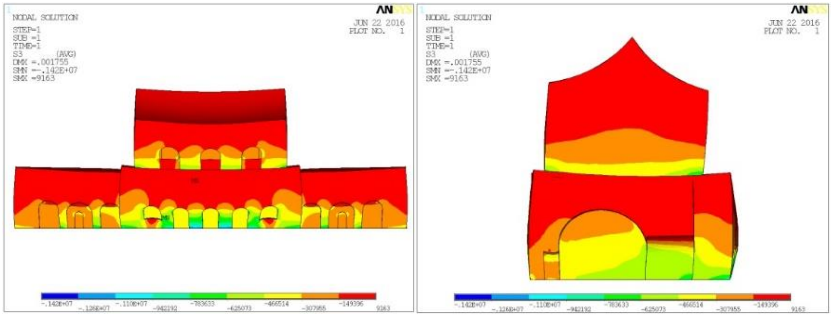
(a) North elevation (b) Transverse section



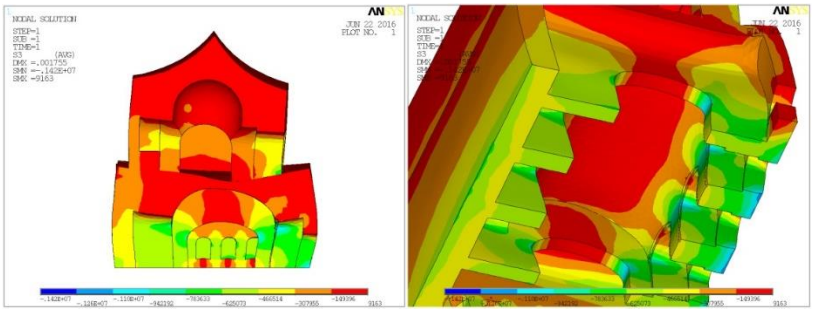
(c) The first floor section (d) The second floor section

Figure 5: The first principal stress diagrams of the brick-vault hall of Yongzuo Temple

The calculation results of the third principal stresses of the brick-vault hall of Yongzuo Temple under the vertical load is shown in Figure.6. The maximum value of the third principal stress is 1.42 MPa, and the compressive strength is 1.35 MPa. The position where the third principal stress exceeds the compressive strength is easy to break. According to the analysis results, under the limited vertical load, the foot of the door arch at the north side is most prone to break.



(a) North elevation (b) East elevation



(c) Transverse section (d) The first floor arches

Figure 6: The third principal stress diagrams of the brick-vault hall of Yongzuo Temple

3.2 Structural performance of this building under the earthquake load

Yongzuo Temple is located in Taiyuan, Shanxi Province, where its seismic fortification intensity is 8 degree, and the design basic seismic acceleration value is 0.2g. The EL Centro earthquake wave was used to analyze the seismic performance of this building along the north-south direction which has a less stiffness. The seismic wave information was shown in Fig 7. The maximum values of the seismic acceleration time history of 8-degree frequent earthquake, design earthquake, and rare earthquake are 0.70 m / s^2, 2.00 m / s^2, and 3.90 m / s^2, respectively [12].

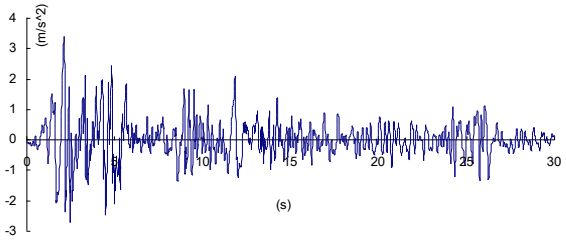
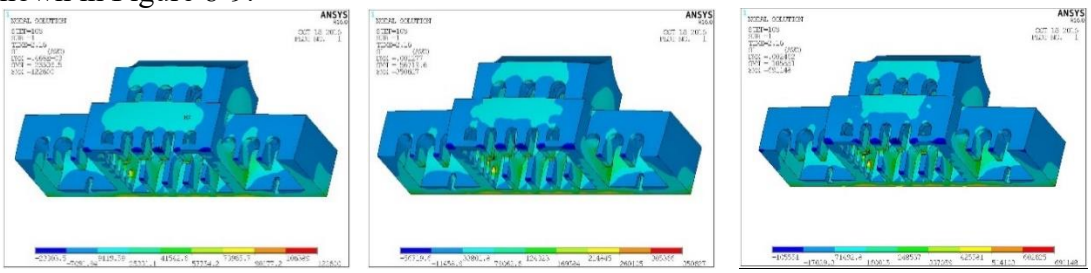


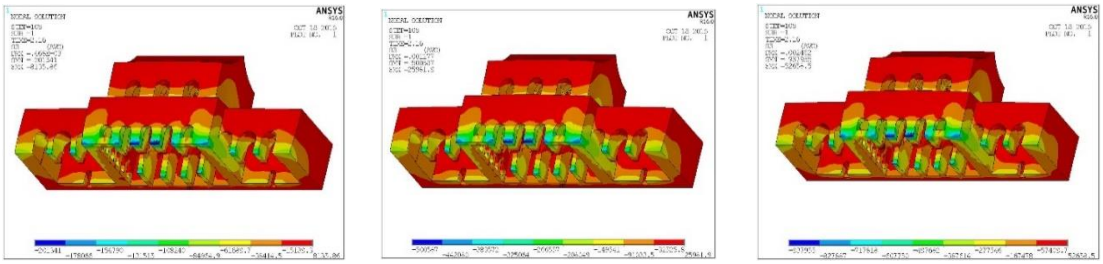
Figure 7 : EL Centro earthquake wave

In this study, a linear time-history analysis of the brick-vault hall of Yongzuo Temple under the 8-degree earthquake was carried out. Because the maximum seismic response occurred at 2.16s, so this time was selected to study the maximum first principal stress and the minimum third principal stress of the brick-vault hall of Yongzuo Temple, the stress diagrams are shown in Figure 8-9.



(a) frequent earthquake (b) design earthquake (c) rare earthquake

Figure 8: the first principal stress diagrams



(a) frequent earthquake (b) design earthquake (c) rare earthquake

Figure 9: The third principal stress diagrams

The calculation results show that the third principal stresses of this building under the 8-degree frequent earthquake, the 8-degree design earthquake and the 8-degree rare earthquake are all less than the compressive strength, which means there is no risk of compressive failure under the 8-degree frequent earthquake, the 8-degree design earthquake and the 8-degree rare earthquake. Under the 8-degree frequent earthquake, the first principal stress of this building is less than the tensile strength, so there will be no cracks occurred in this building. However, under the 8-degree design earthquake and rare earthquake, the tensile stresses of some positions in this building exceed the tensile strength, which may cause cracks occurred in this building. The weak positions of the first floor are the north corner of the exterior wall, the bottom of the arch at the south side, the top of the arch of the central bay. The weak positions of the second floor are the foot of the exterior wall at the north side, the foot of the door arch at the south side, the top of the central arch.

4 CONCLUSIONS

The brick-vault hall of Yongzuo Temple is a very typical case of the brick-vault hall building built in the Ming Dynasty. In this study, the architectural form and structural performance of this building was studied, some conclusions can be drawn as follows:

- According to the analysis of the architectural form, the roof height of this building is 3.820 m, the roof span between the front eave purlin and the back eave purlin is 10.870 m, the ratio of height to span is 3.820/10.870=1:2.85, which is within the range of 1/3.2 ~ 1/2.7 of the traditional official-type timber buildings of the Ming Dynasty, the result shows that the architectural form of this type of brick-vault hall building is very similar with that of the traditional timber building at that time.
- Under the limited vertical load, the top of the partition vault between the intermediate arch and the side arch is most prone to crack, the foot of the door arch at the north side is most prone to break.
- There is no risk of compressive failure under the 8-degree frequent earthquake, the 8-degree design earthquake and the 8-degree rare earthquake. Under the 8-degree frequent earthquake, the first principal stress of this building is less than the tensile strength, so there will be no cracks occurred in this building. However, under the 8-

degree design earthquake and rare earthquake, the tensile stresses of some positions in this building exceed the tensile strength, which may cause cracks occurred in this building.

Acknowledgements. This study was supported by National Natural Science Foundation of China (Grant No. 51778122).

REFERENCES

[1] Gong Kai. Research on brick-vault halls of Ming Dynasty. Master Degree Thesis of Nanjing Institute of Technology. 1988.
[2] Guo Yunling. Research on the types of Wuliang halls in the Beijing area. Master Degree Thesis of Nanjing Normal University. 2014.
[3] Zhu Fuyi. The Decorative Art of Buddhist Architecture in Ming Dynasty Brick Sculptures of Longchang Monastery. *Traditional Chinese Architecture and Gardens*, (2015)**03**:45-48.
[4] Wang Xueqin, Zhao Xin. Research on the architectural decorative art of the brick-vault halls of Ming Dynasty, a case of the brick-vault hall of Longchang Temple. *Movie Review, (*2012) **15**:91-94
[5] Chang Qing. On the evolution of ancient Chinese brick and stone vaulted buildings in the Yuan and Ming Dynasties. *Studies in the History of Natural Sciences.* 12(1993) **2**:192-200.
[6] Jin Zhiqiang. Architecture and Architects at the Yongzuo Temple. *Traditional Chinese Architecture and Gardens*, (2001)**01**:61-64.
[7] Ma Linyu. Study on the Arch Structure System of Chinese Folk House. Master Degree Thesis of Xi'an University of Architecture and Technology.2007.
[8] Madalena Pontea, Rita Bento, Silva Daniel Vaz. A Multi-Disciplinary Approach to the Seismic Assessment of the National Palace of Sintra. *International Journal of Architectural Heritage,* DOI: 10.1080/15583058.2019.1648587.
[9] Gunes Baris, Cosgun Turgay, Sayin Baris, Ceylan Oguz.Structural rehabilitation of a Middle Byzantine ruin and the masonry building constructed above the ruin. Part I: The ruin. *Engineering Failure Analysis*, 105(2019) **11**:503-517.
[10] Gunes Baris, Cosgun Turgay, Sayin Baris, Ceylan Oguz.Structural rehabilitation of a middle byzantine ruin and the masonry building constructed above the ruin. Part II: The building. *Engineering Failure Analysis*, 105(2019) **11**:527-544.
[11] Valente Marco, Milani, Gabriele. Damage survey, simplified assessment, and advanced seismic analyses of two masonry churches after the 2012 Emilia earthquake. *International Journal of Architectural Heritage,* (2001)**13**:901-924.
[12] China Academy of Building Research. Code for seismic design of buildings (2016 revision) GB50011-2010. 2016. China Architecture & Building Press. Beijing

12th International Conference on Structural Analysis of Historical Constructions
SAHC 2020
P. Roca, L. Pelà and C. Molins (Eds.)

RESTORATION AUTHENTICITY OR REALITY - A CASE STUDY

DAVID T. BIGGS

Biggs Consulting Engineering
26F Congress St. #305
Saratoga Springs, New York, USA
e-mail: biggsconsulting@att.net

Keywords: Restoration, Heritage, Masonry, Venice Charter, Authenticity

Abstract. *In recent decades, the Venice Charter of 1964 [1] has provided the guiding principles for the conservation and restoration of ancient monuments. However, many interpret these principles as applying to historic structures in general, and not just monuments.*

The articles in the Restoration section of the Charter have several interesting statements (underlines are for emphasis) that are open to interpretation. In many cases, these statements cause a conflict of priorities, especially with funding being the overriding issue. In addition, local and national heritage agencies sometimes take a more liberal approach to restoration, particularly regarding authenticity.

The statements under discussion are:

"ARTICLE 9. The process of restoration is a highly specialized operation. Its aim is to preserve and reveal the aesthetic and historic value of the monument and is based on respect for original material and authentic documents. It must stop at the point where conjecture begins, and in this case moreover any extra work which is indispensable must be distinct from the architectural composition and must bear a contemporary stamp."

"ARTICLE 10. Where traditional techniques prove inadequate, the consolidation of a monument can be achieved by the use of any modem technique for conservation and construction, the efficacy of which has been shown by scientific data and proved by experience."

"ARTICLE 12. Replacements of missing parts must integrate harmoniously with the whole, but at the same time must be distinguishable from the original so that restoration does not falsify the artistic or historic evidence."

Each of these statements affects the authenticity of the restoration. But, maintaining authenticity of the restoration has to be balanced with the reality of maintaining our heritage buildings on limited resources. Can it be done?

This paper discusses these challenges in the context of the 1996 restoration of a three-story, 19th century brownstone. The paper will include the conflicts with recommendations for an authentic restoration in accordance with the Charter principles. The work was performed on a limited budget and attempted to address the Owner's desire for an aesthetic solution. Finally, an assessment of the restoration after 23 years will be included.

1 INTRODUCTION

The question of authenticity in preservation has been debated for decades. Prior to 1964 there was no general consensus of what degree of authenticity was appropriate. What first was conservation of cultural heritage has expanded to be considered historic preservation. The forms include such objects as archaeological sites, artistic sculptures and paintings, cultural landscapes, buildings, and monuments.

Boito in 1883 presented a series of preferences for dealing with cultural properties to an Italian technical congress of architects and engineers [2]. The preferences adopted included a top priority to consolidation over repair. Next in priority would be repair rather than restoration. Proposed interventions were to be both identifiable and labelled as modern. Any elements or features that were to be removed should be documented and preserved for display at the site. He acknowledged that there may have already been renovations or additions subsequent to the original construction that now was a part of the history of site. Those renovation and additions might be deemed inferior or effectively hiding the original construction.

1.1 1931 Athens Charter

Followers of Boito were instrumental in creating the first Athens Charter in 1931 [3] which adopted many of Boito's ideas. Specifically, Section IV. - RESTORATION OF MONUMENTS states:

"The experts heard various communications concerning the use of modern materials for the consolidation of ancient monuments. They approved the judicious use of all the resources at the disposal of modern technique and more especially of reinforced concrete.

They specified that this work of consolidation should whenever possible be concealed in order that the aspect and character of the restored monument may be preserved.

They recommended their adoption more particularly in cases where their use makes it possible to avoid the dangers of dismantling and reinstating the portions to be preserved."

No specific techniques or methods were proposed but highlighted their concern over the potential damaging use of reinforced concrete. They did recommend "That, in each country, the architects and curators of monuments should collaborate with specialists in the physical, chemical, and natural sciences with a view to determining the methods to be adopted in specific cases;". Scientific determination was essential to deciding a course of action. Interestingly, authenticity is not discussed.

1.2 1964 Venice Charter

Possibly reacting to the reconstruction of buildings and monuments following two world wars, the 1964 Venice Charter [1] professed to save our heritage through preservation authenticity. It provided a tool for fervent preservationists to limit uncontrolled development.

Generally, only preservationists study such documents. Since they are not legally binding, local implementation is highly dependent on local advocates.

The Restoration articles set new standards for preservation and authenticity.

"ARTICLE 9. The process of restoration is a highly specialized operation. Its aim is to preserve and reveal the aesthetic and historic value of the monument and is based on respect for original material and authentic documents. It must stop at the point where conjecture begins, and in this case moreover any extra work which is indispensable must be distinct from the architectural composition and must bear a contemporary stamp."

"ARTICLE 10. Where traditional techniques prove inadequate, the consolidation of a monument can be achieved by the use of any modem technique for conservation and construction, the efficacy of which has been shown by scientific data and proved by experience."

"ARTICLE 12. Replacements of missing parts must integrate harmoniously with the whole, but at the same time must be distinguishable from the original so that restoration does not falsify the artistic or historic evidence."

Subsequently numerous efforts have been made to refine the intent of authenticity including the 1965 UNESCO Archaeological Guidelines, the Burra Charter, the Declaration of Oaxaca, the Florence Charter, the Washington Charter, the Nara Document, the Charter of Brasilia, this Declaration of San Antonio, etc. Several of these are discussed in the following sections.

1.2 1994 Nara Document on Authenticity

In 1994, authenticity was the topic at the Nara (Japan) conference organized by the Japanese government in cooperation with the United Nations Educational, Scientific and Cultural Organization (UNESCO), International Centre for the Study of the Preservation and Restoration of Cultural Property (ICCROM) and International Council on Monuments and Sites (ICOMOS). It criticized the Venice charter and authenticity. The document [6] addresses authenticity "in response to the expanding scope of heritage concerns and interests in our contemporary world".

Article 11 states "All judgements about values attributed to cultural properties as well as the credibility of related information sources may differ from culture to culture, and even within the same culture. It is thus not possible to base judgements of values and authenticity within fixed criteria. On the contrary, the respect due to all cultures requires that heritage properties must be considered and judged within the cultural contexts to which they belong."

It nearly removes authenticity from the requirements for cultural context. From this, countries were encouraged to develop their own criteria for dealing with preservation and authenticity.

1.4 1996 Declaration of San Antonio

In March 1996, the InterAmerican Symposium on Authenticity in the Conservation and Management of the Cultural Heritage was held in San Antonio, Texas, USA by the ICOMOS National Committees of the Americas to address the meaning of authenticity in preservation in the Americas. The Nara document was reviewed and critiqued. Recommendations were made to modify it by issuing a declaration [7].

When discussing authenticity and materials, it was stated that "..there are important sectors of our patrimony that are built of perishable materials that require periodic replacement in accordance with traditional crafts to ensure continued use. Similarly, there are

heritage sites built of durable materials but that are subject to damage caused by periodic natural catastrophes, such as earthquakes, floods and hurricanes. In these cases, we also assert the validity of using traditional techniques for their repair, especially when those techniques are still in use in the region, or when more sophisticated approaches would be economically prohibitive." Thus there was an affirmation of protecting cultural heritage without limiting to authentic restorations.

2 RESTORATION IN THE UNITED STATES

The United States has numerous agencies that oversee historic preservation. At the national level, the National Park Service of the U.S. Department of the Interior controls historic preservation of national sites through the National Trust for Historic Preservation. Generally, each state has its own agency for state historical sites and finally local governments can have a regional agency. Often, determining the appropriate agency and designation is a challenge for any consultant. Several agencies are discussed as follows. Each has taken a local pragmatic approach to preservation.

2.1 New York City

The Landmarks Preservation Commission is a charter-mandated New York City commission. It is the largest municipal preservation agency in the United States. Created in 1965, it was formed to combat losses of historically significant buildings in New York City. According to the Landmarks Law [4], "the purpose of safeguarding the buildings and places that represent New York City's cultural, social, economic, political, and architectural history is to:

- Stabilize and improve property values
- Foster civic pride
- Protect and enhance the City's attractions to tourists
- Strengthen the economy of the City
- Promote the use of historic districts, landmarks, interior landmarks, and scenic landmarks for the education, pleasure and welfare of the people of the City."

The 1964 Venice Charter is not mentioned in the law creating the commission although advocates probably were aware of its existence. Yet, there is no mention of maintaining authenticity as the leading component of preservation. It emphasizes financial reasons as a major driving force.

The commission operates under a set of rules [5]. Section 2-11 includes Repair, Restoration, Replacement and Re-Creation of Building Façades and Related Exterior Elements. Authenticity is addressed in Subsection (b)(3) "In all cases, except where noted, the repair, restoration, replacement or re-creation must match the original or historic materials and features in terms of its physical and aesthetic characteristics, including design, detail, profile, dimension, material, texture, tooling, dressing, color and finish, as applicable." In Subsection (b)(2), it states "Where replacement of large quantities of materials and/or significant architectural features is proposed, the applicant must provide an assessment of the deteriorated conditions warranting such replacement(s). Repair will be given priority over replacement if feasible." So, priority is given to repair over replacement but the rules provide a path to replacement.

Subsection (d)(1) requires “Replacement materials and features should match the original or historic material or feature in terms of physical and aesthetic characteristics. For purposes of this subdivision, this means that replacement material should be “in-kind” in terms of using the actual original or historic material and installation techniques. In-kind replacement should be prioritized and fully considered prior to proposing substitute materials.” While in-kind materials are a priority for replacement, substitute materials are allowed under another section.

2.2 Chicago

Chicago is another major US city with a history of protecting its historic structures. The Commission on Chicago Landmarks was created in 1968. The program [8] addresses exterior qualities of buildings that are “significant historical or architectural features”.
Chicago took the approach of basing its guidelines on the U.S. Secretary of the Interior's Standards for Rehabilitation of Historic Buildings [9] and extending them. Among their objectives they list “To identify, preserve, protect, enhance, and encourage continued utilization and the rehabilitation of such areas, districts, places, buildings, structures, works of art, and other objects having a special historical, community, architectural, or aesthetic interest or value to the City of Chicago and its citizens”.

Several specific aspects of the standards include:

“Distinctive features, finishes, and construction techniques or examples of craftsmanship that characterize a historic property shall be preserved.

Deteriorated historic features shall be repaired rather than replaced. Where the severity of deterioration requires replacement of a distinctive feature, the new feature shall match the old in design, color, texture, and other visual qualities and, where possible, materials. Replacement of missing features shall be substantiated by documentary, physical, or pictorial evidence.

Chemical or physical treatments, such as sandblasting, that cause damage to historic materials shall not be used. The surface cleaning of structures, if appropriate, shall be undertaken using the gentlest means possible.”

As with New York, we see a desire to prioritize the preservation of historic features. However for replacement of deteriorated features, both cities chose to require the imitation of the original features and not distinguish them as was proposed in the Venice Charter. This is in keeping with both the Nara Document and the San Antonio Declaration which essentially suggest self-determination of authenticity.

3 CASE STUDY- FAÇADE RESTORATION OF 1889 BROWNSTONE

This project was completed in 1996. It occurred during a time period when the Nara Document and the San Antonio Declaration were redefining whether restorations needed to be authentic. It is not clear whether the redefinition by these organizations was ground breaking or actually a reflection of what communities and cultures were already doing.

Specifically, the city and state where this project occurred had been requiring authentic restoration; repairs were to be performed using original materials and original techniques. This project was the first known departure from authentic with an historic residential property.

Figure 1 shows its building in 1996 and in its current condition. The primary difference is attributed to the photography and daylight. The restoration was documented previously [10].

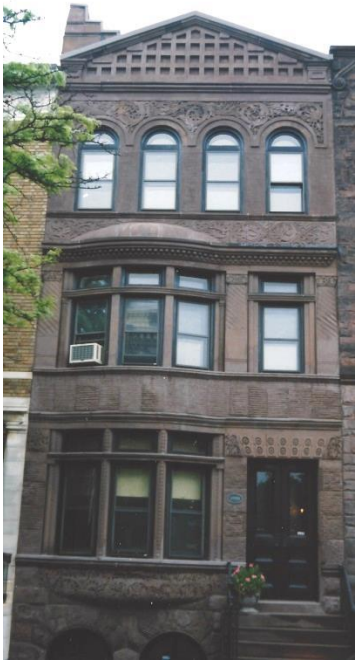


Figure 1a: Facade 1996



Figure 1b: Facade 2019

3.1 Background

The building received local historic status in the 1970s. It has ornate stone carving from base to the roof that is unique. The brownstone is ornamental and overlays a brick structure.

The Owner purchased the building c. 1973 but by 1991, pieces of the brownstone (sandstone) elements had fallen from the building and safety concerns were growing. The Owner started inquiries as to how to restore the façade. Aided by HAF, the local preservation organization, efforts were made to obtain grant funding but with no success. However in 1992, HAF was able to attract a number of preservation specialists to a Sandstone Colloquium which included a hands-on assessment of the building.

Following a day of façade examination by the specialists, over 50 attendees met to discuss the specialists' findings. To the dismay of the Owner, there were many ideas and the predominant recommendation was to add sidewalk protection in the short term. Long term they proposed that most of the brownstone be removed and replaced with new carved pieces. The projected repair cost was $250,000 to $500,000 which greatly exceeded the building value. This was beyond the means of the retired Owner on a pension.

The sidewalk scaffolding was quickly added and the Owner continued to seek funding. Finally in 1995, the deterioration accelerated and material losses were far worse; the Owner became desperate. City building officials were demanding action.

A mason restoration contractor who attended the initial symposium and who provided the sidewalk protection stepped in to offer assistance by meeting with HAF and the building officials.

Historic buildings were expected to be restored using original materials and techniques. But the cost was beyond the Owner's ability to fund so negotiations with the city officials yielded an option:

Remove the brownstone and plaster coat the brick without any ornamentation.

The intent was to provide a safe façade even if it meant losing the aesthetic character of the facade. The contractor estimated this might cost $50,000 to $60,000. The Owner agreed to this level of funding for a budget.

Contrary to local practice, the contractor proposed an alternate solution with the budget of $60,000. They would first remove the severely deteriorated brownstone and stabilize the areas still intact. Then they would re-evaluate the budget. The remaining funds would be dedicated to replacing the deteriorated brownstone with a brownstone patching material that could be carved to replicate the ornamentation. Patches would be anchored with stainless steel pins and wire. If funding was insufficient, plaster would be used as proposed by the city and some aesthetic features would be lost. This would met the city officials' goal to stabilize the façade yet restore some of the features. The city officials approved this concept and gave its first-ever building permit for a project which they did not know what the final appearance of the building would be.

3.2 Restoration

The Contractor recommended the Owner hire the author as her restoration engineer and the team was created. Scaffolding was first erected and a hands-on survey was performed. The problems discovered were related to inferior stone from the quarry and long-term deterioration. Figure 2 shows a sampling of the damage a) sill damage, b) exfoliation of vertical pier, c) underside of sill, and d) dentil damage. The damage was removed to sound material and patched. Damage was scattered throughout the façade. Details were developed cooperatively between the Engineer, Contractor and the material supplier [11] selected. The Owner anxiously watched the work proceed daily from across the street.



Figure 2: Representative problems from 1996

The mason craftworker that installed and carved the patches was quite expert. He replicated the details exactly. In the end, the restoration contractor was able to repair all the deteriorated areas within the budget. The Owner, the HAF, and city officials were very pleased with the results. Their leap of faith in trusting the contractor was justified.

3.3 Performance

The façade condition in Figure 3 shows that the restoration has performed well for over 23 years. There is deterioration visible below a window sill (arrow, Figure 4). The brownstone is delaminating at the interface with the patches; it's likely the original deteriorated brownstone might not have been removed deep enough before installing the patch at this location. The current deterioration will need repairs in the coming years.

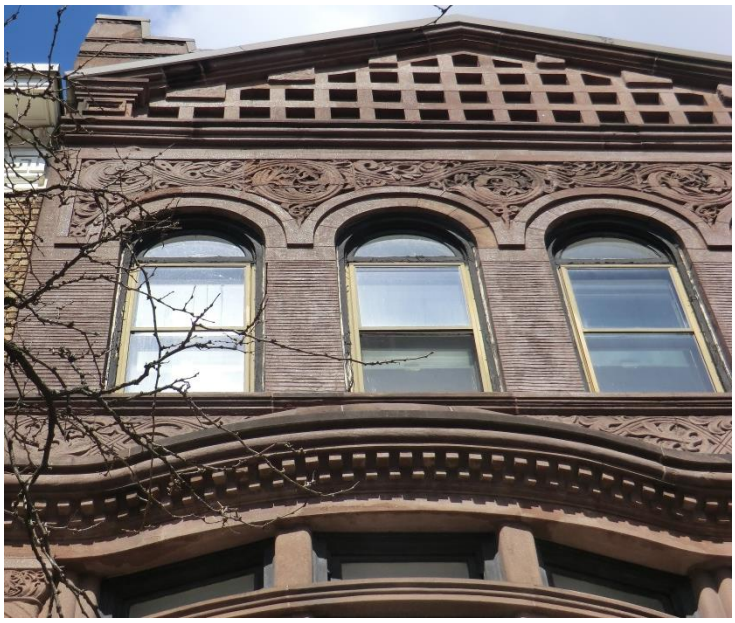


Figure 3: Façade 2019



Figure 4: Sill deterioration 2019

The ornamentation of the synthetically-patched façade is nearly undetectable under most climatic conditions. During rainy weather, the patches are evident since they do not absorb water the same as the brownstone (slightly visible in Figure 3). However since the façade faces the sun, it dries relatively quickly and the patches blend in again.

4 SUMMARY/LESSONS LEARNED

- While the case study demonstrates a successful synthetic restoration that has performed well for over two decades, the real point here is that the concept of maintaining authenticity was challenged for practical reasons. Authentic replacement was cost prohibitive and the Owner did not want to have a non-descript face for her building. Reality for the Owner was that she wanted to enjoy her building and that meant restoring the façade aesthetics even if they were not be authentic.
- The restored facade maintains the value of the property and fits within the historic context of the neighborhood. Simply stabilizing the façade would have maintained public safety but would not have produced a culturally acceptable solution.
- As a society, authenticity should be the highest priority for our restorations. But, not at the expense of losing the very fabric of the buildings and monuments that we enjoy. As previously noted, this project coincidentally occurred within the time period where authenticity was being challenged by the principles of the Nara Document and the San Antonio Declaration. Communities (like New York City and Chicago for example) and owners were deciding what was important culturally and allowing alternate materials and modern techniques to be used in restorations. This self-determination now seems to be a mainstay of most preservation regulations in the United States.
- Today, there are synthetic restoration products that have decades of use for which to be judged. That was not the case in the 1990s.
- From my experience, engineers are not qualified to make an informed decision on accepting new materials that don't have a long history of use without the assistance of specialists. This case study project had a chemist as the owner of the company supplying the patching material who provided the material expertise and an expert restoration contractor who could assess the material. They were integral to the judging the restoration design and making the best decisions given the limited budget.
- Judging the success of a restoration project can only be done through time. While heralded as a success in 1996, time has given us more data. Today, we know more about various synthetic products and proper installation techniques. The material used on this restoration has proven itself on numerous projects over the years and continues to be selected by restoration professionals.

Acknowledgements. Mr. Wil Ganem, Ganem Contracting Corp., and his team made the Owner's dream come true. Michael Edison, Edison Coatings Inc., provided the products and chemistry expertise for the patching system.

REFERENCES

[1] The International Charter for the Conservation and Restoration of Monuments and Sites (Venice Charter), Association for Preservation Technology International Bulletin: The Journal of Preservation Technology, Vol. 37, No. 4, p. 51, (2006).

[2] Starn, R. Authenticity and historic preservation: towards an authentic history. History Of The Human Sciences Vol. 15 No. 1, SAGE Publications (London, Thousand Oaks, CA and New Delhi) pp. 1–16, [0952-6951(200202)15:1;1–16; 021070], 2002

[3] First International Congress of Architects and Technicians of Historic Monuments, Athens 1931.

[4] New York City Administrative Code, Title 25, Chapter 3, http://library.amlegal.com/nxt/gateway.dll/New%20York/admin/title25landuse/chapter3landmarkspreservationpreservatio?f=templates$fn=default.htm$3.0$vid=amlegal:newyork_ny$anc=JD_T25C003

[5] Rules of New York City Landmarks Preservation commission, Title 63, Rules of City of New York, January 22, 2019, https://www1.nyc.gov/assets/lpc/downloads/pdf/Rules/Rules%20of%20the%20NYC%20Landmarks%20Preservation%20Commission_01.22.2019.pdf

[6] Nara Conference on Authenticity in Relation to the World Heritage Convention, Nara, Japan, 1-6 November 1994, https://www.icomos.org/charters/nara-e.pdf

[7] InterAmerican Symposium on Authenticity in the Conservation and Management of the Cultural Heritage, San Antonio, TX, 27-30,March 1996, https://www.icomos.org/en/charters-and-texts/179-articles-en-francais/ressources/charters-and-standards/188-the-declaration-of-san-antonio

[8] Guidelines For Alterations to Historic Buildings and New Construction, March 4, 1992, https://www.chicago.gov/content/dam/city/depts/zlup/Historic_Preservation/Publications/Standards_for_Rehab_2015.pdf

[9] Secretary of the Interior's Standards for Rehabilitation of Historic Buildings, National Park Service, Department of the Interior, https://www.nps.gov/tps/standards/rehabilitation/rehab/stand.htm

[10] Façade Restoration of an 1889 Brownstone, Proceedings of the 8th Canadian Masonry Symposium, Jasper, Alberta, pp.2226-275, 1998

[11] Custom SYSTEM 45 Masonry Patching & Coating, Edison Coatings Inc., Plainville, CT.

12th International Conference on Structural Analysis of Historical Constructions
SAHC 2020
P. Roca, L. Pelà and C. Molins (Eds.)

RESTORATION OF THE QUEEN VICTORIA MARKET SHEDS E-F AND J-M, MELBOURNE, AUSTRALIA

JUSTIN C. HETTINGA[1*]

[1]Robert Bird Group Pty Ltd
Tower 4 Collins Square, Level 19 727 Collins Street, Melbourne VIC 3008 Australia
e-mail: justin.hettinga@robertbird.com.au, www.robertbird.com (*corresponding author)

Keywords: Historical Structure, Conservation and Restoration, Case Study, 19th Century Architectural Heritage, 20th Century Architectural Heritage

Abstract. *This paper discusses the investigations, analysis, and proposed strengthening to Sheds E-F and J-M of the Queen Victoria Market in Melbourne, Australia. The sheds were visually inspected and measured, a point cloud survey was carried out, wind tunnel testing determined design pressures, and timber samples determined species, grade and extent of deterioration. Strengthening designs were in accordance with the Burra Charter – The Australia ICOMOS Charter for Places of Cultural Significance 2013.*

1 INTRODUCTION

The City of Melbourne became aware of potential structural deficiencies of sheds at the Queen Victoria Market and decided to undertake a full assessment of all heritage structures at the site to ensure their safety and longevity. Robert Bird Group was engaged to perform a structural assessment of selected sheds and design any required strengthening.

In this paper a brief history and chronology of the site is provided, followed by a description of the investigations, testing, monitoring and analysis that was carried out. The results and proposed strengthening are described, followed by commentary on the project.

2 HISTORICAL OVERVIEW

2.1 Historical significance

The Queen Victoria Market is a major landmark and tourist attraction in Melbourne, Victoria, Australia, and at seven hectares is the largest open-air market in the southern hemisphere. It has been in continual operation since the 1870s and from a group of central markets built by the corporation of the City of Melbourne during this period, it is the only one surviving.

The site also served as Melbourne's first official cemetery, Melbourne Cemetery, and was in use from 1837 to 1854, then intermittently until being closed in 1917. It is listed on the Victorian Heritage Register, in part due to its importance to the course of Victoria's cultural Heritage. [1]

As an estimated 6,500 to 9,000 burials remain on the site, it is of archaeological significance and has the potential to provide information about Aboriginal and European communities and

their burial practices and customs in early Melbourne. [1]

The site is valued for its demonstration of the principle characteristics of a class of cultural places and objects, namely the produce market. The purpose-built nineteenth and early twentieth century buildings are largely intact, and the predominately utilitarian style adopted for marketplaces at the time is evident.

Due to its ongoing use and continued popularity as a fresh food market and meeting place for locals and tourists, the market is considered socially significant.

2.2 Chronology

Prior to European settlement, the area where Melbourne is now located was home to the Kulin people. Their ancestors lived in the area for an estimated 40,000 years and the population was estimated to be under 20,000. [2] European exploration occurred between 1797 and 1834, and in 1835 John Batman explored large areas of what is now Melbourne. On 6 June 1835, he signed a treaty with the indigenous Wurundjeri elders, purportedly buying 600,000 acres of land around Melbourne. [3] Settlement of the area followed, and two years later in 1837 ten acres of land were set aside for what would become the Melbourne Cemetery. The Cemetery was surveyed by Robert Hoddle, who also surveyed and laid out the central business district of Melbourne. It had sections for Presbyterian, Episcopalian, Roman Catholic, Wesleyan, Jewish, Independent, Society of Friends (Quaker) and Aboriginal burials.

In 1853, the Melbourne General Cemetery in Carlton opened, allowing for the closure of Melbourne Cemetery in 1854 due to concerns over people living increasingly closer to it as the city grew. Following its closure, people who had claims on family plots were allowed to continue burials until 1917. Between 1837 and 1917, an estimated 8,000 to 10,000 people were buried in the cemetery. [1]

The eastern triangular block was granted to Melbourne Town Council in March 1859 for use as a market, and a meat and produce retail market started operating on the site in 1874. Sheds H and I were built for fruit and vegetable growers to operate, and in 1877, legislation granted the market permission to take over part of the cemetery land. In 1878, 45 burials were exhumed, and sheds A-F were constructed. Sheds A-E were open on all sides, and shed F had a brick wall constructed on its southern side to divide the market from the remainder of the cemetery. [1]

In March 1878, the market was officially opened as ‘Queen Victoria Market.’ In 1884 two-storey terrace shop buildings were built along Elizabeth Street, then in 1887 along Victoria Street. Between 1890 and 1905, additional shops were constructed along Victoria Street, and subsequently under 1917 legislation the remainder of the cemetery was acquired by the market. [1]

From 1920 to 1922, 914 bodies were exhumed and relocated, including the remains of John Batman, to Fawkner Cemetery. Sheds K and L were constructed in 1923, the Dairy Produce Hall was constructed in 1928, and the two rows of sixty brick stores comprising Market Square were constructed in 1929-1930 to provide storage for market traders. Shed M was constructed in 1936 and Shed J was constructed in 1991. [1]

A layout of the sheds is shown in Figure 1.

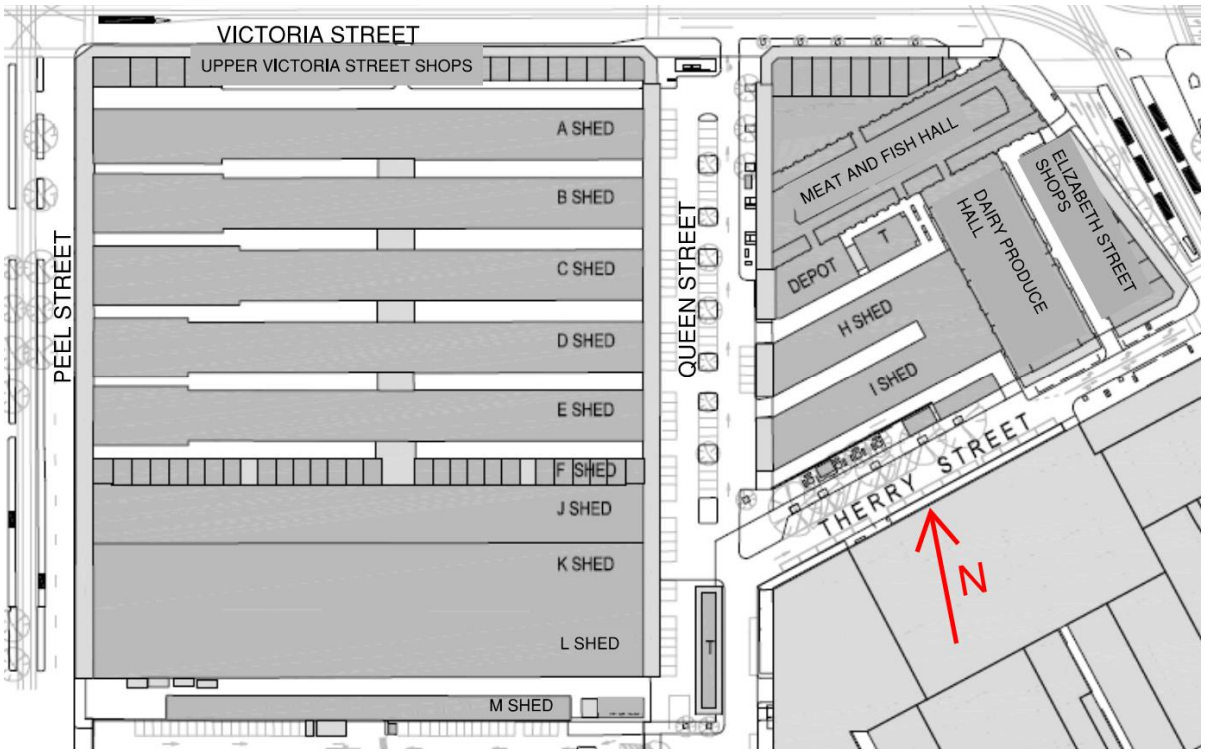


Figure 1: Queen Victoria Market shed layout [4]

3 DESCRIPTION OF THE STRUCTURES

Sections of the sheds looking east are shown in Figures 2 through 5.

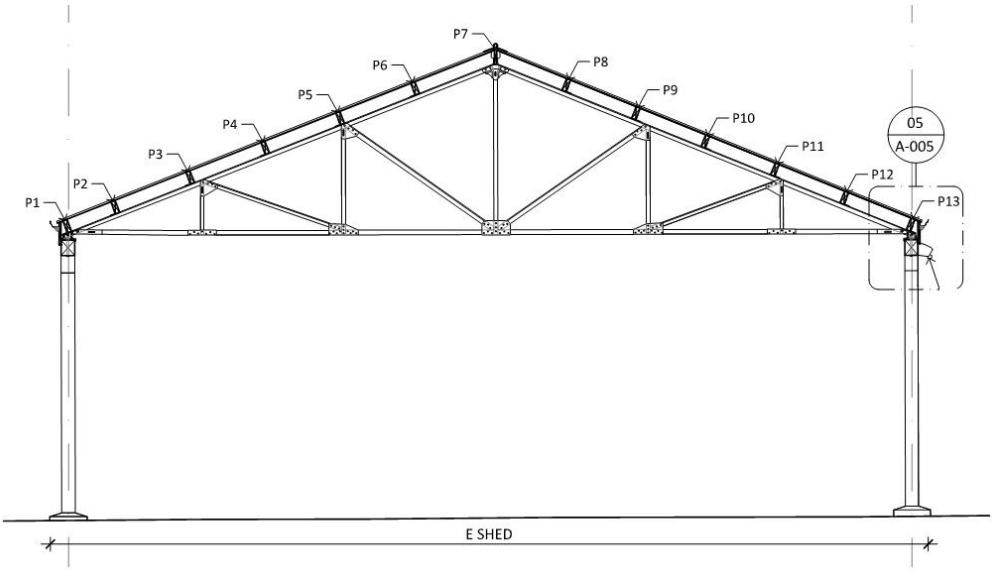


Figure 2: Shed E framing elevation [5]

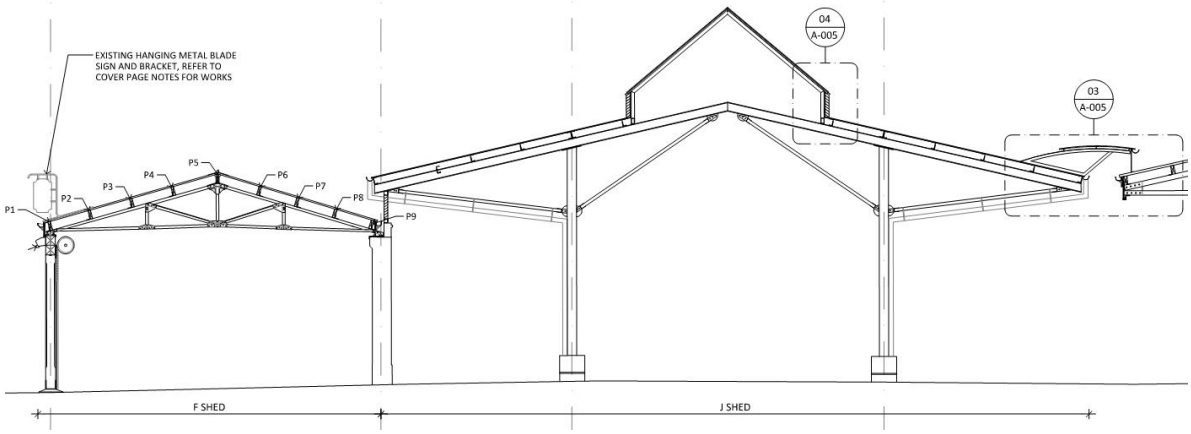


Figure 3: Shed F and J framing elevation [5]

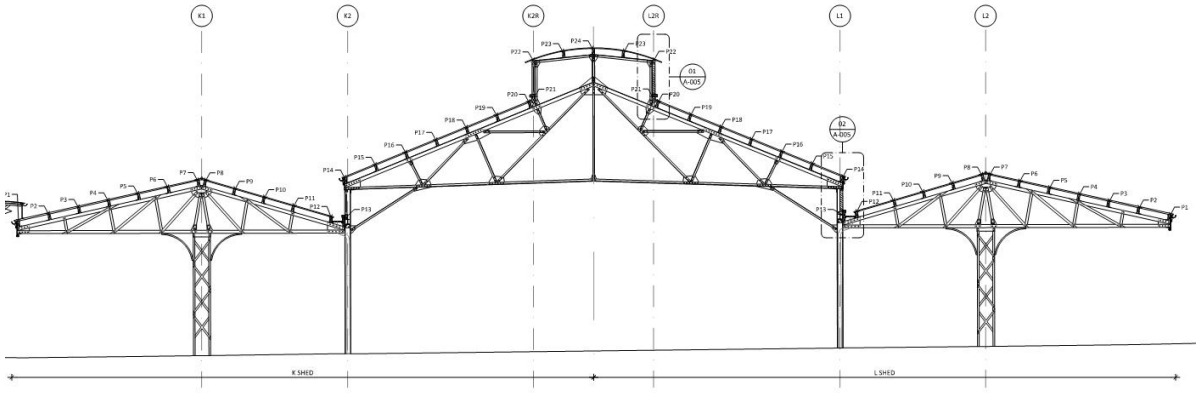


Figure 4: Shed K and L framing elevation [5]

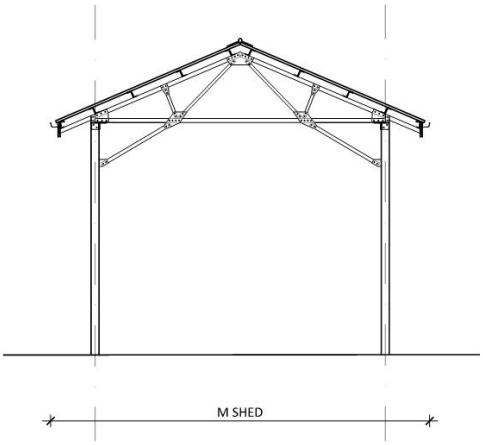


Figure 5: Shed M framing elevation [5]

Shed E has metal roof sheeting supported by timber purlins, steel roof trusses, timber beams, timber posts and pad footings and is shown in Figure 2. The metal roof sheeting and shallow

footings are common across all sheds.

Shed F has the same framing as Shed E, apart from the southern wall which is unreinforced brick masonry on a strip footing instead of timber beams and posts on pad footings. An elevation of Shed F looking east is shown in Figure 3.

In the north-south direction of Shed E, knee-bracing on every second truss provides lateral stability. Shed F has timber framed infill walls between tenancies and therefore does not have knee-bracing. In the east-west direction of both sheds, portal frame action was achieved from the bolts and haunch at the beam-column connection, shown in Figure 6.

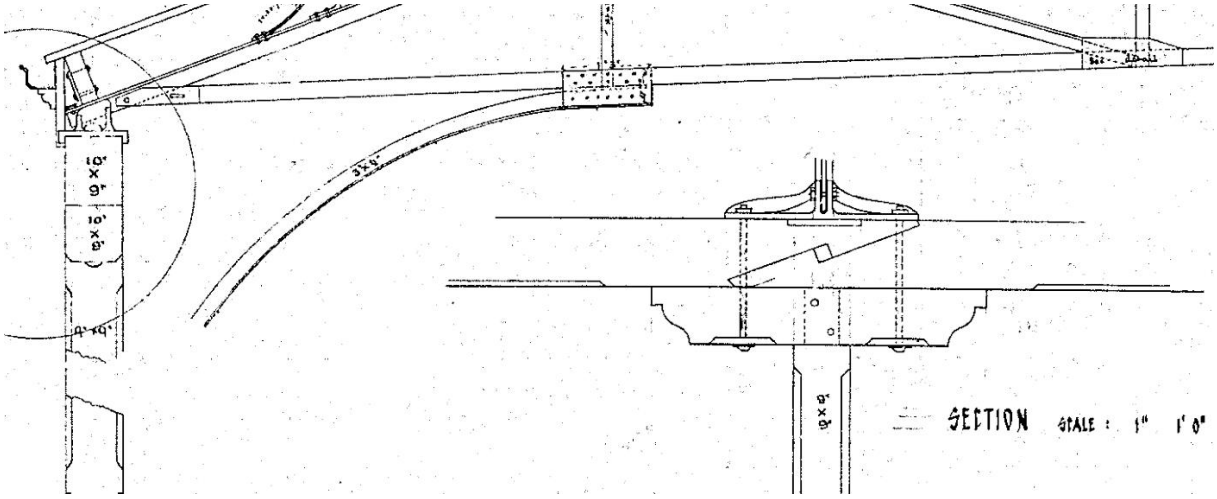


Figure 6: Shed E knee bracing and post to beam connection detail for Sheds E and F

Shed J has steel purlins supported by steel trusses and steel posts and is shown in Figure 3.

Sheds K and L have timber purlins supported by steel trusses. The outer trusses are supported by channels with latticed steel plates connected by rivets, while the inner larger truss is supported by steel posts. An elevation of Sheds K and L looking east are shown in Figure 4. The delineation between Sheds K and L is the peak of the central truss, such that half of the central truss is in Shed K and the other half in Shed L. This delineation is solely for the layout of market stalls.

Shed M has steel purlins on steel trusses supported by steel posts and is shown in Figure 5.

All sheds act independently and are structurally isolated from one another, except for Sheds K and L which together form one structure.

Short canopies constructed with steel purlins, beams and posts provide shade to the footpath along the ends of the sheds, along both Peel Street and Queen Street.

4 INVESTIGATIONS AND DATA COLLECTION

4.1 Determination of applicable building code and level of compliance

Previously, Sheds A to D were analysed as part of a separate project which determined they had insufficient structural capacity and could pose a safety risk. The site owner and custodian therefore decided to assess all the sheds across the market, resulting in this project. To mitigate the risk to a measurable level, a building surveyor was engaged to determine the required level

of compliance.

The building surveyor selected the current Australian building code, the National Construction Code 2019 (NCC), for use on the project in accordance with relevant building legislation. They provided a concession on the structural adequacy requirements by setting the level of required compliance at 80% of code values. This concession took into consideration that building codes differed at the time of construction.

As the NCC uses limit states design, the reduction was applied to the wind loading pressures as it was deemed to be the most appropriate method.

4.2 Existing drawing search

The National Archives of Australia were accessed, and a building plan and documentation search was conducted at the City of Melbourne to locate available drawings.

Structural drawings of Shed F, architectural drawings of Shed J, structural drawings of Sheds K and L, and an architectural section of Sheds K and L were supplied.

4.3 Visual survey and measurements

A full visual survey and measurement was carried out of the existing structures. The roof trusses and canopy roof framing of the sheds are exposed on the underside and easily accessed with boom and scissor lifts. A tape measure, laser measure, and caliper were used to measure member spans and sizes. Damage and deterioration to members were recorded with the aid of a marking plan to denote location.

4.4 Point cloud survey

A point cloud survey provided a full three-dimensional model of the buildings. The benefits of the survey were that structural framing geometry and dimensions taken from site could be verified in the office and any photos or measurements that were missed during the investigation phase didn't require another site visit to obtain the information. The survey could not be used to locate deterioration of the members such as rust on steel members or rot for timber, nor was it to the degree of detail required to measure cross sectional dimensions of slender members and connections. A screenshot from the point cloud survey is shown in Figure 7.

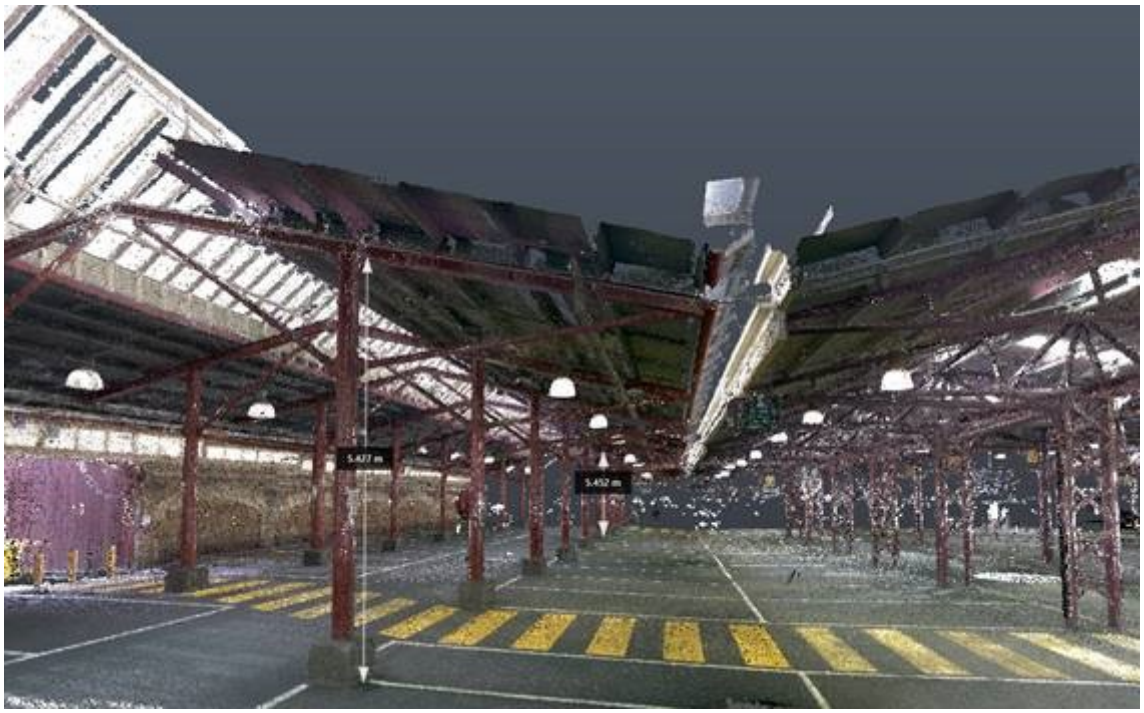


Figure 7: Point cloud generated image. From left to right the back wall of Shed F, Shed J, and the north end of Shed K are shown

4.5 Wind tunnel testing

Wind tunnel testing was conducted to determine accurate wind pressures on the sheds, as the wind loadings from the Australian Standard *AS 1170.4-2011 Structural design actions – Part 2: Wind actions* are prescriptive and therefore often conservative. Design downward pressures were reduced from 0.31 kPa to 0.23 kPa, and uplift pressures reduced from 0.59 kPa to 0.39 kPa by using wind tunnel results in lieu of the code-based approach.

4.6 Investigation of timber members

Timber specialists from the University of Tasmania conducted a full assessment of the structural timber members across the sheds. Columns were identified as River Red Gum (E. camaldulensis) and beams and purlins were identified as Douglas Fir (Pseudotsuga menziesii). Species identification was confirmed by laboratory testing of samples. Members were graded to Australian Standards *AS 2082-2007 Timber – Hardwood – Visually stress-graded for structural purposes* and *AS 2858-2008 Timber – Softwood – Visually stress-graded for structural purposes*, and the majority were determined to be Structural Grade No. 1. The corresponding stress grade for beams, purlins and columns was determined to be F17, which defines the bending strength, tension strength, compression parallel to grain strength and short duration modulus of elasticity values.

Timber members with damage or deterioration were identified by the timber specialist and where required, the depth of damage was determined with a small diameter core sample.

4.7 Structural analysis

Sheds were analyzed using Space Gass finite element analysis software using both two and three-dimensional models as applicable. Results were independently verified with hand calculations.

5 RESULTS AND INTERVENTIONS

5.1 Analysis results

Overall, the sheds were found to be structurally compliant to the 80% of code value limit set out by the building surveyor, with the exception of the lateral stability of Sheds E and F in the north-south direction, and the trusses of Sheds E, F and J under wind uplift loading.

The sheds were all built before seismic design requirements were introduced in the 1994 Building Code of Australia. However, as the sheds have little mass wind loads governed in all cases except for the Shed F masonry wall.

5.2 Sheds E and F lateral stability

Building drift under wind load exceeded code recommendations but was deemed to not be of concern.

The lateral capacity of the sheds in the east-west direction was found to be insufficient as the bending moments in the connections exceeded their design strength. To rectify this, a modification to the connection using steel angles and through bolts was designed, as shown in Figure 8.

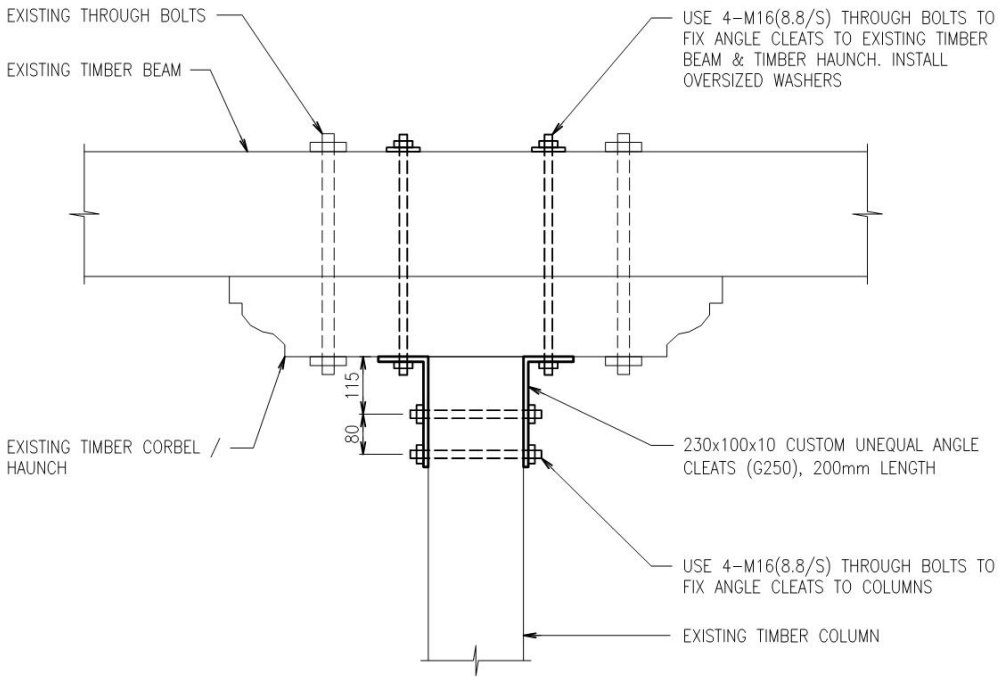


Figure 8: Strengthening detail for Sheds E and F timber haunch

5.3 Shed F masonry wall stability

The masonry wall at the back of Shed F was visibly out of plumb and leaning towards the south, which was confirmed by the point cloud survey. Monthly surveys were undertaken over a six-month period, which determined that no further movement was occurring. Figure 9 shows the survey results for lateral displacement of the top of the wall.

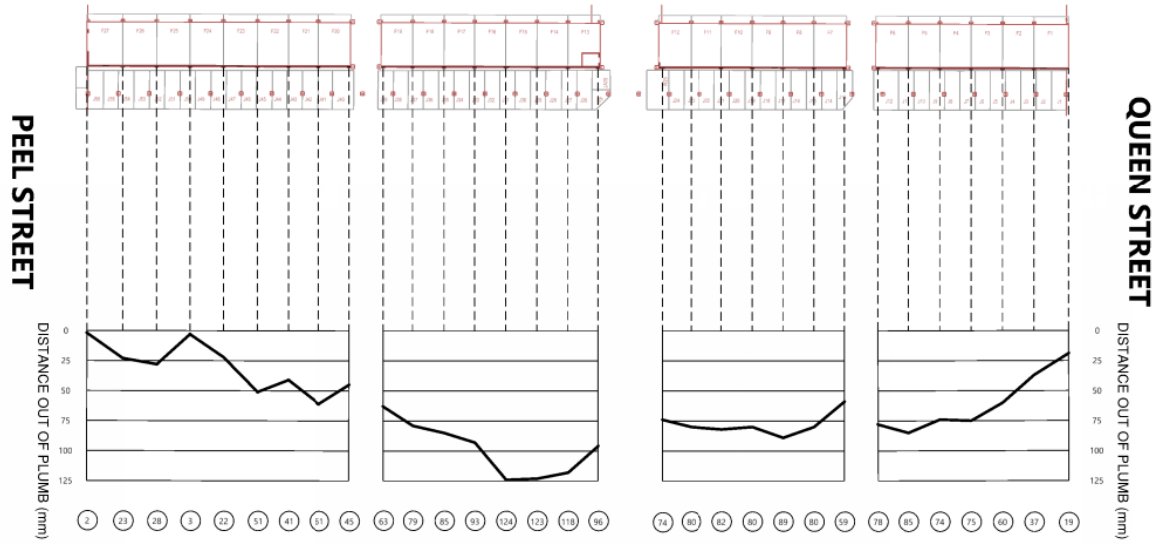


Figure 9: Survey results for the masonry wall at back of Shed F [6]

Non-linear push-over analysis determined that the back wall of Shed F required strengthening to comply with NCC requirements in locations where it was out of plumb by more than 90mm. The concession from the building surveyor to reduce compliance to 80% for structural adequacy removed the need for strengthening to the wall. However, the design originally proposed is described below.

Buttresses on the south side of the masonry wall were designed so that the wall would bear on them in an earthquake. The buttresses would be on the exterior of Shed F to avoid interfering with the tenancies and have shallow pad footings extending partially above ground to avoid interfering with graves. The buttress to wall interface was detailed with rubber bearing pads such that the wall could lean against the buttresses without any physical attachment between them, making the proposed intervention entirely reversable.

5.4 Sheds E, F and J wind uplift case

The trusses were found to be structurally inadequate under the wind uplift design case, as the uplift pressures were enough to put the bottom chords of the trusses into compression. As the bottom chords were tension-only flat-plate members, they did not have any appreciable compression capacity.

The metal roof sheeting requires replacement as it has reached the end of its design life and was deemed to be unrepairable by the heritage consultant. By adding layers of plywood and fibre cement sheet between two layers of metal sheeting, the new panels add weight onto the trusses to prevent compression from occurring in the truss bottom chords in a wind uplift event.

The design masses of the replacement roof sheeting varied depending on the shed, with the maximum being 40 kg/m^2. The secondary benefit of the built-up roof panel is that insulation can be provided to the sheds, increasing occupant comfort during summer days when temperatures around 40 degrees Celsius are not uncommon.

Other than the roof sheeting, there were no other lateral stability elements in the plane of the roof. The replacement roof sheeting build-up was therefore designed as a diaphragm. In Australia, steel cladding systems are commonly made from thin high strength steel, and steel design codes do not currently provide guidelines for the design of crest-fixed steel roof or wall claddings. [7] As the steel roof sheeting is being custom-made for this project, it was designed and specified using *CAN/CSA-S136-01 North American Specification for the Design of Cold-Formed Steel Structural Members*. The crest-fixing of the composite roof decking panel to the purlins resulted in the screw being placed in bending, which was accounted for in the design. A detail of the roof build-up at the metal deck splice location is shown in Figure 10.

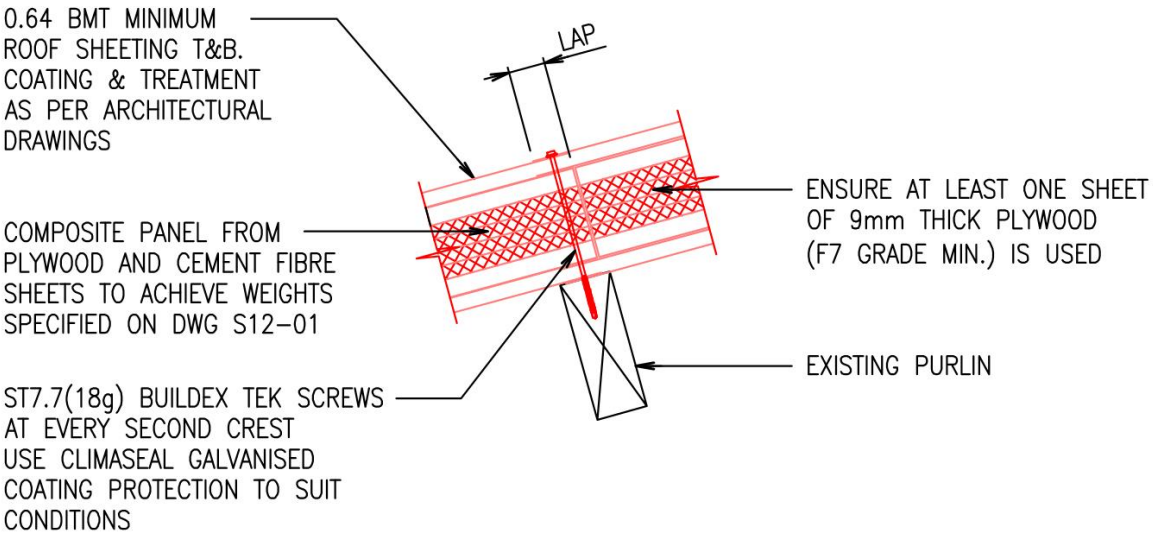


Figure 10: Replacement roof sheeting detail at purlins

5.5 End walls of Sheds K and L

Lightweight sheeting encloses the ends of Sheds K and L between the top of the end truss and canopy roof. To verify structural capacity of this partial end wall under wind load, including preventing out of plane buckling of the truss, the columns were checked as cantilevering off the canopy roof diaphragm as shown in Figure 11, and found to be sufficient.



Figure 11: West end of Sheds K and L

5.6 Replacement of damaged members

Given its use as a busy market, there are numerous locations of local damage to the structure. The sheds are used as a car park on non-market days, forklifts transport goods through the sheds for market set up, and various lights, sound equipment, and other items are hung from the trusses regularly. Vehicle damage is evident on multiple vertical supports. There are also locations where members have been locally cut to allow for services like downpipes to be installed.

During the visual inspection, a register of members to be repaired or replaced was created.

5.7 Timber member repairs

A few timber columns require partial replacement due to significant rot and deterioration. The cause of the deterioration in most cases was a broken downpipe, which resulted in the base of the column undergoing multiple wet-dry cycles over time. Repair of downpipes is being undertaken in conjunction with the partial post replacements.

6 CONCLUSIONS

In order to minimize interventions, close collaboration across the project team was required. The wind tunnel testing was instrumental in reducing the design loads and strengthening.

The concession from the building surveyor to reduce the compliance level from the modern building code was equally important.

Replacement of the roof sheeting with heavier built-up sections was not a favorable outcome due to it being a change to the original design. However, it was preferred when compared to the extensive strengthening that would be required in the form of welding steel plates to existing truss members, had it not occurred. The new built-up roof panels have the same metal roof sheeting profile as the originals but are an observable replacement of the original upon close inspection.

At the time of writing, the tender period for the project is underway and construction works are planned to commence in mid-2020.

Drawings of the project will be stored on file at city council and will remain accessible to the general public like other existing drawings of the market.

ACKNOWLEDGEMENTS. The project team is acknowledged for their expertise and close collaboration on the project:

Heritage consultant and architect: Lovell Chen
Owner and site custodian: City of Melbourne
Timber specialist: University of Tasmania
Building surveyor: Du Chateau Chun
Wind consultant: Mel Consultants
Robert Bird Group project team: Michael Grey, Granil Guerra and Robert Dragwidge

REFERENCES

[1] Heritage Council Victoria. Victoria Heritage Database. *Queen Victoria Market*. [Accessed 2019 December 8]. https://vhd.heritagecouncil.vic.gov.au/places/1211.

[2] Gary, P. *The First Residents of Melbourne's Western Region*, (revised edition). Harriland Press, (1997) ISBN 0-646-33150-7.

[3] Isabel E. and Peter C. *People of the Merri Merri, The Wurundjeri in Colonial Days.* Merri Creek Management Committee, (2001) ISBN 0-9577728-0-7.

[4] City of Melbourne. QVPR Program Conservation Architect and Heritage Consultant Services. Statement of Works - MSA #3575, (2019) pp. 9.

[5] Lovell Chen Pty Ltd. Queen Victoria Market Sheds E, F, J, K, L & M, Project No. 7947, Drawing No. A-004, Revision HV1, (February 2019).

[6] Reeds Consulting. Queen Victoria Market Cemetery Wall Monitoring February Survey, (21 February 2019) Ref. 22524-A.

[7] Mahaarachchi, D. Behaviour and Design of Profiled Steel Cladding Systems Subject to Pull-through Failures, School of Civil Engineering, Queensland University of Technology, (2003).

SEISMIC VULNERABILITY ASSESSMENT OF A 17TH CENTURY COLONIAL ADOBE CHURCH IN THE CENTRAL VALLEY OF CHILE

N. C. PALAZZI[1,2*], G. MISSERI[3], L. ROVERO[3] AND J.C. DE LA LLERA[1,2]

[1]Research Center for Integrated Disaster Risk Management (CIGIDEN),
[2]Pontificia UnivesidadCatolica de Chile
Avda. Vicuña Mackenna 4860, Macul, Santiago, Chile
e-mail: nuriachiara.palazzi@cigiden.cl (*corresponding author), jcllera@puc.ch
[3]Department of Architecture, University of Florence
Piazza Brunelleschi, 6, 50121, Firenze, Italy
e-mail: giulia.misseri@unifi.it, luisa.roveo@unifi.it

Keywords: Historical Structure, Unreinforced Adobe Masonry, Seismic Vulnerability

Abstract. *This paper focuses on the seismic vulnerability assessment of the San Judas Tadeo´s church in Malloa (Chile), an iconic example of Colonial Chilean architecture. This small adobe structure is a single-nave building consisting of the main nave, a bell-tower located in the façade, two external wooden galleries and additional units such as the sacristy, chapel, and two services areas.*

The Church has survived several strong earthquakes larger than Mw>8. Besides, after the February 27th, 2010 Maule event it showed remarkable resilience due to the implementation of traditional timber retrofits inserted in the earthen walls. The use of traditional wooden devices such as bond beams, corner keys, and wooden gables, proved to be effective solutions against strong earthquakes.

Therefore, this church appears as a relevant case of the use of seismic resistant constructive techniques of the17th century colonial architecture and the study of its seismic behaviour holds great interest and relevance.
Aimed to assess the seismic performance of the monument, a complete preliminary study of the church was carried out using a multi-level approach comprising historical research, in situ surveys, crack pattern analysis, physical and mechanical characterization of materials, and structural analyses. In particular as part of an ongoing research, linear and incremental kinematic approaches of limit analyses have been employed with the aim of interpreting the local mechanisms activated during the 2010 Maule earthquake. In these models, the effect of friction on masonry-to-masonry and timber-to-masonry interfaces was considered with promising outcomes.
This study results prove the general validity in the field of timber seismic retrofitting of unreinforced adobe buildings.

1 INTRODUCTION

San Judas Tadeo is the parish of the community of Malloa (-34.442247, -70.943377), a rural village of 12,000 inhabitants located in Cachapoal Province, Libertador General Bernardo O'Higgins region (VI), at 113 km south of Santiago.

The first parish was erected in 1635 and was completely destroyed by the May 13, 1647 (Ms~8) Santiago earthquake [1]. The current parish was founded in 1845 under the avocation of San Juan Batista, but years later the devotion to San Judas Tadeo prompted a name change. The fervor of the community for this saint, known as the employer of the difficult causes, arose in 1887 during an epidemic of cholera. The tragedy touched the citizenry and settled in the collective memory of the village. Thus, the San Judas Tadeo church became a significant religious and civil Landmark of Malloa. It was declared Historic Conservation Zone (ZCH) according to Art. 60 of the General Urban Planning and Buildings Law; and it is now acknowledged as Historical Monument according to Law Nº17.288 of National Monuments [2]. This parish was constructed following the typical architectural, constructive and structural features of Colonial style of the Chilean central valley [3, 4]. The morphology of the structure consists of an austere rectangular plane of a single-nave, and additional units built later. The plane is 45.1m long in the longitudinal direction, 9.9m wide in the transversal direction, with a maximum roof height of 9.92m, accommodating 500 people.

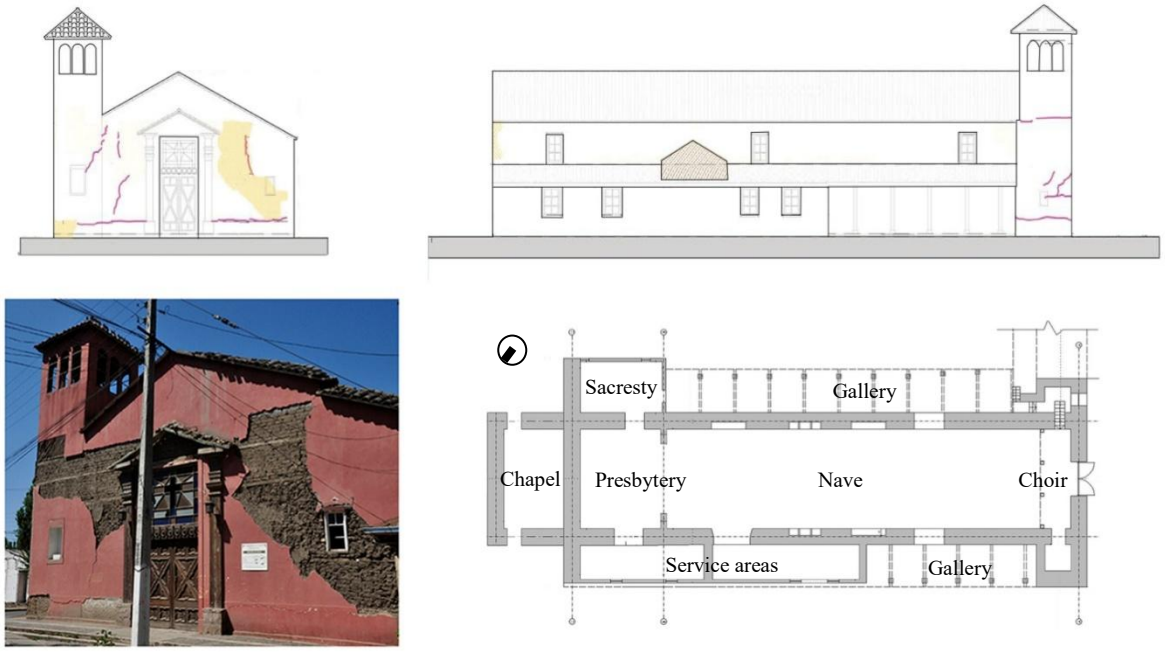


Figure 1: View of the façade of the church and current plan, façade and lateral view[5]

The church has an area of 815.84 m^2, and it features a central rectangular space oriented north-east south-west, a sacristy adjacent to the western wall, and two additional service areas located respectively on the northern and eastern walls. The main nave is divided in three sectors (choir, nave and presbytery, Fig. 1), and has undergone several modifications over the time thus different construction techniques and materials are distinguishable.

2 CONSTRUCTION PHASES AND MAIN INTERVENTIONS

Malloa village is located in the territory of an indigenous village which motivated the installation of Franciscan convent which back to 1635 and was dedicated to San Antonio, one of the oldest in the VI region. The first temple was completely destroyed by the 1647 earthquake and a new Parish was erected in 1662, under the invocation of San Antonio de Papua. The first records date back to1824. The current building was founded on the 17thNovember 1845, although there is no documentation indicating which parts of the1662 temple were reused. After the 1928 Talca earthquake (7.6Mw), the complex suffered from considerable damage, and in the same year it was restored [1]. Despite the lack of historical information about the parish, during direct surveying activities carried out by the authors, it was possible to recognize the original structure and the main subsequent construction phases. In fact, through the detection of construction techniques corresponding to specific historical periods and the survey of structural discontinuities, three main construction phases have been identified.

The first period corresponds to the original block composed by the main nave (choir loft, nave and presbytery) and the base of the bell tower at the side of the facade (dated back 1662-1824).

The second construction phase corresponds to the parish enlargement with northern and eastern service areas attached to the main block. These areas were built with *adobillo*, a system originated in the Valparaiso region in the middle of 19thcentury [6].

Finally, during the third construction phase (undated) a chapel and a sacristy were erected with adobe masonry walls, simply juxtaposed to the rear and west walls, respectively. The actual configuration of the Parish is the result of seismic consolidation interventions and reconstructions during the past centuries characterized by different building techniques and materials, which present different structural behaviors. Probably after the 1985 Valparaiso earthquake (Mw8.0), the parish suffered considerable damage in the façade and bell tower, which were then reconstructed by wooden walls and reinforced through timber ring beams in the upper part. After the 2010 Maule earthquake (Mw 8.8), the church incurred in significant damages due to severe crack pattern that induced separation among walls. Structural damage amplified due to rising damp and local deformation. In 2016, Arias Arquitectos carried out a wide conservation project that addressed the whole parish [1].

3 ARCHITECTURAL ELEMENTS AND PROPERTIES OF MATERIALS

The parish has undergone several modifications over the time. Consequently, different construction techniques and materials are observable. According to the historical analysis, three traditional constructive systems for masonry walls were recognizable: (i) 4-wythe English bond with the insertion of timber elements, named W01; (ii) *adobillo,* which is a mixed wooden-earth technique where a thin timber frame interlocks a single-wythe shiner bond, named W02; and (iii) stacked 2-wythe masonry with header bond, labelledW03. The central nave walls (W01) are adobe masonry with the insertion of timber elements within the thickness, which are traditional seismic resistant technique of the local colonial culture. These timber reinforcements are composed of horizontal and transversal elements.

The wooden horizontal-elements run along the walls of the central nave and the base of bell tower, and transversal-elements across the full whole thickness. The horizontal elements have

a section of 10x20cm located about every 1.8-2.7m, while the wooden transversal ones are about 5x10cm every 2.25m. This traditional construction practice exploits the mechanical proprieties of wood, improving the out-of-plane bending capacity and in-plane shear resistance of adobe walls. The woodworking joints constitute the main seismic weakness of this system when subjected to the seismic motion. In San Tadeo parish there are two types of joints: *hooked scarf* and *halved joints*.

The *hooked scarf joint*, which is employed to connect the wooden horizontal elements, is a traditional method of joining two members end-to-end. This technique offers remarkable capacity in the longitudinal direction because it extends resistive area of the joint, thus maximum allowed force heightens, but the link mostly depends on the mechanical fastener employed to keep the joint closed, Fig. 2a.

The *halved joint*, another traditional link, is used to join two orthogonal members by removing material from each at the point of insertion so that they overlap, Fig. 2b. The amount of material removed is equal to half of the width, so the connections are weak and prone to split.

Following the 2010 Maule earthquake, the failure of the joint interlocking between wooden elements is observed in particular for the hooked scarf joint. The link failures are shown by the slippage between the wooden elements in the horizontal direction, determining the propagation of vertical and diagonal cracks along the entire height of the wall, see Fig.2a.

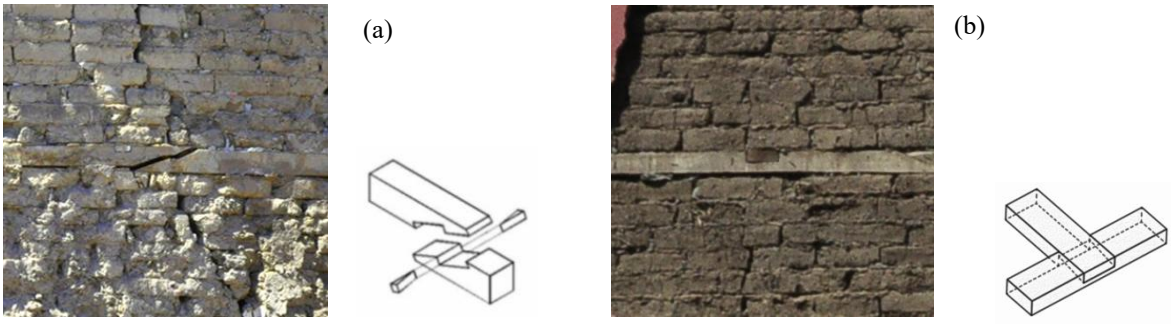


Figure 2: Traditional timber joints in Malloa parish: (a) hooked scarf joint, and (b) halved joint

The W01 walls of the central nave (thickness 1.45m) are made of 4-wythe earthen wall, of adobe brick with dimensions 35x60x15cm, bond by an earth mortar. The connections among orthogonal walls of the central nave, despite the absence of bond, consist of using wooden *corner keys* and *bond beams*. These traditional strengthening solutions induce walls working together even when the bonds between perpendicular walls crack during an earthquake [7], as it has been observed after 2010 Maule earthquake in the rear wall of central nave of Malloa church.

The slender walls of two service areas located on lateral northern wall of central nave are made of *adobillo,* another traditional mixed wood-earth single-leaf wall (W02). The *adobillo* wall of Malloa parish is the result of traditional local anti-seismic techniques and modern materials introduced in 19th century. It is composed by vertical wooden logs (10x10cm) every 75cm, horizontal wooden twigs (10x30cm), adobe blocks (60x30x10cm) of shiner course, and interior and exterior earth plaster with diagonal steel wires. This constructive system, originated in Valparaiso, generally, uses a particularly shaped earth

blocks having two 1'x1' notches in the headers of block that allow to fix the *adobillo* to wooden logs [6]. However, these efficient links between earthen blocks and wooden elements are absent in the *adobillo* walls of San Tadeo Parish.

Finally, the masonries of chapel and sacristy, adjacent to the presbytery walls, were built with adobe masonry W03, block dimensions of 35x70x15cm. The W03 is double-leaf masonry without blocks crossing the whole thickness which can generate a transversal locking, the *diatones*. Consequently, the wall is composed into sections simply positioned one next to the other, very vulnerable to the out-of-plane seismic actions. Furthermore, this adobe masonry is characterized by a head bond resulting in lower shear strength than a monolithic panel and an inadequate seismic behavior[8].

In order to define the mechanical proprieties of adobe blocks, the values suggested by Chilean Standard [9] for adobe structures have been used. The Young's modulus E=200 MPa, compressive strength f'_m=0.6 MPa, and shear strength v'=0.025 MPa of adobe masonry are assumed. The wooden trusses of the roof structures consist of oak elements *(Nothofagus oblique)*, with density (γ=624kg/m^3), compressive strength ($f'_{m,medium}$=46.65MPa), and shear strength ($v'_{0,medium}$=6.08MPa).Finally, to the aim of characterizing the soil mechanics and the foundation type, four excavations located near the west wall of the north chapel [E1], the south area of parish house [E2], the north area of parish house [E3], and the inner courtyard [E4], with a depth of 3m, 2.6m, 3m, and 3m respectively were carried out by [10]. Based on the Chilean Code NCH433of 96 [11] and D.S.61, 2011[12]the soil, having medium dense soil, Vs30 = 332 ms^{-1}, and shear strength non-drained minor of 0.05MPa, was classified as soil type D, with soil coefficient S=1.

3 ASSESSMENT OF CRACK PATTERN

The San Juan Tadeo parish has suffered severe damage after the 2010 Maule earthquake. In particular, different seismic behaviors depending on the construction techniques were observed in the main block (W01), the service areas (W02), and the sacristy and rear chapel (W03). The main block of Malloa parish consists of heavy and thick walls (slenderness H/t=6.8, where H and t are the height and thickness of wall respectively), wooden beam bonds within the thickness and corner keys. Despite this, the traditional anti-seismic system, based on the use of timber, keeps the walls working together (*box-behavior)*. In the main façade, the failure of joints, which used to attach (kink) end-to-end two horizontal members, aided the propagation of deep vertical cracks. The compound overturning of the thick façade (H/t=5.2) is highlighted by vertical cracks passing through the wall thickness (Fig.3a-b) and the disconnections between the façade and the longitudinal side walls, internally observable. Furthermore, the presence of timber corner keys provides reinforcement improving the post-elastic behavior of the walls. Thus, a part of the longitudinal side walls and the façade continue to work together. The diagonal cracks observed in the longitudinal walls highlight the activation of an overturning mechanism that involved the façade and triangular portions (two side wings) of the longitudinal walls around a horizontal hinge, located at 72cm above the ground level. The shape of façade macro-element depends on several factors, mainly: the length and number of corner keys, the masonry-wood friction, and the distance between openings and wall-corner. Significant vertical cracks are also visible in the upper part of longitudinal side walls of the nave, mainly near the openings of windows

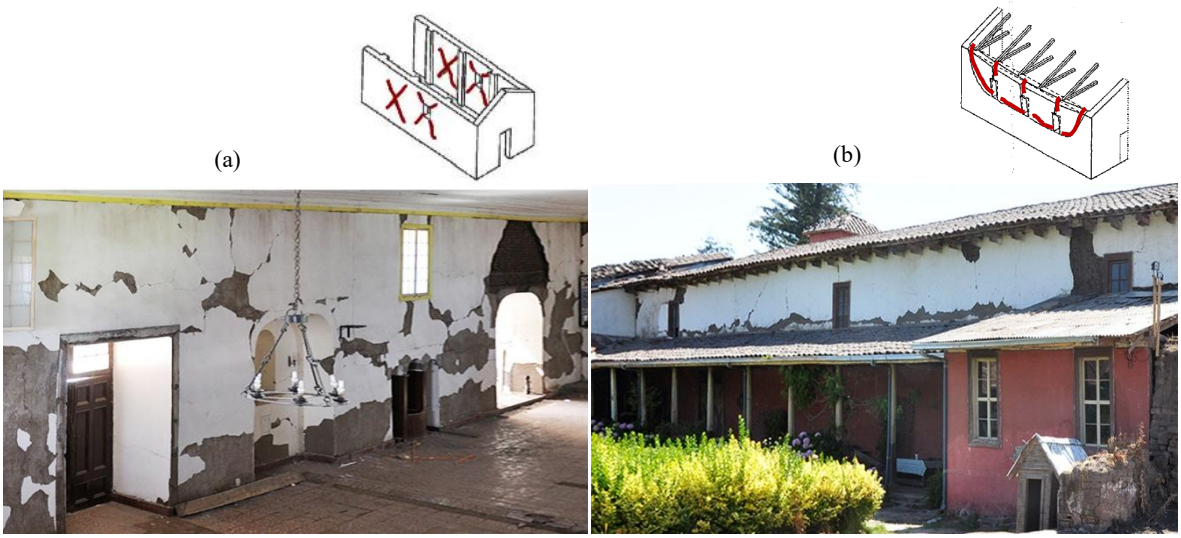
and doors. This crack pattern, observable in the internal (Fig. 4a) and external (Fig. 4b) elevations of side walls, suggests the activation of out-of-plane failure mechanisms, triggered by horizontal flexure of the wall, and involving the upper part of the discretized longitudinal walls between the openings (Fig. 4). The rotation towards the outside occurs around a horizontal hinge defined by the crack in correspondence of the wooden horizontal reinforcements of the W01, located at 4.6m above ground level.



(a) (b)

Figure 3: Deep vertical cracks in the main façade[5]

Diagonal shear cracks caused by the seismic action along the in-plane direction of the wall nave were observed near the openings, in correspondence with the spandrels.



(a) (b)

Figure 4: Deep cracks observable in the (a) internal and (b) external elevations of side walls [5]

The influence of the carpentry links (Fig.2a) on the global seismic behavior of the structure is often neglected. Nevertheless, as demonstrated by the activation of the local failures in the façade and side walls of the parish, it is essential to analyze these particular behaviors in order

to reach a complete understanding. Concerning the presbytery wall, the level of connections obtained through the corner keys at different heights is sufficient to generate restrain with the longitudinal walls. Nevertheless,localized vertical crushing in the corner occurs due to the absence of masonry bonds. The fracture lines are in correspondence of longitudinal wall planes. With respect to the chapel, several local collapses involving the external leaf of the two-leaf adobe masonry (W03) were observed. Two double-leaf-wall overturning mechanisms triggered, determining the collapse of the external leaf, with trapezoidal shape in the upper part of the wall. The low quality of W03 masonry, the absence of good bond, and the presence of big openings close to the wall corner affected the shape of the macro-element. Furthermore, the collapse of the corner of sacristy was observed.The timber consolidation interventions of bell-tower cell and façade gable avoided local collapses and significant damage, guaranteeing ductility and allowing oscillation without loss of equilibrium. These traditional strengthening techniques showed high efficacy in avoiding compete loss and collapses after the several earthquakes that have hit the church.

4 STRUCTURAL ANALYSIS THROUGH LOCAL MECHANISMS

The results described in previous Sections (2 and 3) suggest that preliminary structural analyses should be focused on the recurring failure mechanisms of the observed macro-elements, which have exhibited significant damage during the past earthquakes. With the aim of assessing the vulnerability levels of identified macro-elements, considering the out-of-plane behavior, linear kinematic analyses (LKA) were conducted according toChilean Codes[9], [11] and [12]combined with the prevision of the Italian Code NTC2008[13], and the Guidelines of Cultural Heritage [14]. Firstly, the layout of the mechanisms that are most likely to be activated in the Parish has been defined for the current state. The results of LKA (Kinematic multiplier λ_0, Participating Mass M^*, Mechanism Activation Acceleration a_0^*, the Demand Acceleration at ground and elevated levels) are shown in Table1.

The Parish damage can be interpreted as the activation of the out-of-plane collapse mechanisms that involved: (i) the main façade; (ii) the side walls of main nave, and (iii) the walls of the sacristy and chapel.

(i) Concerning the main building, all detected out-of-plane mechanisms are simple overturning of rigid sub-blocks that actived onthe west and east lateral walls around a cylinder hinge placed 4.6m off the groud levelconsidering the basic treatment of limited compressive strength, LWe1, LWe2, LWe3, LWe4, LWe5, and LWw1, LWw2, LWw3, LWw4, LWw5. All mechanisms are shown in Table1.

(ii) Only in the case of the sacresty walls the triggered mechanisms involved the external leaf of masonry, which collapsed; these mechanisms are labelled LWw5 LWe6 and LWe7. The overturning of the external leafof a masonry is one of the weakest mechanism since the stabilizing action of the weigth can be reduced up to 4 times if compared to a monolitic block.

(iii)Finally, different mechanism types for the out-of-plane behavior of main façade, FA, have been considered. In particular, compound overturning with basic treatment of limited compressive strength (CO-FA), simple overturning with sliding of timber elements hindered by masonry-to-timber frictional forces (SO-FA)and the compound overturning with cohesionless Coulomb failure criteria (COC-FA) have been analyzed.

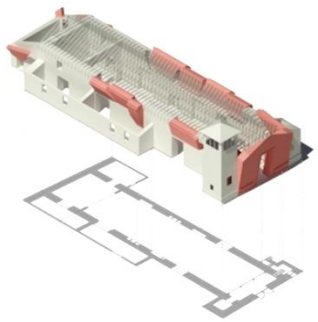
4.1 Out-of-plane failure assessment through standard limit analysis

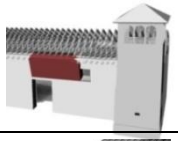
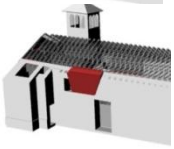
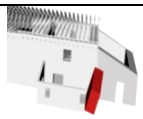
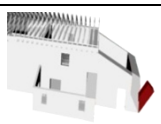
After the identification of the layout of the failure modes and the forces involved in the mechanisms, the kinematic multiplier of the horizontal equivalent forces producing the activation of the mechanisms, λ, has been determined and shown in Table1. Consequently, the λ has been converted into acceleration capacity a_0^*, according to codified procedures[14] and[15] based on the hypotheses of absence of tensile strength of masonry; absence of sliding between the interconnected rigid blocks; and limited compressive strength of masonry.

$$\lambda(\sum_{i=1}^{n} P_i \cdot \delta_{xi}) = \sum_{i=1}^{n} P_i \cdot \delta_{yi} \cdot \delta_{yi}; \qquad a_0^* = \frac{\lambda \sum_{i=1}^{n+m} P_i}{M^*}; \qquad M^* = \frac{(\sum_{i=1}^{n} P_i \cdot \delta_{xi})^2}{g \cdot (\sum_{i=1}^{n} P_i \cdot \delta_{xi}{}^2)} \tag{1}$$

where: λ is the kinematic multiplier; P_i is the i-th load; δ_{xi} is the virtual horizontal displacement of the gravity center of the i-th load P_i; $\delta_{yi}$is the virtual vertical displacement of the gravity centers of the i-th load P_i; $M^*$is the participating mass; anda_0^* is the acceleration capacity;.

Table 1: Results of Linear Kinematic Analysis of current state: Kinematic multiplier λ, Participating Mass M^*, Mechanism Activation Acceleration a_0*, equ. (2) for the Demand Acceleration (DA) at ground level Dag equ. (3) for the Demand Acceleration at an elevated level, Dal; and safety index Is_{IKA}evaluated as $\boldsymbol{a_0^*/DA}$.



ID	State Current	M^* [kN]	λ_i	a_0^* [m/s^2]	DA [m/s^2]	Is_{IKA} [-]
Fa-CO		2286	λ=0.263	1.92	D_{ag}=5.3	0.362
LW1w		328	λ=0.397	3.46		0.65
LW2w		239	λ=0.212	1.99	D_{ag}=5.3	0.38
LW3w		201	λ=0.362	4.87	D_{al}=4.1	0.92
LW4w		212	λ=0.445	4.25		0.80
LW5w		134	λ=0.183	1.34	D_{ag}=5.3 D_{al}=3.1	0.25
LW1e		235	λ=0.378	3.25		0.61
LW2e		312	λ=0.411	3.7	D_{ag}=5.3	0.7
LW3e		262	λ=0.384	3.39	D_{al}=4.1	0.64
LW4e		268	λ=0.367	4.01		0.75
LW5e		397	λ=0.334	2.92	D_{ag}=5.3	0.55
LW6e		95.6	λ=0.099	0.722	D_{ag}=5.3 D_{al}=3.2	0.14
LW7e		47.4	λ=0.242	1.756	D_{ag}=5.3	0.33

For a more realistic simulation in computing the kinematic multiplierλ, the limited state due to masonry crushing for compressive stress (f_m=1.2MPa) has been considered assuming the inward displacement of the cylinder hinge, $t = 0.05\sum_{i=1}^{n} W_i\,(f_d\,l)^{-1}$, which depends on i-th self-weight, W_i, the width of the wall, l, and the design compressive strength, $f_{d=}f_m(\gamma_M)^{-1}$.

The safety conditions require that the structural capacity (α_0^*, equ.1) must be equal or greater than the seismic demand D_{ag} [m/s^2], calculated according to the NCh433 Chilean Code (for soil type D). When the masonry macro-element is placed at the ground level it imposes:

$$a_0^* \geq a_g(P_{VR})Sq^{-1}=5.3\ \text{ms}^{-2} \quad (2)$$

Thus, D_{ag} depends on $a_g(P_{VR})$, the peak ground acceleration with an exceeding probability of 10% in 50 years; S, the sub-soil factor (here assumed equal to 1); and q, the behavior factor to account for energy dissipation capacity of the unreiforced masonry structure, equal to 1.5 according to [15]. In the case of the macro-elements placed higher than ground level, a further check must impose the input demand amplified by the effect of height D_{al} [m/s^2]:

$$a_0^* \geq S_e(T_1)\Psi(Z)\gamma \quad (3)$$

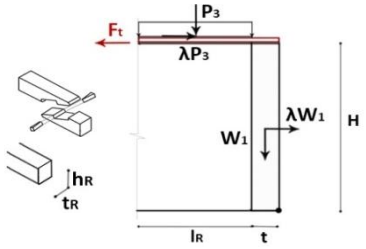
It is in dependence on the design spectrum acceleration, $S_e(T_1)$, with respect to the first vibration period of the macro-block T_1, being T_1=0.09 $H^{3/4}$ (characterizing the adobe buildings, [16].Finally$\psi(z)=Z/H$ is a function depending on the height from the foundation of the centroid of the weight forces applied on the rigid bodies, Z, on the total height of the building from the foundation, H, and on $\gamma=3N/(2N+1)$, which corresponds to a modal participation coefficient, depending on N number of floors.

4.2 Out-of-plane failure assessment through non-standard limit analysis

4.2.1 Simple overturning of main façade considering sliding at timber-masonry interface

Kinematic multiplier for the simple overturning of façade has been also calculated considering that restraining forces at timber-masonry interfacedue to frictional mechanisms can arise, in case the uppermost ring beam is not well anchored to the masonry. The resistive friction force,F_t= 2 μ p t_R $l_R$depends on the dimensions ofthe restraining device(Table2), as proposed in [17].In the expression of Ft,μ_t is the friction coefficient between timber and earth masonry; p is the force per unit surface of the slab;t_R is the thickness of the longitudinal timber element, l_R is the unit-length of the reinforcement (*ring beam*).

Table 2: Simple overturning of main façade (SO-FA) considering sliding at timber-masonry interface



ID	M* [kN]	λ_t	a_0* [m/s^2]	DA [m/s^2]	Is_{IKA} [-]
SO-FA	1691	0.167 (μ=0.3)	1.63	D_{ag}=5.3	0.308
		0.168 (μ=0.5)	1.64		0.31
		0.169 (μ=0.6)	1.65		0.311

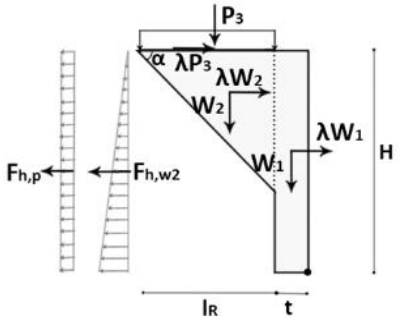
According to [18] different values of the wooden-masonry friction coefficient have been considered, μ=0.3, 0.5 and 0.6, as shown in Table2. It is relevant to note that the

contribution of the ring-beam is significant when a good anchoring of timber joints exists, i.e. when the timber end-to-end joints are working well since l_R significantly increases and consequently also λ_t. The values obtained for λ_t constitute and upper (unsafe) threshold to the corresponding value of λ.

4.2.2 Compound overturning of main façade considering the cohesionless Coulomb's failure criterion

The crack pattern of the Malloa façade, in which diagonal cracks (inclination of the crack slopeto the vertical equal to β = 1.052rad ~ 60.25 °) are visible on the orthogonal walls, denotes a good interlocking among them.The constribution of the timber reinforcement is considered and slope to the horizontal that fracture forms is identified through the minimum angleα.The constribution of friction in the analyisis of façade compound overturning is considered according to [17, 19, and 20] through limit analysis applied to non-standard materials.An added system of forces [17, 19, and 20] acting in the direction opposed to that of the earthquake action, and proportional to self-weights and overburden loads through the friction coefficient has been modelled: $F_{h,w2}$, the horizontal force offered by dry friction and due to self-weight, which depends on the compression found at each block interface and equal to $F_{h,w2} = \{[H(H\,tan\,\theta + t)]/2\}\,\gamma\; b\;\mu$; and $F_{h,p}$, the contribution offered by dry friction due to overburden loads, and equal to $F_{h,p} = p\;H\;\;tan\,\theta\;\;b\,\mu$, where γ is the specific weight of masonry; μ is the friction coefficientrelated to masonry; H is the height of the façade macro-element; b is the thickness of the considered wall; θ =v/t is the staggering ratio angle with v overlapping length among two blocks and t block thickness; and p is the force per unit surface of the slab (Table3).

Table 3: Compound overturning of main façade (COC-FA) considering the cohesionless Coulomb's failure criterion with frictional capacity expressed at all bed joints identifying the crack.



ID	M* [kN]	$\lambda_{t-\mu}$	a_0* [m/s^2]	DA [m/s^2]	Is_{IKA} [-]
COC -FA	2141.8	0.809(μ=0.2)	6.4	D_{ag}=5.3	1.19
		0.949(μ=0.3)	7.4		1.4
		1.032(μ=0.4)	8.1		1.52

The inclinations of crack slopes to the horizontal, characterising mechanism layouts and identified through complementary angles of α. For μ= 0.2, 0.3 and 0.4, the complementary angles of α obtained minimizing $\lambda_{t-\mu}$ are respectively 1.176rad (≅67°), 0.833rad (≅48°) and 0.670rad (≅38). Considering the case of lower friction coeff (μ= 0.2,) which already leads to non-conservative values, it can be observed that the mechanism layout is remarkably close to the staggering mechanism (θ=1.165rad≅67°), showing that the contribution of friction might be less relevant. This consideration supports the hypothesis that the resistive forces necessary to understand the actual mechanism are cohesive forces as investigated in [17].

5. CONCLUSIONS

In this paper a preliminary analysis of the seismic performance of a timber-reinforced colonal church that survived strong earthquakes, the Malloa parish, has been assessed. All OOP failures, detected during survery activieties following the 2010 Maule earthqueke, were assessed through standard limit analysis (LKA) considering the basic treatment of limited compressive strength. Results of LKA for OOP failure of compound façade offered an unsatisfactory safety assessment, safety index Is_{IKA}=0.362. Regarding the OOP simple overturning of west and east lateral walls of central nave offered safety indexesbetween $0.33 \leq Is_{IKA} \leq 0.92$. While, for the overturning mechanisms of external leaf of masonry walls (LW5w and LW6e), the safety indexes are between $0.14 \leq Is_{IKA} \leq 0.25$. In this case the collapse has already occurred during 2010 Maule earthquake.

For a more realistic simulation in computing of the kinematic multiplier, λ, non-standard limit analyses have been also carried out. Simple overturning of main façade has been also calculated considering that restraining forces at timber-masonry interface due to frictional mechanisms can arise, in case the uppermost ring beam is not well anchored to the masonry. The results show that the contribution of the ring-beam is significant when a good anchoring of timber joints exists, i.e. when the timber end-to-end joints are working well since l_R significantly increases and consequently also λ_t. The values obtained for $\lambda_t$constitute and upper (unsafe) threshold to the corresponding value of λ.

Moreover, constribution of friction in the analyisis of façade compound overturning is considered through limit analysis applied to non-standard materials, take into account: the horizontal force offered by dry friction and proportional to self-weights and overburden loads. Although offering reasonable mechanism layout (i.e. surveyed) values of the load multiplier provide a non-conservative estimation of the vulnerability.

Local-level analysis have provieded a reliable assessment of the OOP mechanisms of main façade, lateral walls and chapels. Results suggest that vulnerability could have been successfully reduced through punctual interventions that make use of traditional retrofitting technologies based on the use of wood, instead of extensive and invasive solutions somehow partially incompatible

Acknowledgements.This work was supported by the Research Center for Integrated Disaster Risk Management (CIGIDEN), CONICYT/FONDAP/15110017, and by the SIBER-RISK Regular Fondecyt project CONICYT/FONDECYT/1170836.

REFERENCES

[1] Arias Arquitectos, and Fercovic, G. 2011. Ficha técnica de daño y oferta de servicios. Informe de la Evaluación Preliminar de Daños Provocados por el sismo de 2010, Chile: Ilustre municipalidad de Malloa, Departamento de Proyecto.

[2] Consejo de Monumentos Nacionales, (CMN) Ministerio de 900 Educación. 2011. Chilean law of monuments 17.288. Accessed March 23, 2017. http://monumentos.cl

[3] Palazzi, N. C., Rovero, L., De La Llera, J. C., Sandoval, C. (2019). Preliminary Assessment on Seismic Vulnerability of Masonry Churches in Central Chile. International Journal of Architectural Heritage, 1-20

[4] Palazzi, N. C., Favier, P., Rovero, L., Sandoval, C., & de la Llera, J. C. (2020). Seismic damage and fragility assessment of ancient masonry churches located in central Chile. Bulletin of Earthquake Engineering, 1-25.
[5] Surtierra (2011). Recuperación de la Iglesia San Juda Tadeo de Malloa. Informe Final. Santiago: Oficina de Arquitectura Surtierra – in Spanish.
[6] Correia, M., Dipasquale, L., & Mecca, S. (2014). VERSUS: Heritage for Tomorrow. Firenze University Press
[7] Ortega, J., Vasconcelos,G., Rodrigues, H., Correia, M., Lourenço, P.B. (2017). Traditional earthquake resistant techniques for vernacular architecture and local seismic cultures: a literature review.Journal of Cultural Heritage 27, 181-196
[8] Borri, A., Corradi, M., Castori, G., & De Maria, A. (2015). A method for the analysis and classification of historic masonry. Bulletin of Earthquake Engineering, 13(9), 2647-2665.
[9] Instituto Nacional de Normalización (INN), 2013. Estructuras –Intervención de construcciones patrimoniales de tierra cruda– Requisitos del Proyecto Estructural. Santiago, Chile NCh3332.Of2013.
[10] R&V Ingeniero, (2012). Informe de mecánica de suelos. Iglesia San Judas Tadeo. VI región del Liberator Bernardo O'Higgins
[11] Ministerio de Vivienda y Urbanismo – MINVU (Chile). 2011. Reglamento que fija el diseño sísmico de edificios y deroga D.S. N°117 MINVU of 2010.
[12] Instituto Nacional de Normalización (INN), 1996. Earthquake resistant design of buildings, Official Chilean Code NCh433.Of96.
[13] D. M. LL. PP., (2008), Norme Tecniche per le Costruzioni, 14 Gennaio, Roma (in Italian).
[14] G.U. no.55, 7/03/2006. Approval of forms for the seismic damage assessment of cultural heritage buildings, Decree of the Prime Minister, Rome 23/02/2006. (in Italian).^
[15] Eurocode 8, (2004). Design of structures for earthquake resistance – Part 1: General rules, seismic actions, and rules for buildings (EN 1998-1), European Committee of Standardization. Brussels, Belgium; 2004.
[16] Tarque, N. (2011). Numerical modelling of the seismic behaviour of adobe buildings. de Ph. D., University of Pavia.
[17] Misseri, G., Palazzi, N.C., Rovero, L.(2020) Seismic vulnerability of timber-reinforced earthen structures through standard and non–standard limit analysis. Engineering Structures.
[18] Barbisan, U., & Laner, F. (2000). Capriate e tetti in legno: progetto e recupero: tipologie, esempi di dimensionamento, particolari costruttivi, criteri e tecnologie per il recupero, manti di copertura (Vol. 3). FrancoAngeli.
[19] Casapulla, C., Cascini, L., Portioli, F., & Landolfo, R. (2014). 3D macro and micro-block models for limit analysis of out-of-plane loaded masonry walls with non-associative Coulomb friction. *Meccanica*, 49(7), 1653-1678.
[20] Casapulla, C., & Argiento, L. U. (2018). In-plane frictional resistances in dry block masonry walls and rocking-sliding failure modes revisited and experimentally validated. *Composites Part B: Engineering*, 132, 197-213.

12th International Conference on Structural Analysis of Historical Constructions
SAHC 2020
P. Roca, L. Pelà and C. Molins (Eds.)

SLOW-MOVING LANDSLIDE DAMAGE ASSESSMENT OF HISTORIC MASONRY CHURCHES: SOME CASE-STUDIES IN ITALY

CHIARA FERRERO[1,2*], LUDOVICA CAMBIAGGI[1], ANDREA FENIALDI[1], PERE ROCA[2], RITA VECCHIATTINI[3] AND CHIARA CALDERINI[1]

[1] Department of Civil, Chemical and Environmental Engineering
University of Genoa
Via Montallegro 1, 16145 Genoa, Italy
email: e-mail: chiara.ferrero@edu.unige.it, ludovica.cambiaggi@edu.unige.it, andrea.fenialdi@gmail.com, chiara.calderini@unige.it (*corresponding author)

[2] Department of Civil and Environmental Engineering
Technical University of Catalonia (UPC-BarcelonaTech)
Jordi Girona 1-3, 08034 Barcelona, Spain
e-mail: pere.roca.fabregat@upc.edu

[3] Department of Architecture and Design, University of Genoa
Stradone S. Agostino 37, 16123 Genoa, Italy
e-mail: rvecchiattini@unige.it

Keywords: Historic churches, Masonry, Slow-moving landslides, Damage mechanisms.

Abstract. *This paper presents a contribution for the damage assessment of historic masonry churches exposed to slow-moving landslides. In particular, the authors identified four global damage mechanisms, which are presented here by means of the critical damage assessment of four case studies located in the Liguria region (Italy) in areas affected by slow-moving landslides. For each church, a correlation between the damage patterns observed on-site and the ground movements induced by landslide phenomena was sought by means of visual inspections and crack interpretation. As a result, each damage mechanism was associated to a different pattern of ground movements produced by slow-moving landslides.*

1 INTRODUCTION

Historic masonry churches are significant parts of world cultural heritage; thus, their conservation should be a primary goal for preservation engineers. Although these buildings may be potentially exposed to a number of natural (i.e. earthquakes, floods, landslides, etc.) and anthropic hazards (such as subsidence and tunneling), so far only the damage produced by seismic actions has been systematically investigated. Past and recent earthquakes showed in fact that historic masonry churches are particularly vulnerable to horizontal actions, which induce severe damage usually related to the out-of-plane collapse of building portions called macroelements [2, 3, 4]. In the last decades several studies were devoted to the damage and

vulnerability assessment of historic masonry churches and led to the identification of their collapse mechanisms under seismic actions (e.g. [3, 4]).

On the contrary, as described in [1], the response of historic masonry churches to soil displacements produced by phenomena like subsidence, foundation settlements and landslides has never been systematically analyzed. In particular, so far, in the literature attention was mainly paid to investigate the effects of vertical ground movements on single case studies (e.g. [5, 6]). Conversely, the effects and damages induced to churches by phenomena like landslides, which produce a combination of both vertical and horizontal soil displacements [7], has not yet been explored.

With the aim to fill such a gap of information, the authors performed a damage survey campaign (described in detail in [1]) in 33 historic masonry churches located in the Liguria region (Italy) in areas affected by slow-moving landslides. Despite these latter are characterized by movement rates of the order of only some mm/year [8], severe and extensive damage congruent with the direction of slope movements was observed in several buildings of the sample, thus proving the vulnerability of historic masonry churches to slow-moving landslides. Some recurrent types of damage and damage mechanisms induced to churches by slow-moving landslides were also identified.

This paper presents the four global damage mechanisms identified in [1] by means of the critical damage assessment of four case studies chosen among the 33 churches considered. For each church, firstly, the damage pattern detected during on-site inspections was analyzed in detail and interpreted in terms of damage mechanisms. Then, all available data regarding landslide movements were collected, analyzed and cross-compared with the damage patterns observed on-site. In this respect, it is important to highlight that the authors were able to gather information about state of activity, type and estimated direction of landslide movements, while almost no information was found about magnitude, rate and dominant component (vertical or horizontal). These latter types of data can be obtained by means of advanced satellite techniques (such as the differential SAR interferometry [9]) or inclinometers, the latter providing a profile of subsurface horizontal deformation. However, in the case of the Liguria region, good-quality displacement data can hardly be derived from interferometry due the morphological setting of the territory, which consists primarily of mountainous and hilly areas covered in woods [10]. Furthermore, most of the landslide-affected areas have never been monitored by means of inclinometers. For these reasons, with the aim of coping with such a lack of information, in this paper cracks and deformations observed on-site were used as indicators of ground movements. As a result, the damage patterns corresponding to each damage mechanism could be attributed to specific soil displacement patterns produced by slow-moving landslides.

2 DAMAGE MECHANISMS

In general, the damage assessment presented in [1] proved that churches respond to slow-moving landslides with a global behavior where the different structural components (walls, arches, vaults, etc.) contribute jointly to accommodate soil displacements. This behavior is significantly different from the response by independent macroelements exhibited by churches under seismic actions.

In particular, the following four global damage mechanisms were identified (Figure 1):

a. **Hogging**. This damage mechanism can be attributed to a concave-upward bending (hogging) of the structure produced by an incremental vertical ground movement in the direction of the longitudinal axis of the church (Figure 1a). The structure exhibits vertical cracks in longitudinal walls, repeated in each bay. Such cracks progress over the entire height of the wall, increasing in width with height, and continue up into arches and vaults, cutting them transversally. No significant cracks or gaps are observed in the floor.
b. **Shear deformation**. This damage mechanism can be attributed to a shear deformation of the structure produced by vertical ground movements along the longitudinal axis of the church (Figure 1b). Severe diagonal cracks propagating from the level of the ground are observed in longitudinal walls. A crack/gap in the floor can propagate between the cracks occurring in the opposite longitudinal walls.
c. **Global rigid rotation**. This mechanism is related to an incremental vertical ground movement along the transversal axis of the church (Figure 1c). Along this direction, the church is quite stiff and tends to rotate as a rigid body. There may be cracks, but the most relevant effects are (i) the out-of-plumb of longitudinal walls, (ii) the distortion of transverse arches, and (iii) the inclination of horizontal elements such as tie-rods, balustrades, steps and floors.
d. **Extension**. This mechanism is related to the horizontal component of landslide movement (Figure 1d). In this case, the structure exhibits multiple parallel diagonal cracks in vaults and floors, oriented in the same direction. In addition, severe vertical cracks occur in walls in planes perpendicular to the landslide direction. It is observed that these cracks propagate from the level of the ground and cut the structure over its entire height from floor to vaults, thus indicating that the church suffered extension in the direction of the acting landslide.

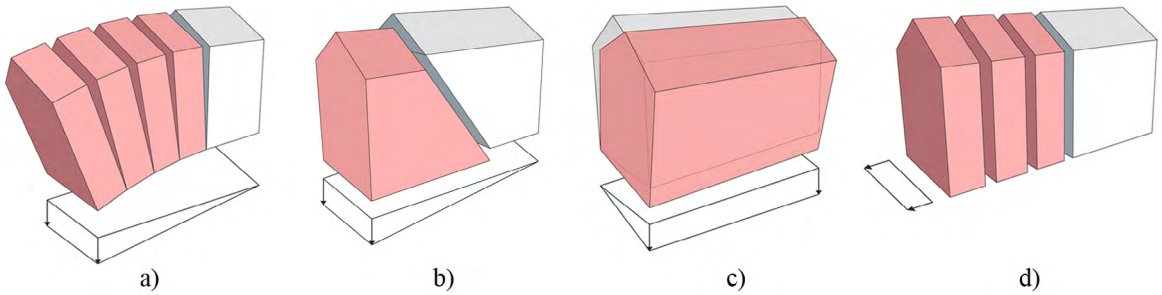


Figure 1: Global damage mechanisms identified in [1]: a) Hogging, b) Shear deformation, c) Global rigid rotation, d) Extension.

It should be highlighted that various combinations of these mechanisms may occur in churches according to (i) the magnitude of vertical and horizontal soil displacements, (ii) the direction of the landslide movement with respect to the church axes, and (iii) the church geometry and structural configuration. Concerning this last point, it is worth noting that, given the same ground movement (an incremental vertical ground movement in the longitudinal direction of the church (Figure 1a-b), the occurrence of mechanism a) or b) may depend on the length/height ratio of longitudinal walls: mechanism a) prevails for high ratio (slender walls), mechanisms b) prevails for low ratio (squat walls).

2 CASE STUDIES

This section presents the analysis of the four case studies under consideration, namely (i) San Martino church in Cembrano, (ii) San Bernardo da Mentone church in Ascona, (iii) San Lorenzo church in Sorbolo, and (iv) Santa Margherita church in Diano Arentino. These churches are representative examples, respectively, of the *hogging*, *shear deformation, global rigid rotation,* and *extension* mechanism. In the case of San Martino church in Cembrano, a combination between the *hogging* and *extension* mechanism was found.

For each church, this section provides a brief description of the main historical, geometric and constructive features as well as a detailed description of the crack patterns and deformations observed on-site. All the collected information about landslides movements as well as morphological setting of the soil are also reported. The data regarding landslide type, state of activity and estimated direction were derived from (i) the landslide maps of the basins plans of the Liguria region [11] [12], (ii) the *Atlante dei Centri Abitati Instabili della Liguria* (hereafter called Atlante [13]), and (iii) the maps of the *Geoportale Nazionale* (National Geo-portal) [14]. The contour curves of the slope were also considered in order to estimate landslide direction. Regarding landslide state of activity (active or dormant), it is important to point out that it is not relevant for the purposes of this work. Indeed, landslides that are currently classified as dormant were necessarily active at a certain point of their evolution over time. Thus, they could have caused the damage observed in the churches investigated.

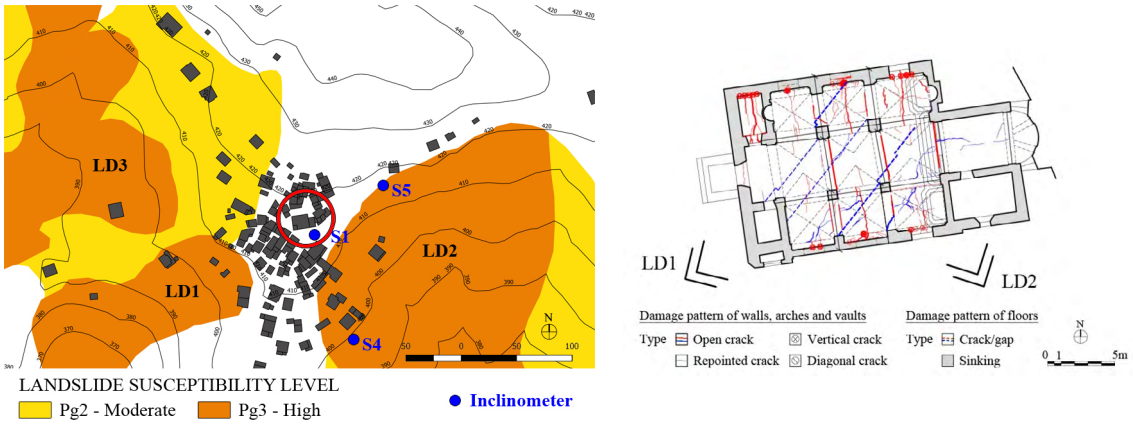
With the aim of obtaining information about magnitude, rate and dominant component of landslide movement, by using the *Geoportale Nazionale* [14] the authors verified (i) the availability of SAR data and (ii) the presence of inclinometers installed within the framework of the REMOVER monitoring project of the Liguria region. However, regarding SAR data, quantitative displacement data useful for the purposes of this work could not be obtained. Indeed, the churches under consideration are located in hilly and scarcely urbanized areas characterized by low distributions of targeted ground points (used by satellites to acquire interferometric data) [10]. Furthermore, the information necessary to decompose into vertical and horizontal displacements the components of motion registered by the satellite along the slope is not available. As for inclinometers, only in the case of San Martino church in Cembrano, the landslide-affected area surrounding the church has been monitored by means of inclinometers.

3.1 San Martino church in Cembrano

San Martino church is located in Cembrano in the municipality of Maissana (La Spezia province). The first documented information regarding the existence of Cembrano parish dates back to 1236; however, the exact date of construction of the church is unknown. In the nineteenth century some structural changes were performed: in particular, the left nave was added, and the original bell-tower was demolished and rebuilt. The masonry church, which is about 29 m and 14 m wide, consists of three naves with presbytery and semicircular apse. A triumphal arch separates the central nave from the presbytery. The central nave is covered by barrel vaults with lunettes, while the lateral naves present cross vaults and the presbytery is covered by a barrel vault. All the vaults are made of brick masonry.

The village of Cembrano as well as the church under consideration are located in a plan area surrounded by three dormant landslides (indicated as landslide LD1, LD2 and LD3 in Figure

2a). In particular, the church is located at a distance of 68 m, 39 m and 125 m from landslides LD1, LD2 and LD3, respectively. Landslide LD3 was not considered for the purpose of this work since it is believed that it cannot affect the church due to its direction and distance from the building.

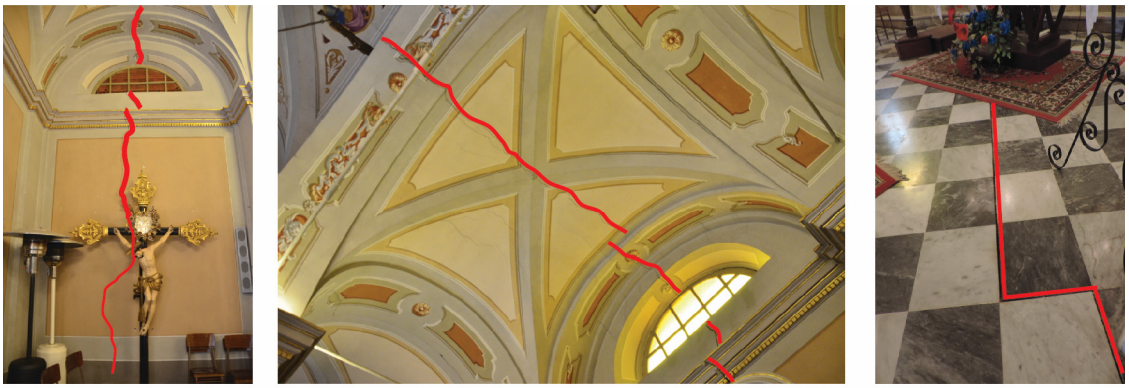


a) b)

Figure 2: San Martino church in Cembrano: a) position of the church and inclinometers on landslide maps, b) damage pattern.

Between 2010 and 2016 the landslides LD1 and LD2, which are classified as slow-earth flows, were monitored by a system of inclinometers installed in the area within the framework of the REMOVER monitoring project (Figure 2a). Inclinometer S1, which is located next to the church, proved the absence of active landslides in the surrounding area. Indeed, negligible values of horizontal displacements were recorded. Conversely, inclinometers S4 and S5 indicated the occurrence of mass movements. In particular, inclinometer S4, located along the east flank of landslide LD2, recorded a displacement of about 6 mm in 6 year in the south-east direction, while inclinometer S5, located on the highest part of the main scarp of landslide LD2, registered a displacement of about 56 mm in 6 year in the south direction.

The crack pattern surveyed in San Martino church is reported in Figure 2b. Extensive and severe damage is observed throughout the building. Significant cracks are present in the longitudinal walls in the middle of each bay (Figure 3a). In the first two bays behind the façade cracks are vertical, while in the third bay they exhibit a diagonal orientation up to the window and then they become vertical. These cracks progress along almost the entire height of the wall, increasing in width with height, and continue up into the arches and vaults above, cutting them transversally (Figure 3b). Conversely, no continuity is observed with the gaps of the floor. Since cracks propagate downwards with descending closure, such a crack pattern (colored in red in Figure 2b) can be associated with tensile stresses occurring in the upper walls due a concave-upward bending (hogging) of the structure along the longitudinal axis of the church. Such a hogging mechanism is consequence of incremental vertical ground movements in the longitudinal direction of the building. Since landslide LD1 moves in this direction, it is reasonable to assume that this one caused the observed hogging mechanism and corresponding crack pattern.



a) b) c)

Figure 3: Damage observed in San Martino church in Cembrano: a) vertical cracks in the longitudinal walls, b) cracks continuing up into arches and vaults, c) parallel oblique gaps in the floor.

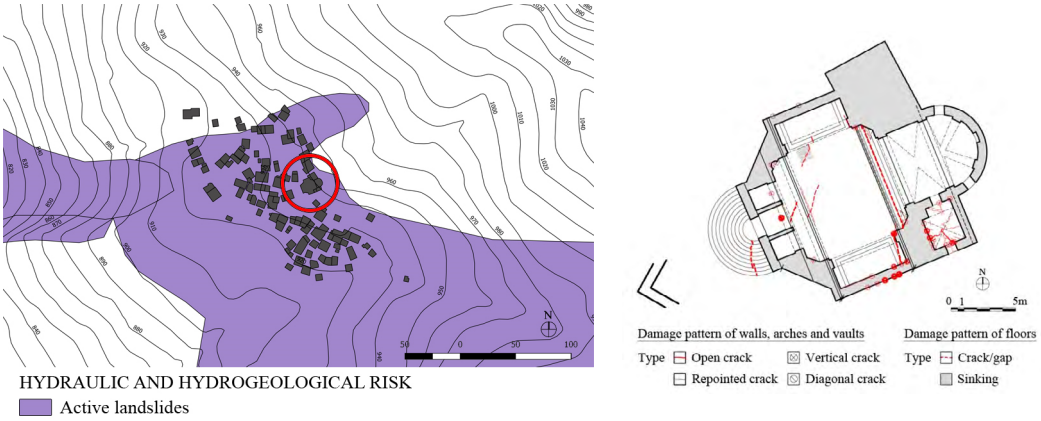
In addition to the damage pattern described above, the presence of three parallel gaps (i.e. separations developing at the joints among tiles [1]) cutting diagonally the entire floor is observed (Figure 3c). Gap width ranges from 3 mm to 10 mm, for a total of 24 mm along the entire length of the naves. Diagonal cracks are also observed in some vaults of the central and left nave, oriented in the same direction as the gaps of the floor. One of these cracks also continues into the barrel vault of the presbytery at mid-span. The horizontal separation among tiles, amounting in total to 24 mm, suggests that the church was subjected to a horizontal movement in the direction perpendicular to the gaps of floors (and cracks of vaults). As shown in Figure 2b, the latter corresponds to the direction of movement of landslide LD2. Consequently, the crack pattern shown in blue in Figure 2b can be associated to an extension mechanism produced by landslide LD2. It is important to highlight that this outcome does not conflict with the negligible values of horizontal displacements recorded by inclinometer S1 between 2010 and 2016. Indeed, the landslide was monitored for a very short time compared to the history of church. Furthermore, it is known that the cracks currently visible can be dated back at least to 2012, thus they probably occurred before the monitoring system was installed. On the other hand, the significant horizontal displacements measured by inclinometer S5 indicates that landslide LD2 is characterized by a significant component of horizontal movement, which is congruent with the crack pattern observed in the church.

3.2 San Bernardo da Mentone church in Ascona

San Bernardo da Mentone church is located in Ascona village in the municipality of Santo Stefano d'Aveto (Genova province). Built between 1827 and 1837, the church is the only building in the surroundings with a Greek cross plan. The church, which is 19 m long and 15 m wide, consists of a single nave with presbytery and semicircular apse. The bell-tower and the canonical house are placed against the presbytery on the left and right side, respectively. The nave is covered by a central sail vault surrounded by 4 lateral barrel vaults with lunettes. The presbytery is covered by a barrel vault with lunettes, while the apse presents an umbrella vault.

San Bernardo da Mentone church is located in a steep area characterized by an average slope angle of 20°. In particular, the church is situated along the right flank (as viewed from the

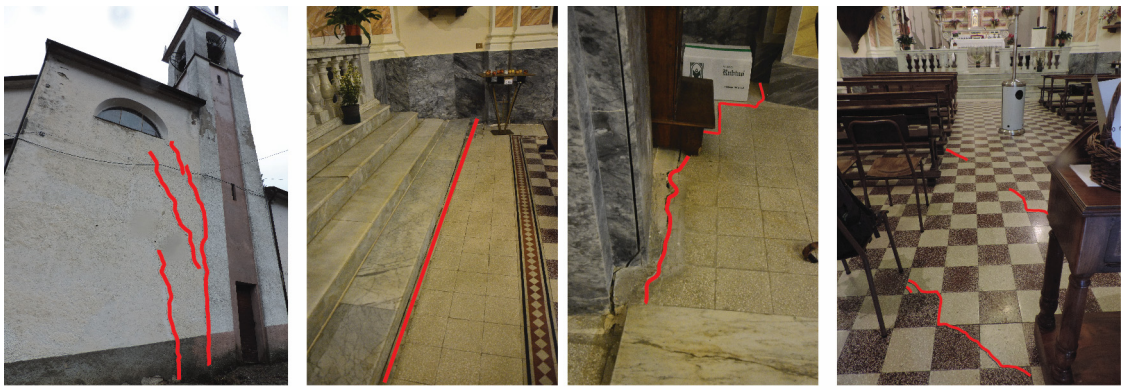
crown) of an active landslide classified as complex (Figure 4a). As shown in Figure 4b, the direction of the landslide movement is parallel to the longitudinal axis of the church.



a) b)

Figure 4: San Bernardo da Mentone church in Ascona: a) position on landslide maps, b) damage pattern.

The crack pattern observed in San Bernardo da Mentone church is depicted in Figure 4b. Both longitudinal walls present large diagonal cracks extending from the ground level and propagating upwards towards the façade (Figure 5a). A large gap crosses transversally the entire floor at the intersection between nave and presbytery (Figure 5b). It is observed that this gap propagates between the cracks of the longitudinal walls. A series of parallel oblique cracks is also detected in the floor (Figure 5c). Furthermore, minor cracks can be observed in the walls and vaults of the canonical house.



a) b) c)

Figure 5: Damage observed in San Bernardo da Mentone church in Ascona: a) diagonal cracks in longitudinal walls, b) large gap/crack in the floor, c) parallel oblique cracks in the floor.

The diagonal cracks occurring in the longitudinal walls at both sides of the church suggest that the building suffered a shear deformation due to differential vertical ground movements in the direction of the longitudinal axis of the church. On the other hand, the large separation among tiles present in the floor at the intersection between nave and presbytery indicates the presence of horizontal displacements. Since both components of ground movements are

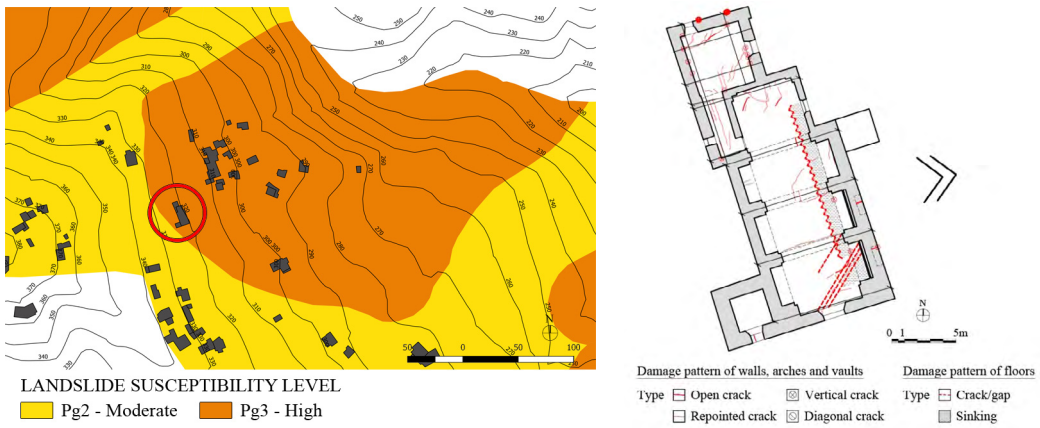
present, it can be assumed that the damage observed in the building was produced by the landslide acting in the area. In this respect, it can also be observed that the crack pattern is congruent with landslide direction since cracks occur in planes orthogonal to the slope movement. It is important to point out that the significant slope of the area where the church is located can contribute to the presence of both vertical and horizontal soil displacements of significant magnitude.

The crack pattern observed in the church also suggests the presence of a separation between the nave and the presbytery. This can be associated either to a different response of the two parts of the building to soil displacements or to the presence of soil discontinuities, which can produce localized differential ground movements when triggered by landslide phenomena.

3.3 San Lorenzo church in Sorbolo

San Lorenzo church is located in the village of Sorbolo in the municipality of Follo (La Spezia province). The construction of the church dates back to the end of the seventeenth century. The church, which is 25 m long and 9 m wide, consists of a single nave, terminating in an almost squared apse, and a sacristy. The access to the sacristy is possible through a corridor connected to the apse area. A bell-tower is located on the left side of the façade. The nave is covered by a barrel vault with lunettes, while the apse presents an umbrella vault. The sacristy and the corridor are covered by a pavilion vault and a barrel vault, respectively. In the last decades the church was subjected to some structural interventions aimed to strengthen the foundations (i.e. micropiles along the external walls) and repair the significant damage produced by slope movements and worsened by floods. The floor was also refurbished.

San Lorenzo church is located on a steep slope characterized by an average slope angle of 24°. In particular, the church stands on a terrace bounded to the east by a retaining wall. As shown in Figure 6a, the area where the church is located is characterized by a high level of landslide susceptibility [11] and is affected by the presence of a rotational and translational dormant landslide. As shown in Figure 6b, the estimated landslide direction is almost perpendicular to the longitudinal axis of the church.



a) b)

Figure 6: San Lorenzo church in Sorbolo: a) position on landslide maps, b) damage pattern.

The crack survey of San Lorenzo church is depicted in Figure 6b. It is important to point out that the authors reported the damage currently visible in walls and vaults, while the damage of floor, which was refurbished, was reconstructed thanks to some pictures dating back to 1994. The floor presented extensive damage in the form of gaps among tiles and sinking. In particular, close to the right longitudinal wall, the floor was affected by a saw-tooth gap extending longitudinally over almost the entire length of the nave and presbytery (Figure 7a). In that area, a significant sinking of the floor could also be observed. Furthermore, multiple parallel oblique gaps accompanied by sinking were noticed in the floor of the first bay behind the façade. Damage of walls is localized in the sacristy, which exhibits two large cracks in the north external wall. Regarding vaults, only few minor open cracks can be observed in both the nave and sacristy.



a) b) c)

Figure 7: Damage observed in San Lorenzo church in Sorbolo: a) saw-tooth longitudinal gap and sinking, b) out-of-plumbness of longitudinal walls, c) distortion of transverse arches and loss of horizontality of tie-rods.

The most significant damage observed in the church are large deformations. Indeed, the building experienced a global rigid rotation downhill along its transverse axis. This can be easily seen from the presence of out-of-plumbness of the both longitudinal walls in the same direction (Figure 7b), distortion of transverse arches (Figure 7c) and loss of horizontality of tie-rods (Figure 7c). These deformations as well as the sinking of the floor on the downstream side of the church suggest that the building was subjected to incremental vertical ground movements in the direction of the transverse axis of the church. Such movements can be reasonably attributed to the landslide acting in the area since the latter is oriented parallel to the transverse axis of the building. Furthermore, such a global mechanism affecting the whole church can hardly be attributed to local subsidence or foundation settlements, which usually produce more localized damage in historical structures. Conversely, slow-moving landslides are associated to large mass movements that can affect the church in its entirety.

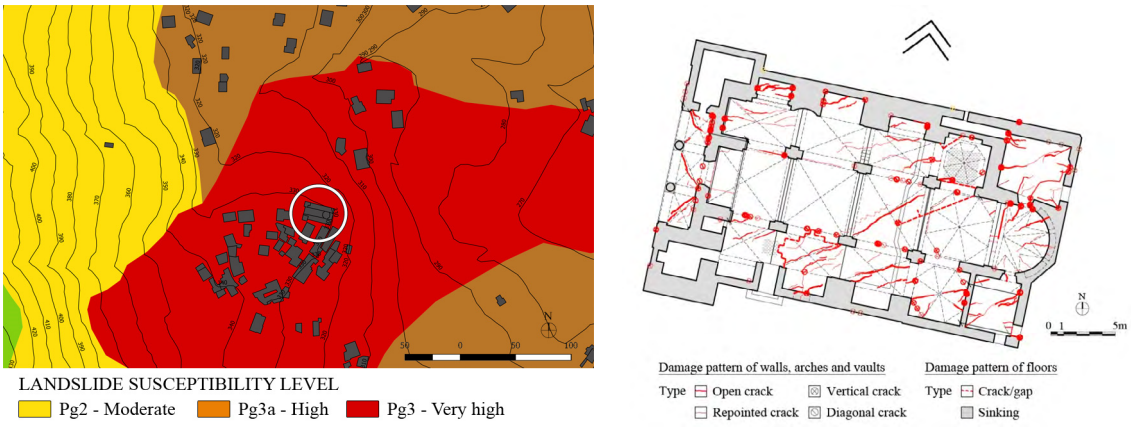
Finally, the horizontal separation between tiles observed in the floor indicates that there is also a component of horizontal movement, which is always present in the case of a landslide.

3.4 Santa Margherita church in Diano Arentino

Santa Margherita church is located in the municipality of Diano Arentino (Imperia province). The church is currently closed since it was declared not usable due to the severe damage exhibited. The church was built in the fifteenth century above the remains of a pre-existing

church. Several structural changes were performed over the centuries: in particular, the two lateral domes, the pronaos and the right bell-tower were added later. The church is 30 m large and 17 m wide. The plan consists of three naves with lateral chapels, presbytery, semicircular apse and two sacristies. The façade has a pronaos consisting of a giant colonnade and two corner towers. The central nave and lateral naves are covered by cross vaults; the transept presents three octagonal domes; the apse is covered by an umbrella vault and the sacristies present wattle pavilion vaults.

Santa Margherita church is located on slope characterized by an average slope angle of 17°. The church is situated on a large active rotational and translational landslide with an area of 23.4 hectares (Figure 8a). From the maps of the *Atlante* [13], it can be observed that in the surroundings of the church the landslide direction is almost perpendicular to the longitudinal axis of the church (Figure 8b).



a) b)

Figure 8: Santa Margherita church in Diano Arentino: a) position on landslide maps, b) damage pattern.

The crack pattern of Santa Margherita church is reported in Figure 8b. The church exhibits extensive and severe damage. The floor presents a series of parallel oblique gaps affecting both the central nave and the lateral naves. Such gaps are very large, reaching a width of some centimeters (Figure 9a). Moderate to severe damage can be observed throughout the vaults. In particular, the vaults of the central nave, lateral naves, sacristies, apse as well as the right lateral dome of the transept exhibit diagonal shear cracks (Figure 9b), all oriented in the same direction and parallel to the gaps of the floor (Figure 8b). Cracks are also visible in the transverse arches at mid-span. Severe vertical cracks can be observed in the lateral walls as well as in left side of the façade wall. These cracks progress upwards from the level of the ground and cut the structure over its entire height, continuing up into vaults (Figure 9c).

Comparing the crack pattern surveyed with landslide direction, it can be observed that vaults and floor present cracks oriented almost perpendicular to the direction of the slope movement (a certain discrepancy is obviously acceptable since the landslide direction indicated in the maps is approximate). Similarly, the cracks in the walls occur in planes perpendicular to the landslide direction. The congruence between damage pattern and landslide direction leads to the conclusion that the slow-moving landslide acting in the area is the cause of the damage experienced by the church.



a) b) c)

Figure 9: Damage observed in Santa Margherita church in Diano Arentino: a) large gap in the floor, b) diagonal shear cracks of vaults, c) vertical crack progressing over the entire height of the wall from floor to vaults.

Although no information is available regarding the magnitude of the vertical and horizontal components of movement produced by the landslide, the damage pattern observed in the church suggests the presence of a significant component of horizontal displacement. Indeed, the large gaps observed in the floor clearly indicate that tiles moved apart in the horizontal direction. Furthermore, the presence of cracks cutting the structure over the entire height, from floor to vaults, suggests that the church experienced an extension in the landslide direction. The presence of a significant component of horizontal movement again confirms that the damage observed in the church was induced by a landslide. Indeed, phenomena like subsidence or foundation settlements only produce vertical ground movements.

4 CONCLUSIONS

This paper discusses the damage mechanisms identified by the authors in historic masonry churches exposed to slow-moving landslide phenomena. Four case studies located in the Liguria region (Italy) in slow-moving landslides-affected areas were investigated. In particular, the damage patterns observed on-site were interpreted in terms of global damage mechanisms and were then correlated with the available information regarding landslide movements. The aim was to demonstrate how each damage mechanism and corresponding damage pattern can be attributed to a specific soil displacement pattern. To this end, firstly the authors assessed the congruence of the damage patterns with estimate landslide direction. This was the first step to attribute the damage observed in the churches to landslide phenomena. Then, cracks and deformations were used to identify the dominant component (horizontal or vertical) of landslide movement. This was necessary since such information was not available from advanced satellite techniques or inclinometers. In particular, the cracks of the floors were found to be good indicators of ground movements. Indeed, sinking and large separations among tiles clearly indicate the presence of vertical and horizontal soil displacements, respectively. As a result, for each of the four churches investigated, it was possible to attribute the damage mechanism to primarily vertical or horizontal ground movements along one of the main axes of the church. In the case of San Martino church in Cembrano, it was interesting to observe how the presence of two landslides acting in different directions in the surrounding area produced a combination of two different damage mechanisms.

In conclusion, this paper provides a first interpretation in terms of global damage mechanisms of the crack patterns and deformations induced to historic masonry churches by

slow-moving landslides. Future works should include structural analysis to support and verify the assumptions regarding soil displacement patterns made on the basis of visual inspections and crack interpretation.

Acknowledgements. The financial support of PRIN 2015 Program by the Italian Ministry of Education, University and Research (MIUR) is gratefully acknowledged for funding the research project "Protecting the Cultural Heritage from water-soil interaction related threats" (Prot. No. 2015EAM9S5), which is the main framework of the study presented in this article.

REFERENCES

[1] Ferrero, C., Cambiaggi, L., Vecchiattini, R and Calderini, C. Damage assessment of historic masonry churches exposed to slow-moving landslides. *Int. J. Archit. Herit.* (2020). *In press.*
[2] da Porto, F., Silva B., Costa C. and C. Modena. Macro-scale analysis of damage to churches after earthquake in Abruzzo (Italy) on April 6, 2009. *J. Earthq. Eng.* (2019) **16**(6): 739-758.
[3] Lagomarsino, S. and Podestà S. Seismic vulnerability of ancient churches. Part 1: damage assessment and emergency planning. *Earthq. Spectra* (2004a) **20** (2): 377–394.
[4] Doglioni, F., A. Moretti, and V. Petrini. *Le chiese e il terremoto.* National Research Council, Trieste, IT: Lint Press (1994) (in Italian).
[5] Saloustros S., Pelà L., Roca p. and J. Portal. Numerical analysis of structural damage in the church of the Poblet Monastery, *Eng. Fail. Anal*. (2015) **48**: 41–61.
[6] Sánchez A. R., Meli R., and Chávez M. M. Structural monitoring of the Mexico City cathedral (1990-2014), *Int. J. Archit. Herit* (2016) **10** (2-3): 254-6.
[7] Cooper A. H. The classification, recording, databasing and use of information about building damage due to subsidence and landslides. *Q. J. Eng. Geol. Hydrogeol.* (2008) **41**:3.
[8] Cruden, D.M. and Varnes D.J. 1996. Landslide types and processes. In: *Landslides: investigation and mitigation*, Transportation Research Board, Special Report 247 (1996), pp. 36-75. Washington, D.C.: National Academy of Sciences.
[9] Cascini L., Fornaro G. and D. Peduto Analysis at medium scale of low-resolution DInSAR data in slow-moving landslide-affected areas. *ISPRS J. Photogramm. Remote Sens* (2009) **64**: 598-611
[10] ARPA Piemonte (Agenzia Regionale per la Protezione Ambientale). Linee guida all'interpreazione dei dati satellitari PSInsar^{TM} in Piemonte (2008).
[11] Piano di Bacino Stralcio per l'Assetto Idrogeologico, Regione Liguria, 2017. Carte della Suscettività al Dissesto (Landslide Susceptibility Maps). Accessed October 25, 2018. http://www.pianidibacino.ambienteinliguria.it/
[12] Piano Stralcio per l'Assetto Idrogeologico, Autorità di bacino distrettuale del fiume Po, 2017. Atlante dei Rischi Idraulici e Idrogeologici (At.las of Hydraulic and Hydrogeological Risks). Accessed October 25, 2018. http://www.pai.adbpo.it/.
[13] Federici, P.R. and Chelli A. *Atlante dei Centri Abitati Instabili della Liguria. IV. Provincia di Imperia*. Regione Liguria (2007).
[14] MATTM. Geoportale Nazionale. Accessed February 13, 2020. http://www.pcn.minambiente.it/mattm/visualizzatori/

12th International Conference on Structural Analysis of Historical Constructions
SAHC 2020
P. Roca, L. Pelà and C. Molins (Eds.)

SOIL SETTLEMENT AND UPLIFT DAMAGE TO ARCHITECTURAL HERITAGE STRUCTURES IN BELGIUM: COUNTRY-SCALE RESULTS FROM AN INSAR-BASED ANALYSIS

ANASTASIOS DROUGKAS[1*], ELS VERSTRYNGE[1*], KOENRAAD VAN BALEN[1], MICHAL SHIMONI[2], THIBAULD CROONENBORGHS[2], ROALD HAYEN[3], PIERRE-YVES DECLERCQ[4] AND JAN WALSTRA[4]

[1] Civil Engineering Department, KU Leuven
Kasteelpark Arenberg 40 Box 2448, B-3001 Heverlee, Belgium
Email: {anastasios.drougkas,els.vestrynge,koenraad.vanbalen}@kuleuven.be – Web page: bwk.kuleuven.be/mat (*corresponding author)

[2] Signal and Image Centre, Royal Military Academy
Avenue de la Renaissancelaan, 30,B-1000 Brussels, Belgium
Email: {Michal.Shimoni,Thibauld.Croonenborghs}@rma.ac.be - Web page: http://www.sic.rma.ac.be/

[3] Royal Institute for Cultural Heritage
Parc du Cinquantenaire 1, B-1000 Brussels, Belgium
Email: roald.hayen@kikirpa.be – Web page: http://www.kikirpa.be

[4] Geological Survey of Belgium, Royal Belgian Institute of Natural Sciences
Jennerstreet, 13, 1000 Brussels, Belgium
Email: {pydeclercq, jwalstra}@naturalsciences.be – Web page: https://www.naturalsciences.be/en/science/do/25

Keywords: InSAR, Soil-Structure Interaction, Building Damage, Structural Monitoring, Data Analysis

Abstract. *Soil movement may be induced by a wide variety of natural and anthropogenic causes, which are detectable in the local scale, but may influence the movement of the soil over vast geographical expanses. Space borne interferometric synthetic aperture radar (InSAR) measurements of ground movement provide a method for the remote sensing of soil settlement and uplift over wide geographic areas. Based on this settlement and uplift evaluation, the assessment of the potential damage to architectural heritage structures is possible. In this paper an interdisciplinary monitoring and analysis method is presented that processes satellite, cadastral, patrimonial and building geometry data, used for the calculation of settlement and uplift damage to architectural heritage structures in Belgium. It uses processed InSAR data for the determination of the soil movement profile around each case study, of which the typology is determined from patrimonial information databases and the geometry is calculated from digital elevation models. The impact on the historic structures is calculated from the determined soil movement profile based on various soil-structure interaction models for buildings. The*

resulting damage is presented in terms of a numerical index illustrating its severity according to different criteria. In this way the potential soil movement damage is quantified in a large number of buildings in an easily interpretable and user-friendly fashion. The processing of InSAR data collected over the previous 3 decades allows the determination of the progress of settlement- and uplift-induced damage in this time period. With the integration of newly acquired and more accurate data, the methodology will continue to produce results in the coming years, both for the evaluation of soil settlement and uplift in Belgium as for introducing related damage risk data for existing architectural heritage buildings. Results of the analysis chain are presented in terms of potential current damage for selected areas and buildings.

1 INTRODUCTION

The investigation of the response of building structures to soil subsidence and uplift is of great importance [1]. Historic buildings, which are often inherently lacking in ductility and left without effective maintenance, are especially vulnerable to damage induced by soil movement. It is therefore critical to develop analysis techniques specifically for existing and historic structures.

In the study of individual structures, it is possible to adopt finite element modelling for the analysis of the structure, since computational cost is not a critical issue [2]. Analysis of larger numbers of buildings over a wider area require the adoption of different strategies for the determination of the loading and the analysis of the buildings [3]. When dealing with country-scale assessment, a level which can affect decision-making and strategy at higher administrative echelons, a different approach needs to be adopted for analysis and result presentation. Space-borne Synthetic Aperture Interferometry (InSAR) methods are a powerful tool for the determination of soil subsidence and uplift profiles [4]. Such methods can be used for the analysis of anything from a single building or small clusters of buildings to entire cities. Application in soil-structure interaction thus far has been mostly limited to the analysis over relatively limited geographic areas [5].

Major difficulties arise in attempting to determine soil movement profiles for individual buildings using InSAR over wide geographic areas. Data point density may be too low for the accurate determination of the soil movement in the area of a particular building. Therefore, the calculation of soil movement intensity parameters commonly used in analytical models [6] may be problematic.

This paper presents a method for the country-scale analysis of buildings subjected to soil subsidence- and uplift-induced damage over an extended time-period. The method consists in country-scale processing of InSAR data, the processing of patrimonial and cadastral data, the calculation of soil movement intensity parameters from limited data and the calculation of damage potentially induced over the investigated period. The method is applied in the entirety of Belgium, involving thousands of architectural heritage buildings.

2 SATELLITE DATA ACQUISITION

2.1 Data Acquisition

Ground displacement, such as subsidence, uplift and horizontal movement can be calculated using InSAR. These methods rely on the measurement of distance change between emission

antennas and points on the ground between successive satellite passages. This distance is calculated through the phase difference of the signal emitted by the antenna, reflected on the point on the ground and finally received by the antenna.
The reflection points on the ground are called Persistent Scatterers (PS) and are characterized by high amplitude of reflection and good temporal [7] and spatial [8] correlation. These points are often located on buildings or other human-made constructions (e.g. at the roofs of buildings) and provide info on the vertical velocity at which a point is subsiding or uplifting.

2.2 Data Processing

PS data is processed using the StaMPS processing chain [9]. PS data collected over 26 years is used in this study, covering the period 1992-2018. This data was collected by three satellites covering the entirety of Belgium at different time periods: ERS 1/2, EnviSAT and Sentinel 1. The number of PS identified for each time period varies, but an average of 800 PS/Km^2 was attained in urban areas where the largest number of potential reflectors is located. For the construction of ground movement velocity fields over the area of Belgium, the PS velocity data is interpolated through inverse distance weighing with a grid spacing of 10 m.

3 BUILDING DATA

3.1 Identification of Analysis Cases

The buildings to be analysed are identified through data mined from the patrimonial databases of the three federal regions of Belgium: Brussels, Flanders and Wallonia. These databases contain basic information on the age, typology and function of every registered object. Several database entries refer to objects which cannot be considered buildings or that are not affected by soil movement. These entries include natural objects, parks and sculptures or public art. Through analysis of this data it is possible to isolate entries which should be considered for analysis.
Different typologies feature different capacity for deformation under induced ground movement. Bare frames are more ductile than infilled frames, which are in turn more ductile than masonry buildings. Data extracted from the databases allows the allocation of each building to one of these three types.
Overall, 269194 analysis cases were identified for Belgium, corresponding to roughly 70% of all patrimonial database entries.

3.2 Building Polygons

Through cross-processing of the patrimonial and cadastral databases of Belgium, the plan of each building was determined, represented by a polygon on the surface of the ground. The height of every building was calculated from subtraction of the digital terrain model from the digital surface model of the country.
In the study of soil-structure interaction, the movement of soil within a certain distance of a building can induce deformation on the superstructure. In order to consider this effect, an area of influence for each polygon was calculated, consisting in an outward offset of 10 m. The PS and interpolated grid values which fall within the area of interest are considered for the calculation of potential damage in each analysis case. Due to the grid spacing of 10 m, every

analysis case is guaranteed to include several grid velocity data points. This is critical for damage calculation due to soil subsidence and uplift, which is a function of the ground deformation gradient in an area rather than simply its magnitude.

4 SOIL DEFORMATION PROFILE

4.1 Calculation of Soil Deformation Surface

Country-scale processing of InSAR data results in a low density of PS due to processing power limitations. Therefore, it is not generally possible to extract detailed soil deformation profiles from the InSAR data available. In order to overcome this problem, an approach capable of calculating a simplified soil deformation profile from limited data is presented here.
A minimum of three data points in R^3 space is required for the calculation of a three-dimensional linear surface f. By assuming that the dip direction of the surface coincides with the direction of the vector connecting two points, then only these two points are required for the calculation of the surface. In the present context, each point is defined by two geographic coordinates and a value of vertical displacement. These points are provided by the PS or interpolated grid data. Based on these parameters, a surface of the type:

$$f(x,y) = a + bx + cy \tag{1}$$

where (x, y) are geographical coordinates and f is the vertical displacement, can be calculated from two points. This simple surface allows the calculation of the vertical displacement at every coordinate pair. When more than two data points are available, the surface f is calculated from the pair of points that yields the maximum tilt ω. Tilt is defined as the ratio of relative vertical distance s to horizontal distance d:

$$\omega = \frac{s}{d} \tag{2}$$

This calculation is executed for each of the building polygons of the analysis cases. The combination of the 10 m interpolation grid with the assumption of the dip direction of f ensures that f can be calculated for every analysis case regardless of PS density in the area of the polygon.
Considering the maximum tilt for the analysis is a conservative assumption. However, this assumption is supported by two facts: a) the number of PS per building polygon is low, even in urban areas where there is an abundance of reflectors, b) the maximum tilt approach can assist in highlighting local effects near the individual buildings which might otherwise be smeared out in a country-scale evaluation of InSAR data.

4.2 Calculation of Building Polygon Loading

By substituting the coordinates of the vertices of each building polygon to function f it is possible to determine the vertical movement each vertex. Since PS data provides info on the vertical velocity, the vertical displacement is calculated by multiplication of the velocity with

the length of time of the investigated period.
By substituting the relative vertical displacement values s for the vertices of each polygon edge to eq. (2) and dividing by the length d of the edge, the tilt ω for every edge is calculated. It is thus possible to calculate the damage at different parts of the structure according to the direction of tilting in the area near each building.

5 DAMAGE MODELLING

Each structure considered for analysis was placed in one of three categories depending on structural typology: a) masonry, b) infilled frame and c) bare frame structures. These typologies generally present very different sensitivity to soil movement, with masonry being the most sensitive and bare frames being the least sensitive to subsidence and uplift.
For the calculation of potential damage of the buildings, an approach of limits on the tilt is adopted. In this approach, the tilt of all the edges in every polygon is calculated according to eq. (2). The maximum tilt among the edges of the polygon is translated to a damage index I in the range of $[0,3]$. Based on this damage index, four damage levels are considered: a) null to negligible for $I \in [0, 1)$, b) slight to light for $I \in [1, 2)$, c) moderate to severe for $I \in [2, 3)$ and d) very severe for $I = 3$. These damage levels correspond to indicative crack widths [10] as presented in Table 1.

Table 1: Correspondance between damage index, damage level and crack width in masonry strutures.

Damage index	Damage class	Crack width (mm)
0.5	Negligible	0.0 – 0.1
1.0	Slight	0.1 – 1.0
1.5	Light	1.0 – 5.0
2.0	Moderate	5.0 – 15.0
2.5	Severe	15.0 – 25.0
3.0	Very severe	>25.0

Based on the tilt limits proposed by Fischer [11], the damage index I in masonry or infilled frames as a function of the tilt ω is:

$$I(\omega) = \begin{cases} 0.75\left(0 + \dfrac{\omega - 0.000}{0.001 - 0.000}\right) & if \quad 0.000 \le \omega \le 0.001 \\ 0.75\left(1 + \dfrac{\omega - 0.001}{0.002 - 0.001}\right) & if \quad 0.001 \le \omega \le 0.002 \\ 0.75\left(2 + \dfrac{\omega - 0.002}{0.003 - 0.002}\right) & if \quad 0.002 \le \omega \le 0.003 \\ 0.75\left(3 + \dfrac{\omega - 0.003}{0.005 - 0.003}\right) & if \quad 0.003 \le \omega \le 0.005 \\ 3 & if \quad 0.005 \le \omega \end{cases} \tag{3}$$

Considering the relatively higher ductility of bare frames compared to masonry or infilled frames [12], the damage index I for bare frames reads:

$$I(\omega) = \begin{cases} 0.75\left(0 + \dfrac{\omega - 0.000}{0.002 - 0.000}\right) & if \quad 0.000 \le \omega \le 0.002 \\ 0.75\left(1 + \dfrac{\omega - 0.002}{0.004 - 0.002}\right) & if \quad 0.002 \le \omega \le 0.004 \\ 0.75\left(2 + \dfrac{\omega - 0.004}{0.006 - 0.004}\right) & if \quad 0.004 \le \omega \le 0.006 \\ 0.75\left(3 + \dfrac{\omega - 0.006}{0.010 - 0.006}\right) & if \quad 0.006 \le \omega \le 0.010 \\ 3 & if \quad 0.010 \le \omega \end{cases} \tag{4}$$

It is assumed, as shown in eq. (3), that infilled frames present the same sensitivity to subsidence and uplift as masonry structures. This assumption is supported by the fact that masonry infills are the most sensitive part of infilled frames and the location where the majority of damage in infilled frame buildings subjected to soil-movement develops. The curves of eq. (3) and (4) are plotted in **Figure 1**.

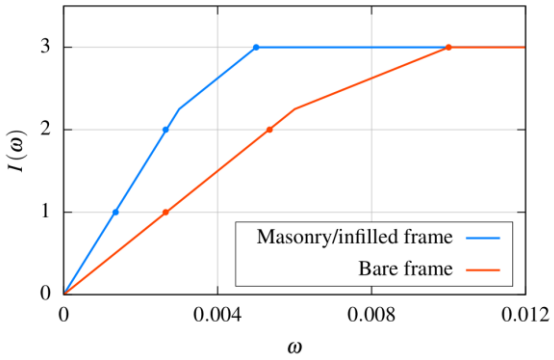


Figure 1: Damage models for tilt ω vs. damage index I.

The damage calculation is performed by accumulating the tilt that occurs during the different measurement periods. The model cannot consider damage that occurred before the beginning of the measurement in 1992. However, when manually working on individual cases, an initial damage index can be introduced, the calculation further increasing the damage index from accumulated tilt due to soil subsidence and uplift.

For the validation of the damage model, the building cases summarized by Namazi and Mohamad are used [13]. The building typology has been reported, along with a qualitative description of the damage reported. Only the cases where the tilt was directly reported were considered in this validation, amounting to 10 cases. The considered cases and the analysis results are presented in Table 2. The comparison of the reported with the predicted damage reveals that the employed damage model results in a generally accurate qualitative prediction of the damage. A small underestimation of the predicted damage is obtained in 2 cases with reported severe damage and a small overestimation is obtained in one case with moderate reported damage.

Table 2: Validation of damage model based on case studies from literature: comparison of reported with predicted damage levels. Accurate damage prediction highlighted in green, overestimation in blue and underestimation in red.

No.	Ref.	Building type	Reported damage	ω	$I(\omega)$	Predicted damage
1	[15]	RC	Severe	1/361	2.078	Moderate
2	[16]	RC	Negligible	1/900	0.833	Slight
3	[16]	Masonry	Very severe	1/240	2.688	Severe
4	[17]	Masonry	Very slight	1/520	1.442	Slight
5	[17]	Masonry	Slight	1/3330	0.225	Negligible
6	[18]	RC	Negligible	1/8333	0.090	Negligible
7	[19]	Masonry	Slight	1/388	1.933	Light
8	[22]	Masonry	Moderate	1/225	2.792	Severe
9	[23]	Masonry	Very severe	1/278	2.474	Moderate
10	[24]	RC	Slight	1/435	1.724	Light

6 ANALYSIS RESULTS

6.1 Potential Damage Calculation

The results of the analysis for the entirety of Belgium are plotted in **Figure 2**. The figure shows the number of buildings for each damage level at the end of the measurement period. The results are presented separately for each federal region and in the totals for the country.
Overall, thousands of buildings are identified as reaching or exceeding a damage index I of 0.5, which corresponds to negligible damage. While not detrimental to the structural safety of structures, distributed cracking of this type can affect durability. The number of buildings with a damage index I of 1.0, indicating slight damage, is in the several hundreds.
There is a foreseen drop in the number of buildings with potential light and moderate damage compared to the buildings with slight or negligible damage. However, there is a noticeable increase in the number of buildings with severe to very severe damage in all regions except Flanders, compared to the number of lightly to moderately damaged buildings. This is a possible effect of the conservative adoption of the maximum tilt curve f. This effect is more pronounced in Brussels, which is characterised by high-density InSAR data.
The majority of buildings with potential damage are located in Flanders, which also features the most populated patrimonial database. The number of potentially damaged buildings in Wallonia is low, yet in percentage compared to the total number of listed buildings, results are comparable among the three regions.

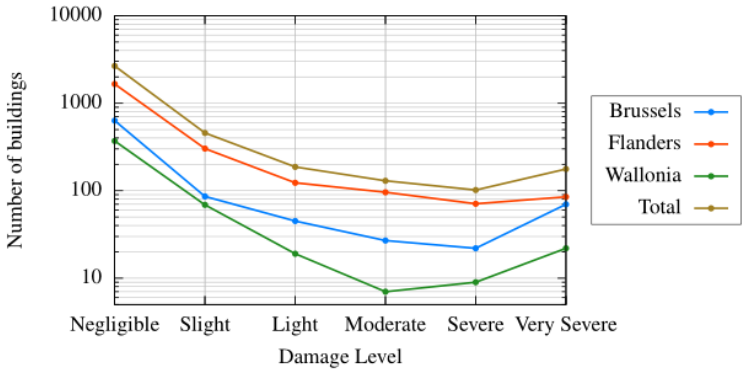


Figure 2: Potential damage analysis results for Belgium.

6.2 Verification and Evaluation of Analysis Results

The verification of the analysis results is accomplished through a sample inspection of selected buildings. Sixteen buildings were identified in the region of Limburg (Flanders) for inspection. The results of the analysis are summarised in Table 3.

Table 3: Potential damage prediction results for selected case studies.

No.	Case type	City	Building type	$I(\omega)$	Inspection
1	residential building block	Hasselt	Masonry	0.19	Negligible
2	large school building	Hasselt	Masonry	0.12	Negligible
3	public building (court house)	Hasselt	Masonry	0.32	Slight
4	public building (government)	Hasselt	Masonry	0.08	Slight
5	town house	Hasselt	Masonry	0.07	Slight
6	church and monastery	Hasselt	Masonry	0.38	Slight
7	hospital and monastery	Hasselt	Masonry	0.24	Negligible
8	industrial heritage (mining concession)	Genk	Masonry + RC	0.15	Moderate
9	public building (swimming pool)	Genk	RC	0.08	Negligible
10	church	Meeuwen	Masonry	0.21	Light
11	industrial heritage (mining concession)	Koersel	RC	0.17	Negligible
12	industrial heritage (mining concession)	Koersel	RC	0.17	Negligible
13	church with cemetery	Donk	Masonry	0.05	Negligible
14	town house	Leuven	Masonry	3.00	Severe*
15	workers' housing	Leuven	Masonry	3.00	Severe
16	coupled town houses	Leuven	Masonry	2.48	Moderate*

* Undergone structural renovation during measurement period

Despite having higher registered tilt values than other buildings in the immediate vicinity, the calculated potential damage was mostly negligible. Site inspection revealed no apparent damage for half of these structures. The other half presented slight to moderate damage, which,

according to the inspection, was sustained and repaired before the measurement period. Therefore, the analysis results are considered to be in agreement with or more conservative than the site findings. Further, three buildings were singled-out for inspection in the city of Leuven. According to the analysis results, the potential damage in one of the buildings is moderate, while in the remaining two the potential damage is severe. One of the structures with predicted severe damage presented substantial ground movement-induced damage. The other building with predicted severe damage and the building with predicted moderate damage have undergone extensive structural renovation during the measurement period. Whether the interventions were due to ground movement damage, or whether the interventions themselves are responsible for the acquired measurements, is unclear. Regardless, the acquired data was able to reflect the movement on the building.
Due to the wide scope of the analysis, the total number of buildings affected by soil movement, namely buildings with any level of potential damage, is very high. It is noted, however, that some of these damages may have already been detected and repaired in the past. Nevertheless, potential damage that has arisen in more recent periods, as well as registered high intensity soil deformation, can assist in directing and focusing site inspection and structural movement monitoring efforts.

7 CONCLUSIONS

This paper presents a method for the acquisition and processing of InSAR and patrimonial data for their use in the calculation of potential damage on existing buildings due to soil subsidence and uplift. The method is designed to be usable in cases of sparsity of InSAR data, to be practical for country-scale assessment involving thousands of analysis cases and to be applicable in cases of arbitrary soil movement profiles.
A large number of potentially damaged buildings are detected. Site inspections are in general agreement with the analysis results.
Due to its flexibility, the proposed method is in principle equally applicable to smaller-scale assessment as it is at the country-scale. It is also suitable for manual calculations in individual buildings, where pre-existing damage can be included in the analysis.

Acknowledgements. The authors wish to acknowledge the funding received by BRAIN.be, BelSPO in support of the GEPATAR research project (“GEotechnical and Patrimonial Archives Toolbox for ARchitectural conservation in Belgium” BR/132/A6/Gepatar).

REFERENCES

[1] A. Amorosi, D. Boldini, G. de Felice, M. Malena, M. Sebastianelli, Tunnelling-induced deformation and damage on historical masonry structures, Géotechnique. 64 (2014) 118–130. doi:10.1680/geot.13.P.032.

[2] A. Drougkas, E. Verstrynge, P. Szekér, G. Heirman, L.-E. Bejarano-Urrego, G. Giardina, K. Van Balen, Numerical Modeling of a Church Nave Wall Subjected to Differential Settlements: Soil-Structure Interaction, Time-Dependence and Sensitivity Analysis, Int. J. Archit. Herit. (2020). doi:10.1080/15583058.2019.1602682.

[3] D. Peduto, G. Nicodemo, J. Maccabiani, S. Ferlisi, Multi-scale analysis of settlement-induced building damage using damage surveys and DInSAR data: A case study in The

Netherlands, Eng. Geol. 218 (2017) 117–133. doi:10.1016/j.enggeo.2016.12.018.
[4] J. Walstra, C. Barbier, L.-E. Bejarano-Urrego, P.-Y. Declercq, D. Derauw, A. Drougkas, R. Hayen, F.-P. Hocquet, J.-F. Lopez, M. Shimoni, K. Van Balen, E. Verstrynge, The GEPATAR project: GEotechnical and Patrimonial Archives Toolbox for ARchitectural conservation in Belgium, in: Eur. Geosci. Union Gen. Assem. Vienna, 2018: p. 15918.
[5] P. Milillo, G. Giardina, M.J. DeJong, D. Perissin, G. Milillo, Multi-temporal InSAR structural damage assessment: The London crossrail case study, Remote Sens. 10 (2018) 20–22. doi:10.3390/rs10020287.
[6] D. Peduto, M. Korff, G. Nicodemo, A. Marchese, S. Ferlisi, Empirical fragility curves for settlement-affected buildings: Analysis of different intensity parameters for seven hundred masonry buildings in The Netherlands, Soils Found. 59 (2019) 380–397. doi:10.1016/j.sandf.2018.12.009.
[7] A. Ferretti, C. Prati, F. Rocca, Permanent scatterers in SAR interferometry, IEEE Trans. Geosci. Remote Sens. 39 (2001) 8–20. doi:10.1109/36.898661.
[8] A. Hooper, H. Zebker, P. Segall, B. Kampes, A new method for measuring deformation on volcanoes and other natural terrains using InSAR persistent scatterers, Geophys. Res. Lett. 31 (2004) 1–5. doi:10.1029/2004GL021737.
[9] A. Hooper, D. Bekaert, K. Spaans, M. Arikan, Recent advances in SAR interferometry time series analysis for measuring crustal deformation, Tectonophysics. 514 (2012) 1–13. doi:10.1016/j.tecto.2011.10.013.
[10] J.B. Burland, C.P. Wroth, Settlement of buildings and associated damage, in: Settl. Struct. Proc. Conf. Br. Geotech. Soc., 1974: pp. 611–654.
[11] D. Fischer, Interaktion zwischen Baugrund und Bauwerk, PhD dissertation, 2009.
[12] ASCE, ASCE/SEI 41-06: Seismic Rehabilitation of Existing Buildings, ASCE, Reston, Viriginia, 2007.
[13] E. Namazi, H. Mohamad, Potential damage assessment in buildings undergoing tilt, Proc. Inst. Civ. Eng. - Geotech. Eng. 166 (2013) 365–374. doi:10.1680/geng.14.00020.
[14] H. Netzel, Building Response Due To Ground Movements, PhD dissertation, 2009.
[15] A.W. Skempton, D.H. MacDonald, The allowable settlement of buildings, Proc. Inst. Civ. Eng. 5 (1956) 727–768.
[16] H. Breth, G. Chambosse, Settlement behavior of buildings above subway tunnels in Frankfurt clay, in: Proc. Conf. Os Settl. Struct., 1974: pp. 329–333.
[17] M.D. Boscardin, E.J. Cording, Building Response to Excavation-Induced Settlement, J. Geotech. Eng. 115 (1989) 1–21.
[18] J.R. Standing, Elizabeth House, Waterloo, in: J.B. Burland, J.R. Standing, F.M. Jardine (Eds.), Case Stud. from Constr. Jubil. Line Extension, London, Thomas Telford, London, 2001: pp. 547–612.
[19] J. Anketell-Jones, J.B. Burland, The Mansion House Revisited, in: Proc. Int. Conf. Response Build. to Excav. Gr. Movements, 2003: pp. 165–176.
[20] R.J. Finno, F.T. Voss, E. Rossow, J.T. Blackburn, Evaluating Damage Potential in Buildings Affected by Excavations, J. Geotech. Geoenvironmental Eng. 131 (2005) 1199–1210. doi:10.1061/(ASCE)1090-0241(2005)131:10(1199).
[21] I.A. Macleod, J.G. Paul, Settlement monitoring of buildings in Central Scotland, Geotechnique. 34 (1984) 99–117.

[22] J. Li, D.A. Cameron, Case Study of Courtyard House Damaged by Expansive Soils, J. Perform. Constr. Facil. 16 (2002) 169–175.
[23] J. Li, Case Study of Movement and Damage to a Residential Building Founded on Expansive Clays, in: Geotech. Eng. Disaster Mitig. Rehabil., 2008: pp. 689–694.
[24] C. Ou, J. Liao, W. Cheng, Building response and ground movements induced by a deep excavation, Géotechnique. 50 (2000) 209–220.

12th International Conference on Structural Analysis of Historical Constructions
SAHC 2020
P. Roca, L. Pelà and C. Molins (Eds.)

STANDARD GRAVITY AND WIND LOAD ANALYSIS ON 103 YEARS OLD UNREINFORCED MASONRY BUILDING

A. KUMAR[1*], AND K. PALLAV[2]

[1]Research Scholar Civil Engineering Department, Motilal Nehru National Institute of Technology Allahabad-211004, Uttar Pradesh, India

email: ambar006@gmail.com

[2]Senior Lecturer, Department of Civil Engineering and Surveying, Cape Peninsula University of Technology, Bellville, Cape Town, 7530, South Africa

email: kumarp@cput.ac.za

Keywords: Ancient structure, masonry building, In-situ survey, Cracks, Finite element modelling, Static analysis

Abstract.

Finite element modelling and analysis has been performed on 103-years old unreinforced masonry Senate hall building (SHB), Allahabad University, India. It is an Indo-Saracenic style of architecture which was built in 1915. An in-situ survey is conducted to know the present condition of the SHB. The major and minor cracks are visible, and construction material has deteriorated at various part of the SHB. The old documents, reports, on-site measurement, and photographs are used to gather the historical data and prepared the accurate model of the SHB on Ansys workbench (ANSYS 14.0) tool. Macro and homogenisation approach has used in the modelling of the SHB. The standard gravity and wind load analysis is performed with a fixed boundary condition on its based of SHB. In gravity analysis, maximum stress (5.69MPa) has been observed at the connections of the ground floor and maximum deformation (7.8mm) on the crown of the arch of the first-floor. The maximum stress and deformation 14.286MPa and 12.491mm have been observed under live load analysis. Further, the maximum stress and deformation obtained under wind load analysis are 4.10MPa and 8.07mm, respectively. The finite element simulation and visual inspection of the SHB are in good agreement with the present condition of the structure.

1 INTRODUCTION

The Allahabad is one of the very famous and holy cities of Uttar Pradesh, India [1]. The city is located on the confluence of three holy rivers Ganga, Yamuna, and invisible Saraswati which is also known as SANGAM. The unwritten record of history has preserved in buildings like temples, churches, fortresses, mosques, sanctuaries, and cities built of brick and stone. Early efforts to build permanent shelter were limited to the materials. These materials afforded an only primitive opportunity for protection, security, and defence of the shelter. But the stone and brick were used in many architectural remains to date as far back as the ancient walls of 8000 B.C. The study of old historical structures is a very challenging and challenging task due to unknown history, plans, construction techniques, materials, renovation/retrofitting in the past. The engineering study on the old structures is very limited in context to Indian scenario [2-4].

The Senate Hall Building (SHB) is an excellent example of Mughal and British techniques like as architectural style, construction techniques and structural elements. *Allahabad University* is established on 23rd September 1887, and it is the fourth oldest university of India after Calcutta, Bombay and Madras universities. The university building was designed by *William Emerson*, who has also designed *Victoria Memorial* in Calcutta and *Crawford Market* in Mumbai, in a combination of *Indo-Saracenic, Egyptian* and *Gothic styles*. Sir Swinton Jacob designed the building in 1909, and after one the year 1910 construction has been permitted. The foundation of the building was laid on 17th January 1910 by Chancellor *Sir John Havett*. The construction of the building was started in 1910, and they were finished in 1915. The SHB is an excellent example of the *Indo-Saracenic style of architecture,* as shown in Fig. 1. In SHB, the mixture of both as detailing and craftsmanship of yellow sandstone presents a wonderful view.

The two-storey building is built upon 1.07m thick plinth level with a load-bearing wall of cellular wall arrangement. The building supports large halls, wide verandah, naves, and jack arch roof. The entire SHB has been built up to second-floor level, and only towers are built up to higher levels. The SHB is symmetrical in the plan at the ground and first-floor level. More than one hundred respected officers and staffs are working in this building. The building is composed of thick walls, arches, towers, columns, vaults, and domes. The three large halls are built on the ground floor level *viz*., *Meeting hall (ME), Examination Hall (EH)* and *central hall* (*CH*). The geometrical dimensions of the *ME* and *EH* are same, and these halls are situated on both side of the *CH. CH* is the biggest hall among all three halls. The CH is spacious with twelve doors and sixteen windows are situated at North, South, East, and West masonry walls on the ground floor level. The SHB is used for meeting, examination, convocation, conferences, social and cultural activities. Figure 1 shows that the brick masonry is coloured with yellow and stone materials is coloured with red.



Figure 1: Senate Hall Building, Allahabad university

2 GEOMETRICAL PLAN

The engineer-in-charge of the university has provided all the details on the geometrical plan and its past repair and renovation background of the SHB. The geometrical model is prepared with the assistance of the old documentation, visual inspection and photographs of the building. The geometrical dimensions of the SHB are measured from Disto meter, and tape. Figure 2 shows the drawn plan of SHB with all the dimensions.

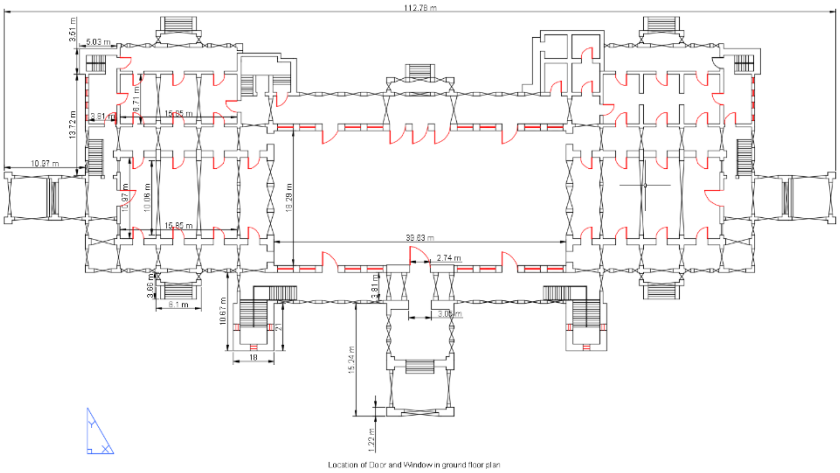


Figure 2: Geometrical plan of the SHB

3 DAMAGES OF THE SHB

The SHB has undergone two great earthquakes such as the Bihar-Nepal earthquake 1934 and Nepal earthquake 2015. The reconnaissance survey and visual inspection of the SHB were started on 17th August 2015, and this was the year of devastating 25th April 2015 Nepal earthquake. The major and minor cracks are visible on the ground floor and the second floor of the building, as shown in Fig. 3 to Fig 5. The minor cracks (approx. 1mm-5mm) are visible on the masonry wall, stone facades, crown of the arches, and connections of the ground floor. The major cracks (approx. 5mm-20mm) are visible on the stone arches through the ground floor to the second floor (Fig 3). Fig 4 shows the deteriorated plaster of ground floor and first floor of the building. The second-floor portion of the building has mostly damaged due to material deteriorating during the 2015 earthquake. The second-floor roof has been repaired time to time from concrete plaster. Approximately 2.5-inch-thick concrete plaster layer was on the east and west verandah of the second-floor level. The meeting halls roof has coated from the tar coal layer to arrest the moisture and seepage in the building. The structural elements of the building such as doors, windows, arches, ventilators and openings, were decorated for the architectural purpose.

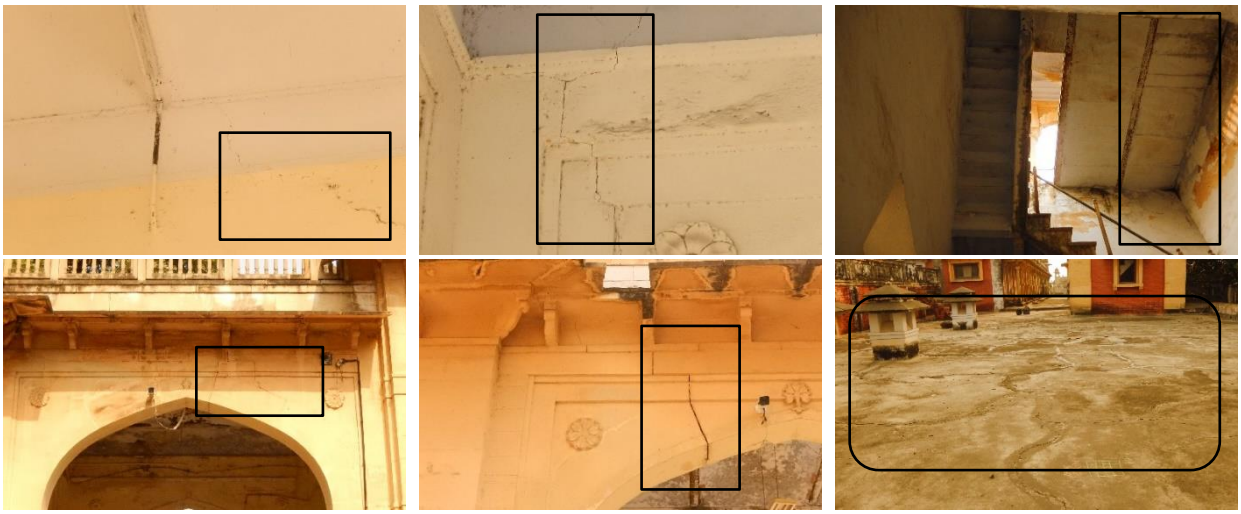


Figure 3: Major cracks (5mm-15mm) visible in the building

Fig.3 shows the deteriorated portion of the structural element in the rectangular black box. Most of the damages and failures are visible in the towers and boundary wall. The decorating element of the building is a failure in north, south and east entrance porches. The entrance of MH and EH of the building is visible major cracks on the ground floor, and first-floor level are closed from brick walls on both side entrance of the portions. Internal side plaster is deteriorated on the stairs and domes due to the effect of seepage, moisture, atmospheric variations. The Central hall bricks wall on the second floor is also deteriorated, and there is a major crack in the octagonal stone columns.



Figure 4: Material deteriorated on different structural components of the SHB

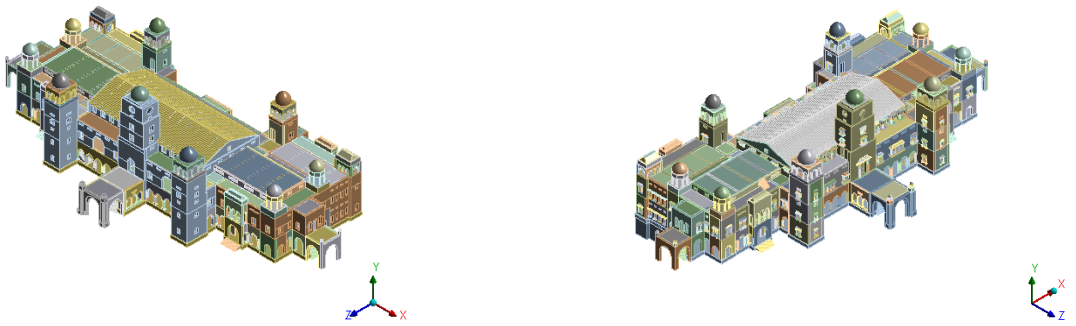
The major cracks are visible in the stone arches and columns of the SHB (Fig. 4). The administration restricts the access of the second-floor portion of the SHB due to damages roof. The meeting hall roof is covered with approximate 2.5mm thick tar-coal coating layer. The front and back verandah of the second-floor level is covered with approximately 2.5-inch thick concrete plaster, but this concrete plaster is not compatible with the old material and it is spalling out. The small plants are visible between the joints of the walls and roofs of the second-floor level.



Figure 5: Material deterioration of the SHB

4 FINITE ELEMENT MODELLING

The exact modelling of the old historical monument is difficult tasks due to unknown background knowledge *viz.*, geometry, materials, construction techniques, cracking and damages, renovation, retrofitting of the building. The macro and homogenization techniques is used in preparing the FEM model of the SHB. In the model, only structural elements have been modelled on the Ansys workbench tool (ANSYS 14.0), as shown in Fig. 6. The brick masonry and stone materials have been modelled separately in the FE model of the building. The homogenous condition has been used for masonry and stone materials of the masonry walls and arches elements. The decorating materials have not considered during the modelling and analysis of the SHB building due to microstructural components and material assign difficulties. The 3D finite element model of the SHB is shown in Fig. 6a. The convergence criteria are used for reasonably adjusting the mesh size for entire SHB (Fig. 6b). The mesh size used for masonry wall is 600mm for masonry walls, roofs 160mm, dome elements 120mm and for stone arches 100mm. Altogether, 12,85,779 nodes and 4,73,994 solid elements are created for the modelled SHB. The elements used for solid and surface element in the model are SOLID 186, SOLID 187 and SURF 154 elements. The elements in the model are joined through TARGE 170 and CONTA 174 by using bonded behaviour. SOLID 186 and Solid 187 are 3-D, 20-noded and 10-noded higher order solid element respectively. This element behaviour exhibited quadratic displacement of each node. The irregular mesh modelling is suited for quadratic displacement behaviour of SOLID 187 element. Both elements defined by ten and twenty noded elements with 3-DOF at each node: x, y, and z directions translations. The material behaviour of these elements (SOLID 186 and SOLID 187) have stress stiffening, large deflection, plasticity, creep, hyperelasticity and large strain capabilities. The simulated stresses and deformations capabilities have mix formulation such as incompressible elastoplastic materials and fully incompressible hyperelastic materials. The SURF154 is used in a surface element in the building model for accurate effect during the loading. The element applies to 3-D structural analyses. It may be overlaid on to an area face of any 3-D element.



(a) 3D finite element modelling of the SHB



(b) Meshed model of entire SHB

Figure 6: Finite element modelling of the SHB

5 ANALYSIS

The analysis of old historical structures is a challenging task due to unknown material properties, connections, hidden cracks, damages, etc. In the present model, cracks and damages are not being modelled. The evaluation of mechanical properties of ancient structures is challenging, and only non-destructive testing is one source for evaluating the mechanical properties. The building has been analyzed for three different loading conditions as given by the Bureau of Indian standard *viz* gravity [18]; live load [19]; and wind load [20]. The major portions of the first and second floor of the building are closed due to damages of the structural element. The live load has been considered for accessible and non-accessible portions on the building. The wind pressure has been calculated from the Indian code and distributed along with the height of the building (Table 1). The prominent wind direction for the towers is from the south and west direction. The analysis of the SHB has been considered for a fixed base. Table 2 shows the material properties evaluated through NDT testing (Rebound hammer, Rebar Locator and Ultrasonic Pulse Velocity Test). The analyses show the maximum von-Mises stress and deformation of the SHB building. The analyses show the observed weak connections, maximum stresses positions, to suggest for strengthening and retrofitting of structural elements and joints.

Table 1: Variation of the wind pressure of the SHB

Height (m)	Terrain Category 3 class B	Design wind speed (m/s)	Design wind pressure (N/m^2)
10 m	0.88	44.26	391.71
15 m	0.94	47.27	446.94
20 m	0.98	49.28	485.78
30 m	1.03	57.80	536.62
50 m	1.09	54.52	600.96

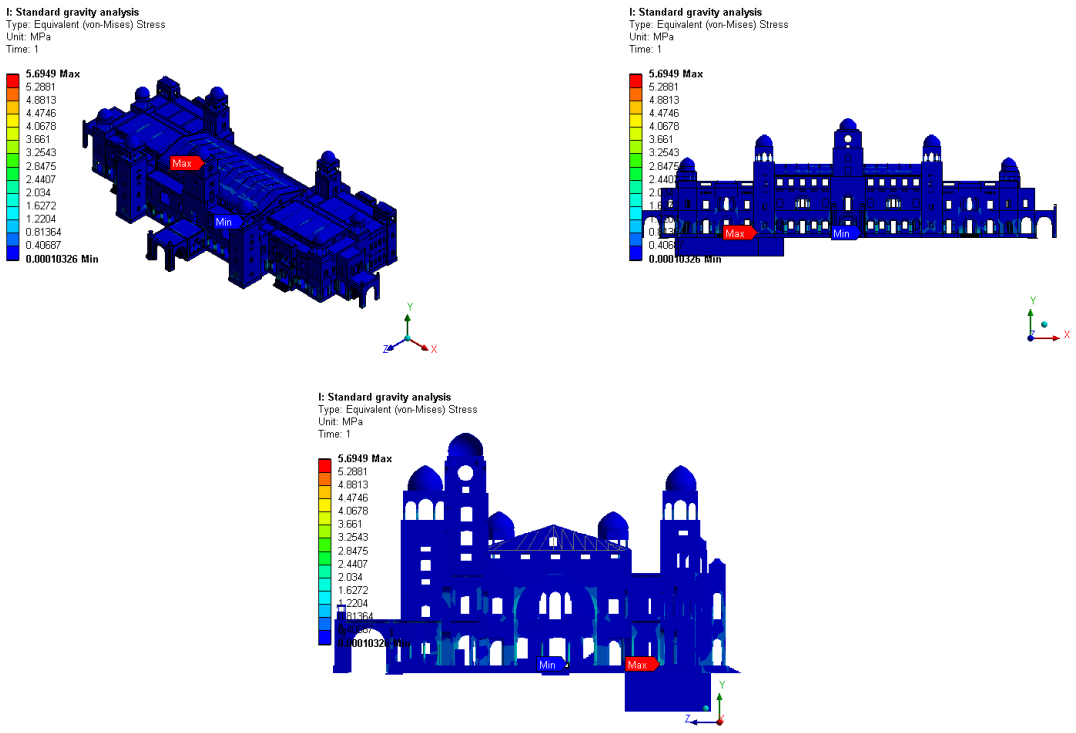
Table 2: Mechanical properties of the SHB

Floor	Density ρ (kg/m^3)	Young's Modulus E (MPa)	Poisson's ratio (μ)
Brick masonry	2100	2400	0.2
Stone	2400	6470	0.2

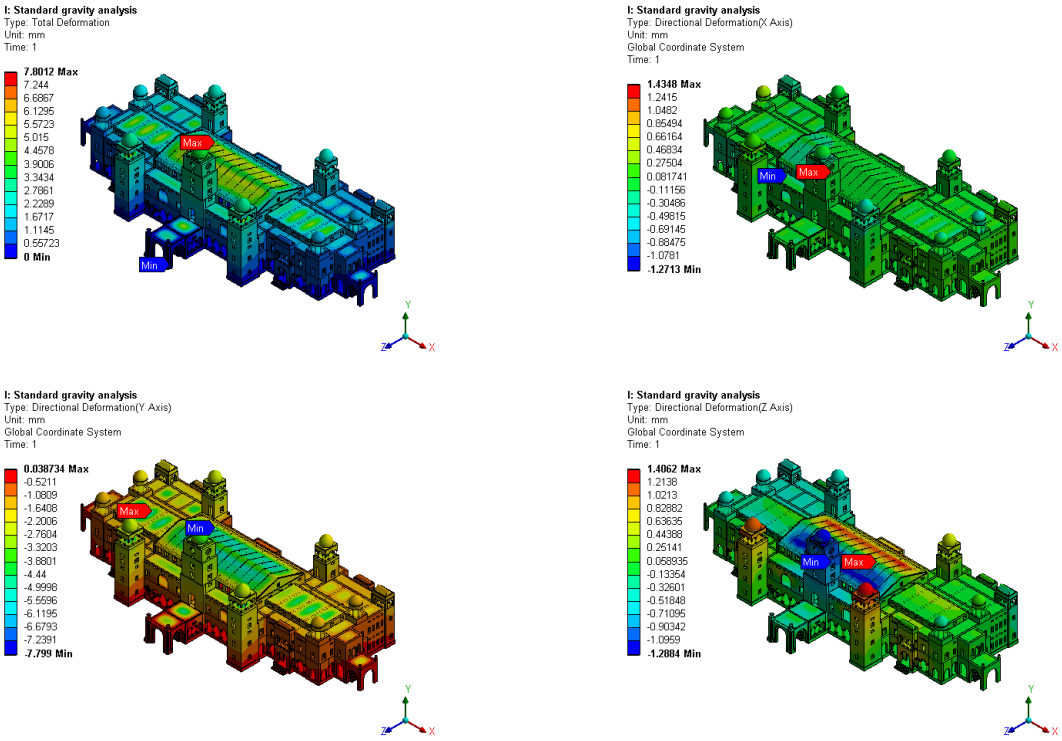
6 RESULTS AND DISCUSSION

Fig. 7 shows the stress and deformation response to gravity load analysis. The maximum stress of 5.69MPa is observed on the connection between the back verandah wall and the ground floor of the stair tower. The stress is negligible on the ground floor masonry walls, and this may be due to its thickness that provides a large area to transfer the building load. The brick masonry walls of the central hall and side halls on the ground floor perform better than the stone masonry walls. The observed stress on the internal portion of stone arches, columns and facades of the meeting and examination hall are in the range of 1.62MPa to 2.03MPa and it is shown in Fig. 7a. The major stress has affected the connection between wall to wall, wall to the roof, roof to the tower of the building from the ground floor to the second floor. The maximum deformation of 7.80mm is observed at the second-floor of south facade wall of the central hall. The directional deformation of the entire building has observed negligible. The longitudinal and transverse directional deformation of the building is observed approximately similar to 1.4mm, but vertical directional deformation of 0.03mm is observed at first-floor wall of the meeting hall. The overall deformation response of the SHB is shown in Fig. 7b. The deformation of the clock tower and side stair tower is observed in the range of 3.9mm to 4.45mm from the third floor to sixth-floor level.

Fig. 8 shows the stress and deformation response of the SHB due to live load. The maximum stress 14.28MPa has been observed on the openings of the window and connections between wall and roof joint of the second-floor level. The in-situ survey of the SHB shows the major cracks and damages on the stone columns, arches and walls on the position of critical stresses. The stresses on stone arches of the meeting hall and examination hall are observed in the range of 5.1MPa to 6.1MPa, respectively. The maximum deformation of 12.49mm has observed on the floor of second-floor and at the roof of the central hall in the building. The truss sections are designed from I-section; the access of these portions is restricted.



(a) von Mises stress behaviour of the SH building

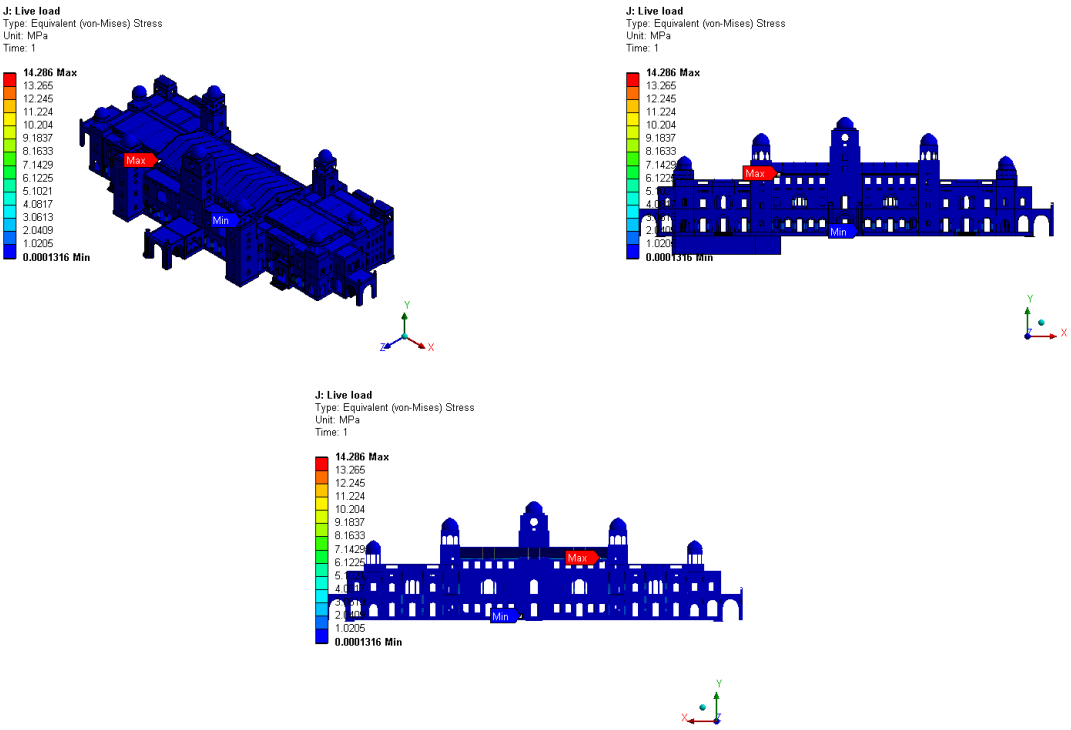


(b) Deformation behaviour of the SH building

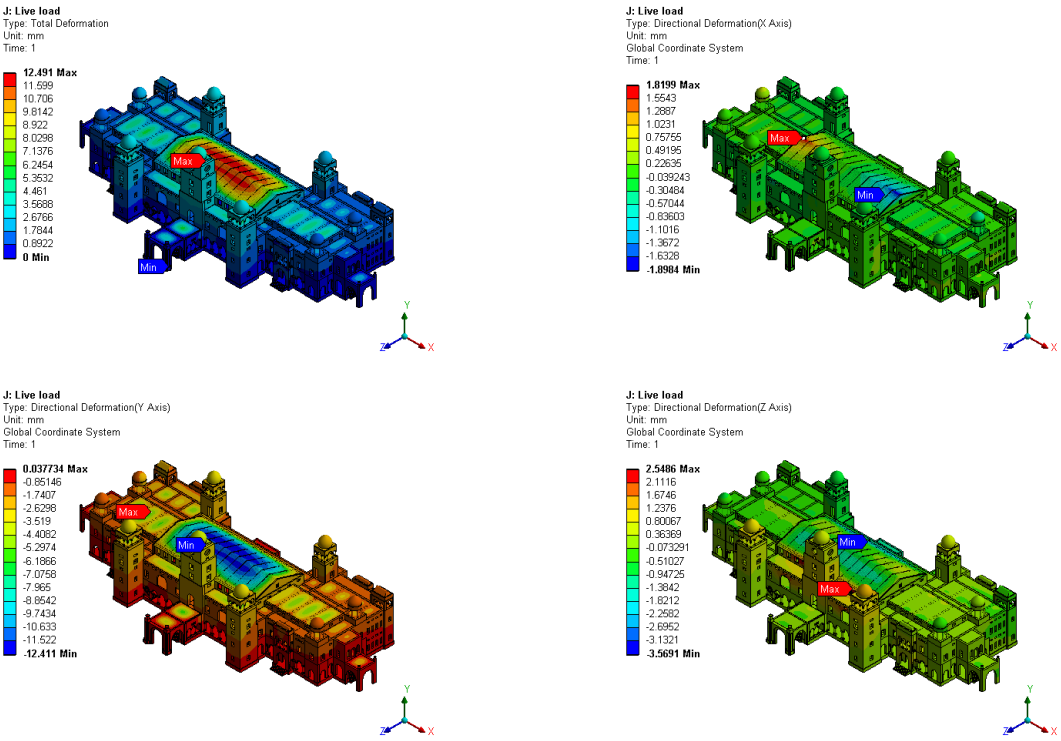
Figure 7: von Mises stress and deformation behaviour during gravity analysis

The longitudinal and transverse deformation has been observed on the second floor as 1.51mm and 2.54mm on the South-central hall wall and North stair tower, respectively. The vertical deformation of 0.03mm is observed on the second-floor masonry roof at the examination hall. The tower of the SHB building is geometrically stable for gravity and live load. The masonry walls are performing better than arches and roof elements of the building.

Further, to know the stress generated through the lateral load; wind analysis has been performed on the SHB building. The maximum stress of 4.10MPa is observed on the wall of the ground floor level between the central hall and examination hall verandah. The stress range on the octagonal columns, domes, tile roof, the balcony from 0.87MPa to 1.17MPa. Front corner tower has observed the stress 1.75MPa to 2.05MPa at the ground and first-floor level. The maximum deflection 8.07mm is observed on the verandah (backside) of the second-floor. The longitudinal and transverse direction deformation is estimated as 1.30mm and 1.33mm, respectively. The vertical directional deformation 0.04mm of the building has observed as negligible at the second-floor level.

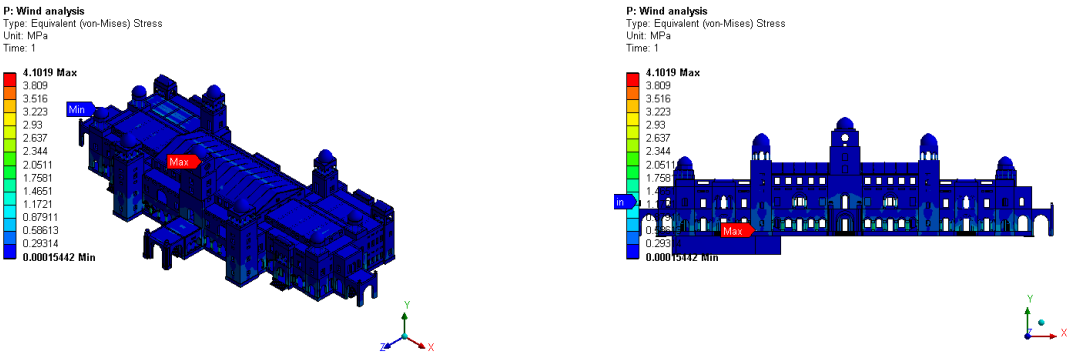


(a) von Mises stress behaviour of the SH building

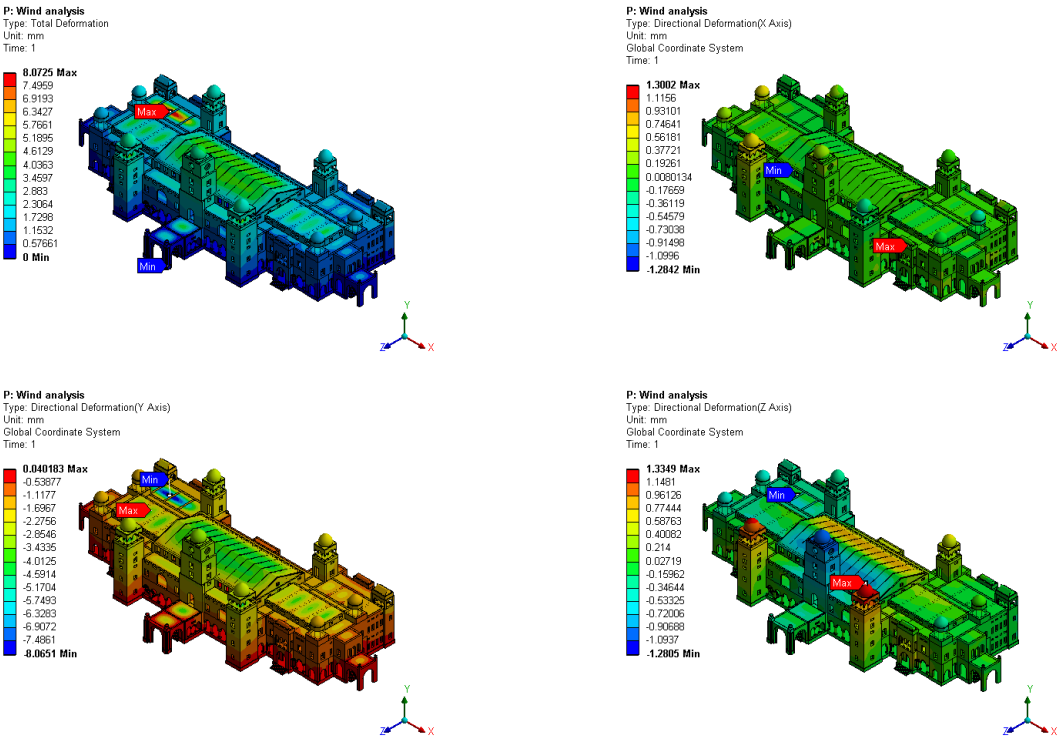


(b) Deformation behaviour of the SH building

Figure 8: von Mises stress and deformation behaviour during live load analysis



(a) von Mises stress behaviour of the SH building



(b) Deformation behaviour of the SH building

Figure 9: von Mises stress and deformation behaviour during wind analysis

7 CONCLUSION

The paper has presented a finite element approach for an unreinforced historical building of Allahabad University which is an excellent example of the Indo-Saracenic style of architecture. The in-situ investigation and retrofitting solutions are suggested to conduct computationally expensive instruments (e.g., time history method, kinematic analysis and pushover analysis) with more sophisticated ones (e.g., microelement approach) can offer proper indications in the structure. The study on the senate hall building leads to the following conclusions. The building is massive in its configuration which provides adequate stability to the structure. In a reconnaissance survey, the major cracks and damages are shown on various structural elements and the openings of the building due to previous earthquakes events and weathering effect. The structural configuration of the building is adequate to withstand the vertical and horizontal loads during the gravity and wind

loads. The entrance porches of the building are more vulnerable on the ground floor level. The analysis suggests that most of the elements of the building need retrofitting and also connections needs to repair between the element. Most of the portion of the building is renovated with new material.

Acknowledgements. The authors would like to thanks Mr Naveen Kumar civil engineer and their staff, who very graciously provided access to the building and gratefully acknowledged for making possible the cooperation between the knowledge about the geometric survey, renovation and retrofitting of the SHB.

REFERENCES

[1] MISRA, R.N., "Architectural Triveni of Allahabad and Asphyxiation of a Monumental Dream (P.K. Acharya and his Manasara)". https://goo.gl/9VGxvy

[2] Dubey, R.N., Thakkar, S.K., Gupta, A., "Seismic analysis for safety evaluation of Taj Mahal Monuments", Eleventh Would Conference on Earthquake Engineering, ISBN: 0080428223.

[3] Ramos, L.F., Casarin, F., Algeri, C., Lourenco, P.B., Modena, C., (2006), "Investigation Techniques Carried out on the Qutb Minar, New Delhi, India", *Structural Analysis of Historical Constructions*, New Delhi. https://bit.ly/2WS3jeS

[4] Pena, F., Lourenco, P.B., Mendes, (2008), "Seismic Assessment of the Qutb Minar in Delhi, India", 14th World Conference on Earthquake Engineering October 12-17, Beijing, China. https://bit.ly/2w89IXI

[5] Cakir, F., Uckan, E., Shen, J., Seker, B.S., Akbas, B., (2015), "Seismic damage evaluation of historical structures during Van earthquake, October 23, 2011", *Engineering Failure Analysis*, 58, 249-266.

[6] Mosoarca, M., and Gioncu, V., (2013), "Failure mechanisms for historical religious buildings in Romanian seismic areas", *Journal of Cultural Heritage*, 14S, 65-72.

[7] Shakya, M., and Kawan, C.K., (2016), "Reconnaissance based damage survey of buildings in Kathmandu valley: An aftermath of 7.8 Mw, 25 April 2015 Gorkha (Nepal) earthquake", *Engineering Failure Analysis*, 59, 161-184.

[8] Lirola, J.M., Castaneda, E., Lauret, B., Khayet, M., (2017), "A review on experimental research using scale models for buildings: Application and methodologies", *Energy and Buildings*, 142, 72-110.

[9] Sassoni, E., Mazzotti, C., Pagliai, G., (2014), "Comparison between experimental methods for evaluating the compressive strength of existing masonry buildings", *Construction and Building Materials*, 68, 206-219.

[10] Gracia, V.P., Caselles, J.O., Clapes, J., Martinez, G., Osorio, R., (2013), "Non-destructive analysis in cultural heritage buildings: Evaluating the Mallorca cathedral supporting structures", *NDT&E International*, 59, 40-47.

[11] Casarin, F., and Modena, C., (2008), "Seismic assessment of complex historical buildings: application to Reggio Emilia cathedral, Italy", *International Journal of Architectural Heritage*, 2, 304-327.

[12] Brandonisio, G., Mazziotti, A., Lucibello, G., Mele, E., Luca, A.D., (2014), "Seismic behaviour of four Italian masonry buildings: comparison between different modelling", SAHC2014-9th International Conference on Structural Analysis of Historical Constructions, Mexico City, Mexico, 14-17 October.

[13] Kumar, A., and Pallav, K., (2017), "Static and Dynamic analysis of Masonry tower of Allahabad University, India", VIII ECCOMAS Thematic conference on Smart Structures and materials (SMART-2017), 5th – 8th June Madrid, Spain. https://goo.gl/RYpBj1

[14] Kumar, A., Pallav, K., and Singh, D.K., (2017), "Static and dynamic analysis of stone arch of Allahabad University", International Conference on Recent Innovations in Engineering and Technology (ICRIET-2017), 18th - 19th Feb. 2017, Jaipur. [ISBN: 978-93-86291-63-9] https://bit.ly/2LRm5RD

[15] Kumar, A., and Pallav, K., (2018), "Static and dynamic analysis of unreinforced masonry wall using finite element modeling in senate hall building", The 2018 Structures Congress (Structures18) Songdo Convensia, Incheon, Korea, August 27 - 31, 2018. https://bit.ly/2STF3I5

[16] Valente, M., and Milani, G., (2016), "Non-linear dynamic and static analyses on eight historical masonry towers in the North-East of Italy", *Engineering Structures*, 114, 241-270.

[17] Milani, G., Casolo, S., Naliato, A., Tralli, A., (2012), "Seismic Assessment of a Medieval Masonry Tower in Northern Italy by Limit, Nonlinear Static, and Full Dynamic Analyses", *International Journal of Architectural Heritage*, 6, 489-524.

[18] IS:875 (Part-1) 1987, Code of practice for design dead loads for building and structures, Bureau of Indian Standards, New Delhi.

[19] IS:875 (Part-2) 1987, Code of practice for design live loads for buildings and structures. (imposed load)", second revision, part-1, Bureau of Indian Standards, New Delhi.

[20] IS:875 (Part-3) 2015, Code of practice for design wind loads for buildings and structures, Bureau of Indian Standards, New Delhi.

[21] Sivaraja, S.S., Thandavamoorthy, T.S., Vijayakumar, S., Aranganathan, S.M., Dasarathy, A.K., (2013), "Preservation of Historical Monumental Structures using Fibre Reinforced Polymer (FRP) - Case Studies", *Procedia Engineering*, 54, 472-479.

[22] Akcay, C., Bozkurt, T.S., Sayin, B., Yildizlar, B., (2016), "Seismic retrofitting of the historical masonry structures using numerical approach", *Construction and Building Materials*, 113, 752-763.

[23] Hegazy, S.M., (2015), "Conservation of historical buildings-The Omani–French museum as a case study", *Housing and Building National Research Center (HBRC) Journal*, 11, 264-274.

12th International Conference on Structural Analysis of Historical Constructions
SAHC 2020
P. Roca, L. Pelà and C. Molins (Eds.)

STATIC ANALYSIS OF A MASONRY ARCHED AND BUTTRESSED RETAINING WALL

DEFNE DOGU[1*], CLIMENT MOLINS[2] AND NIRVAN MAKOOND[2]

[1] Department of Civil and Environmental Engineering
Universitat Politècnica de Catalunya (UPC-BarcelonaTech)
Campus Nord UPC, 08034 Barcelona, Spain
e-mail: defnedogu193@gmail.com

[2] Department of Civil and Environmental Engineering
Universitat Politècnica de Catalunya
Campus Nord UPC, 08034 Barcelona, Spain
e-mail: climent.molins@upc.edu, nirvan.makoond@upc.edu

Keywords: Historical Retaining Wall, Masonry Arches and Buttresses, Photogrammetry, Stability Analysis, Lower Bound Theorem

Abstract: *The wall of Casa Salvans is a masonry arched and buttressed retaining wall which was built in 1909 and located in Terrassa, Catalonia. It contains a series of 11 arches of unique shapes, dimensions and inclinations that are supported on buttresses. Despite being a common retaining wall typology, it can be very challenging to assess the stability of such structures given the variability of their geometry. As such, a systematic methodology for the stability assessment of such walls was developed and applied to the case of the wall of Casa Salvans. Self-produced photogrammetry survey enabled creating accurate three-dimensional models of the front of the wall that were later combined with available information from a topographic survey to build cross sections of the wall for analysis. Modern retaining wall design principles evaluating the stability against overturning and sliding were used to assess the condition of the wall. As a consequence of the uncertainties related to the soil parameters and buried elements of the wall, the stability factors could not comply with modern design criterion. Some parametric analyses were carried out on the shear strength parameters of the backfill, revealing that slight increases in the soil internal friction and wall friction angles enhance the stability factors significantly. Since reasonable soil internal and wall friction angles justifying the stability of the wall were obtained, carrying out a geotechnical survey to determine the actual values was recommended. The in-plane stability of the arches was also verified according to the Lower Bound Theorem by locating a thrust line that fits within all the boundaries despite very conservative geometric assumptions.*

1 INTRODUCTION

The wall of Casa Salvans, located in Terrassa, Catalonia, was built in 1909 by the architect Lluís Muncunill i Parellada. It is a spectacular example of a common retaining wall typology that restrain hard, unsaturated soils through a series of arches connected at buttresses. The

masonry retaining wall, made of pebble stones bonded by mortar, has a total length of 144 m and a maximum height of 11.5 m. This study is focused on the section of the wall that contains 11 arches of varying shapes and dimensions, connected by buttresses. The arches have an instrumental role in load transmission to the buttresses, which are significantly thicker than the wall, enabling the use of less material throughout the wall.

The height, the span and the thickness of the arches increase as one follows the descending slope of the adjacent path (Figure 1) The enumeration of the arches adopted throughout the study imply that Arch 1 has the smallest dimensions while Arch 10 has the largest and Arch 11 is the half arch at the end.

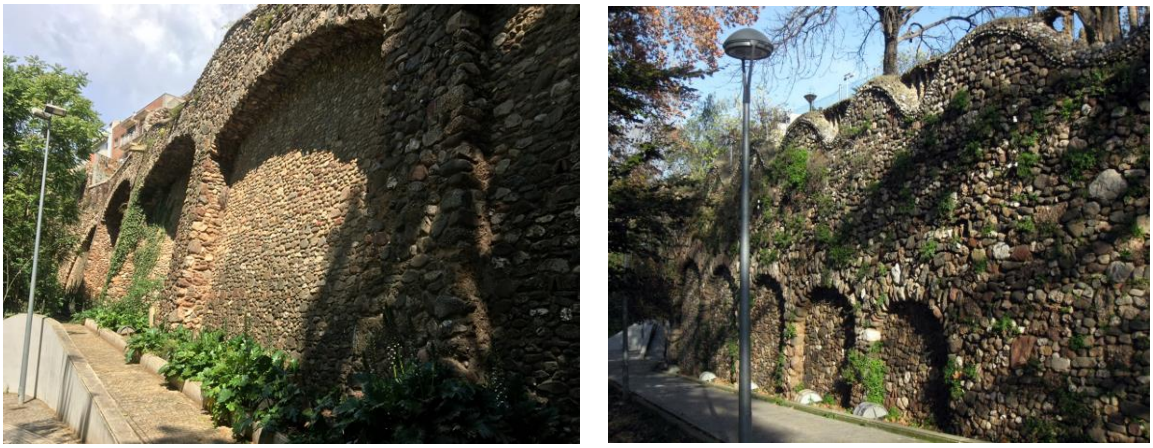


Figure 1: Bigger arches of the wall of Casa Salvans on the left, smaller arches on the right.

As a consequence of the uncertainties related to hidden morphology and soil characteristics, the stability assessment of the wall can be challenging. This study presents a systematic methodology used to address this issue. Firstly, a photogrammetry survey was carried out. Measurements made from the resulting models were then combined with available information to build an idealized geometric representation of the structure. Since no large cracks or detached parts could be found during visual inspections, partial collapse mechanisms were not considered. An initial stability analysis, based on the estimates of the soil parameters, is followed by a sensitivity analysis which aims to comprehend the effect of key geotechnical parameters on the overall stability. Finally, the in-plane stability of the wall is verified according to the Lower Bound Theorem of Limit Analysis.

2 AVAILABLE INFORMATION

2.1 Detailed drawings

Municipality of Terrassa provided detailed plan and elevation drawings obtained through previously performed laser scanning (Figure 2). The precise drawings of the unburied parts of the front and back faces of the wall include elevations and provide useful two - dimensional information.

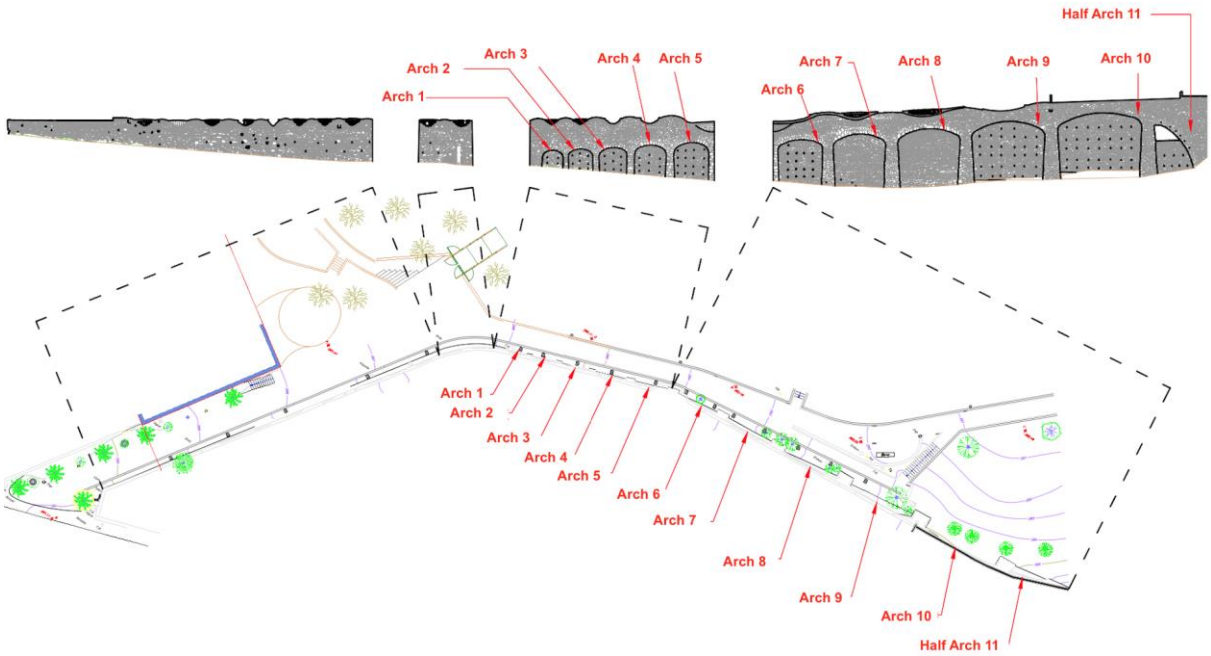


Figure 2: Elevation drawing of the front surface and plan view of the wall of Casa Salvans.

2.2 Topographic survey and exploration pits and holes

In order to gather information on the buried parts of the wall, 20 exploration pits in the ground as well as 5 exploration holes in the wall were made. A topographic survey was also carried out by the Municipality of Terrassa. The 20 exploration pits were located at the base and at the top of the wall on the buttresses and the keys of the arches.

The wall thickness below Arches 8, 9 and 10 was determined to be 0.6 m from the corresponding exploration holes. Therefore, the thickness below arch level was assumed to be constant for Arches 6 – 10 for structural calculations. From the exploration pits at the top of the wall, the extrados of Arches 6 – 9 were located at approximately 0.55 m depth. Based on these measurements, the key of Arch 10 was also assumed to be located at the same depth for the calculations.

A concrete enlargement, acting as a foundation, was located at the base of the wall below Arches 8, 9 and 10. The distance by which the concrete foundation protrudes outwards from the wall was determined to vary between 0.2 m and 0.4 m. At the bases of Arches 1 – 7, the excavations were terminated at shallower depths due to land restrictions.

2.3 Geotechnical survey

Upon request of Municipality of Terrassa, a geotechnical survey was carried out on May 2003 by the company Gesond S.A. Four boreholes of depths 14.5 m to 15 m were executed in the area behind the wall in order to determine the soil profiles, characteristics of the sub-layers and the location of the water table (Figure 3). Nine Standard Penetration Tests (SPT) were carried out at different layers and four samples were taken to be tested in the laboratory.

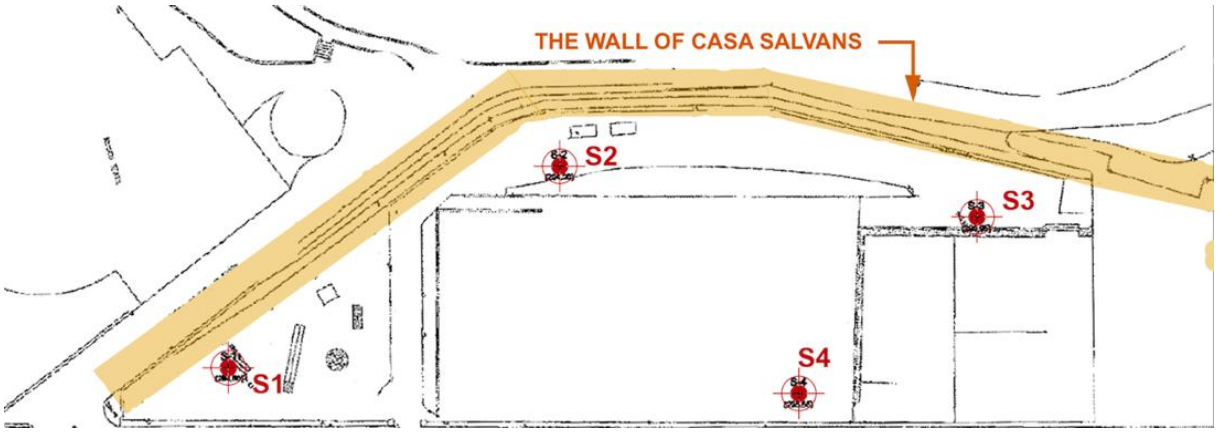


Figure 3: Location of the boreholes relative to the wall of Casa Salvans.

Three predominant layers were determined, of which the characteristics are tabulated in Table 1. Shear strength parameters, cohesion and internal friction angle, ϕ were obtained through correlations with SPT numbers of respective layers.

Table 1: Characteristics and locations of soil layers.

Layer	Characteristics	Depth(m)	γ(kN/m^3)	c_u(kPa)	Φ(°)
R	Backfill material consisting of silty sands	0.8-1.2	19	0	24
A	Alluvial soil consisting of clayey sand	10-10.2	19-21	<10	30
B	Sandy clays with layers of salt and gravel *(saturated below depths of 13.5-14 m)*	10.2 -	21	29	28

The geotechnical cross-sections derived from the stratigraphic profiles were used to estimate the prevalent soil layers throughout the wall. The geotechnical cross-sections were overlaid on the elevation drawing based on relative locations of the boreholes and matching elevations as shown in Figure 4. Considering the assumptions on the extent of the base of the wall, which will be discussed later in Section 5.1, it can be appreciated that the wall under the larger arches is resting on Layer B. At the time of the survey, the water table was located at a lower level than the wall in all boreholes enabling to neglect the effect of pore water pressure.

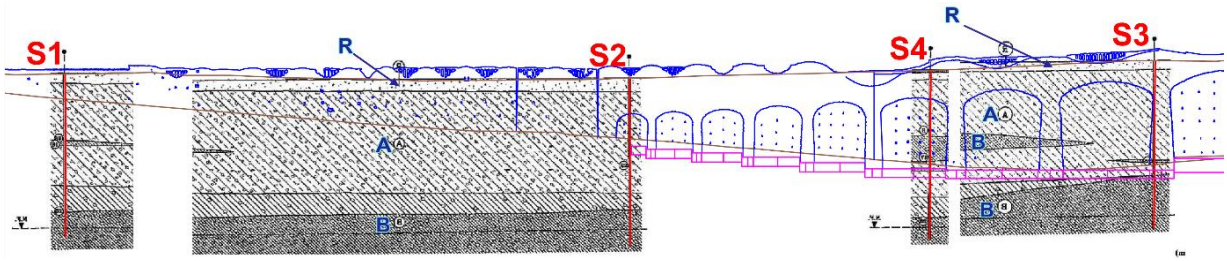


Figure 4: The approximate projection of geotechnical cross-sections on elevation drawing of the wall.

Although it can be suggested that Layer B exists at the bases of Arches 6 – 10, it is not possible to estimate the depth of the layer in contact with the wall. For these arches, Layer B

was assumed to be present only at the level of foundation base while for Arches 1 – 5, Layer A was assumed to prevail through the wall height.

3 PHOTOGRAMMETRY

As mentioned earlier, the wall of Casa Salvans has arches and buttresses of unique shapes and dimensions. Another key aspect of the wall is the front surface having an inclination that varies throughout the wall. For the structural analysis to be representative of reality, three-dimensional characteristics of the wall must be considered in the calculations. Since the available drawings only provide two-dimensional information, a photogrammetry survey was carried out to determine the three-dimensional characteristics of the visible geometry.

Photogrammetry is the science of making reliable measurements from photographs. This is usually achieved through the creation of 3D models of objects of interest. There are several factors affecting the accuracy of the final model such as the quality of the photos and the ability to capture large overlapping areas of the structure in the images. Therefore, it is crucial to take measurements during the survey in order to calibrate and validate the resulting model.

3D models of different parts of the wall of Casa Salvans, which were built using ReCap Photo [1], yielded a mean error of less than 1% over 38 distance measurements. Photogrammetry model of the part of the wall including Arch 10 can be seen in Figure 5. During the survey, markers were placed on the sides of the buttresses, providing a straight line in between, to be considered as the global x-axis in the models. In addition, the inclination of the wall at different locations was verified through inclination measurements taken on site using a plumb line.



Figure 5: Photogrammetry model of Arch 10.

4 IDEALISED GEOMETRY

The stability calculations assume that the concrete enlargement detected at several locations at the base of the wall is prevalent throughout the wall, acting as a foundation and protruding outwards by 0.30 m. Considering the common construction practices of foundations, it was deemed as appropriate to assume the same enlargement at the heel of the base.

The buttresses of Arches 8, 9 and 10 were extended by the depths measured on site. The foundation of an arch was assumed to be at the same level as its shallower adjacent buttress (Figure 6). For Arches 1 – 7, where there were no available measurements due to restricted excavations, the part of a buttress buried under ground was assumed to be 0.75 m, corresponding to the shallowest depth measured on site. The aforementioned trend was also assumed for the foundations of smaller arches.

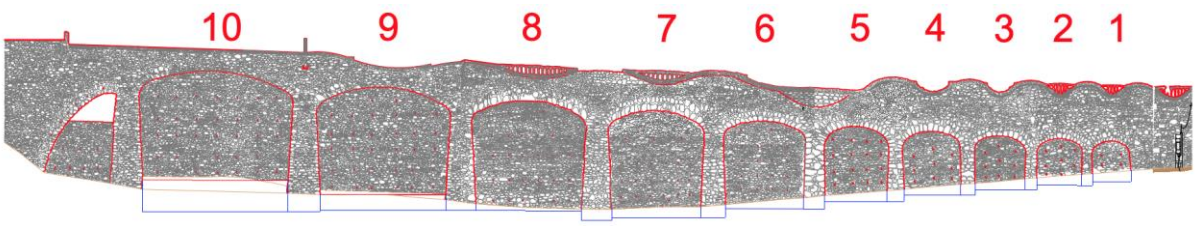


Figure 6: Assumed foundation configuration.

For Arches 1 – 5, the visible arch widths, the distance an arch protrudes from the wall beneath it, are compatible within each other, having a mean of 22 cm with a standard deviation of only 2 cm. Furthermore, the front surface of this part of the wall has a uniform inclination with a mean of 85.6° and a standard deviation of 0.5°. Therefore, it can be suggested that Arches 1 – 5 are non-structural arches that were built for decorative purposes. Thus, it was assumed that this part of the wall behaves as a traditional gravity retaining wall (Figure 7). The back surface of the wall was assumed to have a uniform inclination, as determined at the exploration pit above Arch 3.

The part of the wall consisting of Arches 6 – 10 was idealized based on elevation drawings, the photogrammetry model and the measurements from exploration pits and holes. The excavations revealed that the back surface of the wall is vertical, thus, it was assumed to be vertical until the arch level. The level of the arches as well as their buried widths and thicknesses were obtained from the topographic survey outcomes. Arches were assumed to have rectangular cross-sections.

In order to be conservative, the rear edge of the wall below the arches was assumed to be parallel to the front (Figure 7). Similarly, buttresses were assumed to have parallelogram cross-sections until the arch level. The height of each buttress was taken as the height up to which it already had sufficient thickness to be compatible with the thicker arch connecting to it. The measured buried thickness of 0.6 m was used both for the parts of the wall under the arches and the buttresses.

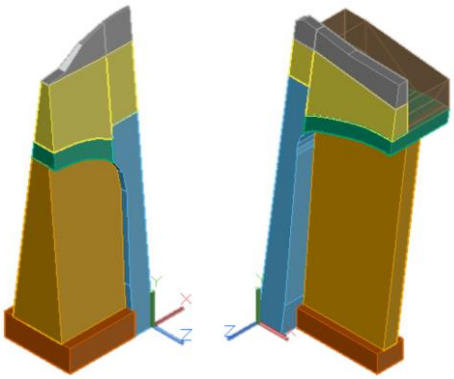


Figure 7: Assumed morphology of the wall for the part consisting of Arches 1 – 5 on the left, for the part consisting of Arches 6 – 10 on the right.

There is a reinforced concrete cantilever section, having a quarter ellipsoid shape, protruding outwards from the wall on the buttress between Arches 5 and 6 (Figure 8). An equivalent of the

visible section was assumed to be present at the back of the wall supporting the cantilever. Figure 8 demonstrates the idealized front and back surfaces of the wall.

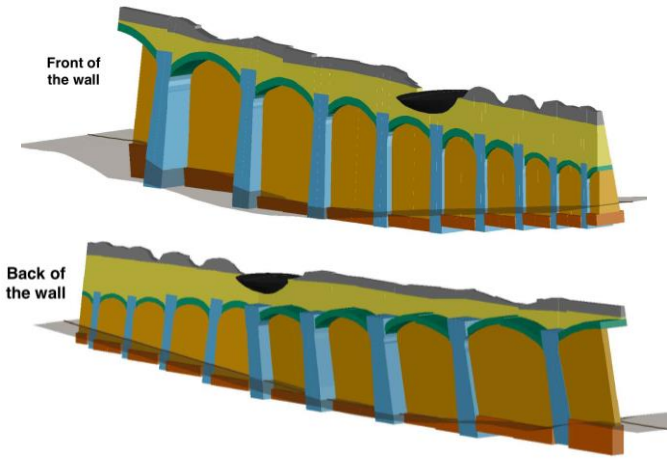


Figure 8: Idealized geometry of the wall from the front view on top, from the rear view on bottom.

5 STABILITY ANALYSIS

5.1 Methodology and assumptions

For the part of the wall consisting of Arches 6 – 10, the failure would be expected due to collapse of individual buttresses as a consequence of the conceivable load transmission path. Loads from the keys of the two adjacent arches are transferred to the buttress, making it the most vulnerable structural element in terms of stability. Hence, the stability of the wall can be evaluated by analyzing sections spanning between the keys of arches on either side of each buttress. Since each arch and buttress are unique in terms of shape and dimensions, assigning a single cross-section to a unit consisting of two half arches and a buttress is inappropriate. By means of the symmetry of an arch and a buttress about their center lines, the section spanning from the key of an arch to the center line of each buttress was defined as the unit section to be analyzed. Considering the geometrical variations throughout the wall, the stability of 18 half-arch sections were evaluated with respect to overturning and sliding (Figure 9). The sections are labelled according to the arch they contain with a suffix of "a" for the right half-arch section and a suffix of "b" for the left half-arch section.

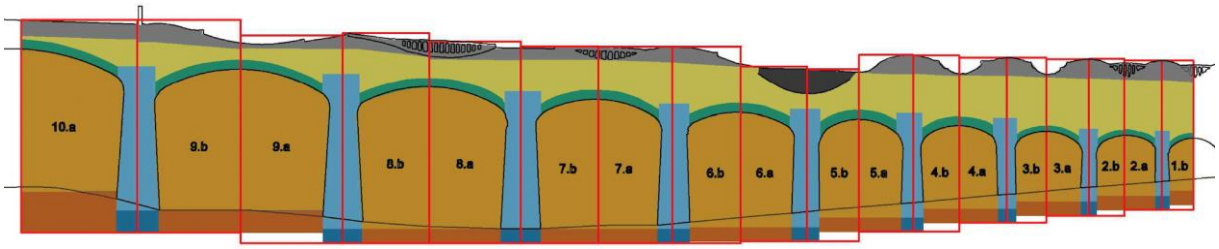


Figure 9: Sections analyzed to assess the stability of the wall of Casa Salvans.

The forces acting on a cross-section of the retaining wall are the weight of the structure, the weight of soil above arch level for Arches 6 – 10 and the forces due to lateral earth pressures. Figure 10 illustrates the forces acting on a section of the wall from the part consisting of Arches

1 – 5. The lateral earth pressures acting on a unit section are the active pressure, P_a applied by the retained soil at the back of the wall and the passive pressure, P_p exerted by the soil at the front of the wall. The forces due to lateral earth pressures were calculated by using Coulomb's Theory of Lateral Earth Pressure. The ground level behind the wall, which was used in the active pressure calculations, was taken as the average ground level within the section. Since pipelines were uncovered at a depth of 0.4 m in some of the pits, the ground level at the front of the wall was assumed to be 0.55 m lower than the actual ground level for the passive pressure calculations.

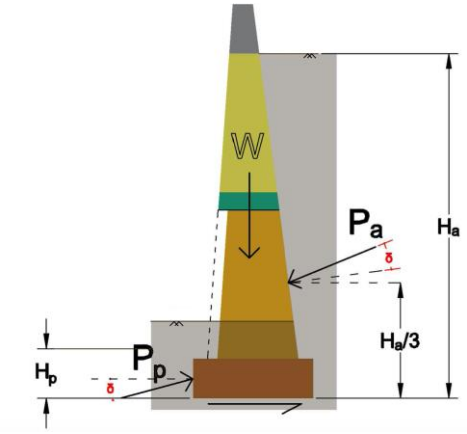


Figure 10: The forces acting on a unit section of the wall from the part consisting of Arches 1 – 5.

The internal friction angle of the soil (ϕ), the friction angle between masonry surface and soil (δ), the ground inclination and the inclination of the back surface of the wall are the parameters used to calculate Coulomb's lateral earth pressure coefficients. The geotechnical survey revealed that most of the retained soil acting on the wall is likely to consist of Layer A. Thus, the parameters defined for the corresponding layer, a specific weight of 19 kN/m^3 and an internal friction angle of 30° were adopted for all computations. According to some literature sources, typical values for the friction angle between stone masonry and soil (δ) varies from 16.4° to 26.3° for clayey earth and from 26.4° to 30.6° for sand and gravel [2]. Since the analysis aims to be representative of the reality, an initial δ value of 20° was assumed instead of correlation to internal soil friction angle, which is the common practice in modern retaining wall design procedures [3].

For Layer A, the undrained cohesion, c_u was determined to be smaller than 10 kPa. In order to be conservative and facilitate the application of Coulomb's Theory, c_u was neglected except for sliding calculations. While estimating the stability against sliding, it was taken as 10 kPa to provide adequate shear resistance. For Arches 6 – 10, a cohesion value of 29 kPa was assumed since it is plausible that the base of the wall rests on Layer B in this part.

After determining the active and passive earth pressures, the total stabilizing vertical load was calculated by multiplying every volume constituting a section by the corresponding specific weight. The specific weight of masonry was taken as 22 kN/m^3 while that of concrete was taken as 23 kN/m^3 [4]. Sections 6a to 10b have an additional stabilizing load due to the weight of the soil lying above the arches and the buttress.

Once all the loads acting on a cross-section have been computed, the factor against overturning, $F_{overturning}$ was determined as the ratio of the stabilizing moments to the overturning

ones, around the toe of the buttress. Similarly, the factor against sliding, $F_{sliding}$ was determined as the ratio of the sum of the sliding forces to the sum of the resisting forces. For both of the factors, being greater than or equal to one indicates that a stable equilibrium condition exists against the corresponding phenomena.

5.2 Discussion of results

The factors against overturning and sliding of all sections are reported in Figure 11 and Figure 12 respectively. As mentioned earlier, Sections 1b to 5b compose the part of the wall that limited information was available on the buried structure, thus it was assumed to behave as a traditional retaining wall with non-structural arches. Considering Section 6a shares the load of the reinforced concrete cantilever, from Section 6a to 10a, the overturning stability enhances as the weight of the section increases. Furthermore, the effect of a change of the soil layer to the more cohesive one at the foundation base can be appreciated in Figure 12 through the sharp increase of the sliding factors when wall adhesion is considered.

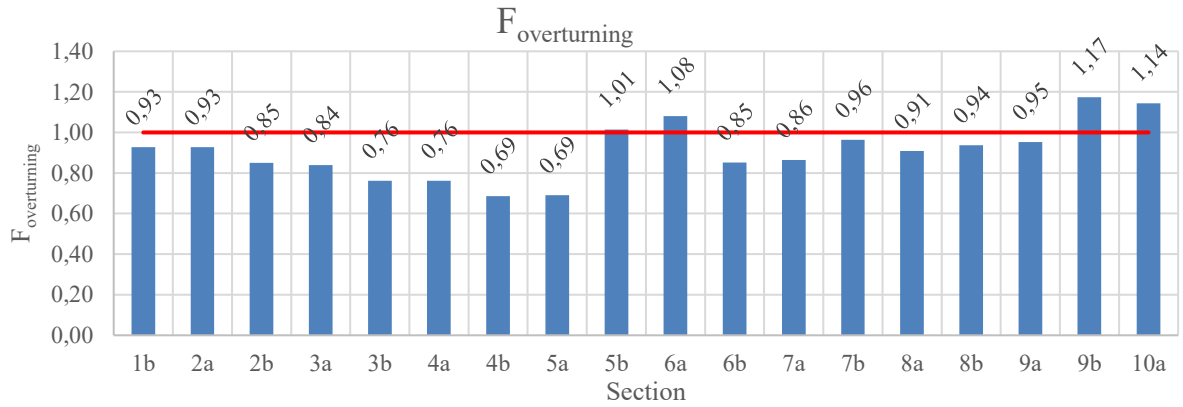


Figure 11: Factors against overturning.

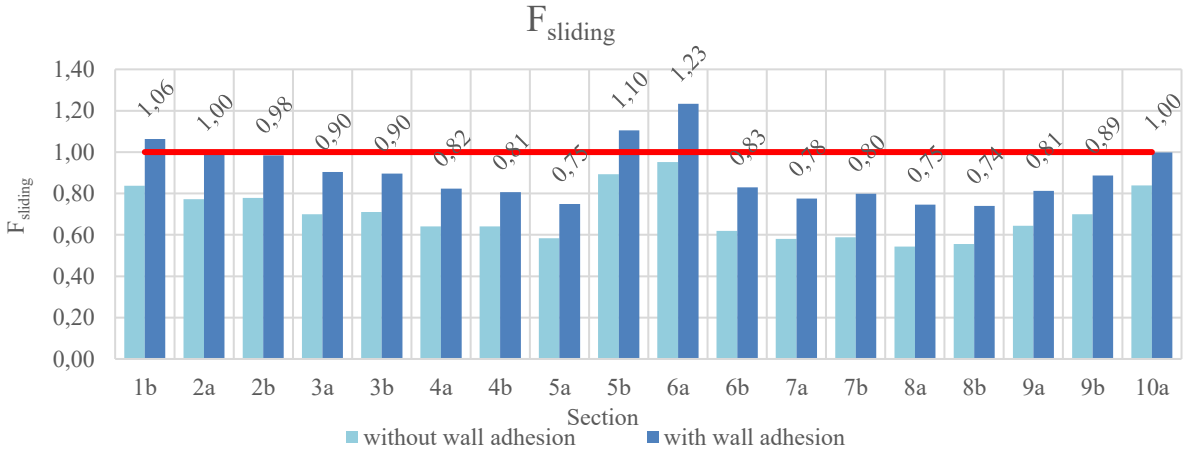


Figure 12: Factors against sliding.

It should be noted that a comprehensive structural verification of a retaining wall would also include the computation of the base pressures and a comparison with the ultimate bearing

capacity of the soil layer. However, based on the assumed geotechnical parameters, the analysis results in an unreliable equilibrium state and the base pressures cannot be computed for most of the sections as they are overturning.

The results indicate that the stability of the wall of Casa Salvans cannot be justified based on the current assumptions. Since the wall has been stable for 100 years and does not present any signs of damage, the factors should not necessarily be interpreted as the wall being unsafe. The shear strength parameters of the soil having been obtained through correlations to SPT-N values evokes uncertainties on the parameters. Therefore, some parametric analyses were carried out to determine the sensitivity of the results to key uncertain parameters.

6 SENSITIVITY ANALYSIS ON GEOTECHNICAL PARAMETERS

Sensitivity analysis was performed on the factors against overturning and sliding of Section 6b by modifying the internal friction angle of the soil, ϕ, and the wall friction angle between the masonry surface and the soil, δ. Section 6b was chosen as the representative unit as it presents relatively low factors compared to the other sections of the assumed cross-section typology. The analysis verified that the evaluation of stability is highly dependent on the aforementioned geotechnical parameters. The effect of different combinations of ϕ and δ ranging from 10° to 40° on the overturning and sliding factors is shown in Figure 13 and Figure 14.

$F_{overturning}$

φ [°]	15	20	25	30	35	40
δ [°]						
10	0.38	0.45	0.53	0.64	0.79	1.00
15	0.47	0.54	0.63	0.75	0.90	1.11
20	0.57	0.64	0.73	0.85	1.01	1.22
25	0.67	0.74	0.84	0.96	1.12	1.35
30	0.77	0.85	0.95	1.08	1.25	1.48

Figure 13: Sensitivity of $F_{overturning}$ of Section 6b to geotechnical parameters.

$F_{sliding}$

φ [°]	15	20	25	30	35	40
δ [°]						
10	0.24	0.29	0.36	0.45	0.59	0.78
15	0.34	0.41	0.50	0.62	0.80	1.05
20	0.47	0.56	0.67	0.83	1.05	1.39
25	0.63	0.74	0.88	1.08	1.35	1.80
30	0.84	0.97	1.14	1.37	1.72	2.35

Figure 14: Sensitivity of $F_{sliding}$ of Section 6b to geotechnical parameters.

Increasing φ enhances the stability of the section against both actions significantly. The effects of changing δ for different φ values on both factors are illustrated in Figure 15 and Figure 16. Increasing δ alters the factor against overturning by a similar trend regardless of the soil internal friction angle. However, the increase in the factor against sliding due to the increase of δ is higher as the soil friction angle gets higher.

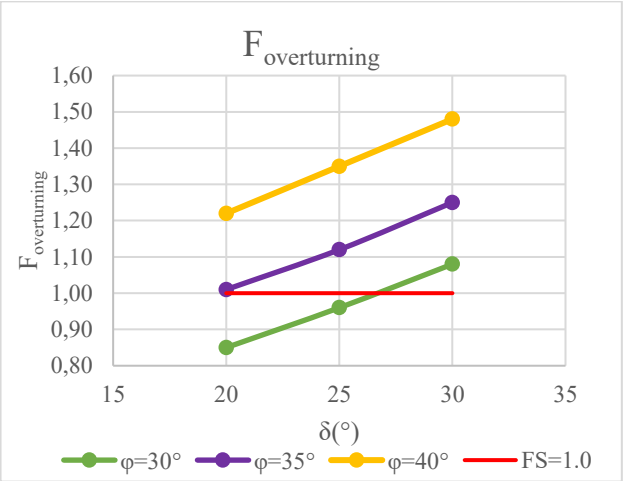


Figure 15: $F_{overturning}$ of Section 6b for different values of φ and δ.

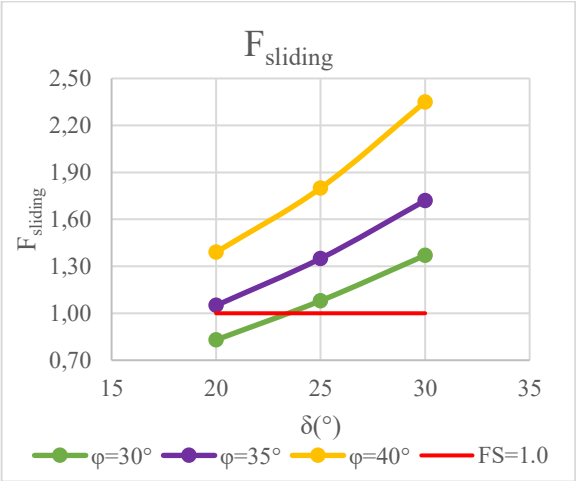


Figure 16: $F_{sliding}$ of Section 6b for different values of φ and δ.

The analysis verified that there are reasonable combinations of ϕ and δ, such as 35° and 20° respectively, which would allow the stability of the wall to be justified in terms of both overturning and sliding. Therefore, it is crucial to determine the actual values of these parameters in order to properly evaluate the stability of the wall.

7 IN-PLANE STABILITY OF ARCHES

In addition to the ability of the wall to resist overturning and sliding caused by lateral pressure of the retained soil, a complete stability verification also involves verifying the in-plane stability of the arches to stand in equilibrium. Unreinforced masonry arches are prone to fail due to stability problems. A structural analysis technique based on plastic theory, Lower Bound Theorem of Limit Analysis, was utilized to evaluate the equilibrium of the arches of the wall of Casa Salvans.

The analysis assumes that masonry has no tensile strength while it has unlimited compressive strength due to stresses being low and that failure may not occur due to sliding. Graphic statics can then be used to locate thrust lines within the boundaries of the arches. A thrust line is a possible load path along the arch that is composed of the resultant compressive forces in equilibrium with the weight of the unit blocks of the arch, in an inverted catenary shape. The Lower Bound Theorem states that an arch can be deemed safe if a thrust line can be found lying entirely within the geometry.

The elevation drawing of the front surface of the wall and the same dimensions used to assess the overturning and sliding stability for the buttresses and arches were used to apply graphic statics on the arch series. The estimated loads acting on the buttresses and the arches were computed based on the estimated volumes of wall elements and soil lying above the arches. The part of the wall below the arches was ignored in order not to enhance the stability of the arches.

In spite of profoundly conservative assumptions on the geometry, a thrust line was found to lie within all boundaries verifying the in-plane stability of the wall (Figure 17). Although

Arches 1 – 5 were assumed to be merely decorative, the initial graphic statics analysis demonstrated that this part of the wall would be more than capable of resisting the thrust transmitted from the bigger arches.

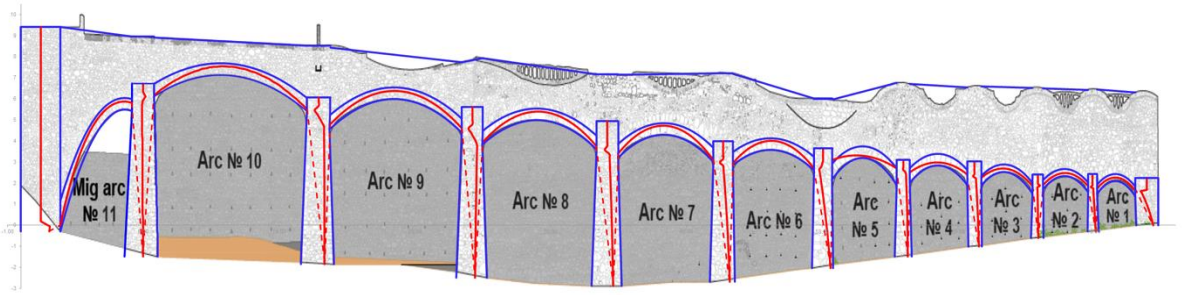


Figure 17: Graphic statics application on the wall of Casa Salvans.

8 CONCLUSIONS

This paper presented the systematic methodology employed for the stability assessment of a masonry arched and buttressed retaining wall. The procedure first involved creating an idealised three-dimensional geometry of the wall by combining information from photogrammetry, excavation pits and holes and detailed elevation drawings. The geometry of the wall is then subdivided into individual analysis sections based on the conceivable load transmission path. After estimates of the lateral earth pressure are computed, the stability of each analysis section against sliding and overturning is verified. Finally, the in-plane stability of the arches is verified using the Lower Bound Theorem of Limit Analysis applied to the idealised geometry. In the case of the wall of Casa Salvans, the stability of the wall against overturning and sliding could not be justified on the basis of the idealized geometry and the estimates of geotechnical parameters obtained through indirect methods. However, the parametric analysis carried out on the effect of the soil internal friction and wall friction angles showed that there are reasonable combinations of the two for which the stability of the wall can be verified in terms of both overturning and sliding. Hence, determining the actual ϕ and δ values is of vital importance to better understand the actual stability condition. In this case, it is therefore highly recommended to carry out a comprehensive geotechnical survey to obtain geotechnical parameters through direct test methods instead of correlations. The in-plane stability of the arches of the wall of Casa Salvans was verified according to the Lower Bound Theorem through graphic statics application.

9 REFERENCES

[1] Autodesk, “ReCap Photo.” Autodesk, 2019.
[2] J. A. J. Dvořák, L. Novák, *Soil conservation and silviculture*. Elsevier, 1994.
[3] R. F. Craig, *Craig’s Soil Mechanics*, 7th Editio. London: Spon Pres, 2004.
[4] B. S. I. BSI, “EC1: Part 1.1: Densities, self-weight, imposed loads for buildings,” *Structural Engineer*, vol. 82, no. 2. European Comittee For Standardization, London, p. 44, 2002.
[5] S. Huerta, “Mechanics of masonry vaults: the equilibrium approach,” in *1st Int. Congr. Struct. Anal. Hist. Constr.*, 2001, pp. 47–70.

12th International Conference on Structural Analysis of Historical Constructions
SAHC 2020
P. Roca, L. Pelà and C. Molins (Eds.)

STATIC AND DYNAMIC LOAD TESTS OF LIBEŇ BRIDGE OVER VLTAVA RIVER IN PRAGUE AND CONCEPT OF REPAIR

PETR TEJ*, JAN MOUREK[1] AND MAREK BLANK[1]

[1]Klokner institute
Czech Technical University in Prague (CTU)
Šolínova 7, 160 00 Prague 6, Czech Republic
e-mail: petr.tej@cvut.cz, www.klok.cvut.cz (*corresponding author)

Keywords: Concrete, arch bridge, historical structure, load tests, reconstruction

Abstract. *The Libeň bridge in Prague is a cultural and technical heritage of concrete construction of the beginning from the twentieth century. The bridge was designed by architect Pavel Janák, the founder of cubism in architecture. According to experts, the Libeň bridge is the only example of cubist morphology application on the bridge structure. Evaluation of Libeň bridge structural condition is an up-to-date topic leading to decision whether this bridge should be repaired or replaced by a new bridge. This article deals with the static and dynamic load testing in comparison with following creation and validation of the FEA model for load carrying capacity assessment of the Libeň Bridge and possible way of reconstruction. Paper deals with crucial procedures for FEA model validation of this backfilled arched concrete structure with a focus on the static characteristic of the structure. Article deals with reconstruction of the vault part of the Libeň Bridge using R-UHPFRC in terms of static operation. It focuses on the two basic problems of the bridge, the solution to increase the bearing capacity of the vault arches and to increase the bearing capacity of the foundations under pillars. The concept of repair is based on extensive diagnostic surveys conducted in 2017. The concept of structural enhancement is based on adding new thin layer of R-UHPFRC (reinforced, ultra-high performance concrete) on the upper vault surface. Concrete bridge structures are exposed to extreme effects of aggressive environmental influences, especially chlorides, which leads to damaging of most exposed bridge components a long time before their service life. UHPFRC material is suitable for repairs of these structures and especially due to its impermeability and high resistance.*

1 INTRODUCTION

The Libeň Bridge (Figure 1) was built between 1924-1928 according to the design by architect Pavel Janák. The structure was designed by Ing. František Mencl, who was the author of the arch part of the. The bridge was opened to the public on 29 October 1928 on the 10th anniversary of the Czechoslovak Republic with the participation of President Tomas G. Masaryk. Arched spans of three joints from plain concrete are considered to be the highest value of the construction.

The bridge carries urban traffic across inundation area. The width of the communication on the bridge is 14.5 m (lanes + tram), both sidewalks have a width of 3.25 m. The road cover is

made of asphalt concrete, the pavements have cast asphalt surface, the tram body is made of concrete panels.

The supporting structure of the arches consists of monolithic concrete segments made of plain concrete with embedded reinforced concrete joints. The vaults are in cross-section divided into 4 segments with a width of 4.85 m. The thickness of the segments is variable - about 0.9 - 1.1 m. The vaults are designed as three-joint arches, 2 joints are always located on the cantilever about 3 m from the edge of the pillars, 1 joint is at the top.

This article focuses on load tests and subsequent assessments of the arched part of the bridge made up of five vaults with backfill. The static action of the vaults is simple – joints at the top and bottom of the vault. In cross-section, the load-bearing structure consists of four vault strips with an approximate width of 4.85 m. The front walls are based on the outer strips, which support the pavement brackets with the railings. In the area above the pillars, the front walls are stiffened by ribs.

Experience with static and dynamic measurement compared to computational models resulting from similar measurements made at the author's workplace on Libeň bridge and similar bridge structures [1]-[4]. Experience with designing of bridge structures author obtained participating on several tasks detailly published in articles [5-10].



Figure 1: Libeň bridge

2 STATIC LOADING TESTS

Two freight four-axle vehicles with a weight of 40 t have been designed as a test load. The vehicles were placed according to symmetrical load bridge by two lorries at the top of the arcs. Load 2 x 40 t in the middle of the span in each arc for all 5 arrays x 4 passes, i.e. 20 load cases. In addition, crossings with a vehicle weighing 40 tons were made, in each of the vault strips 3x back and forth, i.e. 120 crossings.

During the load states the vehicles were in the position as shown in Figure 2, 3 No.1 vehicle (mass 37 t), the vehicle No. 2 (mass 41 t) always points in the same direction - ending towards each other and facing to one end of the bridge. For vehicle crossings, both vehicles were used, alternating in the rides individually.

Within the load test, the primary set of measuring points was monitored, which was designed to track field deflections. Secondary set of measuring points, designed to measure support drops, locating movements in support areas, swiveling and pushing and shearing on joints. With the exception of measuring the drops of the supports, all measurements were made electronically (mostly by different variants of inductive sensors).



Figure 2: Vehicles during static load test – static



Figure 3: Vehicles during static load test – crossing

2.1 Conclusion of static load test

The supporting structure of the test spans behaved flexibly before, during and after the static loading and no new unexpected defects or faults were detected. Static measurements in all spans clearly con-firmed the interaction of all four arched strips, that are longitudinally elastically interconnected. In this sense, the influence of the o hopper (including concrete slabs in the upper part) and the road and tram-way cover, which contribute to the interaction of arched strips and the overall space load distribution in the supporting structure, is significant.

3 STATIC ANALYSIS OF THE STRUCTURE

The computational models were developed in Midas software (Figure 4). The model for assessing the load carrying capacity of vault strips is created using rod, flat, and bulk elements so as to simulate the behavior and dimensions of the structure as close as possible. Due to the complexity of the bridge construction, the overall model is divided into individual vaults, which are then independently assessed.

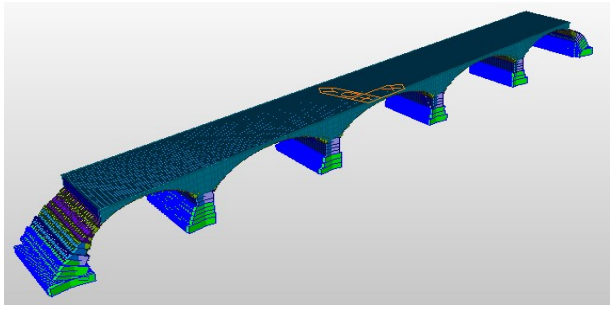


Figure 4: The overall model before dividing into individual parts

3.1 Validation of the model

Validation for temperature effects:

According to the measurements made by precise geodetic measurements, the vertical movement at the top of the longest vault is ± 8 mm when the structure is warmed / cooled by 10 ° C. The bridge construction was loaded with the same ΔT in the computational model and the vertical deformations at the top of the vault were monitored. The following figures 5, 6 show the values found. From their presentation it is evident that the deformation at the top of the vault exactly corresponds to the measured deformations ± 8 mm for the longest vaults 3 and 4.

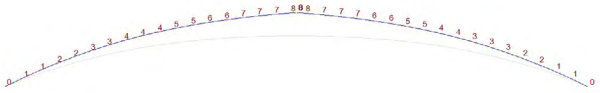


Figure 5: Deformation after the structure is warmed by + 10 ° C on the longest vault



Figure 6: Deformation after cooling of the structure by -10 ° C on the longest vault

Validation of deflection:

The models were validated by adjusting the material characteristics for the individual vault strips, especially the validation concerns modification of the modulus of elasticity of the concrete at a maximum value of 5 %. At the same time, it was necessary to modify the rigidity of the upper slab of the road cover in the area of the middle and the outermost strips at the top arches of the vault. It is obvious that there is a discontinuity in the top plate at this point.

Table 1: The deviation between the measured and observed deflections vault 3

Loaded strip	Deflection measured [mm]	Deflection calculated [mm]	Deviation [%]
1	1,720	1,940	11,3
2	1,975	1,945	-1,5
3	1,945	1,890	-2,9
4	1,945	1,914	-1,6

Table 2: The deviation between the measured and observed deflections vault 4

Loaded strip	Deflection measured [mm]	Deflection calculated [mm]	Deviation [%]
1	1,285	1,761	27
2	1,455	1,564	7
3	1,745	1,523	-14,6
4	1,570	1,741	98

3.2 Conclusion of static analysis

For temperature loads, the produced models behave in accordance with the measured values. Comparing the deflections measured in the static loading test and calculated in the static analysis of the structure, the different parts of the bridge have differently accurate results. For the vault 3 a very good agreement was reached, for the vault 4 there are more marked differences. The conclusions of the static analysis show the functionality of the joints of the structure and the inconsistency of the material properties for the individual parts of the bridge.

4 DYNAMIC LOADING TESTS

To excite the forced oscillation of the bridge structure in shapes close to the theoretical oscillation mode shapes (mode shapes cannot be excited, it is a dimensionless mathematical fictitious shape), a hydraulic INSET vibration exciter (Figure 7) was used in the harmonic excitation mode. During the tests, the excitor was placed on the bridge (or on the tramway) in three positions. These positions were designed for measurements on individual vaults in spans 1, 2 and 5. The theoretical location of the exciter was half the span of the bridge in the longitudinal direction and on the tramline. At these locations, the excitation was in the position for horizontal transverse excitation (relative to the axis of the bridge) and for vertical excitation.

The bridge response to the dynamic loading was monitored in a detailed network of measurement points in which the oscillation velocities were monitored in the vertical, horizontal, transverse and horizontal longitudinal directions. The set of measurement points served to measure the oscillation of the bridge structure in absolute terms. On all the measured fields, the installation and installation of the sensors were identical.

The measurements were made at all measuring points using electrodynamic sensors. Dynamic deflections (or vibration velocities) were measured using triaxial oscillator speed sensors. The measuring line also included two thermometers to monitor the surface temperature of the structure and the air temperature and the anemometer to monitor wind velocities and directions.



Figure 7: The vibration exciter installed on the tramline

4.1 Conclusion of dynamic loading test

The bearing structure of the tested vaults has behaved flexibly before, during and after the dynamic loading and no new unexpected defects or faults have been detected. The amplitude frequency spectra obtained on individual vaults do not show sharp spectral peaks, as is common with compact constructions, but the spectral peaks are rounded and include narrow bandwidth. This effect is due to the effect of different geometric and material characteristics and boundary conditions on individual vaults and their individual parts, both in the longitudinal and transverse directions.

Detected oscillation shapes corresponding to their own oscillation shapes. At the lowest frequencies we find global shapes where the main supporting structure oscillates as a whole, or as two units in portions separated by a vertex joint. Only at higher frequencies vault strips are separated, which then oscillate in pairs.

5 DYNAMIC ANALYSIS OF THE STRUCTURE

The modal analysis model is based on diagnostic measurements on the design and the dynamic load test. The loading test was performed for the vault 1,2 and 5. The vaults 1 and 5 are influenced by the frame constructions, which would burden the other model with another unknown and increase the calculation inaccuracy. For this reason, modal analysis deals with vault number 2. The model was created in Scia Engineer 15 software.

5.1 Model description and results

Construction of the model is composed of individual vault strips of plain concrete C16 / 20 with a mod-ulus of elasticity E = 21 GPa. These elements are modeled with sloping and variable thickness. The top and toe joints are simplified by a sloped line. A joint support is introduced at the heel of the vault. At the top, the joint is replaced with a low stiffness element (E = 1 GPa). The wall elements forming the front wall (E = 19 GPa) and the overhang (E = 3 GPa) are attached to these vault strips. Interaction of the individual strips is ensured by a slab simulating the road cover (according to the diagnostic conclusions it is a concrete slab with a thickness of 500 mm and bituminous cover with a thickness of 200 mm, E = 10GPa). This slab is provided with boundary conditions ensuring the continuity of the structure (non-moving joints). In this model, where the upper slab behaves like a strained membrane that limits the oscillation of the structure, two identical oscillations have been found for measured frequencies of 7.23 and 11.92 Hz (Figure 8, 9).

In case we for this model partially release the boundary conditions for the top plate by inserting resilient supports with a stiffness of 100 MN / m^2, the loosening of the wall linkage over the top joint vertically (flexible support with a stiffness of 100 MN / m2) and by adjusting the stiffness of the left 19 GPa) and right (23 GPa) of the half of the arc to take into account the diversity of materials and possible discontinuities, we obtain another consistent shape of oscillation of the structure for the measured 6.46 Hz (Figure 10).

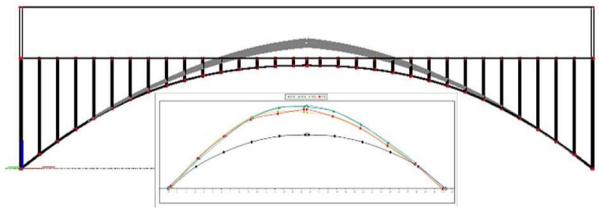
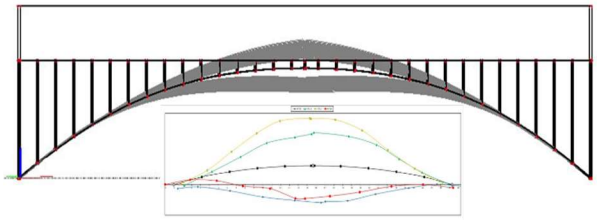


Figure 8: Measured and calculated oscillation shape for 7.23 Hz



4

Figure 9: Measured and calculated oscillation shape for 11.92 Hz

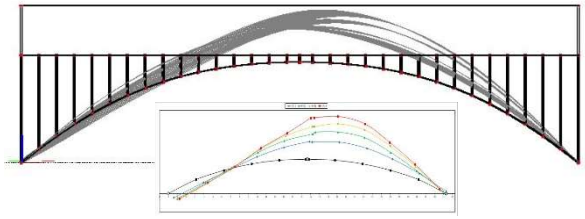


Figure 10: Measured and calculated oscillation shape for 6.46 Hz

5.2 Conclusion of dynamic analysis

Modal analysis has demonstrated the functionality of the joints of the structure. It pointed out the possible discontinuities for the upper concrete slab and the different material properties in the various portions of the supporting strips of the plain concrete vault. The results of the dynamic analysis of the vaults are heavily influenced by the complexity of the entire structure, particularly upper concrete slab and the upper filling.

Table 3 compares the measured and calculated frequencies and their deviation is determined according to [1]. Consequently, the calculated frequencies show a good match with the frequencies measured.

$$\Delta = \frac{f_{theor} - f_{obs}}{f_{theor}} \cdot 100 \quad (1)$$

Table 3: Frequency comparison

Frequencies measured [Hz]	Frequencies calculated [Hz]	Deviation [%]
6,46	6,64	2,7
7,23	8,5	14,9
11,92	10,46	-13,9

6 RECONSTRUCTION OF BRIDGE

The project deals with the possibilities of reconstruction of the vault part of the Libeň Bridge, frame structures and staircases in terms of static operation and durability. In the framework of the vault part, it focuses on two basic problems of the bridge, the solution of increasing the bearing capacity of vault arched strips and increasing the bearing capacity of foundation pillars.

For any bridge work to be used in accordance with current standards in the City of Prague, two basic requirements must be observed:

- static reliability and design safety with specified design load carrying capacity;
- durability and lifetime of the structure.

For this reason, the works were focused on the possibilities and ways to meet these two basic requirements also in the case of the main bridge V009 of the Libeň region, even in the case of a cultural monument, i.e. in order to preserve as much existing structures as possible.

From diagnostics and static analyzes is obvious, that it is necessary to either perform a complex and highly demanding reconstruction aimed at the extensive static solution of the non-compliant parts of the bridge, or the construction of a completely new bridge without using the existing supports and pillars as planned in the 2005 project according to the required load (including tramway operation in both directions) .

Ensuring the durability of the materials as well as the bridge according to the requirements of the current standards will be ensured only by building a new bridge. In the case of complex reconstruction, it must be assumed that such a lifetime cannot be guaranteed by any remediation methods.

6.1 The vault part of the Bridge

The resulting variant of the reconstruction, which seems to be the most appropriate, is to ensure the static reliability and the full load carrying capacity of the bridge, is the solution of strengthening existing vaults with additional concrete layer of UHPFRC (Ultra-High Performance Fiber Reinforced Concrete) in 100 mm thickness. Using of UHPFRC is perspective method for strengthening of existing structures. Very important is also the impact of the bond between UHPFRC and steel reinforcement in coupling surface.

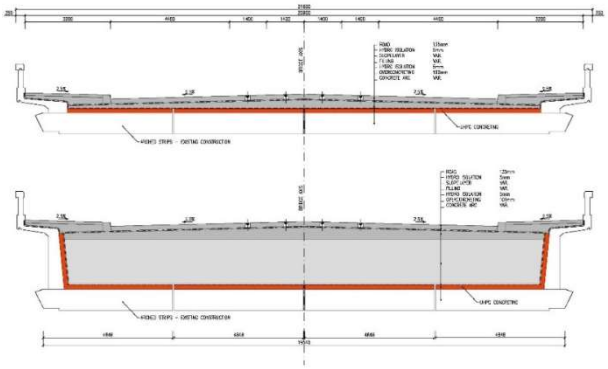


Figure 11: Cross section of the bridge at the top and at the foot of the vault. The UHPFRC layer is marked in red.

Designed reinforcement of the existing vault belts of the Libeň Bridge by an over concreting of 100 mm thick UHPFRC layer.

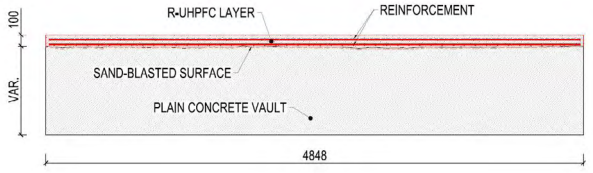


Figure 12: Cross section of reinforced arched strip of Libeň Bridge

Table 4: Comparison of cross-sectional characteristics before and after reinforcement

	area [m^2]	centre of gravity from the lower face [m]	Moment of inertia [m^4]
Original cross-section	3,878	0,5*H	0,207
Ideal cross-section	5,008	0,63*H	0,385
Comparison	+ 29,1 %	0,13*H up movement	+ 86,0 %

From the calculated results, it is evident that by over-concreting only 100 mm of R-UHPFRC material, the cross-sectional characteristics of the arched belts will be significantly improved due to its unique material properties, particularly the high secant modulus of elasticity E_{cm}. The results are calculated for a reference cross-section of 800 mm high and 4850 mm wide.

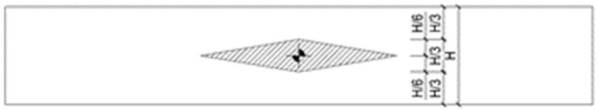


Figure 13: Core of the original cross-section

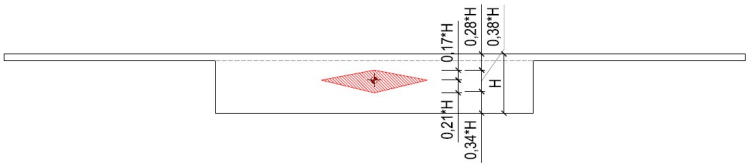


Figure 14: Core of ideal reinforced cross-section

The disadvantage of the reinforcement of the structure is the introduction of the load from the shrinkage of the over concreting. In the case of the possibility of symmetrical double-sided reinforcement of the structure, this load is not a problem, as the result of these forces will be approximately normal compressive force, which is generally well tolerated by concrete structures. In the more frequent case of the possibility of one-sided reinforcement of the structure (over concreting on the upper surface), it is necessary to consider the additional bending moment stress of the supporting structure.

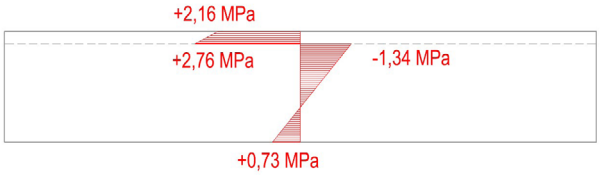


Figure 15: Effects of excess shrinkage on total stress in cross-section

Thickening of the cross-section will increase the cross-sectional area of the cross-section. In the direction of the vertical Z axis (bending around Y-Y) the core height is increased by 29.6%.

The results of the diagnostics of vault foundations show that the structure of the foundation is strongly degraded by sulphate corrosion and regarding its reinforcement it is necessary to proceed with its repair. This repair is based on covering the existing foundation with reinforced concrete envelope.

Unfortunately, this repair does not stop but only reduces the sulphate corrosion process. Predicting the rate of sulfate corrosion without long-term monitoring is not possible. In the case of a complex reconstruction, it will be necessary to monitor and test the condition of the concrete foundations and pillars for a long time. As part of the proposal, it will also be necessary to set up a plan for tracking and monitoring the bridge for reconstruction.

6.2 The frame part of the Bridge

From the point of view of possible static reinforcement, it is necessary to consider the character of structures - these are frame reinforced concrete constructions based on the mutual interaction and cohesion of concrete structures with the steel reinforcement. It is also necessary to consider the stress of the individual elements - these are elements stressed by bending, pressure, shear and their mutual combination.

In terms of possible reinforcement of elements designed from the time of construction with lower bearing capacity - frame construction "B" and part of frame construction "D" as a replacement make new constructions. The static calculation showed insufficient load capacity of the whole structure not only in the local section. Possible reinforcement eg external reinforcement or concreting seems to be technically almost impossible to do, by enhancing the construction they would lose their original character, shape and appearance.

From the point of view of the overall repair, it is recommended the complete replacement of the frame constructions. Regarding the existing damaged frame constructions, it is not reasonably possible to statically increase the durability, functionality and stability of these structures.

7 CONCLUSIONS

Static and dynamic load tests of a considerable scale were carried out on the structure, in which the behavior of the structure of plain concrete vaults was verified. Based on the results, numerical models were developed to perform a static and dynamic analysis of the structure.

A static load test and static analysis has demonstrated the functionality of the structure. It pointed out the possible discontinuities for the upper concrete slab and the different material properties in the various portions of the supporting strips of the plain concrete vault. The dynamic load test and dynamic analysis of the structure confirmed these findings.

From diagnostics and static analysis, it has been shown that for the operation of the bridge to the required load according to the currently valid standards it is necessary to carry out either:

- complex and demanding reconstruction focused on the extensive static solution of the non-compliant parts of the bridge, including the stabilization of the foundations, or
- building a completely new bridge

From obtained results is clear that by reconstruction based only on partial static interventions and "cosmetic" repairs of the surfaces without substantial and complex static intervention (ideally see be-low), the bridge will only be operated with permanent traffic restrictions.

Ensuring the durability of the bridge according to the requirements of the current standards (design value of at least 100 years) can only be provided by building a new bridge. In the case of a complex reconstruction, it is to be assumed that such a lifetime will not be permanently secured by any remediation methods. But regarding the reconstruction of historic buildings this is predictable and usual. With this fact it is necessary to count in the specification of the repair, the requirements for the final parameters of the reconstruction and the subsequent maintenance of the bridge.

Based on the acquired knowledge and information on the state of the bridge and the possibilities of its reconstruction and repairs, the following main conclusions can be found:
The load carrying capacity of the bridge required by the currently valid ČSN 73 6222 can be ensured in two ways:

- The complex reconstruction of the bridge, which includes the following major interventions:
  - Securing the foundations of the vault bridge (fixing in terms of sulphurous corrosion).
  - Replacement of two central vault strips (three-joint arches) in all five vaults with new reinforced concrete belts (again three-joint arches).
  - Repair and rehabilitation of the structures and their surfaces, including putting them into the required appearance.
  - Secondary surface protection to increase service life and durability.
  - Complete replacement of frame structures and staircases with new constructions, including the appearance of concretes in staircases.
  - Implementation of new waterproofing, drainage systems, embankments and bridge superstructure.
  - Regular specialized and long-term (permanent) monitoring of the bridge as well as degradation processes in the foundations and evaluation of the results found in relation to the state - the functional capability of the object.
- Construction of a completely new bridge without the use of the underground structure (foundations and supports) of the existing bridge.

The reconstructed bridge will need to be more closely monitored. It can be assumed that the maintenance and operation costs of the reconstructed bridge will be higher compared to the new construction.

Acknowledgements. Theoretical basis for the presented results were obtained under the support of the research project GAČR 17-22796S.

REFERENCES

[1] Mourek, J., Tej, P., Kral, J., Kolisko, J. "Assessment of structural condition of steel bridge in Brandys nad Orlici." MATEC Web of Conferences 107, doi: 10.1051/matecconf/201710700003

[2] Tej, P., Kral, J., Tejova, A., Markova, J.. "Long-Term Monitoring of a Composite Steel-Concrete Bridge on the Prague Ring Road." Applied Mechanics and Materials, doi: 10.4028/www.scientific.net/AMM.617.13

[3] Čech, J., Tej, P., Kolísko, J., Král, J. 2017. "Structural condition assessment of the bridge in Ostrava." MATEC Web of Conferences 107, doi: 10.1051/matecconf/201710700001

[4] Kněž, P., Čech, J., Tej, P., Blank, M. 2017. "Assessment of structural condition of Libeň Bridge." MATEC Web of Conferences 107, doi: 10.1051/matecconf/201710700002

[5] Knez, P., Tej, P., Citek, D., Kolisko, J. 2017 "Design of footbridge with double curvature made of UHPC", IOP Conference Series-Materials Science and Engineering 246, doi: 10.1088/1757-899X/246/1/012042

[6] Kolísko, J., Čítek, D., Tej, P., Rydval, M. 2017 "Production of footbridge with double curvature made of UHPC", IOP Conference Series-Materials Science and Engineering 246, doi: 10.1088/1757-899X/246/1/012009

[7] Kolisko, J., Cech, J., Tej, P., Knez, P. 2017 "UHPC panels utilized as permanent formwork of in-situ cast reinforced concrete deck bridges." IOP Conference Series-Materials Science and Engineering 246, doi: 10.1088/1757-899X/246/1/012043

[8] Tej, P., Kolisko, J., Knez, P., Cech, J. 2017. "The Overall Research Results of Prestressed I-beams Made of Ultra-high Performance Concrete." IOP Conference Series-Materials Science and Engineering 246, doi: 10.1088/1757-899X/246/1/012051

[9] Tej, P., Kněž, P., Kolísko, J., Vráblík, L. 2017. "Modal analysis of cable-stayed UHPC bridge." MATEC Web of Conferences 107, doi: 10.1051/matecconf/201710700007

[10] Blank, M., Tej, P., Kolísko, J., Vráblík, L. 2016. "Design of Experimental Suspended Footbridge with Deck Made of UHPC." MATEC Web of Conferences 77, doi: 10.1051/matecconf/20167708005

[11] Pokorny, P., Tej, P., Kouřil, M. 2017. "Evaluation of the impact of corrosion of hot-dip galvanized reinforcement on bond strength with concrete - A review", Construction and Building materials 132, p. 271-289.

[12] Pokorny, P., Tej, P., Szelag, P. 2016. "Chromate conversion coatings and their current application", Metalurgija 55, p. 253-256.

[13] Pokorny, P., Tej, P., Szelag, P. 2016. "Discussion about magnesium phosphating", Metalurgija 55, p. 507-510.

[14] Brozek, V, Kolisko, J. et all. 2015."Boronized stainless steels with zirconia coatings", Metal 2015:24th International Conference on Metallurgy and Materials, Tanger Ltd, p. 1069-1074

12th International Conference on Structural Analysis of Historical Constructions
SAHC 2020
P. Roca, L. Pelà and C. Molins (Eds.)

STRUCTURAL ASSESSMENT OF CULTURAL HERITAGE BUILDINGS USING HBIM AND VIBRATION-BASED SYSTEM IDENTIFICATION

ALFREDO CALÌ[1*], ANTONELLA SAISI[1] AND CARMELO GENTILE[1]

[1]Department of Architecture, Built environment and Construction engineering (DABC)
Politecnico di Milano, Milan, Italy
Piazza Leonardo da Vinci, 32 - 20133 Milan, Italy
e-mail: {alfredo.cali, antonella.saisi, carmelo.gentile}@polimi.it (*corresponding author)

Keywords: Historical Structure, Masonry, Monitoring, Non-Destructive Inspection

Abstract. *The paper exemplifies the application of the methodology involving historic and architectural research complemented by HBIM and operational modal testing in the structural modelling of a heritage palace, the Galleria degli Antichi in the historic town of Sabbioneta (Italy), included in the UNESCO World Heritage list since 2008. This monumental building was built in the 16th century. Full details on the history of the building and the information obtained in the non-destructive survey are given in the paper. The good knowledge of the structural geometry, along with the complete inspection carried out and the large number of identified vibration modes, allowed to establish a numerical model of the monumental building for a first quantitative assessment of its structural condition.*

1 INTRODUCTION

The structural analysis of historic masonry structures is a complex task, involving the collection of data from a wide range of sources and the subsequent merging process. Research underlines the significance of an accurate planning of such activities in order to get reliable information about the structural characteristics supporting the structural modeling [1].

Starting from [2] to more recent versions, the Italian Seismic Code bases the structural modeling and the seismic assessment on such multi-cultural approach. The novelty and the importance of such a methodology was assumed and reaffirmed by the ISCARSAH – ICOMOS Committee in a general document concerning the analysis and the structural restoration of architectural heritage [3]. Therefore, the structural modeling requires a process involving historic research, geometric survey, direct inspection supplemented by tests on sampled materials and local non-destructive and minor-destructive tests. The methodology highly recommends the monitoring of the recognized structural pathologies [1].

The structural analysis of historic masonry building is commonly performed in the elastic range (see e.g. [4]) due to the high level of uncertainties about the non-linear properties of the materials. Nevertheless, even linear elastic analysis might be affected by uncertainties and lack of information. Dynamic tests in operational conditions provide quantitative parameters (i.e., resonant frequencies, mode shapes and damping ratios), which are representative of the structural condition and remarkably contribute to the knowledge of the building and to the model calibration and validation [5-6]. In addition, ambient vibration tests are especially suitable to historic buildings for the fully non-destructive way of testing, that is a priority for

the architectural heritage.

It is further recalled that various software codes nowadays implement the Building Information Modeling (BIM) methodology (see e.g. [7]), which describes collaborative processes for production and management of structured electronic information. BIM is generally aimed at creating interactive database collectors for the elaboration of architectural projects, including structural characteristics. Similarly, the information collected in the assessment of historic buildings might be summarized through the creation of a Heritage Building Information Model (H-BIM) [8-9].

Current studies on H-BIM are mainly aimed at improving the geometric description of the "as-built" configuration of heritage buildings through geomatic survey (i.e., laser scanning and photogrammetry) and the organization of the data sources, whereas only few examples are available in the literature on the use of H-BIM in combination with Finite Element (FE) analysis [10]. In [11], the H-BIM potential role in the structural analysis and decision making for restoration and rehabilitation proposals is also pointed out. Furthermore, the integration between BIM, diagnostics and monitoring is suggested in [12], with the discussion including dynamic testing and FE analysis to assess the structural health condition.

In the present paper, a H-BIM workflow was developed to improve the knowledge of an important historical palace; the workflow has been established to manage and merge the information collected through documentary research, geometric survey and description, direct inspection, FE modeling, operational modal testing and analysis. The historic building named *Galleria degli Antichi* [13-14] in Sabbioneta (Italy) was selected to demonstrate the adopted multidisciplinary workflow. The H-BIM workflow consists of the following steps:

(1) Information acquisition from different sources;
(2) Data management and creation of the H-BIM model;
(3) Transfer of information from H-BIM to FE;
(4) Preliminary FE modal analysis to estimate the dynamic characteristics of the building and design of (ambient) vibration testing;
(5) Validation of the entire H-BIM workflow through comparison between numerical and experimental modal parameters. It should be noticed that the outcome of this last step might be considered as positive when one-to-one correlation exists between numerical and experimental mode shapes with limited discrepancy between natural frequencies. Of course, correlation between operational modal analysis (OMA) and Finite Element analysis (FEA) might be further improved through model updating procedures [5-6].

2 H-BIM FOR STRUCTURAL ASSESSMENT: THE *GALLERIA DEGLI ANTICHI*

The presented H-BIM workflow was applied to the *Galleria degli Antichi* in Sabbioneta, Italy. This impressive building, with the main dimension of almost 100 m, was built in the 16th century. On site inspections and tests carried out by the authors, along with the processing of existing geometric surveys [13-14], allowed to define the main characteristics of the heritage building and the subsequent implementation within the H-BIM framework.

2.1 Historic and documentary research

The analysis of several historic documents was the first step of the building investigation [13-14]. Documentary research was carried out in several archives, collecting documents aimed

at pointing out the evolution of the buildings in the 20th century as well as the sequence of interventions and changes of use [14].

The town of Sabbioneta, included in the UNESCO World Heritage list in 2008, was built by Vespasiano Gonzaga in the 16th century to establish the capital of his duchy. In about 35 years, the traces of the ancient settlements were transformed into a fortified Ideal City, recognized as one of the higher examples of the Renaissance principles in urban planning. The *Galleria degli Antichi* (Fig. 1), probably designed by Giuseppe Dattaro and built between 1583 and 1584 to host the art collection of the Duke, was one of the several palaces of the capital. The *Galleria degli Antichi* is connected through a flyover passage (Fig. 1f) to a former building named *Palazzo Giardino*. At present, the flyover is the only access to the building so that visitors have to cross the ground and first floor of the *Palazzo Giardino*, to reach the first floor of the *Galleria degli Antichi* [13-14].



Figure 1. Historic (a) and current (b) views of *Galleria degli Antichi* and *Palazzo Giardino.* Historic (c-d) and current (e-g) views of different parts of *Galleria degli Antichi*.

The *Galleria degli Antichi* is characterized by a long open arcade at the ground floor with 27 couple of massive squared columns made by brick masonry (Fig. 1e) supporting cross-vaults. The structure of the gallery is made by brick masonry (Figs. 1a, 1b and 1e). At the first floor, the building has a long gallery with 26 windows each side (Fig. 1). The gallery walls were

frescoed and stuccoed in a very refined way by famous painters and craftsman of the time (Figs. 1c, 1d and 1g) [13-14]. The gallery is covered by wooden lacunar ceiling with panels richly decorated but apparently in a low state of preservation (Fig. 1g).

The construction is currently used as a museum, but the evidence of several changes of function has been found in the archives [14]. For example, in 1927 troops billeted in the palaces as previously happened with the Napoleon Army (1806). In 1928, the building hosted the offices and the meeting rooms of the fascist party. In 1947 some halls at the ground floor of *Palazzo Giardino* were used as food shop with a kitchen and in 1948 an organization – involved in social, cultural and free-time activities for the workers – rent some rooms. In 1975 and 1990 *Palazzo Giardino* and *Galleria degli Antichi* hosted the antique market.

The archive research also documents several repair interventions, which systematically followed each misuse of the building. The restorations concerned mainly the surfaces, the frescoes and the stuccos [14]. Similarly, other interventions were carried out in 1935, 1953, 1966, 1989, 2001 to repair the effect of the water leakage due to the roof damage. Metal ties restraining the crossing vaults were probably inserted during the works carried out in 1950. Substantial interventions to the structure were performed in 1952, including the rebuilding of the flyover passage. The descriptions of the damages and of the interventions in the archive records are in general very accurate, documenting the presence of cracks, as well. This last information is very important in order to define the real entity of the damage caused by the 2012 earthquake [13-14]. Furthermore, the available historical pictures (Fig. 1) are of utmost importance to identify damage, as well as the transformations occurred to the buildings.

After the 2012 earthquake, both *Galleria degli Antichi* and *Palazzo Giardino* underwent structural interventions. In this intervention, steel ties were inserted at the level of the first floor and roof levels and anchored to the masonry walls. At the extrados of the lacunar wooden ceiling, steel beams where anchored to the masonry pillars. Steel beams were connected by a system of diagonal and transversal steel ties. In addition, timber tie beams were introduced in such anchoring system, probably to distribute the axial compressive stresses.

2.2 On site inspection and geometric survey

On site inspection is carried out to collect data on the as-built state of the heritage construction. Thematic surveys resumes the information according to the specific research objectives (i.e., the surface materials with their decay, the crack pattern or the connection type between the structural elements, etc.). Careful and systematic comparison between the information gathered from archive documents with the visual inspection of the building surface improves the knowledge of the current state of heritage buildings [1, 13].

A relevant complementary activity is the geometric survey, particularly when ortho-pictures of the fronts are available. Furthermore, geometric surveys could be carried out by photogrammetry and laser scanning reconstructions.

The survey of *Galleria degli Antichi* was carried out by HE.SU.Tech Politecnico di Milano, Campus of Mantua. The point cloud, developed using Autodesk Recap® software, was obtained with the Laser Scanner and Theodolite tools. The processed file was imported in AutoCAD, where vector drawings were extracted and saved in DWG format (Fig. 2).

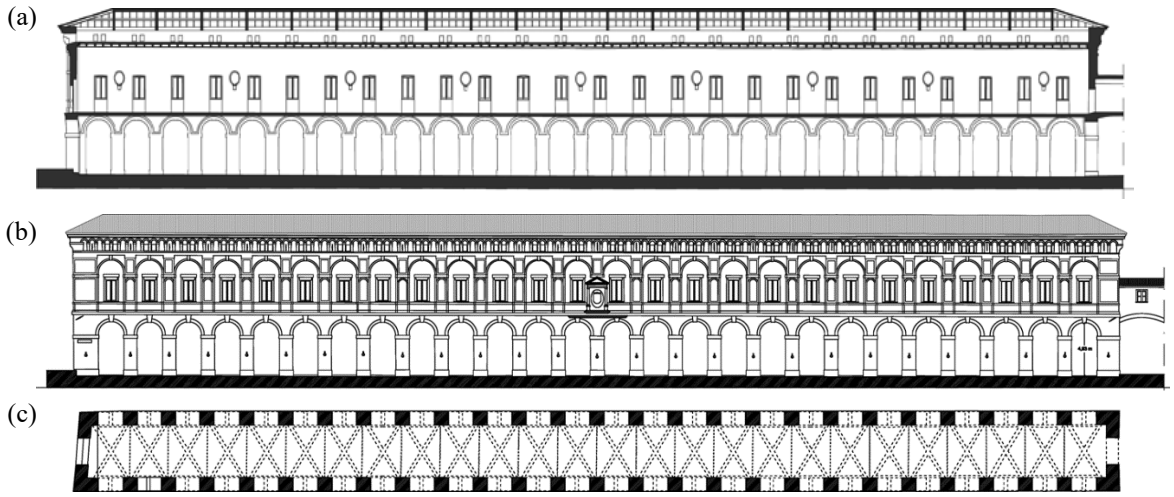


Figure 2. *Galleria degli Antichi*: (a) Longitudinal section; (b) West front; (c) Plan of the ground floor [14].

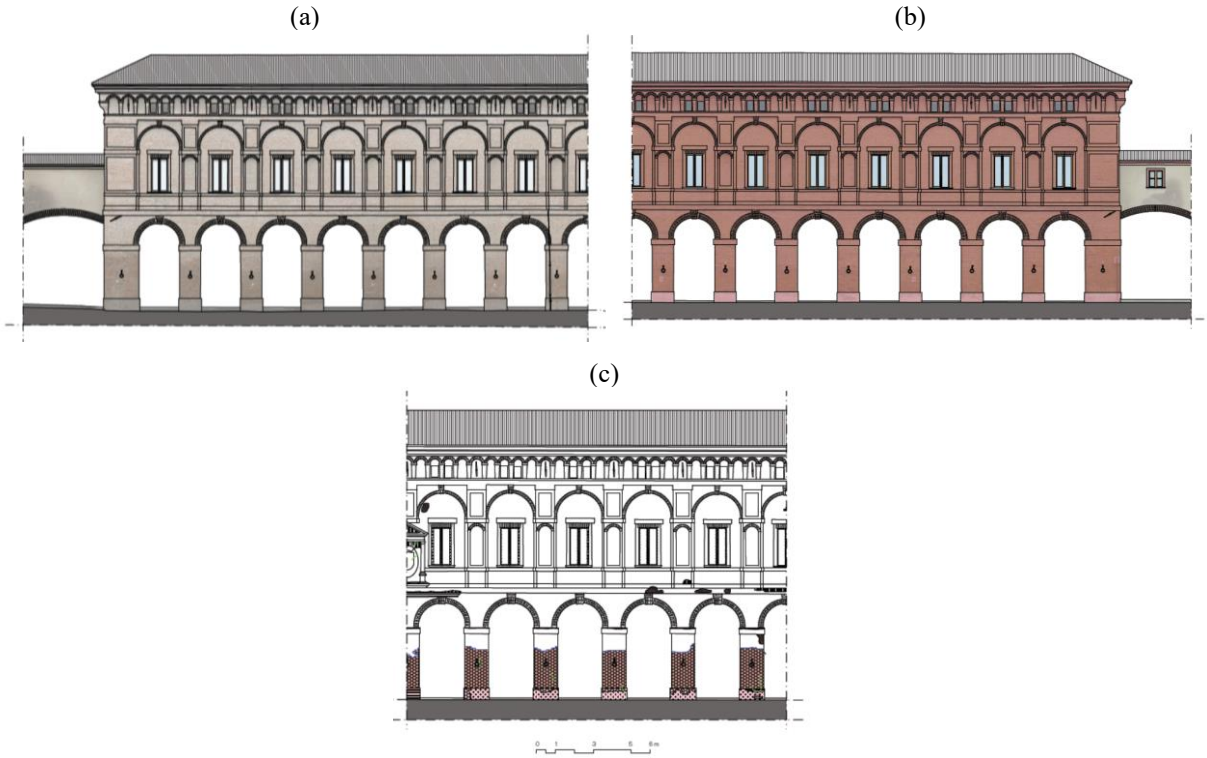


Figure 3. *Galleria degli Antichi*: (a) Geometric survey; (b) Material survey and (c) Material decay survey [14].

Such DWG files represent the summary of geometric survey, which is the base source upon the information collected by comparing the archive documents with on inspections of the buildings. Geometric and thematic surveys have a primary importance in buildings because it helps resuming the investigation carried out in the construction [1] (Fig. 3). Most of the decay problems of the façade of the investigated building are caused by the rising damp: Fig. 2c describes the height of the dampness level and the typical decay of masonry. In the interior of

the building, traces of surface decay are explicable mainly to past leakages occurred from the damaged roof. The water leakage from the roof damaged the ceiling structure as well. Furthermore, during heavy rain the water leaks from the windows of the building, damaging the decoration.

2.3 Historic building information modelling

The previous steps of historical research, geometric and material survey, decay survey and the on site investigation allow defining the main characteristic of the heritage building. The collected information are imported, represented and summarized in the H-BIM model. Although H-BIM can be developed from point clouds, the authors preferred to use the 2D DWG files since the availability of technical 2D drawings is currently more common.

In the model, the building consists of 3D objects (walls, openings, beams, etc.) and those 3D objects are used as database for the information management. The objects collect data about physical and mechanical characteristics of the material, structural connections, boundary conditions and loads; updating of the object characteristics is possible when new information are acquired, without a time-consuming effort during the modification process. Furthermore, each object is defined and dated according to the constructive phase evolution obtained from the historic research.

After the H-BIM model has been completed, the appropriate selection of structural elements allows to define an intermediate "analytical model" (containing all the relevant geometric and structural information on each element) to be exported into a FE software.

2.4 From H-BIM to FEM

In the present application, the "analytical model" is exported in Autodesk Robot Structural Analysis® software [15]. The Robot software allows the user to define the finite elements meshing discretization, that in Revit® is not customizable [15]. The type of finite element automatically chosen during the exportation from Revit® to Robot® is the shell element [15]. It is worth noting that shell elements are not always fully suitable to represent a heritage building but are appropriate when simplified modeling and preliminary assessment of the structure is needed. On the other hand, the compatibility between the two software codes allows easy updating both architectural and structural models at a later stage [15].

In the FE model, the wall middle planes are represented by thick-shell elements, which are defined as 4-node quadrilateral elements (Q4). The beams are modeled as linear beam elements, with 6 degrees of freedom at each node. Regarding the behavior of Q4 shell elements in connection with beam elements – perpendicular to the plane of finite elements, pinned connections are generated [15]. The selected mesh type is Delaunay, with a 0.2 m element size. Such a meshing process led the FE model to have 69179 nodes, with 67169 plane elements and 2676 bar elements; the total number of degrees of freedom is 412482.

3 FE MODAL ANALYSIS AND PLANNING OF AMBIENT VIBRATION TESTS

In the structural assessment of historical constructions, linear elastic analysis is always performed, prior to the application of more refined approaches. In establishing the FE model, the following initial assumptions were introduced for the masonry: (a) homogeneous distribution of the masonry elastic properties; (b) the weight per unit volume of the masonry

and the Poisson's ratio of the masonry were assumed as 18.0 kN/m^3 and 0.20, respectively; (c) the average Young's modulus E was set equal to 1.8 GPa. Furthermore, the building foundations were supposed as fixed.

The geometric characteristics of the load-bearing walls and pillars were modeled according to the results of geometric survey and direct inspections: (i) at ground level, the masonry pillars have a thickness of 1.275 m; (ii) at first floor, the masonry walls have a thickness of 0.85 m; (iii) at the upper level, walls are characterized by masonry arches on the façade (Figs. 1-3) and a constant equivalent thickness of 1.20 m was assumed.

In the lacunar wooden ceilings, the absence of rigid connections between wall-beam and beam-beam elements allows to assume that supports are pinned. The wooden and steel tie beams introduced during the 2012s interventions were represented in Revit® according to their geometries and positions and modeled in Robot® as truss elements.

Selected mode shapes and natural frequencies of the FE model are reported in Fig. 4. As it has to be expected, most of vibration modes involves bending in the transversal direction of the building and the overall structure exhibits a sequence of normal modes similar to the one of a beam supported by springs (Fig. 4).

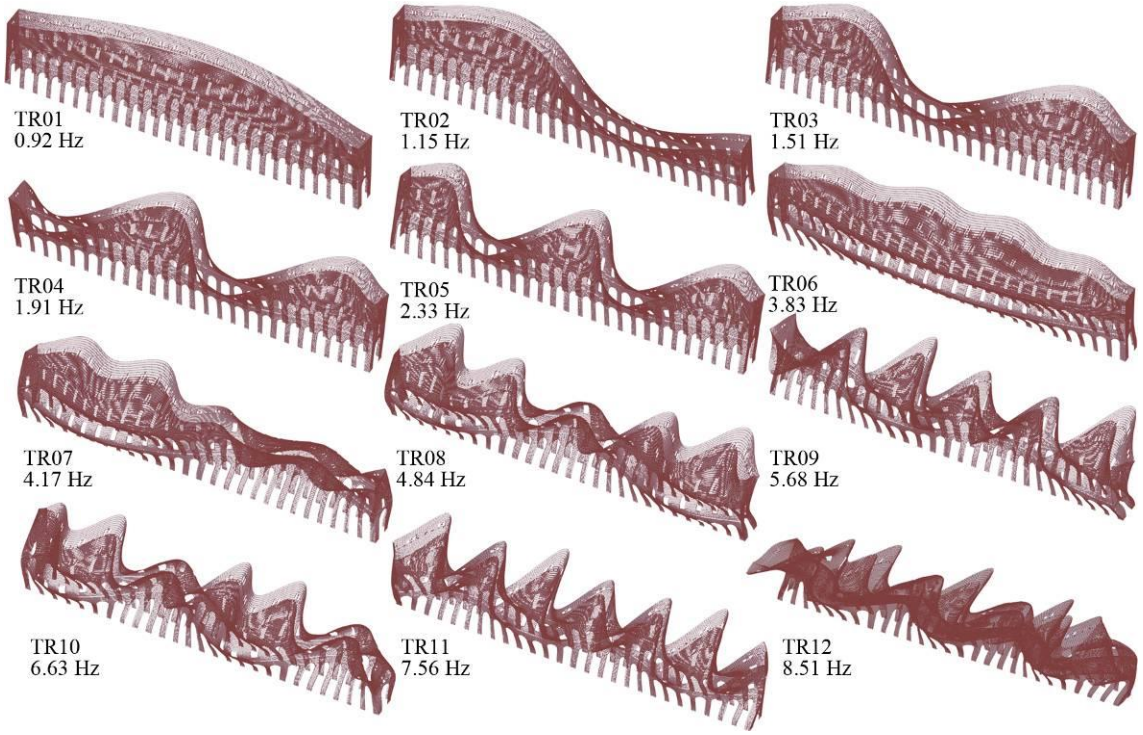


Figure 4. Selected (transverse) vibration modes of the FE model.

3.1 Ambient Vibration tests and Operation Modal Analysis

In order to obtain a validation of the FE model and of the adopted H-BIM workflow, ambient vibration tests (AVTs) were performed. The first floor level was extensively instrumented and a series of two set-ups was required to cover the selected 23 measurement points (Fig. 5): 15 accelerometers were used in each set-up and 7 sensors were held stationary as reference transducers (Fig. 5).

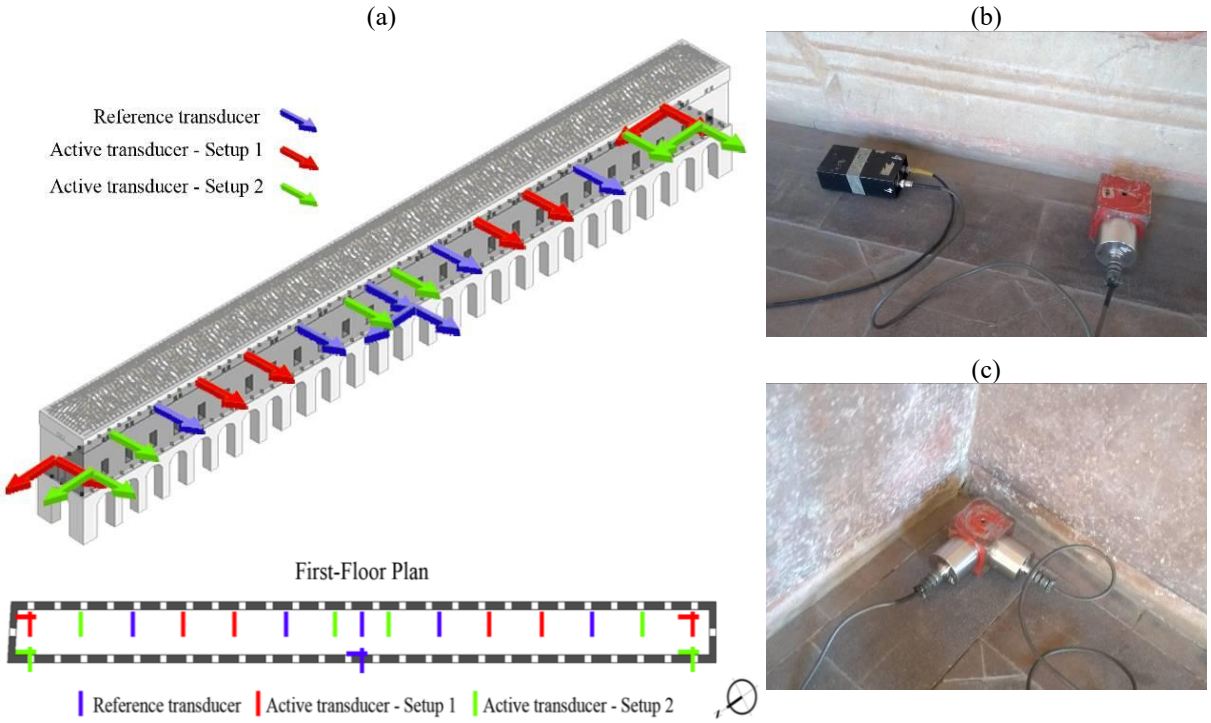


Figure 5. (a) Accelerometers layout and set-ups adopted in ambient vibration tests; Piezoelectric accelerometers in uniaxial (b) or bi-axial configuration (c).

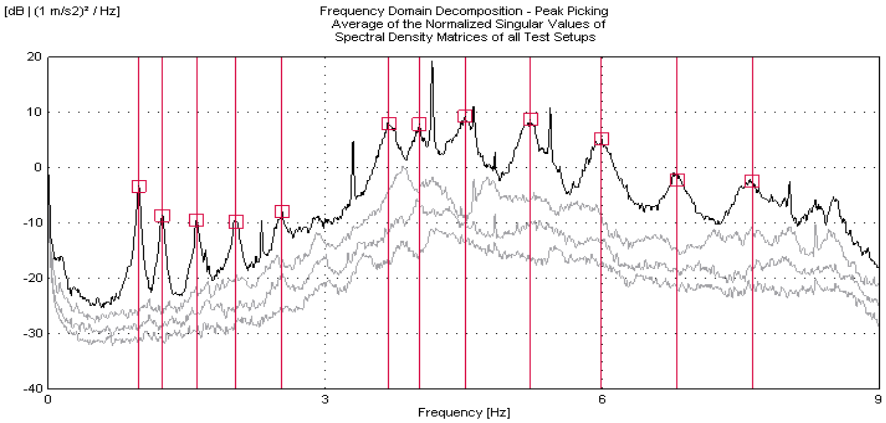


Figure 6. First singular value lines and identification of natural frequencies (FDD).

The AVTs were performed on February 2019 by using the following devices: (i) an acquisition laptop Panasonic Toughbook CF-F9; (b) a multi-channel acquisition system with NI9234 modules (24-bit resolution, 102 dB dynamic range and anti-aliasing filters); (c) 15 WR731A piezoelectric accelerometers (10 V/g sensitivity and ±0.50g of peak acceleration, Figs. 5b and 5c); (d) 15 WR P31 power unit amplifiers (Fig. 5b). The amplifiers were aimed at enhancing the performance of the acquisition chain, providing a constant current to power the internal amplifier, signal amplification and selective filtering. The sampling frequency adopted was equal to 200 Hz, which is more than enough for the investigated building structure whose expected dominant frequencies (Fig. 4) are below 10 Hz. Therefore, low pass filtering and

decimation were applied to down-sample the data to 40 Hz, obtaining a Nyquist frequency of 20 Hz.

The application of the Frequency Domain Decomposition (FDD) technique [16] implemented in the commercial software ARTeMIS [17] to the collected time series led to the identification of 12 transverse vibration modes in the frequency range of 0-9 Hz. The results of OMA in terms of natural frequencies can be summarized through the plot of Fig. 6, showing the first singular value lines (SV) of the spectral matrix. The inspection of Fig. 6 clearly highlights that the FDD technique provides a clear indication of the building modes through well-defined local maxima in the first SV. The corresponding mode shapes are shown in the upper part of Fig. 7.

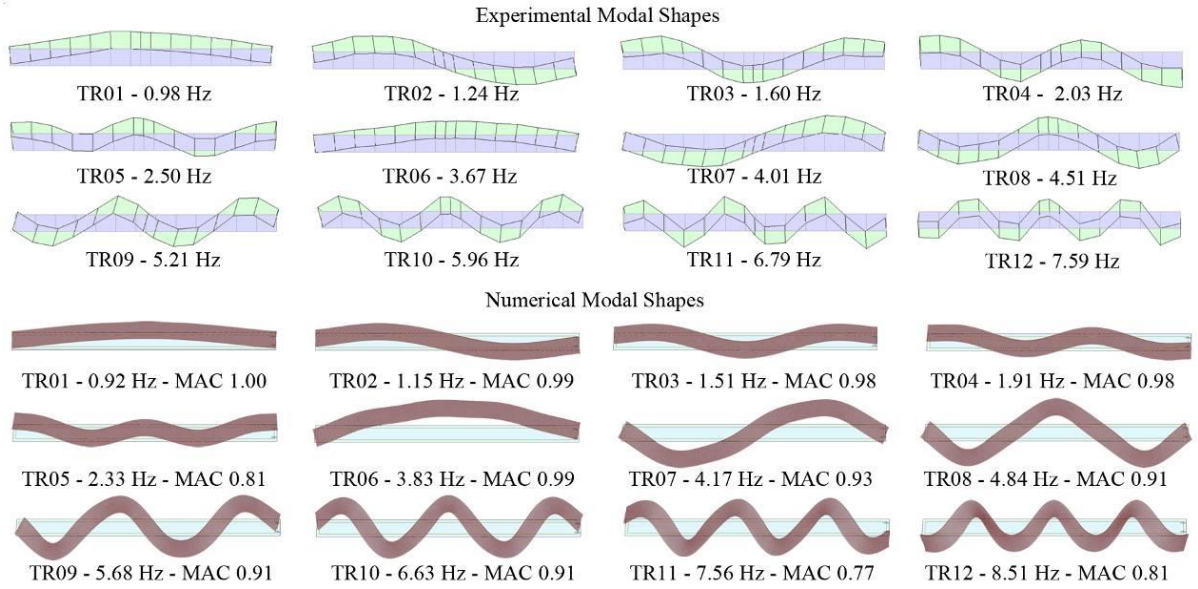


Figure 7. Comparisons between experimental and numerical mode shapes at the first-floor level.

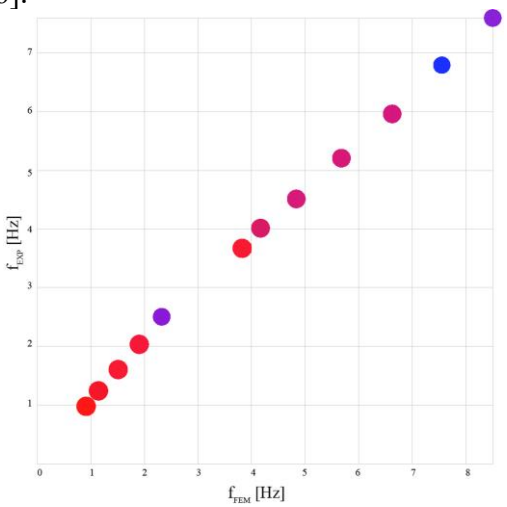
3.2 Validation of the FE model and the H-BIM workflow

Once the dynamic characteristics of the heritage building were identified through AVT and OMA, a comparison with the FEA results is carried out. As usual, such a comparison is aimed at assessing if the geometric, physical and mechanical assumptions adopted in establishing the FE model have been chosen with a reasonable degree of approximation; on the other hand, since the FE model was implemented through a H-BIM workflow, validating the numerical model also provides a validation of the entire methodology.

The Modal Assurance Criterion (MAC) [18] and the combined frequencies and MAC parameters (FMAC) were used to compare the experimental and numerical modal characteristics. The correlation between the dynamic characteristics of the base FE model and the experimental results is shown in Figs. 7 and 8. Figure 8 shows imperfect correlation, with frequency discrepancy DF [$=100\cdot(f_{FEM}-f_{EXP})/f_{EXP}$] ranging up to about 12% and an average distance between experimental and natural frequencies of 7.76%. However, the correlation between theoretical and experimental behavior, notwithstanding its roughness, seems to provide a sufficient verification of the model main assumptions (and hence of the whole H-BIM workflow), being a one-to-one correspondence between the mode shapes, with the worst

MAC value being 0.77.

The imperfect correlation between the FE model and the experimental results is conceivably due to the very simplified assumptions on the to the elastic properties of the masonry and should be improved by updating the distribution of the masonry Young's modulus over the building [5-6].



Mode	f_{EXP}	f_{FEM}	MAC	DF
TR01	0.977	0.916	0.997	-6.17%
TR02	1.240	1.146	0.989	-7.61%
TR03	1.602	1.514	0.983	-6.08%
TR04	2.031	1.908	0.978	-6.92%
TR05	2.500	2.327	0.809	-6.92%
TR06	3.672	3.829	0.986	4.27%
TR07	4.014	4.172	0.931	3.95%
TR08	4.512	4.840	0.913	7.27%
TR09	5.205	5.682	0.914	9.16%
TR10	5.957	6.630	0.906	11.29%
TR11	6.787	7.556	0.769	11.32%
TR12	7.588	8.507	0.809	12.11%
		Average	0.915	7.76%

Figure 8. Modal Assurance Criterion (MAC) and frequency discrepancy (DF) between experimental and numerical modes.

4 CONCLUSIONS

In the paper, the methodology involving historic and architectural research complemented by H-BIM and operational modal testing has been applied to an important heritage building. In more details, the adopted H-BIM workflow includes the following tasks: (1) information acquisition from documentary research and architectural surveys; (2) data organization and creation of the H-BIM model; (3) transfer of information from H-BIM to FE software; (4) preliminary modal analysis in the FE software; (5) operational modal testing and analysis; (6) validation of the FE model and of the H-BIM procedures adopted to develop the FE model through comparison between numerical and experimental modal parameters.

The experience collected in the present investigation allows to draws some conclusions:

- On site inspections, thematic surveys and the comparison of the archive documents with the visual inspection resumed within the H-BIM model improve the knowledge of heritage buildings;
- Dynamic tests in operational conditions provide quantitative parameters (resonant frequencies and mode shapes and damping ratios), which are representative of the structural condition and remarkably contribute to the knowledge of the building. Furthermore, merging the information collected by historic/architectural research, H-BIM and dynamic tests should allow to solve the main uncertainties in establishing numerical models and to assess the structural state of preservation of the building in a fully non-destructive way.

REFERENCES

[1] Binda, L., Saisi, A. and Tiraboschi, C. Investigation procedures for the diagnosis of historic masonries. *Constr. Build. Mater.* (2000) **14**(4): 199-233.

[2] Italian Ministry for Cultural Heritage. *Guidelines for evaluating and mitigation of seismic risk to cultural heritage* (in Italian). Gangemi Editore, Rome (1997).
[3] ICOMOS-ISCARASAH. *Recommendations for the analysis, conservation and structural restoration of architectural heritage*. (2003).
[4] Roca, P., Cervera, M. and Gariup, G. Structural analysis of masonry historical constructions. Classical and advanced approaches. *Arch. Comput. Methods Eng.* (2010) **17**(3): 299-325.
[5] Gentile, C. and Saisi, A. Ambient vibration testing of historic masonry towers for structural identification and damage assessment. *Constr. Build. Mater.* (2007) **21**(6): 1311-1321.
[6] Gentile, C., Saisi, A. and Cabboi, A. Structural identification of a masonry tower based on operational modal analysis. International Journal of Architectural Heritage, (2015) **9**(2): 98-110.
[7] Volk, R., Stengel, J. and Schultmann, F. Building Information Modeling (BIM) for existing buildings. Literature review and future needs. *Automat. Constr.* (2014) **38**: 109-127.
[8] Murphy, M., McGovern, E. and Pavia, S. Historic building information modelling (HBIM). *Structural Survey* (2009) **27**(4): 311-327.
[9] Calì, A., Do Valle, Â., and Dias De Moraes, P. Building Information Modeling and Structural Analysis in the Knowledge Path of a Historical Construction. In: R. Aguilar et al. (Eds.): *Structural Analysis of Historical Constructions*, RILEM Bookseries 18 (2019), pp. 2071-2079.
[10] Barazzetti, L., Banfi, F., Brumana, R., Gusmeroli, G. Previtali, M. and Schiantarelli, G. Cloud-to-BIM-to-FEM: Structural simulation with accurate historic BIM from laser scans. *Simul. Model. Pract. Th.* (2015) 57: 71-87.
[11] Brumana, R., Della Torre, S., Previtali, M., Barazzetti, L. Cantini, L., Oreni, D. and Banfi, F. Generative HBIM modelling to embody complexity (LOD, LOG, LOA, LOI): surveying, preservation, site intervention – The Basilica di Collemaggio (L'Aquila). *Appl. Geomat.* (2018) **10**(4), 545-567.
[12] Bruno, S., De Fino, M. and Fatiguso, F. Historic Building Information Modelling: performance assessment for diagnosis-aided information modelling and management. *Automat. Constr.* (2018) **86**: 256-276.
[13] Saisi, A. and Terenzoni, S. Galleria degli Antichi and Palazzo Giardino at Sabbioneta: Remarks from archive research and direct survey. In: G. Milani et al. (Eds.): *10th International Masonry Conference,* International Masonry Society (2018), pp. 907-916.
[14] Dal Barco, G., Perobelli, S. and Sartor T. *Palazzo del Giardino e Galleria degli Antichi a Sabbioneta*. MSc Thesis, Politecnico di Milano, Milan, Italy (2016).
[15] Autodesk Inc. *Integrating Revit Structure and Robot Structural Analysis Professional Workflows* (2010).
[16] Brincker, R., Zhang, L. and Andersen, P. Modal identification of output-only systems using frequency domain decomposition. *Smart Mater. Struct.* (2001) 10(3):441-445.
[17] Structural Vibration Solutions (SVS). ARTeMIS Extractor 2010. Aalborg, Denmark (2010).
[18] Allemang, R.J. and Brown, D.L. Correlation coefficient for modal vector analysis. In: *Proceedings 1st International Modal Analysis Conference* (1983), pp. 110-116.

STUDY ON CAUSATIVE AGENTS OF DAMAGE IN THE COSTA RICAN CARIBBEAN ARCHITECTURE FROM A MULTIDISCIPLINARY PERSPECTIVE

GARCÍA-BALTODANO, K., [1*]**, PORRAS-ALFARO, D.** [2] **AND HERNÁNDEZ-SALAZAR, I.**[2]

[1] Escuela de Arquitectura y Urbanismo
Instituto Tecnológico de Costa Rica
Campus Tecnológico Local San José, San José, Costa Rica
e-mail: kgarcia@tec.ac.cr, www.tec.ac.cr

[2] Instituto Tecnológico de Costa Rica
Campus Tecnológico Local San José, San José, Costa Rica
e-mail: dporras@tec.ac.cr, ihernandez@tec.ac.cr, www.tec.ac.cr

Keywords: vernacular architecture; Limón, Costa Rica; pathologies in buildings; inventory

Abstract. *The aim of this communication is to analyze the architectural, historic and construction values of the Costa Rican Caribbean architecture, which constitutes an architectural typology of the identity of the city of Limón. Damages linked to biological agents in these buildings were identified based on the multidisciplinary research project titled "Conservation of the Costa Rican Caribbean architecture by applying advanced techniques for studying the causative agents of damage in the buildings".*
An inventory of the study area was conducted in order to identify predominant elements of this type of architecture, as well as to quantify and georeference, through a Geographic Information System, the buildings that are still preserved; the identification of damage-causing agents within the inventory was also part of the process. As a second stage, samples taken from the buildings will be analyzed in the biological sciences laboratory to identify biological agents that were potentially responsible for damage.
Thirty representative buildings of the Costa Rican Caribbean architecture were identified, for which inventory records were made that included information about architectural and building aspects, as well as damage identification and classification, and types of causative agents. Based on a multi-criteria evaluation, Capitanía de Puerto, Casa Misionera de la Iglesia Bautista and other edifications were selected as the buildings to conduct the inventory of biological damage, sampling, and environmental monitoring.

1. INTRODUCTION

Costa Rica outstands for its diversity, including geographical as well as cultural and ethnical aspects. Despite being a small country, its regions are manifestly different from one another, which influences the way constructions for inhabiting the different spaces are made.

Costa Rican Caribbean architecture is an example of vernacular architecture which, although based on imported models, constitutes an adaptation to the spatial and bioclimatic needs of a particular zone of the country. Caribbean architecture in Costa Rica was developed

especially in the city of Limón, between 1870 and 1940, closely linked to settlement and growth processes of this area.

For a long time, the city of Limón was the main port in Costa Rica. It was originally planned to facilitate exportation of coffee beans and was used later for banana exportation. The city was established during a period of economic booming and it was designed to accomplish ideals of modernization and hygienization associated to the prevailing liberal ideology of the time.

This city was the operations center of the United Fruit Company, a multinational company that dominated the banana market at international level. This company also created an enclave in the whole province of Limón by taking advantage of its links to the Northern Railway Company, who led the construction of the Atlantic railway and to whom Costa Rica's government granted a large extension of land as payment for the work [1].

The United Fruit Company imported catalogue buildings for a good part of the edifications, which were influenced by the Victorian Caribbean architecture. However, because of the weather conditions in Limón, of high humidity and temperature and constant rain throughout the year, these buildings required some modifications for enhanced comfort.

With time, the inhabitants of the area, Costa Ricans and afro descendants from the Antilles brought to build the railway, adopted the style, making their own adaptations to the construction of their homes. The center of Limón and its first expansion, known as Jamaica Town, were the two first areas where this type of vernacular architecture was developed.

Costa Rican Caribbean architecture is characterized for using timber material for the structure and enclosures, in which the "balloon frame" system stands out [2]. Large corridors and galleries, steep-sloped zinc roofing, double eaves, constructed high up on concrete or wooden piles, are its outstanding architectonic elements. In addition, this architecture presents decorations of Victorian influence, such as railings, lattices, wooden grilles or *petatillos* and corbels. Although constructions for mixed, commercial, religious and institutional use were made, single-family and multifamily constructions were predominant [3].

In the past, these buildings proliferated in the city of Limón, clearly declining over the years and putting at risk the identity of the area. Although this type of architecture is characteristic of the Caribbean in Costa Rica and is linked to the historical urban landscape of the city of Limón, research on this topic has so far been scarce.

Hardly any literature regarding this topic is available, nor previous inventories to know the number and conditions of the constructions. Added to this, few buildings are protected by the government, which increases their risk of disappearing.

In addition to vulnerability to anthropic agents, these buildings are exposed to biodeterioration, being wood the main construction material, subjected to environmental conditions of high precipitation, humidity and temperature, as mentioned above. From this perspective, we focus on this topic as no previous work has been done in the country in terms of Costa Rican Caribbean architecture.

Since 2018, the Instituto Tecnológico de Costa Rica (TEC), through its schools of Architecture and Urbanism and Forest Engineering, together with the School of Biological Sciences at Western Illinois University (WIU), have been collaborating in the research project "Conservation of the Costa Rican Caribbean architecture by applying advanced techniques for the study of the causative agents of deterioration of buildings". The main objective of this project is "to promote the conservation of Costa Rican Caribbean architecture built within the urban historical center of the city of Limón (historical center and first expansion) between the period 1871-1940, based on the inventory, characterization and diagnosis of the causative

agents of damage in the buildings". To this end, four specific objectives have been proposed to be developed over a period of four years, which are:

- Identify the Costa Rican Caribbean architecture within the temporal (between 1871-1940) and spatial delimitation (historical center and Jamaica Town neighborhood) proposed for research.
- Diagnose the signs of deterioration of the buildings selected.
- Analyze the causative agents of pathological processes detected in the laboratory.
- Propose alternatives for treating the damage detected using a pilot testing project.

This paper presents partial results of the research project. It focuses on showing the architectural, historic and constructive values of Costa Rican Caribbean architecture, as well as advancements with respect to identification of damage associated with biological agents in these buildings.

2. METHODOLOGY

The study and conservation of vernacular architecture requires a process that addresses two aspects: first, understanding its architectural and constructive elements; and secondly, developing a better knowledge of the causative agents that influences its deterioration. From a multidisciplinary vision, this research expects to raise awareness on a type of architecture that has long been undervalued, and at the same time, find possible solutions to its preservation. The steps carried out between 2018 and 2019 corresponding to the first three objectives are detailed below:

2.1. Review of available sources

One of the first tasks of the research consisted in the elaboration of conceptual framework regarding the Costa Rican Caribbean architecture, for which a series of primary and secondary sources were consulted, such as books, magazines, catalogues, newsletters, maps, historical and administrative archives, photographs, expressions of folk art such as paintings and stories, final graduation papers, among others. Mainly sources were consulted from public libraries in San José and Limón, National Archive of Costa Rica, National Library of Costa Rica, Library of ICOMOS Costa Rica, Centre for Research and Conservation of Cultural Heritage and university libraries.

Additionally, the cultural statistics of the Ministry of Culture and Youth linked to the subject of heritage were consulted to identify data on the situation regarding use of and state of conservation of the buildings under study, especially those declared Architectural Historical Heritage.

A review of literature related to biodeterioration and the protocols for the analysis of biological agents was also made.

2.2. Systematization of the information

The project was developed using a collaborative work methodology in which each one of the members contributed to the research according to their expertise. For this purpose, an online platform has been used (Google Drive), fed by all team members for the storage of information

obtained and creation of a database where materials such as photographs, cartography, bibliographic references, etc. are stored.

On the other hand, the information obtained during the first two years of the project was used to create graphic material showing the characteristic elements identified of Costa Rican Caribbean architecture.

2.3. Survey of on-site information and building inventory

Between 2018 and 2019 a series of field trips were made to the city of Limón. The purpose was to gather on-site information to conduct the inventory of Costa Rican Caribbean architecture. Beforehand, a guide to gather information and the strategy to be followed during the fieldwork was designed. Next, the information collected was systematized in records.

2.3.1. Initial listing

A list of the buildings was made that compiled the fundamental characteristics of Costa Rican Caribbean architecture identified using the conceptual framework. Records were used to gather this information and the premises were georeferenced using the on-line software tool My Maps (https://www.google.com/intl/es/maps/about/mymaps/), which allowed including text and photographic information.

2.3.2. Categorization of buildings

Once the initial listing was completed, the buildings were categorized according to legibility and conservation of the characteristics of Costa Rican Caribbean architecture. The typologies presented were:

- Type 1: Non-transformed or slightly transformed building, mostly complying with the characteristics of Costa Rican Caribbean architecture.
- Type 2: Building with some transformations, partially complying with the characteristics of Costa Rican Caribbean architecture.
- Type 3: Very transformed building, conserves few characteristics of Costa Rican Caribbean architecture.
- Type 4: Does not correspond to the object of study.

This activity allowed to establish a filter to identify the buildings that should be inventoried.

2.3.3 Inventory

The inventory included the buildings classified as types 1 and 2. The inventory records designed allowed collection of major information of each building in relation to the research objectives of the project. Among the data featured are: location; proprietors; architectonical, constructive and material characteristics; state of conservation; among others.

2.3.4. Preliminary survey of damages and biological agents.

Records were developed to survey the damage and biological agents present in the buildings inventoried. In addition, photographic records of the elements identified were made.

2.3.5. Data organization

Final records were prepared with the information obtained from the inventory and the preliminary survey of damages and biological agents, with the intention of documenting each of the buildings and to generate a formal document that compiles the inventory.

2.3.6. Inventory revision

A thorough inventory revision process has been carried out and in some cases involved a second visit to the field site to rectify information collected in the first visit and the new updated data was incorporated in the data files.

2.3.7. Database

The information of the inventory and the preliminary survey of damages and biological agents allowed the construction of a database of the buildings of Costa Rican Caribbean architecture present in the historical center of Limón and in Jamaica Town. This tool, in addition to facilitate information management, provides input to develop a multi-criteria evaluation and the creation of a Geographic Information System to support the selection of buildings for sampling and laboratory analysis.

2.4. Identification of deterioration agents

The process of identifying deterioration agents required the selection of a representative sample of the buildings initially identified as part of the inventory. To this end, a multi-criteria evaluation was carried out to prioritize the buildings.

Once the buildings were selected, sampling was performed to continue the study at the Forest Pathology Laboratory of the Forestry Engineering School at TEC and at the Laboratory of Fungal Ecology of WIU.

2.4.1. Multi-criteria evaluation

Multi-criteria evaluation consists of a set of techniques focused on decision making by investigating a number of possible options resulting from multiple criteria and objectives [4]. The ultimate end of this tool is to arrive to concrete decisions after considering information, objects and relationships [5].

The following criteria were established in the present work, and were assigned different percentages according to the interests of the project, weighing the value according to the building:

a) Legibility of the Costa Rican Caribbean architecture characteristics (30%): In order to promote the conservation of this type of architecture, the proper reading of its characteristics is essential, so the first criterion is related to the categorization of previously addressed buildings. Buildings types 1 and 2 were used as they are the ones that best preserve the characteristics. Weighing was performed in conformance with the following aspects:

- Type 1: Non-transformed or slightly transformed building, mostly complying with the characteristics of Costa Rican Caribbean architecture (2 points).
- Type 2: Building with some transformations, partially complying with the characteristics of Costa Rican Caribbean architecture (1 point).

b) Architectural Historical Heritage Declaration (20%): This legal concept, contemplated in Law No. 7555 of Costa Rica, which identifies the country's buildings, public or private, whose cultural and historical significance makes their conservation important.

- Without declaration (0 points).
- With declaration (1 point).

c) Conservation state (30%): As a result of the inventory process, the record incorporated an in-depth assessment of the building components of the edifice. According to the list of the elements and their assessment, a higher score was given to those buildings with the greatest need for intervention.

- Good: The element is in good condition, conserves all or most of the formal and material characteristics of the time (1 point).
- Regular: The element exists but its state is inadequate, with some damage and signs of deterioration and modifications that are not consistent with the time (2 points).
- Bad: The element is in very bad condition, presenting damage and signs of deterioration. Its state needs immediate intervention (3 points).

d) Accessibility to the building (20%): This criterion incorporates the possibility of going deeper into the study of the building.

- Access only to the exterior of the building (1 point).
- Access to the interior of the building (2 points).
- Access to the interior of the building and ease to carry out research (3 points).



Figure 1. Antigua Capitanía de Puerto and the Casa Misionera de la Iglesia Bautista.

2.4.2. Sampling and environmental monitoring

Once the buildings were selected, and with the permission of the owners, the samples of areas with damage by potential biological agents were collected. As of December 2019, the sampling was carried out in the Antigua Capitanía de Puerto and in the Casa Misionera de la

Iglesia Bautista (figure 1). Both buildings have a declaration of Architectural Historical Heritage. We plan to carry out this work in the other selected buildings in the first half of 2020.

Two samples were taken per damaged area using sterile cotton swabs and another one by collecting approximately 1g by scratching the exposed material. As part of the protocol, the damaged areas were sterilized with 70% alcohol. The samples were identified and stored for future use in the laboratory.

2.4.3. Sampling processing in the laboratory

The samples weighing 1g were divided into two (0.5g each) in order to perform two types of analysis. The first procedure consisted in the isolating the microorganisms and the second was extraction of DNA for microbial identification, which is to be performed at Western Illinois University. The sample was stored at -20°C to be sent later to the United States in DNA extraction buffer.

The samples were sterilized in a laminar flow chamber by soaking them into 1% sodium hypochlorite for a period of 30 seconds; then in 96% ethanol for 30 seconds; lastly, the sample was washed in sterile distilled water for one minute.

2.4.4. Microorganism isolation

The sterile samples were subdivided into three and placed on petri dishes with three types of culture media: potato dextrose agar (PDA), nutrient agar (NA) and Sabouraud agar (SA). These cultures were incubated for eight days at 25°C; once incubation finished, the petri dishes were evaluated and hyphal tips were taken to perform a subculture of each fungus found until obtaining an axenic culture of each isolated fungus.

2.4.5 Microorganism identification

The axenic cultures obtained were characterized morphologically; in addition, their DNA will be extracted using a commercial kit DNeasy (Qiagen). Next, molecular identification will be performed using fungal specific primers at the Fungal Ecology Laboratory at WIU.

2.4.6. Environmental monitoring

Devices for environmental monitoring (dataloggers) were placed in each selected building to analyze variations in humidity and temperature throughout the research. In addition, measurements with a thermo-hygrometer and a laser measurer of surface temperature have been carried out during each visit to the buildings to complement datalogger information. The information thus gathered is expected to help establish relationships between humidity and temperature, and the presence of biological agents.

2.5. Participatory process and community awareness

As part of the project's tasks carried out, focal groups have been formed with social agents of the community that, because of their professional profile or connection with buildings of interest for the research, may be able to validate the information or contribute new data. In total, three focal groups were formed during the second semester of 2018 and the first semester of 2019.

Additionally, an exhibition called "Limón Port: Valuing the Costa Rican Caribbean architecture" was produced, to present some of the first results from the research. Its purpose was to raise awareness in the population with respect to vernacular architecture.

3. RESULTS

Despite having performed an exhaustive bibliographic and documentary review of the relevant topics for the project, both the information found in primary and secondary sources and at documentation centers, archives and libraries, was scarce and lacked specialization in the subject addressed in the project. In this regard, there is a clear need to develop additional materials to address the topic of Costa Rican Caribbean architecture and give it the relevance it has as an identity element of this culturally diverse geographic region.

Nevertheless, the information gathered allowed a better understanding of the evolution of Limón's historical center and first urban expansion, and recognize the milestones in the development of the city and their relationship with the emergence of buildings with similar architectonic and construction characteristics. Hence, conceptual framework and a timeline were produced with respect to this topic in order to facilitate the interpretation and understanding the city's evolution.

Review of documents, among which the contributions of [6, 7, 8, 9] stand out, and the contrast between these and the information gathered in the site allowed to identify a series of essential characteristics linked to Costa Rican Caribbean architecture, as follows:

- Use of timber as the main construction material.
- Use of wooden or concrete piles, exposed or covered with little walls in the main facade.
- Presence of attics.
- Windows or air vents on the roof of the building.
- Outdoor corridors or galleries.
- Presence of balconies.
- Stairs located in the corridors.
- Use of eaves and similar structures in other areas separated from the roof, including windows.
- Portico or covered lobby preceding the main access.
- Fretted wood decorations or gingerbread in the facade.
- Roofs with steep slopes.
- Use of corrugated metal sheets for the roofs.
- Strong colors in walls (mainly turquoise, green and pink).
- Wooden latticeworks (wooden grilles or *petatillos*) in the windows and in the upper part of the walls for cross air ventilation.
- Use of shutters.
- Central location of the building in the lot to leave free space at least in three of the sides, which is convenient for collecting rainwater and achieve improved ventilation.
- Thermal control chamber for insolation (monitor).
- Use of metal sheets as wall facings.
- Use of balloon frames.

On the other hand, the information obtained allowed to establish the categories that would be used to classify the buildings found in the study area (figure 2). In this regard, it was found that, of all inventoried buildings, only 12% are type 1, that is, they fully maintain the characteristics of Costa Rican Caribbean architecture since the interventions they present have not affected their image or spatial configuration. Part of this category are the Antigua Capitanía de Puerto and the Casa Misionera de la Iglesia Bautista, both buildings protected by the declaration of Architectural Historical Heritage.

Among the buildings, 23% were classified as type 2, as they have been partially intervened and have, to some extent, transformed their historical image. Some of them even suffered partial alteration of their materials with the addition of modern materials. Type 3 included 28% of the buildings, which have been noticeably transformed and in some cases are given a different use from the original; some elements have been replaced, have suffered partial demolitions or have been intervened with modern materials, with only a few characteristics of Costa Rican Caribbean architecture remaining.

Type 4 included 19% of the buildings as they were not part of the object of study, despite being built with wood, they were from a more recent construction period than the established timeline for the project. The remaining 19% of the buildings were not considered for inventory due to lack of information about them or access limitations.

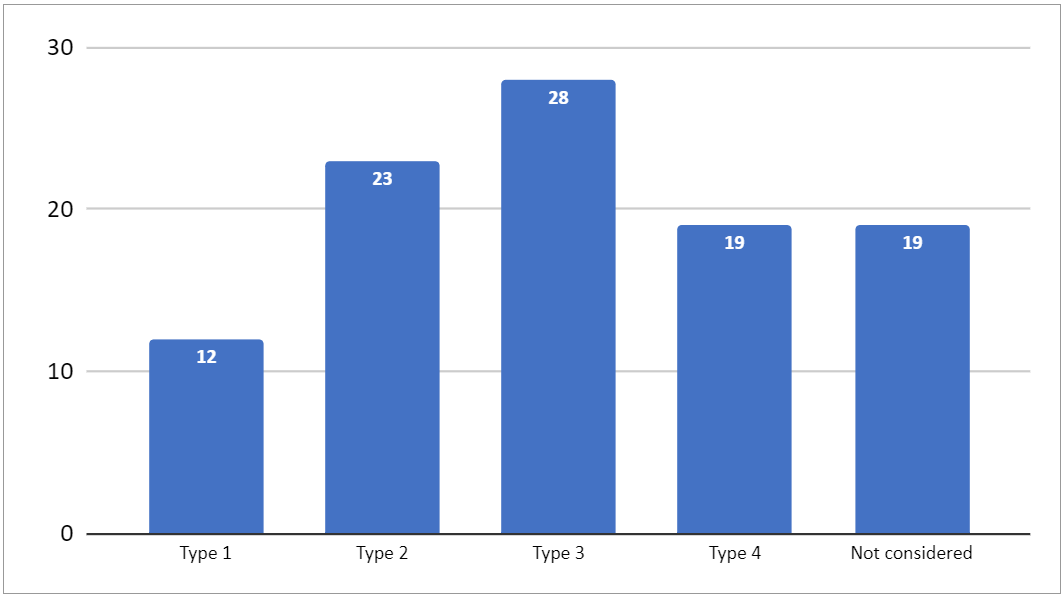


Figure 2. Classification of buildings found in the study area.

The building inventory of Costa Rican Caribbean architecture was carried out only with buildings types 1 and 2. In total, 30 buildings were recorded (figure 3). Each one of the records provides information about the state of conservation, architectural characteristics, types of damage found and causative agents.

The information in the inventory records and the database helped perform the multi-criteria evaluation to choose the buildings in which the sampling and environmental monitoring would be carried out. The multi-criteria evaluation helped determine the buildings of greatest interest for research and plan the sampling by prioritizing. The first five positions were taken by: Casa

Misionera de la Iglesia Bautista (W-tipo1-01), Antigua Capitanía de Puerto (AAA-tipo1-01), Casa Garvey (TT-tipo1-01), multi-familiar housing (TT-tipo1-02) and multi-familiar housing (P-tipo1-01).

The process of sampling and monitoring has already begun in the first two buildings indicated. As of December 2019, a damage survey concerning biodeterioration agents had been carried out. This survey allowed the identification of at least 15 areas showing biological damaged in the Antigua Capitanía de Puerto and 24 in the Casa Misionera de la Iglesia Bautista.

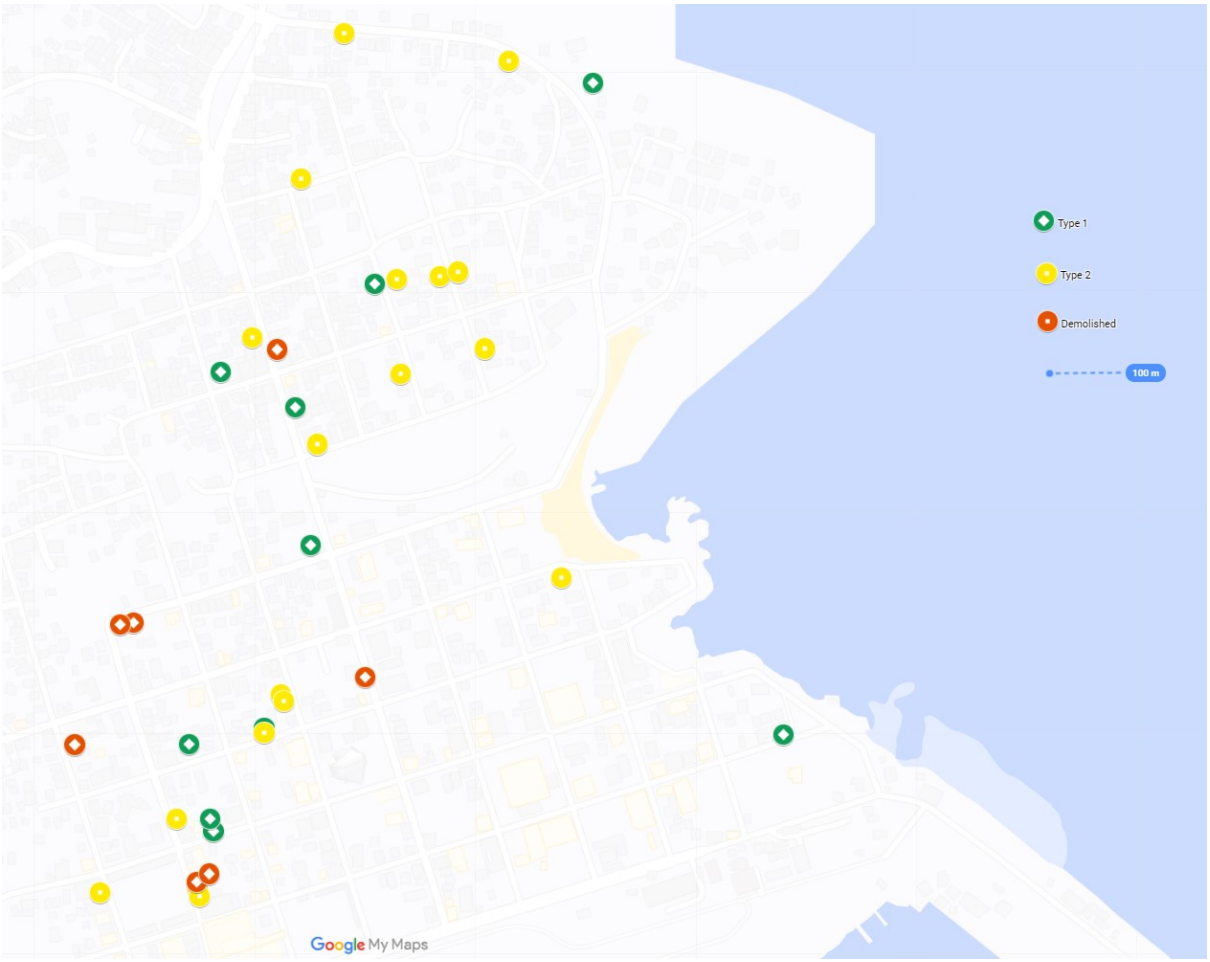


Figure 3. Map of inventoried buildings.

In total, 25 samples were collected in both buildings (11 and 14, respectively). As for the study of fungi associated with these damage structures, these are through a process of isolation and DNA extraction to be later identified. Although it was determined that both buildings are affected by termites, so far it has not been possible to find a living insect. DNA sequencing and analysis of the samples taken is being conducted by researchers at WIU, who are in the process of identifying the microorganisms, at the morphological and molecular level.

Dataloggers have already been placed in the two buildings and continuous environmental monitoring work is being carried out. The data has been collected and added to the project database for use in future stages.

During these first two years of development, the project has generated a large amount of information that has been systematized into three main inputs: a 3D modelling of the buildings with heritage declaration and three private homes; an illustrated glossary of architectural terms and a guide with features of Costa Rican Caribbean architecture; the two latter ones aim to promote the use of technical language to refer to the different building elements and to graphically raise awareness on the particularities of this type of buildings. On the other hand, three-dimensional modelling will simplify the analysis of the climatic conditions of the buildings through the use of specialized software, while allowing the documentation of the buildings.

In order to promote appreciation of this architecture and appropriate the knowledge generated with this research, the exhibition "Limón Port: Valuing the Costa Rican Caribbean architecture" was produced. After this activity was organized, stakeholders have shown interest in launching initiatives related to the tourism sector to allow generation of endogenous development by valuing heritage resources; precisely at this point, an important relationship has been established with a new extension project also developed by TEC in relation to valuing heritage resources.

Lastly, during the development of this research the need arose to identify the varieties of wood present in the different building elements of the inventoried buildings; this process began during the second half of 2019 with the visit of specialists from the TEC School of Forestry Engineering; however, the work of identification will continue over the remaining implementation time of the project.

4. CONCLUSIONS

The limited information and lack of knowledge on Costa Rican Caribbean architecture makes its recognition at the professional level difficult. The same occurs with the processes of awareness and appropriation by the community. Research is required on this type of vernacular architecture from the historic, social and architectural perspectives.

During the period in which the research has been carried out, the demolition of seven type 1 and 2 buildings has already been recorded, as a result of poor state of conservation and pressures from urban development. Of these, five buildings could be documented in the initial listing and two of them have inventory records; thus, the vulnerability of this architecture remains exposed.

Of the 30 buildings inventoried by the project only two have a declaration of Architectural Historical Heritage, which means they are protected by the Government; however, this has not guaranteed their conservation either. The remaining buildings, according to the inventory carried out and the multi-criteria analysis, show that most of them are in a bad or regular condition. This should serve to call attention on preserving and valuing these buildings, looking for options to promote the search for solutions from a multidisciplinary perspective that also contemplates the in-depth study of causative agents of damage.

The progress of the research has made it possible to identify a number of microorganisms potentially associated with biodeterioration. The next stage of the project will delve deeper into the morphological and molecular analysis of these microorganisms in order to propose solutions to the pathological processes detected.

Acknowledgements. We thank the Vicerrectoría de Investigación y Extensión of the Instituto Tecnológico de Costa Rica for their support to this project. We also thank the rest of the research team (Ing. Dawa Méndez-Álvarez, PhD. Andrea Porras-Alfaro, Arch. Dominique Chang-Albizurez, Arch. Enmanuel Salazar-Ceciliano and Arch. Mauricio Guevara-Murillo) and assistant students (Fernando Agüero-Bravo, Sofía Rivera-Villareal, Gerald Cordero-Arias, Rafael Hidalgo-Campos, Gabriela Delgado-Hernández, Rebeca Gómez-Oviedo, Alejandro Varela-Fonseca, Carolina Jiménez-Vargas, Angie Rodríguez-Rosales) who have actively worked in the development of the research activities.

REFERENCES

[1] García, K. *El patrimonio cultural como base para un modelo de desarrollo endógeno. La herencia cultural del Período Liberal en Costa Rica (1870-1940) como capital cultural. Un estudio de caso.* Tesis Doctoral. Universidad Autónoma de Madrid, (2016).

[2] Sanou, O. y Quesada, F. Orden, progreso y civilización (1871-1914). Transformaciones urbanas y arquitectónicas. En E. Fonseca y J. Garnier (Eds.): Historia de la Arquitectura de Costa Rica. Museos del Banco Central y Centro de Investigaciones Históricas de Centroamérica (1998).pp. 219-317.

[3] Woodbridge, R. *Historia de la arquitectura en Costa Rica*. Editorial Tecnológica de Costa Rica, (2003).

[4] Barredo, J. *Sistemas de Información Geográfica y Evaluación Multicriterio en la Ordenación del Territorio.* Editorial Ra-Ma. I edición, (1996).

[5] Munda, G. *Teoría de Evaluación Multicriterio: una breve perspectiva general. Maestría en Economía Ecológica y Gestión Ambiental.* Ed. Universidad Autónoma de Barcelona, (1998).

[6] Gutiérrez, S. *Arquitectura caribeña: Puerto Limón, Bocas del Toro.* Escala, (1991).

[7] Barascout, E. *Anteproyecto de Revitalización del Centro Histórico de Limón*. ICOMOS, (1995).

[8] Vives, I. Arquitectura de la Época de la "United" 1890-1930. *Patrimonio* (2004) 4: 95-109. San José: Centro de Investigación y Conservación del Patrimonio Cultural. 95-114.

[9] Sanou, O. *Guía de arquitectura y paisaje de Costa Rica*. Junta de Andalucía, (2010).

12th International Conference on Structural Analysis of Historical Constructions
SAHC 2020
P. Roca, L. Pelà and C. Molins (Eds.)

STUDYING A MASONRY SAIL VAULT BY ANTONIO DA SANGALLO THE ELDER IN THE *FORTEZZA VECCHIA* IN LIVORNO

F. BARSI[1*], D. AITA[1], R. BARSOTTI[1], D. ULIVIERI[2] AND S. BENNATI[1]

[1]Department of Civil and Industrial Engineering
University of Pisa
Largo Lucio Lazzarino 2, 56126 Pisa, Italy
e-mail: francescobarsi@gmail.com, danila.aita@unipi.it, r.barsotti@ing.unipi.it, bennati.stefano@gmail.com

[2]Department of Energy, Systems, Territory and Construction Engineering
University of Pisa
Largo Lucio Lazzarino 2, 56126 Pisa, Italy
e-mail: denise.ulivieri@unipi.it

Keywords: Masonry sail vault, Limit analysis, Durand-Claye's method.

Abstract. *The present contribution aims to illustrate some first results obtained from ongoing research on a 16th-century masonry sail vault in the Fortezza Vecchia (the Old Fortress) in Livorno (Italy). A multidisciplinary research is currently ongoing. The information collected by means of geometric surveys and experimental tests are being used as input data for the different analytical and numerical models expressly developed to study the vault's structural response. The structural analysis has been performed using two analytical models set within the framework of limit analysis. The first considers the vault as a thin shell, and suitable sets of statically admissible stresses are built; the second model is a modern reinterpretation of Durand-Claye's method for domes. As an additional term of comparison, numerical analyses are carried out by means of FE models. The study is still under development, and a first set of results has been obtained by limiting the analysis to vertical loads accounting for the self-weight of the vault and that of the overlying soil layers.*

1 INTRODUCTION

The present contribution aims at illustrating a preliminary study of the mechanical response of a subterranean sail vault covering a quadrilateral room located in the Canaviglia bastion of the Fortezza Vecchia (the Old Fortress) in Livorno. The Fortezza Vecchia is a maritime castle of great historical interest representative of 15th- and 16th- century Tuscan architecture, built on behalf of the Florentine government. The study is framed within a research project (PRA 2017 – "Tuscan Renaissance architecture: case studies between historical investigation, survey and structural analysis"), promoted by the University of Pisa. Some results obtained in the first phase of the research are illustrated in [1-2].

2 THE "FORTEZZA VECCHIA" IN LIVORNO

The Fortezza Vecchia (Old Fortress) in Livorno is one of the most significant "*alla moderna*" military garrisons in Tuscany. Pisa and later Firenze choose this site located on the sea at the eastern end of Livorno as a management center for port activities.

Between 1369 and 1376 the "Rocca Nuova" was built, then called "Quadratura dei Pisani". In 1421 Florence purchased Livorno for 100,000 gold florins, while Pisa, already sold to Florence in 1405, strongly opposed the Florentine domination. Livorno became "*la pupilla dell'occhio del dominio Fiorentino*" (the pupil of the eye of the Florentine dominion) [3, p. 69] and began to fortify.

In 1506, Antonio da Sangallo the Elder (c. 1455-1534) arrives in Livorno. As chronicled by Giorgio Vasari, Antonio da Sangallo's drawing of the Livorno Fortress was not "entirely executed, nor in the way Antonio had drawn it" [4, IV, p. 288]. The Livorno citadel is a work stylistically similar to that in Pisa, on which Antonio began work in 1509. However, in August of the same year management of the site was taken over by Giuliano, who drew up the final plans [5, p. 685]. At the Livorno construction site, several engineers, technicians and experts oversaw the various stages of construction.

The Livorno Fortress contains some imposing medieval buildings - the Square Tower, the Keep, the Quadratura dei Pisani. Medieval tradition played a considerable role in the drafting of the plans for Livorno. The layout of the Livorno fort was not geometrically regular because of the massive medieval structures it incorporated, and its peculiar position completely surrounded by the sea [5, p. 685-686].

As early as 1519 "the foundations were dug" for the Livorno walls. In 1520 construction work began on the new seaward bastion, called the '*catena*' (chain), later called Cavaniglia, and later still Caviniglia. As the foundations had to be laid directly in the water, a wooden formwork was made, though not without difficulty [5, p. 686; 3, pp. 47–53]. In 1525 the Fortress became an island reachable from land by a boat pulled by cable fixed to an anchoring stone. Between 1546 and 1547, Cosimo I de' Medici, decided to build a palace for his family right inside the fortress. The building stood above the Quadratura dei Pisani and included the medieval Keep [6].

3 THE SAIL VAULT BY ANTONIO DA SANGALLO THE ELDER IN THE CANAVIGLIA BASTION OF THE FORTEZZA VECCHIA

The contour of the Canaviglia bastion is very wide; the throat instead contains the facades of both the quadrangular medieval tower and the contiguous corner of the Quadratura. The west flank is connected to the corner of the Quadratura dei Pisani, which works as the seaward curtain, by a short stretch of wall 16 cubits long. This section contains the inspired addition of an unusual trapezoidal room, covered by a sail vault with an octagonal central ventilation oculus, which links the concave retired flank with the square tower and the medieval stronghold (Figure 1). This room represents a structure of great interest, in which we can recognize the Sangallo brothers' research into "ancient spatial concepts filtered and mediated by Brunelleschi's inventions" [5, p. 688].

The data collected via a TLS survey of the entire fortress (inside and out) has been made available by the administrative bodies (Autorità di Sistema Portuale del Mar Tirreno

Settentrionale – North Tyrrhenian Sea Port Authority). The survey, available as a point cloud, features a density of about 3 points per square centimeter. The point clouds were recorded in a single reference system and were furnished in Autodesk ReCap format. The Autodesk environment made it easy to extract the geometries needed for structural analysis.



Figure 1: Canaviglia bastion, trapezoidal room covered by a sail vault with octagonal central oculus. Image by Photographic Laboratory, Department of Civilizations and Forms of Knowledge, University of Pisa.

3.1 The structural scheme of the sail vault

Point clouds are not well suited for structural analyses. Hence, a representative subset of points was selected from the survey. The coordinates of these points have been used as input data to find the best approximating surface of the vault intrados. A spherical shape has been chosen a priori as approximating surface. The search for the optimal parameters values has been performed by means of a simplified numerical optimization procedure, illustrated in [1]. The ideal surface thusly determined, which turned to be very close to the survey points, is a sphere of 5.5-meter radius.

The vault thickness has been estimated by means of the results of the still ongoing experimental campaign. More precisely, the internal stratigraphy of the vault was investigated by performing 16 endoscopic tests which enabled verifying that the vault is made of seemingly uniform brick masonry. The vault thickness is minimum at the top, where it is equal to 50 cm, and gradually increases as the vault approaches the lateral walls. In order to build a simple structural scheme of the vault that is on the safe side, a uniform thickness of 50 cm has been adopted in the analyses for the resisting part of the vault (Figure 2). The part of the vault that exceeds 50 cm has been considered as a dead load.

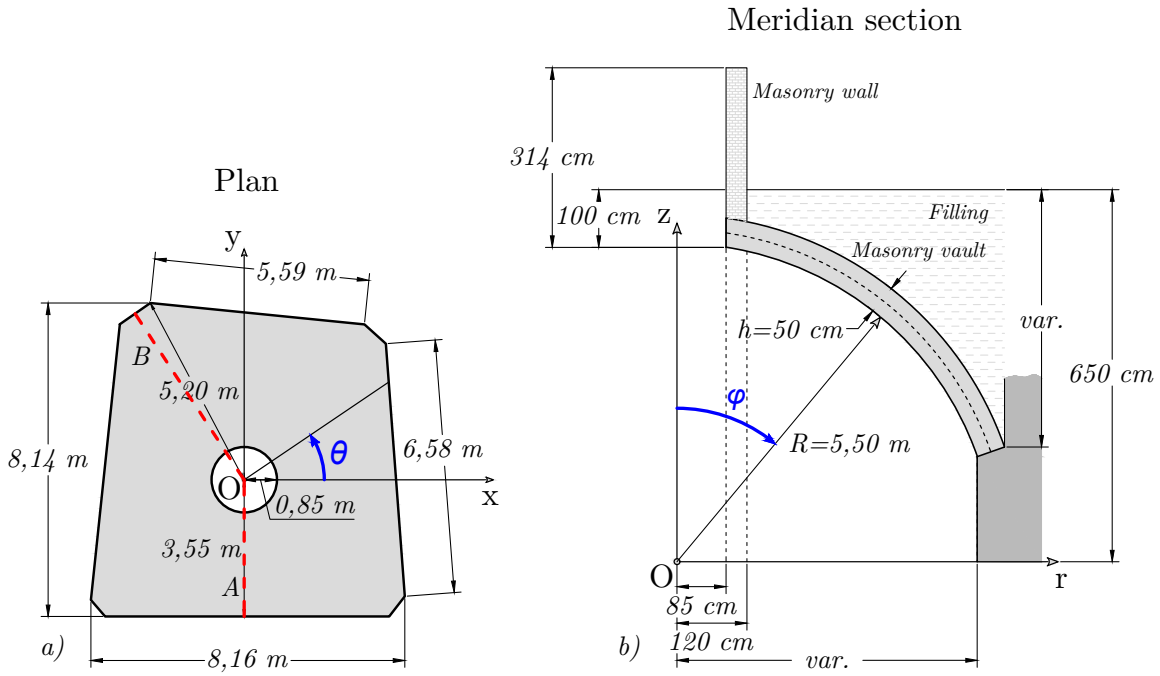


Figure 2: Geometry of the vault: plan (left) and vertical section along a meridian (right).

4 STRUCTURAL ANALYSIS OF THE SAIL VAULT

The structural analysis has been performed by following a methodology already applied by some of the authors to a recent study that addressed the dome of Pisa Cathedral [7]. Two analytical models are used that are set within the framework of limit analysis. The first considers the vault as a thin shell, and suitable sets of statically admissible stresses are built; the second model is a modern reinterpretation of Durand-Claye's method for domes.

In all the analyses, the loads considered are the self-weight of the vault, the weight of the filling material and that of the masonry wall around the oculus. A specific weight of 18 kN/m^3 has been adopted for the masonry and filling. By hypotheses, the walls are considered to be perfect constraints for the vault.

Structural analysis of the sail vault against the vertical loads represents just a first preliminary step toward the evaluation of the vault safety level. The vault as well as the whole Fortezza is a massive masonry construction built for defensive reasons; hence, no structural problem is to be expected as far as vertical loads are concerned. In the following some preliminary results are illustrated obtained by considering the effect of vertical loads. The effect of more severe actions such as internal explosions, bombing and cannon shots from enemy ships will be considered in the next phase of the research.

4.1 Modeling the vault as a masonry shell: statically admissible internal forces distributions

The analysis is aimed at determining statically admissible stress fields within the vault, which is modelled as a masonry shell. For the sake of simplicity, we limit the analysis to axial-symmetric distributions. In order to provide a first estimation of the safety level of the vault,

two different safety factors may be introduced: the geometrical and mechanical safety factors. When geometrical safety factor is considered, the masonry compressive strength is assumed to be unbounded, and safety becomes a matter of geometry. The geometrical safety factor is defined as the ratio between the actual thickness of the vault and the minimum thickness for which it is possible to find a statically admissible stress field. When the mechanical safety factor is considered, the masonry's compressive strength is taken into account. The mechanical safety factor is defined as the ratio between the masonry compressive strength and the maximum stress in the vault.

Since the sail vault at hand is of considerable thickness, the geometric safety factor for vertical loads turns out to be very high. The calculations performed, which are not shown here for the sake of brevity, enable estimating a geometric safety factor of at least 40.

As per the mechanical safety factor, a statically admissible distribution of the internal forces within the masonry shell is built by allowing bending stresses along the whole meridian and compressive hoop forces in the parallels near the top of the vault, within a region of given width (Figure 3). By optimizing the width of the region in which compressive hoop forces are present, the masonry strength assuring a mechanical safety factor of 3 can be made as low as 0.98 MPa.

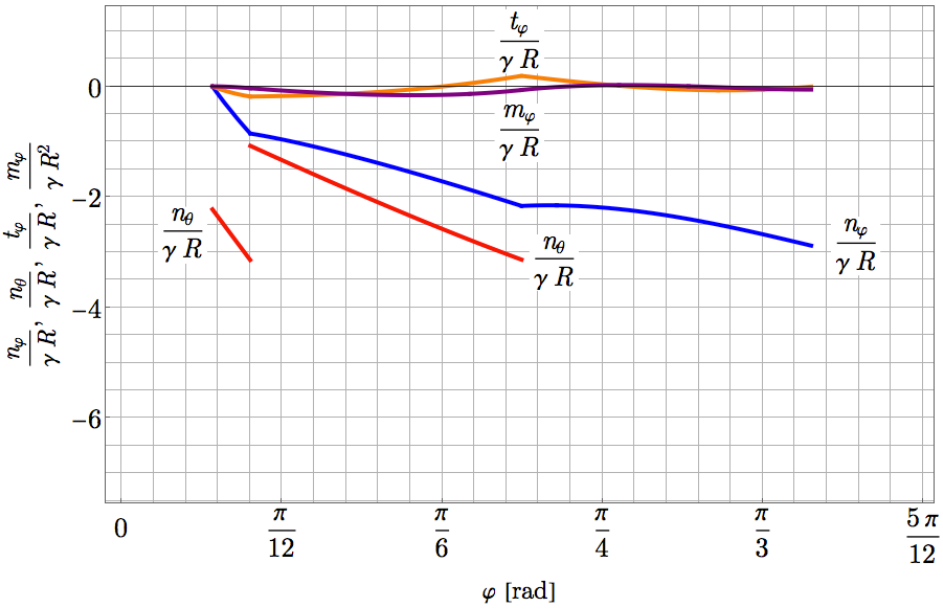


Figure 3: Dimensionless forces per unit length, (n_θ, n_φ = axial force in parallels and meridians; t_φ, m_φ = shear and bending moment in the meridians).

4.2 Equilibrium analysis of the sail vault through a modern re-edition of Durand Claye's method

In this section a revised version of Durand-Claye's method [8, 9] will be applied in order to perform a first evaluation of the stability of the sail vault. In previous papers, the authors have proposed a modern version of Durand-Claye's method by translating the complex graphical construction into a suitable set of equations in terms of the internal forces [10]. Furthermore, the method has been re-edited for domes in order to adequately take into account the influence

of hoop forces and some kinematic aspects at collapse [11-12].

As illustrated more in detail in [2], a first equilibrium assessment can be conducted by applying the slicing technique. In this regard, Durand-Claye's method is applied to two lunes of embrace angle equal to $\varphi = 40.11°$ and $\varphi = 70.79°$, corresponding respectively to the dashed lines A and B in Figure 2, left. An infinite compressive strength is considered for the masonry. The top region near the central oculus is considered to be a rigid annulus of infinite strength. The red and blue curves in Figure 4 correspond to the attainment of a positive or negative limit bending moment at some joint in the radial direction: the stability area is the hatched area bounded by the aforementioned limit curves. Using the same notation adopted in [10-13], it is defined as the locus of the points (P, e) corresponding to statically admissible solutions under the hypothesis of nil hoop forces. Since both stability areas in Figure 4 are extended, the lunes under examination are in equilibrium even if compressive hoop forces are assumed to be nil. The thrust lines corresponding to the maximum (points B, D) and minimum (points A, C) values of the horizontal thrust P are shown in Figure 5. Coherently with the stability area results, they are all contained within the lune's thickness.

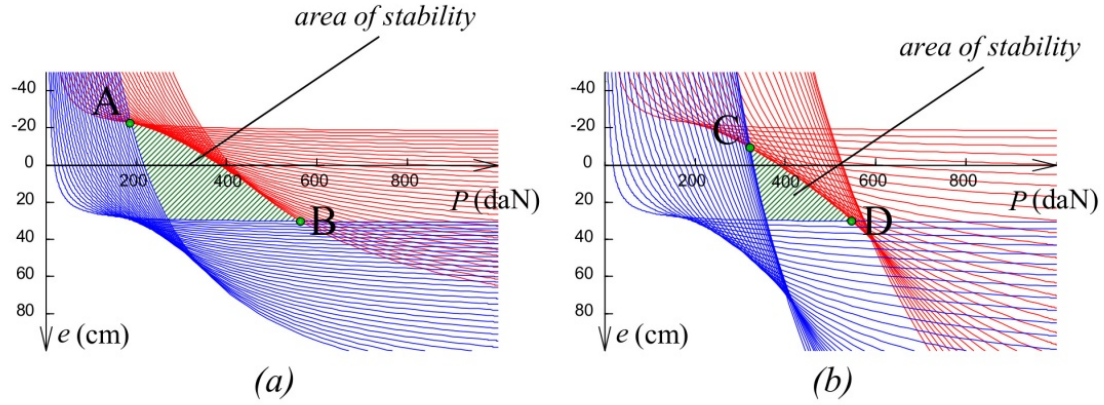


Figure 4: The stability area related to the dome defined by $\varphi = 40.11°$ (a); the stability area related to the pendentive of maximum embrace angle $\varphi = 70.79°$ (b).

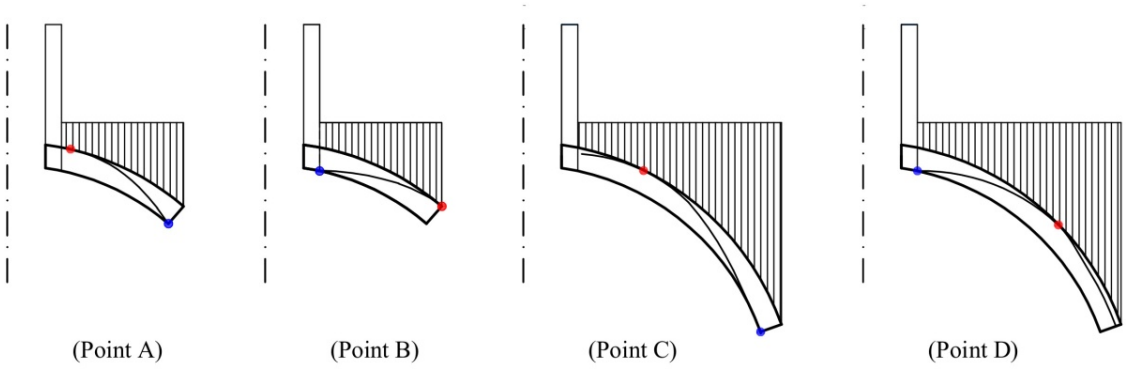


Figure 5: The maximum and minimum thrust lines related to points A, B, C, and D of the stability areas plotted in Figure 4.

As expected, the Fortezza Vecchia sail vault is quite far from any collapse condition. Moreover, even if the stability area were reduced to a single point by progressively reducing the lune's thickness, this would not lead to a limit condition, since the collapse mechanism identified by the vanishing of the stability area would not be a kinematically admissible mechanism for the dome considered as a whole. In this case, the lateral surfaces of each lune would act as constraints by preventing inwards motion.

5 CONCLUSIONS

- The present contribution illustrates some first results of an ongoing research project aimed at studying the structural behavior of the subterranean brick masonry sail vault covering a trapezoidal room in the "Canaviglia" bastion in the Livorno "Fortezza Vecchia". The interdisciplinary analysis aims to take into account historical, geometrical, mechanical and construction aspects.
- A detailed survey of the intrados surface has been carried out by means of a range-based (laser scanning) survey methodology. A post-processing procedure has been adopted in order to obtain the vault's intrados sections in CAD format and the analytically determined 'best' approximating smooth surface.
- Structural analysis of the vault has been performed by means of two different models set within the framework of limit analysis. The first model yielded a preliminary estimate of both the geometrical and mechanical safety factor by considering the masonry vault as a thin shell unable to transmit any tensile stress. The second model made use of a revised version of Durand-Claye's method, by appropriately slicing the sail vault into "lunes". The analyses show that, as it was expected, a considerable safety margin can be estimated for the vault subjected to vertical loads.
- Further analyses will be performed within the next step of the research program. Experimental investigations are going to be performed on the vault and walls so as to fully determine their main geometrical and mechanical parameters. Further study will address the more significant loading condition produced by bombing or internal explosion by also taking into fully account the three-dimensional structural behavior of the sail vault.

Acknowledgements. Financial support from the University of Pisa under programme PRA 2017, project "Architetture toscane rinascimentali: casi studio fra indagine storica, rilievo e analisi strutturale" is gratefully acknowledged. The collaboration of the Port System Authority of the Northern Tyrrhenian Sea is gratefully acknowledged.

AUTHOR CONTRIBUTIONS

I. FB, RB, SB; II. DU; III. FB, RB, DU, SB; IV. FB, DA, RB, SB; V. FB, DA, RB, DU, SB.

REFERENCES

[1] Barsi, F., Barsotti, R. and Bennati, S. Equilibrium of masonry sail vaults: the case study of a subterranean vault by Antonio da Sangallo the elder in the "Fortezza Vecchia" in Livorno. Submitted to the XXIV AIMETA Conf., Rome, Italy, 15-19 September 2019.

[2] Aita, D., Barsotti, R. and Bennati, S. Equilibrium analysis of a sail vault in Livorno's

Fortezza Vecchia through a modern re-edition of the stability area method. Submitted to the XXIV AIMETA Conf., Rome, Italy, 15-19 September 2019.

[3] Frattarelli Fischer, L. *L'Arcano del mare - Un porto nella prima età globale: Livorno*. Pisa (2018).

[4] Vasari, G. *Le vite de' più eccellenti architetti, pittori, et scultori italiani, da Cimabue insino a' tempi nostri*. Firenze: Lorenzo Torrentino (1550).

[5] Ulivieri, D. Fortezza Vecchia in Livorno. *Nexus Network J.* (2014) **16** (3):675-697.

[6] Bevilacqua, M.G., Caroti, G., Piemonte, A. and Ulivieri, D. Reconstruction of lost architectural volumes by integration of photogrammetry from archive imagery with 3-D models of the status quo. Int. Arch. Photogramm. Remote Sens. Spatial Inf. Sci., XLII-2/W9, 119-125, DOI 10.5194/isprs-archives-XLII-2-W9-119-2019 (2019).

[7] Bennati, S., Aita, D., Barsotti, R., Caroti, G., Chellini, G., Piemonte, A., Barsi, F. and Traverso, C., (*in press*), Survey, experimental tests and mechanical modeling of the dome of Pisa Cathedral: a multidisciplinary study. *International Journal of Masonry Research and Innovation*.

[8] Durand-Claye, A. Note sur la vérification de la stabilité des voûtes en maçonnerie et sur l'emploi des courbes de pression. *Ann. des Ponts et Chaussées* (1867) **13**:63-93.

[9] Durand-Claye, A. Vérification de la stabilité des voûtes et des arcs. Applications aux voûtes sphériques. *Ann. des Ponts et Chaussées* (1880) **19** I sem.:416-440.

[10] Aita, D., Barsotti, R. and Bennati, S. A modern reinterpretation of Durand-Claye's method for the study of equilibrium conditions of masonry domes. Proc. XXIII AIMETA Conf., Salerno, L. Ascione, V. Berardi, L. Feo, F. Fraternali and A. M. Tralli (eds.), Gechi Edizioni, Mediglia (MI), 1459-1471 (2017).

[11] Aita, D., Barsotti, R. and Bennati, S. Looking at the collapse modes of circular and pointed masonry arches through the lens of Durand-Claye's stability area method. *Archive of Applied Mechanics* (2019) **89** (8):1537-1554.

[12] Aita, D., Barsotti, R. and Bennati, S. A parametric study of masonry domes equilibrium via a revisitation of the Durand-Claye method. Proc. COMPDYN 2019, Crete, Greece, 24-26 June 2019, M. Papadrakakis, M. Fragiadakis (eds.) (2019).

[13] Aita, D., Barsotti, R., Bennati S. Studying the dome of Pisa cathedral via a modern reinterpretation of Durand-Claye's method, *JoMMS* (2019) **14**(5): 603–619, DOI: 10.2140/jomms.2019.14.603.

12th International Conference on Structural Analysis of Historical Constructions
SAHC 2020
P. Roca, L. Pelà and C. Molins (Eds.)

THE BRIDGE OVER THE ADDA RIVER IN BRIVIO: HISTORY, FULL-SCALE TESTING AND FE MODELLING

GIACOMO ZONNO[1*], CARMELO GENTILE[1]

[1]Department of Architecture, Built environment and Construction engineering (DABC)
Politecnico di Milano, Piazza Leonardo da Vinci 32, 20133 Milan, Italy
e-mail: giacomo.zonno@polimi.it (*corresponding author), carmelo.gentile@polimi.it

Keywords: Reinforced Concrete Arch Bridge, Operational Modal Analysis, Finite Element Modeling and Updating, Non-Destructive techniques.

Abstract. *Selected results from the investigation program of a historic R.C. bridge are presented in the paper. The bridge, crossing the Adda river between the Municipalities of Brivio and Cisano Bergamasco, consists of three tied arch spans, about 44.0 m length each, and represents a crucial node for the vehicular traffic of the region. After a maintenance intervention performed on one pier, the local Authorities committed to Politecnico di Milano an extensive investigation including: (i) documentary research and review of the bridge history; (ii) visual inspection and geometric survey of each span; (iii) full-scale load tests and ambient vibration tests; (iv) FE modelling of each span and validation of the numerical models (through comparison with the available experimental results) and (v) structural assessment of the bridge in its present condition. After a concise review of the bridge history, the paper summarizes the complete results of the experimental tests performed on one span (visual inspection, geometric survey, full-scale load tests and dynamic tests) as well as the development of numerical models.*

1 INTRODUCTION

Historic bridges are an important part of the national heritage and often represent essential nodes of the contemporary road and railway network. A great number of historic reinforced concrete (R.C.) arch bridges was erected in Italy in the first half of the 20th century, as the concrete arch was the most common solution adopted for bridges spanning over 40.0 m or more [1]. Of course, many of these bridges, which were designed according to what today are considered outdated code regulations, are still in service, and their structural assessment is of increasing concern. As a matter of fact, these structures require a special attention because are exposed to several potential damage causes, such as aging of the materials, effects of pollution, lack of maintenance, inappropriate use, increase of traffic vibrations and natural hazards.

The procedure to assess the structural condition of a historic bridge involves several tasks, according to the multidisciplinary approach presented in the modern guidelines of restoration and conservation of historic structures [2]: documentary research in the archives, on-site full-scale testing and finite element (FE) modelling are some of these important tasks to track the health state of a historic structure [3-4]. The documentary research can provide useful

information about the construction phases, structural details and any changes that may have occurred in the life of the structure. Direct inspection and on-site full-scale tests can provide information about the current state and can increase the knowledge about the material properties and the actual structural response. FE models based on the original design drawings, geometric survey and on-site tests can play a fundamental role in the correct assessment of the investigated structures [5-7]. Moreover, the process of developing FE models involves assumptions and simplifications (about the boundary conditions, the characteristics of materials, the presence of damaged areas, etc.) that may induce remarkable errors in predicting the actual response of a "as-built" bridge. Even refined FE models often fail to predict resonant frequencies and modes shapes with a sufficient level of accuracy, as a consequence of both modelling and material uncertainties. A good practice to reduce the gap between the actual behaviour of a full-scale structure and its model is to perform operational modal testing and the consequent validation/calibration of the numerical model by minimizing a measure of the difference between experimental and numerical parameters [1].

Within this context, the present paper summarizes the investigation carried out on the Brivio bridge, built in 1917 and consisting of three R.C. tied arch spans. The investigation involves documentary research, visual inspection and geometric survey, load tests and ambient vibration tests, FE modelling and model updating. The paper is structured as follows. Section 2 describes the main characteristics of the Brivio bridge. Section 3 describes the experimental investigations carried out to assess the heath state of the analysed bridge. Section 4 describes the implemented FE models in detail, and section 5 concludes the paper.

2 DESCIPTION OF THE BRIDGE

The historic Brivio Bridge is located between the municipalities of Brivio (province of Lecco) and of Cisano Bergamasco (province of Bergamo), about 50 km North-East of Milan, in the Lombardia region, northern Italy. The bridge, designed by the Italian engineer Giuseppe Banfi [8], was built between June 1912 and May 1917 (Fig. 1) and crosses the Adda river. The overall structure consists of three R.C. spans with parabolic arches, that are supported by two piers – whose foundation is built in the river bed – and two end abutments.

The documentary research in the archives allowed to find almost complete information on the bridge design, so that important data are available through original drawings (Fig. 2a), static calculation of the arches (Fig. 2b), structural details of reinforcement and foundation system (Fig. 2a), construction materials and code regulation adopted in the bridge design [9].

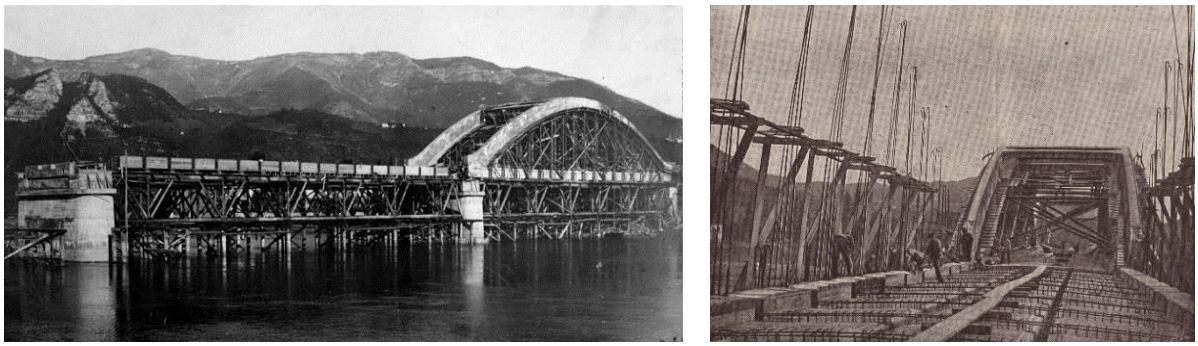
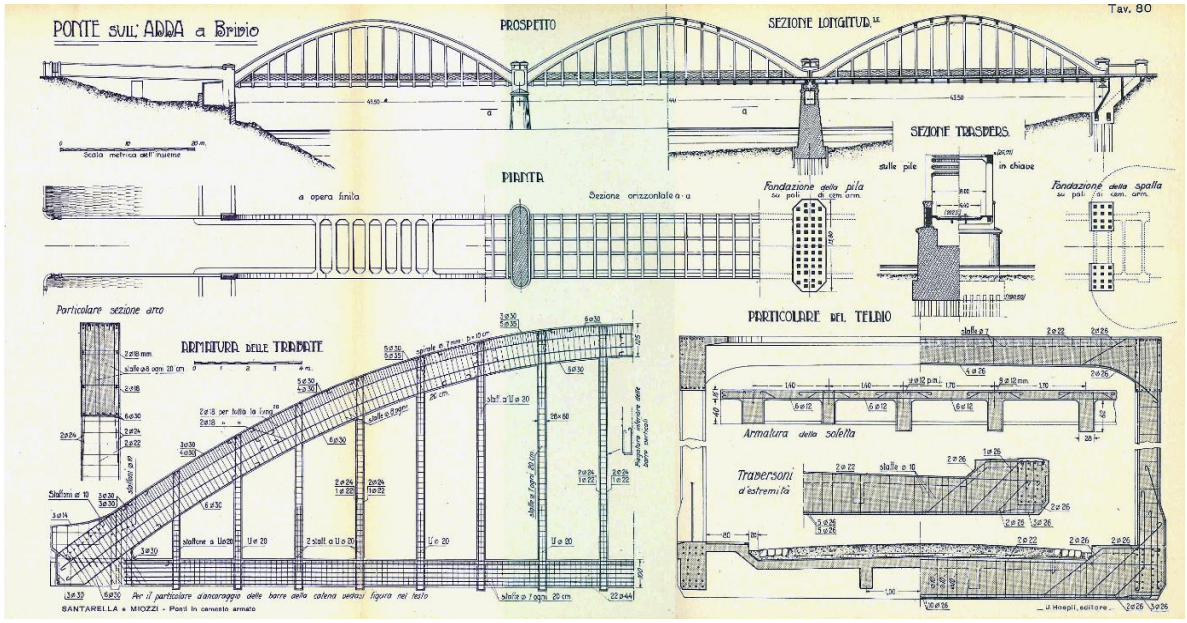


Figure 1: Pictures of the construction phases of the Brivio bridge.

(a)



(b)

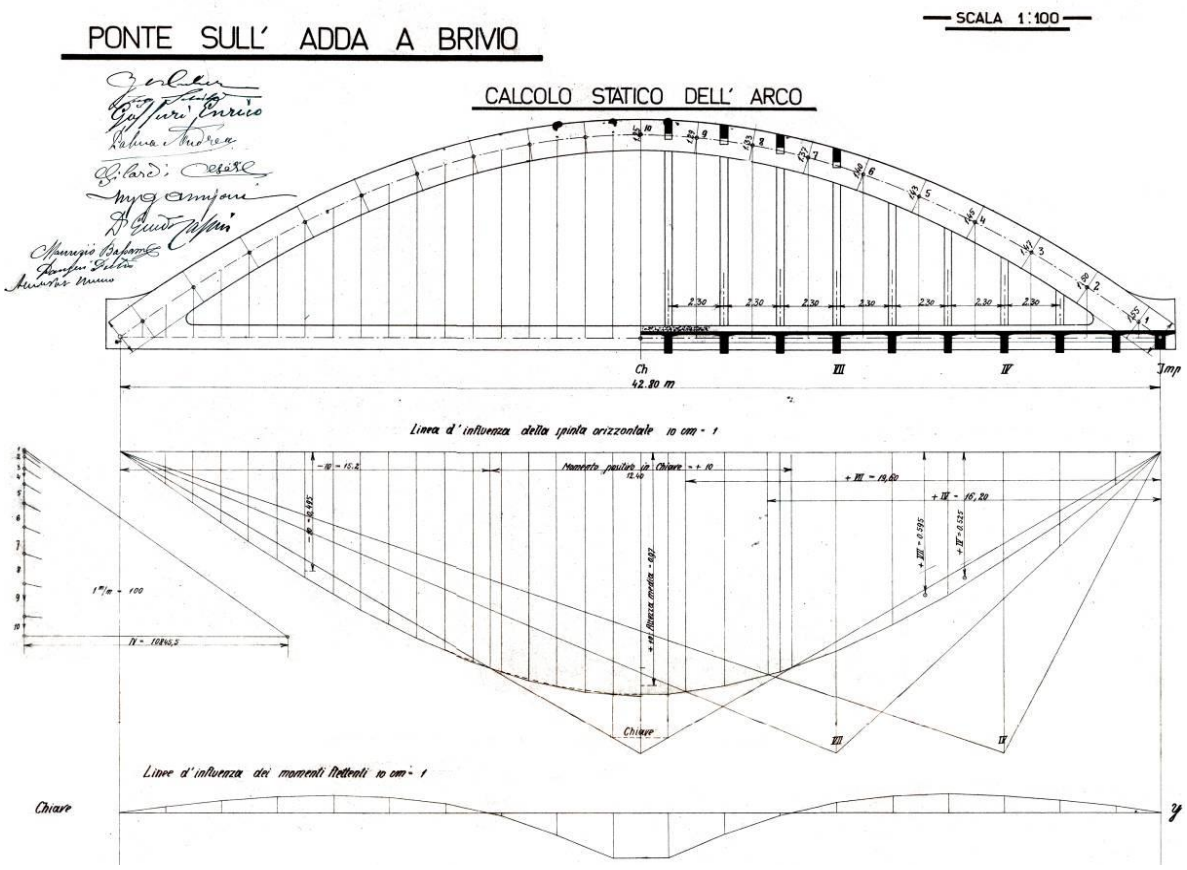


Figure 2: Brivio bridge: (a) Original design drawings [8], and (b) Static calculation of the arch.

In particular, design documents revealed that the steel bars were designed for a maximum tension of 100 MPa, whereas the maximum compression in the concrete was set equal to 4 MPa (with the exception of a few cross-sections where a higher compression of 7 MPa was assumed as allowable). The documentary research also provided information on the issues met during the construction and especially related to the search of workmen and raw materials in some periods of the First World War and the proof load test performed before the bridge opening.

An upstream front view of the bridge is shown in Fig. 3. The Cisano Bergamasco (Bergamo) side is on left bank, whereas Brivio (Lecco) side on the right bank. In this paper, the closest span to Bergamo side was identified as Span 01, the central span as Span 02, and the closest span to Lecco side as Span 03.

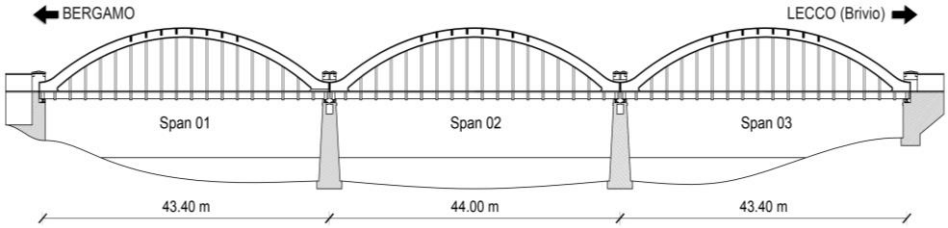


Figure 3: General arrangement of the Brivio bridge.

The bridge underwent several maintenance works during its lifetime. The last interventions date back to:

(a) the 80s, involving the replacement of the support bearings and the increase of the thickness of the deck slab (but few details about these works were found and uncertainty affects the actual thickness of the deck slab);
(b) 2014, involving the pier between Span 01 and Span 02 with the introduction of sheet piles to protect it against the erosive action of water.

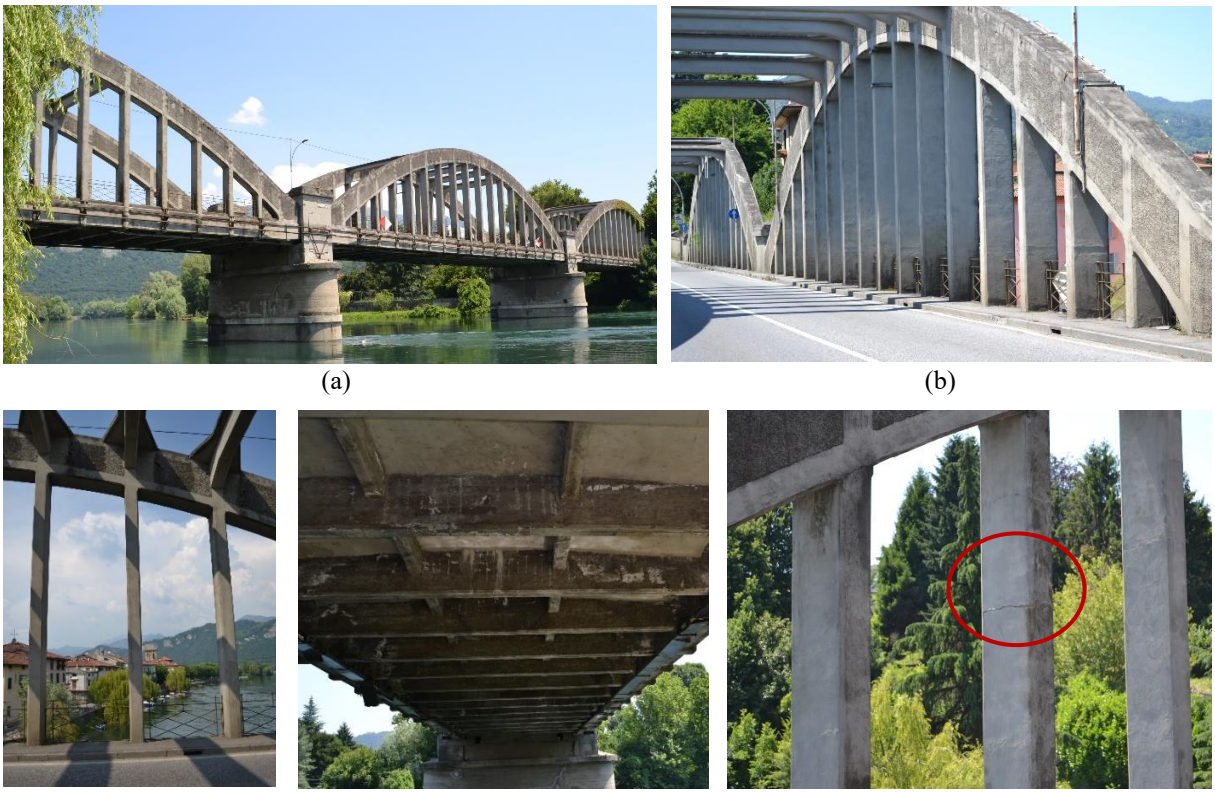
The bridge (Fig. 3) is 130.80 m long and crosses the Adda river. The central span is 44.00 m long while the length of lateral spans is 43.40 m. Each span is symmetric with respect to its mid-longitudinal plane and consists of a horizontal deck, 2 arches and 32 vertical hangers (1 arch and 16 hangers per side).

The deck, 9.2 m wide, hosts two roadway lanes (each 3.8 m wide) and two sidewalks (Fig. 4a) and it is composed by a concrete slab supported by a grid of longitudinal and transversal beams. The deck cross section includes two main girders (0.45×1.00 m^2) and two secondary longitudinal beams (0.20×0.40 m^2); the girders are spaced 8.60 m center to center and includes 22ϕ44 steel bars of reinforcement, whereas the secondary beams are spaced 2.00 m center to center. Both elements (girders and beams) are symmetrically located with respect to the vertical longitudinal plane of the bridge (Fig. 4d). The R.C. slab was originally 14 cm thick, but after the strengthening of the 80s, even if no drawings are available, the owner reports the increase to 20 cm. However, the R.C. slab is also supported by transversal beams, equally spaced every 2.30 m (in correspondence of each vertical hanger).

The arches exhibit a rise of about 8.00 m at the keystone and a rectangular cross section, 0.60 m wide and of height varying between 1.25 m and 1.50 m. The arches of each span are transversally connected with eight struts of 0.35×0.50 m^2 section (Figs. 4b and 4c).

Two concrete tapered piers support the deck into the river bed. Each pier, with a maximum dimension at the base of 3.80×12.80 m^2 (Fig. 4a), is supported by forty-eight piles of "Considère" type, ranging from 13.00 m to 16.00 m in depth.

During the visual inspection, the concrete of the bridge shows diffuse whitish efflorescence and clear signs of carbonation. Furthermore, some horizontal cracks were observed in the vertical R.C. hangers (Fig. 4e).



(a) (b)

(c) (d) (e)

Figure 4: Brivio bridge: (a) General view of the bridge, (b) Detail of the arches, (c) Detail of the vertical hangers, (d) Detail of the longitudinal beams, and (e) View of one horizontal crack detected on a hanger.

3 TESTING AND SYSTEM IDENTIFICATION OF THE BRIDGE

Direct inspection and experimental tests were carried out to assess the bridge current state. Most of those tests were performed on June 2014 (i.e. geometrical survey of arches and hangers, visual inspection and ambient vibration tests) whereas static load tests were performed on September 2014. The experimental investigation was carried out for all the spans of the bridge [10], but in the present paper only the results of the Span 01 will be described.

In the case of ambient vibration tests (AVT), the structural response to ambient and operational excitation was acquired with sixteen vertical measuring positions according to the sensors layout shown in Fig. 5a. Eight cross-sections were instrumented in correspondence of the vertical hangers with two accelerometers placed on both sides of the deck. Two different setups were carried out, considering two sensors as reference transducers, which were kept at the same locations in both setups (see the blue arrows in Fig. 5a). For each setup, ten high-

sensitivity uniaxial accelerometers (WR 731A, 10 V/g sensitivity and ±0.50 g measuring range) connected to a WR P31 power unit/amplifier (Fig. 5b) and a multi-channel acquisition system with 3 DAQ modules (NI 9234, 24-bit resolution, 102 dB dynamic range and anti-aliasing filters) were used. The structural response was acquired at a sampling frequency of 200 Hz and a sampling time of 7200 s.

The modal identification was carried out applying the Frequency Domain Decomposition (FDD) technique [11], and the first four singular value lines (SV) of the Span 01 are shown in Fig. 5c. In the frequency range 2-18 Hz, seven vibration modes were identified, and the corresponding mode shapes are shown in Fig. 6. In particular, f_1, f_2, f_4 and f_6 are bending modes, while f_3, f_5 and f_7 are torsion modes.

The load test was carried out on September 8th, 2014 and a Topcon GPT 3003 total station (angle measurement accuracy of 0.3 mgon and maximum distance measurement of 3000 m) was used to measure the vertical displacement of selected points of the bridge during the tests. Two two-axle trucks (average weight of 336 kN) and two three-axle trucks (average weight of 434 kN) were used as test vehicles.

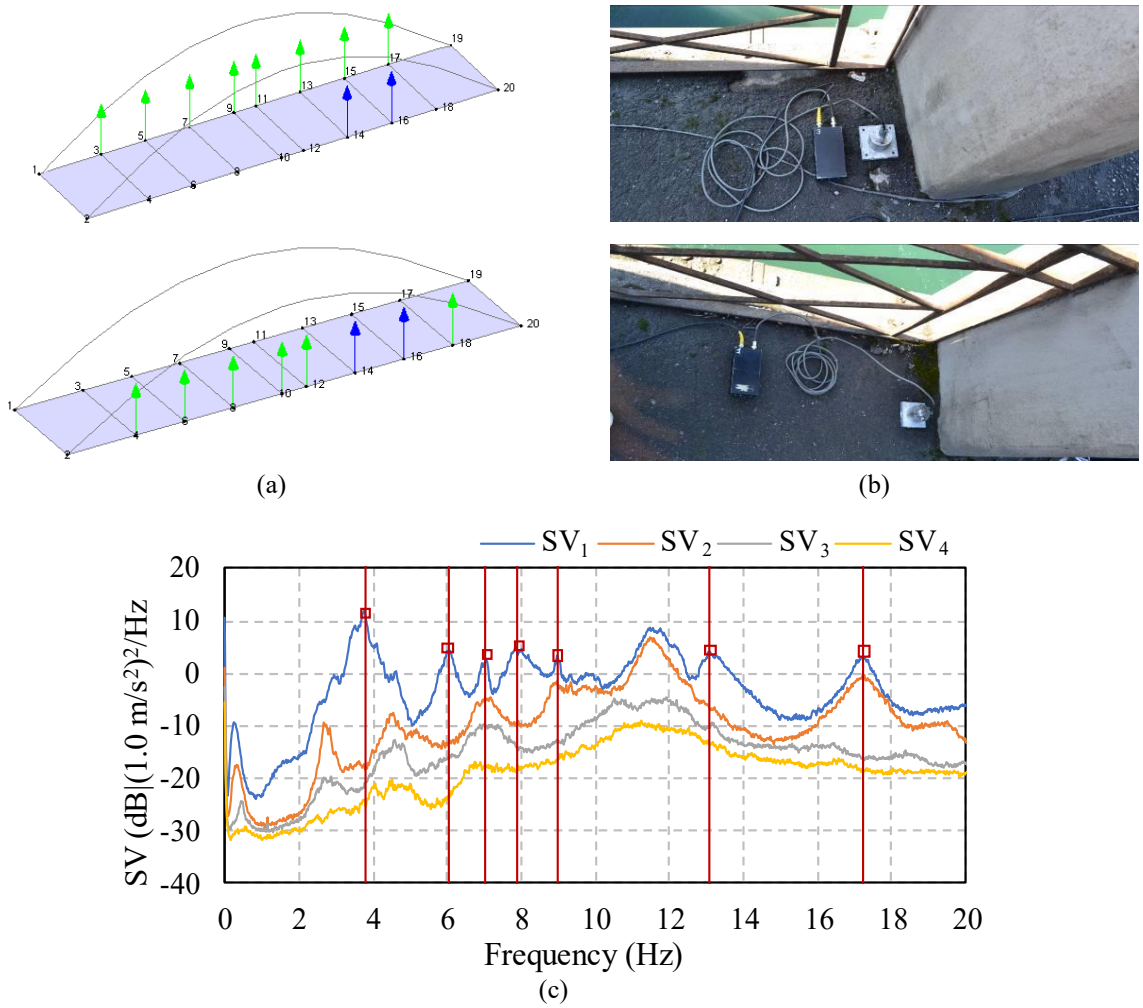


Figure 5: Ambient vibration test: (a) Sensors layout, (b) WR 731A accelerometer and WR P31 amplifier, and (c) Singular value lines (SV) and identification (FDD) of resonant frequencies of Span 01.

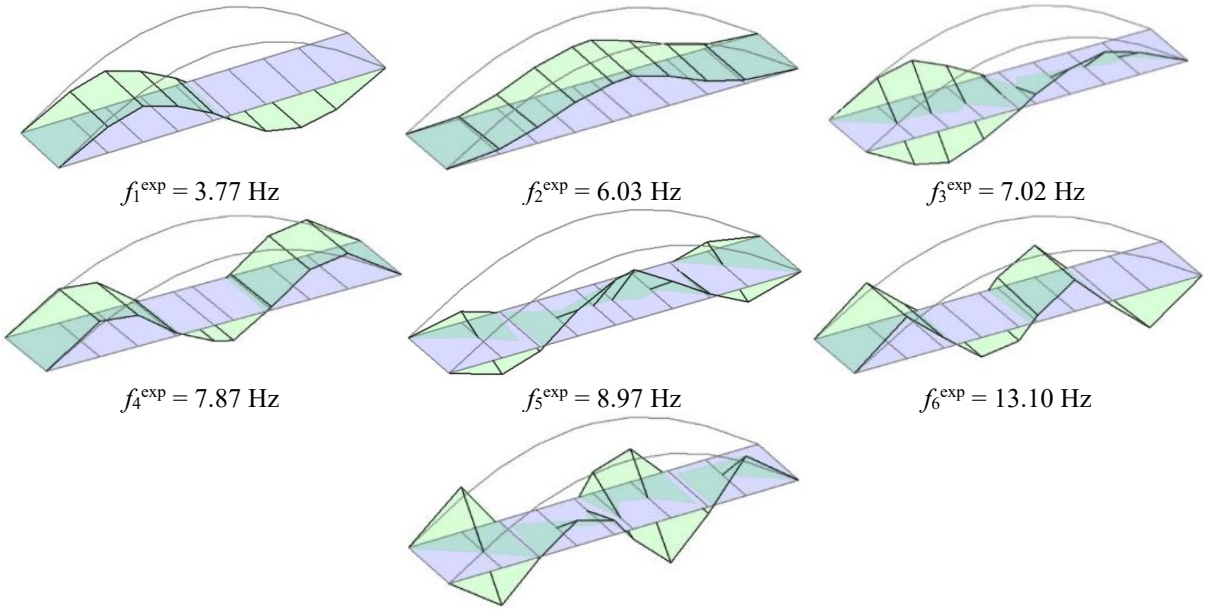


Figure 6: Vibration modes of Span 01 identified (FDD) from AVT.

Two load configurations were carried out. The first configuration is aimed at investigating the effects of an almost uniformly distributed load along the longitudinal axis of the bridge and the test vehicles were positioned in one row, with the three-axle trucks loading the central part of the bridge (Fig. 7). The second configuration consists in applying the test vehicles in the center of the span along two parallel rows (Fig. 8b). Since the load tests were performed just after the strengthening of the pier (on Bergamo side) supporting Span 01 and Span 02, the tests of those spans involved both load conditions, whereas only the first one was adopted in testing Span 03.

The results of the load tests show a regular behavior of the bridge, with the maximum displacements being very low (i.e., less than ten thousandth of the span length). Figure 8c shows the deformed shape of Span 01 under the load condition characterized by two rows of test vehicles: the loaded span exhibited a maximum vertical displacement of 3.2 mm.



Figure 7: Trucks used during the load test of Span 02.

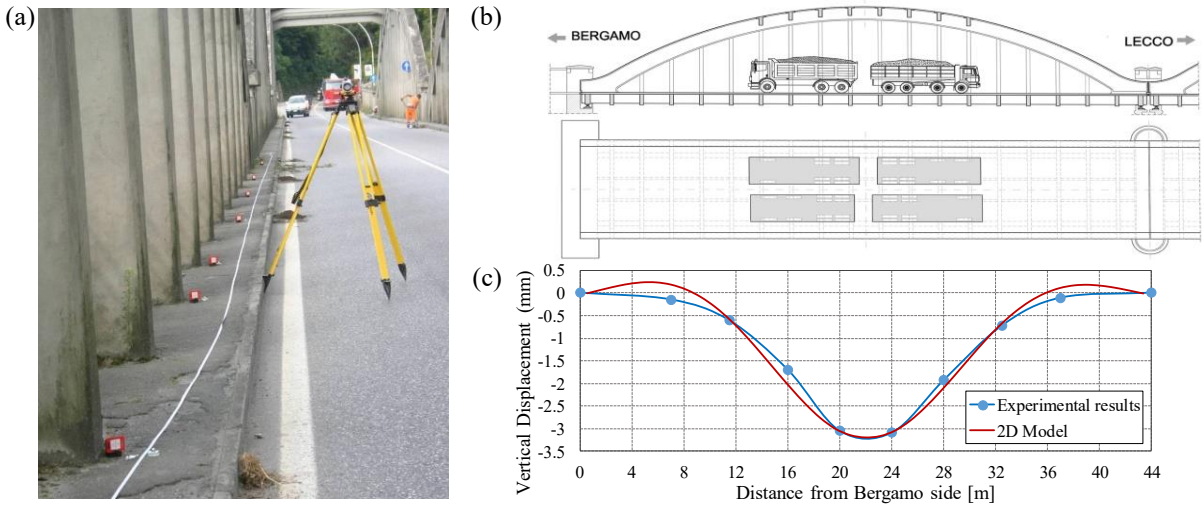


Figure 8: Load tests: (a) View of the bridge during the tests; (b) Second load configuration of Span 01; (c) Deformed shape of Span 01 and comparison with the prediction of 2D model.

4 FEM MODELLING AND UPDATING

The experimental program of field tests was complemented by the development of 2D (Fig.9a) and 3D (Fig.9b) FE models, based on the available geometric survey.

The simplified 2D model was developed and, subsequently, calibrated with the results of the AVT with the main objective of quickly obtaining a reasonable prediction of the vertical displacements during the load tests. After the live load, the 3D numerical model was developed to better investigate the reliability of some assumptions on the geometry of the structure and the interventions that have partially modified the bridge over the years.

The numerical 2D model consists of 126 linear beam elements used to represent the deck, the arches and the vertical hangers (Fig.9a). The deck was simulated with a horizontal beam representing the geometric characteristics – in terms of area and inertia – of the whole cross section of the bridge (i.e., the equivalent cross-section includes the upper concrete slab, the main girders and the secondary longitudinal beams). Seventeen tapered beam elements were used to model the arch: the rectangular cross section is 1.20 m width (equal to the sum of the width of the two side arches) and exhibits varying heights (the height decreases from the end to the top of the arch and vice versa). The sixteen hangers were simulated as vertical beams with a rectangular cross section. Furthermore, only one end of the deck was restrained to the horizontal translation, while springs were added to account for the vertical deformability of the pier and of the abutment supporting the span.

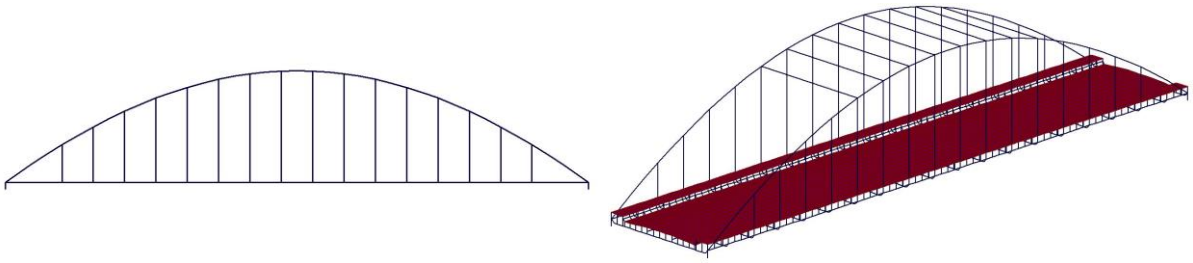
The weight per unit volume was assumed equal to 25 kN/m^3 for the entire structure, and the Poisson's ratio of 0.20 was also held constant. The masses of the elements whose axes lie out of the plane of the model (namely, the floor beams of the deck and the transversal struts connecting the arches) have been lumped at the corresponding nodal positions.

The Young's moduli of deck (E_{deck}), arches (E_{arch}) and hangers (E_{hanger}) and the constant of the vertical springs (k_s) were considered as uncertain parameters and their value were estimated by minimizing the difference between numerical and experimental natural frequencies. The simple system identification procedure proposed in [12] was used to solve the inverse problem. According to [12], each natural frequency of the model is approximated

by a simple polynomial expression $f_i^*(\boldsymbol{X})$, depending on the uncertain parameters (or updating parameters) collected in the vector $\boldsymbol{X}$. After a few FE runs needed to evaluate the polynomials $f_i^*(\boldsymbol{X})$, the updating parameters are computed by minimizing the following objective function:

$$J(\boldsymbol{X}) = \sum_{i=1}^{M} w_i [f_i^{\exp} - f_i^*(\boldsymbol{X})]^2 \tag{1}$$

where w_i (i=1, 2,…, M) are weighting constant (which were set equal to 1 in the present case) and $f_i^{\exp}$ represents the i-th experimentally identified frequency.



(a) (b)

Figure 9: FE models: (a) 2D model, and (b) 3D model.

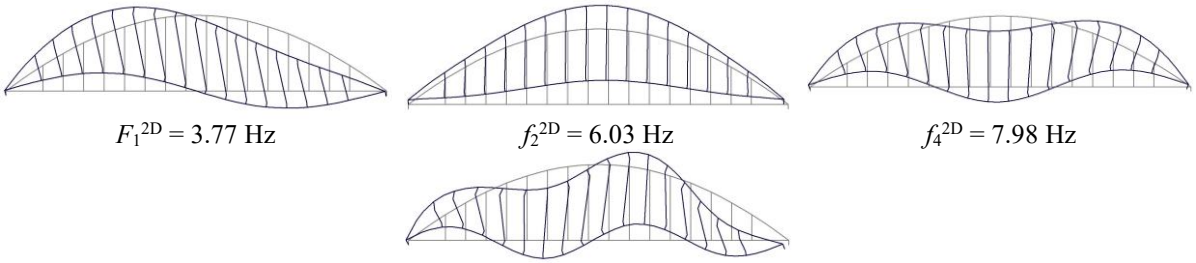


Figure 10: Vertical vibration modes of the updated 2D model.

The selected base values of the unknown parameters to apply the method are: E_{deck}=40 GPa, E_{arch}=35 GPa, E_{hanger}=35 GPa and k_s=2.0×10^6 kN/m. The optimal values of those parameters are reported in Table 1, whereas the lower mode shapes of the updated 2D model are shown in Fig. 10. The comparison between the natural frequencies of the simplified model and the experimental ones is summarized in Table 2. It should be noticed that, despite the simplified nature of the 2D model, a good correlation is obtained in terms of both natural frequencies and mode shapes (Fig. 10): in terms of frequency discrepancy (defined as $\Delta f_i = 100 \cdot |f_i^{\exp} - f_i^{FEM}| / f_i^{\exp}$), the maximum and average discrepancy turned out to be 1.29% and 0.36%, respectively (Table 2).

Furthermore, since the 2D model was mainly established to obtain a quick prediction of the results of static load tests, Fig. 8c exemplifies the match between predicted and measured displacements in the second load condition performed on Span 01.

After the full-scale tests, the numerical 3D model was developed. In this model 1980 beam elements were used to represent the longitudinal and transversal beams, the arches and the vertical hangers, whereas 1184 shells were used to simulate the concrete slab. The arches and the vertical hangers were modeled according to the available geometric survey, and

furthermore, eight transversal beams were added to connect the top part of the arches. The deck was modeled as a grid of beams with four longitudinal beams, sixteen transverse beams (one for each vertical hanger) and an upper concrete slab 0.20 m thick. An equivalent section equal to 0.35×0.80 m^2 was attributed to the slab transversal beams. Concerning the boundary conditions, the model was considered as simply supported in longitudinal and transversal directions, while vertical springs were added to simulate the vertical deformability of pier and abutment of Span 01.

Similarly to the 2D model, the weight per unit volume and the Poisson's ratio of the reinforced concrete was assumed equal to 25 kN/m^3 and 0.20, respectively. The structural parameters selected in the updating procedure are: the Young's modulus of the two edge girders (E_{girder}), the Young's modulus of the grid (E_{grid}), the Young's modulus of the arches (E_{arch}), the Young's modulus of the hangers (E_{hanger}) and the constant (k_s) of the vertical springs supporting the span. Table 1 summarizes the optimal estimates of the updating parameters, whereas the mode shapes of the updated 3D model (corresponding to the experimental ones, see Fig. 6) are shown in Fig. 11. The comparison between the natural frequencies of the model and the experimental ones is reported in Table 2.

The inspection of Fig. 11 and Table 2 highlights an excellent correlation between the optimal 3D model and the experimental results, with the average and maximum frequency discrepancy being equal to 1.61% and 3.52%, respectively; furthermore, Figs. 6 and 11 shows a fairly good correspondence of mode shapes, as well.

Finally, the analysis of results in Table 1 suggests that the updated parameters of the 2D and 3D models exhibit a fairly good consistency.

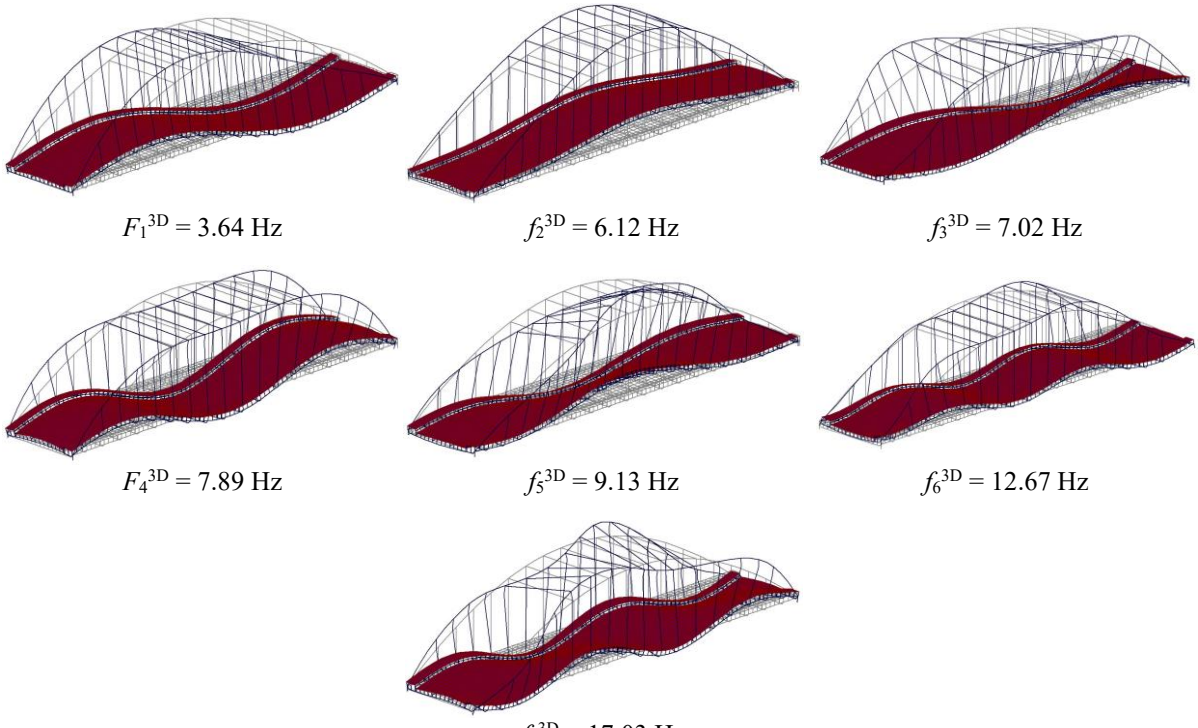


Figure 11: Vertical and torsion vibration modes of the updated 3D model.

Table 1: Optimal structural parameters of 2D and 3D models

Parameter		2D model	3D model
E_{deck} (GPa)	E_{girder}	44.	42.
	E_{grid}		35.
E_{hanger} (GPa)		31.	28.
E_{arch} (GPa)		36.	42.
k_s (kN/m)		1.69×10^6	2.20×10^6

Table 2: Comparison between experimental and numerical (2D and 3D updated model) frequencies

f^{exp} (Hz)	2D model		3D model	
	f^{FEM} (Hz)	Δf (%)	f^{FEM} (Hz)	Δf (%)
3.772	3.774	0.05	3.639	3.52
6.030	6.025	0.08	6.123	1.54
7.019	–	–	7.019	–
7.874	7.975	1.29	7.889	0.19
8.972	–	–	9.127	1.73
13.100	13.096	0.03	12.667	3.21
17.210	–	–	17.029	1.06

$$\Delta f = 100 \cdot \left| (f^{exp} - f^{FEM}) / f^{exp} \right|$$

5 CONCLUSIONS

The paper focuses on the preliminary structural assessment of the Brivio bridge. After the maintenance intervention performed on one pier, an extensive investigation of the bridge was carried out, including documentary research, visual inspection and geometric survey of each span, full-scale load tests, ambient vibration tests and FE models development. Based on the results presented in the paper, the following conclusions can be drawn:

- The historic research has provided valuable information on structural details and changes occurred to the structure;
- The visual inspection and the on-site geometric survey has provided information about the current geometry and heath state of the bridge;
- 7 vibration modes were identified from ambient vibration tests in the frequency range 0-20 Hz;
- The collected information allowed the development and validation of 2D and 3D FE models;
- The calibrated 2D model was successfully used to predict the vertical displacements measured in load tests (that, in turn, demonstrated a regular behavior of the bridge).

The investigation herein presented turned out to be of utmost importance in enhancing the knowledge of the bridge structural behavior. However, further investigation (involving coring tests of materials and continuous dynamic monitoring) have been recently scheduled.

Acknowledgements. The support of the Province of Lecco is gratefully acknowledged. The authors would like to thank M. Cucchi (LPM, Politecnico di Milano) for the assistance in conducting the field tests.

REFERENCES

[1] Gentile, C. Modal and structural identification of a RC arch bridge. *Struct. Eng. Mech.* (2006) **22**(1): 53-70.

[2] ICOMOS/ISCARSAH Committee. *Recommendations for the analysis, conservation and structural restoration of architectural heritage* (2005). https://www.icomos.org/en/documentation-center.com.

[3] Zonno, G., Aguilar, R., Boroschek, R. and Lourenço, P. B. Analysis of the long and short-term effects of temperature and humidity on the structural properties of adobe buildings using continuous monitoring. *Eng. Struct.* (2019) **196**: 109299.

[4] Saisi, A., Gentile, C. and Ruccolo, A. Continuous monitoring of a challenging heritage tower in Monza, Italy. *J. Civ. Struct. Health Monit.* (2018) **8**(1): 77-90.

[5] Deger, Y., Cantieni, R. and Pietrzko, S. Modal analysis of an arch bridge: experiment, finite element analysis and link. *In proceedings-spie the international society for optical engineering* (1994), pp. 425-425

[6] Sena-Cruz, J., Ferreira, R. M., Ramos, L. F., Fernandes, F., Miranda, T. and Castro, F. Luiz Bandeira bridge: assessment of a historical reinforced concrete (RC) bridge. *Int. J. Archit. Herit.* (2013). **7**(6): 628-652.

[7] Türker, T. and Bayraktar, A. Structural safety assessment of bowstring type RC arch bridges using ambient vibration testing and finite element model calibration. *Measurement* (2014) **58**: 33-45.

[8] Santarella, L. and Miozzi, E. *Italian bridges in reinforced concrete* (in Italian). Hoepli, Milan (1924).

[9] *Decreto Ministeriale 10 Gennaio 1907* (in Italian), Gazzetta Ufficiale 2 Febbraio 1907 n.28 (1907).

[10] Ferrari, R., Froio, D., Rizzi, E., Gentile, C. and Chatzi, E.N. Model updating of a historic concrete bridge by sensitivity-and global optimization-based Latin Hypercube Sampling. *Eng. Struct.* (2019) **179**: 139-160.

[11] Brincker, R., Zhang, L.M. and Andersen, P. Modal identification of output-only systems using frequency domain decomposition. *Smart Mater. Struct.* (2001) **10**(3): 441-445.

[12] Douglas, B.M., Reid, W.H. Dynamic tests and system identification of bridges. *ASCE J. Struct. Eng.* (1982) **108**(10): 2295-312.

12th International Conference on Structural Analysis of Historical Constructions
SAHC 2020
P. Roca, L. Pelà and C. Molins (Eds.)

THE COLUMN-LESS STAIR IN LORETTO CHAPEL IN SANTA FE, NEW MEXICO: STRENGTH ANALYSIS

ANITA SUMALI[1]

[1]Biomedical Engineering Department
Texas A&M University
College Station, TX 77843, USA
e-mail: asumali@tamu.edu (*corresponding author)

Keywords: Historical Structure, Finite Element Analysis, Spiral Staircase

Abstract. *A spiral staircase in Loretto Chapel in Santa Fe, New Mexico, has no center column to provide structural strength and stability. Some estimates say that the stair should have collapsed at first use. Yet, the stair has been used daily since its genesis in 1878. Explanations of the strength of the structure varied from "basic mechanics" to "miracle". This article presents a stress analysis of the stair using a finite element model. The loading is 16 persons on steps 1, 3, 5, …, 31 of the stair (as shown in an old photograph), the weight of the stair, and the weight of the railing. Stress computation was performed with a finite element model built and run in Abaqus CAE (Dassault Systemme, 2016). The analysis shows that the center spiral is severely stressed. The maximum Von Mises stress, which occurs near the top of the center spiral, is 1.7MPa. The ultimate strength of strong Engelmann spruce is 2.0MPa. The absence of the center column is significant because a center column would reduce the maximum stress in the stair to about 0.3MPa.*

1 INTRODUCTION

The Loretto Chapel in Santa Fe, the capital of New Mexico, has a spiral staircase with no center column to provide structural strength and stability. Some estimates say that the stair should have collapsed at first use (Bullock, 1978). Yet, the stair has been used daily since its genesis in 1878. Explanations of the source of the structural integrity ranges from simple 'physics' (e.g., Carter, 2010) to attribution to miracle. A landmark in the historic Old Town area of Santa Fe, the staircase has been the subject of many articles. A popular story about the genesis of the stair has been re-enacted in television shows and movies including "Unsolved Mysteries" and the 1998 television movie entitled "The Staircase" (Bobbin, 1998). The author of this present work did not find any numerical explanation of how the stair can support its own weight and the load that it carries. A good numerical explanation can be in the form of stress calculation using finite element analysis and comparison against material strengths. Many related examples of this kind of analysis for wooden structures include Invernizzi (2016).

This article provides finite element calculations to show: 1) The stresses in the staircase structure under heavy loading, 2) Which parts of the structure may be stressed most heavily, and 3) How a center column would reduce the stress.

Figure 1 shows the structure of the stair. The figure is an artist's rendering; but the only difference between the figure and photographs of the actual stair is that the figure eliminates the railing to provide clear view of the structure of the stair. The strength analysis in this paper will include the railing as a load, not part of the load-bearing structure. For the first two years of its use, the stair had no railing (Black, 2014). Making two turns of 360-degree spirals, the stair has a total of 32 steps, the 33rd 'step' being the balcony floor. (The number 33 is said to be the age of Jesus Christ when he was crucified.) Table 1 shows data used in the strength analysis. Specific weight is used to calculate the loading of the stair structure due to its own weight. The ultimate strength and the shear strength of the material (assumed here to be Engelmann spruce) are used not in the calculation but instead compared to the maximum stress in the stair structure.



Figure 1: Staircase structure. (Black, 2014)

2 DATA

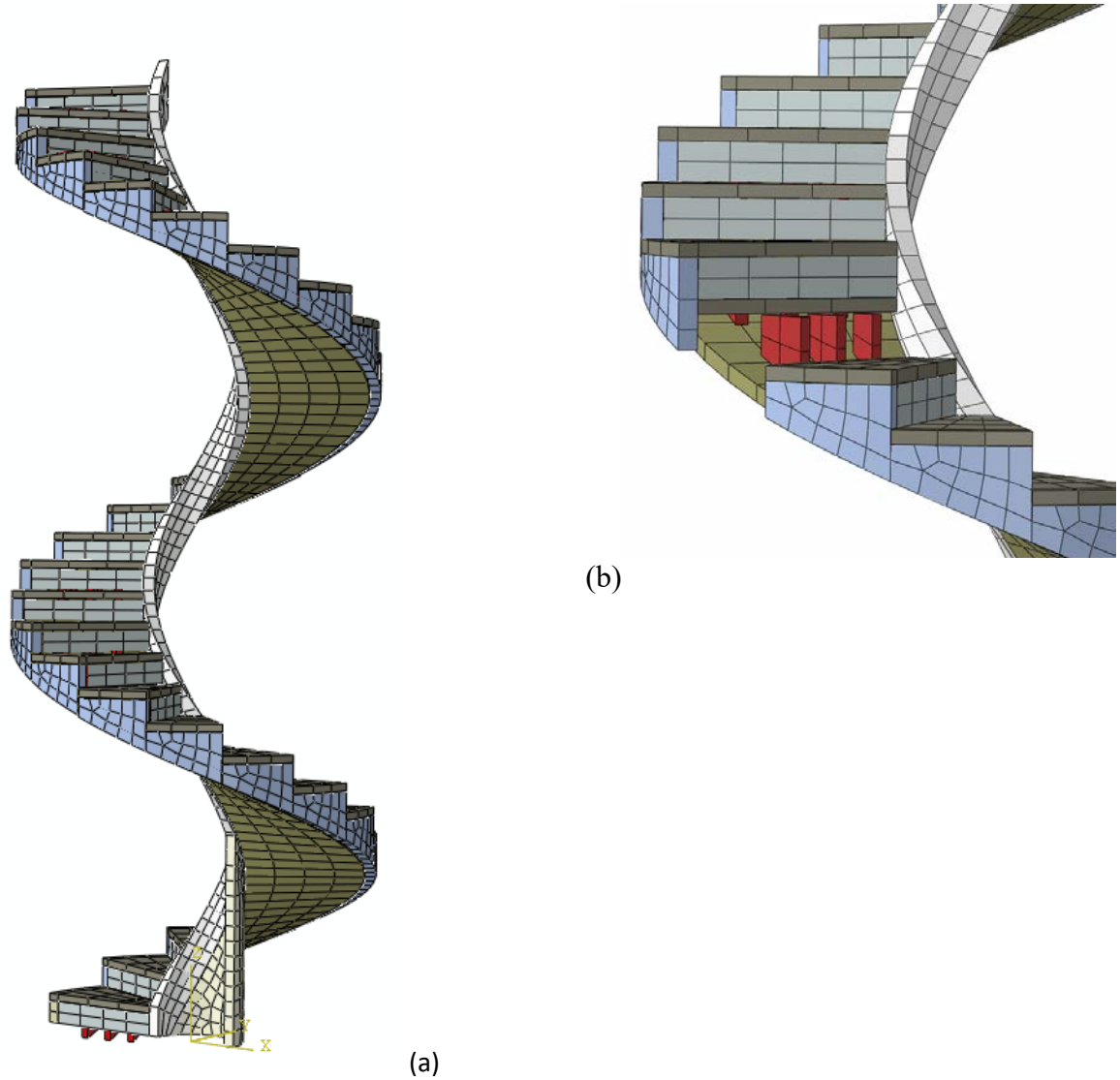
Table 1 shows data used in the strength analysis. Specific weight is used to calculate the loading of the stair structure due to its own weight. The ultimate strength and the shear strength of the material (assumed here to be Engelmann spruce) are used not in the calculation but instead compared to the maximum stress in the stair structure.

Table 1: Data used in strength analysis

Parameter, unit	Value	Notes
Height, m	6.706	
Outside radius, m	1.224	Excludes railing structure
Inside radius, m	0.300	Excludes railing structure
Number of steps	32	The 33rd step is the balcony floor
Thickness of boards, mm	50.8	Assumed for all boards
Thickness of inner and outer helices, mm	76.2	
Weight of railing structure, N/m	200	Rough estimate. Small load.
Number of persons on stair	16	Heavy load based on Fig. 3
Weight of each person, N	800	Conservatively heavier than persons in Fig. 3

3 METHOD OF ANALYSIS

The results of the calculations presented in this article are in the forms of stress. In particular, Von Mises stress is a good overall measure to show the relative distribution of stresses throughout the stair structure. Compressive stress will be compared to the compressive strength of the material; and shear stress will be compared to the shear strength of the material. The stresses that the stair material has to endure is calculated below with a finite element model built and run in Abaqus CAE (Dassault Systeme, 2016). A mesh (Fig. 2) was created from the geometry of the stair, and used throughout this analysis. Figure 3 is a photograph illustrating a heavy loading scenario. Figure 4 is a model of the loads used in the stress analysis: Sixteen persons weighing 800N each stand on steps number 1, 3, 5, 7, …, 31. The weight of each person is assumed evenly distributed over the tread. The stair is also loaded by its own weight, plus the weight of the railings.



(b)

(a)

Figure 2: a) Mesh of the stair, b) Cut-outs showing internal braces.



Figure 3: Photograph used to estimate loads.

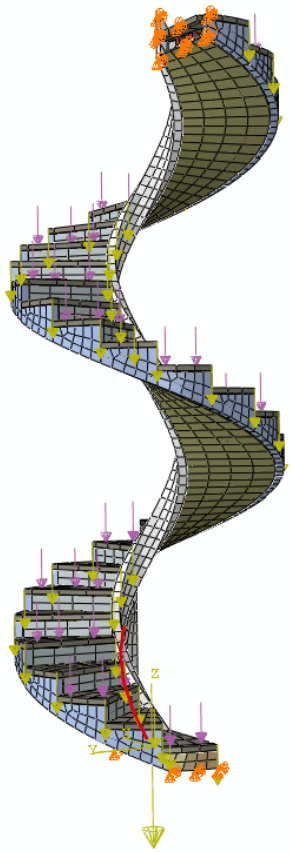


Figure 4: Boundary conditions: Fixed on the top and bottom of the stair. Loading: one person each on steps 1, 3, 5, …, 31; gravity (weight of stair), and weight of railings.

4 STRESS CAUSED BY THE LOADING

Figure 5 shows that the center helix is heavily stressed. At the location with the highest stress, near the top of the inner helix, the Von Mises stress is about 1.7 MPa. The strength of wood is very anisotropic: fracture depends on the alignment between the stress components and the direction of the wood grains. High compression (negative normal stress) in the direction of the wood grains can cause separation of grains (Fig. 6a). Shearing stress parallel to the direction of the grains (see Fig. 6b) also can cause separation of grains. Because anisotropy is important in wood, the compressive and shear stresses are calculated and shown in Fig. 7. The greatest compressive stress is 1.4 MPa. The location of the greatest compressive stress is again in the center helix. The greatest shear stress is 0.75 MPa. The location of the greatest compressive stress is also in the center helix.

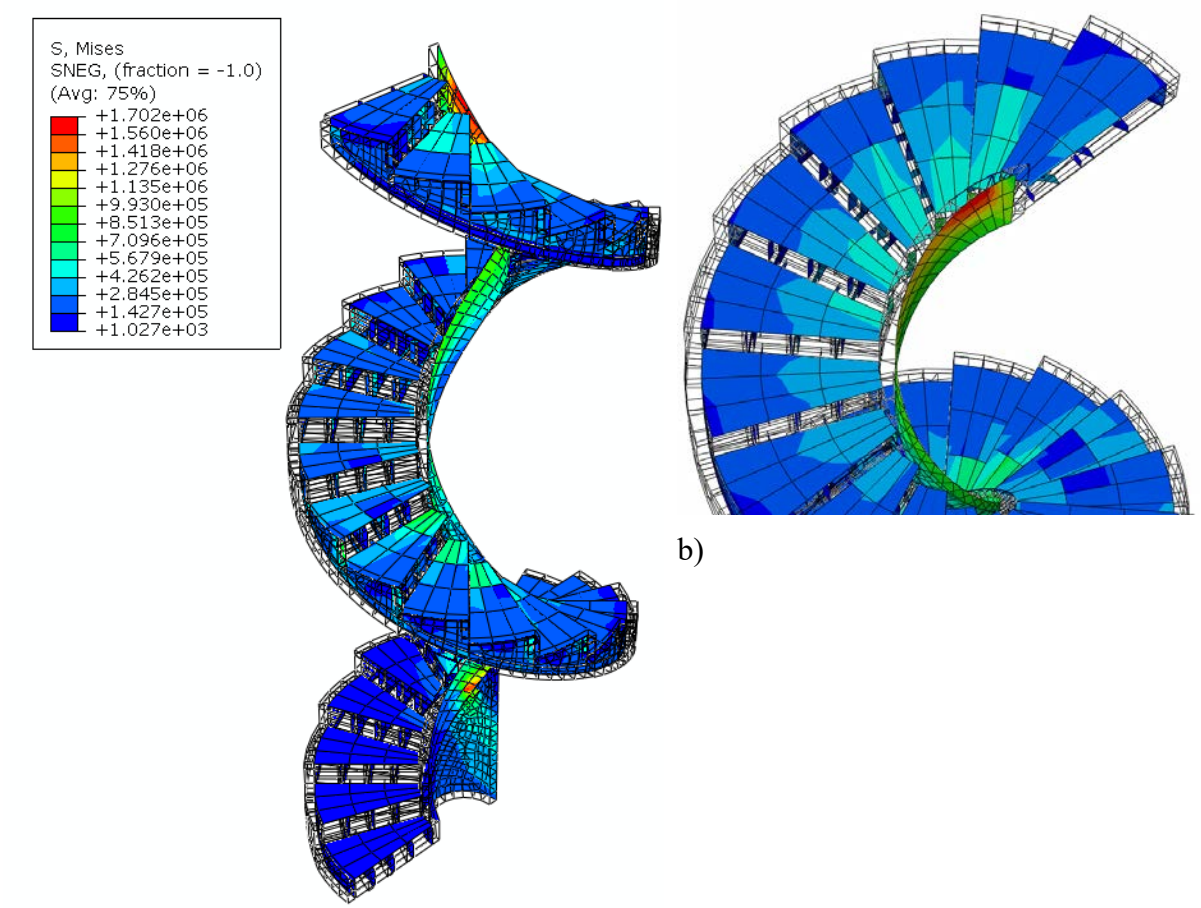
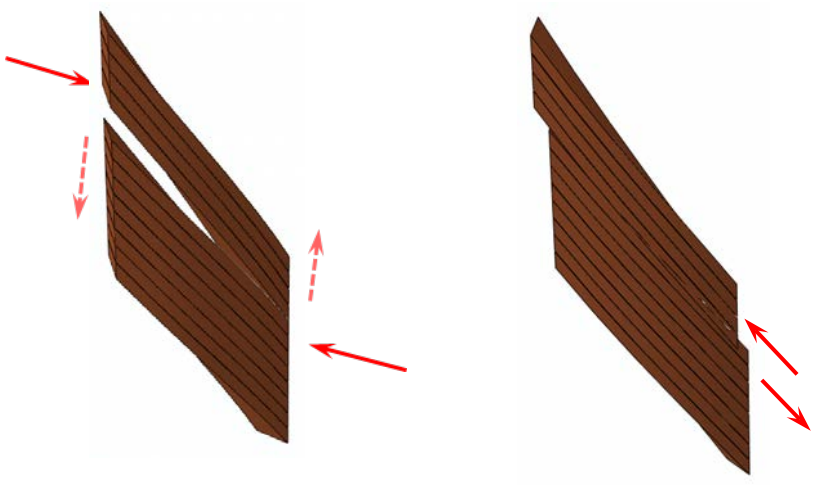
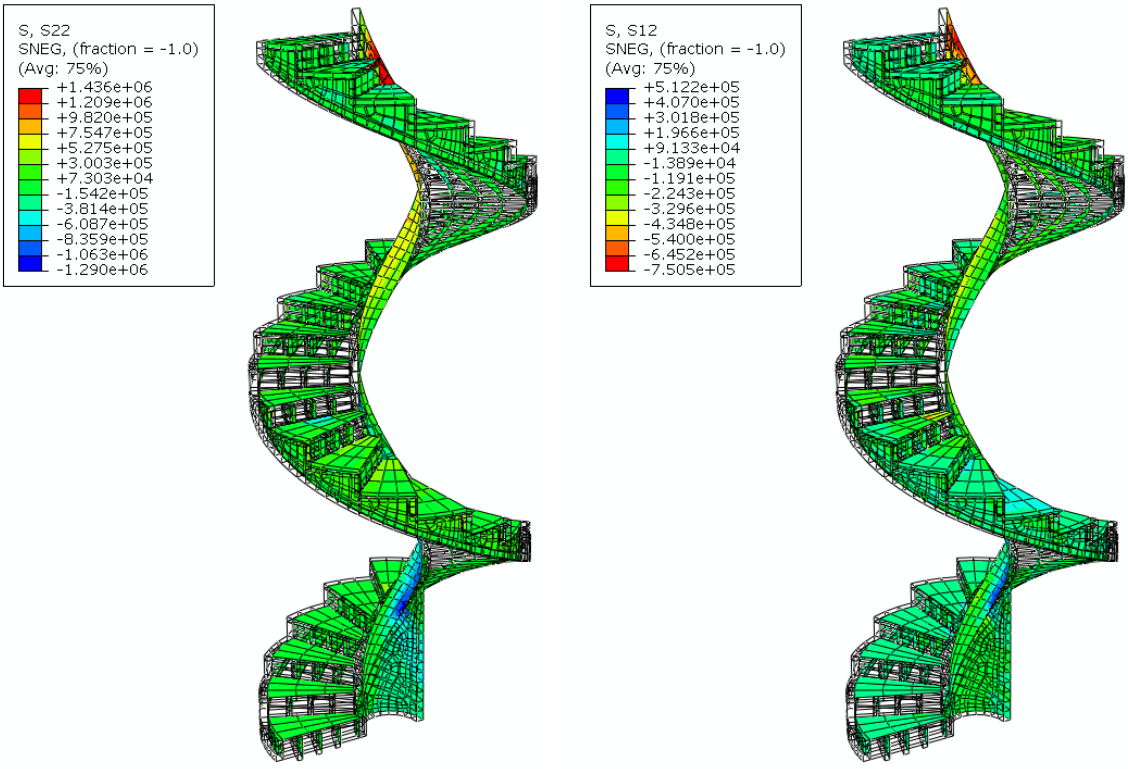


Figure 5: Von Mises stress a) Side View; b) View from above



a) b)

Figure 6: Wood fracture caused by a) Compressive stress; b) Shear stress



a) b)

Figure 7: Damaging stress a) Compression; b) Shear

The material of the stair must be strong enough to withstand the above stresses. Knight (1997) investigated the material and concluded that it was a sub-species of spruce. If the material is Engelmann spruce (which is stronger than most other spruces), it would break at its ultimate strength of 2.0MPa if compressed in the direction of the grains (which is the most damaging stress loading. Wood is much stronger in other loading directions.) If more weights load the stair (for example, a heavy person on each step), it is quite possible that the weights of the persons and the weight of the stair together will break the stair structure. The most likely location of the fracture is the center helix. It is also possible that the stair material is an even stronger Sitka spruce whose ultimate strength is 4.0MPa (Green, 2001). However, the cold location where Sitka spruce grows is many hundreds of miles away from Santa Fe, and it would have been difficult in the 1870's to transport the wood to Santa Fe. On the other hand, Engelmann spruce grows in New Mexico (Green, 2001).

The high stresses from the analysis confirm the assessment that it is difficult for the stair to bear the load (about 14kN from 16 persons plus the railings) plus the stair's own weight (6014N). Thus, the concern that the stair might have collapsed upon loading was justified. A spiral stair without a center column was not only rare but also difficult to design. A center column would serve well as a backbone to the stair. Though downplayed by some experts (e.g. Carter, 2010), the absence of a center column may well be significant.

5 THE IMPORTANCE OF A CENTER COLUMN

Figure 5 shows that the center helix, especially the top part of it, is by far the most heavily stressed part of the stair. Suppose, then, that the center helix were replaced by a more complete hollow column that supports the stair from the ground, as illustrated in Fig. 8. Then, this support would reduce the stresses around the center of the stair. The stress reduction would give a numerical value to the importance of a center column. Below, the above analysis process is applied to the hypothetical design in Fig. 8. The boundary conditions and loads are the same as those shown in Fig. 4.

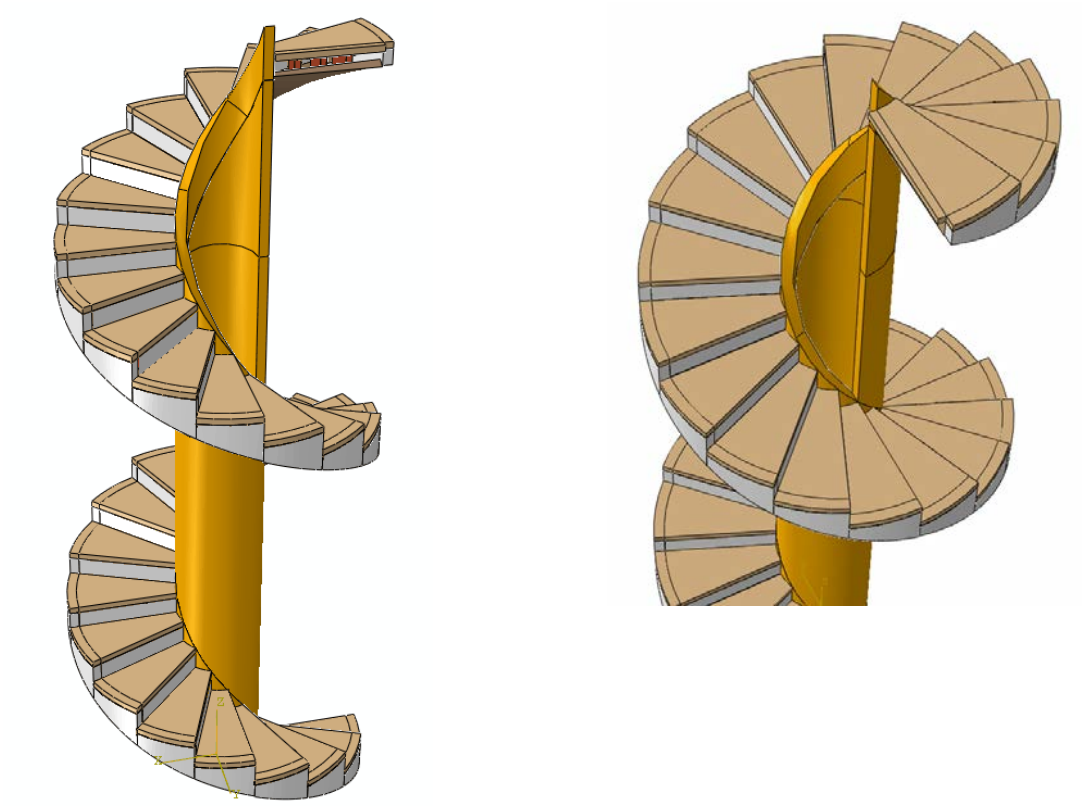
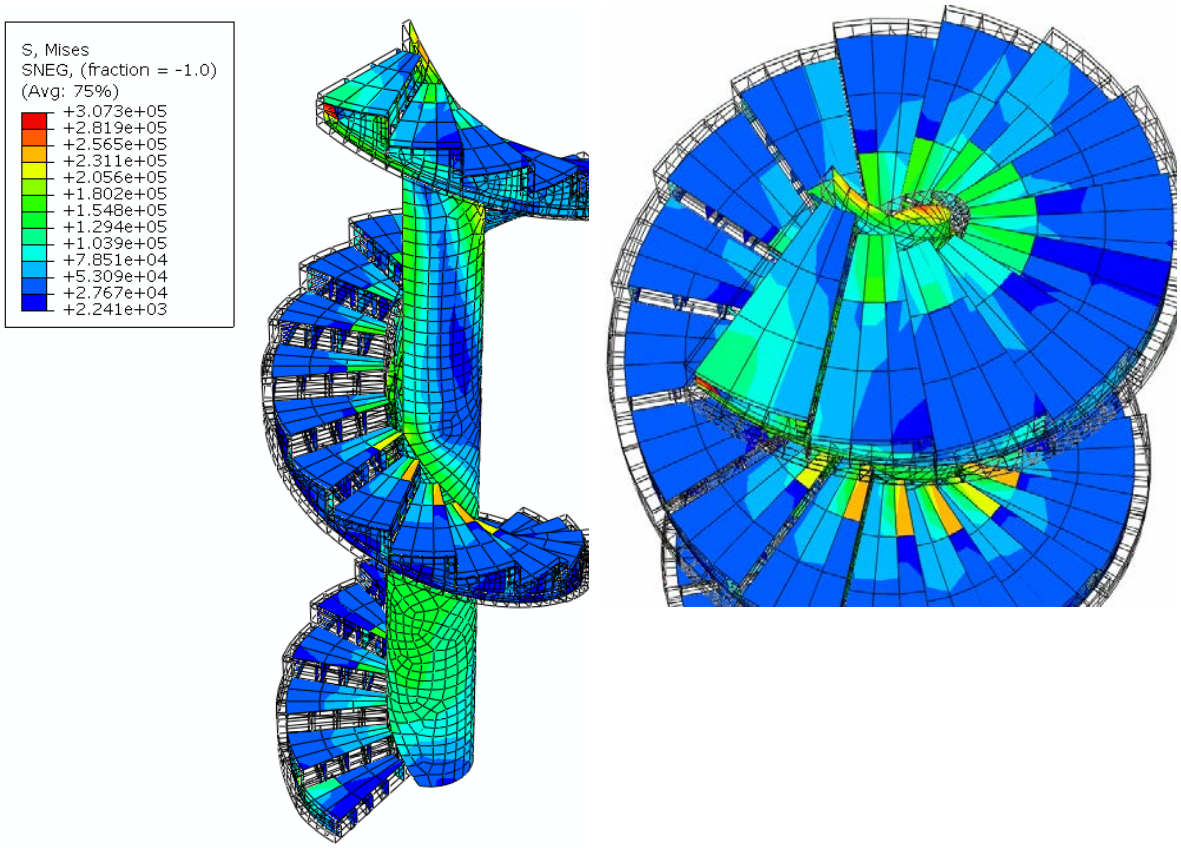


Figure 8: A hypothetical design, the same as the original design but with a center column.

Figure 9 shows that, with a center column, the highest stress in the stair is now around 0.3MPa. The location of the highest stress is on the outside wall at the top of the stair, near the place where the balcony supports the stair. The highest Von Mises stress, which occurs around the center of the stair, is just around 0.28 MPa. Those stresses are about eight times lower than the stress around the center helix of the stair without center column. Thus, the stair without a center column is about eight times weaker than an equivalent stair with a center column. This analysis shows that a center column is very important to the strength of the spiral stair.



a) b)

Figure 9: Von Mises stress in a stair with center column: a) Side view; b) A view from above.

6 CONCLUSION

When loaded with one person every other step, the column-less stair is heavily stressed. The center helix sustains the heaviest stress, especially at the top where the stair is attached to the balcony. The highest stress is about 1.7MPa. Thus, the center helix material must be a strong wood like Engelmann spruce which can sustain stresses up to about 2.0MPa, or a stronger wood. If more weights load the stair (for example, a heavy person on each step), it is quite possible that those weights and the weight of the stair together will break the stair structure. The absence of a center supporting column is quite significant. When loaded with the same load as the column-less stair, a similar stair design with a center column would be stressed to just about 0.3MPa maximum.

Although spiral staircases are common in architectural heritage buildings, few lack both a center column and a stair well that supports the stair from the ground. Most spiral staircases have a center column. The Bramante Staircase at Vatican's St. Peter museum lacks a center column but has a stair well. So does the triple helical staircase of the convent of San Domingos in the Bonaval district of Santiago de Compostela. Angelillo (2016) published an elegant proof of the stability of that staircase – evidence that a stair well that supports the stair from the ground would significantly strengthen a spiral stair.

REFERENCES

Angelillo, M. 2016. The Equilibrium of Helical Stairs Made of Monolithic Steps. International Journal of Architectural Heritage, 10(6):675-87.

Bobbin, J. 1998. “The Staircase” Review in TV Topics. The Buffalo News, April 12.

Bullock, A. 1978. Loretto and the Miraculous Staircase. Santa Fe, N.M.: Sunstone Press.

Carter, T. 2010. The Loretto Chapel staircase: A lesson in physics, not miracles. The Washington Post. January 16.

Dassault Systeme. 2016. Abaqus Student Edition. Software downloaded from https://academy.3ds.com/en/software/abaqus-student-edition

Green, D.W. 2001. Wood: Strength and Stiffness. In Encyclopedia of Materials: Science and Technology, Forest Products Laboratory. Elsevier.

Invernizzi, S. 2016. Numerical Modeling and Assessment of the Ebe Schooner-Brig. International Journal of Architectural Heritage, 6(5):453-77.

Knight, C. 1997. Just What Kind of Wood? Wall Street Journal, October 22.

Matweb. “North American Engelman Spruce Wood”. 2017. http://www.matweb.com/search/DataSheet.aspx?MatGUID=972210a797e2437982460bd800c31dc3 . Accessed Oct. 1, 2017.

12th International Conference on Structural Analysis of Historical Constructions
SAHC 2020
P. Roca, L. Pelà and C. Molins (Eds.)

THE DAR AL CONSUL COMPLEX IN JERUSALEM: IMPROVING THE LIVING CONDITIONS AND THE STRUCTURAL CAPACITY

FILIPPO CASARIN[1*], LEONARDO DI MARCO[2], MARCO MOCELLINI[1], RAMZI SIDAWI[2], PHILIP DAHABREH[2] AND AMJAD K. TAWEEL[3]

[1] Expin srl – Spin-off of the University of Padua
Via Pisacane 34, 35138 – Padova, Italy
email: casarin@expin.it, http://www.expin.it (*corresponding author)

[2] Custodia Terrae Sanctae
St. Saviour's Monastery, P.O.B. 186 9100101 Jerusalem
email: technical_office@custodia.org, https://www.custodia.org

[3] UN-Habitat - Special Human Settlements Programme for the Palestinian People
Ramallah, UCI Building, 17 Nizar Qabbani Street, Al-Masyoun
email: amjad.taweel@un.org, https://unhabitat.org/

Keywords: Jerusalem, Historical Structure, Masonry, Investigation techniques

Abstract. *The Custody of the Holy Land, with own and EU funds, and in Partnership with UN-Habitat, is implementing a comprehensive rehabilitation Project in Dar Al Consul civic and residential complex, which is one of the Custody properties in the heart of the Old City of Jerusalem. The complex, which corresponds to a urban block of relevant dimensions (80 x 50 m x 5 levels above and below the ground) and intersects the Roman Cardo, consists of 40 Houses and a basement floor used as a closed storage at the street level, besides sharing part of its ground floor with the old city market. Prior to the planned rehabilitation works in the houses - to improve the living conditions – and in the basement - to be reused as public space - the Custody intended to conduct a safety assessment of the complex for both static and seismic loads, in order to integrate any needed strengthening work within the planned restoration activities. A series of technical activities were then carried out aimed at evaluating the safety conditions of the structures. A comprehensive investigation campaign was planned and executed in order to characterize the structural materials and define the constructive techniques. Several modelling strategies of the structures, which resulted particularly complex for the historical stratification of the site, were then used. By means of numerical modelling, the stresses were defined in the masonry elements by weight and by occurrence of a seismic event, allowing to highlight the insufficient safety conditions of the main resisting elements of the basement and subsequently to define adequate structural consolidation strategies. During the works, the need for archaeological excavation implied further engineering efforts in order to allow deep excavations avoiding any harm to the above positioned levels and structural portions.*

1 FOREWORD

The Custody of the Holy Land is a fraternity of the Order of Friars Minor, a religious order in the Catholic Church, the Franciscans. The Custody preserves, studies and values the places where the Christian faith originated. It also provides social and housing services to the communities who live in the Holy Land. The Custody, in partnership with UN-Habitat and with own and UE funds, is implementing a comprehensive rehabilitation project in the Dar al Consul civic and residential complex, which is one of the Custody properties in the Old city of Jerusalem. Such complex consists of 40 houses and a basement floor used – at the beginning of the works – as a closed storage at the street level. The project intends to rehabilitate the houses to improve the living conditions of the local community, upgrade the open spaces among the houses and to rehabilitate and confer a new use to the basement as a public space [1].

The building complex covers about 2'400 sq. m divided into 6 buildings, bounded by Khan El Zeit Street, where there are shops of the Jerusalem Souk, and El Tikkyeh Street, where the entrances are. The height of the buildings is variable and reaches a maximum of about 15m from the street level, with 3 floors besides the basement floor (Figure 1).

In parallel with the intended aims of the project, the Custody requested a thorough study for understanding the structural behavior of the built environment in order to couple the necessary rehabilitation interventions with the necessary structural strengthening actions.

2 SITE HISTORY, "DAR AL CONSUL"

The building was named after the Prussian Consul who resided in the building around the middle of the 19th century [2], [3], [4]. The Prussian Consulate purchased a large building in the Muslim quarter to serve as an important German center in the city, and rented another adjacent building that was converted to a Prussian hospice [5].

The property of the building was then transferred to the Latin Patriarchate in Jerusalem around the year 1882. The upper floors of the building were used as a political and cultural center for Prussian activities and for around three decades it was a major site in the Old city. The upper floors have been drastically changed since then and additional buildings were constructed, changing the original shape. The building is one of a chain of huge buildings located on the eastern side of the Bab Khan az-Zait Market (Suq Khan az-Zait). The current extension of the Khan az-Zait Market can be traced back to the second century AD.

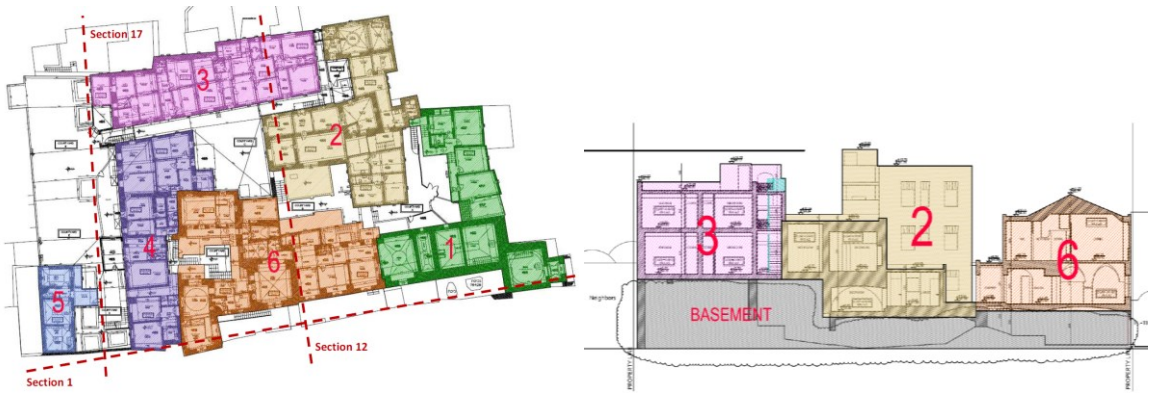


Figure 1: plan view and cross section of the Dar al Consul structural complex in the old city of Jerusalem

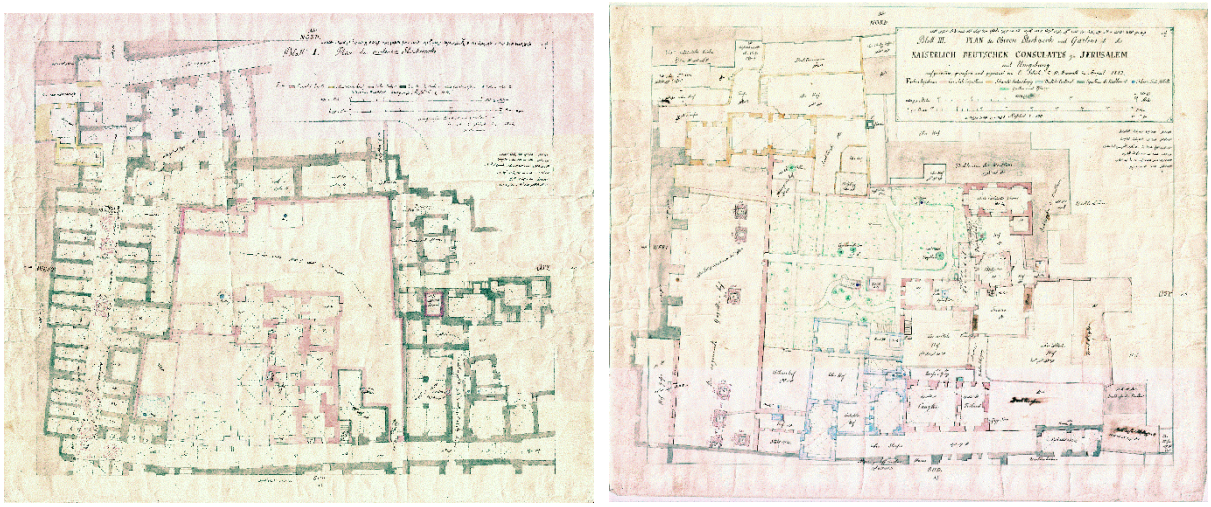


Figure 2: Architectural plans of the building dated August 1882 and January 1883, C.Schick - K.W.Baurath,

This was part of the *Cardo Maximus*, constructed by the Roman Emperor Hadrian as the main colonnade street of "Aelia Capitolina" (the roman name for Jerusalem) in the second century AD. The whole Suq Khan az-Zait and the eastern alleys connected to it were engaged in soap production as well as several olive-oil and sesame presses (ma'asir simsim). These kinds of productions can be traced back to the 10th century AD., or even earlier. It seems that the production of soap had also continued in the Crusader period, flourishing and reaching its peak in both the Mamluk and the Ottoman periods.

3 STRUCTURAL INVESTIGATIONS

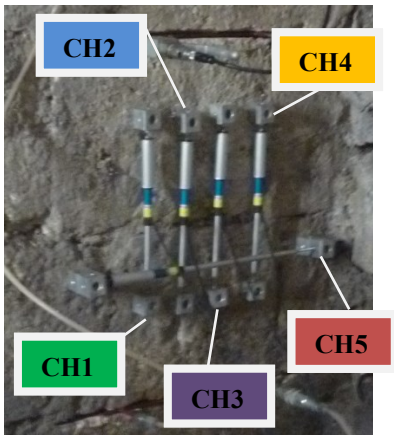
From the 1st to the 5th of December 2014, a wide experimental campaign was carried out in the Dar Al Consul site [6]. The campaign was carried out to determine the main characteristics of masonry, such as the type and soundness of walls, materials and construction techniques, and of the reinforced concrete structures, including mechanical characterization of the major structural elements. Several non-destructive and slightly destructive tests were performed on masonry walls and columns, such as single and double flat jack tests to obtain information on the mechanical characteristics of masonry, sonic tests to identify the compositional characteristics of masonry by measuring the velocity of mechanical waves propagating within the structural elements, videoscope surveys to determine the constitution of the structural elements and the material features, mortar and stone collection for laboratory tests aimed at the determination of their chemical-physical-mechanical properties, providing useful information on the analyzed structural materials. Also tests on reinforced concrete elements of the XX c. buildings were performed, including magnetometric surveys with covermeter aimed at the determination of the position of the rebars in the r.c. elements, with estimation of the concrete cover of the reinforcement, Schmidt-hammer together with ultrasonic tests, aimed to the estimation of the characteristics of the concrete with the SonReb method, compressive strength tests on concrete cores extracted, tensile testing of samples of reinforcing bars in laboratory aimed at the determination of the mechanical characteristics of the steel.

3.1 Obtained results

Results obtained from the tests carried out highlighted a marked vulnerability of the substructures of the complex, and acceptable mechanical characteristics of the structural elements in the upper floors, especially of the most recent buildings.

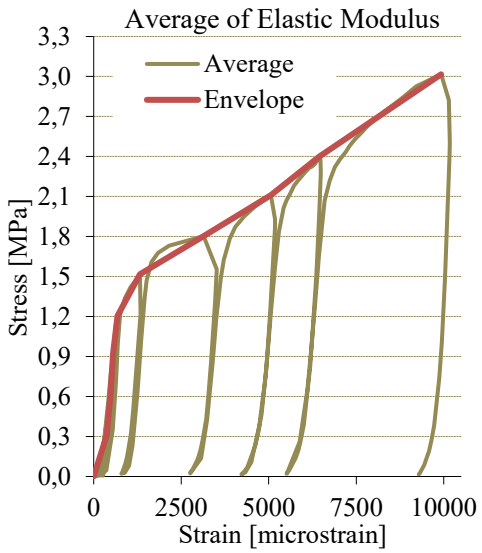
According to the visual surveys, the masonry typology of the basement may correspond to "Masonry with roughly arranged stones, made up with external leaves of limited thickness and internal infill" (table C8A.2.1, [8]), with Young modulus E - to be considered for stability calculations - in the range 1'020 – 1'440 N/mm^2. The comparison with the obtained results shows that the modulus of elasticity in the unloading branches is similar, even if quite scattered, for several tests carried out. However, in the loading branch calculation, a visible stiffness reduction is evident for low value of compressive stress, denoting a reduced value with respect to similar masonry typology found in the area [7]. Moreover, the sampled mortar is remarkably poor and with a substantial presence of organic material.

Sonic tests indicate generally reduced values, especially those carried out in the basement. The walls denoted to have quite low sonic velocities on the ground floor, possibly indicating reduced mechanical characteristics and/or presence of internal loose infill, cavities or inconsistencies. In the upper level velocities are higher, however with variable velocity values. Velocity remarkably increase in presence of diatones or other stones that cover the entire thickness of the wall.



Sensors' layout – test FJ2

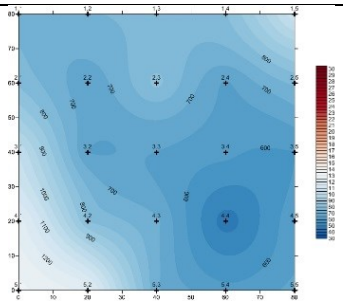
σ_{max} [N/mm^2]	3.00
E_{sec} [N/mm^2]	$\Delta(\sigma)$ [N/mm^2]
832	0.00-0.30
2743	0.30-0.60
4141	0.60-0.90
2292	0.90-1.20
487	1.20-1.50
158	1.50-1.80
160	1.80-2.10
208	2.10-2.40
177	2.40-3.00



Test n° *SON1*

Floor *ground*

Average velocity *790 m/s*



Test n° *SON2*

Floor *ground*

Average velocity *616 m/s*

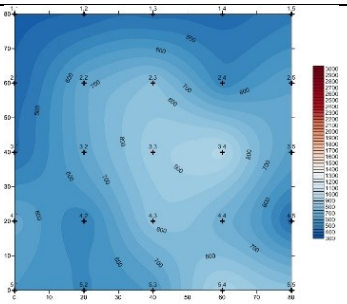


Figure 3: investigation campaign results, basement: (above) Flat Jack test nr.2; (below) sonic tests SON 1 & 2

Direct visual inspections executed through video endoscopy on masonry elements made possible to identify the inner characteristics of walls, floors and vaults, indicating different state of material compactness and arrangement for the several surveys carried out. The surveys allowed the direct inspection of the inner composition of walls, mainly composed by stone masonry with joints of considerable size.

4 STRUCTURAL MODELING – SAFETY CONDITIONS

4.1 The modeling strategy

Considered the structural complexity of the site, a multi-modelling approach was chosen, trying to overcome the limits of any modelling strategy by a combination of methodologies, relying on both global and local models. Linear FE modelling is considered a reliable procedure for the definition of the vertical stress distribution (self-weight analysis) on masonry structures, since the Finite Elements method allows modelling very complex geometries in a quite precise manner. Limits of this methodology emerge when performing the seismic analysis, introducing remarkable shear and tensile stresses, given the (fictitious) hypothesis of linear behavior of structural materials. For this reason and in general in historic masonry buildings, dynamic linear analyses should be more used for understanding the general dynamic behavior (initial frequencies, mode shapes, relevant areas from a dynamic point of view…) rather for defining the structural safety at the Ultimate Limit State. A non-linear equivalent frame approach is indeed suggested for the seismic analysis of masonry buildings, employing a static non-linear (pushover) analysis, since this modelling strategy, however quite simplified, allows considering the strongly non-linear behavior of masonry, redistributing stresses and deformations accordingly, even if accepting some limitations (relevant geometrical simplification). Limit analysis is considered the standard procedure – also given its simple applicability – to define the seismic response of existing masonry buildings when subjected to loads acting out of the plane of the resisting masonry panels, being the most relevant damage scenario experienced by such class of structures in case of earthquakes.

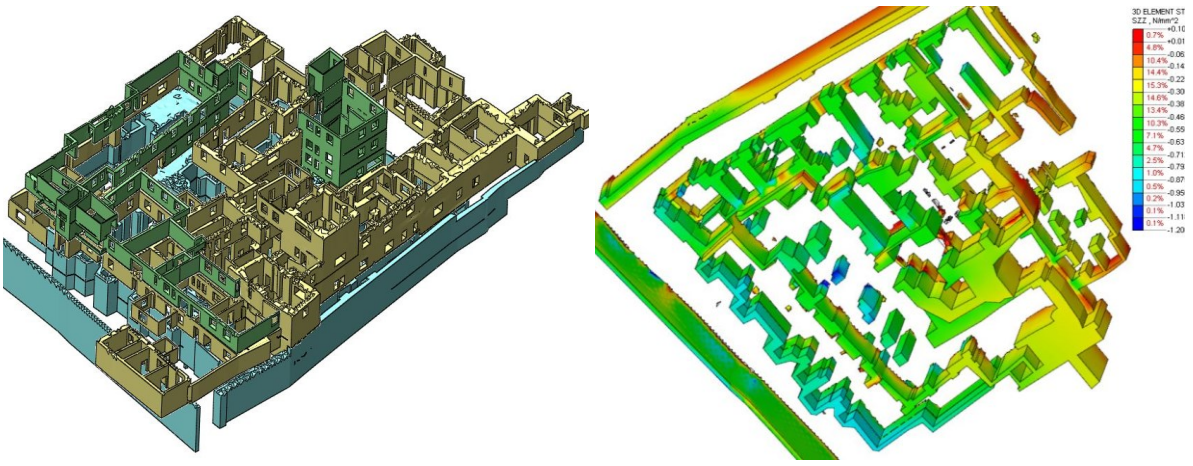


Figure 4: the Dar al Consul global FE model (left) and results of the self-weight analysis at the basement (right)

For the definition of the structural safety level of the Dar al Consul site, the following analysis methodologies were then used: Numerical modelling (Finite Element method), for the assessment of the static and seismic response of the whole complex, by using a static and modal (seismic response) analyses. Numerical modelling (Equivalent Frame approach), for the evaluation of the seismic response of the most significant portions of the residential buildings. Limit analysis, for the ULS safety evaluation of individual structural portions resisting by equilibrium conditions to the seismic inertial forces.

4.2 Obtained results

A tridimensional FE model of the Dar al Consul structural complex was created in order to evaluate the stress and deformation patterns in the masonry and concrete elements [9]. The model is bounded to the ground with fixed restraints, and it is composed by 430'291 tetrahedral 3D elements and 891 beams. The typical size of the tetrahedral 3D element is 0,5 m.
The self-weight analysis was carried out according to the Israeli Standard SI 412 basic combination [10]. Results obtained in terms of σ_{ZZ} stress (compression) indicate that the average value of compressive stress at the ground (basement) level corresponds to approximately 0,5-0,6 N/mm^2. In the upper floors the stresses decrease to 0,25-0,35 N/mm^2. The maximum compressive stress locates at the basement level, where the poorest masonry quality was found, in the main pillars supporting building nr.4. An average compressive stress of approximately 1,0 N/mm^2 or slightly higher is found in the pillars subject to higher compressive forces. Considered the reduced masonry strength at the basement, and from the stability checks carried out, unsafe conditions emerge for the most stressed elements of the basement, namely the pillars sustaining the building nr. 4, but also for linear elements (walls) subjected to less load but with possible lower strength. The average value of stress found from the analysis is in line with the material strength as prescribed by the standards, and sign of cracks / lack of maintenance – and previous strengthening interventions by r.c. jacketing of the pillars – are present in this area, indicating this part of the complex as one of the most vulnerable from a structural point of view.

The seismic analysis of the Dar al Consul complex was carried out by using three different modeling strategies, relying on a numerical approach, with a linear (Finite Element Method) and nonlinear (Equivalent Frame) methodology, and on limit analysis, bearing in mind that the use of an elastic model for determining the seismic response of an existing masonry structure can be misleading since the stress redistribution following the relevant (real) non-linear material behavior in occurrence of an earthquake cannot be properly simulated.

In a first step, the FEM model proposed the analysis of the natural frequencies and associated modes of the structural complex, describing its linear dynamic behavior. The strong degree of compactness of the structural complex, as well as the confining action of the adjacent buildings, stiffen the structural dynamics of the complex, and only relatively few well identified modes were clearly identified, all of them related to the upper levels.
Results of the spectral response analysis, by employing the design response spectrum prescribed by the Israeli Standard SI 413 [11], indicate presence of non-negligible shear stresses in the masonry of the upper levels, following the mode shapes distribution. The shear values are however generally limited, reaching only in few points values non-compatible with the material strength, indicating possible damage concentration areas, in case of the design earthquake.

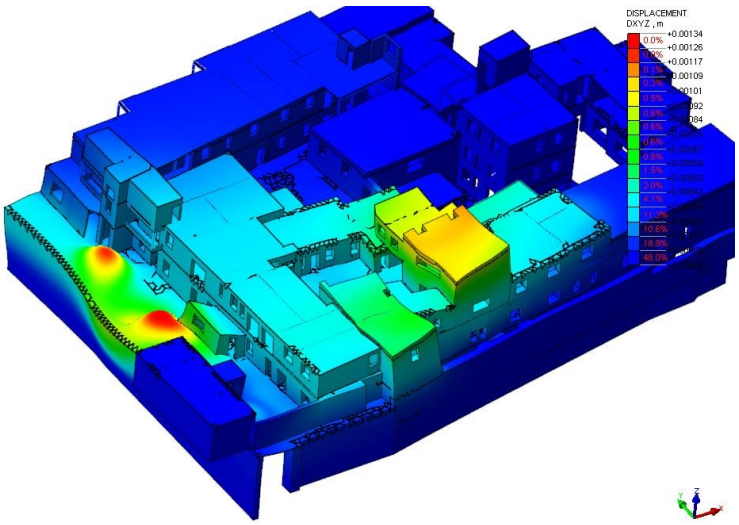
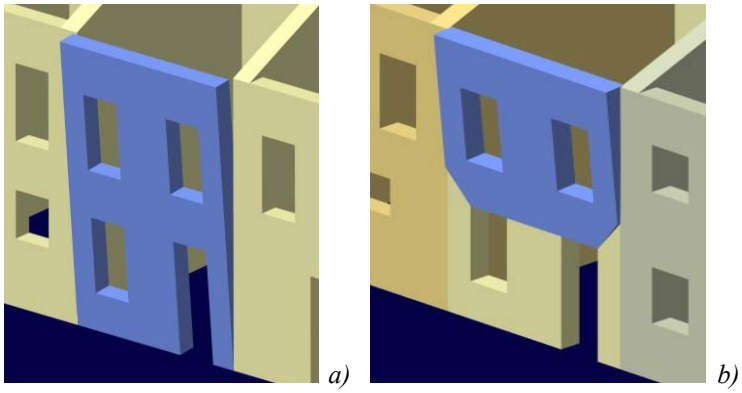


Figure 5: 3D FE model: a) mode nr.10 – f = 6,10 Hz – 31% of mass participation, dir.X

The large number of resisting walls in the two directions at the ground (basement) level together with the limited site seismic hazard, results in limited shear forces at the base of the complex.

Four Equivalent Frame (sub)models were implemented for the execution of the seismic analysis of the upper buildings of the structural complex, named building 1-6, building 2, building 3 and building 4. The analyses carried out per each sub-model indicate that the structural response can be considered adequate, by employing the elastic response spectrum prescribed by the Israeli Standard SI 413. However, considering the soil amplification factor as prescribed by the Italian Standard, it emerges that models building 1-6 and building 3 present some deficiencies, mainly due to lack of resisting walls in the Y direction, denoting a structural seismic vulnerability in the range of 70% (100% corresponds to a satisfactory response).

The limit analysis approach, considered the standard procedure to define the seismic response of existing masonry buildings when subjected to loads acting out of the plane of the resisting masonry panels, was finally applied. The kinematic models, implemented to define the stability of the masonry panels under the seismic actions, were applied to a relevant number of masonry panels of the structural complex, whose stability was assessed in accordance with the Italian regulations, considering both linear and non-linear formulations [8].



a) *b)*

Figure 6: global overturning and upper overturning local collapse mechanism

For each possible significant local mechanism, a part of the construction becomes a labile system (kinematic chain), through the identification of rigid bodies able to rotate between them (mechanism of damage or collapse), usually defined on the basis of typically seismic induced shear surfaces (cracks). The seismic action is then schematized as an equivalent static force given by the product of the mass of the wall and of the vertical loads, times the seismic acceleration, regarded as constant along the height of the wall. The procedure continues with the evaluation of the multiplier of loads (ratio of horizontal forces applied and weight of the masses) which activates the mechanism, that is to say that equals the stabilizing (loads of structural elements) and unstabilizing (inertial seismic) forces. Out-of-plane mechanisms relative to vertical strips of masonry were studied, involving the overturning of the whole wall (Figure 6a) and of the upper level/s of the same wall (Figure 6b).

The checks indicate a general unsafe situation (see typical graphical representation in Figure 7), mainly for lack of adequate connection devices. The greater vulnerability corresponds to the presence of unrestrained vaults, domes and thin masonry in the upper floors of buildings, with their relevant horizontal thrust at the abutments.

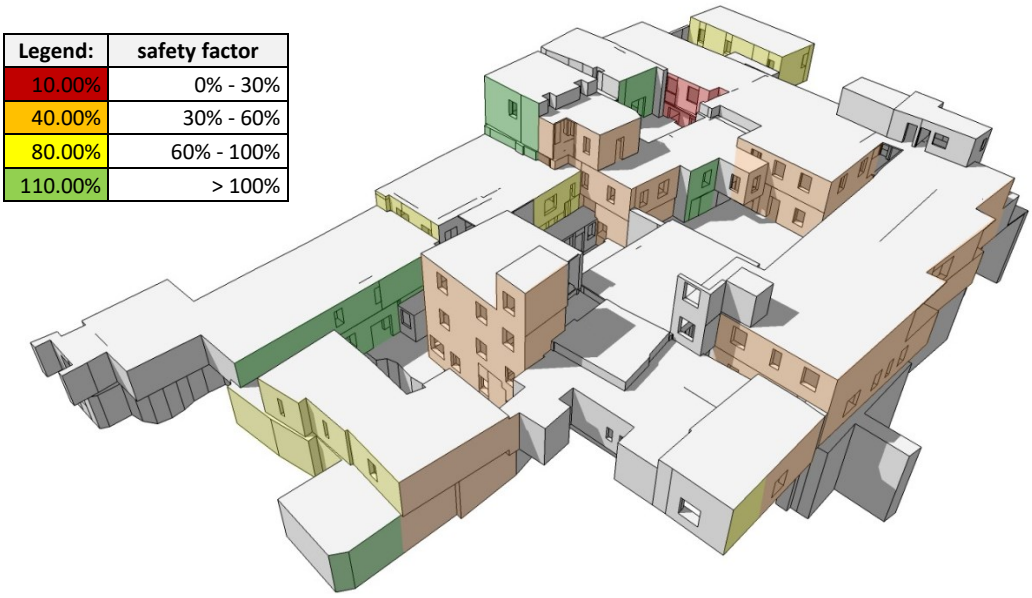


Figure 7: the Dar Al Consul complex North-East view, graphical representation of the safety factor

5 THE REHABILITATION AND STRENGTHENING INTERVENTIONS

A comprehensive architectural and structural intervention is being carried out since 2014, and it is still ongoing, entailing both the rehabilitation of the houses and public spaces of the complex and its structural strengthening and seismic upgrading. The interventions aim at upgrading the living conditions of the residential buildings in the upper levels, at the same time introducing elements for the seismic strengthening (e.g. tie beams), and to reconfigure and strengthen and preserve the basement spaces, that with the passing of time lost their residential / commercial function, finding a balance between conservation and changed architectural needs. Moreover, safety issues are further concerned considered the excavation needs of the site, for

both functional and archaeological needs.

5.1 Interventions in the basement

It is noted a generalized lack of structural consistency in several areas of the basement resisting structures, for intrinsic reasons and for lack of maintenance interventions for relevant periods. The encountered masonry typology of the basement corresponds to irregular stone masonry, thus indicative of a structural vulnerability, worsened by the poor mortar quality. The results of the structural analysis indicated furthermore relevant stress values in the basement, especially in some vertical elements, where previous strengthening interventions were already introduced. For this reason it was considered critical – besides providing a generalized improvement of the mechanical characteristics of the stone masonry structures (hydraulic lime grout injections, deep repointing), to locally intervene to strengthen the most heavily loaded pillars, subjected to excessive compressive values with reference to the actual masonry capacity. Interventions such as "confinement" or "stitching" were designed and applied – together with the overall interventions of hydraulic lime grout injections and deep repointing – to provide an increased strength to such structures, consequently increasing their "safety" conditions.



Figure 8: general layout of the interventions in the basement structures, strengthening intervention on pillars

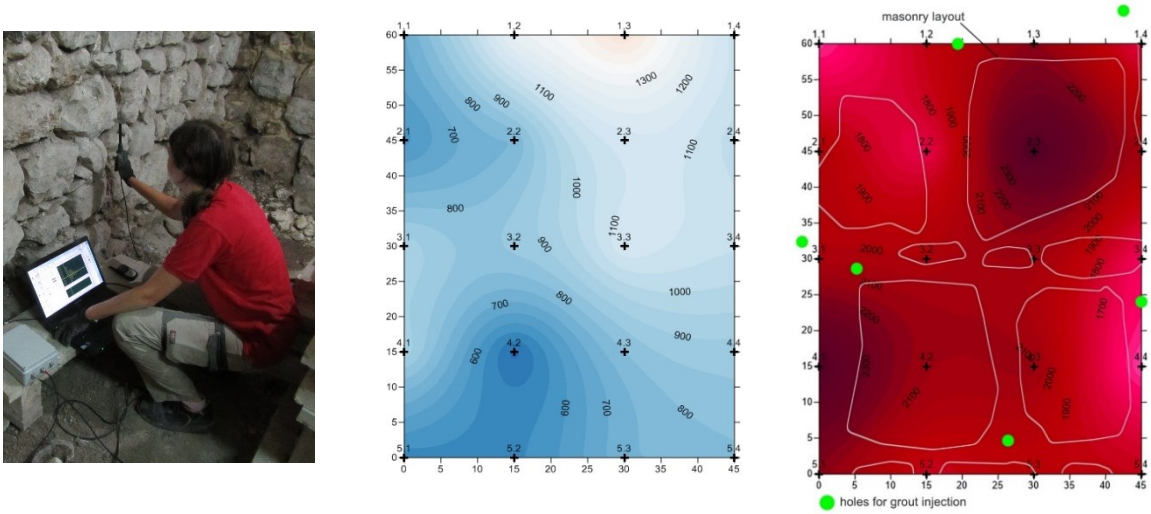


Figure 9: sonic test SON4/SON4i, comparison of velocity before (avg. 800 m/s) and after (avg. 2000 m/s) the injection intervention, graphic representation between sonic velocities (face view of the acquisition grid)

"Traditional" intervention methods were hence employed, always employing compatible materials as hydraulic lime mortar, as deep repointing in masonry walls and pillars, together with more recent techniques which proved their effectiveness, specifically in case of low resistance stone masonry elements. Between these, grout injections in masonry walls and pillars, executed with a high absorption ratio and validated through further investigation activities (direct sonic tests, **Figure 9**), since an overall increase of the velocities measured was widely found (in case of test SON4, an increase of 220% was recorded). Other methods employed were the confinement of masonry pillars and walls transverse tying, in areas of stress concentration, as emerged from the structural modelling. In cases in which there was lack of material, stone integration/reconstruction was considered, highlighting the newly introduced from the original material.



Figure 10: geometrical survey of the basement in 2014 (left) and today (right), with a relevant increase in area and excavations depth

A relevant part of the activities finally corresponded to the excavations in the basement soil, which, year after year, gave the possibility to reach lower levels and find buried structures, also with relevant historical and archaeological findings (e.g. tombs, roman era shops), see **Figure 10**. From an engineering point of view, it was, and it still is a challenge to support the superstructures with uncertain soil conditions, given the difficult execution of geotechnical investigations, the diffuse presence of cisterns in the bedrock and the chaotic stratification of the historical layers of the underground Jerusalem.

6 CONCLUSIONS

- A wide study was carried out to define the structural safety levels of the Dar al Consul complex in Jerusalem. To this aim, several analytical methodologies were employed, since the assessment of the safety state of an historical masonry building is a remarkably complex task, and a single methodology may not be adequate to properly describe the structural response;
- A comprehensive on-site investigation campaign was carried out in order to characterize the resisting structures of the residential complex. Tests carried out highlighted the vulnerability of the masonry structures, especially in the basement;
- Several behavioral models of the structure were implemented, obtaining results of the linear FEM (static and dynamic), non-linear static (equivalent frame approach - seismic), and linear and non-linear limit (local collapse mechanisms) analyses;
- The self-weight analysis indicates that the maximum compressive stress locates at the basement level, where the poorest masonry quality was found, in the main pillars supporting building nr.4. An average compressive stress of approximately 1,0 N/mm2 or slightly above is found in the pillars subject to higher compressive forces. Considered the reduced masonry strength at the basement, and from the stability checks carried out, unsafe conditions emerge for the most stressed elements of the basement;
- Results of the seismic analysis indicate presence of non-negligible shear stresses in the masonry of the upper levels, following the mode shapes distribution. The shear forces are however generally limited, reaching only in few points values non-compatible with the material strength, indicating possible damage concentration areas, in case of the design earthquake. The large number of resisting walls in the two directions at the ground (basement) level together with the limited site seismic hazard, results in limited shear forces at the base of the complex.
- The strengthening intervention arising from the investigation and structural assessment phases, still ongoing, relies on traditional and present-day intervention methods, aiming at the material capacity increase (strengthening of masonry elements) especially in isolated elements or where high stress ratios are found;
- Activities in the Dar al Consul site are currently progressing towards completion, entailing – after the thorough structural strengthening phase – the architectural and conservative detailed design.

Acknowledgements. The Dar al Consul Rehabilitation project is carried out through a partnership between the Custody of the Holy Land (site owner) and the UN-Habitat, with funds coming from the owner and the European Union.

REFERENCES

[1] Dar Counsel Rehabilitation Project Old city Analysis report *STRUCTURAL ASSESSMENT Investigation and tests* (2014) - unpublished
[2] Jubeh N. *Dar al-Qunsul archaeological report* (2015) – unpublished
[3] Arce, A. *Ratisbonne y el santuario del Ecce Homo.* Tierra Santa, tomo 33 – n. 354 (1958), p. 201
[4] Recio Veganzones, A. *Dos inscripciones de Beyrouth conservadas en Jerusalén.* Liber annuus 20 (1970), pp. 118-137
[5] Kark R. and Oren-Nordheim M., *Jerusalem and its Environs*, (2001), p. 58
[6] Casarin, F. *Dal al Consul, Old City Jerusalem, EXPIN technical report – investigation campaign on the structures* (2015) – unpublished.
[7] Casarin F. et al. (2019) *Mechanical Characterization of Masonry Typologies in Israel via Flat Jack Tests*. In: Aguilar R., Torrealva D., Moreira S., Pando M.A., Ramos L.F. (eds) Structural Analysis of Historical Constructions. RILEM Bookseries, vol 18. Springer, Cham
[8] Italian Technical Standards for Constructions, Ministerial Decree 17 jan 2018 and related explicative circular (Infrastructure & Transportation Ministry) 21 jan 2019, n. 7
[9] Casarin, F. *Dal al Consul, Old City Jerusalem, EXPIN technical report – structural analysis – current state* (2015) – unpublished.
[10] Israel standard SI 413 – June 1995 – *Design provisions for earthquake resistance of structures* – The standards institution of Israel;
[11] Israel standard SI 412 – May 1992 – *Loads on structures: characteristics loads* – The standards institution of Israel;

12th International Conference on Structural Analysis of Historical Constructions
SAHC 2020
P. Roca, L. Pelà and C. Molins (Eds.)

THE EVANGELICAL CHURCH OF PEACE IN ŚWIDNICA, POLAND. SEVERAL COMMENTS ON ITS WOODEN CONSTRUCTION AND BUILDING TECHNOLOGY IN THE MIDDLE OF THE 17TH CENTURY

ULRICH SCHAAF

Nicolaus Copernicus University in Toruń, Faculty of Fine Arts
ul. Sienkiewicza 30/31, 87-100 Toruń, Poland
e-mail: u.schaaf@uni.torun.pl, www.konserwatorstwo.umk.pl

Keywords: Early Modern Period, Silesia, Protestant Architecture, Church of Peace, Timber Frame Construction, Building Technique

Abstract. *As a result of the provisions of the Westphalian Peace ending the Thirty Year´s War in 1648, three Protestant churches of timber frame construction, of a previously unknown size, were built in Silesia, outside the walls of the towns of Głogów (Glogau), Jawor (Jauer) and Świdnica (Schweidnitz) in the middle of the seventeenth century. The churches in Świdnica and Jawor, preserved until today, were entered in the UNESCO World Heritage List in 2001 owing, among other things, to the use of pioneering architectural and constructional solutions.*

Answers to questions about the supporting structure designed by military engineer Albrecht von Sebisch in 1656 for the Church of Peace in Świdnica and what construction techniques were selected by master carpenters Andreas Gamper, and Kaspar König, master bricklayer Hans Zöller, and an unknown clay mason in the years 1656-7 for the von Sebisch project, have been sought on the basis of a detailed analysis focused on the following research aspects: construction layout and carpentry joints, carpenters' marks, building material and its processing, materials used to fill the frame fields, and external colour. This analysis has been supplemented by a study of the sources, the literature, and by dendrochronological and technological research.

It has turned out that the main load-bearing system of the church is a system of longitudinal and transverse frames reaching in height through all the floors from the foundation to the top plate under the lean-to roofs above the aisles, or under the gable roof above the nave. Two storeys of the matroneum that encircle the entire interior were directly integrated into this system. The whole is crowned with an orchid truss both over the central nave of the main body and over both parts of the central nave of the transept. As joinery connections, mortise and tenon joints, scarf joints face halved, and cogged joints were used in different variants, depending on their function. Except for oak sill plates and down braces, only softwood was used. Only the whole trees were used, machined initially with an axe, and smoothed with a broadaxe. The fields created by the frame were filled with clay on staffs and plastered. The frame structure was painted dark grey, and the fillings whitewashed.

A comparative analysis with other seventeenth- and eighteenth-century objects on the frame architecture of Lower Silesia shows that the scale of the Church of Peace is unique, while the construction techniques used do not differ from the solutions of that time.

1 INTRODUCTION

The history of the Churches of Peace in Głogów (Glogau), Jawor (Jauer), and Świdnica (Schweidnitz) begins with the Peace of Westphalia of 1648, ending the Thirty Years War. The results of the peace negotiations concerning Silesia are contained in paragraphs 38-41 of article 5 of the peace agreement. In paragraph 38, the Augsburg Lutheran princes of Brzeg (Brieg), Legnica (Liegnitz), Ziębice (Münsterberg), and Oleśnica (Oels), and the city of Wrocław (Breslau) were guaranteed religious freedom under the pre-war privileges, however not under the law, but from the emperor's act of grace. In accordance with paragraph 39, neither the Protestant princes nor their subjects in the Duchy subordinate to the king, referred to as hereditary, were forced to leave the country on account of their religion, provided they kept social tranquillity. In addition, they were granted the right to participate in Evangelical services in places outside the country. Paragraph 40 additionally permitted the followers of the Augsburg faith in hereditary duchies to build three churches outside the city walls: Świdnica, Jawor, and Głogów, if they so demanded. In the last paragraph (41) Sweden and the Protestant states of the Reich received the right to intervene in the Silesian Protestants' matters at the sessions of the Reich Parliament [1, pp. 123-4].

Further restrictions for the Protestants occurred in the years 1651 and 1652 relating to the building of the Churches of Peace: they could be made only of wood and clay [2, pp. 51-52]. In addition, under the order of Ferdinand III 1653, Protestants were deprived of all churches in Catholic Silesia under the so-called reduction of churches, including 254 churches in the Duchy of Jawor and Świdnica [3, pp. 145-230].

After collecting money in the Protestant territories of the Reich and in the neighbouring countries for the construction of the Churches of Peace, it was possible to start their execution: first, in the years 1651-2, in Głogów, then, in the years 1654-6, in Jawor, and, finally, in the years 1656-7, in Świdnica (Fig. 1-2). According to the conditions imposed by the Habsburg authorities, the churches were placed outside the city walls. They were characterized by half-timbered construction and were of enormous scale, which was not common before, as they had to have enough space to house the faithful from the whole duchy at once. The first church of Głogów collapsed during the storm of 1654, but was rebuilt in the a following year. However, in 1758, the second church, built in a half-timbered construction, was destroyed by fire. In the 2nd half of the 17th century and the beginning of the 18th century on, the churches in Jawor and Świdnica were extended by the boxes for the nobles and guilds, vestries, and church bell towers. From the middle of the 18th century both churches underwent numerous repairs and restoration works, mainly on the occasion of jubilees. The churches in Świdnica and Jawor, preserved until today, were entered in the UNESCO World Heritage List in 2001 owing, among other things, to the use of pioneering architectural and constructional solutions [4].

This distinction became the motivation for undertaking detailed research on the building history, architecture, and half-timbered construction of both of the churches in Świdnica [5] and in Jawor [6]. The subject of this article is the Church of Peace in Świdnica, which will be focused on two research questions. The first of these will refer to the load-bearing frame construction designed by military engineer Albrecht von Sebisch in 1656. The second question will concern the construction technique used to build the church in the mid-

seventeenth century by carpentry masters Andreas Gamper and Kaspar König, bricklayer master Hans Zöllner, and a clay masonry master of an unknown name. Based on the reconstruction of the original half-timbered construction, the following issues were presented in order of appearance: the structural system and carpentry joints, the system of carpentry assembly marks, the building material and its processing, the materials used to fill the panels, and external colours. Some of these topics have already been raised in publications [7], [8], [9], while this article is the first attempt at a synthetic discussion of all of the above-mentioned issues. The author, however, is aware that the aspects taken into account do not cover all the issues related to the construction and building technique of the Świdnica church in its entirety.

2 THE ORIGINAL CONSTRUCTION AND BUILDING TECHNOLOGY OF THE CHURCH

2.1 Construction layout

The drawing reconstruction shows that the original church was built on a cross plan with the same length of the longer arms of the body and of the shorter arms of the transept (Fig. 3). Both the three-aisle body and the three-aisle transept were made in a basilica layout, with gabled roofs above the nave and mono-pitched roofs over the side aisles. (Fig. 4).

The architecture of the individual façades is shaped by the half-timbered construction (Fig. 5). The walls are divided by posts into repeating bays, by sill plates, inter-storey rails, extreme ceiling beams and top plates into panels, and by studs and intermediate rails - into fields. A horizontal accent in the composition of the façade is formed by braces crossing on several levels, emphasizing the internal spatial layout. There are neither decorative elements nor woodcarving decorations in the façades.

Two storeys of the matronea consistently run around the interior of the church, clearly emphasizing the central spatial arrangement. They occupy the space of the aisles and are supported by an additional structure within the naves. While the naves were covered with a flat ceiling, the space in the aisles under the mono-pitched roofs was used for the upper matroneum.

The body of the church is about 44.75 m long and about 20.50 m wide, and in the southern and northern arm of the transept - about 5.5 m long and also about 20.50 m wide. The height to the ceiling is about 9.25 m in the body and transept in the aisles, and about 15.00 m in the nave.

The original main supporting construction of the church, still well visible today, consists in the body in the longitudinal direction of four frames reaching the length of the entire church and two frames found only within the matroneum. The axial distance between them is on average about 4.20 m. In the transverse direction there were ten frames. The axial distance between them ranges from about 3.90 m to about 4.35 m.

The transept consists of six longitudinal frames and two transverse frames. Of the longitudinal frames only the outermost frames are independent with their own posts adjacent to the posts of the body. The use of duplicated posts eliminated the threat of significant weakening of a single corner post by multiple carpentry joints. The other frames connect with the main posts of the longitudinal frames of the nave body and form a homogeneous construction with it. The axial distance between the longitudinal frames varies from approx.

3.90 m to 4.25 m, and the axial distance between the transverse frames is approx. 5.50 m.

Initially, all the posts reached the full height of the half-timbered construction, joining with top plates above. The results of architectural studies indicate that the current structure around the lower fragments of the posts and sill plates is secondary everywhere. It can only be concluded from the preserved fragments of the original sill plates that they were originally in the form of a rail between the posts, and that these posts reached a little deeper [5, vol. II, pp. 84-85. There is a lack of material traces to reconstruct reliably the structural solutions below the sill plates, and the only clue is the reconstruction contained in Fritsch's article from 1886, which was based on oral communications [10, p. 603]. The reconstruction presents one post, which reaches about 2 m deep, where it connects with the sill plate. The whole was stiffened with two down braces. The construction with posts reaching deep into the ground was an outdated solution in the mid-seventeenth century, but its use is supported not only by information about the ends of the posts damaged six years after the construction [11, p. 52], but also by von Sebisch's quest for better stability [5, vol. I, pp. 104-5].

The rafter-collar, mono-pitched roofs have identical construction over the aisles of both the nave body and transept. Full trusses coincide with transverse frames of the frame structure, while there are incomplete trusses with beams between these frames. The roof structure over the central naves of the body and transept is a double collar-beam truss with a post structure lying on the lower floor and a central king post strut construction on the upper floor of the truss. Full and incomplete trusses coincide essentially with the structural transverse frames and the entablatures between them. The exceptions to this rule are: the central full truss of the aisle body above the intersection and the second and third full trusses of the southern and northern arms of the transept.

While the aisle body and transept form a uniform construction, the trusses over their central aisles are separate systems: Full and incomplete trusses of the aisle body are fully developed even above the crossing of the aisles, and incomplete trusses of both arms of the transept reach only the body truss.

Individual wooden elements are connected with each other by means of tenons, lap joints and cogged joints in various variants. Tenons are used, among other purposes, to connect elements located in one plane and in contact at a right angle (for example, main posts with sill plates and top plates), or in a diagonal contact (for example, flat sloping upper braces with posts below the beams). Lap joints were also used in the same systems. They predominate in the case of joining the stiffening braces together (e.g. crossing braces) or other vertical and horizontal elements (e.g. posts and truss beams). Lap joints are also used to lengthen the elements in one plane (for example, an oblique overlay joint to lengthen the sill plates and capping beams). To connect two elements that were not in one plane together, cogged joints (e.g. floor beams and truss beams with binding beams and capping beams) were used.

2.2 Carpenter´s marks

The timber framing of individual church construction assemblies, e.g. walls or roof trusses, was performed on the so-called carpentry workbench. Temporary storage of timber-framed assemblies and their transport to the place of construction of the church before erecting the half-timbered construction, as well as the need to distinguish during the assembly of individual elements similar to each other required appropriate marking. When analysing the

system used in the mid-17th century by carpenters, the method of marking structural elements in three directions: in breadth, length, and height was taken into account.

The marking of the transverse trusses of the body is as follows (Fig. 6): the trusses have, counting from the western gable to the intersection of the naves, assembly marks based on the Roman system of writing numbers: I, V, VIII, XI, XV, XVIII, XXI, and XXV (Fig. 7-8), and counting from the eastern gable, assembly marks in the form of round notches: 1, 5, and 8, all made with a chisel. The transverse frame between the frames marked XXV and the round marks in the number 8 have a carpentry mark in the form of semicircular notches in the number 11 adjacent to a thin line. Owing to the fact that the longitudinal frames of the transept are an extension of the middle transverse frames of the body, they are marked in the same way. The transverse frames in the northern arm of the transept have marks in the form of triangular notches made with a chisel, adjacent to a thin line: one triangle in the gable frame, six triangles in the other transverse frame, directly adjacent to the longitudinal body. The transverse frames in the southern arm of the transept are generally marked in the same way, but with the difference that instead of marks in the form of triangles a circular mark made exclusively with a chisel was used. Ceiling beams and truss beams between the frames complete the missing numbers. For example, between the frames marked with Roman numerals I and V, there are ceiling beams and truss beams numbered II, III, and IIII. Inside the individual transverse frames of the body and transept, all the elements have the same mark, for example, Roman I in the western gable façade. No distinctions in the marks of the elements on either side of the axis of symmetry or between individual bays created by the posts were found.

However, in the case of the longitudinal frames of the body, it turned out that the façades of the elements of each bay were given different carpentry marks each. In these bays there are the following marks from the west: I, V, VIII, etc., and from the east round marks of increasing numbers. Despite the fact that they were partially exposed, no assembly marks were found on the structural elements of the internal longitudinal frames.

Altitude distinction exists only in the southern and northern gable walls of the transept and in the western bay of the southern wall of the aisle. Rails and braces in them are marked from the bottom up, up to the level of the mono-pitched roofs above the aisles, with semi-circular or triangular marks numbered one to seven in the gable façades, and Roman marks from I to IIIIIII in the southern wall of the aisle.

The use of such a simple system of carpentry assembly marks when framing the half-timbered construction of a church, in which many similar elements have the same carpentry mark, was probably possible because the carpentry site was also a construction site, which made possible the proper storage of these elements and their direct assembly.

2.3 Construction timber and its precessing

The analysis of the surface of the structural elements shows that only whole trees were used to build the church. Neither half wood nor cross wood was found. Basically, the logs were pre-treated with an axe, and then smoothed with a broadaxe, often leaving the wane to save wood and achieve maximum cross-section (Fig. 8). Only some elements were smoothed with an adze instead of a broadaxe.

All structural elements are straight, without any curves visible to the naked eye, and their

edges run essentially parallel, which testifies to both careful selection of trees in the forest and precise machining of them at a carpentry site. Only in the case of very long elements, for example posts, has a decrease in cross-section upwards been found.

The aforementioned desire to achieve the maximum cross-section of building material is also evidenced by uneven cross-sections within one type of structural elements. For example, the dimensions of inter-storey girths range from 27x32 cm to 30x35 cm. However, regardless of these differences, it can be concluded that building material with four diameters was used, depending on the function of wooden elements in the supporting construction of the church:

- very thick lumber, about 52 cm in diameter (i.e. about 20 inches), from which the posts were made;
- thick lumber, with a diameter of about 42 cm (i.e. about 16 inches), from which sill plates, inter-storey girths, binding beams and top plates were made;
- medium-sized lumber, about 31-34 cm in diameter (i.e. about 12-13 inches), from which, among other things, ceiling and truss beams, rails, studs (except for the gables of the mono-pitched roofs), and down braces in the internal supporting construction were made;
- small lumber, about 21-24 cm in diameter (i.e. about 8-13 inches), from which, among other things, braces, rails, studs in the gables of the mono-pitched roofs, and rafters were made;

Dendrochronological tests have made it possible to determine the types of wood used as well as the year and season at the time of felling trees [12]. These tests prove that for the building of the church oak wood was used for sill plates and for down braces and down passing braces (connecting to the sill plates), and coniferous fir and spruce wood was used for all other structural elements. The trees were felled from the turn of 1652 and 1653 to the summer of 1656. These results seem reasonably reliable owing to the fact that from the moment of obtaining the building permit in 1652, the parish applied for financial and material aid [5, vol. I, pp. 53-57], and in the spring of 1657, the setting of the frame of the church began [5, vol. I, pp. 59-62]. The analysed samples have shown that the logging took place mostly in the winter, when the trees do not grow, they have less juices and, therefore, shrink and crack less, but summer logging also occurred. The processing of the logs itself began at least partly in newer wood, as evidenced by cracks passing through the carpentry assembly marks (Fig. 6).

2.4 Materials used to fill the panels

As already mentioned above [2], according to the church building permit, it was allowed to use only wood and clay for its construction, which also conditioned the way of filling the panels with clay mixed with straw on wooden poles. Their construction was analysed in detail during the last restoration of the church, when some of the fillings were partially exposed or removed in order to repair the structure.

Single notches for fixing the poles in the half-timbered construction were made, using a chisel, on the bottom side of horizontal elements (rails, outermost ceiling beams, and top plates (Fig. 9) or a longitudinal V-shaped groove was made parallel to the side edges. On the upper side of the horizontal elements, only the said longitudinal groove was made (Fig. 10). On this side, an oblique recess was additionally cut out in each element, reaching from the

lateral inner edge of the element to the longitudinal groove, which made possible the assembly and fixing of a pole after the half-timbered construction had been set.

The wedge-shaped poles were obtained by the radial splitting of round trunks with a diameter of about 20 cm. They are made of hardwood with a rough surface that gives clay better adhesion. The width of the poles on the wider side is about 5-7 cm, with their length adapted to the differing height of the panels. At both ends, the poles are narrowed to fit better in the single notches or longitudinal grooves. The axial distance between the poles in the inside diameter is about 8-10 cm.

Clay to fill the panels was mined on site in the municipal clay pit [13, p. 9]. It was mixed with straw bundles about 30-40 cm long and about 15 cm thick, and the poles were entwined with them each time using two to three pieces. Later, both sides of the construction prepared in such a way were coated with clay, mixed with straw cut short, which gave the clay greater flexibility and cohesion, and reduced cracking in the dry state. The type of straw used was not studied, but the analysis of historical sources suggests that it was rye straw [14, p. 87], [15, p. 23]. While still fresh, small recesses with a diameter of about 1.5 cm and a depth of about 2-3 cm were made in the clay, which were to ensure better adhesion for the future plaster (Fig. 11).

Smooth lime plastering was used to plaster the fillings, which on the side of timber framing was rendered flush with structural elements. Technological analyses prove that the ratio of binder to aggregate ranges from 1:3 to 1:5.5. Various types of animal fibre, including sheep fleece and rabbit hair, were added to the plaster as “reinforcement” [16, Domasłowski, p. 24-25].

2.5 The colour of the external walls of the half-timbered construction

Studies have shown that the original colours of the church façade survived only in fragments in the area of the upper windows on the north-west side, which was probably boarded as soon as a few years after the completion of construction [5, vol. I, p 62]. The traces preserved under the boarding will, however, make both the reconstruction of the painting process and the determination of colouring possible (Fig. 12). First, the plastered fillings of the panels were whitewashed, and then the structural elements were coated in grey-black colour. This grey-black colour slightly covered the plaster of the filling, thus optically levelling any unevenness in the cross-section and inaccuracies in the treatment of individual structural elements. The grey-black levelling stripes were later encircled by a contour that masks the inaccuracies in their execution. Finally, the fillings were encircled by an additional thin grey-black line, the so-called accompanying line, about 5-7 cm from the contour. These lines reach the contour in the corners, crossing each other. The contour line and the accompanying line are almost straight, allowing us to conclude that the so-called mahlstick, or a straight stick, was used to make them, along which, holding it a few centimetres from the filling, the lines were painted using a brush.

A specialist analysis showed that soot mixed with lime was used as a pigment, thus resulting in a grey-black colour [16, Domasłowski. p. 28-30].

4 CONCLUSIONS

Architectural studies in conjunction with accompanying research, i.e. dendrochronological

and technological, as well as a study of sources and literature, have made it possible to prepare a drawing reconstruction of the original half-timbered construction of the Church of Peace in Świdnica and the construction technique used for its erection.

The half-timbered construction designed by Albrecht von Sebisch and implemented by craft masters, has performed well, as is attested by its survival, to a great extent, up to the present day. The only weak point in the original load-carrying system was the above-discussed foundation of the posts in the ground, as evidenced by the replacement of the lower ends of all studs and placing them on single stone foundations just above the floor only six years after the church was completed.

Requirements for the parish, designer, and contractors were exceptional because they had to build a church with a half-timbered construction for the protestants from the entire Duchy of Świdnica. The selected load-carrying structure, i.e. the plan of the cross with a three-nave base building and a transept, as well as galleries structurally integrated with the aisles, and the size of the church (it has a capacity of 3,000 seats), meet these requirements. Excluding the Churches of Peace in Głogów and Jawor, it turns out that in comparison with the other half-timbered construction buildings in Lower Silesia and its borderlands from the second half of the 17th century, e.g. with the churches in Szlichtyngowa (Schlichtingsheim - Fig. 13) and Sułów Wielki (Groß Saul - Fig. 14), the load-carrying structure used in Świdnica is innovative.

Such a comparison also shows that the construction technique used is typical for this region and time. This is illustrated, for example, by the way of dividing the structural span of the façade into segments using one or two studs, stiffening the façade with single or crossed braces with lap joints on several levels, the use of building material from a whole tree hewn with an axe and a broadaxe, filling the panels with clay mixed with straw on poles, and the selected grey-black colour version with soot used as a pigment.

REFERENCES

[1] Hutter-Wolandt, U., Das Zeitalter der Reformation. In: G. A. U. Benrath, U. Hutter-Wolandt, D. Meyer, L. Petry, H. Weigelt (Eds.), *Quellenbuch zur Geschichte der evangelischen Kirche in Schlesien*, München: Oldenbourg, (1992), pp. 101-155.

[2] Heuber, G., *Die Evangelische Friedenskirche in Jauer genannt zum heiligen Geist. Festschrift zur Feier des 250jährigen Bestehens der Kirche,* Jauer: Verlag der Hermannischen Buchhandlung, (1906).

[3] Berg, J., *Die Geschichte der gewaltsamen Wegnahme der evangelischen Kirchen und Kirchengüter in den Fürstenthümern Schweidnitz und Jauer während des 17. Jahrhunderts. Mit zum großen Teil noch ungedruckten Urkunden*, Breslau: Selbstverlag, (1854).

[4] Churches of Peace in Jawor and Świdnica, https://whc.unesco.org/en/list/1054, Accessed: June 26, 2019.

[5] Schaaf, U., „Kościół Pokoju w Świdnicy. Dzieje budowy w świetle badań architektonicznych przystosowanych do analizy konstrukcji szkieletowej oraz studium historycznego", vol. I-III, unpublished.

[6] Schaaf, U., *Die Baugeschichte der Friedenskirche Jauer im Spiegel des bautechnischen Befundes sowie der schriftlichen und bildlichen Quellen. Ein Beitrag zur Entwicklung*

einer arteigenen Methode der Erforschung historischer Fachwerkbauten, Toruń: Wydawnictwo Naukowe Uniwersytetu Mikołaja Kopernika, Vol. I-II, (2019).
[7] Schaaf, U., System ciesielskich znaków montażowych jako źródło wiedzy o warsztacie ciesielskim i autentycznej substancji zabytku na przykładzie Kościoła Pokoju w Świdnicy. In: E. Okon (Ed.): *Zabytkowe budowle drewniane i stolarka architektoniczna wobec współczesnych zagrożeń*, Toruń: Wydawnictwo Naukowe Uniwersytetu Mikołaja Kopernika w Toruniu, (2005), pp. 113-32.
[8] Schaaf, U., Kolorystyka elewacji kościoła Pokoju w Świdnicy poprzez wieku w porównaniu z ogólnymi tendencjami opracowań kolorystycznych budynków o konstrukcji szkieletowej. In: *Architektura ryglowa – wspólne dziedzictwo*, Szczecin, (2005), pp. 411-20.
[9] Schaaf, U., Kościoły Pokoju w Jaworze i Świdnicy w drugiej połowie lat 50. XVII wieku. Rekonstrukcja dziejów budowy i formy architektonicznej. In: *Rocznik Historii Sztuki*, XLII (2017), pp. 115-136.
[10] Fritsch, K. E. O., Aus der schlesischen Renaissance des 17. Jahrhunderts (die evangelischen Friedenskirchen zu Glogau, Jauer und Schweidnitz). In: *Deutsche Bauzeitung*, 20 (1886), pp. 577-82, 601-7.
[11] Goguel, E., *Geschichtliche Denkschrift, betreffend die evangelische Friedenskirche „zur heiligen Dreifaltigkeit" vor Schweidnitz*, Schweidnitz: Ludwig Heege, (1852).
[12] Ważny, T., „Analiza dendrochronologiczna drewna ze świątyni Pokoju w Świdnicy", unpublished.
[13] Nowotny, S., *Historia Kościoła Pokoju w Świdnicy*, Świdnica: Pikgroup, (2003).
[14] Krünitz, J., G., *Oekonomische Encyklopädie*, Bd. 70, (1796).
[15] Penther, J., F., *Bau-Anschlag*, 3. Aufl., Augsburg: Pfeffel, (1765).
[16] Domasłowski, W., Kęsy-Lewandowska, M., Łukaszewicz, J., "Badania tynków I wypełnienia ścian konstrukcji szkieletowej kościoła Pokoju pod wezwaniem Świętej Trójcy w Świdnicy", unpublished.



Figure 1: Świdnica, Church of Peace, view from the south-west side, engraving by F. B. Werner, before 1735.



Figure 2: Świdnica, Church of Peace, interior with a view to the altar and pulpit.

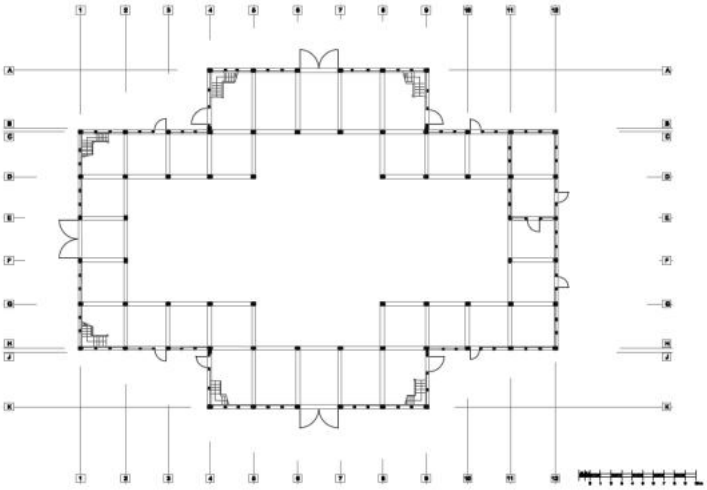


Figure 3: Świdnica, Church of Peace, reconstruction of the original building, ground floor [5]

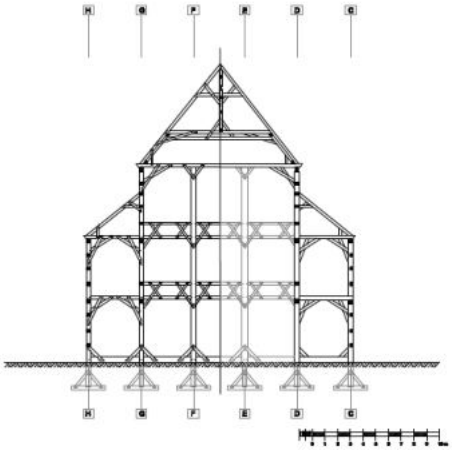


Figure 4: Świdnica, Church of Peace, reconstruction of the original building, cross section [5]

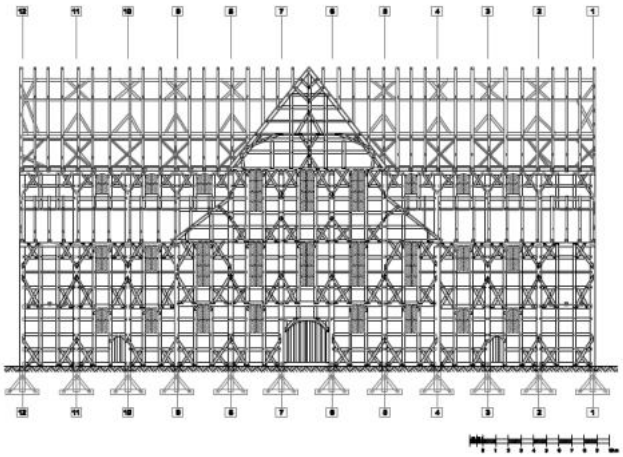


Figure 5: Świdnica, Church of Peace, reconstruction of the original building, cross section [5]

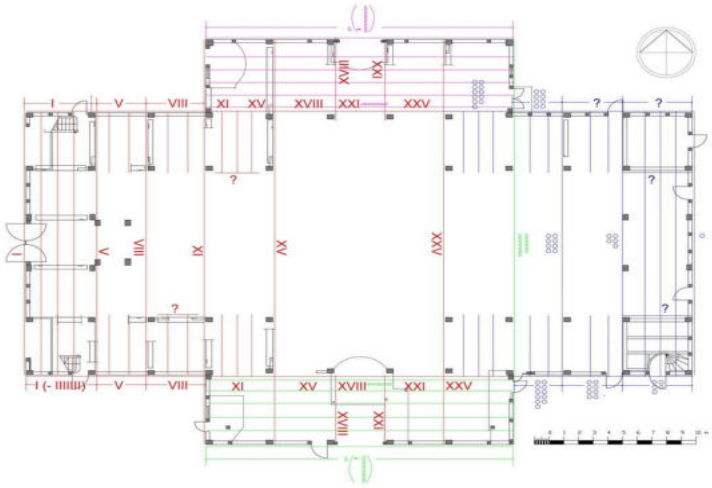


Figure 6: Świdnica, Church of Peace, reconstruction of the carpentry assembly marks system [5]

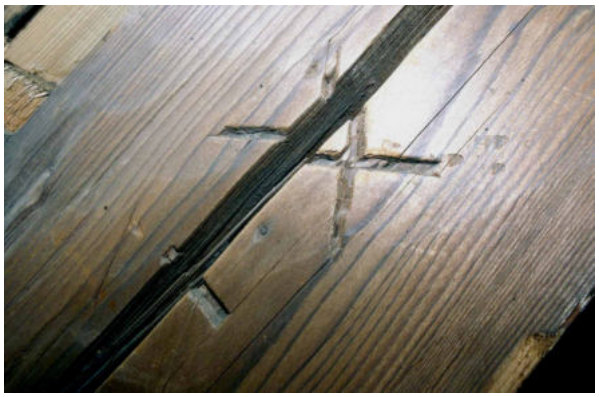


Figure 7: Świdnica, Church of Peace, carpenters` mark



Figure 8: Świdnica, Church of Peace, carpenters` mark, traces of machining with an broadaxe



Figure 9: Świdnica, Church of Peace, notches on the bottom side of the rails and poles covered with clay and straw



Figure 10: Świdnica, Church of Peace, longitudinal groove and oblique cavity at the top of the rail



Figure 11: Świdnica, Church of Peace, clay filling with single cavities



Figure 12: Świdnica, Church of Peace, fragment of the original colours of the external walls

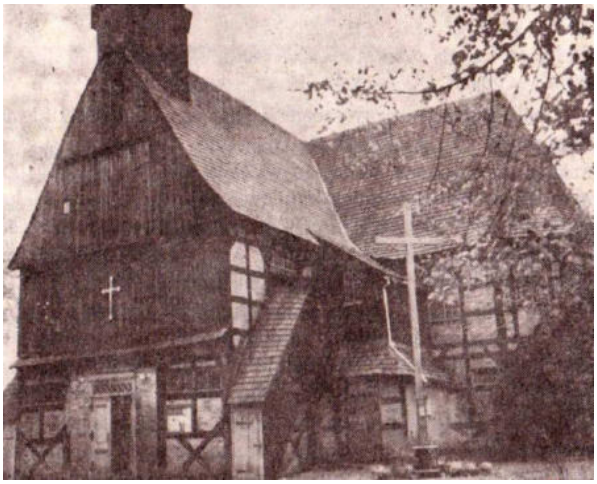


Figure 13: Szlichtyngowa, half-timbered construction church on a cross plan, 1645



Figure 14: Sułów Wielki, half-timbered construction church on a cross plan, 1656-73

12th International Conference on Structural Analysis of Historical Constructions
SAHC 2020
P. Roca, L. Pelà and C. Molins (Eds.)

THE INFLUENCE OF CIVIL WORKS ON HERITAGE ARCHITECTURE, EL VERGEL, CUENCA - ECUADOR

MARÍA G. BARSALLO[1]; FAUSTO A. CARDOSO[2]; EDISÓN R. SINCHI[3]; TATIANA E. RODAS[4]; MARÍA C. ACHIG-BALAREZO[5]

World Heritage City Project, Faculty of Architecture and Urbanism,
University of Cuenca, Cuenca, Ecuador,
[1]gabriela.barsallo@hotmail.com; [2]faustocardosomartinez@gmail.com; [3]edison.sinchit@ucuenca.edu.ec;
[4]tyrodasa@hotmail.com; [5]cecilia_achig@hotmail.com

Keywords: Conservation, Civil Works, Earthen Architecture, Damages, Las Herrerias.

Abstract. *In urban and rural areas of the Andean cities of Ecuador, construction based on earthen technologies has been an important alternative, which are carried out through ancestral customs, such as the minga, which benefit the cohesion of the community. Against this background, the World Heritage City Project of the University of Cuenca (Ecuador) has since the year 2011 undertaken interventions in heritage buildings inspired by the minga, so called Maintenance Campaigns, where the collective efforts of various actors (community, academy and organizations) are joined to recover buildings in highly vulnerable heritage neighborhoods, promoting preventive conservation, maintenance and monitoring of vernacular buildings.*

The fourth campaign, which was carried out in 2018, took place in the Las Herrerias Street in the historical El Vergel neighborhood of Cuenca, a World Heritage City since 1999. The methodology applied in the previous campaigns was essentially maintained, gaining experience and innovating at every opportunity. As a special aspect, the Las Herrerias Campaign was characterized by the existence of buildings with structures that were already affected by civil works previously carried out, such as re-pavements, drinking water installations, various services, etc.

This research proposes to establish conservation strategies of vernacular heritage buildings and to mitigate the effects of poorly carried out civil works. The buildings intervened in the 2018 campaign are taken as reference, specifically those whose damages are the result of civil works. First, a review of bibliographic sources is undertaken to reveal historical data about the neighborhood and the civil works that have been carried out. The research continues with a diagnosis of the condition of the buildings before the Maintenance Campaign. Next, the daily maintenance records and the experience of the participants of the Campaign are investigated to identify and analyze those buildings affected by bad civil works practices and their impact on the damages of their structures. Subsequently, the condition of the buildings after the Campaign is evaluated.

Finally, strategies are proposed that must be considered for the interventions of vernacular heritage architecture, built with traditional earth and wood systems. Furthermore, civil works guidelines are defined for these types of interventions. Accordingly, the preservation for future generations of the wealth of material as well as immaterial heritage is encouraged.

1 INTRODUCTION

The Las Herrerias Street is located in El Vergel, a peripheral neighbourhood within the UNESCO area of the city of Cuenca (see figure 1), declared a World Heritage Site in 1999. This street is of high historical importance, since it used to be the main entrance to the pre-Hispanic city of Tomebamba. Indeed, through this neighbourhood passed the so-called Qhapaq Ñan, the Inca road system, which connected the two most important cities of the Inca Empire: Tomebamba and Cusco.

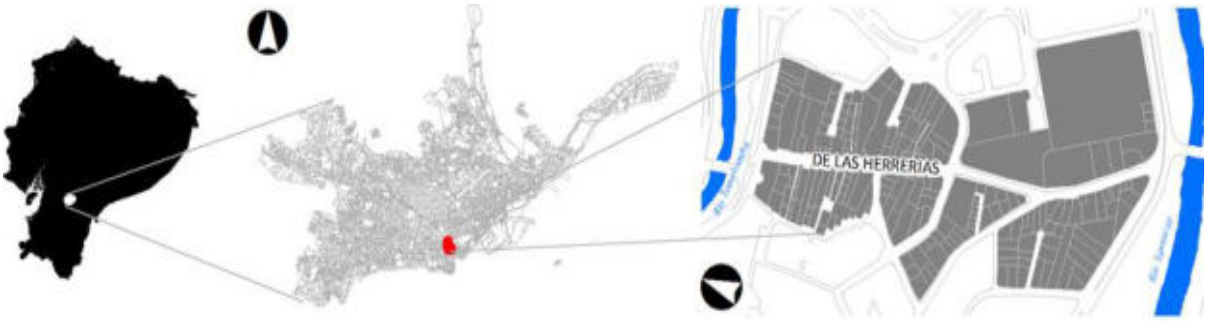


Figure 1: The location of the city of Cuenca, Ecuador, and the Las Herrerias Street.
Source: Municipality of Cuenca

At the time of the Spanish colony blacksmiths settled in this street, in compliance with the socio-economic division of the population created at the end of the 18th century, which distinguished between three zones: 1) the city center, 2) the parish of the natives and 3) the suburban neighborhoods (El Ejido, Barrio El Vergel) [1]. From this emerged a reorganization of the traditional neighborhoods: in the west of the city the potters, in the north the saddlers, in the south the bakers and in the southeast the blacksmiths [2].

The street, then called Antonio Valdivieso, changed its name to Las Herrerias Street in the nineteen-seventies, in reference to the iron forging workshops that offered their services to the people passing through this street.

The architectural landscape is made up of vernacular buildings of adobe or bahareque, roofs of straw and clay and wooden structures covered with handmade tiles. These buildings formed the setting where the modest blacksmith workshops and small commercial shops operated in harmony with their residential use. The typologies of several of these buildings is made up of an interior or exterior portal and rooms derived from the need to work, exhibit, ventilate and live.

Being this a strategic entrance and exit of the city, the horse and mule riders left their animals attached to the portals, while going to the city center to sell and buy products. In this lapse of time the blacksmiths often repaired the horseshoes [3]. However, over time, the blacksmiths diversified into other products, such as locks, gates, nails, hinges, crosses, etc.

Furthermore, from the end of the 19th century, they started to make architectural products, such as handrails and windows, in tune with the new styles being used in the architecture in Cuenca. Today, several vernacular buildings are still present, but the economic activity of the blacksmith has declined in favor of restaurants and tourism.

2 THE LAS HERRERIAS STREET AND ITS INTERVENTIONS

The high growth experienced by Cuenca since the second half of the 20th century brought with it the implementation of small to large civil works, which guaranteed better living conditions for its inhabitants [4]. This improvement of infrastructure and services caused a new challenge to the good conservation of buildings in the middle of an asynchronous reality. Although on one hand, it was important to improve the infrastructure and services with early actions, on the other, concerns about built heritage values only began to be explicit, discussed and applied half a century later. At the time of the execution of the major infrastructure works (re-pavements, drinking water installations, various services) the economic and heritage values of the buildings, from the planners 'and builders' perspective, were so low that without any objection the heights of the streets were drastically increased to give room to the new pavements required by the new guest of the historical city, the automobile. With its arrival, the streets were widened, leading to sidewalks and shoulders being pushed back and causing physical changes to many of the existing buildings. In addition, the elevation of the streets meant that the entrances to the buildings, which supposedly benefited from the new infrastructure, became exposed to flooding on rainy days with water entering the buildings from the street and the slow action of humidity through capillarity. Furthermore, several entrance doors were blocked. When getting wet, the earthen walls lost strength and collapsed one after another. In heritage terms, the price paid for the arrival of the automobile to the city was extremely high.

These interventions, which are normally assumed as the triumph of modernity over the modest earthen architecture, imminently destined for demolition, caused real traumas in the historical centers of Ecuadoran villages and cities.

One of the works that most affected the Las Herrerias Street was carried out in the year 1961. Several portals were removed and the level of the buildings relative to the street was changed, due to the widening and paving of the new street, causing a considerable change in the neighborhood. Figure 2 shows how the level of the sidewalk ascends above the lower level of the building, causing the door to be cut off, water filtrations, danger of tripping over when entering and leaving the building, and a general change of its appearance.



a) b)

Figure 2: a) Vernacular building in the Las Herrerias Street before the street was paved
Source: a) Photographical archive of the Municipal Foundation "El Barranco"
b) Vernacular building in the Las Herrerias Street after the street was paved
Source: b) Photographical archive of the World City Heritage Projecct

This is how public and private works have weighed on life in the cities. Due to the own dynamics of these processes the changes come about slowly, almost unnoticeable and with an aura of benefit to the neighborhood, causing them to be accepted without complaints nor critics by its own inhabitants. That is why the comparison of current with historical photos can be a very valuable tool to analyze and study the landscape.

The need for sidewalks also contributed to alter the environment due to the different materials used. At the beginning of the 20th century were introduced materials such as hexagonal cement bricks and unfinished concrete that are still being used today [5].

With the arrival of electrical and telephone services, and more recently cable TV and the internet, a new problem appeared for the historical centers: the destruction of the urban landscape. Enormous posts with swarms of devices and dozens of wires that enter and exit chaotically were placed in various parts of the neighborhood, occupying pedestrian space. Many of these wires are, in technical terms, dead wires, since they are no longer being used and have not been removed by the responsible companies. Although the need for public space illumination improves the safety in the neighborhood, it is necessary to carry out a detailed architectural landscape analysis to reduce the impact of this infrastructure on the landscape.

Additionally, with the consumerist emphasis of current societies, publicity also gained a position in the public space. Encouraged by the unfortunate idea of the bigger and more luminous the publicity the more successful the result, bit by bit appeared signs, advertisements and billboards that partially crown or cover many buildings, turning the urban historical landscape into a chaotic and disorganized scenery, in which the publicity is the true image of the city.

Finally, it should be noted that on several occasions the Municipality of Cuenca tried to work in the Las Herrerías Street, socializing various projects, including paving the street and the sidewalks (which included the burial of cables), which never materialized [6]. During the years 2017 and 2018, the University of Cuenca made an intervention proposal through a new Maintenance Campaign for the heritage buildings of the traditional neighborhood El Vergel, which was successfully carried out between May and August 2018.

3 MAINTENANCE CAMPAIGN OF THE HERITAGE BUILDINGS OF THE NEIGHBORHOOD EL VERGEL, LAS HERRERIAS STREET

Since the year 2001, the World Heritage City Project (CPM)[1], with its focus on heritage conservation, has been applying Maintenance Campaigns of built heritage. These campaigns are aimed at the recovery of heritage buildings in vulnerable sectors through the collaboration of various social actors. These initiatives start off with an in-depth analysis by professors, students and researchers to identify the buildings to be intervened, determine their values, their damages and the activities to be developed. This work is carried out through participative workshops with the residents of the neighborhood and the support of various public and private entities, in order to forge commitments that are reflected in works, according to the expertise of each actor: the academy as leader and coordinator, organizations as strategic allies (institutions, foundations, associations and companies), the community, owners and neighbors

[1] The vlirCPM project (Vlaamse Interuniversitaire Raad - City Preservation Management), in coordination with a consortium of Flemish Universities, lasted from the year 2007 until 2018. Its objective was to develop scientific foundations and provide education in order to improve the management of heritage sites in southern Ecuador, through the creation of management tools and the diffusion of knowledge. Currently the project is known as the CPM Project (City Preservation Management)

in search of greater social involvement and cohesion of the neighborhood [7].

The first Campaign was applied in the year 2011 on 48 houses in the rural parish of Susudel and two years later a Campaign was carried out on the cemetery of Susudel. In the year 2014, a Campaign was carried out in an urban area in Cuenca, the neighborhood of San Roque, which is one of the neighborhoods of the city's UNESCO area [8]. Finally, in the year 2018, the Maintenance Campaign of the heritage buildings in the Las Herrerias Street of the El Vergel neighborhood was started. Based on this latest experience, during which 21 buildings were intervened, the influence of civil works on heritage architecture has been analyzed.

Without a doubt, the Maintenance Campaign was a challenge, since many of the buildings had considerably deteriorated roofs, columns and facades. The main problems consisted in rotten column bases, leading to a settling of the second floor and affecting the adobe walls as well as the roofs. Furthermore, the landscape was affected by the multitude of wires of different types, use and service [9]. Of a total of 226 damages, rot, stains and detachments account for more than 50%, as shown in figure 3.

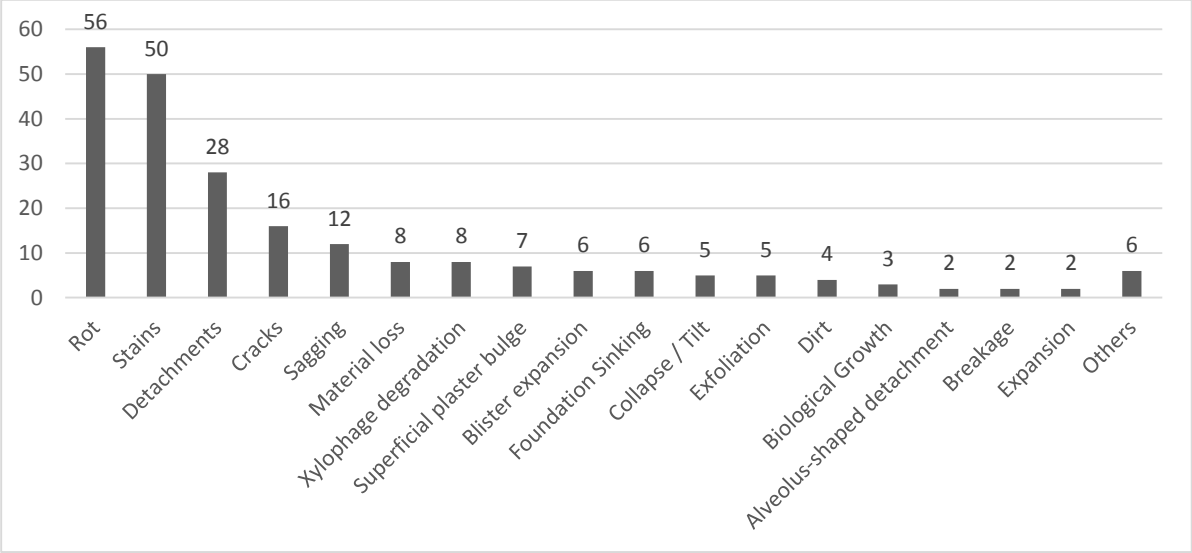


Figure 3: Total number of identified damages before the Maintenance Campaign
Source: World City Heritage Projecct, 2018

This investigation encountered several damages caused by civil works, such as poorly positioned posts, lights and wires as well as changes in the height of the street and sidewalk.

3.1 Civil works as focus of the analysis for the recovery of heritage elements

The effects caused by poorly carried out civil works in the Las Herrerias Street affect the most modest buildings. Especially the columns of the portals got damaged. During the Maintenance Campaign several stone elements, which served as column bases were found buried and as a consequence the wooden columns came into contact with the ground (due to a loss of height of the base) resulting in rot and loss of structural strength. Figure 4 highlights the buildings intervened during the Maintenance Campaign and those with portals. All have

structural problems due to a weakening of their columns. Of the 6 buildings with portals, 5 had columns in direct contact with humidity or with buried bases and all of them were intervened and remedied.



Figure 4: Buildings intervened during the Maintenance Campaign and buildings with portals
Source: World City Heritage Projecct, 2018



a b c d

Figure 5: León House (E204); main facade before the intervention; b) shoirng of the portal during the replacement of the bases; c) original unburied bases; d) columns after the intervention
Source: a, b,c,d) Photographical archive of the World City Heritage Projecct, 2018

A specific example is that of the León House (fig. 4, building E204), which had its stone bases buried several centimeters below the current ground level and replaced by cement coating as shown in photo a). Due to its contact with the ground, this caused an increase of moisture in the columns, leading to the bending of the beams that support the second floor. This type of protection not only affects the strength of the wooden column structure, but there is also a loss of value of the vernacular building due to not maintaining the traditional construction system. Figure 5 shows the situation before, during and after the Campaign.

3.2 Civil works as focus of the analysis for the relocation of urban elements

Electrical installations: the building E204 (figure 5ª) is one of the few buildings that continues to have a vernacular constructive system of adobe on the ground floor and wood on the second floor. In this building the electrical installations were a danger due to the build-up of electrical wires close to its main facade. Similar situations were found in buildings E107 (figure 6a) and O206 (figure 6b), where posts with electrical wires were positioned through their wooden roofs, causing damages to their structures, ceilings, walls and plasters due to rainwater filtration.



a b

Figure 6: Buildings with threats because of electrical installations: a) E204, b) E107 and c) O206
Source: a, b) Photographical archive of the World City Heritage Projecct, 2018

To change this situation, during the Maintenance Campaign the University of Cuenca requested from the local Electricity Utility to study, coordinate and execute the relocation of the 6 involved posts and the burying of its wires. Due to the proximity of the wires to the roofs and the location of the posts in the middle of the sidewalks, this constituted an obstacle both for the access of the owners to their buildings as well as for the free movement of the pedestrians, in addition to directly affecting a window and the aesthetics of the buildings. It is worth mentioning that a Center for the Blind is located in this street, for which the public space needs to offer the necessary facilities. The local Electricity Utility carried out the complementary works of burying the wires within the Maintenance Campaign's intervention area of the street. This also allowed for a coordinated action between the Public Utilities of telecommunications, drinking water, sewage and sanitation to remove the so-called dead wires. In this way, an intervention of the urban space was realized that improved the quality of the services in the area and the image of the neighborhood.

4 STRATEGIES FOR INTERVENTIONS IN VERNACULAR BUILDINGS CONSIDERING PREVIOUS CIVIL WORKS

To develop proposals for the intervention of vernacular heritage buildings, a historical study should be considered. With the results of this study, the type of civil works that have been carried out in the area of interest are identified and it is thus possible to determine guidelines for a better intervention. Thanks to a detailed investigation during the Las Herrerias Maintenance Campaign it was discovered that previously the street was located at a lower level

and that led to the recovery of the stone column bases, which were buried in the sidewalks.

The civil works carried out in the city of Cuenca since the first decades of the 20th century were essential to meet the needs for public health, security and to improve the inhabitants' quality of life. However, these should have been carried out in a properly planned manner, such that they would not have negatively affected the structures of the heritage buildings. In recent years, one can still see how civil works continue to cause damage to heritage buildings. In the year 2016, due to the widening of the Ordoñez Lasso Avenue, in the west of Cuenca, 11 buildings were totally or partially demolished [10]. Some of these were left with rooms of only three walls and out in the open, causing their accelerated deterioration.

The infrastructure civil works in heritage areas is delicate and should involve the presence of a heritage and landscape expert. Electrical, drinking water, sewerage, internet and other infrastructure should preferably be buried. This avoids minor as well as mayor problems, such as those in the Las Herrerias Street, where posts perforated the roof eaves of the heritage buildings and multitudes of wires were left hanging.

Furthermore, the intervention studies of vernacular heritage buildings in historical neighborhoods should be carried out together with the residents of the neighborhood through open, participative and inclusive processes. The suggestion by the Municipality of Cuenca during the first decade of the 20th century to make the Las Herrerias Street and sidewalk at the same level, without sidewalk borders, was rejected by the neighbors, who noted the risk of rainwater entering the buildings, due to the level of the sidewalk being lower than the entrance to their buildings.

12 CONCLUSIONS

The present article shows the analysis of the negative effects on the structures of vernacular heritage buildings caused by civil works, such as the widening of streets, the installation of aerial wires or the installations of drinking water and sewerage.

In the Las Herrerias Maintenance Campaign various problems related to civil works were encountered: an increase of the level of the street, which leads to rotting of columns, the blocking of doors and the entrance of rainwater into the buildings; the location of electricity posts, which form an obstacle for pedestrians and cause the filtration of rainwater into the buildings; the multitude of aerial cables and the proximity of these to the buildings, which damage the aesthetics of the neighborhood and increase the risk of fires. During the Maintenance Campaign, many of these problems were addressed and solved.

A special case in the Las Herrerias Maintenance Campaign is the wooden columns that had their bases buried in the ground when the level of the street was increased, and consequently gradually lost their strength due to humidity. This in turn negatively affected other structural elements, such as beams, roofs and walls. Furthermore, during the intervention of heritage buildings the traditional construction techniques, such as the stone column bases, which function as a separation element between the wooden column and the ground, should be maintained, since these traditional construction techniques are part of the heritage values of buildings and have allowed for the heritage buildings to maintain their importance through time.

It is essential to work together with the neighborhood, to know their opinions as residents, in order to, together with the civil works, improve their quality of life, avoiding problems they had to face in the past, such as the entrance of rainwater into their buildings due to the higher

level of the street.

Without a doubt, the motivations to improve the living conditions of a city go hand in hand with the carrying out of civil works, such as: paving streets to eliminate sand dust and adequate public illumination to improve security. However, they should be carefully planned without affecting the existing heritage buildings and must take into account the different constructive elements and values of the vernacular buildings. This prevents the loss of architectural heritage values, creating a harmony between the civil works, the traditional vernacular architecture and its surroundings.

REFERENCES

[1] Castro, J.D., Muñoz, C., Quizhpe, M. A., Pogo, M. & Tenén, T. *Expediente: "Campaña de mantenimiento de las edificaciones patrimoniales para el barrio El Vergel, calle de las Herrerías".* Noveno ciclo de la opción de Conservación de Monumentos y Sitios. Facultad de Arquitectura y Urbanismo de la Universidad de Cuenca. (2018)

[2] González, I. *Cuenca: barrios de tierra y de fuego: desintegración de los barrios artesanales*, Cuenca, Ecuador: Fundación Paul Rivet. (1991),

[3] Estrella, P. *Cuenca en el siglo XIX: la casa- quinta de Chaguarchimbana*, (Serie Arquitectura y Urbanismo en el Ecuador No. 1) Cuenca, Ecuador: Fundación Paul Rivet. (1992).

[4] Carpio Vintimilla, J.; "Cuenca: Su geografía urbana"; López Monsalve Editores; Cuenca - Ecuador; (1979) pág. 35

[5] Albornoz, B.; Cuenca; *Proyectos de Revitalización urbana 2004 – 2009. Cuenca, Ecuador*: Fundación Municipal "El Barranco". Ilustre Municipalidad de Cuenca. (2009).

[6] Albornoz, B.; *Cuenca, Proyectos de Revitalización urbana 2009 – 2014. Cuenca, Ecuador:* Fundación Municipal "El Barranco". Ilustre Municipalidad de Cuenca. (2014).

[7] Achig-Balarezo, M. C. and Tenze, A.: *The "minga" community participation for the maintenance of vernacular heritage buildings in the historical center of Cuenca, Ecuador*, ISPRS Ann. Photogramm. Remote Sens. Spatial Inf. Sci., IV-2/W6, 9–16, https://doi.org/10.5194/isprs-annals-IV-2-W6-9-2019, (2019).

[8] Cardoso, F., Achig-Balarezo, M., Vázquez, L., Barsallo, G.; *La Conservación Preventiva en Tierra en el sur del Ecuador*. En Terra Lyon 2016, Lyon - France,)2016)., pp. 136

[9] Castro, J.D., Muñoz, C., Quizhpe, M. A., Pogo, M. & Tenén, T. *Expediente: "Campaña de mantenimiento de las edificaciones patrimoniales para el barrio El Vergel, calle de las Herrerías".* Noveno ciclo de la opción de Conservación de Monumentos y Sitios. Facultad de Arquitectura y Urbanismo de la Universidad de Cuenca. (2018)

[10] Tomado del diario El Tiempo. Noticia publicada el 15 de noviembre de 2016. Descargado de: https://www.eltiempo.com.ec/noticias/cuenca/2/casas-de-la-av-ordonez-lasso-seran-demolidas.

THE MODERN IMPOSSIBILITY OF MAKING ART LIKE THAT OF THE PAST. INTERVENTION PROPOSAL FOR THE TEMPLE OF SAN JUAN BAUTISTA, TOCHIMILICO, PUEBLA, MEXICO.

M. ELISA VERA LUNA[1]

[1]Universidad Popular Autónoma del Estado de Puebla (UPAEP)
Facultad de Arquitectura
e-mail: marthaelisa.vera@upaep.mx, www.upaep.mx

Keywords: Historical Structure, restoration theories, earthquake.

Abstract. *Restoration proposal for the Temple of Saint John the Baptist in Tochimilco, Puebla, México, damaged by the earthquake on September 19th, 2017. This proposal is based on the restoration article by the Mexican architect José Villagrán García, his arguments are based on the modification of the architectural values after a restoration project. This must take into account the respect for the authenticity of the original element but must also seek to adapt to the time and requirements of its current environment. Taking these points, a recovery of the space is proposed, consolidating the ruin and using modern materials to fill the gaps left by the earthquake.*

It is sought that this line of restoration be followed more and more in order to identify the historical stages in the life of the monuments.

1 THE EARTHQUAKE

On September 19th, 2017 a 7.1-magnitude earthquake hit central México. The epicenter was located 12 km southeast of the municipality of Axochiapan, close to the boundaries between the states of Morelos and Puebla, and 120 km south from Mexico City. The quake was caused by a rupture within the tectonic plate of Cocos, at a depth of 57 km. Interplate earthquakes aren not common in the region but they are not unusual either.

According to the UNAM's network of seismographs and accelerometers, the quake's maximum acceleration reached 57 gal[1]. Using the seismograms' data, the quake's spectral acceleration can be calculated.

This information provides insight into the behavior of buildings of various heights during the quake. Buildings having between 1 and 12 levels experienced an average acceleration of 119 gal; whilst those having between 12 and 24 levels experienced an acceleration of 60 gal. This data thus explains why the most damaged structures were the ones having between 4 and 7 levels.

The states with most recorded damage caused by this earthquake are Chiapas, Oaxaca, Morelos, Puebla and Mexico City.

2 TEMPLE OF SAINT JOHN THE BAPTIST, TOCHIMILCO

The temple of Saint John the Baptist is located in the municipality of Tochimilco, in the western part of the state of Puebla, close to the state of Morelos, 14 km from the Popocatepetl volcano and 46 km of Axochiapan, Morelos, the epicenter of the earthquake. The temple dates from the end of the XVIII century, though there are maps from 1743 indicating an abandoned shrine in the same location. The shrine was dedicated to Saint John which may mean that some of the original structure was reused to build the existing temple.

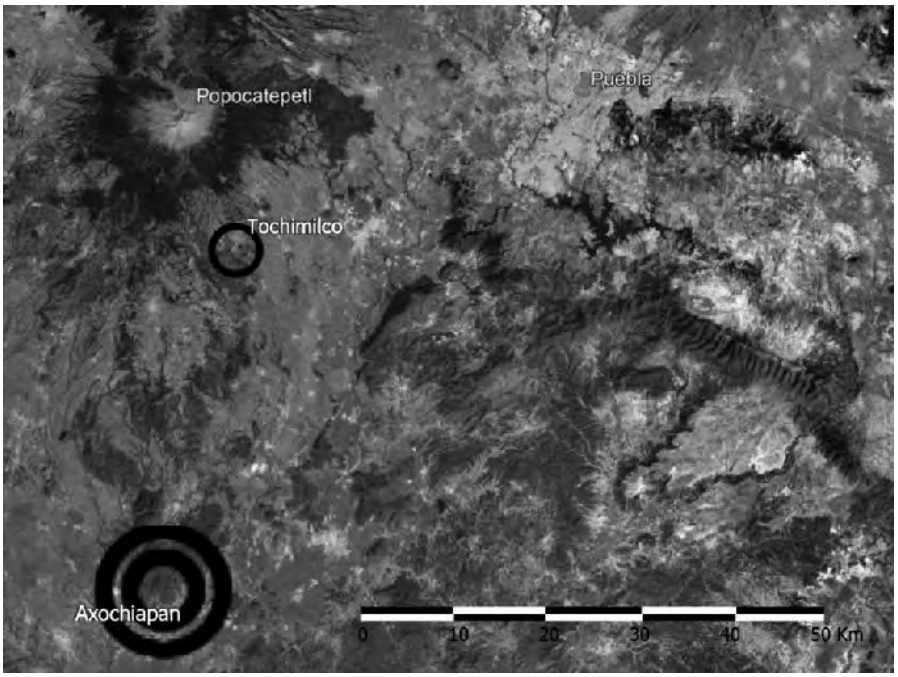


Figure 1. Localization of Tochimilco

The temple is a simple structure with a rectangular base of 7 by 14 meters and a height of approximately 6 meters. It was built over a promontory which is part of a structural block seemingly shaped by a geological fault line and covered with volcanic ashes. The nave is divided into two bodies covered by groin vaults. The north wall is made of irregular stone masonry, earth mortar joints, crowned by two rest arches with rock keystones and, between each keystone, 3 brick courses. The south wall and the façade have a base of approximately 2 meters. The base is of irregular stone masonry and earth joints and continues with a wall of mud bricks and earth mortar joints. The main wall and buttresses are made of irregular stone masonry. The groin vaults are made of stone cyclopean mixture and, unlike the rest of the building, their joints have lime mortar, evidence of them being built at a later date. Attached to the temple and on the north side, there are a sacristy and a warehouse, two rectangular spaces

of 5 by 4 meters each. Their walls are made of irregular stone masonry and the roof cover of square clay and rooftop. A bell tower is also attached to the temple on the north side of its façade. The tower has a base of 3 by 3 meters and a circular core of 2 meters of diameter and 7 meters of height, covered with scrap stone masonry that gives it a rectangular shape. The tower is composed of two bodies crowned by a cupola.

Finally, in recent years a warehouse and a bathroom module were attached to the south façade. They were built with concrete bricks, rebar structures and solid slabs of steel and concrete. The frames were anchored to the temple walls.

3 DAMAGES

The temple of Saint John the Baptist was one of the most affected buildings by the earthquake of September 19th, 2017. Only 30% of the total structure stood after the quake. The amount of damage sparked controversy over the restoration procedures fit for this particular case.

During the quake and due to its slender shape, the bell tower suffered a displacement which led to its collapse. The tower collapse also collapsed the temple's façade. The addition of rooms to the sides of the temple, warehouses on the left and sacristy on the right, strengthened the bases of the walls around the altar. Hence, these walls moved at a different frequency than the first body of the nave, provoking the dismantling of the rest arches, the band and causing the collapse of the vaults. The main wall suffered a vertical fracture, several cracks on the topmost area and loss of material. The buttresses gave way; they cracked in the middle and lost their binding with the main structure.



Figure2. San Juan Bautista after 19 September earthquake.

The sacristy, recently intervened by replacing timber beams with concrete beams, presented minor fractures in its walls and floors. The concrete warehouses, built in recent years, were left under the side walls' debris.
The internal layers were bashed, allowing detailed observation of the construction system as well as the adjustments done to the temple, such as a decommissioned door from the nave to the sacristy and a mural painting on the altar wall. Some defects inside the walls were also revealed.

4 RESTORATION PROJECT

4.1 Theoretical criteria followed by José Villagrán García

The criteria used for this restoration proposal are based on the premises stated by the Mexican architect José Villagrán García. These premises are described in his article *Arquitectura y Restauración de Monumentos* (Architecture and Monument Restoration)[2]. In his text, Villagrán seeks to ignite a reflection on the role played by the architect faced with the restoration of a historic monument, rather than to line up an absolute working theory.

To guide up in that reflection he uses the, apparently contradictory, theories of Ruskin and Viollet-le-Duc. He also emphasizes the precepts set by the 1964 International Charter for the Conservation and Restoration of Monuments and Sites (The Venice Charter).

He takes Ruskin's idea of the importance of consolidating the material to preserve it in its natural state. He then also considers Viollet-le-Duc's concept of restoring the monument to a state in which it could have never existed before; that is, the building material being preserved through interventions that transform its shape into something that did not exist earlier. With these two notions in mind, he defines restoration as "*the art of safeguarding the strength and historic shape-material of the monument employing operations and additions that illustrate its current position and practical purpose*".

This definition is also underpinned by The Venice Charter's articles which state that in any procedure one must prioritize the respect to antique material, clearly marking the intervention in any supplemental work so that historical forgeries are avoided and future generations can easily read the different construction stages. To support that point, the Charter suggests researching exhaustively the building's background and its intervention records.

For Villagrán, the monument to be restored belongs to two architects, the one who initially builds it and the one who is in charge of restoring it, thus becoming the link joining the arts of building and restoring. To proceed with the restoration the architect should take into account four fundamental values of architecture: usefulness, the factological, esthetics, social. After a disaster and mainly after a restoration project those four values are modified. Usefulness, even if potentially maintained, is diminished in order to cover modern needs. As the factological relates to the consistency between the form and its function; it will be necessary to consolidate the building and, in some cases, to change the building materials in order to guarantee the function of the spaces. Esthetic value is most impacted since it is impossible to resurrect what fell apart. In time, it can be reproduced based on previous records, yet this new creation cannot

acquire the value of authenticity from the original. Finally, regarding the social theme, since original parts subsist, the socio-historical value of the monument is evident for the community that envelops it.

The damaged monument becomes the mediator between the culture that sourced it and the current one welcoming it and adapting it to guarantee its continuity. This adaptation would always have to be performed by qualified architects, holding a good grasp of the building materials, the history and the culture that birthed the building and the current needs of the community using it.

4.2 Proposal

Considering the previous criteria and restoration as a multidisciplinary activity needing the expertise of engineers, architects, historians, geo-technicians, etc; studies on the walls' resistance were made for the proposal to respond to the current state of the structure.

The study corroborated that the walls are made of three layers, two external layers of stone secured with earth mortar and a core made of smaller stone mixed with earth and lime. The core has lost cohesion and has started to decouple the external layers causing the collapse in some areas. Furthermore, regions saturated with humidity and cavities were found. This means that the walls are working unevenly and cannot support the structural weight of reintegration with the missing parts and the construction of a vault akin to the original one with the same materials and thickness.

When considering the restoration criteria of Villagrán, the current condition of the materials, the state of the damage and the capacity of the structure to support the structural weight, we propose the consolidation of the ruin by freeing all the elements which could present a health hazard and rehabilitating the space with an independent architectural intervention with state of the art systems whilst keeping the proportions and original shapes.

We aim to be congruent with the original configuration of the building, we plan to supplement the loss of the elements with lightweight construction systems compatible with the original systems that also harmonize with the entire set. In addition, we plan the removal of all the recent elements that do not provide aesthetical value and that concentrate rigidity in some areas of the building.

To consolidate the wall's stumps, we plan to inject slip, a fluid mixture of clay, in the joints, and patching up the cracks when needed. The crowning of the walls, up to the original heights, will be built with mud bricks and plastered with earth mortar. For the roof, we will craft a timber framework covered with clay roof tiles. Such framework will be composed of certified timber, kiln-dried, treated with sealers, flame-retardants, and anti-xylophages. The proposed system consists of a gabled roof with two side-skirts and ridge pitched between 30° y 40° and covered with flat clay roof tiles. To support the roof we propose an internal metallic structure detached from the temple walls so that it can also recreate the geometrical shapes of the arches and groin vaults to facilitate the reading of original elements that are still standing. We propose to build the façade according to the documentation to keep the identity of the temple and to rebuild the

bell tower following the proportions of the original tower but with lesser height to reduce the oscillating motion in future quakes.

This type of intervention reignites the controversy over the usage of original techniques and modern materials. However, on some occasions, it is not possible to correct structural weakness with a traditional solution and lacking qualified labor. Thus we appeal for the usage of modern techniques so that the useful life of this building is prolonged. We reiterate that these actions must be performed by experts and be always bounded by the compatibility of modern and original materials, the durability of the intervention and the feasibility of the removal of additions in the future without affecting the original structure [3].



Figure3. Internal and external views of the proposal.

5 CONCLUSIONS

We seek to discard imitations and historical forgeries lacking insight on the here and now from the original structure. Additionally, we hold a commitment with the future generations; we aim to leave a heritage site true to its story whilst preserving the temple ruins as a homage to the people who built it. We understand building intervention not as a hostile action against historical elements but as a dialogue with the past where we seek to respect its permanence in history whilst imprinting life purpose and constant transformation.

For this proposal, we hold the responsibility of laying it out such that the project becomes a strong link in the constructive historical chain of the community. We aim for this proposal to hold durability standards that can be equated to the one from the initial construction. With these elements in mind, we lay out a proposal only contingent upon the limitations of the original building. Far from silencing the architectural voices of the past, we want to let the original building speak.

Acknowledgements. To the National Institute of Anthropology and History (INAH) and the Architect Teresita Miravete, for their support in the process of restoration of the building, Dr. José Ortega Ramírez and the work team of the Geophysics Laboratory of the National Institute of Anthropology and History to be carried out the study of resistivity, to the architect Antonio Zepeda and the company MIRC for facilitating the architectural surveys and three-dimensional models of the proposal, as well as the permanent access to the restoration

REFERENCES

[1] Cruz, V., Krishna, S., Ordáz, M., *¿Qué ocurrió el 19 de septiembre de 2017 en México? Ciencia UNAM*, recuperado de http://ciencia.unam.mx/leer/652/-que-ocurrio-el-19-de-septiembre-de-2017-en-mexico-. (2017)

[2] Villagrán García, J. *Doctrina de la arquitectura*. El Colegio Nacional, (2007).

[3] Meli, R. *Ingeniería Estructural de los Edificios Históricos*. Fundación ICA, (1998)

12th International Conference on Structural Analysis of Historical Constructions
SAHC 2020
P. Roca, L. Pelà and C. Molins (Eds.)

THE PLASTER CEILINGS OF BUCKINGHAM PALACE AND WINDSOR CASTLE: THEIR CONSTRUCTION, CONDITION AND CONSERVATION

SCOTT BROOKES[1], KEVIN CLARK[1], ROBERT FROSTICK[1*], RICHARD IRELAND[2], LOUIS RANDALL[3]

[1]Alan Conisbee & Associates
1-5 Offord Street, London N1 1DH, United Kingdom
E-mail: robert.frostick@conisbee.co.uk, www.conisbee.co.uk (*corresponding author)

[2]Richard Ireland Plaster & Paint: Consultancy & Conservation of Historic Buildings
100 South Street, Bridport, Dorset DT6 3NW, United Kingdom
E-mail: info@richardireland.net, www.richardireland.net

[3]Louis Randall, The Royal Household Property Section
Buckingham Palace, London SW1 1AA, United Kingdom
E-mail: louis.randall@royal.uk, www.royal.uk

Keywords: Historic structure, Plaster, Ceilings, Nails, Timber, Inspection

Abstract. *Alan Conisbee & Associates and Richard Ireland were engaged by the Royal Household Property Section to inspect and assess the historic plaster ceilings and their supporting structure within Buckingham Palace and Windsor Castle. Following the partial collapse of the Apollo Theatre ceiling in London in 2013 great importance has been placed on the inspection and certification of all historic plaster ceilings throughout the United Kingdom. This paper presents the key challenges of the project included the facilitation of access to constrained spaces, asbestos removal and cleaning of delicate fabric, surveying, digital monitoring, structural and plaster defects. Furthermore we discuss the key project outcomes including lessons learnt and best practice methodologies and practicalities behind inspections of this kind. The paper concludes with an outline of significant discoveries and ongoing laboratory testing of undernailed historic timber connections.*

1 INTRODUCTION

Following the internal collapse of part of the suspended fibrous plaster ceiling (decorative plasterwork composed of plaster of Paris reinforced with hessian) at London's Apollo Theatre (built in 1901) in 2013, an investigation took place which culminated in the release of formal guidance for owners and operators of properties with suspended historic plaster ceilings, produced by the Association of British Theatre Technicians (ABTT). During the investigation by Richard Ireland it was discovered how little was known about the various techniques and materials used in the fabrication of suspended fibrous plaster ceilings and their mechanisms of decay and longevity. This led to an amendment to the ABBT guidance on ceilings which now

recommends a thorough one-off baseline survey by a competent plaster specialist and structural engineer detailing the ceiling and structure fabrication methods, materials, support system and condition. Emphasis is put on the need to physically examine both sides of a ceiling as extensively as practicably possible, requiring access to the ceiling voids and the upper and lower ceiling surfaces.

In 2015 the Royal Household identified the need for a thorough inspection of all suspended ceilings and their supporting structures, subsequently Alan Conisbee & Associates Ltd (Conisbee) were engaged in 2016 by the Royal Household Property Section (RHPS) to assess the condition and structural integrity of the ceilings throughout Buckingham Palace and Windsor Castle. The RHPS acknowledges its duty of care towards those visiting and occupying these buildings and understands the need to undertake detailed inspections and assessments of all suspended plaster ceilings within them in light of the potential risks associated with unchecked deterioration of such fabric. Conisbee's brief was extensive and entailed undertaking structural inspections, managing plaster specialists, surveyors, access consultants and asbestos consultants & contractors, all within the challenging constraints presented by these two unique, historic, working buildings. The following tasks were undertaken:

- Design of permanent safe means of access in advance of surveys and inspections or to ascertain if the current access is safe and suitable for use.
- Survey of all structural and plaster elements for each suspended plaster ceiling throughout Buckingham Palace and Windsor Castle combining inspections from above and below where practicably possible.
- Review of external building fabric likely to impact on each ceiling specifically in terms of age, water damage and/or movement.
- Provision of detailed room specific reports on structural and fabric condition together with prioritised recommendations for repair and ongoing maintenance and inspection, including individual timescales for re-inspection.
- Certification of all ceilings in a condition acceptable for the use of that room and/or area.

Conisbee and plaster specialist Richard Ireland undertook hands-on assessments of 74 ceilings at Ground floor and Principal floor levels at Buckingham Palace equating to approximately 7000m^2 of ceiling surface. Furthermore at Windsor an additional 54 ceilings were deemed sufficiently ornate and culturally significant to require investigation, equating to a further 6000m^2 of ceiling surface, two thirds of this within the State Apartments at Principal floor level..

2 BRIEF HISTORICAL DEVELOPMENT AND CONSTRUCTION

Buckingham Palace is a Grade I listed building in central London and is the principal residence and administrative headquarters of the monarch of the United Kingdom. As well as providing accommodation for the Monarch and the Royal Family it hosts State visits, Investitures, receptions, dinners and many other formal functions, and its State Rooms are open

to the public during the summer months. The core of the present building was begun in 1703 and comprised a large townhouse remodelled and enlarged by John Nash in the 1820's after the site was acquired by King George III[1]. On Queen Victoria's accession in 1837 Buckingham Palace became the principal Royal residence during which it underwent external and internal alterations, notably to the east front and the State Room ceilings, a typical internal view of which is shown in Figure 01.

Windsor Castle is a Grade I listed Scheduled Monument under the Ancient Monuments and Archaeological Areas Act 1979 and contains internationally significant historic fabric from the twelfth to the twentieth centuries. It is one of the most archaeologically complex secular historic buildings in the United Kingdom and the largest continuously occupied castle in the world[2], containing accommodation for the monarch and her family, plus offices, workshops, stores and staff accommodation, and is a hugely popular tourist attraction open 363 days each year. Although Norman and medieval at its core Windsor Castle today is essentially a Georgian and Victorian creation based on extensive neo-Gothic remodelling carried out during the early 19th century.

3 CEILING VOIDS AND SUPPORT STRUCTURE

The Buckingham Palace and Windsor Castle State Apartments are highly significant heritage assets and of great architectural and historical value, both featuring craftsmanship of the highest quality particularly in their decorative aspects. Redecoration and other alterations are usually representative of a change of reign which is also of historic significance. To support these highly enriched ceilings complex iron and timber framing structures were used to create and support their unique shape and form.

At Buckingham Palace the self weight of the plaster ceiling is typically transferred to primary structure through timber laths (thin strips of oak or pine interspaced with narrow gaps) secured with iron nails to small timbers interconnected by a combination of skew nailed butt joints, scarf joints, notched laps and hangers. This timber support frame is typically hung from inverted T section cast iron beams which also support clay pot jack arches integral to the ceiling support system, supporting iron hangers fixed to the primary timber members. A typical example of this is shown below in Figure 02. Where ceilings occur directly below roofs they are generally supported directly by the roof structure (typically timber trusses but occasionally wrought iron of various ages and configurations) spanning between the perimeter walls.

The ceiling support systems at Windsor Castle differ due to the building's much greater age, some of its timber floor and roof structures dating from the 14th century. This structure was retained to support the later lath and plaster ceilings constructed as part of James Wyatt's internal remodelling in the 19th century, with secondary supporting structure typically being integrated into the traditional timber joist and beam floors and trussed timber roof structures in a more direct manner than is the case at Buckingham Palace. The ceilings at both Windsor Castle and Buckingham Palace are predominantly of lime putty mixed with coarse sand and

animal hair, applied by trowel to riven hardwood laths nailed to the undersides of the supporting overhead timber structure.



Figure 01: (Left) Interior view of the Blue Drawing Room 1830's highly enriched lath and plaster ceiling. (Right) KCIIDR baroque painted plaster ceiling by Antonio Verrio dated 1684 at Windsor Castle.



Figure 02: (Left) Internal view above the Blue Drawing Room ceiling, from within the void, highlighting the repeating timber primary beams and typical timber coving structure and back face of the ceiling laths. (Right) KCIIDR rear face, comprising timber floor joists and secondary ceiling members

The earliest ceilings at Windsor Castle are the three surviving oil painted schemes by Antonio Verrio dated 1675-84 which survived George IV's redecoration program of the 1820's, as shown above in Figure 01. Around this time, ceilings at both Windsor Castle and Buckingham Palace were extensively remodelled by James Wyatt and John Nash respectively, both using the plasterer Francis Bernasconi (1762-1841). By the 1800s, pozzolanic additives and gypsum, were used to achieve faster setting lime-based plasters which were typically harder and more brittle, incorporating less hair, and applied in thicker layers to riven or sawn timber laths. This development in materials for plaster ceilings produced a heavier and comparatively less flexible system than earlier periods leading to ceilings characterised by deep compartments created by run-moulded lime plaster ribs and downstand beams, enhanced by the application of cast plaster enrichment fixed with adhesive plaster and ferrous armatures of wire and nails.

4 INSPECTION STRATEGY

Inspections were restricted by the extensive presence of asbestos, debris, dust, detritus, confined spaces and the necessity to preserve historic fabric through minimal intrusive inspection (e.g. significant removal of historic floorboards or areas of plasterwork was neither proposed nor permitted). We therefore implemented a comprehensive but complex process of enabling works prior to our structural and plaster inspections which generally comprised (1) Documentation, (2) Digital Surveying, (3) Access, (4) Cleaning, (5) Inspections, (6) Repairs, (7) Certification and (8) Monitoring and Management.

4.1. Documentation

First, photogrammetric reflected ceiling plans were produced by combining point cloud laser scans with conventional digital photographs, these being essential to record the ceiling condition with a gridded overlay for cross-referencing specific areas during close up visual inspection via Mobile Elevated Working Platform (MEWP). This condition information, including crack patterns, deformation and water staining, serves as a baseline upon which all future condition surveys, assessments and repairs will be based. This may also include monitoring the influence on ceiling condition of nearby construction works.

4.2. Digital Surveying

As well as photogrammetry, laser scanning of the ceiling undersides enabled collation of a 3D point-cloud database for future use including the formation of 3D Revit models, 2D reflected ceiling plans and deformation mapping. To enable deformations to be graphically identified from this baseline scan, coloured, contoured distortion maps of ceiling soffits were produced that illustrate deviations from the plane of an agreed datum plane. A baseline scan was established at the start of our appointment in 2016 and repeated quinquennial scans in the coming years will allow clear and rapid identification of new or ongoing distortions which may require further hands-on investigation. This approach, combined with monitoring of the ceiling, will be utilised to minimise re-inspection requirements and so avoid problematic access into the constrained voids behind the ceilings. The initial data obtained led us to target

key areas such as those outlined in Figure 03. Local distortion of the Ball Supper Room ceiling aided discovery of a failed roof truss bearing which had caused the ceiling to distort, as captured within the scan, and a new stainless steel bracket was subsequently installed to remedy this. The complicated structural arrangement within the Ball Supper Room and its challenging access constraints would have otherwise made this process much more lengthy and challenging.

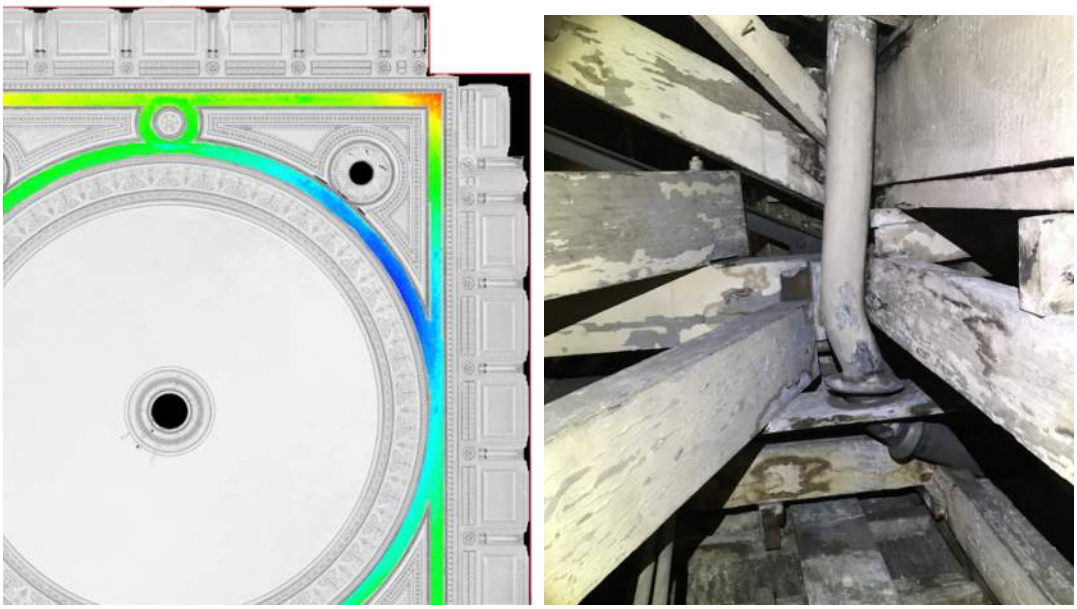


Figure 03: (Left) Distortion mapping of the soffit of the Ball Supper Room. (Right) Photograph of structural defect within the void above, located via the underside distortion. Dropped truss connection was resting on the floorboards and partially supported by a lead drainpipe which has since been repaired.

4.3. Access and Cleaning

An early difficulty was presented by the asbestos within the void spaces and the large amount of dust and debris that had accumulated on the ceiling surfaces, the latter sufficient to obscure the rear surface of the ceiling including the projecting plaster nibs securing the plaster ceiling to the laths, and also the structural connections. At Buckingham Palace alone, 14 individual ceilings above the State Apartments were cleared of 15 tonnes of dust, debris and asbestos to allow safe walkway construction and subsequent structural and plaster inspection and appraisal. Inspection of the topside of ceilings and their supporting structure was carried out above 15 rooms with a requirement for dedicated permanent safe access systems within 7 of these. This process required close collaboration between ourselves, the RHPS, access consultants and asbestos removal contractors to ensure access walkways were constructed safely (some areas posed significant risks of falls from height), as well as managing the health and safety implications of the contaminated environment. Personal air monitoring equipment was used to ensure exposure to asbestos remained at an acceptable level and once walkways were constructed asbestos contractors undertook a fully licensed clean. Trial cleans at targeted

areas were undertaken using a soft head brush to ensure that a licensed clean of the plaster nibs could be achieved without causing damage or loss of the historic fabric.

4.4. Inspections and Repairs

Structural and plaster inspections and repairs are discussed in detail in sections 5 and 6.

4.5. Certification

Conisbee produced detailed reports and documentation of the construction, condition and safety of each ceiling and its supporting structure, plus further documentation outlining material condition, performance, management, access, cleaning requirements and asbestos status. A key project task and ABTT guidance note 20 requirement involved the production of certificates outlining the condition and status of both the plasterwork and structure, a collaborative document produced by Conisbee and the plaster specialist. Each certification took the form of comprehensive condition reports and one-page summary documents for use as quick reference guides outlining the current condition and safety of the ceiling, maintenance requirements and recommended future actions.



Figure 04: (Left) Ball Supper Room ceiling inspections via cherry picker. (Right) Inspection via rope access

4.6. Monitoring and Management

The access constraints were such that it was not practically possible to inspect several ceilings from above, and whilst it is possible to draw a reasonable degree of confidence from underside inspections a further programme of remote underside monitoring is currently being conducted. As part of the early documentation period all ceilings were laser scanned from

below in 2016 to provide a basis for a programme of ongoing monitoring comprising comparative overlaying of repeat scans. Control protocols have also been established for the RHPS which includes regulating access to safe access walkways and other areas above especially sensitive ceilings in order to reduce vibration related damage.

5 STRUCTURAL INSPECTION AND REPAIR

Following completion of our inspections we undertook the structural assessment of each ceiling support structure in general accordance with the following procedure:

- Understanding the structural system (construction, load transfer, integrity, stability).
- Condition assessment of structural members and investigation into the causes of any defects discovered.
- Detailed investigation of structure directly supporting defective areas of plaster as identified in the underside inspections.
- Quantitative and qualitative investigation of structure supporting areas where considerable deviation/deflection of plaster was recorded during underside inspections.

5.1. Undernailed timber connections

Individual vertical undernailed connections between timber members were commonly encountered, directly supporting the ceilings within both Buckingham Palace and Windsor Castle. This form of fixing would doubtless have proven quick and effective when installing the ceiling structure, however their prevalence generates some concerns regarding their structural integrity, specifically the quantified pull out resistance of historic square cross section wrought iron nails from the parent timber in which they are embedded and their ability to effectively withstand tensile loads, especially those applied dynamically.



Figure 05: (Left) Dropped underside nailed connection within Windsor. Similar defects are endemic throughout both the Windsor and Buckingham Palace estate. (Right) Nail sickness and splitting to timber elements in the East Drawing Room, likely accelerated by moisture ingress.

To date our assessment of the adequacy of such connections has been reasonably but wholly based on their historic performance in satisfactorily supporting the dead and imposed loads to which they have been subjected, however this may not accurately reflect their true load capacity. Owing to this, the paucity of relevant codified guidance and the wide variety of variables at play. Conisbee and the RHPS are currently collaborating with the Centre for Engineering Materials at the University of Surrey to undertake in-situ site testing of historic nails. These tests will empirically determine the influence of key variables – embedment, load magnitude and load type – on pull out resistance using original reclaimed historic nails recovered from the Palace and Castle void spaces. Preliminary results suggest that the pull out resistance of such nails is strongly influenced by the timber species, nail embedment and environmental conditions, and further research is in progress which will quantify these factors in detail.

5.2. Insect attack and moisture related decay

One of our key challenges in conserving the historic timber structure lay in justifying the retention of areas affected by insect attack, particularly at Windsor Castle where it was typically more advanced and severe. Generally only the edible sapwood was lost, suggestive of furniture and/or powderpost beetles, and presently assessment is being made at the areas of advanced attack with a view to ensuring the internal condition of the timbers and key connections is not compromised. This work will serve to produce an overview strategy on how to manage the insect damage and appraise its severity and longevity. Similarly, often due to the presence of deep box gutters to the rear of parapet walls decay of timber truss bearings has been an ongoing historic issue and remains an ever present threat to the macro-integrity of the roof and ultimately the ceiling structure. Decay detection drilling has been undertaken in various locations to quantify the extent of section loss, with subsequent calculations to certify the long term adequacy of the timber structure.

5.3. Calculations and analysis

Analysis was typically undertaken through hand calculations to understand the existing stress state of the structural elements and gauge the overall response to imposed loading. Primary timbers are generally of good quality, dense, dry oak and mostly of adequate capacity to perform as intended. Often however modern prescribed serviceability limit states on permitted deflection are not met such that restrictions on access have been imposed to reduce any potential detrimental effect on the ceiling below through bowing, sagging or other similar movement of the timbers that may crack the plasterwork. Unquantified vertical undernailed connections remain an outstanding unknown currently under investigation as discussed previously.

5.4. Structural repairs

In accordance with accepted conservation engineering principles structural repairs typically comprised reversible and distinct simple bolted stainless steel straps or bespoke traditional timber repairs where needed, usually to consolidate failing hangers or connections.

With a view to minimal intervention these have been limited to essential repairs with monitoring and management preferred in lieu of more invasive interventions.

6 PLASTER INSPECTION AND REPAIR

'Plaster' is a generic term describing two entirely different white materials used in building fabrication: lime ($CaCO_3$) from limestone, and gypsum ($CaSO_4$) [1], also known as plaster of Paris, from gypsum and alabaster rock. In the UK and Ireland decorative run mouldings, added to the ceiling flatwork from the early C.16th, were generally executed in lime. By the mid C.18th gypsum was added to accelerate set, and also used to cast solid enrichment. The older methods were gradually ousted during the C.19th by faster setting alternatives including sand and cement based plasters and latterly the invention of 'fibrous plaster' (a gypsum and hessian composite) in 1856. Period and stylistic development are indicators of fabrication material, but only determinable by hands-on inspection of both faces and chemical analysis. The presence and ratio of lime and gypsum is key in determining performance and decay mechanisms. The ceilings at Buckingham Palace and Windsor Castle are mainly of lath and plaster. Lime plaster is trowelled onto a flexible support, in this case riven hardwood laths, forming nibs protruding between and behind the laths. Earlier lime-based plaster ceilings are capable of greater deflection and distortion than later harder setting plasters with added gypsum characterised by less flexible and thicker ceiling plasterwork.

6.1. Common issues and repair measures

Lime plaster performs equally in externally and internally, though the overhead timber support is more sensitive. A common source of ceiling failure is poor exterior rainwater management leading to persistent water penetration causing support failure by fungal and insect attack. Decorative projections such as the large Ballroom ceiling roses at the Buckingham Palace include additional internal support using ferrous armatures of nails or wire and timber - all sensitive to elevated moisture levels which deteriorate in poorly maintained conditions. Good plaster nib formation depends on correctly sized gaps between laths. For this reason, plasterers undertake their own lathing. Gaps too wide or narrow prevent adequate key formation and can lead to failure - especially where a mix weakened by being too wet compromises material integrity.

For lath and lime plaster ceilings, the much used 'builders' method for securing a lath and plaster ceiling considered to be at risk, typically involves wholesale pouring of plaster of Paris over wire mesh or hessian reinforcement laid and secured between bays. This is entirely unsuitable and should have no place in the conservation of sensitive historic decorative lime plasterwork. Poured plaster of Paris has several potentially disastrous drawbacks as it introduces large quantities of heavy wet material to sensitive fabric and furthermore once set the rigidity of the set plaster in turn accentuates any ongoing deflection forces at boundary edges, destabilising otherwise coherent existing plaster.

The preferred method utilises stainless steel washers suspended by wire inserted through small holes drilled through the ceiling plaster and tied off to perforated galvanised band secured between the joists above[4]. The overall goal is to provide additional support to delaminating areas of historic plasterwork. A washer diameter of around 25mm provides a balance between effective support and minimising physical impact to the ceiling plaster. Restraint sites should form a flat seating to maximise washer contact and should be recessed no more than allows subsequent filling and covering. Where access from above is not possible, the use of screws becomes unavoidable. This is less ideal as it is more difficult to accurately determine the location of reliable supporting timber structure and can easily lead to the repeated drilling of the ceiling fabric to locate suitable structures for fixing to. Screws should be of the smallest diameter required with narrow parallel shafts of sufficient length to make a secure fixing in the selected timber. The technique is intended to be used locally in a spirit of minimum intervention and not intended for systematic thoughtless wholesale gridding and is the method being implemented on decorative plaster ceilings and heavy decorative plaster enrichment in both the Buckingham Palace and Windsor Castle where our investigations have identified defects and potential risk of loss.



Figure 06: (Right) Ceiling restraint washers tied back to the timber support structure above via perforated metal band. (Left) Example restraint fixings to plaster ceiling.

7 CONCLUSIONS

We have described in this paper the strategic inspection and assessment of a large number of historic plaster ceilings and their corresponding supporting structure throughout Buckingham Palace and Windsor Castle, each Grade I listed buildings of international significance and importance. Our inspections have implemented the recommendations contained within the latest ABTT guidance and demonstrate the many practical challenges we have encountered when attempting to satisfy these certification requirements. To safely access often restricted, confined, obscured and contaminated spaces located above fragile plasterwork ceilings suspended over rooms in regular use required considerable planning, design and execution. Some of these challenges and limitations are site-specific owing to the special and unique genesis and usage of the buildings, however many are generally and

usefully applicable to a wide range of common building types from all periods. The observed defects and their proposed remedial measures are summarised in Table 01 below:

Table 01: Summary of defects observed and proposed remedial actions

Typical type of defect	Degree of defect	Action
Cracked or distorted plasterwork	Mild	No immediate action; monitor periodically
	Moderate	Inspect corresponding ceiling area above and relevant supporting structure; undertake frequent monitoring or repairs as required.
	Severe	Immediately inspect corresponding ceiling area above and relevant supporting structure; undertake urgent repairs as required.
Waterstained plasterwork	Mild	No immediate action; monitor periodically
	Moderate	Inspect corresponding ceiling area above and relevant supporting structure; undertake further investigations or repairs as required.
	Severe	Inspect corresponding ceiling area above and relevant supporting structure; undertake further investigations or repairs as required.
Distorted or deformed structure	Mild	No immediate action; monitor periodically
	Moderate	Immediately inspect relevant structure at close hand; undertake repairs as required.
	Severe	
Failed structure	Mild	Immediately inspect relevant structure at close hand; undertake repairs as required.
	Moderate	
	Severe	
Fungal or infestation decay of timber structure	Mild	No immediate action; monitor periodically
	Moderate	Inspect relevant structure at close hand; undertake treatment, repairs and monitoring as required.
	Severe	Immediately inspect relevant structure at close hand; undertake treatment, repairs and monitoring as required.
Corrosion of metallic structure	Mild	No immediate action; monitor periodically
	Moderate	Inspect relevant structure at close hand; undertake treatment, repairs and monitoring as required.
	Severe	Immediately inspect relevant structure at close hand; undertake treatment, repairs and monitoring as required.

Acknowledgements. All photographs have been made available for publication by and in collaboration with the Royal Household Property Section. The team thanks the Royal Household for approval to publish this important case study in the hope further discussion and research is conducted into plaster ceiling conservation and best practise approach. Photo acknowledgements: Figure 06 copyright Richard Ireland.

REFERENCES

[1] Bradley, A., Pevsner, N., Schofield, J. (2003). *The Buildings of England: London 6: Westminster.*
[2] Colvin, H.M. (1976). *The History of the King's Works.*
[3] Henry, A. and Stewart, J. (2011). *Mortars, renders and plasters*. Farnham: Ashgate.
[4] Ireland, R. (2014). Decorative lime plaster - conservation and repair. *The journal of the building limes forum*, 21, pp.24-39.

12th International Conference on Structural Analysis of Historical Constructions
SAHC 2020
P. Roca, L. Pelà and C. Molins (Eds.)

THE RESTORATION INTERVENTIONS OF "FORTE MARGHERA" IN VENICE

FILIPPO CASARIN[1], RICCARDO CIANCHETTI[2*], TOMMASO DALLA VIA[2], MARTINA MEGGIATO[2] AND MARCO MOCELLINI[1]

[1] R-Struct srl
Via Vigonovese 31, 35127 – Padova, Italy
e-mail: {casarin, mocellini}@rstruct.com - Web page: http://www.rstruct.com

[2] Insula S.p.A.
Santa Croce, 489 - 30135 Venezia, Italy
e-mail: {Riccardo.Cianchetti, Tommaso.DallaVia, Martina.Meggiato}@insula.it - Web page: http://www.insula.it (*corresponding author)

Keywords: Venice Lagoon, military architecture, fort, Marghera

Abstract. *In the framework of the Strategic Masterplan Cultural Heritage 2014-2018 of the Italian Ministry of Culture, a specific attention for the strengthening and constitution of relevant urban cultural centers is sought through the restoration and re-use of structural complexes of great architectural and historic value such as the case of Forte Marghera (Marghera Fort) of Venice. The need to build a fortress at the point where the mainland approached Venice was understood, after the fall of the "Serenissima" Republic (1797), by the Austrian Empire. The fort was therefore built in a marshy area on the edge of the Venice lagoon, crossed by a maze of canals. The works started in 1805. On the area there was already the old village of Malghera, home to warehouses and customs, which was incorporated into the Fort. However, the return of Napoleon's troops in 1806 surprised the works still in a early stage. The fortified work was then revised according to the plans of the French architect Marescò and conducted under the guidance of the general and military engineer François-Joseph Chaussegros de Léry and later the Chasseloup. The most significant buildings still present in the fortress – object of the current restoration works - are the two French barracks (1805-1814), located on the front near the dock. They are two-storey brickwork masonry structures with a 83x15 m rectangular plan and perimeter walls reaching a 3 m thickness, provided with decorative elements made of Istria stone. Visible decay is present in both two massive buildings, due to differential settlements mainly visible the long sides of both buildings, especially affecting the West one, also partially subjected to local collapse. A wide investigation campaign, aiming to the adequate characterization of the constituting materials and building techniques, was carried out in order to properly feed the design of conservative restoration interventions. Results indicate the use of good quality materials and proper layout also in the foundation system, indicating in the poor soil mechanical characteristics the main structural deficiency leading to the visible settlements. To date, the detailed design stage was reached for just one of the three buildings involved in the restoration, while the two remaining buildings are still in a preliminary design phase.*

1 FOREWORD

Within the Strategic Masterplan "Grandi Progetti Beni Culturali" (*Large Projects Cultural Heritage*) 2017-2018, the MIBACT (Italian Ministry for Cultural Heritage and Tourism) financed the intervention: "*Marghera Fort - museum recovery in the environmental crisis area*" [1]. As the beneficiary of the financing, the Municipality of Venice assigned the development of the project and the site engineering to the in-house company Insula spa [2].

The military fort, acquired from the state by the Municipality of Venice since 2010, houses 78 buildings on a territorial surface of 24 acres, and it is being progressively restored with public funding for cultural purposes and recreational activities (museum / exhibition - Venice Biennale, Civic Museums), and related services. The Municipality of Venice has a strong interest in this location given the central position between Venice and Mestre, between water and land (**Figure 1**, left). The project allocates the overall budget (7M Euro) on the recovery of three buildings: the two 19th century "Austrian" barracks, heritage buildings of considerable historical and monumental interest, facing the marina, besides an early twentieth century ruined building, raised next to the main axis of the *Ridotto Island*, the heart of the Fort, to be possibly reused as exhibition spaces.

2 SITE HISTORY, FORTE MARGHERA

Forte Marghera was conceived and built in different stages from 1797 to 1814. Its construction began in July 1805 on the area of the small village of Marghera, at that time also called Malghera.

Consisting of a church, refreshment venues and storage of goods and served by a bridge, it was the nearest embarkation point to Venice in the communication with the mainland, located between Venice and Mestre. The village and the Marzenego, Osellino and Bottenigo canals (which connected Venice to Liza Fusina) flowed into Marghera between marshes and sandbanks. The conformation of the territory, where the fortress was built was far different from the present one (**Figure 1**, right).



Figure 1: location of Forte Marghera area (left) and historical map of the settlement of "Marghera" (right)

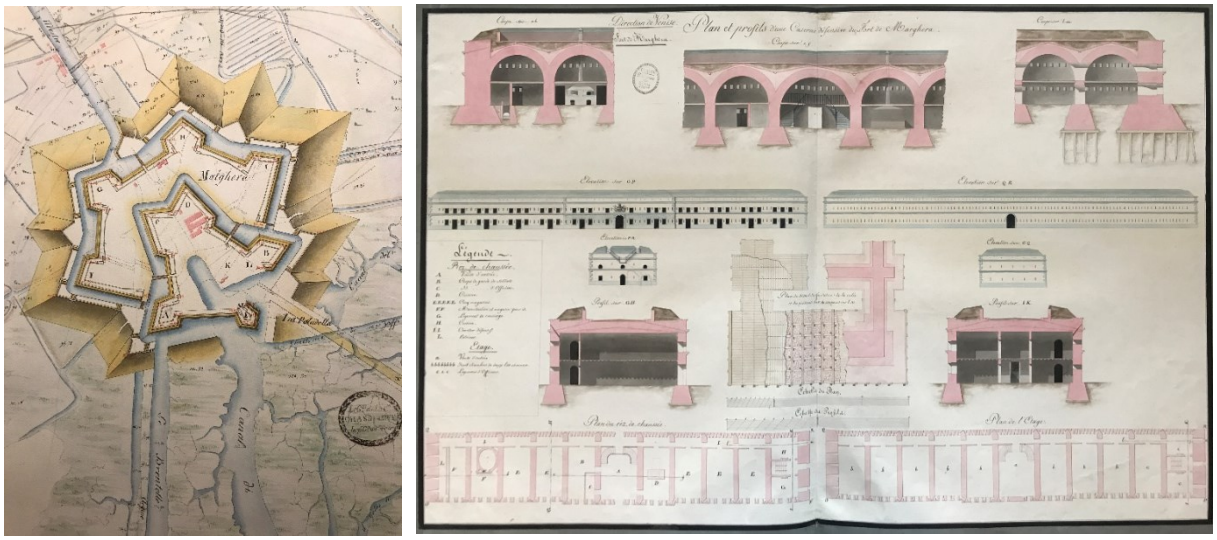


Figure 2: general plan of the Fort (left) and of the French barracks (right)

Following the Salso Canal from the mainland to the lagoon, after the village of Marghera, there was the Anconetta bridge and then the island of San Giuliano. Both in Marghera and San Giuliano there were watchtowers.

The Republic of Venice made the lagoon the main element of defence from its enemies, controlling the most important communication canals linked with the hinterland by blocking them with chains, fences and palisades and a flotilla of armed vessels. Historically, the first line of defence for Venice was on the coast (towers, fortresses), then on the inner islands of the lagoon. Forte Marghera was the first "mainland" garrison to defend the harbour of the city and its very important arsenal was destined to become, in the course of a century, the core of the Campo Trincerato di Mestre (Entrenched Field of Mestre).

The construction of the entrenched field started by the Austrians in the early nineteenth century was completed by the French during the Napoleonic occupation. Its origin dates to the historical period of the fall of the Venetian Republic, when on May 12, 1797, under the force of the Republican armies led by Bonaparte, a pro-French popular government was formed. The French were the first to take a census of the fortifications and to design the Fortress of Marghera above the village. The Austrians, in 1805, began the construction with some requisitions and the construction of some ramparts, and subsequently the French completed it with the construction of the most imposing fortification to defend the city and the consequent disappearance of the ancient village of Marghera.

With the First World War, Forte Marghera, together with the other fortresses of Mestre, was not part of the strategic line of defence, and the weaponry was dismantled and transferred to the front. In recent times, it became an ammunition storage and a weapon repair site, as shown by the buildings used as workshops. Its military function ended on June 30, 1995.

2 STRUCTURAL & GEOTECHNICAL INVESTIGATIONS

A thorough structural investigation campaign was conceived and executed in order to achieve an adequate knowledge level for the design of the interventions for the recovery and restoration of the three historic buildings of Forte Marghera object of intervention (**Figure 3**).



Figure 3: the three buildings object of the intervention: building nr. 8, 9 and 29

These are the two Napoleonic "barracks" located on the lagoon side, called "Building 8" (west) and "Building 9" (east), and a building that has not been covered for years following the collapse of the roof due to deterioration, called "Building 29", located in the center of the islet of the fortress. Tests aimed at the definition of the structural elements' composition (walls and vaults inner arrangement), the geometrical and crack pattern detailed survey (hidden structural portions, foundations) and material characterization (mechanical characteristics). A relevant part of the diagnostic effort was directed to the geotechnical characterization of the soil, being this the obvious suspect of the evident differential settlements pattern resulting in visible structural distortion and masonry walls cracking, especially in the west barrack.

2.1 The investigation campaign

Building nr. 8 has an extensive cracking and deformation pattern, attributable to foundations' differential settlements. From the available documentation, it is noted that buildings 8 and 9 have very large masonry foundations, with the presence of wooden poles to intercept the deeper load-bearing layers (**Figure 4**, left). The study of historical hydrography has however shown that part of building 8 appears to have been partially built over a palaeochannel, subsequently filled with soil for the construction of the fort (**Figure 4**, left). A series of investigations were therefore executed to investigate the nature of the foundation soil in a widespread manner, in order to highlight any difference in the soil capacity or critical issues. A series of electrical piezocone penetration tests CPTu (n. 4 on the North side and n. 4 on the South side of bldg. nr. 8, plus nr. 4 tests along building nr. 9) were performed with depth variable between 15 and 30 meters, together with nr. 5 soil boring at a depth of 20 meters with undisturbed sampling for laboratory tests. Several excavations aimed at highlighting the foundations were also carried out, with execution of sub-vertical surveys aimed at the interception of wooden poles to a depth of 5 meters.

From a structural point of view, different investigation procedures were considered for the two older buildings and the newer one. The two barracks, composed by massive walls and vaults, were subjected to the following structural tests: single and double flat jack tests to obtain information on the local state of stress and the mechanical characteristics of masonry, carried out in the head and inner walls; micro-core drillings with video-endoscopic inspection, for the

evaluation of the internal composition of the walls (head, side and internal walls) and vaults (at the key and at ¼ of the span of two vaults); sonic tests on walls, to identify the compositional characteristics of masonry by measuring the velocity of mechanical waves propagating within the structural elements, especially in the thicker walls; collection of mortar samples for characterization and mineralogical-petrographic study, performed on samples extracted from the core drillings; excavation trenches on the roof, after dismantling the existing cover, to check the exact stratigraphy and state of conservation of the vaults on the extrados; crack pattern survey of the buildings. The more recent building – nr. 29 – already heavily damaged from previous collapse of the roof, was object of the following structural tests: collection of undisturbed samples of single-leaf thick panels for performing nr. 2 diagonal-compression and nr. 2 simple compression tests in the laboratory; micro-core drillings with video-endoscopic inspection, for the evaluation of the internal composition of the pillars; collection of mortar samples for characterization and mineralogical-petrographic study, performed on samples extracted from the core drillings; crack pattern survey of the building.

2.2 Obtained results

The analysis of the crack and deformation pattern of the structures, together with the material decay assessment allowed to identify and map the structural deterioration related to the different pathologies encountered. Besides the identification of the visible cracking of the west barrack, not only in the façade but also in the transverse walls (**Figure 5**), it was indeed possible to appreciate a diffuse material decay (severe degradation of mortars, missing brick units, spalling, pulverization, erosion, rising phenomena and presence of biological attacks), mostly due to the environmental conditions (seaside).

From a mechanical and compositional point of view, the brickwork masonry walls result – notwithstanding the encountered deterioration – sound and properly built, coherently with its military intended robustness.

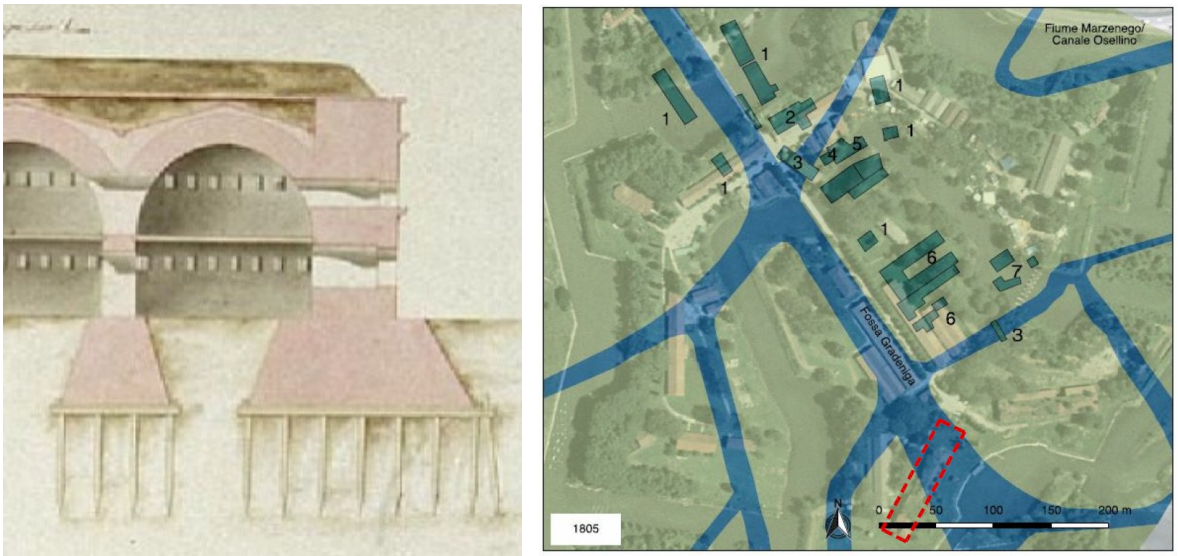


Figure 4: layout of the original French blueprint of the foundation of the head and inner transverse walls (left); map with indication of the palaeochannels in the area of Forte Marghera (right): highlighted in red building nr. 8



Figure 5: crack pattern in building nr. 8: it is highly visible a well-defined differential settlements trend

The inspection of the inner sections of both walls and vaults indicated a properly arranged core, without any loose infill, even for the thicker walls (2,80 m).

Stiffness values emerged from the flat jack tests carried out are compared with those reported in the Italian Standards for the type of masonry observed (brickwork masonry with lime-based mortar). According to Italian Standards [3], the Elastic modulus E is in the range 1.200 – 1.800 N/mm^2 (with reference strength between 2,6 and 4,3 N/mm^2). The comparison with the obtained results shows that the moduli of elasticity obtained onsite match the standard figures. The compressive tests carried out on the wallets extracted from the single-leaf perimeter walls of building nr. 29, being a XX c. building, shown a higher stiffness (and resistance) masonry, equal on average to 7.370 and 5,40 N/mm^2 respectively (**Table 1**).

The sampled mortars composition reflects indeed the constructive periods of the three buildings. Cementitious binder was only found in the sampled material from building 29, dating XX c. the two older buildings, nr. 8 and 9, present mortars using non-hydraulic lime as binder.

Sonic tests carried out widely on the two older buildings (a total of 6+6=12 tests) indicated good to very good values for the sonic velocity through the masonry walls, with relatively homogeneous figures (avg. max/min equal to 1.852 / 2.820 m/s). Higher values were found in building nr. 9 (overall average value of 2.440 m/s) than in building nr. 8, (2.150 m/s), possibly also for the different state of conservation of the two buildings.

The investigations on the foundations and on the soil allowed to confirm the layout as represented in the historical blueprints, with some minor differences (e.g. the foundation width for the massive perimeter walls).

Informative results emerged both from the CPTu and the borehole tests. These last depicted a typical soil stratigraphy of the lagoon of Venice, composed by superficial layers of clayey silt to a depth of -3,00 m, then an alternance of soft layers of silt clay and sand (and a mix between the three) down to a depth of approx. -9,00 m, then the so called “caranto” layer (over

consolidated silty clay) with a thickness of 2 – 2,50 m. below this depth and down to the end of the perforation (-20 m), alternance of sandy silt and again more or less compact silty clay.

The penetrometric tests explained the differential settlements trend encountered in building nr. 9, given the visible change in the soil resistance between -2,0 ÷ -4,0 m, where the foundations / poles find support, between tests nr. 1, 2, 8 (denoting a certain capacity) and 3 to 7, remarkably weaker, approximately located in correspondence of the filled channel.

Table 1: mechanical tests on masonry, on site (flat jack tests) and in laboratory (compressive tests).

Test ID	location	Local stress [N/mm^2]	"Elastic" limit stress [N/mm^2]	Max stress [N/mm^2]	E [N/mm^2]
DFJ 1/8	Head wall, bldg. 8	0,19	3,28	4,22	1.941
DFJ 2/8	Internal wall, blgd. 8	0,64	3,75	4,22	1.408
DFJ 1/9	Head wall, bldg. 9	0,44	2,78	3,25	1.424
DFJ 2/9	Internal wall, blgd. 9	0,41	1,85	3,42	1.072
PM2	Perimeter wall bldg 29	--	--	5,56 [strength]	8.797
PM4	Perimeter wall bldg 29	--	--	5,25 [strength]	5.952

3 STRUCTURAL MODELING – SAFETY CONDITIONS

The two French barracks nr. 8 and 9 have a rectangular plan, 85x15 m in size, and are made by transversal thick walls (about 110 cm thickness the internal walls, more than 280 cm the head walls), which support the barrel vaults (**Figure 6**). The longitudinal facades, also in brick masonry about 110 cm thick, are simply juxtaposed to the vaults, and not clamped to the transverse walls, as highlighted by some cracks visible on site. Walls and vaults are all made in solid bricks masonry, with lime mortar joints.

The buildings are 7 m tall, and originally, they had a roof terrace with perimetral ramparts; nowadays there is a pitched roof made with wooden beams and rooftiles, and the space between the original pavement and the roof is filled with soil.

Building 8 differs from Building 9 for the absence of the central staircase, which is positioned on the East side, where there are intermediate floors that divide the first two vaulted rooms. Barrack 8 presents also a lower part in the north-west corner, due to the collapse of a portion of the barrel vault, currently covered with a wooden roof.

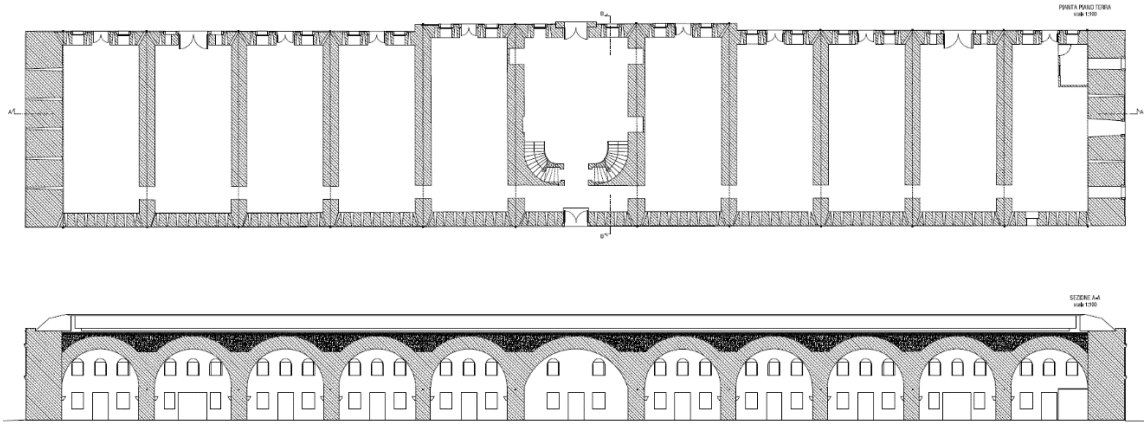


Figure 6: building nr. 9 – plan and cross section

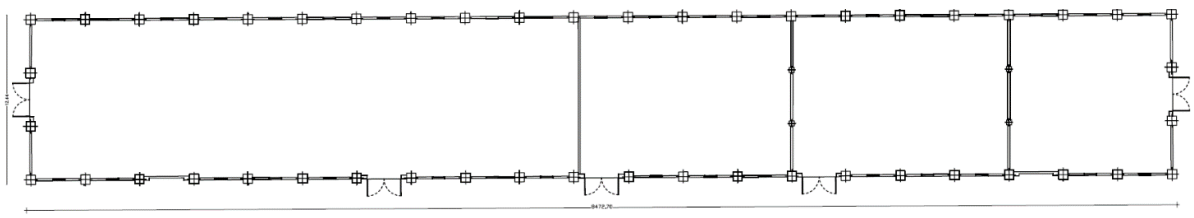


Figure 7: building nr. 29, plan view

The current situation of both buildings highlights a significant state of decay; the external facades are damaged by the growth of vegetation, especially on the top cornices, where some stone pieces are fallen. Vertical walls present cracks in correspondences of the chimneys and diagonal cracks near the entrance portals. There are also systematic cracks between the vaults and the facade walls, due to the absence of connections between facades and transversal walls. Furthermore, the building nr. 8 presents several and evident deformations, with wide cracks on facades and inner walls, remarkably in the central portion which appears lowered than the north-west corner, as described earlier.

The depot building nr. 29, built in the early twentieth century, has completely different structural characteristics (**Figure 7**). This building is made by squared masonry pillars (0.65x0.65m) spaced 4 meters, with bricks masonry single-leaf spandrel walls. It has an elongated rectangular shape, 12.5x85 m, one storey, with pillars high 3,30 m; the roof, currently collapsed, was a wooden pitched roof, with wooden trusses supported by masonry pillars.

3.1 The modelling strategy

Considering the different constructive typologies of the three buildings, different analysis approaches have been chosen.

The two French barracks have been studied using a finite element model, which has been created to define the stress distribution on vertical walls and on foundation soil. The model of each building was processed by the commercial software MIDAS and it is composed by 351’417 tetrahedral 3D elements. The typical size of the tetrahedral 3D element is 0,5m.

Dynamic linear analysis has been used to simulate the seismic behaviour of the massive buildings, considering different level of connection between longitudinal and transversal walls: the two barracks are indeed built with the facades simply juxtaposed to the transversal walls and to the vaults, as often encountered in Venetian historical buildings. Therefore, the facades have been modelled separated from inner walls and vaults, connected to them only by unidirectional (horizontal) springs. This detail also allowed an accurate study of the stresses on foundation soil, avoiding stress distribution on walls that are not directly loaded by the vaults.

The interaction between soil and foundations has been analysed using elastic Winkler springs, calculated according to the geotechnical investigation results. Differences on soil characteristics have been considered using different stiffness value on the springs. Limit analysis was finally used to evaluate the seismic behaviour of vertical walls, in order to check their vulnerability to out-of-plane collapse, including the high horizontal thrust of vaults.

The depot building (nr. 29) was instead analysed with a non-linear equivalent frame model, performing a static non-linear (pushover) analysis and considering the seismic contribution of the longitudinal single-leaf walls between the masonry pillars. Such walls were eventually

reinforced by design in order to consider them as effective bracing elements. The horizontal rigid plane -necessary to distribute the seismic actions to the resistant walls- is ensured by the new steel structures of the roof, with an out-of-context architectural hint. Limit analysis has been used also in this case in order to check the out-of-plane collapse of the vertical walls and to calculate the retaining force which has been applied to the roof structures.

3.2 Obtained results

The global FE models of the barrack buildings (nr. 8 and 9) have been used to perform both static and seismic (dynamic) analysis (**Figure 8**).

The self-weight analysis – carried out according the current Italian Construction Standard NTC2018 – has confirmed the soundness of the vertical structures, built to resist to cannon attacks. The great thickness of vaults and of vertical walls can distribute easily the heavy loads from the roof, made with large layers of soil and with perimetral ramparts.

Results obtained in terms of σ_{ZZ} stress (compression) indicate that the average value of compressive stress at the ground level corresponds to approximately 0,4-0,5 N/mm^2 (**Figure 9**). Average compression stress on vaults is lower than 0,2-0,45 N/mm^2.The seismic behaviour of the building is characterized by the large thickness of masonry walls, which can easily absorb the seismic actions. The main vulnerability is due to the construction method of the facades, which are juxtaposed to the transversal walls and to the barrel vaults and may be subject to hammering effects. Out-of-plane vulnerability is connected only to non-structural elements, such as chimneys or stone cornices. Regarding the interaction between soil and foundation, considering only gravity loads, the inner walls, which are loaded by the vaults, present an average stress about 0,25 N/mm^2, instead in the longitudinal facades, which are loaded only by their self-weight, the calculated stress at the ground level is about 0,18 N/mm^2. This difference in soil stresses, due to the constructive discontinuity between facades and inner walls that do not allow any stress distribution, may have caused differential settlements, which may partially explain the actual crack pattern.

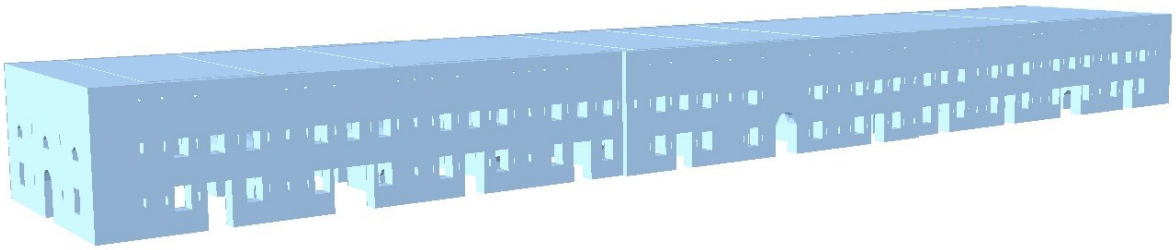


Figure 8: 3D FE model of the barrack buildings

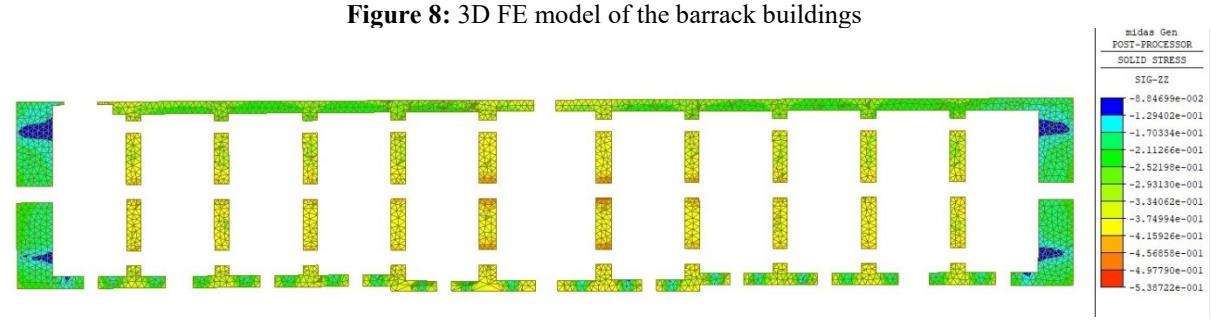


Figure 9: compression stress on masonry walls at the ground level

The depot building (nr. 29) has very different structural characteristics: low thickness walls, one principal resistance direction, collapsed roof. The seismic analysis highlighted a good longitudinal behavior, thanks to very long and regular walls, but a high vulnerability in transversal direction. The limit analysis approach, implemented to define the stability of the masonry panels under the seismic actions, indicated a general unsafe situation, mainly for the very low thickness of the walls that are not retained by the roof structures.

4 THE REHABILITATION AND STRENGTHENING INTERVENTIONS

In agreement with the concerned entities (Municipality of Venice, Ministry of Cultural Heritage central and local offices) and in consideration of the financial resources, the objectives and priorities of the interventions to be performed have been defined:

- Full and functional restoration of the east barrack (nr. 9), for expositions and services;
- Structural strengthening of the west barrack (nr. 8);
- Full and functional restoration of the Depot Building (nr. 29), for expositions use.

Considering the great cultural value of all the buildings, all interventions have been oriented to the maximum conservation of the original characteristics, especially for the two barracks.

The east barrack (nr. 9) intervention will consist in the structural strengthening of the vertical and horizontal elements with seismic upgrading and the realization of new systems (HVAC, electrical, hydraulic). Masonry restoration techniques will be also carried out to achieve a consolidation of the materials in compliance with the historical conservation criteria. The original configuration of the roof will be sought, restoring the roof terrace with perimetral ramparts. The terrace will be accessible by external staircase and lift, in a new steel-made volume separated from the original building. From the structural point-of-view, minimum intervention criteria have been followed; masonry walls and vaults will be restored by traditional interventions, such as structural repointing and cracks sewing by grouting, using natural hydraulic lime mortar. Considered the satisfactory seismic behaviour of the building, the seismic retrofitting will be obtained solving the main vulnerability emerged from the structural analysis, that is the disconnection between façades and inner walls. New stainless steel tie-rods will be inserted in order to connect horizontally the façades, avoiding overturning and hammering effects in case of earthquake; these tie-rods will anyway allow for any vertical displacement between facades and transversal walls, in order to maintain the current static behaviour.

For the west barrack (nr. 8), considered the wide crack pattern and the marked trend of differential settlements, it is planned a strengthening intervention at the foundations level, in order to restore the safety conditions without considering the successive architectural restoration as for building nr. 9. Intervention will consist either on the improvement of the soil mechanic characteristics (e.g. jet grouting) or the insertion of a series of micropiles through the existing masonry foundations in order to connect them to the deeper and stiffer soil layer (over consolidated silty clay) named “caranto”. At the present time, the design outcome is still open: structural and geotechnical modeling will drive the intervention type.

For the depot building (nr. 29), the complete collapse of the roof allowed to propose a new steel roof structure which contribute to the seismic retrofitting of the building at the same time leaving the internal space completely free and unitary so as to promote flexibility of use for temporary exhibitions. The steel structure is made by welded IPE profiles creating a global

reticular beam, acting in its plane as bracing system for the roof and for the masonry walls. Ten new steel columns act as static support for the roof structures and as seismic-resistant elements: the triangular shape columns are connected to the roof profiles by inclined branches, forming seismic portals, fixed at their basis, which can absorb both horizontal and seismic actions.

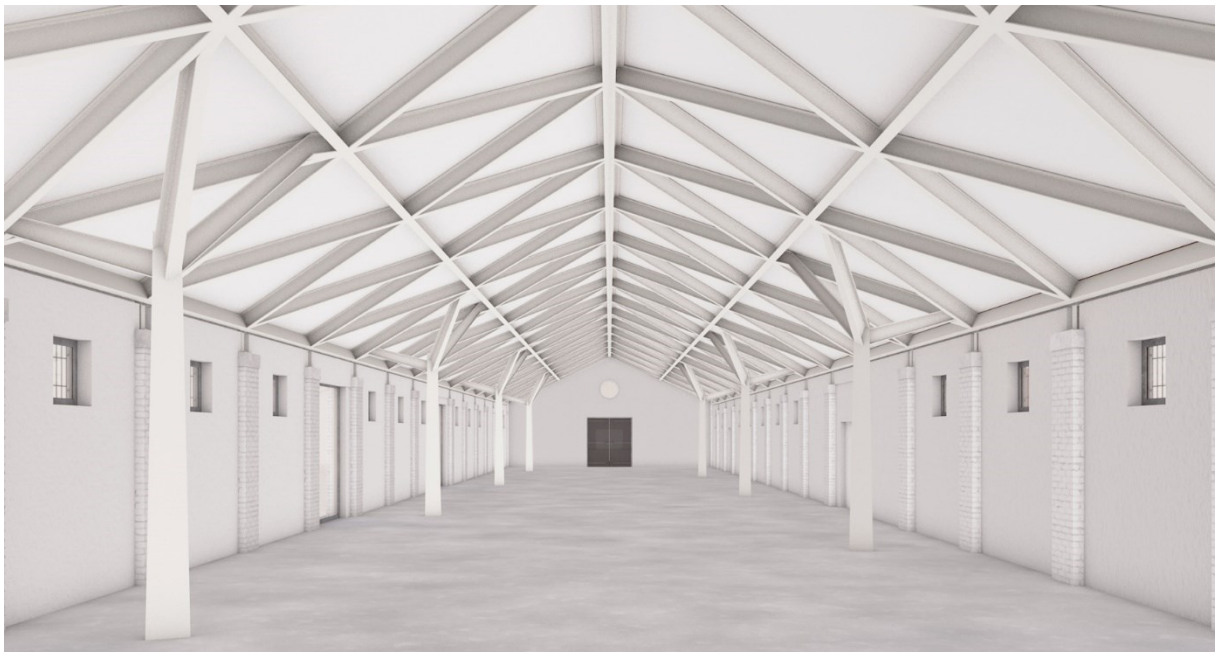


Figure 10: rendered view of the new steel roof structure

As for the original wooden roof, the structural function of the existing masonry pillars is maintained, using them as vertical support for the steel roof; the connection system is studied in order to transfer only vertical actions, avoiding horizontal thrust on masonry, using the original holes of the wooden trusses to center the roof load.

Roof steel elements collaborate with existing masonry walls for the seismic resistance, both in the transverse direction, through the façade walls which are enlarged and connected to the roofing structures, and in the longitudinal direction where the panels between pillars will be reinforced and will become bracing elements. These panels are therefore reinforced by:

- Connections to masonry pillars by the insertion of stainless steel rebars, completely hidden inside the mortar joints;
- Reconstruction of the upper part of the walls, currently collapsed, with reinforced masonry (steel rebars inserted inside the mortar joints);
- Application of steel reinforced strips (FRCM) on the internal side of the panels, using lime mortar, in order to confer tensile resistance to the masonry.

4.1 Future actions

The final design is currently completed for the Building nr. 29 and the approval by Superintendence and Firefighters is pending. For barracks nr. 8 and 9, considering the historical value of the buildings and the interactions between structural requirements and cultural protection needs, a more demanding design phase in terms of restoration is still on-going.

5 CONCLUSIONS

- A very iconic former military area is progressively being reconverted with success to cultural and leisure use at the doors of Venice and its lagoon;
- In this process, in the framework of the Strategic Masterplan Cultural Heritage 2014-2018 of the Italian Ministry of Culture, relevant funding was given for the structural and architectural restoration of two massive historical CH buildings corresponding to Austrian barracks, and a partially collapsed more recent Italian depot building;
- A relevant study was carried out to define the structural safety level of the three buildings, based on thorough structural and geotechnical investigation, in order to design the requested strengthening interventions;
- Structural tests carried out described buildings lacking maintenance with the related problems, however properly built, whit compositional and mechanical good characteristics;
- Geotechnical tests were able to characterize the soil main parameters, stratigraphy and mechanical capacity, also explaining the visible differential settlements of the west barrack, most likely due to unsatisfactory soil compaction in the works of channel filling;
- Interventions were and still are being defined following two different approaches: substantially conservative (with seismic and structural upgrading) for the two seaside barracks, more relevant from a cultural heritage point of view, and introducing a new architectural sign (roof substituting the original one, completely lost) for the more recent Italian depot building.

Acknowledgements. The project of restoration of Forte Marghera is financed through public national funding (Ministry of Cultural Heritage and Tourism - MIBACT) – REF. *Ministerial Decree 556 - 02/12/2016*, with a total amount of 7M€

REFERENCES

[1] *Ministerial Decree 556 - 02/12/2016, Decree of the Ministry of Culture* (MIBACT) approving the "Strategic Masterplan Cultural Heritage", year 2017-2018, funding the intervention "Forte Marghera, museal restoration in the environmental crisis area" (in Italian);

[2] *Agreement for the execution of the intervention signed by the General Secretary* (MIBAC local economic seat) and the Venice Municipality dated 06/02/2016 (in Italian);

[3] Italian Technical Standards for Constructions, Ministerial Decree 17 jan 2018 and related explicative circular (Infrastructure & Transportation Ministry) 21 jan 2019, n. 7

[4] Mocellini M. and Casarin F. (R-Struct, 2018) – *preliminary design of the strengthening and reconstruction intervention of pavilions 8, 9 and 28 of Forte Marghera, Venice, IT* – unpublished, in Italian

12th International Conference on Structural Analysis of Historical Constructions
SAHC 2020
P. Roca, L. Pelà and C. Molins (Eds.)

THE RESTORATION OF THE MEDIEVAL WALLS OF SAN GINESIO: A DEDICATED STUDY FOR THE CONSERVATION, REPAIR AND ENHANCEMENT OF AN IMPORTANT MILITARY FORTIFICATION

M. SARACCO[1*], F. MARIANO[2], A. A. GIULIANO[2], L. PETETTA[2] AND F. PICCININI[2]

[1]Dipartimento di Scienze della Formazione, dei beni culturali e del turismo (Sfbct)
Università di Macerata (UniMC)
P.le Luigi Bertelli, 1 - C.da Vallebona 62100 Macerata
e-mail: mauro.saracco@unimc.it (*corresponding author)

[2] Dipartimento di Ingegneria Civile, Edile e Architettura (DICEA)
Università Politecnica delle Marche (Univpm)
Via Brecce Bianche, 60131 Ancona, Italy
email: {f.mariano, f.piccinini}@univpm.it, {giuliano.andrea, leonardo.petetta}@gmail.com

Keywords: military fortification, analysis, knowledge, conservation

Abstract. *The seismic events that occurred in central Italy in 2016 severely damaged the rich cultural heritage system present in the area hit by the earthquake. Particularly significant is the situation of the Marche Region, here it is necessary to intervene quickly and effectively in order to preserve and secure the damaged historical architectural heritage. Following the agreement signed in 2019 between the administration of the Municipality of San Ginesio and the Marche Polytechnic University, a collaboration has been established, which is the basis of the present research work, aimed at studying and deepening the possible actions to be undertaken to be able to repair, preserve and enhance the medieval walls of the city. The city walls, dating from the fourteenth century A.D., almost completely surround the historic center of the city and are characterized by the presence of a large part of the ancient fortifications such as towers, access doors, defensive walkways, loopholes, etc. Since there is no complete survey of the planimetric configuration and of the elevations of the medieval walls, updated to the situation created after the earthquake, the first phase of the research focused on data acquisition. Combining DJI Spark MMA1 photogrammetric UAV images with cloud point by Mobile laser SLAM Kaarta Stencil, the 3D-dimensional modelling of the walls was obtained with the accuracy related to the output scale of 1:200 and with a detail and complexity useful for the following conservative analysis. Once the data was acquired and processed, it was possible to carry out a complete analysis of the walls structure, identifying the materials and construction techniques, the state of preservation of the materials, the damage situation to the structures, the various construction phases with the consequent relative dating. The analytical phase was concluded, therefore, with the identification and cataloging of the types of walls present. Each of these has been characterized both from a typological and a technical-construction point of view, defining the wall quality (IQM) and the consequent mechanical parameters through the calculation process of the Wall Quality Index.*

1 INTRODUCTION

The seismic events that occurred in central Italy in 2016 severely damaged the rich cultural heritage system present in the area hit by the earthquake. Particularly significant is the situation of the Marche Region, here it is necessary to intervene quickly and effectively in order to preserve and secure the damaged historical architectural heritage.

Following the agreement signed in 2019 between the administration of the Municipality of San Ginesio and the Marche Polytechnic University, a collaboration has been established, which is the basis of the present research work, aimed at studying and deepening the possible actions to be undertaken to be able to repair, preserve and enhance the medieval walls of the city. Specifically, the research program was divided into:

- first phase: acquisition through appropriate geomatical instrumentation of the data necessary for geolocation and three-dimensional reconstruction of the objects under investigation;
- second phase: documentary research for the reconstruction of the historical / construction evolution of the objects being studied and for the identification of the restoration interventions carried out over time;
- third phase: analysis and architectural graphing of the city walls and fortifications being studied by the creation of appropriate technical drawings; study and representation of the state of the materials degradation of surfaces and crack patterns by drafting dedicated thematic maps; definition of the wall quality and the related mechanical parameters of the historical walls through the process of calculating the Wall Quality Index (IQM).

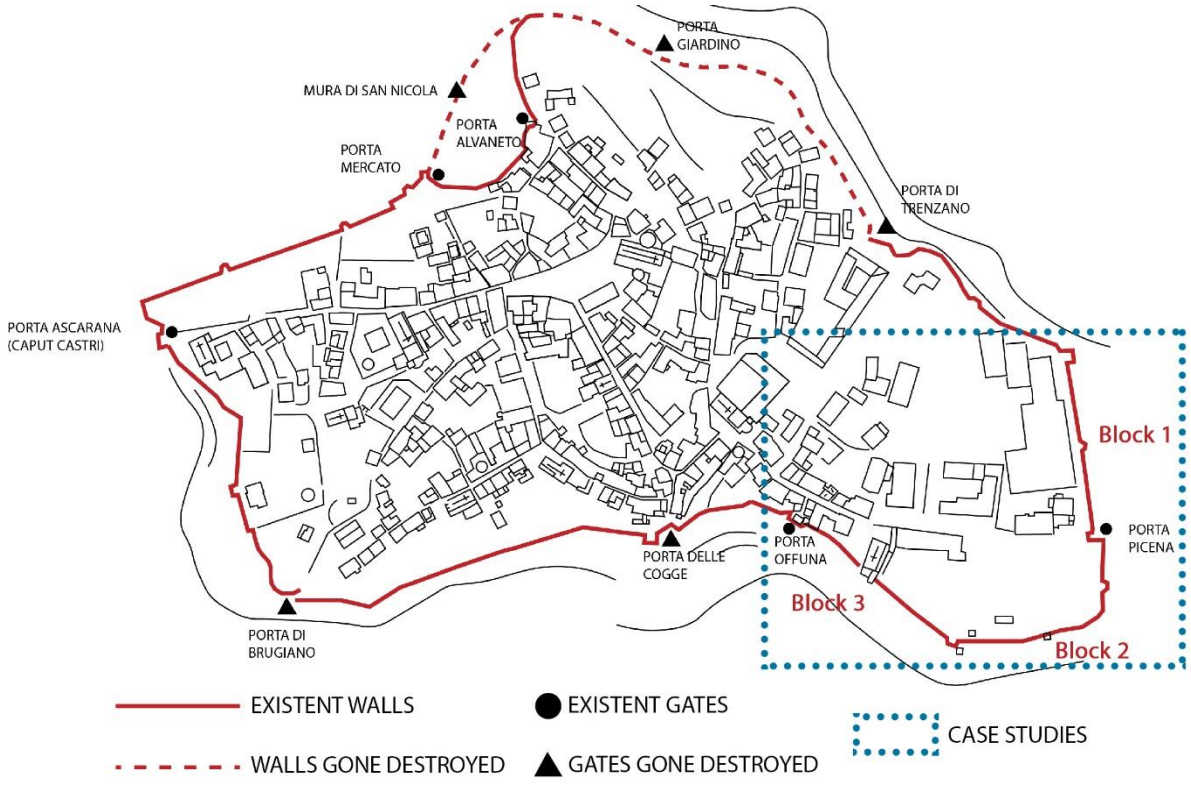


Figure 1: Planimetric diagram of the city walls with identification of case studies

Given the significant planimetric development of the city walls (about 4.5 km in length) and given the presence of vegetation that completely obliterates some portions of the walls, it was decided to operate at first, also in order to validate the methodology described above, on three case studies portions, significant in size and type of the walls themselves. The three case studies, contiguous with each other, are constituted by: "Block 1" that extends from the first tower of the portion of walls placed at the east of the town up to Porta Picena; "Block 2" which continues from Porta Picena to the corner tower of the walls placed in the South; "Block 3" which extends from the latter tower to the Porta Offuna (Fig. 1).

The working group, led by the scientific managers of the research who are Prof. Fabio Mariano and Prof. Eva Savina Malinverni (Univpm), is composed of: Prof. Mauro Saracco (UniMC), Leonardo Petetta and Andrea A. Giuliano (PhD, Univpm), Chiara Mariotti (researcher, Univpm), Stefano Chiappini, Fabio Piccinini, Francesco Di Stefano (PhD Students, Univpm) and by students of the "Architectural Restoration" course (Degree course "Ingegneria Edile-Architettura", Univpm)

2 THE MEDIEVAL WALLS OF SAN GINESIO

2.1 Historical background

The urban layout of San Ginesio is typical of a fortified medieval town whose economy has always been based mainly on trade. The residential buildings, in fact, mainly consist of terraced houses, often with shops in ground floor, that overlooking on the main streets that connect the square to the various city gates. Added to this is the location of San Ginesio along an ancient and important religious pilgrimage route (towards La Santa Casa di Loreto) which led to the construction of numerous religious buildings (churches, convents, monasteries, etc.) and hospitals in the town. The city walls, officially dated from the 14th century AD. [1], almost completely surround the historic center of the city and they are characterized by irregular shapes that are the adaptation to the rough orography of the land. Still today, along the route of the walls, there is the presence of a large part of the ancient fortifications such as towers, access gates, walkways, loopholes, etc. Of particular interest are the shapes and volumes of all surviving access gates (both the original ones and those destroyed and rebuilt in the nineteenth century) that date back to the interventions of the second half of the fourteenth century. The walls, whose official construction date dates back to 1308 as reported by the documents of the Public Council, seem to exist in reality from much earlier, as it emerges from numerous deeds of sale and parchments found that the city was already largely fortified at early 1300. It is supposed, in fact, that the interventions of 1308 did not concern the construction from scratch of the city walls but rather the completion of the missing parts and the restoration of the degraded and / or collapsed portions of the same. Always in the 14th century, a large urban expansion project was also drawn up for the city of San Ginesio, which was to consider the walls too, but due to the wars with the municipality of Fermo and the plague epidemic that hit the city, it was never realized. Throughout the fifteenth century, however, attempts were made to continue at least the project of the walls, so much so that in 1414 the Public Council of the city decided that each new Podestà would have to donate part of his salary proper for the construction of the city walls and even the Papal State, although showing the intention not to invest funds in this part of its territory, authorized the works for the walls and granted tax reliefs

for this purpose. From the eighteenth century there is no more evidence of restoration or maintenance work carried out on the city walls. Over time these deteriorated so much that at the end of the 19th century there was no longer trace of the Porta di Brugiano [2]. We will have to wait until the unification of Italy to see again interest in bringing to light the majesty of this important fortified work. In fact, in the 19th century, operations of complete reconstruction were carried out on entire portions of the walls, such as, for example, for the stretch that goes from Porta Ascarana to Porta Alvaneto [3].

2.2 The restoration work carried out

A documentary research was carried out aimed at the classification and knowledge of the restoration interventions that have occurred over time on the city walls. This operation allowed a correct reading of the state of affairs of the city walls and its fortifications and was indispensable for identifying correctly and effectively the new conservation and restoration interventions to be put in place. Documents regarding the proposals for intervention, the metric calculations and the technical drawings found in the archives of the Soprintendenza Archivistica e Bibliografica dell'Umbria e delle Marche were analyzed. Below The main interventions carried out over time are listed briefly and in chronological order.

1887 - Restoration of Porta Picena and Porta Offuna. The ruins of the Porta Picena's pre-gate were razed to the ground and the crenellated (in Guelph style) crown of Porta Offuna was rebuilt;

1977/1979 - Repair of damage caused by the earthquake to the castle walls through the interventions of: excavation for the realization of sub-foundation carried out by hand; at the points of collapse or landslide, recovery of the masonry with recycled sandstone ashlars and hydraulic lime mortar; grouting of masonry joints with hydraulic mortar; restoration of the balustrade; demolition of masonry incongruous with the original;

1981 - Following the seismic events of 1979, the load-bearing structures of the Porta Picena, especially in the top and roof parts, had lesions in the walls above the openings, in the corner ones and in the internal cover. A similar situation was present in the adjacent walls with detachments in the top part. The repairs works involved: execution of perforations carried out on all walls and positioning of special steel bars blocked with fluid grouts; execution of niches for housing anchoring steel plates inserted inside the masonry such as not to be visible from the outside; repair of all lesions by recessed grouting performed with mortars similar to the existing ones.

1983 - In addition to the interventions of 1981, a technical report was drawn up with which requests were made to increase the resistance of the walls to both vertical and horizontal forces (with the execution of injections of cement-based binders and sewing irons placed every 3 m^2 of wall) and to anchor the corners of the tower in order to reach the necessary resistance to the moments created by the horizontal forces. All this because the masonry was generally in a poor state of conservation with mortars degraded to 80% (if not absent in some sections) and with ramified cracks over the entire surface.

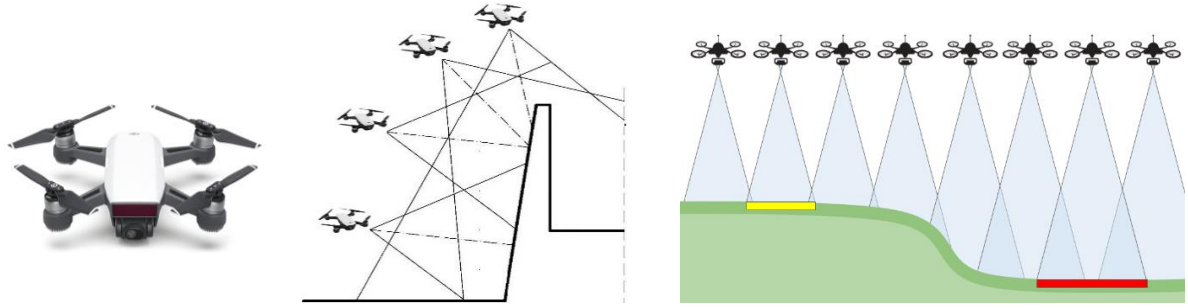
1984 - Reinforcement operations were carried out in the polygonal tower and in the surrounding wall sections by means of perforations of fluid grout reinforced with ribbed steel bars.

1988 - In the portion of the wall that goes from the polygonal tower until it almost reaches Porta Brugiano, restoration and consolidation works were carried out on the structures in relation to

the severe deterioration they were experiencing due to the 1979 earthquake. In particular, the Porta Offuna and the church tower were treated specifically through: removal of the internal covering of Porta Offuna; removal of detrital material on the hospital tower; application of a tarred reinforced sheath; formation of an internal roof covering in Porta Offuna with ancient tiles of which 50% are recovered; formation of waterproof surface grouting with specific mortars; new floorings made by with ancient terracotta tiles in the towers; restoration of water collection and drainage terminals with terracotta pipes; grouting the joints of the existing masonry with hydraulic mortar.
1997 - General consolidation works were carried out following the earthquake of the same year.
2003 - Cleaning and consolidation works were carried out on Porta Offuna, Porta Alvaneto and on some sections of the walls. These works consisted in: hydro-washing of the entire exposed internal and external walls; plastering of the exposed internal and external masonry walls; recovery of the damaged masonry.
2005 - Consolidation works were carried out following the collapse of an entire portion of the walls between Porta Picena and Porta Offuna.
2018 - Following the 2016 seismic events, on Porta Picena and on the portions of neighboring walls, pending the implementation of the definitive repairs, temporary safety measures were carried out. On the top of the walls, the stones not tied to the masonry at risk of collapse were dismantled, with the aim of guarding them and repositioning them with the restoration works. In addition, a containment net fixed to the masonry with mechanical anchors was placed on these points to reduce the risk of falling of the unremoved stone segments. Two towers were, however, surrounded on four sides with harmonic steel strands housed on a frame of vertical wooden beams adjacent to the masonry and with the addition of a wooden paneling to contain the most critical points.

3 FIRST PHASE: DATA ACQUISITION

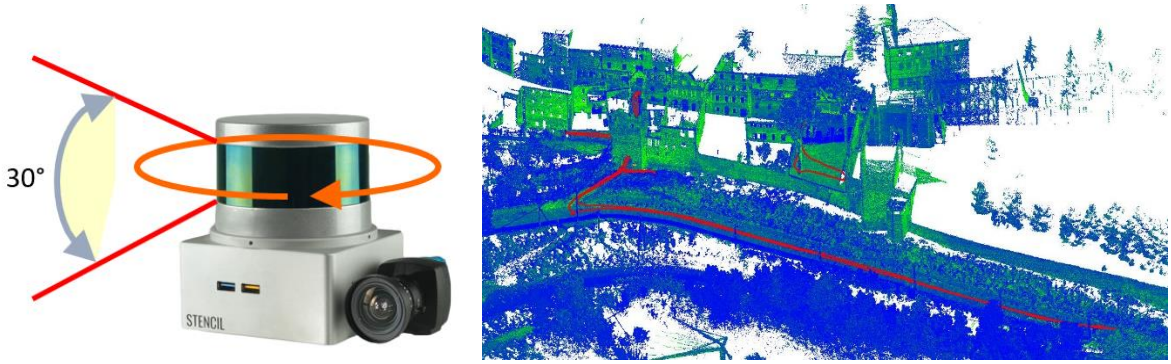
Since there is no complete survey of the planimetric configuration and of the elevations of the medieval walls, updated to the situation created after the recent earthquake, the first phase of the research focused on data acquisition aimed at obtaining a three-dimensional modelling of the walls. In order to create a complete texturized 3D model of the walls, we decided to combine different techniques of acquisition. They include the aerial photogrammetry with UAV (Unmanned Aerial Vehicle) and the mobile laser scanner with a SLAM (Simultaneous Localization and Mapping) technology. This phase began with the definition of a reference system through a topographic survey, useful for the combination of the acquired images and the point clouds in the next data processing step. The photogrammetric survey of the walls was performed using a DJI Spark MMA1 drone and its integrated camera (Fig. 2a) [4]. For each section of the walls different flights were planned. Photos has been shot with the camera at different grades: nadir direction, 30° and 45° from the horizon, and frontal, covering a global field of view of approximatively 180° and guaranteeing a high number of tie points (Fig. 2b). The survey was carried out maintaining the UAV camera at a constant distance of about 30 m from the wall, evaluating carefully both the flight time and the overlapping of the shots (Fig. 2c) required to cover all the wall surface, obtaining an average Ground Sample Distance (GSD) of 4 cm.



a) b) c)

Figure 2: a) DJI Spark MMA1 drone; b) UAV survey positions related to the vertical section of the walls; c) the method of photo overlapping

A survey campaign with the mobile laser scanner KAARTA Stencil 2 [5] was also planned to obtain 3D point clouds of the walls [6]. KAARTA Stencil 2 (Fig. 3a) is a light weight SLAM instrument, with an integrated system of mapping and real-time position estimation: it depends on LiDAR (Light Detection and Ranging) and IMU (Inertial Measurement Unit). The system uses Velodyne VLP-16 that consists on a band of 16 scan lines, with a 360° field of view and a 30° azimuthal opening. A tracker camera is integrated into the device to estimate the trajectory carried out during the acquisition operations. To realize this type of survey characterized by long close-loop paths, the laser scanner was mounted on a small pole held by hand. The progress of the scanning can be monitored in real time via an external monitor attached with a HDMI cable.



a) b)

Figure 3: a) KAARTA Stencil 2; b) the 3D point cloud and the estimated trajectory (red line) made by the mobile laser scanner (right)

The processing phase of the acquired data was conducted in laboratory using specific software. For the image processing, an Agisoft product [7] was used, justified by its good performance on image alignment from different points of view. During the image orientation step, the photos were set in the topographic network using control points for the bundle adjustment and so minimizing the orientation errors. After the images alignment, the resulting dense cloud was obtained through Structure from Motion (SfM) workflow, which allowed the creation of mesh surfaces and textured model. In case of 3D point cloud acquired by mobile laser scanner, the device have automatically processed data during the acquisition phase. Following, CloudCompare [8] is the software for the point cloud analysis that allows the post processing

of the 3D data: registration and alignment of point cloud, manual or automatic cleaning, adoption of some filters to resample the point cloud that becomes lighter and clearly visible. KAARTA Stencil 2 has a strong potentiality to generate a higher number of points composing the 3D point clouds, but does not produce any visible colour information of the 3D points and so the UAV survey is able to compensate for this lack. It is clear that these technologies may be complementary to each other in creating complete high-quality 3D representations (Fig. 4). It is finally important to remark that the 3D model of the walls was realized with the accuracy related to the output scale of 1:200 and with a detail and complexity useful for the analysis and restoration activities.

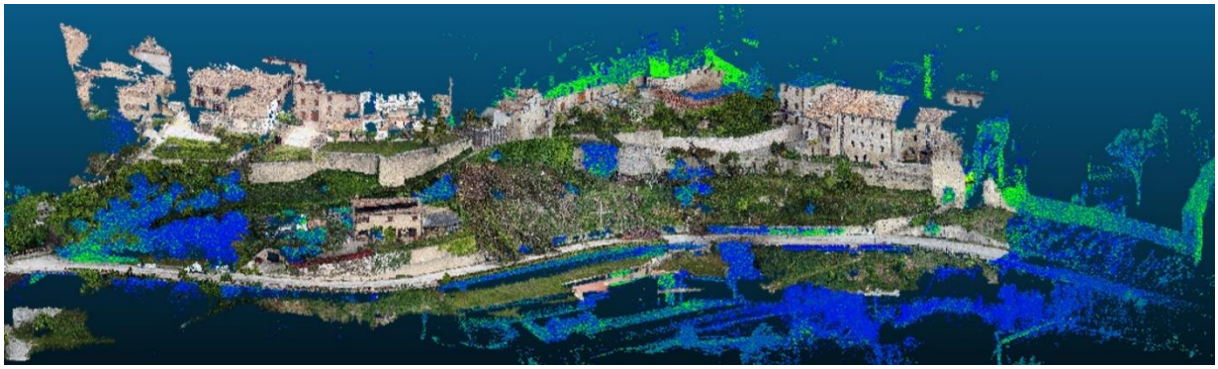


Figure 4: The combination of 3D point clouds obtained by the SLAM and the UAV devices

4 ANALYSIS AND STUDIES

The analysis and studies carried out on walls structure surveyed, have had the objective to identify the types of masonry in work, and then define their characteristics, from a structural point of view, using the method of calculating the Masonry Quality Index (IQM) [9]. On base of this calculation, it was possible to identify and delimit homogeneous portions of walls, which have uniform masonry quality indices and therefore presumed homogeneous structural behaviors. These delimitations allowed to attribute, to the different types of masonry identified, the main mechanical parameters, through the correlations identified by Borri and De Maria [11] between IQM and the classification of the masonry types, defined by the Instructions to the Italian Technical Code (Reference values of the mechanical parameters of the masonry: NTC 2008, tab. C8A.2 - NTC 2018, tab. C8.5.I). The results obtained, will allow to limit the number of invasive tests (double flat jacks) for the instrumental determination of the mechanical parameters, being able to relate the values thus recorded, with those derived from the analysis of the IQM.

4.1 Identification and classification of materials and construction techniques

Once the geometrical survey data was acquired and processed, it was possible to carry out a complete analysis of the walls structure. The first phase of analysis has been focused on the recognition and classification of the types of masonry present; this identification began with a visual survey of a series of parameters, aimed to describe the surface of the masonry, identifying the materials used, the processing of the surface of the blocks, the construction technique and the wall texture. This reconnaissance allowed a first generic subdivision of the walls present,

(macro-type) followed by an in-depth analysis of the parameters deemed useful for their classification; in each macro-type, therefore, were chosen three significant samples, of one square meter, (for a total of 86 samples) and in each, were analyzed the size of the blocks and mortar joints, the presence and quality of the mortar, the methods of laying in works and wall texture (texture in façade and in cross section, existence of transversal connections). As a result, it was possible to classify 35 different types of masonry, in the three sections of walls analyzed. The presence of these numerous types of masonry, is due to different factors often integrated: different construction periods of the parts of the walls, repair works and/or reconstruction of some portions of these as a result of seismic events, overlapping walls of civil buildings or other structures.

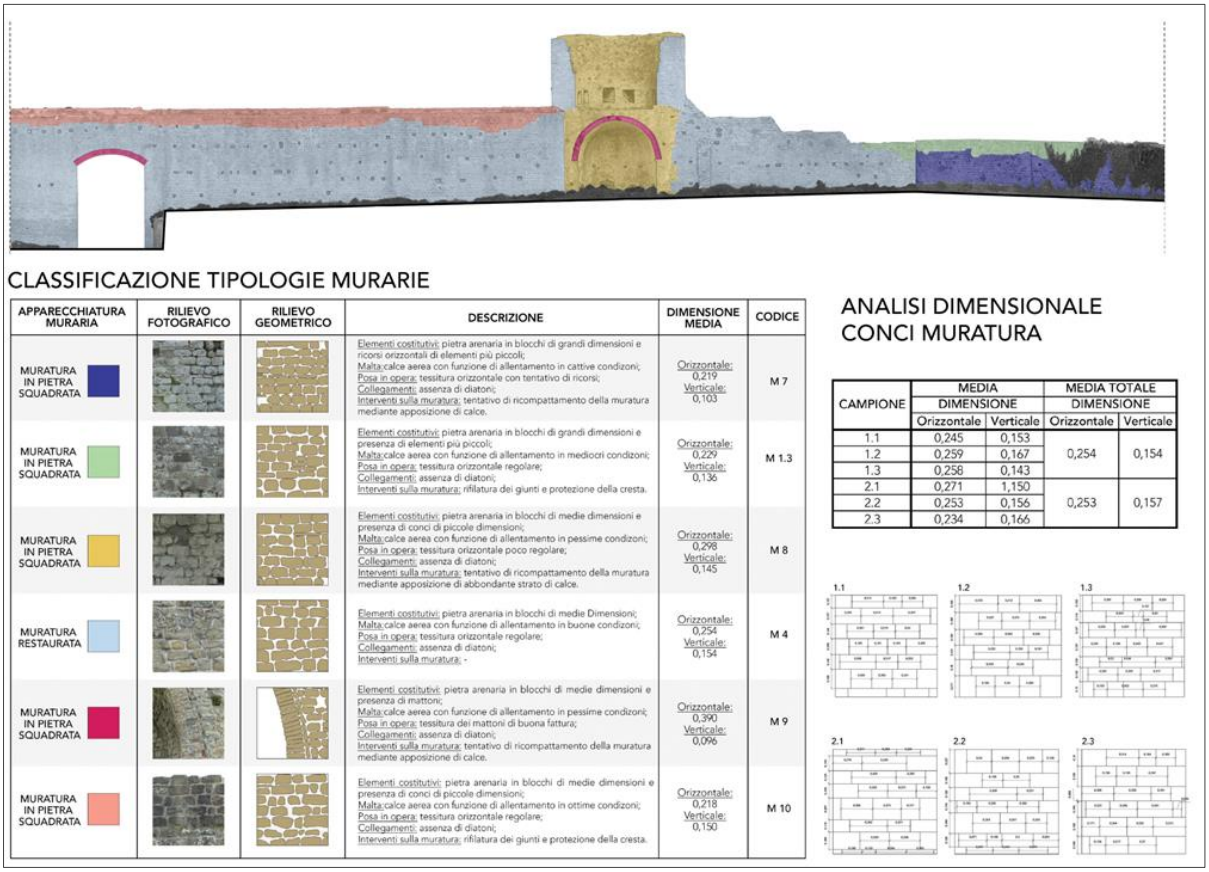


Figure 5: Datasheet for the classification of masonry types. In columns from left to right: type of wall texture, photographic survey of the sample, geometric survey of the sample, description of significant parameters, (constitutive elements, type of mortar, type of laying in work, cross connections) average block size, identification code. On the right, the block size survey and the average size estimate.

The types of masonry identified have been filed in summary tables, assigning each of them an identification code and a color so that they can be easily identified in the survey maps (Fig. 5). The datasheets contain images and the geometric survey of the samples used for classification, annotations relating to the constituent elements, mortars used, laying in the works and the texture of the wall, the possible presence of recent repair and/or restoration work; for this last

aspect, the historical data collected with observations and the relevant data were compared.

4.2 Materials decay and damage situation to the structures

Since the degradation of the materials present in a structure, represents a process of pathological alteration, capable of compromising the chemical and physical-mechanical characteristics of the same, determining the state of preservation of the elements in work, it was essential to assess the strength characteristics of the masonry. It is also important to remember that the IQM calculation method uses qualitative assessment parameters of the conservation status of the mortar and building blocks of the masonry, therefore related to the possible presence of pathological alterations. The analysis of the degradation was carried out, at this stage, through a logical deductive path that, starting from the macroscopic alteration phenomena of the analyzed elements, derived the causes and mechanisms of degradation. The observations made, as indicated, were of a macroscopic type and therefore aimed at identifying forms of pathological alteration that obviously compromise the physical and mechanical characteristics of stone elements and mortar. In this analysis process, the *Lexicon of macroscopic alterations of natural and artificial stone materials* was used, collected in the UNI standard 11182:2006. The classification of the identified degrades, was transferred to the survey papers through a symbolism consisting of alphanumeric codes and colors. The recording of the forms of degradation was completed with the survey of the cracking framework and its interpretation, indicating static failures and the main mechanisms of damage related to dynamic stresses. The main forms of degradation identified, were: the erosion and hurling of the sandstone that constitutes the blocks of masonry and the pulverization of the mortars. These phenomena have been detected in numerous portions of the wall curtain and with particular severity in the base areas and ridges of the masonry. The cracking framework detected, has highlighted portions of masonry affected by rotations out of plane and structural injuries attributable to efforts in the plan, derived from the seismic stresses of 2016.

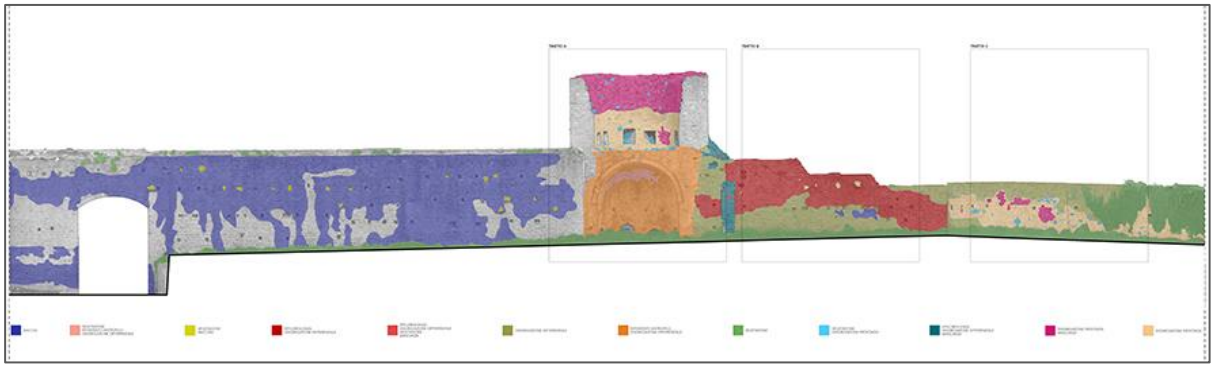
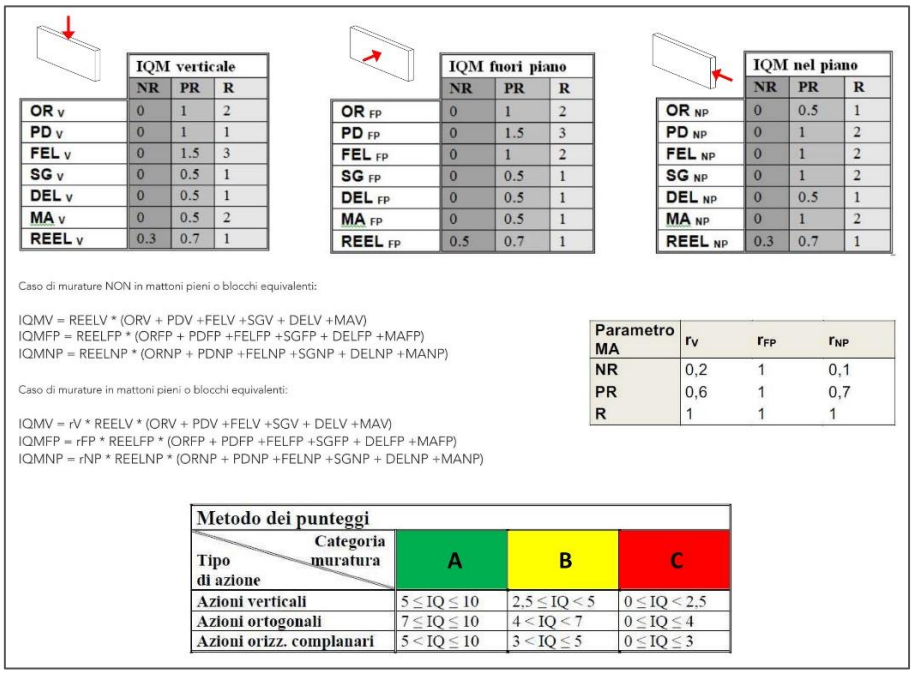


Figure 6: inside front, Block 2. A false-color representation of the main forms of degradation and their extent

4.3 Wall Quality Index (IQM)

The analytical phase was concluded, therefore, with the identification and cataloging of the types of walls present. Each of these has been characterized both from a typological and a technical-construction point of view, defining the wall quality (IQM) and the consequent mechanical parameters through the calculation process of the Wall Quality Index [9]. The

procedure for the assessment of a Masonry Quality Index (IQM) is based on the identification of the masonry buildings typical features, evaluated with respect to the "rules of art" as reported in ancient and modern handbooks; from the visual inspection of masonry texture in façade and in cross section, a numerical evaluation is given to different parameters and a quality index can be obtained [10]. Among the innovations introduced, it is worth highlighting that the evaluation of the IQM is performed by defining the masonry quality as a function of the load type examined: 1) vertical loads; 2) horizontal in-plane loads; 3) horizontal out-of-plane loads [9]. Moreover, a correlation between the masonry quality index and the values of the mechanical parameters proposed in the tab. C8A.2 of the Instructions to the Italian Technical Code 2008 (updated in the tab. C8.5.I, of the Italian Technical Code 2018) has been proposed [11-12]; in particular a relationship aimed to provide values of mechanical parameters "coherent" to those proposed in the two tables mentioned, a function of the IQM has been obtained.



IQM verticale	NR	PR	R
OR $_V$	0	1	2
PD $_V$	0	1	1
FEL $_V$	0	1.5	3
SG $_V$	0	0.5	1
DEL $_V$	0	0.5	1
MA $_V$	0	0.5	2
REEL $_V$	0.3	0.7	1

IQM fuori piano	NR	PR	R
OR $_{FP}$	0	1	2
PD $_{FP}$	0	1.5	3
FEL $_{FP}$	0	1	2
SG $_{FP}$	0	0.5	1
DEL $_{FP}$	0	0.5	1
MA $_{FP}$	0	0.5	1
REEL $_{FP}$	0.5	0.7	1

IQM nel piano	NR	PR	R
OR $_{NP}$	0	0.5	1
PD $_{NP}$	0	1	2
FEL $_{NP}$	0	1	2
SG $_{NP}$	0	1	2
DEL $_{NP}$	0	0.5	1
MA $_{NP}$	0	1	2
REEL $_{NP}$	0.3	0.7	1

Caso di murature NON in mattoni pieni o blocchi equivalenti:

IQMV = REELV * (ORV + PDV +FELV +SGV + DELV +MAV)
IQMFP = REELFP * (ORFP + PDFP +FELFP +SGFP + DELFP +MAFP)
IQMNP = REELNP * (ORNP + PDNP +FELNP +SGNP + DELNP +MANP)

Caso di murature in mattoni pieni o blocchi equivalenti:

IQMV = rV * REELV * (ORV + PDV +FELV +SGV + DELV +MAV)
IQMFP = rFP * REELFP * (ORFP + PDFP +FELFP +SGFP + DELFP +MAFP)
IQMNP = rNP * REELNP * (ORNP + PDNP +FELNP +SGNP + DELNP +MANP)

Parametro MA	r_V	r_{FP}	r_{NP}
NR	0,2	1	0,1
PR	0,6	1	0,7
R	1	1	1

Metodo dei punteggi Tipo di azione \ Categoria muratura	A	B	C
Azioni verticali	$5 \leq IQ \leq 10$	$2,5 \leq IQ < 5$	$0 \leq IQ < 2,5$
Azioni ortogonali	$7 \leq IQ \leq 10$	$4 < IQ < 7$	$0 \leq IQ \leq 4$
Azioni orizz. complanari	$5 < IQ \leq 10$	$3 < IQ \leq 5$	$0 \leq IQ \leq 3$

Figure 7: The IQM is divided according to the direction of the soliciting action into 3 indices: IQM for vertical actions, for horizontal actions out of plane and for horizontal actions in the plane. Based on compliance with the parameters of the "rule of the art", are assigned judgments of partial respect, respect and disrespect, to which some scores are connected. These scores are inserted in formulas that allow to obtain a global value for the three IQM, taking account the corrective parameters linked to the quality of mortar. The last table shows, on the basis of the obtained values, the masonry categories: A, B and C, of which A is the best and C the worst.

The calculation of IQM was carried out on all masonry samples surveyed, (so in three samples for each type of masonry) to obtain representative average values. The results showed low and medium, masonry quality indices in block 1, both for vertical loads, both for those horizontal in-plane and out of plane, while the situation in blocks 2 and 3 was appeared better, since only a single section has obtained a low masonry quality index for all expected loads (vertical, horizontal out of the plane, horizontal in the plane).

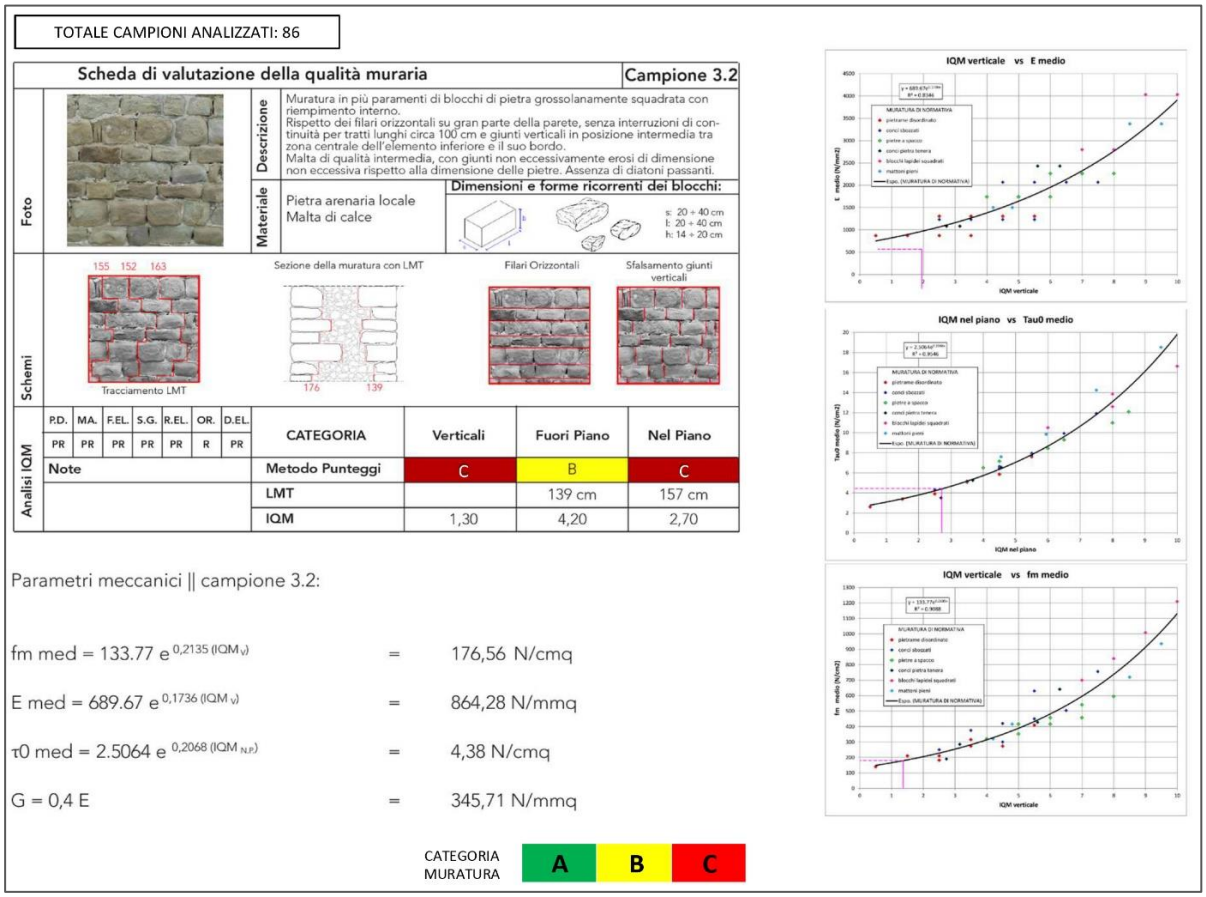


Figure 8: IQM analysis sheet, made for each sample of masonry detected. On the right, the correlation curves with the mechanical values, taken from Italian Technical Code 2008, tab. C8.A.2.

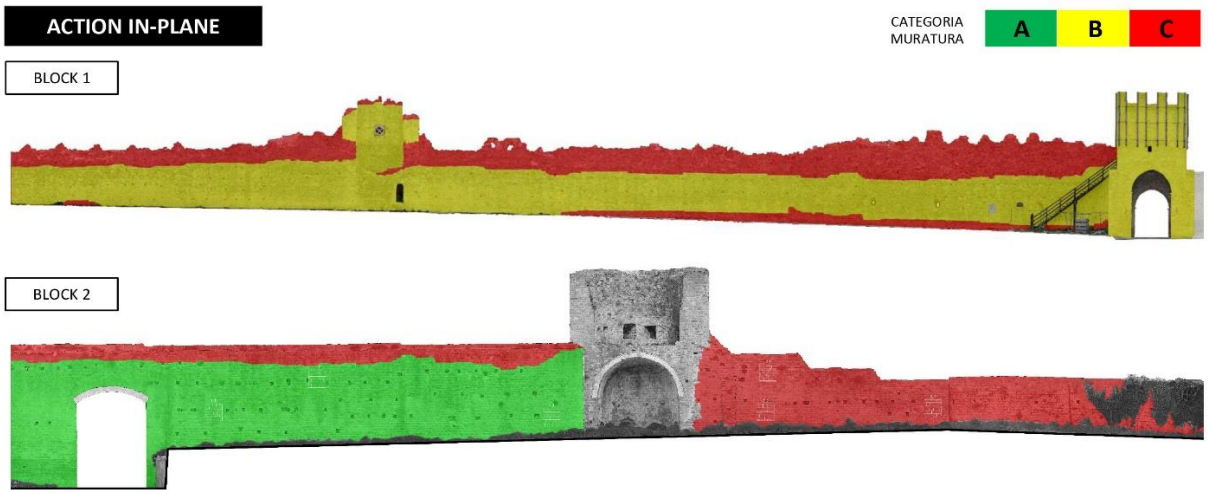


Figure 9: IQM identification of masonry categories

5 CONCLUSIONS

The study allowed to identify the portions of the masonry that have a low quality and therefore a high vulnerability to seismic stresses, since under the effect of dynamic actions, would probably be disintegrated.
This assumption determines the need for a hierarchy of analyses and subsequent interventions, one preparatory to the other. In other words, before carrying out a numerical modeling of the structure, it will be necessary to guarantee a good quality of the masonry structures in order to be able, then, to analyze any local mechanisms or global behaviors. Moreover, the identification of uniform portions of masonry, will be able to limit the number of invasive analyses for the mechanical characterization of the structures. (double flat jacks)

Acknowledgements. Sincere thanks goes to the municipality of San Ginesio. A heartfelt, and special, thanks goes to all the students of the course of "Architectural Restoration" of UnivPM (academic year 2018/2019) for the passion and professionality showed.

REFERENCES

[1] Allevi F., *Il balcone della Sibilla: San Ginesio fra cronaca e storia*. A. Giuffrè, (1960).
[2] Salvi G., *Memorie storiche di Sanginesio (Marche) in relazione con le terre circonvicine*, Tipografia Savini, (1889).
[3] Cortella F., Da incastellamento a città: le mura urbane. In: P.F. Pistilli et al. (Eds.): *La Chiesa Collegiata di San Ginesio. Una storia ritrovata*, Centro Internazionale Studi Gentiliani – Quaderni (2012), pp. 13–48.
[4] https://www.dji.com/it (accessed on 25.05.2019)
[5] https://www.kaarta.com/products/stencil-2-for-rapid-long- range-mobile-mapping/#Specs (accessed on 27.03.2019)
[6] Bronzino, G. P. C., Grasso, N., Matrone, F., Osello, A., and Piras, M., *Laser-Visual-Inertial Odometry based solution for 3D Heritage Modeling: the Sanctuary of the Blessed Virgin of Trompone*, Int. Arch. Photogramm. Remote Sens. Spatial Inf. Sci., XLII-2/W15, 215–222, https://doi.org/10.5194/isprs-archives-XLII-2-W15-215-2019, 2019.
[7] https://www.agisoft.com (accessed on 02.05.2019)
[8] http://www.cloudcompare.org (accessed on 15.04.2019)
[9] Borri A., De Maria A., *Scheda di valutazione dell'IQM (indice di qualità muraria)*, ReLUIS 3rd year report, Annex 3b.1-UR06-1 (2009)
[10] Borri A., De Maria A., *Linee guida per la compilazione della scheda di valutazione dell'IQM*, ReLUIS 3rd year report, Annex 3b.1-UR06-2, (2009)
[11] Borri A., De Maria A. *Indice di qualità muraria (IQM) e correlazione con le caratteristiche meccaniche*, (ReLUIS), (2015) *Report WP1_1-1_2015,UNIPG,*: http://www.reluis.it/images/stories/divulgazione/WP1_1-1_2015UNIPG_IQM_Report.pdf (accessed on 15.01.2020)
[12] Borri A., De Maria A. *Il metodo IQM per la stima delle caratteristiche meccaniche delle murature: allineamento alla circolare n. 7/2019*, Structural n. 222.; https://doi.org/10.12917/STRU222.06 , (accessed on 15.01.2020)

12th International Conference on Structural Analysis of Historical Constructions
SAHC 2020
P. Roca, L. Pelà and C. Molins (Eds.)

THE REUSE OF HOUSING BUILDINGS IN BARCELONA THE VERSATILITY OF OLD CONSTRUCTIVE STRUCTURES

MAGDA MÀRIA[1*], XAVIER MONTEYS[2]

[1]Departament de Projectes Arquitectònics (DPA)
Universitat Politécnica de Catalunya (UPC-BarcelonaTech)
Campus Sud UPC
Av. Diagonal, 649. 5ª. pl. 08028 Barcelona, Spain
e-mail: magda.maria@upc.edu, web page: https://habitar.upc.edu
(*corresponding author)

[2] Departament de Projectes Arquitectònics
Universitat Politècnica de Catalunya
Campus Sud UPC
Av. Diagonal, 649. 5ª. pl. 08028 Barcelona, Spain
e-mail: xavier.monteys@upc.edu, web page: https://habitar.upc.edu

Keywords: reused housing buildings, Barcelona, bearing walls, buildings transformed into housing, adaptive reuse

Abstract.

There are 1,463 buildings in Barcelona, from different times from the first century to the present day, that have changed their functions once or more times throughout their life. This paper analyses those cases in which changes in use relate to housing and it does it in two opposite ways: In one way, examining houses –mostly with building structures of bearing walls– that have endured functional modifications without losing its main attributes. In the opposite way around, studying buildings with other uses than housing – many of them built with isotropic structures or large structural spans– that have been converted into dwellings. On the other hand, and in both cases, the analysis addresses how the urban situation of the building conditions the use to which it will tend to be transformed.

INTRODUCTION

In a recent study, made by our research group on the reuse of buildings in Barcelona, we have identified 1,463 cases of buildings that, from the 1st century to the present [1], have changed their use once or more times. Of all the existing uses – housing, residential, commercial, offices, industrial, sanitary, religious, cultural, recreational, educational, sports and institutional – housing has contributed the most to accommodate new uses: A 55.52%, of the reused buildings in Barcelona were originally homes. It is a high figure compared to a 5.89% of other buildings that, having other original functions, have been converted into housing.

Quantitatively this data has its logic since housing makes up much of the urban fabric of a city; in fact, in Barcelona it entails a 98% of it. However, it is a paradox that structures that respond to domestic requirements have had the capacity to host uses and programs that intrinsically seem to require very different conditions.

Much of the houses in Barcelona are built with wearing walls. Their structural spans delimit stairs, patios and rooms of small or large size, that fit into this structural system. They have constructive and spatial qualities that differ markedly from, for example, those of industrial buildings, composed of large naves and open structures that seem more in line with versatility and, therefore, to house a wide range of functions.

This leads us to believe that the apparent rigidity of the structural system of Barcelona's dwellings does not impede their predisposition to changing use. Furthermore, it induces us to analyze how houses, with their various typologies, have endured functional alterations without losing their main constructive, morphological and spatial attributes.

HOUSING TYPES AND CHANGES OF USE

The Article 272 of the Urban Guidelines of the Metropolitan General Plan of Barcelona distinguishes several kinds of housing: townhouses, masías, palaces, torres-villas and apartment houses [2]. Within them, we establish two large groups: the first includes houses between partition walls, whether they are single-family or multifamily houses: those are *townhouses* and *apartment buildings*; the second, includes freestanding houses: *masías, palaces and torre-villas*.

The *townhouses* are built between partition walls ranging from modest constructions in municipalities added to Barcelona, such as Sant Andreu, Sarrià-Sant Gervasi or Sants, to unique houses in the Eixample or Ciutat Vella. They usually have a back yard and they generally belonged to one family that occupied the entire property. They constitute a 31.1% of the houses that have changed their use and, in their transformation, some of the most outstanding ones have hosted cultural functions, as in the case of the Elizalde house, or the Ametller house; while commercial programs have colonized many others.

The *apartment buildings* are composed of several units, initially for renting and usually with two apartments per floor that occupy the entire depth of the plot. They are mostly built with brick-bearing walls that also support the interior courtyards and stairwells. The rooms are usually very regular, especially in the buildings of the Eixample layout by Cerda. They make up to a 34.0% of the homes that have changed their use and their foreseeable transformation has led them to become residential buildings such as hotels, residences, youth hostels or tourist apartments. An example of this would be the Fuster House, converted into Hotel Casa Fuster.

The *masías* are freestanding constructions, with a three naves structure, that consist of ground floor, main floor and garret. Some have large side galleries added. They were originally destined for housing and, together with the surrounding land, formed productive units linked to agriculture and livestock. Due to the expansion of the city, smaller plots than the original ones currently surround them. They are scattered in the urban fabric, mostly in the strip parallel to the Sierra de Collserola. They make up to the 5.7% of homes that have changed their use, covering very diverse functions: cultural, educational or commercial. An example is Can Cortada, a farmhouse converted into a restaurant.

The *palaces* are buildings intended for housing, built both between partition walls and freestanding. One of their distinctive features is the presence of a central courtyard with a noble staircase of access to the first floor, visually linked to the entrance. They constitute a 6% of the homes that have changed their use, and many of them are concentrated in Ciutat Vella, as the Palacio de la Virreina, converted into a cultural center.

The *torre-villas* are houses built exclusively as freestanding constructions, usually surrounded by a garden. They represent a similar case to that of the palace, but with a more clearly domestic program. They make up to a 23.2% of the houses that have changed their use and their construction is mainly concentrated in the district of Sarrià-Sant Gervasi, in the upper part of Gracia or in Horta-Guinardó. As in the case of the masías, their new functions are very heterogeneous, but they gather similar uses in certain streets or sectors of a district, such as the educational use nearby the Paseo de Sant Gervasi or the Paseo Bonanova.



Figure 1a: Scheme of the different types of housing and its urban location



Figure 1b: Scheme of the different types of housing and its urban location

FROM HOUSING TO OTHER USES

This work considers the affinities between the different types of housing and the uses they have embraced throughout their useful life. But also, comparatively, values buildings that, having other programs in their origin, have become homes. We call this the 'double way of housing use': from housing to other uses and from other uses to housing (Figure 2).

The first “one way of transformation” analyses the 810 dwellings that have changed use in Barcelona. As shown in Figure 3, they have been adapted to all the uses listed in the Metropolitan Master Plan Regulations. However, depending on the type of house/apartment, some final uses predominate over others. This gives us the opportunity to understand the logics that bring the original use to the current one, from the perspective of its typology, its structure and its location in the city.

One of the most frequent affinities between uses is the one between 'housing use' and 'residential use', thus: of the 331 buildings that have been turn into 'residential use', 270 were dwellings (an 81.8%). On the other hand, if we consider that, of the 810 dwellings, 270 have changed its use into a residential one; we find that this is the prevailing program, with a 33.0%, followed by the 'educational use' with a 19% and the 'commercial use' with a 14.3%.

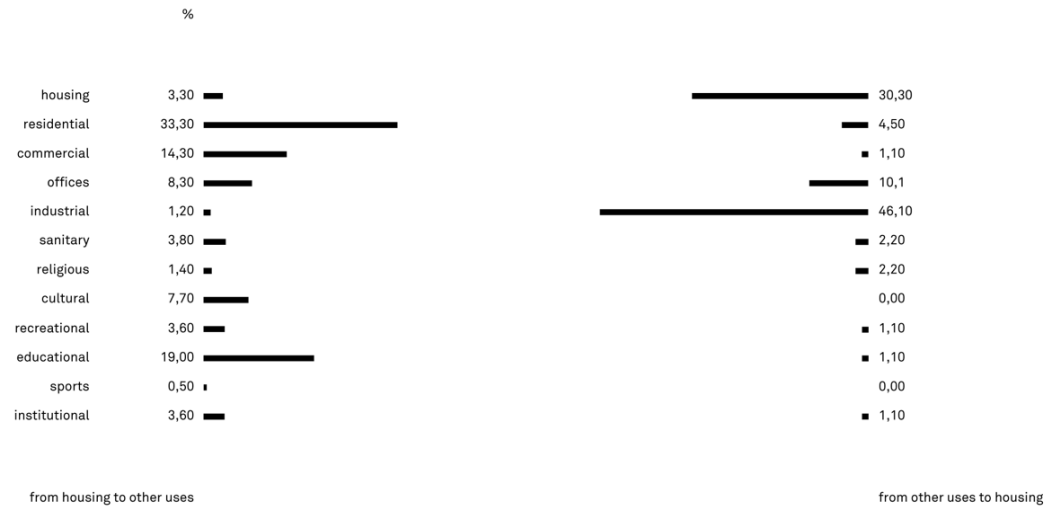


Figure 2: Doble way of housing use

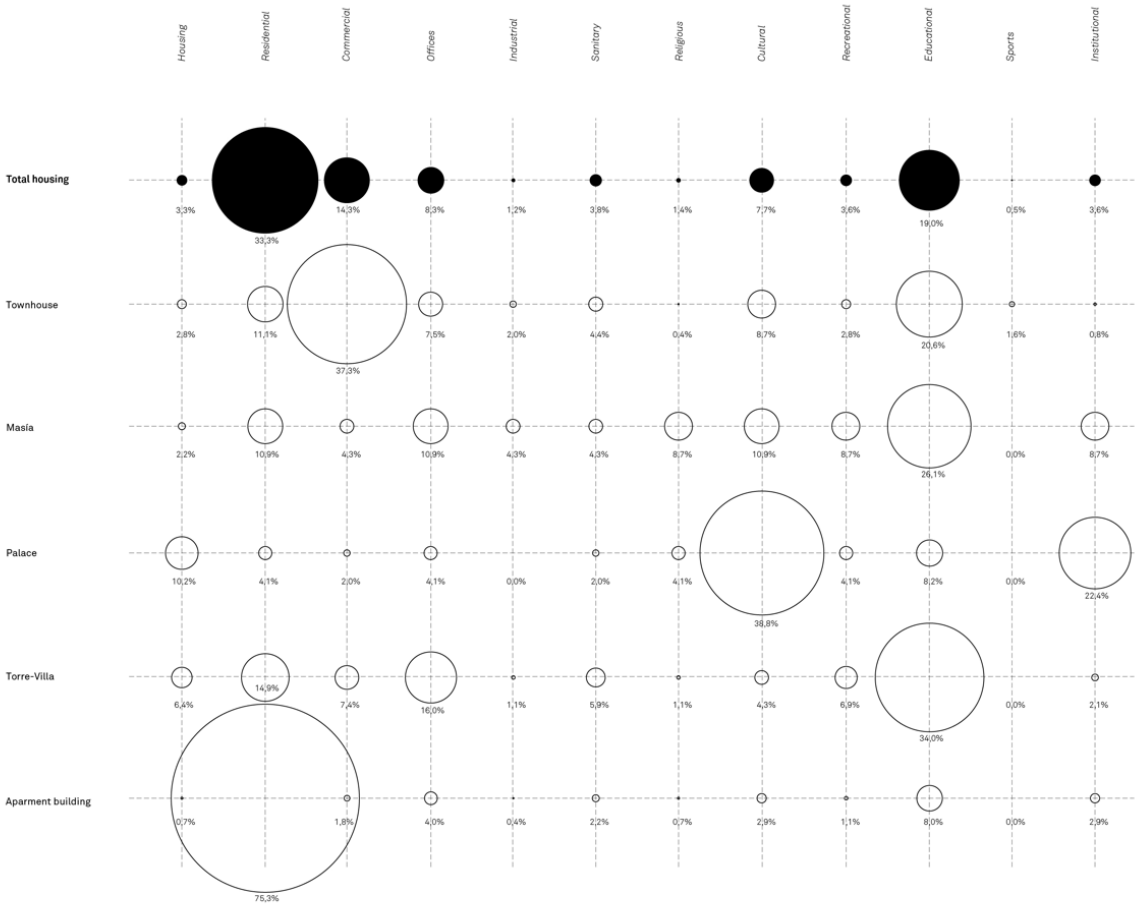


Figure 3: From housing to other uses

We also observe that the *apartment building* typology would represent the greater typological correlation between the established five types of housing and the 'residential use'. A 75.3% of transformed apartment buildings have been converted into hotels, touristic apartments, youth hostels and, to a lesser extent, into geriatric or student residences. Concerning the location, a 44.8%, that is, almost half of the buildings converted into 'residential use' are in Ciutat Vella and a quarter, a 25.6%, are in the Eixample. Another alarming significant statistical figure is, due mostly to the boost of the hotel business in Barcelona, that an 88.3% of the buildings that have moved to 'residential use' - mainly hotels - in Ciutat Vella, come from the 'housing use', and that explains the depopulation of the historic center of the city.

There are many examples of these transformations. Among them, we may highlight the Casa Joan Serra, located in Ciutat Vella, designed in 1867 by Francisco de Paula Villar and converted into the Hotel Montecarlo in 2000, after having been the headquarters of Las Noticias and El Correo Catalán newspapers. Another example is Casa Enric Batlló, located in the Eixample and designed in the late nineteenth century by Josep Vilaseca, with a new hotel use since the mid-1990s, according to Jordi Romeu's design project.

Another significant concordance is that between 'housing use' and 'educational use'. Of the 242 buildings currently hosting educational programs, including schools, academies and universities, 154 have been dwellings before: that is a 63.3%. Among them, the types that have tended the most to adapt their spaces to schools have been the freestanding buildings, the *torre-villas* being the majority type, with a 60.1% over the *masías*.

Concerning their location in the City, of these 154 dwellings transformed into educational buildings, 63 of them (a 40.9%) are in the district of Sarrià-Sant Gervasi. If we compare this data with the maps of the other types of housing locations, we confirm that the 'educational uses' that settle in existing buildings, choose the *torre-villas* first. This is due to the correlation between the interior organization, the size of the pieces, the uniqueness of the building and the presence of a garden, with the spatial needs of a wide range of educational programs.

Some examples that illustrate these changes in use would include the Casa Galvany-Castelló, built in 1890 and converted into the Augusta School; the torre at Muntaner Street, from 1923, transformed into the Nausica School in 1969; or the masía can Fargas, originally from 1300, recently transformed into the Municipal School of Music.

Another remarkable case is that of the palaces. They have been destined firstly for 'cultural use', up to a 38.8%, secondly for 'institutional use'. This may have an explanation in the role they play as part of the city memory, but it is also because of their spatial access features: with a direct link through a patio between the entrance and the noble first floor.

The other type of housing, the urban houses, has tended to transform into 'commercial use', specifically a 37.7% of them. This use includes small shops or restaurants that take advantage of the uniqueness of the property and, in some cases, of the backyard, to adapt its new functions properly.

A notable example of palace that has been turned into 'cultural use' could be the Palace of La Virreina, built on Las Ramblas in 1772, which has been hosting several museum programs since 1935 and that, currently, functions as an Art Center. The Palau Robert as well, built on Paseo de Gracia in 1898, became the Consejería de Cultura of the Generalitat in 1939, and it has ended up being a Cultural Center since 1997.

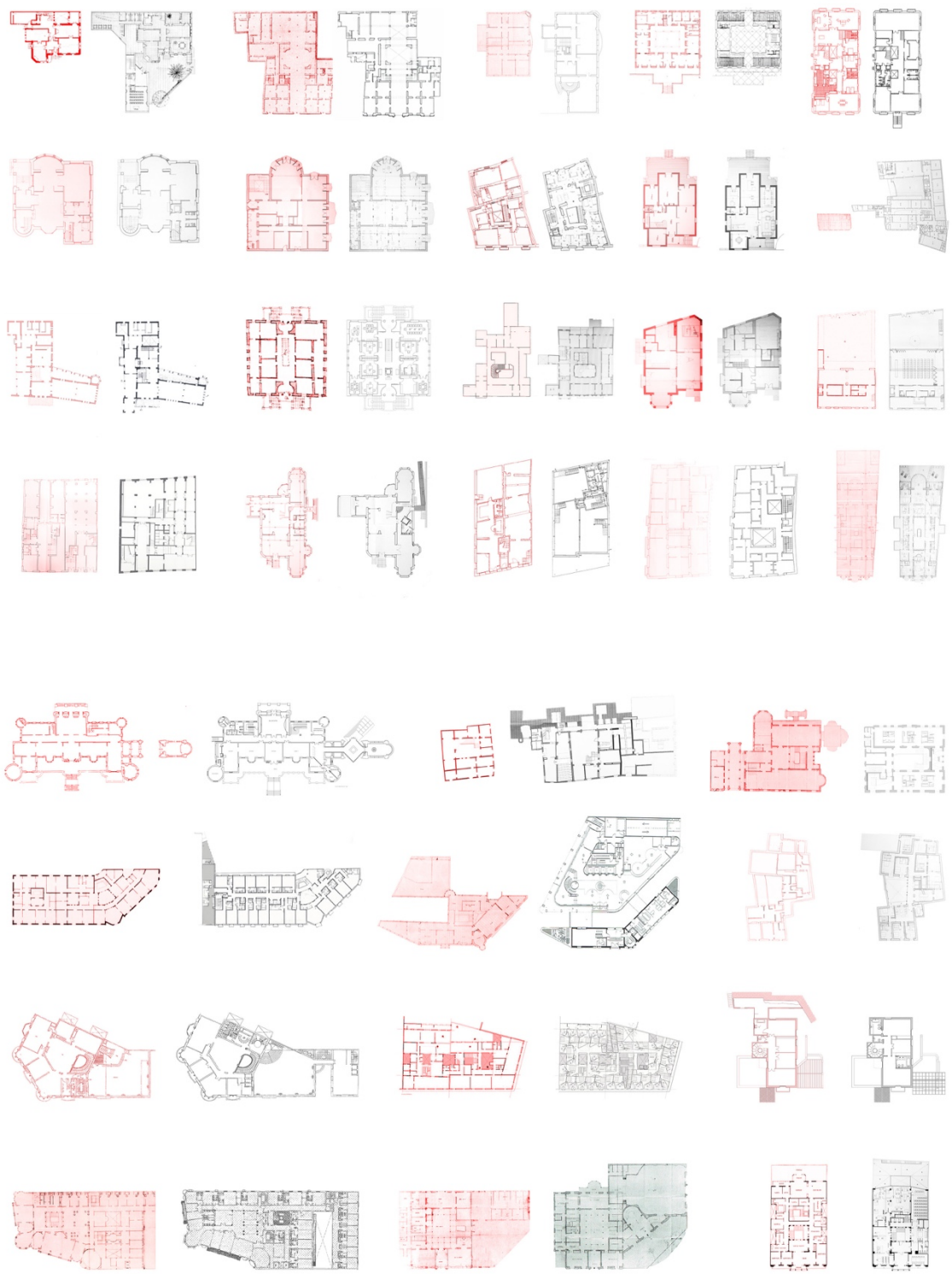


Figure 4: Housing types that have changed their use

FROM OTHER USES TO HOUSING

The second way of the housing change of use, and in opposite direction, analyses those properties that, in origin, had other uses (either residential, commercial, offices, industrial, sanitary, religious, cultural, recreational, educational, sports or institutional) and that, over time, have become housing. The affinities found between the housing building and another functional programs implemented in them are very different from those found in the opposite direction of change of use, that is, the 89 buildings that had other uses and have change to a domestic new program.

In this case, the first thing that is seen is a change that has occurred in the dwelling culture over the last decades: the new ways of life and their link to the decrease in the average occupation of the houses have involved a reduction of the required domestic dimensions. Moreover, the popularization, since the 1990s, of the *loft* typology in Barcelona, has led to interior organizations in which different degrees of intimacy coexist in the same space.

These changes in dwelling culture have led to an easier adaptation of domestic functions to space structures that in the first place related very little to them, such as office buildings, warehouses, or industrial buildings. In fact, a 46% of the buildings that have switched into 'housing use' originally had an 'industrial use'. Most of this 46%, up to a 92.6% of them have done so specifically into apartment buildings and the remaining 7.4%, into urban houses.

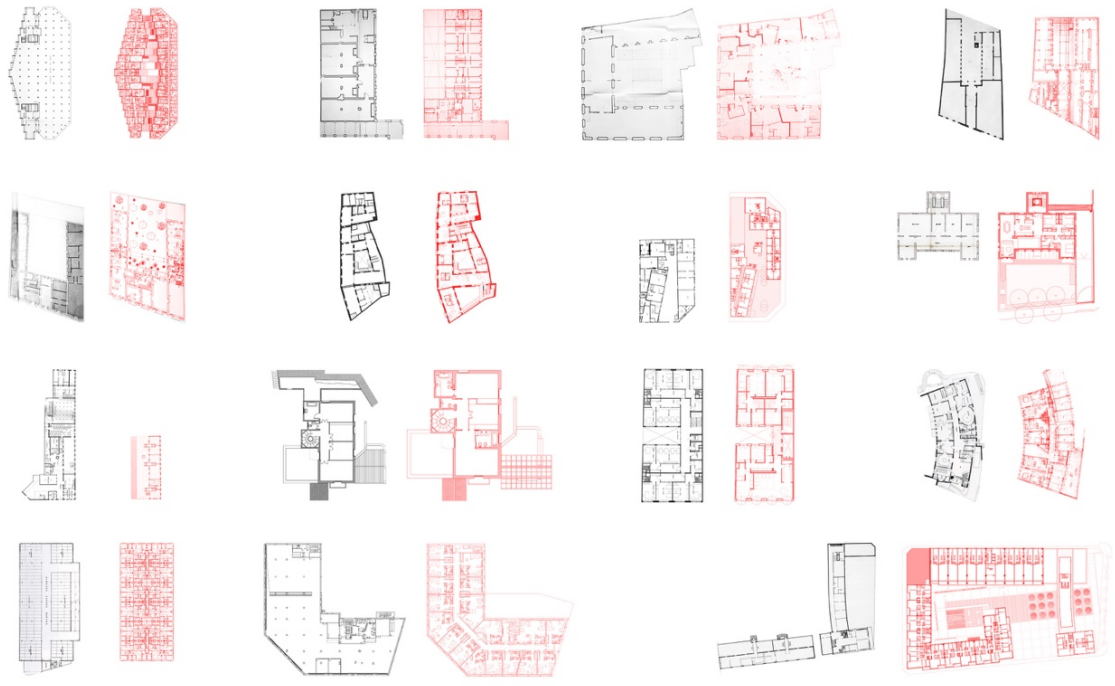


Figure 5: Other types that have become housing

This typological correlation between industrial buildings and housing buildings is very common in the district of Sant Martí, mainly due to the conversion of many factories and warehouses into loft-type dwellings. An example of it would be the Industrias Agrícolas Company, a factory from 1911, converted into Passatge del Sucre lofts by Jordi Garcés in 2010. In addition, we also find other cases in districts such as Ciutat Vella or Gracia, where small industries or workshops have been transformed into domestic spaces.

FIVE LESSONS ON THE "TWO WAYS" OF THE HOUSING USE

The reprogramming potential of these architectures – many of them with equivalent rooms and bearing walls – to suit other functional programs is, at least, equivalent to the definition of 'flexibility' and therefore of 'freedom', as canonized by the Modern Movement. That is why we develop next an intentional analogy through Five Lessons on the "two ways", testing them in parallel with the well-known Le Corbusier's Five Points of a New Architecture' of [4].

The first lesson shows that, in the formal structure of housing, the regularity, repetition or series of some elements must be considered. As the main organizational and structural elements of buildings –such as courtyards or stairs– are crucial for a different use to be coupled in the least traumatic way; the regularity that concerns both the rooms or the parts, as well as the facade or roof elements, plays a decisive role in the preservation of its structural and constructive characteristics.

In most examples of home transformations, the size and repetition of some parts, usually the rooms, have been crucial to the natural adaptation to the new use. This happens in an exemplary way with educational uses. In the antipodes of a 'free plan' organization, these buildings formed by equivalent rooms and some piece of a larger seize demonstrate their suitability to reconcile their various spaces with the activities of classrooms and playtime whatever the pedagogic program or the students' age is.

This also occurs in a similar way in office programs, whether from companies or official organizations, and in sanitary uses, such as medical cabinets, laboratories or small clinics, or in commercials, such as retail sales or catering establishments. All these functions have been coupled to the structure of the house, arranging offices, doctor's cabinets, dining rooms, waiting rooms or meeting rooms inside existing bearing walls' structures.

Qualities as regularity, repetition or series concern not only to the pieces of the dwellings but also to other elements such as windows. In this sense, it is revealing that some of the buildings that have gone from ' offices use ' to ' housing use ' successfully, are built with bearing facades with windows, and not with curtain walls. The window, in these cases, becomes the module that is equivalent to a lounge and that can easily become a room.

The paradox is that, both the regular pieces built by bearing walls, as well as the bearing facades with windows, are the opposite of the diaphanous floors and curtain facades. The latter have an obvious relationship with two of the slogans coined by Le Corbusier in their 'Five points of a new architecture': the free plan and the free facade [4]. Qualities that, without discussion, have been considered for decades as key elements for the versatility of buildings and, obviously, guarantors of their flexibility.

However, the lounges and rooms of a house, prove that they can become classrooms of a school, dining rooms of a restaurant, showrooms of a museum, offices of a company or doctor

offices. If they are not flexible according to the terminology of the modern movement, they are at least, ambiguous and therefore suitable for the requirements of a new use.

The second lesson leads us to recognize that the spatial organization of the house is presented as the most genuine pattern of architecture. We check how the house allows practically all uses, perhaps because we always carry its built-in scheme, especially in terms of the physical relationship with the built space.

In some functional programs, such as schools, this domestic organizational scheme is even beneficial. Pedagogical systems of active education, for example, aim to help children learn to reason for themselves about everyday events. At the same time, attention to their emotional needs requires that the areas where they carry out activities be like domestic ones. These requirements, in terms of space, fit perfectly into a house's functional program, and this explains why many schools have been installed in *torres-villa* or *townhouses*. In this sense, we could say that 'the house educates'. Likewise, these learning systems encourage contact with the outdoors and with nature, which also brings students health benefits. The garden of these urban houses thus becomes a very suitable and appreciated place.

In the third lesson we recognize that the *torre-villas*, *houses* and *palaces* have a special component, sometimes accentuated by their isolated status and because, in many cases, they have become part of the city's history. We can say that all of them are 'singular', and this quality has undoubtedly been one of the requirements for attracting new uses. In relation to this, we realize that the location and the conditions of the urban environment of these unique buildings determine the nature of the new uses to implement in them. The affinities that some functions have in relation to certain parts of the city demonstrates it: Sarrià-Sant Gervasi seems to have specialized in reconverting *torre-villas* and *houses* into schools, and Ciutat Vella presents itself as the district of choice to transform the *palaces* into cultural and institutional uses.

The fourth lesson tells us that the structural, morphological and spatial changes that, to a greater or lesser extent, these houses undergo in their functional re-organization are important factors to consider. In general, when reused, dwellings are stripped off the domestic life's most useful elements and units that hardly fit into other programs: like bathrooms, kitchens, pantries, laundry rooms, etc. This obvious 'cleaning' operation adds up other interventions as well, such as the placement of facilities devices, lifts, or complementary volumes. In many cases, this has distorted the meaning of the original layout, disfiguring the domestic component and eliminating the decoration. However, on the other hand, we must recognize that, without these operations linked to the change of use, many of these buildings would have completely disappeared. In a sense they have not been 'museized', which would equal to 'freezing' their spaces, denying them the ability to remain in use. It would be fair to acknowledge that we can compare these changes to those undertaken by a new homeowner to fit their lifestyle.

Finally, the fifth lesson concerns the second way of 'housing use': The one in which buildings of different programs have become dwellings, and we observe in them, that serial regularity – as in the rooms of a house – is also an important factor. Most strategies for re-use of factories, warehouses, offices, sports facilities or religious institutions are often based on the adaptation of living units – whether rooms, or apartments – to patterns of Repeat. These are often the result of the structural pattern, whether of bearing walls or pillars, of the host building. In addition, the rhythm in the arrangement of the windows in the facades of the host buildings facilitates the coupling of the housing program.

The difference between office or industrial buildings with curtain wall, such as the SEAT car depot in The Plaza Cerda, and the buildings with windows, such as the Caja de Ahorros Provincial at 257 Rosselló Street, or the one at 245 Diputació street, is that in these last two the windows seem to digest better the change to housing. In these cases, the windows are synonymous with opening and their dimensions match those of the rooms, prefiguring the distribution in domestic-sized spaces.

CONCLUSIONS

By reviewing all the cases of the two ways of the 'housing use change' we find that not only the shape and building structure of the properties with various programs – that are transformed into houses – are flexible, but that also the houses themselves are of a great flexibility.

In the first way, it is the 'housing use' that, simply, allows the compartmentalized spaces to be over time other things and host other activities, after all, human. The 'housing use', with its formal patterns of entry, hierarchy of pieces but also the equivalence of rooms, with its activities differentiated by plants, with the central vocation of certain spaces, or with the unquestionable practical idea that they contain services, storage and grooming units predispose a functioning that invites reconciliation with many other uses.

We could say that the house 'educates use'. The house is, making an analogy like the clothes we wear: most of the day are the same, both for work and to carry out social or family activities. This is especially evident in the case of the *torre-villas*, much of them located in the districts of Sarrià-Sant Gervasi, in the upper part of Gracia or in Horta-Guinardó.

In the other way around, although the number of cases is much lower, it is again the 'housing use', especially considered from a contemporary perspective, which allows to be coupled to very heterogeneous spaces. Today, when profound changes are affecting the house – due to the current social structure, economy or lifestyles – the 'housing use' has been simplified and detached from several prejudices. Due to the reduction of dimensions and the tendency to informality, activities such as cooking, eating, working or even sleeping come together in the same space.

On the other hand, in Barcelona, the number of people living alone, as well as those who spend most of their time away from home, has increased. In addition, the city offers a series of services that directly affect the functions we associate with the house. All this makes it possible that, unlike a few decades ago, a series of spaces, that due to their environmental and structural conditions would not have offered the conditions of 'habitability' and the degrees of 'privacy' required, can have a 'housing use' today.

The 'housing use' has quietly carried out a pedagogy that establishes behavioral patterns that can be reproduced anywhere; and a spatial disinhibition that makes it possible to reproduce them in different places, until they become dwellings even temporarily. It is for all this, that we can say that 'the house educates'.

ACKNOWLEDGEMENTS

MINISTERIO DE ECONOMÍA Y COMPETITIVIDAD
Programa Estatal de Investigación, Desarrollo e Innovación Orientada a los Retos de la Sociedad 2014-2017

REFERENCES

[1] X. Monteys, M. Mària, P. Fuertes, R. Sauquet and N. Salvadó. *Atlas del aprovechamiento arquitectónico. Estudio crítico de los edificios reutilizados en Barcelona*, MINECO 2016-2018.

[2] Plan General Metropolitano de Barcelona, 1976.

[3] Los cinco puntos para una nueva arquitectura de Le Corbusier eran: los pilotis, la terraza ajardinada, la planta libre, la ventana alargada y la fachada libre. Ver: Le Corbusier et Pierre Jeanneret (1926): *Les Cinq Points d'une Architecture Nouvelle*

[4] Le Corbusier et Pierre Jeanneret (1926): op. cit.

12th International Conference on Structural Analysis of Historical Constructions
SAHC 2020
P. Roca, L. Pelà and C. Molins (Eds.)

THE USE OF A BUILDING INFORMATION MODEL TO SUPPORT SEISMIC ANALYSIS: APPLICATION TO THE NATIONAL PALACE OF SINTRA, PORTUGAL

M. PONTE[1], R. BENTO[1*], R. MACHETE[1], M. GODINHO[1], A. B. GONÇALVES[1] AND A.P. FALCÃO[1]

[1]Civil Engineering Research and Innovation for Sustainability (CERIS)
Instituto Superior Técnico, Universidade de Lisboa
Av. Rovisco Pais, 1049-001 Lisboa, Portugal
e-mail: {madalenaponte, rita.bento, rita.f.machete}@tecnico.ulisboa.pt, marcia.godinho@gmail.com, {alexandre.goncalves, ana.p.falcao}@tecnico.ulisboa.pt
(*corresponding author)

Keywords: Historical Masonry Buildings, Laser Scanning, H-BIM, Seismic Analysis, Sintra National Palace

Abstract. *This work presents an application of a Building Information Model (BIM) to the National Palace of Sintra, Portugal, a large and complex building composed of different unreinforced masonry buildings that is included in the Cultural Landscape of Sintra, classified under the UNESCO World Heritage list in 1995. The developed H-BIM (Heritage Building Information Modelling) model has the ability to provide the geometric information of the structure of the building, together with its descriptive attributes, such as the mechanical characterization of the building materials, as inputs to the seismic structural analysis. The results of such analyses are also stored as attributes within the H-BIM model, providing an integrated platform usable by the building management. Geometric data was acquired using a Faro Focus^S 70, together with a Topcon Falcon 8+ UAV. The methodology applied in the construction of the H-BIM model was implemented with Autodesk Revit® software. Since the Palace is very complex, its seismic behaviour was studied for the different building units, considering the effect of the adjacent ones, and performing nonlinear static analyses through 3Muri software.*

1 INTRODUCTION

Built Cultural Heritage (CH) sites represent a high value in the definition of cultural identity and it is therefore of the utmost importance to have resources and tools to efficiently support their maintenance and safety. The conservation of buildings' architectural heritage and its maintenance and management are complex tasks since they are the result of historical events, different architectural influences, changes in ownership, and transformations over time [1]. In order to document the important aspects related to the maintenance and conservation of CH buildings or sites, the existence of a complete and coherent database, preserving data of complex systems and capable of answering requests for information demand, is strategic.

The BIM process is well established for new constructions, but not for existing ones, in

particular for CH buildings. For the latter, its implementation faces several problems or challenges such as: the predominance of incomplete or fragmented building information; the complex geometry of most buildings: the need to set up a geometric model that adapts to the parametric representation used by most BIM tools; and the need to represent historical changes in the buildings [2]. In addition, any BIM implementation in the built CH context is strongly related with the purpose for which it has been developed, thus including specificities and capabilities related with the normal maintenance, historical assets, or support for specific studies, for which a multidisciplinary approach is mandatory.

In this paper, a methodology for a BIM-based system implementation for the National Palace of Sintra (Figure 1), in Portugal, is described. The National Palace of Sintra is the most important building in the town centre and one of the most visited palaces in Portugal. It was the royal dwelling of the Portuguese royalty and its value is immeasurable. Given its cultural and social importance, there is undoubtedly the need for its preservation and documentation.

The acquisition of the material properties employed several *in situ* experimental tests – ground-penetration radar (GPR), masonry samples collection, flat-jack tests, ambient vibration tests – as the palace was built using different materials along with its construction from the 11th to early 20th centuries. The experimental results were used to evaluate the structural condition of the palace and to assess its structural safety level, allowing for fine tuning of the strengthening and rehabilitation interventions.

The completed operational model constitutes a useful tool to spatially reference the various tests and essays that are being conducted in the palace, allowing to support the production of adequate structural models and to integrate the results of the structural analyses into the H-BIM database.

The Chapel (Figure 1), on the north side of the palace, is chosen to describe and illustrate the procedures followed in this work.



Figure 1: A top view of the National Palace of Sintra (left); The north view of the palace with the chapel on the right side of the chimneys (right)

2 H-BIM OF NATIONAL PALACE OF SINTRA – METHODOLOGY

2.1 General Description

For the development of the H-BIM model [3], three main steps are highlighted, as

schematically represented in Figure 2. Firstly, the geometry of the palace was acquired with a combination of terrestrial laser scanning (TLS) and unmanned aerial vehicle (UAV) techniques, covering the 11 levels of the palace, which correspond to 244 spaces (e.g. rooms, outdoor gardens, patios) and surrounding environment locations. The two-point clouds datasets were combined into a single coherent H-BIM model and modelled using the Autodesk Revit® software, enabling its conversion to individual surfaces and objects. This model served later as a basis for the construction of the numerical model used in the seismic assessment.

In the H-BIM model, it is possible to include a miscellany of attributes, graphic and non-graphic, with capabilities to represent descriptive characteristics, updated whenever necessary. Some of the attributes may even come from the seismic assessment, such as the identification of the walls vulnerable to the seismic action, and others from the experimental tests. The detailed description of the different steps is provided in the following sections for the Chapel case study.

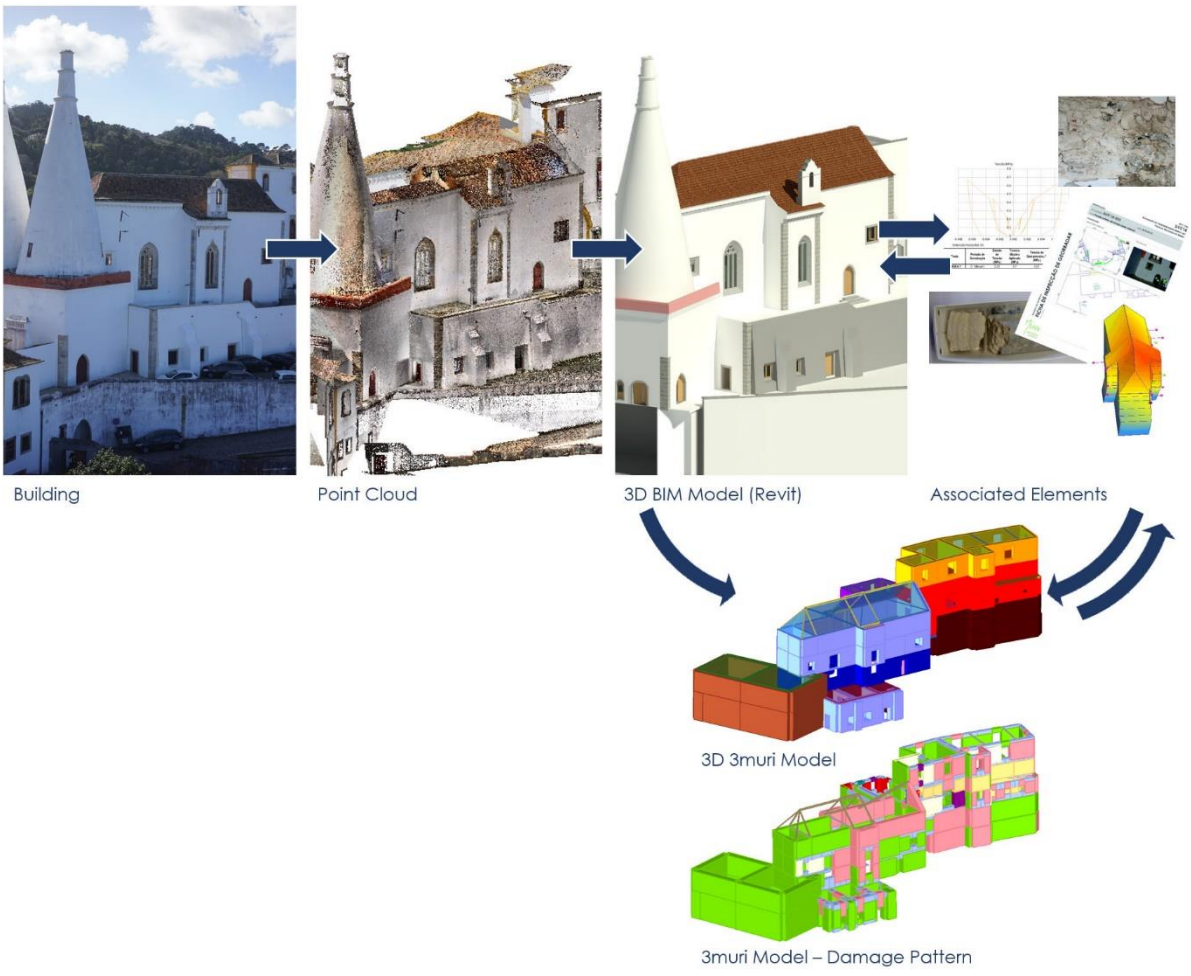


Figure 2: Main steps of H-BIM development process applied to the Chapel

The palace is composed of several connected buildings that were built along the centuries.

Due to the large scale of the monument, the H-BIM model is divided into the main bodies of the palace, thus keeping a reasonable model size. One of the challenges in such complex and culturally important structures is to define the equilibrium between the maximum quality level required versus the time spent and the data size. This problem can appear either while collecting scans or setting up the Revit model.

2.2 National Palace of Sintra

The National Palace of Sintra is a complex structure composed of several masonry buildings, and one of the oldest existing palaces in Portugal, based on Arab foundations. The palace has a special presence in the cultural landscape of the village of Sintra, classified as a World Heritage Site by UNESCO in 1995, mainly due to its two iconic chimneys. In a mixture of Arab and Christian cultures, the construction of the palace has evolved over several ages, becoming one of the rare medieval palaces that have reached our times practically intact, preserving its authenticity. It survived the 1755 earthquake, although small parts were required to be rebuilt at the time, and the 1969 earthquake, which caused some visible damage and floors' settlements in the Bonet building (belonging to the oldest part of the palace).

The Chapel, on the north side of the palace, is chosen to describe and illustrate the procedures that were followed. This chapel still survives today and is one of the oldest parts of the palace (13^{th}-14^{th} centuries). The palace chapel has a tiled floor, walls painted in patterned squares (imitating tiles) and a wooden ceiling decorated in geometrical patterns (Figure 3).

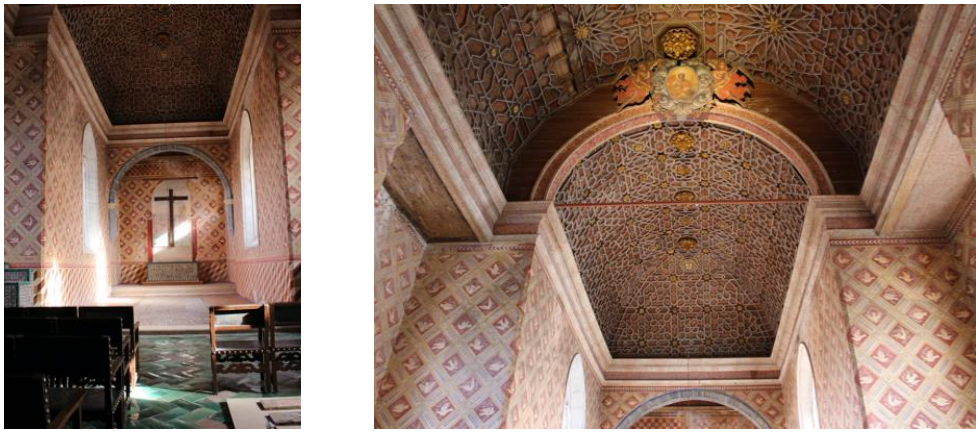


Figure 3: Interior of the Chapel: tiled floor, painted walls and the wooden ceiling

2.3 Data Acquisition

The main aim of this work was to develop an H-BIM model that facilitates spatial reading and a database that is able to include a variety of attributes with capabilities to represent a different type of characteristics, with a large application within heritage management and conservation activities. Requisites were defined to include, beyond the geometry, attribute data to assign to each model element. Attributes that can be assigned are of various types, e.g. historical documentation, the description of materials, construction stages, structural analysis,

other technological aspects, and other information from other inspections, such as experimental *in situ* tests. Thus, two main types of data can be stored or linked to the H-BIM model: geometrical and attribute data.

Geometrical Data

The geometrical survey of the entire palace was performed using a Faro Focus^S 70 and a Topcon Falcon 8+ UAV (Figure 4).



Figure 4: Equipment used for the geometric survey of the PNS: Faro Focus S70 laser (left); Falcon 8+ UAV (middle); generated point cloud (right)

A total of 1397 scans and 13 flights were carried out for the total survey of the palace, indoors and outdoors, as well as the surrounding environment, including 6772 photographs collected, of which 1478 with the UAV.

To scan the entire building and its facades, it was necessary to program the different locations of the scan stations, taking into account the field of view from each one and the necessary overlap with previous and following stations, in order to enable the 3D geometry reconstruction. In the following stage of the process, named co-registration, the point clouds of successive scans are combined into a coherent coordinate reference system through the identification of homologous features (e.g. corner points of architectural objects, plans, marks or checkerboard registration marks) between scans. From the imported point clouds, all the walls, floor, ceiling, columns, doors, windows and other significant elements of architecture were built as BIM elements using plane fitting, or, in the case of the more complex geometries, using parametric modelling where an adequate level of simplification was established.

For the acquisition of outdoor data, namely roofs, terraces, the highest areas of the facades and gardens, the UAV was used (Figure 5) to provide a point cloud produced using photogrammetric processing techniques.

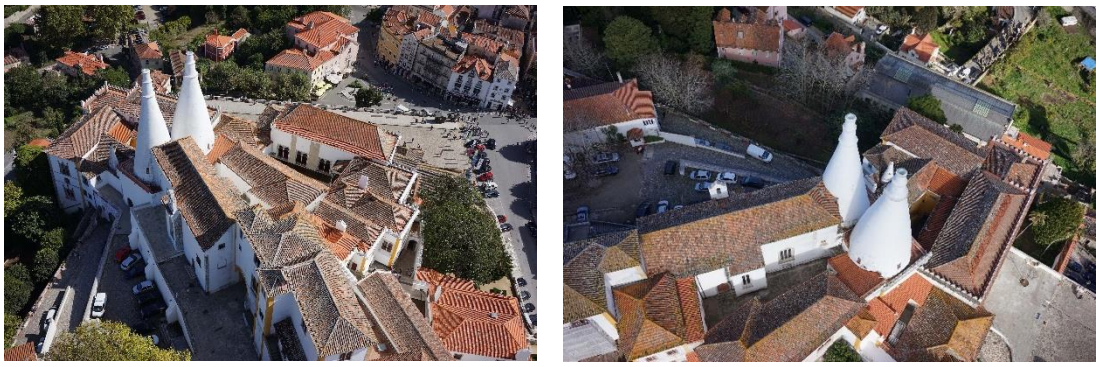


Figure 5: Aerial photograph of the parts of the palace (including the Chapel) collected by the UAV.

Attributes

Historical attributes were filled with information describing the history of each space (such as the rooms, staircases, halls and passageways) or each individual constitutive element (e.g. wall), and its original and current uses. Management attributes record information related to interventions in the building, such as the type of facility or the chronology of the works. Images, text documents and spreadsheet files were the most common data formats in both cases.

To evaluate the seismic safety of the palace and to identify possible structural anomalies and vulnerability factors, an interdisciplinary methodology was developed [4] including an *in situ* experimental campaign. In the framework of the approach described in [5], allowing for an adequate characterization of the structural properties, different types of tests have been conducted, considering Semi-Destructive and Non-Destructive Tests (SDT and NDT, respectively): removal of masonry samples (SDT), flat-jack tests (SDT), ambient vibration tests (NDT) and Ground-Penetrating Radar (GPR) tests (NDT). From the experimental tests, very useful data have been obtained to define and calibrate the structural numerical models developed, thus becoming possible to estimate the actual safety level of the palace and to allow, in the future, the eventual design of the restoration interventions required for the safety of the historical construction.

The locations of the removal of masonry samples, flat-jack tests, ambient vibration tests and GPR tests were defined and represented in the BIM model (Figure 6 and Figure 7). All the main results obtained with experimental *in situ* are linked to the model or added to it as attributes.

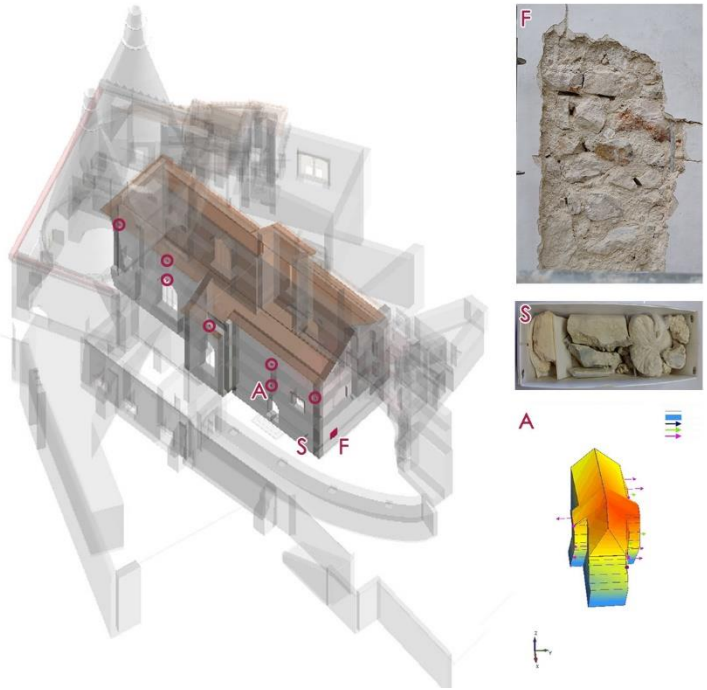


Figure 6: Flat-jack tests, removal of masonry samples and ambient vibration *in situ* tests performed in the Chapel: Survey placement (left) and attributes (right)

In the palace, the locations for the collection of samples and flat-jack tests were chosen on the main structural walls that characterize the main periods of construction, taking into consideration the various limitations, such as the existence of tiles or paintings. Both tests were carried out, whenever possible, on the same wall, or on adjacent walls. Nevertheless, for the case of the chapel, the masonry sample (S, Figure 6) was collected on the north wall, while the flat-jack test was performed on the west wall (F, Figure 6). In fact, the time slice obtained in the north wall from GPR02 test, as shown on the bottom picture of Figure 7, presents a former window that was later filled with a different type of masonry. This result prevented the flat-jack test from being carried out on the same wall as the sample collected, as initially planned.

A campaign of ambient vibration tests was performed in some of the palace's bodies chosen for their structural importance, existent damages and history. The determination of the dynamic behaviour of the structures (frequencies and the modes of vibration) is crucial to calibrate the numerical models. To measure the dynamic response of buildings, force-balance accelerometers of high sensitivity (80V/g) were used: six uniaxial EpiSensor ES-U2 and one triaxial EpiSensor ES-T, from Kinemetrics Inc. To illustrate the type of results reached, in Figure 6 it is possible to observe the fundamental mode of vibration of the chapel (right, bottom), along with the sensors' positions (the circles in red in the BIM model and the red arrows on the right bottom image correspond to the position and the direction of the sensors). The first mode corresponds, as expected, to the vibration of a beam with two ends constrained.

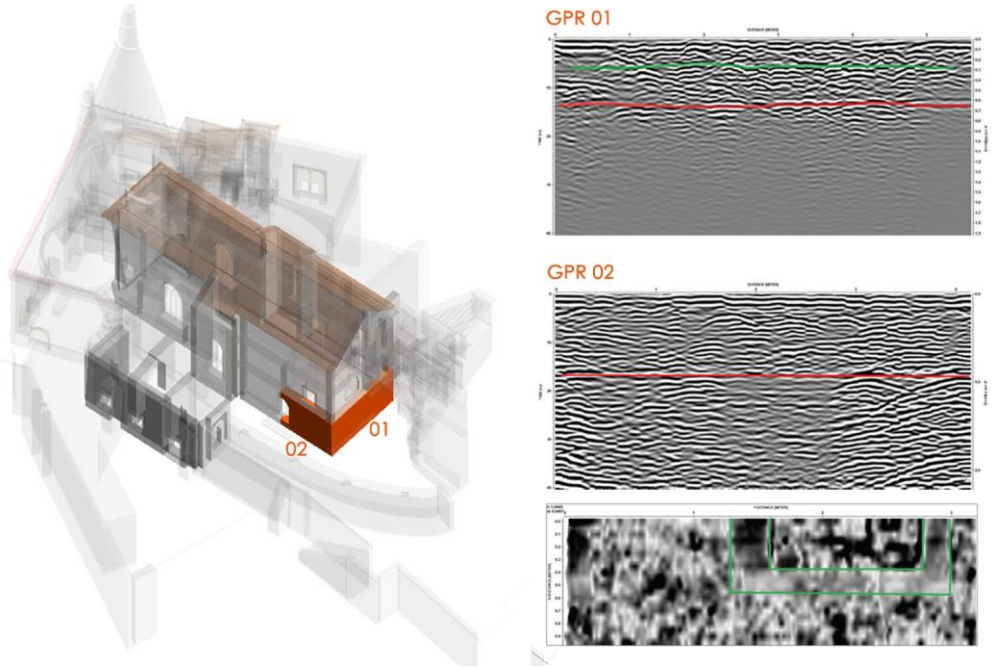


Figure 7: GPR in-situ tests performed in the Chapel: Survey placement (left) and attributes (right)

With the GPR survey it was possible to identify in one of the walls of the chapel two leaves of stone with infilling in between, presenting a thickness of approximately 0.3 m for the exterior leaf. On the horizontal profile shown in Figure 7, corresponding to the GPR1 test (west wall), the limit of the first leaf is shown in green and the total thickness of this wall is presented in red. The results of the north wall, corresponding to the GPR2 test, did not allow to obtain reliable data on the internal structure of the wall. It was only identified a total thickness of approximately 0.95 m and an ancient window, as mentioned before, outlined by stones of 0.3-0.4 m width that was later infilled with a material that is different from the rest of the wall.

3 RESULTS

The final point cloud dataset of the chapel is presented in Figure 8 (left), after cleaning the noise data from features both outside of the palace (e.g. surrounding buildings) and the interior non-structural and non-architectural elements (e.g. furniture). The complete H-BIM model is presented in Figure 8 (right), and in it is possible to access different type of data for individual elements or sections of the building, including horizontal or vertical sections (Figure 9). The detailed geometric representation obtained allows to develop adequate structural models for the seismic assessment, for the identification of vulnerabilities and to recommend eventual future mitigation strategies.



Figure 8: Point cloud dataset (left) and north view of H-BIM model (right)

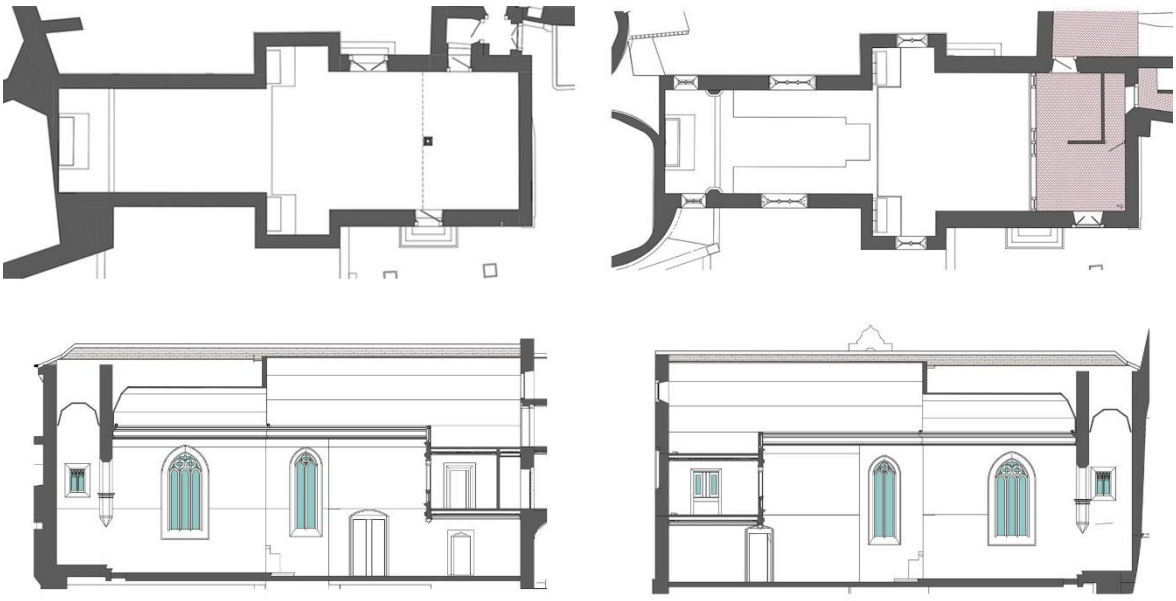


Figure 9: Horizontal sections (top) and vertical sections (bottom) and of the BIM model of the chapel

The H-BIM was used to develop the building's 3D numerical model in the 3Muri [6] software. Lately, the results of the structural analyses performed in 3Muri were introduced in the H-BIM model. The results of ambient vibration tests and flat-jack tests together with the performance of modal analysis and using as reference the values given in Italian Standard [7]

allowed the correct mechanical characterization of the materials, which was after linked to the H-BIM model. Figure 10 illustrates the calibrated mechanical properties of the masonry walls of the chapel.

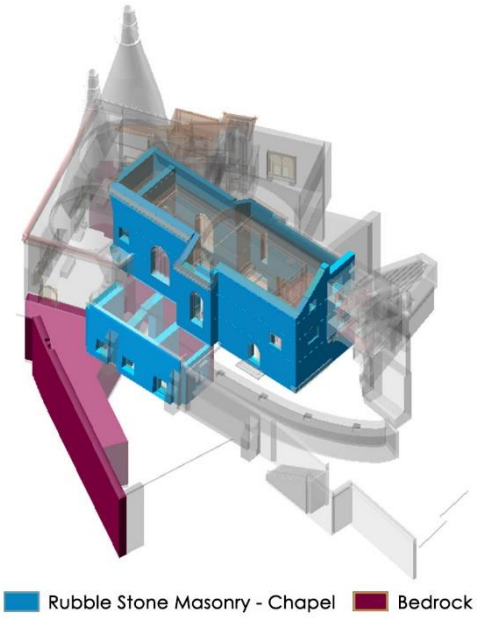


Figure 10: Mechanical properties of the masonry walls

For the seismic assessment of the palace, the in-plane and out-of-plane responses have been carried out by developing nonlinear analyses [4]. However, only the results for the in-plane response are herein represented. 3Muri performs structural and seismic analysis of masonry buildings, is based on the equivalent frame modelling (EFM) approach and allows performing nonlinear analyses of entire 3D building models. In Figure 11, the distribution of the damage of different masonry walls is represented for the near-collapse limit state, as required for monuments according to Part 3 of Eurocode 8 [8]; this extreme situation allows an easy and clear identification of the most vulnerable structural masonry walls and the type of behaviour (shear or bending) which will control their performance. The results shown in Figure 11 were obtained having performed nonlinear static analyses in the two main directions of the chapel [4] and present a combination of the worst outcome of each analysis.

The representation of the distribution of damage in masonry walls through the H-BIM model facilitates spatial reading and enables easy identification of the most vulnerable structural elements and thus the type future interventions to be implemented in the seismic retrofit stage.



Figure 11: Distribution of damage in masonry walls at a near collapse limit state: north view (left) and south view (right)

4 FINAL COMMENTS

The usage of BIM solutions represents a step forward into the management of CH construction, leading to a high level of integration of the information processes that facilitates the flow of data and its continuous revising. This way, a unique platform integrates all geometric and attribute data, and makes it accessible to technicians, architects, historians and public authorities, which is of the utmost importance to coherently manage such spaces.

In this study, a detailed BIM of the National Palace of Sintra, Portugal, has been implemented starting from the points cloud obtained with a laser scanner survey. This work is herein described, and the results obtained for one of the buildings of the palace, the chapel, are presented as illustrative of the model established. The developed system constitutes the central resource for the historical documentation, the description of materials, construction stages, structural analysis, additional technological aspects, and other information from further inspections such as experimental in-situ tests. The latter was obtained for the characterization of the structural elements to then perform the seismic assessment of the palace. The BIM model defined incorporates all this information either in embedded attributes or as external links. Also, the highly detailed geometric representation based on the laser scanning survey allows producing adequate structural models that have been used in the seismic vulnerability assessment procedures and integrates the results of these structural analyses into the BIM database. As such, the main contribution of this work is the presentation of the applicability of the combined use of the attribute storage and geometry database capabilities of heritage BIM through two-way information exchange with structural

analysis software, feeding a circular and continuous dataflow. The information structure that was implemented in the developed solution is prepared to support planning, cost assessment, sustainability evaluation, structural retrofit interventions and building management activities.

The detailed geometric survey of the palace is a valuable resource for management, as it enables future analyses of the building that require comparisons with the current state, e.g., in the result of man-made actions or natural hazardous events.

Additional research will focus on the automatic transformation of the BIM model into an accurate 3D equivalent frame model (EFM), and on the assessment of the usability of the developed system as a keystone for the management of the palace. Currently, the link between the autonomous BIM and EFM system elements follows a loose coupling approach, where data structures are not shared, and information processing is done via external files. According to the process followed, there is no automation in the data sharing and information processing between the two software components. Thus, developments on this particular topic deserve future attention.

A survey on the capacities of the system to cover the needs of data access, update and exchange are also considered for the near future.

Acknowledgements. This project is coordinated by IST and funded by Parques de Sintra-Monte da Lua, S.A.. The authors thank the company Parques de Sintra – Monte da Lua S.A. for supporting this research. The authors also thank Daniel Silva for facilitating the communication between the research team and the National Palace of Sintra management. Lastly, the first author would like to acknowledge the financial support of the Portuguese Foundation for Science and Technology (Ministry of Science and Technology of the Republic of Portugal) through a PhD scholarship [grant number SFRH/BD/145571/2019].

REFERENCES

[1] Osello, A., Lucibello, G., Morgagni, F., HBIM and virtual tools: a new chance to preserve architectural heritage buildings, *Buildings* (2018) **8**(1), 12; doi: 10.3390/buildings8010012

[2] Bruno, N., Roncella, R. A restoration oriented HBIM system for cultural heritage documentation: the case study of Parma Cathedral. In: *The International Archives of the Photogrammetry, Remote Sensing and Spatial Information Sciences*, vol. XLII-2, (2018), ISPRS TC II Mid-term Symposium “Towards Photogrammetry 2020”, Riva del Garda, Italy, 2018. doi: 10.5194/isprs-archives-XLII-2-171-2018

[3] Godinho, M., Machete, R., Ponte, M., Falcão, A.P., Gonçalves, A., Bento, R., BIM as a resource in heritage management: An application for the National Palace of Sintra, Portugal, *Journal of Cultural Heritage* (2019), Elsevier. doi: 10.1016/j.culher.2019.11.010

[4] Ponte, M., Bento, R., Silva, D.V., A multi-disciplinary approach to the seismic assessment of the National Palace of Sintra, *International Journal of Architectural Heritage, Conservation* (2019), Analysis, and Restoration, Taylor & Francis. doi: 10.1080/15583058.2019.1648587

[5] Bento, R., An Interdisciplinary Approach to the Seismic Assessment of Built Cultural Heritage: Case Studies in Lisbon and Outskirts, *Structural Analysis of Historical*

Constructions (2019), Springer International Publishing, Editors: Rafael Aguilar, Daniel Torrealva, Susana Moreira, Miguel A. Pando, Luis F. Ramos, Print ISBN: 978-3-319-99440-6, Electronic ISBN: 978-3-319-99441-3

[6] 3MURI (version 11.5). 2018. Italy: S.T.A. Data

[7] MIT. Circolare n. 617 del 2 febbraio 2009. Istruzioni per l'Applicazione Nuove Norme Tecniche Costruzioni di cui al Decreto Ministeriale 14 gennaio 2008 (2009). (in Italian)

[8] CEN. NP EN 1998-3: Eurocódigo 8 – Projecto de estruturas para resistência ao sismo. Parte 3: Avaliação e Reabilitação de edifícios. Instituto Português da Qualidade. European Committee for Standardization, (2017). Retrieved from www.iso.org/iso/foreword.html. (in Portuguese)

12th International Conference on Structural Analysis of Historical Constructions
SAHC 2020
P. Roca, L. Pelà and C. Molins (Eds.)

THERMAL BEHAVIOR ASSESSMENT OF TWO TYPES OF ROOFS OF THE DOMINICAN VERNACULAR HOUSING

PRIETO-VICIOSO. ESTEBAN[1*], RUIZ-VALERO. LETZAI[2], FLORES-SASSO. VIRGINIA[2]

[1] Universidad Nacional Pedro Henríquez Ureña, UNPHU
Av. John F. Kennedy Km 7 ½, Santo Domingo, Dominican Republic
email: eprieto@unphu.edu.do, http://www.unphu.edu.do (*corresponding author)
[2] Pontificia Universidad Católica Madre y Maestra, PUCMM
Av. Abraham Lincoln esq. Simón Bolívar, Santo Domingo, Dominican Republic
email:{letzairuiz@pucmm.edu.do, virginiaflores@pucmm.edu.do}

Keywords: Vernacular Architecture, Cana Roof, Metal Roof, Infrared Thermography, Monitoring, Dominican Republic.

Abstract. *The Dominican vernacular architecture, based on the indigenous bohio with Spanish influence, is built with natural materials, such as the royal palm (Roystonea Hispaniolana) and the cana palm (Sabal Dominguensis). This model of housing has remained practically unchanged for five centuries, responding adequately to the Caribbean tropical climate. In the twentieth century, start to replace the traditional palm leaf roof by a corrugated sheet zinc, significantly affecting the temperature inside these houses and altering the conditions of living comfort. For this reason, the aim of this research is to evaluate the thermal behavior of two roof types of vernacular housing. One type is a cana palm leaf roof and the other is a corrugated sheet zinc roof. The houses are in the towns of Villa Sombrero and Sabana Buey, Peravia Province, in the southwest of the Dominican Republic, a region with a Tropical savanna climate (Aw) according to the Köppen-Geiger climate classification. The climate is characterized by temperatures from 20°C to 38°C, with rainfall below 500 mm per year. The technique and tools used for this research are: Infrared Thermography (IRT) and digital thermometer for measure of thermal properties of roof materials, a thermometer and hygrometer to measure the relative humidity and temperature inside and outside of the houses, and carbon monoxide (CO) and carbon dioxide (CO2) meter. Passive IRT is used to measures the temperature differences of a structure that are generated under normal conditions. The results indicate that there is a difference in temperature between one type of roofing material and the other. Finding that houses with palm leaf roofs have lower temperature than corrugated sheet zinc roof and present a temperature difference between the interior and exterior.*

1 INTRODUCTION

The use of thatch roof is as ancient as the construction of the first houses. Thatch roofing is a traditional roofing method that involves using dry vegetation. Since the industrial revolution, many thatched roofs have been replaced by metal sheets. From the industrial revolution onwards, many thatched roofs were replaced by metal sheets, which was a new material that promised many advantages over the other. However, when using it, no changes were made in the design and one material was simply replaced for another, affecting the thermal comfort

inside the buildings[1]. For this reason, the aim of this research is to evaluate the thermal behaviour of two roof types of vernacular housing. One type is a cana palm leaf roof and the other is a corrugated sheet zinc roof.

In 2012, Pedro T. Navarro González carried out his doctoral thesis "Study of the roof frames of rural and vernacular construction in Gran Canaria. Structural and constructive analysis"[2], were refers to structural and constructive elements, such as roofs. In 2013, Molina and Fernández carried out a comparative analysis of the thermal envelope and energy demand between two types of housing, the *palloza* and the traditional house, in the mountain area of Os Ancares, in the northwest of Spain, by studying the energy use of straw on roofs[3].

In Peru, the thermal behaviour of the *mojinete* roof was analysed from the particularity of its shape, use of materials and location of openings and its response and adaptation to the local climate at the region of Moquegua that is hot and low rainfall [4]. In Brazil, a thermal study evaluate the thermal efficiency of three roofing materials (fibre cement tile, recycled tile, and thatched roofs) used in shelters for girolando calves and show that the recycled tiles and thatched roofs provided reductions of 18.7 and 14.6% in radiant thermal load [5].

While in 2016, Chandel, Sharma and Marwah, carried out a review of energy efficient features in vernacular architecture for improving indoor thermal comfort conditions, where the main features studied were: built mass design, orientation with respect to sun, space planning, openings, sun space provision, construction techniques, and building and roof materials [6]. In 2018, a doctoral thesis analysed and compared the thermal behaviour of two roofs, one metallic and the other made of concrete, through measurements and simulations, being able to measure their behaviour[7].

2 CASE STUDIES.

Four houses were assessed for this research all located in the Baní Valley, province of Peravia, in the south of Hispaniola Island. Two of them with roofs of cana palm leaves (B-1 and B-2) and two with roofs of corrugated zinc sheets (B-3 and B-4), The B-1 is located in Villa Sombrero and B-2, B-3, B-4 in Sabana Buey (Fig. 1).



Figure 1. The four houses assessed.

Both towns are located on the old Camino Real, which connected the city of Santo Domingo with the west of the island. All the *bohios* were built in the second half of the 19th century, which can be verified by the data offered by the owners and by the presence of cast-iron nails, used before the XX century were began the commercialization of the industrialized nails. The floors of the four houses are made of polished cement. A concrete sidewalk has been placed around all the houses.

2.1. Description.

The *bohios* B-1 and B-2 with a Cana palm leaf roof is a type of vernacular housing commonly used in the Valle de Baní, consisting of a simple volume with a rectangular floor plan, with a gabled roof and small eaves that protect the four facades. Its supporting structure is based on wooden forks, buried in the ground, joined at the top by the sill, on which rests the lock that supports the thick cover of cane palm leaves (*Sabal dominguensis*). The walls of the house and the internal divisions are made of planks of royal palm (*Roystonea hispaniolana*) placed horizontally, overlapping and nailed to the *horcones* or posts, which in this region are usually made of mahogany (*Swietenia mahagoni*) or creole oak (*Catalpa longissima*). For the structure of the roof, we used uncarved sticks or poles from various local timber trees (Fig.2).



Figure 2. *Bohios* (B-1 and B-2) with a cana palm leaf roof.

Both *bohios* have a door in the middle of their main facade and four windows, two on each side of the door. On the back façade facing the patio, they also have a door placed in the center and four windows, two on each side of the door. The spatial distribution of the interior consists of a central area divided by two low walls, called handrails or *balaustres*, which define the living and dining areas. On both sides are the four rooms, one on the right and two on the left side of the *bohio*. The kitchens and latrines are located outside the *bohios*, where there is also usually an *enramada* or covered terrace.

The B-3 and B-4 huts, located in Sabana Buey, have a supporting structure, materials and construction methods similar to those of the B-1 and B-2 huts, but with the difference that the roofs made of cana palm leaves were replaced years ago by corrugated zinc sheets, which are nailed to a structure made of already industrialized wooden rods and belts, usually made of pine. The roofs are gabled with short eaves, with the main facade being somewhat more pronounced (Fig.3). In these houses the zinc roofs are broken to achieve a greater speed in the fall of the water and move them away from the facades. Both cases have an annex at the back,

to integrate the kitchens into the house and add another bedroom. The interior walls, as in B-1 and B-2, remain at the height of the sills, allowing air to flow over them. The B-3 also has fans over the doors, which contribute to the good ventilation of the interior of the hut.



Figure 3. *Bohios* (B-3 and B-4) with corrugated zinc sheets on roofs.

2.2 Dominican climate and the environment condition

Dominican Republic is in the Caribbean, in the tropical zone of the northern hemisphere, at latitude 18°44.142' N and longitude 70°9.759' W. It classified subtropical climate that varies according to the place, due to the topography and the trade winds of the northeast. In general, the geography of the country has created two types of climate: tropical rainforest climate (Af) and tropical savanna climate (Aw), according to the Köppen-Geiger climate classification[8]. The climatic variations are marked, ranging from arid to very humid.

Peravia Province is in the southern region of the country, approximately 60 km west of the city of Santo Domingo, belongs to the coastal plains of the Caribbean. On average, the warmest month is August with a maximum 38.2°C. The lowest months is January with a minimum 20.5°C. The average relative humidity is 65.7% with average precipitation 77.64 mm, and average wind speed 4.375 m/s. (Fig.4). Average monthly hours of sunshine are 9 hours[9]. These climatic conditions (hot and humid) and the properties of the material affect the thermal comfort of buildings, causing a significant increase in the indoor temperature of the building.

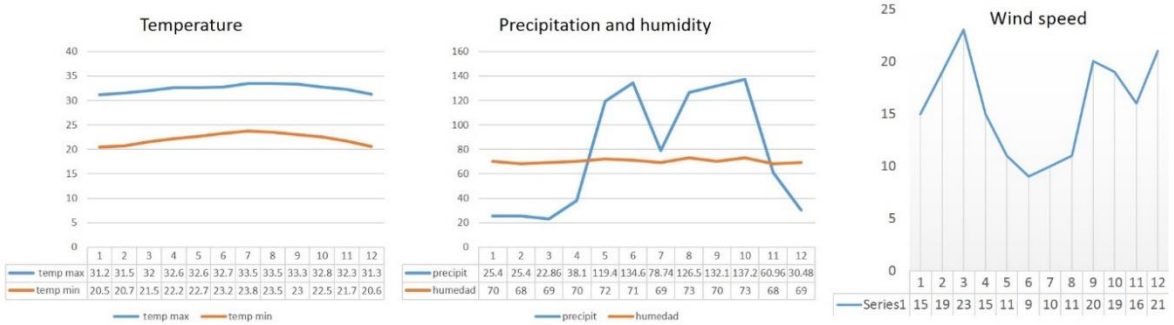


Figure 4. Environmental conditions of Peravia, Dominican Republic.

3. MATERIALS AND METHODS

Non-destructive techniques (NDT) were used to evaluate the houses. The equipment used was hygrometer, Tpi 1010[a] Outdoor/Indoor Air Quality Meter (AQM), Infrared Thermography (IRT) and Surface Temperature. Also, an official weather stations in the vicinity were consulted

and the National Meteorological Office (ONAMET). The measurements were taken during the warmest period, from June 08th to September 28th, 2019. Some additional measurements were taken on June 08th and July 9th, 2019, between 9:30h to 15:40h in a sunny day.

3.1 Environmental condition

The temperature and humidity were measured with an Extech RHT20 Datalogger hygrometer. Four hygrometers were installed in the houses: two inside and two outside the houses. The sampling rate was every 1800 seconds (30 minutes), from 0:21h am to 23:51h. The additional measurements taken on June 08th and July 9th and were done with a Tpi 1010ª Outdoor/Indoor Air Quality Meter (AQM) that measure carbon dioxide (CO2), carbon monoxide (CO), air temperature and relative humidity [10].

3.2 Surface Temperature

Digital Laser Thermometer was used, MASTERGRIP model CM558N. It has a temperature range between -28°C to 482°C and has accuracy +/-2°C or +/-2% (0°C to 482°C) whichever is greater +/-4 degrees C (-28°C to 0°C), with emissivity of 0.95, response time (90%): <0.5 seconds and with a Class II laser pointer. Several measurements were carried out in each roof, one inside and one outside to check the thermal jump effect.

3.3 Infrared Thermography

The study is based on passive thermography, which measures the temperature differences of the roof that are generated under normal conditions [11].Thermography images were used to analyse upper- and lower-surface thermal characteristics for the two roofing materials. The measures were taken with an infrared camera FLIR SYSTEMS model T420, FOL 18mm lens and 240 × 320 pixels IR resolution. The camera has a spectral range 7.5 to 13 micron and a field of view (FOV) of 25°x19°/0.4 meters and spatial resolution (IFOV) of 1.36 milliradians. Have an adjustable thermal range from -20°C to 650°C and for this project was set at -20°C to 120°C. The camera used for this survey meets the requirements of UNE-EN 13187:1998. The emissivity values for cana palm leaves roof are 0,75 and for corrugated zinc sheet are 0,20 (Table 1). For thermal images, an iron colour palette mode was used using reference colours: blue for coldest temperature range and yellow for warmest temperature range. This way, the coldest point can be identified on each image.

Table 1. Energy parameters of roofing materials

Material	Thickness (mm)	Roof slope	Emissivity values	Thermal transmittance U (W/m^2K)	Thermal resistance R (m^2K/W)	Thermal conductivity λ (W/mK)	Density ρ (kg/m^3)	Specific heat cp (J/kg·°C)
Cana palm leaves	600	45°	0,75	0.35	11.1 14.3	0,04 - 0,07	240	180
Corrugated zinc sheet	0,7	20%	0,20	2,20	0,0001	60 112,2	7,18	0.3898

National Society of Master Thatchers (NSMT), 2012 [12] / Fluke Corporation, Emissivity values of common materials, 2007 [13]

4 RESULTS AND DISCUSSION

4.1 Environmental Conditions

The recorded outdoor temperatures were maximum 38.2°C @08/18/19 at 12:21:01 in Sabana Buey; minimum 24.2°C @09/18/19 06:51:01 in Villa Sombrero; with an average of

30.6°C. The recorded outdoor Relative Humidity (RH) was maximum 88.7%RH @09/10/19 at 01:51:01, minimum 37.7%RH @08/21/19 at 12:51:01, average 65%RH. The recorded indoor temperatures were maximum 36.8°C @08/21/19 at 13:21:01, minimum 22.5°C @09/18/19 06:51:01, average 28.8°C. The recorded indoor Relative Humidity (RH) was maximum 83.5%RH @08/28/19 at 22:51:01, minimum 41.0%RH @07/09/19 at 13:21:01, and average 62.6% RH (Table 2).

Table 2. Average of environmental conditions indoor/outdoor

	Indoor			Outdoor			Indoor			Outdoor		
	Temp. Max. °C	**Temp. Min.** °C	**Temp. Avg.** °C	**Temp. Max.** °C	**Temp. Min.** °C	**Temp. Avg.** °C	**RH Max.** %	**RH Min.** %	**RH Avg.** %	**RH Max.** %	**RH Min.** %	**RH Avg.** %
B-1	32.8	22.5	27.7	37.7	24.2	30.3	82.4	53.7	68.9	74.8	39.8	65.7
B-2	32.2	23.8	28.1	38.2	24.4	30.7	83.5	53.1	67.1	88.7	37.7	64.7
B-3	36.8	26.1	30.1	38.2	24.4	30.7	78.5	45.7	61.4	88.7	37.7	64.7
B-4	34.8	25.5	29.3	38.2	24.4	30.7	74.9	41.0	53.1	88.7	37.7	64.7
			28.8			**30.6**			**62.6**			**65.0**

Air quality measurements indicate that B-1 has a higher concentration of CO2 indoors than other samples. It is possible that this is because the house is closed all day, which prevents it from renewing air. But in general, all the houses have great amount of co2 in comparison with the outside (Table 3).

Table 3. Outdoor/Indoor Air Quality CO2

Samples	Indoor	Outdoor	Range
B-1	1930 ppm	1612 ppm	350-1,000 ppm: typical level found in occupied spaces with good air exchange
B-2	1918 ppm	1743 ppm	1,000-2,000 ppm: level associated with complaints of drowsiness and poor air
B-3	1888 ppm	1753 ppm	
B-4	1899 ppm	1748 ppm	2,000-5,000 ppm: level associated with headaches, sleepiness, and stagnant, stale, stuffy air; poor concentration, loss of attention, increased heart rate and slight nausea may also be present.
Average	**1909 ppm**	**1714 ppm**	

4.2 Surface Temperature

The average outside surface temperature of the cana palm leaf roof was B-1: 38.5°C, B-2: 46.5°C and inside B-1: 30.1°C, B-2: 32.3°C., and the average outside surface temperature of corrugated zinc sheet was B-3: 47.5°C, B-4: 49.2°C, and inside B-3: 50.5°C, B-4: 48.5°C. We can observe the differences surfaces temperatures between the cana palm leaf and corrugated zinc sheet.

4.3 Infrared Thermography

Through thermal images (Fig. 5) we can observe some variations in temperatures of both upper and lower surfaces. In the case of the cana palm roof in B-1, the maximum outside temperature is 44.3°C and inside temperature is 31.8°C, with a difference of 12.5°C, while the minimum outside temperature is 34.8°C and the inside temperature is 27.5°C, with a difference of 7.3°C. B-2 present the maximum outside temperature in 54.9°C and inside temperature is 33.4°C, with a difference of 21.5°C, while the minimum outside temperature is 36.2°C and the inside temperature is 30.2°C, with a difference of 6°C.

On the other hand, in the case of corrugated zinc sheet in B-3, the maximum outside

temperature is 51.6°C and the minimum inside temperature is 50.5°C, with a difference of 1.1°C, while the minimum outside temperature is 42.5°C and the inside temperature is 35.4°C, with a difference of 7.1°C. B-4 present the maximum outside temperature in 55.5°C and inside temperature is 54.2°C, with a difference of 1.3°C, while the minimum outside temperature is 41.4°C and the inside temperature is 36.9°C, with a difference of 4.5°C.

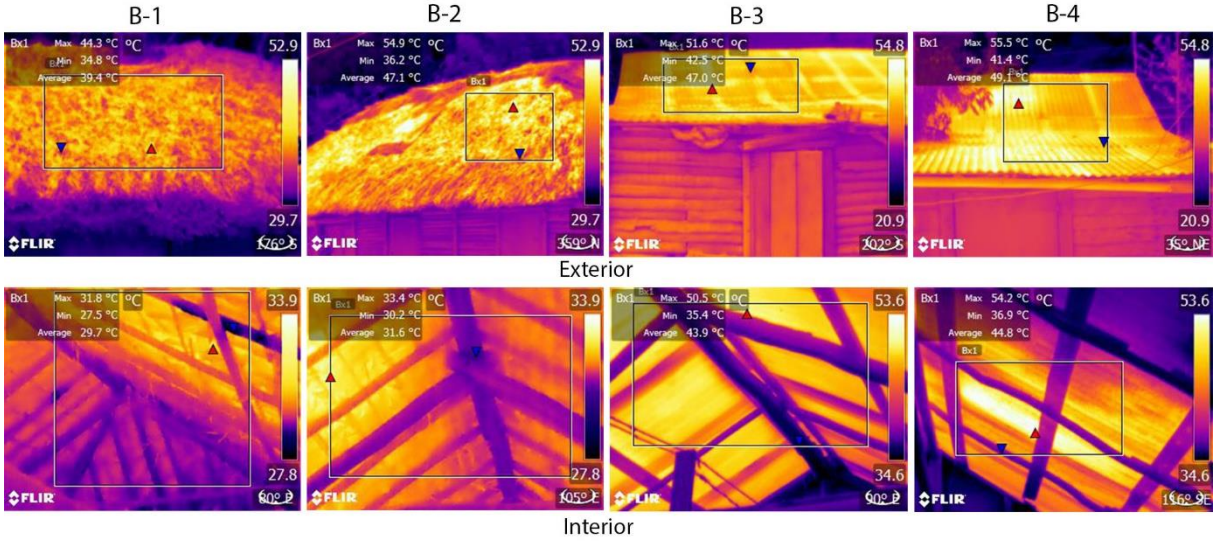


Figure 5. Exterior – interior thermal images of the roof

5 CONCLUSIONS

The cana palm leaf showed better thermal efficiency than corrugated zinc sheet, providing lower values of radiant heat load and surface temperatures, as well as lower temperatures inside the houses. In the case of cana palm roof the maximum difference temperature between outside and inside is 12.5°C and 21.5°C, while in the corrugated zinc sheet this difference is 1.1°C and 1.3°C, obtaining in the interior practically the same temperature as in the exterior.

We can observe that the indoor ambient temperature at B-1 and B-2 is similar to the maximum surface temperature of the roof material. In the case of B-3 and B-4 there is a great difference between these temperatures, due to the construction system that creates some openings between the sills and the roof, allowing the inside ventilation.

Using infrared thermography, it was possible to produce heat maps to quantify surface temperatures and thus observe and evaluate the thermal efficiency of both materials. This process helped to understand the processes of heat transfer between surfaces, confirming in this research that the thatch roof is much cooler and transmits less heat to the interior than the metal roof.

Acknowledgements. The authors would like to thank *Oficina de la Obra y Museos de la Catedral de Santo Domingo*.

REFERENCES

[1] Prieto Vicioso, Esteban. “Dominican bohio. Origins and evolution”, in *Vernacular Architecture Reflections. Challenges and future,* editorial coordination by Marwa Dabaieh and

Valeria Prieto, CIAV-Icomos, pp. 88−109, 2016.
[2] Navarro González, P. *Estudio de los armazones de cubierta de la construccion rural y vernacular de Gran Canaria. Aanalisis Estructural y constructive*. Tesis doctoral, Universidad de Las Palmas de Gran Canaria, 2012.
[3] Molina Huelva, M. & Fernández Ans, P. "Evolution of Thermal Behavior in Stone and Thatched Roof Traditional Houses. Enhancement of a Sustainable Model in Northwest Spain", in *Revista de la Construcción*, Vol. 12 No 2, 2013.
[4] Guevara Lactayo, M. A. & Román Chipoco, L. E. "El techo de Mojinete como parte de la arquitectura vernácula y su connotación térmica, Moquegua, Perú", in 16° Seminario Iberoamericano de Arquitectura y Construcción con Tierra (SIACOT), 2017
[5] De Almeida, G.; Pandorfi, H.; Baptista,F.; Guiselini, C.; Barnabé, J. "Thermal efficiency of individual shelters for Girolando calves in Brazilian semi-arid regions", in *Journal of the Brazilian Association of Agricultural Engineering (Eng. Agríc.)*, Jaboticabal, V.36, No.1, Jan. /Feb. 2016, p.13-23. Doi:http://dx.doi.org/10.1590/1809-4430-Eng.Agric.v36n1p13-23/2016
[6] Chandel, S.S.; Sharma, V. and Marwah, B. M. "Review of energy efficient features in vernacular architecture for improving indoor thermal comfort conditions", *Renewable and Sustainable Energy Reviews*, 65 (2016) 459-477. http://dx.doi.org/10.1016/j.rser.2016.07.038
[7] Torres Quezada, J. E. *Comportamiento térmico de la cubierta en clima cálido húmedo. Repercusión energética del edificio*. Tesis doctoral. Universidad Politécnica de Cataluña, 2018
[8] McKnight, T.; Hess, D. "Climate Zones and Types". Physical Geography: A Landscape Appreciation. Upper Saddle River, NJ: Prentice Hall. 2000.
[9] Ministerio de Medio Ambiente y Recursos Naturales RD. Informe GEO: Capítulo 1, Contexto Geográfico y Socio Económico. MEPYD, RD, 2009.
[10] Tpi USA. 1010a, Indoor Air Quality Meter. https://www.testproductsintl.com.
[11] Kylili, A., Fokaides, P.A., Christou, P. & Kalogirou, S.A. Infrared thermography (IRT) applications for building diagnostics: A review. *Applied Energy*. ELSEVIER. Volume 134, 2014, pp. 531–549. https://doi.org/10.1016/j.apenergy.2014.08.005
[12] National Society of Master Thatchers (NSMT), 2012
[13] Fluke Corporation, Emissivity values of common materials, 2007

12th International Conference on Structural Analysis of Historical Constructions
SAHC 2020
P. Roca, L. Pelà and C. Molins (Eds.)

TO REACH THE LIGHT: THE MONUMENTAL BYZANTINE STAIRS OF CAESAREA, A CONSERVATION AND RESTORATION PROJECT

N. MAKLADA[1*], S. HADID[2], D. ABUHATSIRA[3], P. GENDELMAN[4], Y. OZ[5], AND D. SIBONI[6]

[1] Conservation Researcher, Conservation Department, Israel Antiquities Authority (IAA)
Rockefeller Musem, P.O.B 586, Jerusalem 91004, Israel
e-mail: nabe26@gmail.com

[2] Rappaport Faculty of Medicine, Technion-Israel Institute of Technology

[3] Conservation Planning Office, 3 Har Shlomo, St, Or Akiva 306000, Israel

[4] Archaeological Research Department, Israel Antiquities Authority

[5] Schaffer & Ronen, Conservation Engineering, 33 Jaffa St, Jerusalem 94221, Israel

[6] Conservation Manager, Conservation Department, Israel Antiquities Authority

Keywords: Caesarea, Byzantine Staircase, Maintenance, Sandstone, arch bridge, vault.

Abstract. *Ancient Caesarea has founded in the years 25-10 BC and named after Emperor Augustus. Throughout history, from the early Roman until the Byzantine period, Caesarea was a major city and one of the largest and most important port cities in the Mediterranean. During the Byzantine period, the city encompassed an area three times larger than that delimited by the Herodian wall and became an important center of Christianity. The monumental stairs led to the Byzantine Octagonal Church built upon giant arch above the remains of the enormous Roman stairs of Augustus temple. Stairs led a large number of people from the vast harbor, to the Temple platform. The Byzantine arch located 17 meters from the ancient quay, is 8 meters width and 4-meter long, built with specific technology from local sandstone named Kurkar. The arch fall after the Byzantine period and the staircases severely damaged due to the long exposure of almost 1500 years and environmental conditions such as capillary rise, daily winds carrying sand, high temperature, moisture, salts, and deliberate destruction, for instance, stones robber and collapse parts from the wall. The characteristics of the Kurkar with sustained deterioration and this environmental condition have led to different conservation problems, at various levels of severity erosion, the disintegration in both bonding materials and stones. The conservation measures' purpose is to stop the ongoing weathering process and prevent a deterioration state of the staircases, to restore the arch and stabilize the structure of the stairs to carry 48 tons of the restore arch. The findings of the project show that a suitable solution to ensure effective and sustainable protection of complicated staircases structure from destruction and various weathering condition to carry new massive arch depends on understanding the*

ancient application of building technologies and techniques, the use of original bonding material, integrated monitoring, and ongoing maintenance.

1 INTRODUCTION

The city of Caesarea was founded adjacent to the Mediterranean Sea between Jaffa and Dor (Fig. 1), on the site of the abandoned Hellenistic town "Straton's Tower". Herod king of Judea under Roman aegis made Caesarea the administrative capital and the main harbor of his vast kingdom. The city was named after Caesar Augustus, Herod's patron, the first Roman emperor. It continued to develop and prosper even more in the Byzantine period. In this magnificent port city and its rural hinterland, "prices are low, their abundance obtains" (Jerusalem Talmud, Kil'ayim 9:4, 32c; Ketubot 12:3, 35d).

In the Byzantine era, the city reached its ultimate expansion and encompassed an area three times larger than that delimited by the Herodian wall. The archaeologist Patrich (2018) noted that Until the fifth century, the city developed and spread beyond the course of the Herodian wall without having an outer defense wall and covered an area of some 275 acres.

The Roman temple has built on a Kurkar hill rising high in the center of the city above the port. The foundation remains of the rectangular temple were placed in it faced the port. The architectural elements found dispersed, enable the researchers to reconstruct a Corinthian temple with six columns on the front (*hexastyle*) [3]. With the spread of Christianity and the oppression of paganism, in the middle of the fourth century, the temple was no longer in use, and his stones slowly looted for other building projects, so all that remained were walls of the foundation level [2]. In the year 500, an *octagonal church* enclosed by a square has erected on the ravaged site. Like the octagonal church on Mount Gerizim, this may also have been the church of Mary *Theotokos* [1]. Discernible in the foundations of two octagons, an external one that bore the walls and an internal that supported the columns.

The Temple and after that, the Octagonal church situated on an elevated platform formed the sacred precinct (*temenos*). A wonderful view of the harbor seen from the octagonal church [3]. The eastern retaining wall was curvilinear, the western one ran parallel to the harbor quay, the south and north retaining walls ran perpendicular to it boundaries a large area. The Temple platform was expanded and leveled by a network of walls and a longitudinal vault system on the platform west side [1]. Four large one on the north and south side in dimensions of 25x5 m, and six smaller massive east-west vaults 20x2.5 m, on the front of the temple, adjacent to the altar, and part of the construction staircase system on the temple's central axis, proceeding to the temple above [3]. It was founded on bedrock and built of finely dressed Kurkar ashlars with draft margins surrounding a high or shallow central boss.

At the edge of the piazza in the Roman era adjacent to the quay and on the temple's symmetrical axis, was a massive pier, 20-meter width, and 10-meter length, that housed a staircase leading up to the temple platform [1]. Access to it was from the eastern side of the pier. Thus, the rise began from east to west and continued higher at 180 (degree) turn from west to east. This massive pier supported a bridge with two vaults that existed in the interval between the visible pier and the western (*temenos*) wall, leading to the temple platform. This massive Roman pier disassembled in the Byzantine period, and a new staircase pier system built in its place, the new system included one vault and elongated pier from east to west in dimensions of 10-meter width and 20 meters long [3]. The Byzantine staircase built in the center of the piazza

and went 8 meters inside the quay climbing the stairs begins from the new extension at the western side to the east this massive pier supported a bridge of vault leaning against six east-west vaults from the Roman period and continued higher proceeding to the church above the platform.



Figure 1: Caesarea antiquities heading north. Mites to Michael Peleg, Israel Antiquities Authority, 2019.

The proximity to the sea with dunes and sandstone ridges covers the area, creates a unique climatic condition that accelerates deterioration factors. The ongoing exposure to severe weathering and erosion eventually led to considerable damage. No scientific study has been done on the durability of conservation intervention influence found in harsh climatic conditions like Caesarea ruins. The findings in the field show that understanding the ancient application of building technologies and techniques combined with the use of original bonding material and traditional building technologies reduces damage to various elements and stabilizes the structure to carry a new massive arch, in addition to the need for constant maintenance.

The monumental Byzantine stairs Conservation project started in 2017, applying original bonding materials and traditional building techniques that were implemented with analysis of the archeological and architectural findings to deal with the deterioration and conservation intervention. This case study aimed to resuscitate and stabilize the (*temenos*) wall with the pier and stop the weathering factors by keeping a complicated structure consisted of Kurkar stone; each one endures centuries of history.

2 BUILDING TECHNOLOGY

Caesarea city built from local sandstone named Kurkar 2000 years ago, the stone hewn from the hills around the city. In Israel, the sandstone ridges existing near the Mediterranean Sea and parallel to it, from the north to the south. The ancient architectures and engineers use the local stone to build the city and plaster it with white plaster [3].

The monumental staircase led to the Byzantine Octagonal Church built from two different

structures; an enormous pair on the west side near the quay and six smaller massive east-west vaults 20x2.5 m in the east side adjacent to the alter on the front of the Church central axis. The structures connected with a giant arch in dimensions; 8 meters width, 8-meter-high, and 4-meter long (Fig. 2).



Figure 1: The monumental stairs, arch bridge, and the six small massive vault in the east side. Mites to Danial Siboni, Israel Antiquities Authority, 2020.

The enormous, elongated pier is 20-meter long and, 10-meter width from east to the west leading up to the arch bridge, constructed gradually in rows from huge decorative parts of the Roman dismantled Temple. This massive pier supports a bridge of arch against the western (*temenos*) wall of the six east-west vaults.

The six massive vaults from the Roman period continue to be in use without any change in structure also in the Byzantine period. This vaults system bounded with four big vaults 25x5 m on both the north and south sides supported the Roman Temple platform (Fig. 2). These vaults were founded on bedrock and built of finely dressed Kurkar ashlars [1]. The surrounded wall is 2.6 m in thickness and constructs from ashlars stones with draft margins surrounding a high or shallow central boss on the exterior side and ashlars stone without boss internal. The vaults built above the wall in width 1.5 m and including passages with two arches in each wall the arch width of 2.3 m construct from ashlar stones, each one of the vault entrance and windows to the port at the west side. These walls and vaults built with different construction technology using ashlar stone integrated with lime, earth, and rubble casting, a similar technique on the first five vaults the casting incorporated in the carried wall its begins and ends at the height range of the aisles arch, despite the last vaults casting together with the carried wall (Fig. 2).

The following table illustrate the carried walls number and the different on construction technology, from top to bottom.

Table 1: The table demonstrate the six vault construction material order from top to bottom.

Carried wall	*1 and 2*	*3 and 4*	*5*
Vault	Stone	Stone	Casting
Ashlar stone	4 lines	1 line	-
Casting	80-90 cm	180-200 cm	200 cm
Ashlar stone	6 lines	6 lines	6 lines

2 ASSESSMENT PROCESS

Considering approaches to restore, conserve, or other forms of change, it is vital and fundamental to the conservation planning process to understand the significance of a historic building or objects and the values that contribute it, tangible and intangible.

The condition survey should include an investigation work to determine the original construction and materials, archaeological analysis, causes of decay and deterioration, evaluate threats, and identify priorities for intervention.

Determining conservation and restoration requirements adopted decisions taken regarding appropriate types and levels of intervention depend upon sufficient information being gathered during the assessment process to grant long-term care for the heritage properties**.**

2.1 Environmental problems

Structures, elements, and ruins face gradual deterioration agents from use and weathering factors that determine the decay of building materials. The primary influence on a building typically is very complex and depends on the environmental problems to which it is exposed since it includes suffering from accidental or deliberate damage as previous inappropriate repairs. Also, they are in danger of sudden events such as natural disasters.

Try to understand patterns of complex environmental problems, for example, storm damage, pollution, moisture, salts, flooding, or traffic vibration. The position, construction, and even the materials of the building should consider into account. As a result, the exterior environment of any building will always be unique [6].

2.1.1 Moisture

Water is one of the most critical factors in the deterioration of the stone. Like all porous building materials, the stone is hygroscopic, meaning it has a strong attraction to water and will absorb moisture from the atmosphere or the ground until it reaches equilibrium with its environment [2]. Inside a block of stone, water can exist as a liquid, as a vapor, or as ice in cold condition. While atmospheric humidity increases, porous stones absorb water vapor readily, which it will release as the humidity drops. If the stone is coldish and the air is damp, water vapor will condense to form a film of liquid water on the surface or inside the pores.

Groundwater can be drawn into stone by capillary action, and rainwater can penetrate through building flaws such as open joints, cracks, or soil [4]. In the winter, the source of moisture is a catastrophic event such as a storm, flood, and sea waves. It is critical to many deterioration processes, no matter how they penetrate to stone masonry – through the bonding material or the stone itself. The most common consequences are:

- Transport and crystallization of salts on and within the stone.

- Swelling of clay minerals that can lead to splitting and cracking.
- Growth of plants.

2.1.2 Salts

Contaminants existing in all building stones, and soluble salts are one of the most commons. Their origin is different, including soils, bonding material, biological matter decayed, sea spray, waves, and pollution.

Some will be inherent in the stone, having been incorporated during formation or carried in later by percolation, others may have been absorbed during construction or repair, chiefly from mortars, but most are carried in after building by rain, groundwater, and waves [2]. Liquid water can travel rapidly within the pores at the stones and bonding material, or the surface of the stone. They were dissolving salt and carrying them through the rock fabric and depositing them wherever the liquid flow stopped. Surface crystallization 'Efflorescence' can be unsightly, usually made up of very soluble salts. Less-soluble salt may crystallize within the pores 'Cryptoflorescence', breaking apart the stone, crumbling bonding material, causing powdering and flaking. Cryptoflorescence may also occur where there is rapid drying, such as on the corners where the wind is faster [6].

Damage to stone is worst where there frequent wetting and drying, resulting in cycles of crystallization and dissolution. Salt damage will tend to be apparent in the evaporation zone: the various area between being damp to dissolve the salts and dry enough for them to crystallize [5]. These salts may dissolve again when the available moisture level rises. The location of such zones will often give a clue to the source of the moisture.

Salt affected by many factors, including the chemical components of the salt, the physical characteristics of the pores, the pore moisture content, the humidity and temperature of the ambient air, the temperature of the stone, and the rate of evaporation. Despite these factors, salt behavior is still not wholly understood regarding the differences in salt mixtures behavior. Generally, salt problems will often be active over a wide range of ambient conditions.

2.1.3 Vegetation

It is unquestionably that vegetation in certain circumstances may be masonry protective; indeed, it is benign in several cases where plant growth does damage to the stone. Plants are one of the most common problems in the masonry, existing different plants in various sizes growing on the monuments [6]. Annual and seasonal plants proliferate in cracks but usually die before reaching a large extent, do not cause them, and will not grow in a way that causes more damage. Woody and perennials founded on vertical and horizontal surfaces can be vigorous, producing masses of stems that can dislodge the stone.

Usually, vegetation presence can be indicative of a problem such as open joints, cracks, and water ingress. Trees and shrubs can damage masonry if they are allowed to establish themselves. Plants grow in the soil adjacent, and on the top of the masonry, the roots entered the bonding material between the stones, which is the relatively soft material, disassembled and pushed the rocks around them and expedited the process of weathering.

2.1.4 Maritime environment

Waves can be devastating since it arrives with no warning. It can introduce soluble salts and

other contaminants into the masonry. The greatest danger arises from the drying-out period after the stream. The Mediterranean Sea waves caused by coastal storm-surge are a significant weathering factor. During the winter, waves crash over the masonry causing erosion of mortar and stones, also bring lots of salts into the ruins [5].

Wind with sand and salt causes rapid and increased erosion of bonding materials and stones. Fragments of water splashed into the air from waves able to reach considerable distances carried on the winds. This maritime environment has to be taken into account when trying to understand a problem related to chlorides.

Temperature plays a significant role in several decay processes, such as salt crystallization damage caused by quick evaporation in saturated porous stone, differential expansion and contraction of dense salt-laden crusts on sandstones and limestones.

Deterioration and destruction factors mentioned above, cause erosion and crumbling bonding material, including stones. There is essential to think from a comprehensive perspective about these various conservation problems in order to find suitable solutions.

3 CARE AND MAINTENANCE

The successful repair of stone relies on understanding the practical issues relating to the material and its environment, also considering those within the context of its historical and cultural significance. The priority of a stone conservation program is to deal with the causes of any ongoing deterioration; this may well involve work to other parts of the building and require the input of specialists other than stone conservation or masons. Once the underlying causes of deterioration are detected, treatment and repair options can consider.



Figure 3: The stairs and the arch bridge heading south. Mites to Danial Siboni, Israel Antiquities Authority, 2020.

3.1 Vegetation Uprooting

Seeds germinate quickly in open joints, wall tops, and any surfaces where soil can accumulate. Although many smaller and non-invasive climbers are harmless to masonry walls,

some mature creepers, shrubs, and trees will cause irreversible damage. The most effective treatment is proper maintenance, but there are many situations where vegetation has already been established and should remove. The plants should be trim close to the wall face or the ground so the condition can adequately check, and root systems can then poison. When plant roots rot away into walls, voids will manufacture, this allows water penetration, and eventually, masonry becomes loose. In this case, it is essential to perform treatment; it may require some excavation of joints, grouting, and pointing. Vegetation clearing is a crucial stage for preservation.

3.2 Pointing

Existing pointing can provide evidence about the materials and techniques used in the construction and later interventions. Repointing is the most common intervention on masonry because even the best mortar may tend to erode and need replacement. Although pointing may amount to as little as 5% of the surface area, it will affect the total appearance and behavior of the masonry. Repointing should match the original in color, texture, design, and application.

Table 2: Material used in the project inside the structure walls was in ratio of 1 lime to 2.75 aggregates.

Materials	*Amount (ratio)*	*Aggregate size [mm]*
Lime Putty	1	0-1
Chalk Powder	0.5	0-2
Quarry Sand	1	1-2
Arad Sand	0.5	1-3
Washed Sea Gravel	0.5	2-4
Crushed Charcoal	0.25	0-2

Light gray mortar with flecks of charcoal and shell pieces served as the bonding element with the bedrock inside the staircase walls (Table 2) on the façade between the ashlar stones bonding material is whiter (Beige) and harder to be durable to the environmental factors (Table 3).

3.2.1 Preparing the joints

The existing mortar should remove to a depth of at least 25 mm, or twice the joint width to provide sufficient space. Notably, for thin joints, this rule may need to be modified, but it is always essential to have adequate depth to allow the new mortar to function effectively. Loose dust needs brushing away, and joints flushed out with clean water.

3.2.2 Applying the pointing

The wall should be damp to encourage good bonding between the new mortar and the stone. The material should be placed carefully and pressed well into the joint until overfilled, keeping it away from the face of the masonry. Deep and wide joints may need pre-wetted shards of Kurkar stone or pieces of pottery pushed into the mortar. The weather must be suitable; high temperatures or high winds will dry the material too quickly, inhibiting carbonation. The wall should cover with damp canvas and plastic sheeting during the process and for some time

afterward to slow drying the new pointing.

3.2.3 Surface finishing

When the material is no longer wet, but before it has dried up, it should be pressed back into the joint using the appropriate pointing tool to ensure a good bond with the masonry. At that point, when the material is leather-hard, the surface can finish by beating it with a stiff bristle brush to expose the aggregates and perforate it. This action will give not only visually appropriate open texture but also helps water evaporation and allows air to ger into the material to aid carbonation.

3.2.4 The main stage in successful repointing:

- Removal old and precarious pointing.
- Cleaning out the joint using a hand-held blower.
- Wet the joints thoroughly.
- Apply the pointing.
- Compress the material with a pointing tool of suitable width.
- Allow mortar to take an additional set.
- Cut back the material to a slight recess around the stones.
- Strike the surface with a churn brush.

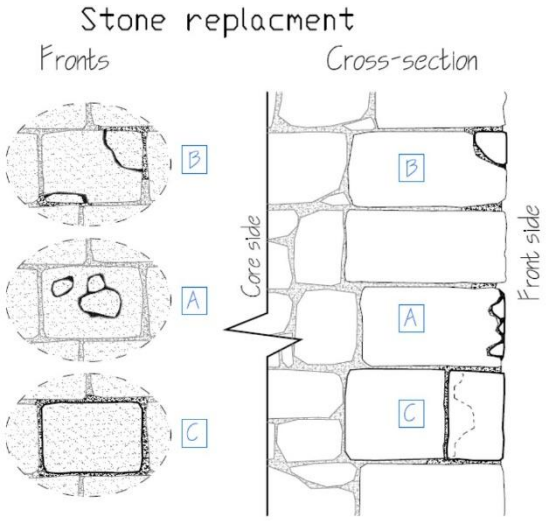


Figure 4: Sketch summarizes the intervention in stone.

3.3 Stone replacement

The replacement of stones has always been a fundamental part of historic building repair. The requirement for authenticity demands that proposals for replacement of stone are carefully and rigorously justified [4]. Repairing stone elements *in situ* plays a substantial role in building conservation. Its design to prolong the survival of stonework by stabilizing faults, filling voids or cracks, and protecting the building architectural from current and historical decay. For

example, crack encouraging and accelerating further deterioration when the moisture gets in and widens as debris accumulates within them. Eventually, these changes may lead to major structural weaknesses. As a general rule, replacement stone should be the same geological type and appearance, both in color and texture, as the original [5].

The aesthetic effects of replacing stone can also be significant. It is essential to be accurate when taking templates and working the stone. Good mason will help the diminishing contrast between the new part and the original around it (Fig. 3) by ensuring that joint widths around the new stone match the original and that the surface has an appropriate finish. Stone intervention in the monumental stairs project divides into three categories [5] (Fig. 4).

A: A lightly weathered stone with 7-12 cm façade cavities.

B: Stone with edge cavities from 12 cm to half stone façade.

C: A severely damaged stone, over a half-face is missing.

The process of replacement starts with removing the old stone minimum amount of decayed should be removed, with particular care taken to save the adjacent material. Sharp chisels and stone saws used to cut out small parts, but for larger ones and complete stone, it is necessary to use a non-percussive drill, an electric hammer, or an angle grinder. Once the stone removes, all debris in the cavity must be clean. The process of replacement starts with removing the old stone minimum amount of decayed should be removed, with particular care taken to save the adjacent material. Sharp chisels and stone saws used to cut out small parts, but for larger ones and complete stone, it is necessary to use a non-percussive drill, an electric hammer, or an angle grinder. Once the stone removes, all debris in the cavity must be clean. The next step in the process is cutting the new replacement stone to the required size ('sawn six sides') from the appropriate antique stone. Restoration of historic stonework detail requires some hand-cutting by chisel and hammer.

Eventually, to install the new replacement stone, the cavity should be well damp, and then a bed of mortar (Table 3) is applied to the back of the hewn space, base, and other side joints. Previous to being into place, the replacement stone should be quite wetted to stop it sucking moisture from the material, especially with the Kurkar sandstone, which absorbs large amounts of water. If necessary, lead, stone fragments, or pottery can be set into the joints to maintain the position of the new stone and prevent the mortar from slumping. The process of stone replacement differs from one category to another: (Fig. 4).

A: complete small cavities in the stone façade with paired stone.

B: fill cavities at the edges using a stone with a straight face and sides.

C: removing the front of the damaged stone to a depth of 25-30 cm and complete it with antique ashlar stone.

Table 3: Material used in replasing stones was in a ration of 1 lime to 2.5 aggregates.

Materials	*Amount (ratio)*	*Aggregate Size [mm]*
Lime Putty	1	0-1
Chalk Powder	0.5	0-2
Quarry Sand	1	1-2
Arad Sand	0.5	1-3
Sea Gravel	0.5	2-4

3.4 The arch bridge restoration

Casting technique gives the structure flexibility and elasticity an example of this; the carried vaults wall stands firm 2000 years to these days. The arch bridge was constructed in the interval between the apparent massive pier and the western (*temenos*) wall, holding the stairs leading up to the Church platform. In the Byzantine period, the arch built lower than the Roman one, the carve into the temenos wall 35-40 cm in-depth, and built the arch bridge with the stairs above it. The new restorer arch built from new ashlar sandstone made of the same geological type the architect divided the arch bridge into seven-line of stone from each side and line number eight as a keystone.

The arch bridge restoration project starts with placing iron mold to hold the stones every one weighs an average of 400 pounds carried out by a crane while the aggregate weight of the arch is 45 tones. The construction began on one side and continue the following day on the other side to make a balance, every day we built one line of stone, each one needed to be adjusted, occasionally cut, and rubbed [7]. We have to be very precise to construct an arch stone should be balanced and facing towards the center point of the arc and located at the same radius distance. Keystone should be placed in one day to lock the arch and start shifting the weights aside and down to the walls.

Bonding material used to connect the arch stone is a hydraulic mortar based on natural hydraulic lime (NHL 5) mixed with 2.5 well-graded aggregate, sand, and crushed stone. To aid workability Lime Putty added up to a maximum of 10 % to the mixture.

4 SUMMARY

The monumental Byzantine stairs are one of the remarkable architectural and archeological findings in the administrative area of Caesarea ancient city. The cultural and archeological significance of the project besides revives the place spirit that is the central concern in Caesarea's historic fabric. Proper planning, monitoring, and ongoing effective maintenance are vital to the stone building long-term preservation, obviate the need for more disturbing and costly intervention also sustain the heritage values of the building: a principal aim of conservation.

The goal of the project presented in this article is dealing with severe damage to the staircase caused by ongoing exposure to harsh weathering conditions, either stabilize and capability the stairs structure to restore the massive bright arch. The project involved detailed documentation of the staircase: assessment of the stones' current condition, detailed treatment program, investigation on stone deterioration state, also adjusted and detailed restoration program.

The findings of the project show that to deal with restore a new bridge arch, a challenge that the Roman and Byzantian faced thousand years ago and overcame it with the knowledge and technology that was available then, it is vital to bring to life and use traditional building technologies either original bonding materials integration with contemporary technology and information. Through experience and in-depth observation of things, we can overcome the challenge we face today.

Since it is not possible to avoid deterioration, a regular inspection and maintenance program is an essential and suitable solution. The new intervention must adopt the conservation principles to be durable and stable against environmental conditions, either identified and reversible.

We cannot think about existence without history and tradition that have defined roles. We are responsible for balance history and modern technology in professional ways. With all these heritage values around us, we have to be curious about discovering new knowledge that will help us to develop. There is a vast heritage to look after, to carve memory, and to preserve for the next generation. Thanks to conservation work and restoration of Byzantine period visual integrity for reviving the spirit of the place, the staircase structure that has disassembled and was in a coma for 1380 years brought to life.

REFERENCES

[1] Ayolon, E. and Izdarechet, A. *Caesarea Treasures*. Jerusalem, Vol. I., (2011), pp. 93-96, Vol. II. (2011), pp.169-180.
[2] Fuhrmann, N.Y. and Porath, Y. *Ancient Caesarea: Conservation and Development of a Heritage site.* Israel Antiquities Authority, Jerusalem (2017), pp. 3-7.
[3] Joseph, P. *A Walk to Caesarea: A Historical Archaeological Perspective.* Jerusalem (2018), pp. 1-8, 30-40.
[4] Maklada, N. Caesarea: Conservation of the South Wall. *Conservation of Cultural Heritage*. Conservation Administration, Israel Antiquities Authority, Jerusalem, Vol. I., (2018), pp. 48-52 (In Hebrew).
[5] Maklada, N., Saad, Y., Schaffer, Y., Gendelman, P., Sha'altiel, Y., Greenfeld, E. and Rosental, I. The Crusader Wall of Caesarea Resurrected: A Conservation Stonework Project, In: Siegesmund, S. and Middendorf, B. (Eds.): Monument Future: Decay and Conservation of Stone, Proceedings of the 14th International Congress on Deterioration and Conservation of Stone, Vol. I., and Vol. II, Mitteldeutscher Verlag (2020), pp. 817-822.
[6] Odgers, D., Henry, A., Martin, B. and Wood, C. *Stone: Practical Building Conservation*. English Heritage. Ashgate Publishing Limited, Farnham, UK, (2012), pp. 47-67.
[7] William, R.P. *Practical Masonry*. Fifth Edition, London, (1904), pp. 11-18.

Acknowledgements. The conservation and restoration work in Caesarea National Park were held due to the Caesarea Development Corporation and funding from the Edmond de Rothschild Foundation for their generous donation which enabled the operation of this project. Many thanks also to the Israel Antiquities Authorities and the Conservation Department for management the archeological excavation with conservation and restoration the archeological ruins. Last thanks to my amazing wife for constant support and encouragement that never ends and Shada Hadid for the spelling checking.

12th International Conference on Structural Analysis of Historical Constructions
SAHC 2020
P. Roca, L. Pelà and C. Molins (Eds.)

TYPOLOGICAL CHARACTERIZATION OF ANCIENT TOWN WALLS FOR DISASTER PREVENTION AND MITIGATION: THE MO.M.U. PROJECT

ANNA DE FALCO[1], FRANCESCA GIULIANI[1]*, DANIELA LADIANA[2], LEDIANA RJOLLI[1], DAVIDE BORDO[1], FRANCESCA GAGLIO[1] AND MICHELE DI SIVO[1]

[1] Department of Engineering of Energy, Systems, Territory and Construction,
University of Pisa, Largo Lucio Lazzarino, Pisa 56122, Italy, www.destec.unipi.it/

[2] Department of Architecture, University of Chieti-Pescara, Viale Pindaro 42, 65127 Pescara, Italy,
www.dda.unich.it/

*Corresponding author e-mail: francesca.giuliani@ing.unipi.it

Keywords: Town Walls, Masonry Structures, Risk Prioritisation, Heritage Conservation.

Abstract. *The problem raised by the steadily increasing number of failures in ancient town walls has recently attracted much interest. This typology of cultural heritage has always played a critical role in shaping local identities and still holds great potential as a cultural resource but poses substantial challenges in management terms. In fact, multi-disciplinary methodologies for their study and analysis are missing. The MO.M.U. project aims to safeguard ancient town walls in Tuscany (Italy) by introducing an integrated framework for their knowledge, diagnostic, assessment, monitoring and management. The proposed approach employs innovative non-invasive technologies and introduces a multi-hazard risk prioritisation methodology to address preventive conservation and programme interventions.*

1 INTRODUCTION

Nowadays there is a growing awareness of the vulnerabilities and exposure of Italian cultural heritage to natural hazards and human-induced threats. Approaches to risk analysis and reduction of immovable cultural heritage are usually based on typological considerations, thus identifying several architectural classes (e.g. ordinary buildings, churches, towers, palaces) accounting for their different response to any hazardous event. A peculiar class of historical constructions involves masonry town walls built as a defence system of the inner historic centre.

Ancient town walls play a critical role in shaping local identities and still hold great potential as cultural resources but pose substantial challenges in management terms. Although national regulations have been issued to improve the structural safety of heritage-listed monuments and buildings [1], a systematic strategy for Disaster Risk Reduction (DRR) of town walls is missing and actions for their preservation are still occasional. Recent damage suffered by historical town walls in the Region of Tuscany, specifically in the historic settlements of Volterra (2014), Magliano in Toscana (2012 - 2014), Pistoia (2011 - 2020),

Cana di Roccalbegna (2013 - 2020), Poggio a Caiano (2017) and San Gimignano (2018), have raised attention on the growing vulnerability of heritage of urban fortifications.

Preventive and planned conservation entails the protection of architectural heritage and is founded on the attentive identification of situations of risk and the systematic planning of minimally invasive interventions [2]. The knowledge of materials, technologies, stratifications and contexts is paramount and is able to favour a systemic approach. These aspects affect the correctness of risk analysis that requires a critical judgment founded on a reading and interpretation of the object to be preserved and the phenomena to which it is subjected. In the architectural heritage domain, simplified multi-hazard approaches represent a significant step forward in the prioritisation of risk reduction measures [3] [4] [5]. Moreover, qualitative index-based methodologies can identify situations when detailed assessments are needed [6].

Starting from 2019, the Regional Government of Tuscany is promoting a systemic research regarding walled historic centres with the objective to develop a fit-for-purpose methodology to inform risk governance in its territory. The MO.M.U. (MOnitoraggio delle Mura Urbane – monitoring of town walls) project brings an innovative contribution towards the analysis of ancient town walls in Italy, focusing on defining methods, technologies and tools for their multi-hazard risk analysis and monitoring. The project herein presented adopts a systemic approach to the organization of processes, ranging from the territorial scale to the more minute scale of individual elements, thus allowing for the multi-level risk prioritisation, preventive conservation, and maintenance. This paper explores the main failure events recently occurred in town walls with the objective to identify their root causes and the parameters affecting the risk assessment. Then, it presents the adopted methodological framework and the ongoing research activities, ranging from territorial to local level investigations. The research activities comprise the implementation of a GIS platform that allows for storing and elaborating diverse types of data. The architecture of the database has been defined according to the research scope and supports knowledge management for risk assessment and governance. The proposed procedure allows analysing risk and designing the layout of a monitoring system, thus allowing for the multi-level risk prioritisation, preventive conservation, and management of maintenance.

2 MOTIVATION AND AIMS OF THE PROJECT

2.1 Failure of town walls in Tuscany

Since 2011, numerous events regarded the collapse of town walls in Tuscany. The main events occurred in Pistoia (PT), Magliano in Toscana (GR), Cana di Roccalbegna (GR), Volterra (PI), Poggio a Caiano (PO) and San Gimignano (SI). In some cases, the collapse recurred after a few years.

Pistoia is an important city that still shows traces of its Gallic, Ligurian, Etruscan and Roman past. On September 19, 2011, a portion of about 25 meters of medieval town walls outwardly collapsed. The curtain wall facing the city centre remained standing and the outer layer crumbled (Fig. 1). The consequence did not result in deaths or injuries, but debris fell on some greenhouses, causing economic losses to agricultural activities. The collapse was triggered by heavy rain in an already critical situation. The main factors influencing the

collapse were the wall slenderness, its height, the difference between the floor levels on the two sides of the wall and the poor quality of the masonry. Walls are made of river pebbles and are weakened by texture irregularity, traces of poorly chosen interventions and lack of maintenance [7]. In September 2020, the same curtain completely collapsed for a length of 30 m. In this case, no extreme climatic events preceded the disaster.



Figure 1: Collapse of the city walls of Pistoia (September 19, 2011). On the left: the failure seen from the outer side; on the right: the failure seen from the city centre.

On November 13, 2012, the south-western tower of the medieval town walls of Magliano in Toscana collapsed. After the middle of the XVII century, they were no longer used for military purposes and their maintenance was neglected. This situation has favoured the construction of new masonry buildings adjacent to the curtain that was thus used as a load bearing wall. The so-called Torrione, about 20 m high and 9 m wide, was made of a stone masonry curtain covering a rocky outcrop in the lower part and containing the earth in the upper part. The structure suddenly collapsed following an extreme meteorological event. The upper part of the tower and the stone masonry debris fell on the road that luckily was not occupied by vehicles (Fig. 2). Consolidation works had been completed just before the disaster: the large and numerous full-height cracks had been closed and the joints repointed. The closure of these natural drainage holes probably caused the collapse during an exceptional rainfall, when the weep holes at the base were obstructed by a great amount of soil accumulated in the inner part of the tower.

After just two years, on December 15, 2014, a second collapse affected a portion of the curtain in the south-western area, following a further rainy event of considerable intensity and duration. The structure was a retaining stone masonry wall of about 8 m height and 17 m length. The collapse was caused by the water pressure on the back of the wall, due to the poor drainage system. The event was preceded by cracks and deformations that appeared on the wall since the previous July. Nevertheless, it was not possible to avoid the collapse which, however, took place without consequences, thanks to the preventive countermeasure provided in proximity of the road.

On October 5, 2013 about 13 meters of town walls collapsed during a heavy rainfall in an ancient small town, Cana di Roccalbegna (Fig. 3). The system was made of a stone masonry retaining wall dating back to the XV century, surmounted by a reinforced concrete slab which formed the base of a panoramic viewpoint square. The masonry was inhomogeneous in terms

of material and construction techniques. The failure was caused by the erosion due to incorrect water drainage and increase of hydrostatic pressure behind the wall during the heavy rainfall event. The rubble reached a building, which fortunately was only hit by minute debris, and the street below, where a parked car was buried. On 21 August 2020 the reinforced concrete slab suddenly broke during the execution of the consolidation works. Four houses have been evacuated and a part of the village has become inaccessible due to debris.



Figure 2: The collapse of city walls of Magliano in Toscana (November 13, 2012). On the left: the "Torrione" before the consolidation; on the right: the "Torrione" after the failure.



Figure 3: Collapse of the city walls in Cana di Roccalbegna (October 5, 2013). On the left: the collapse seen from below; on the right: the debris near the building below the wall.

On January 31, 2014 about 35 meters of the town walls in the south-western side of Volterra suddenly collapsed, after a series of heavy rainfall events. Volterra is a walled hilltop town in Tuscany, one of the most important Etruscan settlements, successively developed as a medieval centre. The failure involved a 9.5 m high segment of a stone masonry retaining wall that embraces the city centre, laying bare the foundations of the historical masonry buildings above (Fig. 4). Luckily, there were no casualties, but the buildings located at a distance of a few meters from the wall were slightly damaged. The main causes of the collapse are the incoherent sandy terrain behind the curtain wall weakened by previous repeated water infiltrations due to the old sewer system of the historic centre, and the water from the heavy rains of January, which increased the hydrostatic pressure on the curtain [8]. Added to this is the intrinsic weakness of the masonry of the collapsed portion, due to the significant and repeated restorations during time, from the middle age up to now. On March 3, 2014 another

failure affected the unstable wall corner located about two hundred meters from the above-mentioned portion toward the South. The collapse was preceded by some cracks on the irregular and inhomogeneous masonry wall. In that circumstance, a part of the embankment slid downwards, despite the remedial works with steel anchors.



Figure 4: The collapse of the city walls of Volterra (January 31, 2014).

As emerges from these emblematic cases, climate change and natural events are seriously affecting historical town walls, but even local technological ruptures can potentially cause the collapse of great sections. Two different hazard conditions can be thus identified: the first is associated to ordinary conditions, such as pollution, wind erosion, capillarity dampness, ground subsidence, and depends on the continuous and progressing actions of the ravages of time; and the second is associated with isolated adverse events, among which landslides, floods, earthquakes, lifelines failures have proven to be more frequent in Tuscany.

2.2 The MO.M.U. project: aims and activities

In the framework of the preservation priorities set by the Region of Tuscany, the two general aims of the MO.M.U. project are as follows:

- to strengthen the role of Local Governments in the preventive and planned conservation of ancient town walls and to raise awareness of the importance of disaster risk governance in the architectural heritage domain.
- to establish a regional multi-hazard risk prioritisation framework for the safeguard of town walls, applying knowledge from multiple disciplines.

Based on these general objectives, seven specific aims are established:

- to create a digital archive that documents the town walls' history, building technologies, construction phases, alterations and modifications, structural materials, past restoration and maintenance works.
- to define fit-for-purpose forms for data collection and organisation and to identify the most effective tools and technologies for the documentation of town walls.
- to identify typical deterioration and damage patterns of historical town walls, and to create a portfolio that accounts for the different materials (mainly stone and brick), architectural typologies (retaining, isolated and massive walls), territorial topography (coast, valley, plain, mountain), century-old transformations. The step requires a preliminary definition of a diagnosis methodology.

- to develop, calibrate and test a multi-level large-scale methodological model to assess the risks of ancient town walls based on specifically formulated performance demands.
- to create a GIS-based system for managing and elaborating georeferenced data and documents from diverse sources, as well as conducting risk assessments of town walls.
- to conduct benchmarking activities on a set of case studies by means of site inspections, surveys, documentation, risk assessment activities in order to test the overall framework.
- to define monitoring actions and intervention measures for planned and preventive conservation, using conventional and innovative technologies, such as Geographical Information Systems (GIS), GPS-based photogrammetry, interferometric Synthetic Aperture Radar (SAR) techniques.

3 METHODOLOGY

The procedure developed within the MO.M.U. project consists in a simplified approach to multi-hazard risk analysis and governance that can be used by officials and administrators in Local or Regional Governments who are not experts in the field(s).

Town walls are deeply integrated into the urban fabric and their accessibility can be difficult since many constructions, even private housing units, have been progressively reusing their structural elements. Besides, the application of invasive tests is not feasible due to the heritage value and the impossibility to alter the physical aspect. Therefore, digital non-invasive technologies have been included into the procedure due to their ability to support the data acquisition, collection, management and elaboration. The combination of traditional geometric surveys and more innovative techniques, e.g. GPS-enabled digital cameras, allows for a complete and extensive photogrammetric documentation of the town walls. Additionally, mobile applications facilitate the recording and collection of data during field surveys [9]. Emphasis is given to the development of a GIS platform that was specifically designed to offer a multi-level reading of the walled system, as well as enable risk evaluations [10]. Finally, interferometric synthetic aperture radar (InSAR) techniques, both space-borne and terrestrial, have shown their effectiveness in providing measurements of ground displacements [8].

The proposed multi-level methodology consists of four phases (Fig. 5) characterised by an increasing level of knowledge, detail and investigation effort. Each level is connected to the previous one and only the progression to the last level allows for establishing monitoring and intervention activities.

The ‘Level 0 - Inventory and geolocalisation’ phase aims to collect data on the town walls located into the Tuscany Regional territory and thus to gain large-scale knowledge on the overall number and main features for their management. Each walled system is analysed as a whole and documented accounting for previous studies, historical information and archival material. A specific GIS-based form, the ‘level 0 census form’, is developed for the purpose. It describes several relevant aspects of the walls, such as the orography, hydrography and topography of the territory, the construction typology, morphology, technologies and materials, the construction and transformation phases, and also the previous restoration and maintenance works. The form is organized in nine sections: (1) localisation and geomorphological data of the site; (2) general information and legal status of protection; (3)

general description and photographic archive; (4) current state; (5) accessibility and usability; (6) history and historical documents; (7) documentation of past interventions; (8) description of the context; (9) decomposition into homogeneous subsystems.

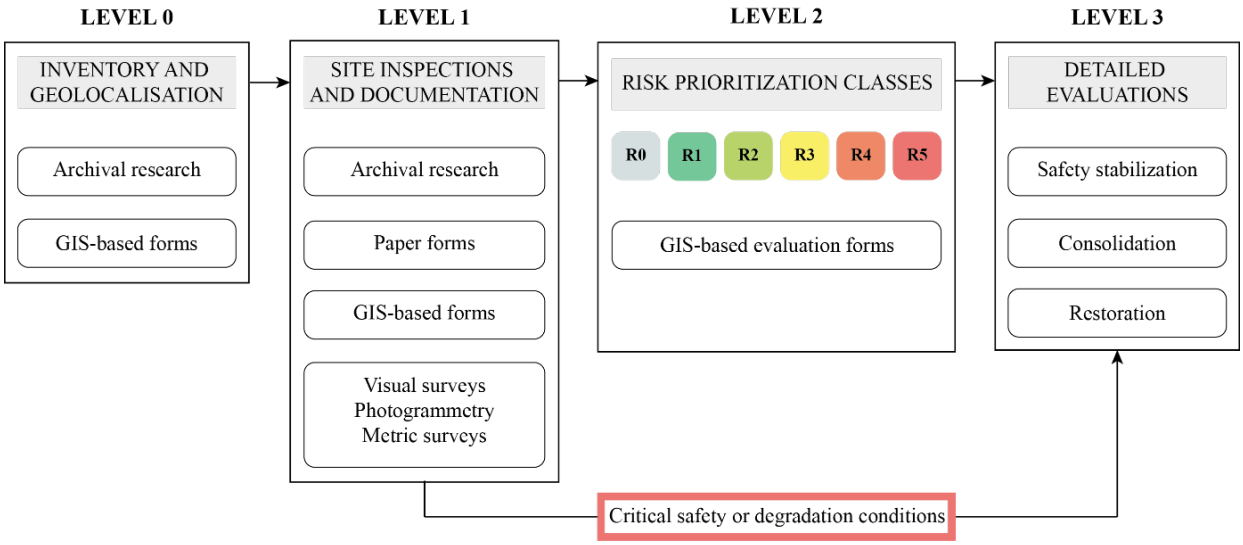


Figure 5: Multi-level methodology for the risk prioritisation and management.

The 'Level 1 - Site inspections and documentation' aims to investigate the town walls as subsystems corresponding to the morphological elements, namely identifying walls, towers, gates, bastions, etc. The knowledge of each element is improved by acquiring specific documents and conducting field surveys (metric, photogrammetric or visual) that can validate, correct and integrate the data collected for Level 0. Finally, this step allows for identifying critical safety or degradation conditions of the element. Their mitigation requires a rapid intervention or the activation of a diagnostic process, thus moving forward directly to Level 3 (Fig. 5). A 'level 1 documentation form' is developed entailing a detailed analysis of the elements, both on-site and off-site. To this end, the form can be filled in either on paper or on the GIS platform, perhaps using mobile GIS applications. The form comprises seven sections: (1) localisation; (2) historical, morphological, typological, geometrical and current state characterisation; (3) accessibility and usability; (4) material archive (masonry materials, stratigraphy units); (5) documentation of past interventions; (6) description of the context and hazardous conditions; (7) critical conditions to activate the diagnostic process and the intervention.

The 'Level 2 - Risk prioritisation classes' aims to evaluate risks on town walls by means of a simplified procedure that depends on six performance demands. The performances have been identified taking into account the heritage significance and past failures of Tuscan town walls. Risk is assessed as a function of hazards, vulnerability, and exposure [11], whose characterisation varies according to the performance demand, as specified in Tab. 1. Hazards account for progressive and catastrophic actions and can be identified according to hazard maps and data on past events in the area. Vulnerabilities are associated to ordinary or extraordinary conditions. The first ones are assessed by means of a fit-for-purpose form

regarding the surveyed degradation and damage processes that are scored with two parameters, magnitude and extension. Instead, extraordinary conditions are evaluated by means of hazard-specific forms that entail a preliminary identification of the elements exposed to each hazard. Finally, exposure refers to the walled system itself as cultural heritage, as well as people, objects, buildings, roads or any element that can be potentially damaged by the failure of the town walls. Six risk classes have been considered, ranging from R0 to R5 [5]: R0 is assigned to units that are not exposed to any hazard; R1 and R2 are associated with acceptable levels of risk requiring on-site inspections; R3 is at the limit of acceptability and therefore requires regular monitoring actions; R4 and R5 are associated to unacceptable and critically unacceptable levels, respectively. Each element is subdivided into a number of units on which the evaluation is performed by means of several GIS-based forms.

Table 1: Performance demands and risk factors of town walls.

Performance demands	**Description**	**Risk factors (H, V, E)**	
Safety and conservation	Material degradation and local stability	H_{sc}	weathering conditions, pollution, land subsidence
		V_{sc}	degradation and damage
		E_{sc}	town walls
Static safety	Stability under static loads and ordinary actions	H_s	weathering conditions, land subsidence
		V_s	degradation and damage, masonry quality, structural inhomogeneities, geometry, connections to adjacent elements, terre-plein, soil type
		E_s	town walls, people, physical assets
Seismic safety	Stability under seismic actions	H_{se}	earthquake
		V_{se}	masonry quality, structural inhomogeneities, geometry, connections to adjacent elements, terre-plein, soil type, openings, wall slenderness, reinforcements, adjacent buildings, topography
		E_{se}	town walls, people, physical assets
Flood safety	Stability under hydraulic actions	H_f	flood hazard
		V_f	soil type, type and depth of foundations
		E_f	town walls, people, physical assets
Landslide safety	Stability under geomorphological loadings	H_l	geo-morphological hazards
		V_l	connections to adjacent elements, type and depth of foundations, topography
		E_l	town walls, people, physical assets
Heavy rainfall safety	Stability under extreme meteorological loadings	H_r	precipitations
		V_r	soil type, drainage and water control systems, masonry quality, terre-plein
		E_r	town walls, people, physical assets
Lifelines rupture safety	Stability under actions induced by technological failures	H_{lr}	lifelines rupture
		V_{lr}	drainage and water control systems, masonry quality, terre-plein
		E_{lr}	town walls, people, physical assets

At first, the evaluator is asked to fill in the 'level 2 degradation and damage patterns form', which is based on the portfolio of typical damage and degradation patterns of Tuscan town walls. For each unit of the walled system, this form allows for defining a vulnerability index as the normalised weighted sum of the products between magnitude and extension scores. Then, specific vulnerability forms (V_{sc}, V_s, V_{se}, V_f, V_l, V_r, V_{lr}) are introduced to account for the liability of walls to be damaged under different actions (H_{sc}, H_s, H_{se}, H_f, H_l, H_r, H_{lr}), as defined by the performance demands (Tab. 1). The overall degradation and damage state is the basis for the vulnerability evaluation in every performance. Exposure is distinguished between the safety and conservation case (E_{sc}) regarding only the town walls and the other cases (E_s, E_{se}, E_f, E_l, E_r, E_{lr}) regarding town walls, people, and physical assets.

The 'Level 3 - detailed evaluations' involves detailed investigations and monitoring activities on town walls subjected to risk levels R3, R4, and R5. The step is mandatory to conduct safety stabilisation, restoration or consolidation works.

4 RESEARCH ACTIVITIES

4.1 Territorial census of Tuscan town walls (Level 0)

The territorial-level census regards 140 ancient town walls (Fig. 6) in Tuscany that are under investigation with the cooperation of regional and local authorities who are in charge of their preservation. The regional GIS-platform collects and georeferences the information requested by the Level 0 census form, such as archival documents, previous studies, historical images and recent photographs.

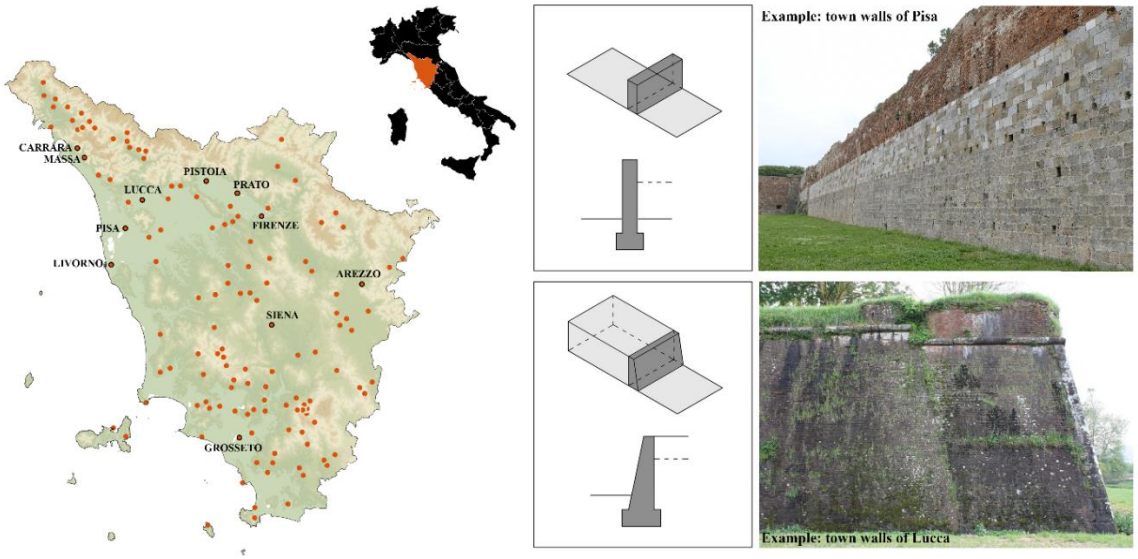


Figure 6: Multi-level methodology for the risk prioritisation and management.

The comparative analysis highlights a quite complex and varied picture, with similarities in the building techniques within geographical areas that were fortified in the same period by common governments, often over pre-existing defence systems. The configuration of the

walls is strongly affected by the territorial topography, particularly in mountain areas where fortifications were built as retaining walls over slopes and cliffs. Conversely, town walls located on valleys and plains present more regular shapes. Most walled systems date back to Medieval times, in some cases incorporating the more ancient defensive systems, particularly Etruscan in the Southern part of Tuscany.
A lower number of cases present Modern fortifications built approximately from the second half of the XV century. Medieval walled systems are usually composed of isolated, slender walls connecting high-rise towers, whereas Modern ones present thicker scarp-shaped sections and bastions, with terre-pleins behind the walls. Town walls are made of stone masonry (mainly Medieval walls) and brick masonry (mainly Modern walls) whose composition, geometry and arrangement depend on local materials and workmanship. Materials are often varied, and several building techniques can be found along the walled system, with many local alterations that can be difficult to identify. The current state is the product of century-old transformations that affect the structural homogeneity and the flow of internal forces within the structure. The wall texture bears signs of these changes, as well as past collapses and alterations, and may reveal the quality of the masonry and its attitude to crumble, especially under seismic actions.

4.2 Local investigations (Level 1 and Level 2): the town walls of Pisa

The town walls of Pisa date back to Medieval times, they were constructed starting from the XII century, using local materials, techniques and workmanship [12]. The overall length is approximately 7 km, the average height of the curtain walls is 11 m, and the mean thickness is 2.20 m. The structure is made of multi-leaf masonry, with two brick and stone outer-leaves and the inner core of rubble masonry. Today, the outer side of the town walls is fully accessible and unimpeded, except for localised areas where the sight is hindered by trees. Conversely, the inner side is almost entirely included in private properties and thus inaccessible.

The walled system comprises different morphological elements, such as curtains (codified as CUR), towers (TOR), gates (GATE), and bastions (BAS). Each element has been deeply investigated thanks to the Level 0 and Level 1 forms. Due to the massive dimensions of town walls, a rapid photogrammetric surveying workflow has been adopted in order to obtain results of the entire investigated portion in a reasonable time. Photographs were acquired using an iPhone 11 camera having a resolution of 12 MP and a 1/2.55-inch sensor, with GPS on. The acquisition was done over several days at different times, to have uniform illumination, avoiding strong direct lights and hard shadows. Ortho-images have been processed from 3D photogrammetry models.

The state of conservation and the structural conditions of the town walls of Pisa are quite varied and tend to be better in touristic areas with public accessibility. Some areas present critical conditions that may affect the structural performance, such as vertical cracks, out of plumbs, and corner failure mechanisms mainly caused by ground subsidence. The presence of differential land subsidence in critical areas is confirmed by InSAR vertical displacement measures that provide punctual time series of the last 5 years. Common degradation patterns concern higher plants, vegetation, superficial loss of materials, moisture and efflorescence.

Partial results are illustrated in Fig. 7, which shows the ortho-image of the portion including GATE.13 and CUR.27. The element is divided into units (labelled from 21 to 30) having a length of 2 m that have been evaluated by means of the Level 2 forms. Coloured stripes identify different risk levels: green squares are characterised by lower risk levels, while red ones present higher risk levels. Two sample performance levels are considered, namely 'safety and conservation' and 'static safety'. The first one involves the preliminary evaluation of degradation and damage patterns, highlighting the worst conditions determined by the presence of moisture, vegetation (both on the wall surface and the top), cracks among joints, and block's erosion. The second performance level entails the assessment of exposure in the facing area having a minimum width equal to the height of the wall. Significant parameters are human flows, material assets, road type, parked vehicles.

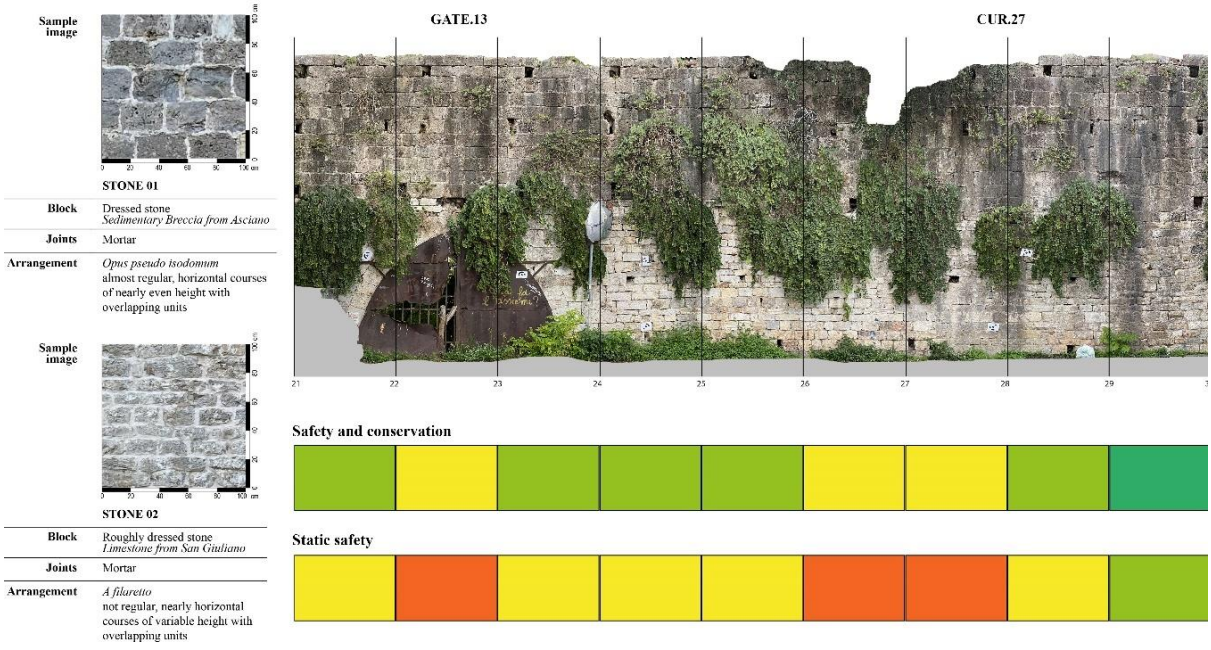


Figure 7: The town walls of Pisa. Masonry typologies and evaluation of risks (Level 2) in two sample performance levels. The coloured stripes recall the six risk levels presented in Fig. 5.

6 CONCLUSIONS

This paper introduced the MO.M.U. project and presented a general overview on the methodology developed for the research scope. Structural safety and risk analysis are rooted in the acquisition of knowledge about the construction under investigation, specifically the geometry, building techniques, materials, damage state, century-old evolutions, material stratifications and territorial context. Starting from the presentation of the main failure events recently occurred in Tuscan town walls, we presented the root causes and parameters affecting the risk assessment. Then, a multi-level methodology has been proposed and applied to the Regional basin. Territorial investigations allowed for characterising the main typological features in the area. Besides, the multi-hazard risk prioritisation procedure is a

first attempt to introduce a simplified quantification of physical vulnerability and exposure. Benchmarking studies concerned the application of the index-based risk prioritisation procedure on the town walls of Pisa. Once calibrated and validated, this approach to risk analysis and governance will be used by governmental officials and administrators. The procedure has potential to be applied to different typologies of historic walls located in diverse geographical areas. In this way, they can achieve planned and preventive conservation that entails a periodic knowledge updating to determine the evolution of risk factors.

Acknowledgements. The authors wish to acknowledge the Tuscany Region and the Consorzio LaMMA (Laboratorio Monitoraggio e Modellistica Ambientale) for the support.

REFERENCES

[1] Presidenza del Consiglio dei Ministri. *Direttiva del Presidente del Consiglio dei Ministri per valutazione e riduzione del rischio sismico del patrimonio culturale con riferimento alle norme tecniche per le costruzioni*. G.U. n. 47 (2011).

[2] Della Torre, S. Italian perspective on the planned preventive conservation of architectural heritage. *Frontiers of Architectural Research* (2020).

[3] Giuliani, F., De Falco, A., Cutini, V., and Di Sivo, M. A simplified methodology for risk analysis of historic centers: the World Heritage Site of San Gimignano, Italy. *International Journal of Disaster Resilience in the Built Environment* (2020).

[4] Sevieri, G., Galasso, C., D'Ayala, D., De Jesus, R., Oreta, A., Grio, M. E. D. A., and Ibabao, R. A multi-hazard risk prioritisation framework for cultural heritage assets. *Natural Hazards and Earth System Sciences* (2020) **20**(5): 1391-1391.

[5] Moratti, M., Gaia, F., Martini, S. *et al.* A methodology for the seismic multilevel assessment of unreinforced masonry church inventories in the Groningen area. *Bull Earthquake Eng* (2019) **17**: 4625–4650.

[6] Romão, X., Paupério, E., and Pereira, N. A framework for the simplified risk analysis of cultural heritage assets. *Journal of Cultural Heritage* 20 (2016): 696-708.

[7] Andreini, M., De Falco, A., Giresini, L., and Sassu, M. Collapse of the historic city walls of Pistoia (Italy): causes and possible interventions. In: *Advances in Civil Structures. Applied Mechanics and Materials* (2013) **352**: 1389-1392, Trans Tech Publication.

[8] Pratesi, F., Nolesini, T., Bianchini, S., Leva D., Lombardi L., Fanti R., and Casagli N. Early Warning GBInSAR-Based Method for Monitoring Volterra (Tuscany, Italy) City Walls. *IEEE Journal of Selected Topics in Applied Earth Observations and Remote Sensing* (2015) **8**(4): 1753-1762.

[9] Nowak, M. M., Dziób, K., Ludwisiak, Ł., and Chmiel, J. Mobile GIS applications for environmental field surveys: A state of the art, *Global Ecology and Conservation* (2020) 23: e01089.

[10] Moreno, M., P. Ortiz, and R. Ortiz. "Vulnerability Study of Earth Walls in Urban Fortifications Using Cause-Effect Matrixes and GIS: the Case of Seville, Carmona and Estepa Defensive Fences." *Mediterranean Archaeology and Archaeometry* (2019) **19**(3): 119-138.

[11] Birkmann, J., Cardona, O.D., Carreño, M.L. *et al.* "Framing vulnerability, risk and societal responses: the MOVE framework." *Nat Hazards* **67** (2013)**,** 193–211. DOI: 10.1007/s11069-013-0558-5

[12] Bevilacqua, M.G., Caciagli, C. and Salotti, C. *Le mura di Pisa: fortificazioni, ammodernamenti e modificazioni dal XII al XIX secolo*. Edizioni ETS (2011).

12th International Conference on Structural Analysis of Historical Constructions
SAHC 2020
P. Roca, L. Pelà and C. Molins (Eds.)

VULNERABILITY ASSESSMENT OF ITALIAN RATIONALIST ARCHITECTURE: TWO CASE STUDIES

P. BERNARDI[1], R. CERIONI[1], E. COÏSSON[1] AND E. MICHELINI[1*]

[1]Department of Engineering and Architecture
University of Parma
Parco Area delle Scienze 181/A, 43124 Parma, Italy
e-mail: {patrizia.bernardi, roberto.cerioni, eva.coisson, elena.michelini}@unipr.it, https://dia.unipr.it
(*corresponding author)

Keywords: Masonry Buildings, Knowledge Process, In Situ Surveys, Static and Seismic Assessment, Rationalist Architecture

Abstract. *The work is focused on the structural vulnerability assessment of two historical constructions, chosen as case-studies representative of a recurrent typology of Italian rationalist architecture, dating back to the Fascist period, often hosting public offices. Both examined buildings have similar dimensions and geometry, being characterised by five/six storeys and by an almost square plan with an inner courtyard, and are located in Emilia-Romagna, in zones of medium seismic hazard. The older building, dating back to the Thirties and located in Ravenna, has a mixed masonry-reinforced concrete structure, while the other one, built in the late forties and located in Parma, is characterised by an unreinforced masonry structure with some limited reinforced concrete elements. For the vulnerability assessment of the two buildings, a multi-disciplinary approach was followed, including the historical documents search concerning both the investigated buildings and the surrounding areas, the detailed geometrical and structural survey, the identification of materials, and in situ and laboratory tests to evaluate materials mechanical properties. These activities allowed reaching an adequate level of knowledge about the present conditions of the structures and their critical deficiencies. This knowledge path is not only necessary for the subsequent numerical analyses, but is also important as it allows targeting the repairing interventions, possibly reducing their final costs, in agreement with the "minimum intervention" approach for heritage buildings.*

1 INTRODUCTION

In Italy all public buildings older than 70 years are *ope legis* considered enlisted buildings, protected by the Ministry of Cultural heritage [1]. This normative prescription is producing more and more enlisted buildings every year, including lately also the period of post WWII. The buildings that have been added to the Superintendency lists in the last decades date back to a period in which the building typologies, the technical solutions, the materials features evolved very rapidly. International organizations like DOCOMOMO, ICOMOS, Getty

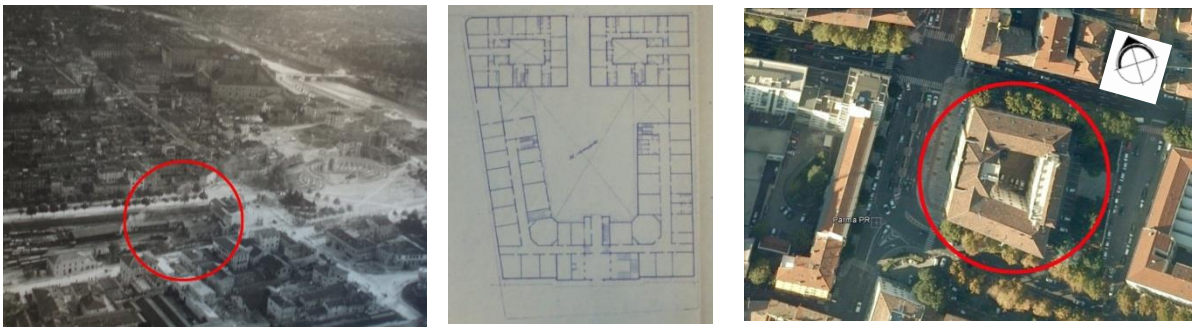
Foundation and World Monument Fund are devoting attention and specific documents to the conservation of these newly defined monuments, but in Italy the Rationalist architecture, earlier subjected to a *damnatio memoriae* due to its Fascist commissioning, is getting only recently more attention and value recognition, which is at the base of a restoration-based approach [2]. Moreover, while the experience on analyzing and restoring older typical masonry structures is large, for these more recent constructions, knowledge is lacking and a correct approach to its analysis is still to be defined. Often these buildings are a mixture of masonry and concrete structures, but the details of reinforced concrete elements are different from todays' ones and – on the other side – bricks and mortars composing the masonry parts are different from traditional ones. In order to carry out a structural analysis on these modern structures, as for all existing buildings, surveys, inspections and on site tests are mandatory and should always take into account also non-structural elements, frequently underestimated in numerical analyses. Real safety comes from deep knowledge, rather than from advanced calculations. The empirical/experimental method developed in the end of the 20th century for historical masonry buildings [3] should also be applied to these more recent and mixed structures, in order to identify the most probable and dangerous mechanisms. To this aim, the analysis of two case studies appears to be meaningful for a better definition of the correct study path.

2 CRITICAL HISTORY ANALYSIS AND DESCRIPTION OF THE BUILDINGS

In case of existing buildings – even if not so old – a thorough knowledge process is required before starting any assessment of the structural safety or planning possible retrofit interventions [4]. The first step of this knowledge process usually consists in historical investigations, which can provide useful information about the building structure, its construction sequence, and building vicissitudes over the years. This first operation, which requires the research and consultation of several archival and bibliographical documents, may sometimes appear expensive and time consuming, but, actually, it is crucial to optimize the planning of surveys and it may have a direct influence on the safety assessment of the building, influencing the modeling choices. Even in case of historical building belonging to an aggregate, the knowledge process is mandatory in order to identify correctly those structural units having a unitary response against seismic actions, as also suggested in [5–7].

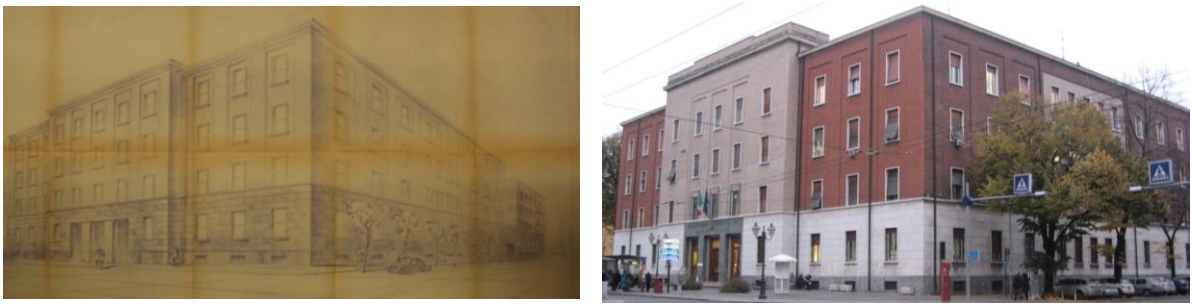
2.1 The "Ex-Magistrato per il Po e Genio Civile" building in Parma (Italy)

The "Ex-Magistrato per il Po e Genio Civile" building, briefly named in the following as "MagisPo", is located in Parma and currently hosts public offices. The draft of the building dates back to the early second post-war period. Building works started in 1947 and lasted until 1959. The building was erected in an urban area – bombed during WWII – between the railway station and the main square of the town (Fig. 1a). The structure of the building and its geometrical configuration underwent some major changes during the construction works, so they do not correspond completely to the 1947 drawings, as can be seen in Figures 1b,c and 2a,b. These drawings show indeed the plans for three main separate buildings, arranged around a common inner courtyard (see Fig. 1b). As can be seen from Figure 1c, only the front building was instead erected, and its original U-shape was modified by connecting the two lateral wings with a rear façade (Figs. 1c and 3d), thus forming an internal closed court.



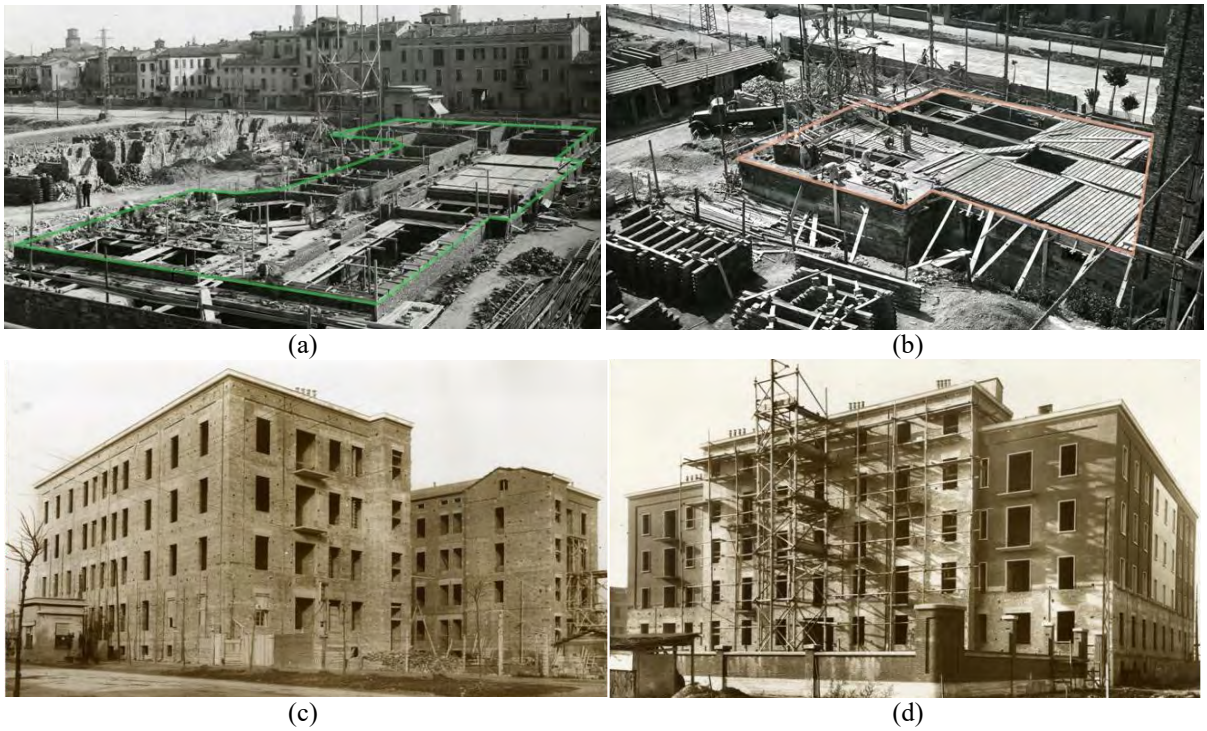
(a) (b) (c)

Figure 1: (a) Aerial view of Parma at the end of the 19th century, with indication of the analyzed area; (b) plan of the building taken from the draft of 1947; (c) aerial view of the MagisPo building from a satellite



(a) (b)

Figure 2: (a) Axonometric view of the MagisPo building taken from the first draft of 1947; (b) general view of the current main façade of the building



(a) (b)

(c) (d)

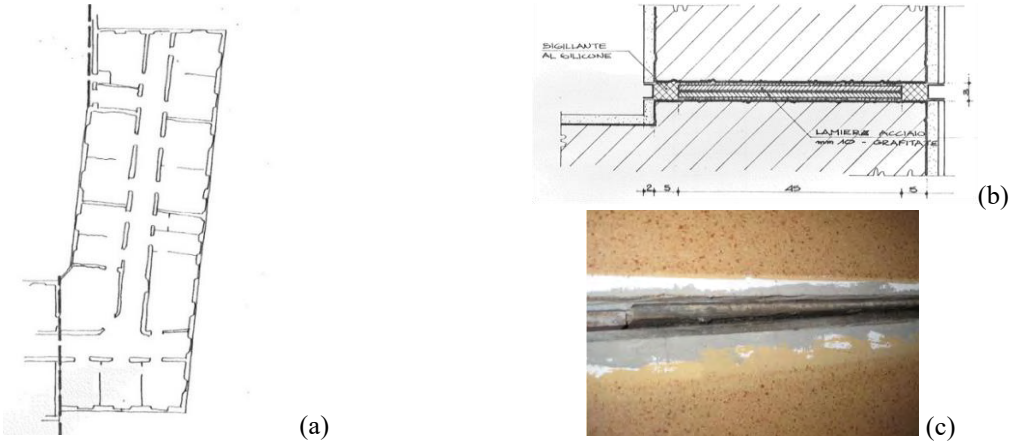
Figure 3: Historical photos documenting the construction stages of MagisPo: (a) erection of the main façade (1948); (b) erection of the east wing (1950); (c) view of the building at mid-Fifties (main façade and the two wings completed); (d) addition of the rear façade (1957)

The construction of the building took place in four subsequent stages, as proved by the historical pictures taken during the works (Fig. 3). The plan was divided into three parts, each one completed before the erection of the next one: the main façade was realized first (Fig.3a), then the two lateral wings (Figs. 3b,c), and finally the rear façade was added (Fig. 3d). To join the adjacent parts together, overhanging masonry teeth were inserted along the height, with a spacing of about 1m (Fig. 4a). The same technique is still visible also in other buildings nearby, dating back to the same period (Fig. 4b). During the following years, the building was subjected to important differential soil settlements that were measured by means of a topographic survey (Fig. 4c). For this reason, in the Eighties the East wing was retrofitted and separated from the rest of the building through the creation of a static joint (Fig. 5a), formed by two graphite steel layers in contact with each other (Figs. 5b,c), and designed by Prof. Cestelli-Guidi in order to allow vertical relative displacements and block horizontal ones.



(a) (b) (c)

Figure 4: (a) Detail of the connection technique adopted in MagisPo building, with overhanging masonry teeth; (b) application of a similar technique in another coeval building nearby; (c) differential settlements at the third level of the building, as resulting from in-situ surveys



(a) (b) (c)

Figure 5: (a) Static joint separating the East wing from the rest of the building; (b) sketch and (c) realization of the joint

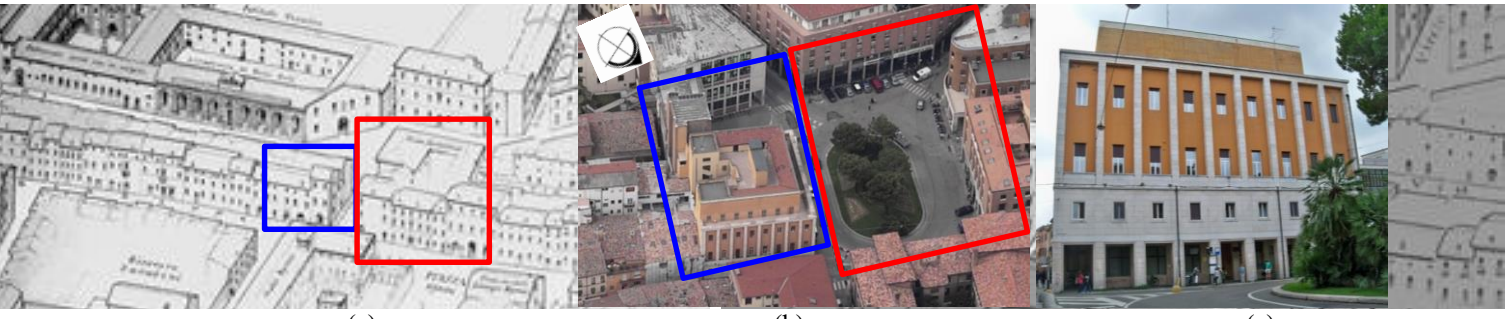
Nowadays the structure has a rectangular hollow floor plan, about 56m x 40m, with a squared inner court. In elevation, there is an underground floor, four floors above ground, and an attic in the rear portion only, reaching 23 m. The load bearing structure is made of masonry walls in

solid bricks and lime mortar, with a very limited number of concrete elements located near the two entrances on the main and rear façades. Most of the floors are realized with reinforced hollow clay blocks (i.e. SAP-like lightweight floors), but some rooms with larger spans are covered through reinforced concrete joists and interposed hollow clay blocks. The floor stratigraphy is completed by an unreinforced concrete deck, 35 to 90 mm thick. A limited number of floors is constituted by NP 120 steel beams, with interposed bricks and an upper concrete deck.

2.2 The "Guilds' Palace" building in Ravenna (Italy)

The Guilds' Palace in Ravenna also hosts public offices. It is part of an urban aggregate, which was partially demolished in the latest Twenties of the last century to allow the realization of "Piazza del Littorio": this was intended to be one of the preeminent examples of the Fascist architecture in Ravenna (Fig. 7). The buildings overlooking the square - i.e. the INA and the Littorio Palaces (Fig. 7a), the Province Palace, and the Guilds' Palace (Fig. 7b) -, realized between 1928 and 1943, were conceived according to the principles of Rationalist architecture, in an ideal connection to the Roman past: the main façades were designed according to a sort of "simplified neoclassicism", with classical architectural details with claddings in marble slabs, rhythmic arcades, columns, arches. The examined building (Fig. 6b,c), designed by architect Emanuele Mongiovì, was built between 1939 and 1942.

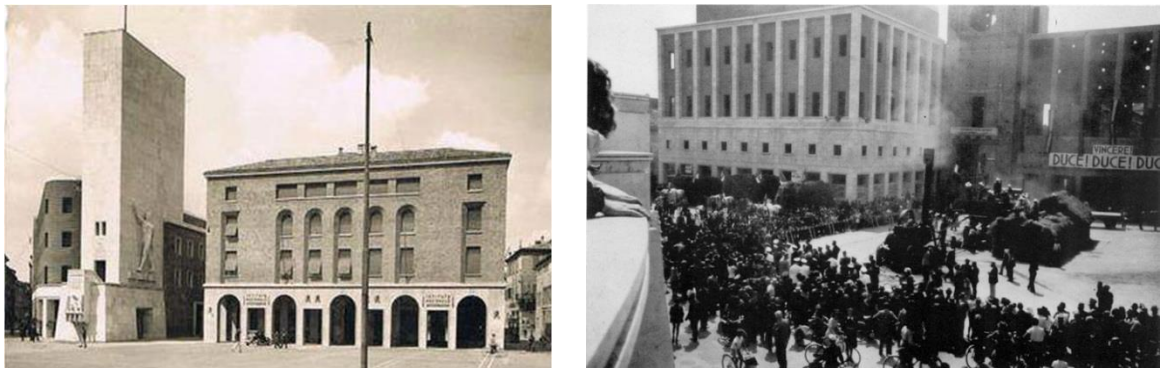
The dismantlement works of the head portion of the aggregate (within the blue box in Fig. 6a) are documented in the historical photos reported in Figure 8. As can be seen, the wall separating the West wing of the Guilds' Palace from the neighboring building (green box in Fig. 8c) was completely demolished and rebuilt (Fig. 8a), while that separating the East wing from the aggregate (red box in fig. 8c) was preserved from dismantlement (Fig. 8b). The project of the Guilds' Palace also included the neighboring tower (Fig. 7b), which was separated from the main building by means of a static joint. In 1947, the Guilds' Palace was owned by the State, and in the following 4 years, the building was subjected to several renovation works, which also included the reconstruction of some floors (mainly at the ground level), as well as some demolitions and reconstructions of masonry walls. Nowadays the structure has an almost square floor plan, about 29 m x 26 m, with a small internal court (Fig. 8c), and consists in an underground floor of limited extension (originally hosting an air-raid shelter, accessible through a trapdoor) and six floors above ground, reaching a maximum height of about 25 m.



(a) (b) (c)

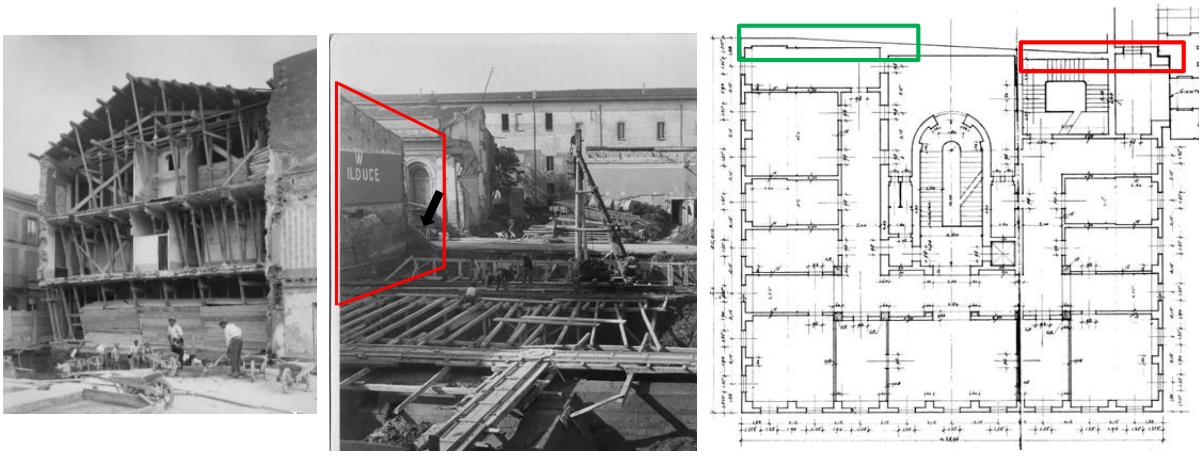
Figure 6: (a) Drawing of G. Savini of the area nearby the Guilds'Palace, dating back to the end of the 19th century; (b) aerial view of Piazza Caduti della Libertà (ex- Piazza del Littorio) and of the Guilds' Palace; (c) main façade of the Guilds' Palace

The building has a mixed masonry – Reinforced Concrete (RC) structure. Besides the RC columns of the arcade running along the building perimeter at the ground floor (Figs. 6c, 7b), most of the remaining frames are located at the front of the palace at the lower levels, while at the upper ones they are replaced by masonry columns and walls. Between the 3rd and the 4th levels, the floorplan of the building becomes narrower, to allow the realization of a terrace running along the whole perimeter. For this reason, the corresponding floor is characterized by the presence of a grid of RC beams (Fig. 9a), which support the above masonry walls. Masonry walls are generally constituted by solid bricks and lime mortar, but hollow bricks were also found at the upper levels of the building (see Fig. 10c). Most of the floors are realized with RC joists and interposed hollow clay blocks, with a 50 mm unreinforced concrete deck. The floor right above the main entrance is instead characterized by a bidirectional grid of RC joists with two layers of interposed hollow clay blocks (Fig. 9b), while the two rooms near the corners of the building, between the ground and the 1st floor, are covered by a lightened slab with radial reinforcement.



(a) (b)

Figure 7: Historical photos documenting the realization of Piazza del Littorio and of the surrounding palaces: (a) Palazzo del Littorio; (b) Guilds' Palace during "threshing of wheat grown in the war gardens" in 1942



(a) (b) (c)

Figure 8: Historical photos documenting the dismantlement of the aggregate in the late Twenties: (a) demolition of the wall in correspondence of Guilds' Palace West wing (green box in Fig. 8c), (b) wall neighboring with the East wing of the palace (red box in Fig. 8c); (c) floorplan of the building, taken from the draft of Arch. Mongiovì



(a) (b)

Figure 9: Historical photos documenting the construction works of the Guilds' Palace: (a) grid of reinforced concrete beams, at the 3rd floor; (b) floor between the ground and the 1st level, with bidirectional concrete joists and interposed hollow clay blocks

3 IN SITU SURVEYS

In situ survey encompasses all those activities that allow the identification of the load bearing structure of an existing building, the loads acting on it, and the existence of possible pathologies. The information collected in this knowledge phase, concerning the geometry of the building, the type and dimensions of structural elements, the construction details, the crack pattern, the presence of structural and non-structural vulnerabilities, as well as material properties and geotechnical aspects, are the basis for subsequent structural analyses and exert a deep influence on the related modelling choices.

This Section provides a general overview of performed activities, common to both the investigated structures, while the following subsections deepen the specific choices related to each single case study. For the two considered buildings, a complete geometric and architectural survey was first performed. Despite the availability of the historical drawings, several discrepancies were found indeed between the original drafts and the present appearance of both palaces. For the MagisPo building, a detailed topographic survey of the differential settlements at different floors was also carried out (Fig. 4c), in order to compare it with the one carried out before the retrofit intervention.

Historical documents were a source of valuable information for the identification of the load bearing structure and of the different materials adopted during the construction of both palaces. Available data were analyzed and used for the planning of in situ essays, which were carried out by using both non-destructive and partially destructive techniques. The removal of plaster portions of about 1 m^2 (Fig. 10) allowed to identify masonry typology and texture, its possible degradation, the quality of the connections between perpendicular walls and between walls and floors (Fig. 10b,c), as well as the possible presence of concrete joists and lintels above the openings. These essays were distributed at different locations of the floorplan – according to the historical evolution – and were repeated at the different levels, in an extensive and systematic way. The quality of transverse connections within masonry thickness was verified at predefined locations through the removal of single bricks (Fig. 10a,b), which were subsequently delivered to the Laboratory of Materials and Structures of the University of Parma, for the determination of their compressive strength (Fig. 11a,b). During this operation, it was also possible to examine the quality of the mortar and to take a sample for subsequent

mineralogical and petrographic analyses (Fig. 11c). Wall thickness was verified by means of small drill holes.



(a) (b) (c)

Figure 10: Removal of plaster portions at different locations of the Guilds' Palace: (a) internal masonry wall at the 1st floor; (b) connection between two perpendicular external walls at the 2nd floor; (c) connection between perpendicular walls and the ceiling at the 5th floor



(a) (b) (c)

Figure 11: (a) Cutting operations to obtain cubic samples from the removed solid brick; (b) execution of compression test on cubic sample; (c) image of a mortar sample at the optical microscope



(a) (b) (c)

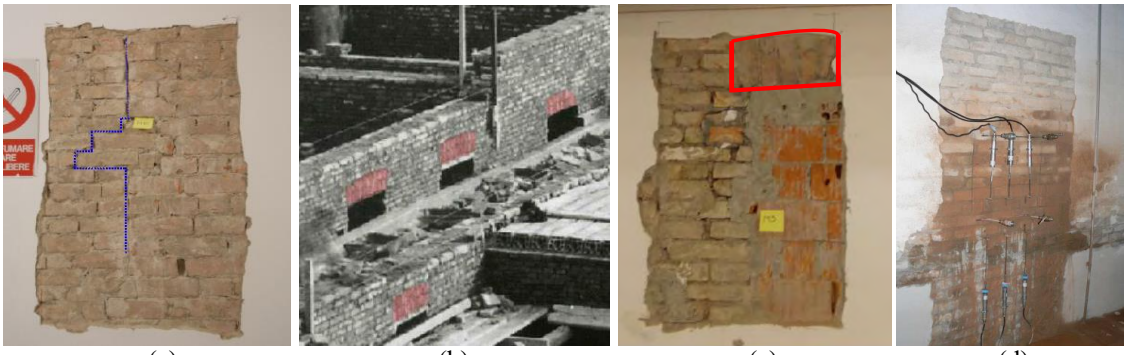
Figure 12: In situ survey on floors: (a) thermographic analysis; (b) removal of plaster layer and concrete cover; (c) core drilling at floor extrados

The direction and typology of floors were checked by means of visual inspections and non-destructive techniques, like thermographic (Fig. 12a) and pacometric analyses, supported by semi-destructive local essays (Fig. 12b), consisting in the removal of plaster layer and concrete cover, and in the measurement of rebar diameters and spacing. Floor stratigraphy was deduced by means of coring at floor extrados (Fig. 12c), while its thickness was measured by performing small drill cores. Similar techniques were also adopted for RC elements (beams, concrete ring

beams, columns). The information deduced from original historic documents were first verified through a simulated design according to the Code Standard in force at the time. Rebars distribution and diameters were then verified through extensive pacometric investigations, further integrated by local essays requiring the removal of plaster and concrete cover.

3.1 The "MagisPo" building in Parma

Since building construction took place in three subsequent phases, in situ survey on masonry was organized so to have a minimum number of essays for each part, and at every level. For each part, plaster was removed to characterize the main masonry typologies, individuated on the basis of their position (internal/external wall) and thickness (from 150 to 550 mm). Some essays were also performed in correspondence of the junctions between the different parts, to confirm the presence of overhanging masonry teeth (Figs. 4a, 13a). A specific survey was also planned near the static joint realized in the Eighties, during the retrofitting works. The availability of several photos documenting the construction phases was also useful to identify different materials and construction techniques (i.e. flat arches above the openings in the underground floor and RC lintels at the other levels; presence of lightly reinforced concrete ring beams, the bearing structure of stairs, etc.), which were verified in situ through targeted interventions. A total of 19 essays were carried out for the determination of masonry typology, with the removal of 7 bricks and 11 mortar samples.



(a) (b) (c) (d)

Figure 13: In situ survey: (a) connection between two wall portions realized at different times; presence of flat arches above the openings at the underground floor from (b) historical photos and (c) direct essays; (d) double flat jack test on a masonry pier of the underground floor

Compressive tests were carried out on cubes with 50 mm side obtained from bricks extracted from the building walls (approximately 4 or 5 cubes for each brick, Figs. 11a,b). These tests provided an average strength value of 23 MPa. Lower compressive strengths were found for those samples taken from the underground level, where different, lower quality bricks, characterized by a paler color, were used. From laboratory tests, mortar was classified as poor. A masonry pier located at the underground floor was chosen to perform a double flat jack test (Fig. 13d), which provided a masonry compressive strength value of about 2.4 MPa. This value corresponds to the minimum value suggested in the commentary document [8] joined to the current Italian Code [9] for the category "solid brick masonry with lime mortar". Considering an intermediate level of knowledge [9, 10] achieved through the in situ survey, and taking into account that the results of the double flat jack test were referred to the masonry with the poorer

quality in all the building (concentrated at the underground level), the central values of the interval reported in [8] for masonry strengths were adopted. These values were further reduced through the application of the confidence factor, according to the followed Standard Codes [9,10].

3.2 The Guilds' Palace

As for the MagisPo building, in situ survey on the Guilds' Palace were planned to verify the reliability of the information collected during the historical research, and to deepen the less clear aspects. In this case, great attention was paid to the investigation of the relations between the studied building and the adjacent ones belonging to the pre-existing aggregate, as well as to the neighboring tower, carrying out visual inspections also in these adjacent structures, to understand better possible interactions, especially during earthquake.

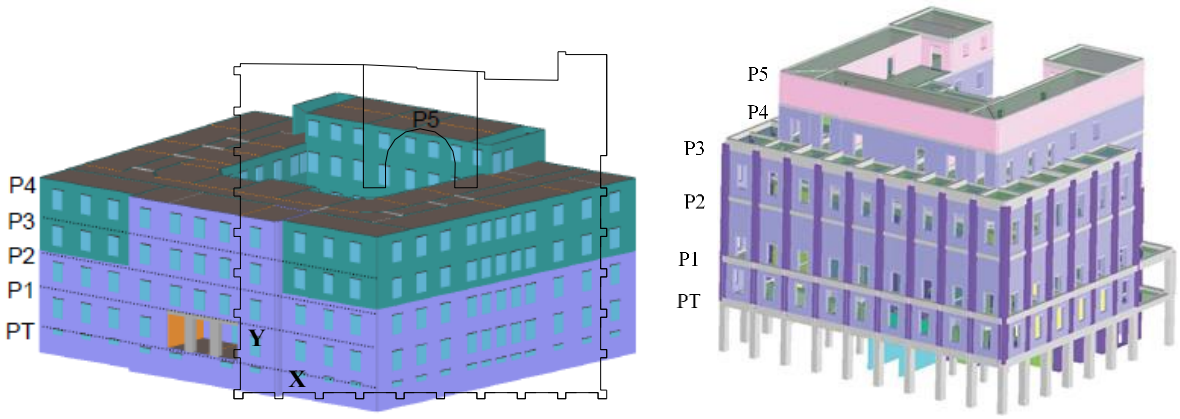
A total of 25 inspections on masonry quality and texture were planned, by examining walls with different position (external/internal) and thicknesses at different levels, and performing a higher number of essays on the wall separating the Guilds' Palace from the aggregate. 14 solid bricks were collected for the determination of material properties through laboratory tests. Compressive tests on cubic samples with 50 mm side obtained from the bricks provided an average compressive strength of 24.5 MPa, but were quite dispersed, even for cubes belonging to the same batch. Lime mortar was characterized by a poor quality. Considering an intermediate level of knowledge [9, 10] achieved through the in situ survey, the central values of the interval reported in [8] for the category "solid brick masonry with lime mortar" were adopted for material strength calculation. These values were further reduced through the application of the confidence factor, which was in this case calculated according to the procedure suggested in [11] for heritage buildings, as it is in the examined case. A value of 1.23, very similar to that suggested in [8] for an intermediate knowledge level, was found.

For concrete elements, strength values were mainly derived from original documents, Code Standard prescriptions in force at the time of its construction, and to a limited number of non-destructive tests. Several semi-destructive essays were originally planned, but their execution was not possible for the negative advice of the Superintendence and of the Property.

4 VULNERABILITY ASSESSMENT OF THE TWO CONSIDERED BUILDINGS

The information collected during the knowledge phase were used as basis for the structural modelling. The effectiveness of connections between perpendicular walls and between walls and floors, the presence of concrete ring beams at floor levels, and the lack of important crack patterns denoting clear out-of-plane mechanisms in both the examined palaces, made reasonable the choice of analyzing the behavior of the whole building, by considering a 3D model. In both cases, the underground floor was not included in numerical simulations (Fig. 14a,b). To achieve a good compromise between accuracy of the results and computational effort, an equivalent-frame macro-element approach was adopted [12]. As a first step, linear analyses under gravity load were performed. In this way, it was possible to easily check the accuracy of the geometric layout and of the assumed applied loads, through the comparison between numerical stress values and those deriving from simple manual calculations, as well as from experimental data (i.e. provided by flat jacks). For the vulnerability assessment of the buildings behavior under seismic loads, the nonlinear static (pushover) analysis was chosen,

since it is currently considered the best-established method for masonry structures, and it is frequently used in case of historical constructions [13, 14]. Based on the available information on the foundation soil, a soil category C according to [9,10] was assumed in both cases without any topographic amplification.



(a) (b)

Figure 14: View of the 3D model adopted for (a) the MagisPo building and (b) the Guilds' Palace

Different models were considered for both the structures examined. Besides a general model of the whole building (Fig. 14), other possible scenarios were investigated, based on the relevant information collected for each case study. For the MagisPo, the behavior of the two portions separated by the joint (realized during the retrofitting intervention dating back to the '80s) was also investigated. It was generally found that the weaker direction for the building under seismic action was that parallel to the main façades, for the presence of two RC frames at the ground floor, interrupting the continuity of shearwalls. Another problem highlighted in the analyses was represented by masonry spandrels, which were weakened by the presence of niches hosting the shutters and the heaters. The return period of the maximum seismic action sustainable by the whole building was found to be slightly lower than 350 years, while it was almost halved when considering the building split into two independent portions. However, this latter scenario seems to be less realistic, since documental findings and in situ survey have proved that the joint between the two parts is more effective with regards to vertical loads than horizontal ones.

For the Guilds' Palace, two separate models were analyzed, by including or not a limited portion of the aggregate behind it. In both cases, it was found that the weaker direction for the building under seismic action was that parallel to the main façade, due to the limited number of shearwalls continuous along the building height. As already observed, shearwalls are lacking in the portion of the ground floor near the main entrance, where RC frames were preferred. The return period of the maximum seismic action sustainable by the whole building was found to be approximately equal to 150 years, and this results is only slightly modified when including an aggregate portion.

5 CONCLUSIONS

The importance of the knowledge path in order to approach correctly the analysis of an existing structure is a self-evident concept. Less evident is how to carry out this knowledge path on buildings – like the ones dating back to the mid-twentieth century – that are not made like

present-day structures but are neither traditional buildings with a long and well-studied experience. The two analyzed case studies focus on the methodology for the structural analysis of this type of buildings, highlighting the need of a strict relation between historical research, on-site surveys and numerical analyses. In particular, the identification of construction phases, changes occurred in time, and earlier structural retrofit interventions have proved to be meaningful information for the definition of the bearing schemes of the buildings and, as a consequence, of their numerical models. In case of uncertainties, like for connections effectiveness in aggregate structures, different conditions have been modeled to check their influence on the global behavior, supplying an idea of the possible variability of the results. The final aim is increasing not only theoretical sensitiveness but also technical awareness of the specificities of the structural analysis on modern architecture.

REFERENCES

[1] Codice dei Beni Culturali, D.L. n.42, 22/91/2004. In G.U.R.I. n.45, 24/2/2004 (in Italian).
[2] Brandi, C., *Theory of restoration*. Translation by Cynthia Rockwell. Florence: Nardini.
[3] Giuffrè, A., Carocci, C., Statica e dinamica delle costruzioni murarie storiche. In: *Proc. CNR Int Congress "Le pietre da costruzione: il tufo calcareo e la pietra leccese"*, Mario Adda Editore, Bari, (1993): 539-598 (in Italian).
[4] Ceroni, F., Pecce, M., Sica, S. and Garofano, A. Assessment of seismic vulnerability of a historical masonry building. *Buildings* (2012) **2**: 332–358.
[5] Lagomarsino, S., Cattari, S., Degli Abbati, S. and Ottonelli, D. Seismic assessment of complex monumental buildings in aggregate: the case study of Palazzo del Podestà in Mantua (Italy). In: F. Peña et al. (Eds.): *SAHC2014—9th international conference on structural analysis of historical constructions, Mexico City, Mexico* (2014).
[6] Caprili, S. and Puncello, I. Knowledge-Based Approach for the Structural Assessment of Monumental Buildings: Application to Case Studies. Front. *Built Env.* (2019) **5**: 52.
[7] Boschi, S., Borghini, A., Pintucchi, B. and Zani, N. Seismic vulnerability of historic masonry buildings: A case study in the center of Lucca. *Procedia Struct. Integr.* (2018) **11**: 169–176.
[8] Circolare n. 617. *Instructions for the application of "Nuove norme tecniche per le costruzioni di cui al D.M. 14 gennaio 2008"*, (in Italian), 2009.
[9] NTC 2008. *Norme Tecniche per le Costruzioni*, D. M. 14/01/2008. In G.U.R.I., 29, 04/02/2008 (in Italian).
[10] UNI EN 1998-3. *Eurocode 8. Design of structures for Earthquake resistance – Part 3: Assessment and Retrofitting of Buildings* (2005).
[11] *Guidelines for the assessment and reduction of seismic risk for cultural heritage according to Italian Standard (D.M. 14 Jan 2008)*, (in Italian), 2011
[12] Penna, A., Lagomarsino, S. and Galasco, A. A nonlinear macro-element model for the seismic analysis of masonry buildings. *Earthq Eng Struct Dyn* (2014) **43**(2):159–179.
[13] Bracchi, S., Rota, M., Penna, A. and Magenes, G. Consideration of modelling uncertainties in the seismic assessment of masonry buildings by equivalent-frame approach. *Bull Earthquake Eng* (2015) **13**: 3423-3448.
[14] Ceroni, F., Pecce, M., Manfredi, G. Modelling and seismic assessment of the bell Tower of Santa Maria del Carmine: Problems and solutions. *J. Earthq. Eng*. (2010) **14**: 30–56.

12th International Conference on Structural Analysis of Historical Constructions
SAHC 2020
P. Roca, L. Pelà and C. Molins (Eds.)

BRITISH COLONIAL ERA'S RELIGIOUS BUILT HERITAGE IN YORUBALAND, NIGERIA: KEY CONSERVATION PROBLEMATICS AND THE STATE OF KNOW-HOW

REYHAN SABRI[1*] AND OLUSEYI A. OLAGOKE[2]

[1]Assistant Professor, Department of Architectural Engineering, College of Engineering
University of Sharjah
University City, Sharjah, UAE
e-mail: rsabri@sharjah.ac.ae, www.sharjah.ac.ae (*corresponding author)

[2] Independent Researcher
Osogbo, Osun State, Nigeria
email: oluseyiolagoke@gmail.com

Keywords: Religious Built Heritage, Conservation Problematics, Spatial Requirements, Modification of Original Fabric, Adaptive Reuse

Abstract. *Colonial-era buildings' conservation is now viewed in a more positive light as part of the urban fabric, however the conservation state of colonial-era built heritage has received scant research attention. There are major challenges especially for the preservation of religious buildings erected in the former European colonial territories in the non-Western world. This paper is the outcome of ongoing fieldwork-based research, which aims to identify and locate the mosque and church structures built during the British colonial era in Yorubaland (South Western Nigeria) and investigates their conservation state. This research adopts a mixed methods approach, employing physical observations and semi-structured interviews with heritage practitioners. The analysis of the fieldwork data initiates a discussion on the challenges and threats that result from the spatial requirements of a growing number of congregations which have lead to physical interventions on the original fabric, ranging from minor to major modifications and demolitions. The deficiencies in institutional conservation know-how in addressing the emerging spatial requirements in theoretically and technically appropriate ways are revealed.*

1 INTRODUCTION

Protection of the architectural legacies of the modern European colonial era is a multi-faceted issue, underpinned by various socio-political, functional, financial, and technological considerations. However, studies since the beginning of the 21st century have indicated how the absence of a balanced representation of the architectural heritage of the modern era, especially of the colonial period, will leave a gap in knowledge about the evolution of architectural and urban fabrics[1]. One negleced topic is the conservation state of religious buildings of the

indigenous communities in the European colonial territories. In several parts of colonized sub-Saharan Africa, church and mosque buildings emerged as monumental structures constituting a new layer of urban fabric [2, 3, 4, 5]. They are evidence of transcultural knowledge transfer via the introduction of Western design and construction skills and their adaptation to local conditions, however the conservation of these structures has not received much academic attention or governmental priority.

Recent research has indicated how in the absence of heritage management policy and governmental and institutional reluctance to heritagize both Islamic and Christian religious structures has accelerated their deterioration and loss [5, 6]. This paper is one of the outcomes of a fieldwork-based research project that aims to identify, document and analyze the conservation state of British colonial era built religious heritage in Yorubaland (Figure 1). The fieldwork was conducted over several trips in a period between June 2017 and December 2019. This paper widens the discussion by looking into the existing conservation knowledge separately for mosques and churches, aiming to reveal comparative insights. By employing participant observation and semi-structured interviews with the members of the Building Committees of the surveyed mosque and church structures, it specifically investigates the problems underlying physical modifications on the fabric of buildings and examines the solutions adopted.



Figure 1: Map of Yorubaland showing the towns/cities surveyed for British colonial-era built religious architecture

2 CONTEXTUAL BACKGROUND: IDENTIFICATION OF RELIGIOUS BUILDINGS ERECTED DURING THE BRITISH COLONIAL-ERA IN YORUBALAND

Islam and Christianity gained a foothold in Yorubaland mainly during the 19th century. Although there had been small numbers of Muslims in Yorubaland since the 17th-century, Islam's presence gained momentum after the Fulani Jihan in 1830s [7, 8]. This was followed by Christianity in the early 1840s, when the abolition of slavery and Britain's intensified presence in West Africa in the heyday of the British Empire introduced led to the introduction of Christian missionaries and instigated a radical change in religious space [9, 10]. Both Islam and Christianity increasingly became the major religions in Yorubaland replacing by the beginning of the 20th century the hitherto prevailing African traditional religions. By then, unlike the unpretentious religious spaces belonging to African traditional religious sites[11], architectural aesthetics had gained a significant role in designing both the mosques and churches[12, 13].

2.1 Typology and morphology of Afro-Brazilian mosques in colonial Yorubaland

Until the late-19th-century mosques in Yorubaland were small-scale and unadorned mud-and-thatch structures, often without minarets [7, 8]. Contact with the wider world from the second half of the 19th century led to the building of more impressive mosques in West Africa [4]. This coincided with the return of freed Africans who were enslaved in Latin America, especially in Brazil. The design of Afro-Brazilian mosques imitated the 17th to 18th-century Baroque churches in Bahia in Brazil, with a longitudinal plan layout similar to Catholic churches, a pedimented central structure and bell towers [3]. To meet the requirements of Islamic worship a mihrab was installed on the Qibla wall, and the bell-tower became a minaret.

These Afro-Brazilian style mosques introduced the first monumental scale mosques in Yorubaland. The earliest ones were erected in Lagos, in the late 19th century, and they set the architectural vocabulary for several chief congregational mosques in Yoruba cities, with most surviving examples from the 1930s and 1940s in various Yoruba towns. The oldest surviving mosque structure is the Shitta Bey Mosque in Lagos, built in 1891-94 [5]. This architectural language included a pedimented central structure, with single or double minaret-towers situated on the front or rear façade; in both cases having the similar longitudinal plan layout. The details and ornaments changes drastically depending on the repertoire of the master-builders, including: pediment crowned with scrolls, round or elliptical oculi and arched openings with stucco surrounds, stringcourse that extends horizontally on the façades, engaged columns, pilasters and plinths, and various stucco decorations, emphasized quoins, rectangular windows topped with decorated blind arches or floral motifs, ornate balustrades surmounting the minaret-towers and roof lines, and Baroque style dormers on the roof level of the side facades (Figure 2).



Figure 2: Shitta Bey Mosque in Lagos (left), and Central Mosque in Abeokuta (right)

2.2 Typology and morphology of missionary churches in colonial Yorubaland

The emergence of church structures in Yorubaland started with the establishment of the first formal church, St Peter's Church in Ake, Abeokuta in 1847 [14]. While the early churches in Yorubaland were erected under the directives of the missionaries, these were mainly mud-and-thatch structures which did not survive. Similarly to mosques, churches with durable materials, mainly brick, stone and metal roofing sheets, started to emerge in the last quarter of the 19th century. The 20th century witnessed the reconstruction of these structures in larger scales to accommodate their growing congregations. The oldest surviving church building is the St. Peter's Church in Ake, built during 1898-1900. While initially the hall-type dominated, from the 1910s until the end of the colonial era, churches were designed mostly in Basilica layout. Neo-Gothic style, both in European versions and in simplified-localised versions, dominated the morphology and aesthetics of the churches from the late 19th century, including: pointed arches, lancet windows with Gothic style mullions, oculi, archivolts, stringcourses, nave arcades with compound piers supporting pointed arches (Figure 3).



Figure 3: Christ Church Cathedral (left), and Holy Cross Church Cathedral (right) in Lagos

3 HERITAGE MANAGEMENT, KEY CONSERVATION PROBLEMATICS AND THE STATE OF KNOW-HOW

Form early on, construction of mosques and churches has been the responsibility of their respective communities, erected and maintained through funds, services and with

construction/finishing materials endowed by charitable citizens. During our fieldwork, we observed that both churches and mosques are self-sustained autonomous entities, and hence the upkeep and maintenance of religious space is under their leaderships' autonomy. In both institutions, each individual church parish and mosque community establishes their respective Building Committee with persons selected from their members to manage the upkeep and maintenance works. However, semi-structured interviews with members of various committees revealed that while there are architects/ engineers in building committees, they are not experts in architectural conservation. It is too simplistic to argue that their selection is intentionally based solely on their loyalty to the respective institution's administration. There is also the reality that the number of heritage management and conservation experts is rather low in Yorubaland (and in fact in Nigeria) due to the near absence of the discipline both in formal and vocational education.

Another problem is the absence of religious heritage belonging to Islam and Christianity in the national heritage legislation, namely the Decree No: 17 of 1979 (Ordinance of 1979) [6]. While there are only three mosque sites listed in the national heritage list, there are no churches included in it yet. This is a situation which lends the leadership of religious buildings a free hand in undertaking decisions regarding physical interventions on the buildings' fabric and sometimes even to make controversial decisions. Exemplifying this is the case of the Central Mosque in Lagos: being one of the earliest Afro-Brazilian style mosques, designed in 1897 as the chief mosque of the country, the Central Mosque in Lagos was inspirational in the design of others around Yorubaland [5]. Following its demolition in 1980, a colossal post-modern structure was built in its place, which was surprisingly (and ironically) later declared an ancient monument in the heritage list of the State of Lagos (Chapter L86), as a 'modern architectural masterpiece, built to replace the old mosque' [15].

Our extensive fieldwork in Yorubaland has revealed several key reasons underlying physical interventions on the religious structures. These include spatial requirements for growing congregations, material deterioration, structural decay, cosmetic interventions for aesthetic reasons, and installing/renewing building services. This paper focuses specifically in the issue of spatial requirements and examines the solutions adopted.

4 SPATIAL REQUIREMENTS FOR GROWING CONGREGATIONS AND THE SOLUTIONS ADOPTED

Both in mosques and churches, increased congregation numbers have prompted attempts to create larger spaces. This is usually achieved in three ways: either by demolishing the old structure to make space for a new one, expanding the old structure, or building a new structure on the site and adapting the old one to a new use.

4.1 Demolishing the old mosques and churches to make space for new and larger ones

In several cases, lack of space at the religious site prompts the demolition of the original structure to create space for a new and larger one. This is especially the case in crowded urban areas such as Lagos, where plot sizes are relatively small. Sadly, several early mosques and churches such as the old Central Mosque, the First Baptist Church, and the Ebenezer Church in Lagos have been demolished for this reason. Colossal post-modern structures now occupy the sites.

4.2 Expansion of the old mosque and church structures by the addition of new spaces

The expansion of the old structure by adding to one or both sides is among the most popular solutions both for mosques and churches. In some cases, such as the Central Mosque in Abeokuta or Christ Church in Ijebu-Ode, the expansión remains in harmony with the existing part both morphologically and in terms of its size. There are several cases however where massive expansions have been built, such as the extension of the southerly façade of the Ode-Omu Central Mosque adding two slender minarets, with an external gallery around the old and new mosque. This extensión from c.1980s, destroyed the original facades, and little of the front pediment, flanking the minaret-tower and some of the rear pediment, has survived (Figure 4). On the other hand, the expansion of the Central Mosque in Offa, where it has been extended on its lateral sides, tripling the total closed área, was more thoughfully carried out. With large domes on top, surmounted by crenellated parapets with slender minarets, and two new polygonal towers on the main façade of the original building, provide an eclectic example of Middle-Eastern mosque architecture. The original building is now constricted by the expansion, started in c.1980s and eventually finished in c.2010 (Figure 4). In another case, at the Central Mosque in Ijebu Ode, an extension in the style of the old facade has been continuing since c.1990s, making it hard to tell the old and new elements apart. Two hemispherical domes were built in front of the pedimented gable, obliterating it (Figure 4).



Figure 4: Expansions on Central Mosque in Ode-Omu (above), Ijebu Ode (below, left), and Offa (below, right).

Among the most radical modifications are the addition of towers in addition to congregation and administrative spaces. For the mosques, a case in point is the Central Mosque of Osogbo, where two new minaret-towers were added to the existing tower and single hall layout mosque in ongoing extension work started c.1995. The new square minaret-towers are similar to the original tower (Figure 5). However, a massive dome was installed as an afterthought to the expanded section which does not suit the building. The facades of the original mosque have been obliterated as the building was expanded. Overall, the expansion is too massive and the morphology of the new additions cause confusion rather than harmonious integration. In a similar vein, a new hall and a bell-tower was added to the originally two-bell-towered Holy Trinity Church in Abeokuta, replicating the existing ones, and making it difficult to differentiate the newly added parts from the originally existing ones (Figure 5).



Figure 5: Modifications on Central Mosque in Osogbo (left), and Holy Trinity Church in Abeokuta (right)

4.3 Constructing a new structure and adapting the old one for new purposes

Adaptive reuse is prevelant on the church sites when a new church is built on the site next to the old one. There is rarely any attempt to create a harmony of architectural languages between the old and new. Exemplifying adaptive reuse are the St Peter's Church in Abeokuta, St. James's Church in Ibadan, Aatan Baptist Church in Oyo, Our Saviour's Church in Ijebu Ode and St. Philip's Church in Ile Ife. While the last one has remained unused since 2014, awaiting final decisións about its future use, in all other cases the old building has been adapted to be for church related functions. Note that, in all cases, the old buildings show signs of material deterioration and structural decay due to the lack of upkeep and maintenance.

In a different approach, when more space was needed for congregations at the Our Saviour's Church in Lagos and a new structure was built surrounding the old one, the latter remained in use in its original function (as a suplementary church space). However, while the facades of the new structures replicate the windows of those at the old church, creating a somehow succesful harmony, the scale of the new structures are massive, dwarfing the old building (Figure 6).



Figure 6: Our Savious' Church (Lagos), cramped in recently constructed new church buildings

5 DISCUSSION AND CONCLUSION

Colonial-era religious built heritage in Yorubaland, which includes Afro-Brazilian mosques and missionary churches, are significant layers of urban fabric. They bear witness to an era of transculturation, during when the Western construction technology and design understandings were imported to the región in part by the Western community and in part by the Africans themselves. Yet, our investigation has pointed to a rapid erosión and loss of this unique layer from the urban fabrics.

This paper has shed light on how spatial requirements instigate modifications to the buildings' fabric. Both in the case of Afro-Brazilian mosques and missionary churches, a common key problem is that these buildings are living religious structures and spatial requirements for providing larger space for the growing number of congregations creates pressure for irreversible extensive modifications on the religious structures' fabric. In the denser urban áreas, like in Lagos, due to the small sizes of the church or mosque sites, the religious communities favor demolition or massive expansions. In the cases when the old building is kept, the new structures often do not integrate respectfully with it. Either they dwarf it or create confusing volumetric expressions. On the other hand, in less populated urban areas the availability of space on the site allows for new constructions, opening the way for adaptive reuse for the old church or mosque structure, although these are seldom protected as heritage structures. In any case, whether the structure is used in its original function or it is adapted for reuse, the material and structural problems are addressed as normal construction works.

The current lack of institutional heritage management policy and conservation expertise, coupled with the implicit absence of religious buildings belonging to Islam and Christianity from the national preservationist legislation, suggests what may lay ahead for these heritage structures. Protection of the remaining examples depends on actions that need to be taken at governmental, institutional, and inter-institutional levels. While the de-centralized and community-based management system of both the church and the mosque institutions is a strength to build on, it is obvious that these systems need to be embedded with heritage capacity/mechanism and monitored from the top (the local and federal government). The best way forward should start with identifying, locating, and listing the remaining colonial-era

religious buildings and tailoring a heritage management policy to protect them while also ensuring their continuing use as religious sites under the control of their respective religious communities.

REFERENCES

[1] van Roosmalen, P. Changing Views on Colonial Heritage. In: R. van Oers and S. Haraguchi (Eds.): *Identification and Documentation of Modern Heritage*, *World Heritage Papers no 5*, UNESCO (2003), pp.122-129.

[2] Bremner, G. A. *Imperial Gothic: Religious Architecture and High Anglican Culture in the British Empire*. Yale University Press (2013).

[3] Hallen, B. Afro-Brazilian Mosques. *Mimar: Architecture in Development* (1988) 29:16-23.

[4] Cantone C. *Making and Remaking Mosques in Senegal*. Brill (2012).

[5] Sabri, R. and Olagoke, O.A. Rethinking the Conservation of Afro-Brazilian Mosque Legacy. *Journal of Architectural Conservation* (2019) 25 (1-2): 49-71.

[6] Sabri, R. and Olagoke, O. A. Predicaments in the Management of Religious Heritage Buildings and Sites in Nigeria. *Conservation and Management of Archaeological Sites* (2019) 21(1): 45-65.

[7] Jawondo, I.A. Architectural History of Ilorin Mosques in the Nineteenth and Twentieth Centuries. *Social Dynamics* (2012) 38(2): 303-312.

[8] Dmochowski, Z. R. *An Introduction to Nigerian Traditional Architecture: Northern Nigeria*. Ethnographica, Vol. I, (1990).

[9] Osifodunrin, P. *The First Church in Lagos: History of Holy Trinity Church, Ebute-Ero 1852-2016*. Ibadan University Press (2018).

[10] Ogundipe, S. A. *A Handbook of History: The Premier Diocese of the Church of Nigeria (Anglican Communion): The Diocese of Lagos 1919-2019*. Rehoboth Publishing (2019).

[11] Probst, P. Picturing the Past. Heritage, Photography, and the Politics of Appearance in a Yoruba Town. In: M. Rowlands & F. de Jong (Eds.) *Reclaiming Heritage. Alternative Imaginaries of Memory*. Left Coast Press (2007), pp. 99-125.

[12] J. Picton. Keeping the Faith: Islam and West African Art History in the Nineteenth Century. In: D. Behrens-Abouseif and S. Vernoit (Eds.) *Islamic Art in the 19th Century*. Koninklijke Brill NV (2006), pp. 191-230.

[13] A. Vaughan-Richards. Le Nigeria. In: J. Soulillou (Ed.) *Rives Coloniales. Architectures, de Saint-Louis À Douala*. Editions de l'OR5TOM (1993), pp. 245-88.

[14] The Cathedral Standing Committee. *The Cathedral of St. Peter, Ake, and Christianity in Nigeria: Chronicle of History 1843-2013*. Oba Oyebade Lipede Christian Books Centre, Abeokuta (2013).

[15] Chapter L86: A law to provide for the preservation, protection and restoration of historical properties and cultural heritage sites in Lagos state and for connected purposes. Listed Sites (Preservation) Law. Lagos State of Assembly, 27 June 2011.

12th International Conference on Structural Analysis of Historical Constructions
SAHC 2020
P. Roca, L. Pelà and C. Molins (Eds.)

CONSERVATION OF ARCHITECTURAL COMPLEX OF MANGUINHOS, IN RIO DE JANEIRO, BRAZIL

BENEDITO TADEU DE OLIVEIRA

Oswaldo Cruz Foundation - René Rachou Institute – Fiocruz Minas
Av. Augusto de Lima, 1715 - Barro Preto, Belo Horizonte - MG, 30190-002, Brazil
Email: beneditoo@uaigiga.com.br - Web page: http:// https://portal.fiocruz.br/

Keywords: Restoration, Conservation, Historic, Scientific, Cultural, Heritage

Abstract. *The aim of this paper is to report on the history and conservation interventions of the historic architectural complex of Manguinhos, in Rio de Janeiro, one of the most significant and symbolic architectural ensembles in Brazil. It is the headquarters of the Oswaldo Cruz Foundation – Fiocruz, under the supervision of the Brazilian Ministry of Health, the most prominent institution of science and technology on health in Latin America. It was protected by the National Historic and Artistic Heritage Institute (IPHAN) in 1980. The construction of the complex started in 1904 on the initiative of the renowned Brazilian scientist Oswaldo Cruz and was designed by the Portuguese architect Luiz Moraes Júnior. The main monument of the architectural complex, the Moorish Pavilion, received varied influences of styles and the décor is a reference to Alhambra. An architectural reading of the complex of Manguinhos will be made, examining the architectural language adopted on the historical buildings in particular the Moorish Pavilion; the material and building systems used in its construction; its meaning for the city and the heritage designation process, the surrounding environment in various periods, and the physical, functional and visual relationship with the city. Regarding the restoration works method, the following will be examined: causes of deterioration; diagnosis and state of conservation; interventions performed over the years; and the project and methodology and the latest intervention works. The conclusion, will analyze the interventions undertaken in the light of modern principles of cultural heritage preservation, the importance of the restoration works of the complex of Manguinhos, and its use as a public cultural and scientific space for the city.*

1. INTRODUCTION

The former Federal Serotherapeutic Institute was created in 1900, in the neighborhood named Manguinhos, in the city of Rio de Janeiro, Brazil. It was composed of a small number of traditional constructions, with brick walls and ceramic tiles roofs. In the same setting there was also an old garbage incinerator that belonged to the municipal administration, comprising the chimney, garbage incinerator and incinerator deposit [1]. By the end of 1902, the scientist and sanitarian physician Oswaldo Cruz became the director of the Federal Serotherapeutic Institute and on March 23, 1903 he was appointed by the President of Brazil, Rodrigues Alves, as head of the Directory-General of Public Health (DGPC), where he remained until November 1909.

His mission was to implement a modernizing model of public health, with the purpose of breaking through the insalubrious reality originated in the Imperial period of Brasil. The priority of the sanitarian reform project was to eradicate the three main pestilential diseases of the time:

smallpox, yellow fever and bubonic plague. In order to respond to the new demands and modernize the premises of the Federal Serotherapeutic Institute, Oswaldo Cruz started the construction of Manguinhos Architectural Complex. This conjuncture was decisive for Manguinhos − whose definition was inspired on the French Pasteur Institute − to become its tropical version and start the production of medicaments, scientific research, and activities related to public health [2].

2. A BRIEF HISTORIC AND ARCHITECTURAL ANALYSIS

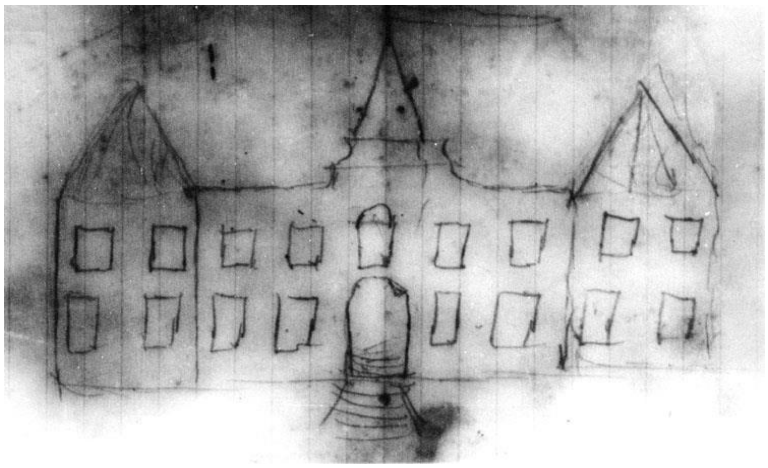


Figure 1. First sketch of the Moorish Pavilion made by Oswaldo Cruz himself (c. 1905). DAD-COC-Fiocruz archives. Photograph by J. Pinto.

The arrangement of Manguinhos Architectural Complex followed a layout that provided good ventilation and insolation of the buildings, and the highest area of the terrain was chosen for the main building to ensure a good visibility of the complex. The Moorish Pavilion, or Moorish Castle, with the front garden in the French style, stands out for its privileged setting, like the Greek temples and Portuguese colonial churches; the front of the building faces the view of the Guanabara bay. Due to its setting, shape and rich decorative details, the Moorish Pavilion is the largest building, standing out among the others in the complex, and therefore it represents the apex of the project. The buildings were arranged as to create a plaza, currently named Pasteur; on one side there is the Horse Stables; on the other side, the Quinine and the Moorish Pavilion; the Plague Pavilion closes the plaza on the back side. Behind this building, on a higher level, there is the Saltwater Aquarium. Separated from this arrangement, on the other hill of the campus, there are the Oswaldo Cruz Hospital, currently named Evandro Chagas Hospital; a vivarium for small animals, named Pigeonry; and the Vaccines Pavilion, built in the 1920s. These two last buildings are placed on the way between the two hills [3].The projects of the buildings that compose Manguinhos Architectural Complex were commissioned to the Portuguese architect and engineer Luiz Moraes Júnior [2].

The first building of Manguinhos Architectural Complex was the Plague Pavilion, built in 1904 in a style that resembles the English industrial and railway stations constructions. It was meant for the preparation of serums and anti-pestilence vaccines, horse inoculation tests, and research on plague. In that same year, the Horse Stables was built in the Tudor style, meant for the inoculation of virulent material and other operations performed on horses, with the purpose of obtaining serum, except for the anti-plague serum; and the Pigeonry was built as a vivarium for small animals. The Moorish Pavilion started to be built in 1905, when the two first buildings

were ready. In the following decade, the Saltwater Aquarium and the Quinine were built, this one meant for the production of official medicaments, and for research and laboratory of chemistry. The constructive system used in Manguinhos Architectural Complex consisted of a foundation made from a track filled with stones, cement and sand, over which were laid load-bearing walls of stones and bricks. The roofs were covered with tiles imported from Marseille, France, that were set on metal structures, in the case of the Horse Stables, and on wooden structures in the cases of the Plague Pavilion and the Quinine. For the Moorish Pavilion, the solution adopted was roof terraces paved with ceramics, also imported from Marseille. The terraces were built from metallic structural profiles, having the hollows filled with perforated bricks, and are surrounded by crenels and turrets – ornaments molded with cement and sand. On the two towers, that are crowning elements of the Moorish Pavilion, a metallic structure was used to sustain the 33 different types of ornaments made of cement and sand, and spherical shaped cupolas covered with copper. For the construction of the Moorish Pavilion large excavations were made on Manguinhos hill, into which large granite blocks were placed and set with cement and sand in the proportion 1:3 originating self-supporting walls of one-meter width. The materials used in the construction of Manguinhos Architectural Complex, such as soil, wood, sand, gravel and stone, were extracted from the estate's terrain. The other materials were imported: mosaics, tiles, bricks, and floor ceramics from Marseille, France; from Germany, lamps, steel, windows and doors, and wall tiles England; marble, from Carrara, Italy; and the tile ceramics (Bordallo Pinheiro), from Portugal [3].The construction works were directed by the Italian master builder Basílio Silvestre Aor, who commanded Portuguese, Italian and Spanish craftsmen specialized in joinery, masonry, painting and stucco. Oswaldo Cruz participated actively in the conception of the projects and followed the construction works development.

The Moorish Pavilion, main edifice of the complex, had its first sketch made by Oswaldo Cruz himself. It was a set of floor plans and elevations that served as a base for Luiz Moraes' projects. On the first project, dated 1905, the Moorish Pavilion had only three floors above the ground floor. On the project dated 1907, also with three floors, the architect added two side-towers to the building, probably influenced by the Montsouris Observatory in Paris. It was only in 1908, when the construction works were already ongoing, that Luiz Moraes elaborated the final project with five floors. All the projects presented a neo-Moorish style.

The buildings designed by Luiz Moraes present an eclectic architectural language, in which the composition is conceived according to the classical principles of frontality, axiality, and symmetry, but there is an ornamental treatment in which two or more styles and decoration tendencies are mixed together. The Plague Pavilion was inspired on the English railway stations, most likely due to the architect's background in railway engineering. The English architectural language used on the main complex - Horse Stables, Quinine, Plague, and Moorish Pavilions – is present together with the Portuguese and Arabic architectural languages. The English style appears both in the architecture of the Horse Stables Pavilion and in the iron elements of stairs, stalls, railings, bars, lamps etc.; also in the equipment, such as scales and elevators, and in the composition and finishing materials, such as granite and solid bricks.

Portuguese, Moorish and English languages are masterly combined in the Moorish Pavilion, Manguinho's headquarters. The English architecture influence in the Moorish Pavilion conception is found in the adoption of the "H" floor plan, with a large stairway in the richly decorated central entrance hall. These are some of the characteristics of the Elizabethan architecture predominant in England in the second half of the 16th century, during the reign of Elizabeth I (1558-1603). Another explanation for the floor plan used at the Moorish Pavilion relates to the Portuguese influence, namely in the adoption of the typical floor plan of 17th

century Portuguese mansions, whose major contribution to the evolution of residences in Portugal was the introduction of the "U" floor plan, with an open patio at the building's back-side. The distribution of spaces is symmetrical, drawing from a central axis, where there is a large hall with stairs, either in the interior or the exterior of the building, or an internal enclosed patio. In the case of the Moorish Pavilion, the distribution of the rooms is made from the central hall and internal stairs, richly decorated. The symmetry is especially present on the façades, where the decorative elements follow a rigorous composition. Another significant characteristic of the Portuguese tradition can be identified on the placement of the lavatories in a tower virtually isolated from the main body of the building.

The decoration follows yet another aesthetic orientation. The adopted language of Arabic origin follows the movement of medieval architecture revalorization that occurred in Europe in the first half of the 19th century as a reaction to the classicist predominance, in an attempt to retrieve the artistic memory of past eras of notable constructive splendor.

The idea of a 'Palace of Science' imagined by Oswaldo Cruz for the Institute's main building was achieved, in the interpretation of its architect, with the use of the language influenced by the architecture of Alhambra, in Spain, thus demonstrating the Iberian cultural heritage of its designer. The first sketch imagined by Oswaldo Cruz, though, revealed a medieval aesthetics, with two triangular-shape towers, therefore distant from the final design implemented by Luiz Moraes.The rich decoration of the main areas of the building, namely the principal stairway hall, the last floor hall, the library reading room, and the verandas, where rich finishing materials were used, besides the handcrafted panels in plaster and wood, contrasts with the extremely simple and functional laboratories, with plain walls with no decoration and covered with white tiles, with rounded corners at the junction of walls and floor [3].

The Pigeonry was built far away from the other buildings of the complex and perhaps for this reason it represents a significant contrast. Its composition and ground floor are also symmetrical; however, it is considered the freest project designed by Luiz Moraes Junior. Small pavilions in geometrical lines and a central tower form a light, harmonious and unpretentious ensemble; the few ornaments are decorative details in concrete, like roof ends and stairs banisters imitating tree trunks as in the gardens of French inspiration [4].

In September 1907, Brazil participated in the 14th International Congress of Hygiene and Demography, held in Berlin, and presented the architectural projects being implemented in Manguinhos. The Brazilian section was awarded the Gold Medal, which was handed to Oswaldo Cruz. In March 19, 1909, the institution was named Oswaldo Cruz Institute, currently Oswaldo Cruz Foundation – Fiocruz, https://portal.fiocruz.br/.

At the closure of the first decade of the 20th century, the first and second floors of the Moorish Pavilion were occupied by operating laboratories, while the construction works continued on the upper floors. The Horse Stables and Plague Pavilion were concluded and operating with activities to obtain serum from horses inoculation with virulent material. The Plague Pavilion, currently named the Clock Pavilion, was used exclusively to obtain antiplague serum. The Pigeonry was already occupied with small-size guinea-pigs. Other buildings concluded in that period were less sophisticated, such as the pergola that originated the Tea House and its annex.

The program of construction and modernization of the Institute's premises continued to be implemented in 1912, including the beginning of the Oswaldo Cruz Hospital, currently Evandro Chagas Hospital. This pavilion integrated a hospital complex originally designed with six unities, of which only one was built, being inaugurated in 1918. The purpose of selecting the other hill to build the Evandro Chagas Hospital was to isolate it from the Institute's laboratorial areas. The building has two floors and the spatial arrangement distributes centrally the basic

services areas and at the extremities the support areas, as kitchen, laundry etc. Interconnecting these areas there are two wards. Externally, the building has a sober, symmetrical solution, in which the ornamental elements are restricted to the verandas that surround the wards, providing internal environmental comfort [5].

The year of 1915 marked the beginning of the construction of the Saltwater Aquarium, which at that time had direct connection with the sea (Guanabara Bay) and was meant for the study of the aquatic microorganisms. Its architecture of art nouveau inspiration contrasted with the other buildings of the complex; it was one of the few attempts of Moraes to adopt a more contemporaneous architectural language [3].

In February 14, 1917, due to Oswaldo Cruz's health problems, the direction of Oswaldo Cruz Institute was assigned to Carlos Chagas, also a physician and scientist, who gave continuity to the construction of Manguinhos Architectural Complex [6].

From 1910 onwards, the inner walls of the third, fourth and fifth floors of the Moorish Pavilion were built, and the following years the terraces and towers too. In 1918 the museum and the library had been installed on the third floor; the ornamentation works of the hall and the library's noble room had been concluded, as well as the external ornaments made of cement and sand. In that same year, the laboratory equipment and electric, thermic, telephone and telegraphic installations had been implemented. Most of the equipment was supplied by the German firm Siemens & Halske.

Oswaldo Cruz died prematurely on February 11, 1917, before the conclusion of the entire architectural complex. The last projects designed by Luiz Moraes for the Institute − the Quinine and the Vaccine Pavilion − were concluded in the 1920s, under Carlos Chagas' administration.

The construction works of the Quinine started in 1919; its purpose was to house the Official Medicaments Service. It was designed to be entirely harmonized with its surrounding, and the volumetry, proportions, composition and façades treatment are similar to the Horse Stables; but is the only building with a polygonal floor plan, which creates an inner patio through which the circulation is made.

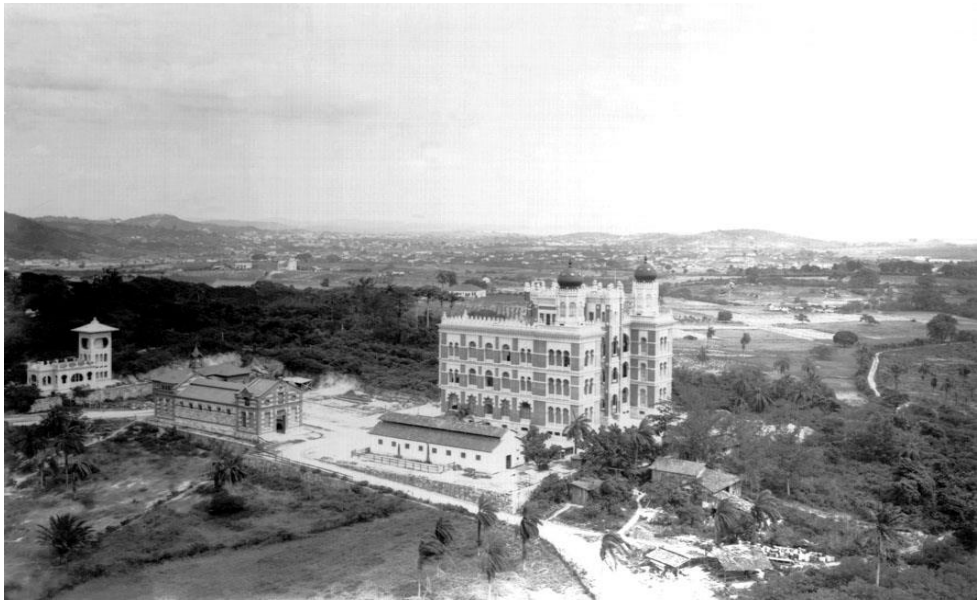


Figure 2. Manguinhos Historical Architectural Ensemble. From left to right: Saltwater Aquarium, Horse Stables Pavilion, old stables, and above the Moorish Pavilion (c. 1918). The Plague Pavilion is behind the Horse Stables Pavilion. DAD-COC-Fiocruz archives. Photograph by J. Pinto.

When concluded in 1922, the Quinine, with two floors, together with the Horse Stables and the Plague Pavilion, these with one floor each, formed a harmonious group of buildings around the Pasteur Plaza, with the Moorish Pavilion, with five floors, presenting the greatest monumentality. This ensemble has always been the highlight of Manguinhos campus due to the architectural styles, the materials used and the constructive systems adopted [3].

No other facilities were built in the complex that could equal these buildings in terms of the construction quality, which was the result of the craftsmanship, techniques, and materials used.

This can be verified in the design, also by Luiz Moraes, of the Vaccine Pavilion, built in 1922, which did not present the same monumentality as the previous ones. The building originally had a floor plan in a "U" shape, with an open patio; conventional constructive systems were adopted, with regular brick walls set with mortar made of lime, sand and cement, and roofs made of a wooden structure covered with French ceramic tiles. Less noble materials were used and the façades, covered with roughcast, are composed of a sequence of large wooden windows, marked by projecting elements.

The premises of Manguinhos Architectural Complex, especially the Moorish Pavilion, were built with the latest technological sophistication available in the country in the early 20th century [3].

3. TRANSFORMATION THROUGH TIME

From the 1930s onwards, major changes occurred within the limits of Manguinhos campus. In 1939−1940 there was the demolition of the old chimney of the garbage incineration furnaces of the Municipality of Rio de Janeiro; it had been the last construction contemporaneous to the Federal Serotherapeutic Institute. Several pavilions were built, notably the Pavilion of Courses and the Central Restaurant, with the application of the 'Five Points for a New Architecture' conceived by the Swiss-born French architect Le Corbusier: pilotis, roof-gardens, glass curtain walls on the façade, free floor plans. The construction materials and the structural constructive system characteristic of the modern movement featured reinforced concrete, ceramic tiles walls, glass curtain walls on the façade, roof-terraces with ceramic pavement, and roofs covered with amianthus tiles.

Designed by the Brazilian architect Jorge Ferreira, with decorative tiles panels by Paulo Osir Rossi, the project of the Central Restaurant was awarded the Special Mention of the jury of the 1st International Architecture Biennale held in São Paulo in 1951. Even more creative, the project of the Pavilion of Courses, by the same architect, had the collaboration of Roberto Burle Marx - author of the landscape architecture and the wall tiles panel, with aquatic microorganisms motif. Jorge Ferreira's architecture is among the most remarkable works produced in Brazil from the 1930s onwards, which gained international repercussion due to the creative reinterpretation of modern architecture principles. However, as will be exposed further in the text, not all the modern buildings constructed in Manguinhos campus have a good architectural quality nor were they all adequately implemented [3].

It was in the 1940s, marked by the consolidation of Manguinhos campus limits and the introduction of modern architecture at Fiocruz, that occurred the first mischaracterizations of the architectural ensemble conceived by Oswaldo Cruz and Luiz Moraes Junior. In 1936, more space for laboratories was evidently need in the Quinine; besides, the possibility of installing an elevator and constructing one more pavement was under study. In 1943, a project by Nabor Forster was approved by Luiz Moraes and two more pavements were constructed at the Quinine, therefore altering the harmonious relation that existed between the buildings around Pasteur

Plaza. As the project was supervised by Luiz Moraes himself, the final outcome was still well composed in its ensemble, though there was a loss in the relation between the previously existing scale and volume. A thorough observation of the currently existing façades and some internal construction details reveals the differences between the original floors and those that were added. This construction works also made changes on the staircase column and the placement of toilets. This would be one of the last participations of Luiz Moraes Junior at Fiocruz [3].

The construction of the old refectory and the Adolfo Lutz Pavilion (1949-1953) also altered the ambience of Manguinhos Historical Architectural Ensemble, due to the styles and construction materials used, and moreover due to the proximity with it. The construction of Carlos Chagas Pavilion (1944−1950), Bio-Manguinhos (1956−1965) and Leônidas Deane (from 1956 onwards), despite not being direct interventions in this historical ensemble, did in fact alter its relation with the surroundings. The Carlos Chagas Pavilion disputes the silhouette and partially blocks some of the main lines of sight of the architectural ensemble, namely the sight from the bordering Avenida Brasil (Brazil Avenue, a main highway in the city of Rio de Janeiro) direction south, and the sight from the road from Ilha do Fundão (Fundão Island) in Manguinhos direction. The Bio-Manguinhos building disputes the silhouette and partially blocks the line of site of the architectural ensemble of those who drive on Brazil Avenue direction north [4]. The Leônidas Deane Pavilion was designed with modern and ample installations to substitute the current Evandro Chagas Hospital, which since the 1930s had shown signs of being too small for the scientific researches in the experimental medicine. The new building was conceived with volumes in not much elaborate proportions, non-harmonious, and it was incorrectly placed. Its large dimensions are incompatible with its setting on the hilltop and there is an excessive proximity to Evandro Chagas Hospital, since its ground floor is too near from the old building.

The Seawater Aquarium lost its function with the construction of Brazil Avenue (1939-1946) when the connection with the sea through an earthenware pipe was interrupted; since then it turned into ruins and was demolished probably in 1958. In 1962, the Gomes de Farias Pavilion was constructed over the ruins of the aquarium, with no concern about its adequacy to the built environment. On the contrary, with its architectural characteristics and placement, it altered the ambience of Manguinhos Historical Architectural Ensemble. Another incorrect intervention carried out in the 1960s was the construction of an energy substation next to the Clock Pavilion.

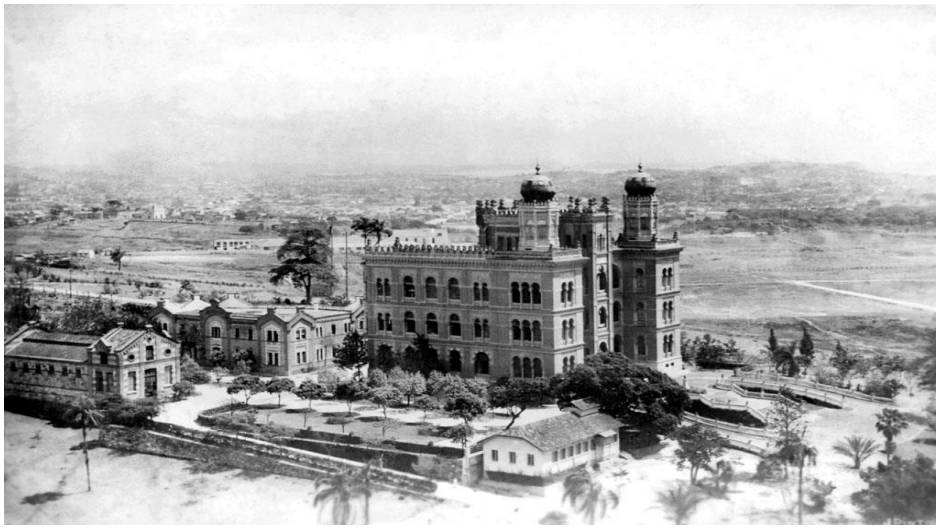


Figure 3. Manguinhos Historical Architectural Ensemble. From left to right: Saltwater Aquarium, Horse Stables Pavilion, Tea House annex, above Quinine and Moorish Pavilion (n.d.). DAD-COC-Fiocruz. Photograph by J. Pinto.

The institutional crisis during the military dictatorship (1964-1985) that in the 1960s culminated in the abrogation of ten scientists also affected Manguinhos campus' buildings, which became totally disregarded, some of them in ruins, remaining virtually only deteriorated service networks and obsolete equipment [7]. In December 1977, several pavilions were retrieved and re-inaugurated, among which the Quinine and the Vaccine Pavilion, this one adapted to become the Residential Village, currently known as the Yellow House. In this period, the Didactic Historical Museum was created; it was placed on the first floor of the Moorish Pavilion and was not conceived and implemented according to modern museology criteria.

PROTECTION MEASURES AND RESTAURATION AND CONSERVATION INTERVENTIONS

In January 1981 the Ministry of Culture homologated the process of heritage listing of Manguinhos Historical Architectural Ensemble through the Institute of Historical and Artistic National Heritage (IPHAN), at that time Secretary of Historical and Artistic National Heritage (SPHAN) [4]. This listed ensemble comprises the Moorish, Plague, Horse Stables Pavilions; the Pigeonry; and Evandro Chagas Hospital. In 1986, there was the demarcation of an extensive green and environment preservation area in the surroundings of this architectural ensemble.

In 1985, with the re-democratization occurring in the country, the institute started a process of revitalization and democratization through the creation of new scientific-technological unities and the introduction of a new management model, since then characterized as democratic and participative. The unity named Oswaldo Cruz House (COC) was created in 1985 with the purpose of retrieving and preserving the memory of biomedical and health science in Brazil, the development of historical research and museology activities, and the restauration and conservation of the historical architectural heritage of Fiocruz [3].

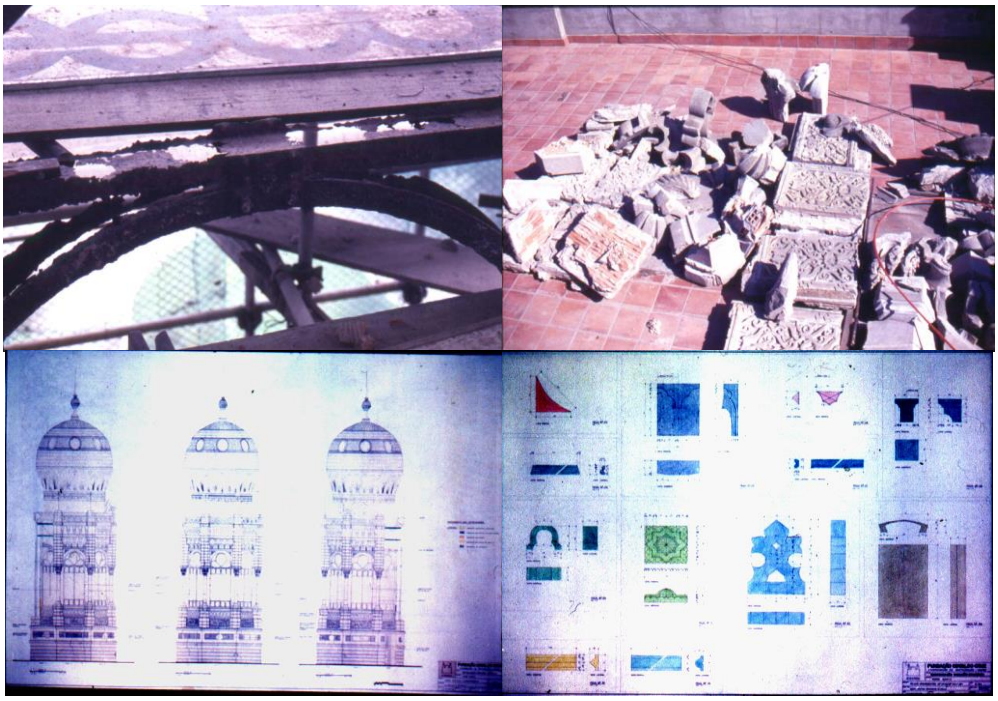


Figure 4. Interventions on the Manguinhos Historical Architectural Ensemble. From left to right: metallic structure, ornaments made of cement and sand, drawings of the façades, and ornaments of the towers of the Moorish Pavilion (1990s). DPH-COC-Fiocruz archives. Photograph by Benedito Tadeu de Oliveira

With the creation of Oswaldo Cruz House (COC) http://www.coc.fiocruz.br/index.php/pt/, the Clock Pavilion was renovated in order to become the seat of the unity; the Didactic Museum was transferred from the first floor of the Moorish Pavilion to the Horse Stables. In 1989, due to the increasing restoration works after the institution was listed as National Heritage, the Department of Historical Heritage (DPH) of COC was created and became responsible for the conservation, restoration and valorization of the historical architectural heritage of Fiocruz, in conformity with the modern principles of cultural goods safeguarding. The DPH also became responsible for researches on the relationship between heritage, architecture, urbanism, and health considering the historical and technological dimensions. Following a global planning, the stages of this work have been carried out according to financial resources availability and priorities established under criteria regarding safety and integrity of the materials [3].

The DPH is responsible for the implementation of preservation projects that are based on the outcomes of historical, stylistic, techniques and materials researches; mapping of damages, diagnoses and intervention methodology; supervision of conservation works, coordination of the systematics of preventive and corrective conservation, adaptation of spaces for new functions; development of a program of education and capacitation of skilled workers in the traditional arts and crafts in the area of cultural heritage conservation.

The different degradation degrees of Manguinhos Historical Architectural Ensemble occurred due to the following factors: wear and degradation of construction materials, lack of preventive maintenance, and wrong interventions suffered along the years. There was no major use incompatibility in these buildings; therefore, this was not an important factor for the degradation [8]. In general lines, the restoration interventions performed on the buildings of Manguinhos Historical Architectural Ensemble were as follows: impermeabilization and restoration of roof-terraces; treatment and reinforcement of metallic structures; restoration of ornaments made of cement and sand, restoration of wall tiles; wall painting restoration; restoration and gaps filling on original coverings; restoration of metallic and wooden windows and doors; substitution of hydro-sanitary, telephone, and electrical installations, and installation of central air-conditioning system, all in compliance with listed buildings[8].

The development of COC, with activities in the areas of research, archive and scientific museum, led DPH's architects to design new premises, always with the concern of keeping to an architectural language in harmony with the historical buildings.

In the last decade of the 20th century several new buildings were inaugurated at Fiocruz, such as Manguinhos Library, the Factory of Vaccines, the Reception Center, and the Museum of Life Pavilions. http://www.museudavida.fiocruz.br/

The Museum of Life was created by Oswaldo Cruz House in 1993 with the objective of bringing science nearer to the population and broadening science and health education to the public, by stimulating the understanding and participation in scientific and sanitarian issues. There is a peculiarity in the fact that the museum is inside Fiocruz campus, which is a scientific structure par excellence. This insertion enables the reflection on historical, territorial and cultural references of the institution's community of scientists and technicians, counting on the vast knowledge produced in its laboratories and scientific collections.

The inauguration of the Museum of Life was in May 1999, opening the celebrations of the Centenary of Fiocruz; since then it has been attracting hundreds of visitors monthly. The first circuit is made on the 'Train of Science', circulating through the following spaces: Reception Center, Science Park, Pyramid, Epidaurus, Butterflies Vivarium, Science on Scene Tent, Temporary Exhibitions Room, Horse Stables Pavilion, Clock Pavilion and Moorish Pavilion.

The construction of the new buildings within the listed perimeter raised the concern about

their adequacy to Manguinhos architectural universe; several constructive techniques were adopted, with the use of steel structural profiles, ceramic bricks on walls as finishing material, ceramic tiles on roof coverages, and the option of designing semi-underground constructions as not to interfere with the visibility of the listed buildings.

At the Reception Center of the Museum of Life there was an attempt to refer to Luiz de Moraes Junior's architecture, adopting a contemporary architectural language but using construction materials as granite and Portuguese stonework on pedestrian pavements, architectural elements as a clock tower, solutions as the wall panel mosaic by the Brazilian artist Glauco Rodrigues portraying historic moments of Fiocruz, besides constructive systems similar to those used on the early 20th century buildings [9]. The final outcome has a good insertion in the surrounding environment and dialogs with Manguinhos Historical Architectural Ensemble. The building is inspired on the railway stations architecture of the 19th century, there is a predominance of empty over full wall-surfaces, and the project's strength is on the steel structure with simple and functional design. The adoption of the architectural language of railway stations is due to the fact that visitors are transported to the other Museum of Life pavilions on a stylized train on wheels. Another intervention made with the same concern is the Annex of the Horse Stables, which is part of the Space of Biodiscovery. The Annex's façades have similarities with the Horse Stables Pavilion in the shape of the openings, treatment of surfaces and construction materials. The new construction was built below the level of the Horse Stables with the purpose of not interfering with its architectural sight, and vegetation was planted on the roof-terrace to integrate it with the environment.

In parallel with the construction works of the facilities needed to meet the new demands for space, Fiocruz continued to carry out the program of restoration and conservation of the Manguinhos Historical Architectural Ensemble, with the support of all the presidencies of the institution from 1987 onwards. Restoration works included the verandas of Evandro Chagas Hospital, façades of the Quinine, and the entirety of the Pigeonry, the Horse Stables and the Clock Pavilion [10]. In 1995, on the centenary of death of the French scientist Louis Pasteur, the monumental illumination of Manguinhos Historical Architectural Ensemble was inaugurated, as well as the restoration works of Pasteur Plaza.

Due to the dimensions and architectural characteristics, the Moorish Pavilion requires complex interventions, which were initiated in 1987 and continue to be carried out in the present; the works have considered the availability of free spaces and the degree of urgency of interventions [11]. The restoration of the Moorish Pavilion, which is occupied by of Presidency of Fiocruz, has always been carried out by parts, equivalent to the half floor area, which are released and occupied successively shortly after completion of the works. The most complex interventions were those of the restoration of crenels and turrets, and of the north and south bow windows, which required the removal of the ornaments for the treatment of the metallic structures. The restoration works of the Moorish Pavilion, which is occupied by the Presidency of Fiocruz, have been carried out in parts and will be the object of future specific publication. There are reports of all the interventions, illustrated with photographs, historical documentation, and are registered on U-matic with statements of technicians and crafts workers involved in the works. The full restoration project comprises architectural survey, mapping of damages, analysis of construction materials, study of deterioration causes, diagnosis, and intervention project [12].

In 1998 the actions of cultural heritage preservation of Fiocruz were extended to the modernist pavilions. In that year, the Central Refectory and the Pavilion of Courses, designed by architect Jorge Ferreira, were listed by the Institute of Cultural Heritage of the State of Rio de



Figure 5. Interventions on the Manguinhos Historical Architectural Ensemble.From left to right: Clock Pavilion, Quinine, Moorish Pavilion and Horse Stables Pavilion (1990s). DPH-COC-Fiocruz archives. Photograph by Benedito Tadeu de Oliveira.

Janeiro (INEPAC/RJ). The restoration of the wall tiles panel created by Burle Marx at the Pavilion of Courses was the first intervention, carried out from 2016 onwards.

Despite the accelerated process of constructions in Fiocruz in the 1990s, the area delimitated in 1986 was virtually preserved. The few interventions carried out respected the surrounding environment and the historical heritage.

4. CONCLUSIONS

The Oswaldo Cruz Foundation, linked to the Ministry of Health, is the largest biomedical research institution in Latin America and it is internationally recognized. It is a public and strategic health institution, with the following missions: to produce, disseminate and share knowledge and technology directed to the strengthening and consolidation of the Brazilian Unified Health System (SUS). The defense of the right to health and to ample citizenship is a central value of Fiocruz.

The campus of Oswaldo Cruz Foundation, comprising approximately 850,000 m^2, is a large green area which presently has circa 160 buildings, with significant architectural examples of various periods. But it is the Manguinhos Historical Architectural Ensemble, especially the Moorish Pavilion, the institution's highest symbol, which remains as the highlight in the Cultural Landscape of Fiocruz. Several factors have contributed to the preservation of the architectural ensemble, such as the solidity of the constructions ensured by the construction systems and materials used; the symbolism of the buildings that was consolidated during almost 120 years of existence of Fiocruz; and the care of the institution with its cultural heritage.

The creation of Oswaldo Cruz House, dedicated to the activities of research, education, documentation and diffusion of the history of public health and biomedical sciences in Brazil, was fundamental to the preservation of Fiocruz's memory. Other Brazilian institutions initiated and implemented some cultural preservation actions, but for different reasons they were not as

successful as Fiocruz, which is currently a reference in its purpose and original areas of activities, but also in the preservation of Brazilian cultural heritage.

The creation of the Department of Historical Heritage (DPH) within Oswaldo Cruz House (COC) has been of utmost importance for the preservation of Manguinhos Architectural Complex, which gathers historical, cultural, and scientific values to apply as a candidate as UNESCO World Cultural Heritage.



Figure 6. Aerial view of Fiocruz campus (c. 2000). CCS-Fiocruz archives.

REFERENCES

[1] Dias, E. O Instituto Oswaldo Cruz - resumo histórico (1899-1918). Rio de Janeiro: Manguinhos, (1918).

[2] Benchimol, J.L. (coord.). Manguinhos do sonho à vida: a ciência na Belle Époque. Rio de Janeiro: COC, Fundação Oswaldo Cruz, (1990).

[3] Oliveira B.T. (coord.), Costa, R. da G.R. e A. J. de S. Pessoa. Um lugar para a ciência: a formação do *campus* de Manguinhos. Rio de Janeiro: Editora Fiocruz, (2003).

[4] Alcântara, P. (coord.). Processo de tombamento do Conjunto Arquitetônico de Manguinhos. Rio de Janeiro: IPHAN, (1980).

[5] Aragão H. B. de. Notícia Histórica sobre a Fundação do Instituto Oswaldo Cruz, *in* Memórias do Instituto Oswaldo Cruz. Tomo 48, (1950), Rio de Janeiro: Serviço Gráfico do IBGE.

[6] Chagas C. F. Meu Pai. Rio de Janeiro: COC, Fundação Oswaldo Cruz, (1993).

[7] Lent H. O Massacre de Manguinhos. Rio de Janeiro: Avenir, (1968).

[8] Oliveira, B.T. e Costa, R. da G. Patrimônio – Manguinhos, Fiocruz. São Paulo, Revista Arquitetura e Urbanismo, 44 (1992), pp.52-53.

[9] Oliveira, B.T. e Costa, R. da G. R. Centro de Recepção do Museu da Vida, Manguinhos, Rio de Janeiro. São Paulo, Revista Projeto Design, 243 (2000), pp.61-63.

[10] Oliveira, B.T. Restauração em Manguinhos - Pavilhão do Relógio. São Paulo, Revista Projeto, 160 (1993), p.55.

[11] Oliveira, B.T. A restauração do Castelo de Manguinhos. São Paulo, Revista Projeto, 136 (1990), pp.122-124.

[12] Oliveira, B.T. O processo de recuperação do Castelo de Manguinhos. São Paulo, Revista Projeto, 120 (1989), pp.154-155.

12th International Conference on Structural Analysis of Historical Constructions
SAHC 2020
P. Roca, L. Pelà and C. Molins (Eds.)

DACIAN FORTRESSES IN ORASTIE MOUNTAINS: MANAGEMENT OF HERITAGE STRUCTURES

GABRIELA PAȘCU[1*], ALEXANDRA KELLER[2] AND CĂTĂLINA BOCAN[3*]

[1] Lecturer, Faculty of Architecture and Urban Planning, Politehnica University Timișoara - UPT, 2A Traian Lalescu street, 300223 Timișoara, Romania,
e-mail: gabriela.pascu@upt.ro

[2] Teaching Assistant, Faculty of Architecture and Urban Planning, Politehnica University Timișoara - UPT, 2A Traian Lalescu street, 300223 Timișoara, Romania, e-mail: alexandra.keller@upt.ro

[3] Associate Professor, Faculty of Architecture and Urban Planning, Politehnica University Timișoara - UPT, 2A Traian Lalescu street, 300223 Timișoara, Romania,
e-mail: catalina.bocan@upt.ro

Keywords: Archaeological sites, heritage management, preservation

Abstract. *The protection of the built and archaeological heritage is an increasingly debated topic in recent years. In order to protect these valuable historic structures and preserve them for the future, holistic approaches are necessary. These generally involves a wide range of specialists and collaborators, multidisciplinary way of developing conservation strategies, while maintaining their original features.*

However, recent studies highlight the fact that the management of heritage sites and buildings is far more than the simple aesthetic and structural repair. It means acknowledging the role of societies and communities in maintaining the importance of these structures and the risk of environmental factors (climate change challenges or earthquake risk) on their state of conservation and the effect of unauthorized interventions over time.

Therefore, based on the case study of Orastioara, a commune in Hunedoara County, Romania, where 3 UNESCO heritage sites (from a total of 6 UNESCO sites in the area) can be found and numerous monuments of national and local importance, the study is presenting the challenges encountered during the development of the general urban plan of the commune, in relation with all the establishments that conserve Dacian fortresses – sites UNESCO; and also a proposal for the future management plan of the protected sites. Since the heritage structures have been neglected over the years, the paper comprises a general overview of the complexity of the developed conservation strategy, in order to be able to manage the heritage structures while taking the particularities of their context into consideration.

1 INTRODUCTION

UNESCO has established, since 1972, a framework for the protection and conservation of cultural and natural heritage and the world heritage list. To these treaties over the years, some particularly important documents, such as Nara Document of Authenticity, were added. To these, 193 states joined including Romania. What was emphasized by this, was that the cultural heritage exceeds the borders of an area or country, standing out in certain cases by exceptional values. These sites are part of everyone's heritage.

1.1 UNESCO sites in Romania

According to the latest statistics from the UNESCO site, there are 1221 cultural and natural heritage sites, with an unequal distribution across continents. Associated with them are many debates because even if they are under extraordinary protection, their threat continues to be imminent. The concepts always taken into consideration are: protection, preservation of authenticity, integration of heritage in context, management and promotion.

Romania joined the World Heritage Convention in 1990, but the actual implementation began to take place only in 2000, when a legislative document was issued regarding the establishment of measures for the protection of historical monuments belonging to the World Heritage List. In the last years, Romania has elaborated various laws and rules of management of the UNESCO heritage, but surely any procedure can be improved.

By 2017, Romania has registered eight sites: (1) Danube Delta (1991, natural site), (2) Beech and virgin forests in the Carpathians and other regions of Europe (2017, natural site), (3) Moldova's Churches (1993), (4) Horezu Monastery (1993), (5) The villages with fortified churches in Transylvania (1993), (6) The Dacian Fortresses from the Orastie Mountains (1999), (7) The historical centre of Sighisoara (1999) and (8) The wooden churches from Maramureș (1999). Regarding Romania, there is also an indicative list, completed in 2017 by the National Institute of Heritage, which includes 18 cultural sites and a natural one [1]. UNESCO sites in Romania are monitored periodically and are decisive territorial factors when developing new General Urban Plans.

1.2 The Orăștioara commune

In such a situation is the Orăștioara commune, situated in the east of the Hunedoara county. The commune is formed by eight villages: Bucium, Costești, Costești – Deal, Grădiștea de Munte, Ludeștii de Jos, Ludeștii de Sus, Ocolișu Mic și Orăștioara de Sus (being the main component village). It has 2079 inhabitants. Within the administrative territory of the commune, there are three UNESCO sites (from a total of 6 Dacian Fortresses from the Orastie Mountains) – that must be integrated and highlighted in the next general urban plan. Their integration implies a proactive management, plan not easy to do in a small commune with a low financial income. In this situation are all the establishments included in this UNESCO Dacian archaeological site.

From this point of view, the realization of the plan should take into account all the six UNESCO sites – Dacian fortresses existing in the area (commune Orăștioara de Sus – Sarmizegetusa Regia site, Costești – Cetățuie site, Costești – Blidaru site; commune Săsciori – Căpâlna site; commune Bănița – Bănița site; commune Boșorod – Luncani site). This UNESCO landscape covers two counties: Hunedoara and Alba.

The establishments and their archaeological sites are situated in the cultural landscape geographically determined by the Șureanu Mountains and the Orăștie river, therefore in a very powerful context from a historical, architectural, archaeological and natural point of view.

1.3 Cultural framing and significance of the Dacian Fortresses from the Orastiei Mountains

Of all the Romanian UNESCO sites, the Dacian Fortresses from the Orăștie Mountains are the only ones that best preserve and highlight the roots and formative evolution of the Romanian people. The name Dacia was mentioned for the first time during the reign of Emperor Augustus, in the writings of M. Vipsanius Agrippa (De mensuratio provinciarum). All ancient authors (Pliny the Eider and Tacitus) considered Dacia to be in the north - Danubian territories (Figure 1a). The Hercynian Forest was considered the northern boundary of the territory inhabited by the Dacians (Julius Caesar, De bello Gall.), an opinion sustained as well by Strabon's writings.

Throughout the former Dacian territory, there are indications of a high-level civilization. Between 100 in. - 106 AD, during the classic period of the Geto-Dacian civilization, the Dacian state formed in the Orăștie Mountains, with the capital at Sarmizegetusa Regia (the city from Grădiștea Muncelului). Oltenia, Banat and central Transylvania were part of the Dacian state.

In 82 BC - Burebista's era. The most important leader of the Dacians was Burebista, which was made king of a large territory and "(…) the first and the greatest of the Thracian kings, ruler of all the lands and thither the Danube (IGB, I2 13). in 44 B.C. In his time fortresses were built with squared stone walls in the area of the Șureanu Mountains, approx. 70 fortifications in Dacia (among which: Blidaru, Piatra Roșie, Costești, etc.).

After 44 BC - the kingdom is breaking down. The settlement from Sarmizegetusa becomes more important, and the population's residence move here.

Towards the end of the 1st century, in this region at least four important settlements are mentioned: Costesti, Ceata, Fețele Albe, Sarmizegetusa Regia, numerous scattered households and seasonal settlements from Rudele, Tâmpu and Meleia.

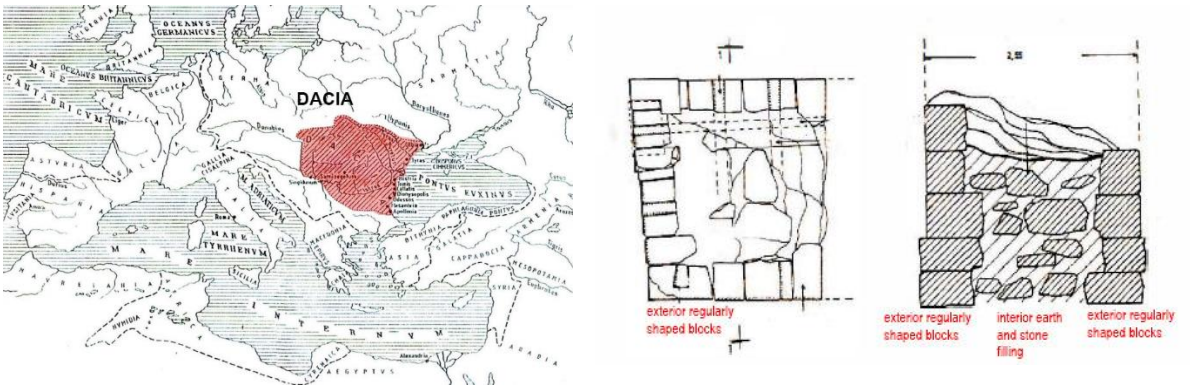
In 88 the Dacians are defeated at Tapea, and in 98 the emperor Traian denounces peace.

101 - 102 is the period of the first Dacian war. This first war resulted in the conquest of the Costești - Cetățuie fortresses, the siege of Blidaru fortress and Fețele Albe.

105 - 106 is the period of the second Dacian war. This second war ends with the burning of the fortresses Piatra Roșie, Blidaru, Cetățuie, Hulpe peak and the settlements in Costești, Ceata, Fețele Albe. The king Decebal commits suicide at Ranisstorum.

106 - 271 is the period of the Roman conquest when the infrastructure of the territory was strengthened, the capital of the new provinces was founded (Colonia Ulpia Traiana Augusta Dacica), Trajan's column was inaugurated in Rome.

At the time of the Roman conquest, a whole series of cities, temples, urban settlements and fortifications were destroyed. The population was mostly relocated to what is now called the Hateg Depression, where a new city - Sarmizegetusa (Ulpia Traiana) was built. Mostly on the territory occupied by the Dacians, the Roman army left a population of shepherds and subsistence farmers. Roman garrisons were installed at the most important points. After the withdrawal of the Roman administration, this area was characterized by a rather rural population.



a) b)

Figure 1: a) Map of Dacia, under king Burebista; b) Murus Dacicus (after [2])

Following this short historical thread, it was observed that the fortresses from Orăștie Mountains were built to defend the territory against the Romans. Based on existing documents and existing research (which is an ongoing process), the following conclusions can be drawn about the character and role of each fortress.

- *Costești – Cetățuie* and its civil settlement. It's the oldest fortress discovered in Orăștie Mountains, dated by the researchers between 2nd century B.C. and the beginning of the following century.
- *Sarmizegetusa Regia*. It became the capital of the Dacian territory, but there is also a hypothesis, according to which, in the same place, before the development of Sarmizegetusa, in the first half of the I century B.C, a cult centre existed, named The Holy Mountain of the Dacians (Kogaionon).
- *Costești – Blidaru and Luncani – Piatra Roșie* were considered to be residences of high military leaders, built in a Hellenistic style (like Costești – Cetățuie).
- *Bănița and Capâlna* – "(…) were annexed to the fortress ensemble from Orăștie Mountains, as an outpost of the defensive system of the Dacian capital." [2].

These fortresses with stone enclosure walls, represented at the end and of the first Christian era, one of the greatest and most important achievements of the military architecture, outside the Roman Empire.

2 THE CONTEXT OF THE ORAȘTIEI MOUNTAINS AND THE LOCATION ARGUMENTS OF THE FORTRESS IN THIS AREA

This densification of the fortresses and settlements in this area is due to the peculiarities of the Șureanu Mountains, more specific the Orăștie Mountains. They are in the southern part of the Mureș Pass and are formed of medium mountains, forested, with narrow valleys, branched and twisted (Figure 2). This whole framework made the region difficult to reach, and therefore provided the cities and settlements an additional defence. At the same time, the Șureanu Mountains have a depressing border with valleys and peaks favourable for living and the best agricultural lands and communication channels. The villages from the valleys, lived in close collaboration with the mountain settlements, between them being a permanent exchange and valorisation of resources.

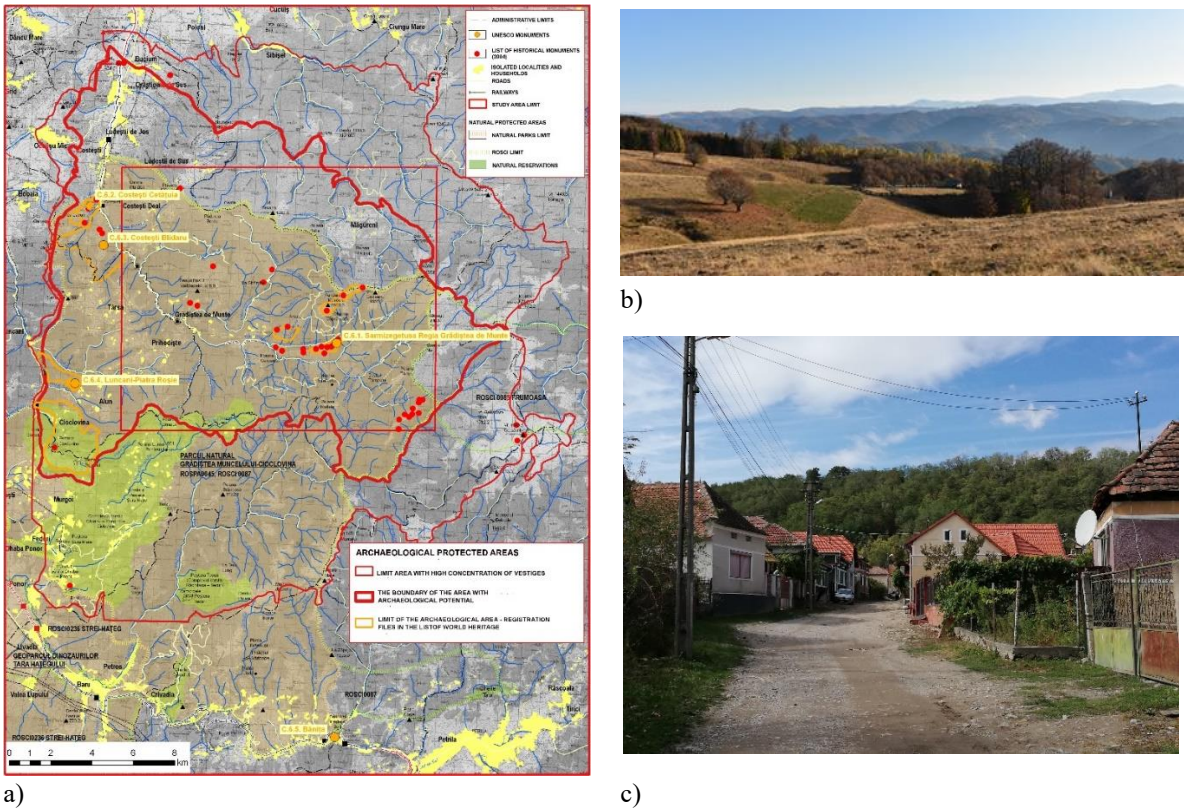


Figure 2: a) Present urbanistic context and UNESCO site position [3]; b) The Orăștie Mountains – the landscape context of Dacian fortresses (© Gabriela Pașcu); c) Orăștioara de Sus village (© Gabriela Pașcu).

Apart from the geographical features of the area, the main argument for the development of Dacian settlements is the presence of iron deposits, the only place of this type known to the Dacians. Other arguments would be the temperatures, which are 1 - 3 degrees higher, compared to the other points of the mountains, easy connections through the hydrographic network with the other areas and the arrangement of the valleys, which allowed simultaneous access to the northern lanes and communication paths [4].

These fortresses were well organized. The main access in the region was dominated and controlled by the main habitat, Sarmizegetusa, located on the top of Grădiștea Hill (part of the Godeanu massif) at 1200 m altitude. From these, a series of fortresses and defence towers continued upstream Apa Grădiștei river. Of these, the most important were the Costești Cetățuie and Costești – Blidaru fortresses. The northeast access was defended by Cugir and Grădiștea de Munte (Vârful lui Hulpe fortification). The fortress Capâlna was also a part of the group being situated in Sebeș Valley. From the south-west, a possible attack was stoped and spot out from the Cioclovina – Ponorici fortification; and from the south-east by Luncani – Piatra Roșie fortress. Another pass was possible through the Vâlcan and Merișor, but these routes were monitored by the Bănița fortress.

The only way left without enough defence to Sarmizegetusa – Grădiștea de Munte was a

very difficult one (downstream the valley of Jiu river) and for this reason, it has been used by the Roman army in the 101 – 102 war. The connection between the fortresses was assured by a very complex network of surveillance towers and residence points. All this system of approximately 150 km^2, was built to protect the Dacian Kingdom centre of power – Sarmizegetusa Regia.

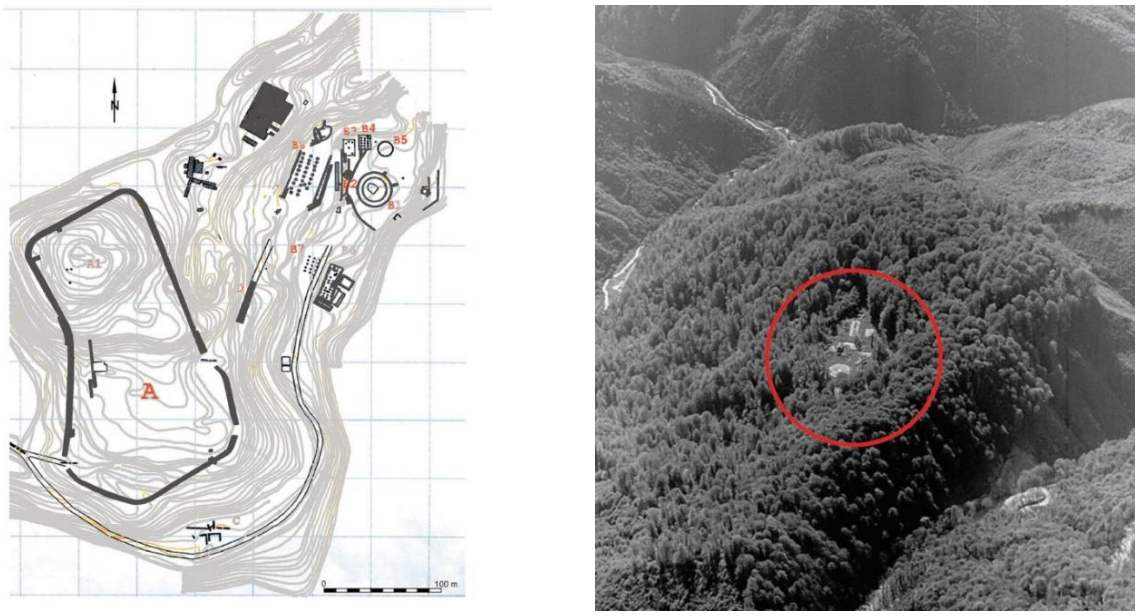
2.1 The historical – urban, architectural and structural features of the sites

The site ***Grădiștea Muncelului – Sarmizegestusa Regia*** (village Grădiștea de Munte) is today a site is the property of the Romanian state, through the national management of forests and is part of the administrative territory of Oraștioara de Sus settlement (Figure 3).

The first information about the ruins from Grădiştea de Munte date from the beginning of the 19th century, when the Austrian administration sent representatives to investigate the phenomenon of the emergence of precious metal treasures in the area. The imperial envoys recorded in their official reports the existence of the fortification and of several stone constructions, besides the numerous pieces discovered. During the 19th century, Grădiştea de Munte came to the attention of scholars and antique collectors. Some of them also dug at different points of the ancient settlement. The first systematic excavations began after World War I, in 1922-1924, when the professor D. M. Teodorescu investigated the fortification and the large circular temple. In 1950 he started the archaeological research project of the site, under the leadership of Professor Constantin Daicoviciu. Since then, fortification elements, cult buildings, metallurgical workshops, water collection and distribution facilities, houses and their annexes have been brought to light [5].

The site can be recognized as an ancient city due to its important religious and defensive character. At the beginning, it had a symbolic and religious value, but in time it grew to have an important economic and defensive role. It is approximated by researchers to have had about 5000 inhabitants. Concerning the urban and architectural characteristics "[…] terraces flourishing workshops, imposing and monumental sanctuaries, strong and domineering walls rising out of the rock of the mountains, all that looked very imposing at the moment of Roman conquest" [2]. The urban structure was coherent and developed for emphasizing the important constructions of the settlement, without conflicting with the natural characteristics of the site. All the edifices were constructed on artificial terraces (approximately 100) on almost 6 km distance. The defensive walls were hundreds of meters long and 10-12 m high and were built in murus Dacicus technique – "double regularly-shaped blocks walls with emplecton" [2].

In the present the site is composed of 1. the Dacian fortress, 2. the sacred area, 3. circular sanctuaries with a central alter-chamber; 4. the cult altar; 5. circular sanctuaries; 6. rectangular sanctuaries of the alignment type with limestone plinths and andesite plinths; 7. the civil settlements; the ancient road system and water adductions.



a) b)

Figure 3: a) Archaeological site Grădiștea Muncelului; b) Aerial image of the site Grădiștea Muncelului (after [2])

The ***Costești Cetățuie fortress*** is situated in the Orastioara de Sus settlement, in the Costesti village, on the left bank of the Apa Orasului river. It had the role of controlling the direct route to the capital of the Dacian Kingdom, Sarmizegetusa Regia (Figure 4a).

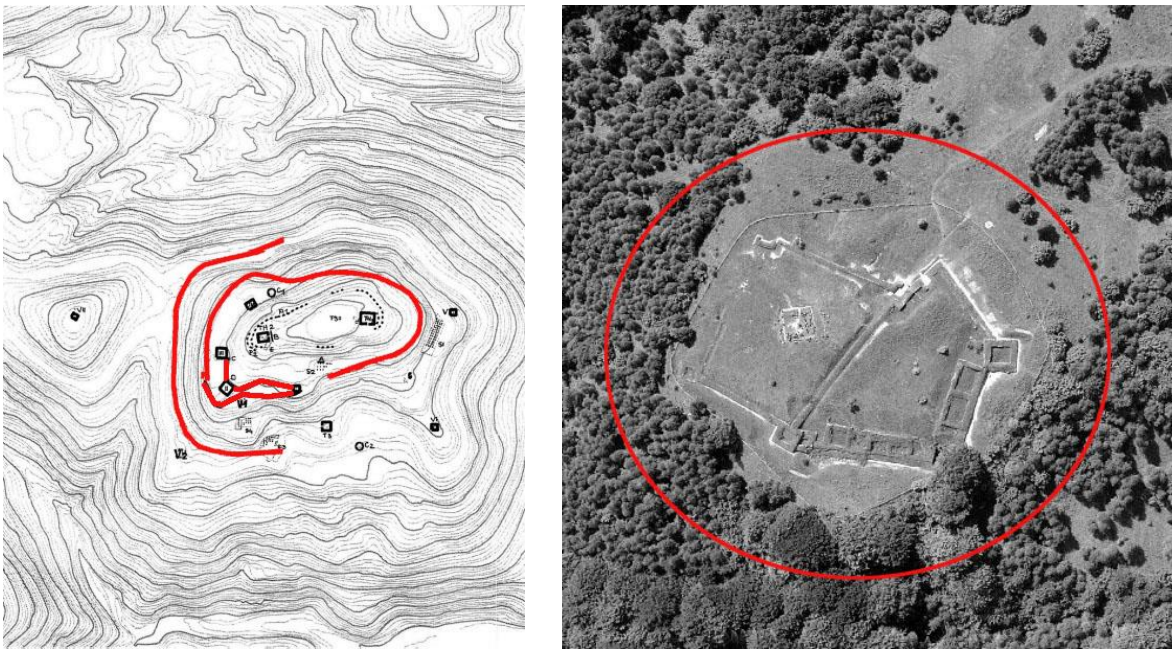
This fortress illustrates the evolution of fortifications made by earthen walls, palisades and ditches, to the fortifications with double stone walls faced enclosures of Hellenistic inspiration.

The superior plateau was protected by an earth wall and was dominated by two massive dwelling towers (palatial towers). The access to the dwelling towers was done through a monumental stairway (3.20 m wide). The site also includes four sanctuaries.

The ***Costesti Blidaru fortress*** is situated on a hill with a 705 m altitude with a large view to the valley of the Mureș river and Sarmizegetusa Regia. From an archaeological point of view, it has a geometrical composition organised around a central element – the dwelling tower (Figure 4b).

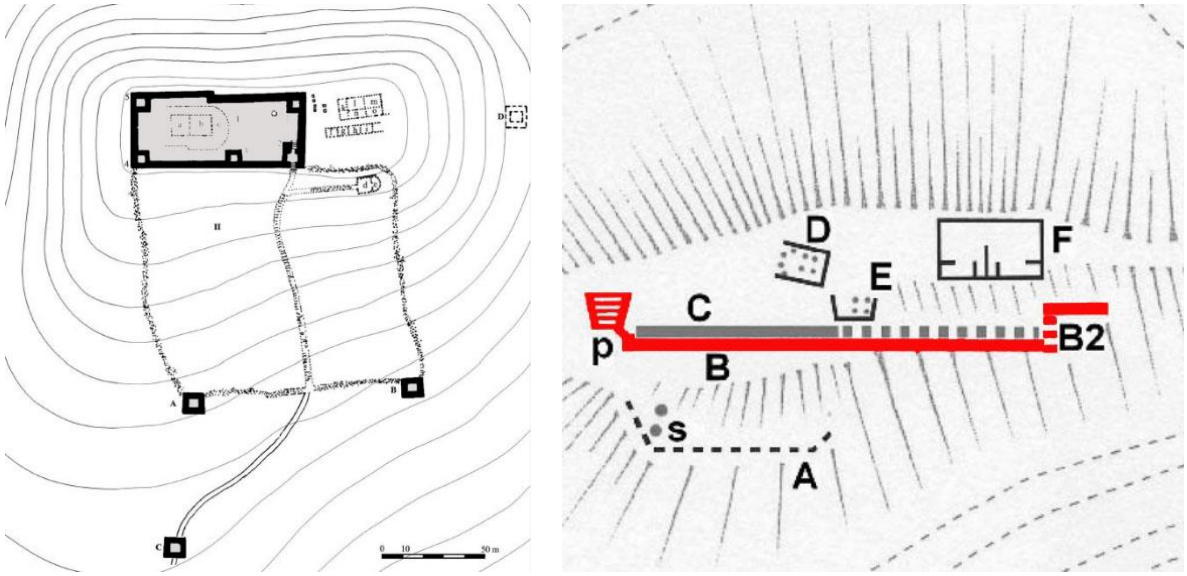
The ***Luncani – Piatra Roșie fortress*** is situated in the Luncani village, Bosorod commune, on the top of the hill bearing the same name. The structure of the defensive elements is of the Hellenistic model and it has inside dimensions of 4.52x5 m and 3.12x3.12 m. The site is composed by the fortifications, five towers, three gates and several edifices (Figure 5a).

The ***Bănița fortress*** is situated in the Hunedoara county, in the commune having the same name. The fortress was built on a raised land called “Dealul Bolii” or “Piatra Cetatii” with a height of 904 m. The fortress is almost inaccessible. This fortification is composed of a series of military construction: enclosure walls, towers, battle platforms, defence banks, etc., built with stone, wood or earth. The first fortification is the 115 m long wall, 2 m thick, using the murus Dacicus technique. The research on this fortress demonstrates its long existence, even without a dominant civilian character (Figure 5b).



a) b)

Figure 4: a) Plan of the archeological site Costești Cetățuie; b) Plan of the archeological site Costești Blidaru (after [2])

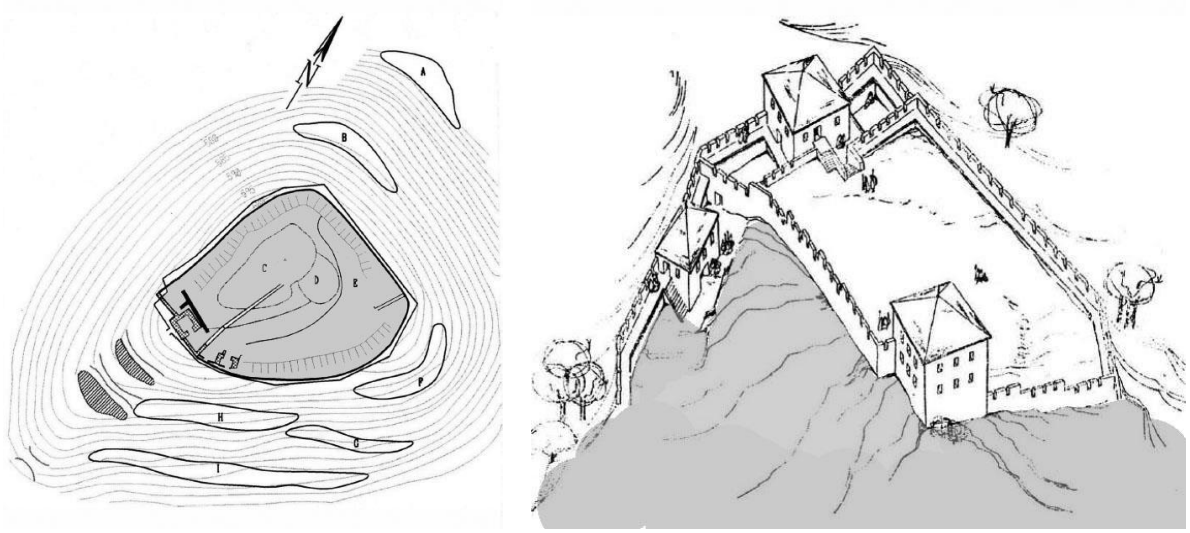


a) b)

Figure 5: a) Plan of archeological site Luncani – Piatra Roșie; b) Plan of archeological site Bănița (after [2])

The ***Căpâlna fortress*** is situated in the valley of the Sebeș River (Căpâlna village) – Săsciori commune, department Alba. It has an isolated position, far from the other Dacian fortresses. The archaeological studies began in the inter-war period. For a good functioning of the fortress, she was placed on the top of Dealul Cetății. For this, terracing works were done on the cliff. This fortress had the role of blocking any access from the east towards Sarmizegetusa Regia.

The plan of the fortification is composed of a ditch, two banks, a dwelling tower and an enclosure (Figure 6).



a) b)

Figure 6: a) Plan of archaeological site Căpâlna.; b) Photographic restitution of Căpâlna site (after [2])

2.2. Current context and site problems

Studies and fieldwork concerning the heritage sites in the Orastie mountains, highlight that there are a series of factors which currently affect the integrity of the sites, but are not brought forward in the various reports concerning the state of conservation of the sites. Besides meteorological factors which are leading to the erosion of the soil around the sites, there are a series of factors related to the general management which ultimately lead to the degradation of the archaeological heritage. Animal grazing and hay growing in the site area (Figure 7a), illegal archaeological diggings, theft, and unsupervised tourism leading to the vandalization of the sites (Figure 7b) and have the most important impact on their state of conservation [1]. Vitalie Barca is also highlighting the fact that these sites are in a bad state of conservation mainly due to the lack of any short or long-term management plan and that it is important to find solutions soon in order to be able to preserve their value for the future [6].

Studies in recent years concerning the management of heritage structures highlight that heritage management must be approached from a multi and interdisciplinary point of view, thus highlighting its holistic nature [7]. Still, they also bring forward that heritage management is not only connected to the preservation of the tangible and intangible value of the site but should also involve local communities [8]. The involvement of local communities and various stakeholders is also highly recommended by the UNESCO Operational Guidelines for the Implementation of the World Heritage Convention [9].

Therefore, it is of utmost importance to develop a comprehensive management plan for the heritage sites from the Orastie mountains sites which could bring forward the significant historical and cultural value of the area and highlight the importance of the sites in the history of Dacian architecture. In the same time, they should ensure the protection of the sites on the short, medium and long-term and be able to evolve and adapt according to continuous studies and investigations of the state of conservation of the sites and current and future threats.



a) b)

Figure 7: Signs of poor management of the heritage sites (a) Haystacks near the archaeological structures; b) vandalization of the heritage site)

3 MANAGEMENT PROPOSAL

The management plan imagined for these UNESCO sites aims to safeguard the outstanding universal value of the archaeological sites, their authenticity and integrity (Table 1). It must be planned both for short term (2 – 5 years) and long term (5 – 30 years). The management plan should be an agreement between all the specialists implicated in the general urban plan of Orăștioara de Sus, Boșorod, Bănița and Săsciori; and in the management plan of the UNESCO sites. Among them are: Romanian Ministry of Culture, local administrations (Orăștioara de Sus, Boșgorod, Bănița and Săsciori), Faculty of Architecture and Urban Planning Timișoara, County Council Hunedoara and Alba, National Heritage Institute, the administration of Natural Park Grădiștea Muncelului – Cioclovina, Museum of Dacian and Roman Civilisation Deva).

The purpose of this management plan for the Dacian Fortresses from the Orăștie Mountains has the purpose of enhancement and integrity conservation. The objectives proposed for the achievement of the purpose must be clearly formulated, so that they can be checked. For every objective, measures must be specified, and their implementation monitored.

Therefore, the following objectives are considered:

1. *Management and identification.*
   (The local communities are supporting the safeguarding and further development of the world heritage, but need to be informed about the urban and architectural actions accepted in these parameters)
2. *Protection and conservation of sites and landscapes integrity.*
   (The Dacian fortresses are preserved as an integral historical complex located in the cultural landscape of Orăștie Mountains – that must be preserved as well)
3. *Sustainable use.*
   (All sites have problems of accessibility, maintenance, minimal weather protection and accessible information's about their extraordinary value. Solving them could mean that the UNESCO site can become an engine for development and improved quality of life)

The basically principals applied are preventive protection, best use of existing laws and responsibilities, participation of the population, sustainable use of the sites, raising awareness and acceptance with respect [10].

Table 1: Overview of the management plan

	OBJECTIVES	MEASURES 2 – 5 years	TASKS	MEASURES 5–30 years
Actors	1.MANAGEMENT AND IDENTIFICATION	1.1 Establishment of a management structure. 1.2 Establishment of effective communication. 1.3 Establishment of a monitoring team. 1.4 Providing information, representing and communicating.	• Overall responsibility and coordination. • Financing. • Monitoring and updating. • Periodic inform of all the actors. • Activation of volunteers for monitoring. • Creation of a site.	Overall responsibility and coordination. Financing. Monitoring and updating. Periodic inform of all the actors. Activation of volunteers for monitoring.
Monuments, sites and landscapes	2.PROTECTION AND CONSERVATION OF SITES AND LANDSCAPE INTEGRITY	2.1 Coordinating and updating. 2.2 Restauration and maintenance. 2.3. Establishment of protection zones and protected context. 2.4. Establishment of a regulation for architectural and landscape intervention in the protected context.	• Monitoring of restauration and action maintenance. • Preparation of a written regulation. • Monitoring of the regulation implementation. • Witness photos • Inspection	Coordinating and updating. Maintenance.
Function and use	3.SUSTAINABLE USE	3.1 Assurance of a better accessibility. 3.2 Tourism organisation.	• Infrastructure improvement. • Marked touristic routes and information panels. • Day tourism. • Overnight stays. • Guided tours.	Day tourism. Overnight stays. Guided tours.

5 CONCLUSIONS

The purpose of this article is to point out the history and the importance of Dacian fortresses – UNESCO sites from Orăștie Mountains. To achieve this purpose the importance of these sites at national and international level, their historical evolution and urban, architectural and structural characteristics were highlighted. Based on this information and research, a management scheme was proposed with three major pillars (management and identification;

protection and conservation; use) with clear tasks to monitor for goals achievements. This plan was designed to fully respect the current UNESCO principles and guidelines concerning the protection of valuable heritage structures while also taking current and future threads to these structures into consideration.

The research and the work for the urban general plan and management plan are on-going, but in the future their will follow and maintain the scheme presented above. This management scheme aims to transform these sites of extraordinary value into engines for community development in which they are located, through a sustainable tourism and not aggressive one, because in the present, their enhancement is minimal compared to their importance.

REFERENCES

[1] Musteata, S., Evaluarea și monitorizarea siturilor înscrise în Lista Patrimoniului Mondial din România. *Plural. History. Culture. Society* (2018) **6**(2):65 -66.

[2] Craciun, C. and Mihai, D., *Dacian Fortresses of Orăștie Mountains*, România – World Heritage, București, (2007).

[3] Quattro Design, *PUZ Zona protejata Sarmizegetusa Regia*, (2009).

[4] Goran, C. *Extras din PUZ Cetățile Dacice, 2010, Secțiune 3.3. Date istorice referitoare la teritoriul studiat*, (2010).

[5] Cetatile Dacice din Muntii Orastiei, *Programul multianual de Cercetări Arheologice din Munții Orăștiei, finanțat de Ministerul Culturii din România și coordonat de către Muzeul Național de Istorie a Transilvaniei din Cluj – Napoca)*, https://www.cetati-dacice.ro/ro/situri/sarmizegetusa-regia/istoricul-cercetarilor

[6] Barca, V. Positive and negative aspects in the management of the Dacian fortresses in the Orăștie mountains listed among UNESCO world heritage sites. *Journal Of Ancient History And Archaeology* (2019) **6**(1):108-148.

[7] Willems, A., Thomas, S., Castillo-Mena, A., Čeginskas, V., Immonen, V., Kalakoski, I., Lähdesmäki, T., Lähdesmäki, U., Gowen-Larsen, M., Marciniak, A., Pérez González, E., White, C. and Mazel, A., Teaching Archaeological Heritage Management. Towards a Change in Paradigms. *Conservation and Management of Archaeological Sites* (2018) **20**(5-6):297-318.

[8] Li, J., Krishnamurthy, S., Roders, A.P. and van Wesemael, P., Community participation in cultural heritage management: A systematic literature review comparing Chinese and international practices. *Cities*, (2020) **96**:102476.

[9] United Nations Educational, Scientific and Cultural Organization, *Operational Guidelines for the Implementation of the World Heritage Convention*, UNESCO World Heritage Centre (2019)

[10] Archäologisches Landesamt Schleswig-Holstein, *Project UNESCO – world Heritage Nomination Hedeby and Danevirke*, (2013)

12th International Conference on Structural Analysis of Historical Constructions
SAHC 2020
P. Roca, L. Pelà and C. Molins (Eds.)

DESIGN CRITERIA AND PROCEDURES FOR ARCHAEOLOGICAL SHELTERS: TOWARDS FLEXIBILITY THANKS TO ALGORITHMIC MODELLING

L. SBROGIÓ[1*], A. BASSO[2], P. BORIN[2], M.R. VALLUZZI[1] AND A. GIORDANO[2]

[1] Department of Cultural Heritage (DBC)
Università degli Studi di Padova
piazza Capitaniato 7, 35139 Padova, Italy
e-mail: luca.sbrogio@unipd.it, mariarosa.valluzzi@unipd.it (*corresponding author)

[2] Department of Civil, Environmental and Architectural Engineering, DICEA
Università degli Studi di Padova
Via Marzolo 9, 35131 Padova, Italy
e-mail: andrea.basso.1@studenti.unipd.it, paolo.borin@unipd.it, andrea.giordano@unipd.it

Keywords: Archaeological shelter, Algorithmic modelling, structural optimization, Flexible design

Abstract. *Many examples of archaeological shelters can be found over sites and a wide range of literature illustrates their features. However, it seems that only a few have passed through a proper assessment phase of their effectiveness and compatibility to the archaeological remains. which is mainly due to proper detailing of the building solution in respect of general conservation criteria. Furthermore, in some cases, shelters have proven to worsen environmental conditions that they are supposed to protect. In this paper design criteria for archaeological shelters are proposed, in respect of the three main themes recognized as crucial: general architectural quality, conservation effectiveness, structural and functional detailing. To deal with the wide range of cases where such criteria must be applied, an innovative tool providing the desired flexibility in the design procedure is taken into consideration. Algorithmic modelling in Grasshopper environment, a plugin for Rhinoceros 3D software, offers the required features thanks to a linear workflow, where the general characteristics of the structure as far as its structural details can be implemented. Every element is represented by a set of parameters in the plugin rather than a single object in the 'parent' modelling tool, thus allowing easy change to the design. Other plugins provide additional tools for specific tasks, such as finite element analysis, safety verifications and structural optimization. The paper presents the methodology for the implementation of the entire workflow and the preliminary assessment of its results, from the structural and architectural point of view, showing good adaptability to several possible design choices (position of pillars, truss number, roof pitch, etc.). Structural optimization is also executed. The future implementation of environmental parameters (e.g. daylight, ventilation, temperature), as an additional set of restraints, will complete the framework on which a final assessment will take place.*

1 INTRODUCTION

The sheltering of archaeological sites has recently been considered more a consolidated practice than the correct response to a clearly stated problem [1]. In fact, shelters, open on the sides, are perceived as less demanding in terms of design and visually less intrusive in archaeological contexts than enclosures. Conversely, enclosures, which are 'permanent' structures completely confined by the means of a roof and walls, are completely designed and, as they encapsulate the vestiges, they substantially alter the perception of the ruins (Fig. 1). Shelters are specifically used for extensive archaeological sites where they cover limited portions of them, like a single house or a few rooms with fragile finishings such as mosaics or paintings. Enclosures are of their most effective with punctual and isolated remains [2].

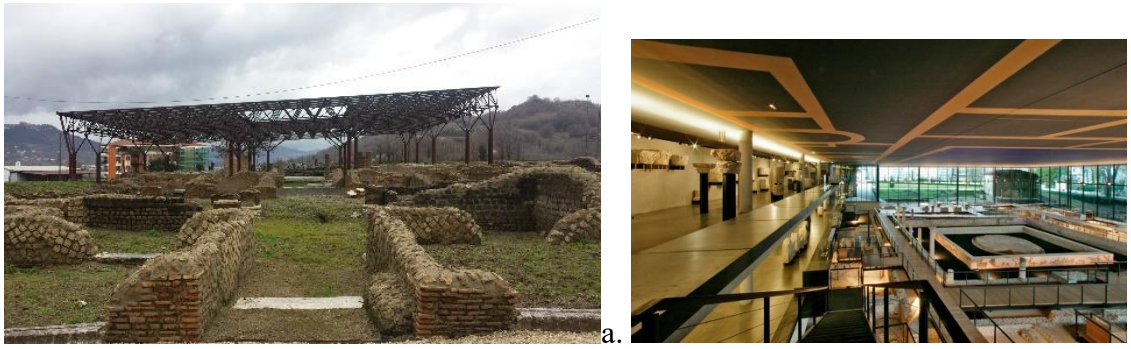


Figure 1: archaeological shelter (a, Civita Atripalda, Avellino, Italy) and archaeological enclosure (b, Vesunna Museum by Jean Nouvel, Periguex, France)

As the following paragraphs will show, the design of those structures is delicate and complex. Two reasons may me stated for that: i) the contradictory nature of the many rules governing shelters' design; ii) the number of rules which must be satisfied: using a traditional 'trial and error' procedure, the 'mechanical' part of the work would be so great that it would impracticable to manage by a single designer/modeller. As a consequence, those rules or 'criteria' should enter a procedure where someone else, say a computer, creates the shape by combining the values that the rules may assume. To that end, the designer should transform the modelling procedure, that is the steps he makes into a modelling software to obtain a specific form, and even the engineering part of the process, that is the structural calculations and verifications, into an algorithm which the computer may follow. The rules become the input variables of the algorithm, but, since many vary within a range, they are better defined as 'parameters'. The computer may then repeat again and again the algorithm in order to find the best solution, the optimum; which is a compromise between the most important criteria.

The paper presents a brief insight (§2) on the reasons of in situ archaeological conservations, the problems that this choice creates, and the criteria that may be used for shelters' design, from an architectural and a structural point of view.

Those criteria are transformed into the input parameters of an algorithm (§ 3), which, for the sake of simplicity, defines a simple structure made of a flat grid of trusses supported by four pillars. Notwithstanding, many other architectural shapes may be defined, such as bidirectional frames, space frames and gridshells (Fig. 2; [3]). On the resulting prototype an optimization analysis, in order to find the combination between the structural shapes and the number of

structural elements is executed (§ 4.2). Finally, each optimized prototype has been calculated and verified for gravity and progressively imposed loads (§ 4.3).

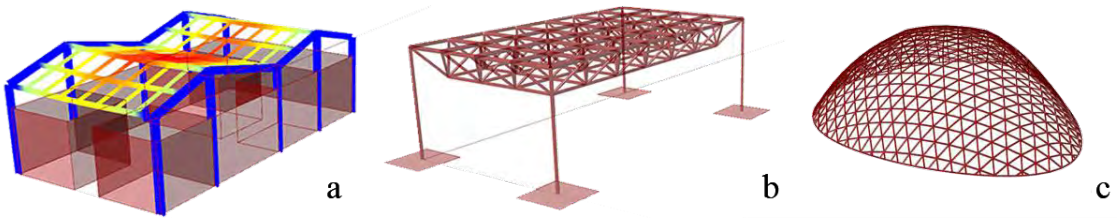


Figure 2: Examples of architectural shapes which may be defined through algorithmic modelling [3].

2 ON SITE CONSERVATION AND DISPLAY OF ARCHAEOLOGICAL SITES

The sheltering or enclosing of archaeological sites has become a common practice since the late 1980s, when the act of moving artefacts and decorative materials into museums from the places where they were found was considered as alteration of the perception of both, the objects and the architectural fragments left on site [4, 5]. In fact, the former lost the environment which they were designed for, the latter were stripped of its characteristic elements. In situ conservation is therefore a powerful means to convey and thus preserve the memories of a place. The visitors' experience of the findings in the actual context of their discovery and of the architecture in its surrounding is an added value which no museum display technique could substitute [4, 5, 6, 7].

However, preserving in situ archaeological materials, may be they either the vestiges of a building or objects or tools, imply a much greater effort than that which may be required for a more traditional museum conservation. In fact, most values in cultural heritage objects deploy on their surface, that which is also the most exposed to variations in temperature and humidity that may be attenuated only through conservation in controlled climatic conditions [8, 9].

The commonest causes of decay of archaeological materials left on site come from different sources [10, 11, 12]: the intrinsic nature of the remains (e.g. stone, wood, masonry, organic materials, etc.); anthropogenic (e.g. unwise handling of objects; vandalism; war conflict etc.); biological (e.g. small animals; vegetation); environmental (e.g. precipitations, temperature, humidity, light and invisible energetic radiation such as ultraviolet and infrared); chemical (e.g. pollution).

In addition, too often shelters and also enclosures have proved responsible for a negative impact on the ancient materials from several points of view. Such situations stem from unfavourable microclimatic conditions determined by the shelter or a premature deterioration of a shelter's structure and/or equipment [1, 13, 14]. The inadequacy of management and development plans on/for the site is another critical factor, which may depend either on the lack of economic resources needed to run them or on the overexposure of the site to contemporary human activities (generally tourism) [15, 16].

Notwithstanding, shelters and enclosures are potentially the best option for preserving archaeological materials since they belong to the field of preventive and corrective measures of conservation, that is they do not touch the fabric of the vestiges directly but work on their 'boundary conditions' [2, 4, 10, 17] while keeping the materials in their original place. In practice however, it seems that these interventions respond more often to either an immediate

psychological need to 'see a roof over the ruins' or to the taste and interpretation of the designer [2, 12]. Therefore, they are either the result of an almost non-existent design procedure or a biased one, where typically more importance is given to formal aspects than conservation. The abundant literature on the whole subject is of little help, since each scholar suggests different criteria or puts emphasis on certain aspects according to his/her own sensibility [18].

In the following, an excerpt of the main criteria will be enough to show the complexity of the subject.

2.1 Decision making in shelter construction

First of all, one has to decide whether a certain archaeological site will be left exposed after its excavation and documentation. The minimum criteria to support this decision are [19]: a) the importance of the archaeological materials; b) the potentiality to communicate the meaning and inform the public about the site; c) the diversity and the attractiveness of the site; d) the accuracy of the available archaeological documentation; e) the associative potential with similar monuments; f) a correct assessment of the site's values. Anyway, the reduction to a 'standard' procedure is impossible; for this reason, the choices relating to the archaeological sites are considered primarily ethical, rather than scientific [20].

Some help may come from looking at the extent of the remains, whether they are ruins and vestiges, where the former have lost their original unity and are now reduced to some walls and/or a pavement, while the latter preserve an echo of the original building. As a result, the former would best be in archaeological documentation, the latter may be recomposed and reconfigured by a shelter [2]. Also, sheltering, and thus altering, decomposed structures which have acquired a proper dignity, structural integrity, and a role in the cultural landscape of a place, would be unjustified [21]. The sheltering may be allowed only if the vestiges are too fragile to be left exposed and at the same time the informative content, which is already enough by itself, may be completed by the shelter [22]. In time, the aim of the shelter has changed, from the museum [23] to the conservation of the fabric [12] and the transmission of values [5]. The ideal situation may be described as the 'living building site', where the information is given to the public as it is extracted from the ground or it is preserved and the public returns the archaeologists with moral and economic support. That is, the archaeological site must play an active role in contemporary society [5, 6, 15, 16].

2.2 Design criteria: general aspects

Since the physical survival of archaeological materials is the main aim of every action taken on any archaeological site, the shelter should reduce and prevent in the long run its degradation, since arresting it would be impossible and conceptually wrong [12].

To this end, some authors express criteria and rules for design [24] while others [12] give indications for assessing the effectiveness of archaeological sheltering which may be translated in rules for design. Since a summary 'manual' many are the sources: i) theoretical approaches to restoration; ii) practical prescriptions for the conservation of objects and artefacts (see e.g [11, 25]); iii) indications for in situ conservation of mosaics or adobe structures, which are the most fragile.

Three main themes may be recognized: general architectural quality, conservation effectiveness, quality and nature of structural and functional detailing. Researches in

conservation [7, 10, 12, 26] detail the following criteria:

- General restoration: respect for authenticity; recognisability of interventions taken; reversibility; minimum intervention; the visitor's ability to understand the ruins;
- Conservation: modification of microclimatic conditions; protection from external climatic agents; flexibility and expandability; natural illumination and ventilation; control of the vegetation (shadows, added humidity, leaves obstructing drainage system, roots); efficient drainage system; control of the greenhouse effect; control of direct illumination of archaeological materials; lateral confinement; lateral overhang;
- Formal and architectural: intrusiveness in the archaeological context; distinguishability from the remains; flexibility and expandability; natural illumination; height; lateral confinement; transparency; number and placement of bearing structure; quality of architectural details;
- Structural: easy conception and easier installation; simpler structural solutions make it easier to find spare parts and to execute maintenance; flexibility and expandability; foundations and footings; type;
- Economic and management: the cost of the structural system and of its installation since they determine reversibility as the willingness to substitute the shelter if it proves inefficacious; the costs of maintenance; ease of maintenance; the cost for a/c and other equipment to keep the indoor climate constant; the long-term availability of financial and human resources to maintain the shelter and to nurture the archaeological site;
- Usability: safety of use; safety from intrusions; protection of the visitor from dangerous parts; protection of the vulnerable parts of the site from the visitors;

2.3 Design criteria: structural aspects

Shelters can be built of a wide range of materials: metal (aluminium or steel) and timber are the most frequently used for structural purposes. The former may be expensive, especially aluminium, and both steel and timber have a limited resistance to corrosion and degradation if left exposed outside with little or no maintenance [27, 28]. For such reasons, the material used in the present proposal are the glass fiber reinforced polymers (GFPR) in the shape of pultruded structural sections [27]. Even though more expensive and rather complicated to be calculated, GFRP is i) almost an 80% lighter than steel; ii) corrosion resistant; iii) designable according to the needs [28].

Since long spans and minimum vertical supports are required, the commonest structural solutions for the covering structures are trusses, space frames, cable-supported structures and, more recently, long-span glued laminated timber beams; however, something that requires a limited number of vertical supports in the middle. The roof sheathing materials may be corrugated steel sheets, clay tiles, polycarbonate or glass panes; lateral confinement is generally provided by timber louvers, masonry walls, expanded metal sheets. As a general rule foundations are supposed to be outside the perimeter of the site but they may also be internal, provided that they do not interfere with the ancient structures, that is they fall along the ancient walls or in places that lack archaeological records [12]. Lightweight and small structures require small foundations and therefore they are more appreciated.

3 ALGORITHMIC MODELLING TOOLS

In a normal 3D modelling process in a computer aided programme, the user has a limited access to the tree of modifiers which he/she adds to the primary objects in the modelling canvas of the software. In contrast, in parametric modelling the user translates the entire sequence of direct manipulations on the primary objects into encoded operations on the parameters and the variables which described the objects [29]. The story of modifications is collected by a Direct Acyclic Graph (DAG) which is a 'code' expressed graphically by the means of boxes ('components'), corresponding to the objects or their modifiers, and cables, which express the relation between the boxes [30]. DAGs allow a linear workflow but not loops. The algorithm works as an 'assembly instruction' which allows the user to focus on the process rather than the product, where inputs streams from the left of the input to the right of the output. Each minimal change in the parameters on the left corresponds to a different output on the right.

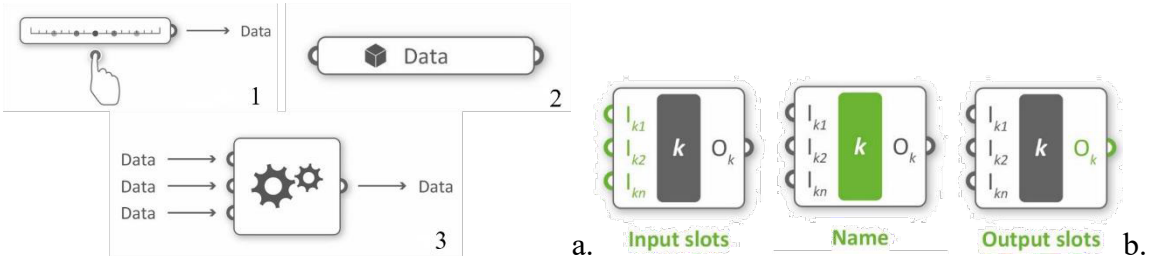


Figure 3: Elements of a DAG: a) type of components 1. slider; 2. Data input; 3. Standard component; b) structure of a component [28]

DAGs are composed by (Fig. 3):

- Input component: they give information within a user's defined list and therefore the basic data for calculation;
- Box component: they allow to memorize certain type of data which may be important to monitor at a certain point of the algorithm
- Standard component: the allow to perform operations on data obtained from the input, representing the minimum step of the overall procedure. They yield a single output as a result of multiple input.

Complex operations may be obtained by combining and clustering single components; the starting value may be a) assigned manually, selecting the value from a drop-down menu; b) obtained by selecting it from and object in the canvas; c) assigned by a cabled connection. Input and output may have different formats (e.g. enter points and then exit segments).

Variations on the parameters may be applied by the user, acting on the input components, or may automatically explored by the computer once an optimization analysis is run. To do so the designer must define an 'objective function' on which one or more variables may have at least a partial impact on it and then the computer performs the combinations in search for the one that best satisfies the function. The rules used to perform the combinations follow the schemes which govern the generation among populations and therefore are known as genetic algorithms [29]. Single or multi parameter optimization analysis is possible according to the piece of software used [31, 32, 33].

4 DESIGN OF THE SHELTER

The parameters are defined as a model's components, with precise features and function within a shelter's structure but whose specification may vary according to the site's characteristics and therefore they are not fixed once for all but may vary to the user's needs. As a result, they are input data - and that is the reason why they appear at the beginning of the algorithm - but they depend on the reasoning already presented.

4.1 Parametric components

The structural parts of the roof and the corresponding logical parts of the algorithm are [3]:

- Pillars: segments obtained by the vertical extrusion (each one independent from the others) of four base points selected by the user. Then those segments are divided in two by a middle point where side panels hang (Fig. 1a);
- Roof: the quadrilateral shape (however sloped) defined by the four base points is subdivided into the local *u* and *v* directions creating the trusses' grid at the lower chord. The points obtained at the intersections are then projected on a plane which may be not parallel to the one already defined, since the top chords may have an inclination different from the bottom ones. Then the base lines in the two directions and in the two planes are subdivided and then linked by segments to define the trusses; their number depends on a slider which grades the spacing between the elements (Fig. 1b);
- Overhangs: they are defined by two points which are projected for the desired distance from the upper extremity of the pillars in the two main direction of the roof. After that the length between two points on the same side is subdivided according with the same spacing used in the quadrilateral of the roof (Fig. 1c);
- Side panels: their extremal nodes are extracted from the points already defined on the pillars and the overhang. Then, the resulting rectangle is once again subdivided according to the roof's grid and the resulting points connected by a polyline obtaining a truss. Each frame is then completed by a stiffening panel (Fig. 1d);
- Secondary elements (roof's corners and bracings): these parts complete the definition of the overhangs at its corners and the introduction of additional bracing elements to stiffen the edges of the roof (Fig. 1e, f).

Since a minimal shelter is made of four pillars, one roof, four overhangs and the corresponding corners and four side panels, similar elements have been grouped together to assign properties (e.g. structural shapes) which are shared within the group. However, this solution is also a matter of commodity when it comes to visualization or if a part/group is not needed (e.g. the side panels).

Each part is not fixed once for all but it has some dynamic features (or parameters) such as its dimensions or the number of elements it includes on in which it is subdivided which are determined by the user simply trough the mean of a slider in the algorithm's routine (Table 1). A change in any parameter affects the whole structure.

Table 1: A shelter's logical-structural parts and corresponding parametric factors

Part (input)	Parameters
Pillars	Height Position in plan Material
Roof	External slope Internal slope Subdivision in *u, v* directions Material
Overhang	Dimension Material
Side panels	Height Distance from the pillars Material
Secondary elements	Dimension Number of bracing elements Material

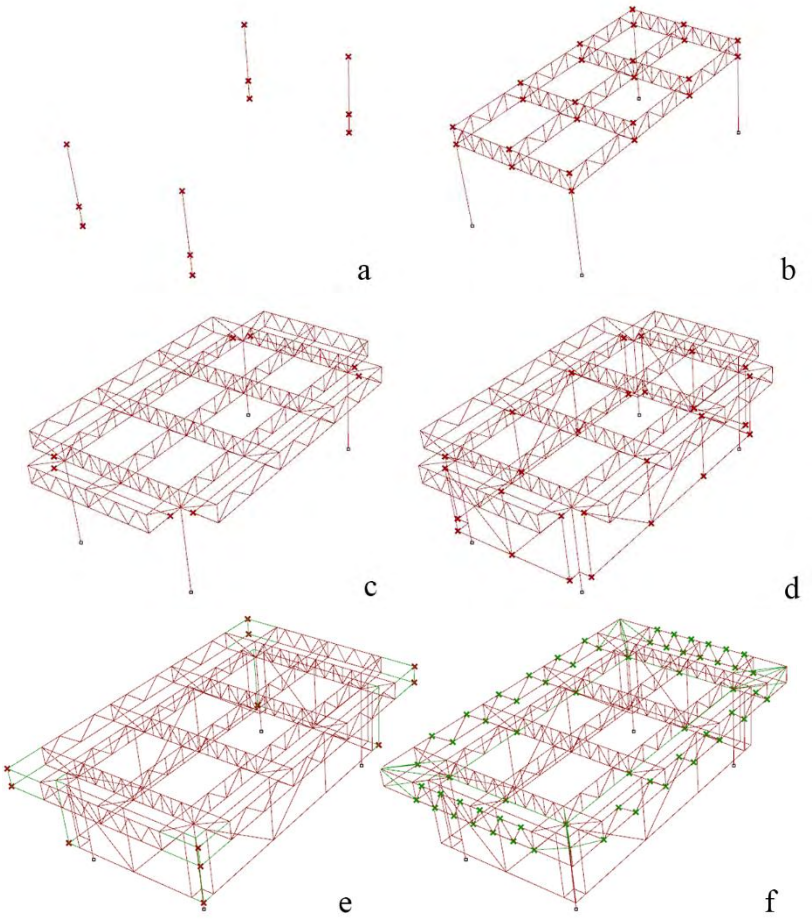


Figure 4: Structural parts of the shelter: a) pillars; b) roof (grid of trusses); c) overhang; d) side panels (only the frame is shown); e) corners; f) bracing stiffening elements [3].

4.2 Finite element analysis and optimization

Structural analysis is possible thanks to a plugin for Grasshopper, Karamba 3D [34], whose potential stays in the real-time structural calculation of t the elements in the parametric model. To that end, however, the geometric model has to be converted into an analytical model, which bears the minimal characteristics to be calculated, through special components. Extremal nodes are then constrained according to the needs; like other FEA tools, in Karamba, internal nodes are considered continuous otherwise specified. Other components of the DAG allow to label each element, in order to distinguish groups and assign the structural shapes (extracted from libraries or used-defined) and the materials (default materials are steel, concrete, timber and aluminium but user-defined properties are also allowed). Finally, one must define the loads: gravity for the self-weight, and the different types of imposed ones. The solution consists mainly of the maximum nodal displacement and the system's deformation energy, but thanks to other components one can manage the model and obtain the forces acting on structural elements, the nodal reactions, nodal displacements etc. (Fig. 2).

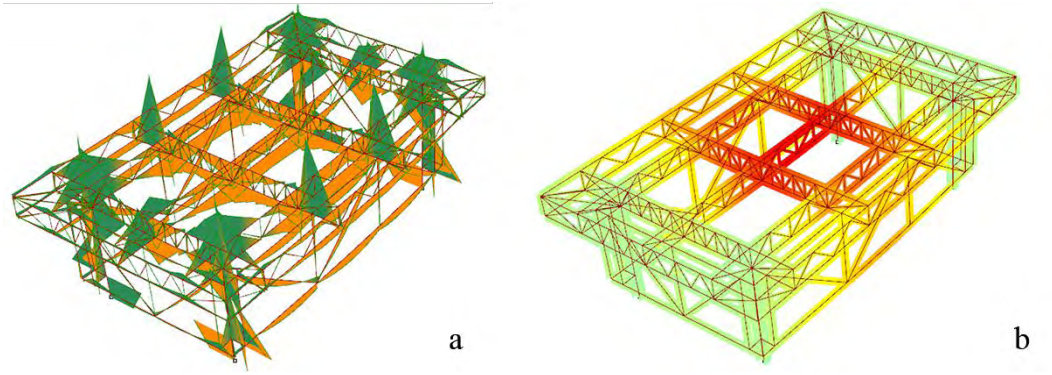


Figure 5: Examples of structural analysis made possible on a model thanks to Karamba plugin: a) bending moment diagram; b) strains (red=maximum, green=minimum) [3].

The search of the best combination of parameters, say the number of trusses in the two directions of the grid, the number of bays within each truss and the structural shapes to be used have been committed to the software. In this case a function relating the mass and the deformation has been defined as suggested by [32, 33] adding a multiplier to scale the effects. Since more than one parameters are involved in the optimization procedure, Octopus plugin has been used.

4.3 Prototypes: structural analysis and structural verifications

For the structural analysis six prototypes have been defined, three of them squared and the other three rectangular with an aspect ratio 1:2, from a minimum of 3x3 m to a maximum of 5x10 m. Other common features are: 3 m intrados height, 0,7 m trusses structural depth, 1,5 m overhang, flat roof (Fig. 3). The structural elements are made of GFRP pultruded shapes, whose orthotropic properties [27, 28] have firstly converted into an equivalent homogenous material [28] and then applied to the model. Previously to structural analysis, each structure has been optimized in Octopus. The applied loads, apart from gravity, which is kept constant, are

incremented at steps of 0,5 kN/m2 until the structural limits at the serviceability limit state (SLS) are reached. calculated according to the formulations proposed in consensual laws [35].

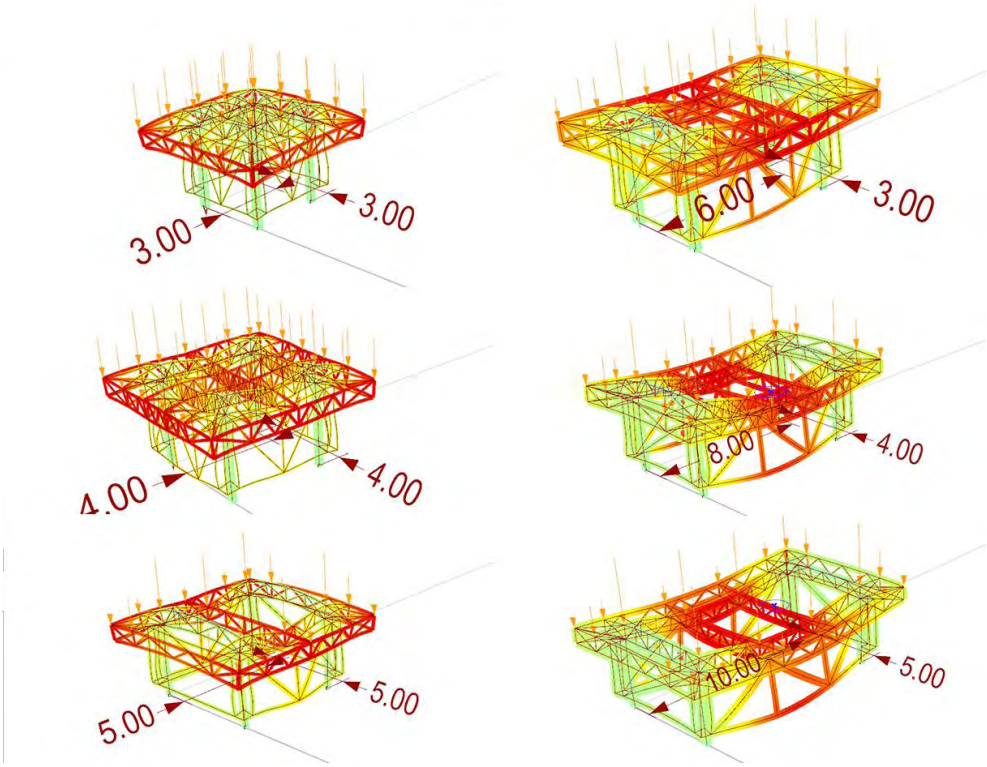


Figure 6: Deformed shape of the prototypes at SLS [3]

5 CONCLUSIONS

The paper presents a first application of algorithmic and parametric modelling to the design of archaeological shelters, and therefore its main results may be described as an evaluation of the possibilities and the potential opened by this approach.

In an ordinary design process, the validation of a proposal in respect to the structural and architectural criteria is done at the end, but, in the case of multiple-constrained tasks, such as the design of an archaeological shelter, this approach is ineffective. As a result, the criteria must become the input variables and the constraints of a process which may respond automatically to their variations, allowing the required flexibility. In Rhinoceros 3D modelling environment, the plugin Grasshopper for algorithmic design offers the needed tools thanks to the visual programming, which is a simplified code writing through the means of objects in a canvas.

In Grasshopper any engineering design process may be translated into an algorithm: the paper presents the logical structure of the procedure to obtain a flat grid of trusses supported by four pillars. The elements (pillars, trusses, overhang, side panels) are chosen and defined according to the criteria while their precise features are parametrically variable and not set once for all. As a result, other sub-plugins (Octopus, Galapagos), which exploit genetic algorithms, can be used to execute an optimization analysis, that is to explore the combinations and permutations of the input parameters in order to find the best solution. In this paper, the

parameters are the number of subdivisions in horizontal structural elements (trusses, overhang) and the structural sections, once the structural heights and the position of the supports are fixed.

The optimization tools work on numerical data, which, in this case, are the internal forces and the deformations of the structure. These data are given by another plugin, Karamba 3D, which executes the structural analysis. The algorithmic modelling has shown its potential also in this case, since, basing on the result of Karamba, a piece of software purposely written assesses the safety of the structure according to the codes.

Thanks to these tools, six real-scale prototypes have been created, optimized and then calculated and assessed within the Grasshopper workflow. Their structural behaviour ath serviceability and ultimate limit states resulted satisfactory for a normal use in an archaeological context even though many improvements are possible both in the details and in the overall functioning.

Further research is also required to add the climatic and energetic criteria to the structural-architectural ones, to control their impact on the design process and one the optimized shape.

REFERENCES

[1] Aslan, Z., Court, S., Teutonico, J.M., Thompson, J. (Eds.) *Protective shelters for archaeological sites*. Los Angeles, (2018).

[2] Di Muzio, A. Rovine protette. *Conservazione e presentazione delle testimonianze archeologiche*. Firenze, (2013).

[3] Basso, A. *Progettazione di sistemi a configurazione variabile per coperture di siti archeologici.* Padova (2018).

[4] Ruggieri Tricoli, M. C. and Sposito C. *I siti archeologici: dalla definizione del valore alla protezione della materia*. Palermo, (2004).

[5] Avrami, E., Mason R. and De La Torre, M. (Eds.) *Values and Heritage Conservation*. Los Angeles, (2010).

[6] Agnew, N. and Brigland, J. (Eds). Of the Past, for the Future: Integrating Archaeology and Conservation. Los Angeles, (2006).

[7] Amendolea, B. (Ed.). *I siti archeologici: un problema di musealizzazione all'aperto*. Roma (1988).

[8] Camuffo, D. *Microclimate for Cultural heritage. Conservation, Restoration and Manteinance of Indoor and Outdoor Monuments*. San Diego, (2014). .

[9] Aslan, Z. Protective structures for the conservation and presentation of archaeological sites. *Conservation and management of archaeological sites* (2001) **5**:73-85.

[10] Panosa, M.I. Musealizing Archaeological Sites. Considerations on Research, Conservation, and Dissemination: A Case Study from the Gavà Mines Archaeological Park. *Conservation and Management of Archaeological Sites*, 17:2, 159-174. (2015)

[11] Pedelì, C. and Pulga S. *Pratiche conservative sullo scavo archeologico. Principi e metodi*. Firenze, (2002).

[12] Laurenti, M.C., (Ed). *La copertura di aree archeologiche*. Museo Aperto. Roma, (2006).

[13] Michaelides, D. (Ed.) Mosaics make a site: the conservation in situ of mosaics in archaeological sites. *Proceedings of the VI international conference of the International Committee for the Conservation of Mosaics* (1996). ICCROM, (2003).

[14] Roby, T. and Demas, M. (Eds.) *Mosaics in situ. An overview of literature on conservation of mosaics in situ*. Los Angeles, (2012).
[15] Palumbo, G. and Teutonico, J. M. (Eds.). M*anagement planning for archaeological sites*. Los Angelese, (2000).
[16] De La Torre, M., (Ed.). *Conservation of Archaeological Sites in the Mediterranean Region*. Los Angeles, (1997).
[17] Brandi, C. *Teoria del Restauro*. Torino, (1977).
[18] Henry Cleere (2010) Management Plans for Archaeological Sites: A World Heritage Template, Conservation and Management of Archaeological Sites, 12:1, 4-12, (2010).
[19] Ruggieri Tricoli, M. C. *Musei sulle rovine. Architetture nel contesto archeologico*. Milano, (2007).
[20] Vaudetti, M., Minucciani V. and Canepa, S. (Eds.). *Mostrare l'archeologia. Per un manuale-atlante degli interventi di valorizzazione*. Torino, (2013).
[21] D'Agostino, S. and A. Melucco Vaccaro A. Il rudere archeologico: un contributo alla conoscenza della sua vulnerabilità. In Biscontin G. e G. Driussi G. (Eds.) *Dal sito archeologico all'archeologia del costruito. Conoscenza Progetto e Conservazione*. Padova, (1996).
[22] Carandini, A. *Storie dalla terra. Manuale di scavo archeologico*. Torino, (2010).
[23] Minissi, F. Ipotesi di impiego di coperture metalliche a protezione di zone archeologiche. *Restauro* 81, (1985).
[24] Sposito, C. Esigenze e requisiti delle coperture. In Sposito A. (Ed.) *Coprire l'antico*. Palermo, (2004).
[25] Huisman, D. J. (Ed.) *Degradation of archaeological remains*. Den Haag, (2009).
[26] Bikai, P. M. e Bikai P. *Caring for the Cultural Heritage: Shelter*. In: ACOR (American Center for Oriental Research) Newsletter 9.1, (1997).
[27] Russo, S. *Strutture in composito. Sperimentazione teoria e applicazioni*. Milano, (2011).
[28] Bank, L.C. *Composite for construction: structural design with FRP materials*. Wiley & Sons, (2006).
[29] Izzo, M. *Exploring the possible role of parametric design in locationing the compositional problem: theory and practice of an evolving approach toward the urban design perspective*. Milano, (2017).
[30] Tedeschi, A. *AAD Algorithms-aided design: Parametric strategies using Grasshopper*, (2014).
[31] Gerbo, E.J. and Salikis, E.P. Optimizing a trussed frame subject to wind using Rhino, Grasshopper, Karamba and Galapagos. In: R.M. Brasil and Pauletti, R.M.O. (Eds.): Shells Membranes and spatial structures: Footprints (2014).
[32] Vierlinger, R. *Multi objective design interface.* Master thesis, Wien (2018).
[33] Bangash, M.Y.H. and Bangash, T. *Elements of spatial structures – Analysis and design*. Telford, (2003).
[34] https://www.karamba3d.com/, last visited on February 15, 2020
[35] Clarke, J.L. (Ed.) Structural design of polymer composites. EUROCOMP design and handbook. EFN SPON, (1996).

12th International Conference on Structural Analysis of Historical Constructions
SAHC 2020
P. Roca, L. Pelà and C. Molins (Eds.)

DIGITIZATION OF CULTURAL HERITAGE BUILDINGS FOR PREVENTIVE CONSERVATION PURPOSES

MARIA-GIOVANNA MASCIOTTA[1*], LUIS SANCHEZ-APARICIO[2,3], SUZY BISHARA[4], DANIEL V. OLIVEIRA[4], DIEGO GONZALEZ-AGUILERA[3] AND JOAQUIN GARCIA-ALVAREZ[5]

[1]*Department of Engineering and Geology (INGEO)
"G. d'Annunzio" University of Chieti–Pescara
Viale Pindaro 42, 65127 Pescara, Italy
e-mail: g.masciotta@unich.it (*corresponding author)

[2] Department of Construction and Technology in Architecture (DCTA)
Escuela Técnica Superior de Arquitectura de Madrid (ETSAM), Universidad Politécnica de Madrid
Av. Juan de Herrera 4, 28040 Madrid, Spain
e-mail: lj.sanchez@upm.es

[3] Department of Cartographic and Land Engineering
University of Salamanca, Higher Polytechnic School of Ávila
Hornos Caleros 50, 05003 Avila, Spain
e-mail: luisj@usal.es; daguilera@usal.es

[4] Department of Civil Engineering
ISISE, University of Minho
Campus de Azurém, 4800-058 Guimarães, Portugal
e-mail: suz.bishara@gmail.com; danvco@civil.uminho.pt

[5] Fundación Santa María la Real del Patrimonio Histórico
Aguilar de Campoo, Palencia, Spain
e-mail: j.garcia@santamarialareal.org

Keywords: Historical Constructions, Preventive Conservation, Digital Documentation, Geospatial Database, PlusCare System, Internet of Things

Abstract. *This work aims at presenting the experimental results obtained by the application of one of the digital protocols developed during the European project HeritageCare: Monitoring and preventive conservation of historical and cultural heritage. These protocols are devoted to the preventive conservation of heritage constructions and its assets. More specifically, the application of the second level of services of the HeritageCare system is presented through two complementary case studies: a large Neo-Manueline church situated nearby Guimarães, Portugal, and a small Romanesque church located in Palencia, Spain. In each case study a different set of digital technologies was employed with the aim of evaluating the flexibility of the developed protocols. This set of technologies comprises the use of in-house*

apps for enhancing the visual inspection together with geomatic techniques based on static and wearable laser scanners as well as digital single-lens reflex and as-built 360º cameras. The results obtained by the application of these digital tools have allowed the creation of a Web-GIS platform for ensuring the proper documentation of cultural heritage and streamlining the management of their conservation process according to a proactive approach.

1 INTRODUCTION

Built heritage is the most important physical evidence of the cultural development and diversity of the humankind. It reflects the historical layers of our society, encompassing various construction systems and materials as well as a wide range of structural typologies, such as cathedrals, palaces, castles, and dwellings, among others. Although representing a significant part of our built environment, following the second world war the maintenance of heritage structures has been set aside in favor of the exponential growth of new constructions, thus increasing their potential for structural damage. Last disasters have demonstrated that there is a clear mismatch between budget spent on constructions or large reactive restorations and budget invested on maintenance. The key to prevent damages and minimize deterioration processes is to adopt a proactive conservation strategy, which means replacing belated and overpriced interventions with timely and affordable condition-based maintenance actions. To be effective and sustainable in the long-term, such an approach must be rooted in systematic documentation and monitoring routines and must be supported by optimized digital workflows that can guarantee the integration, tracking, management and longevity of a huge amount of heterogeneous information [1]. Given the absence of a structured policy and uniform criteria, the European project "HeritageCare - Monitoring and preventive conservation of historic and cultural heritage" (SOE1/P5/P0258) has developed and validated over 60 case studies a multi-level system of services to document and assess the conservation status of the built cultural heritage in Southwestern Europe. By leveraging the latest advances in digitization and smart technologies, this system employs standardized yet flexible data collection protocols (StandardCare, PlusCare and TotalCare) to progressively track the condition of existing heritage and store baseline information for future comparative analysis [2]. In line with the European standards relevant to this field [3], [4], [5], the HeritageCare methodology aims to streamline the conservation process of historical buildings, whether listed or not, by helping the respective owners and managers minimize or prevent damages in their properties with the scheduling of priority-based maintenance actions [6], [7].

The focus of this paper is to present one of the protocols (PlusCare) developed during the HeritageCare project and related Web-GIS tool in order to show the potentialities offered by the combination of Virtual Reality (VR), Internet of Things (IoT) and Geographic Information Systems (GIS) in the field of preventive conservation of cultural heritage and highlight the advantages brought by the digital revolution in capturing, managing and processing "big-data" within a tolerable time from virtually anywhere in the world. To this end, after a brief description of the HeritageCare system and related documentation protocols, the paper discusses the application of the PlusCare tool to two representative case studies selected among the great variety of heritage structures located in South-West Europe: a large Neo-Manueline church situated nearby Guimarães, Portugal, and a small Romanesque church located in Palencia, Spain.

2 A DIGITAL-BASED SYSTEM FOR HERITAGE DOCUMENTATION

2.1 HeritageCare integrated protocols

The HeritageCare system is organized in three complementary service levels (SL), hereafter referred as StandardCare, PlusCare and TotalCare, whose main pillar is the systematic inspection and monitoring of the existing built heritage and related indoor assets. The quantity and complexity of the information collected about the conservation state of the inspected items increase along with the sophistication of the tools employed in each level, being progressively stored into a capable database accessible through a web platform.

Particularly, the StandardCare protocol (SL1) aims at providing a low-cost and rapid condition assessment of the inspected heritage building by identifying its main damages and delivering, in the form of an inspection report, essential information about its primary conservation needs. This protocol relies on the use of a mobile inspection app for uploading and retrieving information directly to/from the HeritageCare database, allowing a real-time digitization of the entire inspection process.

On the other hand, the PlusCare protocol (SL2) provides a more extended knowledge of the heritage ensemble by complementing and integrating the information collected during SL1 with an in-depth documentation of the building state, including detailed inspections of indoor assets, high-resolution surveys, monitoring of relevant parameters and recording of any supplementary data that can contribute to increase the level of knowledge about the actual condition of the buildings/assets (Figure 1). As better described in the next section, the implementation of this protocol relies on a dual Web-GIS tool that allows the integration and georeferentiation of different data sources, while providing an intuitive environment from which the non-expert users (owners and managers) can access the most significant information for the preventive conservation of their buildings.

Finally, the TotalCare protocol (SL3) integrates and manages all data gathered from SL1 and SL2 through the development of interoperable 3D digital models, representative of the inspected buildings. The protocol resorts to the BIM (Building Information Modelling) environment to populate these models with meaningful data and attributes concerning the conservation state of the inspected building, allowing to support informed decision-making and to rationalize the management of the heritage conservation process as information can be easily visualized, controlled, shared and updated.

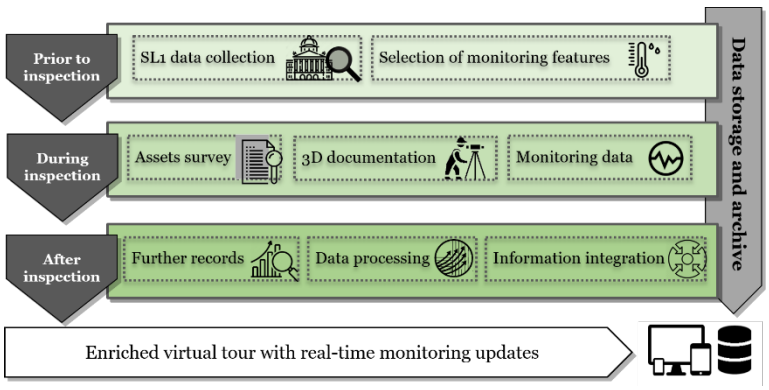


Figure 1: PlusCare protocol of the HeritageCare preventive conservation system.

2.2 The PlusCare tool

The efficient implementation of the PlusCare protocol required the development of a tool able to blend together the latest advances in Virtual Reality (VR), Internet of Things (IoT) and Geographic Information Systems (GIS) in order to integrate and georeference multiple and heterogeneous information coming from different inspection & diagnosis techniques as well as guarantee protocols interoperability. This resulted into a unique Web-GIS tool called PlusCare system, integral part of the HeritageCare platform. This system converges into a dual web-environment, namely one for expert users (inspectors) and one accessible by nonexpert users (owners, stakeholders, etc.) upon successful authentication and authorization.

The main functionality of the expert-user environment is to store into specific tabs all the technical information progressively gathered through the application of the PlusCare protocol, namely: assets condition, panorama photos, monitoring data, point clouds, data records and damages. To facilitate the information transfer between technicians and end-users, the non-expert user environment features a friendly and intuitive interface composed of comprehensive 360° photos of the inspected building across which the owner/manager can virtually navigate and access all the aforementioned information uploaded by the inspectors and enclosed in the virtual tour in the form of georeferenced hotspots. This graphical interface is complemented by a bottom navigation bar that allows to consult high-resolution geometric data via the 3D point cloud as well as the StandardCare condition report. Additionally, if a monitoring network is installed in the building, the PlusCare system is provided with a communication protocol that allows to retrieve real-time information about the monitored parameters and automatically rate their acceptability/degree of risk according to a 3-colour grading scale. All significant information about the conservation state of the inspected constructions and related assets are digitized, integrated, stored and ultimately condensed into this visual output which acts both as a supporting tool to address cost-efficient preventive actions as well as a valuable reference source to facilitate screening activities over time.

3 VALIDATION THROUGH CASE STUDIES

During the project, the HeritageCare protocols and related tools were successfully tested across a notable number of heritage buildings among Portugal, Spain, and Southwestern France. As an example, this section summarizes the application of the PlusCare protocol to two complementary case studies (Figure 2): a large Neo-Manueline church situated nearby Guimarães, Portugal, and a small Romanesque church located in Becerril del Carpio, Palencia, Spain.

3.1 Church of São Torcato, Portugal

São Torcato church is a Neo-Manueline style construction located in the homonymous village in Northern Portugal. The architectural form of the church follows the plan of a Latin cross, with a central nave and a transept, each covered with a barrel vault. The North end of the nave ends with an apse, while at the South end is a gallery entrance with a high choir above. Gabled roofs with wooden trusses protect the vaults beneath. A dome laying on an octagonal tambour sits above the main altar, at the crossing between nave and transept (Figure 2). Side chapels extend along the main nave from the transept to the towers that symmetrically frame the façade. The construction of the church began in 1825 to house the body of São Torcato,

Christian martyr, and stretched over nearly two centuries, involving several building phases. Hence, different materials can be distinguished in the fabric: the walls of towers, nave and transept are made of three-leaf granite masonry with thin mortar joints and inner rubble core, whereas the recently reconstructed dome and apse are made of reinforced concrete (the latter covered with granite veneer).

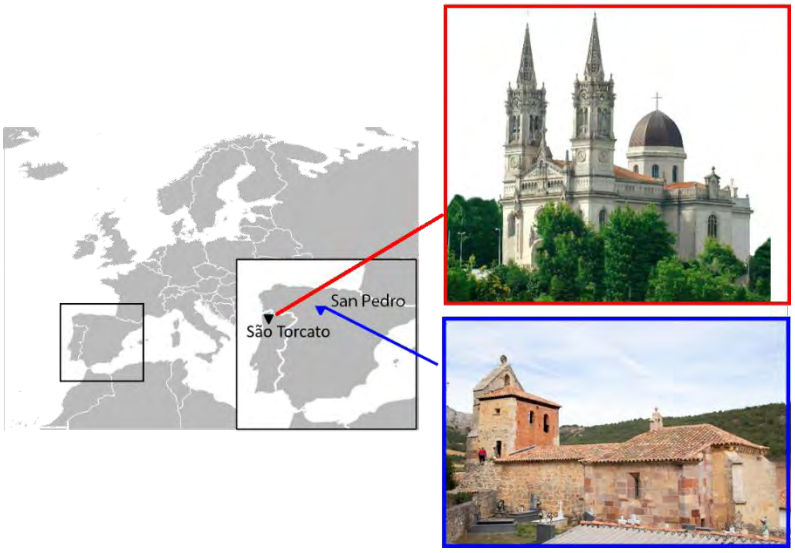


Figure 2: Location and exterior view of the study cases: in red the church of São Torcato and in blue the church of San Pedro.

Extensive visual inspections, monitoring campaigns, as well as topographic and geotechnical surveys were carried out in the church since the 1970s to understand the origin of the deep structural cracks affecting the façade and their possible correlation with the tilting of the towers [8], [9], [10]. It was found that the poor mechanical characteristics of the soil originated differential settlements that progressively led the towers to lean and the façade to crack due to the increasing tensile stresses induced by the towers' movement. As the damage was worsening, the church underwent an in-depth intervention (04/2014–07/2015) that involved the installation of micro-piles to eliminate the differential settlements, the placement of post-stressed tie rods to restrain the towers, and the injection of cracks to restore the material continuity. Before, during and after the intervention, the system's response was tracked by means of a monitoring system, which allowed to supervise the progress of the structural consolidation and assess the effectiveness of the strengthening measures [8].

After a documentary research to collect all existent data about the church, including past diagnostic investigations, a systematic inspection was carried out by the HeritageCare team in order to digitally document the conservation status of the construction a few years after the structural intervention previously described. The HeritageCare mobile e-form was exploited to drive the field work and allow a real-time digitization of the inspection process (Figure 3).

Besides the presence of damages not detrimental to the structural integrity, such as efflorescence and biological microorganisms, especially in the form of lichens both on top of the exterior walls and roof tiles, the condition survey revealed problems of bird infestation in the towers and arcade loggia as well as problems of water infiltration through the roof covering,

walls and openings. Like most of historical stonemasonry structures, the lack of adequate drainage and waterproofing systems played a major role in the development of this type of damages. Surface discolouration processes of diverse nature were also reported on the bottom part of the outer walls of the church. From a structural standpoint, a permanent deformation resulting from the settlements and cracks that affected the church prior to the intervention could be observed in the choir above the entrance. Moreover, new structural cracks were detected on the triumphal arch and along the lateral walls of the nave up to the roof level, pointing out the necessity to install some crack monitoring gauges to understand their actual behaviour and exclude the presence of unstable phenomena. Each damage was accurately documented and assessed according to the HeritageCare damage rating system [1], [6] allowing to identify the primary conservation needs of the church and to assist the owner with the prioritization of remedial measures. To achieve a more detailed knowledge of the building and related indoor assets, this documentation was then integrated by applying the protocol described in Section 2. For the sake of brevity, only the workflow followed for the 3D digitization and virtualization of the church is presented next.

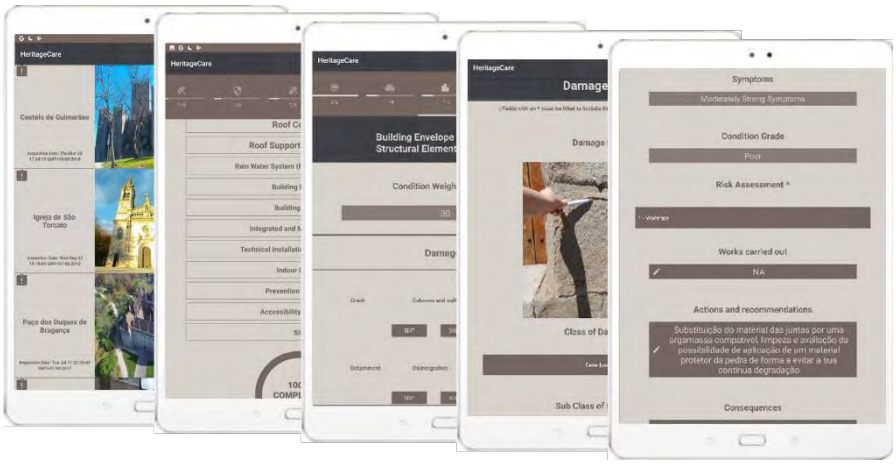


Figure 3: HeritageCare mobile e-form used to document the onsite inspection.

A laser scanner survey was carried out using a Leica ScanStation P20 in order to obtain high-resolution 3D data for accurate geometrical representation and geo-referenced damage mapping. With a maximum capture rate of 1,000,000 points per second, this tool allowed to collect in one working day millions of points carrying precise volumes of information about exterior and interior of the church, thus constituting a valuable reference source of the current conservation state of the heritage (Figure 4). This 3D model required the work of two technicians during 3 weeks and 174 scan stations, obtaining a 3D point cloud made up by 3 billion of points. Then, this point cloud was reduced by different filters to 17 million of points. In parallel, the as-built 360º camera Ricoh theta V camera was employed to take 360° panoramic images both inside and outside. This camera is equipped with two 180º fish-eye lenses that allow to obtain, in a direct way, a 360º panorama. About 110 minutes were necessary to capture 42 panoramas for the virtual environment (2-3 minutes per panorama). Both point cloud and photos were stored into the PlusCare system - along with the rest of information collected about the church - and used as imagery input to create an enriched virtual tour by

means of the low-cost software Pano2VR® as well as the in-house plugin HeritageCare4Pano2VR (Figure 5a). This complement allows to use virtual tours for preventive conservation, adding some extra features that can be consulted in Sánchez-Aparicio et al. [2]. Through this visual tool, the owner was given the possibility to interactively navigate across the church and access fundamental information about its current condition (e.g. type and location of damages, assets condition, geometric details, past monitoring records) through pre-defined hotspots (Figure 5b). It is worth mentioning that each time new data is uploaded to the platform and georeferenced, new hotspots are automatically created inside the virtual tour and linked to the relevant information. Moreover, if a monitoring system is installed, real-time updates of the monitored parameters can be displayed on screen together with the corresponding warning levels to assist the owner in undertaking appropriate condition-based maintenance actions [2].

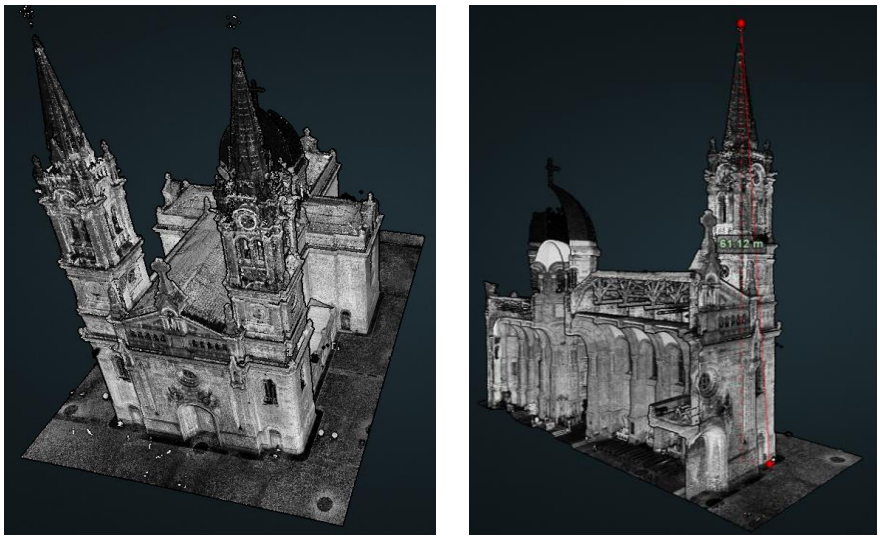
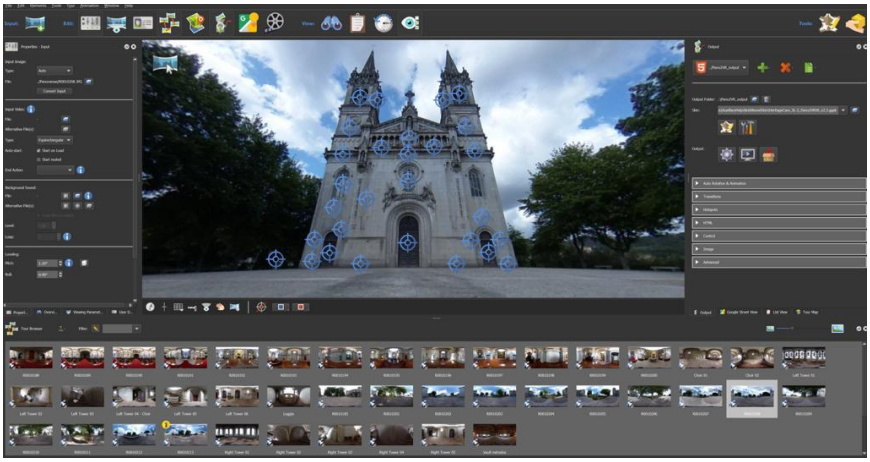


Figure 4: Point clouds of São Torcato church. Exterior view (left) and longitudinal section (right).

a)



b)



Figure 5: PlusCare system: (a) virtual tour creation through HeritageCare4Pano2VR; (b) final output of São Torcato church.

3.2 Church of San Pedro in Becerril del Carpio (Palencia), Spain

The catholic temple of San Pedro is located in the municipality of Becerril del Carpio in Palencia, Spain (Figure 2). This building was originally erected in Romanesque style with a single nave solved by means of a barrel vault, while the apse was erected in Late-Gothic style with a groin vault of eight sides. In the past the church suffered a settlement in the north part of the nave, suffering visible deformations and cracks along the tower, choir, and main nave. During 2007 an extensive diagnostic investigation was carried out with the aim of evaluating the stability of the structure as well as the degradation state of the assets and, during 2011, a major restoration took place. On the one hand, the structure was retrofitted by enlarging the foundations placed below the buttresses in order to reduce the stresses on the soil (this solution was built in reinforced concrete); additionally, the extrados of the vaults covering the main nave were strengthened with a textile reinforced mortar made of basalt fibers and a lime matrix. On the other hand, cleaning and restoration actions were performed on the assets with the aim of enhancing their understanding and avoiding their impairment and loss of value. However, a preventive conservation protocol that could allow to maintain both the structure and its indoor assets in good conditions was not designed.

Thus, in 2019, the church was included within the policies of the HeritageCare project. In a first stage, the StandardCare protocol was applied; to this end, a technician, supported by a tablet provided with the HeritageCare mobile e-form, performed the inspection of the church following the precepts of this service level. Several issues, related with the main damages affecting the church, were highlighted such as: i) presence of detachments and moisture areas on the south wall of the nave; ii) presence of broken tiles on the roof; and iii) widespread biological colonies (major plants and algae). The use of both HeritageCare damage atlas and damage rating system allowed to classify the observed pathologies in accordance with their nature and relevance. All this information, along with other metadata (e.g. construction period, history of the building, previous interventions, etc.), was properly uploaded to the HeritageCare web platform. The detected damages were also rated according to their associated risk, which were included into an easy-to-read report automatically created by the web platform (Figure 6) and delivered to the owner to assist him in the prioritization of the preventive conservation

measures. For instance, it was highlighted the necessity of applying specific short-term actions in order to mitigate the water infiltrations in the north part of the nave, including the removal of plants, the change of some windows and ceramic tiles as well as the repair of detachments.

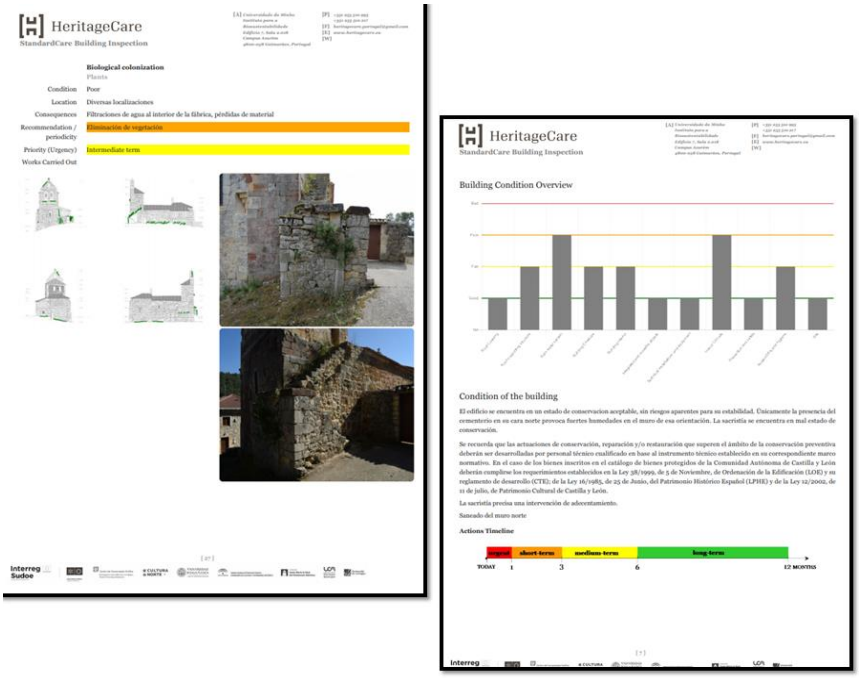


Figure 6: Excerpt from the technical report generated by the HeritageCare platform to support owner's preventive conservation actions in the Church: damage with a moderate risk (left); condition overview in accordance with the risks detected in the inspected building items (right).

Once the first Service Level (SL1) was completed, the HeritageCare team opted for implementing in the church also the PlusCare protocol. This choice was motivated by the necessity of having a deeper knowledge of the current condition of the building (including its assets) and by the necessity of developing a virtual environment that could facilitate the preventive conservation tasks to carry out by the owner. The assets were inspected by following the workflow established within the protocol. Several damages were detected and documented, such as the presence of discolorations or biological colonies. Complementary to this inspection, which was carried out by a unique operator, a digitalization process of the church, comprising virtual environment and 3D point cloud, was performed. In this case, two technicians were required, one for acquiring the 3D point cloud and another one for taking the panoramas to be used as imagery input for the virtualization. The 3D point cloud was captured by using the Wearable Mobile Mapping System (WMMS) Zeb-Revo®. This device is based on the SLAM technology allowing the 3D reconstruction of any environment with a simple walk. A total of 34 mins were required for obtaining the whole 3D point cloud of the church with centimetric accuracy. For more details about the planification and data processing of the digitization the reader can refer to [11]. In parallel to the 3D documentation, the team acquired a total of seventeen 360º panoramas. Each panorama resulted from the stitching of 7 images acquired with a digital single-lens reflex (DSLR) camera, model Canon 700D, equipped with a Sigma 8

mm F3.5 EX DG fish-eye lens. More details about the data acquisition are given in [12]. The stitching process was carried out in the open-source software Hugin® (http://hugin.sourceforge.net/), investing a total of 9 minutes per panorama (2 min for data acquisition and 7 min for processing). Finally, the panoramas were used to generate an enriched virtual tour of the church by employing the same procedure and tools discussed for the case study of São Torcato. Indeed, all the information gathered during the application of this second Service Level (SL2) was uploaded to the HeritageCare server, allowing to output a really intuitive and powerful web-environment based on 360º panoramas linked to a geospatial database (Figure 7a). This latter was conceived to make advanced consults, enabling to filter the information concerning the conservation status of the church by different criteria such as urgency risk, type of damage, location of the assets, monitored parameter, etc. Apart from this, the platform also allows the consultation of the condition report and a virtual navigation across the 3D point cloud to visualize in detail geometric information (Figure 7b).

a)

b)



Figure 7: Appearance of the virtual environment created in the PlusCare system: (a) 360º images linked to the geospatial database; (b) viewer with the metric 3D point cloud of the Church.

4 DISCUSSION AND CONCLUSIONS

This work has presented a digital-based standardized protocol developed within the framework of the European project HeritageCare. More specifically, the digital workflow concerning the second level of services of the HeritageCare preventive conservation system has been discussed in detail. This protocol, called PlusCare, was applied and validated through many case studies in Southwestern Europe, two of which have been reported in this paper to demonstrate the flexibility and scalability of the protocol according to the size and complexity of the heritage object as well as depending on the level of sophistication of the tools used for the digitization process. They are the church of São Torcato in Portugal (medium-size heritage construction) and the church of San Pedro in Spain (small-size heritage construction).

The application of the PlusCare protocol implied the execution of a first level of inspection which was carried out in the same way for both constructions, namely by using the in-house HeritageCare mobile application. This app increases the effectiveness of the onsite inspection work, reducing the time necessary for documenting the observed pathologies and producing a preliminary diagnosis report. In either case, this solution proved to be time-saving in terms of field workload, allowing to document in a few hours the conservation state of each building. With respect to the digitization process featured in the second service level of the HeritageCare system, the current work has shown the application of four different geomatic sensors that can be grouped in two categories: i) the sensor for capturing 360º images; and ii) a wearable mobile sensor for creating the 3D point cloud of the site. Regarding the former, the results obtained from the validation case studies have highlighted two main advantages of the as-built 360º cameras that are worth of mentioning: the great efficiency in capturing and processing panoramas in a short period of time (usually between 2-3 mins) as compared to the DSLR camera that demands a total of 9 mins; the high portability in terms of size and weight. In contrast, the DSLR camera offers better radiometric and geometric quality with a deeper control of the image parameters (i.e. aperture, ISO, etc.), property that results particularly relevant in indoor areas characterized by the absence of proper light. Regarding the second digital technology used for capturing the point cloud of the site, the applicative examples have demonstrated that the WMMS provides an efficient solution for the 3D documentation of built cultural heritage. Given the portability of the device, the process requires a temporal window 10 times lower than its static counterpart. However, this sensor has shown some limitations in terms of range, hindering the capturing of high elements such as towers as well as a centimetric accuracy which could be not enough for monitoring structural movements.

This work was financed by ERDF funds through the V Interreg Sudoe program within the framework of the HeritageCare project (Ref. SOE1/P5/P0258). The authors would like to express their gratitude to the Centre for Computer Graphics of the University of Minho for the web implementation of the platform. Authors also acknowledge the continuous support from the São Torcato Brotherhood and the Diocese of Palencia.

REFERENCES

[1] Masciotta, M.G., Morais, M.J., Ramos, L.F., Oliveira, D.V., Sánchez-Aparicio, L.J., González-Aguilera, D. A digital-based integrated methodology for the preventive conservation of cultural heritage: the experience of HeritageCare project, *International*

Journal of Architectural Heritage (2019), DOI: 10.1080/15583058.2019.1668985.
[2] Sánchez-Aparicio L., Masciotta M.G., García-Alvarez J., Ramos L.F., Oliveira D.V., Martín-Jiménez J.A., González-Aguilera D.A. Monteiro P. Web-GIS approach to preventive conservation of heritage buildings, *Automation in Construction* (2020) 118:103304.
[3] BS EN 15898:2011 Conservation of cultural property – Main general terms and definitions.
[4] UNI EN 16095: 2012 Conservation of cultural property – Condition recording for movable cultural heritage.
[5] UNI EN 16096: 2012 Conservation of cultural property – Condition survey and report of built cultural heritage.
[6] Ramos, L.F., Masciotta, M.G., Morais, M.J., Azenha, M., Ferreira, T., Pereira, E.B., Lourenço, P.B. HeritageCARE: Preventive conservation of built cultural heritage in the South-West Europe, in: *Innovative Built Heritage Models*, Eds. van Balen, K., Vandesande, A., pp. 135-142, London: CRC Press (2018), ISBN: 9781138498617.
[7] Morais, M.J., Masciotta, M.G., Ramos, L.F., Oliveira, D.V., Pereira, E.B., Azenha, M., Lourenço, P.B., Ferreira, T., Monteiro, P. A proactive approach to the conservation of historic and cultural heritage: the HeritageCARE methodology, in: *International Association for Bridge and Structural Engineering Symposium: Towards a Resilience Built Environment – Risk and Asset Management*, Guimarães, Portugal. Zurich: IABSE (2019), pp. 64-71, ISBN: 978-3-85748-163-5.
[8] Masciotta, M.G., Ramos, L.F., Lourenço, P.B. The importance of structural monitoring as a diagnosis and control tool in the restoration process of heritage structures: a case-study in Portugal, *Journal of Cultural Heritage* (2017) 27:36-47.
[9] Sánchez-Aparicio, L.J., Riveiro, B., González-Aguilera, D., Ramos, L.F. The combination of geomatic approaches and operational modal analysis to improve calibration of finite element models: a case of study in Saint Torcato church (Guimarães, Portugal), *Construct. Build. Mater* (2014) 70:118–129.
[10] Masciotta, M.G., Ramos, L.F., Lourenço, P.B., Matos, J.A.C., Development of key performance indicators for the structural assessment of heritage buildings, in: *E-Journal of Non-Destructive Testing - Proc. 8th European Workshop on Structural Health Monitoring (EWSHM 2016)*, 1 (2016), pp. 606-617, NDT.net.
[11] Sánchez-Aparicio, L.J., Conde, B., Maté-González, M.A., Mora, R., Sánchez-Aparicio, M., García-Álvarez, J., and González-Aguilera, D. A comparative study between MMS and TLS for the stability analysis of the San Pedro Church barrel vault by means of the Finite Element Method, *Int. Arch. Photogramm. Remote Sens. Spatial Inf. Sci*., XLII-2/W15, 1047–1054, https://doi.org/10.5194/isprs-archives-XLII-2-W15-1047-2019, 2019.
[12] HeritageCare. 2017. General methodology for the preventive conservation of cultural heritage buildings. Unpublished document, HeritageCARE (Report of the Project Activity 1.2).

12th International Conference on Structural Analysis of Historical Constructions
SAHC 2020
P. Roca, L. Pelà and C. Molins (Eds.)

FILL-IN-GLASS RESTORATION: EXPLORING ISSUES OF COMPATIBILITY FOR THE CASE OF SCHAESBERG CASTLE

L. BAROU[1*], F. OIKONOMOPOULOU[2], T. BRISTOGIANNI[1], F.A. VEER[2] AND R. NIJSSE[1]

[1] Faculty of Civil Engineering and Geosciences
Department of Material, Mechanics, Management and Design (3Md)
Delft University of Technology (TU Delft)
Stevinweg 1, 2628 CN, Delft
*e-mail: l.barou@tudelft.nl, http://www.tudelft.nl

[2] Faculty of Architecture and the Built Environment
Department of Architectural engineering and Technology (AE+T)
Delft University of Technology
Julianalaan 134, 2628 BL, Delft

Keywords: Restoration, Conservation, Structural Glass, Compatibility, Adhesive connections

Abstract. *This paper explores a novel restoration approach for consolidating historic structures using structural glass to substitute for the missing elements, preserving at the same time the structural integrity of the structure. A restoration design is proposed for the hypothetical consolidation of the remaining tower of Schaesberg Castle, in Limburg, The Netherlands. The masonry walls suffer from a significant loss of material and a temporary steel structure currently prevents the tower from collapsing. It is proposed to use stacked float glass to fill the missing parts of the wall. The connection between the old masonry and new glass is the most challenging aspect given the different physical and mechanical properties of the materials, which need to work together in a coherent way. Shear tests of various connecting materials are carried out in order to evaluate the performance of this connection with respect to aspects of compatibility and feasibility.*

1 INTRODUCTION

Materiality appears as one of the most controversial aspects in conservation and restoration practice and during the last centuries it has been interpreted in different ways aiming to reinstate the authentic image of our historic structures. On the one hand, our ambition is to intervene as little as possible to these structures in order to preserve their historical value (*preservation*) and on the other hand we aim to restore them efficiently enough to prolong their life and function in the future (*restoration*). These ambitions often conflict with each other, stressing the choice of materials and the degree of intervention as important aspects of the conservation approach. In practice, the use of traditional materials bears the risk of conjecture between the original and new elements, while modern materials may appear imposing over the existing ones and impair

their authentic image, resulting in irreversible and intrusive interventions. The current conservation and restoration guidelines provide ambiguous recommendations on how to address the issue of materiality, emphasizing aspects of *harmonious integration*, *compatibility* and *reversibility* of any intervention [1,2].

Glass is proposed as a solution in this on-going materiality debate. The aesthetic qualities, durability and mechanical properties of glass are some of the benefits of using it in conservation practices [3]. In particular, a *Fill-in-Glass Restoration* approach introduces glass elements in order not only to complete the missing form of the damaged structure, but also to reinstate its structural integrity (Figure 1). Both the new and old materials work together in an integral way, raising attention to compatibility[1] issues, as the most critical part. The authors address this topic on three interdependent levels; *aesthetic, structural and material compatibility* and demonstrate that the design of the interface between the different materials is the most challenging and yet unknown aspect.



Figure 1: Fill-in-Glass Restoration design proposal for the consolidation of Bembo's bastion in Greece [6].

Towards this direction, this paper aims to explore the structural compatibility of adhesive connections between glass and historic materials, namely clay brick masonry. To demonstrate the feasibility and limitations of the concept, the hypothetical case study of Schaesberg Castle is used for the development of the design. An experimental program is carried out to evaluate the shear bond between float glass elements in stack configuration and clay bricks testing different types of connecting materials.

[1] According to [4,5], *compatibility* expresses the ability of a conservation treatment to avoid any negative consequences that can damage, have negative effects or hinder future treatments of the historic materials.

2 THE CASE STUDY: SCHAESBERG CASTLE

Schaesberg Castle dates back to the 16th century and was built in two phases (1571 and 1616) as the residence of one of the most prominent families of the Cologne-Lower Rhine area (Limburg) in the Netherlands. The castle was made in Mosan Renaissance style, a regional style characterized by stone-framed windows, decorated architraves and alternating layers of brick and stone. The masonry walls are 1 meter thick and consist primarily of a homogeneous core of field fired clay bricks and Kunrade limestone, supplied by a local quarry, for the architectural details such as corners, window frames and horizontal bands.

Over the last centuries the castle slowly fell into decline mainly due to neglect and lack of maintenance. Other causes of decay are WWII and vandalism which resulted in extensive loss of historical materials, such as stones and anchor plates. Previous consolidation attempts, archaeological and geotechnical works, fluctuations of the underground water level and ground porosity are assumed to have contributed to settlement of the soil and consequently the foundations. Today, the remaining tower is temporarily supported by a new steel structure built on top of a concrete ballast, in order to stabilize the walls (Figure 2). Steel tie anchors connect the new structure to the masonry walls at different levels to reinstate stability and counteract the wind loads. The steel structure is accessible through a staircase, which makes the tower functional as viewpoint.



Figure 2: The remaining tower of Schaesberg castle before (left) and after (right) the latest consolidation.

Despite its temporary nature, such structure is rather incompatible with the restoration and conservation principles, as well as visually and physically intrusive to the historic materials. In the context of *Fill-in-Glass Restoration* approach a proposal is made for the permanent consolidation of the remaining tower using structural glass components to reproduce the corner walls of the tower and reinstate their structural integrity. The restoration aims to:

- respect the aesthetic qualities and historic value of the existing structure
- be minimally intrusive to the historic fabric
- ensure compatibility between the old and new materials, minimizing further degradation and allowing for future maintenance
- ensure structural integrity through the design of the connections, which need to act as the weakest link and provide a warning mechanism

3 DESIGN METHODOLOGY

3.1 Materiality

Glass can attain a wide range of aesthetic qualities, which depend on the composition, manufacture technique and configuration. Float, cast and extruded glass elements are the available products used today in various architectural and structural applications. All glass types could potentially be used in restoration and consolidation applications, depending on the materiality of the historic elements, desired degree of transparency and desired degree of resemblance to the original structure [3]. The structural glass assembly needs also to be in harmony with the existing structure and thus satisfy the aesthetic compatibility requirements.

In this context, for the case of Schaesberg Castle a stacked float glass system is explored (Figure 3). The existing construction system of building is based on masonry composed of field fired clay bricks, Kunrade limestone and lime based mortar. The tectonics of the historic construction is defined by this layering of units bonded together with the mortar. Hence, a stacked configuration of float glass elements is chosen to resemble this layering in an abstract way, respecting the principles of the original construction method. The appearance of the glass assembly is more translucent than transparent and depends highly on the glass recipe[2], bonding properties[3] and thickness (Figure 3). In general, the advantages of horizontally stacked float glass configurations are the following:

- high load bearing capacity: the vertical loads (self-weight) are introduced in the middle of the panel and not at the edges, which are weaker [8].
- wide range of architectural possibilities: the panels can be cut in any shape with a waterjet cutting machine
- potential for the connection design of glass to the ruined parts of the structure: easily adjustable to rough, uneven surfaces
- the float glass production line is widely available, so the costs are lower than for glass produced with other production methods

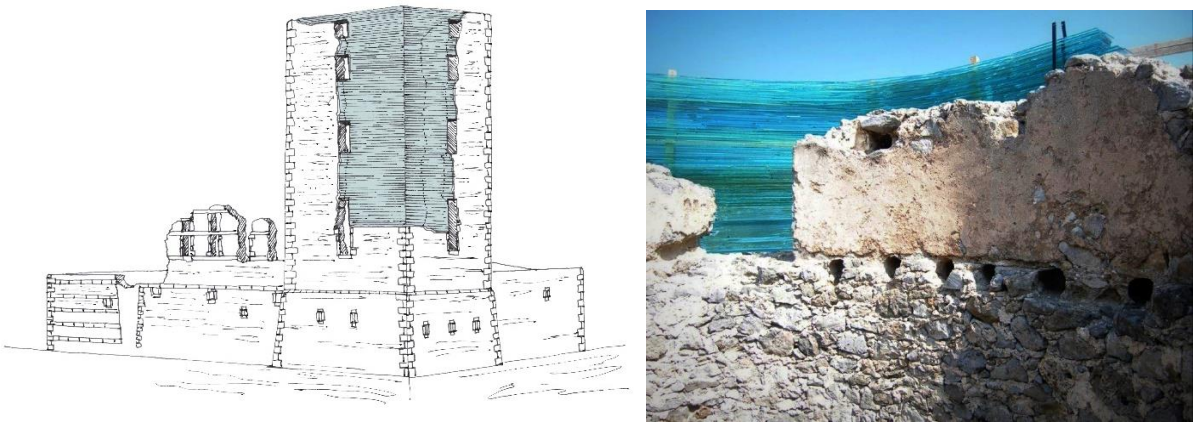


Figure 3: Proposal for the restoration of Schaesberg Castle with horizontally stacked glass elements (left) and the perception of glass and masonry as an artistic installation on a historic flourmill designed by the artist C.Varotsos (right) [9].

[2] The addition of metallic oxides in the glass recipe is responsible for the tint that each glass has. For instance, the most common soda-lime silica glass recipe has a green tint because of the presence of iron oxide [7].
[3] A tint can also be achieved by laminating the glass panels using a colored interlayer (PVB, EVA).

3.2 Stacked float glass assembly

Similar to a common masonry wall, a stacked float glass assembly consists of units and bonding material. Float glass elements with a nominal thickness of 15 mm are horizontally stacked forming elements of 4 layers. Each of these elements represents one layer of the brick masonry and has a minimum weight of 10 kg in order to be easily handled during construction. Along the vertical direction they overlap with each other, similar to a masonry arrangement. Along the horizontal direction they are connected in a tongue and groove interlocking system. The laminated glass elements are bonded together with a transparent double-sized adhesive tape, which works as stabilization mechanism for the entire assembly. The glass assembly consists of annealed glass despite its lower strength[4]. This is the preferred type to use in such a configuration, as it meets the requirements on flatness compared to thermally tempered glass (heat-strengthened or tempered), in which variations in flatness may result in local stress concentrations and failure of the glass.

3.3 Interface design

The role of the interface is to connect the old and new structure in a compatible and least intrusive way. Challenges arise when choosing an effective connecting method for materials with very different physical and mechanical properties (Table 1). Despite the density of the historic materials and glass, which is comparable, the different mechanical and physical properties highlight the importance of a proper interface design in order to achieve not only aesthetic but also mechanical collaboration between the old and new structure. Aspects of stiffness, strength, stress distribution and hygrothermal dilatation appear critical for the connection.

Table 1: Material properties

Properties	Units	Soda-lime glass	Clay brick	Kunrade limestone [d]
Density	Kg/m^3	2500[a]	2200-2800[c]	2320
Young's Modulus	GPa	70[a]	30-35[b]	10-15
Poisson's ratio	-	0.22-0.24[a]	0.21	0.1-0.27
Compressive strength	MPa	300-420[b]	50-70[c]	5-30
Tensile strength	MPa	30-35[b]	5-15 [b]	-
Thermal expansion coefficient	$10^{-6}/K$	9[a]	5-8 [b]	-
Porosity	%	0	7-36[c]	40-50
Water absorption	% by wt	0	4.5-7[c]	-

[a] according to EN572-1:2004
[b] according to [10]
[c] values are for modern fired clay bricks according to [11]
[d] according to [12]

With the aim of intervening as little as possible to the existing structure, adhesive connections are designed and developed for this case study, in order to avoid any loss of the

[4] 6 MPa for permanent loads and 20 MPa for short-term loads (values including safety factors)

historic material (e.g. by drilling holes). Such connections comply also with the existing construction system, which uses mortar to bond the masonry bricks together. More importantly, adhesive connections can achieve a homogeneous load transfer between the old and new structure and accommodate tolerances due to thermal and hygric expansion. Mechanical connections, on the other hand, result in local stress concentrations, which are unfavorable for brittle materials (both masonry and glass) [13]. The requirements for this interface are to:

- accommodate thermal/hygric tolerances
- transfer loads between the old and new
- allow for retreatability in the future
- work as the weakest link between the old and new in order to preserve the historic fabric

The geometry of the interface is highly influenced by this of the historic structure and glass assembly. 3D-scanning technologies in combination with post-processing treatment of glass plates (prior to lamination) with a water-jet cutting machine can result in a glass assembly with the exact imprint of the ruinous surface. Layer by layer, glass follows the geometry of the existing wall (Figure 4). Due to construction and manufacture tolerances a joint thickness that varies between 5 and 30 mm appears realistic and defines the characteristics of the connecting materials. The two main categories of connecting materials that are taken into consideration are mortars, which are already used in masonry structures, and glues, which are widely used in glass applications. The requirements for each of these alternatives are as follows:

Mortars

- Paste consistency (suitable for vertical joints)
- Low shrinkage
- Low pH to avoid alkali-silica reaction to glass

Adhesives (glues):

- Flexible, semi-rigid to allow for large thicknesses
- Medium-high viscosity
- Long setting time
- Weather resistant (UV, moisture, water, salt)

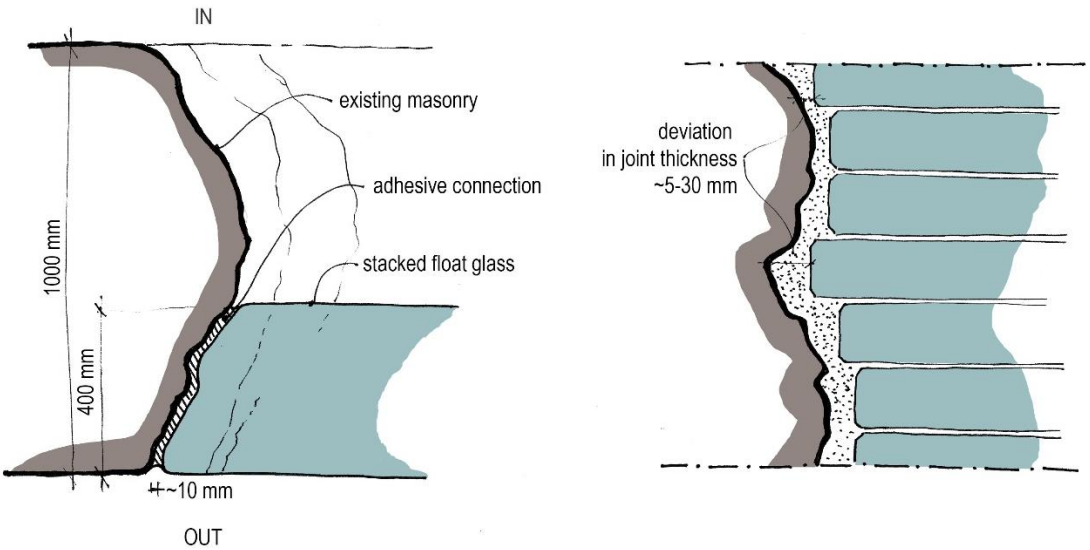


Figure 4: Detail of the interface in plan (left) and section (right).

4 EXPERIMENTAL PROGRAM

4.1 Test specimens

Shear tests are performed in order to evaluate the bonding strength of the aforementioned connection alternatives and demonstrate the potential of this system. In total five different connecting materials are tested: two cement-based materials and three types of glues. The aim of this first experimental program is to observe the:

- failure mode of the joint; specifically whether it results in damage to the brick, which represents the historic material
- effect of the edge geometry of the glass assembly (straight compared to saw-tooth pattern)
- effect of different orientation of the stacked glass assembly (horizontal or vertical stacking)

Table 2 shows an overview of the main properties of the connecting materials. *Remix Multimortar* is a dry multi-purposed cement-based mortar (Class M15), suitable for hollow glass masonries. *Remix Flexible Tile Adhesive* is an all-round cement-based tile adhesive with polymer additives[5], suitable for bonding ceramic and stone materials for indoor and outdoor use. Both of these materials have a consistency suitable for vertical joints. Three different types of glues are chosen, depending on their properties and base technology. *Tec 7* is an MS Polymer-based, strong and permanently elastic adhesive, suitable for glass. *Ottoseal S50* is a silicone-based sealant and *Zwaluw Hybriseal 2PS* is a high-quality professional sealant based on hybrid technology and suitable for bonding glass joints.

Table 2: Properties of the tested connected materials according to suppliers

Material	Base	Shore Hardness	Young's Modulus	Compressive strength	Tensile Strength	Flexural strength
			MPa	MPa	MPa	MPa
Multimortar (Remix)	Cement	-	-	15.7-17.2	-	3.48-4.7
Flexible tile adhesive (Remix)	Cement and dispersible powder	-	-	20.8-30.4	-	4.63-6.03
Tec7 (Tec7)	MS Polymer	A60	1.72	-	2.6 (after 7 days) 2.8 (after 30 days) 3.1 (after 90 days)	-
Ottoseal S50 (Otto-Chemie)	Silicone	A16	0.5	-	1.6	-
Zwaluw Hybriseal 2PS (Den Braven)	Hybrid	A30	0.65	-	1	-

For the preparation of the specimens glass plates of 10 mm thickness are cut in shape and manually ground around the edges to minimize the presence of sharp areas that could initiate

[5] 35% cement; 59.9% fine sand; 3.5% dispersible polymer powder; 2% stabilizer for water retention.

cracks. All glass edges in contact to the connecting materials are machine ground and polished in flat shape. The glass plates are bonded together using a double-sided adhesive tape in order to prevent any movement and be easily handled during the assembly of the joint[6]. The joint thickness is 10 mm for set-up 1 and 3 and 10-30 mm for set-up 2, while the contact area is 4.275 mm^2 on average. A fast drying, solvent-free styroacrylate primer is applied on the glass surface to increase the adherence of *Remix multimortar* to the smooth, non-porous surface of glass. The rest of the materials are applied in direct contact to both glass and brick substrates. All specimens are prepared 2 weeks prior the testing.

4.2 Test set-up

Three different set-ups are used in order to evaluate the shear bond between stacked glass assemblies and brick masonry, as shown in Figure 5. Set-up 1 introduces shear forces perpendicular to the stacking plane, set-up 2 introduces shear forces perpendicular to the stacking plane with the glass plates arranged in a saw-tooth pattern and set-up 3 introduces shear forces parallel to the stacking plane. Set-up 2 aims to create a more realistic representation of the connection compared to set-up 1, with a fluctuation of the thickness joint that is possible to occur due to the rough, uneven surface of the ruin.

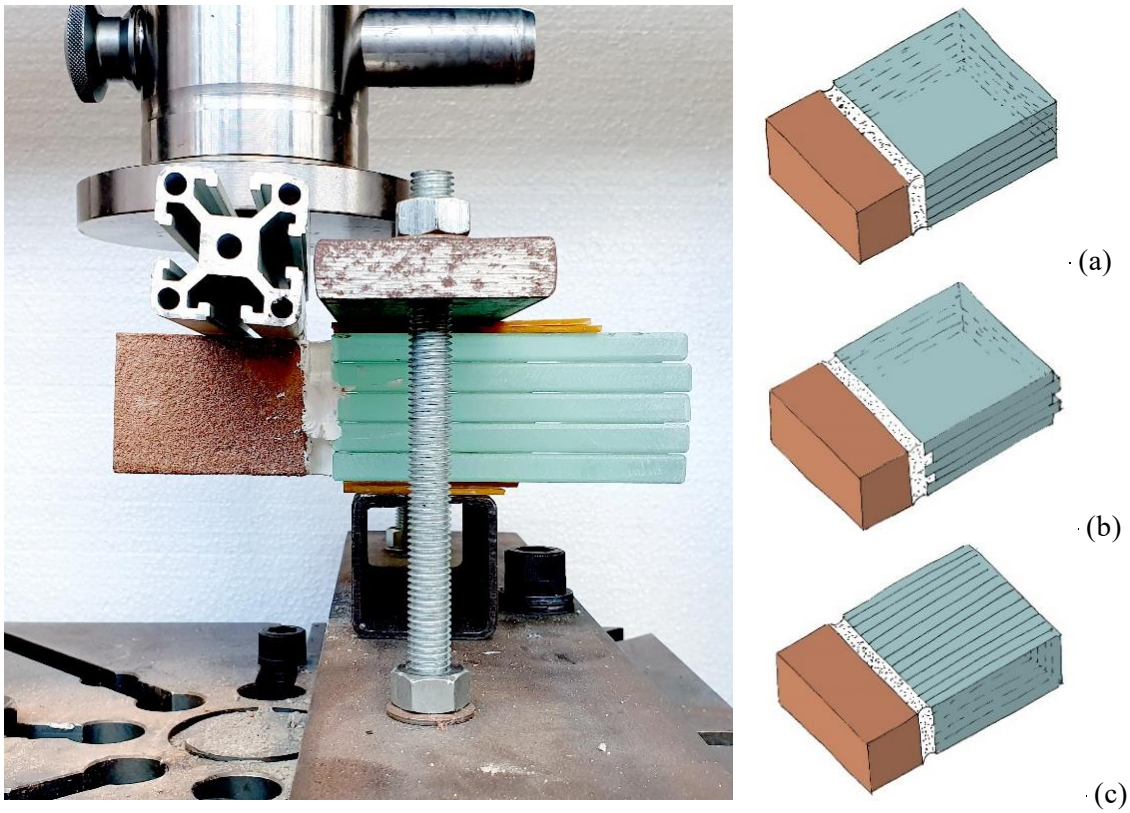


Figure 5: Left: Set-up 1 in testing machine and right: (a) Set-up 1 (glass is stacked horizontally), (b) Set-up 2 (glass is stacked horizontally in a saw-tooth pattern), (c) Set-up 3 (glass is stacked vertically).

[6] This bonding system is developed only for the tests and does not correspond to the actual construction method of the laminated glass elements.

The shear tests are performed in a *Zwick Z100* machine. A specially manufactured steel frame is used to clamp the glass assembly to the base and restrain any movements. Soft PU layers, 3 mm thick, are placed in between glass and steel to avoid the hard contact between the materials and ensure an even load distribution. The vertical load is introduced by the displacement of the crosshead against an aluminum tube and then on the brick in two different speeds: 1mm/min, for the first three materials, and 5mm/min for the following two.

4.3 Discussion

All tested connecting materials show consistent results, which are presented in Table 3 and discussed below according to the aforementioned aims.

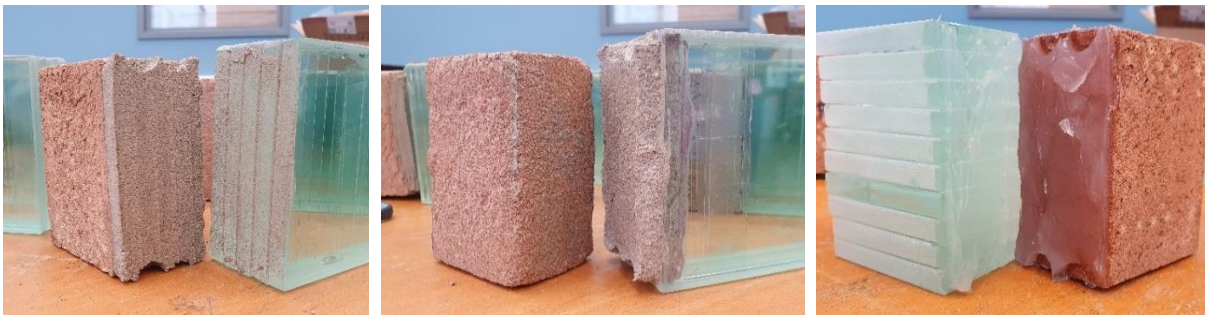
Table 3: Overview of the shear tests

Material	Set-up	F_{max}	Dl at F_{max}	Nominal shear stress τ_{max}	Prevailing failure mode
	#	N	mm	MPa	
Multimortar (Remix)	1	209.25	0.34	0.05	Adhesion to glass
	2	1146.66	1.31	0.15	Adhesion to brick, adhesion to glass, cohesion
	3[a]	0	0	0	-
Flexible tile adhesive (Remix)	1[b]	490.29	1.44	0.12	Adhesion to glass
	2[c]	1683.56	3.71	0.23	Adhesion to glass, cohesion
	3	1209. 82	2.56	0.27	Adhesion to glass
Tec7 (Tec7)	1	1986.43	10.99	0.47	Adhesion to brick
	2	1377.89	7.62	0.17	Adhesion to glass, cohesion
	3	1963.59	11.0	0.47	Adhesion to brick
Ottoseal S50 (Otto-Chemie)	1	527.17	13	0.36	Cohesion
	2	1172	11.11	0.14	Cohesion
	3	1540.33	12.30	0.37	Cohesion
Zwaluw Hybriseal 2PS (Den Braven)	1	1603.34	15.90	0.38	Adhesion to brick
	2	1026.87	12.90	0.13	Adhesion to glass, cohesion
	3	1706.40	16.63	0.39	Adhesion to brick, cohesion

[a] specimens disintegrated during fixture to the machine
[b] results from two specimens; the third is considered unreliable due to rotation of the set-up
[c] results from a single specimen; the other two are considered unreliable due to rotation of the set-up

4.3.1 Failure mode of the connecting materials

All tested materials show favorable failure modes, namely adhesion to glass, adhesion to brick and cohesion, often in combination. Therefore, the connection works as the weakest link and no damage occurs to either the brick or the glass. An overview of the characteristic failure modes and their occurrence is shown in Figure 6. In general and as expected, the mortar and tile adhesive fail in a brittle way, whereas all adhesives (glues) exhibit significant deformation capacity and the ductile behavior of the joint. For the mortar and tile adhesive, failure mostly occurs by delamination of the glass, which indicates the weak adherence bond to the non-porous glass surface. Most of the adhesives (glues) show the opposite result; failure occurs either by cohesion or by delamination of the brick.



34 % 24.5 % 41.5 %

Figure 6: Left: Adhesion to glass, middle: Adhesion to brick, right: Cohesive failure

4.3.2 Influence of glass assembly geometry

The edge geometry of the laminated glass plays a crucial role to the shear bond of the joint. For the first two cases of mortar and tile adhesive, specimens of set-up 2 (saw-tooth geometry) show increased load and maximum displacement compared to these of set-up 1 (straight geometry). The high stiffness of the materials in combination with the interlocking pattern contribute positively to the shear capacity of the joint. In the case of the adhesives (glues) the saw-tooth pattern of the glass had the opposite effect, showing decreased values in terms of force and displacement. This result can be explained by considering the influence of the thickness joint in the shear performance of the adhesives. In this context, the recessed areas in the saw-tooth pattern are, in fact, weak areas that reduce the shear capacity of the joint.

4.3.1 Influence of stacked glass orientation

The orientation of the stacked glass elements (set-up 1 compared to set-up 3) plays an important role for the tile adhesive joints. In set-up 3 both the average maximum vertical force and displacement are significantly increased, whereas the joint demonstrates some ductility. This is evident in the force-displacement diagram as shown in Figure 7. Introducing the shear forces parallel to the stacking plane results in higher deformation capacity of the joint. Set-up 3 shows a consistent increase of the joint stiffness after the first crack occurs, avoiding brittle failure compared to set-up 1.

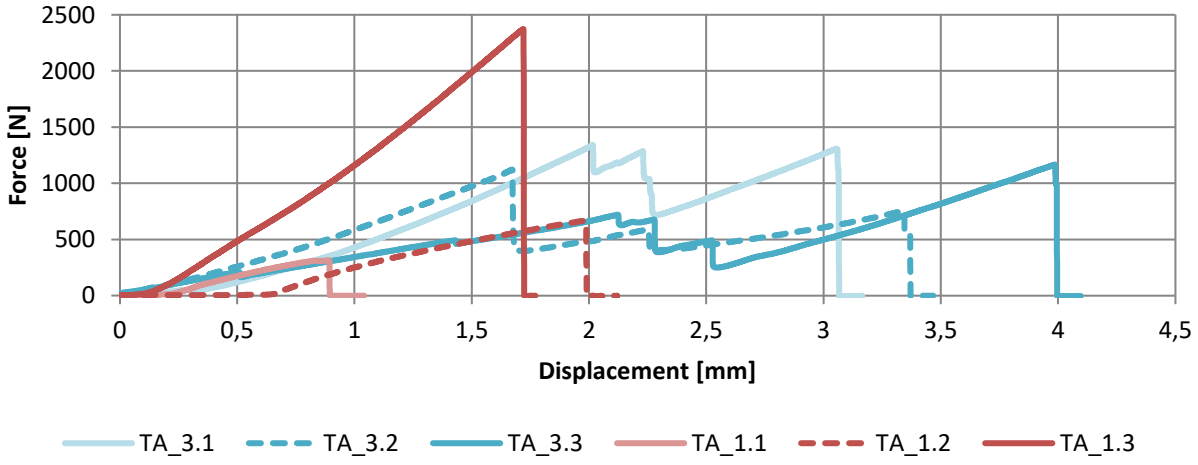


Figure 7: Force-Displacement diagram of tile adhesive joints for set-up 1 (1.1-1.3) and set-up 3 (3.1-3.3).

5 CONCLUSIONS

A novel *Fill-in-Glass Restoration* proposal using structural glass is presented in this paper as a possible answer to the current materiality debate. In the context of exploring the compatibility and feasibility of this concept the case study of Schaesberg Castle is considered. An assembly composed out of horizontally stacked float glass elements completes the missing parts of the historic masonry walls and reinstates its structural integrity. The design of the connection between glass and clay brick masonry is based on materials with adhesive properties. Two cement-based materials and three types of glues are tested in shear order to evaluate the performance of this connection. Although the specimens tested are not sufficient for statistical evaluation and cannot be considered conclusive for establishing mechanical properties, they serve as a first indication of the performance of such system and can be used as basis for future work. Based on the results we can conclude the following:

- All connecting materials exhibit acceptable failure modes that do not result in damaging the historic substructure.
- Specimens bonded with *Tec7* demonstrate the highest shear bond between glass and clay brick, as the most rigid glue. Both mortar and tile adhesive show consistently lower shear strength compared to all types of glues.
- The orientation of the stacked glass elements can influence the shear capacity and ductility of joints with brittle connecting materials, showing potential for cases where shear loading parallel to the stacking plane is dominant (e.g. wind load acting on a horizontally stacked glass assembly).
- The saw-tooth pattern as edge geometry of the glass component is favorable to mortars and tile adhesives and has negative effect on glues.
- The joint thickness fluctuations that occur in the interface due to the geometry of the stacked glass assembly can be better tackled using connecting materials with high stiffness (mortars, tile adhesives) rather than flexible glues.
- Polymer additives are crucial to the shear performance of mortar joints as they increase not only their strength, but also their adherence to the glass surface.

Based on these findings, the most promising direction to continue this study is by researching adhesive connections based on mortar-like materials. Although glued connections demonstrate higher shear capacity and ductile failure compared to ones made by cement-based materials, maintenance and future treatment are challenging issues to take into consideration in restoration applications. After degradation glues are replaced rather than repaired and their life expectancy is debatable[7]. On the contrary, mortars can be easily maintained (e.g. by grouting). The challenge, in this case, is the poor adhesion of mortar to the glass surface. Future work will focus on the adhesive bond between glass and different types of modified mortars to establish their mechanical properties. The glass edge treatment is also crucial for the bonding quality. For this paper, tests of glass elements with flat polished edges were considered, however, edge treatments with increased surface area (e.g. pencil, beveled or sandblasted instead of polished) in combination with a saw-tooth geometry could increase the shear capacity of the joint.

Acknowledgements. This research is carried out in collaboration with ABT bv. The shear tests were carried out at the Faculty of Mechanical, Maritime and Materials Engineering of TU Delft.

[7] Approximately 20-30 years for sealants according to [14].

REFERENCES

[1] ICOMOS. *The Venice Charter: International Charter for the Conservation and Restoration of Monuments and Sites*, art. 4, art. 12, art. 13 (1964)

[2] ICOMOS. *Principles for the Analysis, Conservation and Structural Restoration of Architectural Heritage*, art. 3.7, art. 3.9, art. 3.10 (2003)

[3] Barou, L., Oikonomopoulou, F., Bristogianni, T., Veer, F. and Nijsse, R. *Structural glass: A new remedial tool for the consolidation of historic structures*. HERON 63 (1-2) (2018), pp. 159-197.

[4] Teutonico, J. M., Charola, A. E., De Witte, E., Grasegger, G., Koestler, R. J., Laurenzi Tabasso, M., Sasse, H. R., and Snethlage, R., *Group Report How Can We Ensure the Responsible and Effective Use of Treatments (Cleaning, Consolidation, Protection)?,* Dahlem Workshop on Saving Our Architectural Heritage: Conservation of Historic Stone Structures, Baer, N. S. and Snethlage, R. (Eds), Chichester, John Wiley & Sons, (1997), pp. 293-313.

[5] Van Balen, K., Papayianni, I., Van Hees, R., Binda, L. and Waldum, A. *RILEM TC 167-COM: Characterisation of old mortars with respect to their repair, Introduction to the requirements for and functions and properties of repair mortars, Materials & Structures*. (2005), pp 781-786.

[6] Barou, L.: *Transparent Restoration*. MSc Thesis. Faculty of Architecture and the Built Environment, Technical University of Delft (2016).

[7] Corning Museum of Glass. *What is glass?* (2011) https://www.cmog.org/article/what-is-glass. Accessed on 26 January 2020.

[8] Van Heugten, R.: *Load-bearing Glass Columns: The Stacked Column.* MSc Thesis. Eindhoven: Eindhoven University of Technology (2013).

[9] Varotsos, C. *Geraki-Horizon* (2007). http://www.lakonistas.gr/ena-ergo-toy-varotsou-stin-lakonia-by-lakonistas/. Accessed on 26 January 2020.

[10] Granta Design Limited: CES EduPack 2015. In. Granta Design Limited, Cambridge, (2015)

[11] Theodossopoulos, D. *Structural Design in Building Conservation*. London: Routledge, (2012).

[12] Dubelaar, C. W., Kisters, P. J. M., & Stroucken, J. W. *A natural-stone city walk through Maastricht, the Netherlands.* Netherlands Journal of Geosciences - Geologie en Mijnbouw (2011), 90(2-3), 197–208. Cambridge University Press.

[13] Oikonomopoulou, F, Bristogianni, T, Karron, K, Groot, C, Veer, F & Nijsse, R , Restoring and structurally reinforcing historic monuments by glass. in A Zingoni (ed.), Proceedings of the 6th International Conference on Structural Engineering, Mechanics and Computation: Cape Town, South Africa. 6th International Conference on Structural Engineering, Mechanics and Computation, (2016), Cape Town, South Africa, 5/09/16.

[14] Mayer, P. *Whole life costing: sealants*. (2005) http://www.greenspec.co.uk/building-design/sealants-costs/. Accessed on 30 January 2020

12th International Conference on Structural Analysis of Historical Constructions
SAHC 2020
P. Roca, L. Pelà and C. Molins (Eds.)

INTEGRATED CONSERVATION STRATEGIES IN THE NETHERLANDS

SILVIA NALDINI[1], ROB VAN HEES[2] AND ERNST VAN DER GRIJP[3]

[1]Architectural Engineering + Technology

Delft University of Technology
e-mail: s.naldini@tudelft.nl

[2]Architectural Engineering + Technology

Delft University of Technology & R-Kwadraat MonumentenAdvies
e-mail: r.p.j.vanhees@tudelft.nl

[3]Monumentenwacht Gelderland
e.vandergrijp@monumentenwacht-gld.nl

Keywords: Monumental Buildings, Visual Inspection, Quality in Restoration, Terminology

Abstract. *In the Netherlands a program for the enhancement of quality in the restoration of monumental buildings is presently carried out, stimulated by national authorities and coordinated by the foundation ERM. Guidelines are issued by the branches involved, from architects to masons, under guidance of an experts' committee, to perform interventions on monuments and assess them. The aim of this paper is to discuss the contributions to the program offered by different actors active in the field of conservation, the existing synergies and the potential of using a common language and approach. These are needed to facilitate communication and exchange knowledge. The use of the terminology of MDCS (Monument Diagnosis and Conservation System) can help create a community of stakeholders. Sharing the damage terminology and methodology can help achieving a clear and systematic assessment of damage and its causes. It can further improve the communication among all stakeholders, including owners and laymen, stimulating cooperation, and can allow monitoring of damage and interventions.*

1 INTRODUCTION

In the Netherlands, a program for ensuring Quality in Restoration, stimulated by national authorities, is presently carried out. Its focus lies on the development of guidelines by the various branches, such as contractors, architects and masons, involved in conservation and restoration of monuments. The use of both terms 'restoration' and 'conservation' in the description of the program, are meant to indicate different levels of the interventions. The aim of this paper is to discuss the contributions to the program of different actors active in the field and the existing synergies. In particular attention is focussed on the present role of the system MDCS (Monument Diagnosis and Conservation System) and its potential for facilitating communication and exchange of knowledge [1]. Having clarified the tasks of important actors involved in the conservation of Dutch monuments and their aims, an overview of the situation

in the Netherlands is drawn. Strong points and difficulties are discussed in the strategies for this far-reaching program for the enhancement of the quality of monument conservation in the country.

2 QUALITY IN RESTORATION IN THE NETHERLANDS

Already in the 1970's it became evident that after the restoration of a monumental building, preventive conservation and maintenance were needed. The Monumentenwacht organisation was created - at a provincial level - to carry out regularly inspections, to assess the state of conservation and also to perform minor interventions [2]. The commitment of the organisation concerns Dutch monumental buildings. In the last decades the assistance of Monumentenwacht (MW) in deciding on necessary maintenance activities, has become essential for private owners and for administrators of non-iconic buildings in general. In these cases the decision on the conservation plan is in fact mainly entrusted to the MW inspectors, whereas, in the case of iconic buildings, a restoration team is usually formed including an architect, experts from the Dutch Cultural Heritage Agency (RCE), contractors and often MW inspectors [3]. Subscription to the Monumentenwacht organisation is not mandatory.

Monumentenwacht plays an important role in assessing the work done by contractors, hence contributing to achieve the expected quality in the conservation and maintenance interventions on historic structures. The valuation of the interventions is based on the assessment of the technical and historical compatibility of the work done, in terms of respect for of the historic (original) materials and techniques and their preservation.

Both inspectors and contractors are expected to carry out professional work. It should be noticed that professionalism in conservation is also internationally felt to be an essential goal to reach as already discussed in the TW2018 international conference in Leuven [4].

Creating or enhancing professionalism has become crucial in the policy of RCE since 2009. At that time the policy on the Modernisation of the Monument Care [5] was launched, aiming at the enhancement of the technical quality in restoration and of the ethical approach. These aspects became the focus of the subsequent program on Quality in restoration in 2010 [6], meant to achieve a controllable quality level in restoration of heritage buildings and sites. The program was founded on self-regulation. The Dutch foundation for a recognized restoration standard in the preservation and restoration of monumental buildings and sites, the foundation ERM [6] was created, to co-ordinate the actions of the branches involved in conservation, ranging from the architects and contractors to the masons and the carpenters.

Each of these branches has developed its own guidelines to meet defined quality standards. A committee of experts, created by the foundation ERM, has been appointed to assist and guide this bottom-up initiative. The foundation ERM has also the task of disseminating the execution guidelines, making them accessible online to all interested parties. Further, ERM provides the means for obtaining a certification for the execution of the work and superintends the controls on the work done. It is interesting to notice that any actor in conservation - even those not possessing a certification - can stipulate to perform an intervention in accordance with the execution guidelines.

The ERM guidelines for carrying out visual inspections of monuments [7] are based i.a. on the handbook of Monumentenwacht and the NEN standards [8, 9]. Also other provincial quality regulations refer to the ERM guidelines.

Concerning the already issued ERM guidelines, it was observed that the used terminology for indicating the damage found was not always univocal and clear and it was decided that all guidelines needed to refer to one terminology only, to avoid misunderstandings. The terminology included in the MDCS system (see further) was selected to be used as a reference for the guidelines. The system and the atlases can be found on the online platform Monument*en*Kennis [1] on Monuments (and) knowledge, created by TNO (the Netherlands Organization for Applied Scientific Research), RCE and the faculty of Architecture of TU Delft (Delft University of Technology) [10]. This broad co-operation aims at providing scientific knowledge concerning monuments to all people involved in conservation. The dissemination of the knowledge to non-specialists, including monument owners, is entrusted to Monumentenwacht and other actors in conservation working for owners and laymen-administrators of the monuments [figure 1].

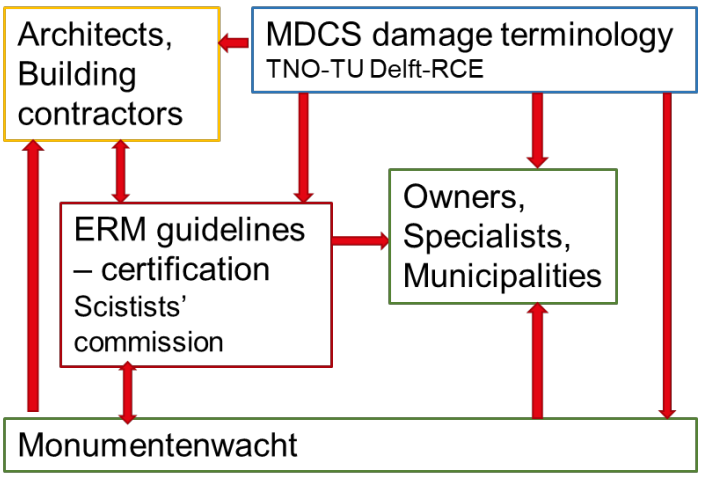


Figure 1: Quality in restoration: synergies between branches/organisations and the potential unifying role the MDCS-terminology can play

2.1 MDCS: identification of damage types for diagnosis and intervention

Already in the 1990's the need was felt for methods to achieve a homogenous approach in conservation. The cooperation of experts from Belgium, the Netherlands, Italy and Germany in the MDDS (Masonry Damage Diagnostic System) project [11] resulted in the development of a system able to guide the user in the subsequent phases of the work, from the visual inspection of historic brick masonry to the diagnosis of the damage found. The part developed for identifying the masonry materials and the damage assessed, became the starting point for the further development to other stone-like materials (such as stone, mortars, plasters, concrete) and even structural damages and proved to be an important means for communication The stand-alone MDDS was further used in national and international projects and became ultimately the web-based 'MDCS'. In a 'wiki' section, additional information can be found and relevant diagnostic and intervention techniques, all presented in a way meant for practical use. On the basis of a sound diagnosis of the causes of damages a plan can be made for a suitable, durable and ethically correct intervention.

The theoretical scientific knowledge made accessible through the MonumentenKennis platform and the MDCS wiki, can be retrieved by all stakeholders, which is in line with the intention of the ERM guidelines. Monumentenwacht and other actors in contact with the owners and the users of building can convey the knowledge to laymen. In order to put the theory into practice, following a methodology is deemed necessary, to clarify the various phases of the conservation process, from the visual inspection and the identification of the materials and the damage found, to the hypotheses on the damage mechanism(s), the control of the hypotheses and the diagnosis (as basis for the intervention).

2.2 Visual inspections

For the visual inspection, MDCS includes atlases for the identification of the materials used in monuments and the damage observed. Each term is unique and furnished with illustrations and a definition. Next to a structural damage atlas with crack patterns and deformations, the atlases concern different masonry materials (e.g. stone, brick, mortar and plaster) as well as historic concrete. The module on historic concrete will benefit from the outcomes of the ongoing international project CONSECH20 [12]. Modules on timber, glass and artificial materials and the forms of deterioration they may show will be added in the future.

Operating in line with the system is leading to the formation of a community of users, talking the same language and using the same approach: damage identification → hypotheses on the causes of damage → control of hypotheses (testing/expert's opinion) → diagnosis → intervention. The use of a common terminology is necessary and makes it possible to understand reports and perform monitoring of the development of the damage. A precise identification of damage and analysis of its cause further lead to consistent interventions: their effectiveness can also be monitored and reported within MDCS.

Conservation practice shows that there is often no agreement with respect to the meaning of a term, or that a damage type is given different names (and interpretations) by different actors.

An example is the difference between salt efflorescence and encrustation. Both are clearly defined and explained in MDCS and illustrated with photos. Salt efflorescence is the result of transport of water and soluble salts via the pore system of a material; encrustation is the result of a process of percolation of water through voids and cracks, in combination with leaching of mortar constituents such as lime, which is subsequently deposited at the surface [figure 2].

A most important consequence of using a univocal damage terminology, is that this allows a clear distinction of phases, the first being that of the identification based on visual assessment and the second being the development of hypotheses on the causes of damage under the given circumstances. When the causes of damage are unclear, this phase ends with an indication of the tests/measurements needed to control the hypotheses and explain the damage.



Figure 2: Salt efflorescence (l) and encrustation due to leaching of mortar constituents (r)

2.3 The potential of Monumentenwacht

The creation of the Monumentenwacht organization in the 1970's marked the moment when the conservation of the built heritage in the Netherlands started to be organized in terms of prevention and to include large numbers of objects. Active at a provincial level, the inspectors of Monumentenwacht perform regular surveys on the state of conservation of monuments and support their owners in maintaining them. According to the Dutch Heritage Legislation [13], the owners are in fact expected to maintain their monumental buildings,

The strong points of the Monumentenwacht concept are the (financially) independent position of the organisation in so far that involvement with the market is not needed, and the way of operating based on prompt detection of damage and control on the quality of the (maintenance-conservation-restoration) interventions, which are possible thanks to the frequent (annual or bi-annual) inspections performed. The inspectors can explain to the owners the value of an ethically and technically correct intervention for preserving the (original) materials. The value of the activities of MW in terms of preventive conservation has been discussed elsewhere [2, 3]. The inspectors further advise the owners to hire contractors preferably working in conformity with the ERM quality guidelines.

2.4 'Monumentenwacht moves'

Because of the growing relevance of the inspectors' advisory task for the owners of a broad range of non-iconic buildings, the project 'Monumentenwacht moves' was started in co-operation with the faculty of Architecture of the TU Delft. This project aims at empowering the inspectors to achieve better structured and deeper analyses of the damage. This means providing them with up to date knowledge, derived from scientific research, and with a better methodology for their investigations. The program involves the Monumentenwacht organisations of the provinces of Gelderland, North Brabant and Limburg and is intended to be spread to the other provinces in future.

In workshops TU Delft organizes for Monumentenwacht, MW-inspectors are made acquainted with the MDCS terminology for visually identifying damage phenomena. Using the MDCS damage atlas as a basis, hypotheses are made on possible causes of damage, according to the method included in the MDCS system. It is of crucial importance that the possibilities, but also the limitations of a visual inspection are clear to the inspectors and consequently to the members

(owners). In the current Monumentenwacht reports definitive conclusions on the causes of damage are often presented (diagnosis), which are in fact mere hypotheses based on the visual inspection and on personal experience.
Instead, the (correct) identification of the visible damage types and the formulation of hypotheses explaining their occurrence need to be clearly separated. The first step, the identification of the damage found, referring to a standardized system, will have an objective character. The formulation of hypotheses needs to be supported by argumentation (e.g. circumstances, information on history and former interventions). This logical line, developed in the MDCS methodology, makes it possible to decide *if/when* the advice of experts or laboratory and further investigations are needed (based on sampling, measuring,...) to evaluate the hypotheses and come to a diagnosis.
The use of the common terminology makes scientific communication possible as well as the comparison between yearly inspection reports. Comparison/monitoring can show the development of not treated damage, but also the effects of interventions on materials and structure.
A passage of a MW report made before the adoption of the new terminology has been selected to show a description of damaged pointing. No reference to the source is given for privacy reasons. The description of the type of damage rises questions: 'especially in the higher part (of the masonry) the pointing is damaged, cracked, has lost adhesion, is detached or washed out'. It is clear for the reader that the pointing is damaged and gone, but in which way? In one piece or through e.g. erosion? It is fundamental to identify the phenomenon in order to better understand the mechanism behind it: for example, in the case of push out, the pointing maintains its cohesion and is indeed pushed by e.g. the formation of a swelling compound or frost action; in the case of erosion the pointing loses particles [figures 3].



Figure 3 Examples of push out of pointing(l) and erosion (r)

The passage of a MW report made before the course concerning a certain location in a building is compared to the passage on the same location based on the MDCS methodology [figures 4, 5].

3.5. Trappen/loopbruggen - bakstenen spiltrap in traptoren 	G				Behoudens enige vochtdoorslag en verpulverde stenen.

Figure 4: Passage of a MW report. The masonry is in a good state (G), with the exception of some moisture penetration and powdering of the stones. (No reference to the source is given for privacy reasons).

3.5. Trappen/loopbruggen - bakstenen spiltrap in traptoren 	G				Plaatselijk redelijk. In de traptoren vertoont het muurwerk door weersinvloeden, vooral aan de weerzijde (west), plaatselijk wat vochtdoorslag en verpoederde bakstenen, Het vochttransport zorgt voor transport en kristallisatie van zouten aan de oppervlakte van het muurwerk. Bij de zachtere bakstenen tekent deze schade zich eerder af.
					Desintegratie, verpoederde bakstenen als gevolg van kristallisatie van zouten.
					Laagvorming en afspringen van baksteen als gevolg van kristallisatie van zouten.

Figure 5: Passage of a MW report concerning the same masonry as in fig. 4, but written on the basis of the MDCS terminology and methodology. The damage is better identified and the damage mechanism explained. (No reference to the source is given for privacy reasons).

In the first example the state of conservation of the masonry of a staircase is described as 'good', with the exception of some moisture penetration and powdering of the bricks. In the following report, MDCS terminology and methodology presented in the course (Monumentenwacht moves) are implemented. The identification of damage and its context is more complete and clear. Although the general state of conservation is rated as good, locally

occurring damage is reported at the west side. The damage is identified as powdering, and moisture penetration is assessed. The mechanism is also explained: due to the moisture penetrated in the wall (soluble) salt is transported and deposited at the surface of the masonry, where it crystallizes causing damage to the 'softer' bricks in the first place. The specific damage found at different locations is disintegration → powdering (second picture) or layering and spalling (third picture). This way of reporting and explaining damage - based on visual assessment, which is inherent to the way of operating of MW – provides the inspector with a basis for planning further investigations (e.g. moisture and salt distribution) or else monitoring the extension and severity of the damage. MW Gelderland is presently developing a tool facilitating the storage of the information on the damage types and interventions. Such a tool would be easy to manage and could be used during (MW) inspections; it is deemed important for recording data, which are presently not always traceable, i.e. data concerning interventions.

2.3 The Quality in Restoration program

The Quality in Restoration program includes theoretical, ethical and technical parts which should to be referred to for carrying out suitable interventions on monuments. The main aim is to encourage the actors involved in the conservation of monumental buildings to develop a correct, professional attitude. The need for a professional recognition was at first felt by the restoration contractors, who started the process.

ERM guidelines have been by now produced by numerous branches active in conservation: in the guidelines, since short, links are made to the MDCS (damage) terminology atlases. In the case of privately-owned buildings, contractors play an important role in deciding on the extent, technique and materials of the interventions, which shows the relevance of acting in conformity with the guidelines.

A co-operation TU Delft – ERM on the revision of the guidelines has shown where critical points lie. Also in the guidelines, like in the reports of MW, the difference should be made clear between what is the visible damage found and what could be the damaging mechanism having caused it (hypothesis). An expression like 'frost damage' in the visual inspection is a good example of an incorrect formulation, where the supposed origin of the damage is used to qualify the type, which is in fact not described. This points at the need of carefully distinguishing the visual form of deterioration (e.g. crumbling, exfoliation) from its (hypothetical) cause (frost action).

3 CO-OPERATION ON DIFFERENT LEVELS: COMMON LANGUAGE

The connection that exists between the knowledge platform Monument*en*Kennis, the ERM Quality in restoration program and the activities of Monumentenwacht reflects the involvement of different actors in the development of conservation strategies at a national level and shows the possibilities of synergies. When this 'system' becomes fully operational, the technical knowledge deriving from the academic world and from scientific research will find its way towards dissemination and use in practice; the quality guidelines created by the branches and related to existing (national and international) standards are meant to create the means for different actors to have the quality of their work recognized.

In order to enhance the use of the common terminology, a damage overview fan deck on damage to stone-like materials has been developed and will be spread by the ERM foundation.

Following the fan deck a MDCS app for smartphones will be developed.

3.1 Sharing knowledge

In a recent PhD research on the improvement of the Quality of conservation interventions, the co-operation among stakeholders based on knowledge sharing is valued as an essential means [14]. The expertise of various people involved in conservation can be thus used to construct a sound basis for the interventions: the relevance of this approach has been addressed as a shared value of the MW organizations of Gelderland, Limburg and North Brabant in a study on methods of operation in practice [15].

The need for sharing knowledge is felt at various levels. A conference with round table sessions was recently organized by the Dutch National Monuments Organization for monument managers of monumental buildings for discussing future ways of co-operating with government on conservation [16]. It was interesting to notice that owners expressed the need of easily finding in a shared website the necessary information to orient, in case of occurrence of damage to the monumental buildings they manage. They pleaded for the creation of a sort of platform where they could share theoretical and practical information. The problem with such an action, wanted by laymen and directed to them, is that the possibility of referring to cases of damage assessment and interventions in a constructive and useful way lies in the completeness of reports, which is often not clear to non-experts. In order to extract useful information from a report this needs to include all details, from the type of materials and structures and their transformation in the course of time, to the damage occurred and the reason and type of intervention. Only when the all the information is available, an assessment of the quality of the conservation process and the success of the intervention is possible, and some data can be extrapolated to help solving problems in other cases. Again, a common terminology and approach lie at the basis of a successful dissemination. This part is often seen as too complex, and yet it is essential. The question arises as to whether and how laymen can profit from the creation of a platform for sharing technical knowledge. It could be interesting to create a community of monument managers, instructed on the values of historic materials and techniques and the needs for their preservation in terms of quality. They could be advised on how to proceed, from the choice of certified inspectors and contractors, to the need of claiming reports including all the steps taken and allowing the assessment of the intervention. In fact Monumentenwacht already gives courses to layman owners on specific subjects. Yet these are their own members, and more (professional) owners should be reached likewise.

3.2 Involvement of owners and users

Owners play a relevant role in the conservation of monumental buildings in the Netherlands [17]. Owners and users of buildings should be encouraged to participate in maintenance and conservation activities. A methodology for involving different stakeholders in conservation practices and maintenance, at different levels, from signalling damage to actually intervening, has been carried out in Portugal. Positive results were obtained in various case studies on intangible and tangible levels: from increased awareness of the relevance of the monumental buildings dealt with, to direct involvement of communities in conservation practices [18, 19].

Empowering laymen stakeholders like owners and users to recognize and signal damage

could be profitable for different reasons: in the first place it would form the basis for starting maintenance activities, and further it can stimulate the emotional attachment of owners and users to their buildings.

4 CONCLUSIONS

In the Netherlands a program on the enhancement of quality in the restoration/conservation of monumental buildings has been promoted by the RCE and coordinated by the foundation ERM. The program has resulted in the creation of guidelines by the involved branches both for obtaining a certification and for performing adequate interventions on monuments. The program is meant to reach all the stakeholders in conservation, from the architects to the masons and the owners and users. The theoretical knowledge provided by various experts should be conveyed to the actors working in practice by MW and other actors. The synergies between the program and the work of different institutions active in the field of conservation can be made stronger through the use of the damage terminology and approach of MDCS, which is a strong tool that can substantially contribute to restoration quality. A clear and univocal identification of the damage, based on a visual assessment, has shown to be a good basis not only for communication and monitoring but also for making well-supported hypotheses on the cause(s) of the damage. Important is the distinction and clarification of the steps leading to the diagnosis. Employing this systematic procedure is expected to contribute to conservation quality and facilitate the creation of a community, where theoretical scientific knowledge can be exchanged and conveyed to practice.

REFERENCES

[1] MDCS https://mdcs.monumentenkennis.nl/ accessed Jan. 2020
[2] Heinemann, H. A., Naldini, S., The role of Monumentenwacht: 40 years theory and practice in the Netherlands, In: Van Balen K. & Vandezande A. (Eds.): *Innovative Built Heritage Models,* bookseries: Reflections on Cultural Heritage Theories and Practices, vol: 3, CRC Press / Balkema, Taylor&Francis Group (2018), pp. 107-116
[3] Naldini, S., Heinemann H. A., Hees, R.P.J. van 2018, Monumentenwacht and Preventive Conservation: Changes, In: Van Balen K. & Vandezande A. (Eds.): *Innovative Built Heritage Models,* bookseries: Reflections on Cultural Heritage Theories and Practices, vol: 3, CRC Press / Balkema, Taylor&Francis Group (2018), pp. 117-124
[4] Naldini S., Hunen van M., Guidelines for quality of interventions in built Cultural Heritage, In: Van Balen K., Vandesande A. (Eds.), *Professionalism in the Built Heritage Sector*, bookseries: Reflections on Cultural Heritage Theories and Practices, vol: 4, CRC Press / Balkema, Taylor & Francis group (2019), pp. 87-93
[5] MOMO, Modernisering Monumentenzorg, https://www.parlementairemonitor.nl/9353000/1/j9vvij5epmj1ey0/vi8y8gd6tkzm, accessed Jan. 2020
[6] ERM http://www.stichtingerm.nl/, accessed Jan. 2020
[7] https://www.stichtingerm.nl/richtlijnen/url2005, accessed Jan. 2020
[8] https://www.stichtingerm.nl/onderhoud-en-restauratie/periodieke-inspecties-van-uw-monument Handboek Monumentenwacht Gelderland, accessed Jan. 2020

[9] NEN 2767 Condition assessment of building and installation components - Part 2: Lists of faults
[10] https://www.monumentenkennis.nl/, accessed Jan. 2020
[11] Franke L., Schumann I., Hees R.P.J. van, Klugt L.J.A.R. van der, Naldini S., Binda L., Baronio G., Balen K.E.P. Van, Mateus J., *Damage Atlas. Classification of Damage Patterns found in Brick Masonry*, Research Report No 8, Vol. 2, European Commission, (1998), Fraunhofer IRB Verlag, ISBN 3-8167-4702-7
[12] https://consech20.eu/ , accessed Jan. 2020
[13] Heritage legislation (Erfgoedwet) 2017, https://wetten.overheid.nl/BWBR0037521/2017-09-01, accessed Jan. 2020
[14] Roy Van N., *Quality Improvement of Repair Interventions on Built Heritage*, PhD thesis KU Leuven (2018)
[15] Naldini S., Varst de G., Koning de S., Grijp van de E., Quality of restoration of monuments: the role of Monumentenwacht, In: Van Balen K., Vandesande A. (Eds.), *Preventive Conservation*, bookseries: Reflections on Cultural Heritage Theories and Practices, CRC Press / Balkema, Taylor & Francis group (in press),
[16] https://erfgoedstem.nl/wp-content/uploads/2019/01/Uitnodiging-NMo-NU-12-Overheid-en-professionele-erfgoedeigenaren.pdf
[17] Kleuver, J. De, Horst, A. Van Der, Özgül, P., Evaluatie stelsel kwaliteitsborging en Stichting ERM, DSP groep - rapport (2017), https://www.rijksoverheid.nl/documenten/rapporten/2017/01/01/evaluatie-stelsel-kwaliteitsborging-en-stichting-erm
[18] Ferreira, T.C, Contributions for the implementation of preventive conservation and maintenance strategies in the Faculty of Architecture of the University of Porto, In: Amoêda, R., Lira, S. and Pinheiro, C. (Eds), *Proceedings 3rd International Conference on Preservation, Maintenance and Rehabilitation of Historical Buildings and Structures*, REHAB, Braga (2017), pp. 255-264.
[19] Ferreira T. C., Bridging planned conservation and community empowerment: Portuguese case studies, *Journal of Cultural Heritage Management and Sustainable Development* (2018): //doi.org/10.1108/JCHMSD-05-2017-0029e

MODERN CONSOLIDATION METHODS FOR CATHOLIC CHURCH IN BAROQUE STYLE FROM ARAD FORTRESS, ROMANIA

ALEXANDRU C. ION[1*] AND MARIUS MOSOARCA[2]

[1]The National Institute of Research and Development URBAN INCERC Timisoara
Str. Traian Lalescu, nr.2, Zip code 300223, Timisoara, Jud. Timis, Romania
e-mail: alexandru.ion86@yahoo.com (*corresponding author)

[2]Polytechnic University of Timisoara, Faculty of Architecture and Urban Planning
Str. Treian Lalescu, nr.2A, Zip code 300223, Timisoara, Jud. Timis, Romania
e-mail: marius.mosoarca@upt.ro

Keywords: masonry, consolidation, church, monument, restoration

Abstract. *This paper presents the results of a study carried on a baroque style Catholic Church, in the field of determining its bearing capacity, restored with reversible materials, technologies and consolidation methods. The Franciscan Monastery is situated in Arad fortress and is an historical building. The structural resistance of the building suffered severe degradation because of the poor maintenance over the years. Two nonlinear analyses were made on the structure that showed that the building may suffer severe structural damage after an earthquake. Based on the results of these analyses some consolidation methods were proposed for the structural elements of the building: walls, arches, vaults, pillars, towers and foundations. Then a third analysis was made using the proposed consolidation methods to determine their efficiency.*

1 INTRODUCTION

Structural consolidation interventions of historical buildings must be reversible and slightly invasive. Because of this it is very difficult to evaluate the efficiency of this sort of punctual interventions on a structure. This paper presents the efficiency of modern and reversible consolidation methods proposed for a baroque style Catholic Church that is an historical building. The study was carried out within the master section entitled "Restoration and Patrimonial Regeneration" within the Faculty of Architecture and Urban Planning at the Polytechnic University of Timisoara.

The historical monument that is the subject of this paper is the Franciscan Monastery from Arad fortress near the city of Arad. The architectural ensemble of Arad fortress is nominated in the list of Historical Monuments of national importance. The fortress is a Vauban type fortification. In the year 1762, the construction of the fortress was ordered by Queen Maria Theresa of Austria. The Franciscan church already existed before the construction of the fortress. The two lateral bodies of the Franciscan Monastery which house the cells of the monks were not built at the same time with the church, but in different stages. During the First and the Second World War and during the communist regime the monastery changed its destination several timesto a prison, stables, bedrooms for the military staff, driving school for soldiers, ammunition deposit. After the year 1989 the Franciscan Monastery was neglected maintenance and has suffered major degradations.

A bibliographic study was made which contain studies made within the master's degree studies [1, 2]. Important research in the field was done as basis for the consolidation methods. A. Narita et al. [3] that describes the behavior and damages of historic buildings that are situated in Banat region in Romania, the same geographic zone as the Franciscan Church. M. Mosoarca et al. [4] studies about the failure mechanisms of Roman Catholic churches and Orthodox churches in seismic area of Banat. A comparison between the two types of failure mechanisms of the churches is also made because the two types of churches have different shapes in plan. M.R. Valluzzi et al. [5] discuss the potentials and limitations of composite materials used in strengthening historical buildings. C. Modena et al. [6] that describe criteria and technologies that can be used for the structural repair and strengthening of architectural heritage.

To determine the bearing capacity of the Franciscan Monastery several nonlinear analysis were conducted with the TreMuri program [7, 8]. In the first analysis the seismic behavior of the individual church was studied. In the second analysis the seismic behavior of the church was studied with the adjacent building bodies forming an aggregate. In the third analysis the seismic behavior of the consolidated individual church was studied.

2 DESCRIPTION OF THE STRUCTURE AND DEGRADATIONS

The Franciscan Monastery (Figure 1) is made out of three different buildings (Figure 2): the Church of the Monastery and two side structures with two floors where the Franciscan monks had their cells. The bearing structure of the church is made out of masonry walls which are 1.5m thick. The foundations of the structure are made out of masonry and are continuous underneath the structure. The thickness of the walls of the towers is also 1.5m. At the entrance of the church there is a masonry vault that is supported by an RC arch, which was an unauthorized intervention, and the wall of the main façade. The RC arch is supported by four 30cm thick RC pillars. The entire church is covered with masonry vaults. Over the vaults there is a wooden bearing structure of the roof and the roof cover. The wooden cover of the roof is made out of props and templets which have the section dimensions of 20cm x 20cm and rafters and braces which have the section dimensions of 15cm x 17cm.

The monk cells structure is made out of a thick compartmentalization with bearing masonry walls which are 30cm thick on the inside and perimeter walls which are 1m thick on the outside. The slabs of the cells are made out of masonry vaults which are 50cm thick on both floors. Over the vaults there is the wooden bearing structure of the roof and the cover of the roof. Underneath parts of the structure of the monk cells there is a basement.



Figure 1: Monastery Façade

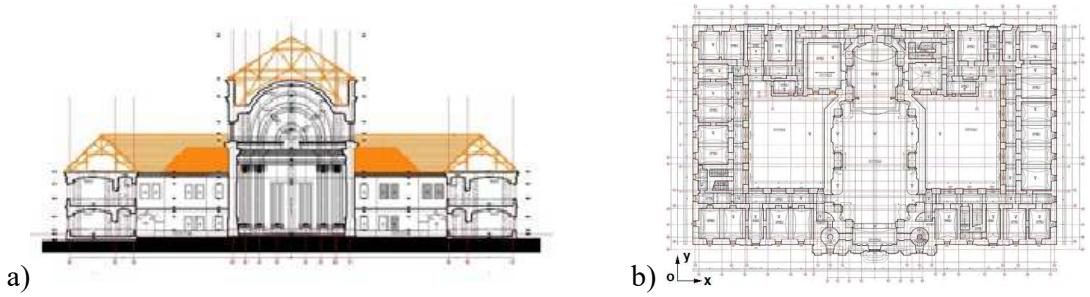


Figure 2: a) Monastery section, b) Monastery plan

The structural strength of the monastery was severely damaged due to lack of maintenance over time. At the on-site examination of the church observations were made of vertical cracks in vaults and arches (Figure 3 b) and inclined cracks at the corners of the buildings which were caused by the subsidence of the foundations. Water infiltration led to the degradation of the masonry, the degradation and the failure of the vaults (Figure 3 a), the peeling of the plaster and the corrosion of concrete and steel bars (Figure 3 c). Also because of the bad maintenance the framing of the roof and the roof covering are almost completely destroyed allowing water infiltration into the building (Figure 3 d) [7].

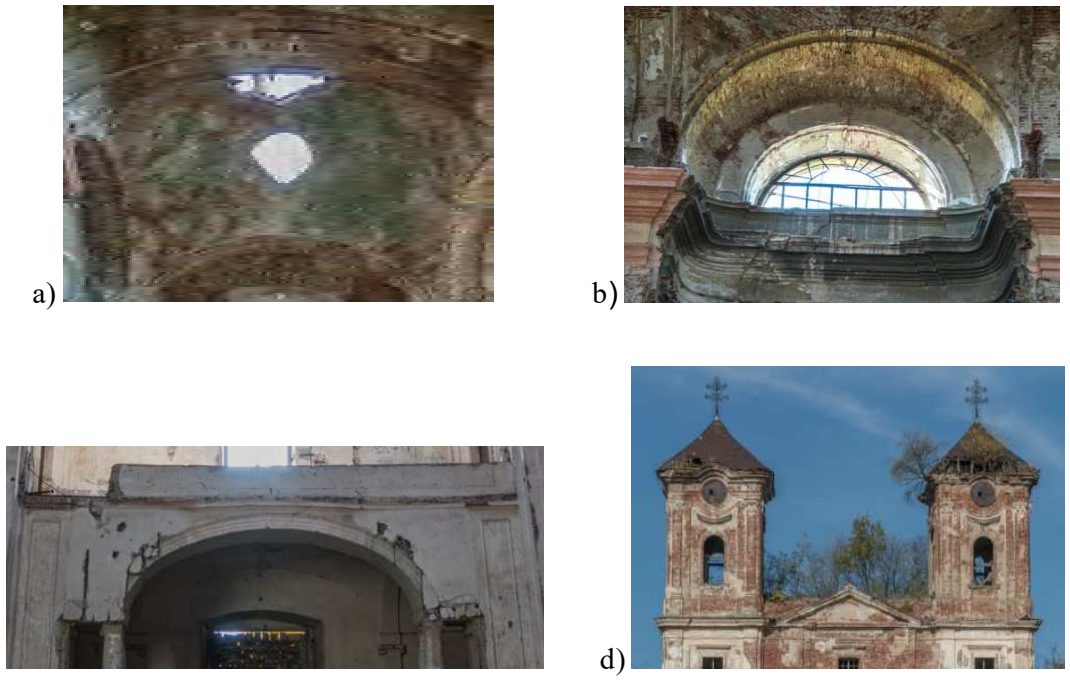


Figure 3: Structural degradation of the church: a) Vault failure, b) Cracked arches, c) Corrosion of the RC arch, d) Roof degradation

Observations were also made of some unauthorized interventions to the structure of the church: two doorway holes on the side walls (Figure 4 a) and the construction of a masonry wall with RC frame to separate the churches apse (Figure 4 b) [7].

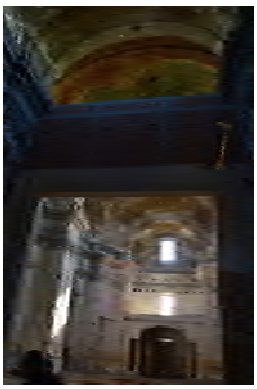
a)  b) 

Figure 4: Unauthorized interventions: a) Doorway hole, b) Masonry wall with RC frame

3 THE DYNAMIC SPATIAL ANALYSIS OF THE UNCONSOLIDATED STRUCTURE

The first step was to realize a push-over analysis of the unconsolidated structure of the church with the help of the TreMuri program to determine the bearing capacity and rigidity of the church. A 3D model of the church is presented in Figure 5 [7, 8].

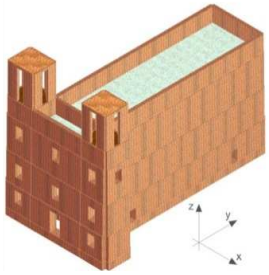


Figure 5: 3D model of the church

The analysis was created for peak ground acceleration of 0.20g according to the Romanian seismic code P100-1/2013. The vibration modes of the structure are shown in Figure 6. The vibration modes of the structure indicate a predominant solicitation of general torsion.

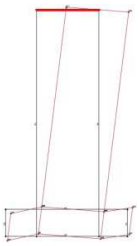
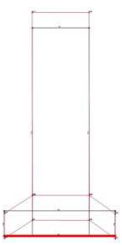
a)  b)  c) 

Figure 6: The vibration modes of the structure: a) the first mode: torsion, Ts=0.518sec, b) the second mode: translation, Ts=0.454sec, c) the third mode: torsion, Ts=0.431sec

On the Ox axis of the church the maximum horizontal displacement of the tower is 2 cm and the maximum shear force is 6200 KN as shown in Figure 7.

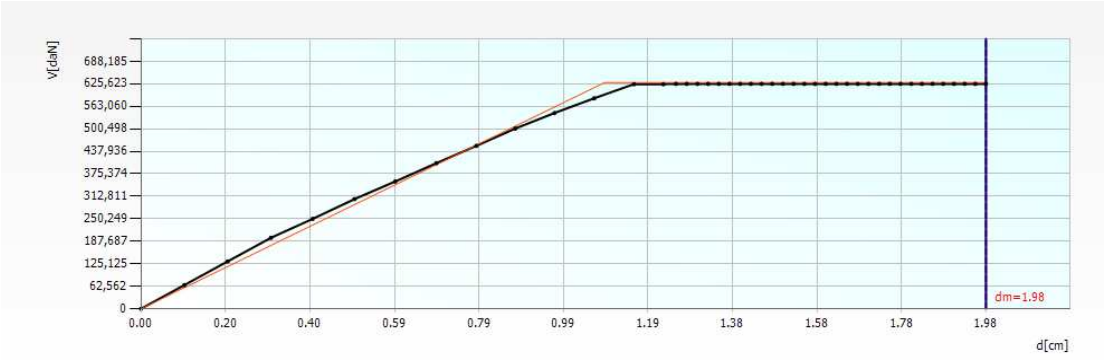


Figure 7: The force-displacement diagram, when the seismic force is applied on the Ox axis

Figure 8 presents the failure mechanisms of the structure on the Ox axis after an earthquake. On the main façade the earthquake produces diagonal cracks in the pears of the tower. On the lateral façade of the church we have diagonal cracks only at the top of the wall and at the tower. Spandrels generally have a ductile yield through bending [7, 8].

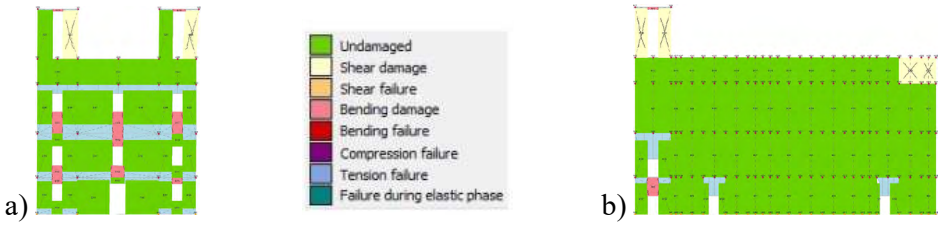


Figure 8: Failure mechanisms of the structure on the ox axis: a) main façade b) lateral façade

On the Oy axis of the church the maximum horizontal displacement of the tower is 5.7 cm and the shear force is approximately 4800 KN as shown in Figure 9.

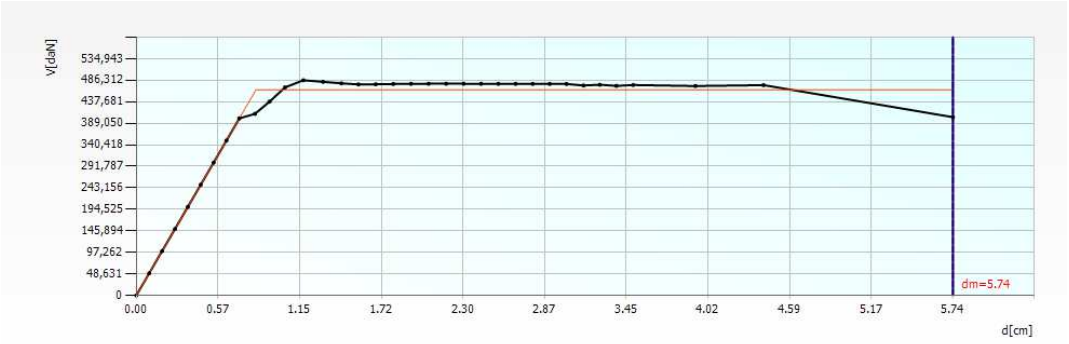


Figure 9: The force-displacement diagram, when the seismic force is applied on the Oy axis

In Figure 10 there are presented the failure mechanisms of the church on the Oy axis after an earthquake. We can see only ductile yielding on the main façade on the spandrels. On the lateral façade we have brittle yielding on the upper side of the structure.

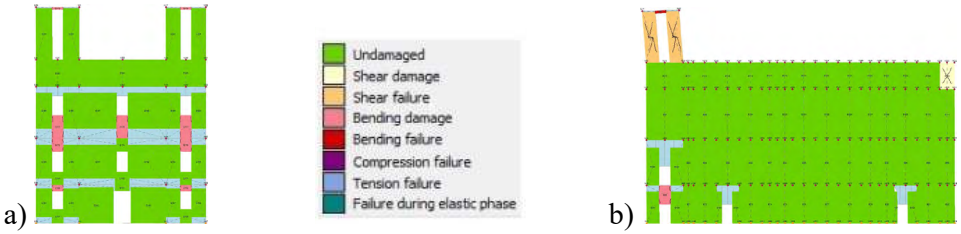


Figure 10: Failure mechanisms of the structure on the Oy axis: a) main façade, b) lateral façade

The second step was to realize another push-over analysis which contains the church in aggregate with the two side buildings that contain the cells of the monks. The 3D model is displayed in Figure 11 [8].

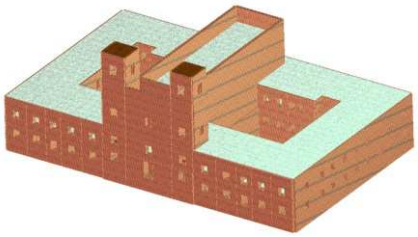


Figure 11: 3D model of the aggregate: church and monk cells

The analysis was made with the same parameters as the analysis where only the church was modeled.

On the Ox axis of the monastery (Figure 12), the maximum displacement of the tower is 1.30 cm and the shear force is 15000 KN. Comparatively to the model where the church is modeled alone the maximum displacement decreased from 2 cm to 1.30 cm and the total shear force raised from 6200 KN to 15000KN.

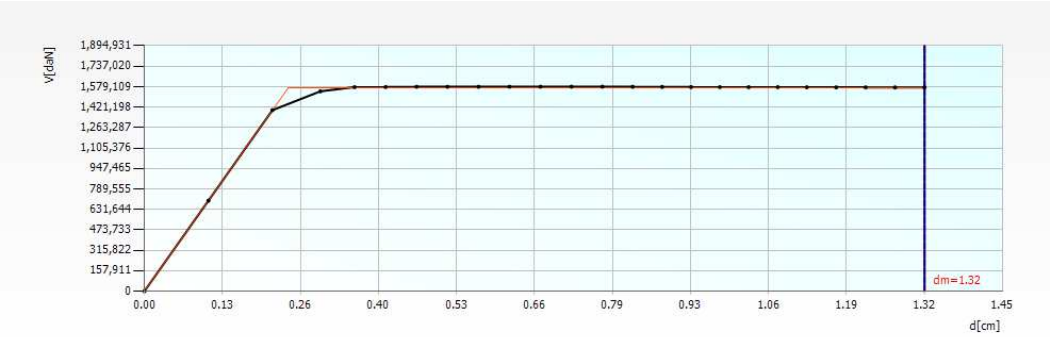


Figure 12: The force-displacement diagram when the seismic force is applied on the Ox axis

As we can see from Figure 13, there are a lot less failure mechanisms compared to the analysis where just the church was modeled. On the main façade we have ductile yielding on the spandrels, but brittle yielding can only be observed at the towers and two spandrels instead of the entire façade like in the first analysis. On the lateral façade we have failure mechanisms only on the towers.



Figure 13: Failure mechanisms on the aggregate structure on Ox axis: a) main façade, b) lateral façade

On the Oy axis of the monastery (Figure 14), the maximum displacement is raised from 5.70 cm to 5.90 cm and the shear force is raised from 4800 KN to 18000 KN.

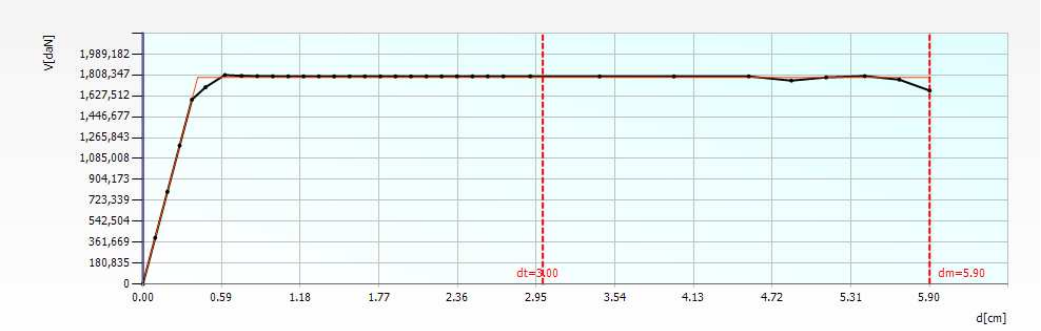


Figure 14: The force-displacement diagram when the seismic force is applied on the Oy axis

The main façade (Figure 15 a) of the monastery has ductile yielding failure mechanisms on the spandrels similar to the analysis where the church was modeled alone. On the lateral façade (Figure 15 b) there is brittle yielding on the tower of the church.



Figure 15: Failure mechanisms of the aggregate structure on Oy axis: a) main façade, b) lateral façade

4 PROPOSED CONSOLIDATION METHODS

After the interpretation of the results from the non-linear analysis, consolidation methods were proposed for each of the elements of the bearing structure. In order to maintain the rigidity of the structure and to increase the bearing capacity, minimal interventions were proposed with composite materials which were produced by Kerakoll Company [7, 9].

The proposal for the arches (Figure 16 a) was that they would be consolidated on the soffit with galvanized steel fibers Geosteel G 1200, mortar GeoCalce G Antiseismico and Steel DryFix 10 connectors.

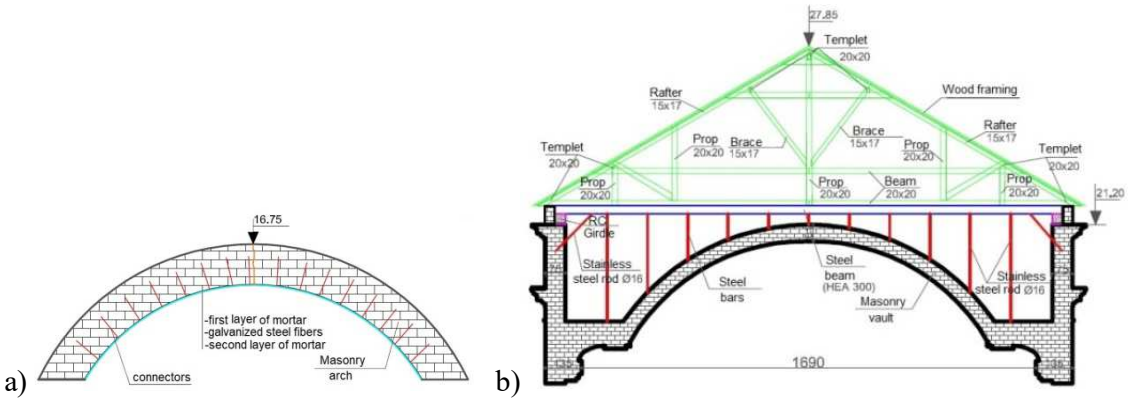


Figure 16: Proposed consolidation methods: a) Consolidation of the arches, b) consolidation of the vaults

The loads from the transversal vaults of the church will be transferred through vertical steel bars to a proposed network of steel beams which lean on the perimeter structural walls (Figure 16 b). This network of beams also transfers the loads from the roof to the structural walls [7, 9].

The consolidation of the altar walls (Figure 17) and the apse walls will be done punctually with galvanized steel fibers Geosteel G 1200, mortar GeoCalce G Antiseismico and Steel DryFix 12 connectors.

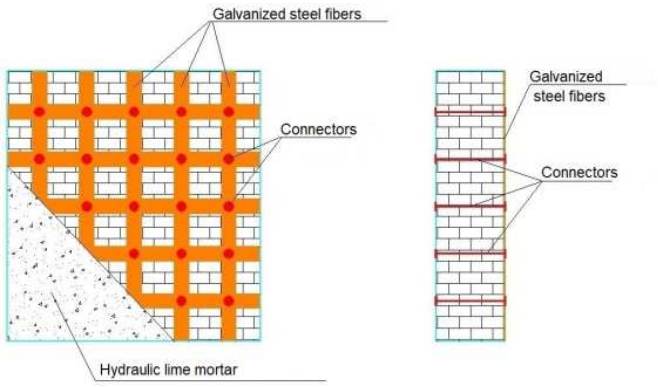


Figure 17: Consolidation of altar walls

For the RC arch and RC pillars (Figure 18) at the entrance of the church, the consolidation with galvanized steel fibers Geosteel G 1200, mortar GeoCalce G Antiseismico and Steel DryFix 12 connectors were chosen.

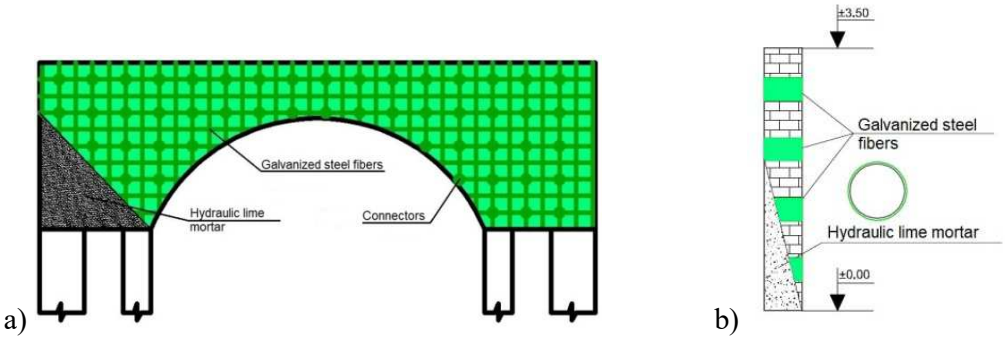


Figure 18: Consolidation of the: a) RC arch, b) RC pillar

The towers of the church (Figure 19 a) will be consolidated on the inside with galvanized steel fibers Geosteel G 1200, mortar GeoCalce G Antiseismico and Steel DryFix 12 connectors.

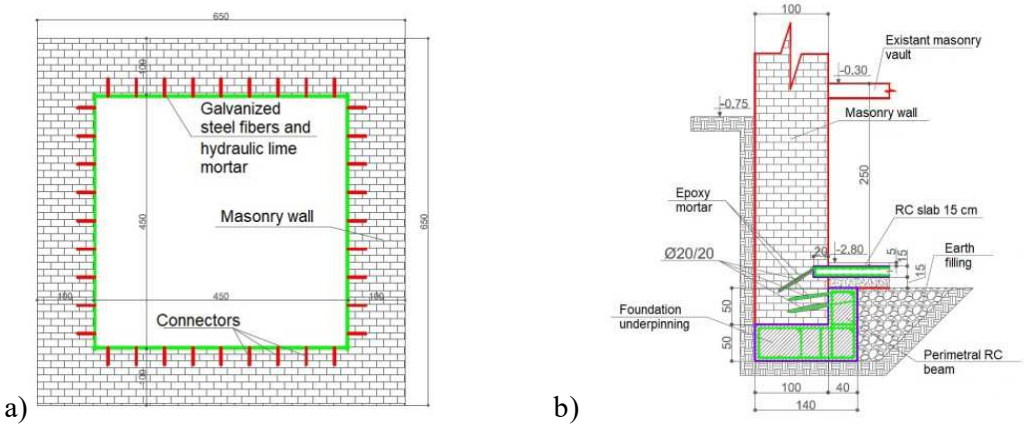


Figure 19: Proposed consolidation methods: a) Consolidation of the tower, b) Consolidation of the foundation

For the foundations an underpinning of the foundation (Figure 19 b) was chosen as the proposed consolidation method that would stop the subsidence of the foundations and the cracking of the structure.

Regarding the unauthorized interventions, it was chosen to demolish the masonry wall with RC frame that separates the apse from the rest of the church. The door holes in the lateral walls will be rebuilt to recreate the structural integrity and the authenticity of the church.

The wood framing and covering of the roof will be remade in its entirety if possible using wood elements from what is left of the existing roof [7, 9].

5 DETERMINING THE EFFICIENCY OF THE CONSOLIDATION METHODS

For the determination of the efficiency of the consolidation methods a third nonlinear analysis was made with the TreMuri program that contain the consolidation methods described above. The analysis was made on the simple model with the church as an independent building [7, 8].

The analysis indicates that on the Ox axis (Figure 20), the shear base force grew to 10800 KN, and the horizontal displacement at the top of the tower went down to 1.60 cm.

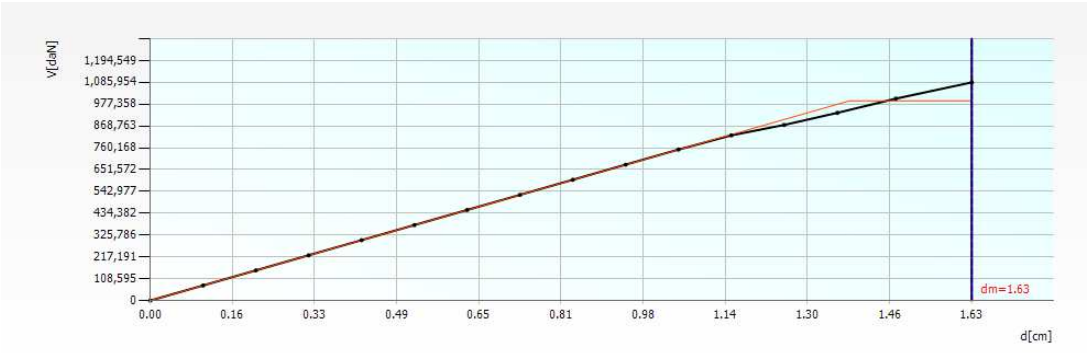


Figure 20: The force-displacement diagram when the seismic force is applied on the Ox axis

On the main façade (Figure 21 a) observations were made that there is a disappearance of failure mechanisms which remain only in the spandrels. There are a few failure mechanisms left on the spandrels. On the lateral façade (Figure 21 b) there are failure mechanisms at the top of the wall and ductile yielding in the spandrels [7, 8].

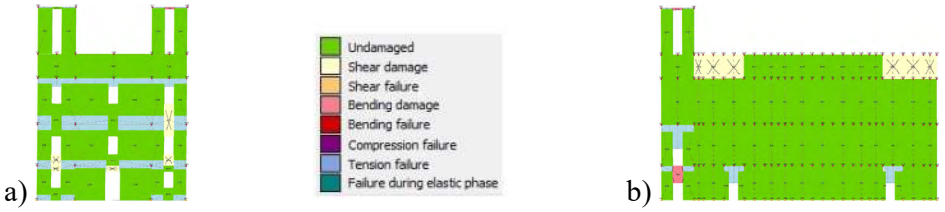


Figure 21: Failure mechanisms of the consolidated structure on Ox axis: a) the main façade b) the lateral façade

On the Oy axis the force-displacement diagram indicates (Figure 22) an increase of the base shear force to 15000 KN and a reduction of the horizontal displacement of the tower to 4.9 cm.

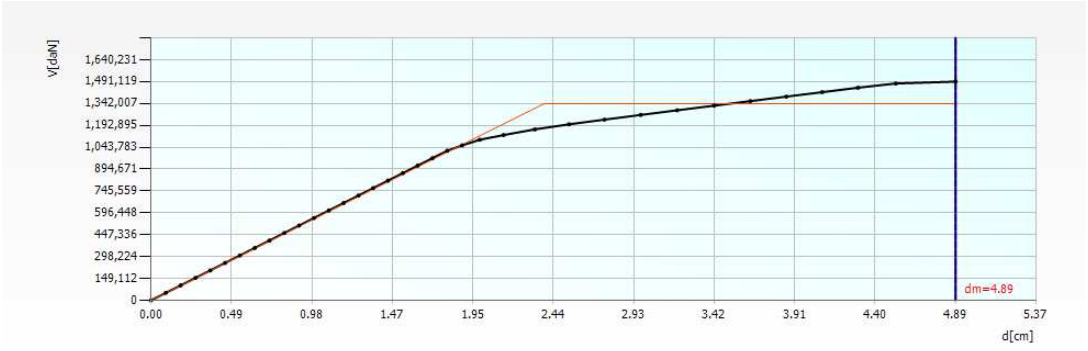


Figure 22: The force-displacement diagram when the seismic force is applied on the Oy axis

On the main façade of the building (Figure 23 a) there are failure mechanisms only at the spandrels of the tower and on the lateral façade (Figure 23 b) multiple failure mechanisms appear along the entire wall.

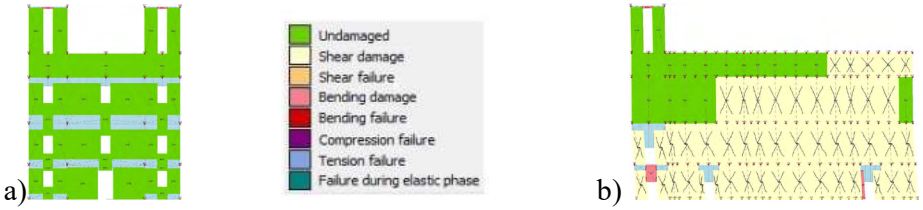


Figure 23: Failure mechanisms of the consolidated structure on Oy axis: a) the main façade, b) the lateral façade

Table 1 represents a comparative study between the results of the non-consolidated structure and the results of the consolidated structure, obtained from TreMuri [7].

Table 1: Comparative table between the results of the non-consolidated and consolidated structure

Axis	Base shear force before consolidation [KN]	Base shear force after consolidation [KN]	**Comparative growth between the base shear forces** [%]	Maximum displacement before consolidation [cm]	Maximum displacement after consolidation [cm]	**Comparative reduction between the maximum displacements [%]**
Transversal x	6200	10800	**74**	2.00	1.60	**20**
Longitudinal y	4800	15000	**213**	5.70	4.90	**14**

Table 2: Comparative table between the vibration modes of the structure

	First mode	Second mode	Third mode
Before consolidation	0.518 s	0.454 s	0.431 s
After consolidation	0.518 s	0.442 s	0.422 s

5 CONCLUSIONS

The Franciscan Monastery is part of the architectural ensemble of the Fortress of Arad and is nominated in the list of Historical Monuments of national importance. The structural health of the buildings from this architectural ensemble, the understanding and the correct utilization, make possible the social reinsertion in this historically urban site.

This paper represents the first time in Romania that a study of the bearing capacity of a historic baroque style church was done. The studies will continue with on-site testing to figure out the exact properties of the materials used in the construction of the church.

The dynamic analysis utilizes to diagnose the Franciscan Church permitted: the identification of the structural strength before and after the consolidation and the identification of the proposed consolidation solutions used to restore the historic architectural surfaces.

The first nonlinear analysis in the TreMuri program indicated that the structure may suffer significant structural damage after an earthquake with the ground acceleration of 0.20g and requires structural consolidation.

The second nonlinear analysis indicated that the building would have a higher structural resistance if the two adjacent bodies would be taken into consideration in the model.

The structural consolidation was made with modern reversible technologies that do not affect the historical value of the building. The unauthorized interventions made to the structure were eliminated to reestablish the structural resistance and the authenticity of the building.

The third nonlinear analysis indicates that the structural resistance of the consolidated building significantly increased compared to the unconsolidated structure. Also this analysis shows us that the number of structural elements in the consolidated area of the towers that suffer failure modes were reduced.

Acknowledgements: I would like to thank Eng. Rares Bradeanu the representative of Kerakoll Company who helped with information about the technology used in the restoration of historical monuments. And also we would like to thank my colleagues Razvan Dinu and Luiza Rosu for their collaboration.

REFERENCES

[1] Rosu, L. *Estetica Mănăstirii Franciscane din Cetatea Aradului*. Dissertation thesis, The Faculty of Architecture and Urban Planning (UPT), Timisoara, Romaina (2018).

[2] Dinu, R. *Repertoriul Decorativ al Bisericii Mănăstirii Franciscane din Arad și Propuneri de Restaurare*. Dissertation thesis, The Faculty of Architecture and Urban Planning (UPT), Timisoara, Romaina (2018).

[3] Narita, A., Mosoarca, M., Modena, C., da Porto, F., Munari, M., Taffarel, S., Marson, C., Valotto, C. and Roverato, M. Behavior of Historic Buildings in Zones with Moderate Seismic Activity. Case Study: Banat Region, Romania. *World Multidisciplinary Civil Engineering-Architecture-Urban Planning Symposium*, Procedia Engineering 161 (2016) 729-737.

[4] Mosoarca, M. and Gioncu, V. Failure Mechanisms for Historical Religious Buildings in Romanian Seismic Areas. *Journal of Cultural Heritage* 145 (2013) e65-e72.

[5] Valluzzi, M.R. and Modena, C. Current Practice and Open Issues in Strengthening Historical Buildings with Composites. *Materials and Structures* (2014) 47: 1971-1985.

[6] Modena, C., da Porto, F., Valluzzi, M.R. and Munari, M. Criteria and Technologies for the Structural Repair and Strengthening of Architectural Heritage. *Rehabilitation and Restoration of Structures Conference* (2013) 51-74.

[7] Ion, A. *Soluții Moderne de Analiză Structurală și Consolidare a Bisericii Franciscane din Cetatea Aradului*. Dissertation thesis, The Faculty of Architecture and Urban Planning (UPT), Timisoara, Romaina (2019).

[8] S.T.A. DATA srl. *TreMuri User Manual Release 10.9.0.* http://www.3muri.com/documenti/brochure/en/3muri10.9.0_eng.pdf(last visit 12.01.2020)

[9] KERAKOLL. *Solutii si produse.* Http://products.kerakoll.com/catalogo.asp?id_lingua=23#(last visit 12.01.2020)

12th International Conference on Structural Analysis of Historical Constructions
SAHC 2020
P. Roca, L. Pelà and C. Molins (Eds.)

PREVENTIVE CONSERVATION FOR BUILT HERITAGE. ANALYSIS OF DIFFERENT MODELS AROUND EUROPE

DALIA STABRAUSKAITE

e-mail: dalstab@gmail.com, https://www.linkedin.com/in/dstabrauskaite/

Keywords: Preventive Conservation, Built Heritage Maintenance, Monumentenwacht

Abstract. *This paper explores how preventive conservation for built heritage is promoted and implemented around Europe, compares the different practices, and identifies some of the necessary conditions for them to be effective and successful. It pulls together a broad range of initiatives including recently launched and lesser known schemes. Since Monumentenwacht was introduced in Netherlands, similar inspection service schemes have been launched in nine European countries. Comparative analysis shows a great diversity in their management, the spectrum of services, sources of income and other aspects. Other important models contributing to the improved maintenance of built environment include heritage centres, databases of contractors, one-off campaigns, conservation manuals, and maintenance enforcement. Interdependencies observed between them suggest that their co-existence is essential for preventive conservation system to be truly effective.*

1 INTRODUCTION

Preventive conservation of built heritage is recognized as an essential part of sustainable heritage management. It can expand the life-span of buildings and their historic fabric, ensure the optimal use of financial, environmental resources and embodied energy, stimulate the market, contribute to the preservation of traditional craftsmanship, increase public safety and bring about many other benefits.

Variety of practices were identified that contribute to the improved maintenance of buildings in Europe. Based on the differences in objectives and methods applied, they were classified into three categories. *Monumentenwacht* type of practices take a hands-on approach and deal with actual historic buildings by providing services such as inspection, monitoring and minor repairs. Measures of education and information (heritage centres, one-off campaigns, databases, conservation manuals) are raising awareness and equipping heritage owners with knowledge of proper repair materials and techniques, qualified specialists in the area, and other relevant information. The third category (combination of support and enforcement) represents the view that maintenance of the built stock should be government and individual responsibility (not a choice) for which supporting legal acts and financial instruments need to be present.

Such spectrum was chosen not to simply list down the different existing initiatives but to get a clear overview of the current practices in the field of preventive conservation for built heritage, to analyse the different approaches and their sustainability. Research methods include a review of literature, desk-based research into projects and policies of different countries, face-to-face interviews and correspondence with heritage professionals, a survey of practical maintenance workshops' participants. This paper is a condensed version of the author's dissertation under the same title.

2 COMPARATIVE ANALYSIS OF *MONUMENTENWACHT* TYPE OF PROJECTS

Monumentenwacht (hereinafter – MW) was set up in the Netherlands back in 1973 as an independent non-profit organisation. The aim was to prevent deterioration of cultural heritage with the means of annual inspection, temporary repairs and provision of professional advice. It started with one part-time team that operated in two provinces and gradually expanded to the whole country [1]. Now the organisation has over 100 employees that inspect more than 13 000 buildings every year [2].

The success of this model inspired a number of other European organisations to implement it in other countries. Nine similar schemes were identified to have been applied since: Monumentenwacht Flanders in Belgium (since 1991), the Bath pilot scheme in England (2002-2003), Monumentendienst in Weser-Ems, Germany (since 2004), Műemlékőr in Hungary (2012-2014), the Traditional Buildings Health Check scheme in Scotland (since 2013) (hereinafter - TBHC), ProMonumenta in Slovakia (since 2014), the Maintenance Plan for the Romanesque Route in Portugal (2014-2018), HeritageCARE in Spain, Portugal and the South of France (since 2016), and FIXUS in Lithuania (since 2019). Some of them have been successfully running for years, others have just been launched, and there are those that seized to exist right after pilot projects were over (see Figure 1).

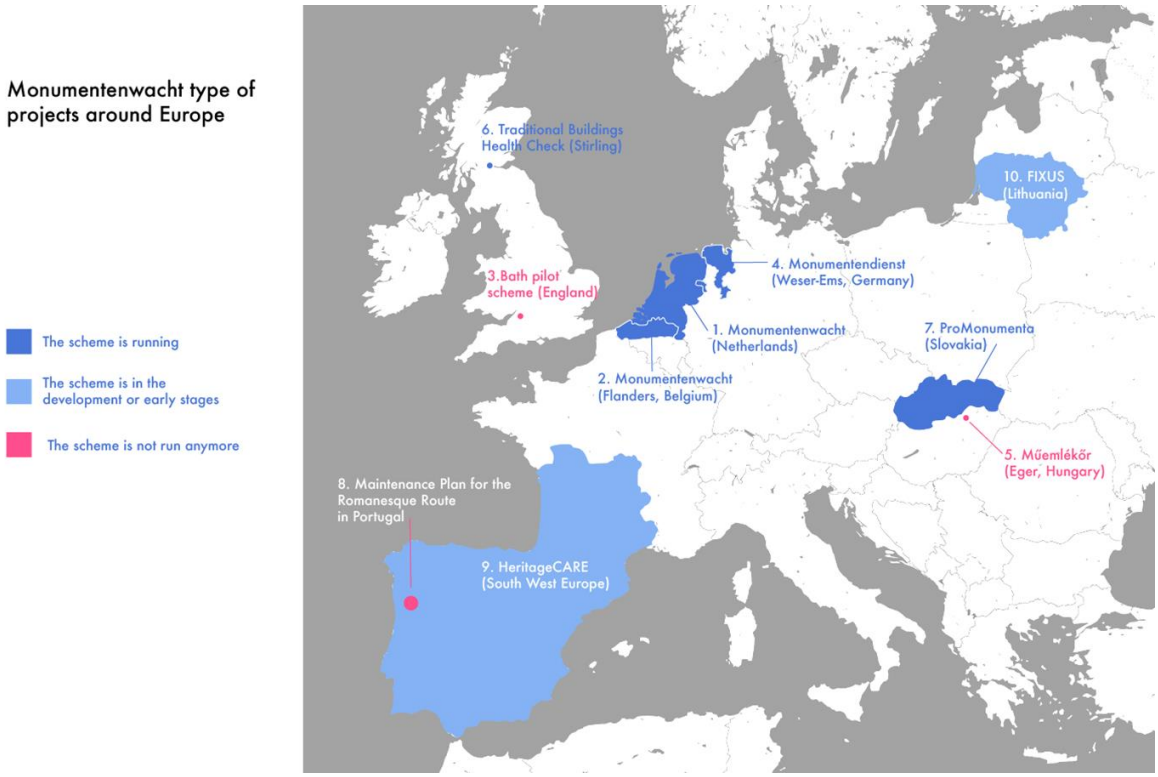


Figure 1: Schemes similar to Monumentenwacht Netherlands found around Europe. Prepared by the author.

Efforts were made to identify and present a full list of such projects in Europe. However, there were some deliberate exceptions made that should be noted. More than one such scheme has been found in Germany but only one was selected (Monumentendienst) as a more prominent example and also for the lack of accessible information about the other ones. Also, there have been attempts to establish similar schemes in Italy and Austria that fell through due to political reasons.

The following subsections are aimed at highlighting these projects' differences and similarities, presenting common trends and challenges, rather than describing each of them individually.

2.1 Services and objects of support

The four main services provided by all 10 organisations analysed are visual inspection, minor but crucial repairs, the provision of maintenance advice, and the delivery of a condition report. Usually, the staff (or someone from the team) would also be able to answer owners' questions related to available funding, legal framework, appropriate energy efficiency measures and similar topics. In some places (e.g. Slovakia; Stirling), the owner cannot apply for a grant without being a member of the scheme and having a recent condition report.

Apart from these core services, some organisations also organise informational or training events; prepare maintenance related manuals; assist in preparing applications for funding; carry out inspections prior purchase or sale of properties; provide guidance during restoration or renovation works; provide tips on how to get comparable quotes from contractors, and provide other services.

Lithuanian project FIXUS stands out among other schemes in that it will carry out laboratory research of samples taken during inspections. Such a service is possible as scientific research of heritage objects is one of the main activities of the project promoter (Centre for Cultural Heritage). Findings (about salts, composition of plasters, types of mould and other) will inform condition reports and recommendations [3].

In Flanders, a fairly new service is the delivery of a Multi-annual Maintenance Cost Analysis report (or Long-term Maintenance Plan). Essentially, it expands recommendations provided in the main report by including the estimation of maintenance costs. Calculations are based on needed materials and man-hours, quantity and frequency of the required interventions and other details. The need for such service was observed during subsequent inspections when some buildings were found in the same or worse condition than before. It turned out that such situation is caused not necessarily by financial difficulties of owners to follow the recommendations but the lack of more specific instructions and cost estimates [4]. Survey carried out in Flanders showed that 92% of members are "strongly interested in further support in maintenance of their valuable heritage, specifically for estimating the costs of the recommended works of preventive conservation" [5].

All of the organisations service historic buildings, however, some only work with listed (protected) properties under public or church ownership, while others (e.g. MW Flanders, Monumentendienst, TBHC, HeritageCARE) also include non-listed and privately owned objects. Non-listed historic buildings are not included in those schemes that are fully funded by public money. MW Flanders and some provinces in Netherlands are exceptional in that they provide services to other objects than buildings as well (movable heritage objects, interiors, maritime objects, in-situ archaeological heritage, historic gardens, cemeteries). They were gradually included as organisations grew in size and experience.

2.2 Organisations and geographical scope

There is a surprising diversity in the type of organisations that initiate and implement this model. In some countries, it is the governmental institutions of state level (in Slovakia, Lithuania) or municipal level (Hungary, Portugal) that take the initiative and assign their subordinate organisations to implement it. In other countries, the scheme is run by one or

several independent non-profit organisations (though financially greatly dependent on public support). They highlight their impartiality as one of the most important traits of the service.

Some of the organisations were established specifically for the purpose (e.g. Monumentendienst Weser-Ems), others expanded their activities (e.g. Stirling City Heritage Trust). Some of the non-profits emerged bottom-up (e.g. MW Netherlands), others had guaranteed governmental support from the start (e.g. MW Flanders). However, the continuity of schemes is not assured by the initial support of governmental institutions. For example, the pilot project in the town of Eger, Hungary (Műemlékőr, en. Monument Guard) was coordinated by the research centre under the Ministry of Human Resources (The Gyula Forster National Centre for Cultural Heritage Management). Despite the success of the pilot, the project was discontinued when the Forster centre was closed due to the changes in political agenda and the reorganization of public administration.

The model has been found to be applied in areas that are very different in size – of a city, a region, a country and even several countries. Projects in cities (Bath, Stirling, Eger) were started as pilot schemes to test this model's feasibility on a small scale first. Schemes in small areas are easier to set up and manage quality wise but they are less economical and more vulnerable to changes in staff. Manager of TBHC explained that it is challenging to balance limited capacity (1 inspection team) with the right amount of marketing and the changing demand for services - periods when there are very few or too many bookings. Under the TBHC scheme, inspection of one building requires around half a day, and then another two days are needed for the preparation of a report (which is around 30 pages long). Thus, one team can only take up around 2 objects per week. Among the researched, there are organisations with less than 5 to over 100 employees.

Schemes in larger areas have the benefits of scale but require effective management systems to ensure the same quality of services, to address logistical and other issues. In Netherlands, an independent organisation exists in every province - they work separately but all of them are affiliated members of an umbrella association. It advocates its members' interests and ensures that the same standards are applied across organisations. In Slovakia, each of the three territorial departments of the Monuments Board has an inspection team (one team consists of 4 persons) to cover different regions.

The project of HeritageCARE is unique in that it covers three bordering countries (South of France, Spain, Portugal) with similar heritage, climatic conditions and common challenges. International and intersectoral collaboration of 19 organisations (universities and research centres, public institutions and private organisations) resulted in the development of progressive methods of inspection and reporting, comprehensive damage atlas and other tools.

2.3 Sources of income

A characteristic common to all the analysed schemes is dependency on public funding. As noted by Zoltán Erő (the managing director of architects' studio Palatium in Hungary), the market would be full of companies offering such maintenance services if it was a profitable business [6].

The three longest running of the analysed schemes (MW Netherlands, MW Flanders, Monumentendienst Weser-Ems) are supported by both local and state level governments with the biggest share coming from the former. It is worth mentioning that in all three countries decentralization policies are applied (especially Germany and Belgium that have federal governments; Netherlands is a decentralized unitary state). That may be one of the reasons why local authorities are more supportive of such schemes.

Exceptional case, in terms of funding, is the Bath pilot scheme, which was grant-aided by three charities. However, the scheme only ran for 12 months and its continuation was considered not possible "without greater promotion and strategic engagement from the conservation authorities, better implementation of existing policy and financial & fiscal stimulus" [7].

All the schemes launched after 2013 (except for TBHC) took advantage of EU/EEA funding. It was used for whether the preparation of the scheme (research) or for its first years of implementation (including acquisition of equipment). The grants were provided under the programmes of Interreg (for HeritageCARE, Muemlekor), EU Structural Funds (MPlan for Romanesque Route), and the EEA Grants (ProMonumenta, FIXUS projects).

The fact that public funding is essential for this model to work is widely discussed but often without the supporting numbers. To get a better understanding of the level of support that is needed, the income generated from the fees was compared with the overall annual budget. The following two membership-based schemes were taken as case studies:

1). The Traditional Buildings Health Check (TBHC) scheme in Stirling covers one small town. From its launch in October 2014 until the summer of 2019, it had attracted around 300 members. The annual budget needed to run the scheme is roughly £170,000. It should be noted that this is the budget of a "normal" year – all the set up costs (purchase of equipment and other) have been incurred in the previous years. Only around £15,000 of this amount is generated from membership fees and inspections, while the rest is the support from the Historic Environment Scotland (public body) [8]. Thus, only 8,8% comes from the direct users of the service (heritage owners and managers).

2). The MW scheme in Noord-Brabant covers one province in Netherlands. It has been operational for 44 years (since 1975) and has over 2000 members. The income planned for 2019 was 1,96 million euros, of which inspection and membership fees were foreseen to constitute 35,5%. The rest was covered by the subsidy from provincial authority (53,6%), the Government (8,7%) and a few other sources [9].

The two examples show what a small proportion of costs is actually covered with the fees collected. Even a well-established organization operating for many years in a relatively big area generates only around a third of its income from members' contributions. The percentage is naturally even lower for a relatively new scheme operating in a small territory of one city.

2.4 Pricing

Majority of MW schemes are based on a membership system under which heritage owners pay an annual member fee and they are also charged for the services provided. However, there is a great variation in pricing policies.

The analysis of different schemes showed that the average annual membership fee is around 40 euros. Manager of TBHC shared that, despite the overall increasing interest in the scheme, 80% of members renew their membership for a second year, only 63% for the third, and 61% for the fourth. That is linked with the low demand (28%) for annual re-inspections which are seen as too frequent [8]. As an incentive, in some provinces of Netherlands, reduced rate is applied when the membership is extended. In Flanders, operators with a large number of heritage objects can purchase a group membership. For example, every heritage owner of Riemst community in Limburg (there are 108 protected objects) can become a member of the scheme for free thanks to the municipal administration that obtained collective membership (for 1000 euros/year). The municipality also subsidizes inspection costs [5].

Fees for services are usually based on hourly rates. The lowest hourly rate amongst the analysed cases was 30 euros/hour (Monumentendienst, Germany). Every provincial organisation in Netherlands has a custom pricing policy. There, rates vary from 31 to 75 euros/hour which is influenced by the different size of support that comes from local authorities. Instead of an hourly rate, TBHC charges 150 to 195 pounds a day. Normally, organisations charge the owners additionally for the materials used on repairs. Some organisations also include travel expenses (whether a fixed "call rate" or based on a distance). In Flanders and Netherlands, services started to be provided to non-members as well but for higher (not subsidized) fees. For example, the usual hourly rate of MW Flanders services is 45 euros but for non-members it's almost twice the amount (80 euros).

There are big differences regarding the value-added tax (VAT) for repair services. In Scotland, the full rate applies, in Germany it's reduced (7%), while in Netherlands such services are exempt from VAT.

In projects that are currently fully funded by the EEA Grants (FIXUS, ProMonumenta) no fees for heritage owners apply. Even after 2022 (the end of EEA supported period), the schemes are planned to be mostly supported by the Government and thus only very small charges are foreseen [10].

To sum up, the schemes that follow the model of MW Netherlands are similar in that they offer the same core services but they are definitely not pure 'copies' of the Dutch practice. There are significant differences in their management, sources of income, the size of geographical area covered and many other aspects.

3 MEASURES OF EDUCATION AND INFORMATION

There are many different educational and informational tools and methods out there aimed at improved maintenance of historic buildings. Four of them stood out to the author as the most common: heritage centres, one-off campaigns, databases of contractors, and conservation manuals. They are distinctly different from each other in terms of form, required budget and staff, the impact that can be achieved, and other aspects. Each is briefly presented in the following sections.

3.1 Heritage centres

A heritage centre, in this context, refers to a non-profit organisation which provides consultations and/or trainings on heritage related topics to heritage owners, specialists and enthusiasts. Most of them are also carrying out activities of heritage research, documentation and dissemination, practical conservation, preparation of condition reports or similar. Such establishments are widespread in the Northern Europe, especially in Norway and Estonia. However, based on personal communication with heritage professionals from Scotland, Central and Western European countries, it seems that little is known about them outside Northern Europe.

Centres that actively provide services to heritage owners and the general public are indicated in the map (see Figure 2). Different colours are used only to signify more clearly to which country the centre belongs. This is not an exhaustive list but most of the important centres in Norway, the Baltics, Scotland and Iceland are believed to have been identified. Those that were considered as very low in activity or inactive were deliberately excluded. Situation in Sweden and Finland has not been investigated enough (due to time limitations

and language barrier). Research done so far has not resulted in the discovery of any prominent centres but it is likely that some exist there as well.

Those centres that mostly focus on the training or the upskilling of craftsmen were also excluded as vocational education is another broad research topic. However, such centres address the issue of skilled workers shortage which directly affects the quality of repairs. In Norway, such training centres can often be found under cultural history and open-air museums (e.g. Buskerud, Midt-Troms, Ryfylke, Husasnotra and other museums).

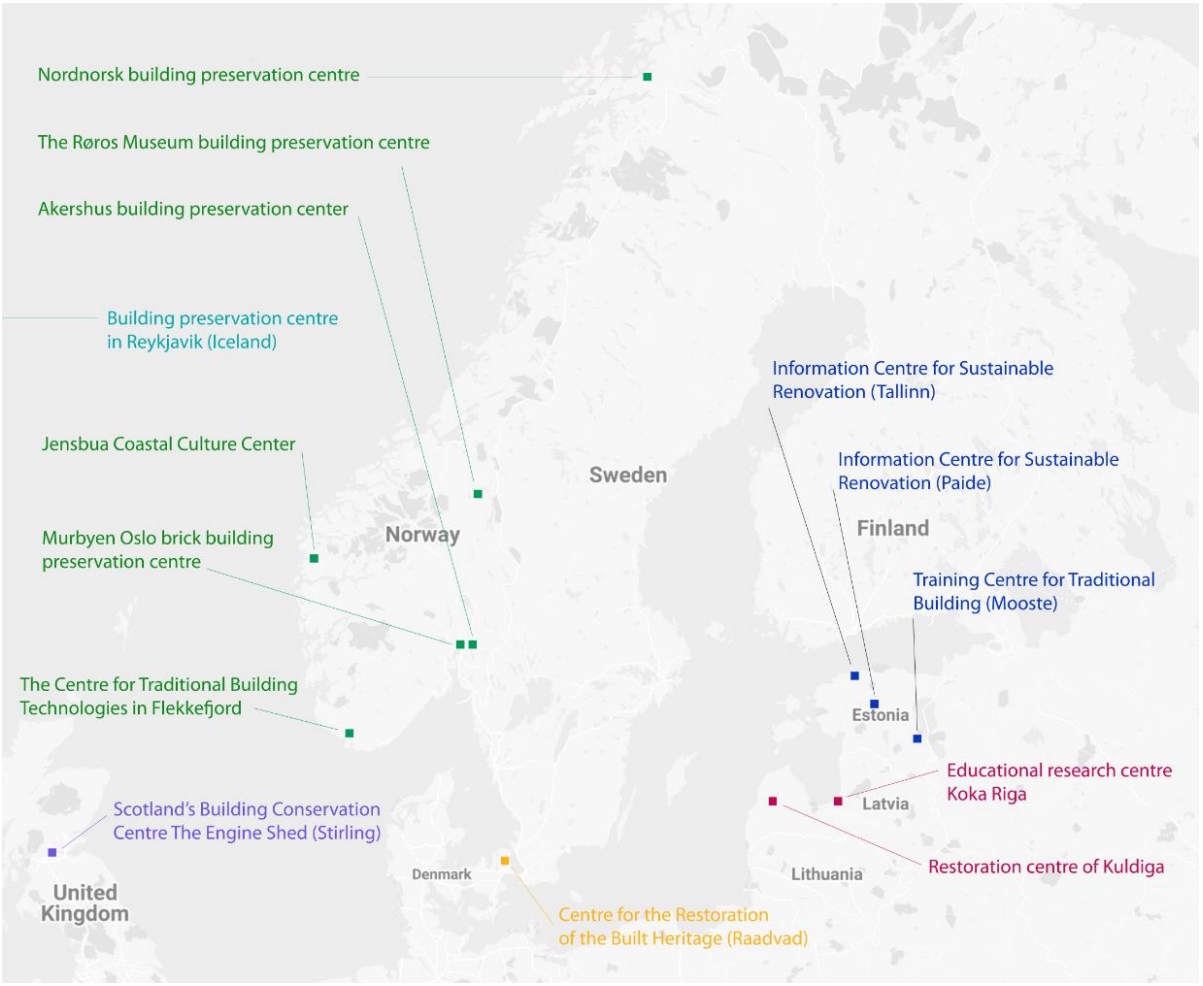


Figure 2: Locations of heritage centres. Prepared by the author.

One of the first centres to appear in the Baltic countries was the Information Centre for Sustainable Renovations (SRIK) established in 2001 in a wooden architecture neighbourhood of Kalamaja in Tallinn. It organizes trainings for heritage owners and specialists, provides consultations, delivers guidance publications and videos, organises various heritage related events. Importantly, in the same building a little shop "Majatohter" is established so heritage owners can easily get appropriate materials for maintenance and repair works. The centre has been supported by the Council (with gradually decreasing funding); it also generates some income from running the shop, from taking part in various international projects and other.

Many of the Nordic centres focus more on wooden architecture (as it is characteristic to the region) but there are exceptions. For example, the Murbyen Oslo centre specializes in historic

brick buildings (that are built around 1850-1930). Its specialists can carry out a free initial inspection to assess the condition of building's facades and common areas. Recommendations on needed works, suitable materials, experienced craftsmen, possible sources of funding are provided in person and in a brief report/ inspection note. The Centre also organizes courses, seminars and city walks. It is financed by the Ministry of Climate and Environment.

The Building Preservation Centre in Reykjavik (operational since 2007) is only open for 2 hours per week. During that time heritage professionals provide free advice on the maintenance and repair of old buildings, there are also samples of suitable products for repairs, books and magazines on architectural conservation. It is the simplest of the analysed centres but a relevant example of how a heritage centre can be run even on a small budget.

3.2 One-off campaigns

There are many examples of one-off campaigns or short-term initiatives around the world for the improved maintenance of heritage. They often emerge as a response to the lack of public attention to a specific problem. Such initiatives can also help to test ideas and their feasibility before bigger investments are made. Normally, a small geographical area and/or a very specific topic is chosen to be tackled.

Events like this are generally considered beneficial but there is not much research measuring their real impact and effectiveness in the long-run (such as application of skills acquired after the workshop is finished). To understand the impact of such short-term initiatives better, one specific case was chosen to be analysed more in depth - a cycle of practical wooden windows conservation workshops for the public that took place in Lithuania in 2016. Each workshop lasted for 4 days so that participants would be introduced to every stage of the process. The size of the group per event was limited to 20-30 persons to ensure hands-on approach. Workshops were led by experienced craftsmen; the programme was complemented with lectures and local excursions related to wooden heritage.

This specific case was chosen for the author had the experience of managing these workshops. That made it possible to get in contact with participants and learn about their experience. An online survey was created and sent in July of 2019. That was perfect timing to collect the data as three years that passed after the workshops is a period long enough to apply such skills and knowledge in practice. 37 out of 70 participants to whom it was sent completed the survey (53%).

More than half of the respondees (57%) felt capable of applying the knowledge and skills gained to repair a window on their own, and 43% actually did apply them. 8% felt that they have applied the knowledge indirectly - in the process of contracting specialists for the repair works and knowing how they want them to be done. These series of events also worked as a platform for networking. A high proportion of respondents made relevant contacts with craftsmen (43%) or used it as an opportunity to get a consultation from craftsmen on topics other than that of the workshop (41%). Around a third made useful and interesting contacts with other participants (32%).

In order to have a somewhat broader and longer lasting impact, an informational video was prepared in which every important stage of the process and recommendations by craftsmen were captured. That turned out to be a very effective measure. First, participants of the workshops found it to be a useful resource to refer to when carrying out the works on their own. Second, the video helped to reach a much broader audience – it has already been viewed over 7 thousand times [11]. Third, the leading craftsman said that a lot of people seeking for professional advice have contacted him after seeing the video and continue to do so.

The survey carried out proved that practical workshops that actively involve participants in every stage of the process can result in improved maintenance of buildings. It is not known what are the actual effects of the more commonly organized "taster sessions", i.e. practical yet shorter events that provide only a brief introduction or skip certain stages of the process.

3.3 Databases of contractors

A common issue around Europe is the lack of qualified contractors that are capable and willing to take up repair works. Many heritage owners and managers encounter difficulties when looking for a good specialist. At the same time, some contractors that are new to the market find it hard to promote their services effectively and reach their target customers. In some European countries specialized databases exist that address these issues.

In addition to the registers of qualified specialists that are more common (e.g. Register of Craftsmen in Norway *Håndverksregisteret*), new types of databases started to appear that include additional services. For example, MaintenanceBooker.org.uk (launched in 2017 by the National Churches Trust) features a competitive tendering system. When the user of the site submits a quote request, various local and national contractors are invited to bid for the job. All the bidders are companies contracted for 4 years through an open tender process in which experience, qualifications and references were taken into consideration.

The Counselling Network for Rural Architecture was created in 2015 to facilitate owners of traditional buildings in rural areas of Estonia in getting professional advice. Its website (www.maamaja.eu/) provides a list of heritage professionals (advisors and craftsmen) classified according to their specialization (e.g. roofs; stone work etc.) and the geographical area in which they operate. Importantly, all the specialists included in the database can also provide a defined counselling service. It consists of the visit to the site, provision of an initial assessment of the building's technical condition and values, recommendations on needed works, appropriate materials, suggestions on where to start, and a brief report. The cost of such subsidized consultation for the owner is set to only 30 euros + VAT + travel expenses, while the Centre of Rural Architecture pays the counsellor 120 eur + VAT. That ensures that the model is viable – financially acceptable to both the owner and the specialist. Most of the Centre's income is the support from the Ministry of Culture, the rest is generated from the organization of trainings and seminars, grants received from different foundations [12].

Such databases have not been found in places where MW services are present. However, members of MW schemes often ask to name specific contractors that could carry out the works indicated in the inspection report. They get disappointed as most of the MW organisations feel that the act of providing such recommendations would compromise their impartiality and reputation. Therefore, the existence of both models would ideally complement each other.

3.4 Conservation manuals

A lot of the information regarding built heritage and conservation is delivered in a very technical language which can discourage wider public to take interest in the subject. However, an increase in publications designed for those without academic and professional background in heritage has been observed in recent years. Among the examples seen, subjects covered include the maintenance of different parts of the building, the use of traditional materials, different types of structures, energy efficiency, guidance on legislative framework.

Their preparation and/or distribution is often one of the functions of *Monumentenwacht* type of organisations and heritage centres. For example, the Engine Shed - building conservation centre in Stirling (run by Historic Environment Scotland) - has an excellent collection of short booklets and some longer publications covering almost every possible topic. Visitors of the centre are welcome to take them free of charge. They are also accessible online on the centre's website. Since the opening of the centre in 2017, a huge number of 34,5 thousand guides has been disseminated (not including e-versions downloaded) [13].

There are also quite interactive online versions such as "Under one roof" launched in Scotland (www.underoneroof.scot) for owners of common properties and their advisers. The website provides practical information and advice on repairs, helps to understand rights, responsibilities and steps to be taken.

Written conservation guidance could be considered as the most passive of the educational - informational methods of encouraging heritage maintenance. Nonetheless, high numbers of copies being distributed show that they are of great interest to the public.

4 COMBINATION OF SUPPORT AND ENFORCEMENT

All the previously mentioned practices try to improve the condition of built environment by raising awareness, informing and educating. However, high percentages of historic buildings in poor condition suggest that such non-obligatory schemes may not be sufficient.

The Scottish House Condition Survey, carried out in 2016, found that almost half (48%) of all dwellings and 67% of pre-1919 buildings (which make up 20% of Scotland's housing stock) have disrepair to critical elements of the building fabric [14]. In Edinburgh, over 20 incidents of falling masonry are reported every month putting public safety at risk [15]. It is evident that similar situation would be found across Europe.

Obligatory maintenance of buildings could be compared to the required periodic technical inspection of vehicles. It is universally agreed that requiring owners to keep their in-use vehicles in good order has apparent benefits to the environment and the public safety. There are façade ordinances in some cities of the United States but similar laws can hardly be found in Europe. Therefore, ongoing discussions and plans to introduce tenement maintenance legislation in Scotland are of great interest in this context.

Three main interlinked proposals put forward by the Scottish Parliamentary Working Group on Tenement Maintenance (established on March 2018) are: 1) Compulsory (not optional) Owners Associations (OA) and their status enhancement to legal entities; 2) Mandatory quinquennial property inspections; 3) Creation of Building Reserve Funds (BRF).

Regular inspections and reports would inform the planning of necessary repairs and expenditure. Reports would be made accessible to existing and prospective owners, as well as tenants, neighbours and policymakers. They would include inspection conclusions, prescribed works under different categories of urgency, indicative costings and information on any grants available. BRF would ensure better control, governance and transparency than OA held funds. It would feature a possibility to invest funds and make loans to owners whose funds are insufficient; ensure long term maintenance through funds being heritable (transmittable to future owners). BRFs would be held in a specially established, national or regional level fund (a form of social investment fund).

Full monitoring of how these laws are being followed could hardly be ensured. However, there are certain control mechanisms foreseen. For example, it would not be possible to sell a tenement flat or to get a grant without an inspection report. Also, if inspection reports were to be connected with Home Reports, the level of maintenance would be visible to potential

tenants. Such situations would naturally force the owner to invest in maintenance and repairs even if not on the intervals required by law.

It is expected that it will take around ten years for this system to be fully launched due to the complexity of legislation to be introduced, the time needed to expand the pool of qualified people for inspections, to ensure the functionality of tools to be used, and to raise public awareness. From the viewpoint of Jocelyn Cunliffe (member of the Tenement Action Group), the assurance of grants' availability is key to the success of the scheme. It would motivate the owners and increase the demand for repairs, which, in turn, would ensure the vitality of the market. Ideally, fiscal incentives (such as the possibility to reclaim VAT for repairs) would also be in place [16].

5 REMARKS ON THE COMMUNICATION OF MAINTENANCE IMPORTANCE

All the discussed schemes are essentially driven by the same motives and the understanding of far-reaching benefits of regular maintenance. However, a review of communication messages in the websites of aforementioned organisations showed that an incomplete picture of preventive conservation impact is presented. Usually, communication evolves around the preservation of buildings' cultural or historical values. Other significant values and benefits (e.g. environmental) are rarely mentioned.

The global focus on climate change brought the attention to the fact that buildings and construction industry are the major drivers of energy demand and CO2 emissions. According to the 2018 data from the United Nations Environment Programme, the manufacture of building materials makes up 11% of total global greenhouse gas emissions [17]. In the heritage sector, these concerns seem to mainly manifest in increased efforts to 1) improve the energy efficiency of existing buildings through the means of insulation, and to 2) apply adaptive reuse on derelict or underused buildings. However, the potential to prolong the lives of buildings that are still in use through preventive conservation methods is not yet fully acknowledged. Aspects of embodied energy, long life-span of many original materials, the carbon footprint of construction could all be used as arguments in favour of regular buildings maintenance.

Apart from the positive impact on the environment, maintenance should also be discussed in connection to public safety, the rising value of historic properties, and the negative impact of many modern materials on human health. Researching and presenting a wider range of preventive conservation benefits would likely make the topic more engaging and relevant to the public and authorities.

5 CONCLUSIONS

Maintenance of historic buildings is being promoted by different types of organisations that apply distinct methods. *Monumentenwacht* type of organisations provide professional inspection services resulting in site specific recommendations. Necessary repairs that they indicate in condition reports require appropriate specialists. Some of the recently launched databases not only list qualified contractors but offer additional features (such as competitive tendering system) that effectively connect specialists with heritage owners. Some of the works can be carried out by the owners themselves but still require some knowledge and skill. They can be sought from heritage centres, conservation manuals and various events for the public. Practical workshops on wooden windows' maintenance were found to not only increase the appreciation of historic buildings but to actually result in improved heritage maintenance as a

large proportion of participants apply the skills in practice. In Scotland, the foreseen legislation is expected to improve generally complicated maintenance of shared properties by enforcing quinquennial inspections among other requirements.

Therefore, all the different methods should be seen as integral parts of preventive conservation system rather than alternative methods. Also, all the models require substantial financial support to be feasible. In order to attract public and private investments, benefits of preventive conservation should be explored and presented beyond the preservation of historic or cultural value.

REFERENCES

[1] Proceedings of the First International Conference Monumentenwacht in Amsterdam, Netherlands held in 2000 (2002).

[2] Monumentenwacht Netherlands. https://www.monumenten.nl Accessed July 2019.

[3] Correspondence with Viltė Janušauskaitė (Head of Projects Department at the state-owned enterprise Lietuvos paminklai; project FIXUS). July-August 2019.

[4] Vandesande, Aziliz. *Preventive Conservation Strategy for Built Heritage Aimed at Sustainable Management and Local Development* (2017), 81.

[5] Goeleven, Carolien. "Monumentenwacht" (2016). http://www.changes-project.eu/wp-content/uploads/2016/01/2016_05_26_Monza_Goedleven.pdf Accessed 30 July 2019.

[6] Proceedings of the conference "Introducing and Running Preventive Maintenance Services for Cultural Heritage Buildings", Budapest, 2014.

[7] Dann, Nigel. "Planned and Preventative Conservation & England: Experiences, Opportunities and Requirements". Preventive and planned conservation conference, Monza, Montova, 2014.

[8] Correspondence with Sonya Linskaill (manager of the TBHC) in July-August 2019, and in person interview in Edinburgh on 8 August 2019.

[9] Monumentenwacht Noord-Brabant. "Noord-Brabant Meerjarenbeleidsplan 2019-2021". https://mwnb.nl/2019/03/08/meerjarenbeleidsplan-2019-2021/ Accessed 19 July 2019.

[10] Correspondence with Viltė Janušauskaitė (manager of FIXUS) and Branislav Reznik (manager of ProMonumenta). July –August 2019.

[11] EEA Grants Lithuania. Medinių langų ir durų restauravimas. https://www.youtube.com/watch?v=UBiTWFtu58g. Accessed on 30 April 2020.

[12] Correspondense with Elo Lutsepp (Head of the Centre of Rural Architecture, Estonian Open Air Museum). August 13, 2019.

[13] Correspondence with Dorothy Hoskins, Technical Outreach and Education Manager with Historic Environment Scotland (HES). July 26, 2019.

[14] Scottish Government. "Scottish house condition survey 2016: key findings". https://www.gov.scot/publications/scottish-house-condition-survey-2016-key-findings/pages/8/ Accessed 5 July 2019.

[15] BBC News. "Very little done since Edinburgh falling masonry death". www.bbc.com/news/uk-scotland-edinburgh-east-fife-48526542 Accessed 25 July 2019.

[16] In-person interview with Jocelyn Cunliffe (architect, member of the Tenement Action Group) in Edinburgh on 30 July 2019.

[17] The European Commission. „Global Status Report 2017". https://ec.europa.eu/energy/sites/ener/files/documents/020_fatih_birol_seif_paris_11-12-17.pdf Accessed 20 July 2019.

12th International Conference on Structural Analysis of Historical Constructions
SAHC 2020
P. Roca, L. Pelà and C. Molins (Eds.)

STRUCTURAL TYPIFICATION OF HERITAGE BUILDINGS USING MODERN TECHNOLOGIES FOR DIGITAL MANAGEMENT AND VISUALIZATION: PRELIMINARY APPLICATIONS IN SOUTHERN PERU

S. HUARANGA[1*], P. PÓRCEL[1], C. YAYA[1], B. CASTAÑEDA[1] AND R. AGUILAR[1]

[1]Engineering Department, Civil Engineering Division
Pontificia Universidad Católica del Perú PUCP
Av. Universitaria 1801, San Miguel, Lima 32, Perú
e-mail: {shuaranga, pporcel}@pucp.pe; {c.yaya, castaneda.b}@pucp.edu.pe and raguilar@pucp.pe

Keywords: Structural typologies, HBIM, Augmented Reality, Andean churches

Abstract. *Structural typologies represent a group of buildings with similar geometrical configuration and seismic performance. These typologies are normally used in the preliminary stages of structural assessment of building stocks since they provide an overview of quick results which guide subsequent studies of cases that resemble the types. This article provides a methodology of structural typification using modern technologies for digitalization and visualization of information based on the study of a representative sample of 22 churches located in the South Andean zone of Peru and considered as part of Peru's Cultural Heritage. For each church, the information has been acquired and digitally modeled through the integration of reverse engineering methods and Heritage Building Information Modelling (HBIM). Furthermore, in order to improve the visualization and interaction experience, a mobile application using Augmented Reality was developed. The use of these modern techniques allowed the management of the information, which enhanced the comprehension of the churches and thus enabled its further structural analyses. As a result, it has been identified 11 structural typologies of Andean churches, based on the material of its load bearing system, their architectural form and some geometrical particularities of its structural elements.*

1 INTRODUCTION

The process of structural typification entails analyzing and classifying building stocks into types, according to relevant elements and geometrical features which influence their seismic behavior and structural capacity [2]. Structural typologies possess common attributes of the group of buildings they represent and their implementation in preliminary seismic assessment evaluations of a macroscale approach generate rapid results and guide further damage analysis [1]. Many post-earthquake studies corroborate that buildings belonging to the same structural typology behave the same manner and, consequently, develop similar collapse mechanisms [3].

To establish representative structural typologies of heritage buildings, it is important to have an adequate and standardized understanding of their structural system [4]. However, on several occasions, this information is non-existent or difficult to access due to the scarce and dispersed documentation recorded of their geometric, architectural and structural characteristics. These difficulties in understanding are intensified in the study of Andean churches because they are considered monumental buildings of complex geometry and architectural features built using multiple materials and no records of construction techniques [5].

2 MODERN MANAGEMENT AND VISUALIZATION TECHNIQUES FOR HERITAGE BUILDINGS

In recent years, rapid advances in technology have promoted the implementation of multidimensional and collaborative techniques in conservation and restoration projects of Cultural Heritage [6]. The use of these tools benefits structural assessment of ancient buildings by improving information management and visualization, which enhance their understanding and facilitates decision-making [7]. In this sense, Heritage Building Information Modelling (HBIM) and Augmented Reality (AR) are recently used in the study of heritage buildings. A proposal of the workflow of its combined employment is presented in Figure 1.

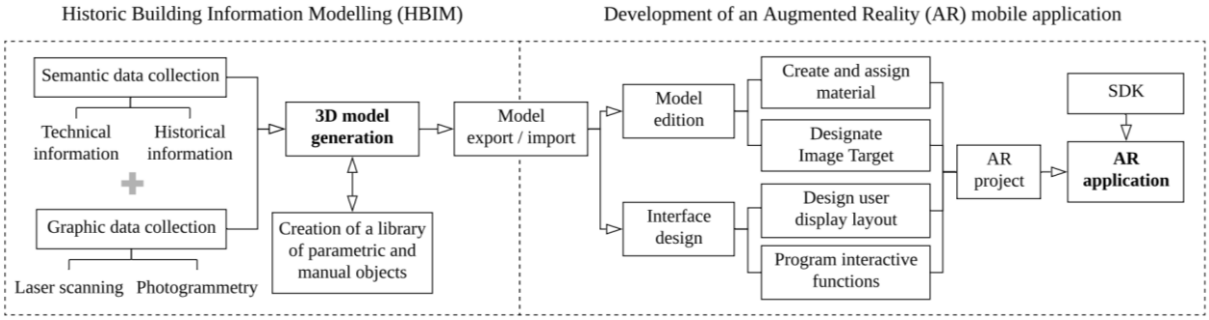


Figure 1: Procedure for digitization and representation using Augmented Reality of information from heritage buildings (adapted from [6])

Heritage Building Information Modelling (HBIM), defined as a process for creating 3D "smart" objects, is used to digitalize information concerning the buildings' architecture, structure and facility systems [7]. These models can also include additional information, such as its construction materials, conservation state or damage patterns [8], which facilitates and integrates the management of the construction processes and the maintenance of their facilities.

The combination of HBIM with reverse engineering procedures for geometrical survey in existent constructions is very attractive. In this aspect, photogrammetry and terrestrial laser scanning are commonly used, complemented with descriptive information from technical and historical sources [9], to obtain point clouds from which objects can be modeled using AEC (Architecture, Engineering, Construction) software [10]. These applications allow a virtual reconstruction of the buildings by the assemblage of smart objects that represent its structural elements. In this process, libraries of 3D objects related to databases can be make up in order to storage relevant information for subsequent analyses.

Augmented Reality (AR) is defined as the overlaying of digital information in the real world environment, improving the perception of the user and promoting real-time interaction [11]. AR can be displayed in handheld mobile devices' screen through the recognition of an Image Target [12]. To develop an AR application, is necessary to import 3D models into display engines and to carry out two steps. Firstly, 3D objects are assigned pre created materials and textures for its rendering and are designated to an Image Target. Secondly, the User Interface is designed by creating the display layout and by programming interactive functions. Software Development Kits, known as SDKs, facilitate the transition of AR projects from graphic engines to mobile operating systems (i.e. iOS or Android) where they will be executed [13]. They also allow their rendering and the tracking and the Image's Target recognition.

3 STRUCTURAL TYPIFICATION USING HBIM AND AUGMENTED REALITY

Peru is recognized as a center of diffusion and reference of the colonial architecture in Andean region [14]. The first churches were the result of the combination of forms and styles imported from the Iberian Peninsula with local contributions, influenced by Peruvian idiosyncrasy and availability of resources in the area [15]. The present investigation is restricted to churches located in the region of Cusco for two reasons. First, Cusco, as the civil, political and ecclesiastical capital of the Spanish viceroyalty, was the main reference and promoter of the development and diffusion of culture, art and architecture in the region [16]-[18]. Second, after the earthquake of 1650 an ecclesiastical provision [17] made official the use of formal architectural and structural models from Cusco as references for the churches to be restored within the city and new constructions in the Andean region [18]. In the present work, a methodology of 3 stages was used for the structural typification of churches (see Figure 2).

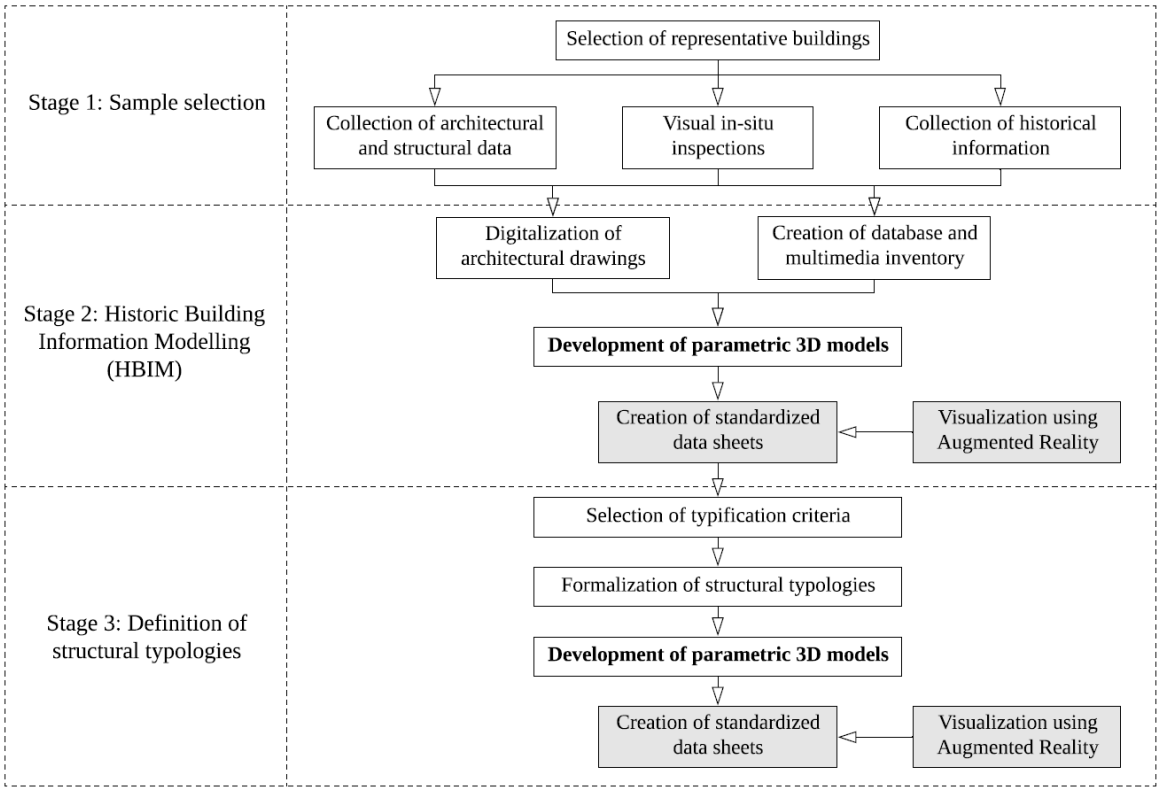


Figure 2: Methodology of structural typification using HBIM and AR

The first stage consisted on collecting information from a sample of 22 Andean churches using bibliography research and in-situ inspections. The information was digitized and stored in databases, which enabled the creation of 3D models of the churches. For each case study, a standardized data sheet including a wide description and documentation of its structural system was generated. In the third stage, the churches were analyzed and, according to three structural criteria, were typified. For each typology, 3D models were created for representing their typical and variable structural elements, which were presented in technical data sheets along with their

description. Simultaneously to these stages, AR applications were developed to visualize and interact with the smart models of both, the churches of the sample and the proposed typologies.

3.1 STAGE 1: SAMPLE SELECTION

A sample of 22 churches located in the region of Cusco was selected due to the existence of historic precedents of their influence in the construction of religious buildings in all the Andean region [15–19]. Because of their importance in the region, these buildings possess available information regarding architecture and structural features, and some of them were object of study of previous structural assessments [20, 21]. Likewise, these temples have a high tourist influx, which provides with extensive photographic records from their inside and outside. In all cases, the missing information was completed with visual inspections which were aimed at updating the architectural and structural information, revision of historical documents, and expanding the photographic record. Within this sample, 70% of the temples are located in the historical city center, while the remaining 30% belong to rural areas.

3.2 STAGE 2: HISTORIC BUILDING INFORMATION MODELLING

The records of architectural drawings obtained were digitalized on CAD and the data collected from historical and touristic sources was condensed on digital databases and multimedia inventories. With these tools, the understanding of the churches was enhanced and thus allowed the creation of standardized data sheets with the descriptions of each case study. The development of smart 3D models was carried out using Revit interface (Autodesk®). A sample of the modelling and implementation process of one data sheet and the descriptive resultant formulary is presented in Figure 3.

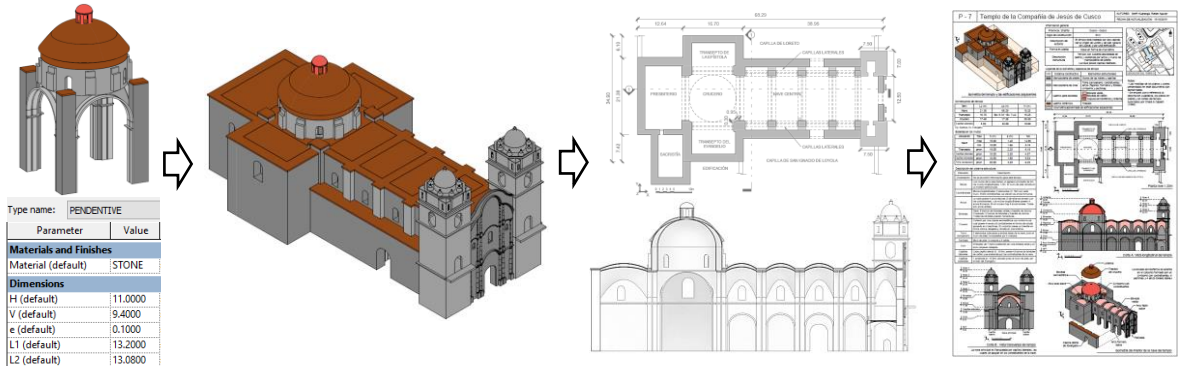
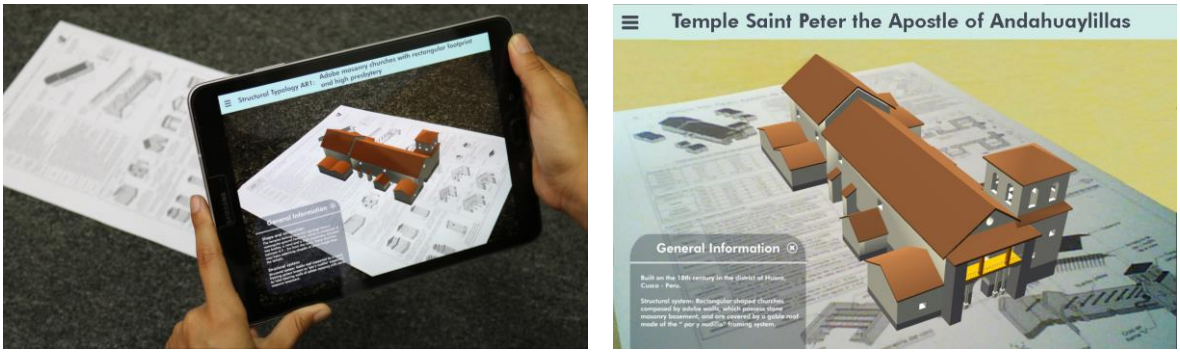


Figure 3: Inventory process of a religious building: the church of the Society of Jesus. (a) Modeling of parametric objects; (b) General 3D modeling; (c) Documentation; (d) Standardized technical data sheets

First, parametric and manual modeling of objects representing structural elements of the church were created according to the recurrence and complexity of its shape. For instance, the most common elements, such as arches or vaults, were modelled parametrically with the aim of using them on further models; whereas, particular elements, such as altarpieces or architectural details, were modeled based on the extrusion of profiles or manual creation of surfaces. The objects were then inserted and assembled in the software, in where they were

grouped according to their structural functionality and type of material. Finally, descriptive data sheets were complemented with the documentation and measures obtained from the 3D model.

The 3D models were imported into Unity [22] for the development of an Augmented Reality experience (AR). They were edited in order to assign colors and textures to its structural elements, differentiating the type of material, and matched to an Image Target, which in this case were the descriptive data sheets. Simultaneously, the user interface, where the user observes and interacts with the structural elements of the 3D model, was developed. For each element two possible interactive functions were designed: the visualization of a pop-up screen where qualitative and quantitative information of the church is displayed, and the displacement in one of the 3D axis. Finally, the engine used Vuforia and Android's SDKs to build the project for Android platform, creating the mobile augmented reality application, as shown in Figure 4.



(a) (b)

Figure 4: Augmented reality application of the church of Saint Peter the Apostle of Andahuaylillas: (a) User view from a handheld mobile device; (b) Graphic interface of the application

3.3 STAGE 3: STRUCTURAL TYPIFICATION

According to the previous survey, it was found that the churches differ mainly in its predominant construction material and in their architectural form. These two criteria influence its seismic performance and thus were selected the structural typification of Andean churches. Regarding its structural system, these buildings are composed of bearing walls made of three types of masonry (see Figure 5).



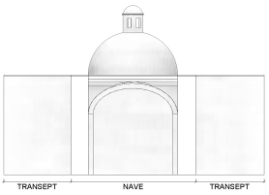
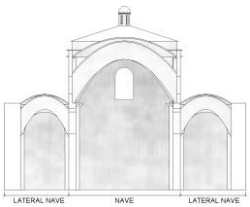
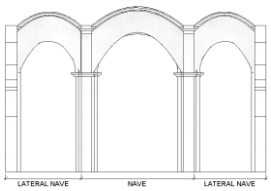
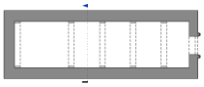
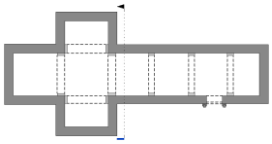
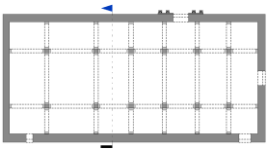
(a) (b) (c)

Figure 5: Types of masonry in Andean churches: (a) Stone masonry in Society of Jesus church; (b) Adobe masonry in St. Peter the Apostle church of Andahuaylillas; (c) Mixed masonry in St. Christopher church

Stone masonry walls are composed of rough or polished stone blocks joined with lime. Adobe masonry walls are composed of adobe blocks joined with mortar, supported by a basement of stone masonry 1-2m high. Finally, mixed masonry is defined as a combination of the two previous types, with a predominance of over 70% of adobe masonry. Within the sample, 50% of the churches possess adobe masonry walls, 32% possess stone masonry walls and 18% possess mixed masonry walls.

Secondly, the field investigation identified four categories of the architecture's distribution according to the buildings' cross section and building plan's shape (see Table 1). Rectangular shaped churches are conformed by a single nave that possess arches that support the vaults along with the bearing walls. The cross-shaped type churches are composed by a rectangular nave crossed perpendicularly by a smaller and rectangular nave called transept. The gallery where the two main axis of the naves crosses is called crossing and is usually covered by a dome, higher that the vaults of other galleries. The Basilical and Hall categories possess a main nave flanked by lateral naves. Basilical shaped churches possess lateral naves almost half of the height of the main nave, whereas Hall shaped temples possess naves with the same height.

Table 1: Categories of churches according to their architectural distribution

	Rectangular	Latin cross	Basilical	Hall
Cross section				
Building plan's shape				

Finally, three particularities of the churches' structural elements were used as final criteria in the typification: vertical irregularities between the nave and the presbytery, variations in mixed masonry and presence of side chapels along longitudinal walls. In the group of adobe rectangular-shaped churches, a subgroup of buildings with the presbytery elevated between 1-2 m above the nave was identified. In this case, the presence of triumphal arches at the intersection of the nave and the presbytery is permanent, whereas elongated nave temples are characterized by occasionally having the triumphal arch. In mixed masonry churches, two possible wall's composition were observed: the existence of high foundations, almost half the height of the wall, and facade walls made entirely of stone masonry. Finally, in stone churches, it was observed that the presence of side chapels, defined as rooms with spans no greater than 1-2m, modify the continuity of the churches' longitudinal walls in order to connect them with the nave. The wall's variation depends on their architectural distribution. For example, rectangular-shaped churches possess walls with a gap at the middle of the nave (see typology SR-2 of Table 2), whereas cross-shaped and hall-shaped churches possess continuous walls with big openings (see typologies SLC-2 and SH of Table 2). In both cases, the load of the roof

at the discontinuous sections are concentrated to the internal arches of the nave, which are normally reinforced in the outside by aligned buttresses.

Based on these criteria, 11 structural typologies were identified within the study sample, as shown in Figure 6 and Table 2. In the schematic 3D views, stone and adobe masonry and bricks are differentiated by the usage of colors that resemble these materials. Moreover, the exterior variable elements of each typology, such as bell towers or adjacent chapels, are set apart from typical structural elements by being colored by a light gray tone. The typologies SR-2, SLC-2 and SH present their adjacent chapels extruded from their original position to show their effect on the continuity of longitudinal walls.

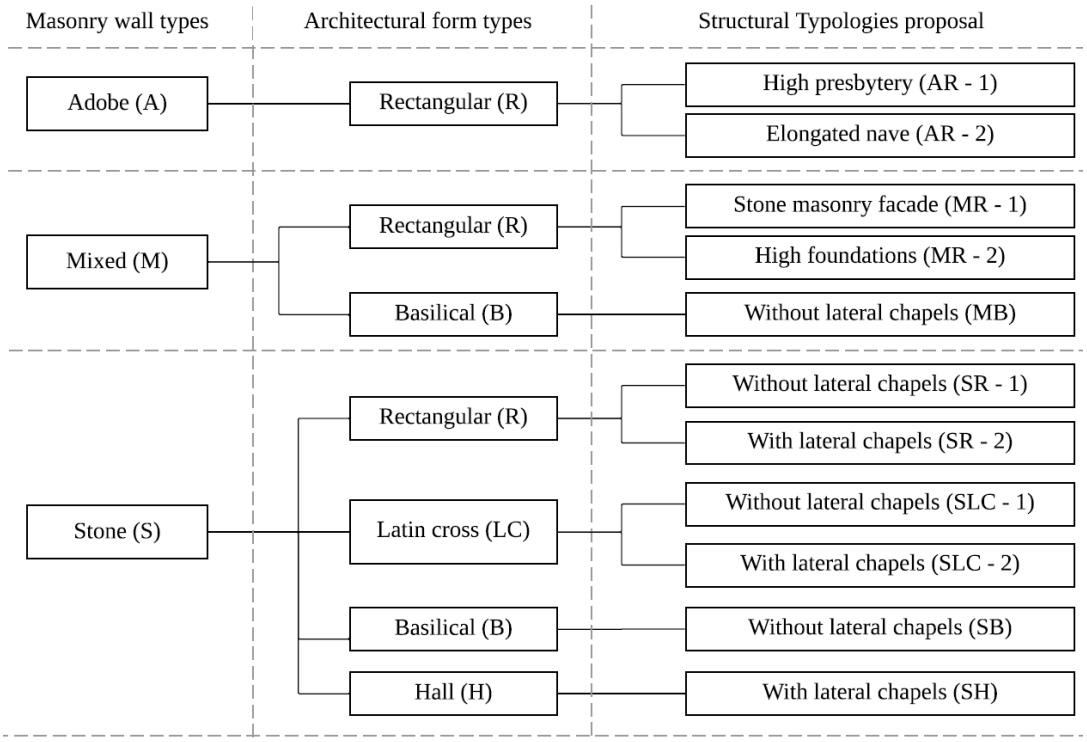
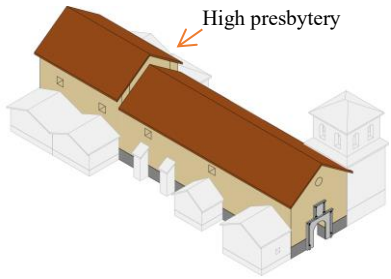
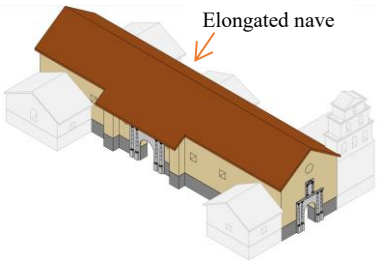
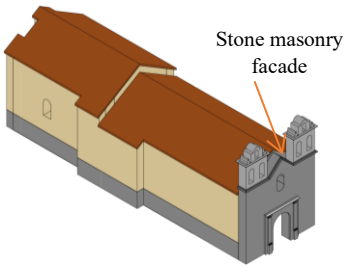
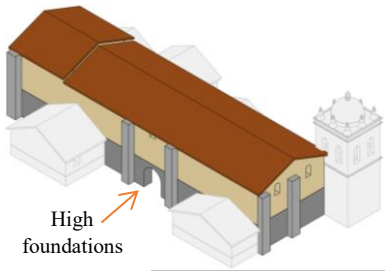
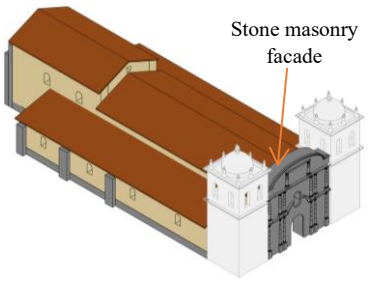
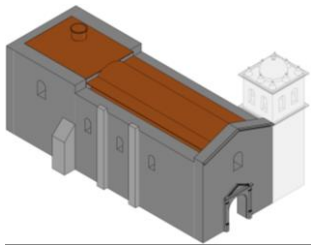
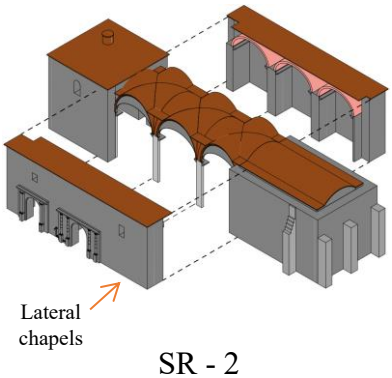
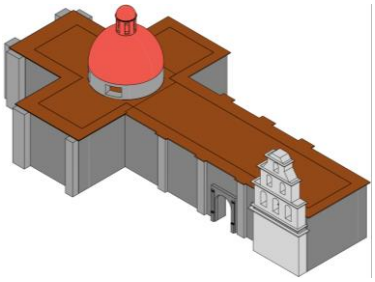
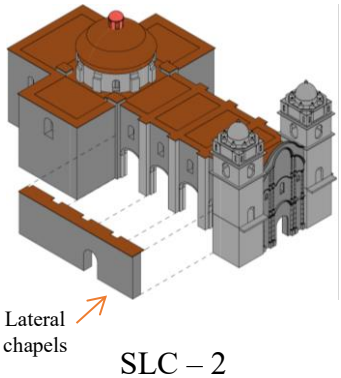
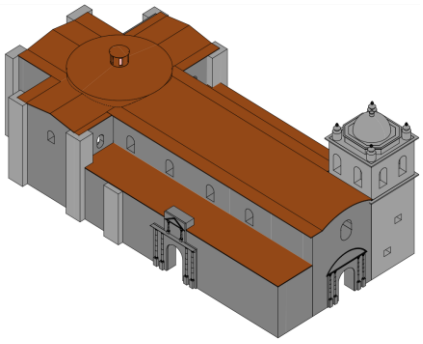
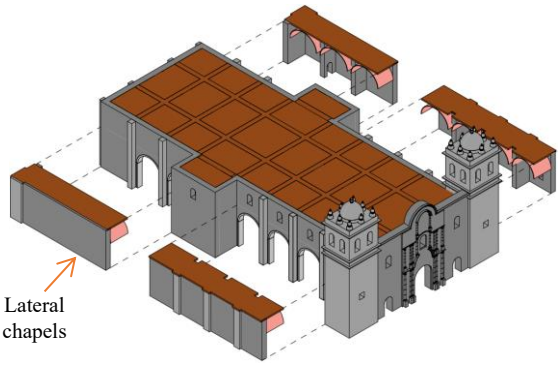


Figure 6: Summary of proposed structural typologies

The process of developing the AR application of the structural typologies is similar to the application made for the 22 sample churches. The differences lie in the interactive functions of the user interface given that the description of structural typologies is more extend due to typical and variable characteristics they represent from their group. The application uses the descriptive standardized sheet as Image Target, as seen in Figure 8a. The general information of the type and the description of its structural elements can be displayed from the main menu, located next to the title of the application. Typical and variable elements of the typologies can be displayed by using it correspond button, as shown in Figure 8b. The names of the structural elements are shown in labels the user can click in order to see more details: a window with further descriptive details appears at one side of the screen and the structural element is highlighted from the rest of the temple (see Figure 8c). In the case of variable structural elements, such as bell towers, choirs or facades, the emergent window includes information and schemes of their possible variations (see Figure 8e).

Table 2: Schematic 3D views of the proposed structural typologies

 AR – 1	 AR - 2	 MR - 1
 MR - 2	 MB	 SR - 1
 SR - 2	 SLC - 1	 SLC – 2
 SB	 SH	

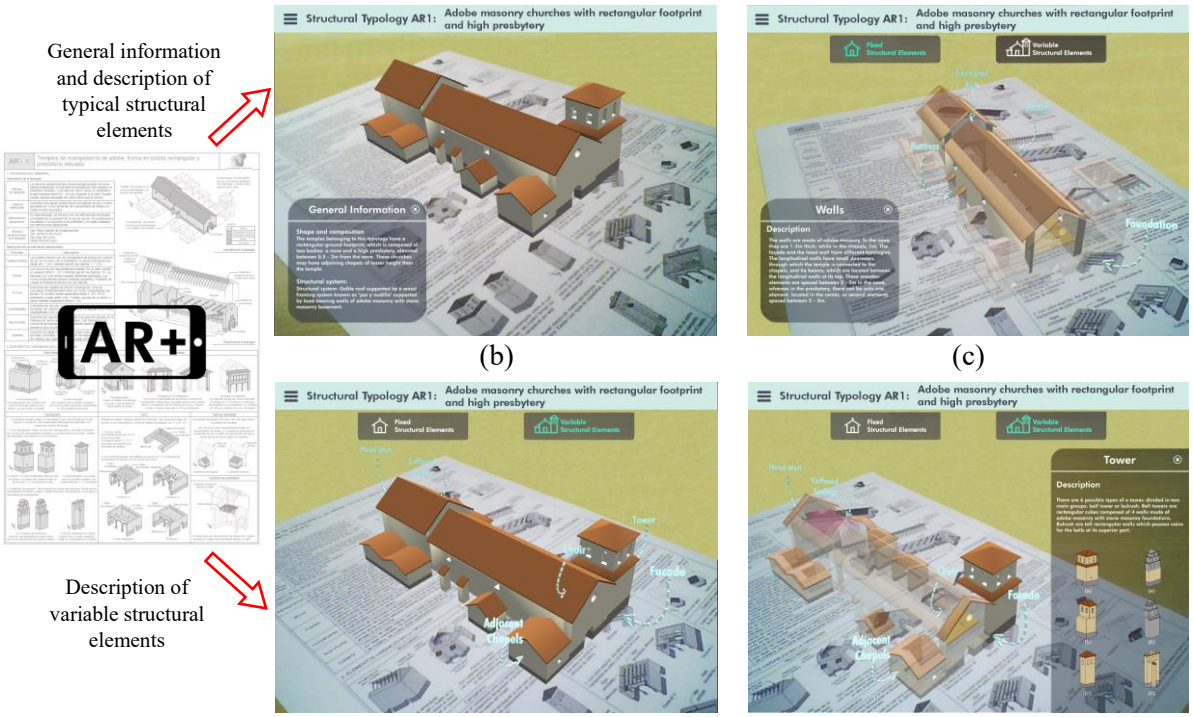


Figure 8: AR application of the structural typology of adobe masonry churches with rectangular shape building plan and high presbytery (AR - 1): (a) Data sheet used as Image Target; (b) General information; (c) Display of typical structural elements - walls; (d) Labels of variable structural elements; (e) Display of variable structural elements – Bell Towers

4 CONCLUSIONS

In preliminary seismic assessment of heritage building stocks, structural typologies are used as classification systems that enable the identification of relevant and frequent building types in national scales. This investigation provides a methodology of structural typification implementing HBIM and Augmented Reality to enhance the information management, description and visualization of heritage buildings. As a result, 11 structural typologies were established, and its typical and variable structural elements were described and documented in standard technical sheets. Furthermore, these sheets were assembled in a condensed repository of data storage interconnected to smart 3D objects' libraries. This investigation adds value to subsequent individual studies of these churches by providing relevant information of their structural system and 3D models that can be used in further numerical evaluations, so manual and time-consuming modelling does not need to be carried out. The development of the Augmented Reality (AR) application was crucial for visual representation and interaction of the digital information modelled. The irregularities and complex morphology of the studied churches can be easily understood by the dynamism and interactivity that the application provides through its user interface and functions. The quantification of the impact of the application on non-specialist users will determine the effectiveness of the method proposed and shall give a lead on the improvement and refinement of the AR application. Future works should

also consider the validation of the proposed structural typologies for its implementation in international scales.

Acknowledgements. This research was performed by the Laboratory of Engineering and Heritage at PUCP. The authors acknowledge the funding provided by DGI-PUCP in the framework of the project Nº 2018-601.

REFERENCES

[1] Rusell, A. Characterization and seismic assessment of unreinforced masonry buildings. PhD thesis, University of Auckland: Auckland, New Zealand (2010).
[2] ICOMOS. Recommendations for the analysis, conservation and structural restoration of architectural heritage. *Paris International Council on Monuments and Sites* (2001).
[3] NIKER (New Integrated Knowledge Based Approaches to the Protection of Cultural heritage from Earthquake-induced Risk). Deliverable 3.1: Inventory of earthquake-induced failure mechanisms related to construction types, structural elements and materials. Università di Padova - European Commission (2010).
[4] ICOMOS. Principles for the analysis, conservation and structural restoration of architectural heritage. *Paris International Council on Monuments and Sites* (2001).
[5] Augusti, G., Ciampoli, M. and Giovenale, P. Seismic vulnerability of monumental buildings. *Structural Safety,* 23 (2001), 3: pp. 253–274.
[6] López, F., Lerones, P., Llamas, J., Gómez-García-Bermejo J. and Zalama E. A review of heritage building information modeling (H-BIM). *Multimodal Technologies and Interaction*, 2 (2018), 2: pp. 21.
[7] Murphy, M., McGovern, E. and Pavia, S. Historic building information modelling - Adding intelligence to laser and image based surveys of European classical architecture. *ISPRS Journal of Photogrammetry and Remote Sensing*, 76 (2013), pp. 89–102.
[8] Pocobelli, D. P., Boehm, J., Bryan, P., Still, J. and Grau-Bové J. BIM for heritage science: a review. *Heritage Science,* 6 (2018), 1: pp. 30.
[9] Yastikli, N. Documentation of cultural heritage using digital photogrammetry and laser scanning. *Journal of Cultural Heritage*, 8 (2007), 4: pp. 423–427.
[10] Logothetis, S., Delinasiou, A. and Stylianidis E. Building information modelling for cultural heritage: a review. In: ISPRS Annals of the Photogrammetry, Remote Sensing and Spatial Information Sciences: *25th International CIPA Symposium,* Taipei (2015).
[11] Van Krevelen, D. W. F. and Poelman, R. A survey of augmented reality technologies, applications and limitations. *Int. Journal of virtual Reality,* 9 (2010) 2: pp. 1–20.
[12] Linowes, J. and Babilinski, K. *Augmented Reality for Developers: Build practical augmented reality applications with Unity, ARCore, ARKit, and Vuforia*. Packt Publishing (2017).
[13] Amin, D. and Govilkar, S. Comparative study of augmented reality SDKs. *Int. Journal on Computational Sciences & Applications,* 5 (2015), 1: pp. 11–26.
[14] Chara, O. *Arquitectura religiosa española en la ciudad del Cusco en los siglos XVI-XVII ('Spanish religious architecture in the city of Cusco in the 16th-17th centuries')*. Cabildo Insular de Fuerteventura Vol II. (1992), 5: pp. 367–388.
[15] Chara, O. and Caparó, V. *Iglesias del Cusco : historia y arquitectura ('Churches of Cusco : history and architecture')*. Universidad Nacional San Antonio Abad del Cusco (1998).

[16] Cosme, C. La influencia hispano árabe en la arquitectura peruana ('The Hispanic-Arabic influence on Peruvian architecture'). *Revista de Arquitectura,* 3 (2016), 1: pp. 99–118.
[17] Municipalidad del Cusco. *Cusco y la herencia del barroco andino ('Cusco and the Andean Baroque heritage')*. Cusco (2013).
[18] Segre, R. *América Latina en su arquitectura ('Latin America in its architecture')*. Siglo XXI editores (1996).
[19] Kubiak, E. La iglesia de los Jesuitas en Cusco como un modelo para la arquitectura de la región ('The church of the Jesuits in Cusco as a model for the architecture of the region'). *Latin American Art, 2* (2012), pp: 35-66.
[20] Marques, R., Ivancic, S., Briceño, C., Aguilar, R., Perucchio, R. and Vargas, J. Study on the seismic behaviour of St. Peter the Apostle Church of Andahuaylillas in Cusco, Peru. In: Proc of the SAHC 2010: *7th International Conference on Structural Analysis of Historical Constructions*, Mexico (2014), pp: 14-17.
[21] Aguilar, R., Noel, M. F. and Ramos, L. Integration of reverse engineering and non-linear numerical analysis for the seismic assessment of historical adobe buildings. *Automation in Construction,* 98 (2019), pp: 1-15.
[22] Unity 2019. Unity Technologies user's Manual, release 2019.2.13f1. United States.

12th International Conference on Structural Analysis of Historical Constructions
SAHC 2020
P. Roca, L. Pelà and C. Molins (Eds.)

THE ISCARSAH GUIDELINES ON THE ANALYSIS, CONSERVATION AND STRUCTURAL RESTORATION OF ARCHITECTURAL HERITAGE

PERE ROCA

On behalf of the ISCARSAH Subcommittee on the Guidelines

Universitat Politécnica de Catalunya (UPC-BarcelonaTech)
Jordi Girona 1-3, mod. C1, 08034 Barcelona, Spain
e-mail: pere.roca.fabregat@upc.edu, www.upc.edu

Keywords: Historical Structure, Architectural Heritage, Structural conservation and restoration

Abstract. *The paper introduces the main concepts and criteria presented in the Guidelines on the Analysis, Conservation and Structural Restoration elaborated by the ICOMOS/ISCARSAH committee. The guidelines have been developed with the aim to provide guidance to experts and practitioners working in the study and conservation of structures or the architectural heritage. The guidelines are based on the ICOMOS Charter on the Principles for he Analysis, Conservation and Structural Restoration of Architectural Heritage elaborated by ISCARSAH and adopted by ICOMOS in 2003. The guidelines are intended to assist the multidisciplinary teams involved in the management of historical structures across all the stages of the study and operation, including the investigation and documentation works, the structural verification and the selection and design of appropriate minimum interventions.*

1 THE ICOMOS /ISCARSAH COMMITTEE AND THE GUIDELINES

The International Scientific Committee on the Analysis and Restoration of Structures of Architectural Heritage (ISCARSAH) was founded by the International Council on Monuments and Sites (ICOMOS) in 1996 as a forum and scientific network of engineers, architects and scientists dealing with the structural dimension of monuments and historical constructions. The committee's focus is on the study and the conservation of the structures of cultural heritage buildings. The committee counts at present with more than one hundred international members.

The committee has been responsible for the elaboration of the ICOMOS Charter on the Principles for he Analysis, Conservation and Structural Restoration of Architectural Heritage [1] (ISCARSAH Principles) adopted by ICOMOS in October 2003. The ISCARSAH Principles, largely disseminated at the international level, have been translated to French, Italian, Spanish, Turkish, Arabic and other languages.

Jointly with the Principles, the ISCARSAH Committee has been working in a set of guidelines oriented to assist researcher and practitioners in the application of the Principles and, more generally, in the study of ancient structures across all its stages, including the investigation and documentation activities, the structural verification and the design of interventions. The

ISCARSAH guidelines have been written with the aim to provide guidance to the multidisciplinary teams involved in the study and conservation of historical structures.

The approval in 2010 of Annex I on Heritage Structures of ISO13822 on Assessment of Existing Structures [2], elaborated with the contribution of ISCARSAH members, constituted an important step towards the dissemination of advanced concepts and practice on the study and restoration of historical structures. The ISCARSAH guidelines have been elaborated taking into account different relevant documents, including the Venice Charter of 1964 [3], the Nara Document of 1994 [4] and ISO13822 [2] along with the ISCARSAH Principles [1].

Following the ISCARSAH Principles and Annex I of ISO13822, the guidelines recognize that historical structures have cultural value in themselves and therefore their conservation must encompass the preservation of all tangible and intangible heritage values that contribute to their authenticity and cultural dimension. The structure is regarded as an essential part of the building's cultural legacy.

The guidelines are based on the premise that a combination of both scientific and cultural insight and knowledge is indispensable for the study and care of the architectural heritage. The necessary insight and knowledge are provided by the different experts integrated in the multidisciplinary team. The guidelines are also based on the understanding that, within such a multidisciplinary approach, structural engineering can provide the technical support necessary to safeguard the structure not only as a functional device but also as a cultural asset.

2 HERITAGE VALUES

It is understood that the conception of the studies and the design of interventions must be based on a previous identification of the heritage values attributable to the historical structure. Therefore, one of the first sections of the guidelines is devoted to the identification of the character defining elements that contribute to the cultural and heritage values of historical structures.

The multidisciplinary team, including architects, engineers, historians, archaeologist and other specialists should be responsible for the identification of the cultural heritage values. As for any cultural resource, the authenticity and the heritage values of a historical structure encompass both tangible and intangible values. Among the tangible character-defining elements, providing heritage value, are the geometry, the materials, the overall structural organization, the construction details and connections, the location and setting (the environment). Imperfections and alterations may be also identified as character-defining elements, and should be respected provided that they do not compromise the safety requirements or the structure's durability. Among the intangible character-defining elements are the construction traditions and techniques, the structural concepts, the original (and subsequent) use and function, and the sources of evidence on ancient knowledge and technology. The spirit and feelings conveyed by the historical construction are also regarded as an intangible character-defining element.

The identification of the character-defining elements and the assessment of the heritage values are of upmost importance for the design of minimum interventions. The evaluation of the impact of the interventions on heritage values is a critical operation in the application of the scientific and engineering approaches presented in the following sections.

3 MINIMUM INTERVENTION

A key concept referred to in the guidelines is that of the minimum intervention. A minimum intervention is the defined as an intervention that optimally combines compliance with structural requirements with the maximum possible protection and enhancement of heritage values and respect to the structure's authenticity. The guidelines provide significant attention to the concepts and procedures concerning investigation and operation which may lead to an adequate minimum intervention. In any case, the definition of minimum intervention involves the need to assess the impact that any intervention will have on the heritage values, which in turn requires to provide criteria on how such evaluation may be performed.

In addition to preserving the structure's authenticity and heritage values, minimum interventions are also desirable for other meaningful reasons. On one hand, excessive unnecessary alteration (incurred by a non-minimum intervention) is not advisable because the modified structure may develop a response difficult to predict, especially in the case of earthquake, with potential undesirable consequences. Furthermore, solutions causing a significant alteration may be very difficult or impossible to remove, therefore compromising later improvements or future new interventions, as dictated by the principles of removability or re-treatability later discussed.

In the guidelines, and based on large previous experience by ISCARSAH members, structural performance and conservation are regarded as complementary conditions leading to convergent optimum operations through the concept of minimum intervention. Rather than being in contradiction, it is understood that, often, the most adequate interventions from a structural point of view are also the ones better respecting the authenticity of the ancient structure.

4 PROPOSED APPROACH

It is understood that an acritical application of codes and standards not specifically oriented to heritage structures may lead to erroneous conclusions on their structural condition and intervention needs. In specific, the rigid application of seismic and geotechnical codes may lead to misinterpret the resistant nature and real capacity of the historical structure and to apply drastic and unnecessary strengthening measures. Similarly, conventional methods for structural analysis oriented to new construction are often based on hypothesis on the structural behaviour that may not be applicable to historical structures.

While the overdesign caused by conservative approaches may be acceptable for new construction, a too conservative approach to structural safety may not be acceptable in the case of heritage structures due to excessive and unjustifiable cost in terms of loss of authenticity and cultural value. Actions that are not indispensable for the safeguarding of the building should be avoided.

In an attempt to overcome the aforementioned difficulties, a different approach is proposed strongly based on the scientific method. The approach proposed integrates qualitative and quantitative evidence through the combination of a set of complementary activities. These activities are:

- Historical research, based on the study of the relevant historical facts on the structure

through the investigation of all kind of documentary sources.
- Inspection consisting in the characterization of the current condition and properties of the materials and structure through surveys and investigations.
- Monitoring, based on the observation of the response of the structure over a period of time.
- Structural analysis, consisting in the quantification of the response of the structure by means of a sufficiently accurate and calibrated structural model. Calibration and validation of the model is done by comparison with empirical information provided by historical investigation, inspection and monitoring according to the approach later described.

These activities are consistently developed across the different phases of the study, which include

(1) the assessment and investigation works, oriented to identify the causes of damage (diagnosis) and to conclude on the structure's conservation condition,
(2) the structural verification, involving the characterization of the structural performance and the identification of the intervention needs, and
(3) the design of the intervention, including the identification and full definition of optimal remedial solutions.

5 ASSESMENT. INVESTIGATION AND DOCUMENTATION WORKS

The first phase of the study includes all the necessary investigations to conclude on the current condition and causes of decay and damage. For this purpose, it is important that the investigating team incorporates the wide range of skills that may be necessary for a sufficiently deep understanding of the structure and its problems. The process leading to the necessary knowledge is based in the integration of the activities mentioned in the previous paragraph (Fig. 1). Historical research may provide precious information on the original features of the structure and latter historical facts or events having had a sensible impact on it. Inspection involves all the necessary activities to characterize the current properties and condition of the structure. Monitoring may provide quantitative information on the evolution of the response of the structure along the monitored period. Finally, structural analysis can contribute to the characterization of the response of the structure for a variety of conditions and actions.

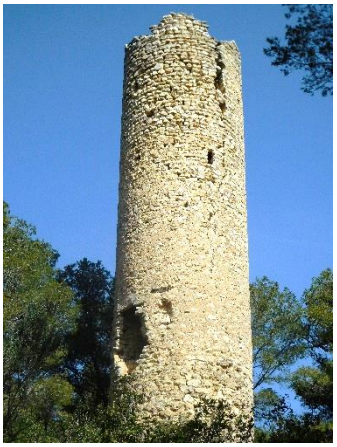
Historical research is regarded as an essential activity that may provide valuable information on the original features of the structure and latter historical events having had impact on it. Aspects to investigate are the stricture's historical and cultural significance, the original construction materials and procedures, the subsequent changes affecting both the structure and its environment, historical natural actions (such as earthquakes) or anthropogenic ones, and past restoration works.

The inspection works can be divided into two different stages, corresponding to (1) the survey of the structure by direct observation and measurements and (2) in situ and laboratory testing. The main objectives of inspection by direct observation include the characterization of the construction and structural features, the identification of ongoing environmental effects and the identification and mapping of damage. The preliminary inspection of the building allows

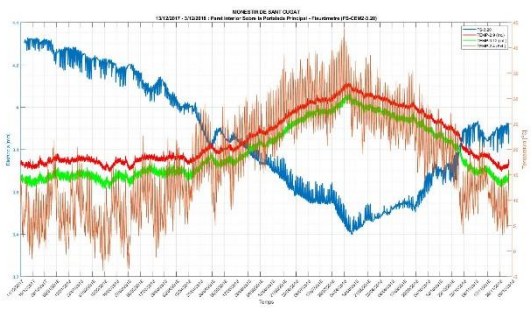
also the location of adequate spots for the performance of geophysical surveys, the execution of Non-Destructive Tests (NDTs) and Minor Destructive Tests (MDTs) and the extraction of samples to be tested in laboratory. As part of the direct observation stage, decisions should be taken on immediate risks and the need for urgent stabilization measures. The second inspection stage (in situ and laboratory testing) involves a detailed characterization of the materials and structure, including their deterioration processes.



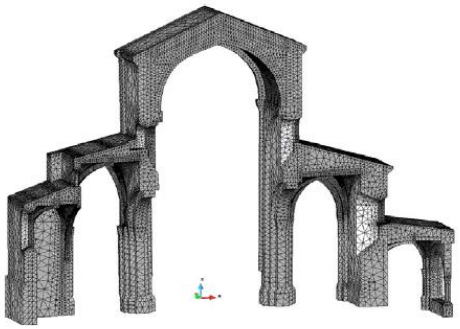
Historical research – Reconstructing the past



Inspection – Charactering the current condition



Inspection – Identifying the current trends



Structural analysis – Simulating past actions

Figure 1: The activities than can be integrated during the investigation and diagnosis phase to draw conclusions on the causes having induced damage and the present structural condition

The guidelines distinguish between static monitoring, consisting in the recording of structural parameters (such as displacements, rotations, crack openings, stresses, etc. …) over a long period of time, and dynamic monitoring, used to record the response of the structure during the occurrence of seismic events, strong wind episodes or other episodic (normally dynamic) actions. Some criteria are provided on how to apply both types of monitoring. In specific, regarding static monitoring, some requirements are mentioned as necessary for an adequate post-processing and interpretation of the registered data. These requirements are (1)

the identification of the critical variables (movements, crack widths), (2) the measurement of not only structural parameters (as crack openings) but also environmental ones (wind speed, temperature and humidity) and (3) a sufficiently long monitored period. Monitoring may be oriented to either survey the evolution of a non-intervened structure or to assess the effectiveness of a possible intervention.

During the diagnosis phase, structural analysis can be utilized to investigate the performance of the structure under past actions. These actions may include gravity loads, earthquake, wind, soil settlements, chemical or physical attack, anthropogenic alterations and thermal cycles, among other. Structural analysis can be utilized to characterize the possible contribution of different actions to existing damage and possible partial collapses. Structural analysis always involves the adoption of a model whose hypotheses and assumptions should be carefully chosen and taken into consideration in the interpretation of the results.

6 ASSESSMENT. STRUCTURAL PERFORMANCE VERIFICATION

The guidelines recognize that the structural verification of a historical structure constitutes a genuine problem posing significant challenges to the analyst. In any case, it is a problem fully encased within engineering understanding and equally solvable by means of engineering approaches, even if the contribution of the multidisciplinary team is of upmost importance. According to the guidelines, the verification of heritage structures involves a multi-dimensional problem in which the conventional and ultimate limit states are considered along with the safeguarding of the possible valuable artistic contents and the preservation of the structure's authenticity and cultural value. Therefore, the adequate performance of the structure must be evaluated taking into account three related targets:

(1) The safety of people at risk
(2) The maximum possible safeguard of valuable immovable cultural and artistic contents
(3) The integrity of the structure as a cultural heritage object

Objectives (1) to (3) will lead to the definition of the acceptable damage levels and the target reliability levels to be considered in the structural verification.

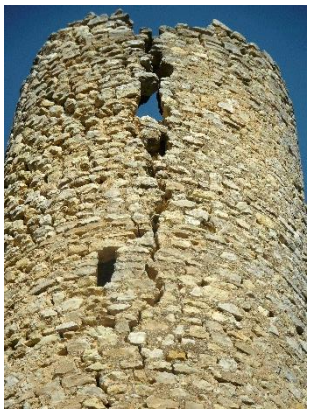
In the presence of very valuable paintings or frescoes fixed to walls or vaults, or other immovable cultural contents, and as suggested by the Annex I of ISO13822, condition (2) may be implemented through the consideration of specific serviceability limit states oriented to control deformation and damage.

In some cases, and as also indicated by Annex I of ISO13822, the protection of the structure's cultural value may lead to the acceptance of reliability levels lower than those implicit in building design codes. In these cases, parallel measures such as restricted use or provision of alternate escape routes must be adopted to limit the consequences of a failure on people. The method presented in section 7.3 provides a certain understanding on the situations that may require the reconsideration of the acceptable reliability levels.

The structural performance verification is also based on the general approach described in section 4 and integrates similar activities. Four different approaches can be considered (Fig.2):

- Historical approach, based on the investigation of the past performance of the structure.

- Qualitative (or comparative) approach, based on the comparison of the structure being analysed with a number of similar constructions whose behaviour is already understood.
- Experimental approach, consisting in the execution of on-site experiments aimed to measure the load capacity of structural members.
- Analytical approach, based on the use of structural analysis to predict the performance of the structure under future actions.



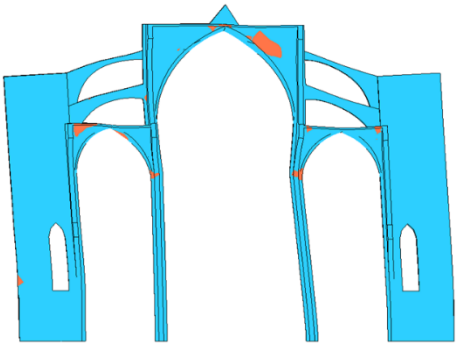
Historical approach –
Investigating the past performance



Qualitative approach –
Learning from similar buildings



Experimental approach –
Carrying out experiments on structural members



Analytical approach –
Modelling to investigate the structural response

Figure 2: Different approaches that can be activated and integrated to conclude on structural performance

In the context of the structural performance verification, structural analysis is regarded as a deductive procedure in which the information on the structure, morphology and actions is invested (as input data) in constructing a structural model which is then used to predict the structural performance under future actions.

It is recognized, however, that structural analysis may suffer from significant uncertainty due to the fact that their reliability depends largely on the representativeness and realism of the adopted mathematical formulations. It is also recognized that data are always limited and liable to uncertainty. Often, the amount of data available are largely insufficient for a complete definition of a model. Due to these uncertainties, models must be always calibrated using the

available evidence on the performance and condition of the structure. This evidence may be provided by historical analysis, inspection and monitoring. However, a full validation is not actually possible and significant uncertainty may remain in spite of the calibration effort. Engineering judgment is therefore necessary to evaluate the feasibility and reliability of the predictions and the correct use of the entire procedure leading to model construction, calibration and prognosis.

The guidelines devote a full section to the approaches and technical possibilities for model calibration. Among other possibilities, this section refers to calibration by comparison of the numerical predictions with existing crack patterns, historical past performance, stress states as measured by means of flat-jack tests (or other procedures), dynamic response or static monitoring response.

The activation of the above four approaches also requires for a methodology or criteria for the integration of their possible outcome. Several criteria are provided on how to combine and integrate the approaches. Such criteria consist on the principles of consistency, completeness and corroboration. Consistency refers to the need for identifying possible contradictions among the information provided by the approaches (the "plausibility check"), in which case improved investigations are needed until the contradictions are explained and solved. Completeness concerns to the need to obtain the necessary and sufficient information on the relevant variables of the problem. Corroboration refers to the convenience or need for redundant evidence provided by the different approaches as a way to confirm the information inferred. When the evidence obtained through the different approaches does not satisfy the above criteria, additional effort may be needed to improve the methods applied and the information obtained. In any case, the process leading to the verdict on the structural performance, based on the synthesis of the approaches, is not formalized and lies strongly on engineering judgment.

7 INTERVENTION

7.1 Intervention criteria

A set of criteria or principles oriented to better identify and develop adequate minimum interventions are provided and discussed. Some of these criteria are in fact well known and are currently adopted in studies or projects on interventions in historical structures. Among them are the principles of *compatibility* with the original material and techniques (including chemical, physical, mechanical, rheological and thermal compatibilities), *durability* of the repair or reinforcing materials, *non-invasiveness* and *removability* of the devices or technologies used for strengthening.

According to the removability criterion, it must be possible to remove and replace the adopted measures. Replacement of the measures may be necessary when the former ones do not prove sufficiently efficient or to implement a more technologically advanced and respectful solution. Removability implies that the dismantlement of the intervention will only generate limited and repairable deterioration on the original construction.

A new criterion, designed as *re-treatability*, is introduced in the guidelines. According to it, any intervention should be designed in such a way that it does not compromise future interventions. This principle is of upmost importance when the technologies utilized do not comply with the aforementioned principles, and especially with non-invasiveness and

removability.

According to the criterion of *controllability*, it must be possible to control the intervention during its execution. Measures that are impossible to control should not be allowed.

Last but not least, the guidelines refer to the principle of *sustainability*, according to which restoration projects should be mostly based on sustainable materials and technologies with low environmental impact during their life cycle.

It is recognized that applying all the mentioned criteria in a simultaneous and strict way may be difficult or impossible in practice. Instead, the criteria should be regarded as convenient guidelines or inspirational principles to be applied to the extent possible in the design of solutions approaching the concept of minimal intervention. For instance, lime mortar grouting for the consolidation of masonry walls may be regarded as an acceptable (even very satisfactory) solution in spite of its invasive character due to its proven durability and compatibility. In turn, strengthening solutions using a material with limited durability (as steel) may be acceptable if they are applied in a non-invasive and removable way and can be regularly inspected and maintained.

7.2 Pro and post natural hazards structural maintainability

The concept of structural maintainability is a novel contribution of the guidelines. The inspiration of the concept lies on real practices undertaken traditionally in seismic regions. In such locations, historical structures have been subjected to repeated repair or strengthening operations during their history. Rather than introducing drastic transformations, the traditional practice has mostly involved regular operations consisting in repair and maintenance. In a similar way, it is understood that the modern approach to seismic resistance of historical structures should base on an extended concept of maintenance allowing the preservation, as far as possible, of the original construction characteristics. Structural maintainability is defined as a continuous maintenance programme involving minimal repair or strengthening operations undertaken after each earthquake. Such interventions should be designed so that they do not hinder future ones. The concept of structural maintainability is intended to facilitate the application of the principle of minimum interventions to the case of buildings affected by earthquake and other natural hazards.

7.3 Proposed engineering approach to the design of the intervention

The proposed approach for the selection and design of interventions is summarized in the flowchart of Fig. 3. The approach is based on the common engineering procedure consisting of envisaging and evaluating a set of alternative solutions. It is also based on the evaluation of the impact of the different alternatives on the heritage values.

After the definition of the reliability levels, a number of alternative solutions may be envisaged satisfying as far as possible the criteria presented in section 7.1. All these solutions should attain the targeted structural reliability levels. In addition, all solutions must be evaluated regarding their impact on the heritage values. Among these solutions, the one causing the minimum impact to heritage values should be selected. If the impact of this solution is sufficiently small (in the sense that its benefit largely surpasses its impact on heritage values), then this solution can be considered as a satisfactory minimum intervention. Otherwise, if the impact on the heritage values is deemed excessive, the adopted structural requirements may be

reconsidered and possibility reduced (which, as mentioned, would require the adoption of complementary measures to avoid inacceptable risk on people). Adopting modified reliability levels means to reinitiate the process and again envisaging possible alternative solutions from which to derive a possible minimum intervention.

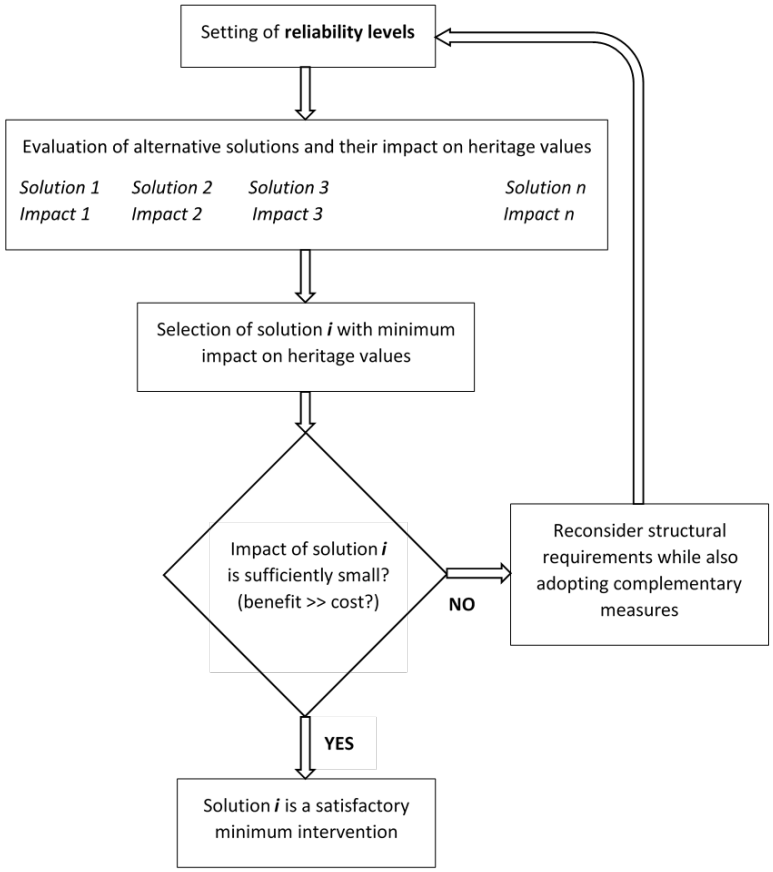


Figure 3: Engineering approach fort the selection of minimum interventions

7.4 Incremental approach

A different strategy towards minimum intervention can result from applying an incremental (or step -by-step) approach beginning with a minimum level of intervention and then followed by possible subsequent supplementary or corrective measures. Observation and monitoring are used to assess the efficiency of each subsequent measures and to evaluate the need for further operation. It must be noted that this approach is applicable to problems involving static loads and cannot be applied to seismic strengthening or interventions against other natural hazards.

7.5 Impact of interventions on heritage values

The engineering approach presented in section 7.3 is based on the evaluation of the impact that possible interventions have on the structure's heritage values. This evaluation can be based on a qualitative classification allowing to categorize the interventions according to their

foreseeable impact. A quantitative evaluation of the impact, while desirable for the sake of objectivity and accuracy, may be difficult to perform due to the multidimensional character of the heritage values and the multiplicity of impacts that interventions may have on them.

As a first approach the guidelines propose a classification in three categories corresponding to low, moderate or high impact ones. It is also acknowledged that interventions may have, in some cases, a positive impact and may even contribute to the cultural value to the historical structure.

The first category includes interventions that have a positive or neutral impact or, if negative, a very low impact on the heritage values. The guidelines provide different criteria for the identification and classification of this type of interventions. In short, they include maintenance, stabilization, repair or strengthening operations that satisfy certain requirements regarding the criteria introduced in section 7.1. Stabilization operations should be fully non-invasive and removable. Repair operations should be based on proven compatible and durable materials (as for instance grouting and injection with adequate mortars or grouts). Strengthening interventions should satisfy several requirements, including the use of non-invasive and removable reinforcing devices (such as tie rods in masonry arches and buildings).

The second category refers to interventions with moderate impact. Included in this category are those based on light, scarcely invasive and mostly removable devices. The damage caused by the implementation or removal of the intervention should be limited and repairable by means of appropriate conventional techniques.

Other interventions that do not satisfy the aforementioned conditions may have a very high impact on the structure's cultural value and are therefore included in the third category. They include, for instance, interventions whose implementation causes significant damage (or even moderate damage if not repairable by means of appropriate conventional techniques), interventions causing a substantial alteration of the structural scheme and resisting mechanisms, or invasive and/or non-removable interventions based on not sufficiently durable or compatible materials.

7.6 Quality assurance

It is recognized that interventions in ancient buildings are generally more complex than in standard construction, and require all involved agents to implement appropriate methods and technologies. The success of interventions is seriously compromised if they are not entrusted to agents with the necessary qualifications in three main areas: (i) studies and design, (ii) inspection and testing, and (iii) execution. The members of the multidisciplinary team should possess the necessary qualifications on training and experience in their areas of expertise.

8 EXPLANATORY REPORT

The guidelines propose that any study and intervention on a historical structure should be completed with an Explanatory Report including a summary with all the findings of the multidisciplinary team. The purpose of the explanatory report is to explain those aspects that cannot be reduced to formal calculations. The report must explicitly present and discuss the reliability of the data, any uncertainties and the hypotheses considered at each stage. Among other aspects, it should include the following items:

- The conclusions of diagnosis on the causes of decay and damage, along with an evaluation of the monument's conservation condition.
- A justified statement on the adopted reliability levels (structural requirements). If these requirements are reduced with respect to the application of current design codes in order to limit excessive intervention, it will be necessary to clearly justify this decision and to explain how adequate safety is provided by alternative means.
- The conclusions on the structural verification, along with the identification of the intervention needs.
- The criteria and procedure considered in the evaluation of the alternative solutions and the selection of the optimal one.
- A detailed description of the selected intervention.

9 CONCLUSIONS

Based in the ICOMOS/ISCARSAH Principles for the Analysis, Restoration and Structural Conservation of Architectural Heritage, the guidelines of the ISCASAH committee are intended to provide insight on the different stages that concern the study and conservation of historical structures, including the investigation and documentation works, the structural verification and the design of intervention. Across of these stages, the guidelines propose the application of a broad and flexible approach strongly based on the scientific method. The proposed approach includes different activities and approaches (such as the historical research, inspection, comparative analysis, monitoring and structural analysis) providing both qualitative and quantitative evidence. The outcome of all the different activities has to be integrated in a consistent way. Possible contradictions (for instance, between historical research and structural analysis) should motivate the reconsideration of the conclusions attained and a more accurate application of approaches and methods.

The proposed engineering approach for the identification of adequate minimum interventions is based on the evaluation (even if only qualitative) of the impact that the envisaged operations (of maintenance, stabilization, repair or strengthening) may have on the heritage values. Criteria are provided to categorize the interventions according to their impact. A distinction is proposed among null to low, moderate and high impact interventions. It is also acknowledged that interventions may have a positive impact on the heritage values.

REFERENCES

[1] Principles for the analysis, conservation and structural restoration of architectural heritage. (2003). ICOMOS / ISCARSAH Committee. Ratified by the ICOMOS 14th General Assembly, in Victoria Falls, Zimbabwe, October 2003

[2] ISO 13822:2010 Bases for Design of Structures – Assessment of Existing Structures. Technical Committee ISO/TC 98, Subcommittee SC2 – Reliability of Structures.

[3] International Charter for the Conservation and Restoration of Monuments and Sites (The Venice Charter, 1064). 2nd. International Congress of Architects and Technicians of Historic Monuments, Venice, 1964. Adopted by ICOMOS in 1065.

[4] The Nara Document on Authenticity (1994) / ICOMOS. Ratified at Nara Conference on Authenticity in Relation to the World Heritage Convention, held at Nara, Japan, from 1-6 November 1994

12th International Conference on Structural Analysis of Historical Constructions
SAHC 2020
P. Roca, L. Pelà and C. Molins (Eds.)

TOWARDS A DIGITAL ARCHITECTURAL HERITAGE KNOWLEDGE MANAGEMENT PLATFORM: PRODUCING THE HBIM MODEL OF BAIT AL NABOODAH IN SHARJAH, UAE

R. SABRI[1*], S. B. ABDALLA[1] AND M. RASHID[1]

Architectural Engineering Department
University of Sharjah
University City, Sharjah, United Arab Emirates (UAE)
e-mail: rsabri@sharjah.ac.ae (*corresponding author),
sabdalla@sharjah.ac.ae, mrashid@sharjah.ac.ae http://www.sharjah.ac.ae

Keywords: Heritage documentation, HBIM, terrestrial laser scanning, scan-to-BIM, point cloud data, Bait Al Naboodah Museum

Abstract. *This paper explores the methodology for the production and integration of Heritage Building Information Modeling (HBIM) into the museum management system of the Emirate of Sharjah, United Arab Emirates (UAE). The historic Bait Al Naboodah Museum is documented as a pilot study using terrestrial laser scanning (TLS) technology. The scanning and modelling processes are explained in a seven-stage workflow: preliminary data acquisition, site surveying and terrestrial laser scanning, processing of the captured cloud point data, post-processing and modelling, quality control, final delivery of the digital model, and its validation. The architectural elements and details of Bait Al Naboodah have been reconstructed in a multi-layered 3D digital model, and its accuracy has been tested. This HBIM model has been conceived as the basis of a shared inter-institutional platform for the Museum's management.*

1 INTRODUCTION

Finding innovative tools for the documentation and conservation of increasingly broad heritage portfolios has dominated heritage conservation research agendas since the beginning of the 21st century. Recently research has focused on various aspects of the configuration and utilisation of digital applications in heritage management [1]. Heritage Building Information modelling (HBIM) has emerged as a significant architectural heritage recording and conservation management tool [2, 3, 4, 5]. Studies from different geographic contexts have revealed important insights regarding the documentation, integration and management of heterogeneous data in digital models [6, 7]. However, this has remained an under-researched heritage topic in the UAE.

The built heritage of the United Arab Emirates consists of examples of traditional architecture of residential, defence, commercial and educational functions, roughly dating from

the early 19th to mid-20th century. The heritage authorities of the Emirate of Sharjah have restored many heritage structures since the 1990s. Many of them are adaptively reused. Several such structures have been re-purposed as museum spaces under the management of the Sharjah Museums Authority (SMA). The conservation management of these structures is the responsibility of the Sharjah Archaeology Authority (SAA). Interviews with relevant officials have revealed that managing museums in heritage structures is challenging as there are multiple tasks and responsibilities. Institutions carry out planning related to conservation management, facilities management, and exhibition management. As these institutions follow a traditional management style, each one has unique documentation and planning methodologies.

While de-centralisation in heritage management has many advantages, overlapping inter-institutional planning for different activities is unavoidable. Clashes in exhibition planning, maintenance works for building services, and conservation works, which disrupts scheduled activities, are examples. Other practical issues include duplication of data by each stakeholder for their institutional requirements. Consequently, resources are wasted to reproduce new architectural drawings or locate existing ones in dispersed archives. It should also be noted that standard sets of architectural drawings of heritage structures are either manually or digitally drawn based on manual measurements; they typically include little detail. Therefore, when architectural data for a part of the building, which is not visible on a standard set of architectural drawings, is required, the technicians need to go back to the building to take new measurements. This happens, for instance, when an exhibitor needs accurate scaled drawings of an exhibition space to plan an exhibition. This research explores the methodology and technical issues for developing a digital model as an effective management platform, where heritage data will be conceptualised and categorised in a semantically enriched system. The research uses Bait al Naboodah Museum in Sharjah as the pilot study. It investigates the methodology of producing an HBIM to be used as a shared management platform by the stakeholder institutions relating to museums in heritage structures.

2 A BRIEF HISTORY OF BAIT AL NABOODAH

Bait Al Naboodah is the oldest and largest surviving traditional courtyard house in Sharjah. This house was originally constructed in c.1845 by Obaid bin Eissa Bin Ali Al Shamsi (aka Al Naboodah), a prominent pearl merchant with international commercial ties [8]. Alazawi notes that there are at least two main construction phases for this partially two-storied courtyard-plan type house: the main entrance and rooms on the East façade as well as the stairs on the North and South which were built in the first stage [9]. This was followed by adding rooms on the other sides of the courtyard and the second floor in several phases of the second stage as the Al Naboodah family grew.

Bait Al Naboodah was subjected to an extensive restoration project from 1990-1995, and it was opened as an ethnographic museum in 1995. Soon after that, the building required extensive conservation work due to continuing material deterioration problems caused by a high water table and termite damage. The building was waterproofed and termite proofed during the conservation works. The work was finalised in 2016, and the museum subsequently reopened (Figure 1). The building was also retrofitted with fire detectors, CCTV, air conditioning, and ramps. Currently, while the SMA manages the museum, the SAA is responsible for its conservation management. The aim of this research is to create an HBIM to be populated with

architectural heritage data and shared by the stakeholder institutions to inform the management of the museum, conservation, and building facilities.



Figure 1: Views from Bait Al Naboodah.

3 DATA ACQUISITION, PROCESSING, AND MODELING

This research utilises terrestrial laser scanning (TLS), also known as terrestrial light detection and ranging (LiDAR), for the architectural documentation of Bait Al Naboodah. TLS measures distance remotely by emitting laser pulses at target points. It is 'regarded as mass data collection technique capable of rapidly collecting millions of points,' making it suitable for generating accurate data [10, 11, 12]. The data collection and processing methodology and workflow is described in the following.

3.1 HBIM methodology and workflow

The process started with acquiring permission from SMA to laser scan Bait Al Naboodah. It continued with site visits in coordination with the SMA officials regarding the scanning process, surveying the heritage structure, and planning for scanning and model making resources. TLS has been planned following SMA's health and safety policy. The workflow is presented in Table 1.

Table 1: Data gathering, processing, modelling, and validation stages.

Stage	Process
1. Site visit and preliminary data acquisition	Pre-study site visits for planning the scanning requirements and coordinating with SMA authorities regarding permission processes.
2. TLS	Spatial data gathering through TLS. Capturing high-quality three-dimensional image of the surroundings in the form of Red Green Blue (RGB) coloured point cloud data.
3. Processing the captured point cloud data	Transferring the point cloud data to a computer environment and initiating the point clouds' cleaning process. Modifications and preparing the point cloud data for further processing.
4. Post-processing and modelling	Transferring point cloud data into Autodesk Revit. Mapping HBIM objects onto point-cloud. Converting the point cloud data into mesh objects. Using Cyclone plugin for Revit to alignment and fitting the image data on the scan data in Revit. Creating customised objects as families in Revit.
5. Quality Control (QC)	Investigating and verifying factors affecting the quality of point cloud data. Validating and checking HBIM submittals
6. Final delivery	Production of an accurate and precise HBIM model, ready to generating: • 2D & 3D plans and coloured-plans. • Elevations. • Sections (2D & 3D). • Animation, rendering and virtual tours. • Maintenance schedules (doors, windows, rooms, columns, etc.). • Bill of quantity/cost estimates.
7. Validation	Site visit for validating the model through: • Visual inspection of functions and spaces. • Random validation of measurements and dimensions.

3.2 Terrestrial laser scanning

We used a single 3D scanner for the TLS, and this means the tripod scanner had to be moved to several locations to capture the larger site from various angles (Figure 2). Therefore, the entire project has been captured using a single tripod-mounted scanner, namely the FARO 3D model X130, which has a scanning range of 130 m. Although using a single scanner slowed down the scanning process, we finalised the scanning in two working days (27-28 October 2019). The chosen 3D laser scanner captures up to one million measurement points per second and generates a precise, high-quality three-dimensional image of its surroundings using an integrated camera. The point cloud data captured by the 3D scanner is a collection of points converted from a range of angular measurements into a common Cartesian (XYZ) coordinate

system and precisely defines the surfaces of the scanned object [13, 14]. The scanner's integrated camera captures high-quality three-dimensional images of its surroundings. However, it produces only one three-dimensional image for each scan, despite each scan containing millions of cloud points. This single image (Figure 2) gives the object the RGB colour, resulting in colourised point clouds.

3.3 Transferring point cloud data and post-processing

The captured point cloud data is a collection of 3D coordinate systems representing the building's exterior surface, including its geometry and colour. After the scanning process, this data has been transferred to a computer environment. However, the captured 3D point clouds are considered raw data at this stage. During the processing stage, the colour of the object surfaces has been added by overlaying imagery from the scanner's integrated camera via Cyclone plugin for Revit (Figure 2).

Usually, further modifications are necessary to prepare for the finished HBIM model. For instance, the point clouds have to be cleaned if there are scan vibrations or dust particles on the lens that may scatter the point cloud data. However, in our case, there were no major issues, except that the surrounding buildings required some cleaning. For our project, the 3D scanner was equipped with an integrated camera to capture high-quality images to aid in point cloud interpretation and provide colourised point clouds (Figure 2).



Figure 2: Colorized Point clouds by RGB color.

3.4 Modeling and mapping HBIM objects onto the point-cloud

The modeling/ mapping processes continued with converting the point cloud data into mesh objects. We built the 3D model of Bait Al Naboodah in Autodesk Revit with the assistance of 'Cyclone plugin for Revit'. This aided in depicting the existing heritage geometry of the

architecture of the heritage structure and producing 3D datasets of the heritage asset in a 3D BIM. However, we had to do some organisations on the point cloud data prior to this stage for the necessary smoothing and proper integrations within the HBIM.

During the 3D modelling process, some objects such as walls, columns, or beams and some doors and windows could be imported directly from Revit libraries. Some others were edited to capture the actual geometric conditions of Bait Al Naboodah. However, due to the complex, non-parametric geometries typically associated with heritage buildings, the digitalisation process involved modelling and customising several objects developed explicitly for this project. Electrical fixture such as lights and lanterns, windows and windows quads, furniture and decorative elements, as well as profiles from roof and facade details, stairs, handrails, and columns, are among the custom created elements for this project (Figure 3). Similarly, some material surfaces had to be created for the project as they were not in the standard Revit libraries (Figure 4).

The customised objects are generated in the same way that existing Revit library objects, i.e. as families. As a result, an object in Revit is associated with a specific family that yields sub-elements, known as classes. For example, all windows have been categorised under one family that branches to various windows (i.e. double light windows, single windows, and top windows). The same has been applied to doors, walls, floors, and decorative elements/details.

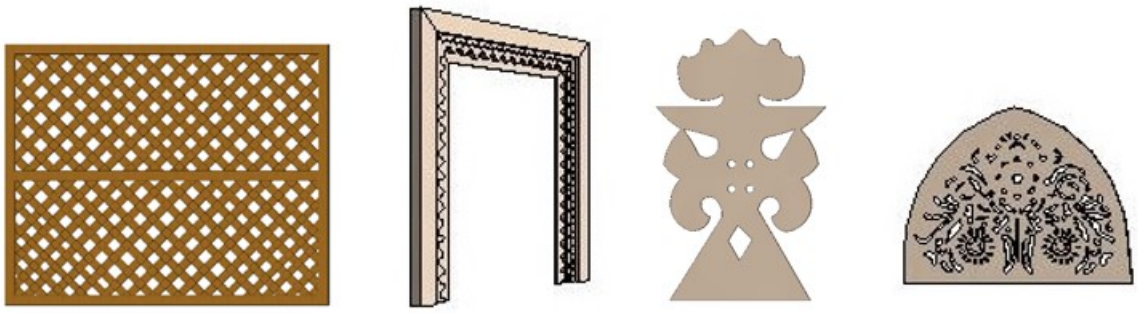


Figure 3: Examples from customised architectural elements created specifically for Bait Al Naboodah HBIM model.

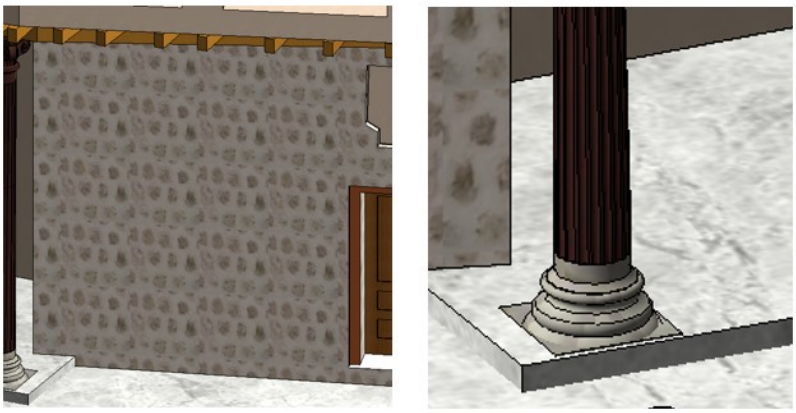


Figure 4: Examples from customised material and mats created specifically for Bait Al Naboodah HBIM model.

3.5 Quality Control (QC)

We investigated and verified the factors that affect the quality of TLS point cloud data at this stage. We verified the HBIM's credibility by point cloud validation, geometry, clash detection, and model coordination. In addition, we reviewed the HBIM model to ensure compliance, accuracy, and a high-quality deliverable to validate the collected data. Revit 2020 allowed for visualisation, walkthroughs, sectioning the model, and the development of plans and schedules. Additionally, Navisworks Manage 2020 was helpful in further reviewing the HBIM's integrity and precise visualisation and review. The QC also included a review of the point cloud data generated by the FARO SCENE LT 2019.2 software. During the QC process, we detected the absent elements and inconsistencies such as a lack of finish material on some façades, missing wood from the ceiling, and missing fixtures and furniture.

3.6 Final HBIM delivery and validation

After correcting the missing parts and modifying the inconsistencies, the final 3D model contained all of the building's architectural components, electrical fixtures, and mechanical components (AC units and toilet fixtures). At this stage, a complete set of floor plans (2D & 3D, elevation, sections (2D & 3D), as well as doors, windows, rooms and columns schedules were generated from the model (Figures 5-7).

We continued verifying its accuracy and precision by taking in-situ measurements and comparing them with the scaled drawings generated from the HBIM model. The validation process was based on taking random measurements at various locations at the building and testing horizontal and vertical measurements against the digitally created HBIM model. The measurements showed accuracy up to +/- 1 mm, indicating that the produced HBIM model is very consistent and accurate up to 99%.

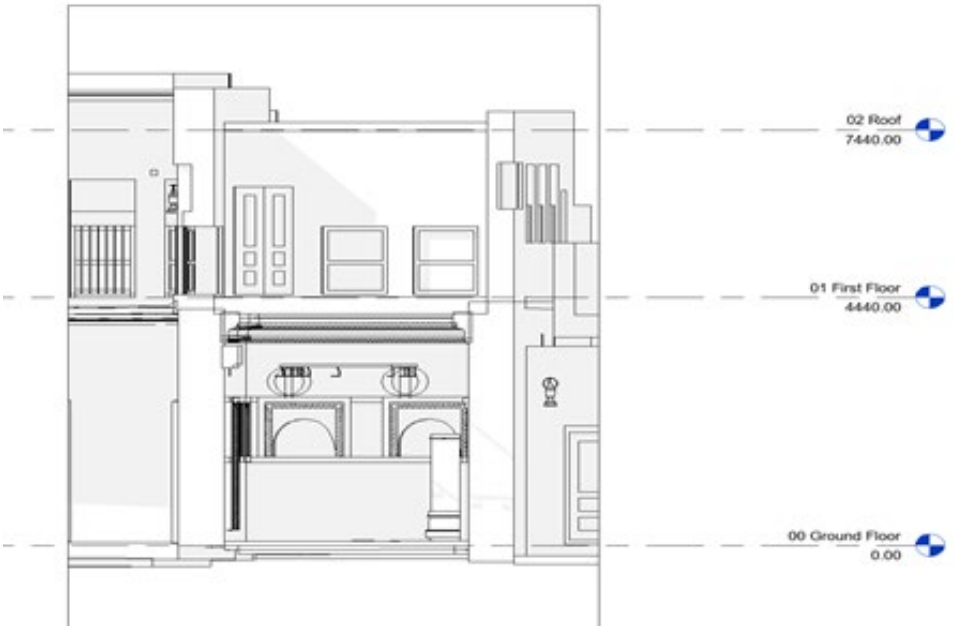


Figure 5: An elevation generated from Bait Al Naboodah HBIM.

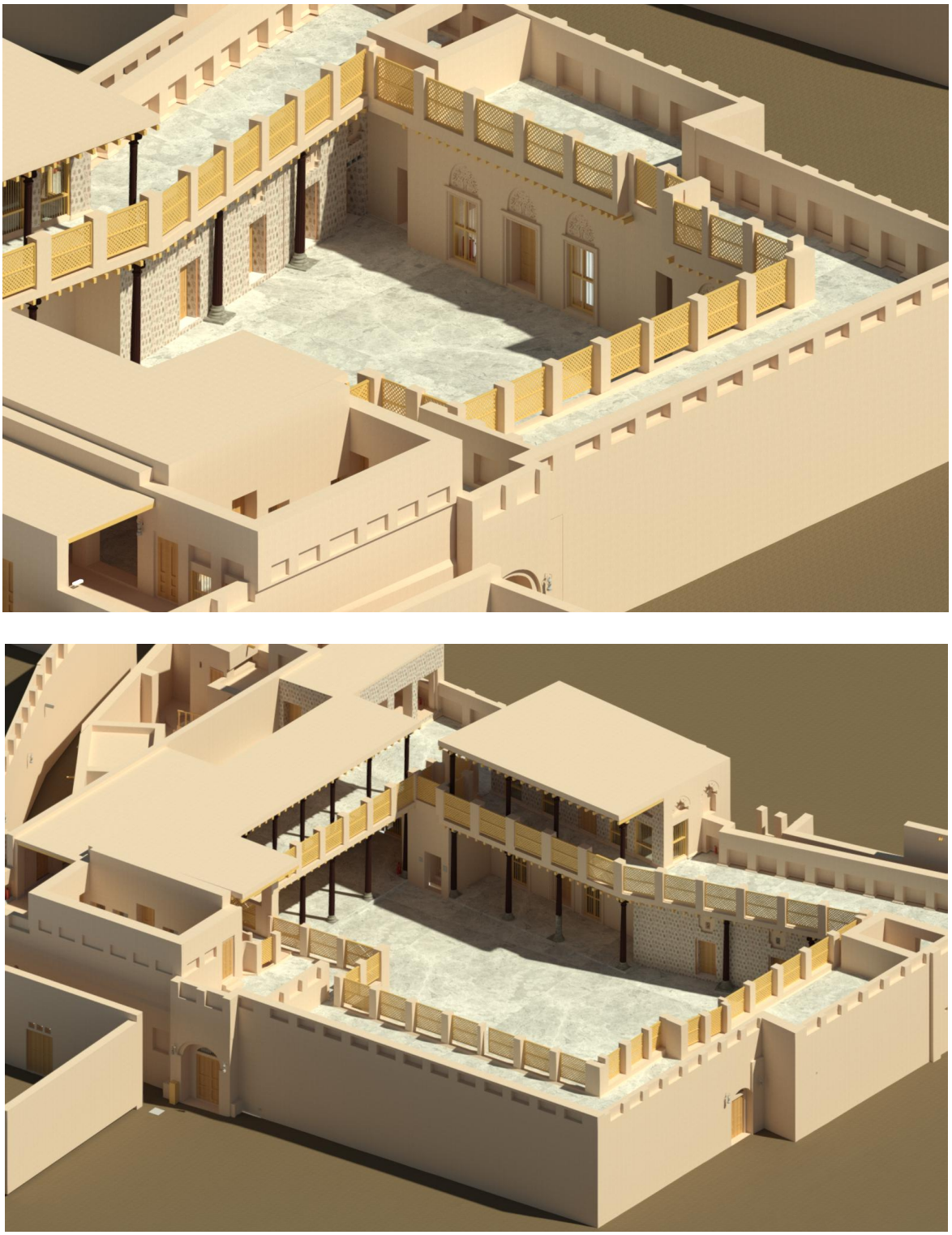


Figure 6: 3D images of the building, generated from Bait Al Naboodah HBIM.



Figure 7: Interior of a temporary exhibition space, generated from Bait Al Naboodah HBIM.

5 CONCLUSION

3D laser scanning and digital architectural heritage knowledge modelling are relatively expensive compared to traditional manual documentation systems. Not only laser scanners are costly, but the scanning and transferring of captured point could data to a computer environment, and its conversion into architectural drawings requires specialised knowledge and expertise. This technology is not widely tested on the heritage structures in the UAE. Our investigation has revealed that the output is invaluable in generating accurately scaled plans, sections, and architectural details for any space and in any numbers. The HBIM, produced for Bait Al Naboodah, using the scan-to-BIM methodology, has proven to be an accurate and efficient architectural documentation method. Scan-to-BIM technology and expertise are available in the UAE's booming construction sector, and this can be efficiently utilised in the heritage sector. The next step of this project is the population of the HBIM model with data to convert it into an inter-institutional digital platform to be used for the management of museum, conservation and building facilities.

Acknowledgements. This research has been financially supported by the University of

Sharjah Research Grant Ref. V.C.R.G. / R. 438/2019. The authors would like to thank the Sharjah Museums Authority and Bait Al Naboodah Museum officials for their support during the laser scanning.

REFERENCES

[1] Arayici, Y., Counsell, J., Mahdjoubi, L., Nagy, G. A., Hawas, S., and Dweidar, K. (Eds.). *Heritage building information modelling*. Routledge (2017).

[2] Quattrini, R., Pierdicca, R. and Morbidoni, C. Knowledge-based data enrichment for HBIM: Exploring high-quality models using the semantic-web. *J. of Cultural Herit*. (2017) 28: 129-139.

[3] Jordan-Palomar, I., Tzortzopoulos, P., García-Valldecabres, J., and Pellicer, E. Protocol to Manage Heritage-Building Interventions Using Heritage Building Information Modelling (HBIM). *Sustainability* (2018) 10, 908.

[4] Bruno, N. and Roncella, R. HBIM for Conservation: A New Proposal for Information Modeling. *Remote Sens*. (2019) 11, 1751.

[5] Andriasyan, M., Moyano, J., Nieto-Julián, J.E., & Antón, D. From Point Cloud Data to Building Information Modelling: An Automatic Parametric Workflow for Heritage. *Remote Sens*. (2020) 12, 1094.

[6] Tucci, G., Conti, A., Fiorini, L., Corongiu, M., Valdambrini, N., and Matta, C. (2019). M-BIM: a new tool for the Galleria dell'Accademia di Firenze. *Virt. Arch. Rev*. (2019), 10(21): 40–55.

[7] López, F. J, Lerones, P. M., Llamas, J., Gómez-García-Bermejo, J. and Zalama, E. A Framework for Using Point Cloud Data of Heritage Buildings Toward Geometry Modeling in A BIM Context: A Case Study on Santa Maria La Real De Mave Church, Int. J. Arch. Her. (2017) 11 (7): 965-986.

[8] Sharjah Museums Authority. Bait Al Naboodah. https://www.sharjahmuseums.ae/en-US/Museums/Bait-Al-Naboodah.

[9] Alazawi, A.S. Sharjah Institute for Heritage, Sharjah, UAE. Personal communication, 16 September 2019.

[10] Rocha, G., Mateus, L., Fernandez, J. and Ferreira, V., 2020. A Scan-to-BIM Methodology Applied to Heritage Buildings. *Heritage*. (2020) 3(1): 47-67.

[11] Boardman, C. *3D Laser Scanning for Heritage Advice and Guidance on the Use of Laser Scanning in Archaeology and Architecture*. Historic England (2018). https://historicengland.org.uk/images-books/publications/3d-laser-scanning-heritage/

[12] Sztwiertnia, D., Ochałek, A., Tama, A. and Lewińska, P. HBIM (heritage Building Information Modell) of the Wang Stave Church in Karpacz - Case Study. *Int. J. of Arch. Herit*. (2021). 15(5): 713-727.

[13] FARO (2021) https://www.faro.com/en/Products/Hardware/Focus-Laser-Scanners

[14] Moyano, J., Odriozola, C. P., Nieto-Julián, J. E., Vargas, J. M., Barrera, J. A., and León, J. (2020). Bringing BIM to archaeological heritage: Interdisciplinary method/strategy and accuracy applied to a megalithic monument of the copper age. *J. of Cultural. Herit*. (2020), 45: 303-314.

12thInternational Conference on Structural Analysis of Historical Constructions
SAHC 2020
P. Roca, L. Pelà and C. Molins (Eds.)

UNREINFORCED MASONRY STRUCTURES' SEISMIC IMPROVEMENT WITH F.R.C.M. : THE EXPERIENCE OF THE VANVITELLIAN PALAZZO MURENA OF PERUGIA

RICCARDO LIBEROTTI[1*], FEDERICO CLUNI[1] AND VITTORIO GUSELLA[1]
[1]Department of Civil and Environmental Engineering
University of Perugia (Italy)
Via Duranti, 06125 - Perugia, Italy
e-mail: riccardo.liberotti@unipg.it (*corresponding author), federico.cluni@unipg.it, vittorio.gusella@unipg.it

Keywords: Heritage Structures, Masonry Building, Numerical Modelling, F.R.C.M. Details

Abstract. *The aim of the contribution is to illustrate strengthening design in regard to the conservation of Palazzo Murena in Perugia, designed in the eighteenth century by the prominent Architect Luigi Vanvitelli. Starting from an accurate historical analysis and taking into account experimental campaign and results of numerical analysis, the vulnerable elements of the construction have been highlighted. A local reinforcement intervention is proposed with the aim of retain the historical value of the architectural characteristics; this consists of the application of plaster with Fiber Reinforced Cementitious Matrix, F.R.C.M., to achieve an adequate strength, without adding supplemental weight to the masonry structure and therefore avoiding an increase of the seismic vulnerability. The benefits of the application of F.R.C.M. materials, also with respect to different reinforcement techniques are broaden.*

1 INTRODUCTION

Owing to the recent earthquakes that affected central Italy, in particular the Umbria region, the University of Perugia activated a research program aimed at the seismic vulnerability assessment of historic buildings under its ownership and management. This activity also involved the architectural complex of Palazzo Murena that hosts the headquarters of the University of Perugia, Fig. 1. This aggregate is composed by three adjacent buildings: Palazzo Murena (former monastic complex), the ex-accountancy office and the church of Montemorcino Nuovo or church of the University, Fig. 2. With reference to Palazzo Murena, in a previous contribution [1] the basic correlations among the historical knowledge, the seismic vulnerability assessment and the widespread experimental tests campaigns have been addressed in the framework of the safeguard of this iconic building. The seismic analysis [1], by macro-element, proved the good global behaviour of the existing masonry structure anyway highlighting, according to the Italian Building Code [2, 3], that Palazzo Murena ranks in a state deserving to be seismic improved in order to enhance its safety. In addition, during the analysis, the presence of a peculiar structural shape in elevation, influencing the building's seismic behaviour, has been observed and addressed as a possible trigger to the activation of local mechanisms. The present work is aimed to illustrate the proposal of reinforcement with F.R.C.M. composite materials. The contribution has been organized as follows. In Sec. 2 the

outcomes of a depth historical investigation of Palazzo Murena, in relation to the design criteria of Luigi Vanvitelli, are reported. The outcomes of a survey and experimental campaign are reported in Sec. 3. From these studies and also considering the result of a vulnerability analysis [1] the interventions conceived in order to increase the safety level regarding the seismic behaviour of Palazzo Murena are described in Sec.4.



Figure 1: Current view of the architectural complex of Palazzo Murena



Figure 2: Composition of the architectural complex: 1) Palazzo Murena; 2) University Church; 3) Ex-Accountancy

2 HISTORICAL INSIGHTS

Palazzo Murena was once an Olivetan monastic complex, called Monte Morcino Nuovo following the transfer from its former seat of Monte Morcino Vecchio, outside Santa Susanna, to the current University's square. The monastery and the church of the Olivetans have been designed by Luigi Vanvitelli and completed by his pupil Carlo Murena, from whom the palace takes its current name. The Vanvitellian contribution to the project of the Monte Morcino Nuovo is witnessed by various bibliographical and archival historical sources [4-7]; between these stands out the biography, dedicated to the architect, that was written by the eponymous nephew in the early years of the nineteenth century [4] in which it is listed, among the works carried out by Vanvitelli, the façades project of the church and monastery of Perugia. In addition, it is reported that the Architect was called to Perugia to build the church and monastery of the Olivetans while he was still working in Ancona and so the palace, whose drawings are

still preserved in Caserta, was later completed by the aforementioned Carlo Murena. In 1740 the works began and concluded in 1762 a few years before the confiscation of the monastery in favour of the University of Perugia; the total expenses were around *68.500 scudi* (far from what initially planned). In 1810 the monastery passed to the University and in 1813 also the Drawing Academy found space within the monastery. With the return of the papal government in 1814, the University had to defend itself from the charge of usurpation and pleaded the Pope not to reclaim the building. Later Pius VII confirmed the University's property entrusting its management to the professors Luigi Canali and Pietro Vermiglioni in exchange, however, of a regular annual tribute of *200 scudi* to be paid to the Olivetans. With the "*Regolamento degli studi*", issued by Leone XII in 1824, the University of Perugia became a State's University with Rector Luigi Canali. In 1860 the University passed to the Italian Government and its neighbourhood was thus evolving into a true "university campus" conditioning also the viability and the typology of the urban settlements [5], Fig. 3.

A considerable number of earthquakes occurred in the area of Perugia since the construction of Palazzo Murena; on this issue, considering the last centuries, a complete report has been drawn [1]. After the seismic event of 1997, the building was interested by reinforcement interventions primarily aimed at the consolidation of its northwest portion. During time, the building has been affected by variations, also in its end use, which reshaped its architectural-structural asset many times. Currently the palace is the "headquarter" of the University of Perugia and of the administrative offices.

3 SURVEY CAMPAIGNS

The research for symbolic-perceptive values emerges observing the geographical position of Palazzo Murena: it is located on a slope within the historical centre of Perugia. That sort of "spur", on the best exposed side of the neighbourhood, guarantees to the palace an extraordinary inter-visibility even from the Perugia's old town. The principal façade of entrance has been conceived in a single architectural composition with the inherent University's Church. Regarding its vertical arrangement, the palace's façade is marked outwardly by the string-courses corresponding to the floors, reflecting some of the proportions and locations of the inner masonry elements (vaults' position, wall's heights etc.).



Figure 3: Picture postcard of Perugia's view in the early of 900th; in the center stands out Palazzo Murena. Extracted by the private collection of Alterocca (Terni)

The ground floor is a hollow rectangle with external dimensions about *60 m x 48 m* and inner dimensions, due to the presence of the cloister, about *30 m x 33 m*. The heights of the different levels are: *4.80 m* for the third basement, *4.10 m* for the second basement, *3.80 m* for the first basement, *4.75 m* for the ground floor, *3.10* m for the mezzanine floor and *6.00 m* for the first floor. Therefore, the layout extension of the building varies from level to level, indicating an accentuated vertical asymmetry especially regarding the composition in elevation of the south and east wings of the palace. Indeed, the ground floor plus the mezzanine floor encumber a total height comparable to the lateral corridor's one. This masonry cluster of vaulted rooms, combining such different floors' heights, creates situations, in the mezzanine, marked out by the presence of some carrying walls resting on the top of the barrel vaults, Fig. 4. This peculiarity, that once housed the monks' cells and the relative corridor of distribution, is not the result of a supplements following the original realization of the building factory but, thanks to the historical investigations conducted in the state archive of Perugia [7], it has proved to be perfectly coeval with the design genesis operated by Luigi Vanvitelli. The structure proposed is an example of the creative flair and of the constructive expertise of the Architect; in that case study the need to satisfy a design objective has entailed, on Vanvitelli's path, the design of an astonishing structural expedient.

Only the main formal relationships and most pertinent ones to the object of the present paper were reported, but many others could be observed in relation to the architectural distribution of the internal compartments e.g. in the inner main corridor can be observed that the inception of the ample string-course in stucco, highlighting the floor of the mezzanine, is proportioned to the corridor's rise. Speaking of the architectural hierarchy, it is interesting to note how great significance is attributed to the serving environments such as the hallways; probably a sign of how the previous monastic use required the attribution of more relevance to common spaces rather than the personal ones, Fig. 5a.

Fractures on the masonry vaults of the main corridor of Palazzo Murena are observable. On this a monitoring system was implemented and permitted to figure out that, to date, the damage pattern appears to be stabilized and that no arising deformation processes are in place for the building and its foundations; please refer to [1] for further details.

The palace appears simple and rigorous by its bricks facades, based on rational splitting norms by means of openings and string-course, but instead lavish on the inside spaces adorned with frescoes, stuccos and extremely fine marble grit floorings, Fig. 5. In fact, above all, the PhD's hall, located on the noble floor of Palazzo Murena (the second one), and its vault have been completely frescoed by two Perugian painters in the 18th century: Giovanni Bevilacqua for the decorative parts and Vincenzo Monotti for the figurative features, Fig. 6. About the floorings, including those of the mezzanine floor, they are made of marble grit, a technique much appreciated and requested throughout the 19th century for the paving of architectural esteem buildings. They are characterized, in this case, by high joints (at the same level as the floor's surface) and by narrow grout lines combined with sharp edged square tiles in order to visually hide the mortar joints achieving a final result closer to the classic one entirely in marble and so without joints). Those choices, however, entails an almost "perfect" installation as any coplanar defects, even minor ones, could not be accepted either for aesthetic (emerging edges) or for functional reasons (steps in the flooring) denoting that this valuable flooring has been made by old craftsmen who were highly qualified, Fig. 5b.

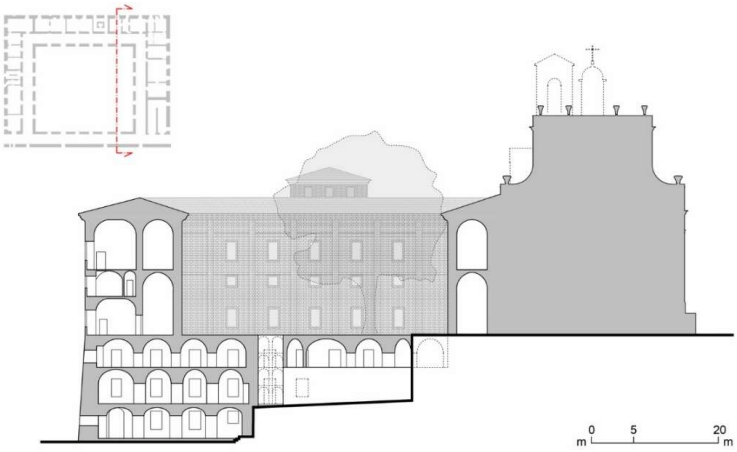


Figure 4: Cross-section of Palazzo Murena



(a) (b)

Figure 5: Architectural arrangement of Palazzo Murena: a) detail of vaults and arcades covering the ground floor; b) view of the marble floorings at the mezzanine floor

4 INTERVENTION OF STRUCTURAL STRENGTHENING

In order to estimate the vulnerability of Palazzo Murena has been recently activated a research program. In a previous contribution [1] a preliminary seismic global analysis on a F.M.E. model (frame by macro-element), created using the data gained by means of innovative survey instrumentations, has allowed to identify in advance the most vulnerable portions of this ancient masonry building and to consequently finalize (and so reduce) the successive execution of the onerous and invasive investigation methodologies (like drills, endoscopies, flat jack tests etc.).

An experimental testing campaign has been conducted in order to assess the mechanical proprieties of the materials; moreover, a monitoring system has been implemented to check the mechanical behaviour of the building under environmental loading.



Figure 6: Ceiling of the PhD's hall of Palazzo Murena

On the basis of the increased level of knowledge deriving from the aforementioned experimental campaign, the preliminary numerical modelling has been refined in order to tune up the global seismic evaluation of the masonry building in its actual state. According to the Italian Standard Codes [2, 3], the subsequent push-over analysis revealed the sufficient safety from global point of view but, at the same time, the presence of high local vulnerable sub-structures. This is the case of mezzanine floor that represent a large geometric irregularity and it is the source of a huge difference in the distribution of the structural masses; moreover, it is vulnerable since it consists of load bearing masonry walls resting, in turn, on the underlying brick vaults and therefore not vertically continuous to the foundation. Eventually, by means of a numerical model, based on the previous outcomes, the application of F.R.C.M. composite materials has been evaluated, leading to a positive influence on the global seismic response of the masonry structures. Given the constructive specificities and architectural uniqueness previously described, the structural strengthening has to assure the building's survival without penalize the role and the meaning it stood for during the centuries. In this framework in order to envisage intervention of structural strengthening the design approach, here proposed, is to not burden the masonry structure with extended interventions but rather in the localized retrofitting of only the most vulnerable structural elements. On this, the composite materials, that can be studied by analytical approach, with classical and non-classical theories [12, 13] or by numerical modelling, allow to fulfil the strengthening of ancient masonry buildings in compliance with their environmental, cultural and social value.

In response to such outcomes, a real reinforcement plan, conceiving the design of F.R.C.M. reinforcements, is proposed without put on the line socio-architectural prestige of the building; circumstance also linked to the accessibility and to the function of such a strategic edifice. The intervention consists in a high performance fiber mesh coupled with an inorganic matrix (mortar), used instead of the traditional epoxy resins, proper of fiber reinforced plastics (F.R.P. systems), in order to obtain a real reinforced plaster [3, 9, 10].

On heritage buildings, the importance of the structural strengthening runs no deeper than the preservation of architectural value of the artefacts; also in the present case the uniqueness of masonries, especially with respect to arches [11], conditioned and inspired the intervention strategies. Focusing the attention on the walls of the mezzanine floor, made of bricks and lime mortar, the application of the composite material allows to avoid the burden of the existing masonry structures with the additional weight and to avert damages to fine marble flooring and other valuable elements during the building work. In particular, the localization of F.R.C.M. on those inner walls guarantees to strength them regarding the bending and the shear actions, Fig. 7. Regarding the design and verification criteria, the technical guidelines provided by the CNR [8] have been followed; in particular the rules described in the paragraph *§ 4.1.1* of the same. In addition the implementation steps and criteria have been thrust toward the innovative design rules promoted by the scientific and technical literature [14, 15, 16]. For design and verification purposes the materials of the Kimia S.p.A. [14], and the relative mechanical parameters Tabs. 1-2, were taken as reference including the use of the bi-directional basaltic net *KIMITECH BS ST 400*, the matrix in mortar M15/F. In addition, the use of transversal connectors known as "fiocchi", one for each *4-5* m^2, in order to create artificial through stones within the walls, and to create a sandwich masonry-reinforced plaster panel was intended, Fig. 8a. With respect to such element the product *Kimisteel FIOCCO GLV* has been chosen, the latter is composed by a "sock" containing unidirectional galvanized steel-zinc filaments. For such element the designed diameters is ϕ *12 [mm]*; entailing for its insertion the creation of wall drills of diameter of between *16* and *20 [mm]* for a minimum depth (L_a) of *20 [cm]*. By reference to the specific locations of the different walls, in comparison to the external masonry casing, different implementation modalities have been conceived, Fig. 8b-c-d; the thickness of the intervention will be inferior to 30 *[mm]*, including the final regularization layer.

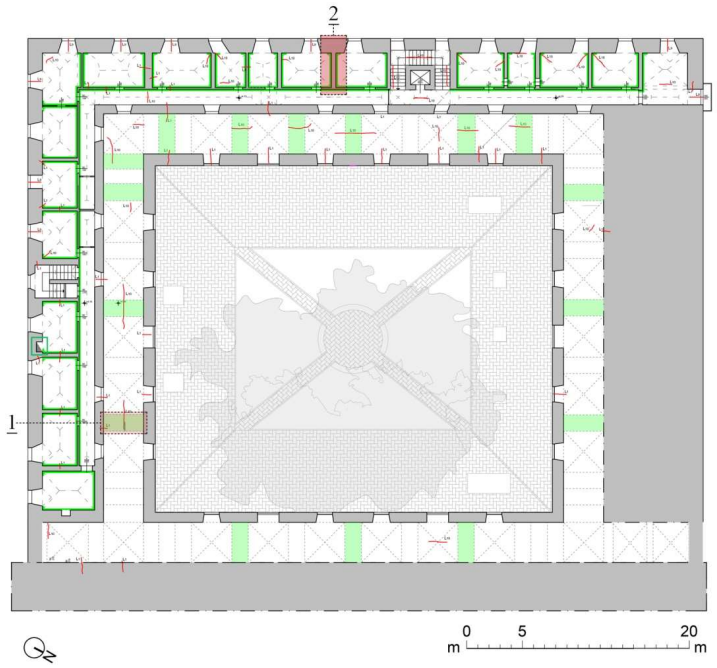


Figure 7: Plan of the mezzanine floor with the proposed interventions in F.R.C.M. (characterized in green). 1) Interventions on the arcades covering the main aisle; 2) Interventions on the inner walls of the mezzanine floor

As observed during the survey, the main corridor on the ground floor is covered by cross vaults spaced out by decorated arcades. In addition, a stucco moulding, placed at the height of springer, runs along the entire length of the building and furthermore the walls are adorned by half pilasters which also develop on the arches giving rhythm to the inner walls of the building. During the monitoring, which is always an important item when dealing with historical structures [17], it was possible to observe how the crack pattern detected on the vaults covering the quadrangular corridor is not representing a state of danger, however its presence testifies the memory of the numerous earthquakes that in past and recently times involved the structure [1]. On this, in a future excerpt of the intervention plan their renewal will be foreseen in the perspective of a re-garnish of whole Palazzo Murena. Aiming at the reinforcement of the arcades the application of F.R.C.M. was envisaged according to a specific designed method, taking into account the architectural value of the mouldings, which refers to the design tips published by the CNR [8] and to the latest analytical and experimental outcomes available in the scientific literature [18, 19].

Table 1: Mechanical properties of the bidirectional basaltic fiber net, *KIMITECH BS ST 400*: ρ_{fib} *[g/cm³]* density, *E [GPa]* elastic modulus, σ_u *[MPa]* ultimate tensile strength, ε *[%]* breaking strain, *g [g/mq]*grammage,w_s *[g/mq]* weigth of tissue starching, D_m *[mm]* dimension of the mesh, *t [mm]* thickness of the net, t_f* *[mm]* equivalent thickness of the net, A_r *[mmq/m]* resistant area, *Q [kN/m]* tensile breaking load of the warp, b_f *[mm]* single strip width. *Intended for each warp direction

ρ_{fib}	E	σ_u	ε	g	w_s	D_m	t	t_f*	A_r *	*Q*	b_f
2,67	89±2	3100	<8	414	61	20x20	1,15	0,065	65	>120	1000

Table 2: Mechanical properties of the matrix M15/F

Element	Material	Particle size distribution	Compression strength [MPa]	Bending strength [MPa]	Shear strength [MPa]	E [MPa]
Mortar - Matrix	Lime inorganic mortar M15/F	maximum 1,20 mm	at 7 dd >9 at 14 dd >12 at 28 dd >15	at 7 dd >3,8 at 14 dd >3,9 at 28 dd >4	0,15 (with masonry - EN 711)	9600

Each arch presents a tripartite moulding; the first phase of the proposed design plan consists of the removal of a small stucco-band from the two most protruding portions of the decoration in order to reach the resistant part of the arch constituted by the masonry. Then, with the same superficial treatment described previously, the F.R.C.M. material is applied in the groove using the aforementioned mortar but employing, this time, a unidirectional stainless steel fiber reinforcement fabric, *Kimisteel INOX 800*, located with respect to its frame along the arch's profile; its high-strength properties are reported within Tab. 3. Regarding the arcades the thickness of the reinforcement intervention should be around *6/7 [mm*] and requires the use of the aforementioned typology of connector in order to provide the coupling to the masonry supports. Finally, for each garnish, the two lateral stucco strips, remainders of the pre-existing decoration, will be used by restorers as reference in order to restore the mouldings in their

entirety, guaranteeing an exterior appearance akin to the original result, Fig. 9. It should be noted that this intervention plan, aimed at the safeguard of this architectural asset, is conceived with methods and technologies which allow to not penalize the strategic function of this building during the F.R.C.M. application phases.

In fact, unlike other strategies of structural intervention, the designed strengthening actions do not lead to the total closure of the University "headquarter" and its offices. In turn some offices, at the mezzanine floor, or part of the main corridor at the ground floor will be close and by the time installations are completed the small construction sites will move to the next spaces; permitting to reopen each time few retrofitted portion of structure in order to accommodate the public, the students and the employees.

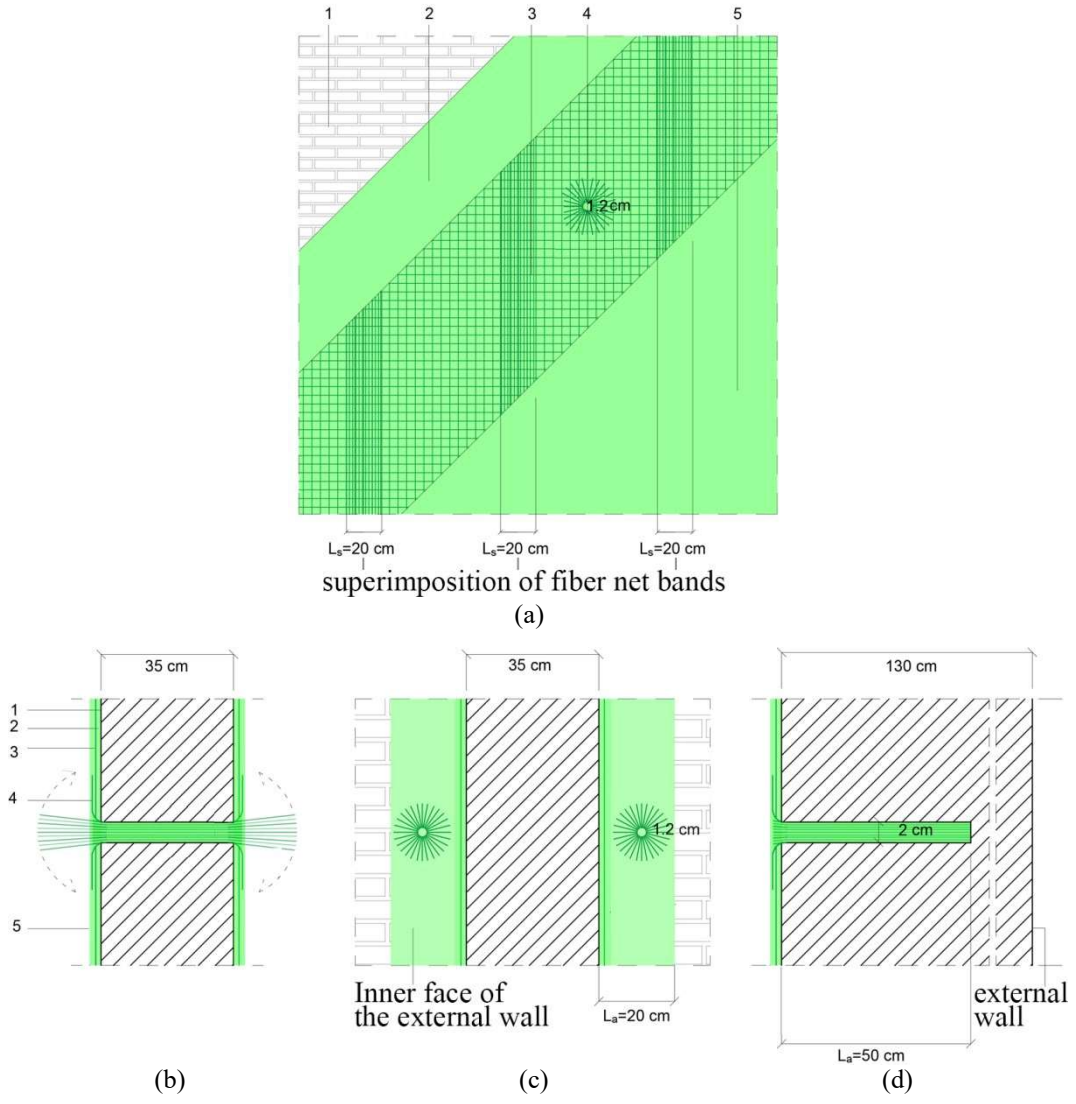
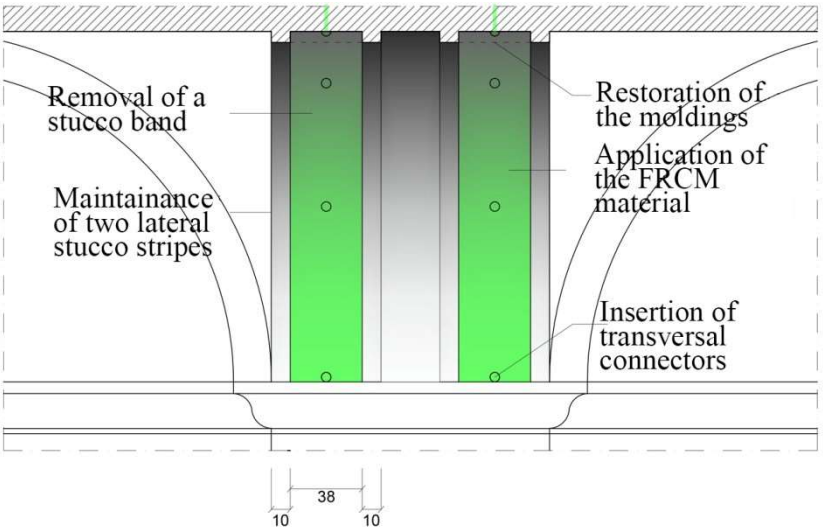


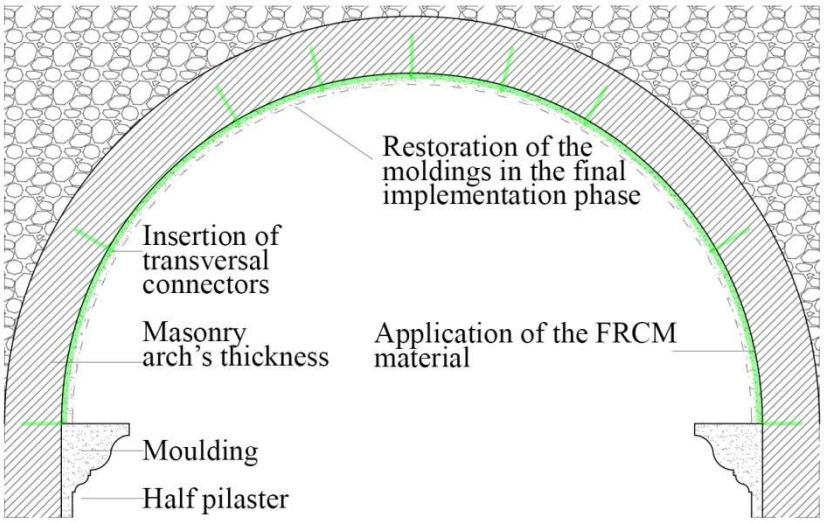
Figure 8: Improvement intervention with F.R.C.M. a) Application procedure, scale 1:40. Technical details of the reinforced walls, scale 1:20: b) General section of a reinforced internal wall with transversal connectors; c) Section of a reinforced internal wall; d) Section of an external wall highlighting the corner joints between reinforced internal walls and perimetral one

Table 3: Unidirectional high-strength stainless steel fiber fabric, *Kimisteel INOX 800 ST1-0619*: *ρ [g/cm³]* density, *E_w [GPa]* elastic modulus of wires, *R_{wire} [MPa]* wire resistance, *ε [%]* breaking strain, N_y number of yelds for each wire, *D_s [mm] diameter of strands, A_s [mmq]* strands resistant area, *Q_w [N]* wire minimum breaking load, *b_f [mm]* single strip width, *g [g/mq]* grammage, *w_s [g/mq]* weigth of tissue starching, *D_m [mm]* dimension of the mesh, *t_t [mm]* steel theoric thickness, *t_f* [mm]* equivalent thickness of the net, *A_{ru} [mmq/m]* resistant area for units of length, *R_u [N/mm]* unitary resistance for units of fabric

ρ	E_w	R_w	ε	N_y	D_s	A_s	Q_{min}	b_f	g	D_m	t_t	A_{ru}	R_u
7,85	210	2000	0,95	16	1	0,483	930	100-300	800	20x20	0,07	77.338	160



(a)



(b)

Figure 9: Improvement intervention with F.R.C.M. and its application procedure technical detail of the reinforced plaster with fiber transversal connector, scale 1:40. a) Transversal section of an arch; b) Longitudinal section of an arch

5 CONCLUSIONS

- Starting from a historical study and accurate survey and taking into account the results of vulnerability analysis, in the present paper a strengthening design approach in regard to the conservation of Palazzo Murena in Perugia has been illustrated;
- In order to preserve the constructive specificities and architectural uniqueness of the building, a local reinforcement intervention is proposed for the walls of the mezzanine floor and for the arches of the main corridor on the ground floor. This consists of the application of F.R.C.M. to obtain a reinforced plaster which assure an adequate strength, without increasing the weight of the masonry structure and therefore without increase of the seismic vulnerability;
- The ongoing research will take into account experimental testing and numerical analyses to check the effectiveness of the proposed strengthening interventions also with respect to the implementation modalities.

Acknowledgments. The support received from the University of Perugia and the collaboration of its Technical Office, represented by L. Palma and B. Buonforte, are thanked.

REFERENCES

[1] Liberotti, R., Cluni, F. and Gusella V. Vulnerability and seismic improvement of architectural heritage: the case of Palazzo Murena. *Earthquakes and Structures* (2020) **18** (3): 321–335.

[2] NTC 2018. Decreto Ministeriale 14 Gennaio2018, Aggiornamento delle «Norme tecniche per le costruzioni», Supplemento ordinario alla "Gazzetta Ufficiale,, n. 42 del 20 febbraio 2018 - Serie generale, Ministero delle Infrastrutture e dei Trasporti; Roma, Italy.

[3] Circ. No7 (2019)*, Circolare del Ministero delle infrastrutture e dei trasporti 21 gennaio 2019, n. 7 C.S.LL.PP.,* Istruzioni per l'applicazione dell'«Aggiornamento delle "Norme tecniche per le costruzioni"» di cui al decreto ministeriale 17 gennaio 2018., Supplemento ordinario alla "Gazzetta Ufficiale" n. 35 del 11 febbraio 2019 - Serie generale, Ministero delle Infrastrutture e dei Trasporti; Roma, Italy.

[4] Rotili M. *Vita di Luigi Vanvitelli*. Timawo e Burgo, Napoli, Italy, (1975).

[5] Chiacchella R. *Un quartiere e la sua storia: La Conca di Perugia. La Conca di Perugia itinerario per una conoscenza e una proposta*. Quaderni Regione dell'Umbria, Perugia: 97–100, (1975).

[6] Dozza, G. *Università Di Perugia. Sette Secoli Di Modernità 1308-1976*. Delta Editrice, Perugia, Italy, (1975).

[7] Sorignani, C. *UNI|TECA Progetto architettonico di trasformazione in Gipsoteca dell'edificio sede dell'ufficio Economato dell'Università degli Studi di Perugia*. Master thesis, University of Perugia, Perugia, Italy, (2018).

[8] CNR-DT 215/2018, Istruzioni per la Progettazione, l'Esecuzione ed il Controllo di Interventi di Consolidamento Statico mediante l'utilizzo di Compositi Fibrorinforzati a Matrice Inorganica, CNR, 2018.

[9] Lignola, G.P., Di Ludovico, M., Prota, A., Aiello, M. A. and Varum H. Design rules for in-plane shear strengthening of masonry with FRCM. *9th International Conference on FRP Composites in Civil Engineering CICE 2018*, Paris, France, July.

[10] Lourenço, P.B., Oliveira, D.V., Leite, J.C., Ingham J.M., Modena, C. and da Porto, F. Simplified indexes for the seismic assessment of masonry buildings: International database and validation. *Engineering Failure Analysis* (2013) **34**: 508–605. https://doi.org/10.1016/j.engfailanal.2013.02.014

[11] Cavalagli, N., Gusella, V. and Liberotti, R. The Role of Shape Irregularities on the Lateral Loads Bearing Capacity of Circular Masonry Arches. In: Carcaterra A., Paolone A., Graziani G. (Eds) *Proceedings of XXIV AIMETA Conference 2019. AIMETA 2019. Lecture Notes in Mechanical Engineering*. Springer, Cham, (2020), pp. 2069–2081.

[12] Autuori, G., Cluni, F., Gusella, V. and Pucci, P. Effects of the fractional laplacian order on the nonlocal elastic rod response. *ASCE-ASME Journal of Risk and Uncertainty in Engineering Systems, Part B: Mechanical Engineering* **3** (3) (2017) September, Article number 030902

[13] Autuori, G., Cluni, F., Gusella, V. and Pucci, P. Mathematical models for nonlocal elastic Composite materials. *Advan. Nonlin. Anal.* (2017) **6** (4): 355–382. https://doi.org/10.1515/anona-2016-0186.

[14] Kimia (2019), Interventi-strutturali-resine-tessuti-pultrusi/frcm; Kimia S.p.a., P.te Felcino (Perugia), Italy. www.kimia.it

[15] Pourfalah S., Cotsovos D.M. and Suryanto B. Modelling the out-of-plane behaviour of masonry walls retrofitted with engineered cementitious composites. *Computers and Structures* (2018) **201**: 58–79.

[16] D'Ambra, C., Lignola, G.P., Prota, A., Sacco E. and Fabbrocino F. Experimental performance of FRCM retrofit on out-of-plane behaviour of clay brick walls. *Composites Part B* (2018) **148**: 198–206.

[17] Gioffré, M., Gusella, V. and Cluni, F. Performance evaluation of monumental bridges: Testing and monitoring 'Ponte delle Torri' in Spoleto. *Structure and Infrastructure Engineering* (2008) **4** (2): 95–106.

[18] Zampieri, P., Gonzalez-Libreros, J., Simoncello, N. and Pellegrino C. Strengthening of Masonry Arches with FRCM Composites: A Review. *Key Engineering Materials* (2019) **817**: 251–258. https://doi.org/10.4028/www.scientific.net/kem.817.251.

[19] Alecci, V., Focacci, F., Rovero, L., Stipo, G., Mantegazza, G. and de Stefano M. FRCM Composites for Strengthening of Brick Masonry Arches. *Key Engineering Materials* (2017) **747**: 174–181. https://doi.org/10.4028/www.scientific.net/kem.747.174.

12th International Conference on Structural Analysis of Historical Constructions
SAHC 2020
P. Roca, L. Pelà and C. Molins (Eds.)

USING INFORMATION TECHNOLOGIES FOR BRIDGE MANAGEMENT IN MEXICO'S ROYAL ROADS BUILT BETWEEN XVI AND XVIII CENTURY

ANDRÉS A. TORRES-ACOSTA[1*], JOEL BUSTAMANTE-ALTAMIRANO[2] AND ALICIA ESPARZA-CARRILLO[2]

[1]Instituto Tecnológico de Estudios Superiores de Monterrey, Campus Querétaro (ITESM)
Campus Querétaro Epigmenio González 500, San Pablo 76130, Santiago de Querétaro, Qro., México.
e-mail: atorresa@tec.mx , www.tec.mx/en/queretaro (*corresponding author)

[2] SATELSA SA de CV
Paseo de la Reforma 184, Lomas del Marqués 76146, Santiago de Querétaro, Qro., México.
email: joel.bustamante@satelsa.com.mx, alice_ec7@hotmail.com, www.satelsa.com.mx/

Keywords: Historical bridges, Royal Road, Information Technologies

Abstract. *After the establishment of the Viceroyalty of New Spain in the 16th century, the interest in precious metals and the mining activities would influence the emerging economic activities and the communications network of the New Spain. All the communications were built based on two mutually perpendicular axes. The first axis, East to West, between Veracruz-Mexico-Acapulco and the other axis, north to South, linked the northern region of the Viceroyalty with Mexico City and to Oaxaca and Guatemala. As part of the road infrastructure needed to get a continuous flow of goods, bridges were very important for crossing rivers, cliffs, and mountains. The fabrication of these structural elements were mainly made using the roman old school. The geometry, length, and materials used were varied, depending on the technical improvements of the time, and local labour expertise. The Vice-regal bridge vestiges are now scattered in the 2 million square km of the Mexican territory. Most of them are still in use, but others were forgotten in the old Royal Roads when they went out of use. This investigation deals with the methodology used (based on information technologies) to create a web-based management system for Vice-regal bridges, that is now available to be used in Mexico by the three government levels (Municipality, State, and Federal) and research institutions.*

1 INTRODUCTION

1.1 Royal Roads

Mexican pre-Columbian societies mainly used footpaths for trade and to move to different places. Since they ignored the usage of the wheel and pack animals, their means of transportation was by foot. The *tamemes* were in charge of transporting any items or merchandise from one place to the other by foot; they could lift around 23 kilograms in their backs and could reach as far as Guatemala.

When central Mexico was conquered by a small group of Spaniards, an extensive period of conquest began in the land. The Conquistadors opened bridle paths made of dirt in order to

reach the different indigenous populations with their horses and subdue them to the Spanish crown. In these early stages, they were content with merely broadening the existing pre-Columbian roads so that the horses, then unknown in the New World, could transit.

During the Viceroyalty (16^{th}-18^{th} centuries), the interest for different products, substantially modified the network of exchange and drove the conquerors to open new roads to be able to travel to regions of difficult access. During this period, the most prominent case was the mining activity and mainly the extraction of silver. New regions were turned into colonies and road networks were shaped according to the locations of the mining *reales* or centers, with the purpose of exporting the products from the mines. As part of this process, other activities (agriculture, ranching, certain types of manufacture needed for the daily life and trade) surfaced as they were indispensable for the continued exploitation at the mining sites since they provided consumption goods for the workers and the raw materials for the mining activities. As new seams were discovered or as mining centers were consolidated, population centers emerged and roads with their corresponding branches were opened around them. [1]

From the 16th century, when the conquerors settled in the different regions of the New Spain, the New Kingdom of Galicia, New Biscay, New Santander and the New Kingdom of León, new routes for the transport of merchandise were opened. Communications during the Vice-regal period were built based upon two perpendicular axes. The first one was outlined from Orient to Occident, between Veracruz- México- Acapulco/ Navidad and it constituted a colossal bridge between the Atlantic and Pacific oceans, known back then as the North Sea and the South Sea, respectively. The other axis, North-South, united the norther regions of the Viceroyalty with Mexico City as well as with Oaxaca and Guatemala. Once opened, these axes of communication were called *Caminos Reales* or Royal Roads; in total, four main channels were built and they were known as:

Royal Road of México-Veracruz or "Viceroys Royal Road"

Royal Road of México-Acapulco or "Royal Road of the Orient"

Royal Road of México-Santa Fe or "Interior Land Royal Road" and

Royal Road of México-Guatemala or "Royal Road to the Salazones (salted meat)". [2]

Military campaigns, missionaries, merchants, stockmen and expeditionary forces streamed from these roads carrying seeds, creeds, customs, culinary traditions, rituals, ideas and knowledge that came from different places and they established in the New Spain and its provinces a complex economic and cultural system that resulted in the building of cities, villages, baserris, haciendas, ranches, presidiums, hospitals, convents, and mining centers from where the precious metals, that for a long time supported the economy of the old continent, were extracted.

In the beginning, the means of transportation were the same people that travelled the roads (*tamemes* and armies) then, after the arrival of the conquerors, the usage of draught animals (horses, mules, oxen, etc.) were responsible for the radical modifications that the outline and the constructive system of the roads underwent. In a similar manner, this modernization in the field of land communications did not only modify the outline of the roads but also their outfitting.

The clash between the pre-Columbian and the European cultures, the shifts in economic activities and the introduction of different means of transportation resulted in changes to the road network existing prior to the conquest; these changes went beyond the creation of new roads. The outfitting of the Royal Roads corresponded to the purposes these roads served (e.g.

transport of minerals, raw materials, foodstuffs, textiles and many other products; transit of people for cultural and religious purposes).

The Royal Roads are of considerable extension that stretches through an ample variety of physical settings and weathers (the Royal Road of the Interior Land is the longest of the Royal Roads with a length of 2 600 km, spread over 11 states); conflicts with the indigenous population persisted throughout the Viceroyalty in different regions surrounding the roads. In short, the outfitting of these roads needed to provide safety both for the travelers and their loads, shelter from the elements and for rest and points were provisions could be found. The lodging structures so that the travelers could rest, spend the night, change mules, and get provisions consisted of *ventas*, *mesones*, and inns; the outfitting on the road itself consisted of abreuvoirs, watch posts, post houses, fortifications, check points and bridges. [3]

1.2 Bridges

It is believed that the first bridges used by humans were natural formations, subsequently imitated by humans in their processes of settlement and movement through the land: rock formations of fortunate shapes, dimensions and placements, fallen tree trunks and protruding tree roots. In Mexico, a notable example of such bridges is Puente de Dios (God's Bridge) which is a rock formation at 80 m over river Amajac in the state of Hidalgo. [4]

The pre-Columbian footpaths were transited by people and therefore were gradually flattened and shaped by the passage of the travelers; it didn't matter if the routes were not straight or with pronounced slopes and the bridges that existed in these roads were very simple, made out of the materials at hand to solve immediate obstacles and often consisted in the natural formations. However, there is evidence of more sophisticated structures, such as the *calzadas* or roads found in the city of Tenochtitlan, the center of the Aztec Empire. These calzadas were outfitted with bridges that allowed the connection between the different urban sectors whilst maintaining the hierarchic urban order. Some collapsible bridges served as protection of the city. Bridges played an important role in the conquest of the city and the exploration of unknown, and often treacherous, territories. Simple bridges were built for expeditions on foot and by horse. [5]

With the establishment of the Viceroyalty of New Spain and other kingdoms within the Spanish Empire new ways of life emerged in the territory. These changes covered all aspects of life: religion, art, cuisine, economic activities, technology and the road networks. The arrival of horses, pack mules and carts came to substitute the *tamemes* during the 16th century and both roads and bridges had to be widened, reinforced and built with subtler slopes so that the pack animals could go through easily, thus ensuring the safety of the travelers and their loads. [6]

In modern times, transformations in the roads, highways and their outfitting are still ongoing as an updating process to the network of roads in the country. In these updates, new roads are frequently outlined, the number of lanes are widened in the existing roads, and materials initially used for the construction are modified and/or replaced. [7] Communities and communication infrastructure (such as bridges) emerge into the spotlight and vanish or lose prominence as the ever-shifting needs of the population demand a constant updating of the roads. The road infrastructure can be used as an analytical element to trace the social, economic and technical changes within a society; the bridges are especially significant because they exhibit the evolution and refinement of constructive systems and the cunning of human beings

to solve the obstacles present in the physical setting. On top of that, bridges often display the prevailing aesthetic elements of a society within a specific time frame through the architecture, craftsmanship, the materials used for construction, and ornamentation. [8]

The Royal Roads are regarded as the communication arteries of the Vice-regal society for the cultural and economic impact they had on the general society of the New Spain through the centuries of its existence. The bridges, being part of these road's infrastructure, played an important role in the flow of merchandise, people, customs, creeds and knowledge through the territory of the New Spain.

The information that Vice-regal bridges could provide to diverse fields of knowledge and disciplines is one of the main reasons for performing a research on them but also in an effort to preserve this constructions and their legacy, highlighting their cultural and historic value through research and the dissemination of the results.

2 PROBLEM STATEMENT

In Mexico, property with historical value is regulated by the INAH (National Institute of Anthropology and History, by its acronym in Spanish), an institution directly dependent on the federal government of Mexico. This institute owns information regarding all the historical properties in the country and such information is deposited in an inventory generated by each INAH office (being 31 offices in total, one for each of the 31 states in Mexico). Bridges built during the Vice-regal period (16^{th} to 18^{th}) are some of the structures included in the INAH's inventory.

This inventory includes fields of information such as location, sketches or architectural outlines, photos (no more than a dozen) and some historical details; unfortunately, some of the properties included lack specific geographic coordinates and their historical details are relegated to an observations field that can be sparse.

The inventories generated by each of the 31 states are kept in each of their INAH's Regional Centers as well as in the General Co-ordination of Historical Monuments of the INAH, in Mexico City. Nowadays, the organizations in charge of harboring the assets of cultural interest, have diverse typologies and capacities, which leaves them in the position of having to manage them in an effective way with very limited resources. The information they have is diversified, decentralized and, fundamentally, in paper support and, rarely, in digital support. In the latter's case, it is not always under standardized formats and safeguarded by one entity.

While an investigation regarding the Vice-regal bridges in the Royal Roads could prove very useful for any potential initiatives of salvaging and/or repurposing these historic bridges as well as to generate other research projects related, it is difficult to gather and process all the information for its subsequent analysis, also the data contained in the inventories can be either incomplete, obsolete, incorrect and sparse in many cases. The changes that the road networks undergo through the years usually result in leaving communities, stretches of roads and structures to fall into oblivion with outcomes such as disrepair and, in many cases, complete loss of the structures and thus no material evidence of their existence.

It is a central necessity to build an updated inventory of these bridges using both the information provided in the inventories and the usage of digital resources, spatial research and georeferencing to complete the existing information and generate new, important information regarding these structures. Information and Communications Technologies will be employed

with the purpose of divulging the results to the general public, research institutions and government agencies and thus be able to safeguard and broadcast the heritage that these historical bridges have to offer.

3 THE RESEARCH PROJECT

The project starts in 2011 as an independent initiative with the objective of creating a catalog/ inventory of the bridges constructed in the Vice-regal period (16^{th} to 18^{th} century) and determine which bridges are located on the route of the Royal Road of the Interior Land or the Silver Route. The project started with the reconnaissance of few bridges, most of them in the State of Querétaro: Bridge of Calesa, Bridge of Juárez, Bridge of Sauz (Pedro Escobedo), Bridge of History (San Juan del Río), as well as two other bridges outside of this state: Bridge of Atongo (Tepeji del Río, Hidalgo) and Bridge of Tres Guerras (Celaya, Guanajuato). For this reconnaissance, trips were conducted over the corresponding stretches in the Royal Road and information, such as geographic coordinates, construction materials, physical state of the structure and photographic evidence, was collected.

During these trips, some bridges of which there was no previous knowledge were found as well as others whose current state was in disrepair and were out of use. For this reason, a request was issued to the INAH in the matter of obtaining a catalog of the bridges in Mexico to get acquainted with their condition and location. The provided information includes around 850 fact sheets of registered bridges.

While a transcription of the obtained data was underway, a situation regarding the scarcity of information or precise details that would allow a correct location of the bridges came to light. In terms of location, there is basic information such as: state, city and street in which the structure can be found. Geographic coordinates are not included and a handful of handmade sketches that provide additional information regarding the spatial location are provided in some of the work sheets, however, without the coordinates these sketches are insufficient to pinpoint the structures' precise location.

The next step was the location of the structures in order to start the creation of the catalog; it was determined that only structures catalogued under the Vice-regal period (16^{th} to 18^{th}) would be identified and worked on. Since the project is an independent initiative and the information collected is of national level there weren't enough resources to perform a direct search (fieldwork) and georeferencing of most of the registered bridges.

Another limitation for a direct reconnaissance of some the bridges is the accessibility to the structures since they may be covered from view by excess of weed; passable roads may not be available and other blockages such as barbed wire and fences for cattle may be present. There are cases in which there are no vestiges of the structures to be found or the structure could be inside private property or restricted government property thus making it inaccessible to the general public.

For the cases in which direct georeferencing is out of question, a researcher with knowledge and experience in the use of information technologies such as GIS applications, was tasked with locating each of the bridges using primarily the satellite maps and information on roads and highways contained in the Google Earth program. All the considered structures were individually tracked using the information provided by the INAH regarding all matters of their location. Information gathered from historical manuscripts, statistical memoirs, books

specialized in historical and cultural properties in the country, travel journals from the 18th, 19th and 20th centuries as well as historical cartography was collected and reviewed to complement the information in the fact sheets and aid in the location of some of these bridges.

3.1 Remote location and georeferencing of the bridges

A classification system was determined based on a range of accuracy of location present in the georeferencing of each bridge. First, a starting point is determined using the information provided in the fact sheets or by using the satellite maps and the tools included in Google Earth. This classification is based on a range of distance from the starting point, in which the structure can be found, and it is the following:

In GREEN are the identified bridges that can be found in a 100m radius from the starting point. These bridges may or may not be visible in the satellite map but using tools such as Street View it is possible to establish a point where the bridge is or was constructed. Some of these bridges may be completely hidden from sight because they are surrounded or covered by modern structures.

In ORANGE are the bridges that could not be identified via satellite maps at first instance and significant information on them in other sources could not be found, other than the information provided by the fact sheets. This information was used to establish the starting point. It was determined that these structures could be located within a 101-500 m radius from the starting point.

In RED, all the remaining bridges whose location couldn't be properly established and only the minimal data could be found such as community, neighborhood, some incorrectly captured street names and sketches. Since there is not a precise location to place the starting point it was determined that the point should be placed in the center of the community or neighborhood or any referenced street.

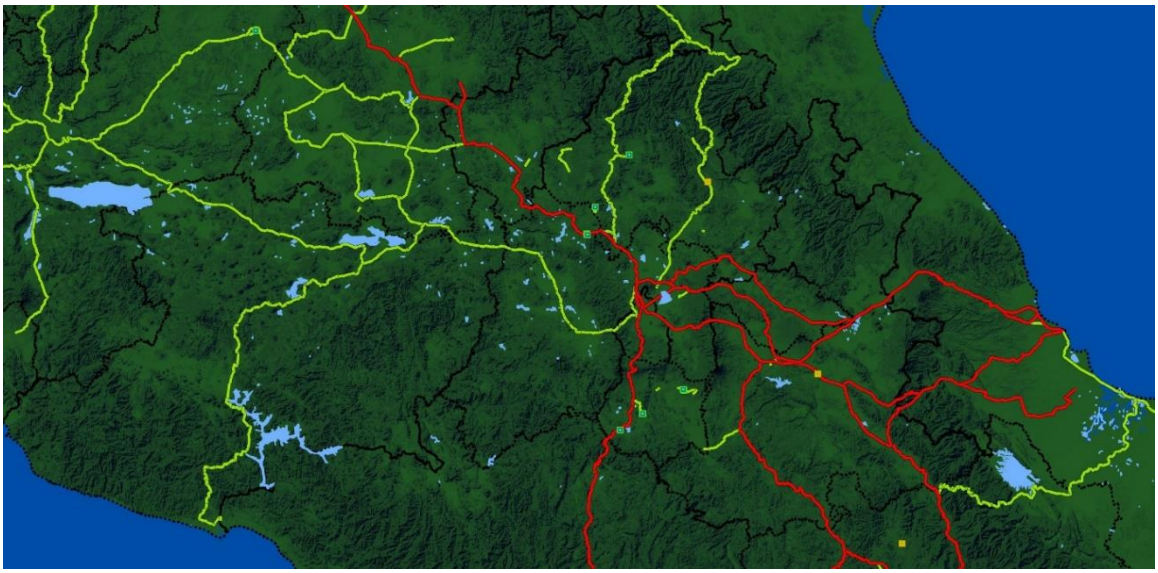


Figure 1. 16th century bridges. The red lines indicate the Royal Roads and the green lines indicate transversal roads. The bridges built during the 16th century and that could be identified with varying accuracy are marked in

squares. The squares employ the color classification system previously mentioned. There is a total of 15 identified bridges built during the 16th century.

It can be noted that many of the bridges marked in green can be found near modern roads and highways. Some of these bridges are still in use and in other cases, modern bridges and structures were built near the old bridges for their replacement, making their preservation possible. A notable case is the Bridge of la Laja or Bridge of Tres Guerras in the entrance of Celaya, Guanajuato.

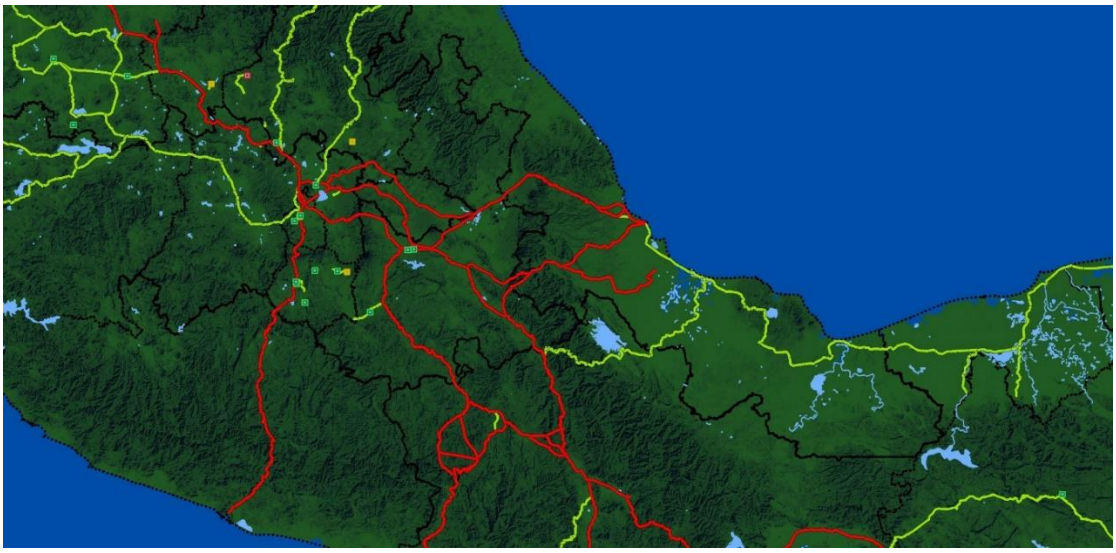


Figure 2. 17th century bridges. Red lines indicate the Royal Roads and the green lines indicate transversal roads. The bridges built during the 17th century and that could be identified with varying accuracy are marked in squares. The squares employ the color classification system previously mentioned. There is a total of 23 identified bridges built during the 17th century.

One of the objectives of this project is to share with the general public the catalogue of Vice-regal bridges that exist or existed in the country. Each registry in the catalogue is meant to include information regarding their construction and materials used, their present condition, geographic coordinates, and photographs. For this objective, the use of a digital platform based in GUI interface with properties for the management of geographic information was considered. Subsequently, testing began with the commercial software ArcGis, from ESRI Company.

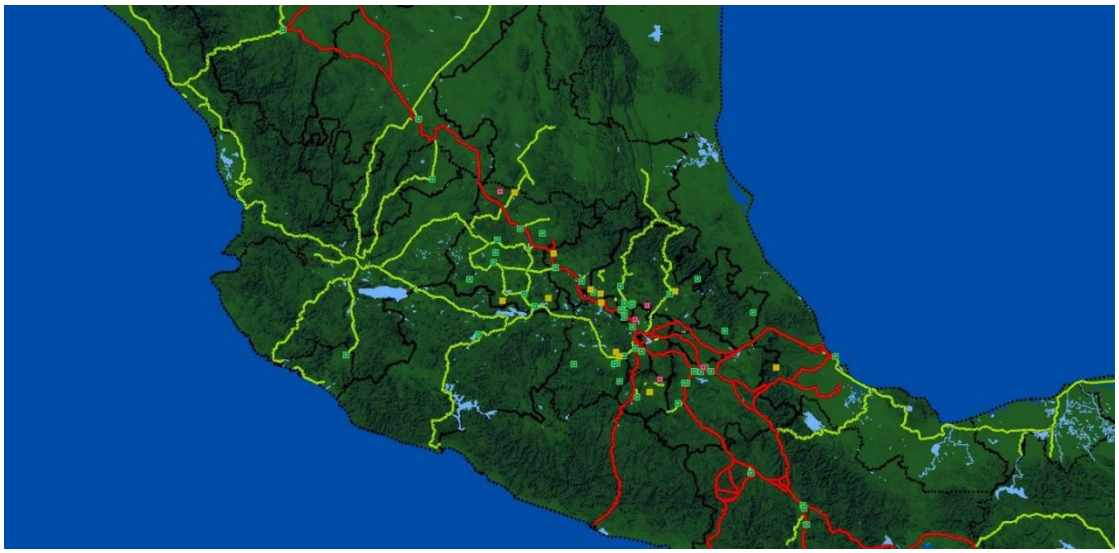


Figure 3. 18th century bridges. The red lines indicate the Royal Roads and the green lines indicate transversal roads. The bridges built during the 18th century and that could be identified with varying accuracy are marked in squares. The squares employ the color classification system previously mentioned. There is a total of 81 identified bridges built during the 18th century.

3.2 Platform generation

Once the graphic interface was developed with the fields to be used, the definitions for each layer corresponding administrative divisions, terrain, federal highways, etc., the information collected from the work sheets and through remote location was transferred to the table format operating in the software (DBF) to subsequently be linked to the section of queries and results. This information can be consulted by applying filters regarding the century of the bridge's construction and location by state. Afterwards the structure of interest can be selected from a list of results obtained in the search. By selecting the desired structure, a complementary screen is displayed which includes all the information available on the selected structure, such as: general observations on the structure, commentaries made by the local population, bridge's condition, type of structure, entity to which it belongs (government or private) and any other detail obtained as well as the photographic archive, if available.

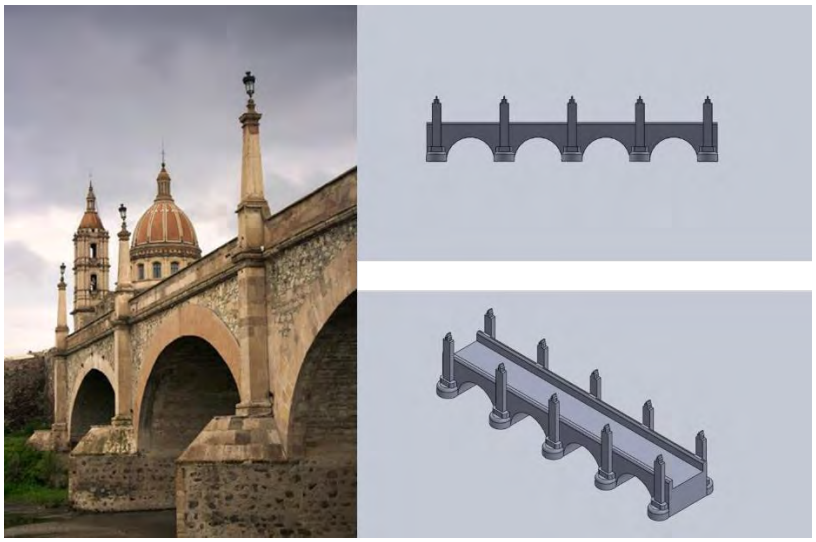


Figure 4. Bridge of Lagos. Built during the 16th century built in the city of Lagos de Moreno, in the municipality of Lagos de Moreno in Jalisco. At the top right is the elevation projection of the bridge drawn for this project and at the bottom right is the isometric projection.



Figure 5. "Puente Grande" or Big Bridge. Built during the 18th century in the city of Acámbaro in the municipality of Acámbaro in Guanajuato. In the bottom is the elevation projection of the bridge.

During the testing stage, the downsides of this software became evident.

- ArcGis is a commercial software that requires a license per computer for personal use and a special license for online usage.

- Aside from the high cost that obtaining and using the sofware implies, its usage requires a certain degree of previous knowledge on the software.

Both situations are incompatible with the contemplated objective of making the results of this project available to the general public or any person interested in the Vice-regal bridges leaving this tool to be discarded while alternatives were searched for. The best option came to be the development of a web based application of free access that can be consulted by means of any electronic mobile device and in which the information displayed can be supoorted by the majority of browsers.

Using technology such as Apache Web Server as setting to host all the information gathered, web pages, images, 3D models and others. MySQL was used as the engine to manage the information in Database, PHP was used for the dynamic handling and structure of the site; JQuery and JS were used for the dynamic handling but from the user's perspective. By using all of these technologies, it is not necessary to be limited to an specific operating system like Linux, Windows or Mac.

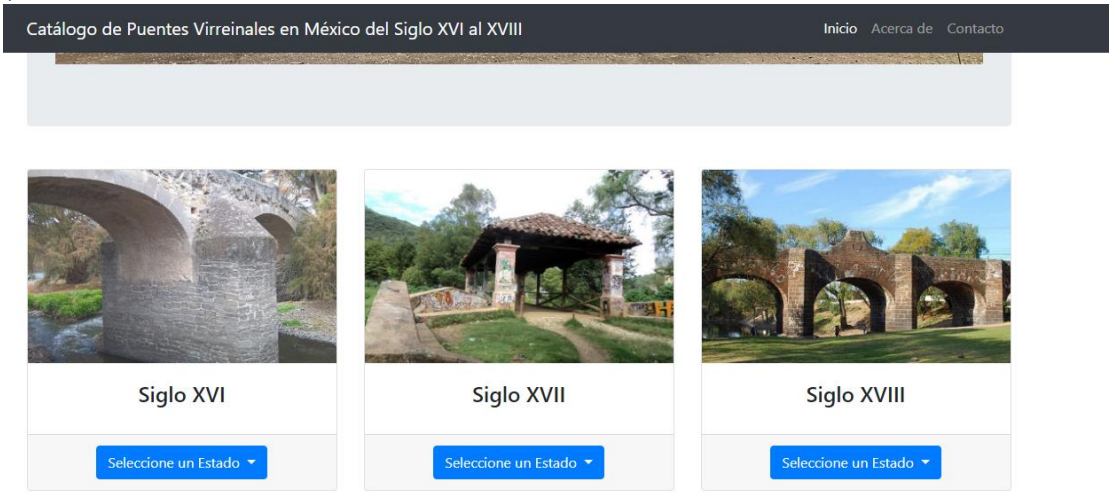


Figure 6. Main page of the website. The user can select information from the 16th, 17th and 18th centuries.

The web-based application development phase of the project is ongoing in order to provide the user with the most information possible. However a site has already been set up and it contains some of the information collected.

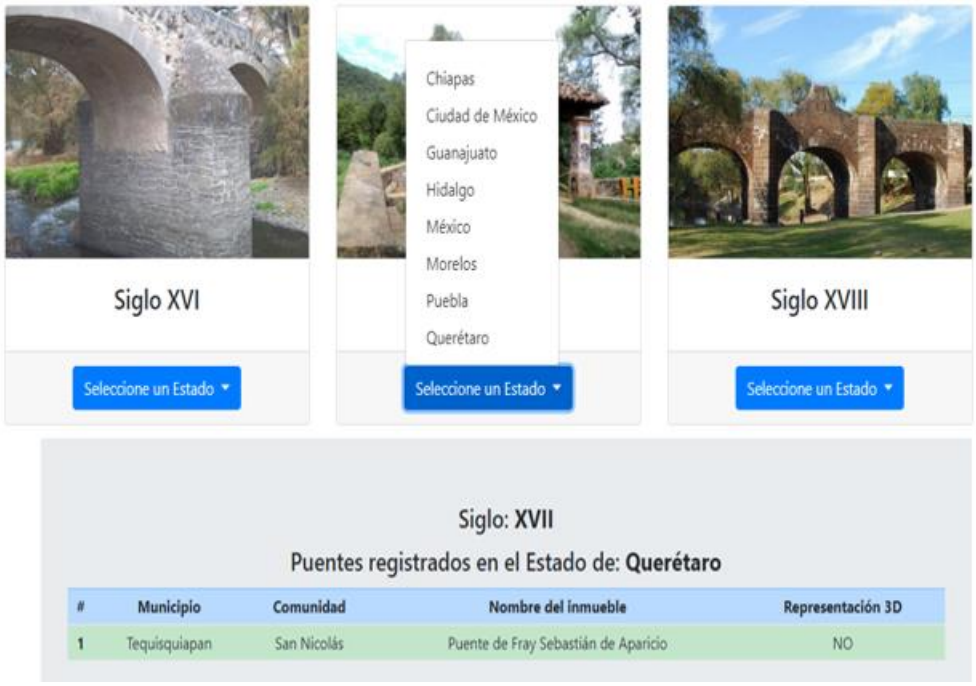


Figure 7. Drop-down list displaying the states available for browsing regarding bridges from the 17th century. Also pictured is the result obtained by selecting the state of Querétaro.

It is intended that the platform be an interactive space where the public can share information in the platform either through a blog or a forum thus enlarging, improving and updating the information.



Figure 8. Page displaying the information of the Bridge of Fray Sebastián de Aparicio in the municipality of Tequisquiapan, Querétaro. The panel on the left side provides the browsing options: information (which includes, when available, oral and documentary data as well as any details of interest noted by the researchers such as inscriptions and physical state of the structure), geographic location- coordinates, 3D rendering and photographic gallery.

The site can be accessed and consulted through the following link: http://sgpa.desacomp.com and any comment or suggestion can be submitted to the address: joel.bustamante@satelsa.com.mx

4 CONCLUSIONS

Providing the obtained information as well as providing means of interaction with the public will not only serve to complement the information presented but to link the public to the historic bridges, considering their artistic, social, and cultural importance. If the public, along with the government institutions and other organizations involved with historic and cultural heritage, are aware of the heritage still standing in the country and its value, perhaps an invigorated interest in the repurpose and preservation of these structures could arise.

Acknowledgements. Authors acknowledge collaboration from the Grupo Camino Real de Tierra Adentro en Querétaro: Rosa Estela Reyes, Virginia Guzmán Monroy, García, Cynthia Leija Sánchez, Eva Lilia Acosta Garnica, Centro INAH Qro; Frida Sarete Orozco Loeza, José Ignacio Urquiola Permisán, Marja González Juárez, Gaspar Real Cabello, Universidad Autónoma de Querétaro. The authors greatly acknowledge the funding provided by SATELSA SA de CV as economical support given to the project since 2009. The opinions and findings in this paper are those of the author and not necessarily those of the funding agencies.

REFERENCES

[1] Tutino, J. *Making a New World. Founding Capitalism in the Bajío and Spanish North America.* Duke University Press (2011), pp. 159-208
[2] Escalante, P. Los Caminos del México Antiguo. In: Cramaussel, C. (Ed.): *Rutas de la Nueva España*, El Colegio de Michoacán (2006), pp. 28-36
[3] Cramaussel, C. El Camino Real de Tierra Adentro. De México a Santa Fe. In: Cramaussel, C. (Ed.): *Rutas de la Nueva España*, El Colegio de Michoacán (2006), pp. 301-303, 314-323
[4] Ortiz, J., Hernández, J., González, J. and Esteva P. *Puentes de México, Arte e Historia*. Grupo Tolteca (1988), pp.7-10
[5] Ortiz, J., Hernández, J., González, J. and Esteva P. *Puentes de México, Arte e Historia.* Grupo Tolteca (1988), pp. 30-39
[6] Ortiz, J., Hernández, J., González, J. and Esteva P. *Puentes de México, Arte e Historia*. Grupo Tolteca (1988), pp. 69-73
[7] González de Cosio, F. *Historia de la Obras Públicas en México*, Volume I, Secretaría de Obras Públicas (1971), pp. 483-484.
[8] Avilés, M. and Brambila R. La puerta del camino a tierra adentro. En busca de evidencias materiales. In: Cramaussel, C. (Ed.): *Rutas de la Nueva España*, El Colegio de Michoacán (2006), pp. 330-337

12th International Conference on Structural Analysis of Historical Constructions
SAHC 2020
P. Roca, L. Pelà and C. Molins (Eds.)

3D FE MODELING OF MULTI-SPAN STONE MASONRY ARCH BRIDGES FOR THE ASSESSMENT OF LOAD CARRYING CAPACITY: THE CASE OF JUSTINIAN'S BRIDGE

VILDAN G. MENTESE[1*] AND OGUZ C. CELIK[2]

[1]M.Sc. Civil Engineer
Formerly, M.Sc., Department of Architecture, Istanbul Technical University (ITU)
34810 Istanbul, Turkey
e-mail: v.gizem.mentese@gmail.com

[2] Professor of Structural&Earthquake Engineering
Faculty of Architecture, Istanbul Technical University (ITU)
Taskisla, 34437 Istanbul, Turkey
email: celikoguz@itu.edu.tr

Keywords: Justinian's Bridge, Masonry Arch Bridges, Collapse Mechanism, Finite Element Analysis (FEA), Three Dimensional Modeling, Inelastic Behavior.

Abstract. *Substantial part of heritage structures in Turkey is historic masonry arch bridges. To explore modeling issues, a numerical work has been initiated to better understand and preserve/transfer this heritage to the next eras. This paper specifically describes the influence of tensile fracture energy of stone material in determining their true load carrying capacities. A case study is presented to explain the modeling issues. With its historical background, current situation, geometric and material properties, this work focuses on numerical investigation of the historic multi-span stone masonry arch Justinian's (or Sangarius) Bridge located in the city of Sakarya in Turkey over the Sakarya River.*

Numerical results show that the value of fracture energy in tension significantly affect the load carrying capacity and failure mechanism of multi-span masonry arch bridges. A more realistic nonlinear response has been obtained for an upper value of the tensile fracture energy of the stone masonry. The bridge model collapses by a-three-hinge mechanism occuring at the loaded arch in the upper value of the tensile fracture energy. The most critical loading point of the bridge is determined as the quarter-span.

1 INTRODUCTION

Masonry arch bridges are complex and nonlinear structures which consist of barrel vaults, spandrel walls, backfill, infill, piers, flood splitters, and wing walls. Finite element method (FEM) is one of the powerful and most commonly used methods in the investigation of structural behavior and failure mechanisms of such structures. Even though performing a nonlinear static analysis (NSA) by FEM requires additional time and effort, the benefits in understanding the structural behavior of this type of structures are fairly high [1].

Masonry is a heterogeneous assemblage that consists of stone and/or brick units and the mortar joints between the units. This complex material displays directional mechanical differences due to the weakness of mortar joints. Existing modeling approaches focus on micro-modeling of the individual component (unit such as stone and mortar) or the macro (composite) modeling of masonry [2]. Based on the desired level of accuracy and allowed computational time, two dimensional (2D) and/or three-dimensional (3D) FE models of masonry arch bridges could be developed by both modeling approaches. The micro modeling should be preferred to understand the collapse mechanism and to observe the hinge formation in the detailed investigation of the masonry bridges. However, the composite modeling based on the homogenization technique [3] is often used due to modeling difficulties of the multi-span masonry arch bridges.

There is a wide range of references [4~10] on the nonlinear behavior and possible collapse mechanisms of masonry arch bridges under vertical static loads by using FEM. Each research has made a considerable contribution to the understanding of failure mechanisms of such bridges which have different arch geometry and material properties. Elastic and inelastic mechanical properties of masonry, infill and backfill effect, boundary conditions, modeling approaches, and imposed loads on bridge significantly affect nonlinear response of such structures. To predict the actual behavior of masonry arch bridges, it is essential to integrate nonlinear response of fill material with crushing and cracking behavior of masonry [5~7]. Detailed FE models which consider discontinuities in the joints between voussoirs have generated the reasonable results about the collapse load and corresponding hinge mechanisms of masonry arch bridges [8~10].

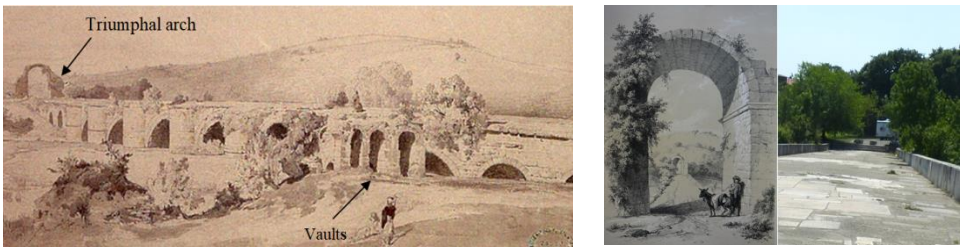
This paper presents numerical results from an investigation of the multi-span masonry arch Justinian's Bridge as a case study. The aim of this work is to search nonlinear structural behavior of the bridge by the finite element method and to investigate the influence of the tensile fracture energy of masonry on the collapse mechanism and load carrying capacity of the bridge.

2 CASE STUDY

2.1 Historical significance

The Justinian's Bridge (also known as the Historical Beşköprü or Sangarius Bridge) was erected to connect Constantinople (today's Istanbul), the capital of the Empire, and the east provinces. The bridge was built in between the years of 553-562 A.D within the 6th century by order of Emperor Justinian (A.D 523-567) of the East-Roman Empire [11]. The bridge takes place over the Sakarya River, in the city of Sakarya in Turkey located on the North-West region of Anatolia according to the available registers.

The Justinian's Bridge is a significant sample of bridge heritage that has reached to the present day from the Byzantine Era. There was a triumphal arch until the 19th century in the western entrance of the bridge [11]. This triumphal arch is seen in Jules Lauren's drawing dated 1859 in Fig.1a and in Texier's engraving dated 1838 in Fig.1b. Nowadays, this part has completely vanished (Fig.1b). Today, the bridge is on a dry valley because the wide Sakarya River laid to 3 km to the East (Fig.2a) and Çark stream, which flows from the nearby Sapanca Lake, flows from a bay of the bridge [15]. The bridge is an unprecedented structure in terms of either its gigantic piers and the apse structures around the bridge (Figs.2a, 2b).



(a) (b)

Figure 1: Justinian's Bridge; (a) painting by Jules Laurens [12], (b) Texier's the lost triumphal arch [13].



(a) (b)

Figure 2: Justinian's Bridge; (a) view of the bridge today [14], (b) apse structure [16].

2.2 Past repair interventions and current damages

The known last restoration of the bridge was conducted in 1995 and carried out by the Republic of Turkey General Directorate of Highways. Some deteriorated stones belonging to spandrel walls were replaced with the new ones and the parapets were constructed. However, the work could not have been completed and the bridge was closed to vehicle traffic.

There is no serious misalignment and obliquity in the horizontal line of the walling. A major crack occurred through the intrados of the arch numbered as 4 at an unknown time [15]. Site investigations made in 2016 revealed that there have been some material losses on the components of the bridge such as parapet, slab, and vaults (Fig.3). Besides, a wide shear crack occurred at the South pier of the apse possibly due to past devastating earthquakes (Fig.3c). Note that the bridge under consideration is located in a highly active seismic zone.



(a) (b) (c)

Figure 3: Current damages [16]; (a) lost parapet part, (b) material loss in vaults, and (c) shear crack in the apse.

In 2018, the current restoration work was initiated by the Republic of Turkey General Directorate of Highways and the work has continued to the date. The Justinian's Bridge has been inscribed on the United Nations Educational, Scientific and Cultural Organization (UNESCO) World Heritage Tentative List since 2018 [17].

2.3 Bridge geometry

The Justinian's Bridge which is a continuous arched masonry bridge has a total length of 429 m in plan (Fig.4). All arch forms of the bridge are semi-circular in Texier's bridge sketch dated 1838 (Fig.4). The bridge has 12 spans, labeled as A1 to A12 and has 7 piers labeled as P1 to P7. The seven arches, which are main load bearing arches and labeled as A4~A10, are double-layered and the average thicknesses of the first (inner) and second (outer) arches are 1.0 m and 0.40 m, respectively. The arches labeled as A5, A7, and A8 have maximum spans of L=24.5 m. Spans of the arches A4, A6, A9, and A10 vary from 19.5 m to 24 m. Other arches possess smaller spans ranging from 3m to 9 m. The main arches were modeled as spans given in Fig.5b because a small part of the bridge sunk into the existing soil nowadays.

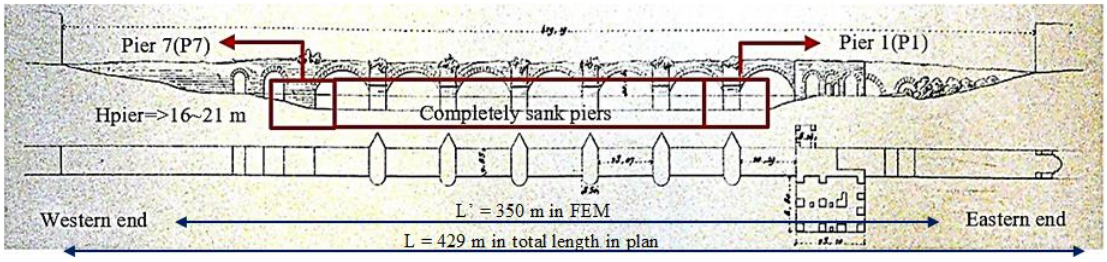


Figure 4: Texier's bridge sketch dated 1838 [13].

Width of the bridge is B=18 m together with the total pier. However, the clear width of the bridge and each flood splitter are 10 m and 4m, respectively. Thickness of each one of spandrel walls is about 2.0 m. The average slab thickness is 0.40 m. The bridge has a maximum clear height of about 9 m together with its visible piers. Section of the piers has a pointed shape at the North facade and a semi-circular shaped at the South facade as given in Fig.5a. The thickness and height of the parapets are 0.50 m and 0.80 m, respectively.

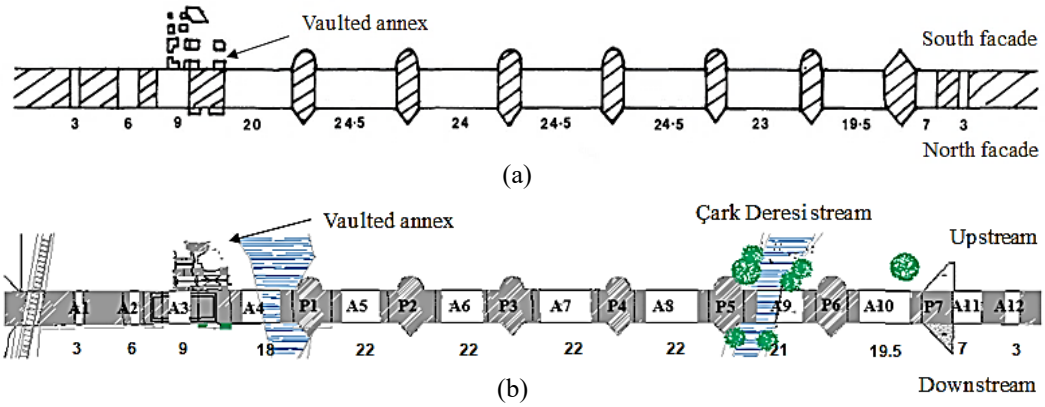


Figure 5: (a) Plan of the Justinian's Bridge after Texier [11], (b) spans adopted in FEM of the bridge.

3 NUMERICAL MODELING

3.1 Material property

Justinian's Bridge was constructed with natural limestone units and brick dust mortar. Rubble stone with mortar was used for backfill (over the arches) and infill (between exterior spandrel walls). The most possible material properties were sought in the well-known references especially focusing on mechanical behavior of masonry bridges since no material tests could have been conducted for the bridge.

Nonlinear behavior of masonry was modeled by adopting the total strain fixed crack model (TSFCM) simulating both compression and tensile behavior of the material, based on the results of a comprehensive study carried out on 3D nonlinear modeling and testing [16]. An exponential softening behavior in tension and parabolic hardening behavior followed by parabolic/exponential softening in compression were chosen. The fill medium was modeled as a cohesive–frictional material by the isotropic Mohr-Coulomb plasticity criterion [7, 8].

Young's modulus (i.e. E modulus) varies from 3000 MPa to 5000 MPa for cut stone masonry with wide joints or substantial rubble masonry [5]. Additionally, the Poisson's ratio (ν) was assumed to be the same (0.20) both for main structural elements, which are piers, arches, spandrel walls, and for secondary structural elements such as flood splitters, backfill, infill, slab, and parapet. Table 1 presents the elastic material properties utilized in the numerical implementation of the bridge.

Table 1: Elastic material properties adopted for the Justinian's Bridge.

	Density, γ [kg/m^3]	Young's modulus, E [N/mm^2]	Poisson's ratio, ν [-]
Arch	2100	3500	0.20
Spandrel wall	2100	3000	0.20
Flood splitter	2100	2500	0.20
Pier	2100	3500	0.20
Backfill & Infill	1900	500	0.20
Slab	1500	1000	0.20

A recommended value of 8 N/mm^2 was considered for the compressive strength of the masonry material frequently seen in such ancient structures [5]. In the condition that compressive strength of masonry is lower than 12 N/mm^2, the ductility factor for compression is recommended to be 1.6 mm [18]. The fracture energy in compression was calculated as 12.8 N/mm for the compressive strength of 8 N/mm^2 and for the ductility index of 1.6 mm. A numerical value of 0.20 N/mm^2 is adopted for tensile strength of overall masonry [16]. The ductility index for tension, which is the ratio between tensile fracture energy and tensile strength, is recommended to be 0.029 mm for stone material [18]. In this study, this value was calculated to be 0.01 N/mm and was considered as a lower value of tensile fracture energy. However, an average value of 0.10 N/mm was adopted for the upper bound of this parameter [1, 7]. The plasticity parameters of the fill material were chosen based on a comparison and discussion of the information given in the current literature [7, 10, 23]. Inelastic properties of the masonry and the fill material are presented in Table 2.

Table 2: Inelastic material properties adopted for Justinian's Bridge.

Masonry material			
f_t	0.20	[N/mm^2]	Tensile strength
Gf^l : Lower value	0.01	[N/mm]	Tensile fracture energy
Gf^l : Upper value	0.10	[N/mm]	Tensile fracture energy
f_c	8.00	[N/mm^2]	Compressive strength
Gf_c	12.8	[N/mm]	Compressive fracture energy
Backfill & Infill			
c	0.05	[N/mm^2]	Cohesion
φ	20	[°]	Friction angle
ψ	5	[°]	Dilatancy angle

3.2 Three-dimensional (3D) finite element modeling (FEM)

A 3D FE model of the bridge was generated in DIANA FEA software [19] using isotropic solid elements, making the use of homogenization technique [3]. All components of the bridge, which are the piers, the inner and outer arches, the spandrel walls, the fill material, the slab and the parapets were individually modeled in the macro-modeling strategy as composite [2]. The FE model of the bridge is shown in Figs.6, 7. The bridge was modeled with a total 39863 solid mesh elements which are eight-noded brick elements used for each component and six-noded wedge elements used throughout the arch ring due to the bridge geometry. It was assumed that the piers of the bridge were fixed to the soil. In order to simulate the sunken parts of piers and side walls of the bridge, the rotational motion was released whereas the axial motion was restrained in all directions.

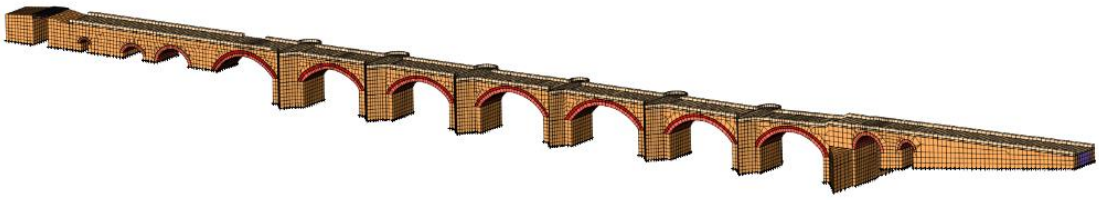


Figure 6: The Justinian's bridge – finite element model.

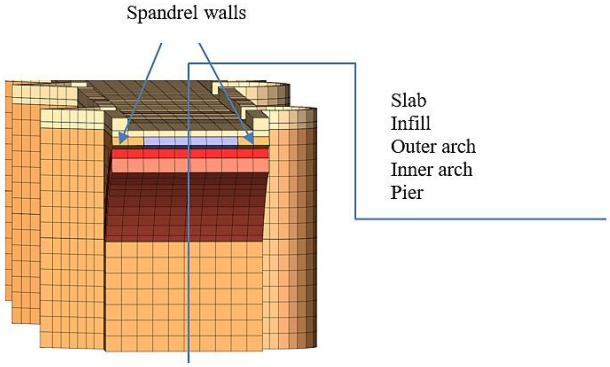


Figure 7: Cross-section view of a typical span of the bridge.

3.3 Load cases

In order to assess the failure mechanism and the critical loading position, the bridge was loaded at three positions of the arch numbered A8 which has the largest span that the maximum displacements and stresses obtained in the linear elastic analyses [20]. Self-weight of the bridge was applied as automatically by the software. Subsequently, the live loads were applied in increments of 200 kN in the vertical direction [21]. The uniformly distributed load was applied to the road surface throughout the full width between the parapets. The loading was then carried out at the quarter (1/4L), one third (1/3L), and middle-span (crown, 1/2L) of the span, respectively as shown in Fig.8.

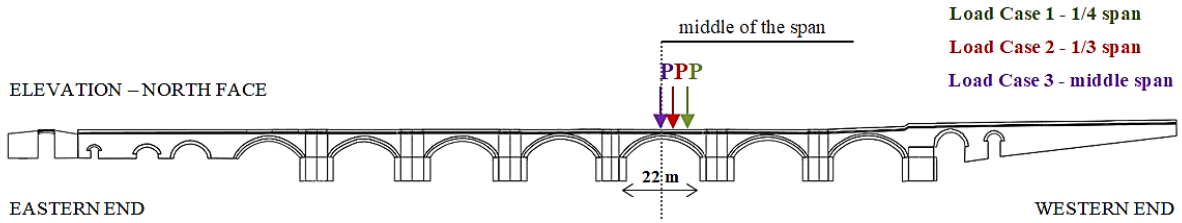


Figure 8: Load cases.

3.4 Nonlinear analysis procedures

Self-weight of the bridge was applied first, followed by the application of the incremental live loads up to failure for each load case. In the numerical implementation, the incremental loading was controlled with force, displacement and residual norms because at least three norms should be satisfied together in the convergence criterion for softening behavior of masonry [19]. In each step of the incremental loading, the iterations were performed with the modified Newton-Raphson method by integrating the line search method in DIANA [19].

4 NONLINEAR STATIC ANALYSIS (NSA) RESULTS

4.1 Influence of tensile fracture energy Gf^I

A series of analysis was carried out for lower and upper values of fracture energy in tension to evaluate the collapse mechanism of the bridge for each load case. The vertical load-vertical deflection curves obtained from the nonlinear static analyses (NSAs) of the bridge are given in Fig.9. Each deflection was monitored after obtaining an equilibrium state in each step of incremental loading. Additionally, upper limit loads are calculated via RING 3.1 [22] and depicted in Figure 9 as well, revealing that the maximum vertical load values obtained from the macro-modeling are close to the ones obtained from the simplified limit analysis.

The numerical results obtained for each load case showed that a lower value of tensile fracture energy cause a weakly nonlinear failure of the bridge. Note that similar results have been reported in other related previous works [7, 16, 23]. The most critical loading position was obtained in the case of middle-span loading for lower value of tensile fracture energy. The failure mechanism occurred by the formation of one-hinge under the middle-span loading of the bridge is given Fig.10 with the presentation of maximum principal stresses. The failure mechanism is relevant around the key stone.

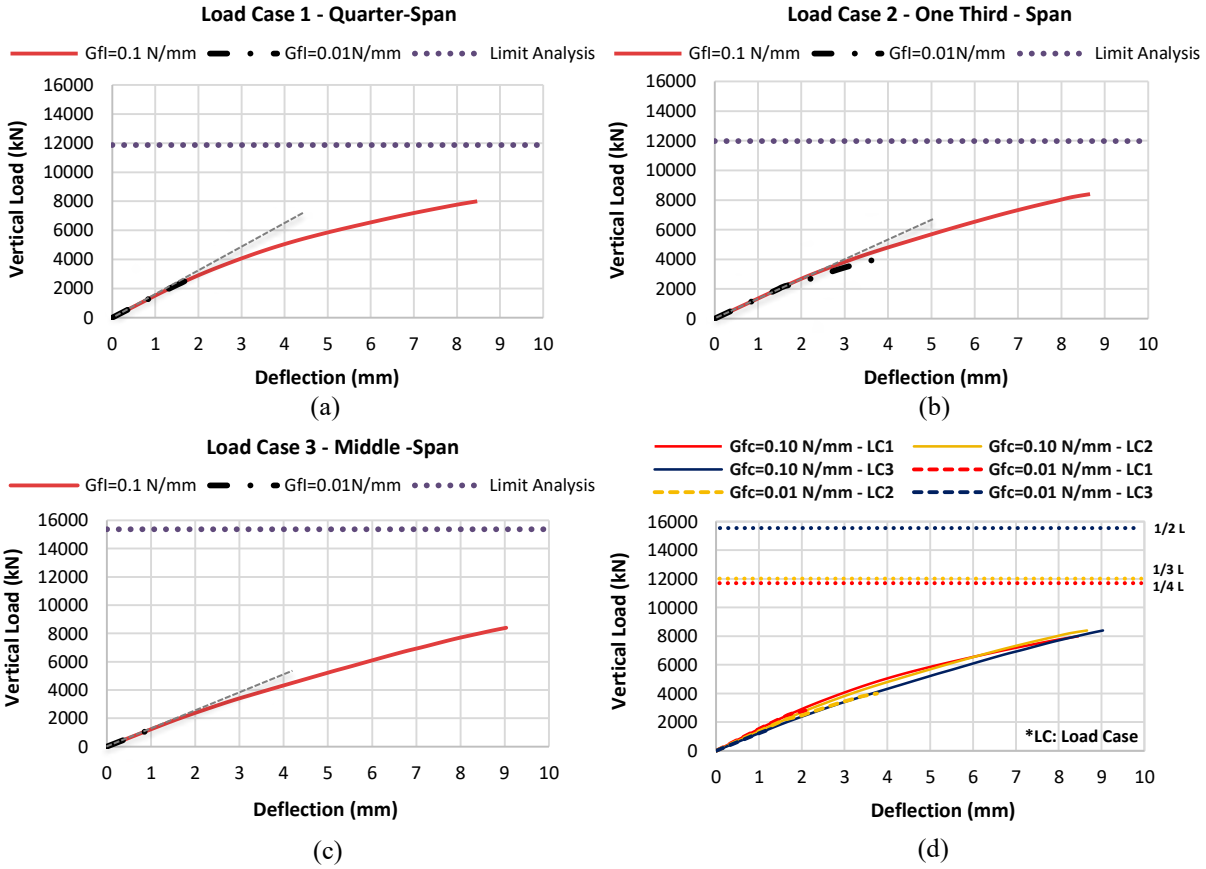


Figure 9: Load-deflection curves obtained for (a) quarter-span, b) one third-span, (c) middle-span, (d) all.

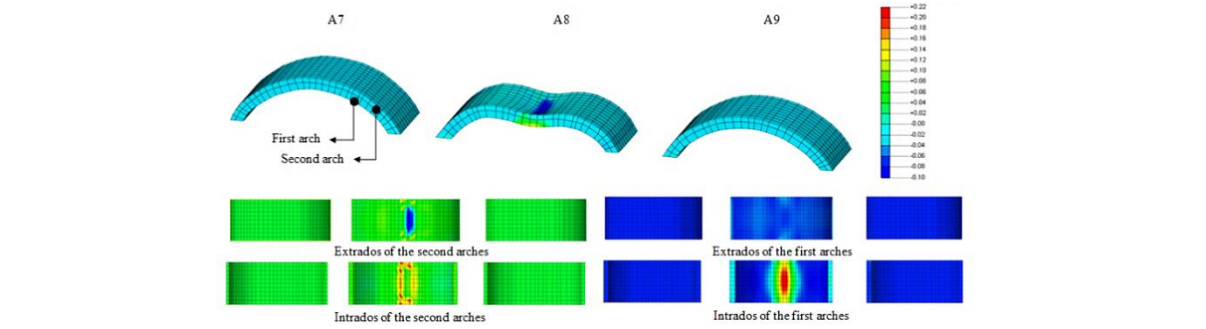


Figure 10: Failure mechanism obtained from the 'middle-span' loading performed for Gf^{I}=0.01 N/mm with the presentation of maximum principal stresses (Scale: -0.10/+0.22 N/mm^2).

For the upper value of tensile fracture energy, the bridge showed a strongly nonlinear behavior and collapsed resulting in larger vertical deflections at a higher load. Note that this is an expected failure type for such structures. The failure loads obtained from the nonlinear static and limit analyses are represented in Table 3. Increasing the value of the fracture energy by 10 times causes 65, 55, and 83 percent increases in the load carrying capacity of the bridge for the loading cases of 1/4, 1/3, and1/2 of the span, respectively.

Table 3: Failure loads obtained for both fracture enegy values in tension.

Load Position	Failure Load (kN)		Difference (%)	Limit Analysis
	Gf^I=0.01 N/mm	Gf^I=0.10 N/mm		
Quarter-span	2800	8000	65	11865
One third-span	3800	8400	55	11978
Middle-span	1400	8400	83	15368

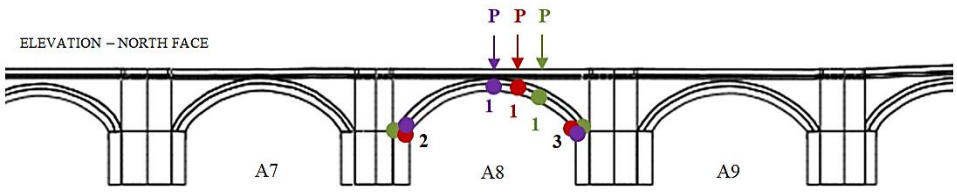
4.2 Comparison of NSA results for Gf^I =0.10 N/mm

Nonlinear responses obtained for the upper value of tensile fracture energy are represented in Table 4 for the three load cases. In each loading position, the bridge showed linear behavior up to one third of the ultimate load (Fig.9) and afterwards collapsed by the generation of 3-hinge mechanism. Fig.11 illustrates the obtained failure mechanisms and the corresponding plastic hinge formations under different load cases.

Table 4: Nonlinear responses obtained for Gf^I=0.10 N/mm.

Load Position	$d_{Z,loaded\ point}$ (mm)	Failure Load (kN)	Hinge Mechanism
Quarter-span	8.5	8000	3
One third-span	8.7	8400	3
Middle-span	9.0	8400	3

It is concluded that the most critical loading position is 'the quarter-span' of the bridge because the lower load carrying capacity was obtained at failure of the bridge. 3D failure patterns of the bridge for the quarter-span load case are given in Figs.12. It is seen in Fig. 12a that cracking was initiated and the three plastic hinges are developed where the principal stresses have reached at the tensile strength of the masonry. Plastic hinges occurred at the loaded span, the East and West springings of the arch, respectively. The critical vertical deflection under the load was obtained to be 8.5 mm.



Hinge No	Load Case 1 - 1/4 span	Load Case 2 - 1/3 span	Load Case 3 - middle span
1	5400	7800	5600
2	7800	8000	7200
3	8000	8400	8400

Figure 11: Failure mechanisms for (a) the quarter-span, (b) the one third-span, (c) the middle-span.

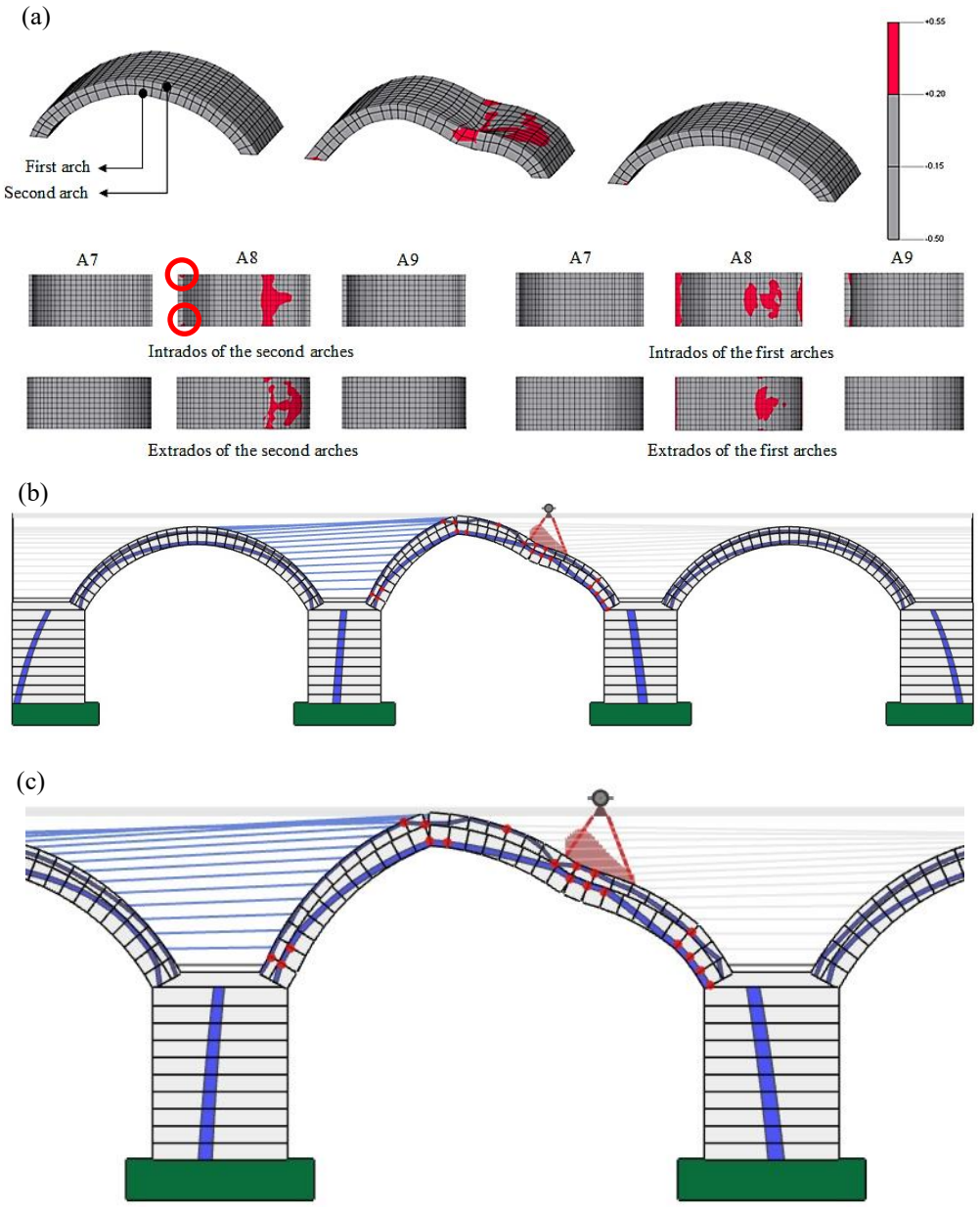


Figure 12: Failure mechanism obtained from the most critical loading position 'quarter-span': (a) finite element model with the presentation of maximum principal stresses for G_f^I=0.10 N/mm (Scale: -0.50/+0.55 N/mm^2), (b) rigid block limit analysis model, (c) close-up view of hinge mechanism in rigid block limit analysis model.

5 CONCLUSIONS

The existing Justinian's Bridge, located in the city of Sakarya in Turkey, has been investigated to assess the possible collapse mechanism and corresponding load capacity. A 3D structural model for the bridge was developed for this purpose. The bridge was loaded at the quarter, one third, and middle-span of the arch numbered 8 (the largest span). A series of nonlinear static FE analyses were performed for the selected lower and upper values of tensile fracture energy of the stone material.

Numerical results show that the value of tensile fracture energy considered for masonry material significantly affects the load carrying capacity and collapse mechanism of Justinian's Bridge. In an upper value of 0.10 N/mm of tensile fracture energy, the bridge behaves strongly nonlinear and failed by generating the hinge mechanism occurring in the loaded arch for all of the assumed three load cases. Note that no visible damage occurred in both arches adjacent to the collapsed arch. The most critical loading position for the Justinian's Bridge under incremental static loads was obtained at the quarter-span of the loaded arch. The results of rigid block limit analysis carried out for the bridge sufficiently close to the results of nonlinear static analysis. Limit analysis calculations show that the most critical loading position again occurred at the quarter span of the bridge. This significant result confirms the widely accepted testing procedure followed in many research [24, 25].

As a result of the nonlinear finite element analyses, under elastic conditions, the allowable vertical load for the bridge was obtained to be 2400 kN (30% of the ultimate load) for the upper value of tensile fracture energy. Ultimate load capacity of the bridge was found to be 8000 kN in which the bridge collapsed by the formation of three plastic hinges. It seems that the plastic hinges occurred at the quarter-span, the east, and west springings where the maximum principal stresses have exceeded the existing tensile strength of masonry.

It is concluded that increasing the value of the fracture energy causes an increase in load carrying capacity of such masonry bridges. Finally, in future works, the influence of greater values of tensile fracture energy and the relation between the tensile strength and tensile fracture energy on the load carrying capacity of masonry arch bridges could be investigated by performing sensitivity analyses.

Acknowledgements. This work has been carried out with the financial support from the Scientific and Technological Research Council of Turkey (TUBITAK) under the assigned project number of 114M305.

REFERENCES

[1] Lourenço, P.B. Analysis of Historical Constructions from Thrust-lines to Advanced Simulations, In P.B. Lourenço and P. Roca (Eds.): *Historical Constructions: Possibilities of Numerical and Experimental Techniques,* Proceedings of the Third International Seminar (2001).

[2] Lourenço, P.B. Computational Strategies for Masonry Structures. Ph.D Thesis, University of Minho, Braga, Portugal: PhD dissertation (1996).

[3] Lourenço, P.B., Milani, G., Tralli, A., and Zucchini, A. Analysis of masonry structures: review of and recent trends in homogenization techniques. *Canadian Journal of Civil Engineering* (2007) **34:**1443-1457.

[4] Cavicchi, A., and Gambarotta, L. Two-dimensional finite element upper bound limit analysis of masonry bridges. *Computers and Structures* (2006)*,* **84**: 2316-2328.

[5] Fanning, P.J., Boothby, T.E. Three-dimensional modeling and full-scale testing of stone arch bridges. *Computers and Structures* (2001) **79:** 2645-2662.

[6] Frunzio, G., Monaco, M. and Gesualdo, A. 3D F.E.M Analysis of a Roman Arch Bridge. In P.B. Lourenço and P. Roca (Eds.): *Historical Constructions: Possibilities of Numerical and Experimental Techniques,* Proceedings of the Third International Seminar (2001), pp.591-598.

[7] Conde, B., Ramos, L. F., Oliveira, D. V., Riveiro, B., and Solla, M. Structural assessment of masonry arch bridges by combination of non-destructive testing tecniques and three-dimensional numerical modeling: Application to Vilanova bridge. *Engineering Structures* (2017) **148**: 621-638.
[8] Milani, G., and Lourenço, P.B. 3D non-linear behavior of masonry arch bridges. *Computer and Structures* (2012) **110-111**: 133-150.
[9] Costa, C., Arede, A., Morais, M., and Anibal, A. Detailed FE and DE modeling of stone masonry arch bridges for the assessment of load-carrying capacity. *Procedia Engineering* (2015*)* **114**: 854-861.
[10] Diaz, J., Romera, L., and Hernandez, S. Non-linear Finite Element Analysis and Limit Analysis Comparison of the Caaveiro Stone Arch Bridge. In C.A. Brebbia (Ed.): *Studies, Repairs and Maintenance of Heritage Architecture,* WIT Press (2007), pp.556-575.
[11] Whitby, M. Justinian's Bridge over the Sangarius and the date of Procopius'de Aedificiis. *The Journal of Hellenic Studies* (1985) **105**: 129-148.
[12] <*http://kantaratlas.blogspot.com.tr/* >, date retrieved 27.05.2018.
[13] <*https://en.wikipedia.org/wiki/Sangarius_Bridge*>, date retrieved 29.06.2016.
[14] <*http://www.sakaryakulturturizm.gov.tr*>, date retrieved 29.06.2016.
[15] Ozcan, Z. Tarihi Sangarius Köprüsü'nde hasar belirlenmesi ve güçlendirme önerileri. *3. Köprüler ve Viyadükler Sempozyumu,* Istanbul, Turkey, 8-10 Mayıs, 2015.
[16] Mentese, V.G. 3D Nonlinear Modeling and Testing of Historic Stone Masonry Arch Bridges: The Case of Justinian's Bridge. Istanbul Technical University, Istanbul, Turkey: M.Sc. Thesis (2018).
[17] <whc.unesco.org/en/tentativelists/6347/>, date retrieved 02.05.2018.
[18] Angelillo, M., Lourenço, P.B., Milani, G. Masonry Behaviour and Modelling. In M. Angelillo (Ed.): *Mechanics of Masonry Structures*, Springer (2014), pp.13-27.
[19] TNO DIANA 9.6. Diana Finite Element Analysis. Delft, The Netherlands: 2014.
[20] Mentese, V.G., Gedik, Y.H., Gunes, O., and Korkmaz, K.A. Structural Investigation on Justinianus Bridge in Sakarya city of Turkey. *1st Istanbul Bridge Conference,* Istanbul, Turkey, August 8-9, 2016.
[21] Page, J. *Load tests to collapse on two arch bridges at Preston, Shropshire and Prestwood, Staffordshire* (Report No. 110). UK: The Report of Transport and Road Research Laboratory (TRRL), Department of Transport (1987).
[22] LimitState: RING 3.1. Masonry Arch Analysis Software. Sheffield, the UK: 2014.
[23] Pulatsu, B., Erdogmus, E., and Bretas, E. Parametric study on masonry arches using 2D discrete element modeling. *Journal of Architectural Engineering* (2018). **24(2)**.
[24] Page, J. Load Tests to Collapse on Masonry Arch Bridges. In T. Telford and C. Melbourne (Eds.): *Arch Bridges,* Thomas Telford, UK: London (1995), pp.289-298.
[25] Brencich, A., and De Francesco, U. Assessment of multispan masonry arch bridges. II: Examples and applications. *Journal of Bridge Engineering* (2004) **9(6)**: 591-598.

12th International Conference on Structural Analysis of Historical Constructions
SAHC 2020
P. Roca, L. Pelà and C. Molins (Eds.)

A COMPARISON BETWEEN TRADITIONAL AND MODERN APPROACHES FOR THE STRUCTURAL MODELLING OF BRICK MASONRY BARREL VAULTS

EVA COÏSSON[1*], DANIELE FERRETTI[1] AND FEDERICO PAGLIARI[1]

[1]Department of Engineering and Architecture, University of Parma
Parco Area delle Scienze 181/A, 43124 Parma, Italy
*e-mail: eva.coisson@unipr.it, daniele.ferretti@unipr.it, federico.pagliari@studenti.unipr.it
web page: http://www.dia.unipr.it
(*corresponding author)

Keywords: Historical Structure, Masonry, Modelling, Barrel Vaults

Abstract. *Masonry vaults are widespread and characteristic structural elements of our built heritage since many centuries, but for a very long time they were built only based upon the experience and the proportional analysis of previous positive examples. Since the Hooke's observations, in 17th century, about the shape of the catenary, and the first graphical analyses of 18th century, the tools for their "scientific" calculation have developed quickly [1], mainly to assess the stability of already existing structures rather than for the prevision of the future behaviour of new vaults. Despite the great progress in this field, ordinary programs for the static and seismic assessment of masonry buildings often disregard the vaults structural role and the professionals sometimes underestimate it, also due to the lack of attention dedicated to these structures by the technical codes. Therefore it seems now important to reconnect the elements of this modelling historical evolution, to compare the different methods and to find an equilibrium between complexity and reliability, making it accessible also to the common professional use, whose effects on preservation are important.*

To this aim, a pavilion vault was chosen as a reference, with given geometries and materials features, and the different methods were applied. On one side, traditional methods were chosen: the graphic Méry method [2] and the static theorem of limit analysis [3] have been applied to a system of 2D arches composing the vault. On the other side, a 2D Finite Element Model and the edge cutting ChronoEngine Distinct Element Model [4] have been also tested, under the same conditions. The influence of the brick pattern on the structural behaviour have been considered, conveniently defining the arches decomposition in the traditional methods and the blocks division in the Distinct Element Method. In all cases, calculations have been made changing both values and positions of the loads. The results are compared both in terms of stresses inside the masonry and in terms of deformation of the structural elements, evaluating the types of information and detail that the different approaches can supply. The results of the advanced numerical methods allow to assess the validity of the traditional approaches. On the other side, the possible contribution of the traditional methods to the calibration of the parameters for the numerical models is also discussed.

1 INTRODUCTION

Since the introduction of the first known arched masonry structures in Egypt and Mesopotamia, at least in the 4th millennium b.C. [1], arches, vaults and domes have spread and characterized our historical built heritage with the adoption of various shapes and technologies, typical of each area and each historical period. As for all constructions – and for masonry structures in particular – until very recently also the curved masonry elements were built only based upon the experience and the proportional analysis of previous positive examples: the main concern of the builders was to have supports large enough to sustain the thrusts, rather than defining the thickness and shape of the vault itself. It was only in the 17th century that Hooke made his observations about the shape of the catenary, concentrating the attention on the shape of the arch and its relation to the carried loads. Then, the first graphical analyses were developed in the 18th century and since then the tools for the calculation of curved masonry structures in a scientific sense have developed quickly [2]. Despite the great progress in this field, and the advanced computation instruments available to date, most of the programs ordinarily adopted by the professionals for the static and seismic assessment of masonry buildings disregard the vaults structural role, involving an underestimation of their stability and a consequent overestimation of the needed structural interventions, in contrast with the required minimum intervention principle for historical buildings. Already in 1945 the architect and engineer Gustavo Giovannoni wrote that "the concept of limiting the strengthening interventions to the minimum needed entails the exploitation of the resource schemes developed in the building statics without altering them" [3], but to exploit these resources, which are intrinsic to the historical structures, we need to know them and also to quantify them efficiently: to this aim, a comparison among methods for the static analysis of barrel vaults with different, progressive levels of refinement are here reported to assess their reliability as instruments for the knowledge and preservation of these irreplaceable architectural elements.

2 STATE OF THE ART

Because of their geometry, barrel vaults are usually modelled as elemental parallel arches; of these, they inherit the different methods of analysis ([6], [26]). The methods for the assessment of arches and vaults can be roughly divided in two categories. To the first category includes the methods based on the graphical tracing of the thrust-line (i.e. the set of points corresponding to the position of the resultant of normal stresses in each cross section of the arch). To this category belong the well-known Mery's method [5] and Heyman's method [6]. The approach has also been extended from 2D to 3D by replacing the thrust-line with a thrust-network of forces ([19], [20], [21]) but for barrel vaults usually this is not necessary. The second category includes numerical approaches mainly based on finite element or discrete element methods. Each of them has pros and cons [2]. Because of the vastness of the subject matter, we will only describe the methods used in this paper.

2.1 Méry's method

Mery's method [5], already reported in the 19th century treatises [22], is one of the simplest methods and perhaps for this reason it is widespread in design practice of small

vaults. Mery assumes that a barrel vault can be studied as an arch made up of infinite non-tensile voussoirs that do not slide between each other. The method is based on the plotting of the line-of-thrust and the study of its position within the thickness of the arch. Based on experimental observations, it is assumed that in a round arch the line-of-thrust passes through the upper middle-third in the key section and at the lower middle-third in cross sections at 30° and 150° with respect to a horizontal line passing through the center of curvature. The arch is safe if the line-of-thrust does not cause tensile stresses, i.e. it is comprised in the cross-section core.

2.2 Line-of-thrust with minimum stress

Mery's method, not allowing the formation of cracks, is quite conservative. Other methods impose less strict conditions on the position of the line-of-thrust, usually adopting lower-bound theorem of limit analysis ([2],[6]). Among these, the approach implemented in the freeware software ARCO [10], computes the position of the line-of-thrust that minimizes the maximum stress in the sections. The stress, which is determined with a no-tension linear elastic model, is compared with the material strength to avoid compression failure. The approach has been used in this work because it is very common in Italian design practice and it adapts well to the stress checks required by the Italian code standard.

2.3 Finite Element Method

Vaults have been extensively studied with non-linear finite element models [2]. For instance, Creazza et al. [24] modelled a barrel vault in 3D using a nonlinear damage model. D'Altri et al. [17] modelled a gothic barrel vault using solid finite elements bricks interacting with contacts. Cavicchi and Gambarotta [25] proposed a two-dimensional finite element upper bound limit analysis that permits to model also the infill. If the infill is taken into account with equivalent forces, it is possible to model the arch with 2D nonlinear fiber beam elements, as proposed by de Felice [23]. This approach has been used in the present work because, despite its simplicity, it represents well the states of stress and the deformation of the arch.

2.4 Discrete Element Method

Discrete Element Method (DEM) has been widely used to model masonry vaults. By means of DEM, portions of vault or single bricks are modelled as blocks interacting each other by means of springs and dashpots. For a comprehensive review of the method, see [27]. Different authors used the software 3DEC to analyze the behavior of cross vaults [28][29][30] and barrel vaults [29] subjected to settlements of the imposts. In typical DEM the equations ruling the problem are solved using time-step explicit integration algorithms which are computationally intensive because of the small time-steps required. To reduce the computational effort, a particular type of DEM, called Non Smooth Contact Dynamics (NSCD), was proposed by Moreau and Jean [31][32]. In this case the equations ruling the problem are solved using implicit integration algorithms that permit larger time-step. This method was implemented in the software LMGC90 [33] and was used to study masonry arches and vaults [34][35][36][37]. An independent implementation of NSCD was proposed by Tasora et al. with the ProjectChrono open source library [7]. The library, originally

developed for mechanical engineering, was applied to study masonry arches and domes [38][39]. The seismic behavior of local mechanisms in a castle were analyzed in [40] while Ferretti et al. [9] used the library to study masonry barrel vaults considering both the presence of linear elastic iron ties and filling, which is modelled with spheres.

Because of its features, the library Project Chrono was adopted in the present work.

3 CASE STUDY

In order to analyse and compare the potentialities, the effectiveness and also the limits of each of the aforementioned methods for the analyses of masonry barrel vaults, a case study was chosen from a real historical structure: the Pilotta Palace, in Parma (Italy). In particular, a barrel vault with pavilion heads, covering the atrium of the Farnese Palace, was chosen: the limited surveys and tests carried out allowed to hypothesize a structure made in brick masonry with a thickness varying between 12 and 24 cm (more details about the conformation of the analysed vaults can be found in [8]). Over the vault, a large room (8 m wide and 22 m long) is located, whose future uses are now under discussion, also in consideration of the structural capabilities of the vault itself [11]. The structural analyses started with the classical methods: the graphic statics of Mery's method and the more recent limit state analysis, conducted through the ARCO software. Since the deformability of the vault is not taken into account by these methods, the analysis was repeated using both Finite Elements Method (FEM) and Discrete Elements Method (DEM) in order to consider the consequences of geometry variations and the behavior of the tie and the supporting walls.



Figure 1: Analysed vault and overlying room

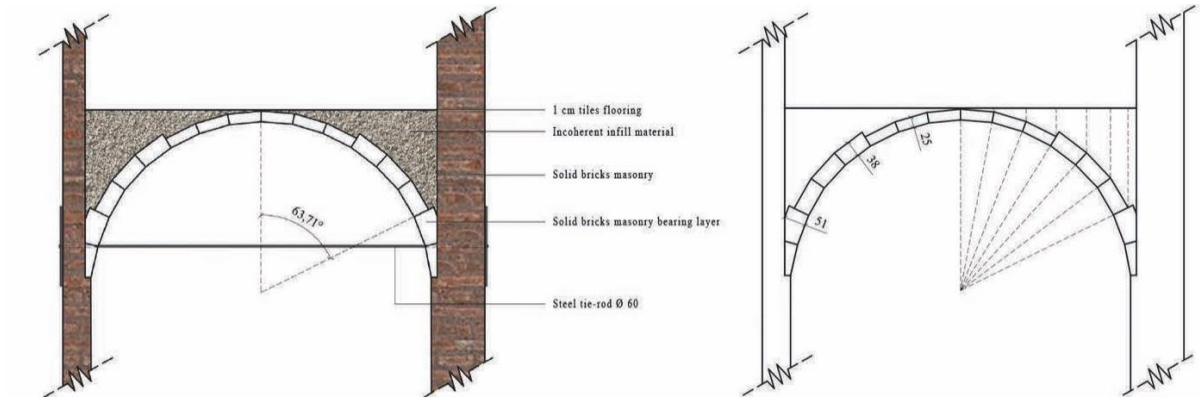


Figure 2: Structural scheme of the vault.

3.1 Méry's graphic method

The first tool used to analyse the vault is based upon the graphic statics: the Mèry's Method. Likewise other classical analysis models, it does not take in to account the deformability of the materials. A 1 m wide arch placed in a representative section of the considered vault, obtained by a detailed laserscanner architectural survey, was chosen to represent the whole structure. The specific weight for masonry and infill was assumed of 18 kN/m^3 and 14 kN/m^3 respectively. The analysis was performed with three load conditions: dead loads (g_k only), dead loads plus variable loads corresponding to reading room use category (q_k = 3 kN/m^2) and the same case with the introduction of the partial coefficients for the action's effect (γ) imposed by the Italian technical code in the Ultimate Limit States assessment. In particular, their values correspond to 1.0 for masonry and infill (γ_{G1}) and to 1.5 for flooring and variable loads (γ_{G2} and γ_Q). Moreover, the collapse condition was determined without partial coefficients, using an iterative procedure. The value of the mean compressive strength of masonry has been assumed equal to f_m = 3.2 MPa and the corresponding design compressive strength was f_d = 2.78 MPa (reduced to 0.93 MPa when taking into account the γ coefficients), following the Italian Code [4]. According to Mèry's method hypotheses, the round arch symmetrically loaded is studied with three plastic hinges located at 30°, 150° (haunches) and 90° (keystone) from the horizontal line passing through the centre of curvature. In fact, the only portion that was analyzed was the one comprised between 30° and 150° and it was divided into 12 voussoirs (Figure 2). The polygon of the forces, represented in Figure 3, is constrained to pass through the upper and lower limit of the cross section core at the keystone section and at the haunches sections respectively. Horizontal thrust component H values are shown in Table 1.

3.2 Line-of-thrust with minimum stress

The analysis was repeated using an approach based on the Line-of-thrust with minimum stress. The chosen tool was the software ARCO [10]: it varies iteratively the eccentricity of the line of thrust, aiming to achieve the lowest possible value of the stresses in the cross sections under the given scheme of vertical loads. The geometry was unchanged compared to the Mèry's method. Results are reported in Figure 3 and Table 1.

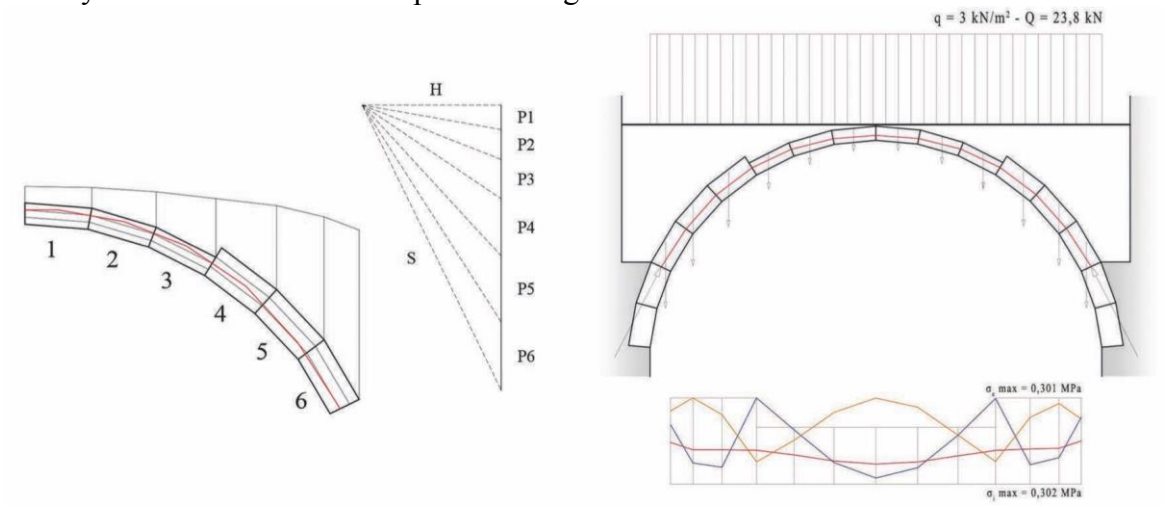


Figure 3: Analysis with Mèry's method (left) and ARCO software (right).

3.3 Finite Element Method

The tool used for the FEM analysis was the software Abaqus from Dassault Systèmes; the same geometry used in the classic methods was modeled with 2D fiber-beam finite elements. Dead and variable loads were rendered by concentrated forces applied in the centre of gravity of the elements. The collapse condition of the structure was obtained with the application of variable loads increased per-step. The mechanical behavior of masonry was modeled using the nonlinear material model "Concrete Damage Plasticity" (CDP), with Young modulus E = 1500 MPa and Poisson coefficient ν = 0.2. The adopted CDP model parameters are: Dilatancy angle: 10°; Eccentricity: 0.1; f_{b0}/f_{c0}: 1.16; K: 0.667; Viscosity parameter: 0.002. For the stress-strain relationship in compression, the relationship proposed in [12] was used. Mortar's compressive strength was assumed prudently equal to f_m = 1 MPa, while the same value for the blocks was taken equal to f_b = 15 MPa. The obtained stress-strain curve (Figure 4) was rescaled to include plastic strain only. The tensile constitutive law refers to the experiences reported in [13] (Figure 5). The first batch of analyses was carried out with the vault constrained at the spring in order to better match the layout of the classic models. The values of the maximum compressive stress in the three cases are reported in Table 1, together with the horizontal thrust component H.

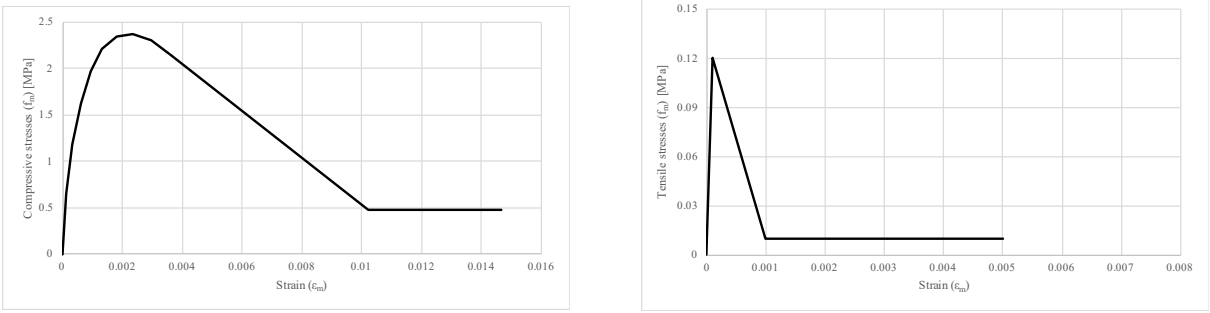


Figure 4 and 5: Compressive and tensile constitutive laws.

The second batch of analyses brings in the contributions of the supporting walls and of the metal tie-rods, 60 mm in diameter, both modelled with beam elements. Mechanical properties were deducted from previous studies regarding historical architectural tie-rods [14]. Considered values were Young modulus E_s = 130 GPa and maximum tensile strength R_m = 281 MPa; the corresponding strain is equal to ε_m = 6.5 %. This layout of the model takes into account only the situation of actual loads (dead loads), with both fixed anchors of the tie-rod and anchors penetrating into the masonry; this condition was simulated by a thermal elongation of the tie-rod calibrated on the value measured in the real case study. In this second case the horizontal thrust H decreases: this evidence means that due to the higher deformability of the tie, a portion of the forces at the haunches discharges on the supporting walls. When anchors penetration is present, plastic deformations develop at about 58° from the vault's axis (Figure 6), approximately in the section where the Mèry's method hypothesis expects the development of plastic hinges. In both cases, plasticization of the tie-rod was not observed. Horizontal displacements are concentrated on the left side of the structure (Figure 6), where supporting walls are thinner (Figure 1). Collapse occurs due to compressive failure of the masonry, with the tie-rod still working in elastic field. The maximum compressive stresses in the cross sections are 1.49 MPa and 0.42 MPa, depending on the fact that anchors

penetration into the masonry was considered or not. This evidence highlights the connection between the deformability of the structure and its stress state under the same loading conditions.

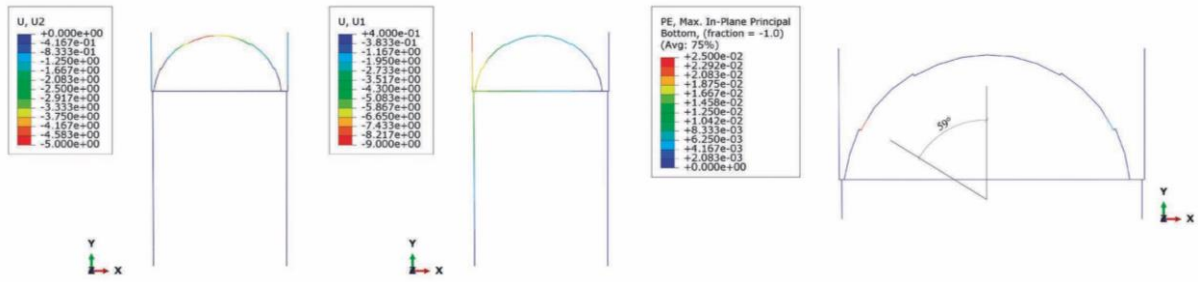


Figure 6: FEM analysis: vertical displacements, horizontal displacements and stresses.

3.4 Discrete Element Method

The analysis was then repeated with the DEM approach: the voussoirs were represented by macro-blocks with the same shape adopted in the previous methods, in order to preserve modelling homogeneity. Infill, flooring and variable loads were considered like concentrated forces applied in the centre of gravity of the elements, in order to reduce the computational burden, except for the case of collapse condition, in which infill was modelled with approximately 780 spheres. Real infill density was increased by a 1.5 factor in order to take into account the empty space among adjacent spheres. The geometry remains unchanged compared to previous analyses.

The software chosen for DEM analyses was ChronoEngine[7], an open source C++ library often used to study masonry architectural structures [9]. Contact forces among blocks and motion laws for each block are ruled by Coulomb's friction law, Newton's Second Law (in the gravitational field) and spring/dashpots reactions. A model based on springs and dashpots, if properly calibrated, can render mortar joints deformability and the resulting deformation of the vault. As a first attempt for calibration, values from [6] were adopted: damping was set at 0.2 kg/s, while compliance was 10-8 N/m. This second parameter was subsequently recalibrated for each different layout of the model, by iteratively matching displacements in a reference point obtained with a corresponding FEM model. The software does not directly provide values of compressive stresses.

Firstly, the 1 m wide arch representing the vault was modelled adopting fixed constrains at the spring, disregarding the contributions of the tie-rods and of the supporting walls. This configuration ensures a consistent comparison with the results obtained with classical methods (Table 1). The collapse condition, obtained using an increasing overload applied upon the flooring blocks in form of vertical concentrated loads, shows a very high lowering of the key section before the loss of bearing capacity of the structure.

The model was then improved with the introduction of the tie-rods and of the supporting walls (Figure 7). Walls were modelled as monolithic blocks, while the tie-rod was approximated with a linear-elastic spring, whose elastic properties are the same previously adopted in the FEM approach (the software does not allow an elasto-plastic behavior). The penetration of the anchors into the masonry was simulated thanks to a two-step analysis: the first one was conducted with a fictitious spring constant k', calibrated with a similar FEM

model, in order to obtain the desired elongation and the deformed configuration of the structure. In the second step, a tie-rod with the real spring constant k was added to the deformed vault obtained in the first step. When the infill is used, it produces a horizontal pressure that modifies the behavior of the model: an overturning mechanism of the upper wall is triggered (Figure 7), and the structure loses its bearing capacity even without the addition of increasing overloads. Displacement values computed in the various models configurations are shown in Table 2.

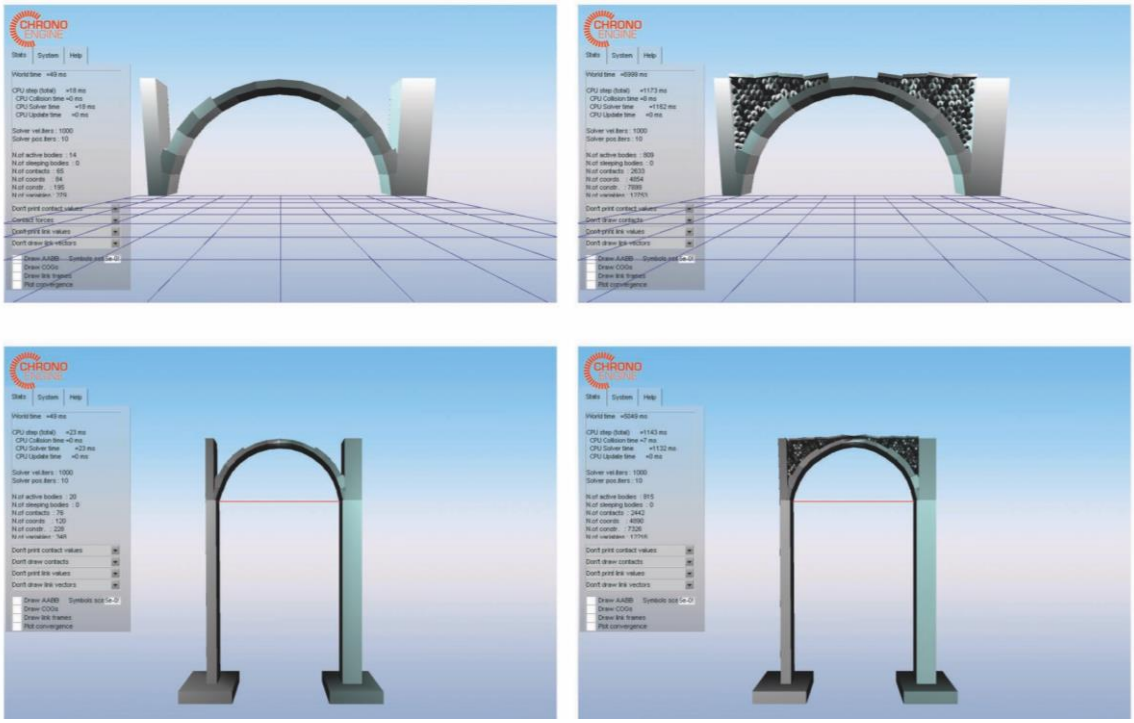


Figure 7: DEM analysis: vault constrained at the spring and model with tie-rod and supporting walls

4 RESULTS AND DISCUSSION

The results obtained with the four different methods are here discussed both in terms of forces and in terms of displacements (the latter, obviously, only for the numerical methods).

4.1 Horizontal thrust and compression stresses

Table 1 reports the horizontal thrust H and the compression stress obtained with the four different methods and with the four different load conditions (dead loads, dead loads plus live loads for reading room use, Ultimate Limit State, collapse condition). Their comparison allow to make some observations about the compliance of the different methods and about their reliability for a static safety assessment of the vaults.

The maximum values of compressive stresses in the first three load cases obtained with the Mery's method are 0.486 MPa, 0.445 MPa and 0.546 MPa respectively. The value in collapse condition is equal to the design compressive strength value. The higher stress value in the case of dead loads only shows a positive impact of the variable loads on the vault stability. The results obtained with the ARCO software confirm the same trend observed in the previous approach; in fact the values for the maximum compressive stresses in the cross

sections are 0.306 MPa, 0.301 MPa and 0.313 MPa for dead loads, reading room and Ultimate Limit States assessment respectively. Due to the optimization of the hinges position exploited by the software in order to minimize eccentricity values, those results are significantly lower with respect to those obtained from the Mèry's method. Nevertheless, the horizontal thrusts computed with ARCO are slightly larger than the ones obtained with Mery's method. FEM results in terms of thrust appear to be more similar to the Mery's ones, while the thrusts computed with the adopted DEM approach are larger also than the ARCO ones. The horizontal thrust at collapse are surprisingly close in Mery, FEM and DEM cases, while it is more than double if computed with ARCO, thus demonstrating that a widespread instrument adopted by professionals is prone to overestimate largely the thrust and thus possibly induces heavier interventions than really needed. From a static safety assessment point of view, in the case of the reading room live loads, the vault is verified with wide margins in the case of null or limited deformations (classical methods and numerical methods with constraints at the spring). However, when the deformability of the structure increases with the addition of supporting walls and tie-rods, this margin become thinner: the maximum overload that the structure can stand calculated with FEM results in 3.36 kN/m^2, only marginally bigger than the value of 3 kN/m^2 imposed by the Italian technical code for this intended use.

Table 1: Comparison of the results in terms of thrust and stress among the four adopted methods.

Method	Dead loads		Reading room		Limit state assessment		Collapse	
	H (kN)	Max comp. st. (MPa)	H (kN)	Max comp. st. (MPa)	H (kN)	max comp. st. (MPa)	H (kN)	max comp. st. (MPa)
Mèry	27.9	0.486	36.7	0.445	41.3	0.546	109.5	2.770
Safe theorem	30.4	0.306	40.4	0.301	45.8	0.313	278.4	2.780
FEM	31.7	0.385	40.7	0.391	45.4	0.394	102.6	1.326
FEM w. Sup.	29.5	0.421	-	-	-	-	-	-
FEM A. Ret.	24.5	1.493	-	-	-	-	35.5	1.495
DEM	38.1	-	45.2	-	50.1	-	104.3	-
DEM w. Sup.	67.9	-	-	-	-	-	-	-
DEM A. Ret.	15.7	-	-	-	-	-	-	-

4.2 Horizontal and vertical displacements

As already stated, only numerical methods produce results that take into account displacements and deformations. In Table 2, the horizontal displacements of the springing points Δh and the vertical displacements of the keystone are reported for each of the four load cases and for the two adopted numerical methods (FEM and DEM). Vertical deformations calculated with both FEM and DEM approaches are generally lower than the maximum observed value in the case study (estimated in about 90 mm): however, when the whole structure is taken into account (including anchors penetrating into the masonry) the expected drops in the keystone section are in the same order of magnitude. With regards to the DEM approach, occasional anomalies such as the very high keystone drop in collapse conditions without tie-rods and supporting walls could be explained with the difficulty in the calibration of the contact springs through the compliance parameter: in fact, it seems to mostly depend on the layout of the single model than on the overall mechanical properties of the masonry.

Table 2: Comparison of the results in terms of horizontal and vertical displacements among the 4 adopted methods.

Method	**Dead loads**		**Reading room**		**Limit state assessment**		**Collapse**	
	Δh (mm)	key lowering (mm)	Δh (mm)	key lowering (mm)	Δh (mm)	key lowering (mm)	Δh (mm)	key lowering (mm)
FEM	-	0.76	-	2.05	-	2.75	-	3.16
FEM w. Sup.	3.39	6.77	-	-	-	-	-	-
FEM A. Ret.	58.99	40.05	-	-	-	-	-	42.86
DEM	-	-1.03	-	0.62	-	1.36	-	680.68
DEM w. Sup.	7.02	39.20	-	-	-	-	-	-
DEM A. Ret.	58.40	53.40	-	-	-	-	-	-

12 CONCLUSIONS

Trying to reconnect the elements of the historical evolution of arches and vaults structural modelling, the present paper compares four different methods – two classical graphic ones and two modern numerical ones – looking for an equilibrium between complexity and reliability, for the common professional use. The main results can be summarized as follows:

- Good agreement in terms of thrust forces between graphical and numerical methods demonstrate that classical methods are trustworthy, altogether with a more straightforward application
- Classical methods do not take into account deformability, which is important when thin supporting walls or thin vaults are concerned: the results more consistent with the real observed ones were obtained with the finite elements method
- DEM method does not provide the state of stress in the blocks, therefore comparison with compressive strength of masonry is cumbersome and must be done in the post-processing phase.
- Calibration of the DEM is very delicate and case dependent, thus suitable mainly for edge cutting research case studies.

Acknowledgements. The contributions of Federica Ottoni to the analysis of the case study, of Claudio Boni to the calibration of the Discrete Element Method and of Alessandro Tasora to the ChronoEngine development are also gratefully acknowledged.

REFERENCES

[1] Bettini S., L'architettura di San Marco, Padova, 1946; s.v. Arco, in Enciclopedia dell'arte antica, Secondo Supplemento 1971, Roma, 1994, pp. 344-354 (in Italian).

[2] A. Tralli, C. Alessandri & G. Milani. Computational methods for masonry vaults: a review of recent results. *The Open Civil Engineering Journal*, 8-1(2014) 272-287.

[3] Giovannoni G., Il restauro dei monumenti, Tipografia Editrice Italia, Roma, 1945 (in Italian).

[4] NTC2018 "Aggiornamento delle norme tecniche delle costruzioni", Ministero delle Infrastrutture e dei Trasporti, D.M. 17-01-2018. (in Italian).

[5] E. Méry, Mémoire sur l'équilibre des voutes en berçeau, *Annales des Ponts et Chaussées*, s.1, 1e trim., t. XIX (1840) 50-70.

[6] J. Heyman, *The masonry Arch*, Chichester: Ellis Horwood, 1982.

[7] "Project Chrono", URL: https://projectchrono.org Accessed January 2020.

[8] E. Coïsson, D. Ferretti, C. Boni & A. Tasora, Defining the structurally compatible uses of ancient vaults: a comparison between traditional and modern modelling approaches, in *6th International Conference on Mechanics of Masonry Structures Strengthened With Composite Materials (MuRiCo6),* Bologna, Italy*,* June 26-28, 2019.

[9] D. Ferretti, E. Coisson & Rozzi, M. A new numerical approach to the structural analysis of masonry vaults, Key Engineering Materials, 747(2017) 52-59.

[10] "Arco", URL: http://gelfi.unibs.it/arco.htm Accessed January 2020.

[11] E. Coisson, F. Ottoni, F. Pagliari, Istanze strutturali nella definizione di usi compatibili: un caso studio nel complesso monumentale della Pilotta, in: Il Patrimonio culturale in mutamento. Le sfide dell'uso, XIII convegno Scienza e Beni Culturali, Bressanone, 2019.

[12] Kaushik, H. B., Rai, D. C., & Jain, S. K. (2007). Stress-strain characteristics of clay brick masonry under uniaxial compression. *Journal of materials in Civil Engineering*, 19(9), 728-739.

[13] A. Lorenzelli, The seismic vulnerability of bell-towers' spires: damage analysis and modeling, thesis in Engineering, University of Parma, supervisors D. Ferretti, E. Coïsson, A.Y. 2016/2017

[14] Calderini, C., Vecchiattini, R., Battini, C., & Piccardo, P. (2016, September). Mechanical and metallographic characterization of iron tie-rods in masonry buildings: An experimental study. In *10th International Conference Structural Analysis of Historical Constructions*, Leuven, Belgium, September (Vol. 13, p. 15).

[15] G. de Felice, Assessment of the load-carrying capacity of multi-span masonry arch bridges using fibre beam elements, Engineering Structures, Volume 31, Issue 8, 2009, Pages 1634-1647.

[16] Demi L. Fang, Rebecca K. Napolitano, Tim L. Michiels & Sigrid M. Adriaenssens (2019) Assessing the stability of unreinforced masonry arches and vaults: a comparison of analytical and numerical strategies, International Journal of Architectural Heritage, 13:5, 648-662.

[17] Antonio Maria D'Altri, Stefano De Miranda, Giovanni Castellazzi, Vasilis Sarhosis, Jamie Hudson & Dimitris Theodossopoulos (2019): Historic Barrel Vaults Undergoing Differential Settlements, International Journal of Architectural Heritage.

[18] P. Gelfi, Role of horizontal backfill passive pressure on the stability of masonry vaults. International Journal for Restoration of Buildings and Monuments 8-6 (2002) 573-590.

[19] D. O'Dwyer, "Funicular analysis of masonry vaults," Computers & Structures, vol. 73, pp. 187-197, 10 1999.

[20] P. Block, T. Ciblac and J. Ochsendorf, "Real-time limit analysis of vaulted masonry buildings," Computers & Structures, vol. 84, pp. 1841-1852, 11 2006.

[21] A. Andreu, L. Gil and P. Roca, "Computational analysis of masonry structures with a funicular model," Journal of Engineering Mechanics, vol. 133, pp. 473-480, 2007.

[22] Chaix, Jacques. 1890. Traité des ponts: première par-tie: ponts en maçonnerie et tunnels: Tome II. Paris: Fanchon et Artus.

[23] G. de Felice (2009). Assessment of load-carrying capacity of multi-span masonry arch bridges using fibre beam elements, Engineering Structures 31, 1634-1647.

[24] G. Creazza, R. Matteazzi, A. Saetta, R. Vitaliani (2002) Analyses of masonry vaults: A macro approach based on three-dimensional damage model. Journal of Structural Engineering,128(5): 646–654

[25] A. Cavicchi, L. Gambarotta (2006) Two-dimensional finite element upper bound limit analysis of masonry bridges. Computers and Structures, 84: 2316-2328.

[26] M. Como, (2013). Statics of historic masonry constructions (Vol. 1). Berlin: Springer.

[27] J. V. Lemos, "Discrete element modeling of masonry structures," *International Journal of Architectural Heritage*, vol. 1, pp. 190-213, 2007.

[28] J. McInerney and M. J. DeJong, "Discrete Element Modeling of Groin Vault Displacement Capacity," *International Journal of Architectural Heritage*, vol. 9, pp. 1037-1049, 11 2014.

[29] G. Lengyel, "Discrete element analysis of gothic masonry vaults for self-weight and horizontal support displacement," Engineering Structures, vol. 148, pp. 195-209, 10 2017.

[30] D. Foti, V. Vacca and I. Facchini, "DEM modeling and experimental analysis of the static behavior of a dry-joints masonry cross vaults," Construction and Building Materials, vol. 170, pp. 111-120, 2018.

[31] M. Jean, "The non-smooth contact dynamics method", *Computer methods in applied mechanics and engineering*, vol. 177, pp. 235-257, 1999.

[32] J. J. Moreau, "Unilateral contact and dry friction in finite freedom dynamics", in *Nonsmooth mechanics and Applications*, Springer, 1988, pp. 1-82.

[33] F. Dubois and M. Jean, "The non smooth contact dynamic method: recent LMGC90 software developments and application," in Analysis and simulation of contact problems, Springer, 2006, pp. 375-378.

[34] G. Lancioni, S. Lenci, Q. Piattoni and E. Quagliarini, "Dynamics and failure mechanisms of ancient masonry churches subjected to seismic actions by using the NSCD method: The case of the medieval church of S. Maria in Portuno", Engineering Structures,vol.56, pp.1527-1546, 2013.

[35] B. Chetouane, F. Dubois, M. Vinches and C. Bohatier, "NSCD discrete element method for modelling masonry structures", International journal for numerical methods in engineering, vol. 64, pp. 65-94, 2005.

[36] A. Rafiee and M. Vinches, "Mechanical behaviour of a stone masonry bridge assessed using an implicit discrete element method," Engineering Structures, vol. 48, pp. 739-749, 2013.

[37] A. Rafiee and M. Vinches, "Implicit discrete element analysis of a masonry cupola under seismic loads," International Journal of Civil Engineering, vol. 14, pp. 357-367, 2016.

[38] V. Beatini, G. Royer-Carfagni and A. Tasora, "A regularized non-smooth contact dynamics approach for architectural masonry structures," Computers & Structures,vol.187,pp.88-100, 2017.

[39] V. Beatini, G. Royer-Carfagni and A. Tasora, "Modeling the shear failure of segmental arches," International Journal of Solids and Structures, vol. 158, pp. 21-39, 2019.

[40] E. Coïsson, L. Ferrari, D. Ferretti and M. Rozzi, "Non-smooth dynamic analysis of local seismic damage mechanisms of the San Felice Fortress in Northern Italy," Procedia Engineering, vol. 161, pp. 451-457, 2016.

12th International Conference on Structural Analysis of Historical Constructions
SAHC 2020
P. Roca, L. Pelà and C. Molins (Eds.)

A CONSTITUTIVE MODEL FOR RUBBLE MASONRY ALLOWING FOR SPREAD MICRO-CRACKS AND LOCALIZED MACRO-CRACKS

MANUELA A. SCAMARDO[1*], ALBERTO FRANCHI[2] AND PIETRO G. CRESPI[2]

[1] Department of Architecture, Built Environment and Construction Engineering
Politecnico di Milano
Piazza Leonardo da Vinci 32, 20133 Milano, Italy
e-mail: manuela.scamardo@polimi.it (*corresponding author)

[2] Department of Architecture, Built Environment and Construction Engineering
Politecnico di Milano
Piazza Leonardo da Vinci 32, 20133 Milano, Italy
email: {alberto.franchi, pietro.crespi}@polimi.it

Keywords: Masonry, Cracking, Plasticity, Softening, Finite Elements, PLCP

Abstract. *Starting from a discussion on the experimental results obtained from diagonal compression tests executed on in-situ masonry panels, the paper presents a constitutive model, together with a numerical formulation, to describe the cracking phenomena in rubble masonry structures. A classical finite element discretization is assumed with the hypothesis of a homogenous continuum material. The adopted constitutive model identifies three different phases: (i) the elastic phase; (ii) the micro-cracking phase, in which the formation of micro-cracks, spread in the structural members, is accounted assuming a plastic material with a strain hardening stable behavior; (iii) the macro-cracks phase, in which the formation of macro-cracks, developing along the edges of finite elements, are simulated by means of localized softening plastic deformation. While the numerical description of spread plasticity in the finite element framework is a topic that has been widely addressed in the past, the representation of localized plastic deformation and its implementation in a finite element code is an original contribution of the authors. From a computational point of view, the value of plastic deformations (i.e. crack openings) is found by solving a parametric linear complementarity problem (LCP) using mathematical programming algorithms. The main advantage of using an LCP method is its ability to deal also with configurations in which instability and a multiplicity of solutions are possible (e.g. softening behavior). The numerical simulation of a diagonal compression test and the comparison of the results with the experimental evidence are presented to validate the model.*

1 INTRODUCTION

The performance of masonry structures under seismic actions is strongly influenced by cracking phenomena that must be considered to obtain a reliable evaluation of the structure's capacity. As experimentally observed, masonry shows signs of damage since the early stages of loading. From a microscopic point of view, when the tensile damage begins, spread and stable micro-cracks start to develop. Once the cracks growth becomes unstable, strain

localization occurs, and macro-cracks develop. The initial phase of damage (i.e. micro-cracking) has an important role in the masonry modelling because affects the analysis results in terms of stiffness and ductility. At the same time, the detection of macro-cracks is fundamental to understand potential collapse mechanisms.

In general, there are two main approaches adopted for masonry modelling [1]: (i) the micro-modelling approach, which usually involves the separate modelling of units, mortar and unit–mortar interfaces but can involve also a lumped representation of the mortar and unit–mortar interface, with potential fracture lines localized at the interfaces; (ii) the macro-modelling approach, which does not make distinction between blocks and joints, and masonry components are smeared into an averaged continuum; the presence of cracks is introduced by changing the mechanical properties of the material. The first approach corresponds to more accurate results but computationally intensive analyses, the second one requires less computational effort but does not account for kinematic discontinuities.

In large analyses, the knowledge of the interaction between units and mortar is negligible for the global behaviour of the structure. Moreover, when the structural problem concerns rubble masonry, the distinction between blocks and joints is not always simple. All this involve the tendency to choose a macro-modelling approach in the practice-oriented analyses, excluding the possibility to realistically describe the formation and propagation of cracks.

Starting from the experimental data obtained from in-situ diagonal compression (DC) tests performed on rubble masonry walls, this study presents an original constitutive model to describe the formation and propagation of cracks in masonry, accounting for both micro and macro fractures. A macro-modelling approach is adopted with a homogeneous and isotropic material. The hypothesis of isotropy can be acceptable when dealing with rubble masonry. Only in-plane behavior is analyzed. The model adopts an innovative finite element structural formulation, enriched with the introduction of mathematical programming algorithms [2, 3]. Both tension and shear cracks are considered. The initial phase of damage, represented by the formation of micro-cracks, is described as irreversible plastic deformations spread all over the elements. Macro-cracks are considered instead as inelastic strains localized at the nodes of potential cracking paths. Softening behavior is considered through a cohesive crack model.

The proposed model is used to simulate a DC test to validate the formulation.

2 EXPERIMENTAL ASPECTS

Non-linear analysis of existing buildings, particularly for seismic loadings, requires the experimental evaluation of the post-peak degradation curve to obtain reliable analytical models. Among the available tests, the DC test is usually adopted for the determination of the shear strength of masonry walls. The in-situ version of the test is usually executed under load control on specimen cut from the existing wall by means of a circular saw or a diamond wire [4].

A special procedure has been adopted by the LPM Lab of Politecnico di Milano to execute several DC tests on the San Filippo Neri historical building in L'Aquila (Italy). The walls tested were made of rubble masonry, very common in the historical buildings of central Italy. The walls exhibit two external layers which are connected by a central infill, less predictable in terms of presence of mortar and size and type of aggregates. This implies a non-homogeneous behavior of the wall section, i.e. it is to be expected that the two external layers move with a certain independence one from the other.



Figure 1: Left, Circular saw cutting the masonry specimen. Right, experimental equipment for the DC test.



Figure 2: Cracking paths on CD01 specimens after the DC test, side 1 and 2.



Figure 3: Cracking paths on CD04 specimens after the DC test, side 1 and 2.

Some pictures about the setting of the test are reported in Figure 1. The experimental equipment was such that the test could be performed by controlling, independently, the two jack forces acting on each masonry external layer.

Figures 2 and 3 show the damage observed at the end of the tests in two different specimens (CD01 and CD04, both sides). The observed damage was generally represented by cracks parallel to the compressed diagonal and sliding phenomena in the vertical/horizontal direction. The crack path was mainly influenced by the location of mortar joints, which represent the weak point of the masonry assemblage.

Figure 4 shows the load vs. displacement curves. The blue and red curves represent the behavior of the two sides of each wall. Significantly different behavior of the two layers have been detected for specimen CD01, while CD04 shows a more homogenous behavior.

Two main facts come out from the observation of the curves: (i) the sharp decrease of the elastic constants in the stable part of the behavior; (ii) the irreversibility of deformations, even at the first stage of the test. It is evident that the initial phase of damage, manifested through the formation of spread micro-cracks, has a fundamental role in the masonry modelling in terms of final maximum displacement and σ-ε plot. At the same time, the analysis of macro-cracks propagation is necessary to realistically evaluate the mechanical capacity of the structure and understand the potential collapse mechanisms. The paper will present an original constitutive model that accounts for both micro and macro-cracks.

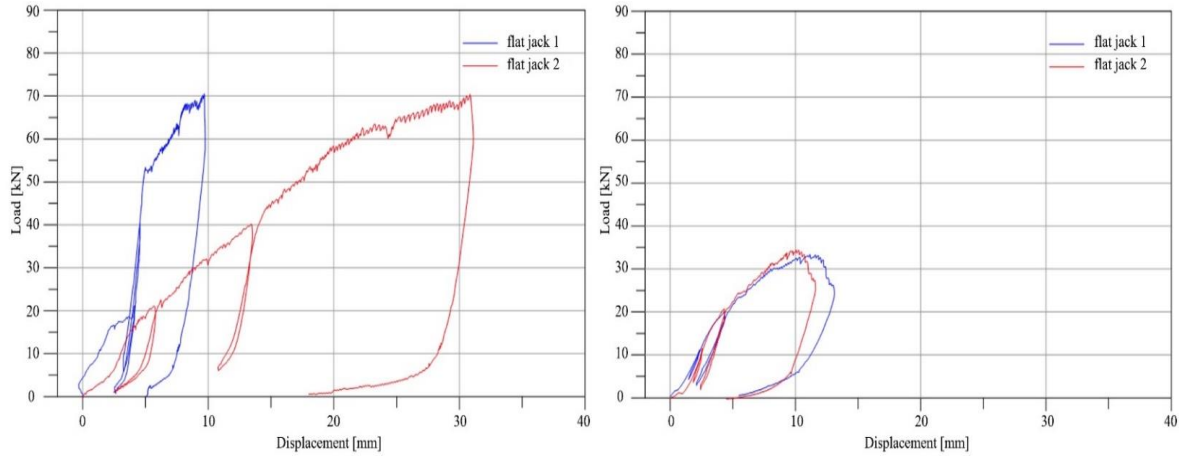


Figure 4: Load vs. displacement curves: left, specimen CD0; right, specimen CD04

3 CONSTITUTIVE ASPECTS

In the following formulation, tensile behavior is considered but shear can be treated analogously. The constitutive model has been subdivided in three phases: (i) undamaged linear elastic phase (Figure 5a), in which the material is considered elastic until the tension σ_y is reached; the value σ_y is a portion of the limit tension σ_t, to be calibrated according to the experimental evidence; (ii) micro-cracking hardening phase (Figure 5b), in which micro-cracks start to propagate following an isotropic hardening law, with hardening parameter h_h, until the limit tension σ_t is reached; (iii) macro-cracking softening phase (Figure 5c), in which the behavior is described by a stress-crack opening displacement constitutive law, with softening parameter h_s and fracture energy G_f. Phases (ii) and (iii) are described in detail in the following.

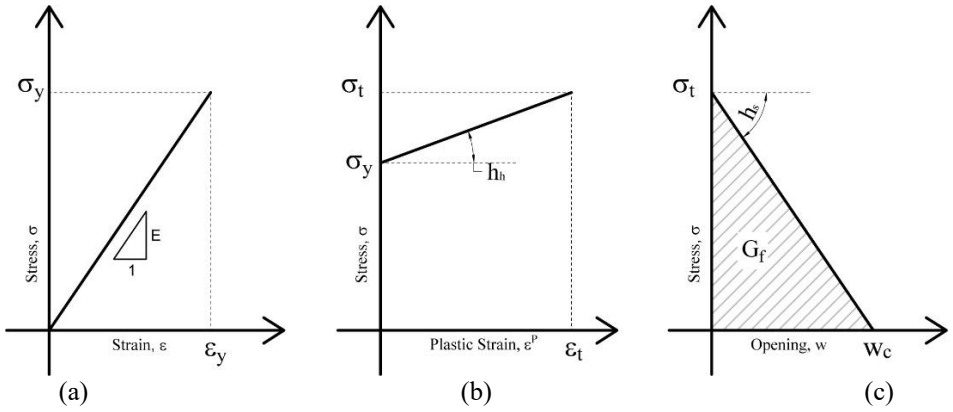


Figure 5: Constitutive law phases: (a) undamaged linear elastic phase, (b) micro-cracking hardening phase and (c) macro-cracking softening phase.

3.1 The micro-cracking hardening phase

The formation of micro-cracks is associated to the "stable" part of the masonry behavior in which irreversible plastic deformations start to accumulate while the load increases. The representation of plastic deformation is made according to the classical theory of plasticity, with the plastic deformation spreading in the finite elements.

Among all the available yield functions proposed in the literature, a Drucker-Prager (DP) criterion [5] has been adopted together with an associated flow-rule. The DP domain is characterized by a regular and smooth limit surface, with obvious computational advantages, and only two parameters to be defined, i.e. the limit stress in uniaxial tension σ_t and uniaxial compression σ_c. It should be remarked that the adopted limit values that active the micro-cracking phase are not the actual limit stresses in tension and compression, but they are lower values to be calibrated on the experimental results. Moreover, only the tension-tension stress regime of the domain will be considered in this specific case.

The governing relations are based on the classical approach developed by Maier [6] and adopted by several authors [7, 8] where the failure surface is a piecewise linear assemblage of linear failure surfaces. An "a posteriori" linearization procedure [9] is adopted, in which the stress points can move on the yield surface along a piecewise linearized path, lying within the bounds of a given maximum violation of the true yield function and consequently having a control on the violation of the flow-rule. The "a posteriori" linearization technique is implemented under the framework of Mathematical Programming (MP) theory and algorithms, with regard to the Linear Complementary Problem (LCP) as already proposed in [7].

Let us consider the yield surface reported in Figure 6,left. For the sake of simplicity and without loss of generality, the yield function has been limited to one parameter convex function. The elastic domain is defined by the stress points which satisfy the relation $\varphi(\boldsymbol{\sigma}, \sigma_0) < 0$, where σ_0 is the given parameter. As soon as the stress point reaches the yield surface $\varphi(\boldsymbol{\sigma}, \sigma_0) = 0$ at point A (Figure 6, right), an approximate elastic domain is defined by the stress points which satisfy the following conditions:

$$\varphi(\boldsymbol{\sigma}, \sigma_0(1+\varepsilon)) < 0 \tag{1}$$

$$\varphi_A = \mathbf{n}_A^T \boldsymbol{\sigma}_A - R_A < 0 \tag{2}$$

where $\mathbf{n_A}$ is the outward unit normal to the yield surface at point A, R_A is the distance of the plane with normal $\mathbf{n_A}$ from the origin and ε is the prescribed tolerance on the violation of the yield surface. The stress point can now move in the elastic domain or along the plane φ_A. If the stress point violates the outer limit surface defined by (1), a back-track procedure is applied that brings the stress point on the inner curve and compute a new tangent plane.

The evolution of the yield surface is governed by an isotropic hardening law with hardening parameter h_h (Figure 7), which represents the initial damage phase where micro-cracks develops.

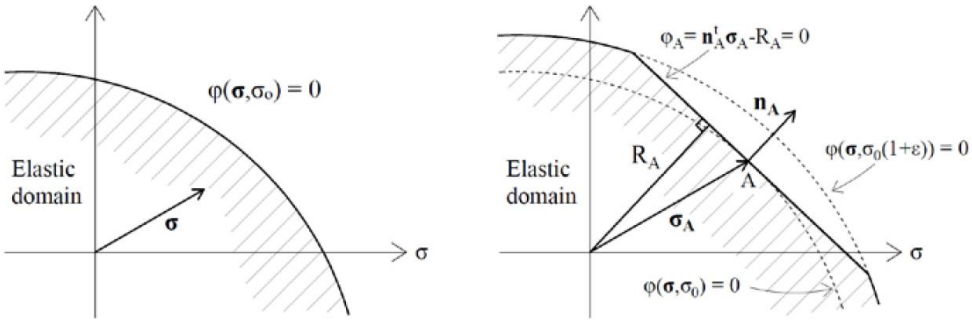


Figure 6: On the left, non-linear failure surface and elastic domain; on the right, stress point reaching the failure surface at point A and introduction of a new yield plane.

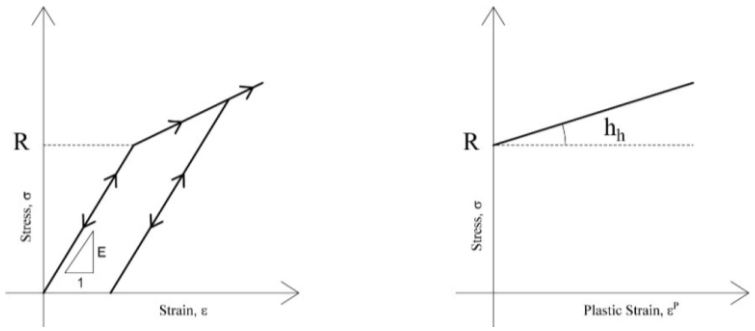


Figure 7: Elastic-plastic strain hardening model to represent the formation of micro-cracks; h_h is the hardening parameter and R the resistance associated to the yield plane.

3.1 The macro-cracking softening phase

When the value of the limit stress in tension is reached, the macro-cracks start to propagate. At this point, in order to provide a good representation of the material behavior, strain softening must be considered. After the limit value is reached, the activated inelastic constitutive law is described as a linear softening branch, according to the cohesive crack model proposed by Hillerborg [10].

Two main assumptions are considered: (i) the crack begins to develop when the ultimate strength is achieved at one node; (ii) the material in the cracked zone is still able to transfer a force dependent on the crack opening displacement. Two parameters must be defined to properly describe the softening behavior: the limit tension σ_t at which the crack starts to open

and the critical crack width w_c at which the normal stress becomes zero. The following relations link the two parameters:

$$w_c = \frac{2G_f}{\sigma_t} \tag{3}$$

$$\sigma_t = -h_s \cdot w_c \tag{4}$$

where h_s is the softening parameter and G_f is the fracture energy.

While in the micro-cracking phase the damage is spread in the elements and the plasticity control is made in terms of actual stresses, in the macro-cracking phase the plastic deformations (i.e. the cracks) are considered as localized at the nodes. The adopted failure surfaces are defined at each node and involves the nodal forces instead of the actual element stresses.

The limit tension σ_t of Figure 5c is then replaced by the limit traction force R_n called resistance (Figure 8, left), calculated at the generic node i as:

$$R_n = \sigma_t \cdot A_i \tag{5}$$

where A_i is the tributary area of the node i. The tributary area of a node is calculated as the product of the tributary length L_i of the node with respect to a predefined crack direction and the thickness of the finite elements. When at one node the resistance R_n is reached, the cohesive crack starts to open. The force at the node begins to decrease following the softening branch. The behavior on the softening branch is non-holonomic. If an unloading occurs, the force decreases following a vertical elastic unloading/reloading branch, keeping unchanged the values of crack width w. When the critical value w_c is reached, the behavior becomes holonomic and the material is considered as elastic perfectly plastic. The crack is fully developed, and it can open and close freely.

3.1 Traction-shear interaction domain

For a realistic description of the damage phenomena, the proposed approach considers the formation of both tensile cracks and shear cracks (i.e. sliding phenomena). What already presented for tension behavior can be easily extended to shear behavior without loss of generality.

At each potential cracking node belonging to a potential crack direction, two independent variables are defined: (i) w, i.e. the traction crack width, that is the normal component of the plastic deformation, and s, i.e. the shear sliding, that is the tangential component of the plastic deformation. A simple maximum stress criterion is adopted both in cases of tension and shear behavior.

The traction-shear domain for a node is represented in Figure 9 where F_n and F_t are respectively the traction and shear component of the nodal force and R_n ad R_t are the limit traction and the limit shear, calculated as the product of the tributary area of the node and the limit stress in tension σ_t and shear τ_{max}, respectively. The parameters σ_t and τ_{max} are defined independently the one from the other.

The plastic deformations (i.e. cracks w and s) develop according to the normality rule. For the sake of simplicity, no interaction between the two variables w and s is considered and they can be activated simultaneously only in the corner point. To make the model closer to reality,

a traction-shear interaction may be considered by introducing a different failure domain (e.g. Mohr Coulomb criterion). This improvement will be treated in future paper.

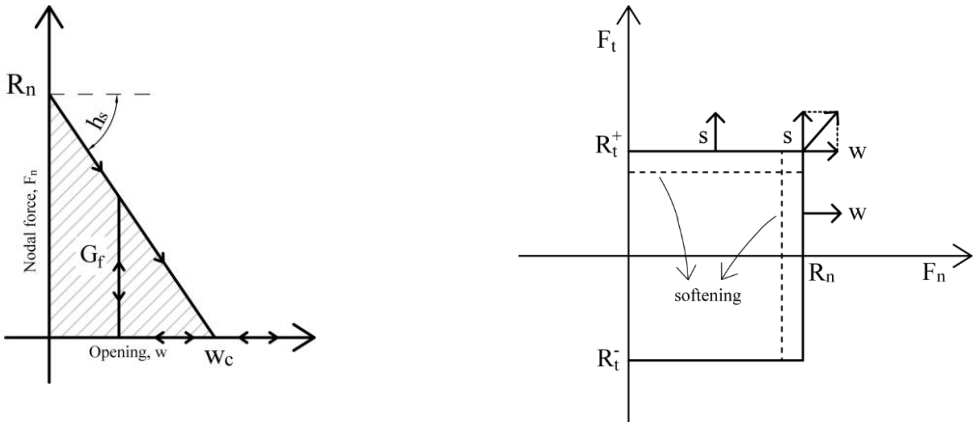


Figure 8: Left, nodal constitutive nodal law. Right, Traction-shear interaction domain.

4 THE MACRO-CRACK MODEL

From a numerical point of view, the macro-cracking model and its implementation in a finite element code represent an original contribution of the authors [2, 3, 11].

Let us consider the FE model in Figure 9 (left) in which a potential cracking path L is identified. If a fracture develops along L, the structure is going to be split into two, identifying on the bottom side the line L^+ and the node I^+ and on the top side L^- and I^-. Focusing the attention on the node I^+ (Fig. 9, middle), an outward unit normal $\mathbf{n_I}^+$ associated to the crack line L^+ can be defined. The vector force $\mathbf{F_I}^+$ at node I^+ is equilibrated with the stresses of the adjacent elements Q_j, Q_k and Q_m. The projection of $\mathbf{F_I}^+$ on $\mathbf{n_I}^+$ must satisfy the following plasticity condition at the node I^+:

$$\mathbf{n_I}^{+\mathbf{T}} \cdot \mathbf{F_I}^{+\mathbf{T}} \leq R_I^+ \tag{6}$$

where R_I^+ is the limit tensile force, calculated as the product of the limit tension σ_t times the influence area of the considered node A_i.

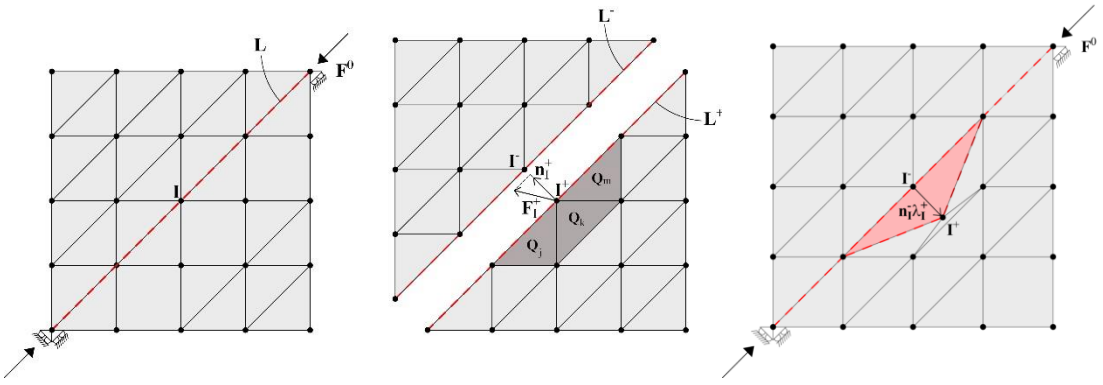


Figure 9: Left: FE model of a plane stress problem. The dashed red line L identifies a potential crack path. Middle: dal force $\mathbf{F_I}^+$ at I^+ equilibrated with $\mathbf{Q_a}$, $\mathbf{Q_b}$, $\mathbf{Q_c}$. Right: Opening of the crack at node I.

The satisfaction of the yield criteria is ensured by considering suitable imposed localized strain $\mathbf{n_I}^-\lambda_I^+$ that represents the displacement associated to the crack opening and obeys to the normality flow rule of plasticity. When the plasticity condition is violated, the crack opens by splitting the node I into two: one belonging to L^-, which remains fixed, and one belonging to L^+, which moves in the direction of $\mathbf{n_I}^-$ opening the crack λ_I^+, named plastic/crack multiplier (Fig. 9, right). The crack opening affects only the bottom half structure (or better, the elements of the bottom half structure around the node I^+). The same procedure can be repeated for any potential cracking node, along any possible direction.

Let us define a vector $\boldsymbol{\lambda}^+$ that collects the crack multipliers $\boldsymbol{\lambda_I}^+$ associated to the nodes on the crack line L^+, with a number of components equal to the number of potentially activable planes. A matrix $\mathbf{N}^-$ is defined which collects, in diagonal form, the outward unit normal vectors $\mathbf{n_I}^-$ of each node (analogously $\mathbf{N}^+$ can be defined for the outward unit normal vectors $\mathbf{n_I}^+$). The problem to be solved is to find the elastic-plastic response of the structure under the external load $\mathbf{F^0}$ and the prescribed inelastic crack openings $\mathbf{N}^-\boldsymbol{\lambda}^+$.

According to the Colonnetti's approach [12], the elastic-plastic response of the structure is obtained as the superposition of: (i) the linear-elastic response of the structure to the given external actions; (ii) the linear-elastic response of the structure subjected to the unknown imposed strains $\mathbf{N}^-\boldsymbol{\lambda}^+$. For a clear definition of response (ii), a sub-structure has to be defined made by the elements, around the considered node, lying on one side of the crack (e.g. for the node I, the dark gray elements in Figure 9, middle). Response (ii) is the superposition of: (a) the linear-elastic response of the sub-structure, considered with fixed nodes, to the imposed displacement $\mathbf{N}^-\boldsymbol{\lambda}^+$, in which all the nodal displacements are zero except the crack opening; the nodal reactions are called $\mathbf{F_{R,i}}$; (b) the linear-elastic response of the structure subjected to $-\mathbf{F_{R,i}}$.

Considering the softening behavior and recalling the plasticity condition (6), a plastic potential vector $\boldsymbol{\Phi}^+$ can be defined on the crack line L^+, as:

$$\boldsymbol{\Phi}^+ = -\mathbf{N}^{+\mathbf{t}}\mathbf{F}^+ + \mathbf{R}^+ + \mathbf{H}\boldsymbol{\lambda}^+ \geq \mathbf{0} \tag{7}$$

where $\mathbf{F}^+$ is the vector of nodal surface forces along L^+, $\mathbf{R}^+$ is the vector that collects the surface resistances of each node and $\mathbf{H}$ is a square matrix with the softening parameter $h_s < 0$ along the main diagonal, that has as many rows and columns as the total number of yield planes. The introduction of the matrix $\mathbf{H}$ describes how the original yield surface changes during the development of cracks. If a failure plane is activated, the corresponding potential function is zero. The governing equations of the structural problem can be expressed as a linear complementary problem (LCP) [11]:

$$\boldsymbol{\Phi}^+ = (\mathbf{A} + \mathbf{H})\boldsymbol{\lambda}^+ - \mathbf{b} + \mathbf{R}^+ \geq \mathbf{0} \tag{8}$$

together with the so-called complementary conditions:

$$\boldsymbol{\lambda}^+ \geq \mathbf{0}\,,\ \boldsymbol{\Phi}^{+\mathrm{T}}\boldsymbol{\lambda}^+ = 0 \tag{9}$$

In case of irreversible inelastic deformations (i.e. non-holonomic problem), in order to capture some critical events like unloading, the conditions (9) must be expressed in rate form as follows:

$$\dot{\boldsymbol{\lambda}}^+ \geq \mathbf{0}\,,\ \boldsymbol{\Phi}^{+\mathrm{T}}\dot{\boldsymbol{\lambda}}^+ = 0 \tag{10}$$

Matrix $\mathbf{A}$ and vector $\mathbf{b}$ describe the behavior of the structure under imposed strains and given

loads, respectively. The Hessian matrix **A**, which governs the global behavior of the structure, is symmetric and semi-definite positive. If softening is considered by the introduction of **H**, the problem may become indefinite. Respect to the standard structural stiffness matrix, the matrix **A** is endowed with sophisticated mathematical features able to easily perform checks about the existence and the uniqueness of the solution [13, 14]. Matrix **A** and vector **b** can be computed in full before the procedure is started as a series of elastic calculations which do not require the expensive computation of the inverse of the stiffness matrix **K**, difficult to be determined in case of singular yield functions.

4 COMPUTATIONAL PROCEDURES

The LCP that governs the evolution of the system may exhibit an indefinite Hessian matrix (i.e. **A**+**H**) meaning that a multiplicity of solutions may be admitted on the equilibrium path due to softening-related bifurcation phenomena or loss of stability. Commercial finite element codes show serious difficulties in managing indefinite problem; MP algorithms have instead proved their ability to capture the whole set of possible alternative equilibrium paths and always find a solution, if it exists [14].

Solving the LCP (8) together with (9) or (10) is equivalent to solve a parametric linear complementary problem (PLCP) by introducing a scalar parameter α called load factor [15]:

$$\mathbf{\Phi} = (\mathbf{A} + \mathbf{H})\boldsymbol{\lambda}^{+} - \boldsymbol{\alpha}\mathbf{b} + \mathbf{R}^{+} \geq 0 \tag{11}$$

The solution of the problem is found in incremental steps, by varying the value of α. Each step and the relative α value are automatically defined when a crack multiplier is scaled to the next inelastic point or until it reaches a critical value. Since the holonomic solution, represented by a system of linear equations, is simpler to be found than the non-holonomic one, the adopted procedure assumes basically holonomic behavior and solves ad-hoc defined LCPs only when non-holonomic constraints are violated [11].

The sequence of solutions follows the evolution of plastic deformation (i.e. the cracking evolution) in the structure and the sequence terminates when a "unique" solution is found or an unbounded solution (i.e. collapse) is found or α decreases down to zero. The solution of each step is computed using a numerical code specifically developed for this purpose and which refers to the pivot theory proposed by Lemke [16].

5 NUMERICAL SIMULATIONS

A simulation of the in-situ diagonal compression test of sample CD04 (see paragraph 2) has been performed using the proposed constitutive model. The specimen dimensions are 1200 x 1200 mm with a thickness of 420 mm as the panel tested in the experimental campaign. The adopted mechanical parameters are reported in Table 1. Poisson's ratio $\nu = 0.2$ and fracture energy $G_F = 0.035$ N/mm are typical values adopted in other numerical works [17]. The other parameters, i.e. Young's modulus E = 1500 MPa and tensile strength $\sigma_t = 0.12$ MPa, have been quantified by calibration of the numerical and experimental results and the obtained values are consistent with typical values of historical masonry. The compression strength has been calculated as $\sigma_c = 10 \cdot \sigma_t$. The adopted FE model is reported in Figure 12.

Figure 13 (left) shows the comparison in terms of load vs. displacement curve. The displacements of the experimental curve are calculated as the mean of the displacements of the

two layers of wall, while the load as the sum of the loads.

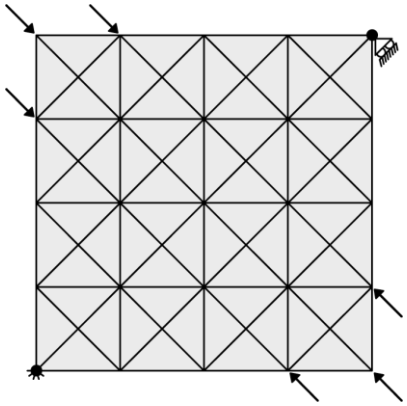


Figure 10: FE model of the masonry panel under diagonal compression

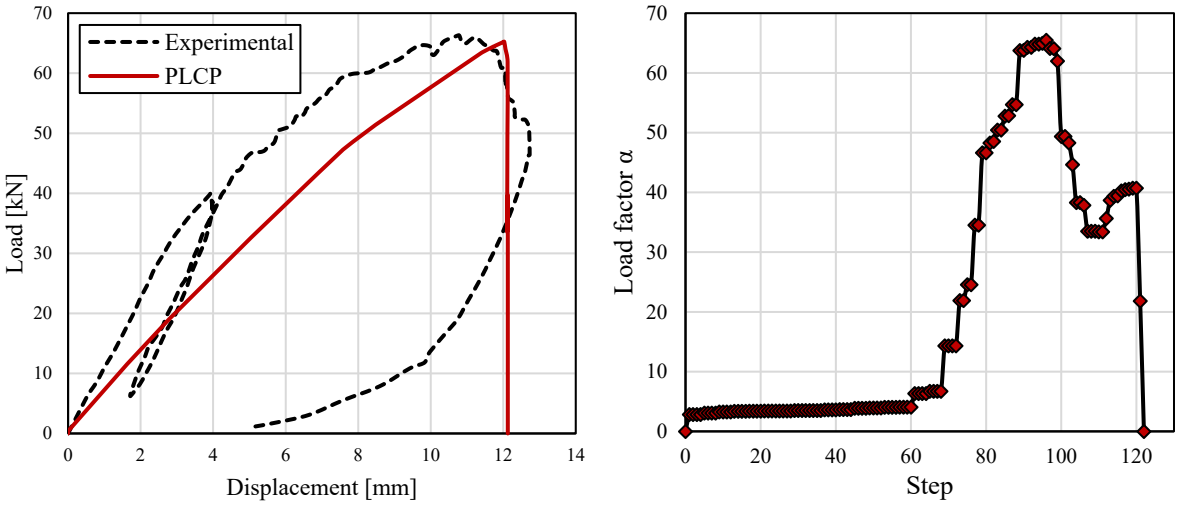


Figure 11: Left, Load vs. displacement curves comparison. Right, Load factor vs. step.

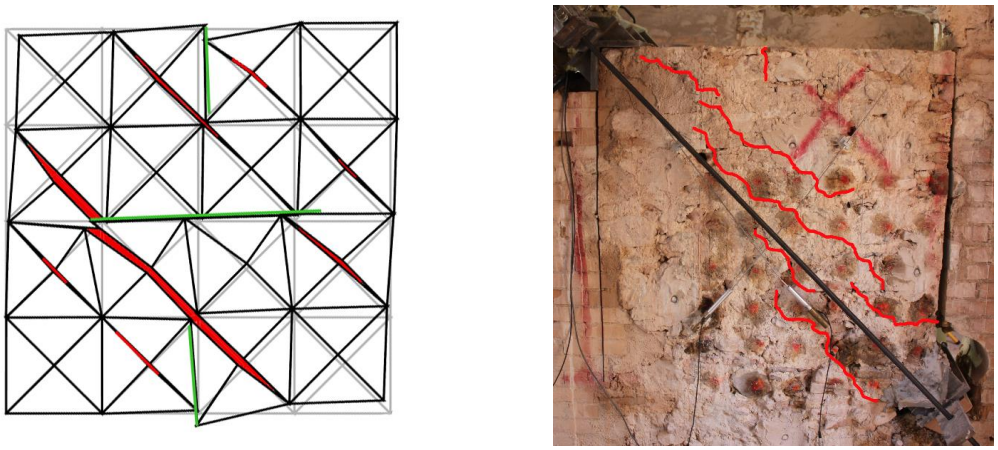


Figure 12: Left, Deformed shape at collapse with traction cracks in red and the slidings in green. Right, Experimental crack pattern.

In the experimental curve it is possible to observe that the plasticization of the material happens already at the first steps of the test (there is no evident change of slope before the unloading/reloading and the values of stiffness are very low). The elastic limit in the numerical simulation has been set to a very low value (1% of the failure in tension) after which the hardening branch starts, allowing a stiffness degradation able to approximate the experimental evidence. The numerical simulation catches the right value of the peak-load and the maximum displacement. The slope of the curve (PLCP), from the beginning to the peak, represents an average stiffness between the two points. A way to make the stiffness closer to the experimental one might be to modify the value of the hardening parameter during the loading history to reproduce the multi-branch hardening. However, this approach would make more complex the mathematical model.

As reported in Figure 13 (right), the load factor α changes during the evolutive non-holonomic analysis. The linear elastic behavior is represented by the first step. The flat section of the curve right after is the non-linear phase in which the spread plastic deformation is collected in the elements. A significant increment of the load factor is recorded when the limit tension is reached at the first node and macro-crack starts. The load factor continues to increase according to the activation of the non-holonomic softening modes at several nodes. When the critical width is reached at the first node, the problem is indefinite, the slope of the curve becomes negative and the load factor starts to decrease. Going forward with the analysis, a positive slope is recorded again meaning that the problem, from indefinite, became positive-definite again. When the load factor becomes zero, the procedure stops.

The final deformed shape of the structure is reported in Figure 14 (left) where tension cracks have developed mainly along the compressed diagonal. Also sliding phenomena in the vertical and horizontal direction are evident. As comparison, a picture of the masonry panel after the test is reported in Figure 14 (right) and a good agreement in terms of cracks pattern is found.

6 CONCLUSIONS

A constitutive model to describe fracture process in masonry has been proposed. The formulation takes its cue from the evidence of experimental tests performed on historical masonry walls. The model describes the cracking phenomenon as the succession of two phases: the micro-cracking hardening phase, with cracks represented by spread plastic deformations, and the macro-cracking softening phase, with cracks represented by localized deformations at the element edges. A non-standard finite element formulation has been adopted to find the solution of the nonlinear structural problem, taking advantage of the ability of mathematical programming algorithms to manage the computational instabilities of softening materials.

The simulation of an the in-situ diagonal compression test has been performed with reference to the results of an experimental campaign conducted on a historical masonry compound in the city center of L'Aquila (Italy). Some mechanical parameters (i.e. Poisson's ratio and fracture energy) has been chosen according to typical values adopted in other scientific works. Some others (i.e. Young's modulus, tensile and compressive strength) has been quantified by calibration of the numerical and experimental results. The numerical simulation was able to catch the value of peak-load and the maximum displacement. The cracking pattern showed cracks developing mainly along the diagonal directions, together with sliding phenomena in vertical and horizontal directions, analogously to what observed after the experimental test.

The validation test has given encouraging results; however, further research work is needed in order achieve the same results also for complex and large-scale structures.

REFERENCES

[1] Lourenço, P.B., Rots, J.G., Blaauwendraad, J., Two approaches for the analysis of masonry structures - micro and macro-modeling. *Heron* (1995), *40*, 313–340.

[2] Scamardo, M., Franchi, A., Crespi, P., An innovative approach for the finite element modelling of masonry cracking, in: *Proceedings of the 10th International Masonry Conference*, The International Masonry Society, Milano (2018), pp. 132–144.

[3] Scamardo, M.A., Franchi, A., Crespi, P.G., Fe modeling of fracture in quasi-brittle material, in: *Advances in Engineering Materials, Structures and Systems: Innovations, Mechanics and Applications - Proceedings of the 7th International Conference on Structural Engineering, Mechanics and Computation, 2019*, (2019).

[4] Corradi, M., Borri, A., Vignoli, A., Experimental study on the determination of strength of masonry walls. *Constr. Build. Mater.* (2003), *17*, 325–337.

[5] Drucker, D.C., Prager, W., Soil mechanics and plastic analysis or limit design. *Q. Appl. Math.* (1952), *10*, 157–165.

[6] Capurso, M., Maier, G., Incremental elastoplastic analysis and quadratic optimization. *Meccanica* (1970), *5*, 107–116.

[7] Cohn, M.Z., Franchi, A., Structural plasticity computer system: STRUPL. *ASCE J Struct Div* (1979), *105*, 789–804.

[8] Tin-Loi, F., A Yield Surface Linearization Procedure in Limit Analysis∗. *Mech. Struct. Mach.* (1990), *18*, 135–149.

[9] Hodge Jr., P.G., Automatic piecewise linearization in ideal plasticity. *Comput. Methods Appl. Mech. Eng.* (1977), *10*, 249–272.

[10] Hillerborg, A., Modeer, M., Petersson, P.E., Analysis of crack formation and crack growth in concrete by means of fracture mechanics and finite elements. *Cem. Concr. Res.* (1976), *6*, 733–781.

[11] Scamardo, M.A., A PLCP finite element crack model for the in-plane analysis of masonry, PhD Thesis, Politecnico di Milano (2020).

[12] Colonnetti, G., Elastic equilibrium in the presence of permanent set. *Q. Appl. Math.* (1950), *7*, 353–362.

[13] Franchi, A., Cohn, M.Z., Computer analysis of elastic-plastic structures. *Comput. Methods Appl. Mech. Eng.* (1980), *21*, 271–294.

[14] Franchi, A., Genna, F., Corradi, L., On the determination of bifurcation and limit points. *J. Eng. Mech.* (1998), *124*, 866–874.

[15] Patrizi, G., The equivalence of an LCP to a parametric linear program with a scalar parameter. *Eur. J. Oper. Res.* (1991), *51*, 367–386.

[16] Lemke, C.E., On Complementary Pivot Theory, in: *Mathematics of the Decision Sciences: Part 1*, (1968), pp. 95–114.

[17] Milosevic, J., Lopes, M., Gago, A.S., Bento, R., Testing and modeling the diagonal tension strength of rubble stone masonry panels. *Eng. Struct.* (2013), *52*, 581–591.

12th International Conference on Structural Analysis of Historical Constructions
SAHC 2020
P. Roca, L. Pelà and C. Molins (Eds.)

A MACHINE-LEARNING MODEL FOR THE DETERMINATION OF MACRO-SCALE MASONRY PROPERTIES BASED ON A VIRTUAL LABORATORY AT MICRO-SCALE

PHILIP KALKBRENNER[1], LUCA PELÀ[1] AND RICCARDO ROSSI[1]

[1]Department of Civil and Environmental Engineering
Universitat Politécnica de Catalunya (UPC-BarcelonaTech)
08034 Barcelona, Spain
e-mail: philip.kalkbrenner@upc.edu, luca.pela@upc.edu, rrossi@cimne.upc.edu

Keywords: Machine-learning, Historical Structure, Masonry, Virtual Laboratory, Representative Volume Element, Micro-scale, Macro-scale, Homogenization Technique

Abstract. *Cutting-edge methods in the computational analysis of structures have been developed over the last decades. Such modern tools are helpful to assess the safety of existing buildings. Multi-scale techniques have been proposed to combine the accuracy of micro-modelling and the computational efficiency of macro-modelling. Machine-learning tools have been utilized successfully to train specific models by feeding big source data from different fields, e.g. autonomous driving, face recognition, etc. This research proposes a continuous nonlinear material law that can reproduce data from micro-scale analysis. The proposed method is based on a machine-learning tool that links the two scales of the analysis by training a macro-model smeared damage constitutive law through benchmark data from numerical tests derived from micro-models.*

1 INTRODUCTION

Building with masonry is one of the oldest construction techniques and a majority of the building stock worldwide is constructed using this component material. Due to its social and cultural value the construction type and assessment tools for masonry must be preserved.

Nowadays numerical methods are considered as a commodity in structural engineering. Computer analysis techniques have been proved successful in assessing the complex behaviour of masonry structures. Two main lines of research can be identified, each with benefits and drawbacks: *macro-modelling* and *micro-modelling*.

Masonry is a heterogeneous material composed of brick units and mortar joints. Each material has different properties. Micro-scale modelling approaches, which are based on the idea of distinguishing between the masonry components, have been proved to be very accurate [1 - 3]. The associated modelling and computation cost is however too high in application to large structures. Macro-modelling [4 - 7] represents the masonry material as a homogenized continuum and thus offers wide applicability to real scale structures. The weakness of macro-modelling approaches is intrinsic to the idea of smearing the behaviours of the masonry components into a single continuum. The advantage is of course that the small

computational cost allows the modelling of large scale structures.

Given both the advantages and disadvantages of the modelling techniques, *multi-scale modelling* approach has the aim to provide a direct relationship between both scales. This approach requires a homogenization technique to scale strain and stress states from the micro to the macro level. Petracca et al. [8] have analysed the *classical first order computational homogenization* as an advanced technique applied to the analysis of masonry structures.

This approach consists of three steps, as defined in [8]. *Down-scaling* transfers the strains from the macro scale and applies them as boundary conditions to a representative volume element (RVE) at the micro-scale. *Solution of the boundary value problem* consists in solving the RVE analysis at micro-scale. *Up-scaling* transfers the stresses from micro-scale to macro-scale by computing a volume average of the micro-scale stresses. The described procedure has been carried out successfully and gives accurate results when compared with experimental tests on masonry structures [8, 9].

However, performing the homogenization at each gauss point of the macro scale model brings along a huge computational effort. Hence, an appropriate alternative to the classical computational homogenization that disconnects the above described steps must be found. A recent investigation presents the concept of smart constitutive laws trained by machine-learning tools [10]. The outcome of such models is a constitutive model that can be applied for numerical analysis of heterogeneous materials in terms of macro scale analysis.

The motivation of the present investigation is to train a machine-learning model that transfers the complex micro-structural behaviour of masonry to a macro model approach. Benchmark data for the machine-learning training procedure are derived from numerical nonlinear tests on masonry micro-models in a virtual laboratory.

The paper is organized as follows. Section 2 presents the general homogenization procedure. Section 3 summarizes the constitutive model applied in the virtual laboratory and for the machine-learning model. Section 4 introduces the machine-learning model, the optimization procedure and application to the present constitutive law. Section 5 explains the idea of the virtual laboratory as a data factory for the machine-learning model. In Section 6 the entire procedure is applied to an in plane loaded masonry wall.

2 THE MACHINE-LEARNING COMPUTATIONAL HOMOGENIZATION TECHNIQUE

"Classical" computational homogenization techniques like first order computational homogenization allow representing the microscopic behaviour of the heterogeneous masonry material very accurately. Such techniques are based on utilizing representative volume elements (RVEs) in order to analyse the material's micro mechanical behaviour. However, they still do not disconnect the micro and the macro-scale at the solving stage. When used together with the Finite Element Method, the procedure transforms strains at the gauss point of the macro-scale into a boundary value problem of the RVE at the micro scale. Thus, a boundary value problem of an entire RVE is solved in order to obtain stress results for only one gauss point at the macro-scale. The computational cost becomes tremendous, the larger the macro-scale models are.

Researches made in [11] introduce an off-line technique to avoid solving the RVE at each analysis step. The strains at the macro scales are not sent to a micro model RVE, but to a large

database. The creation of this database includes the strain and stress results of previously performed analyses on a RVE. Thus, the strains coming from the macro-scale can "choose" their corresponding stress state from the database by comparing the incoming strains with the ones of the database. The works made in [11] contribute substantially to the approach of the present investigations, since a virtual laboratory is used to construct the database. However, the method still implies jumping away from the macro-scale at the solving stage.
The idea of the present research is to avoid hopping around at multiple scales. The key issue is then finding a single homogeneous continuum damage model for the macro scale analysis of masonry that takes into account the masonry's heterogeneity. This research focuses on utilizing a machine-learning model to train the parameters of such a homogeneous continuum damage model for masonry structures. The following sections give an overview of the novel homogenization technique that consists of the following main steps. First, the derivation of a machine-learning model including a homogeneous constitutive law. Second, the construction of a virtual laboratory as a training data factory by running multiple tests on a representative volume element. Third, training and evaluation of the machine-learning model parameters. The fundamental ideas behind and the proper application of each step is presented in the following three sections.

3 CONSTITUTIVE MODEL

3.1 Constitutive Law

According with the theory of Continuum Damage Mechanics, an effective stress definition is adopted to distinguish between damaged/undamaged/loading and unloading stages. It is based on the principle of strain equivalence that assumes the comparison between damaged and undamaged configurations by strain consideration with reference to the elastic material behaviour [12].

$$\overline{\boldsymbol{\sigma}} = \boldsymbol{C} : \boldsymbol{\epsilon} \tag{1}$$

Where $\overline{\boldsymbol{\sigma}}$ is the effective stress tensor, $\boldsymbol{\epsilon}$ the strain tensor and $\boldsymbol{C}$ is the fourth order elasticity tensor. The works of [13 - 15] introduce separated internal damage variables to use damage scalar models for tensile and compressive stress contributions and define the stress tensor $\boldsymbol{\sigma}$ as follows

$$\boldsymbol{\sigma} = (1 - d^{+})\,\overline{\boldsymbol{\sigma}}^{+} + (1 - d^{-})\,\overline{\boldsymbol{\sigma}}^{-} \tag{2}$$

The internal damage variables d^{+} and d^{-} indicate the grade of damage in tension and compression, respectively ($d^{\pm} \in [0,1]$). The tensors $\overline{\boldsymbol{\sigma}}^{+}$ and $\overline{\boldsymbol{\sigma}}^{-}$ are the positive and negative parts of the effective stress tensor and account for different nonlinear behaviours in tension and compression. The decomposition of the effective stress tensor $\overline{\boldsymbol{\sigma}}$ is performed according to [15, 16].

3.2 Yield Criteria

Lubliner et al. [17] proposed a proper yield criterion that considers two scalar values that reflect different material behaviours in tension and compression. The values τ^{+}(tension) and τ^{-}(compression) indicate the equivalent uniaxial stress. This research includes a modified

Lubliner yield criterion [8] in compression and a Rankine yield criterion in tension. The scalars are then defined as follows

$$\tau^+ = \langle \bar{\sigma}_{max} \rangle \ (Rankine) \tag{3}$$

$$\tau^- = H(-\bar{\sigma}_{min}) \left[\frac{1}{1-\alpha} \left(\alpha \bar{I}_1 + \sqrt{3\bar{J}_2} + \kappa\beta \langle \bar{\sigma}_{max} \rangle \right) \right] \tag{4}$$

The constant κ aims to better control the effect of the compression surface on the shear strength of the model. It leads from 0 (→ Drucker-Prager surface) to 1 (→ Lubliner surface). To better understand the meaning of each entity in the equations, the authors advise to read carefully the explanations made in [3].

3.3 Damage Evolution

A threshold value must be introduced to distinguish between an undamaged and a damaged state of the material. At the same time, the threshold must indicate if the model undergoes loading/unloading or reloading, since the damage is an irreversible process. Thus, two additional scalar values are introduced. The actual threshold $r_n^{\pm}$ is defined as follows

$$r_n^{\pm} = \max\left\{ r_0^{\pm}, \max_{t_0 \le n \le t_e} \tau_n^{\pm} \right\} \tag{5}$$

Further information on the damage criteria can be found in Petracca et al. [3]. This research also introduces a combination of an exponential softening law in tension and a quadratic hardening and softening law in compression that fits very well for the numerical analysis of masonry structures. Figure 1 displays the tensile and compressive constitutive behaviours of the law described in [3]. Equations (7) and (8) provide the mathematical rules for damage in tension and compression.



(a) (b)

Figure 1: Uniaxial damage laws for (a) exponential softening and (b) quadratic hardening and softening

$$d^-(r^-) = 1 - \frac{\Psi(\xi^-)}{r^-} \tag{6}$$

$$d^+(r^+) = 1 - \frac{r_0^+}{r^+} exp\left\{ 2H_{dis} \left(\frac{r_0^+ - r^+}{r_0^+} \right) \right\} \tag{7}$$

Where $\Psi(\xi^-)$ depends on the damaged state (hardening or softening) and on a strain-like counterpart ξ^-. A detailed description of $\Psi(\xi^-)$, and the energy regularization in tension and

compression can be found in reference [3].

4 THE SUPERVISED MACHINE-LEARNING MODEL

4.1 Fundamentals

Machine-learning tools are very useful to support computations when a certain task is extremely difficult to program. The general idea is to collect data and utilize them to train a model to solve a task. This way of learning connects a set of inputs I_{true} and a set of outputs O_{true} by searching a function F so that $F(I_{true}) = O_{true}$. The function aims to fit the inputs to the outputs.

The goal of such a fitting is to adjust the machine-learning model parameters $\boldsymbol{\Theta}$ so that the given inputs I_{true} fit to the given outputs O_{true} as accurately as possible. The given outputs O_{true} are compared with predicted outputs O_{pred} in a loss function $\mathcal{L}(\boldsymbol{\Theta})$. If the loss function does not fulfill a predefined loss minimum, an adjustment of the models parameters $\boldsymbol{\Theta}$ is carried out to approximate the outputs O_{pred} of the model to the given outputs O_{true}.

The most popular algorithms to perform such optimizations are gradient descent operators. A detailed overview is given in [18]. The present research applies the *Adam optimizer* [19].

The loss function counts the machine-learning prediction error. A classical computation of the loss is the $\mathcal{L}_2$ loss function that computes a mean square error. The entire loss function applied to the gradient descent optimization for a batch of inputs and outputs of size m can be written as follows:

$$\mathcal{L}(\boldsymbol{\Theta}) = \frac{1}{m}\sum_{i=1}^{m}\left(O_{true} - O_{pred}(\boldsymbol{\Theta}, I_{true})\right)^2 \tag{8}$$

4.2 Present Application Procedure

This Section presents the construction of the specific machine-learning model applied in this research. In order to apply the machine-learning approach its procedure must be mapped to the present scientific issue. Thus the fundamental questions are what are the coupled input and output items, and which mathematical formulation connects them.

- ***The function*** $F(I_{true})$: This research aims to find a correlation between strains and stresses for a homogenized material. For any material, constitutive laws can define such a correlation. Thus the here considered mathematical formulation for the machine-learning model is derived from a constitutive law and is defined as function $\boldsymbol{\Gamma}(I_{true})$.
- ***The input*** I_{true} and ***output*** O_{true}: The constitutive law presented in Section 3 is based on strain equivalence. Then the input I_{true} of the function is a set of strain states $\boldsymbol{\varepsilon}_{true}$. In order to perform the supervised learning, the model requires the reference true output stresses $\boldsymbol{\sigma}_{true}$.
- ***The parameters*** $\boldsymbol{\Theta}$: The strains $\boldsymbol{\varepsilon}_{true}$ run through the model and are adjusted by the constitutive law material parameters which act as the trainable variables of the machine-learning model.
- ***The predicted output*** O_{pred}: The predicted output O_{pred} of the machine-learning model are the stresses $\boldsymbol{\sigma}_{pred}$ computed by the constitutive law.

After having introduced the machine-learning model's participating entities, the general mathematical formulation of the optimization process can be stated as follows:

$$\boldsymbol{\Gamma}(\boldsymbol{\varepsilon}_{true}, \boldsymbol{\Theta}) \approx \boldsymbol{\sigma}_{true} \tag{9}$$

The model searches a modification of the parameters $\boldsymbol{\Theta}$ of the constitutive model $\boldsymbol{\Gamma}$, so that by inputting strain states $\boldsymbol{\varepsilon}_{true}$ an accurate approximation to the reference stresses $\boldsymbol{\sigma}_{true}$ can be achieved. A predefined learning criterion checks the error value of the actual optimization state. If the error value is less or equal to the learning criterion, the optimization finishes and stores the actual modification of the parameters $\boldsymbol{\Theta}$ as the optimized model parameters $\boldsymbol{\Theta}^*$. Then the model can be utilized to predict stresses $\boldsymbol{\sigma}_{pred}$ by entering any strain state $\tilde{\boldsymbol{\varepsilon}}$. It follows:

$$\boldsymbol{\Gamma}(\tilde{\boldsymbol{\varepsilon}}, \boldsymbol{\Theta}^*) = \boldsymbol{\sigma}_{pred} \tag{10}$$

The implementation of the machine-learning model takes place in the python-based open source framework *TensorFlow [20]*. It offers a variety of already implemented optimizers including the above mentioned. The machine-learning model flow inside TensorFlow is based on a computation graph consisting of nodes where each node performs a mathematical operation.

5 VIRTUAL LABORATORY

The here presented technique targets the homogenization of a heterogeneous material. Thus, the material's heterogeneity must be represented in a carefully constructed micro-model. Such a model takes into account the constitutive behaviour of the material's components. It is called a representative volume element (RVE). RVEs can be exposed to boundary conditions, in order to analyse the heterogeneous material's behaviour. Catching this behaviour is essential for any homogenization technique. The here investigated technique necessitates a space where boundary conditions can be applied to a properly micro-modelled RVE in order to determinate its behaviour. This space is called virtual laboratory (VL).

The accuracy of the machine-learning homogenization technique is based on two operational needs: a) a large amount of data and b) a broad data representation. Need a) is crucial for any machine-learning model: the more input data in learning, the more accurate its prediction. Need b) is crucial for the homogenization technique. The data should represent the nonlinear and heterogeneous behaviour of the RVE in order to be able to consider it in the homogenization technique. This can be achieved by performing the virtual experiment up to failure and by carrying out multiple virtual experiments on the same RVE, each taking into account a different boundary condition. This leads to a variety of deformations of the RVE.

5.1 The Boundary Value Problem of the Representative Volume Element

This Section explains the fundamental part of the VL: the representative volume element (RVE) and the solution of its boundary value problem. It is illustrated for a two dimensional RVE but can analogously be applied to a three dimensional one. This work applies the Finite Element (FE) method as numerical tool. Figure 2 shows the schematic view of a micro model RVE of a masonry wall.

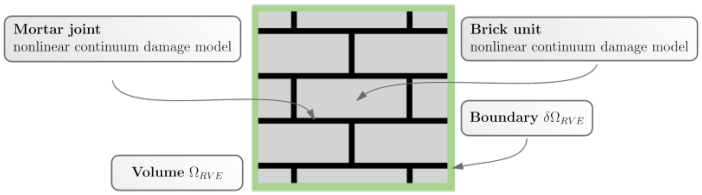


Figure 2: Example of a micro-scale modelled representative volume element $\boldsymbol{\Omega_{RVE}}$ for the virtual laboratory with boundary $\boldsymbol{\partial\Omega_{RVE}}$

In order to solve the boundary value problem of the RVE, boundary conditions must be defined. This can be done by applying a displacement fluctuation field to the RVE. The research done in [8] summarizes several fluctuation fields that can be implemented to RVE analyses. In the present monotonically increasing displacements are applied to the RVE's boundary $\partial\Omega_{RVE}$ as follows:

$$d_x = \left(\varepsilon_{xx} \cdot x + \varepsilon_{xy} \cdot y\right) \cdot t, \qquad d_y = \left(\varepsilon_{yy} \cdot y + \varepsilon_{xy} \cdot x\right) \cdot t \tag{11}$$

Where d_x and d_y are the displacements applied to the FE nodes of the RVE's boundary in x- and y-direction, respectively. The factor $t \in [t_0, t_e]$ describes the time instance of the actual analysis step and increases monotonically. The constants ε_{xx}, ε_{yy} and ε_{xy} are the components of a previously defined strain state $\boldsymbol{\varepsilon}$ in Voigt's notation. Modifying them allows performing a variety of virtual experiments. Investigations made by Zaghi et al. [11] show that all possible strain states can be defined as the coordinates of a three dimensional sphere in a Cartesian coordinate system with each component being an axis:

$$\boldsymbol{\varepsilon} = \begin{pmatrix} \varepsilon_{xx} \\ \varepsilon_{yy} \\ \varepsilon_{xy} \end{pmatrix} = \begin{pmatrix} \lambda \cdot \cos\Theta \\ \lambda \cdot \sin\Theta \cdot \cos\varphi \\ \lambda \cdot \sin\Theta \cdot \cos\varphi \end{pmatrix}, \quad with\ \lambda = \|\boldsymbol{\varepsilon}\| = \sqrt{\varepsilon_{xx}^2 + \varepsilon_{yy}^2 + \varepsilon_{xy}^2} \tag{12}$$

Where λ, Θ and φ are parameters that define the coordinates of the sphere. By modifying angles Θ and φ in interval $[-\pi, \pi]$, all possible strain configurations can be obtained.

A numerical non-linear finite element analysis solves the boundary value problem for each virtual experiment. The open source framework KRATOS *Multiphysics* [21] is utilized. It enables to program a loop over all the considered cases in the virtual laboratory.

While solving the boundary value problem, a procedure ensures to store the stresses at each gauss point of the analysis. The transition from micro to macro-scale takes place by computing an average of the saved RVE stresses at each step. The applied general computation of the up-scaled stress $\hat{\boldsymbol{\sigma}}$ for two-dimensional elements is as follows:

$$\hat{\boldsymbol{\sigma}} = \frac{1}{A_{RVE}} \sum_{i=1}^{n} \left[\frac{A_i}{k_i} \sum_{j=1}^{k_i} \boldsymbol{\sigma}_{i,j} \right] \tag{13}$$

Where n is the total number of elements of the RVE, A_{RVE} is the area of the total RVE, A_i is the area of the *i-th* element, k_i is the number of gauss points of the *i-th* element, $\boldsymbol{\sigma}_{i,j}$ is the stress vector of the *i-th* element at its *j-th* gauss point. The corresponding up-scaled strain $\hat{\boldsymbol{\varepsilon}}$ can be derived by transforming the applied boundary strain $\boldsymbol{\varepsilon}$ to the engineering notation.

5.2 Isotropic Mapping of Up-scaled States

The introduced homogenization technique includes the training of an isotropic constitutive law. Thus an isotropic relation between the up-scaled strain $\hat{\boldsymbol{\varepsilon}}$ and the up-scaled stress $\hat{\boldsymbol{\sigma}}$ must be ensured. This is not the case if stresses of a non-isotropic RVE are averaged. In this research the assumption holds, that the elasticity between both the up-scaled entities from the RVE follows an orthotropic relation.

Pelà et al. [6] apply a concept of *mapped stress tensor* to the nonlinear damage analysis of masonry structures. The idea is that a linear mapping can be found which transforms an initially anisotropic behaviour into an isotropic one. Provided such mapping is known, one can map the input strain onto the isotropic space, operate onto it to obtain an isotropic stress and then inverse map the obtained stress to obtain an equivalent anisotropic behaviour.

This is best explained in symbols, by providing a technique for the construction of the mapping operator. Let $\boldsymbol{C}$ be a generic elasticity tensor and $\boldsymbol{C}^*$ the *closest* isotropic tensor (see e.g. [22] for a discussion on the determination of $\boldsymbol{C}^*$)**.** Provided that $\boldsymbol{C}$ is Symmetric Positive Definite (SPD), something that should be guaranteed for any elasticity tensor. A linear operator **T** can be found such that **C**= $\boldsymbol{T^t C^* T}$**.** A simple constructive proof of this can be found in [23]. Since $\boldsymbol{\sigma} = \boldsymbol{C}:\boldsymbol{\epsilon}$ it follows that $\boldsymbol{\sigma} = \boldsymbol{T^t C^* T \epsilon}$**.** Premultiplying by $\boldsymbol{T^{-t}}$ we obtain $\boldsymbol{T^{-t}\sigma} = \boldsymbol{C^*(T\epsilon)}$**.** If we now define the "mapped" quantities $\boldsymbol{\sigma^*} = \boldsymbol{T^{-t}\sigma}$ and $\boldsymbol{\epsilon^*} = \boldsymbol{T\epsilon}$ we can observe that the relation $\boldsymbol{\sigma^*} = \boldsymbol{C^*\epsilon^*}$ is isotropic, that is, that the matrix $\boldsymbol{T}$ defines the mapping operator we were looking for. $\boldsymbol{C}$ can be approximated by taking into account the results from the RVE analysis. Values are extracted from the linear range at the first analysis step t_0 of each virtual experiment. The stress and strain states are then stored in a matrix, respectively.

$$\tilde{\boldsymbol{\varepsilon}}_{\boldsymbol{t_0}} = [\ \hat{\boldsymbol{\varepsilon}}_{\boldsymbol{1},\boldsymbol{t_0}} \quad \hat{\boldsymbol{\varepsilon}}_{\boldsymbol{2},\boldsymbol{t_0}} \quad \cdots \quad \hat{\boldsymbol{\varepsilon}}_{\boldsymbol{n},\boldsymbol{t_0}}\ ], \qquad \tilde{\boldsymbol{\sigma}}_{\boldsymbol{t_0}} = [\ \hat{\boldsymbol{\sigma}}_{\boldsymbol{1},\boldsymbol{t_0}} \quad \hat{\boldsymbol{\sigma}}_{\boldsymbol{2},\boldsymbol{t_0}} \quad \cdots \quad \hat{\boldsymbol{\sigma}}_{\boldsymbol{n},\boldsymbol{t_0}}\ ] \tag{14}$$

Where $\boldsymbol{n}$ is the number of virtual experiments. The approximated orthotropic elasticity matrix for the two dimensional case can then be computed by applying

$$\boldsymbol{C} = \tilde{\boldsymbol{\sigma}}_{\boldsymbol{t_0}} : \tilde{\boldsymbol{\varepsilon}}_{\boldsymbol{t_0}}{}^{+} \tag{15}$$

Where $\tilde{\boldsymbol{\varepsilon}}_{\boldsymbol{t_0}}{}^{+}$ is the *Moore-Penrose Inverse* of $\tilde{\boldsymbol{\varepsilon}}_{\boldsymbol{t_0}}$. The application of Equation (12) requires that the number of virtual experiments $\boldsymbol{n} > 1$, by definition the Moore Penrose Inverse is supporting the least squares solution to the problem $\tilde{\boldsymbol{\sigma}}_{\boldsymbol{t_0}} = \boldsymbol{C}\tilde{\boldsymbol{\varepsilon}}_{\boldsymbol{t_0}}$.

In order to define $\boldsymbol{C}^*$ as the isotorpic matrix, the research presented here considers a optimization procedure that finds the closest isotropic matrix to an orthotropic one by searching the minimum of the Frobenius norm of both the isotropic and the orthotropic matrix. This optimization includes the modification of the isotropic elastic constants E and ν.

The machine-learning procedure is then performed according to the following steps: i) computation of the anisotropic elasticity matrix $\boldsymbol{C}$ by Moore Penrose; ii) computation of the closest isotropic matrix $\boldsymbol{C}^*$; iii) computation of the transformation matrix $\boldsymbol{T}$; iv) mapping of the training data to the isotropic level; v) train the isotropic constitutive damage model.

Once then isotropic constitutive model is trained, in order to use it, one would follow the steps: i) given the anisotropic strains $\boldsymbol{\epsilon}$ compute the isotropic strains $\boldsymbol{\epsilon^*}$; ii) apply the trained constitutive law to obtain the isotropic stress $\boldsymbol{\sigma^*}$; iii) map $\boldsymbol{\sigma^*}$ onto $\boldsymbol{\sigma}$ into the real anisotropic space.

6 APPLICATION

This Section presents the application of the machine-learning homogenization technique to a two dimensional masonry wall. Figure 3a shows the RVE of the virtual laboratory and its boundary. The wall is build up by bricks of size $0.309\,m \times 0.1475\,m \times 0.045\,m$. The thickness of the vertical and horizontal mortar joints is 0.012 m. These dimensions allow a spatial allocation of the bricks and mortar equal to the "Flemish Bond". The RVE's total dimensions are $0.53\,m$ in x- and y-directions, respectively.



a) b)

Figure 3: Virtual laboratory: a) Micro model of the representative volume element showing the brick units, the mortar joints and the boundary; b) generated strain database for the boundary displacement application

The FE modelling was carried out by utilizing the program *GiD Pre- and Postprocessor* [24]. The average element size counts $0.006\,m$ so that the mortar layer is modelled by two elements in its thickness direction. Exceptionally quadrilateral elements with 4 gauss point integration have been used for the FE mesh. The total number of elements counts 6160.

The FE mesh is passed to the python based FE program *KRATOS Multiphysics*. Both the brick units and mortar joints are assigned with the strain driven d^+/d^- damage constitutive model introduced in Section 3. Table 1 shows the properties assigned to both the materials.

Table 1: Material data for the brick units and the mortar joints applied to the masonry RVE

	E	ν	f_p^+	G^+	f_0^-	f_p^-	f_k^-	f_r^-	G^-	ε_p^-	c_1^-	c_2^-	c_3^-	k_b	κ
	$[GPa]$	$[-]$	$[MPa]$	$[N/m]$	$[MPa]$	$[MPa]$	$[MPa]$	$[MPa]$	$[N/m]$	$[10^{-2}]$	$[-]$	$[-]$	$[-]$	$[-]$	$[-]$
Brick	7.0	0.2	1.5	48.0	2.	6.0	4.6	2.0	3600.0	1.0	0.65	0.5	1.5	1.2	0.16
Mortar	1.8	0.2	0.15	20.0	2.0	6.0	4.6	2.0	3600.0	1.0	0.65	0.5	1.5	1.2	0.16

For the generation of boundary conditions 26 cases are considered. Figure 3b displays the database of strain states $\boldsymbol{\varepsilon}$ for the virtual laboratory (generated from Equation (10)). A single virtual experiment then consists of a nonlinear analysis of the RVE by monotonically increasing the displacement configuration.

By applying the mapping procedure of Section 5 the transformation matrices and the isotropic linear elastic material data for the homogenized material can be derived. The linear elastic isotropic constants are $E = 4.46\,GPa$ and $= 0.187$.

After having finalized the entire procedure explained in Section 5, the training of the machine-learning model starts. In order to simplify the machine-learning procedure the entire

training set is split into three sets. Then a 3 phased optimization can be performed by only training selected variables that correlate to the material behaviour represented in each set. Each set trains selected variables only in its assigned training set. Figure 4 shows the training progression of each variable during the optimization, furthermore it shows the training loss. Table 2 shows the optimized results for the parameters of a homogenized material model for masonry.

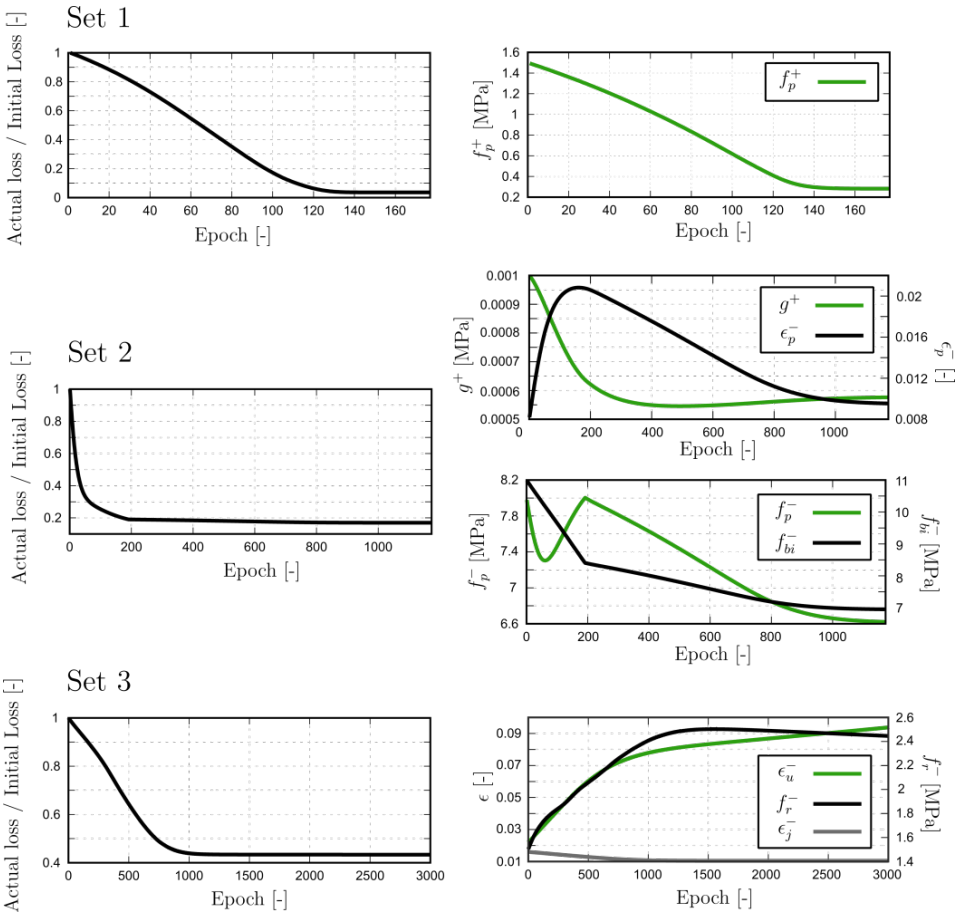


Figure 4: Example of a micro-scale modelled representative volume element $\boldsymbol{\Omega_{RVE}}$ for the virtual laboratory with boundary $\boldsymbol{\partial\Omega_{RVE}}$

Table 2: Values obtained from the machine-learning optimization technique at the isotropic level for a masonry wall with bricks allocated according to the Flemish bond

Homogenized Constitutive Model	f_p^+	G^+	f_0^-	f_p^-	f_{bi}^-	f_r^-	ε_p^-	c_1^-	c_2^-	c_3^-
	$[MPa]$	$[N/mm]$	$[MPa]$	$[MPa]$	$[MPa]$	$[MPa]$	$[-]$	$[-]$	$[-]$	$[-]$
	0.28	0.30	1.0	6.62	6.95	2.45	0.0095	0.5	0.06	7.53

7 CONCLUSIONS

This research has presented a novel homogenization technique for heterogeneous materials. The method deviates from classical homogenization procedures by utilizing a

machine-learning model. Machine-learning model can detect the link between coupled inputs and outputs by searching it in a mathematical formulation. In this work, the mathematical formulation is constricted to be a strain driven non-linear constitutive law.

This research has introduced a virtual laboratory for training data production. In the virtual laboratory a representative volume element (RVE) of the considered heterogeneous material is built up. While running a large amount of different nonlinear numerical analyses on the RVE, data are stored as coupled strain and stress states in order to train the parameters of a machine-learning model. The procedure also respects the orthotropic material behaviour by applying a mapping transformation from an orthotropic to an isotropic state. The presented procedure is applied to a two dimensional masonry wall. A properly constructed micro model RVE of the wall was constructed as a finite element model. A large amount of different boundary conditions were applied to the nonlinear analysis of the RVE in the virtual laboratory. The machine-learning model of the application case is a properly defined nonlinear $d^+/\ d^-$ damage constitutive law that has shown to present the brittle behaviour of masonry structures efficiently. At the optimization stage, the parameters of the constitutive law were trained in order to be able to predict the stress states as approximately as possible.

The future step of this research is the implementation of the trained constitutive law to a FE software. This also includes the transformation procedure. Then the applicability and the accuracy of the trained model can be tested for the analysis at the macro scale.

Acknowledgements. The authors gratefully acknowledge the financial support from the Ministry of Science, Innovation and Universities (MCIU) of the Spanish Government, the State Agency of Research (AEI) and the European Regional Development Fund (ERDF) through the SEVERUS project ("Multilevel evaluation of seismic vulnerability and risk mitigation of masonry buildings in resilient historical urban centres", ref. num. RTI2018-099589-BI00). Support from Secretaria d'Universitats i Investigació de la Generalitat de Catalunya through a predoctoral grant awarded to the first author is gratefully acknowledged.

REFERENCES

[1] Oliveira, D.V. and Lourenço, P.B. Implementation and Validation of a constitutive model for the cyclic behaviour of interface elements, Computers and Structures, vol.28 (2004), pp.1451-1461

[2] Drougkas, A., Roca, P. and Molins, C. *Analytical micro-modellingof masonry periodic unit cells – Elastic properties,*International Journal of Solids and Structures,vol.69-70 (2015), pp.169-188

[3] Petracca, M., Pelà, L., Rossi, R., Zaghi, S., Camata, G. and Spacone, E. *Micro-scale Continuos and Discrete Numerical Models for Nonlinear Analysis of Masonry Shear Walls,* Construction and Building Materials, vol. 149 (2017), pp. 296-314

[4] Saloustros, S., Pelà, L., Roca, P. and Portal, J. *Numerical analysis of Structural Damage in the Church of the Poblet Monastery,* Engineering Failure Analysis, vol. 48 (2015), pp.41-61

[5] Lotfi, H. and Shing, P. *An Appraisal of Smeared Crack Models for Masonry Shear Wall Analysis,* Computers & Structures, vol. 41 (1991), pp.413-425

[6] Pelà, L., Cervera, M. and Roca, P *An orthotropic damage model for the analysis of*

masonry structures, Construction and Building Materials, vol. 41 (2013), pp.957-967[12]
[7] Kalkbrenner, P., Pelà, L. and Sandoval, C. Multi Directional Pushover Analysis of Irregular Masonry Buildings without Box Behaviour, Engineering Structures, vol. 201 (2019)
[8] Petracca, M., Pelà, L., Rossi, R., Oller, S., Camata, G. and Spacone, E. *Regularization of first order computational homogenization for multi-scale analysis of masonry structures,* Computational Mechanics, vol.57 (2016), no.2, pp.257-276
[9] Petracca, M., Pelà, L., Rossi, R., Oller, S., Camata, G. and Spacone, E. *Multiscale computational first order homogenization of thick shells for the analysis of out-of-plane loaded masonry walls,* Computer Methods in Applied Mechanics and Engineering, vol. 315 (2017), pp.273-301
[10] Logarzo H.J., Capuano G., Rimoli J.J., *Smart constitutive laws: Inelastic homogenization through machine-learning*, Computer methods in applied mechanics and engineering, vol. 373 (2021)
[11] Zaghi, S., Martinez, M., Rossi, R. and Petracca, M. *Adaptive and Off-line Techniques for Non-linear Multiscale Analysis,* Composite Structures, vol. 206 (2018), pp.215-233
[12] Woody Ju, J.W., Chaboche, J.L. and Voyiadjis, G.Z. *Damage Mechanics in Engineering Materials*. Elsevier Science Ltd., 1998.
[13] Cervera, M., Oliver, J. and Faria, R. *Seismic Evaluation of concrete dams via continuum damage models.* International Journal of Solids and Structures, vol.24 (1995), no.9, pp. 1225-1245.
[14] Faria, R., Oliver, J. and Cervera, M. *A strain-based plastic viscous- damage model for massive conscrete structures,* International Journal of Solids and Structures, vol.43(1998), no.14, pp.1533-1558.
[15] Wu, J.Y., Li, J. and Faria, R. *An energy release rate-based plastic damage model for concrete,* International Journal of Solids and Structures, vol.43(2006), no.3-4, pp.583-612
[16] Faria, R., Oliver, J. and Cervera, M. *An Isotropic Scalar Damage Models for the Numerical Analysis of Concrete Structures,* CIMNE Monograph, vol December (2000), no.198
[17] Lubliner, J., Oliver, J., Oller, S. and Oñate, E. *A plastic damage model for concrete,* International Journal of Solids and Structures, vol.25 (1989), no.3, pp.299-326
[18] Ruder, S. An overview of gradient descent optimization algorithms, arXiv preprint arXiv:1609.04747 (2016)
[19] Kingma, D.P. and Lei Ba, J. *Adam: A Method For Stochastic Optimization,* paper submitted to: International Conference on Learning Representations (2015)
[20] https://www.tensorflow.org/
[21] Dadvand, P., Rossi, R. and Oñate, E. *An Object-oriented Environment for Developing Finite Element Codes for Multi-disciplinary Applications,* Archives of Computational Methods in Engineering, vol.17 (2010), no.2, pp.253-297
[22] Norris A., *The isotropic material closest to a given anisotropic material*, Journal of Mechanics of Materials and Structures 1 (2005)
[23] Rossi R., Zorilla R., Codina R., *A stabilised displacemen-volumetric strain formulation for nearly incompressible and anisotropic materials*, CMAME, 2020
[24] Melendo A., Coll A., Pasenau M., Escolano E., Monros A., www.gidhome.com, (2016)

12th International Conference on Structural Analysis of Historical Constructions
SAHC 2020
P. Roca, L. Pelà and C. Molins (Eds.)

A MACROSCALE MODELLING APPROACH FOR NONLINEAR ANALYSIS OF MASONRY ARCH BRIDGES

B. PANTO'[1], C. CHISARI[2], L. MACORINI[1*], B.A. IZZUDDIN[1]

[1]Department of Civil and Environmental Engineering, Imperial College London
South Kensington Campus, London SW7 2AZ, UK
e-mail: { b.panto, l.macorini*, b.izzuddin}@imperial.ac.uk (*corresponding author)

[2]Department of Architecture and Industrial Design, Università della Campania "Luigi Vanvitelli"
via San Lorenzo – Abazia di San Lorenzo, Aversa (CE), Italy
e-mail: corrado.chisari@unicampania.it

Keywords: Nonlinear Analysis, Macromodels, Mesoscale Approach, Masonry Arch Bridges.

Abstract. *Masonry arches represent the most important structural components of masonry arch bridges. Their response is strongly affected by material nonlinearity which is associated with the masonry texture. For this reason, the use of mesoscale models, where units and mortar joints are individually represented, enables accurate response predictions under different loading conditions. However, these detailed models can be very computationally demanding and unsuitable for practical assessments of large structures. In this regard, the use of macro-models, based on simplified homogenised continuum representations for masonry, can be preferable as it leads to a drastic reduction of the computational burden. On the other hand, the latter modelling approach requires accurate calibration of the model parameters to correctly allow for masonry bond. In the present paper, a simplified macro-modelling strategy, particularly suitable for nonlinear analysis of multi-ring brick-masonry arches, is proposed and validated. A numerical calibration procedure, based on genetic algorithms, is used to evaluate the macro-model parameters from the results of meso-scale "virtual" tests. The proposed macroscale description and the calibration procedure are applied to simulate the nonlinear behaviour up to collapse of two multi-ring arches previously tested in laboratory and then to predict the response of masonry arches interacting with backfill material. The numerical results confirm the ability of the proposed modelling strategy for masonry arches to predict the actual nonlinear response and complex failure mechanisms, also induced by ring separation, with a reduced computational cost compared to detailed mesoscale models.*

1 INTRODUCTION

Old masonry arch bridges belong to the cultural and architectural heritage and still play a critical role within railway and roadway networks in Europe and worldwide. These structures were built following empirical rules and were not designed to resist current traffic loading and extreme events, such as earthquakes. An accurate assessment of the ultimate performance of these complex structural systems represents a crucial step to prevent future failures and preserve such historical masonry structures for the next generations.

Masonry arch barrels are the key structural components of masonry arch bridges. Their nonlinear behaviour is strongly influenced by the mechanical properties of the two constituents, masonry units and mortar joints, and their arrangement to form the brickwork of the arch (i.e. masonry bond). Two main categories of masonry arch bridges can be identified: stone masonry and brick masonry bridges. In the first group, the arches are built from large voussoirs organised in a single arch ring [1] (Figure 1a). Conversely, in the case of brick masonry bridges, a multi-ring arrangement is usually utilised, where the number of rings depends on the span length of the arch. The rings are typically bonded together using the stretcher method [2] (Figure 1b), where the connection between adjoining rings is guaranteed by continuous mortar joints. Numerous laboratory and in-situ tests were performed to investigate the failure mechanisms of masonry arches and bridges, considering also the influence of backfill and spandrel walls under monotonic and cyclic loading conditions [3]. Moreover, specific studies focused on multi-ring arches pointed out the high influence of the detachment and sliding along the ring joints on the ultimate strength and failure mode of the arch [4].

In previous research, different numerical strategies have been proposed to simulate the nonlinear behaviour of masonry arches and bridge [3]. Generally, approaches based upon limit analysis principles can be effectively used to estimate the ultimate load capacity [5]. However, such strategies do not provide information about the nonlinear response before collapse, and they are often based upon crude assumptions, e.g. the representation of masonry as a no-tension material, which may lead to underestimating the ultimate resistance of masonry arches. Previous studies comprise also simplified 2D finite element (FE) limit-analysis descriptions to simulate the arch-backfill interaction [6][7] and 3D nonlinear FE strategies with elasto-plastic solid elements [1][8][9], where masonry is assumed as a homogeneous isotropic material disregarding its anisotropic nature. More recent numerical models for masonry arched structures and bridges include the micro-model strategy proposed by Milani et al. [10] using triangular rigid elements and nonlinear links, the Discrete Macro-Element method (DMEM) [11][12][13] and the Distinct Element Method (DEM) [14][15].

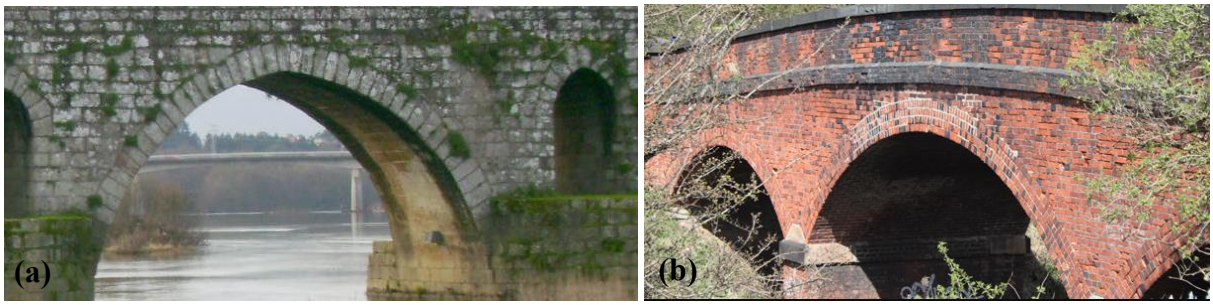


Figure 1: (a) Roman stone-bridge over the Limia river (Portugal) and (b) Brick Rail bridge, Stapleford (UK).

A detailed 3D mesoscale modelling strategy for masonry arch bridges has been previously developed at Imperial College [16][17], which is considered for the calibration of the macroscale approach proposed in the current paper. According to this strategy, the masonry parts of the bridge are simulated by using linear solid elements and 2D nonlinear interface elements to explicitly allow for the masonry bond [18]. The backfill is modelled by elasto-plastic solid elements, and the connection between the masonry components and the backfill

is modelled through nonlinear interfaces representing the actual frictional interaction. This approach generally leads to accurate response predictions, including under extreme loading, but it is associated with significant computational cost which may prevent its use in the practical assessment of real large structures.
This paper proposes a more efficient macroscale strategy for masonry arches and bridges. Elasto-plastic 3D continuum elements interacting with 2D nonlinear interfaces are employed to model a masonry arch but, as opposed to the mesoscale strategy, the mesh characteristics do not depend on the size of the masonry units as the masonry bond is not explicitly represented. The damage-plasticity model proposed in [19] and a multi-surface frictional model [20] are employed for solid and interface elements. The mechanical parameters of the two models are evaluated by solving a multi-object optimization problem by means of a genetic algorithm [21], considering mesoscale predictions of virtual numerical experiments on small masonry components. The model is validated based on the response of two multi-ring masonry arches also interacting with backfill.

2 PROPOSED MACRO-MODEL

In the proposed FE modelling strategy, the arch is discretised by a regular mesh of nonlinear 20-noded 3D solid continuum elements. In addition, 2D nonlinear zero-thickness interface elements are arranged along the circumferential mid-thickness surface of the arch to simulate damage associated with potential ring separation (Figure 2), where each interface lumps the linear deformability and non-linear behaviour of n-1 ring joints (with n the number of rings forming the physical arch). Importantly, the characteristics of the FE mesh with solid elements are not directly linked to the masonry bond. Thus, an arbitrary number of solid elements can be employed along the length of the arch, according to the desired level of response detail, but at least two solid elements should be arranged along the thickness of the arch to accommodate the mid-thickness nonlinear interfaces. In the proposed macroscale representation implemented in ADAPTIC [23], the isotropic plastic-damage material model presented in [19] is used for the 20-noded solid elements. A standard decomposition of total strains ($\boldsymbol{\varepsilon}$) in elastic ($\boldsymbol{\varepsilon_e}$) and plastic ($\boldsymbol{\varepsilon_p}$) components is considered, and the stress tensor ($\boldsymbol{\sigma}$) is obtained from the effective stress tensor ($\bar{\boldsymbol{\sigma}}$) and a scalar damage variable $d(\bar{\boldsymbol{\sigma}}, \kappa_t, \kappa_c)$. The latter variable depends on the stress state and two historical variables (κ_t, κ_c) representing the evolution of plastic strains in tension and in compression.

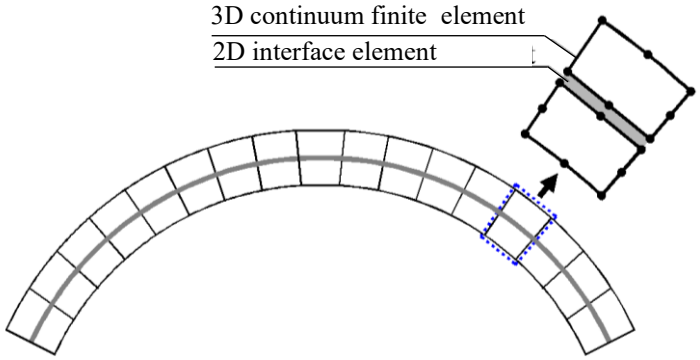


Figure 2: Illustrative FE mesh for proposed macroscale description with solid elements and nonlinear interfaces.

The material relationship is expressed analytically by: $\boldsymbol{\sigma} = (1-d)\,\bar{\boldsymbol{\sigma}} = (1-d)\,\boldsymbol{K_0}\,(\boldsymbol{\varepsilon}-\boldsymbol{\varepsilon_p})$ where, $\boldsymbol{K_0}$ is the fourth-order isotropic elastic tensor. The local hardening plastic problem is solved at each integration point to evaluate the effective stress, adopting a non-associated elasto-plastic constitutive law with Drucker-Prager-like plastic flow potential.
2D 16-noded interface elements [18] are employed for the mid-thickness circumferential interfaces, using the plasticity-damage constitutive model proposed in [20]. According to this model, the stress and strain fields are composed of a normal component in the direction orthogonal to the interface and two tangential components on the plane of the interface. The effective stresses are evaluated at each Gauss point by solving a linear hardening elasto-plastic problem considering three-surface plastic yield domain to simulate the tensile, sliding and compressive failures. Then, the nominal stresses are obtained by multiplying the effective stresses with damage matrix **D**, containing the damage index in traction, shear and compression ranging from 0 (no-damage) to 1 (complete damage).

2.1 Model calibration

The mechanical calibration of the proposed model requires the determination of several material parameters defining the linear and nonlinear behaviour of the solid elements and the 2D interfaces, as described in [19] and [20]. For this reason, an objective and robust calibration procedure represents a fundamental step to guarantee the model accuracy and applicability. In this study, the unknown model parameters are evaluated by enforcing an energy equivalence between a detailed mesoscale model of the periodic cell of the arch (Figure 3a), subjected to specific boundary/loading conditions (also called *virtual* test), and its equivalent representation by the proposed macroscale description. An *m*-objective optimisation problem (where *m* is the number of virtual test employed in the calibration), based on Non-Dominated Sorting Genetic Algorithm [21], is solved by TOSCA-TS software [22] to minimise the discrepancy between the virtual test and the corresponding macro-model responses in terms of global strain energy.

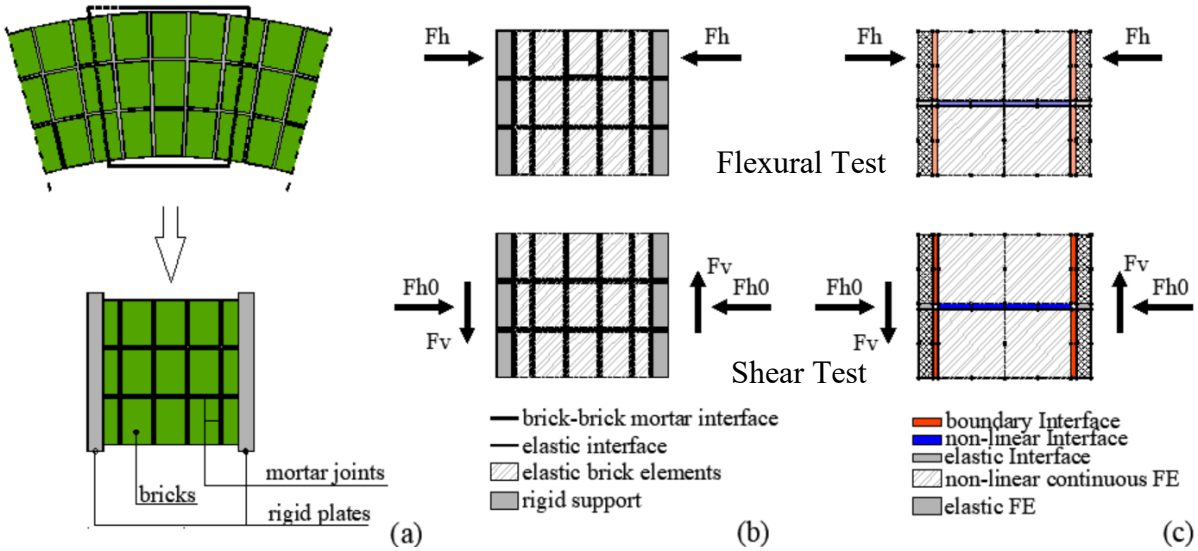


Figure 3: Calibration procedure: (a) elementary cell; (b) mesoscale virtual test; and (c) equivalent macromodel.

In the following, two virtual tests are considered: *i*) a flexural test, in which an eccentric axial force (F_h) is applied with increasing amplitude; *ii*) a shear test, where an increasing shear force (F_v) is applied after an initial axial force (F_{h0}) which is maintained constant during the analyses. In both tests, two rigid plates are modelled to transfer the loads uniformly to the masonry specimens. One plate is fully restrained while the other is free in the flexural test and restrained against rotation in the shear test. The plates are connected to the masonry by elastic interfaces with high normal and shear stiffness, in the case of the shear test, and with high normal stiffness and low shear stiffness, in the case of the flexural test. Illustrations of the mesoscale (virtual test) and the equivalent macromodel descriptions are shown in Figure 3b and Figure 3c.

3 NUMERICAL APPLICATIONS

In this section, the proposed macromodel and the calibration procedure presented in Section 2 are applied to simulate the response of two brick-masonry arches with stretcher bond tested by Melbourne et al. [24], namely Arch G and Arch T specimens. Arch G is a two-ring arch with 3m span, 215mm thickness, 455mm width and strong bricks. Arch T is characterised by three rings, 5m span, 1250mm rise, 330mm thickness, 675mm width and weak bricks. Two initial vertical forces, equal to 10kN for Arch G and 22.5kN for Arch T, were applied at the quarter and three-quarter span and kept constant during the test. Subsequently, a vertical force at quarter span was increased up to collapse under force control.

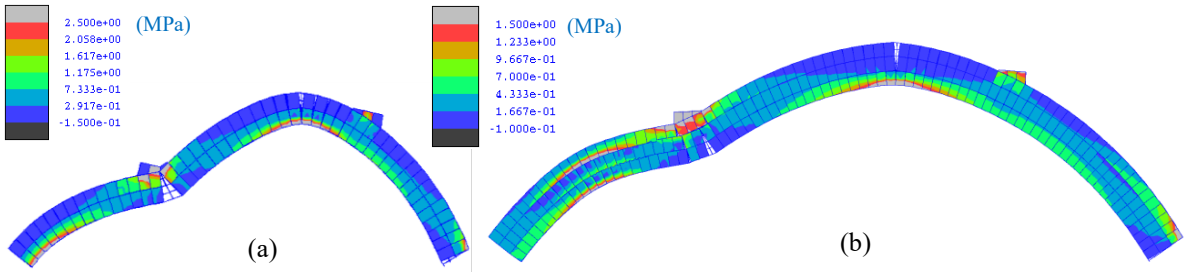


Figure 4: Final deformed shapes with Von-Mises stress of (a) Arch G, and (b) and Arch T.

The responses at failure of the two arches were different. While Arch G experienced a typical 4-hinge mechanism due to the formation of four large radial cracks, Arch T showed a more complex ultimate response characterised also by sliding separation between adjacent rings.
The two arches have been simulated using the detailed mesoscale model and the proposed calibrated macroscale description. As the available experimental material data are not sufficient to fully characterise the mesoscale model, the unknown mesoscale mechanical properties have been evaluated according to [16] to fit the experimental results. The complete set of parameters, adopted in the analyses, are reported in Table 1, where E_b and ν are Young's modulus and Poisson's ratio of the bricks; k_n and k_t are the normal and tangential stiffness of the interfaces; f_t, f_t and c are the tensile, compressive strengths and cohesion of the interfaces; G_t, G_s, G_c are the fracture energies in traction, compression and sliding; $tg\phi$ and $tg\phi_b$ are the factors governing the yield-surface and plastic potential functions. Figure 4 shows the deformed shapes at failure obtained by the mesoscale models for the two arches with the Von-Mises stress. The numerical failure modes are in good agreement with those observed during the experiments [24].

3.1 Arch G

The material parameters of the 3D continuum model for solid elements (Table 2) used in the proposed macroscale approach have been calibrated applying the procedure described in Section 2, adopting for the interface elements the parameters used in the mesoscale counterpart for the masonry joints (Table 1). The latter assumption is justified by the fact that in Arch G the interfaces coincide with the actual ring-to-ring mortar joints. The loading-displacement curves of the meso- and macromodel are compared in Figures 5a and 5b for the flexural and shear tests, respectively. The curves are expressed in terms of relative displacement of the plates versus the applied shear force for the shear test, and in terms of relative rotation versus the external moment for the flexural test. Figure 6 shows the final damage patterns in the interface elements of the mesoscale model (e.g. tension damage and sliding damage for the flexural and shear test, respectively) and in the solid elements of the macro-model (e.g. global damage). The load-displacement curves for Arch G are provided in Figure 7, where the results obtained by the detailed mesoscale and the proposed macroscale models are compared against the experimental data. The curves are expressed in terms of vertical (Figure 7a) and horizontal (Figure 7b) displacements at the quarter span versus the applied vertical load (F). A satisfactory agreement can be observed between the macro-model and the meso-scale response, which is very close to the experimental curve both in terms of initial stiffness and nonlinear response up to collapse.

Table 1: Mechanical parameters of the meso scale model

Masonry	E_b [MPa]	ν [–]	$k_n - k_t$ [N/mm]	$f_t - f_c - c$ [MPa]	$G_t - G_s - G_c$ [N/mm]	$tg\phi - tg\phi_g$
Arch T	6000	0.15	60.0 - 30.0	0.05 - 9.1 - 0.082	0.02 - 0.25 - 5.0	0.5 - 0.0
Arch G	16000	0.15	90.0 - 40.0	0.10 - 24.0 - 0.40	0.12 - 0.12 - 0.5	0.5 - 0.0

Table 2: Mechanical parameters of the 3D plasticity-damage model adopted in the tanalyses of Arch G

3D plasticity-damage model														
E [MPa]	ν [-]	$\tilde{f}_{b0}$ [-]	$\tilde{f}_y$ [-]	ψ [°]	ϵ [-]	k_c [-]	f_t [MPa]	f_c [MPa]	G_t [N/mm]	μ [-]	$k_{c,fc}$ [-]	ρ_c [-]	w_c [-]	w_t [-]
3800	0.15	1.12	0.4	30	0.1	0.66	0.12	24.0	0.045	0.2	1.0E-3	1.0	0.2	0.0
2D Interface material														
k_n [N/mm]	k_s [N/mm]	f_t [MPa]	f_c [MPa]	c [MPa]	ϕ_c [-]	ϕ_g [-]	G_t [N/mm]	G_s [N/mm]	G_c [N/mm]	μ [-]				
100.0	100.0	0.10	24.0	0.39	0.5	0.0	0.042	0.044	5.0	1E-3				

Table 3: Mechanical parameters adopted in the analyses of Arch T

3D plasticity-damage model														
E [MPa]	ν [-]	$\tilde{f}_{b0}$ [-]	$\tilde{f}_y$ [-]	ψ [°]	ϵ [-]	k_c [-]	f_t [MPa]	f_c [MPa]	G_t [N/mm]	μ [-]	$k_{c,fc}$ [-]	ρ_c [-]	w_c [-]	w_t [-]
2571	0.15	1.23	1.0	35	0.13	0.66	0.05	1.25	0.01	0.2	1.5E-3	1.0	0.2	0.0
2D Interface material														
k_n [N/mm]	k_s [N/mm]	f_t [MPa]	f_c [MPa]	c [MPa]	ϕ_c [-]	ϕ_g [-]	G_t [N/mm]	G_s [N/mm]	G_c [N/mm]	μ [-]				
60.0	30.0	0.05	9.1	0.085	0.5	0.0	0.02	0.01	5.0	1E-3				

However, the macro-model overestimates the peak-load by 20 % approximately. The ultimate deformed shape of the macro-model with the Von-Mises stress and the damage index, are shown respectively in Figure 8a and Figure 8b. Both the stress and damage patterns predicted by the macro-model are compatible with the meso-scale prediction (Figure 4a), confirming the ability of the macromodel to predict the main features of the arch response up to failure.

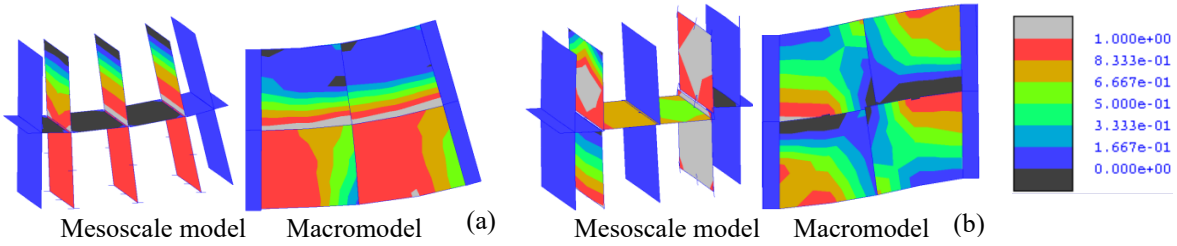


Figure 5: Damage pattern at the last step of the analysis of the flexural (a) and shear (b) virtual test.

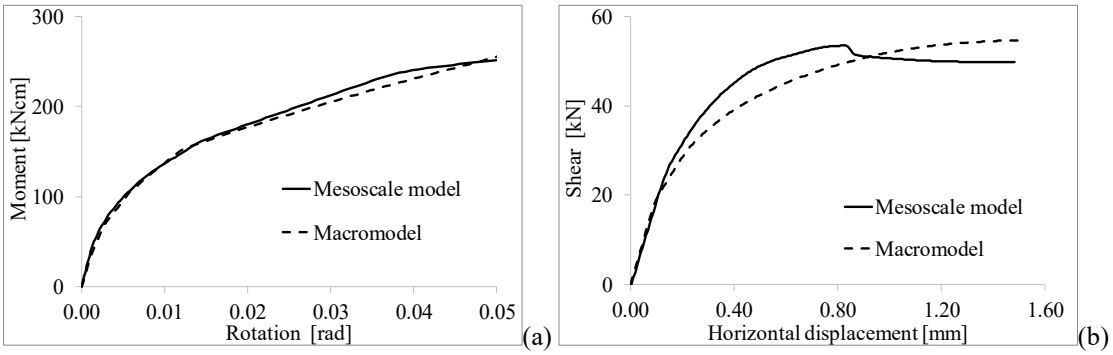


Figure 6: Response of the flexural (a) and shear (b) virtual test for Arch G.

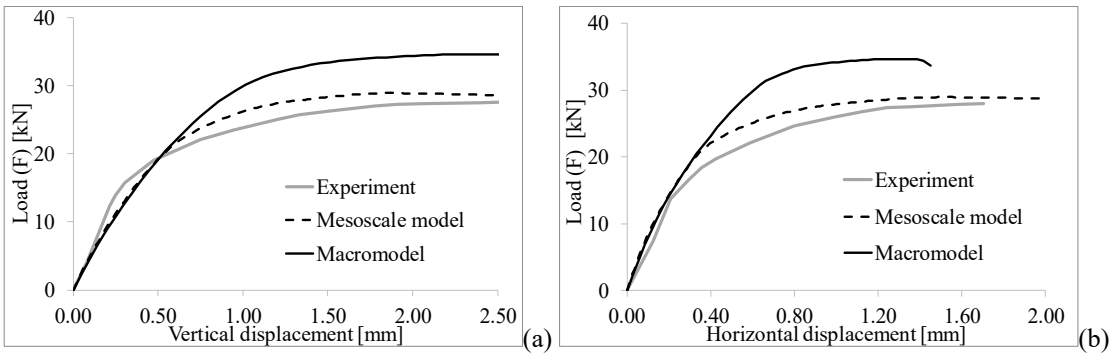


Figure 7: Capacity curves of Arch G: vertical (a) and horizontal (b) displacement at the left patch load.

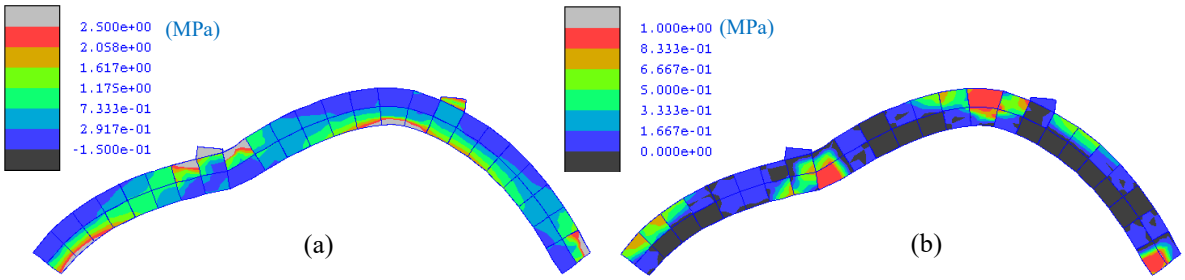


Figure 8: Failure mechanism of Arch G obtained by the macro-model: (a) Von-Mises stress, and (b) damage.

3.2 Arch T

This section reports the results of the numerical simulations performed on the three-ring Arch T, whose collapse behavior is characterized by significant sliding between the rings. The same procedure followed for the two-ring arch in Section 3.1 is applied to estimate both the parameters for the triaxial constitutive law of the 3D continuum elements and for the nonlinear plastic-damage model used for the nonlinear interfaces. The resulting set of macromodel parameters is reported in Table 3. The deformed shapes and load-displacement curves for the flexural and shear virtual tests are reported in Figure 9 and Figure 10. It can be observed that the calibrated macromodel fits well the mesoscale response with a high level of accuracy, both in terms of nonlinear response and damage pattern. The load displacement curves for Arch T are shown in Figure 11. As in the previous example, the numerical curves obtained using the calibrated macromodel are compared against the mesoscale predictions and the experimental results. In this case, the macroscale model slightly overestimates the elastic stiffness of the arch, but it provides a good prediction of the ultimate load capacity.

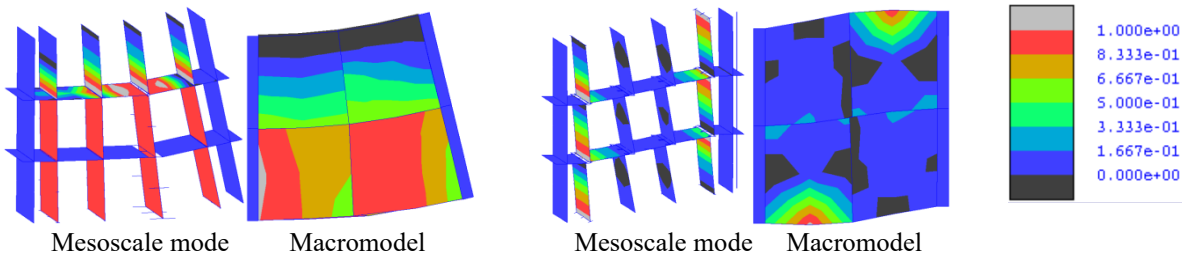


Figure 9: Deformed shapes and distribution of damage: flexural (a) and shear (b) virtual test.

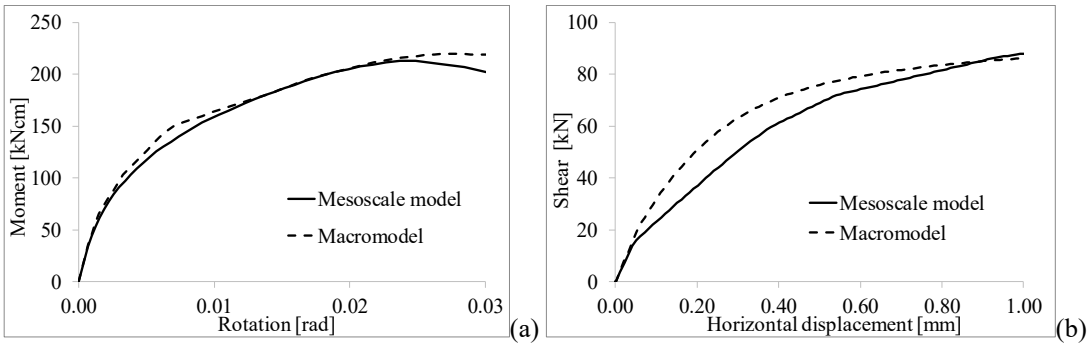


Figure 10: Response of the flexural (a) and shear (b) virtual test for Arch T.

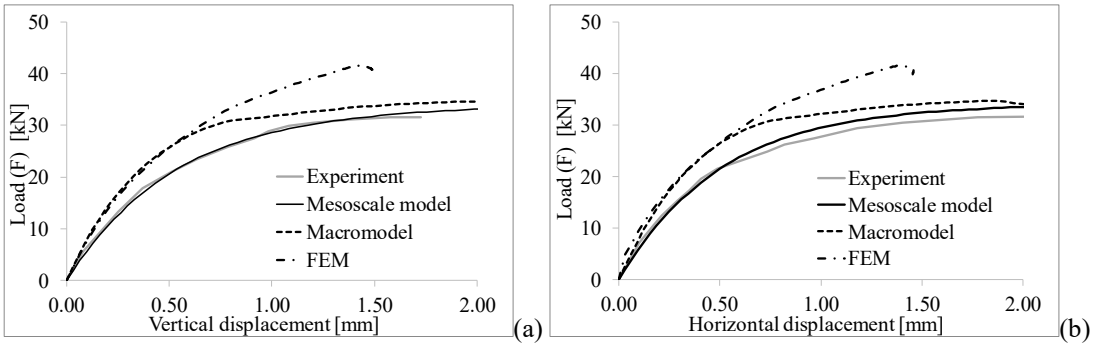


Figure 11: Capacity curves of the Arch T: vertical (a) and horizontal (b) displacement at the left patch load.

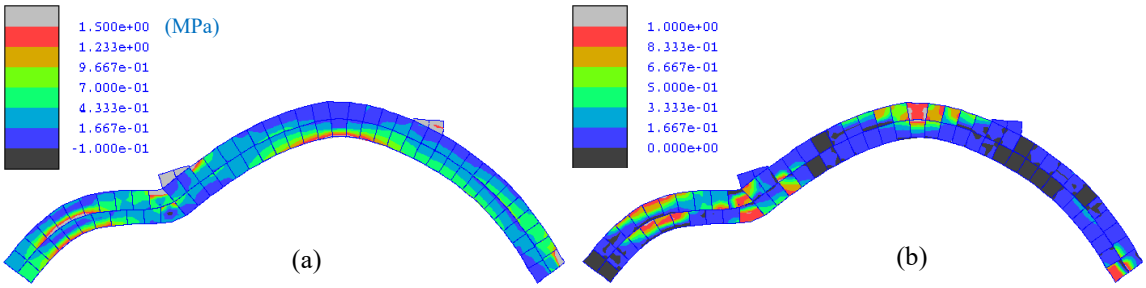


Figure 12: Failure mechanism of Arch T obtained by the macro-model: (a) Von-Mises stress, and (b) damage.

The failure mechanism is depicted in Figure 12, correlated with the Von-Mises stress (Figure 12a) and damage (Figure 12b) patterns. The activation of two plastic hinges can be observed, which are located approximately at the three quarter span and at the right skewback. Large sliding between the rings is also observed between the section where the load is applied and the left skewback. The latter results are substantially consistent to what is predicted by the mesoscale model and observed in the physical tests [24].

To investigate the role played by the nonlinear interfaces within the macromodel, additional simulations have been conducted using a full 3D continuum model (FEM), which does not utilise 2D interface elements, with the calibrated material parameters in Table 3, where the results are shown in Figure 11. It can be observed, that for small displacements (up to 0.05mm vertical and horizontal displacements) the FEM model and the proposed macromodel show the same response. After this point, the two responses diverge due to the sliding activation in the mid-thickness interfaces. The FEM model overestimates the ultimate strength of the arch with an ultimate load prediction 20% higher than the proposed macromodel and 25% higher than the detailed mesoscale model, which provides a very close estimate of the ultimate load capacity to the value measured in the test.

4 ARCH-BACKINFILL INTERACTION

Further numerical simulations are carried out to explore the ability of the proposed macroscale modelling strategy to predict the behaviour of masonry arches interacting with backfill, as in real masonry bridges. The arch specimens, Arch G and Arch T, are analysed connecting the extrados of the two arches to a backfill domain.

In the models for the two specimens with backfill, the backfill with density 22kN/m^3 extends horizontally 2460mm from the two supports of the arches and 300mm vertically above the crown. The strip model is 2880mm wide. A uniform vertical line load is applied at the top surface of the backfill at the three-quarter arch span. Full support is assumed at the base of the arch and the backfill and on the two vertical sides of the backfill. Moreover, the horizontal displacements on the two lateral faces of the arch and backfill are restrained to represent a plane strain condition. The backfill is modelled using a FE discretization with 15-noded tetrahedral elements. According to [17], an elasto-plastic material model with a modified Drucker-Prager yield criterion is employed assuming Young's modulus E_b=500MPa, cohesion c_b=0.001MPa, friction and dilatancy coefficients $tg\phi_b$=0.95 and $tg\psi_b$=0.45. The interaction between the arch and the backfill is simulated by introducing nonlinear interfaces at the extrados with tensile strength f_{fi}=0.002MPa, cohesion c_i=0.0029MPa, friction coefficient $tg\phi_i$=0.6 and zero dilatancy.

The load-displacement curves obtained using mesoscale and macroscale models are shown in Figure 13. A very good agreement up to collapse can be observed. Similar failure mechanisms are predicted by the two modelling strategies as shown by the ultimate deformed shapes and damage contours in Figures 14, 15 and 16. It should be noted that the masonry material properties for the macroscale models have been calibrated based on the virtual tests for the two arches (Tables 1,2 and 3). The results obtained confirm the potential of the proposed modelling strategy with calibrated macroelements in providing accurate predictions of the response of masonry arches and bridges.

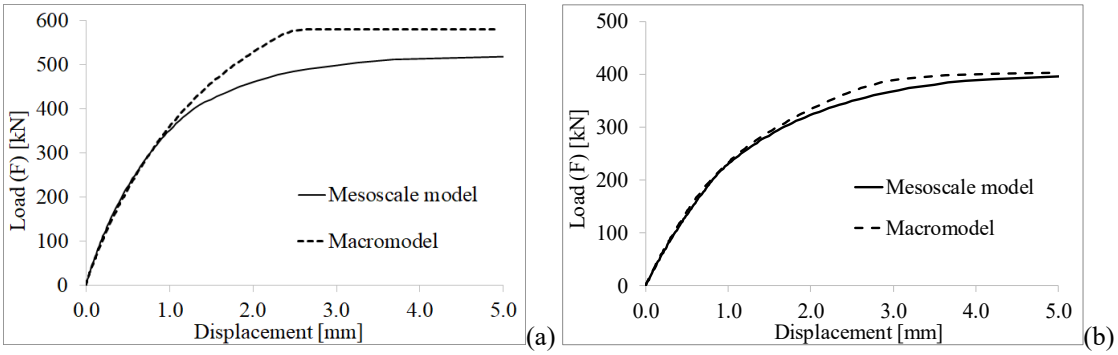


Figure 13: Capacity curves of the arches with backfill: (a) Arch G, and (b) Arch T.

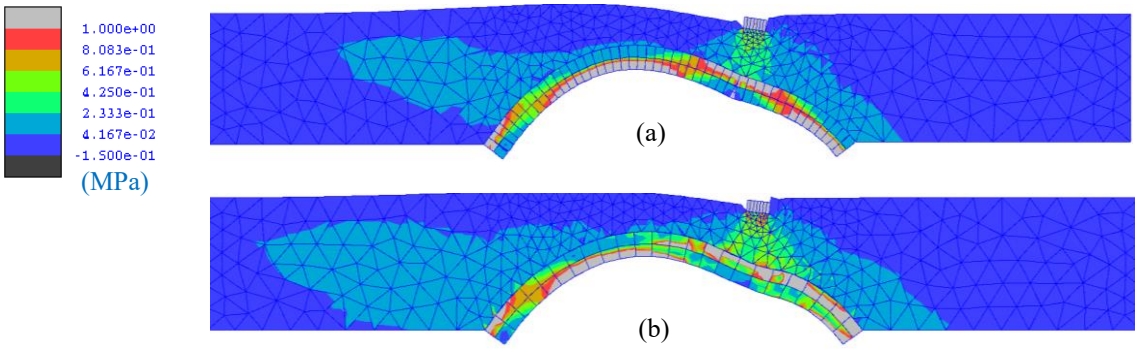


Figure 14: Failure mode and Von-Mises stress of Arch G with backfill: (a) mesoscale model; (b) macromodel.

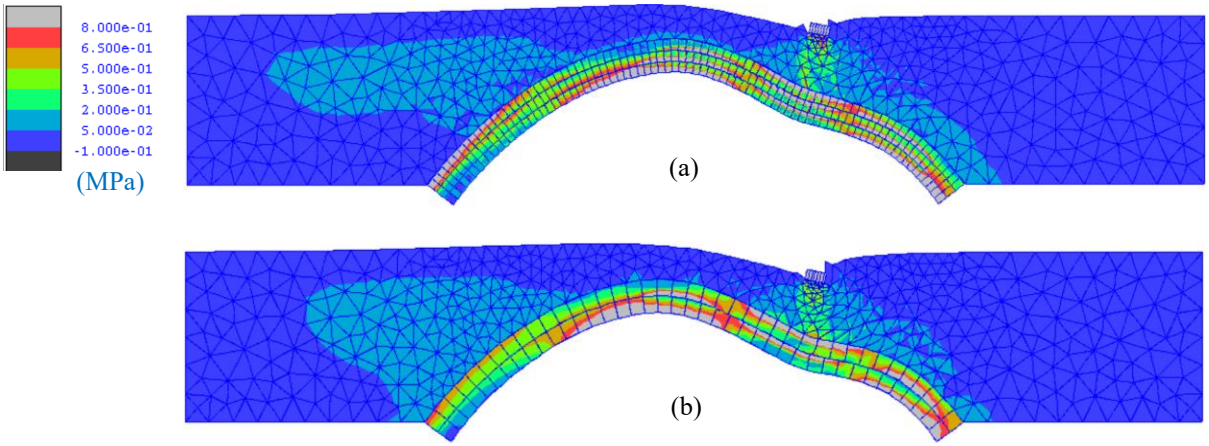


Figure 15: Failure mode and Von-Mises stress of Arch T with backfill: (a) mesoscale model; (b) macromodel.

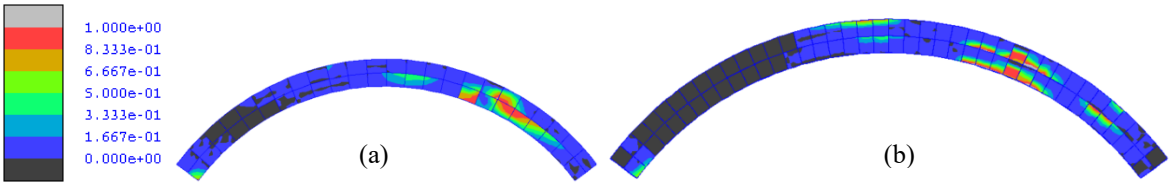


Figure 16: Macro-model damage in (a) Arch G, and (b) Arch T.

CONCLUSIONS

In this study a macro-modelling strategy for brick-masonry multi-ring arches is proposed. This modelling approach benefits from enhanced efficiency compared to detailed mesoscale descriptions, since the adopted FE mesh is independent of the actual masonry bond. A hybrid strategy is followed in which the arch is modelled by 3D elasto-plastic continuum solid elements and 2D zero-thickness nonlinear interfaces arranged along the mid-thickness circumferential surface to simulate potential ring separation. An effective and robust procedure based on genetic algorithms is established to calibrate the macromodel mechanical parameters considering results from mesoscale simulations on virtual experiments. The accuracy and potential of the proposed approach is demonstrated in two numerical examples, based on masonry arches tested in previous research, which are characterised by different failure mechanisms. The results show a very good agreement between the calibrated macromodels and detailed mesoscale descriptions, including arches interacting with backfill as in real masonry bridges, thus demonstrating the potential of the proposed calibrated macro-modelling approach in the practical assessment of masonry arch bridges.

Acknowledgements. This work was supported by the European Commission through the Marie Skłodowska-Curie Individual Fellowship IF ("RAMBEA", Grant Agreement 846061).

REFERENCES

[1] Fanning, P. J., Boothby, T. E., and Roberts, B. J. Longitudinal and transverse effects in masonry arch assessment. *Constr. Build. Mat.* (2001) **15**(1):51-60.

[2] Moreira, V. N., Fernandes, J., Matos, J. C., Oliveira, D.V. Reliability-based assessment of existing masonry arch railway bridges. *Constr. Build. Mat.* (2016) 115, 544-554.

[3] Sarhosis, V., De Santis, S., and De Felice, G. A review of experimental investigations and assessment methods for masonry arch bridges. *Structure and Infrastructure Engineering* (2016) **12**(11):1439-1464.

[4] Melbourne, C. and Gilbert, M. 1995. The behaviour of multi-ring brickwork arch bridges. *Structural Engineer* (1995) **73**(3):39–47.

[5] Gilbert, M., Casapulla, C., and Ahmed, H.M. 2006. Limit analysis of masonry block structures with non-associative frictional joints using linear programming. *Computers and Structures* (2006) **84**:873-887.

[6] Cavicchi, A., and Gambarotta, L. Collapse analysis of masonry bridges taking into account arch–fill interaction. *Engineering Structures*, (2005) **27**(4):605-615.

[7] Smith, C., and Gilbert, M. Application of discontinuity layout optimization to plane plasticity problems. *Proceedings of the Royal Society A: Mathematical, Physical and Engineering Sciences* (2007) **463**(2086):2461-2484.

[8] Conde, B., Ramos, L. F., Oliveira, D. V., Riveiro, B., and Solla, M. (2017). Structural assessment of masonry arch bridges by combination of non-destructive testing techniques and three-dimensional numerical modelling: Application to Vilanova bridge. *Engineering Structures* (2017) **148**:621-638.

[9] Pelà, L., Aprile, A., and Benedetti, A. Comparison of seismic assessment procedures for masonry arch bridges. *Construction and Building Materials*, (2013) **38**:381-394.

[10] Milani, G., and Lourenço, P. B. 3D non-linear behavior of masonry arch bridges. *Computers & Structures* (2012) **110**:133-150.

[11] Caddemi, S., Caliò, I., Cannizzaro, F., D'Urso, D., Occhipinti, G., Pantò, B., ... and Zurlo, R. A 'Parsimonious' 3D Discrete Macro-Element method for masonry arch bridges. *Proceeding of 10th IMC Conference, Milan (Italy)*, 9-11 July (2018)

[12] Cannizzaro, F., Pantò, B., Caddemi, S., and Caliò, I. A Discrete Macro-Element Method (DMEM) for the nonlinear structural assessment of masonry arches. *Engineering Structures* (2018) **168**:243-256.

[13] Pantò, B., Cannizzaro, F., Caddemi, S., Caliò, I., Chácara, C., and Lourenço, P.B. Nonlinear modelling of curved masonry structures after seismic retrofit through FRP reinforcing. *Buildings* (2017) **7**(3), 79.

[14] Pulatsu, B., Erdogmus, E., and Lourenço, P. B. Comparison of in-plane and out-of-plane failure modes of masonry arch bridges using discontinuum analysis. *Engineering Structures*, (2019) **178**:24-36.

[15] Sarhosis, V., Forgács, T., Lemos, J.V. A discrete approach for modelling backfill material in masonry arch bridges. *Computers & Structures* (2019) **224**,106108.

[16] Zhang, Y., Macorini, L. and Izzuddin, B. A. Mesoscale partitioned analysis of brick-masonry arches. *Engineering Structures* (2016) **124**:142-166.

[17] Tubaldi, E., Macorini, L. and Izzuddin, B. A. Three-dimensional mesoscale modelling of multi-span masonry arch bridges subjected to scour. *Eng.Struct.* (2018) **165**: 486-500.

[18] Macorini, L. and Izzuddin, B. A. A non-linear interface element for 3D mesoscale analysis of brick-masonry structures. *International Journal for numerical methods in Engineering*, (2011) **85**(12):1584-1608.

[19] Chisari C, Macorini L, Izzuddin BA, 2020. Multiscale model calibration by inverse analysis for nonlinear simulation of masonry structures under earthquake loading. International *Journal for Multiscale Computational Engineering*, DOI: 10.1615/IntJMultCompEng.2020031740.

[20] Minga, E., Macorini, L. and Izzuddin, B. A. A 3D mesoscale damage-plasticity approach for masonry structures under cyclic loading. *Meccanica* (2018) **53**(7):1591-611.

[21] Deb, K., Pratap, A., Agarwal, S. and Meyarivan, T., A Fast and Elitist Multiobjective Genetic Algorithm: NSGA-II. *IEEE Trans. on Evolut. Comput.* (2002) **6**(2):182-197

[22] Chisari, C., Amadio, C., TOSCA: a Tool for Optimisation in Structural and Civil engineering Analyses. *Int. Journal of Advanced Structural Eng.* (2018) **10**(4):401-419.

[23] Izzuddin, B. A., Nonlinear dynamic analysis of framed structures, PhD, Imperial College London, 1991.

[24] Melbourne, C., Wang, J., Tomor, A., Holm, G., Smith, M., Bengtsson, P. E., Bien, J., Kaminski, T., Rawa, P., Casas, J. R., Roca, P. & Molins, C. (2007) Masonry Arch Bridges Background document D4.7. Sustainable Bridges. Report number: Deliverable D4.7.

12th International Conference on Structural Analysis of Historical Constructions
SAHC 2020
P. Roca, L. Pelà and C. Molins (Eds.)

A METHOD FOR THE STRUCTURAL ANALYSIS AND DESIGN OF ARCHED REINFORCED MASONRY AND/OR CONCRETE STRUCTURES

D. LÓPEZ LÓPEZ[1*], P. ROCA[2], A. LIEW[3], T. VAN MELE[4] AND P. BLOCK[4]

[1] Department of Architectural Technology, Universitat Politècnica de Catalunya
david.lopez.lopez@upc.edu

[2] Department of Civil and Environmental Engineering, Universitat Politècnica de Catalunya

[3] Department of Civil and Structural Engineering, The University of Sheffield

[4] Institute of Technology in Architecture, Block Research Group, ETH Zurich

Keywords: Tile vault, masonry, reinforced brick, formwork, concrete shells, limit analysis, ELARM.

Abstract. *Extraordinary architectural examples of shell structures have been built using reinforced masonry and concrete. The current sparse use of this construction type can be attributed, among other reasons, to a lack of simple design methods, tools and criteria. Extended Limit Analysis of Reinforced Masonry (ELARM) is a new method for the structural analysis and design of reinforced concrete, reinforced masonry or reinforced composite (masonry and concrete) arched structures. It is implemented computationally to create a flexible design and analysis tool, able to provide immediate graphical and intuitive results. The method is based on limit analysis but takes into account the material's limited compressive strength and the vault's cross-sectional bending capacity provided by the reinforcement as an equivalent increase of the thickness. The plastic theorems are then applied considering the new virtual boundaries of the vault's intrados and extrados.*

ELARM is validated through the comparison of its predictions with the results of load tests on two full-scale composite barrel vaults. The vaults feature a structural system composed of a two-layered tile vault as an integrated formwork for a reinforced concrete layer. They were tested under vertical loading up to failure. Both the vertical and horizontal displacements of the vaults were monitored during the tests. The characterisation of the materials composing the vaults was also carried out to introduce the measured material properties and strengths in the equilibrium equations for the computation of the new virtual thickness.

This paper presents the new structural analysis and design method, its experimental validation and some practical design examples to show the potential of the tool. It offers an intuitive process of design in which shape can be adapted and optimised, also having the material properties and thickness, loads and reinforcement quantity and placement as variable parameters. The presented examples include reinforcement optimisation and form-finding procedures and the analysis of a non-compression-dominated structure.

1 INTRODUCTION

The combination of masonry and/or concrete with reinforcement, on its many variants, has produced influential and striking shell structures in the history of architecture [1]. These constructions were particularly in demand from the 1920s to the early 1960s [2]. Nowadays, they are uncommon due to the lack of straightforward structural analysis and design methods and the construction costs, specifically the cost of the formwork [3].

Current formworks for concrete shells are either expensive, complex and wasteful or have formal restrictions. A possible approach to the construction of expressive shells may be provided by the use of tile vaults as stay-in-place formwork for concrete shells [4], which could significantly reduce construction costs and material waste. Furthermore, tile vaults provide a high formal flexibility as they only require formwork at the boundaries, from which the rest of the vault can be built gradually by completing stable sections [5] [6].

The combination of masonry and reinforced concrete creates a new type of composite structure that needs new calculation methods and models to deal with the specific features of the system [7]. This paper presents a method for the structural analysis and design of arched reinforced masonry and/or concrete structures. The method is called Extended Limit Analysis of Reinforced Masonry (ELARM) and is an extension of the work by Roca *et al*. [8]. It is based on the modern formulation of limit analysis for masonry arches by Jacques Heyman in 1966 [9], but takes into account the finite compressive strength of the masonry and concrete as well as the tensile capacity of the embedded reinforcement [4].

ELARM is explained in Section 2 of this paper and its experimental validation is described in Section 3, followed by some examples of different applications of the method in Section 4. The conclusions are presented in Section 5.

2 EXTENDED LIMIT ANALYSIS OF REINFORCED MASONRY OR CONCRETE

The presented method analyses the composite cross-section to obtain its ultimate positive and negative moment for the given axial load, which varies along the structure and is determined by the self-weight and the external loads. The ratio between the ultimate moment and the axial load is equal to the maximum possible eccentricity (Figure 1). The eccentricity related to the positive moment defines the upper limit of the new virtual thickness and the eccentricity related to the negative moment defines the corresponding lower limit. As is done in the classical theory of limit analysis of masonry arches, the structure is divided in a number of virtual voussoirs, which allow the construction of the thrust line and sets the specific sections where axial forces, moments and eccentricities are calculated. ELARM is applicable for reinforced concrete, reinforced masonry and reinforced composite (masonry and concrete) arched structures, provided that the failure mode corresponds to that of a ductile mechanism characterised by the development of a sufficient number of hinges [4].

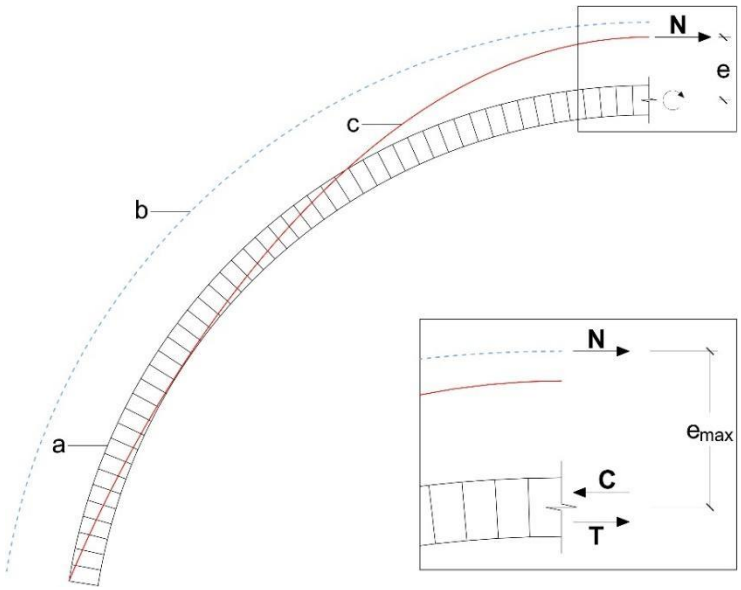


Figure 1: Thrust line located outside of the vault's thickness creating a bending moment; a) reinforced masonry and/or concrete arch, b) upper virtual thickness, and c) thrust line. Lower right) schematic distribution of forces for the ultimate positive bending moment.

The stability of the vault is verified when it is possible to find a thrust line, in equilibrium with the applied loads, that is fully contained within the new virtual thickness of the vault, meaning that the safe theorem is satisfied. The uniqueness theorem can also be applied to obtain the collapse load and mechanism of the composite vault [4].

The support conditions of the vault are of great importance for the definition of the thrust line and the stability of the vault. If the vault is pinned at its supports (Figure 2) with a single contact point, then the thrust line must pass through that point. In the case of a support consisting of a contact surface, unable to take bending moments, the thrust line can pass through any point of the mentioned surface. Finally, in the case of a fixed support (Figure 2a), the limits for the thrust line at the supports coincide with the virtual thickness [4][8]. This method is applicable to reinforced concrete, reinforced masonry and reinforced composite (masonry and concrete) arched structures, provided that the failure mode corresponds to that of a ductile mechanism characterised by the development of a sufficient number of hinges.

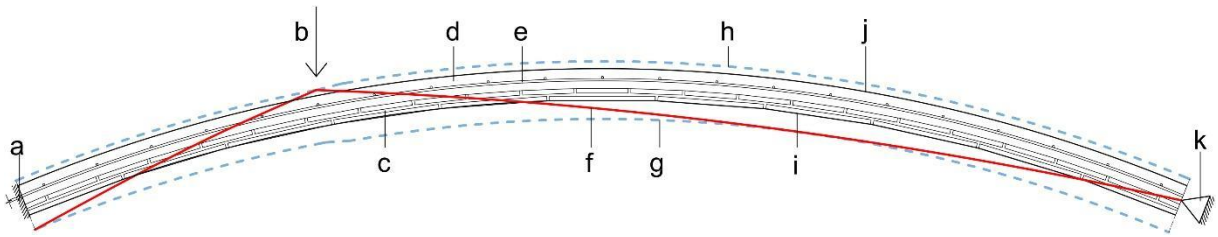


Figure 2: Application of uniqueness theorem with ELARM: a) fixed support, b) applied load, c) tile vault, d) concrete, e) reinforcement, f) thrust line, g) lower virtual thickness, h) upper virtual thickness, i) real lower thickness, j) real upper thickness, k) pinned support.

3 EXPERIMENTAL VALIDATION

The presented method has been experimentally validated by comparing its results with those provided by the load-testing of full-scale prototypes. For these prototypes, the proposed technique of a tile vault as integrated formwork for steel-reinforced concrete was used. They were two composite cylindrical barrel vaults, with a span of 2.78 m, a height of 0.25 m, a width of 1 m and had pinned supports (Figure 3). A vertical load was applied at quarter span to a loading pad with a breath of 115 mm and stretching the entire width of the vault. The peak load for the first prototype was 52.43 kN, while it was 53.15 kN for the second.

The material properties introduced in the model were obtained from compression and tensile tests on samples of the materials composing the vault. Tiles, fast-setting cement, mortar and concrete were tested in compression, whereas steel reinforcement was tested in tension. The compressive strength and unit weight of the tile vault resulted in 13.45 N/mm^2 and 2000 kg/m^3 respectively. Those of the concrete resulted in 22.20 N/mm^2 and 2460 kg/m^3. The mean yield tensile strength of the 6 mm diameter steel reinforcement was 581 N/mm^2 and the Young's Modulus was equal to 207000 N/mm^2. A detailed description of the material characterisation and the load tests can be found in López López *et al*. [4].



Figure 3: Photo of one of the full-scale prototypes.

The geometry of the vaults and the material properties were introduced into the computational model to apply the uniqueness theorem and obtain the ultimate load carrying capacity of the vault (Figure 4). The thrust line's ends were set to the cross-section's centre line to represent the pinned support condition. The vault was divided into 100 voussoirs and the load was applied evenly as point loads onto four voussoirs at quarter span, replicating the 11.5 cm wide loading platform of the experimental tests. The load predicted by the numerical method is 53.6 kN (Figure 4), which is 1.5 % higher than the average of the two values obtained in the experimental tests, 52.8 kN.

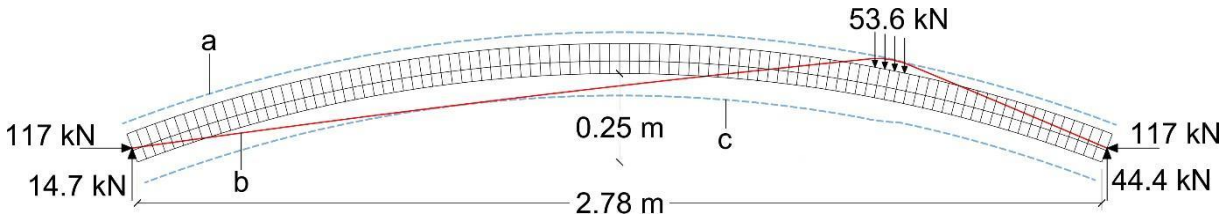


Figure 4: Application of the uniqueness theorem with ELARM to the tested vaults: a) upper virtual thickness, b) thrust line, and c) lower virtual thickness.

4 USING ELARM

The ELARM implementation, coded in Python, results in an interactive tool providing quick structural feedback [4]. As can be expected from any computational implementation, it offers speed, accuracy and the possibility to extend the analysis to similar structures with different sizes or properties. The next subsections describe specific features that this method offers for the design and structural analysis of reinforced masonry/concrete arches. As an example, a 14 m span, arched concrete structure is chosen. Three punctual, asymmetrical and permanent loads of 25 kN are applied at 1/5, 2/5 and 3/5 of the span. The vault is considered simply supported, i.e., each support consists of a contact surface, unable to take bending moments. The compressive strength of the concrete is taken as 40 N/mm^2 with a density of 2400 kg/m^3, and the steel's yield tensile strength for the reinforcement as 500 N/mm^2.

4.1 Reinforcement optimisation

A cross-section optimisation can be carried-out by adjusting the thickness of the structural layers and the amount and positions of the reinforcement, while accounting for different load combinations.

Among the many possibilities for the mentioned structure, Figure 5 and Figure 6 show the case of a 2.5 m rise, 1.0 m wide, 10 cm thick, parabolic arch with reinforcement placed at different levels of the cross-section. This could be the case of an already existing arch that needs reinforcement due to a new loading situation. The position of the reinforcement affects the virtual thickness and thus the possible positions of the thrust line, the final amount of reinforcement and the horizontal thrust. Reinforcement is placed at a distance of 25 mm from the extrados in the case of Figure 5 and at the same distance, but from the intrados, in Figure 6.

Whereas in the case of Figure 5, an amount of reinforcement equivalent to a steel area of 700 mm^2 was sufficient to obtain a solution, in the case of Figure 6, a steel area of 1000 mm^2 is required. However, the option with less steel is, in this case, the one with a bigger horizontal thrust (93 kN), due to a shallower thrust line solution (Figure 5).

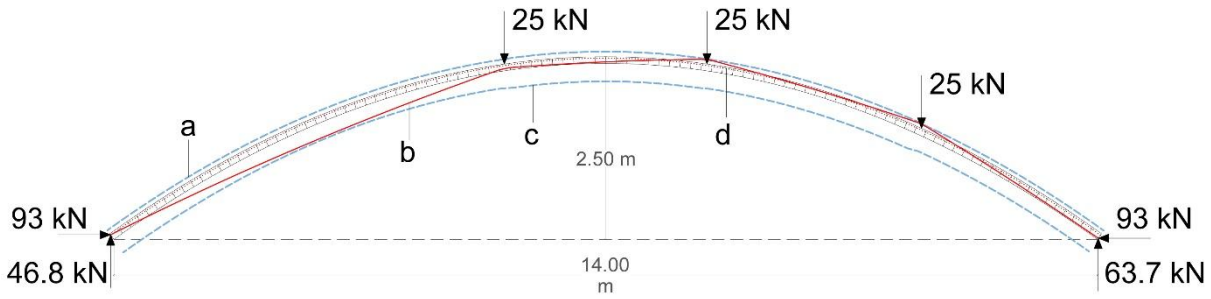


Figure 5: Structure with reinforcement at a distance of 25 mm from the extrados: a) upper virtual thickness, b) thrust line, c) lower virtual thickness, and d) reinforcement.

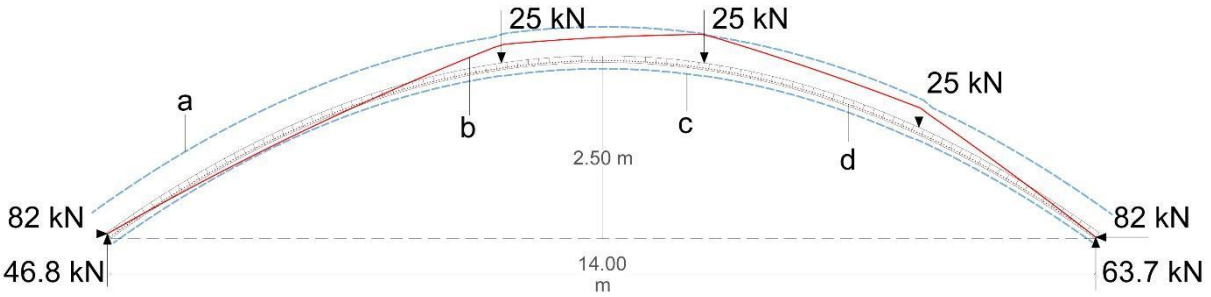


Figure 6: Structure with reinforcement at a distance of 25 mm from the intrados: a) upper virtual thickness, b) thrust line, c) lower virtual thickness, and d) reinforcement.

4.2 Form-finding

The use of the software Rhinoceros and the plug-in Grasshopper for the visualisation of graphical results and for the efficient introduction and modification of input parameters, allows for a fast and user-interactive form-finding process. The starting intrados of the analysed vault can be drawn as a curve in Rhinoceros, which can be easily modified through its control points. As the curve is being adjusted, calculations are computed and graphical updates are provided. The shape and parameters of the vault can be adapted and optimised according to the structural feedback received in near real-time. The presented tool allows the optimisation of the vault´s shape regarding a defined loading condition, e.g. the permanent loads acting on the structure, by modifying the inputs that define the vault's geometry, and then adapting to the tool´s structural feedback. A shape optimized for certain given loads would be one that includes within its virtual thickness boundaries, the thrust line supplied by ELARM with a minimum thickness

and reinforcement. Therefore, instead of starting from an invariable, predefined shape and modifying thickness, material strength and/or reinforcement to increase the virtual boundaries and make the thrust line fit within, a form-finding process consists of modifying the geometrical inputs of the structure to make geometry and thrust line match as much as other design constraints would allow.

For the example of the previous section, maintaining the span and rise and taking into account the permanent and predominant loads, the resulting form-found shape is illustrated in Figure 7. Once a stable unreinforced masonry vault is found, the thickness of the masonry and the steel reinforcement position and amount can be updated considering other loading combinations, including further asymmetric live loads or if a higher safety factor is desired. Figure 8 shows an additional punctual load of 25 kN at 4/5 of the span. Keeping the thickness of 10 cm and adding reinforcement at a distance of 25 mm from the intrados, a steel area of 900 mm^2 is required.

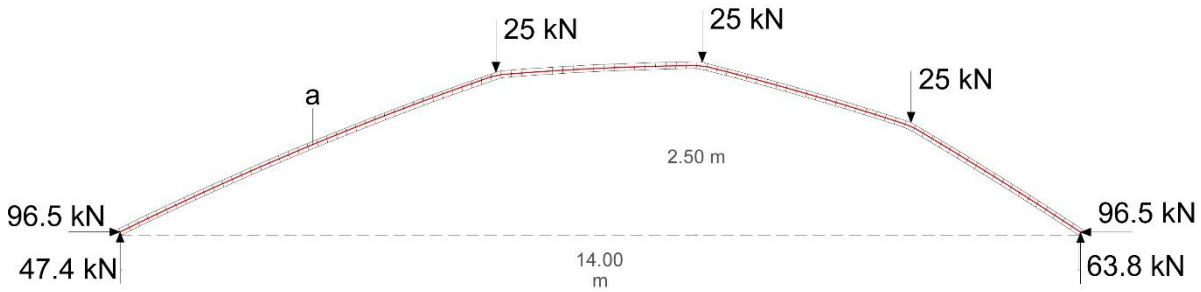


Figure 7: Form-finding with ELARM: a) thrust line.

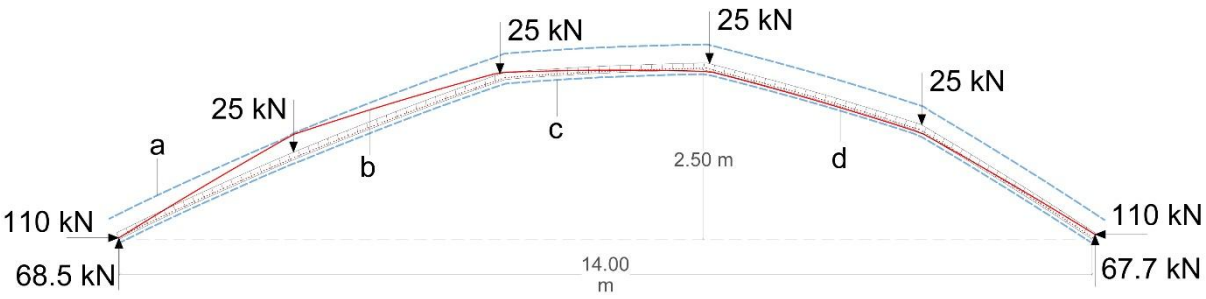


Figure 8: Form-finding with ELARM and an additional load: a) upper virtual thickness, b) thrust line, c) lower virtual thickness, and d) reinforcement.

4.3 Beyond compression-only

The addition of reinforcement to a masonry and/or concrete vault allows for the design of structures that are not restricted to being compression-only. Continuing with the example of the previous subsections, the proposal now is a structure made of three straight segments, being horizontal the middle one (Figure 9, Figure 10 and Figure 11). The advantages of this structure

would be an easier and more economic construction thanks to the possibility to use straight formwork and the functionality of the horizontal surface. The thickness of the concrete structure is increased to 14 cm and reinforcement is placed at a central level of the cross-section.

Figure 9 illustrates the mentioned structure, simply supported and applying the three permanent, punctual loads. An amount of reinforcement equivalent to a steel area of 1400 mm^2 is required to achieve stability. The same structure and conditions are repeated in Figure 10, except for the boundary conditions, which are now fixed supports, i.e., able to take bending moments. This new condition allows a higher range of possible thrust lines, as they must not end at the supports' contact surface, but can be at any point within the virtual thickness. In this case, reinforcement is decreased until 1100 mm^2 (Figure 10). However, this amount of reinforcement would not be enough if an additional punctual load of 25 kN at 4/5 of the span would be included. Figure 11 shows this loading combination, for which a steel area of 1300 mm^2 is required.

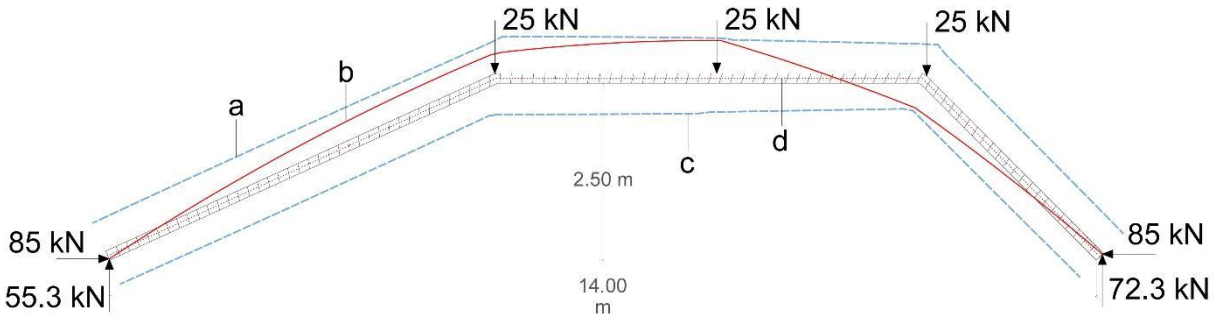


Figure 9: Structure with simply-supported boundary conditions: a) upper virtual thickness, b) thrust line, c) lower virtual thickness, and d) reinforcement.

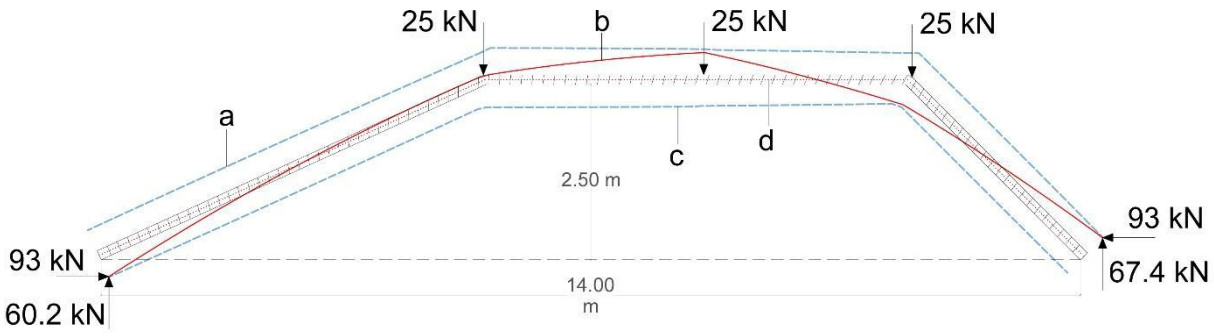


Figure 10: Structure with fixed supports: a) upper virtual thickness, b) thrust line, c) lower virtual thickness, and d) reinforcement.

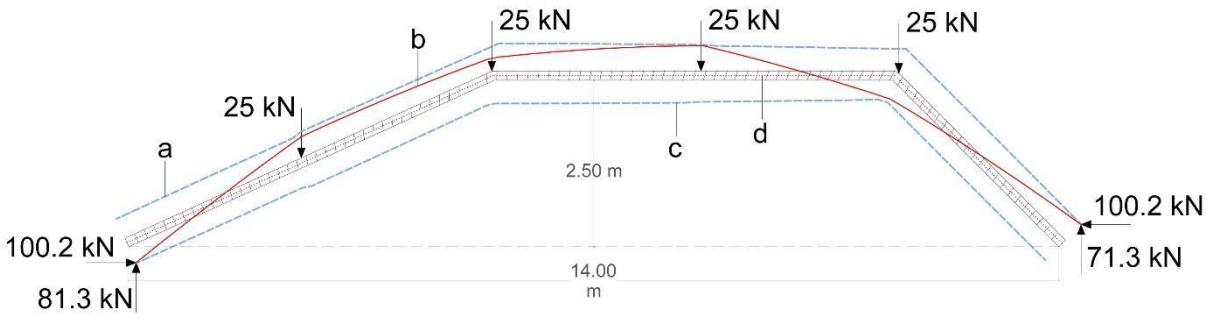


Figure 11: Structure with fixed supports and an additional load: a) upper virtual thickness, b) thrust line, c) lower virtual thickness, and d) reinforcement.

5 CONCLUSIONS

A method for the design and structural analysis of composite (masonry-concrete), arched structures has been presented. The method, called Extended Limit Analysis of Reinforced Masonry (ELARM), is based on traditional limit analysis, but extends it by considering the tensile capacity of the reinforcement and the compressive strength of the masonry and concrete. ELARM can also be applied to other structures with a sufficiently ductile response, such as reinforced masonry or concrete arches and vaults, and similar reinforced composite structures combining masonry and concrete. The method's computational implementation allows for an interactive and user-friendly form-finding process and a straight-forward assessment [4].

The method and the developed computational tool have been validated through experimental research. The applicability and accuracy of the proposed analysis method has been validated through its capacity to predict well the results from the load tests on two full-scale prototypes [4].

Some of the possible applications of ELARM have been shown through an example of a concrete structure with three punctual, permanent, asymmetrical loads. Different solutions have been discussed, including reinforcement optimisation, a form-found shape and a non-compression-only design. ELARM allows the exploration of a large range of possible solutions by modifying the thrust line, the position and amount of reinforcement, the shape of the structure and the load combinations with immediate, responsive, structurally informed feedback

Acknowledgements. This work was supported by the Swiss National Science Foundation (SNSF) [grant number P2EZP2_181591] and the Institute of Technology in Architecture (ITA) at the Swiss Federal Institute of Technology in Zurich (ETH Zurich). It was also sponsored by the construction company URCOTEX, from which Pep Brazo, Antonio Haro and Albert Martí are especially acknowledged. The construction of the prototypes was carried out together with Jordi Domènech, to whom the authors are very thankful.

Experimental support and facilities were kindly offered by the Laboratory for Technological Innovation in Structures and Materials (LITEM) at the Polytechnic University of Catalonia

(UPC), from which Lluís Gil, Ernest Bernat, Christian Escrig and Luis Mercedes are especially acknowledged.

The presentation of this work at the 12th International Conference on Structural Analysis of Historical Constructions (SAHC 2020) was supported by the area of Architectural Structures within the Department of Architectural Technology at the Universitat Politècnica de Catalunya.

REFERENCES

[1] López López, D., Van Mele, T. and Block, P. Dieste, González Zuleta and Sánchez del Río: Three approaches to reinforced-brick shell structures. 10th International Conference on Structural Analysis of Historical Constructions (ed. Van Balen, K., & Verstrynge, E.). London: Taylor & Francis Group (2016).

[2] Meyer C, Sheer M. Do Concrete Shells Deserve Another Look? Concrete International, Oct. 2005: 43-50.

[3] Tang G. An Overview of Historical and Contemporary Concrete Shells, their Construction and Factors in their General Disappearance. International Journal of Space Structures 2015; 30(1).

[4] López López, D., Roca, P., Liew, A., Van Mele, T., & Block, P. (2019b). Tile vaults as integrated formwork for reinforced concrete: Construction, experimental testing and a method for the design and analysis of two-dimensional structures. Engineering Structures, 188, 233-248.

[5] López López D, Domènech M, Palumbo M. "Brick-topia", the thin-tile vaulted pavilion. Case Studies in Structural Engineering 2014; 2: 33-40.

[6] López López D, Van Mele T, Block P. Tile vaulting in the 21st century. Informes de la Construcción 2016; 68(544): e162, DOI: 10.3989/ic.15.169.m15.

[7] López López, D., Van Mele, T., & Block, P. (2019a). The combination of tile vaults with reinforcement and concrete. International Journal of Architectural Heritage, 13:6, 782-798. DOI: 10.1080/15583058.2018.1476606.

[8] Roca P, López-Almansa F, Miquel J, Hanganu A. Limit analysis of reinforced masonry vaults. Engineering Structures 2007; 29: 431-9.

[9] Heyman J. The stone skeleton. International Journal of Solids and Structures 1966; 2: 249–79.

12th International Conference on Structural Analysis of Historical Constructions
SAHC 2020
P. Roca, L. Pelà and C. Molins (Eds.)

A NOVEL NON-LINEAR DISCRETE HOMOGENIZATION APPROACH FOR THE ANALYSIS OF DOUBLE CURVATURE MASONRY STRUCTURES

J. SCACCO[1*], G. MILANI[1] AND P.B. LOURENÇO[2]

[1]Politecnico di Milano, Department of Architecture Built Environment and Construction Engineering ABC, Piazza Leonardo da Vinci 32, 20133 Milan, Italy

e-mail: jacopo.scacco@polimi.it (*corresponding author)
gabriele.milani@polimi.it

[2] Department of Civil Engineering, ISISE, University of Minho,
Azurém, 4800-058 Guimarães, Portugal
email: pbl@civil.uminho.pt

Keywords: Masonry, Dome, Homogenization, Automatic Mesh, Non-linear Analysis

Abstract. *In the context of historical heritage, curved masonry structures as arches, vaults and domes represent the most distinctive and charming feature. Since the 17th century, several approaches have been developed in order to analyze their behavior, achieving nowadays techniques enable to combine ancient and modern methods. However, as these elements act as weak points of the structures during seismic events, the necessity of evaluating their vulnerability and safety level pushed the research to implement new numerical approaches. Although, the behavior of such structures is still not deeply investigated in literature as the high number of variables and uncertainty involved.*

An innovative discrete homogenized model approach is here proposed. The method provides the main features needed for proper simulation of masonry curved structures, including the orthotropy and the typical in-and-out-of-plane coupled behavior exhibited by masonry vaults. Moreover, homogenization procedures directly implemented in the method allows reducing by far the number of variables, leading to non-linear analyses without unpractical computational time.

The model is conceived as an assembly of elastic units joint by non-linear interfaces. These latter are modeled as bricks elements and Concrete Damage Plasticity is used for modeling non-linear mechanical properties, coming from homogenization procedures. The discrete mesh is obtained automatically by means of an ad-hoc script.

With the aim to validate the proposed approach, some non-linear simulations are carried out on examples of an unreinforced dome, of which experimental and numerical data are available, showing the reliability of the method and the accuracy of reproducing the evolution of the damage with a limited computational burden.

1. INTRODUCTION

In the last years increasing efforts have been addressed for evaluating the safety and the

effective behavior of masonry historical buildings. Such constructions spread all over the world as monuments, churches, bridges, aqueducts and even as residential buildings. Due to the fact that such building technology was developed by several countries in different periods of mankind, the level of complexity and variety from the geometrical and material point of view is huge. The most evident features are the composite nature of the material called masonry. Brick or stones are arranged in a different configuration with or without the use of mortar. Both of these components may have a different geological origin or chemical composition, making the application of usual engineer simplifications not straightforward. This complexity is, in a sense, amplified when masonry curved elements are studied. Arches, vaults and domes may be seen as the most identifying features of masonry buildings. However, their beauty is at least equal to their vulnerability, above all when subjected to horizontal seismic loads. In such events, catastrophic human and artistic lost increases the awareness of all technicians and pushed the researchers to carry out more experimental tests and implement innovative numerical approaches. It is important to highlight, as done by Huerta in [1] that, nowadays, vaults and domes are not any more built and the subsequent lack of knowledge have been filled only thank several researchers (see [2-4]) in the last decades. These latter identified, by means of a scientific approach, the effective behavior of curved masonry structures, laying the foundations to more advanced and complex methodologies. In fact, FE based approaches represent certainly the most valid option for properly exploring the performance until the collapse of such complex structures. Non-linear simulations might be carried out by means of micro and macro modeling. The first approach relies on separate modeling of each component of masonry as stones, joints and interfaces (even of the reinforcement when strengthening is simulated [5]). Such an approach ensures a detailed and realistic reproduction of reality. However, the main drawback is obviously the high number of variables involved and the consequent unpractical computational burden. A macro-modeling approach may tackle these issues, leading to easier implementation of the geometrical model and reducing by far the numerical complexity. Some constitutive models were implemented in order to preserve the orthotropy of masonry, requiring though a previous experimental campaign [6]. Even isotropic constitutive models may reproduce well the global behavior of masonry structures [7], but at the same time, they can lead to possible inaccuracy in the evolution of the damage pattern.

Along with non-linear approaches, the kinematic limit analysis combined with FE or with NURBS [8-10] provides a speedy and straightforward approach for identifying the ultimate state at the collapse, allowing fast identification of the safety level. However, no information about the displacement and crack history can be obtained, precluding its application in some scenarios.

In order to address the drawbacks of the above-discussed methods, an innovative methodology for non-linear analysis of curved masonry structures is here proposed. It relies on a discrete model approach coupled with homogenization procedures. Moreover, the non-linear mechanical properties are modeled by means of a generic damage-plasticity constitutive model already available in FE based software as Abaqus. Eventually, experimental and numerical comparisons are provided for assessing the validity of the method and for illustrating its capabilities.

2. FEATURES OF THE PROPOSED METHOD

The method has been implemented with the aim to take into account properly all the aspects peculiar to masonry, preserving at the same time the computational effort, the accuracy and an easy implementation. First of all, a non-linear approach is selected in order to comply with the requirement of international codes that often ask for displacement history of the structure, such as pushover analysis. Then, above all for vaults and domes, due to the great heterogeneity of masonry textures, the orthotropy in the elastic and inelastic range should be reproduced. Moreover, when curved masonry structures are treated, the influence of the membrane state of stress on the out-of-plane behavior is a key aspect of a reliable and predictive method. Last but not least, the number of variables involved has to be kept low, with the way to be easily employed by practitioners. Orthotopy is well reproduced when a micro-modeling approach is selected. However, as mentioned, its use is limited to small scale samples.

A successful way to overcome such limitation is represented by homogenization procedures, often applied to composite materials like masonry. Such procedures are based on the identification of the global structure as a repetition of a representative volume element (RVE), enable to represent accurately the macroscopic behavior. In such a way the efforts required by micro approaches are limited only to a cell level, defining the elastic and inelastic response. Alternatively, a valid and speedy approach at the cell level is the one implemented and presented in [11]. A semi-analytical procedure is described, resulting highly effective and fast through the use of a displacement formulation and a coarse discretization.

At the structural level, following a simplified approach, such homogenized information can be input as an averaged isotropic model. However, with the view of preserving the orthotropic mechanical properties coming out from homogenization procedures, a valid alternative is offered by the so-called discrete methods. In such an approach, elastic or rigid units are linked by interfaces where the non-linearities are lumped. In one of the most commonly used method “RBSM” (Rigid Body Spring Approach), such interfaces are modeled as non-linear springs. Even though such a method proved to be sufficiently accurate, its application has been limited to walls loaded in-plane and out-of-plane, like the impossibility to keep coupled the in-and-out-of-plane effects. Moreover, the implementation of the numerical model may result cumbersome.

The authors believe that a discrete approach along with homogenization procedures may lead to a predictive and straightforward method for modeling of masonry vaults and domes. For this reason, a new method based on the different implementation of the interfaces is here presented. The procedure follows the one described in [12] by the Authors. In this latter, the interfaces have been modeled as flat 3D bricks elements assigning the homogenized non-linear material properties by means of the plastic-damage constitutive model CDP (concrete damage plasticity), already available in Abaqus. The structure is described as a repetition of elastic units, jointed by the interfaces. The choice to assign the elastic properties directly to the cells ensures improved stability when the inelastic range is reached.. Such 3D approach ensures that the influence of the normal stress related to the gravity loads on the non-linear behavior in flexion is automatically taken into account. The number of variables involved in the numerical simulations is very low when compared to micro approaches, opening the way to further application of the method on reinforced structures.

3. METHODOLOGY

The validation of such discrete method on UR and RE out-of-plane-loaded walls is available in [12] where numerical and experimentally comparison is provided, and the interested readers are directed to this research for a point of reference.

The use of Concrete Damage Plasticity for modeling non-linear interfaces leads to easy implementation of the homogenized mechanical parameters along with robust numerical stability. CDP is as isotropic, plasticity-based, damage model, originally conceived for concrete. Successively it has been widely used for modeling masonry structures [13] in the static and dynamic non-linear analysis. A differential behavior in tension (exponential softening) and compression (parabolic softening) is assigned. The progressive decrease of the elastic stiffness is governed by two damage variables dt and dc, which range from 0 (undamaged material) to 1 (completely damaged material).

It is important to highlight that through this approach, despite using a continuum constitutive model, the orthotropy results preserved as the values of non-linear parameters are defined according to the orientation of interfaces. Because of that, its application and a proper simulation of materials like-masonry is possible even in FEM software that does not have in their library orthotropic damage-based models.

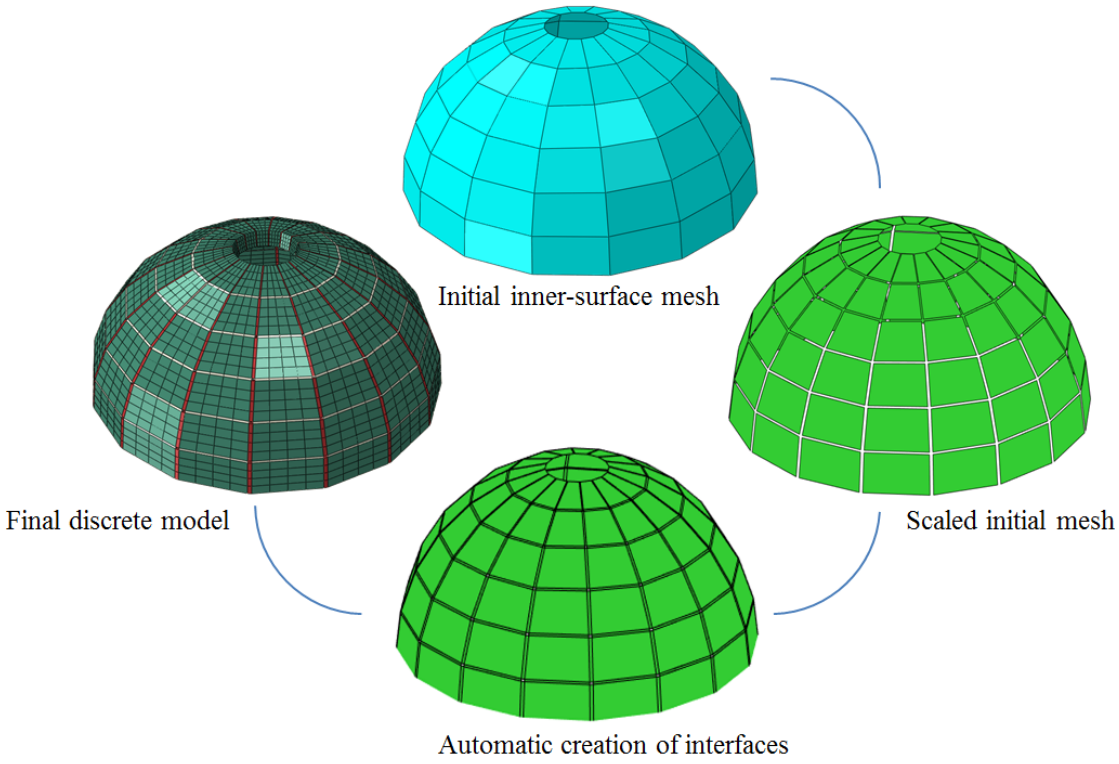


Figure 1: Steps for the automatic implementation of the discrete mesh.

The extension of this method to curved masonry structures is here presented and validated by experimental and numerical comparison of a brick-dome tested by Foraboschi in 2006. Moreover, the method has been improved by means of a MATLAB script that interacts directly with ABAQUS. The script, implemented by the Authors, is able to provide in an

automatic way the discretized mesh and to assign automatically the mechanical homogenized properties to each interface. Such automatic procedure allows the overcoming of some difficulties during the preparation of the numerical method. In fact, the flat 8-noded brick elements employed as interfaces have a thickness that, even though negligible, implies the presence of gaps in the intersections.

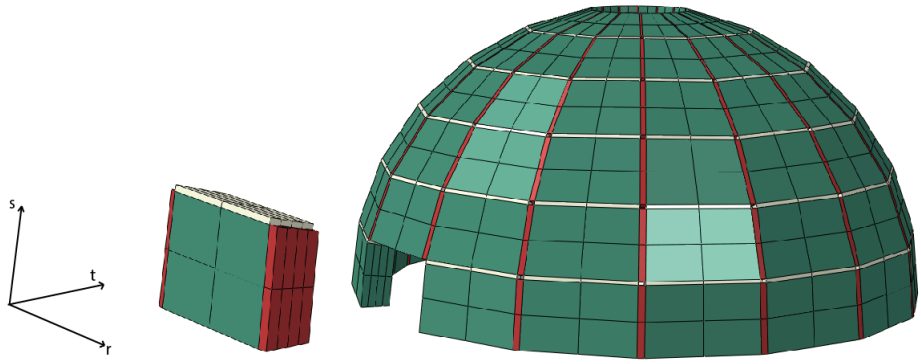


Figure 2: Mesh configuration in detail of the homogenized dome.

The procedure begins with the definition of a coarse but regular mesh of the inner surface of the dome. In such a way each 4-noded shell element generates correspondent elastic units of the final discrete model. In order to accommodate the space needed for interfaces, each element is scaled by a fixed value, by changing the 3D coordinates of four vertices. Then, the elements are automatically joined with the surrounding ones, generating additional 4-noded narrow elements. These latter will be converted to the non-linear interfaces in the final model. After this stage, each 4-noded elements is further subdivided, creating a new mesh for the subsequent discrete model (Fig. 1).

The final model is obtained by an extrusion of the discrete shell mesh. A different quantity can be applied to each node, making possible the modeling of vaults with variable thickness. In this paper, the dome has been modeled with 96 elastic units, providing two different discretizations. The first one with a rough mesh of 4 elements on the plane r-s. The second one, more refined, presents 16 elements on the plane r-s (Fig. 2).

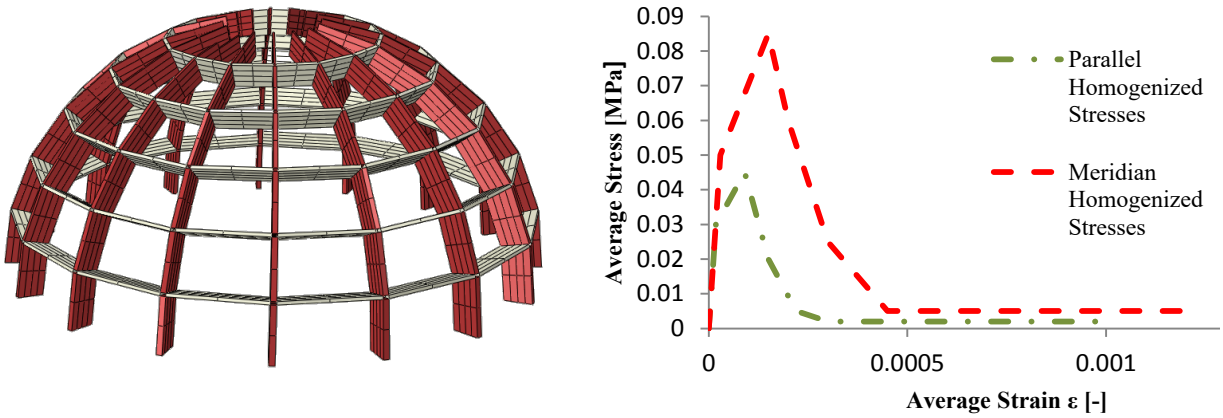


Figure 3: Detail of non-linear interfaces (Left) and relative homogenized stress-strain curve of tensile behavior (Right)

For both models, 4 elements along the thickness of the dome are defined. This choice results sufficiently accurate, according to the experience of the Authors, for reproducing properly the flexural behavior of curved masonry structures. As mentioned, the homogenized mechanical properties are automatically assigned to the interfaces according to their orientation.

This possibility paves the way to a full and comprehensive homogenization procedure, taking advantage of a semi-analytical approaches that may be easily integrated within the script. Such an extension will be a future improvement of the method and the Authors refer to upcoming research the interested readers.

Here the numerical analysis (non-linear and limit analyses) carried out in [14] are taken as references. With the aim to be fully consistent, the homogenized parameters carried out at the cell level of the dome in [14] are re-applied and set by means of a stress-strain input in the Concrete Damage Plasticity (Fig. 3).

4. RESULTS

The dome used as a reference for the numerical analyses was tested by Foraboschi in 2006. It was made of typical Italian bricks with dimensions of 120*250*55 (mm), with an overall dimension of 2.2 m for the inner diameter and a thickness of 120 mm. The dome was tested under the application of an increasing load along the border of the upper hole. The comparison is made in terms of load-displacement curves available from the test ad from previous numerical analyses.

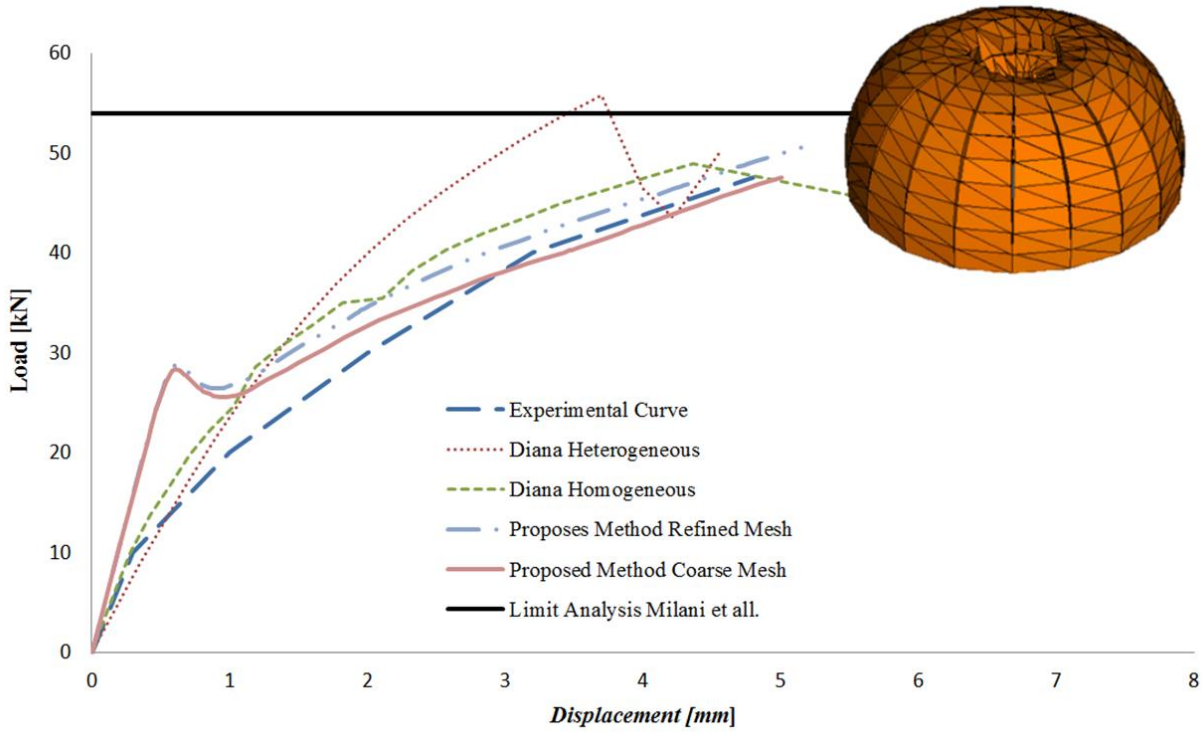


Figure 4: Comparison in terms of load-displacement curves of the proposed method with previous numerical analysis and with experimental reference; Collapse mechanism obtained by means of SQ non-linear analysis by Milani, 2011 (Top right)

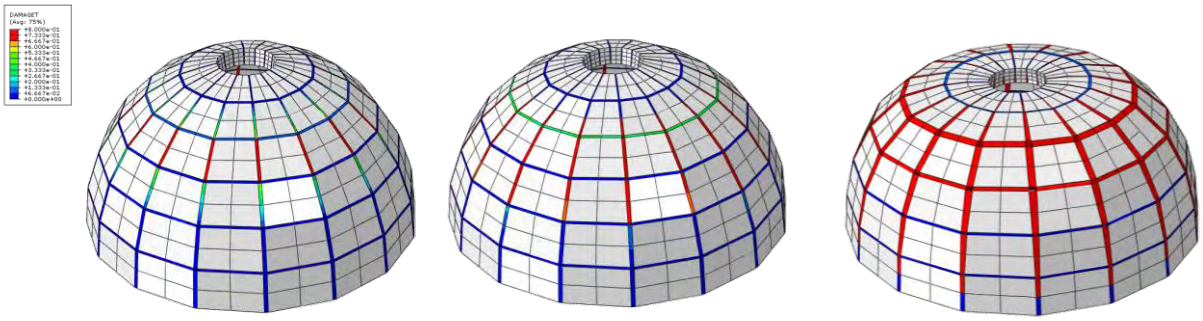


Figure 5: Evolution of damage pattern

The global behavior presents a final displacement around 4.5 mm in correspondence of a peak capacity load nearby to 48 kN (Fig. 4). Concerning the collapse mechanism, the final damage pattern is then compared with the one provided in [14] by the SQ non-linear analysis. As mentioned before, two different mesh configurations have been carried out for the purpose. The coarse one with a number of elements close to 3000 and the more refined one with almost 9000 elements. From Figure 4 it is noticeable how the homogenized outcome has an excellent capacity to reproduce the experimental and advanced numerical results, despite an initial discrepancy in the stiffness.

The damage and its evolution are coherent with what is expected from a symmetric problem. In fact, the cracks start to spread symmetrically along the meridians at 2/3 of the height. Along with meridian cracks, the damage occurs even at the above parallels, leading to the development of a circular flexural hinge (Fig. 5).

5. CONCLUSION

Numerical validation of a 3D discrete homogenized approach for the analysis of curved masonry elements has been presented. The advantages and drawbacks of existing numerical methods have been put in evidence with the aim to justify the implementation of a new method. The required features are so exposed: non-linear approach, low number of variables involved, orthotropic model, accuracy in the simulation of the influence of membrane stress on the flexural behavior. Consequently, a discrete approach coupled with homogenization procedures is suggested as the right methodology for fulfilling all the requirements.

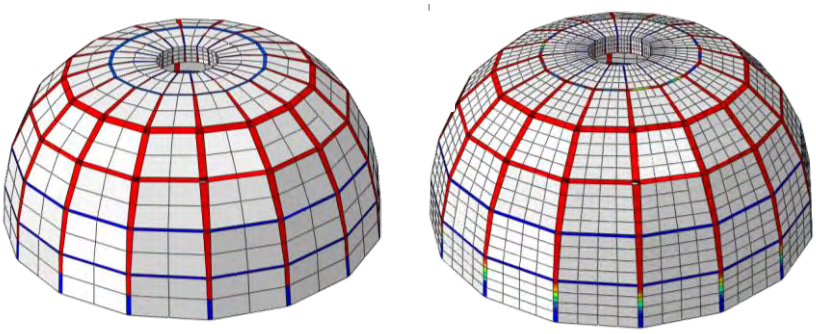


Figure 6: Comparison in terms of crack pattern between two different mesh configuration.

The structure is modeled as repetition of elastic units jointed by non-linear interfaces. These latter are input as flat 8-noded bricks along with plastic, damage based, the constitutive model already available in Abaqus (concrete damage plasticity). In such a way, differential homogenized properties are assigned depending on the orientation of interfaces, preserving the orthotropic behavior. Then, a script for the realization of the geometric discrete model is presented, focusing on the possibility to obtain automatically the discretized mesh and opening the way to future extension.

Finally, the method, already validated on UR and RE out-of-plane-loaded walls [12], is extended to the case of a dome, experimentally tested in 2006 and numerically simulated several times by different approaches. The results obtained show good accuracy in replicating the global behavior in terms of the load-displacement curve, and in terms of damage pattern.

For further application, it is worth noting the negligible difference in the accuracy among the two different mesh configurations (Fig. 5-6). This result ensures the stability and validity of the method even when few variables are involved in the analysis, leading to speedy and reliable applications for practical purposes. Moreover, given the low computational burden, interesting extension to reinforced curved elements may be proposed by the Authors as topic of future works.

REFERENCES

[1] Huerta, S. Mechanics of masonry vaults: the equilibrium approach. In: *Proc. 1st Int. Congr. Struct. Anal. Hist. Constr. Guimaraes*, (2001), pp. 47–70.

[2] Heyman, J. *The stone skeleton*. Cambridge University Press (UK), (1995).

[3] Fanning, P.J., Boothby, T.E. Three dimensional modelling and full scale testing of stone arch bridges. *Comput. Struct.*(2001) **79**: 2645-2662.

[4] Como, M. *Statics of historic masonry costructions.* Springer-Verlag Berlin (Germany), (2013).

[5] Bove, M., Castellano, A., Fraddosio, A., Scacco,J., Milani,G. and Piccioni, M. D. Experimental and Numerical Analysis of FRCM Strengthened Parabolic Tuff Barrel Vault. In *Key Engineering Materials*, 817 (2019), pp. 213–220.

[6] Lourenço, P. B., De Borst, R. and Rots, J. G. A plane stress softening plasticity model for orthotropic materials. *Int. J. Numer. Methods Eng.* (1997) **40**: 4033–4057.

[7] Bianchini, N., Mendes,N. and Lourenco, P.B. Seismic Assessment Of Masonry Cross Vaults Through Numerical Seismic Assessment Of Masonry Cross Vaults Through Numerical Nonlinear Static And Dynamic Analysis. In: *COMPDYN 2019 7th International Conference on Computational Methods in Structural Dynamics and Earthquake Engineering*, (2019).

[8] Grillanda, N., Chiozzi, A., Milani, G. and Tralli, A. Collapse behavior of masonry domes under seismic loads : An adaptive NURBS kinematic limit analysis approach. *Eng. Struct.* (2019) **200**.

[9] Chiozzi, A., Grillanda, N., Milani, G. and Tralli, A. UB-ALMANAC: An adaptive limit analysis NURBS-based program for the automatic assessment of partial failure mechanisms in masonry churches. *Eng. Fail. Anal.* (2018) **85**: 201–220.

[10] Grillanda, N., Chiozzi, A., Milani, G. and Tralli, A. On Collapse Behavior of Reinforced Masonry Domes under Seismic Loads. In *Key Engineering Materials*, 817 (2019), pp. 275–282.
[11] Bertolesi, E., Milani, G. and Lourenço, P. B. Implementation and validation of a total displacement non-linear homogenization approach for in-plane loaded masonry. *Comput. Struct.* (2016) **176**: 13–33.
[12] Scacco, J., Ghiassi, B., Milani, G. and Lourenço, P.B. A fast modeling approach for numerical analysis of unreinforced and FRCM reinforced masonry walls under out-of-plane loading. *Compos. Part B* (2019) **180**.
[13] Valente, M. and Milani, G. Effects of Geometrical Features on the Seismic Response of Historical Masonry Towers. *J. Earthq. Eng.* (2018) **22**: 2-34.
[14] Milani, G. and Tralli, A. A simple meso-macro model based on SQP for the non-linear analysis of masonry double curvature structures. *Int. J. Solids Struct.* (2012) **49**: vol. 808–834.

12th International Conference on Structural Analysis of Historical Constructions
SAHC 2020
P. Roca, L. Pelà and C. Molins (Eds.)

A SIMPLE AND EFFECTIVE RIGID BEAM MODEL FOR STUDYING THE DYNAMIC BEHAVIOUR OF FREESTANDING COLUMNS

DANIELE BARALDI[1*], GABRIELE MILANI[2] AND VASILIS SARHOSIS[3]

[1]Università IUAV di Venezia
Terese, Dorsoduro 2206, 30123, Venezia, Italy
e-mail: danielebaraldi@iuav.it, http://www.iuav.it (*corresponding author)

[2]Department of Architecture, Built Environment and Construction Engineering
Technical University of Milan
Piazza Leonardo Da Vinci 32, 20133, Milano, Italy
e-mail: gabriele.milani@polimi.it, http://www.abc.polimi.it

[3]School of Civil Engineering
University of Leeds
LS2 9JT, Leeds, UK
e-mail: V.Sarhosis@leeds.ac.uk, https://engineering.leeds.ac.uk

Keywords: Masonry, Columns, DEM, Rigid Beam Model, Dynamic response.

Abstract. *In this work, a simple and effective Rigid Beam Model is proposed for studying the dynamic behaviour of ancient freestanding stone columns. As well known, monolithic and multi-drum freestanding columns are historical structural elements typical of ancient temples that still can be found in the Mediterranean area. These columns are particularly prone to collapse in case of seismic actions. The dynamic behaviour of freestanding columns has been studied by many authors in the past [1-3], and it is characterized by a strong nonlinearity due to sliding and rocking between the drums. The Rigid Beam Model here described assumes each drum of the column as a rigid beam element and each interface between the drums as a node of the model able to move horizontally. Similar to Housner [1] approach, this model assumes small displacements and no sliding between blocks. Furthermore, the material nonlinearity is considered by means of a moment-rotation constitutive law slightly modified with respect to the bilinear one introduced by Housner. Numerical simulations were performed on monolithic and multi-drum columns modelled using the proposed Rigid Beam Model approach. Results are compared against simulations of the same columns undertaken by means of the Discrete Element Model, which is able to consider large displacements and the possible sliding between the drums, and it has already proven its effectiveness in simulating column behaviour [2-4].*

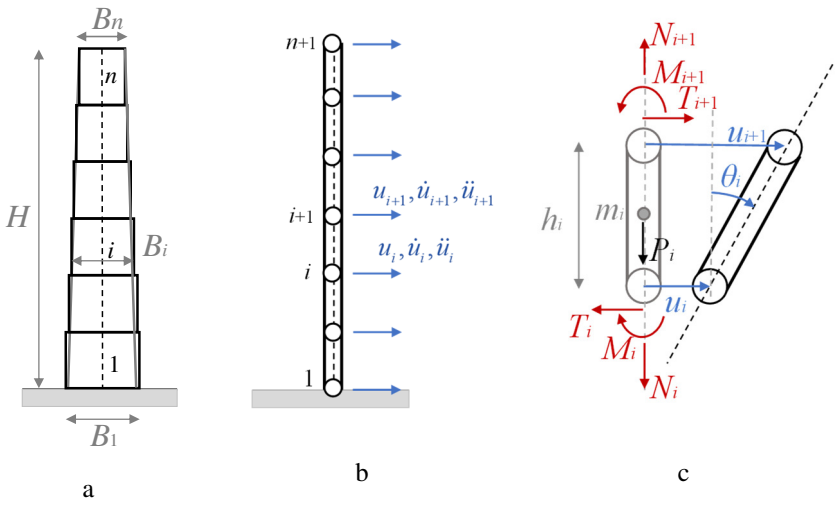
1 INTRODUCTION

Monolithic and multi-drum stone columns are structural elements typical of ancient monuments of the Mediterranean area, built, among the others, by Roman, Greek, and Egyptian civilizations. In the current days, such columns can be often found in freestanding condition, given that the original buildings had been fully or partially destroyed by past earthquakes and other natural or anthropic events. Even if these structural elements survived up to current days,

they are still subjected to seismic actions and they are prone to collapse.
The analytical and numerical assessment of the dynamic behavior of monolithic and multi-drum columns was studied by many researchers (see for instance the references collected in [4]). In particular, the pioneering analytical model proposed by Housner [1] is the first contribution that studied the behavior and the possible overturning of a single rigid block subjected to different types of horizontal actions. The subsequent research activities focused on the assessment of the dynamic behavior of monolithic elements by means of accurate numerical models and with laboratory experiments. Some other research activities focused on the analytical assessment of the dynamic behavior of columns made of a limited number of drums, whereas most of the research activities were dedicated to the use of more or less accurate numerical models for simulating the dynamic behavior of multi-drum columns and more complex stone structures (namely buttresses, arches on columns, trilithic structures). Among the different numerical models adopted for studying monolithic and multi-drum columns, the Discrete Element Method (DEM), introduced for the analysis of soils and rocks [6], has been extensively used, due to the possibility of modelling the column drums as distinct elements, with the possibility to apply dynamic excitations and achieve large displacements.
In this work, a simple and effective numerical Rigid Beam Model, already introduced by authors [5] for studying the dynamic behavior of both monolithic and multi-drum columns, is further investigated. The model considers a multi-drum column as an assemblage of vertically aligned rigid beam elements, with each drum represented by a beam element and each interface represented by a node. Small displacements are considered, and no sliding is assumed at interface level. The effectiveness of the Rigid Beam Model is further validated here by simulating the numerical tests on rigid blocks subjected to harmonic excitations performed by Spanos and Koh [7], and also by applying a half sine-wave ground excitation for reproducing one of the solutions proposed by Housner [1]. Furthermore, a comparison between the results from harmonic analyses on slender monolithic and multi-drum columns obtained from the Rigid Beam Model and the two-dimensional (2D) Discrete Element (DE) code UDEC [8] are provided.

2 RIGID BEAM MODEL

As stated in the introduction, the Rigid Beam Model was introduced by authors in a recent contribution [5] for representing a generic multi-drum column made of n blocks or drums on a rigid ground, having overall height H, lower base width or diameter B_1 and upper width or diameter B_n (Figure 1a). The rigid beam model is defined by assuming a rigid beam element for each drum of the column and considering n+1 nodes at beam element ends, representing the interfaces between the drums (Figure 1b). Sliding between the drums is neglected; hence, the degrees of freedom of the rigid beam model are given by horizontal nodal translations, velocities and accelerations u_i, $\dot{u}_i$ and $\ddot{u}_i$, respectively (Figure 1b). Small displacements are also assumed, hence a generic beam element can be subjected to a rigid rotation depending only on upper and lower nodal displacements and element height: $\theta_i = (u_{i+1} - u_i)/h_i$. Each beam element is also characterized by a mass m_i and by the corresponding weight P_i.



a b c

Figure 1: Multi-drum column (a), corresponding rigid beam model (b), *i*-th beam element (c)

The typical internal forces of the beam element, namely a normal force, a shear force, and a moment N_i, T_i, and M_i, respectively, act at each beam end (Figure 1c). The translational and rotational equations of motion for a beam element may be written as follows:

$$\begin{aligned} m_i(\ddot{u}_{i+1}+\ddot{u}_i)/2 &= T_{i+1}-T_i \\ I_{Gi}\ddot{\theta}_i &= -M_{i+1}+M_i+(T_{i+1}+T_i)h_i/2 \end{aligned} \tag{1}$$

where I_{Gi} is the polar inertia of the drum corresponding to the beam element. The static equilibrium in vertical direction is given by:

$$P_i = N_{i+1}-N_i \tag{2}$$

If the column is subjected to a horizontal ground acceleration $a_g(t)$, equations of motion (1) are subjected to the following boundary conditions at column base and top nodes:

$$\begin{aligned} \ddot{u}_1 &= \ddot{u}_g = a_g(t) \\ T_{n+1} &= 0 \\ M_{n+1} &= 0 \end{aligned} \tag{3}$$

and the equations of motion (1) for the whole column can be written in matrix form as follows:

$$\begin{aligned} \mathbf{T} &= \mathbf{M}_a\ddot{\mathbf{u}}-\mathbf{A}_g \\ \mathbf{M} &= \mathbf{G}\mathbf{T}+\mathbf{I}_G\ddot{\mathbf{u}}-\mathbf{B}_g \end{aligned} \tag{4}$$

where vectors **T** and **M** are nodal shear forces and moments from node i to n: $\mathbf{T} = [T_1\ T_2\ \dots\ T_n]^T$, $\mathbf{M} = [M_1\ M_2\ \dots\ M_n]^T$; vector $\ddot{\mathbf{u}}$ is horizontal accelerations from node 2 to n+1: $\ddot{\mathbf{u}} = [\ddot{u}_2\ \ddot{u}_3\ \dots\ \ddot{u}_{n+1}]^T$. $\mathbf{M}_a$, $\mathbf{G}$, and $\mathbf{I}_G$ can be defined, respectively, as mass coefficient matrix, geometric coefficient matrix, and polar inertia coefficient matrix. $\mathbf{A}_g$ is a vector characterized by null values except the first component, representing the acceleration at the base of the column: $\mathbf{A}_g = [a_g(t)m_1/2\ 0\ \dots\ 0\ 0]^T$; and, similarly, $\mathbf{B}_g = [a_g(t)I_{G1}/h_1\ 0\ \dots\ 0\ 0]^T$. Substituting the

expression of **T** in the expression of **M**, a system of differential equations to be solved for determining the displacements of the multi-drum column is obtained:

$$\mathbf{M} = \mathbf{G}\mathbf{M}_a\ddot{\mathbf{u}} - \mathbf{G}\mathbf{A}_g + \mathbf{I}_G\ddot{\mathbf{u}} - \mathbf{B}_g \tag{5}$$

where $\mathbf{M}=\mathbf{M}(\boldsymbol{\theta})$, since each moment M_i is assumed to depend on the rotation θ_i of the corresponding *i*-th drum by means of a bi- or tri-linear moment-rotation constitutive law, which represents the stabilizing moment for varying block rotation (Figure 2), and it is slightly modified with respect to Housner law by means of an initial elastic bending stiffness $K_{M,i}$ and a smoothing parameter $\xi \leq 1$ for reducing the stabilizing moment $M_{u,i}$ at each interface:

$$M_{u,i} = (B_i / 2)\sum_{j=i}^{n} P_j \tag{6}$$

The system of differential equations in (5) is solved by means of a Runge-Kutta ODE solver.

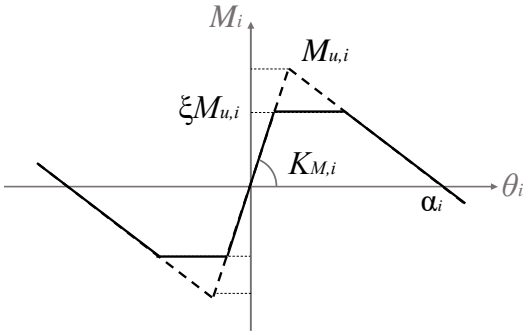


Figure 2: Moment-rotation constitutive law

3 NUMERICAL TESTS

Several numerical tests were performed in order to evaluate the effectiveness of the proposed Rigid Beam Model in simulating the dynamic behavior of freestanding monolithic and multi-drum columns, with respect to existing numerical and analytical solutions. For instance, the numerical tests performed by Spanos and Koh [7] on simple rectangular monolithic blocks subjected to harmonic excitations were considered. Then, the slender column type already adopted by authors in past contributions [4-5] was taken into consideration and a simple half-sine wave excitation and a harmonic one were applied to the ground in order to evaluate the columns' dynamic behavior modelled with Rigid Beams and compared both with Housner solution and numerical results obtained from DEM.

3.1 Monolithic blocks and columns subjected to harmonic excitations

The numerical tests performed by Spanos and Koh [7] on monolithic rectangular columns were considered in this study. A slender and a thick column, having height to width ratio *H*/*B* equal to 4 and 2, were subjected to harmonic excitations with varying input frequency and acceleration amplitude. Such specimens were reproduced by means of the proposed Rigid Beam Model and considering a single rigid beam element. Harmonic excitations were applied for 10 seconds. Starting with the slender column case, Figure 3 shows several deformed configurations

at the end of the numerical tests and Figure 4 collects base and top horizontal displacements versus time. Both the deformed configurations and the horizontal displacements at the top show overturning conditions obtained with 0.5g and 0.5Hz and 1Hz. More information about the possible overturning of the column are collected in Figure 5, which shows the safe-unsafe domain obtained with the Rigid Beam Model compared with that obtained by Spanos and Koh [7], who assumed in this case a restitution coefficient close to 1. Probably due to this condition, the two safe-unsafe-domains are in excellent agreement, both starting with a collapse acceleration equal to 0.25g, corresponding to the static load multiplier for overturning the column, and with an increasing collapse acceleration for increasing frequency, up to 1.5g with 2Hz.

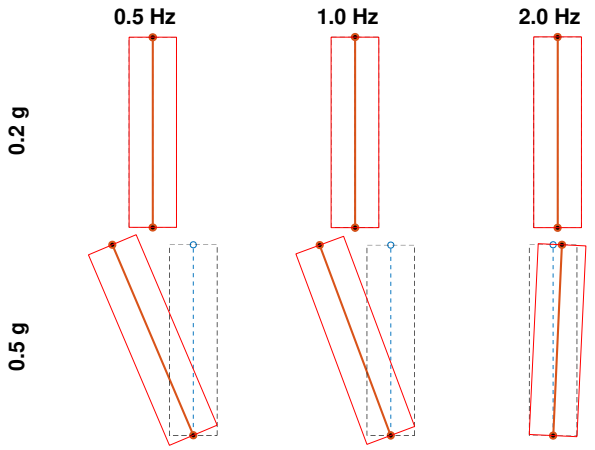


Figure 3: Deformed configurations for a slender monolithic rectangular column (H/B = 4) subjected to several harmonic excitations

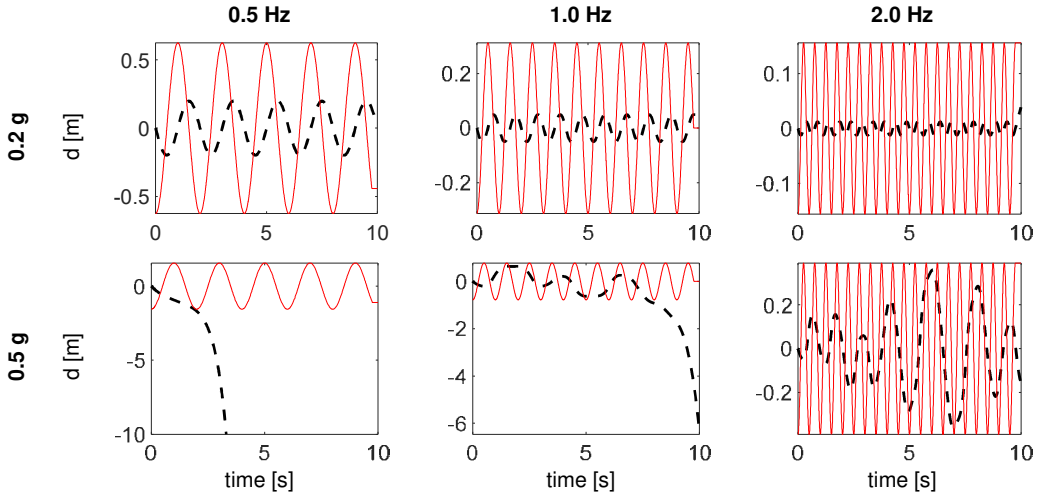


Figure 2: Base (red continuous line) and top (black dashed line) displacements for a slender monolithic rectangular column (H/B = 4) subjected to several harmonic excitations

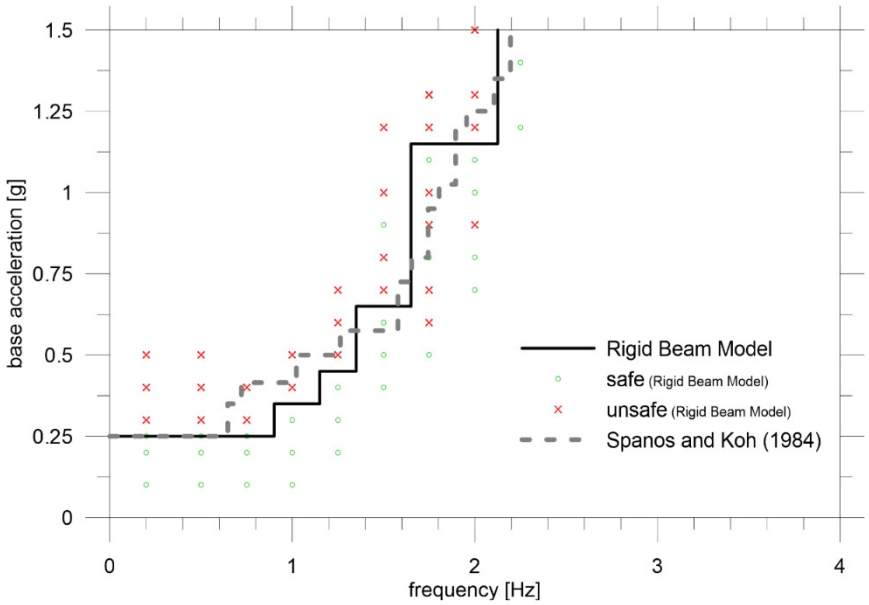


Figure 3: Safe-unsafe domain for a slender monolithic column ($H/B = 4$) subjected to harmonic excitations

Focusing then on the thick column case modelled with the proposed Rigid Beam Model, Figure 6 shows the deformed configurations at the end of the harmonic tests with several values of acceleration and frequency. Also Figure 7 shows the column top and base displacements for the same frequency and acceleration values as before. Overturning conditions in this case were obtained with 0.5g and 1Hz and with 1.0g with frequency values less than 1Hz.

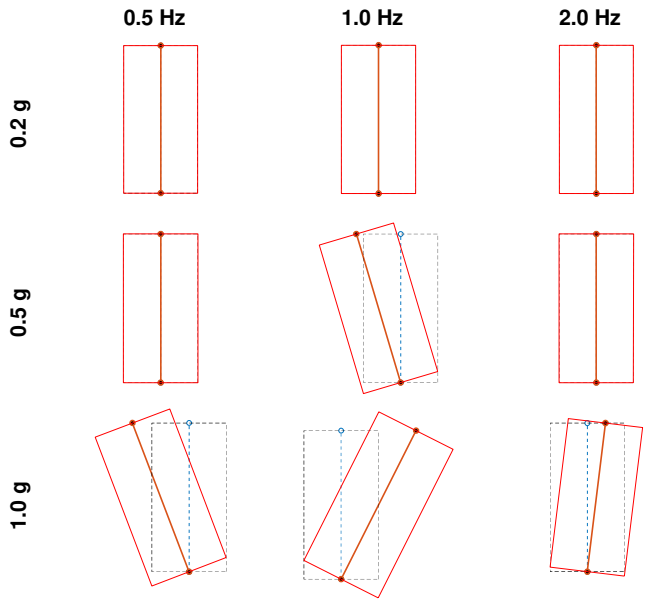


Figure 6: Deformed configurations for a thick monolithic rectangular column ($H/B = 2$) subjected to several harmonic excitations

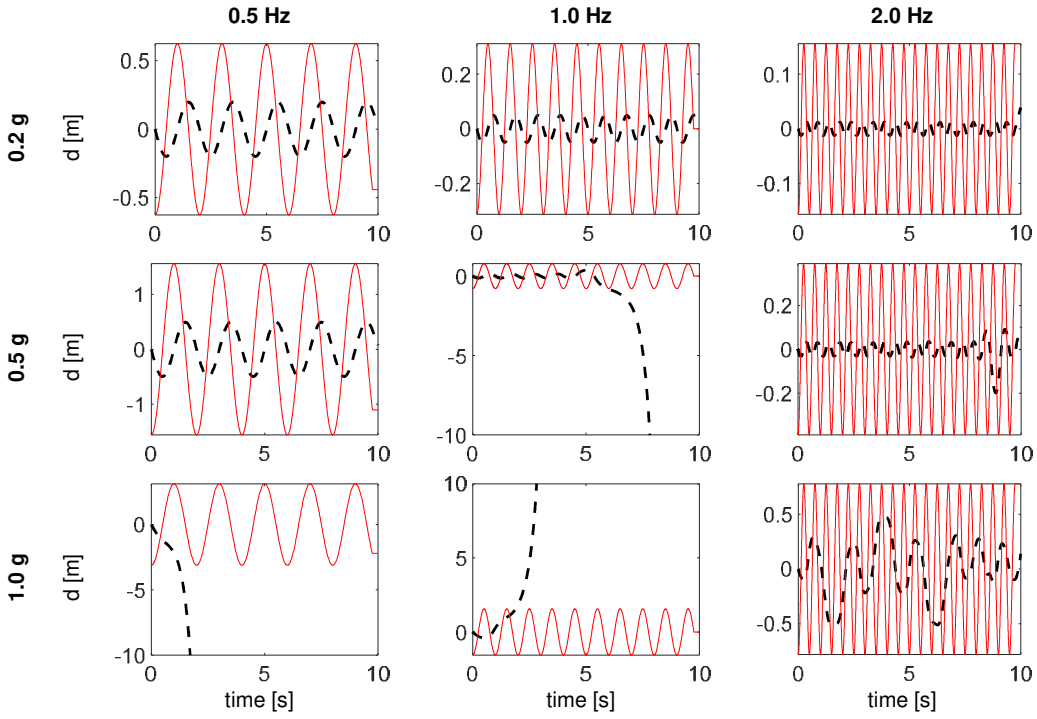


Figure 7: Base (red continuous line) and top (black dashed line) displacements for a thick monolithic rectangular column (H/B = 2) subjected to several harmonic excitations

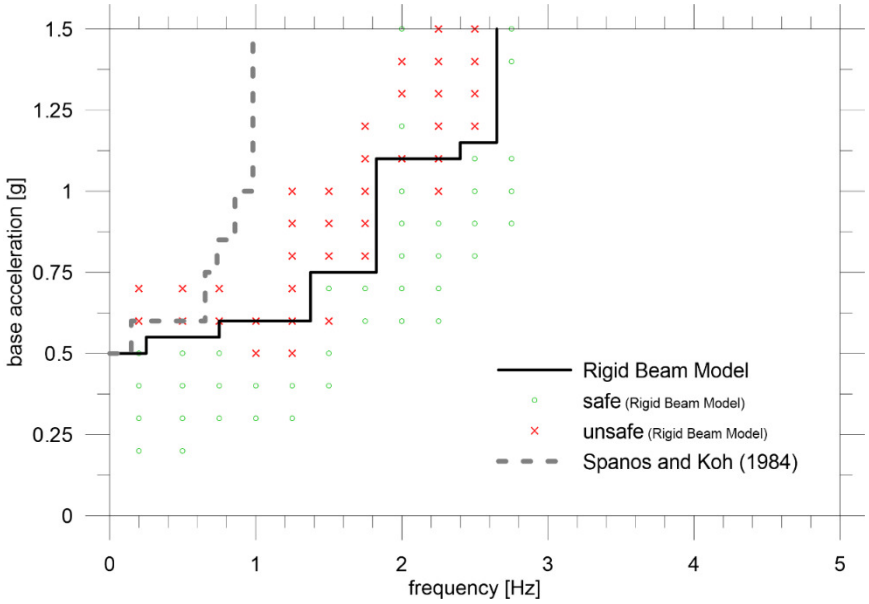


Figure 8: Safe-unsafe domain for a thick monolithic column subjected to harmonic excitations

Figure 8 shows the safe-unsafe domain obtained with the Rigid Beam Model, which is significantly different with respect to that obtained by Spanos and Koh [7], probably due to the small H/B ratio of the case study considered, and also due to the restitution factor close to 0.5

adopted in the reference work. In this case, both domains are characterized by a collapse acceleration equal to 0.5g for small frequency values, which is correctly coincident with the static collapse multiplier of the thick column. For increasing frequency, the Rigid Beam Model allows to obtain overturning accelerations increasing to 1g with 2Hz and 1.5g close to 3Hz, whereas the collapse acceleration values obtained by Spanos and Koh increase rapidly to 1.5g close to 1Hz.

3.2 Monolithic columns subjected to half-sine wave excitations

The slender monolithic column already considered by authors in the previous research [4-5] is here adopted for further validating the proposed Rigid Beam Model. The column has an overall height H=5 m, and lower and upper base width B_1=0.96 m, B_n=0.66 m. A simple half sine wave base excitation is applied to column base by varying the amplitude and the wavelength of the excitation. Overturning accelerations obtained with the proposed model are compared with the well-known Housner solution [1]. For this purpose, the smoothing parameter of the moment-rotation relationship is assumed equal to 1, together with an infinite bending interface stiffness between the ground and the column.

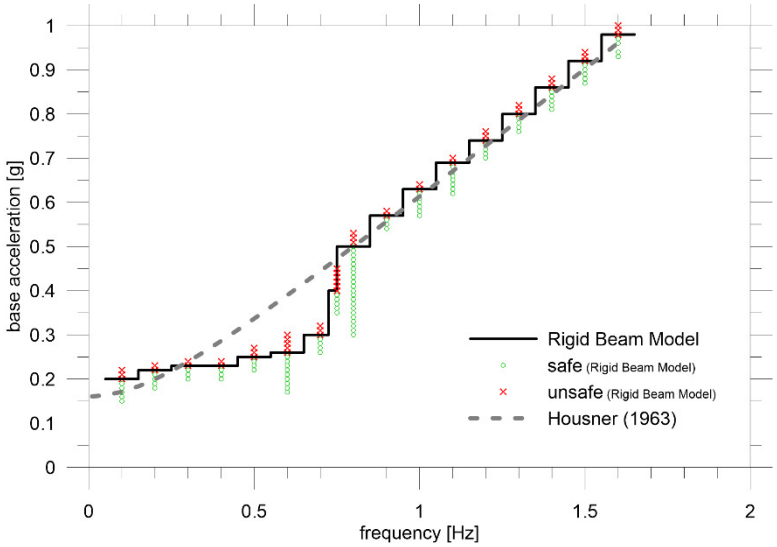


Figure 9: Safe-unsafe domain for a slender monolithic column subjected to half sine-wave excitations

Numerical results obtained with the Rigid Beam Model are in excellent agreement with Housner solution, except for a frequency range between 0.3 and 0.7Hz, characterized by smaller collapse accelerations obtained numerically with respect to the analytic solution. These results are collected in Figure 9.

3.3 Monolithic columns subjected to harmonic excitations

The numerical tests on the slender monolithic column already considered by authors are here updated by adding the column configurations at the end of the analyses or close to the end obtained with the Rigid Beam Model. Collapse mechanisms are evident since they are characterized by large rigid rotations of the column with respect to its base (Figure 10).

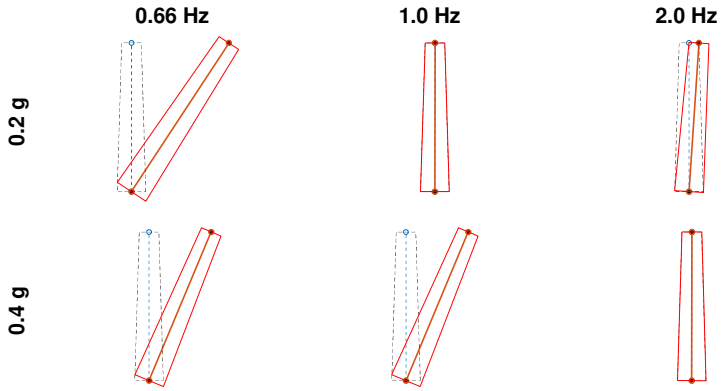


Figure 10: Deformed configurations for a monolithic column subjected to several harmonic excitations

The safe-unsafe domain obtained with the Rigid Beam Model, compared with that obtained with a standard DEM which allows both sliding and rocking of interfaces, shows that the hypothesis of no interface sliding influences the dynamic behavior of a monolithic column, since it reduces the collapse acceleration values for increasing input frequency (Figure 12a).

3.4 Multi-drum columns subjected to harmonic excitations

Similarly to the previous sub-section, the numerical tests on the slender multi-drum column equivalent to the monolithic one already considered by authors [4-5] are here updated by adding the column configurations at the end of the analyses or close to the end obtained with the Rigid Beam Model. Collapse mechanisms are evident since they are characterized by large rigid rotations of an upper part of the column or of the entire column with respect to its base (Figure 11). The safe-unsafe domain obtained with the Rigid Beam Model is slightly updated with further results with respect to the previous proposed results; however, the multi-drum column modelled by means of the Rigid Beam Model is still characterized by small acceleration amplitudes with respect to DEM results, and such amplitudes slightly increase for increasing input frequency (Figure 12b).

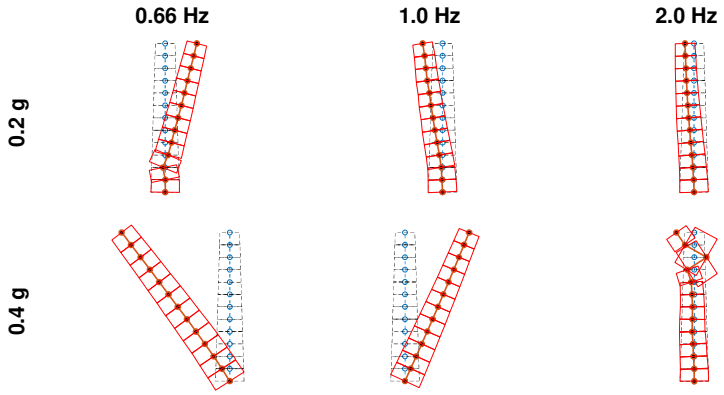


Figure 11: Deformed configurations for a multi-drum column subjected to several harmonic excitations

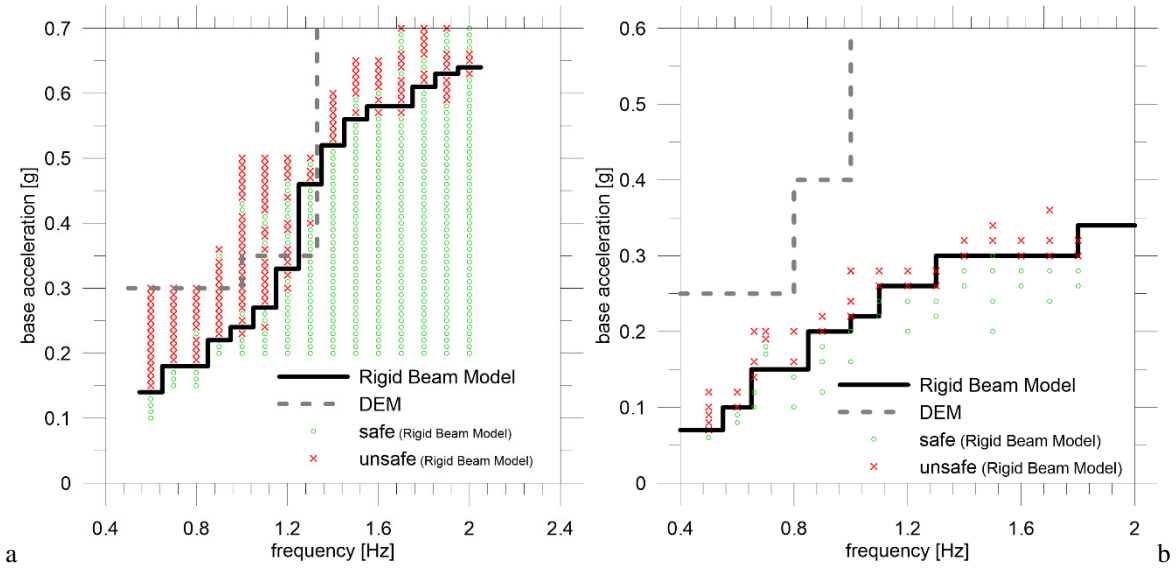


Figure 12: Safe-unsafe domain for a slender monolithic column (a) and an equivalent multi-drum column (b) subjected to harmonic excitations

4 CONCLUSIONS

A simple and effective Rigid Beam Model, recently introduced by authors for studying the dynamic behavior of freestanding monolithic and multi-drum columns [5], has been further investigated with several numerical tests. The model assumes each drum of the column as a rigid beam element and each joint between the drums as a node, in which are lumped the horizontal degrees of freedom of the model. A bi or tri-linear moment-rotation nonlinear law at each joint is also assumed, whereas sliding is neglected. The proposed model turned out to be in excellent agreement with the results of the harmonic analyses performed by Spanos and Koh [6] with the slender column case ($H/B = 4$), whereas a not so good agreement has been obtained with the thick column case ($H/B = 2$), probably due to the small restitution factor adopted in the reference work. The simple case of a ground excitation given by a half sine-wave proposed by Housner [1] has been successfully simulated by the proposed model. Finally, the sufficient agreement of the Rigid Beam Model with respect to the DEM, already showed by authors [5], has been further detailed by performing more harmonic tests on the multi-drum column.
Further developments of the proposed Rigid Beam Model will regard the further comparisons with existing numerical and laboratory results, by considering in some cases real ground motions on monolithic and multi-drum columns.

REFERENCES

[1] Housner, G.W. The behavior of inverted pendulum structures during earthquakes. *Bull. Seismol. Soc. Am.* (1963) **53**(1):403-417.

[2] Psycharis, I.N., Papastamatiou, D.Y. and Alexandris, A.P. Parametric investigation of the stability of classical columns under harmonic and earthquake excitations. *Earthq. Eng.*

Struct. Dyn. (2000) **1**(29):1093-1109.
[3] Papantonopoulos, C., Psycharis, I.N., Papastamatiou, D.Y., Lemos, J.V. and Mouzakis, H.P. Numerical prediction of the earthquake response of classical columns using the distinct element method. *Earthq. Eng. Struct. Dyn.* (2002) **1**(31):1699-1717.
[4] Sarhosis, V. Baraldi, D., Lemos, J. and Milani, G. Dynamic behaviour of ancient freestanding multi-drum and monolithic columns subjected to horizontal and vertical excitations. *Soil Dyn. Earthq. Eng*. (2019) **120**:39-57.
[5] Baraldi, D., Milani, G. and Sarhosis, V. Numerical models for simulating the dynamic behaviour of freestanding ancient columns. *Compdyn 2019 Proceedings* (2019), pp. 1526-1536.
[6] Cundall, P.A., A computer model for simulating progressive large scale movements in blocky rock systems. *Proceedings of the Symposium of the International Society of Rock Mechanics* (1971), Nancy, France.
[7] Spanos, P.D. and Koh, A.-S. Rocking of rigid blocks due to harmonic shaking. *J. Eng. Mech.* (1984) **110**(11):1627-1642.
[8] Itasca. *UDEC - Universal Distinct Element Code manual: theory and background.* Minneapolis, Itasca Consulting Group, (2004).

12th International Conference on Structural Analysis of Historical Constructions
SAHC 2020
P. Roca, L. Pelà and C. Molins (Eds.)

A SIMPLIFIED MODELLING APPROACH FOR THE PRACTICAL ENGINEERING ASSESSMENT OF UNREINFORCED MASONRY STRUCTURES USING LAYERED SHELL ELEMENTS

A. HASSANIEH[1*], M. GHARIB[2] AND M. KING[3]

[1] Corresponding Author. Senior Structural Analyst/Engineer,
Taylor Thomson Whitting, 48 Chandos Street, St Leonards, NSW 2065, Australia.
Email: amir.hassanieh@ttw.com.au

[2] Senior Structural Analyst/Engineer,
Taylor Thomson Whitting, 48 Chandos Street, St Leonards, NSW 2065, Australia.
Email: mahdi.gharib@ttw.com.au

[3] Associate Director,
Taylor Thomson Whitting, 48 Chandos Street, St Leonards, NSW 2065, Australia.
Email: michael.king@ttw.com.au

Keywords: Unreinforced Masonry, Seismic Assessment, Nonlinear Analysis, Layered Shell, Heritage.

Abstract. *Unreinforced Masonry (URM) has been extensively used as a construction material in mass structures with predominant compression load paths. Despite its reasonably established performance under gravity actions, it can be quite vulnerable to seismic loading, predominantly due to its limited tensile strength and associated quasi-brittle failure modes. Therefore, a reliable seismic assessment of URM structures, including heritage buildings, is vital to ensure life safety and minimise their risk of collapse. This can assist in implementing effective remedial measures, if required, to ensure desirable performance level in future events. Despite significant advancements in masonry research, practical assessment of URM has always been a challenge for structural engineers due to the complexity of the mechanics and geometry involved. Different modelling approaches have been trialled so far, which are typically based on equivalent frame, discrete and continuum elements in 2D/3D domains. In this paper, a simplified nonlinear model is introduced within the framework of conventional layered shell elements, which can be easily implemented in commonly used FE packages, e.g. ETABS and SAP2000. In this model, the URM shell element comprises three layers accounting for cohesion and axial-frictional behaviour parallel and perpendicular to the bed joints, where the mechanical properties can be adjusted for various masonry configurations. The performance of the proposed model is validated against several experimental tests available in the literature, where a good correlation with test data is achieved across various design scenarios and loading conditions.*

1 INTRODUCTION

Masonry is one of the oldest construction materials in the world, which has widely been used in buildings, especially low-rise commercial and residential buildings, in different sizes, shapes, and materials. Unreinforced Masonry (URM) is the simplest form of masonry construction and while it is well suited for bearing gravitational loads, it is prone to lateral loads and foundation differential settlement, mainly due to its limited tensile capacity and ductility.

The analysis of URM buildings is a challenging procedure due to geometrical and mechanical complexities, uncertainties associated with material properties, and possible imperfections and cracking in existing buildings. Masonry, by its nature, is a heterogeneous material, and its overall behaviour is characterised by its three constituent components, namely blocks, mortar, and the bond between them [1]. The compressive strength of blocks and mortar is usually higher than their tensile strength. The bond behaviour in shear comprises cohesion and friction mechanisms, while the tensile behaviour is cohesion-only, and generally, the bond strength is weaker than block and mortar. These result in an anisotropic material, where elastic properties, strengths, and post-peak behaviour are directional dependent.

In past studies, significant efforts have been dedicated to the investigation of masonry behaviour through experimental testing. The mechanical properties and failure mechanisms can be assessed at the scale of the masonry components (block, mortar and bond) [2] and structural elements [3]. The experimental tests have been performed on masonry components [4], wallets [5], masonry walls [6], and full-scale masonry structures [7]. It should be noted that the complexities associated with masonry structures extend beyond the mechanical properties alone, and also depend heavily on the structural details and layout, e.g. the connection of walls to horizontal diaphragms, the diaphragms' flexibility, and interaction with return walls that can all significantly affect the behaviour of URM [8].

In conjunction with experimental testing, there has been growing interest among researchers in developing Finite Element (FE) modelling strategies of URM in the past half-century. D'Altri et. al. [1] categorised the modelling techniques into four groups, namely, (a) block- (b) continuum- (c) microelement- and (d) geometry-based models. In the block-based or detailed discrete models, the brick is modelled by block and the mortar is modelled by either an element or a contact behaviour. This model can demonstrate clear representation of failure modes, interaction between simultaneous in-plane and out-of-plane loading, but it requires extensive computational demand. It is generally used for experimental validations and the calibration of standard design equations, making it less suitable for engineering design and assessment of full-scale structures [9], [10]. In the smeared continuum approach, the masonry walls are modelled by a continuum body, in which there is no need to use small mesh discretisation and the mesh size can be larger than the actual block/mortar size by utilising homogeneous constitutive laws. In its preliminary versions, it was assumed that the masonry has no tensile capacity, and a linear-elastic behaviour was assumed for compression [11], [12]. In advancement of this approach, some nonlinear constitutive laws have been proposed based on fracture mechanics, damage mechanics and/or plasticity methods [13], [14]. Several failure criteria have been formulated and utilised for masonry behaviour such as tension cut-off, Coulomb friction, and a compressive cap criterion [15]. Each criterion has been employed to capture a specific failure mode of masonry. The continuum-based methods have been widely used in the modelling of historical masonry buildings, which usually have complex geometry [1]. Despite the variety of the

material models developed in the literature, only some have been successfully validated and implemented in available advanced finite element software, such as DIANA and ABAQUS. In the microelement (lumped plasticity) models, the focus is mainly on global seismic behaviour of the structure. In this method, each wall segment may be categorised as either a pier or a spandrel, whereby piers are akin to columns and carry vertical and lateral loads simultaneously, and spandrels span between two adjacent piers and act more like beams. In this method, linear elastic frame elements have been utilised to model the piers and spandrels, then nonlinear hinges are assigned locally to the member to capture the inelastic behaviour as lumped plasticity [16], [17]. Although the concept of lumped plasticity is simpler and readily incorporated in the common commercial analysis software such as ETABS [18] and SAP2000 [19], it has its own drawbacks. For example, its applications to buildings with arbitrary perforations/openings forming irregular stacks of wall piers and spandrels may not be a straightforward task. Also, it requires some initial indication of the loading, such as the level of axial compression in the member, to properly define the friction properties of the representative shear hinges. Thereby, the distributed plasticity approach in such cases may have a clear advantage over the lumped plasticity approach. In geometry-based models, the structure is modelled as a rigid body. Typically, this kind of modelling is useful to assess equilibrium and collapse mechanics of URM walls [20], [21], but can fall short in capturing masonry behaviour in a progressive loading scenario.

The development of a simplified yet reasonably accurate constitutive framework for the modelling of orthotropic behaviour of masonry structures in commonly used commercial analysis software (e.g. ETABS, SAP2000, Strand7, etc.) holds significant promise for structural engineers and the building industry. This is the subject of this study, and it was achieved by appropriate utilisation of nonlinear layered shell elements for unified modelling of masonry piers, spandrels and even infills panels. The theory of the model is presented in the next section, followed by its implementation in analysis software packages. The model is then validated against several experimental studies available in the literature.

2 MATERIAL MODEL

The structural capacity of historical masonry structures has been generally assessed based on design equations and prescriptive provisions in the international design standards using linear elastic analysis in commercial finite element analysis software. With the introduction of performance-based analysis and design concepts for seismic assessment of existing structures and their successful incorporation into some international provisions by FEMA[22], ASCE [23] and NZSEE [24], explicit nonlinear modelling of historical buildings holds significant merit in the building industry to assess their structural performance under different earthquake records and hazard levels using nonlinear static (Pushover) or dynamic (Time-history) analysis methods. This objective has been achieved by either modelling concentrated/lumped plasticity in potential plastic hinge regions within the members, or by explicit inelastic constitutive modelling commonly known as distributed plasticity. The available guidelines and provisions typically cover the former by characterising nominal plastic hinge properties and performance levels for different actions and members, whereas the latter has been more extensively covered in academic research.

Bed joint sliding is one of the common modes of shear failure in squat piers of low aspect

ratio, which is typically expressed in design standards by a Mohr-Coulomb failure criterion as shown in Figure 1, which is a function of bond and frictional resistance and considered to be a displacement-controlled mode due to the relatively ductile residual component from the sustained friction. The conventional Mohr-Coulomb failure criterion is capped with straight cut-offs limits in tension and/or compression; however, a more realistic criterion would include curved tension/compression caps to account for the possible interactions at high axial stress levels such as that between shear friction and axial compression at high compressive stress states. This results in a reduced frictional component for a combined high axial compression and interface shear stress levels, which can be alternatively expressed by an idealised linear compression cap with a representative slope (ψ) when axial compression stress exceeds a critical limit ($\sigma_{c.lim}$). In lieu of a refined assessment, the so-called dilatation angle may be approximated as $\psi=(\pi-2\varphi)/4$ for a lower bound limit state analysis as given in [25], [26]. On the tension side, a sustained level of cohesion is generally considered for design purposes in international standards [23],[24], which is typically considered as c/2, and the failure line in Figure 1 is thus replaced with the dashed line intersecting the horizontal axis at $f_t=c/(2\mu)$. A similar shear failure mode may also be observed in short spandrels, but the friction component arises from internal actions due to end restraints and/or externally applied load or prestress (if present). However, axial compression can be generated at high chord rotations upon spandrel cracking and degradation of the cohesion mechanism due to the restraints for geometric deformations and the confinement provided by the neighbouring piers. An upper bound estimate for this residual clamping effect is typically obtained by evaluating the axial stress state associated with the diagonal tension failure of the spandrel [3].

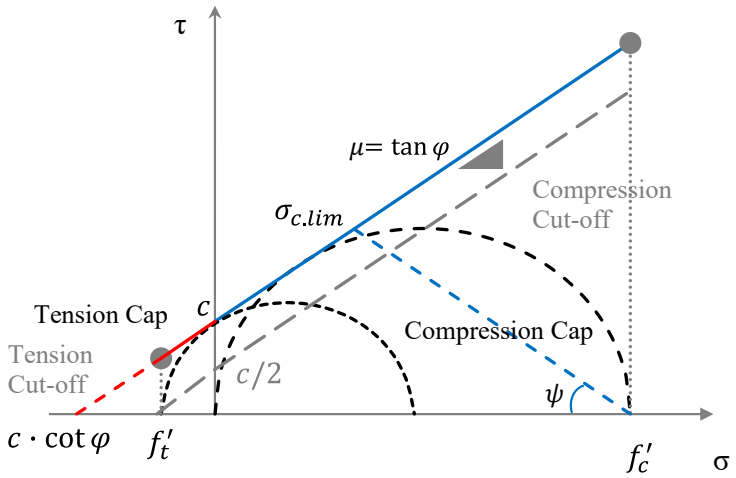


Figure 1 :An adjusted Mohr-Coulomb failure criterion to represent the shear fraction behaviour

In slender piers with high aspect ratio, flexural behaviour is expected to dominate the overall response, which manifests as flexural tensile cracking along the bed joint and typically a rocking mechanism in lightly loaded piers as flexural overturning mode about the toe with an uplift over the heel. This mode is commonly considered to be ductile due to the inherent ductility and prevalent signs of distress. For wall piers with high levels of axial compression, toe crushing may govern the scenario, although it may also be observed at later drift stages of a rocking pier due to the second-order effects. This failure mode is categorised as a brittle mode,

associated with the crushing of the material in a biaxial stress state over the compression stress block zone. The final failure mode under consideration is the diagonal tension cracking in spandrels and even piers, which can appear either in a stair-stepped cracking pattern through mortar, and/or a diagonal cracking pattern through fractured bricks when mortar is stronger. This failure mode is expected to be triggered in piers of intermediate aspect ratio and initiated at half-height of the wall section. Diagonal tension cracking is also considered to be a force-controlled failure mode.

For this study, the commercial FEA software package ETABS was selected for the implementation of the proposed material model due to its common and globally widespread use by structural design engineers, and the contribution of this study to engineering practice is due in part to this fact. The numerical model is implemented using the nonlinear continuum layered shell elements, which make use of properly calibrated directional behaviours to capture the anisotropic behaviour of unreinforced masonry with a reasonable level of accuracy. The proposed framework is equally applicable to SAP2000 or similar FEA software supporting nonlinear layered shell elements with frictional behaviour.

For the axial-flexural response of the masonry elements, it is expected that the adaptation of directional shell layers with representative uniaxial stress-strain curves for different orthogonal material directions, i.e. horizontal and vertical directions for a regular bond pattern, should be able to reasonably capture the expected behaviour and associated failure modes such as toe crushing and rocking in piers, and flexural cracking in long spandrels. This acts like a Rankine (maximum stress) failure criterion for limiting the compressive and tensile capacity in different material directions and stress quadrants, and it neglects the possible interactions such as the favourable effect of confinement in a biaxial stress state. These layers for the axial-flexural response include a shear friction component which accounts for the enhancement in shear resistance due to clamping from normal compression. In addition, a separate nonlinear shell layer is included to represent the cohesive shear bond behaviour and its degradation. The summation of these layers aims to capture the shear response including bond and frictional components. Lastly, a linear plate element with adjusted stiffness (via thickness and/or stiffness modifiers) is overlaid to represent the out-of-plane behaviour of masonry elements, and it is not intended to precisely capture the interactions between in-plane and out-of-plane behaviours if relied upon.

A nonlinear stress-strain curve is considered as shown in Figure 2 for representing the uniaxial behaviour in each direction, which is in line with the recommendations in Eurocode 6 [27]. The behaviour in tension is assumed to be linear elastic up to the masonry's tensile cracking capacity, followed by linear strain-softening depending on the fracture energy and the characteristic length of the FE elements where strain localization occurs. If desired, the linear degradation may be replaced with a bilinear softening that can better resemble an exponential decay. An elastic perfect plastic (EPP) curve may be assumed as a simplified alternative (also shown in Figure 2) for both components, to improve the computational cost and convergence, where the idealised curve is established based on the concept of equivalent strain energy up to the ultimate strain capacity. As can be seen, the equivalent bilinear curve in compression has adjusted initial stiffness and peak compression capacity and requires strain limits (e.g. maximum allowable crushing strain) in place to assess the state of crushing at various structural performance levels. The bilinear tensile behaviour essentially assumes a sustained level of tensile capacity as an idealised yield capacity, which is considered to be half of the peak flexural

tensile capacity in each direction. The vertical tensile capacity (f_{tv}) is generally small due to the horizontal bed joints, and it can be approximated by $f_{tv}\approx 0.5c_{bj}/\mu$ according to Figure 1, where c_{bj} is the masonry bed-joint cohesion and μ is the friction coefficient. However, it is generally neglected for design purposes, especially for a long-term analysis where the formation of cracks along bed joints is highly probable. In contrast, the nominal horizontal tensile capacity (f_{th}) can be significantly higher due to the stair-stepped pattern of the masonry bond and tensile cracking, which in the absence of vertical compression over the bed joint may be approximated as $f_{th}\approx 0.5c_{hj}/\mu+\alpha_s c_{bj}$, where c_{bj} is the masonry head-joint cohesion and α_s is the bond pattern factor taken as the ratio of the sum of horizontal crack length to the sum of vertical crack length.

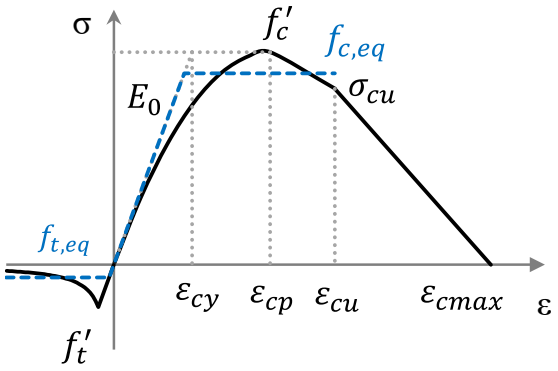
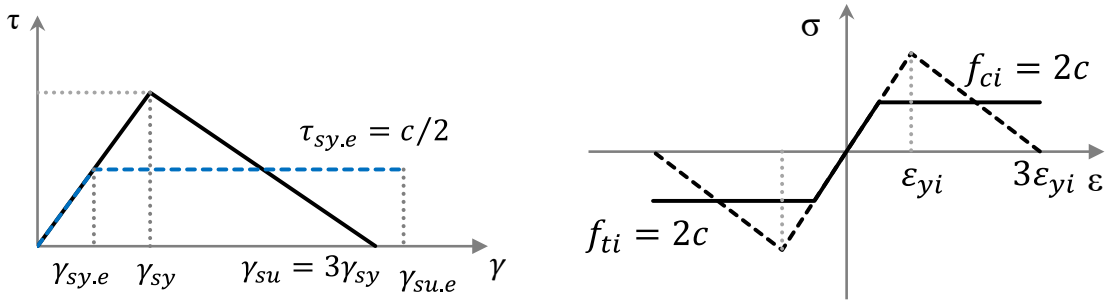


Figure 2 : Schematic illustration of the full and simplified stress-strain curves for uniaxial behaviour in different directions

For the additional cohesive shear layer, a bi-directional shell layer is considered to represent the cohesion capacity and its degradation, which is simply expressed by a linear strain softening here as shown in Figure 3(a) in accordance with NZSEE [24] and ASCE [23]. Similar to tensile behaviour, this can be enhanced with a bilinear softening if desired. An isotropic material with a stress-strain curve per Figure 3(b) must be defined in ETABS such that the desired masonry cohesion capacity (c_m) is obtained based on Mohr's circle for stress as $\tau_{ci}=(f_{ci}+f_{ti})/4$. Therefore, pseudo tensile and compressive capacities are defined as $f_{ci}=f_{ti}=2c_m$ as per Figure 3(b) to capture the target capacity, noting that the initial stiffness must also be adjusted accordingly such that the resultant shear curve yields the expected shear stiffness.



(a) cohesion behaviour (b) shear layer in ETBAS

Figure 3 : Stress-strain curves for the nonlinear shell layer representing cohesive behaviour

Similar to tensile behaviour, an idealised elastic perfect plastic (EPP) curve with an adjusted maximum allowable strain may be considered as shown in Figure 3(b) to resolve the highly probable convergence issues associated with strain softening and the so-called bifurcation

problem when using conventional nonlinear solvers and conventional local continuum formulations. When using such a simplified approach, it is essential to assess the strain levels and ensure the limits associated with different performance levels are not exceeded. This can be checked either locally or globally by the engineer, where the latter for example can be assessed in ETABS by the aid of computational strain gauges for piers and spandrels.

The combination of cohesive and frictional layers is expected to capture the overall shear response as schematically illustrated in Figure *4* and characterised in some international standards, e.g. [23], [24]. The directional layers represent the axial-flexural behaviour. The tensile capacity of the directional layers (if defined properly), alongside the frictional demand, is expected to characterise the orientation of principal stress/strain planes and define the principal tensile stress and the diagonal tension capacity. The probability for this failure mode can be visualised by the contour plots for the principal tensile strain (ε_{11} or ε_{max}), whereas the corresponding capacity can be inspected by the overall principal tensile stress plot (σ_{11} or σ_{max}) which is visualised in ETABS by the contour plot for the resultant principal force F_{max} per unit thickness ($\sigma_{max}=F_{max}/t_w$). Nevertheless, the diagonal tensile capacity (f_{dt}) as a force-controlled component is separately assessed over the course of the analysis by checking the associated shear capacity (V_{dt}) and drift limits for various members (piers/spandrels) in accordance with the available design equations in ASCE [23] and NZSEE [24].

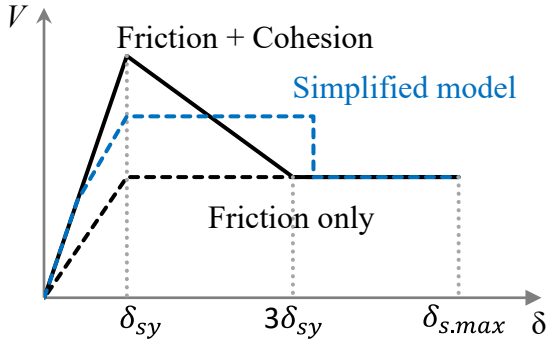


Figure 4 : Overall shear capacity of the member combining cohesive and frictional components

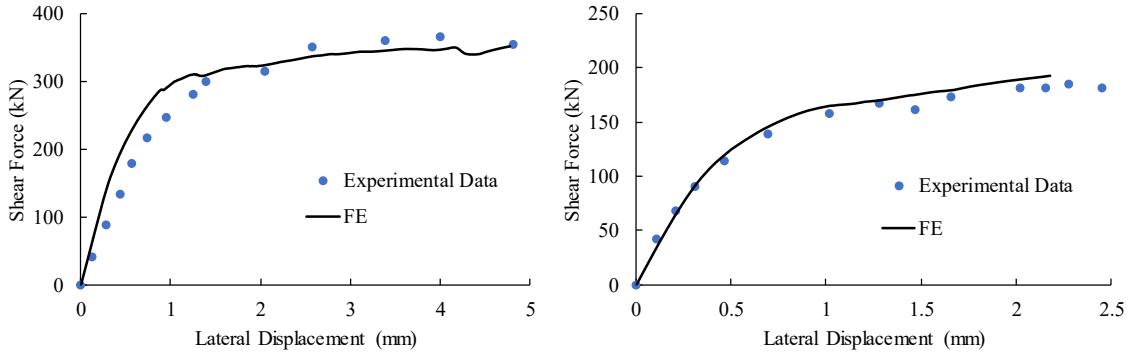
3 VALIDATIONS

In this section, the proposed model has been validated against experimental test results available in the literature including a solid URM wall, a perforated URM a URM wall prototype subjected to footing settlement, and a two-storey frame building under lateral loading.

3.1 Manzouri Tests

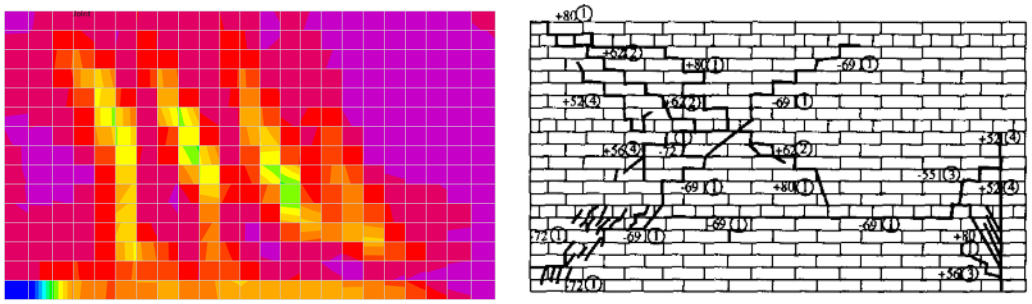
Manzouri *et. al.* [6] performed lateral loading tests on solid and perforated URM walls, specimens W3 and W4, which were subjected to 0.59 and 0.48 MPa overburden, respectively. The mean material properties are provided in Table 1. The aspect ratio of the solid wall was 0.6 and the walls consisted of three wythes of bricks. The walls were modelled in ETABS with the support and loading conditions consistent with the experimental tests. As can be seen in Figure 5, load-displacement responses of the FE simulation show a good correlation with the experimental results. Also, the principal tensile strain contours, as indications of crack locations

and patterns, reasonably agree with the reported crack pattern (See Figure 6 and Figure 7). Due to the unidirectional nature of the nonlinear static analysis performed, it is noted that the combination of expected crack patterns for push in positive and negative directions shall be considered for a better comparison with the experimental pattern from cyclic loading. Toe crushing and diagonal tension cracking were captured in specimen #3, whereas rocking with bed joint sliding were identified in specimen #4.



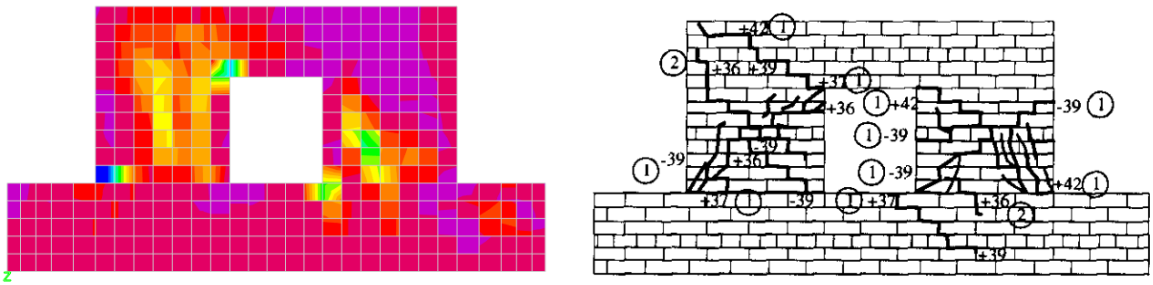
(a) (b)

Figure 5 : Load-displacement of Manzouri tests [6] for W3 and W4 Specimens



(a) (b)

Figure 6 : Tensile strain contour and crack pattern in experimental tests, specimen W3



(a) (b)

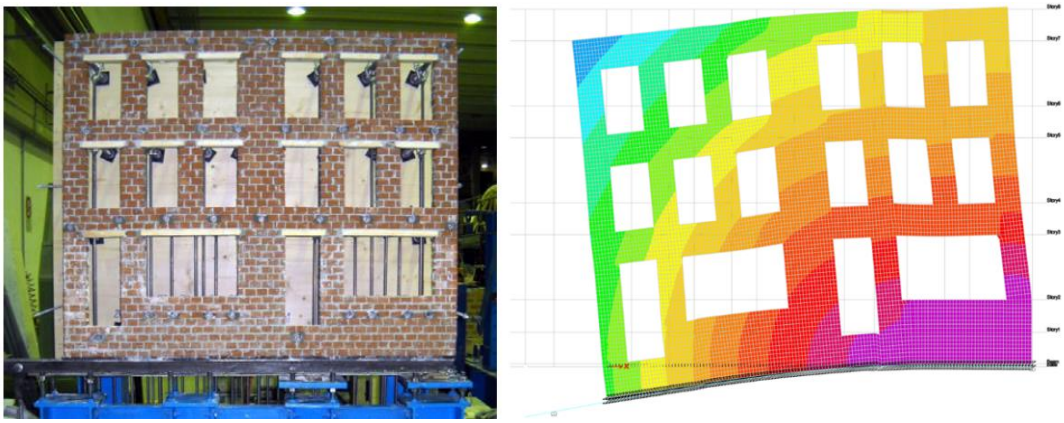
Figure 7 : Tensile strain contour and crack pattern in experimental tests, specimen W4

Table 1 : mean mechanical properties of tested masonry in Manzouri tests [6]

Masonry Compressive Strength (MPa)	Mortar compressive strength (MPa)	Brick compressive strength (MPa)	Brick Modulus of Rupture (MPa)	Brick Tensile Strength (MPa)	Initial Shear strength (MPa)	Friction angle
#W3 18 #W4 11.7	2.6	21.6	3.9	2.6	0.05	50

3.2 Foundation Settlement Test

The effect of soil settlement due to tunnelling excavation on a masonry façade was investigated using experimental tests and numerical modelling performed in [28], [29]. A scaled 1/10 model of a historic Dutch house, as shown in Figure 8(a), was tested under imposed support settlement. The deflections and crack patterns were captured during the test.



(a) (b)

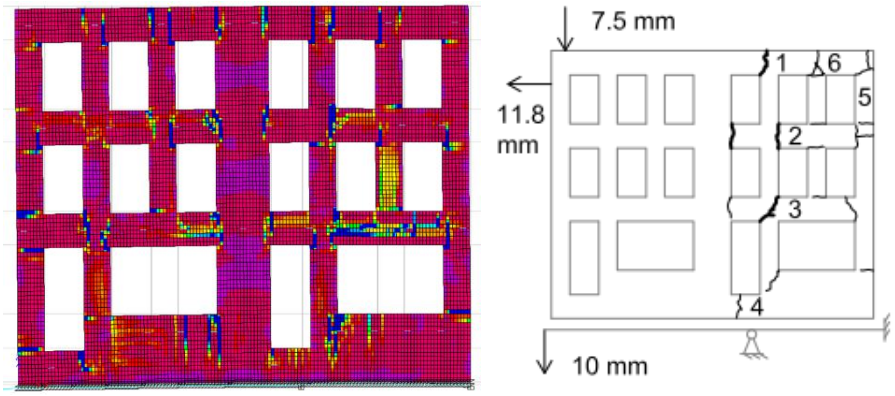
Figure 8 : (a) Scaled specimen test setup and (b) FE model in deformed shape

The mean material properties are listed in

. The deformed shape is demonstrated in Figure 8(b). The contour plot for the maximum principal strain is provided in Figure 9(a), which shows a reasonably good correlation with the crack pattern from the test as shown in Figure 9(b). The model was able to reasonably predict the initiation and propagation of probable cracks as well as different failure modes in the piers and spandrels over the course of testing.

Table 2 : mean mechanical properties of masonry in the settlement test

Compressive Strength (MPa)	Mortar flexural strength (MPa)	Mortar compression strength (MPa)	Brick compressive strength (MPa)	Initial Shear strength (MPa)	Friction angle
11.4	0.31	0.62	14	0.03	37



(a) (b)

Figure 9 : (a) maximum principal tensile strain from FE analysis and (b) crack pattern observed in the test

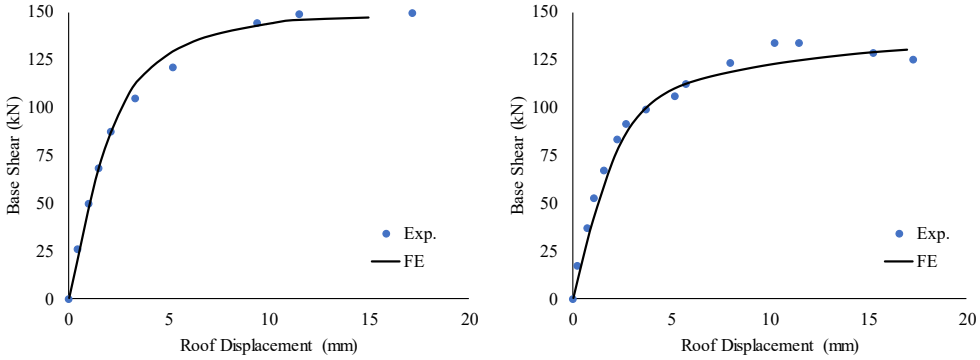
3.3 Full-Scaled Building Tests

Magenes *et. al.* [30] conducted a full-scale test on a two-storey URM building. The building was tested under quasi-static applied displacement. The overburden loads of 240 kN were applied on the floors. The mean mechanical properties of the masonry are listed in Table 3.

Table 3 : Mechanical properties of tested masonry in Magenes' test [30]

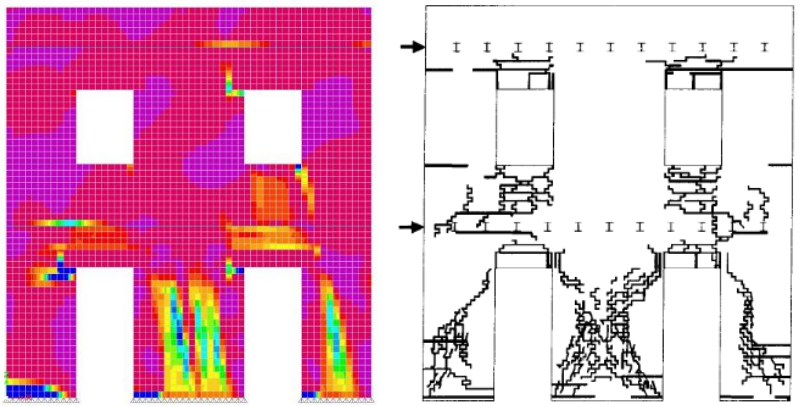
Density (kg/m^3)	Elastic Modulus (MPa)	Compressive strength (MPa)	Tensile Strength (MPa)	Initial Shear strength (MPa)	Coefficient of friction
1652	1491	6.2	0.04	0.23	0.58

As shown in Figure 10, the inelastic capacity curve from FE analysis in terms of base shear vs. roof displacement is compared with the experimental results, which indicates good agreement. The envelope of the cyclic response is used for the sake of comparison. As an indicative example, the crack patterns at the peak base shear load level are shown in Figure 11 for the case with door walls. The numerical simulations were able to roughly indicate different failure mechanics observed during the course of testing for both cases including e.g. bed joint sliding, toe crushing and shear failure of piers and spandrels.



(a) (b)

Figure 10 : Base shear versus roof displacement of (a) door wall and (b) window wall



(a) (b)

Figure 11: Peak load state of door wall: (a) maximum principal tensile strain at from FE analysis and (b) crack pattern observed in the test

4 CONCLUSIONS

In this paper, a simplified method has been proposed for the finite element modelling of unreinforced masonry buildings based on a smeared continuum approach. It was established upon the framework of fibred shell elements with inelastic directional layers, and it was successfully implemented in ETABS software for nonlinear static (Pushover) analysis of buildings; however, it can be potentially applied to any commercial structural analysis software supporting the proposed framework. This method facilitates the modelling process of masonry buildings with complex geometries by using conventional shell elements with some rational yet simple material properties. It can eliminate some of the limitations and difficulties of the commonly used microelement (lumped plasticity) approaches, e.g. presumptive analysis, priori wall discretisation, and complicated modelling for irregular wall stacks and openings, while not significantly affecting the overall computational cost. The proposed approach serves as a practical solution and an easily accessible tool for the structural engineers worldwide to analyse full-scale structures, such as heritage buildings, and assess their structural performance under ultimate loading scenarios including earthquake. The accuracy of the FE model predictions has been verified against several experimental results and showed to be in good correlation. In summary, the proposed model not only can capture the overall structural response in terms of e.g. lateral load-displacement curve, but it can reasonably identify different failure modes in piers and spandrels and their associated cracking pattern as specified in some of the international standards and seismic provisions, e.g. ASCE and NZSEE.

5 REFERENCES

[1] A. M. D'Altri *et al.*, "Modeling Strategies for the Computational Analysis of Unreinforced Masonry Structures: Review and Classification," *Arch. Comput. Methods Eng.*, vol. 27, no. 4, pp. 1153–1185, Sep. 2020.

[2] A. PAGE, "THE BIAXIAL COMPRESSIVE STRENGTH OF BRICK MASONRY.," *Proc. Inst. Civ. Eng.*, vol. 71, no. 3, pp. 893–906, Sep. 1981.

[3] K. Beyer, "Peak and residual strengths of brick masonry spandrels," *Eng. Struct.*, vol. 41, pp. 533–547, 2012.

[4] J. van Elk and D. Doornhof, "Material Characterisation Version 1.3 Report," 2016.

[5] J. A. Thamboo, "Material characterisation of thin layer mortared clay masonry," *Constr. Build. Mater.*, vol. 230, p. 116932, 2020.

[6] T. Manzouri, M. P. Schuller, P. B. Shing, and B. Amadei, "Repair and retrofit of unreinforced masonry structures," *Earthquake Spectra*, vol. 12, no. 4. pp. 903–922, 1996.

[7] L. S. Hogan, I. Giongo, K. Q. Walsh, J. M. Ingham, and D. Dizhur, "Full-scale Experimental Pushover Testing of an Existing URM Building," *Structures*, vol. 15, no. March, pp. 66–81, 2018.

[8] M. Tondelli, M. Rota, A. Penna, and G. Magenes, "Evaluation of Uncertainties in the Seismic Assessment of Existing Masonry Buildings," *J. Earthq. Eng.*, vol. 16, no. sup1, pp. 36–64, Jan. 2012.

[9] A. M. D'Altri, F. Messali, J. Rots, G. Castellazzi, and S. de Miranda, "A damaging block-based model for the analysis of the cyclic behaviour of full-scale masonry structures," *Eng. Fract. Mech.*, vol. 209, pp. 423–448, Mar. 2019.

[10] E. Minga, L. Macorini, and B. A. Izzuddin, "A 3D mesoscale damage-plasticity approach for masonry structures under cyclic loading," *Meccanica*, vol. 53, no. 7, pp. 1591–1611,

May 2018.
[11] G. Maier and A. Nappi, “A theory of no-tension discretized structural systems,” *Eng. Struct.*, vol. 12, no. 4, pp. 227–234, Oct. 1990.
[12] D. Briccola, M. Bruggi, and A. Taliercio, “Analysis of 3D no-tension masonry-like walls,” *J. Mech. Mater. Struct.*, vol. 13, no. 5, pp. 631–646, Dec. 2018.
[13] H. R. Lotfi and P. B. Shing, “An appraisal of smeared crack models for masonry shear wall analysis,” *Comput. Struct.*, vol. 41, no. 3, pp. 413–425, Jan. 1991.
[14] J. Toti, V. Gattulli, and E. Sacco, “Nonlocal damage propagation in the dynamics of masonry elements,” *Comput. Struct.*, vol. 152, pp. 215–227, May 2015.
[15] P. B. Lourenço, *Computational strategies for masonry structures*, vol. 70, no. 08. 1996.
[16] T. Salonikios, C. Karakostas, V. Lekidis, and A. Anthoine, “Comparative inelastic pushover analysis of masonry frames,” *Eng. Struct.*, vol. 25, no. 12, pp. 1515–1523, 2003.
[17] R. Siano *et al.*, “Numerical investigation of non-linear equivalent-frame models for regular masonry walls,” *Eng. Struct.*, vol. 173, no. June, pp. 512–529, 2018.
[18] CSI, “ETABS Analysis and Design of Building Systems.” Computers and Structures Inc, Berkeley, California.
[19] CSI, “SAP2000 Integrated Software for Structural Analysis and Design.” Computers and Structures Inc, Berkeley, California.
[20] J. Heyman, “The stone skeleton,” *Int. J. Solids Struct.*, vol. 2, no. 2, pp. 249–279, Apr. 1966.
[21] K. Doherty, M. C. Griffith, N. Lam, and J. Wilson, “Displacement-based seismic analysis for out-of-plane bending of unreinforced masonry walls,” *Earthq. Eng. Struct. Dyn.*, vol. 31, no. 4, pp. 833–850, 2002.
[22] Federal Emergency Management Agency, “FEMA 440 Improvement of Nonlinear Static Seismic Analysis Procedures,” Redwood City, CA, 2005.
[23] ASCE, *Seismic Evaluation and Retrofit of Existing Buildings ASCE/SEI 41-17*. 2017.
[24] NZSEE, *The Seismic Assessment of Existing Buildings - Initial Seismic Assessment Part B*. 2017.
[25] D. J. Sutcliffe, H. S. Yu, and A. W. Page, “Lower bound limit analysis of unreinforced masonry shear walls,” *Comput. Struct.*, vol. 79, no. 14, pp. 1295–1312, Jun. 2001.
[26] K. Chaimoon and M. M. Attard, “Modeling of unreinforced masonry walls under shear and compression,” *Eng. Struct.*, vol. 29, no. 9, pp. 2056–2068, Sep. 2007.
[27] European Committee for Standardization, “Eurocode 6: Design of masonry structures - Part 1-1: General rules for reinforced and unreinforced masonry structures.” 2005.
[28] G. Giardina, A. Marini, M. A. N. Hendriks, J. G. Rots, F. Rizzardini, and E. Giuriani, “Experimental analysis of a masonry façade subject to tunnelling-induced settlement,” *Eng. Struct.*, vol. 45, pp. 421–434, 2012.
[29] G. Giardina, A. V. van de Graaf, M. A. N. Hendriks, J. G. Rots, and A. Marini, “Numerical analysis of a masonry façade subject to tunnelling-induced settlements,” *Eng. Struct.*, vol. 54, pp. 234–247, 2013.
[30] G. Magenes, G. M. Calvi, and G. R. Kingsley, “Seismic testing of a full-scale, two-storey masonry building: Test procedure and measured experimental response,” *Exp. Numer. Investig. a brick Mason. Build. - Numer. Predict. Exp. Rep. 3.0 - G.N.D.T.*, no. January, pp. 1.1-1.41, 1995.

ADAPTIVE PUSHOVER ANALYSES OF A HERITAGE STRUCTURE: APPLICATION TO A MULTI-TIERED PAGODA TEMPLE

YOHEI. ENDO [1*], YU. KONDO [1], GAKU. IWANAMI [1]

[1]Shinshu University, 4-17-1, Wakasato, Nagano City 380-8553, Japan
e-mail: endii@shinshu-u.ac.jp

Keywords: Adaptive pushover analysis, Historical Structure, Masonry, Multi-tier pagoda, Seismic assessment

Abstract. *The present paper discusses seismic behaviour of multi-tier pagoda temple. The seismic behaviour was examined by different pushover analysis techniques including adaptive pushover analysis. The case study objective is a five-tier pagoda. The studied pagoda is built of timber frameworks and masonry walls. Masonry is composed of burnt solid bricks and earthen mortar. The pushover analyses are conducted, taking into account frictional behaviour between timber and masonry.*
The research challenges two tasks. A first task deals with experiments on interface behaviour between timber and masonry in earthen mortar. The study of the discussed interface behaviour is not straightforward since few tests have been conducted on similar subjects. In the present study, direct shear tests are performed. A second task coves pushover analyses of the five-tier pagoda by means of FE analysis. The paper provides useful experimental data of interface behaviour between timber and masonry in earthen mortar and also suggests efficient strategies of seismic assessment of pagoda-type structures.

1 INTRODUCTION

The paper presents nonlinear static analysis adopted to a multi-tier pagoda structure. Seismic behaviour of historical slender structures has been examined by researchers and practitioners. Among various seismic assessment tools, pushover analyses have been one of frequently used approaches [1]. Initial lateral force distribution patterns significantly influence the results such as maximum responses and damage mechanisms [2]. Recently advanced pushover analyses, including adaptive pushover analysis (APA) and multi-mode pushover analyses, were aimed to be adopted [3,4]. It has been found effective in some cases and however still the analyses encounter issues [5]. Further investigations are essential to apply APA more reliably.

The case study objective is a five-tier pagoda, Kumbeshwar temple in Nepal. The structure was seriously damaged by the 2015 Gorkha earthquake. The studied pagoda structure is composed of masonry walls and timber frameworks. The masonry is composed of solid bricks and earthen mortar. Sal timber is used for frameworks. Timber frameworks are considered to improve the box behaviour. On the other hand, limited experimental investigations have been conducted on interaction between timber elements and masonry walls [6,7]. The present research consists of two phases: experimental and numerical phase. The experimental phase examines interface behaviour between timber and masonry in earthen mortar by direct shear tests. The mechanical characterisation of the timber and masonry materials is conducted in advance of the direct shear tests. As for the numerical phase, taking into account the experimental results, different pushover analyses techniques are conducted on a pagoda structure. A particular attention is given on adaptive pushover analyses. The obtained results are compared with the damage patterns and collapse

mechanisms observed in the real structure. The experiments suggest friction angle and cohesion of interface between timber and masonry in earthen mortar. The paper also aims to contribute to efficient and realistic approaches to the seismic assessment of historical slender structures including multi-tier pagoda type structures.

2 RESEARCH METHODOLOGIES

2.1 Application of different pushover analysis techniques

The present study compares three different seismic analysis methods. They are invariant-force pushover analysis (IPA), adaptive pushover analysis (APA), and nonlinear dynamic analysis (NDA). Comparison is made between IPA, APA and NDA in terms of horizontal base acceleration, displacement and damage patterns. As for IPA, two force distribution patterns were considered. One is proportional to the masses of the structure (m-IPA). The other is proportional to the shape of the fundamental mode of the structure (Φ-IPA). As for APA, the method proposed by Antoniou and Pinho [8] is considered. In the method, the loading pattern at each step is incremented to that of the previous step. The load vector P_t at a load step t is achieved by adding to the load vector of the previous step P_{t-1} (existing loads in equilibrium). The increment is calculated as the product between the current load factor increment λ_t, the current modal scaling vector $\overline{F_t}$ and the nominal load vector P_0, as presented in the equation (1).

$$P_t = P_{t-1} + \Delta\lambda_t \overline{F}_t P_0 \tag{1}$$

2.2 Description of the case study objective

Kumbeshwar temple is a five-tier pagoda. The original temple was built around in 1392 as a two tiered pagoda [9]. Three tiers were added over the two tiers in the 17th century. The dimensions of the ground tier are 7.93×7.59 m^2. The height of the walls of each tier is 7.80, 4.01, 3.38, 2.70, 2.31 m (ground, first, second, third, fourth, respectively). The total height of the pagoda is 23.11 m including the pinnacle (Figure 1a). The pagoda is built of masonry walls and timber frameworks. The masonry consists of solid bricks and earthen mortar. For the frameworks, sal timber is used.

Kumbeshwar temple was severely damaged during the 2015 Gorkha earthquake. The fourth tier was considerably damaged but still survived. The collapse of the fourth tier occurred during the aftershock on May 12, 2015 (Figure 1b,c). The upper three tiers (second, third, fourth) were under reconstruction since they were much more significantly damaged than the lower tiers (first, second). In-situ visual inspection observed that pegs did not exist or lost in connections between timber crossbeams and masonry walls. Description and drawings of the temple are found also in [10,11].

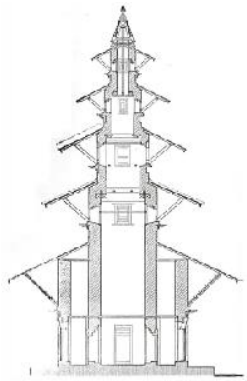
(a)  (b)  (c) 

Figure 1: Kumbeshwar temple: (a) cross section [9], state before the 2015 Gorkha earthquake (b), after the 2015 Gorkha earthquake (c).

3 EXPERIMENTAL STUDIES

3.1 Characterisation tests of masonry materials

Uniaxial compression tests were conducted on bricks in accordance with European standards [12]. The tested bricks were chosen since they had similar surface texture and close density as those used for the studied pagoda. The bulk density was 1,750 kg/m^3. The dimensions of the tested prisms were 40×40×80 mm^3. A 300-kN autograph testing machine was used for the loading [13]. The same testing machine was used for all the tests discussed in the paper. The average compressive strength was 17.8 MPa. The average shape factor of the prisms was 1.08 [12]. The coefficient of deviation (COV) was 17.6%.

Loam was used for the preparation of earthen mortar. Granulometric analysis was conducted on the loam by a hydrometer method according to the Japanese Geotechnical Society [14]. The grain size distribution curve is shown in Figure 2. The observed proportions (sand, silt, clay) were 26.2%, 52.2%, 21.6% by weight.

Mechanical behaviour of earthen mortar was tested. Flexural tests were conducted, taking into account the European standard [16]. Water content is a decisive factor for the strength of earthen mortar [17]. In the tested cases, the water content was set to measure 15.0 cm by a flow-table test. The dimensions of the prisms were 40×40×160 mm^3. The prisms were cured for 56 days. The volumetric shrinkage was 20.3%. Three-point bending tests were conducted. The average flexural strength was 1.35 MPa. COV was 15.20%. The maximum flexural strain was 1.22%. The flexural module at 1/3 of the peak strength was 0.18 GPa in average. Immediately after the bending tests, uniaxial compression tests were carried out on the same prisms. In total, 12 prisms were tested. The compressive strength was 3.82 MPa in average. COV was 13.82%.

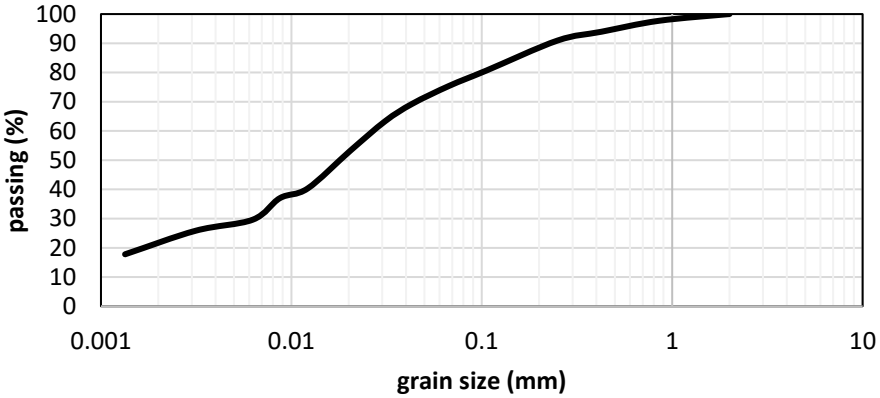


Figure 2: Grain size distribution curve.

3.2 Mechanical characterisation tests of sal timber

Mechanical behaviour of *sal* timber was conducted, referring to the Japanese standard [18]. Two types of tests were conducted as follows: uniaxial compression tests parallel and perpendicular to the grain and three-point bending tests. The uniaxial compression tests were performed on prisms of 30×30×60 mm^2. The three-point bending tests were carried out on prisms of 30×30×420 mm^3. The prisms were 836 kg/m^3 in bulk density.

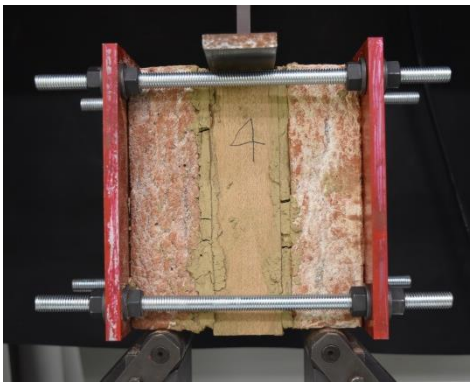
The average compressive strength of two types ($f_{c,0}$, $f_{c,90}$) were 55.1 MPa and 13.3 MPa. COV was 8.23% and 5.86%. The maximum strain was ($\varepsilon_{c,0}$, $\varepsilon_{c,90}$) 2.16% and 9.29%. The modulus of elasticity at 1/3 of the peak strength ($E_{c,0}$, $E_{c,90}$) were 58.9 MPa and 7.4 MPa. The average flexural strength was 125.6 MPa. COV was 5.4%. The maximum strain was 51.5% in average. The average flexural modulus at 1/3 of the peak strength was 11.6 GPa.

3.3 Direct shear tests

Direct shear tests were performed to examine frictional behaviour between *sal* timber and masonry in earthen mortar. The tests were conducted taking into account the European standard for direct shear tests of masonry [19]. The tests aimed to reproduce a possible situation of connections between timber crossbeams and masonry walls of multi-tier pagodas. Thus, it is considered possible that connections between cross beams and walls rely only on friction between two structural elements as discussed in Section 2.2.

The triplet specimens were prepared. The used bricks and *sal* timber were those tested as discussed in Section 3.1, 3.2. In the middle portion of the specimen, a timber block was placed (Figure 3a). The dimensions of the timber blocks were the same as the bricks. The dimensions of the bricks were 50×85×185 mm^3. The thickness of the joint was 10 mm. Three different conditions of pre-compressive stress were considered (0.2 MPa, 0.6 MPa, 1.0 MPa). Three specimens were tested in each condition of the pre-compressive stress. The stress was provided by the jig composed of two steel plates and four steel bolts (see, Figure 3a). One plate was placed at the top of the specimen while the other at the bottom. The steel plates were connected by the four bolts. The value of pre-compressive stress was confirmed by measuring the torque of the nuts. It is noted that the dilatancy of the specimen was considered negligible since the sliding of the timber block occurred at a very low value of the loading.

The average observed shear strength was 0.07, 0.2, 0.33 MPa respectively. All the tested specimens showed shear failure in the mortar bond area on the timber face (Figure 3b).

(a)  (b)

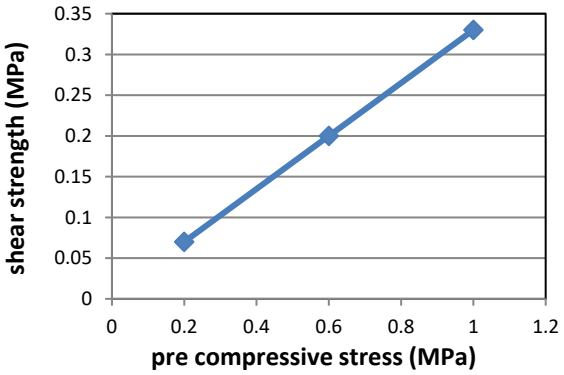


Figure 3: Initial shear strength test: (a) failure of a specimen and (b) normal and shear stress relation.

4 PUSHOVER ANALYSES

4.1 Material models

The considered material parameters for the present study are shown in Table 1. The parameters of the timber were determined, considering the Nepalese building code (NBC) [20] and characterisation tests discussed in Section 3.2. The parameters of the brick masonry were chosen in accordance with the previously conducted masonry material characterisation tests [21] and NBC [15]. Empirical equations were also taken into account [22,23]. To determine the material parameters, sensitivity analyses were carefully performed. Two types of masonry were considered, referring to the construction history and damage state discussed in Section 2.2. They are named type L and R in the present paper. The type L represents masonry of limited strength. The compressive strength is 1.6 MPa. The tensile strength is 5% of fc. The modulus of elasticity is 150 times fc. The type R represents masonry of reasonable strength. The compressive strength is 3.2 MPa. The tensile strength is 5% of fc. The modulus of elasticity is 250 times fc. The masonry walls of the upper three tiers (second, third, fourth) have the properties of type-L masonry. Those of the lower two tiers (ground, first) have the properties of type-R masonry.

As for the failure criteria, the von Mises plasticity model was adopted to the timber in compression and tension. The smeared crack model was adopted to the brick masonry. Drucker-Prager criterion was considered in compression while Rankin criterion in tension. A linear softening curve was considered in tension for uniaxial behaviour. The fracture energy was set as 25 N/m for the masonry type L (50 N/m for type R) in tension.

Interface behaviour was considered between the timber cross beams and masonry walls. The considered interface behaviour was determined in accordance with the tests discussed in Section 3.2. The Mohr Coulomb friction model was adopted. For the normal linear stiffness, 100 N/mm^3 was considered and 50 N/mm^3 for the shear linear stiffness. The considered friction angle was 18.9º ($\tan\phi$=0.33). The value of the tensile strength of the masonry was considered as the value of cohesion. Both geometrical and material nonlinearity were adopted.

Table 1: Adopted material parameters

	brick masonry (type A)	brick masonry (type B)	timber
Modulus of elasticity (GPa)	0.4	0.8	15
Tensile strength (MPa)	0.08	0.16	40
Compressive strength (MPa)	1.6	3.2	40
Poisson ratio (-)	0.2	0.2	0.3
Unit weight (kg/m^3)	1,800	1,800	900

4.2 Description of the FE models

The FE model was created in the software of TNO DIANA [24]. The model is composed of 29,563 nodes, 18,579 eight-node brick solid elements, 2,893 two-node beam elements, 253 four-node shell elements, 64 eight-node shell interface elements and 2,883 mass elements (Figure 4a). The solid elements were used for the masonry walls. The beam elements were for the timber columns and roof members. The shell elements are for timber cross beams. The mass elements were positioned on the beam elements representing the roof rafters as the dead weight of the ceramic tiles, mud and corrugated steel. The timber doors and window panels were not discretised in the model. As for the roof, the timber rafters, joists and beams were only discretised. Taking advantage of the symmetry of the structure, a half model is used. The cross sections of the model were translationally constrained in the Y direction and rotationally constrained around the X and Z direction. The model is fully constrained along the bottom of the structure.

The analyses were adopted to two models of different conditions. One has rigid connections between timber crossbeams and masonry walls of the ground- and first-tier. It is named the rigid connection model (RiC model). The other has frictional interface connections between timber crossbeams and masonry walls of the ground- and first-tier. It is named the frictional interface model (FI model).

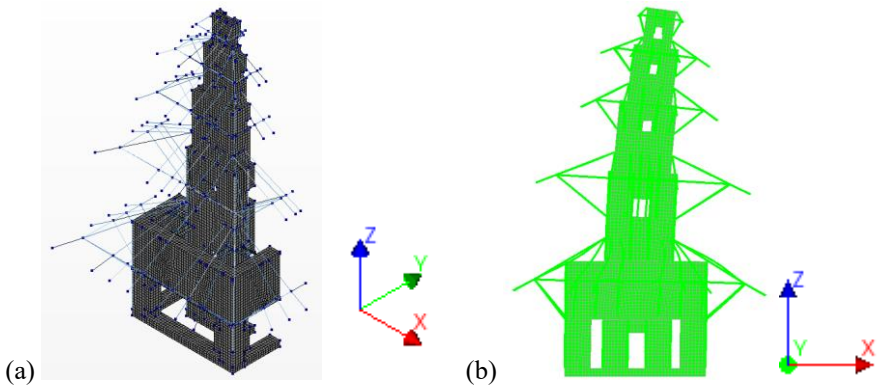


Figure 4: FE model of Kumbeshwar temple: (a) half model and (b) fundamental mode shape.

4.3 Application of invariant-force pushover analyses

Two types of IPA (m-IPA, Φ-IPA) were adopted to the half model of Kumbeshwar temple. Figure 3b shows the shape of the fundamental mode considered for the lateral force distribution patterns of Φ-IPA. As for m-IPA of RiC model, the maximum horizontal base acceleration was equal to 0.227g. The corresponding displacement was 4.19 mm, 14.05 mm, 33.9 mm at the top of the ground-, first- and fourth tier, in turn (Figure 5a-c). Damage of the ground tier indicated out-of-plane movement of the transversal walls and in-plane movement

of the longitudinal walls over the entrance opening (Figure 6a). Damage patterns in the first tier suggest out-of-plane movement of transversal walls. FI model showed lower values of horizontal base acceleration and displacement than RiC model. The observed maximum displacement values were 4.19 mm, 14.0 mm, 34.0 mm at the top of the ground-, first- and fourth tier. The maximum horizontal base acceleration was 0.228g. Both RiC and FI model showed similar damage patterns in the ground- and first-tier in spite of the difference of damage intensity. However, only RiC model presented damage in the third tier (Figure 6b).

As for Φ-IPA of RiC model, the maximum horizontal base acceleration was 0.093g. The observed maximum displacement values were 1.84 mm, 12.5 mm, 67.1 mm at the top of the ground-, first- and fourth tier. Figure 6c shows damage patterns along the corner of ground and first tier due to out-of-plane movement. In-plane damage was also seen in the second and third tier. Regarding FI model, the maximum horizontal base acceleration was 0.088g. The observed maximum displacement values were 1.57 mm, 11.3 mm, 45.6 mm at the top of the ground-, first- and fourth tier. FI model showed damage patterns similar to RiC model although FI model showed lower damage severity (Figure 6d).

Influences of interface behaviour are discussed by comparing the results between RiC and FI model. RiC model presented higher horizontal base acceleration and displacement than FI model by m-IPA and Φ-IPA. Nonetheless, RiC and FI model showed similar damage patterns although RiC model presented much severe damage than FI model.

The observed damage patterns were slightly different between m-IPA and Φ-IPA. As for FI model, Φ-IPA showed damage concentrated in the second tier in addition to the damage in the corner of the ground- and first-tier. On the other hand, m-IPA showed damage only in the corner of the ground- and first-tier. This damage contract would be derived from difference of lateral load distribution patterns. The lateral load patterns of Φ-IPA had more concentration in the upper portion of the structure than those of m-IPA. On the other hand, the ground tier presented close initial stiffness between m-IPA and Φ-IPA. This comes from that the lateral force distributions of m-IPA and Φ-IPA are similar in the ground tier.

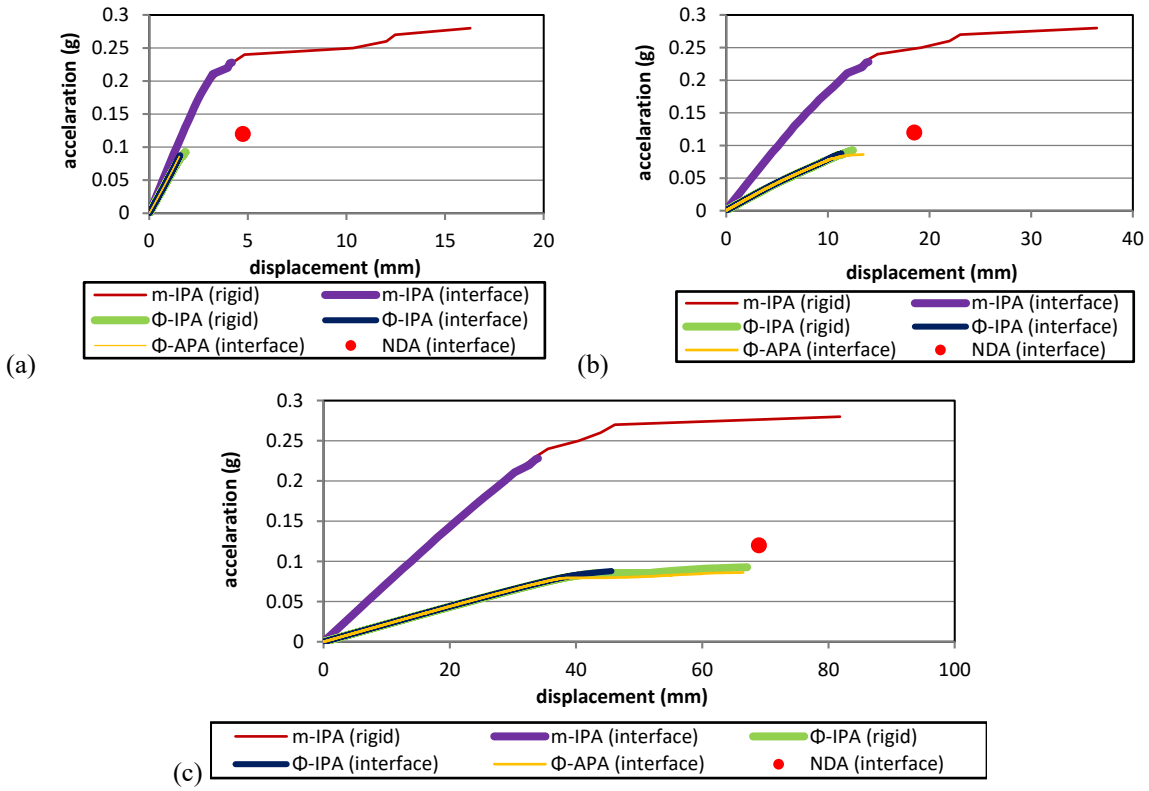


Figure 5: Seismic analyses of Kumbeshwar temple: displacement-horizontal base acceleration relations at the top of the ground tier (a), of the first tier (b), of the fourth tier (c)

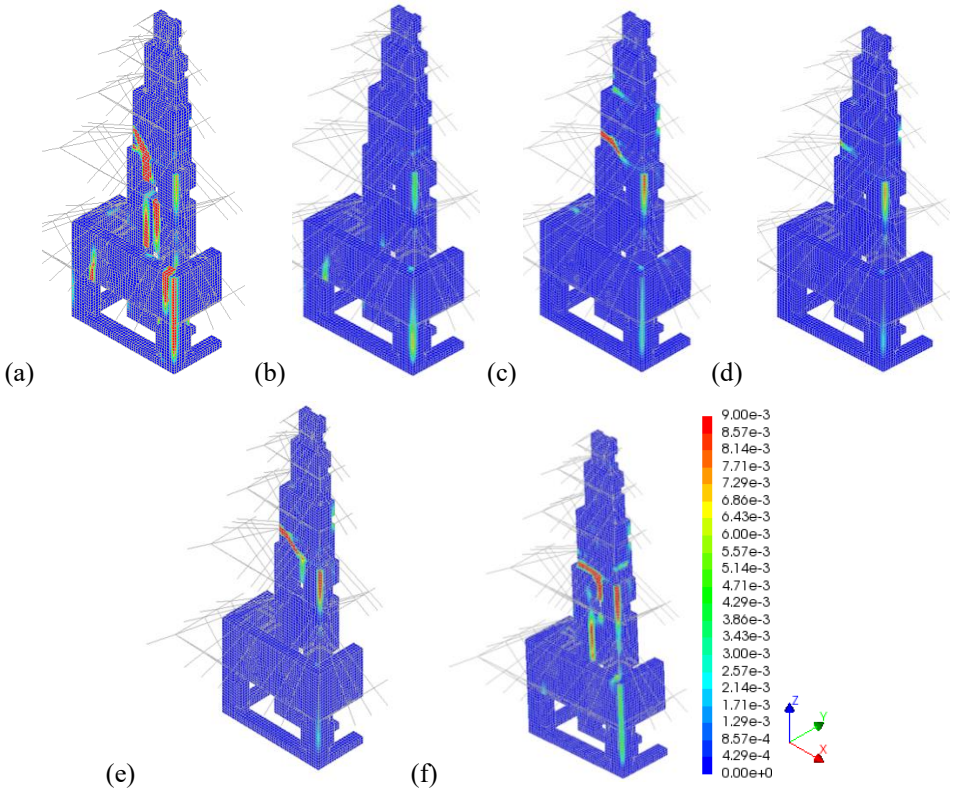


Figure 6: Tensile strain distributions close to the ultimate state: m-IPA of RiC model (a), of FI model (b), of Φ-IPA of RiC model (c), of FI model (d), APA of FI model (e) and NDA of FI model (f).

4.4 Application of adaptive pushover analysis

APA was applied to FI model. The initial lateral load patterns (P_0) were the shape of the fundamental mode of the structure (Figure 4b). The maximum horizontal base acceleration was 0.086g. The corresponding displacement values were 1.5 mm at the top of the ground tier, 13.5 mm at the top of the first tier and 66.5 mm at the top of the fourth tier (Figure 5a-c). The model showed vertical damage in the corner of the ground- and first-tier (Figure 6e). In-plane damage was also observed in the second tier.

APA presented horizontal base acceleration-displacement relations similar to Φ-IPA. However, the observed damage patterns were noticeably different (see Figure 6d,e). APA showed slightly lower initial stiffness than Φ-IPA from the beginning of the application of the lateral forces. It is due to damage caused by dead load. Since the model had limited strength as presented in Section3.1, certain damage already appeared during the application of gravity to the model. It ended in a slight change of the initial stiffness between Φ-IPA and APA.

NDA was adopted to FI model. NDA of Kumbeshwar temple was originally presented in a previously published conference paper [10]. In the present study, NDA was performed on the model presented in Section 4.1, 4.2. The maximum horizontal base acceleration was 0.120g. The observed maximum displacement values were 4.7 mm, 18.5 mm, 69.0 mm. APA and NDA showed vertical damage along the window opening in the first tier (see Figure 6e,f). However, the vertical damage was much extensive in NDA than APA. NDA showed horizontal damage around the base of the second tier. Instead, APA presented diagonal damage in the second tier. The difference of the damage in the second tier would come from loading directions. The loadings of APA were monotonic while those of NDA were dynamic.

5 CONCLUSIONS

Direct shear tests were conducted to examine friction angle and cohesion of interface between timber and masonry in earthen mortar. The tests presented reasonable friction angle for such interface and nearly zero cohesion as expected. The tests were performed, taking into account triplet test procedures for masonry materials. The specimens were composed of two bricks and a timber block in the middle. As further experimental activities, larger-scale specimens will be tested to examine interface behaviour more closely.

In the present study, pushover analyses were carried out on the models with and without frictional behaviour between timber cross beams and masonry walls. Adoption of fictional behaviour avoided overestimation of the capacity of the studied pagoda. However, the conducted pushover analyses implied interface behaviour had to be carefully included in models since the results were unignorably influenced by interface behaviour.

The studied pagoda showed damage due to in-plane and out-of-plane movement. Vulnerabilities to in-plane movement were derived from large openings while vulnerabilities to out-of-plane movement due to limited tensile strength. In the study, the load patterns of APA were the shape of the fundamental mode. APA provided results closer to NDA than IPA in terms of damage distribution patterns. However, it was found that the application of APA was a time-consuming process. Eigenvalue analysis had to be run and load distribution patterns were updated manually at each step accordingly. The initial lateral load patterns were found to be a predominant factor to the analysis results. For the further research of APA, different initial load patterns and updating methods will be studied. In addition for close observations of results between pushover analyses and NDA, the application of N2 method will be considered.

Acknowledgements. The authors would like to acknowledge the Maeda engineering foundation for providing us with the funds for the present research.

6 REFERENCES

[1] Pelà, L., Alessandra A. and Benedetti, A. "Seismic assessment of masonry arch bridges." *Engineering Structures* 31, no. 8 (2009): 1777-1788.
[2] Lagomarsino, S. and Cattari, S. "Seismic performance of historical masonry structures through pushover and nonlinear dynamic analyses." *In Perspectives on European earthquake engineering and seismology*. Springer, Cham (2015): 265-292.
[3] Facchini, L., Betti M., Corazzi, R. and Vladimir, C.K. "Nonlinear seismic behavior of historical masonry towers by means of different numerical models." *Procedia engineering* 199 (2017): 601-606.
[4] Ferraioli, M., Miccoil L., Donato, A.D. and Mandara, A. "Dynamic characterisation and seismic assessment of medieval masonry towers." *Natural Hazards* 86, no.2 (2017): 489-515.
[5] Endo, Y., Pelà, L. and Roca, P. "Review of different pushover analysis methods applied to masonry buildings and comparison with nonlinear dynamic analysis." *Journal of Earthquake Engineering* 21, no.8 (2017): 1234-1255.
[6] Moreira, S., Ramos, L.F., Oliveira, D.V., and Lourenço, P.B. "Experimental behavior of masonry wall-to-timber elements connections strengthened with injection anchors." *Engineering structures* 81 (2014): 98-109.
[7] Vieux-Champagne, F., Sieffert, Y., Grange, S., Polastri, A., Ceccotti, A. and Daudeville, L. "Experimental analysis of seismic resistance of timber- framed structures with stones and earth infill." *Engineering Structures* 69 (2014): 102-115.
[8] Antoniou, S. and Pinho, R. "Development and verification of a displacement-based adaptive pushover procedure." *Journal of earthquake engineering* 8, no. 05 (2004): 643-661.
[9] Shrestha, D.B. and Singh, C.E. "The History of Ancient and Medieval Nepal in a Nutshell" *With Some Comparative Traces of Foreign History*. Vol. 1. (1972).
[10] Center for Applied Research and Development (CARD) *Measured drawing of Kumbeshwar temple.* Institute of Engineering, Pulchowk Lalitpur (2009).
[11] Endo, Y. and Hanazato, T. "Seismic Behaviour of a Historic Five-Tiered Pagoda in Nepal." *In Structural Analysis of Historical Constructions*. Springer, Cham, (2019): 1337-1345.
[12] European Committee of Standardization (CEN), *EN772-1, Methods of Test for Masonry Units–Part 1: Determination of Compressive Strength,* CEN, Brussels, 2011.
[13] Shimadzu Corporation. "*Autograph AGS-X Series*" Shimadzu Corporation (2015).
[14] Japan geotechnical society (JGS) *Basics and guides to soil tests.* Japan geotechnical society: Tokyo, (2002), (Japanese).
[15] Department of Urban Development and Building Construction (DUDBC), *Nepal National Building code (NBC) 203:1994 Guidelines for Earthquake Resistant Building Construction: Low Strength Masonry,* Department of Urban Development and Building Construction, Kathmandu, (1994).
[16] CEN, *EN 1015-11. Methods of test for mortar for masonry–Part 11: Determination of flexural and compressive strength of hardened mortar.* European Committee for Standardization, Brussels. (1999).

[17] Avrami, E., Hubert, G. and Hardy, M. "Terra literature review." *An overview of research in earthen architecture conservation: Los Angeles, The Getty Conservation Institute* (2008).
[18] Japanese Industry Standard (JIS), *Z 2101, Method of test for woods,* Tokyo, (2009), (Japanese).
[19] CEN, *EN 1052-3, Methods of test for masonry-Part 3: Determination of initial shear strength.* Brussels. (2002).
[20] Department of Urban Development and Building Construction, *Nepal National Building code. NBC 112:1994 Timber.* Department of Urban Development and Building Construction, Kathmandu, (1994).
[21] Endo, Y., Yamaguchi, K., Hanazato, T. and Mishra, C. "Characterisation of mechanical behaviour of masonry composed of fired bricks and earthen mortar." *Engineering Failure Analysis* (2019): 104280.
[22] CEN, *Eurocode 6: Design of masonry structures–Part 1-1: General rules for reinforced and unreinforced masonry structures.* European Committee for Standardization, Brussels. (2005).
[23] Kaushik, H.B., Durgesh, C.R. and Sudhir, K.J. "Stress-strain characteristics of clay brick masonry under uniaxial compression." *Journal of materials in Civil Engineering* 19, no. 9 (2007): 728-739.
[24] TNO Diana, *Finite element analysis user's manual-release 10.2'*. (2017).

12th International Conference on Structural Analysis of Historical Constructions
SAHC 2020
P. Roca, L. Pelà and C. Molins (Eds.)

ADVANCED TOOLS FOR FAST MICRO-MODELLING OF MASONRY STRUCTURES

M. PETRACCA[1*], C. MARANO[2], G. CAMATA[2], E. SPACONE[2], AND L. PELÀ[3]

[1]ASDEA Software
Via Breviglieri, 8 - 65128 Pescara, Italy
e-mail: m.petracca@asdea.net, https://asdeasoft.net (*corresponding author)

[2] Università degli Studi G. d'Annunzio Chieti e Pescara
Department of Engineering and Geology (InGeo)
Viale Pindaro, 42 - 65127 Pescara, Italy
email: {corrado.marano, guido.camata}@unich.it

[3] Universitat Politècnica de Catalunya (UPC-BarcelonaTech)
Department of Civil and Environmental Engineering
Jordi Girona 1-3, 08034 Barcelona, Spain
e-mail: luca.pela@upc.edu

Keywords: Masonry, Micro-Modelling, Continuum Damage, IMPLEX

Abstract. *Among all the approaches commonly used to study masonry structures, micro-modelling is the most accurate. Masonry can be seen as a composite material made of bricks and mortar joints. Their different mechanical properties, their geometry and their arrangement inside the micro-structure, lead to very complex behaviours that are often difficult to represent using equivalent homogenous constitutive models commonly available in commercial and research FEM solvers. Micro-modelling can capture the complex non-linear behaviours of masonry by explicitly modelling the micro-structure inside the computational model. Micro-modelling leads to models with a large number of finite elements, thus increasing prohibitively the computational time. This is also due to the problem of solving complex nonlinear solutions involving damage and strain localization, leading to very small time-steps required to achieve convergence. Another issue with micro-modelling is the increased complexity in generating the finite element mesh with all the details of the micro-structure. This work presents some advanced tools that can decrease the high computational time required by micro-modelling. A 2-parameter tension-compression plastic-damage constitutive model is presented as an extension of an existing model previously formulated by some of the authors [1,2,3]. The model is implemented in the open-source FEM code OpenSEES [12] with the IMPL-EX method [5], a mixed implicit-explicit integration method that renders the response of this constitutive model step-wise linear, thus removing the convergence issues typically encountered when dealing with softening responses. This research also presents a tool implemented in the STKO (Scientific ToolKit for OpenSees) pre- and post-processor [4] able to automatically convert a homogeneous CAD geometry of a building into a micro-model.*

1 INTRODUCTION

From a structural point of view masonry can be regarded as a composite material made of bricks and mortar joints. Their constitutive response and their spatial arrangement inside the micro-structure, lead to very complex nonlinear behaviours characterized by different failure mechanisms. Many numerical approaches were proposed in the literature to simulate the structural response of complex masonry buildings, including homogenous continuum models [6], detailed micro-models [1,7], and computational homogenization multi-scale models [2,3,8]. Among all those approaches, micro-modelling is the one that delivers best accuracy. The main advantage of micro-modelling is its good capability of capturing all the complex failure mechanisms that can arise at the micro-structural scale, such as the damage-induced anisotropy, even when simple isotropic constitutive models are used to model the constitutive behaviour of the microscopic components. On the other side, however, micro-modelling has also some drawbacks that often limit its applicability to the simulation of real-life large-scale structure. When used to model large-scale structures, micro-modelling clearly leads to a very large number of finite elements, and consequently to very expensive analyses, both in terms of time and computational power. Furthermore, the presence of constitutive models exhibiting damage growth and strain localization poses the extra issue of poor convergence even when small time steps are used. Last but not least, there is the problem of preparing the geometric model of an entire structure with all the details of the micro-scale. All the aforementioned drawbacks can be however mitigated to a good extent using the right tools, such as parallel computing, special integration algorithms and advanced pre-processing and modelling tools. Section 2 describes briefly the proposed plastic-damage model as an extension to a continuum damage model previously proposed by the authors. Section 3 explains the main concepts and the implementation of the IMPL-EX integration algorithm in the original constitutive model. Section 4 briefly presents an extension tool implemented in the STKO pre- post-processor for OpenSEES that allows the end-user to automatically generate a detailed micro-model starting from a homogeneous surface model of the structure. Finally, Section 5 shows a numerical application to assess the effectiveness of the proposed tools.

2 TENSION-COMPRESSION PLASTIC-DAMAGE MODEL

This section briefly explains the formulation of the proposed tension-compression plastic-damage model, which is an extension to a tension-compression damage model previously formulated by the authors. For more details about the original damage model the user can refer to [1]. In the following, all variables without subscript refer to the current time-step, while those with the n and $n-1$ subscripts refer to the same variables at the two previous (known) time steps.

The d^+/d^- plastic-damage model, is based on the d^+/d^- pure damage model described in [1], with the addition of plasticity. Note however that the main aim of this work is to have a simple and robust constitutive model that accounts for plasticity just as an overall process involving irreversible deformations for a better description of the cyclic behaviour of masonry. For this reason, the typical ingredients of the classical theory of plasticity are not included in the present formulation. Instead, this model recasts the computation of plastic deformations in the same framework of classical continuum damage models.

The nominal stress tensor $\boldsymbol{\sigma}$ is defined as

$$\boldsymbol{\sigma} = (1 - d^{+})\bar{\boldsymbol{\sigma}}^{+} + (1 - d^{-})\bar{\boldsymbol{\sigma}}^{-} \tag{1}$$

where $\bar{\boldsymbol{\sigma}}^{+}$ and $\bar{\boldsymbol{\sigma}}^{-}$ are the positive and negative parts of the effective stress tensor, while d^{+} and d^{-} are the positive and negative cracking damage variables, that account for stress reduction and stiffness degradation from the effective stress space, due to opening of cracks. The effective stress tensor $\bar{\boldsymbol{\sigma}}$ is defined as

$$\bar{\boldsymbol{\sigma}} = \bar{\boldsymbol{\sigma}}^{+} + \bar{\boldsymbol{\sigma}}^{-} \tag{2}$$

$$\bar{\boldsymbol{\sigma}}^{+} = \left(1 - {d_{pl}}^{+}\right)\tilde{\boldsymbol{\sigma}}^{+}\ ;\ \bar{\boldsymbol{\sigma}}^{-} = \left(1 - {d_{pl}}^{-}\right)\tilde{\boldsymbol{\sigma}}^{-} \tag{3}$$

where $\tilde{\boldsymbol{\sigma}}^{+}$ and $\tilde{\boldsymbol{\sigma}}^{-}$ are the positive and negative parts of the trial effective stress tensor $\tilde{\boldsymbol{\sigma}}$, while ${d_{pl}}^{+}$ and ${d_{pl}}^{-}$ are the positive and negative plastic damage variables, that account for stress reduction of the trial effective stress due to plastic flow. The trial effective stress tensor $\tilde{\boldsymbol{\sigma}}$ is defined as

$$\tilde{\boldsymbol{\sigma}} = \bar{\boldsymbol{\sigma}}_{\boldsymbol{n}} + \boldsymbol{C}\colon(\boldsymbol{\varepsilon} - \boldsymbol{\varepsilon}_{\boldsymbol{n}}) \tag{4}$$

$$\tilde{\boldsymbol{\sigma}}^{+} = \sum_{i=1}^{3} \langle \tilde{\sigma}_i \rangle \boldsymbol{p}_i \otimes \boldsymbol{p}_i \tag{5}$$

$$\tilde{\boldsymbol{\sigma}}^{-} = \tilde{\boldsymbol{\sigma}} - \tilde{\boldsymbol{\sigma}}^{+} \tag{6}$$

where $\bar{\boldsymbol{\sigma}}_{\boldsymbol{n}}$ is the effective stress (i.e. only including plasticity) at the previous time step, $\boldsymbol{C}\colon(\boldsymbol{\varepsilon} - \boldsymbol{\varepsilon}_{\boldsymbol{n}})$ is the elastic (trial) stress increment, $\tilde{\sigma}_i$ is the i[th] eigenvalue of $\tilde{\boldsymbol{\sigma}}$, and $\boldsymbol{p}_i$ is its associated eigenvector.

The evolutions of plastic and cracking damage variables are linked together, that is if there is an evolution of the plastic damage, the cracking damage evolves accordingly. The positive and negative failure criteria, or damage surfaces, are similar to each other and are defined as

$$\tau^{-} = H(-\tilde{\sigma}_{min})\left[\frac{1}{1-\alpha}\left(\alpha\tilde{I}_1 + \sqrt{3\tilde{J}_2} + k_1\beta\langle\tilde{\sigma}_{max}\rangle\right)\right] + \frac{{\lambda_n}^{-}}{E} \tag{7}$$

$$\tau^{+} = H(\tilde{\sigma}_{max})\left[\frac{1}{1-\alpha}\left(\alpha\tilde{I}_1 + \sqrt{3\tilde{J}_2} + \beta\langle\tilde{\sigma}_{max}\rangle\right)\frac{f_t}{f_{cp}}\right] + \frac{{\lambda_n}^{+}}{E} \tag{8}$$

τ^{+} and τ^{-} are the so-called equivalent (scalar) positive and negative stresses. The reader can refer to [1] for a more detailed description of each variable that appear the two failure criteria. The Heaviside functions of the minimum and maximum eigenvalues is needed to activate the compressive surface only if at least one eigenvalue is negative, and, accordingly, the tensile surface only if at least one eigenvalue is positive. This is required to avoid tensile damage growth under purely compressive stress states and to avoid compressive damage growth under purely tensile stress states. In fact, even if the positive and negative damage variables affect only the associated positive and negative parts of the stress, their failure surfaces are function of the whole stress tensor.

The last terms in Equations 7 and 8 are functions of the Young's modulus E and the positive and negative equivalent plastic strains ${\lambda_n}^{+}$ and ${\lambda_n}^{-}$ known from the previous time step. These two last terms where not present in the original pure damage model in [1]. In fact, here, due to plasticity, τ^{+} and τ^{-} are function of $\tilde{\boldsymbol{\sigma}}$, which is not the total stress computed from the total

strain. The last two terms in Equations 7 and 8 are included to compute τ^+ and τ^- as if they were computed from the total strain. In this way it can be assured that, in loading conditions, τ^+ and τ^- are always larger than their values at the previous time step.
Figure 1 shows the shape of the two damage surfaces in the principal stress space. The compressive surface is represented for different values of the k_1 parameter.

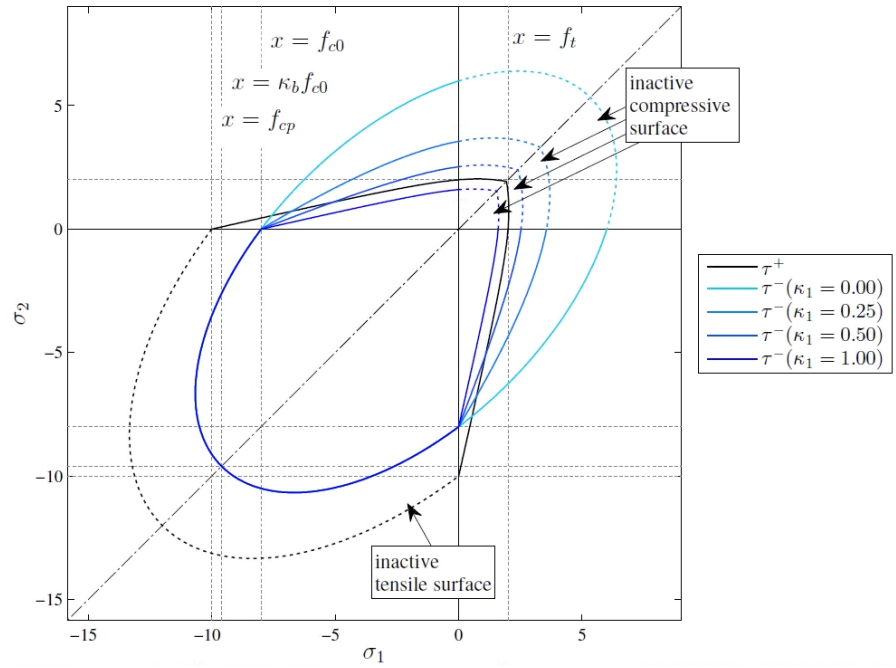


Figure 1: Damage surfaces in the principal stress space (2D plane stress case)

Being the damage and irreversible process, the model introduces the so-called damage thresholds r^+ and r^- , two scalar variables that denote the largest values ever reached by the equivalent stresses τ^+ and τ^- during the entire loading history for each time step t.

$$r^+(t) = \max\left(\underset{s \in [0,t]}{max}\, \tau^+(s)\,; f_t\right) \tag{9}$$

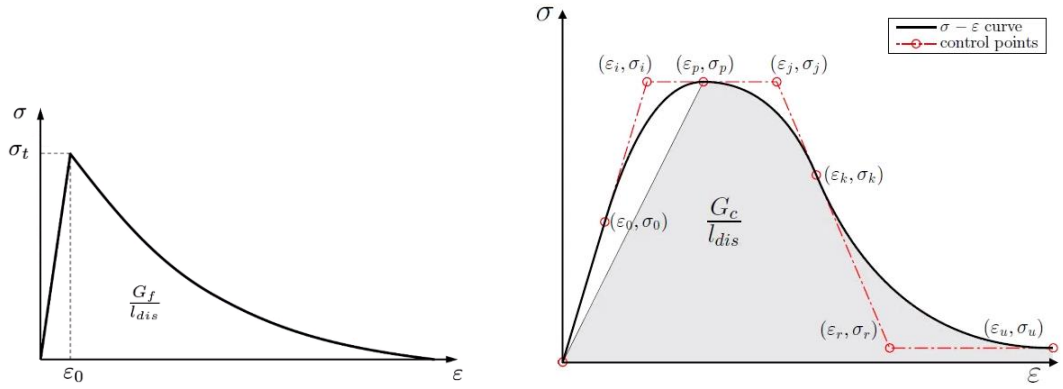
$$r^-(t) = \max\left(\underset{s \in [0,t]}{max}\, \tau^-(s)\,; f_{c0}\right) \tag{10}$$

At this point, in view of the last two terms added in Equations 7 and 8, r^+ and r^- are two scalar measures of the stress tensor as if they were computed from the total strain. In fact, we can compute their total-strain counterparts, and the associated nominal (including the effect of both plasticity and damage) hardening variables, as

$$\varepsilon_{tot}{}^{\mp} = \frac{r^{\mp}}{E} \tag{11}$$

$$q^{\mp} = H^{\mp}\left(\varepsilon_{tot}{}^{\mp}\right) \tag{12}$$

The hardening curves function of $\varepsilon_{tot}{}^{\mp}$ are reported in Figure 2. For a detailed description the reader can refer to [1].



(a) (b)

Figure 2: Tensile (a) and compressive (b) hardening functions

The positive and negative plastic damage variables can be computed as

$$d_{pl}{}^{\mp} = 1 - \frac{q_{pl}{}^{\mp}}{\tilde{r}^{\mp}} \tag{13}$$

$$\tilde{r}^{\mp} = E\left(\varepsilon_{tot}{}^{\mp} - \lambda_n{}^{\mp}\right) \tag{14}$$

$$q_{pl}{}^{\mp} = q^{\mp} + \left(1 - \omega^{\mp}\right)\left(r^{\mp} - q^{\mp}\right) \tag{15}$$

where $\tilde{r}^{\mp}$ are the positive and negative damage thresholds associated to the trial effective stress tensor $\tilde{\boldsymbol{\sigma}}$, $q_{pl}{}^{\mp}$ are the effective (plastic part only) hardening variables, and ω is a plastic-damage factor that can be used to modulate the amount of plasticity to be considered, and it ranges from 0 (pure damage) to 1 (pure plasticity). Once the plastic hardening variables are computed, the cracking damage can be evaluated as

$$d^{\mp} = 1 - \frac{q^{\mp}}{q_{pl}{}^{\mp}} \tag{16}$$

When both plastic and cracking damage variables are computed, the plastic effective stress tensor and the nominal (damaged) stress tensor can be calculated as per Equations (3) and (1) respectively, and the equivalent plastic strains can be updated as

$$\lambda^{\mp} = \varepsilon_{tot}{}^{\mp} - \frac{q_{pl}{}^{\mp}}{E} \tag{17}$$

3 IMPL-EX ALGORITHM

It is well known that nonlinear constitutive models exhibiting strain softening response lead to instabilities and the convergence of the iterative procedure may not be achieved at all. To improve the stability of this kind of analyses, the so called IMPL-EX algorithm originally formulated in [5] was implemented in the proposed tension-compression plastic-damage model. The IMPL-EX algorithm is a mixed implicit/explicit procedure to integrate the constitutive

response. The main idea is that the computation of the constitutive model is divided in two main stages:

- **Explicit integration**. During the iterative procedure the damage thresholds r^+ and r^- at time step t_{n+1} are extrapolated from the previous values at t_{n-1} and t_n which are known from previous time steps as

$$r_{n+1}^{\mp} = r_n^{\mp} + \frac{\Delta t_{n+1}}{\Delta t_n}\left(r_n^{\mp} - r_{n-1}^{\mp}\right) \tag{18}$$

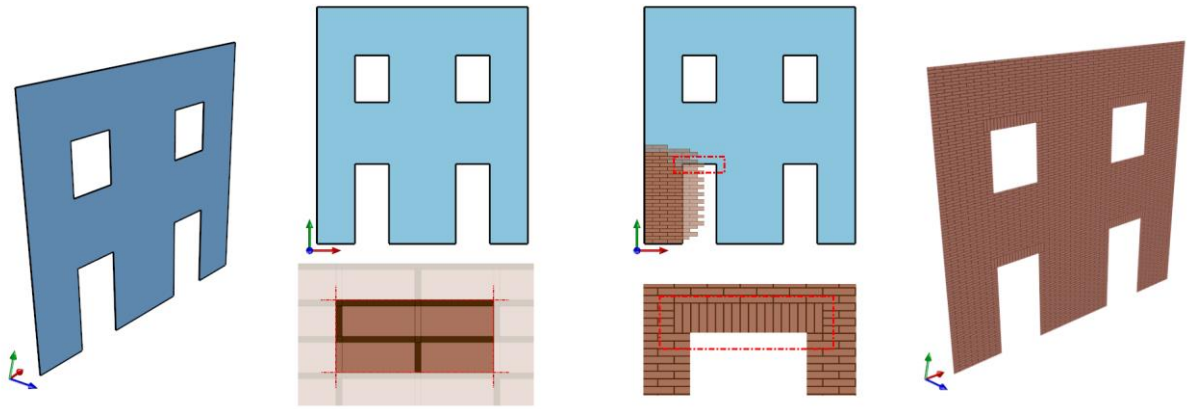
  In this way the solution depends only linearly on the current strain. However, there is another source of nonlinearity, that is the spectral decomposition used to compute the positive and negative parts of the trial effective stress tensor. To avoid this source of nonlinearity, the projection tensors $\boldsymbol{P}^+$ and $\boldsymbol{P}^-$ (as defined in [10]) used to compute the positive and negative parts of the trial stress tensor are those of the previous time step.
- **Implicit correction**. After the equilibrium is achieved the standard implicit evaluation of the internal variables is carried out. In this way this second step can be seen as an implicit correction to the previously described explicit extrapolation.

4 STKO USER INTERFACE AND AUTOMATIC MICRO-MODEL GENERATION

It is well known that one of the limitations of micro-modelling is the excessively high computational time, due to the large number of finite elements required to represent the micro-structure all over the structural model. However, the computational time required by the finite element solver is not the only issue. Preparing a CAD model and a FEM mesh for an entire real-life structure can be challenging. In fact, most of the examples in literature about micro-modelling of masonry, focus on simple shear-walls. This challenge can be overcome if a proper pre-processor is used. This section briefly describes a tool implemented in the STKO pre- post-processor for OpenSEES [4], that allows the analyst to convert a simple 2D or 3D model made of homogeneous surfaces of the walls, into a detailed micro-model.

The procedure, represented in Figure 3, can be summarized in the following steps:

- **User input**. The analyst draws all the surfaces, planar or curves, of the walls of the entire structure, taking care of including holes for the openings. Further, the analyst draws a sample (a repeating unit) of the micro-structure, already equipped with the constitutive models for all micro-structural components (bricks and mortar joints).
- **Reparameterization**. Each generic 3D surface of the structure can be arbitrarily oriented in the space, and does not need to be necessarily planar. Therefore, each surface will be automatically remapped to a 2D parametric space.
- **Fill**. Each surface in the 2D parametric space is filled with the repeating unit of the micro-structure.
- **Cut**. All the pieces of the micro-structure falling into the openings are cut and removed by means of Boolean operation
- **Details**. If necessary, extra details such as arches or lintels on top of the openings are added based on simple user-defined parameters.
- **Remapping**. Finally, each surface filled with the micro-structure is remapped to the 3D space and assembled with the other surfaces of the model.

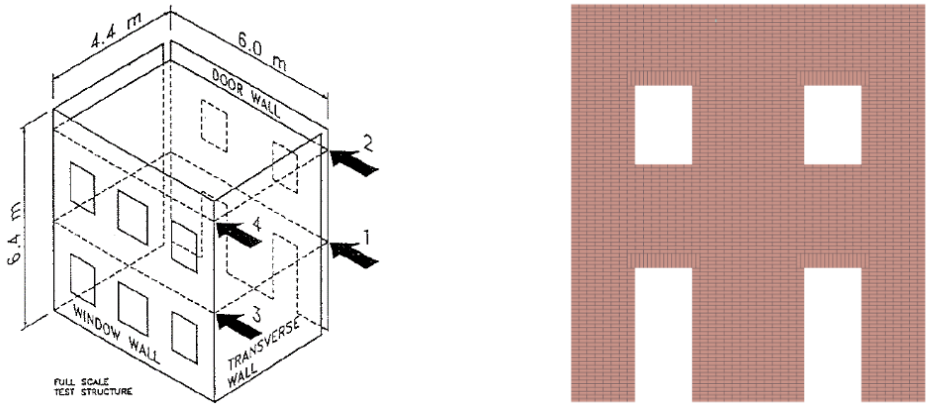


(a) (b) (c) (d)

Figure 3: (a) User input as a homogeneous surface; (b) Reparameterization and micro-sample; (c) Fill, Cut and Details; (d) Remapping to the 3D domain

5 NUMERICAL APPLICATION

In this section a numerical application of the proposed plastic-damage model is presented. A two-story masonry building tested at the university of Pavia, and described in detail in [11], is used and simulated numerically to assess the effectiveness of the proposed plastic-damage model. The numerical model was created in STKO pre- post-processor [4], which automatically produced the TCL input files for the OpenSEES MP parallel solver. The results were obtained from the MPCO Recorder implemented by some of the authors in OpenSEES [12], and visualized in the STKO post-processor. Figure 4 shows a scheme of the tested prototype. Equal loads are applied at the floor levels along the two lateral walls (Door Wall and Window Wall). Since the Door Wall is not connected to the rest of the structure, it was analyzed separately in a 2D model.



(a) (b)

Figure 4: (a) Scheme of the tested building, taken from [11], and (b) numerical micro-model of the Door Wall

Table 1 shows the plastic-damage material parameters used for bricks and mortar joints. Figure 5 shows the obtained load displacement-curve and Figure 6 shows the final crack pattern compared with the one obtained from the experimental test. The results are quite good in terms of maximum strength, crack pattern and cyclic hysteresis loop.

Table 1: Constitutive model parameters for bricks and mortar joints

PARAMETER	DESCRIPTION	UNIT	MORTAR	BRICK
E	Young's modulus	N/mm^2	400.0	2500.0
ν	Poisson's ratio	-	0.18	0.18
ft	Tensile strength	N/mm^2	0.15	1.6
Gt	Tensile fracture energy	N/mm	0.04	0.03
fcp	Compressive strength at peak	N/mm^2	5.0	26.0
εcp	Compressive deformation at peak	-	0.03	0.02
Gc	Compressive fracture energy	N/mm	80.0	20.0

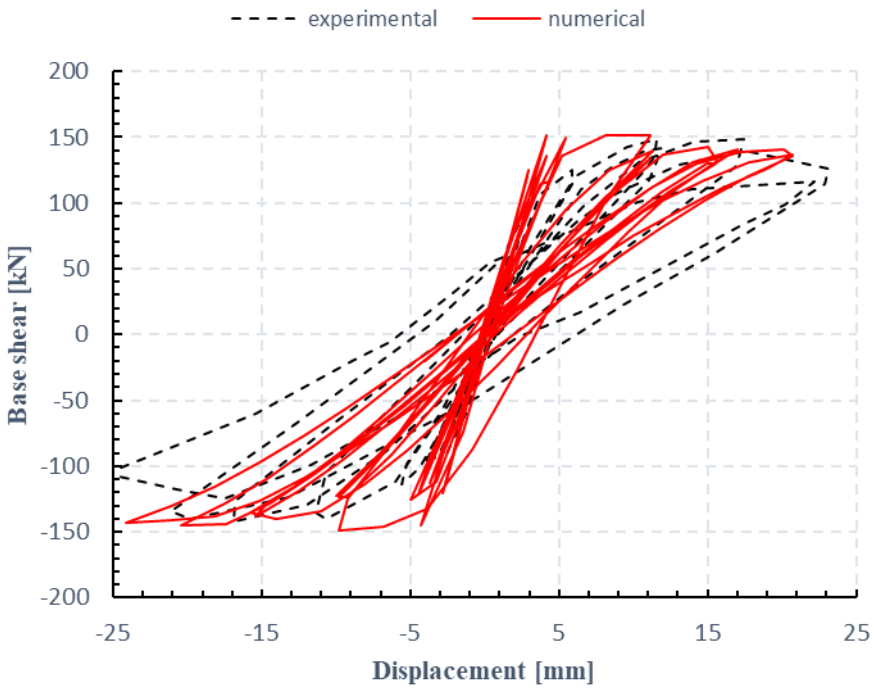


Figure 5: Load-displacement curve for the Door Wall

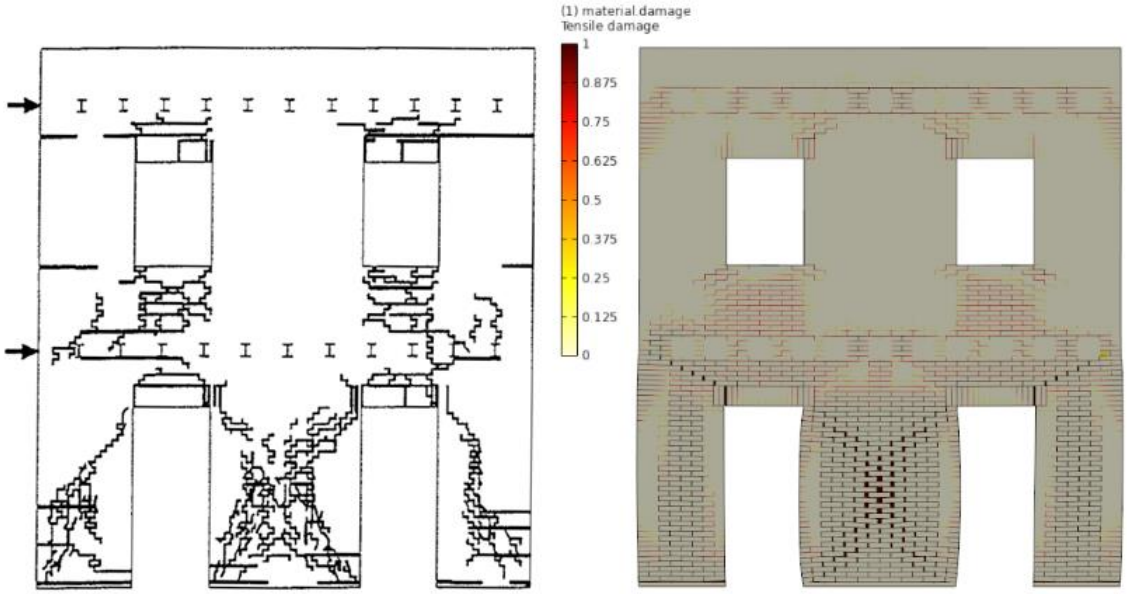


Figure 6: Comparison of the crack pattern at the end of the analysis

6 COMPUTATIONAL COSTS

The entire mesh consists of 16417 nodes (2 DOFs for each node) and 49087 quadrilateral fully-integrated plane-stress elements (4 gauss points for each element). The mesh was partitioned in 6 sub-domains and analyzed with OpenSEES MP. The model ran on an 8-cores Intel Core i7-7700K 4.20 GHz CPU. The analysis was subdivided in 4000 time-steps and ran in less than 25 minutes, thanks to the fact that the IMPL-EX algorithm produces a solution which is step-wise linear, that is, within each time step, the stress response does not depend on the trial strain.

7 CONCLUSIONS

- Micro-modelling is indeed an accurate approach for evaluating the complex nonlinear response of materials such as masonry with a very heterogenous micro-structure where each constituent exhibit highly nonlinear responses. The explicit modelling of the micro-structure captures very well the complex geometric interactions and failure mechanisms that arise at the micro-scale level.
- Unfortunately, the computational cost becomes excessively high, and can drastically increase when standard implicit algorithms are used to solve equilibrium due to the brittle nature of the masonry constituents.
- However, if the right tools are used, the aforementioned drawbacks can be satisfactorily mitigated. Parallel computing offers the first speed up, partitioning the entire domain in many smaller sub-domains that can be analyzed in parallel. The IMPL-EX algorithm removes the strong nonlinearity given by the plastic-damage model, thus improving the convergence, and consequently reducing the computation time. Finally, the burden of creating a complex CAD model such as the micro-model shown in this work, can be overcome using dedicated user interfaces such as STKO.

REFERENCES

[1] Petracca, M., Pelà L., Rossi R., Zaghi S., Camata G. and Spacone E. Micro-scale continuous and discrete numerical models for nonlinear analysis of masonry shear walls. *Construction and Building Materials* (2017), **149**:296-314.

[2] Petracca, M., Pelà L., Rossi R., Oller S., Camata G. and Spacone E. Regularization of first order computational homogenization for multiscale analysis of masonry structures. *Computational Mechanics* (2016) **57**:257-276.

[3] Petracca, M., Pelà L., Rossi R., Oller S., Camata G. and Spacone E. Multiscale computational first order homogenization of thick shells for the analysis of out-of-plane loaded masonry walls. *Computer Methods in Applied Mechanics and Engineering* (2017) **315**: 273-301.

[4] STKO Scientific ToolKit for OpenSees. *https://asdeasoft.net/stko/*

[5] Oliver, J., Huespe, A. E., and Cante, J. C. An implicit/explicit integration scheme to increase computability of non-linear material and contact/friction problems. *Computer Methods in Applied Mechanics and Engineering* (2008), **197**: 1865-1889.

[6] Pelà, L., Cervera, M., and Roca, P., Continuum damage model for orthotropic materials: Application to masonry, *Computer Methods in Applied Mechanics and Engineering* (2011), 917-930

[7] Lourenço, P. B., and Rots, J. G. Multisurface interface model for analysis of masonry structures. *Journal of engineering mechanics* (1997), **123**:660-668.

[8] De Bellis, M. L., and Addessi, D. A Cosserat based multi-scale model for masonry structures. *International Journal for Multiscale Computational Engineering* (2011), **9**: 543

[9] Cervera, M., Oliver, J., and Faria, R. Seismic evaluation of concrete dams via continuum damage models. *Earthquake engineering & structural dynamics* (1995), **24**:1225-1245.

[10] Wu, J. Y., Li, J., and Faria, R. An energy release rate-based plastic-damage model for concrete. *International Journal of Solids and Structures* (2006), **43**:583-612.

[11] Magenes, G., Calvi, G. M., and Kingsley, G. R. Seismic testing of a full-scale, two-story masonry building: Test procedure and measured experimental response. *Experimental and numerical investigation on a brick masonry building prototype - numerical prediction of the experiment, Rep. 3.0. Gruppo Nazionale La Difesa Dai Terremoti, University of Pavia, Pavia, Italy*.

[12] McKenna, F. OpenSees: a framework for earthquake engineering simulation. *Computing in Science & Engineering* (2011), **13**:58-66.

12th International Conference on Structural Analysis of Historical Constructions
SAHC 2020
P. Roca, L. Pelà and C. Molins (Eds.)

ANALYSIS AND ASSESSMENT OF SWEDISH VAULTED MASONRY STRUCTURES USING FUNICULAR METHODS

CARL THELIN[1*] AND FOLKE HÖST[2]

[1]Linnæus University and Tyréns AB
Linnæus University,
351 95 Växjö, Sweden
e-mail: carl.thelin@lnu.se
(*corresponding author)

[2] Tyréns AB
Tyréns AB, Scheelevägen 17
223 70 Lund, Sweden
e-mail: folke.host@tyrens.se

Keywords: Historic masonry structure, masonry vaults, thrust line analysis, funicular analysis, thrust network analysis

Abstract. *Practising structural engineers working with historic masonry structures need access to further developed methods to analyse and assess the structural behaviour of masonry vaults. The aim of this study is to evaluate methods to analyse vaulted masonry structures and to develop a methodology for the application of suitable methods to the work of practising structural engineers. A secondary aim is to use the methods studied to analyse and assess the structural behaviour of three Swedish church buildings of different types and with vaulted structures. The churches are Gökhem church, a small parish church built in the 12th century, and the Lund cathedral, also built in the 12th century; both originally in the Romanesque style but with later alterations. The third church is St Johannes church in Stockholm, built in the neogothic style in the late 19th century. The methods used are parametric graphic statics of thrust line analysis and Thrust Network Analysis (TNA), both based on funicular analysis. The results show the strength of using such methods to assess and evaluate the structural behaviour of historic vaulted masonry structures. They provide a pedagogical description of the structural behaviour of masonry vaults and the conditions that affect their load-carrying capacity. Another result is the implementation of a method to perform the analysis in a feasible and effective way. For the analysed church buildings, the results provide an understanding of their structural behaviour and clearly show how different variables affect the magnitude and impact of the thrusting force. Thrust Network Analysis has great potential to become a very effective method to perform advanced 3d analyses of masonry vaults but needs to be developed in order to enable "best fit solutions" to map the thrust network to the shape of the existing vaults. Such methods are under development.*

1 INTRODUCTION

In the work of practising structural engineers, with a focus on historic masonry buildings, the commissions often relate to structural problems, such as cracking, movement and weathering of materials, or to restoration and reconstruction. Frequently, there are arches and vaults in the buildings and questions concerning their structural behaviour and their impact on the surrounding structures are common. Structural engineers working with historic masonry structures need to have access to further developed methods to analyse and assess the structural behaviour of masonry vaults.

The work initiated by Heyman [1], to apply limit analysis to masonry load-bearing structures, in combination with the rapid development in recent decades of computer-based methods to analyse vaulted masonry structures, has provided a frame-work that entails new possibilities for engineers to assess such buildings.

The main aim of this study is to evaluate methods to analyse vaulted masonry structures. During the work it became evident that there was a need to develop a methodology for the application of suitable methods to the work of practising structural engineers. This became a supplementary aim. With further developed methods it is possible to make more efficient and safer assessments of historic masonry structures. The methods studied are based on funicular analyses, since they are considered suitable [1,2,3] for this field of work. The methods used are *Thrust Network Analysis* [3] and *thrust line analysis using parametric graphic statics* [4,5]. The methods are examined by using three Swedish church buildings with vaulted structures as case studies. A secondary aim is thus to use the studied methods to analyse and assess the structural behaviour of the objects in the case studies. Two types of research questions have driven the work; general research questions concerning the applicability of analysis methods and specific questions concerning the structural behaviour of the historic vaulted masonry structures in the case studies.

2 METHOD

Since the aim of the study is to investigate methods to analyse historic vaulted masonry structures in engineering practice, three masonry buildings have been used as cases to test and develop methods and ways of working. By using real structures with relevant structural problems that consultant engineers have encountered, it is possible to determine how applicable and adaptable the methods are, and their potential and the need to develop them further. In addition, the case studies provide knowledge of how historic masonry structures carry loads as well as other aspects of decisive importance for their structural behaviour. The objects chosen for the case studies represent three different types of historic masonry structures with vaults.

2.1 Capture geometry

In order to analyse the structural behaviour of vaulted masonry structures, a precise description of their geometry is crucial, regardless of the methods used to analyse them. To achieve accurate measures of the vaulted shapes, laser scanning and photo scanning were used [6,7], see Figure 1. The scans need to be carried out on both the intradoses and extradoses of the vaults, and it is also necessary to capture the dimensions of walls, pillars and other relevant geometric information. In many cases, insulation or other obstructing objects on the extradoses of the vaulted structures need to be removed or taken into account in some other way.

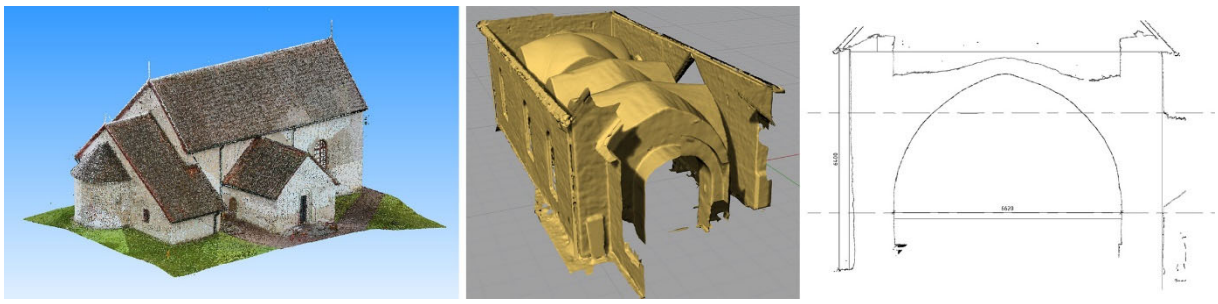


Figure 1: Left: laser-scanned point cloud of the Gökhem church; middle: meshed model of vaults and walls, and right: a section rendered by using the point cloud.

2.2 Thrust Network Analysis

Funicular force networks have been introduced [8] as an extension of the thrust line analysis to also include three-dimensional structures, and has been further developed into Thrust Network Analysis, TNA [3,9]. The Block Research Group at ETH Zürich has developed the RhinoVAULT software to carry out Thrust Network Analyses [10,11]. With RhinoVAULT, Thrust Network Analysis can be carried out within the graphic interface of Rhinoceros [12]. This is an advantage, as the 3d models of vaulted structures produced from the laser scans can be managed easily and effectively in Rhinoceros.

The approach developed for the Thrust Network Analysis in this study consists of nine steps:

1. **Capture the geometry**
   The geometry of the vaults is described by a point cloud generated by laser scanning. The point cloud is used both to create a meshed 3d model to compare with the shape of the thrust network, but also to calculate the loads and their distribution across the vaulted shape.
2. **Creating a meshed 3d model and exporting it to Rhinoceros**
   The point cloud is imported into the 3DReshaper [13] software, where it is processed and divided into different parts in different layers to facilitate the analysis; for example, walls, extradoses of vaults and intradoses of vaults. A meshed 3d model is created in 3DReshaper, exported and then imported into Rhinoceros.
3. **Calculation of loads**
   The main load usually consists of the weight of the vault, determined by its volume and density. In some cases, heavy filling at the haunches of the vaults can provide a considerable load. In cases where the extradoses of the vaults are more or less covered by insulation or some other material, the volume of the vaults has been calculated on the basis of the area of the intradoses and the thickness of the vaults. The thickness can usually be determined by using the point cloud in combinations with an investigation in situ.
4. **Choice of form diagrams for Thrust Network Analysis**
   The Thrust Network Analysis requires the creation of a form diagram. In this project, four different diagrams with different densities have been used. The shape of the vault should guide the choice of the form diagram and it is an advantage if the analyst has an understanding of how the load is carried by the vault.

5. **Determination of points for support**
   Before the height of the thrust network can be calculated, the placing of the support of the thrust network needs to be defined. These points represent locations where the vault is supported by walls or columns. In many cases, there are massive masonry walls and it is not at all obvious at what level and how far within the wall the vault is actually supported. Since the structure is statically indeterminate, it is not possible to know the exact location of the support and extreme possibilities therefore have to be studied to find possible solutions. In this study, a framework with five to seven possible vertical positions in combination with three horizontal positions in a defined grid has been used, see example in Figure 2.
6. **Creation of force and thrust networks in RhinoVAULT**
   The force and thrust networks are created by RhinoVAULT when the supports and form diagrams are given.
7. **Distribution of loads across the geometry of the vault**
   In the Thrust Network Analysis, the total load of the vault and other loads are first given. The load is evenly distributed over the discreet nodes of the thrust network by tributary areas [14] as default. If loads should be positioned in another way, which may be the case with vaults of varying thickness or filling at the haunches, the load must be manually moved to and from the nodes that should carry more or less load.
8. **Fitting of thrust networks relative to vault geometry**
   The lack of an automated "best fit" solution to map possible thrust networks on an existing geometry means that the shape of the network and its fitting to the shape of the vaults need to be carried out by manipulating the force diagram and by using a scale factor for the height of the thrust network. For the fitting of the network, a "target surface" could be used [15]. Such a target surface must also be created in order to achieve best fit solutions. In this study the networks have been fitted in relation to the complete geometry of the vaults and according to the support positions described above.
9. **Results of the Thrust Network Analysis**
   If it is possible to find a solution to the thrust network within the geometry of the vault, the conditions of Heyman [1] are fulfilled and the network presents one possible solution for the structural behaviour of the vault, see example in Figure 2.

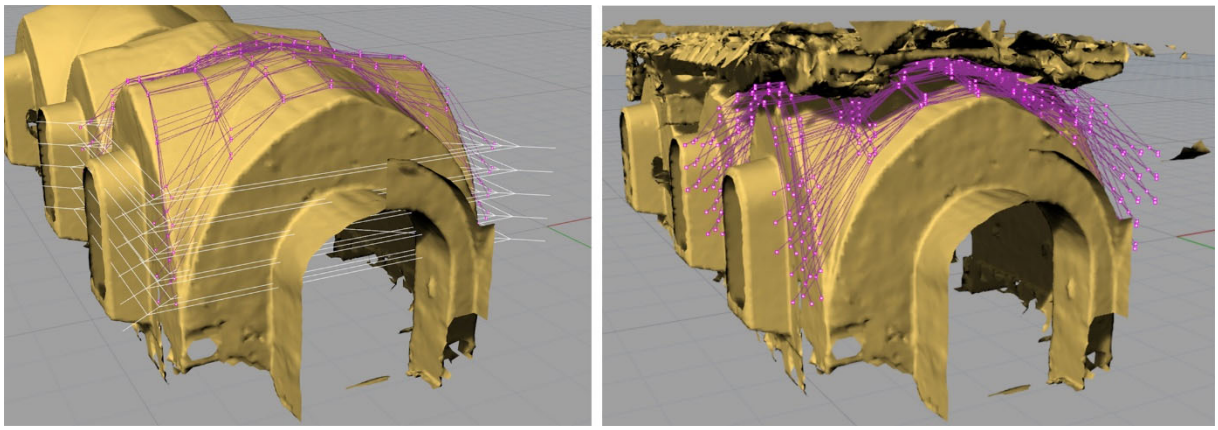


Figure 2: Left: grid for different support positions in the vertical and horizontal direction; right: Possible shapes and positions of thrust networks in a Thrust Network Analysis.

In the available version of RhinoVAULT it is not possible to use "best fit" or "closest fit" solutions for thrust networks on predefined geometries. There are several studies that describe strategies and algorithm to carry out such analyses [15,16,17,18]. Without solutions for best fit analyses the possibilities to fit the thrust networks to thin complex vault geometries are limited, and it is also more difficult to generate the most extreme shapes in the networks that yield minimum and maximum horizontal thrust, respectively. On the other hand, the need to fit the shape of the thrust networks manually by manipulating the force networks leads to an improved understanding of how the structural pattern of forces is controlled within a vaulted structure. In some cases, there have been difficulties in finding the shapes of the networks that converge into a solution that fits the structural shapes. The reason for this is unknown, except in cases where it is simply not possible to fit a thrust network within the geometry of the structure.

2.3 Thrust line analysis using parametric graphic statics

Thrust line analysis using parametric graphic statics has been used and developed previously by the authors [5,7], and has been further developed within this research project. The Geogebra [19] software was used to build the models, see example in Figure 3. The models were used to examine how the thrusting force from the vaults is carried by the building's walls and columns to the foundations by studying appropriate sections where the load from the vaults meets the surrounding structures. Parametric analysis of the vaults using the slicing technique [5] was also carried out in order to compare with the results from the Thrust Network Analysis.

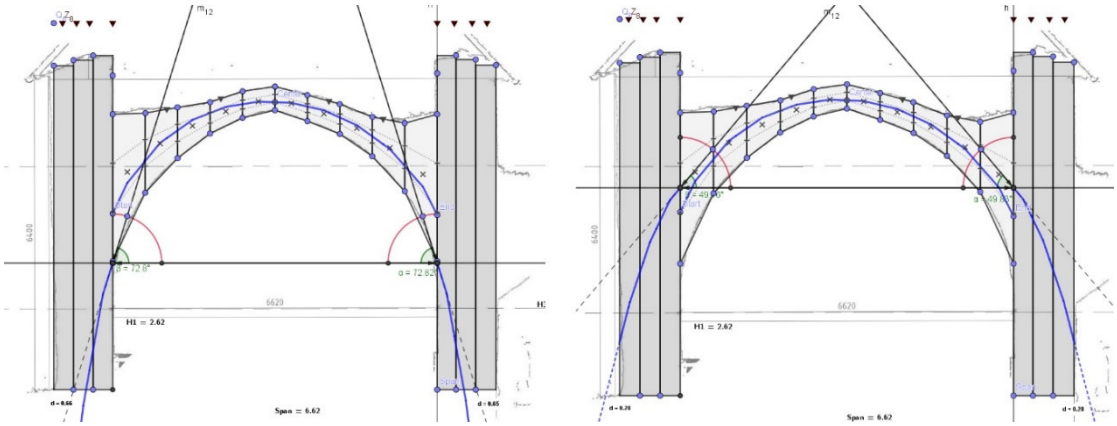


Figure 3: Examples of thrust line analysis using parametric graphic statics.

The approach developed for the parametric thrust line analysis in this study consists of five steps:

1. **Preparation of a section of the building for analysis**
   The section for study is produced from the laser-scanned point cloud using Revit [20] or corresponding software. The sections are dimensioned at strategic places for scaling in Geogebra. The sections can be produced from a drawing based on the point cloud or directly from the point cloud, see example in Figure 1.
2. **Definition of the load-carrying structures of the building**
   In the Geogebra models, the geometry of the different parts of the structure needs to be defined. The depth of the structure; for example, the dimensions of a pillar or the width of the part of a wall that contributes to the load-carrying structure, must be defined. Adjustments to represent different loads from walls with varying thickness or other loads, such as loads from a roof structure, may also be required.
3. **Determination of loads**
   In the model, loads are generated from the geometry by defining the density of the material. Loads from vaults are provided by their magnitude, direction and point of application. Loads from vaults are given by the Thrust Network Analysis or an analysis using the slicing method.
4. **Fitting of thrust line relative to the vault geometry**
   The location of the thrust line within the geometry is manipulated according to the objective of the analysis. Many times, it is desirable to try to fit the thrust line within the middle third of the structure to ensure its safety and minimise the risk of cracking.
5. **Comparisons between different load cases**
   The parametric thrust line analysis enables fast comparisons between different load cases and their impact on the structural behaviour of the building.

The combination of the results from the Thrust Network Analysis of the vaults (or pseudo-3d analysis using the slicing method) and the models for parametric thrust line analysis by appropriate sections gives a description of the complete flow of forces in the analysed buildings. The models provide an understanding of the structural behaviour, an assessment of the safety margins of the load-carrying structure and an understanding of how changes in the load or in the structure affect the structural behaviour.

3 CASE STUDIES

The case studies involved three objects: Gökhem church, Lund cathedral and St Johannes church in Stockholm, see Figure 4. The churches represent three different types of structures with masonry vaults and pose different questions concerning their structural behaviour.

Many questions regarding the structural behaviour of the case study objects was analysed in the study. Here, only a few examples of results are presented.

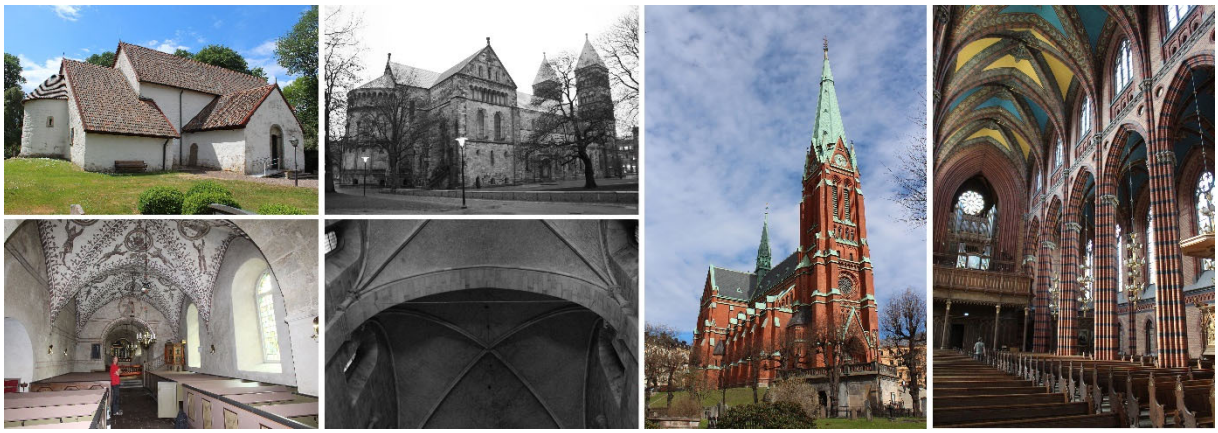


Figure 4: The case study objects: left: Gökhem church; middle: Lund cathedral, and right: St Johannes church.

3.1 Gökhem church

Gökhem is a small parish church built in the 12th century. The building consists of a nave, which was extended to the west already during medieval times, and a lower and narrower choir with an apse to the east. There is a sacristy and a porch at the north of the building. Originally, the building did not have vaults but an open roof structure. The vaults are of limestone and were built in the 15th century.

The building has been the main object for testing of the different methods and comparison of the results. One specific question was how different factors concerning the shape of the vault and its meeting with the supporting wall affect the structural behaviour, and another how different loading situations from the roof structure affect the structural behaviour.

2.3 Lund cathedral

Lund cathedral was first built in the 12th century. The church has three naves, with a transept, a choir and an apse in the Romanesque style. It has been rebuilt and restored several times. The main nave has a total of six rib vaults that were constructed after a fire in 1234. The side aisles have eight vaults each. Buttresses were added during the 16th century. They were later removed during the 19th century and tie rods were installed in the main nave. In the 19th century restoration, the vaults of the main nave were probably partially rebuilt and changed.

Two questions of interest concerning the Lund cathedral is whether the former buttresses with flying buttresses were necessary to support the thrusting forces of the vaults and, consequently, if the current tie rods are equally necessary.

2.4 St Johannes church

St Johannes church in Stockholm was built between 1884 and1890 in the neo-gothic style. It has three naves and a transept. The choir is located to the north and the tower and main entrance to the south. The church is constructed of brick masonry, with details such as tracery, mouldings and sculptures made of concrete. The church has been restored several times. In the restoration carried out in 1970-1974, the vaults were found to have severe cracks and extensive reinforcement of them was required. Measurements were made of the vault geometry and the cracks and a thrust line analysis was carried out. The results showed two types of damages to the vaults. Firstly, they lack the capacity to carry loads to the supports by the diagonal ribs; instead, the load is directly transferred to the adjacent arches. This has led to cracking along the bricks in the upper part of the vaults. This damage was not considered dangerous and was only repaired and not reinforced. Secondly, there was an imbalance between the lower parts of the vaults since the part of the vault adjacent to the walls was much steeper than the ones next to the crossing arches. This had led to severe cracking of the diagonal ribs and a risk of collapse. Reinforcements were introduced to counteract the imbalance of the structure.

One question of interest for St Johannes church is whether it is possible to validate the structural analysis and the described structural behaviour that were presented during the restoration in the early 1970s. Furthermore, questions concerning the importance of the flying buttresses were studied as well as the way in which the load is carried through the structure from the vaults by way of columns, walls and buttresses.

4 RESULTS

4.1 General results

A result of this study is the implementation of a method to carry out analyses of historic masonry vaults based on the funicular methods, Thrust Network Analysis and thrust line analysis using parametric graphic statics in a feasible and effective way for practising structural engineers.

For this study the Thrust Network Analysis has been carried out using the RhinoVAULT software. The main purpose of RhinoVAULT today is to perform form-finding for intuitive creation and exploration of compression-only structures. The program is not adapted to analyse existing structures such as historic masonry vaults. Still, it is possible to carry out analyses of many vaulted structures in the current configuration of the program and many vaults have a shape that make it possible to find several valid solutions within their geometry. The results can also provide information on the structural behaviour, even though it has not been possible to fit thrust networks completely within their geometry. For cases where thrust networks are successfully found within the geometry, it is known from Heyman [1] that the shape of the network represents one possible load path, and this indicate that the vault has a shape that can carry its load by compression only. The results of the Thrust Network Analysis made within this project have thus been the same or more conservative than those obtained by parametric thrust line analysis by means of the slicing method, which was unexpected.

In order to obtain results that are more precise, TNA solutions based on best fit algorithms need to be applied to get a better fit of the thrust networks to predefined geometries. These solutions are not implemented in RhinoVAULT today.

Still, TNA solutions by means of RhinoVAULTS with the methods and the way of working developed in this project make the analysis of the structural behaviour, thrusting forces and studies of how different conditions affect the results much faster than previously. Furthermore, the use of 3d models gives a better understanding of complex vaulted structures.

The models for parametric thrust line analysis make it possible to connect the result of the analysis of the vaults to an analysis of the behaviour of the complete building.

4.2 Case study: Gökhem church

For the Gökhem church structural type with thick vaults it is easy to find, thrust networks that fit within the geometry, and consequently, show possible structural behaviours with TNA, see Figure 5. The parametric thrust line analysis using the slicing method gave solutions with lower thrust than could be found with TNA. This is possibly due to not finding networks with a "deep" enough solution, which would probably have been facilitated by a best fit solution.

The analysis of the vaults of Gökhem church gives a range of valid results of thrust networks that fit within the geometry of the vault. To find possible solutions, the structural behaviour of the complete building needs to be considered to be able to disregard results that give thrusting forces of a magnitude and direction that cannot be supported by the walls.

The results show three factors that interact and are decisive to the magnitude of the horizontal thrusting force: the weight and shape of the vault, the angle of the thrusting force at the location where the vault meets the supporting structure, and the height of this location, which is the location of the structural springing of the vault.

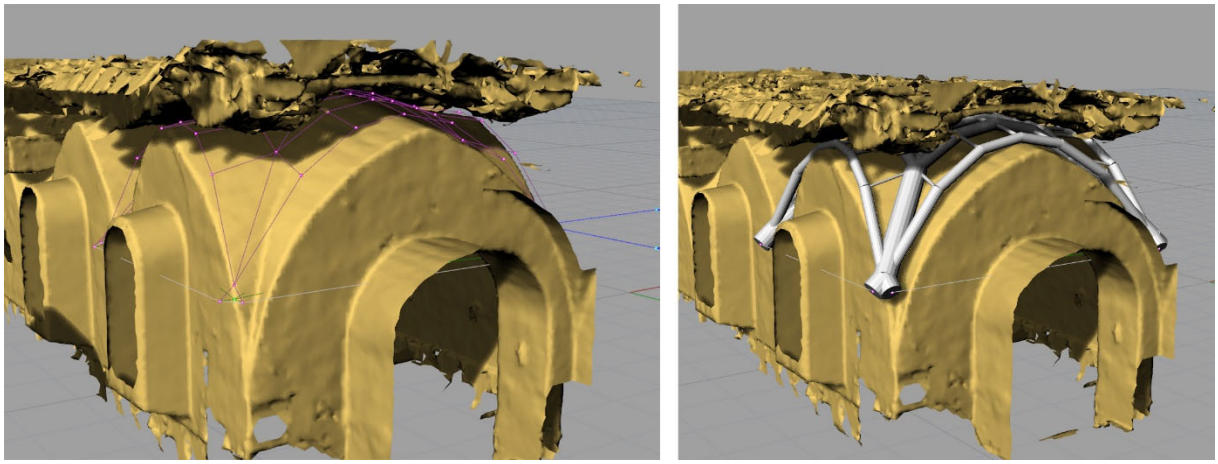


Figure 5: Example of results from thrust network analysis of Gökhem church.

4.3 Case study: Lund cathedral

The thin geometry of the vaults in the main nave of Lund cathedral limited the possibilities to find thrust networks with TNA that fitted the geometry, although it was possible with parametric thrust line analysis and the slicing method. Despite this, it was possible to draw conclusions on the magnitude of the thrusting forces that arise from the vault under different conditions. A comparison between an "almost fit" of a TNA network and parametric thrust line analysis shows good conformity with respect to supporting forces.

The analysis of a section shows that the former buttresses probably had a significant task to

support the thrusting forces from the vaults of the main nave. The tie rods that replaced them in the 19th century are thus important for the structural safety of the building.

4.4 Case study: St Johannes church

Since the vault of the main nave of St Johannes church has an extreme shape and is thin, it was not possible to find thrust networks with TNA that fitted within the geometry, or to find a complete solution using parametric thrust line analysis with the slicing method. The failure to find a TNA-based solution might be attributed to the available methods lacking a best fit solution, but the results indicate that the analysis made in this study, with TNA and parametric thrust line analysis, validates the findings from the earlier analysis that it is not possible to find thrust lines or thrust networks that fit completely within the geometry of the vaults.

The analysis of a section of the church by means of parametric thrust line analysis clearly showed the efficiency of the buttresses and the flying buttresses to counteract different types of loading from the vaults and the roof structure to ensure that the forces in the inner columns of the church are always located at their centre, see Figure 6. The results show the strength of the methods used to describe and study the global force pattern and the clever structure of the flying buttresses to support and allocate the thrusting forces from the vaults and roof structures.

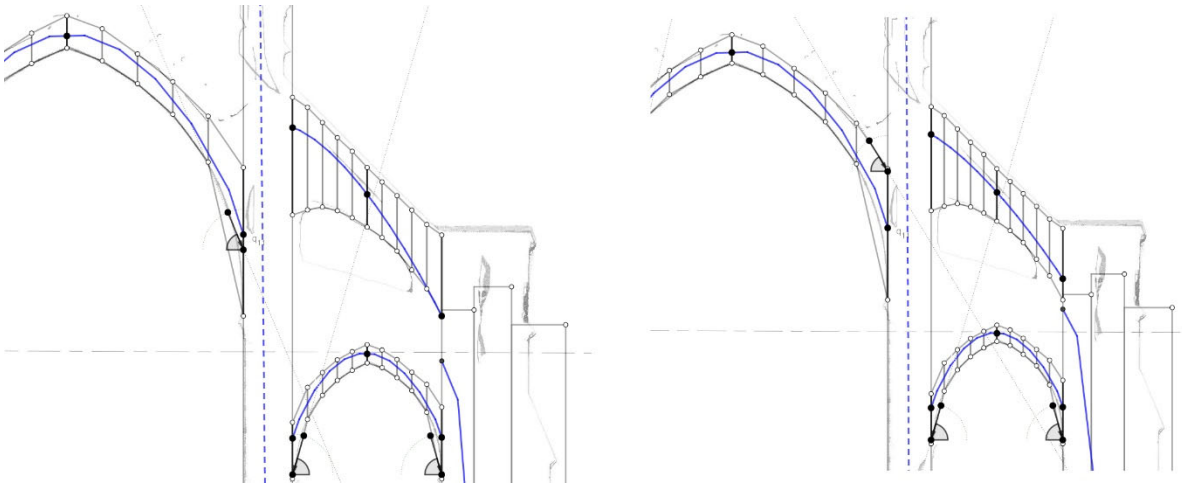


Figure 6: An example of the flexible response of the flying buttresses to different loads. The analysis to left shows the case without wind loading on the roof structure, and the analysis to the right shows the case with wind loading. The increased thrusting force from the central nave is counteracted by the flying buttresses.

5 CONCLUSIONS

The development of computer-based methods to capture complex geometries and to carry out modelling and analyses has created entirely new possibilities to study and assess complex masonry structures. By using the proposed approach to carry out funicular analysis of historic vaulted masonry structures, it is possible to perform analyses and assessments with a reasonable work effort and length of normal project and achieve results of the required quality for practising structural engineers. The methods are efficient for the analysis of complex structures. The methodology also provides a pedagogical description of the structural behaviour of masonry vaults and the decisive factors for their load-carrying capacity. 3d models facilitate the perception and understanding of the analysis and results.

Thrust Network Analysis (TNA) has the potential to become a very useful and efficient tool to analyse historic masonry vaults. For this, a solution to fit the thrust networks to existing geometries is needed. The availability of a best fit solution is also needed to find the most optimal and valid shapes within the geometry of the vaults, depending on the objective of the analysis. Thrust Network Analysis is faster than parametric thrust line analysis by means of the slicing method, and provides the possibility to examine rapidly many different ways that the vaults can carry loads, as well as different loading situations in a sensitivity analysis.

To carry out a thrust line-based analysis for vaulted structures, a target surface needs to be defined in some way. With a best fit-based solution in TNA, a target surface to which the thrust network can be optimised must be defined. The distance from the resulting thrust network and the target surface gives a measure of how well suited the given shape is to be a load-carrying structure for compression only. In analyses of historic masonry vaults, the analyst needs to know which shape is aimed at to describe the structural behaviour of the vaulted structure. The thrust network needs to be located within the geometry of the vaults but, in theory, there can be endless valid variations of its shape. The extremes are given by the flattest possible shape, with the network close to the intrados at the top of the vault and close to the extrados at the support of the vault, and the "deepest" possible shape, with the network close to the extrados at the top of the vault and close to the intrados at the support of the vault. The second case gives the least thrusting force and represents the vault "at rest" and not affected by other forces. Many times, it is desirable to show that the vault has a safe shape and that it is possible to fit a thrust network within the middle third of the geometry. The shape of the target surface therefore needs to be defined according to the questions at hand. The desired shape of a target surface is often far from obvious for vaults with complex shapes. The shape of different target surfaces needs further development and definitions for future studies.

The parametric thrust line analysis is a useful tool to study different load cases and to examine the load paths through the built structure to the foundations. A delimitation of possible structural solutions is obtained by combining thrust line analysis of sections of the buildings with analysis of the vaults´ thrusting forces.

Acknowledgements. The Sven Tyrén trust at Tyréns AB has funded major part of the study presented in this paper. The church of Sweden with the cathedral council in Lund, the Parish of Gökhem and the Parish of St Johannes has provided us with the interesting case studies. The Block Research Group welcomed us to a valuable study visit.

REFERENCES

[1] Heyman, J. *The Stone Skeleton: Structural Engineering of Masonry Structures*. Cambridge University Press, England (1995).

[2] Huerta, S. The Analysis of Masonry Architecture: A Historical Approach. *Architectural Science Review,* Vol. 51.4: 297-328 (2008).

[3] Block, P. *Thrust Network Analysis: Exploring Three-dimensional Equilibrium.* Diss. Massachusetts Institute of Technology, Cambridge, MA, USA. (2009).

[4] Block, P., Ciblac, T. & Ochsendorf J. A. Real-time limit analysis of vaulted masonry buildings. *Computers and Structures* 84 (29-30), 1841-1852. (2006).

[5] Thelin, C., Höst, F. & Rosenberg, C. Att förstå verkningssätt och fånga geometrin i

historiska murverkskonstruktioner, *Bruk av ruiner*, Balksten, K. & Mebus U., eds. (2013), Visby: Fornsalens förlag. (2013).
[6] Historic England, *3D Laser Scanning for Heritage: Advice and Guidance on the Use of Laser Scanning in Archaeology and Architecture*. Swindon. Historic England. (2018).
[7] Thelin, C., Höst, F. & Rosenberg, C. Analysis of historic masonry structures supported by 3D laser scanning. *Proceedings of the 8th International Conference on Structural Analysis of Historic Construction*, Jasiénko, J. (red). SAHC-2012, 15–17 October 2012, Poland. (2012).
[8] O'Dwyer, D.W. Funicular analysis of masonry vaults. *Computers and Structures* 73 (1-5), 187-197 (1999).
[9] Block P., Lachauer L. & Rippmann M. Thrust Network Analysis - Design of a cut-stone masonry vault, *Shell Structures for Architecture: Form Finding and Optimization*, Adriaenssens, S., Block, P., Veenendaal, D. and Williams, C. (editors), Routledge, London. (2014).
[10] Rippmann, M., Lachauer, P., & Block, P. Interactive Vault Design. *International Journal of Space Structures*, Vol 27, No 4: 219-230. (2012).
[11] Rippmann, M. & Block, P. Funicular Shell Design Exploration. *Proceedings of the 33rd Annual Conference of the ACADIA*, Waterloo/Buffalo/Nottingham, Canada. (2013).
[12] Rhinoceros. [Computer program]. http://www.rhino3d.com [2019-03-11]. (2019).
[13] 3DReshaper. [Computer program]. http://www.3dreshaper.com [2019-03-11]. (2019).
[14] Rippmann, M. *Funicular Shell Design: Geometric Approaches to Form Finding and Fabrication of Discrete Funicular Structures*. Diss. ETH Zürich, Schweiz. (2016).
[15] Block, P. & Lachauer, L. Three-dimensional (3D) equilibrium analysis of gothic masonry vaults. *International Journal of Architectural Heritage*, Vol 8: 312-335. (2014).
[16] Block, P. & Lachauer, L. Closest-Fit, Compression-Only Solutions for Free Form Shells, *Proceedings of the IABSE-IASS Symposium 2011*, London, UK. (2011).
[17] Panozzo D., Block P. & Sorkine-Hornung O. Designing Unreinforced Masonry Models, *ACM Transactions on Graphics - SIGGRAPH 2013*,32(4): 91:1-91:12. (2013).
[18] Van Mele, T., Panozzo, D., Sorkine-Hornung, O. & Block P. Best-fit thrust network analysis – Rationalization of freeform meshes, *Shell Structures for Architecture: Form Finding and Optimization*, Adriaenssens, S., Block, P., Veenendaal, D. and Williams, C. (editors), Routledge, London. (2014).
[19] Geogebra. [Computer program]. http://www.geogebra.org [2019-03-11]. (2019).
[20] Revit. [Computer program]. http://www.autodesk.com [2019-03-11]. (2019).

12th International Conference on Structural Analysis of Historical Constructions
SAHC 2020
P. Roca, L. Pelà and C. Molins (Eds.)

APPLICABILITY OF FEM AND PUSHOVER ANALYSIS TO SIMULATE THE SHAKING-TABLE RESPONSE OF A MASONRY BUILDING MODEL WITH TIMBER DIAPHRAGMS

MARIA PIA CIOCCI[1*], RUI MARQUES[2] AND PAULO B. LOURENÇO[2]

[1]Institute for Sustainability and Innovation in Structural Engineering (ISISE),
Department of Civil Engineering, University of Minho,
Campus de Azurém, 4800-058 Guimarães, Portugal
e-mail: mariapiaciocci@gmail.com, web page: https://isise.net (*corresponding author)

[2] Institute for Sustainability and Innovation in Structural Engineering (ISISE) and
Institute of Science and Innovation for Bio-Sustainability (IB-S),
Department of Civil Engineering, University of Minho,
Campus de Azurém, 4800-058 Guimarães, Portugal
e-mail: marquesmnc@sapo.pt, e-mail: pbl@civil.uminho.pt
web page: https://isise.net, web page: http://ib-s.uminho.pt/

Keywords: FE Modelling, Mass-proportional Pushover Analysis, Flexible Diaphragms, Unreinforced Masonry, Wall-to-diaphragm Connections

Abstract. *The seismic behaviour of unreinforced masonry (URM) structures is generally governed by a complex interaction between the out-of-plane and in-plane responses of the walls, depending on the in-plane stiffness of floor/roof diaphragms and the efficiency of wall-to-floor/roof connections. The presence of timber diaphragms, which are typically characterised by low in-plane stiffness and poor connection to the masonry walls, adds challenges to the numerical modelling and analysis, as well as to the structural assessment of URM structures under seismic actions. This work aims at investigating the applicability of refined FE modelling using macro-modelling approach and mass-proportional pushover analysis for simulating the response of URM structures with flexible diaphragms, comparing the results with experimental data obtained from incremental dynamic testing.*

A full-scale two-storey prototype building with timber diaphragms, which was tested in shaking table at the European Centre for Training and Research in Earthquake Engineering (EUCENTRE), in Italy, was considered to perform this study. A refined finite element (FE) model was developed in DIANA software, considering the wall-to-diaphragm (WTD) connections. While the strength values of masonry were adopted according to axial and diagonal compression tests, the modulus of elasticity was calibrated after simulating in-plane cyclic shear tests of masonry piers, which were part of the same experimental program at EUCENTRE. Recommendations from international guidelines were used to derive the assumed material properties for diaphragms and wall-to-diaphragm connections. Mass-proportional pushover analysis was performed and a comparison between numerical and experimental results is presented to investigate the assumptions, advantages and limitations of the presented numerical modelling and analysis approach.

1 INTRODUCTION

Despite the formidable inventory of unreinforced masonry (URM) buildings with a large variety in terms of geometry, materials and construction techniques, they present some common features that make them high vulnerable to earthquakes. Such features include but are not limited to: (1) low material strength; (2) unfavourable geometrical layout; (3) high mass of the masonry structural elements when compared to diaphragms; (4) inappropriate stiffness of diaphragms; (5) poor connection between intersecting walls and between walls and diaphragms. Due to these characteristics, URM buildings frequently collapse in a quasi-brittle way with out-of-plane mechanisms of isolated parts that behave independently from the rest of the structure (i.e. overturning and flexure failure mechanisms). When the premature activation of these failure modes is prevented, an integral structural behaviour can develop with an associated global mechanism of the building which allows to exploit the in-plane capacity of the walls [1].

The timber diaphragms and their connection to masonry walls may have an important role when assessing the seismic response of URM structures, because of their influence on the activation and type of out-of-plane mechanisms. For this reason, their consideration is recommended by several international building codes and guidelines [2–4]. Indeed, when adequate in-plane diaphragm stiffness and efficient wall-to-diaphragm (WTD) connections are provided, the sudden out-of-plane overturning of walls can be prevented. Still, the successful performance of diaphragms and connections does not preclude the possibility of flexural out-of-plane mechanisms, which are however associated with higher performance when compared to wall overturning.

In current practice, the seismic behaviour of URM buildings can be evaluated by performing global analyses on refined finite element (FE) models. However, there are several critical questions which arise when assessing the behaviour of URM buildings, and even more when timber flexible diaphragms are present, such as the choice of modelling strategies and analysis tools. Timber diaphragms are typically implemented while modelling URM structures at the building scale by assuming a linear elastic behaviour, with input material properties calculated according to values and formulas provided by recommendations [3,4] or based on experimental tests at the component level (e.g. [5]). This assumption is corroborated by the fact that prior to the failure of the connections between walls and floors, usually there is no scope for diaphragms to exploit their nonlinear behaviour. As regards WTD connections, very little information is currently available on their structural characteristics and behaviour, leading to simplified assumptions to consider their contribution when assessing the structural behaviour of URM buildings with timber floors. As regards analysis methods, nonlinear static (pushover) analysis is commonly used, especially for refined FE numerical models which are associated to a significant computational burden. However, several aspects involved when pushover analysis is performed (e.g. adequate lateral load pattern) are still open issues for URM structures, particularly in presence of flexible diaphragms.

This paper presents a numerical study aimed to simulate the behaviour of a full-scale two-storey prototype building, representative of existing double-leaf stone masonry buildings with wooden floors and roofs, which was subjected to shaking table testing at the European Centre for Training and Research in Earthquake Engineering (EUCENTRE), in Italy [6,7]. Firstly, numerical simulations of in-plane shear tests of masonry piers were perfomed to calibrate the modulus of elasticity for masonry, and then the model of the prototype building was analysed

by means of mass-proportional pushover analysis. Hence, the modelling strategy and the analysis tool used in this study are evaluated with respect to experimental data.

2 REFERENCE EXPERIMENTAL PROGRAM

The experimental program carried out by [6–8] at EUCENTRE (Italy) was selected as a reference for this study. This program was aimed to investigate the seismic response of URM buildings with timber floors and roofs, and the efficiency of different strengthening interventions to improve diaphragm stiffness and WTD connections. The experimental program included an extensive characterisation of the masonry, comprising uniaxial and diagonal compression tests as well as in-plane shear tests on masonry piers, and shaking table tests on three full-scale prototype buildings. The main features of the reference unstrengthened prototype building (Building 1) and the in-plane cyclic shear tests of masonry piers, which were numerically simulated in this study, are summarised in the following sections.

2.1 Shaking table testing

The prototype building (Building 1) had a rectangular single-room of plan dimensions 5.8 m x 4.4 m, two-storeys and an asymmetrical distribution of openings (Figure 1). The walls were made of double-leaf stone masonry, with a thickness of 0.32 m. As regards the timber floor and roof systems, they consisted of 3 cm thick single layer of planks nailed to joists which were placed every 0.5 m and oriented in the direction of the shortest span, and simply supported on the inner leaf of the masonry walls. The ridge and spread beams of the pitched roof system were weakly connected to the masonry walls. It is noted that additional masses were placed at the floor level, while the roof system was covered with clay tiles.

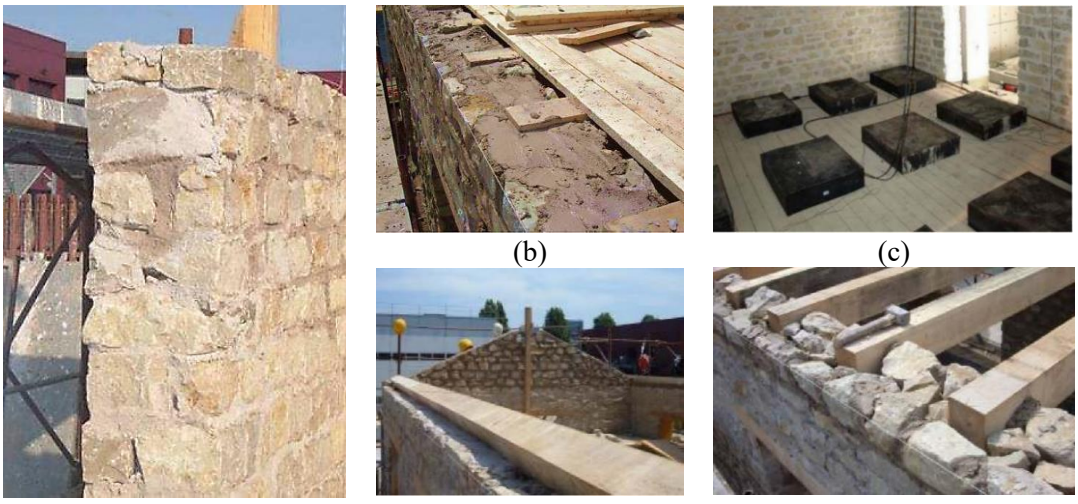


Figure 1: Prototype building (Building 1): (a) masonry wall, (b-c) timber floor, (d-e) timber roof [11]

During shaking table testing, accelerometers were installed at the mid-span and at the corners of the walls at both floor and roof levels in order to monitor the building response. The ground motion recorded during the 1979 Montenegro earthquake was applied to the building prototype in the horizontal direction parallel to the longitudinal walls. The intensity of the ground motion

was gradually increased in each test run, scaling the reference input until a near collapse condition was reached. It should be mentioned that during the final run of the incremental dynamic testing sequence, tie-rods were applied at both diaphragms' levels in order to prevent out-of-plane collapse mechanisms [8].

2.2 In-plane cyclic tests

The experimental program included testing of four masonry piers which were subjected to in-plane reversed horizontal cyclic loading (Figure 2). All specimens were constructed with a nominal thickness of 0.32 m and were 2.5 m high. Two geometric configurations were tested under different levels of axial loading, namely 0.2 and 0.5 MPa. The specimens CT01 and CT02 (squat piers) had a slenderness ratio (h/l) equal to 1, while a slenderness ratio of 2 was assumed for specimens CS01 and CS02 (slender piers). While the vertical axial loading was kept constant, a cyclic horizontal displacement history was applied, both at the top of each specimen. Detailed information about the loading protocol can be found in [10]. As regards boundary conditions, the test setup imposed a double bending configuration by means of a "hybrid" control of the vertical actuators which were forced to apply a constant total axial load as well as to maintain the same vertical displacement.

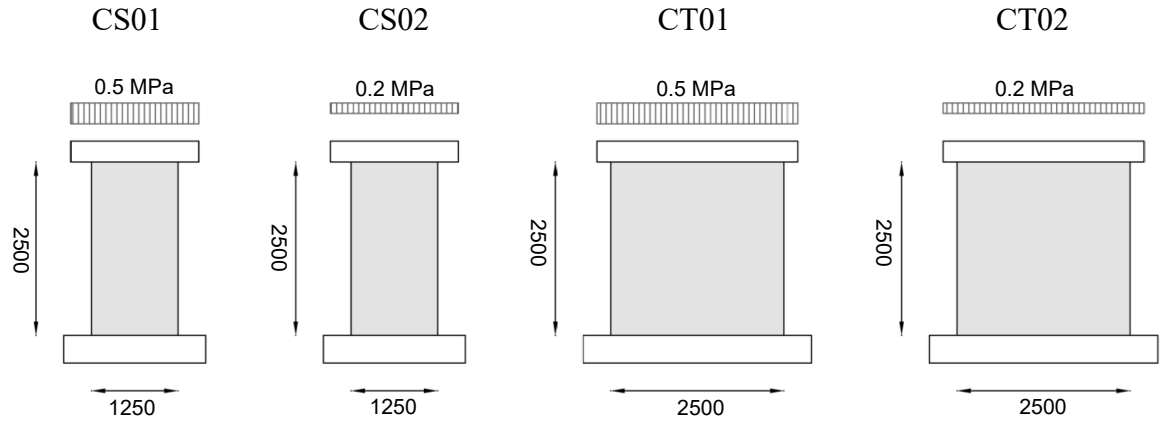


Figure 2: In-plane shear cyclic tests of masonry piers (dimensions in mm)

3 REFERENCE MODEL OF THE BUILDING PROTOTYPE

The FE model of the prototype building was developed in the finite element environment DIANA 10.3 [11]. The masonry walls were modelled with solid elements, while curved shell elements were used for the floor and timber diaphragms. As regards WTD connections at floor level, they were implemented in the model by means of beam elements embedded in the masonry walls. At the roof level, the ridge and spreader beams were modelled as beam elements resting on the walls. It should be noted that the shell elements simulating the diaphragms were connected to the in-plane masonry walls only at nodes corresponding to the location of the WTD connections (Figure 3a).

In order to simulate the mechanical behaviour of masonry, the Total Strain Rotating Crack (TSRC) model was used considering specified compressive and tensile softening behaviour (Figure 3b). The strength values necessary for this model were adopted based on the axial and

diagonal compression tests performed within the same EUCENTRE experimental program [12]. As regards the modulus of elasticity, a value of 2550 MPa was derived from the the axial compression tests. As discussed later in Section 4, this value was subsequently calibrated by performing model updating based on numerical simulation of in-plane shear tests of masonry piers. Fracture energy values which control the softening were not measured experimentally and had to be derived from information available in the literature. A summary of the material properties adopted for masonry is presented in Table 1.

For the shell elements, an equivalent shear modulus was adopted to simulate the timber floor and roof diaphragms. Since limited information was available for these structural components, this value was assumed to be equal to 8.8 MPa, calculated according to recommendations provided in the New Zealand guidelines for a 3 cm thick single straight sheathing diaphragm subjected to loading in the perpendicular direction of joists [3].

Regarding the connection elements between masonry walls and floor joists, the input material properties were evaluated according to EN 338:2016 [13]. An equivalent mass density was assigned to these elements to lump the diaphragms' masses in correspondence to the WTD connections.

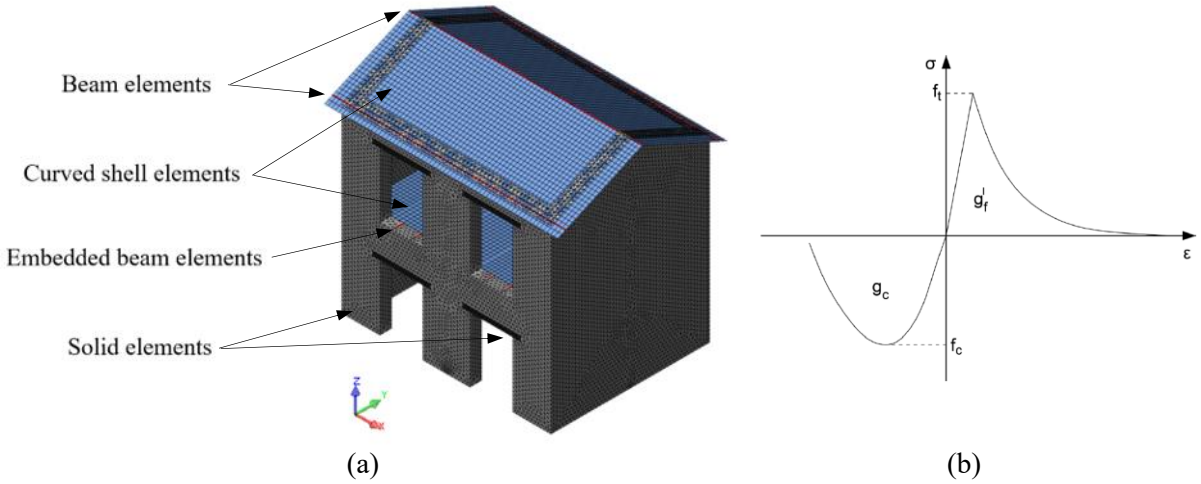


Figure 3: Modelling of the prototype building: (a) FE model, (b) TSRC model

Table 1: Characterisation of masonry material

Masonry material properties	
Modulus of elasticity (MPa)	800*
Poisson ratio (-)	0.20
Compressive strength (MPa)	3.28
Tensile strength (MPa)	0.14
Fracture energy in compression (N/mm)	12.90
Fracture energy in tension (N/mm)	0.012
Specific weight (kN/m^3)	23.0

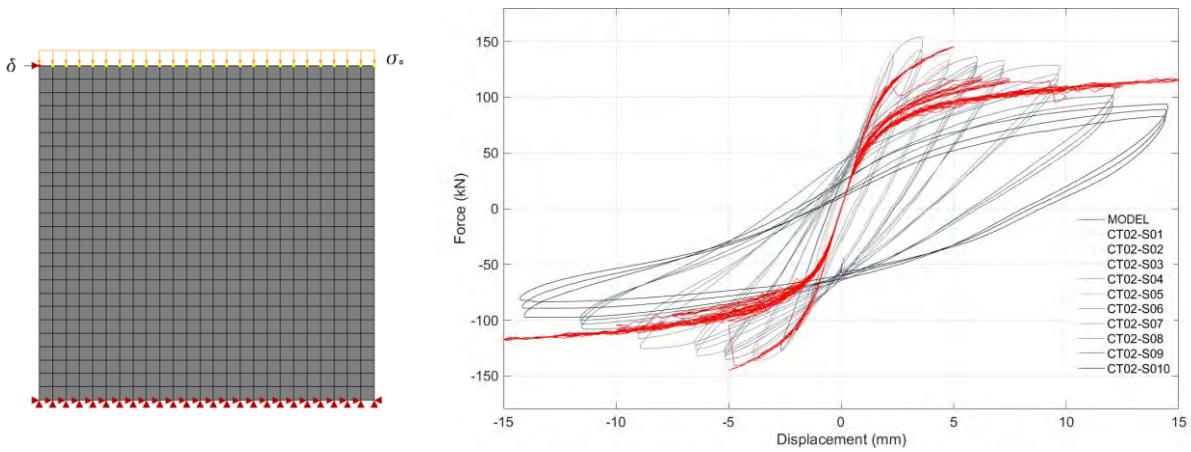
* Calibrated value

4 NUMERICAL SIMULATION OF IN-PLANE CYCLIC TESTS

Eigenvalue analysis performed on the model of the prototype building adopting the value of modulus of elasticity derived from the vertical compression tests, i.e. 2550 MPa, resulted in much higher natural frequencies when compared to the results obtained from dynamic identification tests performed on the specimen before the shaking table test [14]. To investigate better this discrepancy, additional numerical simulations of the in-plane cyclic shear tests presented in Subsection 2.2 were performed. Figure 4a presents the numerical model used to perform this study.

The material properties for masonry were kept with the same values presented in Table 1, except the modulus of elasticity. The vertical axial loading applied at the top of the wall included both the overburden stress load as well as the self-weight of the beam used in the test setup. Proper boundary conditions were implemented in the model to reproduce the double bending configuration assumed in the experimental test, and the loading was applied consistently with the time horizontal displacement history presented in [10]. The results obtained for specimen CT02 are presented in this paper.

Despite the unloading and reloading are simulated by a secant approach in the TSRC model, which leads to an underestimation of energy dissipation under cyclic loading condition [15], the numerical model reasonably simulated the experimental behaviour of the specimen in the scope of this study. As shown in Figure 4b, the initial stiffness was well captured by the model when the modulus of elasticity was assumed to be equal to 800 MPa, comparable with the value obtained from model updating performed on the building model. In terms of strength, the model fairly predicted the experimental value with no need for further calibration. In terms of damage, the model exhibited cracking through the wall diagonals, in agreement with the shear failure observed experimentally. Since consistent results were also obtained for the other specimens, the value of modulus of elasticity was assumed equal to 800 MPa for the model of the prototype building.



(a) (b)

Figure 4: In-plane shear test simulation of specimen CT02: (a) FE model, (b) force-displacement hysteresis

5 NONLINEAR STATIC ANALYSES

The need for nonlinear analysis when dealing with masonry structures is widely recognized. Nonlinear dynamic (time-history) analysis is able to follow the full seismic loading process, considering significant aspects of the structural response; however, it is challenging to perform due to its intrinsic complexity and large computational effort involved. For this reason, nonlinear static (pushover) analysis is usually preferred in common practice, especially for refined FE numerical models which need a significant computational burden.

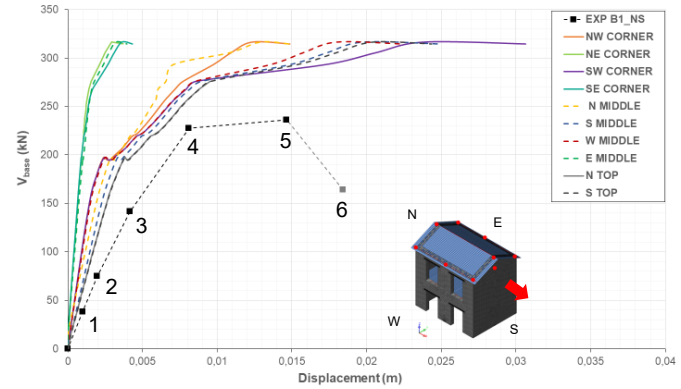
The reference experimental program involved incremental dynamic testing in which the building was subjected to a series of accelerations. Experimentally the structure was inherently subjected to loading spatially distributed as per its mass [16]. Consequently among the various methods of applying the load that can be employed while performing pushover analyses, mass-proportional loading was chosen in this study. Hence, the reference model was analysed performing pushover analyses with loading in the positive (NS) and negative (SN) senses of the longitudinal direction, i.e. the direction of ground motion in the shaking table tests.

Figure 5 presents the comparison between experimental and numerical predictions in terms of capacity curves, i.e. the base shear force-displacement response, plotting the base shear force (V_{base}) versus the horizontal displacement values recordered at nodes at the top level. Moreover, damage obtained in the numerical model is compared to damage documented in the shaking table test. In particular, Figure 6a shows in red cracks occurred in step 5 of the experimental test and in black the ones observed in previous phases.

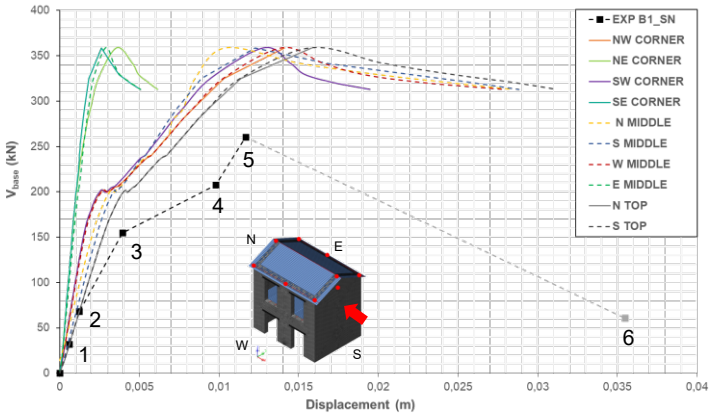
As shown in Figure 5, the numerical response reasonably approximated the linear behaviour of the building prototype until step 2 of the shaking table test. In particular, when comparing the curves obtained for the in-plane walls, the East wall is less flexible than the West wall, which was also observed experimentally [9]. In step 3, a drop in stiffness was observed in the experimental response, which was not captured by the numerical model. In terms of experimental damage, no significant cracks occurred when compared to previous phases, except for cracks due to transportation of the building prototype [9] which were not implemented in the numerical model. In step 4, extensive damage in the upper part of the North wall as well as in the in-plane walls was observed. A good agreement between numerical and experimental predictions was in general obtained for damage in the in-plane walls (Figure 6). As regards the North wall, the numerical model captured the out-of-plane mechanism above the floor level, involving also portions of the in-plane walls. However, some differences were observed in terms of damage pattern. In step 5, the numerical model predicted the vertical crack which occurred in the mid-length of the South wall at the roof level, but it could not properly predict the horizontal crack observed at the base of the South gable wall. It should be noted that 'false-positive' cracks were predicted by the numerical model when compared to experimental results. As shown in Figure 6, vertical cracking occurred at the South-East (SE) and North-East (NE) corners, which were not observed experimentally. Extensive damage was also predicted close to the wall-to-diaphragm connections at roof level, which was not reported in the experimental observations.

In terms of maximum base shear force, the numerical model presents a value which is 35% higher than the experimental one in both positive and negative senses. It should be noted that some contribution to these differences can be related with dissimilar methodologies used when constructing the capacity curves. The numerical responses were defined by considering the base

shear force recorded at the nodes at the base of the model versus the displacement values in the longitudinal direction recorded at the location of the accelerometers in the experimental test. As regards the experimental responses, they represent the envelope of the hysteresis cycles which were evaluated during each testing phase of the building prototype. In particular, the hysteresis behaviour was defined by plotting the inertia force (sum of the product of the measured accelerations by tributary masses assumed as concentrated at each accelerometer location) versus the roof level displacements where the accelerations were recorded.



(a)



(b)

Figure 5: Capacity curves: (a) positive (NS) direction, (b) negative (SN) direction

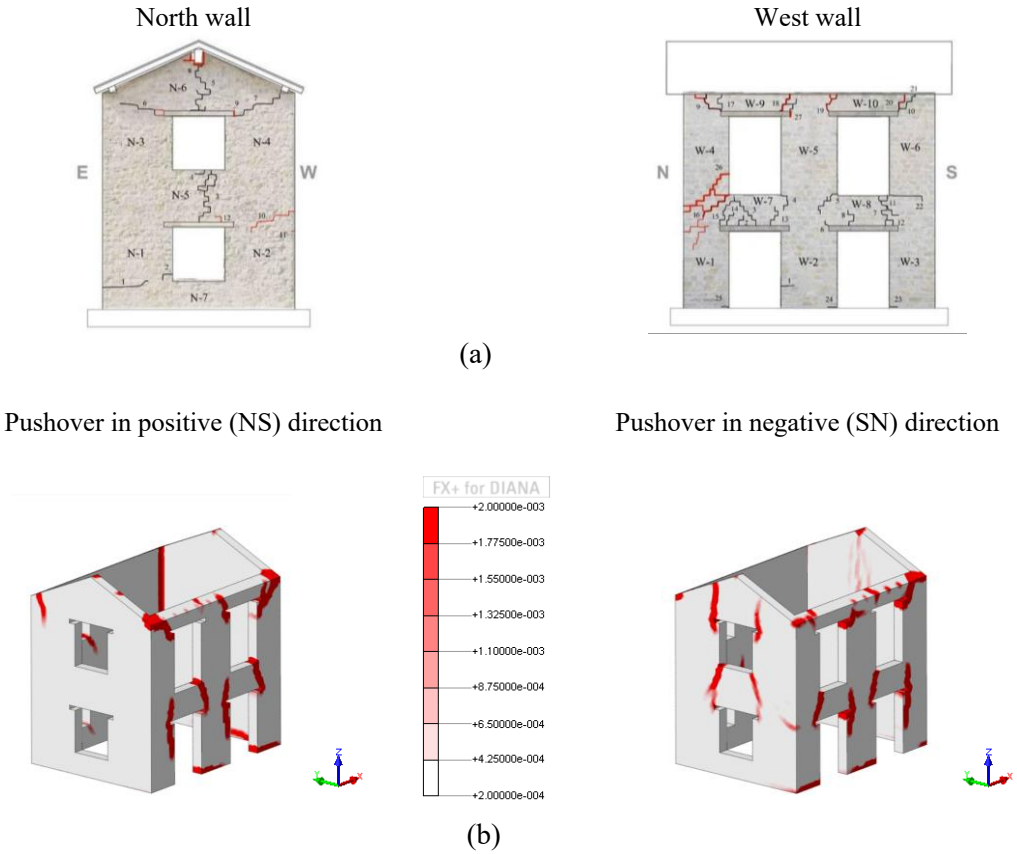


Figure 6: Damage at step 5: (a) experimental observation [9], (b) maximum principal strains in the numerical model

6. CONCLUSIONS

The applicability of refined FE modelling and mass-proportional pushover analysis for simulating the response of a URM structure with flexible diaphragms subjected to incremental dynamic testing was investigated in this paper. The reference experimental program was carried out at EUCENTRE, in Italy, which included extensive characterization testing of the masonry and incremental shaking table testing of three full-scale two-storey prototype buildings. The unstrengthened specimen (Building 1), conceived to reproduce existing double-leaf stone masonry buildings with timber floor and roof systems, weakly connected to walls, was used to perform this work.

For the adopted modelling strategy, the masonry walls were modelled using solid elements, while curved shell elements were used for timber floor/roof diaphragms. The connection of diaphragms to the in-plane walls was modelled by means of beam elements, which were embedded in masonry at floor level. Pushover analyses were performed by applying mass-proportional lateral loading in the longitudinal direction of the building, consistently with the direction of the input ground motion in the incremental shaking table testing.

The results show that the numerical simulations of in-plane cyclic shear tests of masonry piers can be very useful in this work to calibrate the modulus of elasticity for masonryAs regards the numerical model of the building, the base shear force obtained numerically is approximately

35% higher than the experimental one. In terms of damage, the model fairly simulated the main failure mechanisms observed experimentally. However, while damage in the in-plane walls was well captured by the model, the numerical and experimental predictions were not so consistent for the out-of-plane damage. Moreover, when compared to the experimental results the model predicted 'false-positive' cracks at the connection with the transversal walls as well as at WTD connections. The results obtained from the model of the building confirm the need to enhance the contribution of in-plane stiffness of diaphragm and their connection to masonry walls in the building response, which will be pursued in further development of this work.

Acknowledgements. This work was financed by FCT - Portuguese Foundation for Science and Technology, within the INFRARISK PhD program and ISISE (Ref. UID/ECI/04029/2019). The authors would like to acknowledge Prof. Guido Magenes and Dr. Ilaria Senaldi for providing useful information on the experimental program at EUCENTRE.

REFERENCES

[1] Lourenço, P.B., Mendes, N., Ramos, L.F. and Oliveira, D.V. Analysis of masonry structures without box behavior. *Int J Archit Herit* (2011) 5:369-382. https://doi.org/10.1080/15583058.2010.528824.
[2] NTC 2018. *Norme Tecniche per le Costruzioni. Decreto Ministeriale 17/1/2018* (2018).
[3] NZSEE 2017. *The existing Assessment of Existing Buildings. Part C8: Unreinforced Masonry Buildings* (2017).
[4] ASCE/SEI 41-13. *Seismic Evaluation and Retrofit of Existing Buildings* (2014).
[5] Brignola, A., Pampanin, S., Podestà, S. Evaluation and control of the in-plane stiffness of timber floors for the performance-based retrofit of URM buildings. *Bull New Zeal Soc Earthq Eng* (2009). https://doi.org/10.5459/bnzsee.42.3.204-221.
[6] Magenes, G., Penna, A., Senaldi, I., Galasco, A. Shaking Table Test of a Strengthened Full-Scale Stone Masonry Building with Flexible Diaphragms. *Int J Archit Herit* (2014) 8:349–375. https://doi.org/10.1080/15583058.2013.826299.
[7] Senaldi, I., Magenes, G., Penna, A., Galasco, A., Rota, M. The Effect of Stiffened Floor and Roof Diaphragms on the Experimental Seismic Response of a Full-Scale Unreinforced Stone Masonry Building. *J Earthq Eng* (2014) 18:407–43. https://doi.org/10.1080/13632469.2013.876946.
[8] Magenes, G., Penna, A., Galasco, A. A full-scale shaking table test on a two-storey stone masonry building. In: *Proceedings of the 14th European Conference Earthquake Engineering* (2010).
[9] Senaldi, I. *The influence of floor and roof diaphragms on the seismic response of existing masonry buildings*. PhD Thesis, School of Advanced Studies IUSS Pavia, Italy (2012).
[10] Magenes, G., Penna, A., Galasco, A., Da Paré, M. In-plane cyclic shear tests of undressed double-leaf stone masonry panels. In: *Proceedings of the 8th International Masonry Conference* (2010).
[11] DIANA FEA BV. Diana User's Manual, Release 10.3. DIANA FEA BV 2019. https://doi.org/10.1080/15421400600788682.
[12] Magenes, G., Penna, A., Galasco, A., Rota, M. Experimental characterisation of stone masonry mechanical properties. In: *Proceedings of the 8th International Masonry Conference* (2010).

[13] EN 338:2016. *Structural timber - Strength classes*. European Committee for Standardization, Brussels, Belgium.
[14] Kouris, L.A.S., Penna, A., Magenes, G. Dynamic Modification and Damage Propagation of a Two-Storey Full-Scale Masonry Building. *Adv. Civ. Eng* (2019). https://doi.org/10.1155/2019/2396452.
[15] Schreppers, G.M., Garofalo, A., Messali, F., Rots, J. *DIANA Validation report for Masonry modelling* (2017).
[16] Vaculik, J.. *Unreinforced masonry walls subjected to out-of-plane seismic actions*. PhD Thesis, University of Adelaide, Australia (2012).

12th International Conference on Structural Analysis of Historical Constructions
SAHC 2020
P. Roca, L. Pelà and C. Molins (Eds.)

ASSEMBLABILITY CONSTRAINTS IN THE LIMIT ANALYSIS OF 3D MASONRY INTERLOCKING BLOCKS

ELHAM MOUSAVIAN[1*], CLAUDIA CASAPULLA[1]

[1]Department of Structures for Engineering and Architecture (DiSt)
University of Napoli Federico II
Via Forno vecchio, 36 – 80134 Napoli, Italy
e-mail: elham.mousavian@unina.it (*corresponding author)

email: casacla@unina.it

Keywords: Assembling path detection; limit analysis for orthotropic interfaces; structural infeasibility measurement; sliding infeasibility; interlocking blocks

Abstract. *This paper presents a method to analyses the structural feasibility and assemblability of the masonry assemblages composed of interlocking blocks. Interlocking blocks with projections and depressions on their faces have relatively better structural performance comparing to the conventional blocks with flat faces, during and after the construction. Therefore, they can represent proper alternatives to the conventional blocks for the seismic retrofitting of unreinforced masonry structures. Structural soundness and assemblability of a model are both functions of the interlocking block geometry. The proposed methods enable the designer to adjust the shape of the interlocking blocks, while meeting the structural and assembling requirements. The paper first introduces an extension of the limit analysis to the assemblages with corrugated interlocking interfaces having anisotropic sliding behavior. Then, the work reformulates the extended limit analysis to develop a method to measure the structural infeasibility due to the lack of sliding resistance at the interlocking interfaces. This is called sliding infeasibility and the designer can minimize it during the shape exploration. Finally, an assemblability method is presented to check if the designed interlocking blocks can be assembled on the other blocks in contact. This method is added to the extended limit analysis and the sliding infeasibility measurement method in form of a geometric constraint that prevents modeling of un-assemblable structures.*

1 INTRODUCTION

Recently, an exponential scientific interest can be observed in the investigation of the in-plane and out-of-plane behavior of assemblages composed of interlocking blocks. Several studies demonstrate that the static and dynamic load bearing capacities of such assemblages increase when interlocking blocks are used instead of conventional blocks. Many works were carried out to compare the structural performance of different interlocking shapes (corrugated, cross-shaped, etc.) and to find the geometric parameters by which the structural performances are maximized. Liu et al. [1] tested the in-plane capacity of the masonry walls composed of corrugated joints with different cross sections. Totoev [2] and Hossain et al. [3]

experimentally and numerically investigated the in-plane and out-of-plane behavior of the walls with corrugated joints. The out-of-plane behavior of masonry walls with osteomorphic blocks [4,5] and cross-shaped joints [6] were also studied, together with the more conventional interlocking constraints [7-9]. Fang et al. [10], Sassu et al. [11] and Cipollini et al. [12] carried out several interesting numerical and experimental analyses on the structural behavior of wooden joineries with various shapes. Mousavian and Casapulla [13] extended the limit analysis to the corrugated interfaces and performed the structural feasibility of such assemblages as a function of the number and orientation of the locks, i.e., the projections and depressions keeping the blocks together and preventing them from sliding.

Furthermore, interlocking blocks can increase the stability of such assemblages during the construction phase. This can considerably decrease the needed formwork and improve the quality of the workmanship. Therefore, interlocking blocks are good candidates for the retrofitting of masonry structures, provided that the old damaged or missing conventional blocks can be replaced by them. In fact, the insertion of these blocks may be allowed without mortar, which can be lost during the time due to the chemical, physical, and mechanical degradation. In sum, the use of such blocks can strengthen the restored assemblages by increasing their bending and sliding resistances and improve the constructability during the restoration process. To maximize the structural performance and constructability, the optimal shape of each individual interlocking face can be found. The interlocking blocks with the customized shapes can then be manufactured by advanced machines such as CNC mills. This is in the same line of the classical stereotomy, which is a technique to cut each individual block of an assemblage into a particular shape [14]. Finally, interlocking blocks can also improve the thermal response of the walls, aiming to optimize the resources for interventions [15].

In this framework, a plug-in has recently been developed to design assemblages of interlocking blocks with corrugated shape and locks with rectangular cross section [13]. Limit analysis methods, already developed for infinite [16] or finite isotropic associative [17-19] or non-associative [20] conventional frictional joints, was extended to interlocking interfaces with orthotropic sliding behavior [13,21]. This is governed by an associative friction model along the locks and by the lock shear resistance, normally to the locks.

This extended limit analysis is herein reformulated to develop a method to measure the sliding infeasibility (i.e. infeasibility due to violation of sliding constraints) by a numerical value and to introduce assemblability issues. Given the measured sliding infeasibility, the designer can adjust the number and orientation of the locks to minimize this value and reduce the infeasibility in the model. Besides, the lock orientation initially chosen by the designer or adjusted during the shape exploration to reduce the sliding infeasibility, must let the blocks to be assembled or disassembled. When a block can only translate and not rotate, the block in contact with the other blocks is immobilized in some directions, and free-to-move in the others. Choosing the invalid lock orientations, the block can be immobilized (deadlocked) in all directions. Figure 1 shows an example of the deadlocked situation for the central block, which is an invalid model since the blocks cannot be assembled or disassembled.

The developed method follows the Assembly Path Planning (APP) [22] using Non-Directional Blocking Graph (NDBG) developed by Wilson [23]. Given a number of objects in contact, this method describes the directions along which an object cannot move because those directions are blocked by the other objects in contact. When an object is immobilized in

all directions, the object is so-called un-assemblable. Assembly Path Planning (APP) is one of the major fields of the Assembly Planning AP studies in the manufacturing and industrial engineering, investigating the optimal plans to assemble a whole product composed of smaller parts. A comprehensive review on APP has been carried out by Ghandi and Masehian [24].

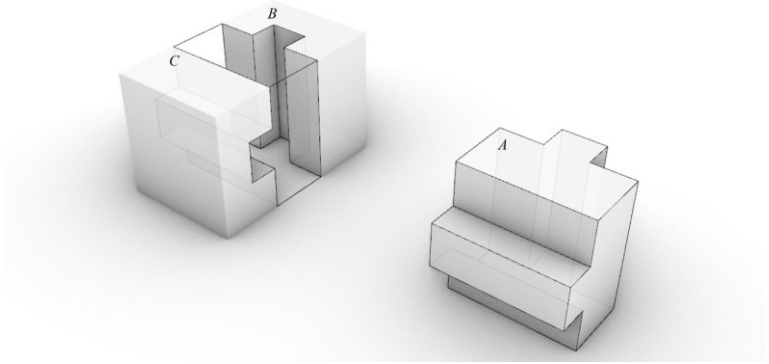


Figure 1: Block *A* cannot be assembled to Blocks *B* and *C* simultaneously.

Given an assembling sequence assigned by the designer, the proposed method finds all the assembling paths along which the block is free to move to be assembled to the other blocks in contact, which were assembled earlier. If no path can be found, the chosen lock orientations for the block faces are detected invalid.

The extended limit analysis and the sliding infeasibility measurement method are briefly introduced in Section 2, while Section 3 proposes a method to analyze the assemblability of the model during the shape exploration, when the lock orientations change to reach the structurally valid model. Some examples are investigated in the same section to demonstrate the performance of the proposed methods. Finally, the conclusions are provided in Section 4.

2 METHOD OF SLIDING INFEASIBILITY MEASUREMENT

Mousavian and Casapulla [13,21] adopted the concave contact model [17,18] to extend limit analysis to the interlocking corrugated interfaces having locks with rectangular cross section (Figure 2a). Such extended limit analysis is herein applied by using the static approach to find one of the possible stable solutions involving associative friction (equivalent to the Coulomb's friction in the static approach) at the contact interfaces. First, at each interlocking interface, two types of failure planes are determined between the locks of two interlocked blocks (dry joints) and between the locks and the main body of the interlocking blocks (fracture planes) (Figure 2b). The locks and the main body of the blocks are considered rigid enough. Merging the dry joint and fracture plane of a single lock, a number of contact points can be distributed on the lock centerline. Internal forces on these points must equilibrate the external forces applied to the block centroids under the following constraints: a) the normal component r^n of each internal force must be in compression, b) the tangential component r^{t1} along the locks must satisfy the associative friction model, c) the tangential component r^{t2} normal to the lock must be less than the shear resistance at each contact point. This resistance is a portion p of the total shear resistance T_0 of the lock, which is considered to be $T_0 = (\tau_k\ s\ b)$, s and b being the lock thickness and length, respectively, and τ_k the material shear strength. The two options for the contact point distribution and shear resistance

definition sketched in Figure 2c are chosen among others [13,21] since they provide the closest shear-torsion behavior to the actual one obtained by a literature experimental test [25].

Solving the linear equilibrium equations under the compression, frictional and shear constraints, the internal forces at the contact points, assumed as variables, are found.The mathematical problem, solved by MATLAB's lsqlin using least square optimization, is formulated as follows:

$$\begin{cases} C_{eq}.\vec{r} + \vec{E} = 0 & Equilibrium\ equation \\ \\ subjected\ to: & \\ \overrightarrow{r^n} \le 0 & compression\ \ constraint \\ \left|\overrightarrow{r^{t1}}\right| \le \mu\left|\overrightarrow{r^n}\right| & friction\ constraint \\ \left|\overrightarrow{r^{t2}}\right| \le \vec{p}\ T_0 & shear\ constraint \end{cases} \quad (1)$$

where C_{eq} is the equilibrium coefficient matrix; $\overrightarrow{r^n}$, $\overrightarrow{r^{t1}}$, $\overrightarrow{r^{t2}}$ are the vectors of the normal and tangential components along the locks, and parallel to them, respectively; $\vec{r}$ is a vector of all the components of the internal forces; $\vec{p}$ is a vector of weights related to the shear resistance at the contact points; $\vec{E}$ is a vector of the external forces and moments. When the solver finds no solution (solver's exit flag is greater than one) the model is recognized structurally infeasible.

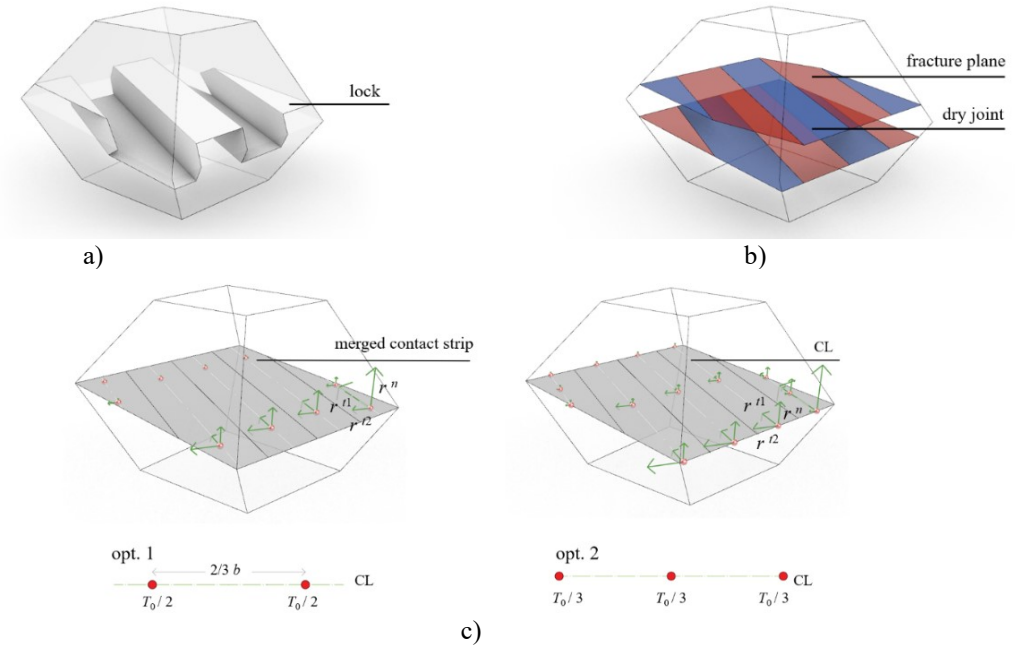


Figure 2: a) Two interlocking blocks with a shared corrugated interface; b) failure planes at the interlocking interface; c) two options for the contact point distribution and shear resistance definition.

The designer can adjust the geometric parameters of the model to remove the structural infeasibility. However, it is usually difficult to guess how to change to parameters to reach a feasible model. If the detected infeasibility can be measured by a numerical value, the

designer can easily tune the parameters to reduce the measured infeasibility to eventually minimize it.

Whiting et al. [25] proposed a method to quantify the structural infeasibility caused by the tensile forces. Similarly, this work measures the infeasibility due to the tangential forces that violate the sliding (friction and shear) constraints, namely sliding infeasibility. Given the measured sliding infeasibility, the designer can adjust the geometric parameters of the interlocking interfaces to minimize it.

The tangential forces can first get any arbitrary value and then the values that are out of the sliding valid ranges are adopted in the optimization process to measure the sliding infeasibility. In this method, however, the internal and external forces are constrained to be in equilibrium and all the normal forces must be in compression.

The extended limit analysis in Eq. (1) is reformulated to develop this method. To this aim, each individual tangential force r^{t} in the vector of variables is replaced by two new variables r^{ta} and r^{tb} so that: $r^{t} = (r^{ta} + r^{tb})$, i.e., r^{t1} parallel to the locks is replaced by the sum of r^{t1a} and r^{t1b}, and similarly r^{t2} normal to the locks is replaced by the sum of r^{t2a} and r^{t2b}. While r^{t1a} and r^{t2a} are respectively constrained to satisfy the friction and shear constraints, r^{t1b} and r^{t2b} can take any arbitrary value.

Then, with the objective function that tries to minimize r^{t1b} and r^{t2b}, the optimization problem is posed as follows:

$$\begin{cases} min \sum_{i=1}^{L} [(r^{t1b})^2 + (r^{t2b})^2] & Objective\ function \\ \\ subjected\ to: & \\ C_{eq}.\vec{r} + \vec{E} = 0 & equilibrium\ equation \\ \overrightarrow{r^{n}} \leq 0 & compression\ \ constraint \\ \left|\overrightarrow{r^{t1a}}\right| \leq \mu \left|\overrightarrow{r^{n}}\right| & friction\ constraint \\ \left|\overrightarrow{r^{t2a}}\right| \leq \vec{p}\ T_0. & shear\ constraint \end{cases} \tag{2}$$

The result of the objective function is defined as the sliding infeasibility measure.

2.1 Validation

The extended limit analysis and the sliding infeasibility measurement method have been implemented to develop a plug-in within the grasshopper (GH) editor, using C# language to model the single layer assemblage with stack bond pattern. The optimization problems are solved by MATLAB solvers which are used as backend. The linear limit analysis and sliding infeasibility measurement problems are solved by MATLAB's lsqlin and fmincon methods, respectively.

To validate the developed plug-in, a semi-circular arch is modeled with 10 m centerline radius, 1 m depth, and 40 blocks under their own weight with 1 N/m^3 density. Figure 3 shows the relation between the minimum thickness of an arch with conventional interfaces and the friction coefficient. It can first be observed that the results obtained by the developed plug-in are in good agreement with the results reported by Gilbert et al. [20] and Casapulla et al. [27]. Then, it is evident that the arch with thickness 1.06 m is structurally infeasible when the

friction coefficient is less than 0.4. In this case, interlocking blocks with large shear strength can be used to increase the sliding resistance of the interfaces.

Table 1, row 1, reports the sliding feasibility of the arch with 1.06 m thickness for different lock orientations, when the friction coefficient μ is 0.33. The results are obtained by the extended limit analysis of Eq. (2). As expected, when the locks are parallel to the arch plane (lock orientation π/2), the assemblage is still infeasible. Changing the lock orientation from π/2 to 0 rad, the sliding resistance of the interfaces increases and eventually the assemblages with lock orientation less than 0.9 rad are recognized feasible.

The second row of Table 1 displays the measured sliding infeasibility of the arch for the different lock orientations. As expected, the infeasibility measure is reduced when the lock orientation changes from π/2 to 0 rad. Considering that the sliding infeasibility measure of a feasible model must be a number very close to zero, the infeasibility measures less than 0.1 reported in Table 1 may represent the feasible arch.

Table 2 reports the sliding feasibility of the arch with friction coefficient equal to 10, using the extended limit analysis and also the sliding infeasibility measures for the different lock orientations. As expected, all the models can be detected structurally feasible and their measured sliding infeasibility is very close to zero.

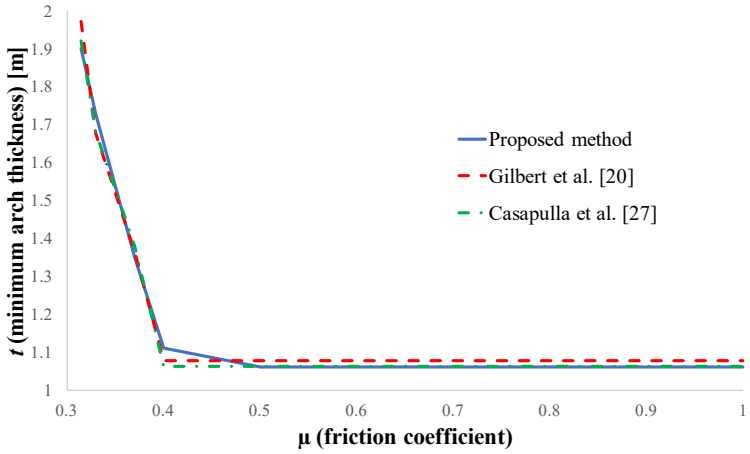


Figure 3: The thinnest semi-circular arch for different friction coefficients reported by the proposed method, Gilbert et al. [20] and Casapulla et al. [27].

Table 1: Measure of sliding infeasibility for μ 0.33; f and i stand for feasibility and infeasibility, respectively.

	μ\orientation (rad)	0	0.3	0.6	0.9	1.2	1.57
limit analysis	0.33	f	f	f	f	i	i
sliding infeasibility measure	0.33	0.026	0.044	0.064	0.084	0.11	0.16

Table 2: Measure of sliding infeasibility for μ 10; f and i stand for feasibility and infeasibility, respectively.

	μ\orientation (rad)	0	0.3	0.6	0.9	1.2	1.57
limit analysis	10	f	f	f	f	f	f
sliding infeasibility measure	10	4×10^{-4}	9×10^{-4}	0.001	0.002	0.007	0.01

3 ASSEMBLABILITY ANALYSIS

This section introduces a method to check the assemblability/disassemblability of a rigid interlocking block. In this work, a block is only allowed to translate and not to rotate and at every assembling sequence, only one block is added to the assemblage. The concept is to investigate if there is at least one translational path through which the block can be assembled or disassembled. Obviously, when a block can be assembled by translating it along a direction, it can be disassembled along the opposite direction. Here, the algorithm detects the disassemblability paths since the demonstration of the directions where an interlocked block is blocked or free to move is more straight-forward.

When two 2D Objects A and B are placed side by side, as in Figure 4, Object A cannot move along all the directions whose terminal points make circular arc $c_A{}^b$ and Object B is blocked by Object A in all the directions whose terminal points make circular arc $c_B{}^b$. Combining these two circular arcs, the Non-Directional Blocking Graph (NDBG) of the whole assembly is modeled. This graph invented by Wilson [23] has been widely used for the Assembly Path Planning.

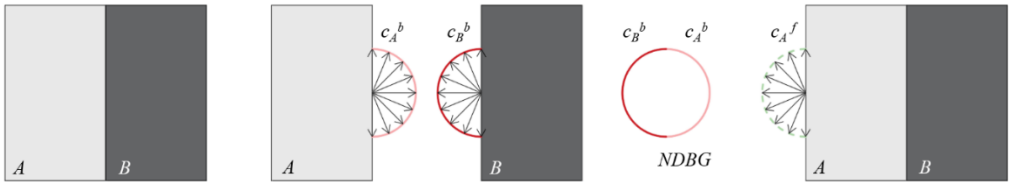


Figure 4: a) Blocking directions for two Objects A and B; b) free to move directions for Objects A.

Alternatively, Non-Directional Free Graph (NDFG) [28] can be used for Assembly Path Planning as well, which is a combination of the circular arcs c^f, representing the directions where the objects are free to move. Assuming that Object B is fixed, Object A can be disassembled from Block B only by translating along one of the directions represented by $c_A{}^f$.

When Objects A and B have two edges in contact (Figure 5), the circular arcs $c_{A1}{}^b$ and $c_{A2}{}^b$ represent the directions along which Object A is blocked by edges E_1 and E_2, respectively. Union of $c_{A1}{}^b$ and $c_{A2}{}^b$ makes $c_A{}^b$ which represents all the directions along which Object A is blocked by Object B. And eventually, subtracting $c_A{}^b$ from a circle, all the directions where Object A is free to move is represented by $c_A{}^f$.

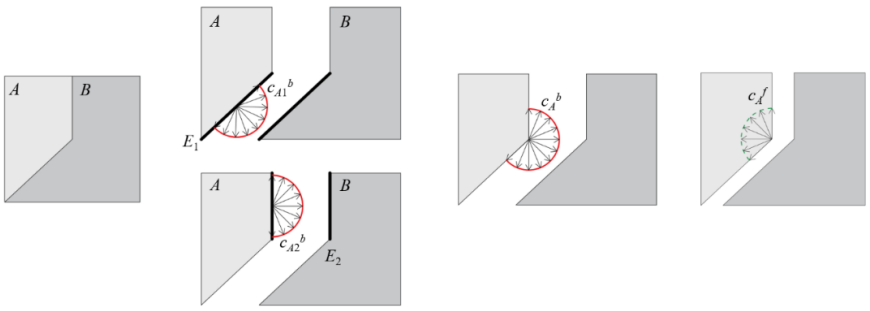


Figure 5: Blocking and free directions for Object A, when Objects A and B have two shared edges.

Similarly, for two 3D Objects A and B with three planar faces in contact (Figure 6), sections of spheres $s_{A1}{}^b$, $s_{A2}{}^b$, and $s_{A3}{}^b$ demonstrate the directions along which Objects A is blocked by Faces F_1, F_2, and F_3, respectively. Union of $s_{A1}{}^b$, $s_{A2}{}^b$, and $s_{A3}{}^b$ makes $s_A{}^b$ which displays all the directions along which Object A is blocked by Object B. Subtracting $s_A{}^b$ from an entire sphere models $s_A{}^f$, which demonstrates the directions along which Object A is free to move. When Object B is fixed, the semi-circular arc $s_A{}^f$ shows all the valid translational paths through which Object A can be disassembled from Object B. It is worth noting that Objects A and B in Figure 6 are interlocking blocks having one lock and increasing the number of the locks, $s_A{}^f$ does not change.

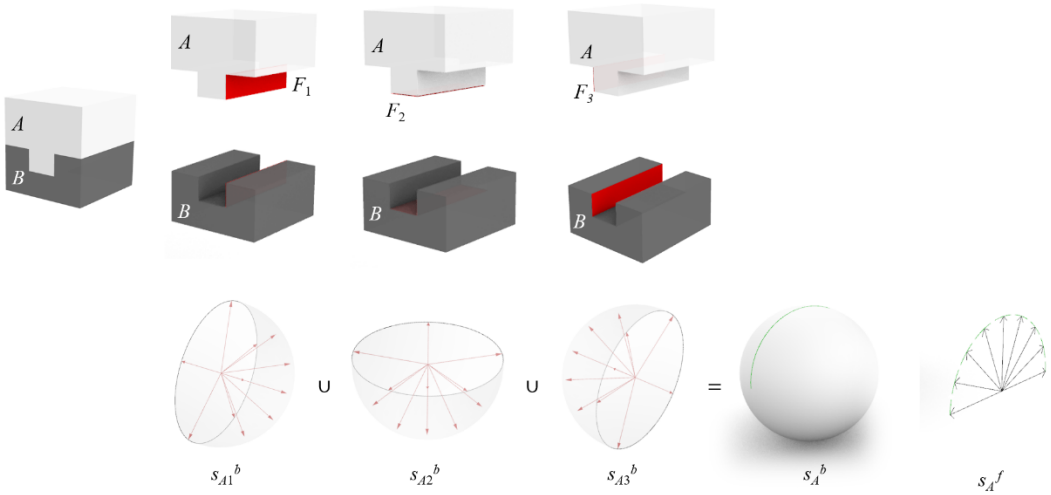
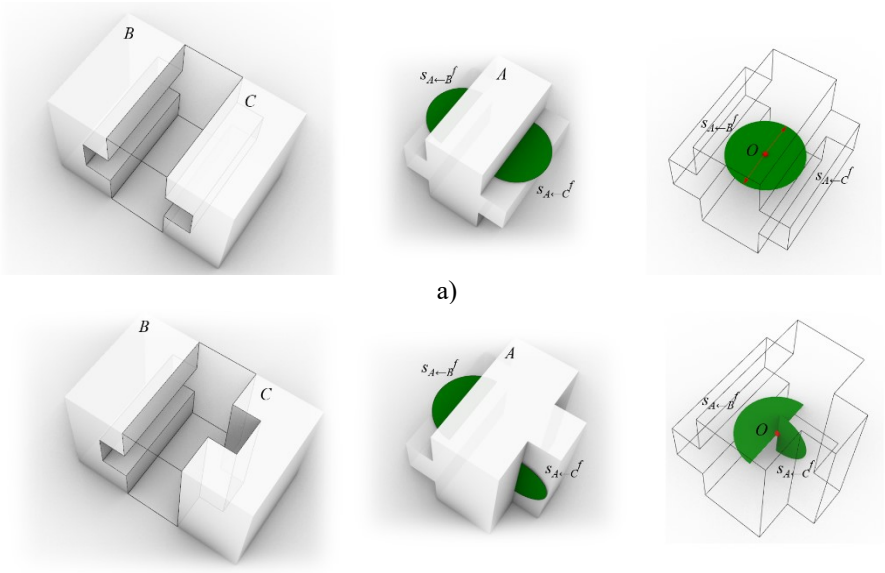


Figure 6: Blocking and free directions for Object A, when Objects A and B have three shared faces.

Moreover, when Object A is in contact with two fixed Objects B and C (Figure 7), two circular arcs $s_{A\leftarrow B}{}^f$ and $s_{A\leftarrow C}{}^f$ displays the directions where Object A is free to move to be disassembled from Objects B and C, respectively. To find all the directions through which Object A can be disassembled from Objects B and C simultaneously, Object A should first be abstracted to its centroid O and then, the arcs $s_{A\leftarrow B}{}^f$ and $s_{A\leftarrow C}{}^f$ can be modeled with their centers passing through O. Intersection of $s_{A\leftarrow B}{}^f$ and $s_{A\leftarrow C}{}^f$ shows the paths along which Object A is free to be disassembled from Objects B and C at the same time. It is evident that Object A can be disassembled from Objects B and C in Figure 7a while it is immobilized in Figure 7b.

This method is extendable to find the directions through which Object i can be separated from fixed Objects 1 to i – 1, where objects are enumerated according to the disassembling sequence assigned by the designer. With reference to Figure 8, arcs $s_{i\leftarrow 1}{}^f$ to $s_{i\leftarrow i-1}{}^f$ displaying the directions where Object i is free to move to be separated from Objects 1 to i - 1, respectively, are first modeled with their centers passing through the centroid of Object i. Then, the intersection of these arcs displays the valid disassembling path for Object i. If the intersection is null (Figure 8a), there is no valid disassembling path, and this shows that the designed model is not assemblable/disassemblable. Therefore, the assemblability constraint can be defined as follows:

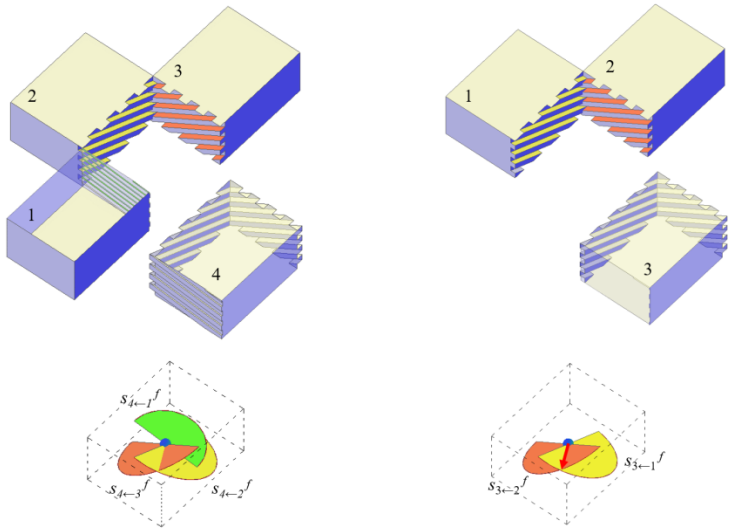
$$\forall\, Object\ i \quad s^f_{i\leftarrow 1} \cap s^f_{i\leftarrow 2} \cap \ldots \cap s^f_{i\leftarrow i-1} \neq \emptyset \tag{3}$$



a)

b)

Figure 7: a) Object A is free to move in two directions displayed by two red arrows; b) Object A is immobilized.



a) b)

Figure 8: a) Object 4 cannot be disassembled from Objects 1, 2, and 3; b) Object 3 can be disassembled from Objects 1, 2 along the red vector.

Introducing this constraint to both extended limit analysis (Eq. (4)) and sliding infeasibility analysis method (Eq. (5)) prevents modeling of structure whose blocks cannot be assembled, and the two formulations can be expressed as:

$$\begin{cases} C_{eq}.\vec{r} + \vec{E} = 0 & Equilibrium\ equation \\ \\ subjected\ to: & \\ \overrightarrow{r^n} \le 0 & compression\ \ constraint \\ \left|\overrightarrow{r^{t1}}\right| \le \mu\left|\overrightarrow{r^n}\right| & friction\ constraint \\ \left|\overrightarrow{r^{t2}}\right| \le \vec{p}\ T_0 & shear\ constraint \\ \forall\ Object\ i \quad s^f_{i\leftarrow 1} \cap s^f_{i\leftarrow 2} \cap \ldots \cap s^f_{i\leftarrow i-1} \neq \emptyset & assemblability\ constraint \end{cases} \tag{4}$$

$$\begin{cases} min \sum_{i=1}^{L} (r^{t1b})^2 + (r^{t2b})^2 & objective\ function \\ \\ subjected\ to: & \\ C_{eq}.\vec{r} + \vec{E} = 0 & equilibrium\ equation \\ \overrightarrow{r^n} \le 0 & compression\ \ constraint \\ \left|\overrightarrow{r^{t1a}}\right| \le \mu\left|\overrightarrow{r^n}\right| & friction\ constraint \\ \left|\overrightarrow{r^{t2a}}\right| \le \vec{p}\ T_0 & shear\ constraint \\ \forall\ Object\ i \quad s^f_{i\leftarrow 1} \cap s^f_{i\leftarrow 2} \cap \ldots \cap s^f_{i\leftarrow i-1} \neq \emptyset & assemblability\ constraint \end{cases} \tag{5}$$

Apparently, changing the disassembling sequence, the assemblability of an assemblage is changed. The ideal disassembling sequence allows the widest range of the lock orientations to model the assemblable assemblage. Finding such ideal sequence will be perused in the future.

4 CONCLUSIONS

This work introduced novel methods to measure the sliding feasibility of an assemblage of interlocking blocks and to check the assemblability of the blocks. It first introduced an extension of limit analysis to the interfaces with orthotropic sliding behavior. The extended limit analysis was then reformulated to develop a method to quantify and measure the sliding infeasibility of a model. This helps the designer to minimize the sliding infeasibility easier. Lastly, the assemblability analysis was described as a method to check if the interlocking blocks can be assembled on the other blocks in contact, when they can only be translated to their final positions in the assemblage. This method was integrated with the limit analysis and the sliding infeasibility measurement methods, preventing the blocks of a structurally sound assemblage to be immobilized, i.e., un-assemblable. In future, the work will be extended to find the optimal assembling sequence by which the widest range of the structurally feasible and assemblable lock orientations can be attained.

Acknowledgements. This project has received funding from the European Union's Horizon 2020 research and innovation programme under the Marie Skłodowska-Curie Grant Agreement No. 791235.

REFERENCES

[1] Liu, H., Liu, P., Lin, K. and Zhao, S. Cyclic behavior of mortarless brick joints with different interlocking shapes. *Materials* (2016) **9(3)**: art. no. 166.

[2] Totoev, Y.Z. Design procedure for semi interlocking masonry. *Journal of Civil Engineering and Architecture* (2015) **9**: 517-525.

[3] Hossain, M. A., Totoev, Y.Z. and Masia, M.J. Friction on Mortar-less Joints in Semi Interlocking Masonry. In: C. Modena et al. (Eds.): *Brick and Block Masonry–Trends, Innovations and Challenges*, CRC Press/Balkema (2016), pp. 1635-1644.

[4] Dyskin, A.V., Pasternak, E. and Estrin, Y. Mortarless structures based on topological interlocking. *Frontiers of Structural and Civil Engineering* (2012) **6(2):**188-197.

[5] Dyskin, A. V., Estrin, Y. and Pasternak, E. Topological Interlocking Materials. In: Y. Estrin, et al. (Eds.). *Architectured Materials in Nature and Engineering*, Springer (2019), pp. 23-49.

[6] Ali, M., Gultom, R.J. and Chouw, N. Capacity of innovative interlocking blocks under monotonic loading. *Construction and Building Materials* (2012) **37**:812-821.

[7] Giresini, L. Design Strategy for the Rocking Stability of Horizontally Restrained Masonry Walls. In: M. Papadrakakis and M. Fragiadakis (Eds.): *Proceedings of the 6th ECCOMAS Thematic Conference on Computational Methods in Structural Dynamics and Earthquake Engineering* (COMPDYN 2017), National Technical University of Athens (2017), pp. 2963-2979.

[8] Giresini, L., Sassu, M. and Sorrentino, L. In situ free-vibration tests on unrestrained and restrained rocking masonry walls. *Earthquake Engineering and Structural Dynamics* (2018) **47(15)**:3006-3025.

[9] Giresini, L., Lourenço, P.B., Puppio, M.L., Sassu, M. Rocking and Kinematic Analysis of Two Masonry Church Façades. In: K. Van Balen and E. Verstrynge (Eds.): *Structural Analysis of Historical Constructions (SAHC 2016)*, CRC Press/Balkema (2016), pp. 1190-1196.

[10] Fang, D., Moradei, J., Brütting, J., Fischer, A., Landez, D.K., Shao, B. and Mueller, C. Modern Timber Design Approaches for Traditional Japanese Architecture: Analytical, Experimental, and Numerical Approaches for the Nuki Joint. In: C. Lázaro et al. (Eds.): *Form and Force (IASS 2019)*, CIMNE (2019), pp. 2911-2918.

[11] Sassu, M., De Falco, A., Giresini, L. and Puppio, M. Structural solutions for low-cost bamboo frames: Experimental tests and constructive assessments. *Materials* (2016) **9(5)**: art. no. 346.

[12] Cipollini, M., Bonannini, E.,Cinotti, M., Sassu, M. Design, production, and installation of wooden walls for the Japan Pavilion at Expo 2015. *Buildings* (2016) **6(4)**: art. no. 43.

[13] Mousavian, E. and Casapulla, C. Structurally informed design of interlocking block assemblages using limit analysis. *Journal of Computational Design and Engineering* (2020) **7(4)**:1-21.

[14] Rippmann M., Curry J., Escobedo D. and Block P. Optimising Stone-Cutting Strategies for Freeform Masonry Vaults. In: J.B. Obrębski and R. Tarczewski (Eds.): *Proceedings of the International Association for Shell and Spatial Structures (IASS) Symposium* (2013), pp. 1-7.

[15] Sassu, M., Stochino, F., Mistretta, F. Assessment method for combined structural and

energy retrofitting in masonry buildings. *Buildings* (2017) **7(3)**: art. no. 71.
[16] Heyman, J. The stone skeleton. *International Journal of solids and structures* (1966) **2(2)**:249-279.
[17] Livesley, R.K. Limit analysis of structures formed from rigid blocks. *International Journal for Numerical Methods in Engineering* (1978) **12(12)**:1853-1871.
[18] Livesley, R.K. A computational model for the limit analysis of three-dimensional masonry structures. *Meccanica* (1992) **27(3)**:161-172.
[19] Casapulla, C. and Maione, A. Modelling the dry-contact interface of rigid blocks under torsion and combined loadings: concavity vs. convexity formulation. *International Journal of Non-Linear Mechanics* (2018) **99**:86-96.
[20] Gilbert, M., Casapulla, C. and Ahmed, H.M. (2006). Limit analysis of masonry block structures with non-associative frictional joints using linear programming. *Computers and Structures* **84(13-14)**:873-887.
[21] Mousavian, E. and Casapulla, C. Limit State Approach for Structurally informed Design of Shells Composed of Interlocking Blocks. In: C. Lázaro et al. (Eds.): *Form and Force (IASS 2019)*, CIMNE (2019), pp. 1610-1618.
[22] Canny, J. *The complexity of robot motion planning*. MIT press (1988).
[23] Wilson, R.H. *On Geometric Assembly Planning*, PhD thesis No. STAN-CS-92-1416 (1992) Stanford University, Department of Computer Science.
[24] Ghandi, S. and Masehian, E. Review and taxonomies of assembly and disassembly path planning problems and approaches. *Computer-Aided Design* (2015) **67**:58-86.
[25] Casapulla, C. and Portioli F. Experimental tests on the limit states of dry-jointed tuff blocks. *Materials and Structures* (2016) **49(3)**:751-767.
[26] Whiting, E., Ochsendorf, J. and Durand, F. Procedural modeling of structurally-sound masonry buildings. *ACM Transactions on Graphics* (2009) **28(5)**:112:1-112:9.
[27] Casapulla, C., Mousavian, E. and Zarghani, M. A digital tool to design structurally feasible semi-circular masonry arches composed of interlocking blocks. *Computers and Structures* (2019) **221**:111-126.
[28] Tai, A.S.C. *Design for assembly: a computational approach to construct interlocking wooden frames*, PhD thesis (2012) Massachusetts Institute of Technology.

12th International Conference on Structural Analysis of Historical Constructions
SAHC 2020
P. Roca, L. Pelà and C. Molins (Eds.)

ASSESSMENT OF STRUCTURAL DAMAGE AND EVOLUTION IN TIME IN HISTORICAL CONSTRUCTIONS USING NUMERICAL MODELS: THE CASE OF THE CHURCH OF SAINT BASSIANO IN PIZZIGHETTONE, CREMONA

GRIGOR ANGJELIU[1*], GIULIANA CARDANI[1] AND DARIO CORONELLI[1]

[1]Department of Civil and Environmental Engineering
Politecnico di Milano (POLIMI)
Piazza Leonardo da Vinci, 32, 20133 Milan, Italy
e-mail: grigor.angjeliu@polimi.it, www.polimi.it (*corresponding author)
email: {giuliana.cardani, dario.coronelli}@polimi.it, www.polimi.it

Keywords: Historical Structure, Masonry, Damage, Lidar survey, Structural evolution, FE model.

Abstract. *This paper investigates the capability of advanced numerical modelling techniques to simulate experimental observations as damage or deformations in complex masonry structures. The case of the church of St. Bassiano in Pizzighettone, Cremona Italy is chosen.*

A multidisciplinary research was set up to collect data as geometric survey with Lidar technology, measurement of axial force in the iron tie rods of the nave, and a monitoring system for crack widths. The data was used as an input to develop and validate a finite element model to study the structural damage and the evolution of the building in time.

The finite element model features a three-dimensional geometry, which is created in part automatically, taking advantage of a parametric model for ribbed masonry vaults, proposed recently by the authors. The FE model results in close adherence with the real building structure, due to the accuracy of the collected data. The simulation model features a continuum plastic damage model to take into consideration the masonry constitutive behaviour.

The results show how the system response is closely related to the structural evolution in time, associated with the dismantling of the chapels on the south side and the addition of the iron tie rods in the nave. The numerical simulations highlight also the important effect of the soil settlements in the present crack pattern. The information obtained using this approach will allow to understand the active mechanisms in the building and to optimise the technical interventions in critical parts of the structure.

1 INTRODUCTION

Changes, transformations and repairs that historical buildings have undergone over the centuries, leave indelible traces in their structure, often affecting the local or even global structural behaviour of the buildings. The actual performance is difficult to be understood and far from that designed at the time of its construction.

The value of architectural heritage is not only related to its aesthetic appearance, but also to

the integrity of materials and structures, as a single product of a constructive technology of a specific historical period and place [1]. Preserving the material component is therefore closely connected with understating the causes of damage and designing compatible repair techniques.

Existing damage in the form of cracks or deformation, may originate from different causes, including: loads, actions, or construction phases which may not be present today [2]. Advanced numerical models are widely proposed in the literature to understand and explain observed damage, understand its evolution in time and design structural strengthening [3]. When considering the complexity of historical buildings, the accurate recording of their geometry and state of conservation are essential to build a structural model correctly representing its structural deficiencies. In this direction, technologies as Lidar scanning have made possible a fast documentation of buildings, in particular remote elements which are difficult to be surveyed manually e.g. vaults. Furthermore, Scan to BIM processes [4] or procedural modelling has made 3D solid models more accessible for FE simulations [5-7].

Particular attention has been lately dedicated to considering the structural evolution in time through the sequential analysis in continuum models. In the Basilica of St. Vitale in Ravenna the detailed 3D FE model was used to investigate the origin of the surveyed crack pattern and concluded that among the causes could be the transformations and repairs in time [8]. Among the first examples of sequential analysis combined with long-term effect analysis was considered in Mallorca Cathedral, to interpret the present damage and current deformations [9]. In Milan Cathedral a correlation was demonstrated between the construction process, settlements in time and the tension force in iron ties [10].

In the present paper we will investigate the possibility to correlate the observed damage through a 3D FE model by considering structural transformation through sequential analysis. The case study is the parish church of St. Bassiano, located in Pizzighettone, Cremona in Italy (Fig.1). It features many construction phases and transformations which make it an ideal case to study the effects of evolution in time in the structural response. The results focus on the interpretation of the observed damage in relation to the removal of the southern chapels and the addition of iron tie rods in the central nave which significantly affected the structural response.


a)


b)

Figure 1: Saint Bassiano church: a) external and b) internal view.

2 CASE STUDY

2.1 Overview

The church of St. Bassiano was built in the 12th century in Lombard-Romanesque style (Fig. 1) It is located in the center of Pizzighettone, a small city in Northern Italy called in Latin language

Piceleo, along the Adda river. The church of St. Bassiano was closed for celebrations and access for visitors in 2012, as the damage observed in the structure increased seriously after the earthquake that hit Emilia Romagna region in 2012.

2.2 Geometric survey

A geometric survey was carried using a high-resolution LiDAR sensor (OS1-64). The configuration during the acquisition phase was set out to a horizontal resolution of 2048 points and a vertical resolution of 64 point at a rotation rate of 10Hz (Fig. 2 - 3).

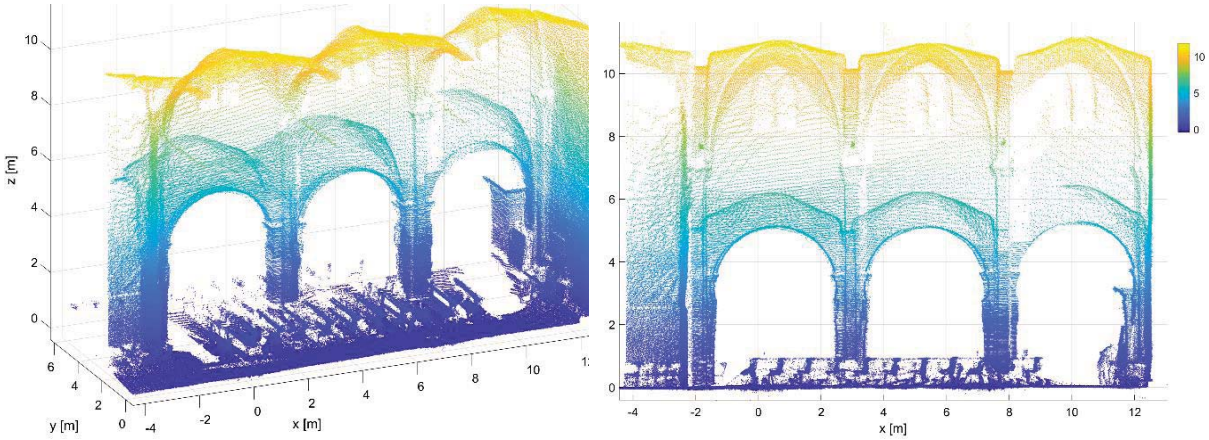


Figure 2: Point cloud measurement of the first 3 bays: a) 3D, b) section.

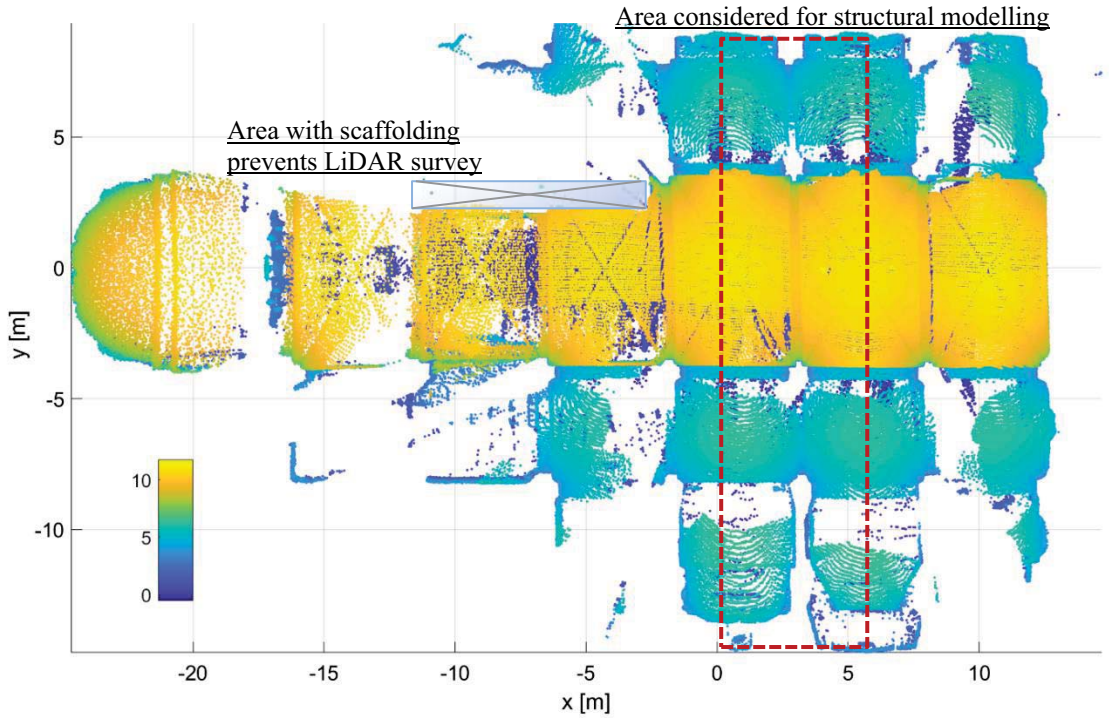


Figure 3: Point cloud measurement of the interior of the church of St. Bassiano.

The survey was focused on the first 3 spans of the church, starting from the facade. It considered a continuous path along the central nave, from which only 12 scans out of 150 where extracted and used to create the final point cloud. The initial alignment was based on the data provided by the Inertial Measurement Unit. A second alignment step was carried out by using the Iterative Closed Point algorithm (ICP) [11]. The final point cloud includes 1 million points and an alignment error of 0.02m (Fig. 2 - 3). The southern part (comprising a part of the nave and aisle) could not be surveyed due to a scaffold present for cleaning paintings.

2.3 Historical notes on the structural evolution

The structural evolution of the church of St. Bassiano is closely connected with historic events between the 15th and 19th centuries, when it was object of many interventions [12]. In the 14th century, Pizzighettone become part of the Milanese domain under the Visconti first and then the Sforza family, who built the masonry town walls [13]. In the beginning of the 16th century, the walled town was invaded by the French and then by the Spanish. In the 18th and 19th centuries the town was gained by the Austrians, and in between by Napoleon's troops, until the unification of Italy in 1861. The following phases can be determined (Fig. 4):

1) The reconstruction of a pre-existing church starting from 1158 and dedicated to Saint Bassiano. The building probably already had three naves and two towers at the place of the two lateral apses.

2) In medieval time cross masonry vaults were added over the three naves and the façade was elevated to cover the increased height of the central nave.

3) In 1456 the Milanese Sforza family radically transformed the architectonical aspect of the church: the façade was elevated, and a rose window was inserted cutting a pre-existing window. Two rows of chapels were added on both external sides of the aisles. A new roof covered Northward the nave and the chapels with only one single roof pitch.

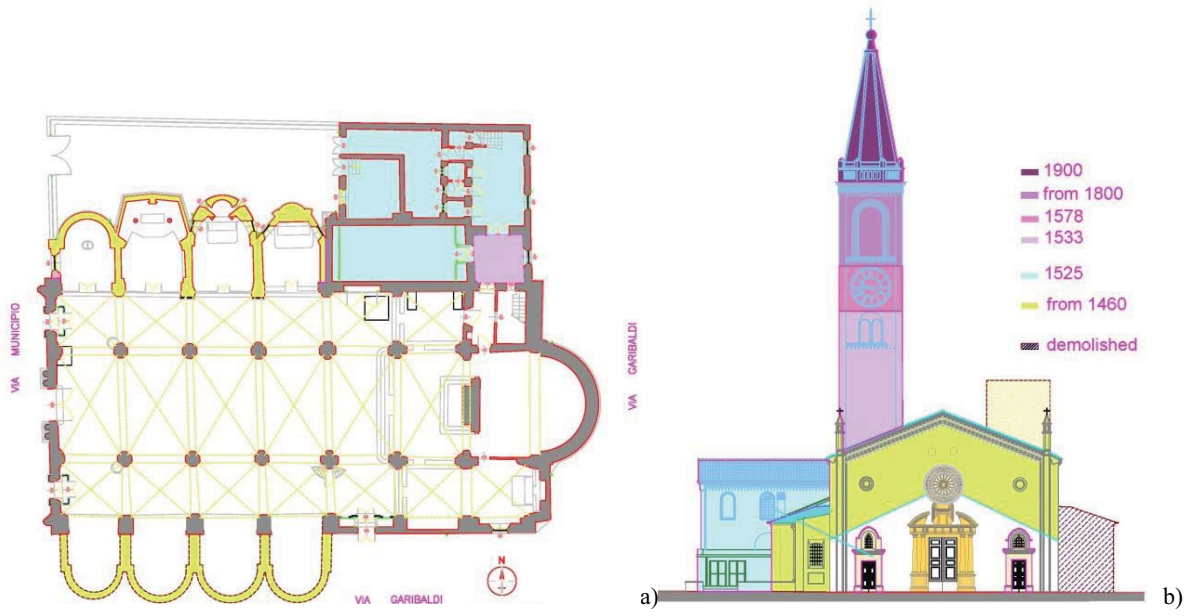


Figure 4: Historical evolution of the St. Bassiano church: a) plan and b) West facade view [12].

4) In late Renaissance time, between 1525 and 1580, additional changes occurred: a) in 1525 the present sacristy was added North-West of the church; in 1533 the bell tower was moved from the South to the North side of the apse and the first part of the present tower was built (Fig. 4); In 1578 the first elevation of the bellfry took place to add a clock.

5) In the 18th century the elevation of the old bellfry on the South side was demolished and the entrance portal probably was added at that time.

6) In the 19th century the facing South chapels were demolished, probably due to the need to widen the adjacent roadway. At this time, iron tie rods were added to the masonry vaults. In 1820 the bellfry on the North side was further elevated and in 1835 the internal church was fully decorated with the present visible style.

7) In the early 20th century the last elevation of the bellfry with octagonal shape was added. In 1963 a restoration made by the architect A. Edallo, changed the roof, partially also with modern reinforced concrete beams and the long single pitch Northward was demolished. Two chapels on the North side were rebuilt in modern style.

2.3 Description of the structural conditions

The crack pattern survey highlighted the serious damage both in the vertical and horizontal structures, weakened by the continuous transformations over the centuries. Almost continuous lines of cracks can be observed in the longitudinal direction along the nave and aisles starting close to the façade and reaching the apse (Fig. 5). Past interventions, supporting directly the roof over the vault, burdened the nave vaults, subsequently increasing their thrust on the aisles and causing many structural cracks on the arches of the central nave. Discontinuities are present also along the chapels and soil settlement effects are recognizable on an internal pillar of the main nave in South-East direction.

The belfry has a poor foundation (in the 1st construction phase it was probably a portico) which caused a relevant out of plumb of about 12 cm towards the North-East side, with resultant crushing on one side and dragging on the other side, with consequences on the sacristy (Fig. 5).

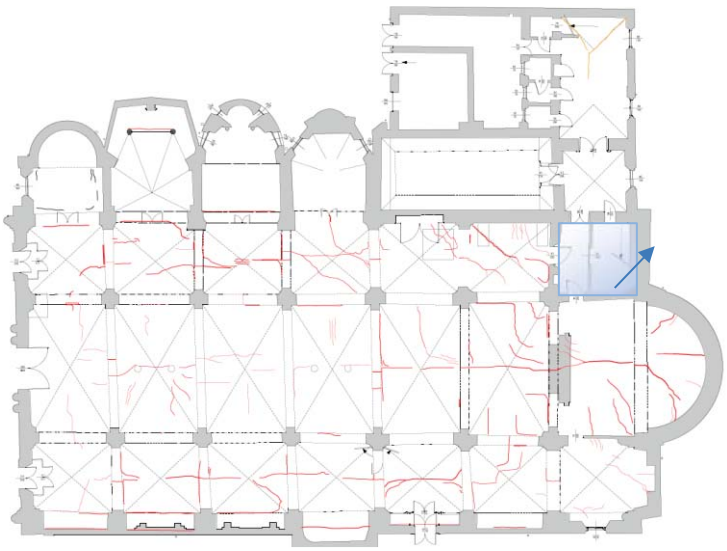


Figure 5: Crack pattern survey of the vaults of St. Bassiano church as of today, and bellfry out of plumb.

The severe structural damage and the needs to replace the damaged roof led then in 2013 to a new general structural strengthening intervention [12] that required the closing of the town church for many years.

The intervention was divided in different phases: the first phase included the complete substitution of the main nave roof from the façade to the apse, with a new timber structure not loading the vaults anymore and with timber trusses, removing the horizontal thrust on the bearing walls. Such intervention stopped the main damage cause affecting the apse, the cross vaults and the main masonry arches of the nave, which were consolidated with FRCM (Fiber Reinforced Cementitious Matrix) composite system, made with a bidirectional mesh of Polybenzoxazole (PBO) fibers [12].

The first phase was considered urgent, allowing the temporary reopening of the church at the end of this step; a second and a third phases (dealing with the aisles, the towers and foundations) were postponed to find the necessary funds and to conclude the works; these at present still need to be executed.

3 STRUCTURAL MODEL

3.1 FE model geometry and meshing

The geometry of the FE model is based on LiDAR scanning of the church interior (see section 2.2). Although, the geometry is based on the scanning of the 2nd bay, the model can be considered as representative of the typical bay.

The FE model includes approximately 300’000 nodes, and a discretization with 122’000 linear tetrahedral elements.

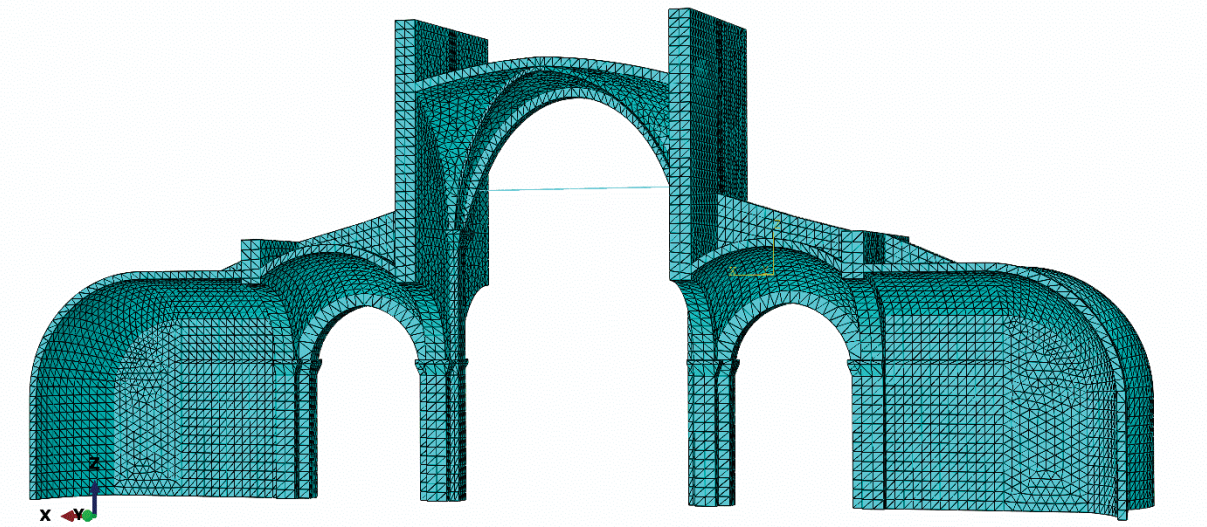


Figure 6: View of St. Bassiano discretized FE model, including also the removed southern chapels

The model considers a parametric geometric modelling procedure, for the vault in the central nave which is the most complex parts of the system[5]. It considers the *tas-de-charge*, ribs, arches, and the vault surcharge [14]. The rest of the structural members (the piers, the buttresses, the walls, and iron tie rods) are modelled manually in Abaqus CAE environment ([15]). The important details of the geometry such as the curvature of the arches, ribs, vault web and characteristics of the geometric rules adopted during the construction are identified.

Finally, the numerical model considers also the southern chapels, removed in the 19th century. This component of the structural system is necessary as an input for the sequential analysis. The geometry of the southern chapel is assumed to be like the one of the northern sides, since no data are available in the moment.

3.2 Constitutive model and material properties

The masonry is modelled with a non-linear plastic damage constitutive model according to the description of Lee and Fenves [16]. The damage variables in tension *dt* and in compression *dc* are taken into consideration by eq. 1 and eq. 2:

$$\sigma_t = (1 - d_t)\, E_0\, (\varepsilon_t - \varepsilon_t^{pl})\ ;\ \ \sigma_c = (1 - d_c)\, E_0\, (\varepsilon_c - \varepsilon_c^{pl}) \tag{1}$$

where: σ_t (, σ_c) is the mono-axial tensile (compressive) stress,
E_0 is the initial elastic modulus,
ε_t (ε_c) is the total strain in tension (compression),
ε^{pl} is the equivalent plastic strain in tension (compression).

Based on similar application in the literature [10] the following choices have been made on the other mechanical parameters necessary in the constitutive model: Dilation angle ψ, 36° ; eccentricity 0.1 ; the ratio of biaxial to uniaxial compression yield strength f_{b0}/f_{c0} , 1.16 ; the ratio between the magnitude of the deviatoric stress in uniaxial tension and compression $K_c = 0.667$ and viscosity parameter is kept at a low level, 0.0002. The data regarding the stress-strain curve are reported in table 1. In the present analysis only one masonry typology is considered. The selected mechanical parameters are chosen based on similar masonry typologies (see table C8A.2.1.in [17]). Although, it is possible to consider more typologies, this could be misleading considering the current level of knowledge. A different choice is clearly made for the rubble fill in the masonry vaults, where the mechanical properties are clearly lower compared to the rest of the structure (Table 1).

Table 1: Mechanical material properties adopted for the numerical analysis.

Properties / Type	γ $\left[\frac{kN}{m^3}\right]$	E $\left[\frac{N}{mm^2}\right]$	ϑ $[-]$	f_c $\left[\frac{N}{mm^2}\right]$	f_t $\left[\frac{N}{mm^2}\right]$	G_f^I $\left[\frac{Nmm}{mm^2}\right]$	G_{fci} $\left[\frac{Nmm}{mm^2}\right]$
Brick masonry	18	2000	0.2	4	0.2	0.012	1.2
Rubble fill masonry	16	800	0.2	2	0.15	0.012	0.5
Steel	79	$2 \cdot 10^5$	0.3	-	-	-	-

3.3 Staged construction analysis

The structural analysis considers a sequential analysis focusing on the interventions in the 19th century where the southern chapels were removed, and the central nave was reinforced with iron ties to contain its horizontal thrust, with average cross section 3,4 x 6 cm. Moreover, as suggested by Angjeliu, et al. [10] also the construction phase of the central nave has been included in order to have an improved prediction of the axial force in the iron ties. The considered stages can be described as follows:

Stage 1: Construction of the aisle and chapels (fig. 7a),

Stage 2: Construction of the central nave (fig. 7b),

Stage 3: Removal of the southern chapel and addition of the iron ties in the nave (fig. 7c).

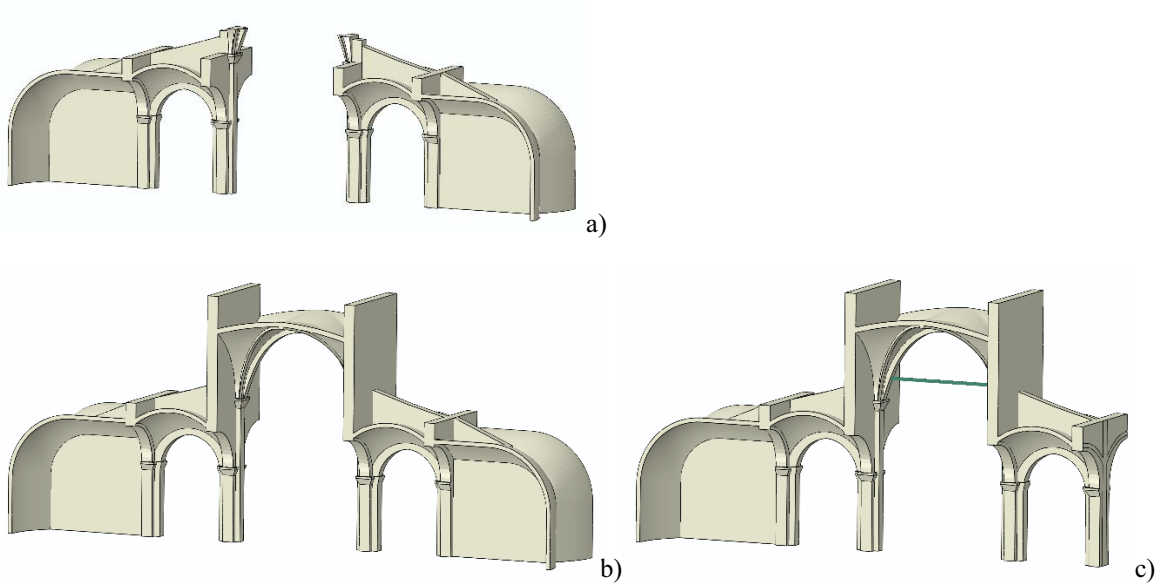


Figure 7: Phases considered during in the sequential analysis

4 RESULTS

In this section the results focus on the interpretation of the observed damage in relation to the documented structural evolution in time of the church of St. Bassiano. In particular, the removal of the southern chapels and the addition of iron tie rods in the central nave changed significantly the structural response.

4.1 Self-weight analysis

The maximal vertical stresses (S33) due to self-weight in the original configuration is approximately 0.79 MPa. These are average values but also typical in masonry constructions. The change of the structural system with the insertion of the steel ties and the removal of the chapels with a buttress role has a significant effect to self-weight vertical stresses which double to 1.76 MPa (Fig. 8).

In particular the results show that the removal of the southern chapel gives rise to damage propagation in the aisle vaults and walls over the arch (Fig. 9). Therefore, the crack in the aisle vaults documented in the recent crack pattern, can be connected clearly with the removal of the

southern chapels in the 19th century (Fig. 5). The inserted iron tie, which in this stage is around 47 kN, is not enough to completely replace the buttressing effect of the previous chapels.

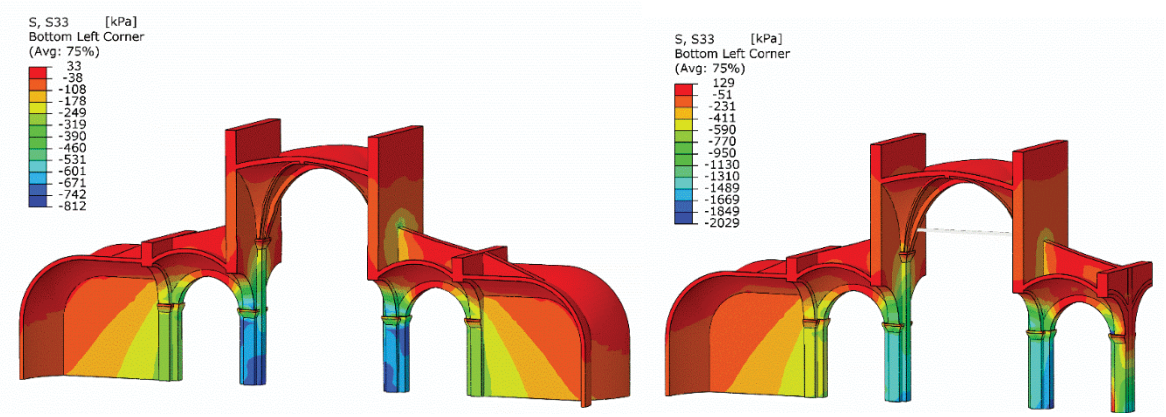


Figure 8: Vertical stresses S33 due to self-weight: a) original configuration, b) current configuration.

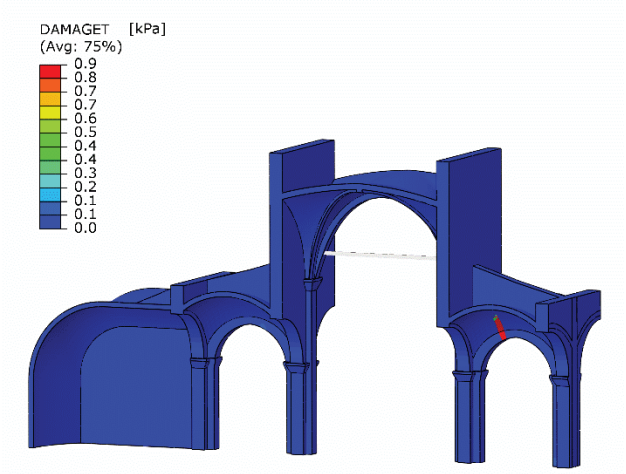


Figure 9: Damage in the southern aisle due to the removal of the chapel in the current configuration

4.2 Settlement analysis

As widely studied in the literature, the soil settlements have a significant effects on damage in historic masonry buildings [18]. In the case of St. Bassiano church, beside the certainty on the presence of soil settlements, there was no information on their specific effects. A set of analysis, considering vertical settlements of 2cm were used to quantify soil settlements effects on the crack pattern. A comparison of the results (Fig. 10) with the observed crack pattern is useful to understand the settlements which actually happened. The preliminary results show that soil settlements in the 2nd and 4th line of piers give a good match between the simulations and the survey crack pattern (Fig. 5). Moreover, the settlements of the 4th line of supports find further confirmation in the values of tension force in the iron ties (see next section 4.3).

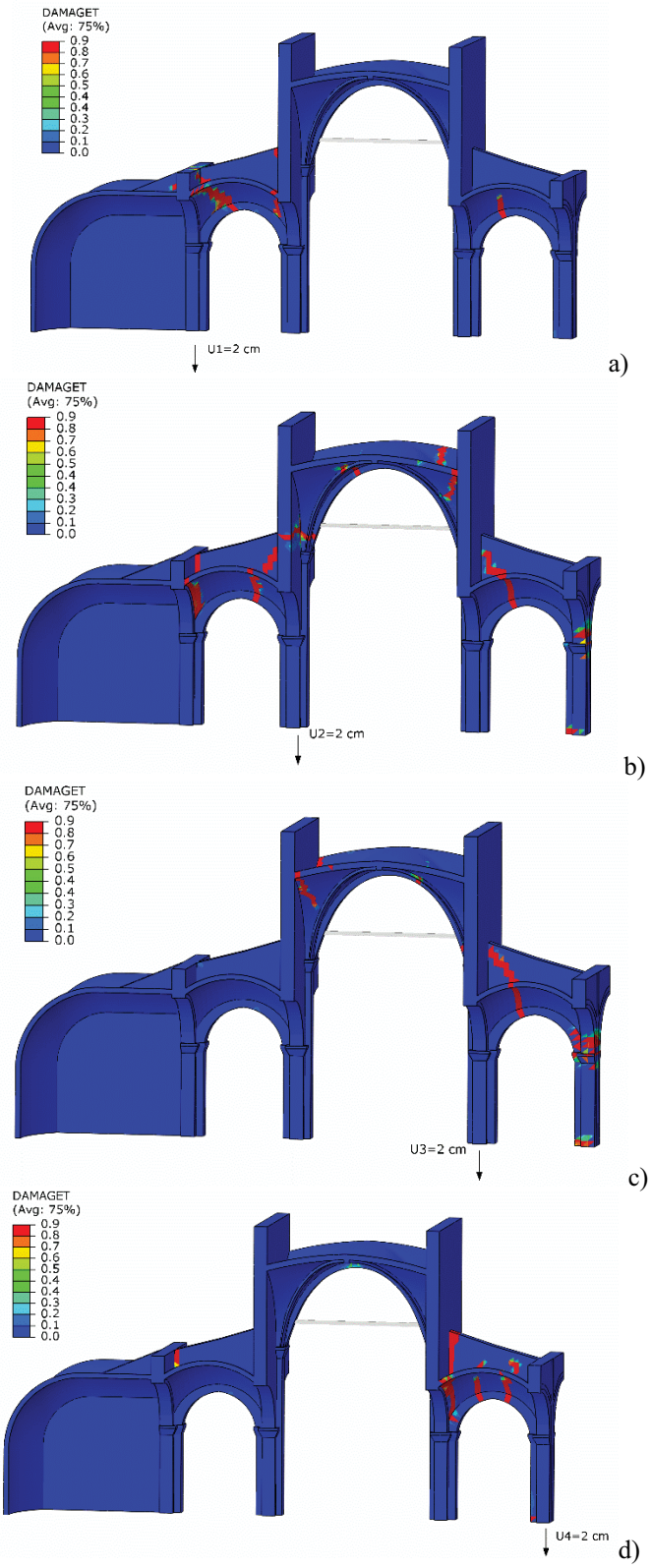


Figure 10: Damage simulation in the current configuration due to settlements a) 1st, b) 2nd, c) 3rd, d) 4th support.

4.3 Analysis of the tension in the iron tie rods

The tension force in the iron tie rods, measured experimentally during a previous diagnostic campaign [12] is used here in combination of the numerical model to understand the effects of the settlements (Fig. 11). The tension force in the iron tie rods from the self-weight is 46.9 kN, which is far from the experimental values, denoting the possibility of settlement effects (as seen in the crack pattern).

The settlements effects produce tension force values in the range 22 kN – 97 kN. In particular the three supports 1 – 3 contribute to lowering the tension tie force. An exception here is only in the 4th support (southern pier) settlement, which doubles the axial force up to 97 kN. This value is particularly close to experimental measurements in the 1st and 3rd bay, which indicates the settlement of the 4th support gives an important contribution in the damage pattern and the tension value in iron ties. Further analysis of these results should allow to understand a more detailed view of the actual combination.

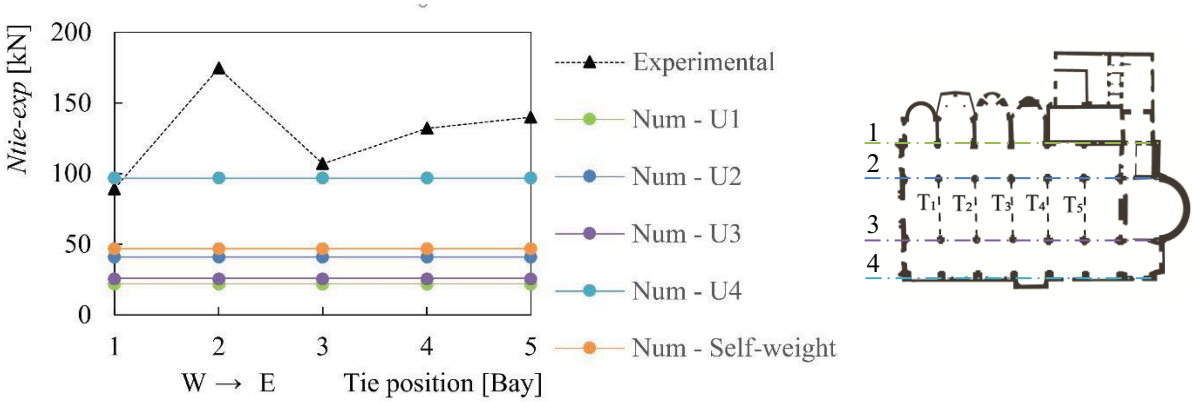


Figure 11: Measurements of the iron tie axial force and the iron tie rod position in plan.

5 CONCLUSIONS

In the present paper the study of the structural damage in relation to construction phases and to soil settlements has been presented. The church of St. Bassiano which has been used as case study features many transformations in the past centuries. This makes it a perfect case to study these phenomena and observations. The conclusions of present study are:

- the importance of the geometry and the survey with LiDAR scanning in the creation of realistic FE structural models;
- the clear connection of the observed damage with the removal of the southern chapels;
- the crack pattern is related to a combination of settlements, where the one affecting the southern pier is particularly important since it produces damage similar to the present crack pattern; this result is relevant for the strengthening intervention – *de facto* one of the future restoration phases will improve the foundations by underpinning.
- the possibility to interpret the measured tie tension as a combination of settlement effects.

Further work could consider: LiDAR scanning of the exterior and updating the FE model accordingly; extraction of structural deformations from the point cloud, calibration and refinement of material properties and a detailed study of the soil settlement effect combination.

Acknowledgements

The authors are grateful to Ouster Inc. who supported our research work by donating a Lidar sensor, used during geometric survey in the church of St. Bassiano. We also thank the Rev. Andrea Bastoni, the Rev. Andrea Lamperti Tornaghi and Eng. Gian Ermes Massetti for the access, help, diagnostic data and support during the study of the church of St. Bassiano in Pizzighettone (Cremona).

REFERENCES

[1] H. Stovel, Origins and influence of the Nara document on authenticity, *APT Bulletin* 39 (2/3) (2008)
[2] S. Saloustros, L. Pelà, P. Roca, J. Portal, Numerical analysis of structural damage in the church of the Poblet Monastery, *Engineering Failure Analysis* 48 (2015) 41-61,
[3] P. Roca, M. Cervera, G. Gariup, L. Pela', Structural Analysis of Masonry Historical Constructions. Classical and Advanced Approaches, *Archives of Computational Methods in Engineering* 17 (3) (2010) 299-325, doi:https://doi.org/10.1007/s11831-010-9046-1.
[4] H. Macher, T. Landes, P. Grussenmeyer, From Point Clouds to Building Information Models: 3D Semi-Automatic Reconstruction of Indoors of Existing Buildings, *Applied Sciences* 7 (10) (2017) 1030
[5] G. Angjeliu, G. Cardani, D. Coronelli, A parametric model for ribbed masonry vaults, *Automation in Construction* 105 (2019) 102785, doi:https://doi.org/10.1016/j.autcon.2019.03.006.
[6] S. Havemann, D.W. Fellner, Generative mesh modeling, University of Braunschweig-Institute of Technology, 2005.
[7] G. Angjeliu, D. Coronelli, G. Cardani, Challenges in Modelling Complex Geometry in Historical Buildings for Numerical Simulations, *Proc. The 18th International Conference on Geometry and Graphics*, Vol. 809, Springer, Milan, Italy, 2019, pp. 1218-1230
[8] A. Taliercio, L. Binda, The Basilica of San Vitale in Ravenna: Investigation on the current structural faults and their mid-term evolution, *Journal of Cultural Heritage* 8 (2) (2007) 99-118,
[9] P. Roca, M. Cervera, L. Pelà, R. Clemente, M. Chiumenti, Continuum FE models for the analysis of Mallorca Cathedral, *Engineering Structures* 46 (2013) 653-670,
[10] G. Angjeliu, D. Coronelli, G. Cardani, T. Boothby, Structural assessment of iron tie rods based on numerical modelling and experimental observations in Milan Cathedral, *Engineering Structures* 206 (2020) 109690, doi:https://doi.org/10.1016/j.engstruct.2019.109690.
[11] P. Glira, N. Pfeifer, C. Briese, C. Ressl, A Correspondence Framework for ALS Strip Adjustments based on Variants of the ICP Algorithm, *Photogrammetrie - Fernerkundung - Geoinformation* 2015 (4) (2015) 275-289, doi:10.1127/pfg/2015/0270.
[12] G. Cardani, G.E. Massetti, When the strengthening of historic masonry buildings should be carried out in different phases: the structural reinforcement and monitoring of the Lombard-Romanesque church of Saint Bassiano, in Pizzighettone (CR), Italy, *Proc. PROHITEC'17-3rd International Conference on Protection of Historical Constructions*, IST Press, Lisbon, 2017, pp. 1-12, isbn:9898481587.
[13] G. Cardani, R. Pizzoli, The town walls of Pizzighettone: A fortified settlement crossed by a river, through six centuries of history, *Sustainable Mediterranean Construction* (1) (2019),
[14] G. Angjeliu, G. Cardani, D. Coronelli, Digital Modelling and Analysis of Masonry Vaults, *ISPRS - International Archives of the Photogrammetry, Remote Sensing and Spatial Information Sciences* XLII-2/W11 (2019) 83-89, doi:https://doi.org/10.5194/isprs-archives-XLII-2-W11-83-2019.
[15] Hibbitt, Karlsson, Sorensen, *ABAQUS Manual*, Dassault Systèmes, 2016.
[16] J.H. Lee, G.L. Fenves, Plastic-damage model for cyclic loading of concrete structures, *Journal of Engineering Mechanics-Asce* 124 (8) (1998) 892-900,
[17] C.S. Ministero delle Infrastrutture d dei Trasporti, Circolare 2 febbraio 2009, n. 617-Istruzioni per l'applicazione delle "Nuove norme tecniche per le costruzioni" di cui al DM 14 gennaio 2008, Gazzetta Ufficiale, 2009.
[18] G. Cardani, D. Coronelli, G. Angjeliu, Damage observation and settlement mechanisms in the naves of the Cathedral of Milan, *Proc. Structural Analysis of Historical Constructions (SAHC)* Leuven, Belgium, 2016.

12th International Conference on Structural Analysis of Historical Constructions
SAHC 2020
P. Roca, L. Pelà and C. Molins (Eds.)

CALIBRATION OF A FEM MODEL WITH COMPLEX GEOMETRY: THE CASE STUDY OF SANTA MARIA MADDALENA CHURCH IN ISCHIA, ITALY

BEATRICE DI NAPOLI[1*], MARIA PIA CIOCCI[1], THOMAS CELANO[2], PAULO B. LOURENÇO[1] AND CLAUDIA CASAPULLA[3]

[1]Institute for Sustainability and Innovation in Structural Engineering (ISISE),
Department of Civil Engineering, University of Minho
Campus de Azurém, 4800-058 Guimarães, Portugal
e-mail: {beatrice.dinapoli1992, mariapiaciocci}@gmail.com, pbl@civil.uminho.pt, www.isise.net
(*corresponding author)

[2]Department of Engineering,
University of Naples Parthenope
Centro Direzionale is.C4, 80143 Napoli, Italy
email: thomas.celano@uniparthenope.it

[3]Department of Structure for Engineering and Architecture
University of Naples Federico II
Via Forno Vecchio, 80143 Napoli, Italy
email: casacla@unina.it

Keywords: FEM model, calibration, OMA, heritage structures, Baraccato system, modeling

Abstract. *The technology of the Bourbonic casa Baraccata is one of the earliest earthquake resisting systems, used since the 18th century across Southern Italy in response to the disastrous earthquakes that hit the region frequently. The church of Santa Maria Maddalena in Casamicciola Terme, Ischia Island, Italy, represents one of the very rare examples, with a unicity lying on the combination of materials adopted. It presents the regular Bourbonic Baraccato walls in the back portion, and tuff-masonry walls embraced in iron frames in the main body. The paper aims at presenting the development of a 3D Finite Element Model (FEM) calibrated taking advantage of ambient vibration tests performed under operational conditions. Sensitivity analyses allowed to inspect and validate several modeling strategies and explore the relevance of the data still unknown to define a reliable numerical model to perform the study on the seismic behavior of the church of Santa Maria Maddalena.*

1 INTRODUCTION

Historical masonry churches are one of the most seismically vulnerable building typologies which need to be preserved considering their value in cultural heritage. Though several in-situ and numerical investigations have been performed in past studies (for example [1]–[5]), the structural behavior of these buildings is still not fully understood to date. The seismic safety assessment of churches is a very complex task due to the numerous irregularities and

uncertainties (geometry, mechanical material properties, historic evolution of the structure, etc.). In particular, these buildings can exhibit numerous failures depending on different parameters such as: mass and stiffness distributions, connection among transversal walls, thrusting roofs, masonry qualities, etc. The failure modes observed for these buildings downstream of seismic events can be divided into a limited group of typical failures. For these reasons, historical masonry structures present a high number of challenges in the safety assessment.

Different conservation methodologies are present in the literature to analyze and retrofit historical masonry construction, as evidenced by [6]. The timber-masonry system represents one of the most used reinforcement strategies in Southern Italy since the catastrophic seismic events of the 18th century. The structural performance of the so-called Bourbonic Baraccato system has been studied by [7] and [8], while investigations on similar systems have been carried out by [9]. This construction system is even more interesting in the case of the church of Santa Maria Maddalena in the Ischia Island (Italy), where it was combined with a mixed iron-masonry solution. A first study on this particular church has been carried out by [10], while open issues on the modeling strategies are still worthy to be addressed.

Non-linear analyses are recommended for the evaluation of the structural behavior of these buildings, requiring a good level of knowledge of the construction such as the mechanical properties of the materials. In common practice, destructive and non-destructive tests can be performed in order to evaluate masonry material properties. In particular, non-destructive tests are mainly used for the evaluation of the elastic properties of the material, such as Young's modulus. Since a calibration of the instruments' curves through the execution of a minimum number of destructive tests is necessary for the determination of reliable values of the mechanical properties, their use in the investigation of the non-linear field of the material is limited. Destructive tests are more suitable to assess the material strength values but they are not recommended, and usually not allowed, for historical buildings due to their high invasiveness. Among non-destructive tests, dynamic identification test is a valuable and reliable tool for the evaluation of the elastic material properties. In fact, the identification of the natural modal shapes and frequencies of the structures can be used for the validation and the calibration of numerical models, in the elastic-field.

This paper presents a methodology for the calibration of a refined numerical model of a case study, the Santa Maria Maddalena church in Ischia, according to the *in-situ* dynamic identification tests presented by [11]. The post-processing results performed in ARTeMIS environment are presented and compared with the eigenvalue analyses results obtained in the numerical model. Lastly, the description of the calibration procedures, obtained through the comparison of the modal shapes and frequencies of the existing structure and the numerical model, enables the validation of some of the adopted modeling strategies and the updating of the Young's moduli of the masonry walls [12]. In addition, the paper presents final remarks regarding the calibration phase and the experimental campaign.

1.1 Description of the case study

Downstream of the moderate seismic event (Mw = 4.2) that hit the Ischia Island on August 21st, 2017, the church of Santa Maria Maddalena in Casamicciola Terme exhibited a relatively low post-seismic damage to the structural system, with distributed crack patterns

mainly detected in the decorative elements, as evidenced by [11].

The building was re-built at the end of the 19th century, after one of the deadliest earthquakes that stroke the Ischia Island in its history, the Casamicciola Terme earthquake of 1883. The construction was designed with one of the most advanced techniques for the seismic risk mitigation at the time and in compliance with the post-seismic recommendations of the municipalities, the adoption of the Bourbonic Baraccato system.

As sketched in Figure 1, the church is composed by the religious spaces arranged with the typical Latin-cross shaped plan configuration (blue), a two-story back part, which hosts some spaces for the parish's activities and the priest's house (green), and the bell tower located in the north-western corner (red). The front part consists of an almost rectangular footprint of dimensions 39.04 m x 20.72 m with five different height levels. The maximum heights of the church are 16.32 m and 22.30 m for the roof top and the bell tower, respectively. It is important to underline that 6 rows of columns are located along the central nave up to the transept. The church covering is supported by a simple system of Palladian timber trusses, aligned along its longitudinal direction.



a) b) c)

Figure 1: a) Volumetric representation, b) external view of the church, c) internal view of the church



a) b)

Figure 2: a) Iron-Baraccato wall panel, b) timber-Baraccato wall panel

The particularity of this building is the use of a mixed system for the load-bearing walls, made of Neapolitan yellow tuff blocks and either chestnut timber or iron elements. In the front part, the church is composed by the mixed iron-masonry technology (Figure 2a), with masonry enveloped in two layers of iron frames which are connected transversally through the

walls thickness. This technology was identified as the so-called 'iron-Baraccato' system for the similarity between the layout of the iron frames and the layout of a regular Baraccato panel ([8], [11]). Some *in-situ* investigations allowed to identify this layout that is presented in Figure 3. The frames encaging the walls constitute a rigid skeleton whose principal advantage to the structural behavior is the connection that they provide between the various structural units. They primarily assure the connection between orthogonal walls, floors and columns. The use of the iron also in these structural units, indeed, enables a structural continuity of the iron frames of the walls and their metallic elements which connection is easily and effectively resolved. Lastly, the presence of a double layer of iron frames tied with each other provides to the walls a certain level of confinement, which increases the overall strength of each wall section.

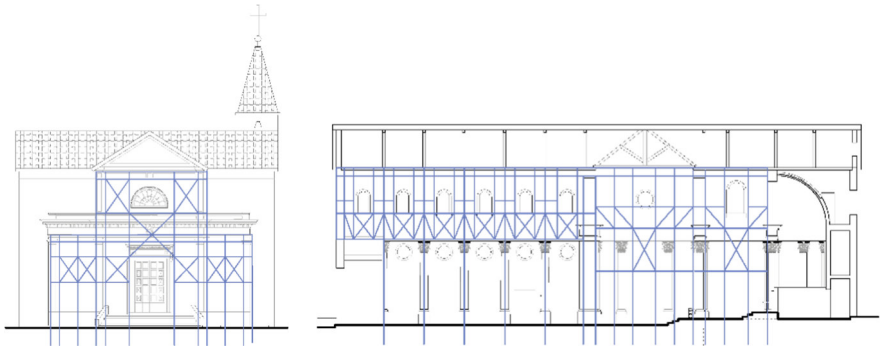


Figure 3: Layouts of the iron frames of the system: a) front façade, b) central nave

Additionally, the use of the traditional Baraccato system (later addressed as 'timber-Baraccato system'), with timber frames embedded inside the masonry texture, was also detected in the back part (Figure 2b). As mentioned above, this constructive system is widespread in Southern Italy as one of the first engineered earthquake resisting systems developed between the 18th and 20th centuries [13]. The use of the two different constructive systems together in a religious building defines the peculiarity of the building itself. The reason for the use of both technologies in the same building is not evident in any reference known to the authors, both were indeed identified by the building regulations as the recommended systems to apply in the reconstruction. However, the use of the iron-Baraccato technology for the main portion of the church and, conversely, the use of the timber-Baraccato one for the rear one may be due to economic reasons.

2 DYNAMIC IDENTIFICATION OF THE CHURCH

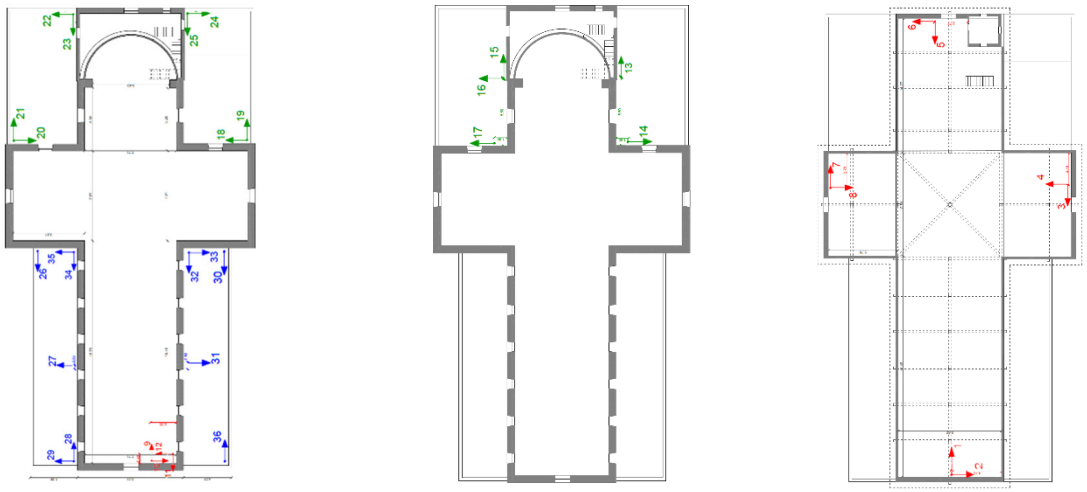
2.1 *In-situ* ambient vibration tests

In-situ ambient vibration tests were performed under operational conditions, under commission of the Campania Regional Directorate for Cultural Heritage (MiBACT), in order to investigate the dynamic response of the structure [11].

Two different test setups were used, with measurement points located at three different levels of the church, as shown in Figure 4. The measurements reported in red color are the ones that were maintained in the same position for the implementation of the two setups, in

green the ones corresponding to the first setup and in blue to the second setup.

The data were collected using ceramic piezoelectric uniaxial accelerometers with high sensitivity (10.0 V/g), low noise (0.13 μg/√Hz), resolution of 10-5 g rms and frequency range of 0.1-200 Hz. They were firmly anchored to the church walls by means of metallic plates avoiding damaged zones and plaster detachments, in order to assure good quality readings. The two setups recorded ambient vibrations for a total time of 3600s with a sampling frequency of 100 Hz. More details can be found in the work of [11].



a) b) c)

Figure 4: Location of the accelerometers at a) +7.35 m level, b) +10.00 m level and c) +11.80 m level

2.2 Operational Modal Analysis (OMA)

The results obtained from the ambient vibration tests were post-processed using ARTeMIS software [14]. The two setups were analyzed both with the Enhanced Frequency Domain Decomposition method (EFDD) and the Stochastic Subspace Identification - Unweighted Principal Components Merged Test Setups method (SSI-UPCX). Since more accurate results were provided by the former method ([10], [11]), only the results obtained by using EFDD are presented in this paper. Figure 5 presents the natural frequencies, modal shapes and damping ratios of the first three modes of vibration which were identified for the structure. In particular, the identified modal shapes can be described as follows:

- Mode I: translational mode in the transversal direction of the church, characterized by major amplitudes of the transept and in-phase displacements between the central nave and the apse walls;
- Mode II: translational mode in the longitudinal direction of the church, characterized by major amplitudes in the central nave and in-phase displacements between the central nave and the apse walls;
- Mode III: mode characterized by the out-of-phase displacements of the longitudinal walls in the transversal direction.

It should be noted that the modal shapes are highly influenced by the geometry implemented in ARTeMIS software, since the representation of the only measured nodes is not enough to clearly understand the effective modes of vibration of the structure. Therefore, the geometrical model of the church was iteratively optimized to compromise between a

sufficiently detailed representation of the building and a sufficiently simplified geometry, taking advantage of the interpolation functions available in ARTeMIS software that were applied to the non-measured nodes to supply the missing information.

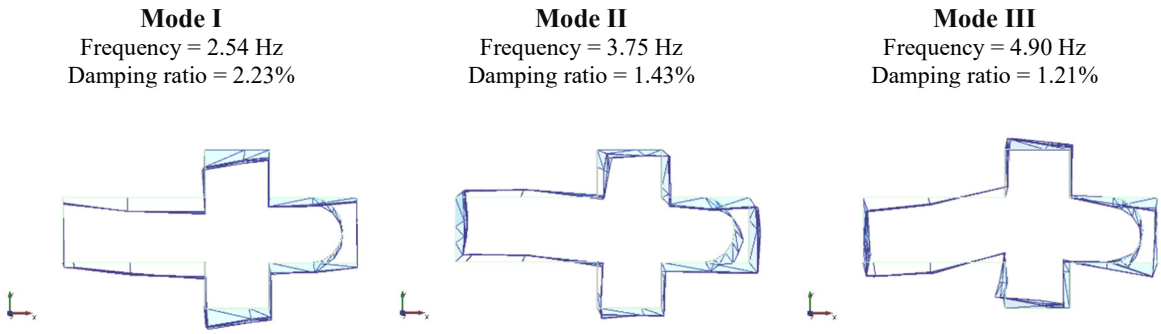


Figure 5: Results obtained by using EFDD method

3 BRIEF DESCRIPTION OF THE FEM MODEL

For the structural assessment of the church a FEM model was prepared in Midas FX+ and DIANA 10.3 (DIsplacement ANAlyser) [15], representing the full relevant structural characteristics of the building.

An initial tentative model was implemented with the following characteristics to be inspected during the calibration phase. In general, the linear elements of the church, i.e. iron and timber frames of the load-bearing walls, columns, timber beams of the apse dome, ties, etc., were represented with 3D beam elements self-standing or embedded in other elements. The two Baraccato walls typologies were modeled with different strategies: a) 3D solid elements with imprinted and embedded 3D beams for the iron-Baraccato walls, b) regular curved shells with imprinted beams for the timber-Baraccato walls. The metallic floor slabs of the building were represented with regular curved shells, implementing orthotropic behavior with relevant stiffness along the beam orientation direction. The roofing system, consisting in a non-thrusting timber system composed of king post trusses, was modeled through the application of an equivalent mass at the top of the model distributed along the roof perimeter. Lastly, as first tentative and not to overweigh the complexity of an already size relevant model, the boundary conditions representing the interaction of the church with the soil were set to perfectly fixed conditions. Figure 6 presents a view of the mesh of the numerical model.

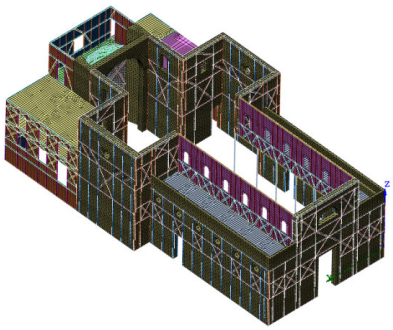


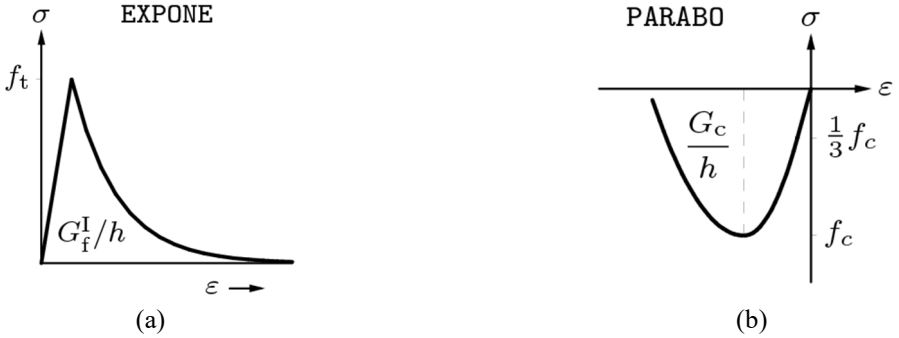
Figure 6: Representation of the 3D FEM model of the church (roof ties omitted) [12]

As for the mechanical characteristics of the materials found in the church, elastic properties were assigned on the base of the literature and code values. The Young's and shear moduli of the orthotropic material implemented for the floor slabs were assigned with simple engineering calculations based on iron properties assumed from the literature and according to [16]. Lastly, masonry was modeled with non-linear properties assuming parabolic behavior in compression and exponential behavior in tension [15] (Figure 7), with strength values estimated as the minimum values recommended by the Italian code [17], reported in Table 1.

Table 1: Elastic material properties of the materials in the model ([10], [12])

WROUGHT IRON [18]			
Material property	**Symbol**	**Value**	**Units**
Density	ρ	7.85	[T/m^3]
Young's modulus	E	154	[GPa]
Poisson's ratio	ν	0.3	[-]
TIMBER – CHESTNUT [19], [20]			
Material property	**Symbol**	**Value**	**Units**
Density	ρ	0.64	[T/m^3]
Young's modulus	E	8000	[MPa]
Poisson's ratio	ν	0.3	[-]
CONCRETE [21]			
Material property	**Symbol**	**Value**	**Units**
Density	ρ	2.4	[T/m^3]
Young's modulus	E	25.3	[GPa]
Poisson's ratio	ν	0.2	[-]
MASONRY [17], [22]			
Material property	**Symbol**	**Value**	**Units**
Density	ρ	14	[T/m^3]
Young's modulus	E	887*	[MPa]
Poisson's ratio	ν	0.2	[-]
Compr. strength	f_c	1400	[kN/m^2]
Tens. strength	f_t	140	[kN/m^2]
Compr. fracture energy [23]	G_c	3.72	[kN/m]
Tens. fracture energy [23]	G_{ft}^I	0.012	[kN/m]

* Young's modulus obtained through modal calibration



(a) (b)

Figure 7: Stress-strain diagrams adopted for the behavior of masonry in a) tension and b) compression

4 CALIBRATION

The described model was implemented with the purpose of including all the complexities of the existing building in order to inspect its global structural and dynamic behavior. To this end, the model construction had to face two challenges: 1) the choice of an appropriate modeling strategy for each structural element, 2) the selection of appropriate mechanical characteristics of the materials involved. Both were overcome by validating the adopted modeling strategies with the results of the OMA introduced in Sect. 2, and by calibrating the relevant elastic mechanical characteristics tuning the natural frequencies of the model with the ones measured in the church. In particular, the process of validation of the modeling strategies consisted of an iterative procedure in which each strategy was inspected by eigenvalue analysis and comparison with the modal parameters obtained with the OMA. On the other hand, due to the great relevance of masonry elastic properties in the definition of the stiffness of the system, its elastic Young's modulus was calibrated to tune the first natural frequency of the FEM model as equal to the first natural frequency of the real structure. This section illustrates the processes that allowed the definition of the final model on which perform the structural analyses ([10], [12]).

4.1 Calibration of the modal shape

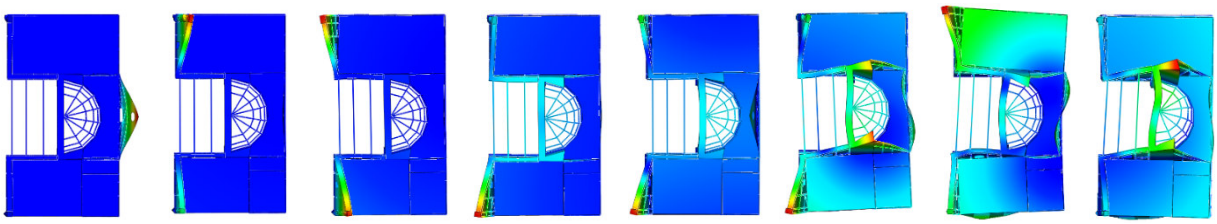
The results of the analysis of the first tentative model evidenced a first global modal shape which mainly involved the transversal deformation of the western section of the transept and a relatively small deformation of the front and the back parts of the church. Even if not corresponding to the experimental results, such a response was expected to some extent. In fact, the difference in the geometrical stiffnesses provided by the western part of the transept, laying partially on the top of the colonnade, and the eastern part, represented by the two L-shaped walls of the transept and the apse, is evident. Conversely, the absence of mobilization of the back portion of the church, witnessing higher stiffness with respect to the main body, needed a more detailed study in order to inspect possible causes. Moreover, the observed dynamic response could also be due to different modeling strategies chosen *a priori*, such as the choice of the boundary conditions to apply to the foundation system and the exclusion of the mass and stiffness contribution given by the roofing system, suppressed in the first tentative model.

For the above-mentioned reasons some alternative models were prepared in order to inspect: a) the influence of the geometrical and mechanical stiffness of the back part, b) the influence of the modeling strategies to apply to the foundation system, c) the influence of the modeling strategies to apply to the roofing system.

4.1.1 Geometrical and mechanical stiffness of the back part

In order to inspect the structural relevance of the rear portion of the building, a partial model was developed by extracting the back portion from the original model (MG_01). This step allowed to highlight, firstly, the great geometrical stiffness of this portion, witnessed by the lack of global modes for frequencies of the order of 10 Hz (Figure 8). Secondly, it was noticed that the modal shape of the church portion is still governed by the L-shaped walls of the transept which do not allow the development of proper translational modal shapes. Lastly, as expected, the layout of the timber frames scarcely influences the modal shapes of the sub-

structures, as evidenced in the analysis of a model with the complete absence of timber elements (MG_02), while having relevance in the modal frequencies as evidenced in Table 2.



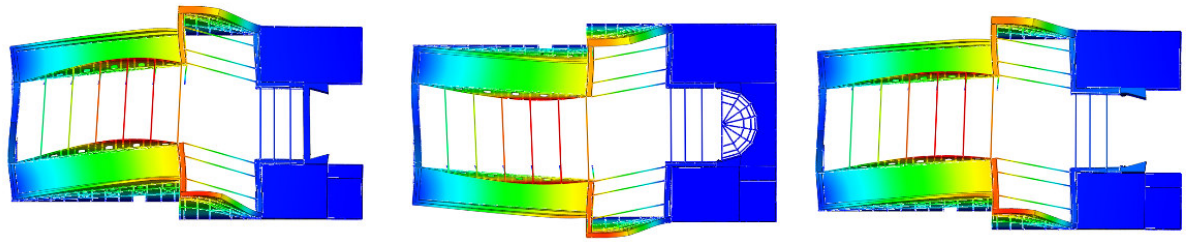
#1 4.07 Hz | #2 5.32 Hz | #3 5.36 Hz | #4 5.99 Hz | #5 7.16 Hz | #6 8.55 Hz | #7 9.93 Hz | #8 10.31 Hz

Figure 8: First eight modal shapes of the MG_01

Table 2: Frequency comparison of the models MG_01 and MG_02

Mode	Frequency [Hz]		Decrease
	MG_01	MG_02	[%]
1	4.071	3.294	19.1
2	5.320	4.926	7.4
3	5.378	5.039	6.3

Besides, the structural stiffness of the rear portion was inspected also with a global model in which the back wall of the canonical house is weakened in various ways: suppression of the central section of the canonical house (MG_03), suppression of the masonry arch at the top of the apse (MG_04), and combination of the two scenarios (MG_05). In fact, the contribution of stiffness of a long wall such as the back wall of the canonical house, along with the apse dome and arch, is relevant to the definition of the global behavior. Conversely, the analyses evidenced that the translational response of the structure is governed by the high stiffness of the western branch of the transept and by the higher deformability of the eastern branch and the naves, so the back wall and apsidal section stiffness contribution is irrelevant (Figure 9). For these reasons and for consistency with the geometrical survey, these elements were kept as original in the final model and further calibration strategies were adopted for the modal shapes.



#1 (f = 3.01 Hz) a) | #1 (f = 3.02 Hz) b) | #1 (f = 3.01 Hz) c)

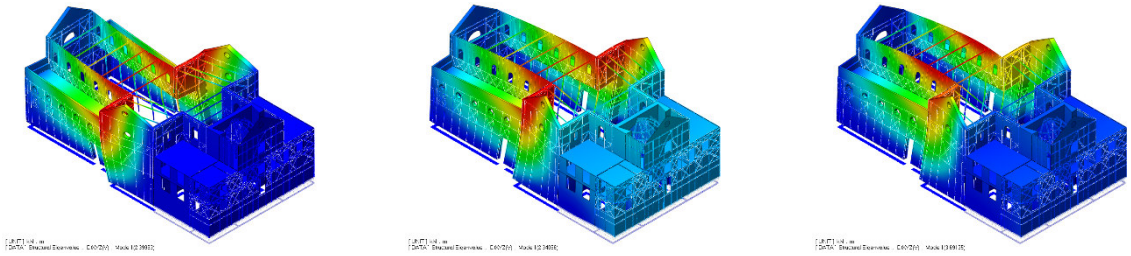
Figure 9: First global modal shapes of the models a) MG_03, b) MG_04, c) MG_05

4.1.2 Foundation stiffness influence

As mentioned above, the modeling strategy for the foundations was the adoption of perfectly rigid boundary conditions. It is well known that in a realistic representation of the

soil-structure interaction some movements are expected. Some analyses were performed (MF_01), by modeling the soil-structure interaction through interface elements with assigned limited stiffness in the vertical direction, according to the Winkler's theory of the elastic soil. It is worth highlighting that such a refined model should be supported by an appropriate level of knowledge about the soil characteristics. In the present case, it was adopted in the scope of inspecting the sensitivity of the dynamic response to these parameters and the need of improving their knowledge. For this reason, the elastic modulus of the soil was esteemed with the literature values (E=120 MPa), considering the edometric modulus equal to 1.15 times the elastic one.

Moreover, since the eigenvalue analyses described so far never involved the translational response of the back portion of the church, an attempt of mobilizing it was carried out by significantly decreasing the mechanical stiffness of the material representing the masonry walls of the canonical house and the stiffness constant of the interface elements below the canonical house (MF_02), also considering optimal characteristics of these two parameters in the main body portion of the church (MF_03). As observed in Figure 10, the influence of these strategies with respect to the dynamic behavior of the church has more relevance in the natural frequencies of the structure rather than in the modal shapes. For this reason, and due to the limited knowledge of the soil characteristics, the interface modeling of the foundations was discarded, and the same value of Young's modulus was kept for all the masonries.



#1 (f = 2.34 Hz) a) #1 (f = 2.40 Hz) b) #1 (f = 3.69 Hz) c)

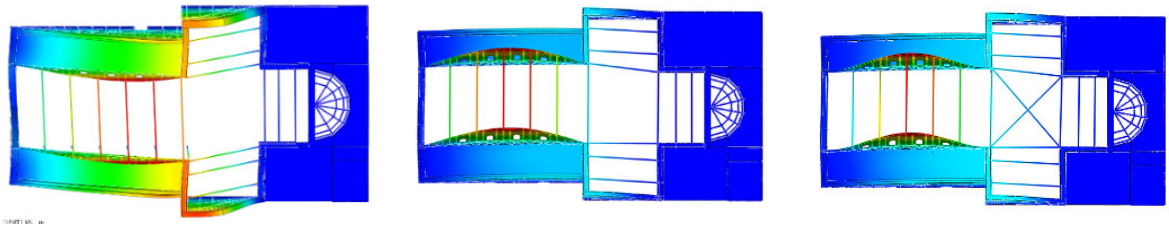
Figure 10: First global modal shapes of the models a) MF_01, b) MF_02, c) MF_03

4.1.3 Roof mass and stiffness influence

With the aim of reducing the model complexity and size, it was initially decided not to include the roofing system in the numerical model, due to the relatively small mass of the timber roof and the relatively high deformability of the attic floor slab. This approach included two simplifications which have great impact in the dynamic response of the structure: a) the suppression of the participating mass of the roof located at the top of the construction; b) the suppression of the stiffness contribution provided at the attic level by the attic floor slab and the roof trusses, which, in particular, enable the redistribution of the horizontal loads at the top of the church walls in case of earthquake.

A further development of an additional model (MR_01), allowed to minimize the error connected to these simplifications, in which the roof mass was applied at the top of the structure as a distributed mass and the timber ties of the roof trusses were simulated with transversal ties over the central nave and the transept. Moreover, more modifications were inspected by inserting additional ties across the cross-shaft (MR_02). The inclusion of these

modifications in the final model allowed a better approximation of the numerical model to the experimental results and to the expected dynamic behavior (Figure 11).



#1 (f = 3.02 Hz) a) #1 (f = 2.16 Hz) b) #1 (f = 2.54 Hz) c)

Figure 11: First global modal shapes in a) the first tentative model, b) MR_01, c) MR_02

However, the modal shapes obtained still hardly correspond to the experimental ones. In fact, the modifications implemented allow a more coherent transversal behavior of the naves, the transept and the back portion, but a relevant deformation of the longitudinal walls of the central nave in the transversal out-of-plane direction is also detected. More studies were performed in order to try to limit the latter behavior by incrementing significantly the stiffness at the roof level, but no significant improvements were found. Conversely, it can be observed that the performed test setup was not able to catch this behavior since no accelerometers were placed at the top-middle location of the second-story walls of the central nave (Figure 4). Hence, the experimental results can only be compared with a partial numerical model in which the upper walls of the central nave are removed, which provide a good shape approximation indeed (Figure 12).

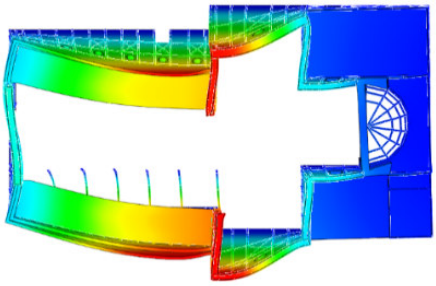


Figure 12: First modal shape of the final model (MR_02) removing the upper walls of the central nave

4.2 Calibration of the modal frequency

Further, the calibration of the elastic properties of the masonry material was carried out, according to [24], through the adaptation of the first numerical global frequency to the first experimental one. The iterative minimization procedure of error on the first frequency led to the estimation of a Young's modulus of the masonry material of 887 MPa, from a first tentative value of 920 MPa. Subsequently, the Modal Assurance Criterion (MAC) was calculated to evaluate the modal shapes of the first three modes, leading to a MAC = 0.74 for the first mode and irrelevant MAC valued for the sequent. It must be pointed out that optimum correlations are represented by MAC≥0.9, good correlations by 0.8≤MAC<0.9 and acceptable correlations by 0.7≤MAC<0.8. MAC values lower than 0.7 are not considered

acceptable for matched modes [24]. The present case is assessed in an acceptable range of values, which was expected since many issues were encountered during the OMA and the calibration of the modal shape.

5 DISCUSSION AND CONCLUSIONS

This paper discusses the methodology applied to an historical building complex in shape, materials and constructive technologies, in order to identify the dynamic properties of the structure and implement a numerical model able to catch its seismic behavior. After the execution of ambient vibration tests on the existing church and the performance of an Operational Modal Analysis to post-process the results, some eigenvalues analyses were performed on alternative versions of the FEM model in order to inspect the influence of the various modeling strategies and mechanical characteristics applied.

In conclusion, it can be observed that the several attempts explored to find a better agreement between the numerical and experimental models well testify the challenging complexity of the structural typology of the church. It was highlighted that the level of knowledge of the structural details and the materials highly influenced the definition of the modeling strategies adopted for the numerical model in the scope of inspecting their relevance in the structural behavior of the building. In this sense, it was observed that simplifications adopted at the beginning of the modeling phase highly influenced the response. Therefore, the modeling strategy and simplifications in the modeling of a complex structure should be taken with great care. The results of the performed ambient vibration tests revealed to be in some cases incomplete in the description of the complex dynamic response of the church, underling the usefulness of preliminary numerical models for defining measurement setup in dynamic identification tests for such complex structures as the Santa Maria Maddalena Church.

Acknowledgements. This work was carried out in the frame of the Advanced Master in Structural Analysis of Historical Constructions and Monuments (SAHC) and partially sponsored by the Italian Civil Protection, through the RELUIS Project - WP4: MAppe di Rischio e Scenari di danno sismico (MARS) (2020). The mentioned *in-situ* analyses were performed under the commission of the Campania Regional Directorate for Cultural Heritage (MiBACT).

REFERENCES

[1] Clementi, F., Gazzani, V., Poiani, M. and Lenci, S. Assessment of seismic behaviour of heritage masonry buildings using numerical modelling. *Journal of Building Engineering* (2016) **8:**29–47.

[2] Betti, M. and Vignoli, A. Numerical assessment of the static and seismic behaviour of the basilica of Santa Maria all'Impruneta (Italy). *Construction and Building Materials* (2011) **25(12)**:4308–4324.

[3] Formisano, A. and Marzo, A. Simplified and refined methods for seismic vulnerability assessment and retrofitting of an Italian cultural heritage masonry building. *Computers and Structures* (2017) **180:**13–26.

[4] Mendes, N. and Lourenço, P.B. Seismic assessment of masonry Gaioleiro buildings in Lisbon, Portugal. *Journal of Earthquake Engineering* (2010) **14(1):**80–101.

[5] Ciocci, M.P., Sharma, S. and Lourenço, P.B. Engineering simulations of a super-complex cultural heritage building: Ica Cathedral in Peru. *Meccanica* (2018) **53(7)**:1931–1958.

[6] Asteris, P.G., Chronopoulos, M.P., Chrysostomou, C.Z., Varum, H., Plevris, V., Kyriakides, N. and Silva, V. Seismic vulnerability assessment of historical masonry structural systems. *Engineering Structures* (2014) **62–63**:118–134.

[7] Galassi, S. and Ruggieri, N. Stability and Stiffness Contribution of the masonry in the Borbone Anti-

seismic System. *9th International Masonry Conference 2014 Guimarães* (2014) 1–9.
[8] Salerno, G., Geremia, F., Pagano, E., Zampilli, M., Ruggieri, N. and Stellacci, S. The Masonry Timber Framed Load Bearing Structure of "Baraccato" System: A Numerical Model. In: H. Cruz et al. (Eds.): *Historical Earthquake-Resistant Timber Frames in the Mediterranean Area,* Springer Netherlands (2015), pp. 205–2013.
[9] Poletti, E., Vasconcelos, G., Lourenço, P.B. and Ciocci, M.P. Numerical Approaches for the Analysis of Timber Frame Walls. In: H. Cruz et al. (Eds.): *Historical Earthquake-Resistant Timber Frames in the Mediterranean Area*, Springer Netherlands (2015), pp. 183–192.
[10] Di Napoli, B. *Modelling and safety assessment of the Church of Santa Maria Maddalena, Ischia, Italy*. Universidade do Minho (2019).
[11] Casapulla, C., Ceroni, F., Rainieri, C., Argiento, L.U., Arcamone, P., Fabbrocino, G. and Carducci, V. Structural assessment of Santa Maria Maddalena church in Ischia (Italy) by experimental modal analysis under operational conditions. In: M. Papadrakakis and M. Fragiadakis (Eds.): *Computational Methods in Structural Dynamics and Earthquake Engineering (COMPDYN 2019),* ECCOMAS Bookseries (2019), pp. 24–26.
[12] Di Napoli, B., Ciocci, M.P., Celano, T., Argiento, L.U., Casapulla, C. and Lourenço, P.B. Seismic behaviour of a mixed iron-masonry church: Santa Maria Maddalena, Ischia (Italy). *Engineering and Computational Mechanics* (2020) (under review)
[13] Ruggieri, N. and Tampone, G. Historical Earthquake-Resistant Timber Frames in the Mediterranean Area. In: N. Ruggieri, R. Zinno and G. Tampone (Eds.): *Historical Earthquake-Resistant Timber Frames in the Mediterranean Area*. Springer Cham (2015).
[14] ARTeMIS Modal v3.5.1.1. *Ambient Response Testing and Modal Identification Software.* (2018).
[15] DIANA FEA BV. *DIANA Finite Element Analysis User's Manual Release 10.3*. DIANA FEA BV (2019).
[16] Li, Y. and Barbič, J. Stable orthotropic materials. In: V. Koltun and E. Sifakis (Eds.): *ACM/Eurographics Symposium on Computer Animation,* The Eurographic Association (2014), pp. 41–46.
[17] C.S.LL.PP. Circolare 21 gennaio 2019 n. 7 *Istruzioni per l'applicazione dell'aggiornamento delle "Norme Tecniche per le Costruzioni" di cui al D.M. 17/01/2018*, Consiglio Superiore dei Lavori Pubblici (2018).
[18] Bussell, M.N. *Appraisal of existing iron and steel structures*. Steel Construction Institute, (1997).
[19] EC-Standards. *EN 338:2003 - Structural timber — Strength classes (updated 2009)*. Ente Nazionale Italiano di Unificazione UNI (2003).
[20] Sousa, H.S., Branco, J.M. and Lourenço, P.B. Characterization of cross sections from old chestnut beams weakened by decay. *International Journal of Cultural Heritage* (2014) **8(3):**436–451.
[21] MIT. Decreto Ministeriale 17 gennaio 2018 n. 8 *Aggiornamento delle «Norme tecniche per le costruzioni».*, Ministero delle Infrastrutture e dei Trasporti (2018).
[22] Calderoni, B., Cordasco, E.A., Guerriero, L., Lenza, P. and Manfredi, G. Mechanical Behaviour of Post-Medieval Tuff masonry of the Naples Area. *Journal of the Intenational Masonry Society* (2009) **21**:85–96.
[23] Lourenço, P.B. Structural masonry analysis: recent developments and prospects. In: University of Newcastle (Australia) (Ed.): *Proceedings of the 14th international brick & block masonry conference,* (2008), Issues: 17-20, pp. 1341–1356.
[24] Mendes, N. Seismic assessment of ancient masonry buildings : Shaking table tests and numerical analysis. *PhD Thesis*, Universidade do Minho (2012).

12th International Conference on Structural Analysis of Historical Constructions
SAHC 2020
P. Roca, L. Pelà and C. Molins (Eds.)

COLLABORATIVE USE OF DEM AND FEM FOR BRICK JOINT SPLITTING IN STRONG EARTHQUAKE GROUND MOTION

TOSHIRO MAEDA[1*], HIROMU TANAKA[2], MIKI SHIRAHASHI[1] AND BUN HIGASHIZAWA[1]

[1]Department of Architecture, Graduate School of Creative Science and Engineering,
Waseda University
3-4-1, Okubo, Shinjuku-ku, Tokyo, 1698555, Japan
e-mail: tmaeda@waseda.jp, www.tmaeda.sci.waseda.ac.jp (*corresponding author)

[2] Structural Design Department, Shimizu Corporation
2-16-1, Kyobashi, Chuo-ku, Tokyo 1048370, Japan
email: hiromu_tanaka@shimz.co.jp

Keywords: Brick wall, Wooden frame, Micro-tremor observation, Excitation test, FEM, DEM

Abstract. *Masonry structures constructed about one hundred and fifty years ago, in the era of the opening of Japan, have been recognized as industrial heritages. Many of them are masonry warehouses made of brick or stone walls framed by wood members. In this research, a two-story warehouse in Tomioka city, a mortar jointed brick masonry with wooden frame reinforcements, was studied for strong earthquake ground motion. Several vibration modes were identified by micro-tremor observations and excitation tests. The three-dimensional FE overall model was constructed and tuned for the distinctive vibration modes. Two DEM local models, one for bending at the center bottom of the wall treated by plane strain, and the other for shear at the upper corner of the wall by plane stress, were constructed to evaluate brick joint splitting. For both models, dynamic displacement response obtained by the three-dimensional FEM were specified at their peripheries via periphery blocks. At the center bottom of the wall, horizontally developing joint splitting in the section was evaluated. At the upper corners, obliquely proceeding joint splitting on the wall was evaluated. In these analyses, the specified displacements were calculated by the FE model for intact brick walls, regardless of the degrading status of the walls. Although this assumption will have to be justified, the results of DEM were consistent with the reported summary of past earthquake damages.*

1 INTRODUCTION

Masonry structures constructed just after the opening of the modern Japan, about one hundred and fifty years ago, have been recognized as industrial heritages. Many of them are masonry warehouses made of brick or stone walls framed by wood members. Though some of them are renovated for modern use, it is indispensable to preserve their original structures for their values. Our research can help renovation design of utilizing their original structural strength. We have been studying collapse mechanisms of masonry structures e.g., a dry masonry Angkor heritage prototype [1 and 2] and a mortar jointed brick chimney in Tokoname [3]. Our strategy constitutes measurements of micro tremor, validation of finite element or

discrete element models, and simulation for unexpected large disturbances.

At this time, a two-story warehouse in Tomioka city shown in Figure 1, a mortar jointed brick masonry with wooden frame reinforcements, was studied for strong earthquake ground motion. It has six bays in longitudinal ridge direction of 33.1 m and two bays in transverse span direction of 7.6 m and the height is 9.7 m. Several vibration modes were identified by micro-tremor observation and 2nd floor excitation, which were accompanied with remarkable out-of-plane deformation of walls. Taking these three-dimensional vibration characteristics into account, we decided to couple three-dimensional finite element analyses with our two-dimensional discrete element method (DEM) software.

The three-dimensional overall FE model was tuned for the distinctive vibration modes by closely evaluating stiffness of wooden structures at roof and 2nd floor levels. Analyses for static horizontal load and dynamic ground motion exhibited that the Von Mises stress was dominated at the centre bottom and at the upper corners of the longer wall in the excitation along the shorter edge direction. The former predominance implied the dominating bending stress and the latter the dominating membrane stress due to the constraining effects of the perpendicular shorter walls.

Two DEM local models were constructed; one for the centre bottom of the wall treated by plane strain and the other for the upper corner of the wall by plane stress. For both models, time-varying dynamic displacement response obtained by the three-dimensional FEM were specified at their peripheries. At the centre bottom of the wall, DEM revealed that the joint splitting was developing horizontally in the section; while at the upper corners, joint splitting was proceeding obliquely on the wall. In these analyses, FEM based overall response with intact brick walls was used regardless of the degrading status of the walls. Although this assumption will have to be justified, the results of DEM were consistent with the reported summary of past earthquake damages.

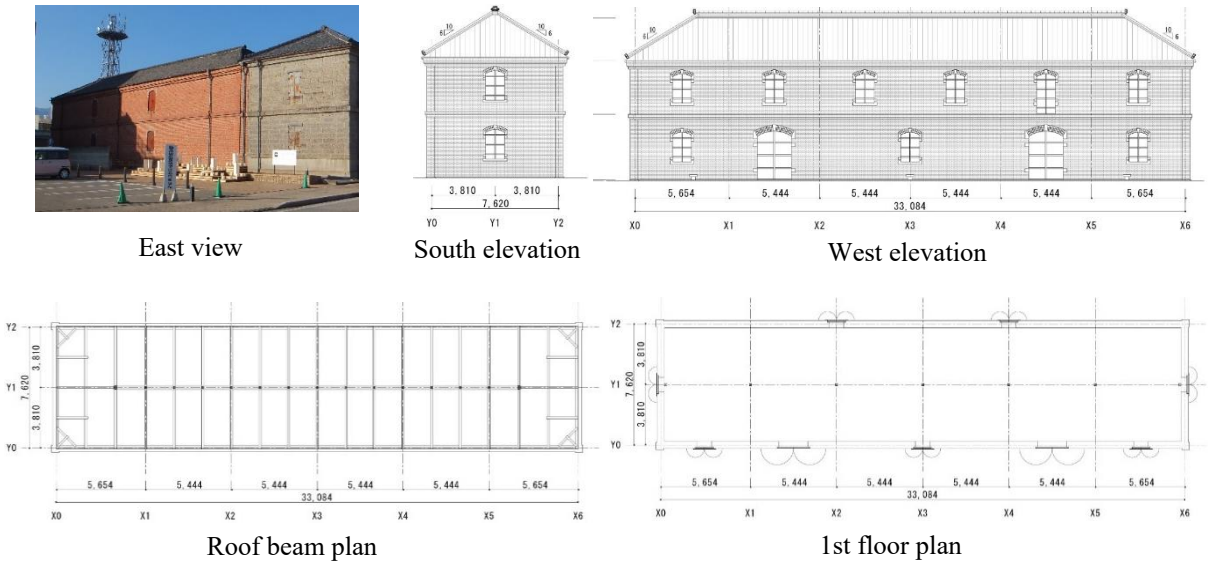


Figure 1: Exterior appearance, plan, section, and elevation of the warehouse

2 MEASUREMENTS AND VIBRATION CHARACTERISTICS

2.1 Measurements and analyses

Micro-tremor observations and excitation tests were carried out to identify natural frequencies and vibration modes of the structure. Servo-type accelerometers of sensitivity 0.3V/(m/s^2) were used with 16-bit data recorder at 1/256 sec sampling and 0.01 V range. The exciter was a linear motor type with a moving mass of 50 kg. The representative locations of accelerometers and the exciter are depicted in Figure 2.

Micro-tremor was measured for 20 minutes and divided into twenty samples of 1 minute, then calculated spectra were ensemble averaged to deduce the transfer functions via FFT. The exciter was operated by two rounds of ascending and descending logarithmic sweep signals from 1 Hz to 30 Hz for two minutes in total. Four of 30 seconds of one-way log-sweep samples were used for the transfer function similar to micro-tremor data. The transfer functions are calculated by H_1 definition, i.e. square norm of cross spectrum divided by products of square roots of auto spectra.

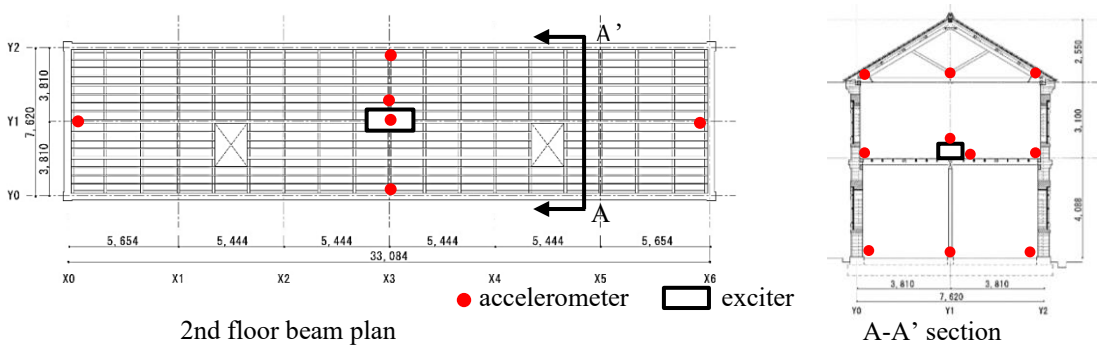


Figure 2: Location of accelerometers and an exciter

2.2 Micro-tremor measurements

Acceleration wave forms and Fourier amplitudes at the center of the 1st floor are shown in Figure 3 for longitudinal and transverse directions. The predominant frequency of 10 Hz is attributable to the reverberation of the subsurface ground.

In Figure 4, transfer functions at the roof level and the 2nd floor level are shown in both directions referring to the 1st floor level. For the transverse direction, the 1st peak at the fundamental frequency 1.95 Hz is followed by several peaks at 4.43, 5.53, 6.87, and 8.37 Hz. Around 5.53Hz and 8.37 Hz, phase relations imply that the corresponding peaks are non-local shear vibration modes. For the longitudinal direction, limited number of peaks are observed. The fundamental frequency is deduced as 7.47 Hz.

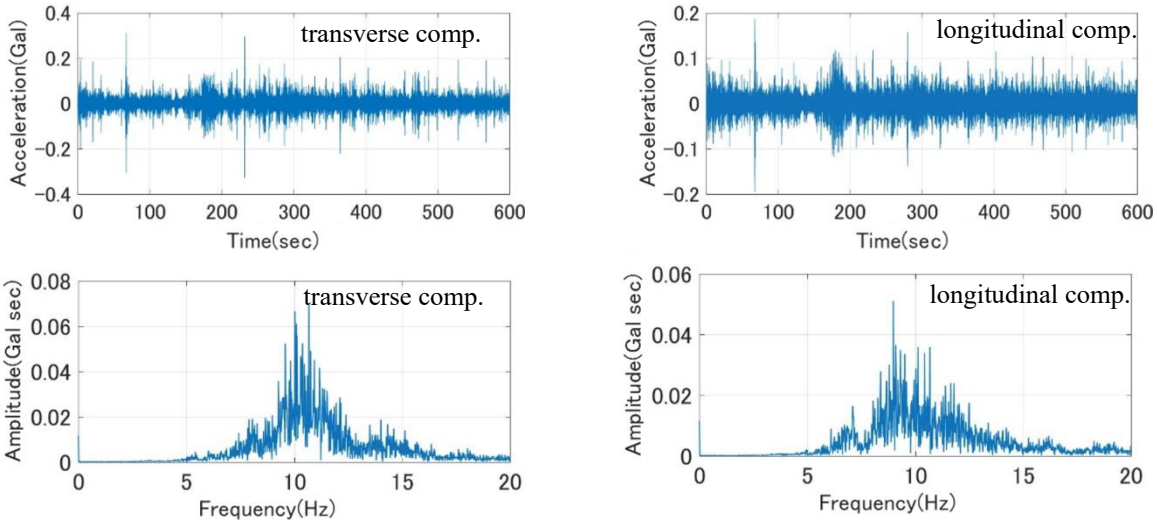
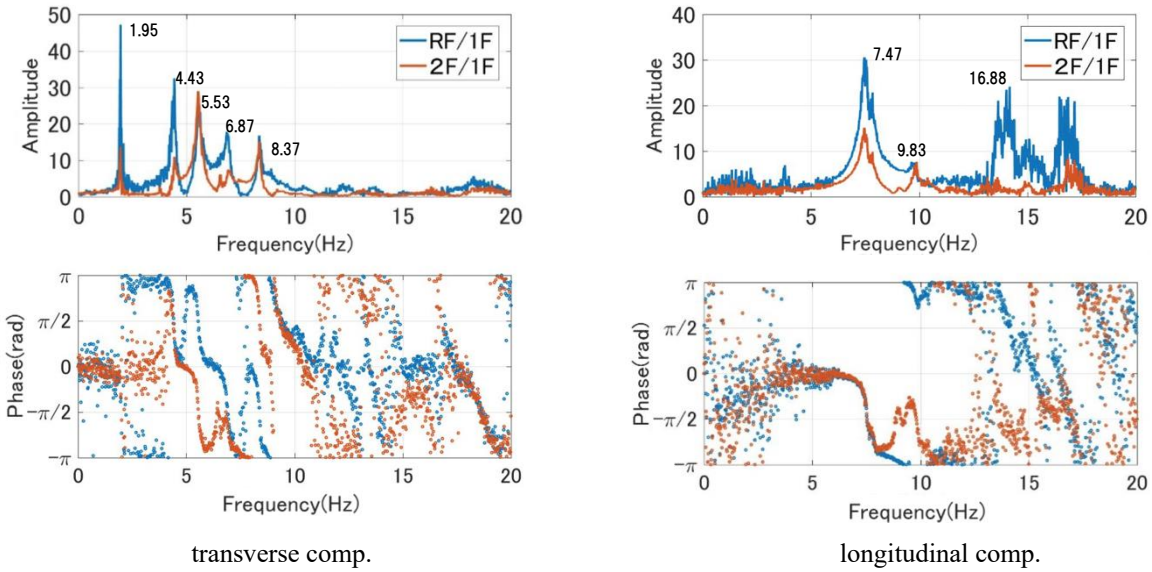


Figure 3: Micro-tremor at the center of the 1st floor

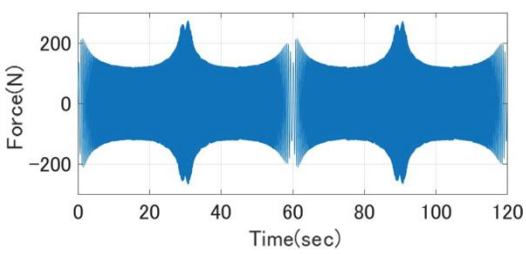


transverse comp. longitudinal comp.

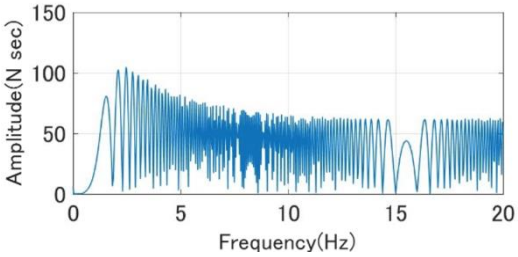
Figure 4: Transfer functions by micro-tremor at the center of the floors

2.3 Excitation by an exciter

The waveform and Fourier amplitude of the log-sweep force are shown in Figure 5. In Figure 6, resonant curves are compared at the roof and the 2nd floor levels. For the transverse direction, the fundamental frequency is 2.03 Hz and the major peaks with resonated phase are seen at 6.00 Hz and 8.63 Hz. In the longitudinal direction, the 1st peak at 7.43 Hz is not dominated and followed by peaks at 10.57Hz and 16.50 Hz.

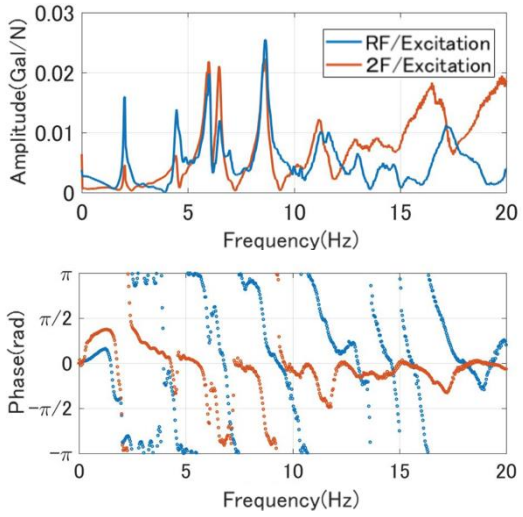


Waveform of log-sweep force

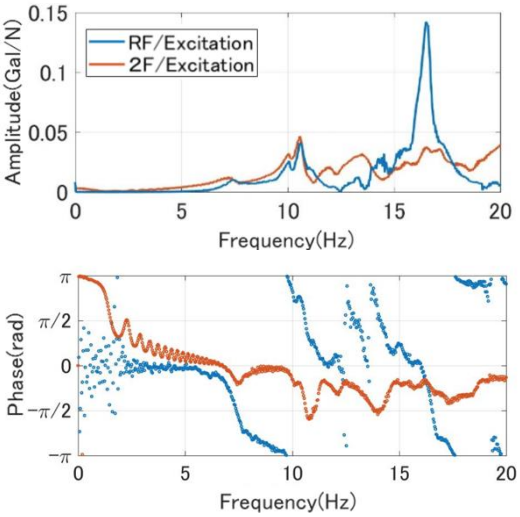


Fourier amp. of log-sweep force

Figure 5: Excitation force at the center of the 2nd floor



transverse comp.

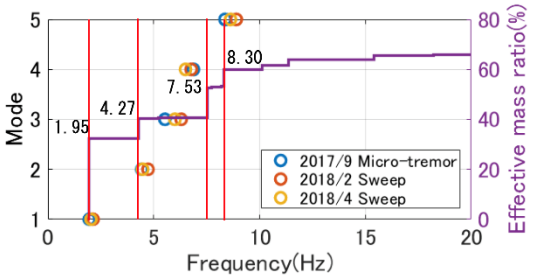


longitudinal comp.

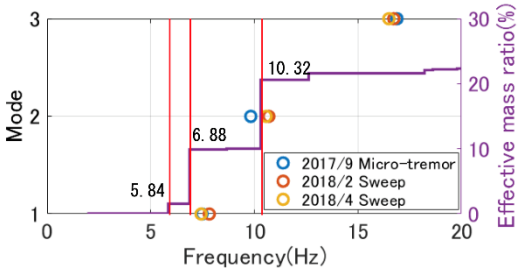
Figure 6: Resonant curves for excitation at the center of the 2nd floor

2.4 Comparison of peak frequencies

Peak frequencies obtained by micro-tremor observation and excitation tests are compared in Figure 7. They are mostly corresponding with each other, which implies that this small size exciter is effective in obtaining resonant curves of this stiff and heavy masonry structure.



transverse comp.



longitudinal comp.

Figure 7: Summary of peak frequencies by measurements and accumulated effective mass ratio by FEM

3 OVERALL FEM MODEL

3.1 Finite element modeling and validation

The finite element model for the masonry warehouse was constructed by combination of isotropic solid elements and beam elements; the former for brick walls and the latter for wooden beams, columns and roof construction. Material constants for beam elements are referred to that of red pine wood obtained by the material test for this project. Poisson's ratio and density for solid elements are typical value for bricks, and Young's modulus for solid elements are set to fit the fundamental frequency of 1.95 Hz in the transverse direction. Damping ratio is 2 %. These material constants are summarized in Table 1. The finite element model is shown in Figure 8. Variation of wall thickness is modelled according to the actual wall configuration as shown in the figure.

Effective mass ratios for natural modes are plotted for natural frequencies and compared with the peak frequencies obtained by micro-tremor observation and excitation tests in Figure7. Peak frequencies are mostly corresponding to the large effective mass ratio.

Table 1: Material constants for brick solid element and wood beam element

	Young's modulus [N/mm^2]	Poisson's ratio	Mass density [g/cm^3]
Brick	2,310	0.2	1.67
Wood	11,830	0.4	0.57

3.2 Simulation analysis (phase in excitation test)

Transfer functions referred to the 1st floor are calculated by time domain FEM linear analysis in each direction as shown in Figure 9. Input acceleration is a 128 sec. portion of measured micro-tremor data on the 1st floor as shown in Figure 3. Similar results for the excitation test are shown in Figure10 where the measured excitation force is used as an input. Comparing these transfer functions with the corresponding experimental ones in Figure 4 and Figure 6, the FEM simulation in the transverse direction is effective up to 5 Hz covering the 1st and 2nd peaks, and in the longitudinal direction up to 10 Hz including the 1st peak.

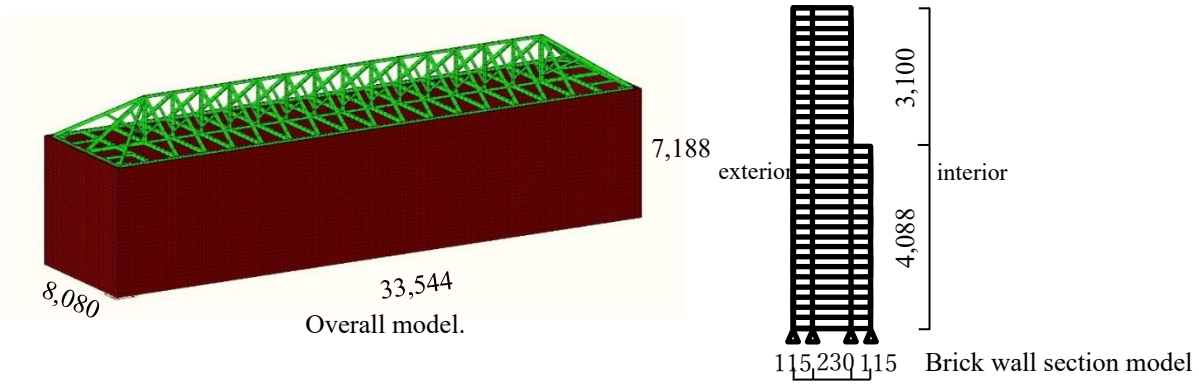
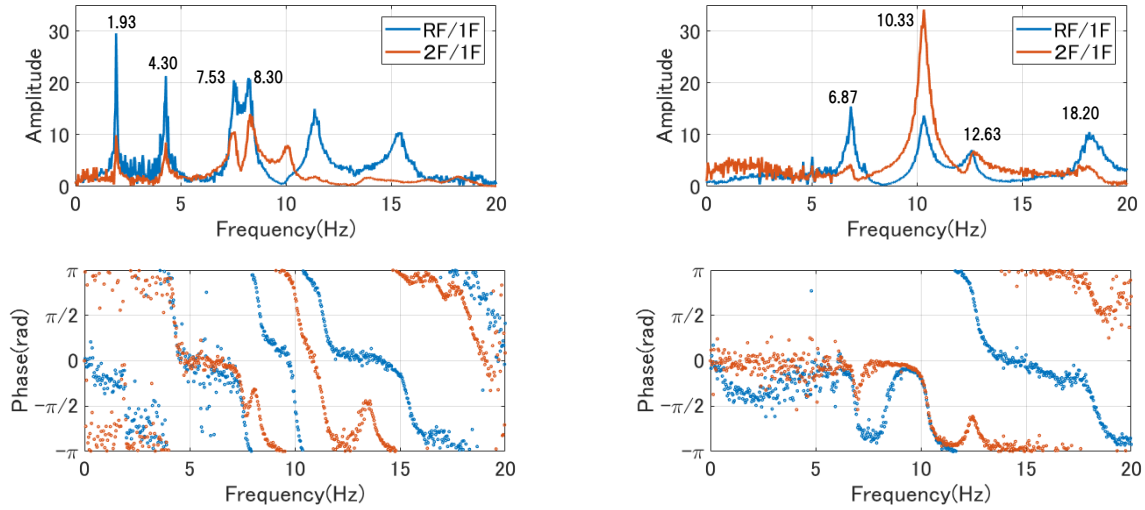
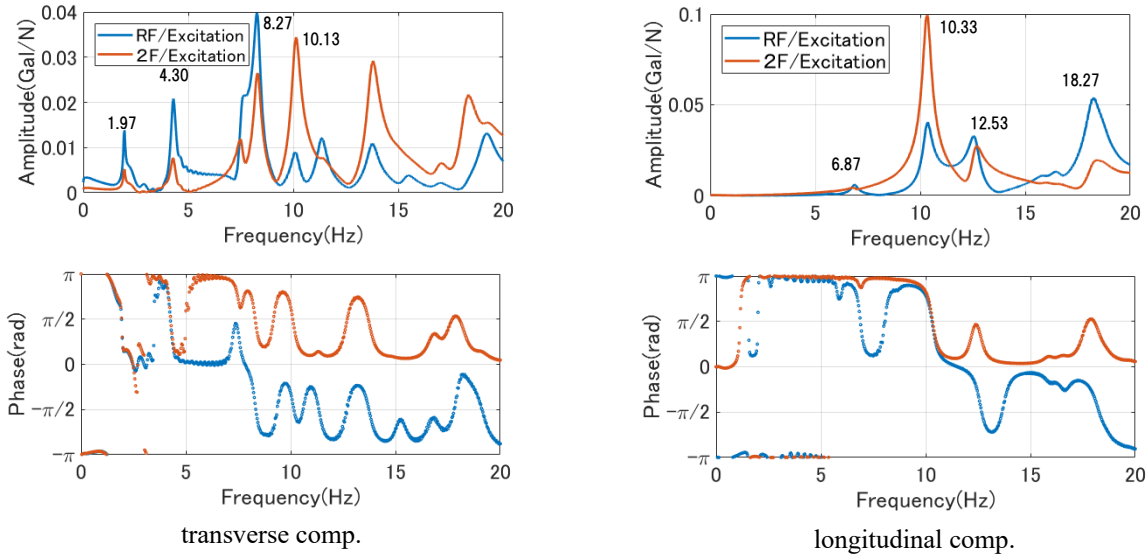


Figure 8: Overall FEM model



transverse comp. longitudinal comp.

Figure 9: Transfer functions for micro-tremor by FEM



transverse comp. longitudinal comp.

Figure 10: Resonant curves for exciter on the 2nd floor by FEM

3.3 Linear static and dynamic stress analyses

Following the shear coefficient design procedure in Japan, static earthquake load corresponding to the base shear coefficient of 0.2 is applied to the finite element model in each direction. In Figure 11, the distributions of deformation, von Mises stress, and relevant stress components are depicted in transverse direction. Deformation is large in the middle of the roof construction and edges of walls nearby. Normal stress σ_{zz} is dominant at the bottom of the longer brick wall due to the out-of-plane bending at the foot of the wall. Membrane shear stress σ_{xz} near the upper corners of the longer brick wall is remarkable.

In Figure 12, these distributions are shown for longitudinal direction. Similar trends are seen in σ_{zz} and σ_{yz}, but not that remarkable. Then, we will focus on behavior in transverse direction hereafter. Stress distribution in the longer wall is similar to that of a gravity-loaded plate with three edges fixed; since base and perpendicular shorter walls play roles of constraints along the three edges of the longer wall. With the same finite element model, a dynamic analysis was carried out with Kobe NS component ground motion in 1995 as shown in Figure 13. The distributions of maximum absolute stress shown in Figure 14 are similar to that of the static loading.

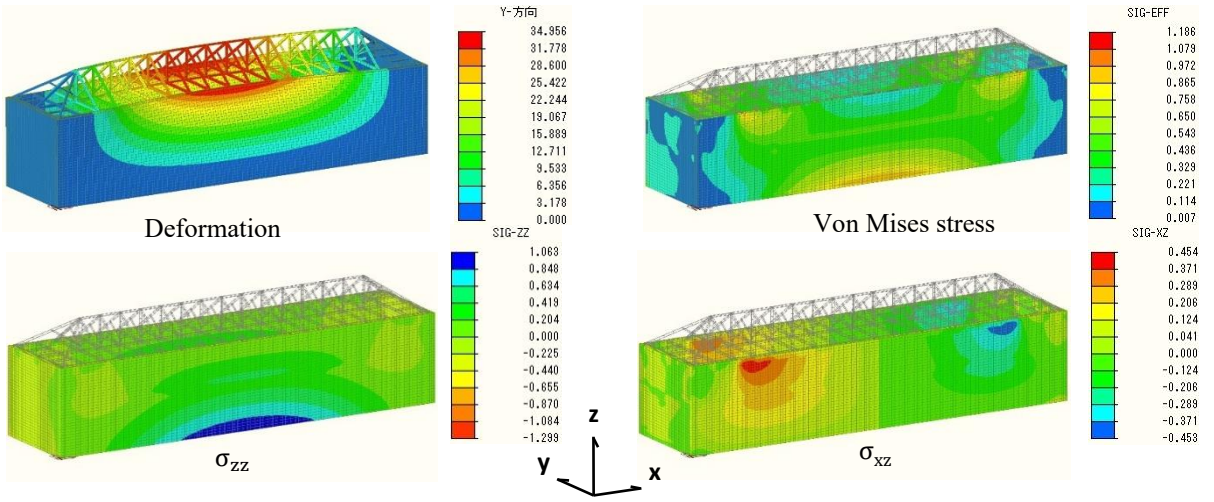


Figure 11: Distribution of deformation and stress components for static load in transverse direction

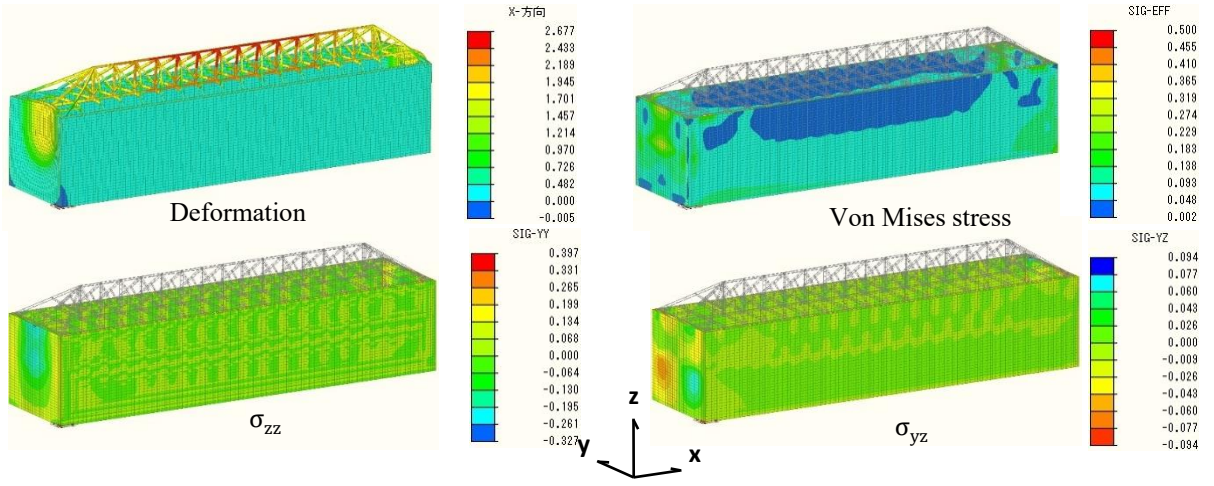


Figure 12: Distribution of deformation and stress components for static load in longitudinal direction

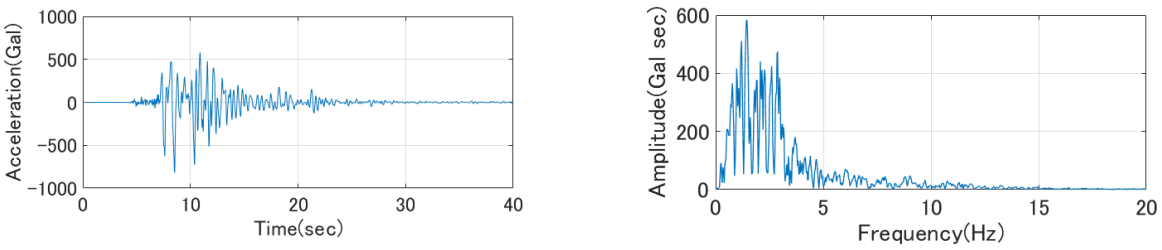


Figure 13: Waveform and Fourier spectrum of input wave, Kobe 1995

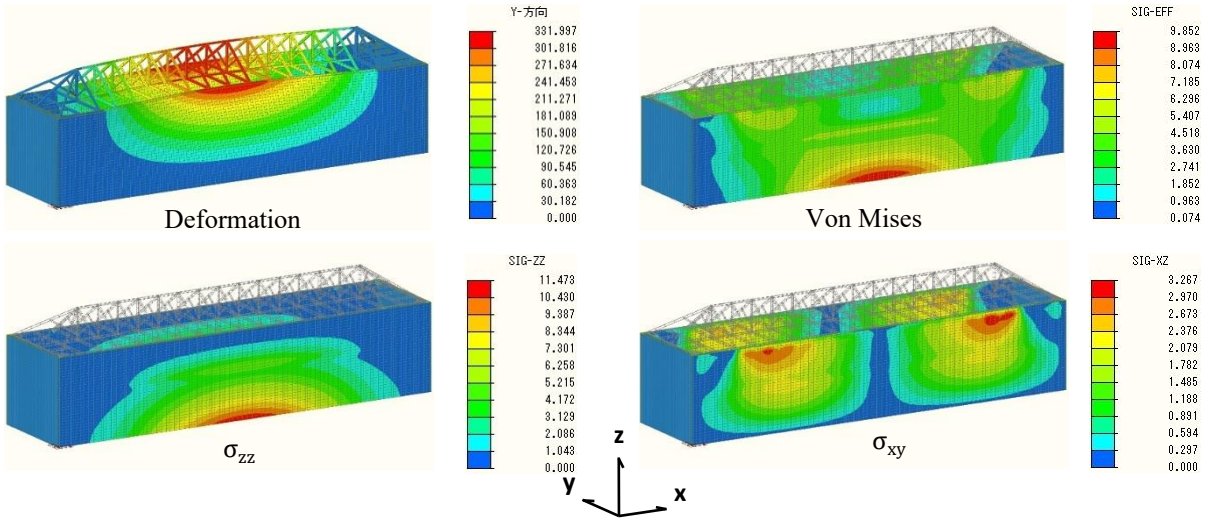


Figure 14: Maximum deformation and stress for Kobe ground motion in transverse direction

4 LOCAL DEM MODELS

4.1 Finite element model and the local discrete element models

Strength of brick wall is governed by the shear strength of its joint. Shear strength and tensile strength of brick joint is much weaker than compressional strength, usually assumed as 1/10 of compressional strength. For the loading in transverse direction, tensile stress at the center bottom and shear stress around upper corners of the longer wall are most significant.

After local crack develops along the joints, brick walls are regarded as discontinuous structure. DEM is a powerful tool to analyze discontinuous structure; the structure is modeled by a set of rigid blocks or deformable blocks moving with each other under external forces and contact conditions. However, it requires long time of computation with large amount of memory to evaluate contact between tremendous number of DOF's of blocks in a three-dimensional discontinuous model. It may be advantageous to incorporate three-dimensional FEM and two-dimensional DEM to predict crack expansion in certain parts of the structure during earthquake ground motion.

We set two DEM local models; one for at the center bottom of the longer wall and the other at the upper edge near the corner of the longer wall as shown in Figure 15. The former model is a part of the wall section modeled by plane strain and designated as bending model. The latter

model is a part of the wall modeled by plane stress and designated as shear model. Both local models are modeled by a set of rigid blocks with normal and shear contact springs along their edges. The normal spring is used to prevent penetration and the shear spring to evaluate shear stress to be used for slip criteria. Contact strengths at interfaces are defined by tensile strength and slip criteria expressed by cohesion and friction angle shown in Table 2. Mass density of blocks is 1.66g/cm^3.

The input motion for the DEM models are the displacements calculated by FEM dynamic analysis. The motion is specified at the peripheries of the DEM models, where special blocks called by the periphery blocks are equipped. The periphery blocks are expressed by double lines along the edges in Figure 16 and Figure 17. Normal contact spring coefficients are assumed by Young's modulus of the brick divided by distance between adjacent block centers as shown in Table 3. Shear contact spring coefficient is specified as 0.0353 N/mm^3, according to the Young's modulus of joint material. Shear and normal contact springs for the periphery blocks are parametrically assumed as 10N/mm^3, 1N/mm^3, and 0.1N/mm^3. In this paper, the result for 10N/mm^3 are shown for space limitation.

Table 2: Strength for brick solid elements

	Tensile strength [N/mm^2]	Cohesion [N/mm^2]	Friction angle [degree]
Interior interface	0.45	0.52	33
Periphery interface	10,000	10,000	89

Table 3: Normal contact spring coefficients for horizontal and vertical joints [N/mm^3]

	Horizontal joint	Vertical center joint	Vertical off-center joint
Bending model	34.48	10.04	13.39
	Horizontal joint	Vertical for long face	Vertical for short face
Shear model	34.48	20.09	10.04

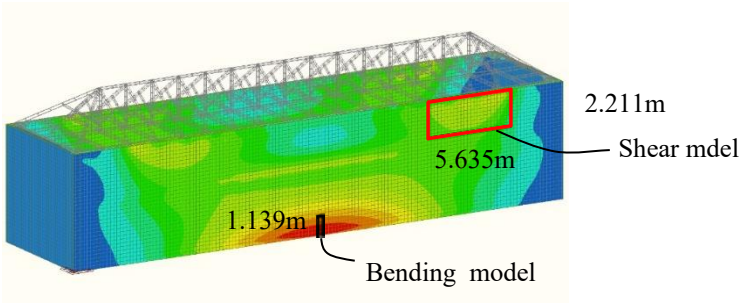


Figure 15: Locations of local DEM models

4.2 Plane strain analysis for bending model

In Figure16, development of cracks at joints in the wall section is shown for the case of 10N/mm^3 periphery block contact spring. Firstly, horizontal cracks appear at the outer face then at the inner face; cracks appear alternatively at both faces while proceeding to interior region and finally several joints penetrating whole thickness of the wall. Cracking pattern depends on

the periphery block contact spring; crack concentration at the middle of the wall for 1N/mm^3 and less cracking for 0.1N/mm^3 (not shown here). The cracking pattern for 10N/mm^3 suits to the summary of empirically inferred collapse mechanism for masonry walls [4].

4.3 Plane stress analysis for shear model

In Figure17, development of cracks at joints on the wall is shown for the case of 10N/mm^3 periphery block contact spring. Crack patterns comprises vertical and diagonal cracks; the vertical cracking is proceeding downward from near the corner of the wall, while the diagonal cracking is proceeding from the lower left corner toward the upper right corner. Similar to the bending model, cracking is less observable for the smaller periphery block contact spring (not shown here).

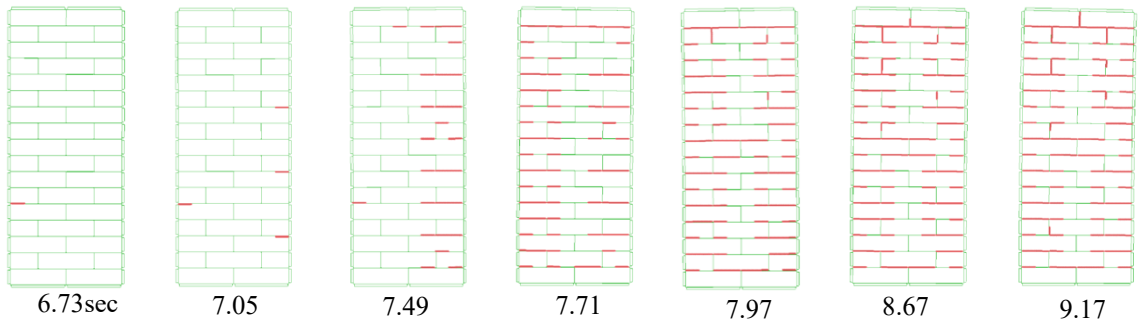


Figure 16: Development of cracks in local bending model for specified motion computed by FEM

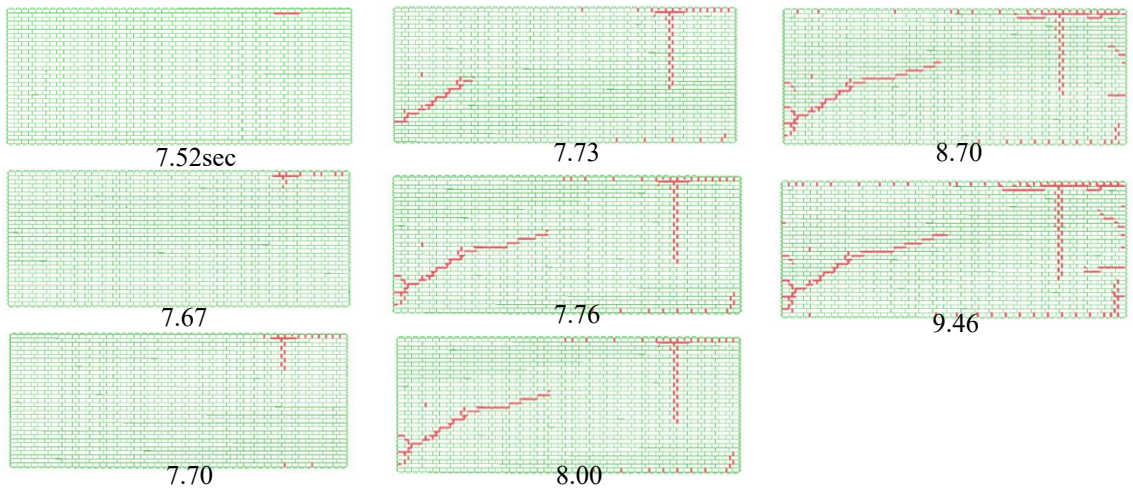


Figure 17: Development of cracks in local shear model for specified motion computed by FEM

5 CONCLUSIONS

Collapse mechanisms of a two-story brick masonry warehouse with wooden frame reinforcements, which is a typical heritage structure in the opening era of the modern Japan, was studied for strong earthquake ground motion by coupling three-dimensional finite element

analysis and two-dimensional discrete element analysis. Three-dimensional vibration characteristics revealed by micro-tremor observation and an exciter test were simulated by a three-dimensional overall FE model; where stiffness of wooden roof and wooden 2nd floor structures were examined for higher vibration modes. The FE analyses for static horizontal load and dynamic ground motion exhibited dominating bending stress at the centre bottom and dominating membrane stress at the upper corners of the longer wall for the transverse excitation. The latter stress distribution is similar to that of a gravity loaded plate with three-edge constraints, since the perpendicular shorter walls function as constraints for the longer walls.

By two-dimensional DEM local models, the dominating bending stress was analysed by plane strain and the dominating membrane stress by plane stress. For both models, time-varying dynamic displacement response obtained by the three-dimensional FE model were specified at their peripheries with periphery contact springs to control the boundary stiffness. At the centre bottom of the wall, DEM revealed that the joint splitting was developing horizontally in the section. At the upper corners, joint splitting was proceeding obliquely on the wall. These collapse mechanisms are in accordance with the summary of empirically inferred collapse mechanism for masonry walls.

Acknowledgements. This paper is based on the 2nd author's Master's Thesis of Waseda University in 2018. This paper is a part of the outcome of research performed under a Waseda University Grant for Special Research Projects (Project number: 2018B-127).

REFERENCES

[1] Hironaka, T., Maeda, T. Araya, M. and Ejiri, N. Safety Evaluation of Inner Gallery in Bayon Temple by DEM with Preliminary Experiments, *10th SAHC* (2016).
[2] Yamashita, Y. and Maeda, T. Simulation of Distinct Element Joint Stiffness of the Historical Masonry Structure Model by Micro-tremor Measurement, *11th SAHC* (2018).
[3] Yamamoto, T. and Maeda, T. Earthquake Safety Assessment of a Tall Brick Chimney in Tokoname Based on the Micro-Tremor Measurement, *14WCEE* (2008), 05-04, 0073.
[4] Minamide ,K. et al. Basic investigation of seismic diagnosis method on historical masonry, Historical masonry prevention committee's report, *Proceedings of Annual meeting for Hokkaido Branch of Architectural Institute of Japan*, (1997), pp.253-256 *in Japanese.*

12th International Conference on Structural Analysis of Historical Constructions
SAHC 2020
P. Roca, L. Pelà and C. Molins (Eds.)

COMBINED SHEAR-FLEXURAL VERIFICATION OF IN PLANE LOADED REINFORCED AND UNREINFORCED MASONRY WALLS

ANDREA BENEDETTI[*1], MIRCO TAROZZI[1] AND LORENZO BENEDETTI[2]

[1]DICAM Department
Università degli Studi di Bologna
2, Viale Risorgimento, 40136 Bologna, Italy
e-mail: andrea.benedetti@unibo.it, www.unibo.it/en (*corresponding author)

[2]STI DESL, Ecole Polytechnique Fédéral Lausanne
ELL 166 Station 11
CH-1015 Lausanne, Switzerland
Web page: https://people.epfl.ch/lorenzo.benedetti?lang=en

Keywords: Masonry panel, in-plane loading, shear-flexural verification, reinforcement design

Abstract. *The safety verification of in-plane loaded masonry panels requires the evaluation of at least three different collapse conditions connected with overturning, shear sliding, and shear – compression failure at the panels' toe. In reinforced panels, the resisting models should even take into consideration the presence of localized or distributed reinforcement.*

In general, the masonry is considered a Mohr-Coulomb type material not resisting tension and plastic in compression, while reinforcement is a brittle elastic material resisting tensile forces only [1].

The ultimate limit state is however linked with a given subset of compressed material inside the panel area. The compressed sections are therefore varying inside the panel as a function of the applied load. The collapse occurs in shear or overturning when one peculiar compressed section reduces to its minimum [2].

By equating the capacity in shear and overturning it is possible to derive an explicit statement of the minimum length of the compressed section which will be activated by a simultaneous failure in shear and overturning. A simple inequality is detecting the real failure mode and this allows directly computing the failure load resultant.

The procedure is very fast and can deal even with localized or distributed reinforcement layers such as fiber strips or mesh reinforced mortars.

Some examples of panels discussed in the literature show the effectiveness of the proposed verification procedure.

1 INTRODUCTION

As is well-known masonry panels under in-plane loading can exhibit several collapse forms

according to the combination of geometry, restraint, axial and shear forces acting on it.

In particular, due to the low tensile capacity of masonry materials, small axial compression forces lead to moderate shear capacities, mainly linked to the cohesion of the material.

If the horizontal displacement demand increases, cracks running on the mortar joints will appear in the masonry panel, reducing thus the length of the compressed zone along the height of the panel. In the cracked condition, the shear is carried on by the compressed area only, producing so a mixed compression-shear state on the masonry. At the shear peak value, the panel can collapse alternately with rocking failure until overturning, or with sliding failure with progressive crack opening.

Collapse by overturning is typical of slender panels under low or moderate axial forces, while shear sliding is typical of very squat walls. When the axial force is very high or the compressive masonry strength is very low, the probability that the panel will fail with shear crushing of the compressed toe increases considerably. In this case, inclined diagonal cracks splitting the bricks arise on the panels.

In this paper, the problem of mixed shear-rocking failure is solved by determining the compressed zone length that makes the shear producing overturning and sliding the same. A closed formula allows computing the ending geometry of stable behavior. Namely, after this point, by decreasing the size of the compressed zone even the shear has to reduce its value in a softening branch. The limit value that results in a shear-crushing of the toe is even expressed in terms of the Mohr-Coulomb failure criterion.

In order to validate the analytical formulation, several experimental campaigns presented in the literature takes as a reference and their findings are discussed in the following.

2 COMBINED SHEAR – FLEXURAL FAILURE OF MASONRY PANELS

Considering a rectangular panel of constant thickness t_M acted on by a linear bending moment distribution it is in any case possible to extract a cantilever part of it which can be considered the part relevant for the failure. The height of this cantilever is given by the ratio of the largest bending moment M_S to the shear force V_S and is equivalent to a shear arm a_v:

$$a_V = \frac{M_S}{V_S} \tag{1}$$

As a consequence of the limited tensile resistance of the masonry texture and beyond a certain shear force, the base section of the cantilever begins to crack, and therefore the equilibrium is guaranteed by the eccentricity of the stress resultant acting on the contact area.

The verification of this incipient failure situation is in general carried out by using different formulas for the possible collapse modes: flexural overturning, shear sliding and shear-compression crushing (according to the Mohr-Coulomb criterion, see [1]).

$$V_{R,fl} = \frac{N_S L}{2a_V}\left(1 - \frac{N_S}{\kappa N_P}\right) \tag{2.a}$$

$$V_{R,sh} = \mu N_S + \beta t_M f_{MV0} \tag{2.b}$$

$$V_{R,MC} = \beta t_M f_{MV0} \sqrt{\left(1+\frac{\sigma_0}{f_{Mt}}\right)\cdot\left(1-\frac{\sigma_0}{f_{Mc}}\right)} \tag{2.c}$$

In the given formulas N_S is the axial force in the panel, L and t are the length and the thickness of the panel' section, f_{Mc} and f_{Mt} are respectively the compressive and tensile strength of the masonry material, β is the length of the compressed area in the base section, κ and μ are the ductility and friction coefficients. The other variables are as follows:

$$N_P = L t_M f_{Mc} \quad , \; f_{MV0} = \frac{f_{Mt}\cdot f_{Mc}}{f_{Mt}+f_{Mc}} \quad , \; \sigma_0 = \frac{N_S}{\beta t_M} . \tag{3}$$

It is to note that the shear-compression failure formula derived in agreement with the Mohr-Coulomb criterion is very similar to the Turnsek-Cacovic formula if the axial stress is not very high:

$$\tau_{R,MC} = \tau_{R,TC} \cdot \sqrt{\left(1-\frac{\sigma_0}{f_{Mc}}\right)} \tag{4}$$

The resisting shear stress is obviously the minimum among the three formulas (2).

Since masonry in compression can be considered an elastic perfectly plastic material [3], the stress distribution at the panel's base is a consequence of the linear strain distribution. By assuming that the ductility D of the material is described by the ratio of the ultimate strain ε_{ult} to the limit elastic one ε_e, the resultant of the stress distribution can be expressed in terms of the compressed area and the ductility ratio D.

If the cantilever is very slender, the failure is occurring by overturning with the minimal length of the contact area:

$$\beta_{\min} = \frac{2D}{2D-1}\cdot\frac{N_S}{t_M f_{Mc}} \tag{5}$$

If the cantilever is sufficiently squat, the failure is occurring by shear with a compressed zone larger than the minimal one. The value of the compressed length at failure can be computed by equating the shear force producing sliding with the one producing overturning:

$$\frac{M_{R,fl}}{a_V} = \frac{N_S}{a_V}\left(\frac{L}{2}-\frac{\bar{\beta}}{n}\right) = \mu N_S + \bar{\beta}\, t_M f_{MV0} = V_{R,sh} \tag{6.a}$$

$$\beta_{\lim} = \bar{\beta} = \frac{n}{2}\frac{N_S\left(L-2\mu a_V\right)}{N_S + n\, a_V t_M f_{MV0}} \geq \beta_{\min} \tag{6.b}$$

The value of the parameter n is defining the adimensional distance of the stress resultant force from the edge of the panel:

$$n = \frac{1+3D\left(D-1\right)}{3D\left(2D-1\right)} \tag{7}$$

Since the deflection of the cantilever can only increase if the shear is increasing and the compressed length is decreasing (in order to guarantee the rotational equilibrium), the limit $\bar{\beta}$ defines even the limit stable displacement of the panel. If the shear - displacement curve of the panel is known, the curve must be cut at $V_{R,\lim}$ given by $\beta_{\lim}$.

Many procedures exist that can allow plotting the shear - displacement curve up to panel overturning (see among the others [4, 5]). One very simple procedure allowing for well-approximated shear displacement curves is the use of hyperbolic functions. As is usual in geotechnics, only two parameters are necessary to build up an effective relationship:

$$V(\delta) = \delta \cdot \left(\frac{1}{K_0} + \frac{\delta}{V_{\lim}} \right)^{-1} \tag{8}$$

In which K_0 is the initial stiffness of the panel and $V_{\lim}$ the maximum resisting shear when the displacement tends toward infinity.

If masonry panels are concern, the initial stiffness is computed from the geometry and the material properties of the panel. The limit shear is computed from the largest panel eccentricity attained at the overturning.

$$\frac{1}{K_0} = \frac{12H^3}{cE_M L^3 t} + \frac{H}{G_M L t} \tag{9}$$

Where E_M and G_M are the elastic and shear moduli of the masonry, and c is a coefficient describing the end rotational restraint of the panel, with values in the range {3;12}.

Once $V_{R,sh} < V_{lim}$ is known, the failure displacement can be computed.

3 SHEAR-FLEXURAL FAILURE OF REINFORCED PANELS

The procedure holding for unreinforced masonry panels can be modified in order to include the effect of fiber reinforcement nets added to the external surfaces of the panel. In general, the flexural reinforcement of masonry elements is carried out by adding fiber strips along the vertical edges of the walls or by using fiber cross braces on the wall faces. The shear reinforcement of the panel instead, is best suited by using mortar coatings and fiber meshes on the faces or by using near-surface mounted bars (NSM) resting on the mortar courses.

The flexural reinforcement is based on the introduction of some tensile resisting force that can carry on a bending moment summing up with the one resisted by the masonry alone. On the contrary, shear reinforcement is mainly thought for increasing the shear capacity of the masonry material.

In what follows a reinforced panel is considered, in which the four vertical edges are equipped with unidirectional strips of fibers externally bonded to the bricks (EBR). Moreover, the panel is reinforced in shear by means of two external thin layers of high strength mortar reinforced with glass fiber meshes.

The CNR-UNI documents 200 and 213 [6, 7] contain the basic theoretical formulation for the strength evaluation of fiber reinforcement systems in which the bonding agent is high strength mortar. A homogenization strategy is presented in [1] able to deal with mortar coatings reinforced with fiber meshes.

Considering the panel presented in figure 1 the aim is the definition of a suitable modification for the formulas presented in the previous section.

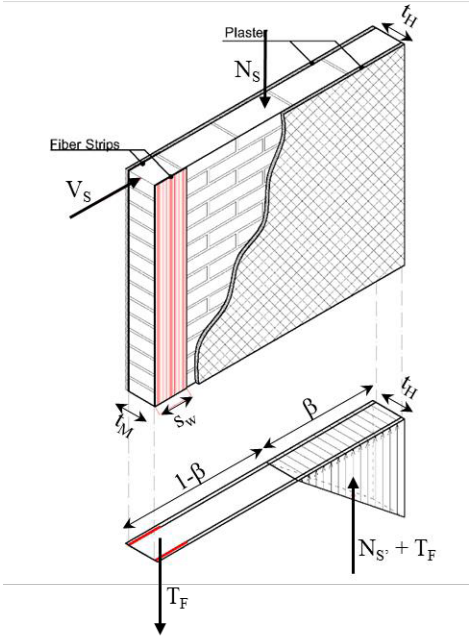


Figure 1: geometry of the considered reinforced panel

By denoting with t_M the thickness of the unreinforced masonry panel, t_L the total thickness of the added reinforcing layers, and with t_H the total thickness of the wall $t_H = t_M + t_L$, it is possible to use the composition rules of series and parallel systems for the calculation of the homogenized shear and compression strength:

$$f_{HV0} = \frac{f_{MV0} t_M + f_{LV0} t_L}{t_M + t_L} \quad , \; f_{Hc} = \frac{f_{Mc} t_M + f_{Lc} t_L}{t_M + t_L} \tag{10}$$

Where f_{Lc} and f_{LV0} are the compressive and shear strength of the reinforcing coatings. The homogenization through the volumetric ratios is possible if the connection between the masonry panel and the reinforced coatings is sufficiently ductile in leading to the full yielding of both materials.

If the flexural capacity of the panel is not sufficient for the rotational equilibrium, added reinforcement strips on the edges can supply the missing resisting moments. By using formulas for EBR or NSM the axial strength T_F of the reinforcement can be computed:

$$T_F = \sqrt{2 E_F G_F A_F s_w} \tag{11}$$

In formula (10) E_F is the reinforcement elastic modulus, G_F is the fracture energy of the interface, A_F is the reinforcement area and s_w is the breadth of the bonding surface [6].

Once the strength of the flexural reinforcement is defined, the formulas (5, 6) can be modified in order to include the effect of the added strength:

$$\lambda_{\min} = \frac{2D}{2D-1}\frac{(N_S + T_F)}{t_H f_{Hc}} \tag{12.a}$$

$$\bar{\lambda} = \frac{n}{2}\frac{N_S L + 2T_F d - 2\mu a_V (N_S + T_F)}{N_S + T_F + n a_V t_H f_{HV0}} \tag{12.b}$$

Where d is the distance of the reinforcement axis to the most compressed fiber.

If $\bar{\lambda}$ is larger than λ_{min} the limit shear force is easily computed as:

$$V_{H,sh} = \mu\left(N_S + T_F\right) + \bar{\lambda}\, t_H f_{HV0} \tag{13}$$

Alternately, if λ_{min} is the smallest length, the limit shear force is computed as:

$$V_{H,fl} = \frac{M_{H,fl}}{a_V} = \frac{1}{a_V}\left[N_S\left(\frac{L}{2} - \frac{\lambda_{\min}}{2}\right) + T_F\left(d - \frac{\lambda_{\min}}{2}\right)\right] \tag{14}$$

4 VERIFICATION OF THE PROPOSED FORMULA

The analysis previously defined is applied to a set of eight brick masonry walls tested by Churilov et Al. [8]. The height of the walls was fixed to 1820 mm, while two different lengths respectively equal to 1420 mm and 2820 mm were chosen investigating the effect of the aspect ratio on the lateral capacity of the wall. Since the purpose of the research was the investigation of the in-plane behavior of both unreinforced and jacketed walls, the whole number of specimens was split into two groups, each of which was made of two slender and two squat walls. The walls of only one group were reinforced through the reinforced concrete (RC) jacketing technique.

The reinforcement was applied to the external faces of the panels by executing transversal connection ties over which the steel wire meshes were welded. then two layers of high strength mortar were poured on forms with a thickness of 25 mm approximately.

Table 1 collects the thicknesses t of the masonry components, their elastic modulus E and their tensile and compressive strength, f_t and f_c, respectively. Concerning brick units, the cylindrical compressive strength was computed as 0.83 times the cubic one, while their tensile strength was evaluated from the flexural tensile strength obtained experimentally.

Elastic moduli of mortar and bricks were estimated starting from their compressive strengths [3]. All these properties were used in this paper to compute the mechanical properties of the masonry walls validating the proposed formulas.

The presented experiments considered very squat panels under a very high axial load and repeated alternated increasing displacement cycles. Therefore they constitute a very sharp reference for testing the prediction capability of formulas dealing with shear-compression failure of masonry panels.

Table 1: Geometrical and mechanical properties of the materials.

	t [mm]	f_c [MPa]	f_t [MPa]	E [MPa]
Brick	65	13.6	1.8	6800
Lime Mortar	10	0.6	0.1	300
Concrete	25	22.7	3.6	20000
Steel Wires	Φ 4.2/10	450	450	200000

In Figure 2 some pictures of the failed panels are presented. The cracking pattern shown by the panels highlights a shear sliding failure under high compressive stress with very large contact zones at the two panel ends.

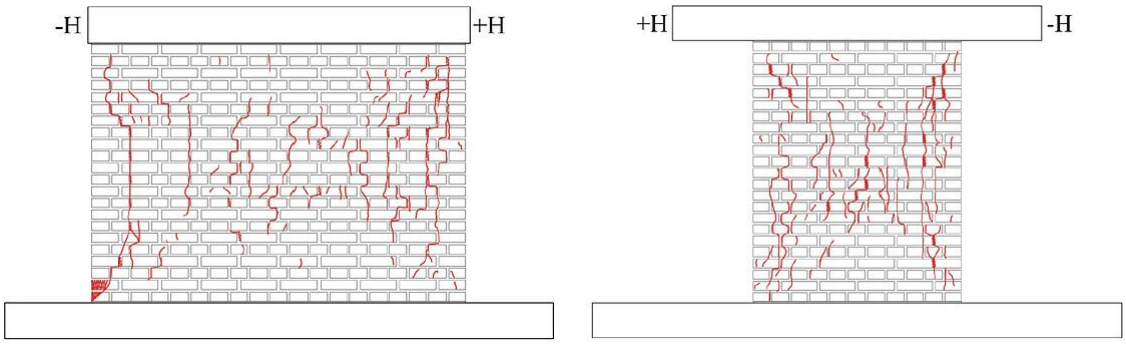


Figure 2: Failure of the panels considered in the Churilov et Al. [8] experimental tests

In what follows the experimental data are compared with the results of the proposed theory in terms of the different possible failure mechanisms, reconstruction of the load-displacement curve and evaluation of the limit displacement at failure. The shear forces V_i are computed through the equations (2.a, 2.b, 2.c) identified by the flexural, the shear, and the crushing-shear failure modes, respectively.

Table 2 presents the comparison of the computed shear forces with the peak forces of the experimental tests of Churilov et Al. [8]. Concerning the displacements, Table 3 collects the maximum displacements δ_{ult} and the percentage drift $\delta_{\%}$ measured in the experimental campaign, compared with the displacements associated with the maximum shear force acting on the wall.

Since the original tests were performed under cyclic loading, two lines described the behavior of the masonry panel along the two opposite directions. For the sake of completeness, both the positive and the negative load-displacement branches were plotted and taken under consideration for the error computation. The maximum analytical displacement $\delta_{V,max}$ provided by the Eq. (8) is the displacement associated with the maximum shear capacity of the wall, assumed as the minimum value among the shears V_1, V_2, V_3 collected in Table 2.

Table 2: Lateral load capacity of URM and SM masonry panels computed for each failure mechanism and under the application of the axial load N.

Units [kN]	URM1	URM2	URM3	URM4	SM1	SM2	SM3	SM4
N	630.00	365.00	315.00	182.50	630.00	365.00	315.00	182.50
V_1	310.22	168.27	179.23	92.12	614.50	311.65	414.61	229.57
V_2	278.72	150.02	157.18	83.02	578.90	288.65	395.41	215.27
V_3	174.14	100.89	139.87	80.96	1056.82	612.28	854.32	494.54
V_{max}	174.14	100.89	139.87	80.96	578.90	288.65	395.41	215.27
V_{exp}	189.14	88.54	157.35	65.46	483.79	227.18	365.15	208.62
$e_{,V}$	9%	-12%	12%	-19%	-16%	-21%	-8%	-3%

Table 3: Experimental [8] and analytical displacements provided for the whole bench of specimens.

Units [mm]	URM1	URM2	URM3	URM4	SM1	SM2	SM3	SM4
δ_{ult}	11.51	16.10	12.86	11.56	12.33	15.05	20.95	21.01
$\delta_{\%}$	0.63	0.88	0.71	0.64	0.68	0.83	1.15	1.15
δ_{peak+}	3.87	6.86	8.13	7.02	2.78	8.40	8.44	16.97
δ_{peak-}	4.43	7.00	8.35	8.96	3.99	8.93	11.96	15.02
E [δ_{peak}]	4.15	6.93	8.24	7.99	3.39	8.67	10.20	16.00
$\delta_{V,max}$	3.10	4.40	5	11.70	20	17.00	17.10	15.4
$e_{,\delta}$	-25%	-37%	-39%	46%	-	96%	68%	-4%

According to what is mentioned before, Figure 3 and Figure 4 illustrate the backbone load-displacement curves of each masonry wall in the two loading directions.

In particular, the solid line describes the lateral capacity of the masonry wall (Eq.8), while red and blue dashed curves are the experimental evolution of the lateral load applied at the top of the wall against the horizontal displacement corresponding to the positive and the negative directions respectively. Two more points are presented in the plots, namely, the triangle identifies the maximum analytical lateral load resisted by the wall, while the circle represents the theoretical maximum displacement given by the existing standards.

The maximum displacements considered by Italian and European standards value are defined as 0.4% and 0.8% of the total height of the panel. Specifically, the first value is associated with the shear-type failure, whereas the other one describes the limit displacement in case of panel overturning.

By observing previous tables and figures, it is very clear that the proposed formula is able to appreciate the maximum value of the lateral load at which the panel fails, even if it is barely accurate only in terms of displacements.

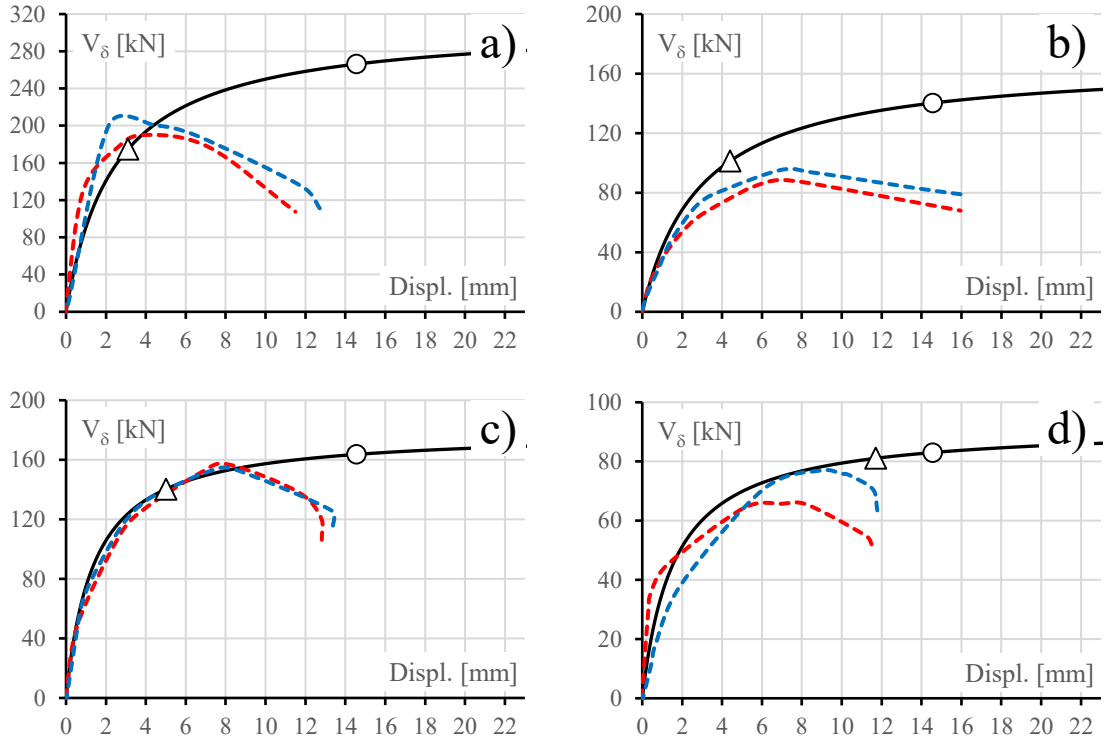


Figure 3: Load-Displacement curves: (a) URM1, (b) URM2, (c) URM3, (d) URM4.

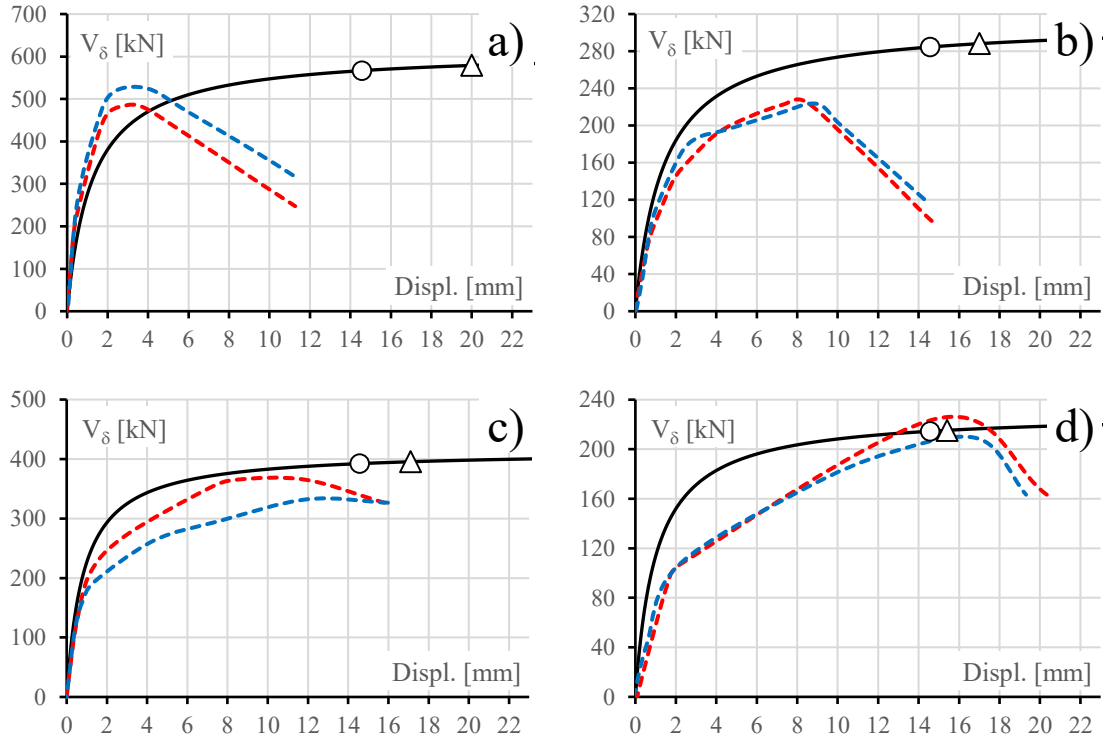


Figure 4: Load-Displacement curves: (a) SM1, (b) SM2, (c) SM3, (d) SM4.

Concerning lateral stiffnesses collected in Table 4, since the hyperbolic curve needs of the value of initial lateral stiffness K_0, its value is computed according to Eq.(9) and it is compared with the value provided experimentally in Churilov et Al [8].

It is to mention that the value of stiffness computed analytically was roughly the double of the secant stiffness obtained experimentally, as previously expected. Consequently, it is extremely important to use the initial stiffness in the load path calculations in order to obtain smaller bias in the estimation of the maximum displacement, as is pointed out by the comparison with the experimental data.

Table 4: Tangential and secant lateral stiffnesses of all the specimens, and their ratio.

Units [kN/mm]	URM1	URM2	URM3	URM4	SM1	SM2	SM3	SM4
K_0	128.93	57.76	128.93	57.76	500.62	224.29	500.62	224.29
K_{exp}	185.610	44.29	74.23	40.30	460.69	102.81	236.28	66.36
ρ_K [-]	0.69	1.30	1.74	1.43	1.09	2.18	2.12	3.38

5 CONCLUSIONS

In the paper, the theoretical framework of the interaction of the failure modes for masonry panels has been discussed in detail. The limit compression zone resulting from the combination of shear and overturning failure has been defined. The shear capacity limitation due to high compression states has been derived in terms of Mohr-Coulomb limit plasticity.

Then, the theoretical framework has been extended to panels reinforced with external coatings of thin FRM layers, and panels reinforced with fiber strips bonded along the vertical edges.

The use of the hyperbolic representation of the load-displacement path allowed the easy construction of the panel' pushover curves. The parameters needed to build the curves were presented and discussed.

By using some experimental results presented in the literature, the effectiveness of the proposed formulation has been demonstrated. The presented results pointed out the importance of considering shear-crushing failure when the axial force has significant value.

The presented procedure is an easy and fast way for the verification and strengthening design of masonry panels subjected to high compression forces, as in monumental buildings.

REFERENCES

[1] Benedetti A. In Plane Behaviour of Masonry Walls Reinforced with Mortar Coatings and Fibre Meshes. *International Journal of Architectural Heritage* (2019) **13**-7:1029-1041, DOI: 10.1080/15583058.2019.1618972

[2] Benedetti A. and Benedetti L. Interaction of shear and flexural collapse modes in the assessment of in-plane capacity of masonry walls. *Proc. of the 12th Canadian Masonry Symposium, Vancouver, Canada, June 2nd -5th, 2013*.

[3] Aprile A, Benedetti A, Grassucci F. 2001. Assessment of Cracking and Collapse for Old Brick Masonry Columns. *Journal of Structural Engineering*, **127**:1427–35. DOI:10.1061/(ASCE)0733-9445(2001)127:12(1427).

[4] Benedetti A, Steli E. Analytical models for shear-displacement curves of unreinforced and FRP reinforced masonry panels. *Construction and Buildings Materials* (2008), **22**(3):175–185. DOI:10.1016/j.conbuildmat.2006.09.005.

[5] Petry S. and Beyer K. Force–displacement response of in-plane-loaded URM walls with a dominating flexural mode, *Earthquake Engng Struct. Dyn.* (2015), DOI: 10.1002/eqe.2597

[6] DT 200-R2. *Guide for the Design and Construction of Externally Bonded FRP Systems for Strengthening Existing Structures*. CNR, Italy (2014).

[7] DT 215. *Istruzioni per la Progettazione, l'Esecuzione ed il Controllo di Interventi di Consolidamento Statico mediante l'utilizzo di Compositi Fibrorinforzati a Matrice Inorganica*. CNR, Italy (2019).

[8] Churilov S., and Dumova-Jovanoska E. In-plane shear behaviour of unreinforced and jacketed brick masonry walls. *Soil Dynamics and Earthquake Engineering* (2013), **50**:85–105. DOI:10.1016/j.soildn.2013.03.006

12th International Conference on Structural Analysis of Historical Constructions
SAHC 2020
P. Roca, L. Pelà and C. Molins (Eds.)

COMPAS MASONRY: A COMPUTATIONAL FRAMEWORK FOR PRACTICAL ASSESSMENT OF UNREINFORCED MASONRY STRUCTURES

A. IANNUZZO[1], A. DELL'ENDICE[1], R. MAIA AVELINO[1], G.T.C. KAO[1], T. VAN MELE[1*] AND P. BLOCK[1]

[1]Institute of Technology in Architecture (ITA), Block Research Group (BRG)
Eidgenössische Technische Hochschule Zürich (ETH - Zurich)
Stefano-Franscini-Platz 1, HIB E, CH-8093 Zurich, Switzerland
email: {iannuzzo, dellendice, maia, kao, van.mele, block}@arch.ethz.ch , www.block.arch.ethz.ch
(*corresponding author)

Keywords: Masonry, Historical Structures, Computational tools, Limit Analysis, Simplified models

Abstract. *In recent years, our (academic/theoretical) understanding of the behaviour of unreinforced masonry (URM) structures has improved significantly, and many advanced technological solutions for conservation have been developed. However, there is still a lack of appropriate methods and tools that can be used for the assessment of URM structures in every day practice. Therefore, since 2018, the Block Research Group has been working on "Practical Stability Assessment Strategies for Vaulted Unreinforced Masonry Structures" with support of the Swiss National Science Foundation (SNSF). The goal of this research project is to create tools suitable for everyday engineering practice and to develop appropriate analysis strategies for diverse contexts and circumstances related to the availability of time, budget and available data. The main outcome is COMPAS Masonry: an open-source, Python-based computational framework for the assessment of URM structures. It provides a general purpose toolbox for working with assemblies (compas_dem) and three custom made open-access solvers that can deal with different aspects of the assessment of masonry structures: compas_tna based on Thrust Network Analysis, compas_prd based on the Piecewise Rigid Displacement method, and compas_rbe based on the Rigid Block Equilibrium.*

1 INTRODUCTION

Unreinforced masonry (URM) is one of humankind's longest-lasting construction methods and forms the structural basis for most of the residential buildings all over the world. The assessment of URM structures is an atypical mechanical problem: constructions are comprised of individual discrete elements; large displacements and deformations are common, and, particularly for historic buildings, material properties and boundary conditions are unknown or unknowable.

Many of the structural analysis tools/software available today were developed for entirely different structural systems with very different materials such as steel, concrete and timber, and

should therefore not be applied to the analysis of masonry structures. Indeed, it is well known that some well-established engineering methods, such as Finite Element Analysis (FEA), do not apply to the assessment of masonry because of their numerical inability to deal with the intrinsic unilateral behaviour of masonry: many of the required mechanical parameters are unknown or even unknowable, and zero-energy modes (ill-conditioned stiffness matrices) related to fractures cannot be taken into account. The reader is referred to e.g. [1, 2], where these aspects have been highlighted. Moreover, even technical regulations are not specifically conceived for URM structures, leaving practitioners the freedom to utilise any method at their disposal. If the masonry knowledge of the practitioner is not in-depth and accurate, the risk of tackling the assessment with non-appropriate tools, and then to wrongly intervene, becomes a certainty. One of the consequences is that many restorations actually compromise the mechanical behaviour of structures that had been standing for centuries.

In 1966, Jacques Heyman [3] gave the theoretical basis to apply Limit Analysis to masonry structures. Still today, his limit analysis theory based on three crude material assumptions, is recognised as one of the best approaches for the assessment of URM structures. Nevertheless, even though the Limit Analysis theory is widely accepted, there is still a lack of user-friendly numerical implementations that can be used by specialists in their everyday activities.

More recently, Discrete Element Modelling (DEM) methods, in particular 3DEC by Itasca [4], have also been successfully applied to the assessment of 3D masonry structures. Currently, they represent the unique alternative to the standard engineering tools conceived for other materials. Unfortunately, since most implementations are only available through (often expensive) proprietary software their use is mainly restricted to academic research.

Since 2018, with the support of the Swiss National Science Foundation (SNSF), the Block Research Group has been developing COMPAS Masonry, a computational framework for "Practical Stability Assessment Strategies for Vaulted Unreinforced Masonry Structures". The goal is to develop better approaches and tools for engineering practice as it relates to the analysis of URM structures.

COMPAS Masonry bundles four Python-based tools: *compas_dem, compas_tna*, *compas_prd*, and *compas_rbe*. The proposed computational framework allows managing complex 3D geometries easily, to work with different loading conditions, to take into account the effects of (large) foundation displacements and, when needed, also mechanical and geometrical imperfections. Furthermore, by making these tools available, this project provides a framework for developing a better understanding of the behaviour of masonry structures which will reflect into more appropriate and less intrusive restoration interventions.

2 COMPUTATIONAL FRAMEWORK

COMPAS Masonry is an open-source, Python-based computational framework for the assessment of URM structures. COMPAS Masonry bundles specific open-access, Python packages and provides benchmark data, protocols and procedures for performing analyses on real-world masonry problems using any combination of the available computational approaches. COMPAS Masonry includes a general purpose toolbox for working with assemblies (*compas_dem*), and three custom solvers that can deal with different aspects of the assessment of masonry: *compas_tna* [5], based on the Thrust Network Analysis (TNA) by Block [6]; *compas_prd* [7], based on the Piecewise Rigid Displacement (PRD) method by

Iannuzzo [8]; and *compas_rbe* which is based on the Rigid Block Equilibrium (RBE) by Withing [9]. *compas_dem* [10] can be used in combination with any of the custom solvers as well as with the commercial DEM solver 3DEC by Itasca [4].

Table 1: Overview of the models, approaches and the numerical procedures adopted in COMPAS Masonry.

Tool	Model	Approach	Solution
3DEC	DEM	Netwton's laws	Explicit dynamics
compas_tna	Heyman	Equilibrium	Nonlinear optimization
compas_prd	Heyman	Energy	Linear optimization
compas_rbe	Livesley (extended)	Equilibrium	Quadratic optimization

As one can see from **Table 1**, including 3DEC, these tools are based on different models/approaches. Specifically, 3DEC uses an explicit dynamics approach, *compas_tna* and *compas_prd* are Limit Analysis-based methods framed within the Heyman's model [3] and *compas_rbe* is based on an extension of Livesley's equilibrium approach [11]. The diverse approaches reflect into different numerical procedures adopted to find solutions: three of them are based on optimisation procedures (linear and nonlinear programming) while 3DEC integrates Newton's second law of motion using the central finite difference method with respect to time.

2.1 General purpose toolbox: *compas_dem*

compas_dem provides tools for the generation of assemblies of discrete elements and especially for the management of relationships between the individual parts. *compas_dem* provides several purposes tools: to generate either parametric or measured 3D geometries; to model/generate mechanical and geometrical imperfections; to detect interfaces in the assembly; to visualize interface forces. Moreover, it provides a common interface for different solvers in the background and tools to post-process and visualise their results.

2.2 Discrete Element Modelling: 3DEC

One of the solvers that can be used in combination with *compas_dem* is 3DEC by Itasca. 3DEC is commercial/proprietary Discrete Element Modelling software, and it is used in this project to benchmark and guide the development of the three other COMPAS Masonry tools. Compared to traditional structural analysis tools DEM software has three main peculiarities: the analysis model consists of separate blocks that can move and deform independently; large displacements are possible; blocks can detach from each other, and new contacts can form. In 3DEC, both rigid and deformable blocks can be considered, and unilateral contact conditions can be defined. In particular, using rigid blocks acting unilaterally and a Mohr-Coulomb criterion, the only mechanical parameters required are: material density, friction angle, Young's and shear moduli (to evaluate the joint stiffnesses). The calibration of these parameters is crucial and, for this purpose, in this project, tests on physical models are performed to calibrate 3DEC parameters and to validate its results [12, 13, 14]. Once the calibration of the mechanical

parameters is done, 3DEC represents a reliable tool for the assessment of URM structures, and it can be used for many assessment problems: stability in a given configuration, load-bearing capacity, displacement capacity, dynamic loading conditions, analysis of the settlements. The downside of the numerical approach (i.e. explicit dynamics, see **Table 1**) is that the computational time needed to solve some typical problems can range from minutes for very simple problems to several hours for problems with more realistic complexity.

2.3 Thrust network analysis (TNA): *compas_tna*

compas_tna provides a base implementation of Thrust Network Analysis (TNA) by Block [6, 15]. TNA works by computing an equilibrated, compressive and admissible thrust network entirely contained within the structural geometry of the masonry. This network is the representation of a one-dimensional, singular, compressive stress field in which the forces are concentrated on the edges and the loads and restraints are applied in the nodes. The method is a direct application of the safe theorem of limit analysis by Heyman [3, 16] since the admissible thrust network corresponds to a lower-bound solution of the limit state of the structure. *compas_tna* sets up and solves a constrained nonlinear optimisation problem [5] searching for a particular stress state of the structure by tuning the objective function and the constraints. Several objective functions are implemented to face different structural problems, such as the search for the minimum and/or maximum thrust and maximum collapse load multiplier. The main constraints of the optimisation problem enforce the heights of the network nodes to be contained within the structural geometry represented by its internal and external surfaces. Additional constraints can also be included to simulate the conditions observed on existing structures, such as simulation of cracks, limits on the reactions of the vault, and openings. By searching among different stress states, TNA can also be used to obtain an estimate of the level of stability of masonry vaults.

2.4 Piecewise rigid displacement (PRD): *compas_prd*

compas_prd is a new computational tool that stems from the piecewise rigid displacement (PRD) method [8]. With the PRD method, a masonry structure is modelled as composed of normal, rigid, no-tension (NRNT) material, which mathematically frames into continuum mechanics Heyman's material assumptions. With PRD both mechanisms and internal forces can be found simultaneously by solving two dual linear programming (LP) problems [17]. The primal LP problem, representing the minimum of the total potential energy in the space of piecewise rigid displacements, returns a rigid macro-blocks partition of the structural domain and thus cracks between adjacent elements, representing singular strain fields. The dual LP problem, that is the minimum of the complementary energy, returns internal and external forces in equilibrium with the external loads and compatible with the crack pattern solving the primal problem. Different mechanical problems can be tackled: stability in the initial configuration, effects of foundation displacements [18]; assessment of the safety under horizontal actions [19]; and, the effects of large foundation displacements [20].

2.5 Rigid block equilibrium (RBE) method: *compas_rbe*

compas_rbe provides a base implementation of Rigid block equilibrium (RBE) by Withing, which is a numerical method for the three-dimensional analysis of equilibrium states of URM

structures modelled as assemblies of distinct rigid blocks. The research of Livesley [11, 21] constitutes one of the basic studies to address RBE. Livesley was the first to solve the equilibrium and mechanism formulations of Limit Analysis using linear programming, and he was also the first to attempt to introduce the mechanism of sliding at the joints. This issue was solved by Gilbert and Melbourne [22], who implemented sliding between joints and incorporated friction into the equilibrium equations. In *compas_rbe* the blocks are considered to be infinitely rigid and to have infinite compressive strength. Interfaces between the blocks are considered to have a finite frictional capacity. *compas_rbe* provides the necessary contact forces (i.e. compression, tension and friction forces) for the assembly to be in equilibrium under given external loads. Furthermore, it extends Livesly's formulation enlarging the space of stress solutions by considering tensile forces in penalty formulation.

3 MODELS AND ASSESSMENT TOOLS: INPUT AND OUTPUT

Master builders constructed masonry not just as chaotic union of bricks but rather as a smart and appropriate assemblage of blocks that prevents sliding failures by ensuring proper connections in each element and in between adjacent elements ("rules of art") [3, 23, 24, 25]. When a masonry construction is structurally sound, it behaves as a whole, its stability depends on its geometry [3, 26, 27, 28, 29] and it can accommodate small external changes with its nucleation into rigid macro-blocks, visible through the fracture pattern. This peculiar behaviour allows masonry structures to be flexible, exhibiting a ductile (elastic) response to the external changes [30].

To understand if the structure to assess responds to this criterium, it is crucial to know some typical aspects: materials and construction phases of the building, history (seismic events, collapses, reconstructions, additions, etc.), stereotomy, construction techniques, and a proper investigation of the geometry. A particular attention needs to be paid to a the exact definition of the relevant crack pattern and measurements of the leaning of the walls and columns. This information is central for understanding the global behaviour of the structure, where each element (e.g. vaults, arches, walls, columns, buttresses, flying buttresses) is a part of a complex mechanical system. After this evaluation, which demands an in-depth knowledge of the specialist, appropriate assessment strategies can be defined and specific tools can be adopted.

3.1 Simplified models

If the structure is structurally sound (*rules of art* [24]), simplified models based on rigid-plastic constitutive relations can be properly adopted [31]. Two of the three solvers available in COMPAS Masonry are based on Heyman's model: *compas_tna* and *compas_prd*. The Heyman model is very crude (no tensile strength, infinite compressive strength, no-sliding failures) not requiring any mechanical parameter but, it represents a robust approach to account for the peculiarities of masonry structures: geometrical stability, unilateral behaviour, fractures, nucleation of the domain into rigid macro-blocks. *compas_rbe*, based on Livesley's formulation, represents an extension of Heyman's model and it requires only one mechanical parameter: the friction angle. Therefore, the solvers of COMPAS Masonry provide a simplified approach to assessment of URM structures that does not require all information about the structure to be known. In the next sections, we highlight, the input data required and the output provided by each COMPAS Masonry tool (see **Table 2**, **Table 3**)

Table 2: Input data required by COMPAS Masonry tools and 3DEC.

Tool	Suitable for	Input	Imperfections	Friction	Other mechanical parameters
3DEC	3D geometry	Stereotomy	✓	✓	✓
compas_tna	3D vaulted structures	External and internal surfaces	✗	✗	✗
compas_prd	2.5D geometry	Geometry or stereotomy	✗	✗	✗
compas_rbe	3D geometry	Stereotomy	✓	✓	✗

The significant benefit in adopting the simplified models provided in COMPAS Masonry is that, beyond accounting for the peculiarities of the masonry with a very crude mechanical characterisation, they provide fast computational solving. In particular, it is well known that for huge mathematical problems (e.g. thousands of unknowns), the linear programming framework offers algorithms able to find a solution in a few seconds. Therefore, solvers based on linear programming (such as *compas_prd*) are useful when we have to face large problems or to approach inverse analysis, where a wide spectrum of solutions is required. Quadratic and, in general, nonlinear optimisation procedures (*compas_tna* and *compas_rbe*) require longer computational time which can range from a few seconds to several minutes. The fast computational solving of the COMPAS Masonry tools constitutes a big advantage over DEM analyses (e.g. 3DEC).

Table 3: Output data provided by COMPAS Masonry tools and 3DEC.

Tool	Forces	Min/Max Thrusts	Displacements	Cracks/ Mechanisms
3DEC	✓	✗	✓	✓
compas_tna	✓	✓	✗	✗
compas_prd	✓	✗	✓	✓
compas_rbe	✓	✗	✗	✗

3.2 *compas_tna*: input/output

compas_tna is especially useful to analyse 3D complex vaulted structures (see **Table 2**). It needs as an input only the internal and external surfaces describing the geometry of the vault. Since it searches for admissible stress solutions for the structure, the output is an equilibrated thrust network of compressive forces entirely contained within the structural geometry. *compas_tna* can directly provide the minimum and maximum thrust exerted by the structure.

3.3 *compas_prd*: input/output

compas_prd it is a direct kinematic-based approach and stands on two dual energy criteria. Currently, it is implemented for 2.5D geometries, that is: the analysis is planar but non-uniform, symmetrical orthogonal depths can be considered. The input required is a discretised geometry of the structure (see **Table 2**). In some cases, the discretisation can coincide with the structural stereotomy while in other cases, the discretisation has to be handled accordingly [32]. Its solutions consist of displacements (i.e. potential mechanisms and cracks) and corresponding internal forces. (see **Table 3**).

3.4 *compas_rbe*: input/output

compas_rbe solves the equilibrium problem for 3D assemblies of rigid, distinct blocks. As input, it requires the stereotomy of the structure and the values describing the friction between the blocks. It can handle geometrical and mechanical imperfections (random distribution of the friction angle), allowing an in-depth investigation of their role in the global mechanical behaviour (see **Table 2**). As solutions, it provides the internal stress states represented by forces acting on the interface between two adjacent blocks. The solution can also involve tensile forces in a penalty formulation and friction forces higher than the one permitted by the actual friction values. This peculiar feature enables the user to understand the main critical regions of the assembly where sliding or detachments can occur.

4 COMPUTATIONAL ANALYSES SCENARIOS

In this section, we discuss the main problems concerning the assessment of historic masonry structures and how they can be tackled within COMPAS Masonry. When we have to assess the safety of masonry buildings, the typical issues are: stability in the reference configuration; load-bearing capacity; effects of settlements; displacement capacity. Horizontal actions (e.g. seismic actions or wind) deserves a special treatment even if they can be framed as a load-bearing capacity case. In **Table 4**, a schematic overview of the assessment problems that can be tackled by each tool is presented.

Table 4: Overview of the problems tackled by COMPAS Masonry tools.

Tool	Stability in ref. configuration	Load-bearing capacity	Horizontal forces	Effects of settlements	Displacement capacity
3DEC	✓	✓	✓	✓	✓
compas_tna	✓	✓	✓	✗	✗
compas_prd	✓	✓	✓	✓	✓
compas_rbe	✓	✓	✓	✗	✗

4.1 Stability in the reference configuration

Assess if a masonry structure is stable in its reference configuration represents one of the most frequent structural problems. A widely accepted approach consists in applying the **Safe Theorem**, that is, to find a compressive stress state lying within the structural geometry and in

equilibrium with the external loads. All the COMPAS Masonry tools are able to address this problem and can explore a wide range of admissible stress states either adopting different objective functions (*compas_tna*) or by adding some further constraints to the initial optimisation problem (*compas_prd* and *compas_rbe*). Outcome of a stability analysis is the safety factor. This number can be defined as an appropriate ratio between a critical position of the flow of forces and an optimal one. All the tools allow the calculation of safety factors in a given configuration by using different approaches.

Anyway, the scenario can get complex if a non-negligible crack pattern is present. This does not constitute an issue for the COMPAS Masonry tools. Indeed, the revealed fractures can be taken into account easily by each tool. In particular, while *compas_prd*, *compas_rbe* can take into account these fractures considering directly a non-perfect initial geometry, *compas_tna* offers robust algorithms to constraint the thrust networks to go throughout certain curves modelling the fracture pattern.

4.2 Load bearing capacity

Every time we are facing the problem of assessing what is the maximum load that a structure can sustain, we are solving a load-bearing capacity problem. Each tool can address this problem. In particular, the approach adopted by the three tools (*compas_tna*, *compas_prd*, *compas_rbe*) is to increment the load until a safe solution can be still found. This procedure gives rise to a set of sequential optimisation (linear and nonlinear) problems. When the load reaches its maximum allowable value, no one solution can be found anymore (for *compas_rbe*, a solution is still possible, but it involves tensile forces). In this way, we obtain the maximum allowable load and its corresponding scale factor. In this last case, *compas_prd* returns also the mechanism and corresponding crack pattern.

4.3 Load bearing capacity, a special case: horizontal forces

Horizontal forces represent a special load-bearing capacity case. When we have to account for the effects of the wind and/or of the seismic actions, one way is to model these actions by considering static, equivalent, horizontal forces All the COMPAS Masonry tools can model horizontal actions as statical forces and can evaluate the horizontal static multiplier following the same procedure exposed in **Section 4.2**.

4.4 Effects of settlements

The effects of settlements represent one of the key issues in the assessment of masonry structures. Most of the time, the crack pattern observed is due to the settlements rather than to overloading. Indeed, in most of the cases these small settlements are due to changes in the boundary conditions (e.g. a change in the thrust's inclination exerted by a pillar can reflect into small foundation displacements). A masonry structure accepts these new boundary conditions through the formation of a crack pattern. These cracks define a decomposition of the structural domain into rigid macro-blocks which allows the structure to displace almost piecewise rigidly. If the settlements are small and cannot grow up anymore, the structure is still stable. *compas_prd* allows for addressing the effects of foundation settlements (see **Table 4**). Furthermore, understanding exactly the causes (e.g. find the shape of the foundation displacements) producing a given crack pattern corresponds to an inverse analysis. Since,

compas_prd can fastly compute a wide range of solutions, it can also be used for conducting this inverse analyse as in [32].

4.5 Displacement capacity

In some cases, foundation displacements can increase affecting strongly the (geometrical) stability of the structure. In some assessment scenarios, it is crucial to know the maximum allowable displacement value for which the structure is still stable. This demands a model which can take into account the evolution of the crack pattern/mechanism used by the structure to accommodate the increasing settlement. In this case, it is important to define a safety factor (in terms of displacement capacity) measuring how far the current structural geometry is from an unstable configuration. *compas_prd* can perform this analysis (see **Table 4**), also accounting for the evolution of the mechanism during the motion (see [20], where it was benchmarked with 3DEC).

5 CONCLUSIONS

In this paper we present an overview of the project in development since 2018 at the Block Research Group entitled "Practical Stability Assessment Strategies for Vaulted Unreinforced Masonry Structures", funded by Swiss National Science Foundation (SNSF). The aim of this project is to provide adequate tools for everyday engineering practice. In particular, one general purpose package (*compas_dem*) and three stand-alone tools (*compas_tna*, *compas_prd* and *compas_rbe*) are provided. The results of this work are shared as COMPAS Masonry, a new open-source, Python-based, computational framework for the assessment of URM structures.

This work shows the potentialities, peculiarities, limitations and applicability range of each tool, referring to specific input data (e.g. geometry, stereotomy, mechanical parameters) and to typical assessment problems (e.g. stability in the reference configuration, load-bearing capacity, effects of settlements and displacement capacity). The individual tools are designed to be as flexible as possible and to provide a simple way to manage complex mechanical and geometrical data.

Beyond benchmark data, protocols and numerical procedures, COMPAS Masonry provides a framework where these four tools can be integrated and applied in different assessment scenarios depending on the availability of information, time and budget. It also provides an easy-to-use mechanical approach, not requiring a detailed mechanical characterisation (zero mechanical parameters for *compas_tna* and *compas_prd*) and offers robust approaches and fast computational solving to account for the peculiarities of URM structures in different assessment scenarios.

Acknowledgements. This work was supported by the Swiss National Science Foundation (SNSF) - project grant #178953: "Practical Stability Assessment Strategies for Vaulted Unreinforced Masonry Structures".

REFERENCES

[1] P. Block, T. Ciblac and J. A. Ochsendorf, "Real-time limit analysis of vaulted masonry buildings," *Computers & structures,* Vols. 84(29-30), pp. 1841-1852, 2006.

[2] H. V. Shin, C. F. Porst, E. Vouga, J. A. Ochsendorf and F. Durand, "Reconciling elastic and equilibrium methods for static analysis," *ACM Transactions on Graphics (TOG),* vol. 35, no. 2, p. 13, 2016.

[3] J. Heyman, "The stone skeleton," *International Journal of solids and structures,* vol. 2(2), pp. 249-279, 1966.

[4] Itasca Consulting Group, Inc (2016) 3DEC, Three-Dimensional Distinct Element Code, Ver. 5.2. Minneapolis: Itasca.

[5] R. Maia Avelino, A. Iannuzzo, T. Van Mele and P. Block, "New strategies to assess the safety of unreinforced masonry structures using Thrust Network Analysis," in *Proceedings of the SAHC Symposium: Barcelona, 2020.*, Barcelona, 2020.

[6] P. Block, Thrust network analysis: exploring three-dimensional equilibrium, Doctoral dissertation, Massachusetts Institute of Technology, 2009.

[7] A. Iannuzzo, T. Van Mele and P. Block, "Stability and load-bearing capacity assessment of a deformed multi-span masonry bridge using the PRD method," *International Journal of Masonry Research and Innovation,* 2021.

[8] A. Iannuzzo, "A new rigid block model for masonry structures," *Ph.D Dissertation, Università degli Studi di Napoli Federico II,* 2017.

[9] E. J. W. Whiting, Design of structurally-sound masonry buildings using 3d static analysis, Doctoral dissertation, Massachusetts Institute of Technology, 2012.

[10] A. Dell'Endice, A. Iannuzzo, T. Van Mele and P. Block, "Influence of settlements and geometrical imperfections on the internal stress state of masonry structures," in *Proceedings of the SAHC Symposium*, Barcelona, 2020.

[11] Livesley, R K, "Limit analysis of structures formed from rigid blocks," *International Journal for Numerical Methods in Engineering,* vol. 12(12), pp. 1853-1871, 1978.

[12] Van Mele, T., McInerney, J., DeJong, M. J., & Block, P., "Physical and computational discrete modeling of masonry vault collapse," *Structural analysis of historical constructions: proceedings of the 8th International Conference on Structural Analysis of Historical Constructions, SAHC 2012, 15-17 October, Wroclaw, Poland,* pp. 2252-2560,DWE, 2012.

[13] C. C. Barentin, T. Van Mele and P. Block, "Robotically controlled scale-model testing of masonry vault collapse," *Meccanica,* vol. 53, no. 7, pp. 1917-1929, 2018.

[14] A. Dell'Endice, A. Iannuzzo, M. DeJong, T. Van Mele and P. Block, "Modelling imperfections in unreinforced masonry structures: Discrete Element simulations and scale model experiments of a pavilion vault," *Engineering Structures,* Vols. 228, 111499, 2021.

[15] P. Block and L. Lachauer, "Three-dimensional funicular analysis of masonry vaults," *Mechanics Research Communications,* vol. 56, pp. 53-60, 2014.

[16] J. Heyman, "The safety of masonry arches," *International Journal of Mechanical Sciences,* vol. 11, no. 4, pp. 363-385, 1969.

[17] A. Iannuzzo, T. Van Mele and P. Block, "Piecewise Rigid Displacement (PRD) method: A limit analysis-based approach to detect mechanisms and internal forces

through two dual energy criteria," *Mechanics Research Communications,* Vols. 107, 103557, no. doi.org/10.1016/j.mechrescom.2020.103557, 2020.

[18] A. Iannuzzo, M. Angelillo, E. De Chiara, F. De Guglielmo, F. De Serio, F. Ribera and A. Gesualdo, "Modelling the cracks produced by settlements in masonry structures.," *Meccanica,* vol. 53(7), pp. 1857-1873, 2018.

[19] A. Iannuzzo, A. De Luca, A. Fortunato, A. Gesualdo and M. Angelillo, "Fractures detection in masonry constructions under horizontal seismic forces," *Ingegneria Sismica,* vol. 35, no. 3, pp. 87-103, 2018.

[20] A. Iannuzzo, A. Dell'Endice, T. Van Mele and P. Block, "Numerical limit analysis-based modelling of masonry structures subjected to large displacements," *Computers & Structures,* Vols. 242, 106372, 2021.

[21] R. K. Livesley, "A computational model for the limit analysis of three-dimensional masonry structures," *Meccanica,* vol. 27, no. 3, pp. 161-172, 1992.

[22] M. Gilbert and C. Melbourne, "Rigid-block analysis of masonry structures," *Structural engineer,* vol. 72, no. 21, 1994.

[23] J. Fitchen, The construction of Gothic cathedrals: a study of medieval vault erection, University of Chicago Press, 1981.

[24] A. Giuffrè, Letture sulla Meccanica delle Murature Storiche, Edizioni Kappa;, 1991.

[25] J. Heyman, "The structural engineer's view of ancient buildings," *Journal of Mechanics of Materials and Structures,* vol. 13, no. 5, pp. 609-615, 2019.

[26] S. Huerta, "Galileo was wrong: the geometrical design of masonry arches," *Nexus Network Journal,* vol. 8(2), pp. 25-52, 2006.

[27] M. Como, Statics of historic masonry constructions, Berlin: Springer, 2013.

[28] S. Huerta Fernández, "Geometry and equilibrium: The gothic theory of structural design," *Structural Engineer,* vol. 84, no. 2, pp. 23-28, 2006.

[29] P. Block, M. DeJong and J. A. Ochsendorf, "As hangs the flexible line: Equilibrium of masonry arches," *Nexus Network Journal,* vol. 8(2), pp. 13-24, 2006.

[30] Angelillo, M., Fortunato, A., Gesualdo, A., Iannuzzo, A., & Zuccaro, G., "Rigid block models for masonry structures," *International Journal of Masonry Research and Innovation,* vol. 3, no. 4, pp. 349-368, 2018.

[31] M. Angelillo, "Practical applications of unilateral models to Masonry Equilibrium," in *Mechanics of Masonry Structures*, M. Angelillo, Ed., Vienna, Springer, 2014, pp. 109-210.

[32] A. Iannuzzo, "Energy based fracture identification in masonry structures: the case study of the church of "Pietà dei Turchini"," *Journal of Mechanics of Materials and Structures,* vol. 14, no. 5, pp. 683-702, December 2019.

[33] T. Van Mele and m. others, "COMPAS: A framework for computational research in architecture and structures.," *https://doi.org/10.5281/zenodo.2594510, http://compas-dev.github.io/,* 2017-2019.

12th International Conference on Structural Analysis of Historical Constructions
SAHC 2020
P. Roca, L. Pelà and C. Molins (Eds.)

CORRELATION STUDIES FOR THE IN-PLANE ANALYSIS OF MASONRY WALLS BASED ON MACROSCOPIC FE MODELS WITH DAMAGE

MARIACARLA NOCERA[1]*, LUIS C. SILVA[2], DANIELA ADDESSI[1] AND PAULO B. LOURENÇO[3]

[1]Department of Structural and Geotechnical Engineering
University of Rome Sapienza
Via Eudossiana 18, 00184 Rome, Italy
e-mail : (mariacarla.nocera, daniela.addessi)@uniroma1.it

[2]Institute for Sustainability and Innovation in Structural Engineering - ISISE
Universidade do Minho
4800-058 Guimarães, Portugal
e-mail : luiscsilva@civil.uminho.pt, web page: www.hms.civil.uminho.pt

[3] Department of Civil Engineering, ISISE, University of Minho
Campus de Azurém 4800-058
Guimarães, Portugal
e-mail : pbl@civil.uminho.pt

Keywords: Masonry structures, Macromechanical finite element, Damage, Crack, Plasticity.

Abstract. *This study explores the use of macro-modelling techniques based on smeared crack and damage-plastic constitutive laws for the cyclic in-plane analysis of masonry panels. The numerical investigation is focused on two material macromechanical models, known as Total Strain Cracking and Crack and Plasticity models. These show some limitations when analysing the behaviour of masonry structures subjected to in-plane cyclic loading. A modified version of the Drucker-Prager model including cohesive softening is introduced to overcome these shortcomings.*
A suite of numerical simulations is performed referring to an experimental campaign on two masonry (squat and slender) panels. A comparison of distinctive features of flexural and shear response of masonry panels is addressed. The results derived from the two FE macro-models are compared with the experimental outcomes, highlighting the effects of geometry, stiffness degradation, and post-peak energy dissipation. Furthermore, a comparison with another macromechanical model is performed.

1 INTRODUCTION

Masonry buildings are a relevant part of the existing civil, architectural and cultural heritage. The preservation of their structural integrity is a very challenging task, requiring the development of accurate and efficient procedures to assess their safety and stability.

Unreinforced masonry structures typically show a high seismic vulnerability and require repairing and strengthening interventions to reduce their collapse risk [1]. An accurate evaluation of the unreinforced structure response is a fundamental step, given the complexity and heterogeneity of masonry material, to design possible efficient interventions. The main aim is to investigate the onset and evolution paths of the damaging mechanisms that can lead to the structural collapse under seismic actions. Several studies were conducted to characterize the different damage mechanisms, which can be caused from various external actions, and study how to provide the safety of these constructions [2]. Analytical and numerical procedures based on different modelling approaches exist in the literature [3]. The main available strategies for masonry structures can be broadly classified as follows: limit analysis, where limit plasticity theorems are applied to evaluate the static response of the structures, macroelement models, where the constructions are idealized in structural components adopting nonlinear constitutive laws, finite element modelling (FEM), where the structures are discretized with different detail scales, and discrete element method, where the buildings are described as an assemblage of distinct blocks interacting along the boundaries. A comprehensive and more detailed review can be found in [4].

Limiting the attention to FEM, different approaches can be recognized as micromechanical and macromechanical formulations. The former approach describes masonry in detail, differentiating between block, mortar and interfaces [5]–[7]. The information on the geometry, texture and constituents is accurately described, as well as their constitutive behaviour. In the latter approach, the real heterogeneous masonry material is substituted by an effective homogeneous continuum medium, where proper phenomenological constitutive laws have to be introduced [8]–[12]. Indeed, several nonlinear constitutive laws have been developed with the aim of reproducing an increasingly realistic description of the structures [13].

Macromechanical finite element models are today the most convenient ones when engineering large to super large problems. The macro constitutive laws for masonry usually rely on a damage and/or plasticity model. Damage models are often combined with a plasticity formulation with the aim of better reproducing the masonry structural response (strongly characterized by energy dissipation). Different approaches were proposed to describe damage from a phenomenological point of view. In particular, models based on the classical theory of Continuum Damage Mechanics [14], in which the material is assumed as a continuum medium, or formulated according to Fracture Mechanics theory, in which discrete cracks of finite size are explicitly modelled, can be distinguished.

In 1968, Rashid introduced the smeared crack formulation, that is a counterpart of the discrete crack concept. This considers the medium, where different cracks are present, as a continuum material [15]. The simplicity of the approach captured the attention of the scientific community and most of the FE codes have adopted this approach. In such a context, this paper investigates the use of macromechanical constitutive models to analyse the nonlinear degrading response of masonry structures. In particular, the study focuses on two material constitutive laws belonging to the class of the so-called Smeared Crack Models (SCM), known as Total Strain Cracking and Crack and Plasticity [15,16]. The results of the experimental campaign conducted by *Anthoine et al.* [18] are numerically reproduced and a comparison on distinctive features amid the flexural and shear responses of masonry panels is addressed. Firstly, monotonic tests are performed to validate the mechanical parameters deduced from literature and prove the model's efficiency to reproduce the real damage mechanisms. Then, the cyclic behaviour of the tested

masonry panels is investigated under in-plane cyclic loading. Some of the limitations of the models are highlighted and, to overcome such restrictions, a modified version of the Drucker-Prager model including cohesive softening is proposed. The effects of the geometry, stiffness degradation, and post-peak energy dissipation are investigated. Comparisons between the adopted macro-models and the experimental outcomes are shown in terms of global in-plane cyclic response of the masonry panels; meaning the envelope capacity curve and the crack mechanisms. Furthermore, the results from a continuum damage-plastic model proposed in *Gatta et al.* [13] is also addressed.

2 MACROMECHANICAL MODELS FOR MASONRY

This section describes the macromechanical finite element models adopted to numerically reproduce the structural response of the masonry panels from the selected experimental campaign. A brief description on the constitutive laws is first stated and the differences between the models are highlighted after. Finally, a short comment on the employed regularization technique to overcome the mesh-dependency of the FE solution is also provided.

2.1 Smeared crack and continuum damage constitutive models

Two smeared crack models implemented in the FE code DIANA [19] are first described, the so-called Total Strain Cracking and Crack and Plasticity models. A modified version of the latter is also presented to better reproduce some features of the nonlinear response of masonry structures. At the end, a macromechanical model based on Continuum Damage Mechanics is introduced [13] with the purpose of comparing the different approaches.

The Total Strain Cracking material models available in DIANA can be categorized into fixed, rotating and fixed multi-directional smeared crack approach [17]. The Total Strain Rotating Crack (TSRC) model is used in this study. This computes the stress as a function of the strain and follows a smeared approach to describe the fracture process. According to the rotating concept, the crack directions are updated to rotate with the principal directions and to be aligned with them during loading history. The basic concept of the TSRC model is that the stress vector is evaluated according to the intrinsic reference system of the crack, given by the axes parallel and orthogonal to the crack. The smeared fracture process is activated when the maximum principal stress, evaluated at a Gauss point of the FE, exceeds the tensile strength. The shape of the tensile softening diagram controls the cracking phenomenon, being governed by the fracture energy parameter of the material that is given by the area under the stress-strain diagram. Two values are introduced for the fracture energy parameters, i.e. g_t and g_c that are associated, respectively, with the tensile and compression behaviours. In this study, an exponential law governs the softening branch in tension and a hardening-softening parabolic law the post-peak response in compression.

The Crack and Plasticity (CP) model is based on the smeared crack approach used to simulate the tensile post-cracking behaviour, whereas the Drucker-Prager plasticity model is adopted to simulate the compressive response. The CP model can be categorized as a multi-fixed smeared crack model with an elastic-plastic constitutive law in compression. According to the multi-fixed crack formulation, and differently from the fixed smeared crack model where only one fixed crack can form at each integration point, more than one crack is allowed to form. In the multi-fixed crack model, the first crack is formed perpendicular to the direction of the maximum

principal stress. After that, another crack is allowed to form if the tensile strength is again violated by the major principal stress and if the angle between the existing crack and direction of the major principal stress exceeds a certain value, i.e. the threshold angle that is usually set to be 30 degrees. As for the TSRC model, the cracking phenomenon is governed by the shape of the tensile softening, defined by the fracture energy g_t. For this study, post-peak tensile stresses decrease following a linear law.

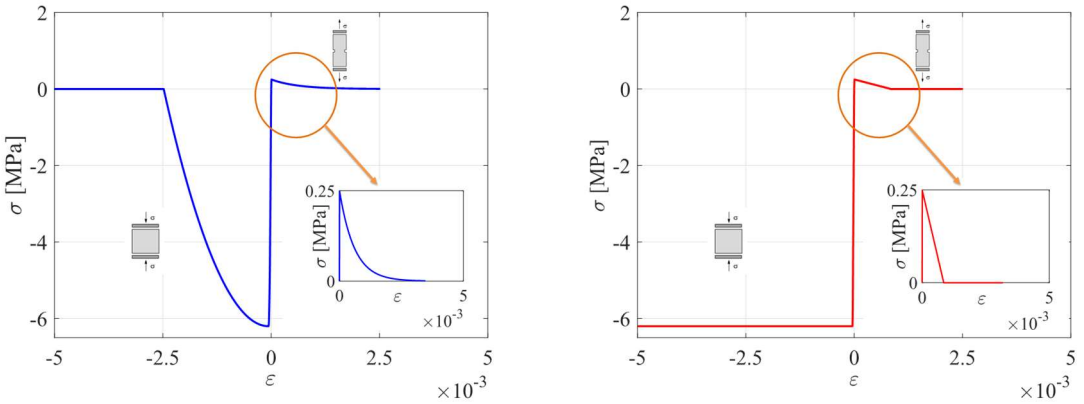


Figure 1: Masonry stress-strain law: TSRC (a) and CP (b) model.

To overcome some shortcomings of the described CP model by its limiting capability of reproducing the real response of masonry, a modified version is here proposed. In particular, with the aim of describing the degrading phenomena also in compression, a cohesive softening is introduced in the Drucker-Prager model, giving rise to the designated Modified Crack and Plasticity model (MCP). The compressive softening law is empirically included in the Drucker-Prager model with strain hardening, whereas the tensile response still follows a bi-linear branch. Consequently, the hardening-cohesion function in Figure 2a is implemented in DIANA, thus modifying the compressive response of the CP model. Figure 2b shows the masonry stress-strain law adopted for the MCP model.

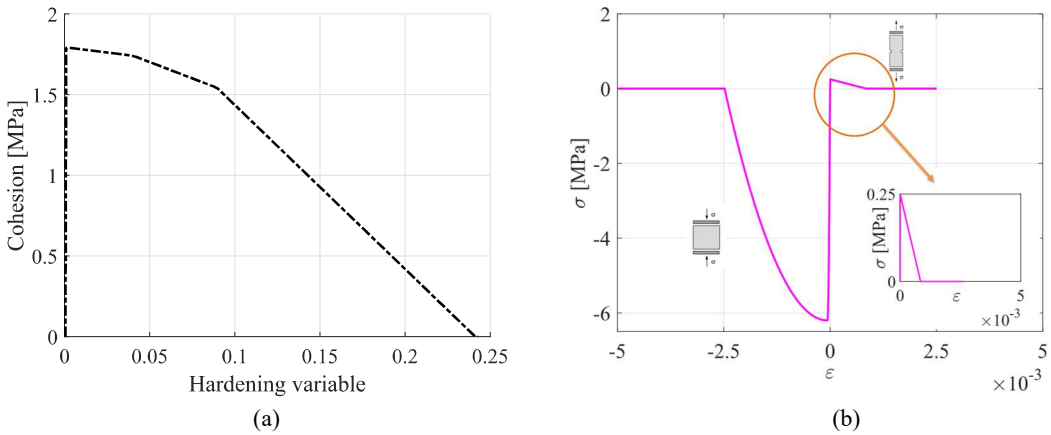


Figure 2: Cohesion hardening function (a) and masonry stress-strain law for MCP model (b).

Finally, a macromechanical model based on the classical theory of Continuum Damage Mechanics is investigated [13], here denoted as CDP (continuum damage-plastic) model. The stress–strain constitutive relationship is based on a damage-plastic model, coupling an isotropic two-variable damage model and the Von Mises plasticity formulation with isotropic and kinematic hardening. This is based on the introduction of two different damage variables, distinguished for prevailing tensile and compressive states, to reproduce the unilateral phenomenon, that is the stiffness recovery due to the cracks re-closure when moving from tension to compression.

2.2 Mesh-dependency and regularization issues

Different techniques can be adopted to overcome the mesh-dependency of the FE solution, when constitutive laws with strain-softening are adopted. For the smeared crack models presented above, TSRC and CP, a fracture energy regularization is used [20] in order to get mesh independent solutions. This relies on the assumption that dissipation within the single element has to be independent from the element size. To this end, the constitutive law is properly modified such that the energy dissipated in the FE is equal to the assigned value G_i with $i = t,c$. For each element, a characteristic length h^e is defined, which depends on the size, shape and interpolation function of the used finite element. Both the mentioned models, that is TSRC and CP, make use of the Rots' element based method [15]. The specific fracture energies g_i, defined as per Eq.(1), is then scaled so that it results $g_i h^e = G_i$ for each element.

$$g_i = \int_{\varepsilon_{0i}}^{\varepsilon_{ui}} \sigma\,(\varepsilon) d\varepsilon + \frac{1}{2}\,\sigma_{0i}\varepsilon_{0i}\,; \quad \text{with } i = t,c \tag{1}$$

Conversely, a regularization technique based on the nonlocal integral approach is adopted for the damage-plastic model CDP [21]. Following this formulation, a nonlocal integral definition of the damage associated variables $Y_{t/c}$, that is those driving the damage evolution process, is introduced in the model. Then, the nonlocal quantities $\bar{Y}_{t/c}$, at the Gauss point **x**, are defined as:

$$\bar{Y}_{t/c}(\boldsymbol{x}) = \frac{1}{\int_A \psi(\boldsymbol{x},\boldsymbol{s}) dA(\boldsymbol{s})} \int_A Y_{t/c}\,(\boldsymbol{s})\,\psi\,(\boldsymbol{x},\boldsymbol{s}) dA(\boldsymbol{s}) \tag{2}$$

in which $Y_{t/c}$ is a local variable at the generic point **s** located in a proper defined neighbourhood of point **x**. The classical Gaussian distribution is assumed as weighting function, with l_c denoting the nonlocal radius of the neighbourhood related to the material internal characteristic length.

3 NUMERICAL APPLICATIONS

The experimental campaign conducted by *Anthoine et. al* [18] is here considered (Figure 3a). Two solid clay panels, characterized by different height/width ratio and assuming identical boundary conditions, are investigated. The bottom side of the walls is completely restrained, while the top side is prevented to rotate. The panels are firstly subjected to a vertical force equal to 150 kN, kept constant during the test, and then a cyclic horizontal displacement history is applied on a steel beam rigidly connected to the top of the walls. The lateral displacement is imposed quasi-statically and characterized by a cyclically increasing amplitude. Two or three

cycles are performed for each amplitude. The geometry of the panels is shown in Figure 3b and 3c with the thickness equal to 250 mm.

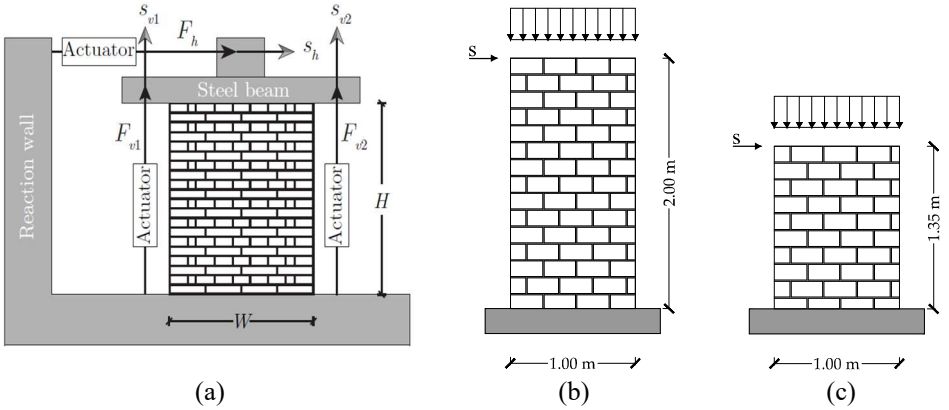


Figure 3: Experimental campaign selected: (a) setup [18], and geometry of the (b) high panel and (c) low panel.

The experimental response of these panels is compared with the numerical prediction of the macromechanical models described before. A plane stress formulation with a 2D four-point quadrilateral FEs and within a 2x2 Gauss integration rule is adopted. A mesh made of 10x20 FEs is used for the high panel, while 10x14 FEs are adopted for the low panel. The mechanical parameters used in the FE models deduced from [22] are contained in Table 1, where E is the Young's modulus, v is the Poisson's ratio, σ_t and σ_c are the tensile and compressive strength values, respectively, G_t and G_c are the value of tensile and compressive fracture energy terms chosen according to [23], and γ is the masonry mass density. For the CP model, other mechanical parameters as the cohesion c (deduced from [19]) need to be defined, see Table 2.

Table 1: Mechanical parametes adopted for the TSRC and CP models.

E[MPa]	v	σ_t[MPa]	σ_c[MPa]	G_t[N/mm]	G_c[N/mm]	γ[T/mm^3]
1700	0.15	0.25	6.2	0.015	1	1.652e-9

Table 2: Mechanical parametes adopted for the CP model.

c[MPa]	Friction angle [rad]	Dilatancy angle [rad]
1.7898	0.5236	0

3.1 Monotonic loading

Following the experimental loading history, a vertical force equal to 150 kN is applied and kept constant during the test. A monotonic horizontal displacement history is imposed on the top of the walls. The results are monitored in terms of global in-plane response curve, meaning the envelope capacity curve, by depicting the total base shear versus the horizontal applied displacement. Figure 4 shows the comparison between the numerically obtained curves (red dashed curves and blue dashed-point curves) and the envelopes (black star symbols) corresponding to the cyclic experimental response for the high (Figure 4a) and low (Figure 4b) panels. Although some differences emerge between the two models, the numerical results are

in quite good agreement with the experimental ones. The TSRC model (blue dashed-point curves) gives a smoother nonlinear response, whereas the CP (red dashed curves) shows sudden drops due to crack's formation. Moreover, in the case of the squat (low) panel, the TSRC also shows a sudden brittle strength loss that is not clear for the CP model.

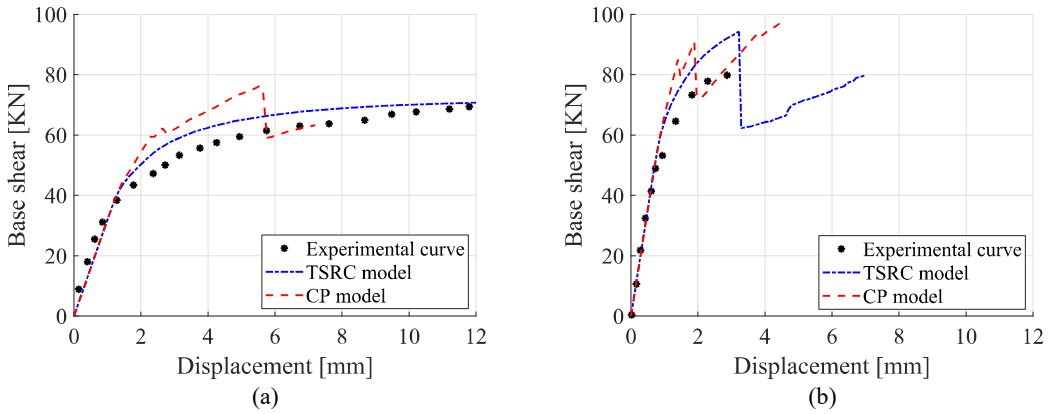


Figure 4: Comparisons between experimental and numerical (TSRC and CP) force-displacement response curve under monotonic loading: (a) high or slender panel, and (b) low or squat panel.

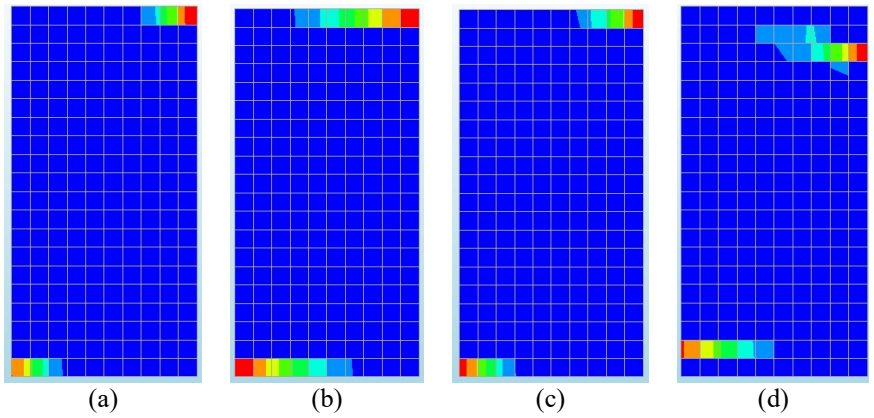


Figure 5: Crack patterns for the high (slender) wall: (a) TSRC for s=2 mm; (b) TSRC for s=12 mm; (c) CP for s=2 mm; and (d) CP for s=6 mm.

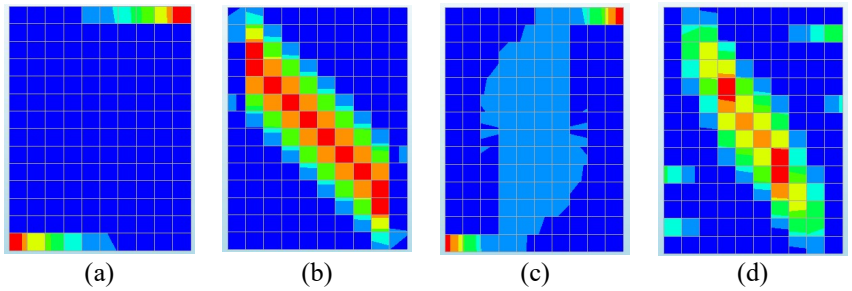


Figure 6: Crack patterns for the low (squat) wall: a) TSRC for s=2 mm, b) TSRC for s=7 mm, c) CP for s=2 mm, d) CP for s=4 mm.

3.2 Cyclic loading

Regarding the cyclic tests performed within the selected experimental campaign (see Figure 3), the cyclic displacement-history shown in Figure 7 is applied to the two panels. The results obtained with the two FE models, the TSRC (blue dashed-point curves) and CP (red dashed curves) models, are presented in Figures 8 and Figure 9 and compared with the experimental outcomes (black star symbols) for high and low panels in terms of force-displacement global curve.

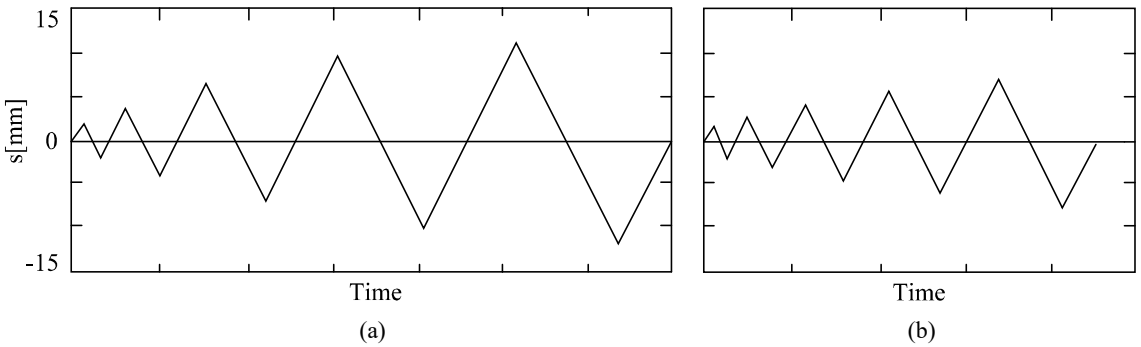


Figure 7: Cyclic displacement history applied to high (a) and low (b) panel.

Figure 8 shows a different trend for the global response curves of both models. It can be explained by the different damage mechanisms that arise during the evolution of the numerical and experimental tests. Indeed, the low wall shows a brittle failure response, with the formation of shear diagonal crack in the middle of the panel. A shear mechanism characterizes the response of the low panel; in converse the high wall shows a flexural failure with the formation of large damaged zones located at the top and bottom sides. Although the monotonic numerical analyses seem to reproduce well the damage mechanisms occurring in the two panels (Figure 5 and 6), the comparison of the numerical and the cyclic experimental results is not very satisfactory. In particular, the numerical models are unable to describe the hysteretic dissipation mechanisms, which is the area under the experimental cyclic curves, particularly relevant for the nonlinear response of the low panel.

To overcome the latter limitation of both models to match the experimental response, the modified version of the CP formulation, i.e. the MCP model, has been adopted as introduced in section 2.1. Figure 10 shows the comparison between the results obtained with the MCP model (magenta dashed curves) and the experimental outcomes (black star symbols) for both the panels. The numerical results obtained for the high panel correlates now better with the experimental response. Yet, the advantage of using the MCP model is less evident in the case of low panel. To be noted is that, in this model, the plasticity evolution is controlled by the cohesion that is, by itself, ruled by the compressive strength. Therefore, starting from an experimental compressive strength value, the effect of plasticity is not properly taken into account during the dissipation process. Instead, starting from an experimental cohesion value, numerical results are more consistent with the experimental ones, although the compressive strength threshold seems to be unrealistic. This issue deserves further investigations.

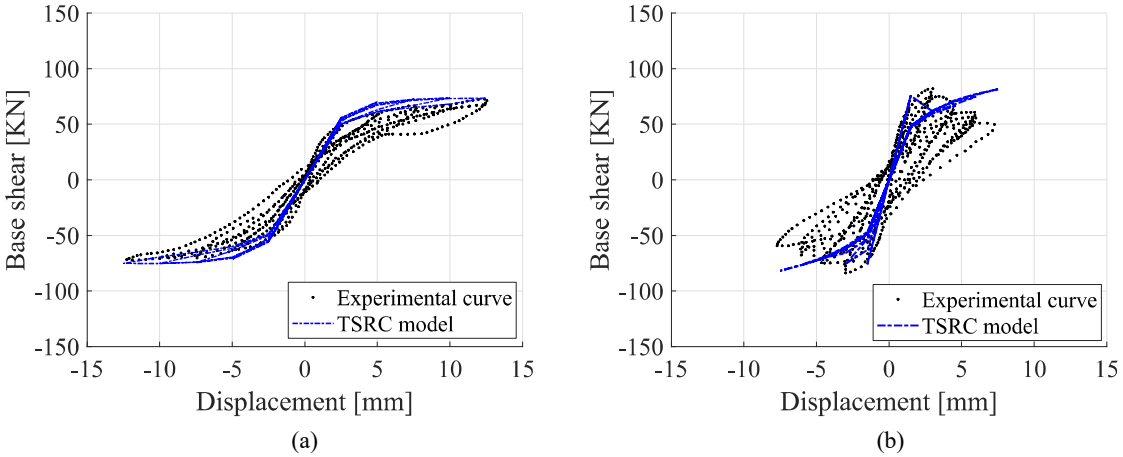


Figure 8: Comparisons between experimental and numerical (TSRC) force-displacement response curve under cyclic loading: a) high and b) low panel.

Furthermore, a comparison with the macromechanical continuum damage-plastic model presented in [13] is performed (Figure 11). The mechanical parameters used for this model are also deduced from [13]. The damage-plastic model reproduces better the experimental responses, especially for the low wall. Indeed, this satisfactorily describes the effect of the energy dissipation due to shear mechanisms occurring in the panel. Regarding the crack patterns (Figure 13), both the latter models are able to describe the distinctive features of flexural and shear response shown by the high and low masonry panels during the experimental campaign, although the continuum damage-plastic model gives more spread damaged in respect to the MCP. This is due to the different way that both models describe the degrading behaviour of masonry, that is by means of the introduction of a continuum damage variable or adopting a smeared crack formulation, as well as to the different regularization technique implemented.

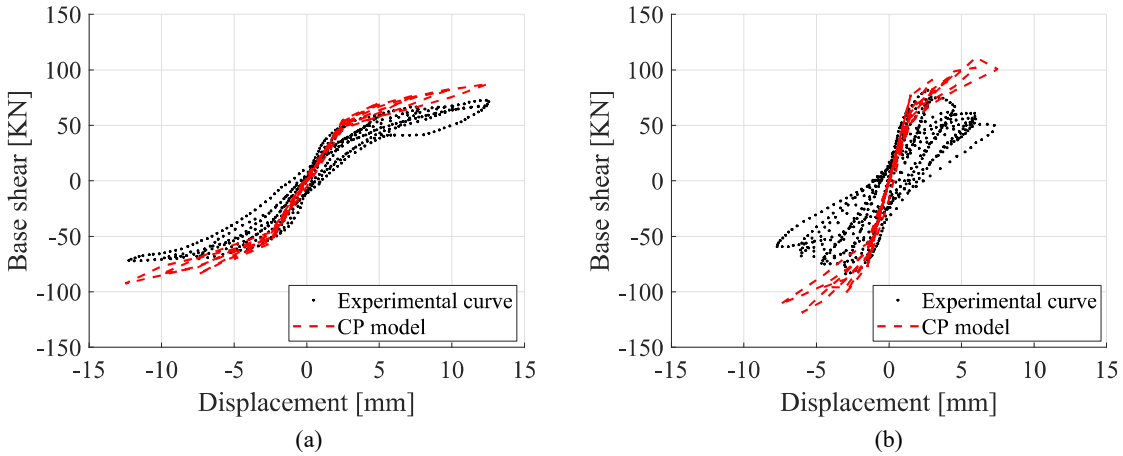


Figure 9: Comparisons between experimental and numerical (CP) force-displacement response curve under cyclic loading: a) high and b) low panel.

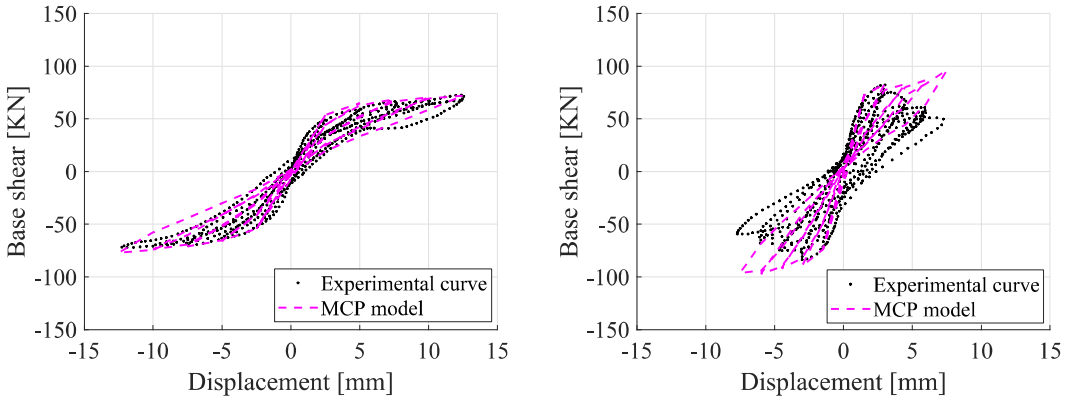


Figure 10: Comparisons between experimental and numerical (CPM) force-displacement response curve under cyclic loading: a) high and b) low panel.

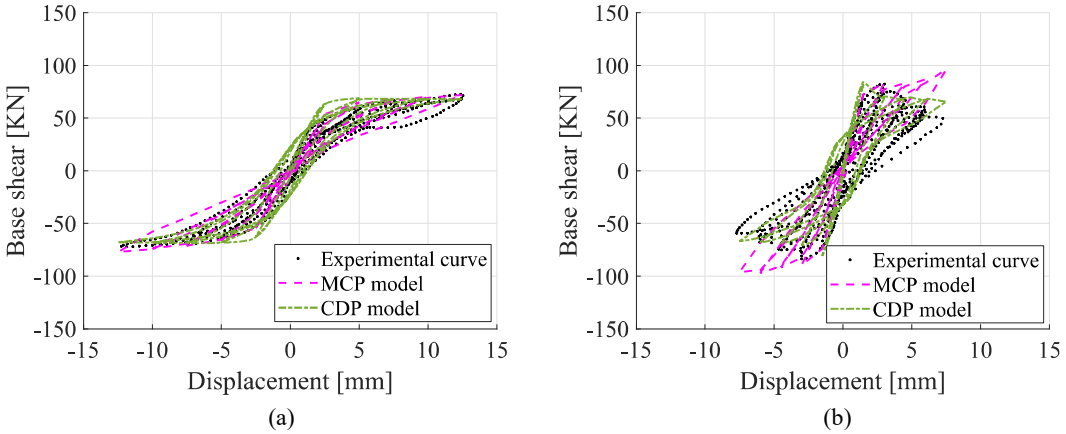


Figure 11: Comparisons between experimental and numerical (MCP and CDP) force-displacement response curve under cyclic loading: a) high and b) low panel.

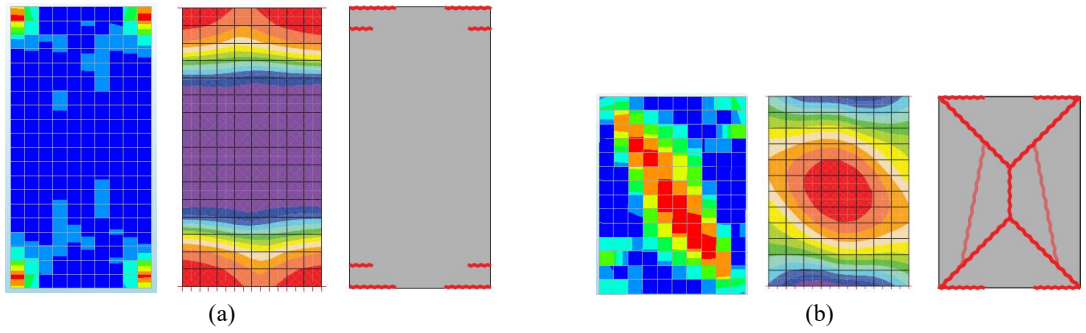


Figure 12: Crack patterns: MCP, CDP and experimental outcomes: a) high and b) low panel.

9 CONCLUSIONS

The structural response of two masonry panels (low or squat and high or slender) experimentally tested by *Anthoine et. al* [18] has been numerically reproduced through different

macromechanical FE models: (i) based on smeared crack approach; and (ii) based on a continuum damage model. In particular, the use of macro-modelling techniques based on smeared crack and coupled damage-plastic constitutive laws for the cyclic in-plane response prediction of these masonry panels was explored. A fracture energy regularization technique was used for the smeared crack models and a nonlocal integral approach for the continuum damage-plastic model.

Two material constitutive macro-models, known as Total Strain Cracking (TSRC) and Crack and Plasticity (CP), have been used to simulate the response of the two panels. These have different geometries and, therefore, different damage paths. Indeed, a shear mechanism characterized the behavior of the low panel. In converse, a flexural rocking response distinguished the high wall with the formation of large damaged zones located at the top and bottom sides. The numerical models have showed some shortcomings, i.e. although the numerical analyses have showed a good agreement reproducing the damage mechanisms, the comparisons in terms of force-displacement curves were not completely satisfactory. Regarding the TSRC model, the numerical results were consistent with the model formulation built just with a cracking constitutive law. Conversely, although the CP model is based on a coupled cracking-plastic constitutive law, its formulation presents some limitations when taking into account the effect of plasticity during the dissipation process. The latter issues were somehow solved through a modified version of the Drucker-Prager model (MCP) by including a cohesive softening law in the existing CP model. For the high wall, the numerical results correlate better with the experimental output with respect to the CP and TSRC models. For the low wall, the correlation was still not very satisfactory and other modifications are required.

Lastly, a comparison between the MCP model, categorized as a smeared crack model, and a CDP macromechanical continuum damage-plastic model [13] was performed. This latter sophisticated model, where damage and plasticity are coupled, proved to be more capable to reproduce the experimental outcomes in terms of force-displacement global curve. Hence, other experimental campaigns on masonry panels and/or larger structures, may be considered to further validate the capabilities of the numerical models to reproduce the masonry response under cyclic-loading conditions and to better understand its advantages and limitations. Furthermore, the analyzed constitutive models can be enriched, in particular the CP formulation, through rigorous mechanically based modifications inspired by continuum damage-plastic models.

REFERENCES

[1] G. Brandonisio, G. Lucibello, E. Mele, and A. De Luca, “Damage and performance evaluation of masonry churches in the 2009 L’Aquila earthquake,” *Eng. Fail. Anal.*, vol. 34, pp. 693–714, 2013.

[2] P. B. Lourenço, N. Mendes, L. F. Ramos, and D. V. Oliveira, “Analysis of Masonry Structures Without Box Behavior,” *Int. J. Archit. Herit.*, vol. 5, no. 4–5, pp. 369–382, Jul. 2011.

[3] E. Sacco, D. Addessi, and K. Sab, “New trends in mechanics of masonry,” *Meccanica*, vol. 53, no. 7, pp. 1565–1569, 2018.

[4] P. Roca, M. Cervera, G. Gariup, and L. Pela’, “Structural Analysis of Masonry Historical Constructions. Classical and Advanced Approaches,” *Arch. Comput. Methods Eng.*, vol.

17, no. 3, pp. 299–325, Jul. 2010.
[5] D. Addessi and E. Sacco, "Nonlinear analysis of masonry panels using a kinematic enriched plane state formulation," *Int. J. Solids Struct.*, vol. 90, pp. 194–214, 2016.
[6] P. B. Lourenço and J. G. Rots, "Multisurface Interface Model for Analysis of Masonry Structures," *J. Eng. Mech.*, vol. 123, no. 7, pp. 660–668, Jul. 1997.
[7] L. C. Silva, P. B. Lourenço, and G. Milani, "Derivation of the out-of-plane behaviour of masonry through homogenization strategies: micro-scale level," *Comput. Struct.*, vol. 209, pp. 30–43, 2018.
[8] L. Karapitta, H. Mouzakis, and P. Carydis, "Explicit finite-element analysis for the in-plane cyclic behavior of unreinforced masonry structures," *Earthq. Eng. Struct. Dyn.*, vol. 40, no. 2, pp. 175–193, 2011.
[9] D. Addessi, "A 2D Cosserat finite element based on a damage-plastic model for brittle materials," *Comput. Struct.*, vol. 135, pp. 20–31, 2014.
[10] L. Pelà, M. Cervera, and P. Roca, "An orthotropic damage model for the analysis of masonry structures," *Constr. Build. Mater.*, vol. 41, pp. 957–967, Apr. 2013.
[11] L. C. Silva, P. B. Lourenço, and G. Milani, "A discrete macro-model using homogenization with strain-rate dependency for the out-of-plane study of masonry panels subjected to impact loading," in *ECCOMAS Thematic Conference on Computational Methods in Structural Dynamics and Earthquake Engineering*, 2017.
[12] L. C. Silva, N. Mendes, P. B. Lourenço, and J. Ingham, "Seismic Structural Assessment of the Christchurch Catholic Basilica, New Zealand," *Structures*, vol. 15, pp. 115–130, 2018.
[13] C. Gatta, D. Addessi, and F. Vestroni, "Static and dynamic nonlinear response of masonry walls," *Int. J. Solids Struct.*, vol. 155, pp. 291–303, 2018.
[14] L. Kachanov, "Rupture time under creep conditions," *Izv. Akad. Nauk SSSR*, vol. 8, pp. 26–31, 1958.
[15] J. G. Rots, "Computational modeling of concrete fracture," 1988.
[16] R. De Borst and P. Nauta, "Non-orthogonal cracks in a smeared finite element model," *Eng. Comput.*, vol. 2, no. 1, pp. 35–46, 1985.
[17] J. G. Rots and J. Blaauwendraad, "Crack models for concrete: discrete or smeared? Fixed multi-directional or rotatin?," *Heron*, vol. 34, no. 1, pp. 3–59, 1989.
[18] A. Anthoine, G. Magonette, and G. Magenes, "Shear-compression testing and analysis of brick masonry walls," in *Proceedings of the 10th European conference on earthquake engineering*, 1995, vol. 3, pp. 1657–1662.
[19] *DIANA, 2019, DIsplacement ANAlyzer finite element software package, version 10, DIANA FEA, Delft, https://dianafea.com*. .
[20] C. Comi and U. Perego, "Fracture energy based bi-dissipative damage model for concrete," *Int. J. Solids Struct.*, vol. 38, no. 36–37, pp. 6427–6454, 2001.
[21] G. Pijaudier-Cabot and Z. P. Bažant, "Nonlocal damage theory," *J. Eng. Mech.*, vol. 113, no. 10, pp. 1512–1533, 1987.
[22] G. Magenes and G. M. Calvi, "In-plane seismic response of brick masonry walls," *Earthq. Eng. Struct. Dyn.*, vol. 26, no. 11, pp. 1091–1112, Nov. 1997.
[23] P. B. Lourenço, "Recent advances in masonry modelling: micromodelling and homogenisation," in *Multiscale modeling in solid mechanics: computational approaches*, World Scientific, 2010, pp. 251–294.

12th International Conference on Structural Analysis of Historical Constructions
SAHC 2020
P. Roca, L. Pelà and C. Molins (Eds.)

DEVELOPMENT OF A NEURAL NETWORK EMBEDDING FOR QUANTIFYING CRACK PATTERN SIMILARITY IN MASONRY STRUCTURES

ÁRPÁD RÓZSÁS [1*], ARTHUR SLOBBE [1], WYKE HUIZINGA[2], MAARTEN KRUITHOF[2] AND GIORGIA GIARDINA[3]

[1]Department of Structural Reliability
Netherlands Organization for Applied Scientific Research (TNO)
Stieltjesweg 1, Delft, The Netherlands
e-mail: [arpad.rozsas, arthur.slobbe]@tno.nl (*corresponding author)

[2] Department of Intelligent Imaging
Netherlands Organization for Applied Scientific Research (TNO
Oude Waalsdorperweg 63, Den Haag, The Netherlands
email: [wyke.pereboom, maarten.kruithof]@tno.nl

[3] Department of Civil Engineering and Geosciences
Delft University of Technology
Stevinweg 1, 2628 CN Delft, The Netherlands
email: g.giardina@tudelft.nl

Keywords: Masonry Structure, Crack Patterns, Similarity Measure, Machine Learning, Deep Neural Network

Abstract. *The degree of similarity between damage patterns often correlates with the likelihood of having similar damage causes. Therefore, deciding whether crack patterns are similar is one of the key steps in assessing the conditions of masonry structures. To our knowledge, no literature has been published regarding masonry crack pattern similarity measures that would correlate well with assessment by structural engineers. Hence, currently, similarity assessments are solely performed by experts and require considerable time and effort. Moreover, it is expensive, limited by the availability of experts, and yields only qualitative answers. In this work, we propose an automated approach that has the potential to overcome the above shortcomings and perform comparably with experts. At its core is a deep neural network embedding that can be used to calculate a numerical distance between crack patterns on comparable façades. The embedding is obtained from fitting a deep neural network to perform a classification task; i.e., to predict the crack pattern archetype label from a crack pattern image. The network is fitted to synthetic crack patterns simulated using a statistics-based approach proposed in this work. The simulation process can account for important crack pattern characteristics such as crack location, orientation, and length. The embedding transforms a crack pattern (raster image) into a 64-dimensional real-valued vector space where the closeness between two vectors is calculated as the cosine of their angle. The proposed approach is tested on 2D façades with and without openings, and with synthetic crack patterns that consist of a single crack and multiple cracks.*

1 INTRODUCTION

1.1 Motivation and background

Every year in the Netherlands, house owners report hundreds of issues concerning cracks in their masonry dwellings. Addressing these problems requires identifying the most likely causes of the observed damage. In these structures, similar causes often manifest through similar crack patterns; thus, quantification of crack pattern similarities is instrumental in understanding masonry damage. Currently, the assessment of similarities between masonry crack patterns relies entirely on experts' judgment. This implies several limitations:

- The quality of the evaluation strongly depends on the experience of the assessor, who needs to correlate the observed crack pattern with previously analyzed and recorded ones;
- The assessment is affected by the expert's understanding of global mechanisms and local conditions;
- Currently, it is not clear how the human brain performs the crack pattern comparison and experts have difficulties in verbalizing and formalizing their decision;
- The process is expensive, limited by the availability of experts, and provides only qualitative assessment.

This leads to a general lack of objectivity in crack analysis as different experts can provide substantially different interpretations for similar crack patterns.

Recent developments in deep neural network embedding have the potential to overcome some of these limitations by providing a tool for automated damage classifications and quantitative measures of crack pattern similarities. While significant effort has been devoted to crack detection and characterization [1,2,3], a consultation with structural masonry experts (forensic engineers and computational mechanics experts) identified a lack of automated tools that could be applied to the practice of damage assessment. Furthermore, only few authors have investigated automated methods to connect masonry damage patterns to their most likely causes [4], and the identification of masonry damage through pattern recognition remains a challenge.

1.2 Aim and objectives

This work addresses the need for a systematic approach to damage classification and quantification of crack pattern similarities in masonry structures by using deep neural network embedding. We focus on two major challenges (Figure 1):

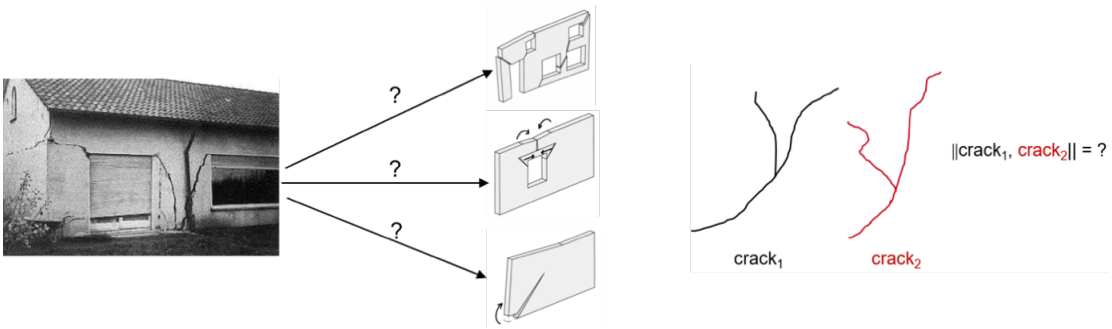


Figure 1: A visual representation of the two major challenges addressed in this paper: crack pattern classification (left) and crack pattern similarity quantification (right).

1. The automated classification of observed crack patterns into damage cause classes (crack pattern archetypes);
2. The quantification of similarities between crack patterns in terms of structural masonry damage in a way that correlates strongly with masonry experts' assessment.

Having an accurate and quantitative similarity measure would enable us to solve both challenges and perform three tasks with high practical relevance:

- Classification of crack patterns into archetypes, such as those proposed by de Vent [5], by calculating the distances between an observed crack pattern and archetype crack patterns. This would allow for a quick and simplified assessment.
- Identification of damage in not directly observed/measured structural components, such as wooden piles, by calculating the distance between an observed crack pattern and simulated (e.g. finite element analysis) crack patterns. This would allow for a more in-depth assessment and understanding the causes of observed damage.
- Automated calibration of finite element models to experts based on matching the similarity between predicted and observed crack patterns.

This paper contributes to develop a fast, cheap, and automated procedure for the assessment of the structural integrity of cracked (damaged) masonry structures by generating synthetic crack patterns using Markov-walks and incorporating expert judgment. The proposed approach is demonstrated on 2D façades with and without an opening, and with crack patterns that consist of a single crack and multiple cracks.

2 METHODOLOGY

The core of our proposed approach is a deep neural network embedding that can be used to calculate a numerical distance between crack patterns on comparable façades. An embedding is a mathematical function that maps a higher dimensional representation to a lower dimensional one while retaining selected essential characteristics of the original representation. In the context of this paper, an embedding maps crack pattern images to a real-valued vector space (i.e., lower dimensional than that needed to represent the images). The challenge is to find such an embedding that produces close-by vector representations for those crack pattern images that are similar by structural engineering standards.

Our working hypothesis is two-fold: first, we assume that crack pattern images and their damage cause/type labels contain sufficient information to find the above described embedding; second, we assume that the embedding can be found by using a deep neural network (a flexible mathematical construct).

The following approach is used to test our hypothesis:

1. Data acquisition: crack pattern images and their damage cause labels.
2. Model definition and fitting: define the mathematical model of the deep neural network and fit its parameters using the data.
3. Model evaluation: comparing the predictions of the fitted model to the damage cause labels for data points not used for the fitting.

Because current deep learning networks are data intensive, we would need at least a few hundreds of crack patterns and corresponding damage causes to test our hypothesis. The highest quality data are real-world cases but those are expensive and time consuming to collect, especially as reliable damage cause labels are needed. Moreover, in real-world cases, multiple damage causes are often present and are difficult to separate even by experts. An alternative

route is to generate synthetic data. This can be done using computational physics to solve the mathematical representation of physical systems (labeled as physics-based approach in this paper), e.g. finite element analysis to solve partial differential equations. Fortunately, our understanding of masonry structures is sufficient to perform crack analysis of them with good accuracy. Still, this approach is relatively time consuming due to the large number and large variety of structures and damage causes needed to be implemented with parameterized models and to perform the analyses and post-processed. Therefore, a cheaper and simpler synthetic data generating approach is used first, which is labeled as a statistics-based approach in this paper and based on Markov-walks guided by rules that encode expert knowledge. Here, a statistics-based synthetic data generating process is used to find the embedding and evaluate its performance. If successful, then it would encourage the acquisition of more realistic but more expensive data sources.

Because the statistics-based approach generates synthetic data and has a random component, an arbitrary number of crack patterns can be simulated once the algorithm is available. Compared with the physics-based simulation approach, it is expected to generate synthetic data an order of magnitude faster; however, the quality of the data is poorer, i.e. less representative of reality.

An approach is proposed and implemented to generate statistical crack patterns resulting from a total of twelve damage causes and for five different façades with and without openings (Section 3). A convolutional neural network (CNN) is fitted to half of the data with the task of classifying the crack patterns into damage cause classes. The first part of the fitted CNN is used as a 64-dimensional embedding of the crack pattern images where the closeness between two vectors is calculated based on the angle between them (Section 4-5). The closeness is interpreted as the similarity between crack pattern images and compared with our experts' judgment.

3 GENERATION OF SYNTHETIC CRACK PATTERNS

A statistics-based simulation approach is developed in order to generate synthetic crack patterns for a wide range of masonry façades and, hence, quickly test the potential of various crack pattern similarity measures. This approach includes an algorithm that generates lines in a pre-defined bounding box (i.e. the geometry of a façade) by means of Markov-walks. The algorithm is generalized so that it can handle a parametric input of the façade and the cracks. This allows control over the dimensions of the façade, and the number, dimensions and position(s) of the openings (doors and windows). It also enables control of the number of cracks, the crack initiation point(s), the crack angle(s), the crack length(s), and how jagged a crack is. Furthermore, structural engineering considerations are imposed in order to increase the resemblance to reality. Though the statistics-based simulation approach is not based on first physical principles, it is able to account for important crack pattern characteristics such as crack location, orientation, and size.

Subsection 3.1 explains the details of the crack pattern generation in masonry wall panels without openings and with a single crack. Subsection 3.2 presents a more realistic case, where crack patterns are generated in longitudinal masonry façades that resemble typical existing dwellings in the Netherlands. These patterns are based on frequently observed damage.

3.1 Case 1: masonry wall panels without openings

To support structural damage diagnosis in masonry structures, de Vent [5] introduced 60 types of crack patterns along with their possible damage causes. In case 1, eight of these are selected as listed in Figure 2. For consistency, the numerical IDs from [5] are used here as well when referring to crack pattern archetypes. The eight archetypes share the following characteristics:

- a single wall panel is considered with a length over height ratio of 1.5;
- a single major crack characterizes the pattern;
- no openings are present;
- a crack is assumed to have unit and constant width.

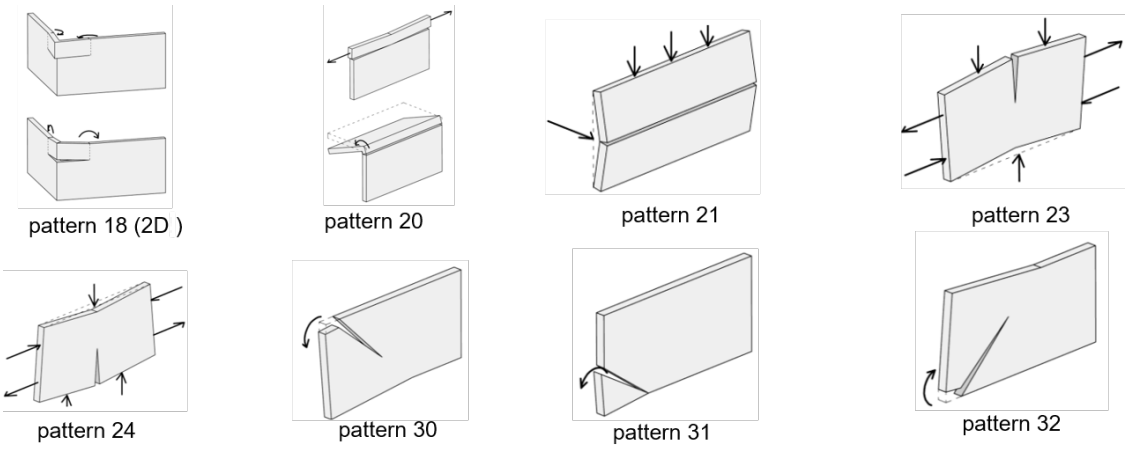


Figure 2: Illustrations of the selected eight crack pattern archetypes [5].

Figure 3 shows the crack parametrization in the wall panels for a normalized (unit square) wall. Each crack is defined by the following parameters: the coordinates of the crack initiation point (x_0, y_0), the crack angle (α), the crack length (l_{crack}), and jaggedness of the crack (σ_{crack}). The first three parameters are randomly and uniformly sampled from an interval that is specified for each crack pattern archetype. For illustrative purposes, the input values of these parameters for the crack pattern archetypes 23, 30, and 31 are summarized in Table 1. In the simulation, the panel is discretized into disjoint rectangles and a crack can propagate only through the cells of this grid, one cell at a time/step. A crack starts from the cell at (x_0, y_0), a random step is taken in either vertical or horizontal direction in a way that the expected global crack angle is α. The average absolute deviation from the expected direction is controlled by σ_{crack}, i.e., 0.5: highest deviation, 0: no deviation. Illustrative realizations of this simulation are presented in Figure 4, one for each case 1 pattern archetype. The simulated patterns illustrate that the proposed statistical approach can simulate realistic-looking and unique (due to the random component) crack patterns. In principle, the current implementation of the algorithm allows for the generation of an unlimited number of unique realizations for the eight selected crack pattern archetypes.

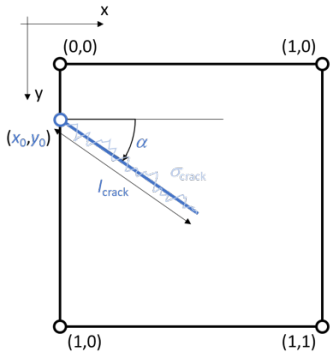


Figure 3: Crack parametrization in the wall panels for a normalized (unit square) wall.

Table 1: Input values in the unit square for the crack pattern archetypes 23, 30 and 31. For explanation of the parameters, see Figure 3.

Pattern ID	x_0, y_0 *	α [deg] *	l_{crack} *	σ_{crack}
23	[0.45, 0.55], [0, 0]	[87, 93]	[0.4, 0.6]	0.5
30	[0.05, 0.20], [0, 0]	[20, 70]	[0.3, 0.5]	0.5
31	[0, 0], [0.60, 0.80]	[20, 70]	2†	0.5

* the lower and upper bounds of the uniform distribution
† to ensure that the crack goes through the entire wall

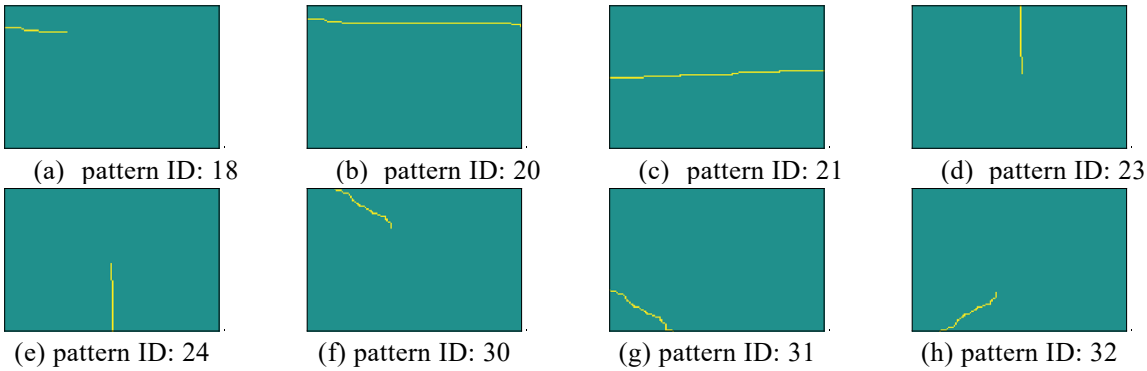


Figure 4: One random crack pattern realization for each damage cause (pattern id) for case 1 (façade with openings). See Figure 2 for the architectural representation of the matching crack patterns.

3.2 Case 2: masonry façades with openings

Every year in the Netherlands, house owners report hundreds of issues concerning cracks that appear in their masonry dwellings. In general, there are two main causes for these cracks: (i) uneven settlements; and (ii) constrained deformation due to temperature effects. The second cause mainly occurs in older masonry dwellings, where dilatation joints are poor or even not present, due to the heating of the roof or when the foundation constrains the façade.

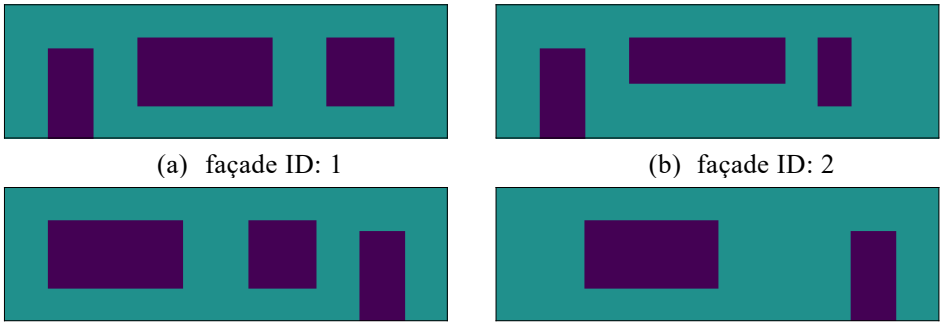
In case 2, random crack pattern are generated in the longitudinal masonry façade of typical Dutch dwellings. Four different geometries are evaluated (Figure 5). One of them is detailed in

Figure 6, showing one door opening and two window openings in the façade. Four crack pattern archetypes are considered based on the following damage causes:

1. Cracking due to uneven settlements with large settlements at the left side (pattern ID: 101);
2. Cracking due to uneven settlements with large settlements at the right side (pattern ID: 102);
3. Cracking due to uneven settlements with large settlements at the middle (pattern ID: 103);
4. Cracking due to high temperature of the roof (pattern ID: 201).

Damage causes 1 and 3 typically result in crack pattern archetypes with a single major crack, whereas damage causes 2 and 4 result in crack pattern archetypes with multiple cracks (we consider two cracks). As in case 1, the cracks are assumed to have unit and constant widths.

The crack pattern realizations are made in a similar fashion as for case 1. For illustrative purposes, parametrization of the two cracks in the façade subjected to damage cause 2 is shown in Figure 7. The parameters of the two cracks are distinguished by the numbers "1" and "2" in their subscripts. Table 2 provides the input values of the crack parameters. The specified intervals of the crack initiation points are relative to the red dots that are indicated in the corners of the right window. The specified intervals of the crack lengths are relative to the length of a fully developed crack (i.e. a crack that has been propagated to the edge of the façade).



(a) façade ID: 1 (b) façade ID: 2

(c) façade ID: 3 (d) façade ID: 4

Figure 5: Overview of the considered façades for case 2. All façades have the same bounding rectangle dimensions. See also Figure 6.

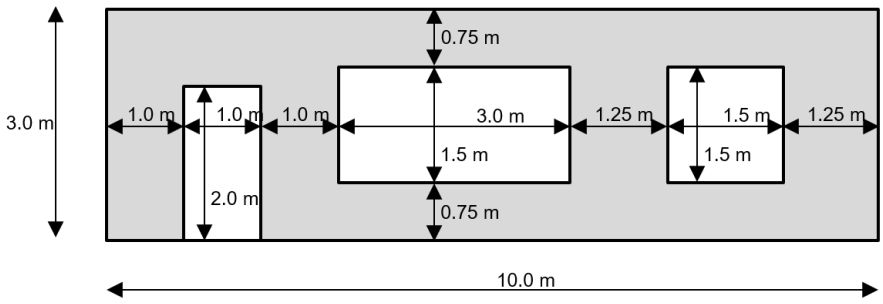


Figure 6: The geometry of the longitudinal façade of a typical Dutch masonry dwelling.

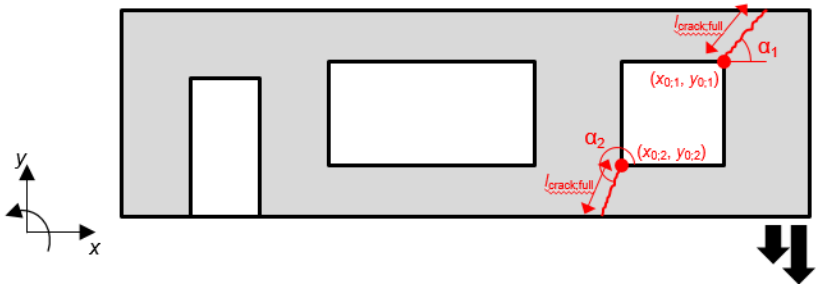


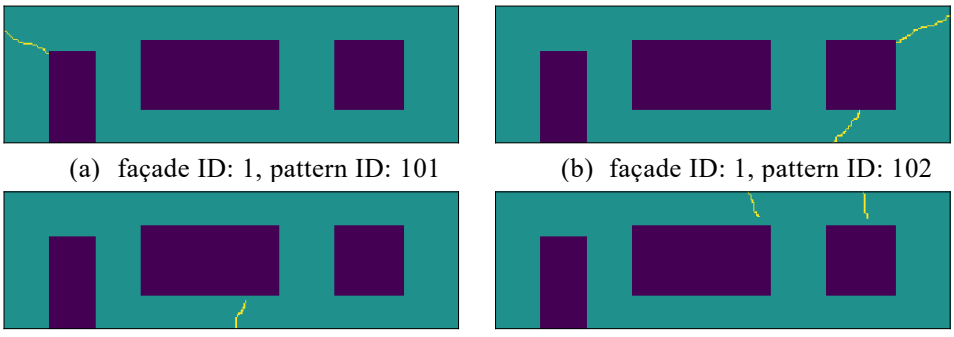
Figure 7: Crack parametrization in the longitudinal façade of a typical Dutch masonry dwelling for damage cause 2.

Table 2: Input values for crack pattern ID 102. For explanation of the parameters, see Figure 7.

$x_{0;1}$, $y_{0;1}$ [cm] *	[-80, 0], [-20, 0] from indicated corner in Figure 7
$x_{0;2}$, $y_{0;2}$ [cm] *	[0, 80], [0, 0] from indicated corner in Figure 7
α_1 [deg] *	[0, 70]
α_2 [deg] *	[225, 270]
$l_{crack;1}$ *	[0.4, 1.0]·$l_{crack;full}$ †
$l_{crack;2}$ *	[0.4, 1.0]·$l_{crack;full}$ †
σ_{crack}	0.5

* the lower and upper bounds of the uniform distribution
† to ensure that the crack goes through the entire wall

Figure 8 shows one illustrative realization for each damage cause. The four images demonstrate that the algorithm is able to generate reasonable crack patterns from a structural engineering point of view, though no physics is explicitly included.



(a) façade ID: 1, pattern ID: 101 (b) façade ID: 1, pattern ID: 102

(c) façade ID: 1, pattern ID: 103 (d) façade ID: 1, pattern ID: 201

Figure 8: One random crack pattern realization for each damage cause (pattern ID) for façade 1 of case 2 (façades with openings).

4 DEEP NEURAL NETWORK

For the analysis of the crack pattern similarity, we used an artificial neural network (ANN) [6]. An ANN is a computational model consisting of nodes that are organized into layers. Each node in a certain layer transmits a weighted signal to the other units in the next layer. A unit in the next layer sums these signals, applies a non-linear function, and sends the result to the units

in the next layer. See Figure 9 for a schematic representation of an ANN.

The model weights are free parameters that are optimized for a certain task. Examples of such tasks are image classification, object detection, or language translation [7]. The performance of the model on a task and dataset is mathematically expressed in an objective function. Under a given dataset, optimization of this objective function with respect to the free parameters is called "fitting" of the model (or "training" in the machine learning community). In our case, we fit the network to classify simulated crack patterns into known crack pattern archetypes. The input of our network is a simulated image of a crack pattern and the output of the model is the class of the crack pattern.

We used a convolutional neural network (CNN) to classify the crack patterns [8]. A CNN takes an image as its input and applies convolutional filters to this image. The values of these convolutional filters are also free model parameters. The filter sizes are hyperparameters and should be set by the user.

The design of the network we used is shown in Figure 10 and consists of eight layers. This model contains $\approx 3 \cdot 10^6$ free parameters. We constructed the network in such a way that the input images are embedded into a 64-dimensional space by the first seven layers. The embedding is used by the last layer to predict the crack class. We used the output of this embedding to calculate the cosine similarity of the different crack images, which we used as a proxy for crack pattern similarity. In other words, the closer the images are in the embedding space, the more similar the crack patterns with respect to their class.

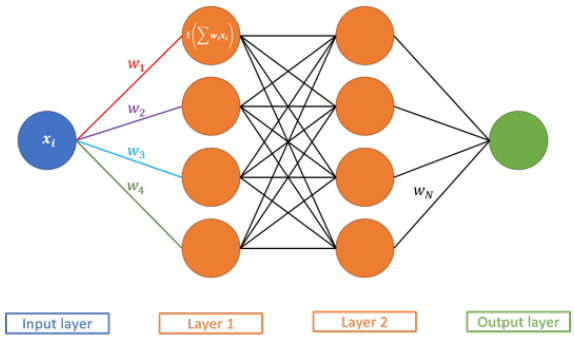


Figure 9: Schematic representation of an ANN. The computational units are represented by the coloured circles. Each of the N connections has a weight w_i and each unit applies a non-linear function to the sum of its weighted input(s): $f(\Sigma w_i x_i)$.

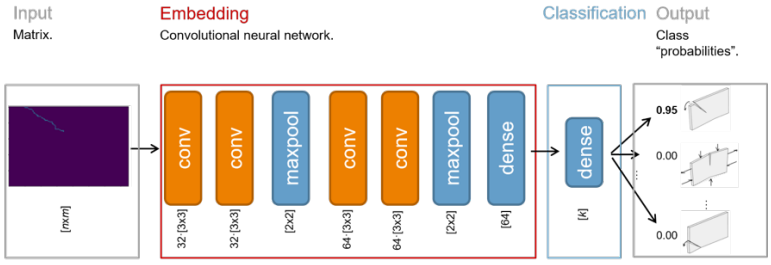


Figure 10: Overview of the neural network used in this work. conv: convolutional layer; maxpool: maxpool layer; dense: fully connected layer.

5 CLASSIFICATION RESULTS AND CRACK PATTERN SIMILARITY

As explained in Section 4, the model is fitted to classify crack pattern images into crack pattern archetypes. We used a randomly chosen subset of the data for fitting and the rest is reserved for testing. The experiments were performed on two data sets: a single façade without openings (case 1) and four façades with openings (case 2). The two sections below describe the results.

5.1 Results for case 1: masonry wall panels without openings

For this case, a total of 4,000 cracks were simulated, with 500 images per class. Here, 2,000 images were used to fit the model and the remaining 2,000 were used for testing. The classification accuracy on the test set is > 99%, which means that the model can almost perfectly classify the eight simulated patterns in their corresponding classes.

We visualize the 64-dimensional embedding space in 2D with a method called t-distributed Stochastic Neighbor Embedding (t-SNE) [9]. This is a widely used method to visualize high dimensional data on a low dimensional subspace. The t-SNE plot in Figure 11 shows that the classes are nicely clustered and perfectly separable in the t-SNE embedding and, therefore, are also separable in the 64-dimensional embedding, which is expected given the high classification accuracy.

We computed the pairwise similarity between all 2,000 simulated crack patterns in the test set with the cosine similarity of the 64-dimensional vectors. This similarity is visualized as a lower-triangular matrix and shown in Figure 12. The rows and columns are sorted on class labels and, as expected, a high similarity is found in blocks at the diagonal of this matrix. A low similarity is found outside these blocks, i.e. between crack patterns of different classes.

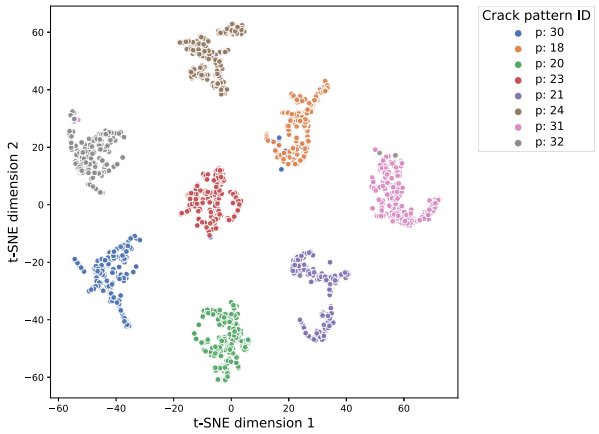


Figure 11: t-SNE scatter plot of the 64-dimensional embedding of case 1 test set crack patterns (façade without openings).

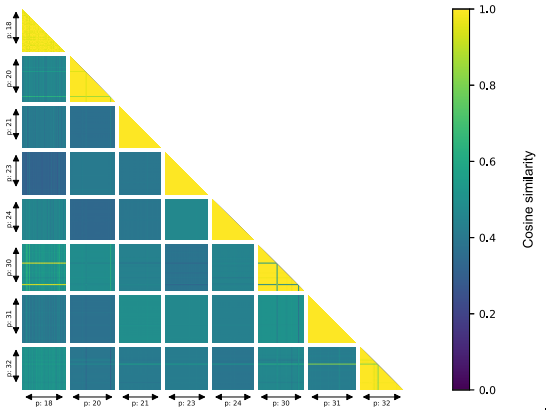


Figure 12: Pairwise cosine similarity of the test set of case 1 (façade without openings).

5.2 Results for case 2: 2D longitudinal façade of typical Dutch dwellings

For this case, a total of 8,000 cracks were simulated: 2,000 images per class, 500 for each unique façade-crack pattern archetype pair. Here, 4,000 images where used to fit the model and 4000 for testing.

Similar to the crack patterns of a masonry wall panel without openings, the classification

accuracy on the crack patterns in the test set of case 2 is >99%. With these data, the model can also almost perfectly classify the eight simulated patterns in their corresponding classes.

The t-SNE plot in Figure 13 shows that also these classes are perfectly separable. Similar to the crack patterns of a masonry wall panel without openings, the pairwise similarity is high for crack patterns of the same class and low for crack patterns from different classes (Figure 14).

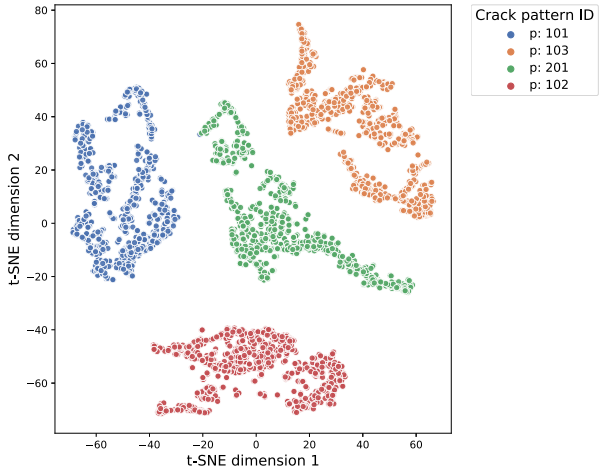


Figure 13: t-SNE scatter plot of the 64-dimensional embedding of case 2 test set crack patterns (facades with openings).

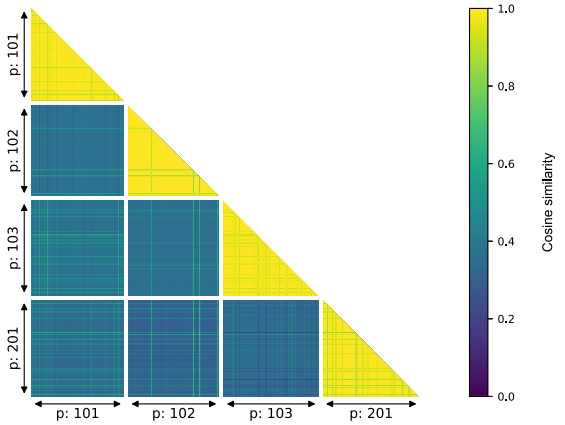


Figure 14: Pairwise cosine similarity of the test set of case 2 (façades with openings). Note that all façades with the same crack pattern ID are assigned to the same group.

6 CONCLUSIONS

This paper addressed the lack of quantitative procedures for the assessment of masonry structure conditions by proposing an automated tool to measure the similarity between crack patterns. We used a deep neural network embedding to calculate a numerical distance between different crack patterns of similar façades. Through Markov-walks guided by expert knowledge, we generated synthetic data that were used to find an embedding and evaluate its performance. We considered twelve damage causes and five façade models, with and without openings, and with single and multiple cracks. The fitted neural network performs exceptionally well in classifying crack patterns that were not used for the fitting: >99% classification accuracy for all considered test cases. The similarity measures calculated using the fitted embedding are in an almost perfect agreement with the experts for between crack pattern class comparisons. A worse performance is observed for within crack pattern class comparisons, i.e. the embedding predicts a very similar low difference for all crack pattern pairs within the same class, while more diversity in the similarity values was expected based on the generated patterns. This is likely due to fact that no information regarding within class similarities are used for fitting the neural network. While the relatively simple simulation process may skew the evaluation of the neural network performance, these results are an encouraging first step towards the development of an automated assessment of damaged masonry structures.

Acknowledgements. We are grateful to Huibert Borsje (TNO) for the valuable discussions on damaged masonry structures and Wessel de Zeeuw (TNO) for his contribution to implementing the computer code to perform the presented analyses.

REFERENCES

[1] Silva, W. and Schwerz de Lucena, D. Concrete cracks detection based on deep learning image classification. In: The Eighteenth International Conference of Experimental Mechanics, Vol. II (2018), pp. 5387.

[2] Chaiyasarn, K., Khan, W., Sharma, M., Brackenbury, D., and DeJong, M. Crack detection in masonry structures using convolutional neural networks and support vector machines. In: Proceedings of the 35th ISARC, Berlin, Germany (2018), pp.118-125.

[3] Dung, C. V. and Anh, L. D. Autonomous concrete crack detection using deep fully convolutional neural network. *Automation in Construction* (2019) **99**:52-58.

[4] Napolitano, R. and Glisic, B. Methodology for diagnosing crack patterns in masonry structures using photogrammetry and distinct element modeling. *Engineering Structures* (2019) **181**:519-528.

[5] de Vent, I. *Prototype of a diagnostic decision support tool for structural damage in masonry*. PhD thesis, Delft University of Technology (2011).

[6] Wang, S.-C. Artificial Neural Network. In: *Interdisciplinary Computing in Java Programming*, Springer US, Boston,MA, (2003), pp. 81-100.

[7] Liu, W., Wang, Z., Liu, X., Zeng, N., Liu, Y., and Alsaadi, F. E. A survey of deep neural network architectures and their applications. *Neurocomputing*, (2017) **234**:11-26.

[8] Arel, I., Rose, D. C., and Karnowski, T. P. Deep machine learning - a new frontier in artificial intelligence research. In: *IEEE Computational Intelligence Magazine*, (2010) **5**(4):13–18.

[9] van der Maaten, L. and Hinton, G. Visualizing data using t-SNE. *Journal of Machine Learning Research*, (2008) **9**:2579–2605.

12th International Conference on Structural Analysis of Historical Constructions
SAHC 2020
P. Roca, L. Pelà and C. Molins (Eds.)

DISCRETE ELEMENT MODELLING OF SINGLE-NAVE CHURCHES DAMAGED AFTER THE 2009 EARTHQUAKE IN L'AQUILA, ITALY

FRANCESCA GOBBIN[1*], REBECCA FUGGER[1] AND GIANMARCO DE FELICE[1]

[1]Department of Engineering, University of Roma Tre
Via Vito Volterra 62, 00146 Rome, Italy
e-mail: francesca.gobbin@uniroma3.it,
rebecca.fugger@uniroma3.it
gianmarco.defelice@uniroma3.it
www.romatrestrutture.eu

Keywords: Churches, Masonry, Distinct Element Method, Rocking domain, Push-over.

Abstract. *The survey of damages after recent earthquakes have shown the fragility of masonry churches against the out-of-plane overturning of the façade. This failure mechanism is currently analyzed having recourse to a rigid body model, using either limit analysis with kinematic approach, or dynamic analysis under rocking motion. However, both the aforementioned methods neglect the interaction with the lateral walls, leading to an underestimation of the effective structural capacity under seismic action. The main goal of this work is therefore to investigate the effect of the interlocking between the façade and the transversal wall and the influence of the quality of masonry in out-of-plane overturning. For this purpose, a refined model of masonry through a Discrete Element Method is developed, based on a detailed recognition of masonry units. The acceleration and displacement capacity are estimated through quasi-static pushover and pulse-based dynamic analyses and compared to those calculated for the rigid body model. The proposed methodology is then applied to a sample of three single-nave masonry churches that suffered damages during the 2009 L'Aquila, Italy earthquake.*

1 INTRODUCTION

Damages experienced during the last seismic events have shown the high vulnerability of masonry churches. These structures, characterized by the absence of horizontal diaphragms connecting the walls, rarely activate a global behavior [1]. Their seismic assessment can be carried out considering distinct macro-elements, having an almost independent structural response under horizontal actions. Indeed, one of the most vulnerable macro-elements is represented by the façade, which may detach from the lateral walls and fail by overturning. Failure may involve the whole height of the façade or only its upper part, due to either a lower connection of the upper part of the façade with the rest of the building or as a consequence of dynamic amplification effects. This mechanism is typical in masonry structures, when the interlocking with side walls is not sufficient to guarantee a box-like behavior. Accordingly, masonry quality and connection with transversal walls play a fundamental role in the structural response under seismic action.

Nowadays, the collapse mechanisms are an effective assessment tool for estimating the seismic acceleration capacity [2], either through the kinematic approach of Limit Analysis [3], or by integrating the equation of rocking motion [4], as well as by considering an equivalent single degree of freedom oscillator. However, all of these models are usually based on the assumption that the façade is detached from the lateral walls and behaves as a rigid body overturning around a hinge at its basis.

Aiming at understanding the role of the connections and their influence on the effective seismic behavior, in the present paper the stabilizing effect of the interaction between the façade and the lateral walls is investigated through a bi-dimensional Distinct Element Method [5]. The effectiveness of the DEM to capture the behavior of masonry structures under seismic loading has already been proved in the Literature [6-16]. In the present case, the model of masonry is based on the assumption that all the non-linearities take place at the contacts among the stones, while these latter can be considered simply as rigid bodies. Three masonry churches that suffered damages from the 2009 L'Aquila (Italy) earthquake are analyzed through both, dynamic pulse-based, and non-linear static analyses. The former provides a stability domain as a function of pulse amplitude and duration that is compared with the unilateral rocking domain of a rigid block [17]. The latter provides the acceleration and displacement capacity under quasi-static horizontal loading, as compared to those obtained according to the rigid block schematization [10,18].

2 THE RIGID BODY MODEL

Consider the façade of the church as the rigid body shown in Figure 1, where b_f, h_f, R, W correspond, respectively, to the thickness, height, semi-diagonal and weight of the façade, while α is the slenderness angle. The dynamic behavior can be analyzed through the inverted pendulum [4], whose configuration is defined by the rotation θ towards the outside. Indeed, the rotation towards the inside is constrained by the lateral walls. For slender blocks ($\alpha < 20°$), the slenderness angle α and the horizontal displacement of the center of gravity u can be approximated, respectively, as:

$$\alpha = \frac{b_f}{h_f}\,; \qquad u = \frac{h_f}{2}\theta \tag{1}$$

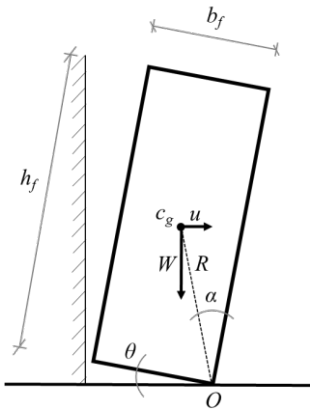


Figure 1: Rigid body model during rocking motion

Let us first consider the structure subjected to a quasi-static horizontal base acceleration a. The motion takes place only when the base acceleration reaches the value $a^* = \alpha g$, which activates the mechanism, where g is the acceleration of gravity. The capacity curve is shown in Figure 2, consisting in an ascending rigid branch corresponding to the absence of motion and a descending branch that, for slender blocks, can be approximated by a linear curve from a^* to the ultimate displacement d_u.

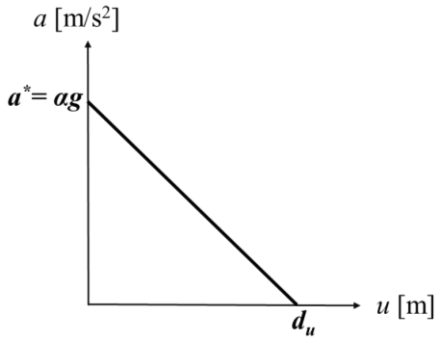


Figure 2: Capacity curve of a rigid body

According to Figure 2, the structure under earthquake base-motion starts rocking when the acceleration reaches the value a^* but does not collapse until the displacement exceeds the ultimate value d_u.

Let us now consider the structure subjected to a semi-sinusoidal pulse, given by the following base acceleration, $a(t)$ acting for a time interval t_0:

$$a(t) = \begin{cases} -a_0 \sin(\omega_0 t + \psi), & t \le t_0 \\ 0, & t > t_0 \end{cases} \tag{2}$$

where $t_0 = \pi/\omega_0$ represents half of the semi-sinusoidal acceleration period.

This schematization of earthquake input has been used in the past, especially in the description of near-fault events [19] and has the advantage of leading to an analytical expression for out-of-plane overturning, as shown hereafter. According to Housner, the equation of motion can be written as:

$$I_o\ddot{\theta} = -WR\sin(\alpha - \theta) + WR\frac{a_0}{g}\sin(\omega_0 t + \psi) \tag{3}$$

Assuming the hypothesis of slender blocks and settling $p^2 = \frac{WR}{I_o}$, the equation of motion becomes:

$$\ddot{\theta} - p^2\theta = \alpha p^2\left[\frac{\sin(\omega_0 t + \psi)}{\sin\psi} - 1\right] \tag{4}$$

By assigning the initial conditions and imposing the equilibrium in the limit configuration $\theta = \alpha$, the following expression is obtained:

$$\frac{a_0}{g\alpha} = \sqrt{1 + \frac{I_o}{WR}{\omega_0}^2} \tag{5}$$

Equation 5 represents the limit condition in terms of pulse amplitude a_0 and duration t_0 beyond which the collapse by overturning takes place.

3 THE NUMERICAL DISCRETE ELEMENT MODEL

The Discrete Element Method was originally proposed for the study of rocks mechanics [20] and then widely applied to the study of the seismic behavior of masonry structures [6-15], thanks to its capability of modeling the cracks and discontinuities taking place at collapse.

In the present paper, the blocks are considered as rigid bodies, while the contacts are modelled as two couples of normal and shear springs. The contact stiffness is determined on the basis of the overall elastic modulus of masonry E_m, which depend on masonry typology. In particular, aiming at lumping in the contact the whole deformability of masonry, the contact normal stiffness depends on the average blocks height h_m simply as the ratio E_m/h_m. The shear contact stiffness can be approximated as half of the normal stiffness. The strength of the contact is controlled by the Coulomb condition $|\tau| \leq \sigma \cdot \tan(\varphi)$, neglecting cohesion and tensile strength, and assuming a friction angle $\varphi = 30°$.

3.1 Mesh modelling

In order to reduce the computational effort of the analysis, a bi-dimensional model has been used. The DEM mesh is based on the survey of masonry, aiming at reproducing, as far as possible, the effective shape of the stones. In order to take into account tridimensional effects, the blocks density and contacts stiffness are affected by the third dimension, i.e. the length of the façade, or the thickness of the lateral wall, as shown in Figure 3. The façade and the side wall heights are respectively denoted as h_f and h_s, while their thickness as b_f and b_s. The façade length is denoted by l_f, while l_s represents the length of the portion of the side wall adjacent to the façade that is explicitly modeled, while the rest of the lateral wall is simply considered as an elastic block. The structure is finally laid on a rigid block, constituting the base to which seismic motion is applied.

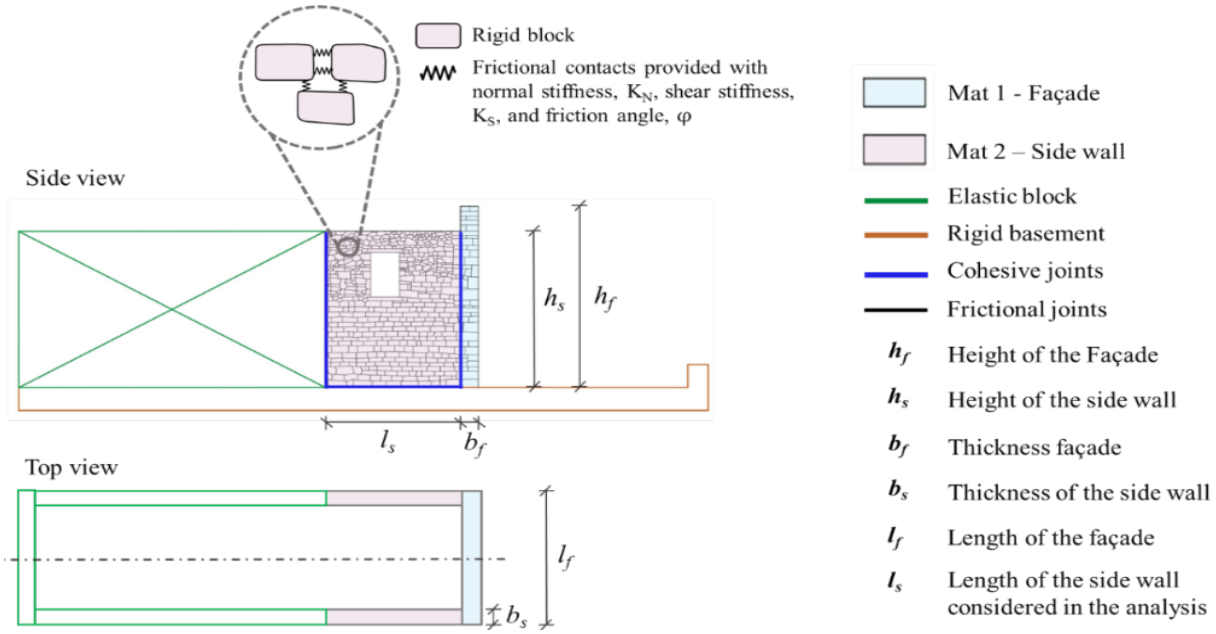


Figure 3: Interface model and framework of the mesh for a bi-dimensional model.

3.3 Seismic Input definition

Both, pushover and pulse-based dynamic analyses have been carried out, where the former consider the artificial damping as implemented in UDEC 6.0, while no damping is considered in the latter.

The algorithm for pushover analysis applies acceleration increments (or decrements) to the centroids of each block, controlling the unbalanced forces and the capacity of the structure to transfer the horizontal action into base shear. Both, the ascending and descending branches of the capacity curve are obtained and, namely, the acceleration which activates the mechanism a^* and the ultimate displacement d_u.

The algorithm for pulse-based analysis applies a semi-sinusoidal acceleration to the centroid of each block in a sequence of analyses for increasing pulse amplitude or duration. The overcoming of the maximum displacement and the consequent collapse of the façade is automatically recognized, providing ultimate displacement capacity and the corresponding pulse action. The unilateral equilibrium rocking domain is finally obtained for varying pulse amplitude a_0 and duration t_0 through an automatic procedure implemented in Fish language [5].

4 CASE OF STUDIES

Three case studies have been considered for the application of the above described procedure for seismic assessment, namely the church of Santa Maria degli Angeli, the church of San Paolo ad Peltuinum and the church of San Sisto, all located in the area surrounding the city of L'Aquila, as shown in Figure 4.

In the next three sections the churches are briefly described, and their geometrical and mechanical properties are provided. Referring to Figures 5-7, l_f & b_f (l_s & b_s) are the length and the thickness of the façade (of the lateral wall) h_f & h_s their height, γ_f & γ_s their specific weight,

K_{Nf} & K_{Ns} their normal joint stiffness, K_{Sf} & K_{Ss} their shear joint stiffness, while the friction angle φ in the contacts is set equal to 30° for all the analyses.



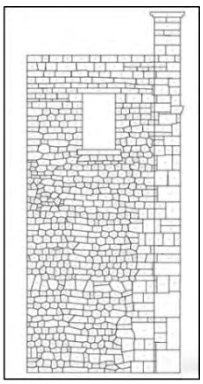
Figure 4: Location of the case studies and the epicenter of the 2009 L'Aquila earthquake.

4.1 Santa Maria degli Angeli

The *Church of Santa Maria degli Angeli* has an almost rectangular plan, with a front width of about 10 m and a length of 16 m. The niches along the nave show the signs of subsequent infill and repeated rearrangements. Two regular rectangular windows can be found on each side, next to the connection with the facade. Masonry is made of small and poorly worked stones (Figure 5).



A)



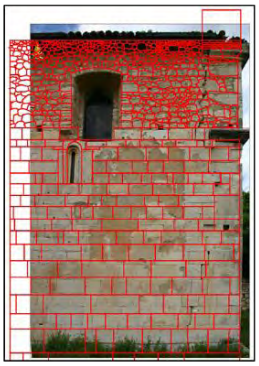
B)

	Façade	Side wall
l_f & b_s [m]	10.00	0.50
l_s & b_f [m]	0.90	4.30
h_f & h_s [m]	10.00	8.80
γ_f & γ_s [Kg/m^3]	2100	2000
K_{Nf} & K_{Ns} [Pa/m]	2.90e10	4.10e10
K_{Sf} & K_{Ss} [Pa/m]	8.31e9	1.35e9
φ [deg]	30°	30°

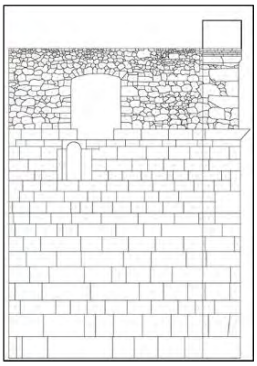
Figure 5: Church of Santa Maria degli Angeli: A) Block masonry recognition; B) Discrete element model; table of the main geometric and mechanical properties

4.2 San Paolo ad Peltuinum

The *Church of San Paolo ad Peltuinum* is located in the municipality of Prata d'Ansidonia (AQ). The structure was probably built between the VII and VIII century a.c. At least five stages of evolution and transformation of the building can be identified, related to the Lombard, Benedictine, Cistercian, Renaissance and eighteenth century influences. The church presents a cross plan with a single nave and a transept. Two different types of masonry can be noticed. The lower part is made of parallelepipedal larges blocks and dates back to medieval period, while the upper part, made of small irregular stones, is the result of a more recent reconstruction (Figure 6).



A)



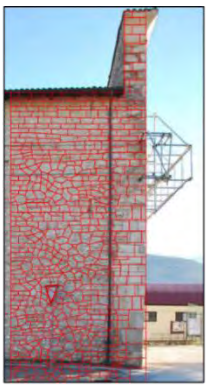
B)

	Façade		Side wall	
	upper	**lower**	**upper**	**lower**
l_f & b_s [m]	8.00		0.80	
l_s & b_f [m]	1.00		5.50	
h_f & h_s [m]	9.60		8.80	
γ_f & γ_s [Kg/m^3]	1900	2200	1900	2200
K_{Nf} & K_{Ns} [Pa/m]	2.19e10	2.69e10	6.96e9	2.85e9
K_{Sf} & K_{Ss} [Pa/m]	7.30e9	8.97e9	2.32e9	9.50e8
φ [deg]	30°	30°	30°	30°

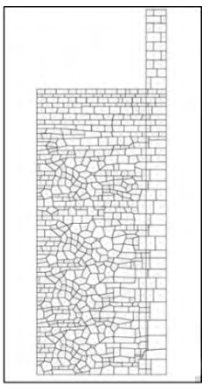
Figure 6: Church of San Paolo: A) Block masonry recognition; B) Discrete element model; table of the main geometric and mechanical properties

4.2 San Sisto

The *Church of San Sisto* dates back to the VIII century a.C. and is located in the city of L'Aquila. The building has a single nave. The façade has a rectangular shape spanning about 10 m in length and 13 m in height, with an horizontal crown. The masonry of the façade has facing in square ashlars, while that of the transversal wall is made of small and poorly worked stones (Figure 7).



A)



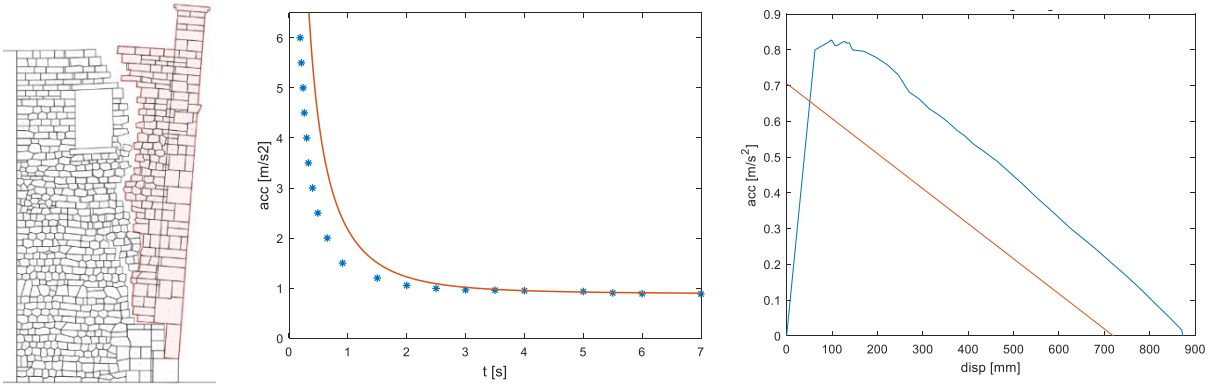
B)

	Façade	**Side wall**
l_f & b_s [m]	9.95	1.40
l_s & b_f [m]	0.75	4.70
h_f & h_s [m]	13.30	10.40
γ_f & γ_s [Kg/m^3]	2200	2100
K_{Nf} & K_{Ns} [Pa/m]	4.05e10	1.64e10
K_{Sf} & K_{Ss} [Pa/m]	1.35e10	5.45e9
φ [deg]	30°	30°

Figure 7: Church of San Sisto: A) Block masonry recognition; B) Discrete element model; table of the main geometric and mechanical properties

4 RESULTS

In this section, the numerical and analytical results obtained for the three cases of study are presented. The stability domain under sinusoidal pulses, and the pushover curve obtained through DEM are compared, respectively, to the analytical rocking domain and to the capacity curve of the rigid block. The comparison shows to what extent the connection with lateral walls may be effective in the seismic assessment of the church against the overturning of the façade.



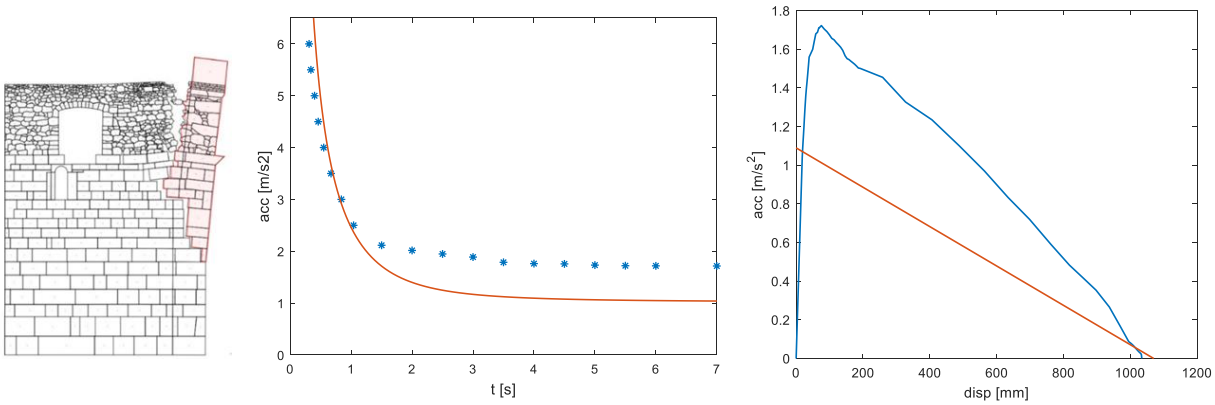
A) B) C)

Figure 8: Church of Santa Maria degli Angeli: A) Predicted crack pattern and failure mechanism according to distinct element analysis, B) rocking domain C) pushover analysis

The numerical analysis of the church of Santa Maria degli Angeli provides an acceleration a^* and a displacement d_u capacities of about 0.8 m/s^2 and 872 mm, respectively, with an increase of about 20% as compared to the rigid block model (Figure 8c). Even though the failure mechanism shows a non-negligible part of the lateral wall involved in the collapse mechanism (Figure 8a), thanks to a good interlocking of the stones, its stabilizing effect is only marginal as a consequence of the small thickness b_s of the lateral wall which is only about 5% of the facade length.

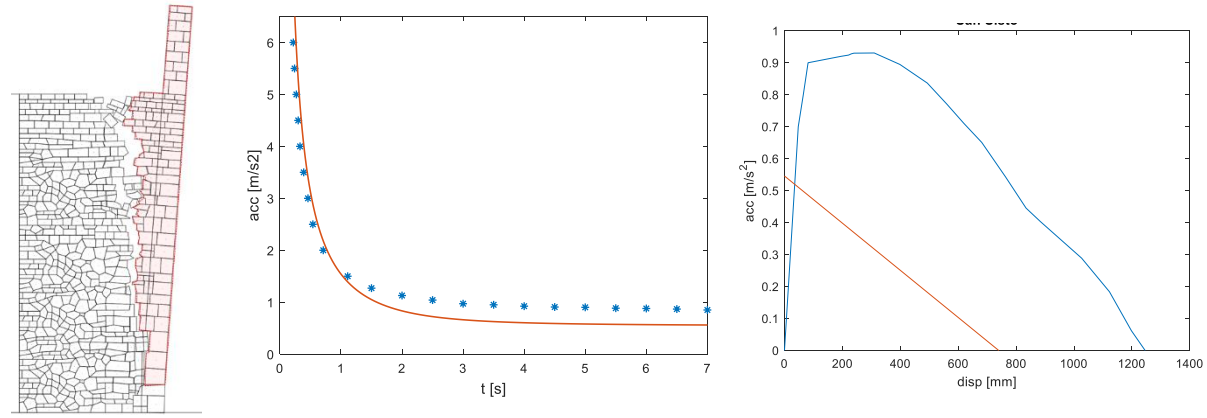
The analysis of the church of San Paolo exhibits a strong increase (of about 50%) in acceleration capacity and almost no increment in displacement capacity when compared to the rigid block. Thanks to the quality of masonry, made of large squared blocks in the basement of the church, the rotation hinge is located at the middle of the façade height (Figure 9a). Therefore, the acceleration capacity increases according to the lower slenderness of the part involved in overturning, while the displacement capacity, which is governed by the façade thickness, remains almost unchanged.

The analysis of the church of San Sisto (Figure 10), shows an increase in both acceleration and displacement capacity of about 65%, thanks to the beneficial effect of the connection between the façade and the transversal wall. Nonetheless, the acceleration capacity a^* determined by the DEM, equal to 0.9 m/s^2 is still low, due to the high slenderness of the façade.



A) B) C)

Figure 9: Church of San Paolo: A) Predicted crack pattern and failure mechanism according to distinct element analysis, B) rocking domain C) pushover analysis.



A) B) C)

Figure 10: Church of San Sisto: A) Predicted crack pattern and failure mechanism according to distinct element analysis, B) rocking domain C) pushover analysis.

The results shown for the three churches under study suggest that the analytical rigid block model generally constitutes a powerful and effective instrument for the seismic assessment of masonry churches. Only when the characteristics of masonry are such as to prevent the complete detachment of the façade, the rigid block only provides a lower bound estimate. In this case, the lateral walls play a non-negligible effect in terms of both, higher hinge position (i.e. lower slenderness of the part undergoing overturning) and stabilizing bending moment against overturning.

5 CONCLUSIONS

In this paper, an approach for modelling the collapse mechanism of historical masonry building and evaluating the reliability of current models used for seismic assessment is outlined. The seismic response of three single-nave churches that suffered damages after the 2009 L'Aquila earthquake is investigated through pulse-based dynamic and quasi-static pushover

analyses, with both analytical and numerical approach. The well-known mechanism of overturning of the façade is considered and the numerical results are compared with those derived neglecting the connections and modelling the façade as a rigid block according to the Housner rocking model.

Through the detailed reconstruction of masonry pattern, the numerical analyses with DEM take into account the effect of connections due to interlocking of stones, resulting in the increase of both acceleration and displacement capacities. The proposed approach succeeds in detecting the expected failure mechanism, which does not change from quasi-static to dynamic loading. Only for short period pulses, the numerical model provides a widespread crack pattern and a slight decrease in seismic acceleration capacity.

Beside the differences that may become relevant for high quality masonry, the rigid block model still represents a powerful and effective tool for the seismic assessment of collapse mechanisms.

Acknowledgements. The present research has been funded by ReLUIS-DPC 2019-2021 and Regione Lazio SICURA research projects. The authors gratefully acknowledge Itasca Consulting Group for providing the web-licenses of UDEC 6.0.

REFERENCES

[1] Lagomarsino, S. and Podestà S., Seismic Vulnerability of Ancient Churches: II. Statistical Analysis of surveyed data and methods for risk analysis. *Earthquake Spectra* (2004), vol. **20**, n. 2, pp. 395-412.

[2] Sorrentino, L., D'Ayala, D., de Felice, G., Griffith, M.C., Lagomarsino, S., Magenes, G. Review of Out-of-Plane Seismic Assessment Techniques Applied To Existing Masonry Buildings. *International Journal of Architectural Heritage* (2017), vol. **11**, pp. 2-21.

[3] Heyman, J. The stone skeleton. *International journal of solids and structures* (1966), vol. **2**, n. 2, pp. 249-79.

[4] Housner, G. W. The behavior of inverted pendulum structures during earthquakes. *Bulletin of the Seismological Society of America* (1963), vol. **53**, n. 2, pp. 403-417.

[5] ITASCA consulting group, UDEC (Universal Distinct Element Code) Version 6.0 (2017), Minneapolis, Minnesota.

[6] Azevedo, J., Sincraian, G., Lemos J.V. Seismic behavior of blocky masonry structures. *Earthquake Spectra* (2000), vol. **16**, n. 2, pp. 337-365.

[7] Lemos, J.V. Discrete Element Modeling of Masonry Structures. *International Journal of Architectural Heritage* (2007), vol. **1**, n. 2, pp. 190-213.

[8] de Felice, G. and Mauro, A. On Overturning of the Façade in Churches with Single Nave: Some Case Studies from L'Aquila, Italy, 2009 Earthquake. Advanced Materials Research (2010), vol. **133-134**, pp. 807-812.

[9] Gobbin, F., Fugger, R. and de Felice, G. Modellazione agli elementi distinti per lo studio dell'interazione della facciata con la parete laterale di alcune chiese nel territorio Aquilano. In: *ANIDIS* (2019).

[10] de Felice, G. Out-of-plane seismic capacity of masonry depending on wall section morphology. *International Journal of Architectural Heritage* (2011), vol. **5**, n. 4-5, pp. 466-482.

[11] Al Shawa, O., de Felice, G., Mauro A., and Sorrentino L. Out-of-plane seismic behaviour

of rocking masonry walls. *Journal of earthquake engineering* (2012), vol. **41**, n. 5, pp. 949-968.

[12] de Felice, G., De Santis, S., Lourenço, P.B., Mendes, N. Methods and Challenges for the Seismic Assessment of Historic Masonry Structures. *International Journal of Architectural Heritage* (2017), vol. **11**, pp. 143-160.

[13] Malomo, D., De Jong, M.J. and Penna, A. Distinct Element modelling of the in-plane cyclic response of URM walls subjected to shear-compression. *Earthquake Engineering and Structural Dynamics* (2019), vol. **48**, n. 12, pp 1322-1344.

[14] Meriggi, P., de Felice, G., De Santis, S., Gobbin, F., Mordanova, A. and Pantò, B. Distinct Element Modelling of masonry walls under out-of-plane seismic loading. *International journal of architectural heritage* (2019), vol. **13**, n. 7, pp. 1110-1123.

[15] Lemos, J.V. Discrete Element Modeling of the Seismic Behaviour of Masonry Constructions. *Buildings* (2019), vol. **9**, n. 2, pp. 43-53.

[16] Malena, M., Portioli, F., Gagliardo, R., Tomaselli, G., Cascini, L. and de Felice, G. Collapse mechanism analysis of historic masonry structures subjected to lateral loads: A comparison between continuous and discrete models. *Computers & Structures* (2019), vol. **220**, pp. 14-31.

[17] Mauro, A., de Felice, G. and De Jong, M. J. The relative dynamic resilience of masonry collapse mechanism. *Engineering Structures* (2015), vol. **85**, pp. 182-194.

[18] Mordanova, A., de Felice, G. Seismic assessment of archaeological heritage using discrete element method. *International Journal of Architectural Heritage* (2018), DOI: 10.1080/15583058.2018.1543482

[19] Makris, N. and Roussos, Y. Rocking response of rigid blocks under near-source ground motions. *Géotechnique* (2009), vol. **50**, n. 3, pp. 243-262.

[20] Cundall, P. A. A computer Model for Simulating Progressive Large-Scale Movements in Blocky Rock Systems. *Proceeding of the Symposium of the International Society of Rock Mechanics* (1971).

12th International Conference on Structural Analysis of Historical Constructions
SAHC 2020
P. Roca, L. Pelà and C. Molins (Eds.)

EQUIVALENT FRAME METHOD COMBINING FLEXURAL AND SHEAR RESPONSES OF MASONRY BUILDINGS

C. MARANO[1*], M. PETRACCA[2], G. CAMATA[1] AND E. SPACONE[1]

[1]Università degli Studi G. d'Annunzio Chieti e Pescara
Department of Engineering and Geology (InGeo)

[2] ASDEA Software
Via Breveglieri, 8 – 65128 Pescara, Italy
web: http://asdeasoft.net

Keywords: Masonry, Pushover Analysis, Equivalent frame, Fiber elements, Vulnerability

Abstract. *This work presents the results of quasi-static non-linear analyses of two masonry buildings using, for the discretization of walls, a macro-element that combines the bending and the in-plane shear responses. The macro-element uses the force-based beam-column element equipped with cross sections discretized in fibers, where the behavior of each fiber is described by uniaxial constitutive models. To describe the shear response of the structural element, the macro-element embeds a shear hinge at mid-span, with a phenomenological non-linear constitutive model calibrated on experimental data. The analyzed buildings are two tangibles examples of un-reinforced and reinforced masonry of the Italian Heritage. The un-reinforced masonry building is a strategic building monitored by the O.S.S., partially damaged by the seismic events in Center Italy in 2016. The reinforced masonry building, a three-storey residential structure, is subject of evaluations carried out in the ReLuis RINTC project, designed as per D.M. 2018.*

1 INTRODUCTION

The seismic events which recently struck the Italian Peninsula have shown the limited earthquake performance of existing masonry structures.

Their high vulnerability is linked to various sources of weakness such as very disparate construction typologies, buildings remodeled over time with interventions without criteria, absence of structural design, architectural modifications, interventions without adequate structural evaluation: most of the existing buildings in masonry are therefore not designed to transfer seismic forces from horizontal to vertical elements.

Nonlinear numerical simulations of existing masonry buildings still represent an open problem in research because it is difficult to develop reliable numerical models of real buildings.

This study presents the results of non-linear pushover analyzes performed on two unreinforced and reinforced masonry buildings. The method, called equivalent frame method (EFM), uses one-dimensional nonlinear macroelements connected through nodal panels considered to be nondeformable and rigid.

The macroelement, originally developed for reinforced concrete structures [1], has been extended in previous works ([2,3,4,5]) to the static and dynamic nonlinear analysis of masonry structures. The macroelement consists of Force Based Elements (FBE) ([6,7]) combined with nonlinear lumped hinges.

The equilibrium between moment and shear is guaranteed at the element level; if properly calibrated, the macroelement is particularly effective in simulating the in plane and out-of-plane response of wall panels of ordinary and reinforced masonry buildings.

The equivalent frame model is implemented in the open source computational platform OpenSees 3.0.3 3 ([8]) with which the numerical analyzes will be conducted together with the pre and post-processor Scientific ToolKit for Opensees, STKO ([9]).

2 EQUIVALENT FRAME METHOD WITH FIBER BASED ELEMENTS AND PHENOMENOLOGICAL LUMPED HINGES

In the simplified approach with EFM, the masonry structures are modeled by assembling equivalent vertical and horizontal one-dimensional elements: piers and spandrels are modeled with appropriate constitutive laws and connected to each other through rigid areas (Figure 1).

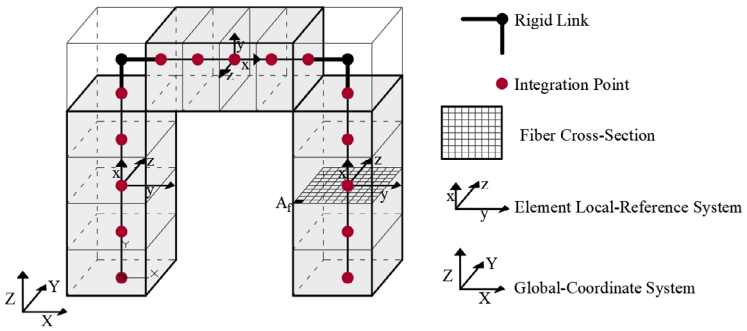


Figure 1*:* EFM discretization

The interaction between axial and flexural behavior is captured by the macroelement using force based fiber elements (Figure 2). The diagonal and sliding shear behavior is captured with a phenomenological law. Flexure and shear interaction is ensured with the equilibrium along the element (Figure 3).

For the unreinforced masonry (URM) building behavior, the uniaxial material "Concrete02" (OpenSees 3.0.3) is used to simulate the masonry. The tensile strength is assumed to be 1/30 of the compressive strength.

For the reinforced masonry (RM) buildings, the masonry behavior is modeled with the uniaxial material "Concrete01" with zero tensile strength an steel bar behavior is modeled with the uniaxial bilinear steel Material "Steel01".

The uniaxial multilinear material of OpenSees 3.0.3 is used to simulate the shear behavior of the wall panels.

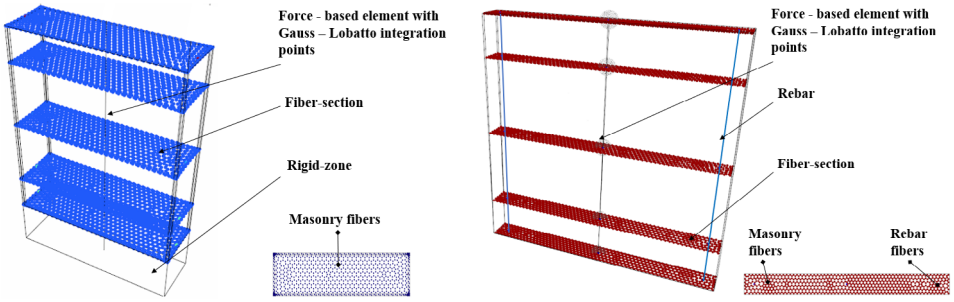


Figure 2: Macroelement formulation

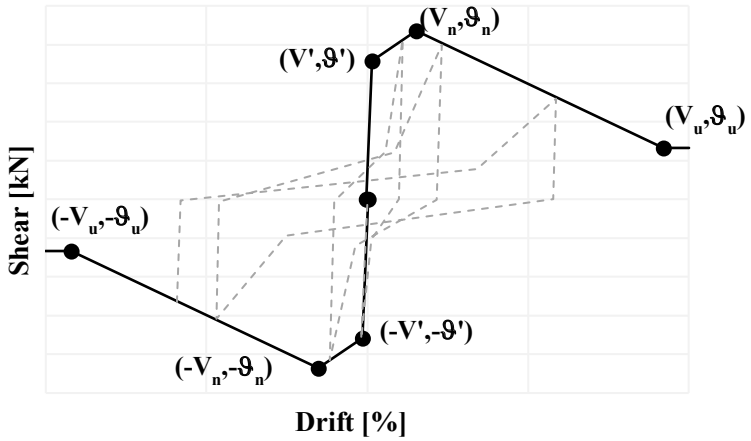


Figure 3: Lumped hinge for shear behavior

The shear strength capacity, V_t ([10]) of URM panels is calculated as:

$$V_t = B \cdot t \frac{f_{tu}}{b} \sqrt{1 + \frac{\sigma}{f_{tu}}} \tag{1}$$

where:

f_{tu} is the masonry tensile strength;
b is equal to 1.5;
B and t t are the length and thickness of the panel, respectively.

The shear strength Vt ([11]) of the RM panels is calculated as the sum of the contributions of the masonry shear capacity $V_{t,M}$ and the reinforcement capacity $V_{t,S}$, according to the following relationships:

$$V_t = V_{t,M} + V_{t,S} \tag{2}$$

$$V_{t,M} = d \cdot t \cdot f_{vd} \tag{3}$$

where:

d is the distance between the extreme compressed fiber and the center of tensile reinforcement;

t is the panel thickness;

f_{vd} is the shear strength of the masonry under compression.

$$V_{t,s} = (0.6 \cdot d \cdot A_{sw} \cdot f_{vd})/s \quad (4)$$

where:

A_{sw} shear strengthening area in the direction of the shear forces

f_{vd} steel design yielding strength;

s spacing among the transversal reinforcement.

In deformation terms, the ultimate angular deformation, ϑ_u of URM panels (URM) at the life safety limit state is assumed to be equal to 0.4% of the panel height [12]; in the case of RM panels, the ultimate angular deformation, ϑ_u is assumed to be 0.6% of the height of the panel [12].

The shear phenomenological law considered in this study does not depend on the axial load N; once the parameters have been set, the law remains constant during the analysis.

The ultimate bending moment, M_u of the masonry spandrels, as indicated in the Italian code DM 2018 [11] is calculated as:

$$M_u = H_p \cdot h_{sp}/2 \cdot [1 - \frac{H_p}{(0{,}85 \cdot f_{hd} \cdot h_{sp} \cdot t_{sp})}] \quad (5)$$

where:

h_{sp} is equal to the spandrel height;

t_{sp} is equal to the spandrel thickness,

The spandrel shear capacity, V, is equal to:

$$V = h_{sp} \cdot t_{sp} \cdot \tau_0 \quad (6)$$

where:

τ_0 masonry shear strength;

h_{sp} masonry spandrel height;

t_{sp} masonry spandrel thickness.

3 PUSH OVER ANALYSES OF TWO LARGE UNREINFORCED AND REINFORCED MASONRY BUILDINGS

3.1 Description of the building investigated

The first case study presented in this work is a pushover analysis conducted on the "Pietro Capuzi" kindergarten school in Visso - Marche - MC - Italy; this is an URM building monitored by the Seismic Observatory on Structures [13] which during the last Italian seismic events (Central Italy - 2016) suffered serious structural damage ([14,15]).

The chosen structure is characterized by a regular distribution of the openings and a predominantly global response with localized damage in the piers and in the masonry spandrels, which can be modeled well with EFM. The plan building was asymmetrical in the two main directions (longitudinal X, transversal Y) and consisted of a mezzanine and a first floor (Figure 4).

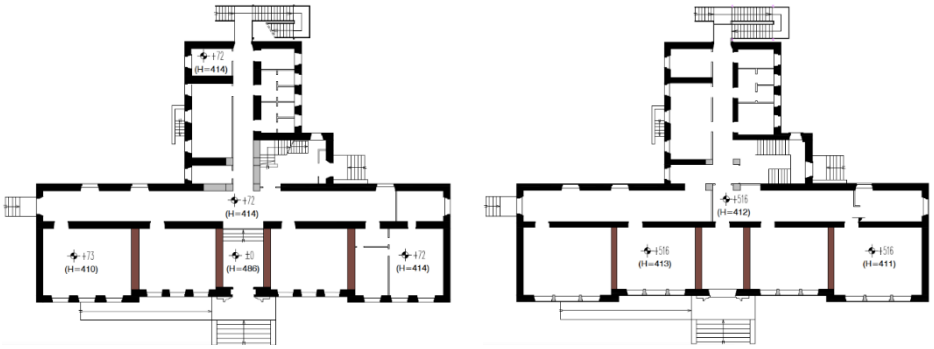


Figure 4: First and second floor plan

The building, as shown in Figure 5, had several cracks caused by in-plane failure mechanism of the piers and spandrels, damage to the infills and non-load-bearing structures ([16]).



Figure 5: Observed damage, adapted from [16]

The second case study presented in this paper is an archetypal building in RM called in this work E8 and calculated according to the Italian design code [17].

The objective of the pushover on the E8 building is to evaluate, through the simplified macroelement model, the building seismic performance as well as detect the damage in the panels and in the steel rebars. The building (Figure 6), designed for L'Aquila (Italy) on type C soil and topography [11] has an axis of symmetry in the direction Y, the height between floors is 3.10 m and slab depth equal to 0.25 m on all levels. All slabs are unidirectional. The wall thickness of the external walls is 0.30 m and of the internal ones is 0.25 m.

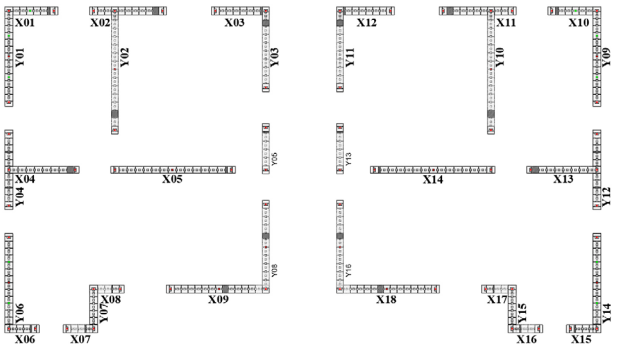


Figure 6: Plan of the E8 building

3.2 Numerical models

The 3D-EFM of the two buildings is shown in Figure 7.

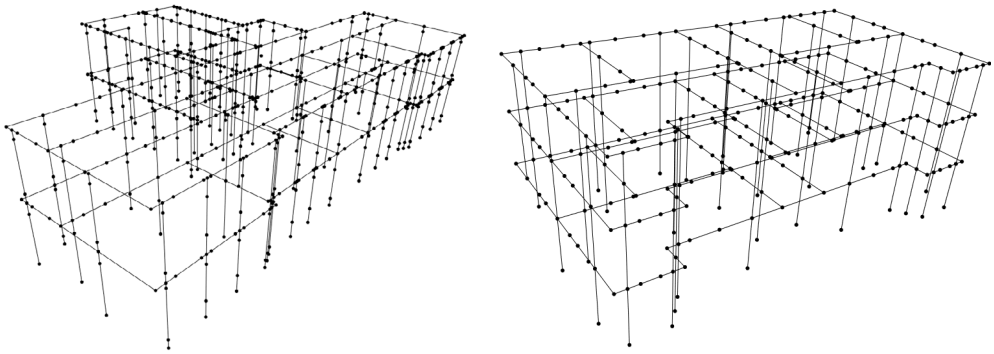


Figure 7: Left EFM of the URM building Right EFM of the RM building

The numerical model of the URM building considers the height of the piers and the length of the panels according to the method proposed by [18].

The mezzanine floor (+4.30 m) and the first floor (+8.70 m) are modeled, while the basement is not considered in the model. The roof and the attic floor are not explicitly modeled but their contribution is taken into account in terms of masses and gravity loads. The curbs are modeled explicitly, while the floors are idealized with kinematic constraints as rigid diaphragms. The piers and the spandrels have a rectangular cross section and the structure is assumed fixed at the base.

The numerical model of the RM building considers the height of the piers equal to the height of the floors. The ground floor (+3.00 m), the first floor (+6.00 m) and the roof (+9.00 m) are modeled. The RC curbs are assumed to behave linearly elastic. The corner reinforcement bars, which are in common with two orthogonal piers, have been distributed equally between the piers considering for each pier a 8 mm diameter bar, the other bars have a diameter of 16 mm. The weight of the elements in both models is applied as distributed load transmitted from the floors to the structural elements.

Table 1 and Table 2 show the mechanical properties assigned to the fiber model: masonry

compressive strength, f_m, masonry tensile strength, f_{tu}, masonry shear strength, f_{vm0}, Elastic Modulus, E_m, Shear Modulus, G, masonry specific weight, W, and steel bar yielding strength, f_{ym}.

Table 1: URM material parameters

f_m	f_{tu}	E_m	G	W
N/mm^2	N/mm^2	N/mm^2	N/mm^2	kN/m^2
4.8	0.14625	2610	870	21.00

Table 2: RM material parameters

f_m	f_{vm0}	E_m	G	W	f_{ym}
N/mm^2	N/mm^2	N/mm^2	N/mm^2	kN/m^2	N/mm^2
6.436	0.2857	5300	2120	9.00	483.871

For both buildings, pushover analysis are performed using displacement control according to a distribution of forces proportional to the masses and using as target displacement a node on the top floor of both buildings. In each step, equilibrium is achieved with a Krylov-Newton iteration process and convergence is accepted with a residual tolerance of 1×10^{-5}.

3.3 URM results

Figure 8 shows the 4 capacity curves and the bi-linearized curves calculated following the indications in [18]. The maximum base shear is 10787 kN for the pushover + X|Uniform at a displacement of 22.30 mm. On the walls aligned in the transversal +Y direction, numerical diagonal cracking failures are observed.

In the longitudinal direction +X direction, the slender wall panels fail in flexure while the squat wall panels fail in shear. The analysis is interrupted due to numerical instability related to the brittle failures of the masonry walls on the mezzanine floor.

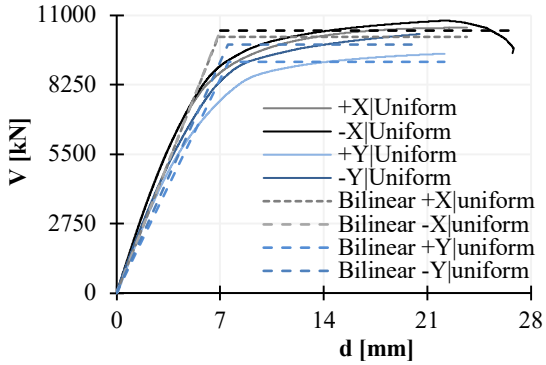


Figure 8: URM capacity curves and bilinearizations

Figure 9 compares the bi-linearized curves and the Acceleration-Displacement Response Spectrum (ADRS), evaluated considering a subsoil Type D category with topography T1 [11].

The seismic risk indicator, ζ_E, defined as the ratio between the capacity and the demand, calculated for the four capacity curves is equal to 0.365, 0.416, 0.346 and 0.281 for the

distribution +X|Uniform, -X|Uniform, +Y|Uniform and -Y|Uniform, respectively. The curves show that the structure has a very limited capacity and it is prone to damage under cyclic loads induced by the earthquake.

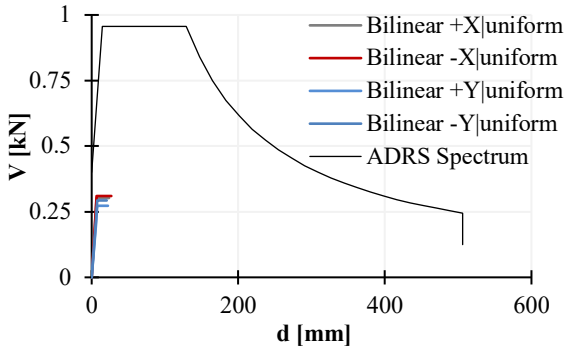


Figure 9: URM Demand vs Capacity URM

Figure 10 shows the comparison between the actual damage observed on site on wall 4 and the numerical damage simulated with OpenSees. The panels at the mezzanine level failed in shear and the wall at the first floor failed because of mixed flexure-shear mechanisms.

Damage is also observed in the spandrels on the mezzanine and first floors. The lumped hinge behavior, V - δ_u extrapolated at the base of the piers highlights a shear numerical failure predicting correctly the actual damage observed. Four piers reached the life-saving limit state ultimate drift, while the other four piers reached the maximum shear capacity but not the ultimate drift). The numerical model reproduces correctly the actual damage observed.

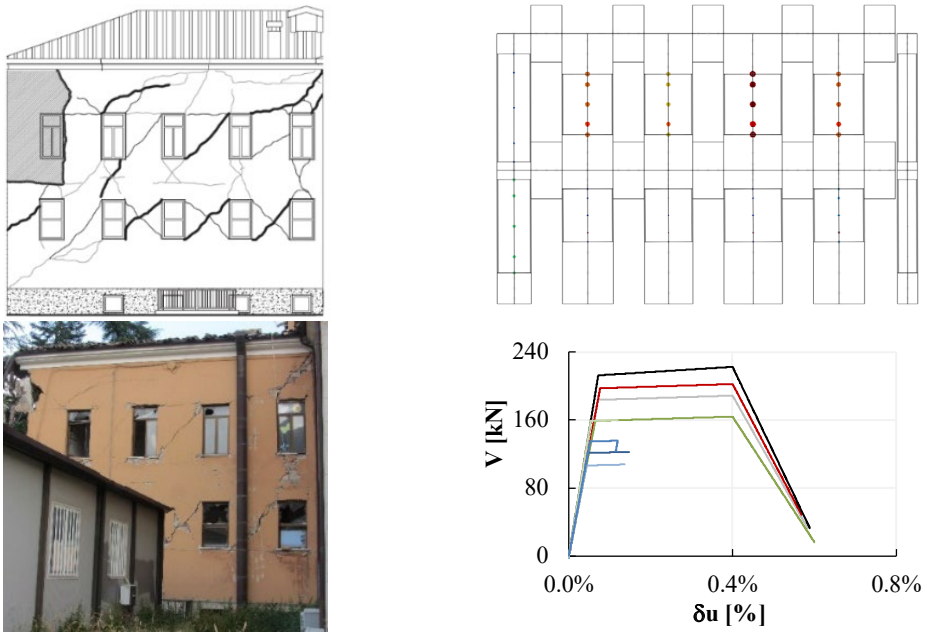


Figure 10: Comparison between numerical and observed damage – wall n°4

3.4 RM results

Figure 11 shows the four capacity curves and the relative bi-linearized curves obtained for the RM building. The maximum base shear capacity is 7415.13 kN for the pushover + Y|Uniform at a horizontal displacement equal to 39.68 mm. The comparison shows an overlap of the curves in the longitudinal direction X due to the perfect symmetry of the building in the direction orthogonal to it. The building collapse is triggered by the panel shear failures on the ground floor in both directions of analysis.

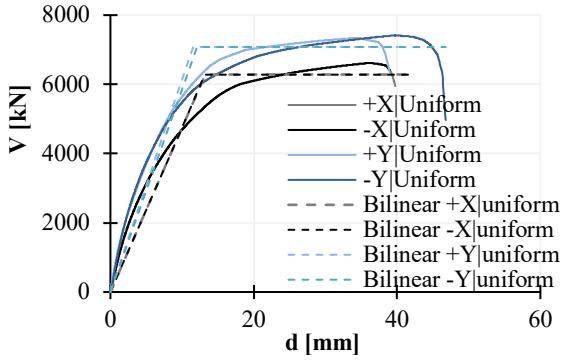


Figure 11: RM capacity curves and bilinearizations

Figure 12 shows a comparison of the bi-linearized curves and the ADRS assuming a type C soil category T1 topography [11].

The seismic risk indicator, ζ_E of the four capacity curves is equal to 1.31, 1.31, 1.625 and 1.803 for the distribution +X|Uniform, -X|Uniform, +Y|Uniform and -Y|Uniform, respectively. Therefore, as expected, the structure capacity complies with the Italian design codes, D.M. 2018.

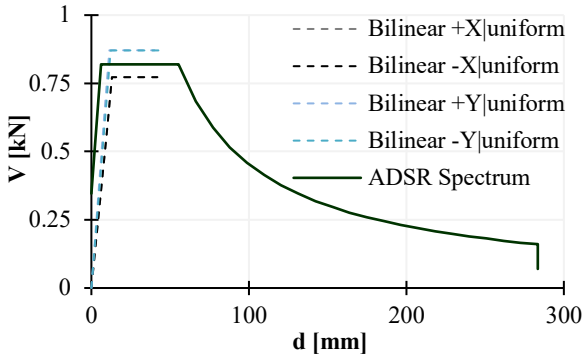


Figure 12: Demand vs Capacity RM

Figure 13 shows, the steel fiber behavior of panel X06 and the Gauss point behavior of panel X14 for the force distribution proportional to the masses in the positive longitudinal direction, +X|Uniform.

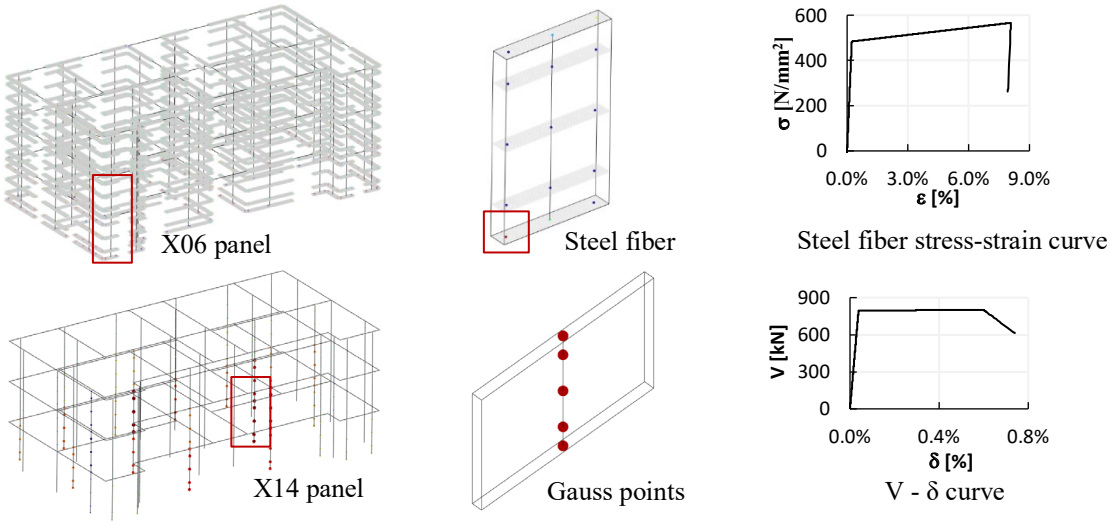


Figure 13: Numerical damage of panel and bars

The results show that the pier on the corner at the ground floor yields because of bar yielding, however the building collapses because of shear failure as indicated by the gauss points.

4 CONCLUSIONS

This work presents the results of pushover analyzes performed on two large URM and RM buildings. The models are developed using the EFM with the open source software OpenSees and the pre and post-processor Scientific ToolKit for OpenSees, STKO.

FBEs are used to describe the axial-bending behavior, while a phenomenological law is used to simulate the shear behavior.

The phenomenological law is calibrated with experimental data to capture correctly the pier and spandrel shear behavior.

In both case studies, URM and RM, the capacity curves are compared with the demands. The results of the analyses on the URM building show that the model is capable to describe correctly the damage occurred and that the URM building is highly vulnerable.

The RM building behaves well under seismic load, the seismic risk ζ_E is higher than 1.31 and therefore the building design complies with the Italian design codes. The EFM proposed in this work ensures to consider correctly the biaxial-bending interaction and to evaluate in depth the steel bar behavior and damage. The quality of the results obtained can be further improved by considering the variation of the axial load to describe the pier shear behavior.

Despite convergence problems that can occur in quasi-brittle materials with softening and the limitations due to the phenomenological shear law, the EFM proposed in this work is particularly efficient and accurate for the non-linear analysis of large-scale masonry structures.

REFERENCES

[1] Marini, A., and Spacone, E. Analysis of reinforced concrete elements including shear effects. *ACI Structural Journal*, 2006, **103.5**: 645.

[2] Raka, E., Spacone, E., Sepe, V., and Camata, G. Advanced frame element for seismic analysis of masonry structures: model formulation and validation. *Earthquake Engineering & Structural Dynamics*, 2015, **44.14**: 2489-2506.

[3] Siano, R., Sepe, V., Camata, G., Spacone, E., Roca, P., and Pelà, L. Analysis of the performance in the linear field of equivalent-frame models for regular and irregular masonry walls. *Engineering Structures*, 2017, **145**: 190-210.

[4] Siano, R., Roca, P., Camata, G., Pelà, L., Sepe, V., Spacone, E., and Petracca, M. Numerical investigation of non-linear equivalent-frame models for regular masonry walls. *Engineering Structures*, 2018, **173**: 512-529.

[5] Peruch, M., Spacone, E., and Camata, G. Nonlinear analysis of masonry structures using fiber-section line elements. *Earthquake Engineering & Structural Dynamics*, 2019, **48.12**: 1345-1364.

[6] Spacone, E., Filippou, F. C., and Taucer, F. F. Fibre beam–column model for non-linear analysis of R/C frames: Part I. Formulation. *Earthquake Engineering & Structural Dynamics*, 1996, **25.7**: 711-725.

[7] Spacone, E., Filippou, F. C., and Taucer, F. F. Fibre beam–column model for non-linear analysis of R/C frames: part II. Applications. *Earthquake Engineering & Structural Dynamics*, 1996, **25.7**: 727-742.

[8] Mazzoni, S., McKenna, F., Scott, M. H., and Fenves, G. L. OpenSees command language manual. *Pacific Earthquake Engineering Research (PEER) Center*, 2006, 264.

[9] Petracca, M., Candeloro, F., and Camata, G.*"STKO user Manual"*. ASDEA Software Tecnology, 2019, Pescara Italy.

[10] Turnšek, V., and Čačovič, F. (1971, December). Some experimental results on the strength of brick masonry walls. In: *Proc. of the 2nd International Brick Masonry Conference*. 1971. p. 149-156.

[11] Aggiornamento delle Norme Tecniche per le Costruzioni (NTC2018). *Ministero delle Infrastrutture e dei Trasporti: Rome, Italy*.

[12] Circolare esplicativa 21/01/2019 n. 7. Istruzioni per l'applicazione dell' «Aggiornamento delle "Norme tecniche per le costruzioni"». DM 17/01/2018 [In Italian].

[13] Dolce, M., Nicoletti, M., De Sortis, A., Marchesini, S., Spina, D., and Talanas, F. Osservatorio sismico delle strutture: the Italian structural seismic monitoring network. *Bulletin of Earthquake Engineering*, 2017, **15.2**: 621-641.

[14] Cattari, S., Degli Abbati, S., Ottonelli, D., Marano, C., Camata, G., Spacone, E., ... and Penna, A. Discussion on data recorded by the Italian structural seismic monitoring network on three masonry structures hit by the 2016-2017 Central Italy earthquake. *Proc. of COMPDYN*, 2019.

[15] Cattari, S., Degli Abbati, S., Ottonelli, D., Sivori, D., Spacone, E., Camata, G., ... and Graziotti, F. Task 4.1 Workgroup_Report di sintesi sulle attività svolte sugli edifici in

muratura monitorati dall'Osservatorio Sismico delle Strutture, Linea Strutture in Muratura. *ReLUIS Report, Rete Dei Laboratori Universitari Di Ingegneria Sismica*, 2017.

[16] Cattari, S., Sivori, D. "*Relazione tecnica scuola dell'infanzia Pietro Capuzi"* (in italian), 2016.

[17] Iervolino, I., Spillatura, A., and Bazzurro, P. RINTC project: assessing the (implicit) seismic risk of code-conforming structures in Italy. *COMPDYN*, 2017.

[18] Lagomarsino, S., Penna, A., Galasco, A., and Cattari, S. TREMURI program: an equivalent frame model for the nonlinear seismic analysis of masonry buildings. *Engineering structures*, 2013, **56**: 1787-1799.

12th International Conference on Structural Analysis of Historical Constructions
SAHC 2020
P. Roca, L. Pelà and C. Molins (Eds.)

ESTIMATION OF THE CLAMPING FORCE OF RIVETED ASSEMBIES THROUGH A THERMOMECHANICAL MODELLING. INFLUENCE OF CLEARANCE AND THICKNESS OF THE CONNECTION

P-J. TISSERAND[1, 2], S. SIRE[3*] AND M. RAGUENEAU[2]

[1]ENS Paris-Saclay, LMT, CNRS
Université Paris Saclay
94235 Cachan, France
e-mail: pierre-jean.tisserand@reseau.sncf.fr

[2]SNCF Réseau, DGII-OA
93210 La Plaine Saint-Denis, France
e-mail: muriel.ragueneau@reseau.sncf.fr

[3]University of Brest, IRDL, CNRS
29200 Brest, France
e-mail: stephane.sire@univ-brest.fr (*corresponding author)

Keywords: Railway bridge, Riveted assembly, Modelling, Clamping force

Abstract. *This study deals with the numerical (FE) modelling of the pre-stress induced by the hot riveting process used in old iron and steel bridges. It aims to provide information to assess old metallic railway bridges. The numerical model presented in this study is developed with Cast3M software. It is used to study the evolution of the pre-stress as a function of the riveted thickness. Mechanical and thermal properties, used for the modelling are depending on temperature. Mechanical and thermal conditions are also taken into account. These include the three types of thermal transfer: the conductivity transfer between the plates and the rivet, the convective and radiative transfer between the rivet and the environment and between the plates and the environment, and the radiative transfer between the rivet and the plates. In order to take into account the induced clearance between the rivet shank and the plates, dedicated riveted specimens were manufactured by the repairing of metal bridges (RPM) team of the SNCF. Clearances were measured for different thicknesses and have been included in the numerical model. The study shows that the assessment of the pre-stress is strongly dependent to the thickness to be assembled. It also shows the importance of the radial clearance of the connection to better estimate this induced pre-stress.*

1 INTRODUCTION

The French railway network includes over 30 000 km of railway tracks and more than 5000 metallic bridges [1]. Some of these bridges were built before the 1900s. At the time, hot riveting was the preferred joining method. Considering the ageing of these constructions, as well as the increasing evolution of traffic in the network, the understanding of the behavior of this type of connection becomes of utmost importance. In particular, the estimation of the clamping stress due to the hot riveting process is important in order to study the mechanical strength over time of these assemblies. The literature shows very significant differences in the estimation of this rivet pre-stress, for instance [2], [3]. But since the riveting process is very dependent on many parameters (for instance; driving pressure and temperature, material characteristics, geometrical parameters), the assessment of the pre-stress is inaccurate. Laboratory tests on riveted connections indeed show scattered mechanical properties, for instance [4]. In order to take into account the influence of geometrical parameters on the pre-stress, a 2D-parametric numerical model (Cast3M software) has been developed. In addition, dedicated assemblies have been manufactured to measure clearances as a function of the thickness to be assembled. These data were included in the FE model.

2 RIVETED ASSEMBLIES FABRICATION

For this study, three rivets assemblies (18mm diameter) have been manufactured taking into account dimensions of riveted connections described in historical technical documentations. Joined plates are 8mm thick and the chosen material is a S235 grade steel. This material has indeed mechanical characteristics similar to those of puddle irons and steels used in the construction of old metal bridges.

Four different connection thicknesses have been studied: 3, 5, 7 and 9 plates. The riveting procedure carried out by the repairing of metal bridges (RMP) team of the SNCF includes seven different steps:

- the drilling then reaming the holes,
- the holding of the plates with screws before riveting,
- the cutting the rivet to the appropriate length, depending on the number of plates to be assembled,
- the heating of the rivet up to 1000°C,
- the insertion of the rivet,
- the pressure on the rivet and the forming of the second rivet head,
- the cooling down of the connection.

The Figure 1 shows the pressure on the heated rivet of the 7-plate assembly (left) , the furnace used by the RPM team with different length rivets (center) and the longitudinal cross-section of a 7-plate assembly for measuring radial clearances (right). Measurements of radial clearances were made, for the 3 rivets of for each assembly (for each assembled thickness), after longitudinal cutting and fine grinding up to grade 2000. Two measurements were made per plate, so the averages of the measured clearances cover 6 measurements for 3-plate (24mm thick) assemblies, 10 for 5-plate (40mm thick) assemblies, 14 for 7-plate (56mm thick) assemblies and 18 for 9-plate (72mm thick) assemblies.



Figure 1: Hot riveting of a 7-plates assembly (left), the furnace with heated rivets (center) and the cross section of a connection showing radial clearances (right)

The Figure 2 shows the evolution of the mean and of the median of the measured clearances for each thickness. It shows that the clearance is variable for a given thickness. Indeed, in the example of the 7-plate assembly (40mm thick), the average radial clearance is 0.09mm and the maximum radial clearance is close to 0.5mm. Moreover, the mean clearance increases with the assembled thickness. It is actually more than three times greater in the case of a 9-plate connection than in the case of a 3-plate assembly.

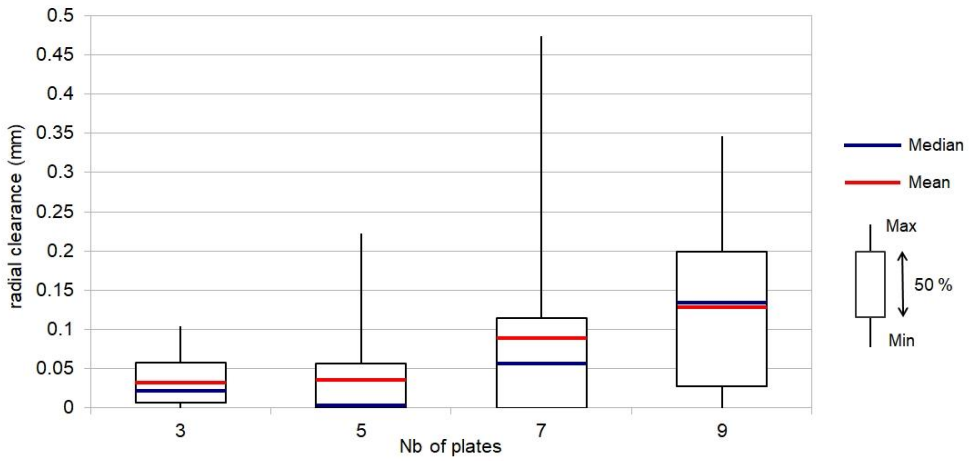


Figure 2: Radial clearance measurements depending on the number of plates (e.g clamp length)

The variation of the radial clearance as a function of the thickness to be assembled is therefore a parameter to be taken into account in the numerical modelling of hot riveted assemblies.

3 NUMERICAL MODEL DESCRIPTION

3.1 Geometry and boundary conditions

A 2D FE parametric model has been developed in the Cast3M software in order to study the clamping pre-stress as a function of the geometrical parameters of the assembly. The following Figure 3 presents the studied geometry, the chosen geometrical parameters for the FE modem (clearance j, rivet diameter d, thickness H) and the planes of symmetry of the model. According to the French 19th century technical documentation, the geometrical characteristics of the rivet heads are dependent on the rivet diameter [5].

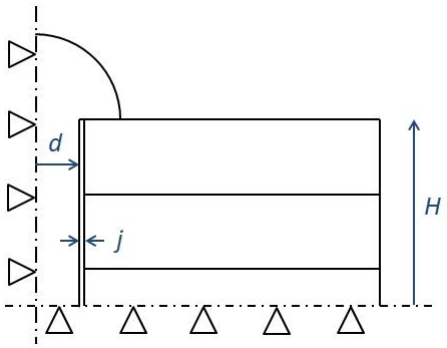


Figure 3: Geometric description of the model, example of a 5-plate connection

3.2 Thermo-mechanical properties

Due to the studied process, the mechanical properties of the materials are temperature-dependent. For this paper, we consider two different real materials used in bridge construction: a material for the plates to be assembled and another for the rivet. This choice corresponds to the data presented in the old technical documentation which specifies the mechanical characteristics that the rivets must respect [6]. The stress-strain relations of the two chosen materials, at room temperature, are shown in the following Figure 4.

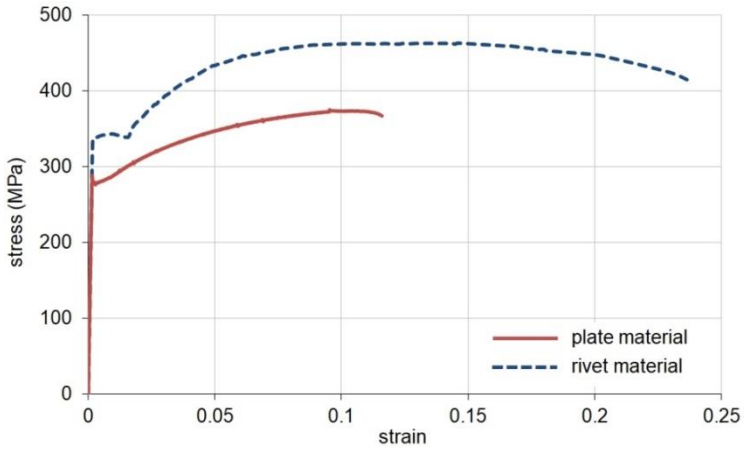


Figure 4: Stress–strain relations for the rivet and plate material in the FE model

During the thermo-mechanical analysis, the hot driven rivet is assumed to be at a uniform 1000°C temperature, then it cools down until it reaches room temperature. At every calculation step during cooling, the mechanical and thermal characteristics (specific heat, thermal expansion coefficient and thermal conductivity coefficient) are updated according to Eurocode 3 part 1-2 for mild steel [7].

3.3 Heat transfer

Three types of heat transfer are considered:

- conductivity transfer: between the plates and the rivet and between the plates themselves,
- convective transfer: between the rivet and the environment and between the plates and the environment,
- radiative transfer: between the rivet and the plates, between the rivet and the environment and between the plates and the environment.

Finally, particular attention is paid to the mesh (TRI3 elements): the mesh is indeed refined at the rivet head / plates contact as high plastic deformations can be generated in this area.

4 RESULTS AND ANALYSIS

4.1 Main results

The following Figure 5 shows the evolution of the clamping stress as a function of thickness; the rivet has a diameter of 18mm, the thickness ranges up to 100mm. For this simulation, a constant radial clearance of 0.1mm has been chosen, corresponding to the values measured and proposed in Figure 2.

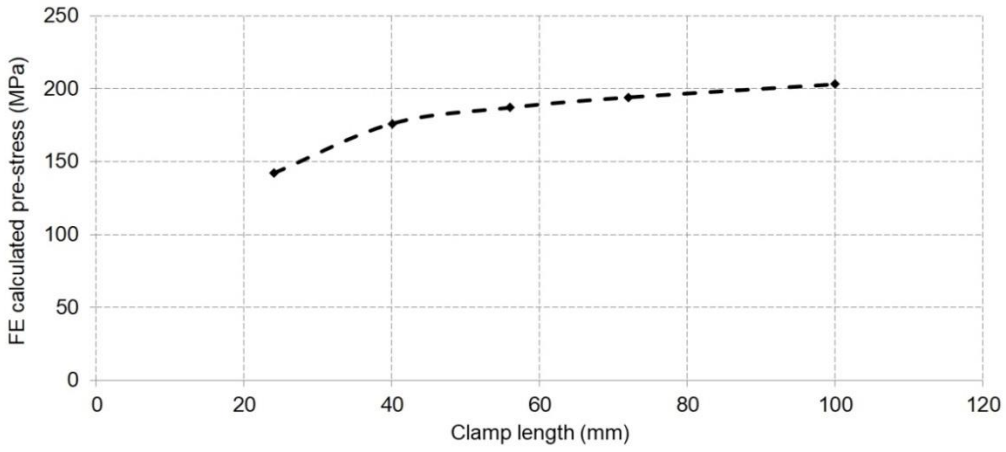


Figure 5: Pre-stress depending on the clamp length of the riveted assembly (18mm rivet, 0.1mm clearance)

Considering that radial clearances can be very different from one rivet to another (see Figure 2 for the same thickness), we have studied the evolution of pre-stress as a function of the clearance. Taking into account the values proposed in Figure 2, we have chosen to study the influence of the clearance up to 0.5 mm. This clearance is assumed to be constant over the length of the rivet shank, as presented in Figure 3.

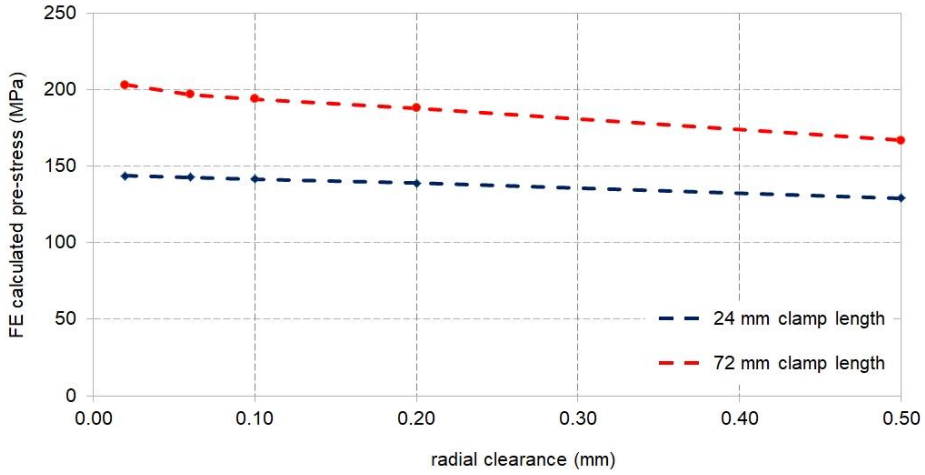


Figure 6: Pre-stress depending on the radial clearance

4.2 Analysis

The calculations show firstly an important influence of the thickness in the pre-stress calculation. The evolution of the results is in line with the literature, for instance [3]. By taking a constant radial clearance for these calculations, it is shown in this study that this stress can increase by more than 30% when changing from a small thickness assembly (24mm) to a larger thickness (72mm). The calculations also show an influence of the radial clearance and particularly as the thickness to be assembled is large. In the two cases studied here (the smallest and the largest joint thicknesses), the more the clearance increases, the more the clamping pre-stress decreases. The selected radial clearances correspond to values measured on the fabricated connections. In the case of the 72mm connection, for a clearance between 0.02mm and 0.5mm, the reduction is about 20%.

For thicknesses larger than those studied experimentally, Figure 1 further shows that the pre-stress can reach magnitudes that could be critical for the mechanical strength of the riveted joint, particularly if the mechanical properties are weak.

5 CONCLUSIONS

In this study, we numerically studied the influence of two geometrical parameters in the estimation of the clamping stress in riveted connections. Indeed, the grip length and a mean radial clearance (depending on this length) were taken into account in a numerical model developed with the Cast3M software. For this, experimental measurements on dedicated assemblies have been used to improve the numerical model. In particular, we show that taking into account a unique clamping stress in a complex multi-rivet assembly can result in an

inaccurate estimation of its behavior given the complexity of this type of assembly.

Acknowledgements. The authors wish to thank the SNCF for the manufacture of the hot-riveted specimens used in the experimental campaign.

REFERENCES

[1] L. Gallegos Mayorga, S. Sire, M. Ragueneau, B.Plu, "Understanding the behaviour of wrought-iron riveted assemblies: manufacture and testing in France", *Proceedings of the Institution of Civil Engineers - Engineering History and Heritage,* Vol. 170, Issue 2, pp. 67-79, (2017).

[2] J. Kafie-Martinez, P.B. Keating, "Finite element modeling for clamping stresses developed in hot-driven steel structural riveted connections", *Int. J. Civil Environ. Struct. Construct. Architect. Eng.*, Vol. 11 (5), pp. 560-565, (2017).

[3] Sustainable bridges, "Condition assessment and inspection of steel railway bridges, including stress measurements in riveted, bolted and welded structures", *Background document SB3.4*, 94 p., (2007).

[4] S. Sire, L. Gallegos Mayorga, B. Plu, "Observation of failure scenarios in riveted assemblies: an innovative experimental strategy", *Procedia Engineering*, 114, pp. 430-436, (2015).

[5] Q. Collette Q, S. Sire, WJ. Vermes, VJ. Mesler, I. Wouters, "Experimental investigations on hot-driven structural rivets in historical French and Belgian wrought-iron structures (1880s–1890s)", *Construction and Building Materials* 54: 258–269, (2014).

[6] Ministère des Travaux Publics aux Préfets, "Circulaire du Ministère des Travaux Publics aux Préfets, 29 Août 1891. Révision de la Circulaire du 9 Juillet 1877", Ministère des Travaux Publics, Paris, France (in French), (1891).

[7] EN 1993-1-2:2005. "Eurocode 3: Design of steel structures – Part1-2: general rules – structural fire design". Brussels: CEN, (2005).

12th International Conference on Structural Analysis of Historical Constructions
SAHC 2020
P. Roca, L. Pelà and C. Molins (Eds.)

EXCESS CAPACITY IN HISTORIC AMERICAN REINFORCED CONCRETE FLOORS

DONALD FRIEDMAN[1*]

[1]Old Structures Engineering
90 Broad Street, New York NY 10004, USA
e-mail: dfriedman@oldstructures.com, www.oldstructures.nyc (*corresponding author)

Keywords: Historical Structure, Reinforced Concrete, Codes

Abstract. *The introduction of reinforced concrete as a structural material in American practice circa 1900 created unique challenges in design and analysis. Engineers and builders had to simultaneously determine proper constituent materials for the concrete, the relation between materials proportions and strength, and formulas for sharing load between steel and concrete. Early on there were only local building codes, which often treated concrete as masonry. This was followed, starting in 1909, by the reports of the "Joint Committee" which served as a de facto national code for concrete; the American Concrete Institute code was first independently published in 1941 and has been updated regularly since.*

All of the early codes, specifically including the Joint Committee report and the ACI code, used allowable-stress design with a linear-elastic model of flexure. Load-and-resistance factor design using an ultimate-strength model was first introduced in the US as an alternate method in the 1956 ACI code, was elevated to equal status with the 1963 code, and was made the standard in the 1971 code with the linear-elastic allowable-stress model as an alternate. Since the ultimate-strength model is generally accepted to more accurately represent flexure in reinforced concrete, the allowable-stress alternate was little used after the transition.

Many details have changed minimally since the 1910s, including provisions for T beams that take advantage of the slab for additional compression flange area. The calculation of shear capacity in both concrete and web reinforcing changed minimally except for the transition from allowable-stress to load-and-resistance-factor design.

Re-analysis of extant concrete structures designed before the 1956 code generally shows a pattern of significant excess capacity in flexure and limited excess capacity in shear. For members that are generally not controlled by one-way (beam) shear (two-way slabs and one-way slabs) the increase in flexure capacity governs; for members where one-way shear is a controlling factor, the small increase, no change, or decrease in shear capacity governs.

Much of the current literature on evaluating the capacity of extant concrete structures focusses on strength degradation from material changes such as rusting rebar and from overall material changes such as carbonation. The presence of excess capacity should also be considered, and it is possible based on review of the governing codes and design methods to determine general patterns as to how much excess capacity may be expected.

1 INTRODUCTION

Accurate of analysis of existing buildings depends in part on understanding their original design. In the case of older buildings with reinforced-concrete structure, there are significant differences between current design and analysis methods and those in use prior to the 1970s. Concrete as a structural material developed later than steel, almost entirely after 1900, which means that processes to create formal standards were in place from the beginning.

The details of material use, construction economics, and design standards differ from one country to another, so this study represent US practice. (The data and formulas used are given in their original units, with metric conversions following in parentheses.) However, it is likely that a similar analysis can be made in any country where reinforced-concrete use began in earnest before 1930.

There is no national building code in the US, as all such laws are enacted at the state level; the *International Building Code* (IBC), starting in 2000, was the first base code generally adopted by states across the entire country. As a result, there were differing standards for structure and other technical issues until national organizations created specific material codes. For example, structural steel was standardized with the 1923 release of the first edition of the *Standard Specification for Structural Steel for Building*s by the American Institute of Steel Construction.

From 1909 to 1941, the most prominent national standard for reinforced-concrete design was a series of reports by the Joint Committee on Standard Specifications for Concrete and Reinforced Concrete. The name "Joint Committee" reflects the fact that no one group was responsible for the specification. The contributors varied over time but generally included the American Society of Civil Engineers (a professional group founded in 1852), the American Railway Engineering Association (an end-user professional group founded 1899), the American Society for Testing Materials (a standards-setting group founded 1898), the American Concrete Institute (an industry-specific group founded as the National Association of Cement Users in 1904 and renamed in 1913), and the Portland Cement Association (an industry-specific group founded 1902). The ages of the organizations are important because they highlight the greater standardization in the US during the 1900s beginning of reinforced-concrete use in buildings compared to the 1870s beginning of steel use in buildings.

The ACI developed and updated its requirements after the Joint Committee had reached a final report in 1921, issuing its "Reinforced Concrete Building Design and Specifications" in 1927 and proposed "Building Regulations for Reinforced Concrete" in 1936. Finally, in 1941, the ACI issued the first version of its full and permanent specification, "Building Regulations for Reinforced Concrete." The current revision of this document is the standard concrete code referenced by the various state and local building codes (and referenced in the national standard IBC.) The ACI code is usually called by the author group (ACI Committee 318) and revision year, so that the current code is ACI 318-19.

One of the most basic questions asked in renovation is the load capacity of an existing floor. Given the changes in beam design from the early Joint Committee specifications to the mid-century ACI code, to the modern ACI code, it cannot be assumed that current codes

accurately reflect the strength of old concrete structures. This paper provides an overall analysis of the changes in design calculations over the course of the twentieth century in order to provide a schematic-level baseline for making decisions about current capacity of the existing concrete building stock.

2 CODE REQUIREMENTS FOR REINFORCED CONCRETE DESIGN

2.1 Before National Standards

Because of the decentralized nature of American building control prior to the 1950s, there are two critical sources of information about the designs standards in use: local codes that had statutory control over design and national standards that were sometimes (and with increasing frequency as time went on) used as references in local codes.

By later standards, the New York City Building Code of 1901 was extremely conservative about the stresses allowed in concrete.[1] Compression was limited to 230 psi (1.6 MPa) maximum in compression, while steel was allowed up to 16,000 psi (110 MPa) tension. No guidance was given on design, and concrete was generally treated as an unreinforced form of mass masonry. While there were various work-arounds for designers, such as applying for a variance for a specific building, the situation was not properly addressed until the 1916 revision of the code, which included provisions similar to those of the Joint Committee.[2]

The Chicago code of 1905 was less conservative than the New York code with respect to concrete itself, allowing flexural compression in concrete of 500 psi (3.4 MPa), and concrete shear of 75 psi (0.52 MPa), but only allowed tension in the steel of 1/3 of the yield stress, or 11,000 to 13,000 psi (76 to 90 MPa) for the steels commonly in use at the time.[3]

The national standards were spread via engineering professional journals and then incorporated into the local and state laws regarding building enforcement. It is not a coincidence that, for example, the 1912 Detroit Building Code has a calculation method and allowable stresses that match the 1909 Joint Committee report.[4]

2.2 The Joint Committee Reports

The preliminary Joint Committee reports of 1909 and 1913 contain essentially the same requirements for beam design as the “final” report of 1916.[5, 6, 7] The important differences are in materials specifications, column analysis, and less common forms of design, as the basics of beam design had been worked out earlier. The 1916 Joint Committee report provides a good summary of the state of reinforced-concrete beam design in the US in the 1910s.[7] There are descriptions of a limited number of possible concrete mixes, as well as a table with a list of ultimate compressive strengths based on the aggregate type and on the fine-to-coarse aggregate proportions. The list of allowable stress is quite simple:

- Maximum allowable flexural compressive stress is 32.5% of the concrete strength.
- Allowable shear stress without shear reinforcing is 2% of the concrete strength.
- Allowable stress in steel is 16000 psi (110 MPa).

The elastic modulus for steel (E_s) was taken as 29,000,000 psi (200,000 MPa). The elastic

modulus for concrete was typically expressed in terms of the modular ratio n (equal to E_s/E_c). The 1916 report gave n=15 for concrete with a compressive strength between 800 and 2200 psi (5.5 and 15 MPa), which covered the bulk of structural reinforced concrete at that time. It also gave n=40 for concrete 800 psi (5.5 MPa) or weaker, n=12 for concrete between 2200 and 2900 psi (15 and 20 MPa), and n=10 for concrete stronger than 2900 psi (20 MPa).

Using the basic design assumptions for a rectangular section beam, (where d is the depth of the beam from the centroid of the tension reinforcement to the top of the beam, b is the width of the beam, A_s is the steel reinforcement area, and p is the steel ratio A_s/bd) the position of the neutral axis is represented by kd, where k is less than 1 and calculated as

$$k = \sqrt{2pn + (pn)^2} - pn \tag{1}$$

The moment arm between the centroids of the steel and the concrete compression is represented by jd, where j is calculated as

$$j = 1 - \frac{k}{3} \tag{2}$$

The calculated maximum stresses in steel and concrete are

$$f_s = \frac{M}{A_s jd} \tag{3}$$

$$f_c = \frac{2M}{jkbd^2}$$

The 1916 report represented a plateau for reinforced-concrete design in the US, but not for research. The basic provisions of that report were in use for roughly 25 years with only minor changes. The same organizations formed a new Joint Committee in 1919 with the purpose of addressing a gap in the 1916 report: creating a specification to accompany the report's design provisions. The 1921 progress report and the 1924 final report of the Joint Committee on Standard Specifications for Concrete and Reinforced Concrete repeated the design provisions of the 1916 report, while adding a great deal of information, in specification form, on the preparation and construction of concrete.[8, 9] The areas of design that were of greatest interest in research, and therefore the areas where changes were most likely to occur, were column design and two-way slab design, neither of which affects the topic of this paper. The last Joint Committee was formed in 1930 to review the 1924 Specification and the 1916 report and bring them up to date as necessary. The report of this committee was issued in 1940, and contained the following notation regarding ordinary beam design: "The standard formulas for rectangular and T-beams and standard notation have become so widely recognized that they are omitted from the Report."[10]

2.3 ACI Standards and Codes

Of the organizations in the Joint Committees, only the American Concrete Institute

(including its years as the National Association of Cement Users) was dedicated to the issues of professional designers. As a new group, it benefited from collaborating with the better-established ASCE. In 1908 the NACU issued its "Report of the Committee on Laws and Ordinances."[11] No analysis equations were provided and the statement that the stress-strain of concrete "may be assumed (a) As a straight line. (b) As a parabola, with its axis vertical and its vertex on the neutral axis of the beam, girder or slab; or (c) As an empirical curve, with an area one-quarter greater than if it were a straight line, and with its center of gravity at the same height as that of the parabolic area assumed in (b)" suggests that the NACU was not settled on linear-elastic analysis. A safety factor of 4 was used against the steel yield stress, assumed to be 32,000 psi (220 MPa), and the concrete ultimate stress, assumed to be 2000 psi (14 MPa). The modular ratio n was taken as 18; the shear stress for unreinforced 2000-psi concrete was taken as 200 psi (1.4 MPa).

The specification was probably not used very much because it came out only a year before the Joint Committee's first report was issued. The Joint Committee had the weight of better-established organizations behind it and was significantly more conservative. There is no way to be certain now to what extent the NACU 1908 code was used, but designs that conform to its outlier criteria - the high allowable shear stress, for example - do not appear to be common, and the values given in the report do not typically appear in local codes of the era.

The NACU abandoned the 1908 report in its 1910 "Standard Building Regulations for the Use of Reinforced Concrete."[12] This is essentially the 1909 Joint Committee report, which is to be expected since the NACU was participating in the Joint Committee. Linear elastic behavior was assumed, but no equations given. Materials assumptions included 2000 psi (14 MPa) concrete, allowable tension (after a safety factor was applied against yield) of 16,000 psi (110 MPa) for "medium steel" equivalent to structural steel and 20,000 psi (140 MPa) for "high elastic steel." Using those materials, they recommend the use of n=15, maximum flexural compression of 650 psi (4.5 MPa), and maximum concrete "web stresses" (i.e. shear) of 40 psi (0.28 MPa). These values are the same as the Joint Committee.

In 1920, the ACI issued Standard Specifications 23, "Standard Building Regulations for the Use of Reinforced Concrete" which is, in form, a building code for reinforced concrete.[13] The general provisions are the same as the 1916 Joint Committee report except as follows:

- Mix proportions were provided for concrete strengths up to 3000 psi (21 MPa).
- Allowable flexural compression was increased to 37.5% of the compressive strength.
- Allowable tensile stress in steel was 16,000 psi (110 MPa), except 18,000 psi (124 MPa) was used when the yield stress was over 50,000 psi (340 MPa).
- Allowable concrete shear stress with only longitudinal reinforcing was 2% of the compressive strength, but could be increased to 3% if the bars were anchored.

The 1920 ACI standard is more detailed and less conservative than the Joint Committee 1916 report, as the ACI was including newer research into the performance of the material. It should be noted that in dealing with analysis of extant buildings designed under the 1920 standard, anchorage of the reinforcing cannot be assumed and is difficult to check, so the unanchored shear provisions should be used.

The ACI's 1927 "Tentative Building Regulations for the Use of Reinforced Concrete," document E-lA-27T, is an update to the 1920 specification.[14] The extent to which linear-elastic flexural analysis was the standard can be seen in the fact that no equations for analysis were given, but the document states "The customary formulas or their equivalent shall be used." The only change to the specifications for the ordinary beam analysis reviewed here is that the allowable flexural compression was increased to 40% of the concrete compressive strength.

The next code version, in 1936, removed "tentative" from the title but kept "T" in the designation ACI 501-36T.[15] (Committee 501 replaced committee E-1.) The statement on flexural analysis was updated to "The accepted theory of flexure as applied to reinforced concrete shall be applied to all members resisting bending." The provisions for beams were the same except that allowable steel tension was generally increased to 20,000 psi (140 MPa); and the modular ration was defined by using 30,000,000 psi (210,000 MPa) as the elastic modulus for steel, and 1000 times the ultimate compressive stress for concrete.

Finally, in 1941, the ACI code, "Building Regulations for Reinforced Concrete (ACI 318-41)" reached its current designation (committee 501 was renamed to 318); all later codes have been based on this version.[16] The only change relative to beam analysis was that the allowable flexural compression was increased to 45% of the concrete compressive strength. The 1947 revision of the code had no changes relative to beam analysis.[17]

The 1951 ACI code revision 318-51 was the same for beam design except that the allowable concrete shear stress was increased to 3% of the compressive strength and the provisions regarding the effect of anchoring longitudinal reinforcing were removed.[18]

The 1956 ACI code had no changes in basic beam provisions but introduced an appendix "Abstract of Report on Ultimate Strength Design."[19] This served more to spur discussion than as a usable option, as it lacked the detail of the main code. The analysis included:

- Compressive stress distribution could take any geometry "which results in ultimate strength in reasonable agreement with comprehensive tests."
- The load factors were 1.2 for dead load and 2.4 for live load; there were no resistance factors stated, so they were effectively 1.0.
- The maximum compressive stress (f'_c) for analysis was 0.85 times the concrete strength.
- The maximum tension (f_y) to be used in analysis was 60,000 psi (410 MPa) or the steel yield stress, whichever was smaller.
- The analysis formulas for flexure were

$$M_u = bd^2 f_c' q(1 - 0.59q) \tag{4}$$

$$q = p\frac{f_y}{f_c'}$$

$$q \le 0.40\frac{f_c'}{f_y}$$

The 1963 ACI code was the pivotal moment in that it gave equal weight to allowable stress (ASD) and ultimate strength designs (USD), with parallel chapters describing each. Some new provisions applied to both methods:[20]

- The elastic modulus for steel was changed to 29,000,000 psi (200,000 MPa).
- The elastic modulus for concrete was to be calculated using the formula

$$E_c = w^{1.5}\,33\sqrt{f'_c} \tag{5}$$

where w was the density of the concrete in lbf per cubic foot and f'_c is expressed in psi. (Note that the ACI formulas typically have hidden embedded units, so that for equation 5 to work, 33 is not simply a numeric constant but carries units of $(psi)^{0.5}/(lbf/ft^3)^{1.5}$.)

The ASD chapters had the same limits on flexural tension and compression as before, but otherwise the shear provisions, with the allowable concrete shear in slabs as

$$f_v = 2\sqrt{f'_c} \tag{6}$$

and the allowable concrete shear in beams as

$$f_v = 1.1\sqrt{f'_c} \tag{7}$$

The USD chapters form the basis of ordinary flexural design per the ACI from this time forwards. The basics of analysis are that the strain in both concrete and steel is proportional to the distance from the cracked neutral axis, and that the maximum allowable compression strain is 0.003. "At ultimate strength, concrete stress is not proportional to strain. The diagram of compressive concrete stress distribution may be assumed to be a rectangle, trapezoid, parabola, or any other shape which results in predictions of ultimate strength in reasonable agreement with the results of comprehensive tests." The recommended stress distribution is a rectangular stress block of $0.85f'_c$ intensity, extending from the compression side of the section to $a=k_1c$ away, where c is the depth to the neutral axis, $k_1=0.85$ for concrete up to 4000 psi (28 MPa) strength and is reduced for greater strengths. k_1 was later renamed β_1.

- The load factors (γ) were 1.5 for dead load and 1.8 for live load.
- The resistance factors (φ) were 0.90 for flexure and 0.85 for shear.
- The moment formula form 1956 was restated with a simpler form:

$$M_u = \phi[bd^2 f'_c q(1-0.59q)] = \phi\left[A_s f_y\left(d-\frac{a}{2}\right)\right] \tag{8}$$

$$p \le 0.75 p_b = \frac{0.85 k_1 f'_c}{f_y}\frac{87{,}000}{87{,}000 + f_y}$$

where p_b is the steel ratio that gives the balanced condition of simultaneous steel and concrete ultimate stress.

- This code has the first ACI statement of factored shear:

$$v_c = \phi\left(1.9\sqrt{f_c'} + 2500\frac{p_w V d}{M}\right) \tag{9}$$

where V and M are the unfactored shear and moment, and p_w is the shear reinforcing ratio, so the second term is zero when considering only concrete shear resistance.

The 1971 ACI code is similar, with a few changes:[21]

- The load factors were reduced to 1.4 for dead load and 1.7 for live load.
- USD was made the base analysis method, with the ASD analysis was reduced to a single section of the "Analysis and Design General Considerations" chapter. This marked the effective end of development of the ASD method by the ACI.
- For normal-weight concrete, a simplified formula was provided for the elastic modulus:

$$E_c = 57{,}000\sqrt{f_c'} \tag{10}$$

No changes were made to these provisions in the 1977, 1983, 1989, 1995, and 1999 ACI code revisions, except that ASD was moved from the main text to an appendix.[22, 23, 24, 25, 26]

The 2002 ACI code was the most recent with changes to these provisions:[27]

- The load factors were reduced to 1.2 for dead load and 1.6 for live load.
- The resistance factor for shear was reduced to 0.75.
- The ASD appendix was removed.

No changes have been made to these provisions in the 2005, 2008, 2011, 2014, and 2019 ACI code revisions.[28, 29, 30, 31, 32]

3 COMPARATIVE ANALYSIS

Since the question at hand is the capacity of ordinary beams, the details of those beams (for example, span length, the ratio of span to depth, or the presence of a slab for T-beam action) only matter if the analysis varies with those details. Similarly, the flexural and shear strength depend on material properties: the compressive strength of the concrete, the tensile strength of the steel, and the elastic moduli of both. In general, the geometry is not important, although extreme cases may have differences: for example, there are shear requirements specific to beams that have an unusually high depth to width ratio. The comparison here uses beams with common geometry, reinforcing, and materials.

For existing buildings, the strength of the concrete is a simple issue, as it can be field tested. In a broad sense, the issue of concrete quality can be treated with visual observation of conditions, although there should be a default assumption that a decades-old building without reported structural problems has concrete of a minimally-acceptable quality. The strength of reinforcing bars can be measured using destructive testing on samples.

In order to keep the analysis focussed, only the provisions for ordinary reinforce-concrete beams and one-way slabs are reviewed, for shear and flexure. The use of T-beams is not considered because the provisions for allowable flange width have hardly changed, so the use of T beams has little or no effect on the comparison of one code to another. The effect of shear reinforcing is not included because (a) slabs almost never include shear reinforcing in

ordinary practice, and (b) determining the amount of shear reinforcing in extant beams can require many more probes than determinant the amount of flexural reinforcement because of the pre-seismic-design practice of eliminating shear stirrups/hoops in the center of beams.

The case studied was a beam 12 inches (0.30m) wide and 28 inches (0.71m) deep, reinforced with 3 #8 bars, 1 inch (25mm) in diameter, using 2000 psi (14 MPa) concrete and 40,000 psi (280 MPa) steel. (Such a beam could not be designed using T-beam analysis if, for example, there were slab openings near mid-span.) The beam has a simple span of 20 feet (6.1m) and supports a total load of 1200 pounds per foot (18kN/m). Three cases were examined, with dead load to live load ratios of 2.0, 1.0, and 0.5. The load ratio does not matter in the ASD analyses, where all loads are treated the same, but affects the results when reviewing older USD designs.

It is not possible to directly compare the analyzed capacity using the different codes because the use of load factors in USD changes the required strength from that used in ASD. Therefore the code-to-code comparison is made using the ratio of demand (applied shears and moments for the example beam using load factors of 1.0 for ASD and those required by code for USD) to capacity (the calculated allowable shears and moments).

The same beam was analyzed under each successive code, and the demand to capacity ratio determined for that code. Since the example beam was chosen to meet the codes, the demand/capacity ratio is less than 1.0 in almost cases, ranging from 0.98 for shear (Joint Committee) to 0.46 for flexure with the 2.0 dead/live load ratio (current ACI code). The only exception is moment under the 1908 NACU code, which has a ratio of 1.72 because of the safety factor of 4 used on the steel. Table 1 shows the demand/capacity ratios, comparing the required moments and shears (M_{reqd} and V_{reqd}) to those provided in design (M_{des} and V_{des}).

Table 1: Demand/Capacity ratios for the same beam under different codes.

	Joint Comm 1909 to 1940	NACU 1908	NACU 1910	ACI 1920	ACI 1927	ACI 1936	ACI 1941, 1947	ACI 1951, ACI 1956 ASD	ACI 1956 USD	ACI 1963 ASD	ACI 1963 USD	ACI 1971 to 1999	ACI 2002 to 2019
DL/LL=2 M_{reqd}/M_{des}	0.86	1.72	0.86	0.85	0.76	0.70	0.68	0.68	0.49	0.68	0.56	0.52	0.46
DL/LL=2 V_{reqd}/V_{des}	0.98	0.20	0.98	0.98	0.98	0.98	0.98	0.65	0.65	0.73	0.86	0.76	0.77
DL/LL=1 M_{reqd}/M_{des}	0.86	1.72	0.86	0.85	0.76	0.70	0.68	0.68	0.59	0.68	0.58	0.55	0.50
DL/LL=1 V_{reqd}/V_{des}	0.98	0.20	0.98	0.98	0.98	0.98	0.98	0.65	0.65	0.73	0.90	0.80	0.83
DL/LL=0.5 M_{reqd}/M_{des}	0.86	1.72	0.86	0.85	0.76	0.70	0.68	0.68	0.69	0.68	0.61	0.58	0.53
DL/LL=0.5 V_{reqd}/V_{des}	0.98	0.20	0.98	0.98	0.98	0.98	0.98	0.65	0.65	0.73	0.94	0.84	0.89

The demand/capacity ratios for each code were then compared to the current code. The moment capacity ratio (original demand/capacity ratio divided by the current demand/ capacity ratio) is always over 1.0 because the calculated moment capacity has increased over time. The ASD moment capacity ratios are quite large, with the smallest (1.28) showing a 28% increase in capacity from re-analyzing under the current code. The USD moment capacity ratios are smaller, but with increase of at least 8%, with the smallest increase for the high-live-load case under the 1971-1999 ACI code.

However, the shear capacity ratios vary widely, generally from 0.74 to 1.27. (Again, the 1908 NACU code is an outlier because of its high allowable shear stress.) In short, the 50 percent increase in ASD shear strengths in the 1951 ACI code resulted in unconservative shear designs for the concrete by current standards. The 2002 reduction of the shear resistance factor from 0.85 to 0.75 means that the even 1971-1999 bare-concrete shear designs are slightly unconservative by current standards. Table 2 shows the shear and moment capacity ratios, comparing original analyses (M_{orig} and V_{orig}) to current (M_{cur} and V_{cur}).

Table 2: Ratio of original to current Demand/Capacity ratios.

		Joint Comm 1909 to 1940	NACU 1908	NACU 1910	ACI 1920	ACI 1927	ACI 1936	ACI 1941, 1947	ACI 1951, ACI 1956 ASD	ACI 1956 USD	ACI 1963 ASD	ACI 1963 USD	ACI 1971 to 1999
DL/LL=2	M_{orig}/M_{cur}	1.86	3.74	1.86	1.85	1.65	1.51	1.48	1.48	1.07	1.48	1.21	1.13
DL/LL=2	V_{orig}/V_{cur}	1.27	0.25	1.27	1.27	1.27	1.27	1.27	0.85	0.85	0.95	1.11	0.99
DL/LL=1	M_{orig}/M_{cur}	1.73	3.47	1.73	1.72	1.53	1.40	1.38	1.38	1.19	1.37	1.18	1.11
DL/LL=1	V_{orig}/V_{cur}	1.18	0.24	1.18	1.18	1.18	1.18	1.18	0.79	0.79	0.88	1.08	0.96
DL/LL=0.5	M_{orig}/M_{cur}	1.61	3.24	1.61	1.60	1.43	1.31	1.28	1.28	1.30	1.28	1.15	1.08
DL/LL=0.5	V_{orig}/V_{cur}	1.10	0.22	1.10	1.10	1.10	1.10	1.10	0.74	0.74	0.82	1.05	0.94

4 CONCLUSIONS

In practice, reuse projects will include analysis of the specific extant beams and slabs. However, an analysis of the type in this paper can be used to give a schematic view of what is to be expected. Existing structure is typically grandfathered against code changes, but if alterations are performed they must meet current code. Therefore knowing that shear capacity is more likely to be a problem in design than moment, the design and investigations can be appropriately focused. Obviously, the capacity of existing shear reinforcing must be a priority,

as is looking for changes to the live load and the live-to-dead-load ratio.

There were two significant changes during the evolution in the calculation of moments: from a linear-elastic model of flexure to an ultimate-strength model, and from allowable stress to the use of load and resistance factors. Because both took place at the same time, they are often conflated, but are actually quite different. Load and resistance factors could be used (rather than a fixed safety factor) to obtaining a safety margin with a linear-elastic model; a fixed safety factor could be used with an ultimate-strength model. The change in model more accurately reflects the actual distribution of stress in a reinforced-concrete beam, and also provides a larger moment capacity, all other factors being equal. On the other hand, the change from a fixed safety factor to combined load and resistance factors can be outcome neutral for some dead-load to live-load ratio. This difference can be seen in the results: shear does not benefit from the model change and therefore has no particular pattern over time, while moment has a general increase in capacity because of the model change.

REFERENCES

1. n.a., *The Building Code of the City of New York*. City of New York (1901).
2. n.a., Building Code of the City of New York. In: *Year-Book of the New York Society of Architects* (1916) 6:49-131.
3. n.a., *An Ordinance Relating to the Department of Buildings…* Chicago City Council (1905), p. 226
4. Schmalzriedt, F. ed., *Complied Ordinances of Detroit of 1912*. City of Detroit (1912), pp. 119-228.
5. n.a., Progress Report of Joint Committee on Concrete and Reinforced Concrete. *Proceedings of the American Society for Testing Materials* (1909) 9:225-262
6. n.a., Report on Concrete and Reinforced Concrete. *Proceedings of the American Society for Testing Materials* (1913) 13:224-281
7. n.a., Final Report of the Joint Committee on Concrete and Reinforced Concrete. *Proceedings of the American Society of Civil Engineers* (1916) 42:1657-1708.
8. n.a., *Progress Report of the Joint Committee on Standard Specifications for Concrete and Reinforced Concrete*. Joint Committee on Standard Specifications for Concrete and Reinforced Concrete (1921).
9. n.a., *Report of the Joint Committee on Standard Specifications for Concrete and Reinforced Concrete*. American Concrete Institute (1924).
10. n.a., *Report of the Joint Committee on Standard Specifications for Concrete and Reinforced Concrete*. American Concrete Institute (1940).
11. Henley, HC, ed. Report of the Committee on Laws and Ordinances. In *Proceedings of the Fourth Annual Convention of the National Association of Cement Users*, National Association of Cement Users (1908), 233-239.
12. n.a., Standard No. 4: Standard Building Regulations for the Use of Reinforced Concrete. *Proceedings of the Sixth Annual Convention of the National Association of Cement Users* (1910) 6:349-361.

13. n.a., American Concrete Institute Standard Specifications No. 23: Standard Building Regulations for the Use of Reinforced Concrete. In *Proceedings of the Sixteenth Annual Convention*, American Concrete Institute, (1920), 283-302
14. n.a., Tentative Building Regulations for the Use of Reinforced Concrete. In *Journal of the American Concrete Institute - Proceedings* (1927) 23:643-677.
15. n.a., Building Regulations for Reinforced Concrete (ACI 501-36T) In *Journal of the American Concrete Institute - Proceedings* (1936) 32:407-444.
16. n.a, *Building Regulations for Reinforced Concrete* (ACI 318-41). American Concrete Institute (1941).
17. n.a., *Building Code Requirements for Reinforced Concrete* (ACI 318-47). American Concrete Institute (1947).
18. n.a., *Building Code Requirements for Reinforced Concrete* (ACI 318-51). American Concrete Institute (1951).
19. n.a., *Building Code Requirements for Reinforced Concrete* (ACI 318-56). American Concrete Institute (1956).
20. n.a, *Building Code Requirements for Reinforced Concrete* (ACI 318-63). American Concrete Institute (1963).
21. n.a., *Building Code Requirements for Reinforced Concrete* (ACI 318-71). American Concrete Institute (1971).
22. n.a., *Building Code Requirements for Reinforced Concrete* (ACI 318-77). American Concrete Institute (1977).
23. n.a., *Building Code Requirements for Reinforced Concrete* (ACI 318-83). American Concrete Institute (1983).
24. n.a., *Building Code Requirements for Reinforced Concrete* (ACI 318-89). American Concrete Institute (1989).
25. n.a., *Building Code Requirements for Structural Concrete* (ACI 318-95). American Concrete Institute (1995).
26. n.a., *Building Code Requirements for Structural Concrete* (ACI 318-99). American Concrete Institute (1999).
27. n.a., *Building Code Requirements for Structural Concrete* (ACI 318-02). American Concrete Institute (2002).
28. n.a, *Building Code Requirements for Structural Concrete* (ACI 318-05). American Concrete Institute (2005).
29. n.a, *Building Code Requirements for Structural Concrete* (ACI 318-08). American Concrete Institute (2008).
30. n.a, *Building Code Requirements for Structural Concrete* (ACI 318-11). American Concrete Institute (2011).
31. n.a, *Building Code Requirements for Structural Concrete* (ACI 318-14). American Concrete Institute (2014).
32. n.a, *Building Code Requirements for Structural Concrete* (ACI 318-19). American Concrete Institute (2019).

12th International Conference on Structural Analysis of Historical Constructions
SAHC 2020
P. Roca, L. Pelà and C. Molins (Eds.)

EXPERIMENTAL DATA FOR THE CALIBRATION OF A NON-LINEAR NUMERICAL MODEL FOR DESCRIBING THE RESPONSE OF MASONRY CONSTRUCTIONS UNDER CYCLIC LOADING

ANNA CASTELLANO[1], AGUINALDO FRADDOSIO [2], MARIO D. PICCIONI [2], ELEONORA RICCI [2*] AND ELIO SACCO [3]

[1]Department of Mechanics, Mathematics and Management (DMMM)
Polytechnic University of Bari
Via Orabona 4, 70125 Bari, Italy
e-mail: anna.castellano@poliba.it

[2]Department of Civil Engineering Sciences and Architecture (DICAR)
Polytechnic University of Bari
Via Orabona 4, 70125 Bari, Italy
email: {aguinaldo.fraddosio, mariodaniele.piccioni}@poliba.it, el.ricci@libero.it (*corresponding author)

[3]Department of Structures for Engineering and Architecture (DiSt)
University of Naples Federico II
Via Claudio 21, 80125 Naples, Italy
email: elio.sacco@unina.it

Keywords: Masonry, Arch, Alternate loading, Stiffness degradation, Experimental.

Abstract. *One of the crucial issues in the still open problem of seismic analyses of masonry constructions is the study of the structural capacity for cyclic loadings; the difficulties are even more pronounced when constructions embedding curved elements like arches, vaults and domes have to be studied. In order to develop effective nonlinear numerical models, the latter have to be capable of representing the relevant aspects of the experimental behavior, and the mechanical parameters of the model have to be carefully calibrated with reference to suitable experimental test results. In this paper the outcomes of experimental tests on a tuff masonry arch under cyclic loading are proposed and discussed, along with the results of experimental tests on the masonry materials (blocks and mortar) aimed at determining the compressive, flexural and shear behavior.*

1 INTRODUCTION

Unreinforced masonry constructions are a large part of the building heritage and are often characterized by a high cultural and historical value. The catastrophic effects of recent earthquakes have highlighted the vulnerability of those construction, and the global relevance of developing suitable approach for the structural analysis under seismic loads.

In this vein, one of the crucial issues in the still open problem of seismic analyses of

masonry constructions is the study of the structural capacity for cyclic alternate loadings [1]. Indeed, because of the very low tensile strength of mortar joints, the mechanical response of masonry constructions under dynamic alternate loads is strongly influenced by the activation of rocking mechanisms between ashlars, and this behavior is very difficult to predict by using numerical models. On the other hand, rocking mechanisms allow for avoiding the collapse of the structure and make overall the structure capable of withstanding horizontal accelerations considerably higher than those predictable by static non-linear analyses [2].

The problem is even more challenging when curved structural elements like arches, vaults and domes are embedded in the construction. Indeed, in recent years a strong research effort has been made towards the development of numerical models aimed at representing the seismic response and or at least the seismic capacity of masonry constructions including arches, vaults and domes.

The problem is still open, and this is testified by the very different approaches proposed in the literature [3], ranging from nonlinear finite element modeling, where the description of the damage plays a crucial role [4,5], to discrete element modeling [6,7]. Other approaches are focused on the determination of estimates of the seismic capacity of curved masonry structures by applying the lower bound theorem [8-10] or the upper bound theorem of limit analysis [11,12].

From the experimental side, whereas recently several very complex full-scale experiments on masonry arches and vaults appeared in the literature (see, e.g., [13,14]), only a few study the structural response under seismic or cyclic loading. This is due to the intrinsic difficulties of performing these tests on large and very heavy structures, and to the problems coming from the possible dispersion of data related to the dependence of the results from the unavoidable defects of the constructions.

Among the few papers on cyclic load tests on masonry arches and vaults, [15] reported the results of dynamic and cyclic load experiments on a brick masonry arch, discussing the related numerical modeling issues by applying a nonlocal damage-plastic constitutive law capable of describing the hysteretic features of the structural behavior. In [16] the results of in-plane cyclic load tests on masonry panels with or without an opening surmounted by a masonry arch are presented, highlighting the higher ductility of the arched panel and studying the stiffness, the strength and the energy dissipation under increasing loads. Moreover, in [17] the results of dynamic tests on unreinforced and FRCM reinforced full-scale masonry arches are proposed, bringing out the peculiar dynamic behavior that can be described as a four link "rocking arch" mechanism and discussing the amplification of the base excitation made by the structure.

In this paper the results of an experiment on a masonry arch under a concentrated eccentric cyclic load applied in displacement control are discussed in view of characterizing an innovative cohesive-frictional interface model for describing the non-linear response of masonry constructions recently proposed in [18] by some of the authors.

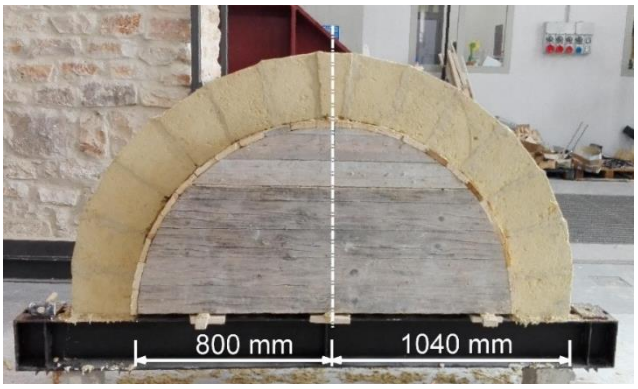
In particular, the examined masonry arch is made of voussoirs of Apulian tuff jointed by hydraulic lime-pozzolan mortar, as it is usual in the construction of the architectural heritage of Apulia. Masonry materials have been characterized in terms of compressive strength (also flexural strength for the mortar) and of shear behavior, by means of shear tests on triplets, aimed at investigating interface behavior of mortar joints.

The overall structural behavior observed shows a number of aspects relevant especially in

view of seismic analyses, to be considered in order to correctly calibrate the mechanical parameters numerical of the model. Among them, the progressive damage and the ductility of the structure.

2 EXPERIMENTAL SETUP

The experimental test here described was performed on a circular arch made of 15 trapezoidal blocks of Apulian tuff. The arch has an internal radius of 800 mm, an external radius of 1040 mm and a thickness of the blocks orthogonally to the plane of the arch is of 140 mm (see Figure 1a).

(a 

(b) 

Figure 1: Geometric configuration of the arch (a) and test setup (b).

In particular, twelve voussoirs were cut by means of a saw from blocks of nominal dimension of 240 mm x 240 mm x 140 mm; two voussoirs were cut with a shape suitable to use them as the imposts of the arch. The keystone was made once the arch was almost completed and had dimensions different from those of the other voussoirs to compensate for the imperfections due to the cut and to the mortar joint thickness. On the second tuff block starting from the keystone a wedge of mortar was made to compensate the inclination of the block due to the arch curvature and provide a support for the loading device (see Figure 2b). The mortar joints have an average thickness of 1 cm.

After about 1 month since the construction, when mortar joints were perfectly hardened, the steel beam used as the arch basis was moved and placed under a steel frame used for supporting the loading device (see Figure 1b).

Here, the arch was subjected to a concentrated vertical load applied at about one fourth of the span, on a steel plate mounted on the top of the mortar wedge showed in Figure 2b. The test was carried out under load control, by performing n. 11 load-unload cycles with progressively increasing displacements of the loaded point. At each cycle a visual inspection was also performed in order to identify eventual cracks in the joints, the formation of eventual hinges and, in this case, to measure the opening of the hinges. The load was applied very slowly using a hydraulic jack with a maximum capacity of 500 kN, fixed on a rigid contrast beam, shown in Figure 1b. A small load cell with a capacity of 5kN has been put between the ball joint of the hydraulic and the wedge on the arch (see Figure 2b).

Six LVDT displacement transducers were used to measure vertical and horizontal displacements. The signal was acquired with a data acquisition system HBM© MGCplus device.

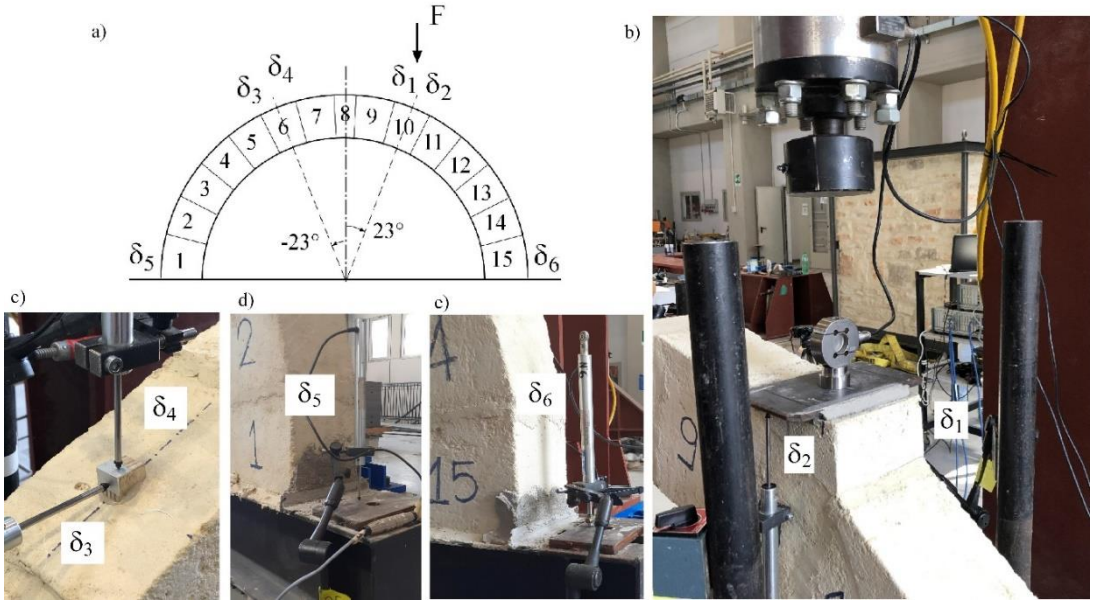


Figure 2: LDTV position and test set-up.

In particular, as showed in Figure 2, two instruments were installed at one fourth of the span on both sides of the block n. 10 where the load was applied in order to measure vertical displacements, δ_1 and δ_2 (Figure 2b). Other two displacement transducers were placed on block n. 6 at a symmetrical position with respect to the load application point; those two instruments measured both horizontal and vertical displacements, δ_3 and δ_4 respectively, of the application point (Figure 2c). At the base of the arch, next to voussoir 1 and 15, two displacement transducers were put to monitor eventual vertical rigid displacements of the support beam, called δ_5 and δ_6, respectively (Figure 2d and 2e). In Figure 2a the location of the LVDT displacement transducers is reported indicating also the angle (±23°) with respect to the vertical axis of symmetry of the arch.

In order to carry out a displacement control test, the oil pressure in the hydraulic jack was constantly adjusted by a feedback system managed by a Labview software. This way the load, measured by the load cell, was promptly adjusted in order to realize the desired target displacement. The very low speed of the test (about $5 \cdot 10^{-3}$ mm/s) was fundamental in order to avoid undesired effects related to the use of a hydraulic instrument in applying the load.

3 MECHANICAL CHARACTERIZATION OF THE COMPONENTS

3.1 Compressive and flexural behavior

A mechanical characterization of the masonry components (tuff bricks and mortar) was performed.

In particular, the compressive strength and Young modulus of the tuff bricks was investigated according to UNI EN 772-1:2011 and UNI EN 1926:2007. Six blocks of Apulian tuff of nominal dimensions of 430x240x150 mm^3 and average mass density of 1400 kg/m^3 were tested under compression using a Metro Com universal testing machine with a load capacity of 600 kN. Those tests provided an average value of the compressive strength of 2.25 MPa and average value of the Young modulus of 637.39 MPa.

The hydraulic lime-pozzolan mortar used for the joints was made by Mapei ("Mape-Antique Allettamento") and is characterized by a mass density of 1883.98 kg/m^3. The compressive and flexural strength were measured according to UNI EN1015-11:2007. The three-point bending test was performed on four 40x40x160 mm mortar prisms after 28 days of curing using an INSTRON 5689 universal with load capacity of 50 kN. The average value of flexural strength was determined equal to 1.91 MPa. Compression strength tests were carried out on the half prisms, giving an average value of the compressible strength of 8.94 MPa. The average value of the mortar Young modulus is 6902.27 MPa.

In the main results are reported in Table 1.

Table 1: Mechanical properties of the tuff and mortar.

	Young's modulus MPa	Compressive strength MPa	Flexural strength MPa
Tuff	637.39	2.25	-
Mortar	6902.27	8.94	1.91

3.1 Shear behavior

According to UNI EN 1052-3:2007, the shear strength of masonry has been determined by shear test on triplets; in particular, this test aims at measuring also the initial shear strength, that is the shear strength under zero compressive stress. Six tuff masonry triplets have been examined by applying shear loads and three different levels of pre-compression load applied normal to bed joint.

During the tests, for each sample (three triplets samples for each pre-compression load), the maximum shear strength $f_{v,i}$ was determined as follows:

$$f_{v,i} = \frac{F_{i,max}}{2A_i}, \tag{1}$$

where $F_{i,max}$ is maximum shear load at failure and A_i is the bed joint area of each sample. The characteristic shear strength f_{vk} was determined as:

$$f_{vk} = 0.7 \cdot f_v \tag{2}$$

with f_v the average shear strength value. Four typical shear failure modes can be observed [19]:

A. a fracture plane localized at one mortar-brick interface due to the attainment of the bonding limit value between the brick and the mortar bed;
B. a vertical crack in the mortar;
C. a fracture plane through a brick;

D. a failure by crushing and/or splitting due to a similar shear strength of both materials, so that the collapse surface cross both the mortar bed and bricks.

Masonry triplets were made by three hand-cut prismatic bricks with a dimension of 240 mm x 240 mm x 245 mm, jointed by two mortar layers 10 mm thick; the overall dimension of each triplet was 740 mm x 240 mm x 245 mm. The triplets were tested after curing of 28 days.

The amount of the normal pre-compressive load, applied during the tests by using an independent horizontal actuator (Figure 3a), was identified as a suitable fraction of the compressive strength of the tuff bricks. In particular, the shear tests have been performed with the following levels of the normal pre-compression σ_p: 0.1 MPa, 0.2 MPa and 0.3 MPa.

(a)  (b) 

Figure 3: Shear test on triplets: setup (a) and failure mode of a specimen (b).

Table 2 summarizes the experimental results and the failure mode observed after shear test for each triplet specimen.

Table 2: Results of shear test on triplets.

ID	σ_p (MPa)	$F_{i,max}$ (kN)	$f_{v,i}$ (MPa)	Failure mode
1_1	0.1	29.3	0.249	A
1_2	0.1	24.2	0.206	A
2_1	0.2	38.9	0.331	A
2_2	0.2	42.9	0.365	A
3_1	0.3	45.3	0.385	A
3_2	0.3	55.8	0.474	A

The only shear failure mode occurred was mode A, involving decohesion along the interface between tuff brick and mortar (Figure 3b).

Starting from the data in Table 2, the characteristic shear strength f_{vk} equal to 0.234 MPa has been determined.

Moreover, by plotting the experimental results in the σ_p-f_v plane (see Figure 4), and by using a linear regression of data, the shear stress with zero normal pre-compression load f_{v0} and the friction coefficient μ by means of Mohr-Coulomb failure criterion:

$$f_v = f_{v0} + \mu\sigma_p \tag{3}$$

have been determined. In particular, it results $\mu = 1.0119$ and $f_{v0} = 0.1327$ MPa.

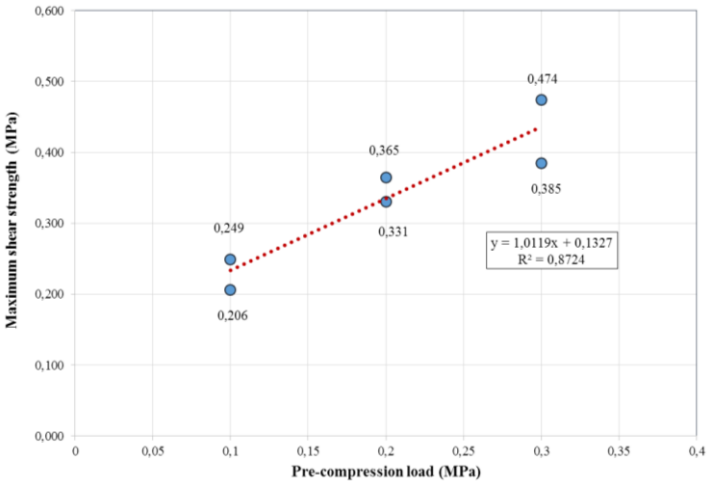


Figure 4: Results of shear test on triplets: shear stress vs pre-compression stress.

4 CYCLIC LOAD TESTS ON MASONRY ARCH

In this section the results obtained for the tested arch are described and analyzed. The experimental test has been conducted until 4 hinges clearly opened, that is, until the arch formed a mechanism. In particular, the collapse mechanism exhibited by the arch was the classic one, with the formation of four alternate hinges, two at the intrados and two at the extrados (see Figure 6).

In Figure 5 the observed experimental behavior is summarized by the superposition of the load-displacement curves obtained in the 11 load-unload cycles performed, where the displacement refer to the load application point and it is obtained by averaging the measures δ_1 and δ_2 (see Sect. 2). Moreover, Figure 6 contains a scheme of the position of the hinges, numbered in order of appearance.

As the load cycles progress, the first joint opening has been observed at the intrados under the application point of the concentrated load, that is, between the voussoirs 9 and 10, during the sixth cycle (C6); this corresponds to the opening of and hinge having the center at the extrados in the position H_1 indicated in Figure 6. Then, in the same load cycle C6 a second hinge H_2 formed at the intrados in a position almost symmetrical with respect to the first hinge H_1; the formation of this hinge corresponds to the opening at the extrados of the joint between the voussoirs 4 and 5. When the second hinge H_2 appeared, a slightly decrease of the load was observed as the displacement increases, until the unload process was started.

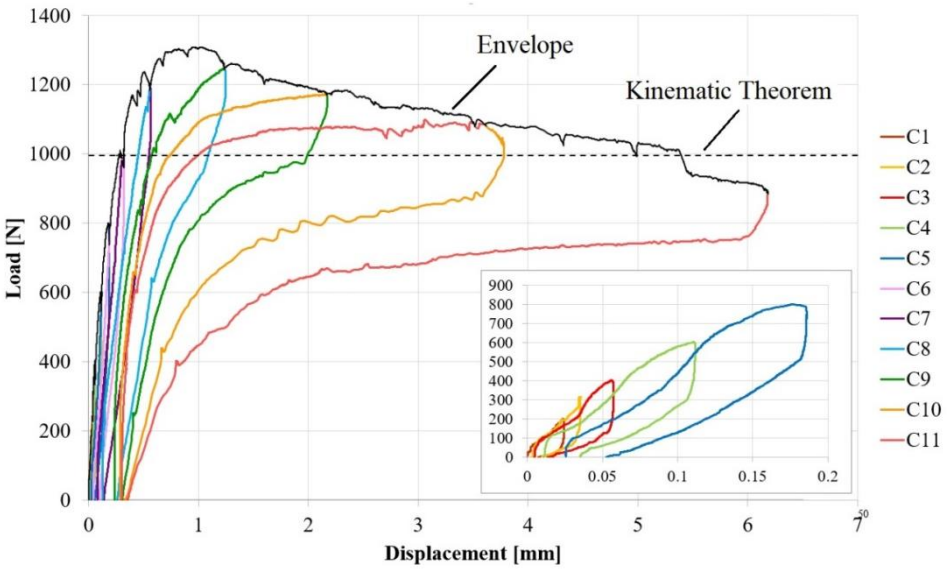


Figure 5: Load-displacement curve and hinge sequence.

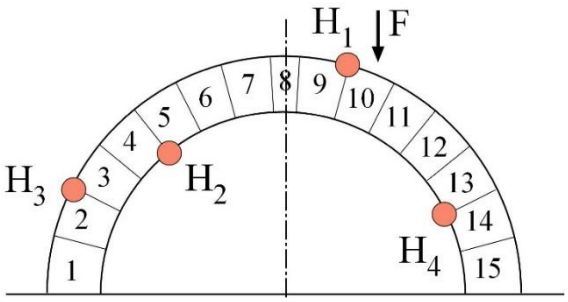


Figure 6: Hinge sequence.



Figure 7: a) First hinge; b) second hinge; c) fourth hinge.

During the seventh cycle (C7) the opening of the joints between the voussoirs 9-10 and 4-5, corresponding to the opening of the hinges H_1 and H_2, was again observed (see Figure 7a and b respectively); moreover, in correspondence of a load of approximately 1210 N, new

fractures occurred between the voussoirs 2-3 and 13-14 (see Figure 7c), perfectly symmetrical one another: thus, also the hinges H_3 and H_4 indicated in Figure 6 formed.

At the peak load of the eighth cycle (C8), equal to about 1310 N, all the above described 4 hinges opened. Figure 5 reports also the collapse load (995.2 N) determined by the kinematic theorem of limit analysis according to the classical Heyman hypotheses: as it is expected, this load is quite similar to the post-peak load in the last cycle, when it is reasonable to assume that the tensile strength of masonry has been practically cancelled by the damage.

Table 3: Maximum load, displacement corresponding to the maximum load, residual displacement and stiffness for each cycle.

Cycle	Maximum Load [N]	Displacement at max load [mm]	Residual displacement [mm]	Stiffness [N/mm]
C1	202.3	0.024	0.0075	6927
C2	312.3	0.035	0.0096	6911
C3	402.7	0.056	0.0133	6543
C4	600.5	0.112	0.0352	5116
C5	794.4	0.183	0.0434	5088
C6	1002.3	0.293	0.0950	4986
C7	1238.6	0.506	0.1359	3613
C8	1309.6	0.945	0.2577	2335
C9	1260.7	1.310	0.3024	-
C10	1184.1	2.330	0.3250	-
C11	1089.9	3.330	0.3513	-

The subsequent three load cycles C9 to C11 were characterized by a progressive reduction of the peak load; moreover, the decrease of the load after the peak as the displacement increases was even more marked. In addition, also the residual displacement at the complete unloading also increases even more. Finally, the opening of the hinges in the last three cycles was even more marked (see Figure 7c).

In the last performed cycle C11, after a peak load of about 1090 N in correspondence of a displacement of 3.330 mm of the loaded point, the test was pushed up a displacement of about 6.2 mm, and a decrease of the load up to 940 N was observed. At this point, the test was stopped because it was clear from the progress of the load-displacement curve that for further increase of the displacement the arch would have collapsed.

In Table 3 a synopsis of the main experimental results obtained from the test is reported, including maximum loads, the correspondent displacement of the loaded point, the residual displacements at complete unloading and initial stiffness for each cycle. The latter was evaluated for each cycle with reference to the loading phase before the peak load, by evaluating the best fitting linear approximation to the load-displacement curve between about 25% and 75% of the peak load.

Notice that since at the cycle C8 the arch already turned in to a mechanism with the formation of all the 4 hinges above described, the initial stiffness was not determined for the last three cycles.

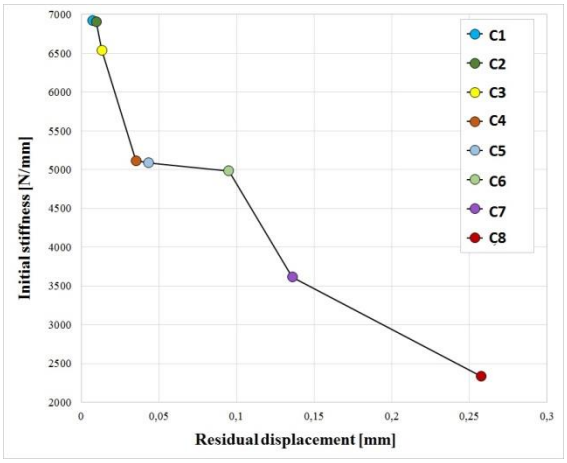


Figure 8: Initial stiffness-residual displacement curve.

In Figure 8 the stiffness values up to the cycle C8 are plotted versus the residual displacement at the complete unloading. The stiffness is practically the same for the first two cycles; correspondingly, the residual displacement is negligible. A sudden decrease of stiffness is noted at the fourth cycle C4, and this corresponds to a jump of the residual displacement from 0.013 to 0.035 mm. This behavior can be ascribed to the formation of some cracks at the joints that involves irreversible deformations and damage with decrease of the stiffness. It is likely that cracks formed at the joints where the first and the second hinges occurred, whereas at the stage C4 these hinges are still not visible. In fact, during each load-unload cycle visual inspections were regularly performed, but visible crack openings were noticed only during the sixth cycle.

From C4 to C6 the residual displacement increases of additional 0.06 mm while the stiffness remains almost the same. After the sixth cycle the stiffness significantly decreases: this indicates the progression of the opening of the joints. The residual displacement reaches a value of 0.2577 mm at the end of cycle C8.

Beyond cycle C8 the load-displacement curves indicate a further decrease of the stiffness of the arch and an additional accumulation of irreversible deformations, denoted by the increase of the residual displacement at the complete unloading.

5 DISCUSSION AND CONCLUSION

The results of the performed experimental test show some peculiar feature of the behavior of masonry arch under cyclic loadings, relevant in view of the modeling of the response of masonry structures embedding arches under seismic loadings.

First, that the stiffness of the arch is constant only for low loads; indeed, as the load increases, the compaction of mortar in the bed joints and the opening of cracks at the joints deteriorate the stiffness, that approaches very low values especially in view of the collapse. This pronounced damage effect is relevant as for the case of masonry panels [20].

A second important aspect is that a masonry arch can sustain cyclic loading even beyond the peak load, and that the softening phase is very progressive, without a marked drop of the load capacity. Moreover, the experimental response highlighted a marked ductility, despite to the fragility of the material components (tuff bricks and mortar): this is due to the particular

arrangement of the masonry, and in particular to the role of the joints, even more relevant in case of masonry curved structures, such as arches and vaults, where the damage localizes practically only in correspondence of the joints.

Furthermore, it should be noted the relatively low value of permanent displacements after the complete unloading, even in the proximity of the collapse, and the narrow shape of the hysteretic loops, indicating the quite low energy dissipation related to the cyclic opening and closing of the hinges.

All the above aspects are very challenging to be modeled and requires nonlinear numerical models capable of accurately describing the damage and the peculiar features of the unloading phase, like the model proposed in [18].

Notice that in the experiment on the arch the shear strength of the interface is never called into play, but its careful characterization is important for describing other kind of structures, like, e.g, a masonry wall even if embedding and arch. In addition, notice that whereas no direct tests have been performed for determining the tensile strength of the masonry, this mechanical parameter can be calculated starting from the cohesion evaluated in shear tests for zero pre-compression stress.

In the next future, the latter will be calibrated starting from the experimental outcomes here described, and then employed for performing non-linear numerical analysis of a masonry wall including both small rectangular openings representing windows recesses and a large opening topped by a masonry arch representing the main door entrance. In particular, the influence of interfacial shear strength of masonry joints on the overall behavior of the masonry structure will be analyzed by a parametric study. Moreover, also FRCM reinforced arches will be taken into account, were an accurate description of the shear behavior of the interfaces play an important role.

REFERENCES

[1] Mallardo, V., Malvezzi, R., Milani, E. and Milani, G. Seismic vulnerability of historical masonry buildings: A case study in Ferrara. *Eng. Struct.* (2008) **30**(8):2223-2241.

[2] Lagomarsino, S. Seismic assessment of rocking masonry structures. *B. Earthq. Eng.* (2015) **1**: 97-128.

[3] D'Altri, A.M., Sarhosis, V., Milani, G., Rots, J., Cattari, S., Lagomarsino, S., Sacco, E., Tralli, A., Castellazzi, G. and de Miranda, S. Modeling Strategies for the Computational Analysis of Unreinforced Masonry Structures: Review and Classification. *Arch. Comput. Method E.* (2019) https://doi.org/10.1007/s11831-019-09351-x.

[4] Pelà, L., Cervera, M. and Roca, P. An orthotropic damage model for the analysis of masonry structures. *Constr. Build. Mat.* (2013) **41**:957-967.

[5] Addessi, D., Marfia, S., Sacco, E. and Toti, J. Modeling approaches for masonry structures. *Open Civil Eng. J.* (2014) **8**(1):288-300.

[6] Lemos, J.V. Discrete element modeling of masonry structures. *Int. J. Archit. Herit.* (2007) **1**(2):190-213.

[7] DeJong, M.J., De Lorenzis, L., Adams, S. and Ochsendorf, J.A. Rocking stability of

masonry arches in seismic regions. *Earthq. Spectra* (2008) **24**(4):847-865.

[8] Fraddosio, A., Lepore, N. and Piccioni M.D. Lower Bound Limit Analysis of Masonry Vaults Under General Load Conditions. In: R. Aguilar et al. (Eds.): *Structural Analysis of Historical Constructions*, RILEM Bookseries 18 (2019), pp. 1090-1098.

[9] Ricci, E., Fraddosio, A., Piccioni M.D. and Sacco, E. A new numerical approach for determining optimal thrust curves of masonry arches. *Eur. J. Mech. A-Solid* (2019) **75**: 426-442.

[10] Fraddosio, A., Lepore, N. and Piccioni M.D. Thrust Surface Method: An innovative approach for the three-dimensional lower bound Limit Analysis of masonry vaults. *Eng. Struct.* (2020) **202**:109846.

[11] Milani, G. and Lourenço, P.B. 3D non-linear behavior of masonry arch bridges. *Comput. Struct.* (2012) **110-111**:133-150.

[12] Chiozzi, A., Milani, G. and Tralli, A. A Genetic Algorithm NURBS-based new approach for fast kinematic limit analysis of masonry vaults. *Comput. Struct.* (2017) **182**:187-204.

[13] De Santis, S., Roscini, F. and de Felice G. Full-scale tests on masonry vaults strengthened with Steel Reinforced Grout. *Compos. Part B-Eng.* (2018) **141**:20-36.

[14] Bove, M., Castellano, A., Fraddosio, A., Scacco, J., Milani, G. and Piccioni M.D. Experimental and numerical analysis of FRCM strengthened parabolic tuff barrel vault. In: A. Di Tommaso et al. (Eds.): *Mechanics of Masonry Structures Strengthened with Composite Materials III*, Key Engineering Materials 817 (2019), pp. 213-220.

[15] Toti, J., Gattulli, V. and Sacco, E. Damage propagation in a masonry arch subjected to slow cyclic and dynamic loadings. *Frattura integr. strutt.* (2014) **29**:166-177.

[16] Karimi, A.H., Karimi, M.S., Kheyroddin, A. and Shahkarami A.A. Experimental and Numerical Study on Seismic Behavior of An Infilled Masonry Wall Compared to An Arched Masonry Wall. *Structures* (2016) **8**:144-153.

[17] Castellano, A., Fraddosio, A., Scacco, J., Milani, G. and Piccioni M.D. Dynamic response of FRCM reinforced masonry arches. In: A. Di Tommaso et al. (Eds.): *Mechanics of Masonry Structures Strengthened with Composite Materials III*, Key Engineering Materials 817 (2019), pp. 285-292.

[18] Serpieri, R., Albarella, M. and Sacco E. A 3D microstructured cohesive–frictional interface model and its rational calibration for the analysis of masonry panels. *Int. J. Solids Struct.* (2017) **122-123**:110-127.

[19] Abdou, L., Ami Saada, R., Meftah, F. and Mebarki, A. Experimental Investigations of the Joint-Mortar Behaviour. *Mech. Res. Commun.* (2006) **33**:370-384.

[20] Rinaldin, G., Amadio, C. and Gattesco, N. Review of experimental cyclic tests on unreinforced and strengthened masonry spandrels and numerical modelling of their cyclic behavior. *Eng. Struct.* (2017) **132**:609-623.

12th International Conference on Structural Analysis of Historical Constructions
SAHC 2020
P. Roca, L. Pelà and C. Molins (Eds.)

FAST SEISMIC VULNERABILITY EVALUATION OF HISTORICAL MASONRY AGGREGATES THROUGH LOCAL ANALYSES: AN ADAPTIVE NURBS-BASED LIMIT ANALYSIS APPROACH

N. GRILLANDA[1*], M. VALENTE[1], G. MILANI[1], F. FORMIGONI[2], A. CHIOZZI[2], A. TRALLI[2]

[1]Department of Architecture, Built Environment and Construction Engineering (ABC), Politecnico di Milano, Piazza Leonardo da Vinci 32, 20133 Milan, Italy
e-mail: nicola.grillanda@polimi.it (*corresponding author), marco.valente@polimi.it, gabriele.milani@polimi.it

[2] Department of Engineering, University of Ferrara, Via Saragat 1, 44122 Ferrara, Italy
email: fabrizio.formigoni@student.unife.it, andrea.chiozzi@unife.it, tra@unife.it

Keywords: local analyses, local mechanism, NURBS, historical masonry aggregates

Abstract. *An efficient computational tool for the local failures analysis in historical masonry aggregates is proposed. A NURBS (Non-Uniform Rational B-Spline) representation of geometry is adopted. NURBS entities, which are common in commercial CAD packages, have the great advantage to describe complex geometries (such as curved elements and walls with a high number of holes) with very few elements. An upper bound limit analysis formulation is implemented, in which the adopted NURBS elements are idealized as rigid bodies with dissipation allowed only along interfaces. The mesh of NURBS elements is progressively adjusted through a genetic algorithm in order to minimize the live load multiplier. This procedure is applied in the evaluation of the horizontal load multiplier associated with the activation of local mechanisms during a seismic event. Some case studies, referring to masonry aggregates located in the historical centers of Arsita (Abruzzo region, Italy) and Sora (Lazio region, Italy), are here presented. A quick evaluation of the seismic vulnerability is performed through the presented NURBS-based computational tool, showing the high importance of the local response in the study of the seismic behavior of masonry aggregates.*

1 INTRODUCTION

Masonry aggregates constitute the great majority of residential buildings in Italian historical centers. Several factors affect the response of these constructions to horizontal loads, such as geometrical irregularities, uncertainties on connections between walls, difficulties on the identification of masonry mechanical parameters, lack of design details, and pre-existent damage, resulting in a seismic behavior quite difficult to predict. Despite difficulties, a tool aimed at studying the structural capacity of masonry aggregates subjected to horizontal load is of great interest, since their high seismic vulnerability has been underlined during past earthquakes (L'Aquila 2009, Emilia Romagna 2012, Central Italy 2016) [1–5].

A lot of different strategies can be found in the technical literature for historical masonry structures [6] and, more specifically, for masonry aggregates. Generally speaking, the commonly adopted approaches can be distinguished in index-based methods [7–11], local failures analyses [12,13], Equivalent Frame-based methods [14–18], and FE static and dynamic non-linear analyses [19–23]. During recent seismic events, the great majority of failures observed was local collapses [24]. It has to be noted that the typical characteristics of masonry aggregates make these structures unable to exibit a global response when subjected to horizontal actions. Therefore, the vulnerability assessment of masonry aggreates cannot leave local analyses out of consideration [25,26] (as also recommended by the Italian code in reference to masonry structures [27,28]).

Local failure analyses are usually performed by using limit analysis techniques. The Heyman model [29], i.e. the classic no-tension material, is usually adopted in order to easily take into account the typical characteristics of the masonry material. However in ancient buildings crushing and shear failures can be frequent, especially in presence of irregular masonry textures. Therefore, more accurate numerical strategies can be followed. Recently, some limit analysis prodecures enriched with homogenization techniques have been presented [30–33]. Homogenization allows representing the heterogeneous masonry material as an equivalent homogeneous material. In this way, fast and efficient methods which take into account heterogeneous and orthotropy through few equivalent parameters have been proposed. Moreover, a novel method for the determination of the homogenized failure surface of a certain masonry texture has been recently proposed [34]. In any case, a refined mesh is always required in the application of these methods.

More recently, a novel limit analysis approach has been presented by some of the Authors [35]. In this method, an upper bound formulation is applied on a masonry structures discretized through few NURBS surfaces (Non-Uniform Rational B-Spline, [36]). The NURBS geometry is commonly adopted in the typical CAD environment and is particularly suited for the representation of complex masonry structures, such as vaults or, more in general, masonry buildings including curved shapes. Each NURBS element is idealized as rigid. Plastic dissipation occurs at interfaces according to a properly defined three-dimensional failure surface, which allows taking into account the main properties of a certain masonry texture. A Genetic Algorithm (GA) mesh adaptation is applied in order to obtain the minimum load muplitplier and the associated collapse mechanism. Some applications to historical masonry constructions have been recently published [37–44].

In this work, the adaptive NURBS limit analysis approach is applied as tool for the local failures analysis of complex historical masonry aggregates. Some case studies taken from the Italian historical centers Arsita (Abruzzo region) [45] and Sora (Lazio region) [19] are presented, providing the potentialities of this method for such a complex structural typology.

2 ADAPTIVE NURBS LOCAL FAILURE ANALYSES ON MASONRY AGGREGATES

This novel limit analysis approach for historical masonry aggregates is based on a discretization of the whole construction through few NURBS (Non-Uniform Rational B-Spline) surfaces. Without going too in details on the theory of NURBS geometrical entities (for which we remand to [36]), the main advantage of NURBS is the possibility to model curved elements,

such as arches, vaults, and circular openings, in easy way and with low computational cost. A NURBS model of a complex aggregate can be realized in Rhinoceros and then imported into the MATLAB environment, where each surface is converted into a 3D macro-element once thickness and offset properties are assigned. Once the model is available in MATLAB, each surface can be eventually subdivided into few elements, each one deriving by a trimmed NURBS surface which is a partition of the initial one.

By assuming the hypotesis of infinitively rigid elements connected by rigid-plastic interfaces, a kinematic limit analysis can be applied. Interfaces are the only zones in which relative velocities can occur and represent the possible fracture lines from which the failure mechanism takes place. In order to properly evaulate the amount of plastic dissipation related to velocity jumps at interfaces, each one is discretized through points in which a local reference system ($\mathbf{n}$, $\mathbf{s}$, $\mathbf{t}$) (Figure 1(a)) is defined, and a three-dimensional failure surfaces (typically a Mohr-Coulomb domain with tension cut-off and linear cap in compression, Figure 1(b)) is assigned. A classic associative plastic flow rule is adopted.

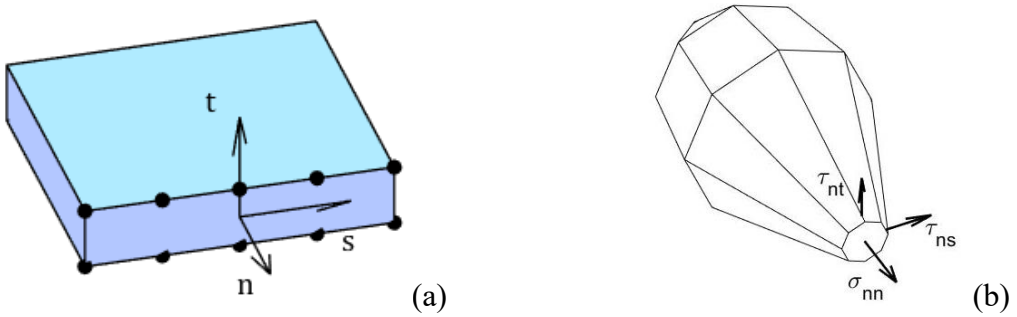


Figure 1. (a) Discretization of interfaces and local reference system, (b) three-dimensional failure surface.

Given a configuration of dead- and live-load (respectively $\mathbf{F}_0$ and $\mathbf{\Gamma}$), the live-load multiplier Γ is found by applying the Principle of Virtual Powers. The procedure can be written according to the following linear programming formulation:

$$\min\left\{\Gamma = \sum_i P_{\text{int}}^i - P_{\mathbf{F}_0}\right\} \text{ such that } \begin{cases}\mathbf{A}_{eq}\mathbf{x} = \mathbf{b}_{eq} \\ \dot{\boldsymbol{\lambda}} \geq 0\end{cases}$$

where:

$\sum_i P_{\text{int}}^i$ is the total amount of internal dissipated power;

$P_{\mathbf{F}_0} + P_{\Gamma}$ is the power dissipated by the external loads;

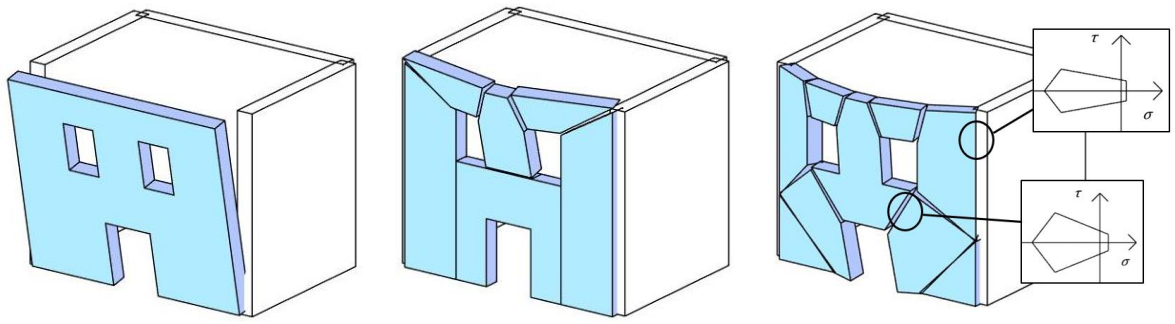
$\mathbf{x}$ is the vector of unknowns, which include the velocity components of each element and the non-negative plastic multipliers $\dot{\boldsymbol{\lambda}}$;

$\mathbf{A}_{eq}$, $\mathbf{b}_{eq}$ are respectively the overall equality constraints matrix (containing geometric constraints, plastic compatibility and normalization condition of live loads power) and the corresponding right-hand side vector.

This is a general procedure for the limit analysis of masonry structures. However, in the specifical case of local failure analyses in masonry aggregates, dead loads represent self-weights and masses applied on each wall, whereas live loads are constituted by a distribution

of horizontal loads proportional to masses (as recommended by the Italian code [27,28]). Therefore, by solving the presented linear programming problem, a horizontal load multiplier α_0 and a mechanism are provided. According to this formulation, the mechanism will depend on the assumed position of fracture lines and the associated horizontal load multiplier will be a upper bound of the collapse multiplier, in agreement with the kinematic theorem of limit analysis. Therefore, the initial mesh has to be adjusted in order to find the real position of fracture lines. A Genetic Algorithm (GA) is here applied for the mesh adaptation procedure, in order to provide a good estimation of the horizontal load multiplier and the collapse mechanism. For more details and applications, the reader is referred to [35,37–44].

This procedure can be applied to evaluate local failure mechanisms in complex historical masonry aggregates. Starting from a model of the whole constructions, some walls (represented by the corresponding NURBS surfaces) can be selected and the code provides automatically the most vulnerable failure mechanism involving these elements. In order to take into account the typical characteristics of masonry aggregates, such as uncertainties on interlocking and eventually, presence of damage, different failure domains can be assigned to contacts between different NURBS surfaces. This assumes a fundamental role in the evaluation of the correct collapse mechanism (see Figure 2).



(a) (b) (c)

Figure 2. Influence of the level of interlocking on the collapse mechanism: examples of (a) low, (b) good, and (c) intermediate level of interlocking.

3 APPLICATIONS TO SOME HISTORICAL MASONRY AGGREGATES

The adaptive NURBS local failure analysis has been applied to some masonry aggregates located in historical centers. Some recent results are here presented. For each example, the parameter values suggested in the Italian code [27,28] have been adopted for each masonry typology observed in the different structural units. For sake of simplicity, all values assumed for the ultimate resistance parameters are summarized in Table 1.

Table 1: Resistance parameters assigned to masonry.

Example	Tensile stress f_t [MPa]	Compressive strength f_c [MPa]	Cohesion c [MPa]	Friction angle Φ [°]	Linear cap in compression ρ [-], Φ_2 [°], [42]
1-The Ortigia case	0	2.6	0.05	22	0.5,45
2-Arsita: Il Torrione	0	1.2 North-East side 1.8 West side 2.0 South side	0.01	37	0.5,45
3-Sora	0	2.6	0.05	22	0.5,45
4-Arsita: Il Corso	0.01 walls 0.05 vaults	2.0	0.035	22	0.5,45

The first example is the Ortigia case [46], a simple masonry building constituted by four walls. This case has been adopted as a trial test for the evaluation of simple local mechanisms. Results are depicted in Figure 3. A good interlocking has been assumed for this case. In addition to overturning mechanisms, for which the adaptive NURBS limit analysis has allowed to determine the exact shape of the participating triangular portions of transversal walls, a horizontal flexure mechanism and a corner overturning have been found. Given the minimum load multiplier equal to 0.106, the lateral walls resulted the most vulnerable elements. However, this example is quite simple and cannot be classified as aggregate of constructions.

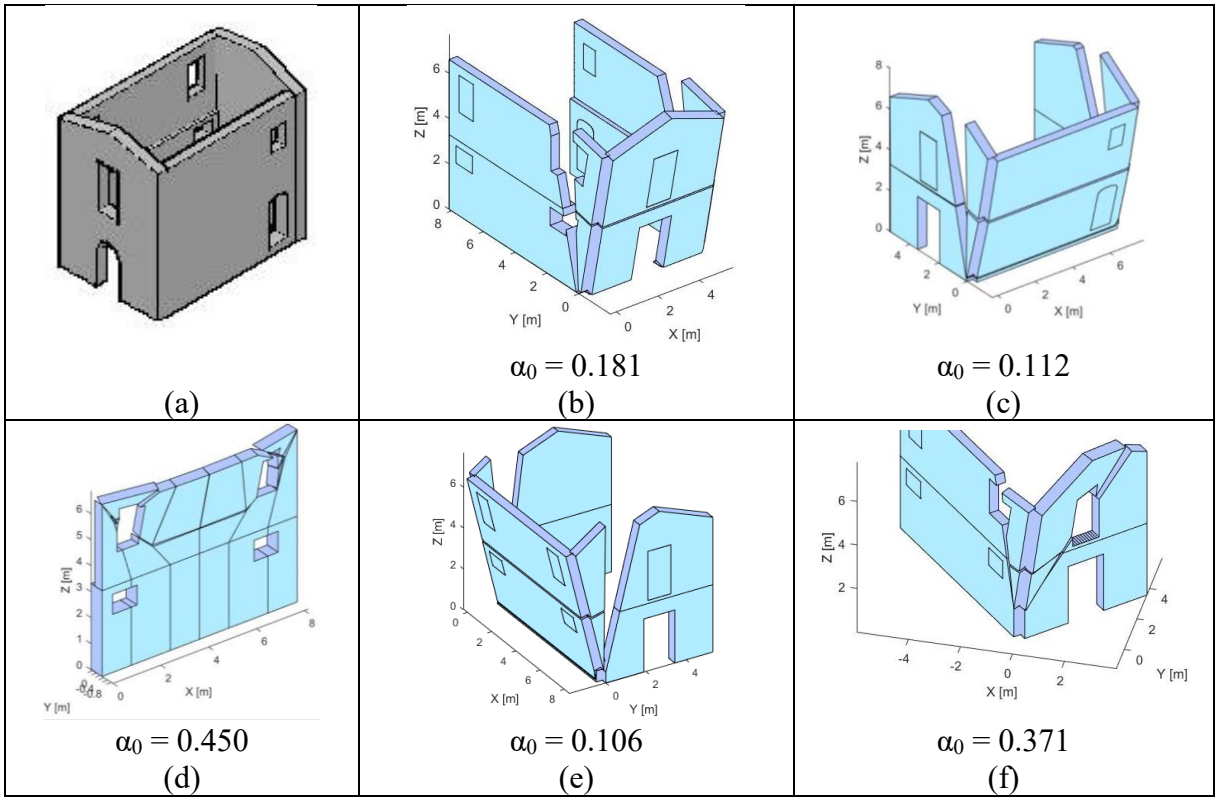


Figure 3. Local mechanisms found for the Ortigia case: (a) 3D model, (b) façade overturning, (c-e) failures in lateral walls, (f) corner mechanism.

Some constructions located in the historical center of Arsita (Abruzzo region, Italy) have been recently analyzed through the proposed tool. Arsita is a small village in the center of Italy which was hit by the 2009 earthquake. Widespread damage has been observed on masonry constructions [1] as a consequence of the seismic event. After the earthquake, a deep investigation has been carried out on the historical center by a scientific team set up by ENEA (Italian National Agency for New Technologies, Energy and Sustainable Economic Development). A total of 17 aggregates have been inspected. As a final output, the Post-Earthquake Reconstruction Plan for the Arsita Municipality has been published [45].

The aggregate number 8, named “Il Torrione”, has been studied through the proposed limit analysis tool. This is a residential building composed of four structural units. The geometry is quite irregular both in the horizontal plan and in height, since it is built on a slope. Three storeys can be observed on the South side, which presents a maximum height equal to about 11.5 m with reference to the ground level. In the North side two storeys are visible with a height equal to 6.5 m, whereas in the East and West side walls are partially covered by the slope. All the different typologies of horizontal floors are characterized by the absence of chains and concrete edgings (according to [45]). The most critical failure mechanisms obtained are reported in Figure 4. Failures include overturning mechanisms, corner mechanisms, and both horizontal and vertical failures. It is worth noting that vertical flexure mechanisms can be obtained once global overturning failures are properly excluded from the automatic research. This can be performed by applying kinematic constraints that represent the presence of chains. As previously mentioned, no chains have been observed on this building. Therefore, these results show how the code allows taking into account even the most typical retrofitting strategies in an easy way. However, the study of masonry aggregates retrofitted by means of chains or strips will be the topic of future papers. As regards walls located in the West side (Figure 4(e, f)), both the cases of no connection and good connection have been studied, resulting in different collapse mechanisms. In any case, the most critical failures are given by the global overturning.

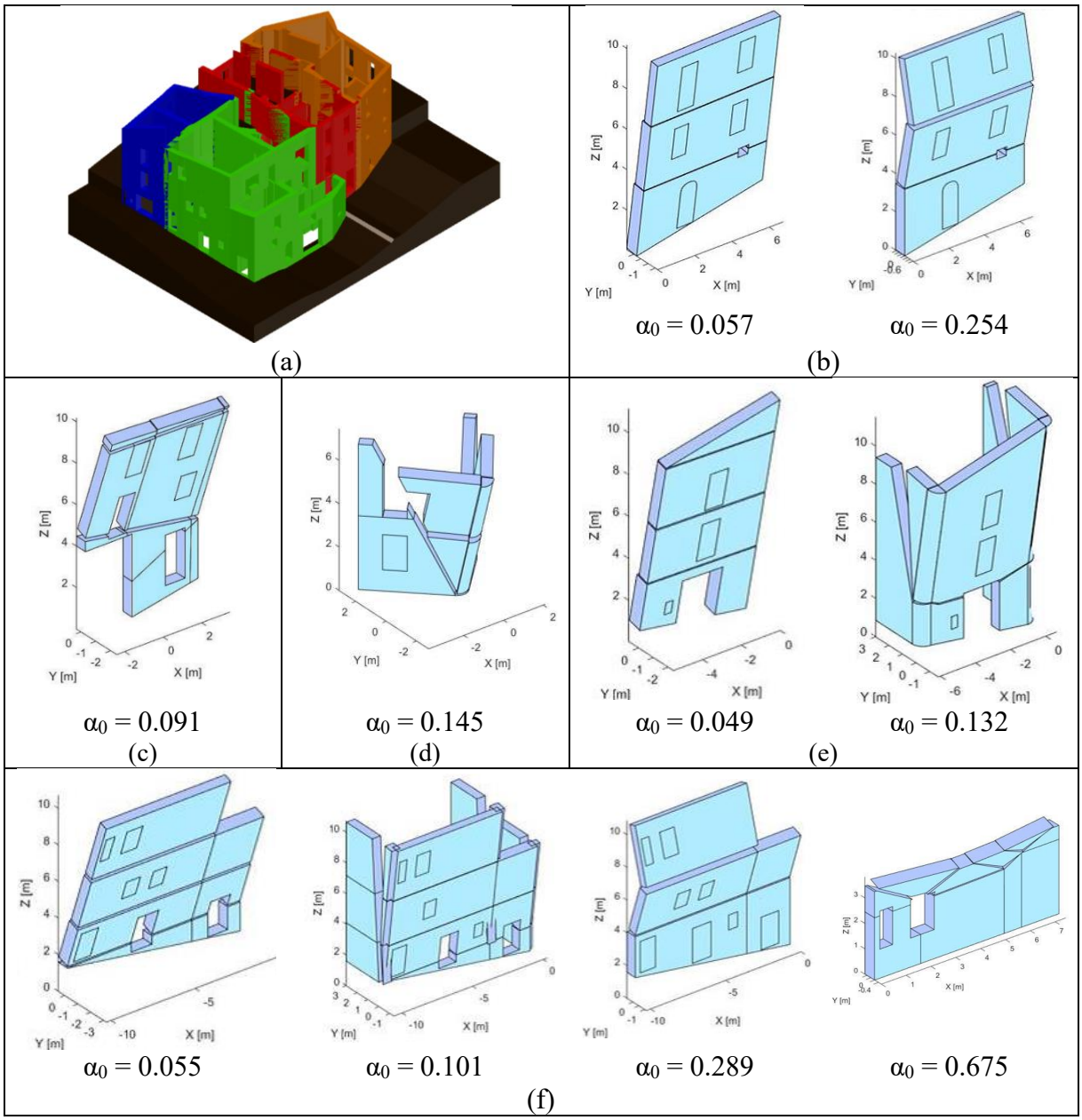


Figure 4. Local mechanism found for the masonry aggregate Il Torrione (Arsita): (a) 3D model, (b, c) failures in the South side, (d) corner failure in the North side, (e, f) failures in the West side.

The next examples regard masonry aggregates that include vaulted elements. A first test has been performed on some aggregates located in Sora (Lazio region, Italy). The local analysis tool has been applied on the perimeter walls of a single structural unit. Some of these walls are connected to another building through a masonry arch (see Figure 5). The result is depicted in Figure 5. As it can be noted, the global overturning of the wall is prevented by the arch, which is not involved into the failure. Therefore, the most vulnerable failure is a partial overturning taking place above the masonry arch. This very simple example has been adopted as trial test before the last case study.

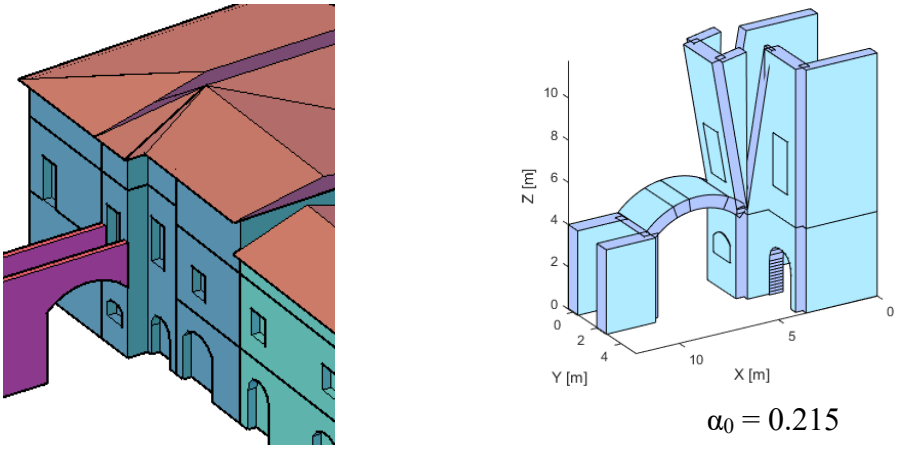


Figure 5. Masonry aggregate in Sora: failure mechanism in presence of a masonry arch.

The last example is the masonry aggregate named "Il Corso", located in Arsita (the number 1 according to [45]). This construction is the final result of the aggregation of three structural units, two residential building and a church (the Church of Santa Vittoria). The whole structure can be inscribed into a rectangle 47 m x 15 m, whereas the maximum height is about 15 m in correspondence of the bell tower. An average thickness of 70 cm has been observed for walls in residential units, whereas in the church even 200 cm thickness value can be found (as for the façade). The presence of several masonry vaults, see for example barrel vaults in the central nave of the church (Figure 6(a)), makes this aggregate a very meaningful example. Generally, a good connection between orthogonal walls has been assumed. Analyses have been performed starting by a 3D model of the whole constructions. It is worth noting that NURBS are particularly suited to this case, not only for a reliable representation of curved geometries, but also for an easy analysis of a 3D model that would implicate a very high computational effort if studied through the traditional FE approaches. The first results on this representative case are here presented. In Figure 6(b-e), failure mechanisms and corresponding horizontal multiplier α_0 and spectral acceleration a_0* (the last one evaluated as suggested in the Italian code [28], §C8.7.1.2.1.3) values are shown. By observing failures obtained in the church (Figure 6(b, c)), it is clear that vaults assume a fundamental role in the collapse. The most critical mechanism is the horizontal response of vaults in the central nave, to which a horizontal load multiplier equal to 0.108 and a corresponding spectral acceleration of 0.084g are assigned. It is worth noting that these complex mechanisms cannot be properly evaluated through the C.I.N.E. application or following standard hand calculations, since the collapse mechanisms are a-priori unknown.

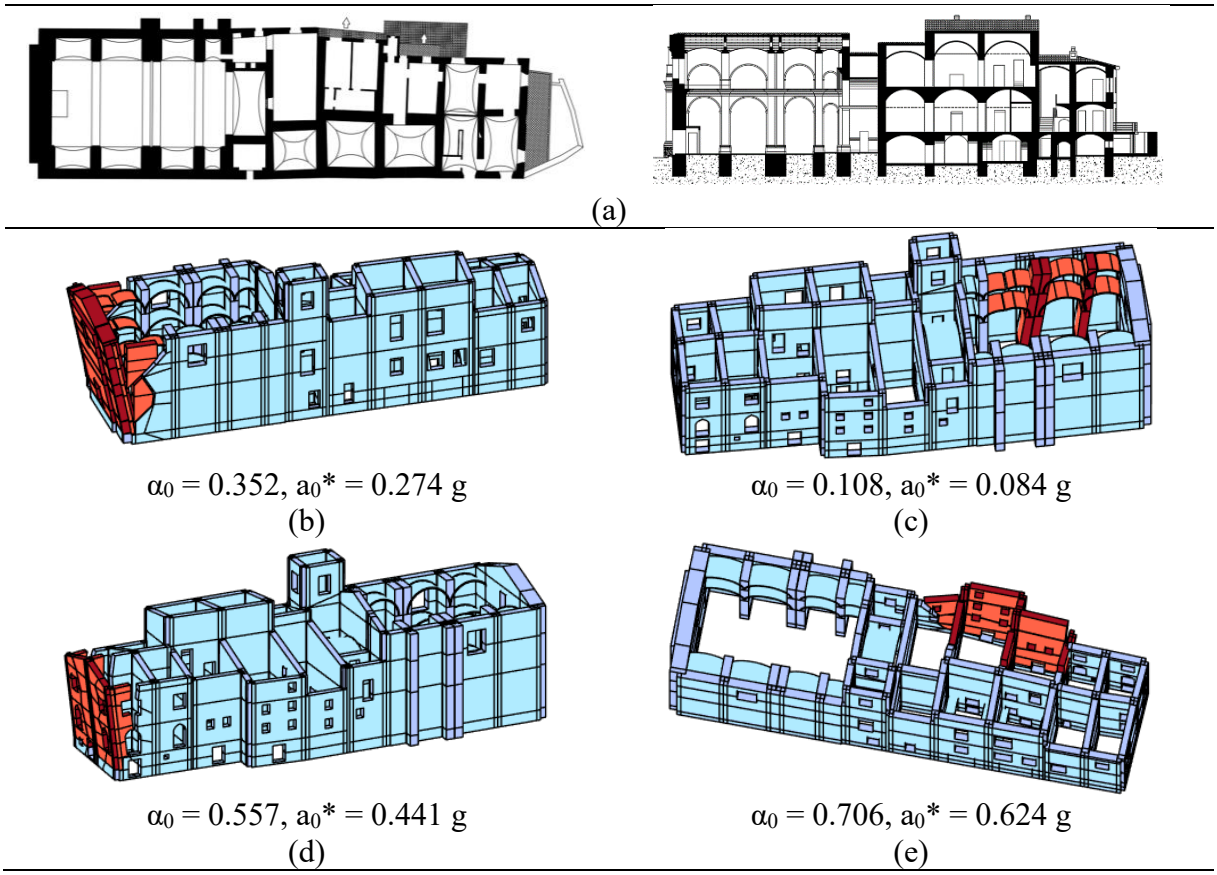


Figure 6. Local mechanisms found for the masonry aggregate Il Corso (Arsita): (a) horizontal plan and section, (b) church façade overturning, (c) failure of vaults in the central nave, (d) façade overturning in the residential structural units, (e) failures in the perimeter walls.

4 CONCLUSIONS

A novel strategy for evaluations of local mechanisms in historical masonry aggregates has been proposed. This method adopts a NURBS discretization of masonry aggregates and applies an upper bound limit analysis with automatic mesh adaptation. Several examples, characterized by different critical situations and increasing complexity, have been here presented.

The use of NURBS resulted particularly suited for historical masonry aggregates, aiming to accurately represent complex geometries by maintaing low the number of elements and, consequently, the computational effort in comparison with the traditional FE approaches. In particular, the effect of the presence of curved elements (see the last two case studies) on the shape of the collapse mechanism is automatically taken into account. Moreover, the use of a mesh adaptation governed by Genetic Algorithm allowed identifying the exact position of fracture lines, avoiding overestimations of the horizontal load multiplier. Thanks to the automatic adjustment of the mesh, the NURBS discretization and the implementation of suited failure domains, the code allowed identifying both classical and non-standard failure mechanisms, which can derive from the presence of vaulted elements interacting with walls, cohexistence of different interlocking conditions, and irregular masonry textures (see in particular the last example).

Good results in terms of local failures and horizontal load multipliers have been found, providing the efficiency of the adaptive NURBS limit analysis in vulnerability evaluations of local failure mechanisms. Therefore, this procedure can be adopted as good alternative to the well-known CINE applications for the evaluation of local failures in complex historical masonry aggregates.

REFERENCES

[1] Formisano, A., Florio, G., Fonti, R., Candigliota, E., Immordino, F., Marzo, A., Moretti, L., Indirli, M., Abate, D., Furini, G., Pierattini, S., Screpanti, A., Angelini, M., Gambatesa, T., and Massaia, C., Seismic vulnerability of historic centres: identification of damage mechanisms occurred in Arsita (TE) after L'Aquila earthquake, 15th World Conference of Earthquake Engineering (15th WCEE). (2012) 24–28.

[2] D'Ayala, D., and Paganoni, S., Assessment and analysis of damage in L'Aquila historic city centre after 6th April 2009, *B. Earthq. Eng.* (2011) **9**:81–104. https://doi.org/10.1007/s10518-010-9224-4.

[3] Carocci, G.F., Small centres damaged by 2009 L'Aquila earthquake: on site analyses of historical masonry aggregates, *B. Earthq. Eng.* (2012) **10**:45–71. https://doi.org/10.1007/s10518-011-9284-0.

[4] Sorrentino, L., and Cattari, S., Seismic behaviour of ordinary masonry buildings during the 2016 central Italy earthquakes, *B. Earthq. Eng.* (2018) **17**:5583–5607. https://doi.org/10.1007/s10518-018-0370-4.

[5] Valente, M., and Milani, G., Seismic response and damage patterns of masonry churches: seven case studies in Ferrara, Italy, *Eng. Struct.* (2018) **177**:809–835. https://doi.org/10.1016/j.engstruct.2018.08.071.

[6] Roca, P., Cervera, M., Gariup, G., and Pelà, L., Structural analysis of masonry historical constructions. Classical and advanced approaches, *Arch. Comput. Method. in E.* (2010) **17**:299–325. https://doi.org/10.1007/s11831-010-9046-1.

[7] Lourenço, P.B., and Roque, J.A., Simplified indexes for the seismic vulnerability of ancient masonry buildings, *Constr. Build. Mater.* (2006) **20**:200–208. https://doi.org/10.1016/j.conbuildmat.2005.08.027.

[8] Formisano, A., Florio, G., Landolfo, R., and Mazzolani, F.M., Numerical calibration of an easy method for seismic behaviour assessment on large scale of masonry building aggregates, *Adv. Eng. Softw.* (2015) **80**:116–138. doi:10.1016/j.advengsoft.2014.09.013.

[9] Formisano, A., Chieffo, N., and Mosoarca, M., Seismic vulnerability and damage speedy estimation of an urban sector within the municipality of San Potito Sannitico (Caserta, Italy), *Op. Civ. Eng. J.* (2017) **11**:1106–1121. https://doi.org/10.2174/1874149501711011106.

[10] Chieffo, N., and Formisano, A., Geo-hazard-based approach for the estimation of seismic vulnerability and damage scenarios of the old city of senerchia (Avellino, Italy), *Geosci.* (2019) **9**. https://doi.org/10.3390/geosciences9020059.

[11] Chieffo, N., and Formisano, A., The influence of geo-hazard effects on the physical vulnerability assessment of the built heritage: An application in a district of Naples, *Build.* (2019) **9**. https://doi.org/10.3390/buildings9010026.

[12] Milano, L., Mannella, A., Morisi, C., and Martinelli, A., Illustration and kinematic analysis of local collapse mechanisms in existing masonry buildings (in Italian), (n.d.).
[13] ReLUIS, DPC, CNR-ITC, C.I.N.E. Condizioni d'Instabilità degli Edifci—Applicativo per le verifche sismiche dei meccanismi di collasso fuori dal piano negli edifci esistenti in muratura mediante analisi cinematica lineare (in Italian), (2009). http://www.reluis.it/doc/emergenza_terremoto_abruzzo/%0ACINE_1.0.4.xls.
[14] Roca, P., Molins, C., and Marí, A.R., Strength capacity of masonry wall structures by the equivalent frame method, Journal of Structural Engineering. (2005) **131**:1601–1610. https://doi.org/10.1061/(ASCE)0733-9445(2005)131:10(1601).
[15] Lagomarsino, S., Penna, A., Galasco, A., and Cattari, S., TREMURI program: An equivalent frame model for the nonlinear seismic analysis of masonry buildings, *Eng. Struct.* (2013) **56**:1787–1799. https://doi.org/10.1016/j.engstruct.2013.08.002.
[16] Formisano, A., and Massimilla, A., A Novel Procedure for Simplified Nonlinear Numerical Modeling of Structural Units in Masonry Aggregates, *Int. J. Archit. Herit.* (2018) **12**:1162–1170. https://doi.org/10.1080/15583058.2018.1503365.
[17] Chieffo, N., and Formisano, A., Comparative Seismic Assessment Methods for Masonry Building Aggregates: A Case Study, *Front. Built Env.* (2019) **5**. https://doi.org/10.3389/fbuil.2019.00123.
[18] Chiumiento, G., and Formisano, A., Simplified and refined analyses for seismic investigation of historical masonry clusters: Comparison of results and influence of the structural units position, *Front. Built Env.* (2019) **5**. https://doi.org/10.3389/fbuil.2019.00084.
[19] Valente, M., Milani, G., Grande, E., and Formisano A., Historical masonry building aggregates: advanced numerical insight for an effective seismic assessment on two row housing compounds, *Eng. Struct.* (2019) **190**:360–379. https://doi.org/10.1016/j.engstruct.2019.04.025.
[20] Habieb, A.B., Valente, M., and Milani, G. 2019a. Effectiveness of different base isolation systems for seismic protection: numerical insights into an existing masonry bell tower, Soil Dyn. Earth. Eng. (2019) **125**(105752). https://doi.org/10.1016/j.soildyn.2019.105752.
[21] Habieb, A.B., Valente, M., and Milani, G. 2019b. Base seismic isolation of a historical masonry church using fiber reinforced elastomeric isolators, *Soil Dyn. Earth. Eng.* (2019) **120**:127-145. https://doi.org/10.1016/j.soildyn.2019.01.022.
[22] Scacco, J., Salazar, G., Bianchini, N., Mendes, N., Cullimore, C., and Jain, L., Seismic assessment of the church of Carmo convent, in: *Congr. Métodos Numéricos Em Eng.*, (2019).
[23] Scacco, J., Ghiassi, B., Milani, G., and Lourenço, P.B., A fast modeling approach for numerical analysis of unreinforced and FRCM reinforced masonry walls under out-of-plane loading, *Compos. Part B Eng.* (2020) **180**. https://doi.org/10.1016/j.compositesb.2019.107553.
[24] Milani, G., Lesson learned after the Emilia-Romagna, Italy, 20–29 May 2012 earthquakes: A limit analysis insight on three masonry churches, *Eng. Fail. Anal.* (2013) **34**:761–778. https://doi.org/10.1016/J.ENGFAILANAL.2013.01.001.
[25] Valente, M., and Milani, G., Advanced numerical insights into failure analysis and strengthening of monumental masonry churches under seismic actions, *Eng. Fail. Anal.*

(2019) **103**:410-430. https://doi.org/10.1016/j.engfailanal.2019.05.009.
[26] Valente, M., and Milani, G., Earthquake-induced damage assessment and partial failure mechanisms of an Italian Medieval castle, *Eng. Fail. Anal.* (2019) **99**:292–309. https://doi.org/10.1016/j.engfailanal.2019.02.008.
[27] NTC2018. D.M. 17/01/2018 Aggiornamento delle «Norme tecniche per le costruzioni». S.O. alla G.U. n. 42 del 20/02/2018; 2018., (n.d.).
[28] CIRCOLARE 21 gennaio 2019, n. 7 C.S.LL.PP. Istruzioni per l'applicazione dell'«Aggiornamento delle "Norme tecniche per le costruzioni"» di cui al decreto ministeriale 17 gennaio 2018., (n.d.).
[29] Heyman, J., The stone skeleton, *Int. J. of Solids Struct.* (1966) **2**:249–256.
[30] Milani, G., Lourenço, P.B., and Tralli, A., Homogenised limit analysis of masonry walls, Part I: Failure surface, *Comput. Struct.* (2006) **84**:166–180. https://doi.org/10.1016/j.compstruc.2005.09.004.
[31] Milani, G., Lourenço, P.B., and Tralli, A., Homogenised limit analysis of masonry walls, Part II: Structural examples, *Comput. Struct.* (2006) **84**:181–195. https://doi.org/10.1016/j.compstruc.2005.09.004.
[32] Milani, G., Lourenço, P.B., and Tralli, A., Homogenized Approach for the Limit Analysis of Out-of-Plane Loaded Masonry Walls, *J. Struct. Eng.* (2006) **132**:1650–1663. https://doi.org/10.1061/(ASCE)0733-9445(2006)132:10(1650).
[33] Milani, G., Lourenço, P.B., and Tralli, A., 3D homogenized limit analysis of masonry buildings under horizontal loads, *Eng. Struct.* (2007) **29**:3134–3148. https://doi.org/10.1016/j.engstruct.2007.03.003.
[34] Tiberti, S., and Milani, G., 2D pixel homogenized limit analysis of non-periodic masonry walls, *Comput. Struct.* (2019) **219**:16–57. https://doi.org/10.1016/j.compstruc.2019.04.002.
[35] Chiozzi, A., Milani, G., and Tralli, A., A Genetic Algorithm NURBS-based new approach for fast kinematic limit analysis of masonry vaults, *Comput. Struct.* (2017) **182**:187–204. https://doi.org/10.1016/j.compstruc.2016.11.003.
[36] Piegl, L., and Tiller, W., *The NURBS Book*, Springer, Berlin, (1995).
[37] Chiozzi, A., Milani, G., Tralli, A., Fast kinematic limit analysis of FRP reinforced masonry vaults through a new genetic algorithm nurbs-based approach, in *Proceedings of the 7th European Congress on Computational Methods in Applied Sciences and Engineering* **3**, 2016: pp. 5326-5339.
[38] Chiozzi, A., Milani, G., Grillanda, N., Tralli, A., Fast kinematic limit analysis of masonry walls with out-of-plane loading, in: *Proceedings of the 6th International Conference on Computational Methods in Structural Dynamics and Earthquake Engineering* **1**, 2017: pp. 2404-2412. https://doi.org/10.7712/120117.5576.17224.
[39] Chiozzi, A., Milani, G., Grillanda, N., and Tralli, A., A fast and general upper-bound limit analysis approach for out-of-plane loaded masonry walls, *Meccanica.* (2018) **53**:1875–1898. https://doi.org/10.1007/s11012-017-0637-x.
[40] Chiozzi, A., Grillanda, N., Milani, G., and Tralli, A., UB-ALMANAC: An adaptive limit analysis NURBS-based program for the automatic assessment of partial failure mechanisms in masonry churches, *Eng. Fail. Anal.* (2018) **85**:201–220. https://doi.org/10.1016/j.engfailanal.2017.11.013.
[41] Grillanda, N., Chiozzi, A., Bondi, F., Tralli, A., Manconi, F., Stochino, F., and Cazzani,

A., Numerical insights on the structural assessment of historical masonry stellar vaults: the case of Santa Maria del Monte in Cagliari, *Continuum Mech. Therm.* (2019) 1–24. https://doi.org/10.1007/s00161-019-00752-8.

[42] Grillanda, N., Chiozzi, A., Milani, G., and Tralli, A., Collapse behavior of masonry domes under seismic loads: an adaptive NURBS kinematic limit analysis approach, *Eng. Struct.* (2019) **200**. https://doi.org/10.1016/j.engstruct.2019.109517.

[43] Chiozzi, A., Grillanda, N., Milani, G., and Tralli, A., NURBS-based kinematic limit analysis of FRP-reinforced masonry walls with out-of-plane loading, *Fratt. Int. Strutt.* (2020) **51**:9–23. https://doi.org/10.3221/IGF-ESIS.51.02.

[44] Grillanda, N., Valente, M., Milani, G., Chiozzi, A., and Tralli, A., Advanced numerical strategies for seismic assessment of historical masonry aggregates, *Eng. Struct.*, 212(110441). https://doi.org/10.1016/j.engstruct.2020.110441.

[45] Indirli, M., Bruni, S., Geremei, F., Marghella, G., Marzo, A., Moretti, L., Formisano, A., Castaldo, C., Esposito, L., Florio, G., Fonti, R., Spacone, E., Biondi, S., Miccadei, E., Vanzi, I., Tralli, A., Vaccaro, C., and Gambatesa, T., The reconstruction plan of the town of Arsita after the 2009 Abruzzo (Italy) seismic event, in: *9th International Conference on Structuctural Analysis of Historical Constructions*, 2014: pp. 14–17.

[46] Giuffrè, A., *Safety and Preservation of Historical Centers: the Ortigia case*, Laterza, (1993). (In Italian)

12th International Conference on Structural Analysis of Historical Constructions
SAHC 2020
P. Roca, L. Pelà and C. Molins (Eds.)

GENERAL THRUST SURFACE OF MASONRY DOMES

ISTVÁN SAJTOS[1*], ORSOLYA GÁSPÁR[2] AND ANDRÁS Á. SIPOS[3]

[1, 2, 3] BME Budapest University of Technology and Economics
Department of Mechanics, Materials and Structures
H-1111 Budapest, Műegytem rkp 3., Hungary
e-mail: [1] sajtos@szt.bme.hu, www.szt.bme.hu (*corresponding author)
email: [2] gaspar@szt.bme.hu, [3] siposa@eik.bme.hu, www.szt.bme.hu

Keywords: Masonry dome, Thrust surface, Catenary-type membrane surface, Funicular-type membrane surface, membrane shell

Abstract. *Masonry domes are shell-like structures with a no-tension type material behavior [1]. The dome geometry, material behavior and the type of the loading define how the dome balances the load. It is known and proved that the dome could balance the load only by forces, without bending moment but cracks may appear since the material does not resist tension. The surface where the balancing forces are acting is called the thrust surface. The paper introduces the idea of the general thrust surface. It is such a balancing surface where the forces are not acting in the tangent plane of the thrust surface and otherwise it is moment free. A method is shown how to find the general thrust surface for a cracked spherical masonry dome. Numerical example illustrates the usefulness and effectiveness of the proposed method to determine the general thrust surface of a spherical dome when radial stereotomy is considered. By the help of the proposed model the safety of the more than 350 years old, cracked dome of Gol Gumbaz, India can be proofed.*

1 INTRODUCTION

Masonry domes are shell-like structures with a no-tension type material behaviour [1]. The dome geometry, material behaviour and the type of the loading define how the dome balances the load. It is known and proved that the masonry dome could balance the load only by forces, without bending moment but cracks may/will appear since the material does not resist tension. The surface where the balancing forces are acting is called the thrust surface. Generally, this is not coincided by the mid-surface of the dome.

If the balancing forces are acting in the tangent plane of the thrust surface than the thrust surface is called *catenary-type membrane/thrust surface*. It is analogous to the envelope of resultant forces in case of masonry arches. If the membrane/thrust surface coincides with the mid-surface of the dome, then the dome is a *funicular-type shell*, i.e. a membrane shell. Otherwise, the masonry dome is safe if the thrust surface is located within the thickness of the dome, nevertheless cracks might form.

The thrust surfaces, mentioned above, can be examined and determined by e.g. thrust network analysis (TNA) [2, 11, 12] or by solving Pucher's equation for membrane shells, that provides the corresponding stress function [3, 4]. If the dome cracks, then the thrust surface

may still be approximated by the series of thrust lines that correspond to the modified model of the cracked dome, i.e. a series of orange-slice arches [1].

It is possible to find a moment-free surface (i.e. thrust surface) to arbitrary dome geometry and loads. However, depending on the stereotomy of the dome, it is not necessarily a membrane surface. This situation is analogous to the general relation between the resultant force vector and the thrust line in the masonry arch [5]. The term *general thrust surface* is introduced to label such a moment-free surface.

The present paper introduces a method to determine the general thrust surface for a spherical dome geometry for radial stereotomy. The load is defined relative to the mid surface of the dome.

Despite the rich literature investigating the phenomena's 2D equivalent (i.e. effect of stereotomy on the thrust line of masonry arches), to the authors knowledge the presented method is a novel approach in the analysis of domes. It may be shown, that both the *catenary-type* and the *funicular-type membrane/thrust surfaces* are special cases of the general thrust surface.

No-tension material behavior and cracks in particular could lead to a general thrust surface. Numerical example illustrates the usefulness and effectiveness of the proposed method to determine the general thrust surface of a spherical dome.

2 GENERAL DESCRIPTION OF THE PROBLEM

Spherical masonry domes are frequently built in the past and so they are considerable part of the architectural heritage. While the sphere, as a form, is architecturally pleasing, then from structural point of view it is not perfect, for the bottom part of it may be cracked in meridional direction for gravity loads. These crack can be avoided if the sphere has special thickness variation. However, this special thickness variation is unrealistic in the vicinity of the bottom of the dome [6].

In case of real domes, it is a general experience that the dome is cracked in meridional direction like in case of the Pantheon [7] or dome of Gol Gumbaz in India [13]. These cracks may be caused by the self-weight or other effects like temperature changing. Independently of the real cause the main question is if the dome is safe in cracked state or not. Obviously the other important question could be how the cracks are developed due to certain loading considering the real, discrete nature of the cracks.

Now our purpose is to examine if a meridional cracked dome could be in equilibrium for its self-weight. We are looking for a thrust surface which provide the possibility to check the safety of the cracked dome. If the thrust surface is enclosed by the thickness of the dome than the equilibrium is possible.

The model considers the real state of dome such that the top cap part is not cracked, only the bottom one, Fig. 1a.

Assumptions:

- The dome has hemispherical mid-surface and it is loaded by its self-weight.
- It is a masonry dome, made of no-tension material i.e. cracks for tension,
- The top, cap part of the dome is not cracked. Its behavior may be described by the membrane state of a spherical shell.
- The bottom part is cracked in meridional direction. The cracks are through cracks

and it is assumed that they are so dense that no any internal force can develop in the circumferential direction Fig. 1b. Its behavior may be described by the bending theory of shells.

- The top and bottom parts are jointed along a circumferential circle at the top end of the cracks. The crack free cap defines the jointing conditions.
- The bottom edge support can resist both vertical and horizontal forces even when they are eccentric i.e. when bending moment is also acting there.



a) b)

Figure 1: a) Masonry dome with real crack distribution, b) Masonry dome model with dense crack distribution.

3 MASONRY DOME WITH CRACKS

The two parts of the masonry dome, the cap and the cracked bottom part has different model corresponding to the different states. The cap is assumed to behave as a membrane shell which is under compression in both, meridional and circumferential, direction too, i.e. it is crack free. The model of the bottom, cracked part is bending shell model, but the meridional cracks cancel the internal forces in the circumferential direction.

The solutions for the two parts are jointed at the top end of the crack. The crack length is not known in advance so it is a free parameter of the problem. Its effect will be discussed in the chapter 3.4.

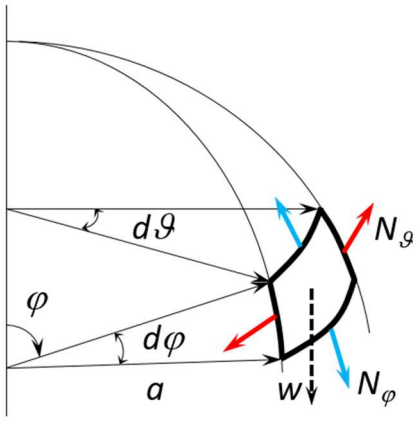


Figure 2: Membrane stet of the cap of the dome

3.1 Solution for the cap of the dome

The cap of the dome is in membrane stress state. The problem is rotationally symmetric as the self-weight as a load is also that kind. There are only two membrane normal forces to balance the load in each, meridional and circumferential, direction, Fig. 2. The equilibrium

equations and its solutions for self-weight is well known in the literature, [8, 9, 10].

It is characteristics for the solution that there is circumferential tension below the so called neutral angle ($\varphi_0 = 51{,}82°$), while the cap part is under compression in both direction, Fig. 3.

So there is a possibility to develop a through, meridional cracks due to circumferential tension even for self-weight. Corresponding to the no-tension material assumption the cracks run up to the neutral angle. Obviously for a real masonry dome material the crack should stop below the neutral angle depending on the tensile strength of the dome material. Otherwise these self-weight caused cracks may propagate further due to other effects like for example temperature changing and traffic caused vibration. Consequently, the cracks may end below or above of the neutral level independently if the self-weight alone could cause it.

That is why it is important to examine and discuss if the cracked dome is in equilibrium in cracked state for any length of the crack.

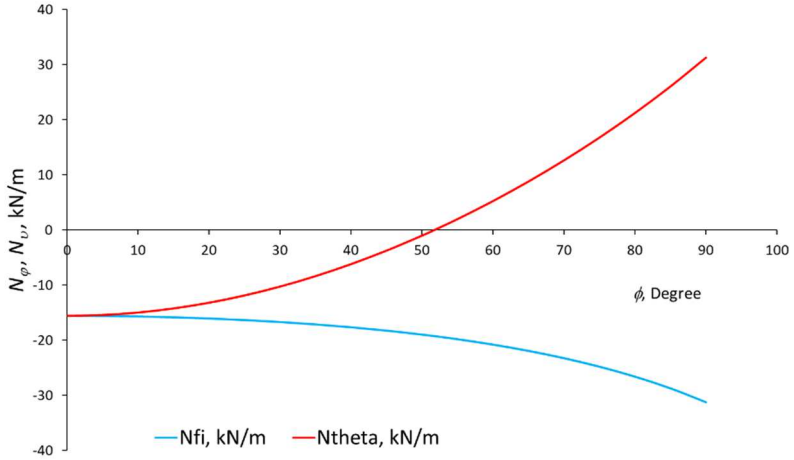


Figure 3: Membrane forces of the dome. a = 5 m, w = 6,25 kN/m^2, t = 38 cm.

3.2 Solution for the bottom, cracked part of the dome

The bottom, cracked part is considered as a bending shell but the meridional, through cracks are so dense that no circumferential internal forces are developed, i.e. there is no resistance into circumferential direction, Fig. 1 and 4. (This is a kind of approximate, "smeared crack" model, although typically there are only 8 -16 discrete cracks in real domes.) However, the bending is effective in the meridional direction and the rotational symmetry of the problem is not altered.

The equilibrium equations of the cracked dome according to the rotationally symmetric bending shell theory are, [8, 10]:

$$\frac{d}{d\varphi}\left(a \sin\varphi\, N_\varphi\right) - a \sin\varphi Q_\varphi + p_\varphi a^2 \sin\varphi = 0, \tag{1}$$

$$a \sin\varphi\, N_\varphi + \frac{d}{d\varphi}\left(a \sin\varphi\, Q_\varphi\right) + p_r a^2 \sin\varphi = 0, \tag{2}$$

$$\frac{d}{d\varphi}\left(a \sin\varphi\, M_\varphi\right) - a^2 \sin\varphi\, Q_\varphi = 0. \tag{3}$$

The equilibrium equation system can be solved without any need of geometrical and

constitutive equation, i.e. *the cracked dome part as a bending shell is statically determinate*.

A closed form solution can be given analytically for self-weight (w, kN/m^2) which is determined by the thickness variation ($t_{(\varphi)}$, cm) and the density of the material of the dome.

For uniform thickness (t) and so for constant self-weight (w), which is the worst case in that sense that the thickness variation is advantageous, the solution is:

$$a \sin\varphi \, N_\varphi = -C_1 \sin\varphi + C_2 \cos\varphi + \tfrac{1}{2} w a^2 \sin 2\varphi, \tag{4}$$

$$a \sin\varphi \, Q_\varphi = -C_1 \sin\varphi - C_2 \cos\varphi + w a^2 \cos^2\varphi, \tag{5}$$

$$a \sin\varphi \, M_\varphi = -C_1 a \sin\varphi + C_2 a \cos\varphi + w a^3 \left(\tfrac{\varphi}{2} + \tfrac{1}{4}\sin 2\varphi\right) + C_3. \tag{6}$$

The C_i-s are integration constants and can be found from the static or natural boundary conditions provided by the cap part of the dome at the top end of the meridional cracks.

For other thickness variations the solutions from (1-3) equations can be found in a similar way.

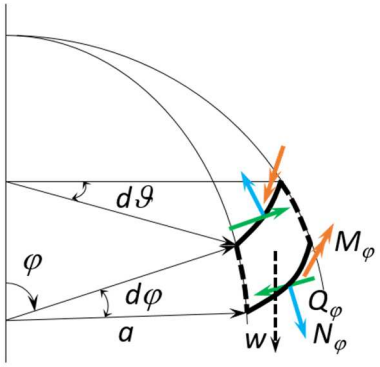


Figure 4: Bending state of the cracked bottom part of the dome

3.3 Jointing the solutions, the effect of crack length on the internal forces

The solution for the cap at the end of the crack gives the boundary conditions for the cracked part. For a chosen crack length ($\varphi = \varphi_0$) the internal forces are determined by the membrane solution. Namely the internal forces of the cracked part at the end of the crack, where $\varphi = \varphi_0$ are: $N_{\varphi(\varphi_0)} = N_{\varphi 0}$, $Q_{\varphi(\varphi_0)} = 0$, and $M_{\varphi(\varphi_0)} = 0$, where $N_{\varphi 0}$ is the membrane meridional force at $\varphi = \varphi_0$.

As it was said earlier the length of the crack, characterized by φ_0, is a parameter of the problem. Keeping in mind that we assumed no tension material behavior the crack end is at the neutral angle. Considering real material behavior with finite tensile strength the crack ends below the neutral level. However due to other effects than self-weight the crack may propagate above the neutral level and the dome must be in equilibrium even in this case too.

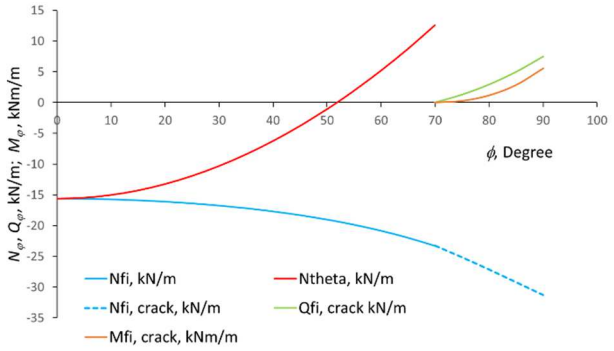
Some numerical results can be seen on Fig. 5 considering all these possibilities. Fig. 5c shows such a case when the crack is longer than what the no-tension case defines. Fig.5b is for the no-tension solution and the Fig. 5a shows the results for finite tensile strength material.

It is a general characteristic of each that the meridional force is not changed considerably for

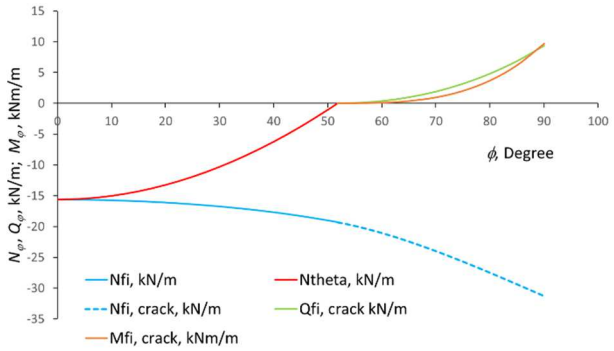
the cracked part. This is due to that the bending shear force is not too large and it is not really effective to balance the load. The meridional bending moment is not too large and it will determine the location of the thrust surface. The transition between the cap and cracked part is "smooth" considering the meridional-, shear force and bending moment. However, the circumferential force has jump at the jointing circle which is a crude estimation of the real behavior.

The connection between the two dome parts in reality is not along a circumferential circle but it is rather a transition zone which is not considered here in the proposed model.

a)



b)



c)

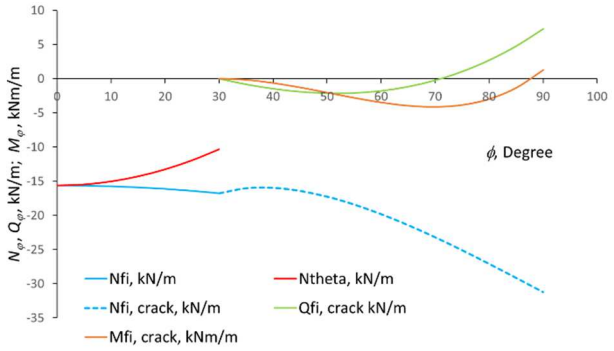


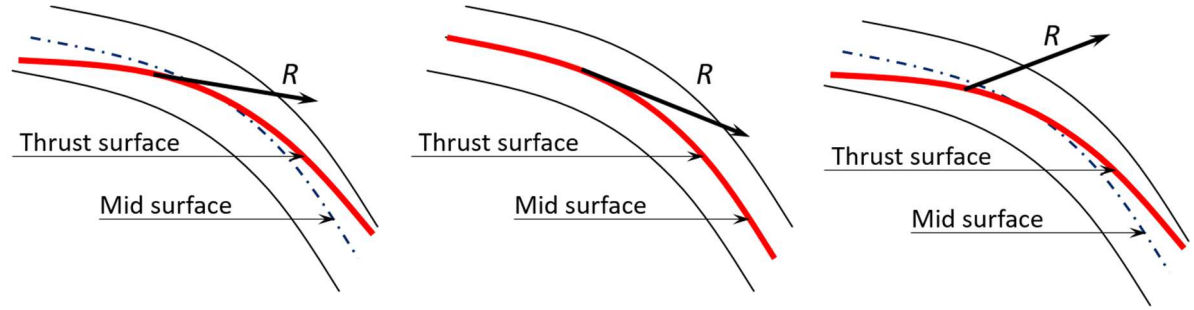
Figure 5: Internal forces of the cracked dome for different crack lengths. a) Crack length is $\varphi = 70°$, b) Crack length is at the neutral angle $\varphi = 51{,}82°$, c) Crack length is $\varphi = 30°$. a = 5 m, w = 6,25 kN/m^2, t = 38 cm.

3.4 Thrust surface of the cracked dome

The thrust line is a commonly used idea and object to examine the safety of masonry arches. The thrust surface is the 3D form of that, and can be understood as such a surface where the resultants of the balancing forces are acting i.e. it is a moment free surface, where only forces are acting. The masonry dome, with no-tension material, is in equilibrium if the thrust surface is inside the thickness of the dome.

Three kind of thrust surface can be distinguished similarly to the thrust lines. If the forces are acting in the tangent plane of the thrust surface than it is called *catenary-type membrane/thrust surface*, Fig. 6a. It is analogous to the envelope of resultant forces in case of masonry arches. If the thrust surface is coincided by the mid surface of the dome and the forces are acting in the tangent plane of the mid surface, then the dome is a funicular-type shell, with *funicular-type membrane/thrust surface*, Fig. 6b, i.e. a membrane shell. If the thrust surface is not coincided by the mid surface of the dome and the forces are not acting in its tangent plane, Fig. 6c, then the thrust surface is called *general thrust surface*.

The shape, location and the type of the thrust surface is influenced by the stereotomy of the dome, i.e. the bonding pattern of the dome masonry. Now we consider only one stereotomy, namely the radial one defined by the polar coordinate system used to give the equilibrium equations of different part of the dome.



a) b) c)

Figure 6: Types of thrust surfaces. a) catenary-type thrust surface, b) funicular-type thrust surface, c) general thrust surface,

Since the cap of the dome is assumed to behave as a membrane shell its thrust surface is a catenary-type thrust surface.

For the cracked part, the thrust surface can be constructed as an eccentricity surface defined by the meridional normal force and bending moment, considering radial cross-sections defined by the polar coordinate-system, Fig. 7. It is a general thrust surface because the resultant of the meridional shear- and normal force is not on the tangent plane of the thrust surface, although it is very close to that.

The Fig. 7 and 8 show the meridional section of the thrust surface for different crack length. It can be seen that (for the assumed dome thickness) the worst crack length is when the crack goes up to the neutral angle. In both other cases when the crack is shorter, or enforced to be longer than the neutral angle is more advantageous in that sense that there is a possibility of the equilibrium for self-weight in cracked state.

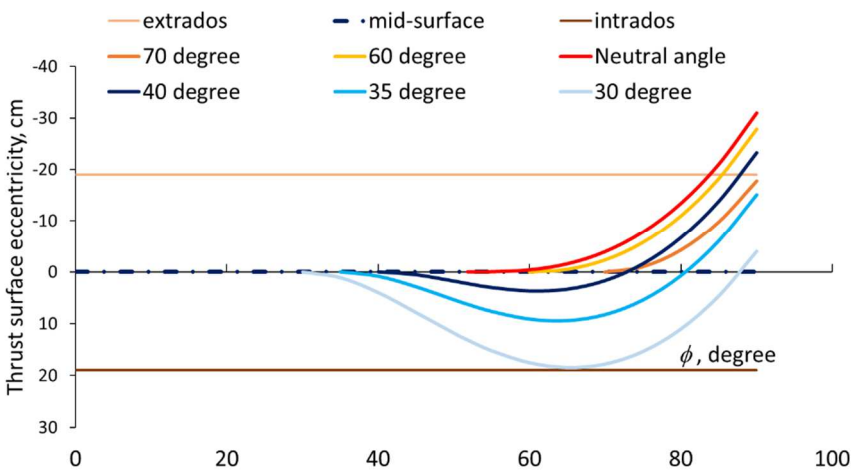


Figure 7: Meridional section of the general thrust surface of the dome for different crack lengths, the thrust surface eccentricity. ($R = 5\ m, t = 38\ cm, w = 6{,}25\ \frac{kN}{m^2}$)

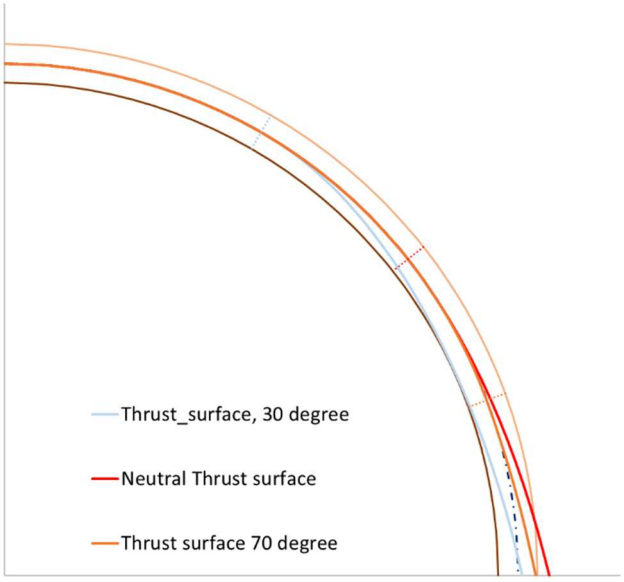


Figure 8: Meridional section of the general thrust surface of the dome for different crack lengths. ($R = 5\ m, t = 38\ cm, w = 6{,}25\ \frac{kN}{m^2}$)

Considering the particular numerical example (Fig. 7 and 8) it may be concluded that the dome is safer than the masonry arch with the same geometry since the development of a (rotational) collapse mechanism has less probability. This is based on that thought (maybe speculation) that if the dome material has tensile strength the crack length is under the neutral level resulting smaller eccentricity at the support. If the eccentricity reaches the extrados i.e. a "plastic" hinge develops at the support, then the crack must move toward the neutral angle.

However, this would increase the eccentricity at the support which is not possible. The only probable possibility that an unstable crack propagation occurs and the crack ends above the neutral angle. This could result an equilibrium state for the dome but there is a possibility to develop another circumferential plastic hinge on the intrados. Nevertheless, this is not probable since only very long cracks make this possibility. Shorter, but ended above neutral level cracks will even close the circumferential plastic hinge crack at the support. A third circumferential plastic hinge would be required to the collapse of the dome which cannot be developed in any case due to self-weight, according to this model.

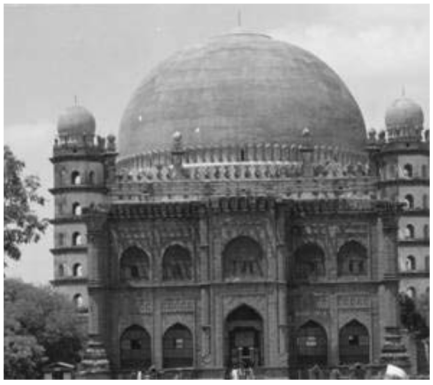


Figure 9: The building and the dome of Gol Gumbaz, India, Bijapur [13]

4 EXAMINATION OF THE DOME OF *GOL GUMBAZ* [13]

The dome of Gol Gumbaz, Bijapur, India was built between 1626 and 1656 (Fig.9). The size of the dome is comparable to the size of the Pantheon. The mid surface radius is 22,1 m and it has a nearly constant thickness, $t = 3{,}0$ m. It is known that there are several meridional cracks on the dome. The cracks end at 4 – 10 m above the terrace level, which is around the springing of the dome. These crack lengths approximately correspond to $\varphi = 70°$ and $\varphi = 80°$ meridional angles, that means the cracks end below the neutral level of the dome according to the membrane theory. This indicates that the tensile strength of the dome material is effective.

The dome was repaired in 1936, after 280 years of construction, certainly having been in cracked state.

The self-weight of the dome is considered to be $60\,\frac{kN}{m^2}$ [13]. The examination of the dome with the given data shows that the experienced cracks result safe equilibrium state for the dome.

Fig. 10. shows the thrust surface eccentricity for the experienced crack lengths. Otherwise Fig. 11. shows the corresponding thrust surfaces. For the shorter cracks the eccentricity is small enough that the dome wall is not cracked in hoop direction. It is suspected that for the longer crack there might be some cracks in hoop direction on the intrados about the springing.

The normal and shear stresses are acceptable and realistic for both crack lengths (see Table 1.) Although there is no information about the strength of the masonry material of the dome it is thought that the masonry made with lime mortar mixed with basalt gravels could easily have at least that strength which is in Table 1.

The calculation clearly proofs the long term experience, that the dome of Gol Gumbaz is safely standing in equilibrium state with the existing meridional cracks.

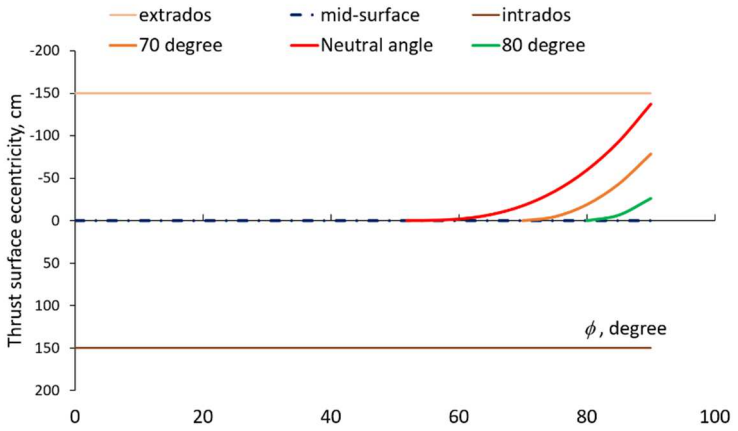
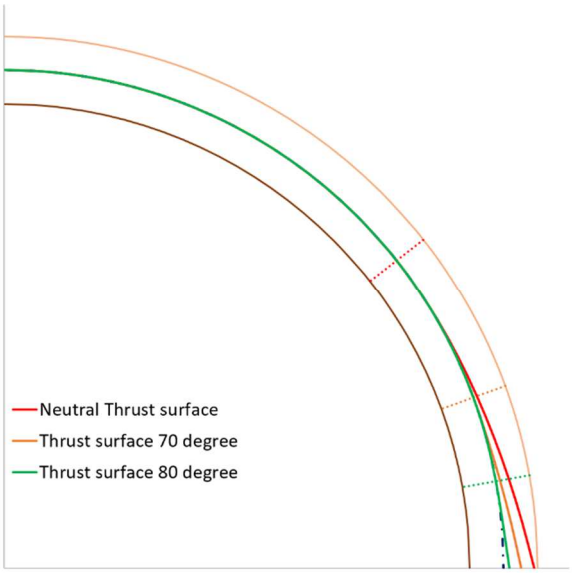


Figure 10: Meridional section of the general thrust surface of the dome of Gol Gumbaz for different crack lengths, the thrust surface eccentricity. ($R = 22{,}1\ m, t = 300\ cm, w = 60\ \frac{kN}{m^2}$)



FiguTable re 11: Meridional section of the general thrust surface of the dome of Gol Gumbaz for different crack lengths, the thrust surface eccentricity. ($R = 22{,}1\ m, t = 300\ cm, w = 60\ \frac{kN}{m^2}$)

Table 1: Calculated data of the dome of Gol Gumbaz, India for existing crack lengths

Crack position ,	e, m	N , kN/m	Q , kN/m	Elastic stress state			Plastic stress state	
				max , kN/m^2	min , kN/m^2	Crack in hoop direction?	$f_{c,req}$, kN/m^2	$f_{v,req}$, kN/m^2
70	0,783	1326	317,5	1233,2	0	**yes**	924,9	147,7
80	0,264	1326	193,2	778,5	314,6	**no**	536,2	64,4

5 CONCLUSIONS

The paper examined the equilibrium of a masonry dome, loaded by its self-weight, in a natural, cracked state. The cracks are meridional through cracks. The cap of the dome was modelled as a membrane shell while the cracked bottom part was considered as a bending shell with a special internal force system related to the meridional cracks. Both parts are statically determinate in that sense that the equilibrium equations alone determine the internal force system. The two solutions were jointed at the end of the meridional cracks.

The internal force system of the cracked dome defines the thrust surface which could be used to examine the safety of the cracked dome.

Three kind of, stereotomy influenced, thrust surfaces may be distinguished: catenary-type, funicular-type and general thrust surface. The paper considers only radial type stereotomy.

Based on the numerical example the following conclusion may be drawn:

- Masonry dome has safe equilibrium state when it is cracked and it may be checked using the thrust surface of the dome,
- The tensile strength of the masonry dome material and the crack length influences or determines the possible, safe equilibrium state,
- It is suspected, based on the suggested model, that there is a possibility of unstable crack propagation in order to reach a safe equilibrium state,
- It seems, that there is no possibility of collapse of the dome for self-weight if the possibility of crack propagation is considered.

The examination of the long term cracked dome of Gol Gumbaz, Bijampur, India gave result corresponding to the more than 300 years of experience. This shows the effectiveness of the proposed simple model.

Finally, the main conclusion could be that the crack propagation process must be considered in order to develop a more precise masonry dome model.

Acknowledgements. The research was supported by the NKFIH Grant 124859 and the FIKP grant of EMMI in the frame of BME FIKP-VÍZ.

REFERENCES

[1] J. Heyman On the shell solution of masonry domes. *Int. J. of Solids Structures* (1967) **3:**227-241.

[2] ed. S Adriaenssens et.al. *Shell structures for architecture. Form finding and optimization.* Routledge, (2014).

[3] F. Fraternali A thrust network approach to the equilibrium problem of unreinforced masonry vaults via polyhedral stress functions. *Mech. Res. Comm.* 37, pp. 198-204 (2010).

[4] A. Baratta, O. Corbi On the statics of no-tension masonry-like vaultas and shells: solution domains, operative treatment and numerical validation", *Ann. of Solid and Struct. Mech.* (2011) **2:**2-4:107-122.

[5] O. Gáspár, A. A. Sipos and I. Sajtos Effect of stereotomy on the lower bound value of minimum thickness of semi-circular masonry arches *Int. J. of Arch. Her.* (2018) **12:**6:899-921.

[6] I. Sajtos, O. Gáspár, A. Á. Sipos Geomery of the crack-free spherical masonry dome. In: C. Lázaro et. al. (eds.) *Form and Force.* Proc. of the 60th Anniversary Symposyum of IASS. CIMNE, Barcelon, Spain (2019), pp.1450-1457.

[7] R. Mark, P. Hucthinson On the structure of the roman Pantheon. *The Art Bulletin* (1986) **68:**1:24-34.

[8] W. Flügge *Stresses in shells.* Springer-Verlag, Berlin, (1960).

[9] P. Csonka *Theory and practice of membrane shells.* Akadémiai Kiadó, Budapest, (1987).

[10] P. L. Gould *Analysis of plates and shells.* Prentice Hall, (1999).

[11] Block, P., & Ochsendorf, J. Thrust network analysis: a new methodology for three-dimensional equilibrium. *Journal of the International Association for Shell and Spatial Structures*, (2007) **48:**3:167-173.

[12] Block, P. Thrust Network Analysis: Exploring Three-dimensional Equilibrium. PhD dissertation, Massachusetts Institute of Technology. Cambridge, USA., (2009).

[13] M. Varma et. al. Stability of masonry dome: Special emphasis on 'Golagumbaz'. In: P.B. Lourenco et. al. (eds.) *Structural Analysis of Historical Constructions. Possibilities of Numerical and Experimental Techniques.* Proc. of the 5th Int. Conf. on Structural Analysis of Historical Constructions, New Delhi, India (2006), pp.1789-1794.

12th International Conference on Structural Analysis of Historical Constructions
SAHC 2020
P. Roca, L. Pelà and C. Molins (Eds.)

GEOMETRIC AND STRUCTURAL INFORMATION FOR THE ANALYSIS OF HISTORICAL DOMES: THE CASE OF THE SS.TRINITÀ CHURCH IN TORINO

GIULIA DE LUCIA[1,3*], **ROSARIO CERAVOLO**[2,3]

[1] Interuniversity Department of Regional and Urban Studies and Planning (DIST)
Politecnico di Torino,
Viale Pier Andrea Mattioli, 39 10125 Torino, Italy
e-mail: giulia.delucia@polito.it

[2] Department of Structural, Geotechnical and Building Engineering (DISEG)
Politecnico di Torino
Corso Duca degli Abruzzi, 24, 10129 Torino, Italy
e-mail: rosario.ceravolo@polito.it

[3]Responsible Risk Resilience Interdipartimental Centre (R3C)
Politecnico di Torino
Viale Pier Andrea Mattioli, 39 10125 Torino, Italy
e-mail: r3c@polito.it

Keywords: Masonry domes, FE models, laser scanner survey, SS. Trinità church

Abstract. *Investigation into the geometric configuration of historical masonry domes is fundamental when studying the structural behaviour of these architectural elements, above all if they have historical and artistic relevance. Indeed, accurate geometric information is essential also for the construction of reliable mechanical models, to monitor the condition state of the building and to plan strengthening and conservation interventions. To this aim, a multidisciplinary approach is required to collate the highest possible amount of data useful for the numerical modelling, including historical and archival research.*

The "SS. Trinità" church is a 16th century building of great historical, architectural and structural significance in the historic centre of Turin. It owes its fame primarily to the architect who built it, Ascanio Vitozzi, and to its large dome, built after the architect's death. The availability of a recently undertaken laser scanner survey of the intrados of the dome made it possible to detect several depressions of the masonry cap. These findings can be either due to construction defects, or to structural problems that developed over centuries, or to the severe fire which struck the dome in 1942.

In this multidisciplinary research, different numerical models of the masonry dome of SS.Trinità church were built. As a first step, a geometric study was based on the point cloud from the laser scanning. Then, structural analyses were conducted on the two different models of the dome-tambour system of the building, in order to try to explain the observed deformation behaviour.

1 INTRODUCTION

Digital technologies are increasingly used in the field of three-dimensional geometric data processing because they permit the integration of several kinds of data and numerous measurements. This is particularly important when dealing with the structural analyses of ancient buildings belonging to the architectural heritage, which are often characterized by complex geometric configurations. Indeed, through current laser scanning technologies, it is possible to design accurate geometric models of buildings and structures, facilitating the design of numerical models to be used for the structural analyses.

By simulating the structural behaviour of a building, numerical models are a very useful tool for planning diagnostic surveys, for evaluating the presence of structural damage or seismic vulnerabilities, and for dimensiong and carrying out conservation and retrofitting interventions. Unfortunately, the design of an accurate numerical model is a complex issue because it requires specific information, strictly related to the historical knowledge of the building, which is hard to be collect and interpret. As far as historical buildings are concerned, uncertainties related to the real geometric shape, the construction techniques or the material characterization often limit the accuracy of the models obtained.

This study regards the structural analyses conducted on the SS. Trinità Church in Torino (Fig. 1) in order to investigate the structural behaviour and the structural health conditions of the building, in particular its masonry dome-tambour system. Masonry domes represent an important element of the Italian architectural heritage, but their conservation is a complex issue due to their geometric and structural complexity. For this reason, the use of accurate numerical models able to simulate their global structural behaviour is a precious tool [1][2][3][4][5]. To this aim, a multidisciplinary approach is required to take into account various kinds of data needed for the most accurate possible design of models. The case study presented is a church with a large masonry dome built at the end of the 16th century under commission from the SS.Trinità confraternity. This is located in the historical centre of the city, near the Royal Palace (ducal palace at that time). The project of the church was requested to the architect Ascanio Vitozzi (1539-1615), a member of the confraternity, who greatly influenced the architectural and urban plan of Torino in the early Baroque age. The church was designed using particular geometric rules based on triangles and hexagons, due to their religious symbolism and referring to the church being dedicated to the Most Holy Trinity. It has a central circular plan, with a main altar and two secondary ones. The cylindrical masonry structure is concluded by a massive cornice which support the dome-tambour system, and the church reaches a height of 50 metres [6][7][8].

This work aims to investigate the structural behaviour of the SS.Trinità church through numerical models designed from an accurate initial knowledge of the building and geometric data acquired by traditional and digital survey technologies. In fact, given the lack of specific archive literature (burnt during the 1942 bombardments), the recent laser scans of the church provide accurate geometric data and information on the current state of the structure.

The subsequent structural analyses allow the structural behaviour of the building to be evaluated and also some preliminary assumptions to be made on the possible causes of the deformations.



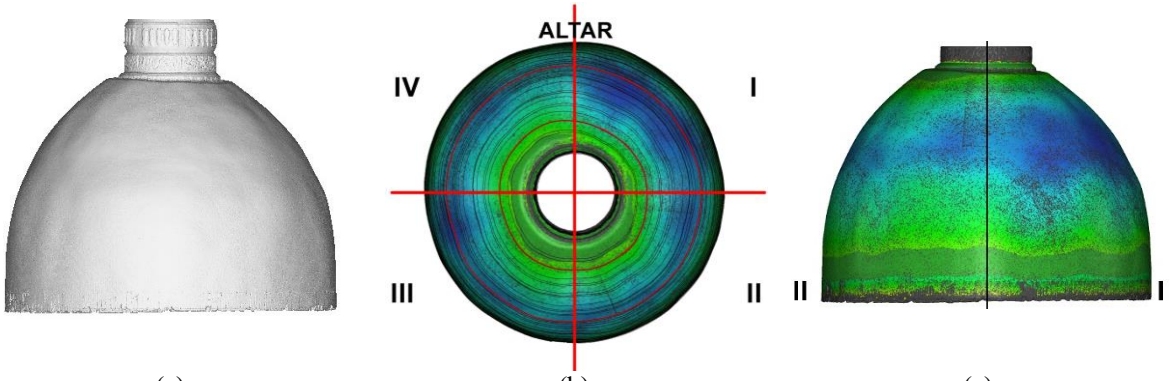
(a) (b)

Figure 1: The SS. Trinità church in Torino: (a) outside view; (b) inside view.

2 THE LASER SCANNER SURVEY OF THE DOME

During the recent restoration work conducted on the church of SS. Trinità, a laser scanner survey of the intrados of the dome was performed. The scanning was conducted using a LEICA BLK360 instrument and the scans were obtained from six measure points with a final resolution of one point for every 5 millimetres. Then, the scans were elaborated as a point cloud. Given access to this point cloud allowed the current shape of the dome to be investigated in this study.

The point cloud was transformed into a mesh, which was the starting point for the design of an accurate geometric model of the dome. The complex geometry of the building and its dome, both in plan and in section, have already been the subject of several geometric studies highlighting the compositional skills of Vitozzi [9]. However, the mesh shows several irregularities and depressions on the intrados of the dome, which are easily visible (Fig.2a). In Figures 2b and 2c, elaborated through 3DReshaper® digital software, the deformations are more evident. They are especially located on the northern side of the dome, to the right of the main altar. For convenience sake, the dome was subdivided in four dials, starting from the main altar, in a clockwise direction. In this scheme, the main deformations are located in the first dial.



(a) (b) (c)

Figure 2: Deformations on the intrados of the dome: (a) the mesh; (b) 3DReshaper elaboration of the deformations, plan view. Red lines indicate the dials subdivision; (c)3DReshaper elaboration of the deformations. Right front view. In blue the areas with the most marked depressions.

In order to have the most complete knowledge possible of the geometry, data from the mesh were compared and integrated with studies conducted on the only one existing archive drawing of the dome. This drawing is not a project drawing but a traditional geometrical survey conducted in 1792 and takes into account only one half of the dome. This cannot be intended as a design drawing but it can be interpreted as a representation of the initial state of the dome. This comparison was useful in order to quantify the deformations of the dome, by considering section line in the drawing and measuring the discrepancies. The discrepancies reach values of 19 cm in some areas of the intrados (Fig. 3) such as in the fourth section (I-III dials). In the same section, the discrepancies on the other side are 10cm.

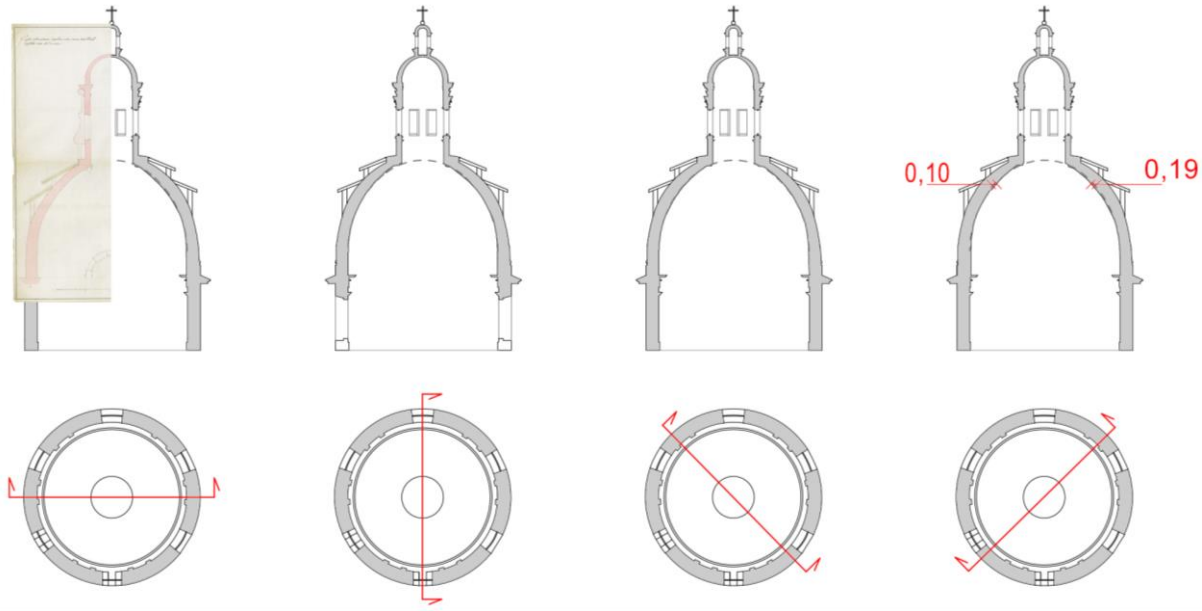


Figure 3: Measuring of the deformations of the intrados in relation to the section line (dropped line). In the first section view, the superposition of the archive drawing can be observed.

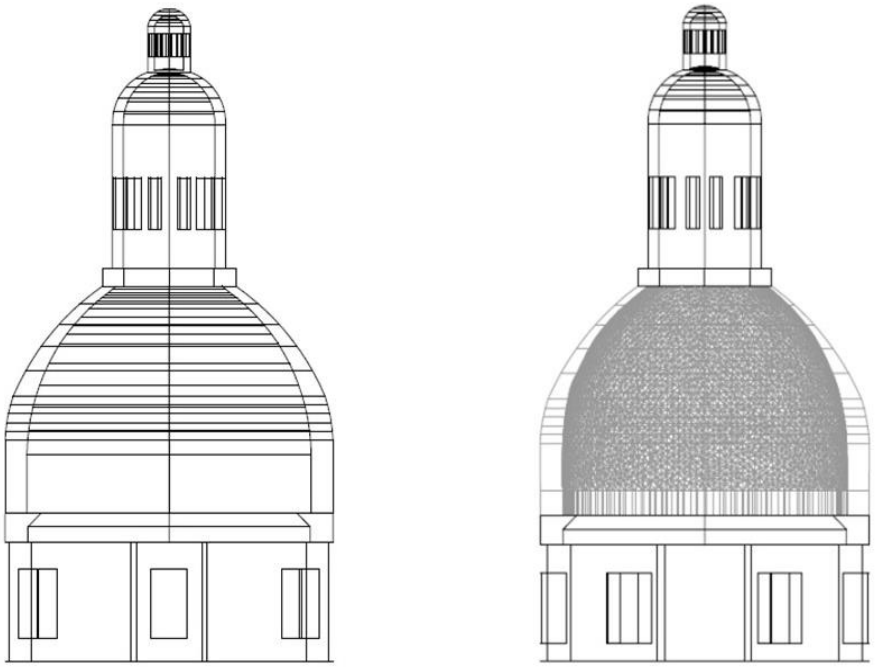
3. THE FE MODELS OF THE DOME

In order to investigate the structural behaviour of the dome-tambour system and to increase knowledge about the deformations observed on the first dial the dome, structural analyses on a numerical model had to be carried out. In this study, two different solid element models were used, both built with a macro-modelling approach and the DIANA code.

The first model is an elastic linear model representing an idealised configuration of the dome, without defects or deformations (model-I). The shape of the dome was created with a simple revolution solid of the profile section obtained from the archive drawing. Then, the model was completed with the tambour and the lantern (Fig.4a). The second model reproduces the current configuration of the dome as resulting from the survey (model-R). This model was created by using directly the geometric information obtained from the scans (Fig.4b). Tambour and the lantern were also added to model-R. They were modelled from simple revolution solids, as in the previous case, because the available scans were referred only to the dome area.

It is worth mentioning that, whenever possible, structural analyses of historical domes should be conducted on models that precisely follow the real configuration of the structures. Indeed, for an accurate investigation of the structural behaviour, possible deformations should not be neglected because they can play an important role.

As far as the material characterisation is concerned, historical masonry requires specific knowledge and investigations on their mechanical characteristic, as well as its production and construction techniques. The mechanical parameters of historical masonry should be evaluated through in situ experimental investigations, but such analyses are often too invasive for buildings that belong to the historical architectural heritage. To this regard, data from the literature can usually be used when dealing with preliminary investigations.



(a) (b)

Figure 4: Geometric models of the dome-tambour system of the SS. Trinità Church: (a) model-I; (b) model-R.

In this study, the parameters of the linear model-I were taken from the study by Pistone and Roccati [10], who conducted the material characterization of the masonry of a building in Torino almost contemporary to this case-study. For the non-linear model-R, a standard elastoplastic model based on the Drucker-Prager (DP) criterion was used, considering the masonry as a material with isotropic behaviour and plastic deformations [11]. Even in this case, data about the elastic phase and resistance of the masonry were taken from the literature [12]. Table 1 shows the mechanical parameters used for the two models.

Then, vertical loads and the snow load were applied to the dome, in addition to the punctual loads related to the two roofs placed on the extrados of the dome. Both models were constrained at the base of the tambour assuming the rest of the building as very stiff.

Table 1: Mechanical parameters used for the masonry of the SS.Trinità church

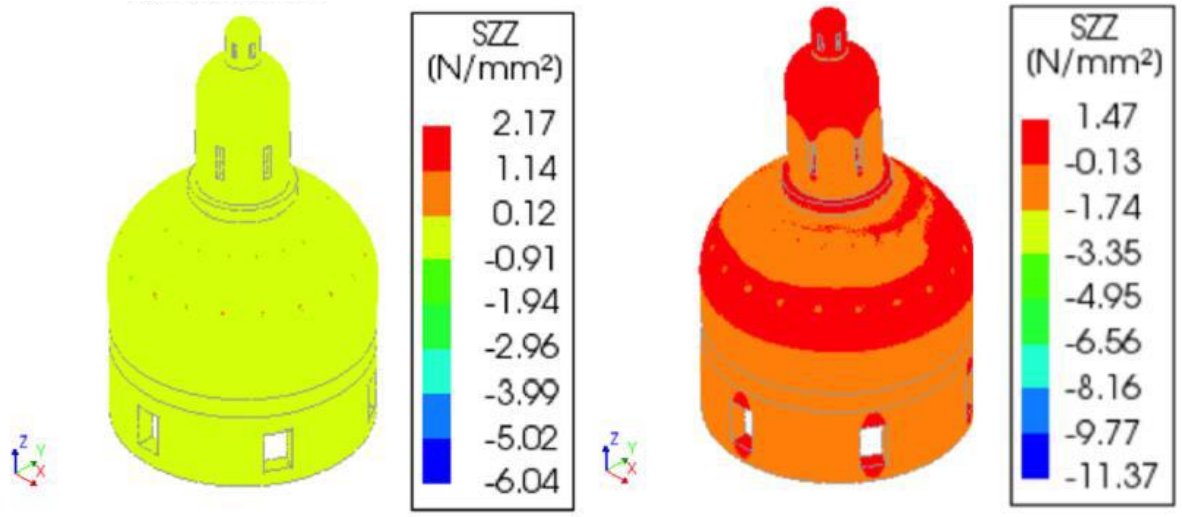
E [MPa]	v[-]	γ [kN/m^3]	c [MPa]	φ [°]	δ [°]	f_c [MPa]	f_t [MPa]
1750	0.25	18	0.24	38	15	4.36	0.24

4. THE STATIC ANALYSES

Static analyses were conducted with the aim of obtaining information about the global structural behaviour of the dome-tambour system and in order to investigate the possible causes of the appearance of the deformations and their influence on the structural state of the building. In fact, the deformations could be due to construction defects and imperfections, to structural problems which appeared over time, or to the severe fire experienced by the dome in 1942. It is important to note that investigations in this field is also deemed to contribute to the historical critical debate. Indeed, some questions about the paternity of the dome, built after Vitozzi's death, still remain unanswered, while doubts remains that the current shape of the dome is that designed by Vitozzi, considering the absence of project drawings [9]. This highlights the importance of a multidisciplinary approach, necessary when dealing with cultural heritage architecture.

Although the assumption of an elastic behaviour for the masonry does not correspond to its real behaviour, such a basic model can be useful in a preliminary stage because it sheds some light on the stress distribution and the displacements affecting the dome. The results of the linear analyses conducted on model-I, and the non-linear analyses conducted on model-R are reported in terms of vertical stress and displacements.

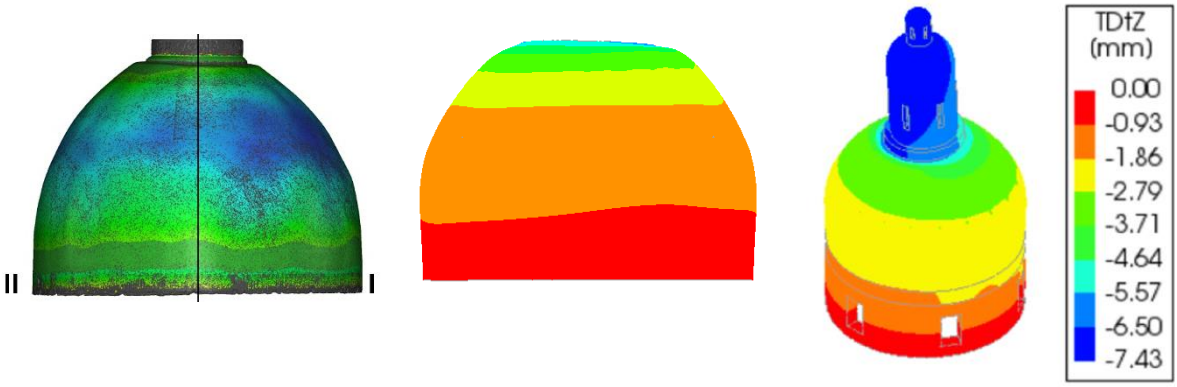
According to both models, the stress state due to the constant vertical loads is moderate: the average compression stress on the extrados of the dome is 1.7 N / mm^2 for the non-linear model and 0.9 N / mm^2 for the linear model. These are expected values in domes and confirm that the structure is able to support the loads to which it is subjected. As far as the representation of the vertical stress is concerned, a horizontal band distribution is visible in linear model-I (Fig. 5a). However, of greater interest is the distribution of the stress state on non-linear model-R. In fact, positive values of stress at the top of the lantern and at the central horizontal band of the dome can be noted, as well as a gradient in the area if the first dial (Fig. 5b). This behaviour is related to the non-linearity of the model which takes into account the real geometry of the dome.



(a) (b)

Figure 5: Representation of the vertical stress: (a) linear model-I; (b) non-linear model-R.

It is also interesting to observe the results of the analyses in terms of vertical displacements. For model-I the vertical displacements obviously have a homogeneous distribution along the parallel of the dome, but for model-R the structural deformations cause an asymmetric displacement field. In particular, higher displacements can be observed at the base of the lantern in the third dial, exactly on the opposite side to the area with the main deformations, to which the eccentricity of the lantern seems to correspond. The effect of this eccentricity is a compression increment at the base of the dome on the third dial and a decompression increment on the first dial. The decompression results in greater inflexion values on the first dial area measured at the same height levels, in particular on the area affected by the largest deformations. This effect is clearly observed in Figure 6.



(a) (b) (c)

Figure 6: (a) representation of the structural deformations on the dome; results of the non-linear analysis in terms of vertical displacements: (b) front view; (b) axonometric view.

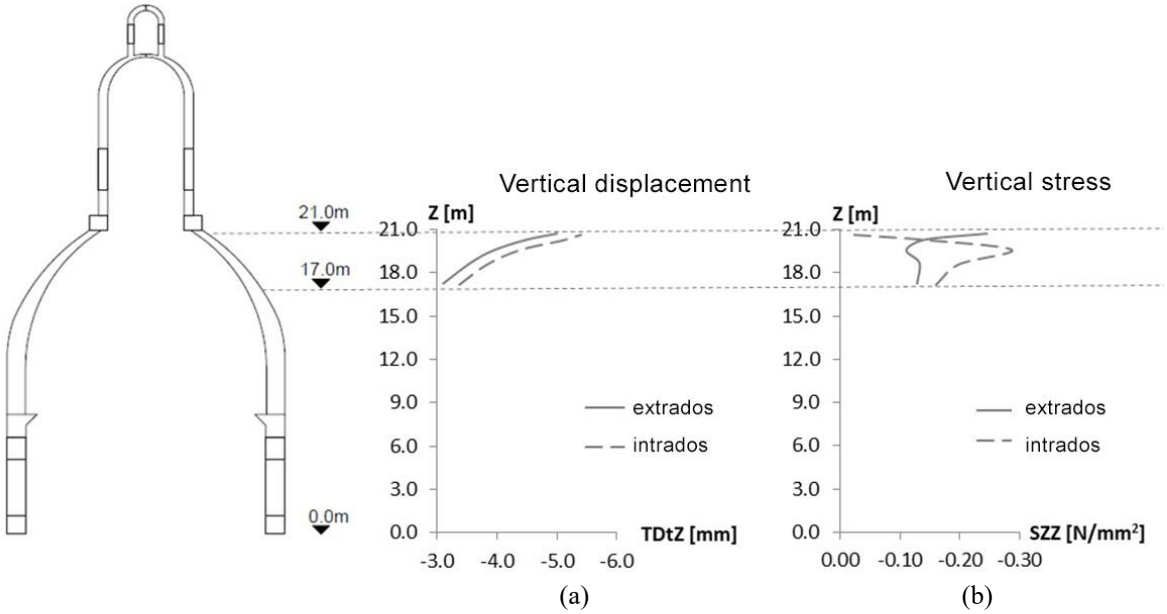
From the plan view, in Figure 7, it is possible to notice the high level of vertical displacements at the base of the lantern on the third dial. This configuration is totally in agreement with what was observed in the scans, where it is easy to note a lateral lowering of the lantern.



(a) (b) (c)

Figure 7: Deformations on the intrados of the dome: (a) the mesh; (b) zoom of the lantern area; (c) results of the non-linear analysis in terms of vertical displacements, top view.

In order to examine in depth the displacement trends by analysing both the internal and external surfaces of the dome, five reference heights were defined, each of which at a relevant increment of displacement value. Then, the vertical displacement and stress values on the nodes located at the intrados and the extrados of the dome were obtained. The detail in Figure 8 shows that, in the area between a height of 17 and 21 metres (measured from the impost of the tambour), the displacement values for both intrados and extrados increase with the increasing height. As far as the vertical stress is concerned, the values measured on the extrados follow the same trend while in contrast they decrease on the intrados.



(a) (b)

Figure 7: Values of vertical displacement (a) and vertical stress (b) for the nodes of the both extrados and intrados in the area of the dome considered between a height of 17 and 21 metres.

4.1 Viscoelastic behaviour of the dome

Simplified viscoelastic analyses (creep) were conducted in order to investigate whether a possible cause of the depressions observed around the dome can be related to the viscous long-term behaviour of masonry.

The method used for plotting long-term displacement curves was taken from the literature [13], assuming the mortar be the viscous phase of the masonry material. The data on the mortar came from constant compression tests reported in the literature [14]. However, the use of a single trend of a mortar test was not sufficient to estimate the viscous behaviour of the masonry. Consequently, a physical model, able to simulate the global behaviour of the material, was deemed necessary.

By setting the viscous phase vs. elastic phase ratio equal to 1:4, the creep function of masonry was obtained. Hence the deformation was calculated accordingly, as a function of the stress history. In order to observe the creep effects on the masonry, the study of the load effect over time in different temporal steps is required. In Figure 9 the evolution over time of the vertical displacement values is shown. They start from a value of shortening equal to 7.6 mm for the first out of 15 steps in a 55-year period, to reach a maximum value of 20.2 mm for the last temporal step.

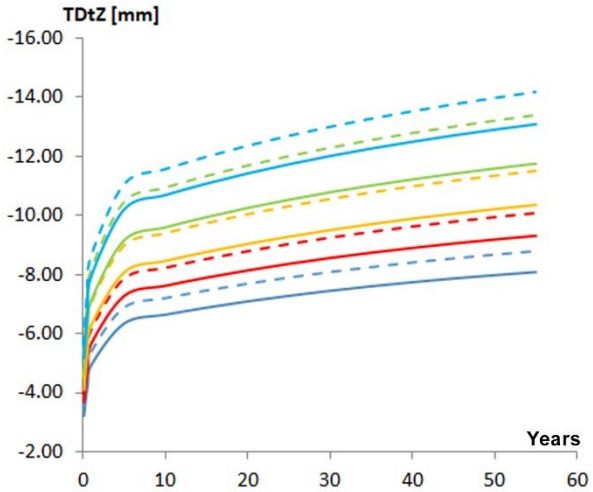
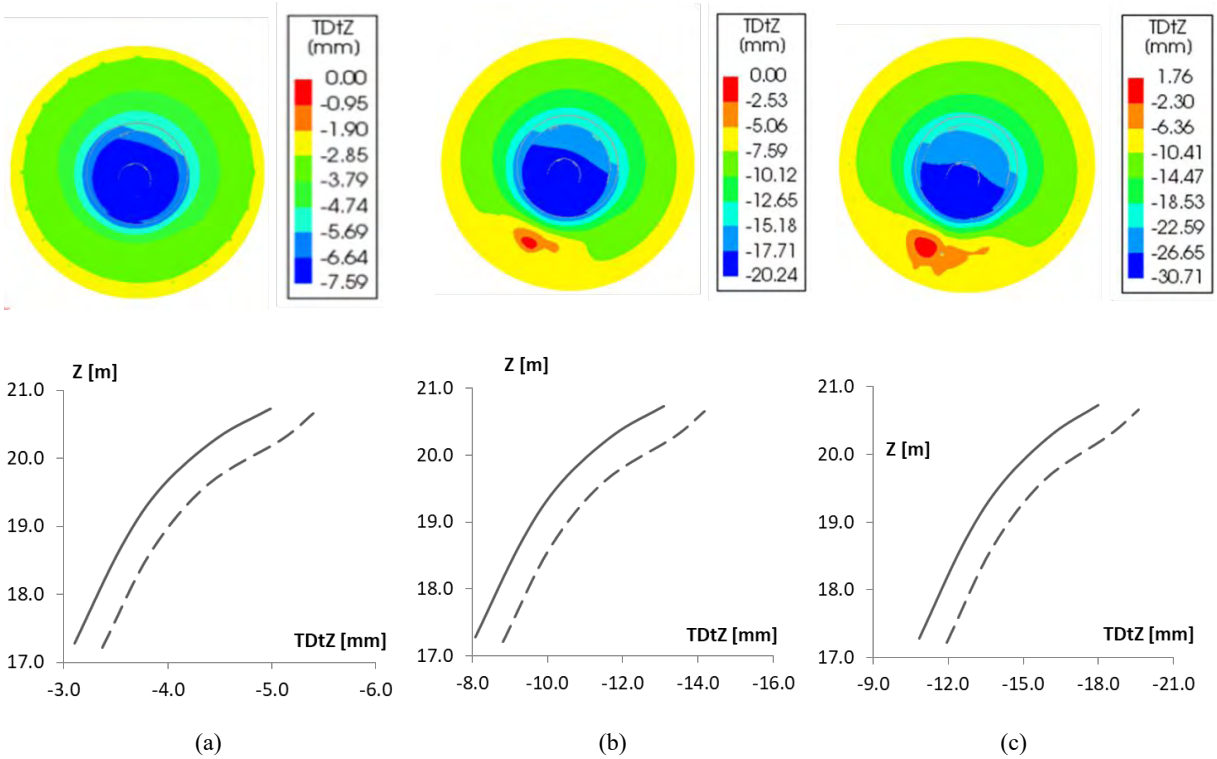


Figure 9: (a) the Vertical displacements over time for the extrados (continuous line) and the intrados (dotted line). The value are measured at five height points (17.2 meters: blue line; 18.7m red line; 19.6 m yellow line; 20.3m green line; 20.7 light blue line).

The model confirms the first dial of the dome to be the more affected by viscous phenomena, in accordance with the observation. In Figure 10, the vertical displacement values are plotted as a function of time, extending the creep analysis to a period of 400 years (approximately the age of the dome). While the deformations measured by the laser scanner survey are in accordance with the elastic and viscoelastic deformations obtained from the creep analyses, these results represent a qualitative value awaiting more in-depth investigations, also due the lack of accurate data on the materials.



(a) (b) (c)

Figure 9: Vertical displacement values as a function of time : (a) 30 days; (b) 55 years; (c) 400 years.

CONCLUSIONS

This study investigated the potentialities of using accurate geometric survey data for the structural analysis of buildings belonging to historical architectural heritage and characterized by complex geometric configuration.

The geometry of the large dome of the SS.Trinità church in Torino was the starting point for creating a realistic mechanical model of the dome-tambour system. Finite element models confirm that geometric deformations observed on the dome are not alarming for the current structural health of the building. Moreover, it was observed that the depressions, possibly due to the construction defects and imperfections can have an important influence on the stress and deformation state of the dome, importantly affecting the global behaviour of the structure. Moreover, creep analyses demonstrated that also viscous deformations can play a role in the static configuration and consequent anomalies. In this specific case, the numerical model showed that the observed leaning of the lantern system, as evidenced by the digital survey, can be the cause of a decompression on a side of the dome, and the consequent depressions in the intrados. Although this research represents only a preliminary study, the results can still support some qualitative, but useful, structural engineering evaluations. It might as well help historians finally resolve the controversy on paternity of this dome, which has long been committed the scientific community. Future studies will address the influence of the fire caused by the World War II events.

REFERENCES

[1] De Lucia, G., Ceravolo, R., Chiorino, M.A., Miraglia G., *The role of structural health monitoring in the seismic protection of monumental structures: the virtual lab of the sanctuary of Vicoforte,*proceeding of VII Structural World Engineering Congress, Istanbul, 24-26 Aprile (2019).

[2] Como, M., *Statica delle costruzioni storiche in muratura*, Rome, Italy, Aracne Editrice, (2010).

[3] Ottoni F,. Dome Strengthening By Encircling Ties: A Monitored Experiment, *Int J Archit Herit*. (2015), **9**:82-95.

[4] Ottoni, F., Blasi C., Hooping as an ancient remedy for conservation of large masonry domes, Int. J. Archit. Herit., (2015), 1**0**:164-181.

[5] Cavalagli N. & Gusella V., Dome of the Basilica of Santa Maria degli Angeli in Assisi: Static and Dynamic Assessement, *Int J Archit Herit* (2015), 9: 157-175.

[6] Scotti, A., *Ascanio Vitozzi. Ingegnere ducale a Torino*, La nuova Italia Editrice, Firenze, (1969), p. 18.

[7] Viglino Davico, M., La chiesa della Santissima Trinità. In Viglino Davico, Ascanio Vitozzi. Ingegnere militare, urbanista, architetto (1539-1615), Quattroemme, Perugia (2003), pp. 231-242.

[8] Ruffino, M. (Eds): *Una chiesa per il Ducato, la Ss. Trinità di Torino,* Torino, CLUT, (2019).

[9] De Lucia, G., Lenticchia E., Ceravolo R., La geometria della cupola della SS.Trinità: dal dato metrico alle valutazioni strutturali, In Ruffino, M. (Eds): *Una chiesa per il Ducato, la Ss. Trinità di Torino,* Torino, CLUT, (2019), pp. 117-142.

[10] Pistone G. and Roccati R., *Testing of large undistributed sample of old masonry*. In Proceeding of the 8th International Brick/Block Masonry Conference, Dublin, 19-21 September (1988).

[11] Drucker D. and Prager W., Soil mechanism and plastic analysis or limit design, *Quarterly of Applied Mathematics*, (1952), **10**:157-165.

[12] Betti, M., Galano, L., Vingoli A., Finite element modelling for seismic assessment of historical masonry buildings. In: D'Amico, S. (Eds), *Earthquakes and their impact on society*, Springer, Switzerland, (2016), pp. 377-413.

[13] Spina, A., *Analisi degli effetti del comportamento a breve e lungo termine di torri in muratura: il caso della torre campanaria del Duomo di Torino.* Thesis in Civil Engineering, Politecnico di Torino, 2018.

[14] Cominelli S., *Comportamento delle murature storiche al collasso: meccanismi di rottura, effetti del confinamento e fenomeni reologici*. PhD Thesis, Università degli studi di Brescia, 2014.

12th International Conference on Structural Analysis of Historical Constructions
SAHC 2020
P. Roca, L. Pelà and C. Molins (Eds.)

IN-PLANE BEHAVIOUR OF AN IRON-FRAMED MASONRY FAÇADE: COMPARISON BETWEEN DIFFERENT MODELLING STRATEGIES

THOMAS CELANO[1*], LUCA U. ARGIENTO[2], BARTOLOMEO PANTÒ[3], FRANCESCA CERONI[1], CLAUDIA CASAPULLA[2], IVO CALIÒ[4], PAULO B. LOURENÇO[5]

[1] Department of Engineering
University of Naples Parthenope
Centro Direzionale is.C4, 80143 Napoli, Italy
*e-mail: thomas.celano@uniparthenope.it
e-mail: francesca.ceroni@uniparthenope.it

[2] Department of Structure for Engineering and Architecture
University of Naples Federico II
Via Forno Vecchio, 80134 Napoli, Italy
e-mail: lucaumberto.argiento@unina.it
e-mail: casacla@unina.it

[3] Department of Civil and Environmental Engineering, Imperial College London,
Exhibition Road, SW7 2AZ London, United Kingdom
e-mail: b.panto@imperial.ac.uk

[4] Department of Civil Engineering and Architecture,
University of Catania,
Via Santa Sofia, 54, 95125 Catania, Italia
e-mail: icalio@dica.unict.it

[5] Institute for Sustainability and Innovation in Structural Engineering (ISISE),
Department of Civil Engineering, University of Minho,
Campus de Azurém, 4800-058 Guimarães, Portugal
e-mail : pbl@civil.uminho.pt

Keywords: Historical Structures, Masonry, Metallic reinforcement, Finite Element Modelling, Discrete Macro-Element Modelling, Non-linear Static Analysis

Abstract. *The 'baraccato' system is a construction technique with genius earthquake resilient features, used for the reconstruction of the historical city centres in the South of Italy after the catastrophic events occurred in the 18th-19th centuries. A very interesting example of such a building typology is represented by the Church of Santa Maria Maddalena, located in the municipality of Casamicciola Terme of the Ischia Island and built in 1896, after the*

catastrophic earthquake of 1883. The church is characterized by a mixed 'baraccato' system mainly made of yellow tuff block masonry walls strengthened by iron profiles or wooden elements. The reduced damage suffered by the church after the seismic event of 21st August 2017 evidenced the good behaviour of such a mixed structural system, especially into avoiding out-of-plane mechanisms. The presence of the iron-framed system is even more challenging in the definition of the modelling strategies for the structural analysis of the church. Thus, the choice of an appropriate numerical strategy to be used for nonlinear simulation should be properly investigated since the interaction between the frame elements and the elements representing the masonry walls has to be considered. As a first step of the structural analysis of the whole church, the in-plane behaviour of the main façade of the Church of Santa Maria Maddalena is analysed in this paper, with the aim to evaluate the efficacy of different modelling strategies. In particular, the study considers different models according to Finite and Discrete Element strategies available within DIANA FEA [1] and 3DMacro [2] software, respectively. Non-linear static analyses are carried out by means of both software and the obtained results are compared and discussed with the aim of extending them to the study of the whole church.

1 INTRODUCTION

After the catastrophic seismic events occurred in Southern Italy in the 18th-19th centuries, the 'baraccato' system was the most accredited construction type imposed by the kings of that time to withstand seismic actions [3]. Other types of mixed timber-masonry buildings can be found throughout the world, such as the 'Pombalino' system in Portugal [4], the 'Dhajji Dewari' in Central Asia [5] or the 'Himis'' system in Turkey [6]. Even in Greece [7] and in other European countries there are mixed structural systems made of timber frames infilled by masonry. The Borbonic "casa baraccata" [8] is certainly an example of the avant-garde engineering of the 18th century. The engineers of that time understood, indeed, that the presence of timber frames as reinforcement elements for masonry buildings allows to obtain mixed systems with greater capacity to resist earthquakes, thanks to an improved global behaviour, i.e. the so-called 'box-behaviour'.

Recent studies on the 'baraccato' system, concerning both experimental tests and numerical modelling [9], have shown the effectiveness of the timber frames in terms of increase of dissipative and resistant capacity in comparison with unreinforced masonry structures. However, due to the high variability of the geometrical configurations, i.e. single square or rectangular modules, presence of one or two diagonals, one or more timber frames, etc., it is not possible to generalize the results for any type of 'baraccato' system. Certainly, the structural behaviour is characterized by an increase in stiffness, strength capacity and ductility. Numerical modelling of the timber-framed masonry system is, therefore, an important research topic worthy to be investigated.

Thanks to the in-situ surveys carried out after the Ischia earthquake of 21st August 2017, several masonry structures made with a 'baraccato' system came into the light, revealing the widespread use of this earthquake-resistant system in the reconstruction of the island after the catastrophic event of 1883. In particular, in Casamicciola Terme, an extraordinary and atypical 'baraccato' system emerged in the church of Santa Maria Maddalena [10, 11]. The church was rebuilt after 1883 using a mixed timber and iron 'baraccato' masonry system, which, thus, makes it as a 'unicum'.

This paper is focused on the study of the in-plane behaviour of the main façade of the Santa Maria Maddalena church through Finite Element and Discrete Macro-Element analyses using the software DIANA FEA and 3DMacro, respectively. In particular, pushover analyses are performed using both software, in order to compare the numerical results and suggest indications about the best modelling strategy for reliably investigating the structural behaviour of the whole church.

2 NUMERICAL MODEL OF THE FAÇADE OF THE SANTA MARIA MADDALENA CHURCH

2.1 The church and the geometry of the façade

The church of Santa Maria Maddalena was built in the Ischia Island (Napoli, Italy) soon after the catastrophic seismic event of 1883, using a mixed construction typology. As shown in Figure 1a, it can be divided into two parts: the main part was realized with an innovative iron 'baraccato' system where the masonry walls are encaged in slender iron frames, while the rear part (sacristy, priest's house, library) was made of a timber 'baraccato' system. While the timber 'baraccato' is more traditional and was diffusely used in the Ischia Island and all over the world, the other was very rare and innovative for that time, also in consideration of the more recent diffusion of iron and steel as structural elements.

The main function required to the iron-framed system was to avoid the out-of-plane mechanisms of the walls and ensure a box-like behaviour of the whole structure. The efficiency of such a mixed 'baraccato' system as earthquake-resistant structure was recently observed after the seismic event of 2017, since the damage in the church only consisted in cracks related to the in-plane response and mainly caused by the expulsion of plaster along the iron reinforcement elements (Figure 1b).

The in-plane behaviour of the iron-framed masonry façade of the church is investigated in the following, starting from the description of its geometry. The façade presents a vertical symmetric axis and two openings, one corresponding to the rose window and the other to the main door of the church (Figure 1c). In elevation, there are two different heights for the central nave and the side aisles. The height of the façade corresponding to the central nave is 15.9 m and 13.1 m, with and without the gable, respectively, while the height of the two parts corresponding to the side aisles is 8.7 m. The width of the central nave is equal to 9.0 m, while the whole façade has a total length of 16.9 m (Figure 2a).

2.2 Materials

The façade is characterized by a mixed 'baraccato' system made of tuff masonry strengthened by iron profiles (Figure 1d). The tuff blocks are rather regular and have dimensions of 0.27 m x 0.23 m in the plane of the wall, and thickness of 0.15 m; the stones are arranged along two faces with an internal core filled with rubble material, following the traditional technique of "sacco" masonries, with a total thickness of about 0.6 m. The vertical iron elements are T-shaped profiles with dimensions 100 mm x 70 mm x 10 mm, while all the other elements (horizontal and diagonal members) have a rectangular cross section with dimensions 50 mm x 20 mm.

Due to the lack of in-situ experimental tests on the materials used in the church, average

values, available in the literature, are assumed in the numerical analyses for the assessment of their mechanical properties. As regards the yellow tuff blocks, a compressive strength of 1.4 MPa [12], a tensile strength of 0.15 MPa, a Young's modulus of 880 MPa, a Poisson's ratio of 0.2, and a specific weight of 14 kN/m^3 are assumed [11]. For the iron elements, a nominal strength of 235 MPa and a Young's modulus of 153000 MPa are assumed in agreement with the range of values reported by [13] for the wrought iron.

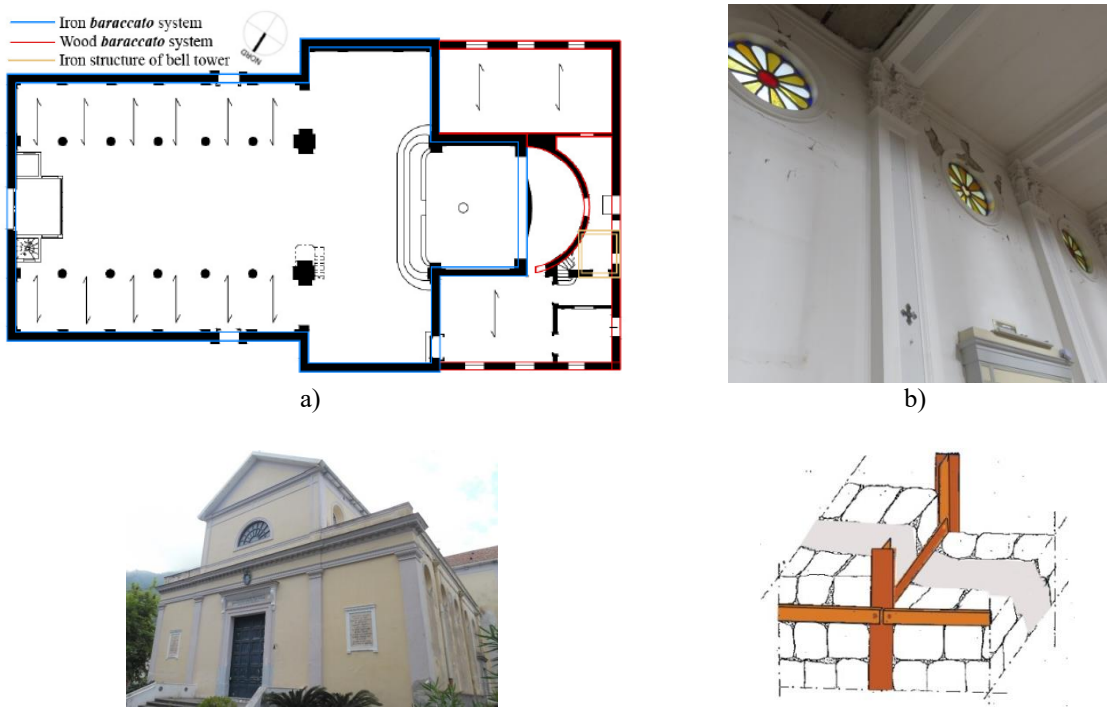


Figure 1: a) Plan of the Santa Maria Maddalena Church with the different construction typologies [10]; b) cracks observed after the seismic event of 2017; c) main façade of the church; d) detail of the iron 'baraccato' system

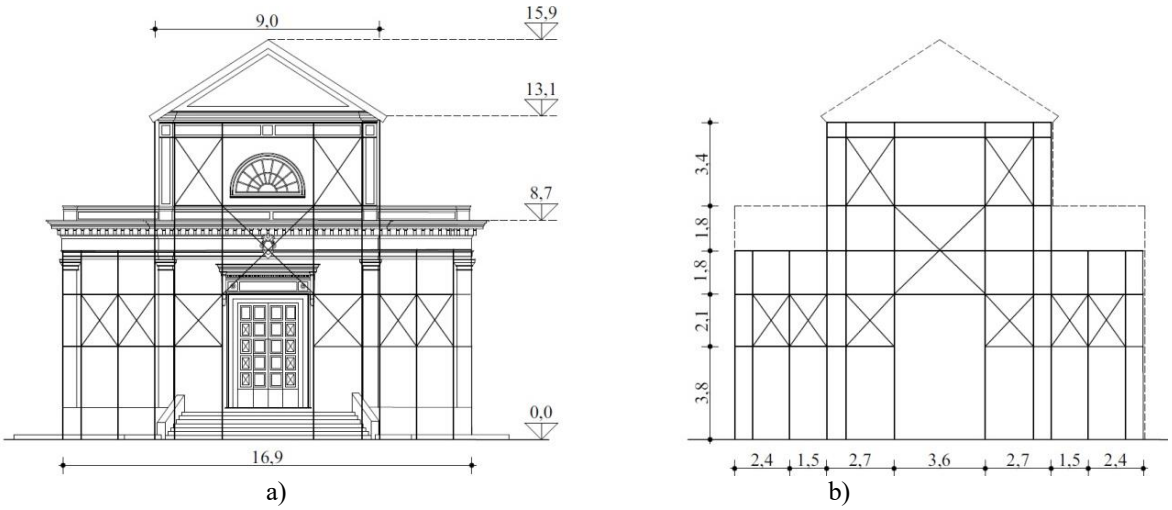


Figure 2: Representation of the geometrical dimensions (in meters) of the: a) façade and b) iron frame

2.3 Loading conditions

The self-weight of the façade is assumed as applied masses and the roof's loads are neglected as they are significantly lower than the self-weight of the façade (the roof trusses are, indeed, in the direction parallel to the façade). The gable is modelled as well as the remaining part of the façade without making further simplifications in the geometric model.

In general, the assessment of the seismic behaviour of buildings through non-linear analysis is based on the use of two force distributions [14]: one is proportional to the masses and the other proportional to the first vibration mode. In this particular case, the analyses evidenced that the two force distributions have a greater relevance in the lower or in the upper part of the façade, if the loads are applied proportional to the masses or to the first vibration mode, respectively. However, in this paper only the results of the non-linear static analyses carried out under the distribution of horizontal forces proportional to the masses are presented.

2.4 Modelling strategies

The main issues for the iron 'baraccato' system are the modelling of the iron profiles and their interaction with the masonry walls, which can be simulated with different modelling strategies. Some non-linear analyses have been performed by [15] on masonry walls strengthened with iron elements with a layout similar to that observed in the Santa Maria Maddalena church. The analyses were aimed to understand both the influence of the iron elements on the overall in-plane behaviour of the masonry walls and the influence of the adopted modelling strategy.

The same two software, DIANA FEA and 3DMacro, used for modelling the masonry walls in [15] are herein used for the façade of the Santa Maria Maddalena church. The first is a Finite Element (FE) software, which allows to perform a refined model based on the detailed discretization of the elements. The second is a Discrete Macro-Element (DME) software, which, being based on a macro-modelling approach, adopts a great simplification of the model, but allows to significantly reduce the computational time effort [16].

The iron elements encaging the masonry walls can be simulated in different ways by both software. 'Beam elements' have both axial and flexural stiffness and they can guarantee or not the perfect adhesion with the solid elements simulating the masonry along the whole length. Conversely, 'truss elements' have only axial stiffness and have no adhesion with the masonry along the whole length, since the connection is active only in the end nodes of the elements. For the façade under study, two cases will be presented in the following, since they can be considered as the most representative of the real conditions of adherence between the two materials:

- Case 1: all iron elements schematized as 'Beam' elements (BEAM model);
- Case 2: horizontal and vertical iron elements modelled as 'Beam' and diagonal elements modelled as 'Truss' (BEAM + TRUSS model).

2.4.1 The model implemented in DIANA software

In the FE model implemented in DIANA, the masonry is modelled by twenty-node isoparametric brick elements based on quadratic interpolation and Gauss integration, named CHX60. An optimization analysis of the size mesh was carried out providing a best value of

0.25 m. The Total Strain Crack Model with an exponential law in tension (Figure 3a) and a parabolic law in compression (Figure 3b) was assumed for masonry.

For the iron profiles, the 'Beam' element, CL18B, is a three-node element, while the 'truss' element, L2TRU, is a two-node directly integrated (1-point) element. A uniaxial elastic-plastic law was assumed in tension for iron, while, in compression, the stress was limited in the elastic field to the buckling value assuming, thus, a brittle model (Figure 3c).

The values of the mechanical properties used in DIANA for the materials are listed in Table 1. Lacking detailed information, the common value $G_t = 0.012$ N/mm was used for the fracture energy in tension, as suggested in [17]. For the fracture energy in compression, the following formulation valid for $f_c < 12$ MPa [17] was adopted:

$$G_c = (2.8 - 0.1 \cdot f_c) \cdot f_c \quad (1)$$

which has a dimension of N/mm and where f_c is the compressive strength of the masonry expressed in N/mm^2.

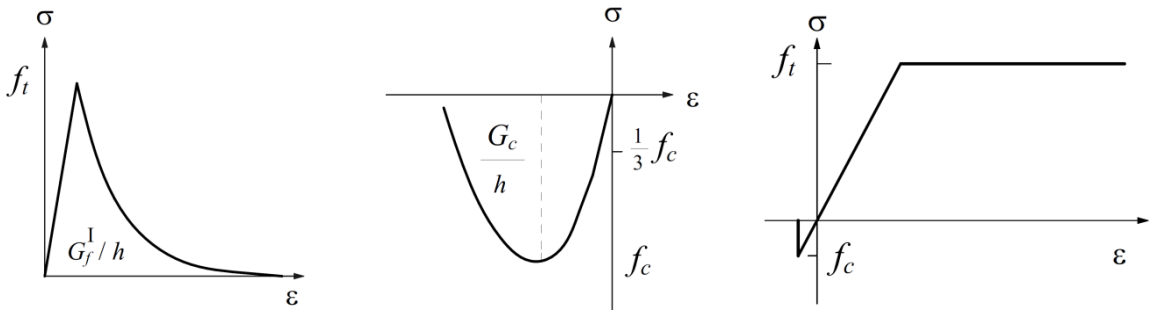


Figure 3: FE Model implemented in DIANA: a) exponential tensile law for masonry; b) parabolic compressive law for masonry; c) uniaxial non-linear elasticity law for iron

Table 1: Mechanical properties used in DIANA FEA

Parameter			*Masonry*	*Iron*
Young's modulus	E	[MPa]	880	153000
Poisson's ratio	ν	-	0.15	0.3
Compressive strength	f_c	[MPa]	1.4	15.1
Tensile strength	f_t	[MPa]	0.15	235
Compressive fracture energy	G_c	[N/mm]	3.724	-
Tensile fracture energy	G_t	[N/mm]	0.012	-

2.4.2 The model implemented in 3DMacro

The Discrete Macro-Element Model (DMEM), implemented in the software 3DMacro, considers the masonry structure as an assemblage of macro-elements [18]. According to this modelling approach, the in-plane behaviour of a masonry panel can be analyzed by means of a two-dimensional macro-element made of four hinges connecting fours rigid edges and two diagonal non-linear springs [19]. The activation of the shear-sliding and flexural failures is controlled by the longitudinal and orthogonal springs at the interface elements, respectively; conversely, the shear-diagonal failure is governed by the diagonal non-linear springs. The

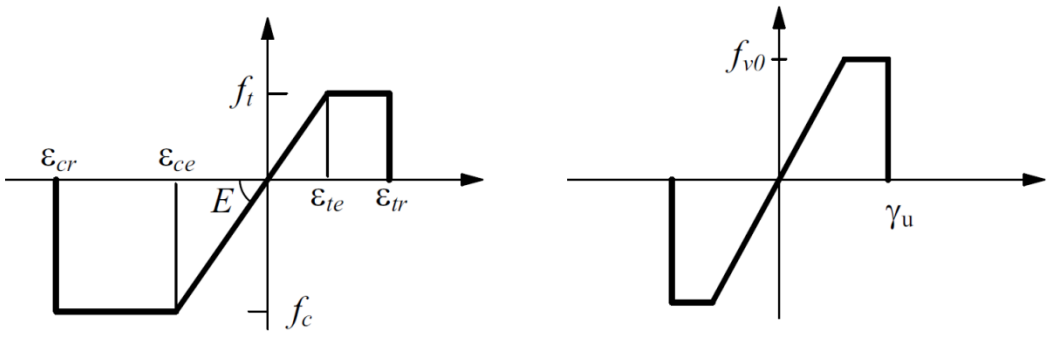
model has been upgraded for the simulation of the in-plane and out-of-plane behaviour of mixed systems in which the masonry interacts with beams elements [18-22].

In this study, the maximum mesh dimension was set on 1 m, while the spacing among the springs at the interface elements was calibrated equal to 20 mm and 100 mm for the unreinforced and reinforced façade, respectively.

Since the two models, FEM and DMEM, adopt different constitutive material approaches, the mechanical parameters in 3DMacro were assessed by means of several parametric analyses. An elastic-plastic law for masonry tensile/compression (Figure 4a) was used in the DMEM to define the ductility in compression and in tension as, respectively:

$$\mu_c=\varepsilon_{cr}/\varepsilon_{ce}; \qquad \mu_t=\varepsilon_{tr}/\varepsilon_{te} \tag{2}$$

The shear-diagonal spring was defined by the shear masonry modulus G and the shear strength f_{v0} (Figure 4b). The Turnšek and Čačovič criterion for the shear-diagonal mechanism was adopted, while the shear strength was defined dividing by 1.5 the tensile strength. Besides, parametric analyses were carried out on the ultimate shear drift, γ_u, in order to provide results consistent with those of the FE model. For the iron elements, the same mechanical properties implemented in DIANA were adopted (Figure 3c). The values of the mechanical parameters used for masonry and iron in the DMEM are listed in Table 2.



a) b)

Figure 4: Constitutive law in: a) tensile/compression and b) diagonal shear

Table 2: Mechanical properties used in 3DMacro DMEM

Parameter			*Masonry*	*Iron*
Young's modulus	E	[MPa]	887	153000
Tangential modulus	G	[MPa]	370	
Compressive strength	f_c	[MPa]	1.4	15.1
Tensile strength	f_t	[MPa]	0.15	235
Compressive ductility	μ_c	-	6.45	-
Tensile ductility	μ_t	-	2.34	-
Shear modulus	G	[MPa]	370	-
Shear strength	f_{v0}	[MPa]	0.10	-
Ultimate shear drift	γ_u	[%]	0.8	-

3 RESULTS OF NUMERICAL ANALYSES

3.1 Unreinforced masonry façade

The study of the unreinforced façade is crucial for assessing the effects of the iron frame. One of the most important results of the non-linear static analysis is the 'capacity curve', generally expressed as the relation between the base shear and the displacement of a control point. In this case, the top point of the gable was chosen as control point.

The first interesting remark is the perfect agreement in terms of initial stiffness between the numerical curves obtained by the two approaches, as shown in Figure 5. The agreement is still satisfactory in terms of strength capacity, though a slight difference specifically due to the different modelling approach (refined and simplified models for DIANA and 3DMacro, respectively). The capacity can also be expressed in terms of the normalised base shear coefficient C_b defined as the ratio of the base shear to the weight of the unreinforced façade (i.e., 1403 kN). In particular, the coefficient C_b corresponding to the displacement of 25 mm is 0.71 and 0.69 for the FE and DME models, respectively.

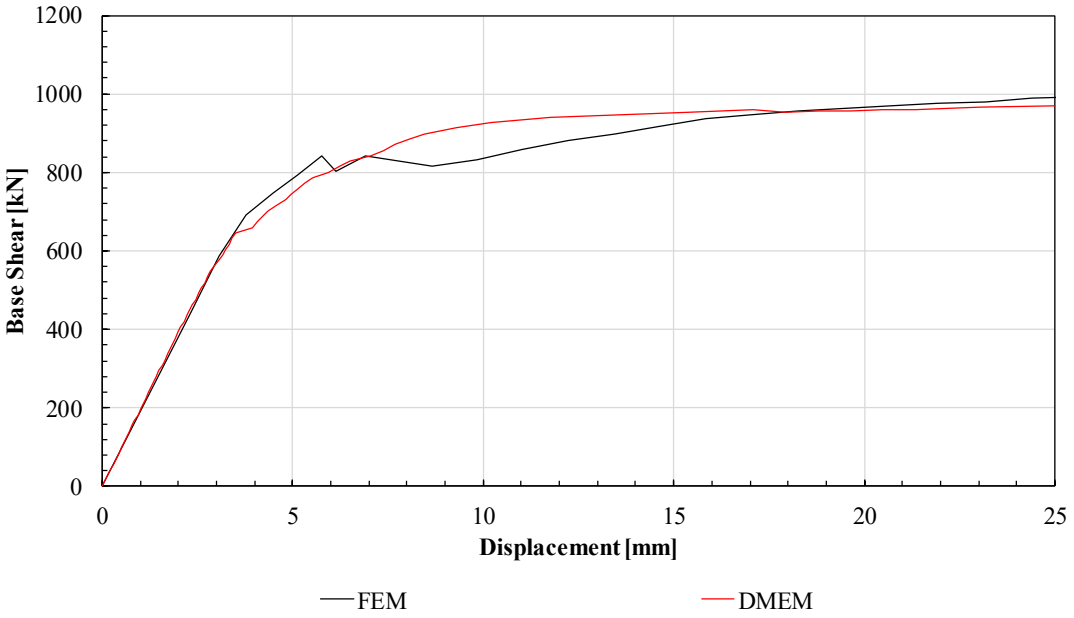
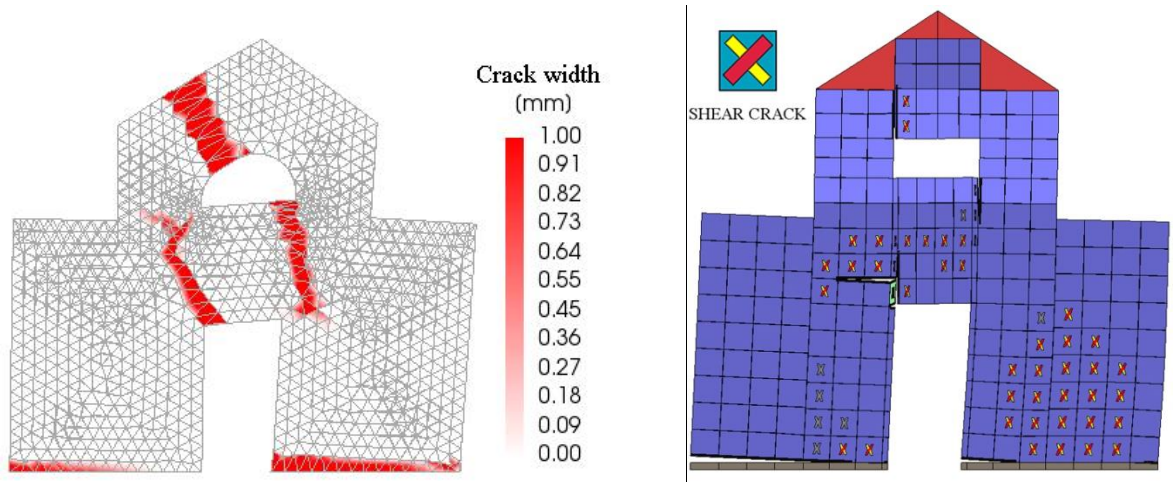


Figure 5: Comparison between the numerical curves of the two models for the unreinforced masonry façade

Moreover, Figure 6 shows a comparison in terms of deformed shape and crack pattern, obtained by the two software at the last step of the analysis. It can be observed that similar failure mechanisms are predicted by the two models. In particular, shear and flexural failures of the masonry portions are localized above the openings and in the bottom part of the façade, respectively.



a) b)

Figure 6: Crack patterns on the unreinforced masonry façade: a) DIANA model; b) 3DMacro model.

3.2 Iron 'baraccato' masonry façade

One of the most relevant issues for the analysis of the iron 'baraccato' system is the modelling of the iron elements and their interaction with the masonry panel. Figure 7 shows the capacity curves for the unreinforced masonry façade and the iron "baraccato" façade furnished by the two software, considering the cases 1 (BEAM model) and 2 (BEAM+TRUSS model) described in section 2.4.

As expected, an increase of both capacity (about 3 times) and stiffness is attained for the reinforced façade compared to the unreinforced one for all the considered cases. In particular, the "BEAM+TRUSS model" in the FEM gives the highest increase of capacity with a slight difference in terms of stiffness with respect to the "BEAM model". Besides, in the 3DMacro approach, the differences between "BEAM" and "BEAM+TRUSS" models are negligible, both in terms of capacity and ductility. Such a results is due to the fact that the 'BEAM' elements in the FEM are actually able to interact with the masonry along the entire length, while in the DMEM the interaction is only restricted to the nodes of the iron frame reinforcing the structure and, thus, the interaction along the whole masonry panel is not taken into account.

Comparing the capacity curves of the two approaches, a satisfactory agreement can be observed, especially when the "BEAM" model is used. However, the maximum base shear value given by the DMEM is in the range of values provided by the FEM capacity curves.

Specifically, the coefficient C_b related to the DME model is equal to 1.88, which is between the minimum (BEAM) and maximum (BEAM+TRUSS) values provided by the FE model, i.e. 1.73 and 2.14, respectively. This coefficient is defined with reference to the reinforced façade weight of 1470 kN and the ultimate displacements of the capacity curves equal to 40 mm and 33 mm for the FE and DME models, respectively (Figure 7). It is worth highlighting that both FEM and DMEM capacity curves cannot run for greater displacements due to numerical convergence issues.

Finally, Figure 8 reports the crack patterns predicted by the DMEM and FEM for the reinforced façade, in perfect agreement as well. In fact, the cracks are mainly localized in the bottom part of the façade in both approaches.

The numerical analyses have evidenced that different modelling approaches, even if

characterized by different level of approximation, can lead to similar results both in terms of capacity curves and damage patterns. Moreover, about the modelling strategies for the iron "baraccato" system, the numerical results of the whole façade seem to be less influenced by the element type adopted for modelling the iron profiles and their interaction with the masonry panels (i.e., TRUSS or BEAM elements) in comparison with what observed in the single masonry panels investigated in [15].

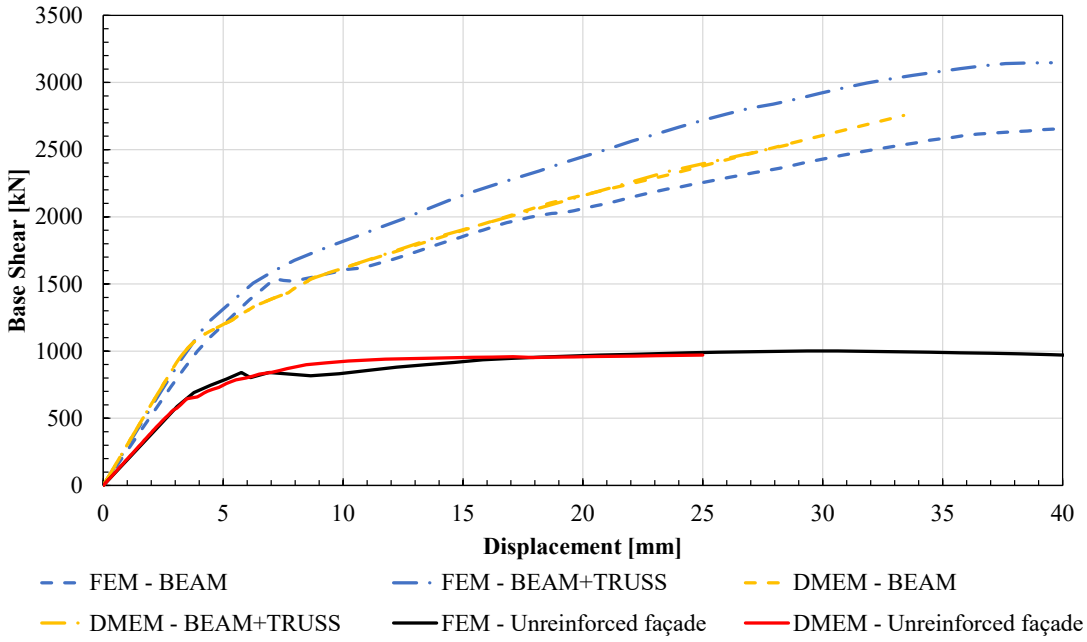


Figure 7: Comparison among the numerical curves of the two models for the iron 'baraccato' masonry façade

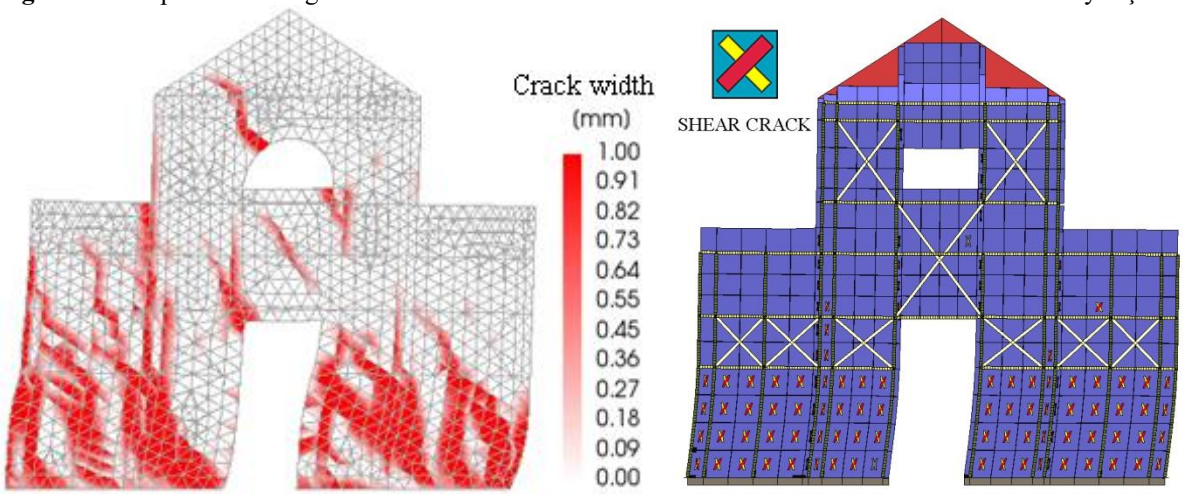


Figure 8: Crack patterns in the façade with 'baraccato' system: a) DIANA model; b) 3DMacro model

4 CONCLUSIONS

The paper presents the results of numerical investigations on the in-plane behaviour of the façade of the Santa Maria Maddalena church, located in the Ischia Island (Italy). As part of the

main body of the church, the façade is made of an atypical "baraccato" system consisting of a tuff masonry wall encaged by iron frames. Since few information is present in the literature regarding the iron "baraccato" system, the study was focused on the identification of the more appropriate modelling strategy for carrying out reliable numerical analyses. In particular, non-linear analysis of the façade under horizontal actions was developed by means of a Finite Element (FE) and Discrete Macro-Element (DME) model, using the DIANA FEA and the 3DMacro software, respectively.

Firstly, the behaviour of the unreinforced masonry façade was investigated by the two approaches, also in order to calibrate the DME model on the FE one. Successively, the non-linear analyses were extended to the same façade reinforced by means of the iron "baraccato" system. The numerical results evidenced a very good agreement between the two approaches both in terms of capacity curves and crack patterns at failure.

The influence of the modelling strategy for the iron profiles was also investigated, with reference to the hypothesis of "BEAM" or "TRUSS" element for the diagonal iron profiles. A slight difference in terms of capacity was observed in the FE model, while, in the DME one, the curves are practically coincident due to the more simplified assumptions considered for the contribute of the diagonal elements.

Despite the good agreement observed between the two approaches, a more detailed investigation on the influence of the mechanical properties on the numerical results will be developed in the future through wide parametric analyses. Successively, the examined modelling approaches will be extended to the study of the whole church taking into account both the in-plane and the out-plane response of the masonry walls.

Acknowledgements. The research has been carried out within the activities of the national Reluis project 2019-2021 "MAppe di Rischio e Scenari di danno sismico (MARS) - Task 4.8 – Modelli e curve di fragilità delle chiese.

REFERENCES

[1] DIANA FEA BV. Diana user's manual, Release 10.3, (2019).
[2] Gruppo sismica S.r.l. 3DMacro. *Il software per le murature (3D computer program for the seismic assessment of masonry buildings)*. Technical report, (2019).
[3] Ruggieri, N. The Borbone "*Istruzioni per gli Ingegnieri*": a historical code for earthquake-resistant constructions. *Int. J. Archit. Herit.* (2017) **11**(2):292-304.
[4] França, J.A. *A reconstrução de Lisboa ea arquitectura Pombalina*. Instituto de cultura portuguesa, (1978).
[5] Hicyilmaz, K.M.O., Wilcock, T., Izatt, C., da Silva, J. and Langenbach, R. Seismic performance of Dhajji Dewari. In: *15th World Conference on Earthquake Engineering*, Sociedade Portuguesa de Engenharia Sismica (SPES), (2012), pp. 24-28.
[6] Cobancaoglu, T. Himis' construction system in traditional Turkish wooden houses. In: P.B. Lourenço and P. Roca (Eds.): *Structural Analysis of Historical Constructions (SAHC 2001)*, (2001), pp. 799-810.
[7] Kouris, L.A.S. and Kappos, A.J. Detailed and simplified non-linear models for timber-framed masonry structures. *J. Cult. Herit.* (2012) **13**(1):47-58.
[8] Cantelmi, F. Un sistema costruttivo antisismico: la casa baraccata. *Geopunto* (2017) **74**:8-

12.
[9] Galassi, S., Ruggieri, N. and Tempesta G. Seismic performance evaluation of timber-framed masonry walls experimental tests and numerical modelling. In: N. Ruggieri et al. (Eds.): *Historic Earthquake-Resistant Timber Frames in the Mediterranean Area*, Springer (2015), pp. 99-103.
[10] Casapulla, C., Ceroni, F., Rainieri, C., Argiento, L.U., Arcamone, P. and Fabbrocino, G. Structural assessment of Santa Maria Maddalena church in Ischia (Italy) by experimental modal analysis under operational conditions. In: M. Papadrakakis and M. Fragiadakis (Eds.): *Computational Methods in Structural Dynamics and Earthquake Engineering (COMPDYN 2019)*, ECCOMAS Bookseries (2019), pp. 1-14.
[11] Di Napoli, B. *Modelling and safety assessment of the Santa Maria Maddalena Church, Ischia, Italy*. Msc. Thesis, Universidade do Minho, Portugal, (2019).
[12] Ceroni, F., Pecce, M., Voto, S. and Manfredi, G. Historical, architectural and structural assessment of the Bell Tower of Santa Maria del Carmine, *International Journal of Architectural Heritage*: Conservation, Analysis, and Restoration, Francis Taylor, Vol. 3, Issue 3, (2009), pp. 169-194.
[13] Brussel, M.N. *Appraisal of existing iron and steel structures*. The Steel Construction Institute, Ascot -Berkshire, (1998).
[14] Ministero delle Infrastrutture e dei Trasporti. *NTC 2018 - Norme Tecniche per le Costruzioni di cui al D.M. 17/ 01/2018*. Italy: Gazzetta Ufficiale N. 42 del 20/02/2018 (2018). (in Italian)
[15] Celano, T., Argiento, L.U., Ceroni, F. and Casapulla, C. In-plane behavior of iron-framed masonry panels: numerical analyses. In: T.P. Tasios et al. (Eds.): *4th International Conference on Protection of Historical Constructions (PROHITECH 2020)*, (2020).
[16] Caddemi, S., Caliò, I., Cannizzaro F. and Pantò, B. New Frontiers on Seismic Modeling of Masonry Structures" *Frontiers in Built Environment* (2017) 3, 39.
[17] Lourenço, P.B. Structural masonry analysis: Recent developments and prospects. In: M. Masi et al. (Eds.): *Proceedings of the 14th International Brick & Block Masonry Conference*, University of Newcastle (2008), pp. 1341–56.
[18] Caliò, I., Marletta, M. and Pantò, B. A new discrete element model for the evaluation of the seismic behaviour of the unreinforced masonry builings. *Eng. Struct.* (2012) **40**:327-338.
[19] Chácara, C., Lourenço, P.B., Pantò, B., Cannizzaro, F. and Caliò, I. Parametric numerical studies on the dynamic response of unreinforced masonry structures. In: K. Van Balen and E. Verstrynge (Eds.): *Structural Analysis of Historical Constructions (SAHC 2016)*, CRC Press (2016), pp. 239-245.
[20] Caliò, I. and Pantò, B. A macro-element modelling approach of Infilled Frame Structures. *Comput. Struct.* (2014) **143**: 91-107.
[21] Pantò, B., Caliò, I. and Lourenço, P. B. A 3D discrete macro-element for modelling the out-of-plane behaviour of infilled frame structures. *Eng. Struct.* (2018) **175**: 371-385.
[22] Pantò, B., Silva, L., Vasconcelos, G. and Lourenço, P. B. Macro-modelling approach for assessment of out-of-plane behavior of brick masonry infill walls. *Eng. Struct.* (2019) **181**: 529-549.

12th International Conference on Structural Analysis of Historical Constructions
SAHC 2020
P. Roca, L. Pelà and C. Molins (Eds.)

INFLUENCE OF SETTLEMENTS AND GEOMETRICAL IMPERFECTIONS ON THE INTERNAL STRESS STATE OF MASONRY STRUCTURES

A. DELL'ENDICE[1*], A. IANNUZZO[1], T. VAN MELE[1] AND P. BLOCK[1]

[1]Institute of Technology in Architecture (ITA), Block Research Group (BRG)
Eidgenössische Technische Hochschule Zürich (ETH - Zurich)
Stefano-Franscini-Platz 1, HIB E, CH-8093 Zurich, Switzerland
email: {dellendice, iannuzzo, block, van.mele}@arch.ethz.ch , www.block.arch.ethz.ch

Keywords: Masonry Structures, Discrete Element Modelling, Geometrical imperfections, Settlements, Internal Stress State

Abstract. *Since a few decades, the Discrete Element Modelling (DEM) method has been adopted by many authors as a reliable tool for the structural assessment of unreinforced masonry (URM) structures. In this paper, through compas_dem and using 3DEC by Itasca as a solver in the background, we investigate the mechanical behaviour of a three-dimensional URM structure combining the effects of foundation displacements and geometrical imperfections. For this purpose, we consider three different models of the above-mentioned structure. The first one is a perfect digital model, while in the other remaining two models, random geometrical imperfections are applied to the perfect model in order to investigate their influence. After post-processing the 3DEC results, the influence of the applied vertical settlement and geometrical imperfections is explored in terms of crack pattern/mechanism, internal stress states, and the thrust exerted on the supports. The aim of this paper is not to find the actual stress state of the highly indeterminate structure, but to investigate the role played by the combined effects of foundation displacement and geometrical imperfections on the internal stress state.*

1 INTRODUCTION

The structural assessment of unreinforced masonry (URM) structures represents one of the most common challenges for engineers in everyday practice. This structural typology is diffused worldwide and includes both historical monuments and residential buildings. In the last century, the essential knowledge for both designing and restoring these structures has been forgotten, and methods and tools for the structural design of reinforced concrete, steel and wooden buildings took over. These methods (e.g. linear or non-linear Finite Element Analysis), even though able of handling complex three-dimensional geometries, are often based on stress/strength approaches and, in order to be applicable to URM, require a refined mechanical characterisation based on parameters that, in most cases, are unknown or unknowable. Furthermore, since it is well known that the stability of masonry structures depends on their geometry rather than on the material's strength [1], these approaches often lead to "unsafe and deceptive results," as explained in [2]. In 1966, Heyman introduced a theoretical framework for

the application of limit analysis to masonry structures through three assumptions that showed the important role of the geometry in the stability of this structural typology. One of the oldest methods used for the assessment of masonry structures that perfectly fits inside the limit analysis framework is the Thrust Line Analysis (TLA). This powerful method is used since centuries and describes the behaviour of the masonry structure very well [3]. Its downside is that is primarily a 2D approach. For the analysis of the 3D behaviour, other limit-analysis methods such as Thrust Network Analysis [4][5], or compressive equilibrium membranes [6][7][8][9], have been developed. Most of these methods apply the Safe Theorem [1], meaning that they assess the stability of masonry structures through lower-bound solutions. Additionally, they have been developed for vaulted geometries, i.e. height fields.

To deal with complex 3D geometries, more generally intricate assemblies, and to account for their typical unilateral behaviour [10], the Discrete Element Modelling (DEM) method developed by [11] can be applied. The DEM method aims to represent the structural behaviour of a system composed of multiple bodies analysed as distinct units in mutual contact at the joints. Several mechanical assessment problems can be tackled: stability in a given configuration, load-bearing capacity, dynamic loading conditions, and the effects of large settlements. Moreover, the possibility offered by the DEM software 3DEC by Itasca [12][13][14] to work in three dimensions helps in the investigation of collapse mechanisms and in understanding the global behaviour of complex geometries [15][16][17][18][19]. The importance to understand the 3D behaviour and the interaction between structural elements of a masonry building is a critical aspect in practice.



Figure 1. Partial collapse of a building after the demolition of the adjacent building (Oct 2019, Andria, Italy).

In many cases, analysis of the global behaviour of the entire building is necessary. Moreover, in historical city centres, intervening on a masonry building often involves the study of several interconnected structures. Sometimes, the negligence in tackling these structural problems can cause sudden collapses (Fig. 1) and the loss of human lives. This paper aims to investigate the influence of vertical settlements and geometrical imperfections on the internal stress state of a buttressed wall structure using the DEM software 3DEC. Even though 3DEC allows

investigating the behaviour of 3D structures, in this paper, the authors provide an extension to what was already available in 3DEC, post-processing the results to visualise the flow of forces within the structure for varying boundary conditions. Finally, the elaboration of the results helps in the analysis of the magnitude and position of the reaction forces at the supports.

2 METHODOLOGY

In this paper, DEM analysis using the software 3DEC by Itasca is performed. In particular, the stability in the initial configuration and the effects of a vertical settlement and geometrical imperfections are investigated. In this section, we provide a short overview of DEM, how we apply imperfections and how we post-process the results.

2.1 Discrete Element Modelling

DEM software has three main peculiarities: the model consists of finite-size bodies able to move and deform independently; large displacements are possible; and the blocks can completely detach from each other, possibly forming new contacts between other blocks. Static and dynamic behaviour can be simulated. The DEM method is widely accepted for the analysis of URM and it can, as stated in [20], approximate Heyman's assumptions [1]. The whole system's deformability, considering rigid blocks, is concentrated at the joints, and it is controlled by two parameters: the normal and shear joint stiffness. Physically, the two values of the joint stiffnesses influence, respectively, the compenetration and the sliding between blocks. High values of joint stiffness should be specified to avoid these two phenomena during the analysis, although this notably increases the computational time. On the other hand, as described in [16] and [19], the values of the joint stiffness could be reduced, within a certain range, without influencing the results of the analysis significantly, hence decreasing the calculation time as well. The two joint stiffness values have been defined as in [18]:

$$J_{kn} = \left(\frac{\frac{E}{h_{block}} + \frac{E}{l_{block}}}{2} \right) \quad , \tag{1}$$

where J_{kn} is the normal joint stiffness, E is the Young's modulus of the material, h_{block} and l_{block} are the average block height and block length, respectively.

For the evaluation of the joint shear stiffness, the Young's modulus E has been replaced by the shear modulus G defined as:

$$G = \frac{E}{2(1+\upsilon)} \quad , \tag{2}$$

where ν is the Poisson's coefficient considered equal to 0.2. Then, the value of the shear joint stiffness has been evaluated as:

$$J_{ks} = \left(\frac{\frac{G}{h_{block}} + \frac{G}{l_{block}}}{2} \right) \quad . \tag{3}$$

Regarding failure at the joints, the Mohr-Coulomb criterion is adopted:

$$\tau = \sigma \tan(\phi) + c \quad , \tag{4}$$

where τ is the shear strength, σ the normal stress, ϕ the friction angle and c the cohesion. In the Mohr-Coulomb criterion, considering Heyman's assumptions, the only parameter needed is the

friction angle, as the value of cohesion is considered equal to zero. Finally, next to the two joint stiffness values and the friction angle, the fourth and last mechanical parameter needed is the density of the block's material. The reduced number of mechanical parameters needed allows limiting the dependency on input data that is based on uncertainty, especially in the assessment of historical masonry structures.

2.2 Geometrical imperfections

Real structures contain imperfections due to element geometry deviations or assembly errors. As shown in [19], imperfections influence the flow of forces within the structure. They redirect the forces accordingly to the imperfect contact conditions between the blocks and have an influence on the displacement capacity or the collapse mechanisms. Using the Python-based package *compas_dem*, part of the COMPAS Masonry framework [21], geometrical imperfections have been applied to the perfect digital model. In particular, element (e.g. due to fabrication) and assembly errors are generated (Fig. 2). For the former, each vertex of the blocks is randomly moved in space, picking the value of the displacement in a specific predefined range using a uniform distribution. For the latter, a random uniform distribution of displacement values, one per block, is generated within a certain range, and each block is moved according to it.

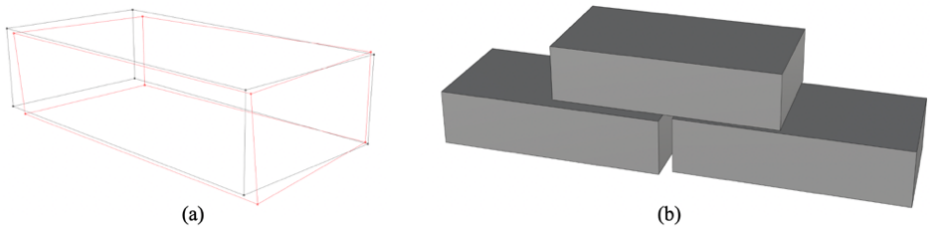


Figure 2. Geometrical imperfections in [19]: element geometry deviations (a); assembly errors (b).

2.3 Post-processing of the results

In this paper, at each step of the analysis, the contact forces calculated by 3DEC are post-processed, and their resultants at each contact interface computed. Then, the resultants are visualised in a CAD software, together with the updated geometry of the digital model. The visualisation of the internal stress state at each step of the calculation allows following the variation due to the changing of the boundary conditions.

3 MODELS

In this paper, we look at the geometry depicted in Fig. 3, representing a typical structural portion of a church in between two buttresses. The structure is 15m tall having openings at different levels. The lateral wall and the pillars are connected in the upper part by two flying buttresses and in the lower part by two walls. The two transversal buttresses also have an opening at the base. Three digital models of the same structure are considered: the first is the perfect digital model, that is, all the blocks have a regular shape resulting in perfect face-to-face contact conditions; the other two models are obtained by applying random distributions of geometrical imperfections of both types.

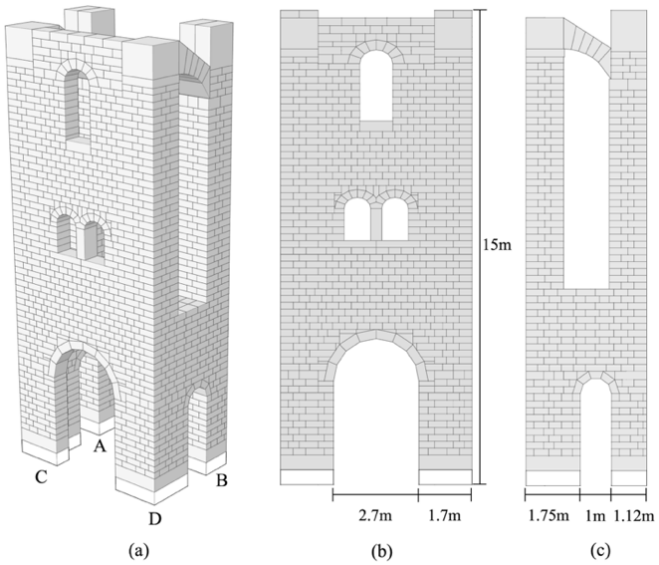


Figure 3. Digital three-dimensional model used in this paper: 3D view (a); front view (b); lateral view (c).

3.1 Geometry and discretisation

The geometry is generated using *compas_dem*, a Python-based package that can manage data structures and create discrete assemblies. A closed mesh represents each block, and through *compas_dem*, geometrical operations can be easily performed. The stereotomy of the model is made with a variable interlocking between the voussoirs. The average dimensions of the blocks are 220mm x 400mm x 600mm. The flying buttresses and all arches at the openings are discretised considering cuts perpendicular to their curvatures. The main structural elements (pillars-wall, buttresses-base, etc.) are linked together through offset/shifted stones.

3.2 Mechanical data

In the analyses, the blocks are considered rigid interacting with their neighbours through unilateral contacts. As explained in Section 2.1, the only mechanical parameters needed by 3DEC to define the mechanical behaviour of the contacts are the friction angle and two joint stiffness values. We consider a material density of 2200Kg/m^3, and a friction angle of 50°. The two joint stiffnesses (normal and shear) have been evaluated using Equations (1) and (3) assuming a Young's modulus of 40GPa, h_{block} equal to 0.22m and l_{block} equal to 0.4m. These two values have then been reduced by a factor of 10 to reduce the calculation time.

3.3 Geometrical imperfections

The two digital, imperfect models are obtained by applying geometrical imperfections to the perfect model shown in Fig. 3. In the first one, named "imperfections 1", only element deviations are applied, that is, each vertex of every single mesh has been moved considering a reasonable arbitrary displacement range of +/- 3mm. In the second imperfect model, named "imperfections 2", both fabrication and assembly errors are considered. The fabrication imperfections are generated using the same range as before (+/- 3mm), while the assembly imperfections are generated considering a reasonable range of +/- 2mm.

4 NUMERICAL ANALYSIS

In this section, the results of the analyses conducted on the three digital models are presented. For each case, the internal stress state in the initial configuration and during the applied vertical settlement is described.

4.1 Perfect digital model

In the initial configuration (self-weight), the flow of forces computed from the post-processed results calculated by 3DEC, showed an internal stress state compatible with the slight displacements allowed by the geometry, which in turn depend by the two joint stiffnesses specified. As shown in Fig. 4.a, in the initial configuration, the flow of forces is quite vertical and deviates around the openings as expected.

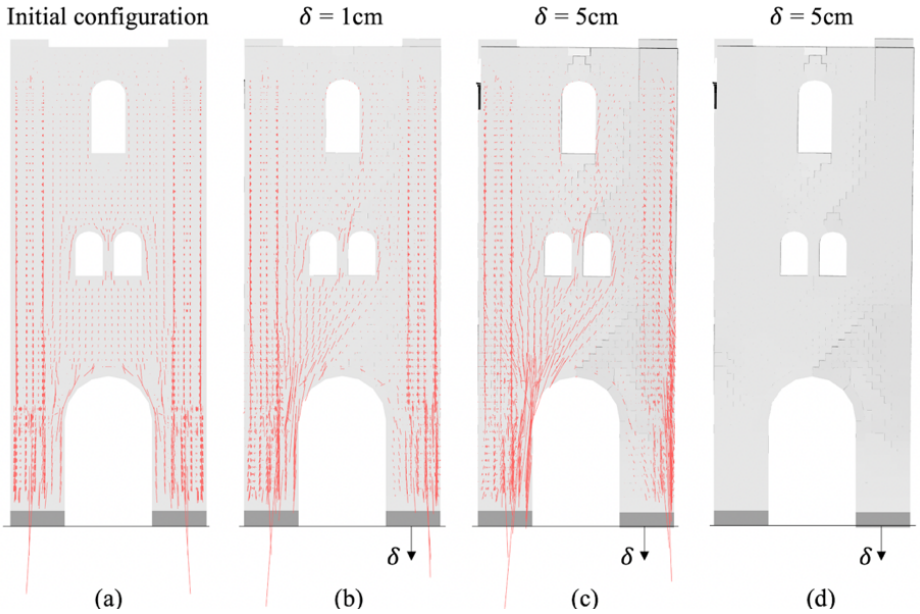


Figure 4. Front view: flow of forces in the initial configuration (a); after 1cm of vertical displacement (b); after 5cm of vertical displacement (c); crack pattern after 5cm of vertical displacement (d).

After the first step of the vertical displacement (1cm), the flow of forces starts changing. Figure 4d shows the crack pattern corresponding to the foundation displacement of 5cm; in particular, diagonal fractures can be easily recognised. Cracks represent a discontinuity in the structure, where contact forces cannot go through. For this reason, the flow of forces changes direction as clearly visible in Figures 4.b-c and 5.b-c. Furthermore, the internal stress state of pillar D, subjected to the vertical settlement, changes, and the forces deviate towards the right corner in the front view and to the left corner in the lateral view. This phenomenon is caused by the combination of the vertical settlement and the thrust exerted by the flying buttress at the top of pillar D.

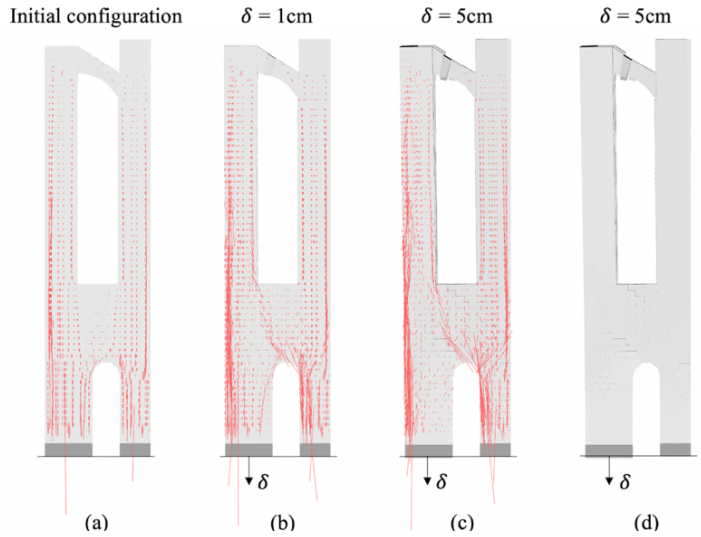


Figure 5. Lateral view: flow of forces in the initial configuration (a); after 1cm of vertical displacement (b); after 5cm of vertical displacement (c); crack pattern after 5cm of vertical displacement (d).

4.2 Digital models with geometrical imperfections

In this section, we present the results of the analyses of the two digital models with geometrical imperfections applied. In Figures 6.b-c, the flow of forces in the initial configuration is compared with the flow of forces in the perfect model (Fig. 6.a). In particular, it is less regular because the geometrical imperfections change the contact conditions between the blocks, i.e. they are no longer interacting face-to-face. Narrow and non-uniformly distributed cracks already appear in the initial configuration.

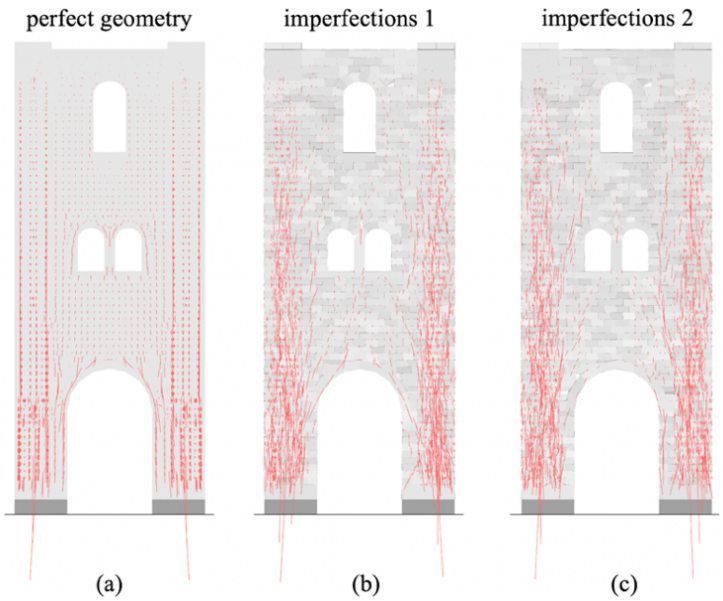


Figure 6. Flow of forces in the initial configuration: perfect digital geometry (a); imperfections 1 (b), and imperfections 2 (c).

The resulting internal stress state is slightly different between the two cases with geometrical imperfections. Arbitrary concentrations of forces are visible, and they have an influence on the distribution of the resultant forces on the four supports as will be discussed in the Section 5.

In Fig. 7, the results of the two models with applied geometrical imperfections subjected to the vertical displacement of pillar D are shown. As soon as the vertical displacement of the pillar occurs, the internal stress state of the structure gets dominated by the effect of the displacement.

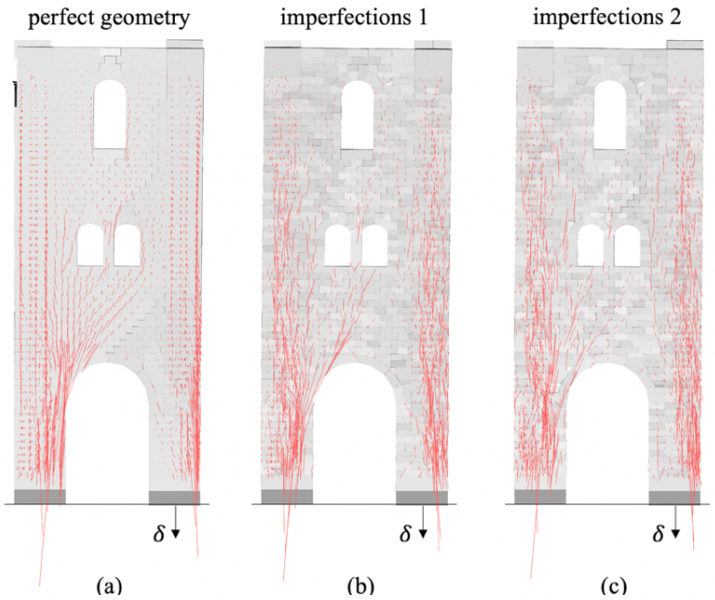


Figure 7. Flow of forces after vertical displacement of 5cm: perfect digital geometry (a); imperfections 1 (b), and imperfections 2 (c).

Specifically, between the three cases showed in Fig. 7, similar deviations in the flow of forces can be easily recognised. Qualitatively, the results are similar, even though, we can state that geometrical imperfections affect the position and the number of the cracks.

5 DISCUSSION

In this section, the results obtained with the perfect and imperfect digital models are compared in terms of stress state (both in the initial and deformed configuration), crack patterns and thrusts exerted on the supports.

5.1 Internal stress state in the initial configuration

In the initial configuration, the perfect model shows a regular distribution of the forces, that flow around the openings in the main wall, compatibly with the boundary conditions. Conversely, the models with geometrical imperfections show a more chaotic distribution but still in accordance with the boundary conditions. This chaotic distribution reflects the non-perfect contacts between the blocks. Since every real structure has a certain amount of imperfections, impossible to reproduce, these results can only give some hints of what could be a more realistic internal stress state. Furthermore, it shows how geometrical imperfections

indirectly represent an irregular distribution of stress-states even in *perfect* (undeformed) initial configurations. Irregularities can concentrate forces in some areas or create non-homogeneous loading conditions even in contiguous blocks, as previously shown in [22].

5.2 Crack patterns

In the second step, when pillar D is subjected to a vertical displacement, cracks open and the internal stress state changes accordingly. In the model with perfect geometry, the cracks are more visible and localised. Based on the experience and on [23], the crack pattern and its inclination were compatible with the type of settlement applied. In the model with geometrical imperfections, smaller cracks open in more locations, shifted to the left or the right compared to the position of the cracks in the perfect geometry, but, keeping the same average inclination. These results provide an important insight and warning for engineers in practice since they show that, due to imperfections, the same settlement can cause different crack patterns.

5.3 Internal stress state after the vertical settlement

For both perfect geometry and the models with geometrical imperfections, the flow of forces deviated to avoid the cracks, going towards pillars C and B. In the initial steps of the displacement, in the model with geometric imperfections, the directions of the resultants on the supports are still influenced by the directions in the initial configuration. With the increasing of the displacement, i.e. increasing reduction of static indeterminacy, the resultants on the supports are less dependent on the local imperfections, but defined by the global macro-block partitions forming. The resulting stress state had the same characteristics observed at step 5cm with perfect geometry.

5.4 Analysis of the resultants on the supports

In Fig. 8, the resultants on the supports for the perfect digital geometry, imperfections 1 and imperfections 2 are presented. For the perfect digital model (first row in Fig. 8), in the initial configuration, because of the symmetry of the model, the self-weight is identically distributed between the left and right pillars, as shown by the percentages. At the base of the two frontal pillars, C and D, the arched openings result in thrusting in the plane of the main wall, with thus resultants directed outwards as well (west and east). Once the vertical displacement starts, after 1cm, a redistribution of the self-weight among the four pillars can be observed. The percentage of self-weight carried by pillar D decreased while the self-weight carried by pillars C and B increased. The resultant of pillar D and its point of application rotated and moved in direction south-east, respectively. The deviation of the flow of forces towards pillars C and B, as mentioned in Section 4.1, is easily to be recognised by looking at the directions of their resultant thrusts, west for pillar C and north for pillar B. With the increasing of the displacement (5cm), the results showed the same trends. Moreover, the application points of the resultants moved towards the south for pillar C, east for pillar B and south-east for pillar D.

In the cases with geometrical imperfections (second and third rows of Fig. 8), the analysis of the resultant thrusts on the supports confirms the clear influence of imperfections in the initial configuration. Their directions and application points are slightly different and the distribution of the self-weight on each pillar is not anymore symmetrical. This difference leads to a different position of the resultants on the supports during the settlement. After the first step of the

displacement, the percentage of self-weight carried by the moving pillar D did not drop by the same amount as for the perfect model, but a bit less, showing how imperfections can mitigate the effects due to the variations of the boundary conditions. Consequently, C and B carried less self-weight than before.

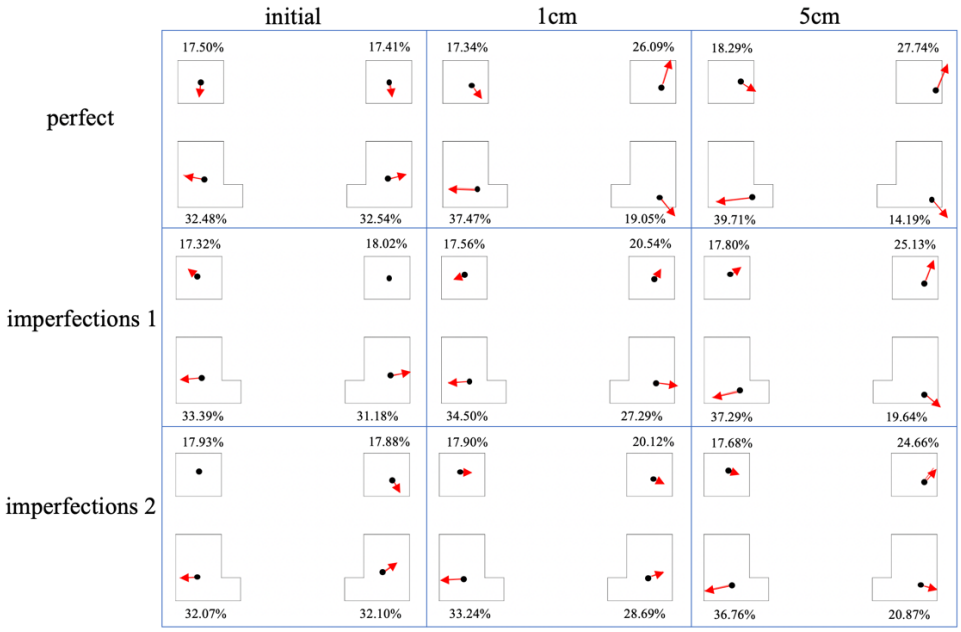


Figure 8. Resultant thrusts at the supports and percentage of self-weight carried by each pillar in the initial configuration, after vertical displacement of 1cm and 5cm: (1st row) perfect geometry; (2nd row) imperfections 1; (3rd row) imperfections 2.

As shown in Fig. 9, in the three cases the self-weight carried by pillar D decreases with the increasing of the displacement, but the magnitude of the decreasing is different in the cases with imperfections.

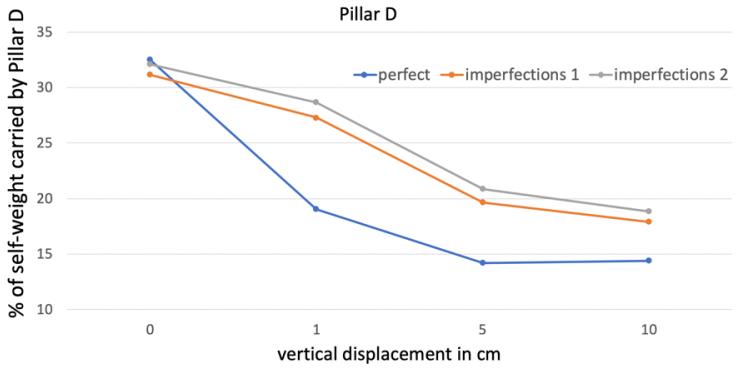


Figure 9. Percentage of self-weight carried by pillar D in the three models, in the initial configuration and after the displacement.

As soon as the displacement increased, at step 5cm, the directions become very similar to the ones observed in the test with perfect geometry, and the further investigation shown in Fig. 9

until step 10cm shows this tendency even for the percentage of self-weight carried by pillar D. This phenomenon showed that at a certain step of the settlement, the global mechanism and displacement dominates the internal stress state more than geometrical imperfections.

6 CONCLUSIONS

This paper investigates the influence of vertical settlements and geometrical imperfections on the internal stress state of a 3D digital model of an URM structure. All the models have been analysed first in their perfect configuration, applying an increasing foundation displacement. In both cases, the crack pattern and the corresponding flow of forces were used to compare the three models. In particular, we noticed that geometrical imperfections mainly influence the initial internal stress state of the structure, and thus, the location and value of the thrusts exerted on the supports. This perfectly fits one of the key points of Limit Analysis as stated in [24], that is, finding the actual stress state in masonry structures is impossible. Geometrical imperfections always belong to real structures and the analyses conducted in this work show that trying to find the actual stress state is worthless. However, though they affect the perfect configuration, as soon as the settlement occurs, the flow of forces is dominated more by the foundation displacement than by geometrical imperfections. Only slight variations locally in the crack pattern are recognisable in the models with imperfections compared to the perfect one. This exploration also suggests another strategy that could be relevant for practical problems in which settlements and specific crack patterns have been observed. In order to calibrate the DEM model, we propose to generate a sufficiently large set of models with imperfections applied, to compare the results with the observed state in reality. The model that matches the best can then be used to do further assessment, as understanding the displacement capacity or the stability after a seismic event. The two typologies of applied imperfections analysed shown a similar effect on the internal stress state, but further investigation is required to understand their respective influence; and, to study the range of stability in the initial configuration due to imperfections, which modify the application points of the resultant thrusts.

Acknowledgements. This work was supported by the Swiss National Science Foundation (SNSF) - project grant #178953: "Practical Stability Assessment Strategies for Vaulted Unreinforced Masonry Structures".

REFERENCES

[1] Heyman, J. The stone skeleton. *Int. J. Solids. Struct.* (1966) **2**:249-279.
[2] Block, P., Ciblac, T. and Ochsendorf, J. Real-time limit analysis of vaulted masonry buildings. *Comput. Struct.* (2006) **84**:1841-52.
[3] Huerta, S. Mechanics of masonry vaults: The equilibrium approach. In: *3rd Int. Semin. Hist. Constr. Guimarães, Port* (2001), pp. 47-70.
[4] Block, P. Thrust Network Analysis: Exploring Three-dimensional Equilibrium. *PhD Thesis* (2009).
[5] Block, P. and Lachauer, L. Three-dimensional funicular analysis of masonry vaults. *Mech. Res. Commun.* (2014) **56**:53–60.
[6] Fraternali, F., Angelillo, M. and Fortunato, A. A lumped stress method for plane elastic problems and the discrete-continuum approximation. *Int. J. Solids. Struct.* (2002)

39:6211-6240.
[7] Fraternali, F. A thrust network approach to the equilibrium problem of unreinforced masonry vaults via polyhedral stress functions. *Mech. Res. Commun.* (2010) **33**:198-204.
[8] Angelillo, M. and Fortunato, A. Equilibrium of masonry vaults. In: *Novel approaches in civil engineering*, Springer, Berlin, Heidelberg (2004), pp.105-111.
[9] Angelillo, M., Babilio, E. and Fortunato, A. Singular stress fields for masonry-like vaults. *Contin. Mech. Thermodyn.* (2013) **25**:423-441.
[10] Angelillo, M., Fortunato, A., Gesualdo, A., Iannuzzo, A. and Zuccaro, G. Rigid block models for masonry structures. *Int. J. Mason. Res. Innov.* (2018) **3(4)**:349-368.
[11] Cundall, P.A. A computer model for simulating progressive large-scale movements in blocky rock systems. *Proocedings Int. Symp. Rock Mech*. Nancy 2 (1971).
[12] Itasca Consulting Group I. 3DEC — Three-Dimensional Distinct Element Code, Ver. 5.2. Minneapolis: Itasca (2016).
[13] Cundall, P.A. Formulation of a three-dimensional distinct element model-Part I. A scheme to detect and represent contacts in a system composed of many polyhedral blocks. *Int. J. Rock Mech. Min. Sci.* (1988) **25(3)**:107-116.
[14] Hart, R., Cundall, P.A. and Lemos, J. Formulation of a three-dimensional distinct element model-Part II. Mechanical calculations for motion and interaction of a system composed of many polyhedral blocks. *Int. J. Rock. Mech. Min. Sci.* (1988) **25(3)**:117-125.
[15] Lemos, J. Discrete Element Modelling of Masonry Structures *Int. J. Archit. Herit.* (2007) **1(2)**:190-213.
[16] Van Mele, T., McInerney, J., DeJong, M.J. and Block, P. Physical and Computational Discrete Modelling of Masonry Vault Collapse. SAHC (2012) 2552–2560.
[17] DeJong, M.J. and Vibert, C. Seismic response of stone masonry spires: Computational and experimental modeling. *Eng. Struct.* (2012) **40**:566-574.
[18] McInerney, J.and DeJong, M.J. Discrete Element Modeling of Groin Vault Displacement Capacity. *Int. J. Archit. Herit.* (2015) **9(8)**:1037-1049.
[19] Dell'Endice, A., Iannuzzo, A., DeJong, M.J., Van Mele, T. and Block, P. Modelling imperfections in unreinforced masonry structures: Discrete Element simulations and scale model experiments of a pavilion vault. *Eng. Struct. (2021) 228: 111499*.
[20] Simon, J.and Bagi, K. Discrete Element Analysis of the Minimum Thickness of Oval Masonry Domes. *Int. J. Archit. Herit.* (2016) **10(4)**:457-475.
[21] Iannuzzo, A., Dell'Endice, A., Maia Avelino, R., Kao, G.T.C., Van Mele, T. and Block, P. COMPAS Masonry: a computational framework for practical assessment of unreinforced masonry structures. In: *Proceedings of the SAHC Symposium*, Barcelona: (2021).
[22] Bigoni, D. and Noselli, G.. Localized stress percolation through dry masonry walls. Part I - Experiments. *Eur. J. Mech. A/Solids* (2010) **29(3)**:291-298.
[23] Mastrodicasa, S. Dissesti statici delle strutture edilizie. Ulrico Hoepli (1978).
[24] Heyman, J. The structural engineer's view of ancient buildings. *J. Mech. Mater. Struct.* (2018) **13**:609–15.

12thInternational Conference on Structural Analysis of Historical Constructions
SAHC 2020
P. Roca, L. Pelà and C. Molins (Eds.)

INFLUENCE OF TEMPERATURE ON THE STRUCTURAL BEHAVIOUR OF MASONRY BUILDINGS

M. GIRARDI[1*], C. PADOVANI[2] AND D. PELLEGRINI[2]

[1]Institute of Information Science and Technologies "A. Faedo", ISTI-CNR
Via Moruzzi, 1, 57126 Pisa (PI)
e-mail: maria.girardi@isti.cnr.it, www.isti.cnr.it (*corresponding author)

[2]Institute of Information Science and Technologies "A. Faedo", ISTI-CNR
Via Moruzzi, 1, 57126 Pisa (PI)
email: {cristina.padovani, daniele.pellegrini}@isti.cnr.it, www.isti.cnr.it

Keywords: Historical Structures, Masonry, Nonlinear analysis, Thermal loads

Abstract. *This paper investigates the mechanical behaviour of heritage structures subjected to seasonal temperature variations. To this end, the constitutive equation of masonry-like materials, which has been embedded in the finite element code NOSA-ITACA (www.nosaitaca.it), is used to model the static and dynamic behaviour of simple arched masonry structures subjected to thermal loads.*

1 INTRODUCTION

Unlike linear elastic materials whose mechanical behaviour in the presence of thermal variations has been investigated in-depth [1], masonry materials under non-isothermal conditions are scarcely explored. A first contribution in this regard was provided in [2], which studied the influence of temperature changes on the displacements and stresses of masonry bridges. More recently, finite element simulations of the static behaviour of the Basilica of San Vitale in Ravenna have been conducted [3], taking seasonal thermal variations into account. Several papers report the presence of cracks in masonry monuments and bridges, which can be ascribed to thermal fluctuations [4, 5]. Moreover, numerous experimental campaigns[6, 7, 8, 9, 10, 11] have demonstrated that the presence of thermal strains affects not only the static behaviour of masonry structures, but also their dynamical properties. Long–term ambient vibration monitoring on masonry towers has proved the influence of environmental parameters such as temperature and humidity on the measured natural frequencies, which generally tend to increase with temperature. Such behaviour is often attributed to the closing of micro–cracks in masonry, due to thermal expansion. Similar effects were also detected in the Mallorca Cathedral and described in [11],which reports frequencies variations on the order of 10 - 20%.

2. THE CONSTITUTIVE EQUATION OF NO-TENSION MATERIALS UNDER NON-ISOTHERMAL CONDITIONS

Masonry is modelled herein as an isotropic nonlinear elastic material with zero tensile strength and infinite compressive strength [12]. This constitutive equation has been

generalized in order to take into account the presence of thermal dilatation, the goal being to model the influence of temperature variations on the stress fields, crack distribution, and modal properties of the structure. Indeed, there are many engineering problems in which the presence of thermal dilatation must be taken into account; relevant examples range from daily and seasonal thermal variations affecting the stress field in masonry constructions, to the thermo-mechanical behaviour of masonry structures under elevated temperatures, such as the refractory linings of vessels and ladles used in the iron and steel industry.

Let us denote by $\theta \in [\theta_1, \theta_2]$ the temperature and by $\theta_0 \in [\theta_1, \theta_2]$ the reference temperature. We assume that the thermal dilatation due to the temperature variation $\Delta\theta = \theta - \theta_0$ is the spherical tensor $\alpha(\theta - \theta_0)\mathbf{I}$, where α is the linear coefficient of thermal expansion and $\mathbf{I}$ the identity tensor. It is possible to prove that for every infinitesimal strain tensor $\mathbf{E}$ and $\theta \in [\theta_1, \theta_2]$, there exists a unique triplet $(\mathbf{T}, \mathbf{E}^e, \mathbf{E}^f)$ of symmetric tensors such that $\mathbf{E} - \alpha(\theta - \theta_0)\mathbf{I}$ is the sum of the elastic strain $\mathbf{E}^e$ and the positive semidefinite fracture strain $\mathbf{E}^f$, and that the Cauchy stress $\mathbf{T}$, negative semi-definite and orthogonal to $\mathbf{E}^f$, depends linearly and isotropically on $\mathbf{E}^e$, through Young's modulus E and Poisson's ratio ν[13]. Here, in view of the modest amplitude of the temperature range considered in the analysis, the elastic constants E and ν, which are generally functions of temperature [14], do not depend on θ. $\mathbf{T}$ is the stress corresponding to strain $\mathbf{E}$ and temperature θ, and masonry-like materials are then characterized by the stress function $\overline{\mathbf{T}}$ given by

$$\overline{\mathbf{T}}(\mathbf{E}, \theta) = \mathbf{T}, \text{ for } \mathbf{E} \text{ symmetric tensor and } \theta \in [\theta_1, \theta_2], \qquad (1)$$

whose explicit expression is reported in [13], along with its derivative $\overline{\mathbf{T}}_{\mathbf{E}}(\mathbf{E}, \theta)$with respect to $\mathbf{E}$.

The equilibrium problem of masonry-like solids subjected to both mechanical and thermal loads is specifically addressed in [13], which describes the procedure implemented in the finite element code NOSA-ITACA (www.nosaitaca.it) with the aim of determining its numerical solution. With regard to the influence of thermal loads on the natural frequencies of masonry constructions, this paper adopts the algorithm presented in [15] and implemented in NOSA-ITACA, which enables calculating the frequencies and mode shapes of masonry constructions while taking into account the presence of cracks due to mechanical and thermal loads. More precisely, given a masonry structure, discretized into finite elements, and given its materials properties, together with the kinematic constraints and loads (both mechanical and thermal), the algorithm is based on a linear perturbation about the solution to the equilibrium problem and calculates the frequencies of the cracked structures by taking into account the tangent stiffness matrix, which is symmetric and positive definite. The algorithm has proved to be able to reproduce the changes measured in the frequencies of masonry structures subjected to reinforcement operations, such as for example, the Mogadouro tower (Portugal) addressed in [16]. Also, the algorithm has been successfully used in [17, 18]to model the changes measured in the frequencies of two masonry towers in Lucca, likely related to seasonal thermal variations. For both the towers considered, frequencies tend to increase with increasing temperature, a trend which was also recognized in numerous experimental campaigns regarding ancient masonry towers [6, 8, 10].

In the following section, we present some analyses conducted on two simple masonry arch models: the first (Model 1) is a round arch with a three-meter span, the second (Model 2) a

masonry arch bridge spanning about 45 m and with a rise-to-span ratio of about 1/7. The influence of temperature variations is examined with regard to both the static and the dynamic behaviour of these structures.

3. MASONRY ARCHES SUBJECTED TO THERMAL LOADS

3.1 Model 1: A round arch

Let us consider the masonry round arch shown in Figure 1, with a span of 3 m and thickness of about 20 cm. It is discretized into 1200 thick shell elements (element 10 of the NOSA-ITACA library), for a total number of 7878 degrees of freedom. The masonry material, which is assumed to have null tensile strength and infinite compressive strength, has Young's modulus E = 3 10^9 Pa, Poisson's ratio $\upsilon = 0.2$, mass density $\rho = 1800$ kg/m^3 and a linear coefficient of thermal expansion $\alpha = 6 \cdot 10^{-6} °C^{-1}$. The mass density of the infill, whose thickness over the arch crown is 0.3 m, is $\rho = 1000$ kg/m^3. The arch, with fixed springers, is first subjected to permanent loads (masonry and infill weights), and then to temperature variations $\Delta\theta$ ranging from -15° C to +15° C. For the sake of comparison, the results obtained via the NOSA-ITACA code are validated against the commercial code MARC [19], using the constitutive law of low tensile materials and setting E_s= 2.0·10^4 N/m^2 [16]. Figures 2 and 3 represent the plot of the normal force N and the bending moment M (assumed positive if the intrados is stretched) per unit width versus the arc length varying from 0 to πR, with R=1.5 m the mean radius of the arch, for the three load conditions ($\Delta\theta = 0°C$ is for the permanent loads only). The curves are shown for both the masonry-like (continuous line) and the linear elastic (dashed line) case. Figure 4 instead plots the eccentricity $e = M/N$ in the arch sections vs. the arc length for the masonry-like (continuous) and the linear elastic case. It is worth noting that the effects of temperature are substantially mitigated by the material nonlinearity, which causes a significant reduction in the stiffness of the arch sections, thus reducing the stresses in the arch with respect to the linear elastic case. This effect is particularly evident for negative thermal variations (cyan lines) and is in agreement with similar results from other studies [20].

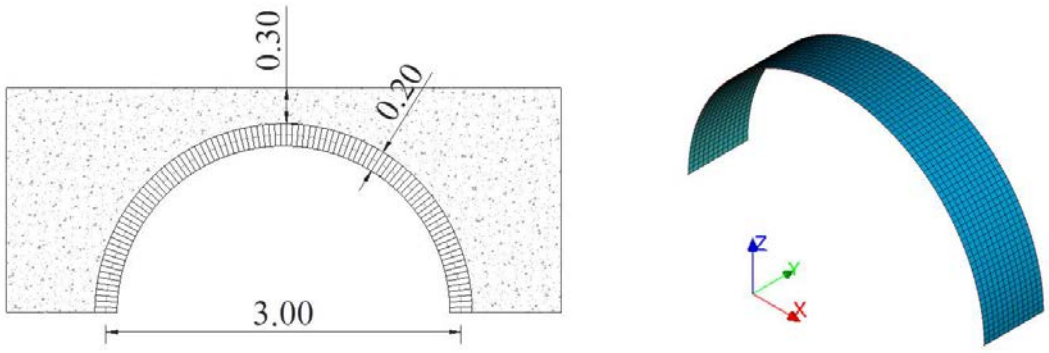


Figure 1: Model 1. Geometry and finite element mesh of the arch.

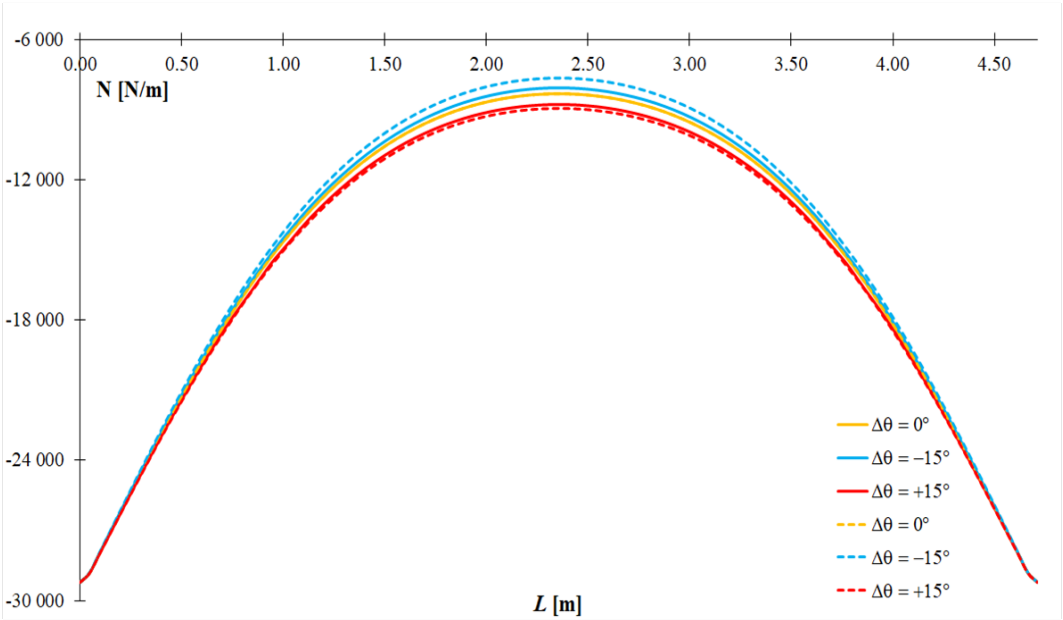


Figure 2: Model 1. Normal force per unit width N [N/m] versus the arc length[m] for $\Delta\theta = 0°C$ (yellow), $\Delta\theta = -15°C$ (cyan) and $\Delta\theta = +15°C$ (red); linear elastic material (dashed) and masonry-like material (continuous).

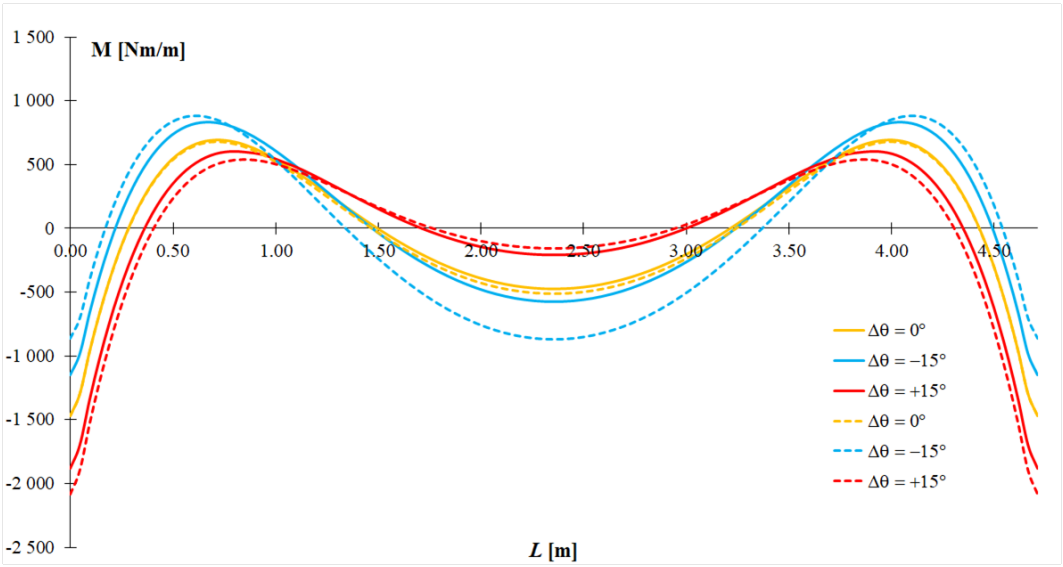


Figure 3.Model 1. Bending moment per unit width M [N m/m] versus the arc length [m] for $\Delta\theta = 0°C$ (yellow), $\Delta\theta = -15°C$ (cyan) and $\Delta\theta = +15°C$ (red); linear elastic material (dashed) and masonry-like material (continuous).

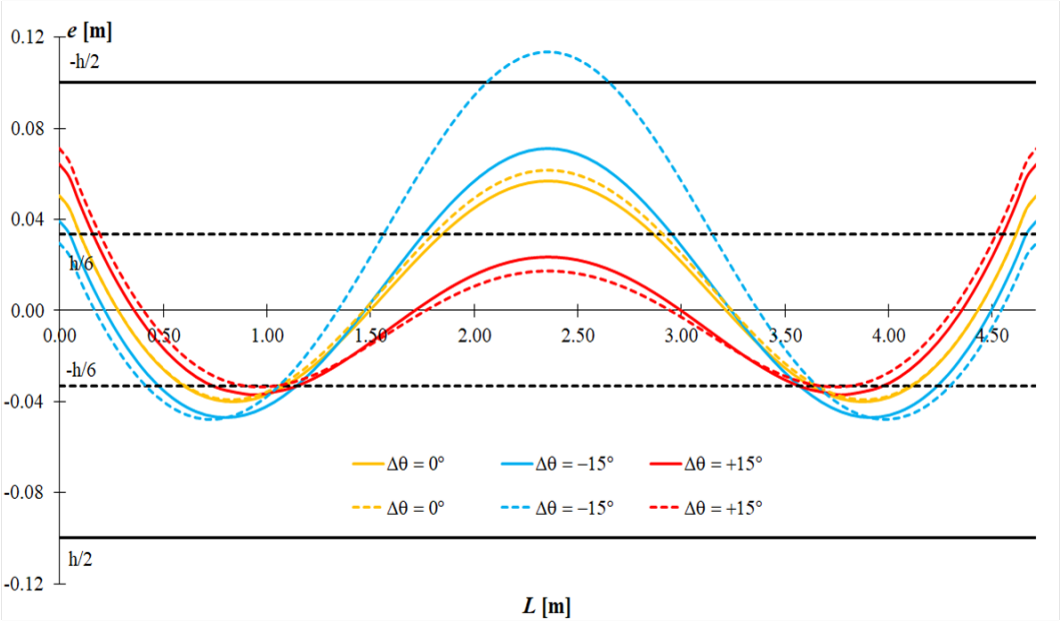


Figure 4. Model 1: Eccentricity e [m] versus the arc length [m] for $\Delta\theta = 0°C$ (yellow line), $\Delta\theta = -15°C$ (cyan) and $\Delta\theta = +15°C$ (red); linear elastic material (dashed) and masonry-like material (continuous).

To investigate how temperature variations affect the dynamic properties of the arch, the procedure described in Section 2 has been followed. Table 1 summarizes the arch frequencies in the linear elastic (f_l) and the nonlinear case (f_{nl}), calculated after application of the permanent loads. The relative differences $\Delta f/f_l$ reported in the table are about8% for the fundamental frequency and 15% for the second frequency. The MACM value [15] measures the correlation between the linear elastic mode shape and the corresponding mode shape of the cracked structure; values close to one indicate that, when transitioning from the linear to the nonlinear case, the eigenvectors remain substantially parallel.

After application of the permanent loads, the arch is subjected to thermal variations $\Delta\theta$, and the first four natural frequencies are calculated, as reported in Table 2. Figure 5 shows a plot of the four frequencies vs. $\Delta\theta$. The second, third and fourth frequencies tend to increase with temperature. The curve of the first frequency, instead, shows a maximum for $\Delta\theta = 0$ and decreases for positive values of $\Delta\theta$. In this case, as shown by the red curves in Figure 4, increasing values of temperature tend to diminish the eccentricity in the central portions of the arch and increase the nonlinearity at the springings. The global result is a decrease inarch stiffness with respect to the horizontal displacements, which are involved particularly in the first mode shape (Figure 6). In general, mode shapes appear much less affected by temperature than frequencies, as proved by the values of the MACM indicator reported in Figure 6 (evaluated for each mode shape between the linear and the corresponding nonlinear eigenvector): all these values are close to one.

Finally, Table 3 shows, for different temperature increments, a comparison between the frequencies calculated by NOSA-ITACA and those calculated using MARC. The small differences at $\Delta\theta = 0$ (on the order of 5%) are attributable to the small tensile strength (not nil as in NOSA-ITACA) assumed in MARC. As shown in the table, despite the different

constitutive equations adopted by the two codes, their results coincide after application of the thermal loads.

Table 1. Model 1. Comparison between linear (f_l) and nonlinear case (f_{nl}); permanent loads ($\Delta\theta$ = 0).

	f_l [Hz]	f_{nl} [Hz]	$\Delta f/f_l$ [%]	MACM
Mode 1	14.704	**13.545**	7.88	0.999
Mode 2	31.991	**27.044**	15.46	0.991
Mode 3	57.138	**51.409**	10.03	0.993
Mode 4	73.048	**64.401**	11.84	0.976

Table 2. Model 1. Effects of temperature variations on the first four mode shapes of the arch. $\Delta f_i(\Delta\theta) = (f_i(\Delta\theta) - f_i(0))/ f_i(0)$.

$\Delta\theta$ [°C]	f_1 [Hz]	Δf_1 [%]	f_2 [Hz]	Δf_2 [%]	f_3 [Hz]	Δf_3 [%]	f_4 [Hz]	Δf_4 [%]
-15	12.932	-4,52	24.347	-9.97	42.235	-17.85	57.033	-11.44
0	**13.545**	0.00	**27.044**	0.00	**51.409**	0.00	**64.401**	0.00
+15	12.164	-10,20	28.730	6.23	53.050	3.19	72.669	12.83

Table 3. Model 1. Comparison of the results obtained via the NOSA-ITACA and the MARC codes for the first four frequencies. For the i-th frequency, $\delta_{i,NM} = |f_{i,NOSA} - f_{i,MARC}|/ f_{i,NOSA}$.

$\Delta\theta$ [°C]	$\delta_{1,NM}$ [%]	$\delta_{2,NM}$ [%]	$\delta_{3,NM}$ [%]	$\delta_{4,NM}$ [%]
-15	3.52	1.87	0.57	1.02
-10	2.00	0.12	0.69	0.92
-5	1.73	0.08	0.53	1.17
0	3.60	7.64	5.76	5.17
5	2.67	2.55	0.37	0.69
10	3.62	1.80	0.49	0.37
15	0.14	0.19	0.81	0.52

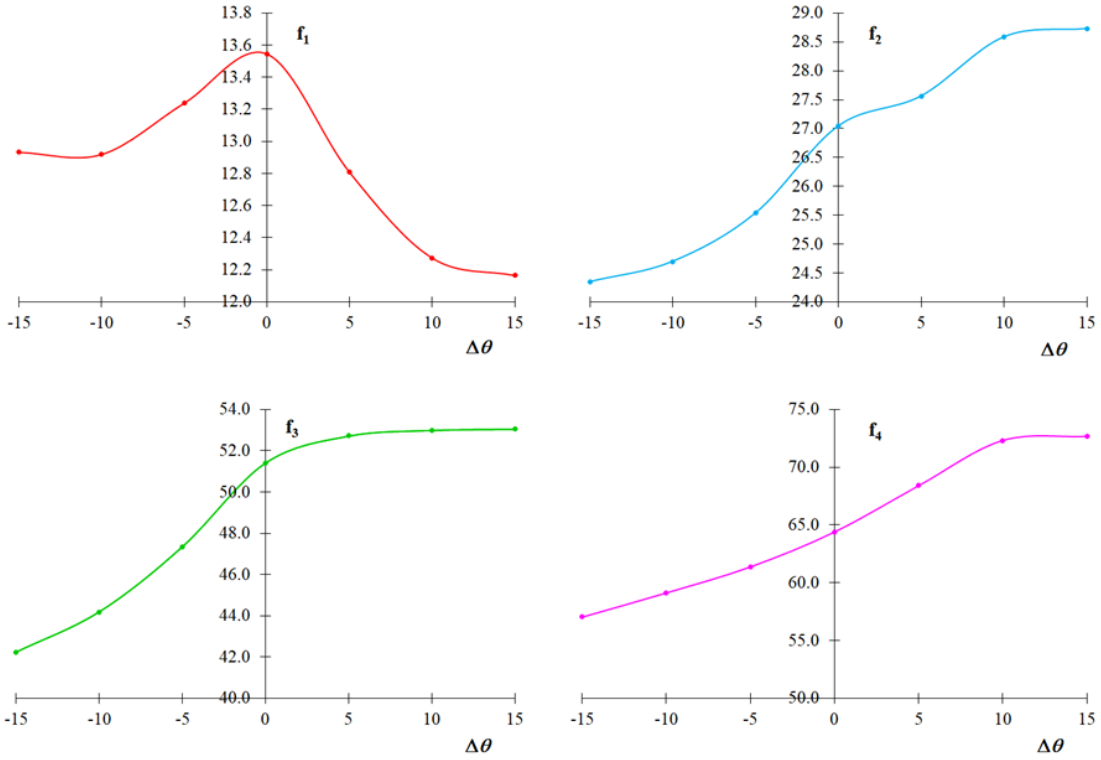


Figure 5. Model 1. The first four arch frequencies [Hz] vs. temperature variations $\Delta\theta$ [°C].

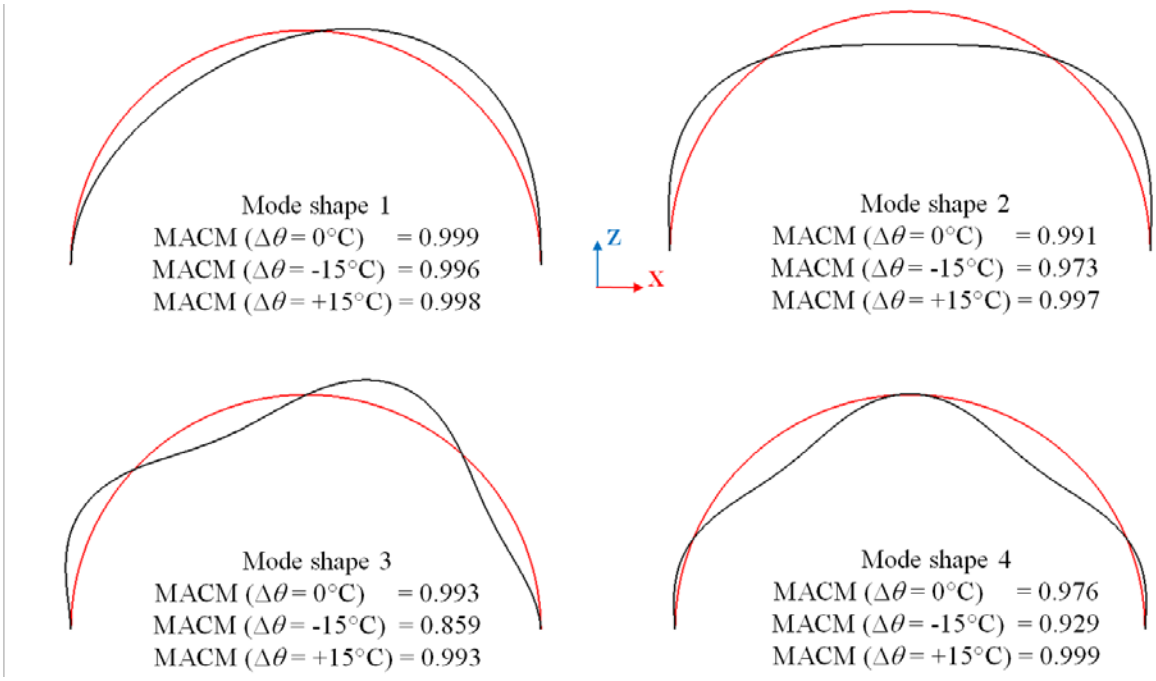


Figure 6. Model 1.The first four mode shapes of the arch.

3.2 Model 2: A masonry arch bridge

Let us consider the masonry arch bridge shown in Figure 7, with a length of 44 m, rise of about 6 m and constant thickness of 1.5 m. It is discretized into 2160 thick shell elements, for a total number of 13650 degrees of freedom. The masonry properties are: Young's modulus E = 4 10^9 Pa, Poisson's ratio $\upsilon = 0.2$, mass density $\rho = 2000$ kg/m^3 and linear thermal expansion coefficient$\alpha = 1 \cdot 10^{-5}°\mathrm{C}^{-1}$. The mass density of the infill, whose thickness over the arch crown is 0.4 m, is$\rho = 2000$ kg/m^3. The arch, with fixed springers, is first subjected to permanent loads (masonry and infill weights) and then to temperature variations $\Delta\theta$ ranging from -10° to +15°.

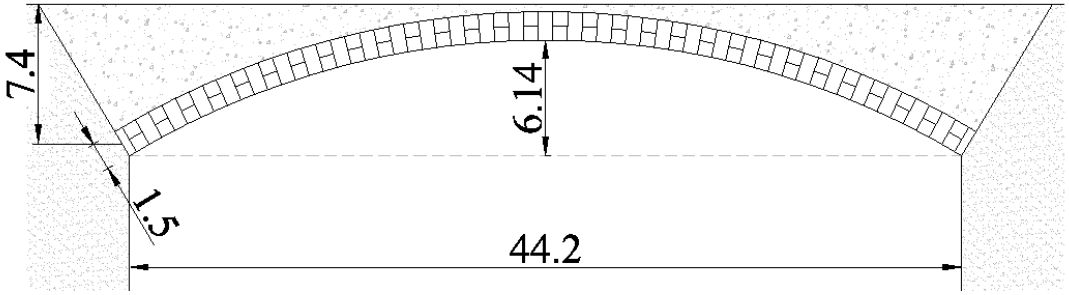


Figure 7. Model 2. Geometry of the masonry arch bridge.

Figure 8shows a plot of the eccentricity e vs. the arc length for the masonry-like case. The arch remains substantially in the linear elastic field, with the exception of the springings, where the eccentricity exceeds one-sixth of the section's height. For a positive thermal variation of 15°, the eccentricity in the mid-section of the arch increases (in absolute value) by about 40%, passing from -9 cm to -13 cm. Correspondingly, the arch's mid-section rises by about 0.5 cm. For $\Delta\theta = -10°$, representing winter conditions, the eccentricity in the mid-section falls from -9 cm to -6.8 cm (24%), and the arch crown undergoes a lowering of about 2.6 cm. Thus, the total displacement of the arch mid-section produced by the considered thermal variations is about 3 cm. These data are in agreement with the experimental evidence, as described in [2], which reports on different cases of masonry arch bridges that present lowering of the crown during winter and its rising during summer. Comparison between Figures 4 and 8 also highlights the role of the span-to-rise ratio on the arches' static behaviour. In fact, Model 1 and Model 2 exhibit very different behaviours even for permanent loads, with opposite signs of the eccentricity.

Regarding the influence of thermal variations on the bridge's modal properties, Table 4 reports the bridge frequencies for different temperature increments. Frequencies at $\Delta\theta$ = 0 are calculated for the permanent loads only. The trend evident in the table is similar to that found for masonry towers: all frequencies tend to increase with increasing temperatures. The frequency variations range from 11% for the fundamental frequency to 0.16 % for the third frequency. As a general remark, the frequency values seem to be more influenced by positive values of $\Delta\theta$: this trend is clearly shown by Figure 9, where the graphs of the four frequencies are plotted vs. temperature increments. As shown in Figure 8, positive values of $\Delta\theta$ tend to

reduce the eccentricity at the springers, which represent the only portions of the arch in the nonlinear field, and thus the structure quickly approaches linear elastic behaviour. Finally, Figure 9 shows the arch's first four mode shapes. As for Model 1, mode shapes are less affected by temperature than frequency, and the values of the MACM indicator (evaluated for each mode shape between the linear and the corresponding nonlinear eigenvector) are all close to one.

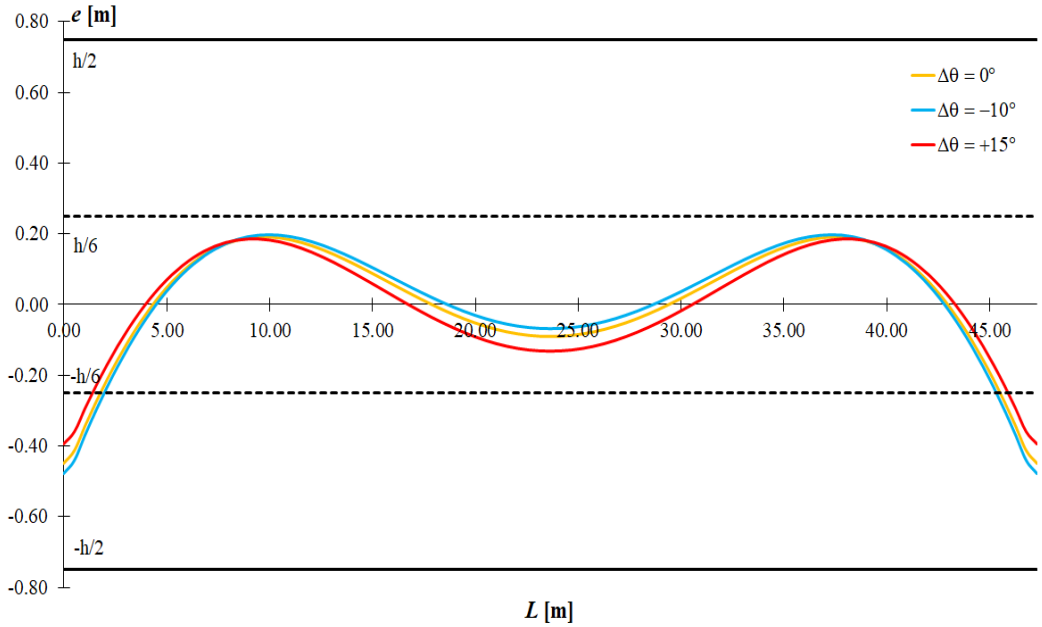


Figure 8. Model 2. Eccentricity e [m] versus the arc length[m] for $\Delta\theta = 0°C$ (yellow), $\Delta\theta = -10°C$ (cyan) and $\Delta\theta = +15°C$ (red), masonry-like material.

Table 4. Model 2. Effects of temperature variations on the arch's first four frequencies; $\Delta f_i(\Delta\theta) = (f_i(\Delta\theta) - f_i(0))/ f_i(0)$.

$\Delta\theta$ [°C]	f_1 [Hz]	Δf_1 [%]	f_2 [Hz]	Δf_2 [%]	f_3 [Hz]	Δf_3 [%]	f_4 [Hz]	Δf_4 [%]
-10	1.435	-1.37	2.758	-1.71	3.624	-0.60	4.813	-1.51
-5	1.444	-0.76	2.788	-0.64	3.645	-0.03	4.869	-0.37
0	**1.455**	0.00	**2.806**	0.00	**3.646**	0.00	**4.887**	0.00
+5	1.519	4.40	2.885	2.82	3.647	0.03	4.997	2.25
+10	1.535	5.50	2.900	3.35	3.648	0.05	5.016	2.64
+15	1.619	11.27	3.018	7.56	3.652	0.16	5.198	6.36

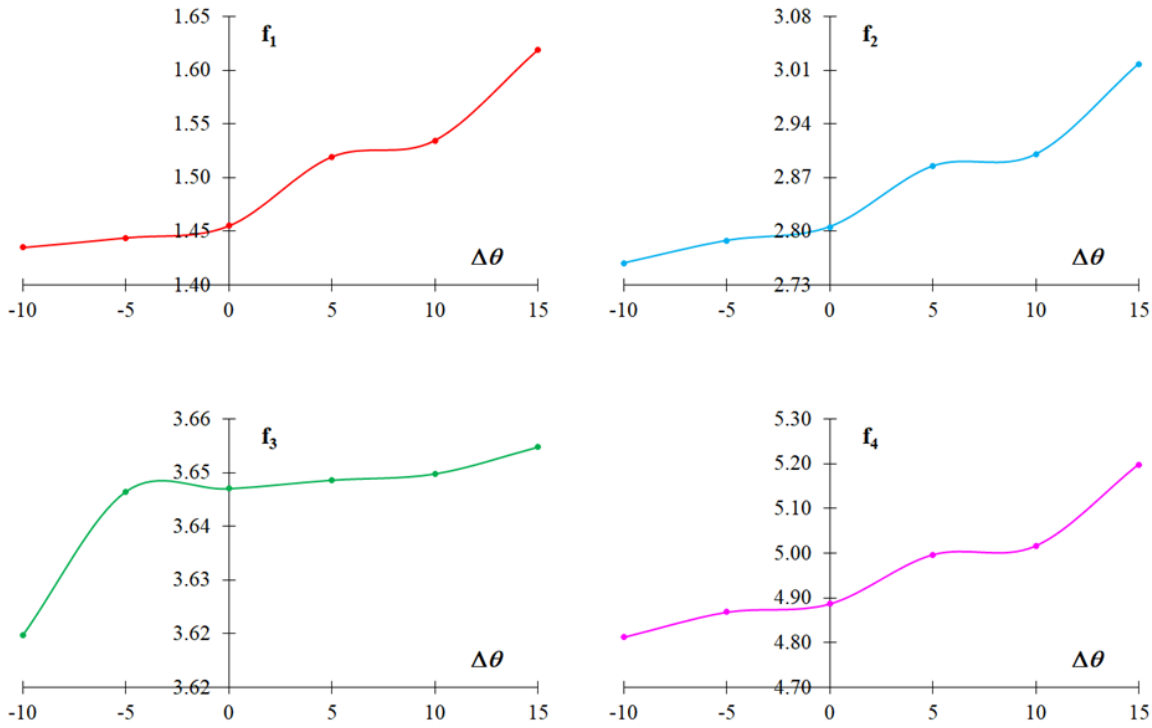


Figure 9. Model 2. The first four frequencies [Hz] of the arch bridge vs. temperature variations $\Delta\theta$ [°C].

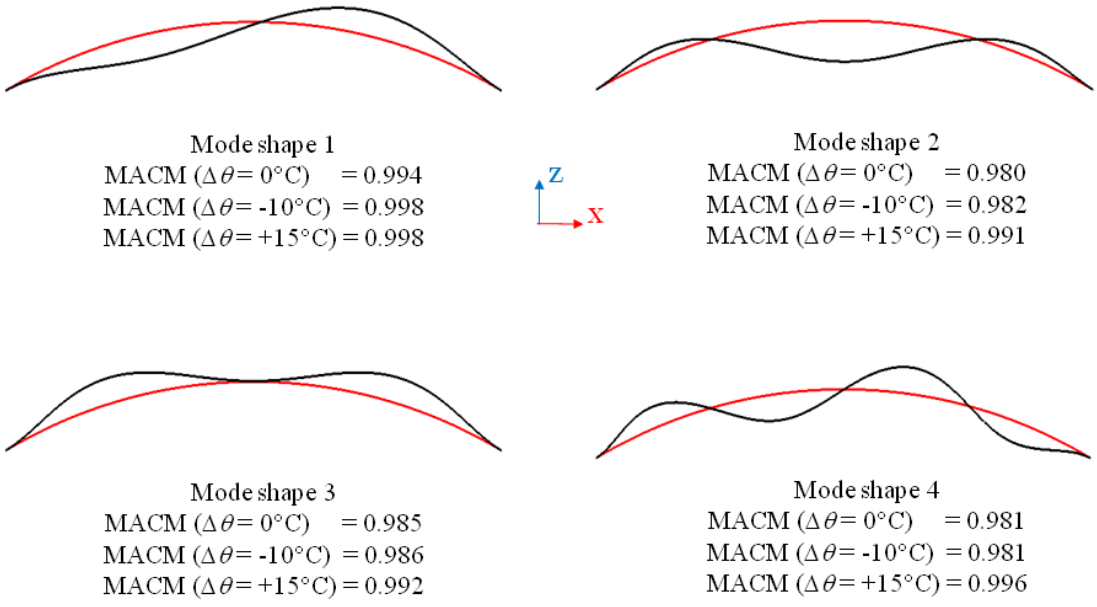


Figure 10. Model 2. The first four mode shapes of the arch bridge.

4 CONCLUSIONS

The paper presents some analyses conducted via the NOSA-ITACA code to assess the influence of temperature variations on the static and dynamic behaviour of masonry structures. The paper extends previous results obtained by the authors on masonry towers subjected to thermal loads.

The case studies analysed in the paper are a round arch and an arch bridge, two structural elements very common in the worldwide architectural heritage. The effects of thermal loads are discussed in terms of the consequent variations in eccentricities and modal properties, with particular regard to natural frequencies. In both cases, when the masonry's scarce capacity to withstand tensile stresses is taken into account (zero or very small tensile strength), thermal loads do not seem to significantly affect the static equilibrium of the arches. In fact, cracking due to the thermal strains causes a reduction in structural stiffness, with consequent mitigation of the stresses induced by the thermal variations. These changes in stiffness in turn affect the arches' modal properties, thus giving rise to significant changes in their natural frequencies.

The numerical results shown in the paper are in agreement with similar outcomes presented in the limited literature available on the topic. Comparisons between numerical and experimental results would be necessary to validate and corroborate the numerical simulations. Experimental tests aimed at investigating the influence of temperature variations on the structural behaviour of masonry arches are being planned for the near future.

Acknowledgements.

This research was partially funded by the Fondazione Cassa di Risparmio di Lucca (Lucca Savings Bank Foundation) within the framework of the project "SOUL - Urban Seismology in the Historic Centre of Lucca", 2019-2022. This support is gratefully acknowledged.

REFERENCES

[1] Timoshenko, S.P. and Goodier, J.N. Theory of elasticity, third Edition, McGraw-Hill Book Company (1970).

[2] Guidi, C. Influenza della temperatura sulle costruzioni murarie. *Atti della Reale Accademia delle Scienze di Torino* (1906) 319-330.

[3] Taliercio, A. and Binda, L. The Basilica of San Vitale in Ravenna: Investigation on the current structural faults and their mid-term evolution. *Journal of Cultural Heritage* (2008) **8**: 99-118.

[4] Blasi, C. and Coisson, *E. The effects of temperature on historical stone masonry structures. Structural Analysis of Historic Construction: Preserving Safety and Significance* (2008) 1271-1276.

[5] Talebinejad, I., Fischer, C., and Ansari, F. A hybrid approach for safety assessment of the double span masonry vaults of the Brooklyn Bridge. *Journal of Civil Structural Health Monitoring* (2011) **1(1-2)**: 3-15.

[6] Azzara, R.M., De Roeck, G., Girardi, M., Padovani, C., Pellegrini, D. and Reynders, E. The influence of environmental parameters on the dynamic behaviour of the San Frediano bell tower in Lucca. *Engineering Structures* (2018) **156**: 175-187.
[7] Dal Cin, A. and Russo, S. Evaluation of static and dynamic long-term structural monitoring for monumental masonry structure. *Journal of Civil Structural Health Monitoring* (2019) **9.2**: 169-182.
[8] Gentile, C., Guidobaldi, M. and Saisi, A. One-year dynamic monitoring of a historic tower: damage detection under changing environment". *Meccanica* (2016) **51**(11): 2873–89.
[9] Gentile, C., Ruccolo, A. and Canali, F. Long-term monitoring for the condition-based structural maintenance of the Milan Cathedral. *Construction and Building Materials* (2019) **228**: 117101 2019.
[10] Ramos, L.F., L. Marques, L:, Lourenco, P.B., De Roeck, G., Campos-Costa, A. and Roque, J. Monitoring historical masonry structures with operational modal analysis: Two case studies", *Mech. Syst. Signal Process* (2010) **24**:1291-1305.
[11] Elyamani, A., Caselles, O., Roca, P. & Clapes, J. Integrated dynamic and thermography investigation of Mallorca Cathedral. *Mediterranean archaeology & archaeometry* (2018) **18**(1): 221-236.
[12] DelPiero, G. Constitutive equation and compatibility of the external loads for linearly-elastic masonry-like materials, *Meccanica* (1989) **24**: 150–162.
[13] Lucchesi, M., Padovani, C., Pasquinelli, G. and Zani, N. *Masonry constructions: mechanical models and numerical applications*. Lecture Notes in Applied and Computational Mechanics, Springer–Verlag, (2008).
[14] Padovani, C., Pasquinelli, G., and Zani, N. A numerical method for solving equilibrium problems of no-tension solids subjected to thermal loads. *Computer methods in applied mechanics and engineering* (2000) **190.1-2**: 55-73.
[15] Girardi, M., Padovani, C., and Pellegrini, D. Modal analysis of masonry structures, *Mathematics and Mechanics of Solids* (2019) **24**(3): 616-636.
[16] Pellegrini, D., Girardi, M., Lourenço, P. B., Masciotta, M. G., Mendes, N., Padovani, C. And Ramos, L. F. Modal analysis of historical masonry structures: Linear perturbation and software benchmarking. *Construction and Building Materials* (2018) **189**:1232-1250.
[17] Azzara, R.M., Girardi, M., Iafolla, V., Padovani, C. and Pellegrini, D. Long-term dynamic monitoring of medieval towers. *Front. Built Environ.* - Earthquake Engineering, (2020), https://doi.org/10.3389/fbuil.2020.00009.
[18] Girardi, M., Padovani, C., and Pellegrini, D. Effects of the stress field on the dynamic properties of masonry bell towers. AIMETA 2017 - *Proceedings of the 23rd Conference of the Italian Association of Theoretical and Applied Mechanics* (2017) **3**: 216-229.
[19] Marc 2014 Volume A: theory and user information. Marc &Mentat (2014) –Marc &Mentat Docs.
[20] Proske, D. and Van Gelder, P. Safety of historical stone arch bridges. Springer Science & Business Media(2009).

12th International Conference on Structural Analysis of Historical Constructions
SAHC 2020
P. Roca, L. Pelà and C. Molins (Eds.)

INFLUENCE OF THE SPATIAL VARIABILITY OF JOINTS CHARACTERISTICS ON THE ELASTIC PROPERTIES OF MASONRY

MARIA LAURA DE BELLIS[1*], VINCENZO SEPE[1] AND MARCELLO VASTA[1]

[1]Department of Engineering and Geology (INGEO)
Università "G. D'Annunzio" di Chieti - Pescara
Viale Pindaro 42, 65127 Pescara, Italy
e-mail: {marialaura.debellis, vincenzo.sepe, marcello.vasta}@unich.it, (*corresponding author)

Keywords: Masonry Structures, Homogenization, Random Uncertainties

Abstract. *Brick masonry is a multicomponent composite material, characterized by a marked inhomogeneity, a highly anisotropic behavior arising from the complex interactions between joints and bricks, and a considerable spatial variability of material properties, particularly relevant in the case of historical masonries. The focus of this paper is on the interdependence between the spatial variability of mechanical properties of joints and the overall homogenized response of a given volume element of masonry. It is assumed that mechanical properties of bed joints may vary according to a fixed probability distribution and correlation function and the mechanical response of the volume element is investigated in terms of the overall elastic stiffness. As confirmed by preliminary results, the spatial variability of the mechanical properties may affect the overall response of a masonry wall.*

1 INTRODUCTION

Experimental and numerical results [1-3], referred either to single constituents or to full-sized masonry walls, have shown remarkable spatial variations of constitutive variables, i.e. Young modulus, tensile and compressive strength among others, also in case of new structures, as well as geometrical variations of the masonry arrangement [4]. In the case of historical masonries, such variability can cause even more relevant effects, especially due to the role of ageing processes, that can locally affect the mechanical characteristics of bed and head mortar joints.

Based on the aforementioned considerations, the focus of this paper is on the interdependence between the spatial variability of mechanical properties of joints and the overall response of a given volume element of the masonry. To this aim, a well established computational homogenization technique is combined with a properly conceived stochastic procedure. It is assumed that elastic properties of bed joints may vary according to a fixed probability distribution and correlation function. The mechanical response, in terms of overall elastic stiffness of the selected volume element, is investigated as a function of mean, variance and correlation length of the elastic properties of the joints, in a realistic range according to values experimentally observed.

2 ELASTIC PROPERTIES OF A VOLUME ELEMENT

Although geometrical and mechanical characteristics of both components of a given volume element and their related uncertainties may play a relevant role on the overall behavior, the most pronounced uncertainties on the global elastic behavior of masonry are likely due to available information about deformability of joints and its spatial variability.

To this aim, for the volume element (Fig. 1, L_0=26 cm) of a regular masonry made of bricks and mortar joints with running bond arrangement, the sensitivity of homogenized elastic properties is investigated as a function of mechanical characteristics of bed mortar joints, varying with a given standard deviation σ_E around a mean value μ_E. A constant value ν=0.2 has instead been assigned to the Poisson coefficient of joints and elastic parameters of bricks have also been considered as constant, E_b=6000 MPa and ν_b=0.2.

Each bed joint (with a total length L_0, see Fig. 1) is discretized in 10 parts (Δx=2.6 cm), assigning to each of them the elastic modulus E in the mean point, as obtained by a random generation of E(x) (see Sect. 3.2) in the interval $0 \leq x \leq L$, with $L >> L_0$ and a sampling step $\delta x=\Delta x/100$.

In the numerical investigation described below a mean value μ_E=500 MPa was assumed, with standard deviation varying between $\sigma_E = 0.07\ \mu_E$ and $\sigma_E = 0.35\ \mu_E$ and six different correlation lengths (L_{c1}=0.26 cm, L_{c2}=0.65 cm, L_{c3}=1.3 cm, L_{c4}=2.6 cm, L_{c5}=5.2 cm, L_{c6}=13 cm).

Namely, for a given σ_E and correlation length L_c, a random realization of E(x) was obtained for L= 1300 cm. From each one of these random realizations, 25 pairs of statistically independent sub-intervals E(x) with the same correlation length were then extracted and assigned as random E(x) to the bed joints of the volume element, while for head joints a constant value $E=\mu_E$ was assumed.

As an example, the random variables E(x) for correlation lengths L_{c1}=0.26 cm and L_{c6}=13 cm are reported in Fig. 2.

The mean and standard deviation of the homogenized elastic parameters (Sect. 3) of the selected volume element, obtained with 25 independent realizations of E(x) on the bed joints, are reported in Sect. 3.2 as a function of standard deviation σ_E and correlation length L_c.

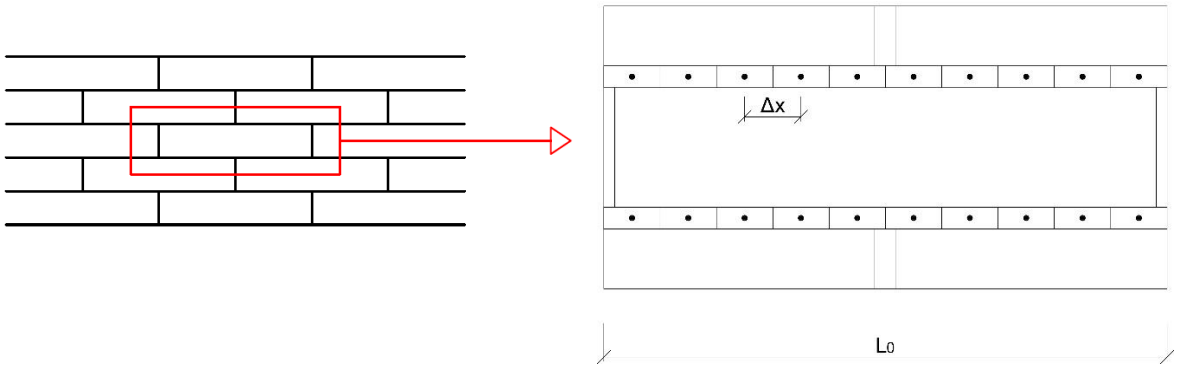
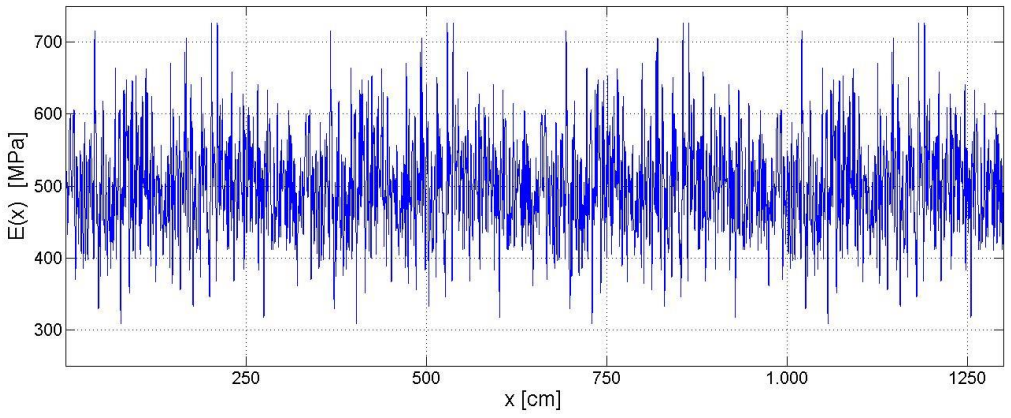
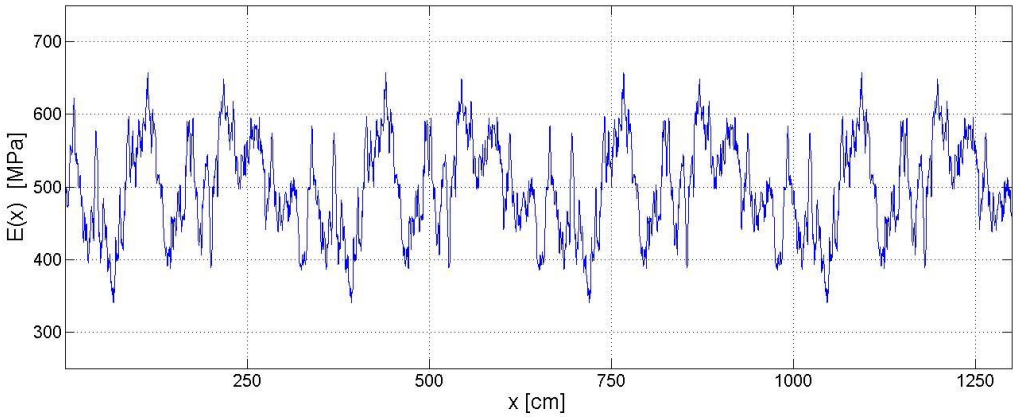


Figure 1: selected volume element: L_0 = 26 cm



(a)



(b)

Figure 2: realizations of the random vector E(x) for two different correlation lengths;

a) L_{c1}=0.26 cm; b) L_{c6}=13 cm

3 HOMOGENEIZED ELASTIC PROPERTIES OF MASONRY ASSEMBLY

The homogenization of the masonry material is performed resorting to a first order computational homogenization technique. Consistently with the classical approach [5-6], the composite material is described at two scales of interest, the microscopic and the macroscopic scale, as a Cauchy continuum. At the microscopic scale, the actual material is thoroughly described, in terms of geometric and constitutive parameters characterizing both blocks and mortar joints, while at the macroscopic one the heterogeneous material is ideally replaced by an equivalent homogeneous material, able to reproduce the overall elastic response of the composite material.

The classical first order multiscale scheme is briefly recalled in the framework of a strain driven approach. FE elastic analyses are exploited to evaluate the effective elastic properties of the masonry characterized by spatial variability of the elastic constants in the mortar joints.

A one to one correspondence is established between a macroscopic point of the first order homogenized continuum and the corresponding material portion at the microscopic scale.

At the typical material point $\mathbf{X} = \{X, Y\}^T$ at the macroscopic level, the displacement vector $\mathbf{U} = \{U, V\}^T$ is defined and the strain vector results as

$$\boldsymbol{E} = \begin{Bmatrix} E_{XX} \\ E_{YY} \\ \Gamma_{XY} \end{Bmatrix} = \mathbf{D} \begin{Bmatrix} U \\ V \end{Bmatrix}, \quad \text{where} \quad \mathbf{D} = \begin{bmatrix} \cdot_{,X} & 0 \\ 0 & \cdot_{,Y} \\ \cdot_{,Y} & \cdot_{,X} \end{bmatrix}, \tag{1}$$

with **D** being the kinematic operator.

The overall linear elastic constitutive equations in the general anisotropic case depends on the overall elasticity tensor **C** as

$$\boldsymbol{\Sigma} = \begin{Bmatrix} \Sigma_{XX} \\ \Sigma_{YY} \\ T_{XY} \end{Bmatrix} = \mathbf{C} \begin{Bmatrix} E_{XX} \\ E_{YY} \\ \Gamma_{XY} \end{Bmatrix}, \quad \text{where} \quad \mathbf{C} = \begin{bmatrix} C_{XXXX} & C_{XXYY} & C_{XXXY} \\ C_{XXYY} & C_{YYYY} & C_{YYXY} \\ C_{XXXY} & C_{YYXY} & C_{XYXY} \end{bmatrix}. \tag{2}$$

On the other hand, at the microscopic scale the corresponding strain $\boldsymbol{\varepsilon}$ and stress $\boldsymbol{\sigma}$ measures are similarly defined together with the local elasticity matrix **c**.

In the case of a periodic continuum the vector $\boldsymbol{E}$ is used as input quantity for the periodic cell and a properly defined boundary value problem is solved with periodic boundary conditions at the microscopic level. By evaluating the local response in terms of stress distributions, it is possible to detect the associated averaged elastic stress components and consistently deriving the components of **C** by exploiting a properly defined macro-homogeneity condition.

Nevertheless, in the case at hand, owing to the random distribution of the Young modulus along the mortar joints, the running bond masonry material is only characterized by geometric periodicity, while it is not periodic with respect to constitutive behavior. In this framework the classical concept of Representative Volume Element (RVE), well established for periodic heterogeneous media, loses its validity. The RVE cannot be a-priori recognized and becomes itself an unknown of the problem, together with the estimation of the homogenized elastic moduli, i.e. the components of **C**.

The RVE can be approached by using a finite size scaling of the so-called statistical volume element (SVE) [7-8] through two hierarchies of constitutive bounds, stemming from the solution of Dirichlet and Neuman boundary value problems at the microscopic level, respectively. The key idea is considering a trial portion of the heterogeneous material of a given characteristic size and keep enlarging such portion until the solution of both of Dirichlet and Neuman boundary value problems have fulfilled a properly defined convergence criterion.

The Dirichlet boundary conditions imposed along the boundary of the SVE can be written as

$$\begin{aligned} u &= E_{XX}x + \Gamma_{XY}y \\ v &= \Gamma_{XY}x + E_{YY}y \end{aligned}, \tag{3}$$

while the Neumann boundary conditions result as

$$t_x = \Sigma_{XX} n_x + T_{XY} n_y$$
$$t_y = T_{XY} n_x + \Sigma_{YY} n_y' \tag{4}$$

with (t_x, t_y) the components of tractions and (n_x, n_y) the components of the outward normal.

The macroscopic stress $\boldsymbol{\Sigma}$ and strain $\boldsymbol{E}$ measures are linked to the respective microscopic ones $\boldsymbol{\sigma}$ and $\boldsymbol{\varepsilon}$ through the so-called spatial averages, as follows

$$\boldsymbol{\Sigma} = \frac{1}{\omega}\int_{\omega} \boldsymbol{\sigma}\, d\omega, \quad \boldsymbol{E} = \frac{1}{\omega}\int_{\omega} \boldsymbol{\varepsilon}\, d\omega, \tag{5}$$

Finally, the homogenized moduli can be obtained via the macro-homogeneity condition, accounting for infinitesimal deformation gradients. Such well-known condition establishes a correspondence between the average internal work over a portion of material at the microscopic level and the mechanical internal work density at the macroscopic point, as

$$\boldsymbol{E}^{\boldsymbol{T}}\boldsymbol{\Sigma} = \frac{1}{\omega}\int_{\omega} \boldsymbol{\varepsilon}^{\boldsymbol{T}}\boldsymbol{\sigma}\, d\omega. \tag{6}$$

In this preliminary work the focus is on the definition of the procedure to evaluate the homogenized elastic moduli valid for the masonry characterized by random distribution of mortar joints elastic moduli, rather than detecting the RVE for such material. This is why we consider only one portion of the heterogeneous material, the one depicted in Figure 1.

Furthermore, in order to obtain a synthetic description of the degree and direction of anisotropic behavior [9-10] of the elastic homogenized response, we evaluate $E_{hom}(\theta)$ and $\nu_{hom}(\theta)$ as a function of the counterclockwise angle θ between the standard basis $(\boldsymbol{e}_x, \boldsymbol{e}_y)$ and the basis $(\boldsymbol{a}_x, \boldsymbol{a}_y)$ rotated of θ about an axis through the origin. More specifically, $E_{hom}(\theta)$ and $\nu_{hom}(\theta)$ are obtained for tension applied along the direction identified by the unit vector $\boldsymbol{a}_x$ inclined at an angle θ with respect to $\boldsymbol{e}_x$.

The homogenized elastic compliance tensor $\boldsymbol{D} = \boldsymbol{C}^{-1}$ in the rotated reference system becomes $\boldsymbol{D}^{\theta}$ and the arising angular variation of the Young modulus and of the Poisson's ratio are consistently evaluated as

$$E_{hom}(\theta) = \frac{1}{D^{\theta}_{XXXX}}, \qquad \nu_{hom}(\theta) = -\frac{D^{\theta}_{XXYY}}{D^{\theta}_{XXXX}}, \tag{7}$$

where D^{θ}_{XXXX} and D^{θ}_{XXYY} are the components of $\boldsymbol{D}^{\theta}$.

The graphical representation of $E_{hom}(\theta)$ and $\nu_{hom}(\theta)$ versus θ is very suitable for an interesting physical interpretation. If the material is isotropic, indeed, the polar plot has the form

of a unitary circle, while deviations from a perfect circle evince the degree and direction of anisotropic behavior.

3.1 Reference case: homogeneous elastic properties of bed and head joints

As a reference case, a constant value $E(x) = \mu_E$ has been assigned to both head and bed joints. The variation of Young modulus $E_0(\theta)$ and Poisson coefficient $\nu(\theta)$ as a function of the angle θ are reported in Figure 3(a) and 3(b), respectively.

As shown by such figures, the equivalent stiffness of the selected volume element attains maximum and minimum values for $\theta = 0$ (stress-strain parallel to the bed joints) and $\theta = \pi/2$ (stress-strain orthogonal to the bed joints), respectively, while maximum values of Poisson coefficient are attained in pseudo-diagonal directions.

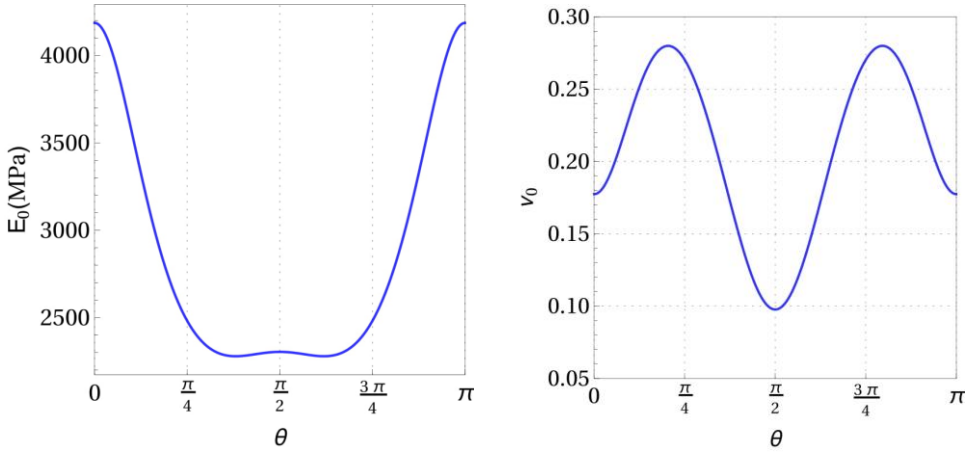


Figure 3: Reference case $E(x)= \mu_E$: Young modulus and Poisson coefficient as a function of θ

3.2 Random elastic properties of bed joints

Stationary Gaussian realizations of the Young modulus

$$E(x) = \bar{E} + e(x) \tag{8}$$

have been generated with $\bar{E}$ the mean value and $e(x)$ a stationary zero mean process obtained as the output of a first order linear scalar stochastic differential equation (Ornstein – Uhlenbeck process) [11]

$$\frac{de(x)}{dx} = -\lambda e(x) + W(x) \tag{9}$$

where $\lambda > 0$ and $W(x)$ a zero mean Gaussian stationary white noise input process with constant spectral density $S_w(\omega)=S_0$ and correlation functions $R_w(l) = \langle W(x)W(x+l)\rangle = 2\pi\, S_0\, \delta(l)$, where $\delta(\cdot)$ stands for the Dirac's delta distribution.

The spectral density $S_e(\omega)$ and the covariance function $C_e(l)$ of the stationary process $e(x)$ are as follows

$$S_e(\omega) = \frac{2\,\pi S_0}{\omega^2 + \lambda^2} \tag{10}$$

$$C_e(l) = \langle e(x)e(x+l)\rangle = \frac{\pi S_0}{\lambda}\exp\left(-\lambda|l|\right) \tag{11}$$

For the same input white noise $W(x)$ different correlated random realizations of $E(x)$ have been obtained for different values of the parameter λ and intensity S_0.

The correlation length L_c is the inverse of λ ($C_E(x) = C_e(x)$)

$$L_c = \frac{1}{C_E(0)}\int_0^{+\infty} C_E(l)dl = \frac{1}{\lambda} \tag{12}$$

while the standard deviation of $E(x)$

$$\sigma_E^2 = C_E(0) = \frac{\pi S_0}{\lambda} \tag{13}$$

As described in Sect.2, for each standard deviation σ_E and correlation length L_c 25 independent realizations of the elastic modulus E(x) of the bed joints have been considered for the volume element in Fig.1.

For each case the elastic tensor of the volume element has been obtained with the homogenization procedure described in Sect. 3 and boundary conditions of the Dirichlet type.

The mean values of the homogenized elastic modulus $E_{hom}(\theta)$ and Poisson coefficient $\nu_{hom}(\theta)$ in the considered set of 25 independent realizations almost coincide, as expected, with the values $E_0(\theta)$ and $\nu_0(\theta)$ of the reference case (Sect. 3.1), independently from the correlation length L_c or the variation coefficient $C_V = \sigma_E/\mu_E$. Therefore they are not reported here.

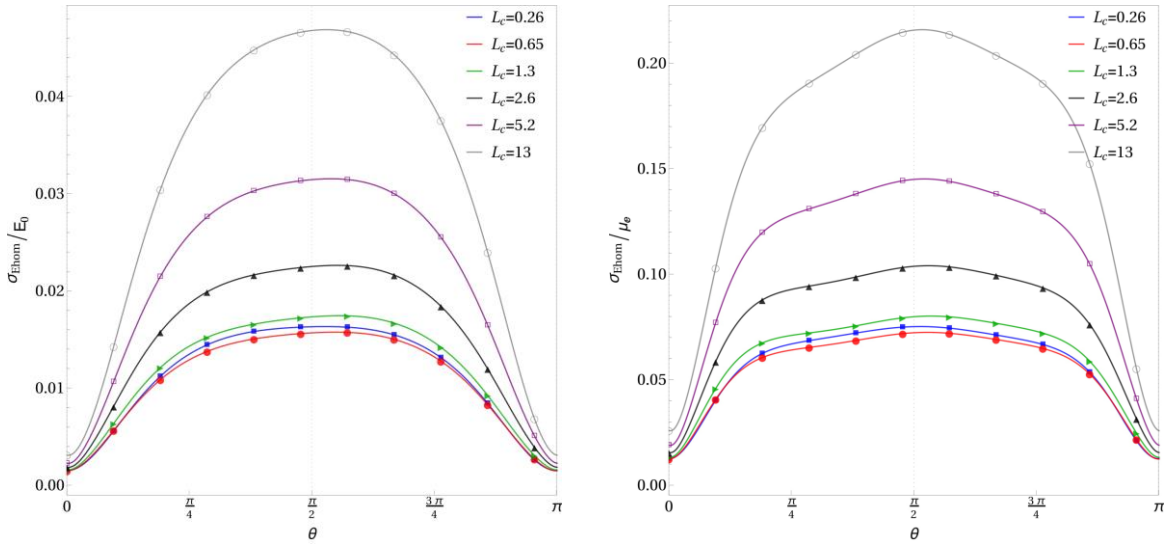
A significant dependence has instead been found for the standard deviation $\sigma_{Ehom}(\theta)$ and $\sigma_{vhom}(\theta)$ of the homogenized elastic modulus $E_{hom}(\theta)$ and Poisson coefficient $\nu_{hom}(\theta)$.

Standard deviations of $E_{hom}(\theta)$ and $\nu_{hom}(\theta)$, normalized with respect to the values $E_0(\theta)$ and $\nu_0(\theta)$ of the reference case (constant $E(x) = \mu_E$, Sect. 3.1) are described below for each angle θ as a function of the correlation length L_c (Fig. 4a, 5a) and of the variation coefficient $C_V = \sigma_E/\mu_E$ of the random variable E(x) (Fig. 6a, and 7a).

Due to the almost perfect coincidence of the mean values of $E_{hom}(\theta)$ and $\nu_{hom}(\theta)$ with $E_0(\theta)$

and $\nu_0(\theta)$, as already discussed, Fig. 4a, 5a, 6a, 7a also represent for each angle θ the ratios between the standard deviations of $E_{hom}(\theta)$ and $\nu_{hom}(\theta)$ and their mean values $\bar{E}_{\mathrm{hom}}(\theta)$ and $\bar{\nu}_{\mathrm{hom}}(\theta)$, respectively.

The same variables $E_{hom}(\theta)$ and $\nu_{hom}(\theta)$ are also shown in Fig. 4b, 5b, 6b, 7b without normalization, with the homogenized elastic modulus $E_{hom}(\theta)$ shown in the non-dimensional form $\sigma_{Ehom}(\theta)/\mu_E$, with μ_E = 500 MPa denoting the mean value of E(x).



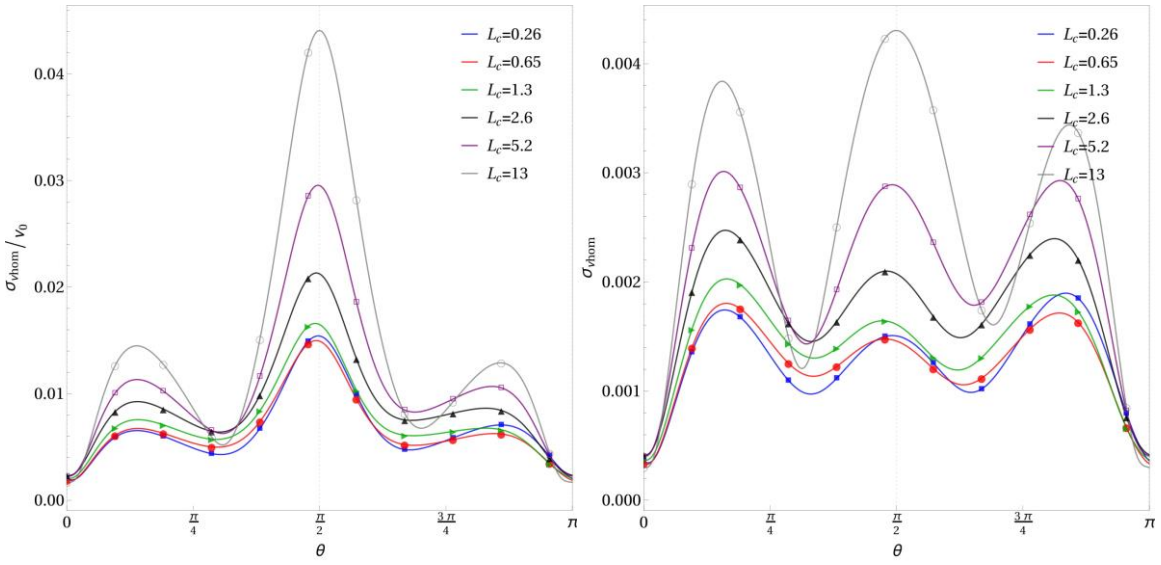
(a) (b)

Figure 4: Standard deviation $\sigma_{Ehom}(\theta)$ of the homogenized Young modulus $E_{hom}(\theta)$ for Dirichlet boundary conditions, for $C_V=\sigma_E/\mu_E$ = 0.14 and different correlation lengths L_C [cm]: a) $\sigma_{Ehom}(\theta)$ normalized with respect to $E_0(\theta)$ of the reference case with constant E(x); b) $\sigma_{Ehom}(\theta)$ normalized with respect to the mean value μ_E of E(x).

It can be observed (Fig. 4a) that for different correlation lengths the standard deviation $\sigma_{Ehom}(\theta)$ of the homogenized Young modulus $E_{hom}(\theta)$ is not negligible with respect to its mean value $\bar{E}_{\mathrm{hom}}(\theta)$, with a maximum of about 5 % for L_c = 13 and θ around π/2. A similar behavior is observed (Fig. 5a) for the standard deviation $\sigma_{vhom}(\theta)$ of the homogenized Poisson coefficient $\nu_{hom}(\theta)$.

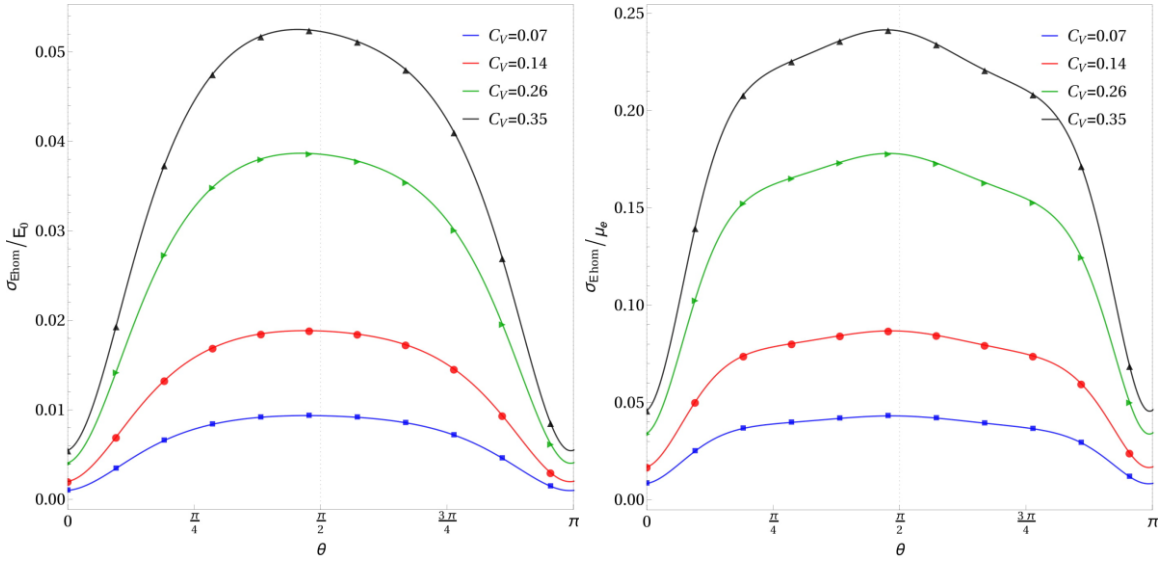
Figures 6a-7a describe the dependence of the homogenized Young modulus and Poisson coefficient on $C_V = \sigma_E/\mu_E$, i.e. the variation coefficient of the random elastic modulus E(x) of the bed joints of the volume element in Figure 1.

As expected, the ratios between the standard deviations $\sigma_{Ehom}(\theta)$, $\sigma_{vhom}(\theta)$ of $E_{hom}(\theta)$ and $\nu_{hom}(\theta)$ and their mean values $\bar{E}_{\mathrm{hom}}(\theta)$ and $\bar{\nu}_{\mathrm{hom}}(\theta)$ increase for an increasing C_V. Maximum values around 5 % have been found for $C_V = \sigma_E/\mu_E$ = 0.35, corresponding to the limit case of a random variable E(x) oscillating between values slightly larger than zero and $2\mu_E$.



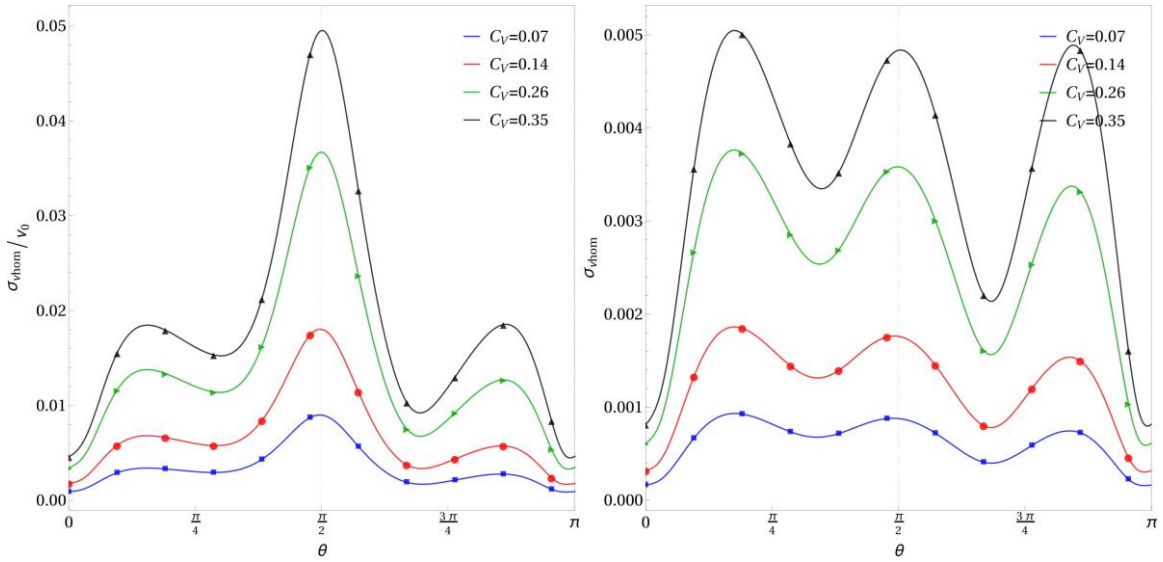
(a) (b)

Figure 5: Standard deviation $\sigma_{vhom}(\theta)$ of the homogenized Poisson coefficient $\nu_{hom}(\theta)$ for Dirichlet boundary conditions, for $\sigma_E/\mu_E = 0.14$ and different correlation lengths L_C [cm]: a) $\sigma_{vhom}(\theta)$ normalized with respect to $\nu_0(\theta)$ of the reference case with constant E(x); b) $\sigma_{vhom}(\theta)$.



(a) (b)

Figure 6: Standard deviation $\sigma_{Ehom}(\theta)$ of the homogenized Young modulus $E_{hom}(\theta)$ for Dirichlet boundary conditions for L_c=0.26 cm and different ratios $C_V=\sigma_E/\mu_E$: a) $\sigma_{Ehom}(\theta)$ normalized with respect to $E_0(\theta)$ of the reference case with constant E(x); b) $\sigma_{Ehom}(\theta)$ normalized with respect to the mean value μ_E of E(x).



(a) (b)

Figure 7: Standard deviation $\sigma_{vhom}(\theta)$ of the homogenized Poisson coefficient $\nu_{hom}(\theta)$ for Dirichlet boundary conditions for L_c=0.26 cm and different ratios $C_V=\sigma_E/\mu_E$: a) $\sigma_{vhom}(\theta)$ normalized with respect to $\nu_0(\theta)$ of the reference case with constant E(x); b) $\sigma_{vhom}(\theta)$.

4 CONCLUSIONS

- The paper examines the interdependence between the spatial variability of mechanical properties of joints and the overall homogenized response of a given volume element of regular masonry.
- Mechanical properties of bed joints is assumed to vary according to a fixed probability distribution and correlation function.
- A well established computational homogenization technique is applied.
- The mechanical response, in terms of overall elastic stiffness of the selected volume element, is investigated as a function of mean, variance and correlation length of the elastic properties of the joints.
- As confirmed by preliminary results, the spatial variability of the mechanical properties may affect the overall response of a masonry wall.
- Such preliminary results encourage further research on historical masonry with larger spatial variability of the elastic properties.

Acknowledgements. The financial support of University ‘‘G. D’Annunzio” of Chieti-Pescara is acknowledged by the authors.

REFERENCES

[1] L. Schueremans, D. Van Gemert, Predicting masonry properties from component properties using probabilistic techniques, *Proceedings of the STRUMAS V, The Fifth International Symposium on Computer Methods in Structural Masonry*, 2001.

[2] R. Zavalis, B. Jonaitis, Lourenco P.B., Analysis of bed joint influence on masonry modulus of elasticity, *Proceedings of the 9 th International Masonry Conference in Guimarães*, 2014.

[3] J. Li, M. J. Masia, M.S. Stewart, Stochastic spatial modelling of material properties and structural strength of unreinforced masonry in two-way bending, *Structure and Infrastructure Engineering*, 1-13, 2016.

[4] V. Gusella, F. Cluni, Random field and homogenization for masonry with nonperiodic microstructure, *Journal of Mechanics of Materials and Structures*, 1 (2): 357-386, 2006

[5] S. Ghosh, K. , S. Moorthy, Two scale analysis of heterogeneous elastic plastic materials with asymptotic homogenisation and Voronoi cell finite element model. *Comput Methods Appl Mech Eng* 132:63–116, 1996.

[6] C. Miehe, Strain-driven homogenization of inelastic microstructures and composites based on an incremental variational formulation. *Int J Numer Methods Eng* 55:1285–322, 2002.

[7] Z. Khisaeva, M. Ostoja-Starzewski, On the size of RVE in finite elasticity of random composites. *J Elast* 85:153–173, 2006

[8] P. Trovalusci, M.L. De Bellis, M. Ostoja-Starzewski, A. Murrali, Particulate random composites homogenized as micropolar materials. *Meccanica* 49, 2719–2727, 2014.

[9] D. Tromans, Elastic anisotropy of hcp metal crystals and polycrystals, *International Journal of Research and Reviews in Applied Sciences,* 6.4, pp.462-463, 2011.

[10] A. Bacigalupo, M.L. De Bellis, Auxetic anti-tetrachiral materials: Equivalent elastic properties and frequency band-gaps, *Composite Structures*, 131: 530-544, 2015.

[11] C.W. Gardiner, *Handbook of Stochastic Methods* (2nd ed.), Springer-Verlag, p. 106, ISBN 978-0-387-15607-1, 1985

12th International Conference on Structural Analysis of Historical Constructions
SAHC 2020
P. Roca, L. Pelà and C. Molins (Eds.)

INSPECTION, DIAGNOSIS AND MODELLING OF AZURARA CHURCH IN THE NORTH OF PORTUGAL

ESTEFANÍA A. CHAVES MORENO[1*], ELLEN T. KEY[1], AMRUTA UPLEKAR[1], OMAR PINO ACUÑA[1], GRAÇA VASCONCELOS[1], JAVIER ORTEGA[1], ELISA POLETTI[1]

[1]University of Minho
Campus of Azurém, 4800-058, Guimarães, Portugal
e-mail: echaves@us.es, ellenkey@ucla.edu, amrutauplekar@gmail.com, opino31@gmail.com, graca@civil.uminho.pt, javier.ortega@civil.uminho.pt, elisapoletti@gmail.com (*corresponding author)

Keywords: Masonry, Non-Destructive Tests, Finite Element Modelling

Abstract. *Santa Maria de Azurara church is a XVI century church in Portugal, classified as a national monument since 1910. The building shows not only the influence of the Manueline architectural style (Portuguese late Gothic style), but also Baroque and Mannerism styles. Presently, the church presents some structural and non-structural problems, so an inspection and diagnosis of the main building pathologies was carried out. This process was assisted by non-destructive testing (NDT) techniques which included sonic tests, ground penetrating radar (GPR) and Schmidt hammer for masonry elements and Pilodyn and ultrasonic pulse velocity for the timber elements. In addition, scanning electron microscope and x-ray diffraction analysis were used for mortar and stone characterization. Furthermore, dynamic identification tests were performed. Numerical analysis was performed to assess the nonlinear behaviour of the structure under different load conditions. In order to create an accurate model, material properties were estimated from the non-destructive tests and the dynamic properties were used to calibrate the model. A nonlinear static analysis (pushover) considering both vertical and horizontal loading was carried out in order to obtain the maximum load factor for the structure.*

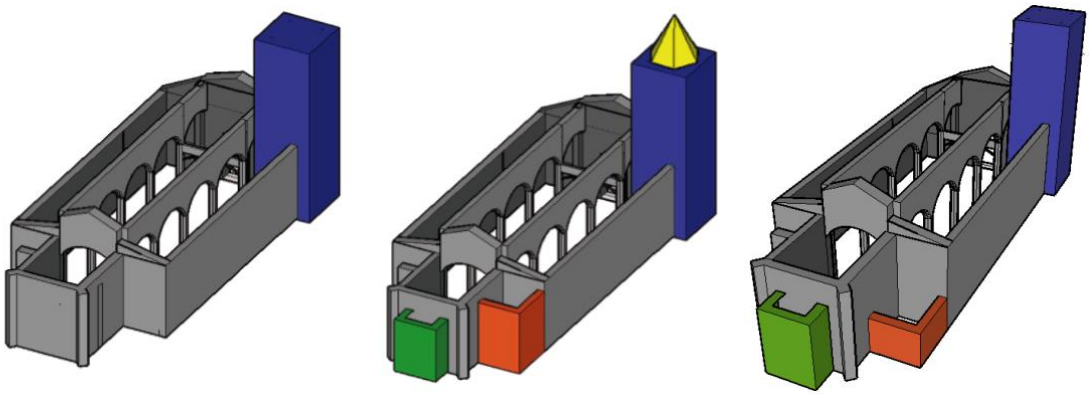
1 INTRODUCTION

Located in the Azurara parish of northwest Portugal, the church of Santa Maria is a local landmark. It is a masonry church dating to the XVI century near the town of Vila do Conde about 25 km north of Porto. Between October 2018 and March 2019, in the scope of the Advanced Master of Structural Analysis of Historical Constructions (SAHC), a team from the University of Minho analysed the church with non-destructive testing, monitoring systems and nonlinear structural analysis using the finite element method. This paper summarizes the work performed and the results.

2 BACKGROUND INFORMATION ON THE CHURCH

The construction of this Catholic church began in 1502 but finished with the apse in 1552, during the reign of King Joao III. For this reason, it could be considered as an example of the Manueline architectural style, a Portuguese style that occurred during the reign of King D. Manuel I between the Gothic and Renaissance styles. During the centuries, several structural changes were made (Figure 1). The church was classified as a national monument in 1910. Interventions in the XX century were made to reduce moisture problems in the floor [1].

The structure of the church is based in massive granite three-leafed walls forming three naves with a timber roof. Octagonal columns and Romanesque arches divide the central and lateral naves. The structural system of the chancel is composed of two stone cross vaults supported in external walls and buttresses. The XVII century tower structure (blue in Figure 1) is composed mainly of very thick external walls. Behind the apse is a small chapel thought to be added in the XVIII century, composed of irregular masonry walls (green in Figure 1).



(a) (b) (c)

Figure 1: Southwest isometric view of the church's structural evolution: (a) XVII century tower construction; (b) late XIX century/early XX century appearance with chapel, sacristy and pyramid; (c) current structure with single-story sacristy and no pyramid on tower

3 DAMAGE SURVEY

Inspection of the church led to the creation of damage maps. First, an in situ visual survey was carried out to identify the damages. This was complemented with a photography survey, where pictures of the damages were taken as well as photos for the creation of a photogrammetry model that would provide information about the geometry and the basis for the creation of the damage maps. The most prevalent types of damage are summarized here, according to ICOMOS guidelines [2]. An overall cause of much of the damage was water infiltration.

3.1 Cracks

The most prevalent appearance of cracks is on the bell tower. Major cracks can be seen on the exterior part of its western facade, under the balcony projection. Also, a major crack is noted on the internal facade which was measured and marked previously in the year 1985 (Figure 2). The crack meter placed there has detected movement since that date.



(a) (b)

Figure 2: Cracks under the balcony of the tower in (a) external west facade and (b) internal east facade.

3.2 Discoloration and deposit

Staining and soiling were present on the exterior walls. Moist areas could be seen in the interior. Efflorescence was densely observed on the lower areas of the internal surface of the walls (Figure 3(a)). It was also observed in areas close to the roof and all the column bases (Figure 3(b),(c)). Clearly, the existing drainage system is not sufficient. The problems in the rainwater system in the roof are the cause of this pathology in the upper part of the walls.



(a) (b) (c)

Figure 3: Efflorescence damage observed in (a) internal wall, (b) areas close to the roof and (c) column bases

3.3 Material loss

Two main types of material loss, erosion and loss of mortar, were observed. Erosion was mainly seen in external decorative elements and extensively on the western facade of the tower. Loss of mortar was seen on all facades in varying degrees.

3.4 Biological colonization

Plants and lichen were observed on the external facades due to inaccessibility, lack of cleanliness and maintenance. Widespread growth of algae can be seen in the interior walls and columns (Figure 4(a),(b)). Algae generally constitute superficial films. However, in the church interior they seem to be growing within the stone rather than on the surface.

The timber altars and roof are heavily infested with termites, wood boring beetles and rot (Figure 4(c),(d)). Termites have infiltrated all of the altars; the small room behind the main altar is the most infested. Trails can be found throughout the building, including in masonry. Holes created by wood boring beetles can mostly be seen on decorative parts of the altars.



(a) (b) (c) (d)

Figure 4: Algae observed on (a) interior walls and (b) column base; (c) termite infestation behind altar; (d) rot in altar

4 MONITORING SYSTEM

Monitoring systems such as crack meters and humidity sensors were installed while thermographic photographs and moisture sensors were used to check the health of the church.

Humidity sensors were placed in four different locations (behind the east altar, on the altar, near the interior face of the north (longitudinal) wall, and in the tower). The period of field work was January to March 2019. During that time, it was found that the tower was the coldest part of the analysed locations and had the greatest fluctuations in relative humidity. To study crack activity, four crack meters have been placed in different locations: two in the tower's interior wall, one on the tower exterior and one in a column adjoining the choir. Continuous monitoring will allow the evaluation of humidity's role in the damage pathologies in the church and the evolution of the cracks.

Thermographic images were taken in various locations and helped to identify areas of moisture, voids, and possible insect attack. They are also helpful in determining if the termites are active or not, but in this case no active termites were found.

A moisture sensor was used to test for moisture at 5, 10, or 30 cm deep in all the columns and the north and south walls. Upon testing it was observed that the readings from the external facade were similar to the internal ones, so it can be observed that even though the external facade appears dry on the surface, it is moist within. It can be inferred that the south wall has higher moisture content than the north wall, correlating with the higher damage seen (efflorescence and biological colonization). From the distribution observed it is clear that the higher moisture concentrations are in the bottom of the walls. The centre of the floor also has extremely high moisture levels.

5 NON-DESTRUCTIVE TESTING

To understand the properties and the behaviour of the church, many tests were performed such as sonic impact tests, rebound hammer, ground penetrating radar as well as some laboratory

tests where some samples were analysed with scanning electron microscopes and X-ray diffraction.

5.1 Stone

Both direct and indirect sonic impact tests were carried out. The masonry in the main body of the church had average Poisson ratio 0.18 and elastic modulus 2.9 GPa, which is comparable to a dressed rectangular stone masonry and higher than the values for a cut stone with good bonding per the Italian building code commentary [3]. The irregular masonry of the tower stairwell and the apse saw the lowest values (2.4 and 1.3 GPa, respectively). The results for the tower walls indicated a very high elastic modulus, over 4 GPa, and Poisson ratio about 0.3.

The rebound hammer test was performed on the face of the stone wall using a Schmidt hammer. Four or five readings were taken at each of five to nine points on each wall. The mean was 40.5 for the main body masonry, 36.2 for the tower and 32.1 for the apse. It can be said that these values are low compared to the literature, possibly due to surficial damages [4].

For ground penetrating radar, the equipment used was the control unit PROEx and an 800 MHz central frequency antenna from Guideline Geo. In walls, horizontal and vertical profiles were carried out. The scans showed that the main body walls have multi-leaf masonry with a relatively regular inner leaf that has properties similar to those of the outer leaves. In columns, only vertical profiles were performed. The stones within a single drum are well-cut and fitted with a thin joint between them, but between drums the fitting does not seem flat.

To investigate the composition of the efflorescence and mortar, some samples of efflorescent salts were obtained from the church column and wall and mortar samples in the south wall. The samples obtained were prepared in the laboratory of the University of Minho for the scanning electron microscope (SEM) and X-ray diffraction (XRD). The salt of the efflorescence collected in the south wall, close to the main altar, corresponds with sodium carbonate ($NaCo_3$), while for the column the salt detected was sodium sulphate (Na_2SO_4). The samples of original mortar indicated the use of non-hydraulic lime mortar, while for repointing the analysis indicated the use of hydraulic mortar.

5.2 Timber

Pilodyn tests found that there was probably little or no decay in the timber roof beams. Direct ultrasonic tests were also performed on the roof beams. The average velocity measured was consistently in the mid-1900s. This uniformity supports the Pilodyn conclusion that there is little or no decay in these timber elements, since decay would not likely be uniform. The tests were not necessary for the timber altars, in which severe decay was clearly visible.

6 DYNAMIC IDENTIFICATION TEST

A representative part of the church was chosen for analysis; namely, the tower and the north walls connected to it. Twelve points of measurement were chosen: five in the bell tower, four in the clerestory wall and three in the external wall (Figure 5). The accelerometers measured the out-of-plane acceleration at every point and in-plane acceleration at one point of each structural element.

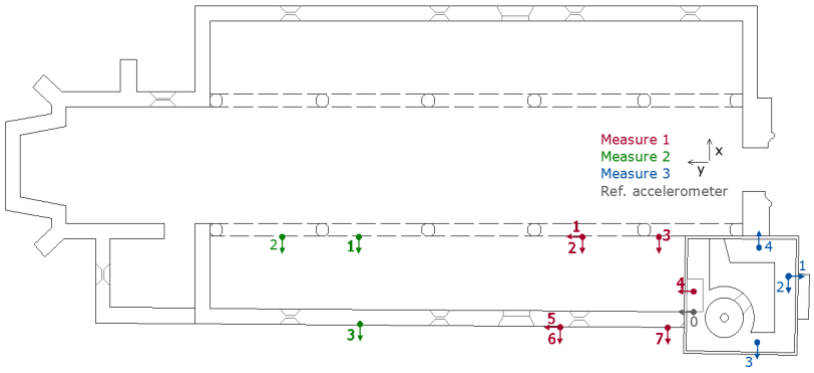


Figure 5: Accelerometer locations for OMA campaign

The information obtained in the campaign was analysed with the program ARTeMIS modal. The software uses two methods of modal identification, and then compares them for validation. Values including damping ratio or complexity of the mode were taken into account as well as the Modal Assurance Criterion values and a visual analysis of the modal shapes; the values are summarised in Table 1. The first four modes were selected for the calibration of the finite element model.

Table 1: Results of the dynamic identification

Mode	EFDD [Hz]	SSI [Hz]	Damping [%]	Complexity [%]	EFDD/SSI freq.	MAC
1	1.733	1.742	1.144	31.947	0.52%	0.652
2	2.678	2.657	0.891	0.103	0.78%	1
3	2.829	2.806	1.058	2.309	0.81%	0.983
4	3.179	3.184	1.227	4.687	0.16%	0.763
5	3.569	3.534	0.14	20.005	0.98%	0.877
6	4.002	4.015	1.039	5.726	0.32%	0.851
7	4.735	4.698	1.185	1.835	0.78%	0.965

7 FINITE ELEMENT MODEL

Finite element analysis was performed with the software Displacement Analyser Finite Element Analysis (DIANA-FEA). Two finite element models were created to analyse the church by importing the AutoCAD models into DIANA-FEA. One was a full shell model (created with 2D elements) created for quicker analyses and one was a solid model (created with primarily 3D and a few 2D elements) for improved accuracy.

For the shell model, the surfaces were defined as regular flat shells in DIANA. The columns were defined as wire elements. For the solid model, objects were defined in DIANA as regular solid elements. Both models included a curved shell vault in the chancel and timber rafters for stiffness and behaviour. The vault is considered a thin shell element, so in DIANA it remained a shell element in both the shell and solid models.

The properties chosen were based on the Italian building code and commentary, the non-destructive testing explained herein, and Model Code 2010 [1,5,6]. Nonlinear properties were

chosen based on several sources in the literature [7,8,9]. Material properties were later modified so that the model matched the dynamic analysis.

Using quadratic mesh order, the mid-side node location was located on shape in order to keep the nodes within the geometry even when the geometry was curved.

Eight-node quadrilateral isoparametric curved shell elements were used for the shell elements (CQ40F). The wire elements were defined as Class-III 3D beam elements, which are curved beam elements with three nodes (CL18B). The solid elements were defined as quadratic/hexagonal mesh elements (primarily the CHX60 twenty-node isoparametric solid brick element) [10].

The roof was not geometrically defined in the model. Rather, the roof structure was considered as a 2 kN/m2 dead load on the walls and the arcades. Supports were defined as fixed translation in all directions at the base of the walls and columns.

7.1 Updating of the model

Once the model was defined, the next step was to use the results from dynamic identification (OMA) to update the model through the comparison of the frequencies and modal shapes.

It was seen in the mode shapes of the dynamic testing campaign that the arcade and the walls were moving together. Therefore, connections between these elements were created. Another facet of the model that was adjusted was the flexibility (elastic modulus) in the connection between the tower's external walls and the west and north facades.

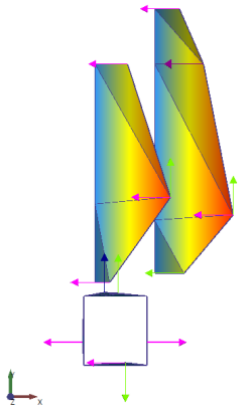
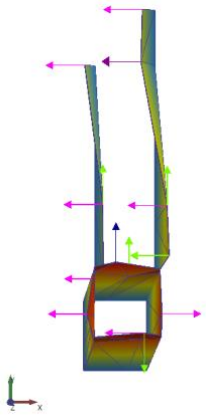
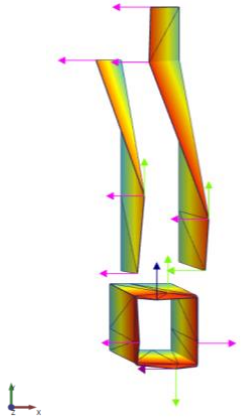
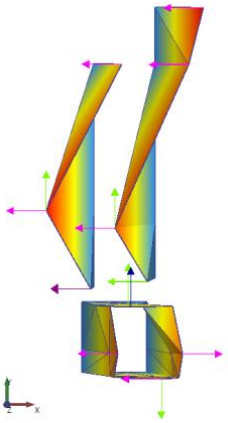
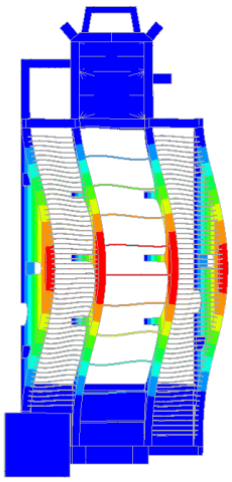
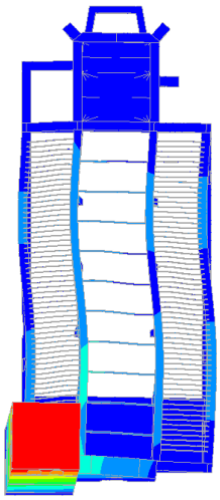
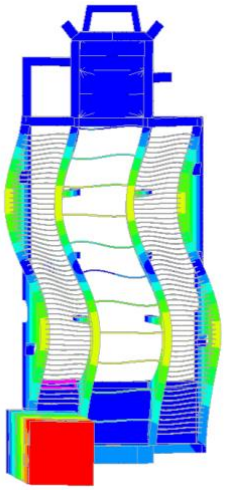
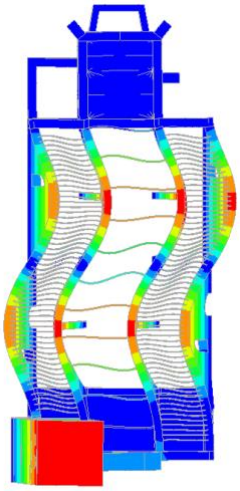
The structural role of the choir slab was not known from initial observations. After modelling, it was determined that to obtain the diagonal mode of the tower, which has a frequency between the modes of direction x and direction y, it was necessary to include the connection of the slab with the tower.

The elastic modulus of the masonry was modified in order to match the values of the frequencies and the modal shapes from the OMA campaign. Then, a MAC comparison was also used. The final properties are listed in Table 2 and the four selected mode shapes are provided in Table 3. Poisson ratio was taken as 0.2, tensile strength as 0.15 MPa, and tensile fracture energy 8 N/m.

Table 2: Material properties assigned in the finite element model

Material type	**Masonry**			**Concrete**	**Timber**
Structural components	Walls of the main nave, arcade, columns, vault	Tower external walls, masonry tower floor	Walls of apse, tower stairwell	Concrete tower floors	Beams and ties
Elastic modulus (GPa)	1.75	1.4	1	30	0.7
Mass density (kg/m3)	2143	2041	1939	2500	700
Compressive strength (MPa)	2.6	1.8	1.0	-	-
Compressive fracture energy (N/mm)	4.16	2.88	1.60	-	-

Table 3: Modal shapes and frequencies of the OMA (ARTeMIS) results and updated FEM

			
OMA Mode 1: 1.73 Hz	OMA Mode 2: 2.68 Hz	OMA Mode 3: 2.83 Hz	OMA Mode 4: 3.18 Hz
			
FEM Mode 1: 1.73 Hz	FEM Mode 2: 2.68 Hz	FEM Mode 3: 2.89 Hz	FEM Mode 4: 3.04 Hz

8 STRUCTURAL ANALYSIS

Nonlinear analysis was performed with a pushover analysis of the 3D solid model in the vertical and horizontal directions.

The first analysis was performed in the vertical direction in order to obtain the maximum load factor for the gravitational load that the structure can support. The capacity curve is shown in Figure 6. Different models were created with different values for the variables that define the nonlinear analysis. Three values for the tensile fracture energy were used, 8, 50 and 1000 N/m. A model without the slab of the choir was also analysed. Model 1 represents the original model whose material properties are defined in the previous section. For Model 2 the slab was removed. Model 3 and Model 4 present higher tensile fracture energy, 50 N/m and 1000 N/m respectively. The results are similar for all the cases, reaching a maximum value for the load factor of 2.3 for the original model. It can be observed that for the current state of loading, the

structure is in the linear range what means that no problems should appear in the structure related to the materials.

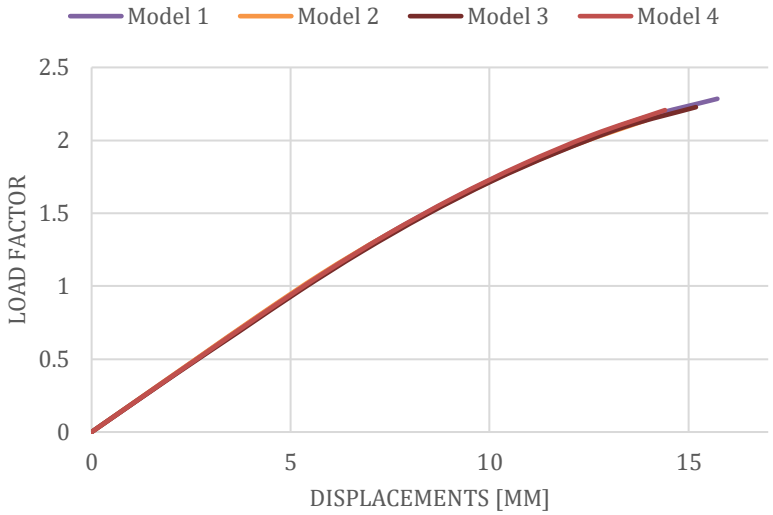


Figure 6: Capacity curve of the incremental vertical analysis

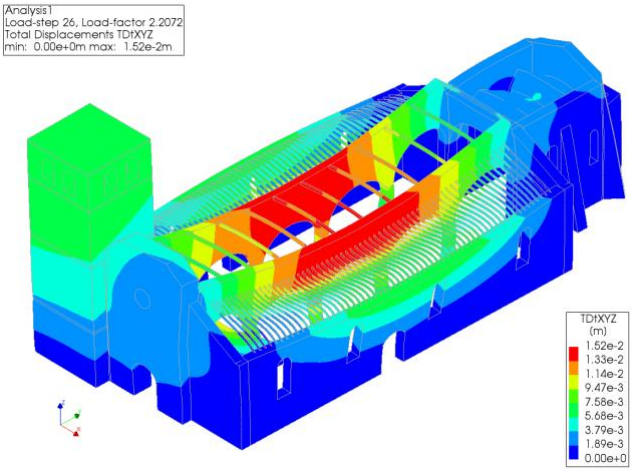


Figure 7: Displacements of the incremental vertical analysis

For the horizontal pushover both the transversal and longitudinal axes were analyzed in one direction. In the case of the transversal direction (X) the church presents a load factor around 0.17 and the capacity curve presents hardening. As expected, in the longitudinal direction (Y) the structure presents higher capacity and the curve reaches a value of 0.3 with an elastic behavior. The nonlinear branch presents softening in this case.

The strain graphs for the pushover in X shows concentrations in the base of the columns and in the connection of the arch of the choir with the lateral wall, see Figure 9. To a lesser extent, strain also appears in the base of the longitudinal walls.

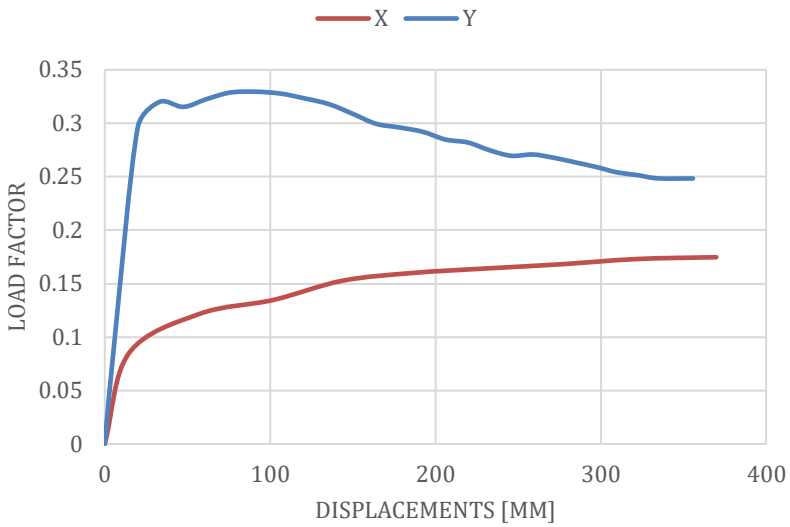


Figure 8: Capacity curves for horizontal pushover

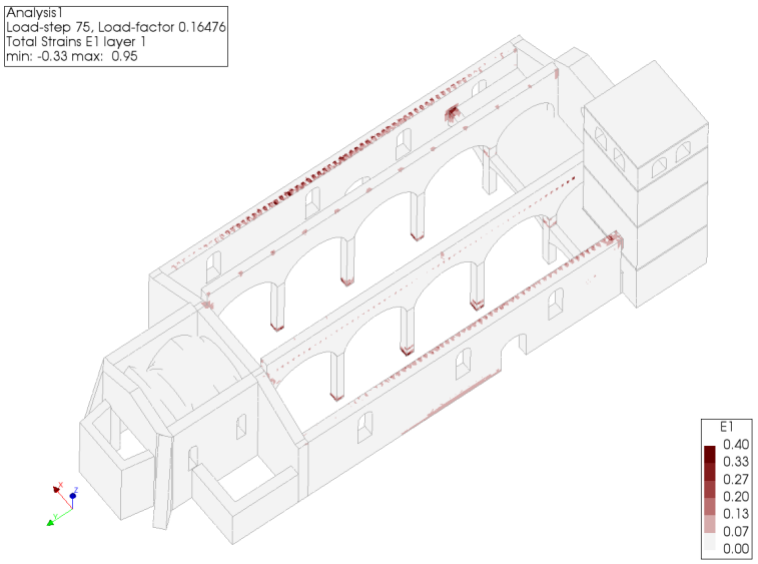


Figure 9: Maximum principal strains E1, x-direction

A different pattern is obtained from the pushover analysis in the y-direction. In this case the strain concentration is located at the base of the tower and the main façade in the shape of horizontal lines (Figure 10(a)), as well as in the connection of the tower with the church walls and in the body of the altar, where the strain pattern is diagonal in the lateral walls and vertical in the wall perpendicular to the force (Figure 10(b)). This diagonal concentration indicates shear failure may happen in the chancel under high loading in the y-direction. Maximum strain values are located in the connection of the arches of the choir with the longitudinal walls.

Since northern Portugal has low earthquake risk (reference peak ground acceleration 0.08g, Portuguese National Annex to Eurocode 8 [11]), it can be concluded that the structure is not likely to surpass the linear range nor sustain much damage in any ground motion events.

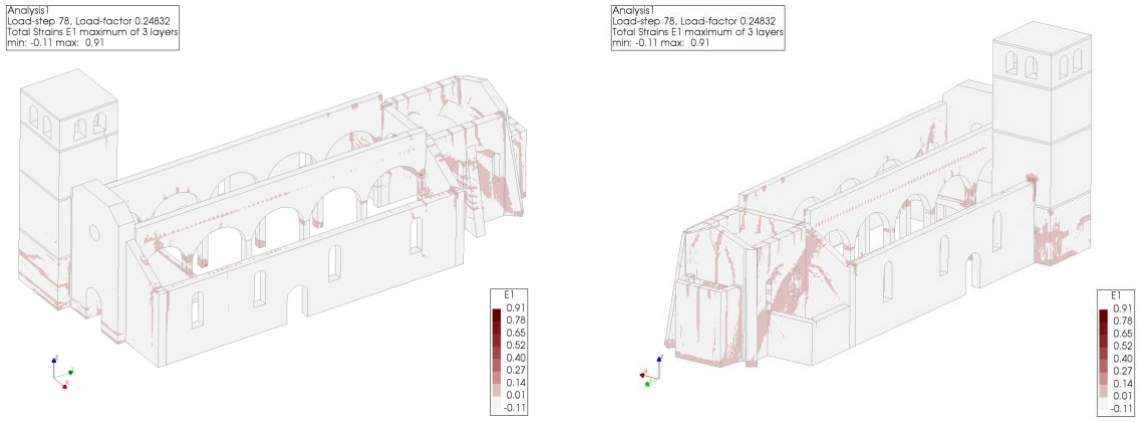


Figure 10: Maximum principal strains E1, y-direction (a) front view; (b) rear view

9 CONCLUSION AND RECOMMENDATIONS

The overall state of conservation of the church is good. No major structural deficiencies were observed. Recommendations include repointing in areas of lost mortar, cleaning of efflorescence and staining, replacing rotted wood, applying a chemical anti-termite barrier in walls and altars, improving ventilation, installing a stormwater drainage system, and performing continued monitoring and maintenance.

The non-destructive tests provided essential information about the conservation states of the materials and the multitude of tests allowed them to be verified against one another. The tests also supplied values of material properties for defining the finite element model.

Finite element analysis provided valuable information about the capacity of the church, both for self weight and horizontal load caused by an earthquake. The vertical loading case raised no concern for the current state of the church. The horizontal loading cases identified areas of possible weakness in case of earthquake, but it is noted that the church is unlikely to experience seriously threatening ground motions.

Acknowledgements. Direção Regional de Cultura do Norte, Dr. Miguel Rodrigues; Igreja de Azurara, Padre Diogo Oliveira, D. Zinha; Francisco and Guideline Geo; Sr. Matos and Structures lab of U. Minho; Nuno Mendes

REFERENCES

[1] I. Sereno, P. Noé, and P. Figueiredo, “Igreja de Azurara/Igreja de Santa Maria,” *Sistema de Informação para o Património Arquitectónico*, 2012. [Online]. Available: http://www.monumentos.gov.pt/Site/APP_PagesUser/SIPA.aspx?id=5240.

[2] ICOMOS-ISCS. (2008). Illustrated glossary on stone deterioration patterns. ICOMOS.

[3] IMIT (2009) Circ. 02.02.2009, n. 617: Istruzioni per l'applicazione delle Nuove Norme Tecniche per le Costruzioni di cui al decreto ministeriale 14 gennaio 2008. Italian Ministry of Infrastructures and Transportation, Rome, Italy (in Italian)
[4] Vasconcelos, Graça, et al. "Prediction of the Mechanical Properties of Granites by Ultrasonic Pulse Velocity and Schmidt Hammer Hardness." *10th North American Masonry Conference, 3-5 June 2007*, no. January 2007, 2007, pp. 980–91.
[5] NTC. Norme Tecniche per le Costruzioni. D.M. 14 gennaio 2008, S.O. No. 30, G.U. No. 29/2008. Rome, Italy; 2008.
[6] The International Federation for Structural Concrete (fib). "Model Code 2010." *Fib Model Code for Concrete Structures 2010*, no. September, 2011, doi:10.1002/9783433604090.ch6.
[7] Kržan, Meta, et al. "Acquiring Reference Parameters of Masonry for the Structural Performance Analysis of Historical Buildings." *Bulletin of Earthquake Engineering*, vol. 13, no. 1, 2015, pp. 203–36, doi:10.1007/s10518-014-9686-x.
[8] Ortega, Javier, et al. "Assessment of the Efficiency of Traditional Earthquake Resistant Techniques for Vernacular Architecture." *Engineering Structures*, vol. 173, no. June, Elsevier, 2018, pp. 1–27, doi:10.1016/j.engstruct.2018.06.101.
[9] EN 1996-1-1 (2005) Eurocode 6: Design of masonry structures – Part 1-1: General rules for buildings – rules for reinforced and unreinforced masonry.
[10] TNO DIANA BV.: DIANA User's Manual -- Release 9.3 -- 2008.
[11] A. Campos Costa, M. L. Sousa, and A. Carvalho, "Seismic Zonation for Portuguese National Annex of Eurocode 8," in *The 14th World Conference on Earthquake Engineering*, 2008.

INVESTIGATION OF THE RESPONSE OF A MASONRY ARCH RAILWAY BRIDGE USING MEMBRANE EQUILIBRIUM ANALYSIS

CARLO OLIVIERI[1*], SAM H. COCKING[2], MAURIZIO ANGELILLO[1] AND MATTHEW J. DEJONG[3]

[1] Department of Civil Engineering (DICIV), University of Salerno, Via Giovanni Paolo II, 132, 84084 Fisciano (SA), Italy
e-mail: colivieri@unisa.it; mangelillo@unisa.it

[2] Department of Engineering, University of Cambridge, Civil Engineering Building, JJ Thomson Avenue 7a, Cambridge, CB3 0FA, UK
e-mail: sc740@cam.ac.uk

[3] Department of Civil & Environmental Engineering, University of California, Berkeley, 777 Davis Hall, Berkeley, CA 94720-1710
e-mail: dejong@berkeley.edu

Keywords: Masonry, Membrane Equilibrium Analysis, Historic Structure, Railway Viaduct

Abstract. *This paper presents an application of Membrane Equilibrium Analysis (MEA) to a historic masonry arch railway bridge in Leeds, United Kingdom. This case study structure is representative of the many masonry arch bridges present on UK and European railway transport networks. It has been chosen because, since 2016, it has been the subject of a detailed Structural Health Monitoring (SHM) campaign, making it an ideal candidate against which to test analytic models. Typically, asset engineers will be responsible for maintaining a large stock of these structures and will lack the time to perform thorough computational analyses. Therefore, simplified approaches, such as MEA, which can offer insight into structural behaviour, have the potential to be highly valuable. This study represents the first step in applying MEA to masonry arch railway bridges.*

1 INTRODUCTION

Masonry arch bridges are important features of railway and road transport networks, throughout the UK and other European countries. However, despite their prevalence, their structural behaviour under working loads is often not understood in detail. As a result, assessments will typically focus on collapse loads, which can be predicted using limit analysis. Serviceability conditions may not be considered directly at all, despite being a driver of structural deterioration.

To address this, asset engineers increasingly prescribe structural health monitoring for their masonry arch structures. One such case is considered here: a masonry railway bridge in Leeds, UK. This bridge has a working life of 150 years and carries a range of local passenger, cross-country, and freight trains. It has experienced historic damage, which was addressed in an intervention in 2015 [1]. Since 2016, two spans, which were the focus of the 2015 remedial works, have been monitored using a range of sensors. These include a network of fibre-optic Fibre Bragg Gratings (FBGs) to measure the distribution of in-plane strains across the arches, in both longitudinal and transverse directions [2].

This sensor network provides detailed measurements of the bridge's response under its working loads, making this an ideal case study for investigating the effectiveness of simplified modelling techniques [3]. One such modelling approach is described here, based on Membrane Equilibrium Analysis (MEA). In this paper, the modelling approach is developed for an arch bridge, based on a

typical span from the viaduct case study, and observations are made on the model's behaviour when typical working loads are applied. Future work will compare this modelling output in detail against the FBG measurements and will include cracking and deformation analysis. The equilibrium solutions produced by MEA, besides being sufficient to prove that the structure is safe, may be used to assess their possible effect on material deterioration, and can be compared with the crack patterns detected in the structure.

In order to model the equilibrium problem for this special example of a masonry vault structure, the unilateral No-Tension (NT) model is applied in this paper. The unilateral model for masonry appears in the literature around the end of the eighteenth century and in the nineteenth century (see Moseley [4]). In the twentieth century, this model was described rationally by Heyman in [5].

Considering the application of unilateral models to vaults, recent available literature is extensive. Our main inspiration come from the work of the school of Salerno, originating in their paper on the Lumped Stress Method [6], and applied to vaults in the papers by Fraternali et al. [7], Angelillo & Fortunato [8], Fraternali [9], and recently by Angelillo et al. in [10] and Gesualdo et al. in [11], where the Membrane Equilibrium Analysis is proposed and applied to some simple cases. We also recall the pioneering work by O'Dwyer [12], and work by Block [13], Block et al. [14], Vouga et al. [15], De Goes et al. [16], Block and Lachauer [17], and Miki et al. [18].

MEA can be used as a tool for finding statically admissible stress fields in masonry structures which can be assumed to exhibit membrane behaviour [10]. Heyman's NT assumption for masonry is enforced by ensuring that the stress potential is concave in form. Starting from a potential which satisfies this constraint and depending on a few parameters, a minimum energy solution for the form is then obtained, through optimization of the parameters, for different load conditions that include the dead load and the moving train loads. The forms which are obtained are contained within the thickness of the arch, even in extreme conditions.

2 DEVELOPMENT OF ANALYTICAL MODEL

2.1 Geometry and equilibrium

A vault can be described by its intrados and extrados surfaces, by the geometry of the filling, and eventually by the form and dimension of the abutments sustaining the vault.

With the present model, it is assumed that the load applied to the vault is transferred and carried by a membrane structure *S*, a surface to which we may think to attach some thickness *s*. The geometry of the membrane *S* is not fixed, in the sense that it can be displaced and distorted, provided that it lays inside the masonry; see Fig.1, to which we refer for notation. For the surface *S* a Monge representation is considered, mapping the position **x** of points belonging to *S* in Cartesian coordinates in the reference shown in Fig.1:

$$\boldsymbol{x} = \{x_1, x_2, f(x_1, x_2)\}\,,\ \{x_1, x_2\} \in \Omega\,, \tag{1}$$

Ω being a two-dimensional connected domain, called the planform of *S,* whose boundary $\partial\Omega$, of outer normal **n**, is composed of a finite number of closed curves; $\{x_1, x_2\}$. By adopting the Monge description, the curvilinear coordinates on *S*, are the Cartesian coordinates of points of *S* in the planform Ω; $x_3 = f(x_1, x_2)$ is the rise of the membrane, and we assume: $f \in C^o(\Omega)$ – that is to say that the surface *S*, which we consider, is continuous but not necessarily smooth.

An efficient way to describe membrane equilibrium of a thin shell under a load q is the formulation by Pucher [19]. Pucher analysis is based on the introduction of the projected stress components, in terms of which two of the three balance equations can be made independent of the membrane shape. The main notation and the Pucher formulation of the equilibrium problem for a membrane, as used here, have been derived using a Differential Geometry approach. The natural and dual base vectors follow from this, and covariant and contravariant tensor components can also be considered. This Differential Geometry approach is especially helpful when converting the projected stress components into physical generalized stress components on the membrane surface.

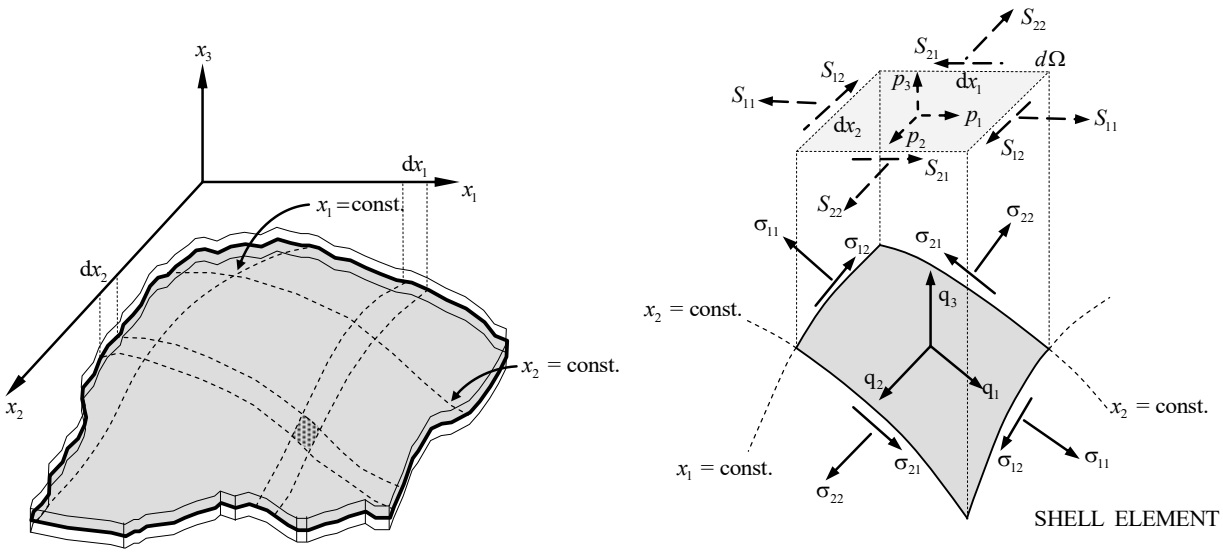


Figure 1: Membrane inside the vault and surface stresses

The projected (Pucher) stress components (see Fig.1) are easily defined in terms of the contravariant components $T^{\alpha\beta}$ of the generalized membrane stress: $S_{\alpha\beta} = JT^{\alpha\beta}$, J being the ratio between the surface area and the projected area. In terms of Pucher stress components, the vector equilibrium equation, projected into the non-orthonormal base $\{\boldsymbol{e}_1, \boldsymbol{e}_2, \boldsymbol{m} = \boldsymbol{a}_3\}$, **m** being the unit normal to *S,* becomes:

$$S_{11,1} + S_{12,2} + p_1 = 0, S_{21,1} + S_{22,2} + p_2 = 0, S_{\alpha\beta} f_{,\alpha\beta} - p_\gamma f_{,\gamma} + p_3 = 0 \,, \tag{2}$$

where $\boldsymbol{p} = J\boldsymbol{q}$ is the load per unit projected area, and $\{p_1, p_2, p_3\}$ are the Cartesian components of $\boldsymbol{p}$ in the given reference. By using the projected stress, the first two equilibrium equations do not depend on the membrane shape and are the same as for the plane stress problem. In the case of pure vertical loading, say $\boldsymbol{p} = \{0,0,-p\}$, the first two equations may be solved introducing an *Airy stress potential* $F(x_1, x_2)$ – that here we only assume to be continuous – in the form:

$$S_{11} = F_{,22}, S_{22} = F_{,11}, S_{12} = S_{21} = -F_{,12}. \tag{3}$$

The third equation of transverse equilibrium expresses the balance of the vertical component of the force $p_3 = -p$ with the scalar product of the Pucher stress matrix times the Hessian of the function *f*. This Hessian matrix is formed by the covariant components of the curvature tensor of the surface. On introducing the Airy stress potential into this equation, we have

$$F_{,22} f_{,11} + F_{,11} f_{,22} - 2F_{,12} f_{,12} = p. \tag{4}$$

2.2 **Unilateral membranes**

A rigid No-Tension (NT) material in the sense of Heyman is assumed, so that the following material restrictions are imposed: the generalized stress **T** is negative semi-definite and does no work for the corresponding strain **E**, that is positive semi-definite:

$$\boldsymbol{T} \in Sym^- \quad , \quad \boldsymbol{E} \in Sym^+ \quad , \quad \boldsymbol{T} \cdot \boldsymbol{E} = 0. \tag{5}$$

The first application of Pucher's transformation for NT masonry vaults can be found in Angelillo and Fortunato [8], where it is shown that, due to the NT constraint, both the surface generalized stress

and the matrix of the projected stresses must be negative semi-definite. In terms of the stress function F, this condition can be written as:

$$F_{,11} + F_{,22} \leq 0, F_{,11}F_{,22} - {F_{,12}}^2 \geq 0\,, \tag{6}$$

hence, $F(x_1, x_2)$ is concave.

2.3 **Singular stress and equilibrium**

If F is only continuous, it may present folds. In this case the projected stress is a line Dirac delta with support along the projection Γ of the fold. The *Hessian* **H** of F is singular transversely to Γ, namely it has a uniaxial singular part parallel to the unit vector **h** normal to Γ. Correspondingly the directional derivative of F in the direction of **h**, called F_h, presents a jump. Therefore, the singular part of the Hessian **H** of F can be written as:

$$\boldsymbol{H}_s = \delta(\Gamma)\Delta F_h \boldsymbol{h} \otimes \boldsymbol{h}, \tag{7}$$

$\delta(\Gamma)$ being the unit line Dirac delta on Γ and ΔF_h the jump of slope along the direction $\boldsymbol{h}$. Therefore, the corresponding projected stress (8) has also a singular part, a line Dirac delta on Γ:

$$\boldsymbol{S}_s = \delta(\Gamma)\Delta F_h \boldsymbol{k} \otimes \boldsymbol{k}\,, \tag{8}$$

where **k** is the unit vector tangent to Γ. The concavity of F implies the concavity of the fold whose projection in the planform is Γ. Then ΔF_h is negative and the corresponding projected singular stress concentrated on Γ is compressive.

In case there is a stress singularity along a line Γ, the equilibrium equation (4),

$$F_{,22}f_{,11} + F_{,11}f_{,22} - 2F_{,12}f_{,12} = p,$$

on that line must be reinterpreted in a weak sense. The main conclusion is that if there is a fold in the stress potential, this gives a concentrated term in the transverse equilibrium equation that, in the absence of any concentrated load p, must be compensated by another concentrated term. Due to the structure of the equation, this compensation term can only be given by an analogous concentrated term, arising from a fold in the surface whose projection must be the same line Γ. Since the stress potential is concave, the two concentrated terms can cancel each other only if the Hessian of the surface along the fold is an indefinite matrix (that is the two principal values of it have different signs).

2.4 **Boundary conditions**

Assuming that the shape of the membrane is given, the equilibrium problem for the unilateral membrane S, under pure vertical loading, consists in finding a concave stress function $F(x_1, x_2)$ satisfying equation (9), with the boundary conditions:

$$F(x_1, x_2) = g(x_1, x_2) \quad \text{or} \quad dF/dn = h(x_1, x_2) \quad \text{on } \partial\Omega \tag{9}$$

being $g(x_1, x_2)$ and $h(x_1, x_2)$ the contact internal moment and axial force produced by the allied tractions, on a beam structure having the same shape as $\partial\Omega$.

Notice that the second order differential equation (4) can be elliptic, parabolic or hyperbolic, depending on the sign of the coefficients, that is whether the shape is locally strictly convex (or concave) or not. If there are regions where the equation is hyperbolic, the characteristics of the equation are real and formulating the problem as a boundary value problem may become impossible.

Since the equilibrium problem is perfectly symmetrical with respect to the two functions

$F(x_1, x_2)$, $f(x_1, x_2)$, we may switch the roles of unknowns and data, thinking that the stress, or similarly the stress potential, is given, and that the shape is unknown. The shape can then be found by solving the second order differential equation (4) with the boundary conditions:

$$f(x_1, x_2) = f^{\circ}(x_1, x_2)\,, \qquad \text{on } \partial\Omega \tag{10}$$

$f^{\circ}(x_1, x_2)$ being the boundary values of the membrane surface. In this case the equation may become at most parabolic, since, due to the No-Tension constraint, the stress potential must be concave.

3 ANALYSIS OF RAILWAY BRIDGE

3.1 Typical span geometry

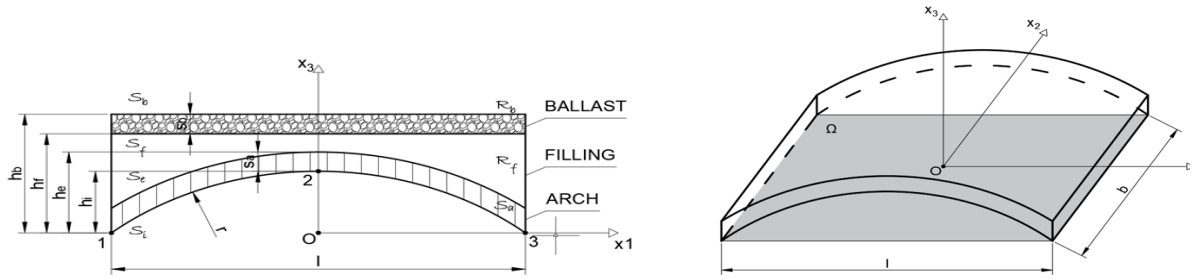


Figure 2: Schematic section of the bridge (a) and a prospective view of the vault structure (b)

Our case study is a masonry railway viaduct in Leeds, UK. This bridge has a working life of 150 years and carries a range of local passenger, cross-country, and freight trains. It has experienced historic damage, which was addressed in an intervention in 2015. Since 2016, it has been monitored using a range of sensors, including a network of fibre-optic Fibre Bragg Gratings (FBGs) to measure the distribution of in-plane strains across the intrados of arches showing notable damage [2].

A schematic section of the bridge is reported in Fig.2a. In Fig.2b a prospective view of the vault structure is depicted. The structure of it is a barrel vault made of bricks sustained by two transverse walls, carrying the dead load of the filling and of the ballast, and the moving load of the trains. The filling is confined by two spandrel walls made of bricks. The main geometrical parameters introduced in Fig.1a have the following values:

$$b = 8.00\ m; l = 7.70\ m; s_a = 0.50\ m; s_b = 0.30\ m;$$
$$h_f = 3.05\ m; h_b = h_f + s_b; h_i = 1.55\ m; h_e = h_i + s_a.$$

3.2 Self-weight and train loads

For the train load we consider, for each train, a total weight $g_t = 327.5kN$, distributed over a small area by considering an exponential distribution (see Fig.3). For the material densities and the gravity acceleration we consider:

$$\rho_a = 1500kg/m^3, \rho_f = 1800kg/m^3, \rho_b = 1600kg/m^3, g = 9.81m/s^2.$$

3.3 Solution (two trains passing on the bridge span)

In this study, we assign a form to the stress potential, which depends on a few parameters, and look for the equilibrium solution for the shape by parametrically solving equation (4). If we consider an elementary arch-like solution, recalling that the projected stress is uniaxial and constant in the direction x_1, the surface which solves the differential equation is a catenary of the load depending on a single parameter: the thrust per unit length. Due to the effect of the intensely localized loads, i.e. the trains, such a surface is not easily fitted inside the intrados and extrados surfaces of the vault and

a four cylindrical-hinge mechanism may be created. The idea here is to consider a biaxial stress regime for the projected stresses which is constant and directed as the Cartesian axes x_1, x_2 and depends on two parameters: the intensity of the normal stress in the x_1 direction and the ratio between the normal stresses in the x_2, x_1 directions.

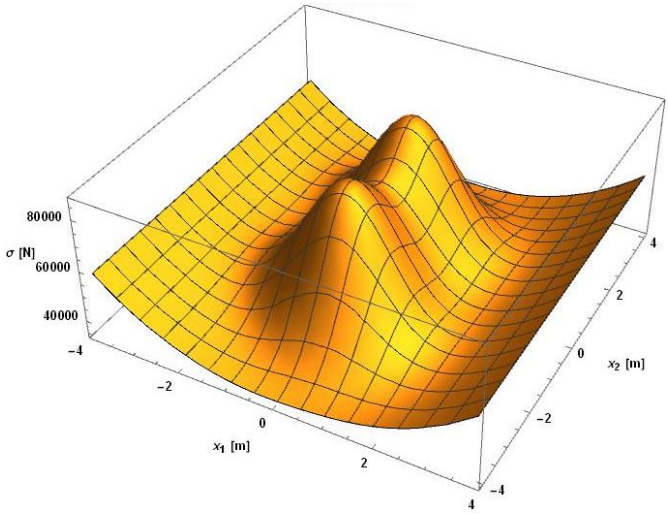


Fig.3: Load profile representing the effect on the membrane of the dead load and the moving load. The moving load due to the train is considered here applied at mid span on both the railways.

Since the two sides of the barrel vault parallel to the x_1 direction are traction free, the x_2 component of the projected normal stress cannot go all the way to the boundary. To take this transverse component and bring it to the abutments we consider that such forces are taken by a 1D structure forming an arch in the planform (see Fig.4).

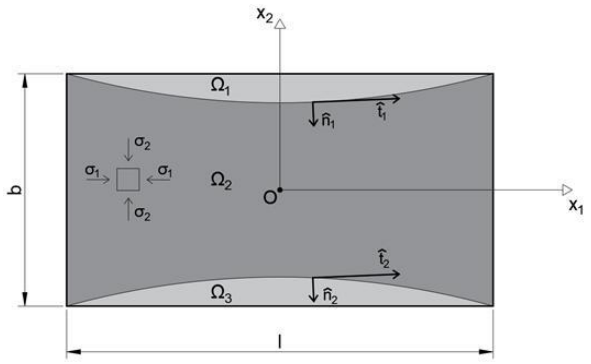


Fig.4: Projected stresses in the planform. The stress is constant and biaxial in the directions of the axes. The jump of the stress across the two curved lines is balanced by a concentrated axial stress acting along them.

To construct this arch and, at the same time, deriving the concentrated axial force along the arch itself, we cut the Airy stress function associated with these stresses, using two symmetric slanted planes, as shown in Fig.5. These planes, parallel to the x_1 direction, are defined by their height H at the origin.

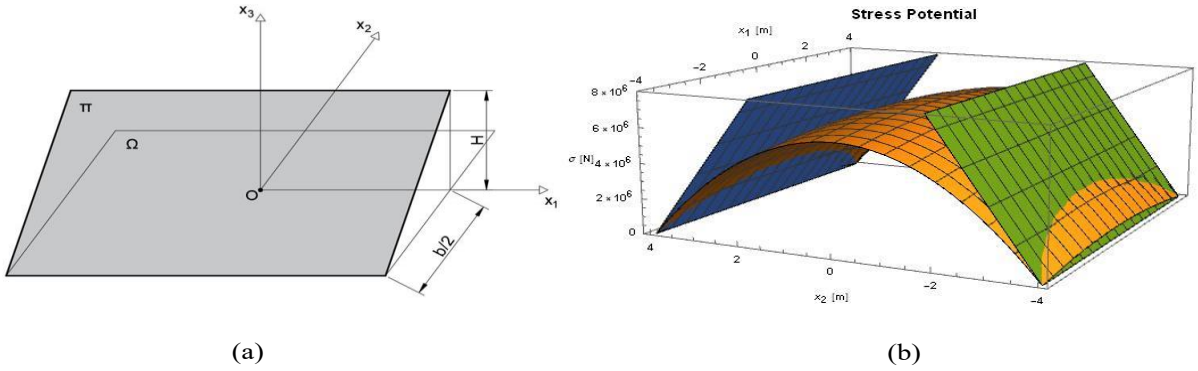


Fig.5: One of the two symmetric planes intersecting the stress function (a) and intersection of the Airy stress function with the two planes (b).

The Airy stress function associated with the biaxial stress regime depicted in Fig. 6 is defined as follows

$$F = \frac{\sigma}{8}([b^2 - 4x_2^2] + \alpha[l^2 - 4x_1^2]), \tag{11}$$

σ and α are two parameters, the first controlling the intensity of the stress and the second controlling the ratio between the two normal stress components. By intersecting this stress potential with the two planes, we obtain two plane curves whose projections on the planform give the two 1D arch structures on which the axial force is attached. These two arches also define the domain Ω (see Fig.6) on which the differential equation is solved.

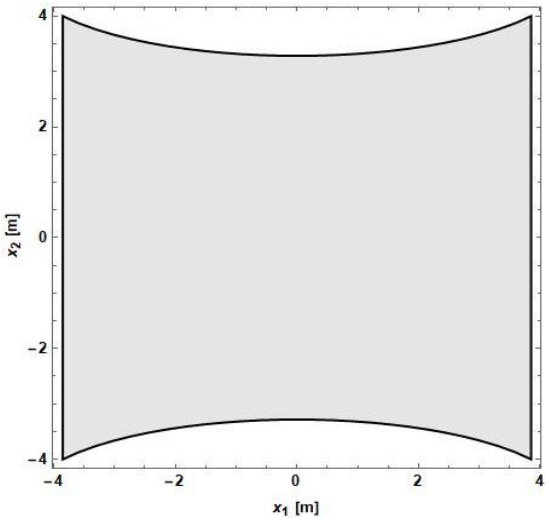


Fig.6: Domain where the transverse equilibrium equation is solved numerically.

We numerically solve the second order (elliptic) differential equation (4) by employing tools in the Wolfram Program Mathematica (see [20]), for finite element solution. We define f_m, a convenient reference surface contained inside the vault, and choose it to be 10% of the thickness (5 cm) above the intrados surface (see Fig.7). In this way, we can consider the thickness of the thrust surface to be 10 cm.

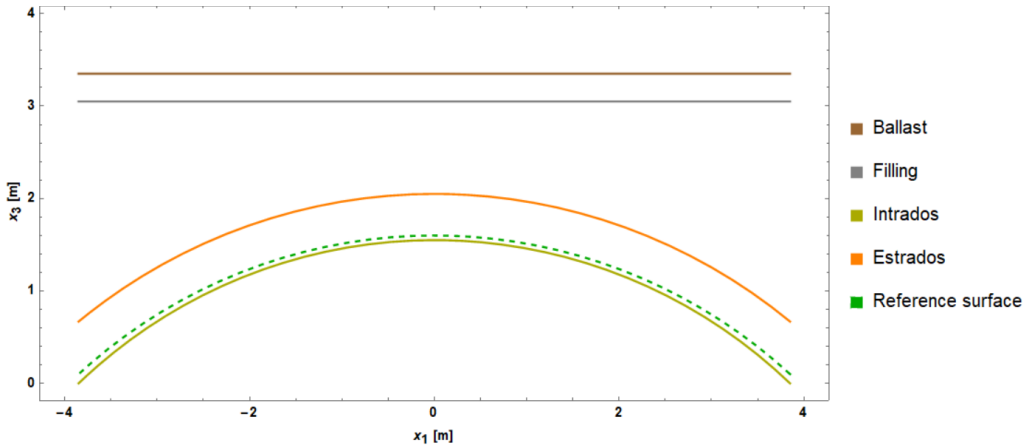


Fig.7: Bridge geometry, axial section.

By using the Finite Element tool in Mathematica, the equation is solved parametrically for the shape f with respect to the parameters σ, α, H, by considering the Dirichelet data for f:

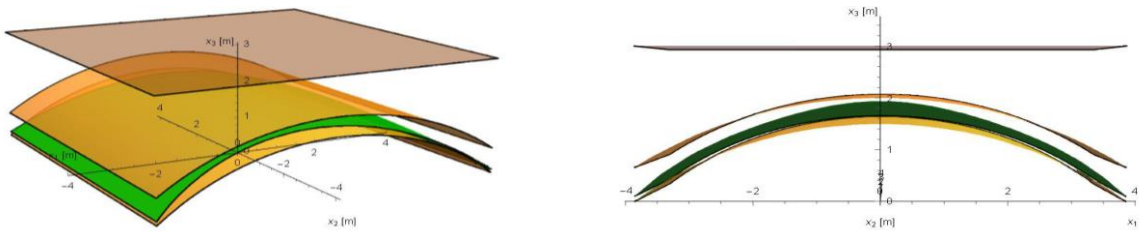
$$f(x_1, x_2) = f_m(x_1, x_2), \quad \forall (x_1, x_2) \in \partial\Omega\,. \tag{12}$$

Finally, the parameters σ, α, H are optimized by minimizing the objective function

$$I = 1/ar(\Omega) \int_\Omega (f(\sigma, \alpha, H) - f_m)^2 dx_1 dx_2, \tag{13}$$

that is the Mean Square Deviation of the shape f from the shape f_m.

The optimized solution, obtained under the loads shown in Fig.3, is shown in Fig.8. It is worth noting that, when considering the axial section at mid-height (x_1 direction, see Fig. 8.b), where the thrust surface is 10 cm from the extrados, the membrane is actually located within the arch thickness (highlighted in orange color in Fig. 8).



(a) (b)

Fig.8: Thrust surface obtained through optimization inside the bridge geometry: perspective view (a) and axial section at mid-height in x_1 direction (b).

This solution gives two constant projected stresses in the x_1, x_2 directions: $\sigma_1 = 763\ kN/m$ and $\sigma_2 = 82\ kN/m$. Considering a thickness of 10 cm, the acting stress inside the arch is 7.6 MPa, which is below the allowable compressive strength of the bricks. The thrust at the four corners of the two arches, $R = 649\ kN$, is inclined at the tangent to the arches at those points. The values of these thrust components in the directions x_1, x_2 are, respectively, $R_1 = 568\ kN$ and $R_2 = 314\ kN$. Note that this is one feasible solution, but further optimization could reduce these forces.

3.4 **Solution (one train passing on the bridge span)**

Now we consider, in addition to the dead load, the weight of a single train on one side of the bridge (see Fig. 9).

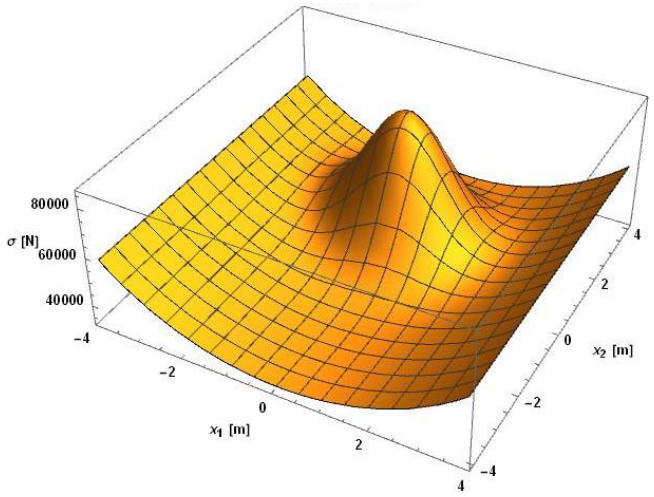
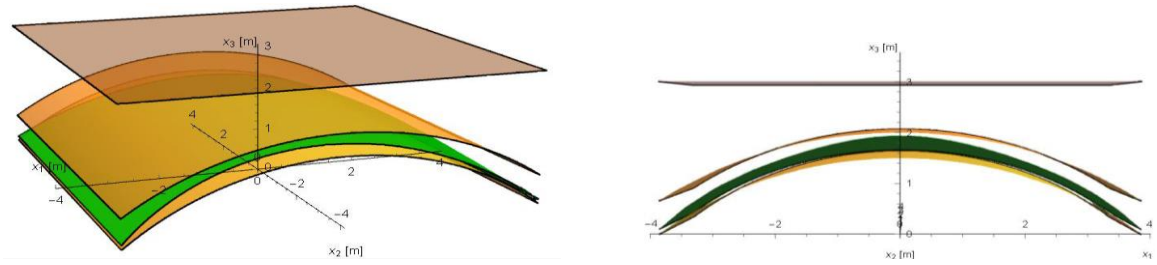


Fig.9: Load profile representing the effect on the membrane of the dead load and the moving load. The moving load due to the train is considered here applied at mid span on one railway.

The optimized solution under the load shown in Fig.9, is shown in Fig.10.



(a) (b)

Fig.10: Thrust surface obtained through optimization inside the bridge geometry: perspective view (a) and axial section at mid-height in x_1 direction (b).

For the load due to a single train, we obtain a similar shape of the thrust surface at a similar distance from the extrados. However, now the solution gives two constant projected stresses in the x_1, x_2 directions: $\sigma_1 = 598\ kN/m$ and $\sigma_2 = 64\ kN/m$. Considering the same thickness of 10 cm, the acting stress inside the arch is now 6.0 MPa, and the thrust at the four corners of the two arches, $R = 509\ kN$, is inclined at the tangent to the arches at those points. The values of these thrust components in the directions x_1, x_2 are, respectively, $R_1 = 446\ kN$ and $R_2 = 246\ kN$.

4 FINAL REMARKS

Analyzing these two solutions, which characterize typical working conditions for this bridge, we observe that, for the same load profile, we can obtain a class of solutions by changing the distance of the reference surface f_m and, consequently, the thickness of the membrane. By increasing this distance, we will certainly find greater projected tensions σ_1 and σ_2 but the consequent increase in thickness will give us lower stresses inside the arch.

Future development might include investigation of the optimum f_m, that gives the true proportion between the position of f_m, the consequent thickness of the membrane, and the stress inside the arch.

Acknowledgements. The authors wish to acknowledge the work of Isabella Elia, who assisted in constructing the analytical model.

References

[1] Alexakis, H., Franza, A., Acikgoz, S. and DeJong, M.J. Monitoring bridge degradation using

dynamic strain, acoustic emission and environmental data. In: *Proceedings of the International Conference on Smart Infrastructure and Construction (ICSIC)*, Cambridge, UK (2019), pp. 523–532. https://doi.org/10.1680/icsic.64669.523

[2] Acikgoz, S., DeJong, M.J., Kechavarzi, K., and Soga, K. Dynamic response of a damaged masonry rail viaduct: Measurement and interpretation. *Engineering Structures* (2018) **168**: 544–558. https://doi.org/10.1016/j.engstruct.2018.04.054

[3] Cocking, S., Acikgoz, S. And DeJong, M.J. Interpretation of the Dynamic Response of a Masonry Arch Rail Viaduct Using Finite-Element Modeling. *J. Archit. Eng.* (2020) **26**(1):05019008. https://doi.org/10.1061/(ASCE)AE.1943-5568.0000369

[4] Moseley, H. On a new principle in statics, called the principle of least pressure. *London and Edinburgh Philosophical Magazine and Journal of Science* (1833), **3**:285-288.

[5] Heyman, J. The stone skeleton. *Int J Solids Struct* (1966), **2**(2):249–279.

[6] Angelillo, M., Fortunato, A., Fraternali, F. The Lumped Stress Method and the Discrete-Continuum Approximation. *Int J Solids Struct* (2002), **39**:6211-6240.

[7] Fraternali, F., Angelillo, M., Rocchetta, G. On the Stress Skeleton of Masonry Vaults and Domes. In: *Proceedings of the Seventh Pan American Congress of Applied Mechanics (PACAM VII)* Temuco, Chile (2002), pp. 369-372.

[8] Angelillo, A., Fortunato, A. Equilibrium of masonry vaults. In: *Lecture notes in applied and computational mechanics, Novel approaches in civil engineering* (Eds Fremond, M., Maceri, F.) (2004), **14**:105-111. Springer, Berlin.

[9] Fraternali, F. A thrust network approach to the equilibrium problem of unreinforced masonry vaults via polyhedral stress functions. *Mech Res Commun* (2010), **37**:198-204.

[10] Angelillo, M., Babilio, E., Fortunato, A. Singular stress fields for masonry-like vaults. *Continuum Mech Therm* (2013), **25**(2-4):423–441.

[11] Gesualdo, A., Brandonisio, G., De Luca, A., Iannuzzo, A., Montanino, A., Olivieri, C. Limit Analysis of cloister vaults: the case study of Palazzo Caracciolo di Avellino. *Journal of Mechanics of Materials and Structures* (2019), Vol.**14**, pp. 739-750.

[12] O'Dwyer, D.W. Funicular analysis of masonry vaults. *Comput Struct* (1999) **73**:187-197.

[13] Block, P. *Thrust Network Analysis: Exploring Three-dimensional Equilibrium* (PhD Dissertation). Massachusetts Institute of Technology, Cambridge, USA (2009).

[14] Block, P., Ciblac, T., Ochsendorf, J. Real-time limit analysis of vaulted masonry buildings. *Comput Struct* (2006), **84**(29-30):1841-1852.

[15] Vouga, E., Hobinger, M., Wallner, J., Pottmann, H. Design of Self-supporting Surfaces. *ACM Trans Graph* (2012), **31**(4): article 87 (11 pages).

[16] De Goes, F., Alliez, P., Owhadi, H., Desbrun, M. On the Equilibrium of Simplicial Masonry Structures. *ACM Trans Graph* (2013) **32**(4): article 93 (10 pages)

[17] Block, P., Lachauer, L. Three-dimensional funicular analysis of masonry vaults. *Mech Res Commun* (2014), **56**: 53-60.

[18] Miki, M., Igarashi, T., Block, P. Parametric Self-supporting Surfaces via Direct Computation of Airy Stress Functions. *ACM Trans Graph* (2015), **34**(4): article 89 (12 pages).

[19] Pucher, A. Über der spannungzustand in gekrümmten flächen. Beton u Eisen (1934), **33**:298-304.

[20] Wolfram, S., *The Mathematica Book*, 5th ed., Wolfram Media (2003).

12th International Conference on Structural Analysis of Historical Constructions
SAHC 2020
P. Roca, L. Pelà and C. Molins (Eds.)

INVESTIGATION ON THE SEISMIC RESPONSE OF A LARGE MONUMENTAL COMPLEX

SILVIA CAPRILI[1], IRENE PUNCELLO[2*] AND PERE ROCA[3]

[1] Department of Civil and Industrial Engineering (DICI)
University of Pisa
Largo L. Lazzarino 1, 56122 Pisa, Italy
e-mail: silvia.caprili@ing.unipi.it - Web page: dici.unipi.it

[2*] Department of Energy, Systems, Territory and Construction Engineering (DESTeC)
University of Pisa
Largo L. Lazzarino 1, 56122 Pisa, Italy
e-mail: irene.puncello@ing.unipi.it - Web page: destec.unipi.it

[3] Department of Civil and Environmental Engineering (DCEE)
Universitat Politècnica de Catalunya
Jordi Girona 1-3, 08034 Barcelona, Spain
e-mail: pere.roca.fabregat@upc.edu -Web page: https://deca.upc.edu

Keywords: Historical masonry building, monumental complex, pushover analysis, Finite Element Modelling, vulnerability assessment

Abstract.
Historical masonry structures are characterised by a high level of seismic vulnerability, as demonstrated by recent and past seismic events. Monumental buildings, in particular, represent a very challenging topic. Their morphological evolution, characterised by transformations, aggregations and modifications developed over the centuries, have given rise to very complex structures that should be considered as structural aggregates rather than single buildings. The present paper briefly summarises the assessment of the structural performance of the monumental complex of the Certosa di Calci (Italy), by applying an in-depth multi-level and multi-disciplinary approach. The morphological evolution of the aggregate was studied by means of critical historical analysis enabling the identification of the structural units composing it. The complex was, besides, subjected to in-situ survey campaigns allowing an adequate knowledge level. Reliable FEM models were elaborated, and non-linear static pushover analyses were performed. The single structural units were initially studied as isolated buildings and then combined evaluating the influence of the in-aggregate behaviour on the overall structural response. Pushover analyses were performed for each evolution configuration, allowing results in terms of capacity curves, load factors and damage distribution. The methodology presented, although used for a specific case study, can be extended to other constructions characterised by similar complexity and features.

1 INTRODUCTION

Masonry structures represent the most widespread existing constructive typology in the European cultural heritage. Seismic events recently occurred evidenced the high seismic vulnerability of historical buildings, highlighting the need for detailed research on their structural response [1, 2]. Among masonry constructions, monumental buildings represent a particularly challenging issue. These structures are characterised by a complex constructive genesis, where the transformations occurred over the centuries determine the coexistence of portions belonging to different ages. Those portions are not always easily recognisable and are often characterised by different construction techniques and by the lack of adequate connections [3]. Many monumental buildings should be considered as structural aggregates rather than as single buildings [4], composed by several Structural Units (SU) not necessarily working together in a global way [5]. To achieve reliable results from structural assessment, deep and accurate investigations are needed, based on detailed knowledge of their history and construction features [6-8]. A sufficient knowledge should be achieved on the base of a well-organised historical analysis able to reconstruct the actual morphology and accounting for the past transformations [9]. Besides, the intrinsic nature of the aggregate requires a detailed identification of its SUs in order to stablish a realistic decomposition into elementary cells mutually interacting [10, 11].

The present paper focuses on the investigation of the structural seismic behaviour of a portion of the *Certosa di Calci* monumental complex (Tuscany, Italy). An accurate multidisciplinary knowledge analysis [12, 13] was carried out to reconstruct the structural evolution of the aggregate. Criteria to subdivide the complex into SUs were envisaged accounting for the realisation period and the different morphology of structural components [14-18]. Relevant SUs were then modelled using the FEM approach to perform non-linear seismic analyses. The pushover analyses allowed a prompt and relatively easy characterisation of the structural behaviour and seismic capacity. A critical review of the mutual interaction between SUs is obviously needed since the morphological evolution and the historical transformations lead to a complex mechanical collaboration among the different units constituting the aggregate. The numerical model, with all the simplifications and assumptions required, represents a useful tool to assess the reliability of the adopted subdivision criteria. The capacity curves and damage predicted by the numerical model allows an accurate investigation and understanding of the structural behaviour of the aggregates taking into account their construction complexity. For this purpose, the elementary cells were firstly analysed as single buildings and then progressively connected with other cells to account for the aggregate morphology. Pushover analyses were thus performed in different configurations, based on the information derived from the historical analysis, in order to evaluate the influence of the interaction between SUs on the overall structural response.

2 HISTORICAL EVOLUTION OF THE MONUMENTAL COMPLEX

The *Certosa di Calci* monumental complex (Figure 1a) is located in Calci, few kilometres far from Pisa, in a strategic position in the South-Western foothill of the Monte Pisano. Benefit from the inheritance of a rich merchant of Pisa and of other private donations, the building process of the monastic complex officially started in 1366. At the beginning, the construction works proceeded fast, allowing the settlement of the first religious family only two years after the foundation. Despite that, the conclusion of the original nucleus, provided with all the spaces essential for the monks' life, could be attested only in the last decade of 14th century.

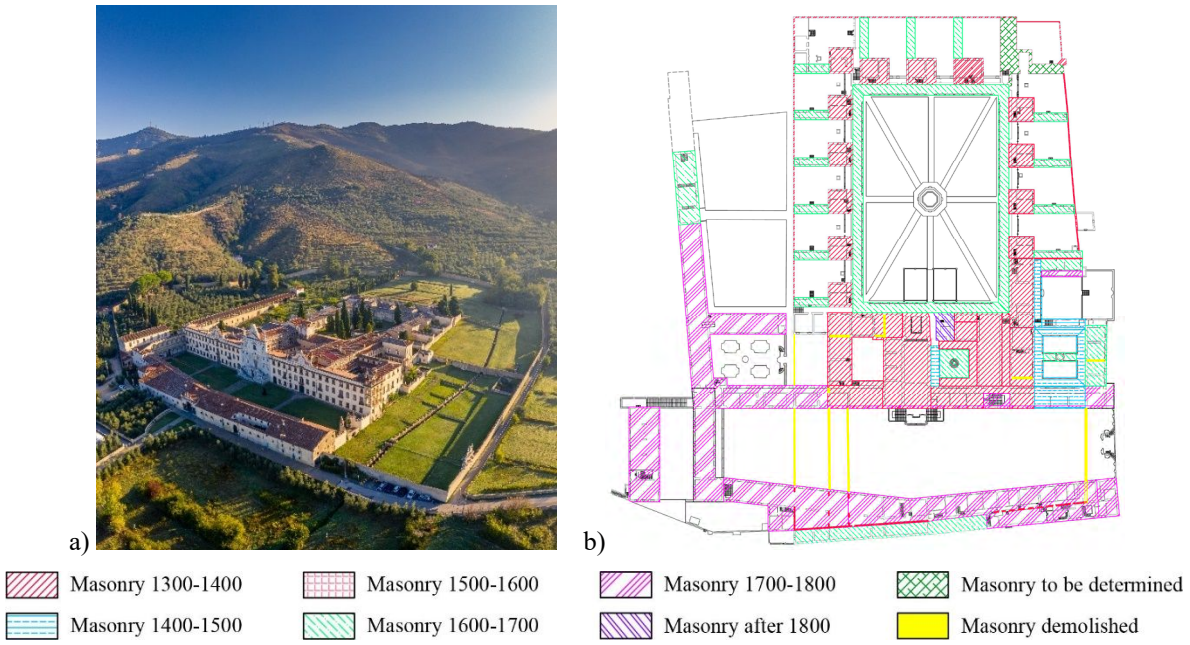


Figure 1: a) View of the *Certosa di Calci*. Photo by courtesy of Guglielmo Giambartolomei; b) plan of the 1st level of the complex with identification of the macro-constructive phases according to the legend.

The building process slowly continued in the 15th and 16th centuries, mostly through local interventions (e.g. addition of porticoes and stairways) and restorations aimed to give a more 'monumental' appearance to the complex. Between the end of the 16th century and the second half of the 17th century, more impactful works were performed including a one-floor addition over most of the first nucleus, important transformations in the main cloister, in the cells and in the cloister on the right of the church, and some additional modifications in the front building (Figure 1b). Nevertheless, the biggest transformations involving *Certosa di Calci* took place at the end of the 18th century, when the structure was considerably enlarged on the northern side, the façade on the courtyard was completed with the addition of the block on the southern corner and several other modifications were realised [19, 20] bringing the building to the current appearance.

3 CERTOSA DI CALCI: STATE OF THE ART

3.1 General description of the building complex

Nowadays, the monumental complex of *Certosa di Calci* shows an irregular shape, the result of the non-homogeneous genesis and of the gradual additions of units to the original nucleus previously mentioned. The different SUs composing the aggregate generally develop on two or three floors, according not only to the importance of the housed function, but also to their position, since the ground level is uphill towards the main cloister.

The different portions are distributed around seven courts (Figure 2), including the main courtyard facing the Church, two little cloisters on its right (i.e. '*chiostro del capitolo*' and '*chiostro della foresteria*'), three gardens/courts on its left and the main cloister. All the cloisters are surrounded by vaulted porticoes, while continuous façades mainly frame gardens and courts.

On the front of the complex, limiting the main courtyard on the East side, the building known

as *'Case Basse'* is located. It developed through subsequent additions to the original surrounding wall and is characterised by a large longitudinal extension with significant structural complexity mainly at the ground floor. The North side of the main court is closed by a two-level block which continues towards the garden and slightly changes its orientation following the sloping ground. Next to the above-mentioned courtyard there is another small court, delimited on the northern side by a quite regular building once housing the barn. The central wing of the monumental complex is composed of several blocks, mainly developed on three levels and organised around four open spaces with the church as central fulcrum. The main cloister shows six cells on the northern and southern side and three cells on the western ones; each cell has its own garden and presents a main squared two-level body and a rectangular one-level body added in the back. The Prior's cell is the only showing higher dimensions and more refined architectural elements.

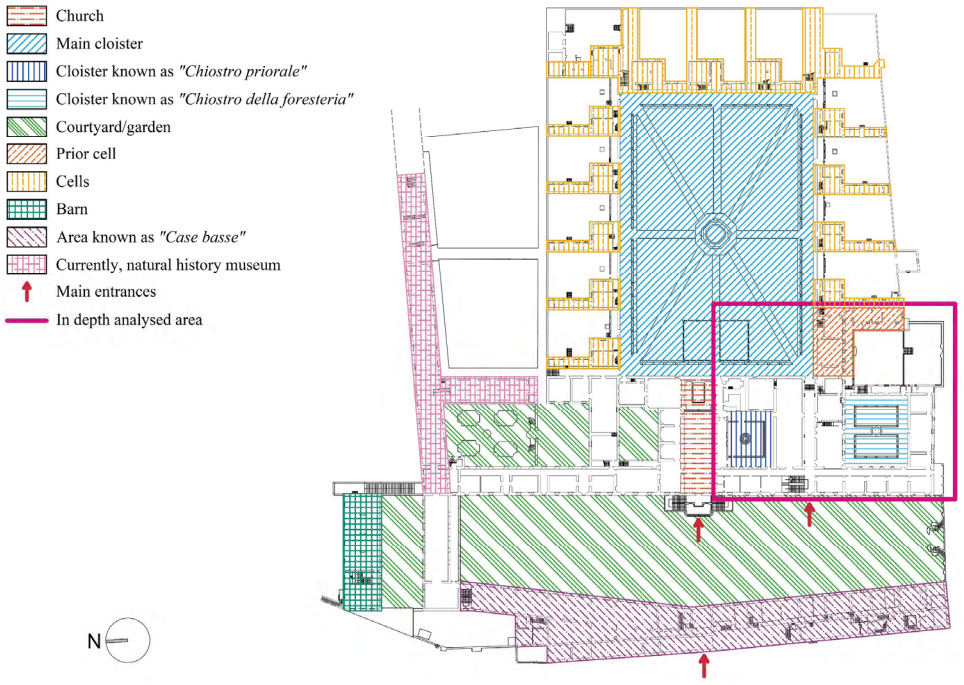


Figure 2: Plan of the first level of the monumental complex with identification of representative areas.

Different functional activities are housed inside the *Certosa*: offices of employees of the Pisa University are spread in different areas, mostly on the 2nd and 3rd floor, while the first two levels on the left of the church host museum spaces. Part of the block on the front of the main courtyard is managed by the Superintendence of Cultural Heritage, as well as part of the 1st floor on the right of the church that is devoted to tourist visits; the cells in the main cloister are mostly used as storages or unused. Due to the large dimensions and to the high heterogeneity of the complex, the in-situ surveys and the following numerical analyses focused on the southern portion marked in Figure 2. This area is one of the most ancient and most articulated due to its highly stratified genesis.

3.2 Geometrical and structural survey

With the cooperation of other research groups of Pisa University, the geometry of the selected area was investigated by means of direct and indirect measurements. The latter ones

were performed through Terrestrial Laser Scanner, able in measuring the position of a great amount of points (the so-called 'point cloud model'), later elaborated in CAD environment to produce plans and sections of all the floors with a high level of accuracy.

An extensive in-situ survey campaign was performed to deeply analyse the current structural condition. Investigations were planned to determine the geometry of structural elements, to define the consistency of walls, vaults and horizontal storeys as well as the connections among different bearing components. Different typologies of vaulted surfaces (e.g. groin, barrel and mirror vaults, some of them with lunettes), with average height between 5 and 6 m, were surveyed in the first two floors. On the contrary, the last level mostly presented wooden storeys with interstorey height equal to about 3-4 m.

The in-situ investigations were spread homogenously around the analysed area achieving a consistent knowledge level, focusing where evident critical points or possible discontinuities were highlighted by the historical analysis (Figure 3). Concerning vertical bearing structures, the textures were analysed by the removal of 50x50 cm plaster portions, with attention to the eventual presence of paintings to be protected. Afterwards, endoscopic investigations aiming to check the inner morphology (e.g. presence of cavities, different adjacent walls, etc.) were performed. Six typologies of masonry pattern were classified. In turn, a general lack of suitable connections between perpendicular walls was observed. No relevant correspondence among the masonry typologies and the historical construction periods was found.

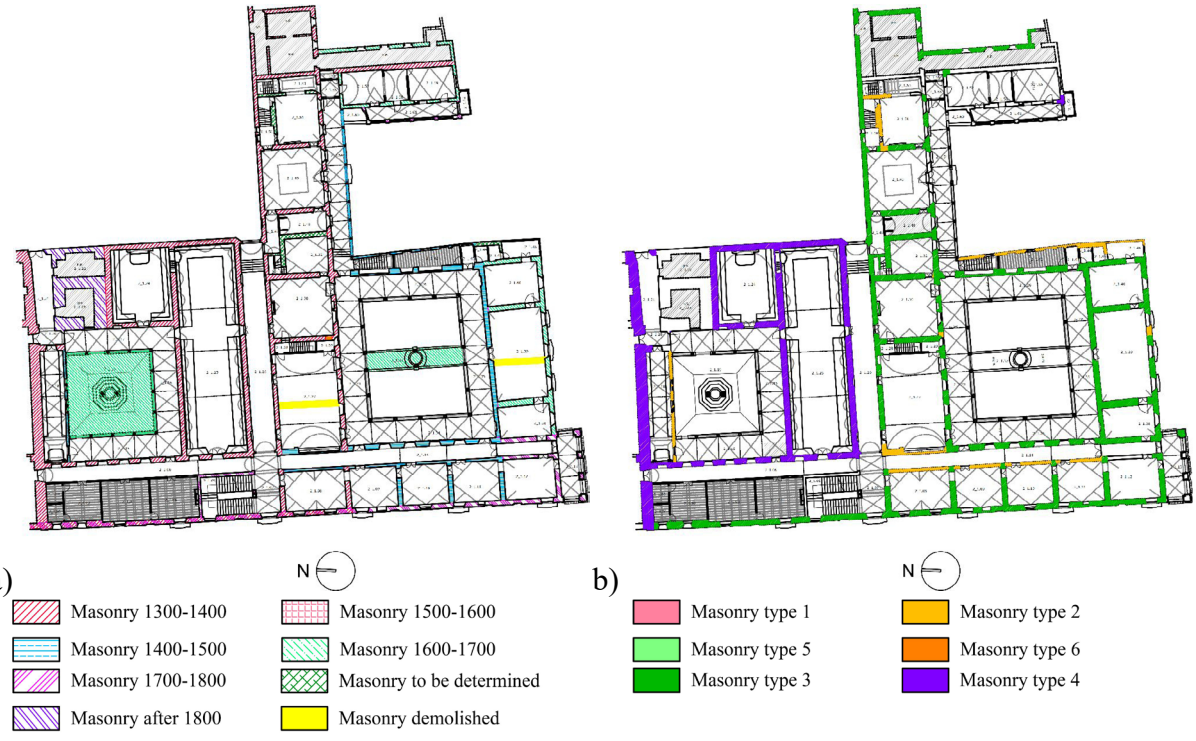


Figure 3: Plans of the first level of the selected area representing: a) the identification of the morphological evolution b) the survey of the masonry typologies.

Plaster removals and endoscopic investigations were also used for the analysis of vaulted surfaces, determining the material composing the load-bearing part, its thickness, the size and

typology of the filling layers. Concerning horizontal storeys, the direct survey was used to determine the size of structural bearing elements and the upper stratigraphy needed to evaluate the resulting permanent loads and masses. In the case of the roof structure, consisting in timber trusses with joists directly supporting the roof covering, inspections were performed only in the accessible areas; consequently, the level of maintenance of the material was assessed thanks to specialised technologists. The survey of the cracking scenario and of the deformation pattern was besides completed both on vertical and horizontal structures; visual inspections and, where needed, removal of plaster portions were performed with the aim of identifying possible local mechanisms, settlement movement or structural deficiency to be in-depth analysed.

3.3 Material properties

For the masonry mechanical properties, values suggested by the current scientific literature were adopted due to the lack of experimental tests results. The masonry textures identified through the in-situ surveys were divided into two macro-categories, correspondent to the '*Muratura in pietrame disordinata'* and '*Muratura in mattoni pieni e malta di calce'* of the table C8.5.I of the Italian Design Code '*Circolare applicativa'* [21]. The latter one was adopted also for the vaults, while for the material of the columns, identified as *serena* stone, the values proposed in [22, 23] were accounted for. Table 1 summarises the adopted material properties.

A specific investigation of the state of maintenance of the iron tie-rods was performed including experimental tests to assess the effective value of tensile strains characterising each element. Concerning timber structures, and as suggested by the results of the in-situ survey, fir wood was considered with an elastic modulus equal to 9500 N/mm^2. Due to the observed maintenance problems and to the lack of specific experimental tests, the most unfavourable fir wood class (S3) according to CNR-DT 206/2007 [24] has been adopted.

Table 1: Mechanical properties of the masonry materials

Masonry typology	General properties			Tensile properties			Compressive properties		
	E	Poisson	w	f_t	G_f	$f_{t\,res}$	f_c	G_f	$f_{c\,res}$
	N/mm^2	-	kN/m^3	N/mm^2	N/mm	N/mm^2	N/mm^2	N/mm	N/mm^2
Uneven masonry	690	0.2	19	0.05	0.0050	0.005	1	1.60	0.1
Masonry composed of solid brick and lime mortar	1200	0.2	18	0.13	0.0097	0.013	2.6	4.16	0.26
Serena stone	1581000	0.2	26.5	5	0.1253	0.5	100	160.00	10

4 NUMERICAL MODELLING AND STRUCTURAL ANALYSIS

4.1 General approach adopted for modelling

To assess its structural performance, the selected portion of the *Certosa di Calci* was firstly disaggregated into its SUs, analysed separately and later re-assembled aiming to understand the effects of mutual interaction of the SUs due to the 'in-aggregate' behaviour. At the moment, only the two limit conditions have been considered, consisting of lack of connection and full connection. The real connection condition may be in fact an intermediate case between these two extremes.

The determination of the SUs took into account several parameters, including the historical constructive period, the variation of the interstorey height and corresponding alignments among

portions, the vertical disposition of bearing masonry walls and thickness' changes, the typology of roof structures, the technological system adopted and, finally, the masonry typology determined through in-situ surveys [12, 17, 18].

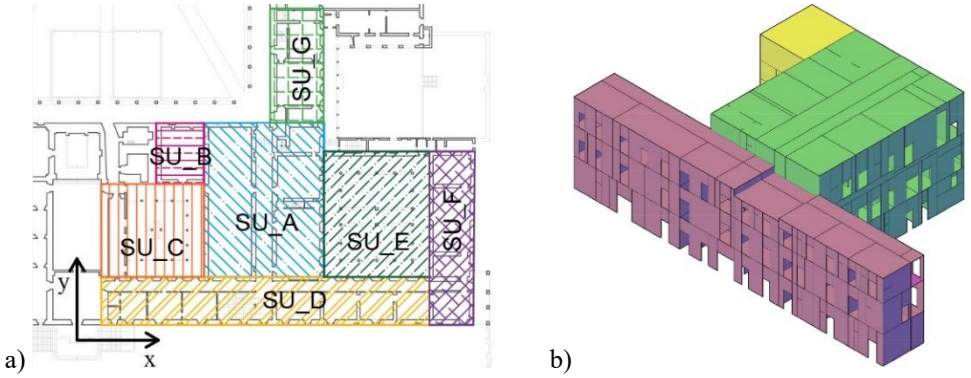


Figure 4: a) tag adopted for the different structural units identified inside the aggregate and indication of the reference system; b) 3D model showing the structural units so far analysed.

Due to the heterogeneity and complexity of the buildings investigated, it was almost impossible to achieve - even within each single SU - a perfect categorization according the listed parameters without reaching an excessive subdivision that would be not really representative of the effective structural behaviour. The pursuing of an 'overall' homogeneity was then preferred, based on the knowledge of the building reached thanks to in-situ surveys. This choice led to the identification of at least seven different SUs in the considered area, as represented in Figure 4a.

So far, only the three SUs represented in Figure 4b were analysed. Considering the differences among them, the two units SU_A and SU_B should belong to the same historical period, even if the construction may not be exactly contemporary as suggested by a structural discontinuity identified in the ground floor. Moreover, SU_B is characterised by the presence of a double volume and its separation from SU_A is marked by a partial wall discontinuity. In turn, SU_D is characterised by lesser homogeneity in the structural features, compared to SU_A, and by a strongly different spatial orientation. The separation between the two SUs is also marked by a different global height and by distinct roof structures.

4.2 Numerical model

A Finite Element Model (FEM) was built by means of the non-linear analysis software DIANA FEA [25]. For all the considered SUs, the same approaches were adopted.

Vaulted surfaces and horizontal floors were modelled as equivalent two-dimensional plane elements [26, 27] by using hexi-quadratic shell elements with eight (CQ40S) and six nodes (CT30S). The same typologies of elements were used to model also masonry walls, while three-node three-dimensional class-III beam elements (CL18B) were adopted for arches. Two-node enhanced-truss element (L6TRU) were used for ties and one-node point masses (PT3T) were employed to simulate the load distribution acting on walls in the case of beam-framed floors. The mesh size varied in proportion with the smallest dimension of each element, with a medium size of 50 cm. Since no specific investigations were performed concerning the foundation system and the soil typology, vertical elements were fully restrained at the base.

For the constitutive model of masonry, the *Total Strain Rotating Crack Model* [25] was used,

able to describe the nonlinear properties of the materials by assuming exponential softening in tension and parabolic hardening followed by softening in compression. The value of the tensile strength, where not directly provided by experimental tests or literature, was evaluated according to suggestions provided by [26, 27], starting from the compressive strength value. The compressive and tensile fracture energy, needed as input parameter in the numerical model, were determined according to [27, 28]. For wooden floors and vaulted structures, a linear elastic orthotropic material model was assumed. The mechanical characteristics were determined according to the principles of equivalence in axial stiffness [29, 30]. For steel components, a linear elastic material model was adopted.

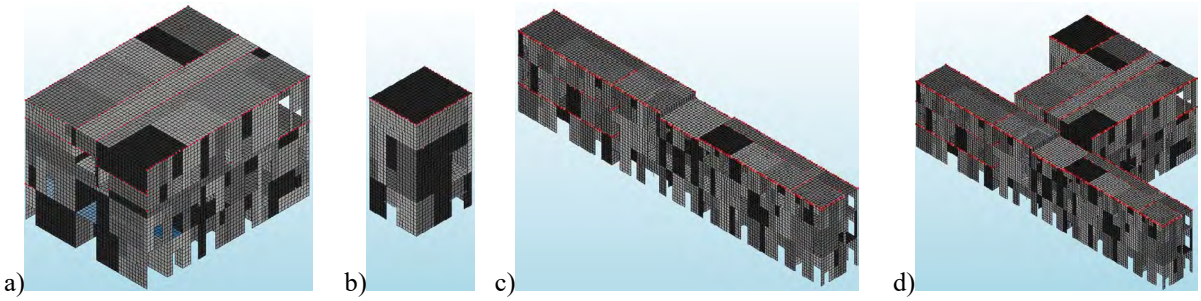


Figure 5: FEM model of Structural Unit SU_A, SU_B, SU_D, SU_A+B+D, respectively in a, b, c and d.

4.3 Non-linear static analysis: methods and first results

The seismic performance of the structural aggregate was analysed by means of nonlinear static analysis. While keeping constant the gravity loads, monotonically increasing horizontal forces, proportional to the mass of the structure, were applied.

Each of the modelled 'single' SUs was analysed separately by investigating the failure modalities and the maximum capacity achieved in terms of acceleration (or base shear force) and displacement. The single-unit analysis allowed an understanding of the individual performance of each portion, including phenomena that would not have been detected if only a global analysis of the entire aggregate had been performed (i.e. local failures, cracking and activation of out-of-plane phenomena of single walls).

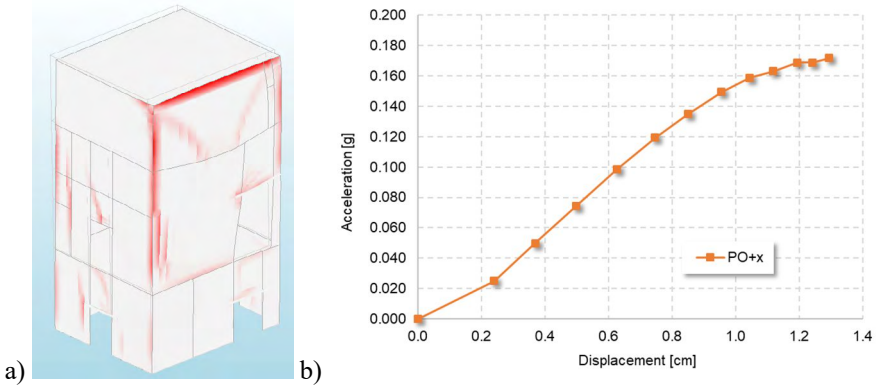


Figure 6: Pushover results for the +x direction: a) tensile strain distribution and b) capacity curve.

As an example, Figure 6a shows the damage distribution due to an out-of-plane local

mechanism for pushover analysis in +x direction on the structural unit SU_B (Figure 4) composed by a double volume. Figure 6b shows the corresponding capacity curve. The same procedure was repeated for all the considered SUs.

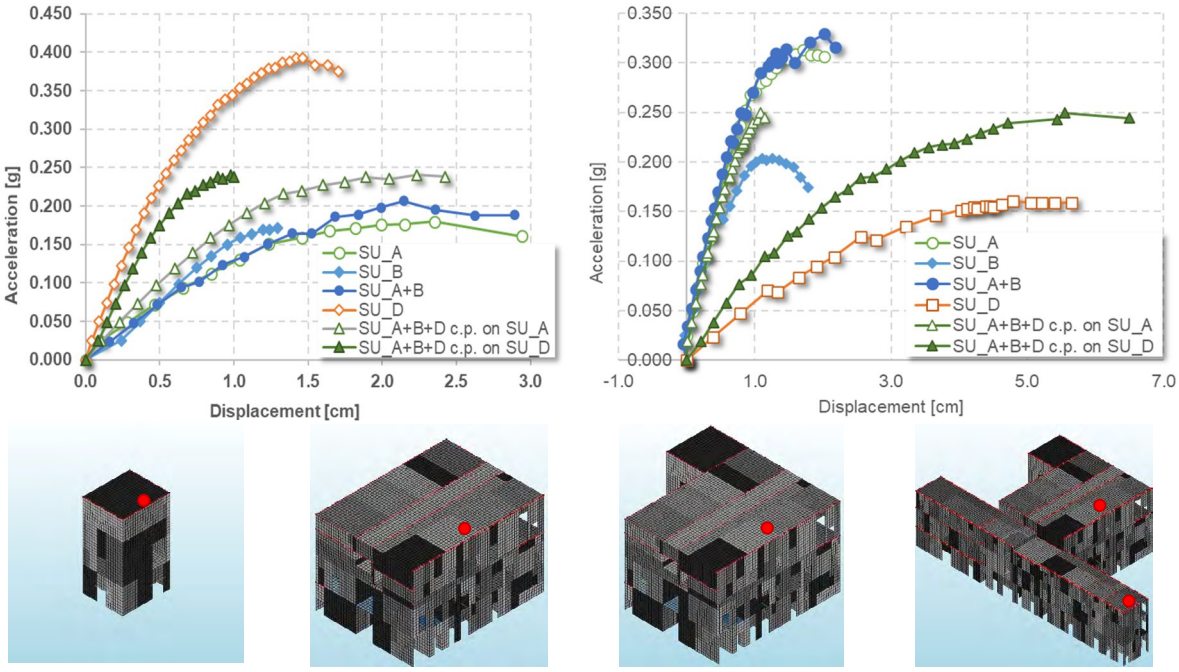


Figure 7: Pushover results in terms of capacity curve for the +x direction (a) and for the +y direction (b), and selected control points.

After analysing the units as isolated buildings, the different portions were progressively connected to each other with the aim of investigating the resulting behaviour due to the "in-aggregate" performance. So far, the adopted procedure has allowed to investigate, for the Certosa monumental complex, the following situations: the connection of two units with very different size and the connection of two units with very different shape. In the former case - SU_A and SU_B - the units were characterised by different capacity related primarily to their dimensions but also to some local phenomena influencing on their performance. In the aggregate configuration, the capacity in +y and -y direction was approximately the same as for the larger unit. Less predictable was the result in +x and -x since the aggregate showed a rather higher capacity than the bigger unit. The smaller unit in fact, despite its limited dimension, was able to mitigate a short pillar effect which was affecting the capacity of the other unit in the isolated configuration. This local phenomenon took place near the connection among the two structures, in a wall of the larger unit which continues in the other one. Consequently, due to the particular location of the local phenomenon, including the smaller unit had a beneficial effect and increased the global capacity.

In the second analysed case - SU_A+B and SU_D - the two units considered as isolated were characterised by higher structural performance in opposite directions due to the very different shape with subsequent different stiffness and resistance. The aggregate configuration revealed, in all the directions, an intermediate capacity among those units analysed as single buildings. Due to their similar dimension, none of the two units was thus able in determining the structural

performance of the aggregate. However, they mutually improved their capacity along the respective weakest directions. This result has been useful also to prove that in these two units the behaviour is not determined by local failures, as otherwise any increment of the global performance would have been hindered by them.

Figure 8 shows the comparison among damage distribution in different SU configurations for comparable accelerations. Cracks development in the connection between the two units can be noticed. Generally, differences in the damage distribution in proximity with the connection area were detected only when the pushover direction was parallel to the connecting surface.

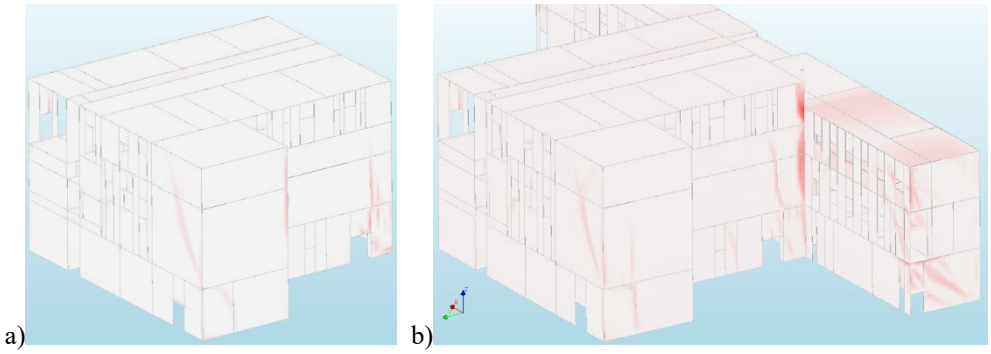


Figure 8: Difference in tensile strain distribution among the structural aggregate composed by SU_A+B (a) and the ones composed by SU_A+B+D (b)

5 CONCLUSIONS AND FUTURE WORKS

The structural assessment of a portion of the monumental historical building *Certosa di Calci* was performed by means of numerical nonlinear static analyses. Due to the high complexity and heterogeneity of the aggregate which included various structural units characterised by different floors and roofs, masonry typologies, material properties and construction periods, the resulting performance of the complex is strongly dependent on the behaviour of the SUs constituting it. The interaction phenomena arising from the combination of the SUs were investigated through the analysis of different historical configurations with increasing complexity. The structural assessment was preceded by a deep multidisciplinary investigation allowing an adequate level of knowledge of the aggregate.

Different SUs were identified and 'extracted' from the monumental complex and their individual seismic response was investigated by means of FEM analyses. In a second phase, the units were progressively connected and pushover analyses were performed for each aggregation in order to study the failure modalities, the interaction phenomena and the modification of the seismic capacity due to the in-aggregate behaviour. It has been noticed that these kinds of analyses, even if oriented to understand the aggregate effect, should consider possible local mechanisms and the reciprocal influence of connected units in the overall behaviour. This phenomena in fact, could partially affect the result even when the structure is characterised by a global behaviour.

Further research is ongoing with the aim of considering a higher number of structurally connected units and also different connection levels among them.

Acknowledgements. The authors are thankful to the Pisa University and to the Superintendence

BAPSAE of Pisa and Livorno for supporting and encouraging this research. The authors would like to thank Prof. M.G. Bevilacqua and his research team for the execution of the Laser Scanner survey, Prof. A. De Falco and her co-workers for the elaboration of the point clouds in CAD environment, for the experimental tests performed on chains and for the collaboration during the in- situ investigations. A special thank is also given to the expert technicians of the *Laboratorio Ufficiale per le Esperienze sui Materiali da Costruzione* of Pisa University for the execution experimental investigations. Finally, the authors' gratitude goes to Guglielmo Giambartolomei for providing the aerial photos of the *Certosa di Calci.*

REFERENCES

[1] Lagomarsino, S. On the vulnerability assessment of monumental buildings. *Bulletin of Earthquake Engineering*. (2006), 4, 445-63.

[2] Clementi, F., Gazzani, V., Poiani, M., Lenci, S. Assessment of seismic behaviour of heritage masonry buildings using numerical modelling. *Journal of Building Engineering*. (2016), 8, 29-47.

[3] Caprili, S., Puncello, I. Knowledge-Based Approach for the Structural Assessment of Monumental Buildings: Application to Case Studies. *Front. Built Environ.* (2019), 5, 52.

[4] Lagomarsino, S., Cattari, S., Degli Abbati, S., Ottonelli, D. Seismic assessment of complex monumental buildings in aggregate: the case study of Palazzo del Podestà in Mantua (Italy). In: *SAHC2014- 9th international conference on structural analysis of historical constructions*, Mexico City, Mexico, (2014), pp. 14-7.

[5] Caprili, S., Mangini, F., Salvatore, W. Numerical modelling, analysis and retrofit of the historical masonry building "La Sapienza". In: *COMPDYN 2015, 5th ECCOMAS Thematic Conference on Computational Methods in Structural Dynamics and Earthquake Engineering*, Crete Island, Greece, (2015), pp. 772-87.

[6] Cattari, S., Degli Abbati, S., Ferretti, D., Lagomarsino, S., Ottonelli, D., Tralli, A. Damage assessment of fortresses after the 2012 Emilia earthquake (Italy). *Bulletin of Earthquake Engineering*. (2014), 12, 2333-65.

[7] Castellazzi, G., D'Altri, A.M., de Miranda, S., Chiozzi, A., Tralli, A. Numerical insights on the seismic behavior of a non-isolated historical masonry tower. *Bulletin of Earthquake Engineering*. (2018), 16, 933-61.

[8] Cattari, S., Lagomarsino, S., Bosiljkov, V., D'Ayala, D. Sensitivity analysis for setting up the investigation protocol and defining proper confidence factors for masonry buildings. *Bulletin of Earthquake Engineering*. (2015), 13, 129-51.

[9] Caprili, S., Mangini, F., Paci, S., Salvatore, W., Bevilacqua, M.G., Karwacka, E., et al. A knowledge-based approach for the structural assessment of cultural heritage, a case study: La Sapienza Palace in Pisa. *Bulletin of Earthquake Engineering*. (2017), 15, 4851-86.

[10] Berto, L., Doria, A., Faccio, P., Saetta, A., Talledo, D. Vulnerability Analysis of Built Cultural Heritage: A Multidisciplinary Approach for Studying the Palladio's Tempietto Barbaro. *International Journal of Architectural Heritage*. (2017), 11, 773-90.

[11] Degli Abbati, S., D'Altri, A., Ottonelli, D., Castellazzi, G., Cattari, S., Miranda, S., et al. Seismic assessment of interacting structural units in complex historic masonry constructions by nonlinear static analyses. *Computers and Structures.* (2018).

[12] Binda, L., Cardani, G., A, S., Valluzzi, M., Munari, M., Modena, C. Multilevel Approach to the Vulnerability Analysis of Historic Buildings in Seismic Areas Part 1: Detection of

Parameters for Vulnerability Analysis through on Site and laboratory Investigations, *Restoration of Buildings and Monuments*, (2007) 13(6), pp. 413-426
[13] Valluzzi, M., Munari, M., Modena, C., Binda, L., Cardani, G., A, S. Multilevel Approach to the Vulnerability Analysis of Historic Buildings in Seismic Areas Part 2: Analytical Interpretation of Mechanisms for Vulnerability Analysis and Structural Improvement, *Restoration of Buildings and Monuments*, (2007) 13(6), pp. 427-442
[14] Carocci, C.F. Small centres damaged by 2009 L'Aquila earthquake: on site analyses of historical masonry aggregates. *Bulletin of earthquake engineering*. (2012), 10, 45-71.
[15] Monti, G., Vailati, M. Analisi di vulnerabilità sismica di edifici in aggregato: un caso esempio. *XIII convegno ANIDIS L'ingegneria Sismica in Italia*. (2009), 28.
[16] Munari, M., Valluzzi, M., Cardani, G., Anzani, A., Binda, L., Modena, C. Seismic vulnerability analyses of masonry aggregate buildings in the historical centre of Sulmona (Italy), (2010).
[17] Formisano, A., Mazzolani, F., Florio, G., Landolfo, R. A quick methodology for seismic vulnerability assessment of historical masonry aggregates. In: *Proc. of the COST Action C26 Final Conference Urban Habitat Constructions under Catastrophic Events*, (2010), pp. 577-82.
[18] Vicente, R., Parodi, S., Lagomarsino, S., Varum, H., Silva, J.A.R.M. Seismic vulnerability and risk assessment: case study of the historic city centre of Coimbra, Portugal. *Bulletin of Earthquake Engineering*. (2011), 9, 1067-96.
[19] Aristo, M. *La Certosa di Pisa*. Mariotti, (1911).
[20] Piombanti, G. *La Certosa di Pisa e dell'isola di Gorgona*. Fabbreschi, (1971).
[21] Circolare. Istruzioni per l'applicazione dell'«Aggiornamento delle 'Norme tecniche per le costruzioni'» di cui al decreto ministeriale 17 gennaio 2018. In: 7, 21/01/2019.
[22] Coli, M., Livi, E., Tanini, C. Pietra Serena mining in Fiesole. Part III: Structural-mechanical characterization and mining. *Journal of mining Science* (2006), 42, 74-84.
[23] Cantisani, E., Garzonio, C., Ricci, M., Vettori, S. Relationships between the petrographical, physical and mechanical properties of some Italian sandstones. *International Journal of Rock Mechanics and Mining Sciences* (2013), 60, 321-32.
[24] CNR, *D. 206/2007 Istruzioni per la progettazione, l'esecuzione ed il controllo delle strutture di Legno*, (2008).
[25] TNO, D. *DIsplacement method ANAlyser. User's manual*, release 10.3. Netherlands, (2019).
[26] Lourenço, P.B., Barros, J., Oliveira, J.T. Shear testing of stack bonded masonry. Construction and Building Materials. 2004, 18, 125-32.
[27] Lourenço, P.B. Recent advances in masonry modelling: micromodelling and homogenisation. In: *Multiscale modeling in solid mechanics: computational approaches*, World Scientific, (2010), pp. 251-94.
[28] Drougkas, A., Roca, P., Molins, C. Numerical prediction of the behavior, strength and elasticity of masonry in compression. *Engineering Structures* (2015), 90, 15-28.
[29] Cattari, S., Lagomarsino, S., Resemini, S. *Il ruolo delle volte nella risposta sismica degli edifici in muratura. Archi e volte in zona sismica- Meccanica delle strutture voltate*. Doppiavoce, Naples, (2012).
[30]Wilson, A., Quenneville, P.J., Ingham, J.M. In-plane orthotropic behavior of timber floor diaphragms in unreinforced masonry buildings. *Journal of Structural Engineering*. (2013), 140, 04013038.

12th International Conference on Structural Analysis of Historical Constructions
SAHC 2020
P. Roca, L. Pelà and C. Molins (Eds.)

LOWER-BOUND LIMIT ANALYSIS OF MASONRY ARCHES WITH MULTIPLE FAILURE SECTIONS

NICOLA A. NODARGI* AND PAOLO BISEGNA

Department of Civil Engineering and Computer Science
University of Rome Tor Vergata
via del Politecnico 1, 00133 Rome, Italy
e-mail: nodargi@ing.uniroma2.it (*corresponding author)

Keywords: Masonry Structures, Limit Analysis, Collapse mechanism, Arch, Linear Programming

Abstract. *A computational method is proposed for the lower-bound limit analysis of masonry arches with multiple failure sections. Main motivation is the observation that, not only the position, but also the orientation of the failure sections in an arch might not be known in advance in practical applications. The lower-bound limit analysis problem is formulated as a straightforward linear programming problem. Numerical simulations highlight the predicting capabilities of the proposed approach, enabling an accurate and safe prediction of the loading capacity of masonry arches.*

1 INTRODUCTION

The structural analysis of masonry structures plays a critical role in the effort to preserve and restore architectural heritage and historical buildings. Many computational approaches have been developed for addressing such a task, at different scales and levels of complexity, including micromechanical approaches (e.g., see [1,2]), multiscale/homogenization approaches (e.g., see [3-6]) and macromechanical/phenomenological approaches (e.g., see [7-11]), to be used in finite element formulations for inelastic structures (e.g., see [12-18]). As an alternative strategy, whose roots trace back to the first discovery by Robert Hook of the analogy between the structural behavior of a masonry arch and that of a catenary, the structural capacity can be computed by a limit analysis approach (e.g., see [19,20]).

In last decades, modern computers and advanced numerical methods have made possible to translate the limit analysis into a powerful tool for the analysis of masonry structures (e.g., see [21,22]. Restricting the attention to masonry arches, a successful approach is the rigid block computational method, originally conceived by Livesley [23], which regards the structure as a discrete system of rigid blocks exchanging unknown forces through their contact interfaces. The method has also been extended to three-dimensional structures (e.g, see [24,25]), non-associative frictional behavior (e.g, see [26-29]) and large displacement regime (e.g, see [30,31]). In a different line of research, several computational approaches resort to the concept of thrust line for performing the lower-bound limit analysis of masonry arches (e.g., see [32-35]) Alternatively, in [36], it has been proposed to numerically integrate



Figure 1: Collapse of masonry arches involving inclined failure sections with respect to the courses of the masonry units, hence calling for a generalization of the classical notion of arch with prescribed stereotomy.

Milankovitch's equilibrium equations [37,38], to characterize the equilibrated stress states of the arch, and then to proceed with the stress state optimization.

Interestingly, the methods mentioned above require, even if in disguise, that a stereotomy of the arch is clearly recognized for a spatial discretization of the problem. Indeed, as already pointed out by Milankovitch [37], the arch stereotomy does not simply allow for a reduction of the problem, but it rather affects its solution, because it implicitly defines the stereotomy sections as the potential failure sections, i.e. the sections where the opening of hinges can take place. Actually, no problem arises in the case of masonry arches constituted by individual voussoirs, as the stereotomy is naturally identified with the physical joints between them. Conversely, when the arch is monolithic or made by small units arranged in a regular or irregular texture, the selection of a stereotomy becomes contrived, and, for each possible selection, a different solution of the lower-bound limit analysis problem is found. Basing on such observation, in [39,40], the non-uniqueness of the thrust line for a monolithic arch is concluded, and a variational formulation is proposed, which is claimed to be "liberated from the concept of the thrust line" [39]. Differently, in [41] it has been suggested to overcome the concept of stereotomy for monolithic masonry arches, and to account for failure sections with arbitrary position and orientation.

Aim of the present work is to propose a computational approach for the lower-bound limit analysis of masonry arches with multiple failure sections. Main motivation is the observation that not only the position, but also the orientation of the failure sections in an arch might not be known in advance in practical applications (Figure 1). Hence, provided a suitable discrete number of potential failure sections is accounted for, the lower-bound limit analysis of a masonry arch is addressed by a straightforward LP problem. It is remarked that, considering multiple potential failure sections allows for an accurate description of the class of its equilibrated and statically admissible stress. Consequently, the resulting solution of the lower-bound limit analysis problem corresponds to the most dangerous stress state that might be induced by the external loads, or, from the dual kinematical standpoint, corresponds to the most dangerous collapse mechanism that might be induced in the structure by the opening of linear cracks. A safer prediction of the structural loading capacity is obtained compared to usual analysis, because taking into account a broader class of potential collapse states. Numerical simulations are presented for investigating the potentialities of the proposed computational approach.

The present paper is organized as follows. In Section 2 the lower-bound limit analysis of masonry arches with multiple failure sections is formulated. Numerical simulations are reported in Section 3 and conclusions are outlined in Section 4.

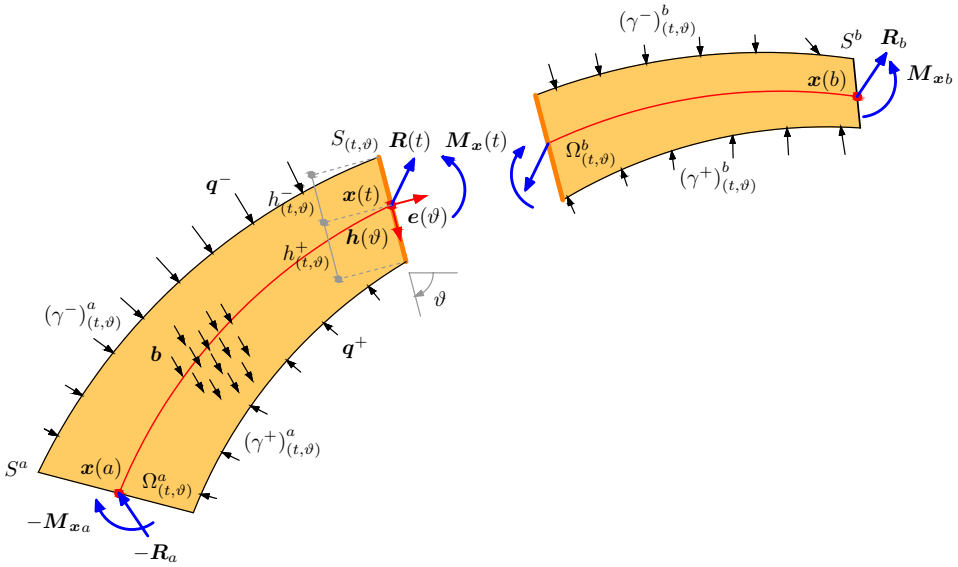


Figure 2: Masonry arch: geometric model, typical potential failure section and positive internal stress resultants are shown.

2 FORMULATION

Let $\Omega \subset \mathbb{R}^2$ be the domain occupied by a masonry arch, as depicted in Figure 2. A Cartesian reference frame $\{O;x,y\}$ is introduced, with $\mathbf{i}$ and $\mathbf{j}$ respectively denoting the unit vectors parallel to the x- and y-coordinate axes, and $\mathbf{k}=\mathbf{i}\times\mathbf{j}$. A reference curve γ is introduced, parameterized by a map $\mathbf{x}\in C^1([a,b])^2$, with the points $\mathbf{x}(a)$ and $\mathbf{x}(b)$ belonging to the two bases of the arch, respectively denoted by S_a and S_b. The intrados [resp., extrados] of the arch is denoted by γ^+ [resp., γ^-]. It is assumed that the arch is clamped at its bases S_a and S_b, that a distribution of body forces $\mathbf{b}$ is applied in Ω, and that a distribution of surface forces $\mathbf{q}^+$ [resp., $\mathbf{q}^-$] acts over γ^+ [resp., γ^-]. In particular, those forces are expressed as $\mathbf{b}=\mathbf{b}^{\mathrm{d}}+\lambda\mathbf{b}^{\mathrm{l}}$ and $\mathbf{q}^{\pm}=(\mathbf{q}^{\pm})^{\mathrm{d}}+\lambda(\mathbf{q}^{\pm})^{\mathrm{l}}$, i.e. split into the sum of dead and live contributions, the latter obtained by amplification of a basic distribution through the load multiplier λ. Furthermore, the arch is assumed to be comprised by a rigid no-tension material (e.g., see [19,20]).

A potential failure section of the arch $S_{(t,\vartheta)}$ is an oriented line segment, which contains the point $\mathbf{x}(t)$, has orientation defined by the polar angle ϑ, and whose initial [resp., final] endpoint is located on the extrados [resp., intrados] curve. The unit vectors $\mathbf{h}(\vartheta)$ and $\mathbf{e}(\vartheta)$, respectively parallel and normal to $S_{(t,\vartheta)}$ are introduced. In addition, the signed distance of the endpoint of the section $S_{(t,\vartheta)}$ on γ^+ [resp., γ^-], measured from $\mathbf{x}(t)$ along $\mathbf{h}(t)$, is denoted by $h^+_{(t,\vartheta)}$ [resp., $h^-_{(t,\vartheta)}$]. It is noticed that the section $S_{(t,\vartheta)}$ cuts the arch into two portions, namely $\Omega^a_{(t,\vartheta)}$ and $\Omega^b_{(t,\vartheta)}$. Let $(\gamma^{\pm})^a_{(t,\vartheta)}$ and $(\gamma^{\pm})^b_{(t,\vartheta)}$ denote the portion of $\gamma^{\pm}$ bounding $\Omega^a_{(t,\vartheta)}$ and $\Omega^b_{(t,\vartheta)}$, respectively.

The (internal) stress resultants $\mathbf{R}(t,\vartheta)$ and $\mathbf{M}_{\mathbf{x}}(t,\vartheta)$ at the potential failure section $S_{(t,\vartheta)}$ are defined by:

$$\begin{aligned}&\mathbf{R}(t,\vartheta)=\mathbf{R}_a-\int_{\Omega^a_{(t,\vartheta)}}\mathbf{b}(\mathbf{p})\mathrm{d}a(\mathbf{p})-\int_{\left(\gamma^{\pm}\right)^a_{(t,\vartheta)}}\mathbf{q}^{\pm}(\mathbf{p})\mathrm{d}\ell(\mathbf{p}),\\&\mathbf{M}_{\mathbf{x}}(t,\vartheta)=\mathbf{M}_{\mathbf{x}a}+\left[\mathbf{x}(a)-\mathbf{x}(t)\right]\times\mathbf{R}_a-\int_{\Omega^a_{(t,\vartheta)}}\left[\mathbf{p}-\mathbf{x}(t)\right]\times\mathbf{b}(\mathbf{p})\mathrm{d}a(\mathbf{p})-\int_{\left(\gamma^{\pm}\right)^a_{(t,\vartheta)}}\left[\mathbf{p}-\mathbf{x}(t)\right]\times\mathbf{q}^{\pm}(\mathbf{p})\mathrm{d}\ell(\mathbf{p}),\end{aligned}\tag{1}$$

where $\mathbf{R}_a$ and $\mathbf{M}_{\mathbf{x}a}$ respectively denote the opposite of the clamp constraint force and moment reactions at the basis S_a, henceforth intended as the static indeterminate reactions of the problem.

The following component-wise representation of the stress resultants is introduced:

$$N(t,\vartheta)=\mathbf{R}(t,\vartheta)\cdot\mathbf{e}(\vartheta),\quad T(t,\vartheta)=\mathbf{R}(t,\vartheta)\cdot\mathbf{h}(\vartheta),\quad M_{\mathbf{x}}(t,\vartheta)=\mathbf{M}_{\mathbf{x}}(t,\vartheta)\cdot\mathbf{k},\tag{2}$$

where $N(t,\vartheta)$, $T(t,\vartheta)$ and $M_{\mathbf{x}}(t,\vartheta)$ can be respectively interpreted as normal force, shear force and bending moment at the potential failure section $S_{(t,\vartheta)}$.

Following the model of no-tension material, the stress resultants $\mathbf{R}(t,\vartheta)$ and $\mathbf{M}_{\mathbf{x}}(t,\vartheta)$ acting over the potential failure section $S_{(t,\vartheta)}$ have to obey suitable static admissibility conditions. Specifically, unilateral conditions are enforced:

$$N(t,\vartheta)\le 0,\quad -M_{\mathbf{x}}(t,\vartheta)+N(t,\vartheta)h^{+}_{(t,\vartheta)}\le 0,\quad M_{\mathbf{x}}(t,\vartheta)-N(t,\vartheta)h^{-}_{(t,\vartheta)}\le 0,\tag{3}$$

implying the normal force to be compressive, and the center of pressure to lie inside the section, coherently with the infinite compressive strength and vanishing tensile strenght of the material. As customary in the analysis of masonry arches, it is assumed that a sufficiently large friction angle is available, such that a no-sliding requirement is tacitly satisfied.

The static theorem of limit analysis requires to maximize the multiplier λ of the basic live loads over the space of equilibrated and statically admissible stress resultants. Indeed, equations (1) supply an explicit characterization of the equilibrated stress resultants acting over the section $S_{(t,\vartheta)}$ in terms of the statically indeterminate reactions $\mathbf{R}_a$ and $\mathbf{M}_{\mathbf{x}a}$. The latter are component-wise collected in the following vector:

$$\mathbf{X}=\left\{H_a,V_a,M_{\mathbf{x}a}\right\},\tag{4}$$

where $H_a=\mathbf{R}_a\cdot\mathbf{i}$, $V_a=\mathbf{R}_a\cdot\mathbf{j}$, $M_{\mathbf{x}a}=\mathbf{M}_{\mathbf{x}a}\cdot\mathbf{k}$, and the semicolon denotes column stacking. On the other hand, by exploiting positions (2), the equilibrated stress resultants (1) can be substituted in the static admissibility conditions (3), which boil down to linear inequalities in the unknowns $\mathbf{X}$ and λ. Hence, the lower-bound limit analysis problem for a masonry arch with multiple failure sections reduces to:

$$\begin{aligned}&\max_{\lambda,\mathbf{X}}\lambda,\\&\text{s.t.}\quad\text{inequalities (3) hold for any } t,\vartheta.\end{aligned}\tag{5}$$

Indeed, for developing a computational solution strategy of problem (5), a suitable discretization is undertaken with respect to the parameters t and ϑ. That amounts at checking

the static admissibility conditions only for a discrete number, say C, of potential failure sections, referred to as control sections. Hence, problem (5) can be finally written in the form:

$$\begin{aligned} &\max_{\lambda,\mathbf{X}} \lambda, \\ &\text{s.t.} \quad \mathbf{A}\mathbf{X} - \mathbf{b}^{\mathrm{l}}\lambda - \mathbf{b}^{\mathrm{d}} \le 0, \end{aligned} \tag{6}$$

where $\mathbf{A}$ is a $3C \times 3$ matrix, and $\mathbf{b}^{\mathrm{d}}$ and $\mathbf{b}^{\mathrm{l}}$ are $3C \times 1$ vectors (for details on the assembling procedure, see [41]). Problem (6) is a Linear Programming (LP) problem, whose solution can be addressed by standard optimization tools.

3 NUMERICAL SIMULATIONS

A pointed arch is considered, as depicted in Figure 3(a). Its geometry is characterized by the radius R, the eccentricity e, the embrace angle β and the thickness h. The intrados and extrados curves of the arch are the union of two arcs of circle, having radius $R \pm h/2$, center at point of coordinates $\left(\pm e, -R\cos(\beta/2)\right)$ and central angle $\beta/2$, measured from the vertical direction. In order to mimic a pseudo-static earthquake loading, it is assumed that the arch is subjected to the self-weight (dead load) and to a distribution of horizontal forces proportional to the self-weight (live load). It is also assumed that the arch is clamped at its springing sections.

The reference curve of the arch is defined as its mid-curve. For investigating how the selection of potential failure sections affects the problem solution, the following choices are considered (Figure 3(b)):

- the solution labeled as "normal" refers to an arch with prescribed normal stereotomy, i.e. with potential failure sections that are normal to the mid-curve of the arch;
- the solution labeled as "multiple, $\eta = 1:n$" refers to an arch made of units with height-to-width ratio η, arranged along the normal direction. Two different case studies are here considered, respectively with $n = 2$ and $n = 4$.

For a discretization, equally spaced control points, at a distance $R\beta/500$ from each other, are first considered along the reference curve of the arch. For the solution with normal stereotomy, normal control sections are selected passing through the control points. For the solution with multiple potential failure sections, a discrete set of orientation angles, geometrically compatible with the texture of the masonry, is preferred to generate potential failure sections. Accordingly, in addition to control sections parallel to the normal direction, also control sections with inclination angles $\vartheta_k = \pm\arctan\left(1/\left(n/2 + kn\right)\right)$, $k = \{0,1\}$, with respect to the normal direction, are considered [41] (Figure 3(b)).

As a preliminary step, a minimum thrust analysis has been conducted to compute the minimum thickness-to-radius ratio $h_{\min}/R$ of the pointed arch for the two values of the eccentricity-to-radius ratio $e/R = \{0.4, 0.6\}$ at varying of the embrace angle β. Relevant results are respectively reported in Tables 1 and 2. Values corresponding to solutions with normal stereotomy are in agreement with the ones reported in [42]. It is noticed that slightly larger values of the minimum thickness-to-radius ratio $h_{\min}/R$ are required when multiple potential failure sections are taken into account.

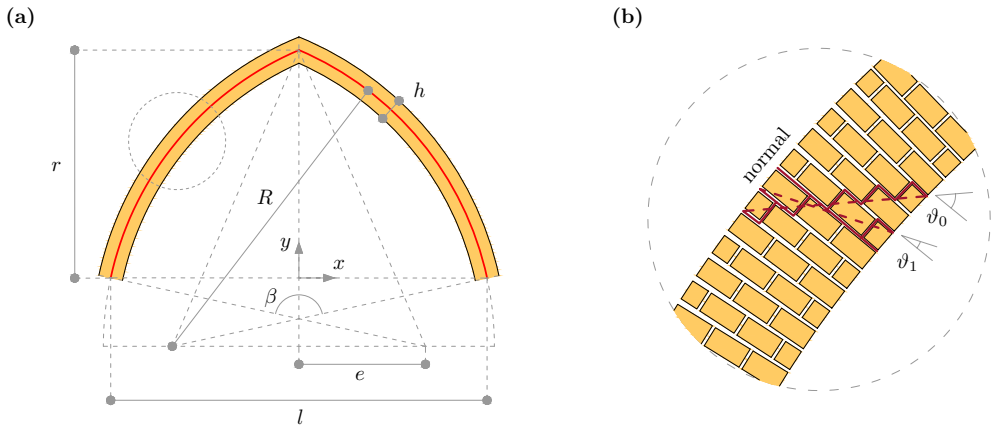


Figure 3: Pointed arch: (a) geometry, with highlighted reference curve, and (b) schematic illustration of the relationship between masonry texture and preferred (i.e. geometrically compatible) orientations of potential failure sections in the solution labeled as "multiple" (units with height-to-width ratio $\eta = 1:2$ are considered).

Table 1: Pointed arch: minimum thickness-to-radius ratio $h_{\min}/R$ for pointed arches with eccentricity-to-radius radio $e/R = 0.4$ and embrace angle β, assuming normal stereotomy or multiple potential failure sections.

Embrace angle β [°]	Normalized minimum thickness $h_{\min}/R$		
	Normal	Multiple	
		$\eta = 1:4$	$\eta = 1:2$
180	0.0468	0.0474	0.0479
160	0.0371	0.0376	0.0384
140	0.0371	0.0376	0.0384
120	0.0364	0.0369	0.0377
100	0.0316	0.0320	0.0326
80	0.0226	0.0228	0.0232
60	0.0099	0.0095	0.0099

Table 2: Pointed arch: minimum thickness-to-radius ratio $h_{\min}/R$ for pointed arches with eccentricity-to-radius radio $e/R = 0.6$ and embrace angle β, assuming normal stereotomy or multiple potential failure sections.

Embrace angle β [°]	Normalized minimum thickness $h_{\min}/R$		
	Normal	Multiple	
		$\eta = 1:4$	$\eta = 1:2$
180	0.0391	0.0401	0.0417
160	0.0390	0.0401	0.0417
140	0.0388	0.0398	0.0414
120	0.0337	0.0346	0.0360
100	0.0226	0.0231	0.0240
80	0.0054	0.0054	0.0051

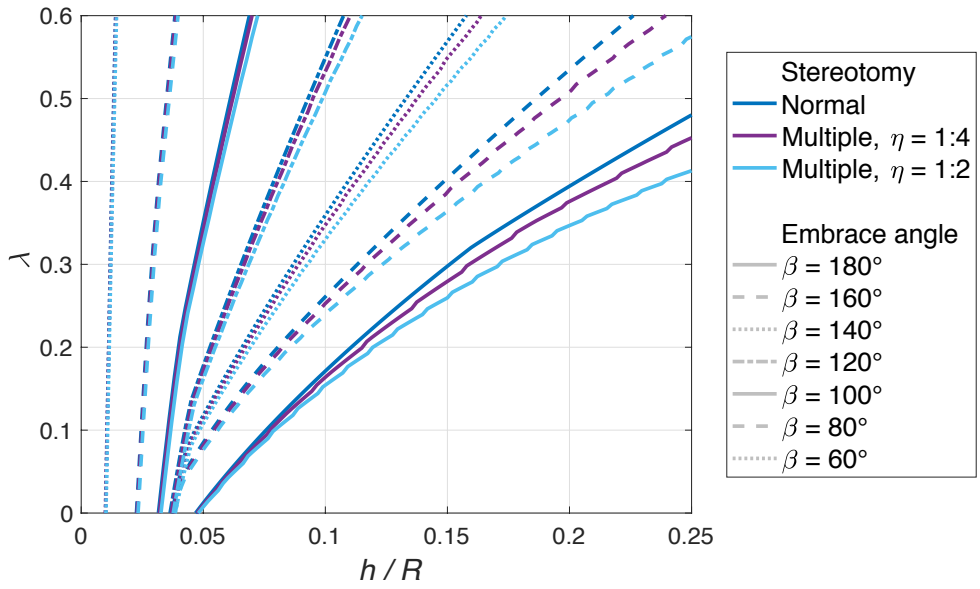


Figure 4: Pointed arch: horizontal forces collapse multiplier λ versus thickness-to-radius radio h/R for pointed arches with eccentricity-to-radius ratio $e/R=0.4$ and embrace angle β, assuming normal stereotomy or multiple potential failure sections.

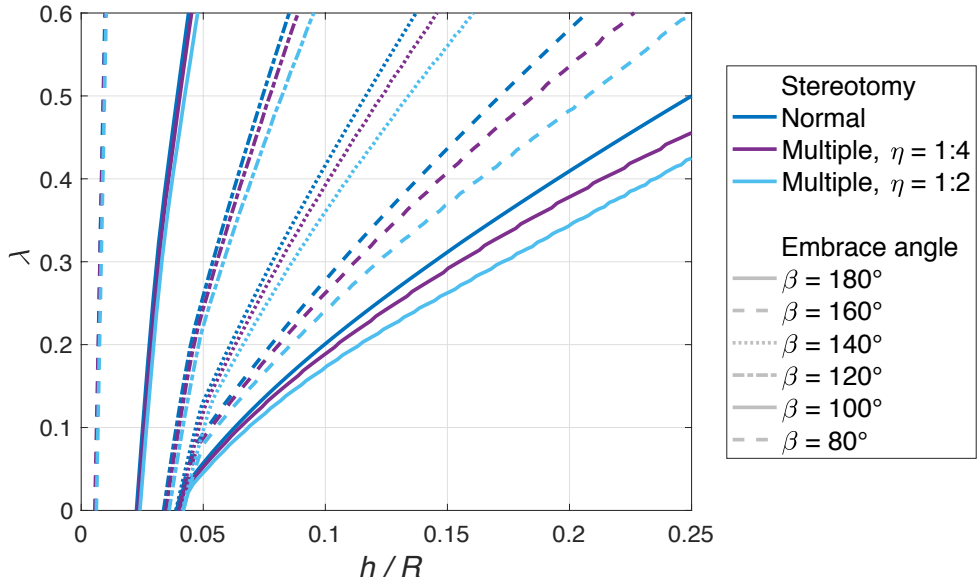


Figure 5: Pointed arch: horizontal forces collapse multiplier λ versus thickness-to-radius radio h/R for pointed arches with eccentricity-to-radius ratio $e/R=0.6$ and embrace angle β, assuming normal stereotomy or multiple potential failure sections.

A parametric analysis on the collapse multiplier λ of the horizontal forces, as a function of the thickness-to-radius ratio h/R, has been carried out for the values of the eccentricity-to-radius ratio $e/R=\{0.4, 0.6\}$, at varying of the embrace angle β. The results are shown in Figures 4 and 5.

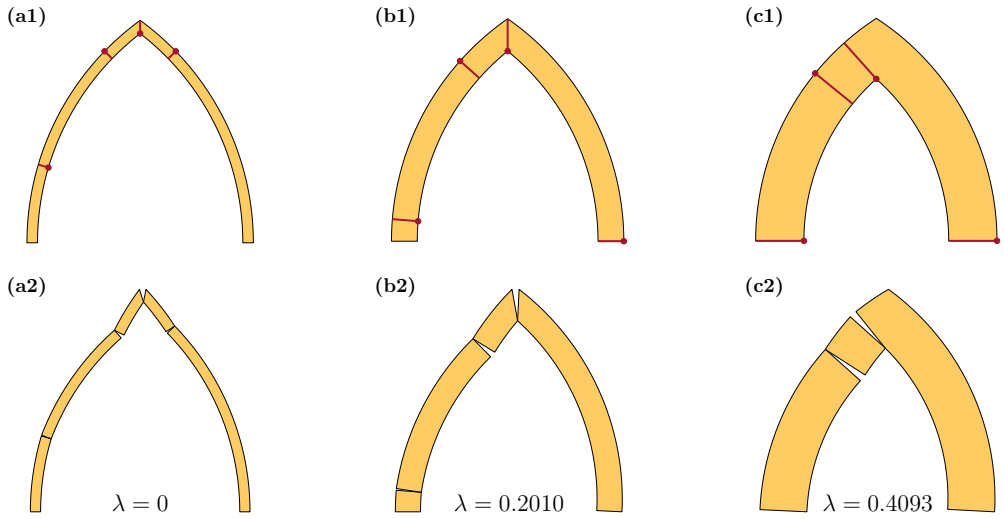


Figure 6: Pointed arch: (a) actual failure sections (first row) and collapse mechanism (second row) under horizontal forces proportional to self-weight, assuming normal stereotomy. Eccentricity-to-radius ratio $e/R = 0.6$, embrace angle $\beta = 180^\circ$, and thickness-to-radius radio (a) $h/R = h_{\min}/R = 0.0391$, (b) $h/R = 0.10$ and (c) $h/R = 0.20$ are considered.

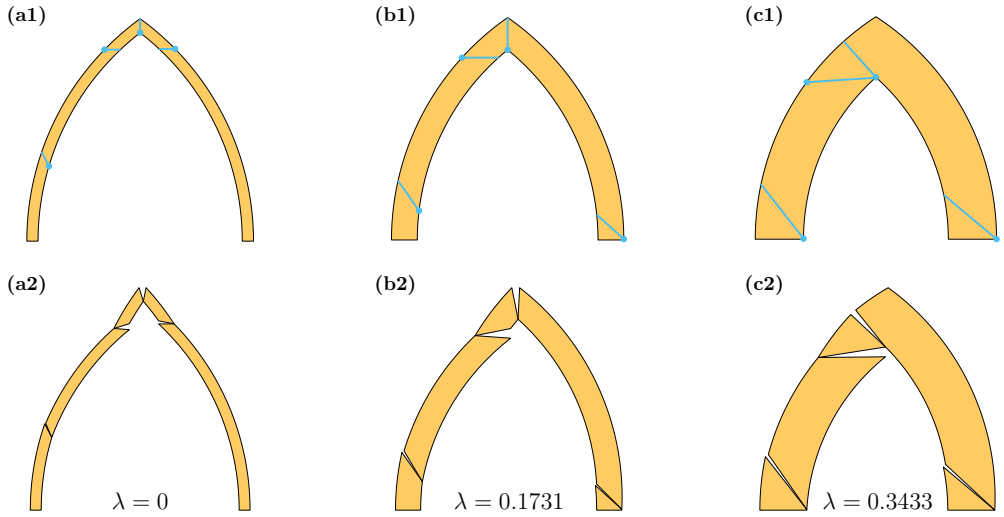


Figure 7: Pointed arch: (a) actual failure sections (first row) and collapse mechanism (second row) under horizontal forces proportional to self-weight, assuming multiple potential failure sections (units with height-to-width ratio $\eta = 1:2$). Eccentricity-to-radius ratio $e/R = 0.6$, embrace angle $\beta = 180^\circ$, and thickness-to-radius radio (a) $h/R = h_{\min}/R = 0.0417$, (b) $h/R = 0.10$ and (c) $h/R = 0.20$ are considered.

As already noted in [42] in regards to the solution with normal stereotomy, for given values of e/R and β, a two-branches curve describes the collapse multiplier λ as a function of the thickness-to-radius ratio h/R. In particular, the first branch, corresponding to small thickness-to-radius ratios h/R, is associated to a four-hinge collapse mechanism in which no right-springing hinge is involved, Figure 6(a). Conversely, a right-springing hinge characterizes the second branch of the curve, corresponding to moderately large or large

thickness-to-radius ratios h/R. In that case, for increasing thickness-to-radius ratios h/R, the most-left hinge smoothly migrates towards the left springing of the arch, with the collapse mechanism shifting from one as in Figure 6(b) to one as in Figure 6(c). Indeed, for small embrace angles β, the second branch of the curve is not developed at all.

Concerning the solution with multiple failure sections, the curves of λ versus h/R have the same general trend as the ones pertaining to the solution labeled as "normal". In fact, collapse mechanisms that are qualitatively similar take place, i.e. four-hinge collapse mechanisms with right-hinge springing or not depending on h/R, as depicted in Figure 7. However, the fact that the actual failure sections may have different orientations with respect to the normal direction implies that the solution with multiple potential failure sections is associated to a reduced loading capacity of the arch with respect to the solution with normal stereotomy. The reduction of the loading capacity of the arch predicted in the case of multiple potential failure sections results to be more pronounced for larger values of the height-to-width ratio η of the units (i.e., for less elongated units), and may be in the order of 15%. As an increase in η is related to an increase in the maximum inclination angle of the potential failure sections with respect to the normal direction, that suggests the maximum inclination angle of the potential failure sections to be a decisive parameter in the determination of the loading capacity of the arch.

In closing, it is remarked that the selection of potential failure sections in the arch has a significant influence in the prediction of its collapse states. Except for arches that are made of individual voussoirs, which can be treated by resorting to the classical notion of element with prescribed stereotomy, a crucial step for a safe assessment of the loading capacity of the arch is to take into consideration at least the preferred potential failure sections (i.e., those that are geometrically compatible with the masonry material under investigation). As a consequence, collapse states that are usually unaccounted for come into light, and more conservative requirements need to be fulfilled by the arch.

4 CONCLUSIONS

A computational method has been proposed for addressing the lower-bound limit analysis of masonry arches with multiple potential failure sections. That model is conceived to generalize the classical notion of masonry arch with prescribed stereotomy, which results insufficient in applications where the orientation of the failure sections, in addition to their position, is not a priori known. In fact considering multiple potential failure sections amounts at taking into account a broader class of potential collapse mechanisms induced by the opening of linear cracks with multiple potential positions and orientations. Provided a finite number of control sections is considered in the arch, the lower-bound limit analysis problem has been formulated as a straightforward linear programming problem. Numerical simulations, also dealing with benchmark problems, have been presented for highlighting the predicting capabilities of the proposed methodology.

REFERENCES

[1] Gambarotta, L. and Lagomarsino, S. Damage models for the seismic response of brick masonry shear walls. Part I: the mortar joint model and its applications. *Earthq. Eng.*

Struct. Dyn. (1997) **26**(4):423-439.
[2] Oliveira, D.V. and Lourenço, P.B. Implementation and validation of a constitutive model for the cyclic behaviour of interface elements. *Comput. Struct.* (2004) **82**(17-19):1451-1461.
[3] Milani, G. Simple homogenization model for the non-linear analysis of in-plane loaded masonry walls. *Comput. Struct.* (2011) **89**(17-18):1586-1601.
[4] Addessi, D. and Sacco, E. A multi-scale enriched model for the analysis of masonry panels. *Int. J. Solids Struct.* (2012) **49**(6):865-880.
[5] Petracca, M., Pelà, L., Rossi, R., Oller, S., Camata, G. and Spacone, E. Regularization of first order computational homogenization for multiscale analysis of masonry structures. *Comput. Mech.* (2016) **57**(2):257-276.
[6] Braides, A. and Nodargi, N.A. Homogenization of cohesive fracture in masonry structures. *Math. Mech. Solids* (2020) **25**(2):181-200.
[7] Pelà, L., Cervera, M. and Roca, P. Continuum damage model for orthotropic materials: Application to masonry. *Comput. Meth. Appl. Mech. Eng.* (2011) **200**(912):917-930.
[8] Pelà, L., Cervera, M. and Roca, P. An orthotropic damage model for the analysis of masonry structures. *Constr. Build. Mater.* (2013) **41**:957-967.
[9] Nodargi, N.A., Artioli, E., Caselli, F. and Bisegna, P. State update algorithm for associative elastic-plastic pressure-insensitive materials by incremental energy minimization. *Fracture and Structural Integrity* (2014) **29**:111-127.
[10] Nodargi, N.A. and Bisegna, P. State update algorithm for isotropic elastoplasticity by incremental energy minimization. *Int. J. Numer. Methods Eng.* (2015) **105**(3):163-196.
[11] Gatta, C., Addessi, D. and Vestroni, F. Static and dynamic nonlinear response of masonry walls. *Int. J. Solids Struct.* (2018) **155**:291-303.
[12] Brasile, S., Casciaro, R. and Formica, G. Finite element formulation for nonlinear analysis of masonry walls. *Comput. Struct.* (2010) **88**(3-4):135-143.
[13] Cervera, M., Chiumenti, M. and Codina, R. Mixed stabilized finite element methods in nonlinear solid mechanics. Part II: Strain localization. *Comput. Meth. Appl. Mech. Eng.* (2010) **199**(37-40):2571-2589.
[14] Nodargi, N.A., Caselli, F., Artioli, E. and Bisegna, P. A mixed tetrahedral element with nodal rotations for large-displacement analysis of inelastic structures. *Int. J. Numer. Methods Eng.* (2016) **108**(7):722-749.
[15] Nodargi, N.A. and Bisegna, P. A novel high-performance mixed membrane finite element for the analysis of inelastic structures. *Comput. Struct.* (2017) **182**:337-353.
[16] Nodargi, N.A. An overview of mixed finite elements for the analysis of inelastic bidimensional structures. *Arch. Comput. Method Eng.* (2019) **26**(4):1117-1151.
[17] Nodargi, N.A. and Bisegna, P. A mixed finite element for the nonlinear analysis of in-plane loaded masonry walls. *Int. J. Numer. Methods Eng.* (2019) **120**(11):1227-1248.
[18] Nodargi, N.A. and Bisegna P. A mixed membrane finite element for masonry structures. In: Carcaterra A. et al. (Eds.): *Proceedings of XXIV AIMETA Conference 2019. AIMETA 2019*, Lecture Notes in Mechanical Engineering. Springer (2020), pp. 1167-1178.
[19] Heyman, J. The stone skeleton. *Int. J. Solids Struct.* (1966) **2**(2):249-279.
[20] Como, M. *Statics of historic masonry constructions*. Springer-Verlag (2016).
[21] Roca, P., Cervera, M., Gariup, G. and Pelà, L. Structural analysis of masonry historical constructions. Classical and advanced approaches, *Arch. Comput. Method Eng.* (2010)

17(3):299-325.
[22] Tralli, A., Alessandri, C. and Milani, G. Computational methods for masonry vaults: a review of recent results, *Open Civ. Eng. J.* (2014) **8**:272–282.
[23] Livesley, R.K. Limit analysis of structures formed from rigid blocks. *Int. J. Numer. Methods Eng.* (1978) **12**(12):1853-1871.
[24] Portioli, F., Casapulla, C. and Cascini, L. An efficient solution procedure for crushing failure in 3D limit analysis of masonry block structures with non-associative frictional joints. *Int. J. Solids Struct.* (2015) **69-70**: 252-266.
[25] Intrigila, C., Nodargi, N.A. and Bisegna P. Frictional behaviour of masonry interfaces: experimental investigation on two dry-jointed tuff blocks. In: Carcaterra A. et al. (Eds.): *Proceedings of XXIV AIMETA Conference 2019. AIMETA 2019*, Lecture Notes in Mechanical Engineering. Springer (2020), pp. 2032-2047.
[26] Baggio, C. and Trovalusci, P. Limit analysis for no-tension and frictional three-dimensional discrete systems. *Mech. Based Des. Struct. Mach.* (1998) **26**(3):287-304.
[27] Ferris, M.C. and Tin-Loi, F. Limit analysis of frictional block assemblies as a mathematical program with complementarity constraints. *Int. J. Mech. Sci.* (2001) **43**(1):209-224.
[28] Gilbert, M., Casapulla, C. and Ahmed, H.M. Limit analysis of masonry block structures with non-associative frictional joints using linear programming. *Comput. Struct.* (2006) **84**(13-14):873-887.
[29] Nodargi, N.A., Intrigila, C. and Bisegna, P. A variational-based fixed-point algorithm for the limit analysis of dry-masonry block structures with non-associative Coulomb friction. *Int. J. Mech. Sci.* (2019) **161-162**:105078.
[30] Portioli, F. and Cascini, L. Large displacement analysis of dry-jointed masonry structures subjected to settlements using rigid block modelling. *Eng. Struct.* (2017) **148**:485-496.
[31] Intrigila, C., Nodargi, N.A. and Bisegna P. Square cross vaults on spreading supports. In: R. Aguilar et al. (Eds.): *Structural Analysis of Historical Constructions*, RILEM Bookseries 18 (2019), pp. 1045-1053.
[32] Block, P., Ciblac, T. and Ochsendorf, J. Real-time limit analysis of vaulted masonry buildings. *Comput. Struct.* (2006) **84**(29-30):1841-1852.
[33] O'Dwyer, D.W. Funicular analysis of masonry vaults. *Comput. Struct.* (1999) **73**(1-5):187-197.
[34] Marmo, F. and Rosati, L. Reformulation and extension of the thrust network analysis. *Comput. Struct.* (2017) **182**:104-118.
[35] Nodargi, N.A. and Bisegna, P. Thrust line analysis revisited and applied to optimization of masonry arches. *Int. J. Mech. Sci.* (2020) **179**:105690.
[36] Ricci, E., Fraddosio, A., Piccioni, M.D. and Sacco, E. A new numerical approach for determining optimal thrust curves of masonry arches. *Eur. J. Mech. A-Solids* (2019) **75**: 426-442.
[37] Milankovitch, M. Theorie der druckkurven. *Zeitschrift für Mathematik und Physik* (1907) **55**:1-27.
[38] Foce, F. Milankovitch's theorie der Druckkurven: Good mechanics for masonry architecture. *Nexus Netw. J.* (2007) **9**(2):185-210.
[39] Alexakis, H. and Makris, N. Minimum thickness of elliptical masonry arches. *Acta Mech.* (2013) **224**(12): 2977-2991.

[40] Alexakis, H. and Makris, N. Limit equilibrium analysis of masonry arches. Arch. Appl. Mech. **85**(9-10): 1363-1381.
[41] Nodargi, N.A. and Bisegna, P. A unifying computational approach for the lower-bound analysis of systems of masonry arches and buttresses. *Submitted* (2020).
[42] Cavalagli, N., Gusella, V. and Severini, L. Lateral loads carrying capacity and minimum thickness of circular and pointed masonry arches. *Int. J. Mech. Sci.* (2016) **115-116**:645-656.

12th International Conference on Structural Analysis of Historical Constructions
SAHC 2020
P. Roca, L. Pelà and C. Molins (Eds.)

MINIMUM THICKNESS AND COLLAPSE CONDITIONS OF THE IRREGULAR MASONRY ARCH SUBJECT TO ITS OWN WEIGTH

N. CAVALAGLI*, V. GUSELLA AND R. LIBEROTTI

Department of Civil and Environmental Engineering
Univrsity of Perugia
Via G. Duranti 93, 06125, Perugia, Italy
e-mail: {nicola.cavalagli,vittorio.gusella,riccardo.liberotti}@unipg.it (*corresponding author)

Keywords: Masonry arch, Irregular geometry, Uncertainties, Minimum thickness

Abstract. *The present paper aims at assessing the shape irregularities influence on the collapse conditions of masonry arches subjected to vertical point force. Surveys campaigns on cultural Heritage buildings often reveal masonry elements with irregular shapes. In order to accurately predict their actual behavior the presence of such features cannot be neglected. The reasons for these non-canonical shapes are manifold e.g. the evolution of degradation processes and the constructive laws. As a first analysis attempt, the geometrical uncertainties tied to the building work criteria are taken into account. A random parametric model is proposed to generate two-dimensional geometry of irregular polycentric arches. Monte Carlo simulations allows estimating the probabilistic density function of the collapse load multiplier evaluated by means of the implemented limit analysis method. The outcomes referred to the masonry arch with nominal geometry are compared to those obtained for the random polycentric arch, highlighting the extent of the load-bearing capacity reduction due to presence of such shape irregularities.*

1 INTRODUCTION

It is well known that the level of knowledge and the in-depth investigations of ancient masonry buildings are the mandatory conditions on which reliable structural safety assessments must be based. Those evaluations derive from an articulated and rather complex process including, in general, historical investigations gathered by direct surveys of the building, also by means of experimental-test campaigns [[1], [2], [3], [4]]. In order to produce vulnerability evaluations on the safe side, the challenge to represent a correct interpretation of the seismic behaviour of historical constructions and in particular masonry bridges (e.g. see Figure 1), in their current state, becomes an essential prerequisite especially in presence of peculiarities, as material degradation and structural damages. In these sense, masonry arches and vaults play a significant role due to their extensive use not only in historical bridges, but also in civil and monumental structures in general. For this reasons, the research activities were continuously devoted to increase the knowledge of their structural behaviour until today [[5], [6], [7], [8], [9], [10], [11], [12], [13]].



Figure 1: Ponte della Mola. Roman aqueduct, sited near Rome, between Tivoli and Palestrina, built from 272 and 262 B.C.

Possible interventions of structural strengthening derive from the knowledge of the constructive specificities and uniqueness of the structure [[14], [15], [16]]. The conceiving of such design actions, that as we know are never predictable or predefined regarding the masonry arched structures the plurality of monuments and infrastructures in terms of construction techniques, size and state of preservation highlights the need to deal with an extraordinarily diversified reality for which it is required to pay the utmost attention not only to the architectural appearance but also to the shape of the basic construction elements e.g. the correspondence between stone blocks and identification of non-original parts [[17], [18]]. Likewise, the phenomena of material degradation, biological patinas, detachment of walls, surface weathering, leaks and erosion must be ascribed as sources of geometrical uncertainties and need to be documented by introducing correlations between causes and effects. In this perspective, in addition, the scientific literature proved to be lacking except from specific papers where the masonry arches have been characterized according to their geometric features [[19], [20]], or where the damage pattern have been analyzed with deterministic or parametric variables [[21], [22]].

In previous contributions proposed by the Authors, the influence of geometrical uncertainties on the structural behaviour of masonry elements has been studied engaging the arches with horizontal actions through static and dynamic approaches [[23], [24], [25]]. Contextually the uncertainties at the voussoirs scale have been introduced, taking into account the randomness of the parameters describing the masonry texture. Those first results proved that for a certain level of irregularities the drop of strength cannot be neglected, as just asserted by several authors in the interpretation of experimental tests. Differently in this paper, the item of the shape

irregularities is treated at a macro scale, defining them as the geometrical variance from the nominal arch, and ascribed to the aprioristic inaccuracies connected to the ancient constructive criteria [26]. This choice founds argumentative roots in the observation of rather articulated historical buildings often composed by masonry clusters combining different floor heights, where some load bearing walls or vaults rest on the underlying arches.

2 DEFINITION OF A MASONRY ARCH WITH IRREGULAR SHAPE

Over architectural and infrastructural heritage of Europe and more, the masonry arch represents the most used constructive system. Its building work requires the installation of temporary scaffoldings and frameworks in order to prop up the structure until it turns into a self-supporting system. The design of such wooden frames, known as centrings, envisages the union of a series of different arc sectors with a view to outline the intrados corresponding with the designed arch. Is thought that this criterion may lead to constructive imprecisions and, for this, within the present contribution this topic is highlighted as a possible source of irregularities in the final shape of the arches. In addition it should be noted that, when composed by several parts for the construction of large structures, the centrings were always built up in situ, resulting in unavoidable geometrical distortions from the nominal geometry, provided by wooden imperfections and manpower activities. The structural influence of such aspect has been addressed within previous contributions [[27], [28]]. The number of the arc sectors which constitute a centring are related to the vernacular building work traditions, the historical period and, above all, of the geometry and dimension supposed for the masonry arch.

In this study, an arch composed by five arc sectors is analyzed, resulting a recurring set up for moderately sized structures. In order to consider the geometrical irregularities affecting the final shape of the arch, a generative model is proposed to obtain geometrical samples of arc sectors affected by uncertainties through a probabilistic approach. The final assembly is therefore composed by the union of five arc sectors as shown in Figure 2(a), assuring the continuity of the tangent function along the development of the arch. The result is a procedure allowing to generate asymmetric polycentric arches derived by predefined random variables of specific geometrical parameters $\tilde{\alpha}_S$ and $\tilde{r}_S$, identifying the angle of embrace and the radius of each arc sector. The obtained line of axis of the polycentric arch is finally scaled in order to have a span l equal to the nominal span value (Figure 2(b)).

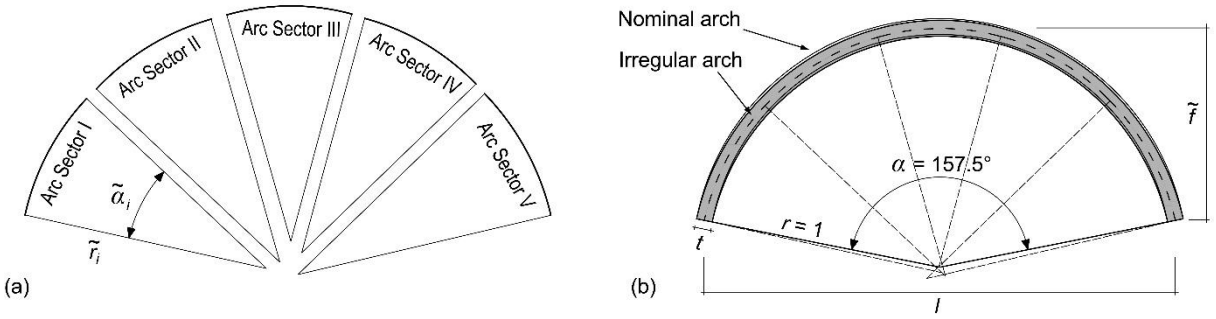


Figure 2: (a) Graphical construction of the arch irregular shape constituted by five random arc sectors. (b) Superimposition between the nominal and irregular arch.

The nominal deterministic geometry analyzed in this work refers to a circular arch defined by the following parameters

$$\begin{cases} \alpha = 157.5° \\ r = 1 \end{cases} \tag{1}$$

being α the angle of embrace and r the radius of the arch; the thickness t is considered constant along all the development of the arch. Given the nominal geometry, the random variables $\tilde{\alpha}_S$ and $\tilde{r}_S$ are defined by the following relations

$$\begin{aligned} \tilde{\alpha}_S &= E[\tilde{\alpha}_S] + \varepsilon\alpha / N_S \cdot \tilde{p}_{\alpha_S} = \alpha / N_S + \varepsilon\alpha / N_S \cdot \tilde{p}_{\alpha_S} \\ \tilde{r}_S &= E[\tilde{r}_S] + \chi r \cdot \tilde{p}_{r_S} = r + \chi r \cdot \tilde{p}_{r_S} \end{aligned} \tag{2}$$

where N_S represents the number of arc sectors (in this case $N_S = 5$ will be considered), ε and χ are defined as geometrical uncertainty coefficients which independently scale the uniform probability density functions $\tilde{p}_{\alpha_S}$ and $\tilde{p}_{r_S}$ respectively (Figure 3). Finally, no variability is considered for the thickness t.

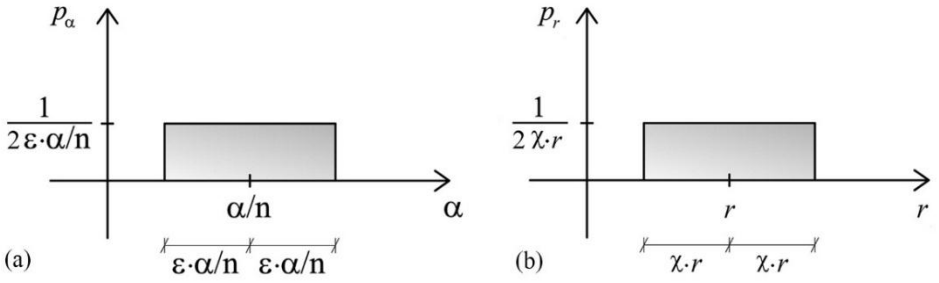


Figure 3: Uniform probability density functions used for the description of the angle of embrace (a) and radius (b) random parameters.

3 MINIMUM THICKNESS OF THE IRREGULAR MASONRY ARCH

3.1 Collapse condition

In the analysis of the minimum thickness of a masonry arch, the collapse condition, generally expressed in terms of collapse load and related mechanism, is strongly dependent on the structural shape and the distribution of the loads applied. It is well known that under its own weight, the collapse condition of a masonry arch is characterized by a symmetric five-hinges mechanism, with two extrados hinges at the imposts, one extrados hinge at the crown and two intrados hinges placed between the imposts and the crown, which position is function of the angle of embrace [29].

On the other hand, an irregular shape significantly affects the position of the hinges, which

lead to the collapse. The introduction of irregularities causes the loss of symmetry both in geometry and in the distribution of the vertical loads. This condition determines an asymmetric collapse mechanism of four-hinges type, characterized by the occurrence of only one hinge at the imposts, alternatively at left or right on the basis of the thrust line shape.

3.2 Work hypothesis and iterative procedure

In this paper, the analysis of the minimum thickness of an arch with irregular shape is carried out through a limit analysis based procedure, aimed at evaluating the collapse load multiplier applied to an auxiliary loads distribution, which leads the structure to the collapse through a four-hinges mechanism. By progressively reducing the thickness of the arch, the collapse load multiplier goes to zero and the contribution of the auxiliary loads vanishes. The thickness associated to a null value of the load multiplier is taken as the minimum thickness of the masonry arch. In this study a distribution of inertial loads was considered as auxiliary load.

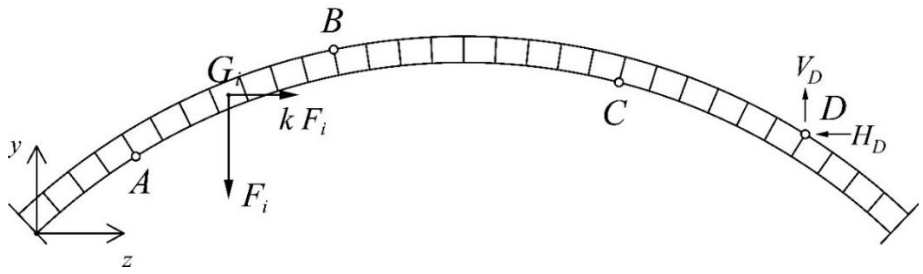


Figure 4: Reference structural model used for the definition of the limit equilibrium procedure.

Let us consider a masonry arch consisting of n voussoirs, on which is acting the self-weight F_i and the horizontal load $F_{S_i} = kF_i$ proportional to the weight by means of the load multiplier k. In the numerical procedure, the horizontal load is assumed directed from left to right, leading the structure to the collapse with a four-hinges mechanism as indicated in Figure 4. The collapse condition, identified by the horizontal load multiplier k and the corresponding hinges position associated to an admissible kinematic mechanism, is evaluated through an iterative procedure. A first attempt position for the collapse hinges A, B, C, D is assigned, i.e. a collapse mechanism is assumed. Then, the equilibrium of moments around the three hinges A, B and C is imposed

$$\begin{cases} H_D(y_A - y_D) + V_D(z_A - z_D) - \sum_{i=1}^{n_{AD}} F_i(z_A - z_{G_i}) - k \cdot \sum_{i=1}^{n_{AD}} F_i(y_A - y_{G_i}) = 0 \\ H_D(y_B - y_D) + V_D(z_B - z_D) - \sum_{i=1}^{n_{BD}} F_i(z_B - z_{G_i}) - k \cdot \sum_{i=1}^{n_{BD}} F_i(y_B - y_{G_i}) = 0 \\ H_D(y_C - y_D) + V_D(z_C - z_D) - \sum_{i=1}^{n_{CD}} F_i(z_C - z_{G_i}) - k \cdot \sum_{i=1}^{n_{CD}} F_i(y_C - y_{G_i}) = 0 \end{cases} \quad (3)$$

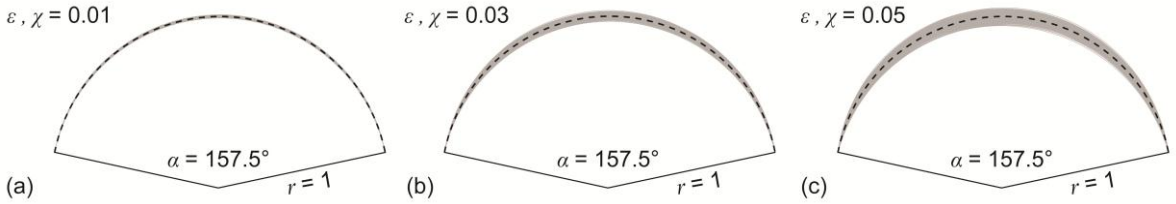


Figure 5: Population of the irregular arches (grey continuous line), generated through uncertainty parameters equal to 0.01 (a), 0.03 (b) and 0.05 (c), compared with the nominal arch (black dashed line).

where n_{AD} n_{BD}, n_{CD}, refer respectively to the number of voussoirs between the hinges *A*, *B*, *C* and *D*. The system of Equations (e) is solved on the three unknowns H_D, V_D and *k*. Finally, the thrust line is determined through the calculation of the joint-by-joint eccentricity e_j of the normal force and assuring the satisfaction of the yielding criterion

$$-\frac{t_j}{2} \le e_j \le +\frac{t_j}{2} \tag{3}$$

If the thrust line is not contained everywhere inside the boundaries of the arch geometry, Equation (3) is not somewhere verified. In this case a new trial configuration of hinges has to be considered and the equilibrium imposed again. The interested reader can see [23] for more details.

As already discussed in the previous Section, the irregular shape of the structure requires to define in advance the weakest mechanism, i.e. if the hinge at the impost occurs at the left or right side. In the application of the proposed procedure, the auxiliary load was previously applied independently from left to right and right to left, achieving two different collapse load multipliers, k_l and k_r respectively. The lower value between them is associated to the weakest mechanism to which corresponds, after the progressive reduction of the thickness, a higher value of the minimum thickness. This value has to be considered the unique admissible as minimum thickness of the irregular arch, due to the occurrence of the collapse.

3.3 Analysis of the results

In this section, the results regarding the estimation of a probabilistic measure of the minimum thickness and the related collapse mechanism of masonry arches affected by three different levels of geometrical irregularities are shown. The analysis was carried out considering a nominal geometry defined by the properties indicated in Equations (1). A population of 1000 samples of random arches was generated according to the roles introduced in Section 2, for each value of the uncertainty coefficients ε and χ. In particular, uncertainty parameters equal to 0.01, 0.03 and 0.05 were considered.

In Figure 5 the line of axis of the generated irregular arches (grey continuous lines) is superimposed to the line of axis of the nominal arch (black dashed line), in order to give an idea of how the uncertainty parameters can affect the structural geometry. A distance measure between the nominal and the generic irregular arch is proposed by introducing the random parameter $\tilde{\rho}(\xi)$ as follows

$$\tilde{\rho}(\xi) = \frac{\tilde{r}_n(\xi) - r}{r} \tag{4}$$

where ξ is the curvilinear abscissa of the of the nominal arch normalized with respect to its total length, $\tilde{r}_n(\xi)$ is the radial distance between the irregular arch and the center of the nominal arch and r is the nominal radius. Figure 6 illustrates the plots of the obtained $\tilde{\rho}(\xi)$ functions at different levels of the uncertainty parameters.

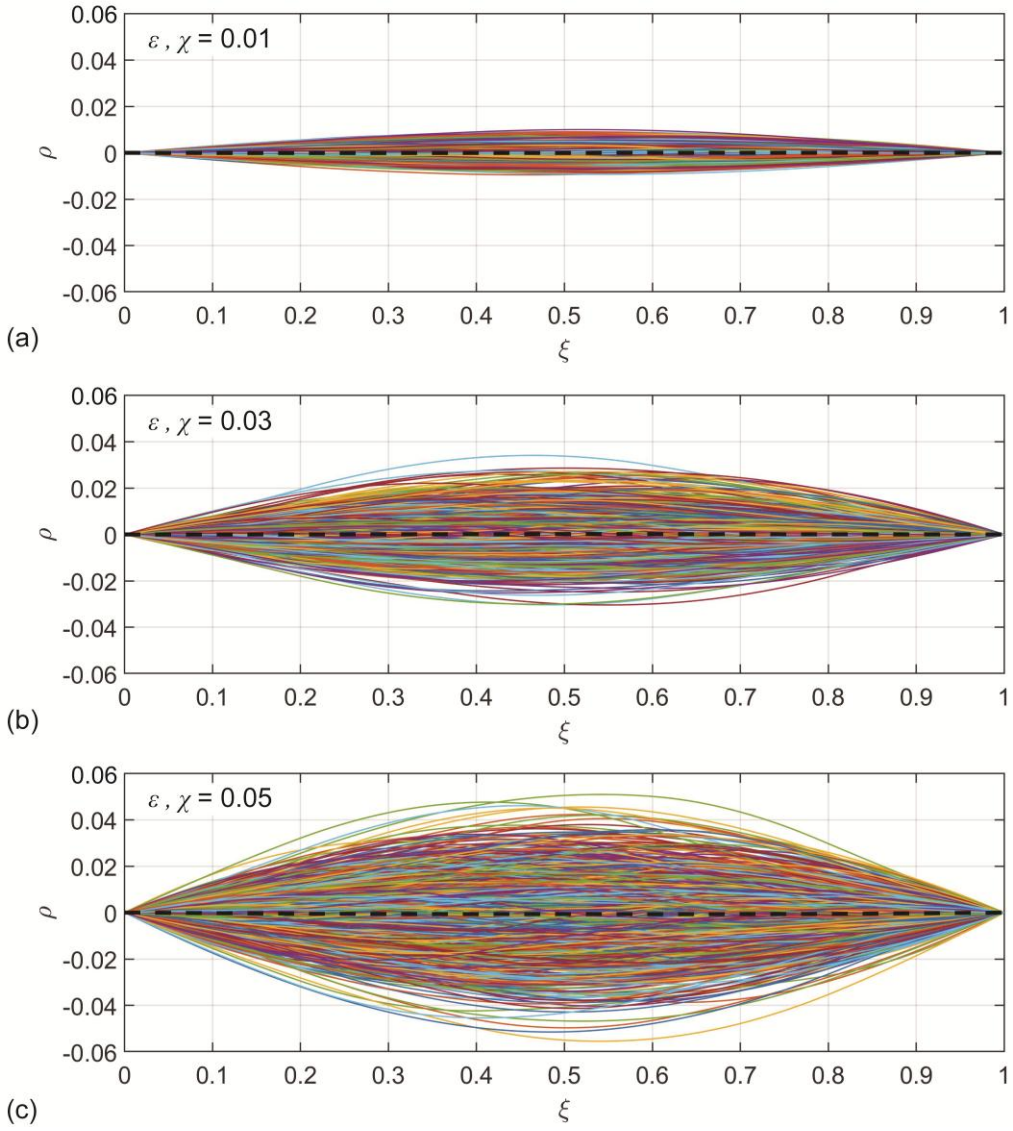


Figure 6: Plots of the radial distances between the irregular and the nominal arches with reference to uncertainty parameters equal to 0.01 (a), 0.03 (b) and 0.05 (c).

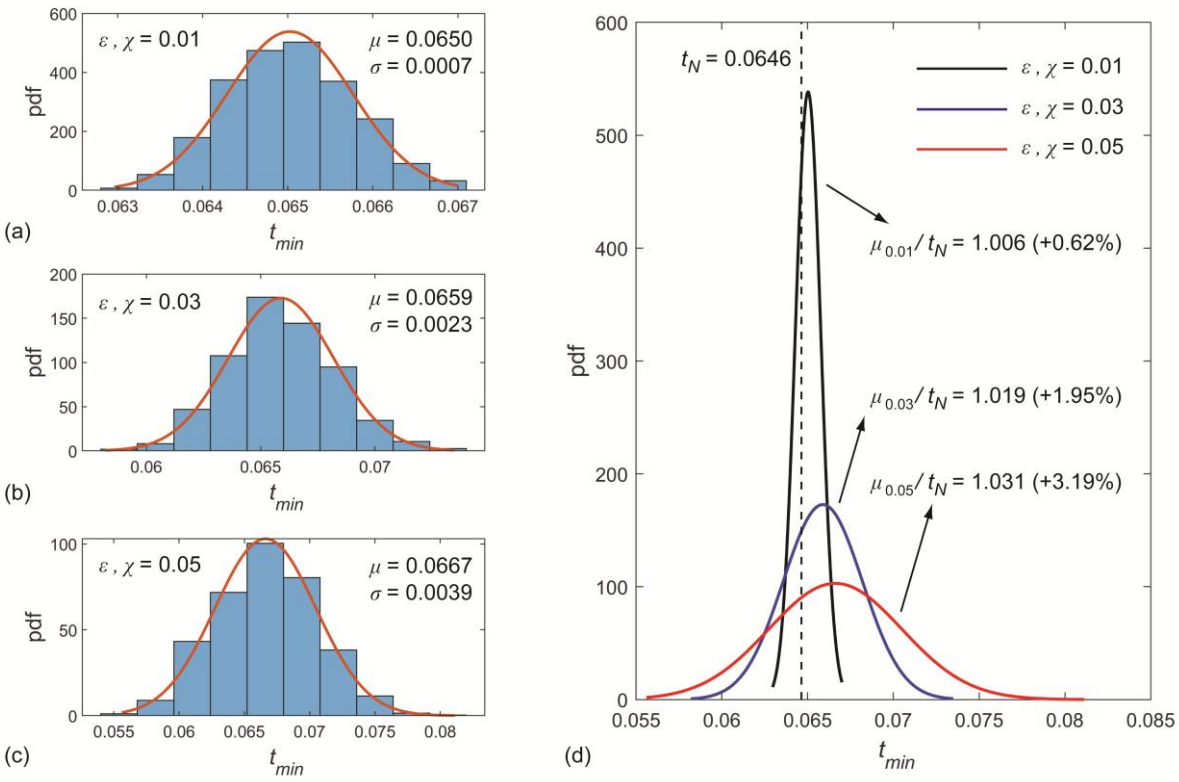


Figure 7: Estimation of the probability density functions of the minimum thickness evaluated on the population of irregular arches characterized by values of uncertainty parameters equal to 0.01 (a), 0.03 (b) and 0.05 (c). (d) Comparison between the probability density functions obtained on the irregular arches and the value of the minimum thickness related to the nominal geometry.

By analyzing the path of the $\tilde{\rho}(\xi)$ functions, it should be noted that in some cases the irregular shape is characterized by values of the radial distance wherever positive or, alternatively, negative, resulting in an arch having a quasi-symmetric shape with a rise higher or lower with reference to the nominal rise. This aspect must be taken into account in the interpretation of the results expressed in terms of the minimum thickness. The presence of quasi-symmetric arches with a rise value lower than the nominal value determines the presence of minimum thicknesses lower than the minimum thickness related to the nominal arch, $t_N = 0.0646$. Figure 7 shows the results obtained in terms of the random values of the minimum thickness $\tilde{t}_{\min}$ at different values of the uncertainty parameters. In particular, an estimation of the probability density function was obtained for ε and χ equal to 0.01, 0.03 and 0.05 (Figure 7(a)-(c)). The mean μ and standard deviation σ values reflect a slight increase of the minimum thickness, up to about 3%, with the increase of the uncertainties and, at the same time, an increase of the values dispersion around the mean value. Figure 7(d) summarizes the comparison between the obtained results highlighting the different probabilistic properties of the irregular arches, with reference to the arch having nominal geometry.

Table 1: Mean (μ) and standard deviation (σ) values of the hinges ($\tilde{\beta}_i$) probabilistic distributions identifying the collapse mechanism.

	$\tilde{\beta}_1$		$\tilde{\beta}_2$		$\tilde{\beta}_3$	
	μ	σ	μ	σ	μ	σ
$\varepsilon, \chi = 0.01$	0.7045	0.0068	1.5705	0.0068	2.4374	0.0068
$\varepsilon, \chi = 0.03$	0.7017	0.0107	1.5709	0.0076	2.4398	0.0106
$\varepsilon, \chi = 0.05$	0.6990	0.0162	1.5706	0.0088	2.4428	0.0163

The irregular shape determines a variability of the results also in the collapse mechanism. As already stated in the previous Section, the symmetric five-hinges kinematic mechanism never occurs due to the asymmetry of the line of axis shape. The mechanism is now characterized by four hinges, among them only one occurs at the impost, either the left or the right with the same probability, i.e. 50%. Regarding the probability distributions of the hinges position along the development of the arch expressed in terms of the angle $\tilde{\beta}_i$, in Table 1 the first statistical moments are reported for the different cases of uncertainty parameters considered. It should be noted that more spread results were obtained for the lateral hinges, $\tilde{\beta}_1$ and $\tilde{\beta}_3$, with respect to the crown hinge $\tilde{\beta}_2$. In particular, with the increase of the uncertainties, the mean values of $\tilde{\beta}_1$ and $\tilde{\beta}_3$ show a slight movement toward the left and right imposts, respectively, and an increase of the standard deviation. The hinge at the crown presents more stable values in terms of both mean and standard deviation. In Figure 8 the histograms of the random variables $\tilde{\beta}_i$ are illustrated for each values of the uncertainty parameters and their range of variability are highlighted with grey fills ($\varepsilon, \chi = 0.01$ dark grey, $\varepsilon, \chi = 0.03$ grey, $\varepsilon, \chi = 0.05$ light grey).

4 CONCLUSIONS

In this paper, the results of an investigation regarding the effect of the geometrical irregularities on the minimum thickness and the collapse mechanism of a masonry arch subject to its own weight have been presented.

For the definition of the irregular shape, a probabilistic generative procedure has been proposed by considering a polycentric arch constituted by five arc sectors described by two random parameters, the angle of embrace and the radius. For each type of random parameters, a unique uniform probability function has been considered. Three levels of uncertainties have been investigated: 1%, 3% and 5% of the nominal value of the considered parameter.

As a reference of nominal geometry, a circular arch of unit radius and angle of embrace of 157.5° has been taken into account. All the samples of random arches generated by the procedure have been scaled in order to have the same span of the arch with nominal geometry. The minimum thickness has been studied as a random variable, obtained through a numerical procedure based on the limit equilibrium analysis.

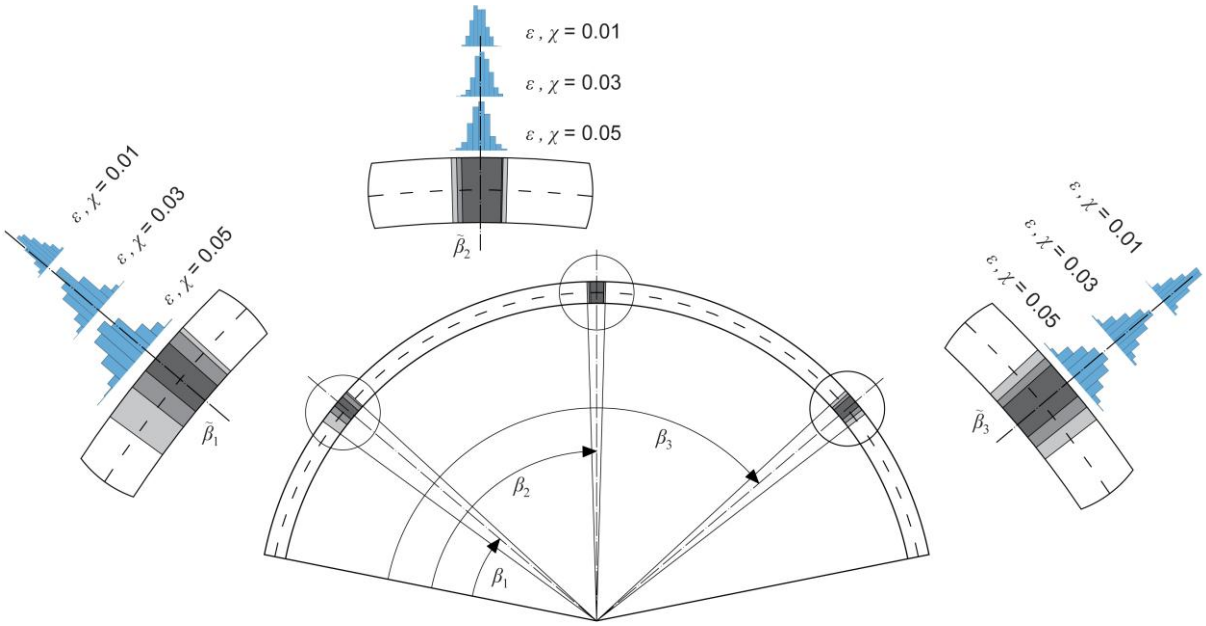


Figure 8: Probabilistic distributions of the hinges $\tilde{\beta}_i$, other than the fourth hinge occurring at one of the impost, identifying the collapse mechanism.

The results have highlighted that, as expected, with the increase of the geometrical irregularities the mean values of the probability density functions estimated by a Monte Carlo approach increase, up to about 3%. The analysis of the collapse mechanisms have induced to highlight that also the hinges position can be considered as random variables, allowing to identify the portion of the arch which have a more high probability to host a collapse hinge.

REFERENCES

[1] Giordano, E., Clementi, F., Nespeca, A. and Lenci, S. Damage assessment by numerical modeling of sant'agostino's sanctuary in offida during the central italy 2016–2017 seismic sequence. *Frontiers in Built Environment* (2019) **4**(7):87.

[2] Cavalagli, N., Kita, A., Castaldo, V.L., Pisello, A.L. and Ubertini, F. Hierarchical environmental risk mapping of material degradation in historic masonry buildings: An integrated approach considering climate change and structural damage. *Construction and Building Materials* (2019) **215**:998-1014.

[3] Grillanda, N., Chiozzi, A., Bondi, F., Tralli, A., Manconi, F., Stochino, F. and Cazzani, A. Numerical insights on the structural assessment of historical masonry stellar vaults: the case of Santa Maria del Monte in Cagliari. *Continuum Mechanics and Thermodynamics* (2019) in press, DOI: 10.1007/s00161-019-00752-8.

[4] Orlando, M., Betti, M. and Spinelli, P. Assessment of structural behaviour and seismic retrofitting for an Italian monumental masonry building. Journal of Building Engineering (2020) **29**:101115.

[5] Cavalagli, N. and Gusella, V. Structural investigation of 18th-century ogival masonry

domes: From Carlo Fontana to Bernardo Vittone. *International Journal of Architectural Heritage* (2015) **9**(3):265-276.
[6] Galassi, S. and Tempesta, G. The Matlab code of the method based on the Full Range Factor for assessing the safety of masonry arches. *MethodsX* (2019) **6**:1521-1542.
[7] Como, M., Di Carlo, F. and Coccia, S. Dynamic response of rocking cracked masonry walls. *Meccanica* (2019) **54**(3):381-398.
[8] Brandonisio, G., Angelillo, M. and De Luca, A. Seismic capacity of buttressed masonry arches. *Engineering Structures* (2020) **215**:110661.
[9] Nodargi, N.A. and Bisegna, P. Thrust line analysis revisited and applied to optimization of masonry arches. *International Journal of Mechanical Sciences* (2020) **179**:105690.
[10] Cocchetti, G. and Rizzi, E. Static Upper/Lower Thrust and Kinematic Work Balance Stationarity for Least-Thickness Circular Masonry Arch Optimization. *Journal of Optimization Theory and Applications* (2020) **187**(3):707-757.
[11] Fraddosio, A., Lepore, N. and Piccioni, M.D. Thrust Surface Method: An innovative approach for the three-dimensional lower bound Limit Analysis of masonry vaults. *Engineering Structures* (2020) **202**:109846.
[12] Grillanda, N., Chiozzi, A., Milani, G. and Tralli, A. Efficient meta-heuristic mesh adaptation strategies for NURBS upper–bound limit analysis of curved three-dimensional masonry structures. *Computers and Structures* (2020) **236**:106271.
[13] Bayraktar, A. and Hökelekli, E. Nonlinear soil deformability effects on the seismic damage mechanisms of brick and stone masonry arch bridges. *International Journal of Damage Mechanics* (2020) in press, DOI: 10.1177/1056789520974423.
[14] Zampieri, P. Horizontal capacity of single-span masonry bridges with intrados FRCM strengthening. *Composite Structures* (2020) **244**:112238.
[15] Rovero, L., Galassi, S. and Misseri, G. Experimental and analytical investigation of bond behavior in glass fiber-reinforced composites based on gypsum and cement matrices. *Composites Part B: Engineering* (2020) **194**:108051.
[16] Bayraktar, A. and Hökelekli, E. Seismic Performances of Different Spandrel Wall Strengthening Techniques in Masonry Arch Bridges. *International Journal of Architectural Heritage* (2020) in press, DOI: 10.1080/15583058.2020.1719234.
[17] Gusella, V. and Liberotti, R. Seismic Vulnerability of Sub-Structures: Vanvitelli's Modulus in Murena Palace. *Buildings* (2020) **10**(9):164.
[18] Lourenço, P.B., Oliveira, D.V., Leite, J.C., Ingham J.M., Modena, C. and da Porto, F. Simplified indexes for the seismic assessment of masonry buildings: International database and validation. *Engineering Failure Analysis* (2013) **34**:508-605.
[19] Tempesta, G. and Galassi S. Safety evaluation of masonry arches. a numerical procedure based on the thrust line closest to the geometrical axis. *International Journal of Mechanical Sciences* (2019) **155**:206-221.
[20] Cazzani, A., Malagù, M. and Turco, E. Isogeometric analysis: a powerful numerical tool for the elastic analysis of historical masonry arches. *Continuum Mechanics and Thermodynamics* (2016) **28**(1-2):139-156.
[21] Zampieri, P., Zanini, M., Faleschini, F. Seismic capacity of masonry arches with irregular abutments and arch thickness. *Construction and Building Materials* (2019) **201**:786–806.
[22] Pepi, C., Cavalagli, N., Gusella, V., and Gioffrè, M. An integrated approach for the numerical modeling of severely damaged historic structures: Application to a masonry

bridge. *Advances in Engineering Software* (2021) **151**:102935.
[23] Cavalagli, N., Gusella, V. and Severini, L. The safety of masonry arches with uncertain geometry. *Computers and Structures* (2017) **188**:17-31.
[24] Zampieri, P., Cavalagli, N., Gusella, V. and Pellegrino, C. Collapse displacements of masonry arch with geometrical uncertainties on spreading supports. Computers and Structures (2018) **208**:118-129.
[25] Severini, L., Cavalagli, N., DeJong, M. and Gusella, V. Dynamic response of masonry arch with geometrical irregularities subjected to a pulse-type ground motion. Nonlinear Dynamics (2018) **91**(1):609-624.
[26] Gusella, V. Geometrical uncertainty in mechanics and random curves in space. *Probabilistic Engineering Mechanics* (2020) **62**:103102.
[27] Cavalagli, N., Gusella, V. and Liberotti, R. Effect of Shape Uncertainties on the Collapse Condition of the Circular Masonry Arch. In: B. Abali and I. Giorgio (Eds.): *Developments and Novel Approaches in Nonlinear Solid Body Mechanics*. Advanced Structured Materials, Springer, Cham 130 (2020), pp. 455-467.
[28] Cavalagli, N., Gusella, V. and Liberotti, R. The Role of Shape Irregularities on the Lateral Loads Bearing Capacity of Circular Masonry Arches. In: A. Carcaterra et al. (Eds.): *Proceedings of XXIV AIMETA Conference 2019. AIMETA 2019*. Lecture Notes in Mechanical Engineering, Springer Cham (2020), pp. 2069-2081.
[29] Heyman, J. (1969) The safety of masonry arches. *International Journal of Mechanical Sciences* (1969) **11**(4):363-382.

12th International Conference on Structural Analysis of Historical Constructions
SAHC 2020
P. Roca, L. Pelà and C. Molins (Eds.)

NEOMUDEJAR ARCHITECTURE AND ANALYSIS OF LOCAL STRESSES OF MASONRY STRUCTURES: THE ESCUELAS AGUIRRE CASE STUDY

JULIÁN GARCÍA-MUÑOZ[1], DAVID MENCÍAS-CARRIZOSA[2*] AND FERNANDO MAGDALENA-LAYOS[1]

[1]Departamento de Construcciones Arquitectónicas y su Control (DCAC)
ETSEM - Universidad Politécnica de Madrid
Av. Juan de Herrera, 6. 28040 Madrid, Spain
e-mail: {julian.garciam, fernando.magadalena}@upm.es,
https://orcid.org/0000-0002-9924-7593 / https://orcid.org/0000-0001-7557-3020

[2]Departamento de Estructuras y Física de Edificación (DEFE)
ETSAM - Universidad Politécnica de Madrid
Av. Juan de Herrera, 4. 28040 Madrid, Spain
e-mail: d.mencias@upm.es, https://orcid.org/0000-0003-1495-5695 (*corresponding author)

Keywords: Historical Structures, Masonry Mechanics, Non-Destructive Inspection

Abstract. *At the end of the 19th century, an architectural style called Neomudéjar became quite popular in some areas of Spain. Very much like other historicist European styles in the same years, the Neomudéjar sought to recreate the local medieval architecture. The use of faced brick façades with complicated bonds -formed by stretchers and headers in and out the main wall plane- lead in term to a wide variety of results that resembled Arabic architecture. The brick façades of the Neomudéjar buildings are ideal case studies for the analysis of the local behaviour of masonry structures, especially regarding problems of stress concentration. There are several methods for studying the global behaviour of masonry structures – from the classic thrust line to the limit analysis tools – but, as the average stresses taken over by structural masonry elements are usually well below the compression strength of the constituent material, the classical methods of analysis are designed to verify only the global stability. Local behaviour, on the other hand, is quite elusive, especially when the properties of the material are uncertain. In such cases stress concentrations might appear, resulting on stress currents and low stress islets. A particular case of these phenomena occurs in the bonding of Neomudéjar façades. Local concentration of stresses is especially likely in these bonds, given the peculiar relative position of some bricks with respect to others. The paper proposed will use one of these buildings, the Aguirre Schools (Rodríguez Ayuso, Madrid, 1886), as a case study to evaluate local behaviour. Starting from a geometrical hypothesis of the internal distribution of the material based on recent photogrammetric surveys, and using conventional software of parametric design, the paper will describe a numerical model based on a non-deterministic random algorithm, although limited in its number of solutions, to discuss later the validity and scope of them. The limitations of the standard hardware in which these design tools are usually handled will also be considered in the discussion.*

1 INTRODUCTION

The geometric complexity of the bonds used in the masonry walls of *neomudejar* buildings makes them interesting case studies for the analysis of one of the least studied particularities of the mechanical behaviour of masonry structures: local phenomena. Several methods allow the analysis of the global behaviour of this type of structures (thrust line, limit analysis, etc.) – being one or the other more or less adequate depending on the characteristics of the material, the available data and the phenomenon studied. However, the analysis of local behaviour is elusive, especially when the properties and even the existence of the joint material is in doubt and the strength of the bond depends on friction.

The fundamental premise of most methods of global analysis is that the average working stresses are always well below the characteristic strengths of the material. This premise is true for most masonry structures; however, local problems arise, especially on irregular elements such as those in the façades of the *neomudejar* buildings (whose specificity lies in the complexity and the variety of the indented brick bonds). These local problems are not related to the average compression values, but to the possible concentrations of stresses in the contacts between blocks. The patterns that characterize the distributions of the blocks of this architecture normally seek to achieve aesthetic effects (rhythms, regularity or irregularity of the surface, etc) or to improve a certain property of the constructive element (ventilation or shading, for example, when it comes to facades), but they are not intended to respond to specific structural problems.

A mathematical model for the analysis of these stress concentrations, designed specifically for geometries of high complexity built in dry-stack masonry, is proposed in this paper. For this purpose, a constructive and geometric description of a case study (the facade of the Las Aguirre School building, in Madrid) is first performed; then the theoretical framework of the proposal (within the studies on percolation in discontinuous media, understood as branching and regrouping of stress currents) is presented; and, finally, a general description of the model (which, from a strictly mathematical point of view, can be considered a stochastic Markovian process in discrete time) and its implementation (carried out by means of graphical-analytical computer tools) are introduced.

2. BACKGROUND AND CASE STUDY

2.1. Case study: the Escuelas Aguirre building

In order to carry out the following analysis, the facade of a building located in Madrid, the Escuelas Aguirre building (Fig. 1a) will be taken as a case study. The building was built between 1881 and 1887 by the architect Emilio Rodríguez Ayuso at the confluence of the streets of Alcalá and O'Donnell. Rodríguez Ayuso, a historicist architect who had already rehearsed the *neomudejar* style in different buildings (such as the disappeared Plaza de Toros de Madrid, 1874) designed for Lucas Aguirre, promoter of the schools, a two-storey building in a rectangular and symmetrical plan, organized around two large covered interior courtyards (initially an open U-floor at the back) and a central core of stairs, which is topped with a tower located in the central part. The masonry façade was built with brick load-bearing walls adorned with abundant recesses and protrusions.

The numerous extensions that the building underwent in the following years, and the

reforms carried out throughout the 20th century, were generally respectful of the *neomudejar* style, to the point of being currently difficult to distinguish from the original construction. A recent study [1] has documented, in addition to the construction in 1896 of the attached pavilions of warehouse and counselling (which were erected following designs by Rodríguez Ayuso), actions of various kinds in 1908-28, 1933, 1999 and 2008. The following analysis is carried out exclusively on the 19th century part of the construction.



Figure 1a. The Escuelas Aguirre building in the 1920s. (Lacoste, circa 1925). **Figures 1b and 1c.** Some views of the brick bonds in different areas of the façade. [1]

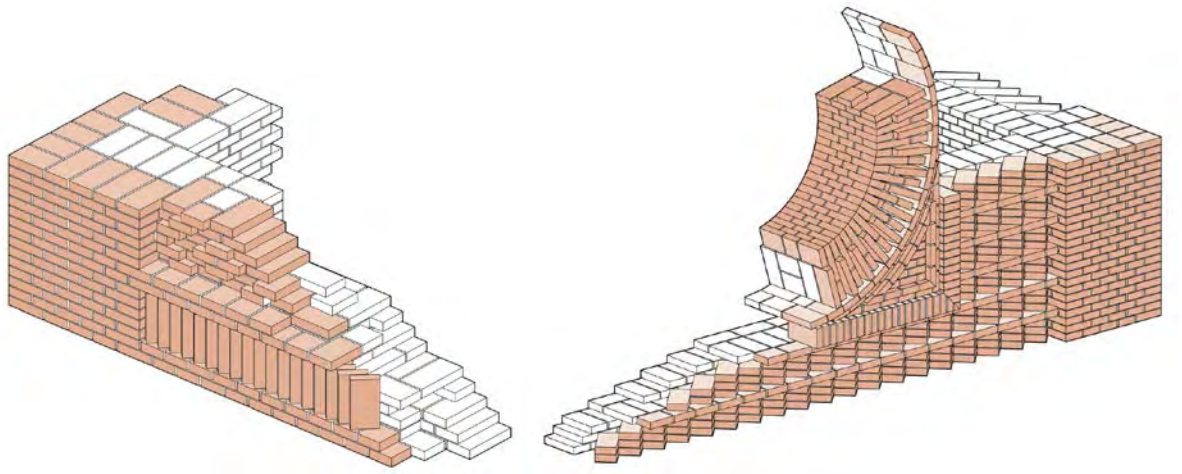
The brick of the main building, brown in colour and 27x13x4.5 cm in measures, is a product of the Jarama riverbank (fig. 1b). It is a piece of regular faces, double frogged, with a special depression on both beds for the placement of the mortar (although it may seem a dry-stack system, this type of masonry rarely is so) that allows the visible joint to be reduced. References to the manufacturer company, SABO [1], appear in the recesses. The bricks of the pavilions, of intense red colour, are mould manufactured and their measures are slightly different, 25.5x12.5x4.8 cm. but the geometry is very similar. The manufacturer's record can also be tracked: in this case it was Eloy Silió's, a factory located in Valladolid [2].

The constructive configuration of the facade is the most common in *neomudejar* buildings. Over the typical headers bond (also called *spanish* in the area) different recesses are made to create diverse figures, mostly rectangular or rhomboid, or to form imposts and cornices (fig. 1c). Jambs and lintels are formed by revoked lintels imitating stone, a mortar line that can also be seen in several impost lines, as well as in the formation of a small decorative bib. The thickness of the wall is variable, decreasing from two and a half bricks (69 cm) on the ground floor, to two (55 cm) on the first floor and lower body of the tower, and to one a half (41 cm) on the Second body of the tower.

The geometric complexity of the bonds used can be noted in figures 2a and 2b. The recesses of the pieces are always proportional to the fourth part of the main dimension of the same. Thus, most common recesses or protrusions are ¼, ½ or ¾ of the main stretcher dimension –that is, the 27 cm. aforementioned. Only occasionally recesses of 1/3 or 1/8, or multiples of these numbers, appear.

2.1. Theoretical framework

This paper attempts to extend the use of methods that have already been used, first in the study of granular media [3] and later in dry-stack masonry, for the analysis of the local behaviour of structures with other types of discontinuities and geometric irregularities caused by the elimination of parts or parts of them and/or by deterioration of the joint material. It is convenient to briefly review some examples of these methods.



Figures 2a and 2b. Brick disposition of the façades of the Escuelas Aguirre. [1]

A large majority of these studies consist of an experimental part, very often carried out by photoelastic tests [4], and some kind of theoretical approach: analytical, or more often numerical, consisting of a simulation of the behaviour of the studied media [5]. Photoelastic tests allow visualizing a locally random behaviour with the appearance of force chains or, more properly, force networks.

The application of these methods to ordered (orthotropic) granular media was carried out, according to Bigoni, first by Rajchenbach [6]. Bigoni's studies on dry masonry walls [7] included not only a photoelastic analysis but also, in a second article, a numerical simulation model compatible with the photoelastic results obtained. In this model, and in order to comply with the equilibrium conditions in each node, a branching occurs, which can be regrouped into subsequent nodes: "The result of the procedure is a form of random cascade admitting random coalescence, in addition to random branching". The photoelastic tests have been partially repeated later by Baig [8] and Magdalena [9], with different objectives and scope, obtaining coincident results.

Although the branching and regrouping model proposed by Bigoni comes to qualitatively similar solutions to the results of photoelastic tests, a later article [10] using a Monte Carlo Simulation through Linear Programming with random contact points, shows, based on the experimental results from a previous load test published by Magdalena [11] that the branching scheme can be improved. However, attempts to transfer this last method to truly three-dimensional cases have so far resulted in high rates of rejection that are excessively expensive from a computational point of view.

This article proposes assuming a model based on percolation, such as that cited by Bigoni or Shahriar's [12]. The concept of percolation corresponds in geology to phenomena such as the slow passage of fluids through a porous medium. The use of the concept of percolation has been extended to a large number of physics topics, as well as other fields: complex networks, epidemiology, etc.

A combinatorial approach is often used to study percolation. This has sometimes materialized as a Random Walk on Graph [13], which implies starting at some vertex and traversing the graph according to a random algorithm. The random walk, a concept introduced by Pearson in a very brief annotation in Nature [14], is a mathematical formalization of the result obtained from taking a series of random steps and has been used in many fields [15]. The concept refers in essence to a unique walk that advances through a series of steps in time.

The formulation proposed below retains the concept of randomness and is based on the resolution of a sequence of equilibrium equations in which the actions are obtained from the results of the previous stage and the reactions are established in a series of points of random application. To meet the equilibrium conditions in each node, a branch can be produced, so the path is not unique but branched in most of them. The procedure refers to an oriented sequence in which the randomness in each stage is conditioned by the results of the previous stage, thus giving a much lower rejection rate than that resulting from the random fixation of the application points independently. In the case of the proposed study, and returning to the percolation image, it is a matter of random diffusion but subjected to the action of the gravity of a system of charges through an orthotropic medium. The name of Directed Stress Percolation [again 13] is applicable, as it has been used, in the field of granular media, to study the transmission of stresses between –grains.

3. MODEL DESCRIPTION

3.1. The constituent element

The constituent element of the model (fig. 3a) is a solid of parallelepiped geometry with sides *A, B* and *C* –the relationship between sides being *A=2B=4C*. In the model described below, each element will be superimposed on another of identical geometry, resting on the larger faces *AB*, at as many heights as necessary, although the basic tool is designed to work in a number of up to 6 to limit the computational cost. The distribution of the element's overlays may vary, of course, depending on the bond of the masonry.

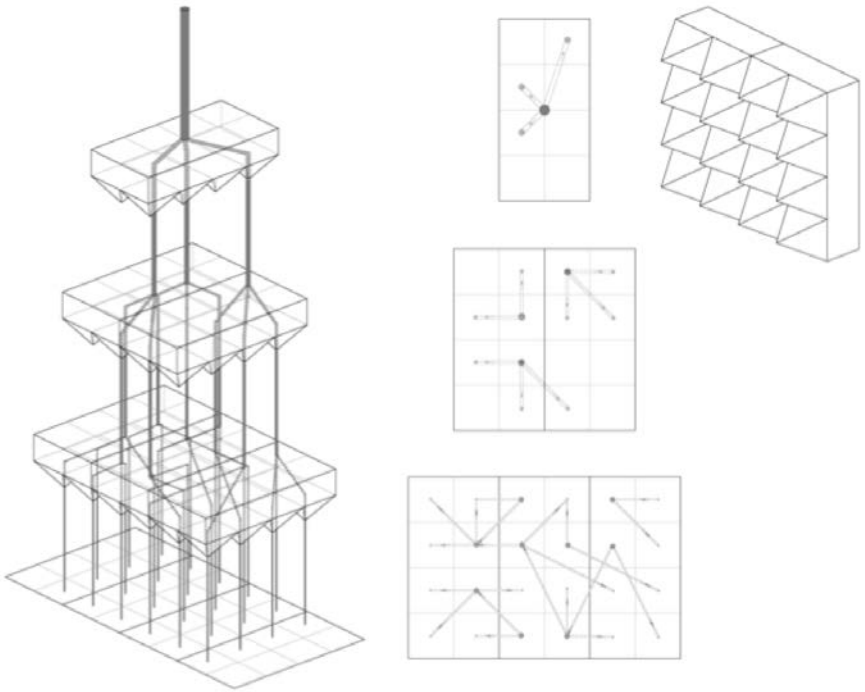
The contact between solids can occur through a limited number of points *n*, located exclusively at the base *AB* of each element. One of the premises of the model is that there is no contact on the *AC* or *BC* side faces. These *n* points are distributed homogeneously on the contact surfaces. To determine *n*, the generator algorithm establishes a grid on the surface *AB* and allows the values of n_a and n_b to be adjusted –both being positive integers. Obviously, the value of *n* is n_ax n_b. Typically, n_a will be of the order of double n_b, (being, as stated, *A*=2*B*) but it should not necessarily be so. The distance *d* between the outer plane of the masonry and the recessed plane cannot be any: it will be determined by the relationship between *A* and n_a, in the form

$$d = p\frac{A}{n_a}$$

p being a number to represent the indentations of the recessed plane, an integer that meets:

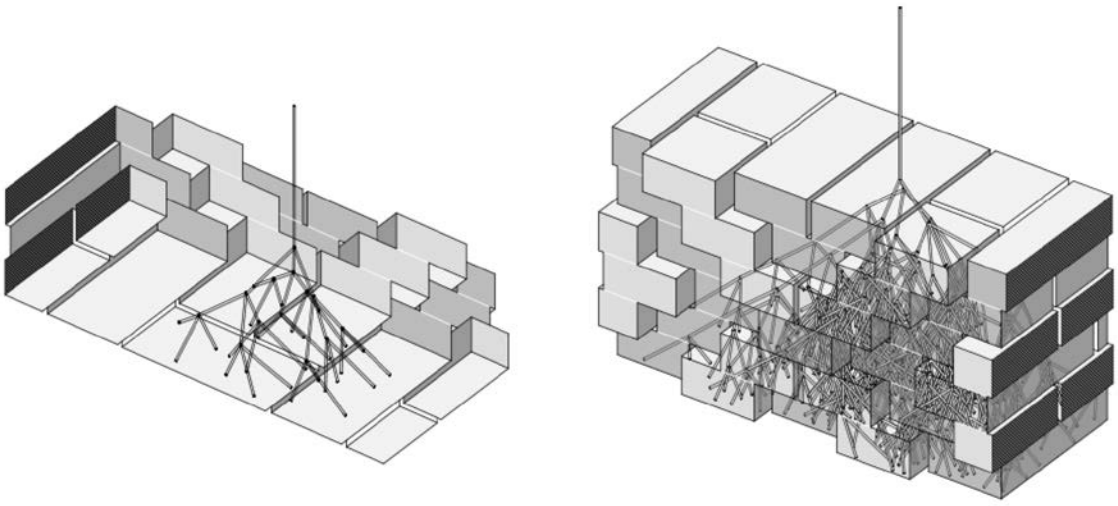
$$0 < p \leq n_a - 2$$

The figures attached (figs. 3a and 3b) are intended to facilitate the physical understanding of the constituent element by representing the possible points of contact as diamond tips. The numerical model does not need to replicate this type of geometry to offer verifiable results. In a physical model, the contact surface at those points would depend on the resistance of the material; in the numerical model, as no limitations for compression stresses are established, this consideration is unnecessary.



Figures 3a y 3b: Description of the constituent element. Contacts points are represented as diamond tips in the lower surfaces of the blocks.

On a finite set of elements such as those described above, stacked vertically and connected through a specific and identical number of points under each block, the proposed model will draw, through a computer algorithm, a tree of paths, a particular case of stochastic process in discrete time in which the time factor is replaced by vertical advance. From a generic point of view, this is a non-deterministic model, although limited in its number of solutions, and subject to various boundary conditions –the fundamental being the one referring to the action and reaction points in the constituent element, since the algorithm forces a certain degree of discretization to always be in one or more of the *n* positions described in the previous section, both on the upper face and in the bottom of the block. This will affect not only the initial punctual action but the entire chain of reactions described below.



Figures 4a y4b: Application to one of the walls in the Escuelas Aguirre building.

The algorithm will start from a value of the initial action Q_y and its position A (which can be entered by the user or self-generated) to randomly search for a triad of points *B, C* and *D* (among the *n* possible contact points described above under the first block) such that the reactions in *B, C* and *D* make possible the static equilibrium of the piece without introducing additional compatibility equations. As is evident, only a limited number of *BCD* triads can offer static equilibrium possibilities against the action exerted on *A*. Once the triad of contacts has been determined, the algorithm automatically assigns the R_B, R_C, and R_D, reactions, that must compensate Q_A so that

$$Q_A = R_B + R_C + R_D$$

A conventional isostatic system would require not only the obvious equilibrium of actions and reactions but also that of the moments resulting from them, $\sum \mathrm{M}_A = 0$. However, this premise cannot be fulfilled for any random point: the position of *A* with respect to *B, C* and *D* should be such that *A* is contained, in plan, in the triangle *BCD* (in the understanding that the reactions R_B, R_C, and R_D must always be of opposite sign to the action; in dry-stack masonry constructions the tensile strength should be considered zero). It is obvious that if *A* is found in one of the corners of the element, the only possible reaction would be at a single point *B*, being $Q_A = R_B$ and *C* and *D* redundant, given that necessarily $R_C=R_D=0$. In the event that *A* was found on one of the faces of the element, a similar situation would occur, although in this case there could be two reactions, so that

$$Q_A = R_B + R_C$$

Only one position, *D*, would be redundant in this case, logically being $R_D = 0$. Thus, the probability of an event occurring is conditioned by the probability of the immediately preceding event. This possibility must be taken into account in bonds such as the one discussed here, given the special arrangement of the blocks (figs. 4a and 4b).

With regard to mechanical analysis, the final model can therefore be considered a set of rigid solids in unilateral, dry and direct contact, with finite friction and following a non-

associative friction-slip law. This model tries to represent a material with compressive strength far superior to that needed to assume the stresses to which it is subjected and reduced tensile strength, although not zero. This last consideration significantly increases the set of statically permissible solutions within the possible combinations.

3.2 Geometric model

The model corresponds to the outer elements of one of facades of the Aguirre Schools, at the height of the second floor (Fig. 5). Six layers have been modelled using computer aided design software Rhinoceros [16]. Each of the bricks is made up of a Brep Box type entity, which is arranged by separating the space corresponding to the joint. The base piece has dimensions of 20 x 10 x 5 cm, with vertical joints 0.5 cm thick and horizontal joints 1 cm thick.

The studied surface has a total dimension of 66 x 23 x 35 cm, composed of both complete pieces and half pieces at the ends (Fig. 5). In the upper part there is a centred piece that will be the one that receives the load in the first place before it is distributed to the rest of the wall.

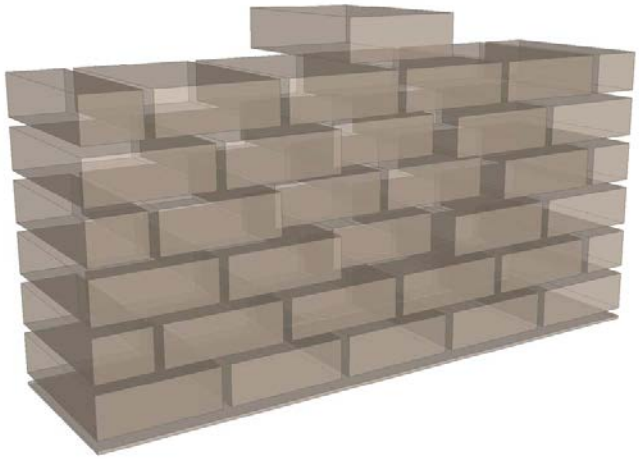


Figure 5: Rhinoceros model of studied piece of wall.

4. IMPLEMENTATION OF THE ALGORITHM

Since the geometric model was made using Rhinoceros, the algorithm implementation to determine the stochastic load path has been programmed using Python language within the Grasshopper parametric design plugin [17] (Fig. 6)

It starts from a piece placed on top of the wall, which receives a vertical load of unit value. This load is distributed among the possible supports that correspond to each of the indentations described in the previous section. The grid of the contact points is parameterized in a number $m \times n$, being $2 \leq n \leq 8$ and $2 \leq m \leq 8$ as well. The number of possible combinations increases very significantly to a greater number of supports –and so does the computing time necessary for processing.

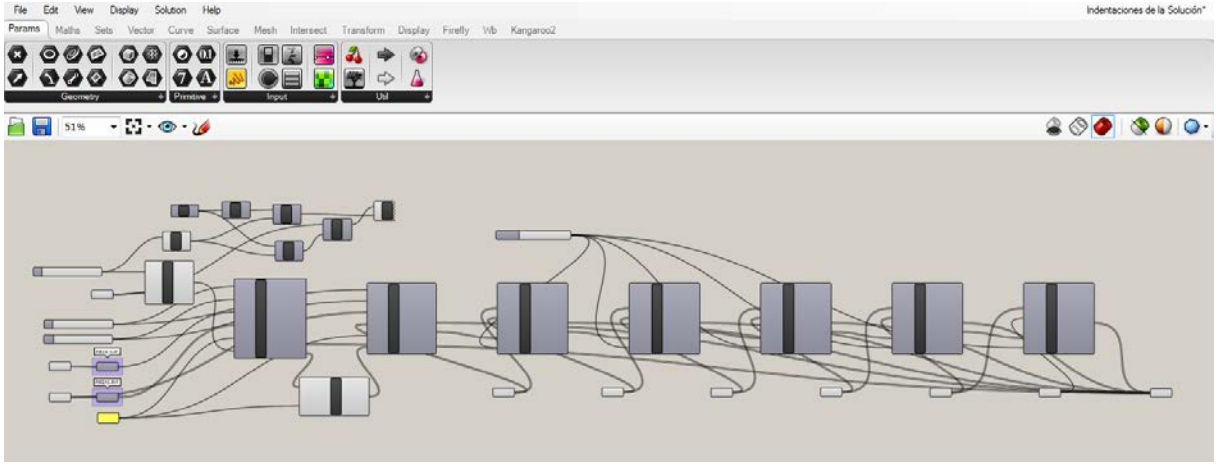


Figure 6: Grasshopper programming scheme.

After establishing these contact points the algorithm evaluates whether it is possible to transmit the load, since some of the blocks can be found in a cantilever and have no support (fig. 7). Once the valid supports under the piece have been determined, one of the combinations that meets the conditions of isostatic equilibrium is randomly assigned (figs. 8a and 8b) These conditions are established based on the equilibrium equations in space, with the additional hypothesis that it is possible to transmit tensile stresses with a maximum value of 10% of the elastic compression limit – a condition that is usual in the regulations and standards for the design of masonry walls.

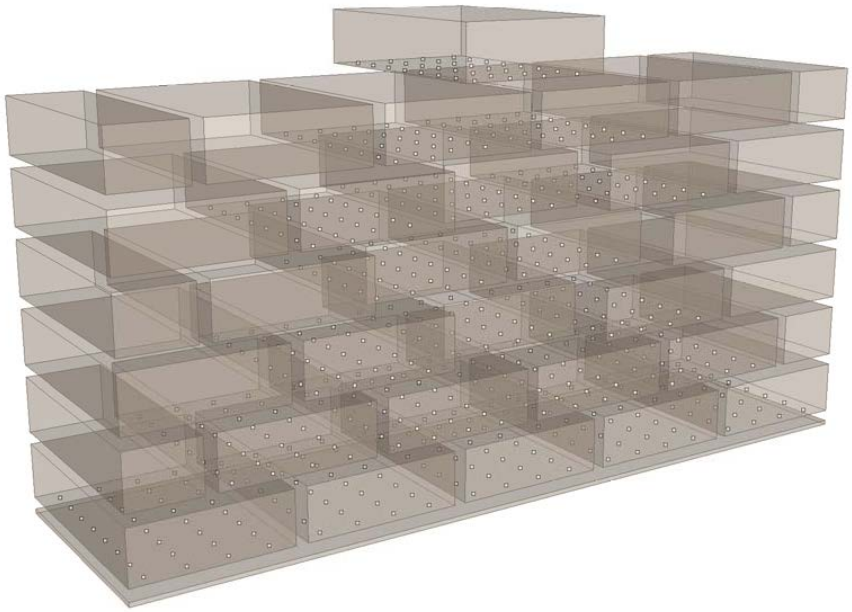
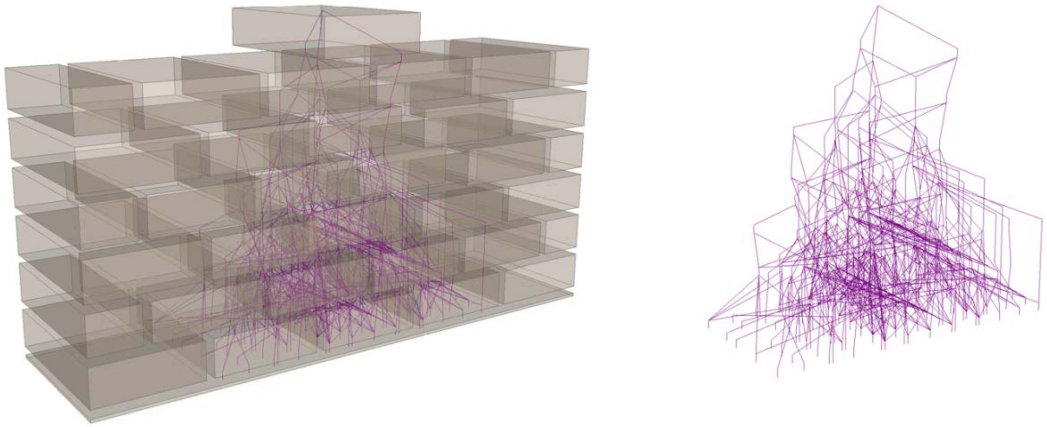


Figure 7: Support possibilities in the Rhinoceros model.

This process is iterated successively in each of the pieces that make up the set studied. In all cases, the load with which the iteration begins is the result of those transmitted on each block in each course, so it is necessary to determine, as the process progresses, the waypoint and the value of the resultant action in each of the pieces.

4. DISCUSSION

From a strictly mathematical point of view, the described model can be considered a stochastic Markov process in discrete time. There are two fundamental reasons for this ascription. On the one hand, the fact that it is not possible to consider each individual itinerary –that is, each line of action– as a strictly random walk: the direction that each line takes will be conditioned by the position and intensity of the rest. On the other hand, a fundamental factor must be taken into account, and it is the possibility of a rejection, which will then force the process to be rearmed at least from the previous level.



Figures 8a y 8b: Scheme of one of the solutions integrated in the wall (left) and isolated (right)

Pearson's classic formulation for a random path does not fit this problem. The Markovian process, however, is more open and contemplates the two singularities mentioned above. The fact that some itineraries have an influence on others falls within the usual considerations of stochastic systems in discrete time, though in the case of the proposed model, of course, there is no time factor in a literal sense, but rather the advance in the vertical load. On the other hand, the possibility of rejection is contemplated in one of the classic continuous time processes, known as the Markov process –as is its implementation from the probabilistic point of view.

With regard to the programming used, the implementation of these systems through graphic tools, as in the one presented in this paper, might limit the range of responses. For the designer it is ideal that the digital tools for the analysis of the local behaviour of this type of structures can be implemented in the same tools that make parametric design possible, as this would allow to contrast the local problems of the structure directly during the design process, and thus anticipate possible stress concentrations in the model prior to its construction, without the need to export the geometry to another tool for its treatment. However, the

performance of the standard hardware with which these design tools are usually handled is limited, and that determines the scope of the analysis.

5 CONCLUSIONS

Masonry structures, and in particular those of buildings such as the neomudéjar façades studied here, are constructive elements of high complexity, whose indented brick bonds are interesting examples of the possibilities offered of combinatorial theory applied to architecture. The façade of the Aguirre Schools has a bond full of these recessions, which produce discontinuities in the volume of the masonry that is capable of conveying the loads paths. It is not, as detailed, a structure consisting of strictly dry-stack blocks, but its complexity makes it an ideal case study to implement the method described above.

These structures often present with local problems, which cannot be studied with the tools commonly used for surveying masonry structures –as its objective is the analysis of global behaviour. The proposed method allows evaluating at least one of the possible load paths compatible with the boundary conditions and the material requirements, also taking into account the geometric discontinuities of this type of masonry elements. The development of this method, and its application in a number of iterations that enable its statistical analysis, can allow detecting the areas where stress concentrations are most likely to occur. This numerical model needs to be complemented by physical tests –which are currently in progress– and statistically contrasted to establish its validity.

The implementation of this model through graphic programming languages –the same ones that make parametric design possible– entails limitations for large-scale statistical analysis. To achieve a sufficient number of iterations it is necessary, of course, to use analytical tools. However, and although these analytical tools are necessary for a general study at the theoretical level, graphic tools can also be useful in the practical one, since problems of local behaviour are frequently due to irregularities, be they geometric or material, in the nearby area.

REFERENCES

[1] del Real Mateos, A. *Estudio Histórico-Constructivo de las Escuelas Aguirre de Madrid.* (2018) Master Thesis. ETS Arquitectura (Universidad Politécnica de Madrid)

[2] Camino Olea, M. S. *Construcción y ornamentación de las fachadas de ladrillo prensado, al descubierto, en la ciudad de Valladolid.* (2001) PhD Thesis. Universidad de Valladolid

[3] Drescher, A., de Josseling de Jong, G. 1972. Photoelastic verification of a mechanical model for the flow of a granular material. Journal of the Mechanics and Physics of Solids, 20(5): 337–340.

[4] Mencías-Carrizosa, D., García, J. and Magdalena, F. Qualitative and quantitative approaches to highly local behaviours of historical masonry structures. In: Van Balen & Verstrynge (Eds.) *Structural Analysis of Historical Constructions – Anamnesis, diagnosis, therapy, controls,* (2016) Taylor & Francis Group

[5] Mencías-Carrizosa, D. *La geometría analítica como herramienta de análisis estructural de fábricas históricas*. (2017) PhD Thesis. ETS Arquitectura (Universidad Politécnica de Madrid). doi:10.20868/UPM.thesis.47167.

[6] Rajchenbach, J. Stress transmission through a cohesionless material. *Material Physics Mechanichs* (2001) 3: 1–4.
[7] Bigoni, D. & Noselli, G. 2010. Localized stress percolation through dry masonry walls. Part I – Experiments & Part II - *Modelling European Journal of Mechanics A/Solids,* 29, 291–298 and 299–307.
[8] Baig, I., Ramesh, K. ans Hariprasad, M. P. Analysis of stress distribution in dry masonry walls using three fringe photoelasticity. *International Conference on experimental Mechanics 2014*. Cambridge: International Society for Optics and Photonic. 93022P–93022P.
[9] Magdalena-Layos, F., García-Muñoz, J. & Mencias-Carrizosa, D. Estructuras de fábrica: enfoques «antiguos» y «modernos» para fenómenos muy locales. *Informes de la Construcción*, 68(542): e150 (2016) doi: 10.3989/ic.16.032.
[10] Magdalena Layos, F. & García Muñoz, J. 2018. Approaches to strongly local phenomena in dry masonry structure. *Int. J. Masonry Research and Innovation*, (2018) Vol. 3, No. 2, doi:10.1504/IJMRI.2018.092460-4
[11] Magdalena, F. Aznar, A. de la Torre and J. F. Hernando, J. I. Recent Results on Sliding Collapse for Masonry Structures Under Static Load Test. *Engineering and Applied Sciences*. Vol. 1, No. 4, 2016, pp. 99-106. doi: 10.11648/j.eas.20160104.14
[12] Shahriar, A. Waldmann, D. Scholzen, F. and Louge, A. Numerical analysis for the determination of stress percolation in dry-stacked wall systems. 2016. Masonry International. 29. pp 27-38
[13] Grimmett G. Hiemer P. Directed Percolation and Random Walk. In: Sidoravicius (ed) *In and Out of Equilibrium. Progress in Probability*, Vol 51, (2002) Birkhäuser, Boston
[14] Pearson, K. The Problem of the Random Walk. *Nature* (1905) 72:294 doi:10.1038/072294b0
[15] Van Kampen, N.G. S*tochastic Processes in Physics and Chemistry*. North-Holland Personal Library. (2007) doi:10.1016/B978-0-444-52965-7.X5000-4
[16] McNeel, Robert. Rhinoceros: *NURBS modeling for Windows* v.5. (2016)
[17] Ruten, D. and McNeel, R. Grasshopper: Generative Modeling with Rhino v.0.9.0076 (2016).

12th International Conference on Structural Analysis of Historical Constructions
SAHC 2020
P. Roca, L. Pelà and C. Molins (Eds.)

NEW STRATEGIES TO ASSESS THE SAFETY OF UNREINFORCED MASONRY STRUCTURES USING THRUST NETWORK ANALYSIS

R. MAIA AVELINO[1*], A. IANNUZZO[1], T. VAN MELE[1] AND P. BLOCK[1]

[1]Institute of Technology in Architecture (ITA), Block Research Group (BRG)
Eidgenössische Technische Hochschule Zürich (ETH - Zurich)
Stefano-Franscini-Platz 1, HIB E, CH-8093 Zurich, Switzerland
email: {maia, iannuzzo, van.mele, block}@arch.ethz.ch, www.block.arch.ethz.ch
(*corresponding author)

Keywords: Masonry Assessment, Thrust Network Analysis, Optimisation, Equilibrium Analysis, Limit Analysis, Geometric Safety Factor.

Abstract. *This work develops new strategies to robustly apply Thrust Network Analysis (TNA) for the assessment of unreinforced masonry (URM) structures studied within the frame of limit analysis. It formulates and solves a nonlinear optimisation problem on thrust networks considering relevant constraints for the assessment of URM structures. Geometrical and force constraints are include such as the consideration of the structural envelope and bounds on the reaction forces. The objective functions studied correspond to the minimum and maximum horizontal thrusts of the vaults. To evaluate the level of stability of an existing structure, this work develops a methodology to estimate the geometric safety factor (GSF) and the minimum thickness of masonry vaults by solving sequential optimisation problems for increasingly tightened geometrical bounds. This procedure is implemented in a Python-based, open-access tool within the COMPAS framework and illustrated here on two- and three-dimensional applications that are relevant for the structural analysis of historical constructions.*

1 INTRODUCTION

Complex unreinforced masonry vaults present a challenge to engineers and scientists aiming to assess their stability and safety. Historically, since Hooke [1] and Poleni [2], the static approach has been used to assess the stability of masonry construction. Its modern formulation was proposed by Heyman [3] with the establishment of limit analysis of masonry structures. According to the safe theorem of limit analysis, if a path of compressive and equilibrated forces is found within the structural geometry, the structure is safe under the applied loads and this set of compressive, internal forces corresponds to a lower-bound equilibrium solution.

For two-dimensional structures, as classically applied to arches, this internal path reduces to a thrust line [4, 5]. O'Dwyer [6] first extended this concept to the assessment of arcuate masonry vaults by modelling the internal stress states as a discrete network constrained to lie inside the envelope defined by the intrados and extrados of the vault.

Block and Ochsendorf [7] introduced Thrust Network Analysis (TNA), in which the force network is described by its vertical projection in plan, named form diagram, and the equilibrium of the horizontal forces is visualised by a reciprocal graph, named force diagram. As elaborated in [8], TNA is an application of the Force Density Method (FDM) as formulated by Linkwitz

and Schek [9,10]; specifically, in TNA, as applied in this paper, the form diagram is considered fixed. More recent publications extend the optimisation procedure with applications to masonry and analysis of the indeterminacy of the networks [11, 12, 13].

Recently, the methodology was revisited by Marmo and Rosati [14] focusing on the form diagram with the introduction of proportional horizontal loads on the network and by Cercadillo-Garcia and Fernández-Cabo [15] also formulating the problem based on the FDM. Alternatives to thrust networks are presented in Fraternali [16] and Angelillo et al. [17] with polyhedral stress functions and in Fraddosio et al. [18] considering membrane solutions.

Even within the state-of-the art of the different approaches briefly mentioned here, there are still a series of limitations that prevent these methods to be largely adopted in practice. These include the lack of a straightforward methodology to compute the level of stability and/or the (geometric) safety factor for a given vaulted structure, the difficulty to deal with non-proportional horizontal loads, and the lack of flexibility to restrain solutions to geometrical features, such as cracks, hinge lines or openings, and force constraints, such as bounds on the reactions and allowance for horizontal reactions along the perimeter of the vault (open edges).

This paper proposes a computation pipeline to robustly apply TNA for the assessment of unreinforced masonry (URM) vaulted structures by efficiently searching for admissible thrust networks for a given structure. The mathematical formulation is taken from [11, 12], and the search is executed by solving a nonlinear constrained optimisation. In particular, as objective functions, the minimum and the maximum of the horizontal thrust for a given form diagram are considered. The constraints of the optimisation problem are enforced on the geometry (heights of the nodes), on the internal forces (compressive) and on the reactions (limited magnitude and inclination). This paper also provides a direct way to verify the level of stability by computing a lower bound of the geometric safety factor (GSF) of the structure. This is done by iteratively tightening the geometrical envelope of the vault while computing minimum and maximum thrust until the structure reaches its minimum thickness and, at this point, these solutions coincide representing the only possible stress state of the structure, i.e. its limit state.

All analyses are performed with a Python-based, open-access tool. This tool implements TNA [8] and is provided through the COMPAS Masonry framework [19], which is a part of a larger research project that aims to develop appropriate and practical analysis strategies and tools for tackling the assessment of URM structures [19].

The organisation of the paper is as follows. In Section 2, the theoretical background is presented. In Section 3, the computational implementation is described. In Section 4, the new solving algorithm is illustrated with two- and three-dimensional examples. Finally, in Section 5, the findings are summarised, pointing to future research.

2 THEORETICAL BACKGROUND

The safe theorem of limit analysis of masonry structures, proved by Heyman [3], states that if any admissible stress field is found for a given structure, then, the structure is safe under the applied loads. A stress field is admissible if it is equilibrated, compressive and fits entirely within the structural geometry of the masonry. In Angelillo et al. [17], the set of statically admissible stress fields H is described. Thus, according to the safe theorem, if H is not void, any solution found in this set can be accepted as a lower-bound solution for the assessment problem. If H includes only one admissible stress field, the structure is in the so-called limit

state. In existing structures, the concern is how far the current state of the structure, considering the self-weight of the structure and the applied loads, is from the limit state condition. In this paper, we are interested stress fields represented by thrust networks that correspond to singular, one-dimensional stress fields having the forces concentrated on the edges of a network.

2.1 Force Densities in thrust networks

As in the mathematical formulation of [8,11], thrust networks are defined by $n=n_i+n_b$ nodes as the sum of n_i internal nodes and n_b restrained nodes. These nodes are connected by m edges according to a connectivity matrix $\mathbf{C}$. The forces are applied on the internal nodes in any direction as the vectors $\mathbf{p}_x$, $\mathbf{p}_y$, $\mathbf{p}_z$. Linkwitz and Schek [9,10] introduce the force-densities q for an edge, corresponding to the ratio between the force f and the length l of the edge. With $\mathbf{C}_i$ and $\mathbf{C}_b$ the columns sliced from $\mathbf{C}$ corresponding to the internal and restrained nodes of the network. The nodal coordinates are $\mathbf{x}$, $\mathbf{y}$, $\mathbf{z}$ and we consider the relations: $\mathbf{U}=\text{diag}(\mathbf{Cx})$ and $\mathbf{V}=\text{diag}(\mathbf{Cy})$. The horizontal equilibrium of the thrust network becomes:

$$\begin{bmatrix}\mathbf{C}_i^T\mathbf{U}\\ \mathbf{C}_i^T\mathbf{V}\end{bmatrix}\mathbf{q}=\begin{bmatrix}\mathbf{p}_x\\ \mathbf{p}_y\end{bmatrix}. \tag{1}$$

Positive qs represent compression. As in [8, 11], the left-hand side of Eq. (1) is considered in the matrix $\mathbf{E}$ of size ($2n_i$ x m) and the vectors $\mathbf{p}_x$ and $\mathbf{p}_y$ of the applied loads on the internal nodes are stacked in the vector $\mathbf{p}_h$ of size $2n_i$, resulting in the horizontal equilibrium as:

$$\mathbf{Eq}=\mathbf{p}_h. \tag{2}$$

For a fixed form diagram, the matrix $\mathbf{E}$ does not change as it depends only on its connectivity and geometry. Therefore, any set of non-negative $\mathbf{q}$ satisfying Eq. (2) will satisfy horizontal equilibrium for the given/chosen fixed form diagram. For such a $\mathbf{q}$ and given the heights of the restrained nodes $\mathbf{z}_b$, one can compute the heights of free-nodes $\mathbf{z}_i$ as:

$$\mathbf{z}_i=(\mathbf{C}_i^T\mathbf{Q}\mathbf{C}_i)^{-1}\left(\mathbf{p}_z-(\mathbf{C}_i^T\mathbf{Q}\mathbf{C}_b)\mathbf{z}_b\right), \tag{3}$$

with $\mathbf{Q}=\text{diag}(\mathbf{q})$ and the vertical loads $\mathbf{p}_z$, often coming from the self-weight of the masonry.

3 COMPUTATIONAL IMPLEMENTATION

The methodology described in Section 2 allows for the computation of thrust networks. This section describes the computational implementation to automate the search for obtaining thrust networks that are solutions to the problem of assessment of URM structures.

3.1 Force indeterminacy of thrust networks

Computing a non-negative vector $\mathbf{q}$ from Eq. (2) is not an easy task since the equilibrium matrix $\mathbf{E}$, for common topologies, is usually ill-conditioned. For that reason, and also to reduce the number of parameters in the system, the problem can be treated in terms of the independent edges [11,20]. The independent edges are the degrees of freedom of the equilibrium system. Therefore, one can take the force densities assigned to the independent edges $\mathbf{q}_{ind}$ as variables to find the force densities for the rest of the dependent edges $\mathbf{q}_{dep}$ with:

$$\mathbf{q}_{dep}=\mathbf{E}_{dep}^{-1}(\mathbf{p}_h-\mathbf{E}_i\mathbf{q}_{ind}). \tag{4}$$

A possible set of independent edges has its indices related to the columns of the matrix **E** that form a base of linearly independent vectors. Finding a set of columns spanning the rank of the matrix **E** can be done by finding a reduced row-echelon form (RREF) of **E** as in [20].

3.2 Minimum and maximum thrust networks

Following the identification of the degrees of freedom of the network, the general optimisation problem is described in terms of the independent edges ($\mathbf{q}_{\text{ind}}$) and the heights of the restrained nodes ($\mathbf{z}_{\text{b}}$) as follows:

$$\begin{aligned} &\textit{minimise} && f(\mathbf{q}_{\text{ind}}) \\ &\textit{subject to} && c_j(\mathbf{q}_{\text{ind}}, \mathbf{z}_{\text{b}}) \geq \mathbf{0} \\ & && h_k(\mathbf{q}_{\text{ind}}, \mathbf{z}_{\text{b}}) = \mathbf{0} \end{aligned} \quad , \tag{5}$$

in which the equality constraint Eq. (5.3) is Eq. (4), ensuring horizontal equilibrium of the fixed form diagram. The inequality constraints Eq. (5.2) will be discussed in Section 3.3. The objective function can be chosen among a great variety of functions relevant to assessment with thrust networks. This paper will discuss the following ones:

$$\textit{minimise} \qquad f(\mathbf{q}_{\text{ind}}) = \pm \sum_{\text{i}}^{\text{n}_\text{b}} \sqrt{\text{R}_{\text{x,i}}^2 + \text{R}_{\text{y,i}}^2} \ , \tag{6}$$

where $\mathbf{R}_{\text{x}} = \mathbf{C}_{\text{b}}^{\text{T}}\mathbf{Q}\mathbf{C}\mathbf{x}_{\text{b}}$ and $\mathbf{R}_{\text{y}} = \mathbf{C}_{\text{b}}^{\text{T}}\mathbf{Q}\mathbf{C}\mathbf{y}_{\text{b}}$ are the vectors containing the reactions in the x- and y-direction, respectively, for the n_b restrained nodes.

This equation, in its positive form, minimises the horizontal components of the thrust, providing the minimum (or passive) thrust state for the vault, for a given form diagram. Eq. (6) is linear and function of the force densities **q** computed from $\mathbf{q}_{\text{ind}}$ by Eq. (4).

If as objective function we consider the negative form of Eq. (6), we maximise the thrust on the structure, rendering the maximum (or active) thrust state, again for the given form diagram.

In both cases we have to solve a nonlinear constrained optimisation, that is dependent on the starting point. For large problems, it has been found that starting from a compression-only solution improves the convergence of the optimisation even if that initial solution does not fit within the geometry of the masonry. To this end, a minimisation of loadpath as in [21] was used as starting point for the examples in Sections 4.2 and 4.3.

3.3 Geometric and force constraints on thrust networks

The first applied force constraint ensures that the force densities are non-negative. The independent edges ($\mathbf{q}_{\text{ind}}$) have their domain directly restrained to $[q_{min}, q_{max}]$, where q_{min} is 0.0 and q_{max} is a virtual bound sufficiently high to restrain the search space without being activated. The remaining $\mathbf{q}_{\text{dep}}$, calculated from Eq. (4), are constrained from below to be non-negative.

To guarantee that the thrust network is entirely contained within the masonry, all nodes of the thrust network have upper and lower bounds constraints assigned to their z coordinate. These bounds can also be modified to model specific observed failures or cracks on the existing structure, forcing the height of specific nodes of the network to lie in a predefined position. These applications are not studied in this paper but will be treated in a forthcoming paper.

Since the projection of the network remains fixed in plan and the heights of the restrained nodes ($\mathbf{z}_{\text{b}}$) are variables of the optimisation, the computed thrust networks can be completely detached from a given reference datum. This can become an issue for studying a self-standing

semi-circular arch (i.e. with no buttressing or fill). This is addressed by constraining the inclination of the reaction forces such as, when extended, the reaction vector still remains inside the masonry geometry. Such a constraint is illustrated in Sections 4.1 and 4.2.

3.4 Optimisation solvers

The examples presented in this paper were solved with an implementation of the sequential linear-quadratic programming available in the open-source Python package PyOpt [22].

3.5 Limit state for lower-bound solution

The main contribution of this paper is to present a methodology for estimating the limit state (or closeness to collapse) of a given structure by computing its geometric safety factor (GSF). The GSF is defined as the proportion of the total depth (t) of the structure's cross-section to the minimum depth (t') of the offset, tightened cross-section required to contain a thrust line [23], or in our case, a thrust network. The procedure developed to obtain the GSF sequentially solves the optimisation for maximum and minimum thrust for a decreasing thickness until the respective results coincide. This condition represents the limit state of the structure, since only one stress state is possible, that is, only one thrust line or network (for a given form diagram) fits in the geometry. At this point, the minimum thickness t', and the GSF = t/t' are computed.

4 NUMERICAL APPLICATIONS

Three applications to URM structures are investigated. First, a semi-circular arch (Section 4.1) is analysed, followed by a dome (Section 4.2) and a rectangular cross vault (Section 4.3).

4.1 Semi-circular arch

The first application looks at a semi-circular arch with base geometry described by a central radius R=1.00m and thickness t=0.20m, i.e. t/R=0.20. The linear form diagram is discretised in 20 nodes equally spaced with regards to the projection onto the circular geometry. The out-of-plane dimension of the arch is 1.00m and the density of the masonry ρ=20kN/m^3. The self-weight is lumped at the nodes. The total vertical loading is W=12.6kN. This problem has three variables: one independent ($\mathbf{q}_{ind}$) and the height of the two restrained nodes ($\mathbf{z}_b$). Eq. (6) is used to find the minimum and maximum thrust on the arch depicted on Figure 1a and b, respectively.

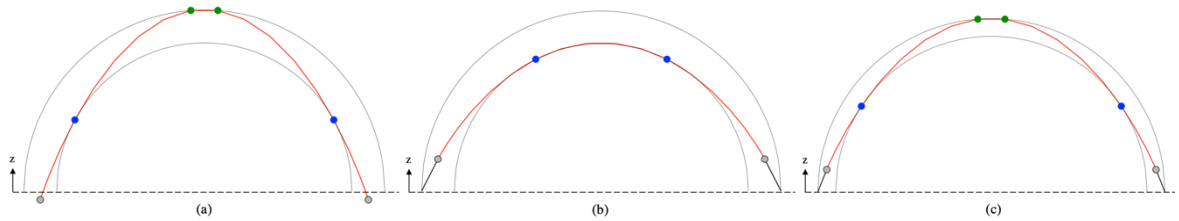


Figure 1: Solutions of minimum (a) and maximum (b) thrust for the semi-circular arch with t/R=0.20 and thrust for the minimum thickness (c) calculated as t'/R=0.1079 after incremental reduction of the thickness.

For the initial configuration t/R=0.20, the ratios of the minimum and maximum thrusts over the self-weight are $(T/W)_{min}$=31.6% and $(T/W)_{max}$=51.2%. The points where the thrust line

touches the intrados and extrados are highlighted in blue and green and the boundary nodes are shown in grey. The segments of the thrust line are depicted in red and the reaction vector is displayed in black when the restrained node is above the reference surface of height z=0.0m. In the solution for the minimum thrust, the restrained nodes go below the reference surface and for the maximum, the restrained nodes go above it and the resultant of the forces touch exactly the extrados of the semi-circular arch (Figure 1b).

Figure 2 visualises the sequential GSF procedure for this example. The optimisation for maximum and minimum is performed reducing t by increments of -0.005m until t=0.110m, and -0.001m afterwards. For each new thickness, minimum and maximum thrust are plotted in Figure 2 until they coincide, representing the limit state where only one thrust line is possible.

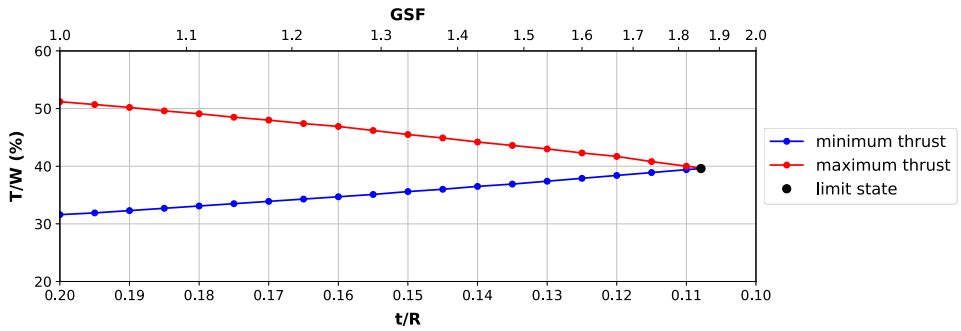


Figure 2. Methodology for deriving the minimum thickness and computing the geometric safety factor (GSF) for the semi-circular arch with t/R=0.20, resulting in t'/R=0.1079 and GSF=1.85.

The minimum thickness t' (or its adimensional t'/R) of the semi-circular arch can be derived as the intersection of the two lines of Figure 2, where we find t'/R=0.1079 and $(T/W)_{limit}$=39.7%. It is known from [5] that the analytical solution for this problem is $(t/R)_{theory}$=0.1075. The error of the proposed methodology is 0.4%, for the discretisation adopted (20 nodes). From this, the GSF can be approximated as the ratio between t and t', resulting in GSF=1.85 (Figure 2).

4.2 Hemispherical dome

For three-dimensional analysis, the assumptions on the force pattern for the masonry vaults become critical. Since the form diagram remains fixed, it should include a logic related to the way that the compressive forces flow to the supports, as in [12]. Therefore, we study two form diagrams to assess a circular dome with a central radius of R=5.0m and thickness t=0.50m, i.e. t/R=0.10 (Figure 3a) under self-weight. The first diagram presents a radial arrangement of the forces to the support; it is composed of 20 meridians and seven circular hoops. As in Section 4.1, the hoops are equally spaced with regards to the base surface and not with the planar projection (Figure 3b). The second form diagram assumes a spiralling force flow (Figure 3c). Both diagrams are composed of 320 edges, have 25 and 18 independent edges respectively that are highlighted in Figure 3. Supports are assigned on the perimeter. The self-weight is assigned according to the 3D tributary area with regards to its projection on the base surface, its thickness t and density ρ=20kN/m^3. The total weight is W=1570kN.

The result for both patterns regarding minimum, maximum thrust and limit thickness are depicted in Figures 4 and 5. Branches with null compressive force are not shown and the

compressive branches have their thickness proportional to the force carried. The points touching the intrados and extrados are marked with blue and green spheres. The same incremental analysis for reduced values of thickness is conducted and the results are plotted in Figure 6.

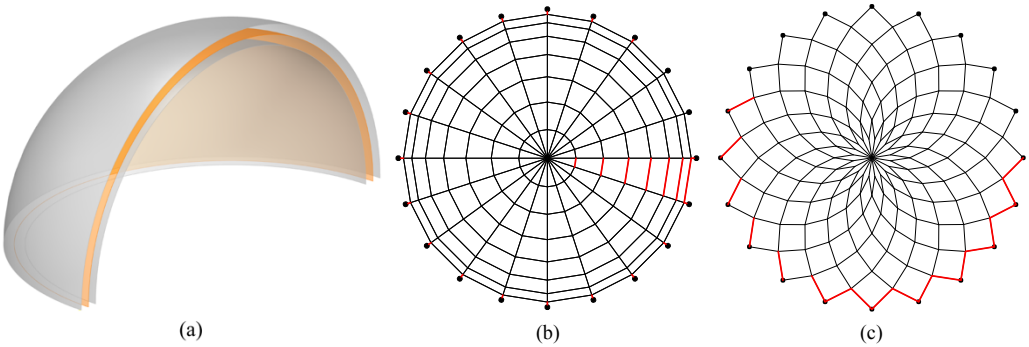


Figure 3. (a) Geometry of the dome with t/R=0.10, showing base surface (orange), intrados and extrados (cut to enhance visualisation); (b) radial form diagram and; (c) spiral form diagram showing independent edges.

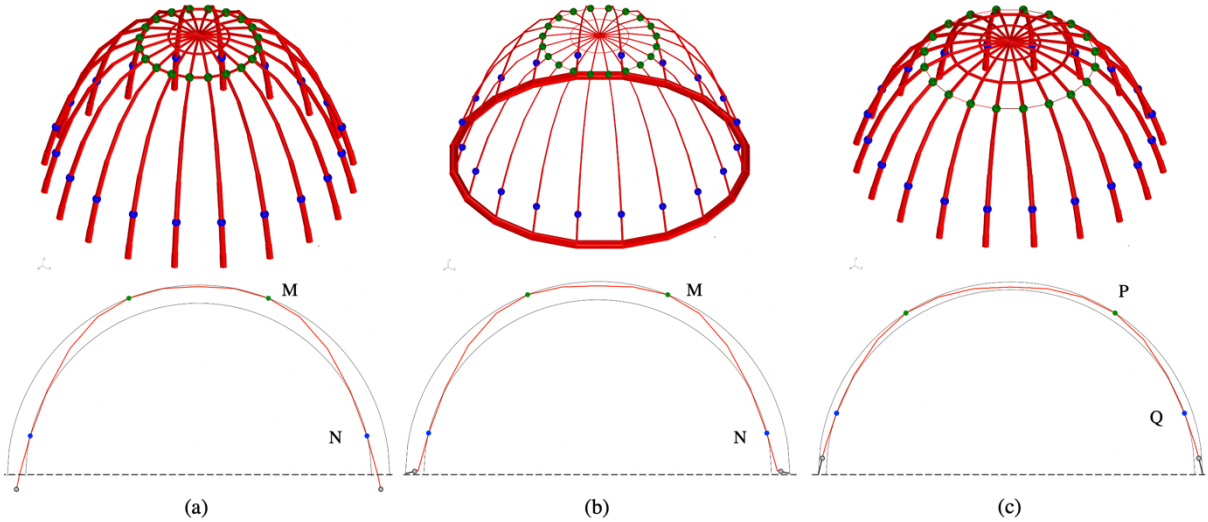


Figure 4. Minimum (a) and maximum (b) thrust solutions for the dome with the radial diagram with t/R=0.10 and with limit thickness (c) achieved (t'/R=0.041). Maximum forces in the plots are 70; 1000; and 72kN.

In the radial diagram, minimum and maximum thrust-over-total-weight ratios for t/R=0.10 are $(T/W)_{min}$=19.8% and $(T/W)_{max}$=430% (Figures 4a-b). The minimum thickness calculated with the radial diagram is t'/R=0.041 where the thrust achieved is $(T/W)_{limit}$=24.4% (Figure 4c). With this result, the safety factor for the dome is estimated as GSF_1=2.42 (Figure 6).

The minimum thrust solution (Figure 4a) shows a bi-axial compressive cap in the upper portion of the dome and an uni-axial stress state towards the supports, where null hoop forces are observed. Looking at a section, the thrust touches the extrados in points M (extrados) and N (intrados) (Figure 4a). Such a stress field is compatible with Heyman's 'orange-slice' mechanism proposed in [23] for an outward (passive) radial displacement of the supports. In this mechanism, cracks form along the meridians where the hoop forces are null and a top cap is preserved uncracked. One can see that while in two dimensions (Section 4.1), the points

touching the intrados and extrados are the only information about cracks (or mechanisms), in the dome, null-forces give additional information about kinematics on the structure.

For the maximum thrust solution (Figure 4b), a compressive ring with high forces is activated in the base of the dome while the magnitude of the forces in the rest of the dome is inferior (see thicknesses of edges). The touchpoints remain in M and N. This suggests that under inward (active) displacement of the supports, a global mechanism for the dome is not activated and the stability is ensured by the compressive ring in the base. This ring creates a discontinuity on the thrust as depicted in the section (Figure 4b), that redirects the reaction force to become almost horizontal. The high difference between maximum and minimum thrust values (22 times greater) gives an idea of the magnitude of the radial pressure supported by the dome.

For the dome in limit thickness condition (Figure 4c) the section and force flow are similar to the minimum thrust with a larger bi-axial cap and section touching in points P (extrados) and Q (intrados). The minimum thickness calculated for the radial diagram is similar to the theoretical $(t/R)_{theory}$=0.042, from [23], with error of 1.4%.

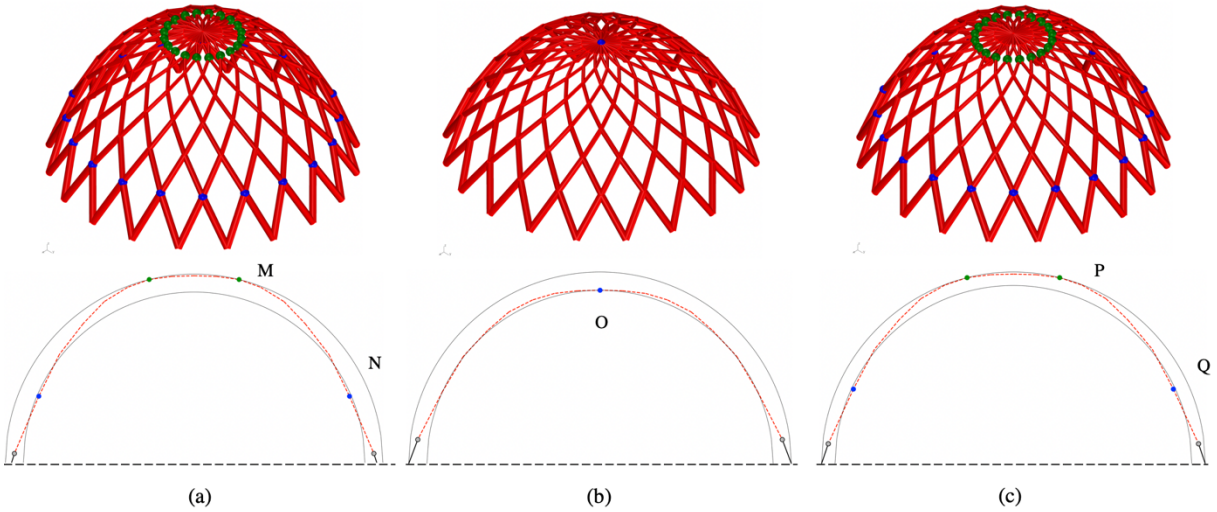


Figure 5. Minimum (a) and maximum (b) thrust solutions for the dome with the spiral diagram with t/R=0.10 and with limit thickness (c) achieved (t'/R=0.073). Maximum forces in the plots are 33; 35; and 34kN.

In the spiral diagram, the minimum and maximum thrust-over-total-weight ratios for t/R=0.10 calculated are $(T/W)_{min}$=31.3% and $(T/W)_{max}$=37.9% (Figure 5a-b). The minimum thickness calculated for this diagram is t'/R=0.073 , with $(T/W)_{limit}$=33.7% (Figure 5c). Such results allow the computation of the safety factor GSF_2=1.37 (Figure 6).

In the spiral diagram, due to its topology, null-force hoops cannot happen; as a consequence, the form diagram will always represent an uncracked solution that does not allow for the 'orange-sliced' mechanism. The GSF_2 found for this pattern is lower, and thus more/over conservative, than for the radial diagram GSF_1. This difference shows the importance of the choice of the form diagram for the assessment with thrust networks. One can also observe that the diagram better aligned with the known pathologies of a dome (radial diagram) resulted in a higher factor of safety and in a further limit state (Figure 6). As expected, refining the diagrams would reduce the errors in the analysis with networks resulting in a slightly higher minimum thickness. However, a sensitivity study on the number of edges is out of the scope of this paper.

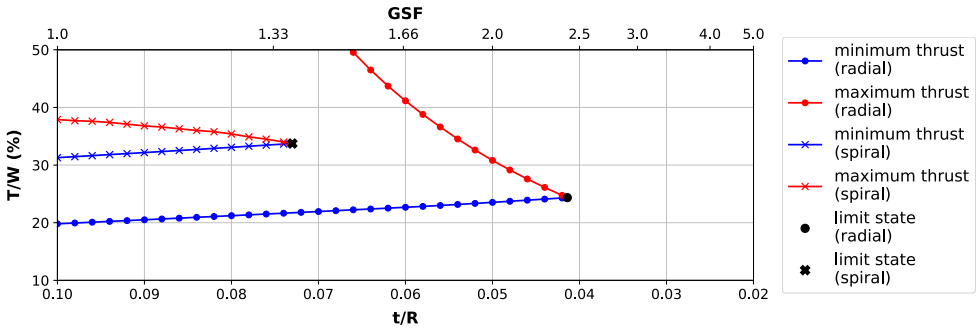


Figure 6. Methodology for deriving the minimum thickness and computing the GSF for the dome (t/R=0.10), the radial diagram resulted in t'/R=0.036 and GSF_1=2.42 and the spiral diagram in t'/R=0.073 and GSF_2=1.37. (Values of T/W higher than 50% not shown for clarity).

4.3 Rectangular cross-vault

We replicate the same analysis for a rectangular rounded cross vault with dimensions 10.0x7.5m and a thickness of t=0.50m. The adimensional parameter is taken with regards to the larger span as t/R=0.10. The geometry is defined by the intersection of two cylinders, the smaller becoming an ellipse. This base geometry is depicted in orange (Figure 7a), with the intrados and extrados for t. Two patterns are proposed referred to as cross- and fan-diagram (Figures 7b-c). The first presents an orthogonal path to the diagonals and then via the groins to the supports, while the second, connects the mid-span to the supports in a straight fashion. The cross diagram has 884 edges, 19 independent edges and the fan has 1024 edges, 36 of which are independent. The self-weight is lumped in the nodes according to the 3D tributary area regarding the projection of the diagrams in the base surface resulting in a total W=902kN for ρ=20kN/m^3. We consider only the four corners of the form diagram to be supported. The results for both patterns regarding minimum, maximum thrust and limit thickness are depicted in Figures 8 and 9. The same incremental analysis is conducted as depicted in Figure 10.

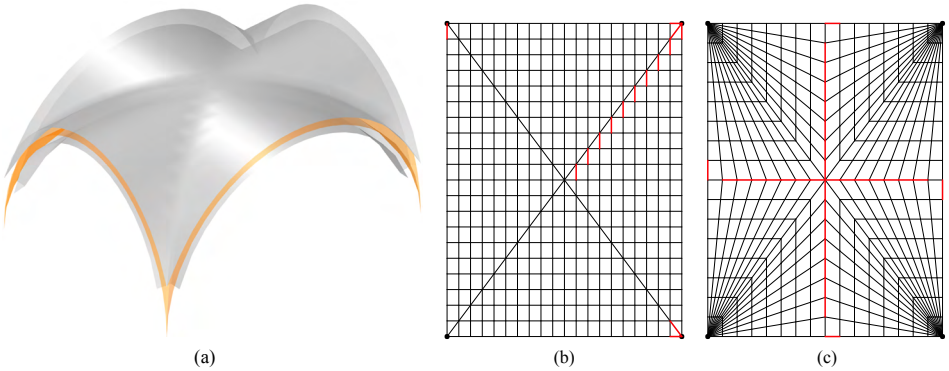


Figure 7. (a) Geometry considered for the rectangular cross-vault (t/R=0.10) , showing base surface (orange), intrados and extrados; (b) cross form diagram and; (c) fan form diagram showing the independent edges.

The adimensional minimum and maximum thrust for the cross diagram are $(T/W)_{min}$=67.5% and $(T/W)_{max}$=96.7% for the initial case t/R=0.10. The minimum thickness calculated in the cross diagram is found to be t'/R=0.061, for a thrust of $(T/W)_{limit}$=76.9%. For the fan diagram,

the difference between the minimum and maximum thrust for t/R=0.10 is smaller, as the optimisation resulted in $(T/W)_{min}$=75.4% and $(T/W)_{max}$=90.9%. The limit state is found for t'/R=0.084, corresponding to a thrust of $(T/W)_{limit}$=80.7%. Based on these values, one can find an estimate to the GSF of the rectangular cross vault studied as GSF_1=1.64 for the cross diagram and GSF_2=1.20 for the fan diagram (Figure 10). This again significant difference, as in the dome example, reaffirms the importance of the form diagram to the present methodology.

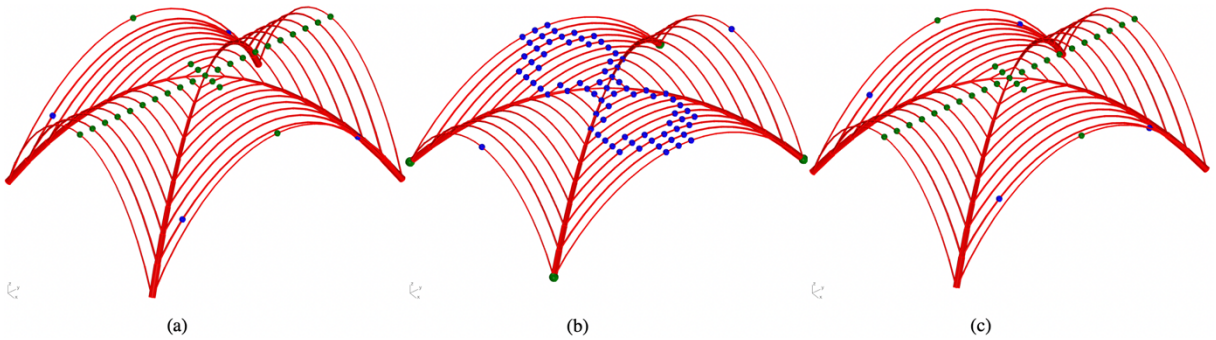


Figure 8. Cross form diagram: minimum (a) and maximum (b) thrust result for t/R=0.10 and thrust for minimum thickness (c) achieved with grid diagram with t'/R=0.061. Maximum forces in plots are 203; 226; and 213kN.

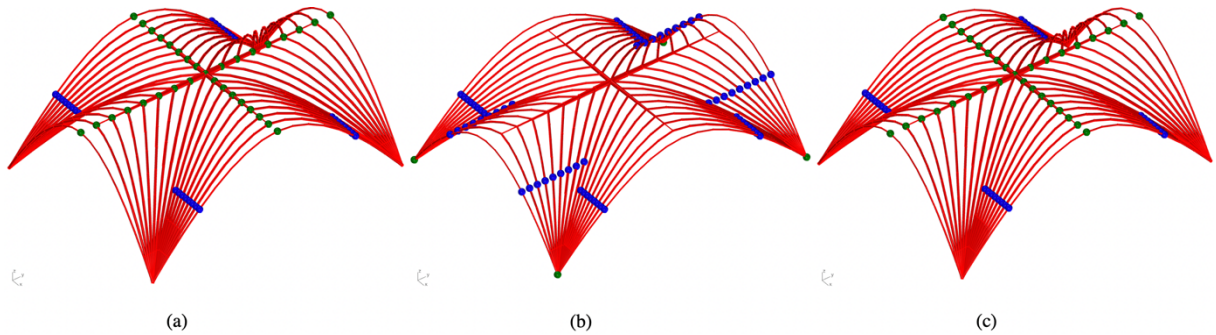


Figure 9. Cross form diagram: minimum (a) and maximum (b) thrust result for t/R=0.10 and thrust for minimum thickness (c) achieved with fan diagram with t'/R=0.084. Maximum forces in plots are 68; 84; and 72kN.

For both diagrams, the minimum thrust touches the extrados in the central portion of the nave, along both spans (Figure 8a and 9a). For the cross diagram, this is more evident in the direction of maximum span (Figure 8a). In the maximum thrust solution, the shallowest thrust is found, which is evident since the network touches the intrados in several points (Figure 8b). For the fan diagram, however, it is observed that the same problem of maximisation did not present such a high number of touching points. Another important difference between the patterns is the fact that for the cross diagram, the forces accumulate along the diagonals, while in the fan diagram, the forces are distributed and the compression force accumulate along the ridges towards the central portion of the vault (Figures 8 and 9).

Regarding the limit analysis, the cross diagram achieved a higher safety factor GSF_1=1.64 against GSF_2=1.20. Similarly to the dome example, the best performing (or less conservative) pattern (i.e. the one with higher GSF) can be seen as a better approximation of the common crack pattern found on cross vaults, known as Sabouret cracks [23] that run parallel to the perimeter of the structure (open edges).

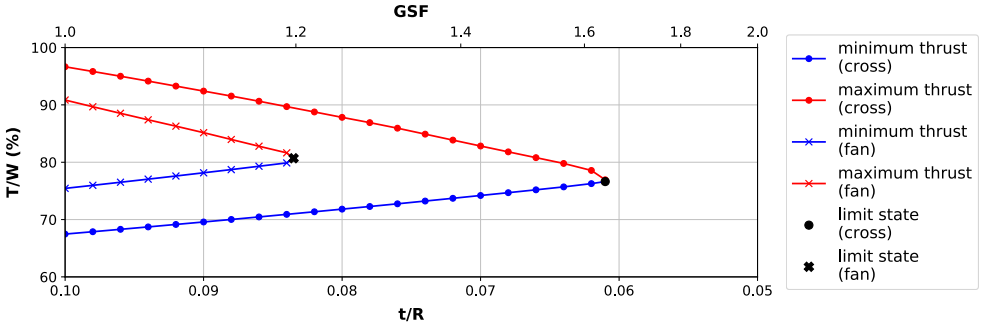


Figure 10. Methodology for deriving the minimum thickness and computing the GSF for the cross vault, cross diagram resulted in t'/R=0.061 and GSF_1=1.64 and the fan diagram in t'/R=0.084 and GSF_2=1.20.

5 CONCLUSION

In the present paper, a methodology to assess masonry structures under vertical loading with thrust networks is developed and implemented in a Python-based tool. A network is described by its fixed projection in plan, the values of its independent force densities $\mathbf{q}_{ind}$ and the heights of the restrained boundary nodes $\mathbf{z}_b$. A nonlinear constrained optimization, with variables $\mathbf{q}_{ind}$ and $\mathbf{z}_b$, is performed yielding the minimum and maximum thrust states for a given masonry vault and form diagram. By sequentially solving for the minimum and maximum thrust networks for decreasing thickness, a methodology for computing the geometric safety factor (GSF) is developed allowing to estimate the closeness to collapse of a given structure. Three applications have been shown: a semi-circular arch, a dome and a cross vault.

A key advantage of the present formulation lies in the fact that it can assess the structure taking as input only the geometry of the intrados and extrados of the vault. On the other hand, the method is built on the formulation of the independent edges, so the solution will be dependent on the given form diagram that cannot change during iterations. This form diagram should be chosen carefully based on assumptions of the flow of forces of the structure to assess. Indeed, it was observed that patterns representing a better approximation of the common crack patterns observed in masonry vaults resulted in higher values of GSF.

Even if not explicitly shown in the examples, the methodology can be extended to estimate the load-bearing capacity under application of additional vertical and horizontal loads. Further development will focus on identifying adapted form diagrams to each problem as even in the presence of an initial, non-perfect (cracked) configuration.

Acknowledgements. This work was supported by the Swiss National Science Foundation (SNSF) - project grant #178953: “Practical Stability Assessment Strategies for Vaulted Unreinforced Masonry Structures”.

REFERENCES

[1] Hooke, R. *A description of helioscopes, and some other instruments*. London: printed by T.R. for John Martyn, (1676).

[2] Poleni, G. *Memorie istoriche della gran cupola del Tempio Vaticano*. Padua: Stamperia del Seminario, (1748).

[3] Heyman, J. The stone skeleton. *Int. J. Solids Struct* (1996) **2(2)**:249-279.

[4] Huerta, S. Mechanics of masonry vaults: The equilibrium approach. In: *3rd Int. Semin. Hist. Constr. Guimarães, Port.* (2001), pp. 47-70.
[5] Ochsendorf, J. Collapse of masonry structures. University of Cambridge, (2002).
[6] O'Dwyer, D. Funicular analysis of masonry vaults. *Comput. Struct.* (1999) **73**:187-197.
[7] Block, P. and Ochesendorf, J. Thrust network analysis: A new methodology for 3D equilibrium. *J. Int. Assoc. Shell Spat. Struct.* (2007) **48(155)**:1-7.
[8] Block, P. Thrust Network Analysis. Massachusetts Institute of Technology, (2009).
[9] Linkwitz K. and Schek, H. Einige Bemerkungen zur Berechnung von vorgespannten Seilnetzkonstruktionen. *Ing. Arch*. (1971) **40**:145-158.
[10] Schek, H. The force density method for form finding and computation of general networks. *Comput. Methods Appl. Mech. Eng.* (1974) **3**:115-134.
[11] Block P. and Lachauer L. Three-dimensional funicular analysis of masonry vaults. *Mech. Res. Commun.* (2014) **56**:53-60.
[12] Block P. and Lachauer, L. Three-dimensional (3D) equilibrium analysis of gothic masonry vaults. *Int. J. Archit. Herit.* (2014) **8(3)**:312-335.
[13] Van Mele, T., Panozzo, D., Sorkine-Hornung, O. and Block, P. Best-fit thrust network analysis: Rationalization of freeform meshes. In: *Shell Structuctures for Archiecture - Form Finding and Optimization*, Routledge (2014), pp. 157-169.
[14] Marmo, F. and Rosati, L. Reformulation and extension of the thrust network analysis. *Comput. Struct.* (2017) **182**:104-118.
[15] Cercadillo-García C. and Fernández-Cabo, J. L. Analytical and Numerical funicular analysis by means of the Parametric Force Density Method. *J. Appl. Res. Technol.* (2016) **14(2)**:108-124.
[16] Fraternali, F. A thrust network approach to the equilibrium problem of unreinforced masonry vaults via polyhedral stress functions. *Mech. Res. Commun.* (2010) **37(2)**:198-204.
[17] Angelillo, M., Babilio, E. and Fortunato, A. Singular stress fields for masonry-like vaults. *Contin. Mech. Thermodyn.* (2013) **25(2)**:423-441.
[18] Fraddosio, A., Lepore, N. and Piccioni, M. D. Thrust Surface Method: An innovative approach for the three-dimensional lower bound Limit Analysis of masonry vaults. *Eng. Struct.* (2019) **202**:109846.
[19] Iannuzzo, A., Dell'Endice, A., Maia Avelino, R., Kao, G.T.C., Van Mele, T. and Block, P. COMPAS Masonry: A Computational Framework for Practical Assessment of Unreinforced Masonry Structures. In: *Proceedings of the SAHC Symposium*, Barcelona, (2021).
[20] Van Mele T. and Block P. Algebraic graph statics. *CAD Comput. Aided Des.* (2014) **53**:104-116.
[21] Liew, A., Avelino, R., Moosavi, V., Van Mele, T. and Block, P. Optimising the load path of compression-only thrust networks through independent sets. *Struct. Multidiscip. Optim.* (2019) **60(1)**:231-244.
[22] Perez, R. E., Jansen, P. W. and Martins, J. R. R. A. pyOpt: A Python-Based Object-Oriented Framework for Nonlinear Constrained Optimization. *Struct. Multidiscip. Optim.* (2012) **45(1)**:101-118.
[23] Heyman, J. *The Stone Skeleton: Structural Engineering of Masonry Architecture*. Cambridge University Press, (1995).

12th International Conference on Structural Analysis of Historical Constructions
SAHC 2020
P. Roca, L. Pelà and C. Molins (Eds.)

NONLINEAR BEHAVIOUR OF TWO-WHYTE STONE WALLS

BURCU DINÇ-ŞENGÖNÜL[1*], YASIN MURAT HOTHOT[2], BILGE DORAN[2], NABI YÜZER[2], SERHAN ULUKAYA[2] AND DİDEM OKTAY[2]

[1]Department of Civil Engineering
Yıldız Technical University
Davutpasa Campus, 34220 Istanbul, Turkey
e-mail: bdinc@yildiz.edu.tr, https://avesis.yildiz.edu.tr/bdinc (*corresponding author)

[2] Department of Civil Engineering
Yıldız Technical University
Davutpasa Campus, 34220 Istanbul, Turkey
email: {yasinmurathothot@gmail.com, doran@yildiz.edu.tr, nyuzer@yildiz.edu.tr, serhanu@yildiz.edu.tr, dyasar@yildiz.edu.tr }

Keywords: Historical Structure, Masonry, Stone Walls, Nonlinear Behaviour

Abstract. *Engineers work hard to convert the highly uncertain and nonlinear behavior of historic masonry structures into something that can be understood with mathematical certainty. Therefore, practical and also accurate structural analysis techniques are still needed for the preserve the historical monuments as a huge cultural heritage. In this context, determining the mechanical properties of historical walls under in-plane and out-of-plane lateral loadings is one of the most important aim. This study aims to investigate the three dimensional (3D) nonlinear behaviour of stone walls subjected to a combination of lateral and vertical loads using approprate constitutive numerical modeling. For this purpose, a simplified micro modeling approach has been proposed for the 3D nonlinear finite element analysis (NLFEA) of stone wall. The dry-stone masonry wall from the literature has been used in the verification step for the proposed model. After that, the new two-whyte stone wall has been constructed in accordance with the original material characteristics derived from the experimental studies and tested under shear compression. Finally, numerical results of NLFEA and experimental results of walls have been compared. It was observed that the numerical analysis results are well matched with the experimental ones.*

1 INTRODUCTION

Masonry historic structures represent architectural cultural heritage of great historical importance in Turkey. They have been used for public and residential buildings in the past several thousand years. A great number of well-preserved old masonry structures still exist proving that this form of construction can successfully resist loads and environmental impact [1]. Conventionally, most major buildings were solid walled structures with the walls bearing directly on the ground. Historical masonry structures are exposed to horizontal and vertical

loads and atmospheric influences throughout their entire life. These structures are composed of many layers and due to the weak connections between the weak materials and gaps, the masonry walls in these structures tend to leave the building. For this reason, damages, cracks, gaps may occur as a result of environmental impacts in historical masonry structures and even dangerous situations can occur [2]. Since these damages are directly related to the loads affecting the structure, it is very important to investigate the complex and nonlinear behavior of the structures by numerical analysis [1,3–5].

The primary aim of this study is to present an effective modeling procedure for the stone masonry walls under shear and compression. For this purpose, in the first part of this study, the mechanical properties of stone and mortar samples provided from a historical masonry structure in Turkey have been determined at laboratory conditions. Then, the two-whyte stone wall which have nominal dimensions 1010x1005x280 mm (lenght x height x width) have been constructed in the laboratory of Yildiz Technical University in accordance with the original material characteristics derived from the experimental studies. In order to evaluate the nonlinear behaviour of two-wyhte stone wall, these wall have been tested under shear-compression. Then this experimental study has been modelled in ABAQUS-6.14 package [6]. An experimental study conducted by Lorenco et. al., which involved dry stone masonry walls under a combination of vertical preloading, and in-plane horizontal shear loading has been selected for the verification of the numerical modeling technique. After that, experimental and numerical results of constructed in laboratory were compared.

2 NUMERICAL AND CONSTITUTIVE MODELING

A number of experimental and analytical studies have been conducted on the behavior of masonry shear walls to reach a comprehensive understanding of complex masonry behavior [[1,3,7–12]]. Proposed theoretical models for implementation to finite element analysis of masonry generally require a large number of material parameters that are difficult to measure easily and reliably. For this reason, several attempts have been made to express the stress-strain relationships of the masonry and its constituents using different modeling techniques such as micro-modeling, homogenization approach and macro-modeling. The common approach is to treat masonry as a continuous medium with the exception of micro-modeling. Micro-modeling should describe the masonry, mortar and the interaction behavior between them. It has been revealed in literature that micro models are more suitable for modeling small structures and the studies in which the interaction between mortar-stone and/or failure modes are important. On the other hand, in macro models, the structural elements are modeled as homogeneous (brick/stone and mortar are modeled together) and the stress-strain relations and fracture surfaces of these elements are described first. Macro models are more useful for larger structures and when the behavior of the entire structure is investigated. In this study, micro modeling technique is addopted for nonlinear analysis of masonry stone walls.

Multi-axial stress states defines the constitutive behavior of the structures such as masonry walls, RC panels, confined columns or elements beyond the elastic range. The basic elastoplastic constitutive models, i.e Mohr-Coulomb (MC) and Drucker-Prager (DP) are widely adopted in constitutive modeling materials, like concretes, soils and rocks [4,13]. Drucker-Prager (DP) yield/break criterion is the most practical mathematical form of the von-Mises criterion used for concrete, metal and stone type materials, and takes into account both

hydrostatic pressure and deviator stress effects at the highest strength (Figure 1)[9]. According to the DP yield criteria, the yield surface can be expressed as follows [6]:

$$f(I_1, J_2) = \alpha . I_1 + \sqrt{J_2} - k = 0 \tag{1}$$

where α and k values are material constants and these values depend on the internal friction angle (ϕ) and cohesion (c) values in the MC criterion. Internal friction angle (ϕ) and cohesion (c) values can be expressed as [6]:

$$\alpha = \frac{2\sin\phi}{\sqrt{3}(3-\sin\phi)}, \qquad k = \frac{6c\cos\phi}{\sqrt{3}(3-\sin\phi)} \tag{2}$$

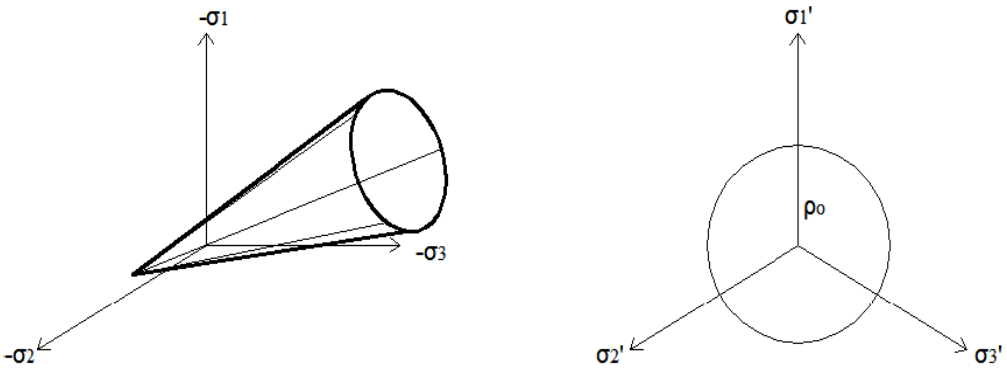


Figure 1: DP criterion:(a) yield surface in the principal stress space;(b) π plane [9]

The MC criterion takes into account the effect of hydrostatic pressure. The MC yield surface is in the form of a hexagonal cone in the deviatoric stress plane. Figure 2 shows yield surface in the principal stress space and π plane [9]:

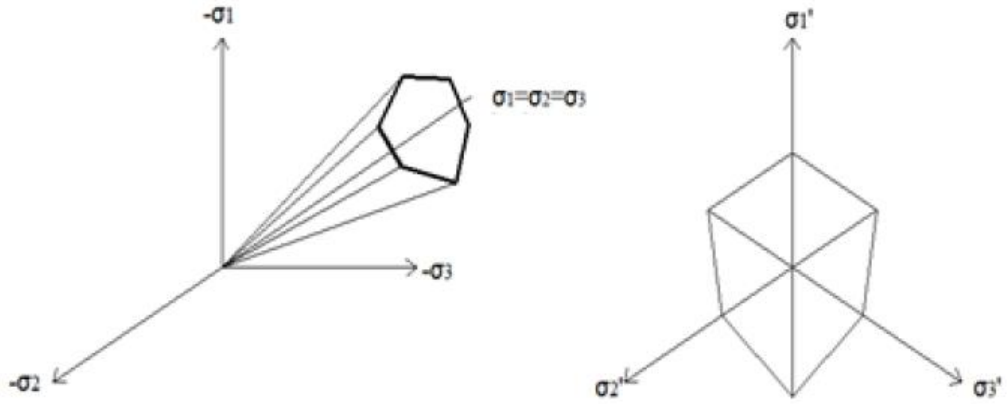


Figure 2: MC criterion:(a) yield surface in the principal stress space;(b) π plane [9]

The MC criterion shows the linear envelope curve obtained from the shear strength of the

material against the applied normal strength [9]. This relationship is expressed as follows [6]:

$$\tau = c - \sigma \tan(\phi) \tag{3}$$

where τ is shear strenght, σ corresponds to normal stress which is negative in compression, c is cohession and ϕ is the internal friction angle. From Mohr's circle [6]:

$$\tau = s\cos\phi \qquad \sigma = \sigma_m + s\sin\phi \tag{4}$$

Substituting for τ and σ, multiplying both sides by $\cos\phi$, and reducing, the Mohr-Coulomb model can be written as [6]:

$$s = \sigma_m \sin\phi - c\cos\phi = 0 \tag{5}$$

where s is half of the difference between the maximum principal stress, σ_1, and the minimum principal stress, σ_3 (and is, therefore, the maximum shear stress),

$$s = \frac{1}{2}(\sigma_1 - \sigma_3) \tag{6}$$

and σ_m is the average of the maximum and minimum principal stresses, and ϕ is the frictional angel [6]:

$$\sigma_m = \frac{1}{2}(\sigma_1 + \sigma_3) \tag{7}$$

3 SOFTWARE IMPLEMENTATION OF PROPOSED CONSTITUTIVE MODEL

Three dimensional (3D) finite element models have been used for stone masonry walls. Masonry constituents, e.g. stone and mortar, are assumed to be isotropic elasto-plastic obeying DP criterion and modeled separately with eight-node brick element (C3D8) [6]. Besides, the mortar thickness and the brick–mortar interface are lumped into a surface to surface interaction while the dimensions of the brick unit are expanded to keep the geometry of a masonry structure unchanged (Figure 3) [6]. In this modeling tecnique, a surface interaction consist of normal behaviour and tangential behaviour [6]. Constitutive model mentioned above has been used for the numerical simulations of sample stone masonry walls.

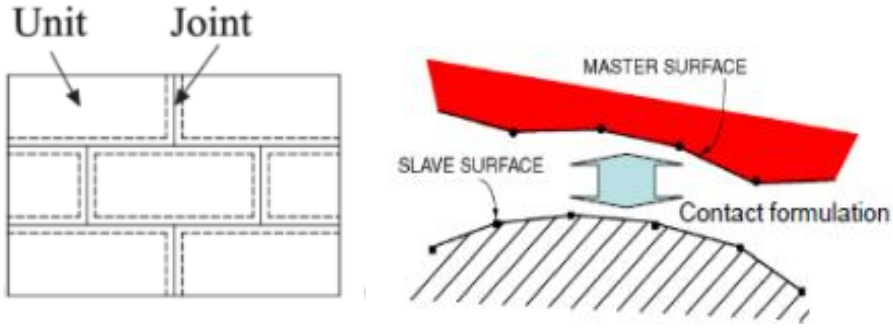


Figure 3: Simplified micro-modeling technique and surface to surface contact [6]

Lourenco et. al. [3], tested 1000x1000x200 mm dry stone masonry walls under a combination of vertical preloading, and in-plane horizontal shear loading (Figure 4). Brick dimensions were used as 200x200x100 mm and 100x100x100 mm in this tests. Two connected hydraulic jacks (N) were placed on the wall while the shear load was applied to the

wall by a horizontal hydraulic jack (P). In this study, the vertical load levels adopted for the tests were 30, 100, 200, and 250 kN. These load values lead to compressive normal stresses of 0.15, 0.50, 1.00, and 1.25 MPa, respectively. A numerical simulation of the tested stone walls was carried out with the Abaqus software [6]. Mechanical properties for test wall and values adopted for FE analyses are given in Table 1, respectively. Both simulation model and laboratory test results agreed very well (Figure 5). Also deformed shape of the experimental and numerical model of the wall was given in Figure 6 [3].

Table 1. Comparison of Experimental and Numerical Parameters

Parameters	Experimental [3]	Numerical
Weight (kN/m^3)	25	25
Young's Modulus (MPa)	1202	2000
Poisson's ratio	0.2	0.2
Friction angles	32	32
Dilatancy angles	0	0
Flow stress ratio	-	0.8
Yield stress (kPa)	-	9000
Friction coefficient	0.39	0.39
Vertical load (kN)	250	250

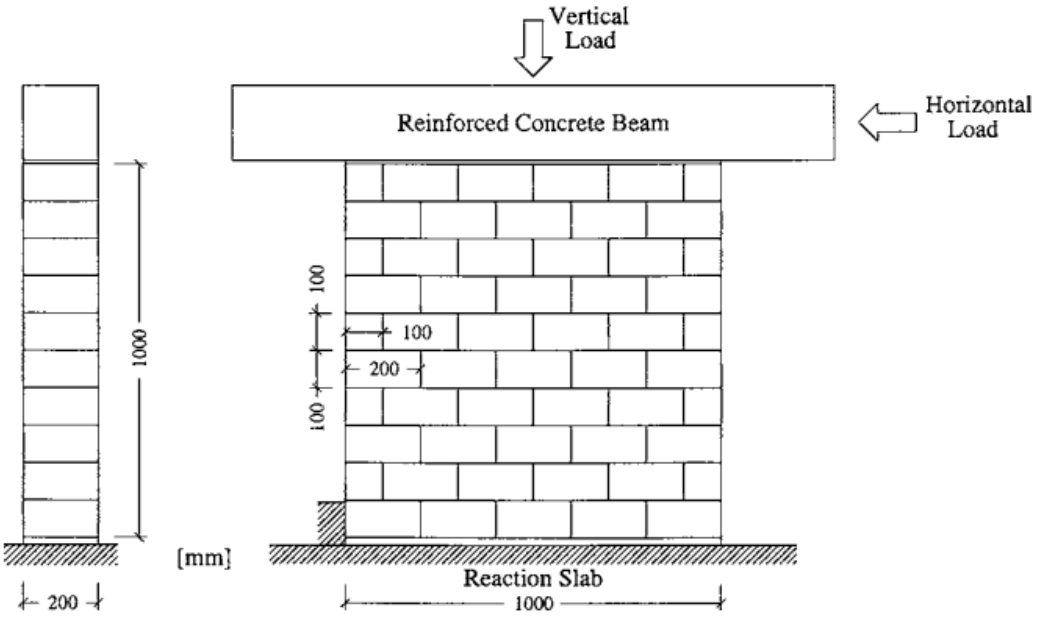


Figure 4: Experimental setup of dry stone masonry wall [3]

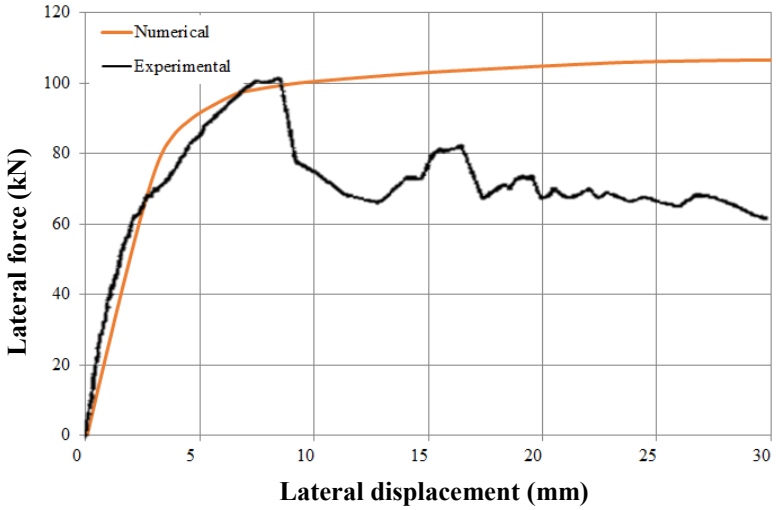


Figure 5: Comparison of experimental and numerical analysis results

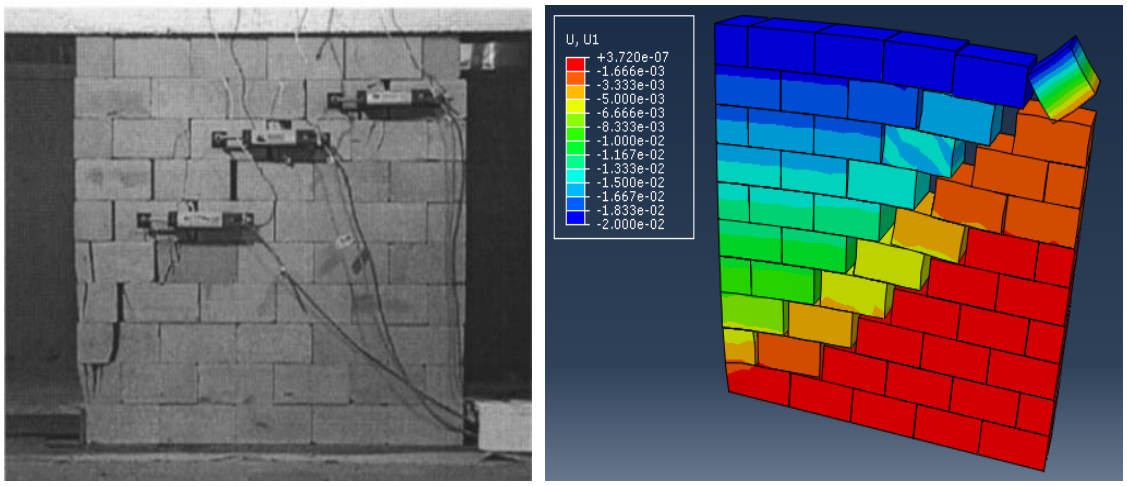


Figure 6: Experimental and numerical comparison of failure mechanism [3]

In the experimental part of this study, the two-whyte stone masonry wall with dimensions of 1010x1005x280 mm were produced in accordance with the orginal material characteristic (Figure 7). The constituents and mix proportions of produced mortar were selected to be compatible with historical lime based mortar specimens. Mechanical parameters of two-whyte stone masonry wall are given in Table 2. The specimen sizes used in mechanical experiments for stone (cylindrical) are different from stone which used in the two-whyte masonry stone model wall. Assuming that the increase in size increases defects (cracks, gaps, etc.) in the specimen, Young's modulus and uniaxial compressive strength values have been decreased in numerical analysis (Table 2).

At the 28th day after the construction, the wall was subjected to increasing lateral load under a constant, uniformly distributed vertical load. The loading apparatus consisted of a

2000 kN and 500 kN capacities hydraulic rams for vertical and horizontal loading, respectively. Instrumentation included two load cells and four displacement transducers (Figure 8). Vertical pre-compression distributed loading of 1.06 MPa was applied to the top surface of a steel plate with a thickness of 3.5 cm located on the center of wall. Lateral loading was then applied at a rate of 0.6±0.1 kN/s. For repairing and strengthening issues, the stone test wall was not loaded to failure (total destruction was not proposed). As shown in Figure 8, when a stair step crack appeared and extended diagonally across the wall, the test was stopped. Finally, experimental and numerical analysis results of two-wyhte masonry wall were compared (Figure 9). Also deformed shape of the numerical model of the two-wyhte masonry wall was given in Figure 10.

Table 2. Experimental and Numerical Parameters of two-whyte stone masonry wall

Parameters	Experimental (stone brick)	Numerical (stone brick+mortar)
Weight (kN/m^3)	25	25
Young's Modulus (MPa)	13000	5000
Poisson's ratio	0.28	0.28
Friction angles	52	52
Dilatancy angles	-	10
Flow stress ratio	-	0.8
Yield stress (kPa)	49000	10000
Friction coefficient	-	0.5

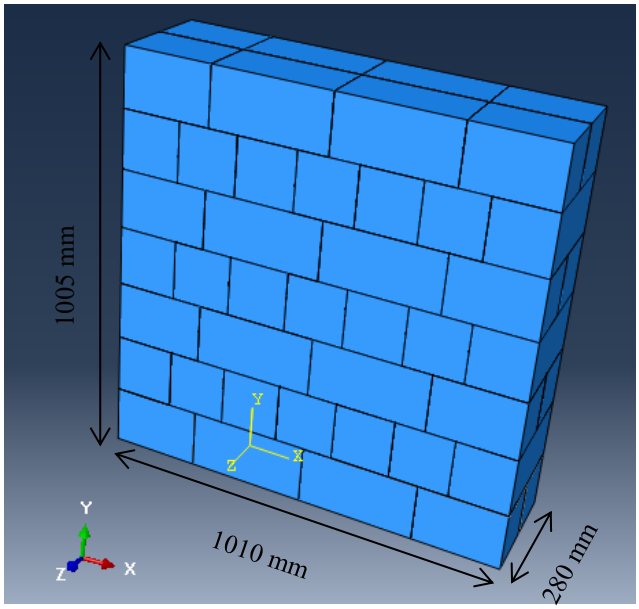


Figure 7: Geometry for the two-whyte stone masonry wall



Figure 8: Experimental set-up

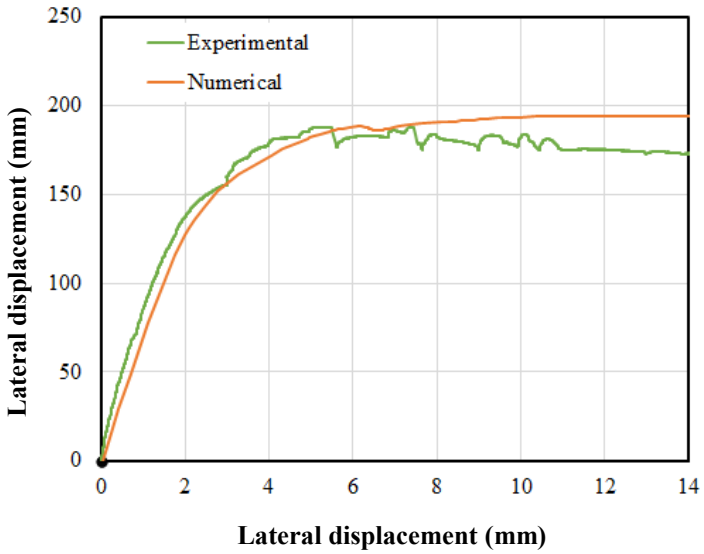


Figure 9: Comparison of experimental and numerical analysis result for two-whyte masonry wall

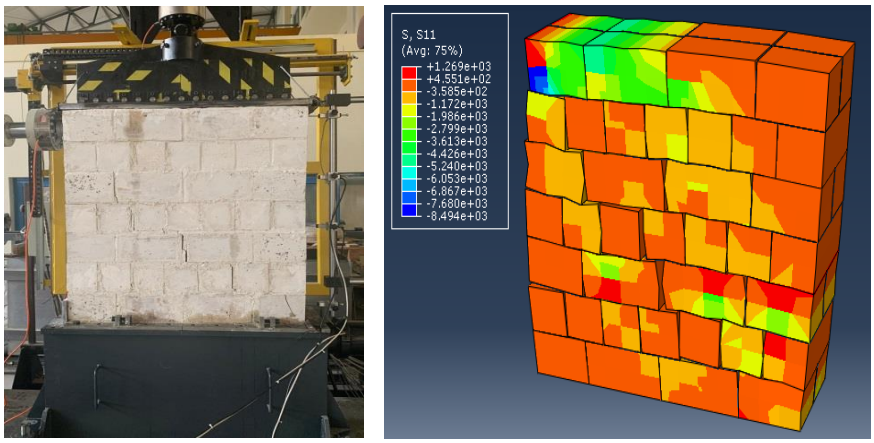


Figure 10: Deformed shape of two-whyte stone wall numerical analysis result

4 CONCLUSIONS

In the present paper, Drucker-Prager (DP) type plasticity is proposed to model the in-plane non-linear structural behavior of stone walls. In order to evaluate the accuracy of proposed simplified micro modeling technique, numerical results of a nonlinear finite element analysis (NLFEA) are compared with the test results of two walls. The following conclusions are drawn from the results:

1. The material parameters of DP criterion for both masonry units and mortar that are considered separately as isotropic and homogeneous materials is expressed in terms of the cohesion and the internal friction angle of Mohr-Coulomb (MC) criterion in this study. Therefore, the surfaces of both DP and MC yield criteria are made to coincide along the compression meridian.
2. For dry stone and two-whyte stone masonry walls, cracks mostly follow along cement mortar joints in a stair step manner.
3. Comparison of the wall responses subjected to vertical and lateral loads between analytical and experimental results, especially for dry stone masonry wall, indicates reasonable agreement except the shape of the load-displacement curves for both mortar joint and dry joint masonry after peak point. The reason for this is that there exists no gradually developing damage defined in the elasto-plastic model.

REFERENCES

[1] Kömürcü, S., Yığma duvarların düzlem içi kırılma mekanizmalarının nümerik olarak belirlenmesi, (In Turkish), MSc. Thesis, İstanbul Technical University (2018).

[2] Baltazar, L.G., Henriques, F.M.A., Cidade, M.T., Experimental study and modeling of rheological and mechanical properties of NHL grouts, 27 (2015) 1–11. https://doi.org/10.1061/(ASCE)MT.1943-5533.0001320.

[3] Lourenço, P.B., Oliveira, D.V., Roca, P., Orduña, A., Dry joint stone masonry walls

subjected to in-plane combined loading, J. Struct. Eng. 131 (2005) 1665–1673. https://doi.org/10.1061/(ASCE)0733-9445(2005)131:11(1665).
[4] Bal, İ.E., Yığma yapılarda doğrusal olmayan artımsal analiz için bir yöntem önerisi,(In Turkish) Dicle Üniversitesi Mühendislik Fakültesi Mühendislik Derg. (2017) 463–474.
[5] Milani, G., Lourenço, P.B., 3D non-linear behavior of masonry arch bridges, Comput. Struct. 110–111 (2012) 133–150. https://doi.org/10.1016/j.compstruc.2012.07.008.
[6] D.S. Simulia, Abaqus 6.14, Analysis User's Guide. (2014).
[7] Doran, B., Orhun Koksal, H., Aktan, S., Ulukaya, S., Oktay, D., Yuzer, N., In-Plane shear behavior of traditional masonry walls, Int. J. Archit. Herit. 11 (2017) 278–291. https://doi.org/10.1080/15583058.2016.1207114.
[8] Doran, B., Yuzer, N., Aktan, S., Oktay, D., Ulukaya, S., Numerical Modeling of Traditional Masonry Walls Strengthened with Grout Injection, Int. J. Archit. Herit. 0 (2019) 1–16. https://doi.org/10.1080/15583058.2019.1618970.
[9] Aktan, S., Düzlem İçi Yükler Etkisindeki Yığma Duvarlarda Bünyesel Modelleme, (In Turkish), PhD. Thesis, Yildiz Technical University (2016).
[10] Oliveira, D.V, Lourenço, P.B., Experimental Behaviour of three-leaf stone masonry walls, Conf. Brok. Event Constr. Asp. Built Herit. Prot. (2006) 355–362.
[11] Corradi, M., Tedeschi, C., Binda, L., Borri, A., Experimental evaluation of shear and compression strength of masonry wall before and after reinforcement: Deep repointing, Constr. Build. Mater. 22 (2008) 463–472. https://doi.org/10.1016/j.conbuildmat.2006.11.021.
[12] Abdulla, K.F., Cunningham, L.S., Gillie, M., Simulating masonry wall behaviour using a simplified micro-model approach, Eng. Struct. 151 (2017) 349–365. https://doi.org/10.1016/j.engstruct.2017.08.021.
[13] Köksal, H.O., Jafarov, O., Doran, B., Aktan, S., Karakoç, C., Computational material modeling of masonry walls strengthened with fiber reinforced polymers, Struct. Eng. Mech. 48 (2013) 737–755. https://doi.org/10.12989/sem.2013.48.5.737.

12th International Conference on Structural Analysis of Historical Constructions
SAHC 2020
P. Roca, L. Pelà and C. Molins (Eds.)

NOVEL CONSTITUTIVE MODELLING APPROACH FOR SHAPE MEMORY ALLOYS VIBRATION CONTROL DEVICES

KACPER WASILEWSKI[1*] AND ARTUR ZBICIAK[2]

[1]Faculty of Civil Engineering
Warsaw University of Technology
16 Armii Ludowej Ave., 00-637 Warsaw, Poland
e-mail: k.wasilewski@il.pw.edu.pl, http://www.il.pw.edu.pl (*corresponding author)

[2] Faculty of Civil Engineering
Warsaw University of Technology
16 Armii Ludowej Ave., 00-637 Warsaw, Poland
e-mail: a.zbiciak@il.pw.edu.pl, http://www.il.pw.edu.pl

Keywords: Shape Memory Alloys, Rheological model, Seismic engineering, Non-linear vibrations

Abstract. *One of the main fields of shape memory alloy application in civil engineering is oriented on mitigation of earthquake effects on structures. Vibration isolators that incorporate elements made of SMA take advantage of its characteristic phenomenon of nonlinear hysteretic response, also known as superelasticity. In this work, authors presents an approach to phenomenological modelling of SMA by using rheological schemes. One of the advantages of this approach is a possibility of formulation of constitutive relationships as a set of explicit differential equations. As an illustration of validity of the formulation, authors present the response of single degree of freedom oscillator that incorporates SMA elements modelled by different existing SMA models. The response obtained based on the model that uses rheological schemes is compared with Lagoudas thermodynamic constitutive SMA model and simplified material model. All of the compered models are found to match well and show important reduction in displacement transmissibility.*

1 INTRODUCTION

Shape memory alloys (SMA) belongs to the family of smart materials being comprehensively studied in recent decades. One of the main fields of its application in civil engineering is oriented on mitigation of earthquake effects on structures. Vibration control devices that incorporate elements made of SMA take advantage of its characteristic phenomenon of nonlinear hysteretic response, also known as superelasticity [1]. Such devices are especially promising for retrofitting and protection of architectural heritage what was verified in several application for strengthening of cultural heritage structures.

In this work, authors present a novel approach to modelling of SMA by using rheological schemes. As an illustration of validity of the formulation, authors present the response of a single degree of freedom oscillator that incorporates SMA elements modeled by different existing SMA models. The response obtained based on the model that uses rheological schemes

is compared with thermodynamic constitutive SMA model developed by Lagoudas et al. [2, 3] and simplified material model also presented by Lagoudas et al. [4].

2 CHARACTERISTICS OF SMA

The first observations of shape memory specific characteristic behaviour were done during the first half of 20th century. First in 1932, Ölander observed "rubber like effect", later named as superelasticity, in an alloy of gold and cadmium [5]. Further studies of this alloy led to observation of "shape recovery", later named as shape memory effect, by Chang and Read in 1951 [6]. The breakthrough event for SMA studies was the discovery of Nitinol, an alloy of nickel and titanium, in 1963 by Buehler and co-workers from U.S. Naval Ordnance Laboratory [7]. Since then it has been discovered that alloys such as copper-zinc-aluminium alloy [8], copper-aluminium-nickel alloy, iron-platinum alloy, iron-palladium or iron-manganese-silicon alloy [9] presents similar unique properties. However, the Nitinol is considered as the alloy that shows the best shape memory properties [10]. SMAs find applications in various fields of engineering such as aeronautics [11], biomedical engineering [12] (especially cardiovascular applications [13]) and structural engineering [14, 15].

The main characteristic of SMAs that benefits for the application in the structural engineering field is superelasticity. This phenomenon can be described based on the graph of the response for the uniaxial tension test of the SMA specimen (Figure 1). After the initial, close to linear, response the superelastic plateau occurs. This kind of response is similar to the one observed during yielding but in this case it is related to stress-induced phase transformation from austenite to martensite (arrow 1 in Figure 1). When the phase transformation completes the further elastic transformation follows the rise of tensile stresses. Upon the stress removal, the reverse phase transformation, from martensite to austenite (arrow 2 in Figure 1) is induced. It results in almost complete strain recovery.

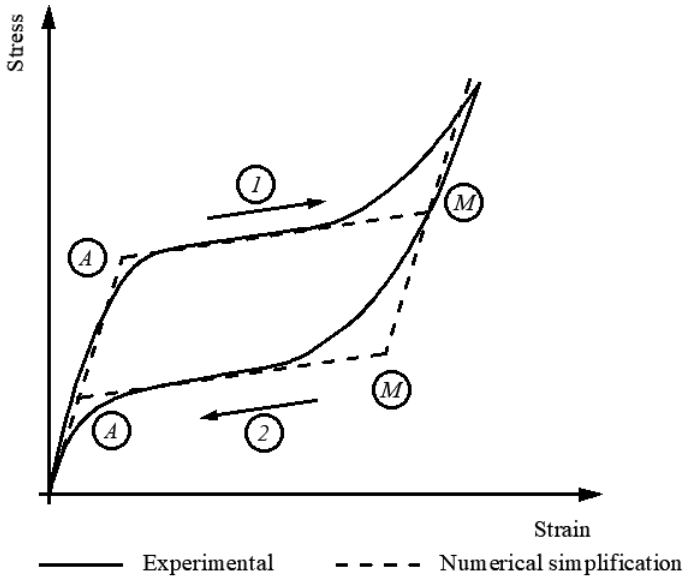


Figure 1: Shape of hysteresis loop of SMA and its numerical simplification

3 SMA IN RETROFITTING OF HISTORICAL STRUCTURES

Applications of SMA in strengthening of cultural heritage structures base on the traditional tying techniques increasing the box-type behaviour of the building. The performance of ties that incorporate SMA elements is enhanced due to the phenomenon of the superelasticity. In case of ground motions with low intensity or other horizontal loads the SMA elements work in the first, elastic branch (Figure 1) what results in behaviour similar to classic (e.g., steel) ties. In case of strong ground motion, SMA elements undergo phase transformation what effects in reduction of stiffness and allowance for controlled displacement of tied members. This phenomenon permits the structure to dissipate part of the energy through a microcracking instead of a dangerous macrocracking. The displacement is later recovered upon the load removal. The noticeable fact is a lower force transmitted to the historical material. Finally, in case of severe ground motion or other extraordinary horizontal load the stiffness of SMA elements increase what helps preventing from excessive displacements [16].

The reinforcement technique for historical structures that incorporates SMA was studied and developed within the ISTECH Project [17]. It based on a device, equipped with wires made of SMA, that reduce the risk of collapse of masonry buildings in case of strong earthquake actions. The trial intervention was implemented in 1999 during restoration of bell tower of San Giorgio church in Trignano after the earthquake in October 1996 which struck the Reggio Emilia and Modena Districts (Italy) [18]. SMA devices were installed as a parts of vertical post-tensioned ties that improve bending and shear resistance (Figure 2a). Despite the numerical and experimental campaign, the application was also verified by another earthquake in June 2000, after which the structure showed no damage of any type. That proved the effectiveness of such a technique.

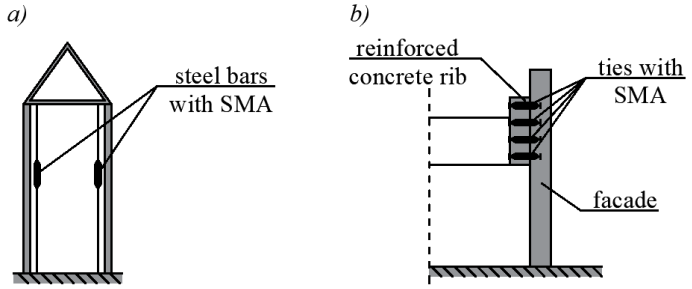


Figure 2: Schemes of the SMA devise arrangements for retrofitting of historical structures – (a) vertical ties in slender structures [18] and (b) horizontal ties for facades [16]

The successful results of the research and exploitation of ISTECH project led to the further application of SMA in restoration of the Basilic of San Francisco in Assisi and the Cathedral of San Feliciano in Foligno [16]. In those cases the strengthening was intended to improve the connection between perpendicular elements (Figure 2b), such as the transept tympanum (in the Basilic of San Francisco) and the façade (in the Cathedral of San Feliciano). Such an intervention aim at the prevention of a out-of-plane collapse of tied elements.

Another investigation was performed by Cardone et al. [19] who examined a behavior of SMA implemented in ties of timber roof trusses. The experimental campaign, that included

thermal behavior and shaking table tests, led to the installation of prototype device in the San Paolo Eremita church in Brindisi.

Presented applications of SMA in historical structures show their several advantages. The improvement of box-type behaviour of buildings, originated from traditional ties, is followed by possibility of controlled displacement that leads to energy dissipation. Moreover, the features of SMA, allow to control the forces in ties not only related to the seismic event but also to changes of temperature, corrosion, and relaxation due to deformation of masonry (creep) [18–20].

4 NUMERICAL MODELLING OF SMA

According to Cisse et al. [21] the constitutive models of SMA could be divided in terms of modelling scale and mathematical structure in the following groups:

- microscopic thermodynamic models,
- micro-macro models and
- macroscopic models.

The models from the first category describe microstructural features in SMA behaviour (e.g., phase nucleation, interface motion, martensite twin growth) at the lattice or grain-crystal levels. The models from the following category rely on micromechanics to describe the material behaviour at the micro or meso scales and then based on a scale transition macroscopic constitutive equations are derived. The last group consists of the models that describe the behaviour of polycrystalline SMAs based on phenomenological considerations, simplified micro-macro thermodynamics or direct experimental data fitting [21].

In case of the analysis of the applications in the field of structural engineering the main goal is to study the influence of SMA elements incorporated in the structure to its response for the excitation. In such a case the most efficient models are the phenomenological macroscopic one.

4.1 SMA vibration control devices modelling with rheological schemes

The concept of modelling SMA as a certain set of rheological elements was earlier discussed by authors in [22–26]. This approach belongs to the group of macroscopic models of SMA and allows to analyse behaviour of structural members without a detailed analysis of the phenomena at the microcrystal level.

The model of a vibration control device can be represented as a single degree of freedom system (Figure 3a) where the mass displacement is given by $X(t)$ and base displacement by $Y(t)$. In this configuration the SMA element is given as a “black box” that expresses the particular set of rheological elements. By the proper configuration of linear elastic springs (characterized by the stiffnesses k_1 and k_2 in Figure 3b), perfectly plastic body (characterized by the force T_0 in Figure 3b) and perfectly elastic body (characterized by the force P_0 in Figure 3b) the hysteretic loop given in Figure 3c can be obtained. In such a configuration the perfectly plastic body is responsible for energy dissipation of the structure, while the perfectly elastic body, along with linear elastic springs, are responsible for energy accumulation. A detailed explanation as well as one-dimensional characteristics of elements are wider discussed in [26].

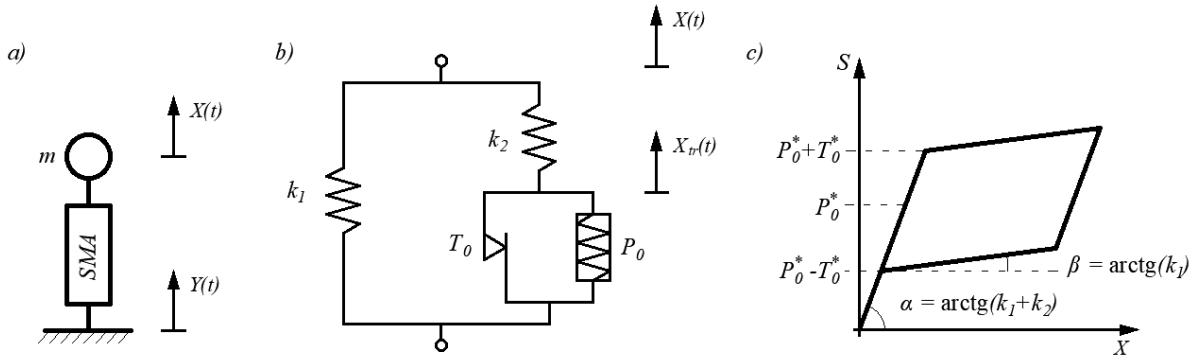


Figure 3: Schematic representation of SMA vibration control device, SMA rheological scheme and the graph of the hysteretic loop

The resultant hysteretic loop (Figure 3c) is characterized by the modified values of forces P_0^* and T_0^*. The correction is a result of kinematic strengthening which is associated with the presence of the k_1 spring in the model. This implicates the increase of the initial value of the internal force at the beginning of the martensitic phase transformation. The correction is given by the equations

$$P_0^* = \frac{k_1 + k_2}{k_2} P_0, \quad T_0^* = \frac{k_1 + k_2}{k_2} T_0 \tag{1}$$

In the structural analysis of buildings subjected to the earthquakes the typical excitation applied to the structure is a ground acceleration related to ground motion. The following equations will be presented following such a kind of excitation. Taking it into consideration the equation of motion of the system shown in Figure 3a is given by the following differential equation

$$m\ddot{X}(t) + S(t) = -m\ddot{Y}(t) \tag{2}$$

where $S(t)$ is a force response of SMA rheological model given by the equation

$$\begin{aligned} S(t) &= S_1(t) + S_2(t) \\ S_1(t) &= k_1 X(t) \\ S_2(t) &= k_2 \left(X(t) - X_{tr}(t) \right) \end{aligned} \tag{3}$$

The rate of deformation of the phase transformation $\dot{X}_{tr}$ is given by

$$\dot{X}_{tr} = f_{SMA}\left(\dot{X}, X, X_{tr} \right) \tag{4}$$

where

$$f_{SMA} = \begin{cases} \dot{X} & \text{if} \quad |S_2| = P_0 + T_0 \text{ and } S_2 \dot{X} > 0 \\ \dot{X} & \text{if} \quad |S_2| = P_0 - T_0 \text{ and } S_2 \dot{X} < 0 \text{ and } S_2 X_{tr} > 0 \\ 0 & \text{otherwise} \end{cases} \tag{5}$$

The above presented set of explicit non-linear differential equations enable to model a

behaviour of SMAs in isothermal conditions in a certain temperature. In different temperatures values of P_0 and T_0 will vary. The generalization of the model for different thermal conditions is possible by determination of the relation between forces P_0 and T_0 and temperature. However this generalization does not influence the character of the presented equations.

5 RESULTS COMPARISON

In order to compare results of the discussed approach to constitutive modelling let consider a SDOF system presented earlier in Figure 3a. The damping of the mass displacements takes place due to stress induced phase transformation of SMA and its hysteretic response.

The considered excitation is a harmonic acceleration applied to the mass. Details of the excitation and material characteristics are given in Table 1. In order to make a comparison those values are based on the numerical example from the work of Lagoudas et al. [4].

Table 1 Design and material parameters

Design parameters		Material model parameters	
Mass	500 kg	k_1	527 N/mm
Amplitude of base excitation	153,4 m/s^2	k_2	14620 N/mm
Frequency of base excitation	50 Hz	P_0	6519 N
		T_0	5761 N

The discussed equations (2) - (5) were implemented in Wolfram Mathematica software. The set of differential equations was numerically solved applying *NDSolve* function by incorporation of forward Euler (*ExplicitEuler*) method. The results are presented below as a set of graphs showing the time history of the mass displacement (Figure 4) as well as the hysteretic loop (Figure 5).

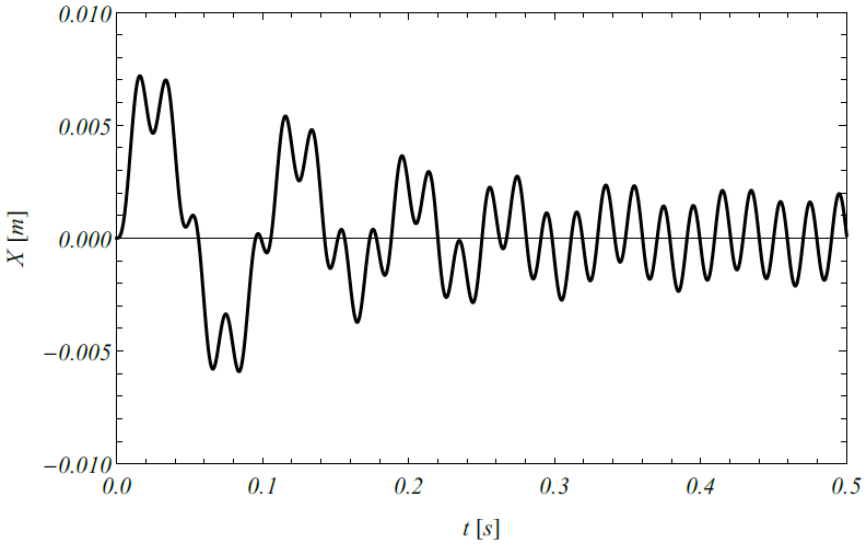


Figure 4 Time history of the mass displacement

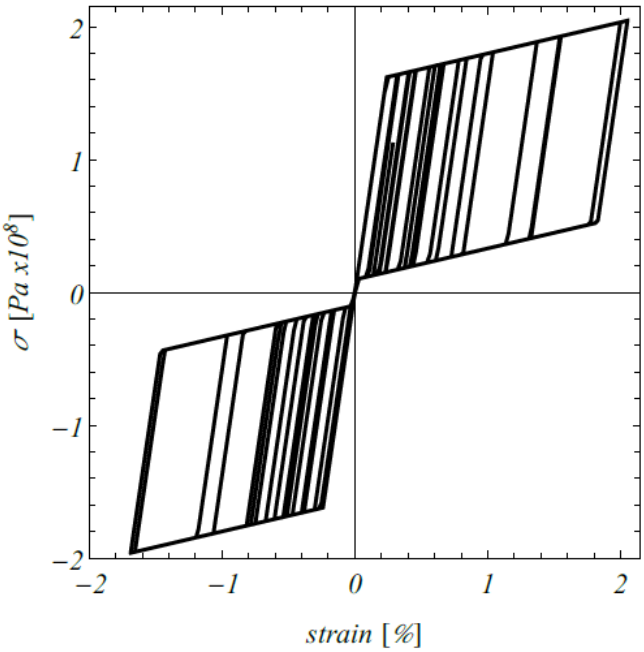


Figure 5 Hysteretic loop of the analyzed SMA device

The graph of the mass displacement history presents noticeable reduction of the amplitudes in the following cycles. The hysteretic loop has a shape characteristic for a superelasticity behaviour of SMA.

Results obtained from basic polynomial model [2] and simplified model [4] obtained by Lagoudas et al. [4] are presented for comparison in Figure 6 and Figure 7. Despite the dissimilarities of maximal and minimal values compared results the character of all of the graphs is coherent. This implicates that the presented formulation stays in agreement with compared models and the differences may result from assumed material parameters.

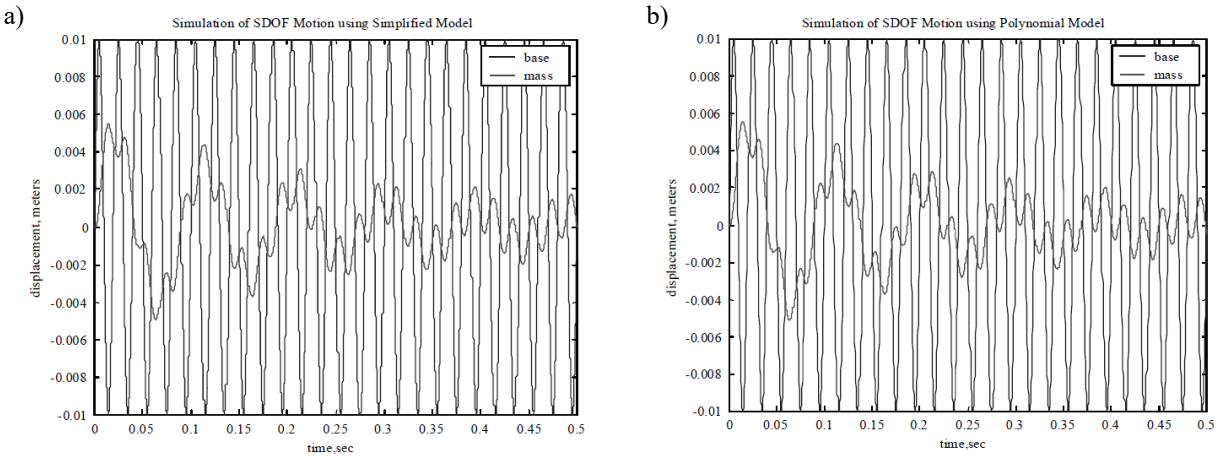


Figure 6 Maps of the displacements for different models of SMA [4] – a) simplified model and b) basic polynomial model

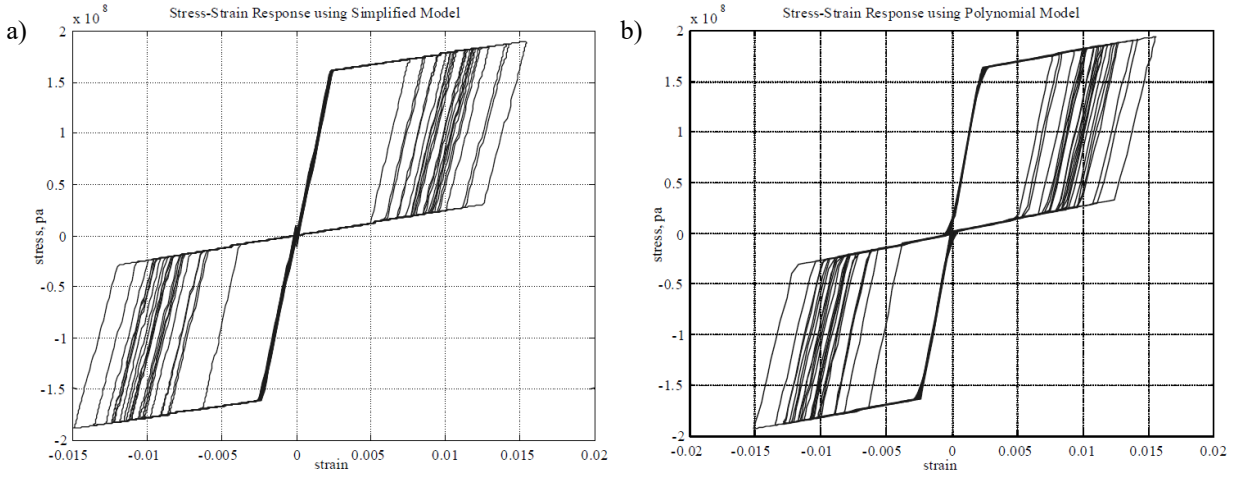


Figure 7 Hysteretic loops for different models of SMA [4] – a) simplified model and b) basic polynomial model

6 CONCLUSIONS

Results of the presented comparison of numerical example show the validity of the formulation. The important fact is that the proposed methodology of the formulation of SMA constitutive equations is based on original rheological schemes. It results in explicit form of differential equations of the presented model. Such a system of equations can be easily implemented in mathematical software. The equations could be directly implemented in the commercial FEM codes as a user's subroutines (e.g. UMAT and VUMAT subroutines in Abaqus [22–24]). Such an implementation may facilitate the analysis of complex structures, such as historical masonry, retrofitted with SMA devices.

REFERENCES

[1] Mohd Jani, J. Leary, M. Subic, A. and Gibson, M.A., A review of shape memory alloy research, applications and opportunities, *Materials and Design* (2014) **56**: pp. 1078–1113.

[2] Lagoudas, D.C. Bo, Z. and Qidwai, M.A., A unified thermodynamic constitutive model for SMA and finite element analysis of active metal matrix composites, *Mechanics of Composite Materials and Structures* (1996) **3**: pp. 153–179.

[3] Qidwai, M.A. and Lagoudas, D.C., Numerical implementation of a shape memory alloy thermomechanical constitutive model using return mapping algorithms, *International Journal for Numerical Methods in Engineering* (2000) **47**: pp. 1123–1168.

[4] Lagoudas, D.C. Mayes, J.J. and Khan, M.M., Simplified shape memory alloy (SMA) material model for vibration isolation, in: Rao, V.S. (Ed.), International Society for Optics and Photonics, 2001: pp. 452–461.

[5] Ölander, A., An electrochemical investigation of solid cadmium-gold alloys, *Journal of the American Chemical Society* (1932) **54**: pp. 3819–3833.

[6] Chang, L.C. and Read, T.A., Plastic Deformation and Diffusionless Phase Changes in Metals — the Gold-Cadmium Beta Phase, *JOM* (1951) **3**: pp. 47–52.

[7] Buehler, W.J. Gilfrich, J. V. and Wiley, R.C., Effect of Low-Temperature Phase Changes

on the Mechanical Properties of Alloys near Composition TiNi, *Journal of Applied Physics* (1963) **34**: pp. 1475–1477.
[8] Asanović, V. and Delijić, K., The mechanical behavior and shape memory recovery of Cu-Zn-Al alloys, *Metalurgija* (2007) **13**: pp. 59–64.
[9] Cladera, A. Weber, B. Leinenbach, C. Czaderski, C. Shahverdi, M. and Motavalli, M., Iron-based shape memory alloys for civil engineering structures: An overview, *Construction and Building Materials* (2014).
[10] Concilio, A. and Lecce, L., Historical Background and Future Perspectives, in: Shape Memory Alloy Engineering, Elsevier Ltd, 2015: pp. 3–30.
[11] Pecora, R. and Dimino, I., SMA for Aeronautics, Elsevier Ltd, 2014.
[12] Auricchio, F. Boatti, E. and Conti, M., SMA Biomedical Applications, Elsevier Ltd, 2014.
[13] Auricchio, F. Boatti, E. and Conti, M., SMA Cardiovascular Applications and Computer-Based Design, Elsevier Ltd, 2014.
[14] Song, G. Ma, N. and Li, H.N., Applications of shape memory alloys in civil structures, *Engineering Structures* (2006) **28**: pp. 1266–1274.
[15] Menna, C. Auricchio, F. and Asprone, D., Applications of Shape Memory Alloys in Structural Engineering, Elsevier Ltd, 2015.
[16] Castellano, M.G. Indirli, M. and Martelli, A., Progress of application, research and development, and design guidelines for shape memory alloy devices for cultural heritage structures in Italy, in: Smart Structures and Materials 2001: Smart Systems for Bridges, Structures, and Highways, 2001: pp. 250–261.
[17] Arato, G.B. Carpani, B. Forni, M. Indirli, M. Martelli, A. Castellano, M.G. and Medeot, R., Application of innovative antiseismic techniques to the seismic retrofit of Italian cultural heritage damaged by recent earthquakes, in: Monument-98, Workshop on Seismic Performance of Monuments, 1998.
[18] Indirli, M. Castellano, M.G. Clemente, P. and Martelli, A., Demo-application of shape memory alloy devices: The rehabilitation of the S. Giorgio Church Bell-Tower, *Proceedings of SPIE - The International Society for Optical Engineering* (2001) **4330**: pp. 262–272.
[19] Cardone, D. Angiuli, R. and Gesualdi, G., Application of Shape Memory Alloys in Historical Constructions, *International Journal of Architectural Heritage* (2019) **13**: pp. 390–401.
[20] Ferretti, E. and Pascale, G., Some of the latest active strengthening techniques for Masonry Buildings: A critical analysis, *Materials* (2019) **12**:.
[21] Cisse, C. Zaki, W. and Ben Zineb, T., A review of constitutive models and modeling techniques for shape memory alloys, *International Journal of Plasticity* (2016) **76**: pp. 244–284.
[22] Grzesikiewicz, W. and Zbiciak, A., Constitutive modelling of pseudoelastic material using Kepes-type rheological element, *Computer Systems Aided Science and Engineering Work in Transport, Mechanics and Electrical Engineering* (2008) **122**: pp. 159–164.
[23] Zbiciak, A., Dynamic analysis of pseudoelastic SMA beam, *International Journal of Mechanical Sciences* (2010) **52**: pp. 56–64.
[24] Grzesikiewicz, W. Wakulicz, A. and Zbiciak, A., Mathematical modelling of rate-

independent pseudoelastic SMA material, *International Journal of Non-Linear Mechanics* (2011) **46**: pp. 870–876.

[25] Zbiciak, A. and Wasilewski, K., Constitutive Modelling and Numerical Implementation of SMA Material with Internal Loops, *Archives of Civil Engineering* (2018) **64**: pp. 211–232.

[26] Zbiciak, A. and Wasilewski, K., Modelling of single degree of freedom SMA oscillators by using rheological schemes, in: MATEC Web of Conferences, 2018.

12th International Conference on Structural Analysis of Historical Constructions
SAHC 2020
P. Roca, L. Pelà and C. Molins (Eds.)

NUMERICAL ANALYSIS OF HISTORICAL REINFORCED CONCRETE SHELL

PETR KNĚŽ[1*], PETR TEJ[1] AND JIŘÍ KOLÍSKO[1]

[1]Czech Technical University in Prague, Klokner institute
Šolínova 7, 160 00, Prague, Czech Republic
e-mail: petr.knez@cvut.cz, www.klok.cvut.cz/en (*corresponding author)
{petr.tej, jiri.kolisko}@cvut.cz

Keywords: Historical Structure, reinforced concrete shell, numerical analysis

Abstract. *This article is focused on the numerical analysis of the historical structure of the reinforced concrete shell. Shells form the roof of the tram depot. It was built in the 50s of the 20th century. The shells are conoid shaped with a control curve in the form of a catenary. The construction of the depot began to show excessive deformation and lose its stability. At present, the depot is out of service and the shells are temporarily supported. This prompted the commissioning of a diagnostic survey and numerical analysis of the structure. The diagnostic research revealed the quality and strength of the concrete, the reinforcement of the structure, the actual thickness of the shells, the structure of the roof cladding and defects in the structure (cracks, etc.) At the same time, the bottom surface of the whole structure was scanned with a 3D scanner and selected points of the structure were measured by geodetic methods. Numerical analysis focused on one shell at the edge of the depot structure. The model was created in Atena 3D software. The main aim of the analysis was to determine the behavior of the structure under load and to predict the ways of its deformation for different loading methods to determine the possible reason for the current deformed shape. Consequently, compare these predicted behaviors with the real deformed structure, whether its deformation corresponds to normal behavior.*

1 INTRODUCTION

The main object of the tram depot Hloubětín consists of a hall with 5 bays. There are 5 parallel tram tracks in each bay, the total number of tracks is 25. On these tracks tram cars were shut down and their maintenance and repairs were carried out.

The load bearing structure of the hall, roofing and construction of rail supports were built in the 1950s. The reinforced concrete monolithic structure of the hall is formed in the longitudinal direction by associated frames - columns and longitudinal girders. In the longitudinal direction, the structure is divided into 3 expansion units of 4, 5 and 4 frames, ie a total of 13 frame constructions = 13 fields. The hall of the depot consists of 6 rows of these frames - 2 outer and 4 inside, which create just 5 bays of tram depot. In the transverse direction, the longitudinal frames are connected by transverse arched girders with a curved rod. It is a sawtooth arrangement of roofing with vertical girders. The areas between longitudinal and transverse girders are covered with reinforced concrete monolithic shells 18.8 m wide and 8.75 m long,

typically 50 mm thick – according to project. These are the shells used to roof the depot instead of the originally designed steel roof structure due to lack of steel at the time of construction. The shells have the shape of a conoid with a control curve in the form of a catenary. In total, the hall is covered with 65 (5x13) shells with total floor plan dimensions ~ 114.25 x 94.0 m (L x W)

Operation of the tram depot Hloubětín was launched on March 10, 1951, all original bays were put into operation at the beginning of 1952.

During the operation of the depot, the insulation of the roof cladding was reconstructed. The original composition of the roof cladding (Heraklit wood fiber insulation + foam concrete with a total thickness of 100 mm) was removed. It was replaced by mechanically anchored thermal insulation thickness ~ 60 mm (polystyrene or mineral fibers) covered with asphalt insulating strips.

The structure was supported by temporary supports and was in disrepair due to excessive deformation of the shells - locally deviating from the ideal shape up to 150 mm, indicating a loss of stability and a change in the behavior of the structure.

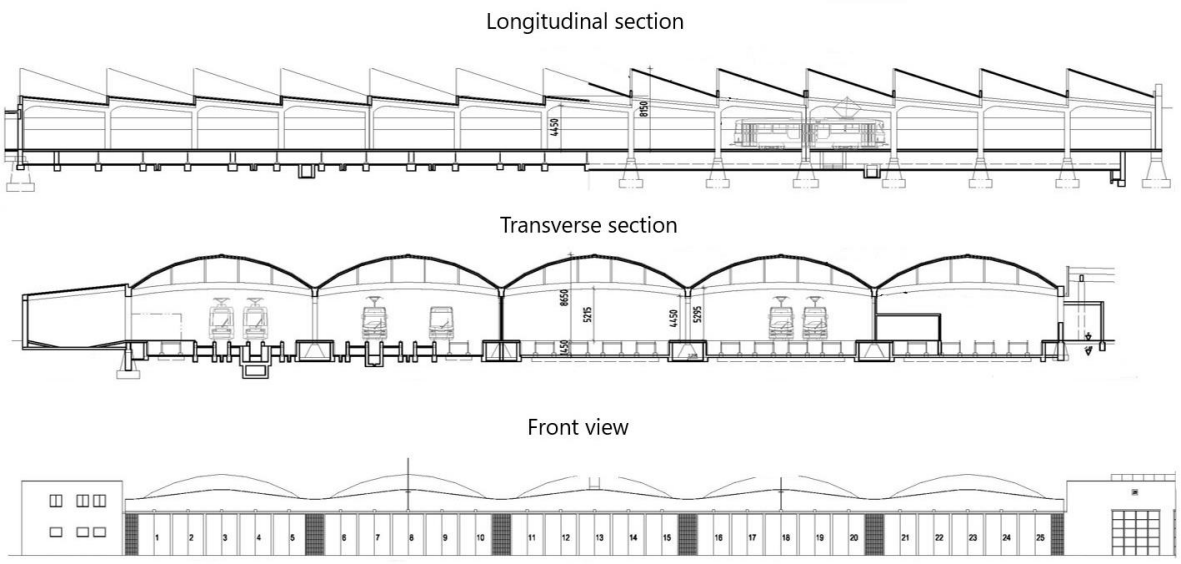


Figure 1: Longitudinal and transverse section and front view of tram depot

The structure was evaluated several times to determine the load-bearing capacity of the structure, but nobody looked in detail at the possible cause of the failure. It has been concluded that the structure does not meet the requirements according to European standards and there is no possibility to improve this situation by possible reinforcement of the structure.

2 CONCLUSION OF DIAGNOSTIC SURVEY

A diagnostic survey was carried out on the construction of the depot. It was focused on finding the material properties of the elements of the load bearing structure – girders, columns and shells. Another important part of the survey was to determine the real reinforcement of shells using destructive and non-destructive methods. Part of the survey was also localization

of detected failures - cracks in concrete, reinforcement corrosion, excessive deformations, etc. The survey was completed with a 3D scan of the bottom surface of all 65 shells.

The diagnostics showed:

- In most cases, the shells exhibit a visually apparent typical deformation manifested by symmetrically placed two 'bent down'.
- Cracks signaling tensile stress were diagnosed at the point of additional support of the shells.

The shells show obvious deformations (Figure 2, 3) and their center line deviates significantly from the ideal shape of the shells from the project. This shape fundamentally affects the unsatisfactory static behavior.

The following facts were recommended for nonlinear calculations:

- Strength of concrete C25/30.
- The reinforcement of the shells is in good agreement with the original project and consists of smooth rods with a diameter of 5.5 mm.
- The recommended design yield strength of the reinforcement is 180 MPa.
- The coverage of the reinforcement when measured from the lower face is very variable and oscillates over a wide range of 5-25 mm.
- The thickness of the shells is also highly variable and oscillates in the range of 35-65 mm.
- The roof cladding consists of 20 mm thick waterproofing, 60 mm thick thermal insulation, which is made of mineral fiber mats at the point of large curvature and in other cases made of EPS (expanded polystyrene), 5 mm vapor barrier.

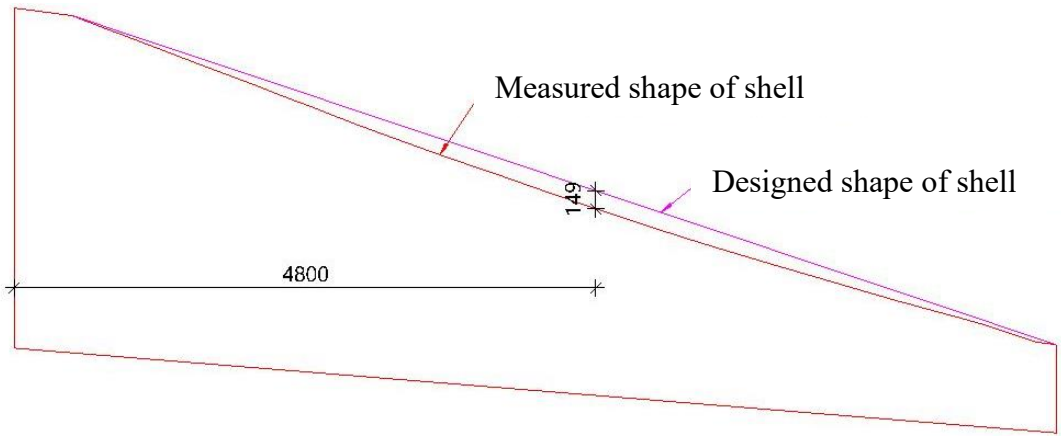


Figure 2: Longitudinal section of the shell at the point of greatest deformation, added shape according to the design

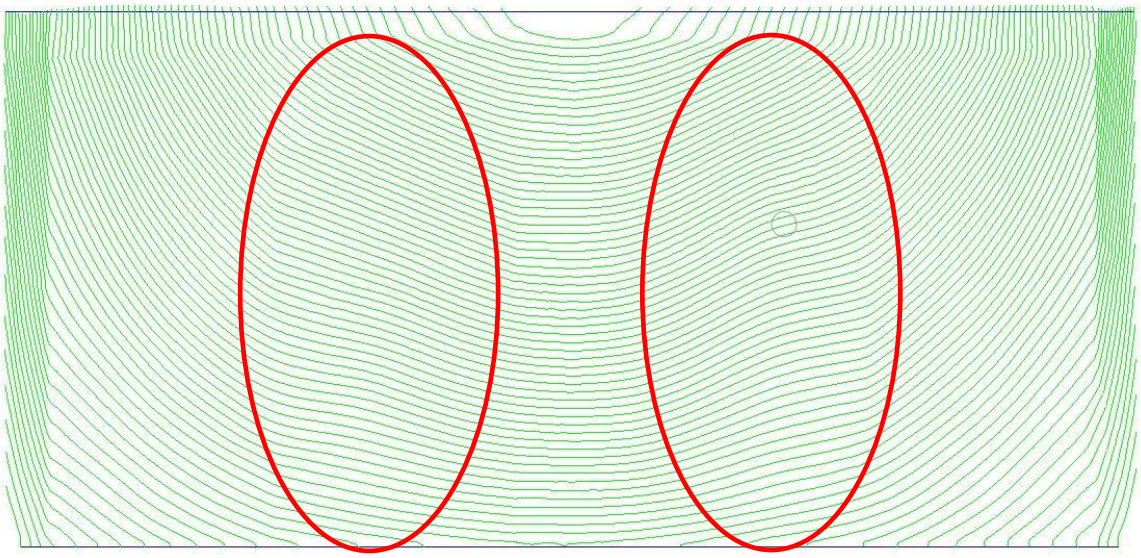


Figure 3: Contour line after scanning the bottom surface of shell shell 7 in field 5 - plan view. Areas with pronounced bulges marked.

3 NUMERICAL ANALYSIS - MODELS

The numerical analysis was carried out on the model of the structure with the ideal shape and also on the model, whose shape was based on the performed 3D scanning. In both cases, a shell lying in the center of the outer bay of the hall was modeled.

3.1 Numerical model of ideal shell shape

Based on the preserved fragments of the original documentation, a 3D model of the structure has been worked out, on the basis of which the computational model of the structure was created in the program Atena 3D.

The model captures one shell, located in the center of the outer bay of the hall. Thus, the calculated structure is prevented in three directions from shifting by the "rest" of the structure and one side may deform. This arrangement is a simplification of the complex relationships that influence the individual elements of the roofing - ideally, it would be possible to have a model of the entire expansion unit, which, given the dimensions of the structure, could not be managed with commonly available computer equipment. The individual shells and the supporting elements interact with each other - bringing additional loads and forced displacements for the part of the structure considered by us that are not taken into account.

The shell is modeled with the thickness by the project - it is 50 mm, which is measured vertically. The shell is double curved, so it is divided into a series of smaller elements to make the mesh element generator able to work with these elements. As a result, the model with the ideal shell shape consists of 320 macroelements (Figure 4).



Figure 4: Model of ideal shell shape

The model is reinforced according to the drawings of the preserved historical documentation. All members are inserted into the model as discrete models (= each member is physically modeled and can show stress). The shell is reinforced with 8Ø5.5 per meter in both directions, and the upper reinforcement is added at the point of attachment. Reinforcing profiles of diameters 14, 16 and 20 mm for longitudinal reinforcement (including bends) and diameters of 5 and 7 mm for stirrups are inserted into the beam members. Typical stirrup spacing is 200 mm. The model contains 2033 bar reinforcements (Figure 5).

The model consists of a finite element mesh with a global mesh edge size of 100 mm. Most of the macroelements are meshed by tetra elements. The model consists of 307 623 finite elements in total (Figure 6).

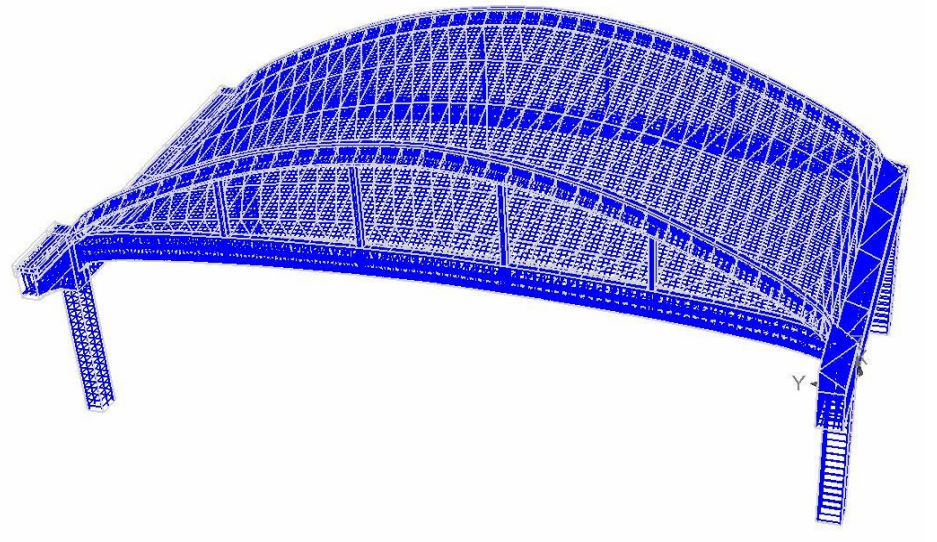


Figure 5: Model with reinforcement



Figure 6: Model with generated finite element mesh

The support of the model is realized as a fixed support on the lower surfaces of the columns, supplemented by the conditions of continuity on the parts of the structure, which are connected to the surrounding parts of the roof – supports, which prevent rotation and horizontal displacement in direction of supported face. (Figure 7).

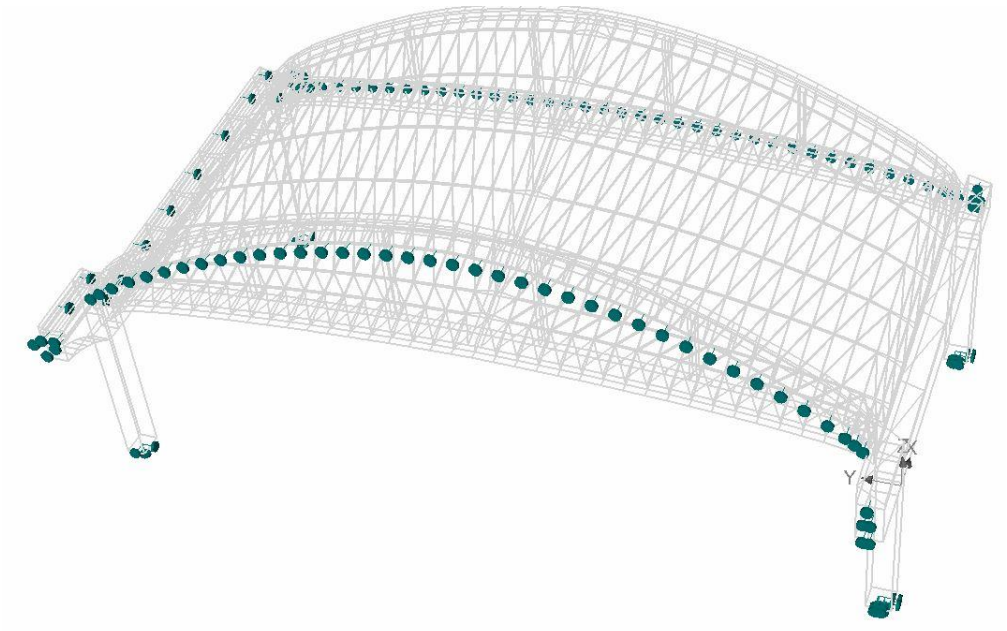


Figure 7: Model with applied supports

The structure is loaded by its own weight, load from the roof cladding, snow (even and windblown) and temperature (±20°C).

3.2 Numerical model of actual shell shape

Based on the measurement of the actual shell shape using a 3D scanner, the shell model was created in Atena 3D. It is a shell placed in the same part of the depot as a model of ideal shell shape. The support elements of the shell are again modeled on the basis of preserved documentation.

Since the already deformed structure is modeled, it is not possible to re-load it with dead loads (self-weight and other dead loads) as they would generate additional deformations that are already part of the model. However, these loads on the structure create some unknown stress state, which has a major impact on results. We tried to take this into account by reducing some of the material properties based on the results on an ideal shape model. Cracks on the actual structure were also detected by diagnostics, which is another parameter that is very difficult to take into account when modeling the structure. However, these cracks affect the rigidity of the structure. Due to the orientation of the cracks, their cause is not most likely to be caused by force loads, but cracks caused by non-force effects (temperature, drop in supports).

The shell is modeled with an average thickness according to the survey - it is 48 mm, which is measured vertically. Shell elements were divided according to the needs of the program into smaller partial parts (shell on parts approx. 0.4x0.4 m - for the possibility of capturing deformations), some elements were divided into triangles (elements of the shell). The model consists of a total of 2116 macroelements (Figure 8).



Figure 8: Model of actual shell shape

The reinforcement of the model is almost the same as the model with the ideal shape. The difference is due only to the unsymetry of the structure. The reinforcement bars of the shell follow the deformed shape. Reinforcement of beams is simplified - instead of bent

reinforcement, straight profiles are used to match the number of reinforcement bars in critical sections. The model contains 974 bar reinforcements (Figure 9).

The finite element mesh is generated according to the same principles as described for the ideal shape model. The model consists of 277 613 finite elements in total. Model supports, snow and temperature loads are also the same (Figure 10).

Only dead loads are not considered, as explained in the introduction to this chapter.

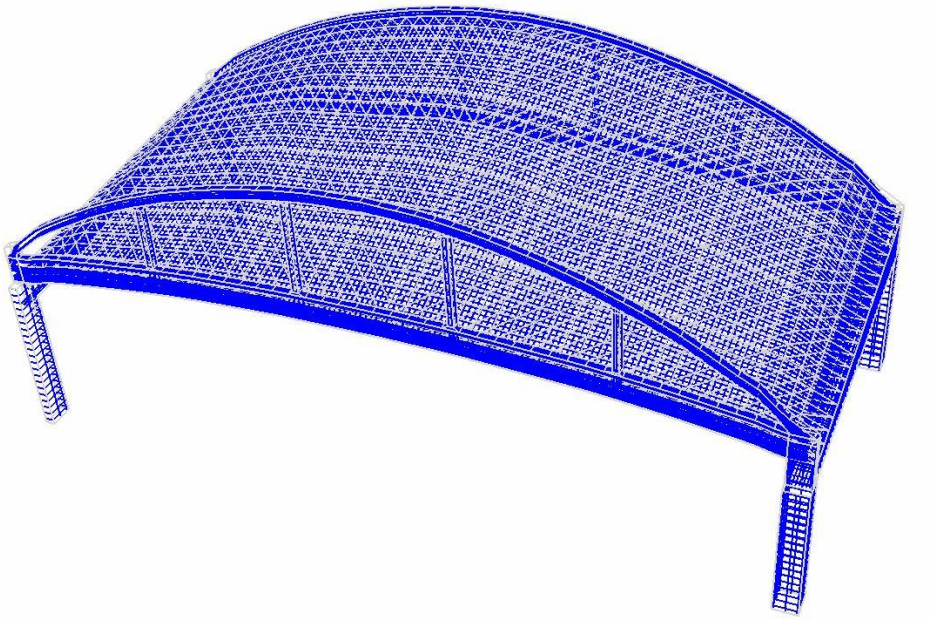


Figure 9: Model with reinforcement



Figure 10: Model with generated finite element mesh

3.3 Materials

The proposed material strengths are not available in the original documentation, so the concrete strengths found in our diagnostic survey are used and the material characteristics of the reinforcement are determined on the basis of tests performed on the cut-outs.

Laboratory tests on concrete samples result in the use of concrete strength class C25/30. Used material model works with mean values of strength and basic values are given in Table 1. This material model is used for the whole model of the ideal shell shape and for the beam elements of the actual shell shape model. The material model used on the model of the actual shell shape is divided into two categories. The first is applied to the most parts of the shell and simulates the initial stress state (Table 2). The second category material model is used in place of cracks found by survey (Table 3).

The material model 3D nonlinear cementitious 2 [1,2,7] was used for the numerical analysis. It takes into account the plastic deformation of concrete and its tensile softening after the crack.

Table 1: Mateial characteristics of concrete class C25/30 Mean

Attribure	Symbol	Value	Units
Modulus of elasticity	E	31000	MPa
Compressive strength	F_c	33	MPa
Tensile strength	F_t	2.6	MPa
Fracture energy	G_f	8.368E-05	MN/m

Table 2: Mateial characteristics of concrete class C25/30 Mean – reduced values for parts without cracks

Attribure	Symbol	Value	Units
Modulus of elasticity	E	16000	MPa
Compressive strength	F_c	33	MPa
Tensile strength	F_t	1.35	MPa
Fracture energy	G_f	4.368E-05	MN/m

Table 3: Mateial characteristics of concrete class C25/30 Mean – reduced values for parts with cracks

Attribure	Symbol	Value	Units
Modulus of elasticity	E	16000	MPa
Compressive strength	F_c	33	MPa
Tensile strength	F_t	0.5	MPa
Fracture energy	G_f	8.368E-06	MN/m

The reinforcement for model of ideal shell shape is modeled using a bilinear material model with hardening with a yield strength of 280 MPa, an ultimate strength of 400 MPa and a maximum elongation of 10%. The reinforcement for model of actual shell shape is modeled using a bilinear material model with hardening with a yield strength of 170 MPa, an ultimate strength of 250 MPa and a maximum elongation of 7% due to initial stress state.

4 NUMERICAL ANALYSIS - RESULTS

4.1 Results for model of ideal shell shape

Calculations have shown that the weak points are in particular the supporting structures, namely the arc tie rod, frame joints and column (Figure 11, 12). The design is strongly influenced by volume changes due to temperature load. The dilatation units are relatively large and the deformations add up. Cooling of the structure results in tensile stress of the elements (a possible source of cracks for both the shell and the beam members), warming then stresses the structure by pressure (potentially there is a loss of stability and buckling of thin-walled elements)

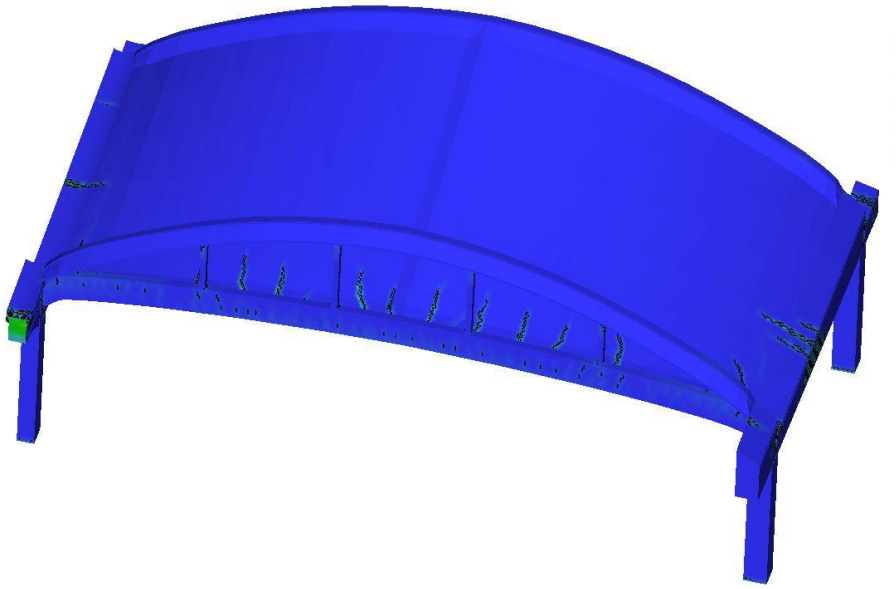


Figure 11: Cracks at ideal shell shape model



Figure 12: Deformed model of ideal shell shape, deformation scale 100:1

4.2 Results for model of actual shell shape

The results are based on the assumptions outlined above and are of an informative nature and very approximate. Generally, it can be stated that tensile stresses occur at the structure at the point of "bulges" and continue to contribute to the deterioration of the current state (Figure 13). According to the survey, deformations of up to 150 mm occur on the structure, a value that indicates a serious problem.

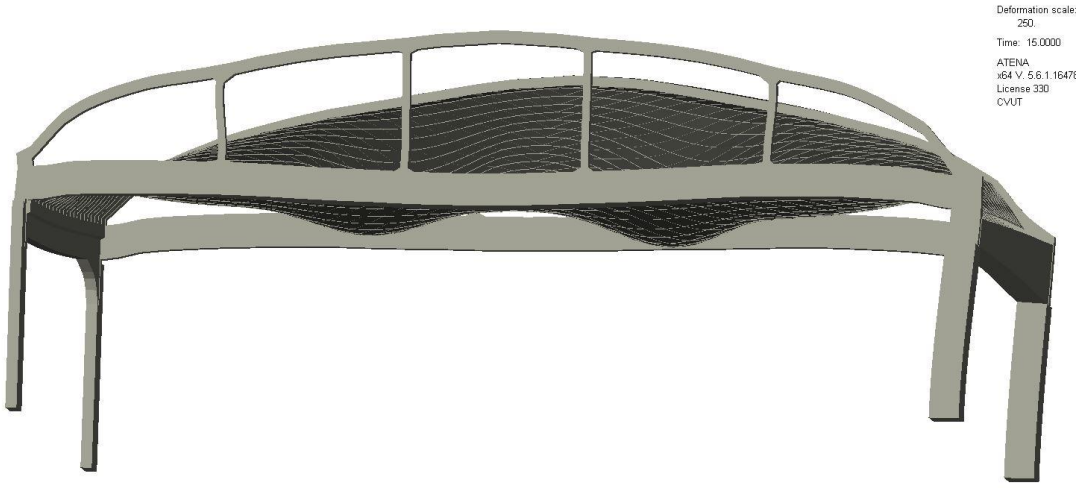


Figure 13: Deformed model of actual shell shape, deformation scale 250:1

5 CONCLUSION

The vast majority of shells typically have a deformed shape formed by two bulges (see Figure 13). The absolute size of the bulges varies from shell to shell. According to the survey, deformations of up to 150 mm occur on the structure, a value that indicates a serious problem.

The assessment of the shell structure in the ideal shape according to the archival documentation did not prove a possible cause of the actual deformations found by the survey. The existing deformed shape of the shells determined by the measurements does not correspond to the deformations resulting from the analysis of the structure (Figure 12). Both in shape and in absolute values of deformation, taking into account creep over time. The shell was loaded with positive and negative temperature, blown snow and local loads possible during the maintenance of the roof in accordance with European standards.

This analysis confirmed only the frequent phenomenon when historic reinforced concrete structures are not sufficiently reinforced when assessed according to current standards. The volume of reinforcement would be sufficient, but due to its lower strength, the result is an unsatisfactory assessment of the ultimate limit state.

The reason for the current atypical deformation of the shells is thus not entirely clear. It is not possible to exclude initial imperfections from the time of construction, which were gradually enhanced by the creep of structures. Alternatively, there could also be local overloading of the shells, eg during the replacement of the roof cladding in 1994. However, damage to the structure during the replacement of the roof cladding seems to be the most likely reason that triggered the degradation of the shells. The original construction of the foam concrete roof cladding would have to be removed very gently, which probably did not happen,

moreover, it was not necessary from a static point of view. The subsequent new roof cladding formed by thermal insulation was mechanically anchored directly into the shell structure, where these anchors pass in a number of places completely through the entire thickness of the shell and are visible from the interior.

However, the final evaluation of the current state of the structure is unchanged regardless of the cause of its origin. There are tensile stresses on the structure at the location of the "bulges", which are unacceptable for this type of structure. The current irregularly deformed shape in combination with an improperly designed support (low stiffness) substantially contributes to a further gradual deterioration of the shells and ultimately their unpredictable behavior.

Acknowledgements.

This project was supported by a grant from the Ministry of Culture of the Czech Republic NAKI II DG20P02OVV005 and a CTU student grant SGS19/138/OHK1/2T/31.

REFERENCES

[1] Červenka, J. and Papanikolaou, V.K. *Three dimensional combined fracture-plastic material model for concrete*. Int. journal of plasticity, 2008
[2] Červenka, V., Červenka ,J.and Pukl, R. *ATENA – a tool for engeneering analysis of fracture in concrete*. Sadhana, 2002
[3] *Model Code for Concree Structures 2010*, Fib, Ernst & Sohn, 2013
[4] *Czech standard ČSN EN 1992, Design of concrete structures*. Czech Standards Institute, 2011
[5] *Czech standard ČSN EN 1991, Actions on structures*. Czech Standards Institute, 2011
[6] Kněž, P., Štemberk, P., Tej, P. and Kolísko, J. *Expert Report, evaluation of the static reliability of shells of the roof construction of the tram depot based on a survey and static non-linear analysis*. Klokner institute, 2019
[7] Červenka, V., Jendele, L. and Červenka, J. *Atena program documentation, Part 1 – Theory.* Cervenka Consulting, 2018

12th International Conference on Structural Analysis of Historical Constructions
SAHC 2020
P. Roca, L. Pelà and C. Molins (Eds.)

NUMERICAL DEVELOPMENT OF A STRENGTHENED WALL-TO-DIAPHRAGM SEISMIC CONNECTION: CALIBRATION AND APPLICATION ON A BUILDING PROTOTYPE

FABIO SOLARINO[1,2*], DANIEL V. OLIVEIRA[1] AND LINDA GIRESINI[2]

[1]ISISE, Institute of Science and Innovation for Bio-Sustainability (IB-S)
Department of Civil Engineering, University of Minho
Campus de Azurém, 4800-058, Guimarães, Portugal
e-mail: solarino.fabio@gmail.com, www.hms.civil.uminho.pt/ (*corresponding author)

[2] Department of Energy, Systems, Territory and Constructions Engineering (DESTEC)
University of Pisa
Largo Lucio Lazzarino, 1, 56126, Pisa (PI) Italy
e-mail: linda.giresini@unipi.it, www.destec.unipi.it/

Keywords: Wall-to-floor connections, URM buildings, Numerical calibration, Nonlinear dynamic analyses, timber floors.

Abstract. *Effective wall-to-floor connections are crucial components of historical buildings to avoid dangerous mechanisms under seismic actions. Existing buildings often present poor friction-based links between timber floor and masonry wall and are not able to ensure the so-called "box behavior", necessary for the correct distribution of seismic forces.*
Nonlinear static analysis is one of the most common tools for the seismic assessment of unreinforced masonry buildings considering advanced nonlinear materials description and allowing for different approaches. The selection of a proper control node, for the definition of the pushover curve, is fundamental and sometimes controversial. Moreover, connections are modelled as simply fixed or absent at all. Dynamic nonlinear analysis seems preferable even suffering from a higher computational effort.

On the bases of previous experimental campaign developed at the University of Minho, the pull-out behavior of a strengthened and unstrengthened masonry-to-timber connection was simulated numerically using OpenSees software. The connection model considers strength degradation and pinching, in agreement with the experimental behavior, and is validated from the energetic point of view, suitable for being included in a global finite element model to study the influence of the hysteretic energy dissipated within the connections on the overall seismic response.

This paper describes the calibration process and the application of the connection model into a unreinforced masonry prototype using nonlinear dynamic analysis under real seismic inputs. Both strengthened and unstrengthened configurations are implemented and results compared. The selected model is part of the blind prediction competition organised within the SERA-AIMS project involving the shaking table test of a half-scaled aggregate.

The main numerical outcomes show that the model is capable to predict typical damage in masonry buildings. The presence of a strengthened wall-diaphragm solution seems to play a secondary role in the overall seismic capacity of the aggregate, probably due to the peculiarity of the building layout, while the absence of the floor can lead to premature damages.

1 INTRODUCTION

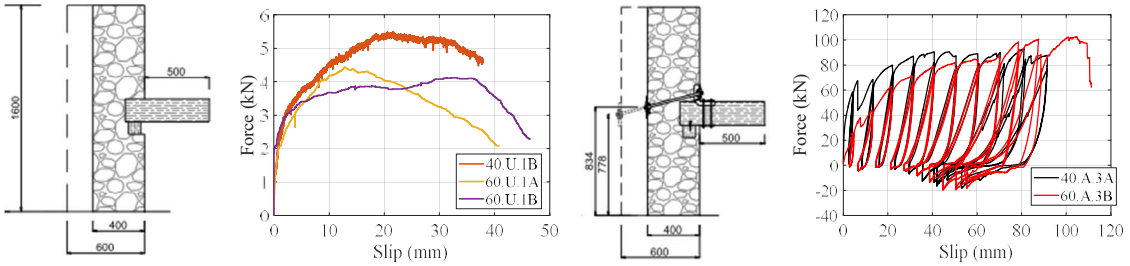
The seismic response of Unreinforced Masonry (URM) buildings is generally weak, mainly due to their intrinsic high inertial forces, but simple and effective characteristics make the structure able to sustain even medium-high intensity ground motions [1]. Despite the geometrical regularities, quality of the materials, masons' expertise play an important role in the capacity of the structure, connections between the walls and between vertical and horizontal elements are crucial for the proper distribution of seismic forces and for preventing dangerous local mechanisms [2].

Finite Element (FE) analysis using homogeneous masonry elements is widely used for seismic assessment of historical structures in spite of unavoidable uncertainties concerning material properties, boundary conditions, value of damping and additional modeling hypothesis [3,4]. Commonly, simplified equivalent-frame, macro-model approaches under nonlinear-static analyses are addressed for the evaluation of the seismic capacity of global structures [5–7], while kinematic analyses are suggested for local analyses of portions of the building as powerful and relatively quick technique well-known among the research community [8–10]. Recently, dynamic nonlinear analyses of simple rigid blocks, also show to be valid tools for the simulation of local mechanisms under ground motion actions, although it is still under development [11,12].

Whatever modeling/analysis approach is taken, accurate simulation of structural connections is crucial for the seismic global and local capacity, as it highly influences the dynamic interaction between the structural components. Common choices involve simplifications both for Wall-to-Wall (WW) and Wall-to-horizontal Diaphragm (WD) connections, depending on the quality/degradation of existing links. Weak WD links may lead to complex interactions concerning frictions or local crushing of masonry, involving possible collapse of the horizontal or/end vertical elements. Strengthened solutions usually comprises metallic components providing a more resistant and ductile behavior [13]. The hysteretic energy of such connections partially influences the overall energy dissipated by the building under seismic forces and should be accounted for in the numerical model. Unfortunately, the experimental knowledge about the force-displacement diagram of these connections is poor and it is difficult to reproduce complicated hysteresis using common modeling techniques. Moreover, WD connections include a large variety of details resulting in several different configurations, hardly to standardize [13].

Recently, Moreira [14] investigated the seismic behavior of rubble stone masonry wall to timber floor beam connections through experimental pull-out tests in both strengthened and unstrengthened specimens (Figure 1), focusing on the monotonic and cyclic tensile behavior. The reinforced connection was seen to be promising for the seismic improvement of existing buildings, often presenting poor friction-based links. This study is considered here as the base for the numerical calibration and validation of the connection model. The monotonic tests of

the unstrengthened connection are useful in order to give an idea of their poor capacity in terms of strength and ultimate displacement, setting the conditions for possible numerical simulations.



(a) (b)

Figure 1: Pull-out tests on WD connections performed by Moreira [14]; (a) unstrengthened; (b) strengthened configuration

While kinematic or rocking approaches allow to include WD connections through simple multi-linear constitutive laws, examples on modeling hysteretical structural connections calibrated on experimental bases can be found for instance in [15–17] developed for connections in Cross Laminated Timber (CLT) members. Moreover, no similar work has been done so far on historical building wall-floor joints. Accurate FE models of the connections are also possible, but not recommended on global buildings with large number of degrees of freedom where the higher computational effort would be unacceptable.

On the base of the experimental work done by Moreira [14] this work develops a simple yet versatile model of the connection between timber beam and masonry wall, which is capable of reproducing the axial hysteretic law as to allow its implementation on global scale models.

2 CALIBRATION OF CONNECTION MODEL

Analytical and numerical developments of experimental data at local level are useful for the evaluation and design of the connection, appropriate path towards the retrofitting of existing buildings under performance- or force-based nonlinear approaches [18,19]. ASCE [20] allows to use cyclic mathematical model when nonlinear dynamic procedures require additional hysteretic parameters and if shape of the experimental hysteresis loop and hysteretic energy is in reasonable agreement with the modelled ones.

Two different types of connections are modeled and calibrated to fit monotonic and hysteretic experimental curves: (i) unstrengthened connection; (ii) strengthened connection. The experimental force-displacement curves, shown in Figure 1, were obtained for different wall thickness and vertical stress levels in order to study the influence of two floor levels. Whilst reinforced connections were tested under both monotonic and cyclic procedures, only monotonic experimental curves are available for unstrengthened configurations. Thus, some hypotheses had to be made about the unloading/reloading shape of the hysteresis curve.

Although the experimental campaign cannot be statistically representative of WD joints, common trend was observed among the typology of connections. In addition, despite the strength capacity significantly increases with reinforcement (about 10 times) when comparing the un-reinforced specimen, the influence of different floor level seems less visible on the

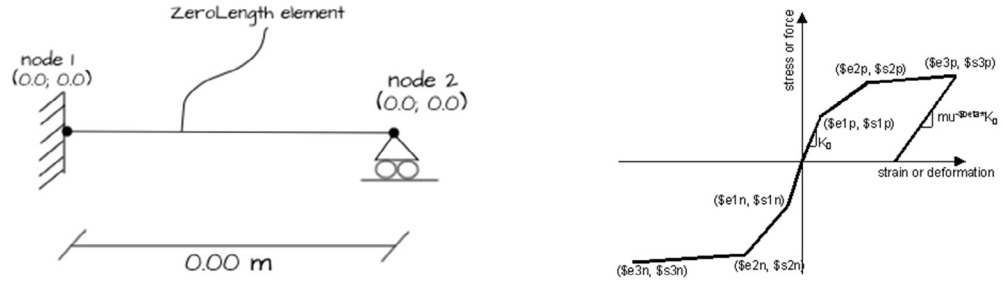
strength, ultimate displacement capacity and shape of hysteretic curves.

Table 1: Summary of experimental tests developed by Moreira [14]; test are labelled using the following criterium: TT.R.NL, where TT is the wall thickness, R is the type of connection (U = unreinforced or A = reinforced), N is the number of the wall and L the location of the connection within the wall

floor level	stress level	wall thickness	connection type	monotonic	cyclic
Upper Level	0.2 MPa	40 cm	unstrengthened	40.U.1A 40.U.1B	-
			strengthened	40.A.1A	40.A.3A 40.A.4A 40.A.4B
Lower Level	0.4 MPa	60 cm	unstrengthened	60.U.1A 60.U.1B	-
			strengthened	60.A.1A	60.A.2B 60.A.3A 60.A.3B

On the base of these considerations, the WD unreinforced connection model is intended to be calibrated based on three monotonic tests (40.U.1B, 60.U.1A, 60.U.1B), while 60.A.3B is selected as the benchmark test for the reinforced connection model, the only one pulled out up to full collapse of the connection (Figure 1).

Within the aim of this work, a single axial spring-like element, calibrated to simulate the overall behavior between the timber floor beam and the masonry wall, is intended to be modelled in a FE environment easy to be implemented in global models. Current experimental tests did not take into account pounding and shear effect, necessary for the full characterization of the coupled axial-shear WD connection under seismic actions, being them solely pull-out uniaxial tensile tests. Therefore, adequate hypotheses have to be developed by the analyst about the remaining unknowns. Inelastic uniaxial material is assigned to a *zeroLength* element [21], representing a two-node spring simply fixed at one end and free to translate to the second end (Figure 2a). *Hysteretic* material model is used to simulate the force-displacement experimental cycles (Figure 2b), accounting for pinching of force and deformation, damage due to deformation and energy, and degraded unloading stiffness based on ductility. The envelope is defined based on three points in each direction and 5 additional parameters governing the cyclic degradation and shape of the curve.



(a) (b)

Figure 2: 1-D connection model developed in OpenSees [22]; (a) model layout; (b) definition of *Hysteretic* material model envelop points

Numerical envelops sufficiently fit the experimental monotonic averaged curves in the case of unstrengthened connections and the backbone curve for the 60.A.3B strengthened configuration (Figure 3). It is worth noting that experimental behavior clearly presents a non-elastic unloading path (i.e. unloading slope is almost vertical if compared to the pre-yielding path, see Figure 1b), while numerical unloading is basically elastic ($K_{unload} = K_0$, for zero unloading degradation). According to the above consideration, the first yielding point P1 with coordinates $(\varepsilon_1, \sigma_1)$, not only defines the elastic limit, but also influences the unloading stiffness, so that two additional points can be devoted to the shape of the envelop curve. While in tension, it is possible to define a very low residual stress, σ_3, simulating the collapse of the connection, indefinitely elastic behavior can be set in compression reproducing the relatively rigid pounding of the beam over the masonry panel. Comparison between the experimental and numerical 60.A.3B hysteresis is shown in Figure 4a, demonstrating sufficient agreement in terms of loading/unloading/reloading paths, ultimate capacity, energy computation (Figure 4b).

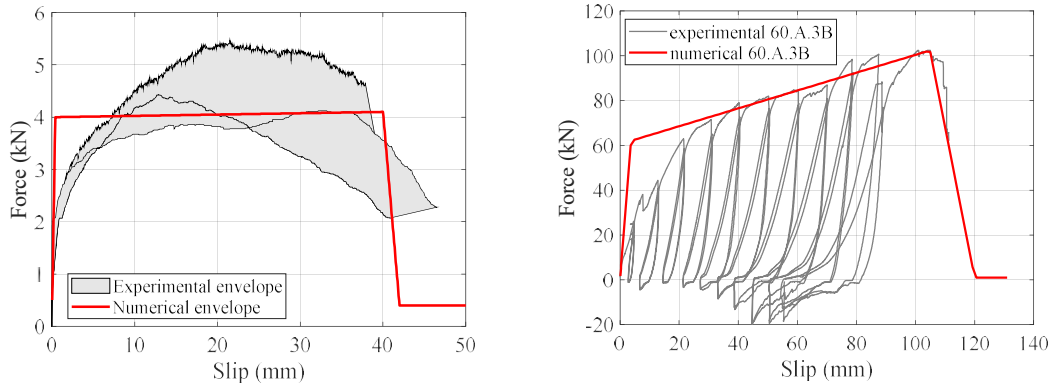


Figure 3: Comparison between numerical and experimental envelope curves of (a) unstrengthened, (b) strengthened 60.A.3B WD connections

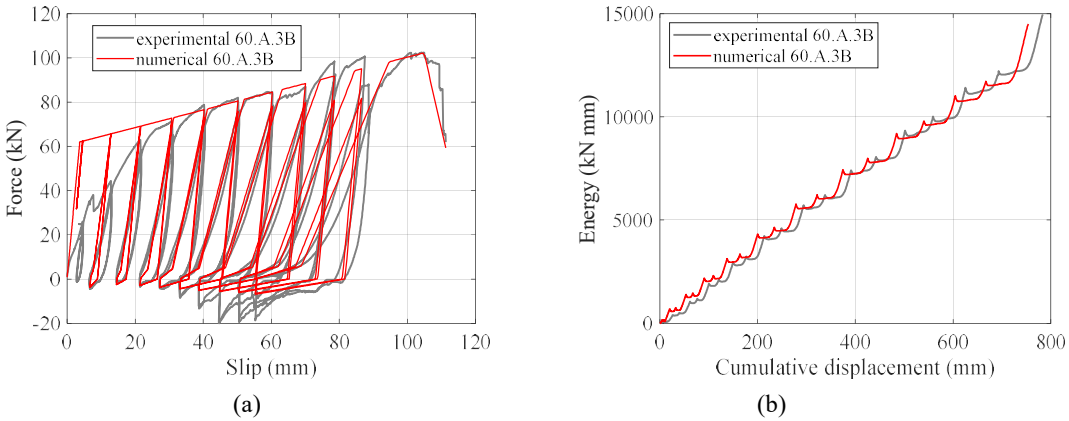


Figure 4: Comparison between numerical and experimental connections (a) 60.A.3B strengthened force-slip curve; (b) total energy

The connections are subjected to reverse cyclic loads to better show the capability of the

model when inverting displacement sign (Figure 5). Only few parameters are necessary to define damage and pinching into the hysteretic model which agrees well with the selected experimental connections. Moreover, despite it is not possible to study the influence of each connection component, setting a limit of the approach, the same calibration procedure can be easily adopted to similar connections, simply modifying few parameters.

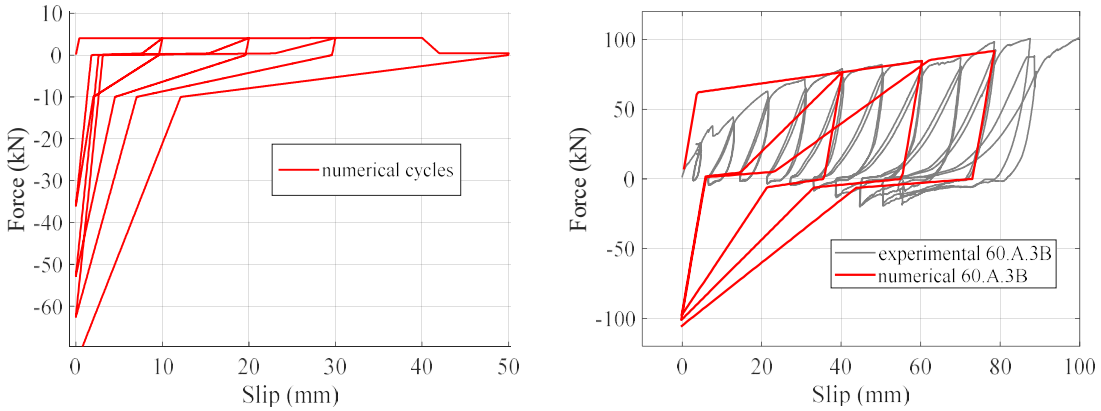
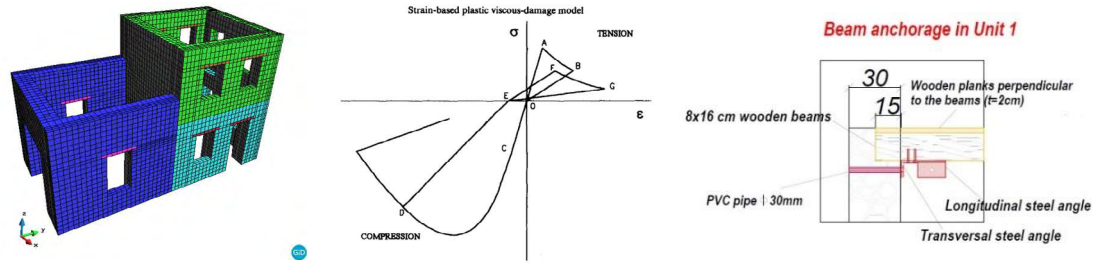


Figure 5: Numerical connection behavior under reverse cycles: (a) unstrengthened model; (b) strengthened 60.A.3B model

3 APPLICATION ON BUILDING PROTOTYPE

3.1 Description of the building

With the aim of better understanding the seismic behavior of stone masonry aggregates, a blind prediction competition has been organized by SERA project AIMS [23] providing experimental results of shake table tests of two half-scaled stone masonry units under two components of horizontal excitations. Research community was invited to develop advanced numerical strategies able to predict the seismic damage of such structures. The geometry is based on typical aggregate layout (Figure 6a), where Unit 1 is a 30 cm thick 2.20 m tall single floor U-shape building, while Unit 2 is a two floor 3.15 m tall rectangular building with decreasing thickness along the height (35 cm at the ground floor and 25 cm at the top floor). Timber beams follow two different orientations and form a relatively weak WD connection, as they are simply infixed and supported into the masonry wall (Figure 6c). Steel angles placed to anchor beams into walls are only present as precaution for later phases of the test and are not activated, thus not expected to influence the behavior of the test buildings. 2 cm thick wooden planks are placed perpendicular to the beams composing a flexible diaphragm. Unit 2 shares one façade with Unit 1; the discontinuity is given by a dry joint connection among the two buildings. A series of 6 cm thick timber lintels are placed above the openings, and reduction of thickness below the openings is considered by using 15 cm thick spandrels. The structure presents symmetry along the Y longitudinal axis.



(a) (b) (c)

Figure 6: (a) 3D FE model– timber beams are not shown for the sake of clarity; (b) masonry material model adopted; (c) detail of WD connection

3.2 Numerical model

3D numerical simulation of the aggregate is performed in OpenSees v.3.0.3 FE framework [22] following a macro-modeling approach where homogeneous masonry material properties need to be assumed. *stBrick* elements (eight-node brick object) have been used for masonry and timber lintels, while *trusses* are adopted for timber beams. The model counts 16688 elements and 22672 nodes, for a total of 66016 degrees of freedom (D.O.F.) (Figure 6a). Two models are developed in order to study the influence of WD connections, namely unreinforced and reinforced connection models. The former is supposed to be the most representative of the actual behavior of experimental specimen, while the second simulates a possible retrofitting solution in agreement with the previously studied strengthened connection (Figure 1). The masonry material model assigned to the brick elements is the Faria1998 damage-plastic model [24], originally developed for concrete and allowing for classical stress-strain envelopes, strength enhancement for confinement, and residual compression strain upon reversal load (Figure 6b). The material was implemented in OpenSees by Tesser (University of Padua) and Talledo (University of Venice), who kindly shared the corresponding routine. Selected masonry material properties (Table 2) are based on preliminary standard tests on masonry wallets.

Table 2: Faria1998 material properties

Young's modulus	E	2.0e6	kPa
Poisson's ratio	ν	0.14	-
Compressive strength	f_c	1300	kPa
Tensile strength	f_t	170	kPa
Damage parameter in compression	A_n	2.0	-
Damage parameter in compression	B_n	0.7	-
Damage parameter in tension	A_p	1.0	-
Plastic deformation coefficient	β	0.4	-

zeroLengthImpact3D [25] elements were used at the interface between the units capable of reproducing pounding/impact, and friction between the walls, based on Hertz and Coulomb theories, respectively. Values of 0.6 friction ratio and 0.0 cohesion were selected as reasonable value for dry stones [26–28]. Previously calibrated *Hysteretic* material is assigned to *zeroLengthElement* (Section 2), simple node-to-node uniaxial springs between trusses and walls, while shear D.O.F. are assumed rigid. Timber beams are modelled using two-nodes *truss*

elements and floor mass is lamped at the beam ends. Base nodes are fixed. The model is meshed following a structured mesh of elements with characteristic length of 5 or 10 cm (Figure 6a).

3.3 Analysis and results

After the application of self-weight, the transient analysis is set using Newmark's integrator, Newton algorithm, energy increments-based convergence test and tolerance of 1e-3 with 100 maximum number of iterations. Damping matrix is specified using Rayleigh damping [29] as a linear combination of stiffness and mass-proportional damping matrices, common in FE dynamic analyses, setting $\alpha_M = 3.9685$, $\beta_K = 0.0001897$ calculated based on 1st and 10th eigenfrequencies in order to account for all important translational and torsional modes and selecting a value of damping ratio of $\xi = 3\%$. It is worth noting that the eigenvalue analysis was performed disconnecting the two units and neglecting floor trusses, in order to evaluate a wide range of reasonable mode shapes.

The model is subjected to two horizontal components of the Montenegro 1979 real record [30], scaled and adapted for the shaking table limits. An Incremental Dynamic Analysis (IDA) is planned considering 25% - 50% - 75% and 100% of the ground motion, reaching the maximum PGA of the shake table (0.875g). According to preliminary analyses, a reduced time-history is performed neglecting the initial 25% sequence, considered to insignificantly damage the structure, thus not justifying the increased computational time. Each level comprises a sequence of 3 substeps: (i) y-direction; (ii) x-direction; (iii) both directions (Figure 7), forming a total of 9 steps, of which 6 are unidirectional, and 3 are bi-directional.

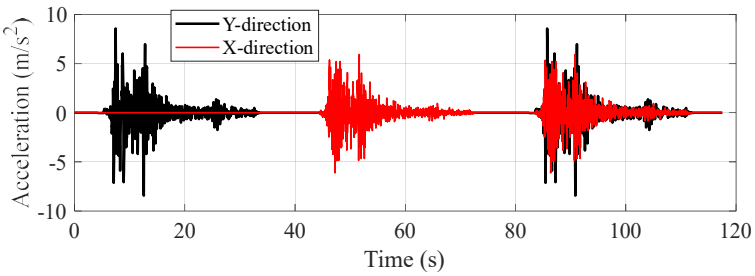
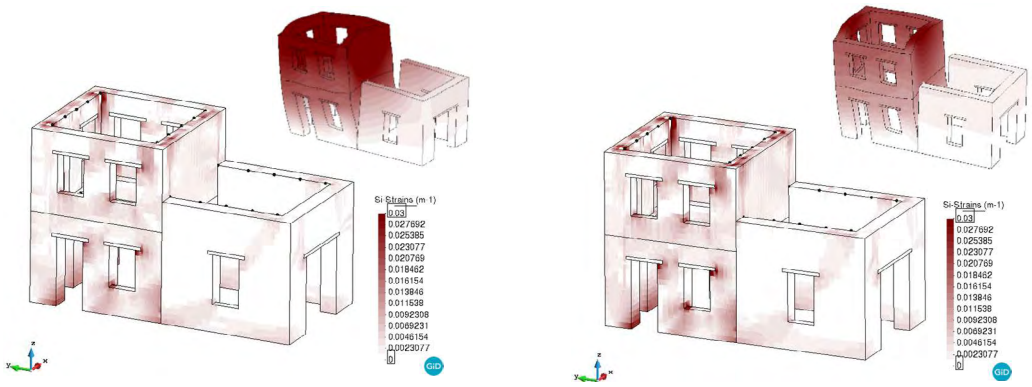


Figure 7: 100% sequence of Montenegro 1979 input ground motion: [Y – X – XY]

Total computational time necessary for the whole sequence (49,844 steps) was about 5 days 13 hours using a Windows-based machine with intel Core i7-9750H CPU (2.60 GHz), and 16 Gb RAM. Damaged models are shown in Figure 8 in terms of principal tensile strains, while time-history results are displayed in Figure 9 in terms of top floor displacements and seismic coefficient, calculated as $\alpha_i = \sum F_i / W$, where i stands for X or Y directions and W is the self-weight of the structure.

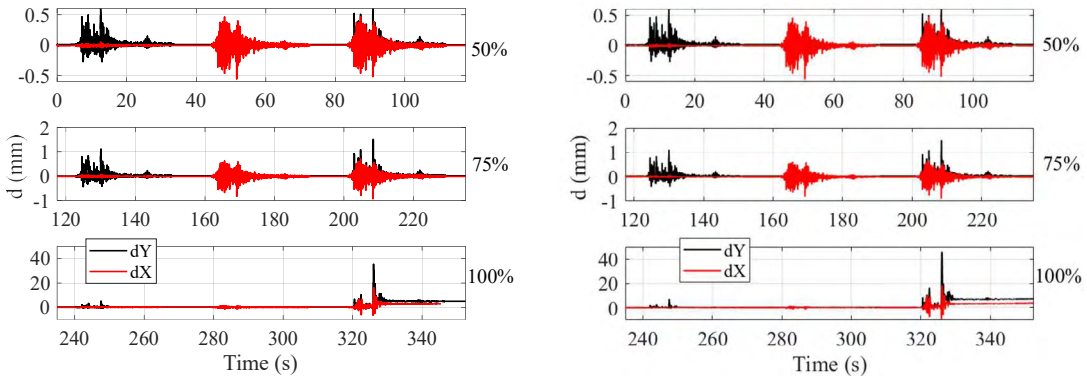
Peak displacements are attained at the last bi-directional step of the 100% sequence. Here, the maximum horizontal displacements in Y-direction at the top corner of unit 2 (46 mm in the strengthened specimen and 35 mm for the unstrengthened model) are about 5 times higher than the displacement under 100% Y (Figure 9). Very few differences can be observed between the unstrengthened connection model and the strengthened one, both in terms of damage and displacements.



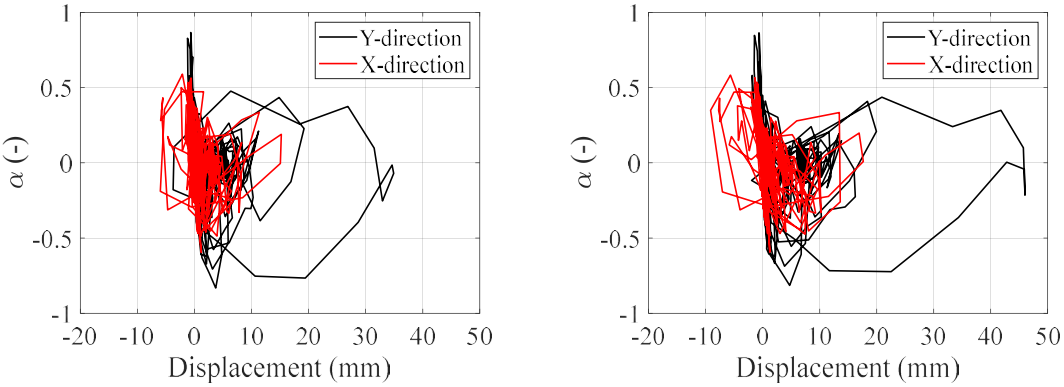
(a) (b)

Figure 8: Tensile principal strains; (a) unreinforced model; (b) reinforced model

The maximum relative beam-wall detachment (calculated as the difference of the beam end and the wall node displacements) is attained in the unstrengthened model without exceeding 1 mm. This is quite a low value, deserving further analysis.



Top floor corner unit 2 time-history displacements along Y and X directions

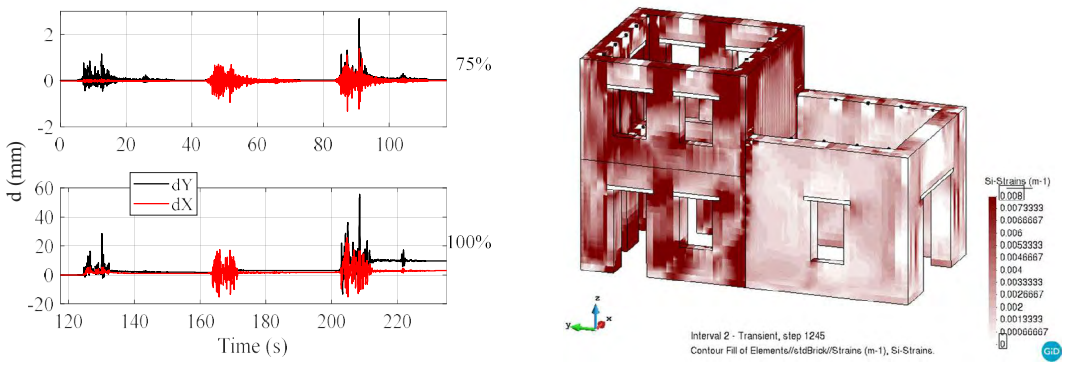


Seismic coefficient vs. horizontal X and Y displacements at the top unit 2 corner

(a) (b)

Figure 9: Dynamic nonlinear analysis results; (a) unreinforced model; (b) reinforced model

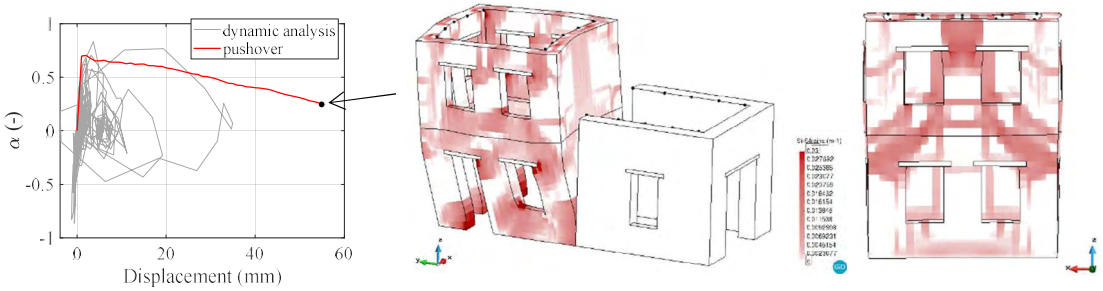
Time history analysis results of same model neglecting timber beams (floor mass is lamped over the wall nodes) are shown in Figure 10 for comparison, demonstrating that buildings with no diaphragm attain higher displacement levels and damages. Compared to the previous models, the building with no floors is expected to be severely damaged since the 100% Y substep, where local and global mechanisms could be activated.



(a) (b)

Figure 10: No-diaphragm model results: (a) displacement time-history of 75% and 100% sequence; (b) tensile principal strains at peak displacement at 100% sequence

Previous results are compared to pushover analysis results (Figure 11). The strength capacity in the positive Y direction predicted by the static analysis is slightly lower than the dynamic prediction (-15%), while the initial static stiffness matches well the dynamic envelope (Figure 11a). Damage patterns at the final step of pushover analysis resemble the ones obtained through dynamic analysis but show major damage suggesting the formation of mechanisms at a lower displacement level. It is worth noting that at about 24 mm displacement, the 20% of the maximum strength capacity is lost, thus further deformations are not trustworthy.



(a) (b)

Figure 11: Static nonlinear analysis results: (a) comparison between static and dynamic capacity curves; (b) principal tensile strains and deformed shape at final step

4 CONCLUSIONS

Nonlinear dynamic time-history analysis is considered one of the most advanced techniques for evaluating the influence of hysteretic wall-to-diaphragm connections on a global URM building in a finite element environment. This work aimed at developing a relatively simple nonlinear numerical connection simulating the complex axial behavior between timber and masonry at floor level. Such connection models are ready to be used in global building models in order to study the influence in a reinforcement perspective.

Two long incremental dynamic analyses were performed on a building prototype, within the scope of a blind prediction competition, in order to predict the behavior of typical aggregate under shake table tests. In-plane and out-of-plane damage is expected especially under the last 100% bidirectional quake, where the model attains the peak deformation of more than 40 mm. No visible improvement is obtained if wall-diaphragm model simulating a strengthened solution is set, probably due to the peculiarity of the buildings and relatively low floors. Local damages are expected especially on Unit 2 façades normal to Y-axis, due to the flexibility of the floor, and bouncing effect at the interface with Unit 1. The same façades are expected to rock out-of-plane, because of the formation of vertical cracks at the connection with transversal walls (Figure 8).

The presence of Unit 1 makes the aggregate more flexible in the positive Y-direction, where the peak displacement is attained (Figure 9). Moreover, unit 2 - ground floor masonry piers are expected to rock along Y-direction, leading to a possible “soft-story” collapse.

The absence of timber floor beams results in a heavily damaged model where premature local mechanisms are expected to appear, demonstrating the well-known importance of adequate horizontal diaphragms.

Finally, a nonlinear static (pushover) analysis was performed and compared to dynamic analysis results only for the unreinforced connection model. The pushover curve agrees well with the dynamic analysis in terms of initial stiffness and strength capacity (being this about 15% lower than the seismic coefficient obtained from dynamic analysis). However, the pushover analysis tends to overestimate the ultimate displacement capacity of about 60% with respect to the dynamic analysis, even if severe damages are expected rather before.

Acknowledgements. This work was partly financed by FEDER funds through the Operational Programme Competitiveness Factors (COMPETE) and by national funds through the Foundation for Science and Technology (FCT) within the scope of project POCI-01-0145-FEDER-007633. The financial support of FCT to the first author, through the PhD grant SFRH/bd/131652/217, is also acknowledged. This work could not be possible without the kind help of Prof. Talledo, from University of Venice, who compiled and shared the necessary OpenSees executable for the analysis.

REFERENCES

[1] M. Tomaževič, Earthquake-Resistant Design of Masonry Buildings, Imperial College Press, London, UK, 1999. https://doi.org/10.1142/9781848160835.

[2] J. Bothara, S. Brzev, A Tutorial: Improving the Seismic Performance of Stone Masonry Buildings, First Edit, Earthquake Engineering Research Institute, Oakland, California,

United States of America, 2011.
[3] J. Ortega, G. Vasconcelos, H. Rodrigues, M. Correia, Assessment of the influence of horizontal diaphragms on the seismic performance of vernacular buildings, Bull. Earthq. Eng. (2018). https://doi.org/10.1007/s10518-018-0318-8.
[4] J. Scacco, N. Bianchini, N. Mendes, C. Cullimore, L. Jain, Seismic assessment of the Church of Carmo Convent, Congr. Métodos Numéricos Em Eng. (2019).
[5] I.E. Senaldi, G. Magenes, A. Penna, A. Galasco, M. Rota, The effect of stiffened floor and roof diaphragms on the experimental seismic response of a full-scale unreinforced stone masonry building, J. Earthq. Eng. 18 (2014) 407–443. https://doi.org/10.1080/13632469.2013.876946.
[6] B. Pantò, F. Cannizzaro, S. Caddemi, I. Caliò, 3D macro-element modelling approach for seismic assessment of historical masonry churches, Adv. Eng. Softw. 97 (2016) 40–59. https://doi.org/10.1016/j.advengsoft.2016.02.009.
[7] C. Casapulla, A. Maione, L.U. Argiento, Seismic analysis of an existing masonry building according to the multi-level approach of the italian guidelines on cultural heritage, Ing. Sismica. 34 (2017) 40–59.
[8] C. Casapulla, L.U. Argiento, Non-Linear Kinematic Analysis of Masonry Walls Out-of-Plane Loaded. the Comparative Role of Friction Between Interlocked Walls, Proc. 6th Int. Conf. Comput. Methods Struct. Dyn. Earthq. Eng. (COMPDYN 2015). (2017) 2301–2311. https://doi.org/10.7712/120117.5568.18332.
[9] Italian Ministry of Infrastructure and Transport, NTC 2018 - D.M. 17.01.18: Aggiornamento delle “Norme Tecniche per le costruzioni,” (2018) 1–198.
[10] C. Casapulla, L. Cascini, F. Portioli, R. Landolfo, 3D macro and micro-block models for limit analysis of out-of-plane loaded masonry walls with non-associative Coulomb friction, Meccanica. 49 (2014) 1653–1678. https://doi.org/10.1007/s11012-014-9943-8.
[11] O. AlShawa, D. Liberatore, L. Sorrentino, Dynamic One-Sided Out-Of-Plane Behavior of Unreinforced-Masonry Wall Restrained by Elasto-Plastic Tie-Rods, Int. J. Archit. Herit. 00 (2019) 1–18. https://doi.org/10.1080/15583058.2018.1563226.
[12] L. Giresini, M. Fragiacomo, M. Sassu, Rocking analysis of masonry walls interacting with roofs, Eng. Struct. 116 (2016) 107–120.
[13] F. Solarino, D. V Oliveira, L. Giresini, Wall-to-horizontal diaphragm connections in historical buildings: a state-of-the-art review, Eng. Struct. (2019).
[14] S.M.T. Moreira, Seismic retrofit of masonry-to-timber connections in historical constructions, Universidade do Minho, 2015.
[15] M. Collins, B. Kasal, P. Paevere, G.C. Foliente, Three-dimensional model of light frame wood buildings. II: Experimental investigation and validation of analytical model, J. Struct. Eng. 131 (2005) 684–692. https://doi.org/10.1061/(ASCE)0733-9445(2005)131:4(684).
[16] G. Rinaldin, C. Amadio, M. Fragiacomo, A component approach for the hysteretic behaviour of connections in cross-laminated wooden structures, Earthq. Eng. Struct. Dyn. 42 (2013) 2023–2042. https://doi.org/10.1002/eqe.2310.
[17] H. Isoda, S. Tesfamariam, Connections for Timber–Concrete Hybrid Building: Experimental and Numerical Model Results, J. Perform. Constr. Facil. 30 (2016) 04016024. https://doi.org/10.1061/(asce)cf.1943-5509.0000849.
[18] American Society of Civil Engineers (ASCE), ASCE/SEI 41-13 : Seismic evaluation and

retrofit of existing buildings, 2013.
[19] EN 1998-3, Eurocode 8: Design of structures for earthquake resistance - Part 3: Assessment and retrofitting of buildings, 2005.
[20] American Society of Civil Engineers (ASCE), Structural Engineering Institute (SEI), ASCE/SEI 41-17 Seismic Evaluation and Retrofit of Existing Buildings, American Society of Civil Engineers, Reston, Virginia, 2017. https://doi.org/10.1061/9780784414859.
[21] G.L. Fenves, ZeroLength Element, Univ. Texas, Austin. (2014). https://opensees.berkeley.edu/wiki/index.php/ZeroLength_Element (accessed January 20, 2020).
[22] F. McKenna, G.L. Fenves, F.C. Filippou, M. Scott, Open system for earthquake engineering simulation (OpenSees), (2000). http://opensees.berkeley.edu.
[23] K. Bayer, I. Tomic, A. Penna, M. Dejong, C. Butenweg, SERA Project: Seismic Testing of Adjacent Interacting Masonry Structures (AIMS), (2019). http://sera-aims.com/.
[24] R. Faria, J. Oliver, M. Cervera, A strain-based plastic viscous-damage model for massive concrete structures, Int. J. Solids Struct. (1998). https://doi.org/10.1016/S0020-7683(97)00119-4.
[25] E. Arash, E. Zaghi, M. Cashany, ZeroLengthImpact3D, Univ. Connect. (2014). https://opensees.berkeley.edu/wiki/index.php/ZeroLengthImpact3D (accessed January 20, 2020).
[26] C. Casapulla, F. Portioli, Experimental tests on the limit states of dry-jointed tuff blocks, Mater. Struct. Constr. 49 (2016) 751–767. https://doi.org/10.1617/s11527-015-0536-3.
[27] G. Vasconcelos, P.B. Lourenço, D. Oliveira, Experimental shear behavior of stone masonry joints, in: Struct. Anal. Hist. Constr. Preserv. Saf. Significance - Proc. 6th Int. Conf. Struct. Anal. Hist. Constr. SAHC08, 2008. https://doi.org/10.1201/9781439828229.ch87.
[28] P.B. Lourenço, L.F. Ramos, Characterization of cyclic behavior of dry masonry joints, J. Struct. Eng. (2004). https://doi.org/10.1061/(ASCE)0733-9445(2004)130:5(779).
[29] A.K. Chopra, Dynamics of Structures 4th Edition, 2019. https://doi.org/10.1017/CBO9781107415324.004.
[30] L. Luzi, R. Puglia, E. Russo, M.D. Amico, G. Lanzano, F. Pacor, C. Felicetta, Engineering Strong-Motion database : a gateway to access European strong motion data, 16th World Conf. Earthq. Eng. Santiago, Chile, 9-13 January. 899 (2017).

12th International Conference on Structural Analysis of Historical Constructions
SAHC 2020
P. Roca, L. Pelà and C. Molins (Eds.)

NUMERICAL MODELLING OF THE SEISMIC PERFORMANCE OF ROMANIAN TRADITIONAL TIMBER-FRAMED BUILDINGS

F. PARISSE[*1], E. POLETTI[1], A. DUTU[2] AND H. RODRIGUES[3]

[1] Institute for Sustainability and Innovation in Structural-Engineering (ISISE)
Department of Civil Engineering, University of Minho
Campus de Azurém, 4800-058 Guimarães, Portugal
e-mail: francescoparisse3@gmail.com and elisapoletti@civil.uminho.pt
web page: https://www.uminho.pt/PT

[2] Department of Civil Buildings, Technical University of Civil Engineering of Bucharest
Bd. Lacul Tei 122-124, 020396 Bucharest, Romania
e-mail: andreea.dutu@utcb.ro - web page: https://utcb.ro/

[3] RISCO
Department of Civil Engineering, Polytechnic of Leiria
Campus 2, 2411-901 Leiria, Portugal
e-mail: hugo.f.rodrigues@ipleiria.pt - web page: https://www.ipleiria.pt

Keywords: Timber-Framed Masonry, Seismic Modeling, Equivalent Frame, Dynamic Identification

Abstract. *Traditional architecture made of timber-framed masonry (TFM) system is widespread around the world and has already been recognized as a unique cultural heritage to be preserved. These structures have shown a good seismic performance compared to other typologies because their configuration and construction details were constantly updated as soon as the builders addressed the causes of damage mechanisms when earthquakes occurred. Regarding this typology, Romanian TFM structures can be considered a representative example also because they experienced several seismic events showing their good earthquake-resistance. Although these buildings are still constructed and inhabited nowadays, no recommendation is provided in the Romanian building code and its structural behaviour is not properly characterized yet. Bearing in mind that the building's global response depends on many parameters such as the performance of its structural elements and their interaction, the calibration of shear walls is crucial to define the non-linear behaviour under cyclic loading. A simplified modelling strategy was chosen to simulate TFM wall response consisting of an equivalent frame with linear elastic elements and non-linearities lumped at the joints by using OpenSees. After calibrating the wall response according to the experimental campaign performed at Technical University of Civil Engineering of Bucharest, the panel was adapted to model a representative Romanian TFM building whose dynamic properties were evaluated by eigenvalue analysis and their potential calibration is proposed based on the ambient vibration tests.*

1. INTRODUCTION

Timber-Framed Masonry (TFM) structures can be found in many seismic countries even though their characteristics may vary according to the available materials, techniques and knowledge resulting in several structural configurations of timber frame (dimensions and arrangement of elements) and type of infill [1]. The system has been iteratively improved by local builders by damage observation after seismic events that let them understand the basic concepts of earthquake engineering [2].

Considering the number of earthquakes, their return period and energy, Romania can be considered as a country with moderate to high seismic risk, especially Vrancea region in the fore-Arc of Carpathians, where the most active tectonic processes are lumped [3]. Many TFM buildings can be observed across this area validating again the correlation between the typology and seismic hazard, and they were classified in five different types during the field investigation in [4].

Although Romanian TFM structures have experienced several earthquakes, their performance is still not properly assessed and neither design nor retrofitting guidelines, are provided by Romanian building codes. The present paper aims at evaluating the dynamic response of a representative Romanian TFM building by applying a simplified modelling strategy consisting of an equivalent frame approach with non-linear springs lumped at the connections. This strategy is reliable since it is based on the initial numerical calibration of the in-plane cyclic behaviour of Romanian masonry panel with the outcomes resulting from the experimental tests in [5], [6], and it is feasible in terms of computational effort.

In this work, the Romanian TFM system is briefly presented by describing the geometrical and structural characteristics of a representative case study [7]. A building is modelled in the software OpenSees by adapting a calibrated mixed panel whose properties are discussed by comparing its local and global response with the experimental results [8]. The building dynamic properties were predicted by eigenvalue analysis and compared to those estimated by ambient vibration tests [7]. A dynamic study and potential calibration was performed as well [8].

2. DESCRIPTION OF A REPRESENTATIVE ROMANIAN TFM BUILDING

The Romanian timber-framed masonry architecture studied in this paper can be defined as a half-timber masonry structure due to the participation of the wooden skeleton to the resisting system not only under dynamic actions but also under static loads [9], [10]. Although the architectural and structural features can vary from structure to structure, this system is characterized in terms of geometry, structural elements, construction details as well as state of conservation by describing a representative building in the Sarbova area, Timis county, which was dismantled and rebuilt in the National Village Museum, Bucharest [7].

The building was a residential house built around 1900-1930 with the typical dimensions of Romanian TFM architecture: one-storey height and rectangular in shape (11.50x6.00 m), but not completely symmetric in plan with respect to the longitudinal and transversal axis [7]. Figure **1** shows the front view and the plan configuration re-elaborated from the drawings by Technical University of Civil Engineering of Bucharest.



(a) (b)

Figure 1: Romanian TFM building: front view (a) and plan configuration (b) [7]

The superstructure is usually raised from the ground to avoid moisture related issues and it is supported by a dry-stacked stone masonry platform or continuous wall-footing with lower beams named "soles" made of hardwood (oak or acacia) which distribute the loads uniformly. Since the building presents timber-framed panels with brick masonry infill, it can be classified as Type 1 according to [4]. This configuration can have bracings not perfectly aligned with the diagonal of each module, and, in this case, they are not restraint by two consecutive vertical posts, Figure 2 and Figure 3. It is worth to stress that diagonal bracings are effective only in compression since they detach from the frame in tension due to the nailed connections. Moreover, they are confined by masonry infill although it can detach from the timber skeleton due to the low adhesion at the interface resulting in potential out-of-plane mechanisms [5], [6]. During the field investigation on TFM buildings across the Vrancea seismic area in [4], a variation of brick masonry bond was also observed due to construction reasons and to increase the friction in the upper part of the wall as well as the stiffness [5]. However, this feature cannot be seen in the case study since a layer of plaster is applied on both sides of the wall to cover the timber skeleton.



(a) (b) (c)

Figure 2: Elevation of TW1 (a), TW2 and TW3 (b), TW4 (c) wall [8]



(a) (b)

Figure 3: Elevation of LW1 (a) and LW2 (b) wall [8]

The horizontal diaphragms consist of timber beams supporting wooden planks or wattle and daub, or sometimes reed and an additional layer of mud plus straw [5] In the case study, primary beams (cross-sectional area about 110x140 mm) are aligned along the transversal direction and transmit loads to the secondary beams on top of each longitudinal wall, Figure

4a. The roofing system is made up of timber as well. The most common configurations are hip or gable roof with king post trusses with no struts [5]. The studied building presents a porch type with loads transmitted to the longitudinal wall LW1 and LW3, Figure 1b. It consists of rafters with a cross-section of around 90x120 mm and a spacing ranging from 90 to 102 cm which support longitudinal timber strips (45x30 mm) nailed to them and applied to fix the upper ceramic tiles, Figure 4b. Diagonal bracings can be also observed in the fields of the roof to increase their in-plane stiffness while the chimney made of clay brick masonry mass may influence the global response of the building due to its non-symmetric location and heavy mass, Figure 4b.



(a) (b)

Figure 4: Primary beams with timber planks (a) and roofing system (b) [7]

The connections between timber elements are similar to those observed during the field investigation already mentioned [4]. The inferior stringers are likely to be laid inside grooves in the continuous wall-footing to prevent any sliding. Vertical posts are driven into the lower beams with mortise and tenon joints, while the latter are half-lap splice type, Figure 5a and b, respectively. Lintels are likely to be simply connected with nails to vertical posts as well as diagonals that sometimes were applied as a propping system during the construction process resulting in fast and unprocessed connections [5]. Cross-halved joints can be observed between primary and secondary beams of the horizontal diaphragm, Figure 5c, but also between rafters and diagonals on the roof fields.



(a) (b) (c)

Figure 5: Mortise and tenon (a), half-lap splice (b) and cross-halved connection [7]

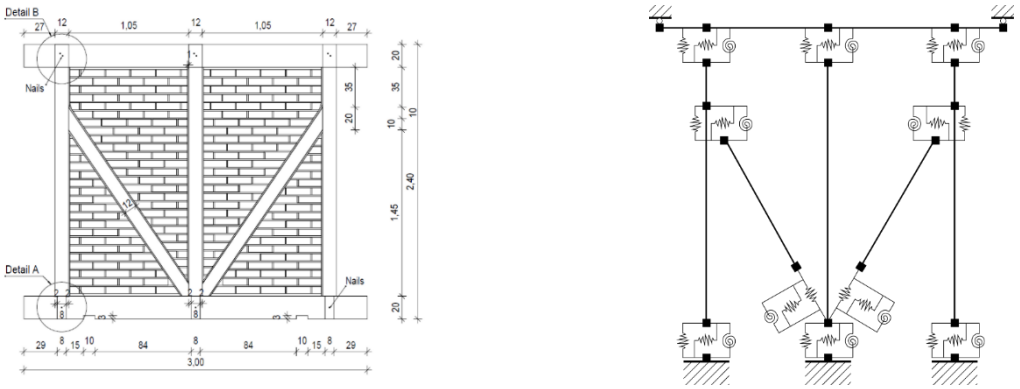
Most of the existing TFM buildings analysed in [4] were in poor conditions due to moisture related problems leading to irreversible decay of timber elements. Since the case study is poorly maintained, it presents the same issues such as biological colonization, coloration, rising damp, minor cracks due to stress concentrations, different construction phases or

excessive shrinkage of infill. These cracks can result in partial detachment of masonry infill also due to the different physical and mechanical properties between the two materials.

3. ROMANIAN TFM WALL CALIBRATION

Although the global response of Romanian TFM buildings is influenced by the previously described structural elements and their connections, the shear walls play an important role and their behaviour was investigated in an experimental campaign, detailed presented in [5], [6], that performed cyclic tests on four mixed panels varying the type of infill and arrangement of diagonals. The results of the timber-framed wall with masonry infill and lower bracings in Figure 6a, S1 in [5], [6], are taken as a reference for the following numerical calibration.

A simplified strategy was used by modelling the panel through an equivalent frame with the non-linear behaviours lumped at the connections, and the model was implemented in OpenSees [11] as proposed in [8], [12]. Figure 6b shows the frame schematization consisting in linear elastic timber elements with translational and rotational springs at their connections. Posts, beams and diagonals are modelled as linear elastic elements since no damage was observed along them during the testing sequence. The choice of neglecting the masonry infill can be validated by the low adhesion at the interface with the timber skeleton, its low mechanical properties and by the presence of lower bracings that mainly control the deformation capacity of the wall [5], [6]. However, the potential underestimation in terms of stiffness due to the confinement effect for both elements and their connections, was considered by modifying the related parameters after the initial calibration of connections based on unconfined configurations. A similar updating procedure was performed for the cumulative dissipated energy that may result lower as well, due to the friction between frame and infill and along the joints. It was increased by making the hysteresis models of each connection larger with a steep slope of the unloading stiffness branch.



(a) (b)

Figure 6: Specimen S1in [5] (a) and its structural scheme (b) [8]

The pure shear behaviour was investigated by restraining the vertical displacements of the upper beam to simulate the pantograph system of the reaction frame, Figure 6b. Moreover, the top beam can be defined as rigid element to make the entire wall move with the same horizontal displacements while bracings are truss elements. It is worth mentioning that the latter ones can slide vertically at the upper connections as observed during the experimental test up to around 65 mm and they can detach at the central lower joint when the tension

exceeds the withdrawal capacity of the slant nailing. The mechanical properties of Romanian fir (parallel modulus of elasticity equal to 8.9 GPa, specific weight of 385 kg/ m^3) and those of masonry infill (specific weight of 19.6 kN/m^3) were assumed consistent with experimental tests performed on similar materials [13]. The difference in total mass between numerical and experimental wall is negligible (less than 0.5%)

3.1 Calibration of connections

Since the global behaviour of TFM walls is mostly controlled by the connections, tee-halved (TH) type at the top and mortise and tenon (MT) type at the bottom, they were calibrated according to representative experimental tests [13], [14], respectively. These campaigns were aimed the study of the moment resisting behaviour and tensile capacity of the joints, but present some differences in terms of geometrical dimensions, types of fasteners and timber species.

Each structural joint was modelled with three springs, one per degree of freedom and aligned according to global or local axis as shown in Figure 6b, considering a 2D model. They are characterized by uniaxial non-linear hysteretic materials such as *SAWS* (developed by Patxi Uriz and converted from FORTRAN, code originally written by Bryan Folz) and *Pinching4* in OpenSees library whose properties resulting from the initial calibration, were iteratively modified to approach the local and global behaviour observed during the experimental tests [5], [6]. Moreover, the central lower connection between post and bracing was characterized by a spring aligned along the diagonal with an *Elastic-No Tension* uniaxial material that allows detachment in tension and prevents overlapping in compression [8]. The vertical spring at the upper joints was modelled to let the bracings slide along the external posts up to the maximum value (around 65 mm) observed during the test.

3.2 Non-linear cyclic analysis

The cyclic response of the simplified numerical model was calibrated with the inverse fitting procedure to approach the local and global behavior of the tested specimen in terms of hysteretic curve, its envelope, the damage mechanisms and the deformed shape. This iterative method consisted in updating the non-linear properties of hysteretic materials at the connections. Non-linear cyclic analysis was performed after pushover analysis to consider the accumulation of damage and degradation effects related to cyclic loadings.

The experimental curve was approached initially in terms of global envelope and then in detail, approximating the reloading and unloading behavior per cycle considering the degradation properties of the non-linear hysteretic materials applied at the connections [8]. Indeed, the wall response is mainly influenced by the moment resisting behavior of the tee-halved and mortise and tenon joint, as well as the sliding effect between diagonals and external posts. Thus, some parameters of their non-linear materials were updated increasing the initial and yielding stiffness from the initial calibration based on representative experimental tests [13], [14]. This modification can be justified by the additional contribution of masonry infill that confines each connection and stiffens the panel. The hysteretic curve resulting from the non-linear cyclic analysis, in red, is overlapped with the experimental one in Figure 7a showing a good approximation between them in terms of maximum base shear per displacement-cycle peak and reloading stiffness even though there are some discrepancies

for the dissipated energy due to the different unloading stiffness and pinching effect. The latter phenomenon relates with the experimental reloading branches that are significantly pinched because the cyclic loading makes the joints weaker with the formation of gaps around the nails due to wood fiber crushing.

It is worth mention that the numerical analysis was performed by applying the same horizontal top displacement vector in positive and negative direction. This assumption eventually resulted in larger differences when the loading reverses in terms of negative peak displacements, shear forces and dissipated energy. The energy calculation is also affected by the non-symmetric behavior in the transition between positive and negative cycles of the experimental hysteretic curve. Figure 7b shows the comparison in terms of absolute cumulative dissipated energy: the numerical curve is always below the experimental one.

The absolute cumulative difference is not perfectly comparable (-36%) even for the maximum drift (5.43%) due to the already mentioned pinching effect and the vertical unloading of the experimental cycles. The different behavior should be investigated in detail to address the causes leading to the change of unloading stiffness in the numerical model. Regarding the lower stiffness of the simplified model, it is due to the initial expert assumption to consider as a reference the third cycle neglecting the first ones mostly influenced by the specimen setting and equipment testing.

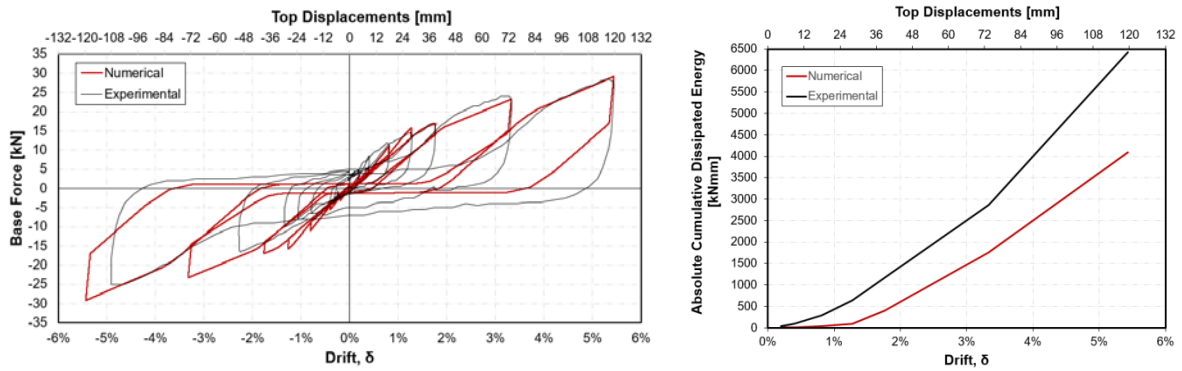
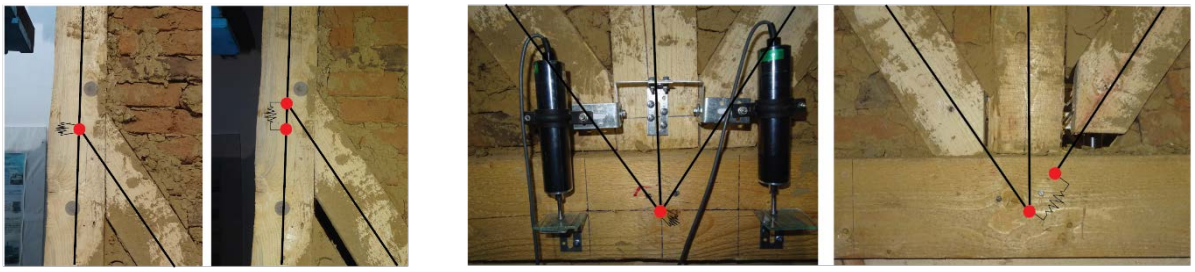


Figure 7: Experimental and numerical hysteretic curve (a) and absolute cumulative dissipated energy (b) [8]

The equivalent frame model shows the same deformed shape of the tested wall with the expected behavior of diagonal bracings. The damage mechanisms are comparable as well. Figure 8a pictures the vertical sliding along the external post whose values (63 mm) are consistent with those observed experimentally (around 65 mm), while the axial detachment at the base is lower than the numerical one (88-107 mm), Figure 8b. This may result from neglecting the withdrawal capacity of the slant nailing and some inaccuracies in the calibration of the upper connections bracing-to-post.



(a) (b)

Figure 8: Vertical sliding along the post (a) and detachment along the diagonal axis (b): initial and final position

4. SEISMIC MODELLING OF THE REPRESENTATIVE ROMANIAN TFM BUILDING

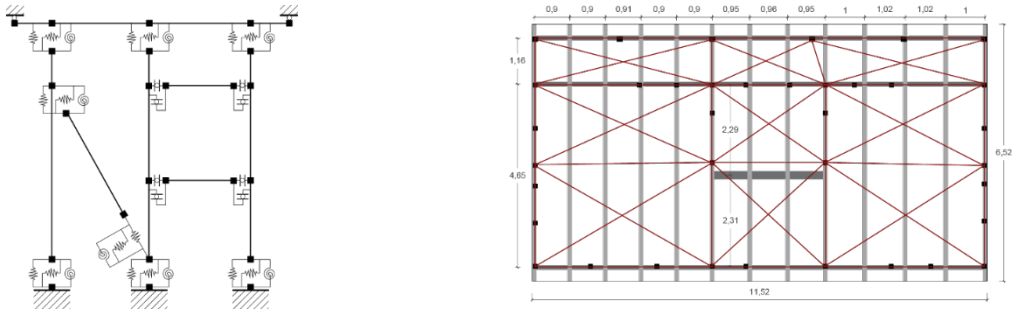
The seismic behavior of the representative Romanian TFM building in the National Village Museum, Bucharest, was predicted by applying the same simplified modeling strategy to compare its dynamic properties with those estimated by ambient vibration tests [7].

Since the global response is influenced by many parameters such as geometry, mass distribution, configuration of structural elements (TFM walls, floor and roofing system) as well as the connections between them and state of conservation, additional expert assumptions and simplifications were made to evaluate the building structural performance. Indeed, the case study presents some differences with the calibrated wall of Section 3 as following:

i. infill made of clay bricks instead of mud bricks;
ii. bracings are not always constraint by two consecutive posts;
iii. presence of openings with related timber lintels;
iv. flexible floor;
v. large variation in mass distribution.

Thus, the representative structural scheme of each wall as well as its boundary conditions were slightly updated as shown in Figure 9a. It is worth mentioning that the set of connections resulting from non-linear static analysis of the wall specimen was applied since the properties of the non-linear hysteretic materials at the springs were updated again to perform non-linear cyclic analysis considering the degradation effects. Moreover, timber lintels are pinned at their ends to the vertical posts, while non-constraint bracings have same connections both at the top and bottom assuming equivalent potential vertical or horizontal sliding, respectively.

The lower nodes are fixed to the ground since neither differential foundation settlements, nor tipping ones, were observed during the field investigation due to the light weight of the structure and its continuous wall-footing. No horizontal sliding was considered as well, but this assumption may not be conservative if the lower beam is not connected to the continuous brick masonry wall footing. Since the confinement and stiffening effect of the masonry infill was considered in the calibration, out-of-plane behavior was neglected as well, even though this mechanism is very likely to occur in case of earthquake due to the low adhesion at the interface between timber frame and infill [5], [6]. Figure 9b shows the horizontal diaphragm modelled as rigid by applying a tying system with high axial stiffness. Vertical uplift was prevented, to be consistent with the wall calibration performed, considering its pure shear behavior.



(a) (b)

Figure 9: Structural scheme of walls (a) and floor (b)

An increased specific weight of masonry infill was defined as 20 kN/m^3 for clay brick instead of 19.6 kN/m^3 for mud brick in S1 specimen in [13] and was distributed along the vertical posts considering their tributary area to simulate the actual mass distribution of each wall. Since timber beams are made of hardwood (oak or acacia), their specific weight is assumed as 600 kg/m^3 and their parallel modulus of elasticity equal to 12 GPa.

Regarding the additional weight of horizontal diaphragm and roofing system, it was concentrated at the structural nodes representing the connections between the transversal primary beams and the secondary ones on top of each longitudinal wall LW1, LW2 and LW3 (Figure 1b) according to their tributary areas. The same procedure was applied to determine vertical loads from the roof trusses considering the actual tributary area of the roof field, not its horizontal projection, due to the steep slope. No horizontal thrust was considered since the roofing system approaches a truss structure with inclined rafters tied at the base by the transversal beams of the floor diaphragm. The presence of the brick masonry chimney and attic walls was considered as lumped weight at its contour posts. Only dead loads were applied to be consistent with the environmental and loading conditions during the dynamic identification. The total weight of numerical model was compared with the one determined by hand calculations resulting in a negligible difference lower than 5%.

The dynamic properties of the simplified model were determined by eigenvalue analysis and compared with those resulting from the dynamic identification. This procedure and the testing equipment are explained in detail in [7], but, in this paper, only the resulting frequencies and mode shapes are presented. Since the calibration procedure was not based on updating neither the non-linear properties of the already calibrated connections, nor the linear material properties due to the state of conservation, it was performed by modifying the elastic stiffness of a fictitious material representing the additional contribution of clay brick masonry infill.

Two simplified models were made to evaluate the differences between two complementary modeling strategies: equivalent frame with non-linear properties lumped at the connections (EF) and the same model infilled with shell elements (EFI), Figure 10a and b. The inverse fitting procedure was performed by modifying the Young's Modulus (E) of infill until the estimated frequencies were obtained. The choice of considering the contribution of a fictitious infill is validated by the higher mechanical properties of clay brick masonry compared to those of mud masonry applied in the wall specimen [8]. Since ambient vibration tests record micro-tremors of structures in their elastic range and the initial stiffness of TFM buildings is

mainly controlled by the characteristics of masonry infill, EF model may result in larger differences in terms of frequencies compared to the estimated ones.



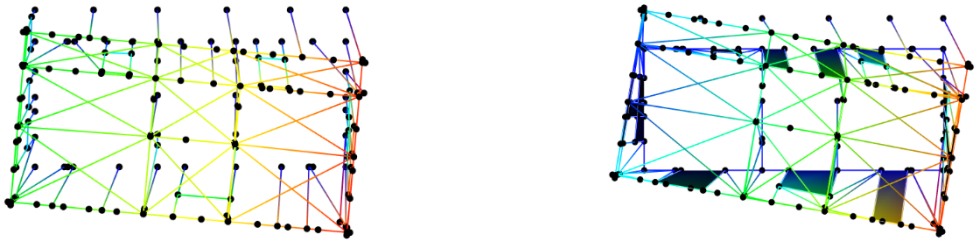
(a) (b)

Figure 10: EF (a) and EFI (b) models

The calibration resulted in the final value of E equal to 58.5 MPa, very low compared to the one related to clay brick masonry (1.2 ÷ 1.8 GPa according to Table C8.5.I in [15]). The value is almost negligible since the numerical model for the wall was already calibrated with the presence of masonry infill. Bearing in mind that the first periods are 0.17 s for the transversal direction and 0.15 s for the longitudinal one and since there are no mode shapes in the already mentioned report [7], the first and second periods with the corresponding mode shapes are compared between EF and EFI models, Table 1, Figure 11 and Figure 12. The periods of EF model are higher than the estimated ones in [7] and the corresponding mode shapes show slight torsional effects due to non-symmetric layout and mass distribution. This effect is even more evident for EFI model where both periods are comparable to those in [7]. Moreover, in EF model, periods and corresponding mode shapes are actually flipped; the highest period is actually longitudinal not transversal and vice versa.

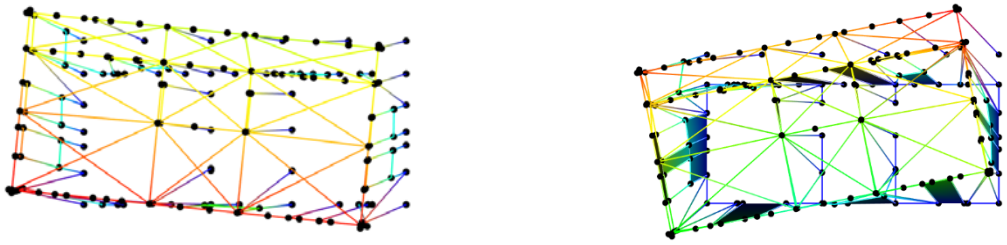
Table 1: Transversal mode shape for EF (a) and EFI (b) models

Model	Mode	Type	Period [s]	Difference [%]	Reference
EF	1	Longitudinal	0.374	220	0.17s (Transversal)
EFI	1	Torsional-Transversal	0.17	-	0.17s (Transversal)
EF	2	Transversal	0.333	222	0.15s (Longitudinal)
EFI	2	Torsional-Longitudinal	0.154	2.6	0.15s (Longitudinal)



(a) (b)

Figure 11: Transversal mode shape for EF (a) and EFI (b) models



(a) (b)

Figure 12: Longitudinal mode shape for EF (a) and EFI (b) models

5. FINAL CONSIDERATIONS

The structural typology with timber skeleton with masonry infill (TFM) has already proven the effectiveness of its seismic performance empirically improved by local builders, but this seismic capacity is still not assessed quantitatively. This research work is aimed at evaluating the seismic behavior of Romanian TFM buildings following the previous studies and existing experimental campaigns in [4]-[7], [10], [13] which determined the non-linear hysteretic response of TFM walls subjected to in-plane cyclic loading.

A representative Romanian TFM building was modelled in the software OpenSees as an equivalent frame structure with non-linear properties lumped at the connections (EF). This model is based on a numerical calibration of the wall specimen S1 tested in [5] by applying the inverse fitting procedure to approach both global and local response [8].

Some additional assumptions were considered to model the Romanian building and estimate its dynamic properties, which were compared to those resulting from ambient-vibration tests. A potential calibration was also proposed by infilling the panel (EFI model) due to the different type of masonry observed in the existing structure, even though the actual objective is to use the most simplified modelling approach to predict the seismic behaviour of Romanian TFM architecture.

The resulting deformed mode shapes of both models showed a significant torsion effect due to non-symmetric mass distribution and layout which should be properly addressed with future analysis. It is worth to mention that the dynamic properties of the equivalent frame model with no infill (EF) are influenced by the connection calibration that presents some limitation of the applied hysteretic materials in the correlation between applied loads and global response, but the wall calibration was performed with a representative vertical load.

The simplified modelling strategy has other limitations such as it does not take into account the interface between the timber frame and masonry infill, but its contribution in terms of dissipated energy was considered in the calibration of connections. In addition, since the masonry infill detaches from the timber frame even in the curing process, the out-of-plane mechanisms are not prevented especially in case of earthquakes, thus a further implementation of the numerical model is required. However, this approach can still provide reliable results, especially for the wall, and allows to capture local failures of connections if the demand exceeds their deformation capacity. The calibration process may even run automatically if the user understands the role of each parameter and connection. Regarding non-linear numerical analysis on simplified models, they may not require a large computational effort thus their application can be feasible to whole buildings.

Acknowledgments

The author wish to thank the University of Minho, where the research was carried out during the Master course in Structural Analysis of Monuments and Historical Constructions (SAHC program), and the Technical University of Civil Engineering of Bucharest – UTCB, where the experimental campaign and the ambient-vibration tests were performed.

References

[1] Bianco, A. *La casa baraccata: guida al progetto e al cantiere di restauro*. Ginevra Bentivoglio EditoriA, Roma, (2010).

[2] Gülkan, P. and Langenbach, R. The earthquake resistance of traditional timber and masonry dwellings in Turkey. *13th World Conference on Earthquake Engineering*, Paper no. 2297 (2004).

[3] Pavel, F., Vacareanu, R., Douglas, J., Radulian, M., Cioflan, C. and Barbat, A. An updated probabilistic seismic hazard assessment for Romania and comparison with the approach and outcomes of the SHARE Project. *Pure and Applied Geophysics* (2016) **173**:1881–1905. https://doi.org/10.1007/s00024-015-1223-6.

[4] Duțu, A., Dima, D. I. and Bulimar, E. G. Materials and techniques for traditional Romanian residential houses. *3rd International Conference on PROTECTION OF HISTORICAL CONTRUCTIONS* (2017).

[5] Dutu, A., Niste, M., Spatarelu, I., Dima, D. I. and Kishiki, S. Seismic evaluation of Romanian traditional buildings with timber frame and mud masonry infills by in-plane static cyclic tests. *Engineering Structures* (2018) **167**:655–670.

[6] Dutu, A., Niste, M. and Spatarelu, I. In-plane static cyclic tests on traditional Romanian houses ' walls. *16th Europeand Conference on Earthquake Engineering* (2018).

[7] Aldea A., Dutu A., Demetriu S. and Dima D.I. *Dynamic properties identification for a timber framed masonry house.* Revista Constructii (under review).

[8] Parisse, F. *Numerical modelling of the seismic performance of romanian traditional timber-framed buildings*. University of Minho (2019). http://hdl.handle.net/1822/62517

[9] Ruggieri, N. An Italian anti-seismic system of the 18th century decay, failure modes and conservation principles. *International Journal of Conservation Science* (2016), **7**:827–838.

[10] Dima, D. I. and Dutu, A. Traditional buildings with timber frame and various infills in Romania. *Proceedings of the WCTE 2016 (World Conference on Timber Engineering)* (2016).

[11] Mazzoni S, McKenna F, Scott MH, Fenves GL. Open system for earthquake engineering simulation user command language manual. Pacific Earthquake Engineering Research Centre, Berkeley: University of California (2006).

[12] Lukic, R., Poletti, E., Rodrigues, H. and Vasconcelos, G. Numerical modelling of the cyclic behavior of timber-framed structures. *Engineering Structures* (2018), **165**: 210–221. https://doi.org/10.1016/j.engstruct.2018.03.039.

[13] Dutu, A., Niste, M., Spatarelu, I., Dima, D. I. TFMRO project (Seismic evaluation of Romanian traditional residential buildings). Scientific Report, Technical University of Civil Engineering of Bucharest (2017). http://tfmro.utcb.ro/.

[14] Sakata, H., Yamazaki, Y. and Ohashi, Y. A study on moment resisting behavior of mortise-tenon joint with dowel or split wedge. *15th World Conference on Earthquake Engineering (15WCEE)* (2012).
[15] Italian Building Code. *Circolare 21 gennaio 2019 n. 7 C.S.LL.PP. Istruzioni per l'applicazione dell'aggiornamento delle "Norme Tecniche per le Costruzioni" di cui al D.M. 17/01/2018*. *Suppl. ord. alla G.U. n. 35 del 11/2/19*, (2019).

12th International Conference on Structural Analysis of Historical Constructions
SAHC 2020
P. Roca, L. Pelà and C. Molins (Eds.)

NUMERICAL SIMULATION OF TRADITIONAL TIMBER-MASONRY BUILDINGS SUBJECTED TO LATERAL LOADS

BELÉN JIMÉNEZ[1*] AND LUCA PELÀ[1]

[1]Department of Civil and Environmental Engineering
Universitat Politécnica de Catalunya (UPC-BarcelonaTech)
Jordi Girona 1-3, 08034 Barcelona, Spain
e-mail: maria.belen.jimenez@upc.edu , luca.pela@upc.edu

Keywords: Nonlinear Static Analysis, Timber Frame, Unreinforced Masonry, Numerical Simulation, Lumped Plasticity Models, Macro-Mechanical FE Models

Abstract. *Existing heritage buildings are often composed of diverse structural typologies, representing a challenge for structural analysis. This work investigates the use of nonlinear static analysis to assess the seismic behaviour of hybrid timber-masonry buildings. The proposed methodology includes the use of Lumped Plasticity Models (LPM) and Macro-Mechanical Finite Element (FE) approaches to simulate the response of structures composed of timber frames and masonry walls. Benchmark experiments on timber and masonry specimens subjected to lateral loads are used to calibrate the constitutive laws governing the behaviour of the proposed models. The calibrated models are used to appraise the seismic response of an existing timber-masonry building located in the historical centre of Valparaíso (Chile). The results predict the nonlinear acceleration-displacement capacity of the buildings, as well as the expected damage of the structure, revealing the potential local and global failure mechanisms.*

1 INTRODUCTION

Hybrid timber-masonry buildings represent a significant amount of the built heritage in seismic prone territories. Past earthquakes demonstrated the good performance of these types of structures against seismic loads, especially for the case of the timber frame typologies. However, the study of hybrid structures is often compromised by a high number of uncertainties due to the variety of the structural typologies, the nature of materials, the complexity of the connections or any singularity, which may influence the response of the structure.

Numerical analyses are increasingly used to assess the seismic behaviour of existing buildings. Available modelling strategies usually deal with timber or masonry structures

separately for the case of homogeneous building typologies. Few research studies could address the modelling of heterogeneous timber-masonry structures in the available literature [1,2].

This research contributes to develop a systematic methodology for the nonlinear static analysis (NSA) of hybrid timber-masonry structural systems subjected to lateral loads. The models were developed with the structural earthquake engineering software SAP2000 v20. The methodology involves a preliminary study of different benchmark experiments used to calibrate the models. An experimental campaign considering bare frame and infilled frame specimens of the Pombalino typology [3] were selected for the numerical calibration of the FE models. A Lumped Plasticity Model (LPM) was proposed for the NSA of timber frame structures. The LPM assumes that nonlinear behaviour is lumped in springs at the members' ends, i.e. where the connections are located, while the timber elements are idealized by using linear elastic isotropic material properties. The infill within the frame was modelled employing the Equivalent Strut Method (ESM). This simplified approach idealizes the infill with a diagonal strut with in-plane strength and stiffness equivalent to that of the uncracked solid masonry panel. Two experimental tests on unreinforced masonry (URM) walls loaded in-plane [5] and out-of-plane [6] were selected to calibrate the macro-mechanical FE models. Such an approach idealized the masonry as a homogeneous material, making no distinction between their components, [7,8]. The nonlinear constitutive law of the masonry material is based on the model proposed by [16], defining the stress-strain behaviour and failure criteria.

The seismic behaviour of a hybrid timber-masonry building existing in the historical centre of Valparaíso (Chile) was simulated using the calibrated models, combining LPMs and macro-mechanical FE models representing the timber and masonry load-bearing systems respectively. The NSA applied in the two main directions of the building allowed to predict the capacity of the structure, as well as the main collapse mechanisms.

2 CALIBRATION OF THE MODEL

3.2 Numerical simulation of experiments on timber frames

The calibration of the timber frame model was developed by simulating two benchmark experimental tests on a bare frame, and an infilled frame of a Portuguese Pombalino wall tested under lateral loads [3]. Both specimens were composed of a main frame of posts and beams braced with St Andrew's crosses, as shown in Figure 2b. Half-lap carpentry joints connected the post and beams of the frame, as well as the diagonals between them, while nails connected the diagonal at the inner sides of main frame elements. The proposed LPM concentrated the nonlinear behaviour of the connections at the ends of the frame members by using either nonlinear hinges or nonlinear springs.

Figure 1a displays the experimentally obtained moment-rotation law of the half-lap connection, as derived from the experimental tests reported in [3]. Nonlinear rotational hinges were assigned at each half-lap connection within the main frame. Due to the lack of experimental data for the diagonal connection, sensitivity analyses were developed to define its axial nonlinear stiffness. Linear elastic models were used to determine the stiffness of the connection by decreasing this value up to reach a good agreement with the global stiffness of

the model. The axial linear stiffness of the connection was estimated as 9050 kN/m. Subsequently, nonlinearities were integrated into the model by defining the maximum capacity of the connection, estimated as 26 kN by performing sensitivity analyses according to the procedure reported in [4]. The deformational relationship governing the response of the connection was defined with an initial linear behaviour up to the maximum capacity, followed by a softening branch, as shown in Figure 1b. The yield displacement of the model d_y was determined following the Equation (1):

$$d_y = F_y / k \tag{1}$$

Where F_y is the maximum capacity and k is the obtained linear stiffness. The ultimate displacement was assumed as the same reached by the half-lap connection in the test (0.05 m), when the central connection failed and the remaining connections no longer worked [3]. Nonlinear axial springs were assigned at each node where the diagonals meet the panel. Moment releases were assigned at the ends of the diagonals to avoid transmission of bending moment to these elements. Linear elastic frame elements were used to represent the timber members using the isotropic linear elastic material properties of the timber specimen specified in [3]. A vertical pre-compression of 25 kN at each post of the frame and a horizontal displacement of 0.1 m at the top beam were applied to simulate the loading conditions of the experiment. The global stiffness of the panel, calculated as 2.60×10^3 kN/m, and the maximum capacity, equal to 55 kN, were properly captured by the model, as shown in Figure 2a. The local and global collapse mechanisms predicted by the model were also in accordance with those occurred in the experiment. The structure entered in the plastic range once the nonlinear axial springs at the end of the diagonals reached their maximum capacity. After that, the connection at the centre of the panel experimented a high shear stress exerted by the diagonals in compression, leading to the ultimate capacity of the rotational hinges at this location, and the total collapse of the frame.

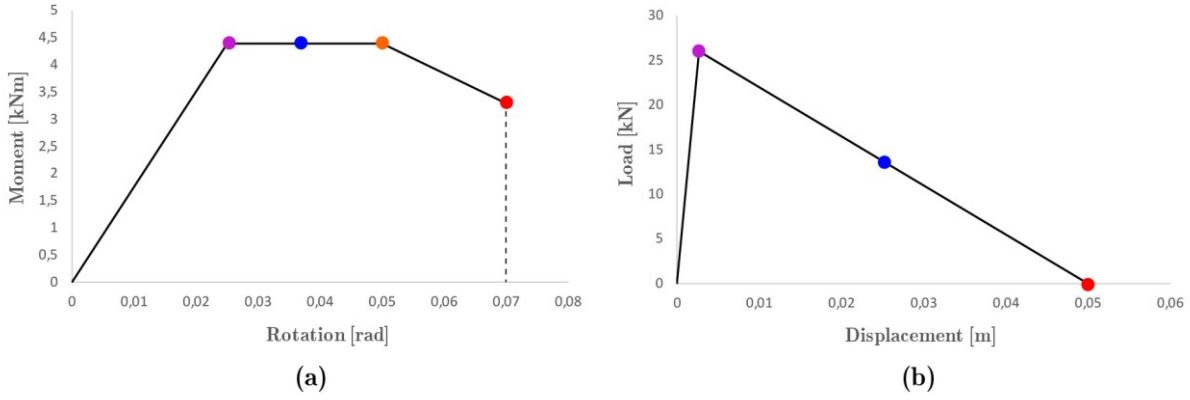


Figure 1: Nonlinear relationships for the connections in the LPM of the Pombalino frame: (a) Half-lap and (b) diagonals.

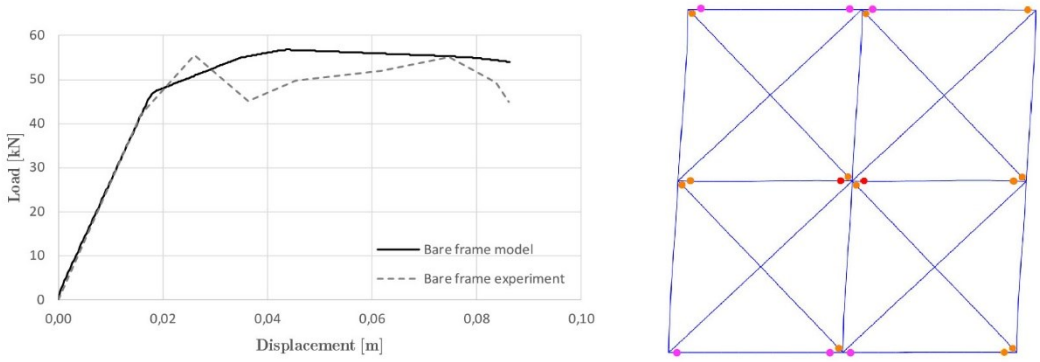


Figure 2: Results of bare frame with the lumped plasticity model: (a) numerical vs experimental capacity curves and (b) collapse mechanisms.

The influence of the infill in the response of the timber frame specimen was simulated applying the ESM proposed by [9, 10]. The ESM assumes that the contribution of the masonry infill panel can be represented by an equivalent compression strut of width ω given by Equation (2).

$$\omega = \left(\frac{k_1}{\lambda_h} + k_2\right) d \tag{2}$$

Where ω is the width of the frame, in m, d is the diagonal length of the infill panel, in m, and λ_h is a relative stiffness coefficient computed by Expression (3). k_1 and k_2 are constant values dependent of λ_h as reported in [11].

$$\lambda_h = \sqrt[4]{\frac{E_m\, e \sin(2\theta)}{4 E_c\, I_{col}\, h_m}}\, h \tag{3}$$

Where E_m is the elastic equivalent modulus of the complete cracking stage on the infill, in kN/m^2; e is the thickness of the infill panel, in m; θ is the angle whose tangent is the infill height-to-length aspect ratio, in rad; E_c is the expected modulus of elasticity of the frame material, in kN/m^2; I_{col} is the moment of inertia of the columns, in m^4; h_m is the height of the infill panel, in m; and h is height of the column measured between centre lines of the beams, in m.

The nonlinear deformation acceptance criterion of the equivalent strut was determined following the methodology described in [11,12]. The lateral load-displacement relationship defined in [11] was adopted to determine the deformational control-scheme of the panel. The stiffness of the strut k_{mfc} corresponding to the complete cracking stage is given by Equation (4).

$$k_{mfc} = \frac{E_m\, e\, \omega}{d} \tag{4}$$

The resistance of the panel is simulated by an equivalent failure compressive strength $(\sigma_{br})_{min}$ which considers the most probable failure mode that may occur in both conventional tests and

real structures subjected to seismic action, as detailed in [11]. The lateral strength of the equivalent strut H_{max} is given by Equation (5).

$$H_{max}=(\sigma_{br})_{min}\, e\, \omega \tag{5}$$

The stiffness coefficient λ_h of the equivalent strut for the infill frame panel was 12.3 considering the geometrical and mechanical properties of the materials defined in [3]. The width of the strut was calculated as 0.21 m considering the coefficients k_1 and k_2 equal to 0.47 and 0.04 respectively. The linear stiffness of the panel k_{mfc} was calculated as 49740 kN/m by applying Expression (4). A characteristic shear diagonal tension failure mode was predicted for the panel with $(\sigma_{br})_{min}$ equal to 240.9 kN/m^2. Lastly, the maximum lateral strength H_{max} resulted as 5.56 kN. Figure 3 displays the obtained load-displacement relationship of the strut based on [12]. The equivalent strut is modelled using linear elastic frame elements pin-connected to the surrounding frame to avoid rotation resistance. Nonlinearities are introduced into the model at the end nodes of the strut using nonlinear axial hinges defined with the load-deformation relationship shown in Figure 3.

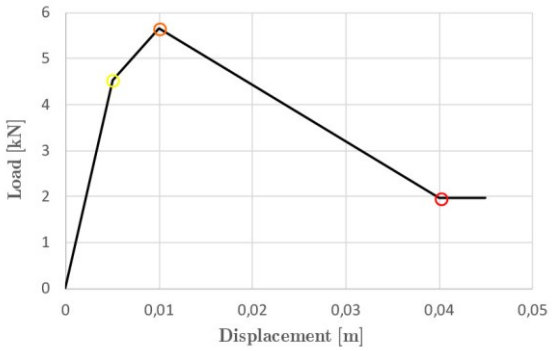


Figure 3: Load-displacement relationship of the equivalent strut model for the infill of Pombalino frame.

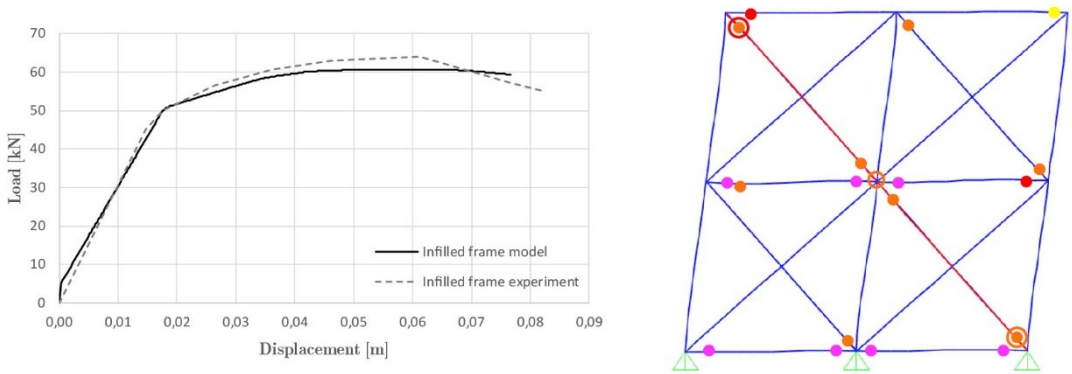


Figure 4: Results of infilled frame with the lumped plasticity model: (a) numerical vs experimental capacity curves and (b) hinges developed.

Figure 4a compares the experimental load-displacement capacity curve with that predicted by the LPM of the Pombalino infilled frame. The model captures properly the global stiffness of the frame, and the maximum capacity is slightly underestimated as shown in Figure 4a. The nonlinearities started to appear when the axial springs of struts and diagonals reached their maximum compressive capacity at the displacement of 0.018 m. After this phase, a progressive failure of the rotational hinges in the main frame occurred until the global collapse of the frame (see Figure 4b). This prediction is consistent with what occurred in the experiment, when the diagonals separated from the main frame inducing the first loss in stiffness, followed by the collapse of the half-lap connections.

2.1 Numerical simulation of experiments on masonry walls

The calibration of the masonry models was developed by simulating two benchmark experiments of in-plane and out-of-plane loaded URM panels. Macro-mechanical FE models were prepared by applying the shell formulation available in the SAP2000 environment. The shells are four-node formulation objects configured by four-point numerical integration to compute the stiffness, and 2-by-2 Gauss integration points to evaluate the stresses, internal forces, and moments at the nodes. This formulation combines membrane and plate behaviour in planar or three-dimensional structures simulating the in-plane and out-of-plane behaviours [13]. Layered shell sections allow the integration of the material nonlinearities in all of the three membrane stress components of each layer. The material model adopted for the simulation of masonry is based on the Darwin-Pecknold theory [14] and the Vecchio-Collins behaviour [15] available in SAP2000 code. The model represents the compression cracking and the shear behaviour considering predetermined stress-strain formulations. A co-axially rotating smeared crack model considers both cracking and crushing of the material. A parabolic stress-strain relationship has been chosen to determine the compressive behaviour of the material, while the tensile response is defined as the 5% of the compressive strength with an exponential softening behaviour. The compressive behaviour of masonry is determined considering the analytical model proposed by [16], as described by Equation (6).

$$\frac{f_m}{f'_m} = A\frac{\varepsilon_m}{\varepsilon'_m} - B\left(\frac{\varepsilon_m}{\varepsilon'_m}\right)^C \tag{6}$$

Where f_m and ε_m are the compressive stress and strain in masonry respectively, and ε'_m is the peak strain corresponding to f'_m A, B, and C are coefficients describing the shape of the curve, being A= 6.4, B=5.4 and C=1.17 [17]. The Coulomb friction model of the material is considered as follows:

$$\tau = c + \sigma \tan\varphi \tag{7}$$

Where c is the cohesion, σ is the normal stress and $\tan\varphi$ is the friction between the elements. A friction angle φ equal to 23º was used to define the shear model as recommended in [17,18]. The FE model is discretized considering a mesh formed by 258 rectangular shell elements of 0.18×0.28 m^2 and 310 nodes. The section of the shells was defined with only one layer of 0.31 m thickness, and four integration points along the thickness direction. Figure 5 shows the uniaxial compression-tension constitutive laws of masonry as defined by the material properties

obtained in [5]. The compressive stress-strain relationship was modified considering a perfectly plastic behaviour (dashed line in Fig. 5a) as suggested in [17], in order to allow the model to reproduce correctly the base rotation of the piers in the experiment. A vertical pre-compression of 200 kN was applied at each pier of the wall, followed by a lateral displacement of 0.03 m applied at a height of 3.00 m on the left side of the wall simulating the experimental loading conditions. All the nodes at the base were restrained in all the DOFs to reproduce the rigid support conditions. NLA was performed to capture the initial yielding and plastic behaviour of the model, and compute the load-displacement curve.

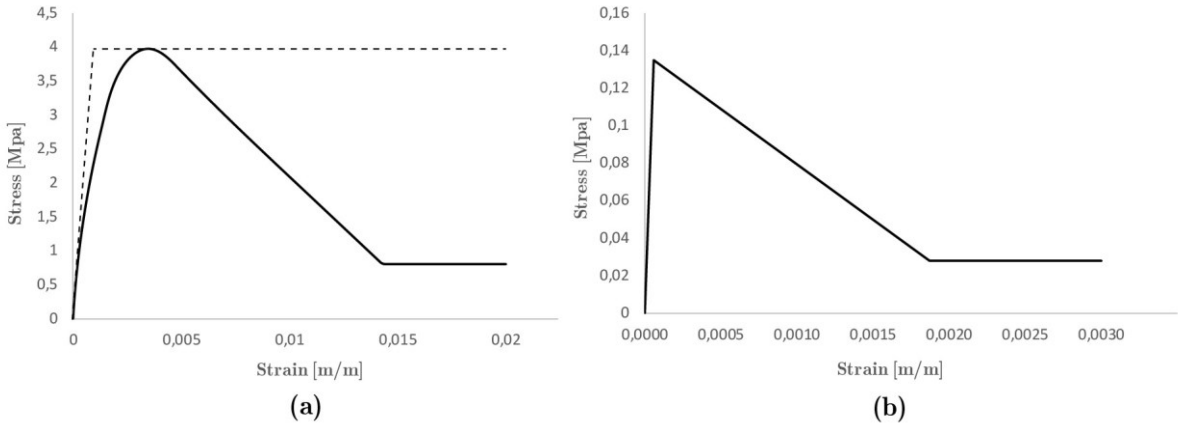


Figure 5: Stress-strain relationships for the in-plane masonry model: (a) compression and (b) tension.

Figure 6a compares the experimental load-displacement response of the wall with the one predicted by the model, revealing a very good agreement in terms of reached stiffness and capacity. The formation of diagonal strut mechanisms at the piers and the spandrel emulated correctly the failure mechanisms occurred in the experiment. Figure 6b shows the principal compressive strain contour of the wall at the end of the test, with the residual resisting mechanism. The diagonal struts and the damage at the piers of the FE model are in agreement with those occurred in the experiment.

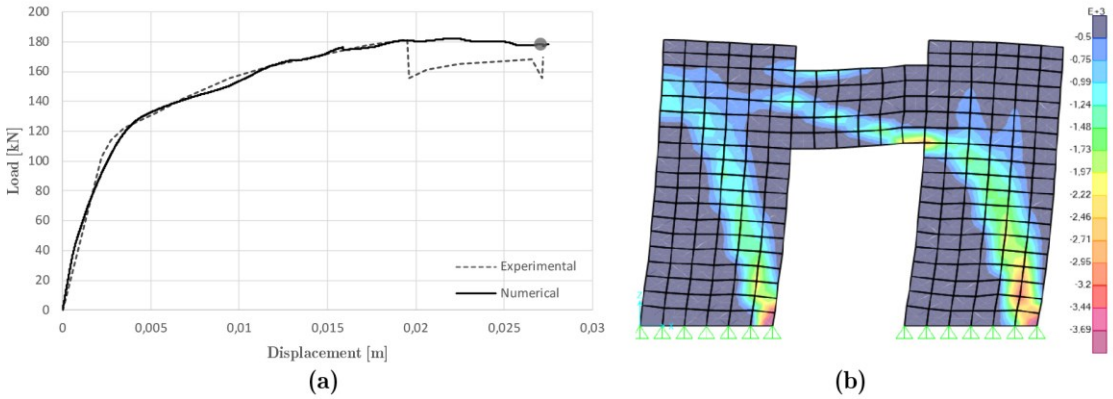


Figure 6. In-plane loaded masonry model results: (a) capacity curve and (b) principal compressive strain contour.

The masonry wall tested under out-of-plane loads [6] corresponds to a solid specimen without openings of 4.00 m width × 2.5 m height × 0.11 m thickness. Return walls of 0.45 m length were built-in at both sides of the specimen to provide a realistic full moment contact along the vertical edges. The wall was subjected to a vertical precompression of 100 kN/m^2 at the top of the wall, followed by a uniform pressure applied under displacement control at the surface of the panel. Given the symmetrical layout of the specimen, only half part of the wall was modeled considering appropriate symmetrical boundary conditions. The model was discretized into 240 shell elements of 0.15 × 0.15 m^2. The section of the shells was set with one layer of 0.11 m and five integration points along the thickness direction. Figure 7 shows the uniaxial compression-tension constitutive laws for masonry considering the mechanical properties obtained by [6].

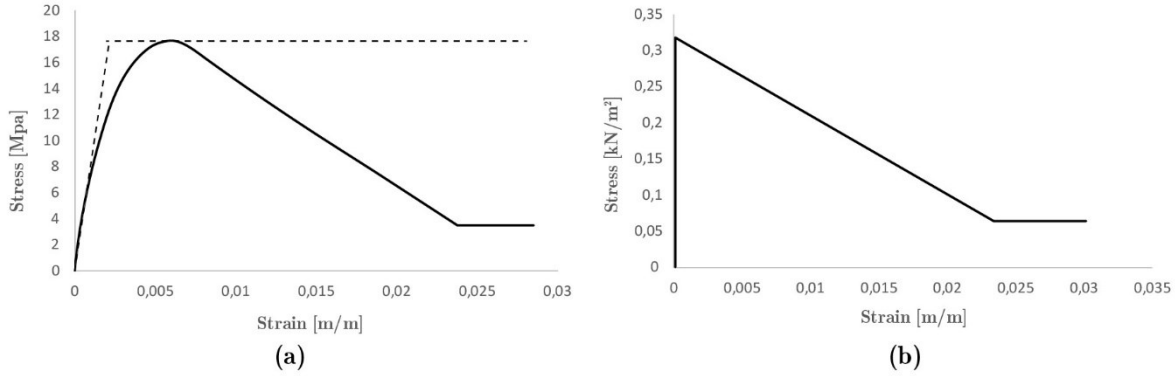


Figure 7: Stress-strain relationships for the out-of-plane model: (a) compression and (b) tension.

NLA was executed under displacement control simulating the load conditions of the experiment. Figure 8 compares the experimental pressure-displacement curve with the one predicted by the FE model, where almost no difference was obtained in terms of initial stiffness and maximum pressure capacity. The predicted damage patterns accurately represent what occurred in the experiment. Diagonal mechanisms due to tensile damage appeared at the surface of the wall once the model reached its maximum capacity. After this point, the damage is concentrated at the central part of the surface, as shown in Figure 8b. Figure 8c showed that vertical cracking occurs also at the intersections of the return walls with the front one. The above mechanisms are in agreement with those occurring in the experiment, where a characteristic “x” shape cracking emerged at the surface of the wall due to bending moment resisted by the diagonal cracks, followed by the progressive opening of the central crack in the middle surface of the panel [6].

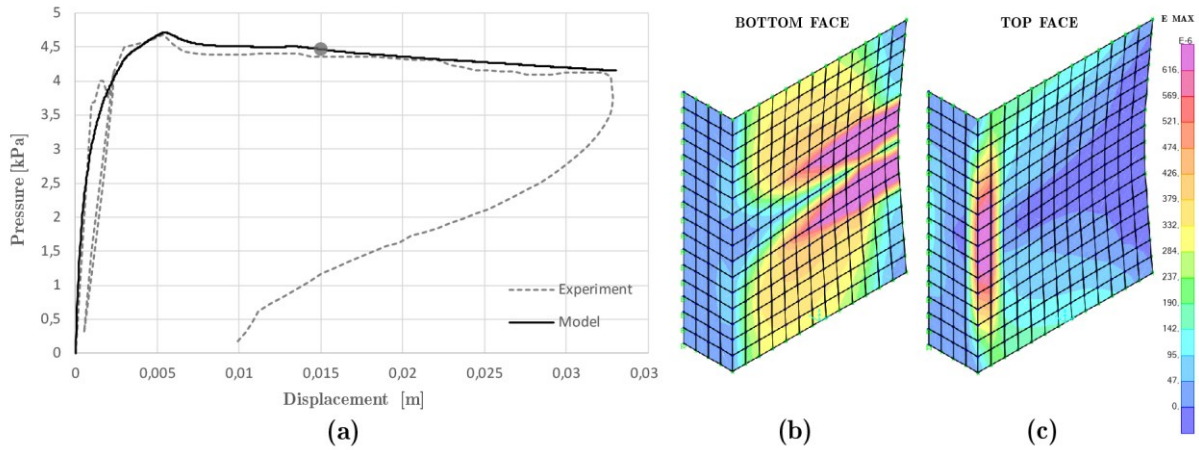


Figure 8: Out-of-plane loaded masonry model results: (a) capacity curve and (b-c) principal tensile strain contour after reaching the maximum load (horizontal displacement of 0.015 m).

3 SEISMIC ASSESSMENT OF A HYBRID TIMBER-MASONRY BUILDING

The calibrated models were used to evaluate the seismic capacity of a hybrid timber-masonry building existing in the historical centre of Valparaíso (Chile). The case-study is composed of timber frame structure following the platform-frame configuration, while two perpendicular sidewalls are made of URM. The timber frame walls are constituted by stud elements of 0.1 × 0.1 m^2 cross-section, spaced 0.4 ÷ 0.6 m each between the top and bottom sills, and braced with diagonal elements. The studs are connected using mortise-and-tenon carpentry connections, while the diagonals are nailed to the posts. Adobe blocks fill the external walls of the façade. The storeys are composed of joists of 0.12 × 0.05 m^2 spaced 0.4 m each other, disposed perpendicularly between parallel walls. The masonry walls have staggered configuration along their elevation, decreasing their sections along the height of the building, and the joists are embedded within the masonry bricks.

Hybrid LPM and macro-mechanical FE models were built to simulate the behaviour of the building under lateral loads. The characteristic mechanical properties of the oak timber were used to define the frame elements. The maximum bending moment of the mortise-and-tenon connection was estimated based on the theoretical model proposed by [19] as 3.6 kNm. The moment-rotation backbone was assumed to be the same as the half-lap model already calibrated in the simulation of the Pombalino frame. Lastly, the diagonal connection was assumed to have the same behaviour of the connection by contact in the Pombalino model too, since they present equivalent configuration and geometry. Nonlinear rotational hinges and axial springs were used to represent the mortise-and-tenon and diagonal connections within the frame, respectively. The material model of masonry was defined using the characteristic mechanical properties of URM proposed by [20].

The results demonstrated that masonry walls had a central role in the lateral response of the building since they contribute to resist a major part of the applied load. However, the overall ductility of the structural system is strictly dependent on the intrinsic fragility of these structural members. Figure 9 displays the acceleration-displacement relationships predicted by the model,

while Figure 10 shows the FE results in the X and Y directions. In the X direction, the model entered in the plastic phase once a tensile crack appeared at the base of the overturning masonry wall perpendicular to the applied load (Figure 10a). Some of the axial hinges of the timber frames parallel to the applied load then started to reach their ultimate capacity. In this case, the total collapse of the building was provoked by the global overturning mechanisms around the base of the masonry walls. The analysis in the Y direction showed the highest stiffness and capacity. In this case, the characteristic global collapse of the model is governed by the shear sliding mechanism formed at the base of the masonry walls parallel to the applied load (Figure 10b), while the hinges of the frame did not reach their ultimate capacity.

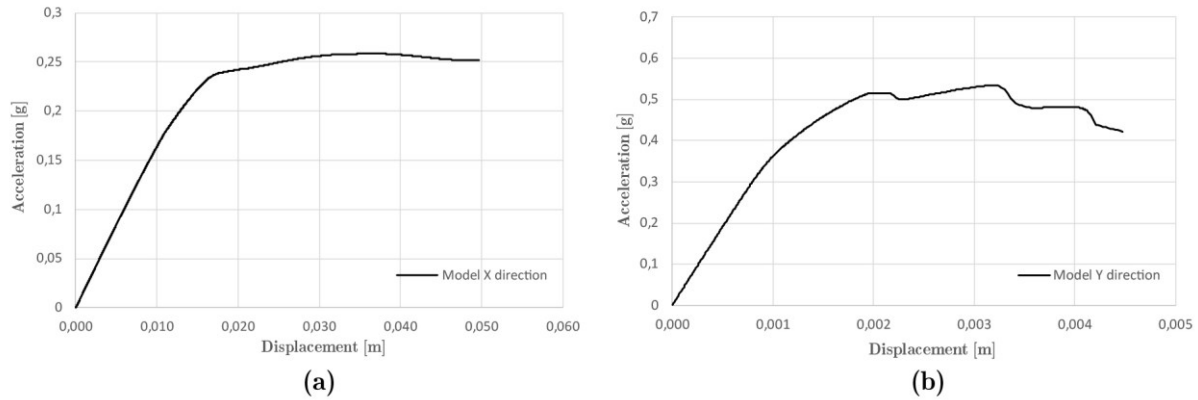


Figure 9: Capacity curves obtained for the hybrid timber-masonry building in Valparaiso, Chile, in the (a) X and (b) Y direction.

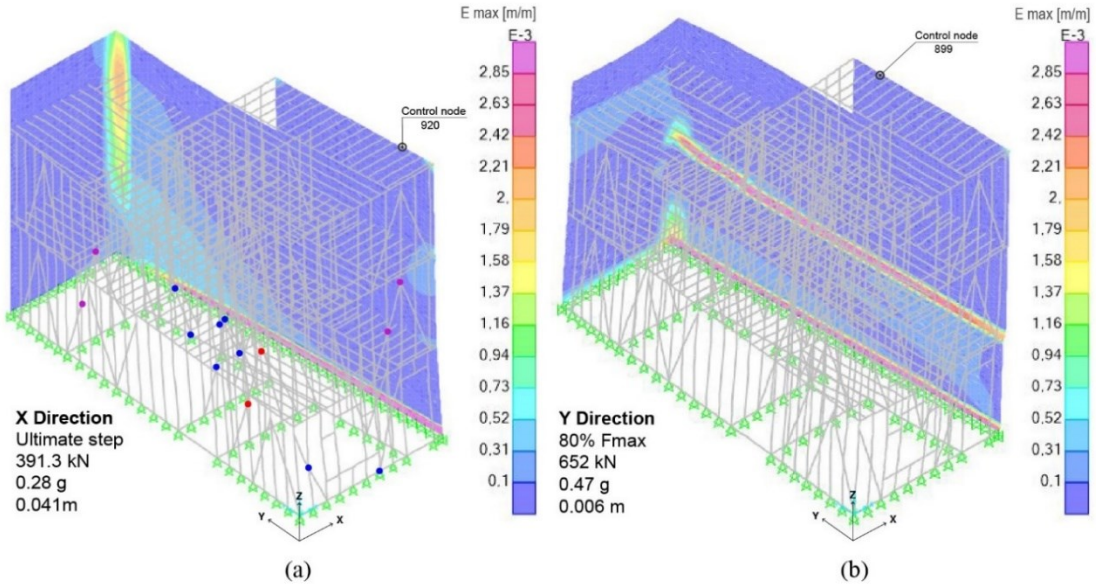


Figure 10. Seismic analysis of a hybrid timber-masonry building in Valparaiso, Chile along the (a) X and (b) Y direction. Principal tensile strain labelled from the maximum to the residual tensile strain capacity, and hinges formation.

4 CONCLUSIONS

This paper has presented a numerical study of timber frame and URM structures subjected to lateral loads, aimed to assess the seismic behaviour of hybrid timber-masonry buildings. A Lumped Plasticity Model (LPM) was calibrated to represent benchmark experiments on timber frames, including infill by means of Equivalent Strut Model (ESM). A macro-mechanical FEM was used to simulate the behaviour of in-plane and out-of-plane loaded masonry tests. The calibrated reference models were used to prepare a hybrid model, including both timber frames and masonry walls, of an existing building located in the historical centre of Valparaíso (Chile). The simulation predicted the collapse mechanisms of the building along its principal directions, showing that masonry walls play an important role in the resisting system. In X direction, the collapse is due to overturning of the largest masonry wall perpendicular to the applied load, with consequent failure of some of the connections in the timber frames. In Y direction, a sliding shear mechanism occurs at the base of the masonry wall parallel to the applied load, with no apparent damage in the timber frame.

Acknowledgements. This research has received the financial support from the ELARCH project (Euro-Latin America partnership in natural Risk Mitigation and protection of the Cultural Heritage), reference number 552129-EM-1-2014-1-IT- ERASMUS MUNDUS EMA21, funded with support of the European Commission. This document reflects the view of the authors, and the Commission cannot be held responsible for any use that may be made of the information contained therein. The authors also gratefully acknowledge the financial support from the Ministry of Science, Innovation and Universities of the Spanish Government (MCIU), the State Agency of Research (AEI), as well as the ERDF (European Regional Development Fund), through the SEVERUS project (Multilevel evaluation of seismic vulnerability and risk mitigation of masonry buildings in resilient historical urban centres, ref. num. RTI2018-099589-B-I00).

REFERENCES

[1] Ciocci, M.P., Sharma, S., and Lourenço, P. Engineering Simulations of a Super-Complex Cultural Heritage Building: Ica Cathedral in Peru. *Meccanica* (2018) 53 (7): 1931-58.

[2] Kouris, L.A.S., and Kappos, A.J. Detailed and Simplified Non-Linear Models for Timber-Framed Masonry Structures. *Journal of Cultural Heritage* (2012) 13 (1): 47-58.

[3] Poletti, E. Characterization of the Seismic Behaviour of Traditional Timber Frame Walls. PhD dissertation (2013). Department of Civil Engineering, University of Minho.

[4] Ciocci, M. P. Structural Analysis of the Timber Structure of Ica Cathedral, Peru. MSc Thesis. (2015). Department of Civil Engineering, University of Minho.

[5] Parisi, F., Ivano, I., Balsamo, A., Augenti, N., and Prota, A. In-Plane Behaviour of Tuff Masonry Strengthened with Inorganic Matrix–Grid Composites. *Composites Part B: Engineering* (2013) 45 (1): 1657-66.

[6] Griffith, M.C., and Vaculik, J. Out-of-Plane Flexural Strength of Unreinforced Clay Brick Masonry Walls. *TMS Journal* (2007): 53–68

[7] Endo, Y., Pelà, L., Roca, P., Da Porto, F., Modena, C. Comparison of Seismic Analysis Methods Applied to a Historical Church Struck by 2009 L'Aquila Earthquake. *Bulletin of Earthquake Engineering* (2015) 13 (12): 3749–78
[8] Pantò, B., Silva, L., Vasconcelos, G., and Lourenço, P. Macro-Modelling Approach for Assessment of out-of-Plane Behaviour of Brick Masonry Infill Walls. *Engineering Structures* (2018): 529–49.
[9] Stafford-Smith, B. Lateral Stiffness of Infilled Frames. *Journal of Structural Division, ASCE* (1963) 88 (6): 183-199.
[10] Bertoldi, S.H., Decanini L.D., and Gavarini, C. Telai Tamponati Soggetti ad Azioni Sismiche Un Modelo Semplificato Confronto Sperimentale e Numerico. *In 6th Convegno Nazionale L'Ingegneria Sismica in Italia* (1993)*:* 815-24.
[11] Decanini, L., Mollaioli, F., Mura, A., Saragoni, R. Seismic Performance of Masonry Infilled R/C Frames*. In 13th World Conference on Earthquake Engineering* (2004).
[12] Sassun, K., Sullivan T. J., Morandi, P., and Cardone D. Characterising the In-Plane Seismic Performance of Infill Masonry. *Bulletin of the New Zealand Society for Earthquake Engineering* (2016) 49 (1): 100–117.
[13] CSI. CSI Analysis Reference Manual (2016).
[14] Darwin, D. and Pecknold, D. A. W. Inelastic Model for Cyclic Biaxial Loading of Reinforced Concrete. Civil Engineering Studies SRS-409 (1974), University of Illinois, Urbana Champaign, Illinois.
[15] Vecchio, F.J. and. Collins, M. P. The Modified Compression-field Theory for Reinforced Concrete Elements Subjected to Shear. *ACI Journal Proceedings* (1986) 83 (2): 219-31.
[16] Kaushik, H. B., Rai D. C., and Jain, S. K. and ASCE, M. Stress-strain Characteristics of Clay Brick Masonry under Uniaxial Compression. *Journal of Materials in Civil Engineering* (2007) 19 (9): 728-39.
[17] D'Ambra, C., Lignola, G. P. and Prota, A. Multi-Scale Analysis of In-plane Behaviour of Tuff Masonry. *The Open Construction and Building Technology Journal* (2016) 10:135-151.
[18] CEN. 2005. EN 1996-1-1: Eurocode 6: Design of Masonry Structures - Part 1-1: General Rules for Reinforced and Unreinforced Masonry Structures.
[19] Chen, C., Qiu, H. and Lu, Y. Flexural behaviour of timber dovetail mortise-tenon joints. *Construction and Building Materials* (2016) 112: 366-377.
[20] NTC. Circolare 21 Gennaio 2019 n. 7 C.S.LL.PP. Istruzioni per l'applicazione Dell'aggiornamento Delle 'Norme Tecniche per Le Costruzioni' Di Cui Al D.M. 17/01/2018." Consiglio Superiore Dei Lavori Pubblici.

12th International Conference on Structural Analysis of Historical Constructions
SAHC 2020
P. Roca, L. Pelà and C. Molins (Eds.)

NUMERICAL STUDY OF THE OUT-OF-PLANE BEHAVIOUR OF TIMBER RETROFITTED MASONRY PRISMS

JAMIU A. DAUDA[1*], LUIS C. SILVA[2], PAULO B. LOURENCO[2]

AND ORNELLA IUORIO[1]

[1] School of Civil Engineering
University of Leeds
Woodhouse Lane, LS2 9JT, Leeds, UK
e-mail: cnjad@leeds.ac.uk (*corresponding author)
oiuorio@leeds.ac.uk

[2] Department of Civil Engineering
University of Minho
Azurém, P-4800-058 Guimarães, Portugal
e-mail: pbl@civil.uminho.pt

Keywords: ABAQUS, Flexure, Masonry, Numerical, OSB

Abstract. *The present study addresses the retrofitting of running-bond masonry walls through the application of oriented strand board (OSB) timber panels aiming to increase the masonry flexural strength and deformation capacity under out-of-plane actions. This paper presents the numerical analysis of masonry prisms to complement the information provided by the experimental campaign developed on flexural performances of timber retrofitted masonries. The numerical model represents the masonry components (brick and mortar) as a three-dimensional volume via volumetric finite elements, i.e. hexahedral 8-node linear brick elements with reduced integration and hourglass control. The nonlinear properties of the mortar joints and the brick units have been calibrated through information that resorts from experimental characterization tests. The numerical damage pattern and load-displacement capacity curve are compared with the experimental observations. A good agreement has been found and, therefore, the calibrated model can be employed in parametric studies, to further analyse the efficiency of the proposed timber masonry retrofit technique, and to more complex structural study cases.*

1 INTRODUCTION

Masonry structures show complex non-linear mechanical behaviour due to its heterogeneous and composite nature [1]. As such, computational numerical analysis of the mechanical behaviour of masonry structures is very complicated. Computational numerical analyses are useful to complement or as an alternative to experimental tests and may be used to predict the behaviour of structures to a given applied load. Numerical analyses are based on different theories such as finite element model (FEM), discrete/distinct element methods (DEM) or

particle flow code (PFC), among others [2, 3 & 4]. FEM-based models are the most widely used due to the availability of many analysis software that operates based on this theory. Therefore, the numerical modelling strategy employed in this paper is based on FEM.

Many researchers who have previously worked on FE modelling of masonry structures [1, 2, 5 & 6] agreed that numerical modelling and analysis of masonry structures posed some of the greatest challenges to structural engineers. The main difficulty has been attributed to the presence of mortar joints which act as planes of weakness, discontinuity, and non-linearity. Besides, the existence of uncertainties in the material and geometrical properties is also another concern when modelling masonry structures [2, 3 & 7]. Despite, quite noteworthy advancements have been made on the application of numerical modelling in the study of mechanical behaviour of masonry structures, numerical analysis of masonry is still a significant area of research [8].

Therefore, this paper presents the numerical analysis on 665 x 215 x 102.5 mm masonry prism to complement the findings in [9]. Here, an accurate finite element model and analysis of the four-point bending test was developed to corroborate the interpretation of the test results obtained from the flexural bond strength test on masonry prism (MP). The main objective of this paper is to develop a concise and efficient nonlinear 3-D finite element analysis to simulate the damage and failure pattern of the masonry prism tested in the laboratory. The developed model was calibrated against the experimental results and analysed to evaluate the performance of the proposed OSB retrofit techniques of MP.

This paper is organised as follows. Section 1 entails the introductory comments as presented above. Section 2 describes the adopted modelling approach and the performed analysis. Section 3 compares the results of the numerical analysis with the experiments and discusses the model behaviour. Section 4 then encloses the paper with conclusions and recommendations.

2 MODELLING APPROACH AND ANALYSIS

Modelling of masonry structures is categorised into three different techniques shown in figure 1 [2]. The detailed micro-modelling is a material level model where masonry structure is considered as a three-phase material. Continuum elements are used to represent the masonry units and mortar joints while interface elements represent the unit–mortar interface. Meanwhile, for the simplified micro-modelling approach, the bricks are represented as fictitious expanded bricks by continuum elements. The mortar joint is then modelled as an interface with zero thickness. Macro-modelling, on the other hand, is a structural level modelling technique where the masonry components (unit and joint) are modelled as one phase material by smearing out masonry units, mortar and unit–mortar interface as a homogeneous continuum [2].

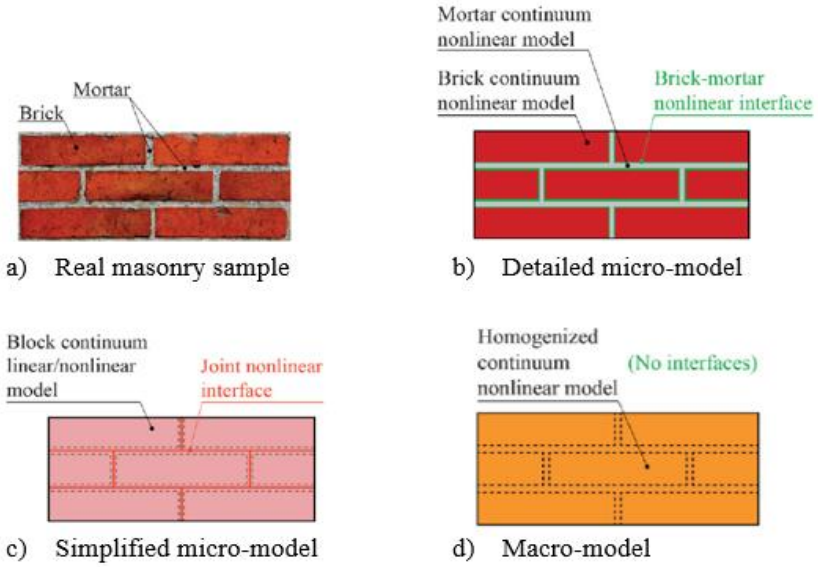


Figure 1: (a) Real masonry sample, (b) detailed micro-model, (c) simplified micro model, and (d) macro model

2.1 Model development and validation

Plain and retrofitted masonry prisms tested in [9] were chosen to verify the behavior prediction of the FE model. The goal is to provide a calibrated numerical model aiming a parametric analysis to evaluate the efficiency of the proposed timber masonry retrofit technique. The adopted model was based on the simplified micro-model technique described in figure 1c. The model was developed by following the steps in figure 2 and using the commercial software ABAQUS FEA. The four-point loading setup was numerically modelled following a detailed description for all the material components to achieve more accurate results. The full description of the numerical model, the assigned material properties and the adopted interactions are described as follows.

Two different models were created for the plain and retrofitted MP, and the models were labelled as MP00-NM and MPOSB-NM respectively. MP00-NM comprises of three components; brick unit, mortar and steel plate for load and support application. The brick unit (215 x 102.5 x 65 mm) and mortar joint (10 mm thick) were represented as three-dimensional deformable parts and meshed with a hexahedral 8-node linear brick, reduced integration, hourglass control (C3D8R) which has an improved convergence. The steel plate for load and support application (5 mm thick) was modelled using a 3-D discrete rigid element and discretised by rigid element R3D4 to represent a part that is stiffer (deformation negligible) than the masonry prism. For MPOSB-NM, two additional parts that are 18 mm thick OSB timber panel and the anchor rod were modelled as 3-D deformable parts and meshed with a hexahedral 8-node linear brick (C3D8R). The OSB timber panel and brick units were drilled at the connection locations as done in the experimental works [9, 10] to apply the retrofit to the MP.

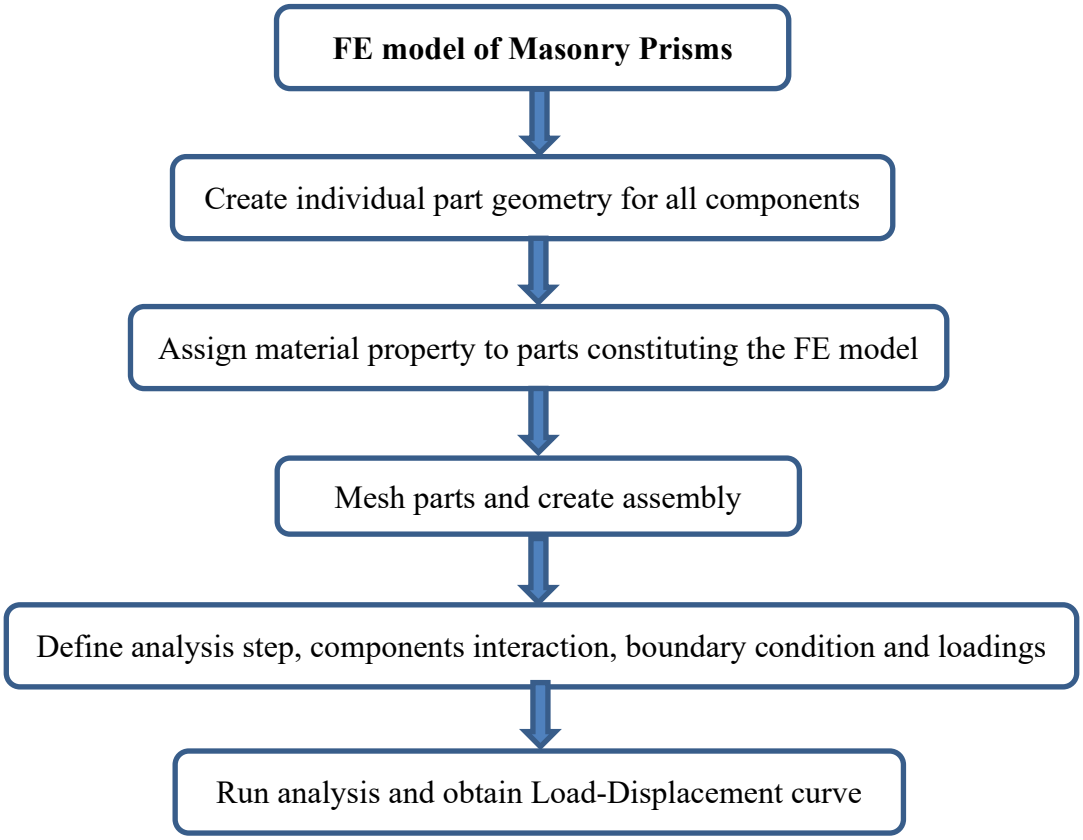


Figure 2: Steps for developing the FE model

The process to build the full model is such that an appropriate interaction and constraints between the model components are implemented to represent the relationship between them. Since the simplified micro modelling strategy is employed here, the brick-mortar bond interface was not specified separately, so the brick continuum and mortar continuum were merged as shown in figure 3a. In order to place the loading at the front face of the model, the surface of the steel plate was tied to the surface of the brick at the 3rd and 7th course using tie constraints (Fig 3b). Similarly, the steel plates were tied to the top and bottom brick at the back of the MP model as shown in figure 3c for the support application. The use of tie constraints ensured that the steel plate could not slip from the brick unit during analysis.

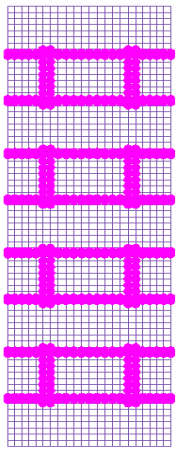
In the retrofitted model, the back-steel plates were tied to the back of the OSB (Fig. 3d). In addition to this, frictional, normal hard contact was specified between the surface of the OSB timber and MP model, as shown in figure 3e. For this analysis, the friction coefficient was taken as 0.5, which is a typical coefficient of friction between timber and brick.

For the anchor connection, the nodes on the surface of the brick around the connection holes were connected to the surface of the anchors using the default contact enforcement in ABAQUS (Fig. 3f). This connection ensures that there is a full adhesive bond between the anchor and the surface of the holes in MP. This kind of connection represents the retrofit system where the OSB timber panel is connected to the MP using adhesive anchor connection [9, 10].

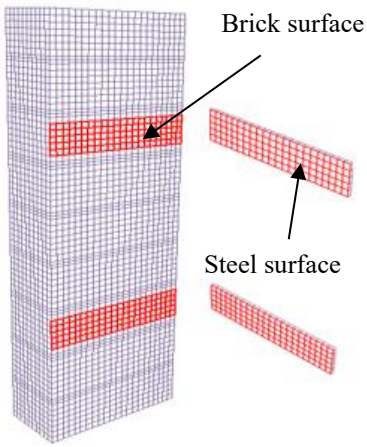
More so, proper consideration of the applied boundary conditions in the numerical simulation was taken. The models were constrained to replicate what was done experimentally

to enable a sound basis for comparison of results. In the created models, the nodes at the middle of the back-steel plate at the top of the MP were restrained in x and z-direction. Also, the plate at the bottom was restrained in all the three directions (x, y, z) at the middle nodes to replicate the support condition of the tested specimen (Fig. 4a).

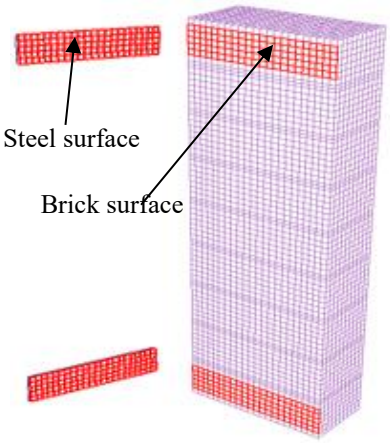
The loads considered in this analysis are self-weight of the model and applied unit load in the out-of-plane direction at the third and seventh course of the model. This loading and support arrangement are a replica of the four-point bending test carried out in the laboratory. The out-of-plane load is applied as a unit uniform distributed load (UDL) on the steel plate tied to the front face of the model (Fig. 4b). The analysis is load control, similar to the test condition. The total load capacity of the model is measured as the load proportionality factor multiplied by the applied load in Newton (N).



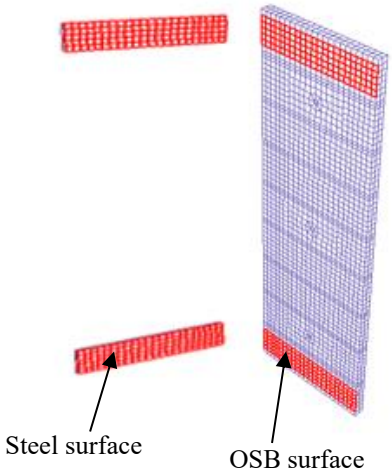
a) Part merging



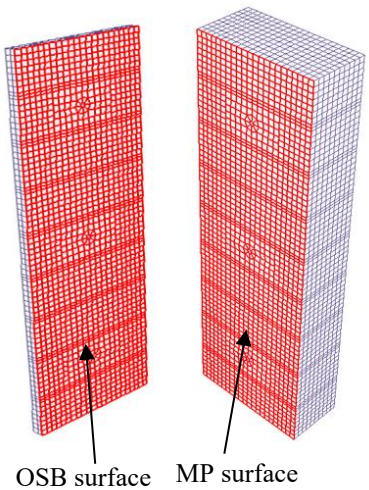
b) Tie constraint between steel surface and brick surface (front)



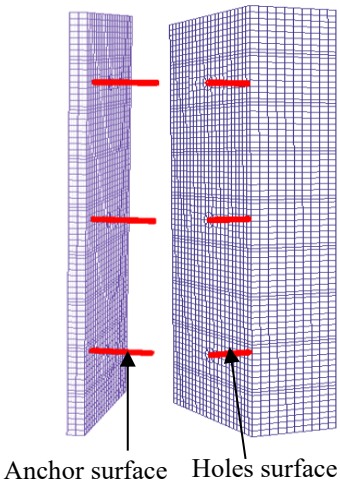
c) Tie constraint between steel surface and brick surface (front)



d) Tie constraint between steel surface and OSB surface

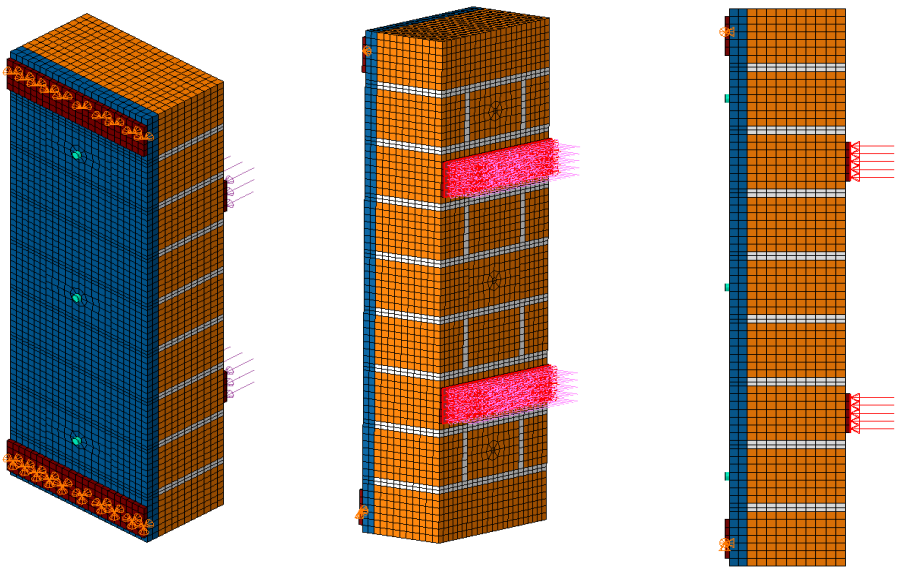


e) Contact interaction between OSB surface and MP surface



f) Adhesive contact interaction between anchor and holes

Figure 3: Applied constraints and interaction in developing the FE model



a) Boundary condition b) Loading c) Loading and BC (side view)

Figure 4: Applied boundary condition and load in the FE model

2.2 Input parameters

The assumed material parameters have been well described in previous work [11]. The Concrete Damage Plasticity (CDP) constitutive model was used to simulate the tensile and compressive non-linear behaviour of the brick unit and mortar. Also, the nonlinear response of the OSB timber panel is represented by an equivalent uniaxial stress-strain curve for both the compressive and tensile stress behaviour. The elastic properties used for the OSB were obtained from the manufacturer specification. The nonlinear behaviour, i.e. the stress-strain constitutive relation of the OSB was derived using existing guidelines [12]. The anchor rods were represented with a linear elastic behaviour, and the steel loading plates as rigid elements. Table 1 presents the abridged mechanical properties of the model components, the full properties, including the plastic-damaging behaviour parameters (Table 2) can be found in [11].

Table 1: Material properties (Elastic)

Properties	Brick	Mortar	OSB	Anchor
Mass density (γ) ton/mm^3	2.2e-9	2.17e-9	0.65e-9	7.85E-09
Young modulus (E) N/mm^2	32470	19850	3500	210000
Poisson ratio (μ)	0.26	0.2	0.24	0.3
Compressive strength (f_c) N/mm^2	87.91	7.1	6.6	
Tensile strength (f_t) N/mm^2	5.93	0.32	0.92	

Table 2: Material properties (Non-linear)

Brick				Mortar			
Compressive Behaviour		Tensile Behaviour		Compressive Behaviour		Tensile Behaviour	
Yield stress (N/mm^2)	Inelastic strain	Yield stress (N/mm^2)	Cracking strain	Yield stress (N/mm^2)	Inelastic strain	Yield stress (N/mm^2)	Cracking strain
26.37	0.00000	5.93	0.00000	1.79	0.00000	0.319	0.00000
68.00	0.00713	4.76	0.00017	3.13	0.00100	0.296	0.01096
78.10	0.01013	3.54	0.00037	4.997	0.00310	0.258	0.02303
84.80	0.01313	2.07	0.00077	5.825	0.00460	0.220	0.03179
87.91	0.01688	0.87	0.00167	6.521	0.00660	0.198	0.04086
72.26	0.02813	0.51	0.00247	6.970	0.00916	0.099	0.05156
36.79	0.03183	0.22	0.00437	7.100	0.01185	0.049	0.06996
19.36	0.03633			5.750	0.02360	0.025	0.09528
11.15	0.04113			3.483	0.03400	0.012	0.11836
				0.710	0.04800	0.006	0.34956

2.3 Analysis method

In this study, the full behaviour of masonry prism model under a continuous increase of load in the form of load-displacement was obtained through a quasi-static analysis. A load control type of analysis has been assumed since the tests were also load controlled. This analysis has been used to perform and validate the model with the obtained experimental data.

To represent softening, the Riks method (arc-length method) has been considered. This method is a robust method for nonlinear analysis, and it allows to properly reproduce the masonry nonlinear response. The adopted CDP model is based on a scalar-based damage model coupled with the plasticity one. Therefore, damage is given in terms of such scalar parameter and addressed separately in terms of compressive (*'damagec'*) and tensile (*'damaget'*) damage.

3 RESULTS AND DISCUSSION

In this section, the results from the numerical analysis are compared with the experimental ones and a brief discussion on the plain and retrofitted models is addressed. Figure 5 and 6 presents the failure of the non-retrofitted and retrofitted models alongside with the actual observed failure modes (tests designated as MP00 and MPOSB, respectively). The comparison

shows that the failure of MP00 occurred in the bed joints within the loading span of the specimen. In the actual test, the total failure occurred in one bed joint, but the numerical model predicts a symmetrical failure on the middle span bed joints. In fact, and from a numerical standpoint, all the mortar joints present the same mechanical properties. In converse, the mechanical properties of the experimentally tested specimen have a spurious and inevitable variation that may be explained, for instance, by construction errors or by the existing dispersion of the material strength values. Hence, the symmetrical joints in the model will experience the same load, and thus the failure will be simultaneous. Whereas, the failure occurs in the weakest joint during the experimental test.

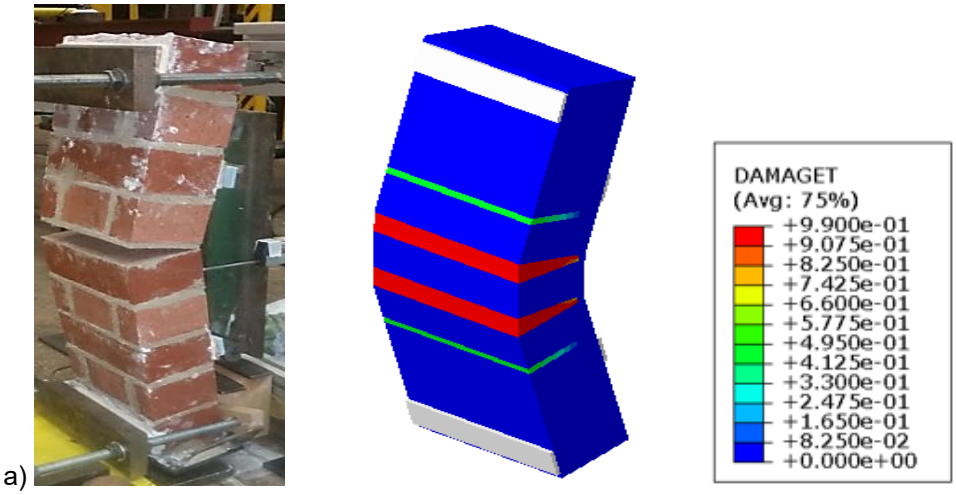


Figure 5: Failure pattern of MP00 (experimental and FE model)

In the case of the retrofitted specimens (MPOSB), the location and type of failure observed in the model output were compared with the experimental observation as highlighted. In the model, the global damage pattern shows all the areas where crack and failure happen occurred in all the tested specimens. References were made to two specimens highlighted for simplification (Fig. 6).

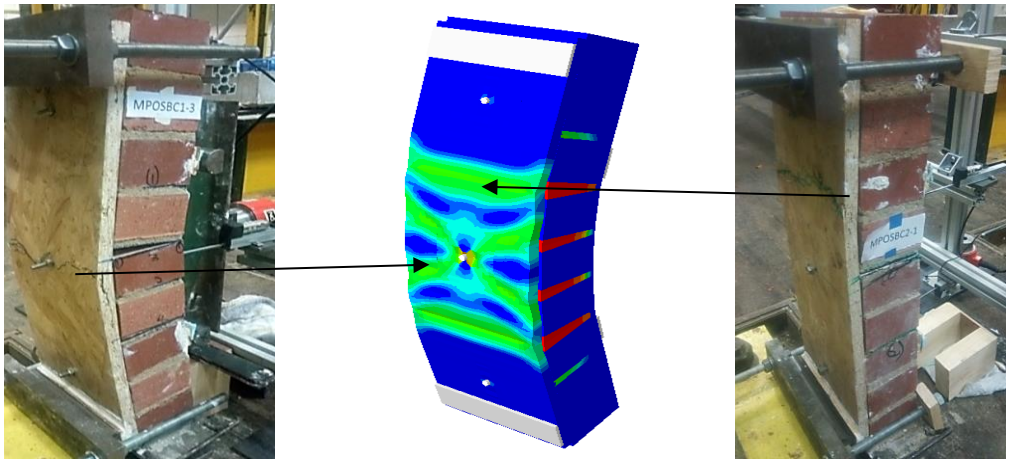
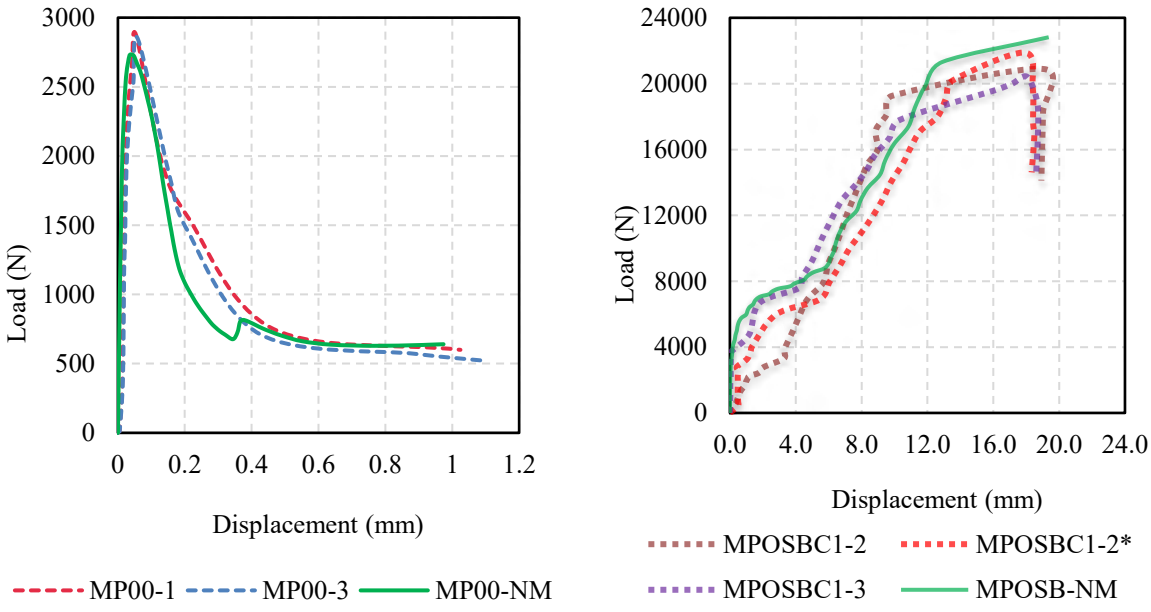


Figure 6: Failure pattern of MPOSB (experimental and FE model)

In terms of the load-displacement capacity curve comparison, Figure 7 shows that the numerical outputs resemble well with the experimental one. The numerical model is able to capture the experimental envelope and predicts the peak load and the corresponding failure to within less than 5% of the average results obtained from the test (Table 2). The curve shows the behaviour of the specimen at the initial elastic phase where the OSB and the masonry are bonded together before the crack initiated at an average load of 3640N for tested specimen and 3842N (5% variation) for the numerical model. This phase then followed by the complete failure of the joint in the masonry prism at an average load of 7982N and 8365N (4% variation) for the test and numerical specimen respectively. The final phase of the curve then presents a region where the masonry part has failed and the OSB is taking the load up to the failure of the OSB.



a) Plain masonry prism (MP00)

b) Retropfitted masonry prism (MPOSB)

Figure 7: Load-displacement curve (experimental and FE model)

Table 2: Comparison of model and test average results

Parameter	MPOO		MPOSB	
	Test	FE model	Test	FE model
Peak load (N)	2857	2723	21890	22820
Displacement (mm)	0.058	0.056	18.74	19.37

4 CONCLUSIONS

This paper presented part of the numerical study conducted to complement the results obtained from experimental tests on small-scale masonry prisms. A simplified detailed-micro model approach was employed to represent the four-point bending test and the advanced software ABAQUS was used. The mechanical properties for brick units and mortar joints have been calibrated from the performed experimental characterization as demonstrated in a previous work by the authors [11]. The Concrete Damage Plasticity (CDP) model available in ABAQUS has been assumed to describe the constitutive relation of the masonry and OSB timber panel. For the strengthened model, the connection between the masonry and the OSB panel is achieved through anchors whose behavior is assumed to be elastic.

Quasi-static analyses on the non-strengthened and strengthened masonry prisms were performed. Capacity curves were derived and represent the relationship among the continuous increasing load and maximum obtained displacement. The comparative analysis of the results with the experimental data confirms that the developed FE models can adequately capture the behaviour of both the plain and retrofitted walls, in terms of ultimate load capacity and damage failure patterns.

Generally, the numerical model predicted the peak load within a 5% deviation from the corresponding failure average load given by the experimental tests. This indicates that the model can be employed to carry out a parametric study to further investigate the performance of the proposed retrofit technique. Hence, parametric studies can be hereafter developed to assess the strengthening technique efficiency when applied to large-scale masonry walls and, as well, to optimize the required thickness of the OSB panels and the connection layout.

REFERENCES

[1] D'Altri, A., de Miranda, S., Castellazzi, G. and Sarhosis, V. (2018). *A 3D Detailed Micro-Model for the In-Plane and Out-Of-Plane Numerical Analysis of Masonry Panels*. Computers & Structures, 206, pp.18-30.

[2] Lourenco, P. (1996). *Computational Strategies for Masonry Structures*. PhD. Delft University of Technology.

[3] Asteris, P., Plevris, V., Sarhosis, V., Papaloizou, L., Mohebkhah, A., Komodromos, P. and Lemos, J. (2015). *Numerical Modeling of Historic Masonry Structures*. In: P. Asteris and V. Plevris, ed., Handbook of Research on Seismic Assessment and Rehabilitation of Historic Structures. IGI Global, pp.213-256.

[4] Zhang, S., Yang, D., Sheng, Y., Garrity, S. and Xu, L. (2017). *Numerical Modelling of FRP-Reinforced Masonry Walls under In-Plane Seismic Loading*. Construction and Building Materials, 134, pp.649-663.

[5] Silva L., Lourenço P. and Milani G. (2018) '*Derivation of the Out-Of-Plane Behaviour of Masonry through Homogenization Strategies: Micro-Scale Level*', Computer and Structures, 209, pp.30-43.

[6] CUR (1994). *Structural Masonry: An Experimental/Numerical Basis for Practical Design Rules (in Dutch).* Report 171, CUR, Gouda, Netherlands.

[7] Dogariu A. (2015) *Numerical Analysis of Steel Wire Mesh Seismic Retrofitting Techniques for Masonry Structures*. [Online] http://www.bipcons.ce.tuiasi.ro/Archive/519.pdf (Accessed 18 May 2017).

[8] Sacco E, Addessi D, Sab K. (2018). *New Trends in Mechanics of Masonry*. Meccanica 2018;53(7):1565–9.

[9] Dauda J., Iuorio O., and Lourenço P. (2019). *Experimental Study of Out-of-Plane Behavior of Timber Retrofitted Masonry Prisms.* In P.B.Dillon & F.S.Fonseca (Eds.), Proceedings of the 13th North American Masonry Conference, Salt Lake City, Utah (pp. 1100–1109).

[10] Dauda, J., Lourenço, P. and Iuorio, O. (in press). *Out-of-Plane Testing of Masonry Walls Retrofitted with Oriented Strand Board Timber Panels.* Proceedings of Institution of Civil-Engineer Structures and Building.

[11] Dauda, J., Iuorio, O. and Lourenço, P. (2020). *Numerical Analysis and Experimental Characterisation of Brick Masonry.* Int. Journal of Masonry Research and Innovation, Vol. 5 Issue: 3, pp.321–347, DOI: 10.1504/IJMRI.2020.10028163.

[12] Chen, G. and He, B. (2017). *Stress-strain Constitutive Relation of OSB under Axial Loading: An Experimental Investigation*. BioResources, 12(3).

12th International Conference on Structural Analysis of Historical Constructions
SAHC 2020
P. Roca, L. Pelà and C. Molins (Eds.)

NUMERICAL STUDY OF PIER-WALL CONNECTIONS IN TYPICAL DUTCH URM BUILDINGS

DANIELA FUSCO[1*], FRANCESCO MESSALI[2], JAN G. ROTS[2], DANIELA ADDESSI[1] AND STEFANO PAMPANIN[1]

[1]Sapienza Università di Roma
Dipartimento di Ingegneria Strutturale e Geotecnica
Via Eudossiana 18, 00184 Rome, Italy
e-mail: d.fusco1994@gmail.com, {daniela.addessi, stefano.pampanin}@uniroma1.it
(*corresponding author)

[2] Delft University of Technology
Department 3MD
Building 23, Stevinweg 1, 2628 CN Delft, The Netherlands
e-mail: {F.Messali, J.G.Rots}@tudelft.nl

Keywords: Glued Connection, Masonry, Seismic, Modelling

Abstract. *In recent years, the seismic risk in the north of the Netherlands has increased due to gas extraction. Since 2014, the Delft University of Technology started a research program to assess the seismic response of unreinforced masonry (URM) buildings. The Dutch URM buildings are characterized by slender piers and transverse walls. In common practice, the connections between piers and transverse walls are often modelled as rigid, but in real structures these connections may exhibit different behaviour. Especially, since the 1980s, calcium silicate element masonry has been commonly used in Dutch buildings, and vertical continuous joints are present between transverse walls. For this reason, it appears essential to assess the connection strength properties, since its failure can significantly reduce the seismic performance of the entire structure. The first part of this work investigates and compares different numerical approaches to describe the nonlinear behaviour of masonry under lateral loads, simulating seismic action. The second part specifically focuses on the critical issues related to the modelling of vertical connections of Dutch URM buildings. A sensitivity study of the frictional parameters is performed to analyze the influence of the strength of the glued connection on the global response of the URM structure.*

1 INTRODUCTION

Typical Dutch Unreinforced Masonry (URM) terraced houses are composed of façades with large openings and slender piers, connected at corners with long transversal walls. The seismic behaviour of the entire structure is determined by the quality of the connections between the transverse wall and piers. In buildings constructed before 1980, which make use of calcium silicate (CS) bricks, the connection is guaranteed by the interlocking of the units. In the 1980s, large CS elements started being used in order to accelerate the construction process, and the connections between the walls and the piers were provided by means of

vertical glued joints with steel ties at the bed-joint level. If this connection fails, the vertical glued joint may slide and open, and the capacity of the structure suddenly decreases [1].

In the past, Raijmakers and Van der Pluijm [2] conducted an experimental research to analyse the failure of the vertical glued connection at the structural element level, i.e. considering only a wall-pier system. Later on, the increasing induced seismicity in the Groningen area has led to a strong interest of Dutch scientific community to the assessment of the seismic vulnerability of Dutch URM structures. Delft University of Technology tested two full-scale two-storey buildings to evaluate the seismic capacity of these structures [3,4,5,6,7].

In recent years, several methods have been developed to analyse and predict the seismic performance of URM buildings [8,9,10]. The nonlinear analysis through the finite element method (FEM) is one of the most common approaches to calculate the seismic capacity of the structure in terms of ultimate displacement and maximum strength. In FEM models, the nonlinear behaviour of the masonry is assigned to the constitutive law of the finite elements. Different approaches can be distinguished and categorised according to the scale of the analysis [11,12,13]. One of the most adopted criteria classifies these as micromechanical, macromechanical, macro-element and multiscale models [14].

This work investigates the appropriate numerical modelling of the vertical glued connections response, in order to study the influence of these connections on the global seismic capacity of the structure. To reach this goal, the first part of the paper focuses on the FE macromechanical modelling of the nonlinear behaviour of masonry structures under lateral loads, simulating seismic actions. In particular, the use of anisotropic or isotropic constitutive laws for masonry is discussed in Section 2. Subsequently, Section 3 compares two different constitutive laws applied in the model to reproduce the possible failure of the vertical glued connection.

2 FINITE ELEMENT MODELS FOR MASONRY

This section focuses on two finite element (FE) models used to assess the seismic capacity of URM structures. In common practice, two different strategies are used to model the nonlinear behaviour of the material: discrete and smeared cracked models [1,12,15]. In discrete crack models, the nonlinear behaviour is lumped in the interface elements located where the crack or the sliding may occur. Instead, in smeared crack models, the crack is smeared out over the finite element and it may occur in any direction. In this work, two different material constitutive laws are compared: the Total Strain Crack Model and the Engineering Masonry Model, both smeared crack model implemented in DIANA FEA [15].

2.1 Constitutive laws

The Total Strain Crack Model (TSCM) assumes a tensile softening behaviour governed by the Mode I fracture energy [1,15]. The compressive behaviour can be defined on the basis of several constitutive functions that describe the hardening-softening compression curves. Regarding the shear behaviour, DIANA permits to fix a reduced shear stiffness after cracking. Some limits of the Total Strain Crack Model are worth to mention, i.e.: the anisotropy of the material is not considered, the shear failure is not distinguished from the tensile failure and the energy dissipation under cyclic loading is underestimated, especially in case of shear failure.

The Engineering Masonry Model (EMM) permits to overcome the mentioned shortcomings of the Total Strain Crack Model. In particular, on the one hand, the Engineering Masonry Model considers the anisotropic property of the masonry and differentiates between tensile and shear failure (implementing the shear failure Coulomb's criterion), and on the other hand it provides a more realistic estimate of the dissipated energy for cyclic analyses in case of shear failure of a pier [15,16].

2.2 Numerical Application: Modelling of a tested two-storey masonry structure

The two constitutive laws described in the previous section are adopted to perform the numerical analysis of the nonlinear structural response of an experimental masonry structure. The aim is to validate the capability of the employed FE procedures to accurately describe the activation and evolution of the nonlinear mechanisms in masonry structures, possibly leading to their collapse.

One of the two two-storey masonry structures tested in 2015 at Delft University of Technology (TU Delft) is considered [3,4]. The specimen, illustrated in Figure 1 (a), is a full-scale masonry assemblage representative of the load-bearing structure of a typical two-storey terraced house built in the Groningen province in the period 1960-1980. These buildings are characterized by small CS bricks and running bond pattern.

The masonry house is modelled with either shell elements or solid elements. Since the structure is symmetric, half of the structure is considered to reduce the computation effort. The slab of the second floor lies up on the walls and the piers via mortar joint, thus this connection can be assumed strong enough to consider shared nodes. The anchors between the first floor and the piers are used to retain any out-of-plane movement of the piers and they are not able to transfer any significant shear load. For this reason, they are modelled with interface elements having non-zero stiffness only in the direction orthogonal to the piers. During the experimental test, a cyclic loading was applied through four actuators coupled in order to maintain the forces equal at the two floors. This loading condition was simulated with a displacement controlled analysis, by adding an auxiliary rigid steel beam with appropriate restrains.

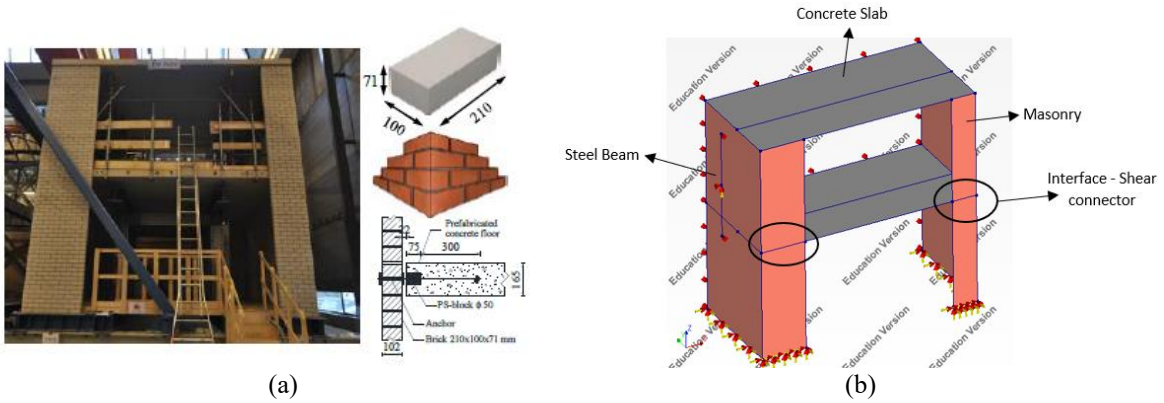


Figure 1: (a) Specimen and construction detail of a typical two-storey terraced house [4] and (b) Simplified modelling schematic.

Three different FE models of the building are implemented and analyzed via the code

DIANA FEA, namely:

- TSCM-Shell: model with shell FEs adopting the Total Strain Crack Model;
- TSCM- Solid: model with solid FEs adopting the Total Strain Crack Model;
- EMM-Shell: model with shell FEs adopting the Engineering Masonry Model;

The material parameters used for the three models, calibrated and adapted on the basis of the material tests performed and reported in [3] and [7], are summarized in Tables 1 and 2.

Table 1: Masonry mechanical parameters: Engineering Masonry Model

Elastic Modulus perpendicular to head joint	E_x	2212	MPa
Elastic Modulus perpendicular to bed joint	E_y	3264	MPa
Shear Modulus	G	1306	MPa
Mass Density	ρ	1805	kg/m^3
Tensile strength normal to bed joint	f_{ty}	0.19	MPa
Minimum strength head-joint	f_{tx}	0.38	MPa
Tensile fracture Energy	G_{ft}	0.0127	N/mm
Angle between stepped diagonal crack and bed joint	θ	0.792	rad
Compression strength	f_c	5.8	MPa
Fracture Energy in compression	G_{fc}	17.4	N/mm
Factor to strain at compressive strength	n	5	
Unloading Factor	λ	0	
Friction angle	γ	0.406	rad
Cohesion	f_{vo}	0.14	MPa

Table 2: Masonry mechanical parameters: Total Strain Crack Model

Elastic Modulus	E	3264	MPa
Poisson's ratio	ν	0.16	
Shear Modulus	G	1306	MPa
Mass Density	ρ	1805	kg/m^3
Crack Orientation		Rotating	
Tensile Curve		Linear- crack energy	
Tensile strength	f_t	0.19	MPa
Tensile fracture Energy	G_{ft}	0.0127	N/mm
Crack bandwidth specification		Rots	
Compression Curve		Parabolic	
Compression strength	f_c	5.8	MPa
Fracture Energy in compression	G_{fc}	17.4	N/mm

A pushover analysis is performed and the capacity curves obtained with the different models are compared with the backbone curve derived from the experimental results [4,5] in Figure 2 (a). The elastic stiffness of the models coincides with that of the experimental curve. After the peak, the stiffness of the structure is significantly reduced, due to the development of the rocking mechanism. During this phase, the cracks are located at the bottom and top of the pier sections, where tensile strains occur. The rocking mechanism occurs in every model, but the maximum base shear is higher in the EMM-Shell model than in the others. The main differences in the results obtained with the different constitutive models emerge in the post-

peak phase. Indeed, the curves evaluated with the TSCM models suddenly decrease resulting in severe softening branches, whereas the EMM model gives a more gradual stiffness and strength degradation. This depends on the observed prevailing failure mechanism. In particular, the loss of capacity in the experimental test was determined by the diagonal cracking of the wide pier (Figure 2 (b)). The same diagonal crack was observed for both the TSCM models (Figure 2 (d) and Figure 3(e)) although this leads to a more brittle failure than that observed in the experiment. On the other hand, the use of EMM constitutive law switches the failure to the toe-crushing of the wide pier, as shown in Figure 2 (c). The use of solid or shell elements affects only the peak strength of the structure, but not the type of failure. The difference also in terms of strength is rather limited for positive displacements, and more significant (yet not very large) for negative displacements.

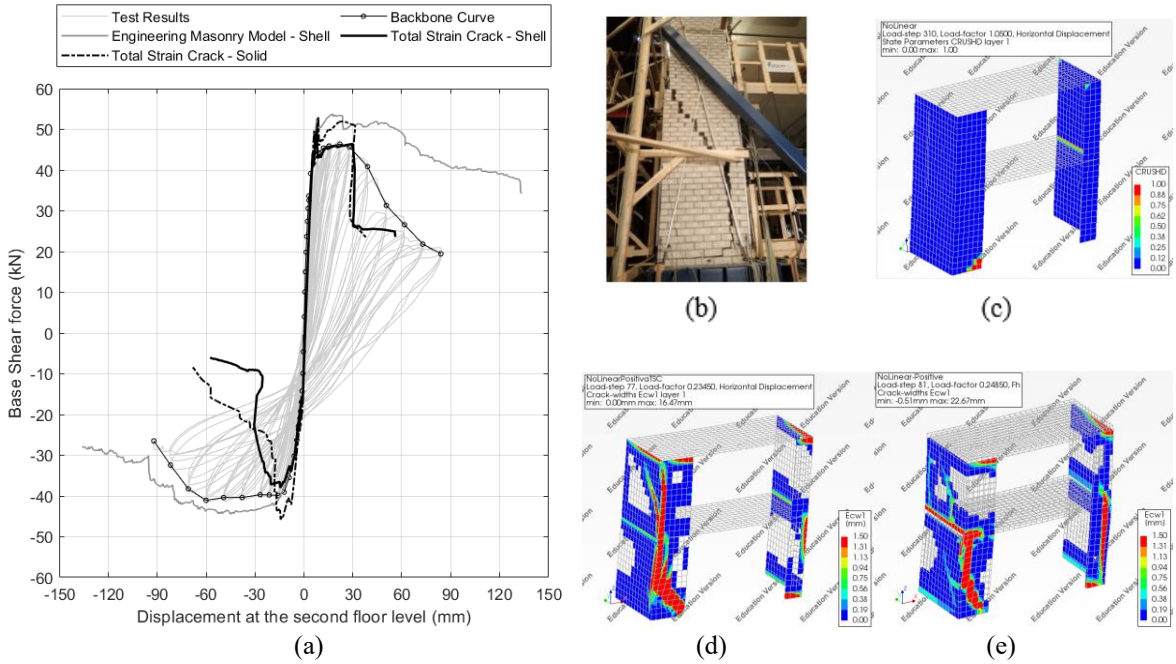


Figure 2: (a) Comparison of the capacity curves: Experimental results, EMM Shell model, TSCM Solid and TSCM Shell. Failure mechanism for each model: (b) Experimental test [Diagonal cracking] [4], (c) EMM Shell model [Toe-crushing], (d) TSCM Shell model [Diagonal cracking] and (e) TSCM Solid model [Diagonal cracking]

3 FINITE ELEMENT MODELLING FOR GLUED VERTICAL CONNECTIONS

As previously mentioned, the seismic capacity of a typical Dutch URM structure is affected by the strength of the vertical connection between the main wall and piers. This was clearly shown by the experimental research performed by Raijmakers and Van der Pluijm [2], which consisted in applying a horizontal load to a U-shaped construction, composed of the main wall and two perpendicular piers. The wall and the pier are composed of calcium silicate element masonry. The results of the test show three possible types of failure mechanisms (Figure 3): the rocking mechanism of the whole structure (a), the diagonal cracking/compression failure of the pier (b), and the shear failure of the wall-pier connection (c). The mechanism (a) can be preliminary to the other two. The mechanism (b) is frequent in

the toothed connection and the mechanism (c) occurs for weaker connection type, as in the case of vertical glued connection. The shear failure of the vertical connection leads to a sudden strength reduction, which affects the seismic capacity of the entire structure [1]. In order to consider this mechanism in the numerical modelling, the vertical glued connection is modelled through interface elements with nonlinear behaviour. Two different constitutive laws, both implemented in DIANA FEA, are considered for the interface: Nonlinear Elastic Model and Coulomb Friction Model.

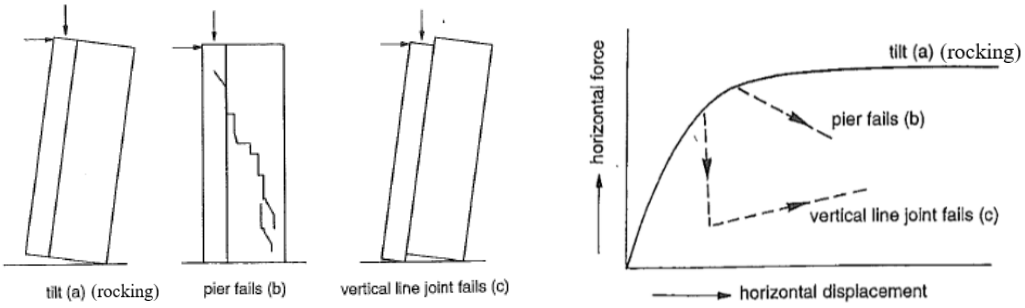


Figure 3: Possible failure mechanisms of a U-Shaped wall [1]

3.1 Constitutive laws for interface elements

The Coulomb friction model for interface elements is based on the Mohr-Coulomb plasticity model, defined by cohesion, friction, dilatancy angle and Mode II energy fracture. In this model, the shear failure depends on the normal stress acting on the interface. The coupled behaviour increases the complexity of the model making more unstable the numerical solution. More details on this type of modelling approach are available in literature [1,12,15].

Alternatively, the nonlinear elastic constitutive law is defined by the relative displacement-traction diagrams both in the normal direction and in the shear direction [15]. In contrast to the Coulomb friction model, the axial (orthogonal to the interface) and shear behaviour are decoupled. The diagonal tangent stiffness matrix with decoupled terms improves the robustness of the model, facilitating the convergence of the analysis.

3.2 Numerical Applications: Modelling at the element and structural level

The modelling in DIANA FEA of the vertical glued connection is analyzed first at the structural element level, i.e. considering only a wall-pier system tested by Raijmakers and Van der Pluijm [2], and then at the structural level on the full-scale two-storey building described in the previous paragraphs.

At the structural element level, two different models, adopting plane stress (2D-Model) and solid elements (3D-Model), were used. The Calcium Silicate masonry is modelled with linear elastic elements. No-tension behaviour was assigned at the base joint, and boundary interface elements were applied between the masonry elements and the fixed supports. An equivalent vertical load, which represents the stabilizing moment given by the weight of the floor, was applied at the top of the wall. The prescribed displacement is applied on the top of the wall, thus performing a displacement-control analysis.

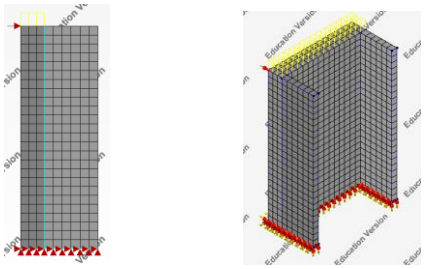
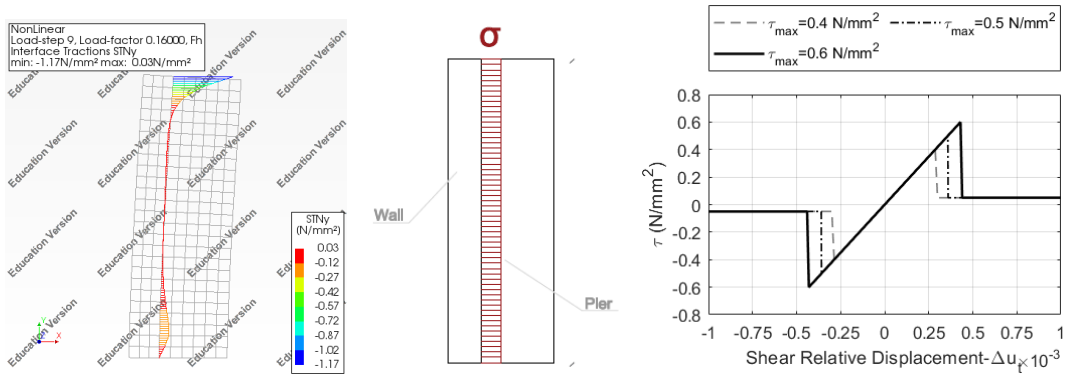


Figure 4: Model of the pier-main wall in DIANA FEA: 2D-Model [Left] and 3D-Model [Right]

The vertical glued connection is modelled through interface elements between the wall and the pier. As previously mentioned, the real behaviour of the interface is governed by the Coulomb friction failure criterion, where the shear strength depends on the normal stress, which varies along the connection, as illustrated in Figure 5 (a). Instead, the nonlinear constitutive law assumes that the shear capacity is equal for each point of the interface. This assumption corresponds to assume a constant normal stress along the interface, as illustrated in Figure 5 (b).

The material parameters for masonry and interface elements are obtained from the literature [1] and summarized in Table 3.

Alternatively, a nonlinear elastic constitutive law is assigned to the structural interface elements, and the relative displacement-shear stress diagrams is defined as illustrated in Figure 5 (c). Three different maximum shear stresses were considered, τ_{max} = 0.4 N/mm^2, 0.5 N/mm^2, 0.6 N/mm^2 (which corresponds to assume a constant distribution of the normal stresses equal to σ=0 N/mm^2, σ=0.13 N/mm^2 and σ=0.27 N/mm^2, respectively).



(a) (b) (c)

Figure 5: Normal stress along the connection: Coulomb Friction Model (a) vs with Nonlinear Elastic Model (b). Relative Displacement - Shear Stress Diagram (c)

Table 3: Vertical interface-Coulomb Friction Model properties [1]

Vertical Joint	Normal Stiffness	k_n	3125	MPa
(Coulomb Friction)	Shear Stiffness	k_t	1395	MPa
	Mode II fracture energy	G_f^{II}	0.05	J/m^2
	Cohesion	c_u	0.4	N/mm^2
	Angle of friction	tanφ	0.75	-

The Coulomb model for the interface generally requires a high computational effort, and it is excessively time-consuming. The analysis converges until the occurrence of the shear failure along the vertical interface, when the shear stress of several nodes reaches the Coulomb strength domain boundary. At that point, the sudden propagation of the crack along the interface leads to instability of the numerical solution and, for the Newton-Raphson iterative method, to lack of convergence of the analysis. Eventually, the Secant (Quasi-Newton) method with a high number of steps was used to follow the post-peak behaviour. The disadvantage is that the initial stiffness reduction, caused by the rocking, is not captured and the curve maintains an elastic behaviour up to the failure of the interface. The analysis performed by Rots [1] using the arc-length method provides a capacity curve similar to that obtained by the experiment. With this method, it is possible to maintain a stable solution during the snap-back, which represents the propagation of the crack along the vertical interface. Figure 6 illustrates the comparison between the three iterative methods. No difference between the modelling with solid elements and plane stress elements is found, except in terms of the computational effort. Besides, it was more difficult to reach convergence in the model with solid elements than in that with plane stress elements.

In case of nonlinear elastic constitutive law, the analysis with Newton-Raphson iteration method is able to provide the failure and post-peak behaviour without any convergence issue. The results of the analyses performed adopting this latter constitutive law for different values of maximum shear stress are compared with those obtained with the Coulomb constitutive law adopting the Arc-Length method in Figure 6. As a displacement-controlled analysis is performed, the snap-back caused by the propagation of the cracking along the vertical interface cannot be captured.

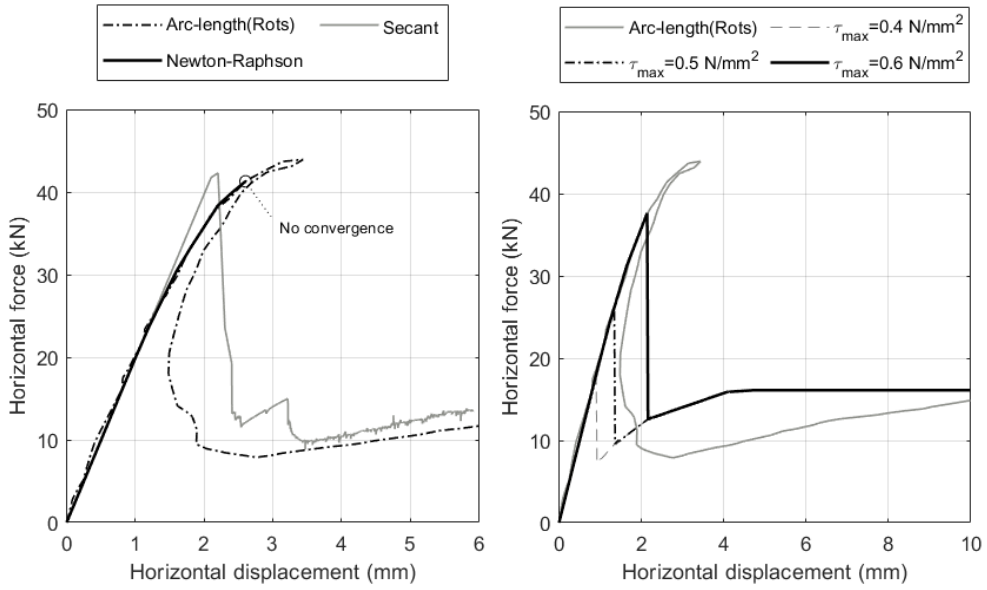


Figure 6: Capacity curves: Coulomb Friction Model [left] vs Nonlinear Elastic Model [right]

At the structural level, the nonlinear behaviour of the vertical glued connection between the pier and the transversal wall has been included in the three models (TSCM-Shell, TSCM-Solid and EMM-Shell) of the two-storey building described in the previous section. A vertical

and a horizontal interfaces were introduced, as illustrated in Figure 7. The first represents the vertical glued connection. The rigid horizontal interface at the top of the pier was used to separate the node at the top of the interface.

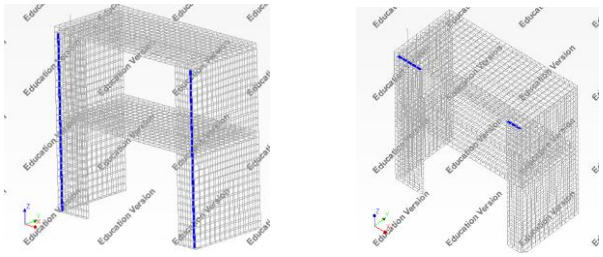


Figure 7: Vertical Interface with nonlinear constitutive law [left] and Rigid Horizontal Interface [right]

First, the connections have been modelled with a vertical interface characterized by the Coulomb friction failure criterion. Using the friction angle ϕ and cohesion of the element pier/wall, no failure of the vertical interface occurs and the results are equal to those obtained for the model without a vertical interface. Then, a sensitivity study was performed by varying the friction angle, to try to capture the failure of the joint. The capacity curves obtained for these variations are illustrated in Figure 8. The results of the sensitivity study show that modelling the vertical interface with Coulomb friction failure criterion leads to instability of the analysis and divergence occurs for small variations of the friction angle. Therefore, it can be stated that this model is not sufficiently robust and it is necessary to adopt a more stable constitutive law for the vertical interface.

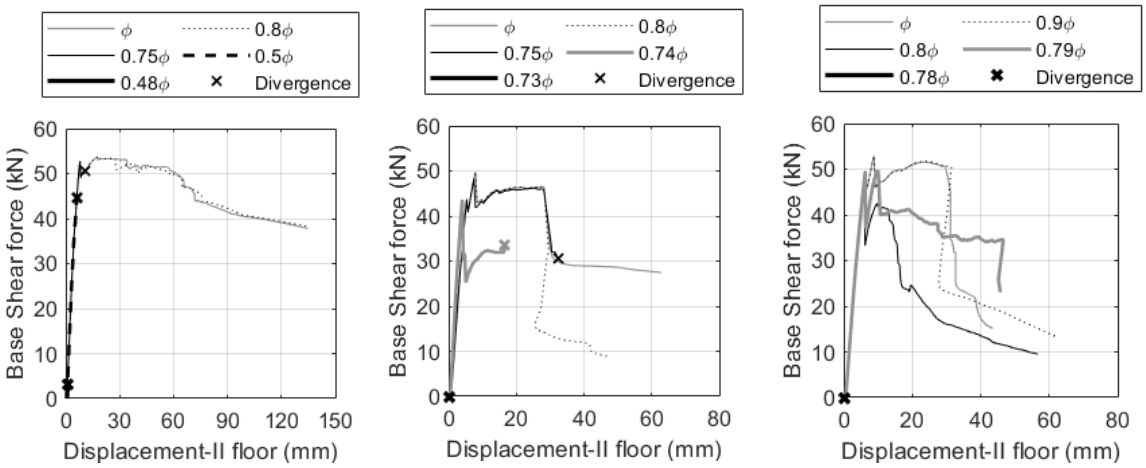


Figure 8: Capacity curves varying the friction for EMM-Shell, TSCM-Shell and TSCM-Solid model, with Coulomb friction model for the vertical connection constitutive law

Subsequently, the nonlinear elastic constitutive law was adopted for the interfaces and introduced in the same three models of the masonry assemblage. A sensitivity study of the influence of maximum and residual shear stress has been performed. The results of this modelling are significantly more stable than those obtained considering a Coulomb friction failure. Figure 9 illustrates the capacity curve of the structure for three different values of the

maximum shear stress (τ_{max}=0.4, 0.5, 0.6 N/mm^2). The global seismic response does not change for larger values of the maximum shear stress. With the decreasing of this value, it is possible to observe that the sudden decrease of the capacity curve occurs for lower values of horizontal displacement. Therefore, the occurrence of failure mechanisms, as the diagonal cracking, depends on the strength of the vertical interface.

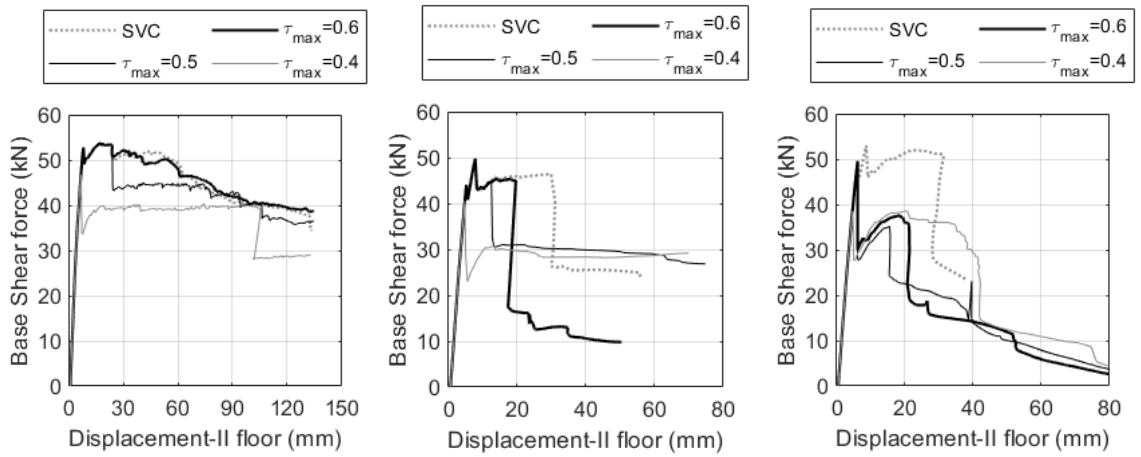


Figure 9: Capacity curves varying the maximum shear stress of EMM-Shell, TSCM-Shell and TSCM-Solid model, with Nonlinear Elastic Model for the vertical connection constitutive law

The sensitivity study varying the residual shear stress (τ_{res}=0.05, 0.025, 0.01 N/mm^2) is illustrated in Figure 9. The results show that the residual shear stress does not influence the peak value, but it rather governs the post-peak behaviour, since the residual capacity reduces at decreasing of this parameter, but the structure is then more ductile. Therefore, in other words, the sliding of the interface prevents the occurrence of further brittle failure, which corresponds to the additional cracking of the wide pier.

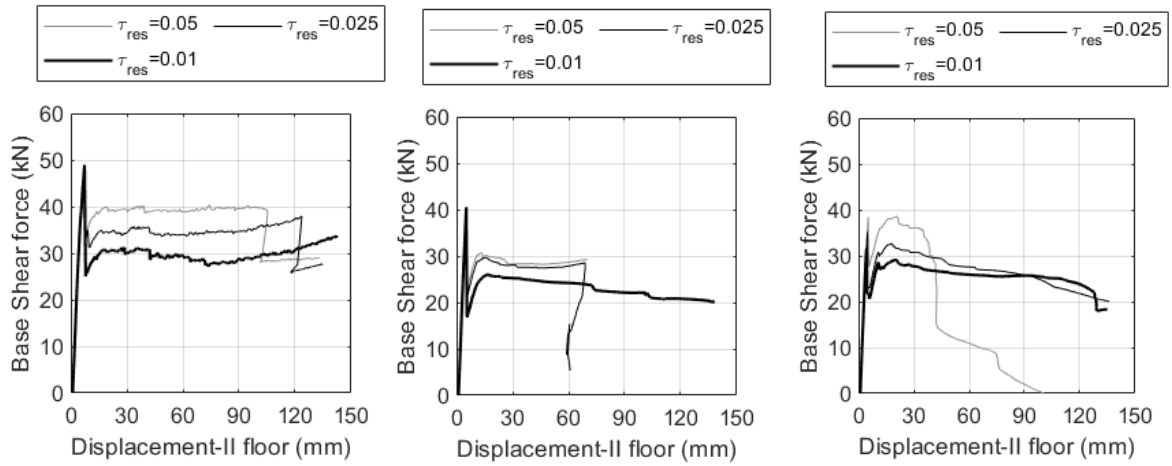


Figure 10: Capacity curves varying the residual shear stress of EMM-Shell, TSCM-Shell and TSCM-Solid model, with Nonlinear Elastic Model for the vertical connection constitutive law

4 CONCLUSIONS

The failure of the vertical glued connections between the wall and pier of the typical Dutch masonry buildings built after the 1980s may reduce the seismic capacity of the entire structure.

The behaviour of such vertical connections is analyzed first at the structural element level, by simulating a wall-pier system, and then at a structural level, by considering a full-scale two-storey building tested at TU Delft. This work shows that the choice of constitutive law is the most critical aspect of the modelling of these structures. The Coulomb-friction criterion is arguably the most representative constitutive law for the real behaviour of the connection, but its use leads to the numerical instability of the solution after the brittle failure of the vertical connection. An alternative modelling is then proposed for the connection by adopting the nonlinear elastic constitutive law defined by the relative displacement-shear stress diagram. In contrast to the Coulomb Friction model, this simplified constitutive law decouples the behaviour in the normal and tangential direction, and this leads to an improvement of the robustness of the model and the stability of the analysis. However, this law requires the calibration of the frictional parameters. Besides, it assumes a constant shear capacity along the height of the connection. When the vertical connection is considered in a complex model, as for example for a real building, the calibration of the parameter in a simpler model, as a pier-main wall model, is suggested. The limitations of this model suggest further investigation to define stable interface elements that may be able to properly represent the evolution of the Coulomb-friction behaviour.

The results of the sensitivity study show that the value of the maximum shear stress governs the occurrence of the shear failure of the interface, whereas the residual shear stress influences the post-peak behaviour. At the structural level, the shear failure of the vertical connection reduces the capacity of the building.

Furthermore, models with different types of elements or constitutive laws are used to assess the seismic capacity of the masonry buildings. The results show that the use of the shell elements or solid elements does not significantly affect the results. On the contrary, different constitutive laws, such as the Engineering Masonry Model or Total Strain Cracked Model, may determine different failure modes of the structure. In particular, when the Total Strain Crack Model is used, the collapse of the structure occurs for smaller lateral deformations.

Acknowledgements. This work has been developed as a jointed research cooperation between Sapienza University of Rome and Delft University of Technology, partly funded by the Sapienza thesis abroad scholarship program, herein gratefully acknowledged.

REFERENCES

[1] Rots, J. *Structural Masonry: An Experimental/Numerical Basis for Practical Design Rules*. A.A Balkema (1997).

[2] Raijmakers, T. M. J. and Van der Pluijm, R. Stability of the calcium silicate piers. *TNOBouw Report BI-91-0219* (1992).

[3] Esposito, R., Terwel, K., Ravenshorst, G., Schipper, R., Messali, F., and Rots, J. Cyclic pushover test on an unreinforced masonry structure reseambling a typical Dutch terraced house. In Proceedings of the *16th World Conference on Earthquake Engineering,*

Santiago, Chile (2017), pp. 1-12.
[4] Esposito, R., Jafari, S., Ravenshorst, G. J. P., Schipper, H. R., and Rots, J. G. Influence of the behavior of calcium silicate brick and element masonry on the lateral capacity of structures. In *10th Australasian Masonry Conference,* Sydney, Australia (2018).
[5] Messali, F., Pari, M., Esposito, R., Rots, J.G., and Den Hertog, D. Blind predictions of a cyclic pushover test on a two-storey masonry assemblage: a comparative study. In Proceedings of the *16th European Conference on Earthquake Engineering*, Thessaloniki, Greece (2018).
[6] Jafari, S., Esposito, R., and Rots, J. G. *From Brick to Element*: *Investigating the Mechanical Properties of Calcium Silicate Masonry*. RILEM Bookseries, 18, (2019), p.p. 596–604.
[7] Ravenshorst G., Esposito R., Schipper R., Messali F., Tsouvalas A., Lourens E-M. and Rots, J. *Structural behaviour of a calcium silicate brick masonry assemblage: quasi-static cyclic pushover and dynamic identification test*. Delft University of Technology, Department of Structural Engineering. Version 5, 21 October 2016 (2016).
[8] Magenes, G., and Penna, A. Seismic Design and Assessment of Masonry Buildings in Europe: Recent Research and Code Development Issues. In Proceedings of *9th Australasian Masonry Conference,* Queenstown, New Zealand (2011).
[9] Calderini, C., Cattari, S., and Lagomarsino, S. In-Plane Strength of Unreinforced Masonry Piers. *Earthquake Engineering and Structural Dynamics* (2008), 38(2), p.p. 243–267.
[10] Sacco, E., Addessi, D., Sab, K., *New trends in mechanics of masonry*, Meccanica, (2018), 53 (7), p.p. 1565-1569.
[11] Lourenço, P.B. *Computations on historic masonry structures.* Prog. Struct. Engng Mater. (2002). 4:301–319.
[12] Lourenço, P.B. *Computational strategies for masonry structures*. PhD Thesis. Delft University of Technology (1996).
[13] Calderini, C., and Lagomarsino, S. Continuum Model for In-Plane Anisotropic Inelastic Behavior of Masonry. *Journal of Structural Engineering (ASCE)*, (2008), 134(2), p.p. 209–220.
[14] Addessi, D., Marfia, S., Sacco, E., Toti, J. Modeling approaches for masonry structures. *Open Civil Engineering Journal*, (2014), 8 (1), pp. 288-300
[15] DIANA FEA User's Manual. TNO Building and Construction Research. (2019).
[16] Mariani, V., Messali, F., Hendriks, M. and Rots, J. Numerical modelling and seismic analysis of Dutch masonry structural components and buildings. In Proceedings of the *16th World Conference on Earthquake Engineering*, Santiago, Chile (2017).

12th International Conference on Structural Analysis of Historical Constructions
SAHC 2020
P. Roca, L. Pelà and C. Molins (Eds.)

SAFE ESTIMATION OF MINIMUM THICKNESS OF CIRCULAR MASONRY ARCHES CONSIDERING STEREOTOMY AND DIFFERENT ROTATIONAL FAILURE MODES

ORSOLYA GÁSPÁR[1*], ISTVÁN SAJTOS[2] AND ANDRÁS Á. SIPOS[3]

[1,2,3] BME Budapest University of Technology and Economics
Department of Mechanics, Materials and Structures
1111 Budapest, Muegytem rkp 3., Hungary
e-mail:[1*] gaspar@szt.bme.hu, [2] sajtos@szt.bme.hu, [3]siposa@eik.bme.hu, www.szt.bme.hu
(*corresponding author)

Keywords: masonry arch, catenary, thrust line, pointed arch, minimum thickness analysis, geometric indeterminacy

Abstract. *Limit state analysis of masonry arches sets to assess the safety of the structure by determining the minimum thickness that just contains a thrust line. Based on the Heymanian assumptions regarding material qualities and the equilibrium approach to the static theorem it has been explicitly proven for semi-circular arches that both the thrust line and the resulting minimum thickness value is subject to stereotomy (brick or stone laying pattern), while present study demonstrates, that the latter statement holds for pointed-circular arches as well. This is not straightforward, since the number- and arrangement of the hinges at limit state vary subject to the geometry in case of pointed-circular arches, resulting a more complex problem. It is also explicitly shown, that stereotomy might also affect the corresponding (rotational) failure mode (for certain arch geometries). Stereotomy of an existing structure is not always known, hence it is relevant to search for a stereotomy related bounding value of minimum thickness for each of the various failure modes. The potential of the envelope of resultants as a thrust line (resulting from vertical stereotomy) leading to bounding value minimum thicknesses is discussed: as shown elsewhere it bounds the family of thrust lines, hence leads to an upper bound value of minimum thickness in case of semi-circular arches. It is demonstrated however, that this cannot be generalized for other rotational failure modes which occur for circular-pointed arches. The envelope of resultants does not necessarily lead to a bounding value of minimum thickness, and even if it does, it can be either an upper or a lower bound. However, it is found that the range of minimum thickness values is bounded in all possible failure mode types. The necessary conditions are provided for each.*

1 INTRODUCTION

Minimum thickness analysis is based on the consideration, that equilibrium of a structure made of no-tension material is only achievable if the thrust line does not exit its boundaries. It determines the smallest possible cross section, that can still fully incorporate the corresponding

thrust line for a given loading and compares it to the actual thickness of the arch. Thrust line is subject to the overall geometry of the structure, its loading and its stereotomy (brick or stone laying pattern). The classical approach (e.g. [1],[2]) for minimum thickness analysis assumes a certain stereotomy (mostly radial) and determines the unique thrust line and/or minimum thickness value for a fixed loading. Moseley, however, already suggested [3] that this set up can be varied. Present study considers the relation of thickness and thrust line fixed (that the latter does not exit the boundaries) and seeks a suitable stereotomy for which the thickness becomes minimal (at which the structure turns into a mechanism). This approach was already applied by the authors in investigating the effect of stereotomy on the minimum thickness of semi-circular arches [4]. It has been shown there and elsewhere [5, 6], that for self-load, the envelope of the resultant force vectors coincides with the thrust line in case of a vertical stereotomy: this is called the catenary-type thrust line. It is rather easily comprehensible that it bounds all other thrust lines corresponding to the same thickness and different stereotomy, if the arch's reference line is convex, see also [4]. Consequently, the catenary type thrust line results in an upper bound minimum thickness value for the semi-circular arch.

Even if the Heymanian assumptions are obeyed, the kinematically admissible (rotational) failure modes (number and arrangement of hinges) vary subject to arch geometry [7, 8, 9]. Nikolić's recent rigorous study [8] on the rotational failure modes of pointed arches provided a reportedly inclusive list of all (altogether 5, see *Figure 1*) possible hinge arrangements subject to the arch geometry. His study suggests, without explicit proof, that 7 is the maximum number of concurrent hinges at the limit state for pointed arches. An *analytical proof* about that maximum was provided by us in [10]. Present paper aims to offer an extension to previous results by investigating the effect of stereotomy on the minimum thickness value of pointed circular arches. Stereotomy of an existing structure is not always known, hence it is relevant to search for a stereotomy related bounding value of minimum thickness for each of the various failure modes, if they exist. The potential of the catenary type thrust line (resulting from vertical stereotomy) leading to bounding value minimum thicknesses is discussed, with special emphasis on the 6 (7)- and 5-hinge type (2a) mechanism (it has already been shown by us in [10] that for 5-hinge type (2b) though it provides a bound, that is a *lower* one, as opposed to the case of 5-hinge type (1), the semi-circular arch (*Figure 1.*)). The complexity of the problems discussed here originates in the geometric indeterminacy of the studied mechanisms: since no hinge is located at either the top (6-h) or the bottom(5-h2a) of the arch, the location of the array of resultants might vary relative to the axis of the arch.

Motivation of present study is further discussed in Section, 2. Modelling, geometry and methodology is treated in Section 3, while results on the effect of stereotomy on the minimum thickness value for pointed arches corresponding to the 6-hinge and 5-hinge type (2a) mechanism are derived in Section 4. Finally, conclusions are drawn in Section 5.

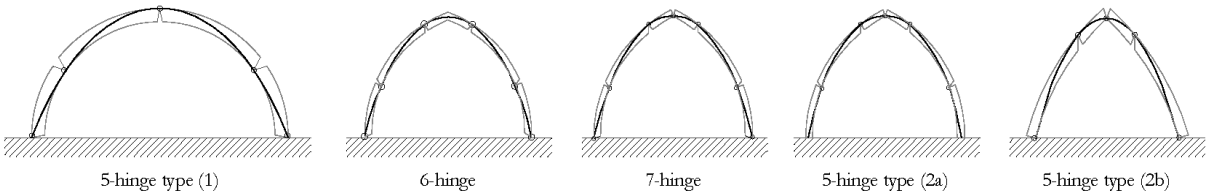


Figure 1. Rotational collapse modes of circular arches, based on [8]

2 MOTIVATION

In particular, we aim to investigate, whether

- the dependence of minimum thickness value on stereotomy is valid for all type of rotational failure modes.
- stereotomy affects the type of failure mode.
- it is relevant to define the stereotomy related bounding value of the minimum thickness for each of the various failure mode types (i.e. arch geometry), if exists. It would substantially simplify the analysis if there was one specific type of the thrust line (i.e. stereotomy), resulting a bounding value for all cases. The catenary type thrust line (linked to a vertical stereotomy) results in an upper bound minimum thickness and hence provides a safe estimation for the semi-circular arch (5-h1 type) – therefor it seems a natural candidate.

3 MODELLING, GEOMETRY AND METHODOLOGY

The applied material model is rigid-plastic, furthermore necessary assumptions proposed by Heyman [1] regarding the constitutive hypotheses are adopted:

- the material has no tensile strength – in specific, *the joints* do not transfer tensile forces,
- the material has infinite compressive strength,
- no sliding occurs between the elements.

The most notable consequence of these assumptions for present research is that only a *rotational failure mode* is considered. The *static approach* of limit state analysis is followed. The *equilibrium condition* is that the thrust line should not exit the boundaries of the arch. The *yield condition* is determined by the eccentricity of the resultant force vector: a plastic hinge forms, if the eccentricity equals half-thickness. Following Heyman's proposal [1], minimum thickness analysis is treated as a plastic design methodology that seeks an optimal geometry. The assumed corresponding rotational failure mode (subject to geometry and loading) determines the arrangement of (plastic) hinges at the limit state, which allows for a *geometric formulation* of the equilibrium and the yield condition: at the limit state the thrust line crosses all hinges (*yield*) and must be tangent to the boundary of the arch at the internal hinges(*equilibrium*). In the following, the equilibrium condition is hence denoted *tangency condition*, in accordance with the geometric formulation.

3.1 Geometry

The arch is modeled as a planar structure made of voussoirs. In order to account for all the theoretically possible arrangements, a continuous model is applied with *sections* (*s*) essentially substituting *joints.* Only constant thickness (*t*) and symmetrical arches are considered, the analysis is hence carried out on a half-arch and symmetry is accounted for in the constraints. (Minimum) thickness is scaled by the radius (*R*) of the arch, hence the notation *t/R* is used. A major simplification of the applied model is that it considers the *loading (self-weight) distributed evenly* along the center line of the arch, which is treated as the reference line (*r*), regardless of the stereotomy. Consequently, the **E** vector (resultant force, see *Figure 3*) field becomes independent of the stereotomy and it seems essential for an analytical study of the problem.

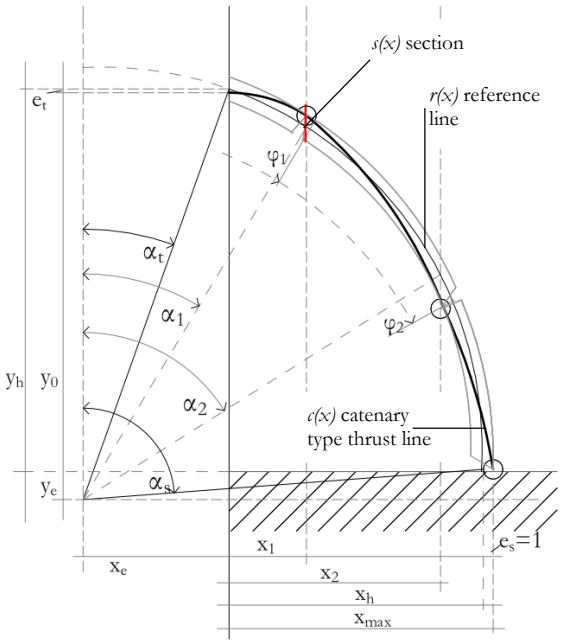


Figure 2. Notation of geometry (*6-h* mechanism)

Depending on the problem discussed, the reference line is either parameterized with respect to the angle to the vertical denoted by α in a polar, or by x in a Cartesian coordinate system. *Stereotomy* is treated as a continuous function ordering the direction of *s* to each point along *r*. The *thrust line* is the set of points of intersection between lines **E** and *s*. Notation is shown in *Figure 2 and 3, right.*

We consider circular-pointed arches with a unit radius (x_e, y_e ϵ [0,1]). We define a deviation function (*d(x)*) in the Cartesian coordinate system as the difference between the center line *r(x)* and the catenary-type thrust line *c(x)*. For a catenary-type thrust line results from a vertical stereotomy, *d(x)* is rather convieniently defined, the applied transformation from the polar system back and forth is straightforward. Depicting *d(x)* corresponds to the vertical projection of *c(x)* and *r(x)*.

$$d(x) := r(x) - c(x). \tag{1}$$

The equation of the envelope of resultants (or the catenary-type thrust line) is obtained based on the vanishing moment:

$$c(x) = y_0 - \frac{\overset{m(x)}{\widetilde{V(x)}}}{H}\big(x - x_V(x)\big), \tag{2}$$

where y_0 denotes the *y*-intercept of *H* at the top, and x_V the *x*-coordinate of the center of mass. While *r(x)* reads

$$r(x) = \sqrt{1 - (x + x_e)^2} - y_e. \tag{3}$$

Thrust line's eccentricity at the top from *r(x)*, denoted e_t, [-1,1] is a unitless quantity, scaled by *t/2R*, half-thickness to radius ratio of the arch. Its eccentricity from *r(x)* at the springing is e_s [-

1,1], analogously to e_t. At the intersections of $\mathbf{E}(x)$ with the intrados (or extrados) (*Figure 2*), the following relations hold (the necessary conversion for angles measured at the extrados is made, though not detailed here, before depicting them on the α-φ plane for φ refers to angles measured at the intrados, see Figure 2, 3):

$$x = \left(1 \pm \frac{1}{2}\frac{t}{R}\right)\sin(\varphi) - \sin(\alpha_t)\,, \tag{4}$$

$$y = \left(1 \pm \frac{1}{2}\frac{t}{R}\right)\cos(\varphi) - \cos(\alpha_s)\,. \tag{5}$$

3.2 Methodology

The methodology of determining the admissible stereotomy functions for a given minimum thickness value is presented in detail in [4] for the case of the semi-circular arch. A very brief outline is given here, while its application to the more general case of pointed arches is to be found in Section 4. As per definition, the stereotomy-dependent thrust line points lay on the resultants (which only depend on the geometry, i.e *r* and *t/R* in the frame of the model), hence those sections of the resultants are inadmissible which are outside (if the arch is sufficiently thin, see [4]) the boundaries of the arch. This allows for the definition of inadmissible ranges of the angle φ for each point along the reference line. Here φ denotes the internal angle to the vertical of intersection of section and *intrados*. The results are depicted on the α-φ plane for a given *t/R* ratio. A visual explanation is given in *Figure 3*. below:

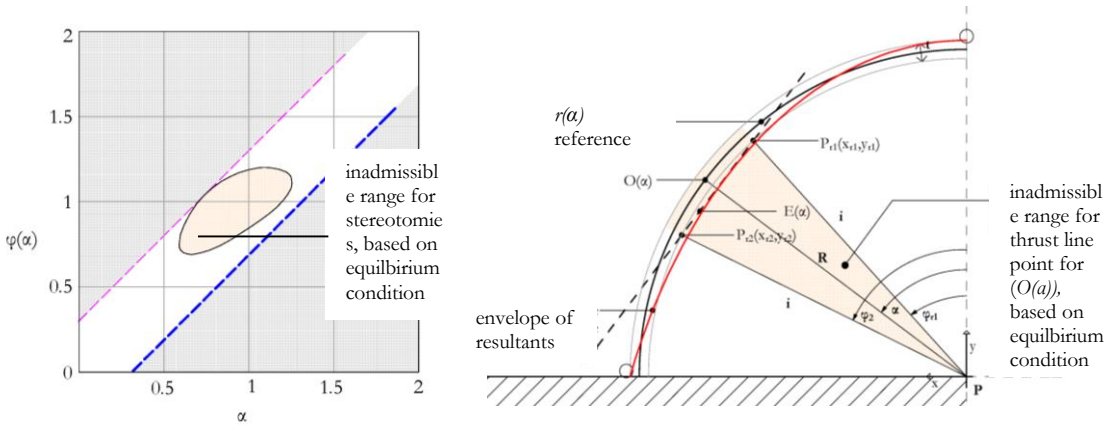


Figure 3. Diagram of admissible stereotomy function-range (left white) in the α-φ plane (*left*), and the explanation of admissible-and inadmissible (orange) ranges on the arch (*right*)

4 EFFECT OF STEREOTOMY ON THE MINIMUM THICKNESS VALUE

Following the initial assumption that the catenary type thrust line leads to a bounding value minimum thickness we start each analysis of an arch (characterized by x_e, y_e, or, equivalently, by α_s and α_t, see *Figure 2*) with a given *r(x)* reference line by determining the *t/R* and the corresponding α-φ diagram depicting the admissible range of stereotomies based on *c(x)*. Determining the minimum thickness value of a pointed-circular arch of given geometry (x_e,y_e) for a *specific stereotomy* is done by solving the following system of non-linear equations:

$$d(x_1) = c(x_1) - r(x_1) = t_{pr}/2R$$
$$d'(x_1) = c'(x_1) - r'(x_1) = 0$$
$$d(x_2) = c(x_2) - r(x_2) = -t_{pr}/2R$$
$$d'(x_2) = c(x_2) - r(x_2) = 0 \qquad (6-9)$$

With x_1 and x_2 denoting the x-coordinate of the internal hinges, and t_{pr} denoting the projection of the half-thickness on the corresponding section. Note that except for the 5-hinge type (1) and (2b) (which are not considered here, see Introduction) always two internal (i.e. between the top and the springing of the arch) hinges appear, one at the intrados, one at the extrados (*Figure 1*). Then, if possible, we modify the value of *t/R* along with the e_t and e_s parameters (see *Figure 2,* note that *r(x) is unaffected!*) and observe the effect on the range of admissible stereotomies (essentially the /modified/ α-φ diagram) and the rotational failure mode, if applicable. Since the equilibrium related constraints are required, we derive the *envelope of resultant* for each new combination. It is important to highlight that we only aim to prove that other stereotomies (and hence minimum thicknesses) are possible, but we do not pursue to derive them for illustration. This also holds for the bounding value minimum thicknesses: we only intend to find the combination that results them (in terms of e_t and/or e_s) and not the corresponding stereotomy (unless, the bounding value is indeed based on the catenary type thrust line).
Results based on *eqs. (6-9)* considering the catenary type thrust line for a selected arch geometry (i.e. failure mode 6-hinge) and its corresponding φ-α diagrams are depicted in *Figure 4*, second row, left. Analyzing the cited diagrams in *Figure 4,* it becomes reasonable to assume that should the *t/R* value be higher, hinge at the intrados would disappear, while for lower *t/R* values, the ranges corresponding to inadmissible points towards the extrados would intersect (hence no admissible stereotomy can be constructed) therefor no stereotomy-related variation in terms of *t/R* exists, see *Figure 4*, first row, middle and right. It is, however, shown below that due to their 'geometric indeterminacy' (parameter e_t *or* e_s influencing the location of the array of resultants) in case of the 6-hinge and 5-hinge type (2a) mechanisms stereotomy related variation still exists: *multiple minimum thickness* values can be derived for the same geometry (i.e. *r(x)*) and moreover the minimum thickness value derived based on *catenary-type thrust line does not provide a bound*.

4.1 6-hinge mechanism

In the case of a 6-hinge mechanism we have 4, linearly independent unknowns for a given geometry (fixed x_e and y_e): *t/R*, e_t, and the locations of the internal hinges, x_1 and x_2. Consequently, if vertical stereotomy is considered (equivalently: catenary type thrust line), solving *eqs. (6-9)*, results a unique 'e_t' value in addition to the location of hinges and *t/R* value for a given geometry. However, relaxing the boundary conditions of the minimum thickness analysis still based on catenary-type thrust line (by instead of *eqs. (6)* and *(8)* enforcing solely the following inequalities on the problem:

$$d_e(x_1) \leq t_{pr}/2R \qquad (10)$$
$$d_i(x_2) \leq -t_{pr}/2R \qquad (11)$$

respectively, opens up a range of admissible values of 'e_t', and allows for stereotomy related variation of minimum thicknesses for the same geometry. Geometrically, condition (*11*) means

that we allow the catenary type thrust line to cross the boundary towards the intrados, while condition (*12*) means it might not even touch extrados (see *Figure 4* second row, middle, left and *Figure* 5). Observe that if both is fulfilled simultaneously alternate admissible stereotomies might exists, as all other members of the thrust line family is 'above' the catenary-type – i.e. one can be found that touches both extrados and intrados. The following questions should then be investigated:

- what is the admissible range of 'e_t'?
- whether an analysis based on the catenary-type thrust line results a bounding minimum thickness value?

The deviation function *d(x)* provides an illustrative tool well suited to investigate these questions:

$$d(x) = \underbrace{y_0 - m(x)\big(x - x_V(x)\big)}_{c(x)} - \overbrace{\sqrt{1-(x_e-x)^2} - y_e}^{r(x)}. \tag{12}$$

r(x) depends on the geometry, hence any changes of the value *t/R* or e_t affects *c(x)* only. *x*, x_v are also independent of these parameters. In order to highlight the effect of any change in these parameters, the following formulation is obtained:

$$d(x) = \underbrace{\overbrace{(\boldsymbol{y_h} - \boldsymbol{y_e} + \boldsymbol{e_t}\frac{\boldsymbol{t}}{\boldsymbol{2R}})}^{\boldsymbol{y_0}}\Big(1 - \frac{V(x)}{V(x_h)\big(\boldsymbol{x_{max}(t/R)} - x_V(x_h)\big)}\big(x - x_V(x)\big)\Big)}_{c(x)} - \overbrace{\sqrt{1-(x_e-x)^2} - y_e}^{r(x)} \tag{13}$$

Note that 'e_t' only affects (directly) the value of y_0. From this formulation it is obvious that for a given *t/R* value reducing the value of e_t results lower *d(x)* values. Hence the admissible range of e_t is found to be:

$$e_{0t} > e_t > -1, \tag{14}$$

where e_{0t} denotes the eccentricity calculated during the determination of minimum thickness considering catenary type thrust line. Note that decreasing *d(x)* means that it moves towards the intrados, at a fixed *t/R*. Hence, it is theoretically possible, to construct arches (by finding admissible stereotomies) for both higher and lower *t/R* values than that defined based on the catenary type thrust line: the corresponding lower and upper bound minimum thickness values can be found based on the assumption that $e_t = -1$.

t/R can be increased as long as $\min(d(x)) \leq t/2R$), whereas it can be reduced as long as $\max(d(x)) \leq t/2R$) – meaning that the envelope of resultant at least touches the intrados, and at most it touches the extrados. The extremities of the range of minimum thickness values hence can be found by solving

$$d_e(x_1) = 0\ ;\ d'_e(x_1) = 0; d_i(x_2) = 0\ while\ e_t = -1 \tag{15}$$

or

$$d_i(x_2) = 0\ ;\ d'_i(x_2) = 0; d_e(x_1) = 0\ while\ e_t = -1 \tag{16}$$

The former resulting lower, the latter the upper bound. **Note that the case of *e* = *-1* turns the originally 6-hinge mechanism into a 7-hinge mechanism** (see *Figure 5*, far left and left)**.**

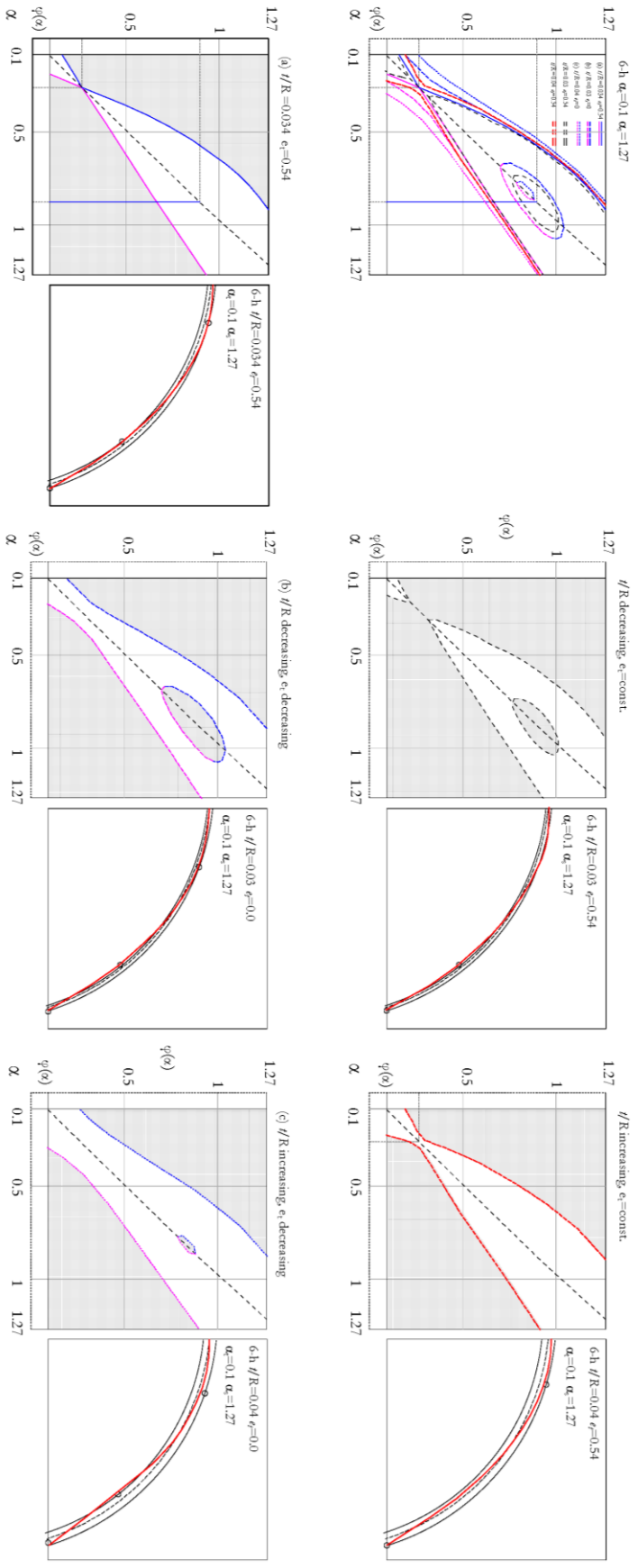
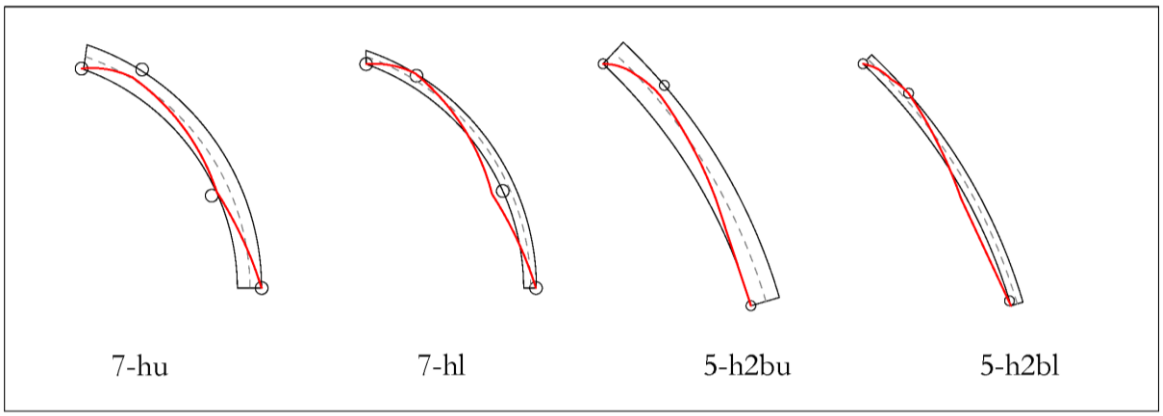


Figure 4. φ-α diagrams of α_b=0.1 α_t=1.27 arches, corresponding to 6-hinge mechanism



** distorted images for clarity*

Figure 5. Hinge arrangement and catenary type thrust line in corresponding limit thickness arches (admissible stereotomy can exist, since all other members of the thrust line family lay above the catenary type thrust line)

Up to this point it has been implicitly assumed that the failure mode is not subject to stereotomy – i.e. only 6-hinge (or in the limit, 7-hinge) mechanisms has been considered. This kept the value of e_s fixed, at 1. However, this is not a necessary condition. Decrease in the value of e_s has a similar, reducing effect on *d(x)* (see below), and it can be activated, if the limit in terms of e_t is achieved (i.e. hinge at the top is at the intrados). This turns the 6-hinge mechanism into a 5-hinge type (2a) or even (b).

4.2 5-hinge type (2a) mechanism

The problem of the 5-hinge mechanism type (2a) is very similar to the above discussed 6-hinge mechanism, except that at the top the thrust line is required to touch the intrados (hinge), while a hinge at the springing is not a necessary condition, hence e_s becomes a parameter. Therefor *eq. (12)* turns into:

$$d(x) = (y_{0(t/R)})\left(1 - \frac{V(x)}{\underbrace{V(x_h)\left(\underbrace{x_h - x_e + e_s\frac{t}{2R}}_{x_{max}} - x_V(x_h)\right)}_{c(x)}}\right)\left(x - x_V(x)\right) - \overbrace{\sqrt{1-(x_e-x)^2} - y_e}^{r(x)} \qquad (17)$$

Clearly, the e_s parameter only affects the value of x_{max}. Note that reducing the value of e_s results similarly to above lower *d(x)* values for arbitrary *x*. Following the same argument (see *Figure 5* right and far right) as for the case of a 6-hinge mechanism it is deductible that a minimum thickness analysis based on catenary type thrust lines *does not* provide any bound for the 5 hinge mechanism type (2a) either (either lower or upper). The admissible range of '*e*' is analogously:

$$e_{0s} > e > -1 \qquad (18)$$

Note that the case of e_s = *-1* turns the originally 5-hinge type (2)a mechanism into a 5-hinge type (2b) mechanism (*Figure 5*).

5 CONCLUSIONS

The most important conclusion of the study above, is that eminently the geometry of the circular pointed arch determines the failure mode, however, it can be modified by the stereotomy, if the failure mode had a geometric indeterminacy (6-hinge, 5-hinge type (2a)) and/or redundancy (7-hinge – this, though not explicitly discussed above, is directly deductible from the cases 6-h and 5-h2a). Furthermore, determination of bounding value of minimum thickness for any geometry is possible if the geometric indeterminacy or the redundancy is resolved. To allow comparison with former results of the literature the outcome of the present work is visualized for a given y_e (0.3) value in *Figure 6*: it contains the resulting minimum thickness values with respect to x_e, for admissible stereotomies. The diagram can be obtained based on *eqs.* (*6-9*). It is clearly demonstrated that in perfect agreement with the findings of Nikolić [8] the 7-hinge mechanism marks a local minimum on the $t/R(x_e)$ function considering both the catenary type thrust line, marked bold red or radial stereotomy (marked bold black) in *Figure 6*. However, if the effect of stereotomy is fully accounted for, the geometry corresponding to the 7-hinge mechanism no longer marks any local minimum. Instead, the observation can be made that lower bound minimum thickness value is to be defined based on the assumption of a 5-hinge type (2b) failure mode. It is important to highlight though that the bounding value minimum thickness (and hence, failure modes) would require unrealistic stereotomies.

The relation of the bold black and red line in the *Figure* also suggests a very important conclusion for *realistic* stereotomies. The formerly proven statement on how considering the catenary type thrust line provides lower bound minimum thickness value for failure mode 5-hinge type (2b) and upper bound for failure mode 5-hinge type (1) can be extended for failure modes with geometric indeterminacy: It provides upper bound for 6-hinge mechanisms, and a lower bound for 5-hinge type (2a) mechanisms.

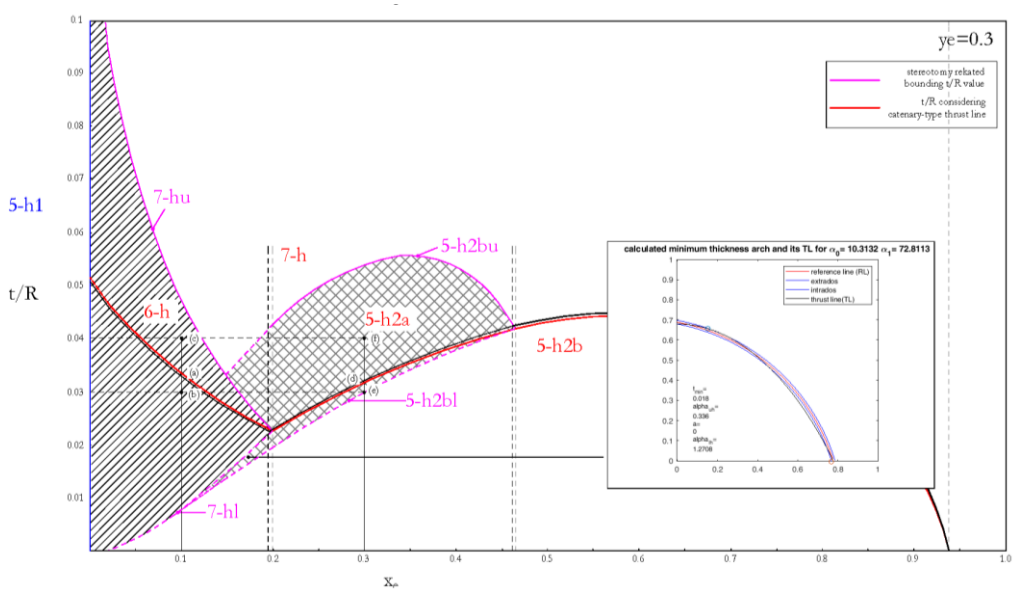


Figure 6. Range of minimum thickness values for y_e=0.3 and the corresponding rotational failure mechanisms

Acknowledgements. The research was supported by the NKFIH Grant 124859 and the FIKP grant of EMMI in the frame of BME FIKP-VÍZ.

REFERENCES

[1] Heyman, J. The safety of masonry arches. *International Journal of Mechanical Sciences*, 11(4) (1969) pp. 363-385.

[2] Cocchetti, G., Colasante, G., Rizzi, E. On the analysis of minimum thickness in circular masonry arches. *Applied Mechanics Review*s,64(5) (2011): 050802.

[3] Moseley, H. On the theory of the arch. In: *The theory, practice and architecture of bridges*, ed. J. Weale. London: Architectural Library, (1843).

[4] Gáspár, O., Sipos, A. Á. and Sajtos, I. Effect of stereotomy on the lower bound value of minimum thickness of semi-circular masonry arches. *International Journal of Architectural Heritage,* (2018) pp. 1-23.

[5] Milankovitch, M. Theorie der Druckkurven. *Zeitschrift für Mathematik und Physik* 55 (1907) pp.1-27.

[6] Alexakis, H.,Makris, N. Limit equilibrium analysis of masonry arches. *Archive of Applied Mechanics*, 85(9-10) (2015) pp. 1363-1381.

[7] Romano, A., Ochsendorf, J. A. The mechanics of gothic masonry arches. *International Journal of Architectural Heritage,* 4(1) (2009) pp. 59-82.

[8] Nikolić, D. Thrust line analysis and the minimum thickness of pointed masonry arches. *Acta Mechanica,* 228(6) (2017) pp. 2219-2236.

[9] Aita, D., Barsotti, R., Bennati, S. Looking at the collapse modes of circular and pointed masonry arches through the lens of Durand-Claye's stability area method. *Archive of Applied Mechanics* (2019), pp. 1-18.

[10] Gáspár, O., Sipos, A. Á., & Sajtos, I. The role of rotational collapse mode and catenary-type thrust lines in the limit state analysis of masonry arches. In *Proceedings of IASS Annual Symposia* 18 (2019), International Association for Shell and Spatial Structures (IASS), pp. 1-8.

12th International Conference on Structural Analysis of Historical Constructions
SAHC 2020
P. Roca, L. Pelà and C. Molins (Eds.)

SAFETY ASSESSMENT OF HISTORIC MASONRY STRUCTURES BY LIMIT ANALYSIS AND DETERMINISTIC PARTIAL SAFETY FACTORS

FERNANDO MAGDALENA[†1], ANTONIO AZNAR[*], JOAQUÍN ANTUÑA[†2] AND JOSÉ I. HERNANDO[†2]

[†1] School of Building Engineering (ETSEM)
Department of Architectural Constructions and their Control
Universidad Politécnica de Madrid
Avda. Juan de Herrera, 6, 28040, Madrid, Spain
e-mail: fernando.magdalena@upm.es

[*, †2] School of Architecture (ETSAM)
Department of Building Structures and Physics
Universidad Politécnica de Madrid
Avda. Juan de Herrera, 4, 28040, Madrid, Spain
e-mail:antonio.aznar@upm.es (*corresponding author)
(orcid.org/0000-0002-1466-0654)

Keywords: Masonry structures, Standard Limit Analysis, Linear Programming, Safety factor, Chebyshev Center.

Abstract. *Safety assessment of historic masonry structures is a complex problem mainly due to the mechanical characteristics of their material. In the 50's it was shown that Standard Limit Analysis is suitable for that type of structures and has proven effectiveness for simplified assessment as long as sliding collapse does not occur. This can be formulated as an optimization problem with the intention of calculating the bounds of the load factor, the maximum for static formulations and the minimum for kinematics. In the static case, it is generally assumed that a load factor lower than the referred of the onset of collapse is a safe load factor, but this assumption is false. The collapse due to the lack of stability may occur by increase or decrease of the load factor.*

This work presents an alternative to load factor determination to evaluate the safety of masonry structures. The possibility to incorporate one or more safety coefficients is presented applying a deterministic partial safety factor method. An important difficulty for this purpose is that usually these partial coefficients are applied to variables that are referred to the origin of coordinates. This would be appropriate for materials with similar mechanical behaviour under tension and compression stresses, but it is not the case for the typical materials employed in masonry structures like stones, bricks or similar. Materials with non-symmetric tension-compression behaviour have the origin of coordinates over the yield surface or very close to it. For this reason, the origin can hardly be considered as a safe reference point.

The method proposed in this work consists of the calculation of the interior point further of the yield surface and considers it as the safest point. Considering that point as the origin of coordinates, the deterministic partial safety factors can be calculated.

1 INTRODUCTION

In 1952 Kooharian [1] proved that Limit Analysis theorems were suitable for masonry structures, although in 1953 Drucker [2] proved that these theorems were not appropriated for cases of sliding collapse. The Standard Limit Analysis is an excellent method to evaluate the resistance and stability of the cases in which sliding do not occur [3], it is especially useful for study in a simplified way the short-time behaviour. In fact, this is probably one of the best methods to evaluate the limit resistance of one structure obtaining the failure strength and the global stability, both of them from basic data as the geometry of the structure and loads. On the contrary, this method is not appropriate to evaluate the mechanical behaviour considering long-time effects, for this issue there are sophisticated tools, although it is important to note that it requires much more specific data.

Heyman has developed "manual" analysis based on these theorems, and he successfully did it because that analysis method perfectly connects with the graphic and non-graphic traditional analysis based on pressure lines.

The Limit Analysis and the linear and non-linear Mathematical Programming have been always closely related. Charnes et al. [4] matched the equivalence between two dual Linear Programming problems with the static and kinematic principles of plastic collapse in trusses. Dorn [5] and Charnes et al. [6] extended the equivalence to structural frames. From the 70's, Limit Analysis using Linear Programming experienced a great development mainly due to the increase of the use of computers. Some examples of this phenomenon can be highlighted, as the application by Anderheggen [7] of a medium continuous with finite elements method of a rigid plastic material, or the application to masonry structures modelled by rigid blocks with unilateral contact by Livesley [8] using a static formulation, or the application of a kinematic formulation by Gilbert et al [9].

The application of lower bound theorem or static method, is used to predict if structures are stables and resistant under specific load case. This is based on the "manual" analysis mentioned above, that consists of obtaining one solution of the equilibrium between whatever internal forces with the load case. It is important to note that this simulated structural response does not have to be the "real" one, but these internal forces cannot violate the constraints of the material at any point. In other words, if a solution that allows to achieve the equilibrium and does not violate the constraints is possible, the structure "finds" it.

It is a different topic how to obtain the variation of the security if the loads or the proprieties of the structure vary. The application of these theorems is not easy if the materials are heterogenous, anisotropic, and with tensile strength values near to zero or even zero. The topic is complicated if the theorems are applied in combination with Mathematic Programming. Their names, lower bound theorem and the upper bound theorem, can be misled.

It is a known fact in these structures that it is more dangerous to reduce the loads than to increase them, nevertheless this phenomenon is sometimes ignored with serious consequences (fig. 1).

From this point, this work is limited to methods with static formulation. In this way, this problem has been approached with "manual" analysis for linear structures with the sole objective of checking the stability using the geometry safety coefficient.

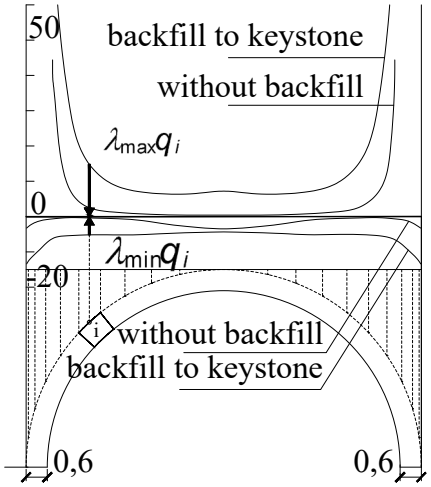


Figure 1: Influence lines for a point load with backfill to keystone and without backfill.

2 STRUCTURE MODELLING

This work proposes a model of a masonry structure with a unilateral material, considering both blocks and the interfaces, with little or no tensile strength, high compressive strength and non-existence or impeded sliding. In the simplest model the tensile strength is voided and in the model of Heyman [10] the compressive strength is not limited. The assumption of considering zero tensile strength has been traditionally applied and it works in favor of the safety. The use of limited compressive resistance considering the possibility of crushing has not been traditional applied, but it appears in researches as Delbecq [11] or Livesley [8]. Respect to the sliding, the Standard Limit Analysis method requires that it be voided. In this way, will be supposed the friction enough to impede the sliding, or the necessary characteristics to avoid it. The sliding collapse has been studied by several authors [12].

Therefore, the mechanical behaviour of the material is modelized as a plastic-rigid, regardless elastic strains. In this way, it is a realistic simplification because the plastic strains that occurs at the point of yield constrains are much superior than elastic ones.

Figure 2 shows an example of axial force (N) and moment (M) applied on a generic section and a stress distribution over this surface. This distribution can be considered for a section, real or virtual, with a unilateral and rigid-plastic material as described before.

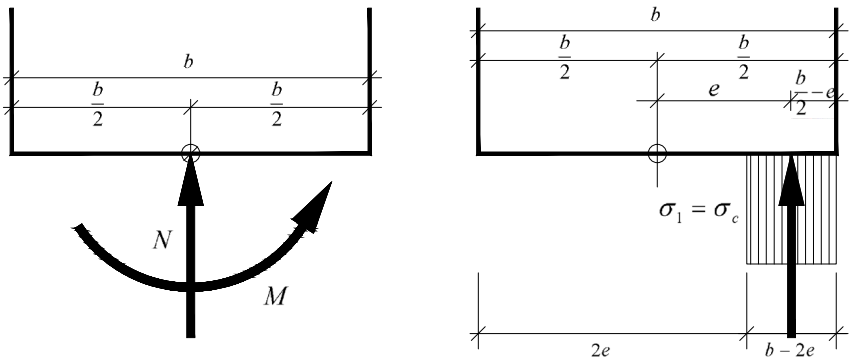


Figure 2: Generalized stresses and stresses in a contact surface of a masonry-like structure**.**

It is possible to define a limit surface or yield surface using the variables of axial force N and moment M, as can be observed in figure 3. The stresses represented into the limit surface

of figure 3 are safe points. In the states represented in the strict limit, the collapse is about to begin. Every stress state outside the yield surface has not physical meaning or, in other words, they are not possible. It is important to note that this limit surface must to be convex so that Limit Analysis can be applied. Further, the elemental deformations produced when the variables reach one point of the limit surface or "plastic multipliers" must be perpendicular to the limit surface in that point.

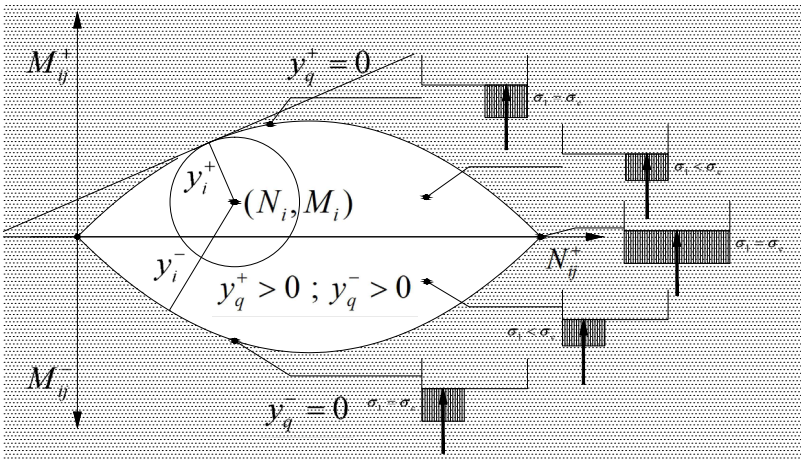


Figure 3: Yield surface M-N of a masonry-like structure.

The effect of the tangential stress V can be incorporated by means of the corresponding yield strength surface N. If this effect produces sliding the Standard Limit Analysis could not be applied. For this reason, as it has been explained before, it is supposed enough friction to impede that the sliding occurs.

The terminology used in this work has been defined below. B^t corresponds to the equilibrium matrix, s is the vector of internal force, g is the vector of permanent loads, λ correspond to the load factor, q is the vector of variable loads, y is the vector of "slack referred to limit stress" and L^t is yield matrix that consist of a matrix of suitable coefficients that relates internal forces to those mentioned slacks. The vector y must to be positive, and from a geometric point of view, corresponds to the distance from one stress point to the limit surface.

The method proposed in this article is based on a static formulation in which every valid solution must be according to Eq. (1).

$$\text{s.a.}\quad \left.\begin{array}{rcl} \mathbf{B^t s} & = & \mathbf{g}+\lambda\mathbf{q} \\ \mathbf{-L^t s} & = & \mathbf{y} \\ \mathbf{y} & \geq & \mathbf{0} \end{array}\right\} \equiv \mathbf{y}\in\{\mathrm{E}_y\} \tag{1}$$

The Standard Limit Analysis can be applied in the cases in which the material is valid according to the previous conditions and the sliding do not conditionate the collapse mode. In these cases, the typical approach to obtain a solution of the problem that shows the collapse mode consists of the calculation of the maximum value of the load factor applicable to live loads, for which the collapse begins Eq.(2) or Eq. (3), and considering that any value of load factor lower than this value is a safe solution. The lower the load factor, the greater the safety. In this way, the maximum load factor does the work of global safety factor over the variable loads. The cases with λ_{max}=0 show the structure is about to collapse with only permanent loads. The cases with λ_{max}=1 show that the structure is about to collapse with concomitant permanent and variable loads without safety coefficients. On the other hand, the cases with λ_{max}>1 show that the structure is able to resist with an increase of variable load before collapse occurs.

$$\max \lambda \quad \text{s.a.} \left\{ \mathbf{B}^t\mathbf{s} = \mathbf{f} = \mathbf{g} + \lambda\mathbf{q} \; ; \; -\mathbf{L}^t\mathbf{s} = \mathbf{y} \; ; \; \mathbf{y} \geq \mathbf{0} \right\} \tag{2}$$

$$\max \lambda \text{ s.a. } \mathbf{y} \in \left\{ \mathrm{E}_y \right\} \tag{3}$$

The second and third constraints of Eq. (2) define a convex polyhedron, and in most closed cases, which are called the yield surface. It is obvious that in problems that include stability there is both an upper and a lower bound for λ, and therefore the methods specifically limited in the obtainment of a λ_{max} are not suitable.

3 THE PROPOSED METHOD

The most advanced method to evaluate the safety of a masonry structure consist of the development of a simulation, for example using Monte Carlo type, with aleatory values of loads, the data of the initial geometry considering the possibility of its variation, and mechanical characteristics. This method is an alternative to use the partial safety factors and corresponds to the probabilistic methods of level III. This possibility is very attractive from a theoretical point of view. However, its real application is difficult due to the lack of data. This is one of the reason why the Limit Analysis is used. In already published works [13] is exposed that would be needed to obtain the distribution of the frequencies of the involved parameters, as loads, resistances, etc. Even in the case to obtain them, it would be necessary to determine the number of replicates per assay to obtain the necessary confidence level.

This article is focused on the evaluation methods with level I of safety. They are deterministic methods in which the results are modified by a safety margin, and sometimes they are developed by means of partial safety coefficients.

The concepts are described below in an example in order to clarify the exposition. The own limitations of the example are obvious, but the clarification and the graphical representation are important advantage. On the contrary, the accuracy is lower.

3.1 Case-Study

This case-study consists of the example of a simple beam of a rigid-plastic material laid on a rigid block, as is show in figure 4. There are one permanent force F_1 and one variable force F_2 applied in both extremes. In this case, the beam is able to resist an ultimate bending moment M_u, that depends on the material. The permanent force is similar to dead loads g and the variable one is similar to live loads q, conditioned by a load factor λ. The geometric dimensions and the location of the forces as can be observed in figure 4.

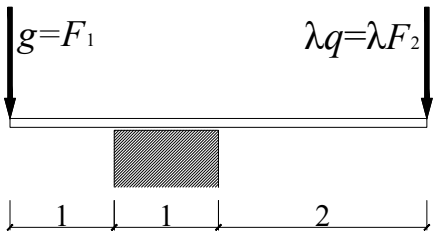


Figure 4: The example of the case-study.

The static variables of this example are de loads g, λq, and the constraints are defined according to the stability limit cases (Eq. 4, 5) and the resistance restrictions (Eq. 6, 7).

These constraints can be graphically represented by the lines that represent the static variables g, λq, as figures 5 shows, limiting two half-spaces: one in white defines the area where constraints are valid, and other one coloured in grey that defines the area where the constraints are unacceptable.

The intersection of all these half-spaces defines a n-dimensional convex polyhedron, in the example a polygon.

$$F_1 \geq \lambda F_2 \tag{4}$$
$$F_1 \leq 3\lambda F_2 \tag{5}$$
$$M_u \geq F_1 \tag{6}$$
$$\frac{M_u}{2} \geq \lambda F_2 \tag{7}$$

Inside this polyhedron which, if it is closed is called a polytope, are all solutions that meet all restrictions, in the example it is the white polygon. In the envelope of the polyhedron are the solutions for which some limit constraints have been reached and, in the case of the example, the collapse is about to begin. Outside, in the gray zone, there are no possible solutions from the physical point of view.

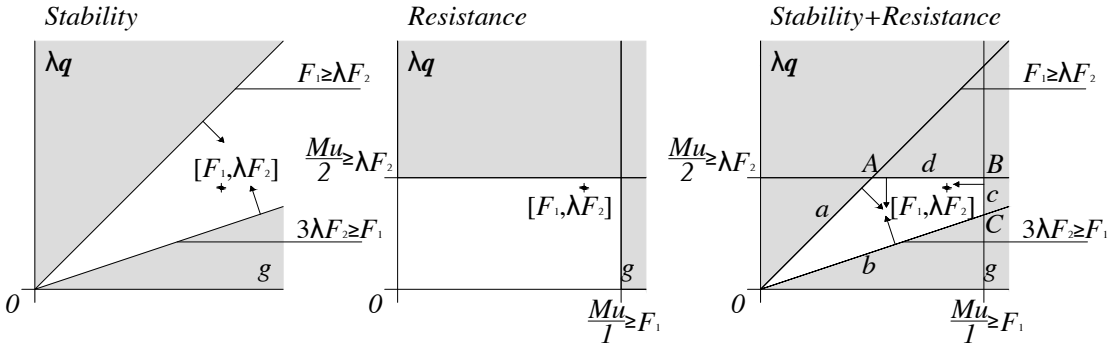


Figure 5: Yield surfaces λq-g of case-study.

3.2 Range of stability

Figure 5 shows that the non-stable solutions coloured in grey can occur both increase and decrease of load factors. The simplest way to obtain both higher and lower limits consists of achieving them according to Eq. 8, 9 and define margin between them (λ_{min}, λ_{max}), thus obtaining the stability range of the system loads.

$$\lambda_{\max} = \max \lambda \quad \text{s.a.} \left\{ \mathbf{B}^t\mathbf{s} = \mathbf{f} = \mathbf{g} + \boldsymbol{\lambda}\mathbf{q} \; ; \; -\mathbf{L}^t\mathbf{s} = \mathbf{y} \; ; \; \mathbf{y} \geq \mathbf{0} \right\} \tag{8}$$

$$\lambda_{\min} = \min \lambda \quad \text{s.a.} \left\{ \mathbf{B}^t\mathbf{s} = \mathbf{f} = \mathbf{g} + \boldsymbol{\lambda}\mathbf{q} \; ; \; -\mathbf{L}^t\mathbf{s} = \mathbf{y} \; ; \; \mathbf{y} \geq \mathbf{0} \right\} \tag{9}$$

This process has been fully developed [12, 14], and it can be graphically represented, as shows figure 6. The straight segment (F_1, $\lambda_{min}F_2$), (F_1, $\lambda_{max}F_2$) builds a polytope with lesser dimensions in this case 1 and inside it, there are all admissible static solutions, where F_1 does not vary.

Any value of load factor into the stability range is a safe solution. The higher distance from the point to the both limits, the greater the safety. In this way it is possible to define a safety coefficient γ for a load factor according to the distance from the point to distances to the average value of the extreme values (Eq. 10).

$$\gamma = \arg\max \left\{ \frac{\lambda_{\max} - \lambda_{\text{med}}}{\lambda - \lambda_{\text{med}}}, \frac{\lambda_{\text{med}} - \lambda_{\min}}{\lambda_{\text{med}} - \lambda} \right\} \tag{10}$$

This method supposes an advance of current knowledge. Although some of the possibilities has been proven before [14], it turns unsafe in cases where the point is near to the yield surface in the direction of another variable than λ.

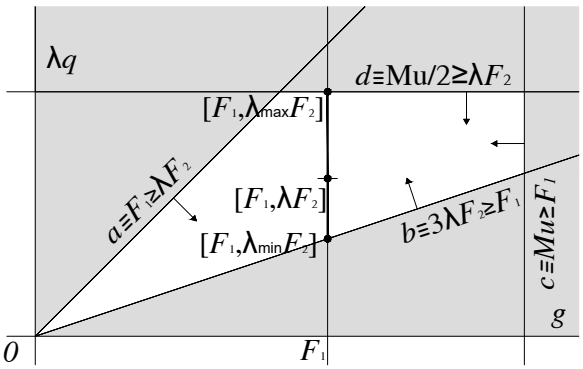


Figure 6: Stability interval.

3.3 Contraction in a fixed value of the yield surface

It is important to have standardized analysis methods. In this way, the safety range of linear structures has been traditionally evaluated using the Geometric Safety Coefficient (GSC) where the evaluation is limited to the stability. This GSC can be interpreted as the possible verification to draw a pressure line between the lines of the own geometry of the contracted structure (figure 7).

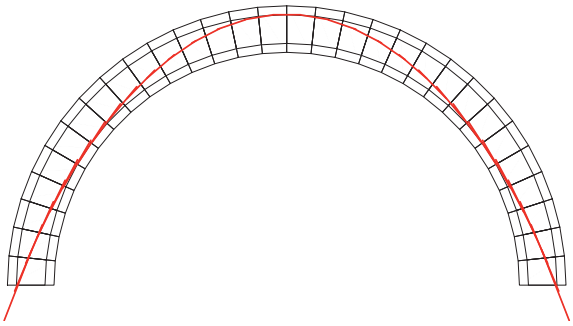


Figure 7: Geometric representation of the Geometric Safety Coefficient.

It is not possible to solve that problem directly with a Linear Program, but it is also possible to solve it iteratively with this tool. It can be achieved increasing and/or reducing the GSC in a process that finishes when the structure remain stable at maximum GSC. In those cases, the resistance is usually checked in the last step.

This article is focused on alternative methods, more general and applicable to any type of structure. Then, from now on this work is oriented to methods about the contraction of the yield surface. In other words, methods based on the distances from a safe stress state point to the yield surface. These types of problems can be solved in the cases of convex envelopes as Convex Optimization problems, and the simplest cases as the case-study with polyhedral envelop can be solved with Linear Programming.

General methods to solve these type of problems have been already described, for example by Boyd et al. [15]. In that work the vector y as the components of the geometric distances from the point of the reference stress to the yield limits is defined, as can be observed in the left of figure 8. This work takes advantage of this vector.

For all these reasons, one alternative easily implementable consists of the calculation of the minimum of the distances that forms a stress point to the nearly point of the yield surface. This calculation can be achieved with a new condition $h \leq y_i$ and solving *max* h and *min* y_i= max h. Eq.(11).

$$\min y_i = \max h \quad \text{s.a.} \quad \left\{ \lambda = \lambda_1; 0 \leq h \leq y_i; \mathbf{B}^t\mathbf{s} = \mathbf{g} + \lambda\mathbf{q} \; ; \; -\mathbf{L}^t\mathbf{s} = \mathbf{y} \; ; \; \mathbf{y} \geq \mathbf{0} \right\} \tag{11}$$

The set of points which $y_i \geq h$ defines a contracted yield surface, as can be observed in the right of figure 8. This envelope is defined by the restriction $y_i = h$.

Every point inside this envelope represents a stress state that is separated at least at a distance h from the nearly limit.

In this way, the method proposed in this work allows with only one Linear Programming problem to guarantee that almost one stress point that corresponds to the load factor $\lambda = \lambda_1$ is separated one distance with respect to the nearly yield surface. Also, this method allows to know which limit constraint is the nearest. The inconvenient of this method is that it does not specify the distance. Thereby, it is not shown if the distance is small or large with respect to the size of the yield surface.

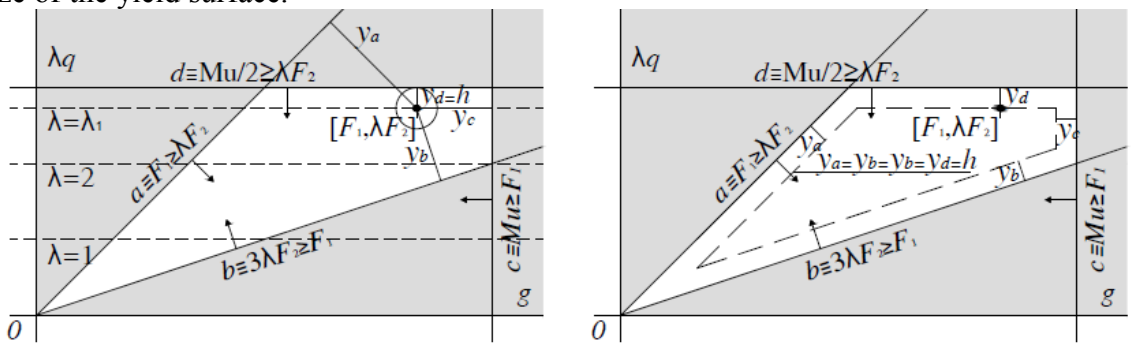


Figure 8: Parallel contraction of the yield surface.

3.4 Homothetic contraction of the yield surface

A most ambitious proposal is based on the implementation of the work of Cervera [16] and it consists of contracting homothetically the yield surface, with the homothetic centre in an interior point that is hypothetically the safest. This proposal is not yet implemented for masonry structures but the idea is very similar with the partial safety factors method, as is described by Ditlevsen [17].

In the left image of figure 9 shows a contracted limit of the yield surface as has already shown[17]. This yield surface, or limit state surface according to Ditlevsen, delimits all the inside points "enough safe" according to the partial safety factors previously established. The main difficulty to apply this methods in masonry structures consists of the ubication of the origin to which to refer the partial safety factors.

In the left image of figure 9 only the resistance restrictions are represented. In this case, the safest static solution is the near to the origin (0,0). Nevertheless, in the right image of figure 9 shows that the safest point (the further of the yield surface) is far from the origin. Generally this occurs including resistance and stability restrictions.

The mode of how to obtain the reference point and how to evaluate the safety of a structure is discussed below.

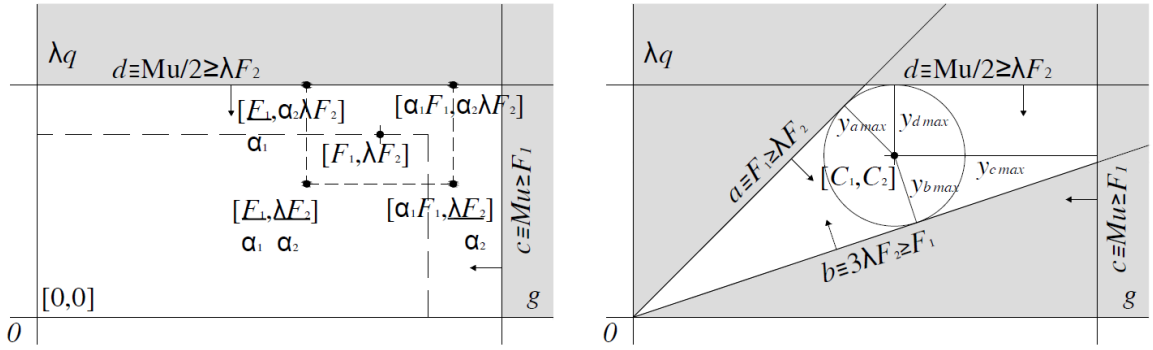


Figure 9: Partial safety factor and point farthest from the yield surface.

3.5 Deterministic partial safety factors

The Chebyshev centre is the inner point that is as far away as possible from a convex envelope, Boyd [15]. It is also the centre of the largest hypersphere, or n-dimensional sphere, contained within this envelope (right image of figure 9) and for that reason it also receives the name of "ball centre". When this envelope is a polyhedron, as in this case, or it can become one by linearization, the problem can be solved by Linear Programming, Eq.(12), very similar to that of Eq.(11). This process consists of the obtainment of the maximum value of h. In this case this value matches with the radio of the maximum hypersphere that can be included into the polyhedron.

$$\max h \;\text{ s.a. } \left\{0 \le h \le y_i;\; -\mathbf{L}^t\mathbf{s} = \mathbf{y}\;;\; \mathbf{y} \ge \mathbf{0}\right\} \tag{12}$$

The solution of the Linear Program will gived both the value of h and the different y_{imax}, these y_{imax} are the maximum distances from the centre that has been used as the origin to the corresponding restrictions. Being this the furthest point from the yield surface and, therefore, the safest.

If the centre of the safe area is known, the maximum distances can be directly obtained replacing the values of the vector s corresponding to the centre of the equation of the vector y. This occurs for example when the yield surface is symmetric with respect to two perpendicular axis. In the same way, it could be obtained for other point referring it as "the most safe point".

According to the left image of figure 9, it can be observed that the safety margins are proportional to some coefficients and to the distance to the origin and, in this case, to the safest point.

This problem can be solved by Linear Program. If a deterministic partial safety factor γ_i is used, that corresponds to a constraint i as the relation between the distance from the centre to the i constraint and the different between this relation with the distance from the selected point to the yield surface. It can be observed in the left of figure 10 and it is represented in equation 13, adding a new variable α_i, according to equation 14. The equation 15 defines the resulting Linear Program.

$$\gamma_i = \frac{y_{i\max}}{y_{i\max} - y_i} \tag{13}$$

$$\alpha_i = \frac{y_i}{y_{i\max}} \;;\; 0 \le \alpha_i \le 1 \tag{14}$$

$$\max h \;\text{ s.a. } \left\{\mathbf{B}^t\mathbf{s} = \mathbf{g} + \lambda\mathbf{q}\;;\; -\mathbf{L}^t\mathbf{s} = \mathbf{y}\;;\; \mathbf{y} \ge \mathbf{0}\;;\; 0 \le h \le \alpha_i\;;\; 0 \le \alpha_i \le 1\right\} \tag{15}$$

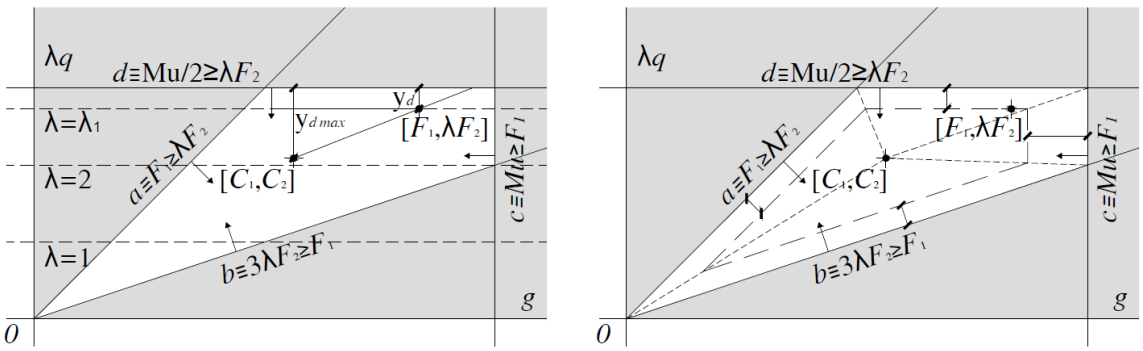


Figure 10: Homothetic contraction of the yield surface.

When the Linear Program is solved the value of h is obtained, along with α_i and together the rest of involved variables. Therefore, the values of γ_i that correspond to each constraint i,

as the global minimum of the deterministic partial safety factor $\gamma_{i\min}$ can be deduced through the equation 16.

$$\gamma_i = \frac{1}{1-\alpha_i} \; ; \; \gamma_{i\min} = \frac{1}{1-h} \tag{16}$$

It is possible to apply a different focus of the same problem. The geometric place of the points with the same γ_{min} coefficient is a homothetic surface with the yield surface, and with the centre of the homothecy, according to Chebyshew, that is represented on the right image of figure 10. It can be applied too in other point considering it as the safest point. It can be established a specific value to the γ_{min} coefficient, in this way a value of h is obtained and hence the separation between the yield surface with the constrained of yield surface. With this "enough safety" surface similar operations could be performed as if it were the original one.

4 DISCUSSION

In order to guarantee that the structure "can find" the solution with higher safety coefficient it is an indispensable requirement that the principles of Standard Limit Analysis are applicable. Thus, if the beginning of the collapse is influenced by sliding, this principles are not applicable.

The implementation of the methods proposed in this work for a yield surface as presented in figure 3 has been carried out. However, its exposition exceeds the objectives of this article.

The work presented in this paper has been focused in the comparison between the maximum safety that can be obtained for a structure for each restriction with the safety referred to in the mentioned case-study. However, this study paradoxically shows that the partial safety factor referred to the rocking constraint decreases when the compressive strength of the material increases. This occurs with the masonry structures typical yield surface.

This work also shows that it is possible to select other points as the centre of the homothecy, or even consider other different coefficients if the case requires it. Both processes have been developed in this article, although in this last case the "enough safety surface" is not a homothetic of the yield surface.

5 CONCLUSIONS

The Limit Analysis by means of Linear Programming consists of the calculation of the maximum of the load factor that increases the live loads to produce the collapse of a structure. In some cases, it is unsafe to evaluate the safety of the masonry structures applying this analysis. When the external variables loads, or any of them, produces a stabilizing phenomenon, a decrease of these loads can produce the collapse of the structure. This is the main conclusion that can be highlighted from this work, because it also affects to other methods that approach the estimation of the safety of masonry structures.

The partial safety coefficients, and specially the lower value of them obtained by the descripted method, guarantee that for a given system of loads (both fixed and variables) there is a solution corresponding.

The method presented in this article underestimates the safety factor in the cases of masonry structures with high compressive strength and in cases in which the collapse mode is the rocking. In spite of the method remains safe, it would be necessary to continue the research for these cases and other similar ones. It could be interesting to expand research about the points that should be considered as the "safest points" and how to estimate the values of the safe coefficients referred to the different collapse modes that can occur in masonry structures.

REFERENCES

[1] A. Kooharian, "Limit Analysis of Voussoir (segmental) and Concrete Arches", *Proceedings of the American Concrete Institute,* 49 (12): 317-328, (1953)

[2] Drucker, D.C. (1953). Coulomb friction, plasticity and limit loads. *Transations of American Society of MechanicalEngineers. 76, 71-74.*

[3] A.Orduña, P.B. Lourenço, "Limit analysis as a tool for the simplified assessment of ancient masonry structures", *Historical Constructions*, 511-520. Guimarães: University of Minho(2001)

[4] Charnes, A., Greenberg, H.J. (1951). Plastic collapse and linear programming.*Bull. Amer. Math. Soo.. 57, 480.*

[5] Dorn, W. S. (1955). *On the Plastic Collapse of Structures and Linear Programming.* Dissertations. Carnegie MellonUniversity. Paper 85.

[6] Charnes, A., Lemke, C. E., Zienkiewiz, O. C. (1959). Virtual Work, Linear Programming and Plastic Limit Analysis. *Proceedings of the Royal Society of London. Series A, Mathematical and Physical Sciences. Vol. 251, No. 1264, 110-116.*

[7] Anderheggen, E., Knopfel, H. (1972). Finite element limit analysis using linear programming. *Int. J. Solids Structures. 8, 1413-1431.*

[8] Livesley, R.K. (1978). Limit analysis of structures formed from rigid blocks. *Int. Journal for Numerical Methods in Engineering. 12, 1853-1871.*

[9] Gilbert, M., Melbourne, C. (1994). Rigid block analysis of masonry structures. *The Structural Engineer. 72, 356-361.*

[10] Heyman, J. (1966) The stone skeleton. International Journal of Solids and Structures, 2, 249-279

[11] Delbecq, Jean-Michel (1982). Les ponts en maçonnerie. Evaluation de la stabilité. SETRA Ministère des transports.

[12] Magdalena, F. (2013) El problema del rozamiento en el análisis de estructuras de fábrica mediante modelos de sólidos rígidos. Tesis de Doctorado. Universidad Politécnica de Madrid.

[13] Magdalena, F.; García, J.; Hernando, J.I.; Magdalena, E. (2017). Safety assessment of masonry structures using ordinal optimization. Proceedings of the 4th WTA International PhD Symposium. Ed. WTA Nederland.

[14] Magdalena,;Aznar, A.; Hernando, J.I.; F.; García, J.(2014). Linear programming as a tool to study the stability of masonry arch bridges Report 37th IABSE Symposium Madrid 2014. International Association for Bridge and Structural Engineering

[15] S.Boyd, L.Vanderberghe, *Convex Optimization*. Cambridge University Press. (2004)

[16] Cervera, J. (2010). Un criterio robusto para la medida del margen -coeficiente- de seguridad. *Informes de la Construcción. Vol.62, 518, 33-42.*

[17] O. Ditlevsen, H.O. Madsen, *Structural Reliability Methods*, Internet edition 2.3.7*,http://od-website.dk/books/OD-HOM-StrucRelMeth-Ed2.3.7.pdf,* (2007)

12th International Conference on Structural Analysis of Historical Constructions
SAHC 2020
P. Roca, L. Pelà and C. Molins (Eds.)

SEISMIC ASSESSMENT OF MASONRY TOWERS: THE CASE OF CASTELLUM AQUAE SYSTEM IN POMPEII

M. SALVALAGGIO[1], V. SABBATINI[2], F. LORENZONI[3]*, M.R. VALLUZZI[1] AND H. WENLIUHAN[4]

[1] Department of Cultural Heritage (DBC)
Università degli Studi di Padova
Piazza Capitaniato 7, 35139 Padova, Italy
e-mail: matteo.salvalaggio@unipd.it, mariarosa.valluzzi@unipd.it

[2] Department of Architecture
Università degli Studi Roma Tre
Largo Giovanni Battista Marzi 10, 00153 Roma, Italy
e-mail: valerio.sabbatini@uniroma3.it

[3] Department of Geoscience
Università degli Studi di Padova
via Gradenigo 6, 35131 Padova, Italy
e-mail: filippo.lorenzoni@unipd.it

[4] Earthquake Engineering Research & Test Center
Guangzhou University
Guang Yuan Zhong Rd. 248, 510405 Guangzhou, China
e-mail: wlh-gd@gzhu.edu.cn

Keywords: historical masonry, towers, Pompeii, finite element modeling

Abstract. *The archaeological site of Pompeii is an extraordinary evidence of Roman architectural heritage which comprehends a large number of masonry constructions, buried after the Vesuvius eruption in 79 AD. They were discovered in the XVIII century when renewed cultural interest induced numerous archaeological excavations. In this scenario, the remains of the Roman aqueduct system, i.e. Castellum Aquae system [1], includes a series of approximately 6 m height masonry water towers (WTs). Among the fourteen surveyed, four free-standing towers (i.e. no. 1, 2, 3 and 4) have been investigated in 2015 by means of non-destructive techniques (sonic pulse velocity tests, ground penetrating radar (GPR), ambient vibration tests), aimed at gathering information on the constructive systems and the current conservation state, as well as data on the overall dynamic behaviour. According to the on-site inspections outcomes, 3D finite element models of the towers were constructed and calibrated on the results of operational modal analysis (OMA) [2]. The model updating procedure was able to describe and simulate the soil-structure interaction, introducing a Winkler elastic soil model, and to define the elastic parameters of masonry.*

This paper describes the seismic vulnerability assessment of the four WTs, considering both

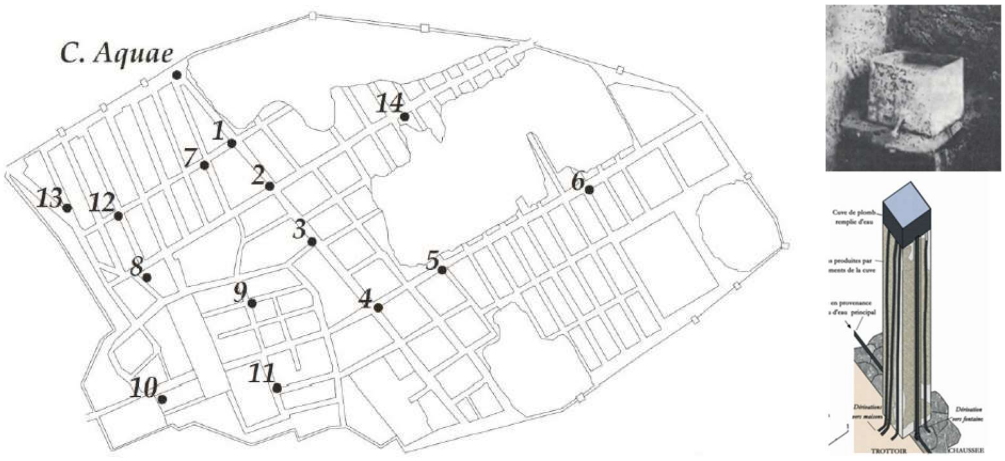
equilibrium capacity and material strength, performing analytical kinematic analyses and numerical finite element modelling.

Aiming at improving the previous studies [3], equivalent modal parameters (i.e. natural frequencies and mode shapes) are used to calibrate analytical models and furtherly refine FE model updating. The numerical models were generated using DIANA software [4], implementing a nonlinear constitutive law for masonry material, i.e. total strain crack model. Afterwards, sensitivity analyses are performed to calibrate both the elastic properties of materials and the Winkler springs' stiffness. Eventually, analytical kinematic approach and FE pushover analyses (with uniform and modal force distribution) are executed to assess the seismic vulnerability of the WTs, according to Italian code [5].

Results of the analyses are presented and discussed. The study was the occasion to compare the results of kinematic and numerical procedures applied to archaeological structures. The results report the FE approach as more conservative than kinematic model. Thus, the importance to adopt a combined global (numerical) and local (limit analysis) approach in the assessment of archaeological structures is stressed.

1 INTRODUCTION

During the archaeological excavation of Pompeii brick and stone masonry water towers, part of the ancient aqueduct system, were discovered. Water towers are located throughout the city and have different heights with the scope of providing water to the whole city. *Castellum Aquae*, i.e. the main water tank, was built at the highest point of the city, closed to Porta Vesuvio, and it controlled the water flow to three pipelines [6]. The hydraulic system comprehended fourteen water towers (as shown in Figure 1) that distributed water and optimized the water pressure reduction [7]. Water towers no. 1, 2, 3 and 4 are free standing while the remaining ten towers are connected to other buildings. Water towers no. 1, 9, 12, 13 and 14 were built around 20-10 BC, before the reconstruction caused by the earthquake of AD 63. Some towers were left uncompleted because of the sudden Vesuvius's eruption of 79 AD that completely buried the city.



a) b)

Figure 1: a) Water towers layout in the Pompeii site[7]; b) original layout of the water tower with the container at the top [7]

According to the archaeological studies, water containers were once placed on top of the WTs to store water [8]. The researches hypothesized that the containers had been part of the water distribution system in the city and used to operate in their time. Olsson [9] advocates the concept of an ancient urban water distribution system and proposed a plausible condition of the original Containers; they are made of lead, the base dimensions are slightly smaller than the those of the water towers, and the height is approximately 1 m.

2 SURVEY AND ON-SITE INSPECTIONS

The water towers are at least 6 m tall with quadrangular base sections of about 1.2 m wide. Part of the masonry volume was removed to place the pipes that carried water from the top lead container to the surrounding buildings. Water tower no. 1 (later called WT1) was built with Nocera tuff masonry; water tower no. 2 (WT2) and no. 3 (WT3) are made of clay bricks with a discontinuity of material in tower no. 2 at 4.3 m from the ground, water tower no. 4 (WT4) is composed of three layers of Sarno limestone from the ground level to 1.6 m in height, Nocera tuff from 1.6 m to 4 m and yellow tuff up to the top. The geometric survey is reported in Figure 3.

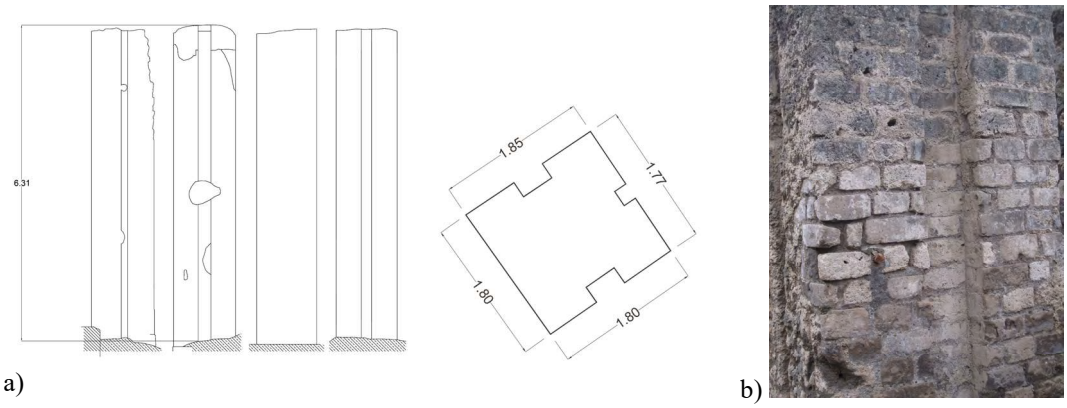


Figure 2. a) Geometric survey of WT1 [7]; b) masonry detail of WT1.

Visual inspections and on-site non-destructive tests were performed by the authors on the four water towers in June 2015. Sonic tomographic tests and ground penetrating radar (GPR) were executed to investigate masonry sections and identify the presence of inner cores and voids/discontinuities. Moreover, dynamic identification tests were carried to characterize the dynamic behaviour of the four towers [2]. Ambient vibrations tests (AVT) and output-only identification techniques were used to extract modal parameters in terms of natural frequencies, damping ratios and mode shapes. Tests were carried out through the recording of three different acceleration time-histories in 6 points for each tower, according to the analysis and interpretation of the expected mode shapes.

The results of dynamic testing and modal analysis are presented in the following table. The dynamic behavior of the four WTs can be related to an inverted pendulum with the first 2 bending modes along the principal horizontal directions (frequencies between 2.6 Hz and 3.1 Hz), 1 torsional mode (frequency between 11Hz and 17 Hz) and 2 second order bending modes (frequency between 14 Hz and 17 Hz).

Table 1. Natural frequencies of the four WTs identified through AVTs

	WT1	WT2	WT3	WT4
Mode no.	f [Hz]	f [Hz]	f [Hz]	f [Hz]
1	2.979	2.783	2.686	3.076
2	3.174	3.125	3.320	3.125
3	16.89	10.94	12.23	14.01
4	17.09	14.4	15.48	15.04
5	17.33	15.48	16.31	15.19

3 KINEMATIC ANALYSIS

The seismic vulnerability assessment of the four water towers was preliminary assessed through the limit analysis method, according to kinematic approach suggested by the Italian Code [5]. Towers were modelled as monolithic rigid blocks, able to rotate on a plastic hinge at the base. The rotation pole translation due to base compressive stresses was calculated, whereas no tensile strength was considered for masonry.

Different collapse mechanisms were studied considering both global overturning (for WT1, WT2, WT3 and WT4) and local overturning (for WT2 and WT4), as shown in Figure 3, due to different construction phases, as detected by [6].

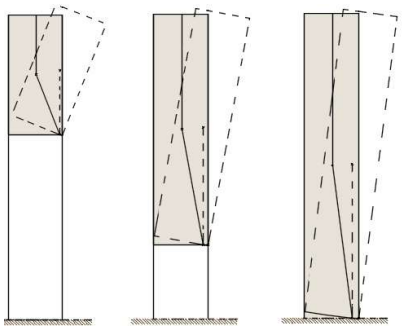


Figure 3. Analyzed collapse mechanisms for WT4

Table 2. Mechanical properties of masonry for the four WTs

			Tuff	Solid Brick	Calculation factors	
Mass density	ρ	[kN/m^3]	16	18	Confidence factor	1.35
Compressive strength	f_m	[N/mm^2]	1.4÷2.4	2.4÷4.0	Material safety coefficient γ_m	2
					Behaviour factor q	2

The mechanical characteristics of materials have been obtained from the Italian code, which provides a range of values for various masonry typologies. Since the inspections phase was performed only through non-destructive testing technique a limited knowledge level was achieved (KL1), corresponding to a confidence factor (CF=1.35) to be applied to the material

mechanical properties. In addition, a safety coefficient of 2 was applied as well as a behavior factor of 2 for the seismic vulnerability assessment (Table 3).

Geological inspections (MASW Multichannel Analysis of Surface Waves) were performed to characterize the soil type for seismic purposes, i.e. determination of the velocity profile for shear waves (Vs). According to the results a soil category C was assigned.

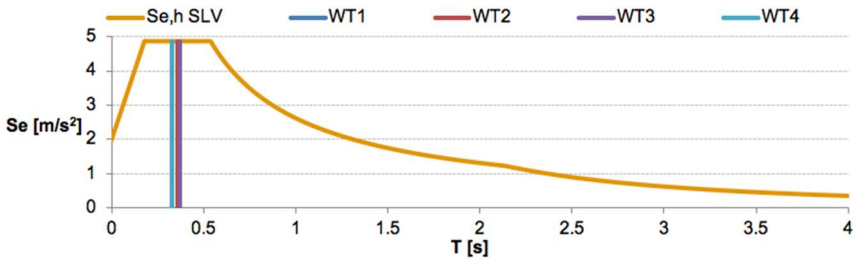


Figure 4 Life-safety limit state elastic response spectrum.

The seismic action used for the assessment of the WTs is defined by the seismic hazard parameters for the site of Pompeii (ag=0.133g for an earthquake return period of 474 years) and the related elastic response spectrum, defined at the Life Safety limit state (Figure 4). Is it possible to notice that the first two principal bending modes of the towers identified by AVTs have a period between 0.3s and 0.4s, which correspond to the maximum amplification in the response spectrum (horizontal branch of the diagram in Figure 4).

The seismic vulnerability of the WTs was determined in the current state and in the original state, with the presence of the water container at the top. This configuration was useful to investigate its role in the reduction of the seismic capacity of the structures. Water container was simulated adding a mass at the top of the tower, considering different level of the water inside, i.e. completely full, half and empty.

The capacity/demand ratio ζ_E was calculated for each configuration and the results are presented in the following histograms.

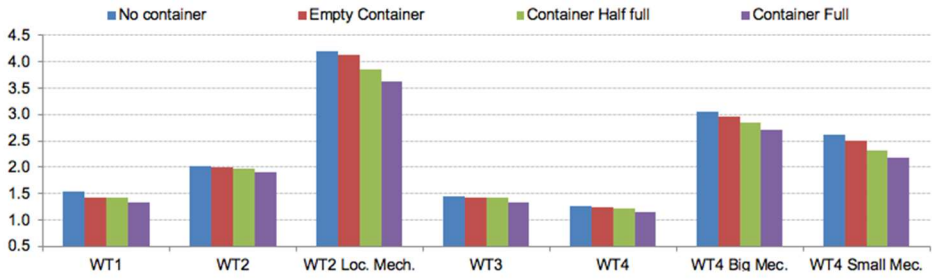


Figure 5. Capacity/demand ratio ζ_E for the four WTs considering different collapse mechanisms

It is clear that for each WT the global overturning with the formation of the hinge at the base is the most vulnerable collapse mechanism. WT4 among the others is the most vulnerable structure (ζ_E=1.27), while WT2 is the less vulnerable one (ζ_E=2). As expected, the presence of the water container at the top reduces the capacity of the structure of a percentage between 4.5%

and 11.3%.

The main parameters involved in the definition of the seismic vulnerability of the water towers were further investigated. Parametric analyses have been performed changing and assessing the following factors: (i) return period and PGA, (ii) behaviour factor q and (iii) soil category. Results are reported in the following graphs.

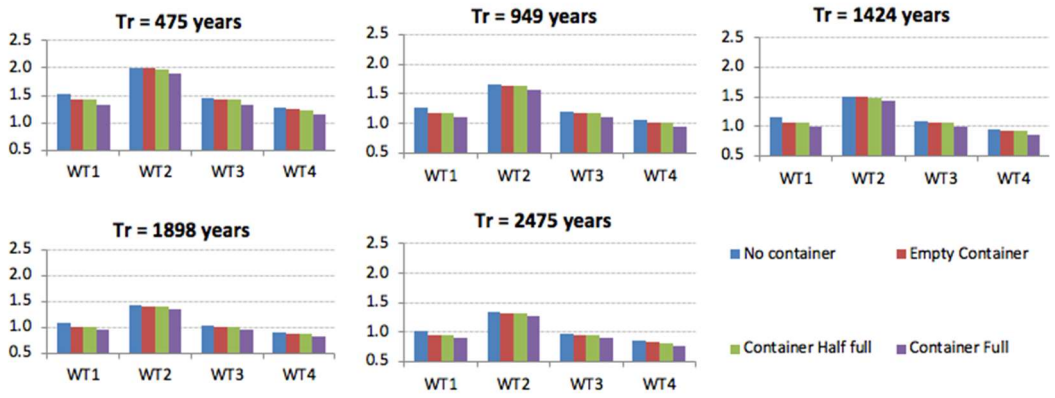


Figure 6. Capacity/demand ratio ζ_E for the four WTs varying the earthquake return period

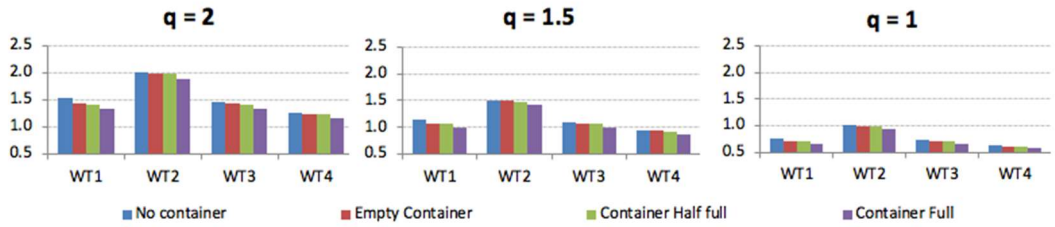


Figure 7. Capacity/demand ratio ζ_E for the four WTs varying the behaviour factor q

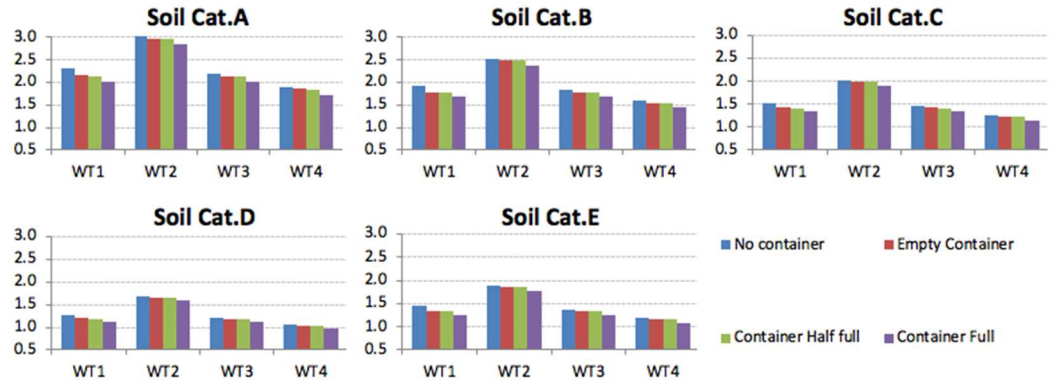


Figure 8. Capacity/demand ratio ζ_E for the four WTs varying the soil type

The study of the collapse mechanisms confirmed that the global overturning of the WTs is the most vulnerable collapse mechanism. The analyses highlighted a higher vulnerability of the WTs with the full water container at the top due to an increase of the overturning moment caused by an additional mass. The most vulnerable tower, according to limit analysis, is WT4,

while the less vulnerable is WT2, able to satisfy the seismic demand for a return period of 2475 years (PGA=0.2196), the highest suggested by Italian code.

4 FINITE ELEMENT ANALYSIS

Numerical analyses were carried out according to finite element approach, with the DIANA FEA 10.3 code [4]. The four towers have been discretized through 15 cm-size 8-noded (HX24L) and 6-noded (TP18L) linear brick elements, with a number of nodes varying from 3700 to 8300 among the towers models (Figure 9).

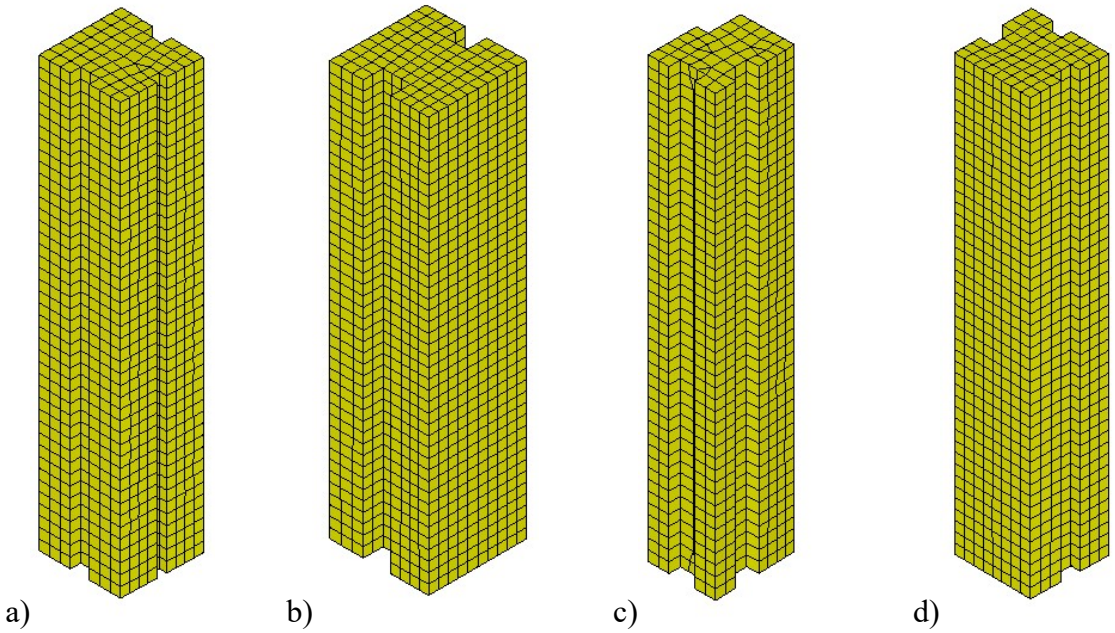


Figure 9. Finite element models of water towers a) 1, b) 2, c) 3, d) 4.

The structural behaviour of a 2000 years old tower is seriously affected by its conservation state, which has been investigated through the described NDT. Thus, on the basis of the work described in [2], the finite element model of water tower no. 1 has been furtherly updated, since the experimental dynamic data collected show a good match with the expected ones, revealing a good conservation status among the four structures. As noticed in [2], rigid constraints at the base are boundary conditions not compatible with an optimal model updating. Thus, according to Winkler model for soil, SP1TR spring elements along main three directions were applied at the base nodes in order to simulate the soil-structure interaction (Figure 10).

The values of modulus of subgrade reaction were based on the ones reported in [9]. The stiffness of the base springs is obtained as the product of modulus of subgrade reaction and influence area of each node. The simulation of soil-structure interaction was furtherly refined considering different influence areas according to the position of nodes in the base (inner section, edge, corner).

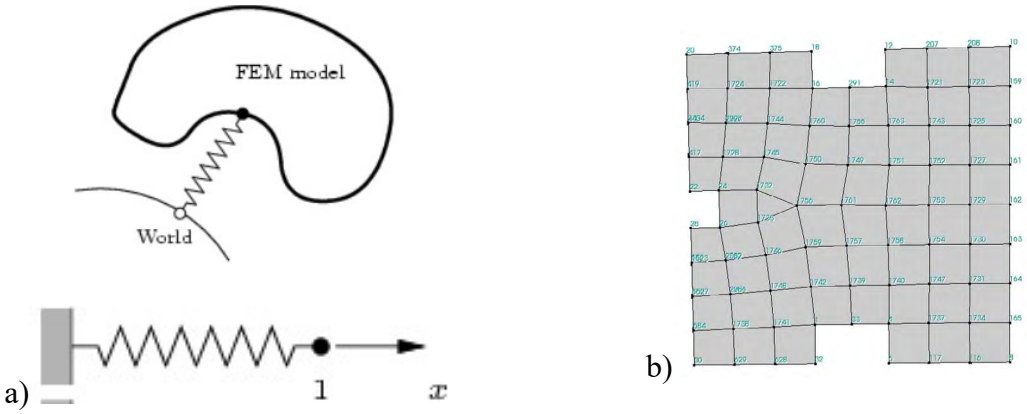


Figure 10. a) One-node SP1TR spring scheme [4]; b) layout of base springs.

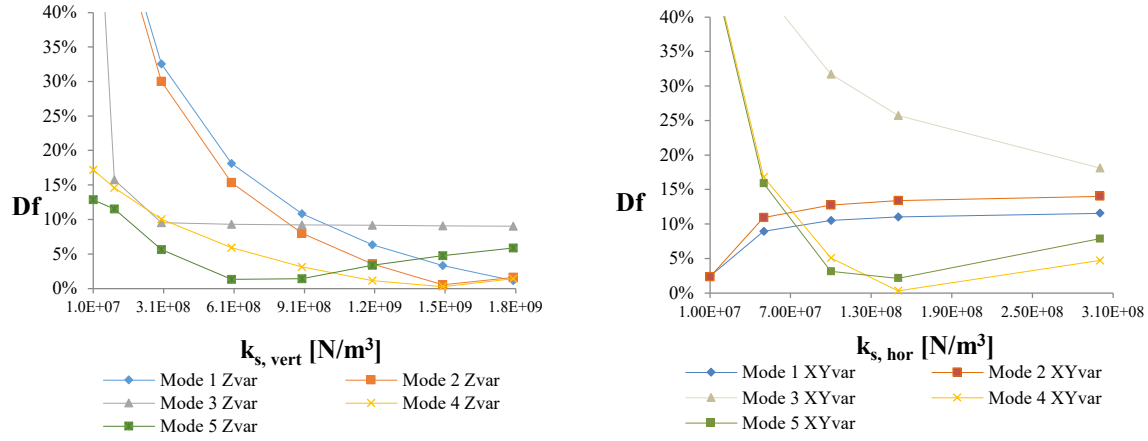
The numerical study was scheduled and performed as follows:

i) Based on the work reported in [4], a sensitivity analysis of the linear properties affecting mode shapes (i.e., mass density and elasticity modulus) have been performed on water tower no. 1, in order to define an updated numerical model;
ii) Once the linear properties of WT1 structural model have been calibrated, a sensitivity analysis aimed at studying the nonlinear properties (i.e. compressive strength, tensile strength, compressive fracture energy, tensile fracture energy) was carried out in terms of quasi-static pushover analysis with uniform load distribution;
iii) The so-defined model is subjected to pushover analyses according to [5], with uniform and modal seismic load distributions. The hypothesis of rigid foundation is also assessed and compared with the elastic foundation one.
iv) The results of the nonlinear calibration are extended to water towers no. 2, 3 and 4, which are analyzed with the same method. Seismic vulnerability assessment of the water towers is thus completed.

5.1 Sensitivity analysis of linear dynamic behavior

The modulus of subgrade reaction is a parameter which takes into account the soil characteristics and the geometry of the foundation system. Unfortunately, neither is available in this case, since geotechnical investigations were carried out only outside the archaeological site and the foundation systems have not been surveyed. Therefore, reference value of the modulus of subgrade reaction, deduced from the one reported in scientific literature [9], were implemented ($k_s = 5 \cdot 10^{10}$ N/m^3).

As reported by [10], stiffnesses along vertical (Z) and horizontal (X, Y) directions are not constant, especially for historical structures. Thus, sensitivity analysis were carried out, keeping fixed the vertical stiffness Z or the horizontal ones X and Y (at $5 \cdot 10^{10}$ N/m^3). Frequency discrepancy D_f percentages between experimental and numerical mode shapes, in function of vertical and horizontal springs stiffnesses, are reported in Figure 11.



a) b)

Figure 11. Frequency discrepancy in function of base springs a) vertical sitffness and b) horizontal stiffness

Based on the results of the sensitivity analysis, linear properties of the numerical models were selected as follows: mass density w = 16.7 kN/m^3, Young's modulus E = 1050 MPa, Poisson's ratio υ = 0.2, whereas modulus of subgrade reaction was fixed equal to $k_{s,vert}$ = 1.5•10^9 N/m^3 for vertical springs, whereas horizontal ones are fixed as one-fifth of them ($k_{s,hor}$ = 3•10^8 N/m^3).

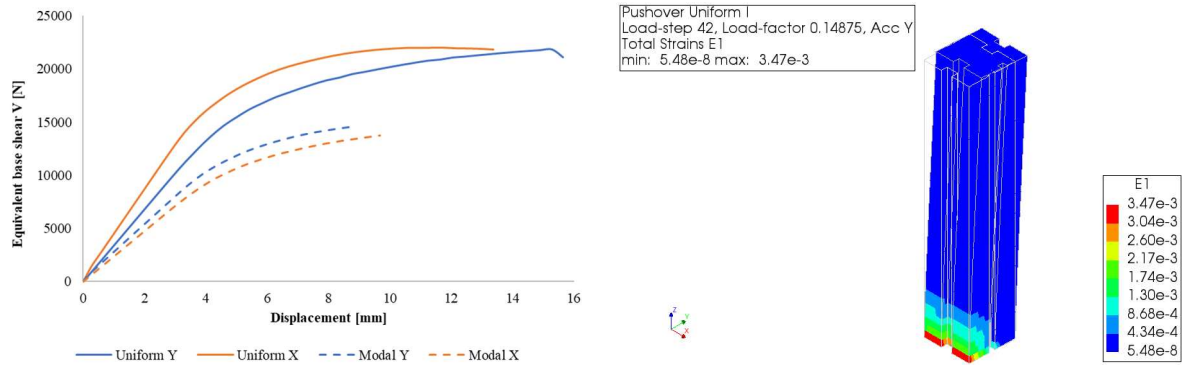
5.1 Pushover analysis

Seismic vulnerability assessment of the water towers is based on static nonlinear analysis (i.e. pushover analysis). Nonlinear constitutive laws were implemented to describe masonry behavior, i.e. the so-called total strain based crack model. A parabolic compressive law and an exponential softening tensile law are described by strength and fracture energy values. Reference value were taken from Italian codes [5] and scientific literature. Tensile strength is derived from Italian code shear strength through Turnsek-Cacovic law. The strength values are obtained after the application of safety coefficient γ=2 and a confidence factor FC=1.35 [5]. The model properties are reported in Table 3.

Table 3. Mechanical parameters of structural material

Element	E [Mpa]	ρ [KN/m^3]	ν	f_c [MPa]	G_{fc} [N/mm]	f_t [MPa]	G_{ft} [N/mm]
WT01	1050	17	0.2	0.52	0.05	0.015	0.01

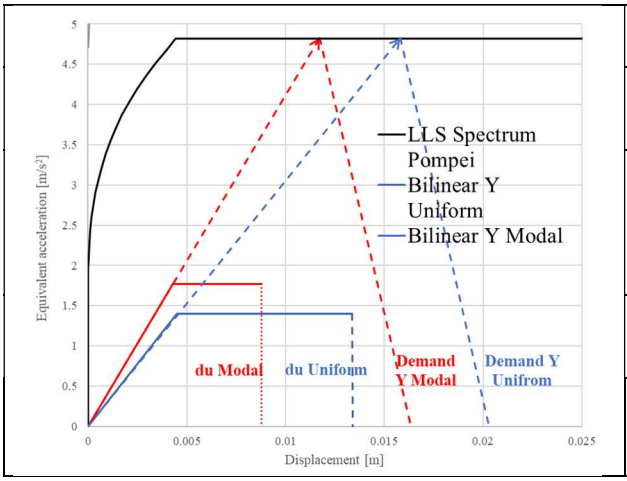
The results of the analyses are elaborated in terms of base shear-displacement capacity curves, reported in Figure 12a. The typical collapse configuration of water tower no. 1 is observable in Figure 12b.



a) b)

Figure 12. a) Capacity curves of water tower no. 1 for uniform and modal lateral loads; b) tensile strain diagram at ultimate load step of uniform Y pushover analysis

The seismic assessment of the water tower no. 1 is performed, according to [5], in terms of displacement capacity based on the ADSR spectrum. Uniform and modal lateral forces distributions, both X and Y directions, were adopted.
The safety verifications are reported in Figure 13.



Safety factor	
X Modal	X Uniform
57.02%	68.56%
Y Modal	Y Uniform
53.69%	65.82%

Figure 13. Safety verification procedure and safety factors.

6 CONCLUSIONS

The research presented within this paper aims at emphasizing the importance of a multidisciplinary approach to the structural and seismic vulnerability assessment of important archaeological structures in Pompeii (Italy). In-situ survey of geometry and crack pattern, historical evolution of the building and on-inspections represent the necessary preliminary steps, fundamental to define correctly all subsequent stages of the seismic evaluation. In particular the use of ambient vibration test and modal analysis was useful to update and calibrate numerical models, since simple estimations from typical values of the building materials (e.g. clay bricks, tuff, limestone, etc.) could lead to an overestimation of the global stiffness. Such a non-destructive test is highly desirable for heritage structures and monuments since it provides

fairly accurate results without having to impose any potential harm to their integrity.

The limit analysis method (macroelements approach) proved to be a reliable tool for the seismic assessment, requiring specific parameters (geometry, damage pattern, etc.), easily derivable from on-site inspections. The implementation of elastic numerical models can be useful to determine the dynamic properties of the structure and perform an initial assessment of the seismic capacity. The integration with more advanced analysis, implementing non-linear constitutive laws of materials, is still a key issue in the correct evaluation of masonry structures.

A brief comparison between the outcomes of kinematic analysis and pushover analysis for WT no. 1 makes clear that the latter one is generally more conservative than the former, as already noticed in [3]. Actually, the seismic verification is successfully passed according to kinematic overturning mechanism, while, according to FE, the displacement capacity of the tower is not enough for seismic demand.

The combined application of global (numerical models) and local (limit analysis) analyses of the response prove to be the correct way to define the most vulnerable structural elements and identify the main structural deficiencies of the water towers.

REFERENCES

[1] C. Ohlig (2001), De aquis Pompeiorum: das Castellum Aquae in Pompeii: Herlunft, Zuleitung und Verteilung des Wassers, Nimègue, 2001.

[2] F. Lorenzoni, M.R. Valluzzi, M. Salvalaggio, A. Minello, C. Modena (2017), Operational modal analysis for the characterization of ancient water towers in Pompeii, In Procedia Engineering, Volume 199, 2017, Pages 3374-3379, ISSN 1877-7058, https://doi.org/10.1016/j.proeng.2017.09.446

[3] A. Pappas, F. da Porto, C. Modena, H. Dessales, "Seismic vulnerability assessment of ancient water towers in Pompeii with kinematic, finite element and discrete element analysis". In: ANIDIS 2013 – L'Ingegneria Sismica in Italia, (2013)

[4] DIANA FEA, *DIANA 10.3 Finite Element Analysis User Guide*, TNO DIANA BV, Delft, 2019

[5] D. M. 17 gennaio 2018, Norme tecniche per le costruzioni, Ministero delle Infrastrutture e dei Trasporti, 2018 (in Italian)

[6] T. L. Heres, "The structures related to the water supply of Pompeii: materials and chronology," Mededelingen Van Het Nederlands Instituut Te Rome, vol. 51/52, pp. 42-61, 1992-1993.

[7] Dessales H. (2008), "D'eau et de pierre. Recherches des laboratoires d'archéologie et de géologie de l'Ecole normale supérieure sur le Réseau hydraulique de Pompéei et son bâti.," 2008.

[8] J. Carlut, H. Dessales, & J. de Sigoyer (2012). D'eau et de pierre: le reseau hydraluique de Pompei et son bati. Paris, France (in French)

[9] Bowles J. E., *Foundation analysis and design*, McGraw-Hill, USA, 1996, pp. 121-127, 501-509

[10] Elyamani A., *Integrated monitoring and structural analysis strategies for the study of large historical construction*. Application to Mallorca cathedral. PhD Thesis. Director. Roca P., Universitat Politecnica de Catlunya, 2015

12th International Conference on Structural Analysis of Historical Constructions
SAHC 2020
P. Roca, L. Pelà and C. Molins (Eds.)

SEISMIC BEHAVIOUR OF DIAPHRAGM ARCHES: CASE STUDIES FROM CATALAN GOTHIC CHURCHES

D. CACACE[1], V. CORLITO[1], M. ZIZI[1], G. DE MATTEIS[1*] AND P. ROCA[2]

[1] Department of Architecture and Industrial Design (DADI)
University of Campania "Luigi Vanvitelli"
San Lorenzo Abbey, 81030 Aversa, Italy
e-mails: {daniela.cacace, valentina.corlito, mattia.zizi}@unicampania.it
gianfranco.dematteis@unicampania.it (*corresponding author)

[2] Department of Civil and Environmental Engineering
Universitat Politècnica de Catalunya
(UPC - Barcelona Tech), 08034 Barcelona, Spain
e-mail: pere.roca.fabregat@upc.edu

Keywords: Masonry Churches, Catalan Gothic, Diaphragm Arches, Seismic Behaviour, Linear Kinematic Analysis

Abstract. *The Gothic style spread, starting from the 12th century, from the Ile-de-France to England and other countries of the Mediterranean area, such as Spain and Italy, according to different configurations and construction techniques, influenced by economic, environmental and social factors. The so-called Catalan Gothic style is not exclusive to the architecture of the Principality of Catalonia but extends to the territories of the Crown of Aragon and Southern France. Its most important characteristics, based on the unitary conception of space and horizontality, had the religious architecture as their major reference. Among other structural elements, the large use of diaphragm arches, built transversally to the longitudinal direction of the nave, has been identified as peculiar both in ecclesiastic and civil Catalan Gothic architecture, although this technique is widely diffused also in the rest of the Mediterranean Europe. The present study focuses on the behaviour of this construction system under horizontal loads. After some brief notes on the history, origins and evolution of diaphragm arches, preliminary outcomes obtained by means of seismic analyses are provided in this paper. In particular, the possible collapse mechanisms of such remarkable curved structures have been firstly investigated by implementing FEM Models derived from real Catalan examples. Therefore, seismic analyses by means of analytical models have been carried out on the detected cases in order to demonstrate the capacity of this kind of structural skeleton, the importance of geometric ratios and the influence that specific typical elements may have in modifying the seismic behaviour of the analysed structures.*

1 INTRODUCTION

During the first half of the 13th century, a form of Gothic architecture different from that typical of the northern France and characterized by its own distinctive characters (deeply influenced by the Romanesque style) appeared in the central-southern France [1], spreading

significantly in Mediterranean European countries.

The churches built according to the so-called *Minor* Gothic style were generally characterized by thicker proportions, with a large frequency of wide-span single naves, massive rib vaults and diaphragm arches [2].

Among other constructive features, the extensive use of diaphragm arches has been identified as peculiar not only in churches, but also in civil architecture [3, 4]. These structural elements, probably derived from the Romanesque construction techniques of northern Italy and related to the Cistercians constructive rules and experimentations [1], made their first appearance in western Europe during the 11th and early 12th centuries, becoming a typical element of the Catalan Gothic architecture.

Different studies have been carried out in order to assess the origins and the evolution of diaphragm arches, as well as to understand the constructive methodology and the behaviour of such a structural skeleton [4-7]. Moreover, some researches [2, 8] specifically justify the structural differences detected in the Mediterranean Gothic buildings by considering the high seismic hazard of the territory in which they were realized and the need to modify the stone skeletons of the cathedrals because of stability reasons.

In this paper, the seismic behaviour of real examples of diaphragm arches present in the Catalan area has been investigated by means of an integrated numerical-analytical approach. Firstly, step-by-step numerical analyses, aimed at defining the possible position of the hinges in the kinematic chains, have been implemented with FEM Models and validated on the basis of studies found in literature. Secondly, and in order to prove the seismic capacity of such a system, limit analyses with a kinematic approach have been carried out, considering both the original configuration of the detected arcades and the modified geometries obtained by progressively removing parts of their specific constitutive elements.

2 THE CATALAN GOTHIC

2.1 General

Catalan architecture features were introduced by Cistercian monks in the second half of the 12th century, but a true diffusion of the style, as we understand it today, only occurred after the 14th century. Several authors [9, 10] put Catalan Gothic architecture in relation with the cultural context of the Mediterranean Gothic, distancing it from the Gothic culture of Northern Europe, to which the Gothic style of many other areas of the Iberian Peninsula belongs. Indeed, this style is not exclusive of the architecture of the Principality, actually extending itself to all the territories of the Crown of Aragon: the kingdoms of Valencia, Mallorca - Rossellón included - Naples and Sicily. According to the type of structural skeleton adopted in the various constructions, two different Gothic models can be identified in Spain [8]: the cathedrals that follow the typical French scheme and a different type (mainly diffused in Catalonia and Andalusia) inspired by the canons of the Mediterranean Gothic.

As far as the religious architecture is concerned, the essential characteristics of Catalan churches are the unitary conception of space and horizontality. Generally, the layouts contemplate the wide aisleless churches and, when the three-nave plan is considered, there is no transept and the side aisles are at almost the same height of the central nave [3]. The weight of the ribbed vaults is often carried by internal buttresses with chapels in the interstices, favouring compact exterior forms.

Despite some differences, mainly related to the number of naves, the disposition and arrangement of buttresses, cross vaults and roofing systems, the extensive use of diaphragm arches can be identified as a peculiar element of this kind of churches.

From a structural point of view, the diaphragm arches act as horizontal bracing elements for the longitudinal walls, concentrating the load at specific points, in correspondence with the buttresses. Moreover, when these elements follow one another at closely spaced intervals, the nave assumes the function of support for the roof.

Obviously, the distance of the diaphragm arches and their geometric configuration influence the conformation of the other structural elements and, in particular, the characteristics of the adopted roofing system. As an instance, the typical use of terraced roofs in the Mediterranean Gothic structures is connected to the regular adoption of flat diaphragm arches along the entire length of the naves.

2.2 Case studies

Different developments of the diaphragm system (concerning also the arrangement of the buttresses) can be identified in the religious buildings belonging to the Mediterranean Gothic style.

In order to investigate the influence of the geometric parameters on the global behaviour of a specific transversal diaphragm, two different geometric coefficients are utilized. These coefficients characterize the relationship between the total height of the diaphragm and the rise of the nave arch at the keystone (the diaphragmatic ratio h_1/h) and between the total height of the nave arch and the total width of the arcade (the rising ratio h/w) can be identified [8, 11].

In Tables 1 and Figure 1, the h_1/h and h/w ratios of some of the main Catalan Gothic cathedrals are shown and compared. In Figure 2, the examples of diaphragm arches specifically analysed in the following sections (i.e. arcades of the Santa Maria del Mar [SMM] and Santa Maria del Pi [SMP] Basilicas in Barcelona, Santa Maria [SMG] Cathedral in Gerona and S. Joan Baptista [SJB] Cathedral in Perpignan) are provided.

Table 1: The h_1/h and h/w ratios for some of the main Catalan Gothic cathedrals.

Cathedral/Basilica	Acronym	Layout	h_1/h	h/w
Santa Creu i Santa Eulàlia (Barcelona)	[SCE]	Three-nave	1.12	0.58
Santa Maria del Mar (Barcelona)	[SMM]	Three-nave	1.02	0.89
Santa Maria (Tortosa)	[SMT]	Three-nave	1.10	0.59
Santa Maria del Pi (Barcelona)	[SMP]	One-nave	1.07	0.97
Santa Maria (Gerona)	[SMG]	One-nave	1.03	1.04
S. Joan Baptista (Perpignan)	[SJB]	One-nave	1.11	0.79
Santa Maria De La Seu (Manresa)	[SMS]	One-nave	1.06	0.75

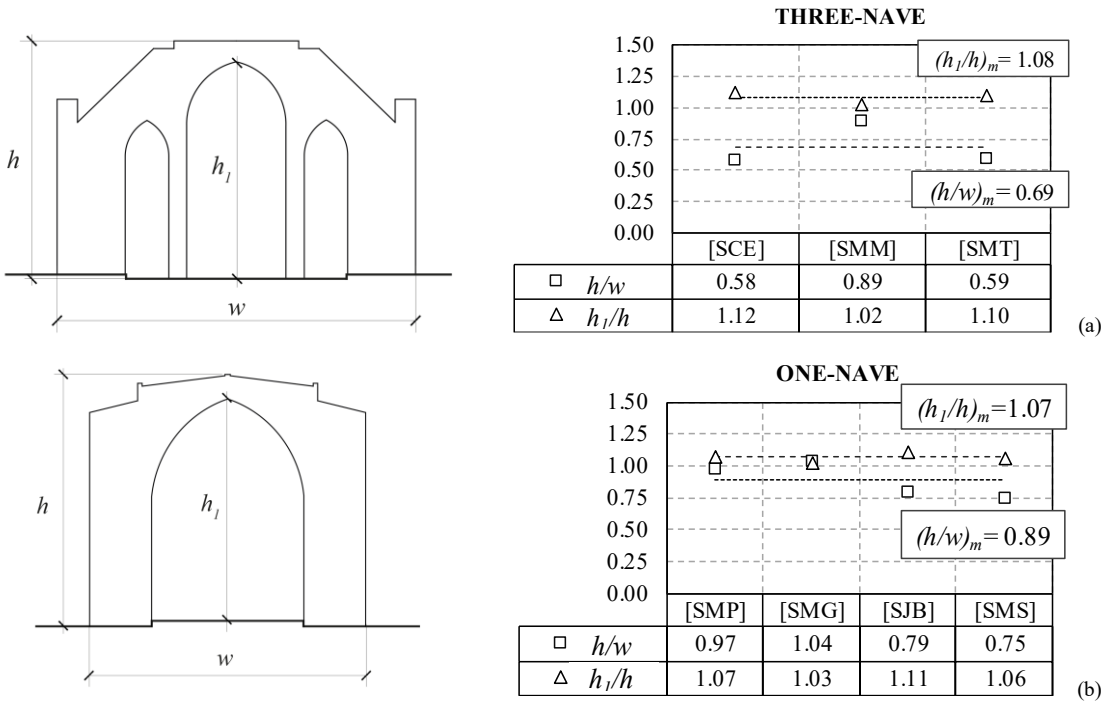


Figure 1: The h_1/h and h/w ratios for some of the main Catalan Gothic Cathedrals with (a) three-nave and (b) one-nave layout

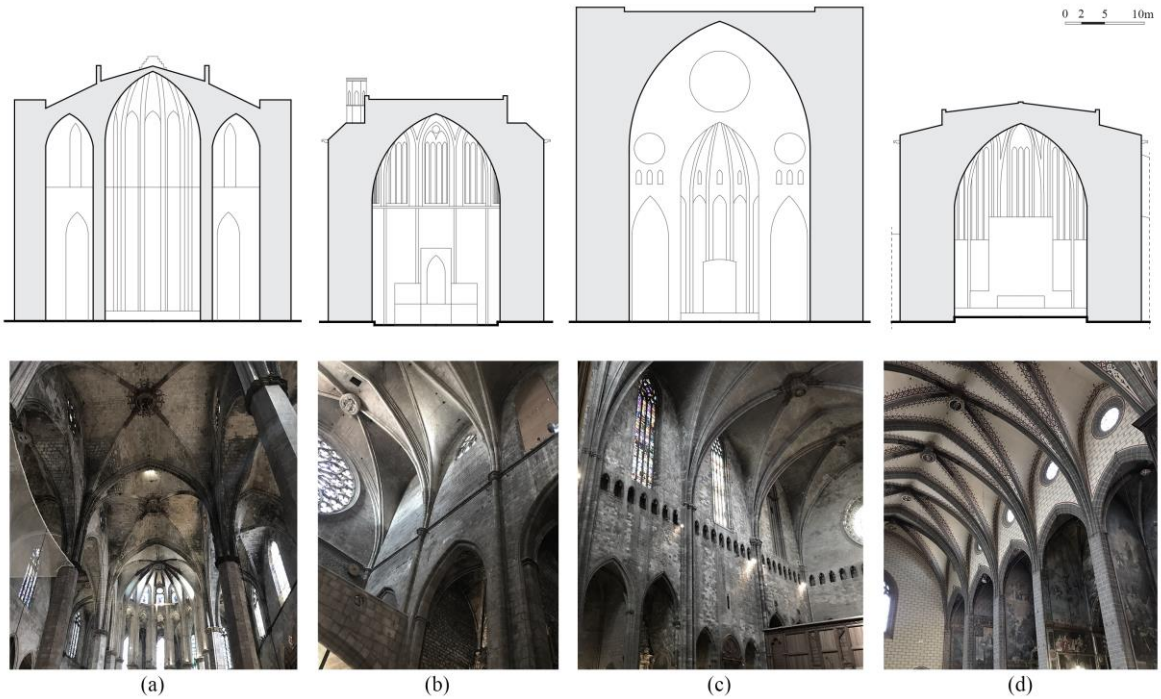


Figure 2: Section of the diaphragm arch and internal photographic survey for (a) Santa Maria del Mar [SMM] Basilica in Barcelona, (b) Santa Maria del Pi [SMP] Basilica in Barcelona, (c) Santa Maria [SMG] Cathedral in Gerona, (d) and S. Joan Baptista [SJB] Cathedral in Perpignan

3 THE LIMIT ANALYSIS WITH KINEMATIC APPROACH

3.1 General

In the following, the seismic behaviour of the diaphragmatic system is investigated by means of limit analyses with a kinematic approach. The proposed approach is considered suitable for the purpose of this study, given the strict dependence of the results on the geometry of the structures, and considering the unavailability of specific mechanical characteristics for the investigated cases.

The limit analysis is based on the Heyman's [12] assumptions for the masonry behaviour, according to which: *i.* masonry has an infinite compressive strength; *ii.* masonry has zero tensile strength; *iii.* sliding failure in masonry cannot occur. Under these assumptions, a masonry element can be considered as an assembly of non-deformable blocks and its failure can be related to the formation of rotational hinges, which induce a displacement distribution into the structure (i.e. kinematic chain).

It is worth noticing that the identification of the position of the hinges is not an easy issue and is not enough for defining the subdivision in rigid blocks, which is influenced by the direction of the potential cracks, too.

The lability of the structure is the sufficient and necessary condition for defining the statically admissible kinematic mechanism. Once that the position of the hinges has been defined, the limit analysis with the kinematic approach provides the calculation of the load multiplier α, by means of the Principle of Virtual Work.

Since external loads have been neglected in the present simplified study, the Eq. (1) has been assumed:

$$\alpha = \frac{-\sum_{i=1}^{n} M_i \cdot g \cdot \delta_{y,i}}{\sum_{i=1}^{n} M_i \cdot g \cdot \delta_{x,i}} \tag{1}$$

where: g is the gravity acceleration, n is the number of non-deformable blocks, M_i is the mass of each block, $\delta_{y,i}$ and $\delta_{x,i}$ are the virtual vertical and horizontal displacements, respectively, evaluated in correspondence of the centroid of the i^{th} block.

According to the graphical method, the kinematic chain has been defined by imposing an infinitesimal rotation to the first rigid block.

3.2 The collapse mechanisms definition

Consistently with the theory of the limit analysis, the definition of the most likely kinematic chain should consist in an iterative procedure aimed at investigating each admissible block subdivision in order to identify the collapse mechanism that returns the minimum value of the load multiplier α.

Such an approach would certainly provide a closed-form result, but it would involve an excessive computational effort, especially if referred to the diaphragm arches, for which both the position of the non-dissipative hinges and the direction of the possible cracks must be defined.

From a mechanical point of view, the rigid-block subdivision corresponds to the definition of a crack pattern, whose development starts from the zones in which the tensile strength of the masonry is overcome toward the most compressed zones, considered as the possible positions of the hinges.

According to these assumptions, a suitable simplified procedure for the definition of the kinematic chain has been implemented and validated on the basis of studies found in literature, carried out on the Basilica of Santa Maria del Mar [SMM] in Barcelona. Such a procedure consists in step-by-step numerical analyses, in which the progressive cracking is introduced in the models by means of mesh subdivisions.

To this purpose, FEM Model of the diaphragm arches have been implemented in *Midas Gen* with a macro-modelling approach. Since the in-plane behaviour is investigated in this study, bi-dimensional elements with a conventional thickness of 1 meter have been assumed for the mesh. For the masonry material, an initial Elastic Modulus E= 8000 MPa, a Poisson's coefficient υ=0.3 and a specific weight γ=2200 kg/m^3 have been considered, according to the values adopted in literature [13] for [SMM]. Finally, the mesh discontinuities have been introduced in the models if the tensile strength (conventionally assumed equal to 0.4 MPa) has been overcome.

The boundary conditions imposed in the step-by-step procedure provides a complete DOF restriction for the base nodes, a vertical gravity acceleration and a uniform horizontal acceleration increasing up to the formation of a sufficient number of hinges.

In particular, the kinematic chain of Figure 3, defined through the formation of 10 non-dissipative hinges located at the base of the piers and at the intradoses and extradoses of the arches, alternatively, has been obtained according to the proposed methodology, returning a horizontal load multiplier α=0.11g.

The defined collapse mechanism results in good agreement with the reference study [14] (as shown in Figure 3b), proving the reliability of the approach, despite the adopted simplified assumptions. The procedure is validated by literature [14, 15] also in a quantitative point of view, by considering the values of the seismic capacity obtained for the considered structure, as shown in Table 2.

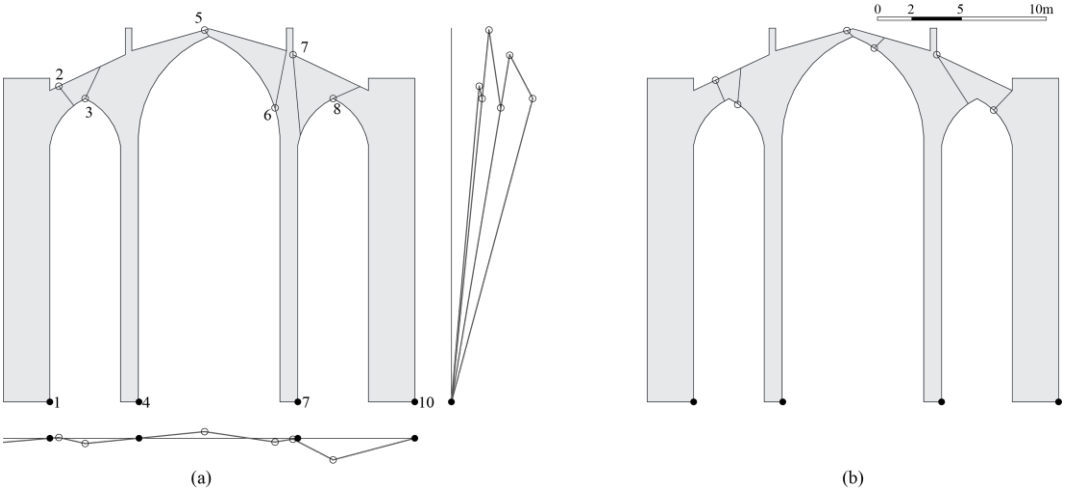


Figure 3: Collapse mechanism of the transversal arcade of [SMM]: (a) kinematic chain obtained in the current study and (b) collapse mechanism from Irizarry et al. (2003) [14]

Table 2: Comparison of the horizontal load multipliers of the transversal arcade of [SMM]

Reference	Type of analysis	α [g]
Current study	Limit analysis with a kinematic approach	0.11
Irizarry et al. (2003) [14]	FE Model	0.13-0.14
	Limit analysis with a kinematic approach	0.11-0.12
Roca (2007) [15]	Limit analysis with a static approach	0.10
	Limit analysis with a kinematic approach	0.10

4 ANALYSIS OF CASE STUDIES

4.1 The kinematic analysis

After having validated the proposed approach, it has been adopted for assessing the seismic capacity of the case studies [SMP], [SMG] and [SJB] introduced in section 2.

The kinematic chains and the collapse mechanisms obtained with the described procedure are shown in Figure 4.

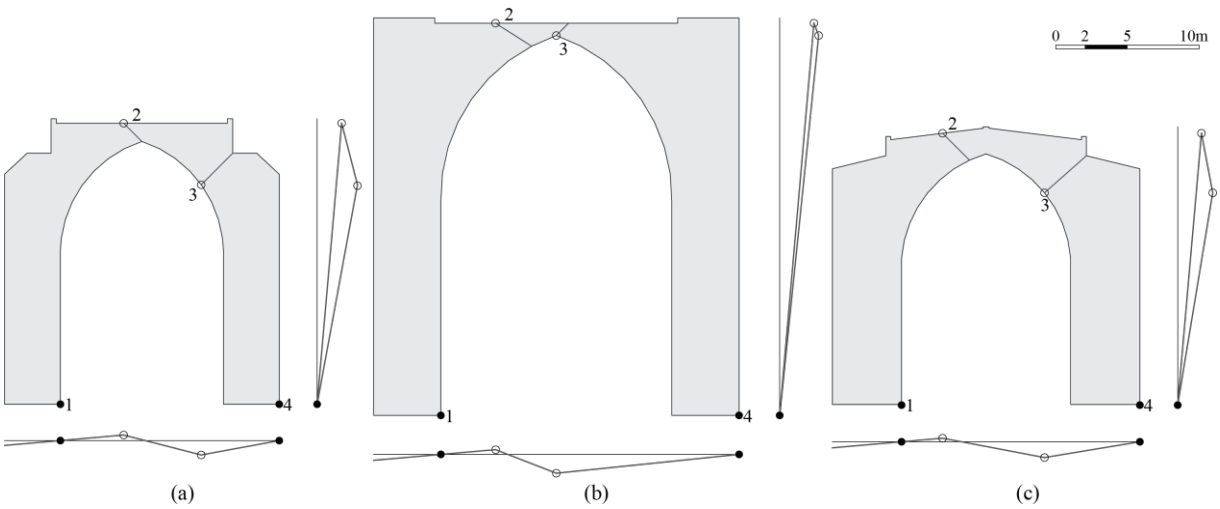


Figure 4: Collapse mechanisms and kinematic chains of the investigated case studies: (a) [SMP], (b) [SMG], (c) [SJB]

As it can be observed, all the investigated cases returned global collapse mechanisms, with the formation of two non-dissipative hinges placed at the base of each pier and two others hinges at the intrados and extrados of the arches, alternatively.

The horizontal load multipliers arisen from the limit analyses are as follows: *i.* [SMP]: α=0.215; *ii.* [SMG]: α=0.162; *iii.* [SJB]: α=0.277.

The obtained horizontal accelerations are shown in Figure 5, where the results are provided as a function of the h/h_1 and h/w ratios defined in section 2, with the linear trend curves.

In particular, in Figure 5b, the results obtained in De Matteis et al. 2019 [11] for the transversal arcades of some of the main European Gothic churches with a three-nave layout are also plotted.

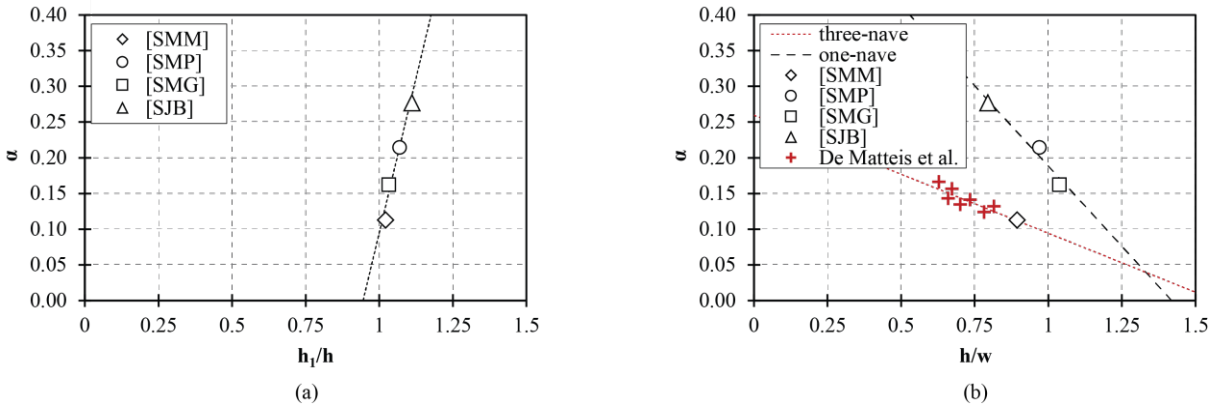


Figure 5: Results of the limit analyses in terms of (a) horizontal load multiplier α - diaphragmatic ratio h_1/h and (b) horizontal load multiplier α - rising ratio h/w (red points and line are referred to De Matteis et al. 2019 [11]).

The depicted results show a linear dependence between the seismic capacity of diaphragm arches and the h_1/h ratio, which means that an increase in the capacity of the structures can be actually observed when the diaphragmatic system is used in churches.

As far as the rising ratio h/w is concerned, it is worth noticing that the value obtained for the three-nave church of [SMM] appears to be consistent with the trend previously obtained in [11] for some Gothic transversal arcades. Moreover, the dependence of the seismic capacity from the h/w ratio is confirmed by the cases with a one-nave layout, despite the different slope of the trend line.

Qualitatively, it could be asserted that the seismic capacity of the diaphragm arches can be strongly influenced by both the diaphragmatic and rising ratio and that a better structural response is generally obtained if the arcade is significantly diaphragmatic and the h/w ratio gives back a small value.

4.2 Diaphragm arches: further considerations on the seismic behaviour

The seismic behaviour of the investigated diaphragm arches has been further assessed by means of additional analyses. In particular, starting from the original geometries of the considered cases, portions of masonry have been progressively removed in order to evaluate the beneficial contribution provided by each structural element on the seismic capacity.

Hence, the geometries of Figure 6 have been investigated, firstly by excluding portions of the lateral buttresses and then by removing the diaphragms.

It is worth mentioning that the portions of the buttresses not removed in the analyses correspond to the real height of the lateral chapels detected in the considered churches by the authors. Moreover, in order to determine the new geometrical configurations, the depths of the arches have been reduced, keeping constant the thickness, which has been obtained by positioning the key of the arch in correspondence of the maximum height of the original diaphragm. In case this value was not included in a thickness-to-span ratio ranging between 1/18 and 1/10, as retrieved from literature [12] and already investigated by the authors [16], it has been modified accordingly.

The modified configurations have been investigated by means of the procedure described and validated in the previous Section.

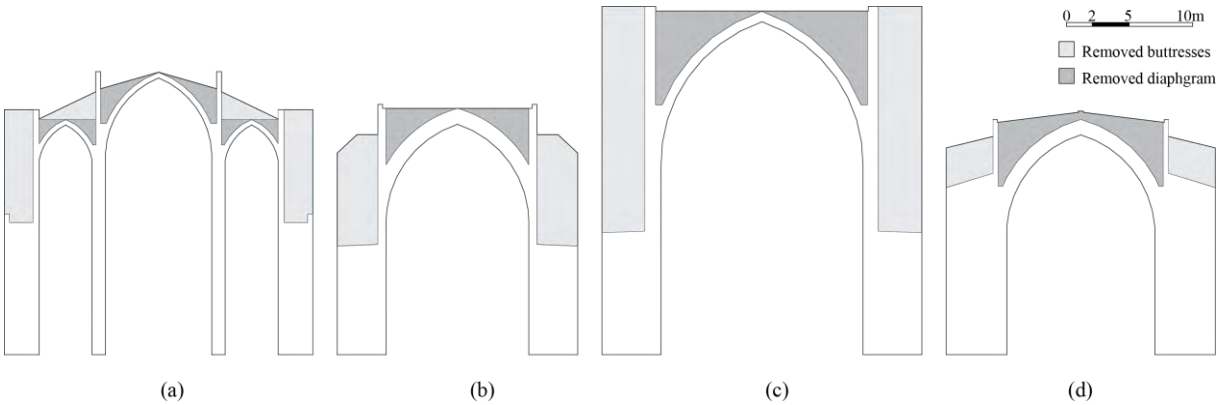


Figure 6: Investigated modified geometries: (a) [SMM], (b) [SMP], (c) [SMG] and (d) [SJB].

The results in terms of kinematic chains are shown in Figure 7 (a-h), while the obtained horizontal load multipliers are plotted in Figure 7j together with those arisen from the original geometries. The results are also summarized in Table 3.

The new limit analyses returned, for almost all the cases, local collapse mechanisms with the hinges occurring only in the thickness of the arches. The only exception is [SJB], whose modified geometries exhibited a global and a semi-global mechanism for the case without buttresses and without buttresses and diaphragm, respectively.

Moreover, the progressive removals of masonry portions from the original geometry have produced a strong decreasing of the seismic capacity of the transversal arcades in the case of [SMM], [SMP] and [SMG]. On the contrary, the case of [SJB] resulted not significantly affected by the absence of the considered reinforcements. This aspect could be related to the original geometry of the arcade, in particular to the large dimension of the lateral buttresses and to the small size of the removed portions. Furthermore, the values of the geometric ratios h/h_1 and h/w reported in Table 1 and Figure 1 show that [SJB] is characterized by proportions that slightly differ from those detected in the other analysed churches.

Despite this exception, the study demonstrates that the diaphragm arches certainly constitute a significant resource, in terms of structural capacity, for the churches and that both the diaphragms and the lateral buttresses can significantly improve the seismic behaviour of this kind of structural skeleton.

Table 3: Results of the limit analyses with the kinematic approach

Analysis	[SMM]	[SMP]	[SMG]	[SJB]
Original Geometry	0.113	0.215	0.162	0.277
No Buttresses	0.048	0.070	0.070	0.312
No Diaphragm	0.043	0.034	0.061	0.285

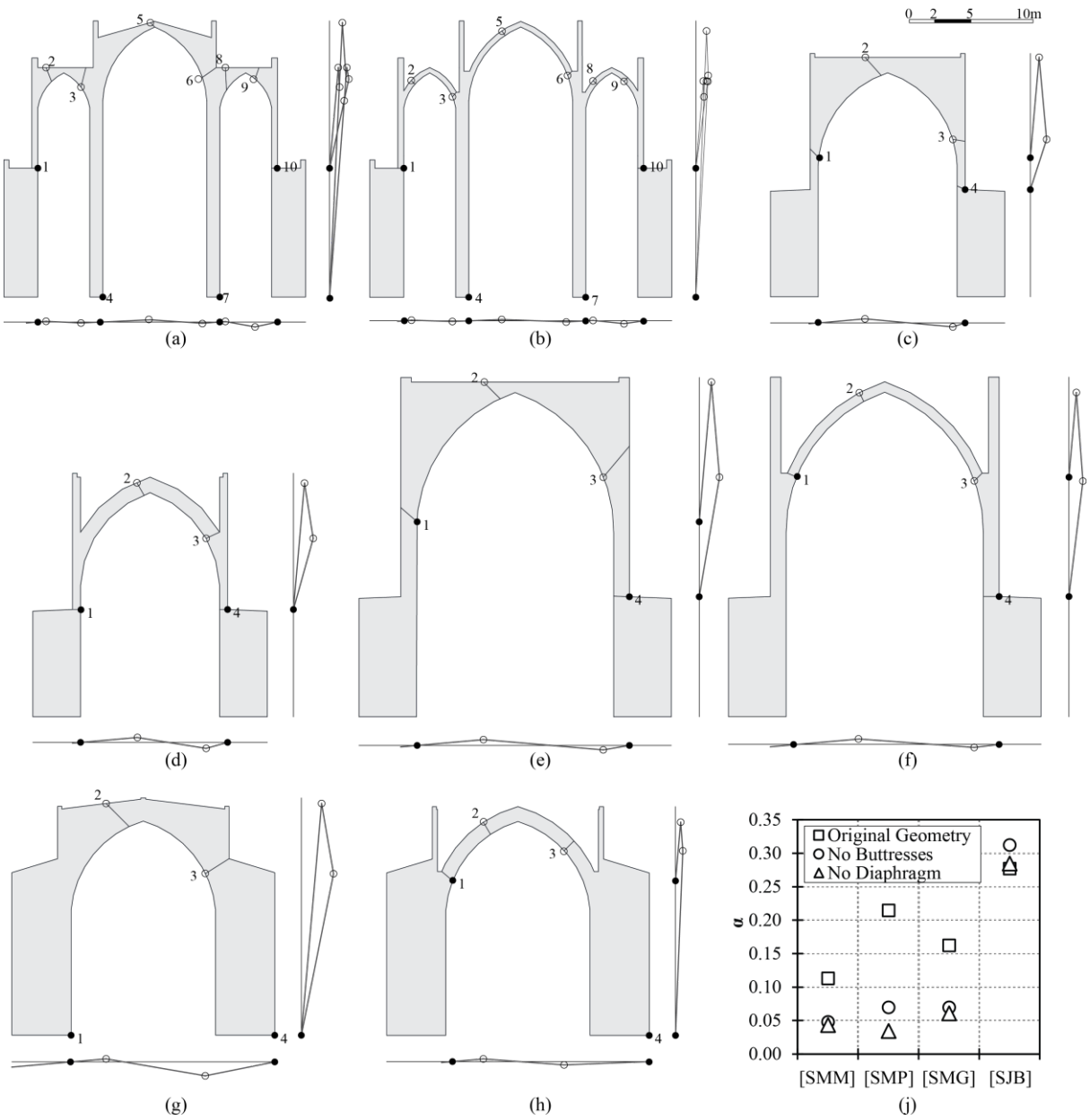


Figure 7: Kinematic chains for the modified geometries: (a) [SMM] without buttresses and (b) without diaphragms; (c) [SMP] without buttresses and (d) without diaphragms; (e) [SMG] without buttresses and (f) without diaphragms; (g) [SJB] without buttresses and (h) without diaphragms. (j) Obtained horizontal load multipliers

5 CONCLUSIONS

In this study, the seismic behaviour of diaphragm arches has been investigated by means of an integrated numerical-analytical approach, which has been validated on the basis of studies carried out in literature on the Basilica of Santa Maria del Mar [SMM] in Barcelona.

In particular, geometries derived from real examples of the Catalan Gothic architecture have been adopted to define simplified FEM Models aimed at identifying the possible position of the

hinges and the collapse mechanisms for each analysed case.

Then, in order to prove the seismic capacity of the diaphragmatic system, limit analyses with a kinematic approach have been implemented for the detected arcades, considered both in their original and modified geometries.

Specific geometric coefficients have been identified in order to investigate the influence of the geometry on the global behaviour of this skeleton, finding an effective incidence of the diaphragmatic (h/h_1) and rising (h/w) ratios on the seismic capacity of the investigated structures. Furthermore, since in almost all cases the modified geometries demonstrated a worse seismic capacity, the study revealed the structural influence of the removed structural elements on the global behaviour of the original arcades.

In general, the present study clearly demonstrates that an increase of the structural capacity can actually be observed when diaphragmatic systems are introduced in churches.

Acknowledgements. The present study has been developed as part of a scholarship funded in the framework of the National Operational Program ESF-ESFR Research and Innovation (PON RI 2014-2020), Action I.1 related to Innovative Industrial Ph.D (Project Code – CUP – B29D17001610006).

REFERENCES

[1] Vivian, P. The Beginnings of Gothic Architecture in Languedoc. *The Art Bulletin*. (1988). 70. 104. 10.2307/3051156.

[2] De Matteis, G. & Mazzolani, F.M. 2010. The Fossanova church: seismic vulnerability assessment by numerical and physical testing. International Journal of Architec-tural Heritage, 4: 222-245.

[3] Roca, P., Pellegrini, L., Oñate, E., Hanganu, A. Analysis of the structure of Gothic Cathedrals. Application to Barcelona Cathedral. In *Structural Analysis of Historical Contruction II*. Possibilities of Numerical and Experimental Techniques, Roca et al. (Eds.), CIMNE, Barcelona, (1998).

[4] Roca, P. Studies on the structure of Gothic Cathedrals. In *Historical Constructions*. P. B. Lourenço and P. Roca (Eds.), University of Guimaraes, Guimaraes, (2001).

[5] Zaragozá Catalán, A. (1990). Iglesias de arcos diafragma y armadura de madera en la arquitectura medieval valenciana. Valencia: Universidad Politécnica de Valencia.

[6] Roca, P., Cervera, M., Pelà, L., Clemente, R., Chiumenti, M. Continuum FE Models for the Analysis of Mallorca Cathedral. *Engineering Structures*, (2013) 46: 653-670, doi: http://dx.doi.org/10.1016/j.engstruct.2012.08.005.

[7] Pulido, V., Alonso-Durá, A., Fenollosa, E., Boquera, A. Análisis constructivo y estructural de la catedral de Valencia. *Informes de la Construcción* (2016) 68, 543, e158, 10.3989/ic.15.102.

[8] Cassinello, P. Influencia de los terremotos históricos en la construcción de las catedrales góticas españolas. *Annali Di Architettura*: Rivista del centro Internazionale di Studi di Architettura "Andrea Palladio" (2005) 17: 9-20.

[9] Lavedan, P., L'Architecture gothique religieuse en Catalogne, Valence et Baléars. Laurens, Paris, 1935

[10] Durliat, M., L'art dans le Royaume de Majorque. Éd. Privat, Toulouse

[11] De Matteis, G., Cacace, D., Rouhi, J., Zizi, M. Seismic behaviour of Gothic transversal

arcades: A preliminary parametric investigation. In Proceedings of SEMC2019, Advances in Engineering Materials, Structures and Systems: Innovations, Mechanics and Applications. (2019) Cape Town, South Africa. ISBN:978-1-138-38696-9.

[12] Heyman, J. The Stone Skeleton: Structural Engineering of Masonry Architecture. (1995) Cambridge University Press.

[13] Murcia-Delso, J., Das, A. K., Roca, P., Cervera, M. Seismic safety analysis of historical masonry structures using a damage constitutive model. In *COMPDYN 2009 - ECCOMAS Thematic Conference on Computational Methods in Structural Dynamics and Earthquake Engineering*. M. Papadrakakis, N.D. Lagaros, M. Fragiadakis (Eds.), Rhodes, Greece (2009).

[14] Irizarry, J., Podestà, S., Resemini, S. Curvas de capacidad para edificios monumentales: la iglesia Santa María del Mar de Barcelona. In proceedings of *2º Congreso Nacional de Ingeniería Sísmica*. 1st-4th April, Malaga, Spain. (2003).

[15] Roca,P. Basílica de Santa Maria del Mar: estudi de l'estructura. Technical University of Catalonia (2007).

[16] Cacace, D., Rouhi, J., Zizi, M. and De Matteis, G. (2019). Vulnerabilità sismica di archi in muratura: uno studio parametrico con approccio cinematico. XVIII Convegno ANIDIS – L'Ingegneria sismica in Italia. Sep. 15-19. Ascoli Piceno, Italy.

12th International Conference on Structural Analysis of Historical Constructions
SAHC 2020
P. Roca, L. Pelà and C. Molins (Eds.)

SENSITIVITY ANALYSIS IN THE REHABILITATION OF HISTORIC TIMBER STRUCTURES ON THE EXAMPLES OF GREEK CATHOLIC CHURCHES IN POLISH SUBCARPATHIA

KATARZYNA SZEPIETOWSKA, IZABELA LUBOWIECKA*

Department of Structural Mechanics, Faculty of Civil and Environmental Engineering
Gdansk University of Technology
Narutowicza 11/12, 80-233 Gdańsk, Poland
e-mail: izabela.lubowiecka@pg.edu.pl (*corresponding author)
katarzyna.szepietowska@pg.edu.pl

Keywords: Historical Structure, Carpentry joints, Structural Analysis, Global sensitivity analysis, Uncertainty quantification

Abstract. *This work concerns structural and sensitivity analysis of carpentry joints used in historic wooden buildings in south-eastern Poland and western Ukraine. These are primarily sacred buildings and the types of joints characteristic for this region are saddle notch and dovetail joints. Thus, in the study the authors focus on these types of corner log joints. Numerical models of the joints are defined and finite element simulations of their statics are carried out. Moreover, a sensitivity analysis is performed in order to describe how the uncertainty of material properties including humidity of some structural members, caused during potential repairs, affect the structural behaviour of the whole connection. This represents the situation when some degraded logs are exchanged into new wood combining old, and often damp, wood with new and dry logs. A non-intrusive probabilistic approach to the sensitivity analysis is applied and regression-based Polynomial Chaos (PC) expansion method is used to propagate uncertainties.*

1 INTRODUCTION

The motivation of the presented research was the survey and the current state of wooden Greek Catholic churches in Polish Subcarpathia (Figure 1), described and analysed in detail in [1]. The susceptibility of wood to rotting and damage reduces the number of those historic buildings, and thus raises the need to preserve this heritage. The construction of this type of structures encourages the authors to deal with their structural elements, like logs and log joints, in terms of their mechanical behaviour. Especially, referring to the situation of repair and replacement of those elements [2].

Nowadays, the necessity of maintenance, renovation and reinforcement of historical structures yields a need for analysis of its mechanical behaviour. Often, the planning for further and more detailed studies is based on basic measurements and structural analysis [3], Finite element method is a common strategy applied to the structural analysis of complex structures [4], [5]. However, one of the problems in the modelling of historic structures are uncertain

parameters that can come from material [6], geometry [7], [8], and boundary conditions. The properties of wood as a natural material exhibit high variability [9], which depend on age, moisture level [10], decay etc. Moreover, an accurate non-invasive measurement on historic monuments is also challenging [7]. Both types of uncertainties, resulting from the material variability and the structure geometry, can be incorporated into the modelling (see e.g., [11]). The influence of the material properties changes and uncertainties on the structural behaviour can be studied in two ways, by local or global sensitivity analysis.



Figure 1: Greek Catholic churches in Polish Subcarpathia:
Cewków (left), Wólka Żmijowska (right)

The global sensitivity analysis can be done by applying probabilistic methods as shown e.g., in[12], [13]. This type of sensitivity of timber structures has been also studied and presented in [14], [15]. The local sensitivity analysis has been employed to timber joints e.g., in [1], where the studied corner joint made of old and new logs was studied. The influence of the change of material parameters on the mechanical behaviour of the joint has been described.

The present study concerns a global sensitivity analysis of corner log joints subjected to lateral load. There are two types of joints taken into consideration, dovetail and saddle notch (Figure 2) as the most common in this type of structures [16]. A special attention is payed to the change of mechanical behaviour of the joints while exchanging their elements, e.g., when a part of damaged old structure is filled with a new wood. This exchange can be represented by the change of material properties of wood that also involves uncertainties referring to the assessment of those properties in existing structures.

The global sensitivity analysis of corner log joints presented in [6] shown how and which of the two considered material paramaters of wood (elastic modulus and friction coefficient) influence the strutural behaviour of the joints. In the present study, the authors are focused on how an exchange of a structural member influences the behaviour of the joints applying a regression based polynomial chaos expansion method [17] to propagate uncertainties of properties of old wet logs and of a new dry log used for replacement.

2 FINITE EMENT MODELLING OF CARPENTRY JOINTS

2.1 Geometry and finite element discretisation

Numerical models of the joints have been defined by means of finite element method. Each of them contain 5 logs (Figure 2) composed in a layout as observed in the churches. Referring to the previous studies, [1], [7], [18], where also some experimental work is addressed, the size of the modelled joints has been scaled 1:2 compared to the real connections. Thus, the 0.7 m long logs have cross-sections of 75 x 135 mm. Geometrically nonlinear static analysis has been performed using MSC.Marc commercial software. The joints were discretised by 37864 (dovetails) and 44008 (saddle notch) of 3D, 8-nodes finite elements with 3 translational dof in each node (Figure 2).

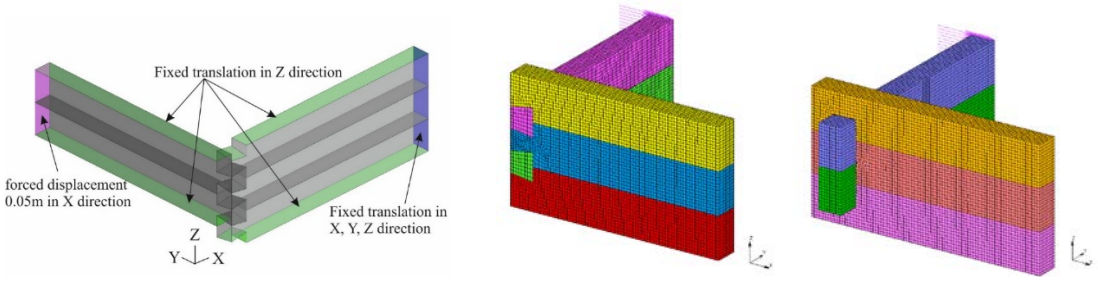


Figure 2: Carpentry corner log joint, topology, boundary conditions and FEM discretization (dovetail – left, saddle notch – right)

The surface-to-surface contact was applied between logs. The three degrees of freedom of each node of the logs cross-sections were fixed on the side of 3 logs while the other two logs were displaced along the x-direction by $u_x = 5$ cm in the global system of coordinates of the model resulting in a change of the corner angle. The bottom and top surfaces of the joints were fixed in the global z-direction (vertical) representing the effect of the foundations and the rest of the wall.

2.2 Material properties

In the analysis, wood has been considered as orthotropic elastic material, where E_L is a longitudinal modulus of elasticity (along the direction of the fibres). Following [19], the moduli of the other directions (radial –R and tangential –T) were calculated in relation to E_L according to the formulae $E_T / E_L = 0.068$, $E_R / E_L = 0.102$, $G_{RT} / E_L = 0.05$, $G_{TL} / E_L = 0.046$, $G_{LR} / E_L = 0.049$, and appropriate Poisson ratios were determined as $\nu_{RT} = 0.469$, $\nu_{TL} = 0.024$, $\nu_{LR} = 0.316$ as described in [15]. It assumed that the joint is made of old wet wood with one middle log replaced by a new dry log.

3 UNCERTAINTY PROPAGATION AND GLOBAL SENSITIVITY ANALYSIS

3.1 Uncertainty propagation

The applied scheme of uncertainty quantification is presented in Figure 3. The methodology applied to carpentry joints in previous research [15] is also used in this study. In order to

propagate uncertainties through models defined in commercial FE system, non-intrusive methods can be applied. Such methods do not require FE code modifications and are based on some number of deterministic calculations. Regression-based polynomial chaos (PC) expansion [17] is one of such methods which requires less simulations than widely-used Monte Carlo method. Truncated PC expansion of the model output Y (quantity of interest) is:

$$Y \approx \sum_{\boldsymbol{\alpha} \in \mathcal{A}} a_{\boldsymbol{\alpha}} \Psi_{\boldsymbol{\alpha}}(\boldsymbol{\xi}), \tag{1}$$

where $\mathcal{A}$ is a truncation set of $\boldsymbol{\alpha}$ M-uplets $(\alpha_1,\ldots,\alpha_M) \in \mathbb{N}^M$ indicating order of polynomials in a multivariate polynomial basis $\Psi_{\boldsymbol{\alpha}}$, $a_{\boldsymbol{\alpha}}$ are the coefficients, and $\boldsymbol{\xi}$ are reduced independent variables. Employed polynomials should be orthonormal with respect to a distribution. Therefore Hermite polynomials are used in case of normal (and lognormal) distribution and Legendre polynomials in case of uniform distribution. In regression based approach, the coefficients are found by solving least square problem. The accuracy depends on the number and choice of regression points for which FE calculations are performed. Based on previous experience, a D-optimal solution from random candidate set is chosen here [20]. Such approach have also resulted in sufficient accuracy in case of modelling of carpentry joints in similar problem [15].

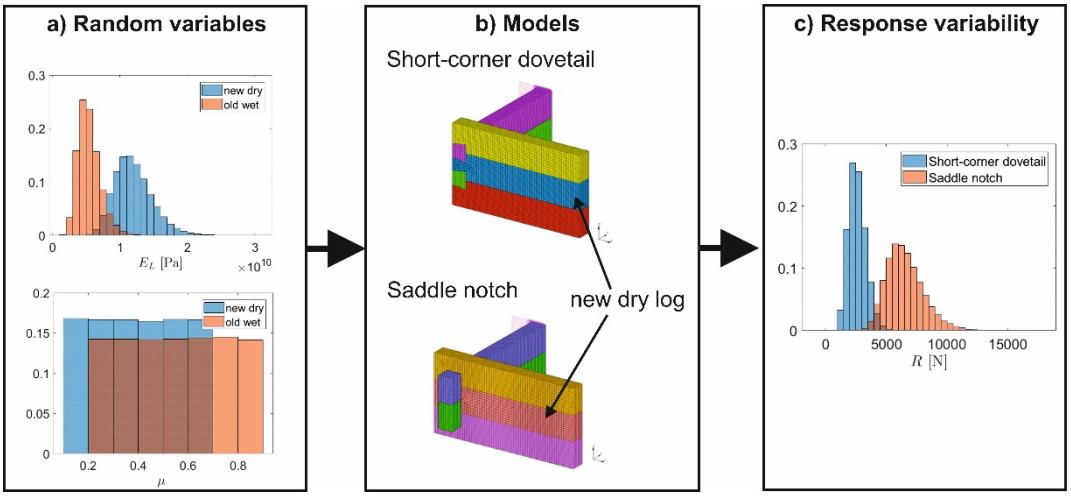


Figure 3: Scheme of uncertainty quantification

3.3 Global sensitivity analysis

In order to study the sensitivity of the quantity of interest to the input uncertainty, Sobol' indices are computed [21]. They are measures of global sensitivity and are based on ANalysis Of VAriance (ANOVA) decomposition. Sobol' index $S_{i_1,\ldots,i_s}$ says how much of the output vriance corresponds to the uncertainty of variables $\xi_{i_1},\ldots,\xi_{i_s}$. Thanks to the othonormality of PC basis, the Sobol' indices can be rapidly calculated with the use of PC coefficients

corresponding to the polynomials depending only on all variables $\xi_{i_1},\ldots,\xi_{i_s}$ [17]:

$$S_{i_1,\ldots,i_s} = \frac{1}{\sum_{\boldsymbol{\alpha}\in\mathcal{A}\setminus\mathbf{0}} a_{\boldsymbol{\alpha}}^2} \sum_{\boldsymbol{\alpha}\in\mathcal{A}_{i_1,\ldots,i_s}} a_{\boldsymbol{\alpha}}^2, \tag{2}$$

where:

$$\mathcal{A}_{i_1,\ldots,i_s} = \{\boldsymbol{\alpha}\in\mathcal{A}: \alpha_k \neq 0 \Leftrightarrow k\in\{i_1,\ldots,i_s\}\}. \tag{3}$$

Total Sobol' index S_i^{Tot} is the sum of all indices including variable *i* and can be calculates as

$$S_i^{Tot} = \frac{1}{\sum_{\boldsymbol{\alpha}\in\mathcal{A}\setminus\mathbf{0}} a_{\boldsymbol{\alpha}}^2} \sum_{\boldsymbol{\alpha}\in\mathcal{A}_i^{Tot}} a_{\boldsymbol{\alpha}}^2, \tag{4}$$

where:

$$\mathcal{A}_i^{Tot} = \{\boldsymbol{\alpha}\in\mathcal{A}: \alpha_i \neq 0\}. \tag{6}$$

3.3 Random variables and quantity of interest

As mentioned before, wood is characterized by high variability of material properties. Therefore, four random variables (Figure 3a) are assumed in both models: dovetail and saddle notch joint.

First, the longitudinal Young modulus of the logs is assumed to be a random variable:

1) $E_L^{new} \sim \mathcal{LN}(23.18, 0.23)$ in case of new dry log (humidity 7-14%) with lognormal distribution fitted to experimental results [15];

2) $E_L^{old} \sim \mathcal{LN}(22.37, 0.30)$ in case of old (XIX century) wet logs (humidity 24-40%) with lognormal distribution fitted to experimental results [1].

Next, the friction coefficient is assumed to be a random variable with uniform distribution in range based on the data taken from literature [22]–[24] in two variants:

3) $\mu^{new} \sim \mathcal{U}([0.1, 0.7])$ - friction between old wet logs;

4) $\mu^{old} \sim \mathcal{U}([0.2, 0.9])$ - friction between new log and old ones.

The quantity of interest, on which the analysis is focused, is a reaction force *R* caused by forced lateral displacement of one side of the joint (Figure 2). The study of uncertainty of this value can bring a crucial information for validation of numerical models of carpentry joints when performed with the use of experimental data [18].

4 RESULTS

The resultant coefficient of variation of reaction force in the models is equal to 28% for dovetail and 23% for saddle notch joint. The histogram of the quantity of interest is shown in Figure 3c. Table 1 presents total Sobol' indices calculated using PC expansion. It can be noticed, that their values are relatively similar between the two models. In case of both models, the influence of uncertainty of E_L^{old} (the highest Sobol' index) is highly dominating. The contribution of E_L^{new} to the output variance is very small and the contribution of friction coefficient is negligible when compared to other variables.

Table 1: Total Sobol' indices obtained by PC order 3

Variable	Dovetail	Saddle notch
E_L^{new}	0.0836	0.0755
E_L^{old}	0.9078	0.9270
μ^{new}	0.0158	0.0000
μ^{old}	0.0178	0.0000

5 CONCLUSIONS

Based on the global sensitivity analysis of old historical carpentry joints made of wet wood with one log replaced by a dry new timber element, the following conclusions can be drawn for both types of considered connections:

- The uncertainty of Young modulus of old wet logs has the highest contribution to the variation of the results; this is also the material dominating in the structure;
- The uncertainty of material properties of only one new log and friction coefficients have negligible influence on the uncertainty of the outcome.

Therefore, the accurate identification of Young modulus of old logs would most effectively decrease uncertainty of the outcome of the models and consequently should be priority in the future studies. What is more, the considered models could be reduced to a smaller number of random variables, omitting the less important ones, which would reduce the number of simulations required to be performed. The information on contribution of each variable to the uncertainty of the model response can be useful in validation of numerical models by comparison with experiments on carpentry joints. The presented work is part of the research aiming to define credible models which can be used in the rehabilitation process of traditional carpentry joints of Greek Catholic churches in Polish Subcarpathia as well as in other historic timber structures.

Acknowledgements. This work was partially supported by the National Science Centre (Poland) [Grant No. 2015/17/B/ST8/03260]. Calculations were carried out at the Academic Computer Centre in Gdańsk.

REFERENCES

[1] I. Lubowiecka, T. Zybała, G. Bukal, M. Krajewski, M. Kujawa, and P. Kłosowski, On the Current State of Dovetail Wall-corner Joints in Wooden Greek Catholic Churches in Polish Subcarpathia with Structural and Sensitivity Analyses, *Int. J. Archit. Herit.* (2019) **00**:1–18.

[2] J. R. Drobiec Łukasz, Pająk Zbigniew, Repair problems of the wooden structure of churches, *J. Herit. Conserv.* (2018) **53**:31–44.

[3] H. Cruz *et al.*, Guidelines for On-Site Assessment of Historic Timber Structures Guidelines for On-Site Assessment of Historic Timber Structures, *Int. J. Archit. Herit.* (2015) **9**:277–289.

[4] J. Milch, J. Tippner, V. Sebera, J. Kunecký, M. Kloiber, and M. Navrátil, The numerical assessment of a full-scale historical truss structure reconstructed with use of traditional all-wooden joints, *J. Cult. Herit.* (2016) **21**:759–766.

[5] I. Bergamasco, A. Gesualdo, A. Iannuzzo, and M. Monaco, An integrated approach to the conservation of the roofing structures in the Pompeian Domus, *J. Cult. Herit.* (2018) **31**:141–151.

[6] M. J. Morales-Conde and J. S. Machado, Evaluation of cross-sectional variation of timber bending modulus of elasticity by stress waves, *Constr. Build. Mater.* (2017) **134**:617–625.

[7] J. Hermida, M. Cabaleiro, B. Riveiro, and J. C. Caamaño, Two-dimensional models of variable inertia from LiDAR data for structural analysis of timber trusses, *Constr. Build. Mater.* (2020) **231**:117072.

[8] P. B. Lourenço, H. S. Sousa, R. D. Brites, and L. C. Neves, In situ measured cross section geometry of old timber structures and its influence on structural safety, *Mater. Struct. Constr.* (2013) **46**:1193–1208.

[9] J. S. Machado, F. Pereira, and T. Quilhó, Assessment of old timber members: Importance of wood species identification and direct tensile test information, *Constr. Build. Mater.* (2019) **207**:651–660.

[10] M. Aydın and T. Yılmaz Aydın, Moisture dependent elastic properties of naturally aged black pine wood, *Constr. Build. Mater.* (2020) **262**:120752.

[11] T. Zybała, K. Szepietowska, G. Bukal, and I. Lubowiecka, Portico farmhouses of the Vistula Delta: architecture, current state and finite element modelling of timber roof truss under material and cross-section uncertainty, *Int. J. Archit. Herit.* (2021), *in press*.

[12] J. Köhler, J. D. Sørensen, and M. H. Faber, Probabilistic modeling of timber structures, *Struct. Saf.* (2007) **29**:255–267.

[13] H. S. Sousa and L. C. Neves, Reliability-based design of interventions in deteriorated timber structures, *Int. J. Archit. Herit.* (2018) **12**:507–515.

[14] P. O. Hristov, F. A. DiazDelaO, E. I. Saavedra Flores, C. F. Guzmán, and U. Farooq, Probabilistic sensitivity analysis to understand the influence of micromechanical properties of wood on its macroscopic response, *Compos. Struct.* (2017) **181**:229–239.

[15] P. Klosowski, I. Lubowiecka, A. Pestka, and K. Szepietowska, Historical carpentry corner log joints-Numerical analysis within stochastic framework, *Eng. Struct.* (2018) **176**:64–73.

[16] J. Jasieńko, T. Nowak, and A. Karolak, Historyczne złącza ciesielskie. (Historical

carpentry joints), *J. Herit. Conserv.* (2014) **40**:58–82.
[17] B. Sudret, Global sensitivity analysis using polynomial chaos expansions, *Reliab. Eng. Syst. Saf.* (2008) **93**:964–979.
[18] P. Kłosowski, A. Pestka, M. Krajewski, and I. Lubowiecka, Experimental and computational study on mechanical behaviour of carpentry corner log joints, *Eng. Struct.* (2020) **213**:110515.
[19] D. W. Green, J. E. Winandy, and D. E. Kretschmann, *Wood handbook – Wood as an Engineering Material.* Forest Products Laboratory, Madison (1999).
[20] K. Szepietowska, B. Magnain, I. Lubowiecka, and E. Florentin, Sensitivity analysis based on non-intrusive regression-based polynomial chaos expansion for surgical mesh modelling, *Struct. Multidiscip. Optim.* (2018) **57**:1391–1409.
[21] I. M. Sobol′, Global sensitivity indices for nonlinear mathematical models and their Monte Carlo estimates, *Math. Comput. Simul.* (2001) **55**:271–280.
[22] P. Grossi, T. Sartori, I. Giongo, and R. Tomasi, Analysis of timber log-house construction system via experimental testing and analytical modelling, *Constr. Build. Mater.* (2016) **102**:1127–1144.
[23] W. M. McKenzie and H. Karpovich, The frictional behaviour of wood, *Wood Sci. Technol.* (1968) **2**:139–152.
[24] M. Xu, L. Li, M. Wang, and B. Luo, Effects of Surface Roughness and Wood Grain on the Friction Coefficient of Wooden Materials for Wood-Wood Frictional Pair, *Tribol. Trans.* (2014) **57**:871–878.

12th International Conference on Structural Analysis of Historical Constructions
SAHC 2020
P. Roca, L. Pelà and C. Molins (Eds.)

SIMPLEX ALGORITHMS FOR 3D LIMIT ANALYSIS OF ROMAN GROIN VAULTS

C. BAGGIO[1*], S. SANTINI[2]

[1]Dipartimento di Architettura
Roma Tre University
Largo Marzi 10, 00153 Rome, Italy
e-mail: carlo.baggio@uniroma3.it (*corresponding author)

[2] Dipartimento di Architettura
Roma Tre University
Largo Marzi 10, 00153 Rome, Italy
email: silvia.santini@uniroma3.it

Keywords: Historical Structure, Masonry, 3D limit analysis

Abstract *In Roman Baths the Romans employed groin vaults of great dimensions, with maximum span more than 20 m; simple tools of structural analysis of ancient wide span vaulted halls are still lacking, due to geometrical and material complexity. In this paper we study the collapse behavior, under horizontal static action, of a corner cross vault of the Baths of Diocletian in Rome (Hall I). In the present modeling, masonry is discretized as a system of interacting rigid bodies in no-tension and frictional contact. The computational code consists in a linear programming approach which make use of a series of optimization packages via lower and upper bound techniques of limit analysis. In the paper, a solution strategy based on a modified simplex algorithm has been introduced in order to manage the large number of contacts given by a 3D block assembly. One more task of the proposed problem consists in a suitable description of the overall 3D geometry, here afforded with a specific pre-processing approach.*

1 INTRODUCTION

During the course of many centuries after the fall of the roman empire the buildings of the Baths underwent a gradual and progressive damage, the site became desolate, wasted and encumbered by ruins, as witnessed by a large number of drawings and engravings by sixteenth century landscapists and artists.

In Italy, the current building code (NTC 2018) requires historical analysis of existing masonry buildings as a pre-requisite for the design of structural conservation; this implies survey of resisting system, collecting data about transformation during life of building, often very long, reconstruction of special events, like seismic ones.

This task was managed by a historical reconstruction of the original vaulted system of the main body of the Baths, by research mainly devoted to collect historical images of ruined portion, trying to establish the sequence of collapses during XVI-XVII centuries (Nizzi &

Baggio 2014).

The structural system of the main body of the baths can be easily understood: larger central groin vaults are counteracted by secondary, peripheral barrel and groin vaults which conduct the thrust action to buttresses and foundations.

Nonetheless a number of questions arise: are the pillars of each vault able enough to resist to thrust or they need also aid from the adjacent walls? How can we measure the relative weakness of the partially ruined vaults?

Thus, in this paper, trying to give a quantitative answer, the authors adopt a numerical procedure based on 3D standard limit analysis according to the Italian Code for masonry structures, in particular for historic masonry and monuments. The limit analysis method for the seismic assessment of masonry structures is well known but application to real vaulted structures is far less common in literature. The proposed procedure is based on a mechanical model already discussed in previous work [Baggio & Trovalusci 2000, 2016]. The main improving, with respect to the previous analyses, concerns geometrical model, pre-processing and solution strategies.



Figure 1: Side photograph of Hall I

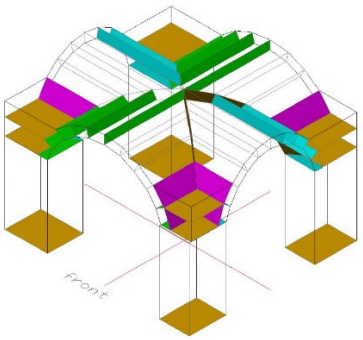


Figure 2: joints: pillar (yellow), abutment (magenta), voussoir (green and cyan), rib (brown)

2 PROPOSED APPROACH

The central body of the Baths is made of a series of seven aisles with semicircular barrel vaults intersecting three aisles; outer groin vaults of minor dimensions provide counteraction of thrust of central vaults. In this study the proposed procedure is applied to the corner groin vault called Hall I (see Figure 1).

The main difficulty in defining the geometrical model consists on a suitable description of the overall 3D assembly; setting up of a 3D mesh with non-trivial geometry becomes rapidly cumbersome and discouraging without the help of a tool to simplify the task. To this aim, the authors in the present work propose a procedure based on the following steps:

- drawing of the vault geometry directly by using AutoCAD;
- modeling of each body or hexahedron as solid element;
- modeling of each interface or joint as ‘region’, that is, an oriented plane surface. Figure 2 illustrates the pillar joints (yellow), the abutment joints (magenta), the

voussoir joints of the vaults (green and cyan) and the rib joints (brown); note that the positive orientation of the local z-axis is represented by color, whereas the rear blank face represents the negative orientation;
- exporting, from AutoCAD model, bodies and regions in a .SAT file which describes the topology of bodies by elementary sub-entities: faces, coedges, edges, vertices and points;
- producing data for the analytical model input, by means of a FORTRAN procedure developed by the authors able to interpret the SAT database. Data extracted by SAT file automatically generate coordinates of the 8 vertices of each hexahedron, mass and center of mass of each body, dimensions, center and orientation of interfaces, preventing data errors and facilitating plotting.

3 LIMIT ANALYSIS AND COLLAPSE MULTIPLIER

Roman masonry should be modeled properly as a continuum material with some resistance in tension; it could hardly be represented as assemblies of blocks with no tension and frictional interfaces. Nevertheless the proposed methodology succeeds in picking out the main characteristics of the behavior of a complex vaulted structure, as shown below.

Masonry assemblages are described as systems of n rigid prismatic blocks connected by no-tension and frictional interfaces through m plane contact surfaces. The blocks can translate and rotate: **u** (6n) is the vector of the generalized blocks displacement. Considering as strain measures of the assembly the relative displacements and the relative rotations between blocks, the kinematic compatibility equations are

$$\boldsymbol{Cu} = \boldsymbol{q} \tag{1}$$

where **q** (6*m*) is the vector of relative joint displacements and **C** is the kinematic matrix.

Vector **q** can be expressed as linear combination of p elementary modes of failure at each interface; typically p for quadrilateral contact surfaces is 14: 4 rotations about four edges, 8 slidings, 2 in-plane rotations

$$\boldsymbol{q} = \boldsymbol{M}\,\boldsymbol{\lambda} \tag{2}$$

where M (6m x pm) is a diagonal matrix containing geometrical coefficients and □ (pm) is the vector of the failure modes. Contact surfaces of different shapes (octagonal for instance) can be also considered simply by suitably varying the matrix of the c-th contact, increasing the number of columns, thence increasing the number of unknowns.

Most of the interfaces have trapezoidal shape varying from one joint to the other, so each contact involves the writing of a specific matrix $\mathbf{M}_c$. Anyway in the most of cases, all the contacts have quadrilateral shape so the number of elementary failure modes p, remains unchanged, equal to 14 for each interface.

The actions on the blocks are permanent loads, represented by the vector of generalized 'dead' loads $\mathbf{f}_0$ (6n), and proportionally increasing loads, represented by the vector $\alpha\mathbf{f}_L$, where $\mathbf{f}_L$ (6n) is the generalized 'live' loads vector and α the unique (non-negative) parameter governing the load increasing. For the sake of clarity, the limit value of α, α_c, is named "collapse multiplier" or "load factor".

The balance equations for the assembly are

$$\boldsymbol{C}^{\mathrm{T}}\boldsymbol{Q} = \boldsymbol{f}_0+\alpha\boldsymbol{f}_{\mathrm{L}} \tag{3}$$

The blocks interact through forces and couples, ordered in the vector of the generalized stresses **Q** (6m). As the joints cannot carry tension and the tangential forces at the interfaces, as well as the in-plane couples (torques), are limited by the friction, bounds on the stress components must be imposed. These bounds define a piece-wise linear yield domain, represented by the inequalities

$$\boldsymbol{\phi} = \boldsymbol{N}^{T}\boldsymbol{Q} \leq \boldsymbol{0} \tag{4}$$

where $\mathbf{N}^{\mathrm{T}}$ (p*m* x 6*m*) is the so-called gradient matrix.
To the 'activation' of a single face of the yield domain a relative displacement corresponds in such a way that

$$\boldsymbol{\phi}^{T}\boldsymbol{\lambda} = 0 \tag{5}$$

In the case of limit bending the vector **q** is normal to the active yield face, while in case of limit shear and limit torque it is not normal to the face (**M** ≠ **N**), so giving rise to a non-standard, non-linear, non convex, problem.

The evaluation of the collapse load and the collapse mechanism of Lagrangian systems of elements interacting through no-tension and frictional contact surfaces corresponds to the Limit Analysis of discretized rigid perfectly-plastic systems with non-associative flow rules. Due to the absence of stability criteria, the solution of the problem of searching the minimum load factor satisfying the Equations (1)-(5) has not unique solution.

In many cases the linearized solution is comparable with the non-linear one, both in terms of collapse mechanism and in terms of collapse multiplier α_c.

From an operating point of view moreover, the introduction of spatial problems highly complicates the numerical task: in systems of blocks connected together in three-dimensional arrangements, the number of contacts per block highly increases, producing a significant overdeterminacy of the kinematic problem. Use of linearized analysis simplifies the numerical task and leads almost always to acceptable results. In this study only LP approach has been used.

A Gauss-Jordan elimination allow to split matrix **C** in two parts: $\mathbf{C}^{\mathrm{I}}$, a square matrix of maximum rank and $\mathbf{C}^{\mathrm{II}}$, together with a correspondent separation of **q** in $\mathbf{q}^{\mathrm{I}}$, $\mathbf{q}^{\mathrm{II}}$ and **Q** in $\mathbf{Q}^{\mathrm{I}}$, $\mathbf{Q}^{\mathrm{II}}$.
Defining two matrices $\mathbf{A}_0$, **A** as

$$\boldsymbol{A}_0 = [(\boldsymbol{C}^{I})^{-1} \;\; \boldsymbol{0}] \qquad\qquad \boldsymbol{A} = [\,-\boldsymbol{C}^{II}(\mathbf{C}^{I})^{-1} \;\; \boldsymbol{I}] \tag{6}$$

from standard algebraic manipulation it follows

$$\boldsymbol{u} = \boldsymbol{A}_0\,\boldsymbol{q} \tag{7}$$

with constraint of kinematic compatibility

$$\boldsymbol{A}\,\boldsymbol{q} = \boldsymbol{0} \tag{8}$$

and

$$\boldsymbol{Q} = \boldsymbol{A}_0^{T}(\boldsymbol{f}_0+\alpha\boldsymbol{f}_L)+\boldsymbol{A}^{T}\boldsymbol{Q}^{II}. \tag{9}$$

A standard limit analysis can be performed by means of upper bound or lower bound approach.
In the first case, upper bound approach, the linear problem (LP) is written as

$$\begin{aligned} &\textit{Determine min } \{\alpha = -\boldsymbol{\lambda}^T(\mathbf{A}_0\mathbf{M})^T\mathbf{f}_0\} \text{ subjected to:} \\ &\mathbf{AM}\boldsymbol{\lambda} = \mathbf{0} \\ &\boldsymbol{\lambda}^T(\mathbf{A}_0\mathbf{M})^T\mathbf{f}_L = 1 \end{aligned} \tag{10}$$

with the unknowns $\boldsymbol{\lambda} \geq \mathbf{0}$, $\alpha \geq 0$. $\mathbf{Q}^{II}$ are obtained as dual unknowns from the optimization routine.
In the second case, lower bound approach, the LP is

$$\begin{aligned} &\textit{Determine max } \{\alpha\} \text{ subjected to:} \\ &(\mathbf{AN})^T\mathbf{Q}^{II} + \alpha(\mathbf{A}_0\mathbf{N})^T\mathbf{f}_L + (\mathbf{A}_0\mathbf{N})^T\mathbf{f}_0 \leq \mathbf{0} \end{aligned} \tag{11}$$

with the unknowns $\mathbf{Q}^{II}$, α.
In this second problem the kinematic unknowns $\boldsymbol{\lambda}$ are obtained by the optimization routine as dual results. Note that for standard limit analysis $\mathbf{M} = \mathbf{N}$.

4 NUMERICAL SIMULATION

4.1 Modeling of masonry vaults by limit analysis

This paper examines only an outer groin vault (covering a corner hall) of minor dimensions, because the larger central vaults are counteracted by a series of barrel vaults on the south-west front and by large pillars or buttresses on the opposite front, towards the 'natatio' (swimming pool).

As part of a research work devoted to assess the safety of the structures of the Baths with particular reference to seismic actions, the live external load, $\mathbf{f}_L$, is represented by horizontal body forces which statically simulate the seismic action.

Hall I is rectangular in plan, so the orthogonal gores show different vault spans: 13.7 m the front span and 10.7 m the orthogonal one, with thickness of about 110 cm. The impost of the vault is 9.7 m above ground level. Dimensions of pillars in plan vary from 3.65 to 5.15 m.

The material of pillars and vaults is 'opus caementicium' that is roman concrete made by an aggregate of tufa rubble stone and a hydraulic mortar of lime and pozzolana.

As said above this material should be modeled properly as a continuum material with some resistance in tension; for future development a moderate tension resistance will be introduced in the 3D model, as already made in 2D models.

However the continuum behavior of this kind of masonry strongly depends on parameters not always easily determinable, so a discrete approach is sometimes preferable.

The model involves 52 bodies or blocks of hexahedral shape and 92 quadrilateral contact faces. This means that in case of upper bound approach the problem has 1288 kinematical unknowns $\boldsymbol{\lambda}$ and 241 constraint equations, otherwise in case of lower bound approach the problem has 240 static unknowns $\mathbf{Q}^{II}$, plus α, i.e. 241 unknowns and 1288 constraints

equations. Exchange between number of constraints and number of unknowns comes from the duality of the two approaches.

Authors know by experience that the LP problem, even if it is linear or linearized, often encounters numerical difficulties in finding correct results; for this reason the number of units chosen to constitute the structure is limited, anyway the very restriction concerns the number of units used to model the gores, whereas the limited number of the pillar blocks doesn't affect the result. Note that abutment units have been inserted in the model since these masses are able to counteract the thrust of the vaults and to stabilize the pillars with their load. At last, the model doesn't take into account masonry walls of minor thickness resting between the bearing pillars.

4.2 Solution strategy

As described above the model data need algebraic manipulation before passing them to an optimization routine; manipulation consists in creation of vectors and matrices, inversion, transposition, binding of matrices and multiplication of matrices by vectors. To speed up the procedure all this operations are automatically performed in sequence by a series of FORTRAN routines. All the process requests a handful of seconds also with large dimension problems.

Above recalled numerical difficulties in optimization process recommend to proceed step-by-step solving, in advance, sub structures, namely parts of the entire vault.

This strategy, moreover, permits to detect and correct errors in the numerical model.

The real Achilles' heel of the whole procedure are the minimization routines: more or less all of the attempted approaches showed to be inefficient in solving problems with a moderately large number of unknowns and constraints.

We tested the 'revised simplex method' in IMSL MATH Library running in FORTRAN and a number of linear optimization routines in the MATLAB environment: these are 'simplex', 'dual simplex', 'interior point legacy' and 'active set' methods.

All of the tested methods failed to reach a solution for the upper bound approach when calculating the optimal point for the larger model, the complete one.

It appeared that the numerical problem was beyond the capacity of all the tested optimization programs. This fact is worthy of discussion.

The simplex method, pretty well known and easy to understand from a theoretical point of view, fails to find a starting point, named 'feasible point', to begin search of the optimal solution and give a warning: 'infeasible problem'; moreover warns about the 'strictness of equality constraints'.

Really, the upper bound approach (see eq. 10) introduces in the algorithm equality constraints, which complicates the finding of a starting 'feasible point'.

So we reverted to use the lower bound technique (see eq. 11) where there are a greater number of constraint equations but these are inequality constraints, so less stringent than in the first case. Finally, an explanation of the difficulties encountered by numerical problem may depend also on the real complexity of the problem; as will be seen below the collapse mechanism activates many faces of the yield domain at the same time, due to the static indeterminacy of the structure, because of a largely greater number of joints with respect to the number of bodies (see for instance Figure 4).

4.3 Results of analyses

The first attempt to carry out an analysis on a substructure is plotted in figure 3: two opposite gores interacting only between joints at the apex of the vault. Direction of horizontal mass action is also depicted in the figure. Due to reduction of number of unknowns and restraints in the model, this numerical problem results easy to be solved by all the optimization routines described above. The kinematic mechanism involves the overturning of two of the four pillars and an arch-like behavior of the two opposite gores. This is, in fact, the standard in-plane behavior of an arch without a steel tie rod, which would oblige the pillars to overturn jointly (Baggio 2009). It can be seen, also, the formation of three cylindrical hinges in the arch at the intrados – extrados – intrados, alternatively, as in an arch, and the fourth hinge at the foot of the right pillar.

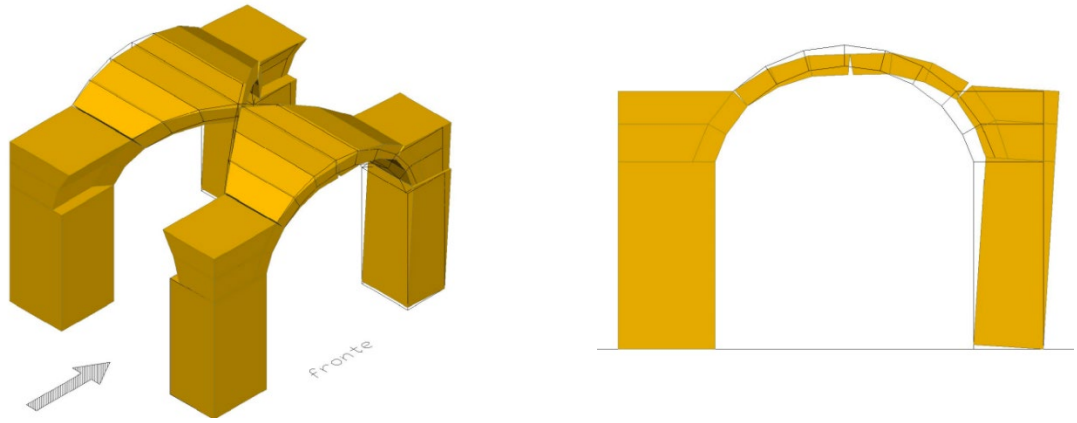


Figure 3: Two opposite gores, axonometric and front view of the collapse mechanism, $\alpha_c = 0.116$

The value of the collapse multiplier $\alpha_c = 0.116$ shows that this structure would be relatively weak, unable to withstand an earthquake as expected in Rome, according to the Italian Building Code.

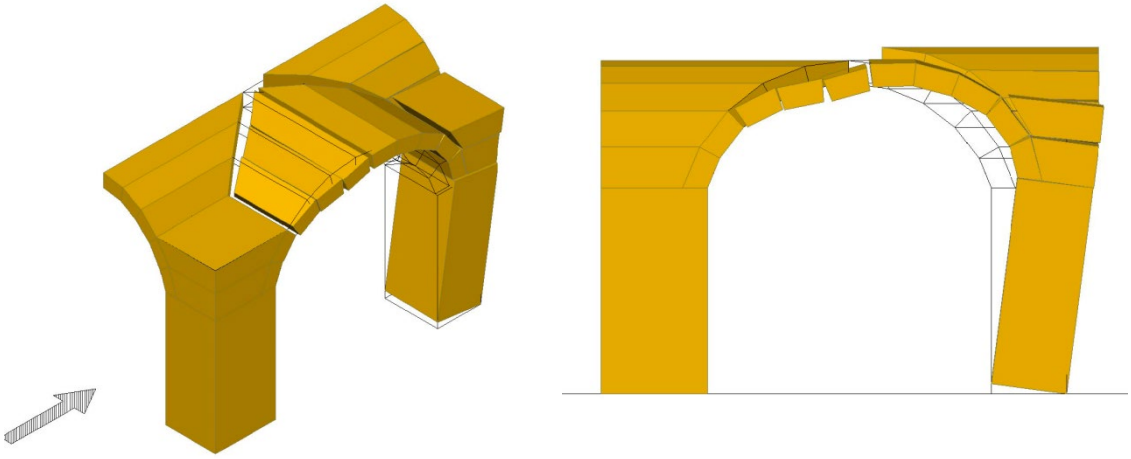


Figure 4: Half symmetric vault: axonometric and front view of the collapse mechanism, $\alpha_c = 0.269$

The second test has been carried out on a symmetric half vault (figure 4). The structure is restrained along the middle axis by external interfaces which act as simple supports with a very low friction coefficient (f = 0.1); again numerical difficulties prevent the reaching of a correct solution when putting to zero the friction in that joints. This fact probably interferes with the collapse mechanism, forcing again an arch-like behavior, but producing a far higher value of the collapse multiplier ($\alpha_c = 0.269$).

In figure 4 can also be observed a number of gaps in some joints; use of linear optimization, as would be correct in presence of associate flow rule implies the introduction of dilatancy in the interfaces. When sliding occurs it give rise to a correspondent normal component of displacement producing the observed gaps. In other words friction is replaced by dilatancy.

The analysis of the complete model in Figure 5 finds out a collapse multiplier α_c comparable with that found for the half model, whereas the mechanism involves the overturning of the four pillars, showing a tridimensional behavior far from in-plane behavior of arches.

A conclusion can also be drawn regarding the safety assessment of the Hall I in the Baths; according to Italian Seismic Code, spectral acceleration required in comparison with the calculated collapse multiplier α_c should vary from 0.12 to 0.20, depending on the accepted return period of the expected earthquake. The complete cross vault analyzed ($\alpha_c = 0.284$) is able to withstand future quakes without need to insert steel tie rods or other strengthening apparatus.

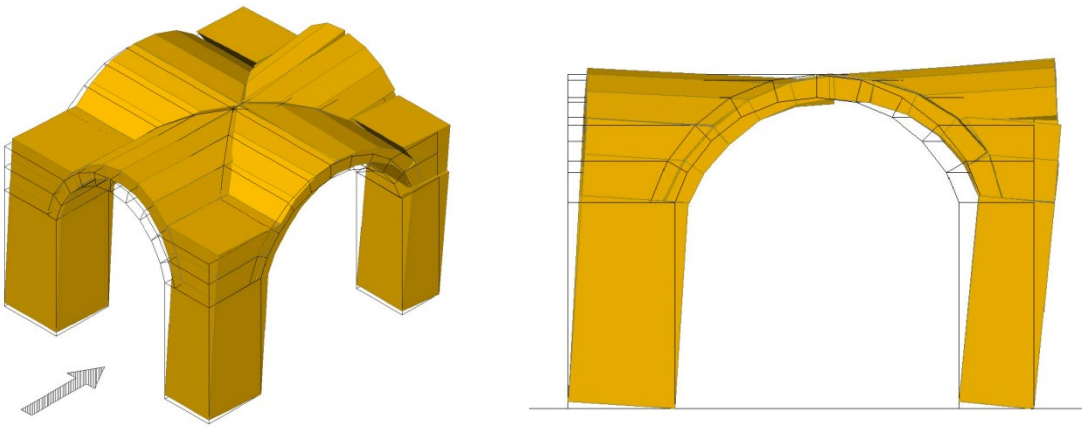


Figure 5: Complete model, axonometric and front view of the collapse mechanism, $\alpha_c = 0.284$

5 A MODIFIED SIMPLEX ALGORITHM

With the attempt to overcome the numerical difficulties due to a large number of blocks and joints, it would be useful to have a proper optimization procedure.

In what follows, in order to specifically deal with the matters concerned, the adopted procedure that makes use of a modified simplex method will be described step by step.
An optimization tableau via the simplex method is usually represented as

$$\begin{vmatrix} 1 & -c^T & 0 \\ 0 & D & b \end{vmatrix} \tag{12}$$

in which the first row defines the objective function and the remaining rows define the constraints. If D can be rearranged to contain an identity matrix I, of maximum range nr (where nr is the number of rows), a tableau in canonical form becomes

$$\begin{vmatrix} 1 & 0 & -\underline{c}^T & z_b \\ 0 & I & E & b \end{vmatrix} \tag{13}$$

The variables corresponding to the columns of **I** are the "basic variables", all other unknowns are the "non-basic variables". The values of the basic variables are easily obtained by setting the non-basic variables equal to zero, in this case the basic variables are equal to the right-hand side **b**. The resulting objective function, even if not optimal, identifies a feasible point anyway.

Unfortunately, this procedure runs only for non-negative values of the right-hand side **b**.

A linear problem not given in canonical form could be managed by introducing *nr* artificial variables, s, named 'slack variables'. A new objective function, z_0, is introduced as first row of the tableau as the sum of the slack variables.

$$\begin{vmatrix} 1 & 0 & 0 & -s^T & 0 \\ 0 & 1 & -c^T & 0 & 0 \\ 0 & 0 & D & I & b \end{vmatrix} \tag{14}$$

By minimizing the new artificial objective function z_0, again with the simplex method, the algorithm ends when $z_0=0$; this means that all the artificial variables assume zero value. As a consequence, the artificial objective function and the slack variables can be eliminated giving rise to a canonical tableau equivalent to the original problem.

In the present formulation, the constraint equations (eq. 10) have the right-hand side **b** which is zero, except for the last one term. This suggested a new approach aimed to obtain a feasible point. The procedure consists in a Gauss elimination on *nr*-1 columns and rows obtaining an identity matrix with range *nr*-1 and non negative b terms, that is a quasi-canonical tableau.

$$\begin{vmatrix} I & E & 0 \\ 0 & e_{nr}^T & 1 \end{vmatrix} \tag{15}$$

Again it is mandatory to introduce an artificial objective function, z_0, but the proposed procedure allows to introduce a single slack variable instead of *nr* ones. So the minimization of z_0 is much more manageable and numerically stable.

The linear problem described can be represented in *tableau form* as follows (Table I); the first two rows and columns correspond respectively to the artificial objective function and to

the true objective function z. The crosshatch identifies matrix **I**, derived from the Gauss elimination.

Table I – Tableau form of the linear problem

	z_0	z	x_1	x_2	x_3	x_4	x_5	x_{nc}	s	RHS
row -1	1	0	0	0	0	0	0	0	-1	0
row 0	0	1	0	0	0	e	e	e	0	0
row 1	0	0	1	0	0	e	e	e	0	0
row 2	0	0	0	1	0	e	e	e	0	0
row 3	0	0	0	0	1	e	e	e	0	0
row nr	0	0	0	0	0	e_{nr}	e_{nr}	e_{nr}	1	1

A row addition of the last row to the first one, called *pricing out,* gives the second tableau (Table II), where the row -1 and the row nr became equal, except for the s column.

Table II – Pricing out

	z_0	z	x_1	x_2	x_3	x_4	x_5	x_{nc}	s	RHS
row -1	1	0	0	0	0	e_{nr}	e_{nr}	e_{nr}	0	1
row 0	0	1	0	0	0	e	e	e	0	0
row 1	0	0	1	0	0	e	e	e	0	0
row 2	0	0	0	1	0	e	e	e	0	0
row 3	0	0	0	0	1	e	e	e	0	0
row nr	0	0	0	0	0	e_{nr}	e_{nr}	e_{nr}	1	1

At this point the phase I begins, aiming to obtaining the minimum value of the z_0 function, indeed equal to 0. The phase I starts by choosing an entering variable, that's to say a new basic column (Table III).

Table III - Choosing an entering variable

	z_0	z	x_1	x_2	x_3	x_4	x_5	x_{nc}	s		RHS
row -1	1	0	0	0	0	e_{nr}	e_{nr}	e_{nr}	0		1
row 0	0	1	0	0	0	e	e	e	0		0
row 1	0	0	1	0	0	e	e	e	0		0
row 2	0	0	0	1	0	e	e	e	0		0
row 3	0	0	0	0	1	e	e	e	0		0
row nr	0	0	0	0	0	e_{nr}	e_{nr}	e_{nr}	1		1

Phase I makes use of the simplex method; the task remains hard owing to the particular structure of the right hand side terms, which, at the beginning represent a degenerate vector (all the terms except one are 0) able to cause stalling or cycling. Numerical methods perform badly often, due to the fact that the matrix includes at the same time numbers too large or too small in magnitude.

The presented method try to avoid initial numerical difficulties performing a Gauss

elimination with full pivoting so that the E matrix contains number not too different in magnitude.

The proposed procedure nonetheless succeeds to reach almost always a correct result. In this case, when $z_0 = 0$, the artificial variable, s, can be eliminated, together with the column -1 and the row -1, producing a canonical tableau equivalent to the original problem (Table IV).

Table IV – Canonical tableau

		z	x_1	x_2	x_3	x_4	x_5	x_{nc}	RHS
objective f.	row 0	1	0	0	0	e	0	e	b_z
constr. eq.	row 1	0	1	0	0	e	0	e	b
"	row 2	0	0	1	0	e	0	e	b
"	row 3	0	0	0	1	e	0	e	b
"	row nr	0	0	0	0	e	1	e	b

The canonical tableau in Table IV represents a *feasible solution*; this one could be passed to a standard simplex routine for Phase II, avoiding the problems described in 3.2. The 3D arch in Figure 6, performing phase I, converges after 2 iterations only. 50 iterations are necessary to complete the phase II, reaching the optimum value of the collapse multiplier α_c.

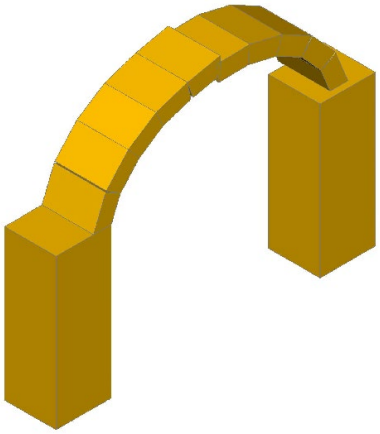


Figure 6: 3D arch model – $\alpha_c = 0.187$

6 CONCLUSIONS

The proposed methodology, even though discrete, succeeds in picking out the main characteristics of the behavior of complex vaulted structure, evaluating and quantifying the relative weakness of ruined cross vaults. It also gives an answer to question posed in the introduction: the pillars of each vault are able to withstand to thrust without contribution from adjacent walls.

In the paper, an original solution strategy aimed to overpass the common difficulties given by the application of linear optimization algorithms has been implemented with satisfactory results in terms of both collapse mechanisms and collapse multipliers. The strategy is based

on a modified simplex algorithm which allows to obtain a quasi-canonical tableau preliminary to the running of the optimization procedure.

A specific preprocessor able to manage the complexity of the overall 3D geometry, has also been developed.

For future work a moderate, or random, tension resistance will be introduced in the model, to better represent roman concrete. Effects of foundation settlements could also be analyzed, simply by varying some constant terms in the eq. 10 and the live load.

Acknowledgements. We wish to express our special thanks to Dr. Rosanna Friggeri past director of the National Roman Museum – Baths of Diocletian, and to Arch. Marina Magnani Cianetti past supervisor of the restoration of the Ludovisi's cloister, recently open to museum visitors.

REFERENCES

[1] Baggio, C. & Trovalusci, P. Collapse behaviour of three-dimensional brick-block systems using non-linear programming. *Structural Engineering and Mechanics* (2000), **10**(2): 181-195.

[2] Murty, Katta G. *Linear programming*, John Wiley & Sons (2000).

[3] Casapulla, C. & D'Ayala, D. Lower-bound approach to the limit analysis of 3D vaulted block masonry structures. In: TG. Hughes & GN. Pande (Eds): *Computer Methods in Structural Masonry*, Vol. *5, Swansea,* Computers & Geotechnics Ltd (2001), pp. 177-183.

[4] Ferris, M. & Tin-Loi, F. Limit analysis of frictional block assemblies as a mathematical program with complementarity constraints. *Int. J. Mech. Sci.* (2001), 43: 209-224.

[5] Baggio, C. Il restauro antisismico dei centri storici e la regola d'arte. *Ricerche di Storia dell'Arte* (2009), 99, 2: 19-29.

[6] Jackson, M. D., Logan, J. M., Marra, F., Scheetz, B. E., Deocampo, D. M., Cawood, C. G. Composizione e caratteristiche meccaniche dei calcestruzzi della grande aula, L. Ungaro, M. P. Del Moro, M. Vitti (Eds), *I mercati di Traiano restituiti – studi e restauri 2005-2007*, Roma, Palombi (2010), pp. 145-153.

[7] Nizzi, I. & Baggio, C. Vulnerabilità sismica delle grandi aule delle terme di Diocleziano. In: A. Centroni & M.G. Filetici (Eds): *Attualità delle aree archeologiche*; Atti del VII Convegno ARCo, Roma, 2014.

[8] Block, P., Lachauer, L. Three-dimensional (3D) equilibrium analysis of gothic masonry vaults. *Int. J. Architectural Heritage (2014)*, 8: 312-335.

[9] Baggio, C. & Trovalusci, P. 3D Limit analysis of Roman groin vaults, IBMAC 2016, Proc. 16th Int. Brick block Masonry Conf., Padua, Italy, CRC Balkema.

12th International Conference on Structural Analysis of Historical Constructions
SAHC 2020
P. Roca, L. Pelà and C. Molins (Eds.)

SIMULATION OF THE OUT-OF-PLANE BEHAVIOUR OF URM WALLS BY MEANS OF DISCRETE MACRO-ELEMENT METHOD

CÉSAR CHÁCARA[1*], BARTOLOMEO PANTÒ[2], FRANCESCO CANNIZZARO[3], DAVIDE RAPICAVOLI[3], IVO CALIÒ[3] AND PAULO B. LOURENÇO[4]

[1] Civil Engineering Division, Department of Engineering,
Pontificia Universidad Católica del Perú (PUCP)
Avenida Universitaria 1801, San Miguel, Lima 15088, Perú
e-mail: c.chacara@pucp.pe, www.pucp.edu.pe (*corresponding author)

[2] Department of Civil and Environmental Engineering, Imperial College London
South Kensington Campus, London SW7 2AZ, United Kingdom
email: bpanto@dica.unict.it, www.imperial.ac.uk

[3] Department of Civil Engineering and Architecture, University of Catania
Viale Andrea Doria 6, 95125 Catania, Italy
e-mail: {francesco.cannizzaro, ivo.calio@unict.it, davide.rapicavoli}@dica.unict.it, www.unict.it

[4] ISISE, Department of Civil Engineering, University of Minho
Azurem, 4800-058 Guimarães, Portugal
email: pbl@civil.uminho.pt, www.uminho.pt

Keywords: Nonlinear dynamic analysis, Parametric assessment, HiStrA software

Abstract. *The seismic response of masonry structures without box-type behaviour is given by a complex interaction between in-plane and out-of-plane behaviours. Previous earthquakes demonstrated that out-of-plane failure mechanisms represent the main cause of structural collapses of UnReinforced Masonry (URM) and historical structures. Previous experimental and analytical studies, investigating the out-of-plane behaviour of URM structures, mostly considered the effects of one-way bending moment. In this regard, recent experimental campaigns and numerical simulations have been conducted in order to investigate the out-of-plane behaviour of masonry walls subjected to two-way bending. These investigations have demonstrated the complexity of this mechanism and stressed the need for accurate numerical tools capable of providing reliable predictions in terms of ultimate strength and failure mechanisms. This paper focuses on the assessment of the dynamic behaviour of a U-shape URM prototype, subjected to shaking table tests, by means of a simplified computational strategy denoted as Discrete Macro-Element Method (DMEM). In this investigation, a comparison between experimental and numerical results was conducted in order to validate the capabilities of the proposed modelling approach. Subsequently, a parametric analysis was carried aiming at determining the influence that masonry mechanical properties, and additional model parameters, have on the out-of-plane nonlinear dynamic response of URM masonry structures.*

1 INTRODUCTION

UnReinforced Masonry (URM) buildings are characterized by a complex behaviour when subjected to dynamic loading. This behaviour is given by the high nonlinearity of the material together with the interaction between in-plane and out-of-plane mechanisms. There is a clear comprehension of the in-plane response of this typology of structures due to the different investigations that have been conducted experimentally, analytically and numerically. The out-of-plane behaviour of URM structures has been investigated by means of analytical and experimental formulations, mainly focusing on the effect of one-way bending loading [1-4]. During the last decades, there has been an increasing interest in understanding the two-way bending out-of-plane behaviour of these structures when subjected to seismic loading, as reported in recent experimental campaigns [5-7]. As reported in [8], numerical simulations were conducted by means of different methods aiming at predicting the response of the two-way bending out-of-plane response of URM structures. However, it was evidenced that this type of behaviour presents a significant complexity due to the diverse results obtained from the numerical simulations. In this sense, there is the necessity of understanding this particular behaviour in order to conduct proper and reliable predictions.

This paper consists of the evaluation of the two-way bending out-of-plane response of an URM structure by means of an original numerical technique known as the Discrete Macro-Element Method (DMEM) [9]. This modelling approach is based on a limited number of elements which allows the application of sophisticated nonlinear analyses with a reduced computational demand. The case study of this investigation corresponded to a U-shape clay brick masonry structure which was subjected to out-of-plane shaking table tests as reported by Graziotti, et al. [7]. Due to the available data of such experimental campaign [10], the numerical model of this structure was subjected to time history analyses based on the application of the signals recorded during the shaking table tests. The comparison between experimental and numerical responses was carried in terms of history of horizontal top displacement. In this investigation, a parametric assessment was conducted in order to determine the influence of some mechanical and model parameters on the nonlinear dynamic response of such a structure.

2 DISCRETE MACRO-ELEMENT METHOD (DMEM)

An innovative computational tool for the assessment of the seismic response of masonry structures, based on a reduced number of DOFs, was initially conceived by Caliò, et al. [11]. The initial formulation of this modelling approach was based on the hypothesis that masonry structures are characterized by a box-type behaviour due to the presence of a rigid diaphragm. Such initial formulation consisted of 2-dimensional panels constituted by hinged rectangles assembled with four rigid edges and two diagonal links. As shown in Figure 1a, the interaction between panels is given by zero-thickness interface elements. These interface elements are composed by a discrete distribution of transversal links (orthogonal to its length) and an additional single longitudinal link. The initial formulation of this modelling approach is capable of accurately simulating the main in-plane mechanisms of this typology of buildings: flexural, shear-diagonal, and shear-sliding. At an interface level, the discrete distribution of transversal links rules the flexural response, whereas the longitudinal link simulates the in-plane shear-sliding response. At an element level, the shear-diagonal response is given by a couple of diagonal links. The kinematic of the initial formulation is described by four DOFs: three related

to the rigid body motion, and the remaining one associated with the in-plane shear deformability.

Nevertheless, the seismic response of most URM buildings and historical constructions is often governed by the interaction of in-plane and out-of-plane mechanisms. As depicted in Figure 1b, this modelling approach was upgraded aiming at accounting for the out-of-plane mechanisms by the introduction of a new interface element [12]. The interface element is composed by a matrix of transversal links which simulate the bi-flexural response, a single link along its length, which governs the in-plane shear-sliding, and a couple of links along its thickness, which rule the out-of-plane shear deformability and torsion responses. In the upgraded version of this modelling approach, the in-plane shear-diagonal response is simulated by a single diagonal link placed at each 3-dimensional panel. The kinematic of the upgraded panel is described by seven DOFs: six associated with translational and rotational rigid body motion, and one related to the in-plane shear deformability. The proper simulation of these mechanisms requires careful calibration procedures for the different sets of links which are thoroughly described in [9].

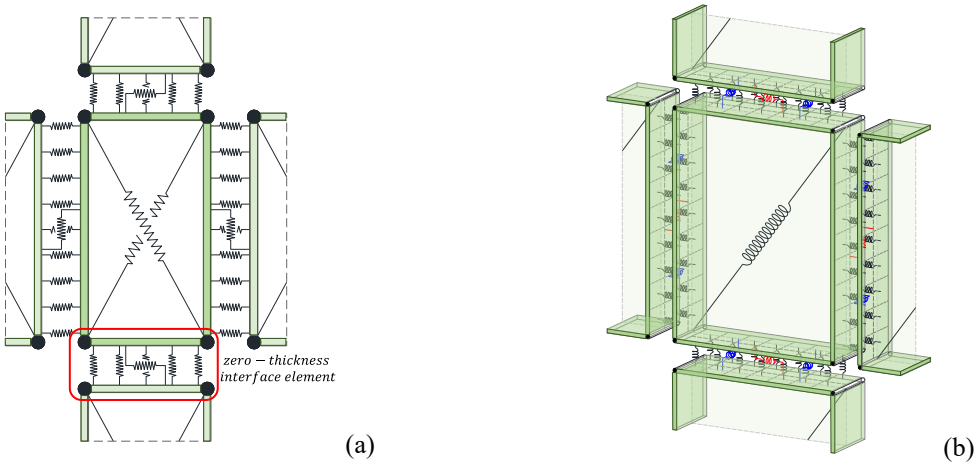
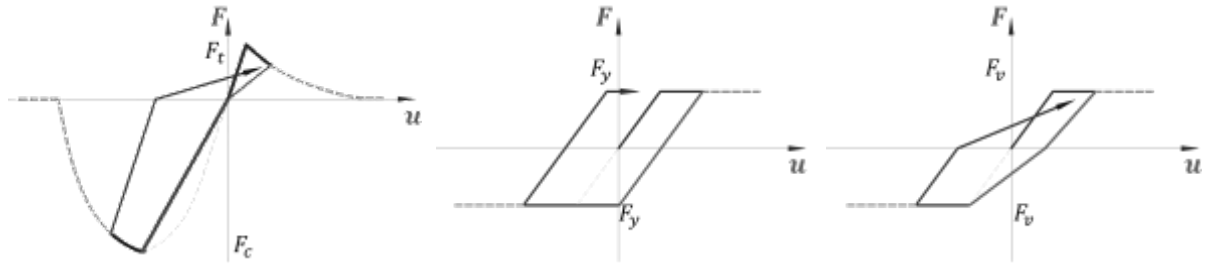


Figure 1: Mechanical scheme of the DME modelling approach: (a) two-, and (b) three-dimensional panels.

In the proposed modelling approach, the nonlinear and cyclic behaviours are focused on the different sets of links. In the case of the transversal links, the tensile response is described by an exponential curve, whereas the compressive response is given by a parabolic curve; both described by a fracture energy approach. The hysteretic behaviour of the transversal links is ruled by a Takeda model [13] (see Figure 2a) which is described by an unloading parameter denoted as β whose value can range between 0 and 1. When β is equal to 1, the unloading cycle is described by a stiffness oriented to the origin, and when β is equal to 0, the unloading cycle is ruled by its initial stiffness. A linear combination between the initial stiffness and the stiffness oriented to the origin is defined when the unloading parameters β presents a value higher than 0 and lower than 1. The nonlinear behaviour of the sliding links is characterized by a Mohr-Coulomb criterion due to the frictional phenomenon of this type of response, and the cyclic behaviour is given by an elasto-plastic hysteretic model (see Figure 2b) Finally, the nonlinear behaviour of the diagonal link can be described by a Mohr-Coulomb or a Turnsek and Cacovic

[14] yielding criterion, whereas its cyclic behaviour is also ruled by a Takeda model (see Figure 2c). A detailed description of the constitutive and hysteretic models of the different sets of links can be found in [15].This modelling approach has been implemented in the software HiStrA (Historical Structure Analysis) [16].



(a) (b) (c)

Figure 2: Cyclic constitutive models of: (a) transversal, (b) sliding, and (c) diagonal nonlinear links.

3 OUT-OF-PLANE URM WALL

The present study consisted on the assessment of the seismic response, by means of the DMEM, of one of the U-shape URM structures reported in the experimental campaign conducted by Graziotti, et al. [7]. In such investigation, calcium silicate and clay brick walls, with different boundary conditions and pre-compression loads, were subjected to a series of shaking table tests aiming at evaluating their out-of-plane behaviour. These walls presented two return walls in order to consider the two-way bending effects on their dynamic response. The clay brick structure, denoted as CL-000-RF in [7], was selected as case study for the present investigation. As illustrated in Figure 3a, this structure presented a main wall with a base of 4.02 m, a height of 2.76 m, and a thickness of 0.10 m, which was restrained by two return walls with a length of 1.00 m which were subjected to a pre-compression load of 0.05 MPa. In this sense, it was considered that the main wall was characterized by a boundary condition in which three edges were fixed, and the remaining one was free (see Figure 3b). The CL-000-RF structure was subjected to 23 shaking table tests aiming at assessing its out-of-plane seismic response as well as the behaviour of the first natural frequency due to cumulative damage.

Graziotti, et al. [7] also conducted a mechanical characterization of this type of clay brick masonry aiming at determining its main mechanical properties such as Young's modulus E, compressive strength f_c, tensile strength f_t, initial shear strength f_{v0}, and friction coefficient μ. This mechanical characterization consisted of the application of simple compression, direct tensile wrench, and triplet shear tests. Additionally, torsional tests were applied for the estimation of additional nonlinear parameters such as initial torsional strength $f_{v0,tor}$, and torsional friction coefficient μ_{tor}. As reported in [7], the total mass of this structure presented a value equal to 2178 kg, which corresponds to a specific weight γ of approximately 13.5 kN/m^3. A summary of the mechanical properties obtained in [7] which were used in this investigation is reported in Table 1.

Table 1: Mechanical properties of the clay brick masonry reported in [7]

E [MPa]	f_c [MPa]	f_t [MPa]	f_{v0} [MPa]	μ [-]	$f_{v0,tor}$ [MPa]	μ_{tor} [-]
7500	17.41	0.41	0.18	0.63	1.13	1.63

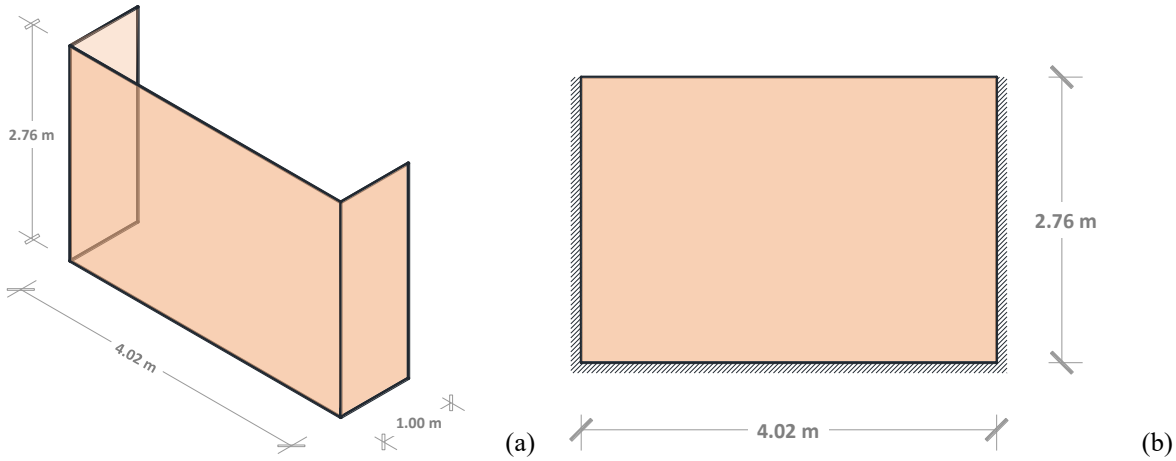


Figure 3: Clay brick structure: (a) geometrical characteristics, and (b) boundary conditions

A calibration of the elastic parameters was conducted with the DME model of the U-shape clay brick structure by initially comparing its first natural frequency with the one that was identified in the experimental campaign. Subsequently, the DME model of this structure was subjected to one dynamic loading with low intensity in order to compare the initial elastic response. Such dynamic loading corresponds to the motion registered at the base of the shaking table during Test #4 [10]. The mesh dependency of the DME model on the estimation of the first natural frequency and on the dynamic response was evaluated by considering three different mesh refinements (see Figure 4). Model A presents the less refined discretization, and it is characterized by 168 DOFs, Model B was described by a medium-mesh refinement with 336 DOFs. Finally, Model C represents the most refined mesh presenting 84 elements, and 588 DOFs.

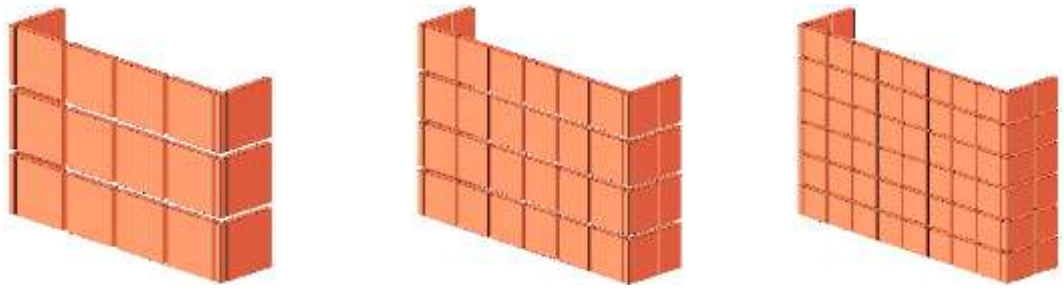


Figure 4: DME models of the U-shape clay brick structures

The experimental first natural frequencies of the undamaged CL-000-RF structure, resulted in 12.80 Hz. The first natural frequency of each model was initially evaluated considering the mean value of Young's modulus (E = 7500 MPa*)* obtained from the material characterization and considering a ratio between shear modulus G and E equal to 0.4 (considering Poisson ratio v equal to 0.25). The numerical frequencies resulted higher than those experimentally observed. The error was about 15% (15.04 Hz) in the case of Model A and increased when considering more discretized mesh refinements. Namely, an error of 21% (16.14 Hz) and 22% (16.46 Hz)

were observed in the case of Model B and Model C, respectively. Hence, it was necessary to decrease the value of the Young's modulus. As reported in Table 2, the dynamic identification was carried out considering two different values of E, and it was possible to determine a satisfactory fitting between numerical and experimental results when E = 5000 MPa.

Table 2: Natural frequencies of the first vibration mode of the Cl-000-RF structure.

Young's modulus E [MPa]	Shear modulus G [MPa]	First natural frequency f [Hz]		
		Model A	Model B	Model C
7500	3000	15.04	16.14	16.46
6250	2500	13.73	14.73	15.03
5000	2000	12.28	13.18	13.44

Subsequently, the numerical models were subjected to the dynamic motion recorded at the base of the shaking table during the Test #4, along the direction perpendicular to the main wall. This signal was characterized by a low amplitude of intensity, allowing the assessment of the elastic response of the structure. In addition, a Rayleigh damping criterion, with a damping ratio of 3%, and a diagonal mass matrix, in accordance with the kinematics of the proposed modelling approach, were taken into consideration for the application of these analyses. The Rayleigh damping parameters were defined by selecting the first and third natural frequencies of the structure for each numerical model. A constant time step discretization Δt = 0.001 sec was adopted for these analyses.

The comparison between numerical and experimental responses, which is illustrated in Figure 5, was focused on the history of horizontal displacement at the top of the main wall. It was observed that Model A presented higher displacements when compared to the experimental ones. These results are due to the large mesh of the models, which does not allow a properly simulation of the torsion effects and the mass distribution. Even though the difference decreased when considering a more refined mesh discretization (Model B), the approximation with the experimental results still lacked a reasonable resemblance. Nonetheless, it was observed that Model C was capable of successfully reproducing the displacements obtained during the experimental campaign; and therefore, this numerical model was selected for the nonlinear parametric assessment.

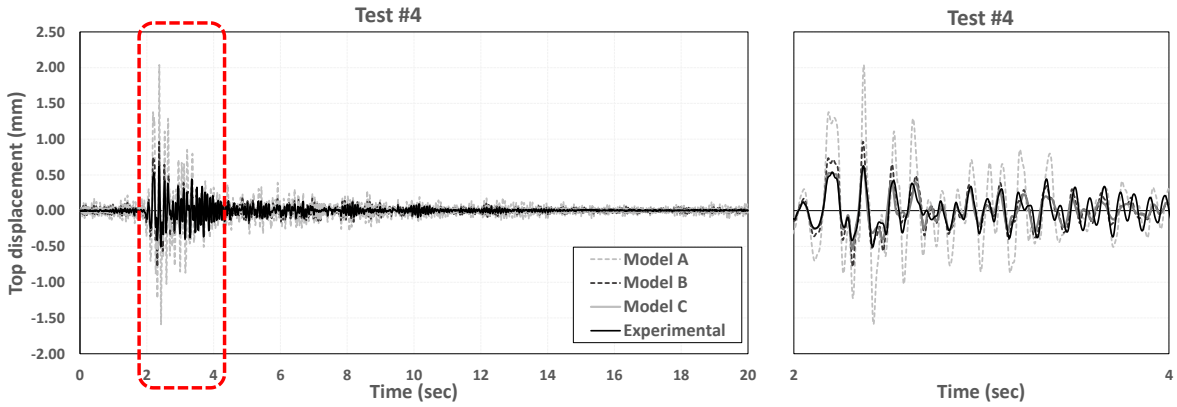


Figure 5: Comparison of horizontal top displacement due to the application of Test #4.

4 PARAMETRIC STUDY

A parametric assessment was conducted to the Model C considering the signals recorded during Test #18 and Test #21, aiming at reproducing the experimental results for high-intensity motions and identifying the parameters that most influence the nonlinear dynamic response of the prototype. The compressive f_c and tensile f_t strengths of masonry were taken from the experimental mechanical characterization, while the cohesion c and the friction coefficient μ ruling the shear-sliding mechanism were defined according to the torsional test conducted on brick joints in the experimental campaign. Finally, the strength f_{y0} associated to the shear-diagonal mechanism was considered equal to the tensile strength. A summary of the mechanical properties defined for the DME model is reported in Table 3.

Table 3: Mechanical properties of Model C for the parametric assessment

Elastic parameters	Young's modulus	E	[MPa]	5000
	Shear modulus	G	[MPa]	1667
	Specific weight	γ	[kN/m^3]	13.50
Flexural parameters	Compressive strength	f_c	[MPa]	17.41
	Compressive fracture energy	G_c	[N/mm]	28.28
	Tensile strength	f_t	[MPa]	0.41
	Tensile fracture energy	G_f	[N/mm]	0.012
Shear-diagonal parameters	Shear strength	f_{y0}	[MPa]	0.41
	Friction coefficient	μ_d	[-]	0.6
Shear-sliding parameters	Cohesion	c	[MPa]	1.13
	Friction coefficient	μ_s	[-]	1.63

An initial value of tensile fracture energy G_f equal to 0.012 N/mm was considered for the application of these analyses. However, it was noted that the response of the numerical model was characterized by significantly larger displacement for Test #18 and Test #21. In order to assess the influence of G_f on the dynamic response of the brick prototype, a parametric analysis was conducted considering three different values: 0.024 N/mm, 0.036 N/mm and 0.048 N/mm. The results of these analyses are illustrated in Figure 6. It was noted that a tensile fracture energy of 0.024 N/mm provided a good approximation in the case of Test #18; however, the fitting between numerical and experimental results of Test #21 was not in good agreement. An acceptable fitting was obtained adopting the value of 0.036 N/mm and 0.048 N/mm, which were assumed as the referring values of tensile fracture energy. It has to be noted that the latter numerical results presented displacements with a slightly lower amplitude to the experimental ones. In addition, the numerical results were still not capable of simulating the residual displacements that the structure experienced during the shaking table test.

A further parametric analysis aimed at investigating the influence of damping on the nonlinear response of this structure. In this sense, a second frequency associated with a higher vibration mode, with a natural frequency of 131.67 Hz and activating the 50% of the total mass, was selected for the definition of the Rayleigh damping parameters. This variation of the second natural frequency also affected the definition of the incremental time step for the time history analyses, presenting a new value of Δt = 0.0005 sec. The comparison between numerical and experimental responses is depicted in Figure 7, with reference to Test #21. It was observed that a significant increment of displacements was obtained when considering G_f = 0.036 N/mm.

This may indicate that the numerical model reached a larger nonlinear response which led to a higher displacement field. On the contrary, this behaviour was not observed when considering G_f = 0.048 N/mm since the increment of top displacement is barely noticeable.

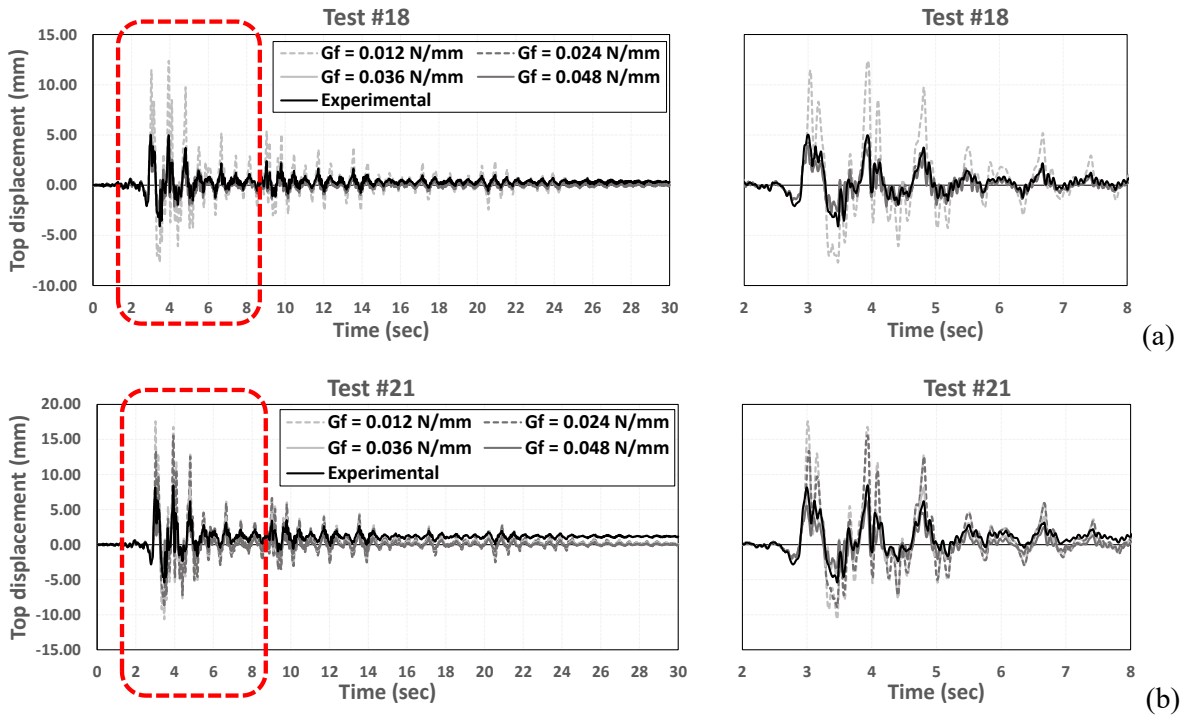


Figure 6: Comparison of horizontal top displacement as a function of tensile fracture energy.

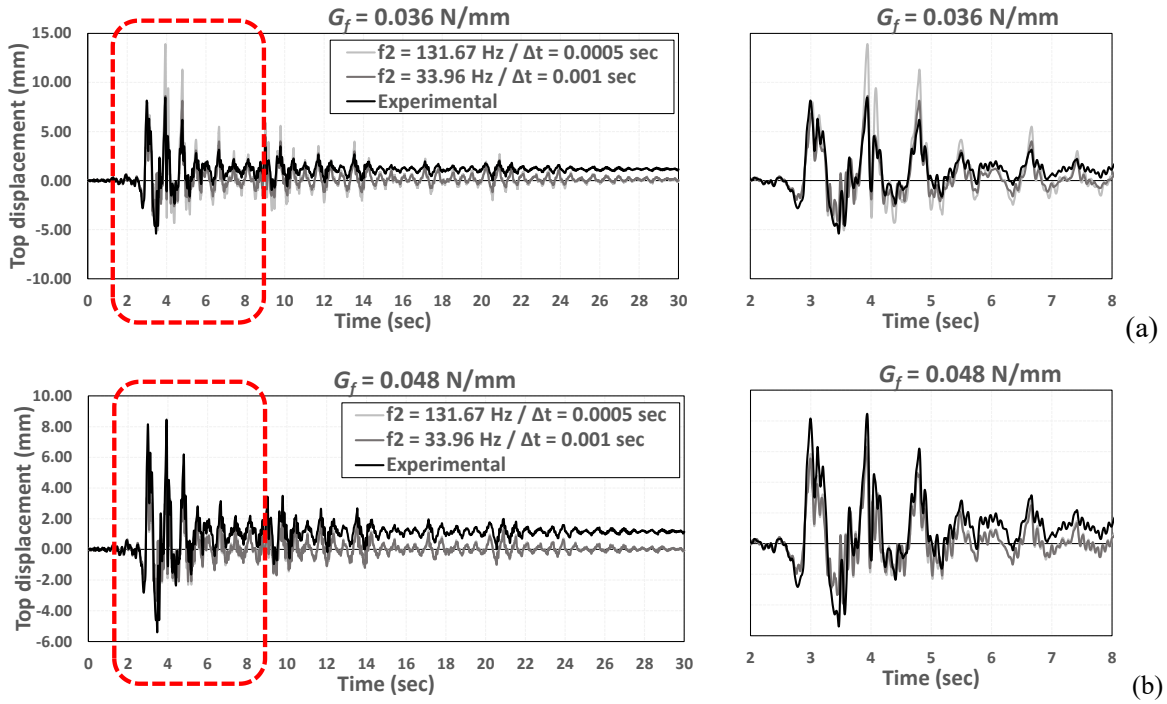


Figure 7: Comparison of horizontal top displacement as a function of damping parameters and time step.

Subsequently, the influence of the hysteretic behaviour of the transversal links on the numerical dynamic response was evaluated. The assessment of the influence of the unloading cycles was carried out considering a tensile fracture energy of 0.048 N/mm since it provided a more stable response. It is worth noting that the previous analyses were conducted considering tensile unloading cycles governed by a secant stiffness (oriented to the origin) with an unloading parameter $\beta = 1$. For this parametric assessment, mixed unloading stiffnesses were considered ($\beta = 0.90$ and $\beta = 0.80$). As shown in Figure 8, the numerical model did not experience significantly larger displacements; however, it was possible to evidence that the unloading cycles influenced the dynamic response of the structure in terms of residual displacement. A closer fitting with the experimental results was obtained when considering a tensile unloading parameter β equal to 0.80.

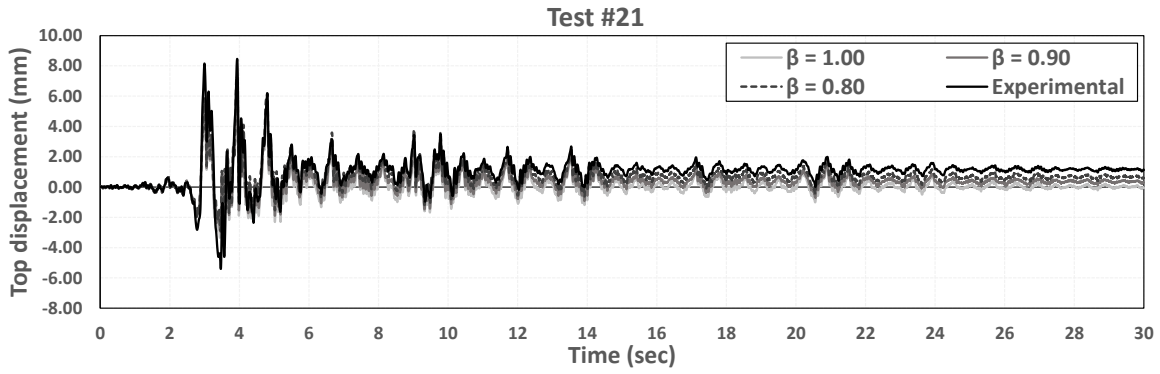


Figure 8: Comparison of horizontal top displacement as a function of tensile unloading cycles.

The final parameters investigated were associated with the shear-sliding response of the interfaces which influence not only the out-of-plane shear deformability and torsion behaviour of masonry but also its in-plane shear sliding mechanism. In this sense, an additional value of cohesion c and friction coefficient μ was considered for this parametric assessment. These values corresponded to those obtained by means of the triplet shear tests during the experimental campaign ($f_{v0} = 0.18$ MPa and $\mu = 0.63$). The variation of the shear-sliding parameters led to a small increment in the horizontal top displacement of the numerical model. In this last parametric assessment, the three tensile unloading conditions were taken into consideration. The one that provided an accurate fitting together with the reduced values of cohesion and friction coefficient corresponded to $\beta = 0.80$ which is illustrated in Figure 9. These results showed a good agreement in terms of residual displacement evidencing the influence on the cyclic constitutive models on the nonlinear dynamic response of URM structures. It is worth to note that the numerical model experienced a slightly larger displacements when compared to the experimental results; however, they are still considered acceptable.

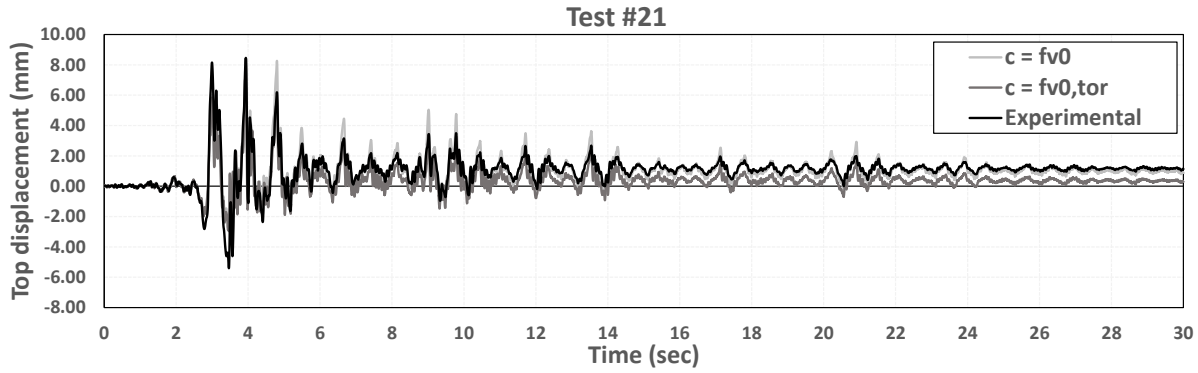


Figure 9: Comparison of horizontal top displacement as a function of shear-sliding parameters.

5 FINAL CONSIDERATIONS

This paper presents the evaluation of the out-of-plane behaviour of one URM structure using an innovative computational tool based on the Discrete Macro-Element Method (DMEM). This structure was subjected to out-of-plane two-way bending seismic loading by means of shaking table tests. The aim of this investigation focused on the simulation of the experimental response of this structure by means of numerical simulations. An initial calibration procedure was carried out in order to determine the elastic mechanical properties of the masonry material in order to reproduce the first natural frequency. In this initial calibration procedure, the dependency of the mesh discretization of the numerical model was also evaluated by the application of a signal recorded at the base of the shaking table during the experimental campaign. Due to the low intensity of this loading, it was possible to assess the response of the numerical models in the linear elastic field; and to determine an adequate model for the simulation of the dynamic response of the URM structure.

Subsequently, a parametric assessment regarding the nonlinear mechanical properties and additional model characteristic was conducted to the numerical model in order to determine the variables that present a significant influence on the out-of-plane nonlinear dynamic response of URM structures. For this purpose, two additional signals recorded during the experimental campaign were applied to the numerical model. These signals presented a higher intensity allowing the evaluation of the dynamic response in the nonlinear field. The variables that were considered for this parametric assessment were the tensile fracture energy, the tensile unloading cycles, the cohesion, friction coefficient, and the Rayleigh damping parameters. It was evidenced that the tensile fracture energy presented a significant influence on the nonlinear dynamic response of the URM structure. Due to the application of both signals, it was noted that a value of tensile fracture energy of 0.048 N/mm provided a good approximation to the experimental results. The variation of the Rayleigh damping parameters and the incremental time step also influenced on the nonlinear dynamic response of the numerical model of the URM structure, especially when considering a tensile fracture energy of 0.036 N/mm. In the case of a tensile fracture energy of 0.048 N/mm, there was a small increment of the displacements and a better representation of the dynamic response. The damping ratio remained constant during all analyses; however, it is worth noting that the influence of this parameter on the dynamic response of URM structure is also being investigated.

Moreover, it was also noted that a variation of the tensile unloading cycles the dynamic response of the URM structure in terms of residual displacements. When reducing the tensile unloading parameter from 1.0 to 0.8, the numerical model experienced larger residual displacements with a reasonable agreement with the experimental results. An alternative solution for the simulation of the residual displacements could be oriented to the definition on unloading cycles which consist on two stages: the first one associated with an initial stiffness, until a certain reduction of the maximum capacity, and a subsequently unloading with a secant stiffness. The last variable evaluated during this parametric assessment corresponded to the nonlinear properties associated with the shear-sliding response. Two values of cohesion and friction coefficient were taken from triplet shear and torsional tests conducted in the mechanical characterization. It was observed that these parameters also presented a slight influence on the nonlinear dynamic response of the URM structure by increasing the horizontal top displacement and also by contributing to the residual displacement of the numerical model. This parametric assessment stressed the need for a reliable mechanical characterization in order to properly predict the complex nonlinear dynamic response of this type of structures.

Finally, it is worth noting additional capabilities of the proposed modelling approach mainly in terms of computational burden. The analyses with an incremental time step of 0.001 sec (30,000 steps) presented a duration of approximately 40 minutes, whereas the ones with an incremental time step of 0.0005 sec (60,000 steps) lasted about 1 hour and 40 minutes using a conventional laptop. Due to the limited number of elements required for a proper simulation of the nonlinear dynamic response of URM structure; and consequently, a reduced computational demand, it was possible to conduct this parametric assessment. This can be extended for the evaluation of the nonlinear dynamic response of more complex structures for practical purposes, which is not feasible with more sophisticated computational tools.

REFERENCES

[1] H. Derakhshan, M. C. Griffith, and J. M. Ingham, "Out-of-Plane Behavior of One-Way Spanning Unreinforced Masonry Walls," *Journal of Engineering Mechanics,* vol. 139, pp. 409-417, (2013).

[2] O. Penner and K. J. Elwood, "Out-of-Plane Dynamic Stability of Unreinforced Masonry Walls in One-Way Bending: Shake Table Testing," *Earthquake Spectra,* vol. 32, pp. 1675–1697, (2016).

[3] T. M. Ferreira, A. A. Costa, R. Vicente, and H. Varum, "A simplified four-branch model for the analytical study of the out-of-plane performance of regular stone URM walls," *Engineering Structures,* vol. 83, pp. 140-153, (2015).

[4] F. Graziotti, U. Tomassetti, A. Penna, and G. Magenes, "Out-of-plane shaking table tests on URM single leaf and cavity walls," *Engineering Structures,* vol. 125, (2016).

[5] P. X. Candeias, A. Campos Costa, N. Mendes, A. A. Costa, and P. B. Lourenço, "Experimental Assessment of the Out-of-Plane Performance of Masonry Buildings Through Shaking Table Tests," *International Journal of Architectural Heritage,* vol. 11, pp. 31-58, (2017).

[6] J. Vaculik and M. C. Griffith, "Out-of-plane shaketable testing of unreinforced masonry walls in two-way bending," *Bulletin of Earthquake Engineering,* vol. 16, pp. 2839–2876, (2017).

[7] F. Graziotti, U. Tomassetti, S. Sharma, L. Grottoli, and G. Magenes, "Experimental response of URM single leaf and cavity walls in out-of-plane two-way bending generated by seismic excitation," *Construction and Building Materials,* vol. 195, pp. 650-670, (2019).

[8] G. de Felice, S. De Santis, P. B. Lourenço, and N. Mendes, "Methods and Challenges for the Seismic Assessment of Historic Masonry Structures," *International Journal of Architectural Heritage,* vol. 11, pp. 143-160, (2017).

[9] F. Cannizzaro, B. Pantò, S. Caddemi, and I. Caliò, "A Discrete Macro-Element Method (DMEM) for the nonlinear structural assessment of masonry arches," *Engineering Structures,* vol. 168, pp. 243-256, (2018).

[10] U. Tomassetti, L. Grottoli, S. Sharma, and F. Graziotti, "Dataset from dynamic shake-table testing of five full-scale single leaf and cavity URM walls subjected to out-of-plane two-way bending," *Data in Brief,* vol. 24, (2019).

[11] I. Caliò, M. Marletta, and B. Pantò, "A new discrete element model for the evaluation of the seismic behaviour of unreinforced masonry buildings," *Engineering Structures,* vol. 40, pp. 237-338, (2012).

[12] B. Pantò, F. Cannizzaro, I. Caliò, and P. B. Lourenço, "Numerical and experimental validation of a 3D macro-model for the in-plane and out-of-plane behaviour of unreinforced masonry walls," *International Journal of Architectural Heritage,* (2017). doi: 10.1080/15583058.2017.1325539

[13] T. Takeda, M. A. Sozen, and N. N. Nielsen, "Reinforced concrete response to simulated earthquakes," *Journal of the Structural Division,* vol. 96, pp. 2557-2573, (1970).

[14] V. Turnsek and F. Cacovic, "Some experimental result on the strength of brick masonry walls," in *2nd International Brick Masonry Conference*, Stoke-on-Trent, UK (1971).

[15] C. Chácara, F. Cannizzaro, B. Pantò, I. Caliò, and P. B. Lourenço, "Assessment of the Dynamic Response of Unreinforced Masonry Structures using a Macro-Element Modelling Approach," *Earthquake Engineering & Structural Dynamics,* vol. 47, pp. 2426-46, (2018).

[16] Gruppo Sismica s.r.l., "HiStrA (Historical Structure Analysis)," (2015), Catania, Italy, Release 17.2.3, http://www.histra.it.

12th International Conference on Structural Analysis of Historical Constructions
SAHC 2020
P. Roca, L. Pelà and C. Molins (Eds.)

STOCHASTIC MICRO-MODELLING OF HISTORIC MASONRY

JOHN ADAMEK[1*] AND PETR KABELE[2]

[1]Buro Happold Engineering
17 Newman Street, Fitzrovia, London, United Kingdom W1T 3EQ
e-mail: john.adamek@burohappold.com (*corresponding author)

[2]Faculty of Civil Engineering, Czech Technical University in Prague
Thákurova 7, 166 29 Prague 6 – Dejvice, Czech Republic
e-mail: petr.kabele@fsv.cvut.cz

Keywords: Historic masonry structures, nonlinear finite element analysis, micro-modelling, spatial variability of material parameters, random fields

Abstract. *The non-linear analysis of historic masonry structures can be difficult to perform due to the highly irregular geometric features, the inherent variability within the materials, as well as the limited amount of experimental data available. The present work details a specific methodology and result for the analysis of the compressive strength of the masonry found in walls of St. Ann's Church in the Czech Republic. A multi-scale 2D finite element modelling approach was adopted. In a mesoscale-level representation of masonry, "small stones" were grouped in with the mortar and treated as a matrix component with homogenized properties, while large stones were treated as discrete inhomogeneities. To characterize this matrix component, microscale-level models were used, in which only the "small stones" and mortar were represented. By simulating uniaxial compression and tension tests on multiple microscale-level models, statistical distributions for compressive and tensile strength, stiffness, and fracture energy were determined. On the mesoscale-level, overall stiffness and compressive strength were determined by simulating uniaxial compression tests on models involving only the large stones embedded in the homogenized matrix. The matrix was considered either as spatially uniform or variable. In the latter case, it was modeled with random fields based on the properties' distributions obtained from the micro-scale model analyses. Furthermore, the multi-scale study was performed for two different threshold sizes defining the "small stones" to compare differences. Approximate qualitative methods were utilized to validate the results.*

Overall, decreasing compressive strength was observed from the plain mortar to the micro-scale model of mortar with "small stones" to the meso-scale model of masonry. Models where matrix variability was represented with random fields exhibited similar failure mechanisms but with strengths 5-6% lower than models with a uniform matrix. Therefore, the effect of the spatial variability of the matrix properties was deemed insignificant.

1 INTRODUCTION

Historic masonry structures are oftentimes highly complex to analyze due to their inherent inhomogeneity on a local and global scale caused by the numerous geometric and material variabilities. While physical experiments offer a good way to estimate load and deformation capacities of masonry structures, they are very limited in scope when compared to the possible formations and variations of built masonry that exist in the world today [1]. The complex geometry and behavior of masonry is often modelled through the finite element method (FEM), where masonry can be idealized into macro-models, meso-models and micro-models [2]. Through recent advances in computer programming, masonry walls can be geometrically analyzed, and random, statistically representative geometries can be generated. Additionally, a few studies have been done reviewing the importance of the spatial variation of micro-parameters of masonry [2,3]. Based on the research done, the pairing of statistical analyses with structural analyses is shown to be beneficial when dealing with unknown materials or materials with highly variable properties, such as masonry [1]. In the present paper, a methodology is presented, which utilizes a multi-scale micro-modelling approach together with a stochastic non-linear analysis to obtain an overall compressive strength and stiffness of masonry, which can eventually be used in a structural-scale analysis of historic buildings. The procedure will be demonstrated on a case study of St. Ann's Church in the Czech Republic.

2 STATE OF ART REVIEW

2.1 Modelling and homogenization

The thesis [2] describes in detail the three main types of modelling for masonry structures: macro-modelling, meso-modelling and micro-modelling. The choice of model used highly depends on the overall goal of the analysis. When used together, these models can reliably mimic the behavior of the global structure as well as the units, mortar and joints, to fully understand masonry behavior in various applications and load cases [2]. Homogenization is the link between macro and micro-modelling of masonry. It is a process which simplifies the material into an equivalent continuum that represents the overall properties but disregards specific details on the units and mortar. Homogenization can be used to evaluate the linear and non-linear behavior of masonry and produces comparable results to that of experimental data [4]. Homogenization can be achieved using a representative volume element (RVE). The size of an RVE should be large enough to contain enough material inhomogeneities when viewed from the smaller-scale perspective (e.g. micro) but also small enough so that overall stress and strain variations within it are negligible when seen in the larger-scale model (e.g. macro). Then, by averaging micro-scale stress and strain fields over an RVE, one can obtain stress and strain in the corresponding material point on the macro-scale. By analyzing the behavior of the RVE under different suitable boundary conditions, the macro-scale stress-strain constitutive relations can be obtained.

Non-periodic masonry is defined as masonry containing units as well as mortar of irregular shapes and dimensions, with the spatial distribution of units and mortar being random. Since many historical structures are characterized by non-periodic masonry, studies such as [4,5,6], have utilized stochastic continuum micro-mechanics in unison with RVEs to determine a homogenized equivalent continuum. In [4], the elastic stiffness tensor of an RVE of a non-

periodic masonry structure was estimated by averaging results obtained from various arbitrarily chosen RVEs with randomized essential and natural boundary conditions. In a further study done in [6], a multitude of finite-sized test windows were made inside of a chosen RVE and an enhanced two-step convergence criterion was utilized, one being probabilistic and another mechanical, to determine if the test windows statistically match the RVE. From the analysis it was determined that a test-window size approximately 5 times the size of the largest dimension of stone was sufficient to statistically limit the geometric difference from the RVE [6].

2.2 Stochastic characterization of irregular geometry and material properties

When dealing with irregular geometry of units and joints, stochastic characterization of masonry can be utilized to account for the irregularities. For example, the authors of [5] applied the theory of random fields to determine the overall elastic properties of irregular masonry. Starting with the digital image processing of an image of the masonry, they evaluated the characteristics of the geometry and obtained statistical information in both the space and frequency domains. Correlation functions were then used to generate random fields to describe the geometric properties of masonry taking into account the deterministic properties of each constituent [5].

Typically, micro-models assume uniform material properties of individual phases. However, due to workmanship factors such as the batching of mortar, filling of joints, and factors effecting the curing of mortar, local material properties exhibit a spatial variation. For example, in [3], auto-correlated random fields were utilized in unison with micro-models to generate the spatial distributions of the strength of mortar and the unit-mortar interface within a masonry structure. The results in [3] showed that the overall force capacity decreased with the increase in correlation length of the random field, meaning that the effect of the spatial variability of the material properties should not be neglected as it may lead to an overestimation of strength [3].

3 METHOLOGY AND APPLICATION

3.1 History

Built in the early 18th century, St. Ann's Church is part of the Broumov Group of Churches located in the Czech Republic. The outer wall is composed of a three-leaf masonry, consisting of locally sourced stone. The external leaves contain irregularly shaped units of highly varying sizes with 5 stone types identified as ignimbrite, yellow sandstone, red sandstone, fine grained red sandstone, and light sandstone. The wall units are bonded together with natural hydraulic lime mortar. The internal leaf is thought to be filled with rubble infill. The walls are 1.2 m thick, with the external and internal layers 0.5 m wide and the infill 0.2 m.

3.2 Geometric statistical analysis

Due to the irregularity in stone size, shape, and placement, the external masonry leaf of St. Ann's Church was statistically analyzed to determine geometric detail of the models to be used for the analysis. The evaluation was completed by analyzing digital images of the front view of 6 sample wall panels with a size of 1 m². The size was approximately 3 times larger than the projected area of the largest stone observed within the structure. Images of two of the wall panels can be seen in Figure 1.



Figure 1: Wall section samples (2 of 6)

Results of the statistical analysis are illustrated in Figure 2. It was found that 80% of the area on average is stone, with the remaining 20% taken up by mortar. Utilizing a cumulative distribution function, it was seen that the size (projected area) of approximately 50% of stone elements was less than 0.001 m², and the size of approximately 68% of stones was less than 0.002 m².

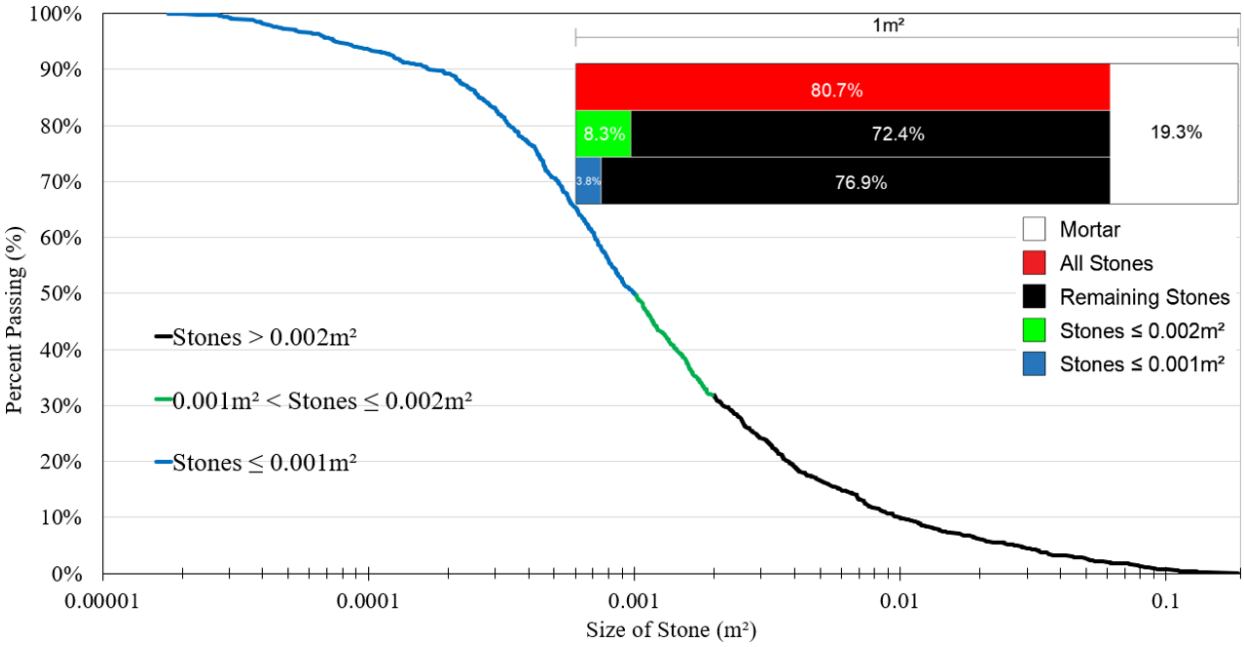


Figure 2: Statistical analysis of geometry of masonry wall sections and cumulative distribution of stone size

3.3 Material properties of masonry constituents

A combination of non-destructive and minor-destructive test methods were utilized to assist in the determination of material properties of the masonry constituents. More specifically, Schmidt hammer testing, masonry coring, SEM analyses, and porosity testing were completed in addition to obtaining expert estimates and reviewing past research [8,9]. A summarized list of values used in the analyses can be found in Table 1.

Table 1: Summary of material properties (values based on expert estimate / research marked by *)

Material	Unit Weight (kN/m³)	Young's Modulus, E (GPa)	Poisson's Ratio	Compressive Strength, f_c (MPa)	Tensile Strength, f_t (MPa)	Fracture Energy, G_f (N/m)	Ultimate Compressive Strain, ε (‰)
Lime Mortar	17.0	0.126*	0.17*	1.5*	0.10*	10*	1.2*
Ignimbrite	21	9.49	0.2	42	4.2*	60*	1.5*
Yellow Sandstone	21	7.51	0.2	29	2.9*	35*	1.5*
F.G. Red Sandstone	21	9.21	0.2	48	4.8*	40*	1.5*
Light Sandstone	21	8.50	0.2	45	4.5*	40*	1.5*
Red Sandstone	21	5.41	0.2	38	3.8*	40*	1.5*

3.4 Multi-scale modelling approach

The goal of the ensuing analyses was to estimate overall stiffness and strength of the front-leaf of the masonry wall by numerically simulating compressive tests, while accounting for its topology (Section 3.2) and the properties of its constituents (Section 3.3). As obvious from Figures 1 and 2, the masonry is highly irregular and consists of stones whose sizes span a broad range. Constructing a compatible finite element (FE) mesh over such a complex geometry proved to be a difficult task, even when using advanced meshing algorithms. Furthermore, the resulting models consisted of a very high number of elements, thus performing non-linear calculations was not feasible. Therefore, a multi-scale modelling approach was used. To this end, three scales with different levels of resolution were defined specifically for the present methodology (Figure 3). These are not to be confused with the micro/meso/macro-modeling approaches reviewed in Section 2.1:

- *Macro-scale* corresponds to the scale of the whole wall, where masonry is represented as equivalent homogenous continuum.
- *Meso-scale* corresponds to the scale of a typical wall panel, where only large stones are treated as distinct inhomogeneities, while the mortar and "small stones" are treated together as one matrix phase.
- *Micro-scale* corresponds to the scale of the joints between the large stones, which consists of "small stones" (as inhomogeneities) and mortar (as matrix).

The feasibility and quality of the meso-scale FE meshing in conjunction with the stones' cumulative frequency in the wall panels were both considered to decide the threshold size below which stones were classified as "small". In order to check sensitivity of the results to the definition of "small stones", analyses were conducted with two threshold size (projected area) values: 0.001 m^2 and 0.002 m^2. These values correspond to 50% and 68% of all the stones, respectively, as was shown in Section 3.2. Furthermore, these stone elements were thought to be small enough in size that they do not extend into the wall along the full depth of the first leaf (0.5 m) and, thus, could be combined with mortar in the 2D model.

The overall homogenized properties on each upper scale were obtained by numerically simulating material tests on representative square samples of the lower-scale structure. To this end, a sliding support was assigned to one edge and uniform normal displacement was applied along the opposite edge of the models (Figures 5a and 6a). Modelling and non-linear analyses were completed utilizing ATENA Science finite element software [10], assuming plane stress

and using triangular elements. A fracture-plastic constitutive material model, called "3D Non-linear Cementitious 2" [10], along with a fixed crack model and an exponential traction-separation law were used both for the matrix and the inhomogeneities (stones) with parameters listed in Table 1. The unit-mortar interfaces were modelled as rigid. The Newton-Raphson method was used to complete the analyses along with an energy error convergence tolerance of 10^{-4}.

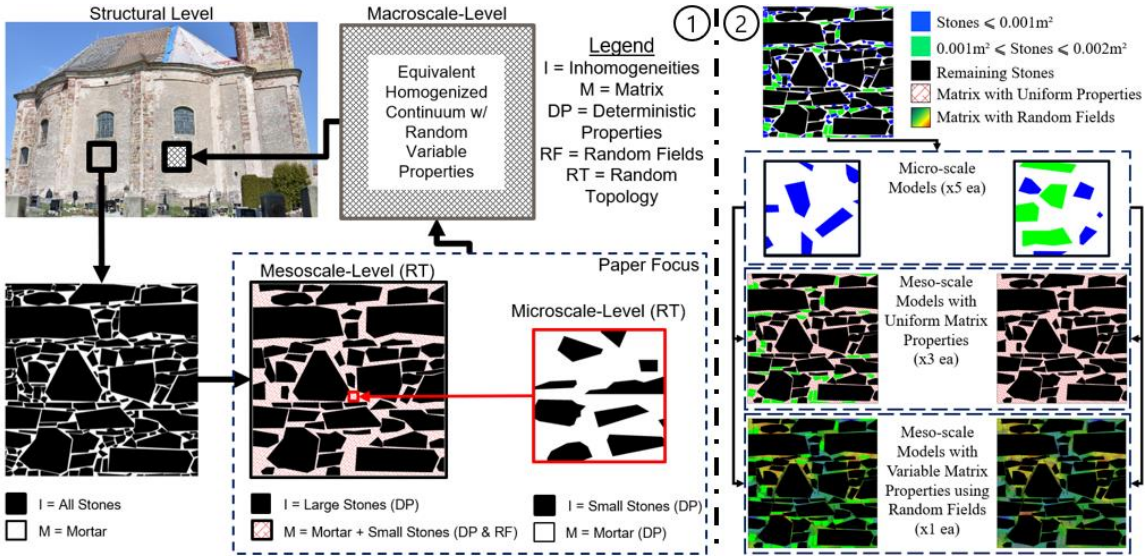


Figure 3: Overview of multi-scale modelling approach (left). Model type and quantity (right).

Multiple micro-scale models were tested in uniaxial compression and uniaxial tension to obtain statistical distributions for four main overall properties, namely Young's modulus (E), compressive strength (f_c), tensile strength (f_t), and fracture energy (G_f). For meso-scale models, only overall stiffness E and strength f_c were evaluated through simulated compressive tests. The overall stiffness was identified from the initial slope of the calculated stress-strain diagrams (Figure 7). Stresses were determined from the reaction forces divided by the cross-sectional area and strains were determined from the applied displacements divided by the length of the specimen. The strengths were determined as the peak attained stresses. The fracture energy was calculated from the area under the softening part of the stress-displacement curves.

The original morphology (Figure 1) did not contain any portion with only "small stones" and mortar that was suitably shaped and sized to allow for a sufficiently large square sample for the micro-scale level virtual testing. Therefore, several separate FE models were built on the micro-scale level using test-windows placed in randomly generated, statistically equivalent morphologies, in which only the "small stones" and mortar were represented. These equivalent morphologies were built by extracting the "small stones" from digitalized images of the sample wall panels and putting them into equivalent area of mortar, thereby ensuring the true area fraction, size and aspect ratio of the stone elements were statistically met. From there, the "small stones" were randomly scattered within the domain utilizing the "SCATTER" function in AutoCAD. Any overlapping stones were manually moved. Test windows were randomly placed using the same function. The windows' size was set to be at least 3 times the size of the largest stone dimension found within the mortar. Since the stones were randomly placed, the smaller

test-windows encompass the spatial variation in overall properties. The complete statistically equivalent morphologies and test windows for the two "small-stone" thresholds can be seen in Figure 4.

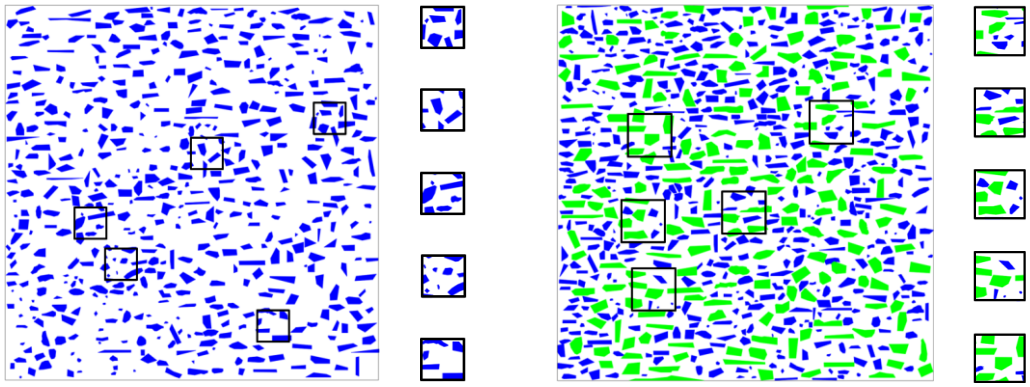


Figure 4: Statistically equivalent morphology and test-windows. Mortar with stones ≤ 0.001 m² (left), mortar with stones ≤ 0.002 m² (right)

The meso-scale models were constructed directly by FE discretization of the vectorized images of the sample wall panels, in which only the large stones were represented. For the meso-scale models, two sets of calculations were done. First, the matrix component was assigned uniform properties using the mean values obtained from the micro-scale models. Second, to capture the variability in the homogenized properties of the matrix component obtained from the micro-scale modelling analysis, random fields generated in FREET/SARA software package [11] were utilized to define each of the matrix properties (E, f_c, f_t, and G_f) in the meso-scale models. No correlation among the properties was assumed. The random fields were generated using the Latin hypercube sampling method assuming Gaussian distributions of the variables. The parameters of the distributions were defined by taking the mean and standard deviation of the values for the homogenized properties found from the micro-scale modelling analysis. The autocorrelation length, which defines the level of variability of the properties in space, was set to match the test window size of the micro-scale models studied. In total, 5 random fields were generated for the matrices of both types of meso-scale model. Due to time constraints only one meso-scale model was analyzed with random fields.

4 RESULTS

4.1 Micro-scale models

Figures 5 and 6 show the stress-strain diagrams and an example of the damage phenomena for the simulated uniaxial compression and tension tests on the micro-scale models. To interpret the failure mode under compression, contour plots for equivalent plastic strain (Figure 5b) and crack width (Figure 5c) before and after the peak stress were compared. In the fracture-plastic model, the plastic strain represents inelastic deformation due to compression. If there was a major jump in crack width without any increase in equivalent plastic strain, then the failure was categorized as tensile splitting. If the limit value of equivalent plastic strain was reached, then

compressive failure occurred due to crushing. The deformed shape (Figure 5d) was also analyzed to help determine if tensile splitting played a major role in failure. For simulated tensile tests, the micro-scale models were analyzed using contour plots for crack width (Figure 6b).

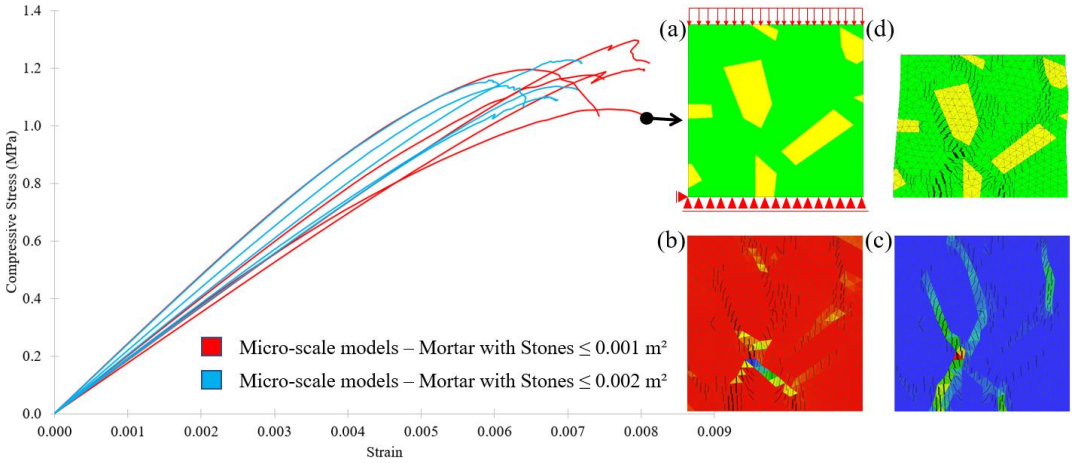


Figure 5: Stress-strain diagrams for micro-scale models under uniaxial compression test. (a) Micro-scale model with applied displacement and boundary conditions. (b) Post-peak equivalent plastic strain, (c) crack width, and (d) deformed shape with cracks after uniaxial compression test.

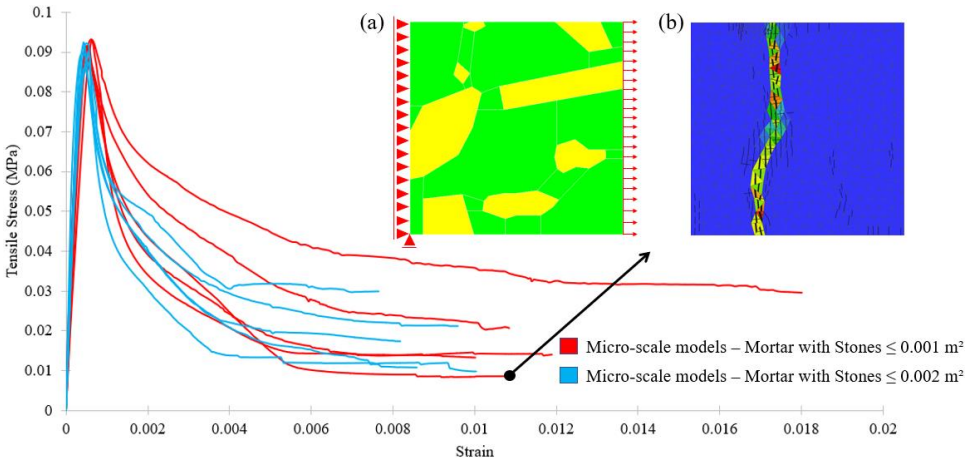


Figure 6: Stress-strain diagrams for micro-scale models under uniaxial tension test. (a) Micro-scale model with applied displacement and boundary conditions. (b) Post-peak crack width after uniaxial tension test.

The formation of cracks initiated the non-linear behaviour of the specimen. For the compressive tests, failure occurred due to compressive crushing, tensile splitting or a combination of both, depending on the sample morphology. Since the models were unrestricted along the vertical sides, they contracted in the vertical direction and expanded in the horizontal direction, which led to the formation of either one or multiple tensile splitting cracks in the mortar. Some of these cracks propagated through the entire height of the specimen leading to splitting failure, while others were constrained by the stones. High plastic strains typically developed in the mortar in the vicinity of the stiffer stones. When these regions spread over

much of the cross section, the compressive crushing failure occurred. For the tensile tests, failure was always caused by a fully formed crack within the mortar which developed along the easiest path around the stones, thus producing a tensile strength of the specimen close to that of the mortar. High fracture energies correlated to extremely tortuous cracks. Table 2 summarizes the homogenized properties determined from the completed analyses for both stone size thresholds.

Table 2: Summary of homogenized values for all micro-scale models

Type of Micro-scale Model	Results	Compressive Strength, f_c (MPa)	Tensile Strength, f_t (MPa)	Young's Modulus, E (MPa)	Fracture Energy, G_f (N/m)
Mortar with Stones ≤ 0.001 m²	Mean	1.18	0.091	199.06	23.90
	St.Dev	0.08	0.002	23.41	5.07
	COV (%)	6.44%	2.05%	11.76%	21.22%
Mortar with Stones ≤ 0.002 m²	Mean	1.15	0.090	208.53	24.82
	St.Dev	0.04	0.002	19.79	2.80
	COV (%)	3.61%	2.54%	9.49%	11.26%

The overall mean values for compressive and tensile strength of the microstructures are lower than those of the plain mortar, with little variability due to different morphologies, proving the models are heavily dependent on the properties initially set for mortar, since that is where the failure is concentrated. Furthermore, the irregular topology is shown to create stress concentrations which reduce the overall compressive strength. The modulus of elasticity and fracture energy both show increases when compared to those of the mortar, which can be attributed to the addition of the highly stiff "small stones" into the mortar. The values for fracture energy increased since the cracks that formed in the mortar were forced to propagate around the "small stones" instead of going through them. When comparing the results of the homogenized properties for the micro-scale models incorporating the two stone thresholds, the differences are very minor.

4.2 Meso-scale models with uniform matrix properties

Figure 7 depicts the stress-strain results of the meso-scale models with uniform matrix properties. The failure mode was analyzed by observing contour plots for equivalent plastic strain (Figure 7b) and crack widths (Figure 7c) before and after peak stress was attained as well as the deformed shape (Figure 7d). The locations of cracks and crack width values were seen to be relatively similar between the same type of meso-model, but there was a slight increase in the number of cracks in the models with a matrix including stones less than 0.001 m². Comparing post-peak equivalent plastic strain, the areas of concentration slightly change, with the models with a matrix including stones less than 0.002 m² having a few additional areas. Based on the deformed shaped, it was observed that the models failed due to a combination of local compressive crushing and tensile splitting within the matrix. In summary, the higher the proportion of the stones modelled as distinct inhomogeneities and not encompassed within the matrix component (i.e. the lower is the "small-stone" threshold value), the more cracks formed due to the increased irregularity in the model topology. Furthermore, a different "small stone" threshold also led to a change in the distribution of equivalent plastic strain. These results were typical for all meso-scale models tested. Table 3 summarizes the compressive strength and stiffness data gained from each of the meso-scale models.

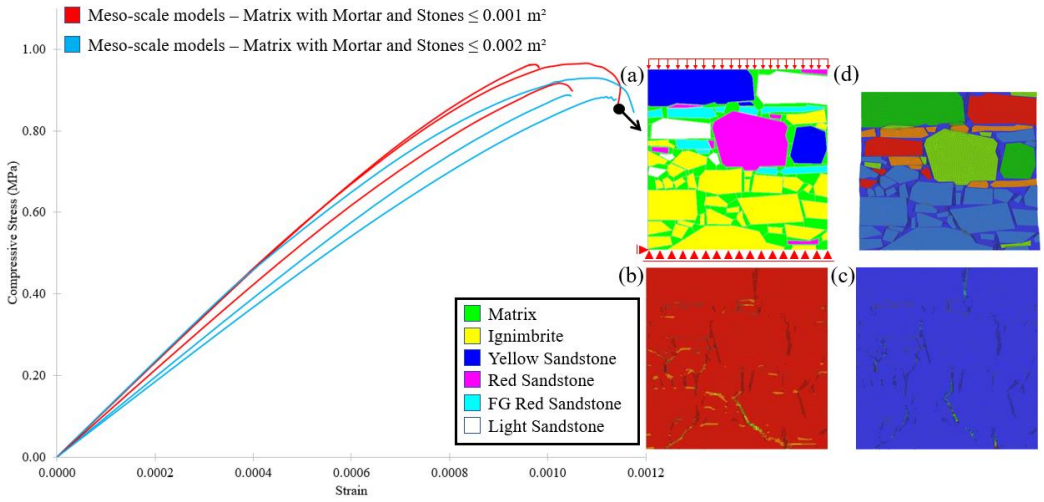


Figure 7: Stress-strain diagrams for meso-scale models with uniform matrix properties under uniaxial compression test. (a) Meso-scale model with applied displacement and boundary conditions. (b) Post-peak equivalent plastic strain, (c) crack width and (d) deformed shape after uniaxial compression test.

Table 3: Compressive strength and Young's modulus for meso-scale models with uniform matrix properties

Meso-scale Models	Wall Panel 1	Wall Panel 2	Wall Panel 3	Average	St. Dev	COV (%)
Compressive Strength, f_c (MPa)						
Matrix with Stones ≤ 0.001 m²	0.96	0.97	0.92	0.95	0.019	2.04%
Matrix with Stones ≤ 0.002 m²	0.89	0.93	0.88	0.90	0.017	1.96%
Young's Modulus, E (GPa)						
Matrix with Stones ≤ 0.001 m²	1.16	1.17	1.07	1.13	0.045	3.97%
Matrix with Stones ≤ 0.002 m²	0.98	1.18	0.92	1.02	0.111	10.83%

Overall, the compressive strength and Young's modulus of models with both "small-stone" threshold values were relatively close in value with a small variance. By observing the failure mechanism for each meso-scale model, it can be concluded that the irregularity in the topology of the wall panels created stress concentrations in the weakest component, in this case being the matrix, where it failed due to combined local crushing and tensile splitting.

4.3 Meso-scale models utilizing random fields

Utilizing the homogenized property distributions obtained from the micro-scale model analyses, random fields were generated for the four variables (f_c, f_t, E, G_f) of the matrix phase for meso-scale models of wall panel 2 considering both of the "small-stone" thresholds. Cracks occurred in the same locations for both models regardless of the spatial variability of the matrix material parameters. This was attributed to the low variability of the matrix strengths f_c and f_t (see COV in Table 2) for each random field realization. Furthermore, by comparing contour plots for the equivalent plastic strain for models with random fields versus models with a uniform matrix, it is seen that the areas of local crushing are similar. Any additional areas of local crushing are due to low compressive strengths produced by the random field for the matrix component in that area. A sample of the generated distributions for compressive strengths for

the two types of models along with post-peak crack locations are illustrated in Figure 8. Compressive strengths from the random field analyses are summarized in Table 4.

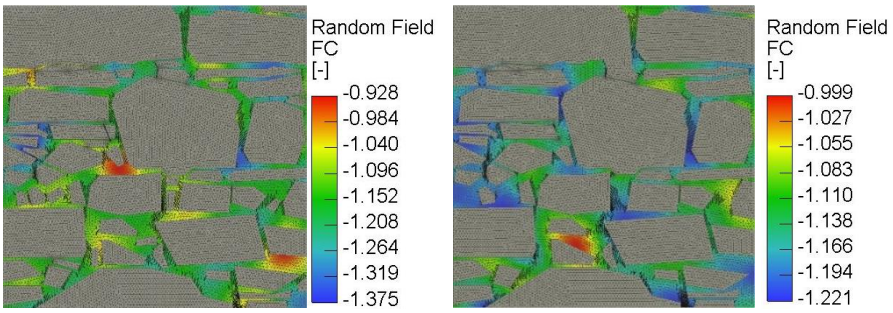


Figure 8: Random fields for f_c and post-peak crack locations. Meso-scale model with distinct stones > 0.001 m² (left), meso-scale model with distinct stones > 0.002 m² (right)

Table 4: Summary of compressive strength (MPa) for wall panel 2

Model	Matrix Incl. Stones ≤ 0.001 m²	Matrix Incl. Stones ≤ 0.002 m²
Model with Uniform Matrix	0.97	0.93
Model with Random Fields (Avg of 5)	0.91	0.88
Mean	0.92	0.89
St. Dev	0.03	0.02
COV (%)	3.50%	1.98%

Based on the results, by considering spatial variability of the matrix, the overall compressive strength of the masonry wall panel was reduced by 0.05 MPa for both matrices containing different thresholds of stone sizes. The spatial variability caused a minor reduction in overall strength when compared to models with a uniform matrix, which is attributed to introduction of weaker properties on a local scale generated by the random fields.

4.4 Verification

To verify sanity of the results, simple comparisons for the overall uniaxial compressive strength were made to literature and other methods for historic masonry structures. First, the Masonry Quality Index (MQI) method as seen in [12], was used to determine the compressive strength based on a qualitative assessment of the walls of St. Ann's Church. Utilizing this method, an MQI of 1.05 was obtained, which correlates with a uniaxial compressive strength of around 1 MPa. Furthermore, reviewing the Italian code for masonry, the uniaxial compressive strength of irregular stone masonry is 1-1.8 MPa [13]. These values are comparable to the values attained from the analyses. Furthermore, the Young's modulus of 1 GPa attained from the meso-scale models lines up with the upper limit given in [13]. The minor difference in strength could be due to the low values that were set for the mortar during the micro-scale modelling analyses.

5 CONCLUSIONS

Based on the multi-scale modelling approach utilized, the uniaxial compressive strength of the front leaf of the masonry walls of St. Ann's Church was determined to be 0.9 MPa. The predicted strength decreased when moving through the respective modelling levels from micro to macro. This decrease was attributed to the non-uniformity of the topology which caused

stress concentrations in the weak material at each level, leading to combined failure mechanisms from both local compressive crushing and tensile splitting. The use of random fields showed minor decreases in compressive strength, with the location of cracks and failure mechanisms remaining similar throughout all meso-scale models. In summary, the results of this study show that the spatial variability of the matrix component can be neglected due to the small variation in the distributions of the homogenized properties obtained but should be reconsidered if the variation become larger after analyzing more randomized micro-scale models. Furthermore, the present modelling approach is shown to produce sound results and allows for the analysis of masonry in full detail by incorporating the effect of the "small stones" without having to explicitly model them on a meso-scale level. Nevertheless, a large number of micro-scale models are required to increase reliability of the statistical distribution, which leads to a time-consuming process and is therefore not recommended for use in a practical setting.

Acknowledgements. This study was completed during the SAHC MSc. program. The authors would like to thank the SAHC Consortium, David Biggs, Prof. Ing. Pavel Kuklík CSc., Ing. Zuzana Slížková Ph.D., and Červenka Consulting for their expertise and guidance.

REFERENCES

[1] Zhang, S., Hofmann, M., & Beyer, K. (2018). A 2D typology generator for historical masonry elements. *Construction and Building Materials*, *184*, 440–453.
[2] Lorenço, P. (1996). *Computational Strategies for Masonry Structures*. Delft University.
[3] Zhang, S., Taheri Mousavi, S. M., Richart, N., Molinari, J. F., & Beyer, K. (2017). Micro-mechanical finite element modeling of diagonal compression test for historical stone masonry structure. *International Journal of Solids and Structures*, *112*, 122–132.
[4] Cluni, F., & Gusella, V. (2004). Homogenization of non-periodic masonry structures. *International Journal of Solids and Structures*, *41*(7), 1911–1923.
[5] Falsone, G., & Lombardo, M. (2007). Stochastic representation of the mechanical properties of irregular masonry structures. *International Journal of Solids and Structures*, *44*(25–26), 8600–8612.
[6] Gusella, V., & Federico, C. (2006). Random Field & Homogenization For Masonry With Nonperiodic Microstructure. *Mechanics of Materials and Structures*, *1*(2), 357–386.
[7] Ostoja-Starzewski, M. (2006). Material spatial randomness: From statistical to representative volume element. *Probabilistic Engineering Mechanics*, *21*(2), 112–132.
[8] Drdácký, M., & Slížková, Z. (2008). Mechanical Characteristics of Historical Mortars from Tests on Small-Sample Non-Standard Specimens, (January).
[9] Válek, J., & Veiga, R. (2005). Characterisation of mechanical properties of historic mortars: testing of irregular samples. *Transactions on the Built Environment*, *83*, 365–374. Retrieved from http://cat.inist.fr/?aModele=afficheN&cpsidt=17545867
[10] Červenka, V., Jendele, L., & Červenka, J. (2018). *ATENA Program Documentation Part 1 Theory*. *Červenka Consulting*. Prague.
[11] Havlasek, Petr, & Pukl, Radomir. (2015). *RLACS Studio Structural Analysis and Reliability Assessment. Červenka Consulting*. Prague.
[12] Borri, A., Corradi, M., Castori, G., & De Maria, A. (2015). Analysis and classification of historic masonry. *Bulletin of Earthquake Engineering*, *13*(9), 2647–2665.
[13] NTC. (2008). Italian Ministry of Infrastructure and Transportation.

12th International Conference on Structural Analysis of Historical Constructions
SAHC 2020
P. Roca, L. Pelà and C. Molins (Eds.)

STRUCTURAL ANALYSIS OF HISTORICAL CONSTRUCTIONS BY GRAPHIC METHODOLOGIES BASED ON FUNICULAR AND PROJECTIVE GEOMETRY

JAVIER SUÁREZ [1*], THOMAS BOOTHBY [2] and JOSE ANTONIO GONZÁLEZ [3]

[1] Department of Mechanic of Structures and Hydraulic Engineering. University of Granada. SPAIN
Edificio politécnico, Campus Fuentenueva s/n 18001 Granada, Spain
e-mail: fjsuarez@ugr.es, https://meih.ugr.es/ (*corresponding author)

[2] Department of Architectural Engineering, Penn State University, PA, US.
104 Engineering Unit A, The Pennsylvania State University, University Park, PA 16802
e-mail: teb2@psu.edu - web page: https://www.ae.psu.edu/

[3] International Graduate School. University of Granada. Spain.
C/ Paz, 18 18071 Granada, Spain. email: jogocaar@ugr.es

Keywords: historical structure, structural analysis, limit analysis; funicular geometry, projective geometry.

Abstract. *This paper presents a graphic methodology for the structural analysis of domes and other surfaces of revolution, based on a combined use of funicular and projective geometry.*
By considering a dome as a network of lines of latitude and longitude, the equilibrium of the network is analyzed in both horizontal and vertical projection. The resulting dual configuration is also a spatial system that can be considered by its projection in a horizontal and a vertical plane.
The dome is divided by latitude and longitude into an arbitrary number of sectors, and the equilibrium is enforced at each node. The tangential forces can be considered for their net effect at each node; the net effect of two tangential forces, equal in magnitude, at a node is a radially directed force in the plane of the line of latitude, acting outwards (compression) or inwards (tension).
Considering their horizontal projection, and its dual form, it is possible to choose the shape of the radial force diagram (the vertical projection and the force diagram), and identify the radial forces associated with it, and thus the tangential forces.
The new methodology is presented through its application to a hemispherical brick dome of small thickness.
The hemispherical brick dome has been also analyzed by applying the slicing technique, considering different hypotheses regarding the structural behavior of the haunch filling, according to its morphological characterization.
The structural analysis of the brick dome using both methodologies allows us to contrast the results obtained.

1 INTRODUCTION

This paper presents a new graphic methodology for the structural analysis of domes and other surfaces of revolution, based on a combined use of funicular and projective geometry.

The new methodology is presented through its application to a hemispherical brick dome of small thickness.

The model used refers to a real dome: the hemispherical brick dome over the transept, in Basilica of San Juan de Dios in Granada (Spain), (figure1). The constructive analysis of the dome was laid out by the authors in [1].

The hemispherical brick dome has been also analyzed by applying the slicing technique, considering different hypotheses regarding the structural behavior of the haunch filling, according to its morphological characterization.

The structural analysis of the brick dome using both methodologies allows us to contrast the results obtained.

2 STRUCTURAL ANALYSIS OF DOMES BY EQUILIBRIUM METHODS

The first contribution to the structural analysis of domes corresponds to Bouguer [2], which solves the theoretical problem of finding the ideal form of a dome, that is, the mathematical equation of the curve which, by revolution, can generate a stable dome, considering the hypothesis that there is no friction between the segments.

Frézier 's stereotomy treatise [3] dedicates a full chapter to the thrust of vaults and divides their study in simple (barrel vaults and lintel vaults) and compound (spherical, ribbed vaults, cloister corner, etc.). Frézier does not analyze specific examples, but he specifies how this analysis should be carried out. He considers the vaults composed of elementary arches, and compares their thrust with the barrel vaults one, which he considers to be known; it is a first version of what is now known as the slicing technique.

The first studies on the stability of existing domes are carried out in the 1740s, commissioned by Pope Benedict XIV, on the occasion of the damages observed in the dome of St. Peter of Rome.

The first study was made by three mathematicians, Le Seur, Jacquier and Boscovich in 1742 [4]. These authors, based on the location of the cracks and the analysis of the movement allowed by them, considered the formation of mechanisms, and established their equilibrium by applying the principle of virtual works. This surprisingly modern approach did not receive the attention it deserved and had no subsequent referrals.

Slicing technique

The second study was conducted by Poleni in 1743 and published in 1748 [5]. Poleni, after making a critical examination of the theories known to date on the stability of the vaults, discards the approach of the three mathematicians, and decides to use the slicing technique, by making a model and considering the theory of the catenary.

The slicing technique consists in considering the dome divided into segments, cutting by meridian planes. Every two opposite segments form an arc. If it is possible to draw a thrust line contained in the thickness of the arc, a possible state of equilibrium of the arch in compression has been found; then the arch is stable, and so is the dome. The brilliant analysis of Poleni barely had any subsequent consequences until the second half of the 19th century.

In the second half of the 18th century, regarding the debate on the stability of the dome of Santa Genoveva in Paris, it is noteworthy the theoretical studies carried out by Gauthey [6] and the experiences on Rondelet models (1802).

In the first half of the 19th century, in the context of *l'École Polytechnique*, *l´École des Ponts et Chaussées*, and the development of the Elasticity Theory, the first rigorous analytical contributions appeared. In 1826 Navier, in his lesson book of *Résistance des Matériaux*, [7],

includes theoretical assumptions for the analysis of domes, groin vaults and cloister vaults. However, the contributions are always theoretical or limited to the verification of the stability of a specific dome or vault.

Graphic methods

In the second half of the 19th century the usual methodology to verify the structural stability of domes was the slicing technique and the manufacture of models with catenaries.

Jean-Victor Poncelet, director engineer of *l'École Polytechnique*, had published his book *Traité des propriétés projectives des figures* [8], in which he developed projective geometry from the work of Gérard Desargues in the 17th century.

Inspired by the work of Poncelet, Karl Culmann publishes his seminal book *Graphic Statics* [9], which meant the appearance of Graphic Static, with enormous influence on the engineers at the time, Maurice Koechlin, Otto Mohr, and Luigi Cremona.

Incorporating Graphic Static to the slicing technique allows the analysis of any type of vault and historical construction, however complex it may be. The analysis of almost all the vaults used in historical architecture can find in [10].

In the early 1900s, graphic methods were widely used to verify previously projected forms following traditional rules of proportion.

The Spanish architect Antoni Gaudí used the graphic methods, not only to analyze already defined projects, but to design using balanced catenary forms.

Eddy´s method

Rankine [11] was the first to develop the membrane equations for revolution domes.

In [12] Henry T. Eddy developed a graphical method of analysis to obtain membrane solutions; it was about graphically determining the horizontal efforts needed for the arc loads to follow a certain trajectory.

Föppl [13] adapted Eddy's method to masonry domes, considering a membrane behavior for the middle surface in the upper section, where there are compression efforts along the parallel rings. When tensions appear (that masonry cannot resist), he considers that loads are transmitted following the funicular of the vertical loads.

Eddy's method became popular thanks to Dunn's publications [14], [15].

In 1909 Rafael Guastavino Jr. applied Eddy's method to calculate a large brick dome on the transept of the Cathedral of St. John the Divine, in New York.

These equilibrium methods were considered approximate by the engineers of that time, who were strongly conditioned by the elastic theory. Although it was possible to analyze an elastic arc, the elastic analysis of spatial structures was beyond the scope of manual calculation. After World War II there was the need to analyze the vaults and ruined buildings before their reconstruction, therefore graphic equilibrium analysis methods were again used; this is the case, for example, of the vaults of the Cathedral of Xanten and of numerous churches and buildings rebuilt by Pieper [16].

In the second half of the 20th century, Heyman [17], [18] presented for the first time the slicing technique and its application in masonry structures, within the theoretical framework of Limit Analysis.

When considering the dome divided into segments by cuts along meridian planes, the slicing technique does not consider the influence of parallel forces on the stability of the dome.

3 BRICK HEMISPHERICAL DOME

This paper presents a new graphic methodology based on combining projective and funicular geometry, for the quantitative determination of efforts in revolution domes, from equilibrium considerations of parallel and meridian efforts.

This methodology is presented through its application to a brick thin dome. The stability of this dome is also assessed with the slicing technique, allowing to contrast the results.

The model considered refers to a real one: the brick dome over the transept in Basilica of San Juan de Dios in Granada (Spain), (figure1).



Figure 1: The Basilica of San Juan de Dios is regarded as a benchmark in Baroque Spanish Architecture.

The dome of San Juan de Dios' Basilica was designed and built as an "encamonada dome", which refers to the arc-shaped timber structure over the rafters, that gives the dome its final outer shape. This typology was implemented in accord with the directions of Fray Lorenzo de San Nicolás's treatise, [19].

Figure 2 shows the following constructive elements of the dome:

- Brick masonry drum, 11.71 m inner diameter, 1.73 m in thickness and 6.7 m height.
- Inner dome with double brick layer, of 8 cm thickness. The dome is built with brick of 3 cm thickness, the bricks were laid in sailor position (with the bed visible). The dome is bearing its own weight (1.4 kN/m^2).
- Filling of the haunch up to 1/3 of the radius of the dome.
- Supporting elements: in the top of the drum masonry wooden elements are embedded, and wooden mudsills are superimposed.
- Wooden structure: formed by curved beams (*camones*) resting on wooden mudsill.
- Planking: 3 cm thick wooden boards nailed on the arches centering, creating a flat surface for the roof tiles, bracing the "camones" and providing a monolithic structure.
- Bonding mortar coat on the planking.
- White and green glazed ceramic roof tiles, on the mortar layer.

The drum of the lantern is made of brick and rests on the wooden structure. Inside the lantern, there is a single layer of brick with which the inner curved surface is achieved. The lantern is surmounted with a spire similarly to the towers. [20].

The structural analysis of the dome through two methodologies, and the contrast of the results obtained, is presented in the following sections.

4 STABILITY ANALYSIS BY APPLYING THE SLICING TECHNIQUE

The stability of the inner brick dome is analyzed by applying the slicing technique developed by Heyman [21] & [22]. The suitability of this methodology to assess the stability of timbrel domes is discussed in [23] and [24].

To apply the theory of Limit Analysis, the following assumptions of masonry behavior are made:

- The material does not have tensile strength.
- For practical purposes, the material can be considered to have unlimited compressive strength.
- Sliding between masonry blocks cannot occur.

If this is the case, the safe theorem establishes that the masonry will be stable if it is possible to find a line of thrust, in equilibrium with the loads, which is entirely included within the section of the masonry.

The geometric safety factor is defined by the ratio between the actual thickness and the minimum thickness of the masonry required to contain the thrust line.

For the current analysis, the dome is divided into fifty spherical spindles (lunes or slices); by checking the stability of each sector, the stability of the entire dome is guaranteed.

Due to symmetry, only one half of each sector is considered. Each sector is considered divided into 19 voussoirs; the weight of the inner brick lantern is added.

The stability of the dome without filling has been analyzed, as well as the stability of the dome with external filling up to a third of the height, as recommended in Fray Lorenzo's treatise.

In [25] the structural behavior of the filling of the vaults is discussed, according to its morphological characterization, distinguishing between rigid filling cemented, solid granular filling, loose granular filling, lightened filling and filling formed by construction rubble.

In this paper, three hypotheses of backfill structural behavior are considered (figure 3):

Hypothesis 1: The filling is made of loose granular material. It has no structural behavior and is considered a dead load on the dome. This hypothesis is modelled by incorporating weights of the filling volumes into the force system, without increasing the section.

Hypothesis 2: The filling is of firm granular material and therefore has a structural function. This hypothesis is modelled by increasing thickness of voussoirs located in the lower third of the height.

Hypothesis 3: The filling is rigidly cemented, preventing the movement of the voussoirs. This hypothesis has been analyzed considering the dome as a shallow dome.

In all cases the weight of the inner brick coating of the lantern was also considered. Thus, four different structural situations have been considered. Each one has been analyzed, by considering different positions of the thrust in the keystone and the reaction in the springer; for each position, the line of thrust has been graphically determined to find a geometry of the line of thrust, in equilibrium with the loads, that is entirely within in the masonry section.

Figure 4 shows the graphical constructions of the thrust line for the hypotheses 2 and 3, considering the weight of the inner brick coating of the lantern.

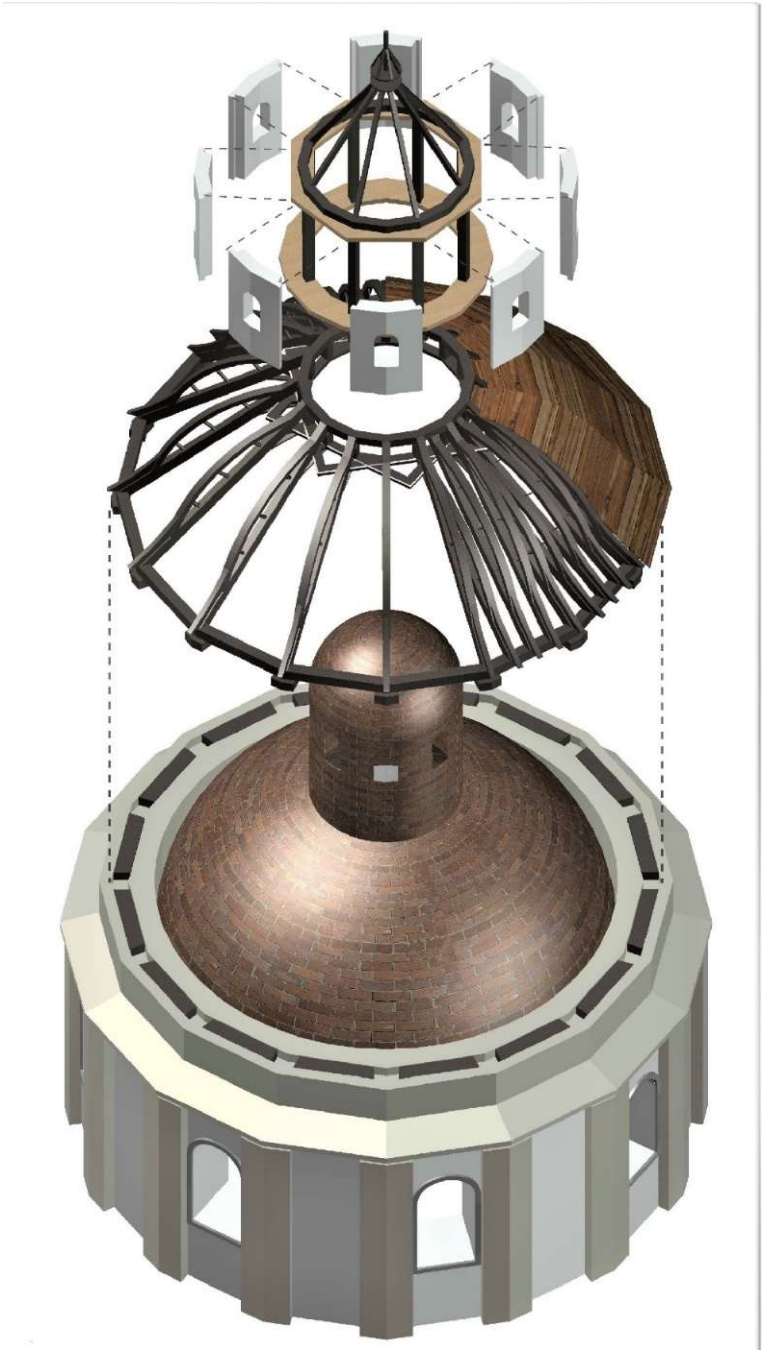


Figure 2. Three-dimensional model of the dome shows how the inner brick coating of the lantern is attached to the brick dome.

Only in hypotheses 2 and 3 and considering the weight of the inner brick coating of the lantern, have resulted a geometry of the thrust line in equilibrium with the loads that is also within the section of the dome masonry. This highlights the importance in the stability of the timbrel dome, of the filling up to one third of the height, as recommended by Fray Lorenzo de San Nicolás.

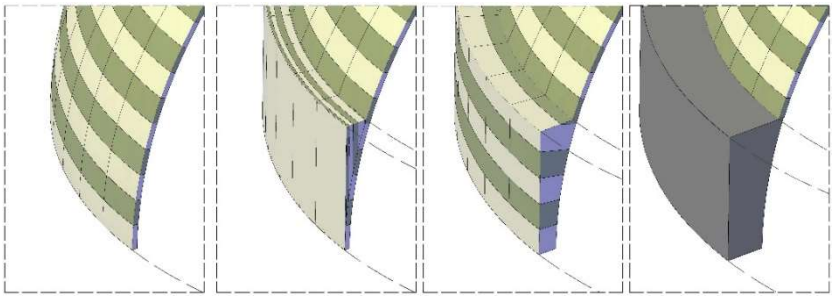


Figure 3. Four hypotheses of structural behavior of filling in the extrados of the dome, have been considered. From left to right; (a) without filling; (b) filling of loose granular material, without structural behavior; (c) filling of firm granular material, with structural function; (d) cemented rigid filling acting as embedment considered as a shallow dome.

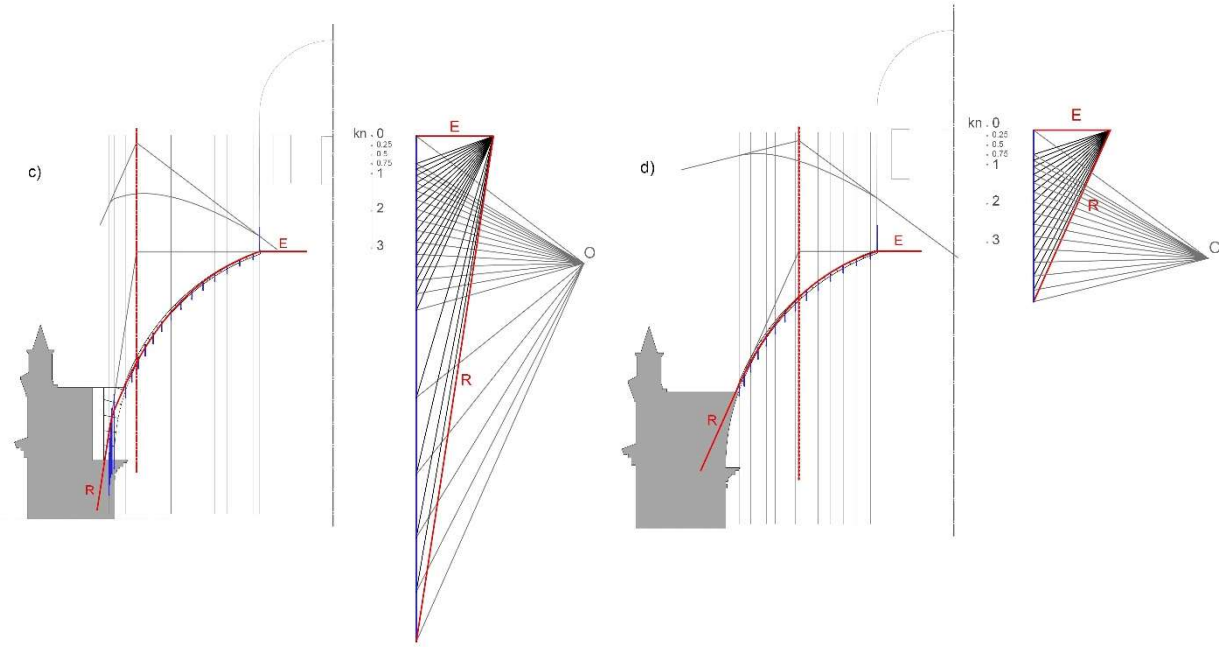


Figure 4. The figure on the left shows' hypothesis 2: filling of firm granular material with structural function. Considering the weight of the lantern, and the horizontal thrust in the keystone located at the top point of the section, and the reaction in the springer 9/10 on the outside of the impost, the position of the line of thrust contained inside the section of the masonry with a geometric safety factor equal to 1.09, a maximum value of compression effort of 13.5 kN is obtained. The figure on the right shows' hypothesis 3: cemented rigid filling, preventing the movement of the masonry. It is considered a shallow dome. Considering the horizontal thrust in the keystone at the 4/5 top point of the section and the reaction in the springer at 5/6 outside the impost, the thrust line located inside the masonry is determined, with a geometric safety factor equal to 1.28; a maximum value of compression effort of 4.8 kN is obtained.

5. GRAPHIC METHODOLOGIES BASED ON FUNICULAR AND PROJECTIVE GEOMETRY.

In this section, a new method is developed for the graphical analysis of domes and other surfaces of revolution, based in Thrust-Network Analysis presented in [26], incorporating other notions from projective geometry to make a more comprehensive method for the analysis of certain classes of structure.

In [26], the forces in a spatial network are solved by the graphical analysis of their horizontal projection: equilibrium of the spatial system is preserved in the plane system. The forces are

analyzed within a dual system in which the forces in equilibrium at each joint are represented by a closed polygon.

In the following, the dome is considered as a network of lines of latitude and longitude; the equilibrium of this network is analyzed in both horizontal and vertical projection. The resulting dual configuration is also a spatial system that can be considered by its projection in a horizontal and a vertical plane. This procedure not only allows the solution of the forces in a system for a given configuration, but also allows an inverse solution of the internal forces that result in a given shape.

The dome is divided by latitude and longitude into an arbitrary number of sectors [figure 5]. Equilibrium can be enforced at each node, that is, at each intersection of latitude and longitude lines. In keeping with [27], [14], [15] and [12], it is noted that the tangential forces can be considered for their net effect at each node: the net effect of two tangential forces, equal in magnitude, at a node is a radially directed force in the plane of the line of latitude: acting outwards (tangential compression) or inwards (tangential tension).

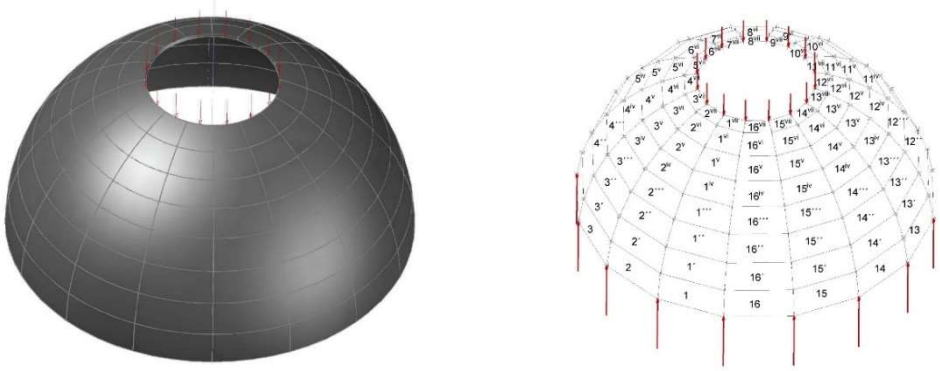


Figure 5. The dome is divided by latitude and longitude into an arbitrary number of sectors (left). Simplified model of the dome: considering the center of gravity and weight of each sector (right).

The lines of longitude and latitude project in a plane through the equator to form a network of forces, as in [26]. These plane forces can be considered in their dual form, which is a similar figure (force polygon) with all of the characteristics reversed: tangential lines on the primal figure are represented by their net radial force in the dual figure, while the radial forces in the primal figure appear as tangential lines in the dual figure. The forces at the exterior of the dome in the primal figure are represented by the center point of the interior of the dual figure, while the forces at the apex of the dome are represented by the lines on perimeter of the dual figure.

Figure 5 represents a simplified model of the dome. The longitude and latitude lines represent the network of discretized membrane forces, in horizontal and vertical projection (figure 6). The spaces between these funicular lines are numbered using Bow's notation; [28].

Figure 7 shows the forces associated with these lines. Each node in the primal system is represented by a quadrilateral of forces in the dual force diagram. Although, sector by sector, the horizontally projected force diagram resembles the funicular diagram, they are different. It is particularly noteworthy that the location distance of the radial forces (represented as tangential lines) from the pole on the dual figure is arbitrary, indicating the high degree of statical indeterminacy of the dome under analysis. On the horizontal projection of the force diagram, on the dual figure, a statically admissible solution can be constructed with practically any position of the ring of radial forces; inward or outward movement of this ring signifies increased or decreased tangential forces.

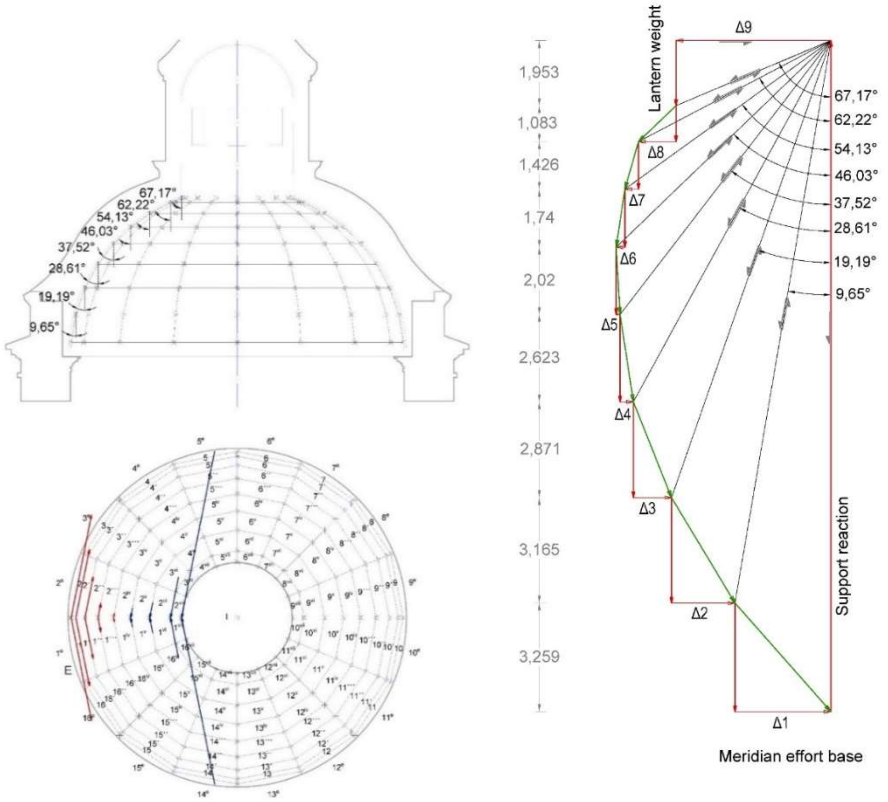


Figure 6. Left: simplified model of the dome, plan, and elevation; in the plan, the tangential forces of tension and compression are also represented. Right: the necessary horizontal increments, in order to, the dome geometry be fit to an antifunicular polygon of the forces system are determined.

On the other hand, by an inverse procedure, as shown in Figures 6 and 7, it is possible to choose the shape of the radial force diagram (the vertical projection of the force diagram), and identify the radial forces associated with it, and thus the tangential forces. This is illustrated in figure 6, where the meridional forces in the dome are shown. The horizontal components of these forces at each node are related to the tangential force components. The angles of the polar rays are chosen so that this polygon matches the shape of the dome exactly. The horizontal forces in the meridional section and hence the tangential forces at each level in the dome are chosen to maintain the proper angles in the funicular polygon. As shown, there is a multiplicity of possible solutions that give exactly this force distribution.

The equilibrium in the vertical plane is assured, by fitting the forces' polygon to the polar rays, so then the dome geometry is an antifunicular of the forces system. The equilibrium of nodal efforts in the horizontal plane is assured by taking the values of the transversal forces from the dual figure.

The result is the construction of a funicular polygon that follows the shape of the dome exactly.

The values obtained by applying of the graphic methodology proposed, measured in Figure 7, are the following:

- maximum value of tension parallel force (fig.7, $F_{1e1} = F_{2e2}$): 7.36 kN (0.09 N/mm^2).
- maximum value of compression parallel force: (fig.7, $F_{1viiI} = F_{2viiI}$): 11.89 kN (0.22 N/mm^2).

- maximum value of meridian force (fig. 6 right): 17.12 kN (0.09 N/mm^2)

In [29] it is considered usual values of brick strength: compressive strength: 15 N/mm^2; tension strength: 1 N/mm^2. In [30] it is exposed that Van der Pluijm [31] used tensile strength values of the masonry unit ranging from 1.5 to 3.5 N/mm^2. Therefore, the values obtained are acceptable for the material.

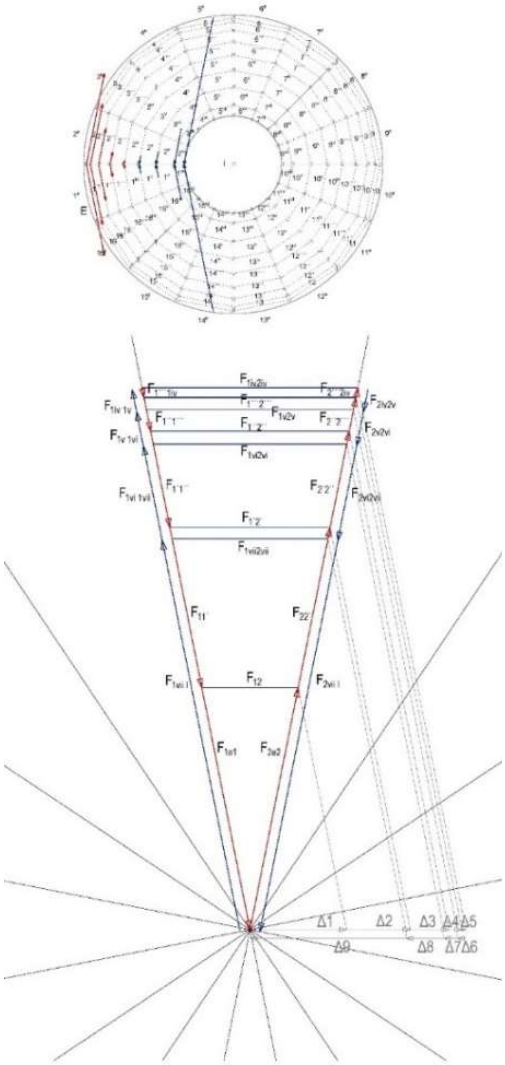


Figure 7. Dual figure: from calculated values of increments, the values of tangential forces in the dome are determined.

6. CONCLUSIONS

This paper presents a new graphic methodology for the structural analysis of domes and other surfaces of revolution, based on combining funicular and projective geometry. It is a new methodology, still in the early stages of its development.

This methodology is presented through its application to a brick dome thin. The stability of this dome is also assessed with the slicing technique, allowing to contrast the results.

The application of the slicing technique, in the frame of limit analysis theorems is a well-known and contrasted technique for the stability analysis of domes, which does not consider the tangential forces. In this work, the results of this analysis highlight the importance in the stability of the timbrel dome of the filling up to one third of the height, as recommended by Fray Lorenzo de San Nicolás.

This new graphic methodology takes into account the tangential forces to determine equilibrium forces solutions in the dome. This equilibrium solution represents one admissible stress state for the dome and leads us to belief that the backfilling of the intrados could be unnecessary.

REFERENCES

[1] Suarez Medina, F.J, Bravo Pareja, R., González Casares, J. A., *Structural and Constructive Analysis of a Faux Vault, the Dome of San Juan de Dios Church, in Granada (SPAIN)*. International Journal of Architectural Heritage. (2019). https://doi.org/10.1080/15583058.2019.1645242.

[2] Bouguer, P., *Sur les lignes courbes qui sont propres à former les voûtes en dôme*. Mémoires de l'Académie Royale de Sciences de Paris, (1734), 149-66.

[3] Frézier, A. F., *La théorie et la pratique de la coupe des pierres et des bois, pour la construction des voûtes... ou Traité de stéréotomie à l'usage de l'architecture* (Vol.1). Jean-Daniel Doulsseker. (1737).

[4] Le Seur, T., Jacquier, F., & Boscovich, R. G. *Parere di Tre Matematici Sopra i danni, che si sono trovati nella cupola di San Pietro.* (1742).

[5] Poleni, J. *Memorie istoriche della gran cupola del tempio Vaticano e de'danni di essa e detristoramenti loro, divisi in libri 5*. *Nella Stamperia del seminario*. (1748).

[6] Gauthey, E. M., *Mémoire sur l'application des principes de la mécanique a la construction des voutes et des dômes, dans lequel on examine le problème proposé par M. Patte, relativement a la construction de la coupole de l'église Sainte-Geneviève de Paris.* Par M. Gauthey de l'imprimerie de louis-Nicolas Frantin. (1771).

[7] Navier, C. L. M. H., *Résumé des leçons données à l'école royale des Ponts et chaussées sur l'application de la mécanique à l'établissement des constructions et des machines (Vol. 1)*. Didot. (1826).

[8] Poncelet, J., *Traité des propriétés projectives des figures, deux volumes*. Bachelier, Paris, 2. (1822).

[9] Culmann, K., *Die Graphische Statik*, Meyer und Zeller. Zürich. (1865).

[10] Körner, C., "Gewölbte Decken." Handbuch der Architectur, Third part 2 (1901): 141-553.

[11] Rankine, W. J. M., *A Manual of Applied Mechanics*. Charles Griffin, London (1858).

[12] Eddy, Henry T., *Research in Graphical Statics*, New York, Van Nostrand. (1878).

[13] Föppl, A., Ausgewählte Capitel der mathematischen Theorie der Bauconstructionen. 1. Theorie der Gewölbe: mit vier Tafeln und vielen Holzschnitten. (1881).

[14] Dunn, W., *Notes on the stress in Framed Spires and Domes.* Journal of the Royal Institute of British Architects. Third Series, vol. 11; (1904). 401- 412.

[15] Dunn, W., *The Principles of Dome Construction*. Architectural Review. (1908). Vol 23: 63-73; 108-112.

[16] Pieper, K., *Sicherung historischer Bauten*. W. Ernst, (1983).

[17] Heyman, J., "*On shell solutions of masonry domes*". International Journal of Solids and Structures, vol. 3, (1967), pp 227.

[18] Heyman, J., *Equilibrium of shell structures*. Oxford University Press, (1977).

[19] Fray Lorenzo de, S.N., *Arte y uso de arquitectura*, Madrid, (1639) first book; (1665) second book.
[20] Isla Mingorance, E., *José de Bada y Navajas, arquitecto andaluz* (1691-1755). Granada, (1977).
[21] Heyman, J., *The Stone Skeleton*. International Journal of Solids and Structures, 2 (2) (1966) 249-279.
[22] Heyman, J., *The Stone Skeleton*. Structural Engineering of Masonry Architecture, Cambridge University Press, Cambridge, (1995).
[23] Huerta Fernández, S., *La mecánica de las bóvedas tabicadas en su contexto histórico: la aportación de los Guastavino, Las bóvedas de Guastavino en América*, Instituto Juan de Herrera. Madrid, (1999).
[24] Redondo Martínez, E., *La bóveda tabicada en España en el siglo XIX: la transformación de un sistema constructivo*. (PhD Thesis). Polytechnique University of Madrid, (2013).
[25] Ramos León, J., *Clasificación morfológica de los rellenos en el trasdós de bóvedas de fábrica.* Informes de la Construcción, 65 (532) (2013). 471-480; https://doi.org/10.3989/ic.12.062.
[26] Block, P. & Ochsendorf, J., *Thrust Network Analysis: A new methodology for three-dimensional equilibrium*. Journal of the international association for shell and spatial structures. Vol. 48. (2007).
[27] Huerta Fernández, S., *The Mechanics of Timbrel Vaults: A Historical outline*, in Essays on the History of Mechanics, ed. Becchi et al. Basel Birkhauser Verlang. (2003).
[28] Bow, R.H., *Economics of construction in relation to frame structures*, Spon,
London, (1873).
[29] Huerta Fernández, S., *Arcos, bóvedas y cúpulas. Geometría y equilibrio en el cálculo tradicional de estructuras de fábrica*, Juan de Herrera Instituto, Madrid, (2004).
[30] Lourenço, P., *Experimental and numerical issues in the modelling of the mechanical behavior of masonry*. Structural Analysis of Historical Constructions II. Barcelona: P. Roca, J.L. González, E. Oñate and P.B. Lourenço (Eds.) CIMNE. (1998).
[31] Pluijm, V. d., *Out of plane bending of masonry: behaviour and strength*. doi:10.6100/IR528212. (1999).

12th International Conference on Structural Analysis of Historical Constructions
SAHC 2020
P. Roca, L. Pelà and C. Molins (Eds.)

STRUCTURAL ASSESSMENT OF THE SEISMIC BEHAVIOR OF THE DOME OF THE TAJ MAHAL

SATWANT RIHAL[1], WILLIAM KOH[2], ANJALI MEHROTRA[3] AND JOHN EDMISTEN[1]

[1]Architectural Engineering Department – College of Architecture & Environmental Design
Cal Poly State University, San Luis Obispo, USA
e-mail: srihal@calpoly.edu (*corresponding author)

[2] Consulting Structural Engineer, Los Angeles, California, USA
e-mail: william@williamkohassociates.com

[3] ISISE, Department of Civil Engineering
University of Minho, Guimaraes, Portugal
e-mail: anjali.a.mehrotra@gmail.com

Keywords: Historical Domes, Taj Mahal, Structural Analysis, Seismic Behavior, Earthquake Resistance

Abstract. *This paper presents the results of a study of the structural assessment of the seismic behavior of the main dome of the Taj Mahal, in Agra, India. Built by the Moghul emperor Shah Jahan between 1632 – 1648 AD, the structure is one of most famous buildings in the world and the finest and most sophisticated symbol of Moghul architecture in India. As it is located in a zone of moderate seismicity, there is an urgent need for ensuring the structural safety and preservation of this iconic cultural heritage for future generations. The objective of this study is to develop a simplified approach to enhance our conceptual understanding of the mechanism of load path/transfer in the dome of the Taj Mahal under both gravity and seismic loads, as well as to better understand the influence of the geometry of the dome on its structural behavior. Using the software SAP2000, a finite element model of the dome is created and analyzed under the action of gravity and seismic loads, with the seismic loading assumed to have a PGA of 0.25g based on the results of a study conducted by the Indian National Disaster Management Authority. The results obtained include plots of the distribution of nodal reactions at selected levels to represent the lateral load behavior of the dome of the Taj, as well as plots illustrating the paths of load transfer under the action of gravity and seismic loads. Free body diagrams of selected rings are also presented to illustrate the 'hoop' forces in the dome, while simplified internal stresses are computed and compared with known material properties. Observations are also presented about the effect of the dome geometry, especially the bulging part of the dome, on the distribution of reactions and the resulting mechanism of load transfer in the structure under both gravity and seismic loading.*

1 INTRODUCTION

World cultural heritage has found rich and creative expression in beautiful and expansive works of domed architecture such as the Pantheon in Rome, built by Emperor Hadrian between 120-124 AD, the Hagia Sophia in Istanbul, Turkey built in 6th century AD and the Taj Mahal in Agra, India built by the Emperor Shah Jahan between 1632-1648 AD. The survival of these structures to this day inspires the fundamental curiosity - how did the ancient builders build such structures with the materials (e.g. stone or brick, and mortar) and knowledge available to them at that time? A lot can be learned from their wisdom, specifically through their understanding of materials, geometry of structural forms, structural stability, and the techniques of construction.



Figure 1: (a) The Taj Mahal in Agra, (b) Humayun's tomb in Delhi and (c) Itmad-Ud-Daulah's tomb in Delhi (CC BY-SA 4.0)

While structures such as the Pantheon and the Hagia Sophia have been the subject of intense curiosity and have received considerable attention and study over the years, the Taj Mahal, on the other hand, has not received the adequate attention and study it deserves. Most studies conducted on the Taj to-date have focused predominantly on architectural, visual, and spatial aspects of the structure as well as on the Moghul gardens that surround it [1-4], while limited studies have been carried out from a structural engineering perspective [5,6,8,9]. In particular, the large, unique onion-shaped dome of the structure invites curiosity and merits further investigation.

This study aims to investigate the behavior of the main dome of the Taj Mahal under gravity and seismic loads in order to enhance our conceptual understanding of the load paths and mechanism of load transfer in the structure; and to better understand the influence of the geometry of the dome on its structural behavior under gravity as well as seismic loads.

In order to do this, the background and construction history of the Taj Mahal are first studied and available drawings, material information and results of previous structural investigations are examined.

Based on these studies, the dome geometry is established, which is subsequently used to generate a finite element (FE) model in SAP2000 [7]. In the first instance, a relatively simple FE model is generated by dividing the dome into a series of circular rings, which are then divided into sixteen radial segments (lunes). This FE model is then analyzed under the action of gravity and seismic loads, with the seismic loading corresponding to the maximum expected PGA on site. The results of this model provide insight into the distribution of forces/reactions in the dome under the action of gravity and seismic loads.

A second more refined FE model of the Taj Mahal dome was then developed in order to investigate the distribution of meridional and hoop stresses in the dome (both over the height and across the dome thickness), under the same loading conditions. The resulting stresses are compared to those reported by previous structural investigations of the Taj Mahal dome [5,6] as well to the material properties of the structure.

2 BACKGROUND

2.1 Design and construction history

The Taj Mahal, considered as one of the most accomplished examples of Moghul architecture in India, was built between 1632 – 1648 AD by the Moghul emperor Shah Jahan in memory of his wife Mumtaz Mahal, who died while giving birth to their fourteenth child.

While designing the structure, Shah Jahan drew inspiration from both traditional Persian architecture as well as classic Mughal architecture as exemplified by structures such as Humayun's tomb and Itmad-Ud-Daulah's tomb (Figures 1b and c). In fact, according to [1], 'Taj Mahal was the logical conclusion and synthesis of several strands that already existed in Moghul architecture'. Various designs were submitted to Shah Jahan and modified according to his own suggestions, and while the identity of the architect of the final structure is heavily debated, it is widely accepted that the principal designer was Ustad Ahmad Lahauri of Lahore. Lahauri, who was a Persian, and said to be heavily involved in the construction of the structure, which was such a colossal venture that it required a whole team of architects, as well as masons, stonecutters, inlayers, carvers, painters, calligraphers, dome builders and other artisans requisitioned from the whole Moghul empire, central Asia and Iran. In fact, it took seventeen years for construction of the entire monumental complex to be completed.

2.2 Plan and configuration

The Taj Mahal has often been described as the embodiment of architectural perfection [4]. It is well recognized that geometry played an everlasting role in its architecture, and the plan layout and configuration of the Taj Mahal has been studied and analyzed extensively by many scholars over the years [1-5].

The tomb, which is the central focus of the entire Taj Mahal complex, is a large white marble-clad structure which stands on a square plinth and consists of a symmetrical building with an iwan (an arch shaped doorway) topped by a large dome and a finial. The base structure is a large multi-chambered cube with chamfered corners forming an unequal octagon that is approximately 54.9 m on each of the four sides. This irregular octagonal plan is a variation of hasht bihisht ('eight paradises') plan, which typically comprises a central chamber surrounded by four chambers at the diagonals and four open fore-halls on the perpendicular axes as illustrated by Figure 2a.

The base structure is surmounted by an inner dome and a cylindrical drum, which in turn is topped by the monumental bulbous dome. While the inner dome keeps the height of the interior space in proportion, the large outer dome helps the structure stand out visually. An elevation drawing illustrating this structural system can be found in Figure 2b [6].

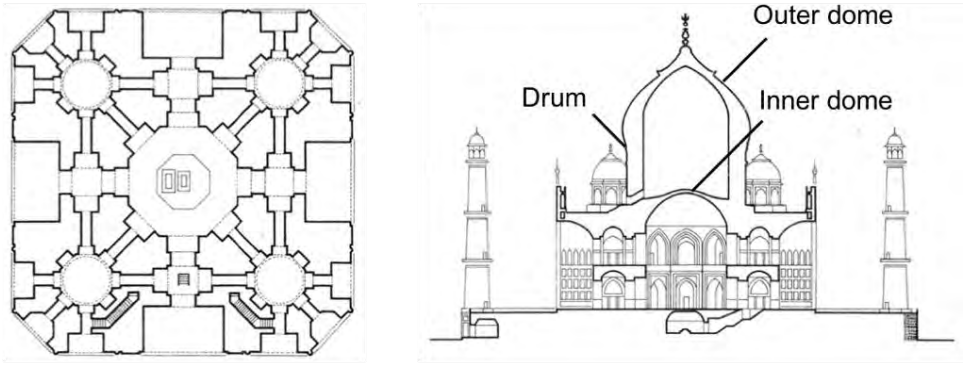


Figure 2: Taj Mahal (a) floor plan and (b) section (source ref. [2])

2.3 Materials used for construction

The materials used for construction of the Taj Mahal were sourced from all over India and Asia, and have been systematically investigated in detail and documented in [3,5,6]. The walls in the complex, many of which are several feet thick, were constructed of bricks with rubble inner cores and façades of either marble or sandstone fastened with iron dowels and clamps. The bricks typically measured 17.8-19.0 x 10.9-12.7 x 1.9-3.0 cm and were combined with lime mortar, while the façade slabs had a thickness of about 15.24 cm. The bricks were fired in local kilns, and the sandstone came from quarries 45 km away near Fatehpur Sikri. The white marble was brought all the way from quarries belonging to Raja Jai Singh in Makrana, Rajasthan, located 402 km away. The interior surface of the dome is finished with polished plaster, made with a combination of burnt lime, ground shells, marble dust, gum, sugar and egg whites, and applied in sequential step process.

2.4 Previous structural investigations

The first known structural investigation of the Taj Mahal, including a thorough examination of the sub-soil conditions and the foundation system, was carried out by Dayalan [5]. The dimensions of the structure were established using precise measurements and detailed drawings made available by the Archaeological Survey of India. Based on these dimensions, the weight of the dome was estimated to be 119,600 kN and the weight of the supporting drum to be 59,800 kN. Dayalan's structural analysis consisted of dividing the dome (up to a height of 22.9 m) into 30 equal sections, constructing a diagram of forces acting at the center of gravity of each of the sections, based on which the stresses were determined. From this analysis, the maximum compressive stress at the base of the dome was determined to be 383.07 kPa, while a maximum compressive stress of 574.54 kPa was recorded at the base of the supporting drum. According to [5] the walls of the cenotaph chamber that carry the weight of the drum and dome are very heavily loaded resulting in a stress level in the cenotaph walls of 766.01 kPa which is almost twice the safe stress limit level for present day bricks with lime mortar. In fact, the signs of crushing detected in the cenotaph chamber are most likely due to the squeezing of mortar (which had likely deteriorated over time) under the action of these superimposed loads.

A more detailed structural analysis of the dome of the Taj under gravity loading was

conducted using finite element modelling in Abaqus FEA [6]. From this analysis it was found that the maximum stresses experienced by the dome in both the hoop and meridional directions were less than the strengths of the brick and mortar, with the over-dimensioning of the structure effectively resulting in a safety factor of 5 for the dome [6]. This compares reasonably well with analyses conducted on the complete Taj Mahal structure using 3D finite element modelling in SESAM, which yielded a safety factor between 4 and 8 for the monument under vertical loading [9].

Studies concerning the seismic analysis and safety of the Taj Mahal have also been conducted at the University of Roorkee, however these make use of relatively simplified models such as the lumped mass and spring model [8].

3 TAJ MAHAL DOME – DIMENSIONS AND GEOMETRY

In order to determine the dimensions of the dome of the Taj Mahal needed to build the computational model for structural analysis, Mehrotra and Glisic [6] established one known reference dimension namely the external dimension of the drum as documented by Dayalan [5]. Using this as a reference dimension, all other defining dimensions were determined relative to this reference dimension. Figure 3a presents the major dimensions of the dome as presented by Mehrotra and Glisic [6]. The dome has a constant thickness of 4 meters, from its base to a height of 15.5 meters above it. Dome thickness varies in the conical portion of the structure (i.e. the top 8 meters of the dome), starting with a thickness of 4.3 meters at the lower end, which increases to 4.8 meters near the top as shown in Figure 3a.

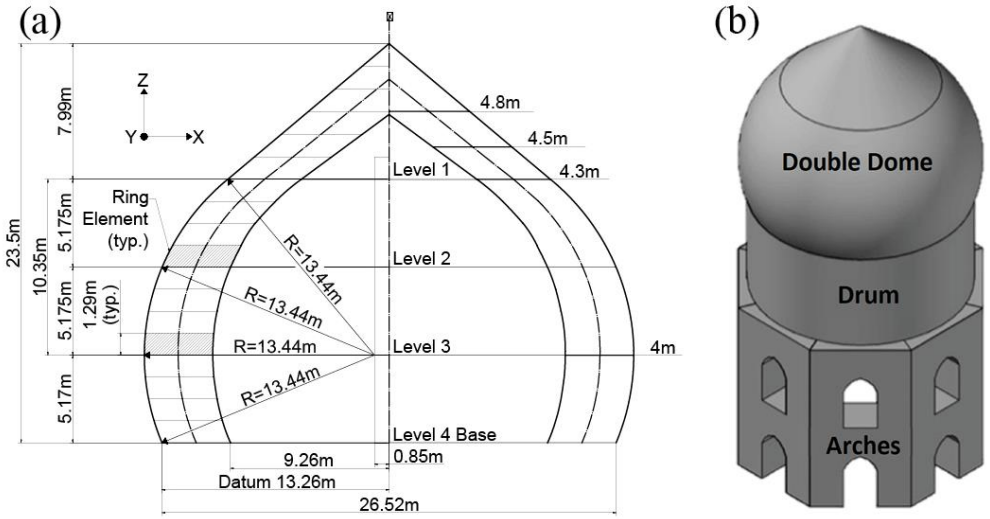


Figure 3: (a) Dome section showing ring dimensions and geometry and (b) Structural System - Taj Mahal

4 STRUCTURAL SYSTEM

The Moghul designers and engineers had developed an innovative structural system for the Taj Mahal consisting of the outer dome supported on a drum, seated on eight massive columns with arches spanning between these columns, as illustrated by Figure 3b (reproduced from [6]). As reported in [5], it is likely that the Taj's outer dome with its bulbous geometrical form must experience a certain amount of tension in the lower part of its structure. In the absence of

reinforcing techniques like outer metal bands during that period, the architects and master builders of the Moghul era managed to creatively achieve stability of the dome by using good quality bricks and mortar, and by gradually increasing the dome thickness [5].

As reported by Dayalan [5] and Viladkar et. al [9], this entire structure rests on a raft/mat 33.5 m thick, which rests on a thick sandy layer 9.1m in depth, overlaying a 63.6 m thick clayey strata, founded on rock.

5 STRUCTURAL ANALYSIS

Dayalan's simplified structural analysis of the Taj Mahal [5] as well as the more detailed structural analysis as carried out by Mehrotra and Glisic [6] only considered gravity loads in the analyses. In this paper, a detailed structural analysis of the Taj Mahal dome has been carried out under the action of both gravity and seismic loads. Ideally it would be desirable to carry out a comprehensive structural analysis of the entire structure, incorporating the entire structural system e.g. the outer dome, inner shallow dome, the drum, and the arched cenotaph and its raft foundation. However, this proved to be infeasible due to modelling complexities and computational constraints, resulting in only the main dome of the structure being considered in this phase of the study.

5.1 Finite Element Analysis – Part I

The objective of the first part of the detailed structural analysis was to investigate the transfer of forces/reactions in the Taj Mahal dome structure. Based on the geometry of the dome presented in Figure 3a, a simple 3D finite element (FE) model of the Taj Mahal dome was first developed using shell elements in the SAP2000. The dome was divided into seventeen rings over its height, which in turn are divided into sixteen radial segments (lunes), resulting in a total of 272 shell elements in the model (17 vertical x 16 radial = 272). Boundary conditions were assumed to be pinned at the base. A 3D view of this model is presented in Figure 4.

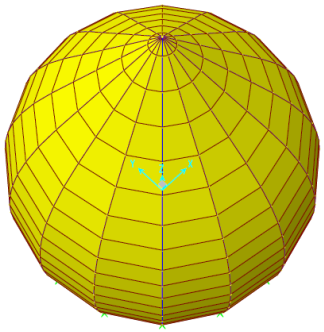


Figure 4: 3D FEA model of the Taj Mahal dome

The material properties adopted for this model are listed in Table 1. Note that the analyses conducted here assume an isotropic material model, which is not the case in reality. However the limited information regarding exactly how the bricks are arranged within the dome (i.e. concentrically/radially/combination of the two), made it challenging to define anisotropic material properties for the model. Thus these effects were neglected in the adopted modelling approach.

Table 1: Material properties assumed for the FE model

Parameter	Value
Density	20.59 kN/m^3
Modulus of elasticity	3447.4 MPa
Poisson's ratio	0.2
Unit compressive strength [11]	2430 kPa
Unit tensile strength [11]	300 kPa
Bond tensile strength [12]	170 kPa

The following three load cases are considered for analysis:

1. Dead load (self-weight only) = 101,705.83 kN
2. Seismic load = 0.25g, as obtained from the results of a study conducted by the Indian National Disaster Management Authority [10]
3. Combined load = Dead + Seismic

and the forces/reactions are studied at four different levels of interest as listed in Table 2 and indicated in Figure 3a.

Table 2: Dome dimensions at the specified levels of interest

Level	Height above Base (m)	Diameter (m)	Dome Thickness (m)
4	0.00	12.90	4.0
3	5.04	13.91	4.0
2	10.08	12.90	4.0
1	15.13	9.19	4.3

Figure 5 presents the distribution of reactions under each of these different load cases. A comparison of the distribution of reactions under the dead load only in the XY plane (Figures 5b and c) illustrates that the forces appear to be pushing outward at the bulging part of the dome (Level 3, Figure 5c) and inward at the base (Level 4, Figure 5b).

A study of dome reactions under seismic loading at the base indicate that the reactions in the direction of the earthquake are maximum at the edges of the dome, and are minimum at the center of the dome in the line of the earthquake. Reactions in a direction normal to the earthquake show bulging in the left half of the dome; and contraction in the right half (Figure 5e). A study of the dome reactions under seismic loading at the bulge (Level 3) indicate that the reactions in the direction of the earthquake are more uniform on both the right and left side of the dome; and that the reactions in the direction normal to the earthquake show lesser bulging and contracting at this level (Figure 5d).

5.2 Finite Element Analysis – Part II

A more refined FEA model was also developed in SAP 2000 using eight node solid elements for investigating the stresses at different levels, and across the thickness of the dome.

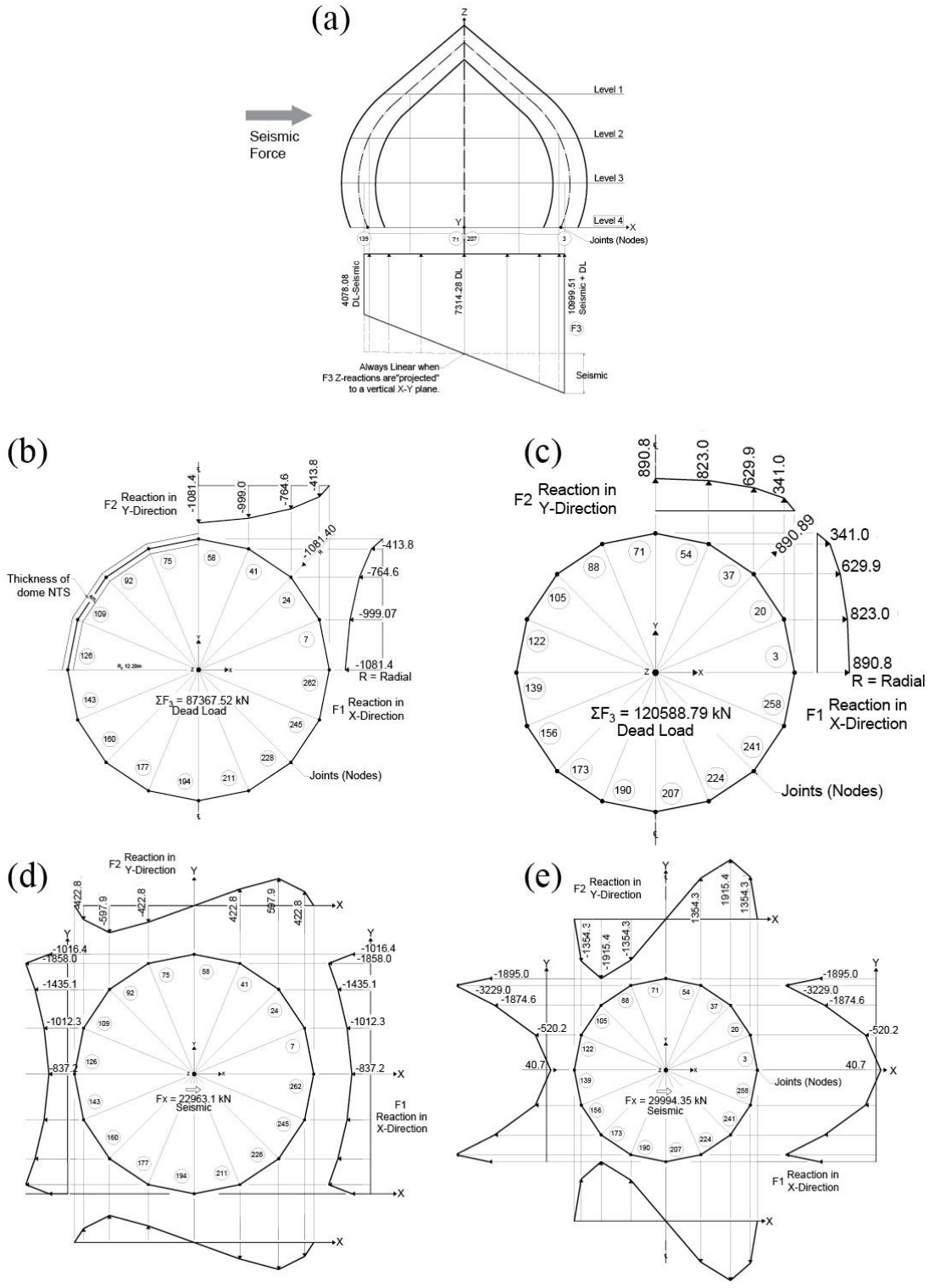


Figure 5: (a) distribution of vertical reactions – dead + seismic; (b) Level 3 (bulge) – XY reactions - dead load - kN; (c) Level 4 (base) – XY reactions - dead load - kN; (d) Level 3 (bulge) – XY reactions - seismic load - kN (e) Level 4 (base) – XY reactions - seismic load – kN

As in the case of the FE shell model, the boundary conditions were modelled as pinned (UX=UY=UZ=0), while the dome was divided into a series of rings over its height, which are then divided into one hundred and twenty radial segments (lunes). The dome was further discretized using solid elements, by dividing the dome thickness into four segments throughout the dome geometry up to 19.5 m above the base of the dome. Above the 19.5 m level, 4 m high solid cone shape elements were generated. The resulting FE model comprises 17644 solid elements, with 23050 joints (Table 3). Note that the material properties and load cases adopted for this model are the same as for the simplified model with the shell elements.

Table 3: Dome dimensions as they relate to SAP 2000 software

Level	No. of segments through dome thickness	No. of vertical divisions	No. of radial divisions	No. of 3D solid elements
4	4	8	120	3840
3	4	8	120	3840
2	4	8	120	3840
1	-	-	120	6124
			Total	17644

Plots of the maximum and minimum principal stress distributions obtained using this model can be found in Figure 6. Under dead load only, the maximum principal stress can be assumed to correspond to the hoop stress, while the minimum principal stress can be assumed to correspond to the meridional stress. It will thus be referred to as such in order to facilitate comparison with the results of other studies.

In general, the study of the hoop stress distributions in the dome of the Taj Mahal under dead load only (Figures 6a) indicates that:

- At level 3 (bulging part of the dome) there is hoop tension which is higher on the outside and lower on the inside of the dome
- At level 4 (at the base of the dome) there is hoop compression on the outer surface of the dome and lower compression on the inside surface of the dome indicating that there is rotation and bulging out even at the base of the dome

A comparison of the maximum hoop and meridional stresses obtained from this structural analysis, with those obtained by Dayalan [5] and Mehrotra & Glisic [6] are presented in Table 4. As Table 4 indicates, under the influence of the dead load only, maximum hoop tensile stress occurs at the outer surface of Level 3 (bulge), with a value of 70.8 kPa. This lies between the maximum hoop tensile stress values reported by Dayalan [5] and Mehrotra & Glisic [6], and is found to be within the safe limits of the 300 kPa tensile strength of brick [11] as well as the 170 kPa tensile bond strength of the brick-mortar interface (perpendicular to the joints, as this is the limiting case) [12]. At the base (Level 4) the hoop stress reverses to compression and varies from -202.0 kPa at the outer dome surface to -39.3 kPa at the inner dome surface, with an average value of -120.6 kPa which is larger than the maximum hoop stresses values reported by Dayalan [5] and Mehrotra & Glisic [6], but still within the safe limits of brick's compressive strength of 2430 kPa [11].

Similarly, a comparison of the meridional stresses under the dead load (Figure 6c) indicates that as in [5,6] the maximum meridional stress is recorded at the outer surface of Level 4 (base)

with a maximum value of -833.4 kPa (compression), which reduces to -168.6 kPa at the inner surface of the dome, resulting in average value of -501.0 kPa which is within the range of the values reported by Dayalan [5] and Mehrotra & Glisic [6] and well within the safe limit of brick's compressive strength.

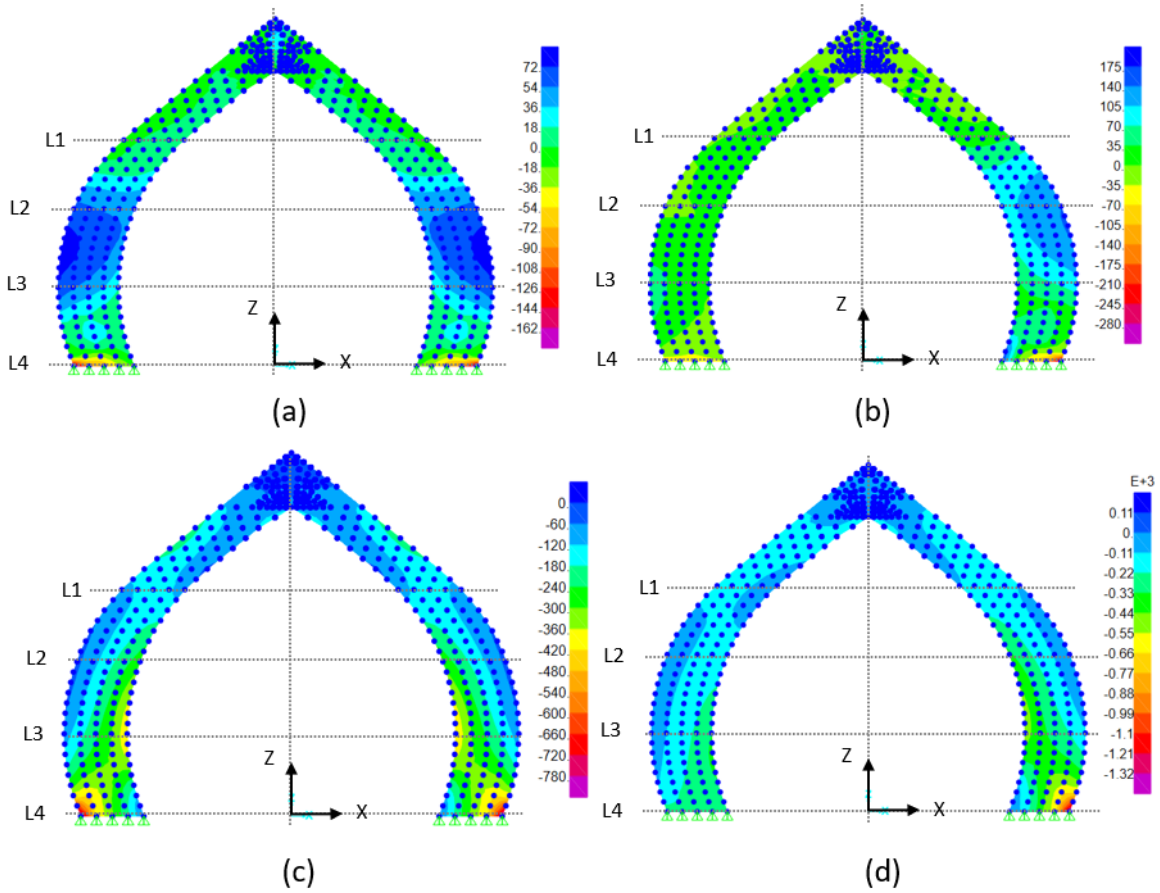


Figure 6: (a) Maximum principal stress - dead load (kPa) (b) maximum principal stress - combined dead + seismic load (kPa) (c) minimum principal stress – dead load (kPa) (d) minimum principal stress – combined dead + seismic load (kPa)

Table 4: Comparison of maximum hoop and meridional stresses obtained under dead load only with those obtained by Dayalan [5] and Mehrotra & Glisic [6]

Level	**Max Hoop Stress (kPa)**				**Max Meridional Stress (kPa)**			
	Dayalan	Mehrotra & Glisic	Outer	Inner	Dayalan	Mehrotra & Glisic	Outer	Inner
4	-65.0	-110.0	-202.0	-39.3	-565.0	-478.7	-833.4	-168.6
3	266.0	40.0	70.8	44.8	-339.0	-75.0	-152.7	-410.3
2	-123.0	-65.0	60.4	51.9	-158.0	-107.6	-94.5	-244.0
1			-66.9	-55.5			-151.1	-105.5

Under the influence of the combined dead and seismic loads, the maximum principal stresses are generally found to be higher on the east side of the dome, and lower on the west side, with the outer surface once again recording larger stresses than the inner surface (Figure 6b). The maximum principal tensile stress is found to migrate from Level 3 (bulge) to Level 2, with a maximum value of 139.8 kPa recorded on the outer surface of the east side of the dome (Table 5). Note that this tensile stress is once again within the limiting tension capacity of both the brick material and the brick-mortar interface.

Similarly, the minimum principal stresses under combined loading (Figure 6d) are generally found to be higher on the east side of the dome and lower on the west side. However, in this case the inner surface tends to record larger stresses than the outer surface (Table 6), with the exception of the base (Level 4) where a compressive stress of -1402 kPa is recorded on the outer surface of the dome. Note that this compressive stress is once again within the 2430 kPa compressive strength of brick. Furthermore, a tensile stress of 170.4 kPa is also recorded on the inner surface of the dome. While this is still less than the tensile strength of the brick unit, it is equal to the 170 kPa tensile strength of the brick-mortar interface, which could result in some cracking of the structure at its base.

Table 5: Maximum principal stress (kPa) under combined dead and seismic load

Level	West Side		East Side	
	Outer	Inner	Outer	Inner
4	-65.3	-61.2	-338.9	28.2
3	43.0	26.2	101.7	67.0
2	-31.0	-17.1	139.8	108.1
1	-133.3	-102.8	35.8	22.1

Table 6: Minimum principal stress (kPa) under combined dead and seismic load

Level	West Side		East Side	
	Outer	Inner	Outer	Inner
4	-266.1	-268.9	-1402.0	170.4
3	-106.7	-321.0	-199.6	-500.6
2	-94.5	-149.4	-95.2	-338.8
1	-162.5	-75.6	-151.9	-136.2

6 CONCLUSIONS

In this paper the results of a seismic analysis of the dome of the Taj Mahal are presented. Results include the mechanism of load transfer, and stress distributions in the dome under gravity and seismic loads. Under the influence of gravity alone (dead load), both the maximum hoop and meridional stresses recorded in the dome are found to be well within the tensile and compressive strengths of brick (safety factors of 4.2 and 2.9 respectively) as well as the tensile bond strength of the masonry (safety factor of 2.4), and compare reasonably well with the results of similar analyses conducted in the literature.

Similarly, under the influence of the combined gravity and seismic loads, the maximum principal tensile stress (139.8 kPa at level 2 at outer surface on the east side) was again found

to be within the limiting tensile capacity of both the brick material and brick-mortar interface, but with the safety factors now reducing to 2.1 and 1.2 respectively. Additionally, the maximum principal tensile stress was found to migrate from level 3 (bulge) to level 2 due to the dome geometry.

Furthermore, under the combined load case, the minimum (maximum magnitude) principal compressive stress (-1402 kPa at level 4 at outer surface on east side) was also found to be less than the compressive strength of the material, but with the safety factor now reducing to 1.7. Additionally, a tensile stress of 170.4 kPa was also recorded on the inner surface of the dome. While this is still less than the limiting tensile capacity of the brick unit, it is however equal to the strength of the brick-mortar interface, which could result in some cracking of the structure at its base. It is proposed to further investigate this potential cracking behavior in the next phase, while also examining the effect of the supporting substructure on the dynamic (seismic) response of the dome.

ACKNOWLEDGEMENTS

The authors acknowledge the valuable assistance of Dr. Ali Roufegarinejad and Mr. Mason Walters S.E. of Forell, Elsesser structural engineers, San Francisco, California during the preparation of this paper. The authors acknowledge the assistance of Alex Limber, fourth year student in the college of architecture and environmental design at Cal Poly State University, San Luis Obispo, California.

REFERENCES

[1] Gascoigne, B. *The Great Moghuls*, Harper and Row, Publishers, New York (1971)

[2] Volwahsen, A. *Living Architecture: Islamic Indian*, Grosset & Dunlap, Publishers, New York, (1970)

[3] Koch, E. *Moghul Architecture*, Oxford University Press, New Delhi, India (2002)

[4] Bunce, F. *Islamic Tombs in India*, D. K. Printworld (P) Ltd., New Delhi, India (2004)

[5] Dayalan, D. *Taj Mahal and Its Conservation*, Abhishek Prakashan, Delhi, India (2009)

[6] Mehrotra, A. and Glisic, B. Deconstructing the Dome: A Structural Analysis of the Taj Mahal, *J. Int. Ass. Shell Spat. Struct*. (2015), **56**(4): 269-284.

[7] Computers and Structures, Inc. *SAP 2000 Software*, Walnut Creek, California (2019)

[8] Dubey, R.N., Thakkar, S.K. and Gupta, A. Seismic Analysis for Safety Evaluation of Taj Mahal Monument. In: *Proceedings of the 11th World Conference on Earthquake Engineering,* (1996).

[9] Viladkar, M.N., Bhandari, N.M., Godbole, P.N. and Trikha, D.N. Three-Dimensional Finite Element Analysis of Taj Mahal Structure. In: *Proceedings of the 5th International Conference on the Structural Analysis of Historical Constructions (SAHC2006),* (2006).

[10] National Disaster Management Authority (NDMA). Development of Probabilistic Seismic Hazard Map of India, Government of India, New Delhi (2011).

[11] Agarwal, P. and Thakkar, S.K. A comparative study of brick masonry house model under quasi-static and dynamic loading, *ISET Journal of Earthquake Technology* (2001), **38**: 103-122.

[12] Singhal, V. and Rai, D.C. Suitability of Half-Scale Burnt Clay Bricks for Shake Table Tests on Masonry Walls, *Journal of Materials in Civil Engineering* (2014), **26**: 644-657.

12th International Conference on Structural Analysis of Historical Constructions
SAHC 2020
P. Roca, L. Pelà and C. Molins (Eds.)

STRUCTURAL EVALUATION OF TYPICAL HISTORICAL MASONRY VAULTS OF CAGLIARI: SENSITIVITY TO BRICKS ARRANGEMENTS

A. CAZZANI[1], N. GRILLANDA[2], G. MILANI[2], V. PINTUS[1] AND E. RECCIA[1*]

[1] Department of Civil and Environmental Engineering and Architecture (DICAAR)
University of Cagliari, Via Marengo 2, 09123 Cagliari, Italy
email: emanuele.reccia@unica.it (*corresponding author)
e-mail: {antonio.cazzani, valentinapintus}@unica.it

[2] Department of Architecture, Built Environment and Construction Engineering (A., B., C.)
Politecnico di Milano, Piazza Leonardo da Vinci 32, 20133 Milan, Italy
e-mail: {nicola.grillanda, gabriele.milani}@polimi.it

Keywords: *Masonry Vaults, Limit Analysis, NURBS, Genetic Algorithm, Laser Scanner Survey, Conservation*

Abstract. *Masonry vaults have a great diffusion in the historical architectural heritage: in this work, their structural behavior is investigated. Attention is focused on lowered sail vaults composed by several brick arrangements, a typical nineteenth-century masonry vault which have great diffusion in Cagliari (Sardinia). The target is evaluating the role played by bricks arrangement in their mechanical behavior. A series of rigorous laser scanner surveys have been performed in order to obtain the effective geometry both at macro-level – the vault shape – and at micro-level – brick patterns. A NURBS (Non-Uniform Rational B-Spline) representation of the geometry is adopted and adaptive upper bound limit analyses are performed. NURBS entities, which are common in commercial CAD packages, have the great advantage to describe complex geometries such as curved elements, with very few elements. An upper bound limit analysis formulation is adopted, in which the NURBS elements forming the mesh are idealized as rigid bodies with dissipation allowed only along interfaces. The mesh constituted by few NURBS elements is progressively adjusted through a genetic algorithm in order to minimize the live load multiplier. Limit analysis is performed initially to determine the collapse multiplier of vertical loads, to assess the load bearing capacity of the vault, then attention is focused on differential settlements, that may be a serious hazard for this structural typology.*

1 INTRODUCTION

Masonry is an ancient structural material and it constitutes most of the historical architectural heritage. It is a composite and heterogeneous material obtained by the assemblage of natural or artificial blocks by means of mortar layers or dry joints. Its internal structure reflects in a complex mechanical behavior, whose understanding represents a challenging research field. During last decades several numerical approaches have been developed: a significant classification can be found in [1].

In this work, attention is pointed out on masonry vaults, that have a wide diffusion in

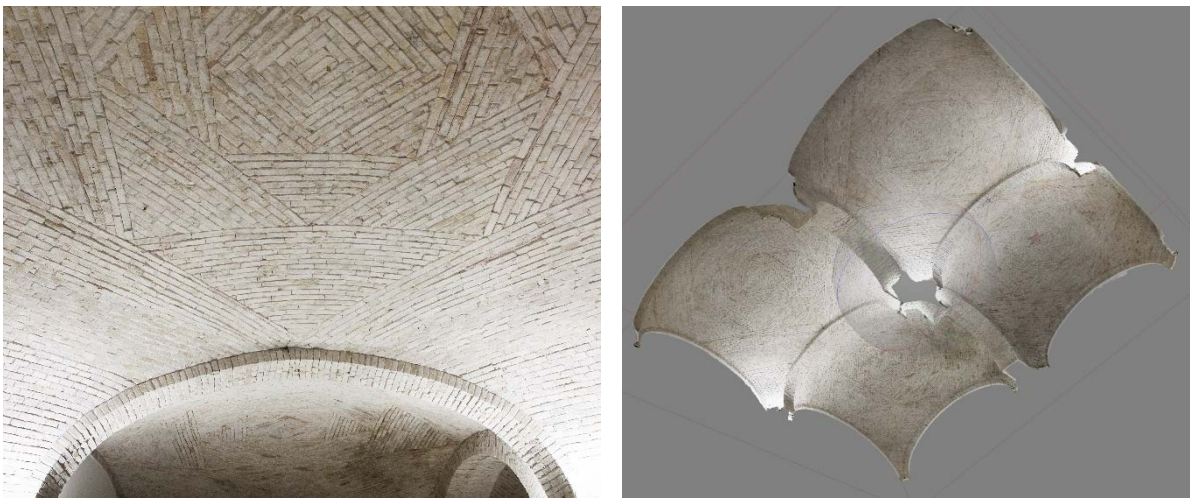
historical buildings. Their structural behavior has been studied for a long time [2,3], but even if a great number of numerical applications has been developed [4], their mechanical behavior is still not fully understood.

Among the different methods that may be found in literature, Limit Analysis is particularly fit to study the collapse behavior of masonry structure [5,6,7]. It is a very effective method for a fast and reliable evaluation of the structural safety of masonry vaults, whose equilibrium is guaranteed when the thrust surface is entirely enclosed within the vault thickness [8]. In literature, both classic upper bound [9,10,11,12] and lower bound theorems [13,14,15] have been applied to study equilibrium and to evaluate failure mechanisms.

Being the behavior of masonry vaults intimately related to their shape, an exact geometric representation is essential in the evaluation of their load-bearing capacity [16,17]. With this aim, geometric reconstructions obtained from point cloud data derived by photogrammetry and/or terrestrial laser scanner may be very useful [18] to provide information both on metrics and on the health status, highlighting cracking and deviation from vertical or horizontal directions [19,20] or from ideal shape, assessed through comparison with parametric [21] or non-parametric models [22].

Here, attention is focused on masonry lowered sail vaults built around the middle of the 19th century with different brick patterns (Figure 1(a)). These vaults have a great diffusion in South Sardinia, and particularly in Cagliari area, but only few studies about them have been carried out, up to now [23]. A series of rigorous laser scanner surveys have been performed on these vaults, in order to obtain the effective geometry both at macro-level, the vault shape, and at micro-level, the brick patterns. A picture of the obtained geometrical outline is reported in (Figure 1(b)).

A NURBS-based upper bound limit analysis approach is adopted to study their collapse behavior under vertical loads and subjected to differential vertical settlements. A preliminary example of the proposed procedure is given by Grillanda et al. [24].



(a) (b)

Figure 1. A typical lowered sail vault in Cagliari (a); geometry obtained by laser scanner survey (b).

2 METHOD: ADAPTIVE NURBS KINEMATIC APPROACH FOR LIMIT ANALYSIS AND STUDY OF SETTLEMENTS ON MASONRY VAULT

For the geometric representation of masonry vaults, the NURBS geometry is one of the more suited modeling techniques. NURBS surfaces (Non-Uniform Rational B-Spline, [25]) are parametric surfaces built from a three-dimensional net of control points and rational B-spline basis functions (the so-called NURBS basis functions). A NURBS surface is defined as follow:

$$\mathbf{S}(u,v) = \sum_{i=0}^{n}\sum_{j=0}^{m} R_{i,j}(u,v)\mathbf{B}_{i,j} \tag{1}$$

in which: u,v are coordinates in the standard parametric domain; $\mathbf{B}_{i,j}$ is a bidirectional net of control points; n,m are the numbers of basis functions respectively along the u- and v-direction; Ri,j are the NURBS basis functions, which are written as follows:

$$R_{i,p}(\xi) = \frac{N_{i,p}(\xi)\cdot w_i}{\sum_{i=1}^{n} N_{i,p}(\xi)\cdot w_i} \tag{2}$$

where: $\Xi=\{\xi1,\xi2,\ldots,\xi\ (n+p+1)\}$ is a non-uniform knots vector; wi $\in \mathbb{R}$ are weight; Ni,p is the i-th B-Spline basis function of degree p.

NURBS surfaces are commonly adopted in the graphic representation of curved geometries. A masonry vault can be easily reproduced by using NURBS surfaces, and the obtained three-dimensional model can be imported into MATLAB through IGES standard file (Figure 2(a,b)). In the MATLAB environment, a subdivision of each surface can be realized by simply partitioning the standard parametric domain. In this way, a mesh composed of trimmed NURBS surfaces is defined: each trimmed surface represents a curved shell-element of the masonry vault (Figure 2(c)). Thanks to the properties of NURBS surfaces, elements of any shapes can be defined. Starting by an initial mesh, mesh adjustment can be applied simply by modifying lines adopted in the subdivision of the standard parametric domain (e.g. moving intersection points or changing slopes, see for example Figure 2(d)).

The trimmed surfaces composing the NURBS model of the vault are here idealized as rigid macro-blocks. In order to take into account non-linearities of masonry material, curved nonlinear interfaces will be defined on elements' edges. Each interface is discretized through points to which the local reference system is defined (Figure 3(a)). A rigid-plastic behavior, defined through a three-dimensional failure surface (typically a Mohr-Coulomb domain with tension cut-off and linear cap in compression, Figure 3(b)) and the associated plastic flow rule, is assigned at each point (we remand to previous works [26] for details on the mathematical formulation). According to this model, in which relative velocities jump can be observed at edges only, interfaces assume the meaning of possible fracture lines to which the mechanism takes place.

A procedure of upper bound limit analysis is adopted on this model. Dead (permanent) loads and live loads (depending on a load multiplier Γ) are defined. The multiplier Γ associated to live loads is determined through the Principle of Virtual Powers, which is computed by means of the following linear programming problem:

$$min\left\{\Gamma = \sum_i P_{int}^i - P_{\mathbf{F}_0}\right\} \text{ such that } \begin{cases}\mathbf{A}_{eq}\mathbf{x} = \mathbf{b}_{eq} \\ \dot{\boldsymbol{\lambda}} \geq 0\end{cases} \tag{3}$$

in which: P_{int}^i is the internal power dissipated at the i-th interface; $P_{\mathbf{F}_0}$ is the external power dissipated by dead loads; $\dot{\boldsymbol{\lambda}}$ are the non-negative plastic multipliers; $\mathbf{x}$ is the vector of unknowns; $\mathbf{A}_{eq}$ and $\mathbf{b}_{eq}$ define the applied equality constraints (i.e. geometrical, compatibility equality constraints and the normality condition).

By solving this linear programming problem, a mechanism and a load multiplier associated with the adopted mesh, i.e. the hypothesized position of fracture lines, are found. In order to optimize the live load multiplier and obtain the real collapse mechanism (according to the kinematic theorem of limit analysis), a procedure of mesh adaptation based on a Genetic Algorithm (GA) is applied (see Figure 4). For details and applications of this adaptive upper bound limit analysis, we refer to [24,27,28,29].

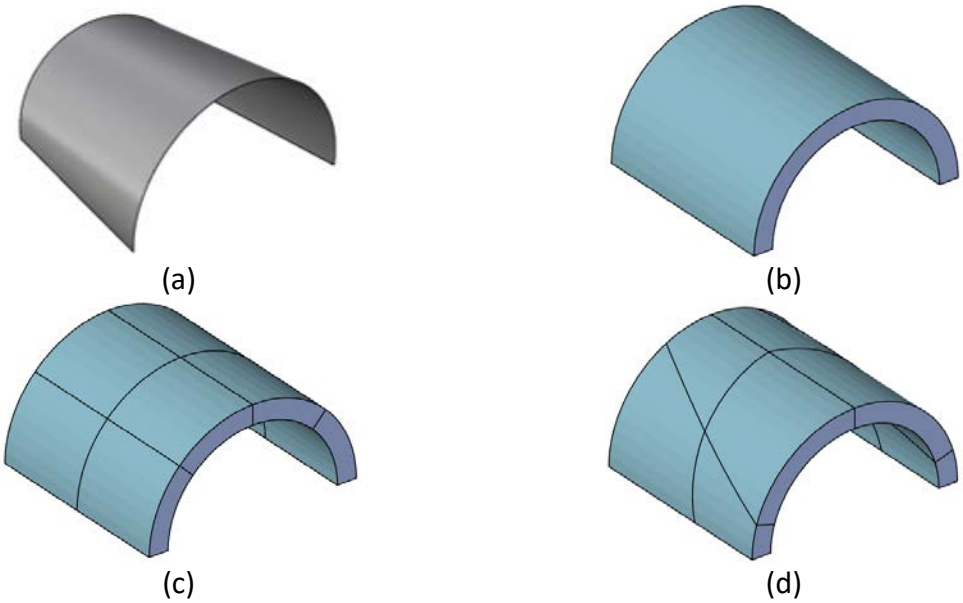


Figure 2. NURBS model generation: (a) NURBS surface in Rhinoceros, (b) NURBS model in MATLAB and its discretization by means of (c) a regular and (d) an irregular mesh.

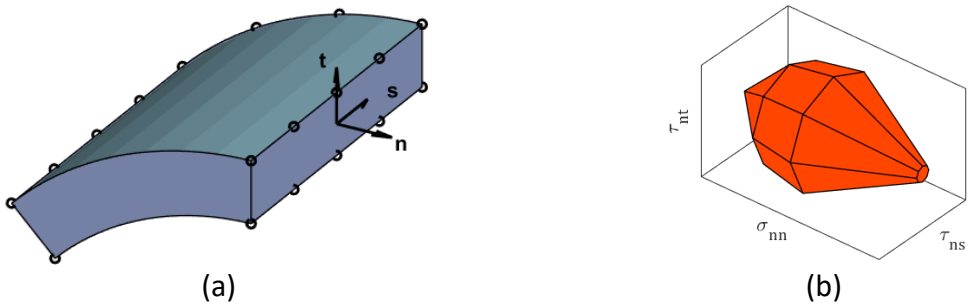


Figure 3. Representation of masonry behavior: masonry-masonry interface and corresponding local reference system (a), and linearized 3D representation of the failure domain (b).

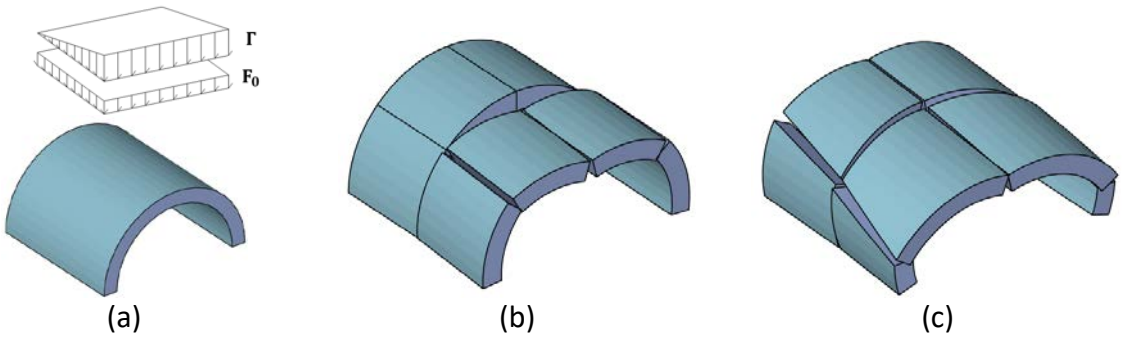


Figure 4. Mesh adaptation procedure: (a) example of load configuration, (b) mechanism associated with the regular mesh, (c) collapse mechanism obtained through GA optimization.

A similar formulation can be adopted in the study of masonry vaults subjected to settlements. Suppose a certain displacement field $\hat{\mathbf{u}}_\mathbf{0}$ is imposed at the external edges of the masonry vault. By discretizing through rigid elements, the crack pattern and displacements induced on the structure can be deduced by solving a unilateral contact problem in which the external work is maximized (see [30]) or, alternatively, the constraint reaction to the settlements is minimized (in agreement with the more recent formulation presented by some of the Authors [31]). If the internal plastic dissipation is assumed on interfaces, the problem can be solved through the Principle of Virtual Work, which can be written according to the following linear programming:

$$min\left\{\sum_i W_{int}^i - W_{\mathbf{F}_0}\right\} \text{ such that } \begin{cases} \mathbf{A}_{eq}\mathbf{x} = \mathbf{b}_{eq} \\ \dot{\boldsymbol{\lambda}} \geq 0 \\ \mathbf{C}_{eq}\mathbf{u} = \hat{\mathbf{u}}_\mathbf{0} \end{cases} \tag{4}$$

in which: W_{int}^i is the internal work at the *i*-th interface; $W_{\mathbf{F}_0}$ is the external work associated with the applied loads; $\mathbf{u}$ is the vector of all displacements of the centroids; $\mathbf{C}_{eq}$ define the equality constraint for the application of the finite displacement $\hat{\mathbf{u}}_\mathbf{0}$.

Therefore, the same adaptive kinematic approach is here applied for the study of the influence of settlements on the masonry vault. By using the same NURBS discretization and the same GA-mesh adaptation, the optimized crack pattern deriving from a defined settlement is properly deduced.

3 NUMERICAL ANALYSES

The structural system involves four vaults (see Figure 1(b)), each one supported on its whole perimeter: the two internal edges between the vaults are supported by masonry arches, while the external edges are supported by masonry walls. In the work, a single vault is analyzed. Arches and external walls are not directly modelled, but they are considered by means of appropriate boundary conditions. The vaults are made by a single brick layer, resulting in a thickness value of about 12 cm along the whole surfaces. The peculiarity of these vaults is the presence of several bricks' arrangements: the vault can be divided in triangular portions characterized by a different orientation of the masonry texture (see Figure 1(a)).

The model has been realized starting from the laser scanner survey: horizontal and vertical

sections of the vault have been extracted (Figure 5 (a)) and then imported in the CAD software Rhinoceros, where an assembly of NURBS surfaces has been created (Figure 5 (b)). A different NURBS has been adopted for each triangular portion of vault: different properties have been assigned to each surface in order to take into account the specific orientation of the masonry texture in the limit analysis. The edge of surfaces between the different triangular portions correspond to possible fracture lines that may develop under vertical loads or due to settlements. The assemble of surfaces has been imported into the MATLAB environment, assigning thickness properties, in order to realize the NURBS model (Figure 5(c)).

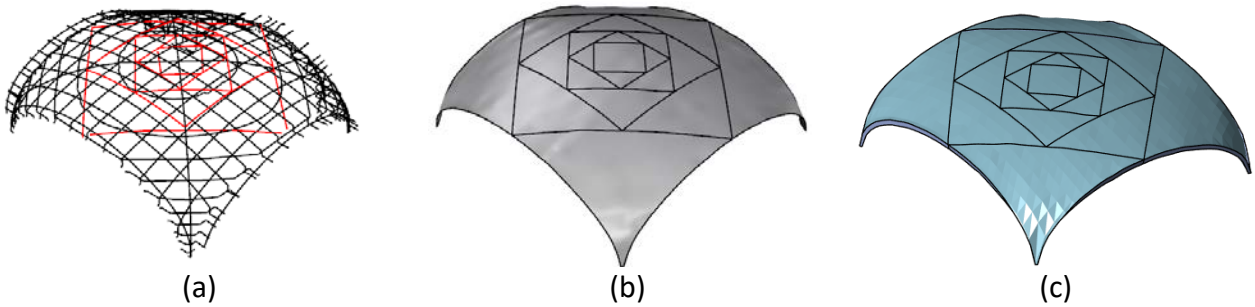


Figure 5. Construction of the NURBS model of the single vault: (a) section lines, (b) assembly of NURBS surfaces in Rhinoceros and (c) obtained NURBS model in MATLAB.

In the first step of analysis cracks may develop only along the initial NURBS surfaces of the model, corresponding to the bed joints between each triangular portions. In this case, the different orientation of bricks inside each part does not play any role in the ultimate load-bearing capacity of the vault, thus a unique value of ultimate stress has been assigned (Table 1).

Table 1: material properties assigned to interfaces between initial NURBS surfaces

Property	*Value*
Specific weight [kN/m^3]	18
Ultimate tensile strength [MPa]	0.2
Ultimate compression strength [MPa]	2.6
Cohesion [MPa]	ft
Friction angle [°]	30

Being the hypothesis of failure only along the triangular portions too simplistic, in the second step of analysis each triangular portions has been subdivided into smaller elements (see Figure 6(a)) chosen taking into account the shape of each surface. The refined mesh is reported in Figure 6(b). In this case, bricks orientation is accounted adopting appropriate values of ultimate stress. A simplified orthotropic model for masonry [32] is adopted: different properties have been assigned to direction 1, parallel to bed joints, and direction 2, orthogonal to the first one (Table 2).

Finally, a third step of analysis is performed applying the mesh adaptation through GA: the refined mesh is adaptively modified in order to find the minimum value of the live load multiplier. In this case, if the orthogonal normal vector is directed along an intermediate direction between 1 and 2, the ultimate stress values are evaluated according to the two main components of the normal vector.

Two analyses are performed: under vertical loads and applying differential settlements.

Table 2: Material properties assigned to interfaces in the refined mesh

Property	*Value*
Specific weight [kN/m3]	18
Ultimate tensile strength - direction 1[MPa]	0.4
Ultimate tensile strength - direction 2 [MPa]	0.2
Ultimate compression strength - direction 1[MPa]	5.2
Ultimate compression strength - direction 2 [MPa]	2.6
Cohesion [MPa]	ft
Friction angle [°]	30

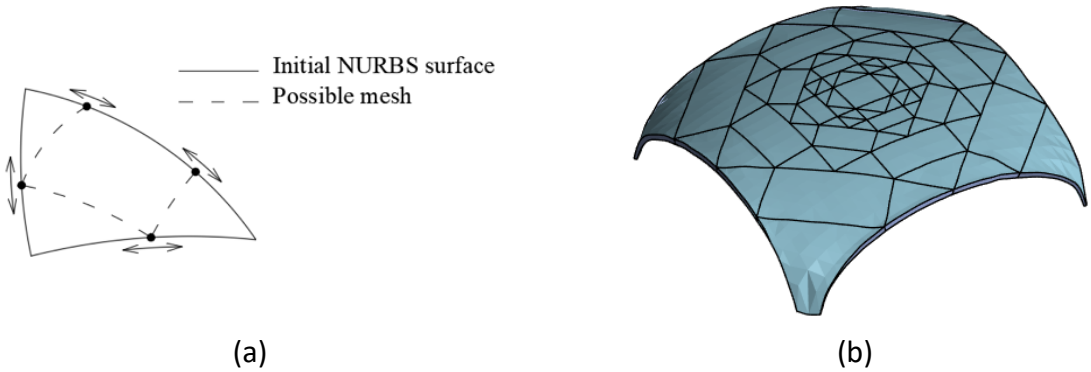


Figure 6. Definition of a possible mesh: (a) schematization of the mesh for the single NURBS surfaces composing the vaults, (b) obtained regular mesh.

3.1 Limit analysis under vertical loads

Two vertical load cases have been considered: Load Case 1 (LC1), in which live load consists of the self-weight only, and load Case 2 (LC2), in which a distributed uniform vertical load has been applied at the extrados of the vault as live load (self-weight is applied as dead load, so it is not affected by the load multiplier). For each load case, a live load multiplier Γ is found. If the final load multiplier is higher than one, as expected, the vault is definitely safe under self-weight (LC1) and under increasing loads (LC2). In order to better compare the results obtained applying the two load cases, the load multiplier obtained in LC2 has been normalized relatively to the total weight of the vault. Results of the three steps of analyses for both load cases, in terms of live load multiplier and collapse mechanism, are reported in the following figures.

In Figure 7 analyses are performed on the initial mesh: live load multipliers Γ are equal to 38.1 and 35.5 respectively for LC1 and LC2. It can be observed that there are no substantial differences between the two collapse mechanisms. The value of the multiplier of LC1 is higher than the one of LC2, and in both cases Γ is considerably higher than one: because of the lowered shape of the vault, crushing assumes a fundamental role in comparison with tensile and shear failures.

A similar trend may be observed in the second step of analysis, reported in Figure 8. The adoption of a refined mesh allows obtaining lower values of the load multipliers Γ, equal to

33.4 and 30.7 respectively for LC1 and LC2. Also in this case, since failure may occur only between the interfaces of the refined mesh, the two mechanisms of collapse are almost the same.

Figure 9 shows the results of the third step of analysis: the mesh adaptation through GA allows to finally obtain the minimum load multipliers, equal to 32.6 and 30.0 respectively for LC1 and LC2. Moreover, in this case, the two mechanisms of collapse obtained by LC1 and LC2 are different.

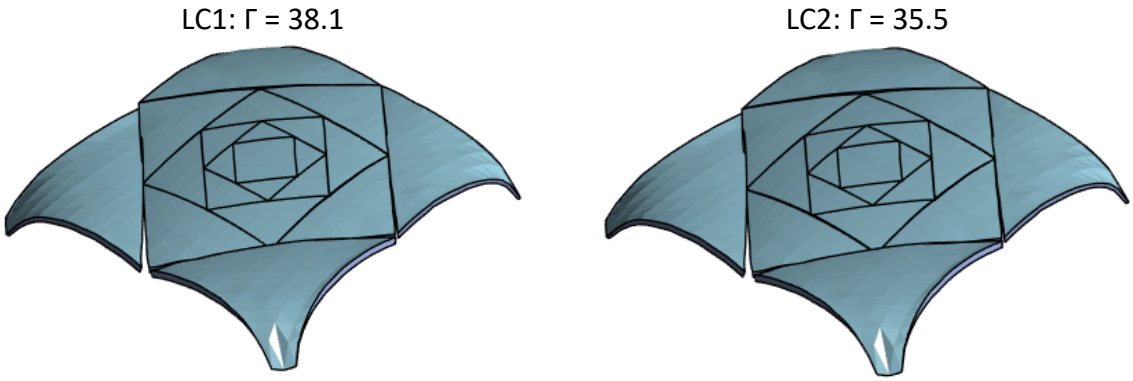


Figure 7: First step of analysis: initial fracture lines.

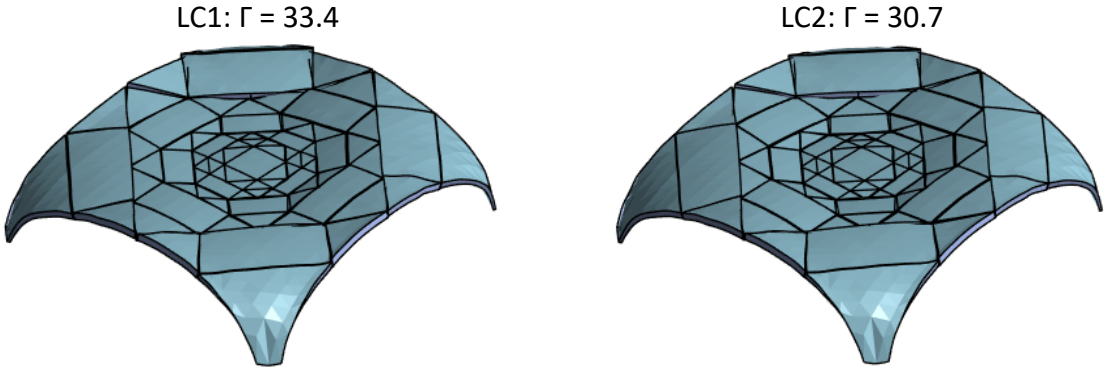


Figure 8: Second step of analyses: refined mesh.

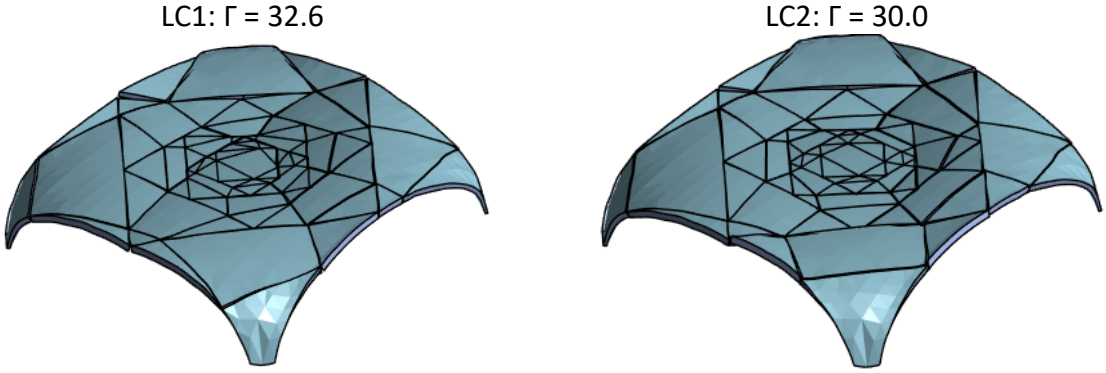


Figure 9: Third step of analyses: mesh adaptation

3.2 Limit analysis whit differential vertical settlements

The crack pattern deriving from an imposed settlement has been determined through the presented procedure. A vertical settlement has been applied along one of the four external edges of the vault (see Figure 10 (a)), as a representation of vertical displacement of the supporting walls. The applied displacement is equal to 1 cm for the whole edge. The same initial mesh has been assumed for each triangular portion of the vault. The final crack pattern and the deformed structure (scaled according to a factor equal to 50) are depicted in Figure 10 (b-d).

As it can be noted, the cracks are mainly localized on the half of the vault subjected to the settlements. Moreover, it is worth noting that the main diagonal cracks follow the mortar joints between the different triangular portions of the vault. This is the natural consequence of the lower resistance parameters assigned to interfaces corresponding to mortar joints.

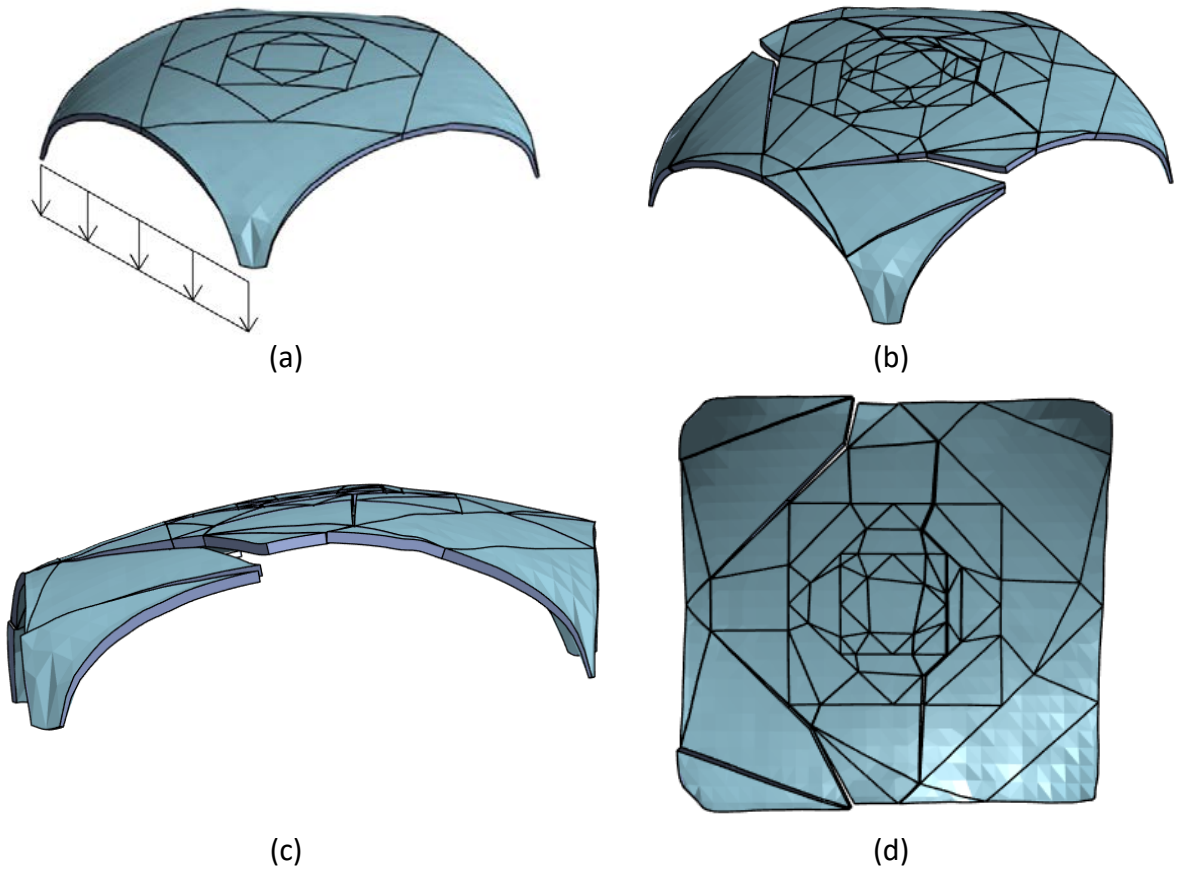


Figure 10. Analysis of the masonry vault subjected to settlements: (a) representation of the applied displacements, (b-d) crack pattern and deformed structure (displacements scaled by 50).

4 CONCLUSIONS

- In the paper, the collapse behavior of masonry vaults has been investigated. Attention has been focused on a lowered sail vaults built with different brick patterns. The geometry of the vaults has been accurately obtained through laser scanner survey and then reconstructed with a 3D NURBS-based model, particularly suited for historical masonry vaults with complex geometry. A limit analysis approach based on an

adaptive NURBS modeling coupled with a genetic algorithm has been performed to obtain the ultimate load of the structure and the associated collapse mechanisms for two different load conditions and in case of differential settlements.

- The use of laser scanner surveys and the adoption of 3D NURBS allow to describe the exact geometry of the vaults. This aspect is essential in the evaluation of their load-bearing capacity, being their behavior intimately related to their shape.
- Because of the lowered shape of the vault, crushing assumes a fundamental role in comparison with tensile and shear failures.
- Differential settlements must be studied: they may be a serious hazard for this structural typology.
- The role played by bricks arrangements must be considered in order to obtain reliable mechanisms of collapse.
- The proposed procedure provides fast and reliable assessment of the collapse behavior of masonry vaults.

REFERENCES

[1] D'Altri, A., Sarhosis, V., Milani, G., Rots, J., Cattari, S., Lagomarsino, S., et al. 2019. Modeling strategies for the computational analysis of unreinforced masonry structures: Review and classification. *Arch. Comput. Method. Eng* doi:10.1007/s11831-019-09351-x

[2] Boothby, T. E. 2001. Analysis of masonry arches and vaults. *Progress in Structural Engineering and materials*, 3(3): 246-256.

[3] Lucchesi, M., Padovani, C., Pasquinelli, G. & Zani N. 2007. Static analysis of masonry vaults, constitutive model and numerical analysis. *J. Mech. Mater. Struct.*, 2(2): 221–2 44.

[4] Tralli, A., Alessandri, C. & Milani, G. 2014. Computational Methods for Masonry Vaults: A Review of Recent Results. *The Open Civil Engineering Journal*, 8: 272-287.

[5] Valente, M., Milani, G., Grande, E., & Formisano, A. 2019. Historical masonry building aggregates: Advanced numerical insight for an effective seismic assessment on two row housing compounds. *Eng. Struct.*, 190, 360-379.

[6] Valente, M., & Milani, G. 2019. Earthquake-induced damage assessment and partial failure mechanisms of an italian medieval castle. *Eng. Fail. Anal.*, 99, 292-309.

[7] Pepe, M., Pingaro, M., Trovalusci, P., Reccia, E., & Leonetti, L. 2020. Micromodels for the in-plane failure analysis of masonry walls: Limit analysis, FEM and FEM/DEM approaches. *Frattura ed Integrita Strutturale*, 14(51), 504-516

[8] Heyman, J. 1969. The safety of masonry arches*, Int. J. Mech. Sci.*, 11 (4): 363-385,

[9] D'Ayala, D. & Casapulla, C. 2001. Limit state analysis of hemispherical domes with finite friction. In *Structural Analysis of Historical Constructions*, Guimarães (Portugal), 2001.

[10] Milani, E., Milani, G. & Tralli, A. 2008. Limit analysis of ma-sonry vaults by means of curved shell finite elements and homogenization, *Int. J. Solids Struct.*, 45: 5258-5288, 2008.

[11] Pavlovic, M., Reccia, E. & Cecchi, A. 2016. A procedure to in-vestigate the collapse behavior of masonry domes: some meaningful cases. *Int. J. Archit. Herit.*, 10(1): 67-83.

[12] Rossi, M., Calderini, C., Di Napoli, B., Cascini, L., & Portioli, F. 2020. Structural analysis of masonry vaulted staircases through rigid block limit analysis. *Structures*, 23, 180-190.

doi:10.1016/j.istruc.2019.10.015

[13] O'Dwyer, D. 1999. Funicular analysis of masonry vaults, *Comp. Struct.*, 73(1-5): pp. 187-197.

[14] Block, P. & Ochserdorf, J.A. 2007. Thrust network analysis: a new methodology for three-dimensional equilibrium, *J. IASS*, 48(3): 167-173.

[15] Angelillo, M, Babilio, E. & Fortunato, A. 2013. Singular stress fields for masonry-like vaults. *Continuum Mech. Thermod*., 25: 423-441.

[16] Cazzani, A., Malagù, M. & Turco, E. 2016. Isogeometric anal-ysis: a powerful numerical tool for the elastic analysis of historical masonry arches, *Continuum Mech. Thermodyn*, 28: 139–156.

[17] Chiozzi, A., Malagù, M., Tralli, A. & Cazzani A. 2016. Arch-NURBS: NURBS-Based Tool for the Structural Safety As-sessment of Masonry Arches in MATLAB, *J. Comput. Civ. Eng*., 30(2): # 04015010-1-11.

[18] Schueremans, L. & Van Genechten, B. 2009. The use of 3D-laser scanning in assessing the safety of masonry vaults. A case study on the church of Saint-Jacobs. *Optics Lasers Eng*., 47: 329-335.

[19] Castellazzi, G., D'Altri, A. M., de Miranda, S. & Ubertini, F. 2017. An innovative numerical modeling strategy for the structural analysis of historical monumental buildings, *Eng. Struct*., 132: 229–248.

[20] Napolitano, R. & Glisic, B. 2019. Methodology for diagnosing crack patterns in masonry structures using photogramme-try and distinct element modeling, *Eng. Struct*., 181: 519–528.

[21] Argiolas, R., Cazzani, A., Reccia, E. & Bagnolo,V. 2019. From LIDAR data towards HBIM for structural evaluation, *IS-PRS Archives*, 42: 125-132.

[22] Armesto, J., Roca-Pardiñas, J., Lorenzo, H. & Arias, P. 2010. Modelling masonry arches shape using terrestrial laser scanning data and nonparametric methods, *Eng. Struct*., 32(2): 607–615.

[23] Cazzani, A., Grillanda, N., Milani, G., Pintus, V. & Reccia, E. Numerical insights on the structural assessment of typical historical masonry vaults of Cagliari, in *Proceedings of 17th International Brick and Block Masonry Conference - 17th IB2MaC 2020*, submitted

[24] N. Grillanda, A. Chiozzi, F. Bondi, A. Tralli, F. Manconi, F. Stochino, and A. Cazzani. Numerical insights on the structural assessment of historical masonry stellar vaults: The case of Santa Maria del Monte in Cagliari, *Continuum Mech. Thermodyn.*, doi:10.1007/s00161-019-00752-8

[25] Piegl L & Tiller W. *The NURBS Book*. Berlin: Springer; 1995.

[26] Chiozzi A, Milani G, Tralli A. 2017. A Genetic Algorithm NURBS-based new approach for fast kinematic limit analysis of masonry vaults. *Comput Struct*; 182:187–204.

[27] Chiozzi A, Milani G, Grillanda N, Tralli A. 2003. Fast and reliable limit analysis approach for the structural assessment of FRP-reinforced masonry arches, *Key Eng. Mater.*, 747:196–203.

[28] Grillanda N, Chiozzi A, Milani G, Tralli A. 2019. Collapse behavior of masonry domes under seismic loads: an adaptive NURBS kinematic limit analysis approach. *Eng. Struct.*, 200: 109517.

[29] Grillanda N, Chiozzi A, Milani G, Tralli A. 2019. On Collapse Behavior of Reinforced Masonry Domes under Seismic Loads. *Key Eng. Mater.*, 817:275–82.

[30] Iannuzzo, A., Angelillo, M., De Chiara, E., De Guglielmo, F., De Serio, F., Ribera, F., et al. 2108. Modelling the cracks produced by settlements in masonry structures, *Meccanica*, 53:1857–73.

[31] Tralli, A., Chiozzi, A., Grillanda, N., & Milani, G. 2109. Masonry structures in the presence of

foundation settlements and unilateral contact problems. *Int. J. Solids Struct.*. doi:10.1016/j.ijsolstr.2019.12.005.

[32] Milani, G., & Taliercio, A. (2015). In-plane failure surfaces for masonry with joints of finite thickness estimated by a method of cells-type approach. *Comp. Struct.*, 150, 34-51

12th International Conference on Structural Analysis of Historical Constructions
SAHC 2020
P. Roca, L. Pelà and C. Molins (Eds.)

STRUCTURAL MODELLING AND NUMERICAL ANALYSIS OF THE PALACE OF SPORTS OF MEXICO CITY

HIRAM BADILLO-ALMARAZ[1*], AGUSTÍN ORDUÑA[2], SERGIO G. DE LA ROSA[1], GEORGIA A. GONZÁLEZ[3] AND GUILLERMO M. ROEDER[2]

[1]Civil Engineering Department
Universidad Autónoma de Zacatecas - UAZ
Av. R. López Velarde No. 801, 98060 Zacatecas, México
e-mail: *hbadillo.civil@uaz.edu.mx, sgdelarosa@uaz.edu.mx, www.uaz.edu.mx

[2] Civil Engineering School
Universidad de Colima -UCOL
Km 9, Colima-Coquimatlan road, 28400 Colima, México
e-mail: aord@ucol.mx, groederc@ucol.mx, www.ucol.mx

[3]Doctoral Program of Development Studies
Universidad Autónoma de Zacatecas - UAZ
Av. Preparatoria S/N, 98065 Zacatecas, México
e-mail: georgi_ara@hotmail.com

Keywords: Historical Structure, Palace of Sports, Numerical Modelling, Finite Element Analysis

Abstract. *The palace of sports represents in many ways the masterpiece from the urban-architectural legacy that was created for the XIX Olympiad in Mexico City in 1968; its uniqueness, from the architectural and structural point of view, makes it one of the most iconic buildings of the city. In this paper the structural modelling and numerical analysis of this iconic building of the Mexican architecture of the second part of the XX century is presented. The numerical modelling is achieved by means of a 3D finite element model in order to obtain preliminary results in terms of dynamic properties and linear and non-linear response of structural elements when subjected to gravity loads. Natural periods of the modes with high participating mass obtained on the numerical model are in well agreement to those of other structures with similar configurations. Nonlinear results show that the structure has a large safety factor under gravitational loads. Finally, recommendations about the improvements that can be applied on the actual FEM model are given based on the results obtained in order to give a better assessment to identify risk scenarios and to prevent them to occur on such iconic structure.*

1 INTRODUCTION

From the urban-architectural legacy constructed for the XIX Olympiad in Mexico City in

1968, one of the most outstanding buildings that were projected for the event is the Palace of Sports, designed by the acclaimed architect Felix Candela in collaboration with architects Enrique Castañeda and Alfonso Peyrí [1]. The building has special features that combine architectural design, structural engineering, urban art, city landscape and cultural identity that made it achieve a value closest to cultural symbolism rather than the simple physical place used for sporting or public events [2].

1.1 Social, cultural and historical context

The year of 1968 in Mexico has been tied to two indissoluble events: a student movement that ended tragically and the XIX Olympic Games. Both events were inserted into a society that struggled to move towards modernity; nevertheless, these events, so far from each other, transformed an entire nation [3].

The sixties represent a period of permanent growing in economic, demographic, and urban terms, to such degree that the Mexican government tried to gain visibility for the country in the international context [4]. Hence, it was essential that México radiated not only through the sporting event but also through culture and art; therefore, the interest to realize a cultural Olympiad at the same time that the games were taking place. According to Pedro Ramírez Vázquez, president of the Olympic Committee, it was necessary to "carry on to everyone the true image of Mexico" [5]. Besides, it would be the first time that the Games would be broadcasted in color television.

The idea of the Mexican government was to project the image of the country through architecture. One of the priorities, was to design outstanding venues where competitions were going to take place, following the idea of creating a *Universopolis* (the new metropolis of the world), as expressed by José Vasconcelos on his book "The cosmic race" [6]. With all these things at stage, Mexico had compromised its prestige, especially given the success of the architecture and structures of the previous achievements in Rome and Tokyo.

Several venues were constructed or upgraded to host the different Olympic disciplines, following the idea of disseminating a national symbolic system that pursued to show the strength of the government whereas trying to renew the image of Mexico [7]; among these were the Olympic stadium, the Mexican Olympic sports center, the Olympic pool and gymnasium, the Olympic velodrome, the Olympic Village, among others. However, among all the facilities built, the Palace of Sports outstands from the rest because of its uniqueness in terms of design and aesthetics. According to several renowned architects, it represents the masterpiece and the greatest exaltation to the monumentality of that period [8].

The Palace of Sports, beyond its qualities in design and construction, is considered the *geosymbol* of the XIX Olympics because works like this not only transcend temporally and spatially but even could give cultural identity to a whole nation.

2 DESCRIPTION OF THE STRUCTURE

2.1 Architectural aspects

The general structure of the building was considered, from the project phase, as the dominant element of the composition, and the determinant factor of its spatial plastic sense [9]. It was projected to achieve an extraordinary design form, far from puerile and ordinary

structures, that could result fascinating from any point of view: exterior and interior, at the pedestrian level and even from the aerial point of view [10].

According to Candela and his collaborators, the constructive solution should be completely realistic, that is, the structure had to be simple and easy to analyze and build, but above all, it would need to agree with the scale. Although the Palace of Sports of Candela, has a clear influence from Pier Luigi Nervi's Palazzo and Palazzetto of Sports, built for the 1960 Summer Olympics in Rome [11], the aforementioned considerations eliminated any chance of applying a concrete shell as roof solution for the Palace of Sports; besides, the building had to meet with the objectives marked by the organizing committee that established that the design proposals should be outstanding but feasible economically.

Due to the low ground resistance of the site, designers decided to adopt spherical dome with an approximate overall area of 27,171 m^2 with a light metal structure (60 kg/m^2 approximately), where the trusses worked basically under axial compression, which makes possible to eliminate the secondary elements.

The supporting structure consists of an almost orthogonal grid of steel trusses with a constant height of 5 m, arranged according to maximum circles of a sphere with and angle of separation of 8° approximately. In Figure 1 an aerial view of the structure is presented. The spherical cover is limited by four maximum circles and divided into 121 squares, whose sides vary from 13 to 10 m. The trusses consist of a central element working under compression, formed by rhombuses, triangulated by radial braces. The upper and lower chords work under tension forces to take positive and negative moments. The central arches have 132 m of span.

The squares that result from the intersection of the trusses are covered with hyperbolic paraboloids consisting of a structure based on an aluminum tube, which, in turn, receives a 38 mm-plywood shell, protected by asphalt waterproofing. The outer surface is lined with a copper tile of 13.5 thousandths of an inch, which eliminates all secondary reinforcements and reduces the dead weight and, therefore, the total cost of the structure [10].

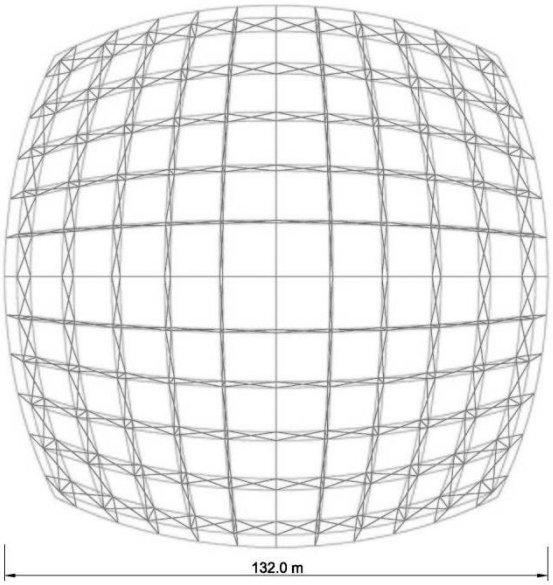
The main reinforcements rest on dices of reinforced concrete that in turn rest on reinforced concrete pillars and inclined buttresses in form of V. Each of the dices and buttresses are joined by connection beams that have the capacity to absorb lateral loads as well as the thrust of the arches.



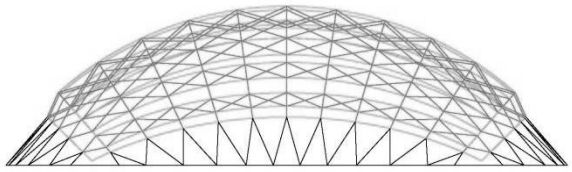
Figure 1: Aerial view of the Palace of Sports

2.2 Structural configuration

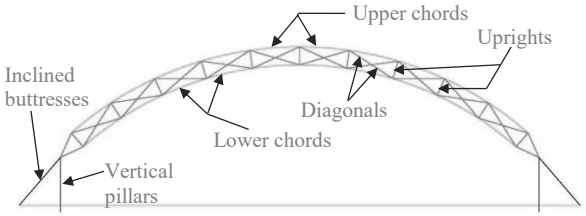
The roof of the Palace of Sports is supported by two sets of circular arches that form a spherical cap of approximately square plan, with an approximate area of 13,700 m² and without any intermediate support. The central axes of the arches are two families of meridians of a sphere of 92.6 m in diameter whose polar axes contained in the same horizontal plane are mutually orthogonal. Figure 2 presents details of the structural configuration of the roof. The structure is limited by four inclined planes that form a dihedral angle of 45° 28' with the two vertical planes of symmetry, in which the polar axes are contained. Each family is composed of 11 arcs separated from each other by varying distances, between 10 and 13 m, so that the grid obtained from the two sets of arches gives as a result areas approximately squared of 12 × 12 m on average, on which hyperbolic paraboloids made with aluminum tubes supported on the main arches have been placed, and on which the roof itself rests, which is formed by plywood and copper foil as mentioned previously [12].



a) Plan view of the roof structure



b) Lateral view of the roof structure including inclined buttresses



c) Geometrical representation of the central arch including inclined buttresses and pillars

Figure 2: Geometry of the roof structure

The arches have a constant height of 5 m measured between the axes of the chords over the entire length, except on the end panels, since they are articulated to the concrete structure that receive them. In Figure 2c, one of the 22 arches that support the roof is shown schematically.

The diagonals were designed as compressed elements to withstand almost all of the normal forces caused by permanent vertical loads, while the chords of the trusses had as basic objective to give the arch the ability to withstand the bending moments produced by wind loads, asymmetric vertical loads, differential settlements, etc.

The analysis of the roof structure was carried out by the renowned structural engineer Oscar de Buen, considering the structure as an arc lattice, formed by 11 elements in each direction, rigidly joined together at their intersections. A structure with 121 knots was

obtained, with a high degree of hyperstaticity. Two simultaneous analyzes were made, using in one of them the method of flexibilities and in the other the stiffness method. In both cases, the effects on the deformations of the normal forces and the bending moments were taken into account. Torsional stiffness of the arches was disregarded, which in addition to introducing notable simplifications in the analysis, is fully justified in structures of this type [12]. Computers were mainly used in the following aspects: structural analysis of the roof, obtaining the detailed geometry of the roof and structural analysis of the ring that receives the arches [13].

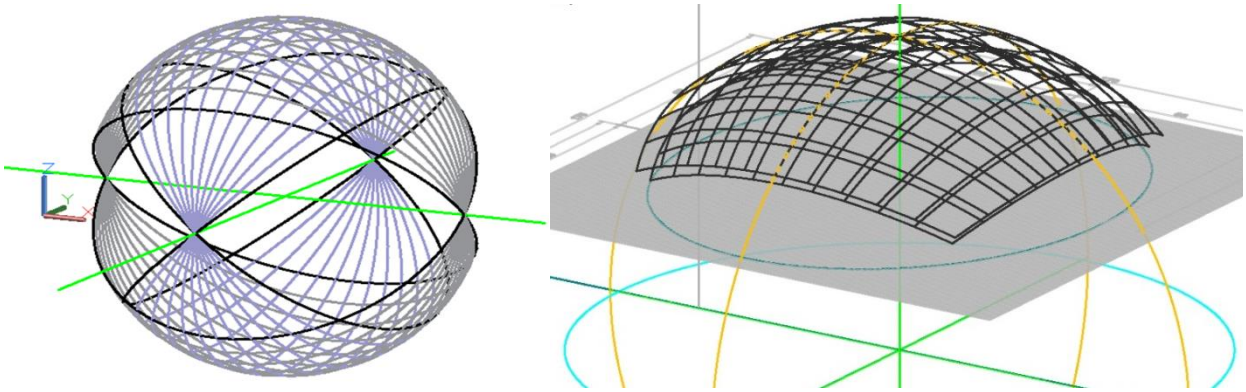
The material used to build the structure was A36 steel, with a yield limit of 250 MPa, except for the tubes that form the chords of the arches, which were made of ASTM A120 steel, with a yield limit is 240 MPa. The diagonals and the uprights are sections H and I formed by three plates welded together. All the joints of the structure were welded together as well.

The profiles used were: circular tube of 21.9 cm of outer diameter, ID 30, thickness 0.70 cm, for the upper and lower chords; section H with flanges of 30 cm of width and 1.6 cm of thickness and web of 30 cm by 1.27 cm for the diagonals; section I with flanges of 15 cm of width and 1.9 cm of thickness and web of 30 cm by 1.27 cm for the uprights.

3 STRUCTURAL MODELLING

3.1 Graphical model

The division of spherical geometry represents an enormous challenge for the analysis of reticular structures. When referring to a geodesic dome as the main geometry form for the modeling of the Palace of Sports, the starting point is a cubic model, projected on a sphere in order to divide it into six squares of equal sections. One of those sections (upper face) will give the initial form of the reticular structure of the Palace of Sports.



a) Central axes which work as boundaries of the guide arches

b) Main grid generated through maximum circles for the internal and external faces

Figure 3: Graphic development of the roof structure

Subsequently, guide arches (maximum circles) will be distributed with spacing with regular revolution angles and fixed to two axes perpendicular to each other (passing from end

to end of the sphere and through the geometric center of it), until a grid of 22 arcs (11 on each direction) is generated as shown in Figure 3a; this will be the main and generating structure of all subsequent geometry. The angle of rotation in which the 11 arches are distributed to generate the grid is 8°16' giving a total measurement of 82°40' between the last and first arch; this causes that all the trusses of each arch will have a different inclination, i.e. none will be parallel. The radial reinforcements are 5 meters high between the family of internal arches and that of the external ones. In Figure 3b the main grid generated through maximum circles for the inner and outer faces of the structure (90.1m and 95.1m of diameter) with 5 m of separation between them is presented.

To define the position of the buttresses and the supports of each arch, the geometry between the grid of arcs will be further prolonged in order to obtain the crossing points with the horizontal plane that will indicate the location of the connecting points of the rooftop cover with the buttresses and of the buttresses with the ground. This grid will need another pair of guide arches on each edge, for the tracing of the supports that will be a transition section between the metal structure and the concrete supports. The buttresses locations are defined as a continuation of the initial geometry of the geodesic dome. Furthermore, uprights and diagonals that connect each of the edges of the uprights are included.

Once the main structure for the dome and buttresses is finished, the same arc geometry will be used for the generation of a third grid that will support the closing substructure of the dome. This intermediate grid passes through each quadrant of the main structure at its midpoints, as it will support part of the aluminum tubular substructure and will shape the pyramids of the roof as shown in Figure 4.

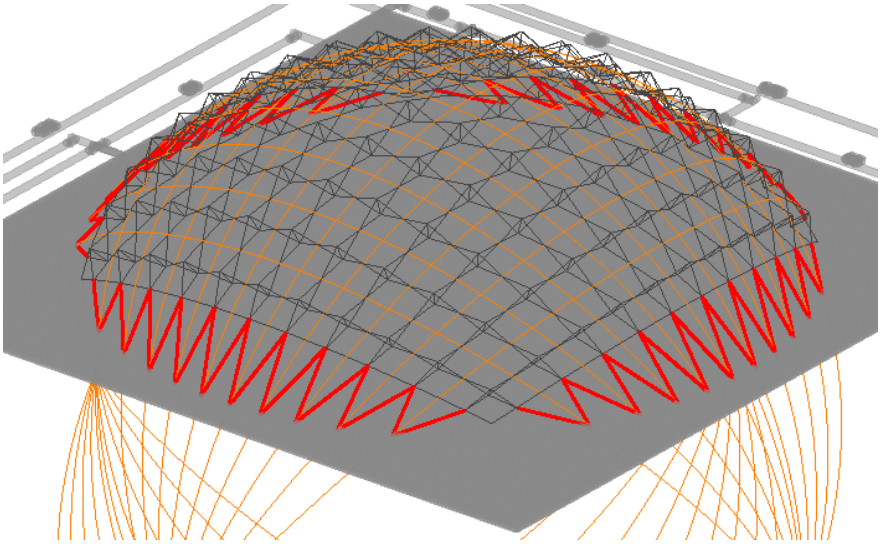
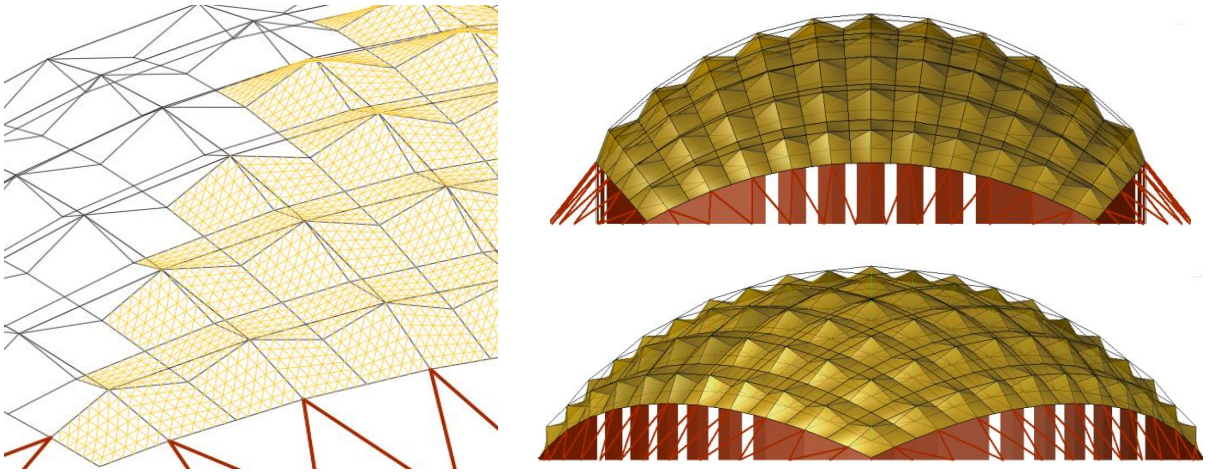


Figure 4: Descriptive geometry of the main structural elements of the Palace of Sports

The rooftop cover of the dome is generated from fragments of hyperbolic paraboloids inserted in the quadrilaterals generated after the subdivision of the dome. Since the hyperbolic paraboloids consist of ruled surfaces, the assembly process was greatly simplified, since the whole cover could be carried out by straight elements without curvature. The characteristic copper finish on the dome sits on wooden boards that are placed on a triangulated grid of

aluminum tubes. The gaps that are formed by the intersection of the grids are approximately 12 x 12 m and were covered with four hyperbolic paraboloid panels based on a three-way grid better known as the triodetic system, which, in turn, receives the plywood cover that forms the dome rooftop enclosure.

The enclosure modules do not hide the structure of spherical arches since they are located between the two concentric spheres. The intersection point of four hyperbolic paraboloid fragments links the metal arches of the dome, making contact with the upper and lower arches alternatively. In this way, the main structure can be appreciated from the inside and from the outside. On Figure 5a, a projection of the aluminum grid over the upper diagonals of the arches is presented (bottom diagonals not shown on the figure). Figure 5b presents a lateral and corner view of the completed graphical model. The graphical model was entirely developed using the software AutoCAD.



a) Projection of the aluminum grid over the upper diagonals of the arches

b) Lateral and corner view of the completed model

Figure 5: Graphical model of the Palace of Sports

3.2 Finite element model

In order to analyze the structural behavior of the Palace of Sports a Finite Element Method (FEM) model was developed based on the graphical model described previously. The model includes the following types of materials: steel, concrete, aluminum and a rooftop cover composite element that comprises the plywood and the cooper foil altogether.

Steel elements are assigned the upper and lower chords (circular tubes), uprights (sections I) and diagonals (sections H) of the trusses; sections H are also used on the boundary elements that define the perimeter of the roof structure. Concrete elements are assigned to the vertical reinforced concrete pillars and inclined buttresses in form of V and on the walls of the perimeter. Aluminum elements are assigned to the contour of the grid of the triodetic system (circular tubes of 95.25 mm of diameter and thickness of 4.1 mm) and to elements of the triodetic system itself (circular tubes of 47.625 mm of diameter and thickness of 2.032 mm). The plywood and the cooper foil composite are assigned to the elements that serve as rooftop cover of the structure. Table 1 shows the mechanical properties of each the materials used in

the numerical analyses. It is important to mention that the density of the rooftop cover composite is modified in order to include, together with the self-mass of the composite, an additional mass of 20 kg/m^2 for installations and another of 20 kg/m^2 for live load.

Table 1: Mechanical properties of the materials used in the numerical analyses

Material	Young's modulus (GPa)	Poisson relation	Yield stress (MPa)	Density (kg/m^3)
STEEL	206	0.28	250	7800
CONCRETE	21.7	0.15	24	2400
ALUMINUM	68.6	0.33	50	2700
ROOFTOP COVER COMPOSITE	10	0.15	N/A	4740

The model was analyzed with the FEM software DIANA-FEA [14]. For the modelling of the vertical reinforced concrete pillars and inclined buttresses, the steel, and aluminum elements a two-node, three-dimensional class-III beam element was used. Meanwhile for the walls of the perimeter and for the rooftop cover composite, four-node quadrilateral isoparametric curved shell elements based on linear interpolation and Gauss integration over the element area were used in combination with three-node triangular isoparametric curved shell elements based on linear interpolation and area integration. The model included 22,199 nodes and 75,062 elements. The boundary conditions of the FEM model are considered as fully constrained on the base of the support elements (vertical pillars, buttresses and walls), since in the actual structure they are connected to a slab that is supported by a compensated foundation of friction and point bearing piles. Figure 6 presents the FEM model with the elements extruded and with the corresponding boundary conditions.

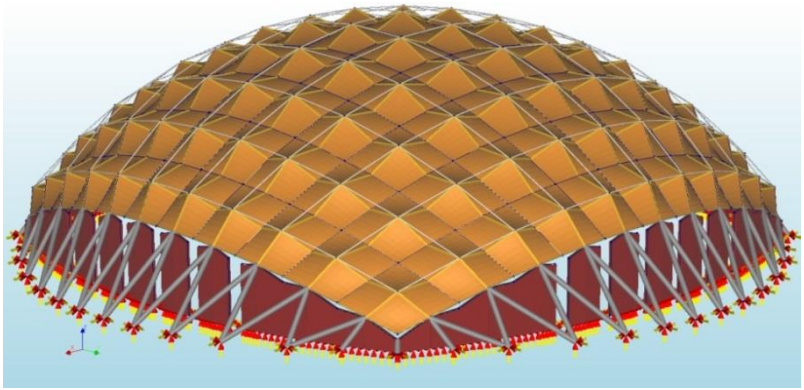


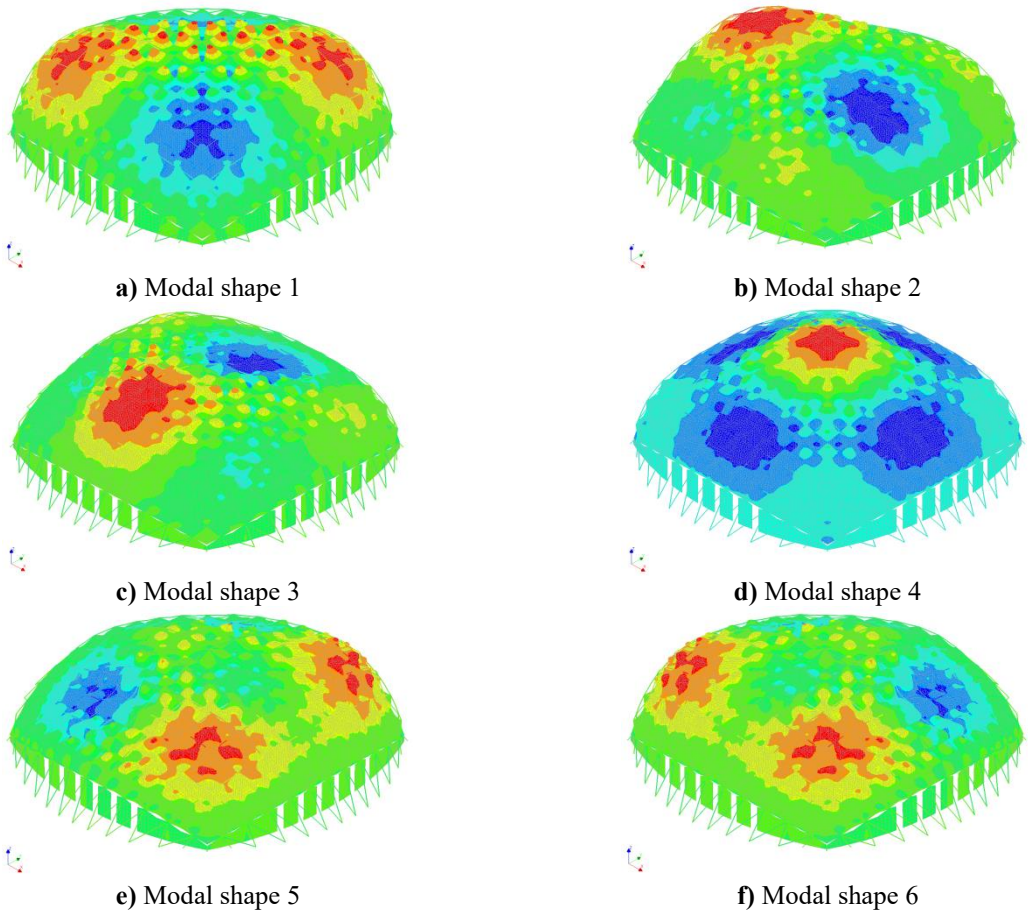
Figure 6: FEM model with extruded elements and boundary conditions

4 RESULTS

The FEM model of the Sports Palace was subjected to a modal analysis in order to obtain the main dynamic properties of the structure. Furthermore, it was also analyzed considering the action of vertical loads taking into account the nonlinear behavior of the steel and aluminum elements of the roof structure.

4.1 Modal Analysis

In order to validate the FEM model, the first 40 natural modes were calculated. Figure 7 shows the six first modal shapes. Color scales represent vertical displacements and go from red for maximum upward displacements, to blue for maximum downward displacements. On this figure it is interesting to observe that, due to the structural symmetry, there are pairs of modes that have equal periods and have essentially the same shape but rotated 90°; for instance, modes 2 and 3, on one hand, and modes, 5 and 6, on the other hand.



a) Modal shape 1 **b)** Modal shape 2

c) Modal shape 3 **d)** Modal shape 4

e) Modal shape 5 **f)** Modal shape 6

Figure 7: First six modal shapes of the Palace of Sports

Table 2: Natural periods of the first ten modes

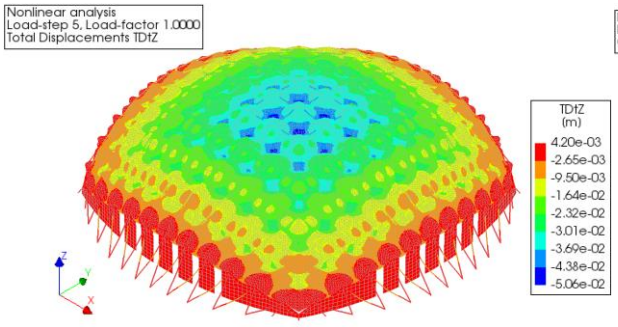
Mode	Period (s)	Mode	Period (s)
1	0.759	6	0.357
2	0.549	7	0.333
3	0.549	8	0.323
4	0.459	9	0.314
5	0.357	10	0.309

Table 2 presents the periods of the first ten modes. The first natural period seems to be very small for a large span structure; nevertheless, it must be taken into account that the roof has a light weight. Similar structures with spatial frames covering large spans present natural vibration periods similar to the ones obtained in this study [15]. The dynamic behavior of the Palace of Sports reflects the structural soundness and stiffness of the building.

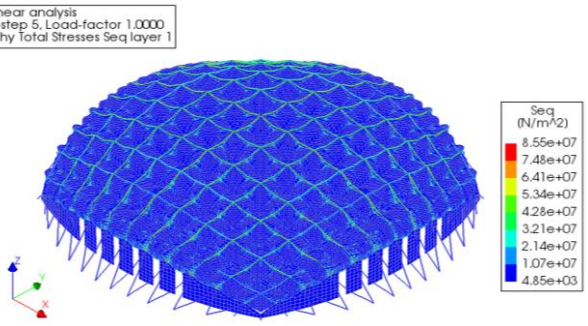
4.2 Nonlinear Analysis with vertical Loads

A nonlinear analysis under gravitational loads is useful to assess the safety of the structure for this action. The dead loads applied are the structure self-weight plus a load of 0.2 kN/m^2 accounting for installations and other objects hanging from the roof. Additionally, a live load of 0.2 kN/m^2 is also included in the analysis. The load factor affects both, the dead and live loads. The analysis takes into account only the nonlinear effects of steel and aluminum elements, according to the yield stresses reported at Table 1.

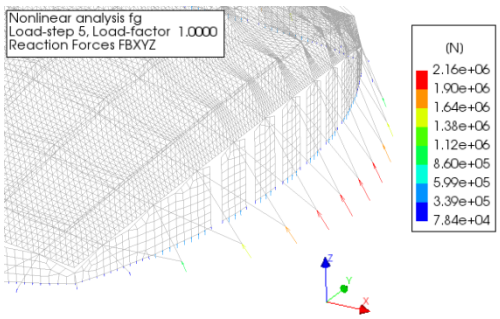
For a unitary load factor, the center of the structure has a displacement of 36 mm; this represents only a 3700th of the span. Figure 8a presents the vertical displacements for this condition; figure 8b presents the Von Mises stresses [14]; and figure 8c shows the reactions at one side of the structure. From figure 8b it is observed that the maximum stress at steel elements is 85 MPa, which represents the 34% of the yield stress. Meanwhile, in Figure 8c, it is observed that the inclined buttresses take most of the load that is transmitted from the roof structure to the ground.



a) Vertical displacements



b) Von Mises stresses



c) Reactions

Figure 8: Behavior under unitary load factor

Figure 9 presents the load factor vs. vertical displacement at the center of the dome. This figure shows that the roof structure behaves linearly until 4 times the loads considered. Also, its maximum capacity is higher than 4.8 times the vertical loads.

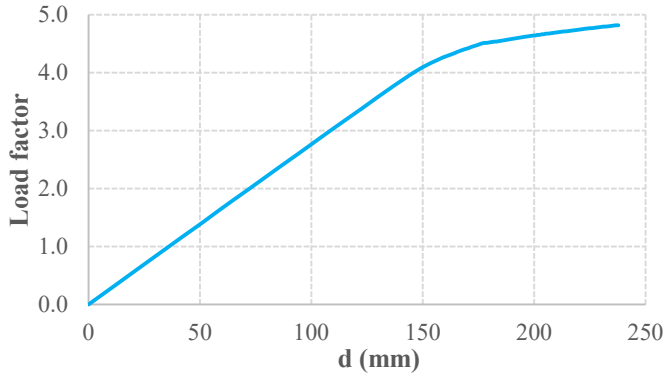
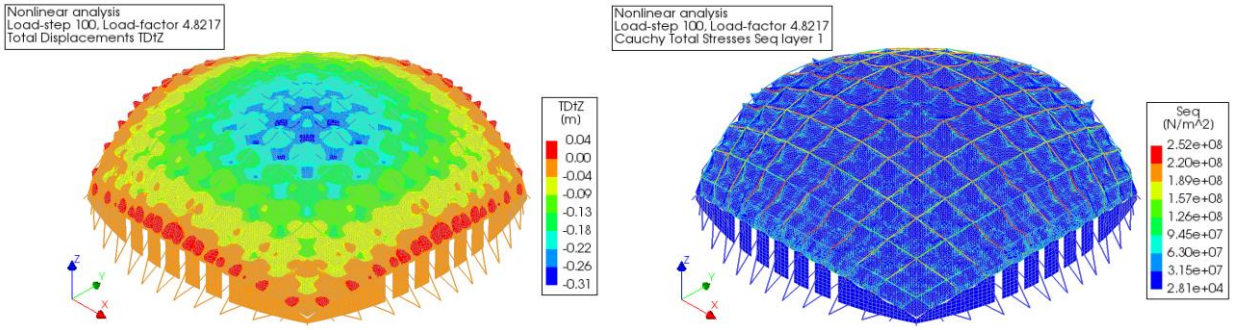


Figure 9: Load-displacement graph for nonlinear analysis

Figure 10 shows the vertical displacements and Von Mises stresses at the last step of the nonlinear analysis for a load factor of 4.8. Figure 10a shows that a maximum vertical displacement downwards of 238 mm has been reached on the center of the rooftop, which represents a 560th of the span; meanwhile Figure 10b illustrates that steel elements have reached their yield stress.



a) Vertical displacements **b)** Von Mises stresses

Figure 10: Behavior under load factor of 4.8

5 CONCLUSIONS

This paper presents a brief review of the historical architectural and structural relevance of the iconic Palace of Sports of Mexico City. The paper also presents the development of geometrical and FEM models. It is important to point out that this is the first advanced structural analysis of this construction since it was designed with rudimentary computational tools. The results in terms of natural modes indicate that this preliminary model is a good approximation of the behavior of the real structure. The dynamic behavior of the Palace of Sports reflects the stiffness and structural soundness of the building. The nonlinear analysis under gravitational loads shows that the structure has a large safety factor for this action.

Tasks to perform in future stages of this project include the determination *in situ* of the natural vibration frequencies of the first natural modes of the structure in order to validate or adjust the properties of the FEM model and performing nonlinear analysis of the model under gravitational loads taking into account mechanical and geometric non-linearities, seismic and wind actions in order to give a safety assessment to identify risk scenarios and to prevent them to occur on such iconic structure.

Acknowledgements. The authors would like to thank to the Public Bureau of Education (Secretaría de Educación Publica) of the Mexican Government for the funds provided to publish this paper through the project "Fortalecimiento de la calidad académica de los programas de licenciatura de la DES de Ingeniería". This support is greatly appreciated.

REFERENCES

[1] Candela, F., Castañeda E. and Peyri A. Palacio de los Deportes. *Arquitectura* (1968) **10-16**:10-13.
[2] García, J.A. and Gallegos, B.M. Patrimonio de la XIX Olimpiada "México 68": los retos para su preservación. *Revista Gremium* (2017) **4-07**:99-114.
[3] Trejo, R. Esos fueron los días. Cultura social, creatividad y libertad en el México de 1968. *Revista Mexicana de Ciencias Políticas y Sociales* (2018) **234**:153-176.
[4] Pozas, R. Los años sesenta en México: la gestación del movimiento social de 1968. *Revista Mexicana de Ciencias Políticas y Sociales* (2018) **234**:111-132.
[5] Ramírez, P. México ante las olimpiadas. *Arquitectura* (1968) **10-116**:2-5.
[6] Vasconcelos, J. *La raza cósmica: misión de la raza iberoamericana*. Espasa, (1948).
[7] Canales, A.F. *La modernidad arquitectónica en México. Una mirada a través del arte y los medios impresos.* Tesis Doctoral, Universidad Politécnica de Madrid, (2013).
[8] De Anda Alanís, E.X. *Historia de la arquitectura mexicana.* Gustavo Gili, (2019).
[9] Candela, F., Peyri A. and Castañeda E. Palacio de los Deportes. *Informes de la Construcción, Consejo Superior de Investigaciones Científicas* (1968) **21-205**:1-7.
[10] Candela, F., Castañeda E. and Peyri A. Proyecto Arquitectónico del Palacio de los Deportes. *Revista Ingeniería, Universidad Nacional Autónoma de México* (1968) **37-4**: 429-433.
[11] Castañeda, L. Image-Machine: Félix Candela's Palacio de los Deportes. *Pidgin* (2010) **8**: 246-257.
[12] De Buen, O. Estructura de acero de la cubierta del palacio de los deportes. *Revista Ingeniería, Universidad Nacional Autónoma de México* (1968) **37-4**: 456-461.
[13] Damy, J. Utilización de las computadoras electrónicas en el análisis del palacio de los deportes. *Revista Ingeniería, Universidad Nacional Autónoma de México* (1968) **37-4**: 462-466.
[14] TNO DIANA. *Finite element analysis user's manual release 10.1*. DIANA FEA BV, Netherlands, (2017).
[15] Wu, J., Zhang, Y. and Geng, X. Dynamic behaviors of two large spatial structures. In: J. F. Abel and J. R. Cooke (Eds.): *IASS-IACM 2008:* "Spanning Nano to Mega" *Computation of Shell and Spatial Structures* (2008).

12th International Conference on Structural Analysis of Historical Constructions
SAHC 2020
P. Roca, L. Pelà and C. Molins (Eds.)

STRUCTURAL PERFORMANCE EVALUATION OF COLUMN-*NUKI* CONNECTION IN TRADITIONAL JAPANESE WOODEN BUILDINGS

SATSUKI MURAI[1*] AND MITSUHIRO MIYAMOTO[2]

[1]Division of Safety Systems Construction, Graduate School of Engineering, Kagawa University
2217-20 Hayashi-cho, Takamatsu, Kagawa 761-0396, Japan
e-mail: s19g407@stu.kagawa-u.ac.jp (*corresponding author)

[2]Department of Engineering and Design, Faculty of Engineering and Design, Kagawa University
2217-20 Hayashi-cho, Takamatsu, Kagawa 761-0396, Japan
email: miyamoto@eng.kagawa-u.ac.jp; Web page: https://www.kagawa-u.ac.jp/kagawa-u_ead/

Keywords: Traditional Japanese wooden buildings, column-*nuki* connection, seismic performance evaluation

Abstract. *Traditional Japanese wooden buildings have been constructed using internal wooden frame structures. Plus-shaped column-nuki connections are important to evaluate the seismic performance of these buildings, and these connections include several joint types, one of which is the oblique scarf joint. However, only very few extant studies have examined column-nuki connections and oblique scarf joints. Consequently, no design equations exist for this combination. Therefore, it is possible that the structural performance of column-nuki connections might be inaccurately evaluated. Thus, this study aims to evaluate the structural performance evaluation of column-nuki connections in traditional Japanese wooden buildings. Full-scale tests were performed on specimens with either the continuous or oblique scarf joint nuki, and results obtained were compared based on parameters, such as the type of connection and number of dimensions. Subsequently, corresponding analytical results were calculated using an extant design equation, and the same were compared against experimental values to determine the validity of using the design equation for column-nuki connections in traditional Japanese wooden buildings. Results obtained in this study demonstrate the initial stiffness to be approximately identical for specimens with continuous or oblique scarf joint nuki. The yield and ultimate bending moment of oblique scarf joint nuki specimens were observed to be approximately 10–70% smaller compared to those corresponding to continuous nuki specimens. In addition, all oblique scarf joint nuki specimens demonstrated an initial cleavage failure followed by multiple failures. Results of these comparisons demonstrate that failure can be partially estimated using the extant design equation considered in this study.*

1 INTRODUCTION

Traditional wooden buildings in Japan, such as temples and shrines, demonstrate high deformability, and they can resist large lateral forces during earthquakes. Since ancient times, these traditional buildings have been constructed using column-*nuki* connections. The construction technique involves building a whole wall around the periphery with the inner structure comprising wooden frames. Column-*nuki* connections used in the construction of Japanese shrines and temples are larger compared to those used in residential houses. Consequently, some walls of ancient Japanese buildings can resist large lateral forces during earthquakes. Thus, column-*nuki* connections can be considered important elements during structural performance evaluation of traditional Japanese buildings. However, as shown in reference [1], very few experiments have been conducted on large column-*nuki* connections and of those, even fewer have been conducted on oblique scarf joint *nuki* connections, a popular connection type, in traditional wooden Japanese buildings. In seismic evaluations of traditional Japanese houses, the extant design equation has been considered only for continuous *nuki*. As shown in reference [2], oblique scarf joint *nuki* are evaluated as 0.5 of the design equation for continuous *nuki* in traditional Japanese houses. Therefore, there exists a possibility that structural-performance evaluations of column-*nuki* connections with oblique scarf joint *nuki* are inaccurate.

The study aims to evaluate the structural performance of column-*nuki* connections in traditional Japanese wooden buildings. To this end, full-scale tests were performed on plus-shaped column-*nuki* connections used in Japanese shrine and temple construction. Results of these tests were compared against those obtained using the relationship between the deformation angle and bending moment as well as failure properties of continuous and oblique scarf joint *nuki*. Details concerning these full-scale tests are described in section 2 of this manuscript, whereas section 3 discusses the validity of estimate equations used for evaluating the said plus-shaped column-*nuki* connection. The said estimate equations were evaluated for comparing analytical results against experimental values pertaining to both continuous and oblique scarf joint *nuki* connections.

2 FULL-SCALE TEST OF PLUS-SHAPED COLUMN–*NUKI* CONNECTION

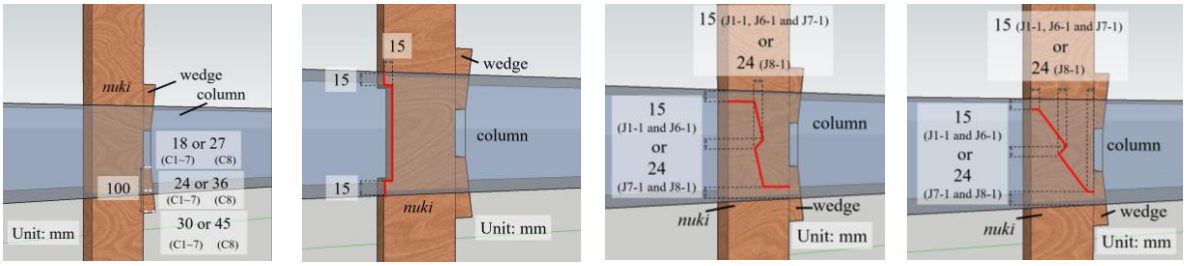
In this study, full-scale tests of specimens with continuous or oblique scarf joint *nuki* were conducted to examine the seismic performance of plus-shaped column-*nuki* connections. The relationship between the bending moment and deformation angle as well as the failure property were investigated. The test parameters were chosen to examine the seismic performance of a plus-shaped column-*nuki* specimen, which had either continuous or oblique scarf joint *nuki*. Both of these have been used for traditional Japanese wooden buildings in the past.

2.1 Outline of full-scale tests

Tables 1 and 2 provide information about the specimens examined in the study. A total of sixteen specimens were tested; eight contained continuous *nuki,* and eight contained oblique scarf joint *nuki*. All specimens were plus shaped, and the lengths of both the *nuki* and the column were 1,400 mm. The test specimens were labeled as C for continuous *nuki* and J for oblique

scarf joint *nuki*. For the continuous *nuki* specimens, one condition was different for each specimen based on C1. Figure 1 (a) depicts a drawing of the continuous *nuki* joint, whereas Figure 1 (b) depicts that corresponding to a continuous *nuki* with cogged C4 joint. All specimens, except C5, have wedges. The oblique scarf joint *nuki* specimens come in two geometries, as shown in Figures 1 (c) and (d). The numbers right after J in the specimens' name correspond to those mentioned in the list of continuous *nuki*s.

The image of the loading device is shown in Figure 2. The specimen was fixed using a jig. In these tests, positive and negative sides are defined as the left and right sides, respectively, and the negative side contains the wedge. The specimen was subjected to cyclic lateral loads, and the apparent shear deformation angle of a *nuki* γ_0 was gradually increased symmetrically from 1/200, 1/150, 1/100, 1/75, 1/50, 1/30, 1/20, 1/15, to 1/10 rad. One cycle of loading was applied. Finally, the specimen was subjected to a lateral load at an angle of 1/7 rad at one end. Figure 3 depicts the full-scale test setup.



(a) Continuous *nuki* (b) Continuous *nuki* with cogged joint (c) Oblique scarf joint *nuki* α (d) Oblique scarf joint *nuki* β

Figure 1: Details concerning connection types used in traditional Japanese buildings

Table 1: Continuous *nuki* specimen specifications

Specimen	Type of connection	Dimensions			Shape of column	Type of wood
		Diameter of column (mm)	Width of *nuki* (mm)	Height of *nuki* (mm)		
C1	Continuous *nuki*	180	50	120	Square	Japanese cypress
C2	Continuous *nuki*	180	50	120	Circle	Japanese cypress
C3	Continuous *nuki*	180	50	120	Square	Japanese cedar
C4	Continuous *nuki* with cogged joint	180	50	120	Square	Japanese cypress
C5	Continuous *nuki* without wedge	180	50	120	Square	Japanese cypress
C6	Continuous *nuki*	180	90	120	Square	Japanese cypress
C7	Continuous *nuki*	240	90	120	Square	Japanese cypress
C8	Continuous *nuki*	240	90	180	Square	Japanese cypress

Table 2: Oblique scarf joint *nuki* specimen specifications

Specimen	Type of connection	Dimensions			Shape of column	Type of wood
		Diameter of column (mm)	Width of *nuki* (mm)	Height of *nuki* (mm)		
J1-1	Oblique scarf joint α *nuki*	180	50	120	Square	Japanese cypress
J1-2	Oblique scarf joint β *nuki*	180	50	120	Square	Japanese cypress
J6-1	Oblique scarf joint α *nuki*	180	90	120	Square	Japanese cypress
J6-2	Oblique scarf joint β *nuki*	180	90	120	Square	Japanese cypress
J7-1	Oblique scarf joint α *nuki*	240	90	120	Square	Japanese cypress
J7-2	Oblique scarf joint β *nuki*	240	90	120	Square	Japanese cypress
J8-1	Oblique scarf joint α *nuki*	240	90	180	Square	Japanese cypress
J8-2	Oblique scarf joint β *nuki*	240	90	180	Square	Japanese cypress

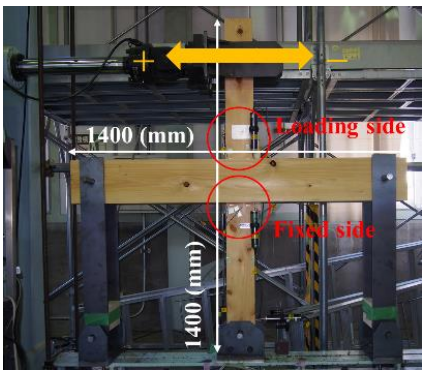


Figure 2: Loading device apparatus



Figure 3: Loading during full-scale tests

2.2 Result and discussion of full-scale tests

Figure 4 illustrates the relationship between the bending moment and deformation angle in the different continuous *nuki* specimens, as determined via full-scale tests performed in this study. The ultimate bending moment corresponds to a deformation angle of 1/10 rad, including a safety factor of 1.5, since the collapse limit of traditional wooden buildings is 1/15 rad.

Images of the failure of continuous *nuki* are shown in Figure 5. Specimens C1 to C7 exhibited cleavage of the wedge. However, the cleavage was not affected by the decrease in bending moment. In C1 and C2, the ultimate bending moments demonstrated approximately the same difference for different column shapes. The initial stiffness of C3 was approximately 70% less than that of C1, and the ultimate bending moment of C3 was approximately 60% smaller than of C1, even though the elastic modulus of C3 was approximately 10% percent than

of C1 in the material test. The ultimate bending moment of C4 was approximately 10% smaller than that of C1, because of the use of the cogged joint. The ultimate bending moment of C1 was approximately 80% larger than that of C5, because of the use of the wedge. Among continuous *nuki* specimens, the ultimate bending moment of C8 was the biggest and the ultimate bending moment increased from C1 to C6 to C7 to C8 because the dimensions of the specimens also increased. It is assumed that the bending moment increased because the dimensions of the specimen increased.

Figure 6 depicts the relationship between the bending moment and deformation angle pertaining to the plus-shaped column-*nuki* connection with a continuous *nuki* and the oblique scarf *nuki*. Results of full-scale tests are depicted in Figures 7. The continuous *nuki* specimen exhibited embedment failure at first; however, all specimens with the oblique scarf *nuki*, except for J8-2 first experienced cleavage failure from the *kama* joint and then bending failure, as shown in Figure 8(a). One *kama* joint was stuck in the other *kama* joint at J8-2, as shown in Figures 8(b). Only the specimen with the oblique scarf joint β *nuki* exhibited shear failure, as shown in Figure 8(c). The initial stiffness of the continuous and oblique scarf joint *nuki* specimens with the same dimensions was approximately the same. Both the yield bending moment and ultimate bending moment were approximately 10 to 70% smaller for the oblique scarf joint *nuki* than for the continuous one. In addition, the specimens with oblique scarf joint β had both a yield bending moment and ultimate bending moment that was 10% smaller than that of the specimens with oblique scarf joint αbecause oblique scarf joint βhas steeper angle than oblique scarf joint α. This suggests that the bending moment tends to be smaller if the *kama* joint connection has steep angle. For the specimens with the oblique scarf *nuki*, the deformation angle was smaller for the load on the positive side than for the load on the negative side until failure.

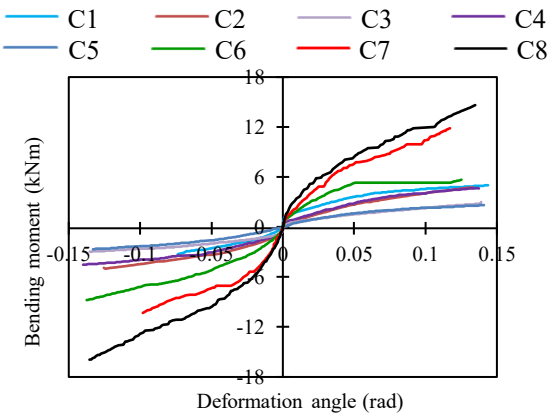
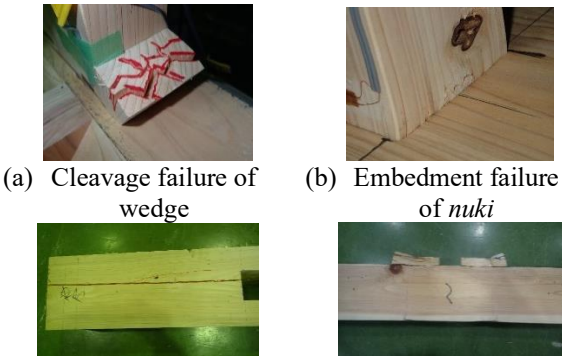


Figure 4: Bending moment vs. deformation angle in full-scale tests (continuous *nuki*)



(a) Cleavage failure of wedge

(b) Embedment failure of *nuki*

(c) Cleavage failure of column

(d) Failure property of *nuki*

Figure 5: Images of failure (continuous *nuki*)

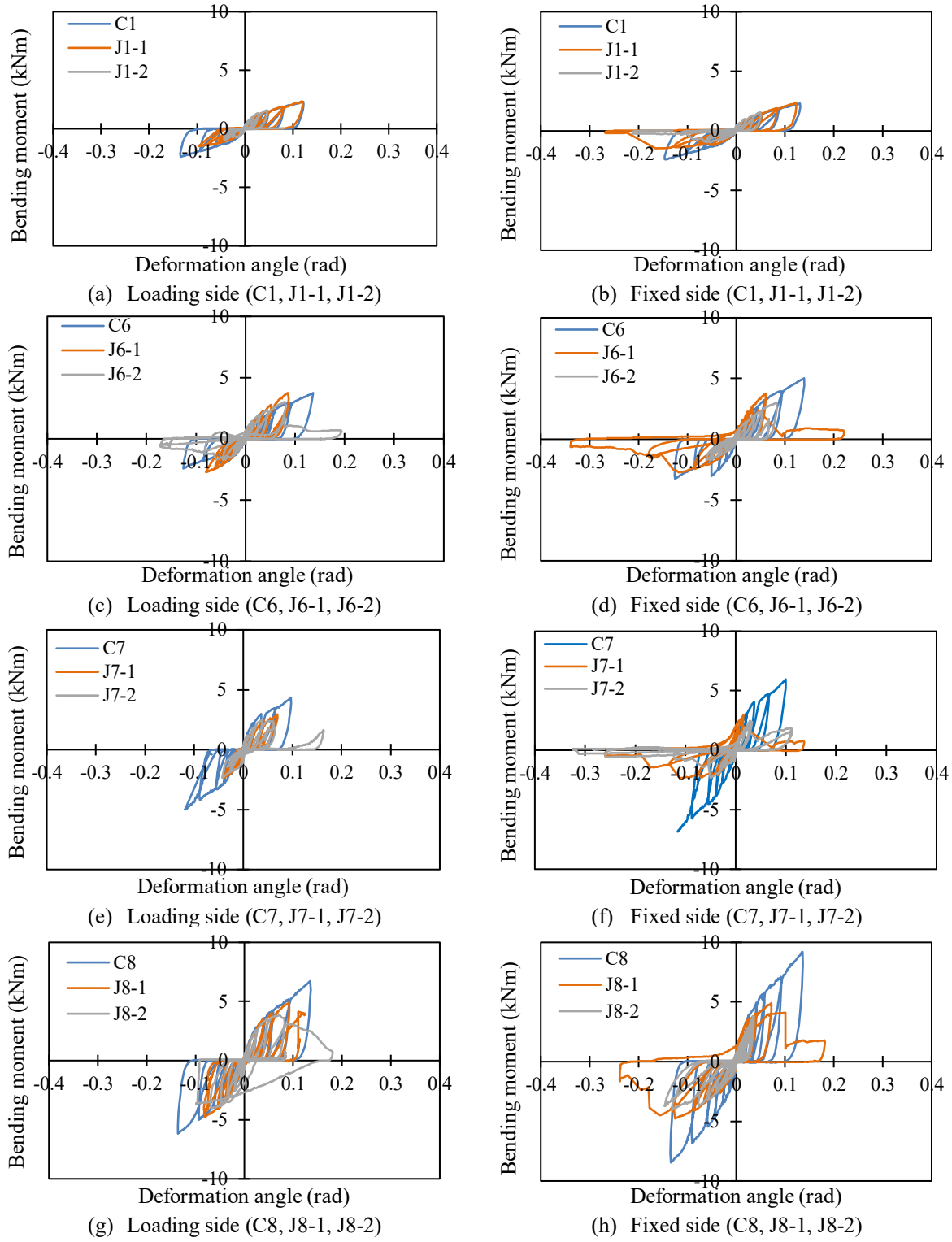
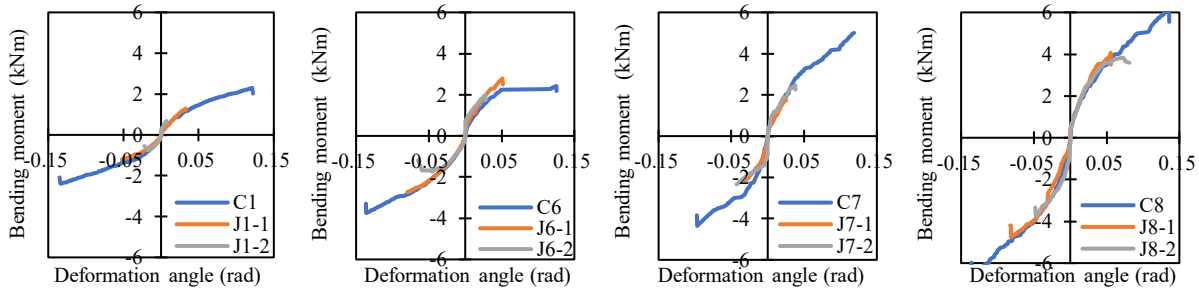
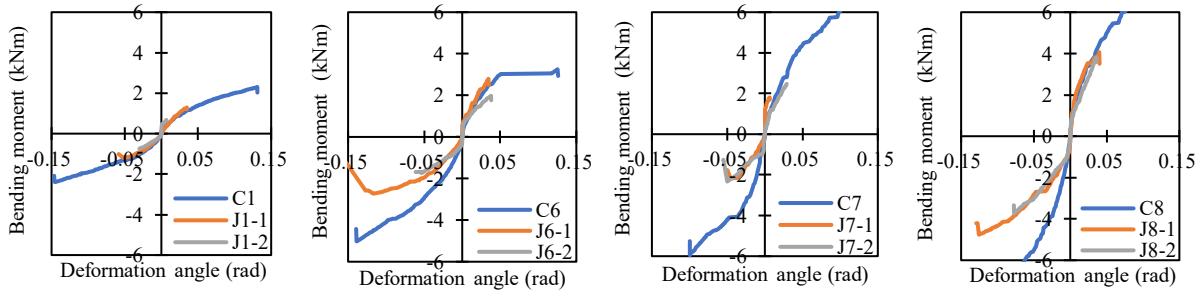


Figure 6: Relationship between the bending moment and deformation angle

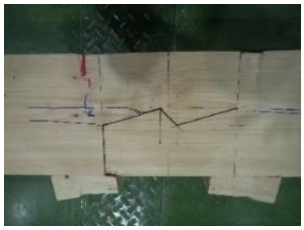


(a) Loading side



(b) Fixed side

Figure 7: Results of full-scale tests



(a) Cleavage failure from *Kama*-joint and bending failure (J8-1)



(b) *Kama*-joint part of the specimen after tests (J8-2)



(c) Shear failure (J1-2)

Figure 8: Failure of oblique scarf joint *nuki*

3 ESTIMATION EQUATION

In this study, theoretical results were calculated using the design equation used for continuous *nuki* in traditional Japanese wooden houses. The rotating stiffness (K_θ) and yield moment (M_y) were evaluated, and the results were compared with those of the full-scale tests.

3.1 Outline of estimate equation for continuous *nuki*

From the design equation of the continuous *nuki* [3], K_θ and M_y are obtained as follows:

$$K_\theta = x_p^2 y_p E_{90} \left\{ \frac{x_p}{Z_0} \left(C_{xm} - \frac{1}{3} \right) + 0.5 \mu C_{xm} \right\} \tag{1}$$

$$M_y = \frac{K_\theta Z_0 F_m}{x_p E_{90} C_{xm} \sqrt{C_{ym}}} \tag{2}$$

$$F_m = \frac{2.4}{3} \times f_{cv} \tag{3}$$

$$C_{xm} = 1 + \frac{4Z_0}{3x_p} \tag{4}$$

$$C_{ym} = 1 + \frac{4Z_0}{3ny_p} \tag{5}$$

$$\theta_y = \frac{M_y}{K_\theta} \tag{6}$$

where x_p is the diameter of half of the column (mm), y_p is the width of the *nuki* (mm), E_{90} is the lateral compressive elastic modulus (N/mm^2), Z_0 is the height of the *nuki* (mm), μ is the coefficient of friction (μ = 0.4 [4]), θ_y is the yield deformation angle (rad), F_m is the embedment yield unit stress (N/mm^2) evaluated from the result of partial compression tests when the edge distance is infinite, f_{cv} is the embedment strength (N/mm^2), C_{xm} and C_{ym} are the embedment growth factors in the *x* and *y* directions, respectively, when the edge distance is infinite, and *n* is the displacement factor between the wood fiber direction and the wood fiber radial direction (n of Japanese cypress is 6, and n of Japanese cedar is 5).

Table 3 provides the material constant which is used for calculation and the ratio of the first and second stiffness from the estimate equation.

The theoretical value of the second stiffness is calculated using the average of the ratio of the first stiffness to the second stiffness from the results of partial compression tests.

Table 3: Material constants

Types of wood	Lateral compressive elastic modulus E_{90} (N/mm^2)	Embedment strength (Partial compressive strength) f_{cv} (N/mm^2)	Embedment yield unit stress f_m (N/mm^2)	Second stiffness / First stiffness (K_2/K_1)
Japanese cypress	239	6.38	5.10	0.094
Japanese cedar	219	4.73	3.78	0.090

3.2 Comparison between theoretical and experimental results obtained for continuous *nuki* specimens

Figure 9 compares the theoretical and experimental values for each continuous *nuki* specimen. The theoretical value was calculated using the average lateral elastic modulus from the results of the material tests. In all continuous *nuki* specimens, the theoretical value of the initial stiffness was greater than the experimental value. This may be caused by the construction tolerances of the specimen and the wood drying shrinkage effect. In addition, the theoretical value, which was calculated using the 50th percentile average of the lateral elastic modulus, was compared with the experimental value to determine the effect of the gap between the column and the *nuki*. As a result, experimental value was between the theoretical values for all

specimens except C5. The gap between the column and the *nuki* in C5 was wider than in the other specimens, because C5 does not have a wedge. Therefore, the experimental results revealed a smaller value than the one that was estimated because the initial stiffness of C5 became smaller than that of the other specimens.

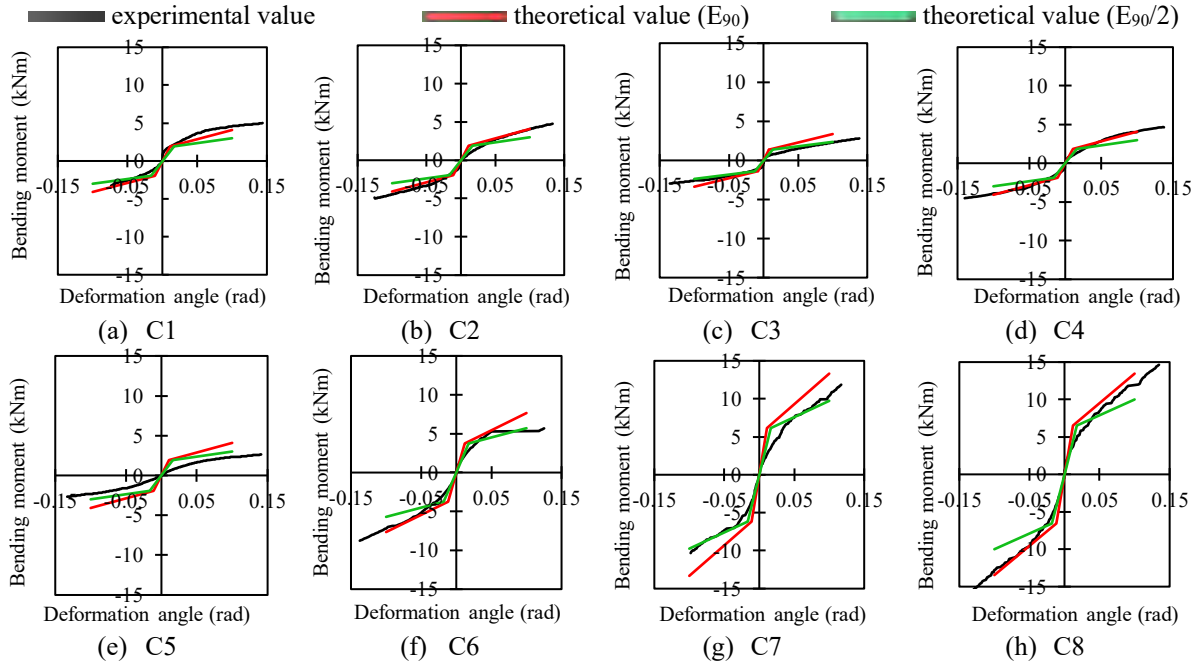


Figure 9: Comparison between theoretical and experimental results obtained for continuous *nuki*

3.3 Estimation equation for oblique scarf joint *nuki*

In the full-scale tests, the specimens with oblique scarf joint *nuki* demonstrated embedment failure, bending failure, shear failure, and cleavage failure. The moment at each failure point was calculated and compared with the corresponding experimental result. Table 4 shows the material constants used for the calculation of the estimation equation.

To calculate the magnitude of the moment that led to the embedment failure, the rotating stiffness K_θ and yield moment M_y were evaluated from the design equation of continuous *nuki*, which was provided by a previous study [3]. This followed the same procedure that was used for the continuous *nuki* (equations (1), (2), (3), (4), (5), and (6)). However, the specimens with oblique scarf joint *nuki* are not symmetrical with respect to the *nuki*. Therefore, the yield moment M_y was divided by two in this case, and the coefficients of friction, μ, were 0.4 and 0.2 on the negative and positive sides, respectively [4].

The moment at the point of bending failure (M_b) was evaluated from the geometrical moment of inertia, I, and bending strength, σ_b, as:

$$M_b = \sigma_b \times \frac{I}{h_e/2} \tag{7}$$

$$I = \frac{y_p \times {h_e}^3}{12} \tag{8}$$

where I is the geometrical moment of inertia (mm^4), σ_b is the bending strength (N/mm^2), and h_e is the distance between an edge of the *nuki* and the shear plane of the oblique scarf joint (mm), as shown in Figure 10.

The moment at the point of shear failure (M_s) was evaluated from the shear strength, τ, as:

$$M_s = \alpha y_p \tau h_e \tag{9}$$

where τ is the shear strength (N/mm^2) and α is the shear distance (mm).

The moment at the point of cleavage failure (M_{uw}) was evaluated using a design equation [5] for cleavage failure if a *nuki* is stressed from the wood fiber and radial direction by equations (10) and (11).

$$M_s = P_{uw} h_e \tag{10}$$

$$P_{uw} = \frac{2}{1} C_r y_p \sqrt{\frac{h_e}{1 - \frac{h_e}{Z_0}}} \tag{11}$$

where P_{uw} is the ultimate strength caused by the cleavage failure and C_r is a cleavage failure constant (N/mm$^{1.5}$) (Japanese cypress $C_r = 10.0$ (N/mm$^{1.5}$)).

Table 4: Material constant

Types of wood	Lateral compressive elastic modulus E_{90} (N/mm^2)	Partial compressive strength F_{cv} (N/mm^2)	Bending strength σ_b (N/mm^2)	Shear strength τ (N/mm^2)
Japanese cypress	250	8.82	72.8	11.7

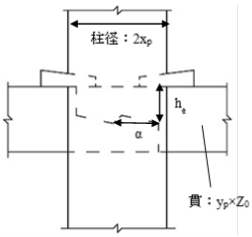


Figure 10: the detail of joint

3.4 Comparison between theoretical and experimental results obtained for oblique scarf joint *nuki* specimens

Figure 11 compares the moments at bending failure, embedment failure, shear failure, and cleavage failure with their associated experimental values for the oblique scarf joint *nuki* specimens. In Figures 11(g) and (h), the moments at the points of bending and shear failure exceeded 10 kNm, and hence these are not shown in the graph.

All specimens with an oblique scarf joint *nuki* first exhibited cleavage failure in the *nuki*, followed by multiple failures. The moment at cleavage failure was the smallest and corresponded to the experimental value. The specimens with an oblique scarf joint *nuki* were already subjected to cleavage failure before the failure was confirmed visually around the *nuki* in the full-scale tests. This was because the cleavage failure occurred in the part of the column–*nuki* joint that is visually inaccessible from the outside. Furthermore, J1-2, J6-2, and J8-2, specimens that exhibited shear failure within the joint after failure, experienced the moment of shear failure.

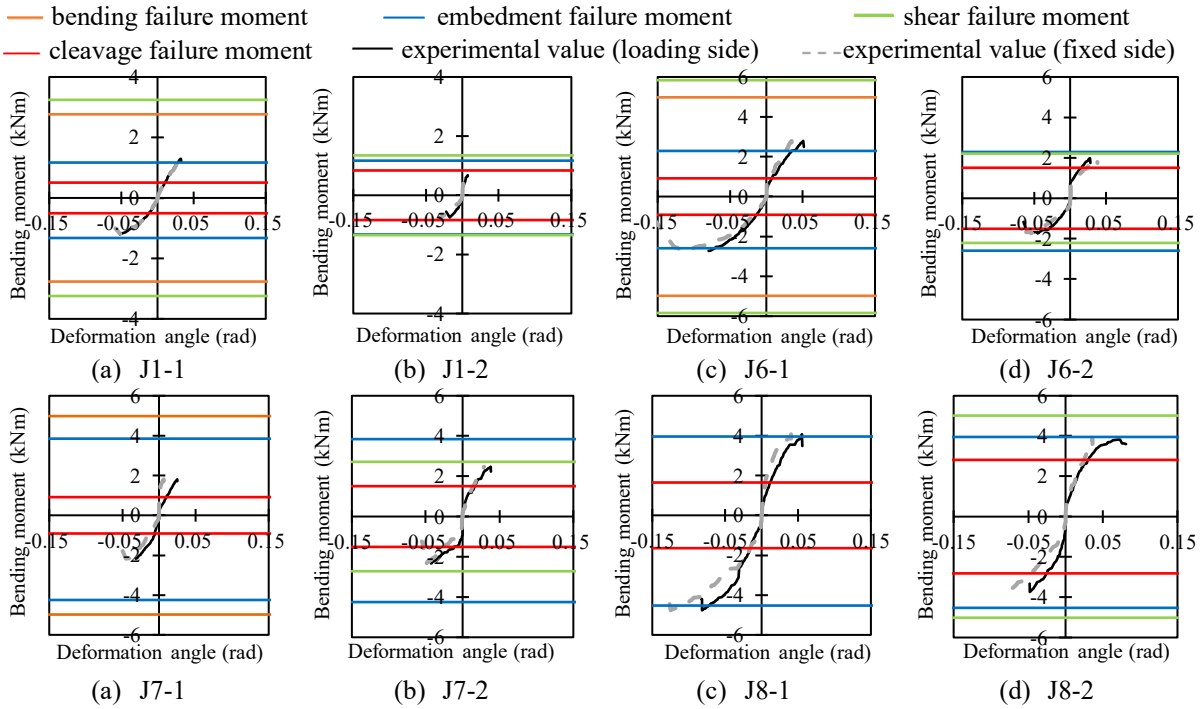


Figure 11: Comparison between theoretical and experimental results obtained for oblique scarf joint *nuki*

4 CONCLUSIONS

We performed full-scale tests to obtain the relationship between the bending moment and deformation angle and failure property of plus-shaped column-*nuki* connections, which of either the continuous or oblique scarf joint *nuki* type. Furthermore, the theoretical values were calculated using the design equation, and the experimental and theoretical values were compared. The main findings of this study are as follows:

- Continuous *nuki* specimens showed cleavage failure at the wedge or column in the full-scale tests; however, this was not affected by the decrease in the bending moment. All oblique scarf joint *nuki* specimens showed cleavage failure first in the *nuki*, followed by multiple failures. The full-scale test results showed that the yield and ultimate bending moment of oblique scarf joint *nuki* specimens were approximately 10 to 70% smaller than those of the corresponding continuous *nuki* specimens.
- In continuous *nuki* specimens, the initial stiffness of the theoretical value was higher

than the experimental one. In addition, the experimental value expected for the C5 specimen without the wedge was within the range of the theoretical values that were calculated using the average lateral elastic modulus and the theoretical values that were calculated using half of the average lateral elastic modulus. The gap between the column and the *nuki* in the specimen without a wedge was bigger than the gap in the other specimens. Therefore, the experimental value of the specimen without the wedge was less than the theoretical one due to the small initial stiffness.

- In the oblique scarf joint *nuki* specimens, the theoretical value of cleavage failure was the smallest, and it coincided with the experimental value. Regarding bending failure and shear failure, the experimental bending moment was smaller than the theoretical value.

The results demonstrated that failure can be partially estimated using the previous design equation by comparing theoretical to experimental values; however, the experimental data on plus-shaped column-*nuki* connections which have oblique scarf joint *nuki* is still insufficient. In the future, more full-scale tests of plus-shaped column-*nuki* connections can be performed, and finite element analysis can be used to create a model which corresponds to various failure properties.

Acknowledgements. This research was supported by the Matsui Kakuhei Memorial Foundation. We gratefully acknowledge this support.

REFERENCES

[1] Kaori Fujita, Isao Sakamoto, Yoshimitsu Ohashi: *A Study on lateral loading test of column and batten (nuki) joint used in traditional wooden architecture (Part 1)*, Summaries of Technical Papers of Annual Meeting, Architectural Institute of Japan, Structures-III, pp. 103-104, 1996.09 (in Japanese)

[2] Editorial Committee for Manual of Seismic Design for Wooden Frame Structures: *Manual of Seismic Design for Wooden Structures Taking Advantage of Traditional Structural Techniques - Methods for Seismic Design and Seismic Reinforcement Design Based on Response-Limit Capacity Analysis* -, Gakugei Shuppan Sha Co. Ltd., Japan, March 2004, pp.79

[3] Architectural Institute of Japan (edited): *Design Manual for Engineered Timber Joints*, Maruzen, Japan, September 2010, pp. 254-257.

[4] Japan Housing and Wood Technology Center: *Project Report about points to consider for design of timber structures* (in Japanese), March 2018, pp. 216-226.

[5] Architectural Institute of Japan (edited): *Standard for Structural Design of Timber Structures*, Maruzen, Japan, March 2009, pp. 36-37.

12th International Conference on Structural Analysis of Historical Constructions
SAHC 2020
P. Roca, L. Pelà and C. Molins (Eds.)

STUDY ON RIGID HOMOGENIZATION METHOD AND MODEL OF MASONRY UNDER DIFFERENT BRICKLAYING METHODS BASED ON REGULAR TESSELLATION THEORY

CHUNXIA YANG*, SHU CHEN, CHENYI LI, AND NAN ZENG

School of architecture and civil engineering
Changsha University of Science and Technology (CSUST)
Changsha, 410114 Hunan, China
e-mail: ycx3346@126.com (*corresponding author)
{874939885, 972898716, 1254453392}@qq.com

Keywords: Masonry Structure, Homogenization Theory, Tessellation Theory, RVE, Anisotropy, Bricklaying Method, Finite Element Method

Abstract. *The brick and tile of the existing masonry structures are precious, so it is not feasible that the components are used as the dismantling unit for maintenance and reinforcement. The homogenization method is an effective multi-scale calculation method, which can be used to establish the analysis model of masonry on the mesoscopic-level. The plane tessellation deconstruction method of masonry structure is proposed, exploring the internal tessellation laws of masonry under different bricklaying methods, and the theoretical system of periodic plane segmentation of masonry is established. Based on regular tessellation theory, the plane segmentation of masonry structures under three kinds of bricklaying methods is periodically carried out through rectangular unit lattice. Deconstructing the smallest element of the tessellation form, the boundary condition of equivalent volume element (RVE) is derived. On the premise of selecting reasonable material parameters, RVE models under three kinds of bricklaying methods are built by finite element software ABAQUS, and the equivalent parameters are obtained to realize the simulation analysis of masonry structure based on micro-mechanics. The results show that the strength of running bonding RVE is higher than that of the other two kinds, and the strength of header bonding RVE is the lowest. The finite element results are compared with the compressive strength results of the specimens under three kinds of bricklaying methods in the existing tests. The results are in good agreement, which shows that the compressive capacity of masonry structures with homogenization simulation under three kinds of bricklaying methods is reliable while homogenization reflects the mechanical characteristics of masonry structure as a whole. The rigid homogenization method based on regular tessellation theory takes brick by brick as components to be dismantled and replaced in the ancient architecture, which opens a new way for the fine analysis of masonry structure. The rigid homogenization method maximizes the protection of the ancient masonry structure, which is of great significance for the protection of human cultural heritage.*

1 INTRODUCTION

Masonry structure, as a composite structure composed of two different materials of brick and mortar, has different deformation and mechanical properties under different brick arrangement modes. As the weak link in masonry structure, mortar, its existence makes the destruction form and mechanical properties of masonry structure more complicated than other building forms. Homogenization method is an effective method to analyze the macro and micro-mechanical properties of composite materials at present. The characteristics of the each material of masonry structure are fused together, equivalent parameters are given to the equivalent volume unit, and then the equivalent volume unit is applied to the whole. Homogenization method can not only study the equivalent properties and deformation of composite materials from the mesoscopic level, but also check the overall response of the structure from the macroscopic level. It has been widely applied in engineering.

The concept of RVE was first proposed in the study of mechanical properties of masonry by L.Gambarotta[1]. Considering the three aspects of bricklaying methods, thickness and homogenization steps, the rigid homogenization theory is put forward to avoid the deficiencies of the gradual homogenization thought by A.Anthoine[2]. The homogenization theory of periodic medium is adopted, and the brick and mortar models are assumed to be of continuous failure type by P.Pegon[3]. In addition, the two assumptions (plane stress assumption and plane strain assumption) are compared, and the differences between the two are obtained. The homogenization method called "Second-order" is proposed by A.Anthoine[4], which can further extend the rigid homogenization theory and apply it to quasi-periodic masonry structures. Masonry homogenization method was first introduced into China by Daquan Wang[5]. Based on the research of composite mechanics theory, the mechanical properties of RVE element are analyzed and periodic boundary conditions are established by Jimei Shen[6]. The influence of different bricklaying methods and different kinds of blocks on the compressive properties of masonry is analyzed by Yalin Li[7].The determination of the minimum basic unit is analyzed, and the selected two-dimensional basic unit is divided in detail by Yaying Wu[8]. RVE model is established and its good reliability is verified by Chenyi Li[9].

Homogenization method can be used as an effective method to study the mechanical properties of unreinforced masonry structures. In the equivalent volume unit with continuous periodicity, the different material properties and bricklaying methods of constituent materials will have different effects on mechanical properties. Therefore, reliable material parameters are selected and the form of separate modeling is adopted. The mechanical properties and deformation properties of RVE selected under common different masonry forms are simulated by ABAQUS analysis software. The stress-strain relationship of each equivalent volume element is analyzed, and the RVE equivalent parameters in all directions are calculated. The RVE isotropic equivalent parameters are applied to the finite element model based on the existing tests. The simulated values are compared with the test values and the error sources are analyzed.

2 THE THEORY OF PERIODIC MASONRY PLANE SEGMENTATION

2.1 Application of Fit Theory

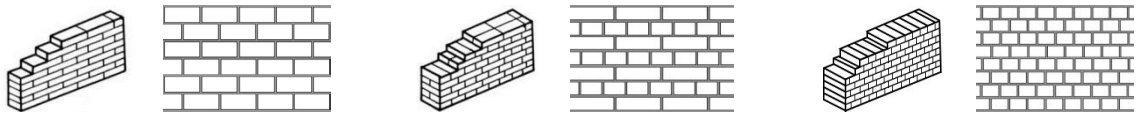
The ancient masonry structure that condensed the wisdom and sweat of the ancient laboring people witnessed the 5000-year civilization and history of China. However, due to man-made destruction and natural erosion, it is imperative for researchers to maintain ancient masonry buildings. Therefore, the conjunction theory is introduced to study the homogenization of masonry structure, in order to provide an effective method for the maintenance of ancient masonry buildings.

Masonry structure, a human creation that has been passed on for thousands of years, has not been taken as a plane division art by predecessors to explore internal tessellation laws. Tessellation composition refers to the regular arrangement of closed graphic objects that have no overlap and no gaps. Tessellation deconstruction refers to the regular plane division of the overall coincidence shape. The former emphasizes that graphic units are used to fill the whole skeleton, while the latter emphasizes that the whole plane is divided by unit graphics. Both are mathematical problems of periodically dividing two-dimensional planes essentially, involving the principle of mathematical symmetry. In the process of tessellation, each graphic element must follow the conditions of edge symbiosis and repeated continuity.

The first step of the masonry homogenization method is to divide the masonry structure periodically. The systematic plane division of the masonry requires a thorough understanding of internal tessellation laws. Therefore, the introduction of tessellation theory to analyze the masonry structure is the premise of the masonry homogenization method.

2.2 Tessellation Laws and Plane Deconstruction Under Three Kinds of Bricklaying Methods

Many practical projects and previous researchers' analysis show that Mechanical properties and deformation properties of masonry structure are affected to varying degrees under different bricklaying methods. There are many types of arrangement and combination of blocks in buildings. The RVE units of masonry under three common kinds of bricklaying methods are selected, as shown in figure 1:



(a) (b) (c)

Figure 1: Three kinds of bricklaying methods selected (respectively running bonding; quarter bonding; header bonding)

The tessellation theory is introduced to analyse masonry structure. The basic unit components move in two different directions. Through translation, rotation, reflection and sliding reflection, a universal tessellation shape, i.e. a complete piece of wall, is generated in the plane. Taking running bonding as a representative to comprehensively consider, it is assumed that the size of the unit basic component of the tessellation shape (as shown in figure 2) is:

$$(xh)\times(yb) \tag{1}$$

Where h stands for the sum of block height and the thickness of horizontal mortar joint in running bonding masonry; l stands for the sum of block length and the thickness of vertical mortar joint in running bonding masonry; d stands for the overlapping amount of masonry walls, and the overlapping amount of running bonding masonry walls is $l/2$; x and y stand for any positive integer.

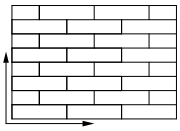


Figure 2: Coordinate system of the tessellation shape

Only when the basic unit components are uniformly and regularly formed into a rectangular, parallelogram, rhombus or regular hexagon array, can the wall be divided into a distributed tessellation shape by plane segmentation laws. For example, when $x = 1$, $y = 1$, there is rectangular basic components for the tessellation shape of running bonding masonry (as shown in figure 3, the half brick and half-thick mortar units surrounding three sides of the brick form a kind of rectangular basic components for the tessellation shape of running bonding masonry). Therefore, all kinds of basic shapes set are periodically divided into the tessellation shape of running bonding masonry. Three kinds of basic segmentation formations are proposed, as shown in figure 4:

(1)The rectangular components $(xh) \times (yd)$ consisting of $2n$ basic shapes with size $h\times b = h\times (l/2)$;

(2)The parallelogram components $(xh) \times (yd)$ consisting of $2n$ basic shapes with size $h\times b = h\times (l/2)$;

(3)The rhombus components $(2xh) \times (yd)$ consisting of $4n^2$ basic shapes with size $h\times b = h\times (l/2)$;

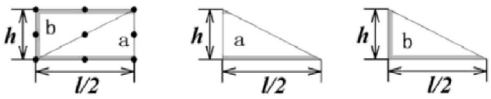
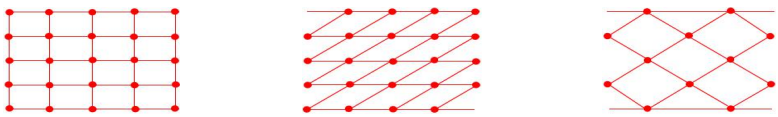


Figure 3: The rectangular components and its basic form of running bonding masonry

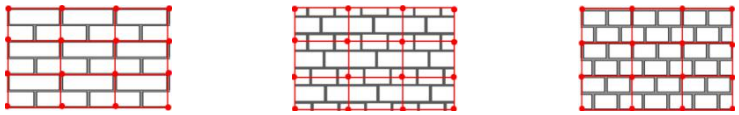


(a) (b) (c)

Figure 4: Three kinds of basic segmentation formation (respectively rectangle; diamond; parallelogram)

When x and y are any positive integers, the basic unit components may not be obtained by the three basic segmentation formations shown in figure 5 after division and division. Therefore, only the whole wall is divided into rectangles, and rectangular basic segmentation

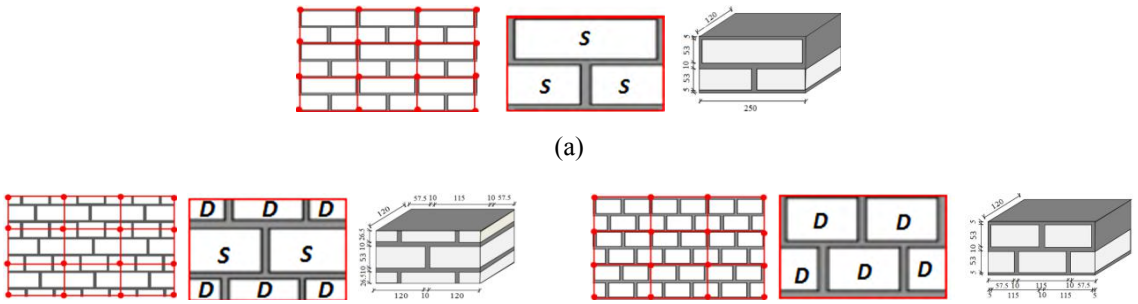
formations are adopted (figure 4(a)). The rectangular segmentation formations of part of the wall under three kinds of bricklaying methods is shown in figure 5:



(a) (b) (c)

Figure 5: Partition of wall sheet matrix lattice in typical bricklaying methods (respectively running bonding; quarter bonding; header bonding)

Referring to the above-mentioned rectangular lattice division, the dimensions of the RVE unit of masonry selected under different assembling methods are shown in figure 6:



(a)

(b) (c)

Figure 6: The sizes of RVE units selected under three kinds of bricklaying methods (respectively running bonding; quarter bonding; header bonding)

2.3 2-D Periodic Description

According to the basic knowledge of mechanics, the stress state in the region Ω of the masonry wall can be obtained. When the load is transferred from one basic component S to another basic component S', the following conditions can be established:

(1) The stress vector is continuous;

(2) The strain in the deformation process is coordinated with each other, and no separation or overlap occurs between basic components.

1) Periodic stress

Condition (1) means that stress is transferred from one side of the same component S to its opposite side to meet the following requirements:

$$\sigma(x+V_\alpha)+n \bullet (x+V_\alpha) = -\sigma(x) \bullet (x) \quad \text{(On opposite sides of } \partial S) \tag{2}$$

Because the outer normal n is anti-periodic symmetric, equation (2) can be simplified as:

$$[\sigma(x+V_\alpha) -\sigma(x)]\cdot n(x) = 0 \tag{3}$$

Therefore, the stress field σ is called a periodic stress field. The stress vector $\sigma \cdot n$ is anti-periodic symmetric on ∂S.

2) Strain-periodic displacement

According to condition (2), opposite sides should completely coincide in shape after

deformation. In other words, the relative displacement field of two opposite sides must be equal to the rigid displacement (translation or/and rotation). The basic component *S* is transformed into the 2-D component shown in figure 7:

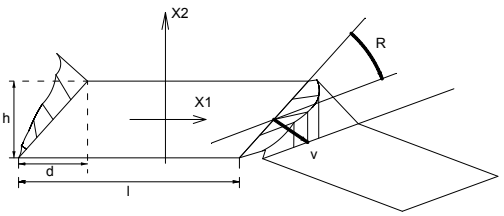


Figure 7: The basic components are compatible with the strain of opposite sides.

In the case of stack bonding pattern, this is expressed by：

$$\begin{aligned} u(x_1 , h)\text{-}u(x_1 , \text{-}h) &= V\text{-}Qx_1e_2 \qquad x_1 \in [\text{-}l , l] \\ u(l , x_2)\text{-}u(\text{-}l , x_2) &= U\text{-}Rx_2e_1 \qquad x_2 \in [\text{-}h , h] \end{aligned} \tag{4}$$

Where *u* and *v* are translation vectors; *R* and *S* are rotation constants.

Similarly, the further conclusion has been proved for running bonding masonry:

$$\begin{aligned} u(l/2+x_1 , h)\text{-}u(\text{-}l+x_1 , \text{-}h) &= V\text{-}Qx_1 \cdot e_2) \qquad x_1 \in [\text{-}l , l] \\ u(l+lx_2/2h , x_2)\text{-}u(\text{-}l+lx2/2h , x_2) &= U\text{-}R(x_2e_1+lx_2/2h \cdot e_2) \qquad x_2 \in [\text{-}h , h] \end{aligned} \tag{5}$$

No matter any angle of the component is regarded as a horizontal or vertical edge, they all undergo the same displacement, which means that equation (5) must be compatible when written for extreme values of x_1, and x_2. When *R* and *S* are both zero constants, the displacements are compatible, so equation (5) is simplified as:

$$\begin{aligned} u(d/2+x_1 , h)\text{-}u(\text{-}d/2+x_1 , \text{-}h) &= Vx_1 \qquad x_1 \in [\text{-}l , l] \\ u(l+dx_2/2h , x_2)\text{-}u(\text{-}l+dx2/2h , x_2) &= U \qquad x_2 \in [\text{-}h , h] \end{aligned} \tag{6}$$

Where *d* is the overlap amount.

Since it leads to a periodic strain field, such a displacement field *u* is called strain-periodic. The strain-periodic displacement field can be expressed in the following form:

$$\begin{aligned} u(x) &= E \cdot x + u^p(x) \\ u_1(x_1 , x_2) &= E_{11}x_1 + E_{12}x_2 + u_1^p(x_1 , x_2) \\ u_2(x_1 , x_2) &= E_{21}x_1 + E_{22}x_2 + u_1^p(x_1 , x_2) \end{aligned} \tag{7}$$

Where $E_{\alpha\beta}$ (α, β = 1 or 2) are four constants; $u^p_{(x)}$ is periodic displacement field with equal values on any set of opposite sides of ∂S:

$$u^p(x+V_\alpha) = u^p(V_\alpha) \quad \text{(On opposite sides of } \partial S) \tag{8}$$

The expression of the strain-periodic displacement field is derived from equations (7) and (8):

$$u(x+V_\alpha)\text{-}u(x) = \mathrm{E} \cdot V_\alpha + \Omega \times V_\alpha \tag{9}$$

As compared with equation (7), equation (9) only involves periodic relative displacement between two points on opposite sides.

2.4 Realization and Application of Homogenization

Because of periodic stress σ (equation (3)) and the strain periodic displacement u (equation (9)) of basic components deduced earlier, it is not necessary to calculate the whole specimen, but to focus on any component in the specimen. In order to obtain σ and u everywhere on the basic component, equilibrium conditions and constitutive relations must be added so that the problem to solve by equation (10) is:

$$\begin{gathered} div\ \sigma = 0 \ \ (\text{on } S) \\ \sigma = f(\varepsilon(u)) \\ \sigma \cdot n \text{ anti-periodic on } \partial S \\ u(x+V_\alpha)-u(x) = \mathrm{E}\cdot V_\alpha+\Omega\times V_\alpha \text{ periodic on } \partial S \\ \langle\sigma\rangle = \Sigma \text{ or } \langle\varepsilon(u)\rangle = E \end{gathered} \tag{10}$$

Where $\langle\sigma\rangle$ and $\langle\varepsilon(u)\rangle$ stand for macroscopic uniform stress and macroscopic uniform strain

Where equation(a) stands for the equilibrium condition, indicating that there is no volumetric force on the basic component S ; equation(b) stands for the constitutive equation of plane stress, and the constitutive relation f is the periodic function of the space variable x, which describes the properties of various materials on the basic component after combination; equation(c) and equation(d) stand for boundary conditions of the basic component derived above; equation(e) stands for the condition for controlling loading, wherein the former controls the loading of stress and the latter controls the loading of strain. Whether controlled stress loading or controlled strain loading is used, the solution of equation (10) is often called "local solution" because microscopic quantities (local quantities) σ and ε (u) are determined by macroscopic quantities (global quantities) E and Σ.

It is worth mentioning that regardless of the material constitution, the average stress and the average strain always conform to Hill's macroscopic homogenization equation, i.e.:

$$\langle\sigma : \varepsilon(u)\rangle = \langle\sigma\rangle : \langle\varepsilon(u)\rangle = \Sigma : E \tag{11}$$

Equation (11) is applicable to any periodic stress field with zero divergence and any strain-periodic displacement field.

Compared with the traditional boundary problem, there are two differences in equation (10):

(1) The load consists in the integral of one field (and not in boundary or body forces);

(2) The boundary conditions are not local.

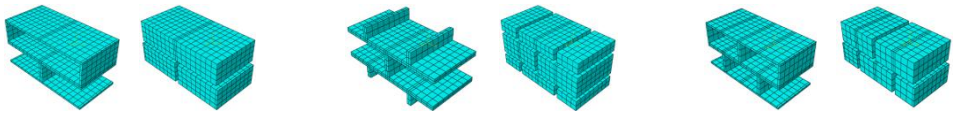
The universal applicability of equation (10) has been proved in various research methods. Even under the action of rigid displacement field. The unique solution (σ, u) can still be obtained by using equation (10) (this has been proved for linear elasticity, perfect plasticity and linear viscoelasticity). Once the local solutions (σ, u) are known, the missing macroscopic quantity E or Σ may be evaluated. The E-Σ relationship, i.e., the global (macroscopic)

constitutive law of the composite material can be built by repeating this process to obtain enough groups of E andΣ.

According to the definition above, if masonry is replaced by the fictitious homogeneous material obeying to this macroscopic constitutive law (homogenized material), the mechanical properties of the specimen subjected to a macroscopical homogeneous loading remain consistent with those of the masonry specimen. This makes it unnecessary to show independent basic components when the finite element software is used to calculate the overall mechanical properties of masonry structures subjected to in-plane loads. Instead, as long as the homogeneous materials are used to build the same structure under the same loading conditions, the an-isotropic homogeneous structure is flexibly meshed (which cannot be realized on the original an-isotropic non-homogeneous masonry structure). The conclusions similar to the original masonry structure are obtained after the appropriate finite elements are selected for calculation.

3 MODEL BUILDING

The reduced integration unit C3D8R is selected. The finite element models of RVE under three kinds of bricklaying methods are shown in figure 8.



(a) (b) (c)

Figure 8: Grid division of RVE models under three kinds of bricklaying methods (respectively running bonding; quarter bonding; header bonding)

To establish the stress-strain relationship by ABAQUS, it is necessary to integrate stresses and strains of the entire RVE. The average stress and average strain obtained as follows:

$$\bar{\sigma}_{ij} = \frac{1}{V}\int_v \sigma_{ij} dV \tag{12}$$

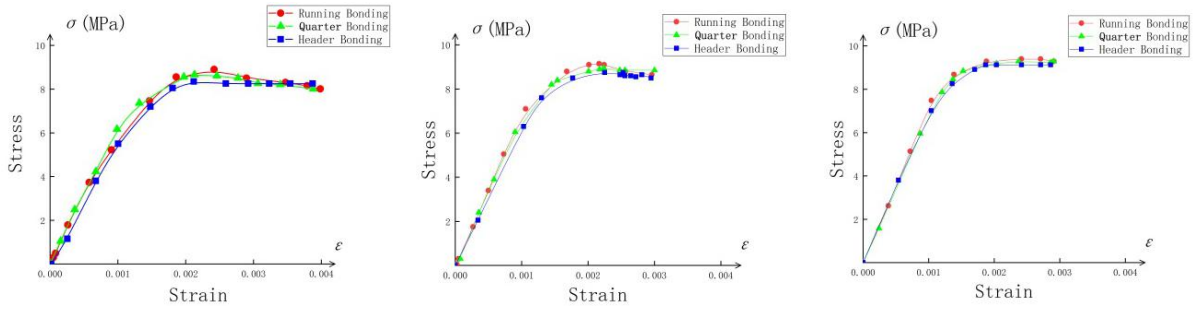
$$\bar{\varepsilon}_{ij} = \frac{1}{V}\int_v \varepsilon_{ij} dV$$

It is approximately believed that the average stress and strain of brick and mortar units are their average values respectively.

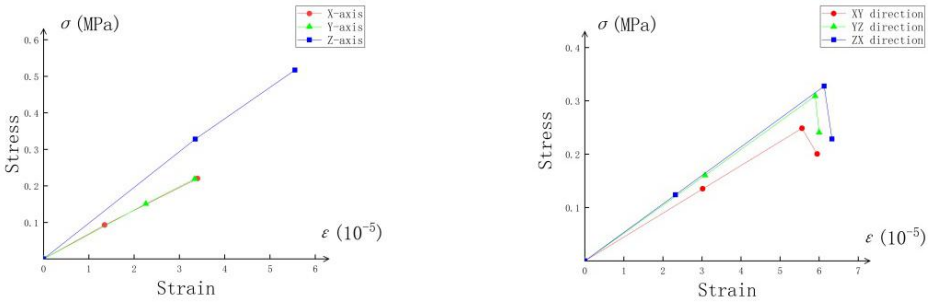
4 EXTRACTION OF EACH EQUIVALENT PARAMETER

4.1 Uniaxial Stress-Strain Curves of RVE Models

Average stress-strain curves of masonry under three kinds of bricklaying methods for uniaxial compression along the x, y and z axes obtained by finite element software ABAQUS are shown in figure 9(a). Average stress-strain curves of the running bonding RVE model for uniaxial tension are shown in figure 9(b). Average stress-strain curves of the quarter bonding RVE model for uniaxial shear are shown in figure 9(c). Peak strains and ultimate strengths are shown in tables 1-3.



(a)



(b) (c)

Figure 9:Stress-strain curve of RVE model for uniaxial stress((a) Stress-strain curves of three kinds of RVE models for uniaxial compression (along x-axis, y-axis and z-axis respectively); (b) Stress-strain curves of running bonding RVE for uniaxial stress; (c) Stress-strain curves of quarter bonding RVE for shear)

Table 1: Comparison of peak stress and strain values for uniaxial compression

Bricklaying methods	X-axis compression		Y-axis compression		Z-axis compression	
	Peak stress (Mpa)	Peak strain	Peak stress (Mpa)	Peak strain	Peak stress (Mpa)	Peak strain
Running bonding	9.17	0.00233	8.98	0.00228	8.77	0.00227
Quarter bonding	8.93	0.00224	8.77	0.00222	8.39	0.00225
Header bonding	9.43	0.00241	9.26	0.00239	9.15	0.00233

Table 2: Comparison of peak stress and strain values for uniaxial tension

Bricklaying methods	X-axis tension		Y-axis tension		Z-axis tension	
	Peak stress (Mpa)	Peak strain	Peak stress (Mpa)	Peak strain	Peak stress (Mpa)	Peak strain
Running bonding	0.219	3.23E-5	0.225	3.38E-5	0.517	5.53E-5
Quarter bonding	0.214	3.23E-5	0.216	3.27 E-5	0.508	5.46E-5
Header bonding	0.201	3.08E-5	0.203	3.11E-5	0.498	5.41E-5

Table 3: Comparison of peak stress values for shear

Bricklaying methods	XY-plane peak stress (Mpa)	YZ-plan peak stress (Mpa)	ZX-plan peak stress (Mpa)
Running bonding	0.29	0.33	0.37
Quarter bonding	0.27	0.30	0.34
Header bonding	0.22	0.29	0.31

4.2 Equivalent Parameters Along Different Axes

When shear stress is not considered, the constitutive relation of elasticity of anisotropic materials is as follows:

$$\begin{Bmatrix} \varepsilon_x \\ \varepsilon_y \\ \varepsilon_z \end{Bmatrix} = \begin{bmatrix} \frac{1}{E_x} & -\frac{\upsilon_{yx}}{E_y} & -\frac{\upsilon_{zx}}{E_z} \\ -\frac{\upsilon_{xy}}{E_x} & \frac{1}{E_y} & -\frac{\upsilon_{zy}}{E_z} \\ -\frac{\upsilon_{xz}}{E_x} & -\frac{\upsilon_{yz}}{E_y} & \frac{1}{E_z} \end{bmatrix} \begin{Bmatrix} \sigma_x \\ \sigma_y \\ \sigma_z \end{Bmatrix} \tag{13}$$

The initial part of the stress-strain curve obtained by finite element analysis is linear elasticity. When there is normal stress along only one axis, the equations for calculating the equivalent elastic modulus and Poisson's ratio along three axes are as follows:

$$\begin{aligned} &\overline{E}_x = \frac{\overline{\sigma}_x}{\overline{\varepsilon}_x}, \quad \overline{\upsilon}_{xy} = -\frac{\overline{\varepsilon}_y}{\overline{\varepsilon}_x}, \quad \overline{\upsilon}_{xz} = \frac{\overline{\varepsilon}_z}{\overline{\varepsilon}_x} \\ &\overline{E}_y = \frac{\overline{\sigma}_y}{\overline{\varepsilon}_y}, \quad \overline{\upsilon}_{yx} = -\frac{\overline{\varepsilon}_x}{\overline{\varepsilon}_y}, \quad \overline{\upsilon}_{yz} = \frac{\overline{\varepsilon}_z}{\overline{\varepsilon}_y} \\ &\overline{E}_z = \frac{\overline{\sigma}_z}{\overline{\varepsilon}_z}, \quad \overline{\upsilon}_{zx} = -\frac{\overline{\varepsilon}_x}{\overline{\varepsilon}_z}, \quad \overline{\upsilon}_{zy} = \frac{\overline{\varepsilon}_y}{\overline{\varepsilon}_z} \end{aligned} \tag{14}$$

For pure shear stress, the shear modulus of three kinds of RVE models along three axes are defined as follows:

$$\overline{G}_{xy} = \frac{\overline{\tau}_{xy}}{\overline{\varepsilon}_{xy}}, \ \overline{G}_{yz} = \frac{\overline{\tau}_{yz}}{\overline{\varepsilon}_{yz}}, \ \overline{G}_{zx} = \frac{\overline{\tau}_{zx}}{\overline{\varepsilon}_{zx}} \tag{15}$$

Table 4: Equivalent parameters of three kinds of RVE models along different axes

Bricklaying methods	The modulus of elasticity			The Poisson's ratio						An-isotropic shear modulus			Percentage of mortar content
	$\overline{E}_x$	$\overline{E}_y$	$\overline{E}_z$	$\overline{\upsilon}_{xy}$	$\overline{\upsilon}_{yz}$	$\overline{\upsilon}_{xz}$	$\overline{\upsilon}_{yx}$	$\overline{\upsilon}_{zy}$	$\overline{\upsilon}_{zx}$	$\overline{G}_{xy}$	$\overline{G}_{yz}$	$\overline{G}_{zx}$	
Running bonding	7134	6538	7579	0.184	0.174	0.180	0.179	0.198	0.196	2547	2603	3219	19.24
Quarter bonding	6842	6317	7263	0.180	0.168	0.175	0.176	0.195	0.193	2538	2592	3112	20.92
Header bonding	6486	6055	6723	0.172	0.165	0.167	0.169	0.187	0.186	2498	2563	3106	22.60

The strengths of running bonding RVE selected are much higher than those of the other two kinds along different axes and the strengths of header bonding RVE selected are the lowest. Mechanical properties of RVE are affected by the placement of mortar joint and the overall volume occupied by mortar joint. In addition, there are some differences in the compressive strength of the three kinds of RVE models along different axes of X, Y and Z,

which is not only related to bricklaying methods, but also related to the sizes along each axis. The compressive stiffness of masonry is inversely proportional to the mortar content. The smaller the mortar content is, the greater the compressive stiffness of masonry, which conforms to the theoretical facts and the variation law of equivalent elastic modulus.

5 ANALYSIS AND SIMULATION OF RVE MODEL

The data of compressive tests in the structural test center of Changsha University of Science and Technology by Zhiwei Hu[10] is used as comparison. Only the running, quarter, and header RVE models are selected for analysis.

5.1 Comparison of Compressive Strength

Simulated and experimental values of the ultimate compressive strength of the three kinds of specimens are respectively shown in table 5:

Table 5: Simulation values (test values) of ultimate compressive strength

Bricklaying methods	Stress area(mm^2)	Failure load (kN)	Compressive strength(MPa)	Error(%)
Quarter bonding	56350	122（113）	2.130（2.005）	7.63
Header bonding	117600	236（220）	2.001（1.871）	6.95
Running bonding	117600	239（214）	2.032（1.820）	11.6

5.2 Comparison of Compressive Strength

Test values and simulation values of elastic modulus are shown in table 6:

Table 6: Comparison of elastic modulus of specimens

Bricklaying methods	Test value (MPa)	Simulation value(MPa)	Error(%)
Quarter bonding	1335	1465	9.7
Header bonding	1066	1152	8.1
Running bonding	1027	1179	14.8

5.2 Results Analysis

The maximum error of compressive strength is 11.6% (less than 15%), which is within the acceptable range, indicating that the homogenization method is reliable for simulating compressive strength of masonry structure under three kinds of bricklaying methods.

From the data comparison, it can be concluded that the general trend of stress-strain simulation curves and test curves is consistent, while test values of the elastic modulus of the specimens under different bricklaying methods are quite different from simulation values. The reason is that strength values itself has certain deviation, and whether the strength is accurate or not directly affects values of the elastic modulus. Moreover, by using homogenization method, although the bond-slip effect at the interface cannot be simulated in the finite element model established by RVE, it can better simulate the mechanical characteristics of masonry structure as a whole.

6 CONCLUSION

- On the premise of the tessellation theory, the whole wall under three common bricklaying methods is divided by using the rectangular division lattice. Three kinds of representative volume element (namely RVE) capable of generating universal tessellation shapes are obtained.
- The theory of periodic masonry plane segmentation is established, and the minimum component of the tessellation shapes is deconstructed, and the boundary conditions of equivalent volume element (RVE) are derived.
- On the premise of selecting reasonable material parameters, RVE models under three kinds of bricklaying methods are established, and the corresponding equivalent parameters are obtained. The results of finite element software are compared with the tests results. The results are in good agreement, which shows that the homogenization method is reliable for simulating compressive strength of masonry structure under three kinds of bricklaying methods and can reflect the stress characteristics of masonry structure as a whole.

Acknowledgements. The research is supported by the National Natural Science Foundation of China (Grant Nos. 51678067, 51808054). This support is gratefully acknowledged.

REFERENCES

[1] L.Gambarotta and S.Lagomarsino. Damage models for the seismic response of brick masonry shear walls. Part I: The mortar joint model and its applications. *Earthquake Engineering and Structural Dynamics*, (1997), **26**(3): 423-439

[2] Anthoine, A. Derivation of the in-plane elastic characteristics of masonry through homogenization theory. *International Journal of Solids and Structures*, (1995)**32**, pp. 137-163.

[3] P.Pegon and A. Anthoine, Numerical strategies for solving continuum damage problems with softening Application to the homogenization of masonry, *Computers and Structures*, (1997)**64**, pp. 623-642, .

[4] A.Anthoine. Second-order homogenization of functionally graded materials. *Inter-nation Journal of Solids and Structures*.(2010)**47**, pp.1477-1489

[5] Daquan Wang. Nonlinear Analysis of Masonry Applying the RVE Homogenization Methods. (2002), pp.45-60

[6] Jimei Shen. Study on Homogenization Process of Masonry and Its Applications Using Numerical Simulation. (2012), pp.29-60

[7] Yalin Li. Study on compressive behavior of cross bore block masonry under different masonry methods. (2015), pp.20-42

[8] Yaying Wu. Research on the Rigid Homogenization Theory of Masonry Structures Based on Regular Tessellation Theory. (2012), pp.33-50

[9] Chengyi Li. Study on the Rigid Homogenization Model of Masonry under Different Masonry Methods (2015), pp.29-63

[10] Zhiwei Hu. The Research on the impact of masonry methods on the brick masonry mechanical properties. (2015), pp.50-66

12thInternational Conference on Structural Analysis of Historical Constructions
SAHC 2020
P. Roca, L. Pelà and C. Molins (Eds.)

STUDY ON SEISMIC PERFORMANCE EVALUATION OF MODERN WOODEN SCHOOL BUILDINGS IN JAPAN

MITSUHIRO MIYAMOTO [1*]

[1]Kagawa University
Faculty of Engineering and Design
2217-20, Hayashi-cho, Takamatsu City, Kagawa Prefecture, Japan
e-mail: miyamoto@eng.kagawa-u.ac.jp

Keywords: Modern Wooden School Building, Static Pushover Analysis, Seismic Performance

Abstract. *Japanese school buildings have been changed from modern wooden structures to reinforced concrete structures after the Building Standard Law was established in 1950. Therefore, only a few modern wooden school buildings exist currently. Ensuring the seismic resilience of these wooden school buildings is essential for their preservation and longevity. In this study, a static pushover analysis was conducted for a modern wooden school building using a 3D frame model to simulate the relationship between lateral load and deformation. This 3D frame model was proposed based on the site investigation and the 2D frame model used in a previous study. From the analysis results, it is found that the bearing capacity was decided by the deformation capacity of the column-to-groundsill connection; therefore, reinforcement to these connections was required to improve the seismic performance of a modern wooden school building.*

1 INTRODUCTION

The structural characteristics of the modern wooden school buildings are different from other Japanese wooden buildings. The main seismic elements are large section braces and knee braces. All braces and knee braces were fixed to the column using steel bolts. The column was connected to the beam or groundsill using metal connectors on each side of a connection.

Several studies in Japan focused on the seismic performance of wooden brace frames. However, only a few studies have focused on the large section brace used in modern wooden school buildings. In addition, a small number of studies have addressed the wooden knee braces. Thus, almost no experimental data are available for evaluating the seismic performance of modern wooden school buildings.

The objective of this paper is to develop a 3D-frame model for the seismic performance evaluation of modern wooden school buildings. In a previous study [1], full-scale static lateral loading tests were conducted for wooden frames, single braces, cross braces, and knee brace specimens to examine the fracture modes and the relationship between the lateral load and deformation. These four specimens were designed based on the site investigation of existing modern wooden school buildings. In addition, a static pushover analysis was carried out for these specimens using a 2D-frame model to simulate the relationship between lateral load and deformation. The analysis models were developed and compared with test results to examine

their validity. The analysis results were in good agreement with the test results.

In the present study, a static pushover analysis was carried out for a modern wooden school building using a 3D-frame model to simulate the relationship between lateral load and deformation. The 3D-frame model was proposed based on the site investigation and 2D-frame model. Based on the analysis results, the bearing capacity and deformation capacity of a modern wooden school building were evaluated.

2 OUTLINE OF A MODERN WOODEN SCHOOL BUILDING

The north and east school buildings of Yashiro Junior High School, which are the target modern wooden school buildings of this study, are wooden structures located in Ehime Prefecture. These buildings were built in 1960 and 1961. The buildings were dismantled recently. However, we were presented with an opportunity to investigate their structural characteristics before they were dismantled. Figure 1 shows the north school building. The main seismic elements are large section braces and knee braces (Figures 2 to 10). The dimensions of the column, groundsill, and the brace are 135 × 135 mm, and those of the beam and knee brace are 135 × 135 mm or 150 × 150 mm and 90 × 90 mm, respectively. All braces and knee braces were fixed to the column using a bolt with a diameter of 12 mm. The column was connected to



Figure 1: Façade of a modern wooden school building



Figure 2: Edge of a timber brace



Figure 3: Overview of a knee brace

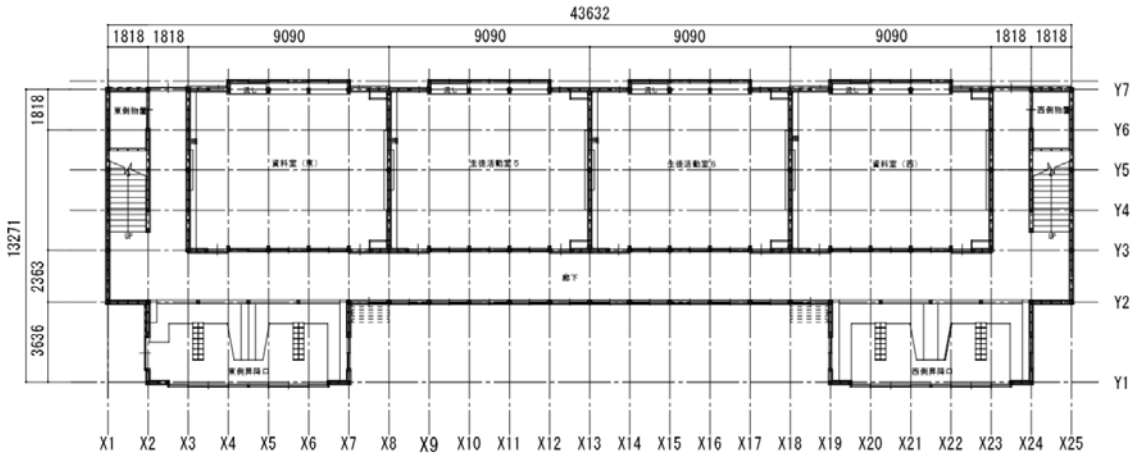


Figure 4: Plan of ground floor

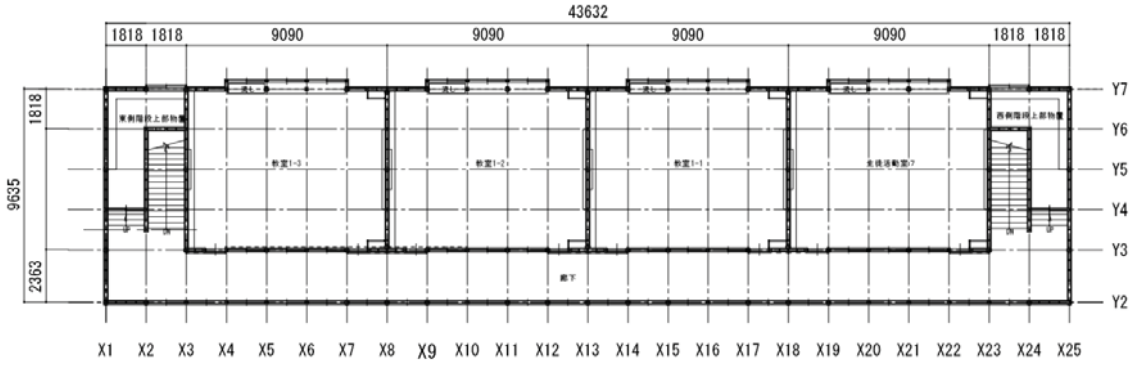


Figure 5: Plan of first floor

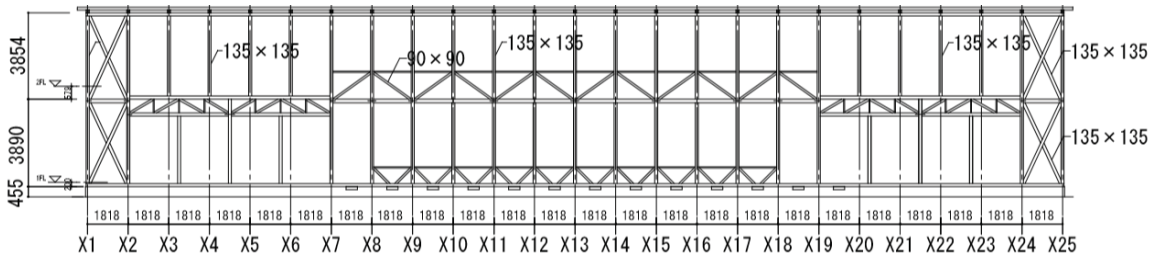


Figure 6: Elevation at Y2 section

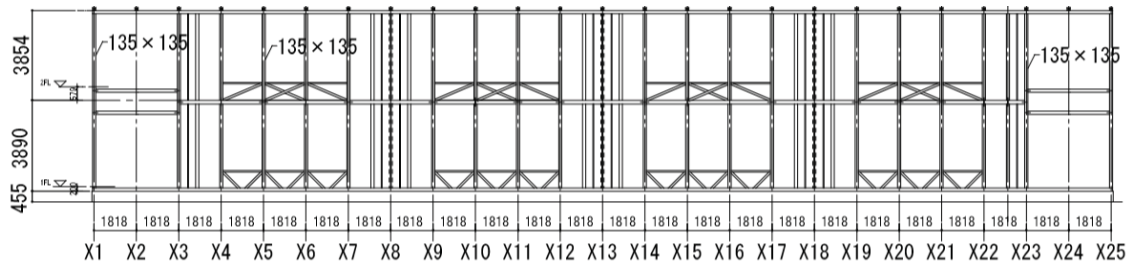


Figure 7: Elevation at Y3 section

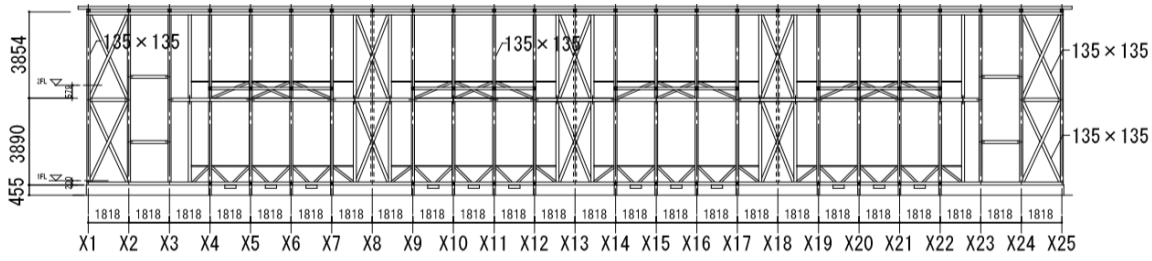


Figure 8: Elevation at Y7 section

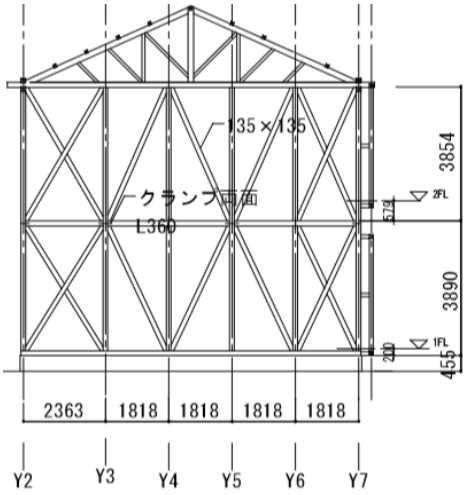


Figure 9: Elevation at X1 and X25 section

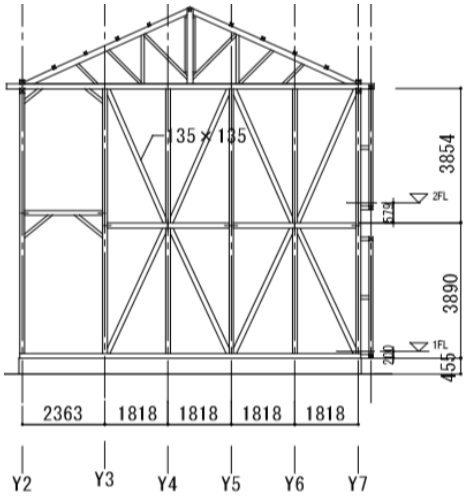


Figure 10: Elevation at X8, X13 and X18 section

the beam or groundsill using metal connectors on each side of a connection.

3 3D FRAME MODEL FOR A MODERN WOODEN SCHOOL BUILDING

The simulation analysis was executed using a 2D-frame model to estimate the relationship between the load and the deformation angle of each specimen in a previous study [1]. The 3D-frame model was proposed based on these 2D frame models.

3.1 Modeling of each seismic element

Four specimens were used for the tests, as shown in Figures 11 to 14. In addition to a wooden frame specimen, single brace, cross brace, and knee brace specimens were also used because they are the main seismic elements in wooden school buildings. One brace in a cross-brace specimen was separated at the intersection. The height and width of each specimen were 2752.5 mm and 1820 mm, respectively. The dimensions of the column, groundsill, and the brace were 135 × 135 mm and those of the beam and knee brace were 135 × 180 mm and 90 × 90 mm, respectively. The column and brace were made of cedar, the beam and knee brace were made of Douglas fir, and the groundsill was made of Japanese cypress. All connections were designed

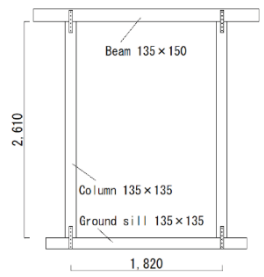


Figure 11: Outline of specimen A

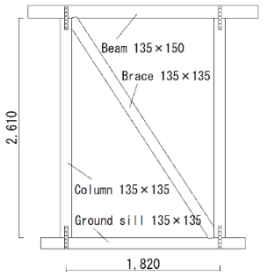


Figure 12: Outline of specimen B

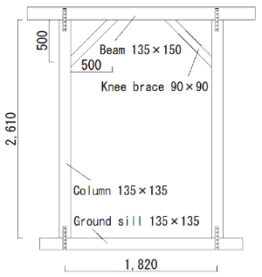


Figure 13: Outline of specimen C

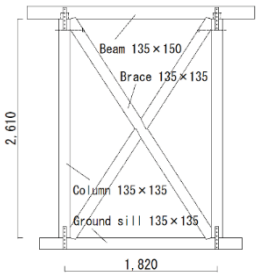


Figure 14: Outline of specimen D

to be the same as those of actual wooden school buildings based on the site investigation. In the column-to-brace connection, the brace was connected to the beam or groundsill with a depth of 15 mm. The column was connected to the beam or groundsill using a short tenon with a height, width, and thickness of 67.5 mm, 90 mm, and 30 mm, respectively. Similarly, in the column-to-knee brace connection, the knee brace was connected to the column with a depth of 15 mm. In addition, metal connectors were fixed on each side of the connection using six nails. The height, width, and thickness of the metal connectors were 270 mm, 40 mm, and 5 mm, respectively. The through brace, separate brace, and knee brace were fixed on the column using a bolt with a diameter of 12 mm. These specimens were subjected to cyclic lateral loads, with the real shear deformation angle being gradually increased symmetrically from 1/450, 1/300, 1/200, 1/150, 1/100, 1/75, 1/50, 1/30, 1/20 to 1/15 rad. Three cyclic loadings were applied. Finally, the specimen was loaded to 1/10 rad at one end.

Figures 15 to 20 show the analysis model used for the static pushover analysis. The analysis models of specimens B and D were assumed to be different because the resistance element of a through brace was different for tensile and compressive braces. The bending resistance at the connection of the metal connector and short tenon was expressed as a rotation spring. The rotation springs of these connections with a through brace on specimens B (compression) and D were excluded because there was a brace to prevent the connection from rotating. The uplift behavior at one side of the column-to-groundsill connection on specimens B (compression) and D was expressed as an axis spring based on the results of following tests. The tensile test for

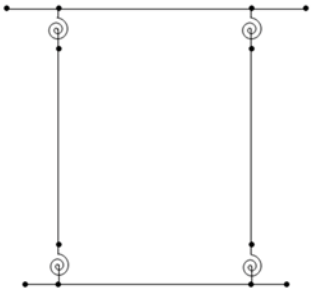


Figure 15: Mechanical model of specimen A

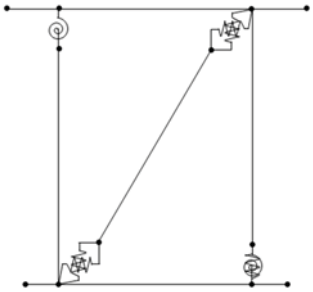


Figure 16: Mechanical model of specimen B (Compression)

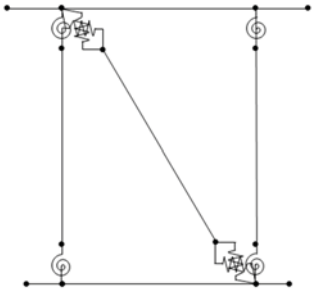


Figure 17: Mechanical model of specimen B (Tensile)

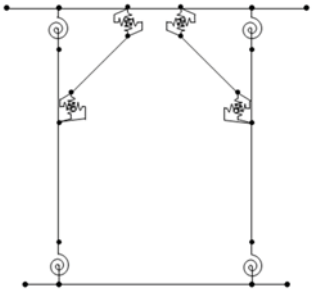


Figure 18: Mechanical model of specimen C

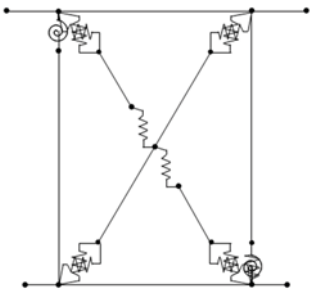


Figure 19: Mechanical model of specimen D (Compression)

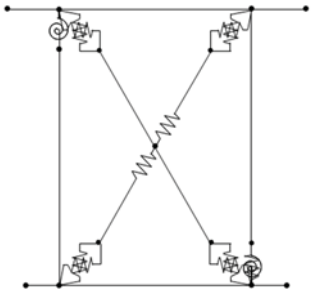


Figure 20: Mechanical model of specimen D (Tensile)

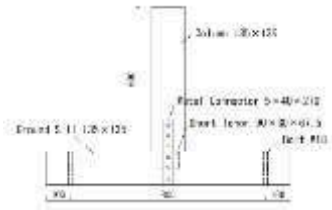


Figure 21: Outline of specimen



Figure 22: Loading instrument

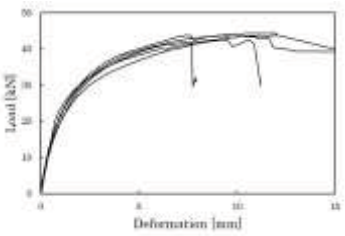


Figure 23: Relationship between load and deformation

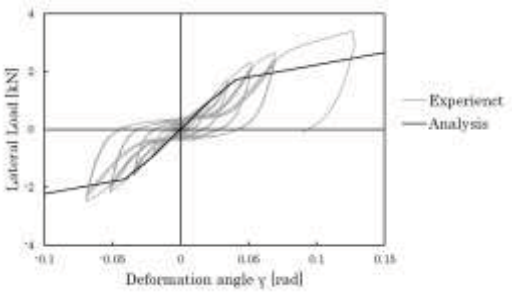


Figure 24: Comparison of experimental and analysis results (specimen A)

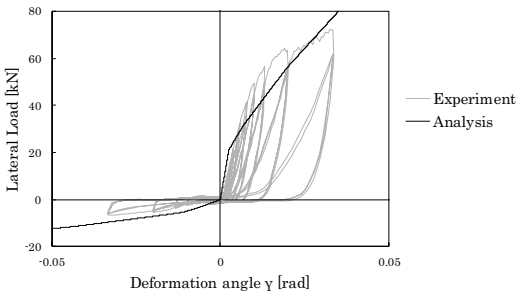


Figure 25: Comparison of experimental and analysis results (specimen B)

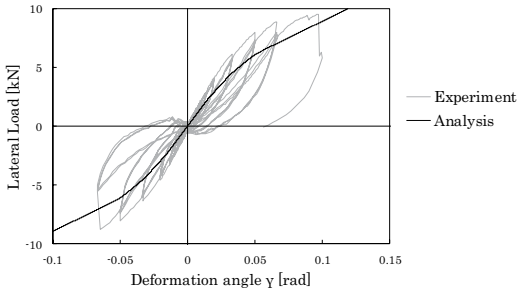


Figure 26: Comparison of experimental and analysis results (specimen C)

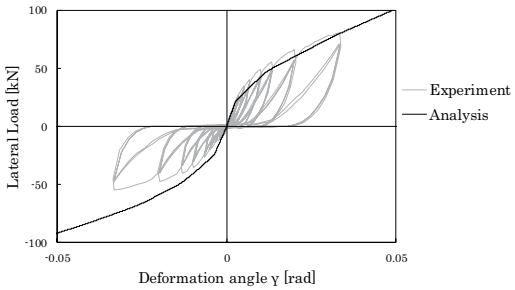


Figure 27: Comparison of experimental and analysis results (specimen D)

column-to-groundsill connection was conducted as shown in Figures 21 to 23. The specimen size was the same as that for the full-scale static lateral loading tests. The number of specimens was five. The embedment resistance at the connection of the through brace, separate brace, or knee brace and the beam, groundsill, or column was expressed as an axis spring. The shear and tensile resistance of a bolt were expressed as an axis spring. A bilinear-hysteresis model was used for each rotation spring and axis spring. The initial stiffness and yield moment or strength were calculated based on a previous study [2] [3]. The material property was estimated through the results of destructive tests for each wooden member based on a previous study [2] [4].

The static pushover analysis was performed using a general-purpose analysis software, i.e., SNAP (Ver. 7). Figures 24 to 27 show the comparison of the relationship between the load and deformation angle of each specimen as obtained from the test and analysis results. The analysis results are in good agreement with the test results for each specimen. The load to the range of a large deformation angle on almost all specimens obtained through the analysis is smaller than that obtained in the tests because the design equations were used for calculation.

3.2 Modeling to a 3D frame

The 3D-frame model was proposed based on the 2D-frame models. Their validity was examined by comparing the test and analysis results. The external walls at X1, X25, Y2, and Y7 were plastered with a mortar and mud wall that were 20 mm and 10 mm thick, respectively. They were not considered as a seismic element due to their small thickness. The small section braces of 90×90 mm were located in the longitudinal direction at Y2, Y3, and Y7 as shown in Figures 6 to 8, but they are not considered as a seismic element because of their dimension

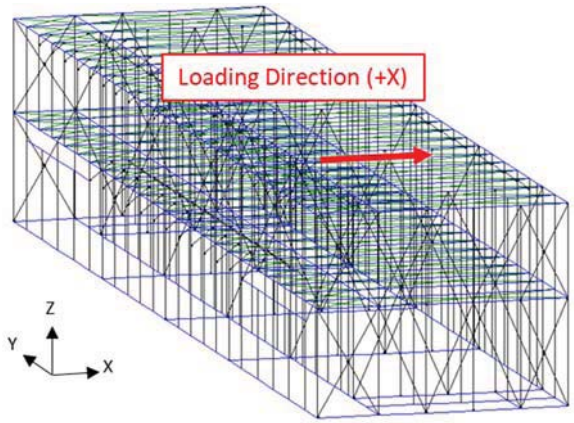


Figure 28: 3D frame model (+X direction)

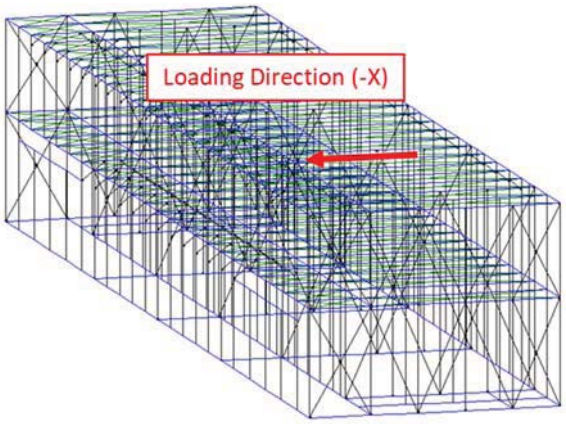


Figure 29: 3D frame model (-X direction)

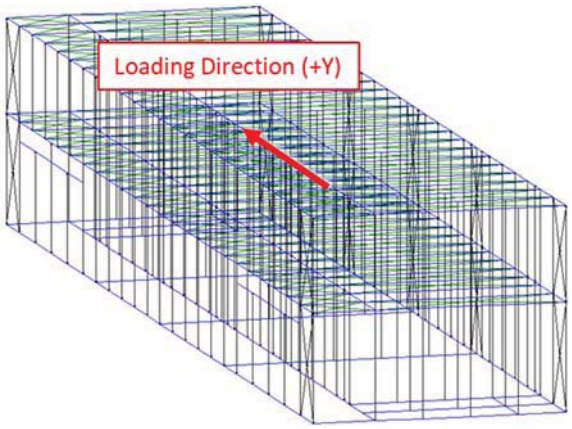


Figure 30: 3D-frame model (+Y direction)

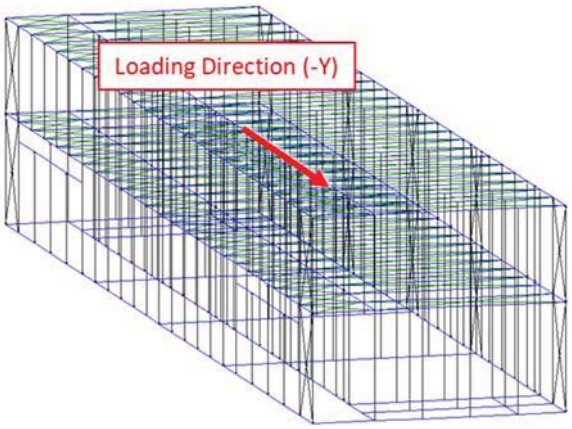


Figure 31: 3D-frame model (-Y direction)

which were smaller than the large section braces of 135 × 135 mm. The axis behavior at the top and bottom of the column-to-groundsill or column-to-beam connections was expressed as an axis spring with a bilinear-hysteresis model. Regarding the embedment behavior, the initial stiffness and yield strength were calculated based on a previous study [2] [3]. Regarding the uplift behavior, the initial stiffness and yield strength were decided based on the results of tensile tests for column-to-groundsill connection as shown in Figures 21 to 23. The material property was estimated based on a previous study [2] and the second stiffness was determined to be $1/8^{th}$ of the initial stiffness.

The 3D-frame model was not including the roof frame because the deformation of roof frame was very small. The horizontal frame such as a floor or roof was expressed as a brace with a bilinear hysteresis model. The initial stiffness and yield strength were estimated based on a previous study [5]. The second stiffness was determined to be 0 of the initial stiffness, i.e., the elastic-perfectly plastic model.

Figures 28 to 31 show the 3D-frame model of the north school buildings of Yashiro Junior High School. Owing to the limitation of the nodal points number in an analytical software, the 3D-frame model was divided into four. For example, +X and –X direction models were considering the seismic elements in the X direction.

4 SEISMIC PERFORMANCE OF A MODERN WOODEN SCHOOL BUILDING

4.1 Outline of static pushover analysis

The static pushover analysis is conducted using 3D-frame models. The ratio between the ground and the first floor-load distribution is decided according to the Distribution coefficient to the vertical direction A_i in Japanese Building Standards Law. In addition, the analysis results are evaluated compared with the Seismic story shear coefficient C_i in Japanese Building Standards Law with Equation (1).

$$C_i = Z \times R_t \times A_i \times C_0 \tag{1}$$

where, Z is Seismic zone coefficient (in case of Ehime Prefecture 0.9). R_t is the Vibration characteristics coefficient calculated by Design first natural period T. C_0 is the Standard shear coefficient (in case of moderate earthquake 0.2 and large earthquake 1.0). Table 1 summarizes the calculation result.

Table 1: Calculation result of the seismic story shear coefficient

Earthquake	Story	Z	R_t	A_i	C_0	C_i
Moderate	2	0.9	1.0	1.43	0.2	0.26
	1			1.00		0.18
Large	2			1.43	1.0	1.3
	1			1.00		0.90

The deformation capacity of a modern wooden school building is evaluated at the top and bottom of the column-to-groundsill or column-to-beam connections. The strength of embedment resistance at the connections continues to increase, on the other hand, the strength of tensile resistance suddenly decreases after the fracture at the connections. Accordingly, the deformation capacity is evaluated by the average yield and ultimate deformation, based on the

results of the tensile test for column-to-groundsill connection. The average yield deformation and the ultimate yield deformation are 4.96 mm and9.38 mm, respectively.

4.2 Results of static pushover analysis

Figures 32 and 33 show the relationship between the story deformation angle and the story shear coefficient from the results of the static pushover analysis. The story shear coefficient is given by the ratio of the story shear force divided by the seismic weight. In these figures, the axis spring deformation at one side of the column-to-groundsill connection reaches a yield deformation of 4.96 mm at the yield point and an ultimate deformation of 9.38 mm at the ultimate point. If the elastic limit of a modern wooden school building is assumed to be 1/120 rad, the story shear coefficient at the ground floor is 0.27 in the X direction and 0.10 in the Y direction, that at the first floor is 0.86 in the X direction and 0.18 in the Y direction. In contrast, the required seismic story shear coefficient C_i for moderate earthquakes is 0.18 at the ground floor and 0.26 at the first floor as shown in Table 1. Therefore, the seismic performance at both floors in the Y direction is insufficient. When the axis spring deformation at one side of the column-to-groundsill connection reaches yield deformation, the story deformation angle reaches 1/31 rad in the X direction and 1/48 rad in the Y direction at the ground floor, and 1/167 rad in the X direction and 1/83 rad in the Y direction at the first floor. The story deformation angle of a modern wooden school building exceeds the elastic limit of 1/120 rad except for the X direction at the first floor. When a modern wooden school building reaches the ultimate limit, the story shear coefficient at the ground floor is 0.80 in the X direction and 0.27 in the Y direction, that at the first floor is 0.89 in the X direction and 0.33 in the Y direction. On the other hand, the required seismic story shear coefficient C_i for large earthquakes is 0.90 at the ground floor and 1.3 at the first floor as shown in Table 1. Therefore, the seismic performance, especially the deformation capacity at the column-to-groundsill connections, at both floors in both directions is insufficient.

5 CONCLUSIONS

In this study, a static pushover analysis was conducted for a modern wooden school building

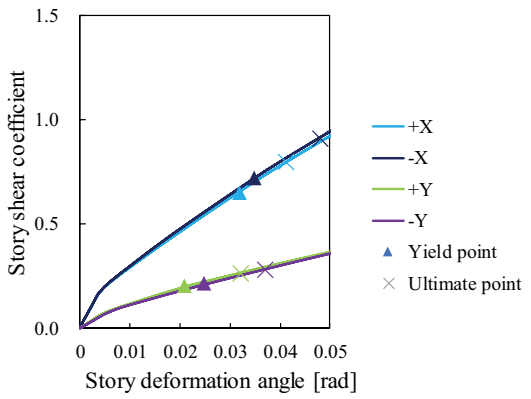


Figure 32: Analysis results (Ground floor)

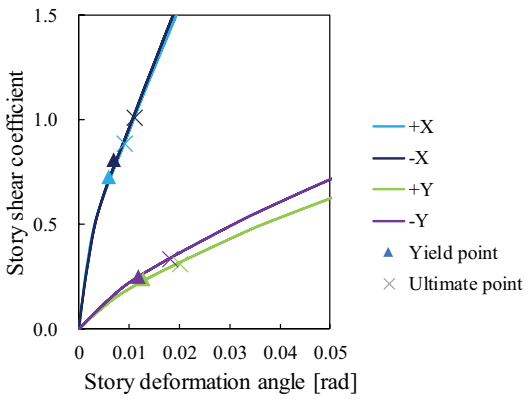


Figure 33: Analysis results (First floor)

using a 3D-frame model to simulate the relationship between lateral load and deformation. This 3D-frame model was proposed based on the site investigation and 2D-frame model in a previous study.

From the analysis results, the required bearing capacity to moderate and large earthquakes was insufficient in the longitudinal direction (Y direction). In the transverse direction (X direction), the required bearing capacity for large earthquakes was insufficient. The bearing capacity was decided by the deformation capacity of the column-to-groundsill connection. Therefore, the reinforcement to these connections were required to improve the seismic performance of a modern wooden school building.

Acknowledgments

This research was partially supported by the Asahi Glass Foundation. We gratefully acknowledge this support.

REFERENCES

[1] Ebisuoka, M., and Miyamoto, M., Study on Seismic Performance of Timber Frame Used for Modern Timber School Building, *AIJ Journal of Structural Engineering*, 64B, 453-461, March 2018.

[2] Architectural Institute of Japan (edited), *Standard for Structural Design of Timber Structures*, Maruzen, Japan, 2006.

[3] Sakata, H., Yamazaki, Y., Udagawa, H., and Ohashi, Y., Experimental Study on Flexural-Shear Behavior of Mortise-Tenon Joint with Dowel, *AIJ Journal of Structural and Construction Engineering*, 77(671), 45-54, January 2012.

[4] Architectural Institute of Japan (edited), *Design Manual for Engineered Timber Joints*, Maruzen, Japan, 2009.

[5] Japan Housing and Wood Technology Center (edited), *The Allowable Stress Design of Conventional Wooden Houses*, Japan Housing and Wood Technology Center, Japan, 2008.

12th International Conference on Structural Analysis of Historical Constructions
SAHC 2020
P. Roca, L. Pelà and C. Molins (Eds.)

THE INFLUENCE OF THE PASSIVE EARTH PRESSURE AND OTHER FACTORS ON THE STABILITY OF THE UNDERGROUND MASONRY VAULTS OF THE PARIS METRO

O. MORENO REGAN[1], E. BOURGEOIS[2], JF. DOUROUX[3] AND A. DESBORDES[3]

[1] setec tpi
Immeuble Central Seine - 42-52 quai de la Rapée 75583 Paris, France
e-mail: omar.moreno-regan@setec.com , www.setec.fr/en/

[2] COSYS-LISIS, Univ Gustave Eiffel, IFSTTAR,
5, boulevard Descartes, Champs sur Marne, F-77454 Marne-la-Vallée, France
email: emmanuel.bourgeois@univ-eiffel.fr , www.univ-gustave-eiffel.fr/en/

[3] RATP
50 Rue Roger Salengro, 94724 Fontenay-sous-bois, France
e-mail: jean-francois.douroux@ratp.fr, alain.desbordes@ratp.fr
www.ratp.fr/en

Keywords: Masonry, Damage, Tunnel, Vault, Metro, FEM

Abstract. *This paper presents an analysis of the behavior of masonry tunnel vaults of the Paris metro when their state of equilibrium is altered. These tunnels were built with a masonry vault combined with sidewalls and a slab made of unreinforced concrete. The main case studied here is that of the spreading of the vault's supports as a result of nearby construction works. Numerical computations are carried out using a specifically developed model for the masonry that combines a homogenization technique with damage models. An interface between the tunnel and the ground allows the study of the soil-structure interaction. The proposed model identifies the possible hinging failure mechanisms and their configuration based on the horizontal displacements and the geometry of the structure. Several other simpler constitutive laws for the masonry are also used and then compared with the proposed model. An analysis on the loss of the passive earth pressure and the deformation of the structure are also provided. Based on the numerical simulations made and real measurements, it was observed that the studied underground masonry vaults may withstand several centimeters of support spreading.*

1 INTRODUCTION

The Paris subway system, operated by the Régie Autonome des Transports Parisiens (RATP), has sixteen lines and carries about 5 million passengers daily. The infrastructure is mostly underground and was built predominantly in the early twentieth century. About 85% of the tunnels comprise a masonry vault. The typical section adopted for the tunnels was built with a masonry vault (blocks of gritstone or *meulière* stone and mortar) and unreinforced concrete sidewalls and ground slab. More details can be found in [1] and [2]. To evaluate the

serviceability state of a tunnel, or the impact of nearby civil engineering works carried out in the vicinity, it is necessary to predict the behavior of the masonry vault and the concrete walls and slab using advanced numerical tools. It is then possible to assess any possible damage to the existing structure. Although the modelling of historical masonry structures has been the subject of many scientific publications [1], there are few references on modelling masonry tunnels. Some studies have been carried out using elastic FEM analysis or limit analysis [1].

This study follows up the model that we developed for masonry vaults [3] and the experimental campaign [2] needed to characterize the materials. This model, as will be discussed later on, uses a homogenization technique and damage mechanics. The issue examined in this paper is that of the spreading of the vault's supports as a result of nearby construction works. Results of the numerical simulation are compared with *in situ* measurements. The proposed model provides a realistic and effective way to analyze the behavior of masonry vaults and gives access to the deformation state of the structure thus allowing the serviceability state and failure load to be evaluated.

2 DESCRIPTION OF THE CASE STUDY

The study deals with the station "Mairie d'Ivry", the southern terminus of the line 7 of the Paris Metro. The three-lane tunnel that forms the station is about 105 m long and it was built with a semi-circular shaped masonry vault supported by two unreinforced concrete sidewalls, bound by a curved unreinforced concrete ground slab. Dimensions are shown in Figure 1 and geology in Figure 2. The construction of the station started in 1938. According to historical records, the method of execution consisted in building initially the sidewalls from the surface as bored piles. Excavation of the tunnel was executed in multiple stages starting with the top heading. Once the sidewalls were finished, the full excavation of the top section and construction of the masonry vault was carried out. Finally, the excavation of the rest of the section (core and bottom) allowed the realization of the curved slab. During the construction, several problems were reported, caused by swelling of the clay layer.

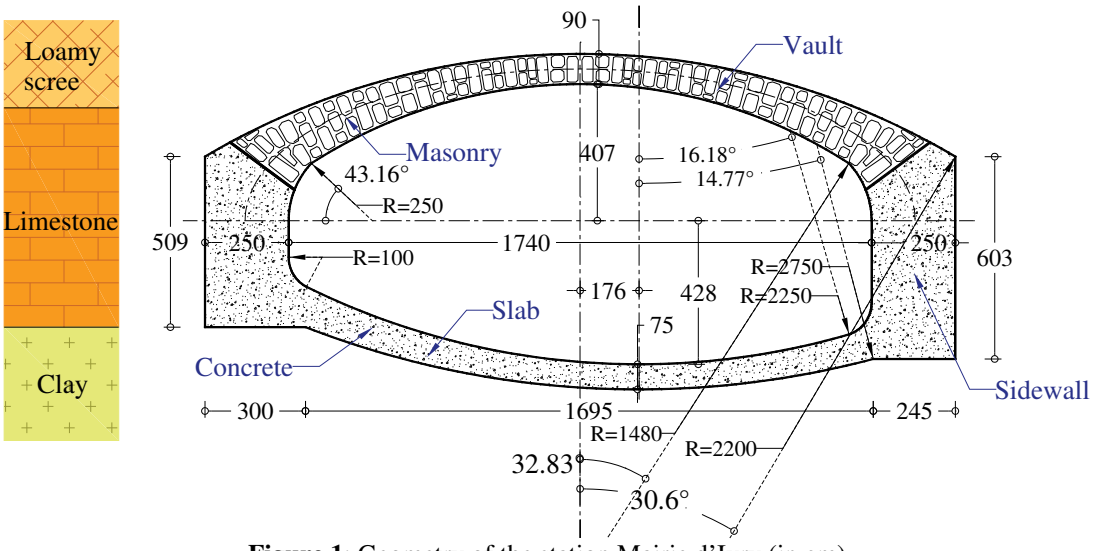


Figure 1: Geometry of the station Mairie d'Ivry (in cm)

Several decades later, the construction of a group of buildings near the station required to perform a deep excavation (Figure 2), which was carried out in a short period of time in 1983.

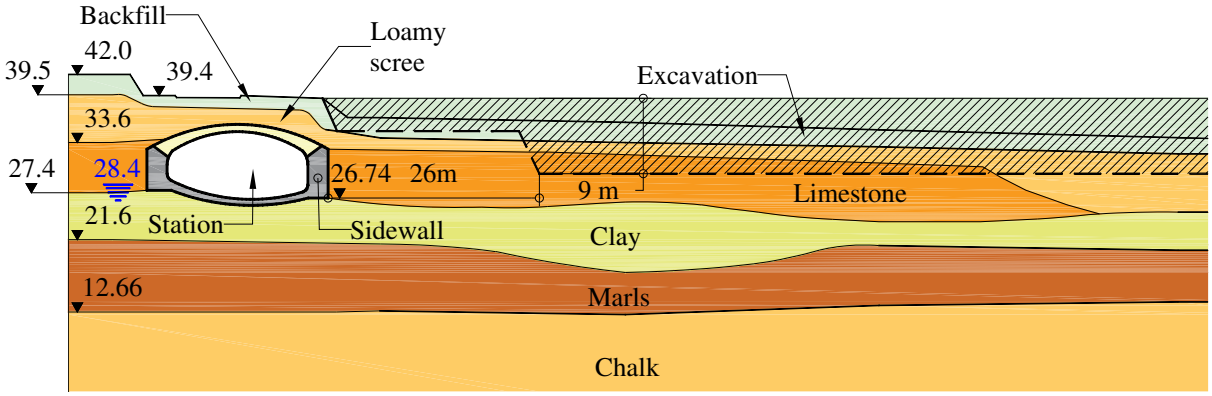


Figure 2: Geology and construction works near the station "Mairie d'Ivry"

Immediately after, numerous structural problems were reported in the station: cracks at the crown and slab (Figure 3), water infiltrations, dislodged tiles, etc. These problems led to the setup of a series of measurements that revealed the subsidence of the masonry vault, the increasing distance between sidewalls and the uplift of the slab. Measurements were taken from 1984 to 2007 (see Figure 6). Several hypotheses were suggested to explain these observations: the decompression and creep of the clay layer; the slight rise of the groundwater table level; the decrease of the passive earth pressure that could be mobilized at the right sidewall, which was needed to ensure stability; amongst others [4]. Also, the clay layer was extremely sensitive to the modification of their state of equilibrium, which may explain the sinking and rotation of the right sidewall; the left sidewall being considered stable.

In order to stabilize the deformations of the structure, a set of reinforcement works was carried out in the tunnel (Figure 3): in 1987 a series of micropiles were installed alongside the right sidewall; and in 1989 the supports of the vault were strengthened with pre-stressed steel tie rods, reducing in this way the thrust of the vault. The tie rods can be seen to this day. Details on the reinforcements can be found in Appendix A and [4].

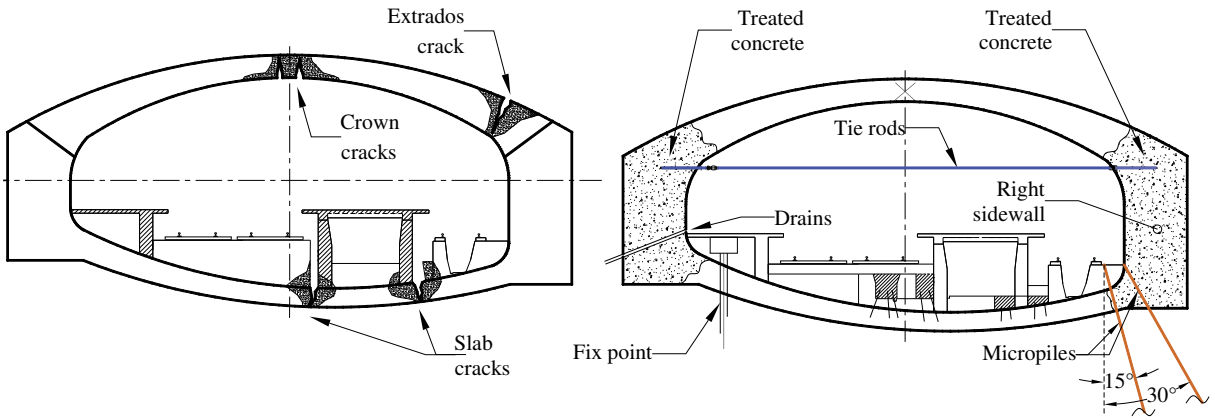


Figure 3: Visible cracks and reinforcement works at the station [4]

3 MODELLING STRATEGY

3.1 General considerations

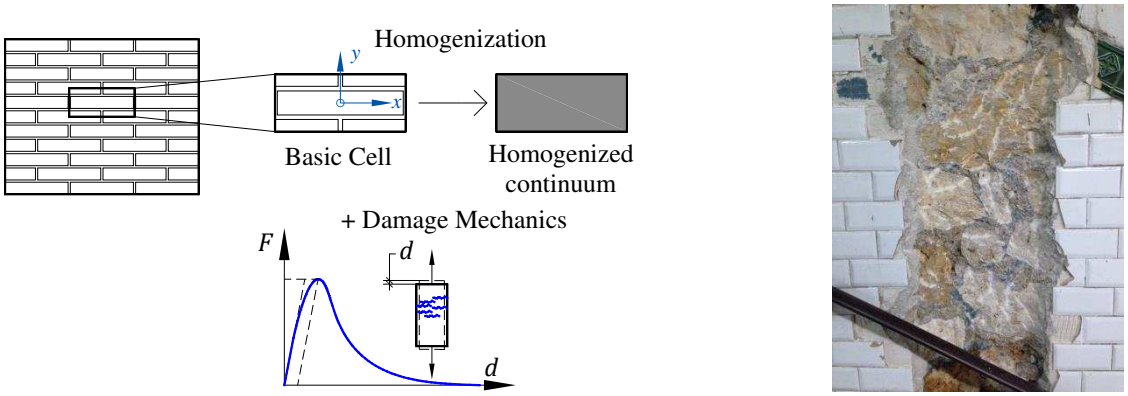
The objective of the study is to reproduce in the most accurate possible way the observed behavior of the tunnel. To this end, a two-dimensional finite element model was built to study the tunnel. Masonry was studied with a specific homogenization-damage model. Soil-structure interaction was modelled through an interface. This model incorporates then several nonlinear material behaviors: tunnel structure, surrounding soil and interface.

In order to study the tunnel problem in 2D we adopted the so-called convergence-confinement method [5][6] to take into account the three-dimensional aspects of the tunneling process in a plane strain analysis. The construction of the tunnel is controlled using a confinement loss parameter λ that ranges from 0 (perfect confinement) to 1 (no confinement). More details are given in §3.4. The groundwater table was modelled implicitly: ground layers below this level were modeled with their effective weight; water pressure was applied to the tunnel assuming that the structure is completely impervious. Stiffness of the initial wood support used to build the tunnel is not taken into account: in the modeling we consider that it no longer exists, and the earth pressure is directly applied to the masonry lining. The calculation was carried out in plane strain and in effective stress.

3.2 Numerical model for the tunnel materials

The model for the masonry incorporates a so-called macro-modelling technique: the masonry is represented by a continuous homogeneous "equivalent" medium. To this end, a homogenization technique is implemented, associated with damage mechanics to represent the non-linearity of the behavior (Figure 4).

In the process of homogenization, it is assumed that the heterogeneous masonry material has a periodic microstructure defined by a "basic cell", whose repetition represents the whole structure. The homogenization procedure is based on the analytical engineering approach proposed by Zucchini & Lourenço [7] for masonry. The geometry of the basic cell (see Appendix A) and the behavior of its components, i.e. blocks and joints, are used to derive the orthotropic constitutive law of the homogenized continuum. The homogenization is carried out within the thickness of the vault.



a) Numerical approach for the masonry b) Typical masonry of the Paris metro tunnels

Figure 4: Homogenization of the masonry.

Coupling homogenization and damage was carried out using the model proposed by Zucchini & Lourenço [8]: a scalar damage variable is associated to each component of the basic cell. The problem is treated in an incremental way: under increasing load, the homogenization technique integrates the damage in each component, and consequently updates the internal stresses and elastic parameters. Here, damage in the components of the masonry is evaluated using a modified version of the isotropic damage model by Mazars [9], with an improved damage criterion and a regularization technique in tension. This damage model was also used for the unreinforced concrete of the sidewalls and ground slab. The variations of the directions of the block-mortar bond in the vault are also considered.

A thorough description of the numerical model can be found in [3]. This coupled model will be referred to as "Damage Model" hereafter. The constitutive law for masonry and concrete was implemented in the finite element code CESAR-LCPC v6 (Solver 6.2.14).

3.3 Material properties

The properties required for the numerical model are presented in Appendix A. Masonry's mortar and *meulière* stone properties led to the following homogenized properties: elastic moduli $E_y = 10\,150$ MPa, $E_x = 14\,620$ MPa, and Poisson's ratio $\nu_{xy} = 0.2$ (see Figure 4a). Concrete elastic properties for the sidewall and the slab are: $E = 8\,500$ MPa and $\nu = 0.21$. Both set of mechanical properties are issued from [2]. The surrounding soil is made up of four layers, modeled with a linear elastic-perfectly plastic model with Mohr-Coulomb criterion. The interface between the tunnel and the soil is modeled with a non-linear behavior; its properties were derived from the soil mechanical properties. Details are presented in Appendix A.

3.4 Initial stress in the masonry vault

In the numerical simulation, the estimation of the initial stress state in the existing tunnel might be a complicated matter. Indeed, the initial stresses in the masonry lining might depend on many factors: stiffness and density of the surrounding ground, stiffness and density of the masonry, ground pressure transmitted to the masonry lining and the construction method; all of these are known only with a certain level of certainty and must be reproduced in the model. Of course, ideally, we would use *in situ* stress measurements in the structure [1]. In most cases though, *in situ* measurements are not available. What we propose here is a trial-error approach in order to produce a reasonable stress state in the vault.

As stated in §3.1, when using the chosen approach, a confinement loss parameter λ must be introduced. Some methods have been proposed in the literature [5][6] to calculate λ for circular tunnels with ground isotropic stress field. Nevertheless, in our study we will introduce a value of λ in such a way that the thrust line position in the structure lies within a distance inferior to $0.3h$ from the mean line (see Figure 5), with h the height of the cross-section. This hypothesis comes from the ultimate limit state verification of unreinforced concrete tunnels [10]. This approach is accurate enough since some similar hypotheses were used when the masonry vaults were conceived [1]. The thrust line here is no other than the eccentricity e of the resultant force:

$$e = M/N \tag{1}$$

where M is the bending moment and N the normal force. The internal forces M and N are calculated in each normal section to the mean line integrating numerically the normal stresses,

assuming elastic behavior for the structure. Taken into account the masonry and soil properties, as well as the construction process (see Table 1), a satisfactory initial thrust in vault is obtained with $\lambda = 0.3$ as illustrated in Figure 5.

It is important to notice that given the construction method, the masonry vault takes direct support on the sidewalls, and these transmit the thrust of the vault to the ground. The soil next to the sidewall is thus compressed and it is found in passive conditions.

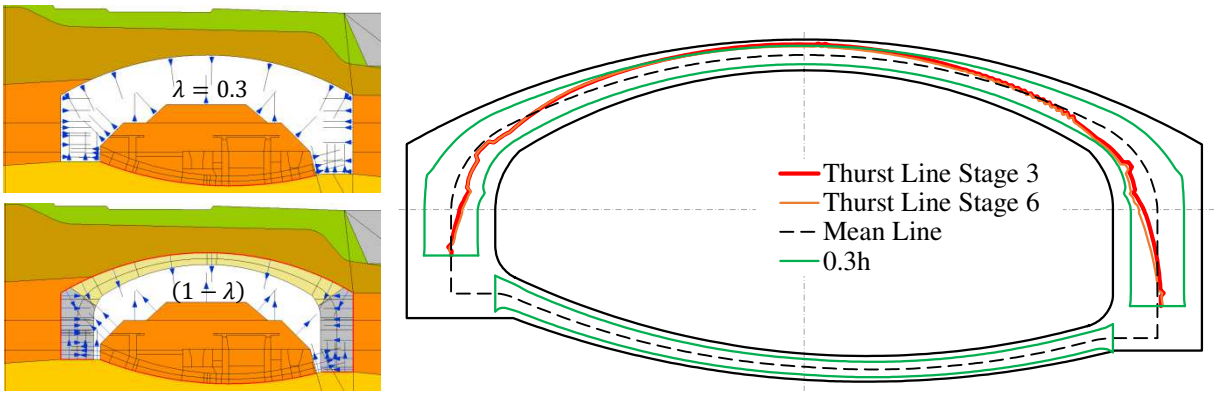


Figure 5: Initial thrust lines in the masonry vault (elastic calculation).

3.5 Modelling stages

We sought to reproduce explicitly the construction method described in §2 as well as the reinforcement works. The model comprises the stages presented in Table 1. The first six stages correspond to the reconstitution of the initial stress in the vault discussed in section 3.4.

Table 1: Modeling stages

Stage	Description	Loads	Comments
1	Initial state: geostatic stress	Soil weight	Groundwater table level is at 26.74
2	Excavation: sidewalls & top section	Forces $\lambda = 0.3$	See §3.4
3	"Construction": vault and sidewalls	Forces $(1 - \lambda)$ & self-weight	See §3.4
4	Excavation: core and bottom	Forces $\lambda = 0.9$	The ground slab was executed at the end, several days later
5	"Construction": Ground slab	Forces $(1 - \lambda)$ & self-weight	-
6	Natural groundwater table level restauration & platform	Water pressure	Groundwater table level is at 28.40. See Figure 2
7	Nearby excavation works	Forces $\lambda = 1$	See Figure 2
8&9	Soil creep: limestone & clay	Creep	See §3.6
10	Setting up: Micropiles	Self-weight	See Figure 3 & Appendix A
11	Soil creep: limestone & clay	Creep	See §3.6
12	Setting up: Tie rods	Pre-stressed force 650 kN @ 2.21m	See Figure 3 & Appendix A
13	Soil creep: limestone & clay	Creep	See §3.6

3.6 Modelling the effects of nearby construction works on the masonry tunnel

As explained in section 2, excavation works carried out near the tunnel together with creep phenomenon on the ground produced high deformations and cracks in the structure. What we

seek in this study is to reproduce what happened in the tunnel and show that the proposed Damage Model may correctly predict the behavior of the existing tunnel. Since the soil next to the sidewall is altered and decompressed due to the construction, it can no longer preserve its initial mechanical properties. A simple approach to simulate the deformation of the soil over time induced by the construction is used: a simplified elastic creep model together with the reduction of the shear strength properties c and $\tan\varphi$ (see Tables 4) of the clay layer under the tunnel and the limestone layer next to the right sidewall. Notice that the objective here is not to give a detailed analysis of the evolution of the soil behavior through time (such a back-analysis would be artificial without proper experimental data). The properties reduction is carried throughout several stages (§3.4). The final properties at stage 13 are given in Tables 4. Properties of the interface (clay and limestone at right sidewall) are also subjected to creep.

4 MASONRY VAULT DEFORMATION AND DAMAGE

The *in situ* convergence measurements were taken with respect to a set of points shown in Figure 6, where the modelling results are plotted in (relative displacements in relation to point 1). Given the set of assumptions taken, it can be observed that the Damage Model manages to reproduce with fair precision the measured deformations of the tunnel (Table 2). The results of simulations with an orthotropic elastic behavior are also presented for comparison. We can clearly see that an elastic calculation completely underestimates the deformations.

Table 2: Comparison of numerical and measured convergences (mm)

Ref.	Measures (mm)	Damage Model (mm)	Elastic Model (mm)
3-5	-54.22	-54.58	-20.01
1-4	19.50	18.04	4.55
2-6	-18.40	-22.48	-8.32
1-2	-4.0	-3.37	-1.69
2-3	5.0	2.31	0.67
3-4	-4.0	-3.56	0.63
2-4	13.0	11.04	4.47

Remark: A positive sign means that the distance between the points increases, and negative signs indicates that it decreases.

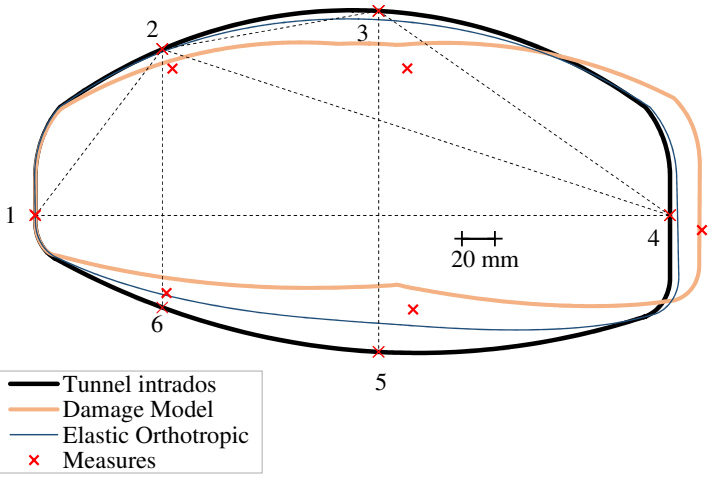


Figure 6: Deformation of the structure

Figure 7 shows the damage state in the tunnel from the numerical model. Damage at the crown of the vault is present from the initial state and evolves to the formation of three damaged zones: mid-span and vault's supports. The spreading of the vault's supports of about 20 mm is close to produce a hinge mechanism and therefore failure. Indeed, we observed that the loss of convergence was close in the numerical model. Hence, a mechanism will eventually form with 6 hinges: three for the vault and three for the slab. Damaged areas observed in the station (Figure 3) are reproduced with good precision by the model in the vault and the slab (Figure 7).

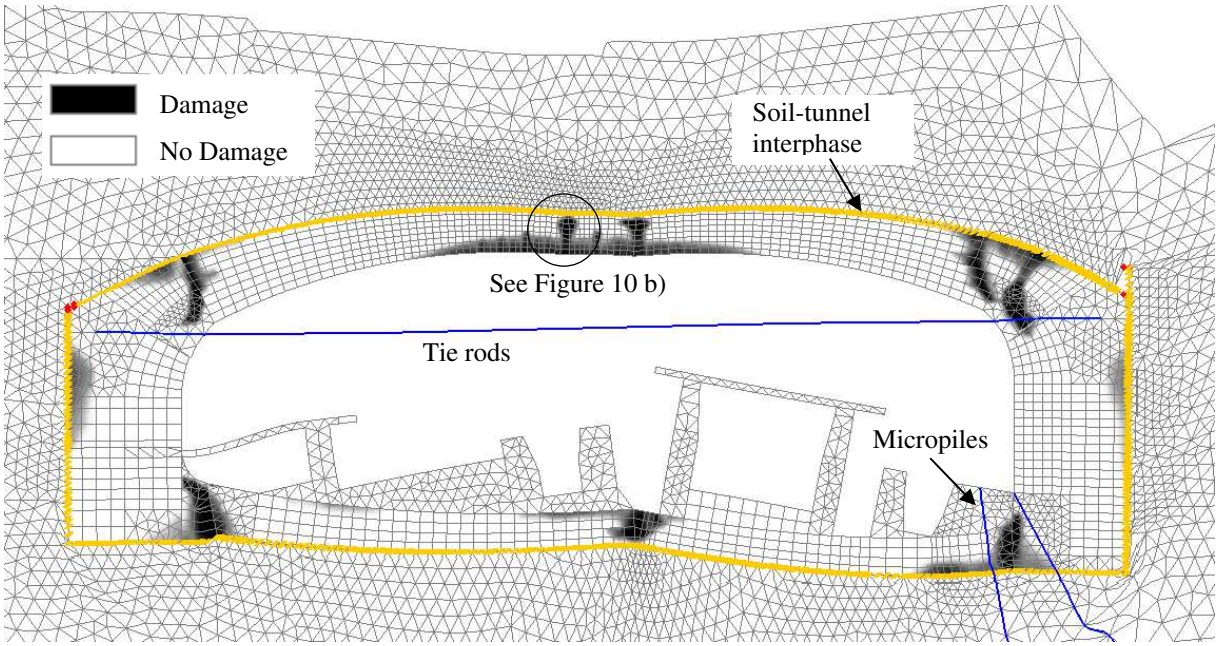


Figure 7: Modelling results: damage in the tunnel structure

5 ANALISYS OF THE PASSIVE EARTH PRESSURE LIMIT STATE

The interaction stresses between soil and structure along the tunnel interface may be of complex nature and difficult to analyze. As a simplification, we consider here that the lateral reaction of the ground necessary to balance the thrust generated by the masonry vault comes only from the contact alongside the sidewalls and that the ground slab plays no role in the structural equilibrium. Since the modification of the equilibrium happens from the right side, we will only study the stress state in the interface at the right sidewall.

We have established that the soil next to the sidewalls is found in passive conditions (§3.4). In order to analyze the passive state of earth pressure and its stability at the right sidewall of the tunnel, as an approximation one may use the approaches commonly used for retaining structures, particularly of those for embedded walls. The limit state of passive earth pressure in a vertical wall may be obtained from Eurocode 7[11] and its French application standard [12]. The passive earth pressure that can be mobilized $p_{\mathrm{b,k}}$ is

$$p_{\mathrm{b,k}}(z) = K_{\mathrm{p}}\sigma'_{\mathrm{v}}(z) + 2c\sqrt{K_{\mathrm{p}}} \quad \text{with} \quad K_{\mathrm{p}} = \tan^2\left(\frac{\pi}{4} + \frac{\varphi}{2}\right) \tag{2}$$

where c is the limestone cohesion (§3.3), σ'_{v} the effective vertical stress in the ground (obtained from the FEM) and K_{p} the coefficient of horizontal passive earth pressure (see Appendix A). The values of c and $\tan\varphi$ of are reduced progressively (§3.6) throughout the subsequent simulation stages. Finally, the force that can be mobilized in the ground $B_{\mathrm{m,k}}$ is obtained by numerical integration of $p_{\mathrm{b,k}}$, calculated only alongside the right sidewall:

$$B_{\mathrm{m,k}} = \int_{\mathrm{bottom}}^{\mathrm{top}} p_{\mathrm{b,k}}(z)\, dz \tag{3}$$

Similarly, the resultant thrust generated by the vault $P_{t,k}$ is obtained from integrating numerically the normal and shear stresses of the interface (§3.1) alongside the sidewall:

$$P_{t,k} = \sqrt{P_x^2 + P_y^2} \quad \text{with} \quad P_x = \int_{\text{bottom}}^{\text{top}} \sigma_n(z)\, dz \quad \text{and} \quad P_y = \int_{\text{bottom}}^{\text{top}} \tau(z)\, dz \tag{4}$$

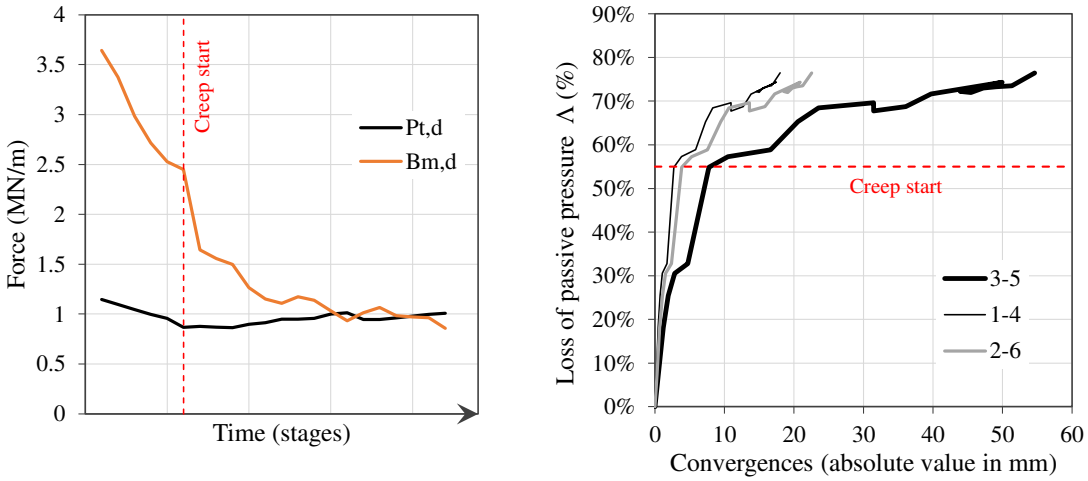
Taken into consideration the limit state in the compressed soil suggested by the standard [12], equilibrium is found if

$$B_{m,d} > P_{t,d} \quad \text{with} \quad B_{m,d} = \frac{B_{m,k}}{1.4} \text{ and } P_{t,d} = 1.35\, P_{t,k} \tag{5}$$

We introduce now Λ as the loss of the passive earth pressure that can be mobilized. This quantity is defined as the reduction of $B_{m,d}$ with respect to a reference initial value $B_{m,d}^{ini}$. In our case, we consider the initial resistance $B_{m,d}^{ini}$ to be the value of $B_{m,d}$ from stage 6 (§3.4), before the excavation carried out in 1983, since we consider this stage as the initial equilibrium state. We have

$$\Lambda = 1 - \frac{B_{m,d}^{ini}}{B_{m,d}} \tag{6}$$

Analyzing now the results from the numerical model, we find that the thrust $P_{t,d}$ generated by the vault remains almost constant at 1 MN/m regardless of the creep, as can be seen in Figure 8a). Although the equilibrium condition (5) is nearly satisfied all of the time, Figure 8b) shows that beyond a certain threshold, convergences in the tunnel reach values larger than 10 mm. This means that even if equilibrium is potentially possible, i.e. no ultimate limit state reached in the tunnel structure, the loss of the resistance of the ground has important structural consequences in the tunnel (cracks, water infiltrations, important deformations), and the serviceability limit state may no longer be satisfied. In this study, a critical threshold is shown when a loss of about $\Lambda = 55\%$ of the passive earth pressure that can be mobilized happens; this also coincides with the start of the elastic creep in the soil (red dotted lines in Figure 8).



a) Evolution of vault thrust b) Tunnel deformation

Figure 8: Loss of the passive earth pressure that can be mobilized

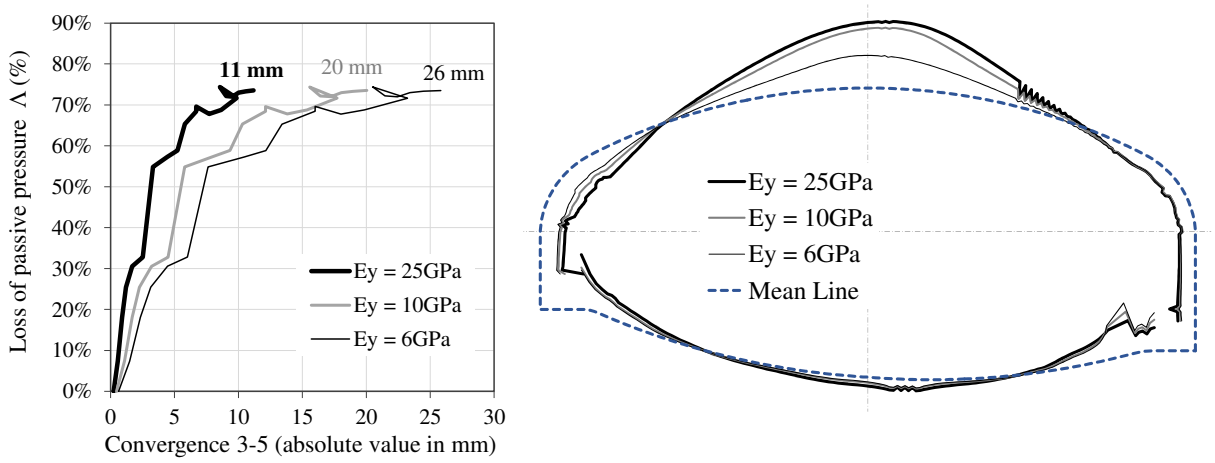
6 MODELLING CHOICES FOR THE MASONRY LINING: CONSTITUTIVE LAW

When external works are carried out nearby an existing tunnel that might affect it, most of the time displacements thresholds are imposed, in order to oversee the impact of the works on the existing structure and guarantee their safety. We will see in this section that the choice of the constitutive law for the materials comprising the tunnel's structure is of capital importance when proposing these thresholds, or simply when evaluating the impacts.

6.1 Elastic domain

When it comes to modeling an old masonry tunnel, in engineering practice, it is common to model it as a linear elastic isotropic material, usually with a very low elastic modulus: a typical value is about 6 GPa [1]. This is done most likely for safety reasons: a low material stiffness can produce large displacements in the model. Nevertheless, this is inaccurate most of the time. Indeed, Figure 9 a) shows that, even with a low elastic modulus, the deformations of the tunnel remain far below the measured values (54 mm for convergence 3-5, see Table 2).

If for some reason the analysis must be carried out in the framework of elasticity for the structure, a low elastic modulus for the lining could be the most unfavorable case, when the safety criterion is measured in displacements only. However, if the objective is to verify the ultimate limit state in terms of internal forces in the structure, the most unfavorable case corresponds to a high elastic modulus of around 20-30 GPa. As it can be seen in Figure 9, a higher elastic modulus will produce higher internal forces in the structure, but lower deformations.



a) Tunnel deformation b) Internal forces: eccentricity of the resultant force (scaled)

Figure 9: Modelling results for different elastic moduli of the tunnel materials (elastic calculation)

6.2 Nonlinear domain

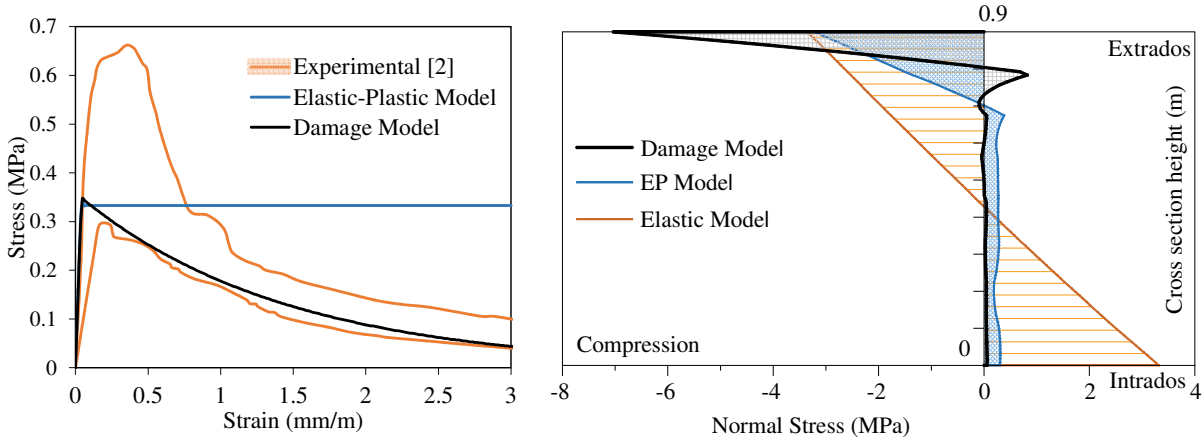
Another commonly used strategy in practice is to model the tunnel materials as a linear elastic-perfectly plastic material, using for instance the Mohr-Coulomb criterion, widely available in civil engineering software. This at least has the advantage to take into account a nonlinear behavior, even if it is not that of the quasi-brittle materials (masonry or unreinforced concrete). The central difference might be seen in the stress-strain evolutions, which are not the same. As it can be seen in Figure 10 a), the damage model is closer to the behavior found

experimentally [2] than the elastic-plastic model. We also observe in Figure 10 b) the diminution of the tensile stress at the crown crack (see Figure 7) and the concentration of the compressive stress at the top, that are not seen in the other models.

Another difficulty raised by this constitutive law is the choice of the mechanical parameters c (cohesion) and φ (friction angle) of the Mohr-Coulomb criterion. Some methods have been proposed [13] to obtain these parameters for concrete structures. In this study, the values of c and φ are proposed in such a way as to respect the Mohr-Coulomb criterion:

$$\frac{\sigma_c}{\sigma_t} = \frac{1+\sin\varphi}{1-\sin\varphi} \quad \text{and} \quad \sigma_t = \frac{2c\cos\varphi}{1+\sin\varphi}, \qquad \sigma_c = -\frac{2c\cos\varphi}{1-\sin\varphi} \tag{7}$$

where σ_t and σ_c are the tensile and compressive elastic limits of the material, respectively. With this approach, we obtain the values shown in Tables 4. It is worth noting that the values obtained for c and φ do not have much physical significance.



a) Uniaxial tensile test for concrete (see Tables 4) b) Normal stress at the crown crack (see Figure 7)

Figure 10: Stress relations for different constitutive laws for the masonry

Modeling results are shown in Table 3 and Figure 11. We can see that the elastic-plastic model produces a better approximation than the elastic model; however, the convergences are lower than those obtained with the damage model, which are closer to the in-situ measures.

Table 3: Comparison of numerical and measured convergences (mm)

Ref.	Measures (mm)	Damage Model (mm)	E-P Model (mm)
3-5	-54.22	-54.58	-40.56
1-4	19.50	18.04	12.72
2-6	-18.40	-22.48	-16.96

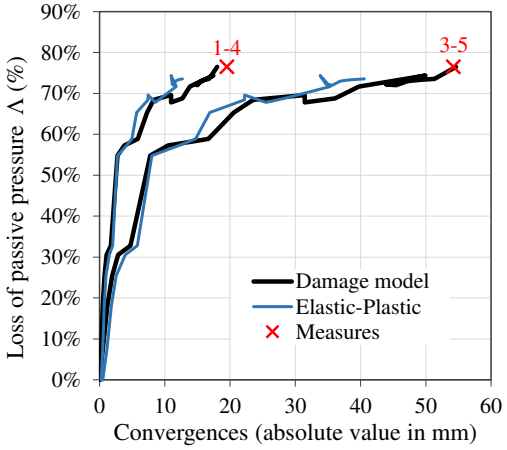


Figure 11: Evolution of the deformation of the structure

7 CONCLUSIONS

We carried out a study on a masonry tunnel of the Paris metro, whose equilibrium state was altered by nearby construction works. A specific damage model for the masonry and concrete was used in the numerical simulations. Given the set of assumptions taken in this study and after analysis of the results, we can conclude the following:

- The proposed model for the tunnel structure reproduces accurately the deformations and cracks in the structure (vertical convergence of about 54 mm);
- The model shows the formation of a hinge mechanism in the tunnel when the spread of the vault's supports is close to a critical value (about 20 mm): three hinges appear in the masonry vault and three in the ground slab.
- From a simplified analytical analysis, we can see that significant deformations and cracks appear in the tunnel when the resistance from the ground available to balance the vault's thrust is reduced by about 50%;
- In all cases, when evaluating numerically the tunnel deformations, a non-linear constitutive law must be used for the tunnel structure; it is clear that an elastic analysis, even with a low elastic modulus, will underestimate the tunnel deformation.
- An elastic-plastic model for the masonry can give better results, but still underestimates the deformations. Also, the constitutive law is not that of the masonry or concrete. The Damage Model is shown to give the best results.
- When performing an elastic analysis, we can see that the most unfavorable case for the displacements is not necessarily the most unfavorable for the internal forces.

Finally, it is worth noting that the setup of a numerical model involving several nonlinear behaviors (masonry, soil and interface) without numerical instabilities remains a very time-consuming task: further improvements of the numerical tools are highly desirable.

REFERENCES

[1] Moreno Regan, O. *Study of the behavior of the masonry tunnels of the Paris subway system* (in French): PhD Thesis, Univ Paris Est, (2016).

[2] Moreno Regan, O., Colas, A., Bourgeois, E., Chatellier, P., Desbordes, A., & Douroux, J. Experimental characterization of the constitutive materials composing an old masonry vaulted tunnel of the Paris subway system. *International Journal of Architectural Heritage* Vol. **12**(2) (2018), 195-215.

[3] Moreno Regan, O., Bourgeois, E., Colas, A., Chatellier, P., Desbordes, A., & Douroux, J. Application of a coupled homogenization-damage model to masonry tunnel vaults. *Computers and Geotechnics* Vol. **83** (2017), pp. 132-141.

[4] Le Bras A. Désordres dans un ouvrage voute de grande ouverture. Démarche suvie pour l'établissement du diagnostic techniques utilisées pour le renforcement. *Tunnels et Ouvrages Souterrains*, no. 113, pp. 229-303, Septembre/Octobre (1992).

[5] AFTES. The convergence-confinement method (GT7R6A1). *Tunnels et Ouvrages Souterrains*, no. 174, pp. 414-424 (2002).

[6] Panet, M. *Le calcul des tunnels par la méthode convergence-confinement*. Presses de l'école nationale des Ponts et chaussées (1995).

[7] Zucchini, A. and Lourenço, P.B. A micro-mechanical model for the homogenisation of masonry," *International Journal of Solids and Structures*, vol. **39**, pp. 3233-3255 (2002).

[8] Zucchini, A. & Lourenço, P.B., A coupled homogenisation-damage model for masonry cracking. *Computers and Structures*, Vol. **82** (11-12), pp.917-29, (2004).
[9] Mazars, J. A description of micro- and macroscale damage of concrete structures. *Engineering Fracture Mechanics*, vol. 25, pp. 729-737 (1986).
[10] AFTES. The use of plain concrete in tunnels (GT7R5A1). *Tunnels et Ouvrages Souterrains*, no. 158 (2000).
[11] NF EN 1997-1. Eurocode 7: Geotechnical design Part 1: General rules (2005).
[12] NF P94-282. Calcul géotechnique Ouvrages de soutènement Écrans (2009).
[13] Hadzijanev Ardiaca, D. Mohr-Coulomb parameters for modelling of concrete structures. *Plaxis Bulletin*. Spring issue 2009

APPENDIX A

In the tables presented in this appendix, the following notations are used:

- ρ Density
- γ Soil density
- γ' Effective soil density
- E Young's modulus
- ν Poisson's ratio
- f_t Tensile strength
- G_{ft} Mode I fracture energy
- f_c Compression strength
- A_c Damage model coefficient for compression
- B_c Damage model coefficient for compression
- ε_{D0} Damage threshold strain
- c Cohesion
- φ Friction angle
- ψ Dilatancy angle

Tables 4: Material properties

Soil Layers

	Backfill	Loamy scree	Limestone	Clay	Marls	Chalk
γ (kN/m³)	18	20	21	20	21	21
γ' (kN/m³)	8	10	11	10	11	11
E' (MPa)	20	250	650	38	43	280
ν	0.333	0.333	0.333	0.333	0.333	0.333
c' (kPa)	15	55	35	20	15	40
φ' (°)	30	39	32	16	32	35
ψ (°)	0	9	2	0	2	5
K_p			3.2546			

Tunnel Materials [2]

	Mortar(1)	*Meulière* stone(1)	Concrete	
ρ (kN/m³)	20.08	20.58	21.60	
E (MPa)	6 000	36 000	8 500	Elastic parameters
ν	0.15	0.30	0.21	
f_t (MPa)	0.300	3.440	0.350	Strength parameters
f_c (MPa)	20.0	25.0	16.0	
G_{ft} (Pa.m)	150	121	250	Damage parameters, see [3] and [9]
A_c	1.1	1.1	1.8	
B_c	585	1500	1174	
ε_{D0}	$5\text{x}10^{-5}$	$9.56\text{x}10^{-5}$	$4.12\text{x}10^{-5}$	

(1)The considered size for the components of the masonry for this study is: mortar joints of 70 mm thickness and meulière stone of 75 mm and 350 mm of height and width, respectively.

Interface (3)

	Loamy scree	Limestone	Clay
δ/φ_{soil}	2/3	2/3	1/3
E_i (MPa)	12 500	32 500	1 900
c_i (kPa)	33.13	21.88	6.50
δ (°)	26.0	21.33	5.33

$$E_i = 50E_{\text{Soil}}$$

$$c_i = \frac{c_{\text{soil}} \tan(\delta)}{\tan(\varphi_{\text{soil}})}$$

Material properties for the Elstic-Plastic model

	c (kPa)	φ (°)	E (MPa)
Masonry	1 466	77.85	12 400
Concrete	1 183	73.174	8 500

Final properties of the soil layers subjected to creep

Soil layer	c (kPa)	φ (°)	E' (MPa)	ν
Limestone	8.5	8.6	20	0.01
Clay	15	12.1	20.5	0.18

(3) Properties of the interface (clay and limestone right sidewall) are also subjected to creep.

Tie-rods(2)	
Ø (mm)	36
E (MPa)	210 000
Spacing	2.21 m
Pre-setress	650 kN

Micropiles(2)	
$Ø_{int}$	127
$Ø_{ext}$	109
E (MPa)	205 000
Spacing	1.0 m

(2) Modelled as elastic bar finite elements (normal effort only)

12th International Conference on Structural Analysis of Historical Constructions
SAHC 2020
P. Roca, L. Pelà and C. Molins (Eds.)

THE SAFETY OF MASONRY ARCHES SUBJECT TO VERTICAL AND HORIZONTAL FORCES. A NUMERICAL METHOD BASED ON THE THRUST LINE CLOSEST TO THE GEOMETRICAL AXIS

S. GALASSI[1*], G. TEMPESTA[2]

[1*]Department of Architecture (DIDA)
University of Florence
Piazza Brunelleschi 6, 50121 Florence, Italy
e-mail: stefano.galassi@unifi.it (*corresponding author)

[2] Department of Architecture (DIDA)
University of Florence
Piazza Brunelleschi 6, 50121 Florence, Italy
email: giacomo.tempesta@unifi.it

Keywords: Masonry Arches, Safety, Seismic Vulnerability, Thrust Line Analysis, Geometrical Factor, Full-Range Factor

Abstract. *In this paper the topic of the safety assessment of masonry arches based upon their geometry is investigated. The theoretical background is the Heymanian master safe theorem along with the no-tension assumption of masonry. The continuous arch is analyzed considering a discrete pattern of vertical loads, such as those of the self-weight and superimposed loads. Among all the lines of thrust contained within the profile of the arch, the one closest to the geometrical axis can be considered to be the best one thanks to the minimum bending moment and shear force present in each cross section. A numerical procedure for computing the line of thrust closest to the geometrical axis of an arch subject to its self-weight has been recently formulated by the authors. This procedure accounts for this line of thrust by minimizing the distances between the geometrical axis of the arch and the thrust line. In order to consider the action of both vertical loads and horizontal forces proportional to the vertical ones, such as those provoked by an earthquake, an extension of this procedure is herein presented. The safety of the arch is finally assessed by computing a domain of equilibrium thrust lines within the profile of the arch which provides, in analogy with the Heymanian geometrical factor of safety, the full range factor of safety. The procedure is described in the paper and illustrated with regards to the analysis of arches subject only to vertical loads and arches subject to also horizontal forces.*

1 INTRODUCTION

In the literature, the mechanical behaviour of masonry arches is investigated using different approaches. With the purpose of computing the actual stress state in an arch, some authors have proposed methodologies that are strictly connected to the need of assessing the properties of masonry and estimating its actual "deformation capacity" [1]. Conversely, other authors, to assess the safety level of an arch or, vice-versa, the vulnerability level, have

formulated methodologies based on the limit analysis principles.

In the context of limit analysis, two approaches can be used: the thrust line method [2-6], based on the static theorem, and the mechanism method [7-12], based on the kinematic theorem. Leaving aside the mechanism method, which requires all the kinematically compatible mechanisms to be defined and which is, therefore, a very computationally expensive method, the thrust line method assesses the safety searching for the existence, within the profile of the arch, of any line of thrust in equilibrium with the loads acting on it, according to the famous assumptions formulated by Heyman [13]: no tensile strength, infinite compressive strength, sliding failure cannot occur due to the presence of friction. Under these assumptions, the material can be considered non-deformable and the arch can be modelled as an assemblage of rigid blocks.

Recently the authors of this paper have formulated a method for the analysis of masonry arches based on the detection of the line of thrust closest to the geometrical axis [14,15], checking at a later stage that it is also within the profile. Among the ∞^3 likely lines of thrust which depict the equilibrium condition between loads and abutment reactions, this is the best one because it corresponds to an internal stress state of almost only compression. Unlike other methods present in the literature, such as that proposed by Heyman in [13], which computes the line of thrust closest to the geometrical axis of an arch exploiting an iterative method that proceeds by trial and errors, and those capable of computing the thrust network or the thrust surface closest to the mid-surface of a 3D-vault [16-20], the method presented herein is a one-step procedure that provides the exact solution in "closed-form", thus reducing the computational time.

In this paper the above mentioned procedure is reformulated and extended in order to account also for a set of horizontal forces, proportional to the vertical ones, capable of simulating the action of an earthquake. Such horizontal forces are computed, in an innovative way, with a reverse method, exploiting the analogy between an inclined plane, on which the structure is "virtually" placed, and the inclination of the resultant actions of the vertical and horizontal loads, thus avoiding the need of inputting them directly in the mechanical model of the structure. The safety of the arch is assessed extending the Full-Range Factor Method (FRS Method) formulated by the authors in [14,15] for the vertical load case to the combination of this load case with the set of horizontal forces, and it is exploited to also compute the seismic factor.

2 LINE OF THRUST CLOSEST TO THE GEOMETRICAL AXIS

Let us consider a continuous arch, subject to a discrete pattern of 'n' vertical loads F_1, F_2,…, F_n. Let us subdivide the arch into 'n' elements (Fig. 1a), in such a way as to apply each load F_i ($1 \le i \le n$) to the centroid G_i of each element. In so doing, in case of a rigid block structure, the elements correspond to the rigid blocks and the lines of separation between the elements correspond to the actual joints.

For the assigned load condition, a family of ∞^3 funicular polygons can be drawn, each one describing a specific condition of equilibrium between loads and abutment reactions. Furthermore, since these funicular polygons must describe the flow of internal forces between the elements of the arch, they are, de facto, the polygons of successive resultants and, therefore, are referred to as lines of thrust as well.

In order to draw a specific line of thrust, three parameters or conditions must be fixed. In the present approach, the parameters that have been fixed are the ordinate of points A and B, through which the first and the last side of the line of thrust must pass respectively, and the value H of the thrust, which is everywhere constant throughout the arch due to the solely presence of vertical loads.

Referring to the generic node 'i' of the line of thrust (Fig. 1b), the equilibrium condition of the vertical forces is provided by Eq. 1:

$$(\tan\alpha - \tan\beta) = \frac{F_i}{H} \tag{1}$$

where α and β are the angles of inclination of the two sides of the line of thrust connected to the node 'i'.

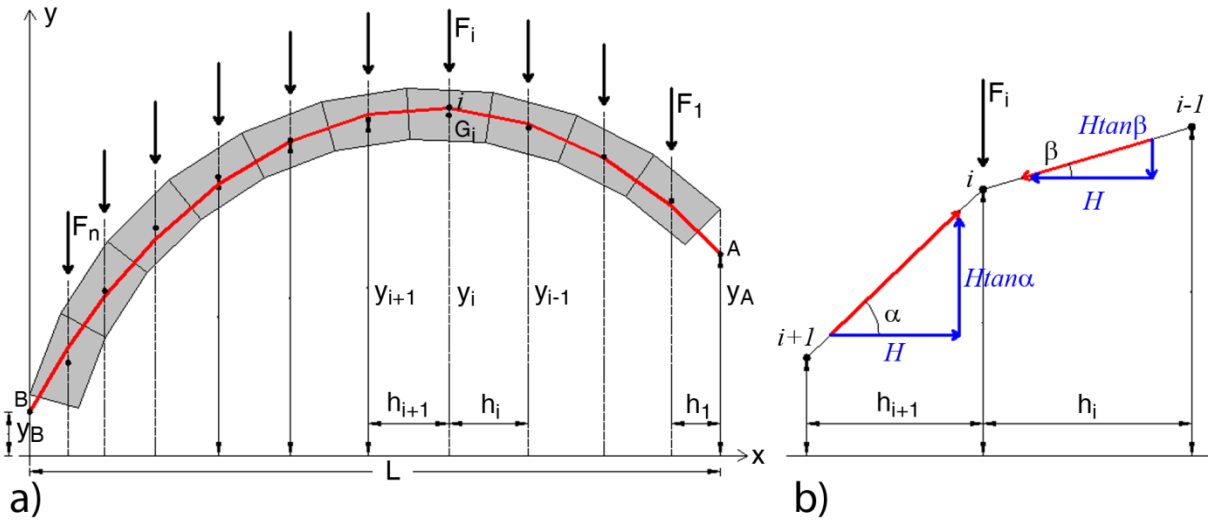


Figure 1: a) Reference discrete arch model; b) detail of the generic node 'i' of the line of thrust

It is worth noting that the equilibrium condition of the horizontal forces is meaningless because, as aforementioned, the thrust H is constant.

The tangents of angles α and β can be expressed, in geometrical form, by Eq. 2:

$$\begin{aligned} \tan\alpha &= \frac{Y_i - Y_{i-1}}{h_i} \\ \tan\beta &= \frac{Y_{i+1} - Y_i}{h_{i+1}} \end{aligned} \tag{2}$$

As a consequence, putting $h_i = x_i - x_{i-1}$ the variable horizontal distance between the centroids of two generic subsequent elements 'i-1' and 'i', that is between the directions of the load vectors F_{i-1} and F_i acting on such elements, Eq. 1 can be replaced by Eq. 3:

$$\left(\frac{-1}{h_i}\right) \cdot Y_{i-1} + \left(\frac{h_i + h_{i+1}}{h_i \cdot h_{i+1}}\right) \cdot Y_i + \left(\frac{-1}{h_{i+1}}\right) \cdot Y_{i+1} = \frac{F_i}{H} \tag{3}$$

Extending Eq. 3 to all nodes of the thrust line, the following system of linear equations is obtained:

$$\begin{cases} \left(\frac{-1}{h_1}\right)\cdot Y_0 + \left(\frac{h_1+h_2}{h_1\cdot h_2}\right)\cdot Y_1 + \left(\frac{-1}{h_2}\right)\cdot Y_2 = \frac{F_1}{H} \\ \left(\frac{-1}{h_2}\right)\cdot Y_1 + \left(\frac{h_2+h_3}{h_2\cdot h_3}\right)\cdot Y_2 + \left(\frac{-1}{h_3}\right)\cdot Y_3 = \frac{F_2}{H} \\ \dots\dots\dots\dots\dots\dots\dots\dots\dots\dots\dots\dots\dots\dots\dots\dots\dots\dots\dots\dots \\ \left(\frac{-1}{h_i}\right)\cdot Y_{i-1} + \left(\frac{h_i+h_{i+1}}{h_i\cdot h_{i+1}}\right)\cdot Y_i + \left(\frac{-1}{h_{i+1}}\right)\cdot Y_{i+1} = \frac{F_i}{H} \\ \dots\dots\dots\dots\dots\dots\dots\dots\dots\dots\dots\dots\dots\dots\dots\dots\dots\dots\dots\dots \\ \left(\frac{-1}{h_n}\right)\cdot Y_{n-1} + \left(\frac{h_n+h_{n+1}}{h_n\cdot h_{n+1}}\right)\cdot Y_n + \left(\frac{-1}{h_{n+1}}\right)\cdot Y_{n+1} = \frac{F_n}{H} \end{cases} \tag{4}$$

where the ordinates Y_i of the nodes 'i' of the line of thrust and the thrust H are the unknowns to be computed.

System of Eq. 4 shows the indeterminacy of the problem of equilibrium of the arch, which is indeed a statically indetermined structure to third degree: there are three more unknowns than the number of equations.

System of Eq. 4 is then rewritten, in matrix form, in such a way as to isolate the three redundant unknowns from the general system, i.e. the thrust H and the ordinates Y_0 and Y_{i+1} of points A and B respectively, and to define three vectors:

- vector T_1, whose entries are the values of loads F_i, which is then multiplied by the constant $K=H^{-1}$;
- vector T_2, whose only non-null entry is the coefficient $1/h_1$ of the unknown Y_0;
- vector T_3, whose only non-null entry is the coefficient $1/h_{n+1}$ of the unknown Y_{n+1}.

Finally, defining D as the matrix of the coefficients of the unknowns, Eq. 4 becomes:

$$[D]\{Y\} = \{T_1\}\cdot K + \{T_2\}\cdot Y_0 + \{T_3\}\cdot Y_{n+1} \tag{5}$$

where:

$$D = \begin{bmatrix} \left(\frac{h_1+h_2}{h_1\cdot h_2}\right) & \left(\frac{-1}{h_2}\right) & 0 & 0 \\ \left(\frac{-1}{h_2}\right) & \left(\frac{h_2+h_3}{h_2\cdot h_3}\right) & \left(\frac{-1}{h_3}\right) & 0 \\ \dots & \dots & \dots & \dots \\ 0 & \left(\frac{-1}{h_i}\right) & \left(\frac{h_i+h_{i+1}}{h_i\cdot h_{i+1}}\right) & \left(\frac{-1}{h_{i+1}}\right) \\ \dots & \dots & \dots & \dots \\ 0 & 0 & \left(\frac{-1}{h_n}\right) & \left(\frac{h_n+h_{n+1}}{h_n\cdot h_{n+1}}\right) \end{bmatrix}, \qquad Y = \begin{Bmatrix} Y_1 \\ Y_2 \\ \dots \\ Y_i \\ \dots \\ Y_n \end{Bmatrix},$$

$$T_1 = \begin{Bmatrix} F_1 \\ F_2 \\ \dots \\ F_i \\ \dots \\ F_n \end{Bmatrix}, \qquad T_2 = \begin{Bmatrix} 1/h_1 \\ 0 \\ \dots \\ 0 \\ \dots \\ 0 \end{Bmatrix}, \qquad T_3 = \begin{Bmatrix} 0 \\ 0 \\ \dots \\ 0 \\ \dots \\ 1/h_{n+1} \end{Bmatrix} \tag{6}$$

Putting $\{R_1\} = [D]^{-1}\{T_1\}$, $\{R_2\} = [D]^{-1}\{T_2\}$, $\{R_3\} = [D]^{-1}\{T_3\}$, the solution of Eq. 5 provides the ordinates of the line of thrust, collected in the entries of vector Y:

$$\{Y\} = \{R_1\}\cdot K + \{R_2\}\cdot Y_0 + \{R_3\}\cdot Y_{n+1} \tag{7}$$

Eq. 7 provides the ordinates of the nodes of all ∞^3 funicular polygons associated to the load condition expressed by vector T_1, depending on the three redundant unknowns mentioned above. Therefore, in order to compute the ordinates of the nodes of the line of thrust closest to the geometrical axis, the three redundant unknowns shall be firstly calculated in such a way as

to respect the above requirement of "closeness". To calculate them, a procedure that minimizes the distances between the nodes of the researched thrust line and the centroids of the elements, is formulated.

In order to make the negative signs of this difference irrelevant in the minimization procedure, the proposed method computes the function S that expresses the square of the sum of the distances ΔY_i between the ordinates Y_i of the nodes 'i' and the ordinates Y_{Gi} of the centroid G_i of the elements, as follows:

$$S = \sum_{i=1}^{n}(\Delta Y_i)^2 = \sum_{i=1}^{n}(Y_i - Y_{Gi})^2 = (\{R_1\} \cdot K + \{R_2\} \cdot Y_0 + \{R_3\} \cdot Y_{n+1} - \{Y_G\})^2 \quad (8)$$

Function S is minimized by expressing the partial derivatives of it, with respect to the three unknowns, equal to zero:

$$\begin{aligned} &\frac{\partial S}{\partial K}(Y_0, Y_{n+1}, K) = 0 \\ &\frac{\partial S}{\partial Y_0}(Y_0, Y_{n+1}, K) = 0 \\ &\frac{\partial S}{\partial Y_{n+1}}(Y_0, Y_{n+1}, K) = 0 \end{aligned} \quad (9)$$

Inputting Eq. 8 into Eq. 9 and solving the partial derivatives, leads to the system of three linear equations that follows:

$$\begin{cases} \{R_1\}^2 \cdot K + \{R_1\}\{R_2\} \cdot Y_0 + \{R_1\}\{R_3\} \cdot Y_{n+1} - \{R_1\}\{Y_G\} = \{0\} \\ \{R_2\}^2 \cdot Y_0 + \{R_1\}\{R_2\} \cdot K + \{R_2\}\{R_3\} \cdot Y_{n+1} - \{R_2\}\{Y_G\} = \{0\} \\ \{R_3\}^2 \cdot Y_{n+1} + \{R_1\}\{R_3\} \cdot K + \{R_2\}\{R_3\} \cdot Y_0 - \{R_3\}\{Y_G\} = \{0\} \end{cases} \quad (10)$$

which can be rewritten in matrix form as:

$$\begin{bmatrix} \{R_1\}^2 & \{R_1\}\{R_2\} & \{R_1\}\{R_3\} \\ \{R_1\}\{R_2\} & \{R_2\}^2 & \{R_2\}\{R_3\} \\ \{R_1\}\{R_3\} & \{R_2\}\{R_3\} & \{R_3\}^2 \end{bmatrix} \cdot \begin{Bmatrix} K \\ Y_0 \\ Y_{n+1} \end{Bmatrix} = \begin{Bmatrix} \{R_1\}\{Y_G\} \\ \{R_2\}\{Y_G\} \\ \{R_3\}\{Y_G\} \end{Bmatrix} \quad (11)$$

or, more compactly as:

$$[N]\{P\} = \{W\} \quad (12)$$

The solution of Eq. 12 provides the value of the three redundant unknowns, stored in vector P:

$$\{P\} = [N]^{-1}\{W\} \quad (13)$$

At this stage, entries of vector Y are reversely computed inputting the values of the three unknowns provided by Eq. 13 into Eq. 7.

Finally, to plot the line of thrust closest to the geometrical axis the abscissa of point A, the abscissas of the centroids G_i of the elements and the abscissa of point B are collected, in sequence, in vector X and the size of vector Y is expanded by concatenating the ordinate Y_0 of point A, inputted in the first entry, the entries stored in the original vector, and, finally, the ordinate Y_{n+1} of point B, inputted in the last entry (Eq. 14):

$$X = \left\{ \begin{matrix} X_0 \\ X_1 \\ \dots \\ X_i \\ \dots \\ X_{n+1} \end{matrix} \right\}, \qquad Y = \left\{ \begin{matrix} Y_0 \\ Y_1 \\ \dots \\ Y_i \\ \dots \\ Y_{n+1} \end{matrix} \right\}, \tag{14}$$

The line of thrust is graphically obtained plotting the poly-line of vertices (X_i,Y_i).

3 EXTENSION TO THE HORIZONTAL LOAD CASE

In the approach of both linear and nonlinear static analysis, the effect of an earthquake can be represented through a pattern of horizontal forces proportional to the vertical ones. The procedure that computes the line of thrust closest to the geometrical axis of an arch under vertical loads is herein extended in order to also consider such horizontal forces.

The procedure takes into account the effect of the horizontal forces by exploiting the analogy between an inclined plane, on which the structure is "virtually" placed, and the inclination of the resultant actions of the vertical and horizontal loads, thus avoiding the horizontal forces to be inputted directly into the mechanical model. According to this analogy, the effect of an horizontal load acting together with a vertical one can be accounted for by rotating the structure at the same angle as that which corresponds to the action line of the resultant.

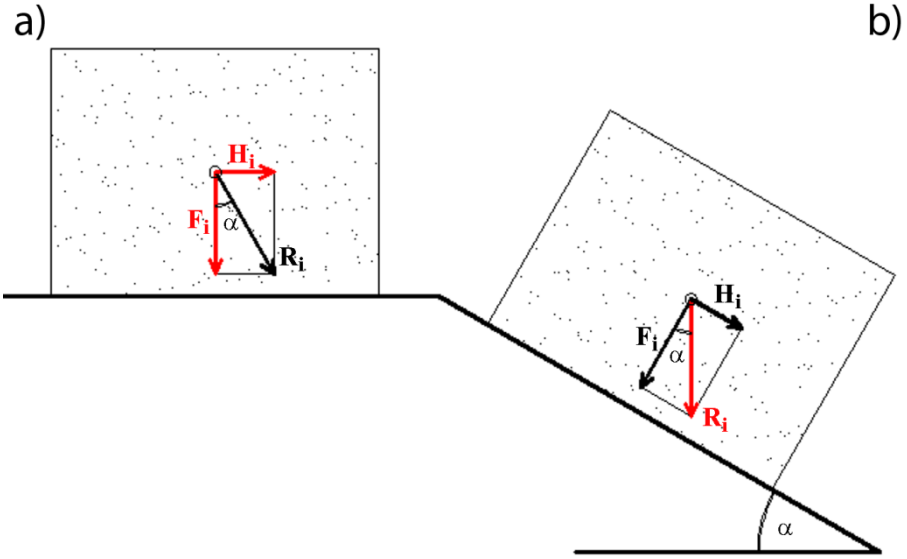


Figure 2: Analogy between inclined plane and seismic effect

Put simply, let us refer to Fig. 2, which shows the generic element 'i' of the mechanical model. Fig. 2a shows the actual position of the element, while Fig. 2b shows the same element placed on an inclined plane rotated at angle α.

In the actual position (Fig. 2a), the element is subject to the joined action of the vertical force F_i and the horizontal action H_i provoked by the earthquake, the horizontal force proportional to the vertical one being computed as:

$$H_i = \lambda F_i \tag{15}$$

where λ is the seismic factor, depending on the seismic zone or the seismicity of the territory.

According to the aforementioned analogy, the joined action of the vertical and horizontal forces can be taken into account by replacing them with a "virtual" vertical force R_i whose length corresponds to the resultant of the forces F_i and H_i (Fig. 2b):

$$R_i = \frac{F_i}{\cos(\alpha)} \tag{16}$$

With this approach, the seismic factor λ corresponds to the tangent of the angle at which the element is rotated:

$$\lambda = \frac{H_i}{F_i} = \tan(\alpha) \tag{17}$$

Therefore, the seismic response of the structure for an assigned seismic factor λ is assessed by rotating the structure at the angle provided by reversing Eq. (17), that is:

$$\alpha = \arctan(\lambda) \tag{18}$$

For clarity, the main steps of the procedure for assessing the seismic response of the structure using the FRS Method (Section 2) are listed below:

1) Compute the angle α (Eq. 18) for the assigned value of the seismic factor λ;
2) Compute the vertical forces R_i (Eq. 16) acting on each element of the structure;
3) Rotate the structure at angle α;
4) Compute the line of thrust closest to the geometrical axis, using the procedure described in Section 2.

4 SAFETY ASSESSMENT

The procedure described in Section 2 and 3 allows one to compute, for any assigned load condition of vertical forces and horizontal forces proportional to the vertical ones, the line of thrust closest to the geometrical axis.

In order to assess if the arch is safe, a comparison between the shape of the line of thrust and the profile of the arch must be carried out. However, the line of thrust closest to the geometrical axis, provided by the computation, could also be somewhere out of the profile of the arch, without mandatorily meaning that the arch is unsafe.

In fact, the line of thrust closest to the geometrical axis is only one of all ∞^3 funicular polygons associated to the load condition. According to the static theorem of limit analysis, it can be vertically shifted in order to check if it stands within the profile of the arch. By doing so, we are exploring all ∞^1 funicular polygons parallel to that provided by the computation.

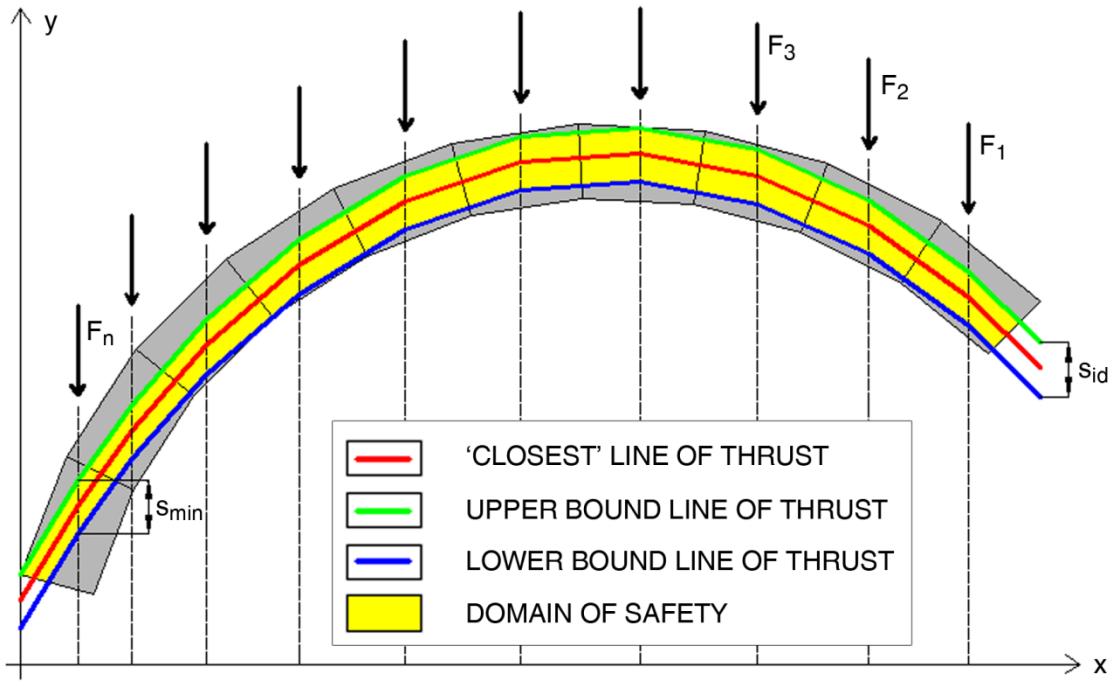


Figure 3: Safety assessment procedure

With this in mind, the authors have developed a procedure to assess the degree of safety of an arch based on the "capacity" of the line of thrust closest to the geometrical axis to be vertically shifted within the profile of the arch (Fig. 3). Two limit positions can be obtained: the lines of thrust, parallel to the original one, tangent to the extrados and intrados of the arch, respectively, in at least one point while still remaining contained within its profile. In authors' formulation, these two polygons identify a domain of admissible lines of thrust (i.e. equilibrium states) and are the upper and lower bound of this region respectively. In other words, this region identifies all the ∞^1 lines of thrust that lie within the profile of the arch and that, as a consequence, describe different safety conditions.

In order to assess the degree of safety with this approach, the "full range factor of safety" has been defined: it is the ratio between the thickness of the domain and the thickness of the arch, in line with the "geometrical factor of safety" proposed by Heyman in [13]. However, in authors' opinion, the factor that best points at the degree of safety of the arch is the reciprocal of such coefficient, that we have denoted as "performance factor":

$$\text{p. f.} = \frac{s_{id}}{s_{min}} \qquad 0 \leq \text{p. f.} \leq 1 \tag{19}$$

It is worth noting that, in line with the formulation of the procedure above described, the thickness s_{min} of the arch to be inputted in Eq. 19 is the minimum vertical thickness among all the thicknesses measured in correspondence to the action lines of loads and that also the thickness of the domain, s_{id}, is vertically measured, and, for this reason, is a constant value.

According to Eq. 19, the safest arch is that in which the line of thrust can be vertically shifted upwards and downwards so that the distance between the upper and lower thrust lines is exactly equal to the thickness of the arch ($s_{id} = s_{min}$). It occurs in the solely case of an

inverted catenary-shaped arch [14] and provides the performance factor equal to 1. Conversely, a performance factor equal to 0 points to an unsafe arch, because the upper bound and the lower bound thrust lines coincide and identify a domain of zero thickness. Therefore, summarizing, the performance factor ranges in the narrow interval [0,1], thus indicating intermediate safety levels.

In the case of an arch subject to a predetermined vertical load condition and horizontal forces computed based on an assigned seismic factor λ, Eq. 19 still holds and the safety level can still be assessed using the FRS approach.

However, in order to assess the seismic vulnerability level of an arch, that is the "seismic capacity" of the structure, the limit value of λ (hereafter referred to as λ_{lim}) is required to be computed.

In the approach of standard limit analysis, λ_{lim} is computed as the load multiplier that activates the collapse mechanism. Instead, with our approach, the seismic factor λ is maximum (i.e. $\lambda = \lambda_{lim}$) when the thickness of the domain of safety is zero:

$$\lambda = \lambda_{lim} \;\rightarrow\; \alpha = \alpha_{max} \;:\; s_{id} = 0 \tag{20}$$

Therefore, in order to compute λ_{lim}, an iterative analysis that runs repeatedly the four-step procedure described at the end of Section 3, is proposed. Such a procedure could be executed increasing, step by step, the angle of the plane on which the arch stands.

However, it is worth noting that the horizontal forces being simulating the seismic action, the seismic factor λ ranges in the interval [0,1] and, in agreement with Eq. 18, the inclination angle of the structure ranges in the interval [0°,45°] accordingly. Therefore, in order to obtain a more accurate value of the limit seismic factor λ_{lim}, we have preferred to use the bisection method in such an interval. The iterative procedure converges when the thickness of the domain becomes zero.

5 NUMERICAL EXAMPLES

5.1 Arch subject to vertical loads

In this section the safety level of a non-symmetric segmental arch is investigated. The arch under study covers a span of 4.70 meters, has an angle of embrace of 135° (with the right abutment positioned at 25° and the left one at 165° from the horizontal reference line), has a constant thickness of 30 cm and is subdivided in 20 elements, each one subject only to its self-weight. Although the specific weight used for the computation is 18kN/m^3, it is also worth noting that this value is irrelevant, since all the elements have the same size.

Figure 4 shows the line of thrust closest to the geometrical axis (the thicker poly-line) which is everywhere within the profile of the arch. Furthermore, the upper and lower bound lines of thrust that border the domain of safety are also shown. The computations, performed with the computer program *ArchiVAULT*, in which the procedure has been implemented, have provided the vertical thickness of the domain of 18.52 cm, the full range factor of safety of 1.6177 and the performance factor of 0.6182, a value that points to a rather safe arch.

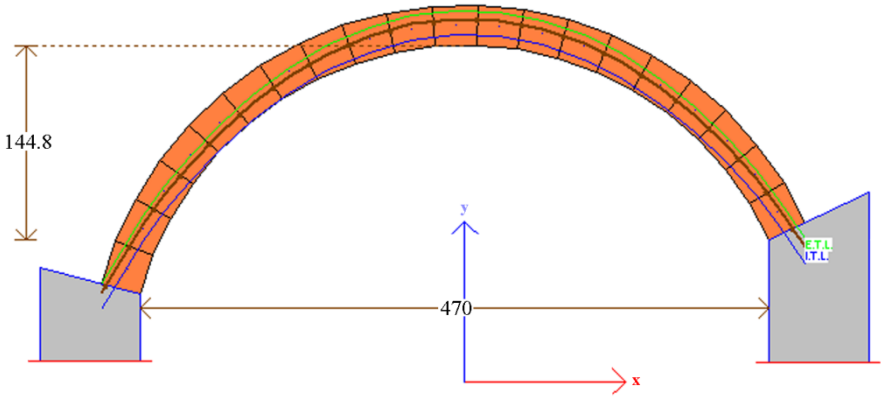


Figure 4: Safety assessment of an arch only subject to its self-weight

5.2 Arch subject to vertical and horizontal forces

According to the value of 0.6182 of the performance factor obtained for the load case of only self-weight in the previous section, the arch seems to be capable of supporting also a pattern of horizontal forces and, therefore, to resist a seismic event.

In this section the safety verification of the arch subject to its self-weight and a set of horizontal forces proportional to it is carried out and the limit value of the seismic factor is computed considering an earthquake acting both in +X and –X direction.

In order to simulate the action of horizontal forces in +X direction, the plane on which the structure stands has been tilted clockwise (Fig. 5a). The maximum angle in correspondence to which the thickness of the domain becomes zero is computed to be 19.88° (indeed, in Fig. 5a the upper and lower bound lines of thrust coincide). It is worth noting that, in correspondence to this value, the performance factor mandatorily becomes zero and the limit seismic factor is 0.3616.

Instead, in order to simulate the action of horizontal forces in -X direction, the plane on which the structure stands has been tilted counterclockwise (Fig. 5b). The maximum angle in correspondence to which the thickness of the domain becomes zero is computed to be 9.88°. Accordingly, the limit seismic factor is 0.1742, a much lower value than that obtained for the rightward forces analysis and, therefore, a much lower seismic capacity is shown.

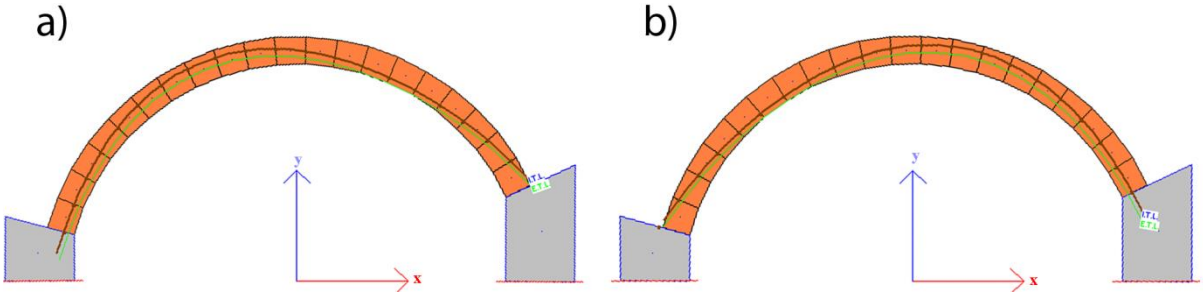


Figure 5: Safety assessment of an arch subject to its self-weight and a horizontal pattern of forces rightward (a) and leftward (b)

6 CONCLUSIONS

- In accordance with Heyman, collapse in masonry arches is not generally provoked by material failure because stresses are always rather small. Accordingly, to assess the safety a procedure based on the comparison between the shape and position of the thrust line and the profile of the arch has been formulated.
- The procedure, denoted as FRS Method, has been developed to compute the line of thrust closest to the geometrical axis of an arch subject to a set of vertical loads, the geometrical axis being represented through the poly-line that joins the element centroids.
- This procedure makes use of the finite difference method to minimize the distance between the ordinates of the element centroids and the ordinates of the nodes of the thrust line.
- Unlike other previous or recent methods in the literature, our method computes the "exact" solution avoiding both proceeding iteratively by trials and errors and the use of optimization techniques.
- Being mainly interested in assessing the behavior of arches in seismic regions, the FRS procedure has been extended in order to include the presence of horizontal forces proportional to the vertical ones.
- The value of the horizontal forces is computed, in an innovative way, exploiting the analogy between the inclined plane on which the structure stands and the inclination of the resultant of the vertical and horizontal forces. Thanks to this trick, the procedure, that minimizes the vertical distances between the ordinates of the element centroids and the ordinates of the nodes of the thrust line, still holds and can easily be exploited also for the seismic verification.
- The safety level of the arch is assessed defining the domain of equilibrium lines of thrust and computing the performance factor (PF), that is the reciprocal of the full range factor of safety (FRS).
- The domain of equilibrium lines of thrust and the FRS are exploited to estimate the seismic vulnerability of an arch by computing the limit seismic factor, which is achieved when the thickness of the domain of safety (i.e.: the PF) becomes zero.

REFERENCES

[1] Alecci, V. Stipo, G. La Brusco, A., De Stefano, M. and Rovero, L. Estimating elastic modulus of tuff and brick masonry: a comparison between on-site and laboratory tests. *Constr. Build. Mater.* (2019) **204**:828-38.

[2] Block, P., Ciblac, T. and Ochsendorf, J. Real-time limit analysis of vaulted masonry buildings. *Comput. Struct.* (2006) **84**:1841-52.

[3] Huerta Fernández, S. Mechanics of masonry vaults: the equilibrium approach. In: Paulo Lourenço and Pere Roca (Eds.): *Proc. of the 3rd International Seminar, Guimarães*, Portugal (2001).

[4] Pugi, F. and Galassi, S. Seismic analysis of masonry voussoir arches according to the Italian building code. *Ing. Sismica-Ital.* (2013) **30,3**:33-55.

[5] Galassi, S., Ruggieri, N. and Tempesta, G. A novel numerical tool for seismic vulnerability analysis of ruins in archaeological sites. *Int. J. Archit. Herit.* (2018) **14(1)**: 1-

22, 10.1080/15583058.2018.1492647.
[6] Galassi, S. Ruggieri, N. and Tempesta, G. Ruins and archaeological artifacts: vulnerabilities analysis for their conservation through the original computer program BrickWORK. In: Aguilar, R., Torrealva, D., Moreira, S., Pando, M., Ramos, L.F. (Eds.), *Proc. of 11th International Conference on structural analysis of historical constructions (SAHC2018),* Cusco, Perù (2018), pp. 1839-1848.
[7] Cavalagli, N. Gusella, V. and Severini, L. Lateral loads carrying capacity and minimum thickness of circular and pointed masonry arches. *Int. J. Mech. Sci.* (2016) **115**:645–56.
[8] Dimitri, R. and Tornabene, F. A parametric investigation of the seismic capacity for masonry arches and portals of different shapes. *Eng. Fail. Anal.* (2015) **52**:1–34.
[9] Zampieri, P., Simoncello, N. and Pellegrino, C. Structural behavior of masonry arch with no-horizontal springing settlement, *Frattura ed Integrità Strutturale* (2018) **43**:182-190, 10.3221/IGF-ESIS.43.14.
[10] Zampieri, P., Simoncello, N. and Pellegrino, C. Seismic capacity of masonry arches with irregular abutments and arch thickness. *Constr. Build. Mater.* (2019) **201**:786-806, 10.1016/j.conbuildmat.2018.12.063.
[11] Zampieri, P., Amoroso, M. and Pellegrino, C. The masonry buttressed arch on spreading support. *Structures* (2019) **20**:226-236, 10.1016/j.istruc.2019.03.008.
[12] Zampieri, P., Cavalagli, N., Gusella, V. and Pellegrino, C. Collapse displacements of masonry arch with geometrical uncertainties on spreading supports. *Comput. Struct.* (2018) **208**:118-129, 10.1016/j.compstruc.2018.07.001.
[13] Heyman, J. The safety of masonry arches. *Int. J. Mech. Sci.* (1969) **11,4**:363-85, 10.1016/0020-7403(69)90070-8.
[14] Tempesta, G. and Galassi, S. Safety evaluation of masonry arches. A numerical procedure based on the thrust line closest to the geometrical axis. *Int. J. Mech. Sci.* (2019) **155**:206-21, 10.1016/j.ijmecsci.2019.02.036.
[15] Galassi, S. and Tempesta, G. The Matlab code of the method based on the Full Range Factor for assessing the safety of masonry arches. *MethodsX* (2019) **6**:1521-42, 10.1016/j.mex.2019.05.033.
[16] O'Dwyer, D. Funicular analysis of masonry vaults, *Comput. Struct.* (1999) **73**:187-197, 10.1016/S0045-7949(98)00279-X.
[17] Block, P. and Ochsendorf, J. Thrust network analysis: a new methodology for three-dimensional equilibrium, *J. Int. Assoc. Shell. Spat. Struct.* (2007) **48(3).**
[18] Marmo, F. and Rosati, L. Reformulation and extension of the thrust network analysis, *Comput. Struct.* (2017) **182**:104-118, 10.1016/j.compstruc.2016.11.016.
[19] Block, P. and Lachauer, L. Three-dimensional funicular analysis of masonry vaults, *Mech. Res. Commun.* (2014) **56**:53-60, 10.1016/j.mechrescom.2013.11.010.
[20] Fraddosio, A., Lepore, N. and Piccioni, M.D. Thrust surface method: An innovative approach for the three-dimensional lower bound Limit Analysis of masonry vaults, *Eng. Struct.* (2020) **202**:109846, 10.1016/j.engstruct.2019.109846.

12th International Conference on Structural Analysis of Historical Constructions
SAHC 2020
P. Roca, L. Pelà and C. Molins (Eds.)

THE UNBUILT MUSMECI PARABOLIC CROSS VAULT REINVENTED AS A DRY-MASONRY STRUCTURE

CLAUDIO INTRIGILA*, NICOLA A. NODARGI AND PAOLO BISEGNA

Department of Civil Engineering and Computer Science (DICII)
University of Rome Tor Vergata
via del Politecnico 1, 00133 Rome, Italy
e-mail: {intrigila*, nodargi, bisegna}@ing.uniroma2.it, www.dicii.uniroma2.it (*corresponding author)

Keywords: Cross Vault, Musmeci Vault, Dry-masonry Structure, Limit Analysis, Parabolic Masonry Arch, Spreading Supports

Abstract. *This paper investigates the unbuilt Musmeci parabolic vault, reinventing the original reinforced concrete structure as a dry-masonry vault. In the framework of rigid no-tension constitutive model with no sliding, the equilibrium analysis is conducted with the aim of evaluating the design thickness of the masonry vault, respecting the original Musmeci shape. A parametric survey is performed to assess the minimum thickness of the vault, and its structural capacity under spreading supports. Attention is focused on the different collapse mechanisms and the corresponding crack patterns. For a better insight into the behaviour of the parabolic vault, the relevant case of the parabolic arch is first analysed and discussed. The numerical results show the feasibility of the project, with a thickness comparable with that proposed by Musmeci.*

1 INTRODUCTION

In 1954 the Italian engineer Sergio Musmeci (1926-1981) conceived a reinforced concrete parabolic cross vault, with a triangular bay, featured by the assembly of three triangular webs. Designed for a small market in southern Italy through a prime structural optimization experiment, the unique vault remained unbuilt [1].

Despite the interesting geometric solution and the pioneering structural optimization procedure, the project remained forgotten and mentioned only in [8] as "exemplary for its modular conception of the structure based on the repetition of cylindrical shells".

In this framework, a novel perspective of the elegant geometry of the Musmeci vault is explored here, revisiting the original reinforced concrete structure. In particular, the possibility of reinventing the original vault as a dry-masonry structure is investigated, adopting the limit analysis theory [2-7].

Aim of this work is, on the one hand, to bring attention to the unique and forgotten geometry proposed by Musmeci, on the other hand, to analyse the structural behaviour of parabolic masonry vaults, still not be researched in detail.

In order to be as faithful as possible to the original geometry proposed by Musmeci, the only free parameter considered in the design process is the vault thickness. Therefore, different

aspects are involved in the proposed procedure.

A first aspect is related to the discretization process of the original geometry as a dry assemblage of blocks, researching on the proper stereotomy of blocks and evaluating their influence on the static admissibility of the vault.

A second aspect is related to estimating a design thickness with a reasonable factor of safety. Accordingly, a set of parametric analyses is conducted to evaluate the influence of the vault thickness on the global response. In particular, the minimum admissible thickness and the minimum thrust of the vault are investigated. Furthermore, since the vault behaviour is deeply influenced by finite displacements at the springing [3,5,7], the Musmeci vault is analysed under horizontal settlements.

According to the Heyman sliced model [2,3,7], the vault is modelled as combination of web arches and ribs and their capacity on spreading supports is evaluated in terms of ultimate displacements and relative thrusts. In this context, attention is focused on the different collapse mechanisms and on the pertaining crack patterns.

The present paper is organized as follows. Section 2 is devoted to a brief review of the Musmeci structural model. The discretization process and the main assumptions of the proposed model are reported in Section 3. Since the behaviour of the parabolic square cross vault is closely connected to the behaviour of its diagonal ribs [7,9], the case of the parabolic arch on spreading supports is first analysed and discussed in Section 4. Then, the minimum thickness of the Musmeci vault and its displacement capacity are analysed in Section 5. Finally, conclusions are outlined in Section 6.

2 THE MUSMECI MODEL: A SYSTEM OF REINFORCED CONCRETE PARABOLIC CROSS VAULTS

Designed in 1954 by Sergio Musmeci in collaboration with the architect Giuseppe Vaccaro, to cover a rural market in southern Italy, the structure is one of the first Musmeci's researches on the minimum structural design criteria [1,8].

The market space has a rhomboidal plan, set on an angle of 120°. The structural elements that compose the cover of the market are the same that determine its shape. It is, indeed, a modular structure consisting of the repetition of 4 tripartite vaults, each one with an equilateral triangular bay. Each vault is formed by three triangular webs with a parabolic profile. The external parabolic arches of the webs have a rise, f, equal to 3.65 m and a span, $2a$, of 12.50 m, as shown in Figure 1. The ribs, generated by the intersection of the 3 webs, are also semi-parabolic arches and form angles of 120° in plan.

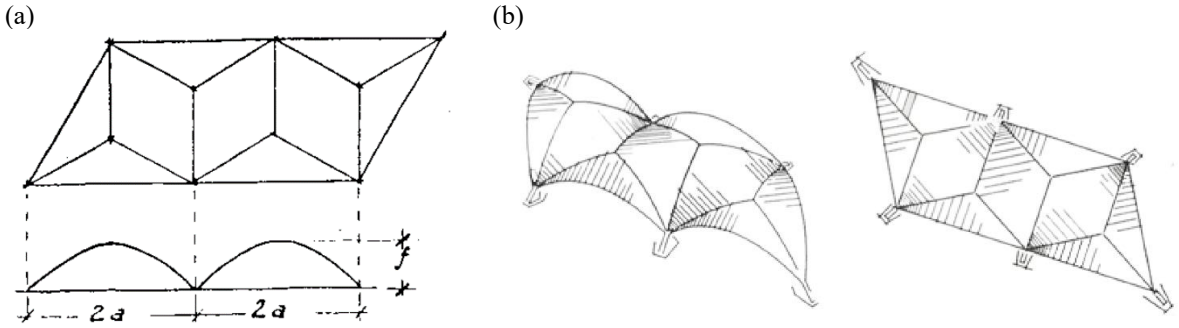


Figure 1: (a) Schematic plan [1], (b) sketch of Musmeci project by Sigel [8]

The structure is designed to be entirely built of reinforced concrete, in which the parabolic webs are self-bearing shells, and the ribs are arches with flexural stiffness that convey loads to the corner abutment pillars [1].

According to Musmeci's idea, the direct correlation between the static functionality and the architectural form of the structure is further represented by the trend of the stresses in the ribs. The ribs are subjected to vertical loads that vary linearly from the crown to the abutment, and to constant horizontal thrusts. Therefore, Musmeci deduced that, though the parabolic centreline of the ribs does not correspond to the funicular line of the vertical loads, since these are not constant, the presence of horizontal thrusts brings the funicular line very close to the parabolic one, thus reducing the maximum eccentricity to few centimetres [1].

2.1 The Musmeci structural model

The Musmeci structural model [1] is here discussed referring to the central surface of a single bay of the tripartite vault. A Cartesian reference system $\{O;x,y,z\}$ with origin O at the crown and positive z-axis downwards is introduced, as depicted in Figure 2.

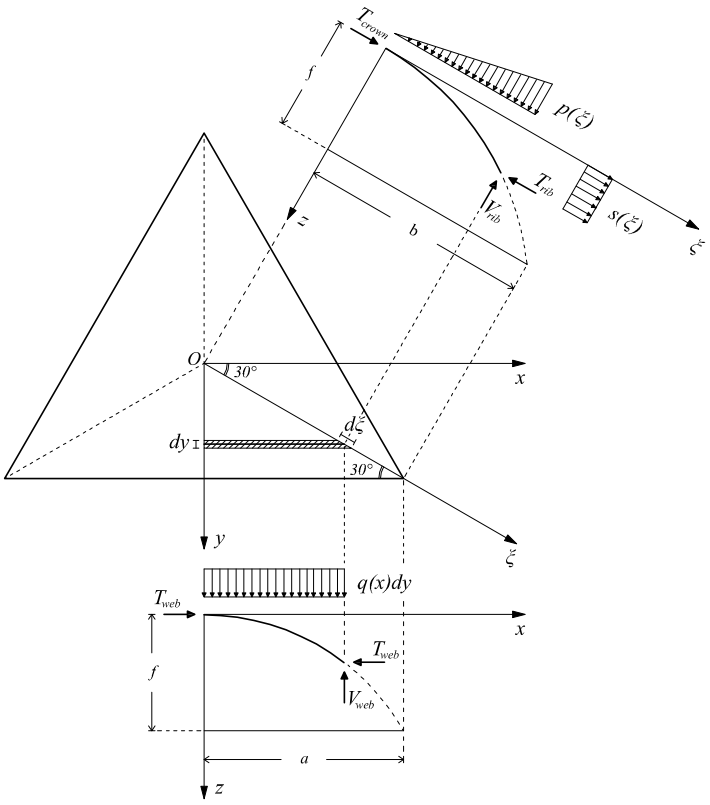


Figure 2: Scheme of the Musmeci structural model

Dividing the webs into arches with infinitesimal width dy, the equation of the arches can be written as:

$$z(x) = \frac{f}{a^2} x^2 , \tag{1}$$

and if q is the vertical load per unit surface in horizontal projection, the thrust is equal to:

$$T_{web} = \frac{qa^2}{2f} dy \,. \tag{2}$$

Rotating by 30° about the *z*-axis the coordinate system and choosing ξ as new abscissa, the equation of the ribs is:

$$z(\xi) = \frac{f}{b^2}\xi^2 = \frac{3f}{4a^2}\xi^2 \tag{3}$$

since the rise is again *f* and the half span is $b = a/\cos(30^\circ) = 2a/\sqrt{3} = 7.22\,m$.

The vertical load acting on the ribs per unit length in horizontal projection is:

$$p(\xi) = 2qxdy = \frac{\sqrt{3}}{2} q\xi \, d\xi \tag{4}$$

and it is accompanied by a horizontal component resulting from the thrust T_{web} of two webs:

$$s(\xi) = 2T_{web}\cos(30^\circ) = \frac{\sqrt{3}}{4}\frac{qa^2}{f} d\xi = \frac{3\sqrt{3}}{16}\frac{qb^2}{f} d\xi \tag{5}$$

Therefore while p varies linearly with ξ, s is constant.

Under these loads, the rib is subjected to bending stresses since its profile does not coincide with their funicular line. In addition, as explained in [1] by Musmeci: "Since the flexural stiffness of rib is practically negligible at the abutment, where the section is theoretically reduced to a point, and at the crown, where the angle between webs becomes zero, the behaviour of the rib can be considered similar to that of a three-hinged semi-arch".

Let V and T respectively denote the vertical and the horizontal reactions at the abutments. In particular, V is equal to:

$$V = \int_0^b p(\xi)\, d\xi = \frac{\sqrt{3}}{4} qb^2 = \frac{\sqrt{3}}{3} qa^2 \,. \tag{6}$$

The moment equilibrium about the crown hinge gives:

$$Vb - \int_0^b p(\xi)\xi \, d\xi + \int_0^b s(\xi) z(\xi)\, d\xi - Tf = 0 \,, \tag{7}$$

which allows immediately to calculate the thrust T:

$$T = \frac{7\sqrt{3}}{48}\frac{qb^3}{f} = \frac{7}{18}\frac{qa^3}{f} \,. \tag{8}$$

At the crown the thrust value is:

$$T_{crown} = T - \int_0^b s(\xi)\, d\xi = T - s(\xi)b = -\frac{\sqrt{3}}{24}\frac{qb^3}{f} = -\frac{qa^3}{9f} \,, \tag{9}$$

and the negative sign indicates the presence of traction in the rib. In particular, since the thrust varies linearly along the rib, it will be zero at $\xi = 2/9\, b = 1.60\,m$. As consequence of traction, a reinforcement is designed as shown in Figure 3 [1].

In the Musmeci project, the vault thickness ranging from 12 to 8 cm, tapering in key, and the webs are connected along the external side by 15 to 22 cm thick edge reinforced curbs, with an almost rectangular section. The ribs have a triangular section with height of 28 cm and are

reinforced in the same way as the curbs. It can be noticed that the longitudinal and transversal bars arrangement along the ribs underlines their structural function as curvilinear beams in the Musmeci model.

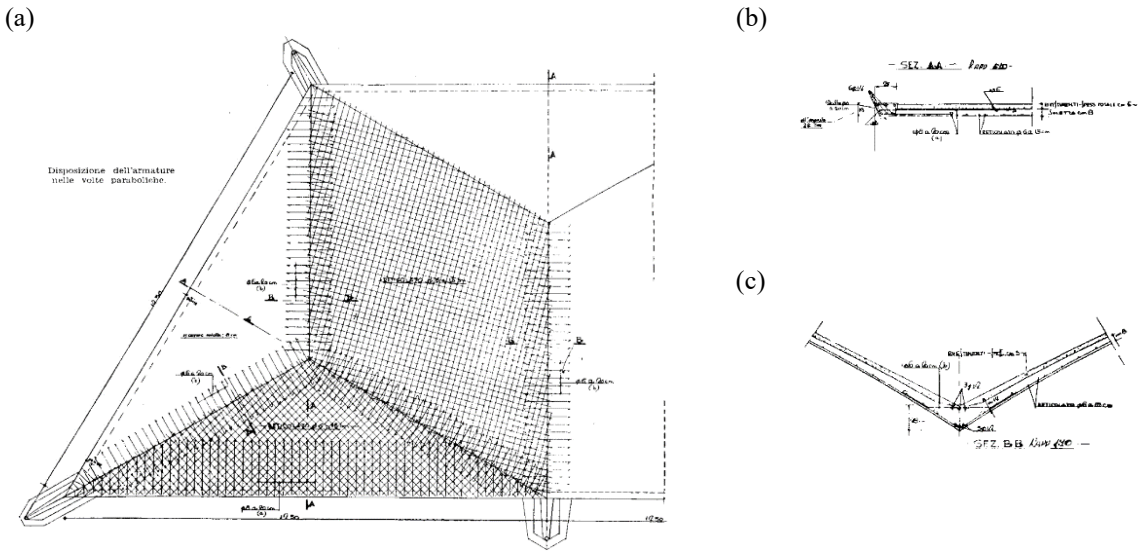


Figure 3: Reinforcement detailing of parabolic vaults [1]: (a) plan view, (b) cross-section of curbs and (c) cross-section of ribs

3 THE MUSMECI VAULT AS A DRY-MASONRY STRUCTURE

In Section 2 the Musmeci approach pertaining to equilibrium analysis of the vault has been introduced. Through the slicing technique, the central surface of the webs is divided into a series of independent parallel arches entirely supported from the diagonal cross-ribs modelled as three-hinged arches.

In the framework of limit analysis applied to masonry structures, the same approach was successively developed by Heyman [3,4] to clarify the path of the forces in masonry domes and masonry cross vaults and to evaluate the thrust value. Furthermore, another link between the presented reinforced concrete vault and classical masonry vaults is pointed out by Musmeci's introduction of the edge curbs. Indeed, the stiffen of external web arches along the free sides of the structure recalls the *formeret* arches in a quadripartite Gothic masonry vault.

In this context, the aim of the present work is to propose in a novel prospective the unbuilt Musmeci vault, reconsidered as a dry-masonry structure. In order to respect the original shape of the vault, the unique design parameter is the thickness t. In detail, the starting point is the discretization of the vault through the research on the appropriate stereotomy of blocks.

The main assumptions are: (i) the webs are coursed in the 'French' way [3] and in the structural model they are divided into a series of parallel arches of variable rise, span and width but with uniform thickness t; (ii) the ideal ribs, generated by the intersection at 120° in plan of two parabolic webs, are modelled as parabolic arches with variable thickness and vanishing width (in particular, at the crown the ribs thickness is equal to t); (iii) all arches are divided into a finite number of voussoirs with joints normal to the curvilinear axis of the web arches (in order to minimize the shear components along the interfaces). Conversely, the ideal voussoirs

of the ribs do not have interface normal to their axes, being generated by the projection of the joints of the web longitudinal courses on diagonal planes of the ribs. Finally, the design voussoir size is investigated in the range between $2.5°$ and $5°$. Two examples of the geometry discretization of the Musmeci vault are shown in Figure 4. Taking advantage of the geometric symmetry, only one-sixth portion of the vault is modelled.

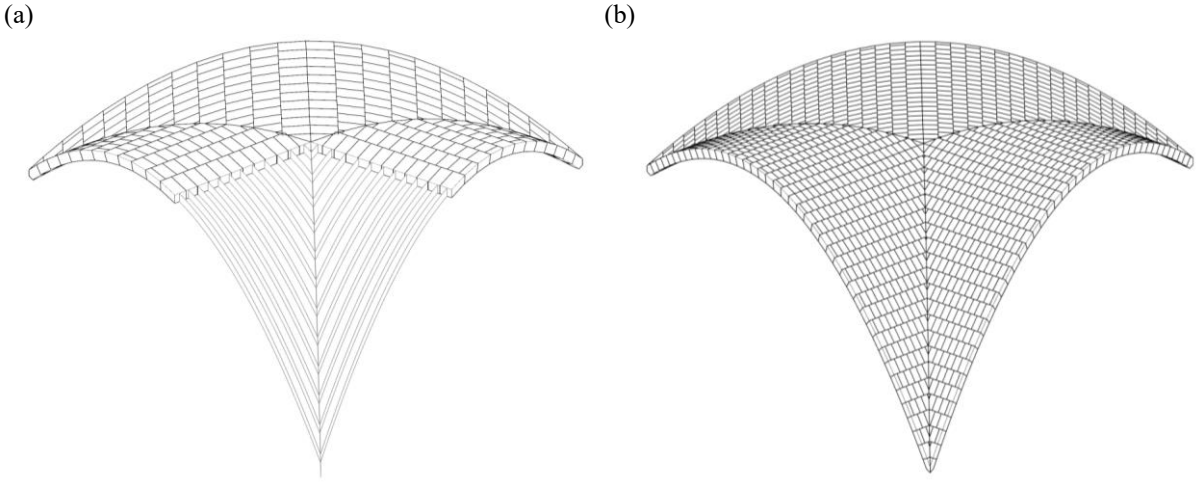


Figure 4: Geometry discretization of Musmeci vault, reconsidered as a dry-masonry structure, with thickness equal to $t = 24\,cm$ and: (a) voussoir size equals to 5° (and the relevant sliced model considered) and (b) to 2.5°

Under the classical assumptions of the limit analysis of masonry structure [2,3] and through the thrust line analysis [4,5,7], the *stability*[1] of the Musmeci masonry vault subjected to gravity loads is investigated, verifying if the thrust line of each arch lies wholly within the masonry.

Compared to Heyman and Musmeci approaches essentially based on membrane solution, with the present approach it is possible to take full advantage of the actual thickness of the vault to carry the self-weight.

First, in the spirit of the minimum structural design criteria, the minimum thickness of the vault is investigated and discussed. Furthermore, adopting the procedure initially proposed for circular masonry arches in [5,7,11] and then considered for square cross vaults in [10], the vault capacity on spreading supports is assessed in terms of ultimate displacements. Since the behaviour of the masonry vault undergoing settlements is deeply connected to the behaviour of its ribs, the case of the parabolic arch is first analysed in Section 4.

4 MASONRY PARABOLIC ARCH ON SPREADING SUPPORTS

This section is devoted to evaluating the behaviour of a masonry parabolic arch undergoing horizontal settlements at the springing. In Section 4.1, attention is focused on the adopted methodology and on compatible mechanisms that can lead the arch to a collapse configuration. In Section 4.2, the least thickness and the minimum thrust of the parabolic arches, generated by the discretization of the Musmeci vault, are analysed for different values of the thickness ratio t/a. Finally, in Section 4.3 the spread limits and the relative thrust at the collapse are discussed and reported. All results have been achieved by means of an inhouse MATLAB® code.

[1] As defined by the Heyman "safe" theorem [2-4].

4.1 Static approach and compatible mechanisms in deformed configuration

The capacity of masonry arches to withstand the actions of the environment, such as differential foundation settlements or earthquakes, lies precisely in the possibility of opening cracks [2]. The cracks are therefore not dangerous but a natural consequence of the aptitude of a masonry structure to absorb the external actions.

In this framework, under the well-known assumptions of standard limit analysis theory adopted for masonry structure [2], the equilibrium approach [5] has been applied to investigate the behaviour of a parabolic arch subjected to self-weight and horizontal displacements at the abutments. In particular, as soon as the centring is removed, the thrust is activated and the supports, being not fixed, undergo a slight yielding. According to [2,7], the small movement causes the formation of three hinges in the arch, at the extrados near the crown, and at the intrados near the haunches, and the thrust at the abutments of the arch is the lowest of all the statically admissible ones. As discussed in [9], the calculation of the minimum thrust T_0 in undeformed configuration can be interpreted as the following linear optimization problem:

$$\min_x f^t x \quad \text{s.t. } Ax \le b, \tag{10}$$

where x is the 2×1 vector collecting the hyperstatic reactions (chosen as the moment and the thrust at the crown section) and f is the 2×1 equilibrium operator such that $f^t x$ gives the thrust at the springing section. Under the assumption of infinite compressive strength of the material, the inequality constraint enforces the pressure points to lie inside the M joint sections of the arch. In detail, A [resp., b] is a $2M\times2$ matrix [resp., $2M\times1$ vector] such that Ax [resp., $-b$] gives the moments of the hyperstatic reactions [resp., the cumulative moments of the gravity loads] with respect to the intrados and extrados points of each joint sections.

Starting from this configuration and increasing the span, the arch deforms according to a rigid body kinematics [5]. Assuming a symmetric mechanism, only half of the arch is considered. In particular as in [9], the half arch is divided into three segments: (i) *Segment I*, from the abutments to the intrados hinge, is subjected to the imposed horizontal settlement; (ii) *Segment II*, placed between the two hinges, is characterized by the same horizontal displacement and by a rotation around the intrados hinge; (iii) *Segment III*, from the extrados hinge to the crown section, is only characterized by a vertical translation. As for semi-circular arches and elliptical arches [5,9], during the displacement of the supports and the consequent kinematic motion, the intrados and extrados hinges might jump in different locations from the starting ones.

A parametric survey is carried out in order to understand the influence of the main geometric parameters on the global response of a parabolic arch. In particular, the external web arch generated by the geometry discretization described in Section 3 and the diagonal arch are considered. In this regard, it should be noticed that the diagonal arch has variable thickness, at the crown equal to t and gradually increasing towards to the support, and a value of rise over span ratio f/a equal to 0.506 (also the diagonal semi-span will be indicated from here on with a) while for the external web arch f/a is equal to 0.584.

Finally, the analyses are performed for different sizes of the voussoirs, but, for space reasons, only the results relating to the case of voussoirs size equal to $2.5°$ (i.e. voussoir length equals to about 31 cm) are reported in the next sections.

4.2 Minimum thickness and minimum thrust of parabolic arch

The minimum thrust T_0, normalized by the total arch weight W, versus the thickness ratio t/a evaluated at the crown section, is plotted in Figure 5 for different values of t/a. The curves start at the least possible thickness. In this situation, the minimum thrust is equal to the maximum one, and the arch reaches a state of limit equilibrium. In particular, the parabolic arches exhibit a behaviour similar to that of flying buttress in the *passive state*, described in the case of uniform thickness in [2,3] and with curved intrados in [11]. Indeed, the thrust line passes through intrados at the crown and at the springing, touching extrados just below the midpoint, as depicted in the red box (diagonal arch) and yellow one (external web arch) of Figure 5.

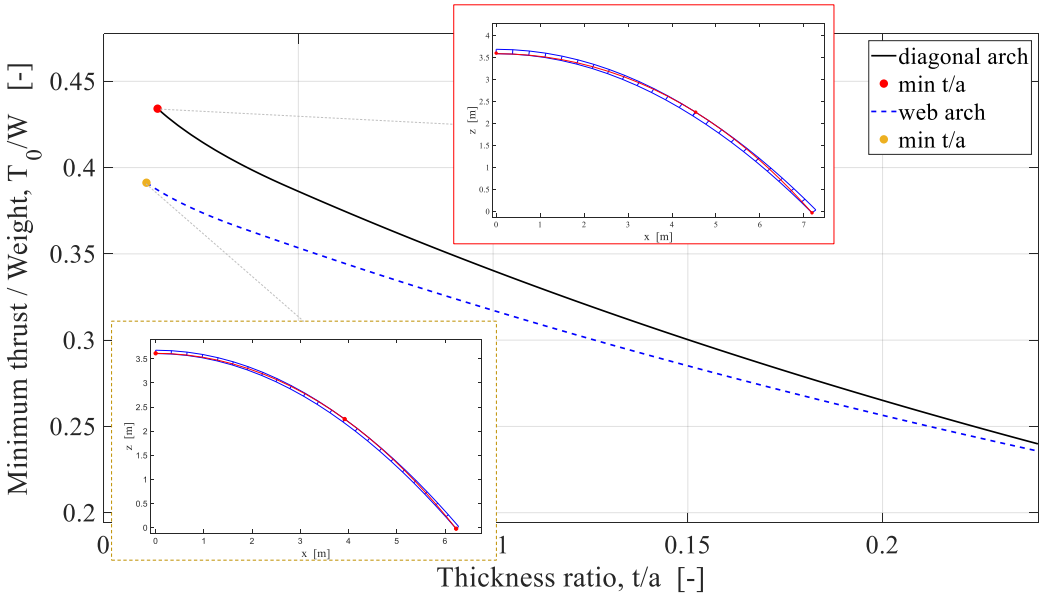


Figure 5: Minimum thrust vs Thickness ratio curves in the undeformed configuration. The red and yellow box inserts show the diagonal and the external web arches at the minimum admissible thickness ratios, respectively

For the diagonal and external web arches, the minimum thickness values are $t/a = 0.014$ and 0.011, i.e. $t = 6.88\,cm$ and $10.10\,cm$, with values of $T_0/W = 0.434$ and 0.391, respectively. Despite the variable thickness, as a consequence of the significant lower value of f/a ratio, the diagonal arch has greater values of T_0/W than the web arch, for each value of t/a. Nevertheless, the smallest admissible value of t/a is attained by the web arch. This result is related to the effect of voussoir stereotomy on the shape of the thrust line [12]. In fact, the discretization through normal cuts of the web arches implies their possibility of accommodating a larger set of thrust lines within their thickness[2].

Moreover, it is worth noticing that the minimum thickness of the web arch is about an order of magnitude lower than the minimum thickness of the elliptical arch with same f/a and t/a

[2] In this regard, the minimum thickness ratio t/a of the same diagonal parabolic arch, with joints normal to its axis, is 0.0075.

ratios [12], since the parabolic profile is closer to the catenary curve.

Finally, as the thickness ratio increases, both curves exhibit a decrease of values of minimum thrust with a trend similar to the one observed for circular arches [10] and elliptical ones [12].

4.3 Collapse displacement and relative thrust of parabolic arch

With the aim to assess the behaviour of the parabolic arch undergoing horizontal displacement at abutments, the cases pertaining to the diagonal and the external web arches are analysed using the limit analysis procedure and their capacity is evaluated in terms of collapse displacement and relative thrust.

As originally proposed for the circular arches in [5], the *thrust increase*, defined as the ratio of the thrust at collapse displacement T_{coll} to the minimum thrust T_0, is plotted versus the thickness ratio t/a in Figure 6a. A practical limit is introduced, i.e. the behaviour of the arches is not investigated when the thrust becomes greater than five times the minimum thrust [9,10].

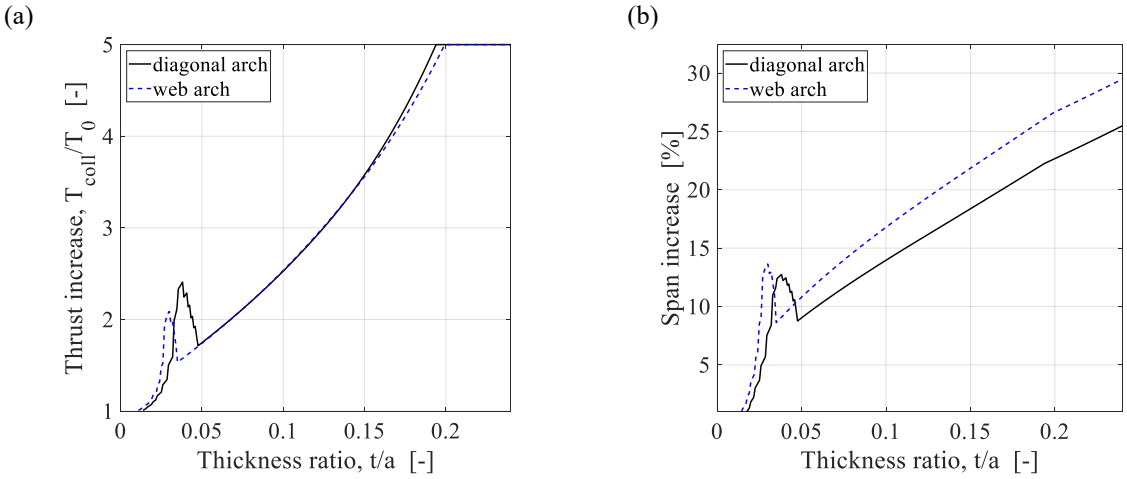


Figure 6: Parabolic arches. (a) Thrust increase vs Thickness ratio curves at collapse configuration. (b) Span increase vs Thickness ratio curves at collapse configuration

The governing failure mechanisms for the parabolic arches on spreading supports can be classified into three types, corresponding to three regions of the curves in Figure 6.

In the first region, for low thickness ratio values until the first peak, both arches fail due to a five-hinge mechanism described in Section 4.2. In particular, the extrados hinge remains located in the same position of the corresponding case of minimum thrust, whereas moving the supports apart the line of pressure touches the intrados at the crown, activating the mechanism.

Increasing the thickness, the location of the initial extrados hinge moves toward the crown of the arch and for small increments of t/a ratio there are large increases in both thrust and corresponding collapse displacement. Unlike the case of flying buttresses described in [11], the formation of the intrados hinge at the crown leads to the failure of the arch, preventing the achieving of the snap-through mechanism.

The second region is within the t/a range of $0.038-0.048$ and $0.030-0.035$, for the diagonal and the web arches, respectively. In details, starting from local peaks, the collapse mechanism changes and jumps of both extrados and intrados hinges occur, modifying the geometry of the

arch and overcoming the static admissibility. Indeed, as presented in [5,9,10], if for a fixed value of the support displacement the line of pressure becomes tangential to two adjacent joints, the gravitational loads cause the closure of the lower hinge and the opening of the upper one. These jumps bring to different collapse configurations, producing discontinuities in the thrust increase clearly visible in the post-peak zone of solid curve of Figure 6a, pertaining to the diagonal arch.

In the third region, the thickness is sufficiently large to accommodate a thrust line passing through the crown at the extrados and through the springing section at the intrados, even in the undeformed configuration. Moving the supports apart, the location of the extrados hinge remains fixed, the arch approaches a classical snap-through failure, but the jump of the intrados hinge causes the failure. The same mechanism has been found for depressed circular arches in [5,10], with a shape of curves very similar to those shown in Figure 6a, for a comparable range of t/a. Finally, for t/a values approximately greater than 0.20, the practical limit is achieved.

The corresponding values of the span increase, defined as the percentage of the ratio of the displacement at collapse to the initial clear span, are depicted in Figure 6b. The trend of the curves is in accordance with the different collapse mechanisms previously described. In particular, it can be noticed that in the third region the slope of the curve is almost linear with a slight slope decrease at values of t/a corresponding to attainments of the practical limit of the thrust increase.

5 THE MUSMECI VAULT UNDERGOING DIAGONAL SETTLEMENT

In this section, the unbuilt Musmeci vault is considered in the new form of dry-masonry structure and its capacity under diagonal settlement is investigated. First, the static and kinematic analyses of the vault are presented in Section 5.1, with attention on different three-dimensional collapse mechanisms. The minimum thickness and the design thickness for both undeformed and deformed configurations are described and discussed in Sections 5.2 and 5.3.

5.1 Static and kinematic analyses

The static analysis of vaults under dead loads is a classical problem in masonry structures, mainly addressed to their conservation and maintenance but recently also as a new method for the design exploration of compression-only structures [14].

Generally, once the support structures have been removed, the activation of the thrust at the supports entails a small settlement, with a slight widening of the ribs and of the webs themselves. Small natural cracks occur, and the minimum thrust state of the vault is activated.

According to [7], the behaviour of the cracked vault can be analysed through the sliced model, under the assumption of rigid no-tension masonry model. As presented in [10], a linear optimization problem, similar to the one in Eq. (10), is solved for the hyperstatic reactions (i.e., the thrust and the moment at the crown of diagonal arch and of each web arch), enforcing the pressure points to lie inside all vault joints. An example of the results of the equilibrium analysis and the corresponding thrust networks is depicted in Figure 7.

Starting from the undeformed configuration, the weight of the vault is divided into the web arches which transmit their horizontal and vertical reactions in the rib plane. The thrusts of the web arches are combined with those of the adjacent web along the diagonal plane and imply a variable horizontal load on the rib where the minimum thrust at the abutment is sought.

Therefore, the initial statically indeterminate problem can be uniquely solved, and a unique hinges pattern in the arches is determined. According to the f/a ratio of each arch and the vault thickness t analysed, a different couple of extrados and intrados hinges can occur in each arch. Since the original geometry of Musmeci vault has low f/a ratio, the thrust lines of each arch passes through the intrados at the springing.

Enforcing a diagonal horizontal displacement at the abutments, the deformed configuration of the vault is analysed. In particular, the deformation of the ribs as a set of rigid bodies (i.e. the three segments introduced in Section 4.1) causes the aperture of cracks that completely split the overlying web. It should be noticed that these mechanisms are able to depict the cracking patterns typically detected for these type of faults [3,7].

As a consequence of the geometric discretization of the vault, each web arch rests on one voussoir of the ribs and undergoes a different possible settlement, according to the pertinent rib segments.

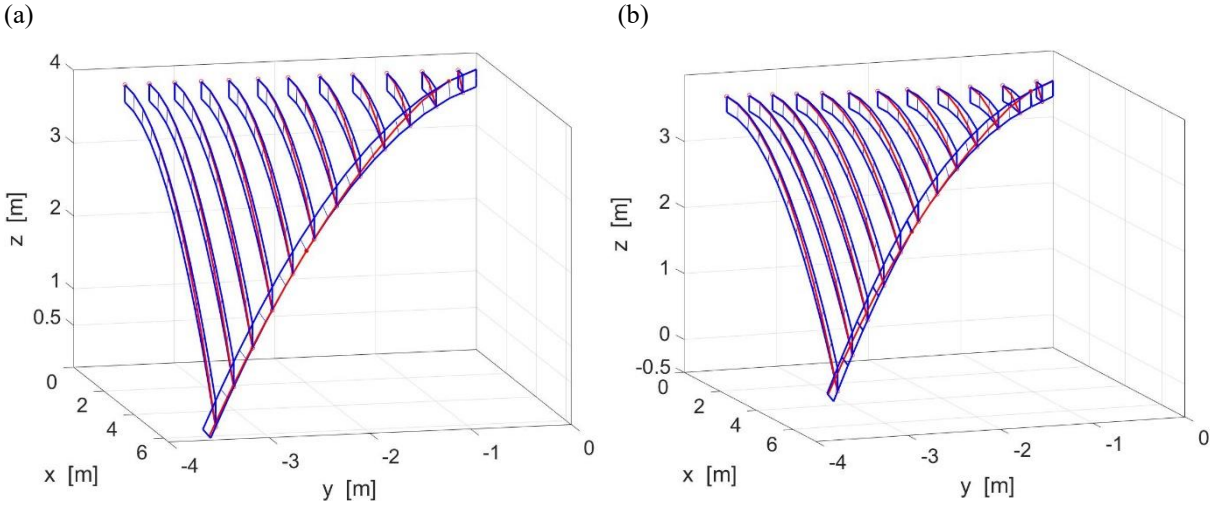


Figure 7: Musmeci vault. Thrust analysis at (a) undeformed configuration and (b) collapse configuration. One sixth of the vault is modelled, with voussoir size of 5° and thickness equal to $t = 24\,cm$, is here considered

Therefore, as presented in [9], the arch webs can be also divided into three classes. *Arches of Class I*, pertinent to the Segments I of the ribs, are in the outer zone of the web and are subject to a horizontal settlement of their springing. *Arches of Class II*, located between the two hinges of the rib, are in contact with the rib only through their intrados hinge and are subject to both vertical and horizontal settlements. Finally, *arches of Class III*, located in the inner zone of the web near the vault key, undergo a vertical translation. Furthermore, in order to have an admissible kinematic mechanism, the Class I and II arches are dragged by a rigid translation orthogonal to their plane. An example of the results of the analysis at collapse displacement is shown in Figure 7b.

5.2 Minimum thickness and minimum thrust of Musmeci vault

In Figure 8, the minimum thrust of the cross vault, normalized with respect to its total weight

is presented for different values of the thickness ratio, t/a.

The trend of the curve is similar to the previous ones shown for the case of the parabolic arch. The curve starts with the minimum thickness ratio (red dot), corresponding to a limit equilibrium state of the vault. In this situation, the mechanism is achieved when the pressure line passes through the extrados at the springing of the diagonal rib, with an incipient five-hinge symmetric mechanism of the ribs. Moreover, it can be noticed that the design thickness ratio t/a, whose choice will be discussed later, is marked with the green square on the curve. In particular, the values of minimum thickness and the design thickness are $t/a = 0.019$ and 0.033, i.e. $t = 14\,cm$ and $24\,cm$, with values of $T_0/W = 0.372$ and 0.350, respectively.

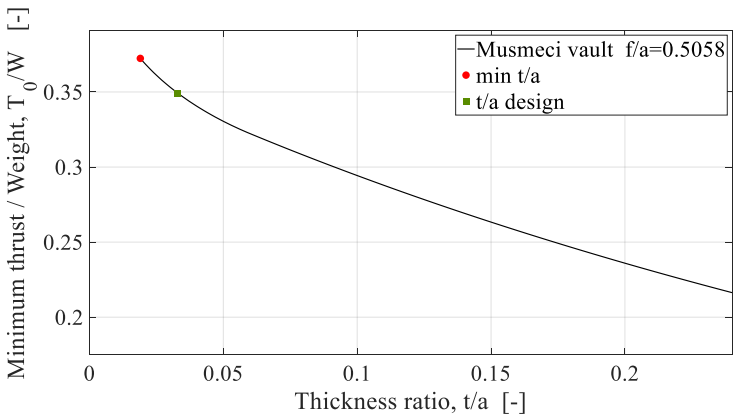


Figure 8: Musmeci vault. Minimum thrust vs Thickness ratio curves in the undeformed configuration

5.3 Displacement capacity of Musmeci vault

In Figure 9a the thrust increase is shown versus the thickness ratio t/a. As before, the curve is truncated when the thrust, at the springing section of the rib, achieves the practical limit.

The failure mechanisms of the cross vault are closely related to the behaviour of their ribs. In particular, for low values of the thickness, the vault collapse is attained due to a five-hinge mechanism in the ribs. Unlike the parabolic arch case (see Section 4.2), it should be noticed that in this case the pressure line touches the intrados towards the haunches and the extrados near the crown and at the supports of the ribs (an example is depicted in Figure 6b). This change in their behaviour is due to the action of the thrusts transmitted by the web arches to the rib.

Increasing the thickness ratio, the initial intrados hinge of the ribs moves from the haunch toward the abutment, involving not only a change in the geometry of the ribs but also a change of the Class of the web arches (see Section 5.1). Moreover, these significant changes in the initial geometry of the vault lead to discontinuities in the values of the increase in thrust, bringing also to a different collapse mechanism pertaining to jumps of the intrados or extrados hinges.

From the value of t/a equal to 0.084 onwards, the initial intrados hinge of the rib remains localized on the springing and the collapse mechanism of the vault approaching to snap-through failure and the practical limit is rapidly achieved.

In Figure 9b the relevant span increase at collapse configuration is reported. The high

displacement capacity of the vault to adapt to horizontal settlements is highlighted by the values of the span increase which grow rapidly up to over 30%. The trend of the curves and the collapse mechanisms are similar than the ones found in [9] for rounded cross vault.

Finally, considering that the original Musmeci structure was designed as a cover for a rural market, without underlying structures, it was chosen as the design thickness of the vault $t = 24\,cm$, with a geometric factor of safety [2] equal to 1.71, accordingly with the minimum structural design criteria of the author. The design size of voussoirs is chosen equal to $2.5°$ as a value near to the standard dimensions of voussoirs used in practice.

An example of the final appearance of the Musmeci vault reconsidered as a dry-masonry structure is depicted in Figure 4b.

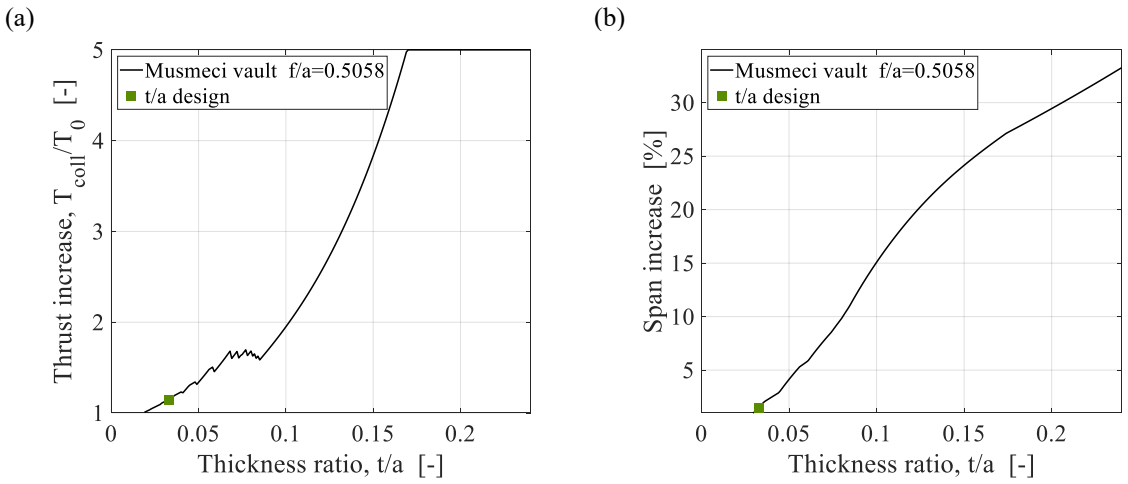


Figure 9: Musmeci vault. (a) Thrust increase vs Thickness ratio curves at collapse configuration. (b) Span increase vs Thickness ratio curves at collapse configuration

5 CONCLUSIONS

The unbuilt parabolic Musmeci cross vault has been proposed in the novel perspective of dry-masonry structure. In order to respect the original shape, the thickness of the vault has been considered as the unique design parameter. First, the geometry discretization of the reinvented vault and the main assumptions of the proposed model have been discussed. Second, the minimum thrust of the vault and its displacement capacity undergoing horizontal settlements have been investigated for different thickness ratio values. The Musmeci vault shows a low value of the minimum thickness and significant span increase at collapse, comparable to the parabolic arch constituting its diagonal rib. In particular, for low thickness ratio values, the failure is due to a five-hinge mechanism. Increasing the thickness, the collapse mechanism approaches a snap-through failure, the thrust increases rapidly and several hinge movements occur. The jump of the hinges involves a sudden change in the deformed configuration that, in some cases, may no longer be statically admissible, consequently leading to a premature collapse of the system. Compared to the original vault of Musmeci, designed to be entirely built in reinforced concrete, the proposed model provides an estimate of a reasonable design thickness of the vault, showing the possibility to bring a new life to this historical and elegant structure, as a dry-masonry vault.

REFERENCES

[1] Musmeci, S. and Vaccaro, G. Copertura a volte paraboliche per un mercato rurale. *L'Ingegnere* (1954) **5**:487-490.

[2] Heyman, J. The stone skeleton. *Int. J. Solids Struct.* (1966) **2**:249-279.

[3] Heyman, J. *The stone skeleton: structural engineering of masonry architecture.* Cambridge University Press, (1997).

[4] Huerta, S. Mechanics of masonry vaults: The equilibrium approach. In: P.B. Lourenco et al. (Eds.): *Historic Constructions*, University of Minho (2001), pp. 47–69.

[5] Ochsendorf, J. A. Collapse of masonry structures. PhD thesis, Department of Engineering, Cambridge University, Cambridge, (2002).

[6] Nodargi, N.A., Intrigila, C. and Bisegna, P. A variational-based fixed-point algorithm for the limit analysis of dry-masonry block structures with non-associative Coulomb friction. *Int. J. Mech. Sci.* (2019) **161** 105078.

[7] Como, M. *Statics of historic masonry constructions*. Springer, Vol. I, (2013), Vol. II, (2016).

[8] Siegel, C. *Strukturformen der modernen Architektur*. Munich, (1961)

[9] Intrigila, C., Nodargi, N.A. and Bisegna, P. Square cross vaults on spreading supports. In: R. Aguilar et al. (Eds.): *Structural Analysis of Historical Constructions*, RILEM Bookseries 18 (2019), pp. 1045–1053.

[10] Coccia, S., Di Carlo, F. and Rinaldi, Z. Collapse displacements for a mechanism of spreading-induced supports in a masonry arch. *Int. J. Adv. Struct. Eng.* (2015) **7**:307–320.

[11] Nikolinakou, M. K., Tallon, A. J., and Ochsendorf, J. A. Structure and form of early Gothic flying buttresses. *Revue européenne de génie civil* (2005) **9**:1191-1217.

[12] Makris, N. and Alexakis, H. The effect of stereotomy on the shape of the thrust-line and the minimum thickness of semicircular masonry arches. *Arch. Appl. Mech.* (2013) **83**:1511-1533.

[13] Alexakis, H. and Makris, N. Minimum thickness of elliptical masonry arches. *Acta Mech.* (2013) **224**: 2977-2991.

[14] Block, P. and Ochsendorf, J.A. Thrust network analysis: a new methodology for three-dimensional equilibrium. *J. Int. Assoc. Shell Spat. Struct.* (2007) **48**:67-173.

A NEW METHOD FOR ASSESSING COMPATIBILITY OF CONSOLIDATION PROCEDURES WITH CONSERVATION PRINCIPLES: INTERVENTION QUALITY INDEX (IQI)

NURIA CHIARA PALAZZI[1,2*], GIULIA MISSERI[3], CRISTIÁN SANDOVAL[2], UGO TONIETTI[3], JUAN CARLOS DE LA LLERA[1,2] AND LUISA ROVERO[3]

[1]Research Center for Integrated Disaster Risk Management (CIGIDEN), ANID/FONDAP/15110017
e-mail: nuriachiara.palazzi@cigiden.cl(*corresponding author)
[2]Pontificia Univesidad Catolica de Chile
Avda. Vicuña Mackenna 4860, Macul, Santiago, Chile
email: jcllera@ing.puc.cl, and csandoval@ing.puc.cl
[3]Department of Architecture, University of Florence
Piazza Brunelleschi, 6, 50121, Firenze, Italy
email: giulia.misseri@unifi.it, u.tonietti@unifi.it, luisa.rovero@unifi.it

Keywords: Built heritage, Masonry, ICOMOS principles, Retrofit interventions

Abstract. *In current times, built heritage is being lost at an alarming rate due to natural and human hazards. Policies for its protection and rehabilitation involve, among other things, challenges related to the refinement of suitable structural strengthening approaches. The arduous balance between gaining acceptable safety levels for occupants without deploying intrusive devices, inconsistent with conservation principles such as those of the ICOMOS charters, is not a simple task. The interest and efforts of the scientific community in this regard have been increasing for decades, but still, it is the structural professional´s responsibility and experience which must define this arduous balance on a case-to-case basis.*

This study addresses the question: How can the quality of structural rehabilitation interventions be assessed in light of conservation principles such as those given by ICOMOS? Here, a preliminary method - called "Intervention Quality Index" (IQI) method is proposed. It assesses the restoration intervention quality in relation to: (i) the level of compliance given by the conservation´s principle score (conservation´s factor, CF); and (ii) the current state of conservation of the monument (safety factor of building considering the seismic intensity, Δ_s). The IQI method considers the compliance level of the designed reinforcement with conservation principle, formalized through the fulfillment of a category, i.e. respected, partially respected, and not respected. Then, these judgments are translated into scores and statistically evaluated. Scores are attributed in relation to the relevance of the fulfillment of a certain conservation principle (authenticity, minimal intervention and intrusiveness, compatibility, recognizability and reversibility) for the seismic structural safety point of view. Preliminary results show that an effective employment of traditional earthquake-resistant practices together with a wise use of modern retrofit strategies allow for the preservation and reinforcement of built heritage without harming its identity.

1 INTRODUCTION

From recent studies of the seismic fragility assessment at macro-scale and single-building-scale of Built heritage [1], [2], [3], [4], [5], and [6], it emerged that several URM monuments, in particular churches, even those consolidated and repaired after a seismic event, demonstrated inadequate performance during sequent ones.
For this reason, several investigations were carried out to develop guidelines and standards for repairing, consolidating and strengthening URM built heritage while respecting ICOMOS conservation philosophy. New Zealand's *Building Seismic Performance* of existing structures [7], the *Building Code Requirements for Masonry Structures* by the American Society of Civil Engineers [8], the *National Peruvian Building Code for earthen structures* [9], the section *Retrofit Design Procedure for existing building* of the European code for *Design of structures for earthquake resistance* [10], the Italian Code *NTC2008* [11] and *Circ.26/2010* [12], and the Chilean *Standard for the Structural Intervention of Earthen Historical Buildings* [13], are some of the outcomes of thisresearchin some of the world's most earthquake-prone countries, in which criteria for strenthening interventions is provided.
Another set of guidelines for conservation and repair of heritage buildings are the*Guidelines for earthquake resistant non-engineered construction* published by UNESCO [14], and *Principles for the analysis, conservation and structural restoration of architectural heritage* [15]. These guidelines present a set of criteria to assess damage types and levels, correlating post-seismic scenarios to possible traditional and modern repair and strengthening techniques.

Although the interest of the scientific community toward this task have been increasing, the arduous balance between achieving acceptable safety levels for occupants without deploying overly intrusive devices, inconsistent with conservation principles such as those of ICOMOS charters, has yet to be resolved. To this aim, a preliminary method called the Intervention Quality Index (IQI) method is proposed.

The paper is organized as follows. After summarising the set of fundamental conservation principles within the framework of structural consolidation interventions, the preliminaly IQI method is presented in Section2. In Section3, stability and strength-based techniques for the reduction of seismic vulnerability of monumental buildings are analyzed through the IQI method which considers the compliance level of each conservation principle.
Then, two case studies on reinforcement interventions are addressed in Section4: the buttresses for improve the stability of San Francisco church's transept walls [16], and the tie-rods for retaining the thrust of external gallery arches of Basilica del Salvador [17]. Both interventions are analyzed through IQI method. Preliminary conclusions are drawn in Section5.

2 ICOMOS PRINCIPLES AND INTERVENTION QUALITY INDEX METHOD

The conservation philosophy has a direct consequence on seismic retrofit projects. The most universal principles of conservation are: *authenticity, minimal intervention and intrusiveness, compatibility, recognizability,* and *reversibility,* [18] and [19]. In the following,

the conservation criteria are stated analyzing the effect that complying with them has on the structural behavior induced by a reinforcement system:

- *Authenticity* [Au] of the original features of the building (materials, geometry), which must be preserved "ensuring that the original mechanical and resisting principles governing the structure response are not altered and original structural elements are not made redundant" [4];
- *Minimal intervention and intrusiveness* [Mi], which consist of an intervention where the human safety and conservation requirements are balanced, througth a cost-benefit analysis that also includes intangible value losses;
- *Compatibility* [Co] between new retrofitting materials and existing elements is related to chemical, physical and mechanical properties. The retrofits and structural elements "not only do no harm to the original ones, but they also act as sacrifical elements in precence of external actions, i.e. they should act as fuses of the structural system" [4]. Furthermore, the *constructive compatibility* allows for reduction of structural discontinuities, which are the preferencial ways of damage in case of seismic motion, and guarantees integration among structural elements and a greater level of monolithicity of masonry walls;
- *Recognizability* [Rc] of retrofitting interventions allows to easily detect the original constructive systems of the building and also possible structural heterogeneities due to post-earthquake repairs (main vulnerability feature in URM structures subject to seismic motions).
- *Reversibility* [Rv] of interventions considers the possibility of removing retrofits if better solutions are found in the future [16] and [21]. Currently, this is one of the most debated conservation issues because new technologies are often invasive and non-reversible. Thus, least harmful solutions should be chosen in accordance with minimum intervention and compatibility principles.

In order to assess the analyzed retrofitting technique/intervention, the degree of agreement with ICOMOS Principles are qualitatively evaluated through a judgement defined as: respect (R), partial respect (PR), and no respect (NR), Table1. These judgement categories (JCs) are directly related to the performance levels (PLs) based on experts' judgment, Table1. Based on the assessment of the fullfilment level between the analyzed intervention and the ICOMOS Principles, a numerical score is assigned to each judgement category. The numerical scores associated with the judgement presented in Table1, are used to evaluate the Intervention Quality Index (IQI) which turns out to provide the level of comformity of new intervention with ICOMOS philosophy. The IQI index is computed by the following equation:

$$\mathrm{IQI} = \Delta_{\mathrm{Is}} \cdot CF \tag{1}$$

Where, Δ_{Is} is the safety index increment and CF is the conservation factor, given respectively by the following expressions:

$$\Delta_{\mathrm{Is}} = \mathrm{I}_{s2} - \mathrm{I}_{s1} \quad (2); \qquad \text{and} \qquad CF = \sum_{\mathrm{k}=1}^{\mathrm{N}} \hat{\gamma}_{\mathrm{PI_k}} = \sum_{\mathrm{k}=1}^{\mathrm{N}} \frac{\gamma_{\mathrm{PI_k}}}{\gamma_{\mathrm{PI_{k,max}}}} \tag{3}$$

Where, I_{s1} and I_{s2} are the safety indexes of the structure before and afterthe intervention, respectively, each obtained as the ratio between spectral seismic acceleration capacity and seismic acceleration demand.

In the conservation factor *CF*, *N* is the number of considered ICOMOS principles (PI), which are Au, Mi, Co, Re, and Rev, and $\gamma_{\mathrm{PI_k}}$ is the *k-th* score, which can range between 0 and 3 according to the judgment category for each considered ICOMOS principle (PI_k). Table1 resports the definition for each conservation principle and the associated score for each judgement. The value of the conservation factor *CF* is thus obtained as the sum of normalized scores, $\hat{\gamma}_{\mathrm{PI_k}}$; normalization of $\gamma_{\mathrm{PI_k}}$ is considered with respect to the corresponding maximum possible score, in this case with $\sum_{k=1}^{N} \gamma_{\mathrm{PI_{k,max}}}$=12 since all five PIs are considered.

Table 1: ICOMOS principle ID, judgement category (JC), conservation´s principle score (γ_{PI_k}) given to each JC, and description for each conservation principlesof performance levels.

ID	JC	γ_{PI_k}	Performance level description
Au	R	2	Original static and dynamic behaviors are not altered.
	PR	1	Original static behavior is not altered, but dynamic behavior is substantially altered
	NR	0	Original static and dynamic behaviors are altered
Min	R	3	Human safety and conservation requirements are balanced. Cost-benefits are balanced
	PR	1.5	Human safety and conservation requirements are partially balanced.
	NR	0	Human safety and conservation requirements are not balanced.
Co	R	3	Retrofitting intervention is compatible mechanically (e.g. stiffness, weight, cohesion and deformability similar to the original structure), physically (e.g. very similar porosity and pore size distribution, very low variation of the moisture transport as absorption and drying rate, no thermal and hygric expansion), and chemically (e.g. identical chemical composition, no harmful chemical reaction, similar solubility) with existing structure.
	PR	1.5	Retrofitting intervention is mechanically compatible with the original ones, but it has slightly or moderately different physically and chemical features (e.g. moderate variation of the porosity and pore size distribution and moderate variation of drying and hygroscopic behavior, different chemical features, no harmful chemical reaction or byproducts).
	NR	0	High level of conflict between the original structure and the retrofitting intervention under dynamic actions, and use of material physically, chemically different from the original ones.
Rec	R	2	Relevant differences between the original structure and new intervention in term of thickness, material, tactile and color consistency.
	PR	1	The features of new intervention are similar to the original, whereas the tactile and color consistency is different.
	NR	0	Thickness, material, tactile and color consistency are similar to the original.
Rev	R	2	New intervention can be completely removed.
	PR	1	New intervention can be removed generating minor damage to the original structure.
	NR	0	New intervention cannot be removed.

To calculate seismic capacity and demand in the case of stability-based techniques, local analyses by damage mechanisms through limit analysis with kinematic approach are suggested (according to [11], [12] and [13]). While to assess the safety indexes before and after a strength-based intervention, which often involves wide areas of the structure, targeted global analyses are recommended.

Based on the value obtained for the IQI index, four categories of fulfillment are defined in the framework of the safety assessment against local damage mechanism

triggering, as shown in Table2: Category A, the intervention meets fully safety requirements and guarantees full compliance with the conservation principles; Category B, the intervention meets partially safety requirements (improvement) and guarantees compliance with the conservation principles; Category C, the intervention meets meets safety requiremts (either fully or partially)but does not guarantee complete compliance with the conservation principles; Category D, the intervention does not meet safety requirements and does not guarantee compliance with the conservation principles.

Table 2: Intervention conformity level to ICOMOS principles

Intervention conformity level			
A	**B**	**C**	**D**
0.75<IQI ≤ 1	0.5<IQI≤ 0.75	0.25<IQI ≤ 0.5	0 <IQI ≤ 0.25

A state of poor conservation of the materials in the structure (i.e. degradation of materials due to continuous exposure to the elements which generates degradation phenomena reducing structural efficiency), the presence of poor quality materials (i.e. irregular textures and/or incoherent and friable mortar), and design errors in the original structure (i.e. lack of wall-to-wall and wall-to-roof connections, excessive slenderness, wall pattern not respectful of the rule-of-the-art etc) inevitably require invasive and consolidation projects which depart from ICOMOS principles. In these cases, the priority is to guarantee the minimum safety level. Therefore, it is necessary to evaluate the invasiveness of the project considering the initial conservation state of the building, and related with the required safety level to the ICOMOS principles. In particular, considering a highly seismic context, a conservation project which is minimally invasive could be insufficient, and hence more invasive solutions might be required. The International Council on Monuments and Sites is aware of the complexity of this issue, and for this reason it is explicit that the principles are non-binding recommendations. Thus, ICOMOS principles are not an absolute requirement, but recommendations for the definiton of optimal retrofit interventions.

3 FROM THE DIAGNOSIS OF VULNERABILITY TO THE CONSERVATION INTERVENTION

The passage from the analytical-diagnostic phases to the intervention project consists of designing a unified intervention strategy considering the identified vulnerabilities and structural deficiencies. The main goals of an anti-seismic reinforcement intervention project are to prevent the activation of local collapse mechanisms both in-plane and out-of-plane, and to guarantee *box-like behavior* while respecting conservation philosophy. The design improvement devices must be able to: (i) collaborate with existing elements and contrast local vulnerability; (ii) systematically increase the displacement capacity of the structure, admitting partial deformations and cracks; (iii) restore the structural resistance of the initial system; (iv) avoid introducing concentrated and relevant stiffness (R.C. slab and injections etc.); and (v) increase the tensile resistant connections.

In [21] two main classes of complementary retrofitting interventions are distinguished: (I) Stability-based techniques, which reduce the deficit connections and thrust of arches and vaults; and (II) Strength-based techniques, which restore and increase the resistance of masonry wall.

3.1 Stability-based techniques

The stability-based techniques reduce deficiency between connections and thrust of structural elements (arches, vaults etc.), stabilizing the structure as a whole, in order to increment *box-like-behavior*. Common stability-based techniques for URM buildings are:
(i) Steel *tie-rod/cross-bracing* [TR- CB], widely used in historical structures to connect wall-to-wall and wall-to-floor and to improve the building integrity; (ii) Wooden ring-beam [RB], placed on top of the walls to guarantee box-like behavior and prevent the activation of out-of-plane mechanisms, providing strength and stiffness against bending; (iii) Brick-masonry enlargement [EN], consisting of a new massive local masonry addition in order to increase the wall section and prevent out-of-plane failures; (iv) Brick-masonry buttresses [BT], generally involving the entire length of the wall and supporting the wall corner and/or projecting from the section of an internal transverse wall, providing resistance to lateral thrusts.

Table 3 – Stability-bases techniques

I) STABILITY-BASED TECHNIQUES															
ID	**[TR- CB]**					**[RB]**					**[EN-BT]**				
Device	Tie-rod and anchor plate or cross bracing					Ring beam (made of reinforced brick masonry, steel)					Enlargement or Buttresses				
Main goal	Prevent the two walls from spreading apart					Prevent overturning, proving strength and stiffness					Improve global behavior and increase the load bearing capacity of wall				
JC	Au	Mi	Co	Rc	Rv	Au	Mi	Co	Rc	Rv	Au	Mi	Co	Rc	Rv
	PR	R	R	R	R	PR	R	R	R	PR	NR	R	R	R	R
CF	11/12 = 0.92					10/12 = 0.83					10/12 = 0.83				

A preliminary validation of the IQI method is carried out assessing each mentioned stability-based technique. Firstly, a qualitative judgment on total, partial or absence of the respect of conservation principles is provided in Table3. Then, the numerical scores associated with the JCs are used in Equ. (3) to calculate *CF*, shown in Table3.
The analyzed stability-based solutions show a high compliance level of each conservation principle (CFs=0.83-0.91). The implementation of restoration solutions using traditional materials (steel TR-CB, wooden RB, masonry EN-BT) is advantageous from a cost and compatibility point of view. However, in highly seismic regions these materials could be insufficient and modern devices might be employed such as systems based on fiber-reinforced composite materials or reinforced-brick-masonry, among others.

3.2 Strength-based techniques

Strength-based techniques improve the strength of walls by providing better “monolithic” behavior to masonry. Common strength-based techniques for URM structures are:
(i) Unstitch-stitch intervention [US], consisting of dismantling and rebuilding a portion of a cracked wall, with the aim of restoring continuity and structural integrity; (ii) bed joint re-pointing [BJR], replacing bad joint mortars with better quality ones; (iii) grout injection [GI], largely applied to fill the holes, cavities and internal voids to reconstitute the structural

continuity and increase the mechanical properties of masonry walls; (iv) artificial headers [AH], which provide transversal locking in wall thickness, connecting the adjacent wall leaves, increasing the monolithicity of masonry panels and the global behavior of structures as well as; (v) Jacketing of masonry [JM]consisting in the use of steel or different fiber, such as CFRP or inorganic matrix, placed on both wall faces and connected thought transversal elements that cross the wall section; (vi) confinement of columns and pillars with composite or steel materials [CN], located in critical sections of vertical elements, generally in the lower part of shafts where vertical cracks are present, to contain transversal dilatation and improve stability of columns and pillar. Also in the case of strength-based techniques, a preliminary validation of the IQI method is carried out. A qualitative judgment regarding the respect of conservation principles is provided in Table4, together with the *CF* values for each mentioned strength solutions.

Table 4: Strength-bases techniques

II) STRENGTH-BASED TECHNIQUES															
ID	**[US]**					**[GI]**					**[BJR]**				
Device	Unstitch-stitch technique for regular brickwork					Grout injection for masonry, stone, adobe and brick made					Bed joint re-pointing for masonry, stone, adobe and brick made				
Main goal	Structural continuity and uniform load distribution					Enhance homogeneity and increase strength					Increase in strength of masonry and prevent water penetration in mortar joints				
JC	Au	Mi	Co	Rc	Rv	Au	Mi	Co	Rc	Rv	Au	Mi	Co	Rc	Rv
	R	R	R*	R	PR	PR	PR	R*	R	NR	R	R	R*	PR	NR
CF	10/12 = 0.83					7.5/12 = 0.62					10/12 = 0.83				

ID	**[AH]**					**[JM]**					**[CF]**				
Device	Artificial headers for masonry, stone, adobe and brick made					Jacketing of masonry with steel or CFRP or inorganic matrix					Confinement of columns and pillars with composite or steel materials				
Main goal	Increase monolithicity of masonry panel and global behavior of structure					Increase strength capacity and ductility of wall					Increase strength capacity and ductility of columns and pillar				
JC	Au	Mi	Co	Rc	Rv	Au	Mi	Co	Rc	Rv	Au	Mi	Co	Rc	Rv
	NR	PR	R	R	PR	PR	PR	PR	R	PR	NR	PR-R**	R	R	PR-R**
CF	7.5/12 = 0.62					7/12 = 0.58					10/12 = 0.83				

* The use of materials with same shape, dimensions, stiffness and strength and compatibles from the chemical, physical and mechanical point of view is implied. **The judgment depends on the used materials.

4. APPLICATION OF IQI METHOD TO TWO CASE STUDIES

In order to further validate the IQI method to assess the quality of structural rehabilitation interventions in light of ICOMOS principles, two case studies have been identified. Both structures have historical and monumental value, are constituted of unreinforced masonry

walls, and are located in a highly seismic contest. For both monuments structural characterization and seismic performance have been widely studied. Thus, the reinforcement interventions of San Francisco church, the oldest ancient monument in Santiago Chile [16], and Basilica del Salvador, neo-gothic architecture in Santiago Chile [17], are analyzed through the IQI method. A description of the application of the method on the two case studies is provided below:

(i) Tie-rods [TR], to contain the arch thrust of Basilica del Salvador external gallery.
The use of [TR] for reinforcing URM structures is a traditional solution compatible with conservation principles, as shown by the conservation factor value, CF=$\sum_{k=1}^{N} \hat{\gamma}_{PI_k}$=0.91, in Table3. Overall ICOMOS principles (Min, Co, Rec and Rev) are achieved with total respect, with exception of Au, partially respected.
In the case of the Basilica del Salvador, the introduction of TRs would effectively counteract the activation of overturning mechanisms involving the outer walls of the external gallery (OWs) in Fig.1. As suggest in Section2, safety indexes of structure after (I_{s2}) and before (I_{s1}) a stability-based intervention shall be calculated through the kinematic approach of limit analysis within a macro-element framework to obtain the safety factor Δ_{Is}, (Equ.2). I_{s2} and I_{s1} are given by the ratio between the spectral seismic acceleration,a_0^*, and seismic demand, D_{ai}. The spectral seismic acceleration is evaluated according to the codified procedures defined in [12]:

$$a_0^* = \frac{\alpha_0 \sum_{i=1}^{n+m} P_i}{M_{eff}}; \qquad \alpha_0 \left(\sum_{i=1}^{n} P_i \cdot \delta_{xi} \right) = \sum_{i=1}^{n} P_i \cdot \delta_{yi} \cdot \delta_{yi}; \quad M_{eff} = \frac{(\sum_{i=1}^{n} P_i \cdot \delta_{xi})^2}{g \cdot (\sum_{i=1}^{n} P_i \cdot {\delta_{xi}}^2)} \qquad (4)$$

Where α_0 is the kinematic multiplier; P_i is the *i-th* load; δ_{xi} is the virtual horizontal displacement of the gravity center of the i-th load P_i; δ_{yi} is the virtual vertical displacement of the gravity centers of the *i-th* load *Pi*; M_{eff} is the participating mass; a_0^* is the acceleration capacity; and *FC* is a confidence factor-related to the knowledge level of the building.

When the analyzed macro-element, i.e. the masonry portion prone to overturn due to the seismic action, is placed at the ground level, the seismic demand D_{ai} is equal to $D_{ai}=D_{ag}=a_g(P_{VR})Sq$, where $a_g(P_{VR})$ is the peak ground acceleration with an exceeding probability of 10% in 50 years; *S,* the sub-soil factor; and *q,* the behavior factor to account for energy dissipation capacity of the unreiforced masonry structure, equal to 1.5 according to[13]. If the macro-element is placed higher than ground level, the seismic demand $D_{ai}=D_{al}=S_e(T_1)\Psi(Z)\gamma$, where $S_e(T_1)$ is a design spectrum acceleration with respect to the first vibration period of the macro-block T_1, being $T_1=0.05H^{3/4}$[13]; $\psi(z)=Z/H$ is a function depending on the height from the foundation of the centroid of the weight forces applied on the macro-element, *Z*, on the total height of the building from the foundation, *H*, and on $\gamma=3N/(2N+1)$, which corresponds to a modal participation coefficient, depending on N number of floors. Considering the structure before the intervention, the kinematic multiplier of the horizontal equivalent forces producing the activation of the mechanisms, α_0, is calculated equal to 0.112 and the corresponding spectral acceleration a_0^* equal to 0.815 m/s^2[17].

Table 5: Tie-rod device to prevent the out-of-plane (OOP) mechanism of external gallery walls (OW) of Basilica del Salvador: $a_0^*{}_1$ and $a_0^*{}_2$ are the mechanism activation accelerations before and after TR intervention;

Is_1 and Is_2 are the safety indexes before and after TR intervention; $\sum_{k=1}^{N} \hat{\gamma}_{PI_k}$ is the conservation factor; Δ_s is the safety factor; IQI index is the intervention quality intervention index; and CL is the conformity level

Macro-elem.ID Mech. ID	$a_{0_1}^*$ [m/s^2]	$a_{0_2}^*$ [m/s^2]	Is_1 [-]	Is_2 [-]	CF [-]	Δ_s [-]	IQI index [-]	CL
OW-OOP	0.815	2.61	0.31	1	0.92	0.69	0.63	**B**

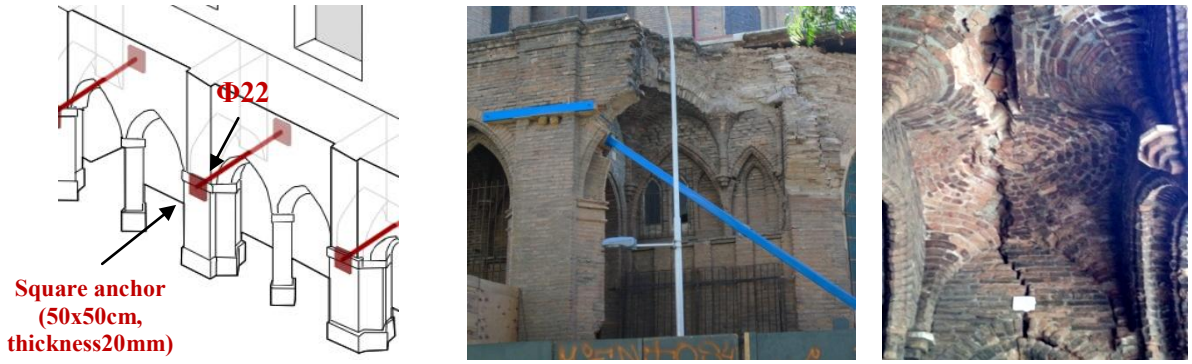


Figure 1: External gallery walls of Basilica del Salvador: (a) Tie-rods device to prevent the OOP mechanism, (b) collapse of external gallery pillars, and (c) deep crack in the arches and vaults.

With the aim of averting the triggering out-of-plane failures of OW macro-blocks, TR introduction is proposed, imposing a_0^* equal to the Demand Acceleration at ground level (D_{ag}=2.61 m/s^2). Considering a circular section of tie (length 5.91m, diameter 22mm), a square anchor (50x50cm, thickness20mm), and steel SS2350 (Young modulus equal to E=2100000daN/cm^2, characteristic strength of steel equal to f_y=2350daN/cm^2, and steel specific weight equal to γ_s=7850daN/m^3) the kinematic multiplier after TR intervention, $\alpha_{0,2}$, is equal to $\alpha_{0,2}$=0.359,considering the tie stress equal to T_{TR}=min (T_t, T_m, T_c) = min (89.3 kN, 344 kN, 86.2kN), where T_t is the failure mechanism related to yielding of the tie rods; T_m is the failure mechanism related to punching of masonry in the anchorage area; and T_c is the failure mechanism related to the resistance of the wall against the penetration of the anchor, due to excess [15]. The comparative analysis of the current state and the state after the retrofitting intervention (Table5) shows a significant improvement of acceleration capacity of the OOP mechanism of OW. This improvement leads to a satisfactory safety assessment, i.e. safety index after the intervention Is_2=1. According to Equ.1, the IQI index for the analyzed intervention is equal to 0.63, leading to an intervention conformity level type “B”.

(ii) Buttresses [BT], to improve the out-of-plane stability of San Francisco´s transept wall. Historically, masonry buttresses were part of the original construction and performed very efficiently during seismic motion. This device increases the wall section and prevents out-of-plane failures providing resistance to lateral thrusts. The BT strengthening efficiency depends on good interlocking between the original and new structure, and mechanical compatibility concerning strength and stiffness of materials employed. Table3 shows that the use of EN-BT as a seismic device in masonry structures guarantees respect for all conservation principles (R) with the exception of *authenticity*. The EN-BT intervention determines the alteration of original static and dynamic behavior, not respecting the Au principle.

As seen in [16], currently the most vulnerable macro-element in the San Francisco church was the transverse arcades of the transept walls (TA). From the historiographical analysis of this structure [16] it emerged that at the beginning of the 20thcentury the buttresses in correspondence of transept walls and aisles were cut.

Thus, with the aim of averting the triggering of OOP failures of the macro-element and in-plane behavior of the transverse arcade, the introduction of buttresses was proposed(Fig.2) according to the specifications provided in the *Guidelines for wall construction with buttresses* and *pilasters* [14]: the buttress thickness must be equal or greater than the wall thickness (t_{wall}); the length of buttress must be equal or larger than $3t_{wall}$; the length (L) between two buttresses must be $L \leq 10\ t_{wall}$ and $L \leq 64\ t_{wall}^2/h$, where h is the height of reinforced wall. Considering a shape coherent with the colonial architectural style (a thickness of 1mx1m, with the same masonry brickwork and mechanical, chemical and physical features of brick and mortar compatible with the original), the current condition of the TA macro-element and the improvement in its the seismic behavior due to the BT device are assessed through LKA analysis (Equ.4) for the northern and southern transept walls. Comparative analyses of the current state and the reinforced state (Table6) show an increase in the safety index (respectively equal to 68% and 75%). These improvements lead to an IQI equal to 0.68 and 0.75 respectively, and an intervention conformity level type “B”.

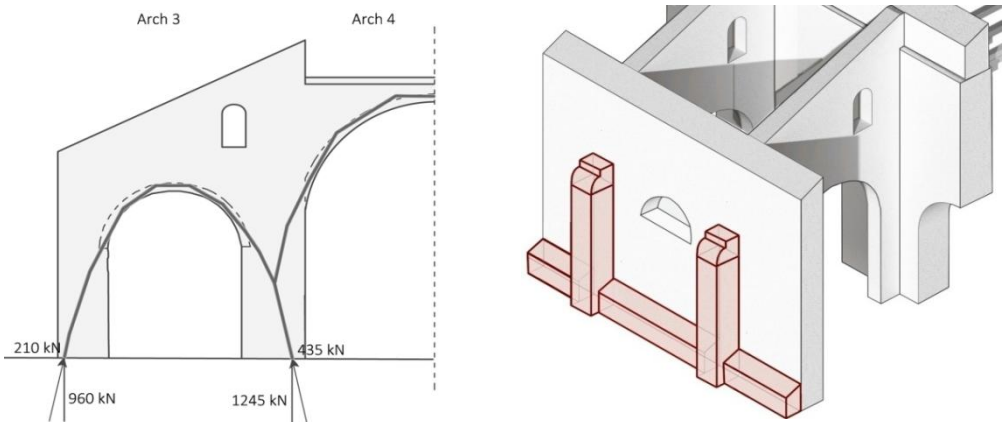


Figure 2: (a) Thrust line for transverse arcades of transept walls and (b) Buttress device to improve the OOP stability of San Francisco’s transept wall.

Table 6: Buttress device to prevent the out-of-plane (OOP) mechanism of transept walls (TR) of San Francisco church: $a_0^*{}_1$ and $a_0^*{}_2$ are the mechanism activation accelerations before and after BR intervention; Is_1 and Is_2 are the safety indexes before and after BR intervention; CF is the conservation factor; Δ_s is the safety factor; IQI index is the intervention quality intervention index; and CL is the conformity level.

Macro-elem. ID Mech. ID	$a_0^*{}_1$ [m/s^2]	$a_0^*{}_2$ [m/s^2]	Is_1 [-]	Is_2 [-]	CF [-]	Δ_s [-]	IQI index [-]	CL
NTA-OOP	0.866	2.34	0.33	1.01	0.83	0.68	0.57	**B**
STA-OOP	1.03	2.63	0.39	1.14	0.83	0.75	0.63	**B**

5. CONCLUSIONS

In this paper, a preliminary proposal to introduce evaluation criteria for the reinforcement interventions in relation to the level of compatibility with the conservation principles was

provided. In order to define the assessment methodology, the conservation ICOMOS principles have been reinterpreted in a purely structural manner considering the impact that a specific retrofit intervention has on the church from a conservation point of view.
The degree of agreement between each retrofit technique and conservation principles has been evaluated through judgement categories (respect, partially respect, and not respect), andthen trasformed into scores. These scores allow to assign a weight relative to the degree of importance that each principle, interpreted in structural terms, assumes in the evaluation procedure. In particular, the respect for *compatibility* and *minimum intervention* principles have been assessed as being more significant than*reversibility* and *recognition*.
The describedmethod represents a preliminary proposal that should be better specified in future works, considering further factors influencing the choice of intervention, such as for example: the required safety levels, the state of conservation of the asset, the symbolic importance and the social value, the costs and the duration of the intervention. Moreover, the method applied here to the Chilean context, must be statistically validated for its application to a wider range of construction contexts. The two case studies have been identified in order to evaluate IQI method, considering specific intervention proposals, such as tie-rods for Basilica del Salvador arches and buttress device to improve the out-of-plane stability of San Francisco transept wall.
Generally, the proposed stability-based techniques arise from the rediscovery of traditional earthquake-resistant practices of Chilean constructive culture (extensively documented in [5], [6] and [17]), while the strength-based techniques arise from the use of modern retrofit strategies.
The obtained results show that the rediscovery of traditional earthquake resistant practices, together with the use of modern retrofit strategies, allow preserving and reinforcing the built heritage without harming its identity. In fact, the application of the IQI method leads to very high values of conservation factor for the stability-based techniques (CF=$\sum_{k=1}^{N} \hat{\gamma}_{PI_k}$ =0.83-0.91), while it leads to lower values and partial assessment relative to the respect of conservation principles for the strength-based techniques(CF=$\sum_{k=1}^{N} \hat{\gamma}_{PI_k}$ = 0.58-0.83).

Acknowledgements.This work was supported by the Research Center for Integrated Disaster Risk Management (CIGIDEN), ANID/FONDAP/15110017, and by the SIBER-RISK Regular Fondecyt project CONICYT/FONDECYT/1170836.

REFERENCES

[1] Cracow Charter, 2000. Signed by representatives of conservation institutions, Proc Int. Conf. On Conservation, Krakow 2000, Krakow, 191–193.
[2] Venice Charter, 1964. International charter for the conservation and restoration of monuments and sites, Proc., 2nd Int. Congress of Architects and Technicians of Historic Monuments, Venice, Italy.
[3] Spence R, D'Ayala D (1999) Damage assessment and analysis of the 1997 Umbria-Marche earthquakes. Struct Eng Int J Int Assoc Bridge Struct Eng 9(3):229–233
[4] Cancino C (2010) Damage assessment of historic earthen sites after the 2007 earthquake in Peru. Adv Mater Res 133–134:665–670

[5] Wilkinson S, Grant D, Williams E, Paganoni S, Fraser S, Boon D, Mason A, Free (2013). Observation and implications of damage from the magnitude Mw 6.3 Christchurch, New Zealand earthquake of 22 February 2011. Bull Earthq Eng 13(1):1–35
[6] D'Ayala, D. (2014). Conservation principles and performance based strengthening of heritage buildings in post-event reconstruction. In Perspectives on European Earthquake Engineering and Seismology (pp. 489-514). Springer, Cham
[7] Palazzi, N. C., Rovero, L., De La Llera, J. C., Sandoval, C. (2019). Preliminary Assessment on Seismic Vulnerability of Masonry Churches in Central Chile. International Journal of Architectural Heritage, 1-20.
[8] Palazzi, N. C., Favier, P., Rovero, L., Sandoval, C., & de la Llera, J. C. (2020). Seismic damage and fragility assessment of ancient masonry churches located in central Chile. Bulletin of Earthquake Engineering, 1-25.
[9] SESOC (2013) Building seismic performance. Submission to the Ministry of Business, Innovation and Employment 8 March 2013.
[10] Masonry Standards Joint Committee, (1999). Building Code Requirements for Masonry Structures, ACI-530-99/ASCE 5-99/TMS 402-99, American Concrete Institute, American Society of Civil Engineers and Masonry Society, Detroit, New York, Boulder.
[11] E.080, (2017). Ministerio de Vivienda, Construcción y Saneamiento. Diseño y construcción con tierra reforzada. Lima, Perú.
[12] Eurocode 8, (2004). Design of structures for earthquake resistance – Part 1: General rules, seismic actions, and rules for buildings (EN 1998-1), European Committee of Standardization. Brussels, Belgium; 2004.
[13] MIT, (2008), Norme Tecniche per le Costruzioni. DM 14 gennaio 2008, Gazzetta Ufficiale, n. 29 del 4 febbraio 2008, Istituto Poligrafico e Zecca dello Stato, Roma.
[14] Circolare n. 26/2010 (2010) Linee Guida per la valutazione e riduzione del rischio sismico del patrimonio culturale, Prot. 10953 del 2 dicembre 2010.
[15] INN, 2013. Estructuras –Intervención de construcciones patrimoniales de tierra cruda– Requisitos del Proyecto Estructural. Santiago, Chile NCh3332.Of2013.
[16] Arya, A. S., Boen, T., & Ishiyama, Y. (2014). Guidelines for earthquake resistant non-engineered construction. UNESCO.
[17] International Council on Monuments and Sites (ICOMOS) Principles for the analysis, conservation and structural restoration of architectural heritage (2003).
[18] Jorquera, N., Misseri, G., Palazzi, N., Rovero, L. and Tonietti, U. (2017). Structural characterization and seismic performance of San Francisco church, the most ancient monument in Santiago, Chile. Intern Jour of Archit Her11(8),1061-1085.
[19] Palazzi, N.C., Rovero, L., Tonietti, U., de la Llera, J.C., Sandoval, C. (2018a). Kinematic limit analysis of Basilica del Salvador, a significant example of the neo-gothic architecture in Santiago, Chile. In 16th European Conference on Earthquake Engineering, Thessalonica, Greece 18-21 june 2018.
[20] Petzet M. (2004). Principles of preservation: an introduction to the international charters for conservation and restoration 40 years after the Venice Charter
[21] Giaretton, M., Dizhur, D., da Porto, F., & Ingham, J. (2016). Seismic assessment and improvement of unreinforced stone masonry buildings: literature review and application to New Zealand.". Bulletin of the New Zealand Society for Earthquake Engineering, 49(2).

12th International Conference on Structural Analysis of Historical Constructions
SAHC 2020
P. Roca, L. Pelà and C. Molins (Eds.)

CHARACTERIZATION OF FRCM- AND FRP-MASONRY BOND BEHAVIOR

CRISTINA GENTILINI[1*], CHRISTIAN CARLONI[2], ROBERTA SANTORO[3] AND ELISA FRANZONI[4]

[1] Department of Architecture (DA), University of Bologna, Viale del Risorgimento 2, 40136 Bologna (Italy)
e-mail: cristina.gentilini@unibo.it, http://www.da.unibo.it (*corresponding author)

[2] Department of Civil Engineering, Case Western Reserve University , 44106 Cleveland, OH (USA)
e-mail: christian.carloni@case.edu, http://engineering.case.edu

[3] Department of Engineering, University of Messina, Villaggio S. Agata, 98166 Messina (Italy)
e-mail: roberta.santoro@unime.it, https://www.unime.it/it/dipartimenti/ingegneria

[4] Department of Civil, Chemical, Environmental and Materials Engineering (DICAM), University of Bologna, Via Terracini 28, 40131 Bologna (Italy)
e-mail: elisa.franzoni@unibo.it, http://www.dicam.unibo.it

Keywords: Masonry, Shear Strength, Pull-off Strength, Failure Mode, Adhesion

Abstract. *Composites made of fibers embedded in organic or inorganic matrices are efficient systems for reinforcing historical masonry structures to provide strength and ductility with a negligible mass increment. As it is well known, the structural performance of the composites mainly relies on their adhesion to the substrate. There are different methods to test the adhesion of the composite to the substrate: in laboratory direct shear test is the most commonly employed, while on-site the bond between the reinforcement and the substrate is checked by the pull-off test. In this paper, the adhesion of different composites to the same substrate made of fired-clay bricks is investigated by both the shear test and the pull-off test to qualitatively assess the difference in the two methods. Additionally, to investigate whether the bond is affected by the presence of water in the pores, half of the specimens were tested in water saturated conditions. Three different types of matrix (based on epoxy resin, natural hydraulic lime and Portland cement) were used for the composite matrix, without changing the geometry, the type of masonry substrate and the fibers (galvanized steel cords).*

1 INTRODUCTION

The effectiveness of externally bonded (EB) composites, both fiber-reinforced polymer (FRP) and fiber-reinforced cementitious matrix (FRCM) composites, applied to masonry structures is governed by the adhesion between the reinforcement and the substrate. The bond behaviour between composites and masonry can be experimentally assessed by means of single-lap shear, double-lap shear, and beam tests [1-3]. The majority of the studies available in literature deals with the direct shear test (and in particular single-lap type), which is

extensively used in laboratory testing. Information on the adhesion between the reinforcement and the substrate and the presence of defects in the application of the composite can be potentially obtained by means of pull-off tests, which are easily performed on site without the burden of building a test fixture necessary to conduct direct shear tests [4]. Although the Mode-II bond behaviour should be studied by performing direct shear tests, the outcomes of pull-off tests could be still valuable in practice. A relationship between the results obtained from the single-lap shear test and those obtained from the pull-off test has not been established, especially for FRCM composites.

In this paper, a comparison between two experimental campaigns is presented. In one experimental program, three groups of masonry blocks made of fired-clay bricks and mortar joints, reinforced by a unidirectional steel fabric embedded in an epoxy resin, in a hydraulic lime-based mortar matrix and in a cement-based mortar matrix were subjected to single-lap shear tests [5-7]. In the other experimental campaign, pull-off tests were conducted on the same type of composites (same fibers and matrices) applied to fired-clay bricks belonging to same batch of bricks employed to manufacture the specimens tested in the first campaign [8]. Results of the single-lap shear test are compared with those obtained in the pull-off test to determine if a relationship exists and whether pull-off test could be a suitable way to obtain information on bond in field applications. This comparison is usually hindered by the fact that composite is applied on the side surface of the bricks for the shear test (the same surface that is actually reinforced on-site), while it is applied in the bed surface for the pull-off test. However, the bricks employed in this study were manufactured by a process similar to that used for historic bricks, namely by pressing, hence the characteristics of the side and one bed surface are very similar. This would be not the case of bricks manufactured by extrusion, for this brick type, the bed and side surfaces are completely different in terms of roughness and characteristics. Additionally, in order to check if the presence of water in the pores may affect the adhesion, half of the specimens were tested in water saturated conditions.

2 MATERIALS AND METHODS

The material used as a substrate in this study is a fired-clay brick of nominal dimensions 250 mm × 120 mm × 55 mm. Three types of composites were considered:

- SRP composite: constituted by steel fibers embedded in an organic matrix, namely a bi-component epoxy resin. The fibers employed are arranged as a unidirectional sheet made of ultra-high strength galvanized steel cords, fixed to a secondary 6 mm-spaced fiberglass micromesh. The cross-sectional area and equivalent thickness of the cord are 0.538 mm^2 and 0.084 mm, respectively. The tensile strength, ultimate strain, and Young's modulus of the steel fibers are 3000 MPa, 2%, and 190 GPa, respectively.
- S-FRLM composite: constituted by the same steel fibers as before embedded in an inorganic matrix [9]. The matrix was a commercially available dry-mix mortar made of natural hydraulic lime (NHL 3.5) and quartz sand, and belongs to the strength class M15 according to EN 998-2 [10].
- S-FRCM composite: constituted by the same steel fibers as before embedded in an inorganic matrix [11]. The matrix was a commercially available dry-mix mortar made of Portland cement binder and quartz sand, with a limited amount of

polymeric admixtures, and compressive strength > 45 MPa according to EN 12190 [12].

2.1 Pull-off specimens

Twenty-four fired-clay bricks were reinforced with composites applied to the 250 mm × 120 mm brick surface. The bricks were cleaned before the application of the composite. A first layer of matrix (2 mm-thick for resin and 4 mm-thick for lime and cementitious mortars) were applied on the surface for S-FRLM and S-FRCM specimens, respectively. After that, sheets of fabric were slightly pressed on them, and a second layer of matrix (having the same thickness of the first one) was applied on the S-FRLM and S-FRCM specimens. The total thickness of the composite was equal to 4 mm (±1mm) for SRP samples and 8 mm (±1mm) for S-FRLM and S-FRCM samples. After curing (1 week for SRP and 1 month for S-FRLM and S-FRCM specimens), two shallow cores perpendicular to the composite surface were drilled in each specimen, leaving the core attached to the brick. The core driller had a diameter equal to 53 mm. In accordance to EN 1542 [13], the cut depth should penetrate 10 mm in the substrate. Steel disks were attached to the external surface of the cores using epoxy adhesive. To investigate if the presence of water in the pores of the substrate may affect the pull-off strength, half of the reinforced bricks were tested after water saturation (suffix 'SATUR' in the label), while the remaining ones were tested in dry conditions (suffix 'DRY' in the label), for comparison purposes. For each type of condition, three tests were carried out.

2.2 Shear test specimens

The performance of the inorganic based composite was determined in terms of adhesion capacity of composite strips applied to a fired-clay brick masonry block. The masonry blocks were constructed with 6 half solid fired-clay bricks (55 × 120 × 125 mm^3) and 5 mortar joints (10 mm thick). The mortar used for the joints was a commercially available dry-mix product made of natural hydraulic lime (compressive strength class NHL 3.5 according to EN 459-1 [14]). Twenty-four 120 × 125 × 380 mm^3 masonry blocks were constructed and left to cure for 1 month at room temperature and humidity. After 1 month, the composite strips were applied to one of the faces of the blocks. The total thickness of the composites was the same as the one for the pull-off specimens. The three groups of reinforced masonry specimens (the group with SRP, the group with FRLM and the group with FRCM) were left to cure for 28 days in laboratory. Twelve composite-masonry joints (4 for each matrix) labeled "DRY" and used as control specimens were tested in dry conditions. Twelve composite-masonry joints (4 for each matrix) were immersed in deionized water for 2 days and then tested in saturated conditions. These specimens were labelled "SATUR".

2.3 Pull-off test setup

The pull-off test was performed in accordance with EN 1542 [13]. A uniaxial direct tensile load was applied perpendicular to the surface of both dry and wet specimens using the pull-off testing device up to failure.

2.4 Shear test setup

Direct shear tests were performed to assess the bond quality between the SRP/S-FRLM/S-FRCM composites and the masonry blocks. Details of the set-up of the single-lap shear tests are reported in [15]. During the tests, the masonry specimens were restrained between two steel plates, while the composite strip was pulled. The load *P* was applied to the end of the bare fibers where an epoxy tab was realized. Two linear variable displacement transformers (LVDTs) were mounted on the face where the composite was applied to measure the displacement of the composite with respect to the masonry surface at the beginning of the bonded area. All tests were conducted in LVDT displacement control at a constant global slip rate equal to 0.84 μm/s until failure.

3 RESULTS AND DISCUSSION

3.1. Mechanical properties of the matrices

The average compressive strength of the cement-based matrix and the natural hydraulic lime-based matrix resulted equal to 46.9 MPa (CV=8.5%) and 13.5 MPa (CV=6.5%), respectively. CEM matrix exhibited a compressive strength more than three times higher compared with the natural lime-based matrix [7, 15]. Epoxy resin had a tensile strength equal to 14 N/mm^2 as reported in the manufacturer data sheet [16].

3.2. Pull-off and shear test results

In general, with the pull-off and shear tests four possible failure modes may occur:

(1) Cohesive failure in the substrate (hereinafter denoted as F1);

(2) Bond failure at the composite/substrate interface (hereinafter denoted as F2);

(3) Interlaminar failure in the composite between the inner layer of matrix and the fabric (hereinafter denoted as F3);

(4) Bond failure at the steel disk/composite interface (hereinafter denoted as F4, this type of failure may occur only in pull-off tests).

Results for the pull-off tests are listed in Table 1 in terms of average strength (calculated as the peak force divided by the area of the disk) and failure modes. As expected, all the SRP specimens failed in the substrate (F1 type) and the decrease in bond strength between a dry and a water saturated substrate was 7.4%. Even if the substrate was involved in the failure surface, its saturated condition led to negligible difference in bond capacity: this is due to the fact that the presence of water in the pores of the brick did not influence significantly its tensile strength, and the substrate in the case of pull-off tests is mainly subjected to a direct traction. In the case of specimens reinforced with lime-based composites (S-FRLM), the failure mode mainly was interlaminar at the interface between the steel sheet and the inner layer of matrix, that remained attached to the substrate. In general, the bond strength was lower with respect to SRP, as usually occurs for these composites (lower than 1 MPa in the case of dry specimens, and lower than 0.8 MPa in the case of water saturated specimens). For this group, the decrease in bond strength between dry and wet specimens is remarkable: around 30%. In Fig. 1, typical failure modes occurred during the pull-off tests for SRP and S-FRLM samples are reported. It should be noted that S-FRCM specimens in this study showed a brittle behavior and most of the samples failed before pull-off testing during curing and/or during the operation of core cutting. This aspect should be better investigated, however it

points out the compatibility issues between such a high strength and stiff matrix and a porous substrate such as fired-clay bricks. Usually, this kind of high strength matrices is employed to strengthen concrete structures, however in certain particular cases, for example in presence of harsh environments these high strength mortars can be employed also for strengthening of masonry structures, leading to compatibility problems with low strength substrates.

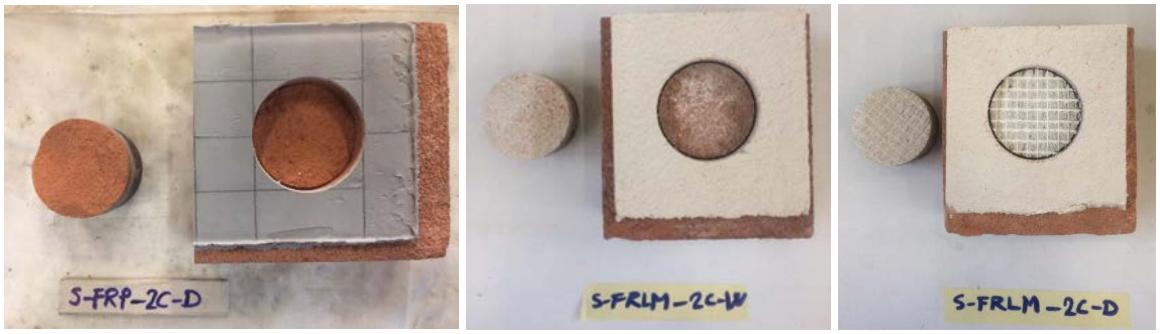


Figure 1. Type F1 failure mode for a SRP specimen on the left, type F2 failure mode for a S-FRLM specimen at the center and type F3 failure mode for a S-FRLM specimen on the right.

Table 1: Results of the mechanical tests: pull-off and shear tests. In parentheses, the coefficient of variation is reported.

Test type	Matrix type	Specimen	Adhesion strength or force	Δ^* [%]	FAILURE MODE
Pull-off test	Epoxy resin	SRP-DRY	1.12 MPa (13.4)	-	F1
		SRP-SATUR	1.04 MPa (12.9)	-7.4	F1
	Natural hydraulic lime based	S-FRLM-DRY	0.99 MPa (14.7)	-	F3
		S-FRLM-SATUR	0.76 MPa (13.4)	-30.1	F3 (in one case F2)
Shear test	Epoxy resin	SRP-DRY	10.72 kN (0.1)	-	F1
		SRP-SATUR	10.16 kN (7.0)	-5.2	F1
	Natural hydraulic lime based	S-FRLM-DRY	6.7 kN (14.9)	-	F3
		S-FRLM-SATUR	5.1 kN (18.0)	-23.5	F3
	Cement based	S-FRCM-DRY	7.5 kN (14.6)	-	F1
		S-FRCM-SATUR	8.6 kN (17.0)	12.8	F1

Results for the shear test in terms of average maximum load for each group of specimens and failure modes are reported in Table 1. All SRP specimens showed a failure mode characterized by debonding with cohesive fracture of the support (F1 type). After cycles in deionized water, SRP specimens exhibited a negligible decrease in bond capacity (-5.2% compared to REF), as appeared from the pull-off tests.

Failure mode of S-FRLM-DRY specimens was interlaminar failure at the matrix-fibers interface (F3 type). As expected, cement-based specimens reached an average peak load that is higher than the lime-based specimens: due to the different mechanical performance of the two mortars. The failure mode that characterized S-FRCM-DRY specimens was debonding at the matrix-substrate interface (F1 type), with a thin layer of masonry that remained attached to

the composite strip, typical failure mode of FRP-masonry joints showing that this mortar is more similar to an organic matrix rather than a mortar. The FRLM specimens tested in water saturated conditions showed a decrease in peak load of about 23%, which is comparable to the one found in the pull-off tests (-30%). It should be noted that the two results in terms of values cannot be compared since one is the average bond strength obtained from a pull-off test and the other is a bond force as obtained in the direct shear test. However, the decrease in terms of adhesion between dry and water saturated conditions is qualitatively similar. Interestingly, the specimens reinforced with cement-based composites show a small increment in the bond force (+12.8%) passing from DRY to SATUR specimens. This increment cannot be compared to the results of the pull-off tests, since as stated before, results for the cement-based specimens are not available.

4 CONCLUSIONS

This work investigated the effects of water presence in the pores of the substrate materials on the bond behavior between composites and fired-clay brick masonry blocks. Both composites applied with organic and inorganic matrices were considered, employing the same type of fibers (galvanized steel cords). Both pull-off tests and shear tests were conducted to compare qualitatively the main results. The following conclusions can be drawn:

- All the specimens reinforced with steel reinforced polymer composites are characterized by a failure mode that involved the substrate (cohesive failure) both tested in dry and in water saturated conditions.
- All the SRP specimens (both pull-off and shear tested) showed adhesion values (strengths and forces) that are higher with respect to specimens reinforced with composites applied with inorganic matrices.
- The decrease in bond strength between dry and water saturated specimens is negligible in the case of SRP (around -6% for both pull-off and shear tests).
- All the specimens reinforced with lime-based composites and steel fibers showed an interlaminar failure mode, i.e. failure plane involved the interface between the inner layer of matrix and the steel sheet.
- All the specimens reinforced with lime-based composites showed a decrease in bond strength (both measured with pull-off and shear tests) between dry and wet conditions (on average around 25%).
- All the specimens reinforced with cement-based composites and steel fibers showed a cohesive failure mode, i.e. failure plane involved the substrate as in the SRP reinforced specimens. In case of shear test, the bonding capacity for saturated specimens showed a small increment with respect to the dry specimens (around 12%). However, this trend cannot be confirmed with the results of the pull-off tests, since all the specimens failed during curing or cutting operations. This last aspect pointed out the compatibility issues between composites having an extremely high rigidity and strength and porous and weaker substrate (the employed cement-based matrix has a compressive strength > 45 MPa, while this value for brick is 17 MPa).

Acknowledgements. Technicians of LISG, LASTM and CIRI-EC laboratories of the University of Bologna and Mr. M. Ghaemi are gratefully acknowledged for their help during

the tests. Kerakoll spa (Italy) is acknowledged for providing the composite materials.

REFERENCES

[1] Babatunde, S.A. Review of strengthening techniques for masonry using fiber reinforced polymers. Compos Struct (2017) 161: 246-255.

[2] Di Tommaso, A., Focacci, F. and Micelli, F. Strengthening historical masonry with FRP or FRCM: Trends in design approach. Key Engineering Materials (2017) 747: 166-173.

[3] Sneed, L.H., D'Antino, T., Carloni, C. and Pellegrino, C. A comparison of the bond behavior of PBO-FRCM composites determined by single-lap and double lap shear tests. Cement Concrete Comp (2015) 64: 37-48.

[4] CNT-DT 215. Istruzioni per la Progettazione, l'Esecuzione ed il Controllo di Interventi di Consolidamento Statico mediante l'utilizzo di Compositi Fibrorinforzati a matrice inorganica, (2018).

[5] Franzoni, E., Gentilini, C., Santandrea, M. and Carloni, C. Effects of rising damp and salt crystallization cycles in FRCM-masonry interfacial debonding: Towards an accelerated laboratory test method. Constr Build Mater (2018) 175: 225-238.

[6] Gentilini, C., Franzoni, E., Santandrea, M. and Carloni, C. Salt-induced deterioration on FRP-Brick masonry bond. In: R. Aguilar et al. (Eds.): Structural Analysis of Historical Constructions, RILEM Bookseries 18 (2019), pp. 1914-1921.

[7] Franzoni, E., Santandrea, M., Gentilini, C., Fregni, A. and Carloni, C. The role of mortar matrix in the bond behavior and salt crystallization resistance of FRCM applied to masonry. Constr Build Mater (2019) 209: 592-605.

[8] Ghaemi Mahdi, Di Tommaso Angelo, Gentilini Cristina. An Experimental Investigation on Pull-Off Tests Conducted on FRP Composites Applied to Brick Units. Key Engineering Materials, 817 KEM, pp. 421-426 (2019).

[9] Technical datasheet of GeoCalce® Fino (Kerakoll S.p.A., Italy).

[10] EN 998-2. Specification for mortar for masonry – Part 2: Masonry mortar (2016).

[11] Technical datasheet of GeoLite® (Kerakoll S.p.A., Italy).

[12] UNI EN 12190. Prodotti e sistemi per la protezione e la riparazione delle strutture di calcestruzzo - Metodi di prova - Determinazione della resistenza a compressione delle malte da riparazione (2000).

[13] UNI EN 1542. Prodotti e sistemi per la protezione e la riparazione delle strutture di calcestruzzo - Metodi di prova - Misurazione dell'aderenza per trazione diretta (2000).

[14] UNI EN 459-1. Calci da costruzione - Parte 1: Definizioni, specifiche e criteri di conformità (2015).

[15] Franzoni, E., Gentilini, C., Santandrea, M., Zanotto, S. and Carloni, C. Durability of steel FRCM-masonry joints: Effect of water and salt crystallization. Mater Struct (2017) 50: Article N. 201.

[16] Technical datasheet of GeoLite® Gel (Kerakoll S.p.A., Italy).

12th International Conference on Structural Analysis of Historical Constructions
SAHC 2020
P. Roca, L. Pelà and C. Molins (Eds.)

COST-EFFECTIVE IMPLEMENTATION OF NITINOL TO IMPROVE THE SEISMIC PERFORMANCE OF AN UNREINFORCED MASONRY BUILDING

TERRENCE F. PARET[1*] AND JEFFREY M. RAUTENBERG[2]

[1]Wiss, Janney, Elstner Associates, Inc. (WJE)
2000 Powell Street, Suite 1650, Emeryville, California, USA 94608
tparet@wje.com, www.wje.com (*corresponding author)

[2] Wiss, Janney, Elstner Associates, Inc. (WJE)
605 Highway 169 N, Suite 1000, Minneapolis, Minnesota, USA 55441
jrautenberg@wje.com, www.wje.com

Keywords: Nitinol, Shape memory, Seismic performance, Seismic retrofit

Abstract. *Congregation Sherith Israel, one of San Francisco's lesser known gems, is an historic unreinforced masonry building with a naturally lighted dome that rises over 100 feet above its centerpiece --- an ornate mural painted vaulted sanctuary that occupies nearly 90 percent of the plan area of the building. Though damaged only modestly by the 1906 earthquake that destroyed many of its unreinforced masonry neighbors, it was subject to a local seismic upgrade ordinance. Various innovative strengthening techniques --- including the first known use in North America of super-elastic nitinol for seismic resistance --- were implemented to supplement the structure's inherent strengths. The design was developed to permit historically significant features to remain virtually undisturbed; construction was completed in 2017.*

The building was required by the municipality to be strengthened to meet seismic safety standards for assembly occupancy. Following years of study, a strengthening plan that was feasible and cost-effective, yet would not harm the historic interiors and exterior, was developed and installed. Construction involved an initial phase of more traditional strengthening in 2010 to maintain occupancy on an interim basis, followed by a second phase of innovative technologies to achieve full compliance.

The strengthening philosophy relied heavily on supplementing, rather than supplanting the existing building's strengths and leveraging its natural dynamic characteristics. The nitinol was designed to provide cost-effective easy-to-install structural "fuses" within an octagonally-configured tension tie system to promote re-centering and control out-of-phase, out-of-plane behavior of the vulnerable gable end walls, parapet and arches that define the main facades. Though the nitinol interconnects all four gable end walls, the octagonal configuration of the system causes no disruption to the domed sanctuary by circumventing the interior dome, and the sanctuary today is in the same condition as before the project. The supplemental seismic work included a fiber reinforced polymer catenary and rocking compression-only pilasters to control displacements without incrementing the demand on its floor-to-wall ties.

1 INTRODUCTION

Tension ties have been employed at least since the Augustan age to supplement the stability of masonry structures. Hoop-type tension rings have been used to resist spreading of masonry vaults and domes since the Middle Ages and through-structure iron ties in direct tension have been in common use to supplement the out-of-plane stability of masonry walls at least since the Renaissance. Such iron ties were often added as retrofit measures after cracking or deformation became concerning but were sometimes installed during original construction [1].

Whether deliberate or not, tension ties in ancient structures participate in the resistance of inertial forces that are generated during earthquake shaking. When they are installed in the upper reaches of masonry walls where local accelerations tend to maximize in any given structure, they can alleviate critical local seismic vulnerabilities, for example, of gabled end walls. Gabled end walls, which are not typically load-bearing and have low gravity-induced compression, are often the first major part of a structure to exhibit severe damage or collapse in earthquakes. However, iron ties are comparatively inflexible relative to the out-of-plane character of masonry walls, meaning that when existing structures are retrofitted with tension ties, local restraints that can be detrimental to the structural response of the masonry can be introduced. Moreover, iron ties are not conducive to promoting re-centering of the masonry; once the iron yields, whatever displacements that caused the yielding are locked-in, and iron is not especially ductile. A structural material with more forgiving properties would therefore be ideal for use in a retrofit tension tie.

Since the architecture of many houses of worship includes gabled end walls, tension ties in these structures are relatively common. Iron tension ties can often be observed transecting the main sanctuary. In addition to the aforementioned potential detrimental interaction, adding ties to a sanctuary that does not have them already can be highly disruptive to the integrity of the space, not to mention to the finishes through which such ties often pass. Means to bypass the sanctuary space without sacrificing the beneficial attributes of tension ties would also therefore be beneficial.

Recently, Sherith Israel, a historic synagogue with a domed sanctuary and gabled end walls in San Francisco, was seismically retrofitted. The centerpiece of that retrofit was an octagonally-configured tension tie system that circumvented the sanctuary space, and the sides of the octagon were connected to the gabled end walls of the structure with nitinol fuses, thus resolving the concerns described above. The system was designed to utilize inexpensive materials and installation methods without compromising performance. The design concept and details are described herein, along with the some of the other strengthening measures implemented in the project, which was completed in 2017.

2 PROJECT CONTEXT

Designed by Albert Pissis, a prominent San Francisco engineer/architect trained at the Ecole de Beaux-Arts in Paris, Sherith Israel was constructed in 1904 and is on the National Register of Historic Places. The exterior shell of the building consists of heavy brick masonry bearing walls that are clad with Colusa sandstone slabs as veneer and rise to roughly 65 feet at the main roof and 75 feet at the gables. At the east, west, and south elevations, these walls are articulated in plan and include large corbelled arch substructures that provide significant out-of-plane stability and support the gable end walls vertically. The building is capped by a steel-framed,

zinc-clad, 60-foot diameter, naturally lighted dome and drum that rise to roughly 120 feet above the street and roughly 100 feet above its centerpiece --- an ornate mural painted vaulted sanctuary that occupies nearly 90 percent of the plan area of the building and is large enough to seat nearly 1400 people. [Figures 1 and 2]



Figure 1: Exterior south and west elevations circa 1910
[photo from OpenSFHistory / wnp4.1507.jpg]



Figure 2: Interior of the sanctuary
[photo by Bruce Schneider Photography, Oakland, California]

The drum and dome are supported on a plan-octagonal system of riveted steel trusses that span to four built-up riveted steel columns; these columns support virtually all of the vertical loads from the wood and steel framing at the roof, the balcony, and the sanctuary levels, except

for a roughly 8-foot strip of floor adjacent to the perimeter walls.

A mural painted lath and plaster inner dome that is partially open to permit light from the drum above to enter the sanctuary rises to the elevation of the peak of the gables and is also supported by the octagonal trusses. The interior steel framing engages the masonry shell at only eight locations on each framing level, two on each elevation. [Figures 3 and 4]



Figure 3: Sherith Israel under construction circa 1904
[photo from OpenSFHistory / wnp14.0971.jpg]

The Great San Francisco Earthquake of 1906 exposed the initial failure modes of the building, causing substantial damage to the gable end walls (some of which remains visible), and loss of parapet coping and detachment of the masonry gable end wall from the roof framing on at least one elevation. [Figure 5]

Substantial cracking of interior plaster partitions, ceilings and the inner dome also resulted [2]. Overall though, the seismic response of Sherith Israel was as laudable as the behavior of other Albert Pissis-designed landmark unreinforced masonry structures in San Francisco, all of which survived the earthquake with little structural damage relative to many other buildings in the community, indicating that unreinforced masonry is not inherently high-risk construction if it is well-configured and constructed with high-quality materials.

In the 1980's, the State of California passed legislation requiring that the seismic risk deriving from unreinforced masonry structures that could not be demonstrated to have certain minimum levels of seismic resistance be mitigated. Effectively, the synagogue's congregation had a choice: demolish its home or strengthen it to comply.

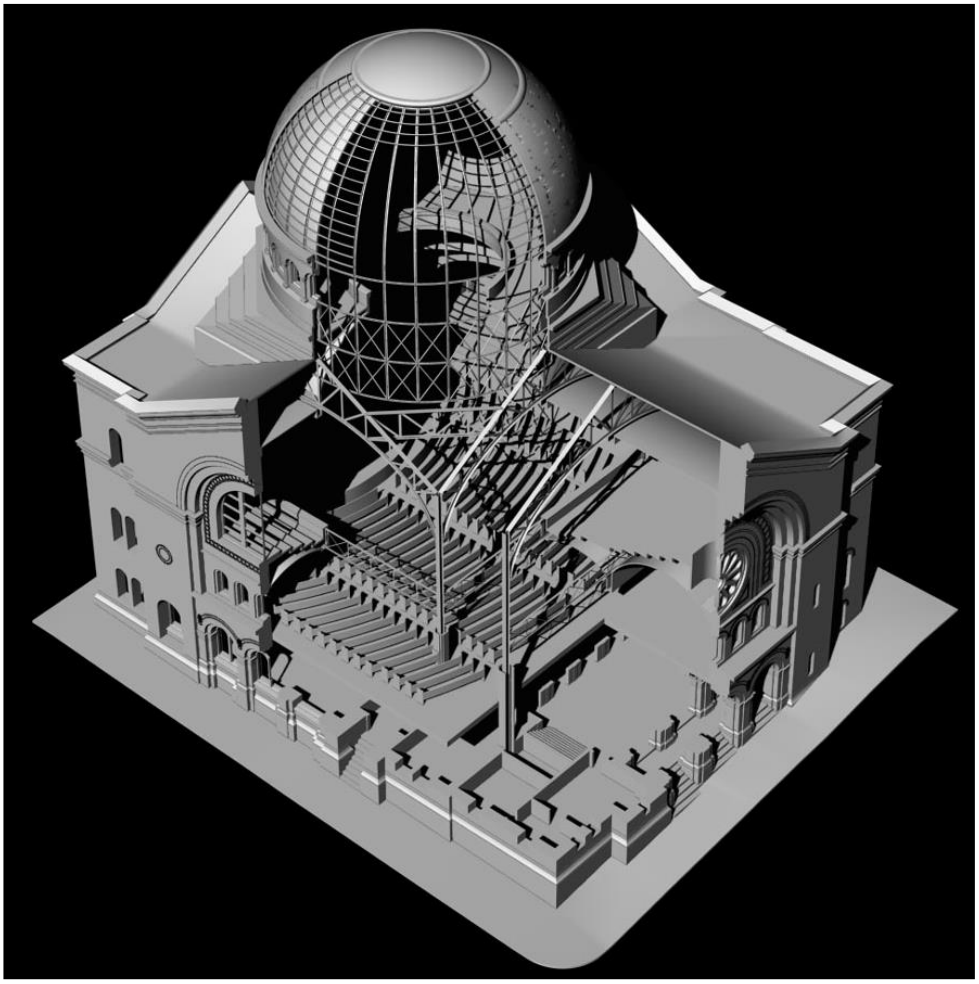


Figure 4: Isometric cut-away model
[rendering by ELS Architecture and Urban Design, Berkeley, California]

3 PROJECT PROGRESSION

The initial stages of the project included substantial documentary research and field investigation to understand the response of the structure to the 1906 shaking and to characterize its constituent construction materials, construction quality and current condition. These efforts will not be described herein beyond noting that aside from localized deterioration from periodic water intrusion during the 20th century, the building was a virtual museum in that many of the manifestations of 1906 ground shaking had gone unrepaired and remained visible in both finished and unfinished portions of the building, which revealed a great deal of empirical data about how this structure responds to ground shaking. The guiding philosophy of the project -- Engineering for Preservation -- has been described elsewhere [3][4].



Figure 5: South cornice undergoing repair after 1906 earthquake
[photo from Bancroft Library, Berkeley, California: https://calisphere.org/item/ark:/13030/hb4m3nb45g/]

3.1 Analysis

Linear dynamic analyses were conducted for various purposes, including to identify primary response modes and dynamic amplification over the building height. These analyses, which were performed using SAP2000 [5], revealed that the structure survived the 1906 earthquake in part due to the dynamic separation between in-plane and out-of-plane response modes of the perimeter masonry walls. These walls contribute roughly 85% of the mass of the entire structure and dominate the building response [6]. This separation results from the flexibility of the diaphragm framing, including the open sanctuary, that permitted a large proportion of the building mass to respond at a fraction of the spectral plateau (i.e., out-of-plane wall behavior). Preservation of this behavior was deemed to be a design priority -- second only to the goal of preserving the historic fabric of the building -- because without dynamic separation between these modes, the in-plane shear strength of the masonry would have needed to be supplemented, which would have itself resulted in widespread disruption of historic materials. The linear dynamic analyses also clearly demonstrated that the dynamic response of the gable end walls is significantly amplified with respect to the input motions and even with respect to the global spectral acceleration. Without explicit consideration of this amplification, the gable end walls would always be vulnerable to earthquake shaking.

Nonlinear adaptive pushover analyses of each of the exterior brick masonry wall elevations were performed using ADINA [7][8]. The analyses improved our understanding of the demands arising from deformation compatibility between the wood floor diaphragms and the plan-articulated masonry walls that is enforced by the diaphragm-to-wall connections necessary to

preclude out-of-plane wall failure. The flexible diaphragms permit substantial out-of-plane response of the masonry, meaning that in plan, the masonry walls are subject to behavior somewhat analogous to catenary action and must lengthen to conform to the lengthening of the diaphragm chords. However, because Sherith Israel's exterior walls are plan-articulated, coincident with lengthening, the walls undergo partial unfolding of the articulations. Understanding this unfolding via nonlinear analysis was judged to be key to designing interventions to maintain the integrity of the masonry during strong shaking. Significant cracking from unfolding during 1906 shaking was still evident in the building attic.

4 PREMISE AND GEOMETRY OF THE TENSION TIE SYSTEM

The design goals for the tension tie system included a variety of considerations, but chief among them were

1. to provide some control on the outward out-of-phase displacement of the gable-end walls and corbelled arch substructures without overly restraining them, i.e. allowing them to deform under inertial loading but limiting the opportunity for the masonry to become unstable;
2. to provide some post-yield re-centering/restorative force such that each cycle of motion would not ratchet the end wall displacement outward, but rather, would encourage the end walls to return to their original position; and
3. to add only relatively marginal cost to the overall seismic improvement project, meaning that the system had to utilize inexpensive components and it had to be readily installable in the attic of the historic synagogue. Sub-requirements for the latter included that all the components of the system had to be light enough to be easily transported to and around the attic, and assembly of the system had to be possible without welding or flame-cutting to avoid risk of fire and without shoring the historic ceilings that also functions as the floor of the attic.

A system composed of steel with nitinol fuses inserted into the load path was deemed to be ideal to accomplish these goals because both the stiffness and the strength of such a system could be readily tuned to the stiffness of the end walls, and because a design was envisioned early on that could use relatively inexpensive nitinol rods and anchoring components. Nitinol, a nickel-titanium alloy, is a superelastic material with heat-activated shape-memory attributes that was developed in the mid-twentieth century.

Until recently, the primary commercial uses of nitinol have been in the optometric and biomedical fields for which nitinol alloys are typically customized and are quite expensive. While structural/seismic uses of nitinol have been explored in university laboratories for decades, until recently, practical applications for nitinol in buildings have been elusive, partly because its hardness makes machining of it both difficult and expensive. After the 1997 Assisi earthquake, nitinol was used to retrofit three ancient structures that were damaged by that earthquake, including the Basilica of San Francisco in Assisi that was the first structure in the world to be retrofitted with a shape-memory alloy device (SMAD) [9][10]**Error! Reference source not found.**. The SMADs deployed on those projects were customized and had to be specially manufactured for their intended use. Since that time, the cost of nitinol -- especially off-the-shelf nitinol product --has become quite affordable considering the great structural advantages it can provide. It is believed that the Sherith Israel project described herein is the

first use of nitinol in North America, and the use of nitinol on this project was specifically designed to use simple off-the-shelf products, rather than devices of special manufacture.

The geometry of the tension tie system in Sherith Israel was dictated by the complex geometry of the roof, which consisted of flat areas at the building corners, steep gables at the approximate center of each of the four building elevations, and an inner lath and plaster dome that completely interrupted the line of sight between opposing gabled end walls. The desire to interconnect opposing walls at a common elevation with linear elements was thus at odds with the design goal to not allow new structural elements to intrude through the historic mural painted plaster finishes and across the sanctuary. In this instance, the design goal of preserving the integrity of the sanctuary space won out, and the tension tie system therefore designed to circumvent the inner dome, meaning that opposing walls could not be directly interconnected, but rather were interconnected via an intermediate element.

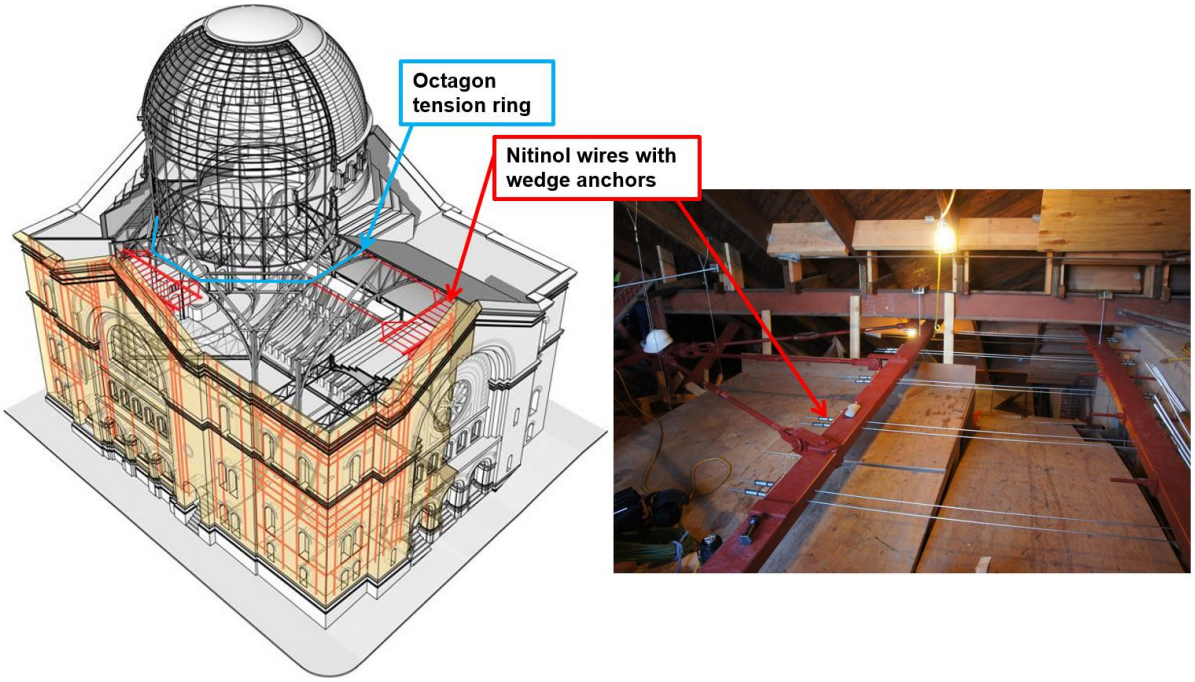


Figure 6: Geometry and installation of the tension tie system
[rendering by ELS Architecture and Urban Design, Berkeley, California]

The intermediate element was an “octagon tension ring” which was comprised of 2-inch diameter Dywidag rods. These rods were selected to balance the requirements of constructability against the desire to make the octagon tension ring as stiff as possible. The ring was located at the single elevation at which any interconnection of the end walls could be accomplished without disrupting the inner dome and still remain within the enclosed attic space; utilizing that elevation necessitated that the interconnecting elements take the form of an octagon that paralleled the existing octagonally-configured truss framing supporting the roof, the drum and the domes. For the tension ring to be installed without penetrating the roof, the new Dywidag rod elements had to be threaded through the only obstacle-free pathways that would allow for interconnection; these were barely large enough for the Dywidags to pass

through. Steel plates were sized and shaped to provide "hubs" for interconnecting the Dywidags to each other at each of the eight nodes of the octagon and for connecting other rods that extended toward the exterior walls, along the path of which were inserted the assemblies that held the nitinol fuses [Figure 6].

The nitinol fuses consisted of arrays of 0.190-inch diameter nitinol wire strung roughly 6 feet between hollow square structural steel tubes and anchored on the backside of each tube with spring-loaded wedge anchors that are typically used for anchoring high strength post-tensioning strand. Two spring-loaded wedge anchors were installed at each end of each wire to provide redundancy in the anchorage. One array was installed adjacent to, and anchored to, each of the four exterior walls, with twenty-four nitinol wires installed in each array. The interior side of each array was connected via steel tension rods to its respective nodes on the octagon tension ring. Given their appearance, the arrays were referred to as looms or harps by project personnel. The 6-foot length of the fuses was selected to allow roughly 4 inches of deformation of the wall to occur before the nitinol would begin to experience any permanent set and the cross-sectional area of nitinol in each fuse was selected such that yield of the fuse would occur at a local end wall acceleration of roughly 50 percent of gravity and one inch of outward displacement. The wire diameter was selected to permit wires to be spread more or less uniformly across the width of the gable end walls at the elevation of the tension tie, just above the top of the corbelled arches. Given the properties of the nitinol and the design configuration, outward wall deformations greater than 8 inches should be readily accommodated by the fuses.

5 NITINOL TESTING AND TUNING OF THE FUSES

Nitinol was selected early on in the design process because of its inherent ability to sustain large deformations while remaining elastic, i.e. providing a re-centering force with each cycle of response. Energy dissipation was a benefit but was not explicitly factored into the selection criteria. In general terms, nitinol's stress-strain relationship includes a linear-elastic range of response to a strain of roughly 1 percent elongation, a superelastic 'flagging' response between about 1 percent and 6 percent elongation, followed by a stiffening nonlinear inelastic response to a failure strain typically around 12 percent [Figure 7]. While nitinol has been increasingly used by the optometric and medical communities, those applications are typically highly specialized (e.g., interventional stents), use relatively expensive medical-grade alloys with highly customized and controlled properties, and employ very small-diameter wires that would be inadequate for structural applications.

The superelastic mechanical properties of nitinol can vary widely as a function of the alloying ratios, heat treatment program, and in-service temperature; as such, a robust testing program was developed so that the global behavior of the nitinol fuses could be appropriately tuned for both strength and stiffness over the superelastic range of response and means for reliably anchoring the nitinol could be verified. The diameters and lengths of the nitinol wires were first roughly sized to achieve the target properties using expected nitinol properties for off-the-shelf product; those parameters were then fine tuned based on the results of the testing program, material availability and cost.

The deformation capacity of the fuses was governed by the overall length and the maximum superelastic strain that could be expected from the nitinol wires. The target 4-inch elastic deformation capacity and the typical 6 percent maximum superelastic strain resulted in the need

for wires with a gage length of about 67 inches; wires with an overall length of 84 inches were ultimately selected to allow for the doubled wedge anchors at each end. This gage length is expected to yield superelastic behavior, energy dissipation, and a net restoring force to the masonry walls over a deflection range up to 4 inches.

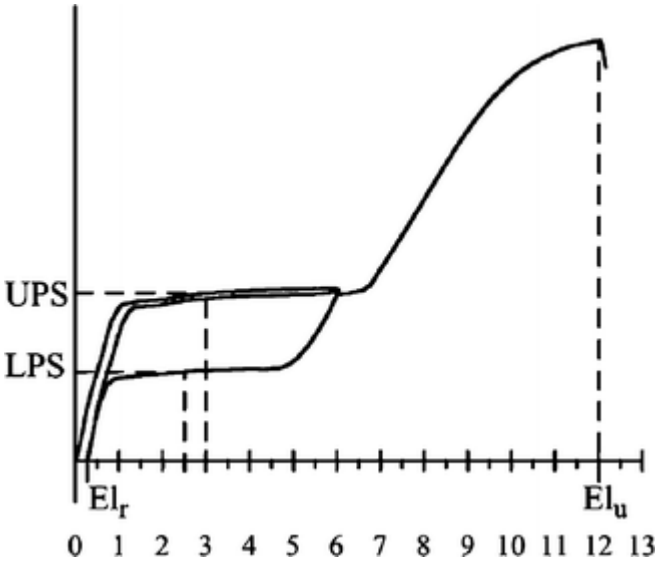


Figure 7: Typical stress-strain behavior of nitinol [11]

The quantity and diameter of nitinol wires that were used in each fuse was selected such that the total force resisted over the superelastic range of response would be roughly equivalent to 50 percent of the weight of the tributary wall area. During the initial design phase, the estimated superelastic upper plateau stress ("UPS" in Figure 7) of 70 ksi --- which is, in actuality, highly dependent on the specific nitinol alloy, the heat treatment process, and the actual ambient temperature --- resulted in the need for twelve ¼-inch-diameter wires at each nitinol fuse.

Testing to confirm and fine tune the preliminary design progressed generally in two phases: an initial feasibility study during the early design phase in 2007, and a later study in 2016 to fine-tune the selection of both diameter and alloy / heat treatment. Both phases of testing included study of means to anchor the nitinol wires, as nitinol is both very hard and difficult to machine. The first round of testing generally included cyclic tension tests of ¼-inch diameter wires to different levels of elongation in the superelastic range of response and at temperature ranges that were expected in the attic of Sherith Israel (45F, 72F, and 90F) [Figure 8]. The results of the testing program confirmed that the length preliminarily chosen for the nitinol wires would provide the anticipated deformation capacity, the diameter and quantity of wires would provide the target restoring force on the perimeter bearing walls, and that wedge anchors would provide a reliable means to transmit the seismic-induced forces into the nitinol. The exact nitinol formulation used in the 2007 testing program was no longer available for the final installation in 2016, so the design using twelve ¼-inch-diameter wires was updated with a design using twenty-four 0.190-inch-diameter wires at each fuse. The 2016 testing program was used to confirm that the actual nitinol wires selected would behave as intended and that the wedge anchors would provide sufficient anchorage at forces and deformations exceeding those expected to occur during an earthquake.

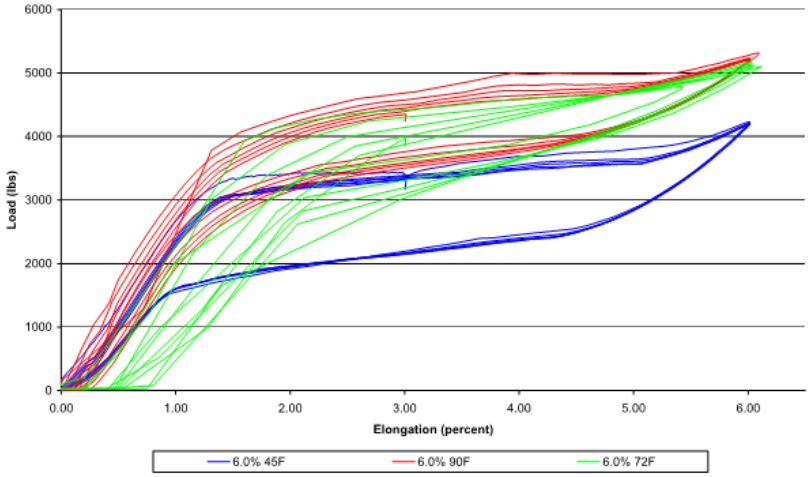


Figure 8: Stress-strain behavior of nitinol wires at a target elongation of 6%

It is worth noting that while the process for selecting and testing of the nitinol wires is described above as being rather neat and linear, the actual selection process was more circuitous. The material that was used during the initial phase of testing in 2007 was no longer available from the original nitinol supplier, so in the later phase of work, an alternate supplier had to be secured; at least three different wedge anchor products were tested and rejected due to inadequate force transfer or slipping of the grips during testing; and the later phase of testing included several different diameters of wire and several different suppliers, as some of the nitinol that was being provided did not achieve the target stress-strain behavior. This selection process served as an important reminder that the use of novel materials or systems requires additional thought and effort prior to implementation.

12 CONCLUSIONS

The historic temple, Congregation Sherith Israel, one of San Francisco's century-old gems, was constructed largely of unreinforced brick and stone masonry circa 1904 and survived the Great San Francisco Earthquake of 1906 with relatively modest damage compared to other nearby buildings, many of which suffered partial or complete collapse. Nonetheless, the structure was recently required by the municipality to be seismically improved. Out-of-plane behavior of the unreinforced masonry perimeter walls and the gabled ends, which were damaged in the earthquake, was confirmed analytically and by on-site observations of the vestiges of damage from historic earthquakes to be one of the primary vulnerabilities of the structure.

Among various other interventions, a novel, highly cost-effective, tension tie system with nitinol fuses was designed to specifically target this primary vulnerability by interconnecting all four perimeter walls to mitigate the propensity of these walls to move outward, and to introduce re-centering attributes into the system. This was the first known seismic application of this superelastic material in the United States. To avoid disruption to the temple's ornate mural painted sanctuary, whose inner dome rose to the elevation of the tops of the gable end walls, the tension tie system was designed to circumvent the inner dome and to be fully contained within the attic space using an octagonal tension ring.

Cost-efficiency and installation-efficiency were primary considerations. All components of the tension tie system were selected such that they could be hand-carried and easily installed without the need for any welding or torch work, and without heavy machinery or disruption of any interior finishes. The nitinol fuses were also designed to use "off-the-shelf" material that required no customization and no machining, and to use readily available means for anchoring.

Based on an extensive laboratory testing program, the individual nitinol rods comprising the fuses were sized both in length and diameter to limit --- but not prevent --- outward deflection of the perimeter walls, while at the same time providing a restoring force to help limit residual wall deflections after an earthquake.

REFERENCES

[1] Petrucci, Enrica, DiLorenzo, Francesco, Tie-Rods and Anchor Plates in Old Buildings: Structural Elements with High Aesthetic Impact. Metalli in Architettura, Scienza E Beni Culturali XXXI. Edizioni Arcadia Ricerche. (2015)

[2] Paret, Terrence F., Freeman, Sigmund A., Searer, Gwenyth, R., Hachem, Mahmoud and Gilmartin, Una M. Using Traditional and Innovative Approaches in the Seismic Evaluation and Strengthening of a Historic Masonry Synagogue. Engineering Structures Volume 30, Number 8 Elsevier B.V. (2008)

[3] Paret, Terrence F. Alternative Seismic Strengthening for Sherith Israel in San Francisco, CA. Association for Preservation Technology International Bulletin, (2012), pp. 21-29

[4] Paret, Terrence F., Searer, Gwenyth, R. and Freeman, Sigmund A. The Seismic Strengthening of Temple Sherith Israel, Structure Magazine National Council of Structural Engineers Associations, Volume 26, Number 5, (2019)

[5] Computers and Structures, Inc. "CSI Analysis Reference Manual" SAP2000 version 9.1, Berkeley, CA (2004)

[6] Paret, Terrence F., Freeman, Sigmund A., Searer, Gwenyth, R., Hachem, Mahmoud and Gilmartin, Una M. Seismic Evaluation and Strengthening of an Historic Synagogue Using Traditional and Innovative Methods and Materials. First European Conference on Earthquake Engineering and Seismology (2006)

[7] Hachem, Mahmoud M., Paret, Terrence F., Searer, G.R., and Freeman, Sigmund A. The Evaluation and Retrofit of a Historic Unreinforced Masonry Building Using Nonlinear Adaptive Pushover and Dynamic Analysis Methods. The 14th World Conference on Earthquake Engineering, Beijing China, (2008)

[8] ADINA R&D Inc. "ADINA: Theory and Modeling Guide", Report ARD 05-07, Watertown, MA, (2005)

[9] Bonci, A. Carluccicio, G. Castellano, M.G., Croci, G., Infanti S., and Visckovic, A. Use of Shock Transmission Units And Shape Memory Alloy Devices for the Seismic Protection of Monuments: The Case of the Upper Basilica of an Francesco at Assisi, In: International Millennium Congress - More than two thousand years in the history of architecture, UNESO-ICOMOS, Paris, Volume II, (2001)

[10] Castellano, M.G. and Infanti, S. Structural Analysis of Historical Constructions - Modena, Lourenco & Roca (eds) Taylor & Francis Group, (2005)

[11] ASTM F2516-2018: Test Method for Tension Testing of Nickel-Titanium Superelastic Materials. ASTM International, (2018).

12th International Conference on Structural Analysis of Historical Constructions
SAHC 2020
P. Roca, L. Pelà and C. Molins (Eds.)

CYCLIC TESTS ON THIN MASONRY VAULTS STRENGTHENED THROUGH COMPOSITE REINFORCED MORTAR

N. GATTESCO[1], I. BOEM[2*]

[1]Department of Engineering and Architecture, University of Trieste
Piazzale Europa 1, Trieste, Italy
e-mail: gattesco@units.it

[2] Department of Engineering and Architecture, University of Trieste
Piazzale Europa 1, Trieste, Italy
e-mail: boem@dicar.units.it (*corresponding author)

Keywords: masonry, seismic retrofitting, composite materials, thin vaults, experimental tests

Abstract. *The paper deals with the strengthening of thin masonry vaults by means of a CRM (Composite Reinforced Mortar) strengthening technique based on Glass Fiber-Reinforced Polymer (GFRP) meshes embedded in a 30 mm thick mortar matrix, applied at the vault extrados or intrados and connected to the masonry abutments through steel bars and GFRP elements. The experimental campaign concerned quasi static cyclic tests performed on four full-scale samples, supporting their self-weight only and subjected to uniform horizontal transversal loading. The results of the tests are described in terms of crack pattern, failure mode and load-displacement graphs, referring both to the horizontal displacement monitored at the crown section and to the sliding at the spring sections. High improvements in terms of both resistance and displacement capacities emerged in respect to the plain masonry and the connection with the abutments resulted fundamental for ensuring the reinforcement effectiveness.*

1 INTRODUCTION

The presence of vaults in traditional masonry buildings of the European architectural heritage is very frequent, with variations that differ for the historical period and the geographical ambit [1]. Among the different typologies, thin vaults, namely the brick "*in folio*" vaults, made of solid bricks laid flatly in a single layer, characterize several historical buildings in Central and Southern Italy [2]. They concern, typically, barrel vaults, cloister vaults and groin vaults and they are used in flooring, ceilings, covering churches aisles, staircases. Actually, the structure construction starts with the progressive bricks overhang to form the abutments of the vault then a sequence of bricks arranged in flat are placed in order to provide the wanted shape (Figure 1a). These elements can be either load-bearing structures, filled with disaggregated material, on which the upper floor insist, or secondary elements constituting the ceiling of a room or other spaces and carrying their own weight only. In this latter case, due to the very high slenderness, the vaults have a high vulnerability to accidental actions and, in particular, to earthquakes [3] - Figure 1b,c, so that strengthening interventions are needed.



(a) (b) (c)

Figure 1: Brick *in folio* masonry vaults: (a) typical configuration and examples of vault failure occurred (b) in the St. Egidio's Church of Guardea, Italy [2] and (c) in the Capuchins' Church of Urbino, Italy (ifg.uniurb.it)

In the past, the jacketing with steel reinforced concrete has been extensively used to improve the resistance and stiffness of the unreinforced vaults, but durability and compatibility drawbacks led to the use of more suitable strategies for the application to historical assets. For example, the introduction of post-tensioned steel ties [4] or the construction of additional layers of brickwork and mortar on the extrados [5]-[6] proved to be effective intervention strategies. Moreover, the coupling of non-corrosive reinforcements (glass or carbon fibers, PBO, stainless steel) with inorganic matrices (including mortars based on natural lime) is gradually becoming a common practice [7]-[9] .

In this ambit, the authors already investigated on the effectiveness of a CRM strengthening technique based on the application, at the vault extrados or intrados, of a 30 mm thick mortar coating with GFRP (Glass Fiber-Reinforced Polymer) meshes embedded [10]-[11]. The previous tests concerned full-scale masonry barrel vaults with laid on edge solid bricks. The paper reports original results concerning a recent experimental campaign on brick *in folio* masonry vaults; a particular attention was devoted to the connection of the CRM layer with the abutments, so to provide adequate resistance against sliding and uplift. Quasi-static cyclic tests, based on uniform horizontal loading, were performed on unreinforced and reinforced vaults built on masonry abutments. Both the reinforcement applied at the extrados and at the intrados were considered. The results are presented, compared and discussed in the paper in terms of crack pattern, failure mode and load-displacement graphs.

2 SAMPLES CHARACTERISTICS

The samples concern masonry barrel vaults made of solid bricks, having a rise-radius ratio $f/r = 0.5$, with radius $r = 2275$ mm, width $w = 770$ mm and thickness $t = 55$ mm (Figure 3). The compressive strength of the bricks was $f_{c,b} = 16$ MPa, that of the lime mortar $f_{c,m} = 3$ MPa. Four samples were tested: one concerned unreinforced masonry (vtNR), one reinforced masonry with the CRM at the extrados (vtRE) and two at the intrados (vtRI and vtRI+).

The CRM strengthening technique consists in the application of a 30 mm thick layer of mortar (mean compressive strength $f_{c,c} = 7$ MPa, Young modulus $E_c = 14$ GPa) with GFRP meshes embedded. To improve the adhesion to the substrate, a scratch coat was applied in samples vtRE and vtRI. Differently, in sample vtRI+, a pre-existing layer of mortar, 15 mm thick (mean compressive strength $f_{c,p} = 5$ MPa), was applied so to represent the cases where the

removal of the existing plaster is unable without the vault damaging and it is therefore preferable to overlay the CRM; the surface was bush-hammered before the CRM application.

The GFRP mesh was produced by twisting the long glass fibers in one direction across the wires in the perpendicular direction, in which the fibers were maintained straight. The wires were coated with a thermo-hardening resin (vinyl ester epoxy and benzoyl peroxide as catalyst). The mesh had a 66x66 mm^2 grid pitch, with a fiber cross area of 3.8 mm^2 in each wire. The twisted fibers wires had a mean tensile strength of 4.5 kN, with stiffness 264 kN, while the tensile strength of the straight fibers wires was 5.6 kN, stiffness 296 kN. In the vault samples, the orientation of the twisted fibers wires followed the arch direction.

In the vaults reinforced at the intrados, L-shaped GFRP connectors (6 per square meter, 7×10mm^2 cross section) were applied by insertion into holes in masonry (12 mm diameter) and injected with vinylester epoxy resin. Square parts (165×165mm^2) of GFRP mesh (33×33mm^2 grid pitch) were introduced to improve the anchorage of the connectors in the mortar layer.

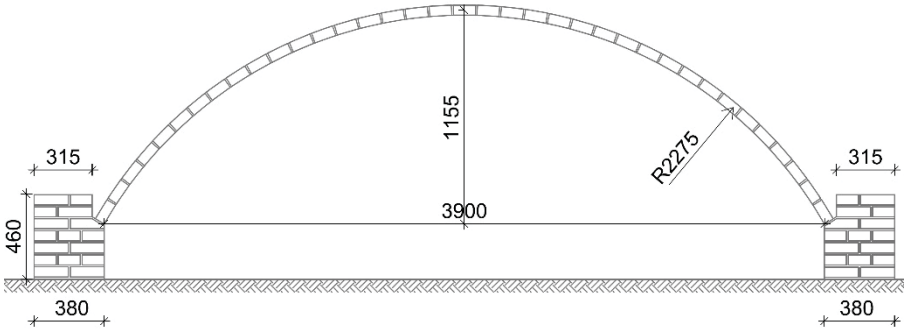


Figure 2: Main geometric characteristics of the thin vaults samples

To connect the CRM reinforcement to the masonry abutments, three stainless steel M6 threated bars, 260 mm spaced, were applied at each end (Figure 3). Each bar was injected in the masonry abutment with tixotropic epoxy resin (300 mm bond length) and embedded in the mortar coating (a minimum bond length of 40 times the bar diameter was ensured), with a nut applied at the end. Moreover, in cases concerning CRM applied at the intrados, the external couples of L-shape GFRP connectors perpendicular to the vault surface were deeply injected in the masonry abutments (Figure 3b).

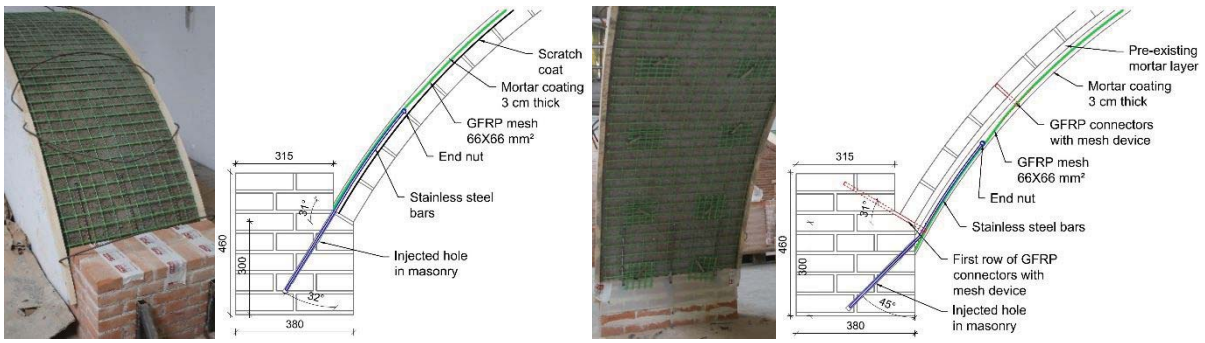


Figure 3: Arrangement of the CRM connection with the abutments for samples reinforced (a) at the extrados and (b) at the intrados

4 TEST SETUP

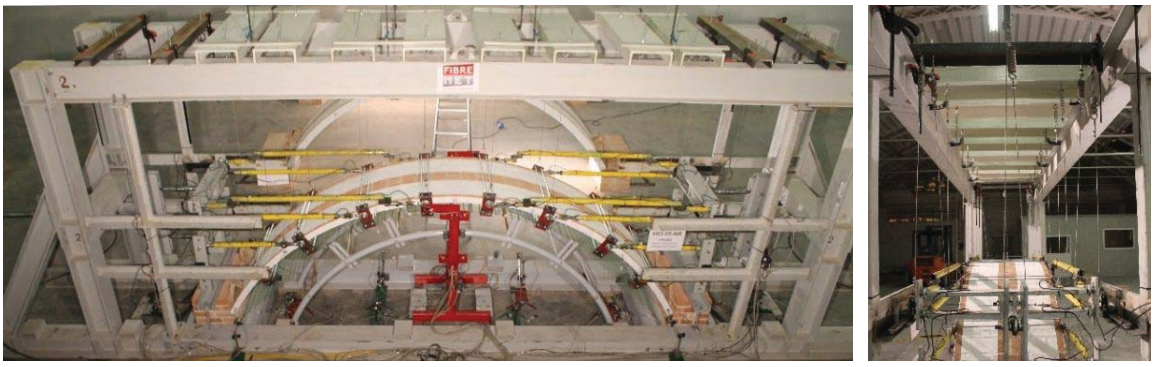
The test setup (Figure 4a) was aimed to reproduce a uniform transversal load pattern representing the effect of the horizontal inertial forces induced by an earthquake on thin masonry vaults supporting their own weight only.

Quasi-static cyclic tests were performed: forces of identical magnitude and direction were applied at eight different points along the vault length, equally spaced, through pinned frame systems installed at the two halves of the vault and supported by sliding guides. The horizontal load was modulated through two hydraulic actuators applied at the opposite sides of the contrast structure and activated by a hand pump. Flow control valves permitted loading, unloading and the inversion of the loading direction.

The steel apparatus was designed adequately stiff, so to assume negligible its deformation in respect to that of the sample; loading cells and potentiometer transducers allowed the real-time monitoring of the load displacement story. More details were reported in [1].

It is observed that, due to the thinness of the vault, the vertical forces transmitted by the loading arms, induced by their weight, can modify significantly the vault stress state, especially in the early stages of the tests, when the horizontal load is low. Thus, the loading arms were hanged on the upper beams of the contrast frame through steel cords equipped with a preloaded tension spring at the upper end (Figure 4b). The initial elongation of each spring was calibrated so to completely counteract the vertical load transmitted to the vault. Similarly, also the pinned frame systems for the load distribution were hanged to avoid friction on the sliding guides.

It is worth to note that, in the early stages of the tests, the variation in the springs elongation is negligible, since the vault deformation is limited, as well as the cords inclination (the cords length was at least 950 mm).



(a) (b)

Figure 4: Test setup for the vaults: (a) global view and (b) detail of the hanging system

3 EXPERIMENTAL RESULTS

During the tests, horizontal cracks opened at the intrados or extrados, due to the flexural tensile failure of the masonry or of the mortar coating. The crack patterns of the vaults are schematized in Figure 5a-Figure 8a, distinguishing cracks formed for the two opposite loading directions (red and blue colors in agreement with the load direction).

Actually, in the unreinforced vault vtNR (Figure 5a,b), the cracks were localized in few sections. At first, in the negative loading direction, three cracks opened in the left vault side:

one at extrados, in an haunch section (Figure 5c) and two at the intrados, at the skewback and near the keystone (Figure 5d). Then, when the loading direction was inversed, one crack at the extrados (at right haunch - Figure 5c) and one at intrados, at the right skewback, formed. The presence of four hinges, in alternate position extrados-intrados, was thus achieved and the vault failure mechanism activated. The maximum load, $F_{h,max}$, equal to 0.55 kN, was attained in correspondence of very small horizontal displacement at the crown section δ_{hK} (<1 mm).

Differently, in the reinforced samples, once four cracks formed in alternate position intrados-extrados (typically, at the two skewback sections and at two opposite haunch sections), the load was maintained and even slightly increased. This was due to the presence of tensile resistant elements such as the GFRP mesh and the connection bars with the abutments, which provided additional bending resistance to the reinforced masonry sections. At the increasing of the vault deformation, a diffuse cracking of the mortar coating generally occurred and several cracks formed on the masonry side.

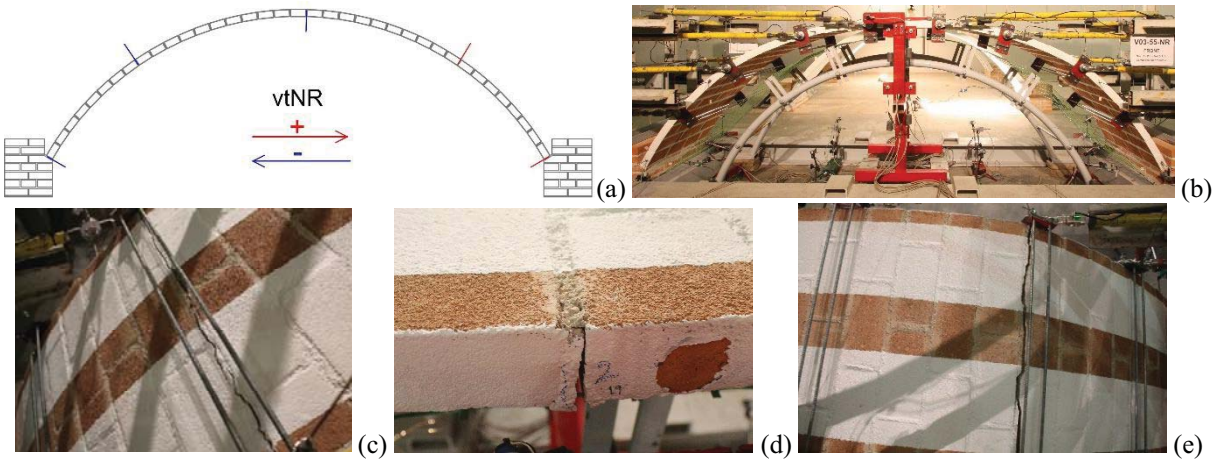


Figure 5: Sample vtNR: (a) crack pattern, (b) global view at the incipient collapse and details of the cracks (c) at the left haunch, (d) in the vicinity of the crown section and (e) at the right haunch

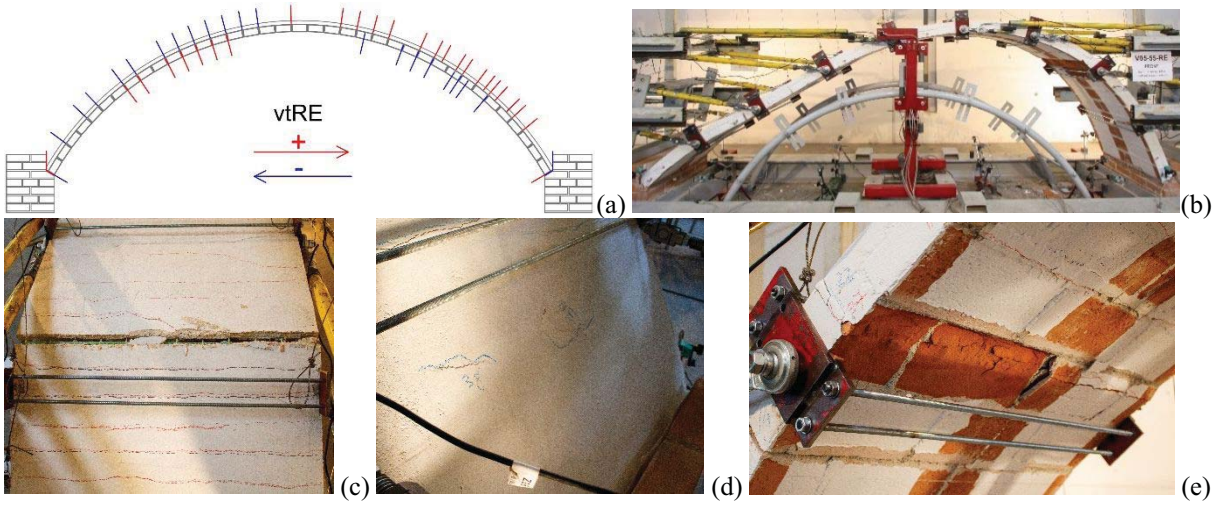


Figure 6: Sample vtRE: (a) crack pattern, (b) global view at the incipient collapse and details (c) of the cracks and GFRP mesh rupture at the extrados of the right haunch, (d) of the mortar local cracking in correspondence of the connection steel bars and (e) of the compressive local failure of some bricks at the intrados of the left haunch

Sample vtRE (Figure 6a,b) reached a maximum load $F_{h,max}$ = +11.8 kN at δ_{hK} = 115.5 mm. The vault collapsed when the rupture of the GFRP wires disposed along the vault occurred at the right haunch section (Figure 6c). During the test, starting from about $\delta_{hK} \cong \pm$ 80 mm, some mortar local damage in the vicinity of the end nut of some steel bars was noted, as likely caused by the occurrence of some slip in the coating (Figure 6d). The bricks compressive failure at the haunches was also observed at very high displacements (δ_{hK} > 110 mm) - Figure 6e.

Sample vtRI (Figure 7a-d), attained to +7.3 kN (at δ_{hK} = +19.6 mm) in the positive direction and then approximately maintained the load, while in the negative, once reached -8.2 kN (at δ_{hK} = -27.9 mm) the load gradually decreased. Some mortar damaging in the vicinity of the GFRP connectors at skewbacks emerged from about $\delta_{hK} \cong \pm$ 45 mm. Moreover, at about $\delta_{hK} \cong \pm$ 70 mm, a conic splinter in correspondence of some steel bars, close to the end nut, evidenced the partial extraction from the coating (Figure 7c). Some inward slip was noted at the spring sections (Figure 7e); while no evident outward slips emerged (Figure 7f).

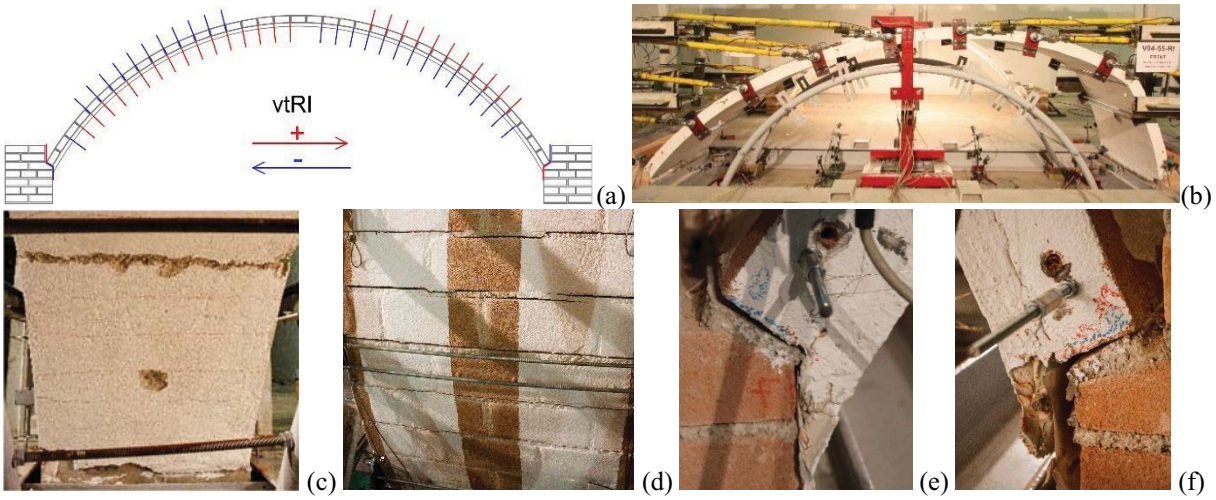


Figure 7: Sample vtRI: (a) crack pattern, (b) global view at the incipient collapse and details of the cracks (c) at the intrados of left haunch, (d) at the extrados of right haunch and at the (e) left and (f) right spring sections

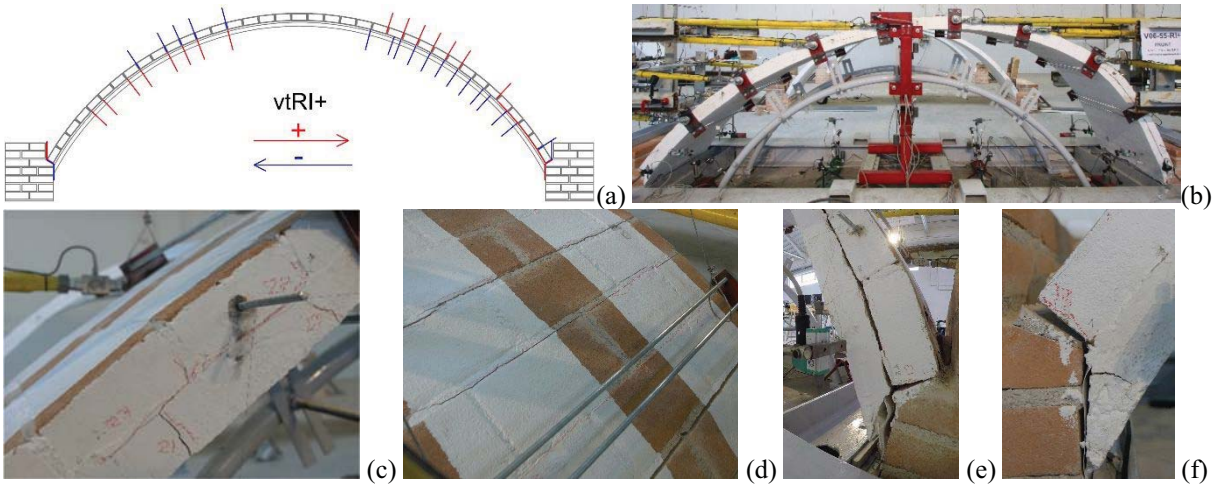


Figure 8: Sample vtRI+: (a) crack pattern, (b) global view at the incipient collapse and details of the cracks (c) at the intrados, left haunch, and (d) at the extrados, right haunch, (e) of the mortar detachment from the masonry at the right end and (f) of the inward slip at the left spring section

Sample vtRi+ (Figure 8a-d) attained to +13.1 kN (at δ_{hK} = +39.0 mm) and to -10.5 kN (at δ_{hK} = -21.0 mm). As the deformations increased, detachment surfaces formed between the pre-existing mortar layer and the masonry substrate (Figure 8c); the most relevant emerged at about δ_{hK} = +40 mm, around the right skewback (Figure 8e) and induced a significand load decrease in both directions. Some inward slip was also noted at the spring sections (Figure 8f).

4 ANALYSIS OF RESULTS

The results of the tests on reinforced masonry vaults are plotted in the graphs of Figure 9-11a, in terms of capacity curves representing the trend of the global horizontal load, F_h, at the varying of the mean horizontal displacement monitored at keystone δ_{hK}. The capacity curve of the unreinforced masonry sample was omitted, due to the very low performances in terms of both resistance and displacements before collapse ($F_{h,max}$ = 0.55 kN, with δ_{hK} <1 mm).

All the reinforced samples achieved significantly high performances in respect to the plain vault, both in terms of horizontal load and displacement capacities. In particular, the resistance ratio resulted about 21.5 for vtRE and 14.9 for vtRI.

The comparison between vtRI+ and vtNR is not proper (an unreinforced masonry vault with a pre-existing mortar layer should be considered). However, vtRi and vtRI+ can be compared: the presence of the pre-existing layer of mortar, reasonably lead to and higher resistance (+60%), due to the thicker cross section, but a premature detachment of the mortar from the masonry substrate, related to the higher stress state, can compromise the reinforcement effectiveness (reduced ductility).

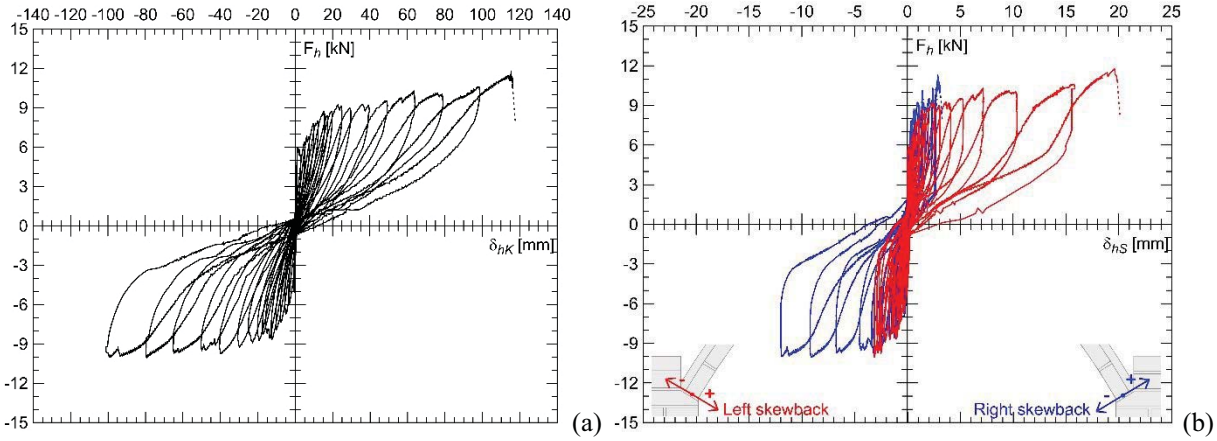
Reasonably, a progressive strength and stiffness degradation in the capacity curves of the reinforced samples would occur in repeating cyclic deformation during the test, due to irreversible damage accumulation related to the cracking and the crushing phenomena in the masonry and in the mortar coating.

The trends of the horizontal load at the varying of the mean tangential displacements δ_{hS} monitored at the skewback sections are plotted in Figure 9-11b. It is observed that, in sample vtRE (Figure 9b), the inward displacements resulted slightly higher in the positive loading direction and reached about +20 mm at the left vault end in correspondence of the peak load. In both loading directions, the outward sliding resulted more limited due to the constraint provided by the masonry abutments; thus, the graphs $F_{h,max}$ - δ_{hS} are asymmetric. In sample vtRI, the inward slides attained to about ±15 mm at the last cycles (Figure 10b); while in sample vtRI+ (Figure 11b) ranged between -8.5 mm and + 17 mm at peak loads. Then, sliding reached –15.5 mm and +25.5 mm; also comparable outward slides emerged in the last cycles.

The configuration with the reinforcement applied at the extrados, vtRE, resulted more effective than that with the reinforcement applied at the intrados, vtRI. In this regard, it is observed that the monitored inward sliding at the spring sections determined, in vtRE, an increasing of the bending at the extrados along the vault, with a better exploitation of the GFRP mesh resisting contribution in tension, as evidenced by the final rupture of the mesh wires. Differently, in vtRI, the inward slide induced a decrease of the bending stress along the vault intrados; in fact, the mesh failure did not occur. However, the resistance increase in respect to the unreinforced configuration is significant, thus the investigated configuration is adequate.

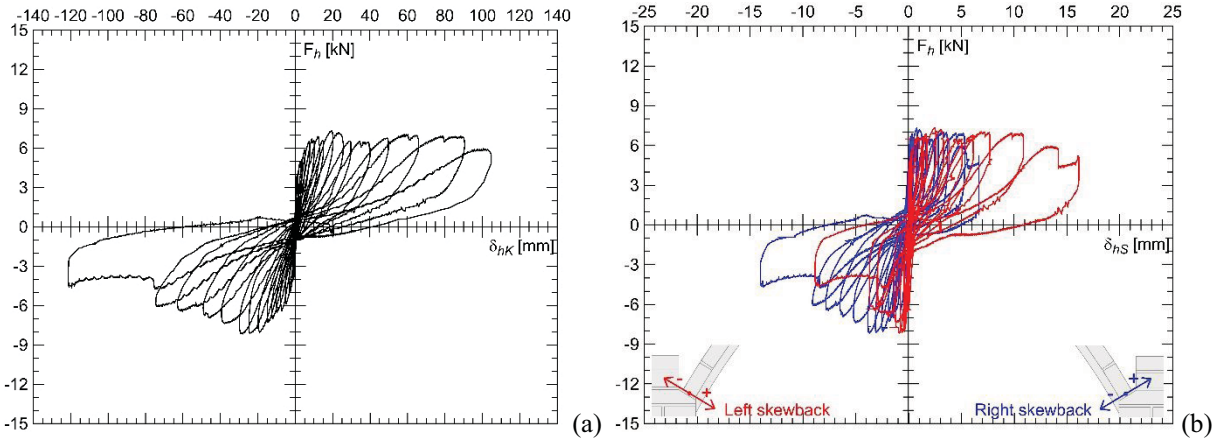
In general, the appropriate design of the connection of the CRM layer with the abutments, (both in resistance and in stiffness), is fundamental for assuring the effectiveness of the

strengthening intervention and avoiding that excessive, premature local movements at the ands compromise the reinforcement contribution.



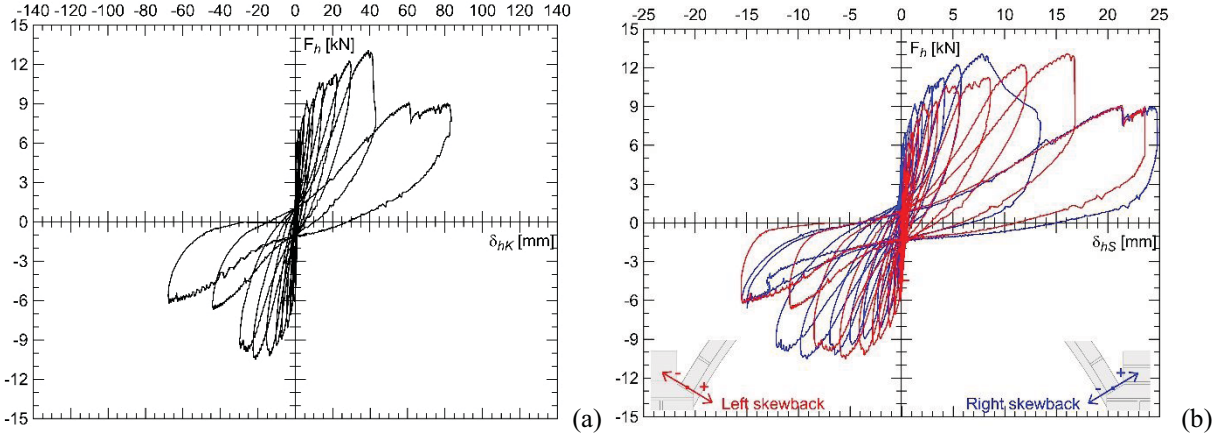
(a) (b)

Figure 9: Sample vtRE - trend of the horizontal load at the varying (a) of the horizontal displacements at the crown section and (b) of the tangential displacement at the skewback sections



(a) (b)

Figure 10: Sample vtRI - trend of the horizontal load at the varying (a) of the horizontal displacements at the crown section and (b) of the tangential displacement at the skewback sections



(a) (b)

Figure 11: Sample vtRI+ - trend of the horizontal load at the varying (a) of the horizontal displacements at the crown section and (b) of the tangential displacement at the skewback sections

9 CONCLUSIONS

The paper reports original results of a recent experimental campaign on thin masonry barrel vaults strengthened with CRM system. It concerned quasi static cyclic tests performed on full-scale samples subjected to horizontal transversal loading, so to reproduce the effects of inertial forces induced by an earthquake on thin vaults supporting their own weight only.

The tests setup is described in the paper, evidencing the strategy adopted to avoid parasitic stresses on the samples, induced by the loading system. The main samples features are reported, focusing on the strategy adopted to connect the reinforced layer to the masonry abutments, based of steel bars and GFRP L-shape connectors.

The results of the tests are described, detailing the crack patterns and the different failure modes of the four tested samples: one unreinforced (vtNR), one with the CRM applied at the extrados (vtRE) and two with the CRM at the intrados (vtRI and vtRI+, in which the presence of a pre-existing mortar layer was also accounted). The experimental curves of the reinforced samples, representing the trend of the horizontal load at the varying of both the horizontal displacement at the crown section and of the sliding at the spring sections, were plotted and compared.

It emerged that the GFRP mesh is able to limit the separation by rotation of the faces of cracked sections, allowing instead a widespread mortar cracking and delaying the activation of the collapse mechanism. High improvements in terms of both resistance and displacement capacities were obtained in respect to the plain masonry: the resistance ratios resulted about 21.5 timer for vtRE and 14.9 for vtRI. The result of sample vtRI+ evidenced that the interface between the pre-existing mortar layer and masonry substrate is a very critical area in which a premature detachment can occur, compromising the effectiveness of the reinforcement (ductility).

The connection with the abutments resulted, in general, fundamental for the reinforcement effectiveness, contrasting the free rotation at the vaults ends and opposing to the inward sliding. It is however observed that the designed connection configurations partially constrained these rotations/displacements, as emerged by the sliding monitored at the spring sections and evidenced by some mortar local damage in the vicinity of some steel bars and of some GFRP connectors.

Numerical investigations are in progress, so to simulate the experimental tests and perform parametric analysis on more configurations. Pull-out characterization tests will allow to calibrate the actual behavior of both the GFRP L-shape connectors and the steel bars and also to evaluate the possible contribution of the bars in contrasting the inward sliding (dowel effect).

Acknowledgements. This paper is based on part of a research project financed by the composite engineering factory Fibre Net SpA, Pavia di Udine (UD), Italy. The authors wish also to thank Allen Dudine, Carlos Passerino and Andrea Miniussi for the useful help provided during the tests.

REFERENCES

[1] Brumana, R., Condoleo, P., Grimoldi, A., Landi, A.G. Shape and construction of brick vaults. Criteria, methods and tools for a possible catalogue. In: *The International Archives of the Photogrammetry, Remote Sensing and Spatial Information Sciences*, Volume XLII-

5/W1 (2017). *Geomatics & Restoration – Conservation of Cultural Heritage in the Digital Era*, 22–24 May 2017, Florence, I.

[2] Nunziata, A., Bianchini, N., D'Andrea, M., E., Serpe. Le volte in foglio e il sisma. Analisi delle chiese nell'area Umbro-Marchigiana. In: *IV Convegno di Ingegneria Forense - VII Convegno su crolli, affidabilità strutturale, consolidamento*, 14-16 September 2017, Milan, I (in Italian).

[3] Indirli, M., Kouris, L.A.S., Formisano, A., Borg, R.P., Mazzolani, F.M. Seismic Damage Assessment of Unreinforced Masonry Structures After The Abruzzo 2009 Earthquake: The Case Study of the Historical Centers of L'Aquila and Castelvecchio Subequo. *International Journal of Architectural Heritage: Conservation, Analysis and Restoration* (2013), **7**(5), 536-578.

[4] Jurina, L. The reinforced arch: a new technique for strengthening masonry arches and vaults using metal tie bars. In: *16th National Congress of the C.T.A.* (1997) Ancona, I.

[5] Capozucca, R., Analysis of thin composite masonry vaults. *Masonry International* (1997) **11**(1): 19-25.

[6] Castori, G., Borri, A., Corradi, M. Behavior of thin masonry arches repaired using composite materials. *Composites Part B: Engineering* (2016) 87:311-321.

[7] Briccoli Bati, S., Rovero, L., Tonietti, U. Strengthening masonry arches with composite materials. *Journal of Composite for Construction* (2007) **11**(1):33–41.

[8] Garmendia, L., Marcos, I., Garbin, E., Valluzzi, MR. Strengthening of masonry arches with Textile-Reinforced Mortar: experimental behaviour and analytical approaches. *Materials and Structures* (2014) 47:2067–80.

[9] Alecci, V,, Focacci, F., Rovero, L., Stipo, G., De Stefano, M. Extrados strengthening of brick masonry arches with PBO–FRCM composites: Experimental and analytical investigations. *Composite Structures* (2016) 149:184–96.

[10] Gattesco, N., Boem, I. Strengthening of masonry vaults through a thin extradoxal layer of fiber reinforced lime mortar. In: *10th International Conference on Structural Analysis of Historical Constructions*, 13-15 September 2016, Leuven, B.

[11] Gattesco, N., Boem, I., Andretta, V. Experimental behaviour of non-structural masonry vaults reinforced through fibre-reinforced mortar coating and subjected to cyclic horizontal loads. *Engineering Structures* (2018) **172**: 419–431.

12th International Conference on Structural Analysis of Historical Constructions
SAHC 2020
P. Roca, L. Pelà and C. Molins (Eds.)

EVALUATION OF PERFORMANCE OF MATURED HYDRAULIC GROUTS: STRENGTH DEVELOPMENT, MICROSTRUCTURAL CHARACTERISTICS AND DURABILITY ISSUES

ANDRONIKI MILTIADOU-FEZANS[1*], MICHAIL DELAGRAMMATIKAS[2], ANNA KALAGRI AND PANAYOTA VASSILIOU[2]

[1]School of Architecture
National Technical University of Athens (NTUA)
Patission42, 10682 Athens, Greece
e-mail: amiltiad@central.ntua.gr(*corresponding author)

[2]School of Chemical Engineering
National Technical University of Athens (NTUA)
Zografou Campus, IroonPolytechneiou9, 15780 Athens, Greece
email: mdel@mail.ntua.gr, pvas@chemeng.ntua.gr

Keywords: Grout, natural hydraulic lime (NHL), pozzolan, performance, mature specimens, durability

Abstract. *The present paper evaluates the performance of matured hydraulic grouts, with respect to their composition and the induced microstructural characteristics. Four different grout compositions were examined; three grouts based on natural hydraulic lime (NHL5), plain and in combination with pozzolan, and a ternary white cement - pozzolan - hydrated lime mixture. Both grout-only specimens and composite injected material have been examined and injected grout - masonry material interaction issues are discussed.*

1 INTRODUCTION

Grouting constitutes one of the most common techniques applied for the repair and strengthening of historic masonry structures or fissured architectural members, when interconnected voids are present. Systematic research has been undertaken for the performance evaluation of various types of grouts and specific design criteria have been developed [1-9]. This technique is also used for the in-situ conservation of detached or cracked mosaics, wall paintings or frescoes and other valuable decorative surfaces [10-13]. Given the fact that it is a non-reversible intervention, a holistic methodology has to be adopted both for the design of the grout and the method of its application [14].

A series of research works for the performance evaluation of natural hydraulic lime (NHL) grouts, realized during the last decades, have proved the mechanical efficiency of this type of grouts for the structural restoration of stone masonry [3, 4, 6, 15-23]. Due to the similarity with the in-situ materials, natural hydraulic lime grouts are favoured in structural restoration of historic masonries, constituting a reliable alternative to higher strength ternary cementitious grouts (with low cement content). Thus, further systematic research for the optimization of NHL-based grouts, with respect to their composition and taking into account both fresh and hardened state properties over time, is of great interest.

The aim of this work is to investigate the performance of three NHL grout compositions along with a ternary mixture, by studying their physicochemical, mechanical and durability characteristics. Fresh state injectability, as well as hardened state mechanical properties at 28, 90 and 365 days are presented first. Subsequently, physicochemical, mechanical, microstructural characteristics and durability to soluble salts of matured specimens of these grouts are studied and commented upon. The paper is concluded with the presentation of the results of representative samples selected from injected mosaic substrata (constructed on wall models, damaged and then consolidated with grouts) and examined by SEM/EDS and XRD, providing data on their penetration capacity and their solidification inside porous media.

2 MATERIALS AND METHODS

2.1 Grouts composition, mixing procedure and fresh state properties

Three different grouts based on natural hydraulic lime NHL5, plain or mixed with pozzolan of type I and a ternary grout, of low alkali and sulphate content white cement, mixed with hydrated lime powder and pozzolan of type II, were examined (Table 1). Both pozzolans are natural, finely ground materials with pozzolanicity of 7.5 N/mm^2 and 5.8 N/mm^2 respectively.

Table 1: Composition of the grouts

Composition (% w/w)	NHL5 (St Astier)	White cement (Aalborg)	Pozzolan Type I	Pozzolan Type II	Lime Powder	Super-plasticizer*	Water*
GR1	100%					[(a)]1%	80%
GR2	90%		10%			[(b)]1%	80%
GR3	80%		20%			[(b)]1.5%	80%
GR4		30%		45%	25%	[(c)]1%	80%

Notes: Superplasticizers are based on (a) modified lignonaphthalene salts (CHEM SPL™, Domylco), (b) polyether carboxylates (CHEMIUM 172™, Domylco) and (c) naphthalenesulfonate polymer (RHEOBUILD™ 5000, Basf); * superplasticizer and water percentage refer to the grout solids total mass.

The design of the grouts was performed with the aim to ensure high injectability under low pressure (~0.075 MPa), even in voids and cracks of nominal minimum width (W_{nom}) equal to 0.2 mm. For this purpose, the penetrability, fluidity and stability characteristics of the suspensions were fully examined. Based on the design criteria proposed in literature [7, 8, 9], a water to solids ratio equal to 0.80 was experimentally determined, together with the adequate type and dosage of superplasticizer. The standardized sand column test method (EN 1771) was applied to check the penetrability and fluidity, along with the determination of the Fluidity Factor (using a Marsh cone of 3 mm nozzle diameter) and the flow time of 500 ml of grout, out of 1000 ml inserted in a Marsh cone of 4.75 mm nozzle diameter (EN445); stability of the suspension was studied using NF P18-359 (Table 2). An ultrasound dispersion mixer of 28 kHz, assisted by simple mechanical stirring at 300 rpm, was employed for the laboratory preparation of the mixtures. The mixing time was 3-4 min for the NHL-based grouts and 6 min for the ternary grout (2 min/solid component).

2.2 Mechanical tests

For the evaluation of the mechanical properties of the grouts, prismatic specimens (40x40x160 mm) were prepared and moulded in the laboratory. The curing conditions were kept constant at 90 ± 5% RH and 20 ^{o}C (EN 459/2) until the execution of the tests at the ages of 28, 90 days and 12 months, using a Tritech 100 kN Wykeham Farrance machine at 0.05 mm/min and 0.1 mm/min loading rate in flexion and compression, respectively (Table 2). For the determination of the flexural strength, three prismatic specimens were tested under a three-point bending arrangement. After a period of about 2 years, during which the specimens were preserved in the environmental chamber, they were removed and kept at 90 ± 5% RH at room temperature up to the age of 14 years. The matured grout specimens were tested in compression using the same apparatus and loading conditions.

2.3 Examination of microstructural characteristics of matured grouts

Porosity and porous size distribution were examined by mercury intrusion porosimetry (MIP) at the age of 14 years using a Quantachrome Autoscan 60 Porosimeter composed of two units, for low (24 psi) and for high (60000 psi) pressure. For the evaluation of large void volumes, polished specimens were examined by SEM/EDS (FEI Quanta 200 coupled with an EDAX detector) at low magnifications and the micrographs were analysed by digital image processing (DIP) using ImageJ FIJI software [24], while the EDS elemental analysis results were used in order to evaluate the cementation index of each composition. Mineralogical analysis was performed X-ray diffraction (XRD) of powdered samples, using a Bruker D8 ADVANCE apparatus, equipped with a Lynxeye detector, at a 0.03˚/0.8 s step.

The water absorption coefficient by capillarity (C) was determined in accordance with NORMAL 11/85. A notable variation from the norm is that prior to the measurements, the grout specimens were dried at a temperature of 45 ± 5 ˚C, as the drying conditions described in the standard are too severe for grouts.

In addition to the cured grout-only specimens, representative samples of two of the examined grout compositions (GR1 and GR4) were retrieved from the injected substrata (lime and OPC based mortars respectively), bearing the mosaics attached on three-leaf wall models, constructed in the framework of a research project for grouting strengthening of three-leaf masonry [4, 6]. These specimens, taken from the injected wallettes -matured indoors until the execution of the mechanical tests and then exposed to outdoors conditions, without any particular curing- were examined by SEM/EDS, XRD and MIP, in order to qualitatively evaluate their preservation state, the penetration capacity of the grout, its bonding with the wall inner materials and the mosaic substrata, as well as its microstructure, chemical and mineralogical composition.

2.4 Durability of grouts to sodium sulphate salt crystallization test

The salt crystallization damage is one of the most common causes of porous building materials deterioration. The mechanisms of crystallization, crystal growth and crystallisation pressure inside the pores of building materials [25], as well as their consequent degradation patterns (crack development, pulverisation, crumbling, flaking etc.) were extensively studied and analysed [26]. A number of factors influence this phenomenon, such as the building

materials porosity, the porous size distribution and morphology, the composition of the salt solution, the wettability of the porous media, as well as environmental parameters.

In the present study sodium sulphate salt durability tests were carried out according to the following procedure: matured grout specimens (cubes 20x20x20 mm) preserved for 14 years, in the same conditions as presented in paragraph 2.2, were impregnated in 10% w/w sodium sulphate (Na_2SO_4) solutions and dried for six cycles at 20°C. After the sixth cycle, half of the specimens were dried at 20°C and the others at 50°C until constant mass was reached.

3 RESULTS AND DISCUSSION

3.1 Rheological, physico-mechanical, chemical and microstructural characteristics

As presented in Table 2, all the grout compositions met the following injectability criteria: the time required for the grout to reach the top of the sand column penetrability test (h = 36 cm) was set to less than 50 s ($T_{36} \leq 50$ s); the Fluidity Factor values had to be higher than $0.7x10^3$ mm/s and the total efflux time of 500 ml of grout out of 1000 ml inserted in the cone (measured with a Marsh cone having a 4.75 mm nozzle diameter) had to be between 20 s and 45 s ($20 \text{ s} \leq t_{d=4.75} \leq 45$ s); the maximum acceptable limit for the bleeding test was set to 5% [1, 7, 8, 9].

Table 2: Rheological, mechanical and hydric characteristics of the grouts

	GR1	GR2	GR3	GR4
T_{36}: Sand column 1.25/2.50 mm (voids: 0.2–0.4 mm)	22.5 s	24 s	26 s	19 s
Fluidity Factor ($x10^3$ mm/s)	0.99	0.88	0.71	1.15
Marsh cone $t_{d=4.75\ mm}$ (500 ml of grout)	22 s	24 s	25 s	20.5 s
Bleeding	2%	1%	< 1%	3%
Flexural Strength (MPa) 40x40x160 mm specimens	1.16 (28 d) 1.75 (90 d) 4.04 (1 y)	1.31 (28 d) 1.90 (90 d) 3.80 (1 y)	1.22 (28 d) nd 3.34 (1 y)	2.14 (28 d) 2.29 (90 d) 3.49 (1 y)
Compressive Strength (MPa) 40x40x40 mm specimens	1.64 (28 d) 4.50 (90 d) 6.80 (1 y) 10.4 (14 y)	2.51 (28 d) 5.34 (90 d) 7.01 (1 y) 11.4 (14 y)	2.11 (28 d) nd 5.47 (1 y) 12.0 (14 y)	3.66 (28 d) 8.16 (90 d) 13.85 (1 y) 18.1 (14 y)
C ($g \cdot cm^{-2} \cdot s^{-0.5}$)	0.010 (14 y)	0.007 (14 y)	0.013 (14 y)	0.005 (14 y)

The mechanical properties of the NHL5-based grouts, especially compressive strength, are generally improved with the addition of pozzolan due to the stable products produced by the pozzolanic reaction, resulting to a pore refinement as indicated by MIP measurements (Table 3). Increasing the addition of pozzolan from 10% to 20% leads to a small decrease of the strength during the early ages, which is probably attributed to the slow rate of the pozzolanic reaction. These results highlight the need for a more systematic research regarding the various component dosage, with the aim to reach an optimization, when complete consumption of

portlandite is sought. Given that the reactivity of a pozzolan is highly dependent on its composition and granulometry, a generalized model of the pozzolanic reactivity cannot exist. Thus, every new pozzolan in the NHL5-pozzolan system requires a different systematic study. Nevertheless, the mechanical properties of matured NHL5-based grouts, measured in the present study, proved to be very satisfactory, indicating that the addition of pozzolan has a significant positive effect to the strength development over time. Unfortunately, there were no matured specimens suitable to test in flexion, so these interesting findings can only be validated, as far compressive strength is concerned.

SEM backscattered electrons micrographs (Fig. 1) show that the grout microstructure at the age of 14 years appears denser in the case of ternary grout and hydraulic lime grouts with 20% pozzolan. The evident reduction of large void volumes with the addition of pozzolan was quantified by DIP (Fig. 2).

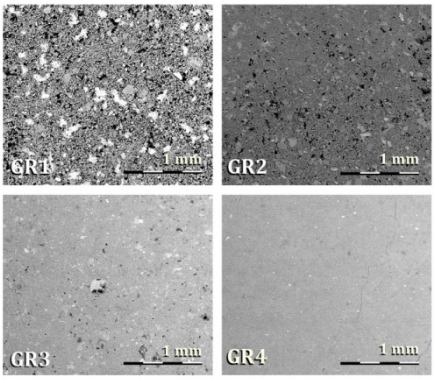


Figure 1: SEM-BS images of the hardened grouts, at low magnification (50x). Large voids appear dark.

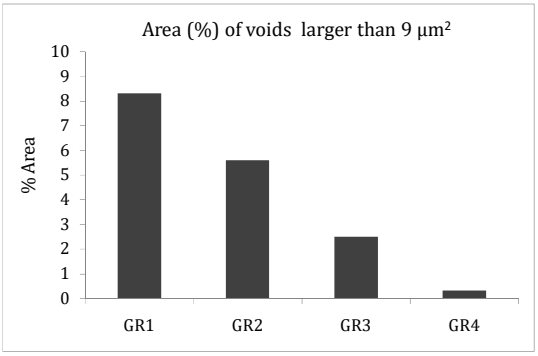


Figure 2: Area (%) of voids larger than 9 square microns estimated by DIP.

Table 3: Microstructural characteristics of the grouts cured up to 14 years based on MIP results.

		GR1	GR2	GR3	GR4
Total Porosity (%)		52.2	47.2	51.4	49.6
Total intruded volume (cm^3/g)		0.556	0.459	0.481	0.458
d_{bulk} (g/cm^3)		0.938	1.029	1.068	1.084
$d_{apparent}$ (g/cm^3)		1.931	1.929	2.168	2.129
Low pressure	Fraction of pores (5-110 μm)	1.4%	1.1%	1.2%	1.1%
	Mean pore radius (μm)	29.93	11.7	11.07	12.6
High pressure	Fraction of pores (0.002-5 μm)	98.6%	98.9%	98.8%	98.9%
	Mean pore radius (μm)	0.022	0.020	0.019	0.015

Water absorption measurements show that the NHL5-based grouts exhibit higher water absorption rates (about twofold) compared to the ternary grout, which is mainly attributed to the presence of pores of large sizes. The addition of 10% pozzolan reduced the rate of absorption compared to the plain NHL5 grout and this is linked to the relative decrease in pore size due to the pozzolanic activity. The opposite is observed for the addition of 20%

pozzolan which leads to higher absorption rate attributed probably to the pore size distribution and their interconnection.

The cementation index (C.I.) based on Boynton equation, was calculated, using the SEM/EDS analysis results, for all the grouts under study at the age of 14years in order to evaluate the hydraulicity of the mixtures. The data of Table 3 reveal that the addition of pozzolan increases the hydraulicity index of the NHL5 grouts. It is notable that the CI value of the grout GR3 and that of the ternary grout GR4 are very similar.

Table 3: Results of SEM-EDS analysis normalized and expressed as element oxides and the calculated cementation index (CI). Concentrations correspond to full frame analysis of the images presented in Figure 1.

Element oxide (% wt)	GR1	GR2	GR3	GR4
Na_2O	0.88	0.78	1.10	1.15
MgO	2.12	2.07	1.14	1.02
Al_2O_3	2.85	4.21	4.90	6.15
SiO_2	25.77	30.28	39.17	41.53
SO_3	0.98	1.89	0.65	0.88
Cl_2O	0.00	0.90	0.70	0.36
K_2O	0.51	0.50	2.06	1.65
CaO	65.72	58.10	49.18	45.82
Fe_2O_3	1.20	1.27	1.11	1.42
C.I.	1.11	1.48	2.28	2.63

The XRD patterns (Fig.4), show that the samples, extracted from the surface of the specimens, of the plain NHL grout (GR1) are not fully carbonated, as is revealed by the presence of portlandite [$Ca(OH)_2$] characteristic peaks. This can be attributed to the formation of well crystallized portlandite that hinders carbonation. Similar samples from NHL5-based grouts containing pozzolan show no (GR3) or just traces (GR2) of portlandite, while portlandite is absent from the ternary grout (GR4), indicating that it has been consumed by pozzolanic reactions and/or has been carbonated. Vaterite [μ-$CaCO_3$], formed in the grouts containing pozzolan, is associated to compositions of higher hydraulicity [27]

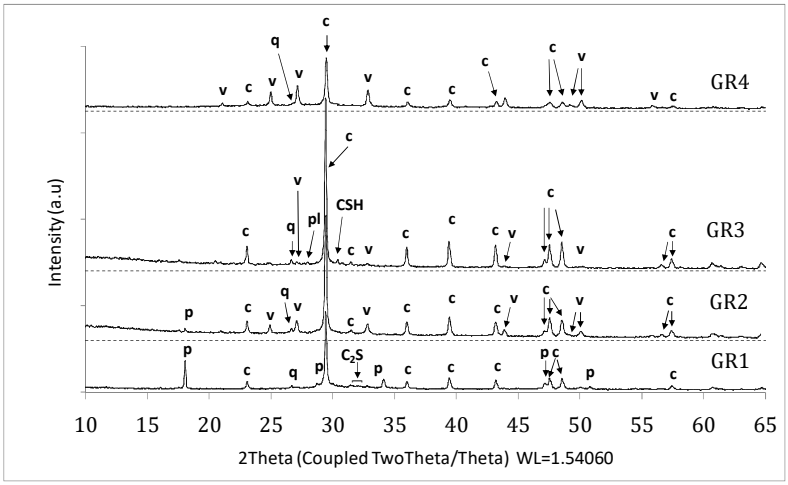


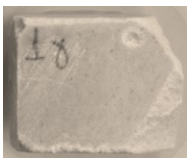
Figure 4: XRD patterns of the grouts at the age of 14 years: **c**: calcite [β-$CaCO_3$]; **v**: vaterite [μ-$CaCO_3$]; **p**: portlandite [$Ca(OH)_2$]; **q**: quartz; **pl**: plagioclase; **CSH**: calcium silicate hydrates; **C_2S**: dicalcium silicate.

3.2 Durability against crystallization of sulphate salts of grout-only specimens

The weight changes of all mixtures during crystallization cycles and the decay pattern are shown in Table 5. In general, all grout compositions exhibited good behaviour against the sodium sulphate attack. However, during the 9th cycle and with drying at 50 ^{o}C, the ternary grout (GR4) exhibited extensive and deep fracturing that led to the destruction of the specimens. Concerning the NHL5 based grouts, GR1 and GR2, containing 0% and 10% pozzolan respectively exhibited similar behaviour, while the grout GR3 (20% pozzolan addition) appear more susceptible to the weathering effects at the same stage, even compared to GR4. However, the durability of all the grouts tested was characterized as satisfactory, as they maintained their characteristics under severe sulphate attack conditions for at least 8 cycles (drying at 50 °C) and for more than 11 cycles when drying was carried out at 20 °C.

Table 5: Mass changes (%) and damage pattern during salt durability tests

Grout	Mass changes until the 6th cycle. Drying at 20^{o}C and high RH	Mass changes from 7th to 11th cycle. Drying at 20^{o}C	Mass changes from 7th to 9th cycle. Drying at 50^{o}C and low RH
GR1	21.1%	-2% (edge rounding and surface losses)	-4.4% (edge rounding)
GR2	13.2%	-2.2% (edge rounding and surface losses)	-5.3% (edge rounding and delamination)
GR3	12%	-4% (delamination)	-8.6% (delamination and edge rounding)
GR4	33%	7% (edge rounding)	8% (fracturing)

	GR1	GR2	GR3	GR4
11th cycle. Drying at 20^{o}C				
9th cycle. Drying at 50^{o}C and low RH				

It is noted here that, unlike stone, mortar or concrete studies, the research related to the durability of grouts in an aggressive environment is very limited; thus, the behaviour of low cement ternary grouts and NHL based grouts, with or without pozzolan, against soluble salts has not yet been systematically studied. Moreover, due to the lack of a testing standard for the durability of grouts, researchers mainly use those referring to stone, modified as to the shape and size of the specimens, the type of the salt and its concentration, the apparatus, the drying temperature etc.; thus difficulties are induced for the comparison of the results. Relatively few works have been contacted on grout-only specimens [1, 10, 16, 17], while the need for developing new test methods, including the evaluation of injected specimens has been already proposed in the literature by Beçir - Şimşir [12], demonstrating that such experiments may be considered more representative of the real field conditions.

3.3 Penetration and solidification of the grout injected into the wall

The SEM examination of representative samples from the injected mosaic substrata of the wall models provides data about the penetration and the solidification of the grout inside the pores, cracks and other discontinuities of a real structure, cured in real environmental conditions for many years. Small pieces were epoxy impregnated and polished cross-sections, imaged by SEM in back-scattered electron (BSE) mode. Figure 4 presents the plain NHL5 grout (GR1) having penetrated into a 1 mm wide crack existing in lime mortar. Near the interfaces with the porous lime mortar, the grout microstructure appears to be denser with finer particles compared to the bulk, which appears less densely packed, with coarser particles. The adhesion to the mortar appears to be good. Presumably upon entering the dry substrate, part of the grout liquid phase (i.e. water rich in Ca ions) is absorbed by the porous surrounding materials, attracting the thinner particles that may move in the open pores for some microns.

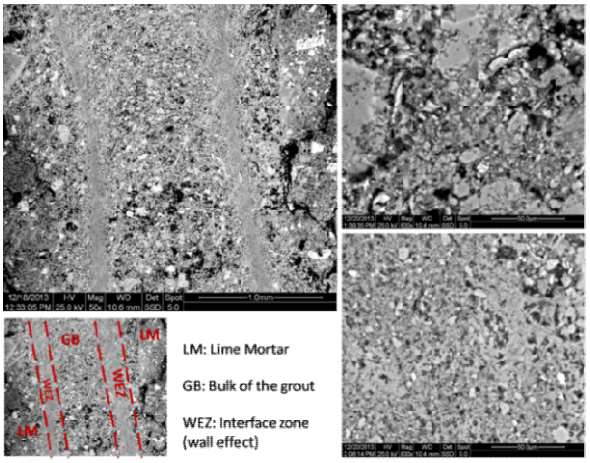


Figure 4: SEM BS images acquired 8 years after the injections. Clockwise from top left: 50x, the plain NHL 5 grout (GR1) penetrating a crack; 800x, the bulk of the grout; 800x, the interface zone between grout and lime based mortar; schematic presentation of the distinct materials and morphologies

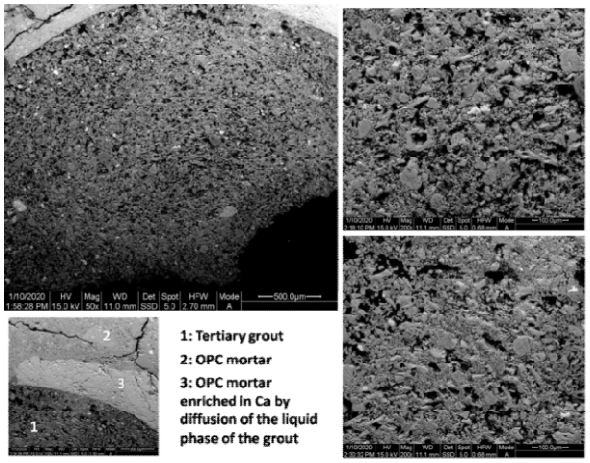


Figure 5: SEM BS images acquired 15 years after the injections. Clockwise from top left: 50x, the ternary grout (GR4) filling a void; 800x the bulk of the grout; 800x the interface between the grout and the OPC based mortar; 100x evidence of diffusion of the Ca rich grout liquid phase in the OPC based mortar.

As stated in the relevant literature the water absorption out of the grout may have a beneficial effect on the adhesion between grout and substrata, provided that the grout solid phase is stable and capable to retain the water necessary for the hydration and the solidification of the grout [1]. Besides this, water absorption causes binder particles to adhere to the wall of the flow channel, but in the rest of the channel the grout that keeps on flowing, retains the same properties as the grout that is injected [15]. Representative results of reduced area EDS analyses showed that these areas are relatively richer in calcium compared to the bulk of the grout (Fig. 6), indicating that in this zone a differential diffusion of ions is likely to occur [2, 28]. The creation of these zones may be attributed to the synergetic effect of absorption of water by the mortar and stones and probably to the wall effect [29], which does not allow larger particles to reach the wall that channels the flow of the grout, creating thus a thickening "wall effect zone".

The observation of the ternary grout in contact with the cement based mortar, from the second wall model (Fig. 5) showed that the aforementioned phenomenon is less pronounced than in the case of the more porous lime based mortar; in this case, the interface area appeared less dense and thus more porous and poorer in calcium than the bulk (Fig. 7). As expected, the adhesion and the phases developed in this area are different, as they strongly depend on the type of grout and the nature and porosity of the substrate, as well as its water absorptivity.

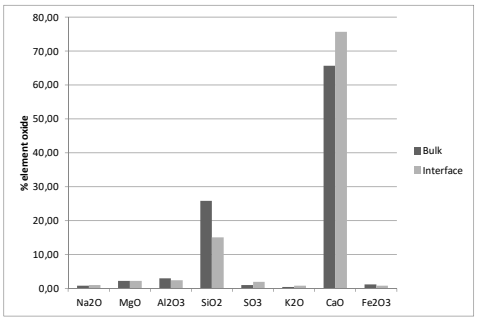


Figure 6: SEM-EDS analysis at the bulk of plain NHL5 grout (GR1) and the interface between the grout and the mosaic substrata lime mortar.

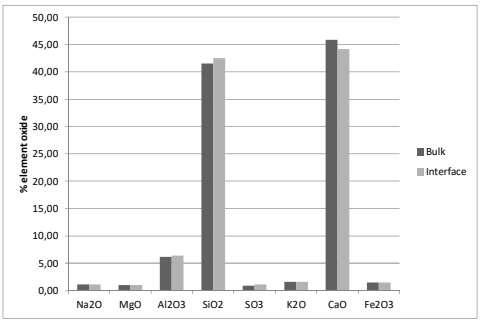


Figure 7: SEM-EDS analysis at the bulk of ternary grout (GR4) and the interface between the grout and the mosaic substrata cement mortar.

In the case of the plain NHL5 grout (GR1), XRD results of the grout samples collected from the injected walls, indicate the presence of portlandite, while the ternary grout (GR4) is fully carbonated to calcite and vaterite (Fig. 8). The presence of non hydrated dicalcium silicate (C_2S) in GR1, may be attributed to the absorption of water from the surrounding wall materials in combination to its slow hydration rate, though traces of C_2S are also present in the grout-only specimen (Fig 4). Conclusive results based on quantitative Rietveld analysis of the minor crystal phases require higher resolution spectra and extensive discussion of the results, which is beyond the scope of this short paper.

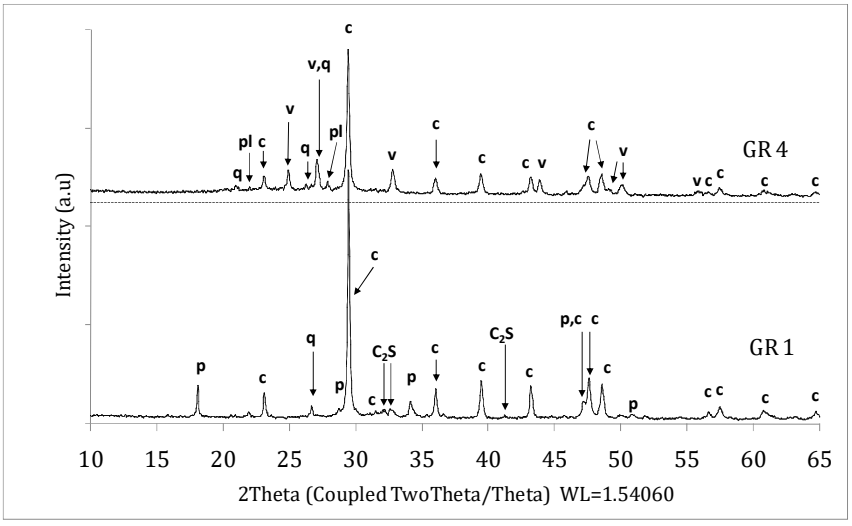


Figure 8: XRD patterns of the ternary (GR4) and the plain NHL5 (GR1) grouts. The samples were collected from the wallettes and tested 14 years after the injections: **c**: calcite [β-$CaCO_3$]; **v**: vaterite [μ-$CaCO_3$]; **p**: portlandite [$Ca(OH)_2$]; **q**: quartz; **pl**: plagioclase; **C_2S**: dicalcium silicate

Table 6 summarizes the results of MIP measurements on samples of the grouts injected and thus cured inside the walls. Comparison with the results of Table 3 (grout-only specimens GR1 and GR4), proves that porosity of the same grouts cured in the wall decreases, as is expected. A refinement in the pore size is also observed for the plain NHL5 grout (GR1).

Table 6: Microstructural characteristics of the grouts cured inside the wall (MIP results).

	Total Porosity	Total intruded volume	Fraction of pores (5-110 μm)	Mean pore radius	Fraction of pores (0.002-5 μm)	Mean pore radius
GR1	40.3%	0.310 cm^3/g	0.2%	13.4 μm	99.8%	0.028 μm
GR4	40.3%	0.263 cm^3/g	1.3%	12.3 μm	98.7%	0.033 μm

4 CONCLUSIONS

The conclusions drawn from the results of this study are as follows:

- All the grout mixtures under study satisfy the injectability requirements set.
- The addition of 10% pozzolan improved the physico-mechanical characteristics of the NHL grouts. The addition of 20% of pozzolan to NHL led to less satisfactory results, indicating that more intermediate dosages are necessary for the optimization of the composition. Moreover, a systematic investigation using various pozzolans and dosages is necessary in order to obtain comparative data on this topic, which is highly depended on the nature and the granulometry of the materials used.
- The addition of pozzolan in the NHL grouts led to the refinement of the pore structure, the reduction of water absorption coefficient and the increase of the hydraulicity index of the mixtures. XRD analysis of the NHL grouts containing pozzolan, reveals the absence -or just traces- of portlandite, indicating that it has been consumed by pozzolanic reaction and/or has been carbonated to calcite and vaterite. A significant amount of portlandite remains after the hardening of the plain NHL5 grout, while carbonation results to the formation of calcite.
- The durability of all tested grouts was characterized as satisfactory. All compositions of grout-only specimens have maintained their characteristics under severe sulphate attack conditions for at least 8 cycles. The mixtures of plain NHL5 and 90% NHL in association with 10% pozzolan showed slightly better resistance to salt crystallization than the ternary grout. A systematic research including both grout-only and injected material specimens, may be more indicative for characterizing the durability of injected structures.
- The observation of hardened grouts injected in wallets revealed interesting phenomena, related to the flow and penetration capacity as well as the setting and the adhesion of the grout to the wall materials. At the interface with the internal discontinuities (cracks, pores, etc) of the injected substrata, a more or less dense zone is observed. Calcium enrichment or depletion, depends on both the grout and the substrate nature.
- The MIP results revealed a lower total porosity for the injected grouts and a slightly different pore size distribution compared to the cured grout-only specimens.

Furthermore, the data provided by this research, highlight the need for developing new testing methods for the study of injected media (composite specimens, i.e. grout and substrata) instead of grout-only specimens, which are more vulnerable to curing conditions

and may probably lead to misleading results, mainly regarding hardened state properties.

Acknowledgements. The authors would like to express their gratitude to Dr. Ioannis Karatasios, researcher at INN/NCSR "Demokritos", and to Dr. Anastasia Michalopoulou for performing the MIP measurements. Equal gratitude is due to Katerina Kastellanou, Urania Tserpeli, Ioanna Maria Papastamati and all the staff of the Directorate of Research and Technical Support for Studies and Restoration Works of the Hellenic Ministry of Culture, for providing access and performing the mechanical testing on the matured grouts.

REFERENCES

[1] Miltiadou, A.E. *Étude des coulis hydrauliques pour la réparation et le renforcement des structures et des monuments historiques en maçonnerie.* Thèse de Doctorat de l'Ecole Nationale des Ponts et Chaussées. Pub. LCPC, Collection Etudes et recherches des Laboratoires des Ponts et Chaussées, série Ouvrages d'art, OA8 ISSN 1161-028X, LCPC, Décembre 1991, Paris, France, (1990), p. 278.

[2] Toumbakari, E.E. *Lime-pozzolan-cement grouts and their structural effects on composite masonry walls.* Ph.D. Thesis, Katholieke Univ. Leuven, (2002).

[3] Valluzzi, M.R. *Comportamento meccanico di murature storiche consolidate con materiali e tecniche a base di calce*. Ph.D. Thesis, Univ. of Trieste, (2000), p. 276.

[4] Miltiadou-Fezans, A., Vintzileou, E., Papadopoulou, E. and Kalagri, A. Mechanical properties of three leaf stone masonry after grouting. In: *Proc. of 5th International Conference on Structural Analysis of Historical Constructions*. New Delhi, India (2006).

[5] Adami, C.E. and Vintzileou, E. Interventions to historic masonries: investigation of the bond mechanism between stones or bricks and grouts. *Mater. Struct.* (2008) **41**:255–267.

[6] Vintzileou, E. and Miltiadou-Fezans, A. Mechanical properties of three-leaf stone masonry grouted with ternary or hydraulic lime-based grouts. *Eng. Struct.* (2008) **30**:2265–2276.

[7] Miltiadou-Fezans, A. and Tassios, T.P. Fluidity of hydraulic grouts for masonry strengthening. *Mater. Struct.* (2012) **45**:1817–1828.

[8] Miltiadou-Fezans, A. and Tassios, T. P. Penetrability of hydraulic grouts. *Mater. Struct.* (2013) **46**:1653–1671.

[9] Miltiadou-Fezans, A. and Tassios, T. P. Stability of hydraulic grouts for masonry strengthening. *Mater. Struct.*(2013) **46**:1631–1652.

[10] Ferragni, D. et al. Injection grouting of mural paintings and mosaics. In: *Proc. of symposium international of adhesives and consolidants*, Paris, 2–8 September, (1984), pp. 110–116.

[11] Biçer-Şimşir, B. and Rainer, L. *Evaluation of Lime-Based Hydraulic Injection Grouts for the Conservation of Architectural Surfaces.* The Getty Conservation Institute, Los Angeles, (2013), p. 105.

[12] Biçer-Şimşir, B. Preliminary Study on the sulfate resistance of lime-based hydraulic injections grouts for the conservation of architectural surfaces. In: I. Papagianni et al. (Eds.): *Proc. 4th Historic Mortars Conference*, Santorini,10-12 October, (2016), pp. 548-555.

[13] Papayianni, I. and Pachta, V. Experimental study on the performance of lime-based grouts used in consolidating historic masonries. *Mater. Struct.* (2015) **48**:2111-2121.

[14] Miltiadou-Fezans, A. and Tassios, T.P. Holistic methodology for the mix design of hydraulic grouts in strengthening historic masonry structures. In: I. Papagianni et al. (Eds.): *Proc. 4th Historic Mortars Conference*, Santorini, 10-12 October, (2016), pp. 580-587.

[15] Van Rickstal, F. *Grout injection of masonry, scientific approach and modeling*. Ph.D. Thesis, Katholieke Univ. Leuven, (2000).

[16] Kalagri, A., Miltiadou-Fezans, A. and Vintzileou E. Design and evaluation of hydraulic lime grouts for the strengthening of stone masonry historic structures. *Mater. Struct.* (2010) **43**: 1135–1146.

[17] Badogiannis, E., Miltiadou, A., Kalagri, A., Ipsilanti, E., Dedeloudis, C. and Vintzileou, E. Mix design and performance evaluation of grouts with super fine natural pozzolan. In: *Proc. of International Conference on Structural Analysis of Historical Constructions, SAHC 2012,* Wroclaw, Poland,15–17 October, (2012), pp. 773-780.

[18] Bras, A. and Henriques, F.M.A. Natural hydraulic lime-based grouts – The selection of grout injection parameters for masonry consolidation. *Constr. Build. Mater.*(2012) **26**:135-144.

[19] Jorne, F. *Injectability of hydraulic lime grouts for old masonry consolidation*. PhD Thesis, Department of Civil Engineering, Univ.de Nova de Lisboa, (2016), p. 207.

[20] Luso, E. and Lourenco, P. Bond strength characterization of commercially available grouts for masonry, *Constr. Build. Mater.*(2017), **144**:317-326.

[21] Mazzon, N. *Influence of Grout Injection on the Dynamic Behaviour of Stone Masonry Buildings*. PhD Thesis, Univ. degli Studi di Padova, (2010), p. 272.

[22] Silva, B., Dalla Benetta, M., da Porto, F. and Valluzzi, M.R. Compression and sonic tests to assess effectiveness of grout injection on three-leaf stone masonry walls. *Int. J. Archit. Herit.* (2014), **8**:408–435

[23] Gökyiğit-Arpaci1, E.Y., Oktay, D., Yüzer, N., Ulukaya, S. and Ekşi-Akbulut, D. Performance Evaluation of Lime-Based Grout Used for Consolidation of Brick Masonry Walls. *J. Mater. Civ. Eng*. (2019), **31**:04019059.

[24] Schindelin, J. et al. Fiji: an open-source platform for biological-image analysis. *Nat. Methods,* (2012), **9**:676-682.

[25] Espinosa-Marzal, R.M. and Scherer, G.W. Advances in understanding damage by salt crystallization. *Accounts Chem. Res*. (2010), **43**:897–905.

[26] Steiger, M. and Asmussen, S. Crystallization of sodium sulfate phases in porous materials: the phase diagram Na_2SO_4–H_2O and the generation of stress. *Geochim. Cosmochim. Act*. (2008), **72**:4291- 306.

[27] Elsen, J., Van Balen, K. and Mertens G. Hydraulicity in historic lime mortars: a review, In: J. Valek et al. (Eds): *Historic Mortars*, Rilem Bookseries, (2012), pp.125-139.

[28] Breton, D., Carles-Gibergues, A., Ballivy, G. and Grandet, J. Contribution to the formation mechanism of the transition zone between rock-cement paste. *Cement Concrete Res.* (1993), **23:**335-346.

[29] Roussel, N. and Gram, A., Physical Phenomena Involved in Flows of Fresh Cementitious Materials. In: N. Roussel, A. Gram (Eds): *Simulation of fresh concrete flow*, STAR RILEM Technical Committee 222-SCF, Springer, (2014), pp. 20-22.

12th International Conference on Structural Analysis of Historical Constructions
SAHC 2020
P. Roca, L. Pelà and C. Molins (Eds.)

EXPERIMENTAL AND NUMERICAL ANALYSES ON SANDSTONE ELEMENTS OBTAINED BY 3D PRINTING

C. SCURO[1*], S. TIBERTI[2], S. PORZIO[3], R. S. OLIVITO[3] AND G. MILANI[2]

[1]Department of Physics
University of Calabria, Rende, Cosenza, Italy
E-mail: carmelo.scuro@unical.it (*corresponding author)

[2]Department of Architecture, Built Environment and Construction Engineering
Technical University of Milan, Italy.
Email: simone.tiberti@polimi.it; gabriele.milani@polimi.it

[3]Department of Civil Engineering
University of Calabria, Rende, Cosenza, Italy
E-mail: saverio.porzio@unical.it; renato.olivito@unical.it

Keywords: Historical Structure, Masonry, Monitoring, Non-Destructive Inspection

Abstract. *The international cultural and historical heritage is often subject to degradation and damage. The main causes contributing to these phenomena are the chemical and mechanical actions due to acid rain, environmental pollution, and earthquakes. Other causes are the cycles of freezing and thawing that induce the manifestation of internal stresses leading to the deterioration of the material and the collapse of structural parts.*

In the field of architectural restoration, this problem has been addressed by two main solutions. The first involves cleaning processes that leave the missing parts visible; the second consists of introducing reproductions of the missing parts, creating a clear distinction between pre-existing and new elements. In both cases, the seismic behavior of the structure is modified; in the second solution, the added elements do not contribute to the structural strength since they are made of plaster or stucco.

This work aims at presenting a preliminary study on the creation of replacements of missing elements within damaged heritage buildings. The work is structured in two distinct phases. In the first phase, specific cubic specimens, created with a 3D printer, are produced and subjected to uniaxial compression tests. The experimental campaign is carried out in order to provide useful information regarding the 3D material engineering constants that are currently absent in the literature. In the second phase, the experimental results are used in a numerical model to calibrate the mechanical properties of an equivalent homogeneous material.

1 INTRODUCTION

Masonry buildings constitute the largest part of the existing historical heritage. These structures often consist of materials with poor mechanical properties, since they date back to different historical periods. Several monumental masonry buildings are still standing despite being located in renowned seismic areas (in Southern Europe and especially in Italy); therefore, such buildings are characterized by a high level of seismic vulnerability. Currently, masonry buildings that are historically and culturally important are safeguarded by specific technical standards aiming at their protection and preservation over time [1-2]. Several detailed and advanced methods have been developed by researchers and engineers alike to investigate these buildings in the knowledge phase, for the assessment of their structural safety against seismic actions, and eventually for enacting possible strengthening and conservation strategies [3].

The cultural and historical heritage is often subject to degradation and damage inducted by the earthquakes and the kinematic mechanisms caused by these phenomena. However, such kind of damage is not the single reason behind the collapse of masonry structures. In fact, other causes can be identified in the chemical and mechanical actions due to acid rain, environmental pollution, and the cycles of freezing and thawing that produce internal stresses leading to the deterioration of the material and the collapse of structural parts [4]. This entails a reduction of the walls' thickness and, subsequently, of the overall structural strength; therefore, a strategy for replacing the missing structural parts must be conceived.

This work aims at studying and characterizing a specific material for the recreation of the missing structural parts, which are 3D-printed bricks consisting of sandstone powder. These elements are created in order to verify if they can withstand structural loads.

To highlight the typical causes of damage due to the aforementioned actions, the Monastery of Santa Maria of Monte Persano is here considered as a case study (Fig. 1). The monastery is located in the town of San Lucido in Calabria along the slopes of Monte Sant'Angelo, and was ostensibly established around the year 1000 by Basilian monks wandering in Southern Italy after the Arab invasion of Sicily [5]. For this building, a classification of the degradation and of the collapse mechanisms observed in the structure are carried out.



a) b)

Figure 1: a) Monastery of Santa Maria of Monte Persano; b) Masonry observed in the construction.

2 CLASSIFICATION OF THE DEGRADATION

The classification of the structure degradation is carried out according to the Italian standard NorMal 1/88, produced by NorMal committee under the auspices of the CNR [6].

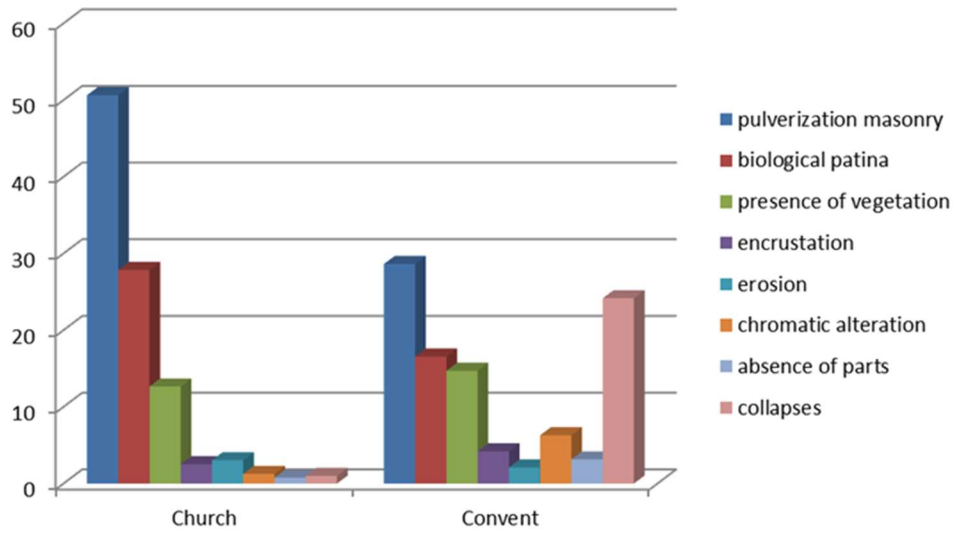


Figure 2: Different typologies of degradation

Fig. 2 shows that the highest percentage of degradation for both the convent and the church is due to the pulverization of the masonry (50% church, 28% convent), followed by biological patina (28% church, 16% convent) and presence of vegetation (13% church, 15% convent); for the convent, the 24% of damage is also due to the detachment and collapses of structural parts.

The action of water and weathering is a major cause of almost all degradation phenomena identified in the structure. There are various preliminary interventions that can reduce the causes of these phenomena, canceling the capillary action of water by reducing its damaging effects on the masonry. For example, the removal of the biological patina can be achieved by applying - up to total absorption - an organic water-repellent solvent in conjunction with biocide herbicides [4].

The complex of Santa Maria is subject to static instability and is characterized by cracks located in some parts of the masonry walls. Apparent damage is observed in the openings, the transverse walls and the vaults of the church, which consist of fictile tubules [7-9]. Moreover, clear detachment cracks can be identified between some vertical elements and their related horizontal elements, which instead have remained intact over time. In general, all these cracks are related to static and seismic phenomena to which the building has been subject over the centuries. Overloads caused by the presence of material due to various collapses of the structure has created widespread damage on the most rigid walls and on the horizontal structures connected to them.

The church façade shows cracks on the vaults and in its square window, creating damage even on the lithic cross; other cracks affect the intrados of the vaulted roof. Conversely, the monastery displays widespread damage in the Southern façade above the main entrance, located

under the window and positioned to the East. This type of damage tends to occur where the wall is weakened by the presence of irregular window holes (as in this case) due to the reduction in thickness of the wall of the sub-window. On the Western side of the same façade, a crack has developed from the inside (through-cracking), caused by the outer wall within the longitudinal rotation mechanism of the convent.



a) b) c)

Figure 3: a) Crack in the transversal wall; b) Cracks caused by the hole in the wall; c) Damage in the vault

Other damage can be identified in the structure: seven cracks affect the transverse wall dividing the various rooms (Fig. 3a), two are caused by improperly large holes created in the past (Fig. 3b), and five more appear on the longitudinal wall, caused by the rotation mechanism. In the ground floor there are other cracks: two again caused by the aforementioned holes, other are visible along the flat intrados surface of the vaulted roof (Fig. 3c). Finally, at the landing level of the staircase, it is possible to observe damage in the transverse wall, which develops from the bottom with a vertical progression and then is tilted.

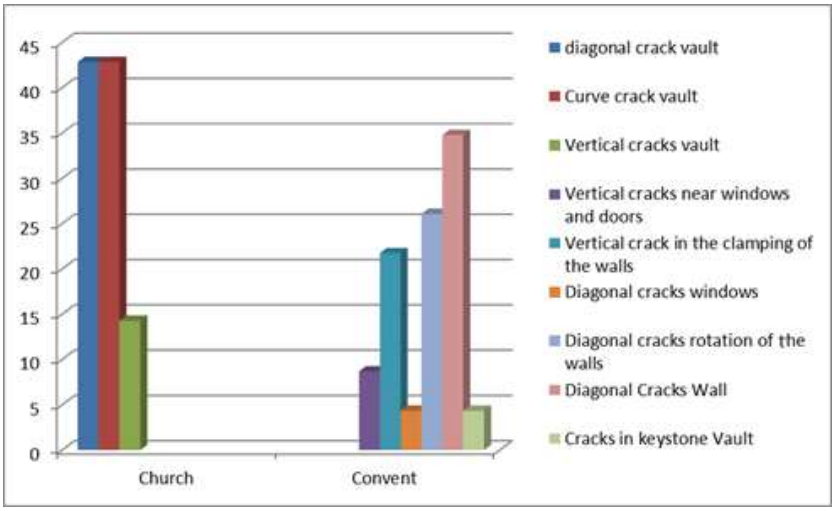


Figure 4: Different typologies of cracks.

Fig. 4 shows the classification of the almost 30 cracks clearly identified in the structure. The church displays in percentage an equal amount of diagonal and curved cracks, the latter located in correspondence of the vaulted roof but also visible on the façade, below the arch of the vault. Different types of failure are instead observed in the convent: the highest percentage belongs to cracks with diagonal development due to improper holes in the walls (34.8%), whereas other relevant percentages belong to diagonal cracks due to the rotation of the walls (26.1%) and to vertical cracks located at the clamping of the walls (21.7%).

The walls consist of masonry with disordered sandstone elements (cobblestone and uneven stone), like the rest of the construction. Protruding stones are visible on the right side of the Southern façade of the monastery, suggesting the continuation of the building to the Eastern side. This is corroborated by the presence of two arches that are located on the Eastern perimeter wall, which together with the four round arches are assumed connected to a supposed cloister.

3 3D PRINTER TECHNOLOGIES

The technologies and operating principles on which 3D printers are based were developed in the late 1980s by S. Scott Crump and the Stratasys Company, which he founded in 1989. The company began manufacturing machines for rapid prototyping, capable of producing real objects from three-dimensional CAD models. The main technologies used for 3D printing are three: Fused Deposition Modeling, StereoLitographic Apparatus, and Selective Laser Sintering [10].

Fused Deposition Modeling: Fused Deposition Modeling (FDM) is a methodology used for modeling and prototyping. It was developed by S. Scott Crump in the late 1980s and was then marketed by Stratasys in the 1990s.

The technology operates on an additive principle, releasing the material in layers. The plastic filament, collected in a reel, is liquefied inside a melting chamber and then released by an extruder nozzle onto the printing plate (bed), according to a pattern of lines that constitute the layers superimposed on the previous ones [11]. The nozzle, which is heated to dissolve the plastic material (specifically PLA), regulates the flow of delivery and moves along the x and y axes, guided by a numerical control mechanism, through the use of a CAM software (computer-aided manufacturing) (Fig. 5a).

StereoLitographic Apparatus: The StereoLitographic Apparatus (SLA) represents the first technique adopted in rapid prototyping. It was created by Charles W. Hull, founder of 3D Systems and inventor, among other things, of the STL format (STereo Lithography interface format or acronym for "Standard Triangulation Language").

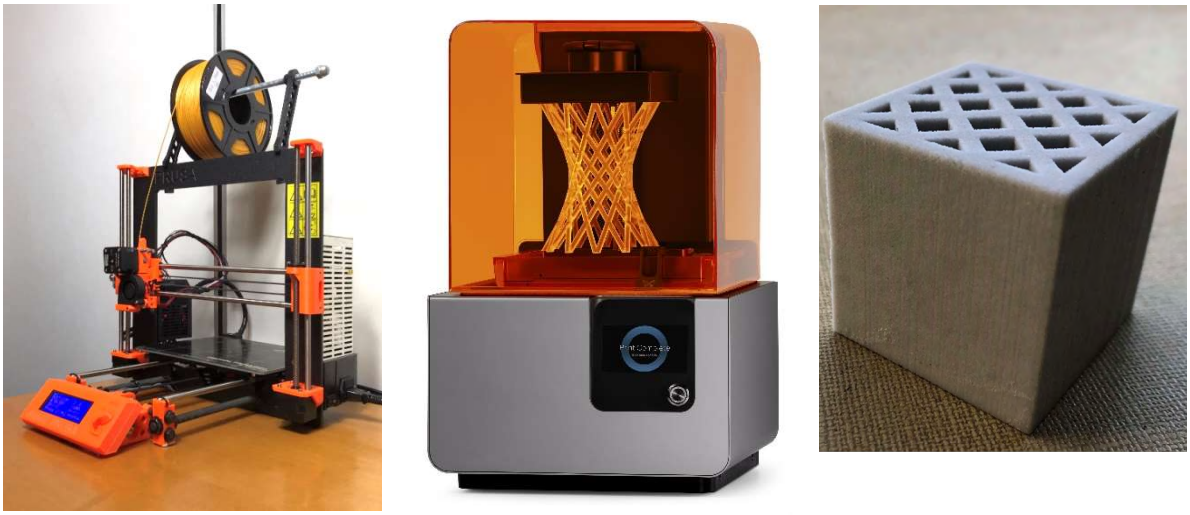
This technique uses a tank containing a special liquid resin capable of polymerizing when hit by light (photopolymerization); the printing plate, called bed, is the surface designed to accommodate the resin and is able to move up and down. A laser beam is projected through a system of mirrors, which shapes the liquid surface and modulates a raster image that is used to reconstruct the first section of the object to be created [10-11]. After the first scan, the bed lowers so that the resin can create a new liquid surface and a subsequent laser scan generates a second section (Fig. 5b). The process is repeated until the desired object is completed.

Selective Laser Sintering: Selective Laser Sintering (SLS), is based on the use of powders that can be thermoplastic, metallic or siliceous. The sintering of the powders, i.e. the compaction and transformation into an indivisible compound, takes place through a laser, thus

generating the prototype to be printed.

The procedure involves spreading a thin layer of powder on the bed, using a special apparatus; at the same time, the laser sinters where necessary. Also in this case the bed is mobile, and lowers down to the desired level to distribute the next layer of powder; everything is repeated until the complete generation of the model. SLS-printing technology is used both for the creation of aesthetic prototypes, with high levels of refinement and accuracy, and for the reasonably fast creation of functional objects [11].

This sintering technology allows the use of different materials, usually mixed with nylon, with which it is possible to obtain objects with different performances of strength, elasticity, and temperature resistance. Finally, after processing, the object is removed and separated from the non-sintered powders, which are partially or totally recovered and then reused in other printing processes (Fig. 5c).



a) b) c)

Figure 5: a) FDM 3D printer; b) SLA 3D printer; c) Specimen printed with the SLS technology.

4 EXPERIMENTAL CAMPAIGN

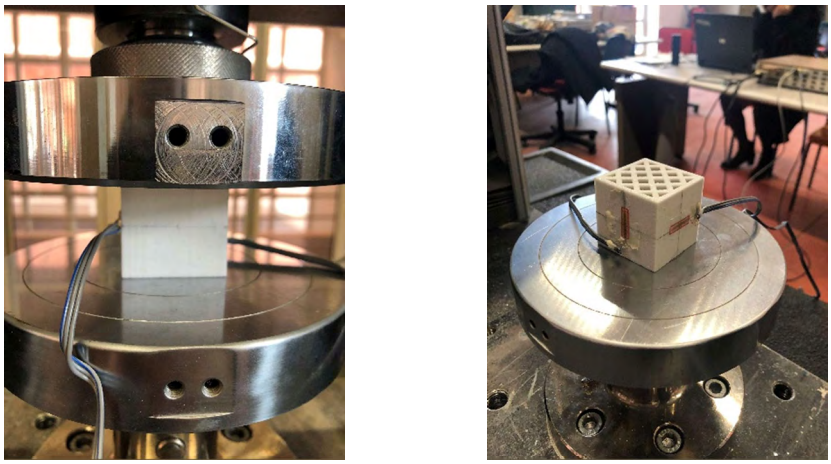
In order to characterize the material used to create the elements, four specimens are 3D-printed using the SLS technique. The samples are cubes with dimensions 40×40×40 mm^3, and are characterized by a partially hollow internal conformation as shown in Fig. 5c. They are printed in this way to reduce costs and ensure lightness. The material used for rapid prototyping of the samples is laser sintered sandstone powder. This type of powder is chosen to ensure compatibility between the 3D-printed element and the support of the existing material in a typical masonry historical construction.

The aim of the experimental program is to investigate the mechanical properties of sandstone powder. All experimental tests are conducted at the Materials and Structures Engineering Laboratory of Civil Department of University of Calabria. The experimental mechanical properties here obtained are later used to calibrate the numerical model of the material.

4.1 Test set-up

Uniaxial compression tests are performed on four cubic bricks printed in 3D NFTs (Fig. 6a). The testing machine used for the tests operates with a displacement control. The position and the lowering of the loading plate is provided at any instant and controlled through displacement sensors connected to the CPU of the test machine control panel [12]. Also, two strain gauges are applied on the lateral surfaces of the specimen to measure the values of vertical and horizontal strain [13] (Fig. 7b).

The compressive tests are performed with a crosshead speed equal to 0.2 mm/min; the load is applied parallel to the printed layers of the object.



a) b)

Figure 6: a) Compression test set-up; b) Application of strain gauges on the lateral surfaces of the specimen.

4.2 Experimental results

The mechanical properties obtained from the experimental tests are the compressive strength and Young's modulus of the 3D-printed cubic bricks. The load-displacement diagrams of the four compressive tests are plotted in Fig. 7. All specimens clearly display a brittle mechanical behavior with a strong linearity before attaining the peak load; the second part of the diagrams is characterized by a small softening branch. Also, the presence of strain gauges allows the evaluation of a constitutive law for the specimens. Fig. 8 shows the compressive stress-strain diagrams related to specimens.

The values of mechanical properties obtained from experimental tests are summarized in Table 1 and are in accordance with values available in literature for sandstone [14].

Table 1: Mechanical properties obtained from experimental tests

Specimen	Peak load [kN]	Compressive strength [MPa]	Young's modulus [MPa]
1	45.04	39.25	5850.2
2	39.39	34.33	5752.8
3	38.87	33.87	8156.9
4	35.82	31.21	7751.0
Average	39.78	34.67	6877.7

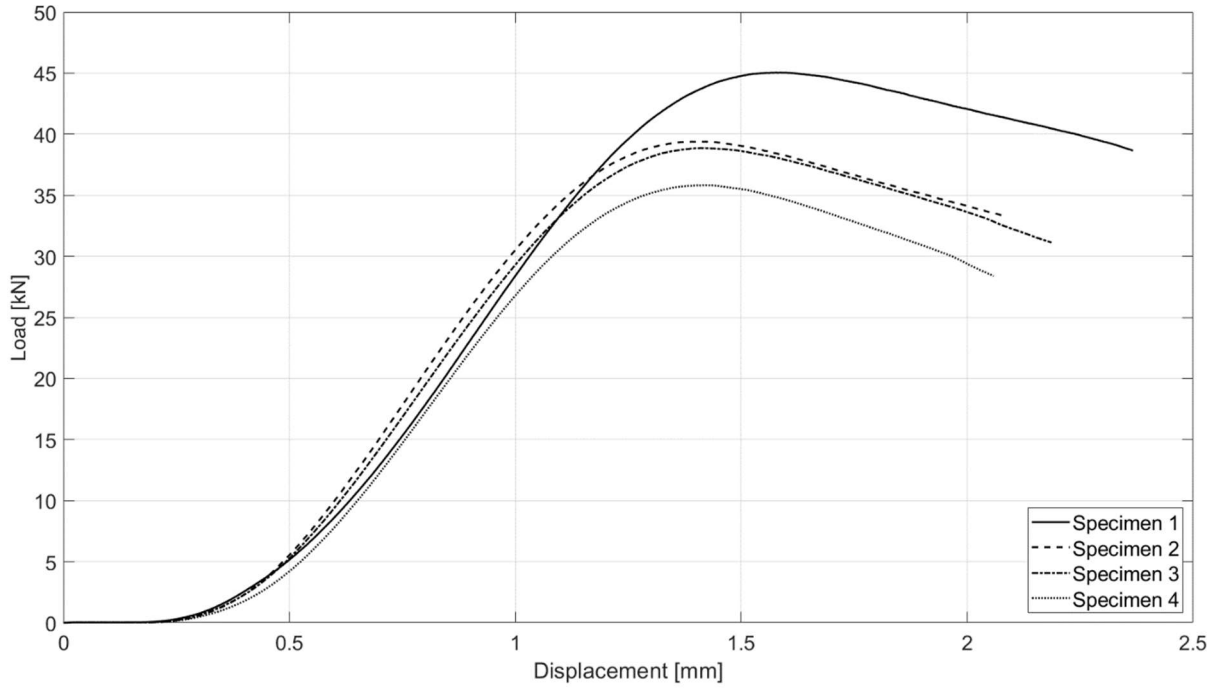


Figure 7: Load-displacement diagrams related to compressive test

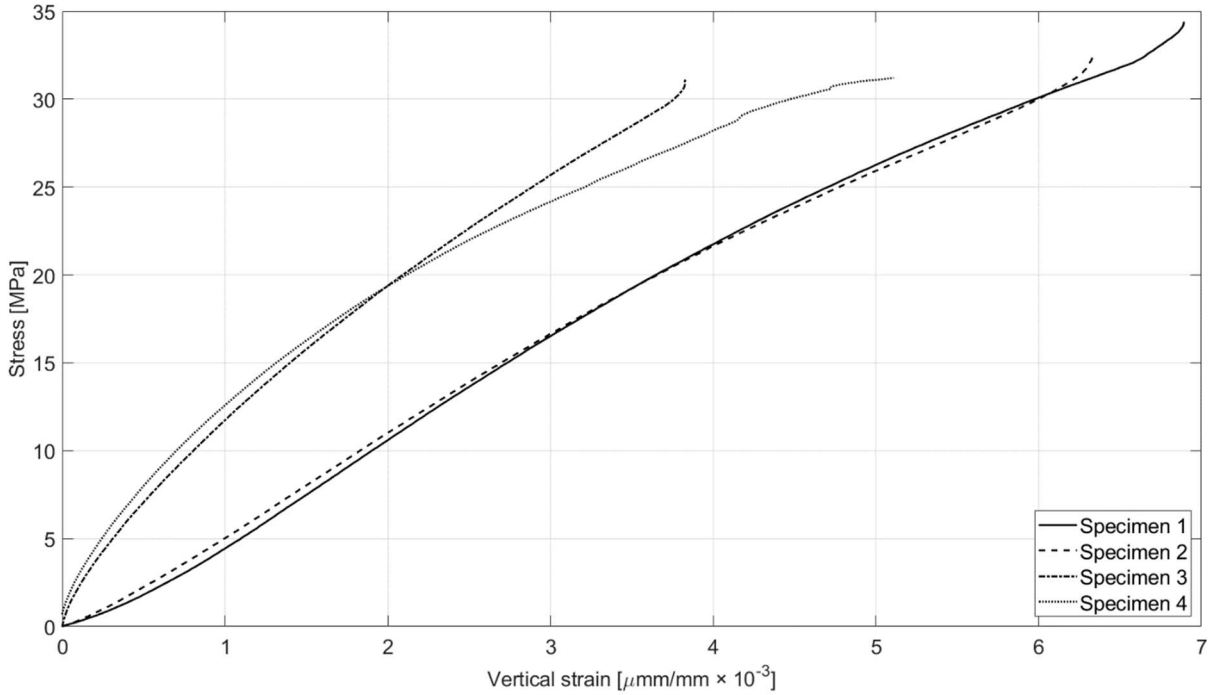


Figure 8: Stress-vertical strain diagrams related to compressive test

5 NUMERICAL MODEL

The results obtained from the experimental campaign are used to calibrate the mechanical properties of an equivalent homogeneous material for use in advanced FE simulations. To this end, a numerical model of the specimen is created in the commercial FE code ABAQUS, sharing the same dimensions of the experimental cube (40×40×40 mm^3) but with no holes. The exclusion of the voids from the numerical model is needed for calibrating the mechanical properties of the equivalent homogeneous material, which accounts for the presence of the voids only from a mechanical point of view, thus without modelling each of them. Then, a finite element mesh is created for the numerical model, consisting of 6773 quadratic tetrahedral elements as shown in Fig. 9.

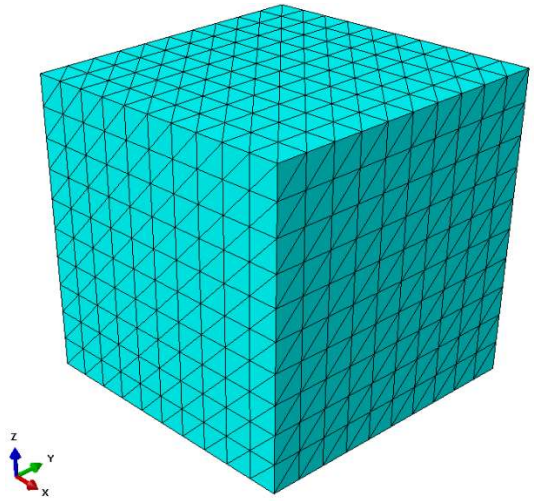


Figure 9: Finite element mesh of the numerical model

The material model employed for the equivalent homogeneous material in ABAQUS is the so-called "Concrete Damaged Plasticity" model (or CDP), which has been successfully used in several applications for representing the mechanical behavior of homogeneous materials due to its great versatility [8]. Here, the mechanical properties of the equivalent homogeneous material are calibrated by performing a series of numerical analyses simulating the experimental compressive test; the mechanical properties employed in the CDP are changed for every analysis until the resulting load-displacement diagram of the numerical compressive tests is contained in the envelope of the experimental ones. For both the compressive and tensile constitutive laws of the equivalent homogeneous materials, an exponential decay law is defined starting from the values of compressive and tensile strength, respectively.

The final result shows that the value of the Young's modulus found in the experimental campaigns can be safely used for the equivalent homogeneous material; the compressive strength must instead be reduced due to the fact that the numerical compressive test is performed on a full cube with no holes, where a larger area is involved in the application of the external load. The values of the mechanical properties of the calibrated equivalent homogeneous model are listed in Table 2. Fig. 10 shows the load-displacement diagram of the numerical model with the calibrated mechanical properties plotted against the envelope of experimental data, where it fits rather satisfactorily.

Table 2: Mechanical properties of the calibrated equivalent homogeneous model

Young's modulus [MPa]	Poisson's ratio [-]	Compressive strength [MPa]	Tensile strength [MPa]
6878	0.29	24.5	2

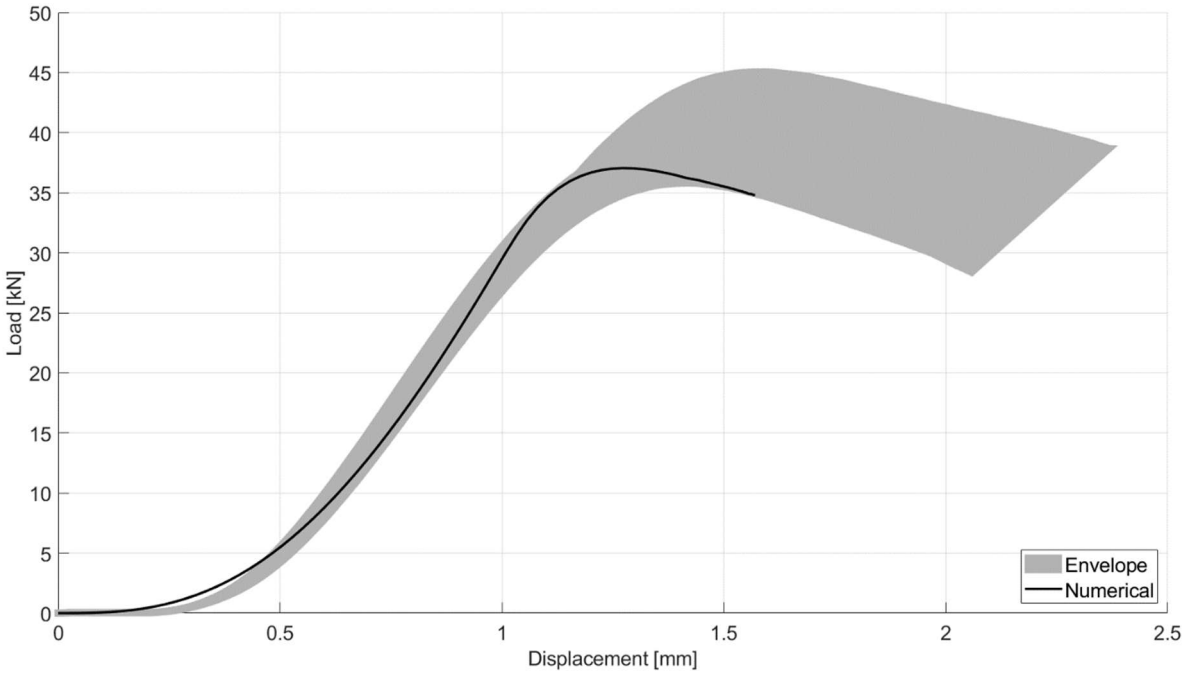


Figure 10: Load-displacement diagram of the calibrated numerical model plotted against the envelope of experimental data

6 CONCLUSIONS

Safeguarding and rehabilitating the Italian cultural and historical heritage is one of the most important issues to address in the context of structural engineering. To date, many structures in the historic centers are degraded and damaged, and often this damage is not only due to seismic actions but also to different factors such as the chemical and mechanical actions induced by acid rain, environmental pollution, and the cycles of freezing and thawing. One of the main consequences is usually the partial collapse of structural elements and the reduction of their mechanical properties.

The main purpose of this paper is to find a solution to this problem. A 3D model is created in a computer graphics software and is subsequently prototyped with a printer employing the SLS technology. The four specimens are subjected to compressive tests to identify their compressive strength and Young's modulus, which are still not available in literature for structural elements created with sandstone powders. The average values obtained from the experimental campaign are 34.67 MPa and 6877.7 MPa for the compressive strength and Young's modulus, respectively. These values are in accordance with those typically found in the literature for classical sandstone, and highlight how the structural elements made with this technique can both replicate the absences in the structure and resist the applied loads. The

experimental data are eventually used to calibrate numerically the mechanical properties of an equivalent homogeneous material that can be used in ABAQUS to reproduce those of the 3D-printed material. This is achieved by performing numerical analyses of the experimental compressive tests on an analytical model of the specimen, tuning the mechanical properties of the equivalent homogeneous material until the numerical load-displacement diagram fits well into the envelope created from the experimental data. The mechanical properties obtained through this calibration can then be used in advanced numerical analyses to simulate the presence of the 3D-printed material in complex analytical models where this material is used to recreate missing structural parts.

REFERENCES

[1] Olivito, R. S., Codispoti, R., & Scuro, C. A seismic analysis for masonry constructions: The different schematization methods of masonry walls. *In AIP Conference Proceedings* (Vol. 1906, No. 1, p. 090007). AIP Publishing, (2017, November).

[2] Tiberti, S., Scuro, C., Codispoti, R., Olivito, R. S., & Milani, G. Experimental and numerical analysis of historical aseismic construction system. *In Structural Analysis of Historical Constructions* (pp. 910-918). Springer, Cham. (2019).

[3] Olivito, R. S., Scuro, C., Porzio, S., Codispoti, R., & Demarco, F. Seismic vulnerability of ancient masonry buildings: The case study of low-rise towers. *In AIP Conference Proceedings* (Vol. 2116, No. 1, p. 420007). AIP Publishing LLC. (2019, July).

[4] Croci, G. *The conservation and structural restoration of architectural heritage*, Vol. 1 (1998). WIT Press.

[5] Martire D. *La Calabria sacra e profana*. (1878). Tip. Migliaccio.

[6] NorMal 1/88, CNR Italy.

[7] Scuro, C., Lamonaca, F., Codispoti, R., Carnì, D. L., & Olivito, R. S Experimental and numerical analysis on masonry arch built with fictile tubules bricks. *Measurement*. (2018), **130**, 246-254.

[8] Scuro, C., Tiberti, S., Codispoti, R., Milani, G., & Olivito, R. S. Fictile tubules: A traditional Mediterranean construction technique for masonry vaulted systems. *Construction and Building Materials*, (2018). **193**, 84-96.

[9] Scuro, C., Tiberti, S., Porzio, S., Olivito, R. S., & Milani, G. (2019, August). Study of the interface behaviour between fictile tubules bricks and mortar: numerical and experimental analysis. *In IOP Conference Series: Materials Science and Engineering* (Vol. 586, No. 1, p. 012027). IOP Publishing.

[10] Schubert, C., Van Langeveld, M. C., & Donoso, L. A. Innovations in 3D printing: a 3D overview from optics to organs. *British Journal of Ophthalmology*, (2014), **98(2)**, 159-161.

[11] Calignano, F., Manfredi, D., Ambrosio, E. P., Biamino, S., Lombardi, M., Atzeni, E., ... & Fino, P. Overview on additive manufacturing technologies. *Proceedings of the IEEE*, (2017).**105(4)**, 593-612.

[12] Tiberti, S., Scuro, C., Codispoti, R., Olivito, R. S., & Milani, G. Traditional masonry arches and domes with fictile tubules in mediterranean seismic areas: advanced numerical models and experimentation. *In 6th ECCOMAS thematic conference on computational methods in structural dynamics and earthquake engineering,* Rhodes Island, Greece

(2017, June) (pp. 2431-2448).
[13] Scuro, C., Sciammarella, P. F., Lamonaca, F., Olivito, R. S., & Carni, D. L. IoT for structural health monitoring. *IEEE Instrumentation & Measurement Magazine*, (2018). **21(6)**, 4-14.
[14] Molina, O., Vilarrasa, V., & Zeidouni, M. Geologic carbon storage for shale gas recovery. *Energy Procedia*, (2017)114, 5748-5760.

12th International Conference on Structural Analysis of Historical Constructions
SAHC 2020
P. Roca, L. Pelà and C. Molins (Eds.)

EXPERIMENTAL AND NUMERICAL ANALYSIS OF A FRCM REINFORCED PARABOLIC TUFF BARREL VAULT

ANNA CASTELLANO[1], JACOPO SCACCO[2], AGUINALDO FRADDOSIO[3*], GABRIELE MILANI[2], MARIO DANIELE PICCIONI[3]

[1] Department of Mechanics, Mathematics and Management (DMMM)
Polytechnic University of Bari
via Re David, 70125 Bari, Italy
e-mail: anna.castellano@poliba.it, www.dmmm.poliba.it
[2] Department of Architecture, Built environment and Construction engineering ABC
Politecnico di Milano
Piazza Leonardo da Vinci 32, 20133, Milan, Italy
e-mail: jacopo.scacco@polimi.it, gabriele.milani@polimi.it, www.abc.polimi.it/
[3] Department of Civil Engineering Sciences and Architecture (DICAR)
Polytechnic University of Bari
via Re David, 70125 Bari, Italy
e-mail: aguinaldo.fraddosio@poliba.it, (*corresponding author) mariodaniele.piccioni@poliba.it, www.dipartimentoicar.it

Keywords: Historical Construction, Masonry, Vaults, Fiber Reinforced Cementitious Matrix (FRCM), Experimental mechanics, Micro-modeling.

Abstract. *An experimental and numerical analysis of the structural behaviour of a barrel tuff masonry vault strengthened by a Fiber Reinforced Cementitious Matrix (FRCM) reinforcement system it is proposed. The geometry and the materials of the vault are representative of some historical constructions in Apulia (Italy). The vault, under the action of the self-weight and of a distributed load representative of the infill, has been first damaged by differential settlement of abutments, and then repaired and strengthened by FRCM composites. Finally the structure has been subjected to a increasing concentrated load on the extrados. A 3D heterogeneous FE Abaqus numerical model describing the above mentioned experimental conditions is carried out in order to reproduce the response of the FRCM reinforced vault. The obtained experimental and numerical results allows for discussing the structural behaviour of the reinforced vault, and then the effectiveness of the employed reinforcement.*

1 INTRODUCTION

The integrity of barrel masonry vaults plays a crucial role in the structural behavior of construction of the architectural heritage like palaces, churches, cloisters and castles. Anyway, settlements of abutments of the vault, for example induced by foundations differential displacement often induce considerable damage [1].

For historical constructions, the presence of damage states induced by foundations

settlements is often the norm rather than the exception. Whereas these damage states can be irrelevant in term structural capacity of withstanding ordinary gravitational loads, they can significantly undermine the load carrying capacity against exceptional loads, first and foremost seismic loads. Thus, it arises the necessity of suitable strengthening interventions, capable of restoring or eventually increasing the structural capacity of the undamaged construction.

In this vein, Fiber Reinforced Cementitious Matrix (FRCM) composites have gained an increasing interest as material for the reinforcement of historical masonry constructions. This is due mostly to the high compatibility with historical masonries, both from the technological and the structural point of view [2], and for the possibility of making diffuse reinforcement interventions.

The study of the structural behavior FRCM reinforced masonry construction is even now an open research issue, especially in the case of curved structures like arches, vaults and domes. Indeed, in the literature there are still too little numerical (see, e.g., [3]) and experimental papers [4-9] on this subject.

The experimental and numerical work here proposed aims at studying the effectiveness of a Fiber Reinforced Cementitious Matrix (FRCM) reinforcement system of a barrel masonry vault in terms of the load carrying capacity.

The geometry and the materials of the masonry vault resemble a typology of masonry vaults common in the historical centers of Apulia (Italy). In particular, a polycentric near parabolic vault was constructed by using Apulian tuff ashlars put together with a lime-cement mortar.

For what concerns the gravitational loads, the vault is subjected, in addition to the self-weight, to a distributed load representative of the weight of the infill.

The experiments consisted in two phases. In the first phase, the unreinforced tuff barrel vault was damaged by lowering only one abutment, simulating a typical damage induced, for example, by foundations settlements.

Once blocked the abutments, and repaired the cracks, the extrados of the vault was reinforced by a FRCM system composed by a fiber-reinforced mortar embedding a basalt fiber net. At this point, the second phase of the experiment consisted in applying a increasing concentrated load to the extrados of the vault along a generatrix in order to study the load carrying capacity of the reinforced vault, and then the effectiveness of the reinforcement.

The experiment, performed on a full-scale vault, required a quite complex experimental setup ad hoc designed [7,8]. In both tests, the masonry vault was continuously monitored through of several sensors placed in appropriate points of the intrados and extrados of the structure. In the second phase, discussed in the present paper, the load was gradually increased by 8 slow loading-unloading cycles. The reprocessing of the experimental data gives very accurate quantitative information on the structural response of the reinforced vault.

A 3D heterogeneous FE Abaqus numerical model reproducing the experimental conditions previously discussed is carried out in order to reproduce the second phase of the experiment. In the FE approach adopted, stones, mortar joints and cementitious matrix are assumed obeying a Concrete Damage Plasticity material model, with softening in both tension and compression, whereas equivalent elasto-damaging trusses are utilized for the fiber net. The FE model is calibrated on the results of experimental tests on the materials used for the vault and for the reinforcement. The numerical results fit with sufficient accuracy the experimental

outcomes, providing a useful reference for future application of FRCM strengthening technique on curved masonry structures.

2 TUFF BARRELL VAULT: GEOMETRY AND MATERIALS

The full-scale barrel masonry vault under test was designed specifically to reproduce both the geometry and the materials of some vaults widespread in historical cities of Apulia (Italy).

In particular, for what concerns the geometry, the vault has a raised, polycentric profile, whose shape is more similar to the parabola than to the circumference [7-7]. The span is 346 cm and the rise 120 cm (Fig. 1-2). For what concerns the materials, the voussoirs were made by cutting blocks of the so-called Apulian tuff, coming from the quarries of Gravina in Puglia. Moreover, for the construction of the vault a lime-cement mortar with low mechanical properties very similar to the properties of mortars used in rural tuff constructions was employed.

The vault was built at Laboratorio Ufficiale Prove Materiali "M. Salvati" of Politecnico di Bari, where experimental tests were carried out. The two supports of the vault are made by steel beams: one support is fixed, while the other can be moved by a hydraulic jack, allowing for controlled vertical displacements of one of the abutments of the vault. Two additional steel beams placed on the top lateral shoulders of the vault give further constraints, avoiding rigid rotations of the whole structure [7,8].

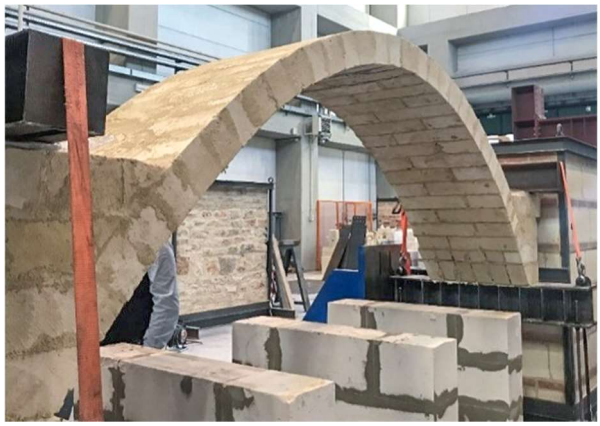


Figure 1: Tuff Barrell Masonry Vault (front)



Figure 2: Tuff Barrell Masonry Vault (back)

The mechanical properties of materials have been determined by mechanical tests in accordance with UNI standards. In particular, according to UNI EN 772-1:2011 and UNI EN 1926:2007 standard compression tests were performed on six cubic tuff samples having nominal dimensions of 430 mm x 240 mm x 150 mm and average mass density 1400 kg/m^3. The samples were tested using a Metro Com universal testing machine with load capacity of 600 kN. From the experimental results, it was possible to determine the average compressive strength f_{bm} = 2.25 MPa, the characteristic compressive strength f_{bk} = 1.87 MPa and the average Young modulus E_m = 637.39 MPa of the bricks. Moreover, according to UNI EN 1015-11:2007 six prismatic samples of the mortar with nominal dimensions of 14 mm x 14 mm x 160 mm and average mass density 1883.98 kg/m^3 were prepared during the construction of the vault. After 28 days of curing these samples were subjected to flexural

tests (three-point bending tests) and compression tests by using an INSTRON 5689 universal testing machine with load capacity of 50 kN. Then, the flexural strength f_{mf} = 1.91 MPa, the compressive strength f_{mc} = 8.94MPa and the average Young modulus E_m = 6902.27 MPa of the mortar has been determined.

The FRCM reinforcement consisted in a basalt fiber mesh (6 mm x 6 mm) embedded in a cement mortar. The basalt fiber net has a tensile strength f_{tB} = 60 kN/m and a Young modulus E_B = 89000 MPa.

3 EXPERIMENTAL TESTS AND RESULTS

3.1 Setup

A quite complex experimental setup was designed and built, in order to control both the vertical displacement of one of the two supports and the concentrated load on a generating line of the extrados of the vault. The complexity is related also to the dimension of the vault, that is a full-scale structure.

After the construction of the vault, 40 sandbags (with total weight 840 kg) were placed on the top of the vault in order to simulate the infill load (Fig 3).

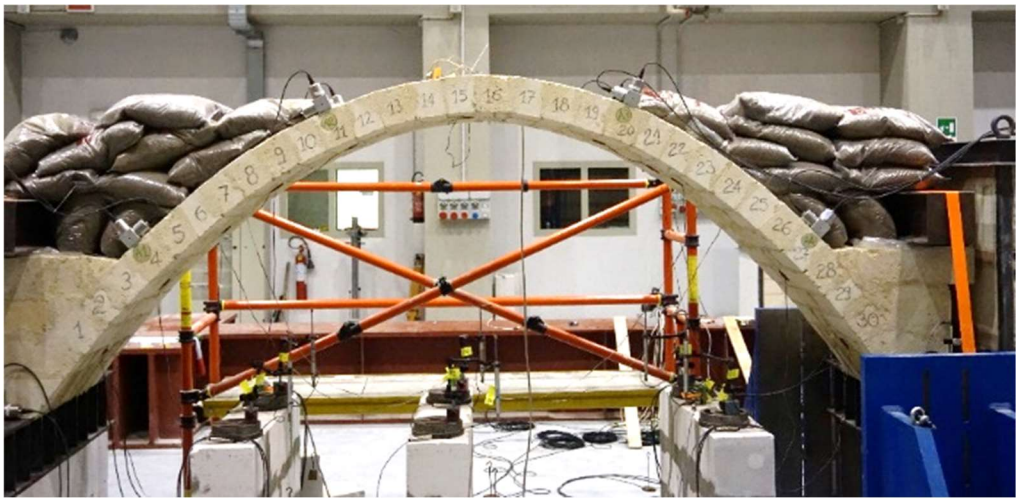


Figure 3: The masonry vault with sandbags in order to simulate the infill load

During both tests, the mechanical response of the vault continuously monitored through different sensors (Fig. 4) placed in suitable points of the vault and on supports [7,8]:

- 9 electrical strain gauges applied to the intrados of the vault along the middle axis (SI1, …, SI9);
- 7 electrical strain gauges applied to the extrados of the vault along the middle axis (SE1, …, SE7);
- 8 pairs of monoaxial accelerometers applied to the extrados of the vault, with measuring directions oriented tangent and orthogonal to the vault, respectively, and placed symmetrically with respect to the middle axis of the vault (A1, …, A8);
- 6 potentiometric displacement transducers connected by 6 plumb-lines to suitable

points of the intrados of the vault (P1, …, P6);

- 2 LVDT displacement transducers (LVDT1, LVDT2) applied on the support steel beam capable of vertical displacements controlled by the jack.



Figure 4: Some sensors placed on the vault and the sensor control station during the tests

3.2 First phase: the unreinforced vault under differential settlements between abutments

Two different experimental campaigns were performed: in the first, the unreinforced vault was damaged by differential vertical settlements between abutments. In particular, in this first phase a hydraulic jack placed under one of the supports of the vault allowing differential vertical settlements between abutments. The test was carried out in displacement control by gradually applying the differential settlements through subsequent increments. At the end of each step, a visual inspection was performed in order to evaluate the opening of cracks; moreover, the dynamic response of the vault under white noise excitation was acquired.

The test was interrupted when the formed cracks transformed the vault in a statically determined structure, thus capable of adapting to differential settlements by rigid body rotations. This happened at the 11th settlement step, corresponding to a relative vertical displacement between abutments of about 17 mm.

The cracking hinges formed in positions compatible to those typical of the collapse mechanism of a circular arch under vertical support settlements without rotations of the abutments (mechanism III in [10]).

In particular, an intrados cracking hinge formed in correspondence of the joint between voussoirs 23 and 24, and two extrados cracking hinges appeared in correspondence of the joint between voussoirs 14 and 15, and of voussoirs 11 and 10, respectively (Fig. 5).

According to the observations in [11], the slight differences from the cited mechanism in

[10] were likely ascribable to the shape of the vault (that have a parabolic profile rather than circular), by the different embrace angle and by the different thickness to radius ratio.

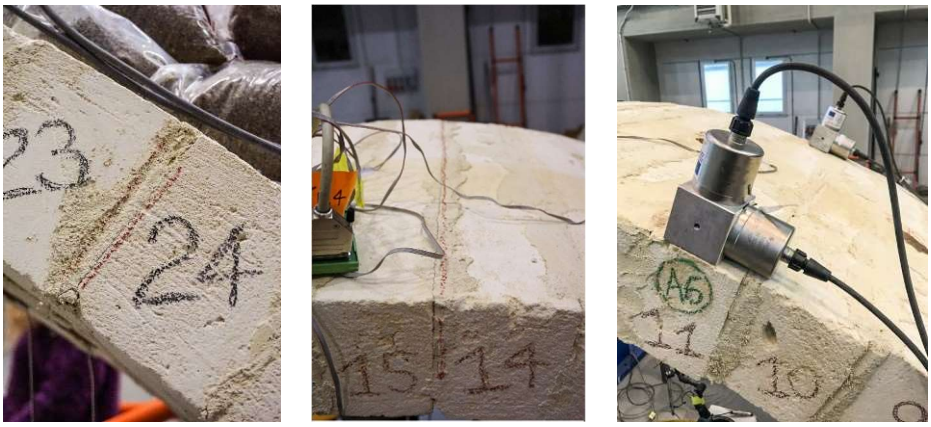


Figure 5: The three crack hinges

3.2 Second phase: FRCM reinforced vault under eccentric concentrated load

After the end of the first phase, the differential settlement of an abutment was blocked, the sandbags have been removed, and the crack hinges were filled by lime-cement mortar. Then, the extrados of the vault was reinforced by a FRCM system composed by a fiber-reinforced mortar embedding a basalt fiber net. In particular, the reinforcement was carachterized by an average overall thickness of 15 mm and a width of 600 mm.



Figure 6: 2nd test. setup

After the curing time of the reinforcement, the sandbags were placed again on the extrados of the vault, and two “double-acting hydraulic return” jacks with maximum load capacity 98 kN were positioned symmetrically with respect of the two faces of the vault (front and back) on a rigid contrast beams system. On each jack a load cell with capacity of 100 kN was

mounted. This system (jacks and load cells) was connected by means of threaded rods to a rigid beam placed on the extrados of the vault in correspondence of voussoir 10, at about ¼ of the span (Fig. 6). This way it was possible to apply an eccentric concentrate load on the reinforced masonry vault in order to evaluate the effectiveness of FRCM reinforcement.

The test was carried out in displacement control, by performing n. 8 loading-unloading cycles with progressively increasing displacements of the loaded voussoir. The low speed of the test was a key factor for actually realize a displacement control test. To this aim, an effective and constant monitoring of the oil pressure in the two hydraulic jacks was obtained by using a feedback system managed by a Labview software.

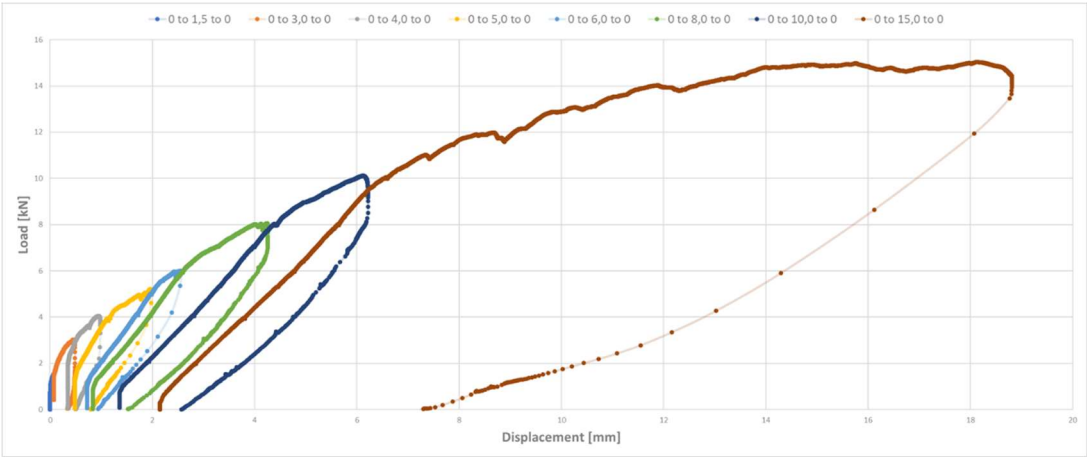


Figure 7: Load – Displacement curve for each cycle

During each load cycle, the mechanical behavior of the reinforced vault was monitored through the described sensors. Moreover, at the end of each cycle a visual inspection was also performed in order to identify the formation of cracks in the joints and hinges, and dynamical measurements were made through the accelerometers by exciting the structure with white noise.

Table 1: Second phase: main results for each loading-unloading cycle.

Cycle	Maximum Load [kN]	Displacement at max load [mm]	Residual displacement [mm]
1	1,5	0,00789	0,07708
2	3	0,47135	0,34425
3	4	0,94575	0,48135
4	5	1,98235	0,24175
5	6	2,47735	0,35400
6	8	3,99235	0,87545
7	10	6,13285	1,8675
8	15	18,10135	6,2245

The second experimental phase has been conducted until the vault was no longer capable

to support additional load increase.

The overall experimental behavior of vault is summarized in Figure 7 by the superposition of the load-displacement curves obtained in the 8 loading-unloading cycles performed; in the diagram, the displacement refer to the load application point (voussoir 10) and it is obtained by averaging the measures provided by two potentiometric displacement transducers applied at the two sides of the loaded voussoir (see Sect. 3.1).

The curves in Figure 7 correspond to data in Table 1 that collects the main overall results obtained during the test: the value of maximum load [kN], the value of displacement at maximum load [mm] and the residual displacement [mm] at complete unloading for each cycle.

(a)  (b) 

Figure 8: The crack hinges: (a) Front view and (b) back view of the masonry vault

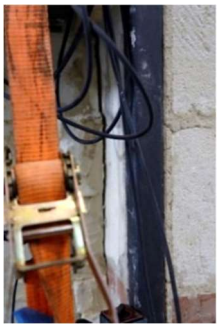
(a)  (b) 

Figure 9: The crack hinges: (a) Front view and (b) back view of the masonry vault

As the load cycles progress, the first crack hinge has been observed at the intrados under the application point of the concentrated load, that is, between the voussoirs 9 and 10 (Fig. 8), during the fourth cycle (corresponding to a maximum load value of 5 kN).

No further cracks were observed in subsequent cycles, proving the effectiveness of the reinforcement system applied to the extrados of the vault.

The test was interrupted at the end of the eighth cycle (corresponds to a maximum load value of 15 kN) when a crack was observed between the vault and one of the lateral supports due to the rotation of the structure (Fig. 9). This rotation substantially prevented for further increase of the load. A reconstruction of the deformed profile of the intrados middle line for

each load step, in the complete unloading state (permanent deformation) is showed in Fig. 10 through the data acquired by the six potentiometric displacement transducers and the two LVDT displacement transducers (see Sect. 3.1).

Further considerations will be possible when the large amount of collected data, including also dynamic measurements, will be completely reprocessed and examined.

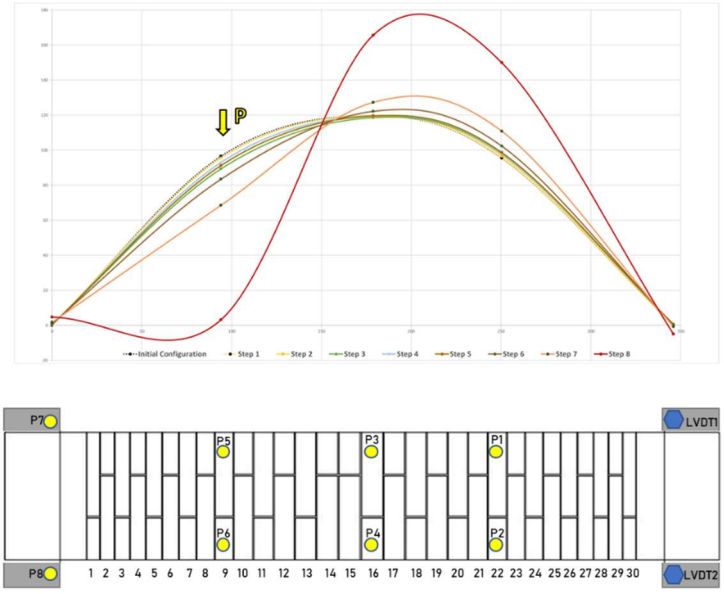


Figure 10: Reconstruction of the deformed profile of the intrados middle line of the vault

4 NUMERICAL MODELLING

The outcomes regarding the second-phase of experimental campaign have been reproduced by advanced non-linear simulation through the FE-based software Abaqus. A 3D heterogeneous approach has been selected in order to model separately all of the components (stones, mortar joints, cementitious matrix, basalt fiber) of the reinforced vault (Fig. 11). The non-linearities are assigned taking advantage of the Concrete Damage Plasticity model, available in the library of Abaqus and already applied with success to masonry structures [12]. Concrete damage plasticity is an isotropic elasto-plastic constitutive model with damage. The degradation of the elastic stiffness is determined by two variables of damage dt and dc, functions of the plastic strains. Such variables vary between a value of 0 for the undamaged material and 1 for the material that has completely lost any stiffness. CDP allows the definition of a distinct behavior under tension and compression, respectively following an exponential softening and a parabolic softening. A 3D approach is preferred in order to ensure a better stability of the model and to avoid some inaccuracy associated to a 2D simplification of the problem. With this aim, only a portion of 100 mm along the thickness is modeled in order to reduce the computational burden. Non-linear properties are assigned to the stones of the vault, the mortar joints, the cementitious matrix and the fibers of the strengthening. These latter have been assigned of an elastic-fragile behavior with a negligible compressive strength in order to avoid unrealistic contribute to the global stiffness.

Regarding the discretization, 8-noded solid bricks are used (Fig. 11). The joints present at least two elements in the thickness, whereas a rougher discretization is addressed to the tuff bricks. The matrix of the reinforcement is modeled as two different layers tied together with a global thickness of 15 mm. The basalt fibers are idealized as 2-noded trusses and embedded in the middle of the cementitious matrix. Seven truss elements are introduced along the depth of 10 mm with an equivalent cross section, following a procedure already suggested in literature [13].

A tie connection is assumed among all the different elements, allowing the use of a differential discretization in the mortar and in the stones. However, in such a way, the detachment of the strengthening from the stone substrate is not modeled, because is considered a failure unlikely to occur in the case of FRCM strengthening. At the same time, also the slipping between the matrix and the fibers is not considered here. The geometrical model has been implemented on the deformed configuration obtained by the analysis reproducing the settlement phase and provided in [8]. Again, following the experimental procedure, the filling made of sandbags and the steel beams located at the spandrels are modeled directly as distributed and concentrated loads.

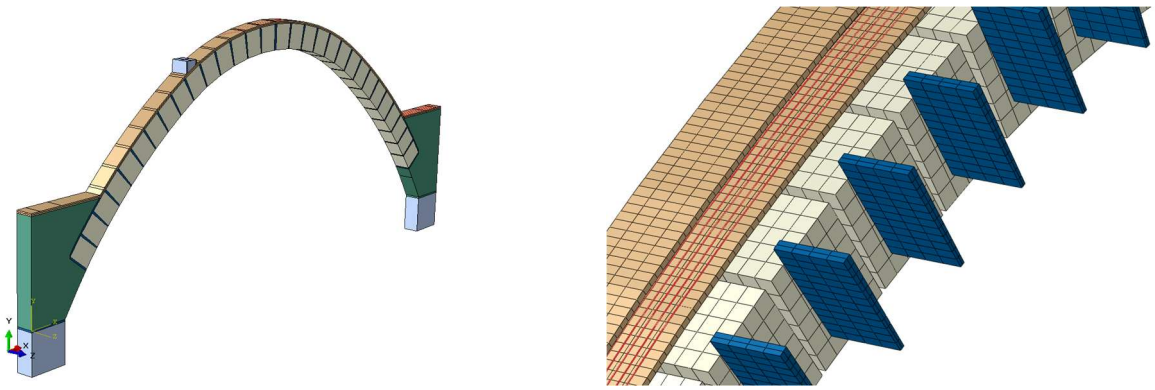


Figure 11: 3D Geometric model of the vault (Left); Mesh detail of each component (Right)

The non-linear analysis is conducted imposing an incremental displacement at the top of voussoir 10 and the first results of the numerical approach are here exposed. As expected, the first crack to occur is the one just under the concentrated load between voussoir 9-10, in correspondence of a load around 6 kN (Fig. 12). Afterward, as noticeable from Figure 13, the load reaches a maximum value nearby 16 kN in correspondence of 19 mm.

Despite of an initial gap in the stiffness in the first stages of the analysis, the global behavior is well reproduced, being able to catch the final displacement and the peak load with adequate accuracy.

Regarding the damage pattern, the crack under the concentrated load and the rotation of the left spandrel are reproduced as well. Although, differently to the experimental observation, more damage occurred in two different location leading to a classic 4-hinges mechanism, even delayed by the presence of the reinforcement. A better fitting of the crack pattern with the experimental results may be the topic of future works by the Authors.

However, the micro-modeling approach succeeds in the simulation of the effectiveness of the FRCM strengthening on the global behavior of the vault, providing a numerical reference

for the validation and the application of this technique even for the practitioners.

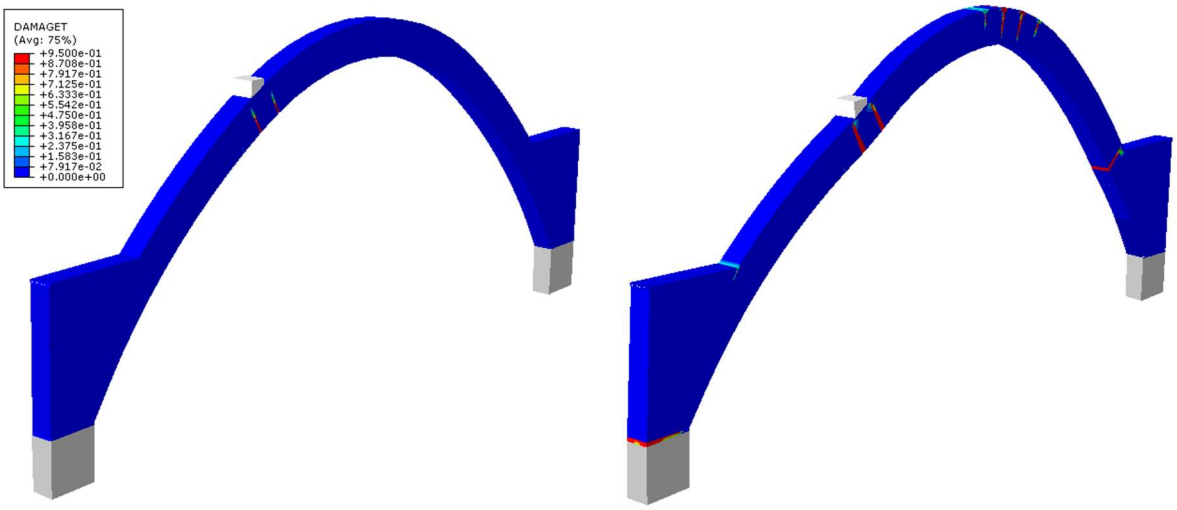


Figure 12: Damage configuration at the occurrence of the first crack (Left); Final damage crack pattern (Right)

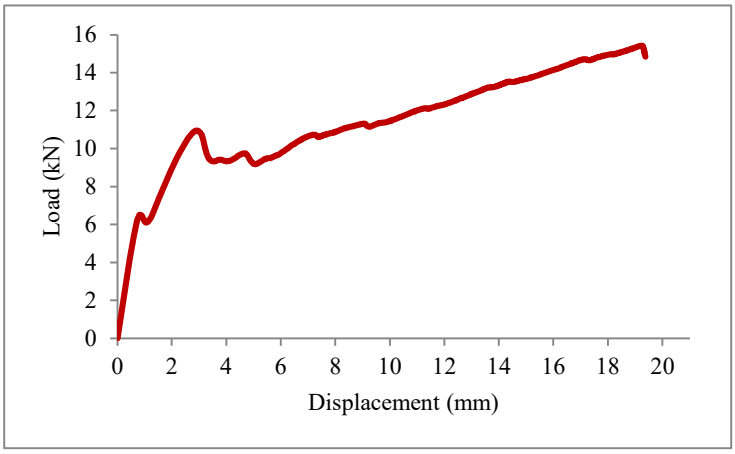


Figure 13: Load-displacement curve of the reinforced vault subjected to a concetrated load

6 CONCLUSIONS

The first result of an experimental and numerical analysis on a FRCM reinforced tuff masonry vault have been proposed. The full scale experiment performed give a broad overview on the complex structural response of the examined structures. The challenging problem of numerical modeling such a highly nonlinear problem has been faced by a micromodeling approach capable of reproducing the overall behaviour of the reinforced structure, although characterized by a relatively low level of complexity. This makes the propose approach interesting also for the employ in practical applications.

REFERENCES

[1] Coccia, S. Di Carlo, F. and Rinaldi Z. Collapse displacements for a mechanism of spreading-induced supports in a masonry arch. *Int. J. Adv. Struct. Eng.* (2017) **7**(3): 307-320.

[2] Carozzi, F.G., Milani, G. and Poggi, C. Mechanical properties and numerical modeling of Fabric Reinforced Cementitious Matrix (FRCM) systems for strengthening of masonry structures. *Compos. Struct.* (2014) **107**:711-725.

[3] Carozzi, F.G., Poggi, C., Bertolesi, E. and Milani, G. Ancient masonry arches and vaults strengthened with TRM, SRG and FRP composites: Numerical analyses. *Compos. Struct.* (2018) **187**: 385-402.

[4] Valvona, F., Toti J., Gattulli, V. and Potenza, V. Effective seismic strengthening and monitoring of a masonry vault by using Glass Fiber Reinforced Cementitious Matrix with embedded Fiber Bragg Grating sensors. *Compos. Part B-Eng.* (2017) **113:** 355-370.

[5] Carozzi, F.G., Poggi, C., Bertolesi, E. and Milani, G. Ancient masonry arches and vaults strengthened with TRM, SRG and FRP composites: Experimental evaluation. *Compos. Struct.* (2018) **187**: 466-480.

[6] Castellano, A., Fraddosio, A., Scacco, J., Milani, G. and Piccioni, M.D. Dynamic response of FRCM reinforced masonry arches. Key Engineering Materials (2019) 817: 285-292.

[7] Scacco, J., Milani, G., Bove, M., Castellano, A., Fraddosio, A. and Piccioni, M.D. Experimental and numerical analysis of the effectiveness of FRCM strengthening on a parabolic tuff barrel vault. AIP Conference Proceedings (2019), 2186. DOI: 10.1063/1.5138011

[8] Bove, M., Castellano, A., Fraddosio, A., Scacco, J., Milani, G. and Piccioni, M.D. Experimental and numerical analysis of FRCM strengthened parabolic tuff barrel vault. *Key Eng. Mater.* (2019) 817 KEM:213-220.

[9] De Santis, S., Roscini, F. and De Felice, G. Retrofitting masonry vaults with basalt textile reinforced mortar. Key Eng. Mater. (2017) 747: 250-257.

[10] Zampieri, P., Faleschini, F., Zanini, M.A. and Simoncello, N. Collapse mechanisms of masonry arches with settled springing. Eng. Struct. (2018) 156: 363-374.

[11] Ochsendorf, J. The masonry arch on spreading supports. Struct. Eng. (2006) 84(2): 29-36.

[12] M. Valente and G. Milani, "Effects of Geometrical Features on the Seismic Response of Historical Masonry Towers," J. Earthq. Eng., vol. 00, no. 00, pp. 1–33, 2017.

[13] J. Scacco, B. Ghiassi, G. Milani, and P. B. Lourenço, "A fast modeling approach for numerical analysis of unreinforced and FRCM reinforced masonry walls under out-of-plane loading," Compos. Part B Eng., vol. 180, no. August 2019, p. 107553, 2020.

12th International Conference on Structural Analysis of Historical Constructions
SAHC 2020
P. Roca, L. Pelà and C. Molins (Eds.)

EXPERIMENTAL ASSESSMENT OF SHEAR RESPONSE OF BRICK MASONRY RETROFITTED WITH TRM

LARISA GARCIA-RAMONDA[1*], LUCA PELÀ[1], PERE ROCA[1] AND GUIDO CAMATA[2]

[1]Department of Civil and Environmental Engineering
Universitat Politécnica de Catalunya (UPC-BarcelonaTech)
Jordi Girona 1-3, Campus Norte UPC, 08034 Barcelona, Spain
e-mail: larisa.garcia.ramonda@upc.edu, luca.pela@upc.edu, pere.roca.fabregat@upc.edu,
www.upc.edu (*corresponding author)

[2]Department of Engineering and Geology
University "G. D'Annunzio" of Chieti Pescara
Viale Pindaro 42, I-65127 Pescara, Italy
e-mail:g.camata@unich.it, www.en.unich.it

Keywords: Masonry, TRM, FRCM, Cyclic shear-compression test, seismic retrofitting, "scuci-cuci" technique.

Abstract. *As one of the main historical construction materials, masonry is abundant among the architectural heritage of earthquake-prone areas of the Mediterranean countries. Earthquake mitigation approaches are now focusing on strengthening solutions based on compatible and environmentally friendly repair materials. These solutions should efficiently improve the in-plane lateral strength and displacement capacity, which are the two most significant parameters considered in the seismic assessment of masonry buildings. This paper reports an experimental programme on masonry walls composed of handmade solid clay brick and hydraulic lime mortar, a recurrent typology for historical buildings. Tests under cyclic in-plane forces were carried out on unreinforced and retrofitted walls. The unreinforced walls were repaired and retrofitted after being damaged in the first test and were then tested again to investigate the recovery of strength. The repair consisted in filling the open cracks and replacing the damaged bricks by following the so-called "scuci-cuci" technique. The retrofitting consisted of externally bonded textile reinforced mortar (TRM). The investigated TRM system was a continuous bidirectional grid of basalt embedded in hydraulic lime mortar. The experimental results show the suitability of the proposed solutions for seismic retrofit and post-earthquake repair of existing masonry buildings. The research results highlight the effectiveness of the investigated systems in increasing the resistance and ductility of unreinforced brick masonry. In addition, the results allow a better understanding of the behaviour of masonry walls subjected to cyclic horizontal displacement.*

1 INTRODUCTION

Clay brick masonry is one of the most recurrent construction materials found in the

Mediterranean built heritage. Owing to the material's almost null tensile strength, among other mechanical features, masonry buildings show large vulnerability to earthquake action. In an attempt to enhance the seismic performance of masonry constructions, a significant research effort has been undertaken during the last decades in order to validate efficient strengthening techniques. Among them, textile reinforced mortar (TRM) has been receiving increased attention due to its mechanical efficiency and satisfactory compatibility with the masonry substrate. This technique is also known in the scientific literature as FRCM (Fibre Reinforced Cementitious Matrix), according to the nomenclature adopted in the American standards [1]. As lime-based matrix is preferred to cementitious one nowadays, the acronym FRCM can be reinterpreted according to the novel definition "Fibre Reinforced Composites in inorganic Matrix" introduced by recent Italian standards CNR-DT 215/2018 [2].

In order to better understand the mechanical behaviour of TRM retrofitted masonry, a series of quasi-static experiments, consisting in shear-compression tests with cyclic loading, were carried out in the Laboratory of Materials and Structural Technology of the Universitat Politécnica de Catalunya (UPC-BarcelonaTech).

The main aim of the experimental programme was to investigate the in-plane performance of TRM strengthened brick masonry walls with focus on the predominant failure modes and deformation capacity. The programme comprised six tests on four walls. Two specimens were tested in the unreinforced configuration and later repaired and retrofitted with low-density basalt TRM (LDB-TRM). The remaining two walls were retrofitted with the same LDB-TRM solution. The walls were tested up to peak loading and beyond until an almost complete exhaustion of its residual bearing capacity in order to determine the drift corresponding to the collapse limit state. The experimental results are compared with the provisions of Eurocode 8 and NTC2018 on limit conditions against earthquake. Eurocode 8 [3] defines two main limit states corresponding to Significant Damage (SD) and a ultimate limit state associated with Near Collapse (NC). The Italian standard NTC2018 [4] defines a Serviceability Limit State (SLE), which includes the Damage Limit State, and a Ultimate Limit State (SLU).

2 SPECIMENS FEATURES

2.1 Material characterization

Four masonry walls with dimensions 1270 × 1270 × 310 mm^3 were built with clay bricks in Flemish bond with 21 courses and 15 mm thick mortar joints. The specimens represent one of the most frequent material combinations in historical masonry, i.e. solid clay brick and lime mortar joints. The handmade solid clay bricks were fired using traditional methods. The mortar was derived from a hydraulic lime-based commercial premix by reducing its compressive strength with limestone filler addition in order to replicate a low strength historical lime mortar [5]. The mechanical properties of the bricks and mortar were measured following standards EN 772-1 and EN 772-6 [6,7]. The measured normalized compressive strength $f_{b,c}$ and flexural strength $f_{b,f}$ of the bricks were equal to 17.99 MPa (with coefficient of variation CV 8.3%) and 2.44 MPa (CV 20.0%) respectively. The compressive strength $f_{m,c}$ and flexural strength $f_{m,f}$ of the mortar were equal to 2.61 MPa (CV 27.5%) and 0.58 MPa (CV 28.4%).

Two specimens were tested in the unreinforced configuration (URM), and later repaired and retrofitted with a bidirectional low-density basalt grid (LDB). The remaining two specimens

were retrofitted with the same LDB. The textile was embedded in a mortar matrix consisting of a premixed NHL 3.5 natural hydraulic lime mortar with compressive strength $f_{mm,c}$ and flexural strength $f_{mm,f}$ equal to 13.18 MPa (CV 9.8%) and 3.26 MPa (CV 2.2%) respectively.

Four LDB sheets with dimensions of 800 × 1270 mm^2 were applied to each specimen. Two sheets were placed on each face of the wall with an overlap of 300 mm in the centre of the wall. The overlapping was chosen according to a previous study indicating that a minimum bond length of 200 mm is required for good performance [8]. The used LDB textile has a Young's Modulus of 90 GPa and an ultimate tensile strength of 1700 MPa.

2.2 Repair and retrofitting

After the initial tests, two unreinforced specimens were repaired using the *"scuci-cuci"* technique, i.e. a local reconstruction of the damaged masonry portions based on fractured bricks replacement and lime mortar repointing. The aim of the repair was to restore the wall's structural continuity along the cracks and to recover its initial stiffness. The materials used for the *scuci-cuci* operation were the same ones utilized for the original construction in order to assure good compatibility in terms of stiffness and resistance. The considered repair technique followed three stages. First, the cracks of the specimens were widened using a rotary hammerdrill accessorized with a 20 mm width flat chisel, and a hand tool 30 mm width flat chisel. Second, the damaged bricks were replaced by new ones, as shown in Figure 1. Finally, the cracks were filled with the same lime-based mortar used for the retrofitting of the walls.



Figure 1: *Scuci-cuci* intervention on the URM tested walls. Removing and replacing of fractured units. Filling of cracks with lime-based mortar for repair.

3 EXPERIMENTAL SET-UP

The samples were laid on a metallic C- profile filled with concrete. This profile allowed the sliding shear failure to potentially occur in the bed joints of the lower course of bricks [9]. This profile was fixed on a stiff steel plate fixed to the strong floor slab of the laboratory by means of post-tensioned steel bars. In turn, a reinforced concrete (RC) beam was placed on top of the wall. This element was used for the application of both uniformly distributed vertical load and horizontal cyclic loading by the corresponding actuators. In addition, a stiff metallic H-profile stiffened with ribs was placed over the RC beam in order to ascertain an even distribution of the applied vertical loading. The vertical load was applied with two jacks with a capacity of 1000 kN each. The jacks reacted against a stiff frame anchored to the strong floor. A 3 mm

thick Teflon sheet and a 3 mm thick PVC sheet were inserted between the RC beam and the metallic profile to provide a smooth horizontal surface and to reduce the friction between both elements. In addition, a layer of cement-based mortar with thickness of 5 to 10 mm was placed between the RC beam and the PVC sheet in order to level the top surface of the beam and guarantee a uniform vertical load transfer.

3.1 Testing procedure

The shear compression tests were performed in two steps. First, the vertical force V was gradually applied under force control. The valves of the jacks were closed once the designed compression stress was reached ($\sigma_v = 0.3$ MPa). With the valves closed, no displacement or rotation of the top of the wall was possible and applying horizontal load induced a double bending condition [10]. Because of the testing mode, the vertical load increased with the application of horizontal load. The increase of vertical load depended upon the stiffness degradation of the wall.

The horizontal shear force H was applied with a hydraulic actuator anchored to a reaction wall. The actuator had a pushing and pulling capacity of 350 kN and 250 kN respectively. Two steel plates (530 × 300 × 30 mm^3) connected by 4 steel rods of 40 mm diameter were mounted aligned with the horizontal actuator. One of the plates was connected to the horizontal actuator by means of a hinge, enabling the application of reversed cyclic loading in the horizontal directions, see Figure 2.

The walls were instrumented with ten linear variable displacement transducers (LVDT) to measure diagonal displacement and control the uplift and relative sliding between the wall and its base. Eight potentiometer displacement transducers were utilized to measure the diagonal and vertical displacement. Finally, two laser sensors measured the imposed horizontal displacement. The vertical load was measured by means of four pressure transducers and the horizontal load by the actuator's inner load cell.

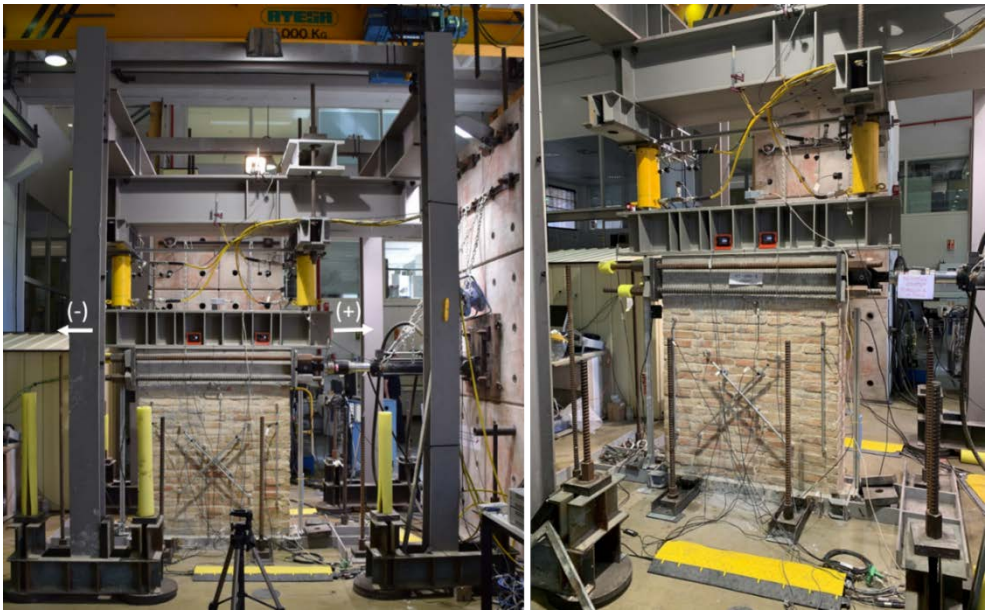


Figure 2: Set-up of the shear compression test

3.2 Loading protocol

The in-plane cyclic loading was displacement-controlled to capture the accumulated damage in the wall and to enable the detection of the failure mechanism. The loading protocol adopted for all test, shown in Figure 3, follows the guidelines provided by FEMA 461 [11]. The loading history consisted of repeated cycles of step-wise increasing deformation amplitudes. Three cycles were completed for each amplitude.

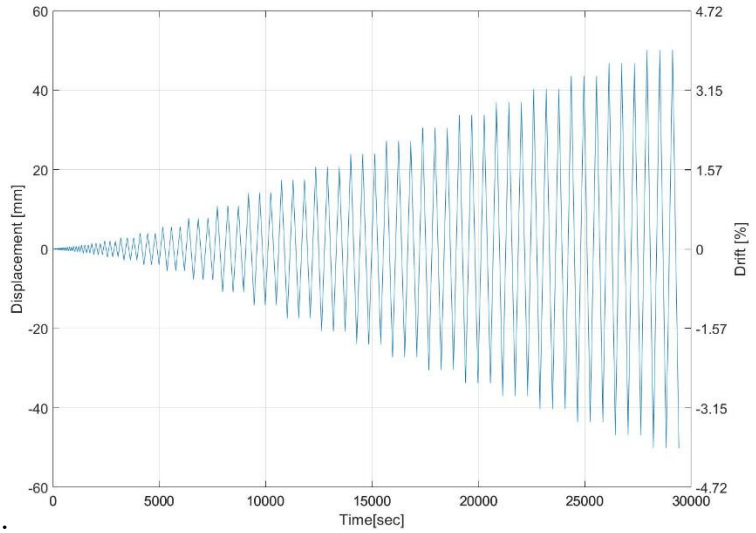


Figure 3: Cyclic loading protocol for the shear compression test

4 EXPERIMENTAL RESULTS

4.1 Failure modes

Figure 4 shows the crack pattern at the end of the test of each specimen. It is noted that data on specimen LDB-TRM (LDB_2) are disregarded due to technical problems experienced by the loading system during this test.

The crack patterns evidence that all the specimens experienced shear failure. Damage in unreinforced specimens was characterised by a stair-step cracking mainly developed through the mortar joints and by tensile splitting of some units. The crack pattern of specimen URM_1 only shows one diagonal crack because the test was not continued beyond the development of this first crack. The load capacity of theses specimens shows significant scattering probably due to the variation of the mechanical properties of the masonry components.

The repaired and retrofitted specimens and the just retrofitted specimens showed also diagonal cracks developed from the centre of the panel with severe damage occurring in the region where the two cracks intersected.

The repaired and retrofitted specimens showed a more diffuse crack pattern in the centre of the panel compared to the just retrofitted one. The LDB grid in the former case had to withstand more displacement cycles, starting at early stages of the test, because of the re-opening of the repaired cracks. The cracks re-opening transferred the tensile stress to the LDB grid, causing the spalling of the mortar and thus the diffuse crack pattern. Despite this particular feature, the

specimens retrofitted with LDB evidenced a more homogeneous response in terms of crack pattern and lateral load capacity compared with the unreinforced ones.

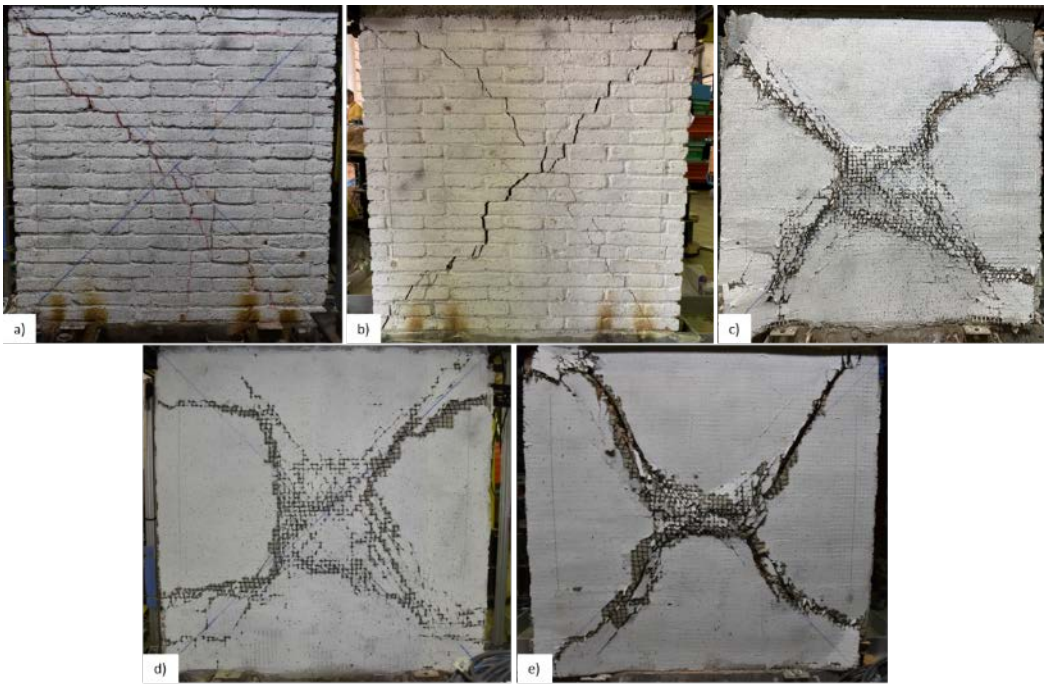


Figure 4: Crack patterns at the end of the test: a) unreinforced wall URM_1, b) unreinforced wall URM_2, c) wall repaired and retrofitted with LDB, URM1_R, d) wall repaired and retrofitted with LDB, URM2_R, e) wall retrofitted with LDB.

No toe-crushing in compression was observed in any of the specimens during the test and up to the largest displacement amplitude attained.

Debonding was detected close to the corners of the specimens where the load was applied. Such debonding, however, was a local phenomenon induced by the metallic plates through which the cyclic load was applied and did not interfere on the attained load or deformation capacities.

4.2 Force-displacement curves

Figure 5 shows the experimental force-displacement curves under cyclic in-plane loading. The experimental force-displacement envelopes are derived from the hysteretic curves and constructed by connecting the peak force at the first cycle of each displacement amplitude. The positive direction is the direction in which the horizontal hydraulic actuator pulls the specimen, whereas the negative one is the direction in which the actuator pushes the specimen (Figure 2).

The experimental curves are characterized by an initial linear branch corresponding to the undamaged behaviour of the structure. At the onset of cracking, and with the development of damage and energy dissipation, the response becomes non-linear, as evidenced by the force-displacement envelope, while at the same time wider hysteretic loops are observed. The hysteretic loops widen progressively as the residual strength decreases until failure. Among the unreinforced specimens, the wider hysteretic loops were seen in URM_2 (see Figure 5 b) in

correspondence with the more severe damage observed in it during and after the test, Figure 4 b. However, and after repair and testing, the same specimen URM2_R showed a more ductile and progressive damage than its pair URM1_R.

The repaired and retrofitted walls showed a moderated improvement in lateral load-bearing capacity. However, the peak loads were reached at a larger displacement compared with the unreinforced ones. Consequently, their global behaviour showed larger deformation capacity and ductility, as seen in Figure 5. The just retrofitted specimens showed a significant increment in both lateral-load bearing and deformation capacity, evidencing the effectiveness of the reinforcement system.

Table 1 summarizes the main parameters of the force-displacement experimental curves for both directions. The cracking load H_{cr} is the one recorded when the first cracks became visible. The peak load H_{max} is the one corresponding to the maximum lateral load attained. The ultimate load H_u is derived from the bilinear idealization as discussed in the following section.

Table 1: Experimental first crack and peak loads. Ultimate load obtained for the bilinear idealization.

Specimen	First crack load [kN]		Peak load [kN]		Ultimate load [kN]		H_{cr} / H_{max}		H_u / H_{max} (-)	
	H_{cr} (-)	H_{cr} (+)	H_{max} (-)	H_{max} (+)	H_u (-)	H_u (+)	(-)	(+)	(-)	(+)
URM_1	-114.46	-	-192.38	150.7	-176.02	-	0.59	-	0.91	-
URM_2	-102.31	104.96	-162.29	151.56	-154.22	146.37	0.63	0.69	0.95	0.97
URM1_R	-120.70	126.05	-175.09	180.08	-161.53	174.42	0.69	0.70	0.92	0.97
URM2_R	-142.20	132.44	-194.56	167.88	-181.99	162.87	0.73	0.79	0.94	0.97
LDB_1	-135.84	146.19	-213.10	207.16	-195.95	202.80	0.64	0.71	0.92	0.98

4.3 Bilinear idealization

The bilinear idealization is a simplified approach used in the study on the in-plane seismic response of masonry walls. The idealization permits the determination of the response spectra in a way similar to linearly elastic systems [3,4]. It this also used in the computation of the ductility [12].

The bilinear approximation of the experimental envelope curves was obtained as described in Figure 6. First, the cracking point was identified along with the peak load. The ultimate displacement δ_u was defined as the displacement at which the lateral strength had dropped to 80% of H_{max}. If such a large drop was not attained, the largest displacement reached during the test was taken as δ_u. The ultimate strength H_u is defined as the maximum load o the bilinear idealization and is calculated taking into account the energy dissipation capacity of the experimental envelope curve. The ultimate strength is determined so as to produce a bilinear curve enveloping the same are below as the experimental curve up to δ_u. For the present application, the bilinear idealization was calculated for both positive and negative directions.

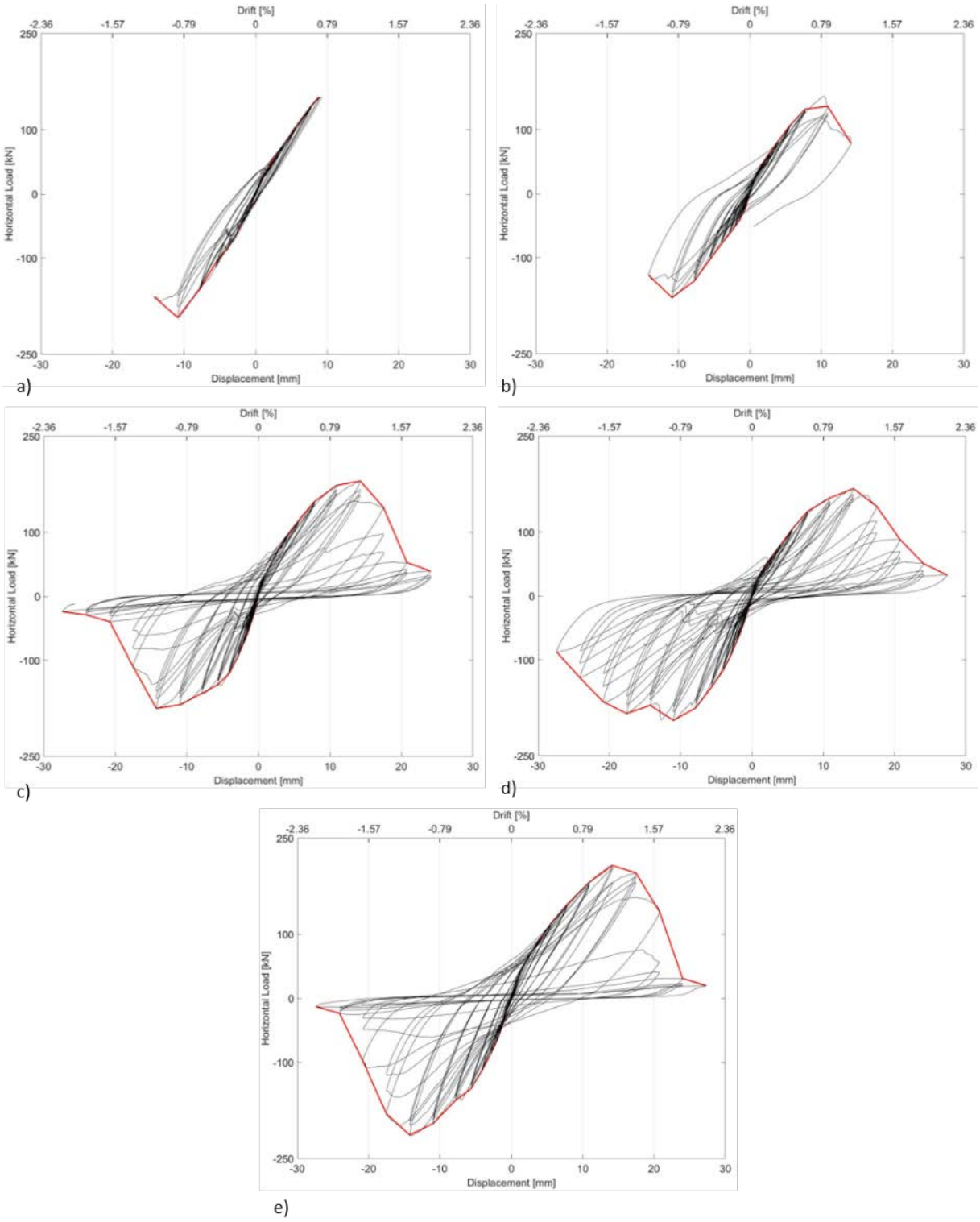


Figure 5: Force-displacement hysteresis curves and envelope curves of tested walls: a) unreinforced wall URM_1, b) unreinforced wall URM_2, c) wall repaired and retrofitted with LDB, URM1_R, d) wall repaired and retrofitted with LDB, URM2_R, e) wall retrofitted with LDB (LDB_1).

Table 1 shows the ratio H_{cr}/H_{max} which on average is equal to 0.69 (CV 8%). This value is consistent with Eurocode 8 [3] and the proposal of Tomaževič [13] and Magenes and Calvi [12] for the bilinear idealization of the hysteretic behaviour of the wall, which propose a H_{cr}/H_{max} value equal to 0.7. However, the ratio H_u/H_{max} yields a higher value than 0.9, which is the value proposed by the aforementioned authors. The value of the ratio for all the tests is on average equal to 0.95 (CV 3%).

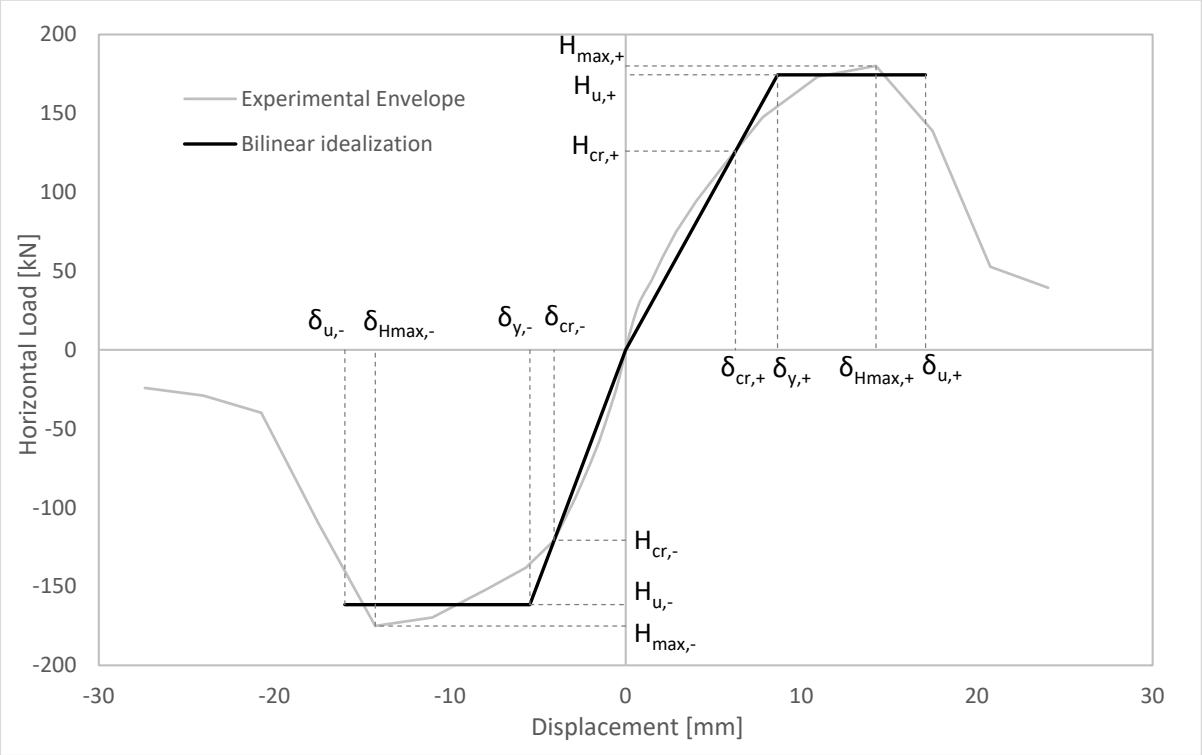


Figure 6: Example of bilinear idealization.

Table 2 and Table 3 show the main limit states analysed following [14,15] in terms of displacement and drift. The aforementioned authors considered five limit states. The displacement at cracking point δ_{cr} corresponds to the displacement for which a load equal to 70% H_{max} is attained. The displacement at yielding δ_y is associated with the ultimate load H_u. The maximum displacement δ_{Hmax} corresponding to the peak load associated to the SD limit state defined by the codes. The ultimate displacement δ_u corresponds to the displacement for which the reduction of the lateral strength is 20% and is associated to the NC limit state introduced by the codes. In addition, [14,15] defines a collapse displacement δ_c as the one corresponding to ta drop of the lateral strength of 50%.

EC8 [3] defines two main limit states corresponding to Significant Damage (SD) and a ultimate limit state associated with Near Collapse (NC). For unreinforced masonry walls failing in shear mode, the limit drifts corresponding to the SD and NC states are set to $\theta_{SD} = 0.4\%$ and $\theta_{NC} = 0.5\%$ respectively. The Italian standard NTC2018 [4] defines a Ultimate Limit State (SLU), equivalent to EC8's NC state, for which the drift limitation is equal to $\theta_{SLU} = 0.5\%$.

When compared with the limit drifts defined by EC8 [3] and the Italian code [4], it is

observed that both standards underestimate the deformation capacity of the unreinforced tested walls by 50%. The average value of drift obtained in the experimental test, considering both directions, for the URM specimen for the SD and NC limit states are 0.8% and 1.1% respectively.

Table 2: Experimental displacements corresponding to different damage levels.

Specimen	Cracking displ. [mm]		Yielding displ. [mm]		Max displ. [mm]		Ultimate displ. [mm]		Collapse displ. [mm]	
	δ_{cr} (-)	δ_{cr} (+)	δ_y (-)	δ_y (+)	δ_{Hmax} (-)	δ_{Hmax} (+)	δ_u (-)	δ_u (+)	δ_c (-)	δ_c (+)
URM_1	-5.55	-	-8.53	-	-10.89	8.94	-14.16	-	-14.16	-
URM_2	-5.56	5.51	-8.38	7.68	-10.90	10.91	-13.95	12.26	-14.18	14.17
URM1_R	-4.08	6.25	-5.45	8.65	-14.26	14.25	-15.99	17.07	-18.54	19.34
URM2_R	-5.62	7.82	-7.19	9.62	-11.01	14.23	-21.71	17.86	-26.59	21.75
LDB_1	-5.61	7.81	-8.09	10.83	-14.22	14.17	-17.89	19.1	20.46	21.75

Table 3: Experimental drift values corresponding to different damage levels.

Specimen	Cracking displ. [mm]		Yielding displ. [mm]		Max displ. [mm]		Ultimate displ. [mm]		Collapse displ. [mm]	
	θ_{cr} (-)	θ_{cr} (+)	θ_y (-)	θ_y (+)	θ_{Hmax} (-)	θ_{Hmax} (+)	θ_u (-)	θ_u (+)	θ_c (-)	θ_c (+)
URM_1	-0.4%	-	-0.7%	-	-0.9%	0.7%	-1.1%	-	-1.1%	-
URM_2	-0.4%	0.4%	-0.7%	0.6%	-0.9%	0.9%	-1.1%	1.0%	-1.1%	1.1%
URM1_R	-0.3%	0.5%	-0.4%	0.7%	-1.1%	1.1%	-1.3%	1.3%	-1.5%	1.5%
URM2_R	-0.4%	0.6%	-0.6%	0.8%	-0.9%	1.1%	-1.7%	1.4%	-2.1%	1.7%
LDB_1	-0.4%	0.6%	-0.6%	0.9%	-1.1%	1.1%	-1.4%	1.5%	-1.6%	1.7%

5 CONCLUSIONS

- The application of a bidirectional basalt grid (LDB) improved the in-plane response of the masonry walls in terms of load-bearing capacity and deformation capacity. When compared with the reference unreinforced ones, the retrofitted walls showed a significantly more ductile behavior with larger lateral displacement and consequently greater deformation capacity.
- The reinforced walls showed a more homogeneous response characterized by very similar crack patterns, failure modes and load capacities. By comparison, the unreinforced ones showed results that are more scattered in terms on lateral load-bearing capacity.
- The scuci-cuci and retrofitting intervention applied to the previously damaged walls, attained a satisfactory repair with full recovery of the initial load-bearing capacity.
- The application of the current codes has led to a significant underestimation of the deformation capacity shown by the tested walls. The underestimation is of 50% for the unreinforced walls.

Acknowledgements. The authors gratefully acknowledge the financial support from the Ministry of Science, Innovation and Universities (MCIU) of the Spanish Government, the State Agency of Research (AEI) and the European Regional Development Fund (ERDF) through the SEVERUS project ("Multilevel evaluation of seismic vulnerability and risk mitigation of masonry buildings in resilient historical urban centres", ref. num. RTI2018-099589-BI00), and from Kerakoll Ibérica S.A. through the RTD project A-01217. Support from Secretaria d'Universitats i Investigació de la Generalitat de Catalunya through a predoctoral grant awarded to the first author is also gratefully acknowledged.

REFERENCES

[1] American Concrete Institute, ACI 549.4R-13 - Guide to Design and Construction of Externally Bonded Fabric-Reinforced Cementitious Matrix (FRCM) Systems for Repair and Strengthening Concrete and Masonry Structures, (2013).

[2] CNR - Consiglio Nazionale delle Ricerche, DT 215/2018 - Istruzioni per la progettazione, l'esecuzione ed il controllo di interventi di consolidamento statico mediante l'utilizzo di compositi fibrorinforzati a matrice inorganica (in Italian), (2018).

[3] European Standard, Eurocode 8 : Design of structures for earthquake resistance — Part 3: Assessment and retrofitting of buildings., 3 (2004).

[4] Ministero delle Infrastrutture e dei Trasporti, DM 17/01/2018 - Aggiornamento delle "Norme Tecniche per le Costruzioni" (in italian), (2018) 1–198.

[5] J. Segura, D. Aponte, L. Pelà, P. Roca, Influence of recycled limestone filler additions on the mechanical behaviour of commercial premixed hydraulic lime based mortars, Constr. Build. Mater. 238 (2020). doi:10.1016/j.conbuildmat.2019.117722.

[6] CEN, EN 772-1, Methods of test for masonry units. Part 1: Determination of compressive strength, Com. Eur. Norm. Brussels. (2011).

[7] CEN, EN 772-6, Methods of test for masonry units. Part 6: Determination of bending tensile strength of aggregate concrete masonry units., Com. Eur. Norm. Brussels. (2002).

[8] M. Santandrea, I.A.. Imohamed, C. Carloni, C. Mazzotti, S. de Miranda, F. Ubertini, A study of the debonding mechanism in steel and basalt FRCM masonry joints, Brick Block Mason. - Trends, Innov. Challenges. (2016) 433–440.

[9] C. Knox, Assessment of Perforated Unreinforced Masonry Walls Responding In Plane, The university of Auckland, 2012.

[10] G. Magenes, G.M. Calvi, Cyclic behaviour of brick masonry walls, in: Balkema (Ed.), Proc. Tenth World Conf. Earthq. Eng. 19-24 July 1992 Madrid, Spain, 1992: pp. 3517–3522.

[11] Applied Technology Council, Interim Testing Protocols for Determining the Seismic Performance Characteristics of Structural and Nonstructural Components - FEMA 461, (2007).

[12] G. Magenes, G.M. Calvi, In-plane seismic response of brick masonry walls, Earthq. Eng. Struct. Dyn. 26 (1997) 1091–1112.

[13] M. Tomaževič, Earthquake-Resistant Design of Masonry Buildings, Imperial Collage Press, 1999. doi:10.1142/9781848160835.

[14] F. Vanin, D. Zaganelli, A. Penna, K. Beyer, Estimates for the stiffness, strength and

drift capacity of stone masonry walls based on 123 quasi-static cyclic tests reported in the literature, Bull. Earthq. Eng. 15 (2017) 5435–5479. doi:10.1007/s10518-017-0188-5.

[15] M. Godio, F. Vanin, S. Zhang, K. Beyer, Quasi-static shear-compression tests on stone masonry walls with plaster: Influence of load history and axial load ratio, Eng. Struct. 192 (2019) 264–278. doi:10.1016/j.engstruct.2019.04.041.

12th International Conference on Structural Analysis of Historical Constructions
SAHC 2020
P. Roca, L. Pelà and C. Molins (Eds.)

EXPERIMENTAL INVESTIGATION OF THE BOND BETWEEN GLASS TEXTILE REINFORCED MORTAR (GTRM) AND MASONRY SUBSTRATE: THE EFFECT OF TEXTILE IMPREGNATION

PARASKEVI D. ASKOUNI[1*] AND CATHERINE G. PAPANICOLAOU[2]

[1]Structural Materials Laboratory (SML)
University of Patras (UP)
Rio Patras, 26504, Achaia, Greece
e-mail: askounip@upatras.gr, http://sml.civil.upatras.gr/ (*corresponding author)

[2]Structural Materials Laboratory (SML)
University of Patras (UP)
Rio Patras, 26504, Achaia, Greece
e-mail: kpapanic@upatras.gr, http://sml.civil.upatras.gr/

Keywords: Textile Reinforced Mortar, Masonry, Bond, Impregnation

Abstract. *Textile Reinforced Mortar (TRM) is an appealing choice for the strengthening of existing structures and especially that of monumental character through application as external reinforcement. In the current study, the TRM-to-masonry bond was experimentally investigated focusing on the parameter of the yarns' treatment, that is none or impregnation with Styrene-Butadiene Rubber – SBR latex. For this purpose, both double-lap/double-prism (DL) and single-lap/single-prism (SL) shear bond test configurations have been employed. Specimens comprised strips of glass fiber textiles (either uncoated – UT or fully impregnated – IT) applied on wall prisms of stack-bonded smooth clay units through a cement-based mortar. TRM strips of DL specimens (with uncoated textile – UT or impregnated textile – IT) had a bond length (BL) equal to 150 mm. This BL was larger than the effective one, i.e. the minimum length needed for the attainment of the maximum TRM bond capacity (with UT). Due to the inadequacy of the DL set-up in capturing specimens' post-peak response, the SL set-up was also opted for. TRM strips of SL specimens (with UT or IT) had various BLs (100 mm, 150 mm and 200 mm) in order to study the combined effect of BL and textile impregnation. According to the results from both set-ups, the maximum bond load, F_{max} of specimens with IT was increased by 40% in comparison with specimens with UT. Additionally, F_{max} of specimens with IT increased with increasing BL.*

1 INTRODUCTION

Textile Reinforced Mortar (TRM) is a composite material comprising fiber grids embedded in an inorganic (typically, cement- or lime-based) matrix. The textiles used consist of dry or coated (partially impregnated) or fully impregnated fiber yarns (although, it is debatable whether such a treatment leads to composites that should be put under the TRM umbrella). TRM systems have been gaining the technical world's acceptance as externally

bonded strengthening means of existing masonry structures (see [1] for a compilation of successful interventions in real-life structures). Especially, in the case of structures of a monumental character, TRMs' compatibility with various substrates, (partial) reversibility of the intervention and substrate breathability render this composite material as an appealing choice for strengthening. However, the efficient use of TRMs significantly depends on both the bond between the composite material and the existing substrate and the bond between the grid and the matrix. Unless certain unfavourable conditions are met, it has been shown that the most vulnerable interface during in-plane shear load transfer from the substrate to the textile is the textile-to-matrix interface in respect to the TRM-to-substrate one [2, 3]. The current study focuses on the effect of the yarns' treatment (impregnation with polymers or lack thereof) on the improvement of textile-to-matrix bond. This type of yarns' treatment can eliminate the well-documented telescopic pull-out phenomenon i.e. the relative slippage of unbonded ('dry') inner filaments in respect to the mortar-bonded sleeve ones during yarns' pull out from the matrix. It is noted that in dry fiber yarns this distinction between inner (or core) filaments and outer (or sleeve) ones is due to partial penetration of the matrix into the yarns; the degree of penetration depends on a multitude of parameters such as the consistency of the matrix, the weight of the yarn and the production method of the TRM.

A previous relevant study is that of [4] who concluded that the bond capacity of a TRM system consisting of a carbon fiber textile embedded in a pozzolanic mortar applied onto clay bricks was improved through a treatment involving yarns' (moderate or complete) impregnation with a flexible epoxy resin combined with quartz sanding. Furthermore, by application of a carbon fiber textile on masonry substrates by means of a lime-based mortar [5] studied the simultaneous effect of TRM bond length and yarns' treatment (complete impregnation with a flexible epoxy resin in combination with quartz sanding). According to the experimental results of the latter study, the matrix-to-textile bond improvement due to textile treatment was more pronounced for increasing bond lengths. In the work of [6], a Round Robin test campaign was undertaken in order to assess the TRM-to-masonry bond capacities of various glass fiber TRM systems comprising textiles with different geometries and yarn treatments and different types of mortars such as lime- or cement-based ones. In particular, the comparison of the maximum axial textile stress of some GTRM systems combining coated or uncoated textiles with lime-based mortars and pre-impregnated textiles with lime- or cement- based mortars ended up to similar stress values concerning the coated and uncoated textiles (however more scattered in the case of dry fibers) and higher stress values concerning the pre-impregnates ones.

Yarn's impregnation (partial or complete) results in: (i) improved matrix-to-yarn bond; (ii) improved stress distribution among both different filaments within the same yarn and different yarns within the same textile layer; and hence (iii) better exploitation of the fibers' tensile capacity [see also 7]. In TRM/masonry joints and in the absence of debonding phenomena along the TRM/masonry interface, this translates into an increase in the load-bearing capacity of the joints under in-plane shear loads. Nevertheless, strength improvements are not always the critical ones, especially when structural upgrading interventions of unreinforced masonry structures against seismic actions are called for. In these cases, energy dissipation of the strengthened structure is a crucial feature. Under this light, dry or coated fiber yarns failing under telescopic pull-out can provide the strengthening system with favourable energy dissipation characteristics. Moreover, yarns' impregnation (or even

coating) with polymers entails some drawbacks, such as: (i) 'stiffening' of the textile resulting in its inability (partial or complete, depending on the impregnation degree achieved and on the type of impregnating means applied, e.g. thermoset polymer or synthetic rubbers) to closely match irregular surfaces; and (ii) thermal decomposition of the polymeric coating/impregnation means at exposure temperatures larger than (roughly) 400°C, leading to matrix-to-textile bond deterioration as shown from pull-out tests run on post-heated/cooled-down textile reinforced concrete specimens [8]. Nevertheless, it should be mentioned that polymers are not the only option as materials for yarns' coating/impregnation; for example, cement slurries or other minerals can be used for this purpose, see [9, 10].

The experimental results presented herein are the products of a campaign focusing on the effect of textile complete impregnation with a Styrene-Butadiene Rubber (SBR) latex emulsion on the bond capacity of AR glass TRM overlays bonded on masonry substrates. The study involved shear bond tests of both the double-lap/double-prism (DL) and the single-lap/single-prism (SL) type. In this work, SBR was used on the basis of its ability to ensure partial pull-out of the core filaments [11] (and, hence, to yield higher energy dissipation composite features) in comparison to epoxy-resins [12] (comparisons made with carbon fiber yarns, though).

2 MATERIALS

2.1 Masonry

Stack-bonded single-brick wall prisms were used for the simulation of masonry substrates. Each wall comprised solid clay bricks with a smooth surface and cement/lime-based mortar joints. The mechanical characteristics of the walls normal to their joints were determined according to the recommendation LUMB1 [13] and were found equal to 26.4 MPa (CoV 10%) and 7.3 GPa (CoV 18%) as per compressive strength and modulus of elasticity, respectively. Bricks measured 200×100×50 mm and were of a compressive strength equal to 20 MPa, according to the producer. Joints were approximately 15 mm thick. For their construction a M5 general purpose masonry mortar, according to the Eurocode 6 [14] classification, was used containing cement (CEM IV 32.5N), lime and sand in proportions 1:2:6, by volume.

2.2 TRM

Two TRM systems were investigated sharing the same cement-based mortar (matrix) and the same AR-glass fiber textile the only difference being in the yarns' treatment: (i) dry, i.e. "as produced", henceforth referred to as UT (uncoated textile) versus (ii) fully impregnated by hand using a Styrene-Butadiene Rubber – SBR latex emulsion, henceforth referred to as IT (impregnated textile). The dry textile (with a balanced arrangement of yarns in two orthogonal directions) had an areal weight and a mid-yarn spacing equal to 320 g/m^2 and 12 mm, respectively. Both textiles were mechanically characterized through tensile tests on 9-yarns' strips; testing was carried out partially according to EN ISO 13934-1 [15]. According to the results, the tensile strength (f_t) and the elastic modulus of UT were equal to 822 MPa (CoV 7%) and 71 GPa (CoV 6%), respectively. The respective values for IT were found equal to

1126 MPa (CoV 1%) and 66 GPa (CoV 1%), respectively. The mortar used as matrix contained polypropylene fibers and a low content (<5%, by weight of cement) of polymeric additives for the avoidance of shrinkage phenomena. The compressive and flexural strengths of the mortar were determined according to EN 1015-11 [16] at 21 days post-production and were found equal to 22.3 MPa (CoV 11%) and 5.2 MPa (CoV 14%), respectively; its elastic modulus was equal to 7.6 GPa (as provided by the manufacturer).

3 EXPERIMENTAL PROGRAM

3.1 Set-ups employed

Both double-lap/double-prism (DL) and single-lap/single-prism (SL) set-ups were employed for reasons explained in the following (see subsection 4.2). Specimens involved in DL tests consisted of two wall prisms connected with a single TRM overlay on each side, (Figure 1). Each TRM overlay was made of two mortar layers of equal thickness (around 3 mm) and a single uncoated or impregnated textile strip sandwiched between them. The total length of the TRM overlay was equal to double the examined bonded length plus the unbonded length, which was equal to 100 mm (50 mm space between the wall prisms plus 2×25 mm starter unbonded lengths introduced for the avoidance of stress concentration phenomena). The TRM overlay was centrally bonded on the walls widthwise and its width was 120 mm comprising 9 longitudinal (load-aligned) yarns. Specimens were moist-cured using wet burlaps for 7 days and then stored in lab conditions for 14 more days until testing. Each wall prism was fitted in a steel frame before testing. Subsequently, both the bottom (fixed) and the top (moving) part of the specimen (Figure 1a) were connected to the machine through centrally-positioned ball joints in regards to the specimen's cross-section in order to ensure self-alignment of the specimen during testing. Activation of the bond mechanism was realized by imposed distancing of the two wall prisms using a servohydraulic system furnished with a 50 kN load cell. Tests were run in a displacement-control mode at a constant piston displacement rate equal to 0.005 mm/s. The instrumentation of each specimen (Figure 1a) consisted of: (i) two digital dial gauges (DDG) placed adjacent to the strip's loaded ends (DDGLE) on each side of the specimen in order to measure the distancing between the two wallettes; (ii) two DDG placed at the strip's free ends (attached on the central textile yarn – DDGFE) on a single side of the specimen (henceforth side A), in order to record the slip of the projecting textile at this position; (iii) three strain gauges along each TRM half-overlay and one at the overlay's unbonded length (side A), mounted on the central yarn of the textile, through slots; (iv) a random pattern of black dots on the opposite side of side A which was previously painted white (henceforth side B) in order to conduct post-test DIC analysis.

Specimens involved in SL tests comprised a single wall prism unilaterally reinforced with a TRM overlay constructed as described for the case of DL specimens. The TRM strip was centrally bonded on the wall widthwise distancing 25 mm from the wall's top edge so that stress concentration phenomena could be avoided. The total length of the TRM overlay was equal to the examined bond length while its width was equal to 120 mm (9 yarns). The textile projected from both the top and the bottom parts of the TRM strip (Figure 1b). Curing conditions of the specimens were the same to those of DL ones. Each wall prism was placed and fixed in a steel frame connected to the moving part of the machine. The projecting textile at the top was connected to the fixed part of the machine through a joint providing full in-

plane and partial out-of-plane rotation capacity. The top end of the textile strip was sandwiched between two fiber-reinforced polymer tabs and fixed between two bolted steel plates. During testing, the projecting textile was being pulled away from the bonded TRM overlay using a servohydraulic testing machine fitted with a 250 kN load-cell; piston displacement was the controlling command at the same rate as that in DL tests. The instrumentation of each specimen (Figure 1b) consisted of: (i) two DDG fixed on the wall acting against an aluminium plate which was glued on the first transversal yarn of the pulled textile close to the strip's loaded end in order to measure the relative displacement of the textile in respect to the wall; (ii) two DDG fixed on the wall acting against an aluminium plate which was glued on the second transversal yarn of the textile close to the strip's free end, in order to record the slip of the textile at this position; (iii) three strain gauges along the TRM overlay mounted on the central yarn of the textile, through slots.

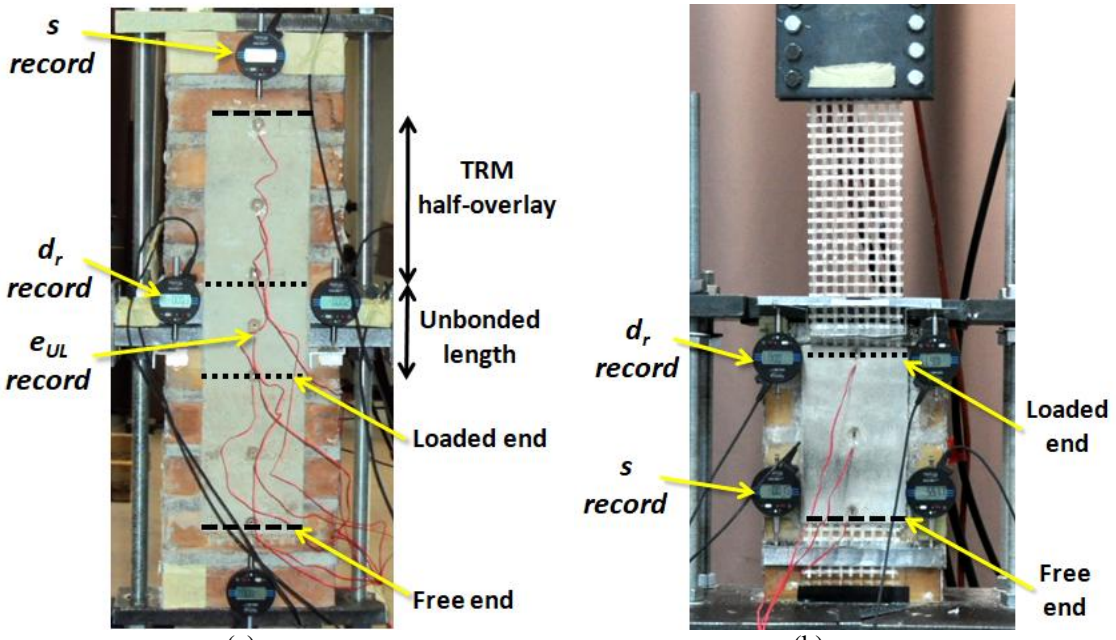


Figure 1: (a) Double-lap/double-prism and (b) Single-lap/single-prism set-up

3.2 Specimens

In total, 5 DL and 12 SL specimens are presented in the current study. In the case of DL specimens, the bond length of the TRM overlays was equal to 150 mm while 3 of them were furnished with UT and the rest with IT. The selected bond length was higher than the one previously determined as the effective bond length of identical TRM/masonry joints with UT (assessed by DL shear bond tests) [3]; the latter was found equal to 125 mm. In the case of SL specimens, half of them were furnished with UT and the remaining with IT while also varying the examined bond lengths (100 mm, 150 mm and 200 mm). Specimens' notation has the form of BLx_y_z_n (see Table 1), where x is the bond length (BL) of the TRM overlay in mm, y is the type of set-up employed (DL or SL), z is the type of textile employed (UT or IT) and n is the specimen number in a group of identical specimens.

4 EXPERIMENTAL RESULTS

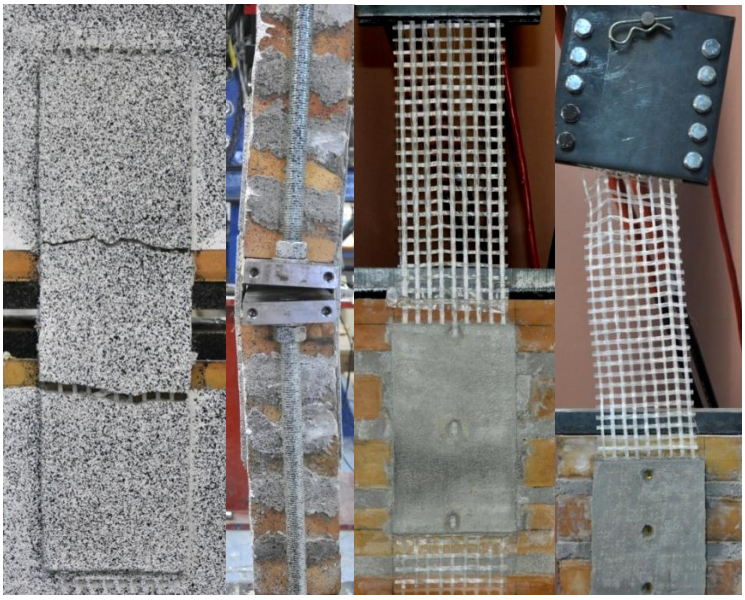
4.1 Response curves and values

The experimental results are listed in Table 1. For the DL specimens, each tabulated value was derived as follows: (i) maximum load of each TRM half-overlay, F_{max}, being equal to half of the piston load at maximum (assuming equal piston load distribution between the two reinforced sides of the specimen due to its symmetry [3]); (ii) maximum textile axial stress, σ_{max}, being equal to the ratio of F_{max} to longitudinal fibers' area A_f (= 6.912 mm^2); (iii) relative displacement of each TRM half-overlay in respect to the wall prism at maximum load, $d_{r,max}$, being equal to one half of the average of the four readings from the DDGLE minus one half of the elongation of the unbonded length per side (taken equal to the strain gauge reading times the unbonded length); (iv) the elongation corresponding to maximum load, e_{BL}, being equal to the mean value of the strain integrals of the TRM half-overlays on Side A; (v) the slippage corresponding to maximum load, s_{BL}, being equal to the difference between the $d_{r,max}$ and e_{BL} values (see also [3]); (vi) textile exploitation degree being equal to the ratio of σ_{max} to f_t. It is noted that both the relative displacement and the slip of the two TRM half-overlays of the same side were assumed to be equal (see also [17]). For the SL specimens, the derivation of the values included in Table 1 was realized as in the case for DL specimens with the following exceptions: (i) maximum load, F_{max}, was equal to the piston maximum load (ii) relative displacement at maximum load, $d_{r,max}$, was equal to the average of the readings from the DDGLE; (iii) elongation at maximum load, e_{BL}, was equal to the strain integral of the TRM overlay. The failure mode of each specimen is also included in Table 1.

All DL and SL specimens receiving UT failed "as usual", that is due to textile slippage from within the matrix. In the case of DL specimens failure (appreciable reduction of load-bearing capacity) was associated to the enlargement of one of the previously formed cracks along the unbonded length (Figure 2a) which in turn led to the out-of-plane rotation of both wall prisms and the loss of specimens' symmetry (Figure 2b). SL specimens with IT failed due to either textile slippage (Figure 2c) or rupture of the projecting textile close to the gripping device (bolted steel plates) due to stress concentration [Figure 2d and (σ_{max} / f_t) values in Table 1, all less than 1). It is clarified that in neither DL nor SL specimens were cracks formed along the bonded part of the overlay or did any interlaminar shear failure or TRM-to-substrate debonding phenomena occur.

Table 1: Experimental results

Specimen	F_{max} (kN)	σ_{max} (MPa)	$d_{r,max}$ (mm)	e_{BL} (mm)	s_{calc} (mm)	σ_{max} / f_t %	Failure mode
BL150_DL_IT_1	3.67	530.96	0.59	0.21	0.37	47.15	Textile slippage
BL150_DL_IT_2	3.04	439.81	0.57			39.06	
BL150_DL_UT_1	2.43	351.56	0.33	0.20	0.06	42.77	
BL150_DL_UT_2	2.27	328.41	0.23			39.95	
BL150_DL_UT_3	2.37	342.88	0.27			41.71	
BL200_SL_IT_1	4.61	667.00	6.71	1.22	5.49	59.24	Textile slippage
BL200_SL_IT_2	5.23	756.65	0.90	0.44	0.46	67.20	Yarns' rupture
BL150_SL_IT_1	3.69	533.85	0.94	0.50	0.65	47.41	Yarns' rupture
BL150_SL_IT_2	3.54	512.15	1.35			45.48	Yarns' rupture
BL100_SL_IT_1	3.25	470.20	0.52	0.30	0.22	41.76	Textile slippage
BL100_SL_IT_2	3.24	468.75	0.72	0.39	0.33	41.63	Yarns' rupture
BL200_SL_UT_1	2.32	335.65	0.45	0.25	0.19	40.83	Textile slippage
BL200_SL_UT_2	2.20	318.29	0.44			38.72	
BL150_SL_UT_1	2.37	342.88	0.70	0.21	0.28	41.71	
BL150_SL_UT_2	2.17	313.95	0.29			38.19	
BL100_SL_UT_1	2.12	306.71	0.44	0.07	0.36	37.31	
BL100_SL_UT_2	1.99	287.91	0.43			35.03	



(a) (b) (c) (d)

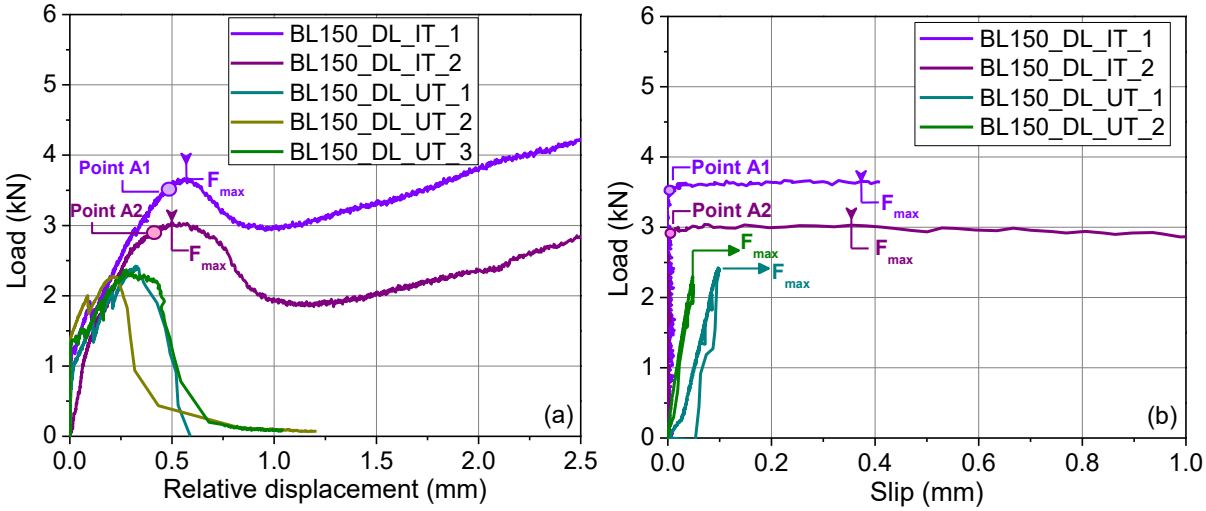
Figure 2: Images after failure depicting: (a) Textile slippage (side B) and (b) out-of-plane rotation of DL specimens, (c) textile slippage and (d) yarns' rupture in SL specimens

4.2 Discussion

The response of DL specimens with both UT and IT is depicted in Figure 3 through the respective curves of load versus relative displacement and load versus slip. Focusing on the former curves presented in Figure 3a, it is revealed that up to the attainment of F_{max} both groups of specimens present a first linear and a second non-linear ascending branch.

Additionally, F_{max} increased by 40% - on average - due to textile impregnation with the SBR latex emulsion. This is attributed to the consolidation of each yarn into a single macro-fiber leading to the absence of fibers' telescopic slippage and to the subsequent increase of the textile tensile strength (see subsection 2.2). In respect to the curves presented in Figure 3b, it is noted that slip values of specimens with UT have been derived from DDGFE records while those of specimens with IT have been computed through DIC analysis. Slip values of IT were almost zero up to points A1 and A2 which correspond to load values lower but close to the maximum one. After these points and up to F_{max} textile slippage increases rapidly due to the progressive debonding of the textile along its bond length. Starting from zero values at test start, slip values of UT kept on increasing up to F_{max}; nevertheless, these values (the ones corresponding to F_{max}) were much lower than the respective ones of the IT due to sleeve fibers' (filaments') rupture which is always present when glass fiber dry yarns are being pulled out from the matrix.

As previously mentioned (see subsection 4.1), DL specimens lost their symmetry in respect to the vertical plane normal to their faces after failure. In the case of UT, sleeve fibers' rupture led to an irrecoverable strength loss (descending branch of the load response curves - Figure 3a) due to the stress (and strain) lag of the core fibers in respect to the sleeve ones (telescopic pull-out effect). As a consequence, both the relative displacement of the fibrous reinforcement in respect to the substrate and the out-of-plane rotation of the specimens (at ultimate ≡ zero load-bearing capacity) were much lower than the respective values derived from counterpart specimens furnished with IT. Indeed, in the case of IT and with the fibers remaining intact for the total duration of the test, the specimens' post-peak response was characterized by a temporary (and rather limited) load drop followed by a steady-rate load increase (Figure 3a). This phenomenon was attributed to the contribution of (extra) friction at the textile-to-matrix interface on the convex side of the assemblage under testing during (and due to) the increase of the out-of-plane rotation of the walls (which, in turn, was owed to the good bonding conditions and the integrity of the fiber yarns). In an attempt to further investigate the effect of yarns' impregnation with SBR, more shear bond tests were designed, this time employing the SL set-up.



(a) (b)

Figure 3: (a) Load vs. relative displacement and (b) load vs. slip curves of DL specimens

The response of SL specimens with UT or IT is depicted in Figure 4 through load versus relative displacement curves. As mentioned before, all SL specimens with UT failed due to textile slippage from within the matrix. However, the dominant failure mode among SL specimens with IT was due to yarns' rupture close to the load introduction area reflected by an abrupt load drop in the respective response curves. Two SL specimens with IT (namely, BL200_SL_IT_1 and BL100_SL_IT_1) failed due to textile slippage (Figure 4a and 4c, respectively). From visual inspection and from the load versus relative displacement curve of specimen BL200_SL_1i it has become clear that the resulting response values have been contaminated by out-of-plane (Mode I) phenomena probably caused by misalignment between the unbonded part of the textile and the face of the specimen. Therefore, this specimen is excluded from the processing of the experimental results.

In Figure 4d, F_{max} values of all specimens tested are presented versus the bond length values considered. The increase of F_{max} due to textile impregnation was also confirmed in the case of SL specimens (though, only for BL = 100 mm, taking into account the specimen with IT failing due to textile pull-out). This increase amounts to approximately 55%. By comparing the F_{max} values of specimens with a bond length of 150 mm furnished with UT, it is inferred that the type of shear bond test set-up employed has negligible effect on F_{max}. This is in accordance to the findings of [18]. Although not too obvious, it is noticed that the F_{max} values of specimens with UT (failing due to textile pull-out) show a load stabilization trend with increasing bond length which can be used (as a 'rule of thumb') for the determination of the effective bond length of the TRM/substrate joint under consideration. On the contrary, the F_{max} values of specimens with IT (failing due to stress concentration-inflicted rupture of the yarns) – or, equivalently the exploitation ratio of the textile's tensile strength – increase for increasing bond length. The increase of the bond length reduces the level of load distribution unevenness between different yarns in the textile layer (for a given value of total textile resisting load) allowing it to undertake higher loads as the textile-to-matrix contact area increases. Failure finally occurs due to the inevitable load distribution unevenness between yarns (at higher load levels for longer bond lengths) manifested through the in-plane rotation of the textile gripping fixture (Figure 2d). By comparison of the F_{max} values of UT- vs. IT-furnished SL specimens for each bond length considered a lower bound of the increase in the shear bond capacity of TRM/masonry joints due to textile impregnation with SBR latex can be determined. This amounts to 40%, 60% and 130% for a bond length of 100 mm, 150 mm and 200 mm, respectively. Hence, the overall minimum increase in the shear bond capacity of TRM/masonry joints due to textile impregnation with SBR latex is equal to 40%.

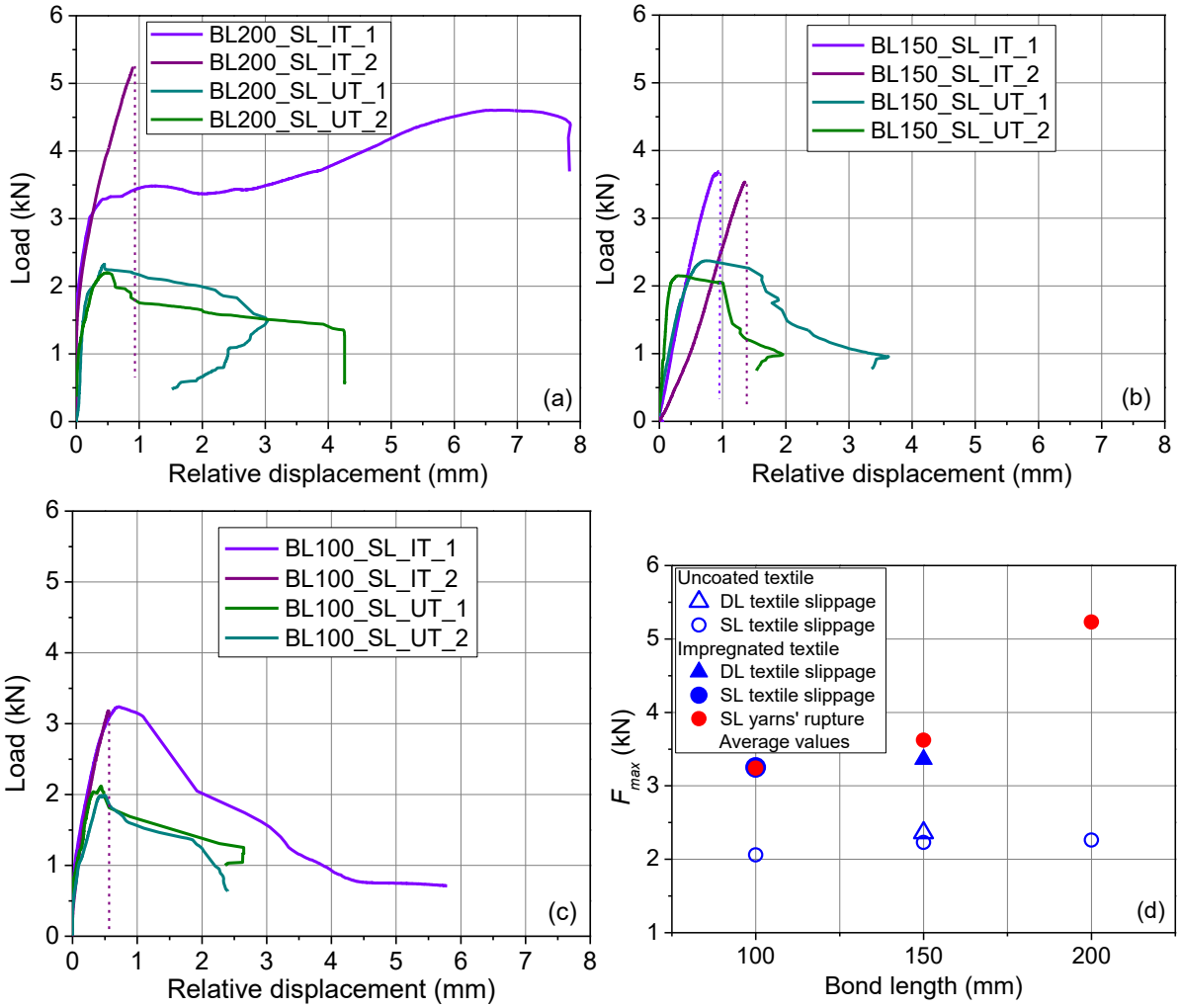


Figure 4: (a)-(c) Load vs. relative displacement curves of SL specimens and (d) F_{max} vs. BL

5 CONCLUSIONS

The currently presented experimental results concern the study of a TRM system consisted of AR-glass fiber textile embedded in cement-based mortar and applied on wall prisms made of smooth clay bricks. The effect of textile's full impregnation with SBR latex on the bond capacity of the TRM system was examined through the application of both DL and SL set-ups.

- The increase of load-bearing capacity of TRM/masonry joints under direct in plane shear loads due to textile impregnation with SBR latex was confirmed by employing both DL and SL set-ups. Depending on the set-up employed, this increase ranges between 40% and 55% for the type of TRM/masonry joints investigated in this work (failing due to textile pull-out from the matrix).
- For SL shear bond test configurations and for the same bond length considered, textile impregnation with SBR latex might result in the change of failure mode (from

textile pull-out to textile rupture). Nevertheless, textile rupture occurs at an exploitation ratio of the textile's tensile strength much lower than 100% due to stress concentration phenomena at the vicinity of the textile gripping fixture. Hence, a lower bound of the increase in the shear bond capacity of TRM/masonry joints due to textile impregnation with SBR latex can be determined (40%, 60% and 130% for a bond length of 100 mm, 150 mm and 200 mm, respectively). The exploitation ratio of the textile's tensile strength also increases with increasing bond lengths.

- It was verified that the type of set-up employed has negligible effect on the maximum transferable in-plane shear load along TRM/masonry interfaces.
- The behavior of IT-furnished DL specimens in terms of load vs. relative displacement response (pseudo-strain-hardening in the post-peak range) can be extrapolated to that of structural members receiving such TRM overlays as a means of flexural strengthening. Therefore, it would be logical to assume that the strengthening system will impart favorable energy dissipation capacity characteristics to the strengthened members.

Acknowledgements. The authors gratefully acknowledge Sika Hellas ABEE for providing the mortar.

REFERENCES

[1] Triantafillou, T. ed. Textile fibre composites in civil engineering. Woodhead Publishing (2016).

[2] D'Ambrisi, A., Feo, L. and Focacci, F. Experimental and analytical investigation on bond between Carbon-FRCM materials and masonry. Composites: Part B 46 (2013), pp. 15–20.

[3] Askouni, P.D. and Papanicolaou, C.G. Experimental investigation of bond between glass textile reinforced mortar overlays and masonry: the effect of bond length. Materials and Structures 50(2) (2017), pp. 164.

[4] Donnini, J., Corinaldesi, V. and Nanni, A. Mechanical properties of FRCM using carbon fabrics with different coating treatments. Composites: Part B, 88 (2016), pp. 220-228.

[5] Donnini, J. and Corinaldesi, V. Mechanical characterization of different FRCM systems for structural reinforcement. Construction and Building Materials 145 (2017), pp. 565-575.

[6] Leone, M., Aiello, M.A., Balsamo, A., Carozzi, F.G., Ceroni, F., Corradi, M., Gams, M., Garbin, E., Gattesco, N., Krajewski, P., Mazzotti, C., Oliveira, D., Papanicolaou, C.G., Ranocchiai, C., Roscini, F. and Saenger, D. Glass fabric reinforced cementitious matrix: Tensile properties and bond performance on masonry substrate. Composites Part B 127 (2017), pp. 196-214.

[7] D'Antino, T. and Papanicolaou, C. Comparison between different tensile test set-ups for the mechanical characterization of inorganic-based composites. Construction and Building Materials 171 (2018), pp. 140–151.

[8] De Andrade Silva, F., Butler, M., Hempel, S., Toledo Filho, R.D. and Mechtcherine, V. Effects of elevated temperatures on the interface properties of carbon textile-reinforced concrete. Cement and Concrete Composites, 48 (2014), pp.26-34.

[9] Aljewifi, H., Fiorio, B. and Gallias, J.L. Characterization of the impregnation by a cementitious matrix of five glass multi-filament yarns. European journal of environmental and civil engineering 14(5) (2010), pp.529-544.
[10] Schneider, K., Michel, A., Liebscher, M., Terreri, L., Hempel, S. and Mechtcherine, V. Mineral-impregnated carbon fibre reinforcement for high temperature resistance of thin-walled concrete structures. Cement and Concrete Composites 97 (2019), pp.68-77.
[11] Lorenz, E., Schütze, E. and Weiland, S. Textile Reinforced Concrete-Properties of the Composite Material. BETON-UND STAHLBETONBAU 110 (2015), pp.29-41.
[12] Rempel, S., Kulas, C. and Hegger, J. Bearing behavior of impregnated textile reinforcement. In: Brameshuber, W. (Ed.), 11th International Symposium on Ferrocement (FERRO-11) and 3rd International Conference on Textile Reinforced Concrete (ICTRC-3), Aachen, Germany, 7-10 June 2015, pp. 71-77.
[13] RILEM TC 76. (1991). "Technical recommendations for testing and use of constructions materials: LUMB1." Chapman & Hall, UK.
[14] (CEN) European Committee for Standardization. (2005). "Design of masonry structures, part 1.1." *Eurocode 6*, Brussels.
[15] British Standard. (1999). "Textiles-Tensile properties of fabrics, part 1." *EN ISO 13934*, UK.
[16] (CEN) European Committee for Standardization. (1993). "Methods of test for mortar for masonry, part 11." *EN 1015*, Brussels.
[17] Sneed, L.H., D'Antino, T., Carloni, C. and Pellegrino, C. A comparison of the bond behavior of PBO-FRCM composites determined by double-lap and single-lap shear tests. Cement and Concrete Composites 64 (2015), pp. 37-48.
[18] Askouni, P.D. and Papanicolaou, C.G. Comparison of double-lap/double-prism and single-lap/single-prism shear tests for the TRM-to-masonry bond assessment, In: Mechtcherine V., Slowik V., Kabele P. (eds) Strain-Hardening Cement-Based Composites, SHCC 2017, RILEM Bookseries 15, Springer, Dordrecht, (2018) 527-534.

12th International Conference on Structural Analysis of Historical Constructions
SAHC 2020
P. Roca, L. Pelà and C. Molins (Eds.)

EXPERIMENTAL STUDY ON THE SHEAR BEHAVIOR OF FRCM STRENGTHENED MASONRY PANELS

FRANCESCA FERRETTI[1*], ANDREA INCERTI[2] AND CLAUDIO MAZZOTTI[1]

[1] Department of Civil, Chemical, Environmental and Materials Engineering (DICAM)
University of Bologna
Viale Risorgimento 2, 40136 Bologna, Italy
e-mail: francesca.ferretti10@unibo.it (*corresponding author), claudio.mazzotti@unibo.it

[2] CIRI Buildings and Construction (CIRI-EC)
University of Bologna
Via del Lazzaretto 15/5, 40131 Bologna, Italy
e-mail: a.incerti@unibo.it

Keywords: Masonry, In-plane Shear Behavior, Brick, FRCM, Strengthening

Abstract. *Innovative strengthening solutions, such as Fiber Reinforced Cementitious Matrix (FRCM), are becoming increasingly diffused for the retrofitting of existing masonry structures with the aim of reducing the seismic vulnerability of these construction typologies. In recent years, many studies have demonstrated the suitability of these materials in enhancing the shear capacity of masonry walls and improve the overall structural behavior, avoiding fragile collapse mechanisms. In the present work, six diagonal compression tests were performed on unstrengthened and FRCM strengthened masonry panels to evaluate the improvements attributable to the presence of the FRCM systems. Two different bidirectional basalt grids were applied to the masonry samples, with and without mechanical anchorages. The tensile and bond properties of the chosen FRCM systems were investigated through laboratory tests. The objective was, indeed, to compare the performances of two textiles, characterized by different densities, and to investigate the role of mechanical anchorages. The experimental results confirmed the efficiency of the FRCM strengthening systems in improving the shear behavior of masonry panels. The FRCM strengthened samples experienced a considerable strength increase and less brittle failure mechanisms. The roles of both the mortar matrix, the fiber grids and the mechanical anchorages were highlighted by analyzing the onset of cracking and the failure propagation within the samples.*

1 INTRODUCTION

The structural performances and the safety of historical masonry building during a seismic event are key aspects to be assessed, since these construction typologies usually show a weak behavior if subject to horizontal loads, characterized by out-of-plane and in-plane collapses [1,2]. Several researches in literature studied different retrofitting systems realized by using composite materials applied to the surface of masonry elements, in order to enhance the structural capacity with respect to the shear actions invoked during an earthquake without

evident changes in stiffness.

In this framework, Fiber Reinforced Polymer (FRP) or Fiber Reinforced Cementitious Matrix (FRCM) systems were introduced and their advantages and drawbacks highlighted [3-5]. The behavior of these innovative materials was broadly analyzed with reference to the resistance, i.e. tensile and bond strength, the influence of the masonry substrate, e.g. presence of mortar joint and brick roughness, their compatibility with the substrate, the sustainability, and the fire resistance [6-13]. Studies were also carried out about the in-plane behavior of masonry walls, made of different masonry substrates, strengthened with composite materials [14-21]. From the structural point of view, the efficiency of these systems was found to be highly significant.

The aim of the present research is to enhance the knowledge about the structural performances and the failure modes of masonry panels, built with clay bricks and lime-based mortar, strengthened with FRCM systems made with bidirectional basalt fiber grids and a lime-based mortar matrix. To this aim, a diagonal compression test setup [22,23] was adopted to analyze the in-plane shear behavior of the wall panels. The experimental results obtained were discussed in terms of load bearing capacity and maximum displacement at collapse, considering the effectiveness of the FRCM strengthening systems with respect to the unreinforced masonry samples.

2 EXPERIMENTAL CAMPAIGN

In the present experimental campaign, two different masonry substrates were investigated, built with the same fired clay bricks and two different mortar mixes (*B-M1* and *B-M2*). The masonry panel dimensions were equal to 1100×1100×250 mm^3 and 1200×1200×250 mm^3 for the *B-M1* and *B-M2* typology, respectively. Six masonry walls were built, three for each substrate type. Subsequently, four panel were retrofitted by FRCM composites, made with a lime-based mortar matrix and bidirectional basalt fiber grids. The characteristics of the tested samples are reported in Table 1, where each specimen is named with a code indicating the wall substrate type (*B-M1* or *B-M2*), the applied FRCM system (basalt fiber grids, *B200* or *B400*, and mortar matrix type, *M3* or *M4*) and the presence of mechanical anchorages (*A*) or not. A continuous layout of the strengthening system was adopted (Figure 1): the bidirectional basalt grids were applied symmetrically on the entire surfaces of the wall panels, adopting an offset of about 20 mm from edges to prevent early debonding phenomena. A single grid layer per side was adopted, embedded in a 6 mm thick layer of mortar. A total number of six diagonal compression tests were performed. The mechanical characterization of the masonry components and the FRCM strengthening systems will be presented in the following Sections.

Table 1: Experimental campaign: characteristics of the tested samples

Specimen ID	FRCM system	Mechanical Anchorages
B-M1_URM	-	-
B-M2_URM	-	-
B-M1_B200-M3-A	Basalt fiber grid + NHL mortar matrix	Yes
B-M2_B200-M4		-
B-M1_B400-M3-A		Yes
B-M2_B400-M4		-

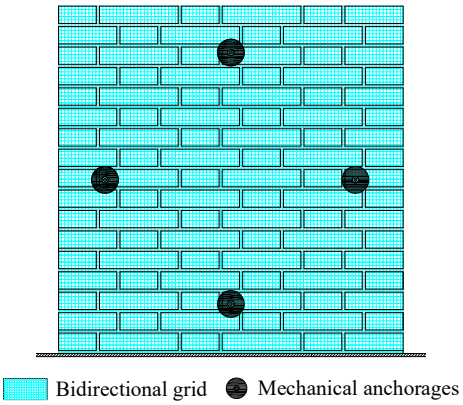


Figure 1: FRCM strengthening system layout

2.1 Masonry constituents

The fired clay bricks adopted for the construction of the masonry panels had dimensions equal to 120×250×55 mm^3. Their mechanical properties were investigated through standard laboratory tests. In particular, uniaxial compressive tests [24] and Brazilian tests [25] were carried out on cylindrical specimens with a unitary aspect ratio, obtaining a compressive strength $f_{c,b}$ equal to 18.7 MPa (CoV = 5%) and a tensile strength $f_{t,b}$ equal to 3.1 MPa (CoV = 15%). Moreover, three-points bending tests [26] were performed on prismatic specimens, having dimensions 40×40×250 mm^3, for the evaluation of the flexural strength $f_{fl,b}$, obtaining 4.8 MPa (CoV = 7%). Finally, also the elastic modulus was determined through cyclic compression tests [27], resulting to be equal to 6850 MPa (CoV = 3.9%).

Concerning the mortar used in the masonry bed joints, two mortar typologies were adopted for the construction of the brick masonry panels (*M1* and *M2*). They were pre-mixed natural hydraulic lime-based mortars and they were subject to standard laboratory tests for the mechanical characterization [28], obtaining the mechanical properties reported in Table 2 in terms of compressive strength ($f_{c,m}$), flexural strength ($f_{fl,m}$) and elastic modulus (E_m).

Table 2: Mechanical properties of the mortars

Mortar	$f_{c,m}$ (MPa)	CoV (%)	$f_{fl,m}$ (MPa)	CoV (%)	E_m (MPa)	CoV (%)
M1	4.8	12	1.5	15	4590	17
M2	2.6	12	1.2	9	4250	18

2.2 Strengthening systems and layout

Two different FRCM retrofitting systems were investigated, constituted of bidirectional symmetrical basalt fiber grids embedded in a natural hydraulic lime-based mortar matrix. The grids were characterized by different density, equal to 200 g/m^2 (*B200*) and 400 g/m^2 (*B400*), and equivalent thicknesses equal to 0.032 mm and 0.064 mm, respectively. Pre-mixed natural hydraulic lime-based mortars were adopted as matrix (*M3* and *M4*), characterized by the mechanical properties reported in Table 3, evaluated through standard tests [28].

At the beginning of the experimental campaign, the adopted FRCM strengthening systems

were subject to direct tensile tests in order to evaluate the tensile strength $f_{t,f}$, the ultimate strain ε_u and the fiber elastic modulus E_f. Moreover, direct shear tests [6] were also performed to determine the bond strength $f_{b,f}$. The experimental outcomes of tensile and bond tests are reported in Table 4 and Table 5, respectively.

The efficiency η of the basalt FRCM systems was evaluated as the ratio between the bond strength and the tensile strength (Table 5): the highest value (91%) was associated to the textile failure due to fiber rupture (*B200*), while the lowest value (64%) was observed for the textile showing a delamination at the matrix-fiber interface (*B400*).

Table 3: Mechanical properties of the mortar matrices

Mortar	$f_{c,m}$ (MPa)	CoV (%)	$f_{fl,m}$ (MPa)	CoV (%)	E_m (MPa)	CoV (%)
M3	12.6	9	2.9	23	9100	14
M4	13.1	5	3.4	5	8675	11

Table 4: FRCM systems: results of the tensile tests

Textile	Fiber type	Specimen dimensions (mm^3)	$f_{t,f}$ (MPa)	ε_u (%)	E_f (GPa)
B200	Basalt grid	400×40×10	1160	2.2	76
B400	Basalt grid	400×40×10	960	1.1	66

Table 5: FRCM systems: results of the direct shear tests

Textile	Masonry prism (mm^3)	Bonded length (mm)	Bonded width (mm)	Thickness (mm)	$f_{b,f}$ (MPa)	η (%)
B200	120×120×445	345	50	8	1060	91
B400	120×120×445	345	50	8	620	64

3 DIAGONAL COMPRESSION (DC) TEST SETUP

The experimental setup used to evaluate the shear capacity of the clay brick masonry walls was a standard setup, following the indications provided by the ASTM E519 and RILEM LUMB6 Standards [22,23]. A servo-hydraulic actuator, equipped with a load cell having a maximum capacity of 500 kN, was used for the application of the diagonal compression displacement. The tests were, indeed, performed under displacement control with a rate equal to 0.01 mm/s to analyze both the pre-peak and the post-peak behavior. The diagonal displacements were measured by four linear potentiometers (50 mm stroke and 1100 mm gage length), positioned on both sides of the masonry panels along the two principal diagonals. The setup of the test is shown in Figure 2. In accordance with the elastic solution of a masonry panel subject to a DC test [29,30], the stress state (σ, τ) in the center of the panel and the masonry tensile strength f_t can be evaluated as:

$$\sigma = 0.56\frac{P}{A_n} \tag{1}$$

$$\tau = 1.05\frac{P}{A_n} \tag{2}$$

$$f_t = 0.5\frac{P_f}{A_n} \tag{3}$$

where P is the diagonal load (P_f at failure) and A_n is the net area of the wall. In this configuration, the directions of the principal stresses are known and coincident with the diagonals of the panels. The shear strain γ can be determined as the sum of the deformations evaluated along the principal directions (ε_c and ε_t), taken as the average between the deformations on the two sides of the specimen. Considering the tangential stress τ *vs* shear strain γ diagram, the shear modulus G can be evaluated as the secant modulus between 1/10 and 1/3 of the maximum tangential stress.

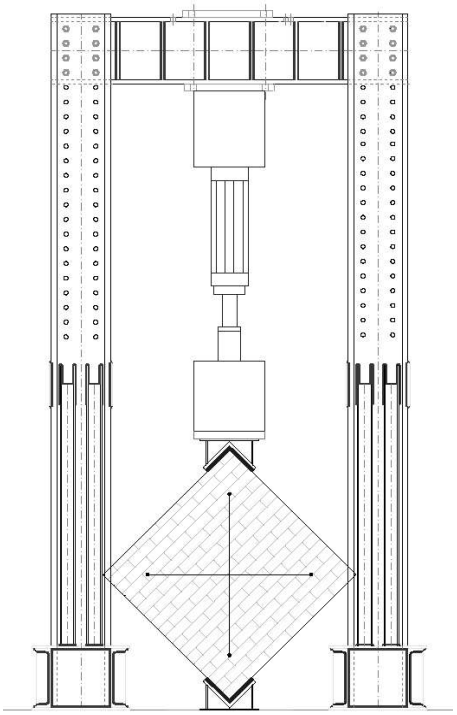


Figure 2: Diagonal compression (DC) test setup.

4 EXPERIMENTAL RESULTS

The experimental results are presented and discussed in this Section in terms of shear behavior, shear capacity and failure mode with the objective of discussing the improvements given by the FRCM composites applied on unreinforced masonry.

4.1 Failure modes

During the DC tests, two different failure modes occurred, reported in Figure 5. In particular, the failure modes of the URM panels were characterized by an evident single fracture line along the compressed diagonal, according to the panel stress state (Figure 5*a*). The FRCM strengthened masonry walls, instead, showed a more widespread cracking pattern on the external surfaces of the reinforcing layers, along the compressed diagonal. With reference to the failure mode of the FRCM reinforcements, it was noticeable that the *B200* basalt grid (Figure 5*b,d*) was characterized by partial delamination and rupture of fibers along the cracking lines (Figure 5*f*), while the failure of the *B400* basalt grid was characterized by delamination phenomena only. This different behavior can be related to the reduced spacing of the *B400* grid, which did not allow the mortar matrix to properly penetrate within the grid itself. The presence of the mechanical anchorages did not significantly influence the overall behavior of the samples in terms of failure mode, but it prevented the grid detachment at the extremities of the wall panels, which was visible for the samples strengthened without the use of anchorages.

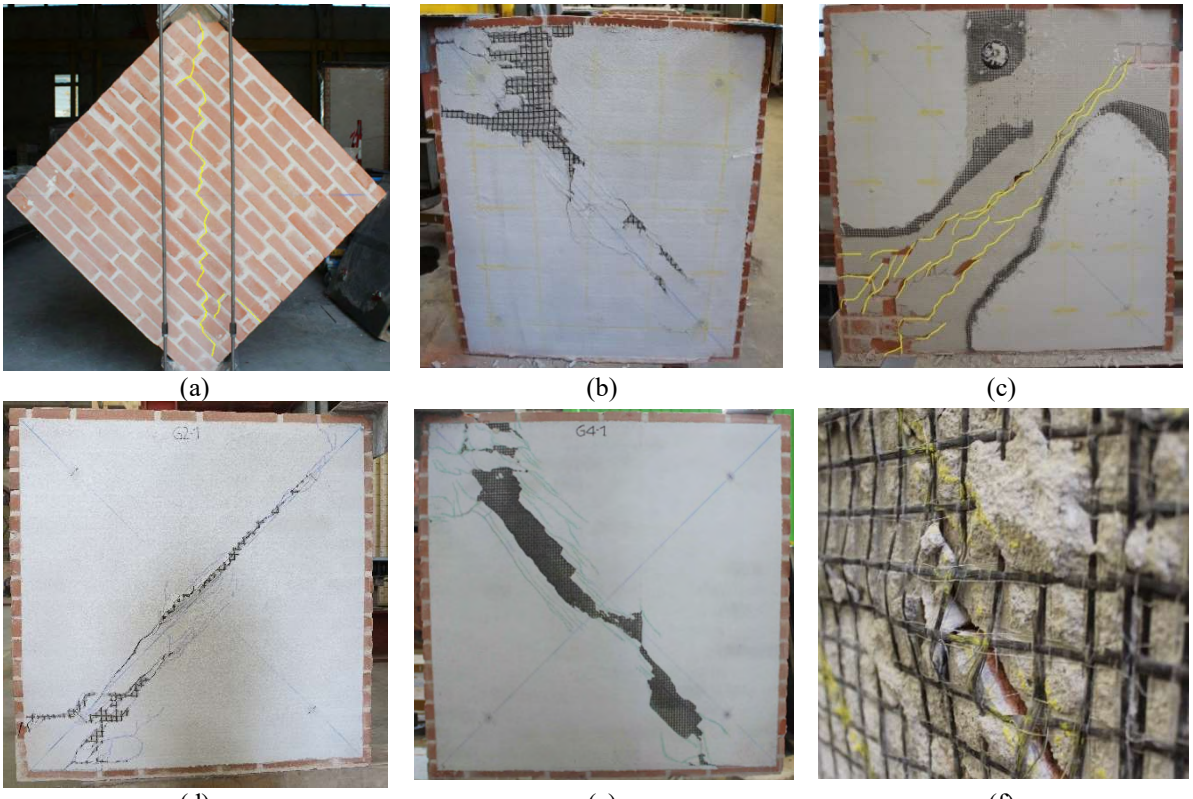


Figure 5: Failure modes in the DC tests: (a) URM panel; (b) B-M1_B200-M3-A; (c) B-M1_B400-M3-A; (d) B-M2_B200-M4; (e) B-M2_B400-M4; (f) delamination and rupture of the *B200* textile.

4.2 Shear behavior and capacity of the FRCM strengthened panels

The load *vs* displacements graphs are reported in Figure 3 and Figure 4 for the *B-M1* and *B-M2* panel series, respectively. A very similar shear behavior was noticed, characterized by an initial linear branch and a first peak load, followed by a drop in the load bearing capacity and by a second peak load. From the experimental observations, it can be stated that the reaching of the first peak load corresponded with the appearance of the first crack in the mortar matrix. The second peak load, instead, can be associated with the failure of the textiles.

The results of the DC tests are summarized in Table 6, in terms of diagonal load at failure P_f, strength increment with respect to URM panel, masonry tensile strength f_t, shear modulus G and pseudo-ductility μ. The latter was determined as the ratio between the ultimate shear strain, taken in correspondence of a 20% reduction in the load bearing capacity after the peak load, and the shear strain corresponding to the same load value along the initial loading branch.

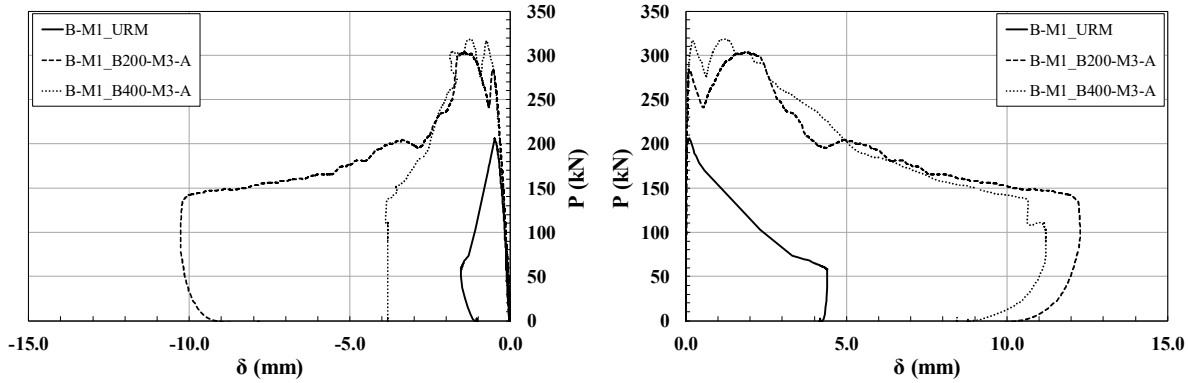


Figure 3: DC test results for *B-M1* panels: (a) Load *vs* vertical displacement graph; (b) Load *vs* horizontal displacement graph

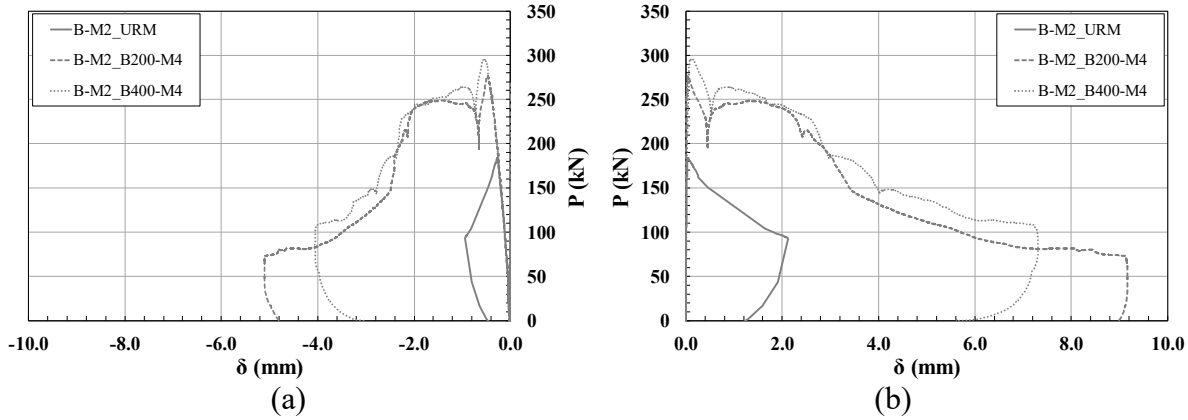


Figure 4: DC test results for *B-M2* panels: (a) Load *vs* vertical displacement graph; (b) Load *vs* horizontal displacement graph

Table 6: Diagonal compression test results.

Sample code	P_f (kN)	Strength Increment (%)	τ_f (MPa)	$f_{t,M}$ (MPa)	$G_{1/10\text{-}1/3}$ (MPa)	μ (-)
B-M1_URM	206.1	-	0.79	0.37	2660	4.0
B-M2_URM	183.7	-	0.64	0.30	3056	4.4
B-M1_B200-M3-A	303.7	47	1.16	0.55	2649	13.9
B-M2_B200-M4	276.7	51	0.96	0.46	3216	13.3
B-M1_B400-M3-A	318.7	55	1.22	0.58	2810	10.9
B-M2_B400-M4	295.8	61	1.04	0.49	2705	10.9

With regards to the results obtained for the two URM panels, the differences observed in the maximum load and, consequently, in the masonry tensile strength, can be associated to the differences in the mechanical properties of the mortar used for the construction of the panels, e.g. $f_{c,m(B\text{-}M1)} > f_{c,m(B\text{-}M2)}$.

With reference to the results obtained for FRCM strengthened samples, it is possible to state that, for both the masonry typologies, significant strength increments were obtained. In particular, similar increments were observed for panels strengthened with the same FRCM system, given that the mortar matrices *M3* and *M4* were characterized by similar mechanical properties. It is worth mentioning that the strength increments obtained for the panels strengthened with the *B400* basalt grid were not as high as expected, given that the *B400* grid was characterized by an amount of fibers doubled with respect to the *B200* grid. It should be considered that the efficiency of the *B400* textile was significantly lower, as reported in Table 5: the bond strength was approximately equal to half the tensile strength of the *B200* grid. This observation could explain why a similar strength increment was registered in the DC tests for the panels strengthened with the two FRCM typologies.

The presence of the mechanical anchorages seems not to significantly affect the value of the first peak load. However, they influenced the behaviour after the first peak. Indeed, the mechanical anchorages, and generally the fiber grids, started working in the second reloading branch. More in detail, the panels strengthened making use of anchorages experienced a higher load increment after the first peak, reaching a second peak load similar or even higher than the first one.

Values of the shear modulus *G* for the masonry panels were quite similar, demonstrating that the structural performances were enhanced by the application of the FRCM retrofitting systems without considerable changes in terms of stiffness, with values ranging between 2649 and 3216 MPa.

Finally, the displacement capacity of the FRCM strengthened samples was significantly higher than the one of the URM samples, which experienced a quasi-brittle failure. Quite high values of the pseudo-ductility factor μ were, indeed, evaluated for all the FRCM strengthened panels. In particular, similar results were obtained for walls strengthened with the same FRCM system. The pseudo-ductility was higher for the panels strengthened by the *B200* textile, most probably for the same reasons introduced above: failure mode and efficiency of the grid.

5 ANALYTICAL FORMULATION

The evaluation of the shear capacity of strengthened walls ($\tau_{t,r}$) can be carried out through the anaytical formulation provided by the Italian CNR Guideline for the design of strengthening interventions using FRCM systems [31]. The formulation is based on an additive approach, considering the contributions of unreinforced masonry ($\tau_{f,URM}$) and of the dry fibers ($\tau_{t,f}$), according to Equation (4):

$$\tau_{t,r} = \tau_{f,URM} + \tau_{t,f} = \tau_{f,URM} + \frac{n_f \cdot t_{Vf} \cdot l_f \cdot \alpha_t \cdot E_f \cdot \varepsilon_{fd}}{\gamma_{Rd} \cdot A_n} \quad (4)$$

where τ_f is here considered equal to the shear strength of the correspondent URM sample, n_f is the number of reinforcing layers, t_{vf} is the textile equivalent thickness, l_f is the width of the FRCM system measured orthogonally to the shear force, α_t is a coefficient, equal to 0.8, accounting for a reduced tensile strength for fibers subjected to shear, E_f is the fiber elastic modulus, ε_{fd} is the design strain of the FRCM system, γ_{Rd} is a safety factor, considered equal to 1 here, and A_n is the net area of the panel cross section. In detail, the design strain is considered equal to the ratio between the bond strength and the elastic modulus E_f of the dry fibers, for the panels strengthened without using mechanical anchorages, while it is multiplied by 1.5 for the panels reinforced with mechanical anchorages, to account for intermediate delamination phenomena.

The analytical and experimental results are compared in Table 7, where the maximum shear stress obtained in the DC test ($\tau_{f,Exp}$) is reported together with the shear capacity of the strengthened walls, calculated according to Equation (4). The analytical formulation generally underestimates the experimental outcomes, even if a quite good agreeement can be noticed between experimental and analytical results. However, it should be mentioned that the proposed analytical formulation does not take into account the role of the mortar matrix, which was found to be crucial in the experimental tests. Indeed, especially for the panel series *B-M2*, the maximum shear stress was reached in correspondence of the first peak load, related to the cracking of the mortar matrix and not to the failure of the textile.

Table 7: Shear capacity of FRCM strengthened panels: analytical *vs* experimental results.

Sample code	$\tau_{f,URM}$ (MPa)	$\tau_{t,f}$ (MPa)	$\tau_{t,r}$ (MPa)	$\tau_{f,Exp.}$ (MPa)	Error (%)
B-M1_B200-M3-A	0.79	0.31	1.10	1.16	-5.2
B-M2_B200-M4	0.64	0.21	0.85	0.96	-11.5
B-M1_B400-M3-A	0.79	0.29	1.07	1.22	-12.3
B-M2_B400-M4	0.64	0.25	0.89	1.04	-14.4

6 CONCLUSIONS

The present research deals with the study of the shear behavior of FRCM strengthened

masonry panels through the execution of DC tests. Six masonry panels were built, and two masonry typologies were considered. Four panels were then strengthened adopting two different FRCM systems, both characterized by the use of basalt bidirectional grids, having different densities, and a lime-based mortar matrix. The effect of the presence of mechanical anchorages on the shear strength of the masonry samples was also analyzed.

The experimental results showed a good efficiency of the strengthening systems, with strength increments ranging from 47% to 61%, with respect to the URM panels. The presence of the FRCM systems did not determine significant stiffness increase of the panels but it influenced their failure mode, which became more ductile if compared to the quasi-brittle failure of the URM samples. The pseudo-ductility factor was indeed evaluated in the experimental campaign.

In general, the shear behavior of the FRCM strengthened samples was characterized by a first peak load, corresponding to the cracking of the mortar matrix, and by a second peak load, associated to the failure of the textiles. The role of the mortar matrix was highlighted since it was found to be crucial in the shear behavior of the strengthened panels. The presence of the mechanical anchorages seemed not to significantly affect the failure mode of the panels and the value of the first peak load. However, the anchorages allowed the textile to better redistribute the tensile stresses and determined a higher load increment after the drop in the load bearing capacity following the first peak load.

A comparison between the experimental results and the analytical formulation provided by the Italian CNR Guideline was carried out, showing a quite good agreement. In particular, the analytical results tended to underestimate the experimental ones. In general, it should be mentioned that the important role of the mortar matrix is not taken into account by the available analytical formulation. Further experimental results are needed to better analyze the matrix contribution and maybe include it in an alternative analytical approach.

Acknowledgements. The financial and technical support of Kerakoll Spa, Sassuolo (MO) Italy, and the financial support of the Italian Department of Civil Protection (ReLUIS 2020 Grant – Innovative Materials) are gratefully acknowledged. The technical staff of the Interdepartmental Centre for Industrial Research (CIRI Buildings & Construction) is gratefully acknowledged for the work during the setup of the tests.

REFERENCES

[1] Penna, A., Morandi, P., Rota, M., Manzini, C.F., da Porto, F. and Magenes G. Performance of masonry buildings during the Emilia 2012 earthquake. Bull. Earthq. Eng. (2014) 12:2255–73. https://doi.org/10.1007/s10518-013-9496-6.

[2] Ferretti, F., Ferracuti, B., Mazzotti, C. and Savoia M. Destructive and minor destructive tests on masonry buildings: Experimental results and comparison between shear failure criteria. *Constr. Build. Mater.* (2019) **199**:12–29. https://doi.org/10.1016/j.conbuildmat.2018.11.246.

[3] Papanicolaou, C., Triantafillou, T., Karlos, K. and Papathanasiou M. Textile-reinforced mortar (TRM) versus FRP as strengthening material of URM walls: in-plane cyclic loading. *Mater. Struct.* (2007) **40**:1081–97. https://doi.org/10.1617/s11527-006-9207-8.

[4] Papanicolaou, C., Triantafillou, T. and Lekka, M. Externally bonded grid as strengthening and seismic retrofitting materials of masonry panels. *Constr. Build. Mater.* (2011) **25**(2):504-514.
[5] Mazzotti, C. and Murgo, F.S. Numerical and experimental study of GFRP-masonry interface behavior: Bond evolution and role of the mortar layers. *Compos. Part B Eng.* (2015) **75**:212–225.
[6] De Felice, G., Aiello, M.A., Caggegi, C., Ceroni, F., De Santis, S., Garbin, E., et al. Recommendation of RILEM Technical Committee 250-CSM: Test method for Textile Reinforced Mortar to substrate bond characterization. *Mater. Struct.* (2018) **51**:95. https://doi.org/10.1617/s11527-018-1216-x.
[7] Valluzzi, M.R., Oliveira, D.V., Caratelli, A., Castori, G., Corradi, M., de Felice, G., et al. Round Robin Test for composite-to-brick shear bond characterization. *Mater. Struct.* (2012) **45**:1761–91. https://doi.org/10.1617/s11527-012-9883-5.
[8] Ceroni, F., de Felice, G., Grande, E., Malena, M., Mazzotti, C., Murgo, F., et al. Analytical and numerical modeling of composite-to-brick bond. *Mater. Struct.* (2014) **47**:1987–2003. https://doi.org/10.1617/s11527-014-0382-8.
[9] de Felice, G., Aiello, M.A., Bellini, A., Ceroni, F., De Santis, S., Garbin, E., et al. Experimental characterization of composite-to-brick masonry shear bond. *Mater. Struct.* (2016) **49**:2581–96. https://doi.org/10.1617/s11527-015-0669-4.
[10] Carozzi, F.G., Bellini, A., D'Antino, T., de Felice, G., Focacci, F., Hojdys, Ł., et al. Experimental investigation of tensile and bond properties of Carbon-FRCM composites for strengthening masonry elements. *Compos. Part B Eng.* (2017) **128**:100–19. https://doi.org/10.1016/j.compositesb.2017.06.018.
[11] Sassoni, E., Andreotti, S., Bellini, A., Mazzanti, B., Bignozzi M.C., Mazzotti, C. and Franzoni E. Influence of mechanical properties, anisotropy, surface roughness and porosity of brick on FRP debonding force. *Compos. Part B* (2017) **108**:257-269.
[12] Lignola, G.P., Caggegi, C., Ceroni, F., De Santis, S., Krajewski, P., Lourenço, P.B., Morganti, M., Papanicolaou, C., Pellegrino, C., Prota, A., and Zuccarino, L. Performance assessment of Basalt FRCM for retrofit applications on masonry. *Compos. Part B* (2017) **128**:1-18.
[13] Bellini, A., Bovo, M. and Mazzotti, C. Experimental and numerical evaluation of fiber-matrix interface behaviour of different FRCM systems. *Compos. Part B* (2019) **161**:411-426.
[14] Faella, C., Martinelli, E., Nigro, E. and Paciello, S. Shear capacity of masonry walls externally strengthened by a cement-based composite material: an experimental campaign. *Constr. Build. Mater.* (2010) **25**:4403–4414.
[15] Babaeidarabad, S., De Caso, F. and Nanni, A. URM Walls Strengthened with Fabric-Reinforced Cementitious Matrix Composite Subjected to Diagonal Compression. *J. Compos. Constr.* (2014) **18**:04013045. https://doi.org/10.1061/(ASCE)CC.1943-5614.0000441.
[16] Ferretti, F., Incerti, A., Ferracuti, B. and Mazzotti, C. FRCM strengthened masonry panels: the role of mechanical anchorages and symmetric layouts. *Key Eng. Mater.* (2017) **747**:334–341.

[17] Incerti, A. Tilocca, A.R., Ferretti, F. and Mazzotti, C. Influence of masonry texture on the shear strength of FRCM reinforced panels. In: R. Aguilar et al. (Eds.): *Structural Analysis of Historical Constructions*, RILEM Bookseries 18 (2019), pp. 1623-1631.
[18] Ferretti, F., Incerti, A., Tilocca, A.R. and Mazzotti, C. In-Plane Shear Behavior of Stone Masonry Panels Strengthened through Grout Injection and Fiber Reinforced Cementitious Matrices. *Int. J. Archit Herit.* (2019). https://doi.org/10.1080/15583058.2019.1675803.
[19] Incerti A., Ferretti F. and Mazzotti C. FRCM strengthening systems efficiency on the shear behavior of pre-damaged masonry panels: an experimental study. *J. Build. Pathol. Rehabil.* (2019) **4**:14. https://doi.org/10.1007/s41024-019-0053-9.
[20] Ferretti F., Incerti A., Ferracuti B., Mazzotti C. FRCM strengthened masonry panels: the role of mechanical anchorages and symmetric layouts. *Key Eng. Mater.* (2017) **747**:334–341.
[21] Del Zoppo M., Di Ludovico M., Prota A. Analysis of FRCM and CRM parameters for the in-plane shear strengthening of different URM types. *Compos. B Eng.* (2019) **171**:20–33.
[22] ASTM E519−15. Standard test method for diagonal tension (shear) in masonry assemblages 2015:4–8. https://doi.org/10.1520/E0519.
[23] RILEM LUMB6. Diagonal tensile strength tests of small wall specimens. *RILEM TC-76 LUM* (1991).
[24] EN 772-1. Methods of test for masonry units - Part 1: Determination of compressive strength (2011).
[25] EN 12390-6:2009. Testing hardened concrete - Part 6: Tensile splitting strength of test specimen (2009).
[26] EN 12390-5:2009. Testing hardened concrete - Part 5: Flexural strength of test specimens (2009).
[27] EN 12390-13. Testing hardened concrete - Determination of secant modulus of elasticity in compression (2013).
[28] EN 1015-11:1999/A1:2006. Methods of test for mortar for masonry - Part 11: Determination of flexural and compressive strength of hardened mortar (2006).
[29] Frocht, M. Recent advances in photoelasticity. *ASME Trans* (1931) **55**:135–53.
[30] Yokel, F.Y. and Fattal, S.G. A Failure hypothesis for masonry shearwalls. J. Struct. Div. - ASCE (1976) **102**:515–32.
[31] CNR-DT 215/2018. Istruzioni per la Progettazione, l'Esecuzione ed il Controllo di Interventi di Consolidamento Statico mediante l'utilizzo di Compositi Fibrorinforzati a Matrice Inorganica (in Italian). *National Research Council (CNR)* (2018).

12thInternational Conference on Structural Analysis of Historical Constructions
SAHC 2020
P. Roca, L. Pelà and C. Molins (Eds.)

EXPERIMENTAL TESTS ON FRCM AND FE MODELLING FOR THE HERITAGE STRUCTURE'S REUSE

RICCARDO LIBEROTTI[1*], NICOLA CAVALAGLI[1] AND VITTORIO GUSELLA[1]

[1]Department of Civil and Environmental Engineering
University of Perugia (Italy)
Via Duranti, 06125 - Perugia, Italy
e-mail: riccardo.liberotti@unipg.it (*corresponding author), nicola.cavalagli@unipg.it, vittorio.gusella@unipg.it

Keywords: Historical Structures, Masonry, FRCM, Experimental test, FE modelling

Abstract. *This paper presents the first results of an ongoing research in partnership with Kimia S.p.A. company (Italy). In particular, experimental tests on masonry specimens reinforced with Fiber Reinforced Cementitious Matrix (FRCM) have been recently conducted by Kimia according to the up-to date guidelines: specifically the single-lap shear test. On the base of the experimental results, a finite element model has been developed in order to reproduce the actual behaviour of the specimens. The results, derived both by the experimental tests and the FE model calibration, constitute the basis for planning an experimental campaign on masonry walls strengthened by FRCM loaded in the plane. The constructive details of the experimental set-up, conceived in order to create a self-balanced system and to bring the specimens to failure, are described together with a preliminary numerical modeling based on the already done test.*

1 INTRODUCTION

It is well known that the level of knowledge and the in-depth investigations regarding ancient masonry buildings are the mandatory conditions on which to base reliable structural safety assessments. Those evaluations derive from an articulated and rather complex process including, in general, historical investigations gathered by direct surveys of the building, also by means of experimental campaigns. In order to assess the vulnerability condition of a structure, the correct interpretation of the seismic behaviour in its current state is essential, especially when dealing with historical constructions built with masonry elements often characterized by structural peculiarities. Possible interventions for structural strengthening derive from the knowledge of the constructive properties and the peculiarities of the buildings. The conceiving of such design actions must prevent the occurrence of damages related to the artifact's survival without jeopardize the role and the meaning they stood for during the centuries.

Nowadays new reinforcement methodologies are including the use of FRCM composite materials that allow to fulfill the strengthening of ancient masonry structures in compliance with the environmental, cultural and social context where the buildings are placed. The FRCM composite system offers multiple benefits with respect to other composites or traditional

reinforced plasters:

- good mechanical properties;
- reduced thickness (minor than 3 cm);
- easy installation thanks to the lightness of the mesh and the building work modalities (e.g. FRP);
- reversibility of the intervention, being the inorganic mortar less aggressive than the epoxy resins used in other composite materials;
- good performance against fire (resulting in part from their inherent non-combustibility);
- possible recyclability of the natural origin nets in function of the characteristics of the matrix.

Even if some guidelines about the design rules have been proposed for the application of such composite [1], the definition of effective numerical strategies is still an open issue, due to the complexity of the interactions among fiber, matrix and masonry, requiring further studies with special attention peculiar applications. Some recent contribution can be found in literature about it based on numerical and/or analytical models [2, 3],

In a previous research, this new-gen. structural reinforcement has been proposed in relation to the structural strengthening of the Vanvitellian Palazzo Murena [4], actual headquarters of the University of Perugia. In this framework, indeed, the peculiar feature of the "*in falso*" bearing walls, masonry panels built without a direct load path to the ground and laying on the below vaults, has been highlighted as a recurrent circumstance in Italian Renaissance architecture and marked as a possible risk factor, Fig. 1.



Figure 1: Cross-section of Palazzo Murena, in red are highlighted some of the "*in falso*" walls

That occurrence, in case of seismic action, could trigger a sort of domino effect, due to possible collapse of the underlying masonry vaults, then compromising the safety of the entire structure. In the perspective of its strengthening, the design of interventions has been necessary to act in compliance with the valuable elements of the building such as marble floors and precious

stuccos, without further increasing the existing structures with the weight of additional non-canonical gears, if compared to the structural genesis of the building. In this context, the reinforcement of the masonry walls through FRCM appears an adequate solution.
This composite system proved many applications in relation to masonry structures and in literature there are several experimental studies [5- 8] carried out on elements reinforced with FRCM systems, as well as modeling strategies primarily based on the finite element methods [2, 3]. However, it should be noted that the investigation for the mechanical behaviour of the proposed application (*wall beam*) is not adequately investigated.

In order to improve the knowledge about such a technology and its application, an experimental campaign, has been started in partnership with Kimia S.p.a.to evaluate the effectiveness of the applications of FRCM to masonry walls regarding the prevention of in-plane collapse.

2 EXPERIMENTAL INVESTIGATIONS

The research program consists in experimental tests to assess the mechanical characteristics of the materials and the composite, and the development of numerical strategies able to reproduce the behaviour of the structural system. In this chapter are partially reported the first tests recently conducted by Kimia S.p.a. company for the preliminary characterization of such composite materials at the mesoscale level. The results have been used to calibrate a numerical model described in the following.

2.1 Single-lap shear test

According to the specific guidelines provided by the Reluis [9] *single-lap shear tests* have been conducted on rectangular walls samples reinforced with FRCM, which geometrical characteristics are reported in Tab. 1. Concerning the composite materials, the fiber net *Kimitech BS ST 200* and the matrix *MALTA M15/F* have been used; the nominal mechanical properties are reported for the net in Tab. 2, and in Tab. 3 for the masonry. The test method (also called *bond test*) consists in applying increasing shear forces between the composite and the support in order to assess the quality of the bonding and of the interaction between the fiber and the matrix.
The sample's preparation required:

- the cleaning of the surface of the masonries substrate and its saturation and wetting (condition s.s.a.);
- application of a first layer of mortar *Basic MALTA M15/F*;
- positioning of the fiber net *Kimitech BS ST 200*;
- application of a second layer of mortar *Basic MALTA M15/F*. After the curing period (at least 28 days) the traction device installation procedures were carried out, Fig. 2;
- the specimen is positioned vertically in a steel support, with a free portion of the fiber net, of a length in the range between *221* and *245 mm*, facing downwards and secured in a vice;
- a mechanic vice keeps the mesh tab stationary, while the crossbar of the test machine goes up, and therefore the reinforced wall, pulling the fiber and engaging the reinforcement with a shear actions.

Table 1: Geometric features of the reinforcemnt net samples: *B [mm]* the witdh, *L [mm]* the total length, L_e *[mm]* the effective length, L_f *[mm]* the free length, *T [mm] the thichness, M [mm x mm] the network sizes,* L_t *[mm]* the reiforcement net witdh, *N* the number of yarns

Fiber	B	L_f	L_e	Lf	T	M	L_t	N
B_01	153,3	305,0	300,0	254,0	10,00	20x20	135,0	7
B_01	156,6	308,0	302,0	220,6	10,00	20x20	135,0	7
B_03	154,0	307,0	304,0	245,3	10,00	20x20	135,0	7



(a) (b)

Figure 2: Sample's preparation: a) Application of the fiber net on the first layer of matrix, b) Fulfilment of the implementation with the second mortar layer according to a reference thickness

Table 2: Mechanical properties of the basaltic fiber: T_e [mm] the equivalent thichness, *Q [N/mm]* tensile breaking load of the warp, *E [GPa]* elastic modulus, ε strain, *G [kg/m²]* grammage, D [kg/m³] density, σ_u *[MPa]* ultimate tensile strength

Fiber	Texture	T_e	Q	E	ε	G	D	σ_u
B	bidir.	0,035	78	89 ±2	<8	0,24	2670	3100

Table 3: Mechanical properties of the matrix

Element	Material	Particle size distribution	Compression strength [MPa]	Bending strength [MPa]	Shear strength [MPa]	E [MPa]
Mortar - Matrix	Lime inorganic mortar M15/F	maximum 1,20 mm	at 7 dd >9 at 14 dd >12 at 28 dd >15	at 7 dd >3,8 at 14 dd >3,9 at 28 dd >4	0,15 (with masonries - EN 711)	9600



(a) (b) (c)

Figure 3: Experimental set-up: a) Testing machine, b) Detail of the pulling vice with the location of one LVDT sensor on the net, c) Cracks' appearance on the external layer of the matrix of one of the samples

Fig. 3 illustrates the experimental set-up carried out through a universal testing machine, on which the installation of LVDTs allowed to obtain the displacement describing the progressive shear failure of the composite. In the present paper the data related to a sensor located at the lower side of the sample are reported, in particular the one attached to the net (Fig. 3 b), with respect to three tests (Tab. 4).

Two tests (Test 01 and Test 02, Fig. 4) have been characterized by the breaking of the fiber while the sample (Test 03, Fig. 4) failed according to a mixed collapse mode. For all the tests the maximum resistance corresponds to the breaking of the fiber within the reinforcement (Failure Mode - FM F – Fig. 4) and with specific reference to third test this condition is preceded by a matrix-substrate detachment to which subsequently followed a break of the fabric on the free scrap; indeed, the matrix-substrate detachment is the cause of the observed ductility (Failure Mode – FM (B/E) F – Fig. 4b). The elaboration of the data gathered by the experimental observation permitted to create a load-displacement diagram for FRCM with basaltic fibers in relation the failure modes reported by the guidelines [9], Fig. 4.

Table 4: Experimental tests' data

	Fiber resistant area [mm^2]	Maximum Load [kN]	Maximum stress [MPa]	Failure Mode FM	Age of testing [dd]
Test 01	5,37	6,48	1207,45	F	74
Test 02	5,48	5,93	1081,46	F	81
Test 03	5,39	6,79	1259,74	(B/E) F	129

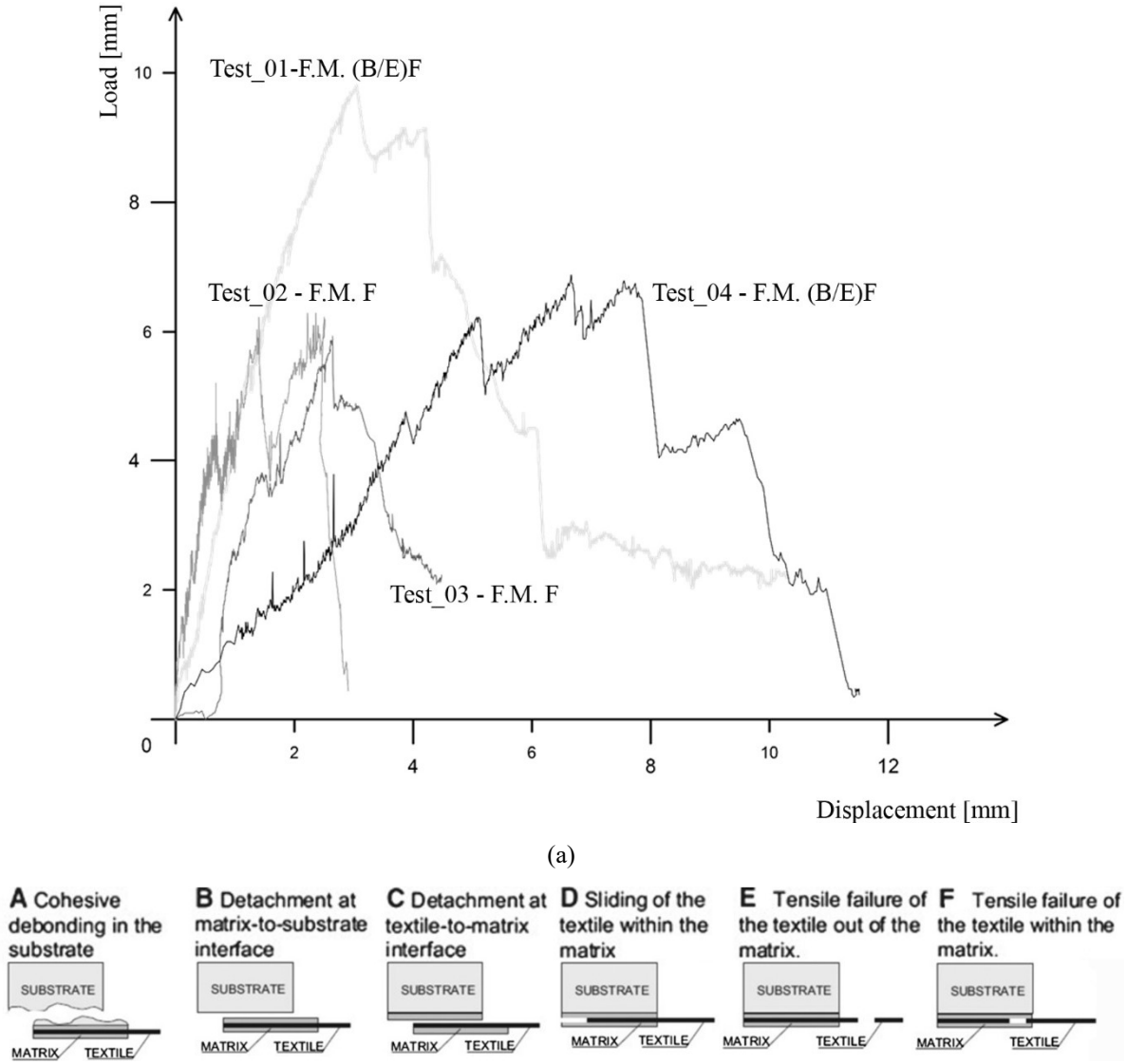


Figure 4: Experimental outcomes: a) Load-displacement diagram for FRCM with basaltic fibers, b) FRCM failure modes (FM) for single-lap shear tests [1]

3 NUMERICAL MODELLING OF THE SINGLE-LAP SHEAR TEST

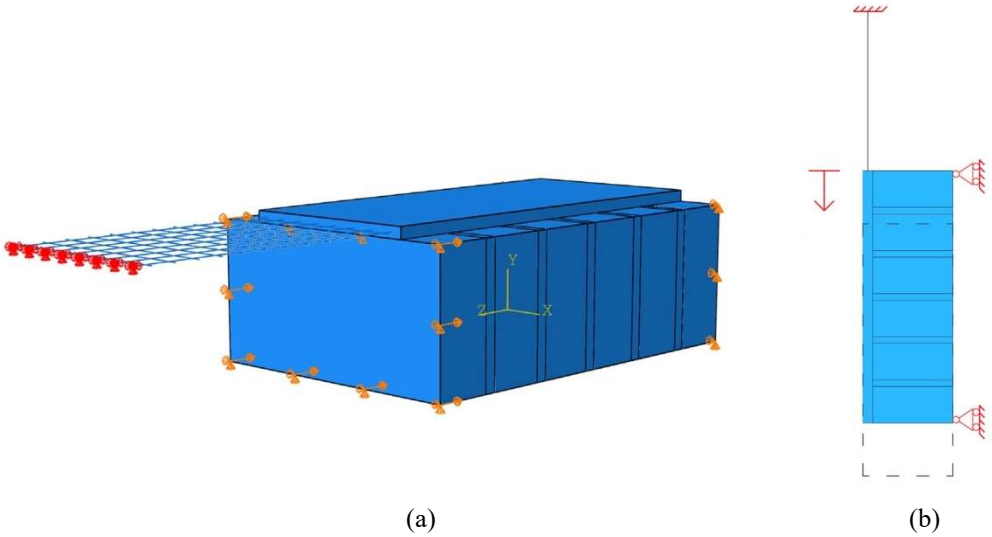
In order to describe the mechanical behaviour of the FRCM strengthening system, a preliminary FE numerical modelling has been developed aiming at reproducing the experimental tests.

The elements that make up the specimens have been modeled as follows:

- bricks, mortar *M10* (masonry joints) and mortar *M15* (matrix) with 8-node solid elements:
- the fiber basaltic net (*20x20 mm* mesh) with 2-nodes linear elements.

Internal constraints have been applied between the mortar joints and bricks, and between the

wallet and matrix, preventing any relative displacement. In this way, the interaction between the matrix and the support has been condensed in the nonlinear behaviour of the matrix itself. Similar kinematic constraints have been applied for the interaction between the matrix and the fiber, which lies embedded into the matrix layers. In relation to the external constraint, in order to reproduce the test modalities, the end portion of net free from matrix has been completely constrained while to one of the terminal surfaces of the masonry wallet incremental displacements has been imposed, Fig. 5.



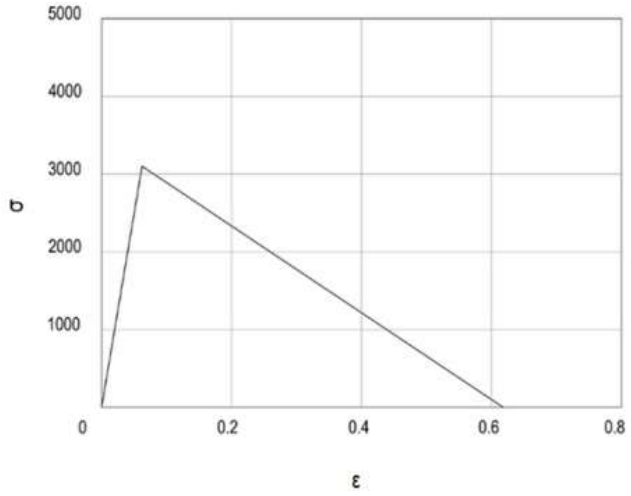
(a) (b)

Figure 5: a) External constraints; b) Modeling hypothesis

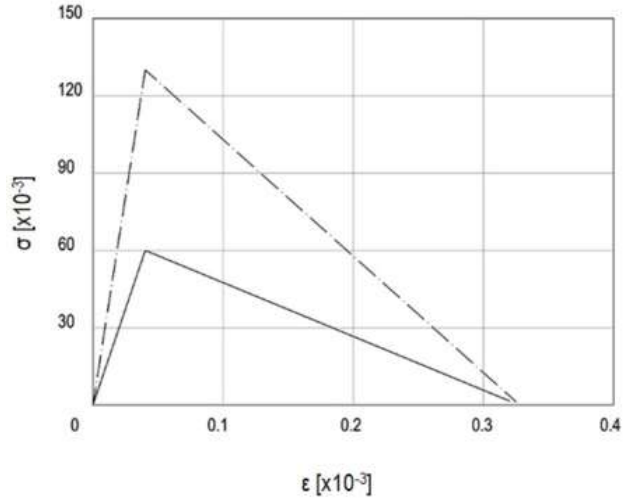
In order to better reproduce the response of the composite (Fig. 6) different models for all the materials composing the sample have been calibrated, especially in the post-peak behaviour, being some mechanical properties known in their nominal values, provided by the Kimia company. Following the approach proposed by [2] an elastic-plastic model with softening has been used for the fiber net, while a concrete model for bricks, mortar joints and the matrix. For the matrix also a tension damage model has been used to describe the evolution of damage observed during the test.

In addition, with the aim of evaluating the effect of each parameter on the structural response, a sensitivity analysis has been carried out by varying the mechanical parameters which significantly affect the response of the specific problem analyzed. Two analyses (FEM_Test_01 and FEM_Test_02) have been conducted in order to simulate the structural behaviour of Test 01 and Test 02; the first has been calibrated in total agreement with the nominal mechanical values and integrated with literature parameters, while the second with reduced stiffness values compared to the nominal ones, Tab. 5-6.

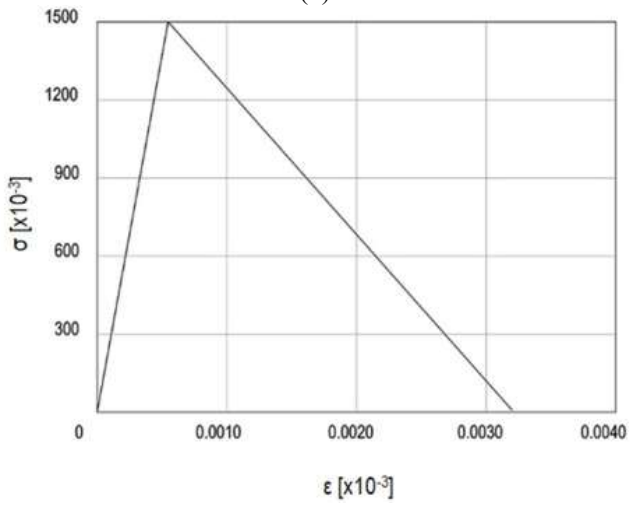
With the aim of further describe the damage behaviour, expressed contextually to Test 03, the damage for mortar matrix has been introduced according to the literature data [8] and the observations gathered by the experimental tests. Also in this case a sensitivity analysis has been carried out, in order to evaluate the influence of the nonlinear and damage parameter on the numerical response. Two models have been considered, FEM_Test_03 and FEM_Test_04 which differ in the mechanical properties according the values reported in Tabs. 7-8.



(a)



(b)



(c)

Figure 6: Constitutive laws in tension used for the constituent materials in terms of σ (stress) [kN/m^2] and ε (strain): a) Basaltic fiber, b) Dash-dotted line bricks, straight-mortar *M10*; c) inorganic matrix *M15*

Table 5: Mechanical properties for the FE modelling: ρ *[t/m^3]* the mass density, *E [KN/m^2]* the Young's modulus, ν the poisson's ratio, θ *[°]* the dilatation angle, *e [KN/m^2]* the eccentricity, f_{b0}/f_{c0} the ratio of initial equibiaxial compressive yield stress to initial uniaxial compressive yield stress; *k* the ratio of the second stress invariant on the tensile meridian to that on the compressive meridian

Material	ρ	E	ν	θ	e	f_{b0}/f_{c0}	K
Brick	1,7	$8x10^6$	0,1	10	0,1	1,16	0,667
Mortar M10	1,85	$1,06x10^7$	0,2	10	0,1	1,16	0,667
Matrix M15	1,9	$1,06x10^7$	0,2	10	0,1	1,16	0,667
Basaltic net	2,67	$8,9x10^7$	0,26	-	-	-	-

Table 6: Mechanical properties used in FEM_Test_01 and FEM_Test_02 regarding the nonlinear characteristics of the concrete model. The Yield stress and the Displecemtent are reported respectively in [*kN/m^2*] and in [*m*]. Between brackets are indicated the values used in FEM_Test_02

	Compression hardening		Tension stiffening	
Material	Yield stress	Cracking strain	Yield stress	Strain or *Displ.
Brick	1000	0	350	0
	10	0,0085	1,3	0,000325
Mortar M10	6000	0	50 (20)	0
	60	0,017	1,6	0,00064
Matrix M15	9000	0	50 (20)	*0
	15000	0,0067	1,6	*0,00224 (0.0005)
	20000	0,0026		
	12600	0,01185		
	90	0,017		

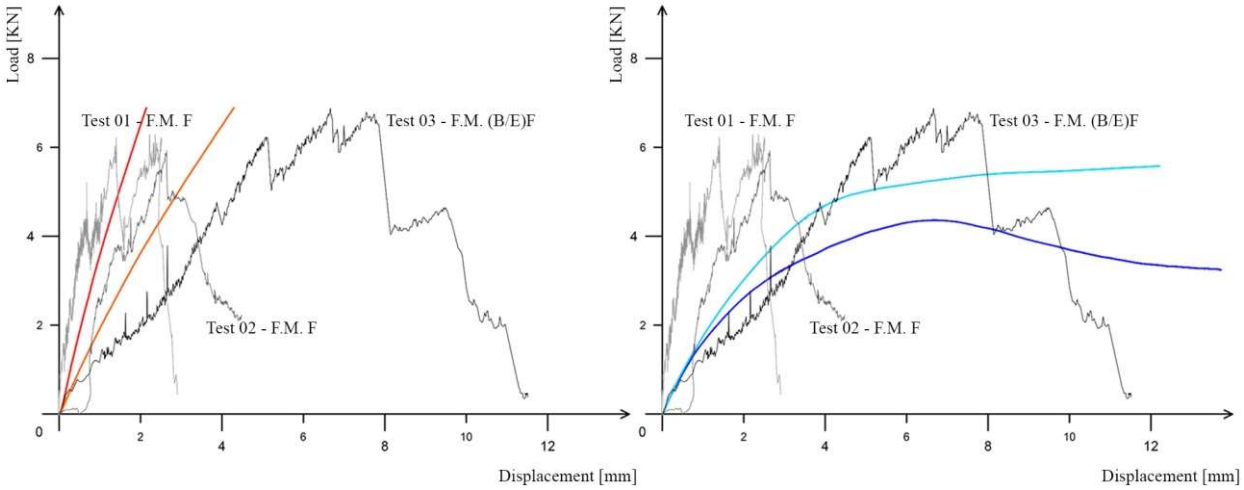
The outcomes (Fig. 7) revealed to be promising and quite consistent to the conducted experimental tests, also with respect to the collapse modes observed during the third one; anyway a better description of the progressive damage of such composite can be obtained through the characterization of the interfaces between the matrix and support.

Table 7: Mechanical properties used in the FEM_Test_03 and FEM_Test_04 (same units of measure of Tab. 5) regarding the elastoplastic behaviour for the numerical models with damage parameter matrix. Between brackets are indicated the values used in FEM_Test_03

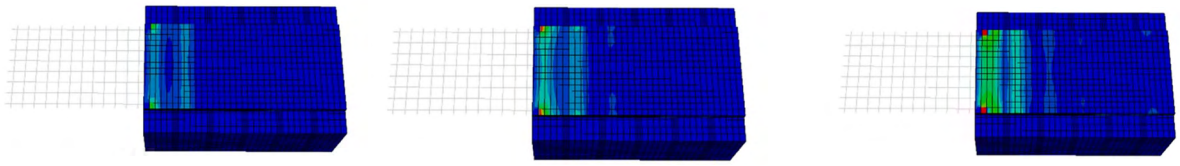
Material	ρ	E	ν	θ	e	f_{b0}/f_{c0}	K
Brick	1,7	$1.5x10^6$	0,1	10	0,1	1,16	0,667
Mortar M10	1,85	($1,06x10^7$) $1,5x10^7$	0,2	10	0,1	1,16	0,667
Matrix M15	1,9	($1,06x10^7$) $1,5x10^7$	0,2	10	0,1	1,16	0,667
Basaltic net	2,67	$8,9x10^7$	0,26	-	-	-	-

Table 8: Mechanical propertiesused in the FEM_Test_03 and FEM_Test_04 (same units of measure of Tab. 6) regarding the concrete damage model. Between brackets are indicated the values used in FEM_Test_03

	Compression hardening		Tension stiffening		Tension damage	
Material	Yield stress	Cracking strain	Yeld stress	Displ.	Damage parameter	Strain or *Displ.
Brick	1000	0	40	0		
	10	0,0085	1,3	0,000325		
Mortar M10	3000	0	60	0		
	30	0,0017	1,6	0,00032		
Matrix M15	3000	0	(80) 60	0	0	*0
	5000	0,0067	1,6	(0,001) 0,00024	0,8	(*0,001) 0,00024
	4200	0,01185				
	30	0,017				



(a) (b)



(c)

Figure 7: Comparisons between experimental and numerical outcomes. a) Models without damage parameters; respectively in red and orange lines FEM_Test 01 and FEM_Test 02 with respect to Tabs. 5-6; b) Models with tension damage model in the matrix, respectively in light-blue and blue lines FEM_Test 03 and FEM_Test 04 with respect to Tabs. 7-8; c) Progressive increasing of the damage pattern in the inorganic matrix (in red the most damaged areas)

4 DESIGN AND PROCEDURE FOR THE EXPERIMENTAL CAMPAIGN ON MASONRY WALLS

The final aim of the experimental campaign planned in partnership with Kimia S.p.a. is to evaluate the incidence of the application of those new-gen composite materials regarding the prevention of the dangerous in plane wall's collapse. On this, a specific set-up has been designed in order to engage life-sized unreinforced and reinforced masonry walls with action similar to the ones ascribed to the condition of *"in falso"* walls. The tests will be conducted on three rectangular walls samples characterized by the same start traits about geometry features, masonry texture and material's mechanical properties: the first one in unreinforced masonry, the second enhanced by a widespread application of the composite material and the last presenting a FRCM strips of in order to configures as a truss beam. Also the experimental setup in terms of loads' application and constraint modalities were equal. With the aim of bringing the specimens to failure, a steel contrast system has been designed to make a self-balanced assembly and the respective breaking loads were applied by mean of a hydraulic flat jack. Furthermore, a monitoring system has been to record the increasing of the applied load and the structures' deformations in relation to the duration of the tests which had as a final moment the complete breaking of the masonry panels, Fig. 8. In addition, the breaking load will be also evaluated in relation to increasing of cracking pattern, (given the presence of the plaster) surveyed thanks to the use of a thermal camera combined with a previously implemented post-processing algorithm aimed at the wall texture damage analysis [10, 11].

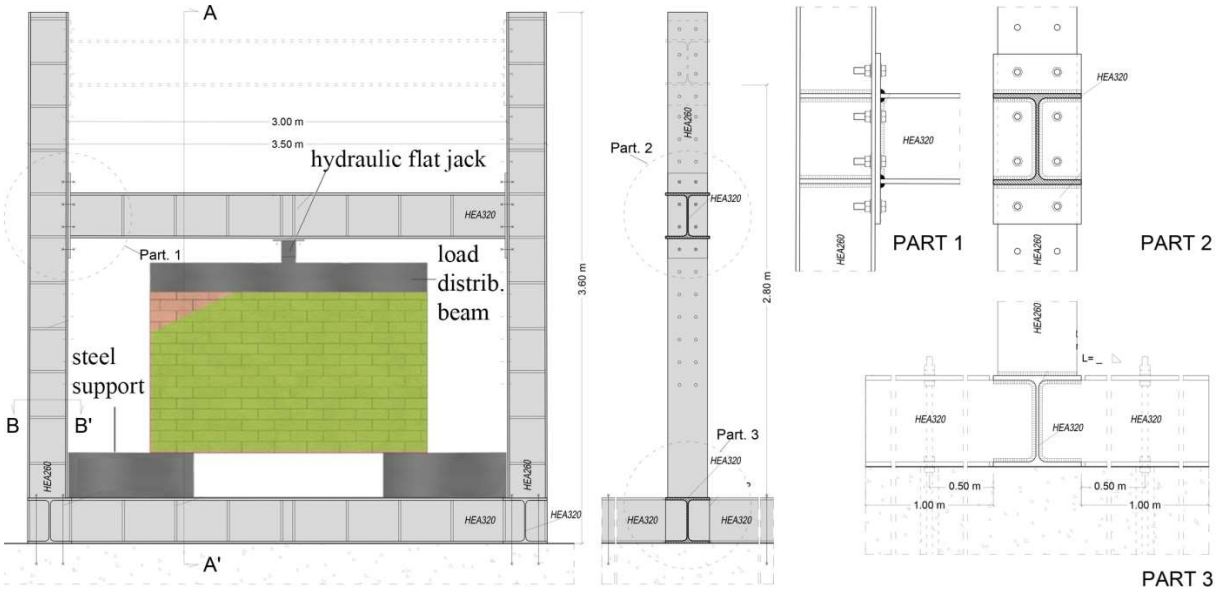


Figure 8: Design details of the steel contrast frame conceived for the near-future experimental campaign

5 CONCLUSIONS

- The results have clarified the experimental behaviour of the FRCM systems, in good compliance with the one of this preliminary numerical modeling referred to the nominal mechanical characteristics of two different materials composing such composite;

- The topic of this ongoing research is to create a model inclusive of the interface between net and matrix in order to replicate the complex failure modes;
- The just planned experimental campaign will be useful to correlate the in-work implementation, time and the skills required for their fulfillment, to the mechanic behaviour of such composite material with respect to the strengthening of masonry walls; subsequently the collected data will be used for a more in deep calibration of a numerical model.

Acknowledgements. Authors gratefully acknowledge Kimia S.p.a. represented by the C.E.O. Eng. Eva Bisciotti, the Technical manager Eng. Stefano Agnetti and the Information and Education manager Dr. Federico Picuti, for their professional and human collaboration. The efforts made by Dr. Gianluca Goracci contextually to his Master Thesis work, are thanked.

REFERENCES

[1] CNR-DT 215/2018, Istruzioni per la Progettazione, l'Esecuzione ed il Controllo di Interventi di Consolidamento Statico mediante l'utilizzo di Compositi Fibrorinforzati a Matrice Inorganica, CNR, 2018.

[2] Bertolesi, E., Milani, G. and Poggi, C. Simple holonomic homogenization model for the non-linear static analysis of in-plane loaded masonry walls strengthened with FRCM composites. *Composite and Structures* (2016) **158**: 291–307.

[3] Pourfalah, S., Cotsovos, D.M. and Suryanto, B. Modelling the out-of-plane behaviour of masonry walls retrofitted with engineered cementitious composites. *Computers and Structures* (2018) **201**: 58–79.

[4] Liberotti, R., Cluni, F. and Gusella, V. Vulnerability and seismic improvement of architectural heritage: the case of Palazzo Murena. *Earthquakes and Structures* (2020) **18** (3): 321–335.

[5] Carozzi, F. G. and Poggi, C. Mechanical properties and debonding strength of Fabric Reinforced Cementitious Matrix (FRCM) systems for masonry strengthening. *Composites: Part B* (2015) **70**: 215–230.

[6] D'Ambra, C., Lignola, G.P., Prota, A., Sacco, E. and Fabbrocino, F. Experimental performance of FRCM retrofit on out-of-plane behaviour of clay brick walls. *Composites Part B* (2018) **148**: 198–206.

[7] De Carvalho Bello, C.B., Boem, I., Cecchi, A., Gattesco, N. and Oliveira, D.V. Experimental tests for the characterization of sisal fiber reinforced cementitious matrix for strengthening masonry structures, *Construction and Building Materials* (2019) **219**: 44–55

[8] Colombi, P. and D'Antino, T. Analytical assessment of the stress-transfer mechanism in FRCM composites, *Composite Structures* (2019) **220**: 961–970.

[9] RELUIS - WP 2, Compositi a matrice cementizia (FRCM) - Prove di distacco di sistemi di rinforzi FRCM da supporto in muratura-Istruzioni per l'esecuzione delle prove, Luglio 2017.

[10] Cluni, F. and Gusella, V. Masonry elastic characteristics assessment by thermographic images. *Meccanica* (2019) **54** (9): 1339–1349.

[11] Cluni, F., Costarelli D., Gusella, V. and Vinti, G. Reliability increase of masonry characteristics estimation by a sampling algorithm applied to thermographic digital images, *Probabilistic Engineering Mechanics*,DOI:10.1016/j.probengmech.2020.103022

12th International Conference on Structural Analysis of Historical Constructions
SAHC 2020
P. Roca, L. Pelà and C. Molins (Eds.)

FIBRE REINFORCED GEOPOLYMERS AS INORGANIC STRENGTHENING COMPOSITES FOR MASONRY STRUCTURES

ENRICO GARBIN[1*], MATTEO PANIZZA[2], SERGIO TAMBURINI[2], MARCO NATALI[2], AND GILBERTO ARTIOLI[3]

[1] Inter-Dept. Research Centre for the Study of Cement Materials and Hydraulic Binders (CIRCe)
University of Padova, Via G. Gradenigo, 6, 35151 Padova, Italy
e-mail: enrico.garbin@unipd.it, http://circe.dicea.unipd.it/ (*corresponding author)

[2] Institute of Condensed Matter Chemistry and Energy Technologies (ICMATE)
Italian National Research Council, C.so Stati Uniti, 4, 35127 Padova, Italy
email: matteo.panizza@icmate.cnr.it,{sergio.tamburini, marcostefano.natali}@cnr.it

[3] Dept. of Geosciences, University of Padova
Via G. Gradenigo, 6, 35151 Padova, Italy
email: gilberto.artioli@unipd.it

Keywords: Geopolymers, Alkali-Activated Materials (AAM), Composite Materials, Strengthening, Masonry structures, FRCM/TRM

Abstract. *The study presents an assessment of externally bonded Fibre-Reinforced GeoPolymers (FRGPs) as strengthening material for masonry structures. Thanks to their tailored chemical and mechanical characteristics, geopolymer matrices can fulfil the restoration criteria for Built Heritage (BH) with the benefit of heat-resistant performances better than those of organic and inorganic matrices used in Externally Bonded Fibre-Reinforced Polymers (EB-FRP) and Fabric-Reinforced Cementitious Matrix (FRCM) materials, respectively. This work is built on the outcomes of a previous investigation that proved the suitability of the developed geopolymer matrix for applications on clay bricks, revealing a good adhesion to masonry substrates and to embedded reinforcements. The behaviour of three FRGPs, including either a bi-directional basalt mesh, a bi-directional carbon mesh or a unidirectional Ultra High Strength Steel (UHSS) fabric, was explored by means of local tests on masonry sub-assemblages made of soft-mud clay bricks and hydraulic lime mortar. In overall, 9 single-lap shear tests on single bricks with a bonded length of 200 mm and 9 three-point bending tests on 2-brick slices, connected by a mortar joint and reinforced at the bottom face, were carried out. Lastly, the behaviour in alkaline environments of each reinforcement was investigated through tensile tests on coupons immersed for 28 days in alkaline solutions simulating the conditions of the geopolimeric matrices. Results confirmed the interesting potential of FRGPs for strengthening masonry elements, highlighting a good performance of steel and carbon reinforcements. On the other hand, precautions should be taken with basalt meshes that, as expected, were more sensitive to alkaline environments.*

1 INTRODUCTION

Existing masonry buildings and Built Heritage (BH) require a permanent maintenance

process to withstand the effects of hazardous natural events and mitigate their effects. This can be accomplished by devoted activities of restoration and structural repair adopting traditional and innovative materials and intervention techniques [1–3]. In the last three decades, the use of Externally Bonded Fibre Reinforced Polymers (EB-FRPs) has grown to be one of the reference interventions for existing buildings and for BH [4–6]. The main advantages of EB-FRPs that fostered their widespread application on existing structures, including also those belonging to the BH, are for instance: their ease and flexibility of application, their fast curing and the related ability in carrying tensile stresses in few hours or days, low weight in comparison to many traditional materials (e.g. steel rods/plates), the high tensile strength and stiffness-to-weight ratio, enhanced fatigue and endurance in aggressive environments [3,5,7]. Nevertheless, FRPs have some compatibility and removability issues with existing and BH masonry structures, mainly due to the adoption of organic matrices [3,8]. In the last decade, research has investigated the replacement of organic (e.g. epoxy) with inorganic matrices made of cement or lime-based mortars [9–13]. The combination of fibres, usually in the form of meshes, with inorganic matrices is currently often labelled with the acronym of Fibre Reinforced Cementitious Matrix (FRCM) [14,15], acronym that also covers for cement-free matrices, while in several former publications the acronym Textile Reinforced Mortars (TRM) was used [3,11,13]. Advantages of FRCMs over FRPs include: better compatibility with masonry substrates and traditional craftsmanship, reversibility, better behaviour under high temperatures and lack of toxic vapours in case of fire, resistance to Ultra-Violet (UV) radiation, water-vapour permeability, applicability over moist substrates, greater deformability and potential lower cost [3,6,8,12,13]. Moreover, inorganic matrices appear particularly suitable for applications to masonry structures, where the bond strength of epoxy matrices can hardly be entirely used due to the inherent mechanical characteristics of the substrate, and for a better compliance with restoration criteria, especially when cement-free matrices are adopted [3,6,12,13]. Nevertheless, traditional lime-based inorganic mortars compatible with BH often show low adhesion to masonry substrates and between the FRCM layers [3,6,13]. To overcome this issue, geopolymers were studied as possible efficient and compatible inorganic matrices for existing masonry substrates and BH [16]. Indeed, geopolymer can meet the dedicated restoration requirements of BH, thanks to their typical chemical composition and porosity which are similar to that of clay bricks [16], while delivering physico-mechanical performances exceeding those of the best inorganic matrices used in FRCMs [16,17].

Geopolymers are relatively recent and emerging inorganic cement-free binders that present a combination of the best characteristics of ceramic and cement-based materials [16,17]. Moreover, they have a clear advantage over EB-FRPs and FRCMs as non-inflammable and heat-resistant matrices for inorganic composites designed to reach temperatures of 1000°C [16,18]. Geopolymers are inorganic quasi-fragile materials produced from aluminosilicates typically activated with alkali hydroxide and/or alkali silicate solutions [16,17]. Several aluminosilicate or calcium-aluminosilicate raw materials can be used, such as dehydroxylated aluminosilicate clay mineral (e.g. metakaolin) and industrial by-products resulting from high temperature processes such as fly ash or ground blast furnace slag, among others [17]. They are also materials suitable for a greener economy, since they can be derived from by-products or from the recycling of industrial waste materials, and they can be produced with up to ten times lower CO_2 emission than Portland cement [17,19]. Geopolymer grouts and mortars can be obtained by charging the geopolymer binder with sand or fine

aggregates [16,17].

Fibre Reinforced GeoPolymer (FRGP) is the combination of a geopolymer grout with fibre meshes or fabrics, similarly to Fibre Reinforced Cementitious Matrix (FRCM) [16]. Several studies were done on geopolymer fibre composites as final product made with both short fibres [20–22] and multiple laminated layers of fabrics [18,23,24], fewer investigations exist on FRGPs for retrofitting structural elements, and most investigations focused on strengthening Reinforced Concrete (RC) beams [25–28]. Whereas, very little contributions on the use of FRGPs as strengthening materials for existing masonry structures are present [16,29]. The mechanical models and the design procedures available for FRCMs [14,15,30,31] can be adopted owing to the inherent quasi-fragile behaviour of the geopolymeric matrix. Lastly, for a successful application of FRPs, their durability should be evaluated. Geopolymers have already shown good resistance towards acid and alkaline environments [16,17]. Therefore, the main durability issue is connected to the endurance of the fibres when embedded in a geopolymeric matrix, which provide an alkaline environment that might result corrosive for certain reinforcements as glass or basalt fibres [32,33]. Indeed, this is a common issue for the glass fibre laths embedded in lime or cement plasters and for any fibre mesh embedded in the cementitious matrices of FRCMs [34].

In this framework, the behaviour of three FRGPs was explored by means of local tests on masonry sub-assemblages made of soft-mud clay bricks and hydraulic lime mortar. The three FRGPs embedded a bi-directional basalt mesh, a bi-directional carbon mesh and a unidirectional Ultra High Strength Steel (UHSS) fabric, respectively. In total, 9 single-lap shear tests on single bricks with a bonded length of 200 mm and 9 three-point bending tests on 2-brick slices, connected by a mortar joint and reinforced at the bottom face, were carried out to evaluate the bond behaviour and the flexural strengthening performances of the three FRGPs. Lastly, the behaviour in alkaline environments of each reinforcement was studied through tensile tests on coupons immersed for 28 days in alkaline solutions, tentatively simulating the pore solution of the geopolymeric matrices.

In this paper, the experimental results about the materials, the durability, the bond behaviour and the flexural behaviour of the strengthened masonry sub-assemblages are presented and discussed. Results confirmed the untapped and interesting potential of FRGPs as strengthening materials, highlighting a good performance of steel and carbon reinforcements. On the other hand, precautions should be taken with un-sized basalt meshes that, as expected, were more sensitive to alkaline environments.

2 MATERIALS AND METHODS

Low-strength 250 × 120 × 55 mm³ soft mud clay bricks, intended to simulate a typical historical masonry unit, were adopted. Their average performance (coefficient of variation – CoV – in brackets) was 17.7 N/mm² (6.2%) in compression and 4.43 N/mm² (10.3%) in bending [35], whereas their apparent density was $1.63 \cdot 10^3$ kg/m³ (1.0%).

The mortar forming the joint of the 2-brick slice bending specimens was a commercially available pre-mixed cement-free pozzolana lime mortar with siliceous sand aggregates, category M15 according to Eurocode 6 [36], with a 28-day average strength of 14.7 N/mm² (2.5%) measured according to standard EN 1015-11 [37].

The geopolymer matrix, extensively described in [16], was prepared with metakaolin and

ground granulated furnace slag as solid precursors, and sodium silicate with molar ratio SiO_2/Na_2O of 1.5 and concentration of 41.3% as liquid activator. The binder embedded fine siliceous sand and wollastonite as inorganic aggregates, resulting in a grout with density of $2.0 \cdot 10^3$ kg/m³ (1.0%), after hardening. The cylinder compressive strength was 44.6 N/mm² (3.0%) and the splitting resistance was 4.4 N/mm² (7.1%) in average, measured on cylindrical specimens with diameter of 35 mm and aspect ratio of 2.

The geopolymer matrix was coupled with 3 types of fibre reinforcements, either a unidirectional steel fabric or two balanced bidirectional fibre meshes, i.e. carbon or basalt, thus generating three Fibre-Reinforced GeoPolymers (FRGP).

The unidirectional steel fabric (STL) was composed by Ultra High Strength Steel (UHSS) strands, mounted on a mesh support, approximately 6 mm spaced apart. The datasheet reports a characteristic tensile strength of 3070 N/mm², an average elastic modulus of $190 \cdot 10^3$ N/mm² and an equivalent thickness of 0.075 mm.

The carbon reinforcement (CAR) was a bidirectional balanced mesh made of uncoated yarns, having a centre-to-centre spacing of about 9 mm, with a surface density of 200 g/m². It has a characteristic tensile strength of 2500 N/mm², an average elastic modulus of $230 \cdot 10^3$ N/mm² and an equivalent thickness of 0.048 mm, according to its technical datasheet.

The basalt reinforcement (BAS) was a bidirectional balanced mesh made of un-sized yarns, having a centre-to-centre spacing of about 8 mm, with a surface density of 300 g/m². It has a characteristic tensile strength of 1735 N/mm², an average elastic modulus of $90 \cdot 10^3$ N/mm² and an equivalent thickness of 0.053 mm, according to its technical datasheet.

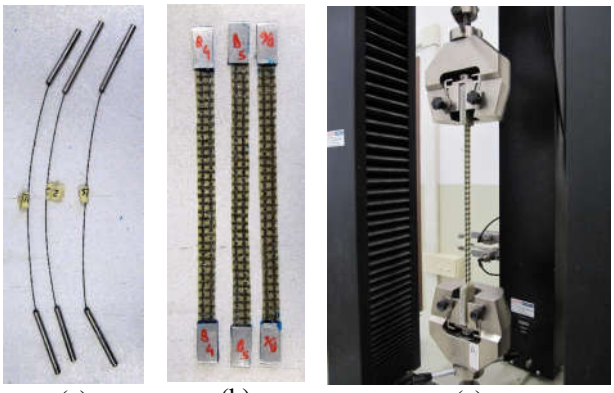
The experimental program herein presented envisaged 3 types of tests, specifically: (i) direct tensile tests carried out on coupons of fibres, either in pristine state or subjected to a 28-day conditioning in 3 different alkaline solutions; (ii) single-lap shear tests performed on FRGPs longitudinally applied to single bricks; and (iii) 3-point bending tests executed on specimens made of 2-brick slices bonded by a mortar joint, either unreinforced or with the FRGP applied to the bottom surface.

2.1 Tensile tests on fabric coupons

Either single strand, in the case of steel, or 2-yarns coupons, in the case of carbon and basalt, were tested in tension in a 25 kN electro-mechanic universal machine. Specimens were 380 mm long to allow a free length of about 280 mm after the application at each end of 2 aluminium tabs (or sleeves in the case of steel) 50 mm long, glued with epoxy resin, which were clamped by the test machine. Carbon and basalt yarns were impregnated with a small amount of epoxy resin to load uniformly the yarns and obtaining the full resistance of the mesh, thus preventing or limiting possible uneven distribution of stresses inside the reinforcement.

Tests were carried out either on pristine samples of reinforcements (C0 condition) or on fibres immersed for 28 days in 3 alkaline solutions to investigate their possible degradation in environments simulating the possible pore solution of the geopolymer matrix. C1 consisted in a 5% aqueous solution of NaOH (corresponding to 1.25M), as provided by the standard ASTM E2098/E2098M [38]. Aqueous solutions of either sodium (the same used as binder activator) or potassium silicate were adopted for C2 and C3. The formulation of the potassium silicate had a molar ratio $SiO_2/K_2O \sim 1.5$, equal to the silica/sodium one, with a solid matter concentration of 46.0%. Silicates were dissolved in water to achieve the same concentration of

Na (or K) atoms of the C1 solution. At least 4 samples for each type of reinforcement and conditioning solution were tested. After the immersion, fibres were rinsed and dried to measure the weight loss by means of an analytical balance.



(a) (b) (c)

Figure 1: Samples of steel (a) and basalt (b) reinforcement for tensile tests, and a coupon ready for testing (c)

2.2 Single-lap shear tests

Specimens consisted in a single brick with the FRGP applied longitudinally onto the wider surface (Fig. 2a) with a bonded area 200 mm long and 60 mm wide, delimited by masking tape during casting. A protruding portion extending for about 220 mm beyond the edge of the brick was used for the connection to the test machine. The reinforcement was embedded inside the geopolymer matrix for the whole length, except in the case of steel strands that were kept bare beyond the edge of the brick. The area of the reinforcement varied according to the type, since the FRGP included either 8 steel strands, 5 carbon or 7 basalt yarns to achieve the desired width.

The test setup (Fig. 2b), designed for a universal electro-mechanic machine, was the same already adopted in several former researches [6,39]. It consisted in two steel plates 50 mm thick connected by 4 threaded bars, two of which fastened to the bottom head of the test machine. The specimen was inserted between those plates, taking care to alignments and contacts, and the protruding reinforcement was glued with quick setting resin to a steel part connected to the upper head of the test machine by means of a ball joint. Four potentiometers were used to monitor displacements, two positioned at the beginning of the bonded length, one in the middle and one at the unloaded end of the FRGP. Tests were carried out in displacement control, with a rate of the movable loading beam progressively incremented from 0.3 mm/min to 1.2 mm/min in the last stages of the tests. Load and displacement values were recorded by an external acquisition system at 10 Hz.

Three specimens per type of reinforcement were tested, for overall of 9 samples.

2.3 Bending tests on 2-brick specimens

Three-point bending tests were carried out on specimens made of 2 slices, about 32 mm thick, cut from single bricks. Those slices were longitudinally aligned and connected by a 10 mm mortar joint, thus obtaining samples approximately 510 mm long (Fig. 3a). Subsequently, the FRGP was centrally applied to the bottom side, extending for about 330 mm. The reinforcement comprised 3 strands or yarns for each type of fibre. The geometry of the

specimens was a trade-off between representativeness and materials availability.

A 50 kN electro-mechanic universal machine equipped with a commercial setup for bending (Fig. 3) was used. The span between the bottom supports was 380 mm, slightly greater than the length of the FRGP. Contacts between sample and steel supports were improved by small rubber inserts. Tests were carried out in displacement control, with a rate of the movable loading beam of 0.5 mm/min. Load and displacements were recorded by the embedded data acquisition of the universal machine.

Three specimens per type of reinforcement were tested, for overall 9 samples. In addition, 3 unreinforced specimens were tested twice at 0.1 mm/min with a 2.5 kN load cell, repairing the failed joint with epoxy resin and testing again the same specimen to measure also the resistance of the strongest mortar-to-brick interface.

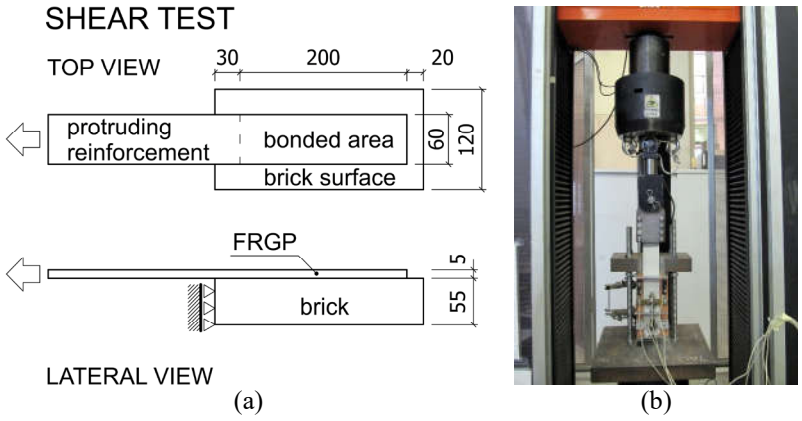


Figure 2: Sketch of a shear test specimen with dimensions in mm (a) and sample ready for testing (b)

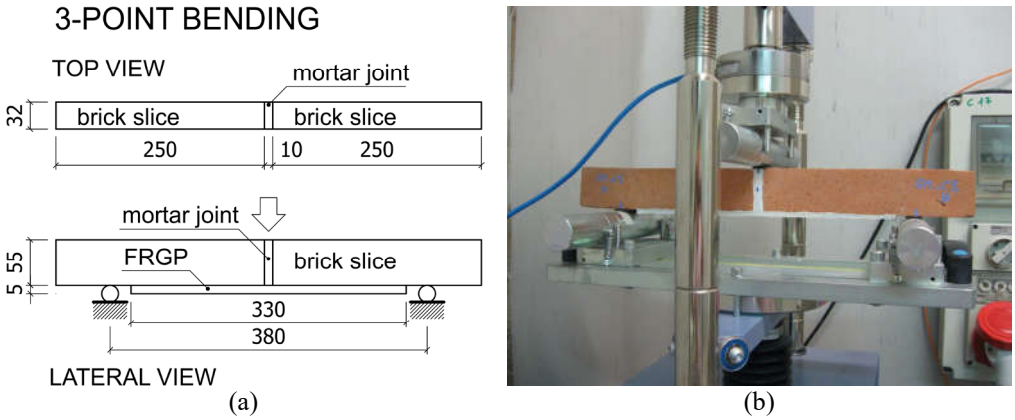


Figure 3: Sketch of a 3-point bending specimen, with dimensions in mm (a) and sample ready for testing (b)

3 RESULTS AND DISCUSSION

3.1 Tensile tests on fabric coupons

Failure was generally as expected, with a fibre tensile rupture localised inside the free length between the anchoring, in some cases close to the tabs. Although few specimens showed an

irregular failure, due to slippage problems at the connection with the test machine or to an imperfect alignment, at least 4 suitable results were included in calculations.

The average tensile strengths $f_{t,avg}$, grouped by fibre and conditioning type, are listed in Table 1 together with their coefficient of variation (CoV). Measured values of weight loss are shown in Figure 4a, whereas tensile strength retentions are shown in Figure 4b.

Steel strands were substantially not affected by the alkaline environment, with a strength loss always lower than 3% that can be considered within a common experimental variability, despite a weight loss that exceeded 3% in two cases, probably due to the loss of the protecting coating without impairing the resisting cross-section. Carbon fibres presented a strength retention of about 93% in sodium hydroxide and sodium silicate solutions and were slightly more sensitive to potassium silicate solutions as proved by a lower strength retention of about 86%. Conversely, they showed the lowest values of weight loss of about 0.2–0.3%. Finally, as expected, the un-sized basal fibres showed the worst degradation, with a strength loss of about 25% in silicate solutions and 45% in sodium hydroxide solution, with a weight loss comprised between 0.7–1.9% (the lowest was measured in NaOH). Strength conversion coefficients for aggressive environments proposed by the Italian guidelines CNR DT200R1 [40] (0.85 for carbon and 0.50 for glass fibres) and CNR DT215 [15] (0.70 regardless of the fibres type), compared to the present experimental results, appear reasonably close where applicable. As observed in [32], there is no apparent correlation between weight loss and strength retention.

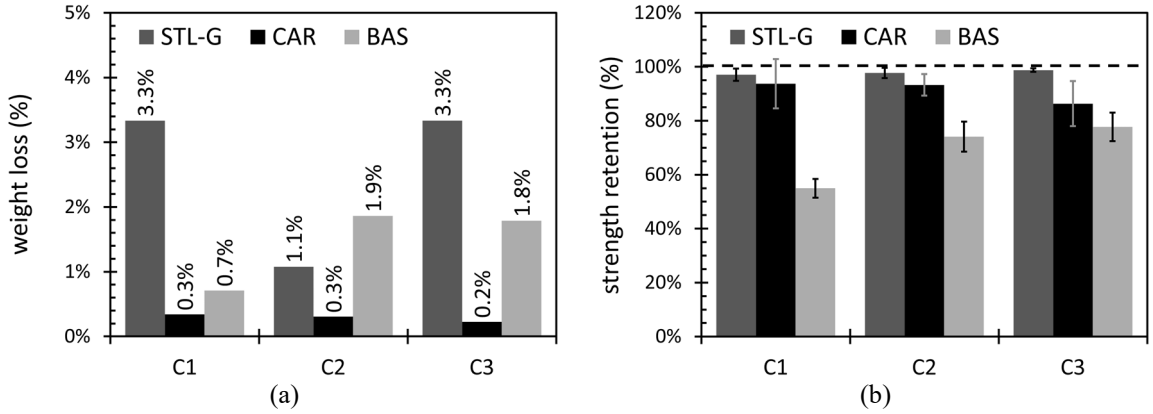


Figure 4: Weight loss (a) and tensile strength retention (b) measured on conditioned fibres

Table 1: average tensile strength in pristine condition (C0) and after treatment in alkalis, with CoV in brackets

Specimen	C0 – $f_{t,avg}$ N/mm²	C1 – $f_{t,avg}$ N/mm²	C2 – $f_{t,avg}$ N/mm²	C3 – $f_{t,avg}$ N/mm²
STL	3125 (0.5%)	3033 (2.4%)	3053 (1.9%)	3086 (0.7%)
CAR	2854 (7.9%)	2675 (9.7%)	2663 (4.3%)	2464 (9.7%)
BAS	1845 (3.2%)	1013 (6.3%)	1367 (7.5%)	1434 (6.8%)

3.2 Single-lap shear tests

Failures were substantially different for each type of FRGP. Steel strands failed in tension in 2 specimens (Fig. 5a), while in one case a partial debonding, about 2/3 of the bonded length, occurred (Fig. 5b). Carbon yarns generally slipped inside the matrix (Fig. 5c), with minor signs

of tensile failure in the most external fibrils and several cracks in the protruding FRGP, about 25-30 mm spaced apart. On the other hand, basalt yarns showed a rather clear tensile rupture with no remarkable sign of slippage (Fig. 5d).

Results, in terms of failure mode, maximum load P_{max} and maximum stress σ_{max}, are given in Table 2, together with the exploitation coefficient η_{ST} calculated as the ratio of σ_{max} and the fibre tensile strength $f_{t,avg}$ measured in pristine conditions (C0). As expected, the effectiveness of the FRGP was in all cases lower than 1, confirming that shear tests, although excluding bond failures, cannot achieve the reference strength of the fibre reinforcements when embedded in inorganic matrices. Nonetheless, in the case of steel, the exploitation was not lower than 0.8, thus suggesting that steel strands are less sensitive to this type of test. Carbon fibres slipped at values comprised between 0.41 and 0.47, while basalt failed at 0.23 and 0.32, cracked specimen excluded. Similar exploitation coefficient η_{ST} are currently obtained for optimal FRCM systems [6,12,13,34].



(a) (b) (c) (d)

Figure 5: Failure modes of shear tests: (a) tensile failure and (b) partial debonding of steel FRGP; (c) slippage of carbon fibres and diffuse cracking of the matrix; and (d) tensile failure of basalt mesh

Table 2: results of single-lap shear tests

Specimen	Main failure	P_{max} N	σ_{max} N/mm²	η_{ST}
ST-STL-1	tensile break	12764	2966	0.95
ST-STL-2	debonding	9214	2141	0.69
ST-STL-3	tensile break	10678	2481	0.79
ST-CAR-1	tensile break/slippage	3271	1140	0.44
ST-CAR-2	tensile break/slippage	3480	1213	0.47
ST-CAR-3	tensile break/slippage	3030	1057	0.41
ST-BAS-1	tensile break (*)	804	271	0.15
ST-BAS-2	tensile break	1285	433	0.23
ST-BAS-3	tensile break	1737	585	0.32

** specimen cracked during handling before the test*

3.3 Bending tests on 2-brick specimens

The failure of the 3 unreinforced specimens was always located at the mortar-brick interface (Fig 5a). They were tested twice, the second time after repair of the failed joint, and showed a

remarkably variable resistance comprised between 37 and 129 N, corresponding to a bond strength, calculated as the ratio of maximum bending moment and section modulus, comprised between 0.22 and 0.81 N/mm². The average strength of the weakest joint of each specimen was 0.41 N/mm², while the average of the strongest ones was 0.62 N/mm².

In the case of steel FRGP, failure was due to a shear crack of the brick that started close to the end of the reinforcement (Fig 5b), after a wedge-like cracking of the portion beneath the applied load. Carbon FRGP failed due to slippage of the fibres (Fig 5c), whereas basalt FRGP broke in tension (Fig 5d), in all cases in correspondence of the main crack that opened at the mortar-brick interface.

Results are listed in Table 3 in terms of failure mode, maximum load P_{max} and maximum stress $\sigma_{max.sb}$, the latter calculated through a section analysis based on the assumption of a stress-block $0.8 \cdot x$ high, being x the neutral axis depth. The exploitation coefficient η_{BT} was calculated similarly to the case of η_{ST}. Steel-reinforced specimens could not attain a fibre effectiveness close to shear test samples, due to the earlier shear failure of the brick. In the case of carbon FRGP, which also showed one shear failure mode, the exploitation η_{BT} of 0.41–0.44 was comparable to η_{ST}. Conversely, basalt FRGP reached relatively high values of η_{BT} (0.60 and 0.71), more than twice the η_{ST} of ST-BAS-2 and ST-BAS-3, probably thanks to the reduced number of yarns and to the bending specimen that allowed an evener stress distribution. Similar exploitation coefficient η_{BT} are currently obtained for optimal FRCM systems [6,10,13,34].



(a) (b) (c) (d)

Figure 5: Failure modes of bending tests: (a) joint failure of unreinforced specimens; (b) brick shear failure in case of steel FRPG; (c) slippage and partial rupture of carbon fibres; and (d) tensile failure of basalt mesh

Table 3: Results of 3-point bending tests

Specimen	Failure	P_{max} N	$\sigma_{max,sb}$ N/mm²	η_{BT}
BT-STL-1	brick shear	1289	1591	0.49
BT-STL-2	brick shear	1425	1799	0.56
BT-STL-3	brick shear	1515	1919	0.59
BT-CAR-1	slippage	1218	1257	0.44
BT-CAR-2	slippage	1119	1170	0.41
BT-CAR-3	slippage / brick shear	1199	1258	0.44
BT-BAS-1	tensile break (*)	321	434	0.24
BT-BAS-2	tensile break	798	1114	0.60
BT-BAS-3	tensile break	927	1302	0.71

** mortar joint cracked before the test, probably due to drying shrinkage of the FRGP*

4 CONCLUSIONS

The paper presented an assessment of the adhesion and durability properties of FRGPs as strengthening material for masonry buildings. The FRGPs were made of an eco-efficient and heat-resistant geopolymeric matrix that has a chemical composition and porosity similar to that of soft-mud clay bricks simulating a typical historical masonry unit. Therefore, the matrix is an interesting inorganic bonding agent for the implementation of removable and compatible composites suitable, not only for exiting masonry buildings, but also for BH. The three FRGPs studied were reinforced either with a bi-directional balanced basalt mesh, a bi-directional balanced carbon mesh or a unidirectional UHSS fabric.

The adhesion and mechanical performances of the three FRGPs were investigated by means of local 9 single-lap shear tests on single bricks with a bonded length of 200 mm and 9 three-point bending tests on two brick slices, connected by a mortar joint and reinforced at the bottom face. The exploitation coefficients derived from the shear and the bending tests are in accordance with the best performances currently obtained by the FRCMs. Nonetheless, FRGPs are provided with an undoubtedly more innovative inorganic matrix.

On the other hand, further studies are necessary to investigate the durability of the FRGPs. In fact, the behaviour in alkaline environments simulating the pore solution of the geopolymeric matrices highlighted the possibility of undesired corrosive outcomes on the fibres, especially when they are un-sized (or they lost part of the sizing) as the basalt mesh used in this paper.

The results confirmed the untapped and interesting potential of FRGPs. In particular, The FRGPs reinforced with the carbon mesh and the UHSS fabric shown interesting result as potential inorganic composites suitable for strengthening exiting masonry buildings and BH.

Acknowledgements. Several industries provided free of charge part of the materials used in this research: Fidia s.r.l. (Perugia, Italy) the basalt mesh, Kerakoll s.p.a. (Sassuolo, Italy) the Ultra High Strength Steel fabric, BASF CC Italia (Treviso, Italy) the carbon mesh and the pozzolana lime mortar, San Marco Terreal Italia (Noale, Italy) the soft mud clay bricks.

REFERENCES

[1] Modena, C., Valluzzi, M.R., da Porto, F., Casarin, F. Structural Aspects of the Conservation of Historic Masonry Constructions in Seismic Areas: Remedial Measures and Emergency Actions. *Int. J. Archit. Herit.* (2011) **5(4-5)**:539-558.

[2] Tomaževič, M. Seismic Resistance of Masonry Buildings in Historic Urban and Rural Nuclei: Lessons Learned in Slovenia. International Journal of Architectural Heritage, *Int. J. Archit. Herit.* (2011) **5(4-5)**:436-465.

[3] Valluzzi, M.R., Modena, C., de Felice, G. Current Practice and Open Issues in Strengthening Historical Buildings with Composites. *Mater. Struct.* (2014) **47(12)**:1971-1985.

[4] Triantafillou, T.C. Strengthening of Masonry Structures Using Epoxy-Bonded FRP Laminates. *J. Compos. Constr.* (1998) **2(2)**:96-104.

[5] Shrive, N.G. The Use of Fibre Reinforced Polymers to Improve Seismic Resistance of Masonry. *Constr. Build. Mater.* (2006) **20(4)**:269-277.

[6] Garbin, E., Panizza, M., Valluzzi, M.R. Experimental Characterization of Glass and Carbon FRCMs for Masonry Retrofitting. *ACI Special Publication*, 324:3.1-3.20. American Concrete Institute (2018).

[7] Hollaway, L.C. A Review of the Present and Future Utilisation of FRP Composites in the Civil

Infrastructure with Reference to Their Important In-service Properties. *Constr. Build. Mater.* (2010) **24(12)**:2419-2445.
[8] Tedeschi C., Kwiecien A., Valluzzi M.R., Zajac B., Garbin E., Binda L. Effect of thermal ageing and salt decay on bond between FRP and masonry. *Mater. Struct.* (2014) **47(12)**:2051–2065.
[9] Papanicolaou, C.G., Triantafillou, T.C., Karlos, K., Papathanasiou, M. Textile-Reinforced Mortar (TRM) Versus FRP as Strengthening Material of URM Walls: In-plane Cyclic Loading. *Mater. Struct.* (2007) **40(10)**:1081-1097.
[10] Papanicolaou, C.G., Triantafillou, T.C., Papathanasiou, M., Karlos, K. Textile Reinforced Mortar (TRM) Versus FRP as Strengthening Material of URM Walls: Out-of-plane Cyclic Loading. *Mater. Struct.* (2008) **41(1)**:143-157.
[11] Garmendia, L., Marcos, I., Garbin E., Valluzzi, M.R. Strengthening of Masonry Arches with Textile-Reinforced Mortar: Experimental Behaviour and Analytical Approaches. *Mater. Struct.* (2014) **47(12)**:2067-2080.
[12] de Felice, G., De Santis, S., Garmendia, L., Ghiassi, G., Larrinaga, P., Lourenço, P.B., Oliveira, D.V., Paolacci, F. and Papanicolaou C.G. Mortar-based systems for externally bonded strengthening of masonry. *Mater. Struct.* (2014), **47(12)**:2021–2037.
[13] Kouris L.A.S. and Triantafillou T.C. State-of-the-art on strengthening of masonry structures with textile reinforced mortar (TRM). *Constr. Build. Mater.* (2018) **188**:1221-1233.
[14] ACI 549.4R-13. *Guide to Design and Construction of Externally Bonded FRCM Systems for Repair and Strengthening Concrete and Masonry Structures*. American Concrete Institute (2013).
[15] CNR DT 215/2018. *Guide for the Design and Construction of Externally Bonded Fibre Reinforced Inorganic Matrix Systems for Strengthening Existing Structures*. Italian National Research Council (2020).
[16] Tamburini, S., Natali, M., Garbin, E., Panizza, M., Favaro, M. and Valluzzi, M.R. Geopolymer matrix for fibre reinforced composites aimed at strengthening masonry structures. *Constr. Build. Mater.* (2017) **141**:542-552.
[17] Provis, L. and van Deventer J.S.J. *Geopolymers: Structure, processing and industrial applications*. Woodhead Publishing in Materials (2009).
[18] Kurz, S., Balaguru, P.N. Comparison of Inorganic and Organic Matrices for Strengthening of RC Beams with Carbon Sheets. *J. Struct. Eng.-ASCE* (2001) **127(1)**:35-42.
[19] Pacheco-Torgal, F. and Jalali S. *Eco-Efficient Construction and Building Materials*. Springer Science+Business Media (2011).
[20] Shaikh, F.U.A. Review of mechanical properties of short fibre reinforced geopolymer composites. *Constr. Build. Mater.* (2013) **43**:37-49.
[21] Welter, M., Schmücker, M., MacKenzie, K.J.D. Evolution of the fibre-matrix interactions in basalt-fibre-reinforced geopolymer-matrix composites after heating, *J. Ceram. Sci. Technol.* (2015) **6(1)**:17–24.
[22] Vickers, L., van Riessen, A., Rickard, W.D.A. *Fire-resistant Geopolymers: Role of fibres and fillers to enhance thermal properties*. Springer Briefs in Materials (2015).
[23] Toutanji, H., Deng, Y. Comparison between organic and inorganic matrices for RC beams strengthened with carbon fiber sheets, *J. Compos. Constr.-ASCE* (2007) **11(5)**:507-513.
[24] Ferone, C., Colangelo, F., Roviello, G., Asprone, D., Menna, D., Balsamo, A., Prota, A., Cioffi, R., Manfredi, G. Application-oriented chemical optimization of a metakaolin based geopolymer. *Materials* (2013) **6(5)**:1920–1939.
[25] Papakonstantinou, C.G., Katakalos, K. Flexural behavior of reinforced concrete beams

strengthened with a hybrid inorganic matrix-steel fibre retrofit system, *Struct. Eng. Mech.* (2009) **31(5)**:567-585

[26] Menna, C., Asprone, D., Ferone, C., Colangelo, F., Balsamo, A., Prota, A., Cioffi, R., Manfredi, G. Use of geopolymers for composite external reinforcement of RC members, *Compos Part B-Eng* (2013) **45(1)**:1667-1676.

[27] Katakalos, K., Papakonstantinou, C.G. Fatigue of reinforced concrete beams strengthened with steel-reinforced inorganic polymers, *J. Compos. Constr.-ASCE* (2009) **13(2)**:103-112.

[28] Carabba, L., Santandrea, M., Carloni, C., Manzi, S., Bignozzi, M.C. Steel fiber reinforced geopolymer matrix (S-FRGM) composites applied to reinforced concrete structures for strengthening applications: A preliminary study. *Compos Part B-Eng* (2017) **128**:83-90.

[29] Garbin, E., Panizza, M., Valluzzi, M.R., Nardon, F., Tamburini, S., Favaro, M., Magro, A., Characterization of Fibre Reinforced Geopolymers as structural strengthening material for historical brick masonry. In: *Proc. of 9th International Masonry Conference*, Guimarães, Portugal, July 7–9 (2014).

[30] Ceroni, F. and Salzano, P. Design provisions for FRCM systems bonded to concrete and masonry elements. *Compos Part B-Eng* (2018) **143**:230-242.

[31] Meriggi, P., de Felice, G., De Santis, S. Design of the out-of-plane strengthening of masonry walls with fabric reinforced cementitious matrix composites. *Constr. Build. Mater.* (2020) **240**: 117946, https://doi.org/10.1016/j.conbuildmat.2019.117946

[32] Tamburini, S., Natali, M., Garbin, E., Valluzzi, M.R., Artioli, G. Comparison of fibres in geopolymer matrix for structural reinforcement of masonry (FRGP): Compatibility, reactivity, durability. In: *ECI Conference on Geopolymers: The route to eliminate waste and emissions in ceramic and cement manufacturing*, Schloss Hernstein (Austria), May 24-29 (2015).

[33] Dhand, V., Mittal, G., Rhee, K.Y., Hui, D. A short review on basalt fiber reinforced polymer composites. *Compos Part B-Eng* (2015) **73**:166-180.

[34] Triantafillou, T. *Textile Fibre Composites in Civil Engineering*. Woodhead Publishing Series in Civil and Structural Engineering (2016).

[35] Girardello, P. *Rinforzo di volte in muratura con materiali compositi innovativi*. Ph.D. Thesis, University of Padova, Italy (2013). In Italian.

[36] EN 1996-1-1. *Eurocode 6: Design of masonry structures – General rules for reinforced and unreinforced masonry structures*. European Committee for Standardization (2005).

[37] EN 1015-11. *Methods of test for mortar for masonry. Determination of flexural and compressive strength of hardened mortar*. European Committee for Standardization (2019).

[38] ASTM Standard E2098/E2098M–13. *Standard Test Method for Determining Tensile Breaking Strength of Glass Fiber Reinforcing Mesh for Use in Class PB Exterior Insulation and Finish Systems (EIFS), after Exposure to a Sodium Hydroxide Solution*. ASTM International, West Conshohocken, PA (2013).

[39] Panizza, M., Garbin, E., Valluzzi, M.R., Modena, C. Experimental comparison of various types of specimens subjected to SL and DL shear bond tests on EB composites applied to bricks. In: *6th Int. Conf. on FRP Composites in Civil Engineering – CICE 2012*, Rome (Italy), June 13-15 (2012).

[40] CNR DT 200R1/2013. *Guide for the Design and Construction of Externally Bonded FRP Systems for Strengthening Existing Structures*. Italian National Research Council (2013).

12th International Conference on Structural Analysis of Historical Constructions
SAHC 2020
P. Roca, L. Pelà and C. Molins (Eds.)

FLEXURAL RESISTANCE OF MASONRY WALL RETROFITTED WITH TIMBER PANEL UNDER OUT-OF-PLANE LOADING

ORNELLA IUORIO[1*], JAMIU A. DAUDA[1] AND PAULO B. LOURENCO[2]

[1] School of Civil Engineering
University of Leeds
Woodhouse Lane, LS2 9JT, Leeds, UK
e-mail: o.iuorio@leeds.ac.uk (*corresponding author)
cnjad@leeds.ac.uk

[2] Department of Civil Engineering
University of Minho
Azurém, P-4800-058 Guimarães, Portugal
e-mail: pbl@civil.uminho.pt

Keywords: Flexure, OSB, Retrofit, Sustainable, URM

Abstract. *Retrofit of unreinforced masonry (URM) structures is incessantly attracting interests of masonry professionals. Because there are enormous URM structure stocks in different parts of the world that have shown vulnerability to damage against out-of-plane actions due to having limited flexural strength and deformation capacity [1]. As such, there is a global trend of promoting the development of sustainable retrofit techniques for URM structures. The authors' previous study [2] has introduced the application of oriented strand board type 3 (OSB/3) as a prospective sustainable retrofit material for URM wall with evidence of improving the flexural performances. This paper presents, for the first time,experimental works on 1115 x 1115 x 215 mm double wythe single leaf URM walls. Specifically, quasi-static out-of-plane loading tests were carried out on two plain specimens, two single-sided retrofitted walls and two double-sided retrofitted walls. The flexural and displacement capacities were evaluated in both plain and retrofitted specimens, and the results substantiated that OSB/3 application improves the flexural capacity of masonry wall. Therefore, the application of OSB/3 for retrofitting URM buildings can be considered as an inexpensive, efficient and sustainable retrofit technique.*

1 INTRODUCTION

Unreiforced masonry structures are among the oldiest type of constructions, and has seen usage worldwide. However, masonry is a complex construction material and the assessment of its structural response and mechanical properties is a challenge [3]. Its behaviour is often influenced by the quality of materials used, workmanship, and the bond pattern [4]. It is quasi-brittle in nature, hefty in self-weight, contains loose components, has low tolerances to oscillation and thus undergoes sudden brittle failure without much warning to the occupants [1 & 5]. Therefore, in case of sudden failure under out-of-plane loading, occupants of URM

structures do not have enough time to run for safety. Hence, detail consideration for retrofit of old URM structures is highly encouraged to ensure that they can perform their highly sought energy absorption and force relieving roles against failures.

The failure of URM wall is mainly against horizontal forces resulting in flexure due to out-of-plane bending and in shear due to in-plane bending [6 & 7]. URM walls have considerable compressive strength under vertical loading, but they are relatively weak in tensile strength to resist lateral (out-of-plane) loads. They are weak against overpressure from blast effect induced by explosion or earthquake, snow-avalanche for habitation in a mountain area, extreme wind, and mostly lateral (out-of-plane) loading. Specifically, the work presented in this paper aims to improve the out-of-plane capacity of URM walls against out-of-plane loading.

Previously, the authors have introduced the application of oriented strand board (OSB) type 3 to retrofit URM walls to increase their structural capacity and flexural resistance [2, 8]. Before the application of the proposed retrofit scheme, an understanding of the mechanical properties of the constituents (i.e. solid fired clay brick and cement-lime mortar) that were used to construct the masonry walls for investigating the efficiency of the proposed retrofit technique was carried out and reported [9, 10]. After that, small-scale test on 215 x 102.5 x 665 mm masonry prisms in the form of four-point bending test was performed to determine the out-of-plane flexural strength [2]. The flexural bond strength test was carried out to provide a simplified means of gathering data on the flexural strength of plain URM prisms and URM prisms retrofitted with 18 mm thick OSB timber panel and the two selected connection types. The test was carried out to help in understanding the behaviour of masonry and the connection between masonry prism and the proposed OSB timber retrofit technique. The test provided an insight into the effectiveness of the OSB panels on the flexural behaviour of masonry prisms. Thus, it is a pedestal for the design and implementation of the larger-scale tests described in this paper and to validate the effectiveness of the proposed retrofit technique.

This paper presents experimental works on a larger-scale (1115 x 1115 x 215 mm) masonry walls to discuss the application of timber-masonry composite in the retrofit of URM walls. The overall experimental program for investigating the proposed techniques includes the first two stages of work that has been described in [2, 9 & 10]. Here, an experimental program involving subjecting both plain and timber retrofitted URM walls to out-of-plane loading using quasi-static (monotonic) loading scheme is presented. The results of the experimental works are also presented and analysed to evaluate the performance of the proposed OSB retrofit techniques of URM walls.

In addition to the introductory information in section 1, this paper entails four other sections, including section 2 for the material properties, section 3 for the test program and test setup. Afterwards, the results of the experimental works were presented and analysed in section 4. The paper ends with conclusions and recommendations in section 5.

2 MATERIALS

The full experimental characterisation of mechanical properties of masonry components (i.e. UK fired solid clay bricks and mortar) has been presented in [9, 10]. The reasons for selecting each material used in this study have also been highlighted in the referenced paper

[9, 10]. However, the most significant properties, brick strength and water absorption for the brick unit and consistency value and compressive strength of mortar are reported hereafter.

2.1 Masonry Components (Brick Unit and Mortar)

The Masonry test specimens were built using an engineering class B fired solid clay bricks with UK standard size 215 x 102.5 x 65 mm (length x thickness x height). The brick unit has an average strength of 88 N/mm^2 (CoV of 2%) and 4% water absorption (CoV of 5%). The unit strength affects the behaviour of the specimens under loading, and the water absorption is important for the bond between the brick and mortar. If the brick water absorption is too high, the mortar dries up quickly causing dry shrinkage in the mortar, and if the bricks absorb more water than recommended it reduces the strength and durability of the specimen. For these reasons, it is important to clarify these two significant properties (brick strength and water absorption).

The mortar used for the construction of all specimens is type N (general purpose) mortar mix with a ratio of 1:1:6 (Type II Cement: aerial lime: sand) by volume. The mix ratio gives an average dropping value of 10.2 mm and average cube strength of 7.1 N/mm^2 at 28 days. For conformity, the mortar was sampled during the construction of all specimens and gave comparable results.

2.2 Retrofit Material (Oriented Strand Board and Connections)

For the retrofit materials, 18 mm thick engineered wood-based panels (OSB type 3) were selected for this study. The board has an average density of 650 kg/m^3, internal bond strength of 0.3 N/mm^2, and modulus of elasticity of 3500 N/mm^2 and 1400N/mm^2 for both bending in major and minor axis respectively [11]. Also, adhesive anchor connections [9], were used. The adhesive anchor connection is a combination of styrene-free vinylester-hybrid injection mortar and A4 anchor rod. The styrene-free vinylester-hybrid mortar is a high-performance injection mortar which is largely used for fixings in both perforated and solid brick. The diameter of the anchor rod is 8 mm with a permissible tensile load of 1.29 kN.

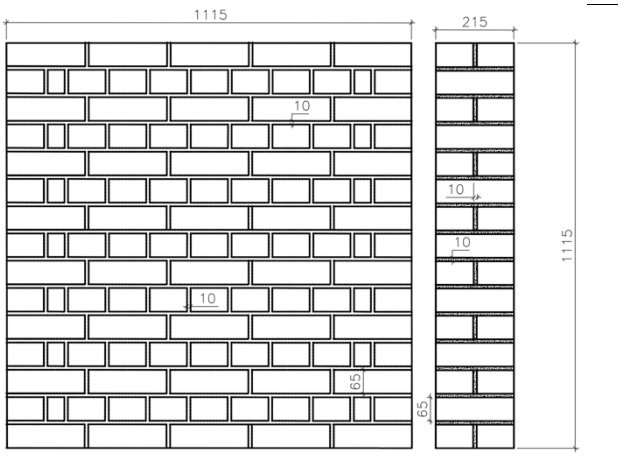
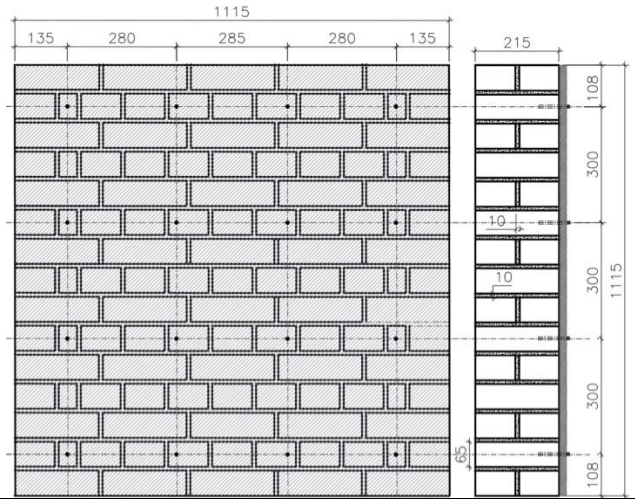
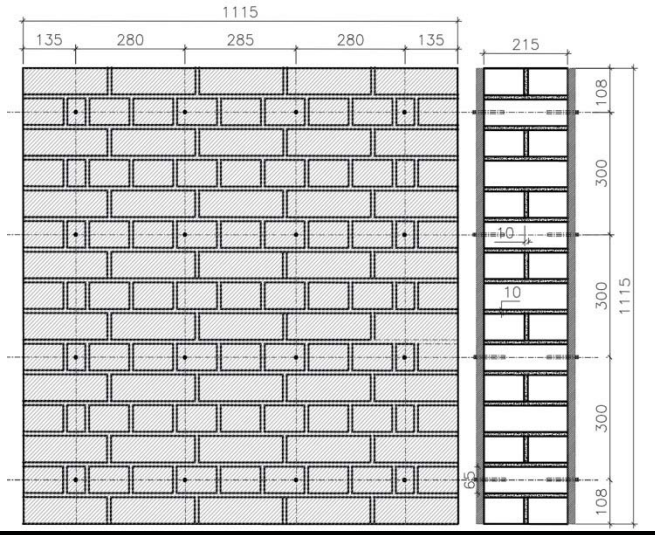
3 METHODS

3.1 Test Program

Six 1115 x 1115 x 215 mm single leaf, double wythe solid URM walls were tested in the laboratory under four-point bending test using quasi-static monotonic loading scheme. The experimental campaign (Table 1) involved testing: (a) two samples as plain wall (PW1115) to serve as reference to measure the effectiveness of the proposed retrofit techniques, (b) two samples each retrofitted with 18 mm thick OSB using adhesive anchor connections on the face in tension (1SRW1115) and, (c) two samples each on both sides of the wall (2SRW1115). The specimens were labelled as follows (table 1):

PW stands for Plain masonry Wall
1SRW stands for Wall Retrofitted with OSB panel on one Side
2SRW stands for wall Retrofitted with OSB panel on two Sides
1115 indicates the wall height,
Suffix number (1 or 2) represents the unique specimen ID.

Table 1: Test program specimen identification

Specimen ID	Description	
PW1115-1	Plain masonry wall	
PW1115-2		
1SRW1115-1	One-sided retrofitted wall	
1SRW1115-2		
2SRW1115-1	Two-sided retrofitted wall	
2SRW1115-2		

3.2 Test Setup

The specimens were tested under four-point loading test arrangement [12] to assess their flexural behaviour. The test was load controlled, and the load was applied to each tested specimen using a hydraulic ram and was distributed through a steel spreader arrangement in the central area of the wall (Fig. 1). All specimens were tested with simply supported boundary condition and a vertical pre-compression load (305 x 305 x 240 UC section amounting to 3 kN load) on top of the wall. The specimen constructed on reinforced concrete footing was rested on 50 mm diameter cylindrical roller with the axis of the roller parallel to the face of the specimen. At the back of the wall, 5mm thick metal plate was fixed across the middle of the top and bottom course of the wall to provide contacts for the simply supports. Similarly, 5mm thick metal plate was fixed at 1/4th and 3/4th of the specimen height at the front side to provide contacts for which the loading rollers rest.

The loading scheme was such that an initial load was applied continuously at a rate of 1kN/min for up to 5kN and then maintained for 5mins period. The purpose of maintaining the applied load was to allow the wall assembly to come to substantial rest before taking the next set of reading [11]. Also, this helped to observe any time-dependent deformation and load redistribution. The load steps were repeated continuously for 10kN, 15kN, 20kN, 25kN, and 30kN load and maintained for 5mins period at each load step. After that, the load was increased continuously to the failure of the specimens. In order to obtain the maximum capacity of the retrofitted walls, the applied load was increased continually after the first crack until additional cracks were formed in the retrofitted specimens and ultimately the timber at the back of the masonry walls were broken. During testing, the applied load on the wall were monitored using a 200KN capacity ring load cell. Also, 8 LVDTs were used to record the deflections of the test specimen along the wall centre, mid-top and the bottom.



Figure 1: Test set up

4 TEST RESULT

4.1 Load-Displacement Curve

The net out of plane displacement in the mid-height of the wall was estimated by deducting the mean displacement recorded at the top and bottom of the specimens from the average mid-height displacement. This deduction accounted for the unexpected displacement at the top and bottom of the wall. Figure 2 shows the load-displacement curves obtained from the experiment. The inference from figure 2 shows that the plain specimens PW1115-1 & PW1115-2 have a quasi-linear behaviour up to about 15000 N loads, which corresponds to the onset of crack formation in the plain wall. After that, the load continuously increased with small increments in the out-of-plane displacement before the specimen failed. At the failure point, the displacement suddenly increased. This increment is due to the brittle nature of the failure pattern. The maximum load attained by PW1115-1 and PW1115-2 is 38330 N and 39720 N respectively. The average of these two value (39025 N) was chosen as a baseline to evaluate the effectiveness of the proposed timber-retrofit technique in both single-sided and double-sided retrofitted walls. For the retrofitted wall specimens, the first crack appeared at an average load of 52750 N and 68714 N for 1SRW1115 and 2SRW1115 respectively. Finally, the average peak load and out-of-plane displacement at the specimens mid-height were estimated as (114622 N, 25.88 mm) and (120559 N, 12.61 mm) for 1SRW1115 and 2SRW1115, respectively. Figure 2 reveals that the proposed retrofit technique has substantially increased the out-of-plane load capacity of retrofitted walls by almost three times when compared to the plain wall.

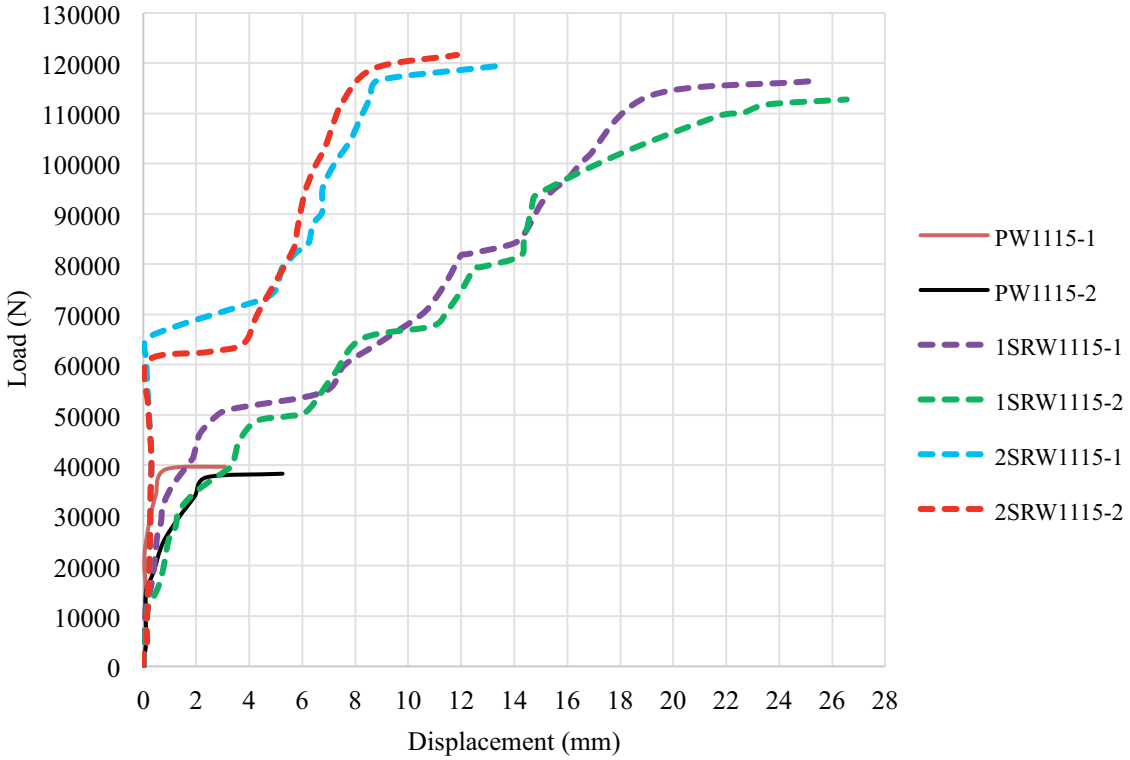


Figure 2: Load vs Displacement curve for specimens

4.2 Failure Pattern

The observed failure pattern in the plain walls is characterised by the sudden formation and rapid opening of the crack in the unit/mortar joint interface throughout the whole wall specimen thickness. The failure of the plain masonry wall is quasi-brittle and always started with the formation of a crack opening in one bed joint at the tensile face of the specimen (i.e. the side opposing the loading face). Subsequently, the crack occurred in the bed joint was propagated through the perpend joint to the next bed joint. The crack occurred throughout the whole thickness of the wall so that the unit-mortar interface was completely separated (Fig 3).

The behaviour of single-sided retrofitted masonry wall (1SRW) shows that the net out-of-plane displacement of the specimens increased with the applied out-of-plane load from the beginning. This behaviour indicates that 1SRW specimens started to deflect while remaining undamaged. The failure of 1SRW began from the tensile face with the first crack occurred in the unit-mortar interface at 54600 N and 50900 N for 1SRW1115-1 and 1SRW1115-2 respectively. But the application of the OSB timber panel at the back of the wall specimens kept the specimens un-separated after the first crack. Therefore the loading increased continuously until other cracks appeared in the bed joints parallel to the first crack still within the inner bearing for 1SRW and 2SRW (Fig. 3b & 3c).

Meanwhile, the double-sided retrofitted wall (2SRW) shows approximately no displacement (0.25 mm) before the first crack occurred in the masonry part at an average load of 68714 N. This implies that the addition of the timber panel on the compression face (i.e. the face where the load was applied) in 2SRW improved the lateral resistance of the 2SRW specimens. So, double-sided application means that the specimen remained undamaged before the first crack occurred at an average load and displacement of 68714 N and 4.18 mm respectively.



a) PW1115-1



PW1115-2



b) 1SRW1115-1



1SRW1115-2





c) 2SRW1115-1 2SRW1115-2

Figure 3. Failure pattern of retrofitted masonry wall

5 CONCLUSION

This paper has presented a larger-scale experimental study to propose the application of oriented stranded board (OSB) type 3 to retrofit masonry wall. In particular, it focused on the effectiveness of the proposed timber-based retrofit technique against out-of-plane failure. Here, six tests have been performed on 1115 x 1115 x 215 mm single leaf, double wythe solid masonry walls. Two of the walls were tested as plain wall (PW), two as single-sided retrofitted masonry wall (1SRW), and the last two as double-sided retrofitted masonry wall (2SRW).

Out-of-plane bending test in the form of four-point loading test was performed on all the six specimens. The aim was to obtain the response of both the plain and retrofitted masonry walls against out-of-plane loading to evaluate the performance of the proposed technique. The aim was achieved by assessing the load-carrying capacities and displacement capacities of both plain and retrofitted walls.

The main conclusion from this study is that oriented strand board (OSB) type 3 can considerably increase the flexural capacity of masonry walls when subjected to out-of-plane loading. An astonishing increase of about 300% load capacity can be achieved in a double wythe masonry wall and can be up to about 500% increase in a more weaker wall such as single leaf masonry wall as previously demonstrated in the earlier study [2].

A limitation of this study is that the results and observations are based on specimens with free boundary conditions that replicate masonry walls without returning walls at the corner,

which is a rarity. However, many experimental works in literature [6,7,12] have shown that tests on panels without corners are a good indication in assessing the out-of-plane capacity of URM wall. Hence, in the future, an extension of this study would be beneficial to investigate the performance of the proposed technique on typical load-bearing walls together with corner walls.

REFERENCES

[1] Lourenço P., Mendes N., Costa A., and Campos-Cost A. *Methods and Challenges on the Out-of-Plane Assessment of Existing Masonry Buildings.* International Journal of Architectural Heritage, 11(1) pp.1.

[2] Dauda J., Iuorio O., and Lourenço P. (2019). *Experimental Study of Out-of-Plane Behavior of Timber Retrofitted Masonry Prisms*. In P.B.Dillon & F.S.Fonseca (Eds.), Proceedings of the Thirteenth North American Masonry Conference, Salt Lake City, Utah (pp. 1100–1109).

[3] Costa, A., Arêde, A., Costa, A. and Oliveira, C. (2011). *Out-of-plane Behaviour of Existing Stone Masonry Buildings: Experimental Evaluation*. Bulletin of Earthquake Engineering, 10(1), pp.93-111.

[4] Wang, C., Forth, J., Nikitas, N. and Sarhosis, V. (2017). *Retrofitting Of Masonry Walls By Using a Mortar Joint Technique: Experiments And Numerical Validation*. Engineering Structures, 117, p.58-70.

[5] Priestley, M. (1985). *Seismic Behaviour of Unreinforced Masonry Walls*. Bulletin of the New Zealand National Society for Earthquake, [online] 18(2), pp.191-205. Available at: http://www.nzsee.org.nz/db/Bulletin/Archive/18 (2)0191.pdf [Accessed 17 Jun. 2017].

[6] Prabaharan, A. (2008). *Seismic Strengthening of Masonry Buildings*. PhD. Anna University Chennai 600 025.

[7] Nazir, S. (2015). *Studies on the Failure of Unreinforced Masonry Shear Walls*. PhD. Queensland University of Technology, Australia.

[8] Dauda J. and Iuorio O. (2019). *Timber-Masonry Composite Systems for Retrofit of Unreinforced Masonry Wall*. In Proceedings of 2019 Society for Earthquake and Civil Engineering Dynamics Conference (SECED), London September 2019.

[9] Dauda J., Iuorio O. and Lourenço P. (2020). *Numerical Analysis and Experimental Characterization of Brick Masonry*. International Journal of Masonry Research and Innovation, Vol. 5 Issue: 3, pp.321–347, DOI: 10.1504/IJMRI.2020.10028163.

[10] Dauda J., Iuorio, O. and Lourenco P. (2018). *Characterization of Brick Masonry: Study towards Retrofitting URM Walls with Timber-Panels.* In: 10th International Masonry Conference (10thIMC). In proceedings of 10th International Masonry Conference (10thIMC), 09-11 Jul 2018, Milan, Italy.

[11] Anon, A. (2018). *Technical Information Sheet for Oriented Strand Board.* [online] Available at: http://www.osb-info.org/Assets/file/EN/OSB_Technical_Information [Accessed 23 Jul. 2018].

[12] ASTM E72 - 15 (2015). *Standard Test Methods of Conducting Strength Tests of Panels for Building Construction*. West Conshohocken, PA: ASTM International.

12th International Conference on Structural Analysis of Historical Constructions
SAHC 2020
P. Roca, L. Pelà and C. Molins (Eds.)

FROM THE CURE OF THE SIMPLE STRUCTURAL ANALYSIS TO THE CONTROL OF THE FINAL TECHNOLOGICAL QUALITY – THE CONSERVATION OF "SANTA MARIA DEGLI ANGELI" ORPHANAGE IN CASTELGRANDE (POTENZA, ITALY)

FRANCESCO P.R. MARINO[1*], GIANLUCA AULETTA[1], FABRIZIO BALDANTONI[1], FELICE C. PONZO[1] AND FILIBERTO LEMBO[1]

[1] Università della Basilicata - School of Engineering (SI-Unibas)
Campus Macchia Romana, 85100 Potenza, Italy
e-mail: francesco.marino@unibas.it*, gianluca.auletta@tiscali.it, fbba6@hotmail.it
felice.ponzo@unibas.it, filiberto.lembo@unibas.it (*corresponding author)

Keywords: Conservation, Durability of the anti-seismic retrofits, Energy Upgrade, *Quercus cerris* glued laminated timber, anti-seismic timber floors

Abstract. *The conservation work carried out on the "Santa Maria degli Angeli" Orphanage in Castelgrande (Potenza, Italy) following the earthquakes of 1980 and 1981 is a good example of the need to evolve and refine the concept of seismic consolidation and upgrade of monumental heritage; this, considering not only the needs of the current structural calculation, but also those related to the design of durability and overall technological quality. Built from 1878 around the original nucleus of a chapel, the seminary, then an orphanage, kindergarten, nursery school, sewing workshop and school, and summer mountain colony, constitute a precise landmark in the landscape of the ancient town of Castelgrande. Severely damaged by the earthquakes, it was declared unfit for use and evicted, and is still abandoned today. Immediately afterwards, radical refurbishment works were carried out on it, with the creation of sub-foundations, injections and tackles with reinforced concrete slabs for the load-bearing walls, replacement of the floors in steel beams and bricks with reinforced concrete floors, replacement of the wooden roofs with others of the same configuration, but in steel beams and clay tables, with a reinforced concrete slab above. The workings were not completed due to lack of funds and those performed so far show today serious pathologies (in particular the corrosion of the reinforcement of the joist of the floors and of the steel beams) as result of the lack of attention to fundamentals of materials science and of durability. Based on the current legislation and calculation methods, the research verified the seismic vulnerability of the building and proposed the necessary corrective actions: in particular, the replacement of the roofs with others, lighter and more durable, made of laminated, conditioned local Quercus cerris wood. A new destination has been proposed, linked to the presence of the Astronomical Observatory, and its upgrade to nZEB has been designed, in respect of its monumental features*.

1 METHODOLOGICAL FRAMEWORK AND RESEARCH OBJECTIVES

The role of structural consolidation in the context of conservative restoration of heritage monuments, through discussions that spanned a period of two hundred years [1], has been enshrined in numerous *Conservation Charters*[1], of national and international importance. Nonetheless, the debate around how to carry out these consolidation interventions is still lively, at least in Italy. On the one hand, there is he who defends the need to safeguard, above all things, the meaning of the work [2, 3]. And, therefore, he urges the use of the same construction techniques used in the construction of historic buildings, refined over millennia of history. And he deepens, also through the Manuals of the time, the ways in which every single component was originally created by pushing himself, for example, to rediscover the use of hot beeswax to waterproof Venetian plaster [4]. On the other, the mainstream philosophy, according to which, after praising Camillo Boito and his "religious scruple" to be adopted towards monuments, every opportunity is good to fill castles, towers and churches with injected armed perforations, micro-piles and Fiber Reinforced Polymers [5].

Thus, while the *Conservation Charters* prescribe the conservation of the "sacrifice layers" (plasters, stuccos) and the coloring of the heritage buildings, then in reality in many Italian regions (but also in other Countries) it has become normal practice that of removing the plaster on churches, monasteries and castles to show facing stones that have never been exposed. And doing so with the approval of the Heritage Protection Bodies, and thus accelerating the degradation and / or ruin of buildings [6, 7]. Likewise, many innovative structural solutions should only be allowed on historic buildings if they are scientifically proven and experienced (according to the provisions of art.10 of the *Venice Charter* 1964: "*Where traditional techniques prove inadequate, the consolidation of a monument can be achieved by the use of any modern technique for conservation and construction, the efficacy of which has been shown by scientific data and proved by experience*"). Instead, they are nonchalantly tested, and prove (after a few years) incompatible with the elements they should consolidate, not bearing the test of that time which the elements to be strengthened resisted. Exemplary is the risk of formation of Ettringite, hydrated sulpho-aluminate, expansive salt, due to the injection of cement grouts inside walls, bonded with lime mortar. A phenomenon known since the 80s, but ignored by those who continued, even after (and in part continues) to inject churches, towers and castles with these products and to publish their reports, as if it were something to boast about [5]. Similarly, for the consolidation of structural elements in wood or stone with epoxy resins, whose fire resistance is almost non-existent [5].

The aim of the research was therefore to document, through a concrete case study, the effectiveness and durability of the structural recipes currently used after the 1980 and 1981 earthquakes in Campania and Basilicata for the consolidation and anti-seismic adaptation of heritage buildings, and propose the necessary modifications and implementations, as part of a general project of reuse of the heritage buildings, economically viable. The methodologies adopted are those offered by the Building Science and the Building Construction Technique,

[1] *Ministerial Decree of 21 July 1882* and related *Fiorelli Circular*; *Athens Charter* 1930*; Venice Charter* 1964*; Italian Restoration Charter 1972; Amsterdam Charter* 1975*; Charter of Conservation and Restoration of objects of art and culture* 1987*,* proposed but never made mandatory*; Washington papers* 1987*; Krakow* 2000 and *Faro* 2005. And, of course, the most recent Italian standard on the matter, Legislative Decree no. 42/2004, *Code of cultural heritage and landscape.*

the Materials Science [8] and the works of the CIB Commission W86 *Building Pathology* [9, 10] and of the joint Commission CIB W80 / RILEM 175-SLM *Methods for service life prediction of building materials and components* [11]. Commissions in which some of the Authors have participated and whose indications are already been used for a general publication on the topic [12] and for many other specific contributions on other case studies.

2 THE "SANTA MARIA DEGLI ANGELI" ORPHANAGE IN CASTELGRANDE (POTENZA, ITALY)

The building object of the research is one of the most relevant monuments and a precise landmark (Fig.1) of an ancient city, Castelgrande (40 ° 46'00 "N, 15 ° 25'00" E), on the border between Basilicata and Campania, and which owes its name to a medieval castle, unfortunately not survived earthquakes.

The Municipality now has about 900 inhabitants (decreasing) and is perched at 950 m a.s.l. on the crest of a hill. The building was built, starting from 1878, at the expense of individuals (the Cianci family and others) on private land, which in previous centuries (1661) housed a cemetery and a small chapel, further downstream than the current Church. The first nucleus of the complex was the easternmost part of the Church, made of brick masonry, consisting of a square-plan room (with a roof of double-pitched bent tiles supported by wooden beams, set on the walls above the transverse arches of a lowered dome) and a small entrance narthex. The building of the Rectory and then of the main building followed immediately afterwards: in 1890 it was under construction as for the ground floor (in stone masonry, vaulted) and the construction of the upper floors (in stone masonry with wooden or steel suspended floors) was authorized, to be used for religious and welcoming purposes. The reconstruction of the roof destroyed in the Second World War was an opportunity to equip the Church with a second span, identical to the first, thus making the nave longer and completing its decoration in continuity with the existing one. Further, a clear expression of the respect, in those years, of the concept of *concinnitas*, as for the reconstruction of the Abbey of Montecassino, of the bridges over the Adige in Verona or of S. Trinita in Florence.

In the years between 1970 and 1980, a new building was built in the south-east end, perpendicular to the main one, raising an existing basement with two floors above ground (Fig.2). It was built with a reinforced concrete frame and placed, without seismic joints, adjacent to the main building. In this period, a house located to the west was annexed to the complex and was then raised by one floor.





Figures 1 and 2: South panorama of Castelgrande and east view of the building object of the research

3 EARTHQUAKES OF 1980-81: DAMAGES AND SUBSEQUENT CONSOLIDATION INTERVENTIONS

The earthquake of 11/23/1980 (90 seconds, 6.9 degrees on the Richter scale) and those of 1981, of less intensity, caused serious damage to the building and to the Church: the collapse of the oldest dome, the pediment and the cornice on the facade (for the hammering of the roof ridge beam); cracks on the main facade and the side walls (for disconnection of the corners and thrust of the transverse arches), with the threat of collapse due to overturning towards the outside; widespread subsidence of foundations. The damage was amplified by a series of contributing factors: the lack of regularity in the plan and in the section of the building; the eccentric position of the stairwell; the absence of bracing walls at the large rooms for dormitories and common activities; the presence of the southeast building, of a different and more deformable structure and not separated by seismic joints; the poor quality of the walls; the lack of retaining elements between floors and walls; the deformability of the floors themselves, in wood and steel; the absence of a roof slab (replaced by a simple false ceiling) and top curbs; the presence of a pushing wooden cover; the absence of effective lintels at the openings and the disordered presence of openings cut into the walls to house wardrobes, fireplaces and more.

An overall anti-seismic consolidation and recovery intervention was necessary. The design was approved by the Heritage Protection Body with the obligation of rigorous maintenance of the existing typological and structural organization, and the elimination of superfetations (the part built in the 70s which, however, was neither demolished nor detached from the main building through a seismic joint). The project therefore envisaged (Fig. 3) the construction of sub-foundations to enlarge and stiffen the seabed of most of the load-bearing walls of the building, through micro-piles and reinforced concrete curbs measuring approximately 0.40 x 0.60 h, connected to each other, under the walls, every 1.5 - 2.00 m. A huge reinforced concrete wall was also built, up to 10 meters high and more than 80 m long, to increase the external space available to the lower basement, which has become an element of strong alteration and degradation of the surrounding urban landscape. The load-bearing walls were consolidated by closing the openings in them, with solid brick walls, with injections of cement grout and with the application of "*10 cm thick concrete slabs reinforced with welded mesh Ø 8 20 x 20 cm, connected to the walls by "dovetail" couplings or simply with steel rods Ø 12*" (from the Project Report [14]). For the vaults of the ground floor, "*by reinforced stitching of the same and subsequent casting on the extrados of a concrete hood with electro-welded mesh Ø 8 20 x 20 cm, effectively anchored, with metal bars, to the perimeter walls and, on the side upstream, to the rock by means of small diameter traction poles*" [14].

For the floors, they were all "*demolished and redone with "Bausta type" joists at a distance of 50 cm with interposed light brick pots and overlying r.c. slab, not less than 4 cm thick* [14] (Fig. 4). It was foreseen that the floors of the building buried on the mountain side were tied to the rock with traction poles placed at the height of the horizontal floors, so as to block them. And that the floors were connected to the walls with curbs of a height not less than that of the floor itself, made in traces or, wherever possible, for the entire width of the walls. As for the roofs, both of the Church and of the rest of the building, the wooden ones were demolished and replaced with pitched floors made of IPE 140 steel beams every meter, clay tables and upper r.c. slab (Fig. 5).

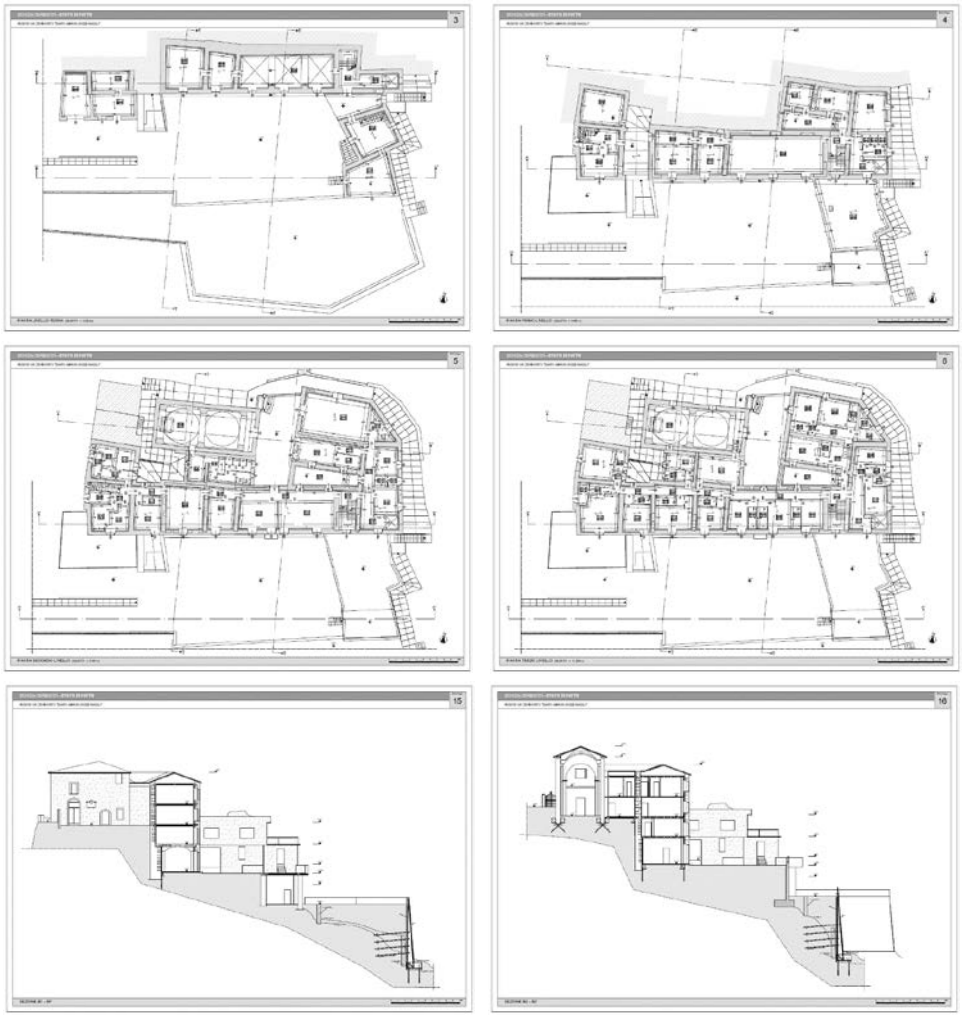
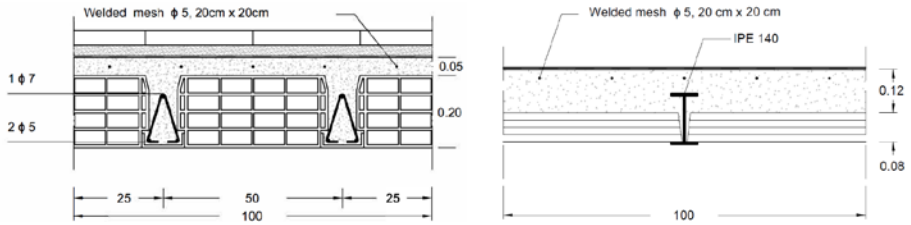


Figure 3: Plans and sections of the consolidation intervention done



Figures 4 and 5: Details of the "Bausta type" floor (left) and of the new pitched roof that replaced the original wooden roof (right), realised in the consolidation intervention

A chain was placed on the extrados of the great central arch of the Church to harness its thrust; the corners were stitched through steel bars in concrete injected perforations. On the top of the main building, the false ceiling was replaced by a reinforced concrete floor, tied to the perimeter curb. All the lintels of the openings were reinforced by applying IPE steel beams "tear" or, when possible, by demolishing the existing arches and replacing them with reinforced concrete castings, connected to the curbs of the floors. The stairs were redone in reinforced

concrete, redesigning them to decrease the height of the steps.

The works were carried out on several occasions and only partially, limited to most of the structural works, and the construction works aimed at the realization of the distribution scheme of an important religious, cultural and social assistance center, according to the building program for: a small seminar; a female and male orphanage with annexed laboratories; a kindergarten and an elementary school; rooms for the summer reception, such as "mountain colony", of n. 60 children. In the end, the public funding provided for by law no. 219/1981 for the reconstruction and development of the territories affected by the seismic events of November 1980 and February 1981 ended and the works were suspended, without the plants and finishing works having been carried out. The building has thus remained completely abandoned and open to the weather since the early 90s. Today the building, owned by the Municipality since 2000, is listed in the municipal list of real estate properties to be disposed of and valorized through a specific intervention plan for it.

4 CURRENT STATE OF THE BUILDING COMPLEX AND OBSERVATIONS ON THE EFFECTIVENESS AND DURABILITY OF THE INTERVENTIONS

Any current recovery hypothesis of the building must start, with all evidence, from the effectiveness of the interventions carried out for the purposes of anti-seismic safety, according to current standards. Preliminarily, it must be observed how at the time the Italian legislation [14] provided for the interventions already carried out, and also provides today, that for the monumental buildings it is not necessary to achieve, in the consolidation interventions, a real "adjustment", i.e. the achievement of the safety levels foreseen by the current standard; but it is sufficient to achieve an "improvement", increasing structural safety, even without necessarily reaching the levels required by the Italian legislation. It must be underlined that, in this regard, the Italian legislation does not set precise values, but they are agreed each time by the designer and by the client according to the performances they intend to achieve.

4.1 Assessment of seismic vulnerability

The study of the structure's seismic vulnerability was carried out by resorting to the use of nonlinear static analysis (Pushover). This choice of analysis was dictated by the fact that it lends itself better to describing the real behavior of masonry structures, unlike linear analyzes. In addition to this type of analysis, which concerns the overall behavior of the structure, local analyzes were also carried out on possible collapse kinematics. The CDmaWin software of the STS Company was chosen and used, a structural CAD aimed at masonry structures and whose calculation module uses a finite element solver [15]. The checks were carried out following the technical standards for construction NTC 2018 and considering a limited "level of knowledge", of the LC1 type, achieved, with the analyzes made on the structure of the building. From the reliefs made, they consist of two types of walls, one of disordered stone type and the other in solid bricks and lime mortar.

The demolition of the south-east building was hypothesized, because it is built in a mixed structure, in adherence to the main building, built in masonry. As foreseen in the 1986 authorization from the Heritage Protection Body, his conservation is not justifiable both for being an element of neglect of the formal apparatus of the building, and for its bad conditions of conservation, and the need to demolish it partially in every case to make seismic joints. The

remaining part of the structural complex was divided into three parts (the Church, the main body and the basement body downstream) and modeled separately. Before performing the nonlinear static analyzes, the dynamics of these three structural bodies were studied; relative modal forms and their own periods were identified (see Fig. 6: above, the three of the Church; in the center, the three of the main building; below, the three of the basements), and the limit equilibrium analysis for local mechanisms in all the most delicate points.

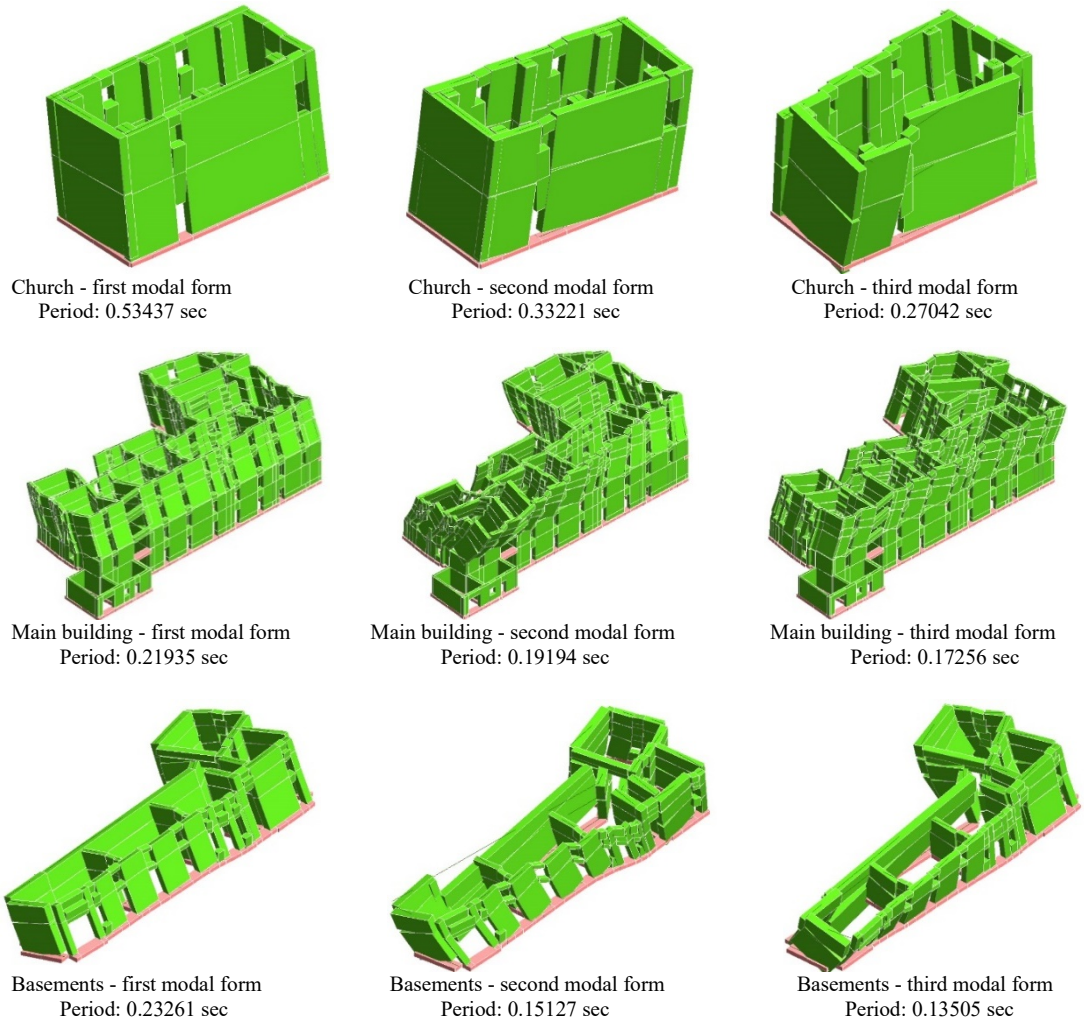


Figure 6: Modal form and periods of Church, main building and basements

After studying the dynamics and calibrating the structural models, we moved on to nonlinear analyzes (Pushover). The structural interventions already present on the building and built after the 1980 Irpinia and Basilicata earthquake were also considered in the modeling. From the study of the capacity curves, the seismic vulnerability indices relating to the three structural bodies were determined. The seismic vulnerability indices express the relationship between the acceleration of capacity of the structure and the acceleration of demand relating to the site in question. The site falls in an area with high seismic risk, the subsoil falls into the A type of the NTC 2018 (rock masses with Vs > 800 m/s^2) and the topography in the T3 type (slope with an

inclination between 15 and 30 degrees). The PGA acceleration corresponding to the SLV (life safeguard limit) is equal to 0.31g, considering a nominal life of 50 years and a class of use III. The seismic vulnerability indexes are respectively 0.51 for the church, 0.55 for the main body and 0.52 for the basement: all slightly greater than 0.5, a value which in any case can be considered acceptable for the type of destination of the structure. Therefore, the interventions carried out have raised the safety level of the entire building complex. Finally, as regards the analysis of the local mechanisms of collapse out of the plane, conducted using the limit analysis method, there were no significant critical issues, as the structures have both covering curbs and metal anchoring bars in the hammer's walls and chains in the arches of the Church.

4.2 Interventions for improving seismic behavior and building durability

Through the analysis, it became clear that the intervention carried out well could have been softer, more rational, and even cheaper, if he had renounced to place the two heavy floors on the top of the main building, the one above the third level and the other the sloping roof slab: they increase significantly, and in the least suitable position, the masses that undergo seismic acceleration. In relation to the conditions of severe exposure to atmospheric agents in which these elements have been found in these thirty years (with the penetration of rainwater through the badly placed bituminous membrane) (Fig. 7) both are severely corroded.



Figure 7: Accelerated degradation of structures due to the design errors illustrated in the text

On closer inspection, there are blatant design errors: the floor in Fig. 4 shows an insufficient concrete cover to ensure its durability, even if it divides internal environments [9]; and that of Fig. 5, in the presence of IPE profiles without any protection, is destined to corrode quickly by differential aeration [9]. The same mistake was repeated for the roofing of the Church, where the heavy roof was built, when light wooden trusses could have been chosen. It is therefore appropriate to remove these heavy floors, leaving only the perimeter curbs in place, which would otherwise be problematic to remove without destroying the upper cornices of the buildings, subject to a specific protection rule. Light reticular wooden trusses can be placed in their place. In this regard, the Authors have devised and developed [16][17][18] a particular thermo-hygrometric conditioning method for a species of hardwood widespread in Basilicata, the *Quercus cerris* (*Turkish Oak*), which allows the production of laminated wood beams with exceptional static performances [17] (Fig. 8). In this regard, even if the latest Standard UNI EN 14080:2013 only reports strength classes from GL 20h to GL 32h, remark that the reference to the resistance class GL 36h "*refers to laminated wood obtained from specific hardwood species based on some provisions of the current European standard*" and following the results of the tests carried out on the *Quercus Cerris* laminated wood specimens typed as a number and size of the lamellas and glue used [16].

Class of resistance			*GL 24h*	*GL 28h*	*GL 32h*	*GL 36h*	*Quercus Cerris*
Flection's characteristic resistance	$f_{m,g,k}$	N/mm^2	24	28	32	36	**102.2**
Parallel traction's characteristic resistance	$f_{t,0,g,k}$	N/mm^2	16.5	19.5	22.5	26	**94.17**
Perpendicular traction's characteristic resistance	$f_{t,90,g,k}$	N/mm^2	0.40	0.45	0.50	0.60	**2.09**
Parallel compression's characteristic resistance	$f_{c,0,g,k}$	N/mm^2	24	26.5	29	31	**89.53**
Perpendicular compression's characteristic resistance	$f_{c,90,g,k}$	N/mm^2	2.7	3.0	3.3	3.6	**9.94**
Cutting's characteristic resistance	$f_{v,g,k}$	N/mm^2	2.7	3.2	3.8	4.3	**9.64**
Mean parallel elastic modulus	$E_{0,g,mean}$	N/mm^2	11600	12600	13700	14700	**23413**
Parallel elastic modulus 5th percentile	$E_{0,g,05}$	N/mm^2	9400	10200	11100	11900	**18953**
Mean perpendicular elastic modulus	$E_{90,g,mean}$	N/mm^2	390	420	460	490	**780**
Modulus of sliding	$G_{g,mean}$	N/mm^2	720	780	850	910	**1460**
Mean density	$\rho_{g,k}$	kg/m^3	380	410	430	450	**815.77**

Figure 8: Performances of the elements developed by the Authors [16] [17], in laminated wood of *Quercus cerris* thermo-hygrometrically conditioned

The relative pitched floor is provided in the same wood, insulated and ventilated and covered with double-roof tiles as well as the original one (see below, Fig. 10). Other interventions are necessary to drain the surface waters at the boundary and under the buildings and limit the phenomena of capillary rise, favoring the evaporation of the water contained in the ground through cavities and floors permeable to steam (see below, Fig. 11).

5 THE REHABILITATION AND REFURBISHMENT HYPOTHESIS

In "Toppo di Castelgrande", at 1250 m asl, in a site particularly favorable for observation due to the absence of light pollution, one of the most important national astronomical observatories has been built since 2007, equipped with a 156 cm diameter mirror telescope and many other related equipment, managed by the National Institute of Astrophysics (INAF). An observatory for amateurs is also operating in a nearby location, equipped with a smaller telescope (Ø 40 cm), which can be used by all astronomy enthusiasts, managed by the Pro Loco; and work is underway for the construction of a Theme Park, entitled "Journey to the Cosmos", which will host a planetarium that will allow a playful-scientific approach to astronomical phenomena. The area of the Municipality of Castelgrande is of great naturalistic interest, for the richness of its chestnut and broad-leaved forests in general, for birdlife and for the intact landscape. We have therefore studied the methods by which to develop religious and welfare hospitality (the reason why the building complex was built), towards the hospitality of the international scientific community and naturalist tourists.

And this with the creation of an "Astronomical Study Center", divided into offices, study rooms, meeting and conference rooms and a library, in addition to the dining area and the hotel. On the first basement floor there would be the main parking lot, deposits and rooms for thermal and electric power plants and systems. It would be connected by a ramp on the ground level (Fig. 9a, top left), which would house the parking for the handicapped, pantry and cellar, kitchen, restaurant in the room covered with cross vaults, the staircase and the elevator for the access to the upper floors. An external walkway, which passes under an arch, connects this level with the higher ones, up to the square around the former church. At the first level (Fig. 9b, top right) would be located: the hotel reception, the internet point, offices and meeting room, toilets, stairs and lift. At the second level (Fig. 9c, bottom left) they would find n. 7 hotel rooms, for n. 13 beds; the library in the former church, with related services; the conference room and its offices and services; stairs and lift. At the third level they would find n. 9 hotel rooms and

one suite, for n. 20 beds and two storage rooms (Fig. 9d, bottom right).

5.1 The thermal upgrade in nZEB

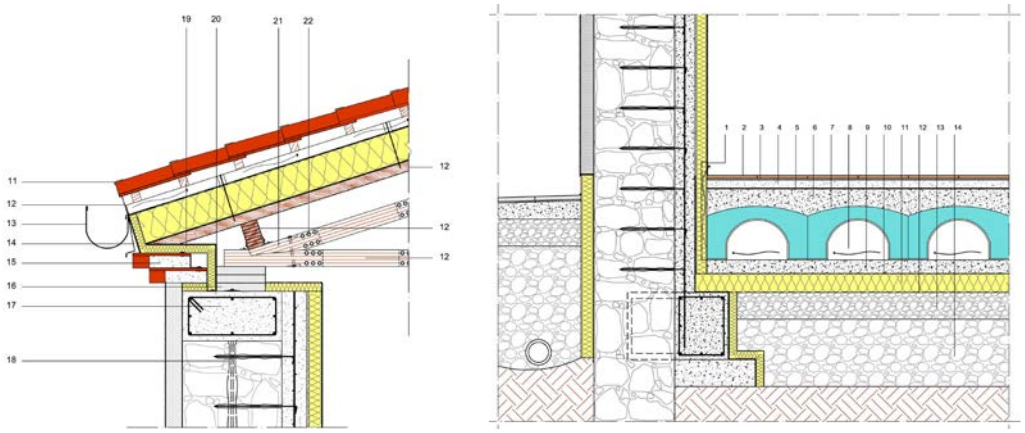
As a result of the Directive 2010/31/EU of the European Parliament and of the Council on the energy performance of buildings, after 31 December 2018 buildings occupied and owned by public authorities, on which 'major renovation' is done, must be 'nearly Zero Energy Buildings' (nZEB). That "*means a building that has a very high energy performance…The nearly zero or very low amount of energy required should be covered to a very significant extent by energy from renewable sources, including energy from renewable sources produced on-site or nearby*" (Article 2, Definitions, of the Directive). The challenge that arises today, when working on cultural heritage buildings, is to reconcile the theories on conservation [1, 2, 3] and the new needs for energy efficiency refurbishment, but not only [7, 19].



Figure 9: Plans of the refunctionalization project in an "Astronomical Study Center" and annexed hotel

The most efficient way to isolate a building is undoubtedly the one from the outside [20]. It avoids the thermal shocks that are produced with the insulation from the inside, following the sudden change in temperature in the insulation thickness, in correspondence with the connection between plug walls or vaults and facade walls. The Ancients had already solved the problem by applying plaster crusts, based on aerial lime and pumice and crushed earthenware chips, one palm thick (8 cm) and beyond, with λ also of 0,5 W/mK. As has happened in many regions of southern Italy, especially in volcanic areas, such as the *Anaktoron* of Torre di Satriano (530 b.C.), a few tens of kilometers from Castelgrande [21]. The industry has developed even more performing mineral insulating plasters (λ = 0,066 W/mK and less), which can be considered the legitimate heirs of the ancient ones, and whose finishes are the lime-based mineral ones of historic buildings. This choice was combined with that of "open diffusion"

insulation from the inside, in expanded perlite (λ = 0,045 W/mK), which is aimed at minimizing energy consumption and contributing decisively to transforming the building in an nZEB. With limestone walls 60 cm thick, plated with the existing reinforced concrete counter-wall, 15 cm thick, the current transmittance is U = 1.93 W/m^{2}K. By adding 10 cm of insulating plaster on the outside and 8 cm of expanded perlite on the inside, the transmittance after the hypothesized intervention becomes U = 0.265 W/m^{2}K (Fig. 10). Cornices and stone windowsills are safeguarded, dismantled and reassembled ten centimeters further out, in order to maintain the same previous ratio with the plane of the walls, connecting them with stainless steel shelves for balconies, like Halfen type. The ground connection of the heated rooms is assumed to be drained, insulated and ventilated through the internal environment (Fig.11) in order to be dehumidified. Its transmittance, which is now U = 3.549 W/m^{2}K, would become U = 0.208 W/m^{2}K. The whole building is assumed to be equipped with Controlled Mechanical Ventilation systems divided by zones and equipped with dehumidification batteries, since the average relative humidity of the external environment only in July and August drops below 60%, and for the rest of the year is much higher, reaching an average of 80% in the winter months. These systems would also dissipate the moisture transmitted by the soil through the ventilated cavities and the wall or floor coverings. The roof, which currently has a transmittance U = 2,723 W/m^{2}K, with the new package, insulated with 20 cm of wood wool and ventilated, would assume a U = 0.176 W/m^{2}K. Photovoltaic tiles substantially indistinguishable from the traditional ones are expected to be placed on the roof slopes correctly oriented to South, for a surface equal to 327.5 m^2, with the possibility of producing 20 kWp. Passive house wooden frames have been hypothesized, with U_w = 0,82 W/m^{2}K.



Figures 10 and 11: Details of the vertical closure-cover node (left) and the ground connection (right)

At present, the building if it still had the original fixtures and heating system, would have a very bad energy classification, in Class G, the worst, with a primary energy index for heating and domestic hot water EPi + EPacs = 696.8 kWh/m^2 year. Following the planned changes, it would go into Class A4 with EPi + EPacs = 24.7 kWh/m^2 year, 28 times lower, and would be fully classified as nZEB. Thanks to the insulation from the outside, it would have a great useful thermal inertia, which would allow it to face the summer seasons without air conditioning systems.

5.2 Lighting and acoustic upgrade

A meticulous study was conducted on the quantity and quality of lighting provided by the existing windows, in relation to the intended destinations, through the study of the Average Daylight Factor (FLDm), referred to by the relevant national regulations (in particular UNI EN 12464-1), and experimental tests were carried out using a Delta OHM luxmeter mod. 4D8501. This has resulted in valuable indications regarding the need in many rooms to integrate existing windows by means of reflective blinds inside the frame and reflective ceilings, translucent over-doors for corridors, Solar tubes and Solar Spots, so as to reduce as much as possible the use of artificial lighting of the rooms. Given the large mass of the wall elements and the high acoustic efficiency of the external fixtures, in a space with little external noise, the attention from the acoustic point of view has turned to the insulation from internal noises, from trampling and from plant and machinery, and to control the reverberation times of the largest and most common rooms. Light multi-layer walls have been provided with internal rock wool insulation, with high and proven efficiency in reducing airborne noise, and heavy doors equipped with effective seals; absorbent floors and screeds on resilient layers with low dynamic rigidity to reduce impact sounds. The widespread use of sound-absorbing plasters with α-Sabine 0.8 and, where necessary (former Church, restaurant, meeting rooms), suspended ceilings with specific characteristics and acoustic performance has been envisaged.

5.3 Sewing of the injury constituted by the large wall against ground

The need to reconstruct the relationship of the building with its environment, altered by the construction of the large wall against the ground downstream, has led to the proposal to create a natural cladding creeper (Hedera helix, Hedera Hibernica, Trachelospermum jasminoides) on a cable network and a layer of non-woven fabric fixed to the wall.

5.4 Color and surface texture

As said, the characteristic color of the building (except the stone frames or the "romanelle" of the upper cornice, destined to remain unchanged) has always been white. There are at least 300 whites, and each of them may appear whiter or grayer, depending on the texture with which it is spread (smooth, with a more or less fine grain size, applied with a float or trowel, with parallel movements or crossed, orange peel or scratched, and so on almost endlessly). The proposed restoration of the original appearance of the building foresees the use of only the white color on the outside, available in two versions: perfectly smooth, and therefore lighter, for the architectural elements (pilasters, cornices), present above all on the external surface of the former church; trowel treated, with a grain size of 2-3 mm, with crossed movements, and therefore more full-bodied and slightly more gray, due to the fields between the architectural elements and the facades of the main building. Just as, moreover, it results from the historical photographic documentation.

6 CONCLUSIONS

The anti-seismic consolidation interventions generally carried out in the 80s-90s of the last century have very often privileged the aspect of pure calculation, rather than considering the technological correctness and durability of the works.

And, the works that involved "Santa Maria degli Angeli" Orphanage of Castelgrande, which are a good example of this way of operating, have not escaped this logic. Thirty years later, the

result is buildings that meet current anti-seismic standards but on which it is necessary to intervene heavily, to ensure its conservation. A vision, at the same time more complex and more precise, extended to the consideration of the relationship with the ground in the different points of the building, of the waterways, of the individual injuries and of the individual subsidence, would probably have allowed to operate in a "lighter" way. Without a single recipe for all parts of the building, but certainly saving resources to use them in the drainage and hydraulic arrangement of the area. The choice to build the downstream wall and the two roofs was undoubtedly useless and harmful, and burned resources that could have been more usefully used to complete or at least cover perfectly and close the building.

More and more, the design tasks ask designers for an overall strategic vision, within which to implement the most appropriate tactics, to be evaluated in cross-comparisons, through which to decide the best one. The search for sustainability pushes to invest in the quality of the solutions and in their durability. It is no longer admissible for a designer to decide on a concrete cover or the technique of using a steel section without asking the question of the durability inherent in the solution.

Authors' contribution. F Lembo coordinated and provided the research objectives. FPR Marino has developed the various aspects of research, the methodological and operational tools and verified the accuracy of research results. G Auletta and FC Ponzo studied the structural aspects and the assessment of seismic vulnerability. F Baldantoni made specific analyzes in his graduation thesis. The authors' contribution in manuscript revision, editing and writing the text of the paper, was the same.

REFERENCES

[1] Marconi, P. *Il restauro e l'architetto. Teoria e pratica in due secoli di dibattito*. Marsilio, Venezia (1988), ISBN 88-317-5759-8.

[2] Marconi, P. *Materia e Significato. La questione del restauro architettonico*. Gius. Laterza & Figli, Roma-Bari (1999), ISBN 88-420-5851-3.

[3] Marconi, P., *Il recupero della bellezza*. Skira, Milano (2005), ISBN 88-7624-484-0.

[4] Scappin, L. Il saper fare gli intonaci "par modo che li stiano bene", dalle fonti scritte alle sperimentazioni. In F. Doglioni et al. (Eds.): *Conoscenza e restauro degli intonaci e delle superfici murarie esterne di Venezia: campionature, esemplificazioni, indirizzi di intervento*, Il Prato, Venezia (2017), pp. 374-423, ISBN-10 8863364036.

[5] AA.VV. *Trattato sul consolidamento*. Mancosu editore, Roma (2003), ISBN 88-87017-069.

[6] Giebeler, G., Krause, H. and Fisch, L. *Refurbishment Manual. Maintenance, Conversions, Extensions*. Basel Birkhäuser Architecture, Detail Construction Manuals, Munich Edition (2009), pp. 208-209 e 210-213.

[7] Lembo, F. *Difendere e diffondere la cultura degli "strati di sacrificio" e del colore dell'edilizia storica*. In: Convegno Architetti e Restauratori dei Beni Culturali, Trento, Italy, 7-8 novembre (2019, in press).

[8] Offenstein, F. *Compatibles, incompatibles – ou comment associer les matériaux de construction*, Editions du Moniteur, Paris (1988).

[9] CIB W 086 Publication 155, 1993. *Building Pathology, A State-of-the-Art Report*. Rotterdam, The Netherlands: CIB Press, 78 p.

[10] CIB W 086 Publication 393, 2013. *A State-of-the-Art Report on Building Pathology.* De Freitas V.P. (edited by). Rotterdam, The Netherlands: CIB Press, 200 p. ISBN 978-90-6363-082-9.

[11] Lacasse, M.A. and Sjostrom, C. *Methods for service life prediction of building materials and components – recent activities of the CIB W80/RILEM 187-SLM*. In: Proceedings of the International Workshop on Management of Durability in the Building Process, Milan, Italy (2003), June 25-26, pp. 1-11.

[12] Lembo, F. and Marino, F.P.R. *Il comportamento nel tempo degli edifici. Cause di degrado e soluzioni progettuali dei sistemi edilizi "tradizionali" ed "industrializzati". Casi di studio*. EPC Libri, Rome, Italy (2002), ISBN: 88-8184-241-6, con ampia bibliografia.

[13] Martone, A. *Relazione al progetto di riparazione antisismica della Casa delle Figlie di Maria Ausiliatrice Salesiane di Don Bosco*, Castelgrande (1986), presso l'Ufficio Tecnico del Comune di Castelgrande.

[14] D. Lgs. 22 gennaio 2004, n. 42 *Codice dei beni culturali e del paesaggio*, art. 29, 4° co. e D. M. 17 gennaio 2018 *Aggiornamento delle "Norme tecniche per le costruzioni"*. In: Supplemento ordinario alla Gazzetta Ufficiale n. 42 del 20 febbraio 2018, punto 8.4.2 "Intervento di miglioramento", pag. 292.

[15] S.T.S. Software Tecnico Scientifico. *CDMa Win: Computer Design of Masonries, software per la verifica di strutture in muratura*. Siracusa, Italia (2018).

[16] F.P.R. Marino, F. Lembo, A. Videtta, C. La Notte. Quercus Cerris glued laminated timber: a novel material derived from wood. Tests on thermoigrometric conditioning, wood adhesives and flexion breakout tension. In: *Sustainable Housing Design Emphasizing Urban Housing - XXXIV IAHS World Congress*, Luciano Editore, Napoli, Italia (2006), Settembre 20-23. ISBN: 9788860260307. http://hdl.handle.net/11563/11205

[17] Lembo, F. and Marino F.P.R. Floors realized in *Quercus Cerris* laminated timber in buildings with structure in masonry, performing anti-seismic functions. In: B.P. Sinha and L. Tanaçan (Eds.): *Proceedings of 8th International Seminar on Structural Masonry*, Çizgi Basim Yayin Ltd. Sti, Istanbul, Turkey (2008), November 05-07, pp. 441-448. ISBN: 9789755613420. http://hdl.handle.net/11563/11203

[18] Lembo F, Marino FPR, Masullo R. Anti-seismic light, ductile, sustainable and reversible timber *Quercus Cerris* floors for reinforcement in conservation design. In: Branco JM, Poletti E, and Sousa HS (Eds.): *Proceedings of 5th International Conference on Structural Health Assessment of Timber Structures* - SHATiS'2019, Universidade do Minho, Escola de Engenharia, Guimarães, Portugal (2019), September 25-27, pp. 829-838. ISBN: 978-989-54496-2-0. http://hdl.handle.net/11563/139675

[19] Petzel, M. and Heilmeyer, F. *Reduce Reuse Recycle. Architecture as Resource.* German Pavillion, Venice 13th International Architecture Exibition, Hatje Cantz (2012).

[20] Lembo, F. *Isolare dall'esterno. Teoria, tecniche e manutenzione*. Volume I *Teoria*. Edizioni C.E.L.I., Faenza, Italia (1990).

[21] Lembo, F. And Marino F.P.R. Ipotesi di ricostruzione del sistema delle coperture dell'*anaktoron* di Torre di Satriano. In: M. Osanna & M. Vullo (Eds.): *Segni del potere - Oggetti di lusso dal Mediterraneo nell'Appennino lucano di età arcaica*, Osanna Edizioni s.r.l., Venosa (PZ), Italia (2013) pp.75-82, ISBN: 9788881674015. http://hdl.handle.net/11563/61523

12th International Conference on Structural Analysis of Historical Constructions
SAHC 2020
P. Roca, L. Pelà and C. Molins (Eds.)

HISTORICAL TIMBER STRUCTURES IN ADANA-TEPEBAĞ SETTLEMENT AND CONSOLIDATION APPROACH WITH MODERN TIMBER PREFABRICATED SYSTEMS

KERİMCAN APAK [1]

[1]Adana Alparslan Türkeş Science and Technology University
Balcalı Mahallesi, Çatalan Caddesi, No:201/1 Sarıçam, 01250
Adana, Turkey
e-mail: kerimcanapak@atu.edu.tr, https://web.atu.edu.tr/kerimcanapak

Keywords: Timber Frame Structure, Brick Masonry, Prefabricated Systems

Abstract. *Adana-Tepebağ settlement is located in the south-east part of the Anatolia close to the Mediterranean Sea. This settlement is located in the center of the city, composed of unique architectural heritage with different plan typologies of historical structures, used of varied materials such as timber, brick, and stone. Traditional timber structural systems are widely used in this area.*

In this research, proposing a consolidation method for traditional timber structures with modern prefabricated systems in the frame of technological prefabrication criteria. Such as several joint details, lifting and storage properties, and fabrication state of the construction element and minimum waste ideal of the timber material [2].

This research is done in a historical settlement in Adana-Tepebağ. The state of the timber structures is in a high damaged condition as a result of the lack of maintenance in an extended period. Consequently, there is a need for a consolidation method for the maintenance of historical structures in that area. These analyzing criteria are applied to a historical timber structure in that settlement on a case study for showing the progress of this methodological approach.

The progress of the methodology is composed of three main steps;

1-The damage and corrosion analysis of skeleton timber structure.

2-The decision method within the frame of technological prefabrication criteria of modern timber prefabricated elements on the damaged parts of this structure.

3-Data's, which are collected from the previous two stages, are analyzed and compared.

This methodological approach expected to be a rational decision method for the consolidation of historical structures in the Tepebağ settlement. Significantly partly damaged timber structures consolidation is very critical in the frame of budget and the authenticity of the building.

1 INTRODUCTION

Tepebağ settlement is located in the center of Adana city, which is placed in the southeast part of Anatolia near the Mediterranean border. This settlement is an important historical area of traditional Turkish houses and Tepebağ tumulus, which is the first settlement of Adana city. In the historical period, Tepebağ is very dominant in Adana city's economic, social, physical, social development. The location is very significant related to its history and the civilizations which are passed through. The first known localized civilization in Adana city is Hittite's in B.C. XV. After this period, one after another, Assyrians, Egyptians, Romans, Seljuks, and Ottomans are settled in Adana [7].

The first organized construction facility of the Adana was done in the Ramazanoğlu seignory period (1352-1517). The most symbolic buildings were constructed at that time. Natural catastrophes of the floating of the Seyhan River and the nomad population were adverse effects of the development of the built environment until the economic revolution of Adana in the 19th century [5,7].

Before the 19th century, adobe construction was frequently used in Adana houses. After the second half of the 19th century, the construction quality of traditional Adana houses was developed, and the traditional architectural style of the region was defined. Durability of the structures get important; therefore, timber skeleton system with masonry walls was used instead of adobe construction [5,7].

The historic urban site of this area is losing its authentic characteristics and importance for the lack of maintenance of the houses in an extended period. The conservation projects of this settlement are prepared with traditional construction techniques that need considerable amounts of workforce, construction cost, and time. Therefore, there is a need for a consolidation method for these historical houses. Prefabricated timber systems and their application on historical timber houses proposed a rational methodology for the consolidation and renewal of those houses.

2 THE PLAN TYPOLOGY AND CONSTRUCTION TECHNIQUES OF TRADITIONAL HOUSES IN ADANA-TEPEBAĞ SETTLEMENT

Until the mid of 19th century, the traditional Adana houses are built upon one-floor mud-brick with earthen built flat roof. With the help of industrialization and commercial movement, street development and housing construction is progressed. At the end of the 19th century and beginning of the 20th century, magnificent traditional houses are built near the Seyhan river and extended all around the area. Tepebağ settlement was located in the historic commercial center of the Adana city (Figure 1). Therefore, the housing units are located around this area. This settlement is very significant and catchy with its narrow adjacent oriented traditional timber houses on curvilinear streets [4,5].

Traditional Tepebağ timber houses were built upon the historical commercial area; for this reason, the units of the houses were changed according to the functional needs. The ground floor is used for storage and cellar. The upper part of the house is used for a residential unit. Some houses are designed with a mezzanine floor which called 'Cihancuma'. The idea of planning 'Cihancuma' is getting a vista from the Seyhan river [4,5].

The houses are designed according to the number of family members. The most important aspects of designing Turkish houses are socio-cultural and socio-economical aspects, as well

as local construction materials and climate. Thus stone, timber, and mud-brick material are frequently used in those buildings. Beside of this, the temperature is another factor for organizing the functional units. Therefore, traditional Adana timber-framed houses are designed and planned in the direction of the prevailing wind. Rooms and sofas are the main functional units that had an identical design and layout of the house. The place of the rooms on the plan is determined by the location sofas [4].

The plan typology of traditional Adana houses is classified according to the placement of the sofa. The functional interpretation of the sofa is an entrance hall for the bedrooms. Gathering activities and entertainment are the main functional specifications of the sofa in the traditional Turkish living routine.

The first type of house; the sofa is located inside of the plan. In this type, the sofa is surrounded by rooms. The balconies are placed in front of the sofas, which are the common space for the family members and common areas for distribution between the functions. In general, in those types of houses, there are leisure spaces for summer on the top of the sofas. In the second type of house, the sofa is located outside of the plan and oriented to the north-south direction. The upper part of the sofas is open to the exterior without any barrier; therefore, the occupants can benefit from the sunlight and prevailing wind. The sofa expanded to the street from its adjacent wall by doors and windows, which brought a visual enrichment to the facade [6,12].

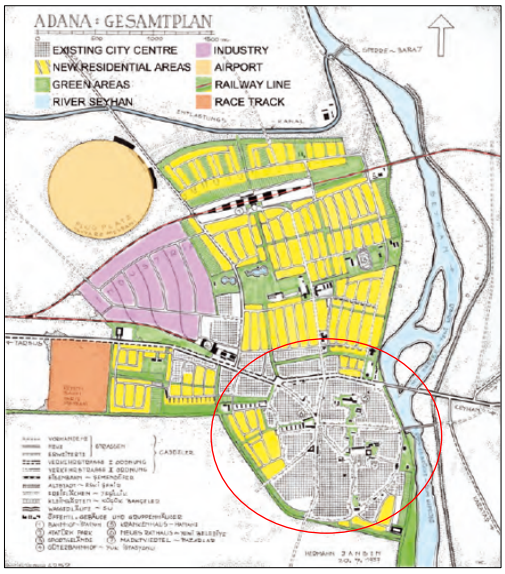


Figure 1: Adana-Tepebağ settlement, the city plan prepared and drawn by Hermann Jansen in 1940 [11]

There are two types of construction systems in traditional timber houses in Adana-Tepebağ. In the first system, the load-bearing stone walls are constructed on the ground floor with 50 cm to 60 cm thick. On the upper floor, the wall is built with a timber-framed filled with mixed brickwork. In the second system, the load-bearing walls are constructed on the ground floor with 50 to 60 cm thick with mixed brickwork masonry supported with timber beams. On the upper floor, the timber-framed walls are filled with mixed brickwork masonry. The height of the masonry walls is approximately 3.5m to 4m. The lap joints are used with timber tie-beam and timber frame elements which are used inside the load-bearing walls [1,10].

Some unique architectural elements, such as cantilevered floors, balconies, oriels, decorative elements, and eaves, are used in traditional Turkish houses in Adana. Oriels are used for visual integration of interior spaces through the street. Besides, cantilevered floors are used for creating an enlarged space in interior areas (Figure 2). In traditional timber Adana houses, the parts of the building, such as staircases, doors-windows, roofs are constructed in unique timber design and construction techniques [1,10].



Figure 2: Adana-Tepebağ case study house, inventory number of the house is 152 [1].

3 DECISION APPROACH OF PREFABRICATED TIMBER SYSTEMS IN HISTORICAL BUILDINGS

The critical argument in the preservation of architectural heritage is to conserve the historical buildings with rational and minimum consolidations. For preserving them against the effects of time, the unique characteristics of the buildings, such as structural features, materials, and construction details, are getting crucial. The necessary starting point of consolidation is to criticize and analyze those features.

The conservation projects of historical timber buildings in Turkey is strictly coherent with the authenticity of building materials and techniques. For the consolidation projects, all the characterization and the analyses are essential parameters. Without those parameters, the consolidation work is not coherent with the authenticity of the building, and it will corrupt the unity of its historical identity. Therefore, consolidation and assembly time for historical buildings with traditional construction techniques are excessively high. Besides, the construction craft needs high professional expertise. Thus, prefabricated timber systems could be a new approach for the conservation of historical timber buildings.

Prefabricated timber construction systems are classified into four types. Post and beam, balloon, structural isolated panels, and platform are the prefabricated timber systems that are used in modern construction assemblies. All those systems have positive and negative technological points that had to be considered while deciding to use them. Historical timber structures have unique construction details and different structural problems. By the direction of this methodological approach, rational timber structural system is decided according to the specific construction details and structural issues of historic timber structures.

For determining the rational prefabricated timber system by the direction of this methodological approach, the damage analysis of the historic building must be identified.

Besides, technological parameters of prefabricated timber structures are compared and examined according to the data of the historic building.

The technical principles of prefabricated timber structures are classified under the headline of four main timber prefabricated structural systems. The technological aspects and their relation with timber structural systems are listed as follows.

3.1 Production of the timber parts

In this criterion, timber parts of the structure are assembled in the construction site or a factory. This criterion affects the construction time and the quality of the details. Factory based production of timber building parts always brings high craft with quality control and minimizing assembly time in construction sites. Besides, adverse atmospheric conditions are not affected by timber parts and not occur any deformations. Also, timber waste material management is done in factory assembly. The suitability of the production criteria of the prefabricated timber structure is parallel with its factory assembly rate [2,8].

3.2 Assembly of the timber parts

The number of prefabricated timber panels which are joined in a construction site or factory and their lifting ease determined the assembly criteria. The number of features and the joint details are increased the time of the construction. Post-beam and balloon systems are mostly constructed in site. Those systems composed of small elements that need a considerable amount of time for assembly. However, structural isolated panels and platform timber systems composed of big construction units such as walls and floor slabs. Assembly work for construction parts of walls and slabs is done in a factory, therefore, joining big construction units in site needs less time compared with other timber prefabricated systems. Besides, lifting ease of prefabricated timber elements are a critical factor for construction. Crane's working area and the dimensions of the timber parts are essential for the assembly [2,8].

3.3 Transportation and storage of the timber parts

According to the construction system, prefabricated timber parts are assembled in factories or construction sites. If the timber parts are joined in a factory, the transportation limits of the highway correlatively the size of the timber parts have to be considered. Besides, if the timber parts are joined in a construction site, the closed storage area and size of timber elements get their importance.

The storage area of the timber parts inside of the construction site is brought an additional cost for the construction. Hence, the prefabricated timber systems which need storage place inside of the construction site are not or less suitable to this parameter [2,8].

Technological parameters of the prefabricated systems and their suitability are compared and matched on the table 1. There are three main considerations for prefabricated timber elements related to technical parameters. If the parameter fills the requirement, it is labeled as 'respected'; if not, it is marked as 'not respected'. If the parameter fills the requirement by preconditions, then it is labeled as 'depended'.

Table 1: Prefabricated timber systems and their suitability with technological parameters [2,8].

	Prefabricated timber systems			
Parameters	Post-beam	Balloon frame	Structural isolated panels	Platform
Production	Not respected	Not respected	Respected	Respected
Assembly	Not respected	Not respected	Respected	Respected
Lifting ease	Respected	Depended	Depended	Depended
Transportation	Respected	Depended	Depended	Depended
Storage	Depended	Depended	Respected	Respected

4 CASE STUDY CONSTRUCTION SYSTEM AND DAMAGE ANALYSIS

For examining and receiving appropriate data for the methodological approach, general structural condition of the case study building, damage status for each floor was analyzed.

4.1 Structural System

The case study of this research is chosen from the historical timber house in Tepebağ-Adana. The inventory number of this building is 152 in the archives of the Adana endowment office. This building is composed of ground, mezzanine and first floor with load-bearing walls. The load-bearing wall is composed of 20cm x10cm x5cm mixed brickwork with 10cm x10cm timber tie beams. Each floor is constructed with timber beams covered with timber finishing plate materials (Figure 3).

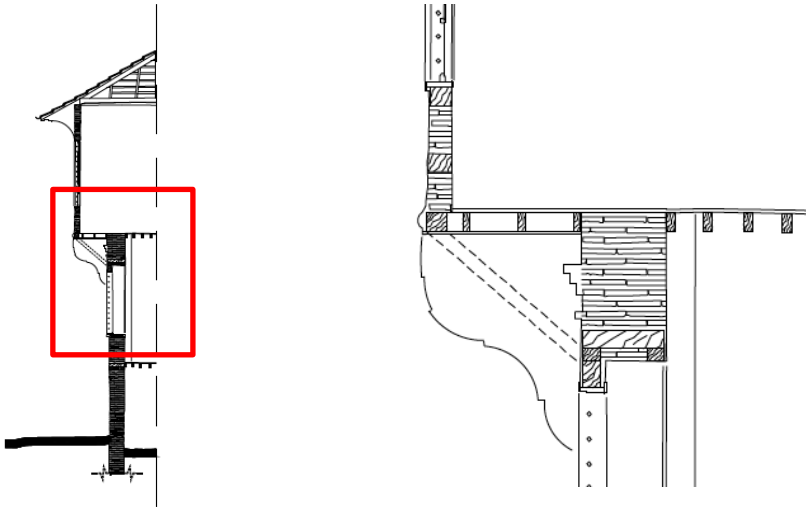


Figure 3: Adana-Tepebağ case study house: On the right, system detail, and on the left timber floor, load-bearing wall and oriel joint detail are shown [1,13].

4.2 Damage Analysis

When we examine the structure, there is no clue for the not decadence of the structure. However, from the past to the recent time, the house is faced so many catastrophic events such as Adana-Ceyhan earth-quake in 1998. Therefore, dynamic forces are directly affecting the

structure, and some of the load-bearing walls got damaged. Timber elements inside of the structure, such as staircases, windows, and doors are decay in time. The structure of the roof got damaged, and the form of the roof is deteriorated as a result of the dynamic forces.

On the ground floor, two rooms are designed on the sides of the plan. The thickness of the masonry walls of the rooms is 40cm thick, constructed with mixed brickwork with timber tie-beam support. There is no structural damage to the load-bearing walls. The ceiling is constructed with a timber structure. Primary timber beams are placed parallel to each other with 3,40cm. distance. Secondary beams that are placed above and perpendicular to the primary beams are constructed 25cm parallel to each other. In initial inspection, there is not decadence on the primary and secondary timber beams. However, there is a considerable humidity exposure inside the structure. Therefore, it could be some decay on the corners of the timber beams which are inside of the masonry walls. Also, on the surface of the floor timber finishing material, there had some decay related to humidity. In areas A, B, C, and D, which is marked with red lines, there is decay on the surface of the masonry walls related to humidity. Also, in area D, which is marked with blue circular lines, four poles connection detail with ground floor had some decay related to humidity (Figure 4-8). Inside the courtyard, there is a reinforced concrete structure that is built afterward of the historical building [1].

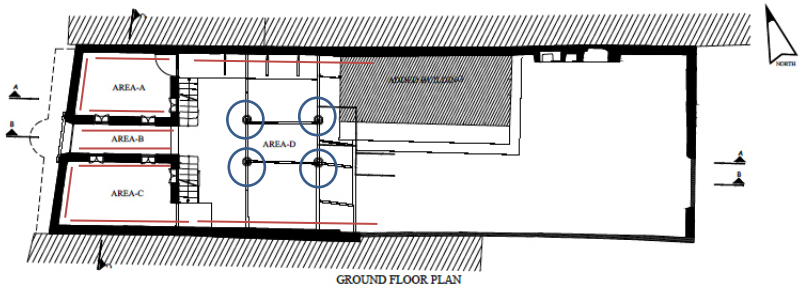


Figure 4: Adana-Tepebağ case study house ground floor plan [1].

On the mezzanine floor, there are cracks and decay on the plasters of the walls, which is marked with red lines. Besides, above the windows and the doors, some deep cracks are related to the load-bearing structure.

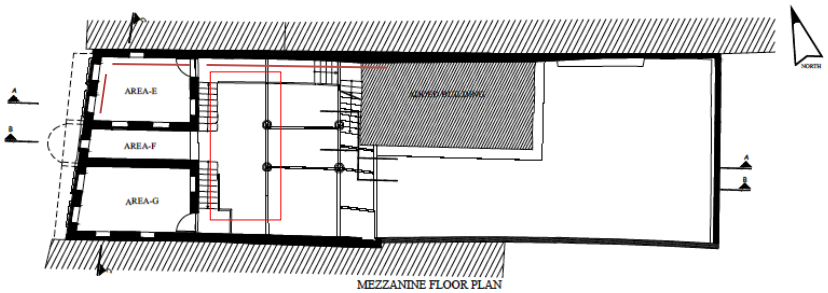


Figure 5: Adana-Tepebağ case study house mezzanine floor plan [1].

The cracks on mezzanine floor are related to the forces which are come in sight with horizontal loads such as seismic activity. Most of the staircases, which are connected ground

and mezzanine floor, had a considerable decay. Therefore, it needs to be renewed. The timber floor of the courtyard had decay related to humidity, which is marked with a red rectangle [1].

The first-floor slab is supported with timber posts that are located inside of the courtyard. These posts are started from the ground floor and continue to the beneath of first-floor slab timber primarily beams. On the first floor, two brick masonry walls are rested on a timber slab, and there is a critical bending that happened on those beams, which are shown in a purple rectangle (Figure 6-8). The walls which are marked with the light blue line have deep cracks and partially collapsed (Figure 6). There are cracks and decay on the plasters of the walls, which is marked with red lines (Figure 6-7) [1].

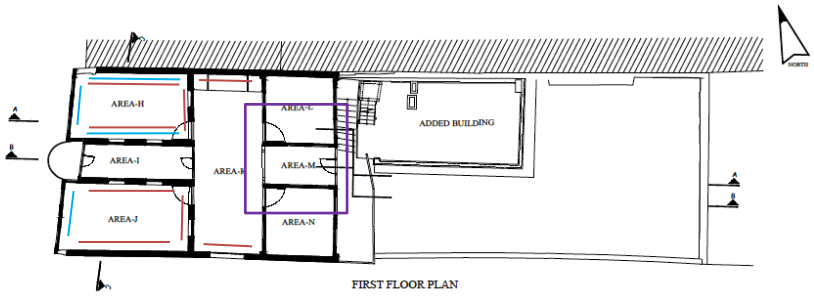


Figure 6: Adana-Tepebağ case study house first-floor plan [1].

On the ground floor, three spaces that are surrounded by masonry walls had some cracks. Those cracks are on the plaster, and they are not getting inside of the load-bearing structural system. However, the masonry walls, which are located on the first floor, especially the north wall, had deep cracks. Those cracks are affected the stability and bearing capacity of the first-floor load-bearing system (Figure 6). The north wall and the side walls are separated from each other, and it caused instability of the structure. These cracks and separations are occurred by seismic activity. Nevertheless, against the seismic forces, diagonal timber beams are used on the north loadbearing brick masonry wall (Figure 2) [1].

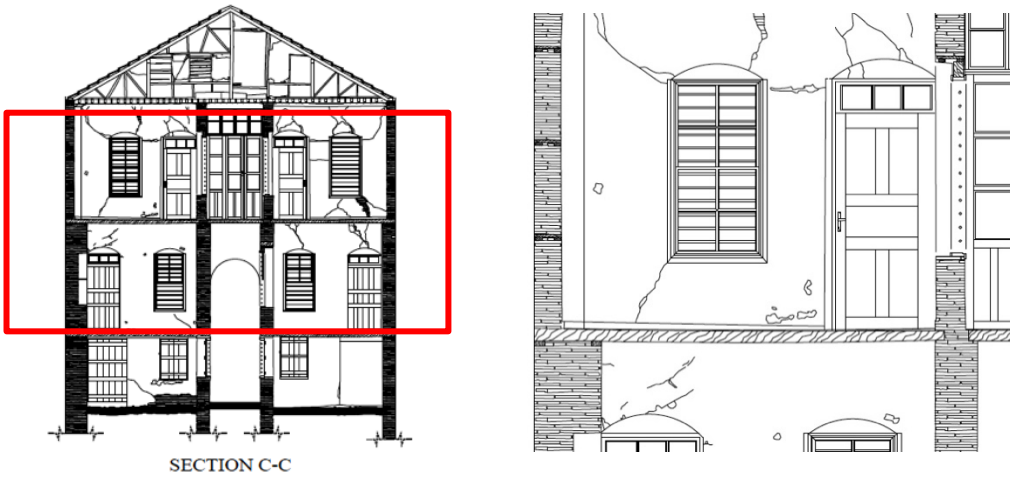


Figure 7: Adana-Tepebağ case study house: On the right section C-C and the left, timber slab, and load-bearing wall joint detail are shown [1].

The structural timber elements of the roof were decayed as a result of water, humidity, and solar radiation. The water on the roof is not drained adequately and get out of the building. Therefore, the whole structure, especially timber, is under the effect of corrosion [1].

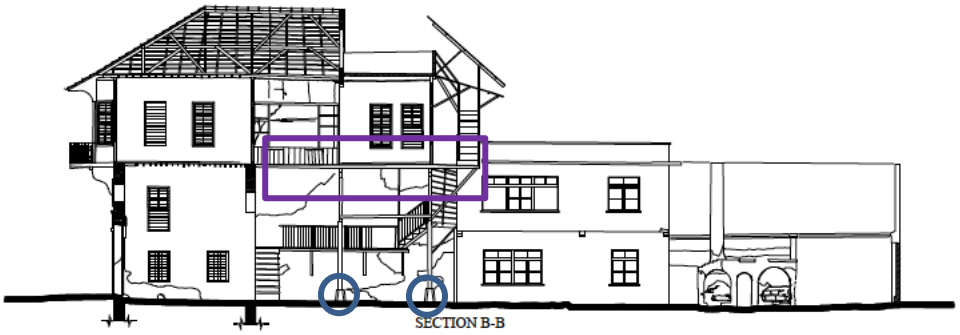


Figure 8: Adana-Tepebağ case study house: On the right section C-C (Adana endowment office) and the left timber slab and load-bearing wall joint detail are shown [1].

5 METHODOLOGICAL APPROACH OF THE CASE STUDY

Damage analysis of the three-floor load-bearing structure constructed with a timber frame filled with mixed brickwork is done in the previous chapter. The proper conservation approach is decided according to data received from damage analysis and technological parameters of the contemporary timber prefabrication with the principles of conservation of wooden built heritage by ICOMOS international wood committee in December 2017, Delhi, India.

According to the ICOMOS, the international wood committee, two main points are entirely related to this research. The first point is an intervention, and the second point is using present-day materials and technologies. Some crucial interventions and present-day materials and technologies criteria of the timber structures by the international wood committee are listed on the following sentences [9].

A-“The strengthening of the structure using traditional or compatible materials and techniques” [9].

B-“Interventions should follow the criteria of the minimal interventions capable of ensuring the survival of the construction, saving as much as possible of its authenticity and integrity, and allowing it to continue to perform its function safely” [9].

C-“Be the minimum necessary to ensure the physical and structural stability and the long-term survival of the structure or site as well as its cultural significance” [9].

D-“Be reversible, if technically possible,” [9].

E- “Repairs carried out-in situ and on original elements would require an unacceptable degree of intervention” [9].

F-“As much as possible of the existing members should be retained” [9].

G-“New members or parts of members may be discreetly marked, so that they can be identified at a later date” [9].

H-“Present-day materials and technologies should be chosen and used the greatest caution and only in cases where the durability and structural behavior of the materials and construction techniques have been satisfactorily proven over a sufficiently long period” [9].

The methodology of conservation with prefabricated timber elements is analyzed with technological criteria's and their suitability with ICCOMOS timber committee ideals. As it is mentioned, in Adana-Tepebağ settlement, traditional historical houses have specific construction details. The structural system of those houses is generally composed of a timber skeleton system with a mix of load-bearing walls. Some of the structural systems are under the effect of big moments, which caused a failure of the parts of those structures. Modern timber prefabricated systems are composed of construction units such as walls, floors, and roofs. Fabricated composite timber beams and columns are considered as prefabricated elements. The units and components can be fabricated in different dimensions and specifications, such as durability and strength. Prefabricated timber systems are essential for decreasing the cost of construction as well as for the conservation in terms of rapid assembly and reaching the high construction quality.

In this methodology, original materials and joint details of the structure are trying to keep. However, for the deteriorated and the loss parts, replacements are done with modern prefabricated units. Modern prefabricated systems are not fit for the compatibility and traceability criteria of the structure. For the reversibility criteria, modern prefabricated structures have possibilities of permeability of intervention with the original one [3].

Using original joints and material is essential for keeping the authenticity of the structure. Modern prefabricated systems are not compatible with this ideal. However, under the risk of loss of significant cultural heritage, this methodology could be a solution. The deteriorated elements could be replaced, and the continuity of the structure is maintained with the use of prefabricated units and components [3].

The proposed intervention for the damage analysis within the frame of technological criteria of prefabricated timber structures and international wood committee principles are shown on the following table 2-4.

Table 2: Proposed intervention of damage 'A'

Damage Analysis 'A'	Highly damaged first floor walls on the front elevation of the house.
Proposed intervention	On the mezzanine floor, masonry has deep cracks on critical points of the walls, such as the upper part of windows and doors. Therefore, first floor damaged walls are proposed to replace with structural insulated panel or platform wall systems for providing a lightness to the entire structure. Also, the proposed wall system provides high strength with adequate thermal isolation parameters, which provide comfort criteria.
Technological principles of prefabricated timber structures	Those systems are compatible with technological principles; however, lightness and the durability of the prefabricated walls are the essential points for decision.
ICOMOS, International Wood Committee Principles	Coherent with the principles.

Table 3: Proposed intervention of damage 'B'

Damage Analysis 'B'	Deflection of first floor primarily timber beams and decay of secondary beam's corners within the sockets of loadbearing structure.
Proposed intervention	Masonry on the first floor is occurring o pointed load up on the timber beams and caused deflection. Therefore, replacing them with structural insulated panel wall or platform wall systems is proposed. This deflection occurs a deformation on primarily timber beams. Deflected primarily timber beams replaced with timber 'I' beams that have high strength ratio and durability. Timber 'I' beams can support secondary timber beams, floor finish materials, and walls that are rested on them. Decay of secondary beams which are lost their support function are replaced with similarly specified beams.
Technological principles of prefabricated timber structures	Those systems are compatible with technical regulations. The usage of timber 'I' beam is brought and present-day material look and high strength and durability. Besides, lightness and the durability of the prefabricated walls are the crucial factors for structure.
ICOMOS, International Wood Committee Principles	Coherent with the principles.

Table 4: Proposed intervention of damage 'C'

Damage Analysis 'C'	Deep and shallow cracks and decay poles.
Proposed intervention	The shallow cracks on the walls are on the plaster, and they are not related to structural behavior. They can maintain easily. However, deep cracks are entirely associated with masonry load-bearing structures. Therefore, replacing timber tie beams are an essential intervention to prevent those cracks. Decay of timber poles are risky for providing a long-term strength for the structure. Those timber poles are very critical for the structure, which is supporting half part of the first floor. Therefore, it is necessary to replace them with impregnated timber beams.
Technological principles of prefabricated timber structures	Timber tie beams can be impregnated for atmospheric conditions. Therefore, they can process in a factory. Thus, timber tie beams and poles are compatible with technological principles.
ICOMOS, International Wood Committee Principles	Coherent with the principles.

6 CONCLUSIONS

The historic urban site of the Tepebağ settlement is losing its authentic characteristics and importance for the lack of maintenance of the traditional timber houses in a long time. The

conservation projects of this settlement are prepared with traditional construction techniques that need considerable amounts of workforce, construction cost, and time. Therefore, there is a need for a consolidation method for these historical houses. According to the methodology, the findings of damage analysis and their examination under the comparison charts, building plans and sectional layouts, judgment about the losses, and their causes are clearly defined. The technological parameters and their comparison chart give a general format and decision method for proper structural systems. All those findings provide a general idea for the conservation of historical structure. However, principles for the conservation of wooden built heritage by the ICOMOS international wood committee, gives the borderlines of conservation. With all of those analysis, parameters, and principles, the proposed materials for maintain and conserve the historical timber structure is decided.

This research is significant and unique for its approach related to contemporary timber materials, assembly techniques, and their usage for conserving traditional load-bearing timber frame houses of Adana-Tepebağ. In the future, this research topic can be expended with instrumental analysis of humidity, temperature, decay of structural elements, and their conservation and maintenance with contemporary timber materials.

REFERENCES

[1] Adana Endowment office, *Documentation related to case study inventory number:152*, (2016).

[2] Apak, K. *Ahşap strüktürel sistem seçim modeli ve geleneksel Kıyıköy konutları üzerinde değerlendirilmesi – Decision methodology of timber structural system and evaluation on Kıyıköy settlement*. PhD Thesis, Mimar Sinan Fine Arts University, (2009).

[3] Croatto, G., Turrini U. *Restoration of historical timber structures -Criteria, innovative solutions and case studies,* Seminario Intervir em construçoes existentes de madeira, (2014).

[4] Çelik, Ç. *XIX. yy'dan günümüze Adana'da konut mimarisinin gelişimi-The evaluation of Adana's dwelling architecture from XIXth century till today*, Ç.Ü. Master Thesis (1999).

[5] Durukan, İ., Karaman, F., Saban, D., Erman, O. *Adana, Inventory of urban cultural heritage (2004-2005)*. TÜBA-KED 7/ (2009).

[6] Eldem, S.H. *Türk evi-Turkish house*, TAÇ Vakfı Yayınları, (1987).

[7] Halaçoğlu, Y. *Adana tarihçesi, Adana köprü başı - History of Adana, Adana köprü başı,* Y.K.Y. Yay, (2000), s.11-12.

[8] Herzog, T., Natterer, J., Schweitzer, R., Volz, M., Winter, W. *Timber construction manual*, Birkhauser, (2004).

[9] ICOMOS International Wood Committee. *Principles for the conservation of wooden built heritage*, Adopted by ICOMOS at the 19th General Assembly in Delhi, India, (2017).

[10] Kafesçioğlu, R. *Kuzey – Batı Anadolu'da ahşap ev yapıları – Timber houses in north-west Anatolia*, İ.T.Ü., (1955).

[11] Ökesli, S.D. *Herman Jansen's planning principles and his urban legacy in Adana,* Metu JFA, (2009), pp.45-67

[12] Özmen, Ö., *Geleneksel Adana evleri, Adana köprü başı – Traditional Adana houses, Adana köprü başı,* Y.K.Y. Yay, (2000).

[13] Umar, N. *Photography inventory related to Adana-Tepebağ*, (2010).

12th International Conference on Structural Analysis of Historical Constructions
SAHC 2020
P. Roca, L. Pelà and C. Molins (Eds.)

NUMERICAL MODELLING OF MASONRY ARCHES STRENGTHENED WITH SFRM

S. CADDEMI[1], I. CALIÒ[1], F. CANNIZZARO[1], D. RAPICAVOLI[1], N. SIMONCELLO[2], P. ZAMPIERI[2], J. GONZALEZ-LIBREROS[3], C. PELLEGRINO[2],

[1] Department of Civil Engineering and Architecture, University of Catania, Via Santa Sofia 64, 95125 Catania, Italy.

[2] Department of Civil, Environmental and Architectural Engineering, University of Padua, Via Marzolo 9, 35131 Padua, Italy.

[3] Department of Civil, Environmental and Natural Resources Engineering, Lulea University of Technology, 97187 Lulea, Sweden.

paolo.zampieri@dicea.unipd.it, (Paolo Zampieri)

Keywords: Masonry arch; Fiber reinforced mortar; steel fibers, discrete macro-element model; HiStrA software, nonlinear static analysis

Abstract. *The adoption of effective strengthening techniques of historical constructions is one of the most widely debated aspects in structural engineering. Within this topic, the application of steel fiber reinforced mortar (SFRM) has been recently proposed as a low invasive and effective way to obtain a considerable structural benefit in the safety of existing masonry structure. To this purpose, in this paper the experimental results obtained on a circular masonry arches are presented. The considered specimens, subjected to a vertical increasing static load, is tested in the unstrengthened and strengthened configurations, and is part of a wider experimental campaign. After presenting and discussing the experimental results, they are compared with those relative to numerical simulations conducted by means of a discrete macro-element (DME) strategy, based on a simple mechanical scheme, able to model the nonlinear behavior of masonry structures with a limited computational effort. Such an approach is here extended to model the SFRM strengthening technique accounting for the main failure mechanisms associated to the combined presence existing masonry and the additional strengthening layer applied at the intrados of the arch. Numerical and experimental results demonstrate the efficacy of the proposed retrofitting strategy both in terms of bearing capacity and increase of ductility.*

1 INTRODUCTION

Masonry arch bridges still in use in the world roadway and railway network represent an important portion of the entire bridge stock and most of them were built more than 100 years ago. Due to their age, the restoration and the conservation of masonry bridge is an important aim of the infrastructure's owners. In many cases, a repair intervention is needed in order to bring the bridge to an adequate structural safety level required by National Standards. Different actions are responsible of the decrement of the structural safety level of the masonry arch bridges; for example: the increased traffic loads, the environmental actions, soil settlements, lack of maintenance, seismic events, etc... Many (traditional and innovative) strengthening techniques [1, 5] have been investigated by scientific community with the aim to repair/maintenance masonry bridges.

Recently, the use of reinforced mortar with short steel fibers as strengthening system applied to concrete or masonry has caught the attention of many researchers. In fact, this composite material has high value of compressive and tensile strengths with a good tensile ductility due to the steel fibers.

In this paper, the effectiveness of steel fiber reinforced mortar (SFRM) for the strengthening of masonry arches is evaluated. A masonry arch previously loaded in order to achieve a specified damage level, was strengthened with a SFRM layer at the intrados and then retested [3]. Numerical simulations have been performed in order to describe the non-linear behavior of the masonry arch in unstrengthened and strengthened condition. The HiStrA software based on a discrete macro-model, already available in the literature, has been used for the numerical analysis that show good agreement with the experimental results.

2 EXPERIMENTAL CAMPAIGN

A single masonry arch (Fig. 1) was tested (UN.ND) under a monotonic force concentrated at the arch crown then it was retested (UN.LD) in order to evaluate the residual strength of the specimen after the first loading. Subsequently, the arch was strengthened using a 30 mm layer of SFRM (Fig. 2) applied at the arch intrados and it was tested again (SFRM.LD).

The arch specimen was comprised of 29 clay bricks disposed in a single layer. The arch rise (f), span length (L), thickness (S), and width (W) were 610 mm, 1430 mm, 110 mm, and 245 mm, respectively as reported in Fig. 1. Standard clay bricks were used in this investigation with nominal dimensions equal to 245x110x60 mm.

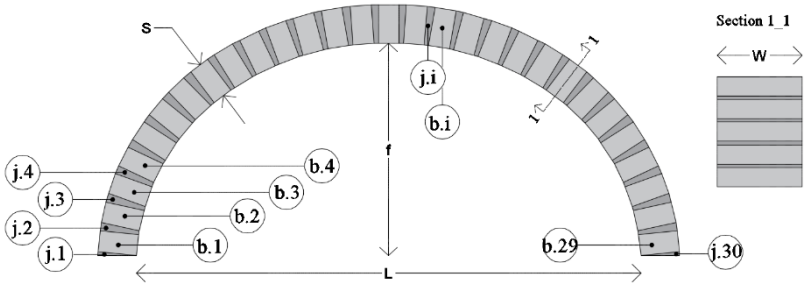


Figure 1. Arch geometry and brick-joint numbering.

A low strength cementitious mortar was used for the arch joints in order to replicate the current condition of existing arches. Standard clay bricks were used in this investigation with nominal dimensions equal to 245x110x60 mm. The SFRM is comprised of a high strength mortar fiber-reinforced with around 2% of hook end steel fibers in volume. The mechanical parameters experimentally evaluate are reported in Simoncello et al 2019 [3].



a) b) c)

Figure 2. Strengthening procedure: a) SFRM dimension, b) Formwork, c) SFRM pouring.

The load was applied through a hydraulic manual jack connected to a load cell with a maximum capacity of 20 kN. The load cell was placed on a 20 mm thickness steel plate on top of brick b.15, as shown in Fig. 2. During tests UN.ND and UN.LD, the arch was loaded past the peak load until the load dropped to 0.25 kN and then unloaded. Test SFRM.LD was ended when failure of the arch was attained. During testing, vertical and horizontal displacements of the arch were monitored by means of seven linear variable differential transducers (LVDTs) positioned as shown in Fig. 3.

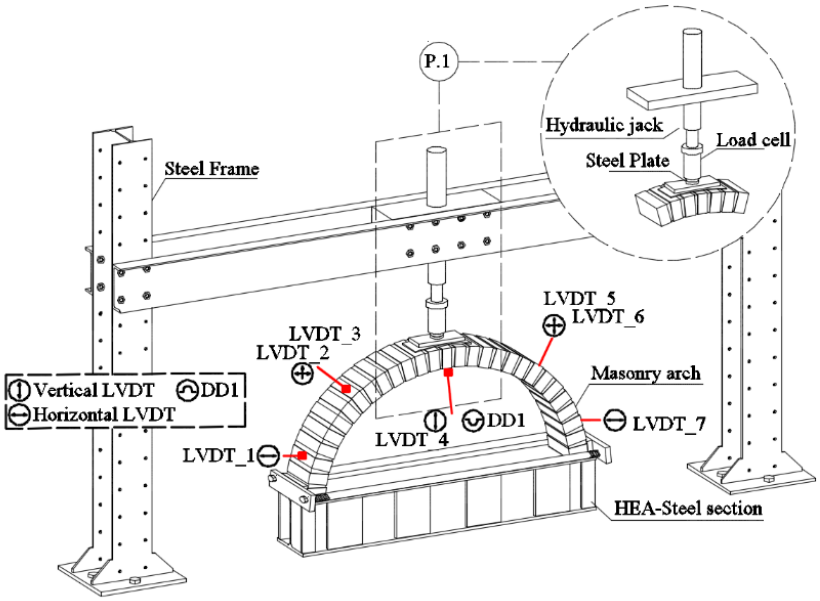


Figure 3. Test setup: applied load system and displacement monitoring.

3 DISCRETE MACRO ELEMENT-BASED NUMERICAL STRATEGY

In this work a numerical strategy based on a discrete macro-model, already available in the literature, is employed for the nonlinear numerical simulations of the considered dome. According to this approach, the masonry is modeled by an equivalent mechanical scheme constituted by a hinged quadrilateral endowed with one or two diagonal links to rule the diagonal shear cracking, and interacting with contiguous elements along its four edges by means of nonlinear discrete interfaces, which govern the flexional and the sliding behaviour. Each discrete interface is made of a single or multiple (according to the model) rows of transversal links for the flexional behaviour and single or multiple (according to the model) sliding links. The different stages of this discrete element are reported in Figure 4. This approach was originally introduced for modeling the in-plane behavior of unreinforced masonry structures [6] (Figure4a). This plane element possesses four degrees of freedom, a single row of transversal links and a single in-plane sliding link, and is able to model the main failure mechanisms of the masonry in its own plane, as long as a proper calibration procedure of the links is adopted. Two subsequent upgrades were achieved to expand the potentialities of the approach. First, the out-of-plane (spatial) behavior, typical of historical constructions, was added [7] by considering additional rows of transversal links and two additional out-of-plane sliding links (able to govern the out of plane shear behaviour and the torsion), thus enabling the out-of-plane degrees of freedom (Figure 4b). Subsequently, a further upgrade was introduced considering a shell macro-element characterized by an irregular geometry, variable thickness along the element and skew interfaces [8] in order to deal with structures with a curved geometry, such as vaults and domes, Figure 4c. The calibration procedures, concerning the mechanical properties of the links, were properly extended in order to account for the more complicated geometry of the element, but keeping the same general philosophy.
Numerical and experimental validations of the proposed approach, with reference to full scale historical structures can be found in [9, 10]; a specific study devoted to the investigation of arched structures is reported in [11].

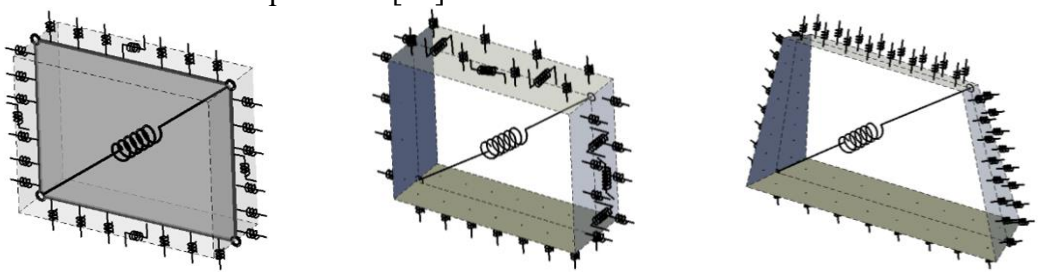


Figure 4. Layout of the macro-element adopted for masonry at its three stages: (a) plane element, (b) spatial regular element and (c) three-dimensional element for curved structures.

In all the above referenced paper applications in the nonlinear static field where proposed. More recently, the proposed approach has been upgraded to account for the presence of fiber-reinforced reinforcements [12], Figure 5. However, none of the studies focused on strengthened structures was devoted to SFRM; in this paper, the proposed methodology is applied for the first time with reference to curved structures reinforced with a SFRM technique.

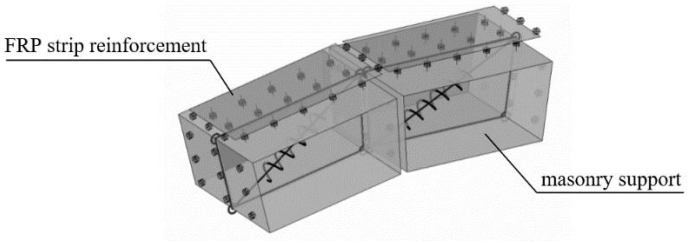


Figure 5. Layout of the interaction between flat FRP discrete element and masonry substrate [9].

4 COMPARISON BETWEEN EXPERIMENTAL AND NUMERICAL RESULTS

The maximum load Pmax, the ratio between the test maximum load and that of the test UN.ND (Pmax/Pmax,UN.ND), and ductility for each test are summarized in Table 1. In this paper, the ductility is computed as the ratio between the ultimate displacement (the displacement at ultimate load, taken as 85% of the maximum load in the descending branch of the applied load vs. arch crown displacement curve) and the displacement at the end of the elastic branch [3].

Table 1. Summary of test results.

SPECIMEN	P_{max} [kN]	$P_{max}/P_{max,UN.ND}$	Ductility
UN.ND	0.44	1.00	12.77
UN.LD	0.34	0.76	11.72
SFRM.LD	14.15	31.87	2.90

The unstrengthened specimens exhibited a typical mechanism characterized by the formation of four alternate hinges, as shown in Fig. 6. For both tests, the location and sequence of the hinges remained the same. Moreover, it is important to underline that due to the randomness of the material the hinge configuration is not symmetrical as well-known from equilibrium theory.

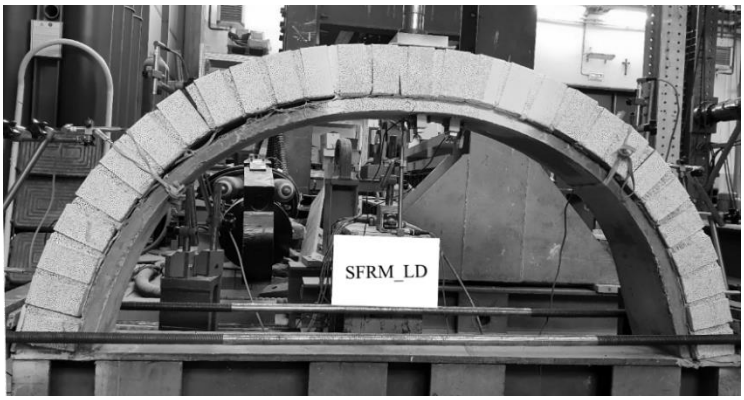


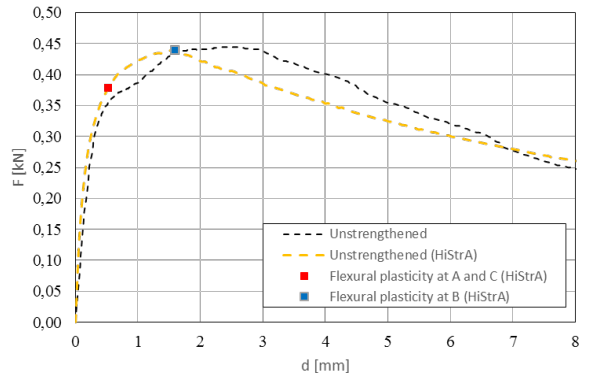
Figure 6. Collapse mechanism for the strengthened condition

A numerical model was implemented in the software environment HiStrA (Historical Stuctures Analysis) which employs the numerical approach described in the previous section. The model is made of 29 elements (which are associated to 116 inplane degrees of freedom), for which the adopted mechanical properties are summarized in Table 2. In particular, the flexural constitutive law is characterized by the Young's modulus E, the compressive σ_c and tensile σ_t strengths and the compressive G_c and tensile G_t fracture energies; the shear diagonal behavior is considered elastic and associated to the shear modulus G; no sliding can occur among the blocks.

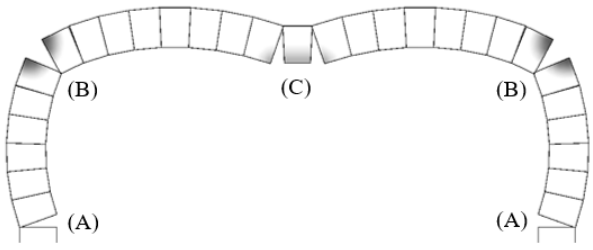
Table 2. Mechanical properties adopted in the numerical model.

Typology	E [MPa]	σ_c [MPa]	G_c [N/mm]	σ_t [MPa]	G_t [N/mm]	G [MPa]	c [MPa]	G_s [N/mm]	w [kN/m^3]
Masonry arch	1000	7.22	3	0.014	0.04	400	-	-	18
SFRM	15000	91.02	1000	10	5	6000	0.2	0.13	24

In Figure 8a, a comparison between numerical and experimental results in terms of capacity curve, is depicted. The results show a good agreement in terms of initial stiffness, peak load and softening branch. The agreement is encountered also in terms of failure mechanism, Figure 8b, which is characterized by the opening of five flexural hinges with symmetric locations. The progression of the opening of the flexural hinges is also identified in the capacity curve.



(a)



(b)

Figure 8. Numerical results of the unstrengthened arch in terms of a) load–arch crown displacement and b) failure mechanism

Since the thickness of the SFRM strengthening is not negligible with respect to the arch thickness, in the numerical model of the strengthened arch it is modelled with an inner ring of 29 discrete elements, which lead to a total amount of degrees of freedom equal to 232. The

inner ring of elements is associated to the mechanical properties reported in Table 2. In particular, the sliding between inner SFRM ring and external masonry arch is enabled and associated to an elastic-plastic behaviour with softening associated to the cohesive strength c and fracture energy G_s. In Figure 9 the results in terms of capacity curve and failure mechanism are reported; as expected, the failure mechanism involves the sliding between the masonry arch and the SFRM reinforcement, which also delays the opening of the flexural hinges. Again, the sequence of opening of the hinges is summarized in the capacity curve thus allowing to reconstruct the progression of the damage in the arch. The numerical results, which are in good agreement with the experimental ones, are able to grasp the beneficial contribution and the effectiveness of the SFRM technique.

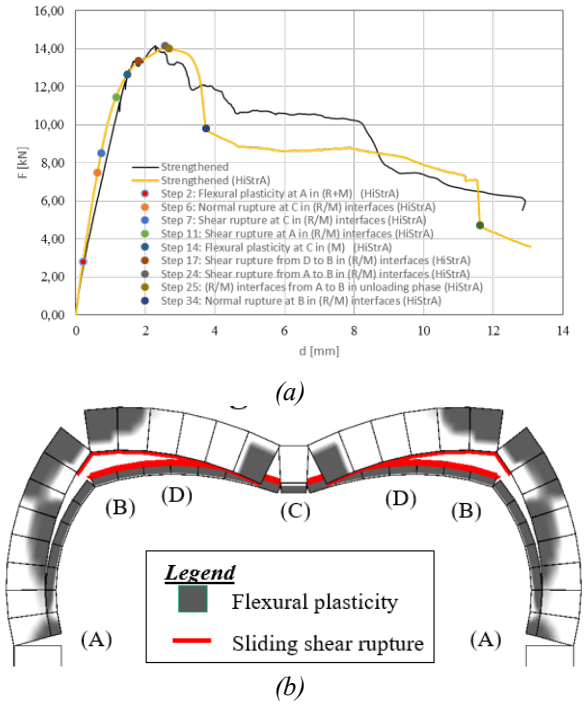


Figure 9. *Numerical results of the strengthened arch in terms of a) load–arch crown displacement and b) failure mechanism*

5 CONCLUSION

In this paper, the destructive experimental tests of a masonry arch (in the unstrengthened condition and in the strengthened with SFRM layer applied to arch intrados condition) have been reported. Results show an increase in term of load-carrying capacity of around 40 times respect to the unstrengthened condition. A simplified numerical strategy based on a Discrete Macro-Element approach, previously adopted for modelling masonry structures, and other strengthening techniques, is here applied for the first time to model arches reinforced with SFRM. The numerical simulations, using a HiStrA software based on a discrete macro-model, show the load-arch crown displacement curve with a good agreement respect to the experimental curves. The failure modes as collapse mechanism for the unstrengthened

condition and the detachment of the SFRM strip for the strengthened condition are in according with the experimental results.

REFERENCES

[1] D. V. Oliveira, I. Basilio, and P. B. Lourenço, "*Experimental Behavior of FRP* Strengthened Masonry Arches," J. Compos. Constr., vol. 14, no. 3, pp. 312–322, 2010.
[2] P. Zampieri, N. Simoncelo, C. D. Tetougueni, and C. Pellegrino, "A review of methods for strengthening of masonry arches with composite materials," Eng. Struct., vol. 171, no. May, pp. 154–169, 2018.
[3] Simoncello N, Zampieri P, Gonzalez-libreros J, Pellegrino C. Experimental behaviour of damaged masonry arches strengthened with steel fiber reinforced mortar (SFRM). Comp. Part B 2019; 177:107386. https://doi.org/10.1016/j.compositesb.2019.107386.
[4] Zampieri, P. Horizontal capacity of single-span masonry bridges with intrados FRCM strengthening (2020) Composite Structures, 244, art. no. 112238, . DOI: 10.1016/j.compstruct.2020.112238.
[5] Zampieri, P., Simoncello, N., Gonzalez-Libreros, J., Pellegrino, C. Evaluation of the vertical load capacity of masonry arch bridges strengthened with FRCM or SFRM by limit analysis (2020) Engineering Structures. DOI: 10.1016/j.engstruct.2020.111135
[6] Caliò, I., Marletta, M., and Pantò, B. (2012). *A new discrete element model for the evaluation of the seismic behaviour of unreinforced masonry buildings*. Eng. Struct. 40, 327–338. doi:10.1016/j.engstruct.2012.02.039
[7] B. Pantò, F. Cannizzaro, I. Caliò, P.B. Lourenço *Numerical and experimental validation of a 3D macro-model for the in-plane and out-of-plane behaviour of unreinforced masonry walls* – (2017) International Journal of Architectural Heritage, 11(7), pp.946-964 doi: 10.1080/15583058.2017.1325539.
[8] I. Caliò, F. Cannizzaro, M. Marletta (2010). *A discrete element for modeling masonry vaults*.7th International Conference on Structural Analysis of Historical Constructions (SAHC2010). Shanghai (China) 6-8 Ottobre 2010.
[9] F. Cannizzaro, P.B. Lourenço, *Simulation of Shake Table Tests on Out-of-Plane Masonry Buildings. Part (VI): Discrete Element Approach – (2017)* International Journal of Architectural Heritage, 11(1), pp. 125-142 doi: http://dx.doi.org/10.1080/15583058.2016.1238973.
[10] Pantò, B., Cannizzaro, F., Caddemi, S., and Caliò, I. (2016). *3D macro-element modelling approach for seismic assessment of historical masonry churches*. Adv. Eng. Softw. 97, 40–59. doi:10.1016/j.advengsoft.2016.02.009
[11] Cannizzaro, F., Pantò, B., Caddemi, S., and Caliò, I. (2016). *A Discrete Macro-Element Method (DMEM) for the nonlinear structural assessment of masonry arches*. Eng. Struct. (2018) 168:243–56
[12] Pantò, B., Cannizzaro, F., Caddemi, S., Caliò, I., Chácara, C. and Lourenço, PB., *Nonlinear modelling of curved masonry structures after seismic retrofit through FRP reinforcing. Buildings* (2017) 7:79.

12th International Conference on Structural Analysis of Historical Constructions
SAHC 2020
P. Roca, L. Pelà and C. Molins (Eds.)

OUT-OF-PLANE BEHAVIOUR OF TUFF AND BRICK MASONRY WALLS STRENGTHENED WITH FRCM COMPOSITE MATERIALS

A. BELLINI[1*], A. INCERTI[1] , A. NANNI[2] AND C. MAZZOTTI[3]

[1]CIRI Buildings and Construction (CIRI-EC)
University of Bologna
Via del Lazzaretto 15/5, 40131 Bologna, Italy
e-mail: alessandro.bellini5@unibo.it (*corresponding author), andrea.incerti3@unibo.it

[2] Department of Civil, Architectural and Environmental Engineering
University of Miami
1251 Memorial Drive, McArthur Engineering Building, Rm. 325, Coral Gables, FL 33146-0630
e-mail: nanni@miami.edu

[3] Department of Civil, Chemical, Environmental and Materials Engineering (DICAM)
University of Bologna
Viale Risorgimento 2, 40136 Bologna, Italy
e-mail: claudio.mazzotti@unibo.it

Keywords: Out-of-plane, Masonry, Brick, Tuff, FRCM, Strengthening

Abstract. *Strengthening with composite materials is becoming more and more an effective solution for increasing the structural safety of masonry buildings, often subjected to severe degradation or potentially vulnerable to seismic events. Structural retrofitting can be performed according to different techniques, based on Fiber Reinforced Polymer (FRP) or Fiber Reinforced Cementitious Matrix (FRCM) strengthening systems. The second group of composite systems is usually preferred nowadays thanks to some important advantages such as better compatibility with the substrate, applicability on wet surfaces, fire resistance, permeability and reversibility. Several experimental and numerical studies can be found in literature concerning masonry panels strengthened with FRP and FRCM systems. The knowledge about the use of the latter, nevertheless, is still partially limited, in particular if the out-of-plane behaviour of walls is taken into account, with the experimental and numerical database available resulting mainly restricted to monotonic cases. In this framework, results of an experimental campaign devoted to the study of the out-of-plane behaviour of tuff and brick masonry walls strengthened with different types of FRCM systems will be presented and discussed in this paper, performing also a comparison with available predictive formulas. Experimental results showed, in general, good performance of FRCM composite materials, with a proper exploitation of their tensile capacity, proving their effectiveness for the out-of-plane strengthening of historical masonry walls.*

1 INTRODUCTION

Historical buildings and civil constructions are commonly made, especially in the Southern Europe area, with stone, brick or tuff elements coupled with hydraulic lime-based mortars, for realizing different types of masonries. The masonry panels behaviour, primarily as a reaction to horizontal actions triggered for example during a seismic event, represents a key issue to be investigated, in order to improve structural safety of the constructions, avoiding local and global failure mechanisms.

In the last years, several studies have been carried out on masonry elements retrofitted with composite materials such as Fiber Reinforced Polymers (FRPs) or Fiber Reinforced Cementitious Matrix (FRCM) systems, highlighting advantages and drawbacks of these two kinds of strengthening techniques, starting from applicability on wet surfaces until fire resistance or compatibility and removability of the strengthening materials used [1-12]. However, only few works are focused on the out-of-plane behaviour of masonry walls built with different masonry substrates and strengthened with composite materials [13-17].

In this framework, the objective of the present study is to improve the knowledge about failure modes and performances of two particular masonry substrates (made with tuff stones and clay bricks) when retrofitted with FRCM systems comprising basalt, aramid-glass fiber grids and steel fiber sheets, using also different layouts during their application to masonry panels. A specific, purposely made experimental set-up, validated during previous laboratory flexural tests [15,16], was used to simulate the effect of a distributed out-of-plane load, such as that generated during a seismic event and the outcomes coming from retrofitted samples were then discussed in terms of maximum bending moment capacity and displacement at failure, highlighting the effects of the FRCM strengthening systems with respect to the reference unreinforced panel.

Finally, predictive formulas, expressed in accordance with ACI 549.4R-13 guideline approach [18], were compared with the experimental outcomes, starting from the preliminary mechanical characterization of the materials used for retrofitting the masonry walls.

2 MATERIALS AND SAMPLES PREPARATION

The experimental campaign carried out for the evaluation of the out-of-plane behaviour of tuff and brick masonry walls strengthened with FRCM composites is summarized in Table 1, where each specimen type is identified with a simple code containing the wall substrate (B = brick or T = tuff masonry), the applied FRCM system (basalt G2, aramid-glass R1, steel G6 or steel G12) and the number of FRCM plies. For each sample type, a single test repetition was performed, for a total number of 12 out-of-plane flexural tests.

Details and mechanical characterization of masonry walls and FRCM strengthening systems will be discussed in the following.

2.1 Masonry walls

The masonry walls tested were built with both clay bricks and tuff blocks using the same low strength natural hydraulic lime (NHL) mortar for bed joints. Clay brick masonry samples were double-leaf panels with dimensions of 1.20×0.25×2.70 m^3, fabricated from standard clay bricks with nominal size 250×120×55 mm^3, adopting a mortar joints thickness of about 10 mm. Tuff block masonry instead was built starting from tuff blocks with nominal size

370×245×105 mm^3, resulting in a masonry panel with total dimensions of 1.13×0.245×2.70 m^3. The samples were cured in laboratory-controlled conditions after construction and before the application of FRCM strengthening systems. Materials characterization was carried out by testing masonry prisms [19] and mortar cubes [20] in compression after 28 days of curing. The obtained average compressive strength of masonry prisms was 8.50 MPa and 2.08 MPa, respectively, for clay brick and tuff masonry, whereas the mean 28 days mortar cubes compressive strength was 2.52 MPa.

Table 1: Experimental campaign.

Specimen ID	Substrate type	FRCM system	n. of plies
B_URM	Brick (B)	-	-
B_G2-1		Basalt G2	1
B_R1-1		Aramid-glass R1	1
B_R1-2		Aramid-glass R1	2
B_G6-1		Steel G6	1
B_G12-1		Steel G12	1
T_URM	Tuff (T)	-	-
T_G2-1		Basalt G2	1
T_R1-1		Aramid-glass R1	1
T_R1-2		Aramid-glass R1	2
T_G6-1		Steel G6	1
T_G12-1		Steel G12	1

2.2 Strengthening systems and layout

Four different types of FRCM strengthening systems were used for performing wall flexural tests on both clay brick and tuff substrates, comprising steel, basalt and aramid-glass fibers. All the strengthening systems were applied using the same natural hydraulic lime (NHL) mortar as FRCM matrix, characterized by a nominal compressive strength of 15 MPa.

Steel G6 system is a unidirectional sheet made of ultra-high strength galvanized steel micro-cords (SRG) characterized by a total mass (inclusive of thermal welding) of 670 g/m^2 and by an equivalent fiber thickness of 0.084 mm.

Steel G12 system is another unidirectional SRG system made of the same ultra-high strength micro-cords, but characterized by a different density (1200 g/m^2) and by an equivalent thickness of 0.169 mm. Steel G6 and G12 systems were applied to the wall by using a discontinuous layout (see Figure 1a), adopting three vertical 100 mm-wide strips, whereas all the other FRCM systems were applied by following the continuous layout shown in Figure 1b.

Aramid-glass R1 system is a bi-directional grid with a nominal spacing of 15 mm and a density of 250 g/m^2 (equivalent dry fiber thickness along the tested direction is 0.031 mm), applied according to two different configurations: single ply (R1-1) or double-ply (R1-2) layout.

Basalt G2 system is instead characterized by the use of a basalt grid with a total density of 200 g/m^2 and a nominal spacing of 17 mm (equivalent dry fiber thickness along each direction

is 0.032 mm). All the FRCM/SRG systems were mechanically characterized at University of Miami according to AC 434 Annex A [21], performing tensile tests in order to evaluate the ultimate tensile strength, the cracked and uncracked moduli of elasticity and the ultimate tensile strain of the strengthening systems. The obtained average values, which will be used for comparison between experimental results coming from wall flexural tests and predictive formulas [18], are summarized in Table 2.

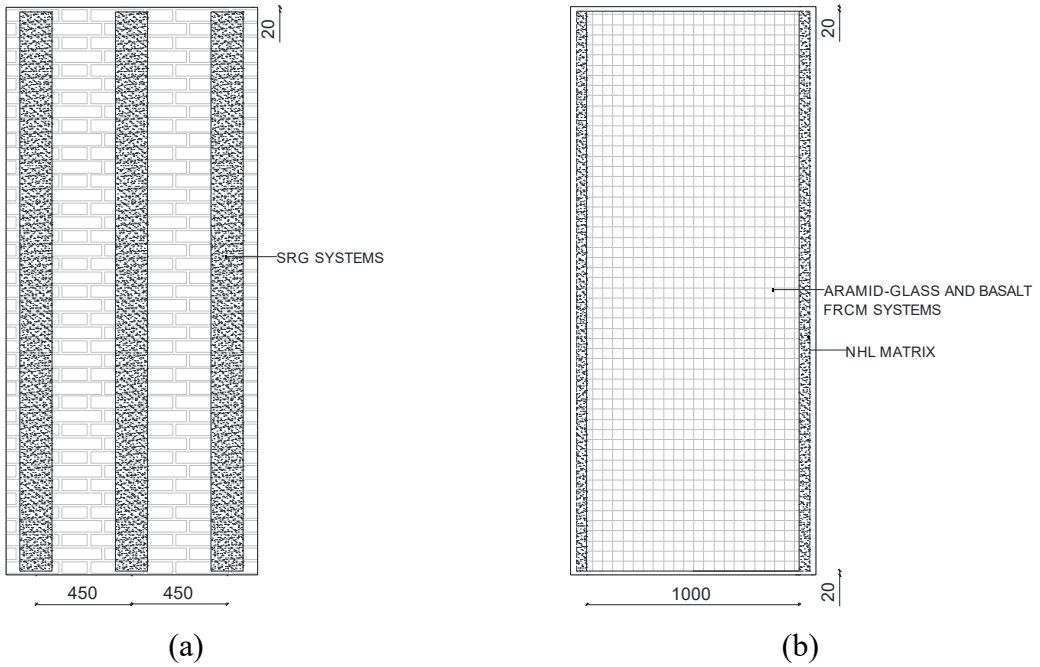


Figure 1: Strengthening systems layout: (a) SRG systems; (b) aramid-glass and basalt systems.

Table 2: Materials characterization: results of tensile tests on FRCM systems according to AC434, Annex A.

Strengthening system	Ultimate stress [MPa]	Cracked modulus of elasticity [GPa]	Uncracked modulus of elasticity [GPa]	Ultimate strain [%]
G6	884.1	58.51	452.9	1.42
G12	617.5	37.27	400.9	1.08
R1	1188.0	30.63	2054.5	2.93
G2	685.2	46.65	1784.5	1.86

3 OUT-OF PLANE TEST SET-UP

The experimental set-up used for evaluating the flexural capacity of clay brick and tuff masonry walls was a purposely designed set-up, able to test full-scale samples, previously validated during several experimental campaigns carried out on FRCM-strengthened masonry panels [15,16].

The set-up, shown in Figure 2, allowed to place the walls following a simply supported

static scheme, adopted to induce flexural failure, and to apply horizontal loads together with a constant uniform vertical compression axial stress (σ = 0.2 MPa for clay brick masonry walls and σ = 0.15 MPa for tuff samples). Out-of-plane forces were applied along four symmetrically distributed positions, generating a bending moment distribution quite similar to that produced by a uniform distributed load. Test walls were anchored to the reaction wall and to the laboratory strong floor by means of steel elements, allowing the panels to bend in the out-of-plane direction.

Pressure transducers were used to measure independently the out-of-plane forces and the vertical stress, applied by using two independent hydraulic circuits. Horizontal displacements at the top, bottom and mid-height of the walls were measured by means of draw-wire displacement transducers (WDTs). Two additional displacement transducers (LVDTs) were used to measure rotation of the bottom hinge.

Further details on the adopted experimental set-up can be found in [15].

Tests were performed under horizontal force control at a rate equal to 2 kN/minute, adopting a data acquisition rate of 2 Hz.

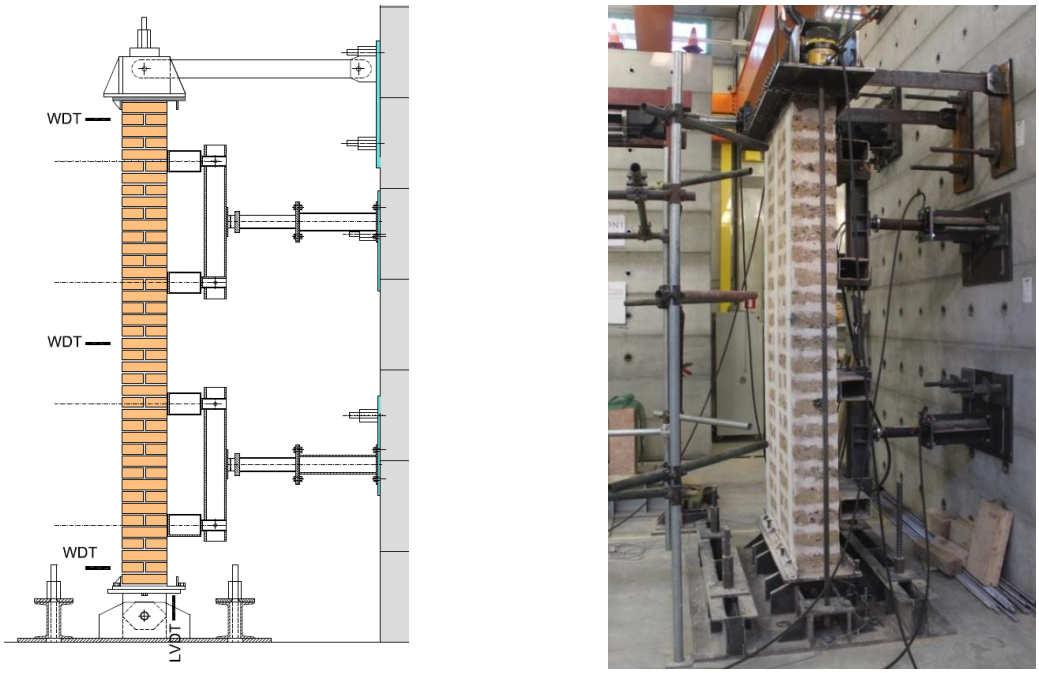


Figure 2: Experimental set-up.

4 EXPERIMENTAL RESULTS

Experimental results in terms of failure modes, maximum capacity and moment-deflection curves will be presented and discussed in this section.

4.1 Failure modes

Table 3 and Table 4 show the results obtained for both clay brick and tuff brick walls.

The two different failure modes identified during out-of-plane tests are shown in Figure 3:

a) flexural failure with fiber tensile rupture (Figure 3a) or *b*) shear failure of the strengthened wall (Figure 3b). In more detail, flexural failure always occurred due to the tensile failure of the FRCM fabric in proximity of the panel mid-height, in a portion of the wall where the bending moment was constant and maximum, and it was always located in correspondence of a previously cracked section of the masonry wall. Shear failure were observed from walls strengthened by high density steel fabric (B_G12-1, T_G12-1) or with low substrate mechanical properties (T_G6-1).

Table 3: Out-of-plane test results: clay brick substrate specimens.

Specimen	Failure mode	Maximum capacity M_{max} [kN m]	Increment [%]	Maximum deflection δ_{max} [mm]
B_URM	Flexure	9.80	-	6.66
B_G2-1	Flexure	14.56	+ 48.57	12.08
B_R1-1	Flexure	22.99	+ 134.59	44.94
B_R1-2	Flexure	31.76	+224.08	47.00
B_G6-1	Flexure	32.35	+230.10	63.92
B_G12-1	Shear	30.69	+213.16	34.07

Table 4: Out-of-plane test results: tuff brick substrate specimens.

Specimen	Failure mode	Maximum capacity M_{max} [kN m]	Increment [%]	Maximum deflection δ_{max} [mm]
T_URM	Flexure	7.77	-	31.39
T_G2-1	Flexure	15.85	+ 103.99	61.69
T_R1-1	Flexure	19.33	+ 148.78	63.26
T_R1-2	Flexure	24.53	+ 215.70	50.17
T_G6-1	Shear	20.80	+ 167.70	47.60
T_G12-1	Shear	16.91	+ 117.63	19.77



(a) (b)

Figure 3: Test results: typical failure modes: (a) flexural failure with fiber tensile rupture; (b) shear failure.

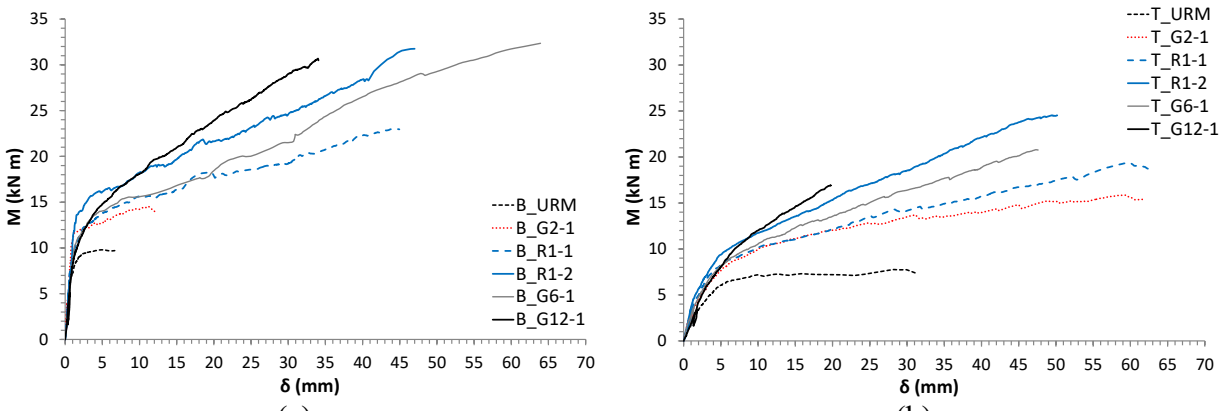
4.2 Out-of-plane capacity and moment-deflection curves

The maximum bending moment M_{max} reached during the out-of-plane experimental tests, in comparison to the unreinforced masonry (URM) walls is indicated in Table 3 and Table 4, respectively, for clay brick and tuff walls, together with the maximum deflection δ_{max}.

Steel (G6 and G12) and aramid-glass (R1) strengthening systems showed the best results, with an optimal efficiency moving from one ply (R1-1) to two plies (R1-2) in the case of aramid-glass samples. All the samples, except for B_G12-1 wall, proved to be able to reach the maximum strengthening system capacity without premature debonding phenomena or shear failure of the substrate. The capacity increment, in comparison to the unreinforced sample, was remarkable for all the brick walls tested, ranging from a minimum of 48% to a maximum of 230%.

The same comparison made for tuff masonry walls highlighted some differences: the premature shear failure of the substrate limited the maximum capacity of SRG strengthened samples, whereas G2 and R1 bidirectional grids reached their mechanical capacity. As for brick samples, a good increment was found passing from one ply to two plies in the case of R1 strengthening system. The difference between strengthened and URM walls was included in the 104 - 216% range, highlighting again the good efficiency of FRCM strengthening systems also in case of substrates with lower mechanical properties.

Figure 4 shows the moment-deflection curves obtained during flexural tests for all the walls tested, including clay brick (Figure 4a) and tuff substrate (Figure 4b). As a general remark, all the strengthened samples showed a typical bilinear behavior, with a first almost linear phase until the onset of cracking (which can be identified as a short non-linear phase characterized by a progressively decreasing slope) and a second branch with an almost constant positive slope. The curves, in general, highlighted not only the remarkable increment in terms of maximum bending moment measured from strengthened samples, but also an evident increment in displacement capacity (see Figure 4 and Tables 3,4).



(a) (b)

Figure 4: Out-of-plane test results: moment-deflection curves: (a) clay brick walls; (b) tuff masonry walls.

4.3 Discussion of experimental results: comparison between brick and tuff masonry

If moment-deflection curves obtained from the two different substrates are compared, considering the same strengthening system type, some general trends can be observed (see Figure 5). First of all, since the out-of-plane capacity depends both on masonry mechanical properties and on the strengthening system efficiency, retrofitted clay brick walls showed, as expected, higher out-of-plane flexural capacity if compared to strengthened tuff masonry walls. If initial stiffness of moment-deflection curves is analyzed, again tuff masonry, characterized by weaker mechanical properties, showed the worst results, independently from the FRCM system type considered. Analyzing maximum displacement capacity of basalt and aramid-glass FRCM systems (Figure 5a), the maximum deflection registered during experimental tests was generally similar or higher for tuff masonry walls. When dealing with G6 and G12 steel systems instead (see Figure 5b), the premature shear failure of masonry substrate caused a completely different trend, with a reduced displacement capacity for tuff samples when compared with similarly strengthened clay-brick walls.

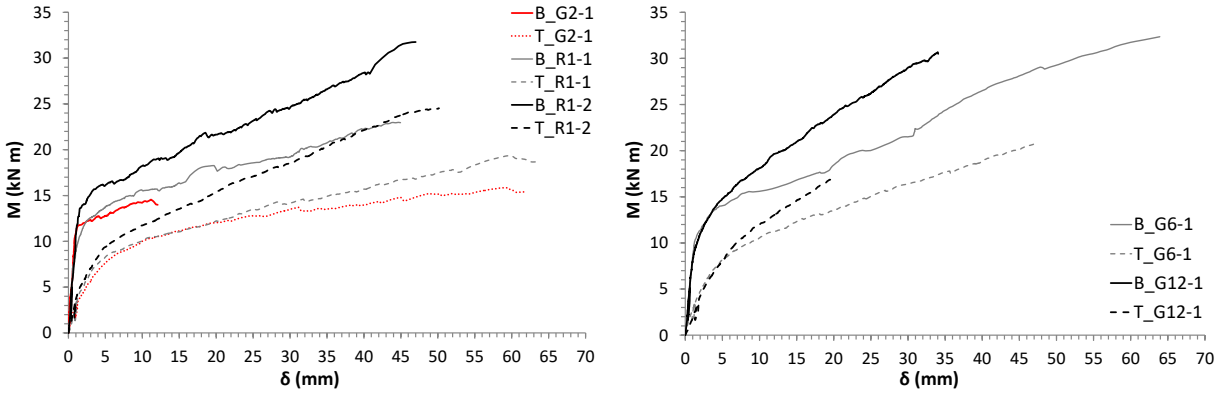


Figure 5: Comparison between moment-deflection curves on different substrates: (a) basalt G2 and aramid-glass R1 systems; (b) G6 and G12 steel systems.

5 COMPARISON WITH PREDICTIVE FORMULAS

Out-of-plane flexural capacity M_n of masonry walls has been also estimated by following the ACI 549.4R-13 approach [18], starting from the definition of the effective tensile strain and stress levels of the composite at failure. Results have been then compared with experimental findings M_{max}.

The effective tensile strain of the FRCM composite material can be evaluated from tensile tests performed according to AC 434 Annex A (Table 2). Since the purpose of the comparison is not to calculate design values, but to compare predictive formulas with experimental results, ultimate strain values reported in Table 2 will be considered as effective tensile strain values ε_{fe}, without the strain limitation $\varepsilon_{fe} \leq 0.012$ contained inside ACI 549.4R-13 [18], suitable for design of the strengthened elements.

Following this approach, the effective tensile stress level at failure f_{fe} is:

$$f_{fe} = E_f \cdot \varepsilon_{fe} \tag{1}$$

where E_f is the tensile modulus of elasticity of the cracked FRCM composite material (see Table 2) and considering the stress limitation $f_{fe} \leq f_{fu}$, where f_{fu} identifies the experimental ultimate tensile strength of the FRCM composite.

Starting from the effective tensile stress at failure and assuming the stress block factors $\beta_1 = 0.7$ and $\gamma = 0.7$, respectively for the extension of the part under compression and the intensity of the uniform stress, equilibrium of forces can be used to calculate the neutral axis depth c. If the failure mode is governed by FRCM failure:

$$c = \frac{Q + n_f \cdot A_f \cdot f_{fe}}{\gamma \cdot f'_m \cdot \beta_1 \cdot B} \tag{2}$$

where Q is the applied axial force, n_f the number of plies of the FRCM system, A_f the FRCM composite area per ply, f'_m the compressive strength of masonry and B the width of the masonry wall. After calculating the neutral axis depth, and indicating with t_w the wall thickness, the nominal flexural strength M_n can be determined as:

$$M_n = \gamma \cdot f'_m \cdot \beta_1 \cdot c \cdot B \cdot \left(\frac{t_w}{2} - \beta_1 \cdot \frac{c}{2}\right) + n_f \cdot A_f \cdot f_{fe} \cdot \frac{t_w}{2} \tag{3}$$

It should then be verified that the compressive strain in the masonry does not exceed the ultimate value ε_{mu}, generally assumed equal to 0.0035:

$$\varepsilon_m = \varepsilon_{fe} \cdot \left(\frac{c}{t_w - c}\right) \leq \varepsilon_{mu} \tag{4}$$

Otherwise, if crushing of masonry is the governing failure mode, in order to calculate the neutral axis depth, the following equation is needed:

$$c^2\left(\gamma \cdot f'_m \cdot \beta_1 \cdot B\right) + c \cdot \left(\varepsilon_{mu} \cdot E_f \cdot A_f - Q\right) - \varepsilon_{mu} \cdot E_f \cdot A_f \cdot t_w = 0 \tag{5}$$

and the nominal flexural strength can be determined as:

$$M_n = \gamma \cdot f'_m \cdot \beta_1 \cdot c \cdot B \cdot \left(\frac{t_w}{2} - \beta_1 \cdot \frac{c}{2}\right) + n_f \cdot A_f \cdot E_f \cdot \varepsilon_f \cdot \frac{t_w}{2} \tag{6}$$

Finally, if this second failure mode occurs, it should be verified that the tensile strain in the fiber does not exceed the ultimate strain value ε_{fu}, determined through mechanical characterization of the FRCM material (see Table 2):

$$\varepsilon_f = \varepsilon_{mu} \cdot \left(\frac{t_w - c}{c}\right) \leq \varepsilon_{fu} \tag{7}$$

The out-of-plane nominal capacity M_n, calculated according to this theoretical formulation, is reported in Table 5 and Table 6, respectively, for clay brick and tuff masonry walls and compared with the experimental capacity M_{max}.

As can be observed from the tables, ACI 549.4R-13 approach provides results that are on the safe side, with ratio M_{max} / M_n ranging from 1.26 to 2.79 for clay brick masonry panels and from 1.88 to 2.75 for strengthened tuff masonry walls. Figure 6a, where experimental and theoretical values of each clay brick masonry specimen are compared, shows, in more detail, a good approximation for G2 basalt samples, but a completely different result, with a larger underestimation of experimental outcomes, in the case of steel and aramid-glass samples with 2 plies. The same trend can be also observed for tuff walls strengthened with basalt and aramid-glass FRCMs (Figure 6b), but cannot be

confirmed for those retrofitted with G6 and G12 steel strengthening systems, where shear failure occurred in masonry before reaching the maximum out-of-plane flexural capacity.

Table 5: Comparison with predictive formulas: clay brick masonry walls.

Specimen	Experimental capacity M_{max} [kN m]	Nominal capacity M_n [kN m]	M_{max} / M_n [ ]
B_URM	9.80	7.25	1.35
B_G2-1	14.56	11.55	1.26
B_R1-1	22.99	9.99	2.30
B_R1-2	31.76	12.72	2.50
B_G6-1	32.35	11.61	2.79
B_G12-1	30.69	12.24	2.51

Table 6: Comparison with predictive formulas: tuff masonry walls.

Specimen	Experimental capacity M_{max} [kN m]	Nominal capacity M_n [kN m]	M_{max} / M_n [ ]
T_URM	7.77	4.56	1.70
T_G2_1	15.85	8.40	1.89
T_R1-1	19.33	7.03	2.75
T_R1-2	24.53	9.41	2.61
T_G6-1	20.80	8.45	2.46
T_G12-1	16.91	9.00	1.88

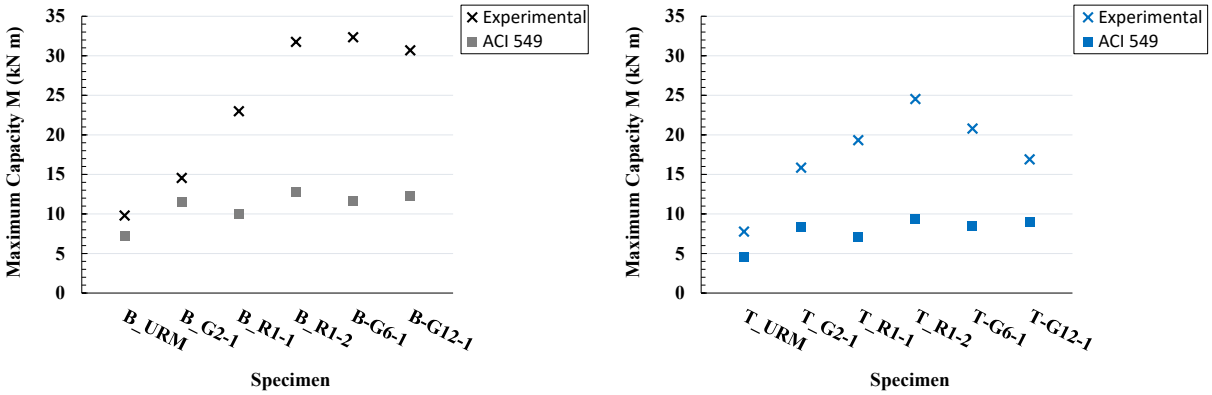


Figure 6: Comparison between experimental results and predictive formulas (ACI 549.4R-13): (a) clay brick masonry walls; (b) tuff masonry walls.

6 CONCLUSIONS

The paper presents the results of an experimental campaign focused on the evaluation of the out-of-plane behaviour of clay brick and tuff masonry walls retrofitted with FRCM composite materials.

Flexural tests were performed by using a purposely design set-up, able to independently apply an axial force and out-of-plane horizontal forces on a full-scale masonry panel, evaluating failure modes and capacity of the strengthened walls. The experimental results showed a good efficiency of the strengthening systems, with capacity increments, in comparison to the URM wall, ranging from 48% to 230% for brick masonry samples and from 104% to 216% for tuff specimens.

The most common failure mode was flexural failure of the wall with final tensile failure of the FRCM reinforcement, with only a few cases of shear failure, involving high density steel strengthening systems.

Tests were also performed on aramid-glass fibers, investigating the effect of a different number of plies and highlighting that a remarkable capacity increment is possible passing from one to two plies, at least for low density fabrics, without changing the failure mode of the strengthened wall.

Finally, starting from mechanical characterization of the FRCM systems, a comparison between experimental capacity and nominal capacity, calculated according to ACI 549.4R-13 [18] approach, was performed, obtaining values of their ratio ranging from 1.26 to 2.79 for clay brick masonry walls and from 1.88 to 2.75 for strengthened tuff specimens and therefore concluding that theoretical values are always on the safe side, with an underestimation of experimental outcomes.

Acknowledgements. The authors would like to thank Kerakoll S.p.A. for providing materials and for strengthening systems application. The financial support of the Italian Department of Civil Protection (ReLUIS 2019-2021 Grant – Innovative Materials) is gratefully acknowledged.

REFERENCES

[1] Carloni, C., and Subramaniam, K.V. FRP-masonry debonding: numerical and experimental study of the role of mortar joints. *J. Compos. Constr.* (2012) **16**:581-589.

[2] Mazzotti, C., Ferracuti, B., and Bellini, A. Experimental bond tests on masonry panels strengthened by FRP. *Composites Part B* (2015) **80**:223-237.

[3] De Felice, G., De Santis, S., Garmendia, L., Ghiassi, B., Larrinaga P., Lourenço, P.B., Oliveira D.V., Paolacci F. and Papanicolau C.G. Mortar-based systems for externally bonded strengthening of masonry. *Materials and Structures* (2014) **47**:2021-2037.

[4] Carozzi, F.G., Bellini, A., D'Antino, T., de Felice, G., Focacci, F., Hojdys, L., Laghi, L., Lanoye, E., Micelli, F., Panizza, M. and Poggi, C. Experimental investigation of tensile and bond properties of Carbon-FRCM composites for strengthening masonry elements. *Composites Part B* (2017) **128**:100-119.

[5] Papanicolaou, C., Triantafillou, T. and Lekka, M. Externally bonded grid as strengthening and seismic retrofitting materials of masonry panels. *Construction and Building Materials* (2011) **25**(2):504-514.

[6] Bellini, A., Bovo, M. and Mazzotti, C. Experimental and numerical evaluation of fiber-matrix interface behaviour of different FRCM systems. *Composites Part B* (2019) **161**:411-426.

[7] Bellini, A., Shahreza, S.K. and Mazzotti, C. Cyclic bond behavior of FRCM composites applied on masonry substrate. *Composites Part B* (2019) **169**:189-199.
[8] Incerti, A. Tilocca, A.R., Ferretti, F. and Mazzotti, C. Influence of masonry texture on the shear strength of FRCM reinforced panels. In: R. Aguilar et al. (Eds.): *Structural Analysis of Historical Constructions*, RILEM Bookseries 18 (2019), pp. 1623-1631.
[9] Incerti, A., Ferretti, F. and Mazzotti, C. FRCM strengthening systems efficiency on the shear behavior of pre-damaged masonry panels: an experimental study. *J Build Rehabil* (2019) **4**: 14. DOI: 10.1007/s41024-019-0053-9.
[10] Ferretti, F., Incerti, A., Tilocca A.R. and Mazzotti, C. In-Plane Shear Behavior of Stone Masonry Panels Strengthened through Grout Injection and Fiber Reinforced Cementitious Matrices. *International Journal of Architectural Heritage* (2019). DOI: 10.1080/15583058.2019.167580.
[11] Sassoni, E., Andreotti, S., Bellini, A., Mazzanti, B., Bignozzi M.C., Mazzotti, C. and Franzoni E. Influence of mechanical properties, anisotropy, surface roughness and porosity of brick on FRP debonding force. *Compos Part B* (2017) **108**:257-269.
[12] Lignola, G.P., Caggegi, C., Ceroni, F., De Santis, S., Krajewski, P., Lourenço, P.B., Morganti, M., Papanicolaou, C., Pellegrino, C., Prota, A., and Zuccarino, L. Performance assessment of Basalt FRCM for retrofit applications on masonry. *Compos Part B* (2017) **128**:1-18.
[13] Babaeidarabad, S., De Caso, F., and Nanni, A. Out-of-plane behavior of URM walls strengthened with Fabric-Reinforced Cementitious Matrix Composite. *J Compos Constr* **18** (2014). DOI 10.1061/(ASCE)CC.1943-5614.0000457.
[14] Harajli, M., ElKhatib, H., and Tomas San-Jose, J. Static and cyclic out-of-plane response of masonry walls strengthened using textile-mortar system. *J Mater Civil Eng* (2010) **22**: 1171-1180.
[15] Bellini, A., Incerti, A., Bovo, M. and Mazzotti, C. Effectiveness of FRCM reinforcement applied to masonry walls subject to axial force and out-of-plane loads evaluated by experimental and numerical studies. *International Journal of Architectural Heritage* (2018) **12**(3):376-394.
[16] Bellini, A., Incerti, A. and Mazzotti, C. Out-of-plane strengthening of masonry walls with FRCM composite materials. *Key Engineering Materials* (2017) **747**:158-165.
[17] De Santis, S., Bellini, A., de Felice, G., Mazzotti, C., and Meriggi, P. Design of the out-of-plane strengthening of masonry walls with textile reinforced mortar composites. *9th International Conference on Fibre-Reinforced Polymer (FRP) Composites in Civil Engineering - CICE 2018*. 17-19 July, Paris, France. 2018.
[18] ACI 549.4R-13. Guide to design and construction of externally bonded Fabric-Reinforced Cementitious Matrix (FRCM) systems for repair and strengthening concrete and masonry structures. 2013.
[19] ASTM C1314-16. Standard Test Method for Compressive Strength of Masonry Prisms. 2016.
[20] ASTM C109/C109M-16a. Standard Test Method for Compressive Strength of Hydraulic Cement Mortars (Using 2-in. or 50-mm Cube Specimens). 2016.
[21] AC 434. Acceptance criteria for masonry and concrete strengthening using Fabric Reinforced Cementitious Matrix (FRCM) and Steel Reinforced Grout (SRG) composite systems. 2016.

12th International Conference on Structural Analysis of Historical Constructions
SAHC 2020
P. Roca, L. Pelà and C. Molins (Eds.)

OVERVIEW OF THE MECHANICAL PROPERTIES OF STEEL REINFORCED GROUT SYSTEMS FOR STRUCTURAL RETROFITTING

FRANCESCA ROSCINI*, STEFANO DE SANTIS, PIETRO MERIGGI AND GIANMARCO DE FELICE

Roma Tre University
Department of Engineering
Via Vito Volterra 62, 00146 Rome, Italy
e-mail: francesca.roscini@uniroma3.it, www.romatrestrutture.eu (*corresponding author)
email: {stefano.desantis, pietro.meriggi, gianmarco.defelice}@uniroma3.it, www.romatrestrutture.eu

Keywords: Steel Reinforced Grout, Composite Material, Experimental Tests, Mechanical Properties

Abstract. *Steel Reinforced Grout (SRG) is a mortar-based composite recently developed for structural retrofitting, which provides high tensile strength with limited increase in mass and in stiffness, and whose effectiveness relies on the good interaction between steel cords and inorganic matrices. Many companies already supply SRG systems for rehabilitation activities and the scientific community has been working intensively on experimental and numerical investigations to demonstrate their effectiveness for structural applications, which also led to the inclusion of SRG in national and international standards for product qualification and design. However, a clear view of the mechanical properties of these systems is still lacking, due to their variability, which, in turn, strongly depends upon cord layout, textile architecture, and characteristics of the matrix. This paper provides an overview of the mechanical properties of SRG composites on the basis of the tests carried out at Roma Tre University and of the other experimental evidences available in the literature. The results of tensile tests on bare textiles and SRG coupons with different inorganic matrices, and of bond tests on masonry and reinforced concrete substrates are collected and the performances of the different SRG systems are compared. The influence of the mortar matrix on crack spacing, ultimate strain and tension stiffening in tensile tests is analysed. The capacity of the steel cords to ensure a proper shear transfer through interlocking within the matrix and the effect of cord density on failure mechanisms in bond tests are also discussed.*

1 INTRODUCTION

Steel Reinforced Grout (SRG) is a class of innovative mortar-based composites, named as Fabric Reinforced Cementitious Matrix (FRCM), developed for structural rehabilitation, as externally bonded reinforcements of existing reinforced concrete and masonry constructions. They can enhance structural capacity without alterations of geometry, mass and stiffness. Similarly to other FRCM systems, SRG may represent a valid solution to traditional techniques, such as the installation of steel tie-bars, the construction of crowning beams or the laying of

reinforced concrete plater overlays, which may be invasive, non-reversible, more expensive and inappropriate for applications to historical buildings. Therefore, they actually are an effective strengthening system first at all for cultural heritage thanks to their high compatibility between mortar matrix and masonry substrate.
SRG specific benefits have been demonstrated by a number of investigations carried out in different application fields. More specifically, experiments showed that the use of steel as reinforcement in FRCM composites provides an improvement of mechanical properties thanks to the ductility [1, 2] and the high tensile strength [3] of the textile. The layout of the cords also ensures a particularly efficient interlocking with mortar matrices, improving the bond at their interface [4, 5, 6, 7]. Finally, connection and anchorage systems can be effectively added to SRG overlays [8, 9, 10], allowing their installation on various structural members [11, 12, 13, 14] and ensuring particularly high gains in load carrying capacity as well [17,18]. On the basis of such investigations, SRG composites are currently included in the testing [19], acceptance [20] and design [21, 22] guides.
This paper collects the most recent research studies on SRG carried out in Roma Tre University according to EAD certification procedure [23], which followed those performed within the RILEM TC-250 CSM (Composites for the Sustainable Strengthening of Masonry) [22]. The most significant mechanical characteristics are compared to discuss the effect of the following parameters: architecture of the single cord, density of the textile, characteristics of the matrix and the substrate materials (concrete, clay bricks and tuff units).

2 MECHANICAL PROPERTIES OF STEEL TEXTILE AND SRG COMPOSITE UNDER DIRECT TENSILE TEST

In this paragraph, results of direct tensile test on bare steel textile and on SRG coupons are collected from Roma Tre University tests and others experimental investigations.



Figure 1.1: Experimental set up for tensile tests on dry textile

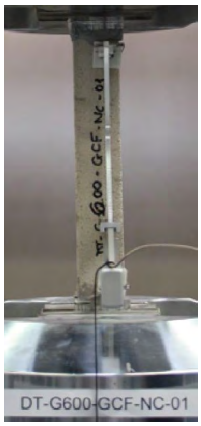


Figure 2.2: Experimental setup for tensile tests on SRG coupons

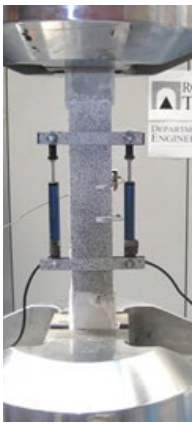




Figure 3.3: Experimental setup for shear bond tests

2.1 Tensile behaviour of steel textile

Direct tensile tests (Figure 1.1) on steel textiles are carried out to obtain peak stress, corresponding strain, and Young's modulus. In particular, in this case are collected properties and results from Roma Tre University(†)[24] and RILEM TC 250-CSM(*) [25, 26, 27]

experimental studies on four typologies of steel textiles:

S1) Galvanized Steel textile, consisting in Ultra High Tensile Strength Steel (UHTSS) cords with 6.35mm spacing, 0.084mm design thickness and 670g/m^2 surface mass density (low density). Each cord (Area=0.538mm^2) is obtained by twisting 2 wires around 3 rectilinear ones, having 0.108mm^2 cross section area.

S2) Galvanized Steel textile, consisting in Ultra High Tensile Strength Steel (UHTSS) cords with 3.18mm spacing, 0.169mm design thickness and 1340g/m^2 surface mass density (low-medium density).

S3) Steel textile, characterized by AISI 304 stainless steel made of cords, with 3.18 mm spacing. Each cord (cross section area=0.595mm^2) is obtained by twisting 5 wires having 0.119 mm^2 cross section area; 0.188mm design thickness and 1500g/m^2 surface mass density.

S4) Steel textile, characterized by AISI 316 stainless steel made of ropes, obtained by twisting several small wires; ropes have a cross section area of 0.69mm^2 each and are spaced 5mm.

Table 1: Geometrical properties and mechanical characteristics of steel textile under direct tensile test

Specimen label	c [cords/mm]	i [mm]	γ [g/m^2]	t [mm]	f_s [N/mm^2]	E_s [kN/mm^2]	ε_s [%]
S1*	0.157	6.35	670	0.084	3191	186	2.19
S2†	0.314	3.18	1340	0.169	3005	184	1.90
S3*	0.315	3.18	1500	0.188	2084	130	2.29
S4*	0.200	5.00	1057	0.138	1150	147	1.18

c = cord density; i = spacing; γ = surface mass density; t = equivalent (design) thickness
f_s= peak stress; E_s= secant Young's modulus ; ε_s =strain corresponding to peak stress;
*= RRT by RILEM TC-250 CSM experimental tests [25, 26, 27]
†= experimental tests recently carried out in Roma Tre University according to EAD [24]

Table 1 reports the main results of direct tensile tests on bare textiles: galvanized steel achieves the maximum tensile stress (around 3000N/mm^2). Stainless steel tensile behaviour assumes Young's modulus lower than galvanized one, which could depend not only on the steel treatment (galvanized vs stainless) but also on the different cord architecture, causing a limited easy handling as well.

2.2 Tensile behaviour of SRG coupons

Direct tensile test provides also the constitutive behaviour of SRG (Figure 1.2). The main mechanical parameters in the un-cracked, cracking, fully cracked stages are collected in this paragraph [22, 23]. In order to make SRG coupons for direct tensile tests, the four abovementioned textiles are combined with the following mortars:

ML) Lime based mortar with geopolymeric binders.

MG) Geopolymeric mortar.

MP) Lime and pozzolana based mortar.

MR) Fibre-reinforced cement mortar with polymeric additives.

Table 2 summarizes and compares the experimental results and failure modes (Figure 2.1), of six SRG systems, from Roma Tre University (†) [24] and Rilem TC 250-CSM (*) experimental investigations [25, 26, 27].

Table 2: Properties of mortars and mechanical characteristics of SRG coupons under direct tensile test

Steel textile	Inorganic mortar				SRG direct tensile results				
Label	Label	f_{cm} [N/mm^2]	E_{cm} [kN/mm^2]	f_{tm} [N/mm^2]	f_t [N/mm^2]	ε_t [%]	E_{1m} [kN/mm^2]	E_{3m} [kN/mm^2]	Failure mode
S1*	ML	20.6	11.42	5.42	3461	2.03	914	184	A-AB
S2†					2918	1.82	1063	187	A
S1*	MG	56.3	22.01	10.31	3365	1.90	1718	186	A-AB
S2†					2964	1.92	1352	195	A
S3*	MP	6.4	6.31	1.24	2448	1.75	547	178	A-AB
S4*	MR	22.7	10.0	11.2	1045	1.23	892	102	B

f_{cm} = compressive strength; E_{cm} = Young's modulus from tests on cubic specimens; f_{tm} = tensile strength from three-point bending tests; f_t= peak stress ε_t =strain corresponding to peak stress; E_{1m}= Young's modulus in un-cracked stage; E_{3m}= Young's modulus in cracked stage.
*= RRT by RILEM TC-250 CSM experimental tests [25, 26, 27]
†= experimental tests recently carried out in Roma Tre University according to EAD [23, 24]

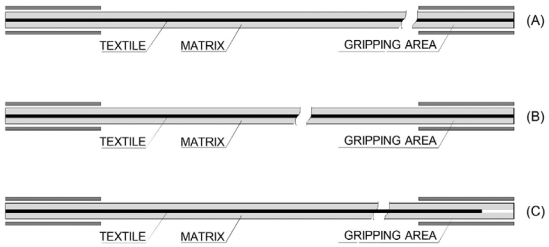


Figure 2.1: Failure mode in direct tensile tests (Rilem procedure)

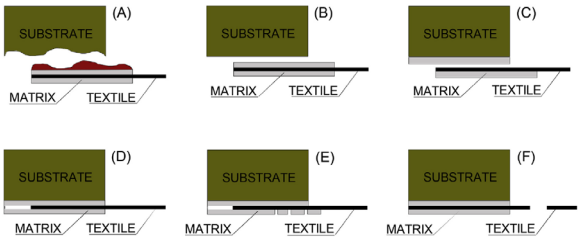


Figure 2.2: Failure mode in shear bond tests (Rilem procedure)

Experimental data collected in Table 2 show that peak stress values (f_t) and Young's modulus at third stage (E_{3m}) are generally very similar to those of bare textiles (f_s , E_s – Table 1). For instance, in SRG systems made by "S1" steel textile, the mortar contribution is calculated up to 8%, definitely more than ones made by "S2".
This phenomenon can be attributed to the fact that the low density of cords well-establishes a stress transfer among mortar layers, promoting the mechanical interlocking between cords surface and mortar. At the same time, the maximum contribution of mortar is detected for "S3-MP" system, in which the SRG peak stress value increases by 18% with respect to the dry steel textile. In this case, mortar improves the loading distribution between steel cords. For each test on SRG carried out under direct tensile, the ultimate strain corresponding to peak stress value is very close to that calculated for bare textiles, with the only exception of "S3-MP".
Concerning the failure modes (Figure 2.1), in general the main failures occur near the gripping areas (Failure mode "A") because of local stress concentration, anticipated by a progressive cracking development along the entire length of the coupon. Ruptures took place in the middle (Failure mode "B") of the coupon only for "S4-MR" system. Failure "C", characterized by cracking in the length of the specimen and fibers slippage, in any case is not observed.
From this test type, tension stiffening could be also clearly observed thanks to the distributed crack pattern. For both systems made by "S2" steel textile, crack spacing (Figure 3) is similar and as a result, the failure mode does not depend on the type of the mortar.

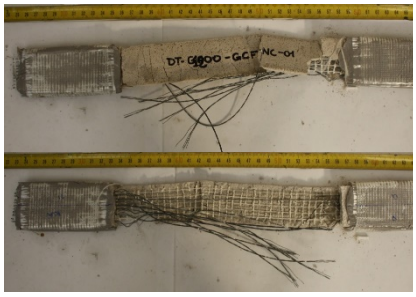
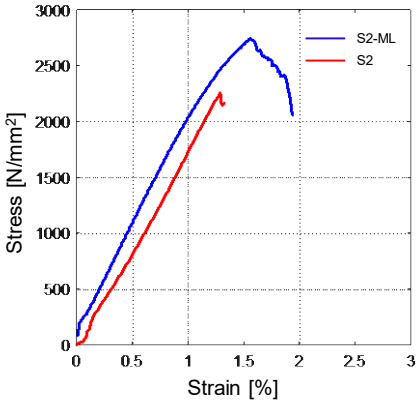
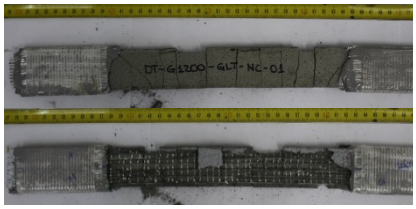
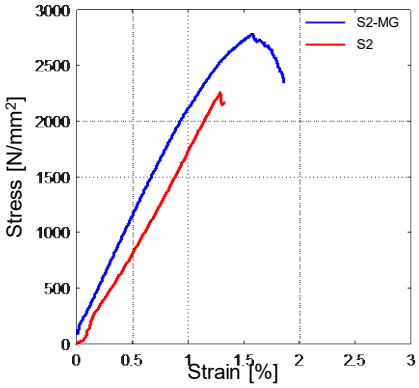
Specimen label	Failure mode	Stress-strain average curve Tensile behaviour
S2-ML†		
S2-MG†		

Figure 3: Failure mode in systems with "S2" steel textile (low-medium density). †= experimental tests recently carried out in Roma Tre University according to EAD [23, 24]

3 SRG-TO SUBSTRATE BOND BEHAVIOUR

Single-lap shear bond test (Figure 1.3) allows studying the SRG-to-substrate stress transfer behaviour, which is represented by the following properties: stress at peak load (f_b), exploitation ratios ($\eta_{dry}= f_b/f_s$, the amount of dry textile tensile strength that is exploited at bond failure; $\eta_{comp}= f_b/f_t$, the amount of SRG tensile strength that is exploited at bond failure). Failure modes are also recognized (Figure 2.2): failure mode "A" corresponds to debonding with cohesive failure of the substrate; failure mode "B" happens when debonding occurs at the matrix-to-substrate interface. For debonding at the textile-to-matrix interface, failure mode is named "C". Failure mode "D" identifies the textile slippage within the mortar matrix. Failure mode "E" occurs when textile slippage within the matrix and cracking of the outer layer of mortar are observed. Tensile rupture of the textile (out of bonded area) is classified in failure mode "F". In the following paragraphs shear bond performances of SRG composites bonded to different substrates (concrete, clay brick masonry and tuff blocks) are discussed. The following sections collect the experimental data provided by Ascione and co-authors [30] for concrete substrate, Round Robin Test RILEM TC 250-CSM procedures [25] for brick masonry, and finally others research documents for tuff substrate [31, 32].

3.1 SRG-to-concrete bond behaviour

The analysis of SRG-to-concrete substrate bond behaviour is illustrated in a recent research available in literature [30], in which different parameters have been investigated. Herein, tests with manufacturing and curing characteristics of SRG similar to Round Robin Test TC 250-CSM procedures are selected. Regarding geometrical dimensions of strengthening strip, the bonded interface length is 300mm, the width dimension is 100mm and the number of layer is chosen equal to 1. The SRG curing is carried out in room temperature for 28 days and then wet clothes are placed on the top of composite surface each day for two weeks. Inorganic mortar assumes these properties: >50MPa is the strength in compression, the tensile strength in bending is evaluated >8 MPa (28days in curing) and the elastic modulus in compression is comprised in a range from 20 to 22GPa. In addition, the properties of concrete prisms are comparable to reinforced concrete in existing buildings (concrete cylindrical strength after 28 days in the range of 13-25MPa). The surface finish (bush hammered and sandblasted) and the density of steel reinforcement ("S1" an "S2") are the only variable parameters.

Table 3: Shear bond tests results for SRG-to-concrete substrate

Specimen label	Substrate – surface finish	f_b [N/mm^2]	η_{dry} [%]	η_{comp} [%]	Failure mode
S1-ML	Concrete – bush hammered	2705	85	78	C or F
S2-ML	Concrete –bush hammered	1035	34	31	C
S1-ML	Concrete – sandblasted	2847	89	82	C or F
S2-ML	Concrete – sandblasted	899	30	28	C

In Table 3, shear bond test results on concrete substrate are collected: stress values at peak load depend on the steel density and not on the surface finish. Indeed, the global response of SRG made of low-density steel textile ("S1") is mainly provided by steel reinforcement and the subsequent failure mode corresponds to steel cords tensile failure. On the other hand, steel textiles with higher density fail at a peak load value which is the half of that achieved by lower density textiles, thus not exploiting all the strength properties of the SRG composite. This is the reason why, in "S2" systems, failure occurs by matrix debonding ("C") within the system, at the steel-mortar interface. For systems made by "S1" steel textile, failure mode "C" is associated to steel cords rupture in the unbonded region ("F" mode).

3.2 SRG-to-masonry bond behaviour

Steel Reinforced Grout-to-masonry substrate bond behaviour was deeply studied in the Round Robin Test initiative organized by the Rilem TC 250-CSM, with laboratories of several research centres from all Europe involved [25].

The maximum value of stress at peak load was recorded for SRG strengthening made by "S1" galvanized steel and lime mortar (Table 4). Failure occurred in the unbonded textile ("F" mode), therefore both exploitation ratios are very close to 100%. S4-MR system also exhibited a good bond performance, as shown by the high values of the exploitation ratio. In this case, textile slippage within the matrix took place (Failure mode "D").

Table 4: Shear bond tests results for SRG-to-masonry substrate

Specimen label	Substrate	f_b [N/mm^2]	η_{dry} [%]	η_{comp} [%]	Failure mode
S1-ML*	Clay brick masonry	3023	95	87	F
S1-MG*	Clay brick masonry	2457	77	71	B or C
S3-MP*	Clay brick masonry	1169	56	48	D
S4-MR*	Clay brick masonry	939	82	89	D

3.3 SRG-to-tuff bond behaviour

In order to investigate the SRG-to-tuff bond behaviour, test data from De Santis and de Felice [31] and Bilotta and co-autohors [32] are analysed in this paragraph. From the first document published in 2015, shear bond test performances regarding tuff unit strengthened with two systems ("S1-ML" and "S1-MG") are reported in this study. At the same time, other two cases are provided by the second research: in particular, two typologies of SRG systems applied to tuff units are analysed. Both the systems are made of the same mortar, named "MH", which is a bi-component premixed pozzolan-based grout also including hydraulic natural lime, sand, polymeric additives and short glass fibers spread in the matrix, having 12.4N/mm^2 compressive strength and 6.2N/mm^2 flexural strength. Two galvanized steels are used: three specimens are manufactured with "S5" steel textile and other three with "S6" steel type. Their properties are reported in Table 5.

Table 5: Geometrical properties and mechanical characteristics of steel textile

Specimen label	c [cords/mm]	t [mm]	φ [mm]	$f_f^{(s)}$ [N/mm^2]	$E_f^{(s)}$ [kN/mm^2]	$\varepsilon_f^{(s)}$ [%]
S5	0.100	0.149	1.38	1570	200	1.10
S6	0.200	0.138	0.93			

c = cord density; t = equivalent (design) thickness; φ = cord diameter; f_f= nominal tensile stress of dry fibers; E_f= Young's modulus ; ε_f = ultimate strain; $^{(s)}$ = data provided by supplier

Table 6: Shear bond tests results for SRG-to-tuff substrate

Specimen label	Substrate	f_b [N/mm^2]	η_{dry} [%]	η_{comp} [%]	Failure mode
S1-ML	Single tuff block	1676	52.6		C
S1-MG	Single tuff block	1876	58.9	-	A-C
S5-MH-1	Single tuff block	183	12	-	B
S5-MH-2	Single tuff block	414	28	-	D
S5-MH-3	Single tuff block	414	24	-	D
S6-MH-1	Single tuff block	1118	71	110	F
S6-MH-2	Single tuff block	1159	74	114	F
S6-MH-3	Single tuff block	476	30	47	B
S6-MH-4	Single tuff block	421	27	41	B

From Table 6, experimental data show the high variability of single-lap shear bond tests

carried out on tuff substrate. SRG systems made by "S1" galvanized steel textile achieve the maximum bond value: in particular, "S1-MG" exhibited a higher value of the bond strength with respect to "S1-ML", because geopolymer mortar is stronger than lime one. On the other hand, the maximum exploitation was achieved only for two tests (η_{dry}=71-74% η_{comp}=110-114%). Generally, in the other tests, a relatively lower bond capacity was observed, because of the weakness of the substrate and inappropriate surface preparation (debonding at tuff-matrix interface, failure mode "B").

3 CONCLUSIONS

The critical review of existing experimental evidences leads to the following observations on the tensile and bond behaviour of SRG composites:

- The rough surface of the steel cords provides an effective load transfer capacity with the mortar, as demonstrated by the distributed cracks developing under tensile loading; on the basis of available results, this is independent from the type of mortar matrix;
- The good interaction between steel cords and mortar matrix contributes to the efficiency of the SRG-to-substrate shear transfer capacity, as demonstrated by the high values of the exploitation ratios (about η=80%) detected in shear bond tests, with failure occurring by either detachment at the textile-to-matrix interface or tensile rupture of the cords.
- On the other hand, the smoother surface of steel ropes may lead to the slippage of the textile associated with a lower bond capacity (about η=50%);
- The development of adequate interlocking between textile and mortar matrix highly relies on the spacing between the steel cords.

The following issues still deserve further research efforts:

- influence on textile-to-matrix bond capacity of diameter and surface of steel cord;
- influence on substrate-to-SRG bond behaviour of substrate preparation, especially on irregular masonry surfaces and on weak substrate materials;
- long-term durability, in terms of both test protocols and results, to be developed in parallel with the research on other mortar-based composites [32, 33, 34, 35, 36].

Acknowledgements. This work was carried out within the Research Project "SICURA Sustainable technologies for the seismic protection of the cultural heritage" (2018-2020) funded by Lazio Region. Funding is also acknowledged from the Italian Ministry of Education, University and Research (MIUR), attributed to the Department of Engineering of Roma Tre University, in the frame of the Departments of Excellence Initiative (2018-2022).

REFERENCES

[1] Wobbe, E. Silva, P. Barton, B.L. Dharani, L.R. Birman, V. Nanni, A. Alkhrdaji, T. Thomas, J. and Tunis, G. Flexural capacity of RC beams externally bonded with SRP and SRG. In: *International SAMPE Technical Conference*, (2004), pp. 3009-3016.

[2] Grande, E. Imbimbo, M. and Sacco, E. Modeling and numerical analysis of the bond behavior of masonry elements strengthened with SRP/SRG. *Composites Part B: Engineering* (2013) **55**: 128–138.

[3] De Santis, S. Napoli, A. de Felice, G. and Realfonzo, R. Strengthening of structures with Steel Reinforced Polymers: A state-of-the-art review. *Composites Part B: Engineering* (2016) **104**: 87-

110.
[4] Razavizadeh, A. Ghiassi, B. and Oliveira, D.V. Bond behavior of SRG-strengthened masonry units: Testing and numerical modeling. *Construction and Building Materials* (2014) **64**: 387–397.
[5] De Santis, S. and De Felice, G. Tensile behaviour of mortar-based composites for externally bonded reinforcement systems. *Composites Part B: Engineering* (2015) **68**: 401-413.
[6] De Santis, S. Bond behaviour of Steel Reinforced Grout for the extrados strengthening of masonry vaults. *Construction and Building Materials* (2017) **150**:367-382.
[7] Malena, M. Closed-form solution to the debonding of mortar based composites on curved substrates. *Composites Part B: Engineering* (2018) Volume **139**: 249-258.
[8] Borri, A. Castori, G. and Corradi, M. Shear behavior of masonry panels strengthened by high strength steel cords. *Construction and Building Materials* (2011) **25**: 494–503.
[9] Thermou, G.E. De Felice, G. De Santis, S. Alotaibi, S. Roscini, F. Hajirasouliha, I. Guadagnini, M. Mechanical characterization of multi-ply steel reinforced grout composites for the strengthening of concrete structures. *9th International Conference on Fibre-Reinforced Polymer (FRP) Composites in Civil Engineering. (CICE 2018)* pp. 298-305.
[10] Thermou, G.E. De Santis, S. de Felice, G. Alotaibi, S. Roscini, F. Hajirasouliha, I. Guadagnini M. Bond behavior of Multi-Ply Steel Reinforced Grout Composites. *Construction & Building Materials*. (To appear)
[11] Huang, X. Birman, V. Nanni, A. and Tunis, G. Properties and potential for application of steel reinforced polymer and steel reinforced grout composites. *Composites Part B: Engineering* (2005) **36**: 73–82.
[12] Da Porto, F. Stivanin, E. Gabim, E. Valluzzi, M.R. SRG applications for structural strengthening of R beams. *ACI Spec Pub* (2012); **286**: 119-132.
[13] Napoli, A., Realfonzo, R. Reinforced concrete beams strengthened with SRP/SRG systems: Experimental investigation. (2015) Construction and Building Materials, 93, pp. 654-677.
[14] Thermou, G.E. and Hajirasouliha, I. Compressive behavior of concrete columns confined with stee-reinforced grout jackets. *Composites Part B: Engineering* (2018); **184**: 56-65.
[15] De Santis, S. Roscini, F. and de Felice, G. Full-scale tests on masonry vaults strengthened with Steel Reinforced Grout. *Composites Part B: Engineering* (2018) **141**: 20-36, ISSN 1359-8368.
[16] De Santis, S. De Canio, G. de Felice, G. Meriggi, P. Roselli, I. Out-of-plane seismic retrofitting of masonry walls with Textile Reinforced Mortar composites. *Bulletin of Earthquake Engineering* (2019) **17**(11):6265-6300.
[17] de Felice, G. De Santis, S. Realfonzo, R.Napoli, A. Ascione, F. Stievanin, E. Cescatti, E. Valluzzi, M.R. Carloni, C. and Camata, G. State of the art of steel reinforced grout applications to strengthen masonry structures. *American Concrete Institute, ACI Special Publication* (2018) June, Issue SP 326.
[18] Carloni, C., Ascione, F., Camata, G., De Felice, G., De Santis, S., Lamberti, M., Napoli, A., Realfonzo, R., Santandrea, M., Stievanin, E., Cescatti, E., Valluzzi, M.R. An overview of the design approach to strengthen existing reinforced concrete structures with SRG (2018) American Concrete Institute, ACI Special Publication, 2018-June (SP 326).
[19] de Felice, G. Aiello, M.A. Caggegi, C. Ceroni, F. De Santis, S. Garbin, E. Gattesco, N. Hojdys, Ł. Krajewski, P. Kwiecień, A. Leone, M. Lignola, G.P. Mazzotti, C. Oliveira, D.V. Papanicolaou, C. Poggi, C. Triantafillou, T. Valluzzi, M.R. Viskovic, A. Recommendation of RILEM TC 250-CSM: Test method for Textile Reinforced Mortar to substrate bond characterization. *Materials and Structures* (2018) **51**(4):95.
[20] ICC-ES (International Code Council - Evaluation Service). (2013). AC434 Acceptance criteria for masonry and concrete strengthening using fiber-reinforced cementitious matrix (FRCM) composite systems. Whittier, CA, US.
[21] CNR (Italian National Research Council). (2019). CNR-DT 215/2018. Istruzioni per la

Progettazione, l'Esecuzione ed il Controllo di Interventi di Consolidamento Statico mediante l'utilizzo di Compositi Fibrorinforzati a Matrice Inorganica. (In Italian).

[22] ACI-RILEM (ACI 549 0L – RILEM TC 250-CSM Liason Committee). (2019). Guide to Design and Construction of Externally Bonded Fabric-Reinforced Cementitious Matrix (FRCM) and Steel-Reinforced Grout (SRG) Systems for Repair and Strengthening Masonry Structures (to appear).

[23] EOTA (European Organization for Technical Assessment). EAD340275-00-0104 Externally-bonded composite systems with inorganic matrix for strengthening of concrete and masonry structures. (to appear)

[24] Roscini, F. Malena, M. and de Felice, G. Experimental evidences and numerical modelling of SRG systems under uniaxial load. *10th International Conference on FRP Composites in Civil Engineering (CICE 2020), Istanbul 1-3 July 2020*

[25] De Santis, S. Ceroni, F. de Felice, G. Fagone, M. Ghiassi, B. Kwiecień, A. Lignola, G.P. Morganti, M. Santandrea, M. Valluzzi, M.R. Viskovic, A. Round Robin Test on tensile and bond behaviour of Steel Reinforced Grout systems. *Composites Part B: Engineering* (2017) **127**:100-120.

[26] De Santis, S. Hadad, H.A. De Caso y Basalo, F.J. de Felice, G. Nanni, A. Acceptance Criteria for Tensile Characterization of Fabric Reinforced Cementitious Matrix (FRCM) Systems for Concrete and Masonry Repair. *Journal of Composites for Construction* (2018) **22**(6):04018048.

[27] de Felice, T. D'Antino, A. De Santis, S. Meriggi, P. Roscini, F. Lessons learned on the tensile and bond behaviour of Fabric Reinforced Cementitious Matrix (FRCM) composites. *Frontiers in Built Environment, section Earthquake Engineering*.

[28] Arboleda, D., Carozzi, F.G. Nanni, A. Poggi, C. Testing Procedures for the Uniaxial Tensile Characterization of Fabric-Reinforced Cementitious Matrix Composites. *Journal of composites for construction* (2016) **20**(3), p.04015063. ISSN: 1090-0268 , 1943-5614.

[29] Roscini, F. De Santis, S. and de Felice, G. Experimental investigation on the mechanical behaviour of mortar-based strengthening systems. *Proceedings of 10th International Conference on Structural Analysis of Historical Constructions (SAHC2016), 12-16 September 2016, Leuven, Be.*

[30] Ascione, F., Lamberti, M. Napoli, A. Realfonzo, R. Experimental bond behavior of Steel Reinforced Grout systems for strengthening concrete elements. *Construction and Building Materials* (2020) **232** 117105.

[31] De Santis, S. and de Felice, G. Steel reinforced grout systems for the strengthening of masonry structures. *Composite Structures* (2015) **134**:533-548.

[32] Bilotta, A. Ceroni, F. Nigro, E. Pecce, M. Experimental tests on FRCM strengthening systems for tuff masonry elements. *Construction and Building Materials* (2017) **138**: 114–133.

[33] Cancelli, A.N. Aiello, M.A. Casadei, P. Experimental investigation on bond properties of SRP/SRG – Masonry systems. *Proc. 8th Int. Symp. on FRPRCS-8* University of Patras, Patras, Greece, July 16-18 (2007).

[34] De Santis, S. Stryszewska, T. Bandini, S. de Felice, G. Hojdys, Ł. Krajewski, P. Kwiecień, A. Roscini, F. Zając, B. Durability of Steel Reinforced Polyurethane-to-substrate bond. *Composites Part B: Engineering* (2018) **153**:194-204.

[35] De Santis, S. Meriggi, P. de Felice, G. Durability of Steel Reinforced Grout composites. *17th International Brick and Block Masonry Conference (IB2MaC 2020)*

[36] Meriggi, P., de Felice, G., De Santis, S., Morganti, M., Roscini F. Durability of Steel Reinforced Grout systems subjected to freezing-and-thawing conditioning. *1st fib Italy YMG Symposium, 15 October 2019, Parma, Italy.*

12th International Conference on Structural Analysis of Historical Constructions
SAHC 2020
P. Roca, L. Pelà and C. Molins (Eds.)

PERFORMANCE ASSESSMENT OF BASALT FRCM FOR THE CONFINEMENT OF CLAY BRICK MASONRY CYLINDERS

J. D'ANNA[1*], G. AMATO[2], J. F. CHEN[3], G. MINAFÒ[1] AND L. LA MENDOLA[1]

[1]University of Palermo
Department of Engineering
Viale delle Scienze Ed. 8, Palermo (Italy)
e-mail: jennifer.danna@unipa.it (*corresponding author), giovanni.minafo@unipa.it, lidia.lamendola@unipa.it

[2] Queen's University Belfast (UK)
School of Natural and Built Environmental, David Keir Building
email: g.amato@qub.ac.uk;

[3] Southern University of Science and Technology (China)
Department of Ocean Science and Engineering
email: chenjf3@sustech.edu.cn

Keywords: Masonry columns, FRCM, Basalt-fibre strengthening, Confinement, Experimental investigation

Abstract. *Fibre Reinforced Cementitious Matrix (FRCM) composites have been proved to be a suitable strengthening material for masonry structures in the last years. Moreover, basalt fibres are increasingly used as reinforcement of composites as a more sustainable alternative to glass fibres. The goal of this work is to investigate the effectiveness of basalt FRCM to confine masonry circular columns. A total of eighteen clay brick masonry cylinders were tested in compression. The specimens were cored from two different masonry assemblies and wrapped with one or two layers of BFRCM composite. The stress-strain curves and the gains of strength and strain capacity of confined cylinders compared to the control specimens are reported together with a description of the failure modes.*

1 INTRODUCTION

Recent earthquakes occurred in the Mediterranean area pointed out the high vulnerability of masonry building heritage, especially when structural details and quality of materials are not adequate. Masonry constitutes the main construction material of a wide part of the world building historical heritage and many of these structures need to be preserved for their cultural, historical and architectural values. Particularly vulnerable structural members are columns or piers, which usually sustain mainly axial loads. When a structure is affected by structural deterioration or undergoes change of designed use causing a variation of the acting compressive forces on columns, brittle crushing failure can arise. As a consequence, the need to repair and upgrade masonry columns constitutes an ongoing demand.

In this context, the use of external wraps made by composite materials represents one of the most popular techniques proven to be effective in upgrading the performance of weak masonry

members [1, 2]. The goal of this method is to increase the axial capacity and the local ductility of the material, producing a passive confinement action. In the last years growing attention has been paid to Fibre Reinforced Cementitious Matrix (FRCM) composites [4, 5], which proved to be suitable for strengthening masonry. The composite inorganic matrix makes the composite compatible to the masonry substrate and ensures durability in aggressive environmental conditions, vapour permeability and low sensitivity to high temperatures.

In regard to reinforcement, basalt textiles proved to be a promising alternative to the most common synthetic fabrics [6], such as carbon or glass fibres.

Currently the majority of published experimental works on FRCM strengthening of masonry columns focuses on square/rectangular columns [1-8]. Although less common, testing of circular columns can provide useful data on the effect of pure confinement. Moreover, the effect of the number of reinforcing layers on the stress-strain response of FRCM-confined columns is investigated only by few studies [8] as the most of experimental works consider only specimens reinforced with one or two grid plies [1-7].

The present paper presents the results of a set of axial tests on clay brick masonry cylinders confined with BFRCM. A preliminary investigation was carried out on the mechanical properties of constituent materials of masonry and the strengthening system. The cylinders were assembled using two different brick arrangements in order to test the influence of the joints on the masonry capacity. The role of the reinforcing ratio was also studied by considering the confining effect of one or two layers of basalt FRCM. The results in terms of compressive strength and strain increments allow drawing some conclusions on the effectiveness of this strengthening system.

2 EXPERIMENTAL PROGRAMME

2.1 Specimen description and preparation

A total of eighteen clay brick masonry cylinders were prepared and tested under uniaxial monotonic compression. The specimens had a diameter of 94 mm and height of 190 mm, and were cored from two different assembly schemes, Scheme I and Scheme II (see Fig. 1). Both schemes provided cylinders with three rows of pressed bricks and 8 mm thick mortar joints. Cylinders cored from Scheme I had only one vertical joint in the middle third (Fig. 1a) while cylinders cored from Scheme II had three staggered vertical joints, one at each level (Fig. 1b). The samples were cored after a curing period of 30 days and then wrapped with one or two BFRCM layers.

The tested specimens were very small in this study. It may be noted that what is important is the confinement pressure, not the surface to volume ratio. Existing studies on FRP-confined concrete columns have shown that there is no significant size effect for circular columns [9].The only issue which might have some effect is that the overlapping zone is more significant compared with circumference in very small columns than larger ones, which would require further research.

Table 1 gives a summary of all the specimens. The tested cylinders were named as CN_SXL, where C stands for cylinder, N refers to the specimen number, S indicates the assembly scheme (W and C for Scheme I and Scheme II respectively), X refers to the number of confinement layers (1 or 2), L means layer. For unconfined samples, the last two letters were substituted by "Un".

Table 1: Compressive tests on BFRCM-confined cylinders

Assembly scheme	Specimen	Number of vertical joints	Number of BFRCM layers
Scheme I	C1_WUn	1	None
	C2_WUn		
	C3_WUn		
	C4_WUn		
	C1M_W1L		1
	C2M_W1L		
	C3M_W1L		
	C4M_W1L		
	C1M_W2L		2
	C2M_W2L		
	C3M_W2L		
Scheme II	C1_CUn	3	None
	C2_CUn		
	C1M_C1L		1
	C2M_C1L		
	C3M_C1L		
	C1M_C2L		2
	C2M_C2L		

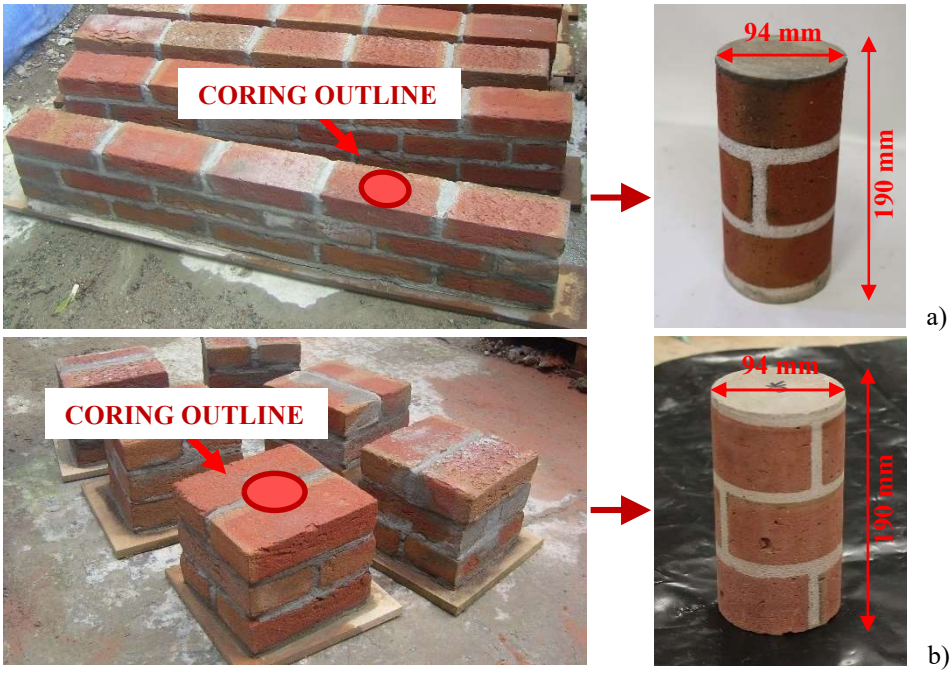


Figure 1: Assembling schemes of cylinders: a) Scheme I (wall); b) Scheme II (column)

2.2 Materials

2.2.1 Components of masonry

Pressed bricks with nominal dimensions 50x100x210 mm were used for assembling walls and columns from which cylinders were cored. In order to characterize the mechanical behaviour of the clay brick units, six cubes with side equal to 50 mm were tested under uniaxial compression (Fig. 2a) according to EN 772-1 [10]. The bricks showed an average compressive strength equal to 42.53 MPa (COV=8.75%).

The mortar used for assembling walls and columns was composed of cement and sand, with a weight ratio of 1/5. Water was added in order to reach the minimum workability. Three-point bending tests were performed on six standard 40x40x160 mm mortar prisms (Fig. 2b) and uniaxial compressive tests were carried out on obtained twelve halves, according to EN 1015-11 [11]. The mortar had an average compressive strength equal to 20.93 MPa (COV=5.52%) and an average tensile strength equal to 5.33 MPa (COV=5.13%).

2.2.2 BFRCM system and components

The grid used to wrap the cylinders was a primed bidirectional grid, having nominal cell size of 6x6mm and equivalent thickness of 0.039 mm. The nominal mechanical characteristics provided by the manufacturer were: unit tensile strength of 60 kN/m, ultimate strain of 1.8% and Young's modulus of 89 GPa. To characterize the tensile behaviour of the basalt mesh, monotonic tensile tests were carried out on a series of twelve strips [13, 14] (Fig. 2c), according to ISO 13934-1 [12]. The recorded average values of strength, strain and Young's modulus are reported in Table 2, along with the coefficient of variation (COV).

The mortar used as matrix of the BFRCM system was a bicomponent cement-based mortar, enriched with short glass fibres. According to the technical data sheet, the mortar had flexural strength of 8 MPa, compressive strength equal to 25 MPa and Young's modulus of 10 GPa. Three-point bending tests were performed on six standard 40x40x160 mm prisms according to EN 1015-11 [11]. The recorder average flexural strength and COV are reported on Table 2.

Additionally, the mechanical behaviour of the composite was characterized under tension. Fourteen BFRCM coupons were manufactured using different reinforcement ratios, according to available regulations [15]. Specimens were tested under displacement control, with a rate of 0.2 mm/min and using Digital Image Correlation (DIC) technique for recording the strain field [13, 14].

Table 2: Mechanical characterization of basalt grid and mortar matrix

BASALT GRID			MORTAR
Average Tensile strength [MPa] and COV	**Average Tensile strain [%] and COV**	**Average Elastic modulus [GPa] and COV**	**Average Flexural strength [MPa] and COV**
2045	2.55	81.91	7.18
10.55%	8.21%	3.48%	2.80%

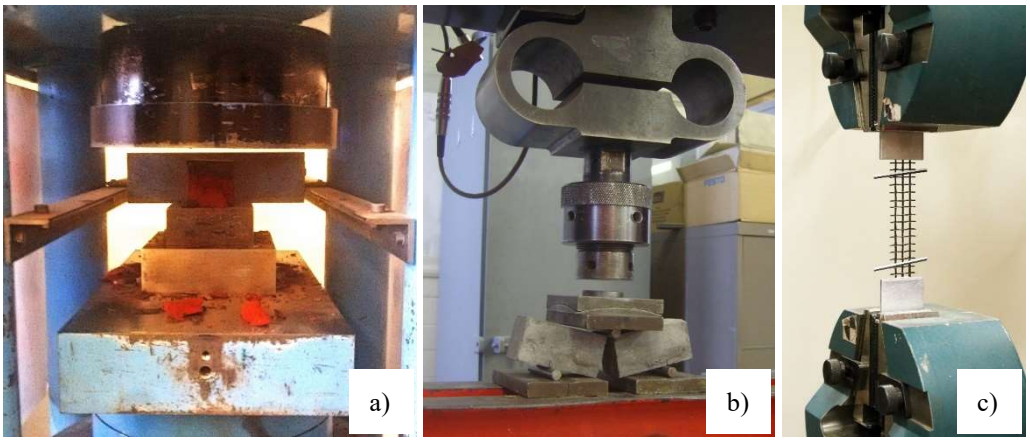


Figure 2: Characterization tests on components: a) compressive tests on brick cubes; b) three-point bending test on mortar; c) tensile test on basalt grid

2.3 Test procedure and instrumentation for compression tests on cylinders

A 600 kN electro-hydraulic loading frame was used to perform monotonic compressive tests on the cylinders. Tests were carried out in displacement control, using a loading rate of 0.002 mm/sec, after applying three loading/unloading cycles under load control up to 40-50 kN.

Six Linear Voltage Differential Transducers (LVDTs) were installed, four to monitor the displacement of the upper loading platen and two at the lower platen (Fig. 3). In order to record the local axial strain in the middle half of the specimens, three extensometers connected to two steel rings placed around the cylinders were also used.

Furthermore, the DIC technique was used to analyze the strain field on the surface of the cylinders [14]. Outcomes of DIC measurements are not reported in this paper for the sake of brevity.



Figure 3: Test setup for compressive tests on masonry cylinders

3 RESULTS AND DISCUSSION

3.1 BFRCM system

The average experimental results of the tensile tests on BFRCM coupons are summarized in Table 3 for the three series of samples reinforced with one, two and three layers respectively. In particular, the outcomes are presented with reference to the three stages typical of the response of FRCM composites tested under tension: un-cracked Stage I, crack development Stage II and cracked Stage III [13].

Table 3: Average results of tensile tests on BFRCM coupons

Series	Stage	Peak load [kN]	Strain [%]
1 Layer	I	1234.11	0.030
	II	1398.03	1.019
	III	2054.93	2.322
2 Layers	I	1448.22	0.035
	II	1855.26	0.448
	III	3538.20	1.912
3 Layers	I	1437.38	0.044
	II	1821.68	0.229
	III	4633.19	1.466

3.2 BFRCM-confined cylinders

The outcomes of monotonic compressive tests are presented in terms of axial stress-strain curves in Fig 4, for unconfined and BFRCM-confined cylinders from Scheme I and Scheme II respectively. The axial strain up to the peak load was obtained considering the displacement recorded over the central half of the cylinders. For the post-peak branch the LVDT readings from top and bottom plate were used since the rings fixed on the cylinders had to be taken off during the last part of the tests. For unconfined cylinders C1_WUn, C2_WUn, and C3_WUn, the strain was evaluated using the LVDTs on the top and bottom plates as the readings in the central area of the cylinders were lost during testing. This explains the different measured value of stiffness of these cylinders in Fig. 4a. The strains of these specimens were not taken into account for the calculation of ε_{m0} and ε_{m0u} in Table 4.

The stress-strain curves of unconfined cylinders present a brittle behaviour, characterized by an almost linear ascending branch and a steep load drop after the peak.

The stress-strain curves of BFRCM-confined cylinders show a linear branch followed by a stress drop due to the failure of the inner masonry core and the formation of first cracks in the external jacket. Afterwards, the curves show a new stress increase up to the peak, which is followed by a descending branch ending in a plateau region (Fig. 4). The full stress-strain curve of cylinder C3M_W2L is not available due to a technical problem during testing.

Table 4 reports the average peak axial stress (f_{m0} - f_{mc}), the axial strain at peak stress (ε_{m0} - ε_{mc}) and the ultimate axial strain corresponding to a 15% stress reduction with respect to the peak value (ε_{m0u} - ε_{mcu}) of tested cylinders, along with the COVs.

In the case of unconfined cylinders, the average peak stress values were 25.19 MPa and

19.85 MPa for Scheme I and Scheme II respectively, pointing out a considerable detrimental effect of the vertical mortar joints.

For one-layer confined cylinders, the average strength increases were equal to 27% and 66% for Scheme I and Scheme II specimens respectively, compared to unconfined cylinders. For cylinders confined with two BFRCM layers, the average strength gain was 38% for Scheme I and 85% for Scheme II. As expected, the effectiveness of BFRCM jacket was higher for the weakest masonry, i.e. in the case of Scheme II cylinders having three vertical joints.

Regarding the strain at peak stress, one-layer reinforced cylinders from Scheme I and Scheme II exhibited the same increase of average strain at peak stress, equal to 45%, compared to control samples. Two-layer strengthened specimens from Scheme I showed an average increase of 57%, while specimens from Scheme II presented an average strain gain of 75%.

In terms of ultimate strain, cylinders from Scheme I showed an average ultimate strain increase of 72% and 97% for one and two-layer confined specimens respectively, in comparison to unconfined ones. For cylinders from Scheme II, the average ultimate strain increased by 96% and 121% respectively for one and two-layer reinforced specimens.

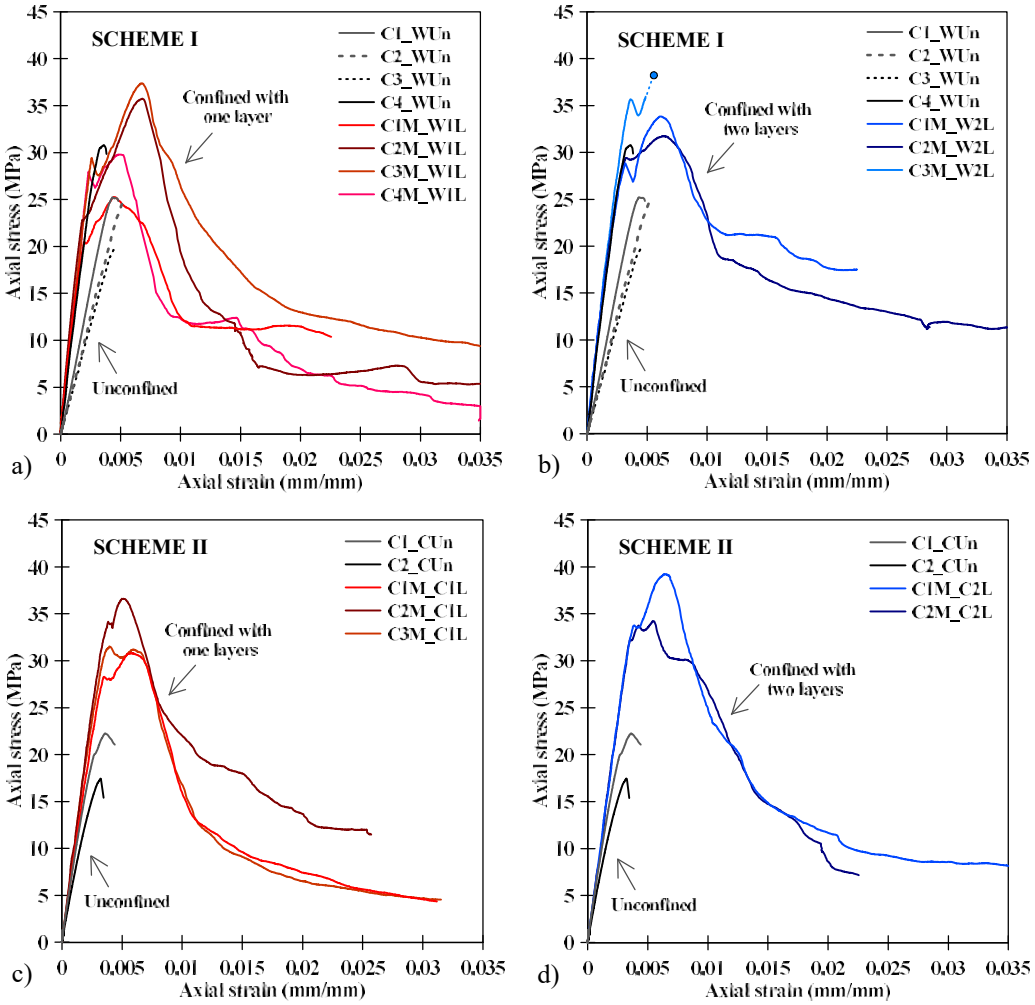


Figure 4: Stress-strain curves of masonry cylinders: a) Scheme I - 1 layer; b) Scheme I - 2 layers; c) Scheme II - 1 layer; d) Scheme II - 2 layers

3.3 Failure modes of masonry cylinders

Figure 5 presents unconfined and confined cylinders at the end of the compression tests.

As expected, the unconfined specimens showed a brittle behaviour and the failure was characterized by the formation of almost vertical cracks along the height. Vertical joints created preferential routes for the development of cracks and the failure involved crushing of masonry with spalling of material through the height of the cylinders (Fig. 5a and b).

Confined cylinders showed similar failure modes and no substantial difference was observed between the different schemes. In all the cases, the ultimate condition was reached by failure of the basalt textile. Vertical cracks developed for the entire length of the samples, producing detachment of the external mortar layer of the jacket in those parts and the loss of material in some areas (Fig. 5c and d).

Table 4: Average results of BFRCM-confined cylinders

Assembly	Confinement	Peak axial stress [MPa] and COV	Peak axial strain [mm/mm] and COV	Ultimate axial strain [mm/mm] and COV
		f_{m0}	ε_{m0}	ε_{m0u}
Scheme I	Unconfined	25.19 17.60%	0.0040 12.41%	0.0043 15.91%
Scheme II	Unconfined	19.85 17.14%	0.0034 8.88%	0.0038 13.56%
		f_{mc}	ε_{mc}	ε_{mcu}
Scheme I	1 Layer	32.04 (17.40 %)	0.0058 (21.27 %)	0.0074 (13.37 %)
	2 Layer	34.78 (10.35 %)	0.0062 (2.75 %)	0.0085 (6.76 %)
Scheme II	1 Layer	32.98 (9.60 %)	0.0050 (18.78 %)	0.0075 (7.07 %)
	2 Layer	36.73 (9.58 %)	0.0060 (12.16 %)	0.0085 (8.90 %)

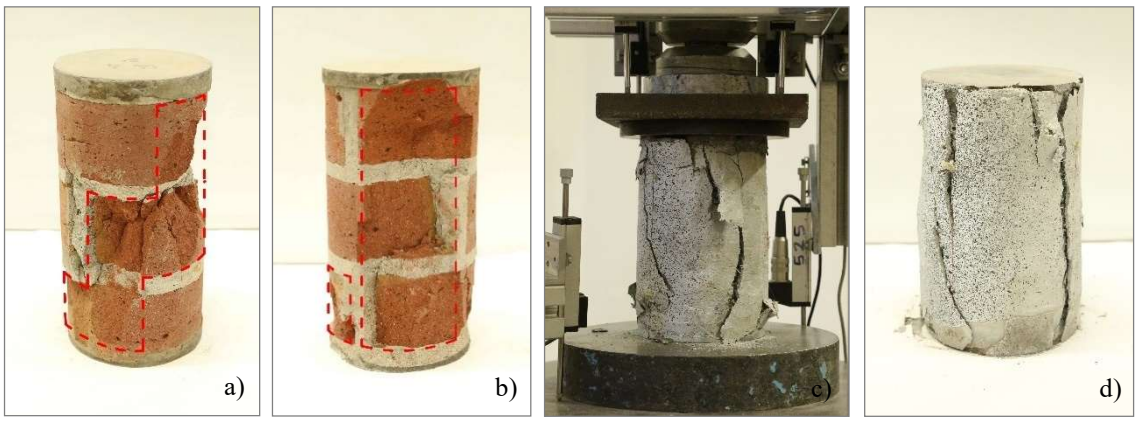


Figure 5: Cylinders after failure: a) unconfined (Scheme I); b) unconfined (Scheme II); c) one-layer BFRCM-confined (Scheme II); two-layer BRFCM-confined (Scheme II)

4 CONCLUSIONS

This paper presented the results of an experimental study on small scale clay brick masonry cylinders, tested under axial compressive load. The cylinders had two different assembly schemes and were confined with one or two BFRCM layers. Considering the experimental results and for the range of variables examined, the following conclusions can be drawn:

- Unconfined cylinders with three vertical mortar joints (Scheme II) presented an average strength reduction of 20% compared with those having one vertical joint (Scheme I);
- For one-layer BFRCM-confined cylinders, the average strength increased 27% and 66% for Schemes I and II specimens respectively, compared to unconfined cylinders. Two-layer confined specimens had an average strength enhancement of 38% for Scheme I and 85% for Scheme II, respectively;
- The confinement due to BFRCM increased considerably the ductility of the specimens. These last showed a softening branch in the compressive stress-strain curves;
- The ultimate condition of confined specimens was reached by failure of the basalt textile, highlighting that the full capacity of the fabric was exploited.

REFERENCES

[1] Micelli, F., Di Ludovico, M., Angiuli, R., Aiello, M. A. Experimental tests on full scale FRP/FRCM confined masonry columns subjected to axial load. *Mater Struct* (2014) **47**(12):2081-2100.

[2] Incerti, A., Vasiliu, A., Ferracuti, B., Mazzotti, C. Uni-Axial compressive tests on masonry columns confined by FRP and FRCM. In Proceedings of the 12th international symposium on fibre reinforced polymers for reinforced concrete structures and the 5th Asia-Pacific conference on fibre reinforced polymers in structures, joint conference, Nanjing, (2015), pp. 14-16.

[3] Alotaibi, K. S. and Galal, K. Axial compressive behaviour of grouted concrete block masonry columns confined by CFRP jackets. *Compos Part B - Eng* (2017) **114**:467-479.

[4] Minafò, G. and La Mendola, L. Experimental investigation on the effect of mortar grade on the compressive behaviour of FRCM confined masonry columns. *Compos Part B – Eng* (2018) **146**:1-12.

[5] Cascardi, A., Micelli, F., Aiello, M. A. FRCM-confined masonry columns: experimental investigation on the effect of the inorganic matrix properties. *Constr Build Mater* (2018) **186**:811-825.

[6] Santandrea, M., Quartarone, G., Carloni, C., Gu, X. L. Confinement of masonry columns with steel and basalt FRCM composites. In *Key Engineering Materials*, Trans Tech Publications 747 (2017), pp. 342-349.

[7] Maddaloni, G., Cascardi, A., Balsamo, A., Di Ludovico, M., Micelli, F., Aiello, M. A., Prota, A. Confinement of full-scale masonry columns with FRCM systems. In *Key Engineering Materials*, Trans Tech Publications 747 (2017), pp. 374-381.

[8] Ombres, L. and Verre, S. Masonry columns strengthened with Steel Fabric Reinforced Cementitious Matrix (S-FRCM) jackets: experimental and numerical analysis. *Measurement* (2018) **127**:238-245.

[9] Guo, Y. C., Gao, W. Y., Zeng, J. J., Duan, Z. J., Ni, X. Y., & Peng, K. D. Compressive behavior of FRP ring-confined concrete in circular columns: Effects of specimen size and a new design-oriented stress-strain model. *Constr Build Mater* (2019) **201**:350-368.
[10] EN 772-1. Method of test for masonry units – Part 1: Determination of compressive strength (2011).
[11] EN 1015-11. Methods of test for mortar for masonry – Part 11: Determination of flexural and compressive strength of hardened mortar (1999).
[12] ISO 13934-1. Textiles – Tensile properties of fabrics – Part 1: Determination of maximum force and elongation at maximum force using the strip method. CEN – European Committee for Standardization (April 2013).
[13] D'Anna, J., Amato, G., Chen, J. F., Minafò, G., & La Mendola, L. On the use of Digital Image Correlation (DIC) for evaluating the tensile behaviour of BFRCM strips. In *Key Engineering Materials*, Trans Tech Publications Ltd 817 (2019), pp. 377-384.
[14] D'Anna, J. Experimental investigation on the effectiveness of basalt-fibre strengthening systems for confining masonry elements (2019).
[15] ICC. AC434. Proposed Acceptance Criteria for Masonry and Concrete Strengthening Using Fibre-reinforced Cementitious Matrix (FRCM) Composite Systems. Whittier, CA: ICC-Evaluation Service (2013).

12th International Conference on Structural Analysis of Historical Constructions
SAHC 2020
P. Roca, L. Pelà and C. Molins (Eds.)

PERFORMANCE OF UNREINFORCED MASONRY STRENGTHENED WITH BED JOINT REINFORCED REPOINTING

LUCIA LICCIARDELLO[1], JAN G. ROTS[2], RITA ESPOSITO[2*]

[1] Researcher; Department of Materials, Mechanics, Management and Design, Delft University of Technology, Stevinweg 1, 2628CN Delft, The Netherlands; l.licciardello@tudelft.nl.
[2] Full Professor; Department of Materials, Mechanics, Management and Design, Delft University of Technology, Stevinweg 1, 2628CN Delft, The Netherlands; j.g.rots@tudelft.nl.
[2]Assistant Professor; Department of Materials, Mechanics, Management and Design, Delft University of Technology, Stevinweg 1, 2628CN Delft, The Netherlands; r.esposito@tudelft.nl.

Keywords: unreinforced masonry (URM), settlement, induced seismicity, bed joint reinforcement, twisted steel bars, in-plane test.

Abstract. *Bed joint reinforced repointing is a strengthening method often used in the Netherlands to counteract settlement damage. This strengthening technique consists of cutting a slot in the mortar joint and installing twisted steel bars embedded in a high-strength repair mortar. Due to the increase in seismic activities, triggered by gas extraction in the region of Groningen (northern part of the Netherlands), it is of interest to investigate whether this strengthening technique is efficient against seismic load.*

In order to characterize the performance of the bed joint reinforced repointing using twisted steel bars, an experimental campaign was conducted at Delft University of Technology. A quasi-static cyclic in-plane test on a full-scale wall was performed; similar tests on unstrengthened specimens were available from a previous experimental campaign [1][2] and were used for comparison. Moreover, small scale pull-out tests were performed to study the interaction between the steel bars and the repair mortar.

By comparing the response of unstrengthened and strengthened masonry specimens, it is observed that the use of bed joint reinforced repointing can provide an increase in terms of ductility and displacement capacity, but not in terms of force capacity. Regarding the serviceability limit state, a reduction in crack width and an increase of load at onset of cracking were observed. The preliminary information obtained for the presented case study provides the ground for futher research as well as benchmark for numerical modelling.

1 INTRODUCTION

The bed joint reinforced repointing technique consists in the insertion of reinforcement (steel, stainless steel or FRP bars) in shovelled mortar bed joints rifilled with repair mortar. This technique does not influence the aesthetic aspect of the building and it can be applied with limited invasiveness; for this reason it is often used to preserve the historical and the artistic aspects of cultural heritage buildings. In the Netherlands, where the buildings' stock is mainly composed of unreinforced masonry, this techniques has been largely applied to counteract settlement damage. During the last years, the phenomena of induced seismicity, due to the gas extraction, considerably increased in the region of Groningen (northern part of the Netherlands), causing damage to the unreinforced masonry buildings. Therefore, it is of

interest to investigate the performance of masonry strengthened with bed joint reinforcement under seismic loading.

Previous studies on reinforced repointing mainly focused on evaluating its effictivness against settlement and creep damage, while less attention has been paid to the seismic performance of masonry strengthened with bed joint reinforcement. Previous researchers [3][4], showed no significant improvement of the strength of masonry, but thanks to the confining action provided by the bed joint reinforcement a reduction of the dilation and a reduced cracks pattern were obtained. In literature, limited information on the seismic performance of masonry strengthened with bed joint reinforcement is available. In this respect, researchers mainly performed diagonal-shear compression tests on wallets. Ismail et al. [5] made a comparison of the bed joint reinforcement with a near-surface mounted technique made by placing steel bars in the vertical direction, being this often done to prevent out-of-plane failure of unreinforced masonry buildings in countries prone to strong intensity seismic events.

To this purpose an experimental campaign was conducted at Delft University of Technology; a quasi-static cyclic in-plane test on a full-scale wall was performed. Within this testing campaign also the performance against settlement damage was investigated by performing four-point bending tests on strengthened and unstrengthened masonry wallettes [6]; however in this paper only the results obtained from the cyclic in-plane test are presented and discussed. The experimental results obtained from the test on the strengthened wall are compared with the results obtained on similar unstrengthened walls obtained from previous experimental campaigns [1],[2]. Section 2 provides a detailed description of the material used, the type of specimen, the test set-up and the loading protocol. Section 3 shows the main results that were obtained from the test on the unstrengthened and the strengthened walls. The results are discussed in section 4 and Section 5 presents the main concluding remarks.

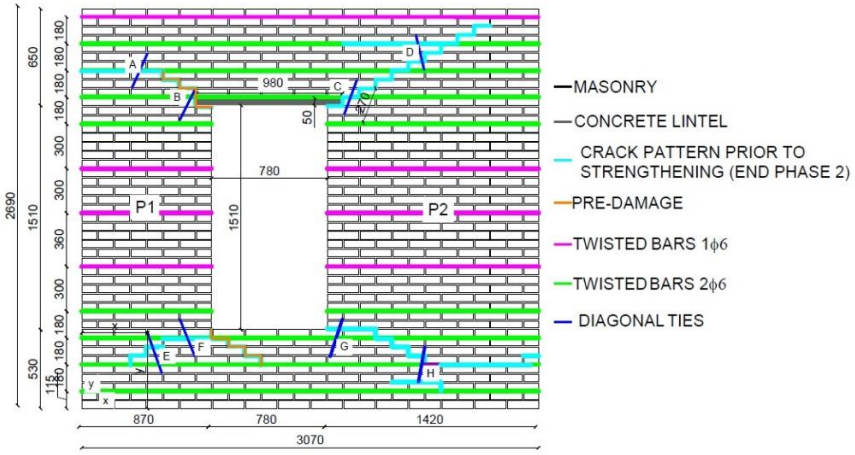
2 MATERIALS AND METHODS

2.1 Description of the specimen

To assess the performance of the bed joint reinforcement with twisted steel bars against seismic load, a quasi-static cyclic in-plane test on a full-scale strengthened wall was performed and compared with available data on unstrengthened walls tested in previous studies [1][2]. Two different walls were considered: a pre-damaged wall TUD-COMP-45 [2] and an undamaged and unstrengthened wall TUD_COMP-41 [1]. The geometry of the wall was the same and was defined based on typical dimensions presents in Dutch detached house [7] (Figure 1a). The walls were made of solid clay single-wythe masonry and built in running bond, Table 1 lists the material properties of the single components and of masonry. Both walls were tested under a cyclic loading protocol [1][2] up to a light damage state in which a maximum crack width around 2 mm was obtained (light blue lines Figure 1a). To reproduce the damage caused by settlement before an earthquake, in the wall TUD_COMP-45 [2] a pre damage was simulated by creating un-bonded brick-joint interfaces using thin plastic strips (orange lines in Figure 1a). Afterwards, only wall TUD_COMP-45 was strengthened (Figure 1a) and re-tested up to light damage state. Eventually, both walls were tested up to near-collapse state. To evaluate the performance of the strengthening measures for the serviecibility limit state, the comparison is made by considering the results obtained for the

light damage state on wall TUD_COMP-45 before and after the strengthening measure was applied, while the considerations for near collapse limit state are drawn from the comparison between the two walls.

The layout of the bed joint reinforcement mainly reflected the application in practice. The areas above and below the window opening are the most prone to vertical damage due to settlement. Consequently, to counteract the settlement damage two twisted steel bars were installed in the mortar joints in the area above and below the window opening every three mortar courses (green lines in Figure 1a); additionally one bar every five/six mortar courses (pink line in Figure 1a) was installed in the piers (vertical masonry portion next to the window opening) and diagonal ties (blue lines in Figure 1a) were installed in correspondence of the existing diagonal cracks at the corners of the window opening. Figure 1b shows the detail of a strengthened section and Table 2 lists the properties of the cement-based repair mortar, twisted steel bars and diagonal ties used for the strengthening.



(a)



(b)

Figure 1: Overview of the adopted specimen and its features: (a) dimensions and strengthening configuration; (b) detail of the strengthened bed joint and execution of the intervention.

Table 1: Material properties of replicated clay brick masonry built in July 2018 [2].

Material properties	Symbol	Unit	Average	C.o.V	No. tests	Standard
Normalised compressive strength of masonry unit (210x100x50-mm)	f_b	MPa	28.31	0.10	9	EN 772-1:2000 [8]
Flexural strength of masonry unit	f_{bt}	MPa	6.31	0.11	8	EN 6790:2015 [9]
Compressive strength of construction mortar (cement:lime:sand ratio of 1:2:9)	f_m	MPa	3.59	0.09	24	EN 1015-11:1999[10]
Flexural strength of construction mortar	f_{mt}	MPa	1.55	0.10	12	
Density of masonry	ρ	kg/m^3	1628	0.01	-	-
Compressive strength of masonry in the direction perpendicular to bed joints	f'_m	MPa	12.93	0.07	3	EN 1052-1:1998[11]
Elastic modulus of masonry in the direction perpendicular to bed joints calculated between 1/3 and 1/10 of the maximum stress	E_3	MPa	3190	0.24		
Flexural bond strength	f_w	MPa	0.08	0.32	10	EN 1052-5:2002[12]
Masonry initial shear strength	f_{v0}	MPa	0.13	-	6	EN 1052-3:2002[13]
Masonry shear friction coefficient	μ	-	0.82	-		

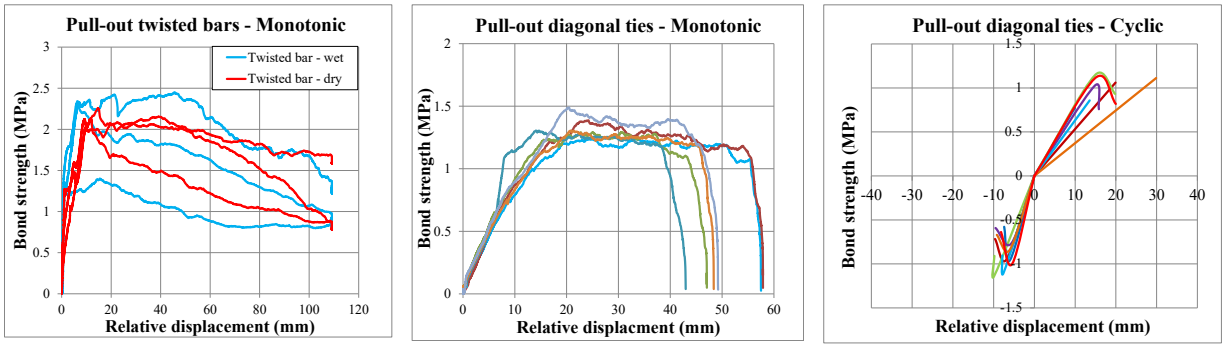
Table 2: Material properties of the materials used for strengthening.

Cement-based repair mortar						
Compressive strength of repair mortar	$f_{m,r}$	MPa	46.42	0.09	16	EN 12190: 2018[14]
Flexural strength of repair mortar	$f_{mt,r}$	MPa	7.68	0.24	9	
Twisted steel bar*						
Ultimate tensile	f_{nu}	MPa	1112	-	-	
Tensile strength	F_{pu}	kN	10	-	-	
0.2% Proof stress	f_{py}	MPa	900	-	-	
Diagonal tie*						
Ultimate tensile	f_{nu}	MPa	1398	-	-	
Tensile strength	F_{pu}	kN	13	-	-	
0.2% Proof stress	f_{py}	MPa	1100	-	-	

*Data provided by producer.

The effectiveness of the bed joint reinforcement depends on the bond behaviour between the mortar and the twisted steel bar, which can be studied with pull-out test [15]. Within this study, the bond behaviour between the twisted steel bars and the repair mortar and between the diagonal ties and the masonry is considered. In the first case, the standar EN 1766 [16] was adopted by embedding the repair mortar and the twisted steel bars in concrete cubes with dimensions 400x400x250-mm. In the second case, diagonal ties were vertically installed in a masonry triplet with dimensions 210x170x100-mm. The set-up used for the two types of test was the same and similar to the one adopted in a previous testing campaign [17]. For the two types of test a monotonic load was applied; in addition for the diagonal ties cyclic pull-out

tests were also performed [17]. Figure 2 shows the experimental results in terms of bond-strenght versus relative displacement curve. For the cyclic tests, the envelope curve was calculated considering the force and the displacement in correspondence of the peak force and in correspondence of a drop of 20% of the maximum force [17]. These curves can serve as input for numerical analyses.



(a) (b) (c)

Figure 2: Bond-strength versus relative displacement curve: (a) monotonic test on twisted steel bars; (b) monotonic test on diagonal ties; (c) cyclic test on diagonal ties.

2.2 Test set-up and loading scheme

Figure 3 shows the set-up adopted to perform the quasi-static cyclic in-plane test. An overburden of 0.12 MPa was applied on top of the wall through two steel beams. The lateral load was applied with a horizontal actuator with a capacity of 100 kN. The positive loading direction is defined when the horizontal actuator is compressed (from right to left in Figure 3). On the front side of the wall, which corresponds to the external side of the wall on which the bed joint reinforcement was installed, Digital Image Correlation (DIC) was applied to detect crack initiations and propagation; the backside of the wall was instrumented with contact sensors.

The walls were tested under a quasi-static cyclic lateral in-plane load in a cantilever configuration by controlling the horizontal displacement of the jack and the net horizontal displacement was calculated as the displacement of the top beam with respect to the external reference excluding possible rotations of the set-up and possible horizontal displacement of the bottom beam with respect to the external reference. In Figure 4 the net horizontal displacement is shown and it is similar for the unstrengthened and strengthened configuration. The lateral load was applied in three phases: phase 1 and phase 2 up to light damage state with the same loading protocol as used in Ref. [2]; phase 3 up to near collapse state with the loading protocol derived from a previous study and representative of a Groningen type earthquake [18]. In phase 1 and 2 each cycle was composed of 30 runs, in phase 3 the first two cycles were composed on 2 runs and the remaning were composed of a single run (Figure 4). A cycle is defined as the time interval in which the same target horizontal displacement was applied with the same rate. A run is defined as the time needed to impose the target displacement in the positive and negative loading direction up to returning to the original position of the wall. During the light damage phase, the lateral load was applied with a

constant rate equal to 0.125 mm/s; during the near-collapse phase, the load-rate varied between 0.03 to 1 mm/s so that each cycle lasted 5 min (except for the last cycle that lasted 4 min because the test was stopped as it is explained in section 3).

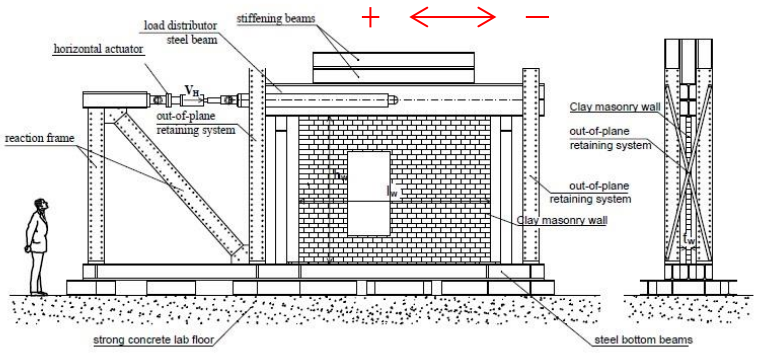
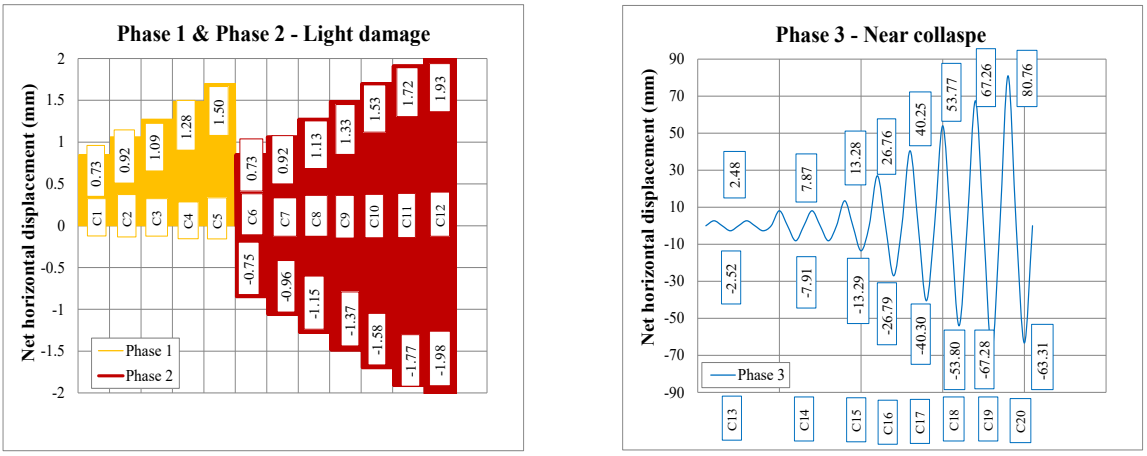


Figure 3: In-plane test set-up.



(a) (b)

Figure 4: Loading scheme: (a) light damage phases 1 and 2; (b) near collapse phase 3.

3 EXPERIMENTAL RESULTS

In this section, the results obtained from the in-plane test on the unstrengthened and strengthened walls are presented in terms of crack pattern and base shear force versus net horizontal displacement (Figure 5).

Considering the unstrentghened case, the response is analysed for specimen TUD_COMP-45 [2] up to light damage state and for specimen TUD_COMP-41 [1][2] up to the near collapse state. The initial stiffness, calculated in the first cycle of phase 1 (C1 d = 0.72 mm) was equal to 29.06 and 26.88 kN/mm for wall TUD_COMP-45 [2] and TUD_COMP-41[1], respectively. A similar response was observed up to the maximum base shear force. The maximum base shear force was equal to 20.72 kN (C15 d=11.11mm) and to -19.54 kN (C14 d=-7.97mm) for the positive and negative loading direction, respectively. For wall

TUD_COMP-41, the ultimate displacement was equal to approximately 40 mm in both loading directions, corresponding to a ultimate drift of 1.61/-1.49 %. Both walls show the formation of diagonal stepwise cracks from the window corners. To highlight the small differences in crack position, for wall TUD_COMP-41 the subscript "a" is added to the crack number. Crack 1 and 2 developed during phase 1 (orange color in Figure 5a) with a stepwise configuration starting from the bottom right and the top left corner of the window opening, respectively. The onset of cracking was in correspondence of cycle C1 (d = 0.72mm) at a load equal to 19.6 kN. During phase 2 (red color in Figure 5a), crack 3 and 4 evolved with a stepwise configuration from the bottom left and top right corner of the window opening, respectively. During Phase 3 (blue color in Figure 5e), existing cracks mainly evolved by increasing their length and width.

Considering the strengthened case, the response is analysed considering the wall TUD_COMP-45 both for the light damage and the near collapse state. The initial stiffness, calculated in the first cycle of Phase 1 (C1 d = 0.73 mm), was equal to 28.78 kN/mm. The maximum base shear force was equal to 25.14 kN (C16 d = 23.08 mm) and to -23.46 kN (C14 d = -7.90mm) for the positive and negative loading direction, respectively. At the end of the near collapse phase, the ultimate displacement was equal approximately to 80 mm and to 60 mm for the positive and negatve loading direction, corresponding to an ultimate drift of 2.99/-2.34 %. The test was stopped because out-of-plane deformation occurred in both piers (vertical masonry portion next to the window opening). Crack 1 developed during Phase 1 (orange color in Figure 5c), with a stepwise configuration from the bottom right corner of the window opening; crack 2* developed horizontally at the top left corner of the window opening in a mortar joint where the reinforcement was not present (a subscript is used to mark the crack because it had a different shape/location with respect to the unstrengthened wall as will be explained in Section 4). The onset of cracking was in correspondence of cycle C1 (d = 0.73mm) at a load equal to 19.7 kN. Crack 3 and 4 developed during phase 2 (red color in Figure 5c) with a stepwise configuration at the bottom left corner and at the top right corner of the window opening, respectively. During phase 3 (blue color in Figure 5g), the cracks in the masonry portion above the window opening developed mainly horizontally in the mortar joints where the reinforcement was not present, while in the portion below the window opening the cracks propagated in the mortar joints forming an arch mechanisms triggered by the bars. Approaching the end of the test, thanks to the progression of damage at cycle C18 (d = 53.77/-53.80 mm) the cracks started also in the bricks at the bottom left corner and at cycle 19 (d = 67.26/-67.28 mm) at the bottom right corner of the window opening.

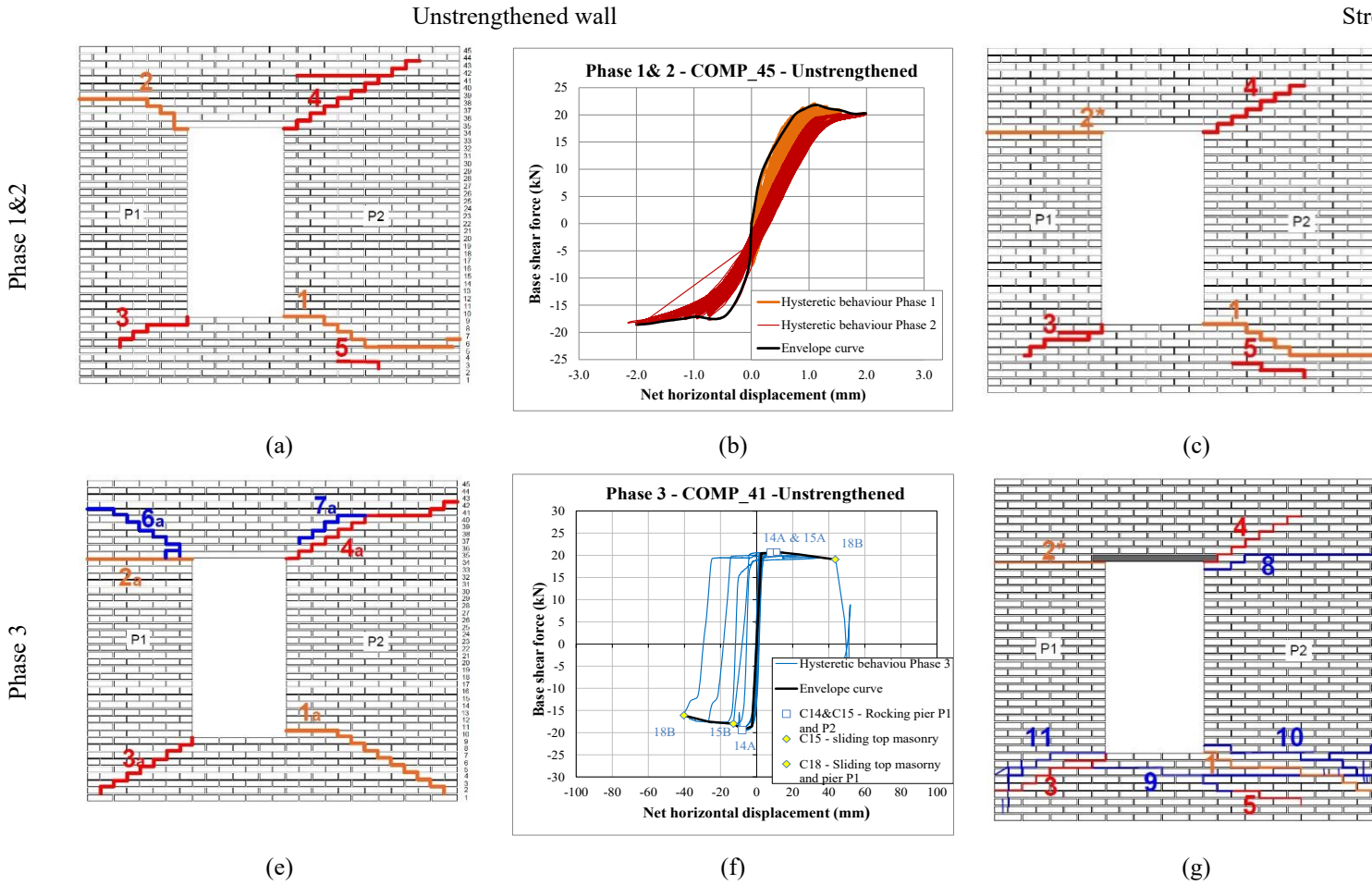


Figure 5: Crack pattern and base shear force versus net horizontal displacement curve: (a)-(b) unstrengthened wall during light damage ph
phase; (e)-(f) unstrengthened wall during near collapse phase; (g)-(h) strengthened wall during near c

4 DISCUSSION OF THE RESULTS

In this section, the comparison between the unstrengthened and the strengthened wall is carried out in terms of crack width and length for the light damage phase, and in terms of failure mechanisms and equivalent bilinear curve [19] for the near collapse phase

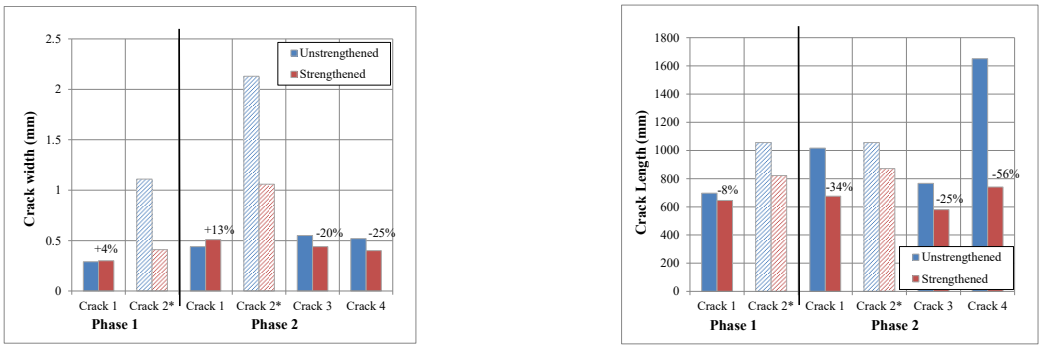
Figure 6 shows the comparison in terms of crack width and length for the four main stepwise cracks formed at the window corners at the end of phase 1 (d = 1.50 mm) and at the end of phase 2 (d = 1.93/-1.98 mm). A reduction in crack width between - 20 and 25% and in crack length between - 25 and 56% was observed. Due to the different shape of Crack 2* for the strengthened wall, horizontal crack rather than stepwise crack, this is not included in the comparison. A delay at the onset of cracking was also observed: during phase 1 crack 2 started at cycle C2 (d = 0.91 mm) and at cycle C4 (d = 1.28 mm) for the unstrengthened and strengthened wall, respectively; during phase 2 crack 3 started at cycle C7 (d = 0.94/-0.96 mm) and at cycle C8 (d = 1.13/-1.15 mm) for the unstrengthened and strengthened configuration, respectively. For the near collapse phase a quantitative comparison in terms of crack width and length cannot be performed since the accuracy of the DIC for crack width larger then 2 mm is significantly reduced. In correspondence of cycle C18 (d = 53.77/-53.80 mm), which corresponds to the end of the test for the unstrengthened configuration, it can be observed qualitatively that the crack width was smaller in the strengthened wall.

Figure 7 shows the failure mechanisms of the masonry components during the near collapse phase (phase 3) for both unstrengthened and strengthened wall. Relevant load levels, corresponding to the occurrence of failure mechanisms, are identified and indicated with markers in Figure 5. Four main failure mechanisms are considered: rocking of one of the piers (marker A), sliding between two part of the wall (marker B), arch mechanism below the window opening (marker C) and toe crushing (marker D). Considering the unstrengthened wall, until cycle C14 (d = 7.89/-7.97 mm) the rocking of the piers was the prevailing mechanisms in both loading directions (point 14-A). At cycle C15 (d = -12.82 mm), sliding of the top masonry portion with respect to the piers (point 15-B) started in the negative loading direction. Until cycle 17 the prevailing mechanisms were rocking of the piers in the positive loading direction and sliding of the top masonry portion with respect to the piers for the negative loading direction. At cycle 18 (d = 43.63 mm) also sliding of the top masonry portion and of the pier P2 occurred with respect to the pier P1 and the bottom masonry portion in the positive loading direction (point 18-B). Considering the strengthened wall, until cycle C17 rocking of the piers was the prevailing mechanism in both loading directions (points 14-A and 15-A). At cycle C18 (d = 53.77/-53.80 mm) an arch mechanism formed in the area below the window opening thanks to the presence of the bars (point 18-C). At cycle 20 (d = 80.96/-63.31 mm) toe crushing (Figure 8a) of the bottom right corner (point 20-D) and sliding of the top masonry portion with respect to the piers (point 20-B) occurred for the positive and negative loading direction, respectively. The test on the strengthened wall was stopped due to excessive out-of-plane deformation of the piers (Figure 8b) .

Figure 9a shows the out-of-plane deformation versus the net horizontal displacement for the unstrengthened (blue triangles) and strengthened wall (red circles). For the unstrengthened wall a maximum out-of-plane deformation of 10 mm was observed in the last cycle C18. For the strengthened wall a similar magnitude of out-of-plane deformation is observed at cycle C15 (d = 13.28/-13.29 mm) especially for the narrow pier P1. In the last cycle (C20, d = -63 mm) both piers experience a significant out-of-plane deformation of approximately 40 mm for

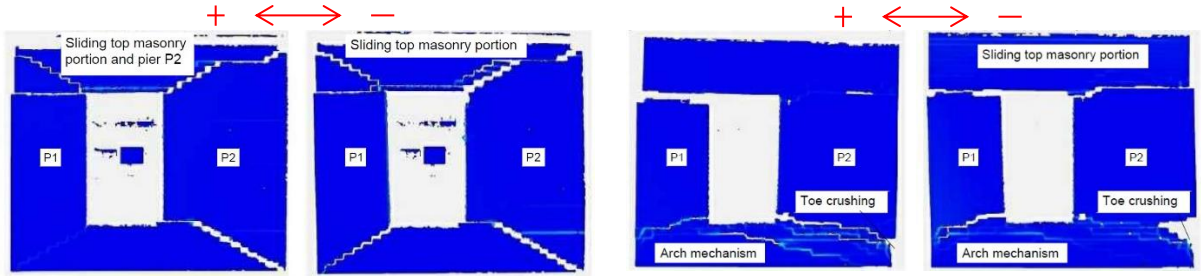
the negative loading direction. The cause of this excessive out-of-plane deformation can be ascribed to the asymmetric position of the twisted steel bars in the thickness of the wall, which becomes of relevance for extensive in plane damage

To compare the seismic performance of the strengthened and unstrengthened wall, the equivalent bilinear curve was adopted [19] (Figure 9b). The strengthened wall showed a slight increment (+15%) in terms of base shear force, but a substantial increment in terms of displacement capacity (+40-45%) and ductility (+30-40%) was observed. The ultimate drift increased from 1.61 to 2.99% and from -1.49 to -2.34% in the positive and negative loading direction, respectively.



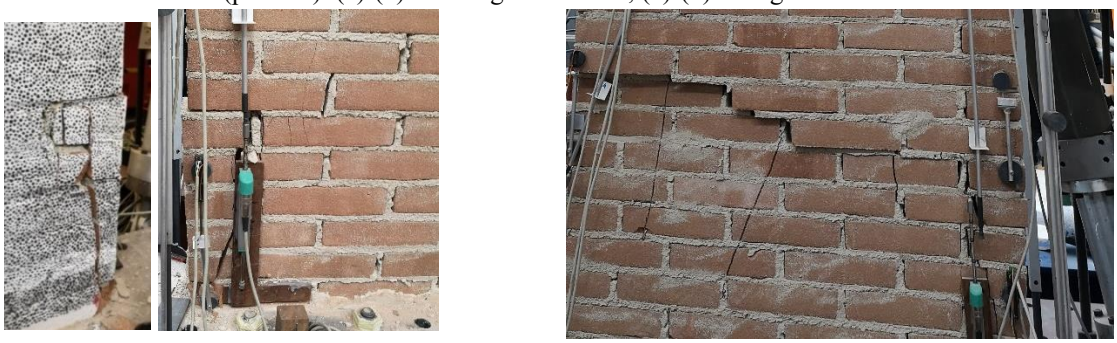
(a) (b)

Figure 6: Performance during light damage phase test in terms of: (a) crack width; (b) crack length.



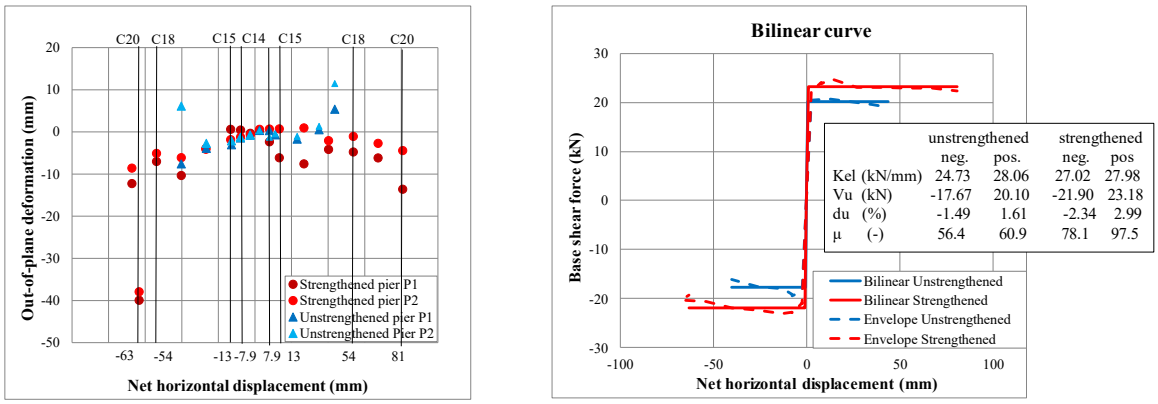
(a) (b) (c) (d)

Figure 7: Relevant failure mechanism observed through DIC analysis at the end of the near collapse phase (phase 3): (a)-(b) unstrengthened wall; (c)-(d) strengthened.



(a) (b)

Figure 8: Detail of some mechanisms: (a) toe crushing and cracks in the brick at bottom right corner; (b) out-of plane of the pier P1 and cracks in the brick at bottom left corner.



(a) (b)

Figure 9: (a) Out-of-plane deformation; (b) bilinear curve.

5 CONCLUDING REMARKS

The bed joint reinforcement is often used in the Netherlands against settlement damage in historical unreinforced masonry buildings, because it does not influence the aesthetic aspect of the buildings. In addition in the last years, the induced seismic events are increasing in the region of Groningen and it is of interest to investigate whether this strengthening method is efficient against seismic load.

To this purpose, a quasi-static in-plane test on a full-scale wall was performed at Delft University of Technology. The selected wall was representative of residential rather than historical buildings since it was single wythe, the adopted mortar was cement and lime-based and the pre-compression load applied was very low; while in historical buildings the walls are generally double wythe and the adopted mortar is generally lime-based. However, the results aim to provide a first analysis of the use of bed joint reinforcement as strengthening method as well as support the validation of numerical models to be used for further studies.

In order to investigate the efficiency of this strengthening method, the obtained results for the strengthened wall were compared with the ones obtained for previously tested unstrengthened walls [1][2]. The main findings can be summeried as follows:

- The presence of bed joint reinforcements prevent the formation of stepwise cracks at window opening and triggers the formation of horizontal cracks in mortar joints where the reinforcement was not present; for large in-plane displacement the twisted steel bars can trigger an arch mechanism below the window opening. Approaching the end of the test, thanks to the progression of damage the cracks developed also in the bricks at the bottom corners of the wall.
- At the end of the light damage phase, crack width (-20÷25%) and length (-25÷55%) reduction were obtained for the strengthened wall.
- For the strengthened wall, a minor increment in terms of base shear (+15%), but a significant increment in displacement capacity (+40÷45%) and in ductility (+30÷40%) was observed.
- The presence of the twisted steel bars leads to a different evolution of failure mechanisms. For the unstrengthened wall the prevailing mechanisms were rocking of the piers together with the masonry portion above the window opening, and sliding of both the masonry portion above the window opening and the pier P2 with respect the rest of the wall. After the maximum capacity of the wall was reached the steel bars started working, bringing to

the formation of an arch mechanism in the area underneath the window opening and to toe crushing at the bottom right corner. An important out-of-plane deformation also occurred in the strengthened wall caused by the asymmetric position of the twisted steel bars in the thickness of the wall.

Although the aforementioned outcomes are based on a limited number of tests and further investigations are needed, the reduction of crack width and length and the significant increase in displacement capacity and ductility of wall subjected to in-plane loading suggest that this method can be suitable to strengthen unreinforced masonry buildings in areas with low intensity earthquakes.

Acknowledgements. This research was found by the Rijksdienst voor het Cultureel Erfgoed (RCE) part of the Ministerie van Onderwijs, Cultuur en Wetenschap (OCW), subsides No. MS-2018-189, which is gratefully acknowledged.

REFERENCES

[1]Korswagen, P., Longo, M. and Meulman, E. Damage sensitivity of Groningen masonry structures – experimental and computational studies. Delft University of Technology. Report no. C31B69WP0-12, version 1, 30 December 2017.

[2]Korswagen, P., Longo, M. and Meulman, E. Damage sensitivity of Groningen masonry structures – experimental and computational studies. Delft University of Technology. Report no. C31B69WP0-13, version 1, 21 December 2018.

[3]Valluzzi M.R., Binda L., Modena C. (2005). Mechanical behaviour of historic masonry structures strengthened by bed joints structural repointing. *Construction and Building Materials,* 19(2005), 63-73.

[4]NIKER (2010), New integrated knowledge based approaches to the protection of cultural heritage from earthquake-induced risk.

[5]Ismail N., Petersen R.B., Masia M.J., Ingham J. (2011). Diagonal shear behaviour of unreinforced masonry wallets strengthened using twisted steel bars. *Construction and Building Materials,* 25(2011), 4386-4393.

[6]Licciardello L., Esposito R. (2019). Experimental study on unreinforced masonry strengthened with bed joint reinforcement. Delft University of Technology. Report no. CM1B07-2, version 1, 28 November 2019.

[7]Kallioras S., Guerrini G., Tomassetti U., Marchesi B., Penna A., Graziotti F., Magenes G. (2017). Experimental seismic performance of a full-scale unreinforced clay-masonry building with flexible timber diaphragms. *Engineering Structures,* 161(2018), 231-249.

[8]EN 772-1 (2000). Methods of test for masonry units - Part 1: Determination of compressive strength. *Nederlands Normalisatie-instituit (NEN).*

[9]NEN 6790 (2005). Technical principles for building structures-TGB 1990- Masonry structures - Basic requirements and calculation methods. *Nederlands Normalisatie-instituit (NEN)*.

[10]EN 1015-11 (1999). Method of test for mortar for masonry – Part 11: Determination of flexural strength of hardened mortar. European Committee for Standardisation (CEN).

[11]EN 1052-1 (1998). Method of test masonry – Part 1: Determination of compressive strength. *Nederlands Normalisatie-institute (NEN).*

[12]EN 1052-5 (2005). Method of test masonry – Part 5: Determination of bond strength by bond wrench method. *Nederlands Normalisatie-institute (NEN).*

[13]EN 1052-3 (2002). Method of test masonry – Part 3: Determination of initial shear strength. *Nederlands Normalisatie-institute (NEN).*

[14]EN 12190 (2018). Products and systems for the protection and repair of concrete structures – Test methods – Determination of compressive strength of repair mortar.

[15]Moreira S., Ramos L.F., Csikai B. (2014). Bond behaviour of twisted stainless steel bars in mortar joints. 9th International Masonry Conference Proceedings, Guimaraes, Portugal.

[16]EN 1766 (2015). Products and systems for the protection and repair of concrete structures -Test methods – Reference concrete for testing. *Nederlands Normalisatie-institute (NEN).*

[17]Skroumpelou G., Messali F., Esposito R., Rots J.G. (2018). Mechanical characterization of wall tie connection in cavity walls. *Proceedings of 10th Australian Masonry Conference*, 11-14 February, Sideny Australia.

[18]Mariani, V. Numerical prediction and sensitivity studies of the shaking table test on EUC-BUILD-2. Delft University of Technology, 17 November 2016

[19]Magenes, G., Morandi, P. and Penna, A. (2008). In-plane cyclic tests of calcium silicate masonry walls. *Proceedings of 12th International Brick/Block Masonry Conference*, 18-20 February, Sydney Australia.

12th International Conference on Structural Analysis of Historical Constructions
SAHC 2020
P. Roca, L. Pelà and C. Molins (Eds.)

REINFORCEMENT AND CONSOLIDATION OF MASONRY STRUCTURES. SUCCESSFUL CASES IMPLEMENTED: FROM THE STUDY TO THE EXECUTION PHASE

JOSE DOBÓN[1*] AND MIGUEL A. SORIA[2]

[1]Civil Engineer
Kerakoll Ibérica S.A.
Carretera de l'Alcora, Km. 10,450, 12006 Castellón de la Plana, Spain
e-mail: jose.dobon@kerakoll.es

[2] Building Engineer
Kerakoll Ibérica S.A.
Carretera de l'Alcora, Km. 10,450, 12006 Castellón de la Plana, Spain
e-mail: miguel.soria@kerakoll.es

Keywords: Masonry, Structural Strengthening, Hydraulic Natural Lime Mortars, Steel Fibers, Basalt Fibers

Abstract. *Traditionally, reinforcement and consolidation of masonry structures has been done according to one of the following approaches, or a combination of them: By using materials with a very different nature and behaviour from the original ones in the reinforced structure or by increasing the section of those structures, increasing, therefore, their hardness. The first approach could unleash serious setbacks in the original structure. Using materials with high elastic modulus on more flexible elements might generate new tensions in the system, which previously did not exist, compromising the reinforcement intervention. The second approach implies increasing significantly the structural geometry and, therefore, its own global hardness.*

The modern approach, which reinforcement and consolidation of masonry structures pursue, is solving both, different nature of materials and sectional increasing. It is done by using compatible materials with the original structure, combining the elastic behavior of them and assuring the original breathability, and implementing low thickness interventions in order to do not modify the original hardness.

The proposal of a reinforcement system compatible with the historic and architectonic nature of the structure, is based on a mineral matrix of hydraulic natural lime, GeoCalce F Antisismico, combined with basalt fiber fabrics (GeoSteel Grid) or galvanized steel unidirectional bands (GeoSteel Hardwire™). With this system typology, it is ensured an improvement in the mechanical resistances of the structure, based on a simple and low thickness application.

The aim of the exposition is introducing a reinforcement and consolidation system for masonry structures developed by Kerakoll and showing several success cases, in Spain and Italy, reinforced with this system. Each case will be explained from the initial study phase to the execution of the intervention, including the calculations to determine the application to be done.

1 INTRODUCTION

The last seismic events in Italy (L'Aquila 2009, Emilia 2012, Italy center 2017) have shown the vulnerability of masonry structures. The majority of existing buildings in Europe were designed without considering seismic loads and/or the changing of usage destination. From the last 20 years, in some cases until now, engineers and architects, when they have worked in existing structures, must have interrupted their structural usage due to two factors: the available strengthening technologies are very invasive and, the most important one, they should use solutions with a wide time of installation commonly related to concrete strengthening, heavy steel profiles and sectional growths. FRCM (Fiber Reinforced Cementitious Mortar), mortar matrix reinforced with fibers and SRG (Steel Reinforced Grout), mortar matrix reinforced with steel fibers, those two systems have become the most popular ones thanks to their excellent ratio strength – weight and their relatively easiness and quickness application compared with traditional technics above-named.

The aim of the present document is demonstrating the validity of the systems already explained on the presentation and developing different successful cases that are done with these strengthening systems.

2 MATERIALS PROPERTIES

2.1 Galvanized steel fiber fabrics

The steel galvanized fiber fabrics are made with galvanized steel micro – cables of high resistance, interlaced forming cordons and installed with welding on a special glass fiber mesh, achieving a highly dimensional stability. This composition allows the fabric be similar to other fiber types of unidirectional fabrics (carbon, aramida or glass), see Figure 1, in addition to their application simplicity.



Figure 1: Page layout

Micro – cables and cordons are made accordingly to ISO/DIS 17832 standard, which describes fabrication technics and the referential parameters. Micro – cables and cordons characteristics are detailed in Table 1.

Table 1: Micro – cable and cordon characteristics

Material	Tensile strength (MPa)	Elastic Modulus (GPa)	Section (mm^2)	ε
Micro – cable	2900	87000	0,1076	-
Cordon 3x2	750	200000	0,538	>1,50%

The micro – cable interlaced allows to maintain unchanged the elastic modulus of the cordon in comparison with the micro –cables, empowering the high resistance and rigidity of steel.

Cordons are galvanized obtaining a material that is not affected by the corrosive agents and it make them appropriate for different exposure environments. Zinc coating is ruled by EN 10244 – 2 being the zinc quantity great to 15,97 g/m^2. In Figure 2, it shows a SEM image of the 40 times augmented filament to determine the thickness and the mineralogy of the zinc coating, in order to do the process quality control.

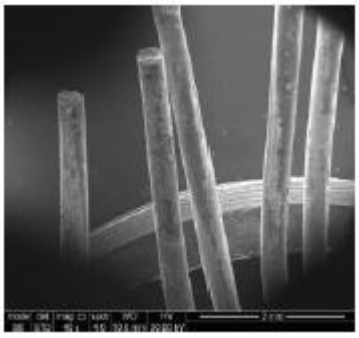


Figure 2: sole cordon SEM image

Steel fiber fabrics are available in four different densities, based on the distances between cordons. The two with the lowest density, 1,57 and 3,19 cordons per fabric centimeter respectively, are adequate to be used with mineral matrix, whereas the two with highest densities, 4,72 and 7,09 cordons per centimeter, must be installed with epoxidic matrix, Figure 3.

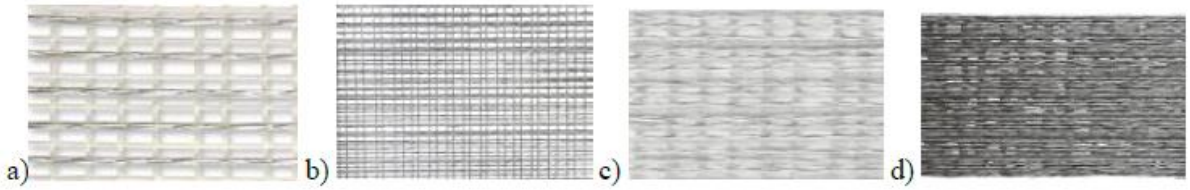


Figure 3: four different steel fiber fabrics densities, cordons per centimetre: a) 1,57; b) 3,19; c) 4,72 and d) 7,09

SRG systems present, among others, a great advantage in front of FRP composed systems: they have a considerable shear resistance when they are subjected to perpendicular actions to their guideline. This last characteristic is exclusively for this kind of fiber.

2.2 Basalt and stainless steel fiber fabrics

Biaxial equilibrated fabrics made of basalt fiber and stainless steel AISI 304 micro – wires, with the same grammage in both directions. The special combination, basalt and stainless steel micro – wires, ensures a high shear strength and abrasion.



Figure 4: Stainless steel and basalt fiber fabric

Basalt fibers are the result of volcanic stone fusion and it ensures excellent mechanical and physicochemical properties in aggressive environments. The hardness of basalt fibers guarantees good tensile and shear strength, which are essential in masonry consolidation. Basalt fibers, used in GeoSteel Grid fabrics, are ruled by the normative UNI 8746 and UNI 9409.

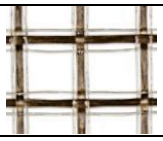
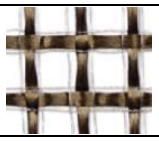
Stainless steel AISI 304 micro – wires are installed in both sides of the basalt fiber, besides its mechanical contribution to the fabric; it balances and stabilizes the fabric in any direction. Using stainless steel provides a greater ductility and shear strength to the fabric, allowing to the strengthening system a greater energy dissipation and ensuring a better security coefficient in the intervention.

Table 2: Stainless steel AISI 304 and basalt fibers characteristics

Material	Tensile strength (MPa)	Elastic Modulus (GPa)
Basalt	2900	87000
Stainless Steel AISI 304	750	200000

GeoSteel fabrics are suitable as frame for low thickness extended structural reinforcements, in combination with high resistance steel fiber connectors GeoSteel or helical stainless steel bars Steel DryFix®. GeoSteel Grid fabrics are developed in three different density; from those different densities, they receive their commercial name: GeoGrid 120, GeoSteel Grid 200 y GeoSteel Grid 400. In Table 3, it is shown technical properties from these three different densities:

Table 3: Technical properties of stainless steel AISI 304 and basalt fibers fabrics

Technical Properties	GeoGrid 120	GeoSteel Grid 200	GeoSteel Grid 400
			
Fabric dimensions (mm)	22 x 22	17 x 17	15 x 15
Density (g/mm^2)	130	200	400
Tensile load per width unity (KN/m)	30	55	110
Tensile characteristic strength (MPa)	1600	1700	1700

The basalt fiber has a special alkali – resistant protector treatment, it consists in a resin in aqueous basis free from solvent, which gives to the fiber an additional protection.

2.3 Natural hydraulic lime matrix

The matrix election is based on the type of support where is going to be the reinforcement done, for this reason, with masonry structures the selected matrix is natural hydraulic lime. The Table 4 shows different mechanical properties of this matrix, being particularly indicated for structural reinforcement in masonry structures. In them, due to their natural origin compounds, it is possible ensure the perfect adhesion, porosity, hygroscopicity and breathability with the original support, achieving a highly compatibility between the original structure and the reinforcement done.

Table 4: Mechanical properties of mineral matrix

Material	Compressive strength (MPa)	Flexional strength (MPa)	Elastic Modulus (GPa)	Adhesion (MPa)
GeoCalce F Antisismico	15	5	9230	0,80

Table 5: Results of experimental tests (% increased in relation to non – reinforced specimens)

Single lap (Shear test) (ASTM D3163)	60% (4 cordons per inch), 30% (8 cordons per inch) for the fibers tensile strength
Masonry walls (diagonal compressive test)	From 230% to 527% (SRG)
Vaults (asymmetric load in a fourth part of the span)	355% (extrados SRG)
Masonry walls in U shape (test in vibrating table, peak acceleration)	520% (anchored with SRG)

3 STUDY CASES

The following study cases represent, among others, FRCM and SRG typical applications of structural reinforcement in masonry structures done in Spain and Italy in the last 5 years. Three study cases are showed: one of them is an extrados reinforcement of the vaults in “Fira de Montjuïc”, other one is an extrados reinforcement of the dome of San Vicenç Church in Saurí and the last one is a wall reinforcement in the Botanic Garden in Pisa.

3.1 Vaults – Fira Montjuïc – Barcelona

The vaults are cracked, they are visible from its intrados and distributed along their ribs. After the analysis, it is determined that the degradation cause is the lack of waterproofing in the vaults affecting to their structural integrity. It is decided to do a structural reinforcement by the extrados vault, due to their intrados can not be covered by esthetical reasons. Together with the intervention, the cause of the degradation is removed by waterproofing the vault with materials capable of ensuring the transpirability balance and with an elastic behavior similar to the original structure.

The procedure for doing the structural reinforcement is as follows:

1. Removal of old coatings
2. Support preparation
3. Application of the structural reinforcement mortar, GeoCalce F Antisismico.

4. Installation of the GeoSteel G600 fabric.
5. Fabric anchor > 30 cm.
6. Application of the structural reinforcement mortar, GeoCalce F Antisismico, in order to cover the fabric.



Figure 5: Vaults extrados

In Figure 5, it is shown the different installation phases of the structural reinforcement and the waterproofing system applied. This treatment ensures the transpirability of the support materials.

3.2 Masonry wall – Botanic Garden - Pisa

The Botanic Garden of Pisa was found the 16th century by Cosimo I of Medici, its extension is 27000 m^2 approximately. It is located close to the Miracles Square. It is encircled by a perimeter wall with a variable height, between 3,50 m. to 4,85 m., it goes through Via Roma and its function is to protect the arboreal species. The structure is coated in both sides, it is a wall made, mainly, with bricks with different constructive layers. The wall width is variable, from 30 cm. in the south zone where we can find a framed structure with concreate, to 41 cm. in the central zone as far as 50 cm. in the crossroads with via Galli Tassi.

The deformation's diagram shows the tipping phenomena up to 9 cm, which are achieved due to the hystoric vegetation located close to the perimeter. Their roots go through the wall foundation and enter into the pavement, even breaking it. In these zones, where the vegetable level is higher than 80 cm, there is humidity over the wall at the outside zone. It degrades the coating and disaggregate the surface (Figure 6).



Figure 6: Perimeter wall status

In July of 2010, a sudden collapsing event took place in a part of wall, in a bordering zone between a private garden and the Botanical Garden. The prominent vulnerability accompanied by the degradation and the clear tipping, mainly related to the vegetable species nearby, were the precursor in the summer of 2011 for the implementation of anti-tipping interventions along the street. It was installed, each three sections of 40 m. approximately, two inclined metallic braces anchored to a micropiles foundation fitted in the Botanic Garden land. The structure support is made by a metallic beams grid, installed over the wall surface.

In 2016, the consolidation intervention was done. The intervention was thought for ensuring the static security of the wall against the tipping danger due to horizontal actions (seismic and wind), meanwhile ensuring a ductile behavior of the masonry in front of plants roots disaggregation actions.

With this purpose, the wall part that goes along Via Roma was reinforced with buttress built in situ, installed every 6 m. in continuity with the original structure and consolidated over the micropiles foundation.

The masonry walls between buttresses were reinforced facing flexional stresses supposing a continue beam diagram. It was made with longitudinal bands, GeoSteel G600, installed with natural lime hydraulic structural mortar, GeoCalce F Antisismico.

This tridimensional calculus model used for the structural analysis made with finites elements is shown at Figure 7. Seismic forces are assessed as equivalent static forces; in the Figure 7, it is also shown the stress diagram.

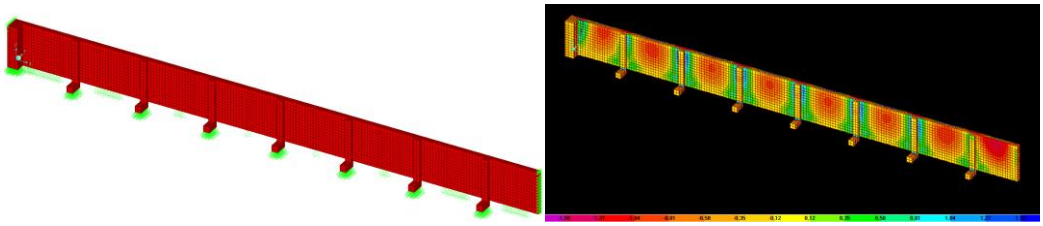


Figure 7: Structure modelling and stress diagram

With the intervention done is ensured the old wall stability of the Botanic Garden against wind forces and it increases the security level against seismic forces.

3.3 Barrel vaults – San Vicenç de Saurí Church - Sort

San Vicenç de Saurí is the parochial church of Saurí village, in the municipal district of Sort, in Pallars Sobirà region. The church construction is estimated around the year 852, its style is Baroque. It is a church with a sole nave, built on stone; in addition, it has the typical Pyrenean bell tower on an octagonal floor plan and a main deck. It is a protected building as a “Bien Cultural de Interés Local”. Moreover, it was aesthetically restored on the inside by Santi Moix, an international artist born in this village.

Together with the restoration work, they studied the old stone structure and its barrel vaults of

an area of 25 m^2 approximately in order to ensuring the structural building stability. From that study, it was determined the need to strengthen the vaults due to its low thickness and the existence of cracks on them.

The proposal done is the one on shown on Figure 8:

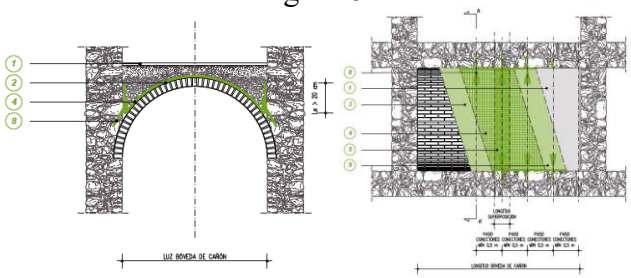


Figure 8: Extended extrados reinforced system for barrel vaults schema

The procedure schemed of the reinforced system is as follows:

1. Removal of old coatings
2. Support preparation
3. Application of the structural reinforcement mortar, GeoCalce F Antisismico.
4. Installation of the GeoSteel Grid 2000 fabric.
5. Overlap length > 30 cm.
6. Anchor length > 20 cm.
7. Overlap anchor length > 30 cm.
8. Mechanical connector done with GeoSteel G600 fabric.Application of the structural reinforcement mortar, GeoCalce F Antisismico, in order to cover the fabric.

The reinforcement done helps to avoid the vaults from the collapsed produced by the plastic joints due to the lack of tensile strength of the masonry. This typology of reinforcement helps improving the structural performance of this kind of structure offering a ductile breaking behavior, besides improving their mechanical resistance. The intervention was done in the following phases, as shows Figure 9:

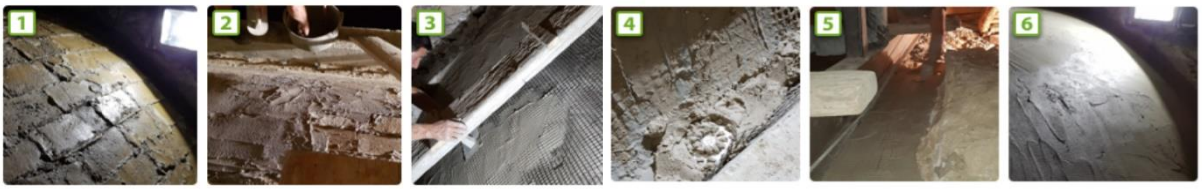


Figure 9: Phases done during the vaults reinforcement application

4 CONCLUSIONS

Since 2004, when using high – resistance steel fiber bands started on civil engineering applications, several studies took place in order to study its mechanical properties and effectiveness as external reinforcement elements. The benefit of installing steel bands or stainless steel and basalt fiber biaxial fabrics in combination with mineral mortars, instead of organic mortars, is that SRG/FRCM systems are a versatile reinforcement technology thanks to

its compatibility with the original structure and its easy application. The interventions explained through this document are a clear example of validity as a structural reinforcement system. It is demonstrated that SRG/FRCM systems, improve the bearing capacity of the structure subjected to different stresses, static as well as dynamic, which are not capable of stand design loads, helping to preserve from deterioration. Moreover, they improve the structural ductility in comparison with other more traditional structural reinforcements, such as FRP systems.

The studies done, as well as the different applications made with these systems, have demonstrated, without doubt, that this new kind of composite materials must be included in the range of composite materials intended for structural reinforcement. At the same time, these systems are used with mineral mortars, offering a better response and compatibility with the original structure.

REFERENCES

[1] Casadei P. and Agneloni E. Advance composites applications on historical structures in Italy: Case studies and future developments 6th International Conference on Structural Analysis of Historical Construction – Preserving Safety and Significance, Bath, United Kingdom, July 2-4, 2008, ISBN Vol.2:978-0-415-48107-6.

[2] Casadei P. and Agneloni E. Case Studies on Advanced Composite Materials for Civil Engineering and Architectural Applications Structural Engineering International, vol.21, 3/ 2011, 271-278.

[3] Casadei P., Nanni A., Alkhrdaji T., Thomas J. Performance of Double-T prestressed concrete beams strengthened with Steel Reinforced Polymer. Adv Struct Eng 2005;8(4):427-442.

[4] Casadei P., Nanni A., Alkhrdaji T. Steel-Reinforced Polymer: an innovative and promising material for strengthening the infrastructures. Concr Eng Int 2005;9(1):54-56.

[5] De Santis S., de Felice G., Napoli A., Realfonzo R Strengthening of Structures with Steel Reinforced Polymers: A state-of-the-art review. Compos Part B: Eng, 2016; 104:87-110

[6] De Santis S., Casadei P., De Canio G., de Felice G., Malena M., Mongelli M., Roselli I. Seismic performance of masonry walls retrofitted with steel reinforced grout. Earthquake Engineering and Structural Dynamics, 2016;45(2):229-251. DOI: 10.1002/eqe.2625.

[7] De Santis S., Casadei P., de Felice G. Tests on the bond performance of mortar based strengthening systems on masonry substrates. Proc. Int. Conf. IMC'14 - 9th International Masonry Conference (Guimarães, Portugal, 7-9 July 2014). ISBN: 978-972-8692-85-8.

[8] Faella C, Napoli A, Realfonzo R. Seismic behaviour of RC beam-column joints strengthened with steel fiber composite materials. In: Proceedings of XVI Convegno ANIDIS, L'Aquila, 2015 (in Italian).

[9] Napoli A., Realfonzo R., Casadei P. Rinforzo a flessione di solette in c.a. con sistemi in SFRP/SFRCM. In: Proceedings of XX Congresso CTE, Milano, Italy, 2014 (in Italian).

[10] Napoli A., Realfonzo R., Petracca M., Candeloro F., Camata G., Casadei P. Flexural strengthening of RC slabs with SRP/SRG: an experimental-numerical comparison. In: Proceedings of ACE 2015, Vietri sul Mare, Salerno, Italy, 2015.

[11] Napoli A., Realfonzo R. Compressive behavior of concrete confined by SRP wraps. Construction and Building Materials 2016 (in press).

12th International Conference on Structural Analysis of Historical Constructions
SAHC 2020
P. Roca, L. Pelà and C. Molins (Eds.)

REPAIR CONNECTION WITH WOODEN WEDGED DOWELS: PRELIMINARY EXPERIMENTAL LABORATORY TESTS AND FEM MODEL FOR THE DESCRIPTION OF THE MECHANICAL BEHAVIOR

E. PERRIA[1*], S. SIEGERT[2], X. LI[1] AND M. SIEDER[1]

[1]Institute of Building Construction and Timber Structures, Technische Universität Braunschweig
Schleinitzstraße 21 A, D-38106 Braunschweig
e-mail: e.perria@tu-braunschweig.de - www.tu-braunschweig.de/ibholz (*corresponding author)
e-mail: xinyi.li@tu-braunschweig.de - www.tu-braunschweig.de/ibholz
e-mail: m.sieder@tu-braunschweig.de - www.tu-braunschweig.de/ibholz

[2] IGP Gockel PartGmbB - Ingenieure und Architektin, Kieler Straße 1, 34225 Baunatal
e-mail: siegert.svenja@gockel-ingenieure.de - www.gockel-ingenieure.de

Keywords: Preservation of monuments, timber, repair techniques, mechanical fasteners, laboratory testing, numerical modeling.

Abstract. *The present paper describes the first steps of the research project by the title "Repair connection with wooden wedged dowels. New and alternative repair method that meets the demands of Monument Protection of built substance's gentle care and material fairness". The project aims to develop guidelines for static-constructive use of wood-wood repair connections with wooden wedged dowels.*
In the research project, the first steps for the description of the mechanical model for the wooden wedged dowels have been approached. Literature about wooden pegs and dowels and built examples of wooden wedged dowels in existing buildings have been analyzed; more, preliminary laboratory tests and FEM simulations have been implemented.
In this paper, the results of the preliminary laboratory tests and the parallel development of a FEM model with the aim of describing the deformation behavior of the wooden wedged dowels for the most used wooden species will be presented. The main aims are: a) Analysis of the distribution of the strains / deformations in the dowel and in the connected building components when inserting the wedge. b) Analysis of the risk of opening of cracks in the materials. c) Analysis of distribution of stresses in the dowel and in the connected building elements utilizing FEM modeling calibrated on the experimental results.
Thanks to the evaluation of deformation behavior in the proposed geometrical configuration and material combinations of wedge, dowel and connected building elements, it has been possible to understand the general framework of deformation behavior and failure modes for different combinations of timber density of the connection components.

1 INTRODUCTION

The ICOMOS Charter of Mexico [1] – worldwide referenced document for the conservation of timber architectural heritage – explicitly asserts that the intervention on traditional and

heritage timber structures must follow traditional carpentry techniques or compatible modern materials and techniques. The prioritization of traditional wood-wood connections aims to protect the material authenticity and integrity of the building and to guarantee the principles of reversibility and minimum intervention. In the Charter it is also specified that the new members or parts of members should aesthetically resemble the whole, but at the same time may be discreetly differenced from the original construction material, so that they can be identified at a later date.

On one side, hand-carved *wooden nails* based on historic examples continue to be used to secure the position of the half-timbered joints in one-to-one replacement of historical connections. On the other side, the situation is different when it comes to replacing damaged timbers, where historically no connection was in place. In these cases metal fasteners are used very often, especially if the repair has to be designed for tensile-stressed structural elements or if a clamping effect is required. In these load-cases, predestined solutions for strengthening measures are based on the use of metallic nails, screws and bolts, mainly for shear and tensile stressed wood joints, or of steel or plastic rods. In these cases, the choice of the metallic mechanical fasteners is almost unique, while the structural engineers cannot provide proof of the repair for alternative techniques or mechanical fasteners because there is no basis for calculation. However, these latter fastening techniques are not to be favored from the point of view of monument preservation's principles [1, 2] for the conservation of wooden built heritage.

The aim of the project is the development of technical knowledge for the repair connection with *wooden wedged dowels*, alternative wooden mechanical fasteners for historical timber structures. The specific aim of the project is to develop a guideline for the static-constructive use of *wooden wedged dowels*, which will allow the appropriate retrofitting or upgrading in line with the requirements of monument protection.

2 BASIC PRINCIPLES: STATE OF THE ART AND *REQUIREMENT MATRIX*

With the aim of development of suitable mechanical models for the *wooden wedged dowels*, existing mechanical models and evaluation of load-bearing capacity for classical *wooden nails* and *dowels* were analyzed; furthermore, selected existing built examples of *wooden wedged dowels* were analyzed. For the analysis and evaluation of the *wooden wedged dowels*, which can be found in built examples, experienced carpenters, who have been using repair connections with *wooden wedged dowels* for decades, were asked about their properties, parameters for manufacturing and construction (*empirical values*).

Extrapolating pieces of information from literature and built references, the most significant parameters for the construction of a mechanical model for the *wooden wedged dowels* were collected in a *requirement matrix*; furthermore, it was identified which parameters could be fixed and which ones could make a significant contribution to a constructive evaluation.

Further boundary conditions were fixed basing on results of preliminary tests (TV).

2.1 State of the art

The majority of existing mechanical models are based on the analysis of historical *dowel-shaped* wooden *fasteners*, mainly wooden *pegs*. The function of such fasteners was to secure the position of the half-timbered joint (withdrawal) and absorb tensile forces perpendicular to

the fastener's axis. The development of *dowel-shaped fasteners* according to [3] and [4] starts from the 10th century onwards with the development of wooden *keys*, *wedges, pegs, pins, nails*, *trenails*, *head nails*, up to *dowels* and *plugs* developed in the 19th century. *Dowel-shaped w*ooden *fasteners* differ for shape in the sense of longitudinal development (slight tapered or cylindrical) and geometric adaptation of the cross section in the peg hole diameter (quadrangular, octagonal or round with or without nail head). Nowadays *dowel-shaped fasteners* are roughly divided into two categories: "wooden nails" for fasteners with octagonal cross-sections and "dowels" for ones with round cross-sections. On the subject "wooden nails*"* there are many publications [5,6,7,8,9,10,11,12], which refer to the assessment of the load-bearing capacity of wooden *pegs, pins, nails* in the historical connection. In his research report, Müller [13] summarized the results of Ehlbeck, Hättich, Kessel, Augustin, Görlacher, Blaas, Ernst, Werner [5-12]. Furthermore, European Standards [14] and [15], provide further design proposals and load-carrying capacity for some kind of *dowel-shaped* wooden *fasteners*.

From the résumé of the state of the art, it is important to conclude that some mechanical models for *dowel-shaped* wooden *fasteners* are valid for specified boundary conditions (minimum spacing, minimum thickness, and fixed diameter or timber species) for connections in single or double-shear. The existing, most complete and flexible mechanical model, suitable for the adaptation for the *wooden wedged dowels,* is the one proposed in [15] based on the approach of [6]. On the basis of preliminary tests, the mentioned model will be implemented with relevant parameters and made suitable for the verification of repair connections with *wooden wedged dowels*.

2.2 Defined parameters for the *wooden wedged dowels*: the *requirement matrix*

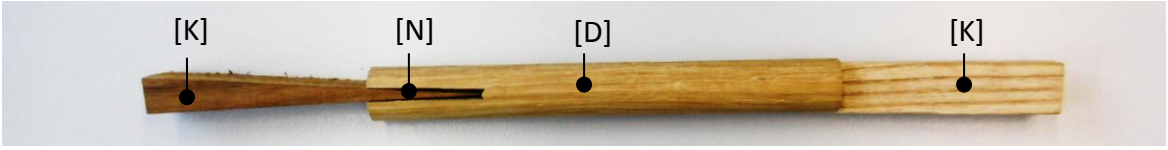


Figure 1: Abbreviations for the parameters in the *wooden wedged dowels*

From the analysis of existing mechanical models and existing built examples of connections with *wooden wedged dowels*, some basis parameters were defined. The representation of following described parameters is also depicted in Figure 1 and Figure 2.

DOWEL [D]:

- Wooden species: European ash (*Fraxinus excelsior*, *L.*) (kiln-dried); European oak (*Quercus sp.*) (kiln-dried).
- Direction of the fibers: longitudinal direction of the fibers = length of the dowel.
- Length of the dowel [l_D]: Variable, equal to the height of building components' cross section [$l_D = h_B$].
- Diameter of the dowel [d_D]: $d_D = 16 - 20 - 24 - 30\ mm$

GROOVE [N]:

- Centered on the diameter of the dowel
- Length of the groove on Side 1 (S1) [$l_{N,1}$] and groove on the Side 2 (S2) [$l_{N,2}$]: each max. $l_N \leq 1/4 \cdot l_D$ and $l_{N,1} = l_{N,2}$

- Thickness of the groove [t_N]: $t_N = 1 - 3\ mm$
  (according to production rule: $t_N = 1/10 \cdot d_D$)
- Length of dowel's core [$l_{D,kern}$]: $l_{D,kern} = l_D - \mathrm{l_{N,1}} - \mathrm{l_{N,2}}$
- Distance between groove's bottom and shear line [$l_{kern,D}/2$]
- Angle θ (parameter T1 in Table 1) between orientation of the groove and direction of annual rings on dowel's cross section: Fixed combination: $= T1 = 0$. According to [16, 17, 18] the maximum strength between tangential and radial is – at least for *Quercus sp.* – along the radial direction, because of the presence of medullary rays.
- Angle φ (parameter T2 in Table 1) between the orientation of the groove on S1 [N,1] and fibers' direction in the building component: Variable orientation for different building component's wooden species.
  → Variable probed in preliminary tests TV1.
- Angle β (parameter G in Table 1) between the orientation of the groove on Side 1 [N,1] and groove on Side 2 [N,2]: Fixed combination: $\beta = \mathrm{G1} = 0$.
  →Variable probed in preliminary tests TV1.

WEDGE [K]:

- Wooden species of the wedge: Oak (*Quercus sp.*) (kiln-dried).
- Direction of the fibers: longitudinal direction of the fibers = length of the wedge.
- Length of the wedge [l_K]: fixed: $l_K = l_N + 10mm$
- Width of the wedge [b_K]: $b_K = d_D$
- Thickness of the wedge (correspondent to dowel's opening) [$t_{K,\mathrm{D}}$]: $t_{K,\mathrm{D}} \cong 5.2mm$.
- Thickness of the wedge at the tip (correspondent to groove's bottom) [$t_{K,1}$]: $t_{K,1} \cong 0mm$
- Angles in the wedge: [$\alpha_{K,a}$; $\alpha_{K,b}$; $\alpha_{K,s}$]. With $\alpha_{K,s}$ = 8°-10° (at the tip).
- Practical manufacturing rule for the angle of the wedge: "per cm length of the (pointed) wedge, the width is up to 2 mm".
- The form of the *ideal* wedge represented in Figure 2 differs from the *real* one, because of the easiness of manufacturing: in the first case $\alpha_{K,a} = \alpha_{K,b}$, while in the second case $\alpha_{K,a} \neq \alpha_{K,b}$, and $\alpha_{K,a} = 90°$.

BUILDING COMPONENTS [B]:

- Connection only in single shear
- Wooden species of repair building component (must be same or similar to the in-situ timber, which bulk density & moisture content have to be proofed):
  - Hardwood: Oak (*Quercus sp.*) or similar density, minimum 5 year air-dried;
  - Softwood: Spruce (*Picea abies*), silver fir (*Abies alba*), European redwood (*Pinus sylvestris*) or similar density, can be kiln-dried.
- Timber moisture content ideally constant: hypothetically fixed at: $u \cong 12 - 13\%$
- Minimum width of the building component [$b_{B,min}$]: $b_{B,min} = 120mm$
  equivalent to 1x row *wooden wedged dowels* $d_{D,min} = 20mm$ with $a_{4,min} = 2{,}5 \cdot d_D$.
- Minimum height of the building components [h_B]: $h_{B,min} = h_{B,1} + h_{B,2} \geq 120mm$ i.e. connection in single shear with $h_{B,1} \geq 60mm$ & $h_{B,2} \geq 60mm$
  equivalent to minimum length of dowel's core [$l_{D,kern,min}$]: $l_{D,kern,min} = 60\mathrm{mm}$

MINIMUM SPACING / DISTANCES IN THE CONNECTION:

- Minimum distance to timber edges [a_4]: $a_{4,min} \geq 2.5 \cdot d_D$
- Minimum distance to timber end [a_3]: $a_{3,min} \geq 4 \cdot d_D$
- Minimum spacing among fasteners [$a_1 = a_2$]: $a_1 = a_2 \geq 2 \cdot d_D$
- Minimum spacing between fasteners and checks (or cracks) in building components [a_r]: $a_r \geq 2 \cdot d_D$.

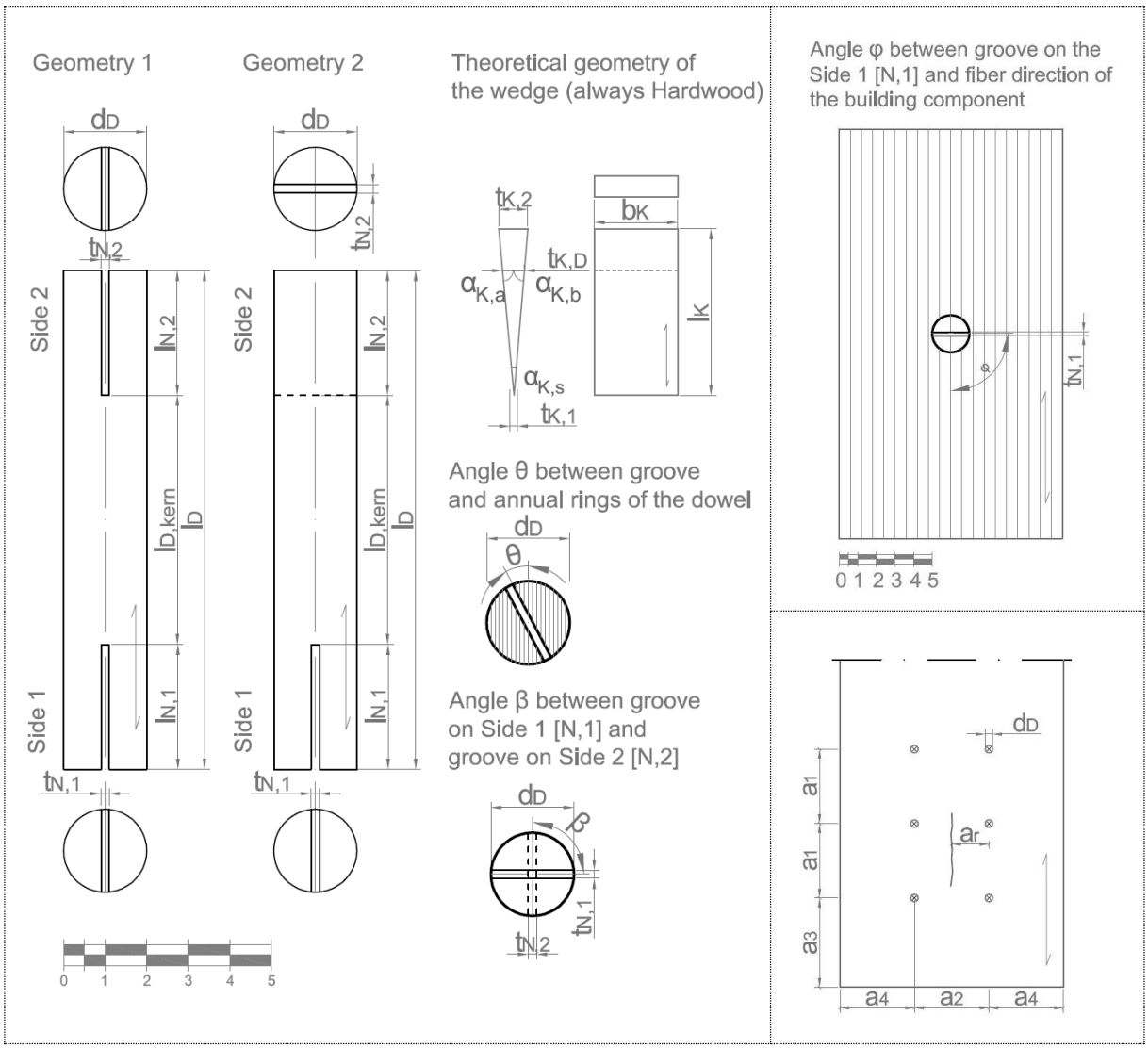


Figure 2: Parameters in the repair connection with *wooden wedged dowels*

3 RESULTS OF EXPERIMENTAL PRELIMINARY INVESTIGATIONS

In order to adapt the already existing models for „wooden nails“ and „dowels“ for the *wooden wedged dowels*, further important constructive and static parameters were analyzed in the preliminary experimental investigations (TV1) and afterwards implemented in the *requirement matrix*.

3.1 Aim

Aim of TV1 was to determine some significant parameters that play a major role in the formation of cracks in the *wooden wedged dowel* and on components' surfaces and to bring forward the most favorable wood and geometrical combinations.

The initial parameters for the design of test specimens for the TV1 were fixed based on the *empirical values* and some relevant constructive parameters were considered as variables.

Specific aims of the preliminary tests TV1 were:

- Analysis of the distribution of strains in the dowel and in the building components as a consequence of introduction of the wedge in the groove;
- Analysis of cracks and failure modes in the materials;
- Fixing relevant parameters;
- Fixing relevant manufacturing rules;
- Collect data for the construction of a FE-Model

3.2 Geometry of specimens

The geometry of test specimens for the TV1 was prepared according to the parameter defined in paragraph 2.2. Some specific parameters and variables for TV1 are listed below.

Fixed geometric parameters:

- Dimension of building components: $(b\ x\ h\ x\ l)\ 120\ x\ (60 + 60)\ x\ 220mm^3$
- Timber species: Dowel: oak; Building components: oak, spruce.
- Dowel diameter: $d_D = 20mm$
- Dowel length: $l_D = 120mm$
- Thickness of the groove: $t_N = 2mm$
- Length of the groove: $\mathrm{l_{N,1}} = \mathrm{l_{N,2}} = 30mm$
- Wedge parameters' $\alpha_{K,a} \neq \alpha_{K,b}$, and $\alpha_{K,a} = 90°$ were produced according to *real* form.
- θ : angle between orientation of the groove with respect to the direction of annual rings on dowel's cross section. For TV1 the parameter was fixed as: $= T1 = 0°$.

Variable geometric parameters:

The analyzed variables are described in detail in Table 1, and briefly listed below:

- H: Timber combinations:
  - H1: Dowel: oak (HW) / Building component: spruce (SW)
  - H2: Dowel: oak (HW) / Building component: oak (HW)
- T2: angle between orientations of the groove with respect to fiber direction of the building component on S1.
- G: angle between orientation of the groove on S1 and on S2. In the existing built examples the dowels were always rotated of $\beta = 90°$ to avoid the feared risk of dowel's core splitting. In the current research project, both the rotated ($\beta = 90°$) and parallel ($\beta = 0°$) arrangement of the groove are probed.

3.3 Materials and methods

The tests consist of the insertion of the wedge on both S1 and S2 by means of a universal testing machine with a strain-controlled test (velocity $= 1\ mm/s$) (Figure 3). The wedge was not introduced – as in real conditions – by means of a hammer. The reason is the attempt to

repeat – for every specimen – the same boundary conditions: velocity, load amount, direction of the load (without natural direction's corrections of a human operator) and centered load on the wedge (in the *real* form: asymmetrical wedge).

Before the tests, the specimens were conditioned minimum 24h in a climatic chamber T=20°C and RH=65%.

Mechanical properties of the test specimens (bulk density, moisture content and bending E-module) were determined for both building components and dowels. Test specimens were divided into groups: specimen produced from the same original initial cross section belonged to the same group. The properties were determined using reference samples for each group.

The superficial visible and non-visible deformation/strain during the tests were recorded with the optical measurement system WM.

Test Steps:

- Step 0: In a first stage, the dowel is installed in the building component.
- In a second stage, the wedge is inserted in the dowel's groove as follows:
- Step 1: introduction of the wedge in the groove up to the maximum depth of penetration ($E.T.$) equal to groove length. $E.T._{max,Step1} = 30mm = l_N$);
- Step 2: further introduction of the wedge up to a defined failure mode (buckling of wedge).

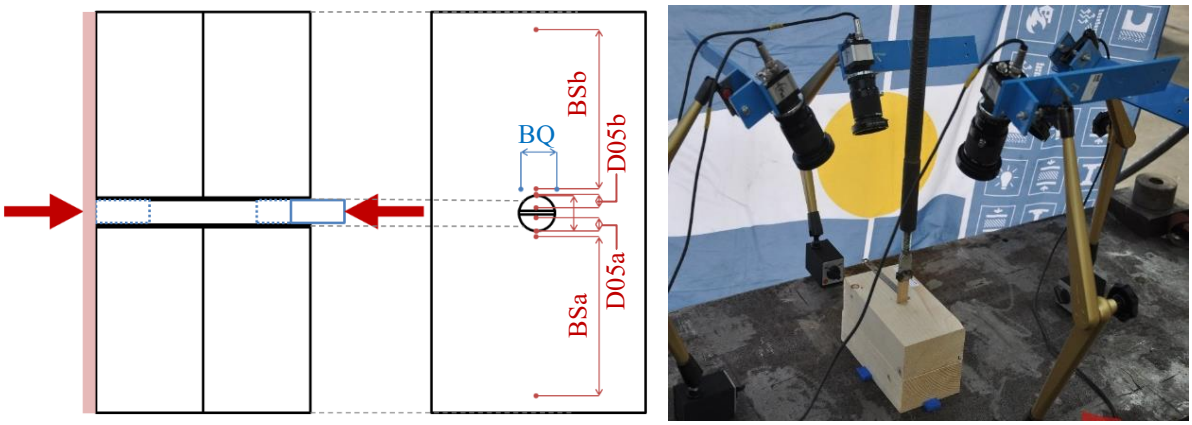


Figure 3: Test setup and optical measurement system WM for measurement of deformation/strain: a) Scheme b) Picture

Table 1: Abbreviations for the variable parameters of the wooden wedged dowel in TV1

H	T1-	T2-	G
Timber combinations	Angle θ between orientation of the groove and the direction of the annual rings on the dowel's cross section	Angle φ between the orientation of the groove on Side 1 [N,1] and fibers' direction in the building component on S1	Angle β between the orientation of the groove on Side 1 [N,1] and groove on Side 2 [N,2]
H1 = SW-HW H2 = HW-HW	T1-0 → θ = 0° T1-45 → θ = 45° T1-90 → θ = 90°	T2-0 → φ = 0° T2-45 → φ = 45° T2-90 → φ = 90°	G1 → orientation of the groove on S2 parallel to orientation on S1 G2 → orientation of the groove on S2 perpendicular to orientation on S1

Table 2: Tested geometric combinations and repetitions for timber combination

Geometric combinations	T2 on:		Repetitions for timber combination	
	S1	S2	H1	H2
T1-0_T2-0_G1	φ = 0°	φ = 0°	1	4
T1-0_T2-45_G1	φ = 45°	φ = 45°	4	0
T1-0_T2-45_G2	φ = 45°	φ = 135°	5	5
T1-0_T2-90_G1	φ = 90°	φ = 90°	5	5
T1-0_T2-90_G2	φ = 90°	φ = 0°	5	5

3.4 Conclusion

After testing, some specimens showed presence of cracks in the dowel in correspondence of groove's bottom and/or on building components' surface(s). Furthermore, for some specimens the penetration of the wedge was registered beyond $E.T. = l_N$. Therefore, dowel's core length after tests $[l'_{D,kern}]$ is to understand as the $l_{D,kern}$ minus crack and penetration length in the dowel after testing. The results of TV1 are following discussed for three cases "results for H1", "results for H2", "general conclusions", and resumed in Table 3.

Results for H1:

T2-0_G1:

- Dowel's core length $l'_{D,kern}$ average after testing is $l'_{D,kern,mean} = 30.00mm$.
- Occurrence of failure in dowel's core is 100%. Occurrence of cracks on the building components' surfaces is 50%.

T2-90_G2 :

- Dowel's core length $l'_{D,kern}$ average after testing is $l'_{D,kern,mean} = 33.25mm$.
- Occurrence of failure in dowel's core is 75%. Occurrence of cracks on the building components' surfaces is 38%. It is important to emphasize that the occurrence of failure on building component's surface increases by 60% and in the dowel by 92% when only S2, i.e. φ=0° is considered.
- The configuration T2-90_G2 will be abandoned because on the average: frequent occurrence of failure (tension perpendicular to the grain) on building component's surface S2 (φ=0°), and reduced dowel's core $l'_{D,kern}$ (deep crack generation at S2 (φ=0°)).

➔ In conclusion, all configurations with φ=0° will be abandoned for the timber combination H1 (T2-0_G1; T2-0_G2; T2-90_G2).

T2-45_G2:

- Dowel's core length $l'_{D,kern}$ average after testing is $l'_{D,kern,mean} = 46.30mm$.
- Occurrence of failure in dowel's core is 17%. Occurrence of cracks on the building components' surfaces is 50%.

T2-45_G1:

- Dowel's core length $l'_{D,kern}$ average after testing is $l'_{D,kern,mean} = 60.00mm$.
- Occurrence of failure in dowel's core is 0%. Occurrence of cracks on the building components' surfaces is 13%.
- Observation: higher bulk density induces on average smaller probability of opening of cracks in dowel's core: T2-45_G2: cracks in dowel's core: 6/12 - $\rho_{DOLLE,mean} = 0.560\ g/cm^3$; T2-45_G1: cracks in dowel's core: 0/16 - $\rho_{DOLLE,mean} = 0.715\ g/cm^3$.

➔ In conclusion, the configuration T2-45_G1 will be kept for next investigations, the

configuration T2-45_G2 will be abandoned.

T2-90_G1:

- Dowel's core length $l'_{D,kern}$ average after testing is $l'_{D,kern,mean} = 60.00mm$.
- Occurrence of failure in dowel's core is 70%. Occurrence of cracks on the building components' surfaces is 0%.
- Explanation: because of different E-moduli of the timber species in the connection, cracks occur in the dowel but not on the building component's surface. It is assumed that spruce has a higher elasticity and a higher capacity to absorb deformations compared to oak.

➔ In conclusion, the configuration T2-90_G1 will be kept for next investigations.

Results for H2:

T2-0_G1:

- Dowel's core length $l'_{D,kern}$ average after testing is $l'_{D,kern,mean} = 60.00mm$.
- Occurrence of failure in dowel's core is 0%. Occurrence of cracks on the building components' surfaces is 0%.

T2-90_G2:

- Dowel's core length $l'_{D,kern}$ average after testing is $l'_{D,kern,mean} = 60.00mm$.
- Occurrence of failure in dowel's core is 19%. Occurrence of cracks on the building components' surfaces is 33%. It is important to emphasize that the occurrence of failure on building component's surface increases by 60% and in the dowel by 25%, when only S2, i.e. φ=0° is considered.
- Observation: higher bulk density induces on average smaller probability of opening of cracks in dowel's core: T2-90_G2: failure of dowel's core on S2: 2/8 - $\rho_{DOLLE,mean} = 0.569\ g/cm^3$; T2-0_G1: failure of dowel's core: 0/16 - $\rho_{DOLLE,mean} = 0.721\ g/cm^3$.

➔ In conclusion, the configuration T2-0_G1 will be kept for next investigations, the configuration T2-90_G2 will be abandoned.

T2-45_G2

- Dowel's core length $l'_{D,kern}$ average after testing is $l'_{D,kern,mean} = 46.30mm$.
- Occurrence of failure in dowel's core is 0%. Occurrence of cracks on the building components' surfaces is 17%.

T2-45_G1

- Dowel's core length $l'_{D,kern}$ average after testing is $l'_{D,kern,mean} = 60.00mm$
- Occurrence of failure in dowel's core is 0%. Occurrence of cracks on the building components' surfaces is 13%.
- In the configuration T2-45 $E.T._{K,mean} = 17.25mm$ i.e. $t_N = b_D > 2mm$. Possible disadvantage: zero expansion of the dowel and no clamping-effect.

➔ In conclusion, the configuration T2-45_G1 will be kept for next investigations, the configuration T2-45_G2 will be abandoned.

T2-90_G1

- Dowel's core length $l'_{D,kern}$ average after testing is $l'_{D,kern,mean} = 42.40$mm.
- Occurrence of failure in dowel's core is 70%. Occurrence of cracks on the building components' surfaces is 0%.
- In the configuration T2-90 $E.T._{K,mean} = 20.75mm$ i.e. $t_N = b_D = 2\,mm$. Possible disadvantage: zero to low expansion of the dowel in T2-90 and no or low clamping-effect.

➔ In conclusion, the configuration T2-90_G1 will be kept for next investigations.

Table 3: Results of TV1 for timber and geometric combinations.

	H1					H2				
	T2-0_G1	T2-90_G1	T2-90_G2	T2-45_G1	T2-45_G2	T2-0_G1	T2-90_G1	T2-90_G2	T2-45_G1	T2-45_G2
$l'_{D,kern,mean}$ $[mm]$	30.00	60.00	33.25	60.00	46.30	60.00	42.40	60.00	60.00	46.30
Dowel's core failure $[\%]$	100	70	75	0	17	0	70	19	0	0
Building components' surfaces failure $[\%]$	50	0	38	13	50	0	0	33	13	17

General conclusions:

- Disadvantage of configuration G2: greater effort in manufacturing.
- Advantage of configuration G1: less effort in manufacturing.
- In correspondence with dowel's core presence of a torsional stress in G2 vs. no-torsional stress in G1 (later confirmed by FEM simulations)
- Dowel's core remains sufficiently free of cracks independently from β.
  ➔ In conclusion, the geometry G1 is preferred.
- T2-90 higher stiffness of the building component (higher strength properties in tension parallel to the grain), i.e. lower penetration depth of the wedge.
- T2-0 smaller stiffness of the building component (smaller strength properties in tension parallel to the grain), i.e. higher penetration depth of the wedge.
- Observation: during the insertion of the dowel in the building component (Step 0), a deviation respect to the intended angle φ is possible. Strength properties of HW are generally higher than SW ones; therefore, the building component of HW offers more resistance, and the deviation is here more probable than in one of SW. The approximated deviation from the intended angle is $\varphi = \mp 45°$.

4 FEM SIMULATIONS

The data collected during the TV1 were used for the development of a FE-Model of the repair connection with *wooden wedged dowels*. FE-simulations were performed with the software COMSOL.

4.1 Aim

The aim of the development of the FE-Model is to obtain a large number of virtual test results that realistically represent the stress / strain in different geometric and material configurations of the repair connection; therefore, a statistical evaluation of the parameters from the totality of the experimental and virtual results is possible. Specifically, in this first simulation series, the model was calibrated on the specimen H2_T1-0_T2-90_G1:d, and the presented results are a comparison between the results in the developed model and experimental results.

4.2 Geometry of the specimen

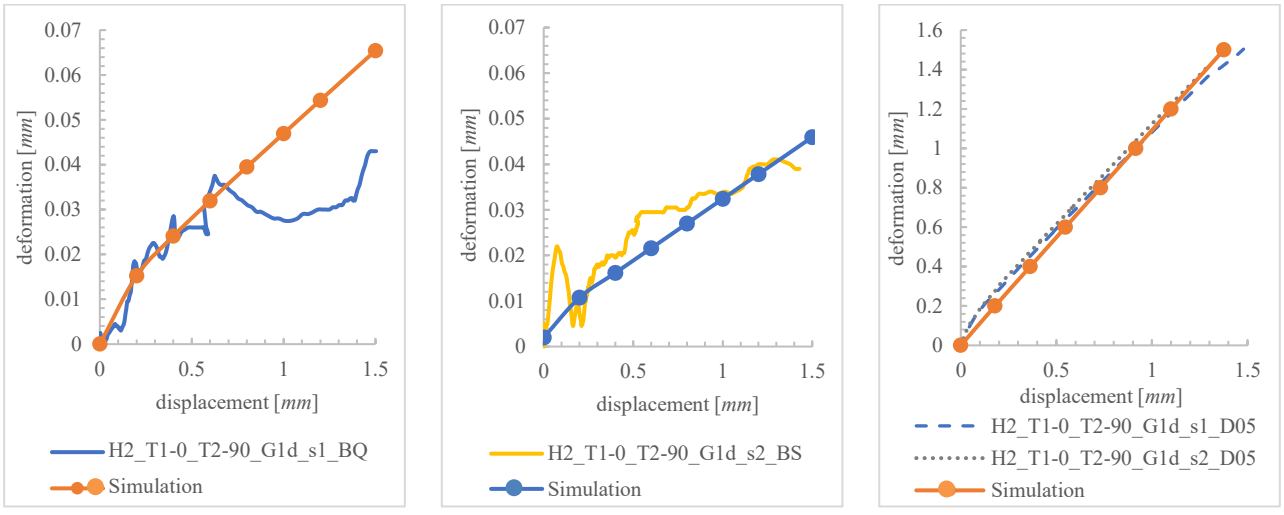
The geometry of the model was chosen according to geometrical properties of the test specimens TV1 (see Paragraph 3.2). In the FE-Model the wedge has no correspondent geometrical element, but is simplified as a change in volume in the groove.

4.3 Materials and Methods

The *actual* material properties Young's modulus ($E_{m,0}$) and bulk density (ρ) of the specimen H2_T1-0_T2-90_G1:d were determined. *Unknown* material properties for the specimen were assigned based on the experimentally ascertained $E_{m,0}$. According to [16], timber strength class D35 was assigned to building components and D27 to the dowel. In the specimen there is a difference between *actual* and *theoretical* properties. The correlation between $E_{B,m,0,EN338}$ and $E_{B,m,0,actual}$ is 96%, while the correlation between $E_{D,m,0,EN338}$ and $E_{D,m,0,actual}$ is 99.5%. Furthermore, difference in density between components and dowel is according to [16] properties: $\Delta_\rho = 40\,Kg/m^3$; however, according to *actual* material properties, the difference in density is approx. $\Delta_\rho = 100\,Kg/m^3$. The linear elasto-plastic behavior of materials was assumed according to [17-19]. Based on bevor mentioned material properties, further *unknowns* in the material model ($E_{c,0}$; $E_{c,90}$; Poisson ratio) were determined by the iteration procedure *FEM-updating*. The material behavior of materials in the FE-Model was calibrated according to the optical measurement results for the test specimen H2_T1-0_T2-90_G1:d (See Figure 3 and Table 4) for following cases:

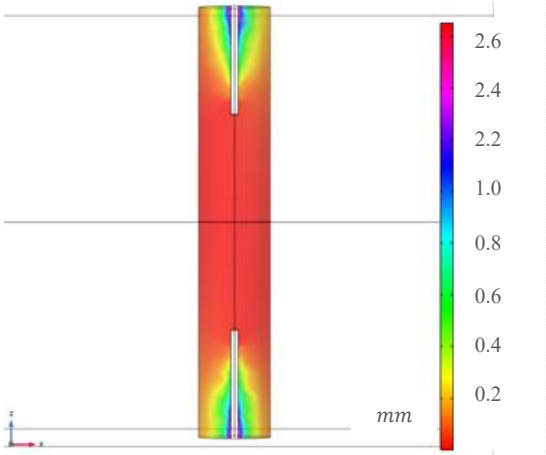
- (Piston) displacement / deformation perpendicular to the fibers (BQ) on building component's surface;
- (Piston) displacement / deformation parallel to the fibers (BS) on building component's surface;
- (Piston) displacement / deformation perpendicular to annual rings on dowel's cross section (D05).

Table 4: Displacement/ deformation diagrams in the specimen H2_T1-0_T2-90_G1d. Comparison between optical measurements and the results of the simulations.

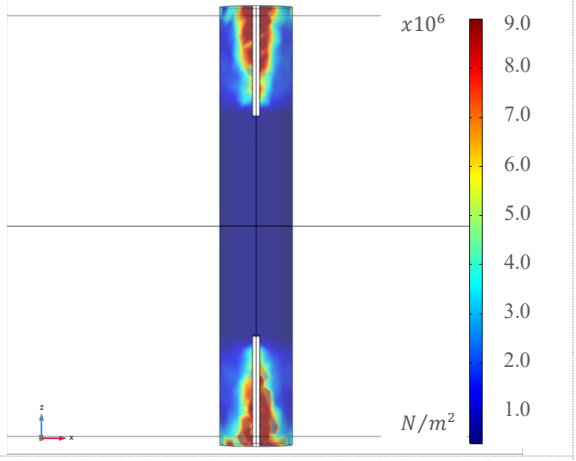


a) b) c)

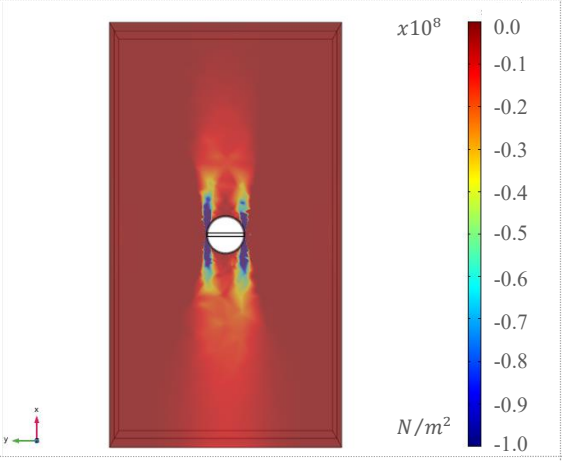
Table 5: Results of FE simulations for H2_T1-0_T2-90_G1 - Case study TV1.



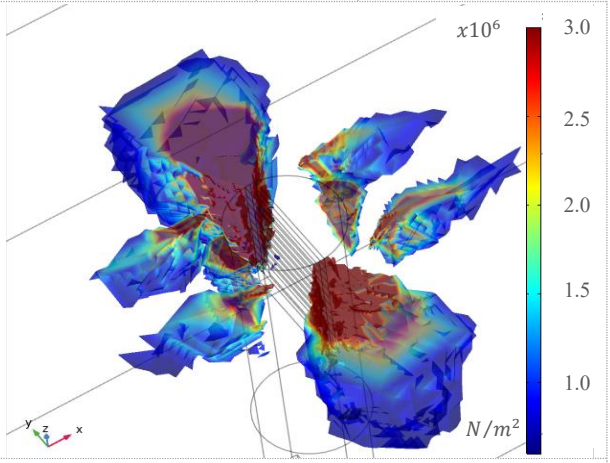
Global deformations in the dowel as a consequence of expansion of wedge's volume in the groove $\Delta_l = 1.5mm$ (x-direction) each side.



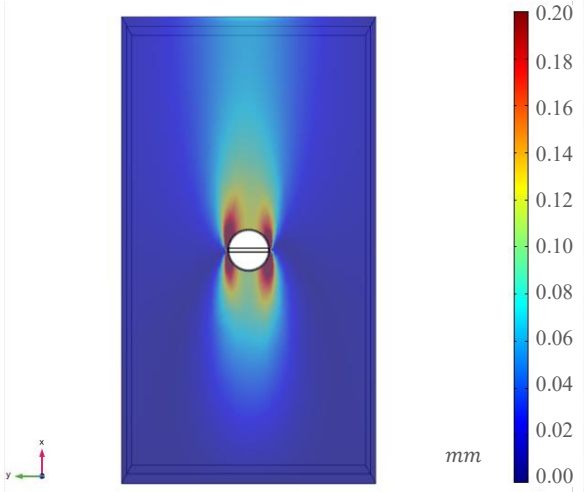
Global stress in the dowel as a consequence of expansion of wedge's volume in the groove $\Delta_l = 1.5mm$ (x-direction) each side.



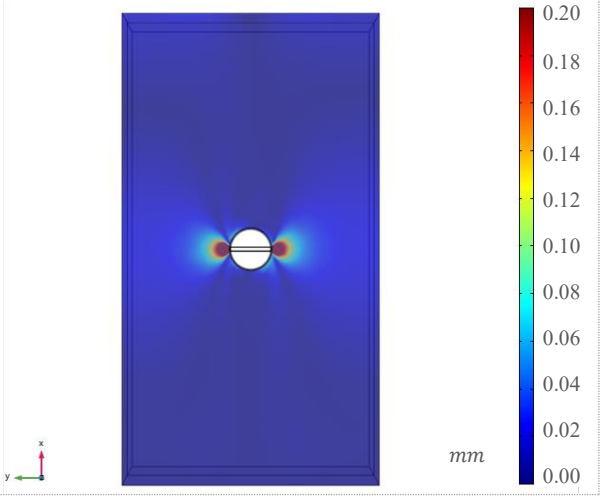
Stress in the building component (x-direction) as a consequence of expansion of wedge's volume in the groove $\Delta_l = 1.5mm$ (x-direction) each side.



Stress in the building component (y-direction) as a consequence of expansion of wedge's volume in the groove $\Delta_l = 1.5mm$ (x-direction) each side.



Strain in the building component (x-direction)



Strain in the building component (y-direction)

The simulations were performed under following assumptions: 1) The "action" in the experimental tests is the application of a load that permits through a displacement of the piston, the introduction of the wedge in the groove. In the FE-Model the introduction of the wedge is simulated as a change / shift in the volume of the groove. The maximum volume-change corresponds to the maximum (x-direction) displacement of the wedge in the performed test 2) The presence of friction and imperfections on the contact surface between wedge and dowel are neglected; 3) Radial and tangential material properties of the wood are the same.

4.4 Conclusions

Results of simulations for the geometry H2_T1-0_T2-90_G1:d are represented in Table 5. Here, distribution of stresses (exceeding $f_{t,90}$) and deformations in the dowel and building component is depicted. The correspondence between simulations and experimental results is the best possible. Nevertheless, due to engineering assumptions in the material model, test results and simulations differ under some aspects: as soon as a crack occurs in the material, FEM results differ from the experimental ones because the idealized linear elasto-plastic behavior of the model (based on Navier theory) does not take into account the loss of energy after failure.

5 CONCLUSIONS

Results of experimental preliminary investigations TV1 permitted to identify the significant parameters that play a major role in formation of cracks in the *wooden wedged dowel* and on components' surfaces. Similarly, it was possible to compose the *requirement matrix*, which contains all determinant constructive and static parameters for the implementation of a numerical model for design of repair connections with *wooden wedged dowels*. Furthermore, results of experimental preliminary investigations permitted to identify the most favorable wood and geometrical combinations for the definition of the axial load-carrying capacity of *wooden wedged dowels*. This second step is already in process with the experimental preliminary investigations TV2. Furthermore, the results of the first FE-Model will be further implemented. In the second update of the FE-model mechanical properties $E_{m,0}$, ρ, $E_{c,0}$, $E_{c,90}$ for building components and dowels will be determined in laboratory conditions according to [20] for different timber species. *Actual* material properties, together with *actual* elasto-plastic behavior of structural components and dowel will be used for the generation of more, realistic results for different timber combinations.

Acknowledgements. The research was financed with funds from the research initiative Zukunft Bau of German Federal Institute for Research on Building, Urban Affairs and Spatial Development (BBSR, BMI) (SWD-10.08.18.7-18.16). Furthermore, the research project was both financially and scientifically supported by: Niedersächsisches Landesamt für Denkmalpflege; IGP Gockel PartGmbB - Ingenieure und Architektin; Werkstätten für Denkmalpflege GmbH Quedlinburg.

6 REFERENCES

[1] ICOMOS ISCARSAH (2017). *Principles for the conservation of wooden built heritage* Adopted by the 19th ICOMOS General Assembly, New Delhi, India, 15 December 2017.

[2] Petzet M. *Grundsätze der Denkmalpflege 1*. ICOMOS, Heft des Deutschen Nationalkomitees, Bd. X, München (1992).

[3] Gerner M. *Entwicklung von Holzverbindungen Forschungs- und Untersuchungs-ergebnisse*, Fraunhofer IRB Verlag, (2000).
[4] Ashurst, J. and N. *English heritage. Practical building conservation. Timber*. Ashgate, 2012.
[5] Blaas H.J., Ehlbeck J., Kreuzinger H., Steck G. *Erläuterungen zu DIN 1052: 2004-08. Entwurf, Berechnung und Bemessung von Holzbauwerken*. 2. Aufl. Deutsche Gesellschaft für Holzforschung. München und Karlsruhe: DGfH Innovations- und Service GmbH, Bruder, (2005).
[6] Blaas H.J., Ernst H., Werner H. Verbindungen mit Holzstiften - Untersuchungen über die Tragfähigkeit. In: *Bauen mit Holz*, 101, (1999), Heft 10, Pp. 45–52.
[7] Ehlbeck J., Hättich R. Tragfähigkeit und Verformungsverhalten von ein- und zweischnittig beanspruchten Holznägeln. In: *Erhalten historisch bedeutsamer Bauwerke* - Jahrbuch 1988, SFB 315, Universität Karlsruhe, Wilhelm Ernst & Sohn Verlag für Architektur und Technische Wissenschaften, Berlin, (1989).
[8] Görlacher R. Empfehlungen für die Praxis. In: *Historische Holztragwerke (Untersuchen, Berechnen und Instandsetzten)*, SFB 315, Universität Karslruhe, (1999).
[9] Holzer S. M. *Statische Beurteilung historischer Tragwerke* - Band 2 | Holzkonstruktionen. Ernst & Sohn, (2015).
[10] Kessel M., Augustin R. *Untersuchung der Tragfähigkeit von Holzverbindungen mit Holznägeln für Sanierung und Rekonstruktion von alter Bausubstanz*. Forschungsbericht, FH Hildesheim/Holzminden, Fachbereich Bauingenieurwesen, Labor für Holztechnik, Hildesheim, (1992).
[11] Kessel M., Augustin R. Untersuchung der Tragfähigkeit von Holzverbindungen mit Holznägeln. In: *Bauen mit Holz*, 96 (1994), Pp. 484–487.
[12] Gehri E. *Holzbau- Tabellen Band 2*. Lignum, Schweizerische Arbeitsgemeinschaft für das Holz, Zürich, (1990).
[13] Müller A., Vogel M, Lang S., Sauser F. *Historische Holzverbindungen. Untersuchung des Trag- und Verformungsverhaltens von Historischen Holzverbindungen und Erstellung eines Leitfadens für die Baupraxis*. Forschungsbericht der Fachhochschule Biel, Institut für Holzbau, Tragwerke und Architektur, (2016).
[14] DIN EN 1995-1-1 / NA: 2013-08 National Annex – Nationally determined parameters – Eurocode 5: Design of timber structures – Part 1.1: General – Common rules and rules for buildings. Normenausschuss Bauwesen (NABau) im DIN, (August 2013).
[15] SIA 269/5:2011, Existing Structures – Timber Structures. Swiss Society of Engineers and Architects, Zurich, Switzerland.
[16] DIN EN 338:2016-07 Structural timber - Strength classes.
[17] Niemz P., Sonderegger W. Holzphysik. Physik des Holzes und der Holzwerkstoffe. Fachbuchverlag Leipzig im Carl Hanser Verlag, (2017). P. 275.
[18] Clorius, C. O., Damkilde, L., Hoffmeyer, P. Fatigue in Wood: An investigation in tension perpendicular to the grain. BYG-Rapport; No. R-038 Kgs. Lyngby, Denmark: Technical University of Denmark (DTU), (2001).
[19] Kollmann F. *Technologie des Holzes und Holzwerkstoffe*. Erster Band. Springer Verlag, (1951). Pp. 667-669.
[20] DIN EN 408:2012-10 Timber structures - Structural timber and glued laminated timber - Determination of some physical and mechanical properties.

12th International Conference on Structural Analysis of Historical Constructions
SAHC 2020
P. Roca, L. Pelà and C. Molins (Eds.)

STABILIZATION AND CONSOLIDATION OF HISTORICAL MULTI-LEAF MASONRY

JIŘÍ WITZANY[1], JIŘÍ BROŽOVSKÝ[2], TOMÁŠ ČEJKA[1], JAN KUBÁT[1] AND RADEK ZIGLER[1*]

[1] Faculty of Civil Engineering (FCE)
Czech Technical University in Prague (CTU in Prague)
Thákurova 7, 166 29 Prague, Czech Republic
e-mail: {witzany, cejka, jan.kubat.2, zigler}@fsv.cvut.cz, kps.fsv.cvut.cz (*corresponding author)

[2] Faculty of Civil Engineering (FAST)
VSB - Technical University of Ostrava (VSB-TUO)
Ludvíka Podéště 1875/17, 708 00 Ostrava-Poruba, Czech Republic
email: jiri.brozovsky@vsb.cz, www.fast.vsb.cz

Keywords: Multi-leaf Masonry, Historical Structures, Failure Mechanism, Stabilization

Abstract. *Historical masonry structures with a greater thickness can often be made as so-called multi-leaf masonry with outer leaves lined with the application of some of the masonry bonding methods and with the inner leave of the so-called cast core formed by fragments of stones of different sizes that are bonded with more mortar. The load capacity, stiffness and the failure mechanism of multi-leaf masonry are influenced by the interaction of individual leaves with different deformation and physico-mechanical properties and the nature of the mutual connection of individual leaves of masonry. The performed analyses showed a significant influence of especially the cast core masonry tensile strength and the contact joint strength between the core masonry and the outer leaves*.

1 INTRODUCTION

Failure mechanism of multi-leaf masonry with outer layers (facing leaves) of coursed masonry of regular (dressed) stone blocks, or of roughly coursed masonry with irregular, partially treated (roughly dressed) quarry stones and with an inner layer, the so-called cast core, consisting of fragments of stones differing in sizes and shapes, which are laid in a larger amount of mortar, is different from the failure mechanism of coursed stone masonry or roughly coursed irregular masonry [1,2]. The determination of the residual compressive loadability of multi-leaf masonry is a demanding task at which the calculation procedures used for single-leaf masonry cannot be fully applied.

Due to the nature of the inner leaf containing a larger amount of binder (e.g. 40-60% of the generally more flexible binder) than the outer masonry leaves (e.g., 15-30% binder), different deformation properties, a different load capacity and failure mechanism of this type of masonry can be expected [3]. The “bonding” of the outer leaves with the inner leaf contributes to the increase in the coherence and integrity of multi-leaf masonry. Also, the natural irregularity of

the inner surface of the outer (facing) leaves made of undressed stones improves the bonding of the outer and inner leaves and increases the resistance of the multi-leaf masonry structure to "splitting", which usually precedes complete failure of masonry.

The process of multi-leaf masonry failure under concentric compressive loads is characterized by the detachment of individual masonry leaves, damage to the masonry cross-section due to transverse (expanding) tensile forces usually caused by the different stiffness of the cast core and the facing leaf masonry [4,5,6].

Historical masonry is characterized by considerable heterogeneity and different properties of its individual components [7,8,9,10]. The study of the influence of different material properties of individual parts of multi-leaf masonry on its failure mechanism is therefore a basic prerequisite for its reliable stabilization and consolidation design.

2 THEORETICAL AND EXPERIMENTAL RESEARCH INTO THE BEHAVIOR OF MULTI-LEAF MASONRY UNDER COMPRESSIVE LAODING

The research projects (NAKI DF12P01OVV037 and NAKI DG16P02M055) involved the theoretical and experimental analysis of the failure mechanism of multi-leaf masonry under concentric compressive load exerted by force or by forced deformation was performed. The theoretical and experimental analysis was carried out on a model of multi-leaf masonry (Fig. 1) with outer (facing) leaves approx. 150 mm thick made up of roughly dressed sandstone blocks (approx. size of 170 x 150 x 120 mm, compressive strength approx. 40 MPa) and a core masonry leaf approx. 300 mm in thickness made up of sandstone fragments with a lime mortar binder (mortar compressive strength of facing leaves of 1.15 MPa in the case of bonded leaves and 1.08 MPa in the case of non-bonded leaves, mortar compressive strength of cast (inner leaf) masonry of 0.92 MPa in the case of bonded leaves and 0.97 MPa in the case of non-bonded leaves).

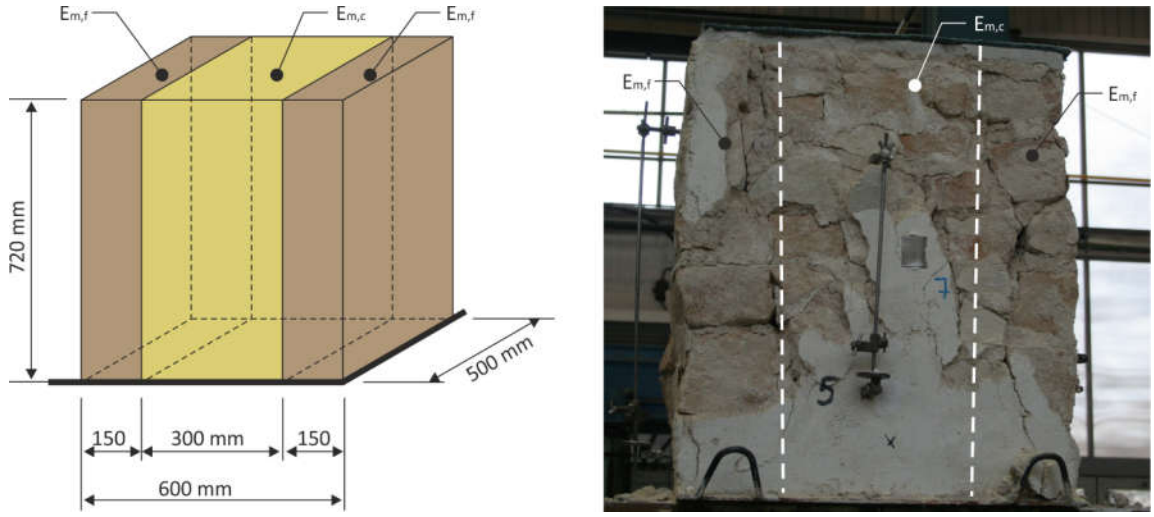


Figure 1: Multi-leaf masonry specimens

Numerical analysis (2D linear finite element analysis) included a total of 7 different arrangements of segments (bodies) of multi-leaf masonry loaded at the upper free end by a uniform vertical compressive load and 7 segments (bodies) loaded at the upper free end by

forced vertical deformation (Fig. 2, Tab. 1). The numerical analysis covered different alternatives of computational models (single-leaf, multi-leaf, bonded and non-bonded leaves) as well as computational load models (force, forced deformation).

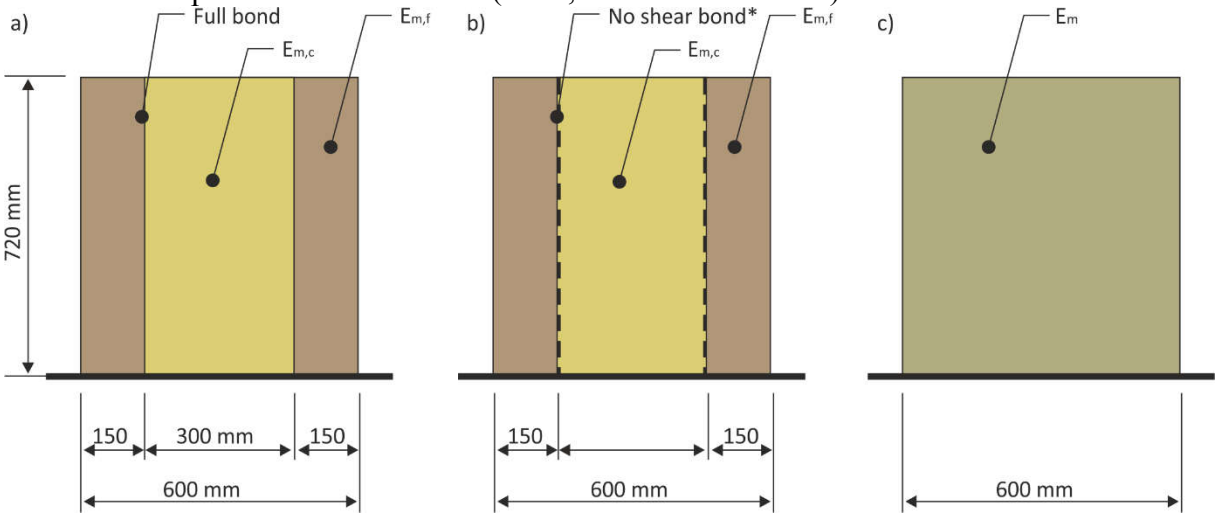


Figure 2: a) Multi-leaf masonry with full bond between leaves, b) Multi-leaf masonry with no shear bond between leaves (*horizontal stresses are transferred), c) Single-leaf masonry

Table 1: Overwiev of theoretically studied cases of multi-leaf masonry

	Geometry	Load type	$E_{m,f}$ [GPa]	$E_{m,c}$ [GPa]
1		Force	3.8	1.6
2			3.8	1.2
3			3.8	3.8
4			1.6	1.6
5			1.2	1.2
6		Deformation	3.8	1.6
7			3.8	1.2
8			3.8	3.8
9			1.6	1.6
10			1.2	1.2
11		Force	3.8	1.6
12			3.8	1.2
13		Deformation	3.8	1.6
14			3.8	1.2

The experimental research was carried out on a total of 6 test specimens of the same dimensions as in the theoretical analysis (width x depth x height - approx. 500 x 600 x 720 mm) loaded by a monotonically increasing compressive force exerted by a hydraulic press with a digital pressure sensing center (manufacturer MFL Germany, load range 0 - 10000 kN, Fig. 3).

Based on the theoretical and experimental analysis of multi-leaf masonry segments, two different failure mechanisms of multi-leaf masonry under concentric compressive load were formulated.

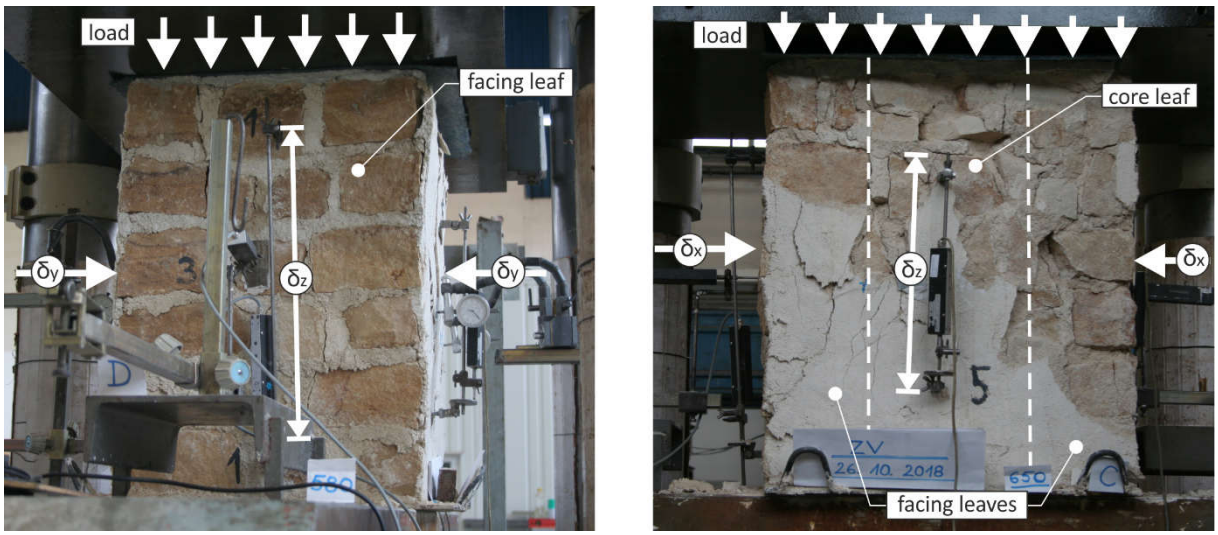


Figure 3: Test specimens of multi-leaf masonry under compressive load

3 MULTI-LEAF MASONRY FAILURE MECHANISM

The failure mechanism of multi-leaf stone masonry of the "coursed facing masonry leaf - cast masonry leaf – coursed facing masonry leaf" composition is characterized by the development of transverse (horizontal) tensile forces with the maximum value in the middle of the masonry and shear forces with the maximum in the joint between the facing masonry leaves and the cast core leaf (Fig. 4).

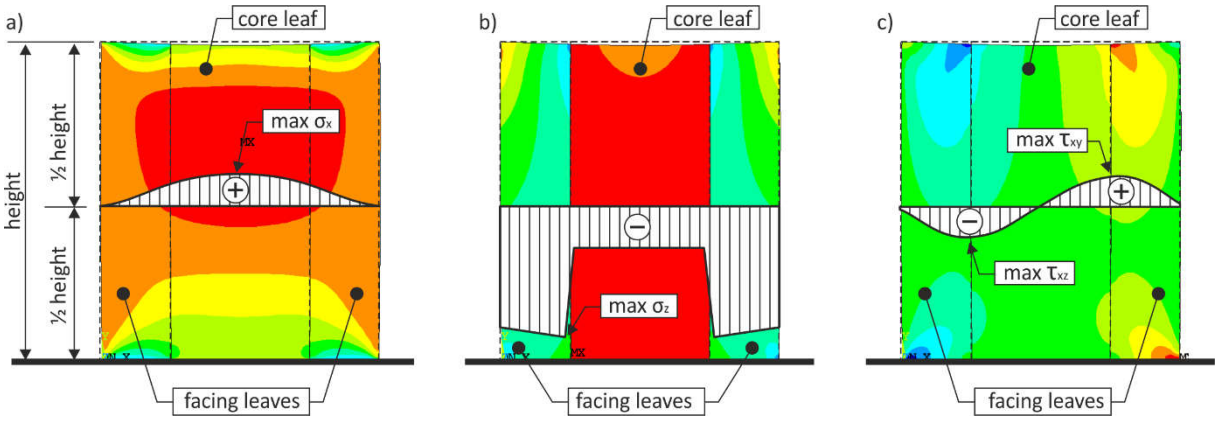


Figure 4: Results of numerical analysis – a) Horizontal stresses, b) Vertical stress, c) Shear stresses

Based on the results of the numerical analysis, deflection of stress trajectories in multi-leaf masonry loaded by concentric compression due to the higher stiffness of facing masonry leaves $E_{m,f}$ (lower compressibility) compared to the stiffness of the core masonry leaf $E_{m,c}$ can be observed. This deflection of the stress trajectories (change from the vertical trajectory in case

of single-leaf masonry or masonry where $E_{m,f} \approx E_{m,c}$ to more complex or inclined stress pattern in case of Em,f ≠ Em,c) is accompanied by the formation of horizontal stresses which increase in size with the increasing difference in the stiffness of the facing and core masonry leaves ($E_{m,f} > E_{m,c}$).

In the case of $E_{m,c}/E_{m,f}$ ration equal to 0.42, the horizontal stresses $+\sigma_x$ reached 646% and 861% in case of facing leaf or core leaf, respectively, compared to a single leaf masonry. In the case of $E_{m,c}/E_{m,f}$ ration equal to 0.32 these stresses reach 769% and 1028% in case of facing leaf or core leaf, respectively, compared to a single leaf masonry (Fig. 5). These additional horizontal tensile stresses, combined with no uniform distribution of vertical stresses $+\sigma_z$ (Fig. 6) can lead to significant crack formation and masonry failure. This mechanism is further enhanced by the increase in shear stresses $+\tau_{xz}$ reaching up to 775%, depending on the $E_{m,c}/E_{m,f}$ ration (Fig. 7).

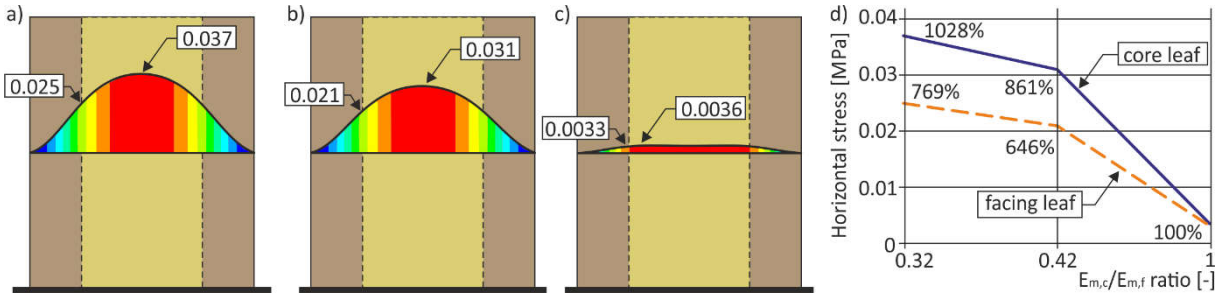


Figure 5: Horizontal stresses $+\sigma_x$ in multi-leaf masonry – a) Ratio of $E_{m,c}/E_{m,f} = 0.32$, b) Ratio of $E_{m,c}/E_{m,f} = 0.42$, c) Ratio of $E_{m,c}/E_{m,f} = 1$, d) Change of horizontal stress due to the $E_{m,c}/E_{m,f}$ ratio

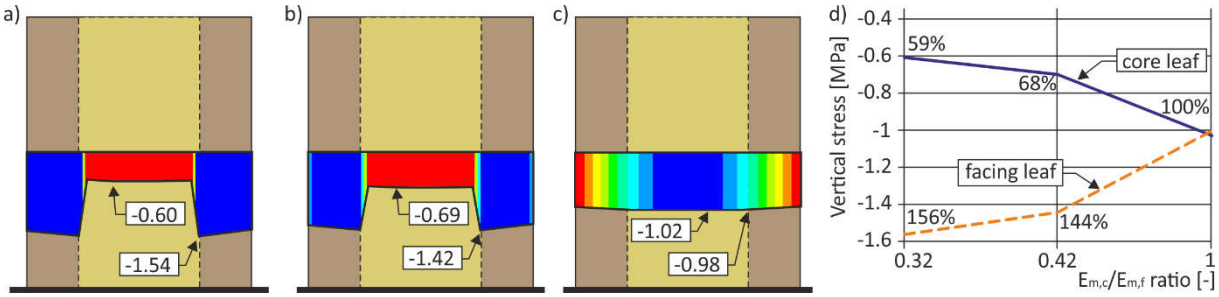


Figure 6: Vertical stresses $+\sigma_z$ in multi-leaf masonry – a) Ratio of $E_{m,c}/E_{m,f} = 0.32$, b) Ratio of $E_{m,c}/E_{m,f} = 0.42$, c) Ratio of $E_{m,c}/E_{m,f} = 1$, d) Change of vertical stress due to the $E_{m,c}/E_{m,f}$ ratio

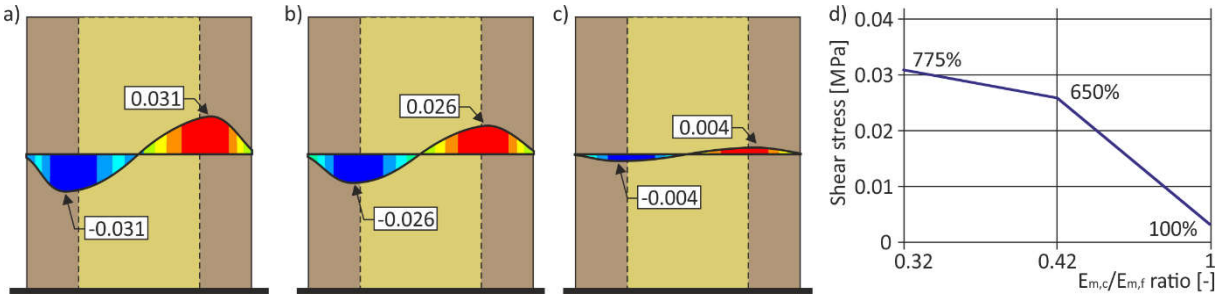


Figure 7: Shear stresses $+\tau_{xz}$ in multi-leaf masonry – a) Ratio of $E_{m,c}/E_{m,f} = 0.32$, b) Ratio of $E_{m,c}/E_{m,f} = 0.42$, c) Ratio of $E_{m,c}/E_{m,f} = 1$, d) Change of shear stress due to the different $E_{m,c}/E_{m,f}$ ratio

Based on the experimental results (Fig. 8 and Fig. 9, Tab. 1 and Tab. 2), it can be stated that the characteristic failure of multi-leaf masonry depends on the tensile strength of the cast core masonry and the strength of the contact joint between the facing and the core masonry leaves.

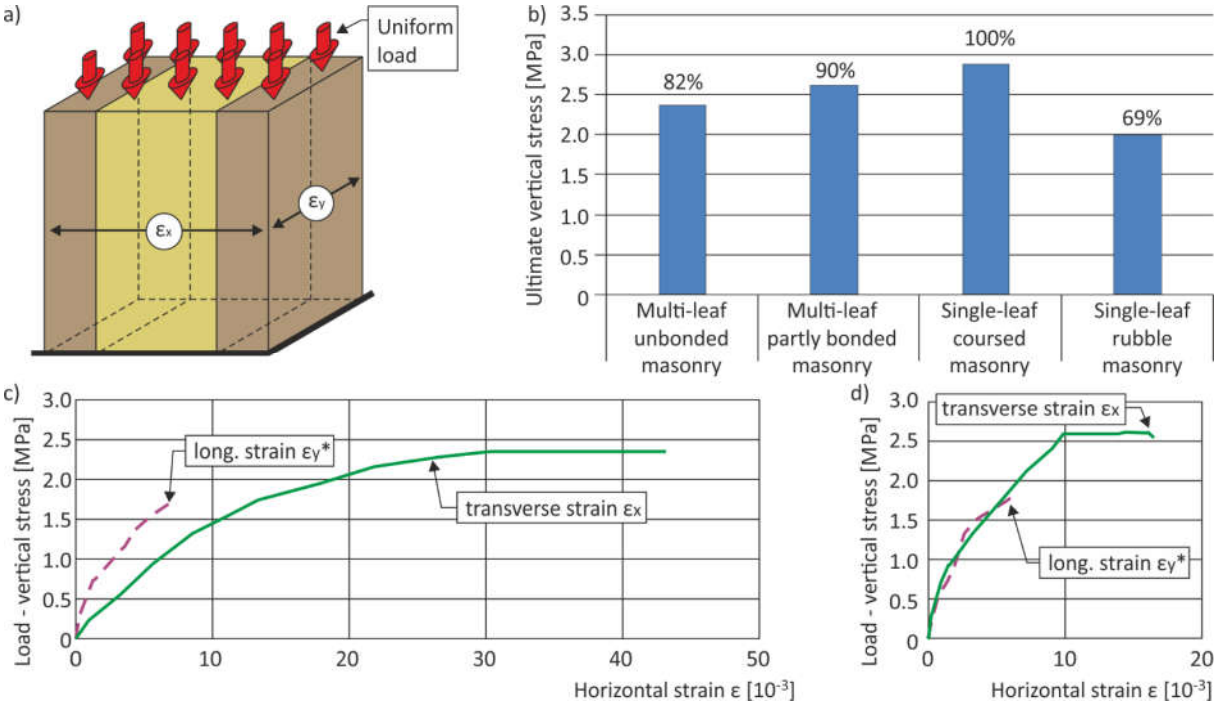


Figure 8: a) Scheme of experimental specimens, b) Ultimate compressive stress, c) Transverse and longitudinal horizontal strains for un-bonded masonry, d) Transverse and longitudinal horizontal strains for bonded masonry, *Note*: Due to test setup, longitudinal strains were not measured up to ultimate load*

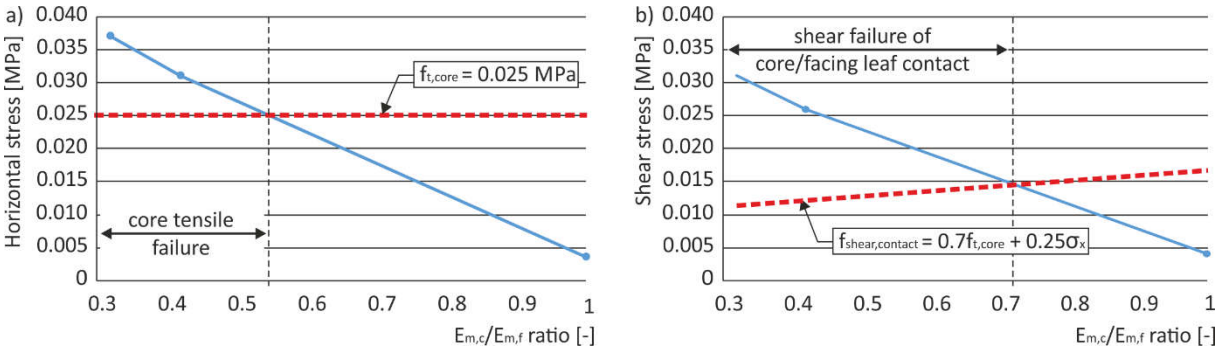


Figure 9: a) The change of tensile stresses due to the $E_{m,f}/E_{m,c}$ and tensile strength of the core leaf (rubble) masonry, b) The change of shear stresses due to the $E_{m,f}/E_{m,c}$ ratio and shear strength of the core/facing leaf contact

In terms of the response and the type of failure of multi-leaf masonry loaded by concentric compressive force, which precedes reaching the limit load, the loss of stability and bearing function of multi-leaf masonry, two different failure mechanisms of multilayer masonry can be distinguished:

a) Failure mechanism of multi-leaf masonry due to reaching the ultimate strength of the core (cast) masonry. This failure mechanism of multi-leaf masonry can be observed in cases where the ultimate tensile strength of the cast core masonry is exceeded due to vertical tensile cracks, which gradually extend from the middle third of the height of the compressed masonry (walls, columns) towards the heel and head. The formation of vertical tensile cracks in the masonry core is subsequently accompanied by an uneven distribution of normal compressive stresses across the cross-section of multi-leaf masonry, which precedes reaching the limit load. The reduction of the stability - buckling strength - of the masonry parts (columns) delimited by individual vertical tensile cracks contributes to the progressiveness of the multi-leaf masonry failure mechanism.
b) Failure mechanism of multi-leaf masonry due to reaching the ultimate shear strength in the contact joint between the facing masonry leaves and the core masonry leaf. This failure mechanism of multi-leaf masonry can be observed in cases where the ultimate shear strength in the "facing leaf – core leaf – facing leaf" contact joint is exceeded and individual masonry leaves become detached. The ultimate compressive strength of multi-leaf masonry at this stage of failure depends primarily on the intensity of the uneven distribution of normal stresses and the buckling strength of the facing leaves.

Table 2: Overview of experimental multi-leaf and single-leaf masonry specimens and their material properties

Masonry type	Masonry units comp. strenght [MPa]	Mortar comp. strenght [Mpa]	Dimensions [mm]		
			Width	Depth	Height
Multi-leaf, un-bonded	46.4	0.95-1.10	510	580	710
Multi-leaf, bonded	46.4	0.93-1.13	510	590	740
Single-leaf, coursed	46.4	1.01	485	595	730
Single-leaf, rubble*	19.51	1.68	540	540	1710

*Note: *Test specimen from another test series (full height specimens), included for comparison*

Table 3: Results of experimental testing of multi-leaf and single leaf masonry specimens

Masonry type	Ultimate vert. stress σ_z [MPa]	Ultimate strains ε [-]		
		Vertical (ε_z)	Transverse horizontal (ε_x)	Longitudinal horizontal (ε_y)
Multi-leaf, un-bonded	2.37	0.0117	0.0302	0.0073*
Multi-leaf, bonded	2.61	0.0164	0.0143	0.0057*
Single-leaf, coursed	2.89	0.0109	0.0169	x
Single-leaf, rubble	1.99	0.0201	0.0342	x

Note: Strains at approx. 75% of ultimate load level (*), strains not measured (x)

4 STABILIZATION AND CONSOLIDATION OF MULTI-LEAF HISTORICAL MASONRY

Stabilization and consolidation measures should be based on the failure mechanisms characterized by masonry splitting accompanied by reduced stability and compressive load capacity. In terms of prevention of the appearance of premature tensile cracks, which result in multi-leaf masonry splitting, the most effective methods that can be recommended, based on the research conducted and authors' experience of in-situ applications, are:

- *In the case of insufficient contact joint strength or damage*
  - Reinforcement of multi-leaf masonry by transverse anchors (connectors) designed on the principle of the so-called "nail" grouting. After the insertion of steel bars (e.g. with periodic surfaces) into transversally drilled holes (slightly sloping inwards – approx. 5°, reaching to approx. 1/2 of the core thickness), pressure grouting (with lime, cement or polymer based binders, resins etc.) is performed. The optimal spacing of individual grouted nail anchors (connectors), which can be arranged in one or several rows one above the other, is less than or equal to the thickness of the facing masonry leaf (Fig. 10a).
  - Pressure grouting aimed at reinforcing the contact joint with grouting mixtures based on polymer or epoxy resins or grouting mixtures based on lime or cement binders. The grouting hole should reach into the core leaf to a maximum depth equal to the thickness of the facing masonry leaf (Fig. 10b).
- *In the case of insufficient strength or quality of the core leaf masonry*
  - Grouting of the cast core masonry with a suitable grouting mixture, depending on the pore system, voids or cavities. In order to increase the efficiency and reliability of grouting, it is advisable to carry out two-stage grouting aimed at increasing the stiffness and strength of the core masonry. Grouting holes should reach to 2/3 - 4/5 of the thickness of the core masonry leaf (Fig. 10c).

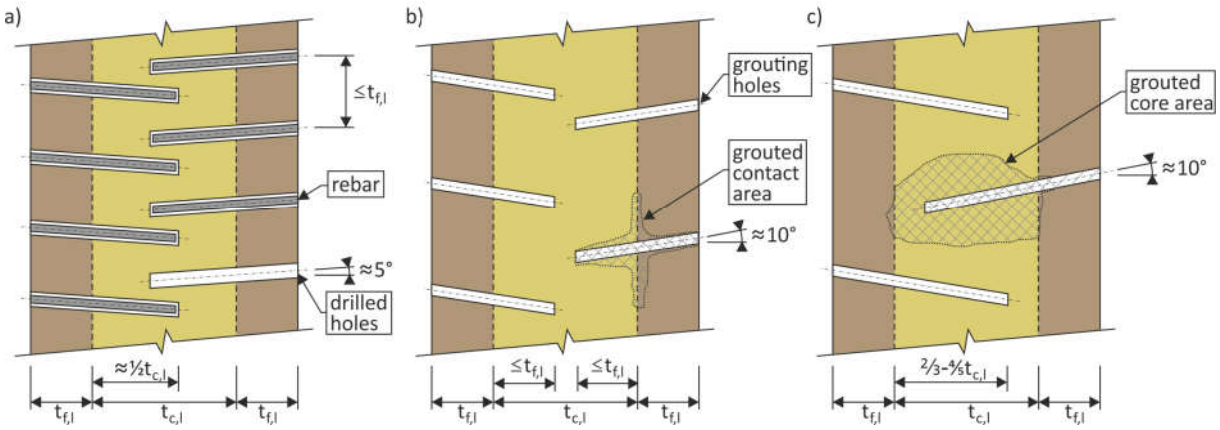


Figure 10: a) Stabilization of multi-leaf masonry by "nail" grouting, b) Stabilization of multi-leaf masonry by contact joint grouting, c) Stabilization of multi-leaf masonry by core grouting

5 CONCLUSIONS

The determination of the residual compressive load capacity of multi-leaf masonry and the design of remediation and reinforcement methods of damaged multi- leaf masonry requires a

specific approach based on the results of detailed research, diagnostic investigations and theoretical analysis. Massive multi-leaf masonry usually shows sufficient reserves in the load capacity due to the magnitude of real loads. The tests and analyses performed, in contrast, pointed out the risk factors of multi-leaf masonry that may be the cause of its sudden failure (collapse).

Acknowledgements. The article was written with support from the NAKI DG16P02M055 project "Development and Research into Materials, Procedures and Technologies for Restoration, Conservation and Strengthening of Historic Masonry Structures and Surfaces and Systems of Preventive Care of Historic and Heritage Buildings Threatened by Anthropogenic and Natural Risks".

REFERENCES

[1] Stavroulaki, M., Papalou, A. Parametric analysis of old multi-leaf masonry walls *International Journal of Conservation Science* (2014) **5(4)**:435-446.

[2] Demir, C., Ilki, A., Characterization of the materials used in the multi-leaf masonry walls of monumental structures in Istanbul, Turkey. *Construction and Building Materials* (2014), **64**:398-413.

[3] Aldreghetti, I., Baraldi, D., Boscato, G., Cecchi, A., Massaria, L., Pavlovic, M., Reccia, E., Tofani, I. Multi-leaf masonry walls with full, damaged and consolidated infill: Experimental and numerical analyses. *Key Engineering Materials* (2017) **747**:488-495

[4] M. R. Valluzzi, F. da Porto, C. Modena, Behaviour of multi-leaf stone masonry walls strengthened by different intervention techniques, In: P.B. Lourenço, P. Roca (Eds.) *Historical Constructions* (2001)

[5] Candela, M., Borri, A., Corradi, M., Righetti, L. Effect of transversal steel connectors on the behavior of rubble stone-masonry walls: Two case studies in Italy. *Brick and Block Masonry: Trends, Innovations and Challenges - Proceedings of the 16th International Brick and Block Masonry Conference*, IBMAC 2016 (2016), pp. 2029-2038.

[6] Corradi, M., Borri, A., Poverello, E., Castori, G. The use of transverse connectors as reinforcement of multi-leaf walls. *Materials and Structures/Materiaux et Constructions* (2017) **50(2)**, art. no. 114

[7] Witzany, J., Čejka, T., Kroftová, K., Šmidtová, M., 2016. The effect of degradation processes on the serviceability of building materials of historic buildings, *The Civil Engineering Journal* **3(10)**, art. no. 11

[8] Witzany, J., Zigler, R., Čejka, T., Pospíšil, P., Holický, M., Kubát, J., Maroušková, A., Kroftová, K., Physical and Mechanical Characteristics of Building Materials of Historic Buildings *The Civil Engineering Journal* (2017) **4(12)**:343-360

[9] Witzany, J., Zigler, R., Kroftová, K., Čejka, T., Kubát, J., Holický, M., Karas, J., The Effect of Pore Distribution in Historic Masonry on the Grouting Method and Grouting Mix Selection, *The Civil Engineering Journal* (2018) **3(10)**:307-329

[10] Witzany, J., Zigler, R., Čejka, T., Libecajtová, A., Polák, A., Kubát, J., 2019. Research into the effect of grouting on physical-mechanical properties of historic masonry, In: A. Zingoni (Ed.) *Advances in Engineering Materials Structures and Systems: Innovations, Mechanics and Applications* (2019). London: Taylor & Francis, p. 617-618.

12th International Conference on Structural Analysis of Historical Constructions
SAHC 2020
P. Roca, L. Pelà and C. Molins (Eds.)

STATIC TEST ON FULL SCALE RAMMED EARTH BUILDING WITH MESH–WRAP RETROFITTING STRATEGY

KSHITIJ C. SHRESTHA[1*], TAKAYOSHI AOKI[2], MITSUHIRO MIYAMOTO[3], NORIYUKI TAKAHASHI[4], JINGYAO ZHANG[5], PHUNTSHO WANGMO[6], NOBORU YUASA[7], SANGCHUL SHIN[7], PEMA[6] AND KUNZANG TENZIN[6]

[1] Nagoya City University
464-0083 Nagoya, Japan
e-mail: kshitij@sda.nagoya-cu.ac.jp, (*corresponding author)

[2] Nagoya City University
464-0083 Nagoya, Japan
e-mail: aoki@sda.nagoya-cu.ac.jp

[3] Kagawa University
761-0396 Takamatsu, Japan
e-mail: miyamoto@eng.kagawa-u.ac.jp

[4] Tohoku University
980–8579 Sendai, Japan
e-mail: ntaka@archi.tohoku.ac.jp

[5] Kyoto University
615–8540 Kyoto, Japan
e-mail: zhang@archi.kyoto-u.ac.jp

[6] Department of Culture, Ministry of Home and Cultural Affairs
133 Thimphu, Bhutan
email: {pwangmo, pema, kunzangt}@mohca.gov.bt

[7] Nihon University
275-8575 Narashino, Japan
email: {yuasa.noboru, shin.sangchul}@nihon-u.ac.jp

Keywords: Rammed Earth Structure, Composite Masonry, Full–scale test, Retrofitting

Abstract. *This paper reports the experimental campaign for static tests performed on unreinforced (URE) and mesh retrofitted (RRE) full scale rammed earth building. Amongst varying building patterns of traditional rammed earth houses found in Bhutan, a two-storied building with a full solid wall (small openings) on the first floor and larger opening in the front facade of the second floor was chosen. The proposed mesh–wrap retrofitting of the walls involved the use of standard mild steel welded mesh as the main mesh, M–Mesh (Ø 1.8 mm and*

34 mm c/c spacing) and light and galvanized welded mesh as a lapping mesh, L–Mesh (Ø 1.45 mm and 28 mm c/c spacing) provided at the corners and along the height of the walls. The static test loading protocol involved the displacement controlled loading with drift-control over the building. Cracks and damage observations were made at the storey drift ratios of: 1/2000, 1/1000, 1/750, 1/500 for URE building. The same URE building was retrofitted afterward and retested as RRE to storey drift ratios of: 1/2000, 1/1000, 1/750, 1/500, 1/250, 1/150, 1/100 and 1/75. The mesh retrofitting is found effective in both damage control as well as strength enhancement over the unreinforced one. The URE specimen showed a clear opening of shear and vertical cracks in the in-plane loaded walls near the openings and Jugshing holes. For the RRE specimen, cracks dispersed over a large region of the in–plane loaded walls. No delamination of mesh–wrap was observed, showing the effectiveness of the proposed technique. The RRE specimen showed enhancement in base shear by 2.5 times, ductility 2.3 times, and energy absorption 12 times the URE counterpart.

1 INTRODUCTION

Rammed earth (RE) construction is one of the most dominant traditional and historical construction practices and is mainly popular in the western part of Bhutan. These traditional buildings represent not only the unique architecture of Bhutan but also expresses the social and economic viability of the community. However, the past earthquake of magnitude M6.9, which occurred on September 18, 2011, near Nepal–India border destroyed remarkable number of rammed earth structures in Bhutan. Several past research works studied the behavior of RE wall components in both in–plane [1,2] and out–of–plane directions [1,3–5]. The research works clearly state the vulnerabilities of RE walls, but the works are limited to element tests of RE wall components.

The present work tries to assess the behavior of a full–scale two–storied rammed earth building through drift–controlled push–over static tests. A clear definition of the limit state for RE is presented to identify the different damage levels in RE building based on the full scale tests. Further, an effective mesh–wrap retrofitting strategy is also proposed to improve the seismic resilience of RE. The proposed work will help to contribute towards strengthening the existing traditional and historical rammed earth houses, which comprises a significant percentage of the current building stock in the country.

2 TEST PROGRAM

2.1 Materials

2.1.1 Rammed earth

The rammed earth (RE) material used in construction was from the nearby local site. The earth soil used for ramming included reddish-white clay with small pebbles. The grain size distribution of the RE used showed a particle size range of 0–10 mm. More details on the soil materials and particle size distribution can be found in Wangmo et al. [3]. For material characterization, RE cylindrical core samples were extracted from the test specimens using core drilling machine with diamond core bits for dry core drilling. In total, twelve of these cylindrical core samples for each specimen type were tested to measure compressive strength (ASTM C39)

and splitting tensile strength (ASTM C496). Table 1 lists the properties of RE from material characterization.

Table 1: Material characterization of rammed earth block

Specimen	URE				RRE			
Unit	ρ_b (kg/m^3)	f_c (MPa)	f_t (MPa)	E (MPa)	ρ_b (kg/m^3)	f_c (MPa)	f_t (MPa)	E (MPa)
Mean	1837	0.94	0.12	249	2024	1.65	0.17	389
Std. Dev.	33	0.12	0.02	58	13	0.15	0.03	55

2.1.2 Timber

Wooden beam joists, 125 mm wide 150 mm deep of mixed conifer found in Bhutan, were used at the floor levels. The material properties for timber can be found in Shrestha et al. [5].

2.1.3 Mesh retrofitting components

Two types of wire mesh were used, standard mild steel welded mesh as the main mesh, M–Mesh (Ø 1.8 mm and 34 mm c/c spacing) and light and galvanized welded mesh as a lapping mesh, L–Mesh (Ø 1.45 mm and 28 mm c/c spacing) at the corners and along the height of the walls. A cement (OPC) plaster of ratio 1:3 (cement: sand) was applied to the RM wall substrate. The average compressive and tensile strength of the cement plaster was 17.38 MPa and 1.59 MPa, respectively. It should be noted authors are already working towards the use of stabilized mud plaster over the cement plaster in their future work. Cement plaster was chosen over stabilized mud plaster for the present work primarily due to limited curing time for the test specimen during the winter season. It may be argued that since the strength of cement plaster (30 mm thick) is far greater than that of rammed earth, there can be a mechanical incompatibility between the two materials. It should be noted that the results reported are for the first set of series of planned tests, and authors will focus their future works to scrutinize these arguments further.

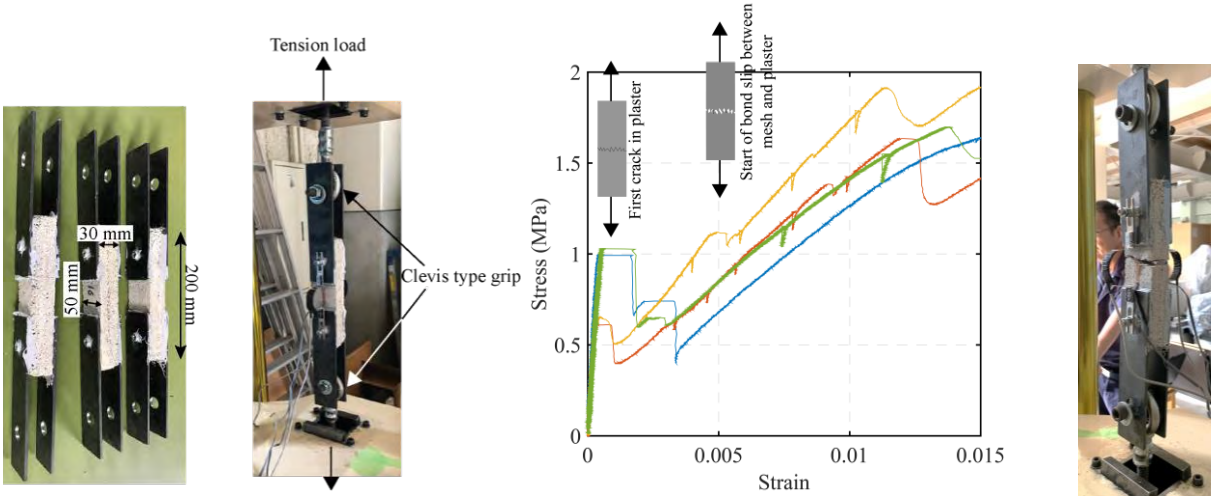
For material characterization of the retrofitting components, test coupons (Figure 1a) 200 mm long, 50 mm wide, and 30 mm thick were prepared for M–Mesh and tested under tensile loading with clevis type grip as shown in Figure 1b. Figures 1c and 1d show the test results for the tensile coupon tests. The plot in Figure 1c shows an initially high stiffness and drop in load at around 0.6–1 MPa stress representing the initial cracking in the mortar. Afterward, the stiffness reduces significantly, and the crack widens with further slip along the length of the coupon (Figure 1d). The authors will generalize these tensile test coupon tests to incorporate in the material characteristics for finite element modeling generation in their future works.

2.2 Test specimen details

2.2.1 Prototype unreinforced rammed earth specimen (URE)

The full–scale tests were carried out on a prototype Bhutanese traditional house. The building represents a traditional residential house of Bhutan following the typical architectural pattern with limited openings at first floor level and a large opening on the second floor of the building's front facade. The prototype has a floor area of 8.1 m × 5.4 m as shown in Figure 2,

with three rooms on each floor. The second floor level has a large opening in the front facade, termed as rabsey. The URE specimen was tested after four months of drying. The drying period was decided based on the authors' previous works [6].



(a) (b) (c) (d)

Figure 1: Material characterization tests for mesh retrofitting component: (a) Test coupons epoxy-bonded at the ends to steel plates, (b) Test set–up with clevis type grips, (c) Tensile stress versus strain plots for tensile coupon tests of M–Mesh, (d) Typical failure mode at the end of coupon test

2.2.2 Mesh–wrap retrofitting and retrofitted rammed earth specimen (RRE)

Figures 2 and 3 show the details of the retrofitting works carried out on the specimen. It should be noted that the retrofitting was started after completion of the first series of tests on the unreinforced specimen, URE. Two types of wire mesh were used, standard mild steel welded mesh as the main mesh, M–mesh (Ø 1.8 mm and 34 mm c/c spacing) and light and galvanized welded mesh as a lapping mesh, L–mesh (Ø 1.45 mm and 28 mm c/c spacing) at the corners and along the height of the walls. A lapping length of 300 mm was provided in the vertical direction in regular intervals, while 600 mm lap was provided in the horizontal direction at the corners. First, the mesh was placed on the walls using U–hooks. This was followed by clamping of mesh to the walls using 12 mm diameter rods inserted through the jugshing holes and bolted with nuts, as shown in Figures 2 and 3a. Finally, a 30 mm thick cement plaster (cement and sand at 1:3) was applied over the mesh. Prior to plastering, the wall's surface was pretreated using cement slurry (thin mix of cement and water). For the floor joist, X–bracing with timber of size 75mm×75mm was provided to connect the floor joists. The X–bracings were bolted to the floor joists at the center and the ends. It should be noted that only the in–plane loaded walls (east and west elevations) were retrofitted as shown in Figure 2, with an extension of the L–mesh to the north and south elevations up to 600 mm. The RRE specimen was tested after three months of curing.

2.3 Test set–up and instrumentations

The test set–up for the static test is illustrated in Figure 4a. Two 1000kN capacity jacks were positioned at the second–floor level (2FL), and the other two of 500kN capacity were placed at

the roof–floor level (RFL). One end of the jack was connected to the reaction wall through the built–up section and the other end to the test specimen's wall face through a 9.5 m long H–section. There were two 9.5 m long H–sections installed at each floor level, resting on support systems that allow them to slide along the support with the jacks. The static jack is a hydraulic system that was manually operated. The instrumentations are illustrated in Figure 4a. The instrumentation involves load cells installed on hydraulic jacks to measure the applied forces. The displacement was measured using 14 displacement transducers: ten laser transducers (Keyence, IL–300) and four strain gauge type transducers (TML SDP–100C, SDP–50C) at three different levels (base, 2FL, and RFL) of the test specimen both at the loading and the free side. A multi–channel dynamic strainmeter DS–50A was used for data logging with the LAN interface setting. The data sampling rate was set at 100 Hz.

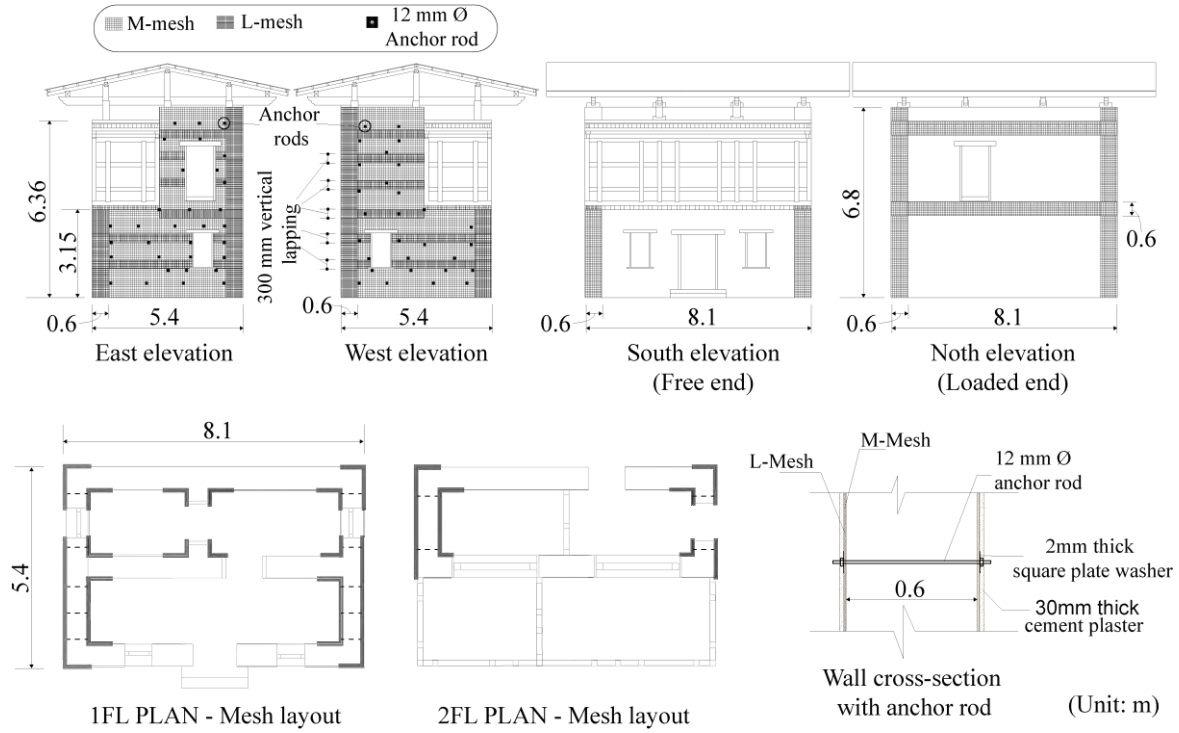


Figure 2: Prototype retrofitted rammed earth building specimen (RRE)

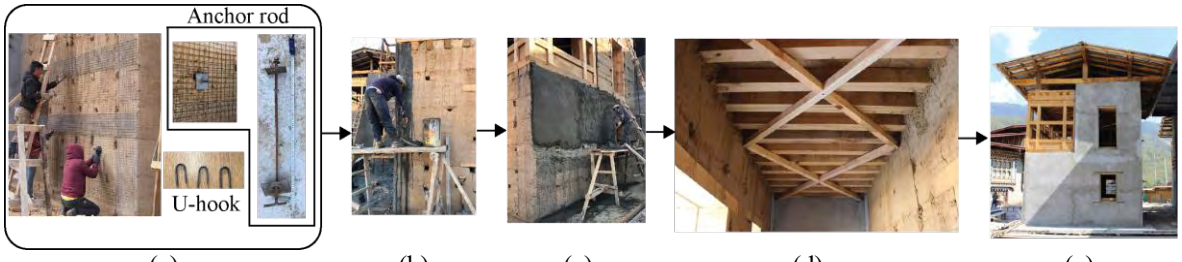
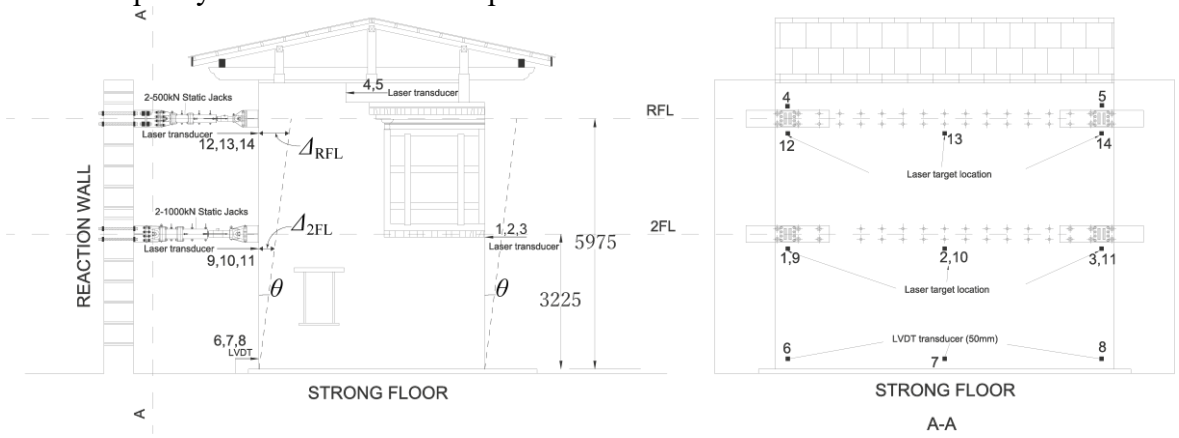


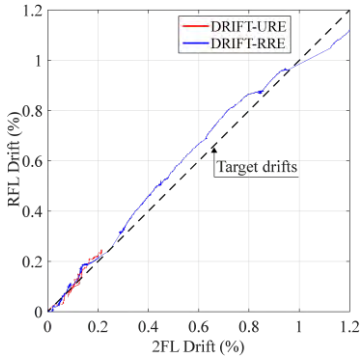
Figure 3: Retrofitting work process: (a) Placement and anchorage of mesh, (b) Application of cement slurry as pretreatment, (c) Cement plastering, (d) Wooden brace for floor rigidity, (e) Final specimen after retrofitting

The static test loading protocol involved the displacement controlled loading with control

over the drift in the building. Each floor level of the specimen was subjected to displacement controlled loading to a specified target storey drift value, followed by observation of cracks and damages to the building. Here, the storey drift ratio, θ, is the ratio of the lateral displacement to the floor height. Cracks and damage observations were done at the storey drift ratios of: 1/2000, 1/1000, 1/750, 1/500 for the prototype unreinforced rammed earth specimen (URE). For retrofitted prototype specimen (RRE), in addition to above drift values, the building was subjected to storey drifts of 1/250, 1/150, 1/100, and 1/75. It should be noted that the loads applied in each storey levels, 2FL and RFL, were displacement controlled through manual synchronization, maintaining the target storey drifts through the monitoring of the drift records at the real–time data logging system. Figure 4b shows the target and the actual storey drifts for the static test, and the actual loading history can be considered satisfactorily closer to the target drift. The load cell measurements and the absolute displacement readings were collected to draw the capacity curves for each test specimen.



(a)



(b)

Figure 4: (a)Test set–up and instrumentation, (b) Actual and target storey drifts

3 RESULTS AND DISCUSSION

3.1 Micro–tremor measurements for dynamic characterization

Micro–tremor measurements for the test structures were made using three–component velocity sensor Model–2205B by Showa Sokki Corporation. The measurements were made to assess the vibrational characteristics of the prototype specimen before the test (no damage) and

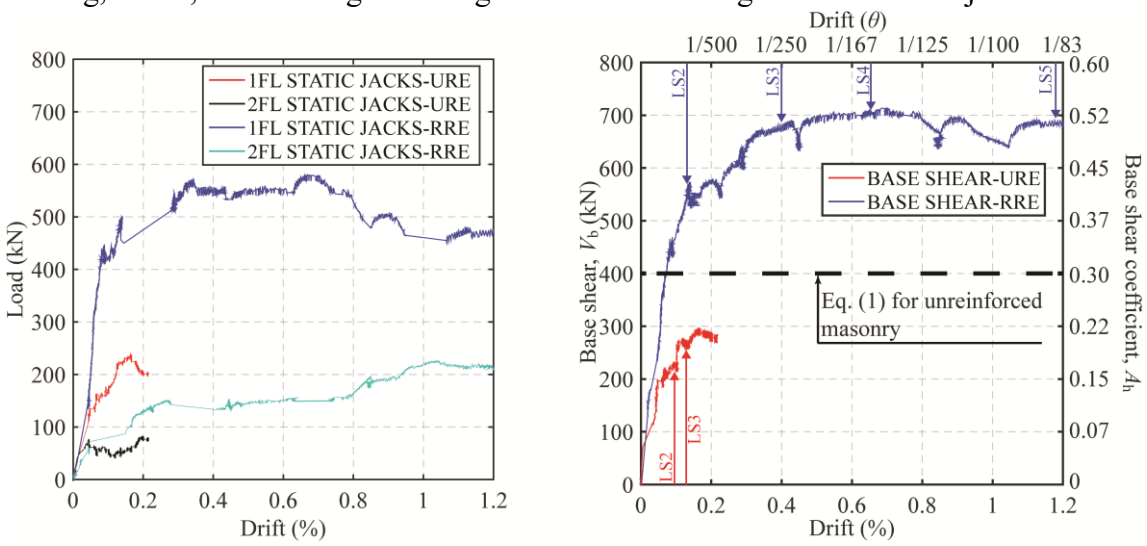
after the test (post damage) and also to study vibrational characteristics' changes after the retrofitting process. The data sampling was done at a frequency of 200 Hz with a recording time of 300 seconds. The measurements were done where the sensor pick–ups were placed at the 1FL, 2FL and RFL of the building specimen. Table 2 lists the first two natural frequencies for both the test specimens estimated using the Stochastic Subspace Identification (SSI) method. The first mode natural frequency for URE (before test) was 5.29 Hz, and this reduced to 4.64 Hz after the test with moderate damage at maximum storey drift of 1/500. Similarly, with the retrofitting measures, the first mode natural frequency increased to 6.03 Hz, which alsosubsequently reduced to 5.22 Hz after the test.

Table 2: Results from micro–tremor measurements

Specimen	Natural frequency (Hz)			
	Mode 1		Mode 2	
	Before test	After test	Before test	After test
URE	5.29	4.64	7.48	6.83
RRE	6.03	5.22	8.49	6.91

3.2 Capacity curve

Figure 5a shows the capacity curves in each floor correlated to the load cell readings for 2FL and RFL static jacks of both the prototypes, the unreinforced specimen, URE, and the retrofitted one, RRE. The presence of a large opening on the second floor and less contributions from the wall in load sharing means that the load recorded for the load cells in RFL was comparatively lower to the ones in 2FL. The first floor level, on the other hand, houses solid walls all around the building, hence, contributing to the higher load cell readings from the static jacks.



(a) (b)

Figure 5: (a) Capacity curves in each floor for both prototype unreinforced and retrofitted specimens, (b) Global capacity curves for both prototype and retrofitted specimens

Figure 5b shows the global capacity curves with cumulative base shears of URE and RRE specimens. It should be noted that the drift (θ) shown in the capacity curves is the roof storey

drift, defined as the absolute displacement of the roof (Sensors 12–14 in Figure 4a) divided by the height of the sensor from the ground. From the global capacity curves, the ultimate strength for RRE specimen (714 kN) was about 2.4 times URE specimen (294 kN), an increment of 420 kN. Further, the roof displacement for RRE (38.5 mm) at the maximum base shear was about 4.2 times for URE (9 mm).

Indian Standard Code IS 1893 [7] provides simple formulations to compute design base shear for unreinforced masonry in the Indian subcontinent, which was for comparison purposes in Figure 5b, represented by dotted lines. The design base shear [7] is given by:

$$V_b^D = A_h W_t \tag{1}$$

where, A_h is the design horizontal base shear coefficient given by $(ZIS_a/g)/(2R)$ and W_t is the seismic weight of the building. Here, Z is the zone factor taken as 0.36 for very severe seismic zone, I is the importance factor taken as 1 for a residential building, S_a/g is the spectral acceleration coefficient taken as 2.5 for a natural time period of 0.2 second, and R is the response reduction factor taken as 1.5. The cumulative base shear of URE was below the design base shear value, and the retrofitted specimen RRE exceeded the design value by 1.8 times.

There were also significant enhancements in ductility and energy absorption for the RRE specimen, as shown in Table 3. Here, the energy absorption (ψ) is given by the area under the global capacity curve until the ultimate base shear, and the corresponding top storey displacement. Ductility is the ratio of top storey displacement at the ultimate base shear to yield displacement. It should be noted that the results reported for unreinforced specimen URE were until the storey drift of 1/500; hence the values reported for energy absorption and ductility for URE can be slightly underestimated.

Table 3: Test results for the prototype unreinforced and retrofitted specimens

Specimen	Ultimate base shear, V_b (kN)	Energy absorption, ψ (kN–mm)	Ductility, μ
URE	294	1813	3.4
RRE	714	22680	7.7

3.3 Damage observations and definition of the limit states

Real–time manual crack documentation was done during the test at the predefined target storey drift ratio through visual observations, and detailed drafting of the cracks was done at a later stage with the support of video recordings. The damage observations for the test specimens are illustrated in detail in Figure 6 for URE and Figure 7 for RRE. Here, cracks for in–plane walls in the loading direction are presented, and relatively smaller cracks for dispensable walls in out–of–plane are excluded.

The damage observed during the tests is also reflected in terms of limit states defined by five different predefined damage states, as illustrated in Table 4. The limit states in Table 4 are modified form of the same proposed by Nabouch et al. [8] for rammed earth walls, based on in–plane shear tests on individual rammed earth walls. Since the present study is on a full–scale structure, the proposed limit states are also more practical and representative of the actual real scale building.

Table 4: Limit states for rammed earth building

Limit states	Damage	Observations in the building
LS1	No damage	No crack observed
LS2	Slight damage	First appearance of cracks
LS3	Moderate damage	Cracks near openings (diagonal cracks); Toe crushing; First observation of fall of earth particles
LS4	Extensive damage	Extension of diagonal cracks; Extensive crushing; Extensive fall of earth particles
LS5	Total collapse	Excessive damage not economically reparable; Visible residual drift

3.3.1 Unreinforced rammed earth specimen (URE)

For URE specimen, the crack documentation, as illustrated in Figure 6 are presented for three storey drifts, 1/1000, 1/750 and 1/500. As reported earlier, the test was stopped at the drift of 1/500 for later retrofitting purposes and re-testing of the same building. The first few hair–line cracks originated near door openings and below the loading point in east elevation, and near lintel and jugshing holes of west elevation when the storey drift was up to 1/1000 (Limit sate: LS2 Slight damage). For the storey drift of 1/750, there was an extension of cracks in the in–plane walls and new cracks were visible within the rammed earth blocks in 1FL (Limit sate: LS3 Moderate damage). At 1/500 storey drift, there was a widening of the previous cracks and new inclined shear cracks within the rammed earth blocks in west elevation. A vertical crack about 1.5 m long also appeared at the far end in west elevation with some earth particles even falling (Limit sate: LS3 Moderate damage). The authors felt the specimen experienced substantial damage to warrant its repair, and the test was stopped at this point since the main aim was to retrofit this building for re-testing purposes.. There was a negligible increment in cumulative base shear for URE specimen with further increment in drift. Therefore, based on authors'observations, limit state of LS4 representing "Extensive damage" will possibly occur for URE at storey drift of 1/250, which may not allow effective retrofitting of the specimen.

3.3.2 Retrofitted rammed earth specimen (RRE)

The crack documentation for RRE specimen is illustrated in Figure 7 for six different storey drift levels with their corresponding damage states defined. There were no cracks observed up to storey drift of 1/1000 (Limit sate: LS1 No damage). At storey drifts of 1/750 and 1/500, hairline cracks started to appear near the lintels of openings. There were also numerous small vertical cracks below the rabsey opening corner, and horizontal cracks also initiated in both floor levels (Limit sate: LS2 Slight damage). It should be noted that all the cracks were hairline cracks up to this load level. For storey drift of 1/250, there was widening and extension of previous cracks at the corner of rabsey opening and clear vertical cracks at the far end from the loading point. There was also crack due to toe crushing near the base of the south face (Limit sate: LS3 Moderate damage). At storey drift of 1/150, there were extensive cracks and slight spalling of plaster (Limit sate: LS4 Extensive damage), with a clear long horizontal crack along the sill level, possibly the lapping region of the mesh. The previous cracks kept extending for storey drift of 1/100, followed by extensive spalling of plaster above the door opening (2FL) and also near the window opening (1FL). There was also plaster crushing at the toe near the

base of the south face (Limit sate: LS4 Extensive damage). At storey drift of 1/75, the cracks opened up significantly wide, and these relatively wide cracks were extending over the whole length of the wall. The spalling of plaster continued, and clear rocking of the entire building was visible. A sharp splitting sound possibly due to the dislocation of timber components was heard. Furthermore, the building also showed clear residual drift post the release of load. Based on the observation, this limit state level was defined as LS5 Near collapse. It should be noted that there was no delamination or separation of the mesh from the specimen throughout the whole test, showing the effectiveness of the anchor rods in keeping the mesh intact even at such adverse damage levels.

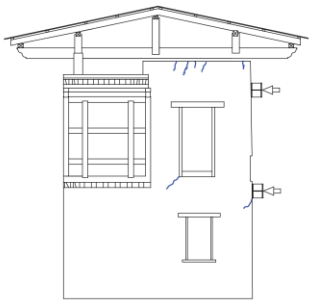
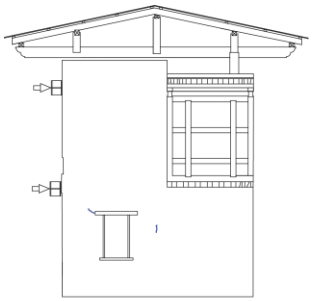
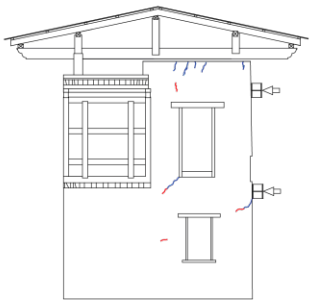
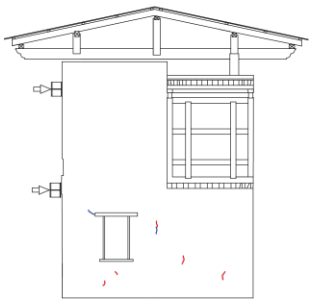
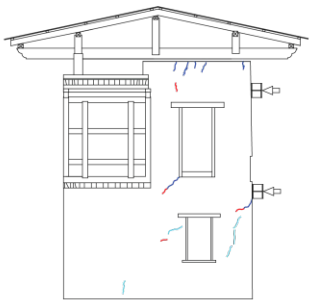
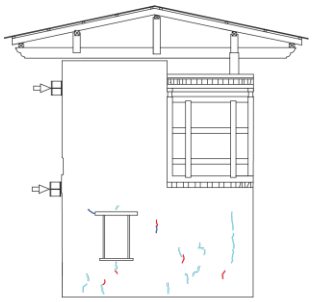
EAST ELEVATION	WEST ELEVATION	REMARKS
		Storey drift, θ = 1/1000 East elevation: - Small cracks below the door opening and the top RE block - Small cracks below the loading point in 2FL West elevation: - Small cracks above the window Limit state: LS2 Slight damage
		Storey drift, θ = 1/750 East elevation: - Extension of the cracks below the door opening as well as blow the loading point in 2FL West elevation: - Small cracks visible within the rammed earth blocks Limit state: LS3 Moderate damage
		Storey drift, θ = 1/500 East elevation: - Widening and extension of the cracks below the loading point in 2FL - New cracks near the window opening West elevation: - Significant number of inclined cracks within the rammed earth blocks below 2FL originating from the Jugshing holes - A vertical crack about 1.5 m long appeared at the far end from loading point Limit state: LS3 Moderate damage

Figure 6: Crack evolution for unreinforced rammed earth (URE) specimen at different load levels and their respective limit states

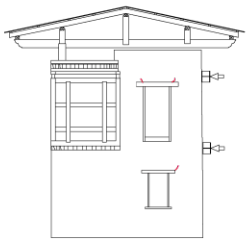
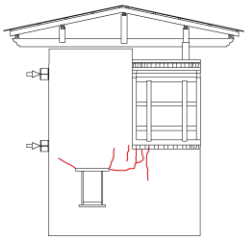
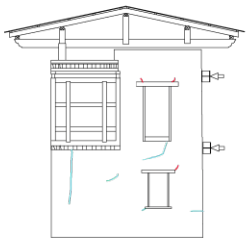
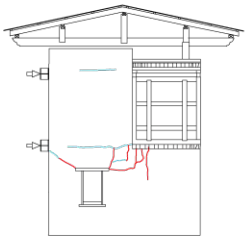
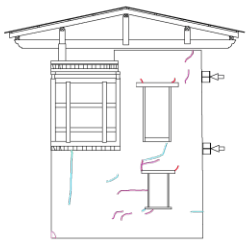
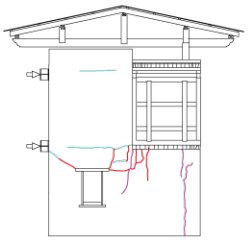
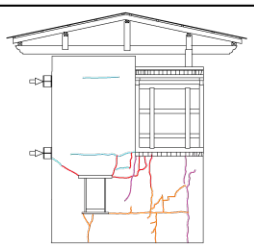
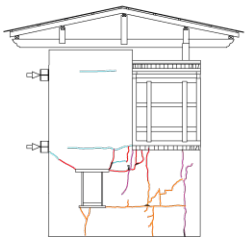
EAST ELEVATION	WEST ELEVATION	REMARKS
		Storey drift, $\theta = 1/750$ - Hairline cracks near the window openings for both East and West elevations - Cracks near the corner of rabsey opening in West elevation Limit state: LS2 Slight damage
		Storey drift, $\theta = 1/500$ -Extension of the previous cracks - Horizontal crack in both floor levels - Hairline vertical crack at the far end near South elevation Limit state: LS2 Slight damage
		Storey drift, $\theta = 1/250$ - Extension and widening of previous cracks - New crack at the corner of rabsey opening - New vertical crack near the South elevation - Crack due to crushing near the base of South face Limit state: LS3 Moderate damage
		Storey drift, $\theta = 1/150$ - Widening of previous cracks - Extensive cracks around the openings with slight spalling of plaster - Horizontal cracks along the sill level (lapping region) Limit state: LS4 Extensive damage
		Storey drift, $\theta = 1/100$ - Deformed shape of the building was visually observed - Extensive spalling of plaster above the door opening and also near the window opening - Plaster crushing at the toe near the base of South face Limit state: LS4 Extensive damage
		Storey drift, $\theta = 1/75$ - Large widening of already opened cracks - The previous cracks were extending towards the loading point - Spalling of the plaster continued - Rocking of the whole building was visible Limit state: LS5 Near collapse

Figure 7: Crack evolution for mesh–retrofitted rammed earth (RRE) specimen at different load levels and their respective limit states

4 CONCLUSIONS

In the context of understanding the vulnerabilities of traditional rammed earth structure and proposing an effective retrofitting strategy, a full–scale static test was designed on a typical prototype two–storied Bhutanese rammed earth building. The test program involved two phases of testing, with the first test on unreinforced rammed earth specimen (URE) and the second phase with the test on the same building after mesh–wrap retrofitting (RRE). The ultimate base shear for RRE was 2.4 times of URE. The energy absorption and ductility index were also significantly enhanced for mesh–wrap retrofitted specimen by 12 and 2.3 times, respectively.

Damage limit states for the prototype rammed earth building is also presented to understand the evolution of damage in rammed earth structure at different storey drifts based on real-scale test results. A set of five limit state values are proposed as a function of storey drift ratios, with a clear definition of the damage levels and damage states visually understandable for both unreinforced and retrofitted rammed earth building.

Acknowledgements. This research was supported by the JST/JICA, SATREPS (Science and Technology Research Partnership for Sustainable Development) project (Grant No. JPMJSA1611). We would also like to acknowledge the technical assistance of Engineer Ugyen Dorji and Technician Lhendup from DoC, MOHCA, The Royal Government of Bhutan.

REFERENCES

[1] Hamilton, H.R., McBride, J. and Grill, J. Cyclic testing of rammed–earth walls containing post–tensioned reinforcement. *Earthquake Spectra* (2006) **22**:937–959.

[2] Miccoli, L., Oliviera, D.V., Silva, R.A., Muller, U. and Schueremans, L. Static behaviour of rammed earth: experimental testing and finite element modelling. *Materials and Structures* (2014) **48**:3443–3456.

[3] Wangmo, P., Shrestha, K.C., Miyamoto, M. and Aoki, T. Assessment of out–of–plane behavior of rammed earth walls by pull–down tests. *International Journal of Architectural Heritage* (2019) **13**:273–287

[4] Shrestha, K.C., Aoki, T., Konishi, T., Miyamoto, M., Zhang, J., Takahashi, N., Wangmo, P., Aramaki, T. and Yuasa, N. Full–Scale Pull–Down Tests on a Two–Storied Rammed Earth Building with Possible Strengthening Interventions. In: R. Aguilar et al. (Eds.): *Structural Analysis of Historical Constructions*, RILEM Bookseries 18 (2019), pp. 1557–1565.

[5] Shrestha, K.C., Aoki, T., Miyamoto, M., Wangmo, P., Pema, Zhang, J. and Takahashi, N. Strengthening of rammed earth structures with simple interventions. *Journal of Building Engineering* (2020) **29**:101179.

[6] Shrestha, K.C., Aoki, T., Miyamoto, M., Wangmo, P. and Pema. In-plane shear resistance between the rammed earth blocks with simple interventions: Experimentation and finite element study. *Buildings* (2020) **10**:57.

[7] Indian Standard 1893 Part 1. *Indian Standard Criteria for earthquake resistant design of structures Part 1 General provisions and buildings*, Bureau of Indian Standards, 5th edition, (2002).

[8] El Nabouch, R., Bui, Q.B., Ple, O. and Perrotin, P. Rammed earth under horizontal loadings: Proposition of limit states. *Construction and Building Materials* (2019) **220**:238-244.

12th International Conference on Structural Analysis of Historical Constructions
SAHC 2020
P. Roca, L. Pelà and C. Molins (Eds.)

STRUCTURAL RESTORATION AND RE-USE OF THE HISTORIC COAL MINE TOWER

DAVID ANĐIĆ[1*], MATEJ HORVAT[2] AND JURAJ POJATINA[2]

[1]Studio Arhing d.o.o.
Ćire Truhelke 49, 10 000 Zagreb , Croatia
e-mail: david.andjic@yahoo.com, www.studio-arhing.hr

[2] Studio Arhing d.o.o.
Ćire Truhelke 49, 10 000 Zagreb , Croatia
e-mail: horvat.matej1@gmail.com, juraj.pojatina@gmail.com, www.studio-arhing.hr

Keywords: historical structure, steel, mine tower, reconstruction

Abstract. The coal mine is located in the town of Labin, Istria peninsula, Croatia. Restoration of the tower is a part of the project that includes thorough restoration and re-use of the Labin mining complex for cultural, tourist and educational purposes. The tower was built in 1938 by Italian authorities as part of the pre-war campaign. It is a 32.5 m high steel structure that once enveloped the elevator to a 200 m deep mine shaft. The structure is a built up Vierendeel truss with four columns / chords connected with horizontal moment resistant beams. Two large steel inclined struts were resisting elevator rope forces connected to the elevator machine building. The mine was shut down in 1988. The assessment of the tower consisted of geometry measurement, cross-section shape determination, steel quality determination, condition of members and connections (rivets and bolts), protective coating condition and underground supports condition. Two samples were taken to laboratory to determine the steel grade with tensile yield test. Structural model with existing members has also been analysed. Different loads were considered comparing the original purpose of the tower and the planned representational purpose. In addition, structural member verification according to Eurocode standards has been done. Load bearing steel structure is geometrically sound, mostly with no visible deformations, deflections or drifts. Foundations are crack free and with no visible subsiding. Lack of maintenance of the anticorrosive coating from 1988 until today caused most of the damage. Due to the significantly aggressive environment, anchoring part of the structure was severely ruined. Lower part of the above ground structure was in the similar condition. Water retention and salt carried from the lower part of the shaft caused significant damage to the steel structure in these areas. Replaced members were built in with original riveting technique. Anchoring structure replacement called for a temporary support structure, which represented the most demanding operation in the whole restoration process. The temporary support structure was a steel truss structure in pyramidal form that allowed complete removal of the lowest segment and reconstruction of the anchoring elements and concrete foundation. According to the evaluation, existing galleries that surrounded the tower had to be completely removed and redesigned with new loads. Future use of the tower with its galleries is primarily of representational purpose. Moreover, a new elevator with its own structure inside the existing tower is considered and it has no influence on the existing

structure. Since the tower is registered as an architectural heritage by the Croatian Ministry of Culture, specific demands regarding structural restoration were issued. The principles of structural analysis and restoration together with multidisciplinary approach have been applied in this project.

1 INTRODUCTION

The coal mine is located in Istrian town of Labin, region that was well known for its mining potential in the past. The tower was built in 1938 by Italian authorities as part of the pre-war campaign. Shaft above which the tower was built was part of the underground complex with pertaining tunnels and shafts that connected nearby mining towns and small ports in that region. The mine was shut down in 1988 and tower rests unused and exposed to weather conditions since then. Restoration of the tower was part of the project that included thorough restoration and re-use of the Labin mining complex for cultural, tourist and educational purposes.

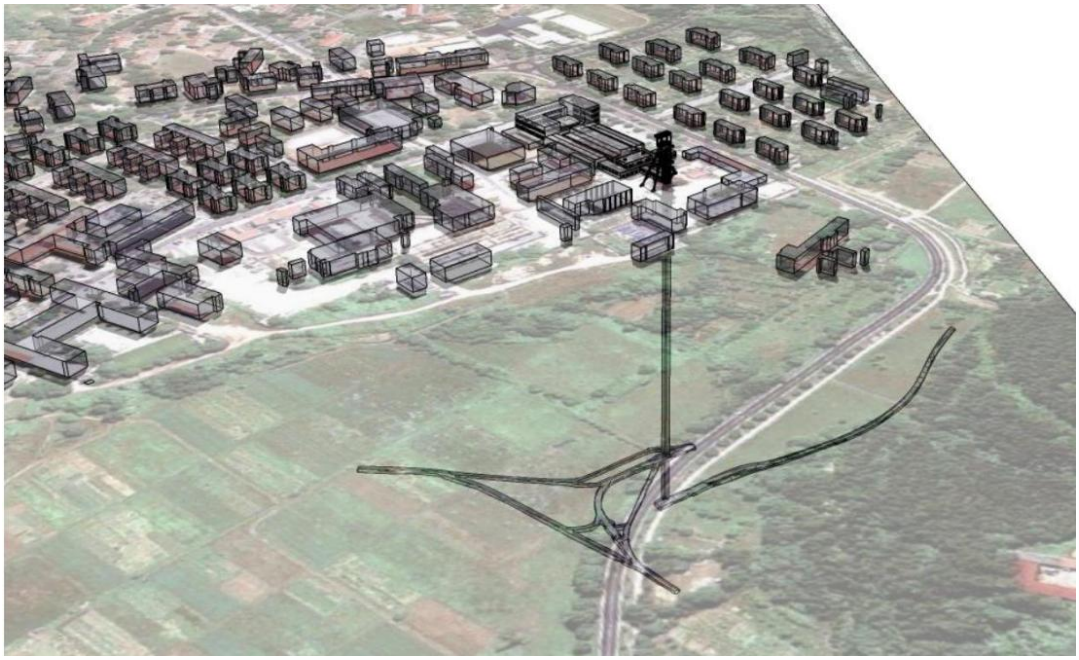


Figure 1: Mine shaft with nearby tunnels 200 m below the surface

Structural restoration of the tower included replacement of corroded members of underground anchoring structure and lower part of the above ground structure which sustained damage too severe to be repaired. Temporary support structure was built to enable removal of the lowest segment and reconstruction of the anchoring elements and concrete foundation. Replaced members were built in with original riveting technique. Existing galleries that surrounded the tower had to be completely removed and redesigned. Installation of the new elevator that leads 200 m down the shaft was also a part of the restoration project in conceptual design phase. The new structure of the elevator inside the existing tower has no influence on the tower structure.

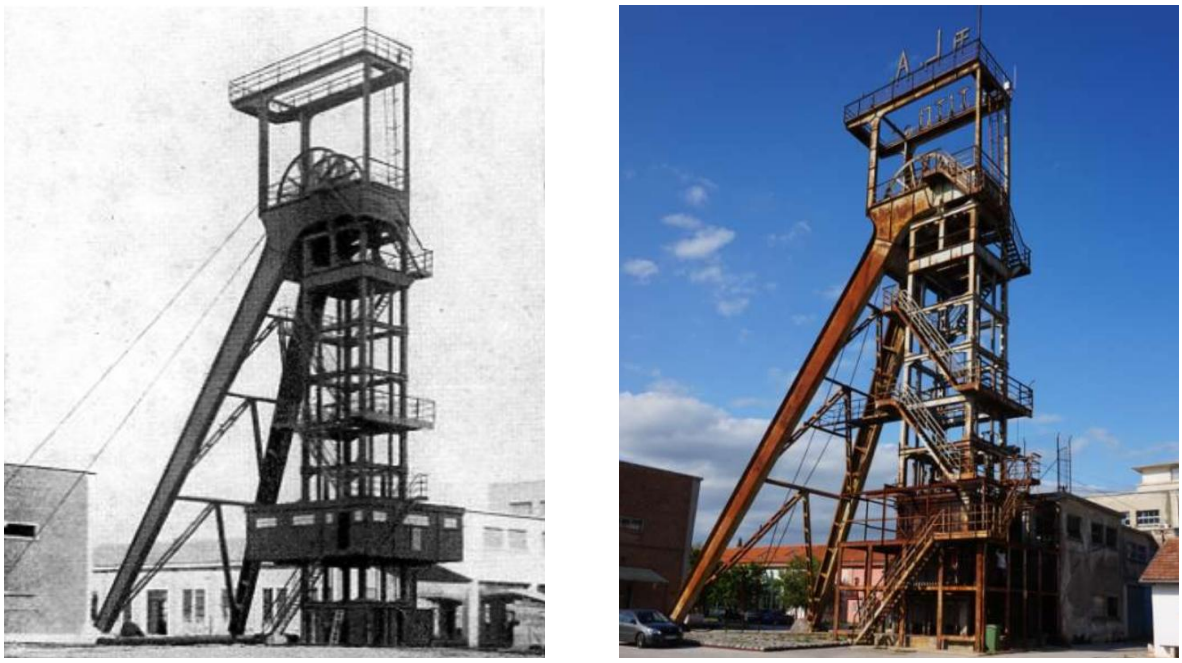


Figure 2: Mine tower and the connecting bridge, as originally built - photo taken in 1942. on the left, mine tower nearly 30 years after shutting down – photo taken in 2015. on the right

Purpose of this paper is to present the results of detailed inspections, laboratory testing and software analysis of tower's condition prior and after restoration. In addition, temporary support structure design and detailing is shown in further text as the most challenging part of the restoration.

2 STRUCTURAL CONCEPT

Tower is a 32.5 m high steel structure that once enveloped the elevator to a 200 m deep mine shaft. All load carrying elements were constructed as riveted built up members. The structure is a built up Vierendeel truss with four columns/chords connected with horizontal moment resistant beams. The tower itself is anchored beneath terrain to the steel transfer beams which directed reactions to the concrete wall of the shaft. Vertical truss structure is 22.0 m high. Layout dimensions of the truss are 4.5×3.7 m. Vertical distance between horizontal beams is 2.4 m – 3.0 m. Inclined part of the structure is connected to the main truss through the pinned joint at the top of the truss and anchored in the concrete footing with bolts. Inclined struts resisted the elevator rope forces connected to the elevator machine building. K form bracing is installed in plane of the struts. On the horizontal top part of the struts, at the height of 24.2 m two pulley wheels (sheaves) with the diameter of 5,0 m were installed. Wheels were constructed as riveted and welded built up members. The top structure above pulley wheels is 7,0 meters high and consists of four columns connected at their top with beams with the inspection deck. Gallery with 2,0 m wide walking deck surrounded the tower at the height of +4.65 m above the terrain level with layout dimension 8.4x7.6 m. Its primary function was to enable communication with miners' building and their transportation via elevator. Steel stairway with pertaining platforms served for inspection and maintenance. It

started at the base of the tower and reached the sheaves level from where the vertical ladder led to the inspection deck on top.

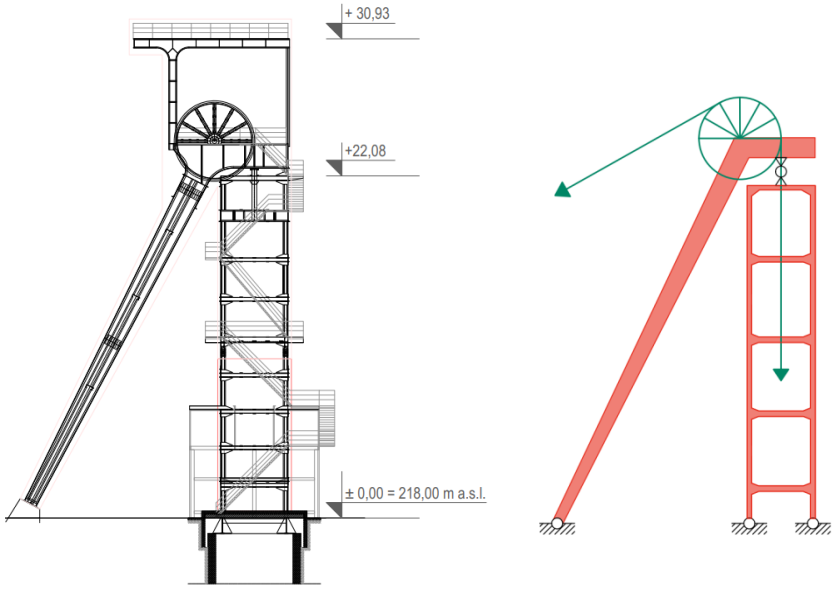


Figure 3: Mine tower drawing prior to restoration on the left, structural scheme with the forces imposed by the elevator mechanism on the right

3 VISUAL INSPECTION

Thorough visual inspection of the tower structure was conducted. Comprehensive photographic documentation was produced for every tower level together with the series of evaluations determining coating conditions elaborated below. Thickness of the protective coating was measured with PCE- CT 28 instrument. Measurements were carried out on five bearing elements partially corroded and they have shown mean value of protective coating thickness of 107.8 µm. The results were taken with reserve given that instrument measured thickness of the coating along with corrosion byproducts. Together with measuring coating thickness, cross hatch adhesion test was conducted with Elcometer 107 cross hatch cutter. Results showed that structure elements above level +11.70 m fall into class 2 and elements below into class 4 determined by ISO 2409 standard. Furthermore, evaluation of the degradation of the coating was made according to standards HRN EN ISO 4628-(2-6).

Table 1: Assesed degree of degradation according to standardards HRN EN 4628-(2-6)

Standard HRN EN ISO 4628-	Structure level	
	Above +11.70 m	Below +11.70 m
-2 Blistering	4(S5)	5(S5)
-3 Rusting	Ri 3(S3-5) and Ri 4(S4-5)	Ri 5(S5)
-4 Cracking	3(S4)c	5(S5)c
-5 Flaking	4(S4)b	5(S5)b
-6 Chalking by tape method	2(S2)	5(S5)

It was concluded that the underground support structure and the lower part of the structure were in extremely deteriorated condition. Therefore, these sections were selected for complete or partial replacement. Members of the upper part of the structure were selected for restoration of the protective coating and minimal repair actions.



Figure 4: Coating condition – lower part of the structure on the left; upper part of the structure on the right

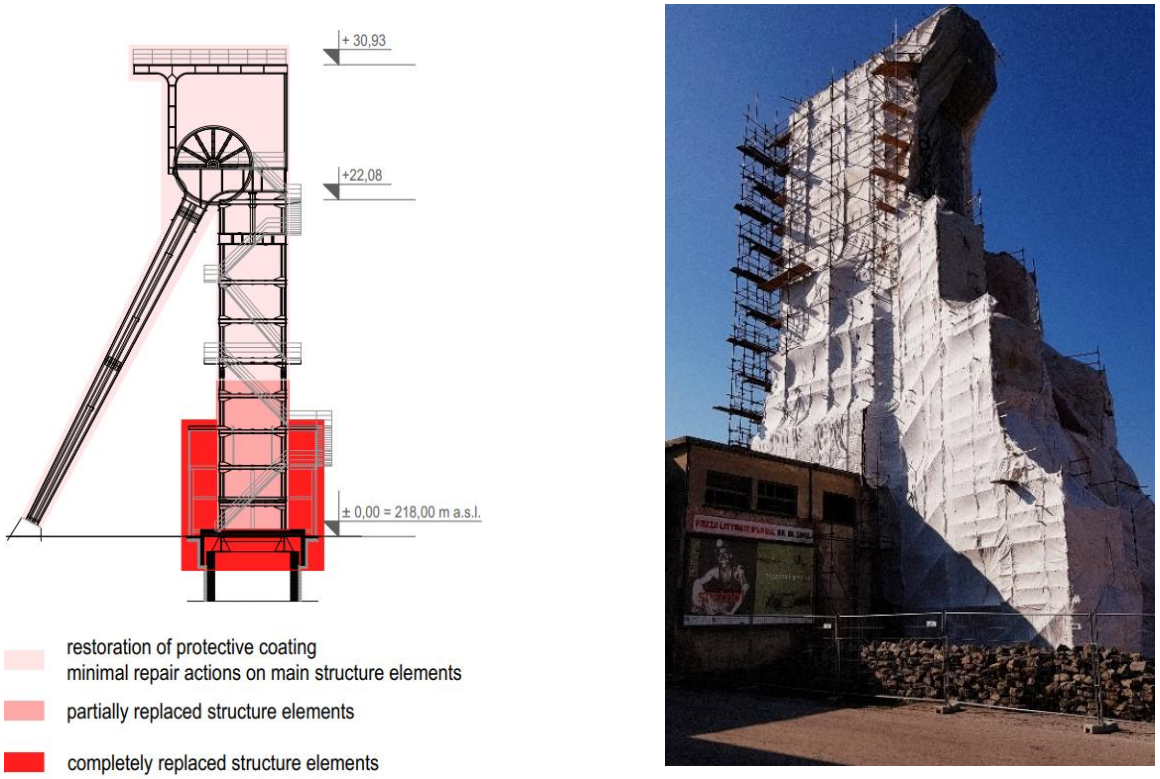


Figure 5: Structure defects and repair actions classification on the left; tower during sandblasting of the upper part of the structure on the right

4 LABORATORY TESTING

In addition to the on-field inspection, tensile test and chemical analysis in laboratory were conducted. The specimens were taken from the field into laboratory for analysis. Although specimens satisfy tensile test for hot rolled type of steel S235 in line with EN 10025:2002, toughness not being tested, chemical analysis has shown that the concentration of impurities is higher than allowed - concentration of P, S and Cu, respectively. Taking the results of chemical analysis into account together with age of structure, built in 1938., specimens fall into St33 type of steel according to DIN 17100, unkilled steel. The aforementioned type of steel matched S185 type of steel according to HRN EN 10025 with remark that lesser welding capability should be taken into account when choosing welding technology. Therefore, only bolted connections were used.

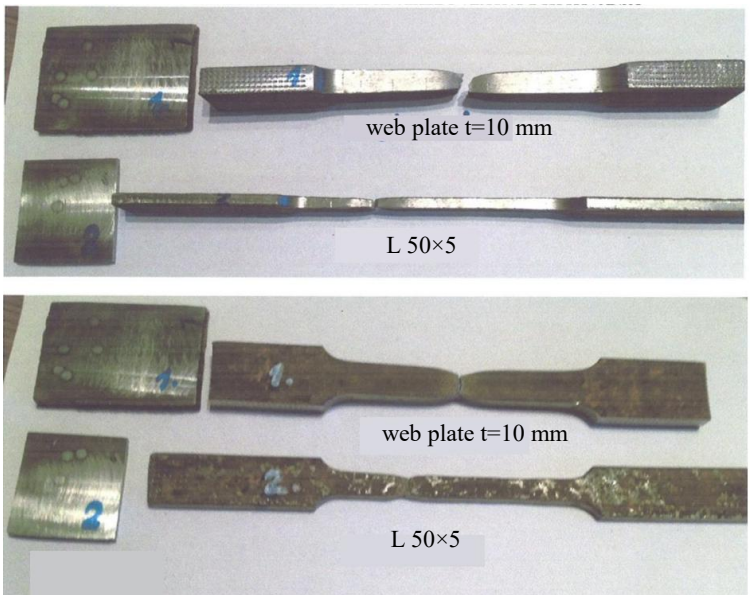


Figure 6: Specimens for chemical analysis on the left and tensile test specimens on the right

Table 2: Results of tensile test

Specimen No.	Specimen description (mm)	Assumed class of material	Cross sectional area of the specimen (mm^2)	Elastic limit (yield strength) R_e (N/mm^2)	Tensile Strength R_m (N/mm^2)	Strain A_5 (%)	Remark
Legitimate for S235 JR				min. 235	360-510	min. 26	
1	web plate t= 10mm	St 33	50	256	368	29	
2	L=50x5mm	St 33	141	249	357	45	

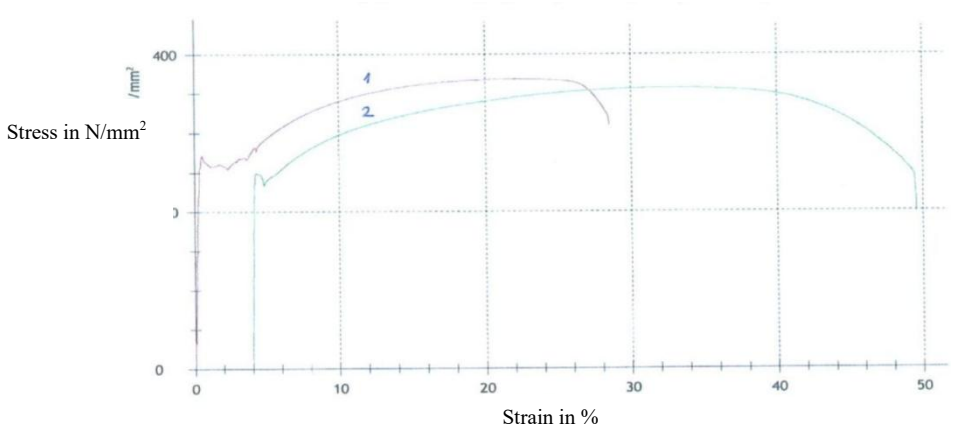


Figure 7: Stress- strain diagram for tested specimens

Table 3: Results of chemical analysis on LECO spectrometer

Specimen No.	Chemical composition in %						
	C	Si	Mn	P	S	Cu	Al
1	0.035	0.000	0.354	0.044	0.020	0.018	0.000
2	0.123	0.003	0.460	0.048	0.042	0.086	0.002
Legitimate for S235 JR according to HRN EN 10025-2	Max. 0.17	-	Max. 1.70	Max. 0.035	Max. 0.035		Min. 0.020

5 CORROSION PROTECTION

Future corrosion protection, as well as existing anticorrosive coating condition was one of the main concerns at the time of the inspection. Due to the condition of the coating, especially in the lower part of the structure, sand blasting to $Sa2^{1/2}$ according to EN ISO 12 944 was proposed. Execution and supervision of the protective coating was done according to EN ISO 12944-1-8:1999. Atmospheric corrodibility category was determined as C5 very high (80-200 µm for a year of exposure). Anticorrosive protection coating was proposed as a combination of two component priming coat with high zinc share (80 µm NDFT), epoxy based intermediate coats (80 µm NDFT) and polyurethane topcoat (80 µm NDFT). Overall nominal dry film thickness was designed as 240 µm.

6 STRUCTURAL ANALYSIS

Structural analysis of existing tower structure was performed with reduced (actual) cross-section dimensions and according to Eurocode standards with loads predicted for the future use. Imposed loads were significantly smaller compared to the loads that the tower was initially built for. Influence of the horizontal loads, wind and seismic loading, was taken into account during design checks. Analysis of the members had shown sufficient load bearing capacity. As the most challenging part of the restoration, temporary structure that enabled reconstruction and replacement of severely damaged sections of the tower, was further elaborated.

6.1 Temporary support structure

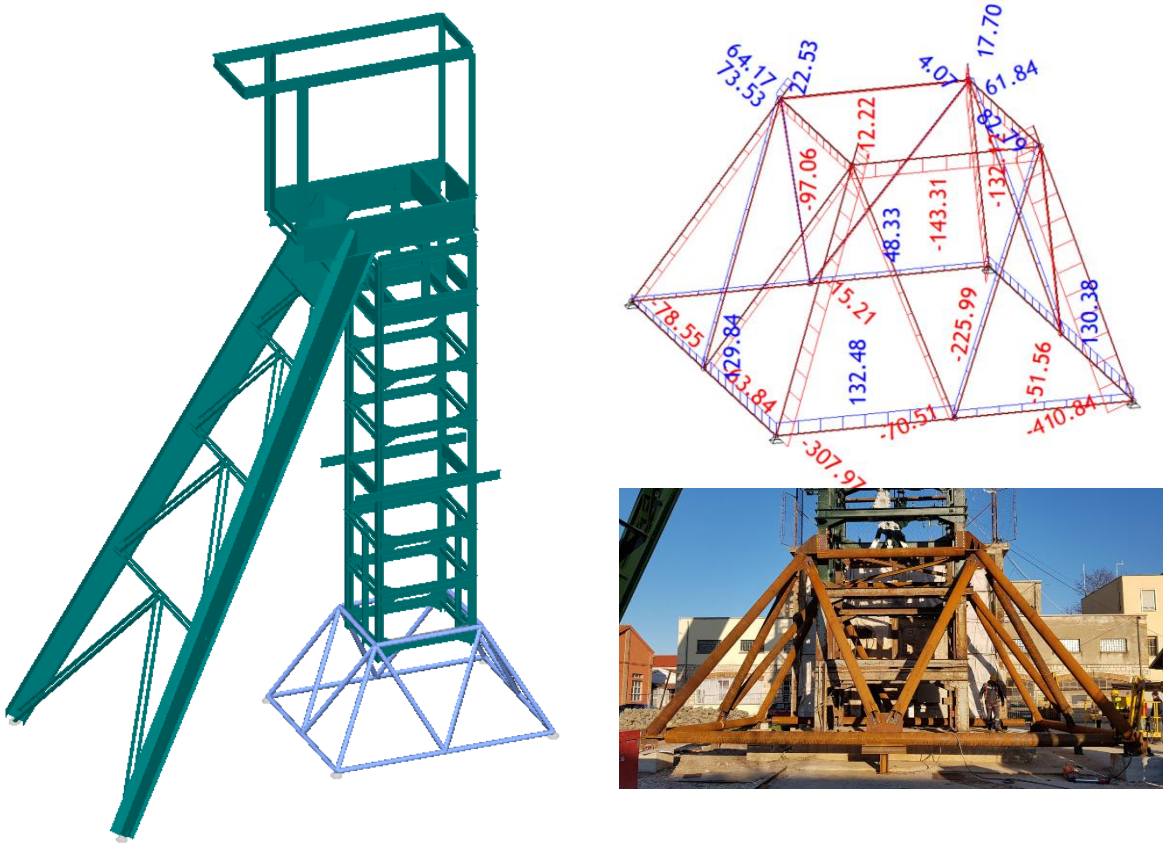


Figure 8: Temporary support structure model on the left; diagrams of longitudinal forces on temporary truss structure on the top right and the same structure constructed on the site on the bottom right

As part of the reconstruction, temporary support structure was designed. Neighbouring structure and existing roads around the site also determined the final outline of the temporary structure. Steel space truss in the form of truncated pyramid was chosen as the optimal structure for given purpose. Truss elements were bolted with circular hollow sections 273.1x10.0mm.

Transfer of the gravitational and horizontal loads from tower to temporary structure was enabled via bolted connection. Forces between two structures were transmitted through 24 M24 bolts and 20 mm thick plate with side stiffeners into the members of the temporary truss structure.

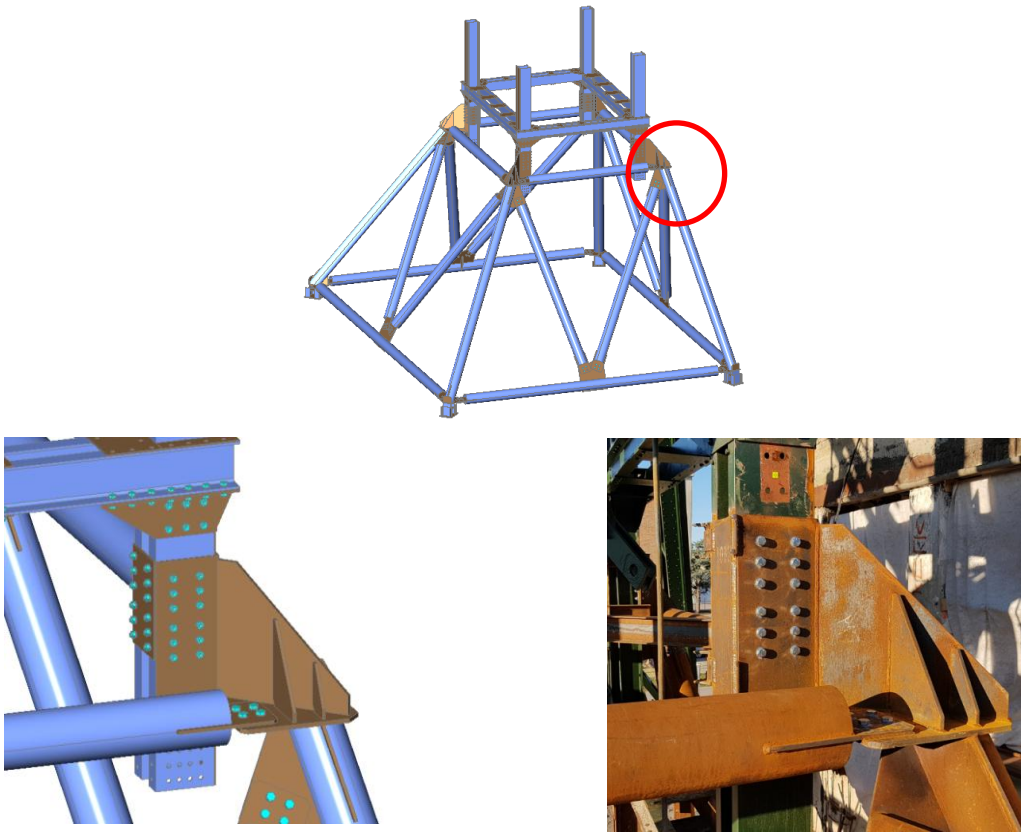


Figure 9: Isometric view of the temporary support structure model in Bentley Prosteel software in the top centre, model of the connection detail of the existing tower structure and temporary support structure on the left, and constructed on-site on the right

Hydraulic pump was installed in the steel bearing connection. Pumps enabled lifting, load releasing and lowering of the structure as well as its accurate positioning. In the course of the design of the temporary structure it was important to properly assign boundary conditions of the supports. Three out of four bearings were designed as movable in horizontal directions while fourth bearing was fixed so the forces in members of the truss could be correctly triggered.



Figure 10: Software design of the steel bearing connection on the left and construted on-site in the right

7 CONCLUSION/RECONSTRUCTION PHASE

The tower structure was severely deteriorated due to years of negligence, deficiency of protective coating and significantly aggressive environment of the underground structure. The principles of structural analysis and restoration of historic steel structures together with a multidisciplinary approach was applied in this project. In addition, unique temporary structure that allowed replacement of the base of the tower was designed and successfully constructed. The next phase of the restoration project is elevator installation.

REFERENCES

[1] J. Pojatina, "Existing structure assessment and analysis", (2015).
[2] J. Pojatina, "Coal mine tower restoration and new elevator design", (2016).
[3] J. Pojatina, "Structural restoration of coal mine tower", (2018).
[4] J. Radić, *Trajnost konstrukcija 1*, Croatian University Edition, 2010
[5] A. Braun, T. Vidović, D. Bačić, "Coal-mining plant Pozzo Littorio near Labin, unknown work of Gustavo Pulitzer Finali in Istria, Prostor. Scientific journal for architecture and urbanism, Vol. 27 No.1 (57): 1330-0652, (2019.), pp. 36-49.
[6] A. Braun, T. Vidović, Coal mining complex Pijacal, Labin-central building and export shaft, (2017.)

THE CLT PANELS IN STRUCTURAL RESTORATION: CHARACTERISTICS AND TECHNICAL REGULATIONS

PROF. ING. GIORGIO FRUNZIO[1*], ING. LUCIANA DI GENNARO[2] ING. LUIGI MASSARO[3] AND ING. FABIO D'ANGELO[4]

[1*]Department of Architecture and Industrial Design
Univesità degli Studi della Campania "Luigi Vanvitelli"
Abbazia di San Lorenzo ad Septimum 81031 Aversa (CE), Italy
e-mail: giorgio.frunzio@unicampania.it - Web page: https://www.unicampania.it

[2] Department of Engineering
Univesità degli Studi della Campania "Luigi Vanvitelli"
Via Roma 29 81031 Aversa (CE), Italy
e-mail: luciana.digennaro@unicampania.it

[3] Soc. M. & P. s.a.s. di Massaro Cesare & C.
Via Ovidio 2 - 81033 - Casal di Principe (CE), Italy
e-mail: ing.luigi.massaro@gmail.com

[4] TECNOLAB srl
Via S. Maria del pianto, 80 – 80143 - Napoli, Italy
e-mail: info@tecnolabnapoli.it - Web page: http://www.tecnolabnapoli.it

Keywords: Wood, CLT panels, Masonry, Historical Structure, laboratory tests

Abstract. *Wood can represent a valid and important alternative to the most commonly used structural materials for the restoration of masonry buildings, with a view to efficient, effective and "conscious" renovation. Today, the modern technologies allows to overcome the structural limits of solid wood due to its own anisotropy. The use of composite wood elements makes possible to obtain excellent mechanical performances that consent to evaluate aspects such as the use of low environmental impact retrofit strategies. The aim of this work is the analysis of mechanical parameters related to CLT (cross laminated timber) panels in order to determine their possible use in the structural restoration of masonry buildings. The CLT panels consist of solid wood planks superimposed so that each layer has the fibres rotated ninety degrees with respect to the adjacent layer. The layers (always in odd number and at least three) can be connected by discrete joints, pins and nails, or glued together. This configuration enables to product large structural elements with considerable thickness. Two different experimental test campaigns were carried out on samples of panels with three and five glued layers. The purpose of experimentation activities was to evaluate the bending deformation of the wooden elements and shear strength of the bonding sections. All the tests were processed according to the provisions contained in the UNI standards. The test results were then compared with different theoretical calculation models to determine the one that best represents the tested material.*
The tests outcomes have shown that some characteristics of the material, such as the remarkable ductility, open different scenarios of use for the CLT panels in the field of structural restoration of masonry buildings.

1. INTRODUCTION

The purpose of this work is to provide some assessments of the possibility of using structural wood-based products such as CLT panels, for the restoration of existing masonry buildings both ordinary that monumental ones. The CLT panels consist of a series of layers of solid wood lamellas placed with the fibres rotated by 90° with respect to the adjacent layers, therefore by their own nature these elements are suitable for interventions to reinforce of the structures in their own plan. It is also considered that these elements can be a valid solution to the reinforcement of the structural elements for actions out of their own plan in order to increase both their resistance than their ductility, using for example prestressing techniques such as PressLam® [2,4], performing fully reversible interventions.

In this note, we intend to study the possible applications of CLT panels in the restoration of masonry buildings both in relation to the techniques used to date than in relation to other future perspectives.

These structural wood-based panels are to date widely used in the structural reinforce of the timber floors in order to increase their strength to the actions that operate in their own plan [5,6,7,8,9,10,11,12,13]. It is considered essential to better know the mechanical properties and laws that govern the behaviour of this material subjected to stress, in order to evaluate the possibility of extending its use to other field of application.

The working group conducted a campaign of tests on CLT panel taking as reference the technical regulations to evaluate the bending resistance (UNI EN 408:2012) and the sliding resistance of the gluing sections (UNI EN 392:1997).

The results of these campaigns are summarised in the following paragraphs.

2. TECHNICAL REGULATIONS

Laminated wood and CLT panels have long since provided a new way of using wood in structures. This means, as with other structural materials, that specific product standards must be drawn up. These standards define the types of structural material, their mechanical properties and estabilish how to determine them.

Below are the regulations in force which seem to be relevant in this case.

2.1. Strutture

- UNI EN 1995-1-1:2014 - Eurocodice 5 - Progettazione delle strutture di legno - Parte 1-1: Regole generali - Regole comuni e regole per gli edifici. (Design of wooden structures - Part 1-1: General regulations - Common regulations and regulations for buildings)
- ETAG 007 - GUIDELINE FOR EUROPEAN TECHNICAL APPROVAL of TIMBER BUILDING KITS
- Norme tecniche per le costruzioni (NTC 2018). D. Min. Infrastrutture e Trasporti 17 gennaio 2018 (Technical standards for construction (NTC 2018))
- CNR-DT 206/2007 Istruzioni per la Progettazione, l'Esecuzione ed il Controllo delle Strutture di Legno (Instructions for Design, Execution and Control of Wooden Structures)

- Circolare 21 gennaio 2019 n.7 ” Istruzioni per l’applicazione dell’«Aggiornamento delle “Norme tecniche per le costruzioni”» di cui al decreto ministeriale 17 gennaio 2018″ (Circular January 21, 2019 n.7 ”Instructions for the application of the «Update of the “Technical standards for construction”» referred to in the Ministerial Decree of 17 January 2018)
- Direttiva del Presidente del Consiglio dei Ministri 9 febbraio 2011 Valutazione e riduzione del rischio sismico del patrimonio culturale con riferimento alle Norme tecniche per le costruzioni di cui al D.M. 14/01/2008. (Assessment and reduction of seismic risk of cultural heritage with reference to the Technical Standards for constructions referred to in D.M. 14/01/2008.)

2.2. Materials

- ISO 16572:2008 Timber structures -- Wood-based panels -- Test methods for structural properties
- ISO 16696-1:2019 Timber structures -- Cross laminated timber Component performance, production requirements and certification scheme
- UNI EN 13017-1,2 :2001 - Pannelli di legno massiccio - Classificazione in base all’aspetto delle facce - Conifere/Latifoglie; (Solid wood panels - classification according to face appearance - coniferous/hardwood)
  This standard is the official Italian version of the European standard EN 13017-1 (edition November 2000). The standard specifies general requirements and appearance classes for both single-layer solid wood panels and multi-layer solid wood panels, the latter having a minimum thickness of the outer layers of 3,5 mm, made from coniferous/hardwood.
- UNI EN 12775:2002 - Pannelli di legno massiccio - Classificazione e terminologia (Solid wood panels - Classification and terminology)
  This standard is the official Italian version of the European standard EN 12775 (January 2001 edition). The standard provides a classification for solid wood panels and defines the terms used.
- UNI EN 13353:2011 - Pannelli di legno massiccio (SWP) – Requisiti. (Solid wood panels (SWP) – Requirements)
  This standard is the official English version of the European standard EN 13353:2008+A1 (May 2011 edition). The standard specifies the requirements for solid wood panels as defined in UNI EN 12775, with a maximum thickness of 80 mm, for use in dry, humid and outdoor environments, as defined by service classes 1, 2 and 3 of UNI EN 1995-1-1.
- UNI EN 14081-3:2012 - Strutture di legno - Legno strutturale con sezione rettangolare classificato secondo la resistenza - Parte 3: Classificazione a macchina; requisiti aggiuntivi per il controllo di produzione in fabbrica. (Structural wood with rectangular cross-section classified according to strength - Part 3: Machine classification; additional requirements for factory production control)
- UNI EN 14080:2013 - Strutture di legno - Legno lamellare incollato e legno massiccio incollato – Requisiti (Wooden structures - Glued lamellar wood and glued solid wood – Requirements)

- UNI EN 14081-2:2013 - Strutture di legno - Legno strutturale con sezione rettangolare classificato secondo la resistenza - Parte 2: Classificazione a macchina - Requisiti aggiuntivi per le prove iniziali di tipo. (Wooden structures - Structural wood with rectangular cross-section classified according to strength - Part 2: Machine classification - Additional requirements for initial type tests.)
- UNI EN 14081-1:2016 - Strutture di legno - Legno strutturale con sezione rettangolare classificato secondo la resistenza - Parte 1: Requisiti generali (Wooden structures - Structural wood with rectangular cross-section classified according to strength - Part 1: General requirements)
- UNI EN 338:2016 - Legno strutturale - Classi di resistenza (Structural wood - Resistance classes)
- UNI EN 14358:2016 Strutture di legno - Calcolo e verifica dei valori caratteristici (Wooden structures - Calculation and verification of characteristic values)

2.3. Laboratory Tests

- ISO 8375:2017 Timber structures -- Glued laminated timber -- Test methods for determination of physical and mechanical properties.
- UNI EN 313-1:1997 - Pannelli di legno compensato. Classificazione e terminologia. Classificazione. (Plywood panels. Classification and terminology. Classification.)
- UNI EN 392:1997 - Legno lamellare incollato. Prova di resistenza a taglio delle superfici di incollaggio. (Glued laminated wood. Resistance to shear test of gluing surfaces.)
- UNI EN 314-1:2005 - Pannelli di legno compensato - Qualità dell'incollaggio - Parte 1: Metodi di prova (Plywood Panels - Gluing Quality - Part 1: Test Methods)
  This standard is the official version of the European standard EN 314-1 (December 2004 edition). The standard specifies the methods for determining the quality of gluing of plywood with veneers, planing boards and lamellar panels by cutting test. The relevant requirements are specified in UNI EN 314-2.
- UNI EN 408:2012 - Strutture di legno - Legno strutturale e legno lamellare incollato - Determinazione di alcune proprietà fisiche e meccaniche. (Structural wood and glued lamellar wood - Determination of certain physical and mechanical properties.)
- UNI EN 384:2016 - Legno strutturale - Determinazione dei valori caratteristici delle proprietà meccaniche e della massa volumica (Structural wood - Determination of characteristic values of mechanical properties and density)
- Linee Guida per la certificazione dell'idoneità tecnica all'impiego di materiali e prodotti innovativi in legno per uso strutturale (DM 14.01.08 – Norme Tecniche per le costruzioni paragrafo 11.1, lettera C) - Guidelines for the certification of technical suitability for the use of innovative wood materials and products for structural use
- UNI EN 16351:2015 Strutture di legno - Pannello di tavole incrociate – Requisiti (Wooden structures - Cross board – Requirements)
- EN 13354:2008 - Solid wood panels (SWP) - Bonding quality - Test method;
  This European Standard specifies a test method for determining the bonding quality of single-layer and multi-layer solid wood panels by a shear test.

From the analysis of the regulations losted above, in order to know the mechanical parameters of the CLT panels, it was considered appropriate to apply the following standards:

- UNI EN 392:1997 - Glued lamellar wood. Trimming resistance test of gluing surfaces.
- UNI EN 408:2012 - Wood structures - Glued structural wood and glulam wood - Determination of certain physical and mechanical properties.

It should be noted that the standards chosen for the tests are not specific for CLT panels.

3. APPLICATIONS

The overcoming of the problems related to the anisotropy of the raw material, and the possibility of reaching remarkable thicknesses and dimensions, have made these panels an important business reality which is forcefully emerging in various construction sectors.
Willing to investigate the possible applications in the structural restoration field, was noted that these panels have often been used for the refurbishment and reinforcement of existing wooden floors and roofs [5,6,7,8,9,10,11,12,13].

Verifications carried out on masonry buildings located seismic areas often reveal a criticism about the timber ceilings, because in order to guarantee a uniform transfer of the loads to the lateral resistant elements, it should be ensured a diaphragm behavior of floors and inclined rooftops. But instead the real condition is that the wooden horizontal structures had a remarkable deformability, and therefore their behavior is clearly far from a diaphragm one. Consequently there is a need to intervene with reinforcement and stiffening measures on these structures. Clearly the possibility of operating on ancient structures carrying out as possible by reversible and dry interventions, becomes increasingly important in structural retrofit strategies.

With this perspective the CLT panels provide an innovative solution to the problem while matching the reinforcement needs with those related to a philosophy of reversibility and low invasiveness of interventions. Numerous scientific studies, experimentations and realizations have demonstrated the effectiveness in terms of reinforcement in the own plan of the structures. This allow therefore to consider at date these panels as a valid alternative to the traditional techniques of reinforcement.

In the literature, several research groups have shown that for CLT-reinforced horizontal structures, increasing loads apllied, the crisis of the system is reached with the crisis of the connection sections. So it were obtained resistance values 7 times higher than the traditional slabs. The reinforcement of wooden roofs both planar or inclined, represent another possible application of CLT panels in structural restoration. In the literature there are several studies about this topic, in particular in order to evaluate the different possibilities of modelling these kind of structures in relation to the potential dissipative effects that the reinforcements with these panels determine. A plausible modelling hypotesis is to consider the connections between panels and trusses as springs characterized by linear or not linear propreties according on the type of analysis carried out [9]. Regardless of whether the dissipative effects are evaluated, also in this case this reinforcement strategy is effective both in terms of seismic response and in terms of reversibility and low invasiveness.

However, studies conducted on other plausible interventions involving the use of CLT panels are very rare.

This type of panels could probably be used for the consolidation of the masonry walls by operating a sort of tackle inside the walls themselves [3]. This type of intervention would allow the original appearance of the buildings to be preserved by operating with an almost complete reversibility perspective in full compliance with the buildings both from the aesthetic that from the constituent materials point of view .

4. EXPERIMENTAL TESTS

4.1. Bending Resistance

In order to investigate the behaviour of the panels, several tests were carried out on samples of panels consisting of 3 and 5 lamellas layers. The 3-layer panels have a height of 100 mm and consist of external lamellae of a height of 25 mm, while the inner layer is made up of a lamella of a height of 50 mm. The 5-layer panels have a height of 120 mm with slats of equal thickness of 24 mm. In both types of panels the lamellae are 300mm long. The results of the experiments were compared with theoretical calculation models. All tests were carried out according to UNI EN 408:2012. The panels used for the tests are made of wood classified C24 according to UNI EN 338 with the following mechanical characteristics:

$$E_0 = 110000 \text{ N/mm}^2; E_{90} = 3700 \text{ N/mm}^2; G = 690 \text{ N/mm}^2$$

The tests were performed by placing the samples on two known centre distance supports by progressively applying the load in the centre.

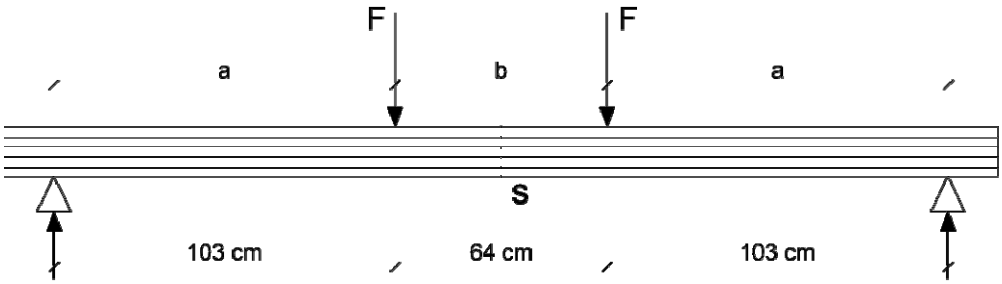


Figure 01: Test load scheme (UNI EN 408:2012)



Figure 02: Load test

Below one of the Force-Displacement diagram is shown:

Load [kg]	Deflection [mm]	Load [kg]	Deflection [mm]
0	0	800	50
100	6	700	42
200	12	600	39
300	20	500	32
400	26	400	26
500	34	300	18
600	39	200	11
700	46	100	6
800	52	0	1

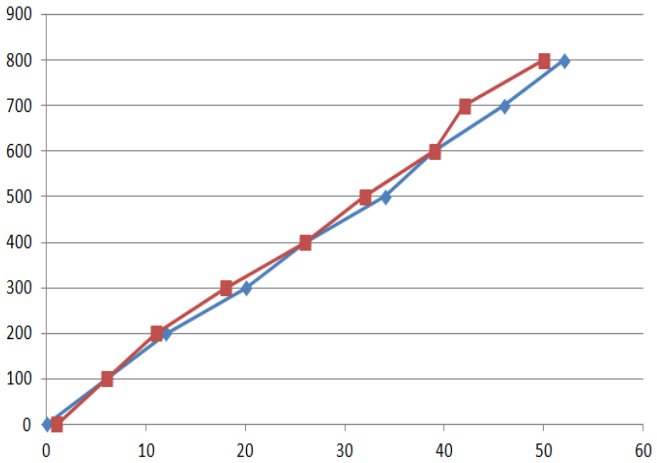


Figure 03: 3-layer panel force-displacement diagram

When the test phase are finished, the theoretical displacement in the centre was calculated using three different models:

- Model 1: the calculation of the maximum displacement was performed by neglecting the contribution of the transverse layers, but giving them the transfer of the shear effort to the adjacent layers while preserving the flat sections;
- Model 2: in compliance with the technical regulations, the calculation of the maximum deflection has been calculated taking into account the cooperation of the transversal elements;
- Model 3: The calculation was performed taking moderately into account the contribution of the transverse layers with their shear deformability.

The following table summarizes the values obtained from the test (with subscript sp) and from the 3 different calculation models (with subscript t):

Table 1: Bending test results

	3-LAYER PANEL			**5-LAYER PANEL**		
	Model 1	***Model 2***	***Model 3***	***Model 1***	***Model 2***	***Model 3***
EI	2,40625E+11	2,41781E+11	2,37537E+11	3,72557E+11	3,72685E+11	2,37537E+11
V_t	24,67	24,55	24,99	13,28	13,28	13,44
V_{sp}	50,5	50,5	50,5	27	27	27

The comparison between the experimental values and the theoretical ones show that the displacements values found during the tests are much higher than those obtained from all the theoretical calculation models. This could be due to an incorrect attribution of the EI value to the material in the three calculation models considered. If it was, starting from the experimental data found, it would be necessary to create a model of the CLT material more responsive to reality. The experiments shown in this work have been carried out on a specific standard for lamellar wood which does not necessarily apply well in this case, it should be

noted.

4.2. SLIPPING

In order to investigate the behavior of the gluing surfaces of the CLT panels, and in the absence of specific technical regulations (ref. § 2), several tests were carried out on different specimens in according to the provisions contained in the UNI EN 392: 1997 standard "Wood glued lamellar. Shear strength test of gluing surfaces ".

This standard doesn't contain specific provision for the orientation of the fibres in relation to the direction of application of the load. That because the field of application of the regulation, is exclusively laminated wood which as is known, is made with lamellas oriented in the same direction.

In order to considerate the mutual 90 degrees rotation of the lamellas, that is of the fibres, constituting CLT panels, the working group carried out the tests by dividing the samples into two families: the first characterized by the central panel fibres oriented parallel to the direction of load application (SAMPLES TYPE A), the second one with the central panel fibres orthogonal to the direction of application of the load (SAMPLES TYPE B).

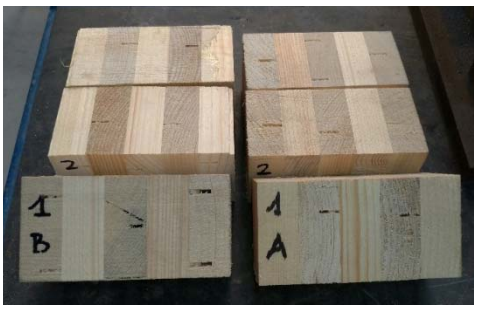
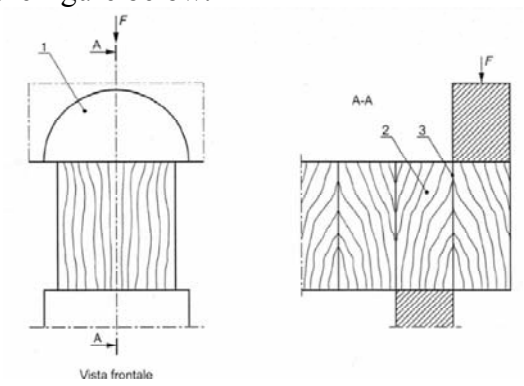


Figure 04: Specimens type A (central layer fibers parallel to the load direction) and type B (central layer fibers orthogonal to the load direction)

The test was carried out on the basis of the scheme described in the standard as shown in the figure below.



a)



b)

Figure 05: a) Representation of the performed test (UNI EN 392:1997) - b) Laboratory test

Ten tests were performed, five for each samples family. The results are shown in the table below:

Table 2: Slipping test results

Specimen	Basis [mm]	Width [mm]	Height [mm]	Mass [Kg]	Specific Weight [Kg/m^3]	Thickness [mm]	Breaking load [KN]	τ [N/mm^2]
1A	60	119	60	0,178	415,500	3	15,273	4,243
2A	60	119	59	0,185	439,159	6	20,223	5,713
3A	60	119	59	0,175	415,420	5	10,888	3,076
4A	60	119	60	0,176	410,831	5	12,512	3,476
5A	60	119	56	0,179	447,679	4	14,987	4,460
1B	60	119	59	0,174	413,047	3	7,464	2,108
2B	60	119	58	0,180	434,657	6	10,928	3,140
3B	60	119	60	0,185	431,839	3	7,709	2,141
4B	60	119	59	0,179	424,916	8	15,934	4,501
5B	60	119	60	0,184	429,505	9	13,769	3,825

Analysis of results indicates that samples B resistance values are clearly lower than those of A family. It means that the τ value for the group A samples are 33% higher than the B group ones.

By studying the breakage mechanisms of the individual specimens, we can observe that while for the A samples the crisis occurs with the failure of the gluing surface, for group B the crisis occurs with the failure of the central layer of the panel and not of the bonding surface. The results described are clear in the figure below



Figure 06: Post test specimens

All in all, we can affirm that from the tests carried out it is clear that the individual layer orientation assumes considerable importance both in terms of strength, Than in terms of "quality" of breakage, when we want to analyze the parameters that govern breakage by stressing the bonding surfaces.

5. CONSIDERATIONS AND CONCLUSIONS

The need to carry out structural restoration interventions that operate according to a philosophy of maximum reversibility and low invasiveness is becoming increasingly important.

In this perspective, the use of wood-based structural products and in particular CLT panels could represent a valid alternative solution to traditional structural restoration methods. In order to meet this requirement, in our opinion, it is necessary to introduce specific technical From the results of the tests shown in this work, it is clear that to date there are still numerous uncertainty factors linked both to the correct choice of the mathematical model to be used to better describe the behavior of the material, than to the presence of a poor regulatory framework related to the tests to be carry out on CLT panels. This work shows therefore that CLT panels cannot be actually tested in the same way as laminated wood.

That is especially in the case with we have to consider the use of CLT panels in the structural restoration for out of their own plan actions

6. REFERENCES

[1] Boscolo Bielo, Marco. La Progettazione delle strutture in legno. (the design of wooden structures) ed. Roma: Legislazione Tecnica s.r.l. 2014

[2] Daniel Moroder, Tobias Smith, Andrew Dunbar, Stefano Pampanin, Andrew Buchanan. Seismic testing of post-tensioned Pres-Lam core walls using cross laminated timber. Engineering Structures ELSEVIER (2018)

[3] Ivan Giongo, Gianni Schiro, Maurizio Piazza. On the use of timber-based panels for the seismic retrofit of masonry structures. Conference: 3rd International Conference on PROTECTION OF HISTORICAL CONSTRUCTIONS Lisbon (2017)

[4] Sandoli Antonio, Pinto Mirko, Pampanin Stefano, Calderoni Bruno. Protezione sismica di edifici esistenti in c.a. mediante l'utilizzo di pareti lignee post-tese. (Seismic protection of existing buildings in reinforced concrete through the use of post-stretched wooden walls) Pistoia: ANDIS 2017

[5] Roensmaens B., Van Parys L., Carpentier O. and Descamps T. (2018) Refurbishment of existing timber floors with screwed CLT panels, International Journal of Architectural Heritage

[6] Gubana, A. (2015) State-of-the-art report on high reversible timber to timber strengthening interventions on wooden floors. Construction & Building Materials,

[7] Gubana, A., Melotto, M. Experimental tests on wood-based in-plane strengthening solutions for the seismic retrofit of traditional timber floors. Construction and Building Materials.

[8] Longarini, N., Crespi, P., Scamardo, M. Numerical approaches for cross-laminated timber roof structure optimization in seismic retrofitting of a historical masonry church. 2019 Bulletin of Earthquake Engineering

[9] Longarini, N., Crespi, P., Zucca, M. Dissipative cross lam roof structure for seismic restoration of historical churches. 2018 REHABEND
[10] Ongaretto, E., Pozza, L., Savoia, M. Wood-based solutions to improve quality and safety against seismic events in conservation of historical buildings. 2016 International Journal for Quality Research
[11] Roensmaens, B., Van Parys, L., Branco, J., Descamps, T. Proposal of a CLT Reinforcement of Old Timber Floors. 2019 RILEM Bookseries
[12] Unuk, Ž., Premrov, M., Žegarac Leskovar, V. Development of an Innovative Approach for the Renovation of Timber Floors with the Application of CLT Panels and Structural Glass Strips. 2019 International Journal of Architectural Heritage
[13] Riggio, M., Tomasi, R., and Piazza M. (2014) Refurbishment of a traditional timber floor with a reversible tech-nique: importance of the investigation campaign for design and control of the intervention. International Journal of Architectural Heritage
[14] Basile Andrea, Frunzio Giorgio, Nicolella Maurizio, Scognamillo Claudio, Analisi LCC per componenti in legno lamellare esposti in esterni. (LCC analysis for laminated wood components exposed to the outside) ISTEA-Re-shaping the construction industry-Maggioli Editore (2017)
[15] Frunzio, Giorgio, Di Gennaro, Luciana: Seismic structural upgrade of historical buildings through wooden deckings strengthening: the case of study of Palazzo Ducale in Parete, Italy. Firenze CINPAR 2018 Structural Integrity PROCEDIA ELSEVIER (2018)
[16] Curlante D. - Progettare strutture in legno lamellare, Dario Flaccovio Editore, 2014.
[17] Bellomo V.- Strutture in legno lamellare , Grafill , 2015
[18] Bergamasco, I., Gesualdo, A., Iannuzzo, A. and Monaco, M. (2018) 'An integrated approach to the conservation of the roofing structures in the Pompeian domus', Journal of Cultural Heritage, DOI: 10.1016/j.culher.2017.12.006.
[19] Frunzio, G., D' Agostino, S. (2015) 'Between mechanics and architecture: the quest for the rules of the art', in Masonry Structures: Between Mechanics and Architecture, pp.1-19, Springer International Publishing
[20] Faggiano, B., Grippa, M.R. and Calderoni, B., 2013. Non-destructive tests and bending tests on chestnut structural timber. In Advanced Materials Research (Vol. 778, pp. 167-174). Trans Tech Publications.
[21] Piazza, M.; Modena, R.; Tomasi, R.., 2005 Strutture in legno. Materiale, calcolo e progetto secondo le nuove normative europee. Hoepli Editore.
[22] De Matteis Gianfranco, Corlito Valentina, Guadagnuolo Mariateresa, Tafuro Anna. 2019. Seismic Vulnerability Assessment and Retrofitting Strategies of Italian Masonry Churches of the Alife-Caiazzo Diocese in Caserta. Int. J. Architectural Heritage – Taylor & Francis
[23] Russo Teresa,Tesi di laurea corso di laurea magistrale in architettura: Costruire con il legno oggi. X-Lam: dal processo produttivo alla sperimentazione in laboratorio. (Master's degree thesis in architecture: Building with wood today. X-Lam: from the production process to laboratory experimentation.) Università degli Studi della Campania LUIGI VANVITELLI 2017/2018 – Relatore Prof. Ing. Frunzio G.

12th International Conference on Structural Analysis of Historical Constructions
SAHC 2020
P. Roca, L. Pelà and C. Molins (Eds.)

TREATMENT FOR RISING DAMP AND NATURAL HYDRODYNAMIC EQUILIBRIUM IN MASONRY WALLS

JOSE DOBÓN[1*] AND MIGUEL Á. SORIA[2]

[1]Civil Engineer
Kerakoll Ibérica S.A.
Carretera de l'Alcora, Km. 10,450, 12006 Castellón de la Plana, Spain
e-mail: jose.dobon@kerakoll.es

[2]Building Engineer
Kerakoll Ibérica S.A.
Carretera de l'Alcora, Km. 10,450, 12006 Castellón de la Plana, Spain
e-mail: miguel.soria@kerakoll.es

Keywords: Masonry, NHL mortar, Historic Heritage, Capillary Moisture, Damp Walls

Abstract. *The water absorption, in the Historic Heritage Restoration, through porous materials of the different constructive elements, is certainly one of the factors that constitute the basis for most pathologies and degenerative phenomena on plastering and masonry walls. Particularly, the most critical humidity comes from the soil, because it contains salts (chlorides, sulphates, nitrates). Those salts impregnate the masonry and unleash humidity rises up to several meters. Humidity varies the physical and chemical behaviour of the wall, increasing the thermic conductivity and limiting the isolation power. In addition, due to surface crystallization of the salts, early disintegration of the building materials and rapid destruction of the wall are generated. A wall saturated with water diminishes its isolation power and favours the formation of mould and bacteria, worsening the healthiness of the environments and the well-being of the people who habit them. In nature, a natural hydrodynamic balance is established between the water absorbed by building materials through capillarity and osmosis, and the water transferred to the atmosphere through evaporation. The constant components within this equilibrium are the absorption of water through capillarity and osmosis of the building materials, and the chemical nature of the aqueous solution absorbed. The variable components are the temperature and relative humidity of the atmosphere. The evaporation surface, composed by masonry mortar, plastering, scraping and painting are the constructive elements on which we might make an intervention. The traditional constructive systems, exclusively based on using natural lime for the manufacture of masonry mortars and rendering, and on using lime paste for coatings and paints, used to create the natural effects of the breathable hydrodynamic balance of the masonry. The challenge is to reproduce today, on site, a range of natural lime products in order to carry out interventions completely comparable to the original construction techniques. The range of naturals products, ensures a natural balance between rising damp and surface humidity evacuation, exploits the natural qualities of microporosity and hygroscopicity of the NHL, and natural pozzolan. The lack of reaction with the salts ensures chemical stability of the rendering and the duration of the entire dehumidifying system. The aim of the paper is to present real cases.*

1 INTRODUCTION

Walls are all potentially absorbent and suffer from contact with water. In particular the most critical form of humidity is that deriving from the ground, as it is loaded with salts (chlorides, sulphates and nitrates) that impregnate the wall and trigger capillary moisture rising that can reach heights of several meters.

Damp changes the physical and chemical behaviour of the wall, increasing thermal conductivity and restricting the insulating capacity. Furthermore, due to the surface crystallisation of the salts, it causes early crumbling of the construction materials and rapid destruction of the wall. A wall that is saturated with water has a lower insulating power and encourages the formation of moulds and bacteria, worsening the health of rooms and the well-being of those living in them.

2 DEHUMIDIFICATION HISTORY

Historically, different systems have been used trying to solve the moisture rising on walls. Leaving aside the well-known “trasdosado” system due to its proven inefficiency, below we chronologically list the different systems employed for dehumidify walls.

2.1 Moisture control with waterproofing (50's)

The first attempts to restore the surface of damp walls by capillary rise were focused on waterproofing the surfaces with the intention of keeping the water inside the wall. The waterproofing agents used were mainly the bitumen spread on the walls before plastering or even the lining of the walls with lead plates to ensure total insulation of the plaster from the wet and saline wall.

The ascending capillary force of the water was not considered which, due to the lack of surface evaporation, went further up the wall until it reached a new level higher than the previous one.

2.2 Mechanical cutting and aerator siphons (60's)

These systems, which seek to prevent moisture to climb the wall upwards, fail to desalinate the wall and therefore leaves it highly hygroscopic, so it does not solve one of the factors that causes mortars degradation.

2.3 Chemical cutting systems (70's)

This system consists of injecting resins into the base of the wall that waterproofs it. As before, this system fails to solve the crystallization of salts on the wall surface and causes the surface degradation of the building elements (renders, mortars, plasters, stons, bricks)

These systems are the precursors of sacrifice mortars

2.4 Macroporous mortars for cortical dehumidification (80's)

A first attempt to dehumidify through the use of semi-breathable aerated cement mortars involved waterproofing the surface of damp walls with the application of osmotic base mortar to reduce (at least "50%") the contribution of humidity and salts. The operation of aerated cement mortars was based on foaming additives which, during the mixing phase, generated macroporosity intended for the crystallization of the salts inside the mortar.

The limited durability of the system depended on the clogging speed of the macropore capacity which saturated allowing the reappearance of salts and moisture on the surface. This is why they were called sacrifice mortars.

2.5 WTA dehumidifying systems (1985)

The technical requirements for cortical restoration mortars are established for the first time. It includes both lime mortars and cement mortars.

2.6 CE mark (2000)

European standard EN 998-1, Specification for mortar for masonry - Part 1: Rendering and plastering mortar. The Type R are the Renovation mortars (the cortical restoration mortars).

This standard establishes tests to determine parameters as: dry bulk density, compressive strength, adhesion and fracture pattern, capillary water absorption, water penetration after capillary water absorption, water vapour permeability coefficient, thermal conductivity and reactions to fire.

2.7 Natural microporous mortars for cortical dehumidification (2005)

In 2005, thanks to the contribution of Kerakoll in research on natural limes and pozzolans, a new naturally breathable, salt-resistant mortar was found which complies with the requirements of the WTA and the EN 998-1 Type R, Biocalce Zoccolatura.

2.8 Biocalce MuroSeco: The first mortar that dries the wall in depth by dehydration (2016)

This special mortar for dehumidification guarantees a natural balance between moisture rising and surface dispersal of the humidity, taking advantage of the natural micro-porosity and hygroscopic qualities of pure NHL lime and natural pozzolan.

The fact that it does not react with the salts ensures that the render is chemically stable and makes the entire dehumidifying system more long-lasting.

The birth of the first natural lime and puzzolan mortar/render for long-term cortical dehumidification.

3 BIOCALCE MUROSECO FEATURES

3.1 The pure natural hydraulic lime that breathes

Nature has taught us the secret of how to make walls breathable. This line of natural mortars are a simple, natural materials whose porosity, breathability and hygroscopic qualities allows a continuous interchange of air and vapour within the wall, keeping the house healthy and in perfect equilibrium.

The quality of the natural hydraulic lime NHL 3.5 and selection of the natural elements gives this mortars greater natural porosity, compared with cement based plasters and renders, acting as a true “hygrometric lung” on the wall and providing a perfect balance between strength and elasticity, making this line of natural products perfectly compatible with even deteriorated walls and increasing indoor liveability



Figure 1. Natural Ingredients

3.2 Compatible with Historical Restoration

In the Historical Restoration, it is intended to return to the building its original conditions, through the appropriate repair and restitution work. Therefore, the selection of suitable materials is very important, so the best approximation regarding the classic binder of the original mortars is natural lime.

Natural lime mortars are easily reversible materials. It will be necessary to take into account when restoring, that this will not be the last, but that in the future there will be maintenance and other interventions in the same heritage.

This naturals mortars is indicated for the Restoration of Historical Heritage since:

1. Respect tradition, ensuring complete affinity with the materials and construction techniques of historical heritage.
2. Its high porosity, low capillary absorption and high breathability make it ideal for the rehabilitation of historic buildings, even in the presence of moisture.
3. It is resistant to salts, thanks to the lime and pozzolan that make the NHL mortar insensitive to the attack of disintegrating salts.
4. Recreate the original colors. Lime colors and natural earth and oxides return to the original tones of the old colors guaranteeing an optimal and complete conservative restoration.

3.3 The secret of its active pore

The size of the ACTIVE MICROPORES in the special dehumidication mortar guarantee high levels of breathability and very low capillary absorption. The small diameter of the capillary channels blocks the passage of water, which does not get into the render, while it allows free passage of the vapour molecules.

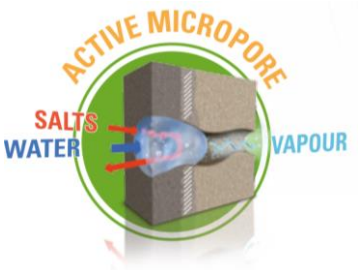


Figure 2. Avtive Micropore

3.4 The natural lime-pozzolan that is insensitive to sulphate attack

Kerakoll's research technicians have managed to identify a natural pozzolan that, thanks to its origin and grain size, makes the natural hydraulic lime nhl 3.5 insensitive to sulphate attack.

The chemical resistance of an hydraulic binder to attack by sulphate salts is determined using an analysis method known as the "ANSTETT TEST".

5. The method involves preparing test samples of binder (which is first hardened in water, dried and then ground) with 33% gypsum (sulphate). Support preparation
6. The new powder mixture is then damped with 6% water and compressed in a special mould to form a cylindrical pellet of standard dimensions (Ø 80 mm).
7. The test sample prepared in this way is placed on a porous septum (ceramic biscuit tile) in permanent contact with water.
8. The reaction to sulphates is checked by measuring the diameter of the pellet at regular intervals using a precision gauge (± 0.01 mm).

The measurement express the percentage increase in diameter from the start of the test.



Figure 3. Anstett Sample

4 STUDY CASES

The following study cases represent some examples of works carried out with the micropore dehumidifying system in 2004 and 2013. Two case studies are shown: one of them is a dehumidification of the barrel vaults of the "Fuerte Victoria Grande" in Mellila (Spain), and the other is a dehumidification of the "Limonaia" building of the Boboli Garden in the Pitti Palace of Florence (Italy).

4.1 Barrel vaults – Fuerte Victoria Grande – Melilla

The Fort Victoria the Great (Military Engineer Juan Martín Zermeño, 1735-1736) and his defensive perimeter is part of the system of the Fourth Precinct Fortified Melilla. It all starts with the intention of rescuing the soul buried under the old prison's debris in the eighteenth century Fortification, incorporating traces that allow us to know part of the life of the building over the time. We develop a historical collage flavoured with the beautiful ruins found in the present archeological finds and hue of contemporaneity that contextualizes the intervention of rehabilitation.

The intervention with this dehumidifying system is concentrated in the barrel vaults that form the galleries of the fort. These vaults are mixed with masonry base and brick arch, and there was moisture, both rising and roof water filtration. After waterproofing the roof, the strength of the support was evaluated and the suitability of the dehumidifying system was confirmed.

After applying the pure NHL lime and pozzolan dehumidifying mortars a lime-based render compatible with the system, was applied. As a decorative and projective layer, it was painted with breathable paint based on pure silicate according to DIN 18363 that guarantees the continuity of dehumidification.



Figure 4. Previous and current status of one of the vaults

4.2 Masonry wall – "Limonaia" of the Boboli Garden – Florence

Built between 1777 and 1778 to a design by Zanobi del Rosso, the *'Limonaia'* is the Boboli Gardens most characteristic building, which has come to us almost intact, thanks to the continuity of use that has been made. The building, in fact, is still used as a shelter of citrus collections (about five hundred pots), highly appreciated by the Medici, both for the therapeutic and aromatic qualities of the fruit, and for its beauty and singularity. The facade, one of the few examples of rococo taste present in Florence, still preserves original mortars and fixtures.

The restoration of the *'Limonaia'* involved the roof, the interior and the main facade of the building and the elevations of the side rooms. Particular attention was paid to the restoration of the main front mortars on which two surveys were carried out with stratigraphic tests in 1997 and 2002, which made it possible to draw up a careful mapping of the degradation and led to the choice of an accurate methodology intervention for mortars and paints, conducted in the same way that guides the restoration of the wall paintings. The philosophy of the intervention was to consolidate and preserve all that was possible to save of the original mortar, avoiding indiscriminate removal and subsequent remaking with new mortars.

It is for this reason that the project was chosen by the European Heritage Laboratory as an example of methodological reference for any safeguard and conservation intervention of plaster of historical value that still exists.

The building facade presented problems of moisture rising with presence of humidity marks, saline efflorescence, fall of mortars and paints, disintegration of mortars, cracks and fissures.

After careful analysis, there natural lime mortars was approved and selected by the "*Soprintendenza per i Beni Architettonici ed il Paesaggio"* of Florence, Pistoia and Prato as the most appropriate solution to guarantee the recovery and conservation of the *'Limonaia'* of the Boboli Garden, in respect of the existing structures and of the original materials.

This natural line of products, based on pure natural lime NHL 3.5, has been proposed as a suitable solution for the conservative restoration of the mortars of historical and monumental buildings, thanks above all to its characteristics of porosity, breathability and hygroscopy that allow a continuous exchange of air and steam inside the masonry.



Figure 5. Limonaia post-restauration 2004

5 CONCLUSIONS

Since the 80's, sacrifice mortars have been used as the best solution available to try to reduce the effects of moisture rising. Many times these mortars have been cement based which have produced irreparable damage to the historical heritage. The use of sacrifice mortars of pure natural lime NHL compatible with historic buildings, thanks to its behavior more similar to the original materials, often managed to delay the appearance of the moisture rising without damaging the heritage but requiring periodic maintenance of the mortars. Only the combination of natural pure lime NHL wisely dosed with natural pozzolan and selected aggregates achieve a highly breathable mortar with a micro-pore configuration that prevents the mechanical attack of salts. On the other hand, this combination of elements is what also makes the mortar resistant to the chemical attack of the salts, thus solving the moisture rising problem in a lasting way without the need to carry out constant maintenance tasks and which, with the over the years, dry the wall affected by moisture rising.

The studies and the different applications carried out with this micropore dehumidifying mortars, have shown, after years of correct behavior in real cases, that this dehumidification system is the most appropriate, not only to solve the problem of moisture rising, but also the more compatible in historic buildings, thanks to its mechanical and performance characteristics very similar to that of the original materials.

REFERENCES

[1] ARKOS, *Il restauro della Limonaia del Gardino di Boboli*. Scienza e restauro dell'Architettura, 15, Florence, Italy, September 2006.

[2] Kerakoll, *Biocalce Tasciugo: il primo intonaco asciuga muro che disidrata in profondità*. Sassuolo (MO), Italy, January 2016.

[3] Mario Lolli Ghetti, *Lo Stanzone Nuovo de' vasi del Real Giardino di Boboli*, in Mario Lolli Ghetti, Giorgio Galletti, Litta Medri, Daria Cervini, *Il Giardino Botanico di Boboli*, Fi, Centro Di, 1996, pp. 3-4.

[4] Loris Stefanini, *La 'fabbrica' della Limonaia tra Sette e Ottocento*, in Paola Grifoni (edited by), *La Limonaia del Giardino di Boboli. Storia e restauro*, Livorno, Sillabe, 2005, pp. 33-35, with previous bibliography.

[5] World Monuments Fund, *Limonaia at Boboli Gardens and Garden of Villa Medici At Castello.* New York, EU. Recovered from http://www.wmf.org

[6] Loris Stefanini, *Modifiche e trasformazioni tra Otto e Novecento*, in Paola Grifoni (edited by), *La Limonaia del Giardino di Boboli. Storia e restauro*, Livorno, Sillabe, 2005, pp. 36-37, with previous bibliography.

[7] Loris Stefanini, *L'intervento di restauro*, in Paola Grifoni (a cura di), *La Limonaia del Giardino di Boboli. Storia e restauro*, Livorno, Sillabe, 2005, pp. 62-73, with previous bibliography.

[8] José Antonio Fernandez Fernandez, *Rehabilitaton Works on the 4th fortification in Melilla: "Victoria Grande fortress" and "Covered Path*", Akros: Revista de Patrimonio, Spain, ISSN 1579-0959, Nº. 14, 2015, págs. 55-62

12th International Conference on Structural Analysis of Historical Constructions
SAHC 2020
P. Roca, L. Pelà and C. Molins (Eds.)

TRM-STRENGTHENED TIMBREL CROSS VAULTS SUBJECTED TO VERTICAL SETTLEMENTS

PEDRO A. CALDERÓN, ELISA BERTOLESI, MANUEL BUITRAGO, JUAN J. MORAGUES AND JOSÉ M. ADAM*

ICITECH, Universitat Politècnica de València, Camino de Vera s/n, 46022 Valencia, Spain
e-mail: pcaldero@upv.es (P.A. Calderón), elber4@upv.es (E. Bertolesi), mabuimo1@upv.es (M. Buitrago), jmorague@upv.es (J.J. Moragues), joadmar@upv.es (J.M. Adam)
(*corresponding author)

Keywords: Textile Reinforced Mortar (TRM), Timbrel Masonry Cross Vaults, Settlement-Induced Damages, Masonry Strengthening.

Abstract. *Two full-scale timbrel cross vaults subjected to vertical settlements in one of their supports were tested at the ICITECH laboratories of the Universitat Politècnica de València. In one of the vaults a support was moved downwards, while the other was subjected to upward-downward displacements in one support. Both tests are described and analysed in detail in Torres et al. [1,2]. Both vaults presented certain levels of post-test damage in the form of cracks and significant displacements. In order to analyse the effectiveness of the reinforcement of previously damaged vaults, both were strengthened with TRM and subjected to further testing in which vertical settlements were applied to one support. The TRM strengthening comprised an extrados layer composed of a 25x25 mm glass grid embedded into two approximately 5 mm thick layers of cementitious matrix. The TRM strengthening was able to withstand higher peak loads and prevent the formation of cracks along the extrados surface of the structure, while as expected, ductility increased. A 3D macro-modelling FE strategy on Abaqus commercial software was also adopted to study the behaviour of the vaults during the tests.*

1 INTRODUCTION

Most historical constructions are made of masonry [1]. During the centuries and depending from the local availability of the row materials, masonry has been constructed using different kind of blocks and type of mortars. As expected, its variety makes assessing a masonry building's safety particularly challenging. In addition, although most of the masonry constructions being part of the architectural heritage have been constructed following rules of thumb, they are currently subjected to different types of loads, for example: overloading, dynamic actions, settlement, in-plane and out-of-plane deformations [1]-[5]. In particular, the damage suffered by many historical churches and buildings after the recent Italian earthquakes [2] has shown that masonry vaulted structures are particularly vulnerable to supports distortion. Differential settlements in the supports may result in deformations, cracking, and cause changes in their geometry, twist and vertical alignment [2][4][5].

Evaluating the consequences associated with foundation or support movements and proposing innovative and compatible retrofitting solutions, are two of the main questions that have attracted the attention of the architects and engineers who have to preserve historical and other types of masonry constructions.

To this scope, cementitious based strengthening materials have attracted the attention of the scientific community as an alternative to Fibre Reinforced Polymer (FRP) composites for repairing historical masonry structures. Similar to FRPs, cement-based materials are lightweight, easy to apply and represent an affordable solution because of their low cost, good applicability to irregular and damp surfaces, resistance to high temperatures, good breathability, low invasiveness [6].

The mechanical properties of the substrates where TRM strengthening materials are applied, play a crucial role, since cement-based composites are often employed to reinforce weak masonries [7]. Various studies have been conducted to identify TRM's mechanical properties [8][9]. Other studies assessed the effectiveness of TRM composites applied to isolated structural elements [10][11]. Pioneering works on simple and biaxial bending TRM reinforced panels were analysed in [12][13], whereas several studies assessed the behaviour of TRM on curved weak masonry supports, including [14].

Due to their prohibitive cost, few studies have analysed the performance of TRM on full-scale structures. [15] studied the dynamic performance of a one-story masonry building tested on a vibrating table and repaired by cement-based materials. Vaults have been found to be particularly vulnerable [1][2] due to their remarkable interaction with their context, so that large differences in lateral stiffness between piers and perimeter walls results in distortions in the supports that have to be absorbed by the masonry vaults.

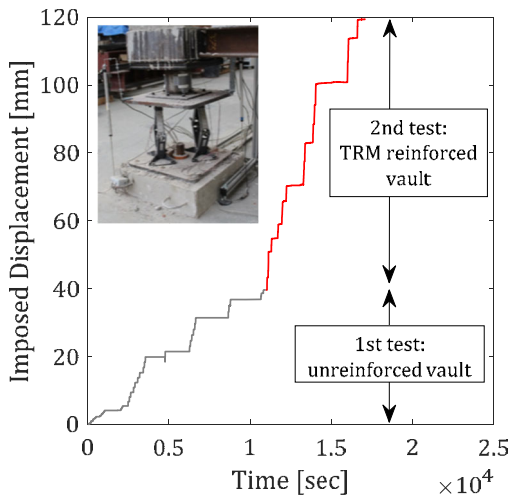
As no experimental studies have so far analysed the behaviour of TRM composites on full-scale cross vaulted structures, the present work was aimed at filling this gap with a double experimental campaign on full-scale masonry timbrel cross vaults damaged by two types of soil settlement and repaired with TRM materials.

2 EXPERIMENTAL INVESTIGATION & LOADING PROTOCOL

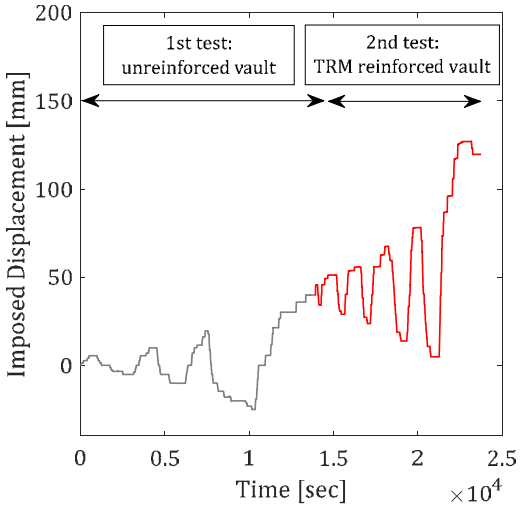
The experimental campaign investigated the behavior of two masonry timbrel vaults reinforced with Textile Reinforced Mortar (TRM) composites when subjected to either monotonic and cyclic vertical settlements. To this scope, two masonry vaults were built at the ICITECH laboratories of the Universitat Politecnica de Valencia (Valencia, Spain). The vaults were pre-damaged in a preliminary step by applying two types of vertical movements to one of the supports [16][17].

The 4x4 m2 square plan vaults with 1.8 m high lateral arches were built with 230x110x26 mm3 clay tiles and approximately 10 mm thick mortar joints. Four cubic concrete supports, S1, S2, S3 and S4, were built on steel bases. The arches were composed of four layers of clay tiles with cement mortar, plaster paste and lime mortar joints. Two vertical support distortions were applied to the damaged masonry cross vaults, i.e. a monotonic downward settlement up to 80 mm and an up and down cyclical displacement. Both settlements were imposed on the deformed vaults with a residual 40 mm downward displacement due to the need to realistically reproduce and analyze in lab conditions the repairs of the damaged masonry structures. Both excitations were imposed statically to support S1 (see **Figure 1**) by means of

two manually synchronized mechanical jacks placed below the steel base. The remaining supports were constrained as follows: support S3 was fixed to the reaction floor. S2 and S4 were only allowed to slide horizontally.



-a



-b

Figure 1: Comparison of displacement protocols applied to the as-built and TRM-reinforced structures: Case A (-a) and Case B (-b).

A steel system composed of 140 mm high HEB girders formed the bracing frame connecting all the supports and providing partial horizontal confinement of the vaults. The girder frame also helped to avoid excessive diagonal distortions of the vault by hinging all the steel bases and allowed the positioning of three load cells to monitor vertical reactions in supports S1, S2 and S4.

The two vaults were strengthened by means of a 10 mm thick layer of TRM material. The glass fiber netting comprised a 25 mm spacing glass grid with an equivalent resistant area of 35.27 mm2/m, ultimate tensile strength 45 kN/m and elastic modulus 72 GPa. The strengthening technique comprised three phases: (i) injection and masonry repointing, (ii) application of a 5 mm thick layer of cement mortar, (iii) placing the fiber glass fabric and (iv) finishing off with the last 5 mm thick mortar layer. After the injection phase, the vault extrados only was reinforced by 500 mm wide radially placed glass TRM strips. Glass strips were not anchored to the concrete supports, nor were spike anchors or connecting devices used.

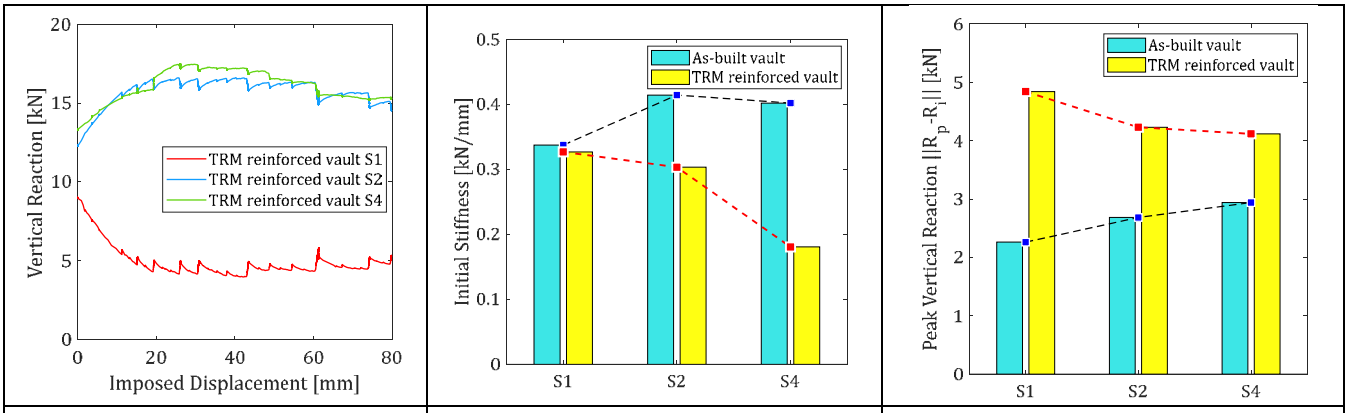
3 EXPERIMENTAL RESULTS: MONOTONIC SETTLEMENT

3.1 Experimental Results

Figure 2-a depicts the reaction force-displacement curves obtained experimentally in supports S1, S2 and S4. As can be seen in **Figure 2**-a, the vault' behavior can be divided into three phases: (i) the initial elastic response was obtained up to 10 mm, (ii) from 10 mm to 30 mm behavior was non-linear until the peak value (Rp), and (iii) in the third phase it became less pronounced with lower reaction forces up to failure at 80 mm. The TRM had a twofold

effect: (i) it helped to extend the elastic phase, which doubled from 5 mm to 10 mm and (ii) considerably increased the displacement capacity at failure, which doubled from 40 to 80 mm. Apart from a few differences, the initial reactions of the TRM-reinforced vault are similar to those monitored at the end of the unreinforced vault test. Considering the as-built structure, there are negligible differences between the three reaction values in all the monitored supports, confirming an approximately equal re-distribution of the vault's weight. Conversely, the second test was performed starting from the deformed vault configuration obtained at the end of the first test and then applying the monotonic settlement. As expected, since the test started with a downward residual displacement of 40 mm in support S1, the equal distribution of the reaction forces in the as-built structure were altered, especially in the initial reactions (Ri) in S2 and S4, which increased almost symmetrically. Unexpectedly, the reaction force in S1 was not altered by the initial deformed vault configuration.

Figure 2-b depicts the initial stiffness values calculated as the slope of the vaults' elastic response (until 5 mm for the as-built and 10 mm for the TRM-reinforced vault) of all the monitored supports. The TRM helped re-establish the original stiffness in S1, while S2 and S4 slightly reduced their initial stiffness. A different trend was found in the effectiveness of TRM on the peak forces throughout the tests. A comparison of the response of the as-built and repaired structures is given in **Figure 2-c**, which shows significantly higher peak reaction forces due to the TRM.



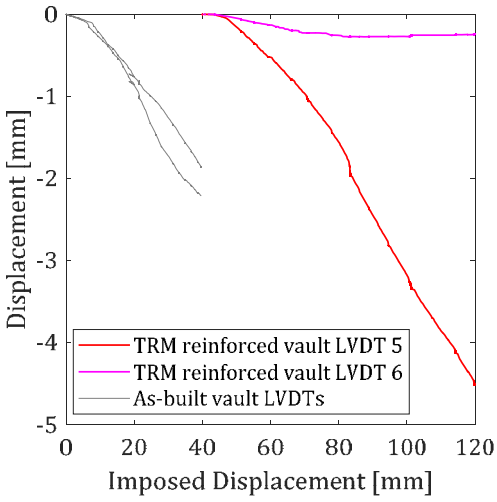
-a -b -c

Figure 2: Reaction forces vs imposed displacement curves obtained experimentally(-a). Comparisons between as-built and TRM reinforced vaults: initial stiffness (-b) and peak forces (-c).

3.2 Crack Pattern

At the end of the first test (unreinforced vault subjected to monotonic settlement) [16], the vault experienced: (i) cracks formed on mortar joints on supports S1 and S3 and on some damaged bricks in S2, (ii) a diagonal curved hinge crack opened on the vault extrados and propagated along the diagonal arch towards S2 and S4. As vault stability was seriously threatened, the authors decided to stop the test and carry out repairs. Despite the injections, the TRM-reinforced vault experienced: (i) the opening of one extrados curved hinge connecting supports S2-S4 and (ii) traditional hinge mechanisms in the lateral arches. Hinges were also detected near S2 and S4. The cracks in the extrados opened mostly in the reinforcing mortar (see **Figure 3-a**). No debonding or fiber-to-matrix slippages were detected

during the whole series of tests. The activated damage mechanism involved the reinforcing mortar matrix but there was no tensile failure of the glass grid. It should be noted that the cracks on lateral arches S4-S1 and S2-S1 attempted to join up with the diagonal hinge between supports S2-S4. This peculiar failure mechanism also occurred in the unreinforced vault [16] (**Figure 3-b**). In details, **Figure 3-a** gives the displacement read by the LVDTs placed on the unreinforced vault (between 0 to 40 mm) and the TRM-repaired vault extrados (between 40 to 120 mm). LVDT 5 monitored the formation of the hinged diagonal crack along supports S2-S4 on the vault extrados, which doubled in size from 2.5 mm in the unreinforced to 5 mm in the reinforced vault.





-a -b

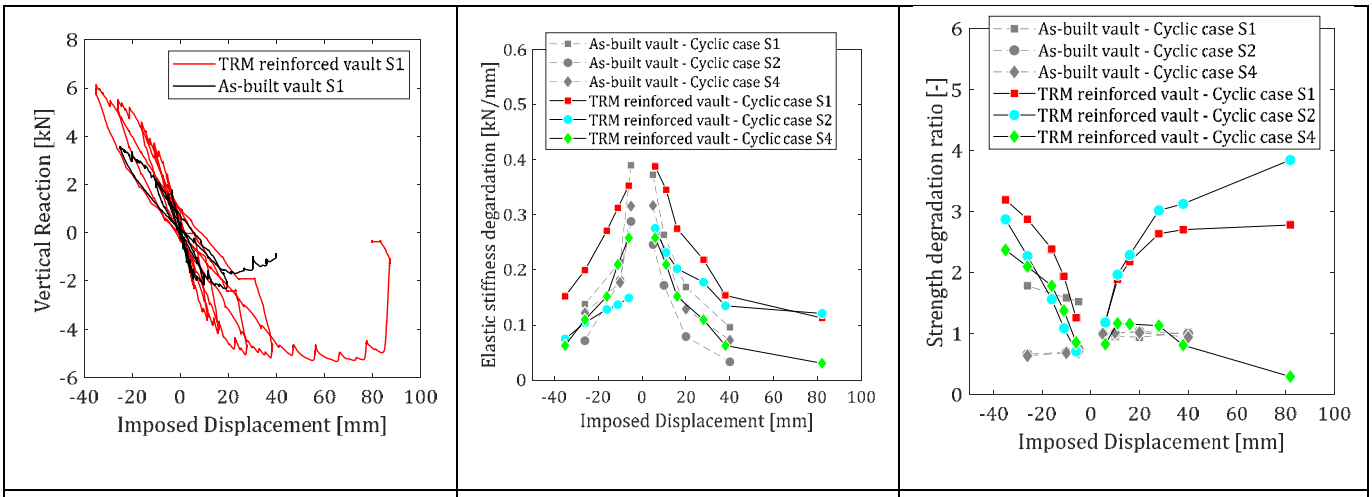
Figure 3: LVDTs placed on the vaults extrados (-a) and cracking mechanism formed on the TRM reinforced vault intrados (view of diagonal arch S3-S1) (-b).

4 EXPERIMENTAL RESULTS: CYCLIC SETTLEMENT

4.1 Experimental Results

Figure 4-a depicts the reaction force-displacement curve obtained in support S1 considering the load increments produced only by the displacement protocols. The curve is traced in the same color as the corresponding support number and superimposed on the unreinforced counterpart. The ultimate bearing capacity of the TRM-reinforced vault is significantly greater than that of the as-built structure, as are the corresponding ultimate displacements. Elastic stiffness degradation (**Figure 4-b**) was computed as the slope of the force-displacement curves monitored in all the cycles of the campaign up to 80% of the peak reaction forces. As expected, in the TRM-reinforced vault the initial elastic stiffness progressively degraded up to a maximum of four times at 80 mm in support S1. The initial stiffness values in the first cycle were quite similar to those of the undamaged unreinforced vault at the beginning of the test. Although negligible differences were detected due to material heterogeneity, the consistency of the values from the beginning of the test confirmed the effectiveness of TRM in recovering the structure's original stiffness. Strength degradation

is another important parameter (**Figure 4-c**). Strength degradation curves were drawn using the peak forces obtained in each cycle of all the monitored supports. The as-built and TRM-reinforced vaults were normalized with those obtained in the first cycle of the unreinforced vault. As can be seen in **Figure 4-c**, the TRM strengthening dramatically changed the unreinforced vault's strength degradation trend found in [17]. Unexpectedly, both up and down movements showed a clear increasing trend common to all the supports in all cycles, except for the last cycle of S4. The reduced strength was detected in S4 before the other supports, indicating a faster entry into the energy-consuming state. The TRM-reinforced vault's behavior was quite symmetric under upward and downward settlements.



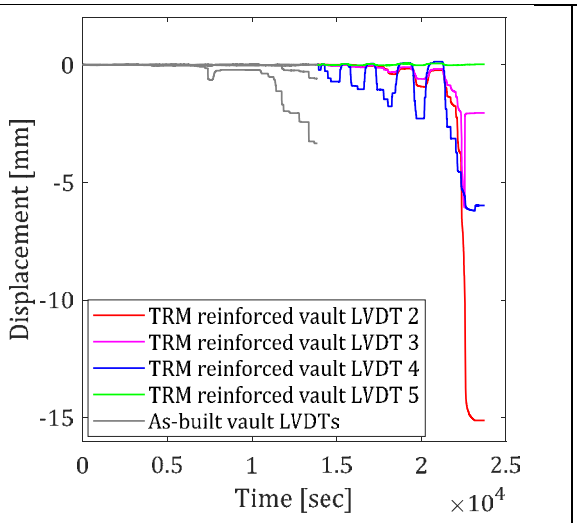
-a -b -c

Figure 4: Reaction force-displacement curves (cyclic settlement) in supports: S1 (-a). Comparison between as-built and TRM reinforced vaults: stiffness degradation (-b) and strength degradation (-c).

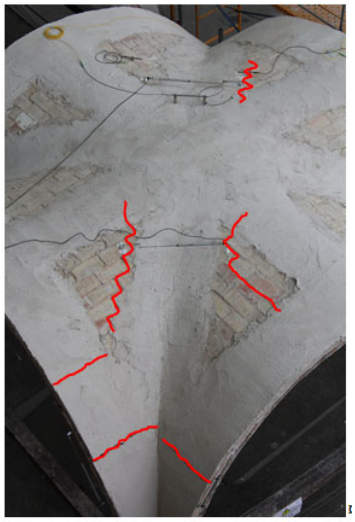
4.2 Crack Patterns

Similarly to the monotonic case, the TRM-reinforced vault subjected to cyclic settlements experienced the formation of hinges in the lateral arches and the widening of a diagonal crack on arch S2-S4. **Figure 5-a** depicts the displacements recorded by the LVDTs close to supports S2-S3 and S4 during the testing of the unreinforced and TRM reinforced vaults. The cracks formed during the first test were relatively narrow (3 mm). In the reinforced vault severe damage was detected on the extrados and intrados of support S2. The base of S2 experienced a deep crack which formed during upward movements. Furthermore, both lateral arches S2-S1 and S2-S3 experienced wide cracks on the extrados which affected the vault's integrity. It is worth mentioning that, those on the former arch opened up to approximately 16 mm. In addition, the TRM experienced preliminary cracking of the reinforcing mortar, followed by the progressive tensile failure of the glass grid. The same failure mechanism was observed in lateral arch S2-S3. In this case, the crack, which propagated across the mortar joints, caused the external layers of masonry to separate. Although a visual inspection showed the crack was similar to the one in arch S2-S1, LVDT 3 could only partially detect it. Only one LVDT tracked the formation of the diagonal hinge that opened between supports S2-S4 on both extrados and intrados due to the cyclic settlement. Thanks to the presence of the TRM

strengthening, the premature separation of the vault into two independent parts was avoided (**Figure 5-b**). **Figure 5-b** shows the crack patterns at the end of the cyclic test in the reinforced vault. The cracks on the extrados were diverted by the reinforcing materials to the masonry away from the retrofitted zones. The TRM radial configuration prevented the crack on the top of the extrados from propagating. The cracks reached a maximum value of 8 mm at the end of the test in the unreinforced vault, or approximately half the width of the opening in the reinforced vault.



-a



-b

Figure 5: Comparison of displacements records by LVDTs placed close to supports S2-S3 and S4 (-a) and crack pattern obtained at the end of the investigation (-b).

5 CONCLUSIONS

The present work describes a double lab test comprising the application of monotonic and cyclic settlements in two masonry timbrel vaults constructed at the *Universitat Politecnica de Valencia* (Spain). The results obtained allow us to draw the following conclusions:

- The paper describes a repair technique to be used for severely damaged masonry cross vaults composed of: injection, masonry repointing and application of TRM composites in a radial pattern on the extrados.
- TRM composites increased the load-bearing capacity of the masonry cross vaults, almost doubling the peak reaction forces in both cases.
- The proposed radial strengthening configuration almost completely restored the initial elastic stiffness of the damaged vaults in both cases.
- TRM strengthening doubled the vaults' elastic phase and ultimate displacements.
- TRM failure in case of monotonic downward settlement comprised the cracking of the reinforcing mortar. No debonding, fibre-to-matrix slippage or tensile failures of the textile grid were detected.
- TRM failure in case of cyclic vertical movement was characterized by the opening of wide cracks in support S2, with the cracking of the mortar matrix and tensile failure of the glass grid.

REFERENCES

[1] Bertolesi E., Adam J.M., Rinaudo P., Calderón P.A. Research and practice on masonry cross vaults – A review, *Engineering Structures* 180 (2019), pp. 67-88.

[2] D'Altri A.M., Castellazzi G., de Miranda S., Tralli A. Seismic-induced damage in historical masonry vaults: A case-study in the 2012 Emilia earthquake-stricken area. *J Build Eng* 13 (2017), pp. 224–43. doi:10.1016/j.jobe.2017.08.005.

[3] Atamturktur S., Bornn L., Hemez F. Vibration characteristics of vaulted masonry monuments undergoing differential support settlement. *Eng Struct* 33 (2011), pp. 2472–84. doi:10.1016/j.engstruct.2011.04.020.

[4] Acikgoz S., Soga K., Woodhams J. Evaluation of the response of a vaulted masonry structure to differential settlements using point cloud data and limit analyses. *Constr Build Mater* 150 (2017), pp. 916–31. doi:10.1016/j.conbuildmat.2017.05.075.

[5] Carfagnini C., Baraccani S., Silvestri S., Theodossopoulos D. The effects of in-plane shear displacements at the springings of Gothic cross vaults. *Constr Build Mater* 186 (2018), pp. 219–32. doi:10.1016/j.conbuildmat.2018.07.055.

[6] Alexandros L., Thanasis S.K., Triantafillou C. State-of-the-art on strengthening of masonry structures with textile reinforced mortar (TRM), *Constr Build Mater* 188 (2018), pp. 1221-1233.

[7] Del Zoppo M., Di Ludovico M., Balsamo A., Prota A. In-plane shear capacity of tuff masonry walls with traditional and innovative Composite Reinforced Mortars (CRM), *Constr Build Mater* 210 (2019), pp. 289-300.

[8] Caggegi C., Lanoye E., Djama K., Bassil A., Gabor A. Tensile behaviour of a basalt TRM strengthening system: influence of mortar and reinforcing textile ratios, *Compos Part B Eng* 130 (2017), pp. 90-102.

[9] Ascione L., De Felice G., De Santis S. A qualification method for externally bonded Fibre Reinforced Cementitious Matrix (FRCM) strengthening systems, *Compos Part B Eng* 78 (2015), pp. 497-506.

[10] Wang X., Lam C.C., PanIu V. Comparison of different types of TRM composites for strengthening masonry panels, *Constr Build Mater* 219, (2019), pp. 184-194.

[11] Augenti N., Parisi F., Prota A., Manfredi G. In-plane lateral response of a full-scale masonry sub-assemblage with and without an inorganic matrix–grid strengthening system, *J Compos Constr* 15 (2011), pp. 578-590.

[12] Kariou F.A., Triantafyllou S.P., Bournas D.A., Koutasc L.N. Out-of-plane response of masonry walls strengthened using textile-mortar system, *Constr Build Mater* 165 (2018), pp. 769-781.

[13] D'Ambra C., Lignola G.P., Prota A., Sacco E., Fabbrocino F. Experimental performance of FRCM retrofit on out-of-plane behaviour of clay brick walls, *Composites Part B* 148 (2018), pp. 198-206.

[14] Giamundo V., Lignola G.P., Maddaloni G., Balsamo A., Prota A., Manfredi G. Experimental investigation of the seismic performances of IMG reinforcement on curved masonry elements, *Composites: Part B* 70 (2015), pp. 53–63.

[15] Maddaloni G., Di Ludovico M., Balsamo A., Maddaloni G., Prota A. Dynamic assessment of innovative retrofit techniques for masonry buildings, *Composites Part B: Engineering* 147 (2018), pp. 147-161.
[16] Torres B., Bertolesi E., Moragues J.J., Calderón P.A., Adam J.M. Experimental investigation of a full-scale timbrel masonry cross vault subjected to vertical settlement, *Constr Build Mater* 221 (2019), pp. 421-432.
[17] Torres B., Bertolesi E., Calderón P.A., Moragues J.J., Adam J.M. A full-scale timbrel cross vault subjected to vertical cyclical displacements in one of its supports, *Engineering Structures* 183 (2019), pp. 791-804.

12th International Conference on Structural Analysis of Historical Constructions
SAHC 2020
P. Roca, L. Pelà and C. Molins (Eds.)

A FRAMEWORK FOR THE DETAILED FLOOD VULNERABILITY MODELLING OF BUILT CULTURAL HERITAGE

RUI FIGUEIREDO[1*], XAVIER ROMÃO[1] AND ESMERALDA PAUPÉRIO[2]

[1] CONSTRUCT-LESE, Faculty of Engineering, University of Porto

Rua Dr. Roberto Frias, s/n, 4200-465 Porto, Portugal
e-mail: {ruifig, xnr}@fe.up.pt (*corresponding author)

[2] Construction Institute, Faculty of Engineering, University of Porto

Rua Dr. Roberto Frias, s/n, 4200-465 Porto, Portugal
e-mail: pauperio@fe.up.pt

Keywords: Cultural Heritage, Flood Vulnerability, Flood Risk, Risk Assessment

Abstract. *Flooding is the most common and damaging of natural hazards at global level, and in a context of climate change, flood risk is expected to increase. This has prompted governments and international agencies to adopt measures towards the reduction of flood risk in recent years. Among them is the development of flood risk assessments and flood risk management plans, with particular emphasis on cultural heritage, not only due to its significance for society, but also because of its particularly high vulnerability to natural hazards, including floods. In order to quantify risk and define prioritization and management plans for a given set of cultural heritage assets, vulnerability models that allow estimating and comparing the impacts of floods at an asset-by-asset level are required. However, there is currently a lack of approaches in the literature to achieve this. This study proposes a component-based synthetic modelling framework to perform detailed vulnerability analyses of cultural heritage assets. The framework is illustrated through an application to a Portuguese church.*

1 INTRODUCTION

Flood risk is expected to increase worldwide in the coming decades due to various socio-economic and environmental factors, including climate change. Minimizing flood risk across any given region requires robust risk management decision-making, which must necessarily be supported by risk assessment studies. These combine flood hazard data for a region of interest with information on exposed assets and models of their vulnerability (i.e. the impact they are expected to undergo as a function of flood actions), and allow computing consistent risk metrics.

The socio-cultural importance of cultural heritage calls for particular attention to this asset type in any flood risk management plan. However, at present, there is a lack of methods in the literature to quantify the flood vulnerability of cultural heritage assets, which hampers the development of flood risk assessments, and consequently informed risk management prioritization and optimization of mitigation measures. This gap can be justified by various underlying difficulties. Firstly, cultural heritage assets tend to differ considerably among themselves, precluding the development and application of common vulnerability models to

portfolios of assets, except in large-scale risk assessments for preliminary screenings of risk. Secondly, empirical approaches commonly adopted for other asset types, such as common residential buildings, are not applicable, because they require datasets of observed damage and/or losses, which are not available for cultural heritage assets. Thirdly, there is no agreed upon method to quantify the value of cultural heritage assets and, consequently, their degree of damage or loss as a result of a disaster [1, 2].

This study aims to address the above issues by proposing a framework to model the flood vulnerability of cultural heritage assets, so that this information may be used within risk assessment studies where an asset-by-asset differentiation of risk is required. The proposed approach is based on a component-based synthetic modelling framework, whereby hypothetical flood scenarios are simulated and the corresponding potential overall damage is estimated as the combination of damage to each component of cultural value comprising an asset. The modelling framework is illustrated through an application to a church in Portugal.

2 METHODOLOGY

For each cultural heritage located in an area of interest, flood risk is defined as the probability that damage will occur as a result of flooding, and is commonly expressed as a function of hazard, vulnerability, and exposure. Within this conceptual framework, hazard represents the intensities and probabilities of occurrence of flood scenarios, exposure expresses the assets' overall values, and vulnerability links flood intensities to potential impacts. This paper specifically addresses the latter, presenting a methodology for the quantification of the vulnerability component of risk for cultural heritage assets. The approach is organized into three steps that are described in the following subsections.

2.1 Surveying and value assessment of exposed components

The specific nature of cultural heritage requires an asset-by-asset characterization of vulnerability when the objective is to develop risk management and prioritization plans with a high level of granularity. This can only be achieved through on-site collection of information. Therefore, the first step of the methodology involves the identification, documentation and value assessment of all the relevant exposed components that comprise a cultural heritage asset and contribute to its overall cultural value. The surveying process should allow collecting the most relevant information for characterizing the flood vulnerability of an asset. Simultaneously, it should also be a simple procedure that can be carried out efficiently without the need to involve significant resources and/or specific engineering skills (to allow surveys to be carried out by local non-technical stakeholders). In this regard, the two fundamental variables that need to be collected are the main material of each component and the height at which it is located.

In order to facilitate the surveying process of a given cultural heritage asset and help ensure that relevant components are not left out, it is useful to establish a taxonomy for such components beforehand. Because this classification scheme could vary significantly between different asset types, specific taxonomies should be defined for each type. For the case of churches, a taxonomy is proposed in Table 1, which was developed to support the application of the framework to the case study described in Section 3, a Portuguese church. The most common material types for each component are also identified to further support the surveying procedure.

Table 1: Proposed component taxonomy for churches, containing the most relevant components commonly found in Portuguese churches and their respective materials.

Group	Designation	Common main materials
1. Building	1.1. External walls	Stone, Concrete, Earth, Wood, Clay brick
	1.2. Internal walls	Stone, Concrete, Earth, Wood, Clay brick
	1.3. Basement walls	Stone, Concrete
	1.4. Wall paintings and coverings	Ceramic tilework, Gilded woodcarving, Murals, Decorative plaster
	1.5. Floors	Stone, Wood, Clay tiles
	1.6. Roofs	Concrete, Wood, Clay brick
	1.7. Doors	Wood, Metal
	1.8. Windows and stained glasses	Glass and Wood/Metal
2. Contents	2.1. Main retable and altar	Wood, Gilded woodcarving
	2.2. Other retables and altars	Wood, Gilded woodcarving
	2.3. Altar table	Stone, Wood, Earth
	2.4. Main altar pulpit	Stone, Wood, Metal
	2.5. Nave pulpit	Stone, Wood, Metal
	2.6. Baptismal font	Stone, Metal
	2.7. Statuary	Wood, Metal, Ceramic, Paper pulp
	2.8. Organ	Various
	2.9. Furniture	Wood
	2.10. Light fittings	Metal, Crystal
	2.11. Tombs	Wall, Stone
	2.12. Metal liturgical implements	Gold, Silver, Brass
	2.13. Textile liturgical paraments and implements	Textile
	2.14. Books	Book paper
	2.15. Candlesticks and lamps	Gold, Silver, Brass
	2.16. Porcelains	Porcelain

After the component survey, it is then necessary to estimate the value of each of the selected components. Given that such values cannot be expressed in absolute economic terms, within the proposed framework, indices of value for the different components of the cultural heritage asset are defined, which reflect their estimated relative value with respect to the other selected components. It is recommended that at least three levels of significance are adopted:

- a low level, for components that are not unique and that contribute in a limited manner to the overall cultural value of the asset;
- an intermediate level, for unique components that have significant cultural value;
- a high level, for unique components with exceptional cultural value, which are determinant for the overall cultural value of the asset.

In order to expedite the surveying procedure, particularly in situations with a large number of components, it is suggested that only components that can be affected by floods up to a certain return period are documented, and that the relative value of those components with respect to the whole set of components (i.e. floodable and non-floodable) is defined in aggregated terms, based on expert judgement.

2.2 Estimation of flood susceptibility for each component

The susceptibility of each component is defined as the level of impact it is expected to undergo as a result of the action of flooding. In order to estimate the susceptibility of different components, a literature review was carried out in order to characterize the effects of floodwater on certain commonly found materials [3–12], taking the taxonomy shown in Table 1 as a reference. A summary is presented in Table 2 for some materials. Based on this analysis, the susceptibility of each material was translated into a scale of indices, as represented in Figure 1. Note that for each material, besides a base level or range of susceptibility indices (represented by the hatched shapes), there are also higher levels of possible impact that are determined by amplifying factors related, for example, to the material condition, inadequate post-event drying or treatment, or the level of floodwater contamination, according to the descriptions presented in Table 2.

Table 2: Effects of exposure to flood water for some of the most commonly found materials in Portuguese churches.

Material	Description
Stone	- Different types of stone can behave differently under the actions of flooding, depending on their softening coefficient and hydric expansion. - The susceptibility of most common types of stone to flooding is generally low. - Negative impacts can increase if walls are not properly treated and dried after an event, if they are in poor state of conservation, or due to harsh weather conditions.
Concrete	- Concrete is not particularly vulnerable to flooding. - Concrete floors may take a long time to dry if appropriate actions are not taken.
Earth construction	- Unbaked earth-wall constructions are particularly vulnerable to water damage, especially if external plaster finishes that may exist are not well maintained.
Timber and woodwork	- Wood generally presents high values of hydric expansion and may swell and distort when wet. It is also vulnerable to fungal and insect infestations, causing rot. - Issues with wood may be minimized if appropriate action is taken following a flood event, and wood is properly ventilated and dried. This is especially true for sound structural timber. - Floorboards and other elements that can buckle require specific post-flood measures.
Metalwork	- Aluminium, bronze, copper and brass objects will not be damaged by immersion in water as long as they are allowed to dry quickly. Iron and steel may rust and expand, but damage can be limited through quick drying.
Wall paintings	- Historic wall paintings, including frescoes, may be damaged by salt crystallisation, paint flaking or mould growth, particularly if an inadequate drying procedure is adopted.
Book paper	- Paper is highly vulnerable to water and requires swift and appropriate post-event recovery actions to prevent destruction. Negative consequences can include rapid development of mould, physical damage, and bleeding of soluble inks and colorants. - Even if treated adequately (which requires expert knowledge), wet books and records generally cannot be fully restored to their pre-damage condition. - Contaminated water can exacerbate the negative impacts of floodwater on paper.

Table 2: Effects of exposure to flood water for some of the most commonly found materials in Portuguese churches (continued).

Paintings on canvas	- Exposure to water can cause immediate damage to most paintings, as well as make the artwork more susceptible to short or long-term damage. Appropriate drying is required to reduce negative impacts. - Water can lead to flaking and loss of image layers, as well as expansion, shrinkage and subsequent deformation of painting supports.
Textiles	- Textiles can present significant variations that determine if and how they can be salvaged after a flood. Damaged textiles can present colour change, bleeding of dyes, shrinkage, watermarks from migrating finishes, and mould. - Certain contaminants will require textiles to be discarded.

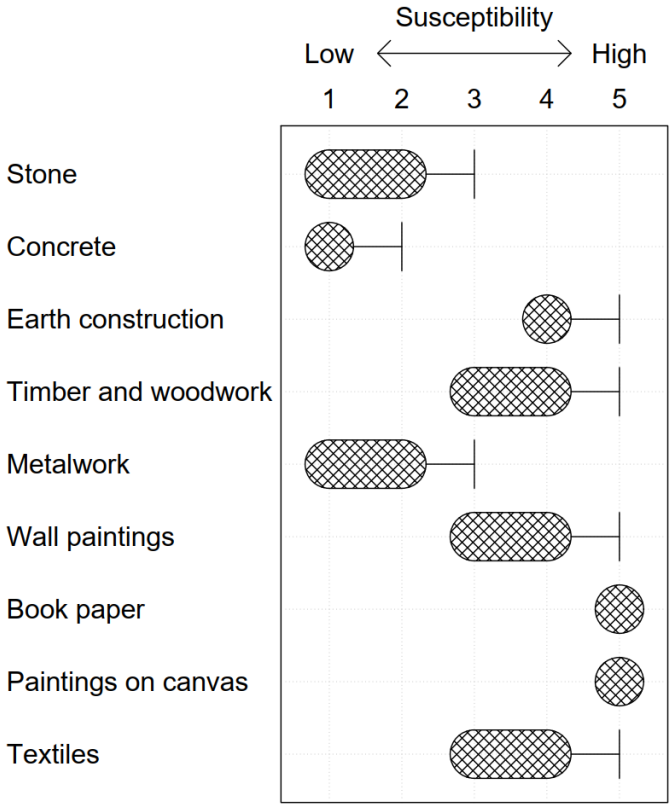


Figure 1: Examples of flood susceptibility indices considered for some materials.

2.3 Definition of the flood vulnerability function

The vulnerability function for a cultural heritage asset can then be defined as a function of the value, susceptibility, and elevation of its components. Given that values and impacts cannot be expressed in absolute terms, the vulnerability function should quantify impacts in relative terms, i.e. as a fraction of the overall cultural value of an asset (which should be defined independently of the quantification of vulnerability, based for example on its listed status). In order to achieve this, a normalization of the above indices is required. The value indices of the asset's components should be scaled such that they sum to one. In this way, the resulting values

will represent the fraction that each component is estimated to contribute to the overall value of the cultural heritage asset. The susceptibility indices should be scaled such that 'no damage' corresponds to 0, while 'damage that is not fully repairable' corresponds to 1. The vulnerability function is then obtained through a what-if analysis, based on a simulated step-by-step inundation of the asset, and in the evaluation of the corresponding damage based on the features described before. The level of damage at each step is given by

$$f(x) = \sum_i g(x) v_i s_i \tag{1}$$

with

$$g(x) = \begin{cases} 1 & if\ x \geq h_i \\ 0 & if\ x < h_i \end{cases} \tag{2}$$

where x is the water depth, i represents each component of the cultural heritage asset, h_i is the height at which the component is located above a reference level (typically the external ground floor level, from which the water depth is also measured), and v_i and h_i are their value and susceptibility indices, respectively.

3 CASE STUDY

3.1 Description

The case study adopted to illustrate the proposed framework is the Igreja da Misericórdia de Esposende (Figure 2), a church located in the municipality of Esposende, in northern Portugal. The church dates back to the end of the 16th century, having received a number of interventions over the centuries, and comprises mannerist, baroque and neoclassical architectural styles. Despite its relatively small size, it contains a very interesting and coherent set of works of art, and is listed as a building of public interest [13, 14].



Figure 2: Main façade of the church.

Based on to the hazard maps developed for Portugal within the scope of the European Floods Directive [15], the church is located within the extents of high-probability flood scenarios, and the water depth associated with an extreme scenario of 1000-year return period (considered herein as the maximum achievable water depth) is 1.38m (Figure 3).

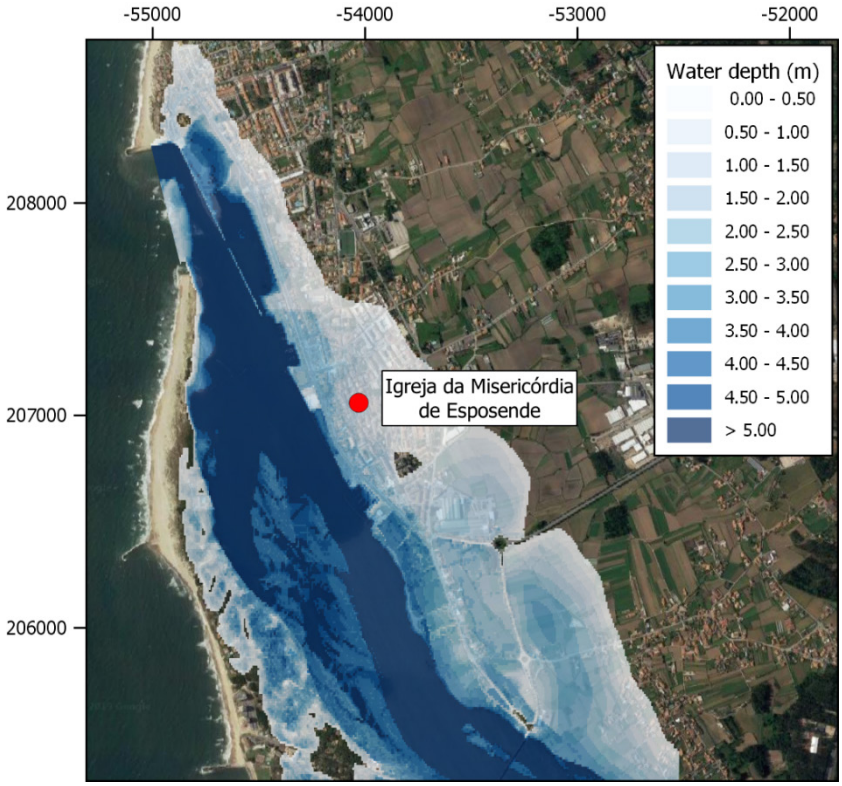


Figure 3: Location of the case study church (Igreja da Misericórdia de Esposende) and hazard map showing water depths for the 1000-year return period flood scenario (CRS: ETRS89 / Portugal TM06).

3.2 Vulnerability assessment results

The church was surveyed by the authors on 3 January 2020 following the general procedure described in Section 2. A detailed inventory was developed for the ground floor only (shown in Figure 4), given that the uppers floors are above the maximum flood level. Still, the entire church was surveyed in order to establish the relative value of the floodable components.

The inventory comprises both building and contents; it includes a total of 79 components and component assemblies, together with their materials, heights from the reference level, and information on whether they are moveable. The latter allows establishing two separate vulnerability functions that consider scenarios with and without the preventive evacuation of moveable items. Three indices of value (1, 3 and 10) were considered for assets with low, substantial, and exceptional significance, respectively. Table 3 presents the inventory referring to the contents of the main chapel, and a photograph of this part of the church is shown in Figure 5. For brevity, only this part of the inventory is presented herein. Finally, the obtained vulnerability function is presented in Figure 6.

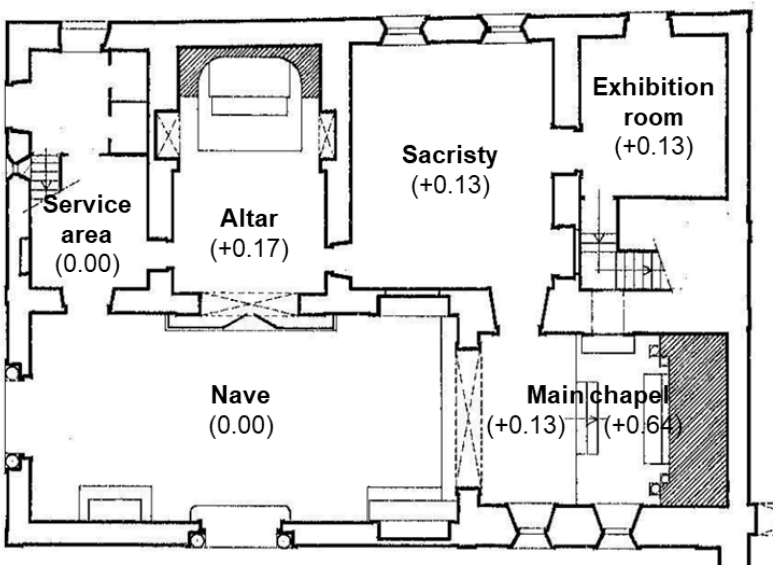


Figure 4: Ground floor plan.

Table 3: Inventory of contents of the main chapel.

Component	Move-able	Material family	Material	Height (m)	Value index	Suscept. index
Plinths (set of 2)		Stone	Granite	0.13	1	1
Statue	✓	Wood	Polychromed wood	1.02	3	4
Statue	✓	Wood	Polychromed wood	1.02	3	4
Kneeling benches (set of 2)	✓	Wood	Blackwood	0.13	1	4
Altar table		Wood	Gilded woodcarving	0.64	3	4
Pulpit	✓	Wood	Gilded woodcarving	0.69	3	4
Altar		Wood	Gilded woodcarving	1.29	3	4
Statue	✓	Wood	Polychromed wood	1.64	10	4
Main altar		Wood	Gilded woodcarving	0.64	10	4
Main retable		Wood	Gilded woodcarving	0.64	10	4
Painting		Canvas	Painting on canvas	2.49	10	5
Candlesticks (set of 2)	✓	Wood	Gilded woodcarving	1.84	1	4
Candlesticks (set of 2)	✓	Metal	Brass	1.84	1	2
Jugs (set of 2)	✓	Ceramic	Porcelain	1.84	1	5
Individual benches (set of 4)	✓	Wood	Blackwood	0.64	1	4
Altar side table	✓	Wood	Gilded woodcarving	0.64	3	4
Chair	✓	Wood	Upholstered blackwood	0.64	1	4



Figure 5: Photograph of the main chapel.

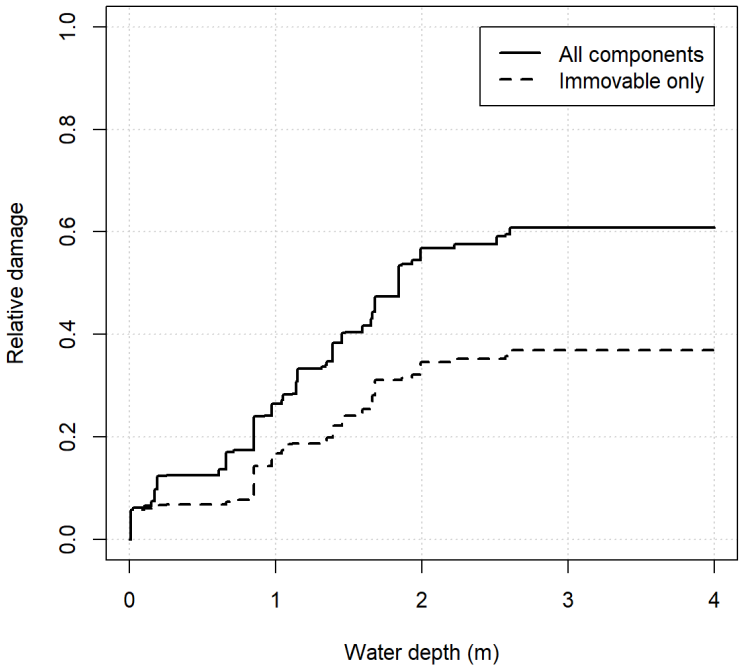


Figure 6: Vulnerability function for Igreja da Misericórdia de Esposende.

4 DISCUSSION

This paper has illustrated a new framework to model the flood vulnerability of cultural heritage assets based on a component-by-component analysis. The main objective of this framework is to provide a vulnerability analysis for risk assessment studies that aim to determine and compare levels of risk among cultural heritage assets, supporting the implementation of risk management plans at a detailed level. Although this inevitably requires site-specific surveying, the framework has been designed to achieve an adequate balance between simplicity and accuracy. Nevertheless, the framework may still be expanded to account for other flood properties besides water depth, such as flood duration and flow velocity, which may be relevant for certain building components.

In this study, the proposed vulnerability modelling framework was showcased for a church in northern Portugal, demonstrating its applicability. Further research will include applications to other churches in order to perform a comparative analysis of risk levels. This is also expected to provide insights about the practicability of aggregating asset-specific vulnerability functions in order to derive functions for asset classes with similar characteristics and quantify the associated uncertainty.

Acknowledgements. The authors would like to thank Câmara Municipal de Esposende and Santa Casa da Misericórdia de Esposende for their availability. This work was financially supported by: Project POCI-01-0145-FEDER-030469 - RIACT - Risk Indicators for the Analysis of Cultural heritage under Threat, funded by FEDER through COMPETE2020 - Programa Operacional Competitividade e Internacionalização (POCI) and by national funds through FCT - Fundação para a Ciência e a Tecnologia; and by Base Funding - UIDB/04708/2020 of CONSTRUCT - Instituto de I&D em Estruturas e Construções, funded by national funds through FCT/MCTES (PIDDAC).

REFERENCES

[1] Figueiredo, R., Romão, X., Paupério, E., Flood risk assessment of cultural heritage at large spatial scales: Framework and application to mainland Portugal. *J. Cult. Herit.* 2019.

[2] Stephenson, V., D'Ayala, D., A new approach to flood vulnerability assessment for historic buildings in England. *Nat. Hazards Earth Syst. Sci.* 2014, *14*, 1035–1048.

[3] Siedel, H., Historic building stones and flooding: Changes of physical properties due to water saturation. *J. Perform. Constr. Facil.* 2010, *24*, 452–461.

[4] English Heritage, Flooding and Historic Buildings. 2015.

[5] Štulc, J., The 2002 Floods in the Czech Republic and their Impact on Built Heritage. *Herit. Risk* 2008, 133–138.

[6] Drdácký, M.F., Flood Damage to Historic Buildings and Structures. *J. Perform. Constr. Facil.* 2010, *24*, 439–445.

[7] Boinas Dias, A.R., Análise de risco de cheia: desenvolvimento de um modelo aplicado ao Património Nacional, Universidade do Porto, 2014.

[8] Northeast Document Conservation Center, Emergency Salvage of Wet Books and

Records. 2019.

[9] Ray, E., The Prague library floods of 2002: Crisis and experimentation. *Libr. Cult. Rec.* 2006, *41*, 381–391.

[10] Klempan, B., Emergency Treatment of Water-damaged Paintings on Canvas – Canadian Conservation Institute (CCI) Notes 10/5, 2017.

[11] Braaten, A., Flood-damaged Textiles: What to Salvage and How to Clean, North Dakota State University, 2009.

[12] Kirby, S., Hammett, W., Cleaning Flooded Upholstered Furniture, Curtains, Bedding, Table Linens and Other Household Textiles, North Carolina State University, 2014.

[13] Afonso, J.F., Martins, S., Rodrigues, R., Calvo, A., et al., Uma Confraria do Mar: A Misericórdia de Esposende entre os Séculos XVI e XIX, Câmara Municipal de Esposende / Santa Casa da Misericórdia de Esposende, 2014.

[14] Direção-Geral do Património Cultural, SIPA – Sistema de Informação para o Património Arquitetónico. 2019.

[15] Brandão, C., Saramago, M.M., Ferreira, T., Cunha, S., et al., Elaboração de Cartografia Especifica sobre Risco de Inundação para Portugal Continental. 2014.

12th International Conference on Structural Analysis of Historical Constructions
SAHC 2020
P. Roca, L. Pelà and C. Molins (Eds.)

ASSESSING THE IMPACT OF SEISMIC RISK MITIGATION AT THE URBAN SCALE ON COMMUNITY RESILIENCE AND HOUSING RECOVERY

A. BASAGLIA[1*], A. APRILE[2], E. SPACONE[1] AND L. PELÀ[3]

[1] Department of Engineering and Geology (INGEO)
University "G. D'Annunzio" of Chieti-Pescara
Viale Pindaro 42, 65127 Pescara, Italy
Email: {alberto.basaglia*, enrico.spacone}@unich.it, www.ingeo.unich.it (*corresponding author)

[2] Department of Engineering
University of Ferrara
Via Saragat 1, 44122 Ferrara, Italy
email: alessandra.aprile@unife.it, www.de.unife.it

[3] Department of Civil and Environmental Engineering
Universitat Politècnica de Catalunya (UPC-BarcelonaTech)
Campus Nord, Carrer de Jordi Girona, 1, 3, 08034 Barcelona, Spain
Email: luca.pela@upc.edu - Web page: http://www.upc.edu

Keywords: Community Resilience, Housing Recovery, Seismic Risk, Risk Mitigation

Abstract. *European historical city centers are particularly prone to natural disasters. This is due to the fragility of structures that often times do not comply with seismic codes; the high constructions' density that causes induced damage; and the historical relevance of buildings that makes difficult the enacting of mitigation strategies.*

In Italy, major earthquake caused extensive damages over the last century. Seismic events have a huge impact on the nation's economy growth due to direct and indirect impacts, such as for example the high reconstruction costs or the business interruption spread out over a long period, respectively. In addition, the duration of recovery can affect the population wellbeing and cause permanent displacement. For this reason, the preventive planning of disaster management strategies are crucial to mitigate the damage and enhance resilience. Proposed strategies have to be effective and economically sustainable.

In this paper, two towns affected by the 2012 Northern Italy Earthquake are chosen to analyze the reconstruction process. Using information published on the town journal, relevant aspects of the community resilience are highlighted. In particular, the housing recovery, i.e. the return of displaced people to a permanent housing solution is investigated.

Then, a suite of seismic mitigation strategies is proposed for both cities, taking into account the peculiarity of the built environment and the damage distribution available thanks to the post-event buildings' inspection. The effectiveness of the proposed strategies is assessed through a cost-benefit analysis, highlighting optimal solutions to reduce the economic and social losses.

1 INTRODUCTION

Major earthquakes are among the deadliest and costliest natural disasters both worldwide [1] and in Europe [2] in the past decades. In Italy, four major seismic sequences occurred since 2009 (L'Aquila 2009, Northern Italy 2012, Central Italy 2016-2017 and Ischia 2017) causing more than 650 casualties and injuring almost 2400 people [3,4,5,6].

The high social impact can be associated to the high vulnerability of the built environment. In fact, the first seismic zonation map, i.e. the identification of the potential seismic hazard and probability of occurrence, covering the entire Italian territory was developed only in 2003 [7] and adopted in the Design Code of 2008 [8]. On the other hand, the vast majority of buildings were designed pre-2003 and therefore without following earthquake-resistant design (ERD) concepts, see Figure 1 [9].

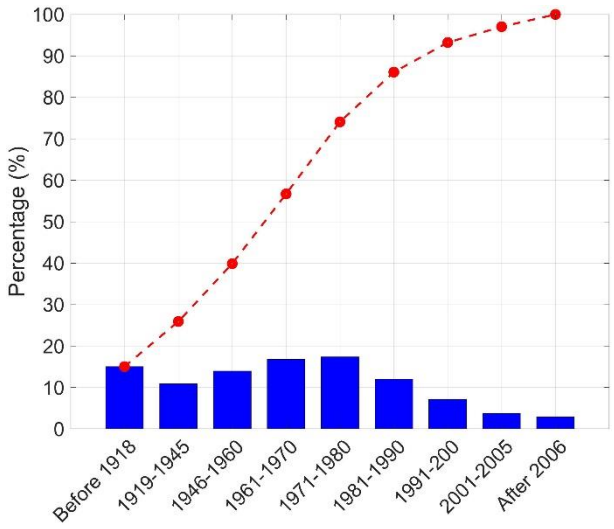


Figure 1. Percentage of Italian buildings per construction period (blue bar) and their comulative sum (red line).

This vulnerability led to significant direct and indirect losses in the occurrence of major earthquakes. Direct losses include the repair and reconstruction costs [10,11], while indirect losses may be referred to the business interruption [12] and the cost of providing temporary housing for the people displaced [13].

In particular, when people are displaced from their home, two different solutions are generally adopted: they are provided with a temporary shelter, called PMAR (*Prefabricated Adaptable and Movable Residences*), or they are given a monetary contribution called CAS (*Contribution for Accommodation Self-determined*) in case they decide to independently find a housing solution. These housing solutions are defined as "temporary", even if they may last for several years, affecting the population wellbeing, causing identity loss [14] or, in extreme cases, the depopulation [15].

All the aforementioned aspects highlight the need of preventive seismic risk mitigation strategies at the urban scale, in order to reduce the socio-economic impact of earthquakes. Recently, the Italian Government issued a tax break called *SismaBonus* [16] up to 85% in 10 years of the cost invested by owners of houses or flats in increasing the seismic performance of the buildings they live in. To easily quantify the actual and target seismic performance of

buildings, guidelines have been introduced that classify buildings into seven classes depending on a safety index $IS-V$ [17], see Table 1. $IS-V$ is evaluated by performing structural analyses according to the Code provisions [18].

Table 1. Risk classification depending on the Safety Index IS-V.

Safety Index	IS-V Class
100% < IS-V	$A^{+}_{IS\text{-}V}$
80% ≤ IS-V < 100%	$A_{IS\text{-}V}$
60% ≤ IS-V < 80%	$B_{IS\text{-}V}$
45% ≤ IS-V < 60%	$C_{IS\text{-}V}$
30% ≤ IS-V < 45%	$D_{IS\text{-}V}$
15% ≤ IS-V < 30%	$E_{IS\text{-}V}$
IS-V < 15%	$F_{IS\text{-}V}$

In this paper, the recovery process of two cities affected by the 2012 Northern Italy earthquake (NIE) is presented. Data are collected through the cities' municipal journal. Then, the effect of preventive seismic mitigation strategies is investigated thanks to the post-seismic buildings' inspection. A cost-benefit analysis is performed considering both socio-economic losses.

2 DOCUMENTING THE HOUSING RECOVERY

Two major seismic events hit the Emilia Romagna Region, Northern Italy on May 20th May 29th, 2012. These earthquakes caused 27 fatalities, injured approximately 400 people and left almost 15000 homeless [19,20]. The high number of people displaced required the Civil Protection Agency to provide PMARs, see Figure 2, or assign CASs so that temporary housing solutions could be found.



Figure 2. PMARs installed after the 2012 NIE.

The area affected by the NIE is highly industrialized and it is reasonable to assume that this aspect significantly contributed to the disaster recovery, as people were able to retain their job. Yet, one of the most important aspects for the recovery is the return to their pre-event home or a permanent housing solution. This is generally referred to as *housing recovery* [13]. Few studies have already evaluated the trend of people living in a PMAR or being assigned a CAS.

For example, Mannella et al. (2017) [21] analyzed the evolution of people displaced after the 2009 L'Aquila earthquake until the end of 2016. Then, Carnelli and Frigerio (2017) [22] studied the number and social indicators of people living in PMARs in the city of Mirandola until mid-2016. It is worth noting that, even considering a time span of seven years, the full recovery was not observed, meaning that the issue of people displaced by major earthquakes may last for a very long time after the event.

In this study, the housing recovery of Concordia sulla Secchia and Mirandola, two cities affected by the 2012 NIE is documented. Data are collected through the municipal journals, the "Concordia Comune" [23] and "Indicatore Mirandolese" [24], see Figure 3, which are freely accessible online.



Figure 3. First issue of the (left) Concordia Comune and (right) Indicatore Mirandolese after the 2012 NIE.

The housing recovery is associated to the number of people either living in a PMAR or being assigned a CAS. No information was found on the number of people staying in a hotel and similar lodging establishments or that decided to move out from the city, and therefore are not included in the study. Results are shown in Figure 4.

After the 2012 NIE occurrence, in the city of Concordia sulla Secchia slightly less than three hundred people (94 households) lived in a PMAR and almost nineteen hundred people (756 households) were assigned a CAS. In the city of Mirandola, the number of homeless was significantly higher, as almost a thousand people (286 households) lived in a PMAR and slightly less than 7500 people (2964 households) were assigned a CAS. In 2017, approximately five years after the NIE, all households living in a PMAR in both cities had returned to a permanent housing solution. On the other hand, 13% and 7% of people displaced were still assigned a CAS in Concordia sulla Secchia and Mirandola, respectively. These findings highlight the very long process of housing recovery that may take several years, causing distress in the population and affecting the community *resilience*, i.e. the return to the pre-event performance [25].

It is worth noting that, despite these data are considered reliable given that they are provided by a journal issued by the municipality itself, they are scattered throughout the years, making it difficult to understand the trends.

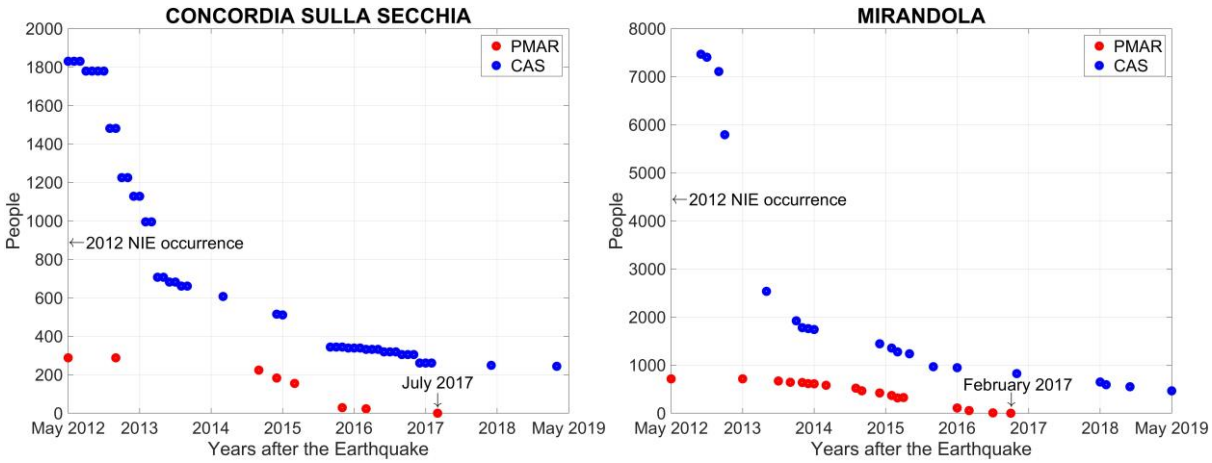


Figure 4. Housing recovery for (left) Concordia sulla Secchia and (right) Mirandola after the 2012 NIE.

Very few information are available regarding the cost of PMARs and CAS. A report states that each PMAR cost approximately 26.000€ [26] while another puts the cost at 125.000€ [24], probably including the money needed for the land expropriation and PMAR installation. Regarding the CAS, some information is drawn again from the municipal journal "Concordia Comune" [22], see Table 2. From 2012 to 2018, more than 6 million Euros have been assigned to the people displaced, with a monthly contribution of approximately 400€ per households.

Table 2. CAS contribution for Concordia sulla Secchia between 2012 and 2018.

Period	CAS [€]	No. Households
May - July 2012	545737	756
August - November 2012	1458690	735
December 2012 - January 2013	651074	612
February - March 2013	546177	506
April - May 2013	497894	466
June - July 2013	411320	411
August - September 2013	322162	292
October - November 2013	309440	282
December - January 2014	299510	273
February - May 2014	441800	194
January - March 2016	120168	142
April - June 2016	119782	140
July - September 2016	117950	137
October - December 2016	114891	132
January - March 2017	108920	126
April - June 2017	96873	108
July - September 2017	86341	105
October - December 2018	71709	101

3 SEISMIC RISK MITIGATION AT THE URBAN SCALE

Given the high impact that major earthquakes have on affected communities, that require several years to recover and have significant associated losses, preventive seismic mitigation strategies become crucial. These strategies have to be effective but also economically sustainable.

As for early 2020, 140.6 and 470.5 million Euros have been assigned for the repair and reconstruction of residential buildings in the city of Concordia sulla Secchia and Mirandola, respectively [27]. Considering the total area of buildings, it leads to an investment of approximately 1500€/m^2 to rebuild or retrofit a structure up to the current Code provision in terms or ERD concepts (class $A_{IS\text{-}V}$ of Table 1). However, for existing buildings that were designed without ERD concepts, the seismic retrofit may not be the optimal solutions in monetary terms. For example, installing bond-beams and/or tied rods to guarantee the box-like behavior of unreinforced masonry (URM) buildings or preventing the shear failure of reinforced concrete (RC) columns with fiber-reinforced polymers may prevent collapse and therefore guarantee a sufficient safety level. This concept can be referred to as *class upgrade* (CU). A CU raise the considered building up a $IS-V$ class and it therefore is expected to undergo a lower damage in the occurrence of an earthquake. Considering the five damage levels defined in the European Macroseismic Scale (EMS-98) [28], CUs are described in Table 3.

Table 3. Summary and description of the considered class upgrades for buildings.

Class Upgrade	IS-V Class	Expected Damage	Example
CU 1	$E_{IS\text{-}V} \rightarrow D_{IS\text{-}V}$	D5 → D4	URM: Reinforced injections and crack repair [29] RC: Concrete cover restoration and crack repair [30]
CU 2	$D_{IS\text{-}V} \rightarrow C_{IS\text{-}V}$	D4 → D3	URM: Application of bond-beams or tie rods [31] RC: FRP wrapping [32] and ETS application [33,34]
CU 3	$C_{IS\text{-}V} \rightarrow B_{IS\text{-}V}$	D3 → D2	URM: Wall-to-wall connection with steel frame RC: Infill walls strengthening [35]
CU 4	$B_{IS\text{-}V} \rightarrow A_{IS\text{-}V}$	D2 → D1	URM: Reduction of in-plan slab flexibility RC: Reduction of in-plan slab flexibility
CU 5	$A_{IS\text{-}V} \rightarrow A^{+}_{IS\text{-}V}$	D1 → D0	URM: Walls reinforcement with TRM [35] RC: Introduction of new resistant system [36]

Damage level D5 is associated to complete collapse and D0 is associated to no damage. Class $F_{IS\text{-}V}$ of Table 1 is not considered as the very poor seismic performance makes it unfeasible to undertake any strengthening work.

For each CU, a nominal cost of 300€/m^2 is assumed based on the Authors' professional experience. Information about the buildings' construction type, floor area and observed damage are available thanks to the Da.D.O. (*Database of Damage Observed*) online database [37] that collects data about the post-event inspections that assess the damage and evaluate the accessibility. Only URM and RC buildings are considered, as they represent almost the entirety of the sample. The structural type and damage distributions for Concordia sulla Secchia and Mirandola are shown in Figure 5.

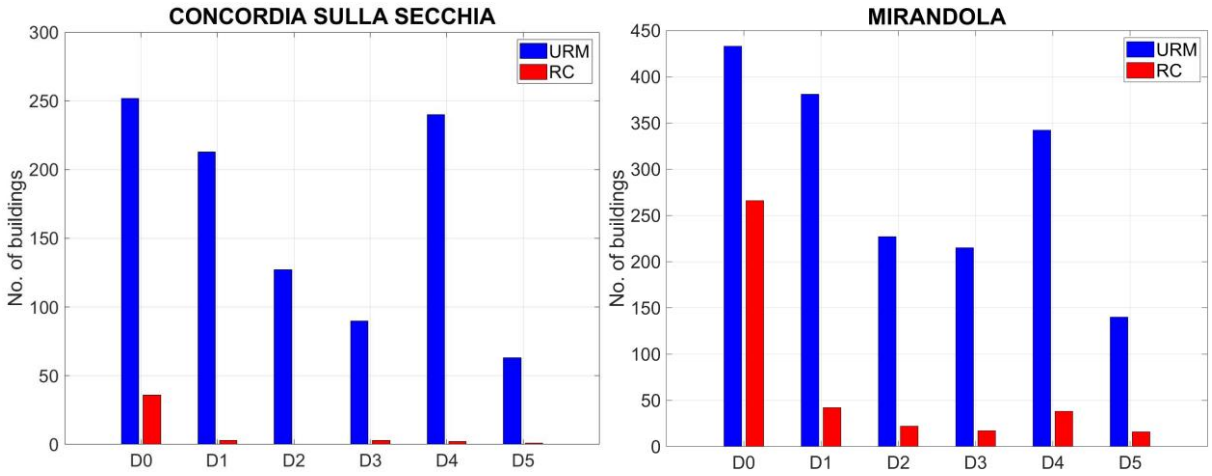


Figure 5. Structural type and damage distribution for (left) Concordia sulla Secchia and (right) Mirandola.

Repair and replacement cost are assumed based on a recent study about the reconstruction after the 2009 L'Aquila earthquakes [38] and are defined for five damage levels, see Table 4.

Table 4. Assumed repair and replacement costs.

Damage Level	Repair/replacement cost [€/m²]
D1	27
D2	135
D3	405
D4	810
D5	1350

A cost-benefit analysis of seismic mitigation strategies is performed for Concordia sulla Secchia and Mirandola by considering the five CUs described in Table 3. At first, only most damages buildings are reinforced and the cost of a preventive strengthening is compared with that of the repair and replacement costs. The analysis is carried on until all buildings have been retrofit so that they are expected not to undergo any damage in the occurrence of an event similar to the NIE. Results of the analysis are shown in Figure 6.

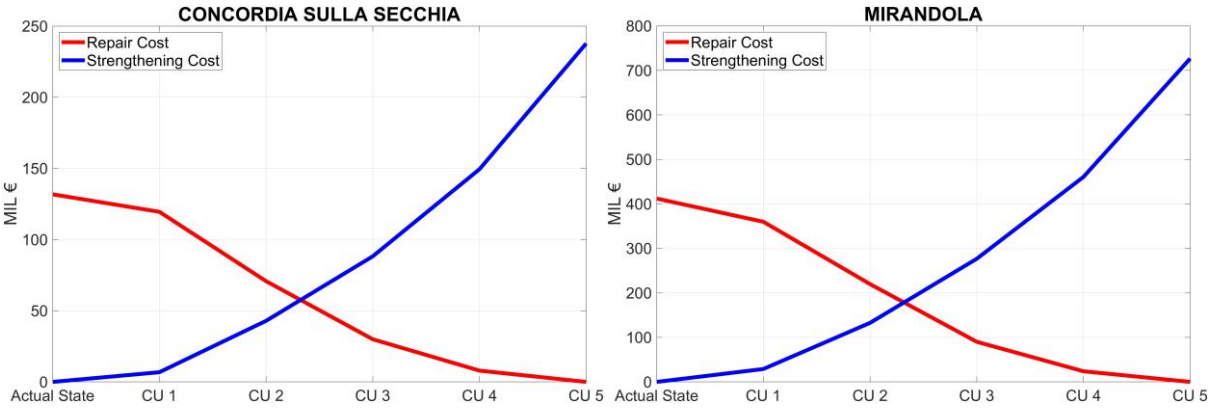


Figure 6. Cost-benefit analysis of various CUs for (left) Concordia sulla Secchia and (right) Mirandola.

Obtained results show that the optimal solution (the point where the strengthening and the repair cost curves meet) is between the 2nd and 3rd CU. In terms of $IS-V$ Class, the optimal solution is between class $C_{IS\text{-}V}$ (45% ≤ IS-V < 60%) and $B_{IS\text{-}V}$ (60% ≤ IS-V < 80%). These findings are in line with provisions of Italian Guidelines [39] that suggest for existing buildings to adopt strengthening works that allow them to withstand up to 60% of the expected seismic actions.

In addition, it is noted that estimated repair and replacement costs for residential buildings of Concordia sulla Secchia and Mirandola, obtained with values of Table 4, are comparable to those actually assigned [27], see Table 5.

Table 5. Comparison between estimated and assigned repair and replacement costs for Concordia sulla Secchia and Mirandola.

City	Estimated repair and replacement costs [MIL €]	Assigned repair and replacement costs [MIL €]
Concordia sulla Secchia	131.8	140.6
Mirandola	412	470.5

The positive effect of seismic mitigation strategies is assessed also in terms of the social impact. In particular, the expected number of injuries and fatalities is evaluated for the same CUs of Figure 6. The casualty estimation is performed using the approach defined by Zuccaro and Cacace (2012) [40]. Results are shown in Figure 7.

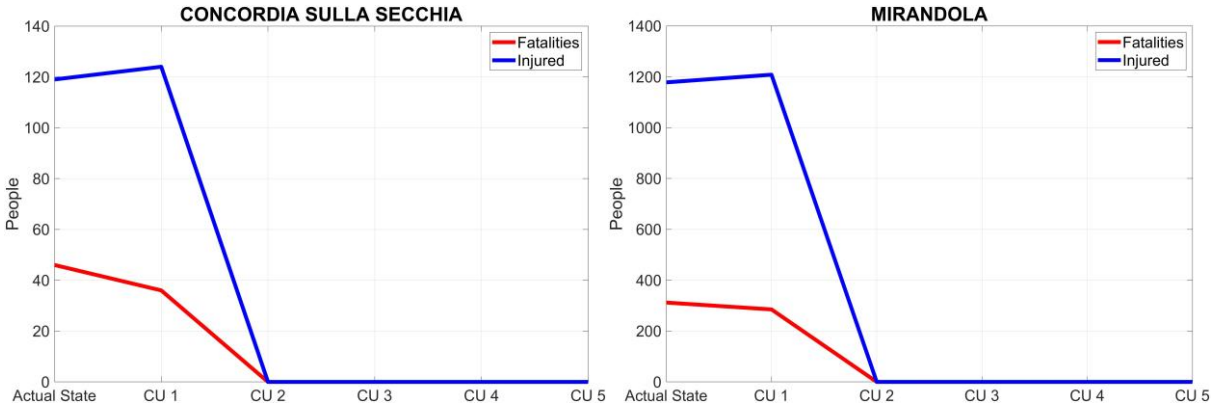


Figure 7. Injuries and fatalities estimation for (left) Concordia sulla Secchia and (right) Mirandola.

Obtained results show that with 2 CUs an event similar to the 2012 NIE is expected not to cause any injury or fatality. These findings further support those obtained with the cost-benefit analysis in Figure 6.

4 SUMMARY AND CONCLUSIONS

In this paper, the benefit of preventive seismic mitigation strategies at the urban scale is presented and evaluated. In Italy, these strategies are crucial due to the age of the built environment, that in most cases is not designed following ERD concepts and therefore may undergo significant damage event with earthquakes of moderate intensities.

Damage is considered in terms of both social and economic losses. Social losses include loss of lives and injuries, but also the people displaced who are in need of a new housing solution. In particular, people displaced may need several years to return to a permanent home, with consequences on their wellbeing and the overall community resilience. Economic losses include both the repair and replacement costs and the business interruption. In order to reduce losses, preventive mitigation strategies have to be implemented. These could range from localized strengthening works to a complete retrofit.

This paper presented a data collection of the housing recovery of two cities affected by the 2012 NIE thanks to the information included in the municipal journals. It is observed that, more than seven years after the earthquake, a considerable portion of the population hasn't returned to a permanent housing solutions yet.

Then, the concept of class upgrade is introduced and used to perform a cost-benefit analysis of a suite of mitigation strategies. By comparing the strengthening and the repair and replacement costs, the optimal solutions is found. This solution is in line with the current Code provision for existing buildings and may be used to enact policies at the Stakeholders' level to promote a "culture of mitigation". A significant contribution in this way is given by the recently introduced *SismaBonus*, a tax break in 10 years for the seismic strengthening of residential buildings that could make the work more affordable. For this reason, the use of risk assessment methods at the urban scale [41] is crucial to clearly identify the more vulnerable areas of a city and in this way prioritize the strengthening works.

Acknowledgements. This work was supported by the University Fund for Research (FAR) program of the University of Ferrara, 2015, "Historical Centers Livable and Sustainable" (HC-LIVE)" and by the scholarship of the University "G. D'Annunzio" Chieti-Pescara, 2019, "Risk Assessment of the Built Heritage at the Urban Scale" (Ref. Num. 0002299). The fourth Author would like to acknowledge the Ministry of Science, Innovation and Universities (MCIU) of the Spanish Government, the State Agency of Research (AEI), and the European Regional Development Fund (ERDF) through the SEVERUS project (Multilevel evaluation of seismic vulnerability and risk mitigation of masonry buildings in resilient historical urban centres, Ref. Num. RTI2018-099589-B-I00).

REFERENCES

[1] CRED. Natural disasters 2018. An opportunity to prepare. Available at: https://www.cred.be/sites/default/files/CREDNaturalDisaster2018.pdf (2019).

[2] PreventionWeb. Europe - Disaster Statistics. Region Profile for Natural Disasters from 1980 – 2008. Available at: https://www.preventionweb.net/english/countries/statistics/index_region.php?rid=3 (2008).

[3] Alexander, D. and Magni, M. Mortality in the L'Aquila (central Italy) earthquake of 6 April 2009. *PLoS Curr* (2013) **5**:e50585b8e6efd1.

[4] Mucciarelli, M., and Liberatore, D. Guest editorial: the Emilia 2012 earthquakes, Italy. *Bull Earthq Eng* (2014) **12**:2111-2116.

[5] Fiorentino, G., Forte, A., Pagano, E., Sabetta, F., Baggio, C., Lavorato, D., Nuti, C. and Santini S. Damage patterns in the town of Amatrice after August 24th 2016 Central Italy earthquakes. *Bull Earthq Eng* (2018) **16**:1399-1423.

[6] Briseghella, B., Demartino, C., Fiore, A., Nuti, C., Sulpizio, C., Vanzi, I., Lavorato, D. and

Fiorentino, G. Preliminary data and field observations of the 21st August 2017 Ischia earthquake. *Bull Earth Eng* (2019) **17**:1221–1256.
[7] Bellicoso, A. Italian Anti-Seismic Legislation and Building Restoration. *Int Journal for Housing Science* (2011) 35: 137-147.
[8] Ministero delle Infrastrutture e dei Trasporti. Norme Tecniche per le Costruzioni. *Gazzetta Ufficiale* (2008) **29**. Italian.
[9] Istat. Edifici residenziali. *Istituto Nazionale di Statistica* (2011). Available at: https://www.istat.it/. Italian.
[10] Di Giacomo, M. I costi dei terremoti in Italia. Centro Studi Consiglio Nazionale Ingegneri (2014). Italian.
[11] Ufficio Valutazione Impatto. Terremoti. L'Aquila, Reggio-Emilia, Centro Italia: politiche e risorse per ricostruire il Paese. *Senato della Repubblica* (2017). Italian.
[12] Rose, A. Defining and measuring economic resilience to disasters. *Disaster Prevention and Management* (2004) **13**: 307-314.
[13] Peacock, W.G., Dash, N., Zhang, Y. and Van Zandt, S. Post-Disaster Sheltering, Temporary Housing and Permanent Housing Recovery. In: H. Rodríguez et al. (Eds): *Handbook of Disaster Research*. Springer, Cham (2018), pp. 569-594.
[14] Giuliani, A.R., Mattei, A., Santilli, F. Well-Being and Perceived Quality of Life in Elderly People Displaced After the Earthquake in L'Aquila, Italy. *J Community Health* (2014) 39: 531–537.
[15] Di Giovanni, G. and Chelleri, L. Why and how to build back better in shrinking territories? *Disaster Prevention and Management* (2019) **28**: 460-473.
[16] Agenzia delle Entrate. Sisma Bonus: Le Detrazioni Per Gli Interventi Antisismici. Available at: https://www.agenziaentrate.gov.it/ (2019). Italian.
[17] Ministero delle Infrastrutture e dei Trasporti. Linee Guida Per La Classificazione Del Rischio Sismico Delle Costruzioni. *Decreto Ministeriale* (2017) **65**. Italian.
[18] Ministero delle Infrastrutture e dei Trasporti. Aggiornamento delle «Norme Tecniche per le Costruzioni». *Gazzetta Ufficiale* (2018) 42. Italian
[19] Rossetto, T., Alexander, D., Verrucci, E., Ioannou, I., Borg, R., Melo, J., Cahill, B. and Kongar, I. The 20th May 2012 Emilia Romagna earthquake (2012) *EPICentre Field observation report*.
[20] Ioannou, I., Borg, R., Novelli, V., Melo, J., Alexander, D., Kongar, I., Verrucci, E., Cahill, B. and Rossetto, T. The 29th May 2012 Emilia Romagna earthquake (2012) *EPICentre Field observation report.*
[21] Mannella, A., Di Ludovico, M., Sabino, A., Prota, A., Dolce, M. and Manfredi, G. Analysis of the population assistance and returning home in the reconstruction process of the 2009 L'Aquila earthquake. *Sustainability* (2017) **9**: 1395.
[22] Carnelli, F. and Frigerio, I. A socio-spatial vulnerability assessment for disaster management: Insights from the 2012 Emilia earthquake (Italy). *Sociologia urbana e rurale* (2016) **11**: 22-44.
[23] Municipality of Concordia sulla Secchia. Concordia Comune. Available at: https://www.comune.concordia.mo.it/. Italian.
[24] Municipality of Mirandola. Indicatore Mirandolese. Available at: http://www.comune.mirandola.mo.it/. Italian.
[25] Bruneau, M., Chang, S.E., Eguchi, R.T., Lee, G.C. et al. A framework to quantitatively

assess and enhance the seismic resilience of communities. *Earthquake spectra* (2003) **19**: 733-752.
[26] Battista C. Ricostruzione, ecco quanto costano i moduli abitativi provvisori. *ModenaToday* (2013). Available at: http://www.modenatoday.it/. Italian.
[27] Regione Emilia-Romagna. Open Ricostruzione. Monitora gli interventi per la ricostruzione in Emilia-Romagna. Available at: https://openricostruzione.regione.emilia-romagna.it/.
[28] Grünthal, G. European Macroseismic Scale 1998. *Cahiers du Centre Européen de Géodynamique et de Séismologie* (1998) **15**.
[29] Modena, C., Valluzzi, M.R., da Porto, F. and Casarin, F. Structural Aspects of The Conservation of Historic Masonry Constructions in Seismic Areas: Remedial Measures and Emergency Actions. *Int Jour of Architectural Heritage* (2001) **5**: 539-558.
[30] Biondini, F., Camnasio, E. and Titi, A. Seismic resilience of concrete structures under corrosion. *Earthquake Engng Struct Dyn* (2015) **44**: 2445-2466.
[31] Frumento, S., Giovinazzi, S., Lagomarsino, S. and Podestà, S. Seismic retrofitting of unreinforced masonry buildings in Italy. In: *Proceedings of the 2006 NZSEE Conference* (2006), Napier, New Zealand.
[32] Perrone, M., Barros, J.A. and Aprile, A. CFRP-based strengthening technique to increase the flexural and energy dissipation capacities of RC columns. *Journal of composites for construction* (2009) **13**: 372-383.
[33] Breveglieri, M., Barros, J.A., Aprile, A. and Ventura-Gouveia, A. Strategies for numerical modeling the behavior of RC beams strengthened in shear using the ETS technique. *Engineering Structures* (2016) **128**:296-315.
[34] Breveglieri, M., Aprile, A. and Barros, J.A. RC beams strengthened in shear using the Embedded Through-Section technique: Experimental results and analytical formulation. *Composites Part B: Engineering* (2016) **89**: 266-281.
[35] Gulinelli, P., Aprile, A., Rizzoni, R., et al. A Fe Model for TRM Reinforced Masonry Walls with Interface Effects. In *Key Engineering Materials* (2019) **817**: 57-64.
[36] Zerbin, M. and Aprile, A. Sustainable retrofit design of RC frames evaluated for different seismic demand. *Earthq. Struct* (2015) **9**: 1337-1353.
[37] Dolce, M., Speranza, E., Giordano, F., Borzi, B., Bocchi, F., Conte, C., Di Meo, A., Faravelli, M. and Pascale, V. Observed damage database of past Italian earthquakes: the Da. DO WebGIS. *Bollettino di Geofisica Teorica ed Applicata* (2019) **60**: 141-164.
[38] De Martino, G., Di Ludovico, M., Prota, A., Moroni, C., Manfredi, G. and Dolce, M. Estimation of repair costs for RC and masonry residential buildings based on damage data collected by post-earthquake visual inspection. *Bull Earthq Eng* (2017) **15**: 1681–1706.
[39] Il Presidente della Repubblica. Decreto legge 6 giugno 2012, n. 74: interventi urgenti per le popolazioni colpite dagli eventi sismici nelle province di Bologna, Modena, Ferrara, Mantova, Reggio Emilia e Rovigo il 20 e il 29 maggio 2012. *Gazzetta Ufficiale* (2012) **131**. Italian.
[40] Zuccaro, G. and Cacace, F. Seismic casualty evaluation: The Italian model, an application to the L'Aquila 2009 event. In: R. Spence et al. (Eds): *Human casualties in earthquakes*. Springer, Dordrecht (2011), pp. 171-184.
[41] Basaglia, A., Aprile, A., Spacone E. and Pilla F. Performance-based Seismic Risk Assessment of Urban Systems. *International Journal of Architectural Heritage* (2018) **12**: 1131-1149.

FIRE PREVENTION IN OTTOMAN AND HABSBURG BUILDING CODES FOR BOSNIA AND THEIR APPLICATION IN TRAVNIK

A. CAROLINE JAEGER-KLEIN[1,2]*, B. AJLA BAJRAMOVIC[2] C. LUKAS STAMPFER[1]

[1] Institute of History of Art, Building Archaeology and Restoration
Technical University if Vienna (TU-Wien), Karlsplatz 13/251-1, 1040 Vienna, Austria
e-mail: jaeger-klein@tuwien.ac.at (*corresponding author), lukas.stampfer@tuwien.ac.at,
www.baugeschichte.tuwien.ac.at

[2] Department of Art History
University of Vienna, Garnisongasse 13, Campus courtyard 9, 1090 Vienna, Austria
e-mail: ajla.bajramovic@univie.ac.at, http://ercbos.univie.ac.at

Keywords: Fireproof Material, Building Regulations, Modernization, Building by Plan, Type-Planning, Identity and Architecture

Abstract. *The city of Travnik, located in central Bosnia, served as an administrative center of the Ottoman province between 1699 and 1851, with only short interruptions. In 1878, the Congress of Berlin awarded the Austro-Hungarian Monarchy rights of occupation for this Ottoman province. The following year, the new administration already faced its first big fire, which wiped out a major part of downtown Sarajevo. A new building code, which tried to minimize future hazard risks and was soon valid for all of Bosnia, was established in 1880.*

In September 1903, two major fires hit Travnik. The Ottoman administrative building used by the new officials was already fire-improved, so it survived the fires without sustaining any serious damage. The same cannot be said for the traditional residential neighborhoods at the foot of Travnik castle, which burnt down to their foundations. The mosques in Travnik that were constructed mostly of wood were damaged severely. Austro-Hungarian administration officials identified the traditional way of building as a serious risk for all of Bosnia and tried to counterbalance by implementing the new regulations rigidly in their post-fire reconstruction program. They seem to have developed a more secure 'mosque building model type', which they implemented in the re-erection of the Lončarica, Zulići, Kahvica and Šumećka mosques. While rebuilding the Varoška and Lukačka mosques, the distinct 'official' style of Habsburg-Bosnia [1], a blend of various architectural elements associated with 'the Orient' that the literature tends to name 'pseudo-Moorish', was used.

1 INTRODUCTION

Located in central Bosnia, Travnik is a charming but sleepy midsized town that, according to the Austro-Hungarian census of 1895, had a population of ca. 5,933 [2]. Travnik enjoys a favourable location on the Lašva River, situated along an important north-south trade, and served as administrative centre of the Ottoman province of Bosnia Herzegovina from 1699 to 1851, with short interruptions in 1827-28 and 1832-36. Ottoman viziers and the consuls of Austria and France left traces in Ivo Andrič's Nobel-prize-winning literature as well as several buildings. The viziers resided and carried out their official duties in a distinct type of building called *konak,* and were buried in various mausoleums, called *türbe* in Turkish. After the take-over of Ottoman-Bosnia by the Habsburg monarchy in 1878, Travnik maintained its role as the capital of one of the six districts (in German named *Kreise*) into which Bosnia and Herzegovina was divided under the former rulers. After the arrival of Austro-Hungarian officials in Travnik, several modern building complexes intended for military, social (health-care, education) and religious infrastructural use were fitted into its existing city-scape. However, the old administrative building, the historic *konak,* was kept as the main administration centre. In October 1893, the Lašva-Donji Vakuf-Jajce/Bugojno railroad project reached Travnik. Its completion meant that Travnik was better connected with nearby towns, but it was exactly this railway's construction that caused a disastrous fire in September 1903.

The Austro-Hungarian government's interesting response to this serious catastrophe, and the previously initiated efforts to implement modern fire-proof building structures according to Austrian standards, are the subject of the following paper. The ERC project titled "Islamic architecture and Orientalizing style in Habsburg Bosnia, 1878-1918" (PI: Maximilian Hartmuth, University of Vienna) intends to identify the specific technical as well as regulatory measures implemented by the Austro-Hungarian authorities. A brief visit to Travnik in the fall of 2018 made clear that this town's legacy in central Bosnia would merit further attention. In May 2019, a joint TU-Vienna and ERC-project research team, together with architecture students, documented the rebuilt mosques destroyed in the great fire of 1903 using combined laser-scan, photogrammetry and hand measurement techniques, with the aim to extract the resilience strategies of the Austro-Hungarian administration for the place. Hence, the post-procession phase is still ongoing.

2 BOSNIAN FIRE HAZARDS AND THE AUSTRIAN BUILDING CODE

The Austro-Hungarian monarchy took over administration of Bosnia and the Hercegovina in the summer of 1878. For complicated matters of foreign and internal politics, "the chief architects of Austria's colonial policy were … civil servants rather than legislators" [3]. The undoubted mastermind of that policy, Benjamin von Kallay, who governed the province from 1882 until 1903, stressed in an interview given to a British newspaper that "rational bureaucracy was the key to Bosnia's future … Administration is our only politics" [4]. In accordance with that motto, officials rapidly implemented new urban planning and structural engineering rules and regulations as soon as they identified the major building security threat caused by Bosnia's traditional construction techniques. The capital of the Habsburg-Empire, Vienna, served as role model.

2.1 A brief history of Austria's building regulations and its fire-care approach

One crucial aspect of security that officials in urban areas have always faced has been to safeguard lives and property threatened by fires in densely populated neighborhoods, sometimes entire cities. Vienna, as the residence of Habsburg emperors since the 16th century and of the Austro-Hungarian Empire since 1866, had overcome a series of city fires between the years 1252 and 1330. Forty percent of its then majority wooden houses were destroyed. In order to avoid the repetition of such disasters, as early as 1534 the authorities implemented systemic regulations in order to counterbalance this specific threat [5]. In the 1720's, a new generation of fire-security regulations laid the grounds

for a first Viennese Building Code. The great empress Maria-Theresa (1717-1780) again reformed the valid fire-regulations. Wooden shingles used for the roofs and timbered staircases were forbidden. Additionally, the profession of the chimneysweeper was created. For the construction business, those first regulations mandating the use of fireproof material meant a fundamental change. To accelerate that process, Maria-Theresa initiated the royal brick industries' foundation at Wienerberg for burnt brick production. Finally, her son, the great reformer Joseph II (1741-1790), launched further fire-regulations in 1782. They were structured into the following four chapters: 1) how to prevent fires, 2) how to deal with the risk of fire, 3) how to fight the fire and 4) what to do with fire-damaged sites and properties [6].

In 1829, the first consolidated Building Code for Vienna was proclaimed; it specifically addressed the administrative process related to building construction. The code regulated the obligations of the building parties before the site was opened, during the erection-phase and after the construction was finished. It also codified the maximum building-height, the minimum width of its corresponding streets and established an office of supervision for all building activities [7]. The Building Code of Vienna served as role model for all of Austria, a tradition that was continued in Bosnia and the Hercegovina. As soon as Sarajevo had its own building regulations, they were instituted for the entire province.

2.2 The first big fire in Habsburg Bosnia and its consequences

Already during their first year of administration, Austro-Hungarian officials were confronted with a fire catastrophe in Sarajevo, the capital. In the night from August eighth to ninth of 1879, the entire western part of the market district (*čaršija*) burnt down to its foundations [8]. Prstojević has described the initial, more easily applied preventive measures concerning the storage of certain inflammable goods and placement of adequate equipment like water-filled buckets or long fire ladders, which had to be available at critical sites such as the bazaar-area with the wooden shops (*dućan*s) [9]. The new Austro-Hungarian administration quickly worked out a building code for Sarajevo and selected other towns and market places in Bosnia and the Hercegovina. On 14 May 1880, this new building code replaced the Ottoman building regulations from 1863, which Habsburg-Bosnia had immediately taken over and proclaimed in German, the new regime's administrative language [10]. The Ottoman code already included directions similar to the Austro-Hungarian ones, but were insufficiently implemented and supervised. The Ottoman code's §24 had already made fireproof chimneys obligatory. §25 forbid building guesthouses in timber structures and §28 required wooden roof-covers to be additionally protected by fire proofed material. For neighborhoods damaged by fire, the Ottoman building code prescribed wider streets and more open places than the traditionally constructed urban fabric would have provided (§12). The Austro-Hungarian administration added to the building code's 1880 version sanctions for not building in accordance with the licensed plan (§14) and completely banned dead-end streets (*Sackgassen*) for new quarters, in addition to the mandated widening and straightening of the streets (§23).

Certainly, those regulations interfered fundamentally with the local town-planning tradition. Dead-end streets were essential features of Ottoman-period residential neighborhoods (*mahale* in Bosnian) and their social control mechanisms. The fire-fighting rationale claimed for such regulations was the need for modern fire-fighting equipment and an adequate number of fire-fighting men to quickly reach the fire's heart and prevent its rapid expansion. Clearly, this was in contradiction to the traditional characteristics of Ottoman towns, where culture and climate ask for narrow, shadowed and hidden, and partially covered semi-public street space. However, as mentioned, the 1863 Ottoman building code already required the same measure as the Austro-Hungarian code from 1880. The ban of dead-end-streets was not a novelty of the new European regime, nor fire-proofed chimneys and roof-coverings.

What *was* definitively new were regulations requiring the use of burnt brick in certain wall-dimensions or stone for public buildings and for residential- and commercial buildings. Existing roofs had to be covered with fireproof material within fifteen years. Based on Vienna's long-term experience — Vienna had avoided major urban fires like the one Sarajevo suffered in 1879 — buildings now had to be separated from each other with fire-proof walls (*Feuermauern*) surpassing the eves and space of the roofs. One stairway of fire-proof material (stone, for instance) had to run through the entire building up into the roof-space. The roof-space had to be divided by an iron door with a fireproof frame (§40, p. 259). Circulation corridors and the uppermost ceiling dividing the residential space from the roof-space had to be from fireproof material. It is not true that the regulations banned wooden or wooden-framework structures. They still could be erected if some space between the building and the neighboring structure was maintained. For structures with just a ground floor, wooden staircases still were allowed.

The 1880 Building Code's §23 regulated street (*Gassen*) width in four determined categories (C*lassen*). To guarantee healthy conditions, in correlation to the width of the streets, the building-height of the neighboring residential houses was fixed by §53. The amendment of 1893 [11] added a fifth class of streets in §23 with a width of 15 meters. For the two widest street categories, permission for a third floor above the basement is given in §48 if such a high building will not disturb harmony with the neighboring structures or the architectural effect within the street-view. No other health or security issues are criteria for the building code, while the argument of aesthetics is added. In general, the 1893 Building Code is more oriented toward city regulation measures, and deals less with fireproof materials and construction techniques. This may already show that the stricter supervision of an efficient administration had led to sufficient structural fireproofing.

Schmid and other contemporary commentators might be right if they described the building safety reality in Bosnia and the Hercegovina before the Austro-Hungarian administration as insufficient. Catastrophes were not the result of inefficient or non-existent Ottoman regulations, and were, instead, more a matter of inefficient Ottoman administration. Schmid summarized building conditions before the Austro-Hungarian occupation by noting that official administrative buildings like the *konak*s, the residential representative buildings of the governors, consisted only partially of rubble stone masonry and mostly of timber framework infilled with mudbrick [12]. Schmid described further that the chimney was often completely lacking and smoke had to exit through a roof hatch. A ceiling did not separate the roof space, and its coverings consisted of straw, rete or, like in central Bosnia, long wooden shingles.

However, many people avoided implementing the new building regulations. The government-appointed building director, Edmund Stix, who was responsible for overseeing all building activities, reported as early as 1887 that modern building regulations nearly led to a standstill in all private building activities [13]. To counterbalance that, the provincial government on 18 May 1880 [14] released an order to exempt objects damaged or destroyed in the fire of 1879 from the housing-tax. If they were repaired or re-erected by November 1, 1884, the tax-relief was valid for 30 years. The exemption from the housing-tax was also valid for new structures or reconstructions outside the before mentioned scene-of fire, but with a more limited duration from five to twenty years. Schmid reports further that with such measures, and through the influence of building companies from other parts of the monarchy, finally the richer strata of Bosnian society could be convinced to equip their old buildings with modern and secure standards [15].

3 AUSTRO-HUNGARIAN FIRE-PREVENTION FOR TRAVNIK AND THE GREAT FIRE OF 1903

Travnik had – and still has – a well-preserved traditional building stock. After the 'era of viziers' ended there in 1851, few building activities took place in the town until the Austro-Hungarian district and county administrations were established. The Habsburg district administration (*Kreisbehörde)* finally settled in the existing Ottoman *konak*, referred to in the official plan documents as the 'great' *konak* (*Großer Konak*) because there also existed a smaller *konak* building. Obviously, the great *konak* needed some adaptations to fit the new administration's requirements. The Travnik Canton's district archive (*Kantonalni arhiv Travnik*) still holds an extant set of plans documenting this functional as well as technical adaptation process. Here, just the enhancement of the structure's fireproofing will be described as it helped to keep the great *konak* intact during the devastating fires of September 1903.

3.1 Fireproof adaption of the existing Ottoman *konak* building

Travnik became the capital of the 1580-founded Ottoman province of Bosnia during the second Battle of Vienna, which started in 1683 and lasted until 1699, when the Treaty of Karlowitz established peace. As the Austrian Prince Eugene of Savoy occupied and demolished Sarajevo in his 1697 assault, the Sultan Mustafa II decided to move the vizier's seat to Travnik, which was safer and in a better strategic position to defend the Ottoman Empire's western border. Between 1699 and 1851, 77 viziers used the *konak* building as their home and operations base. It was erected on the city's western side in the early eighteenth century, and first mentioned in written sources in 1749 [16]. For the former Ottoman *konak* to meet the Austro-Hungarian administration's requirements, the structure needed to be modified according the standards of the 1880 Sarajevo building code. Because the Habsburg administration re-used the former Ottoman structure, it needed to reflect the new government's values; that need ultimately resulted in changes to the *konak*'s appearance.

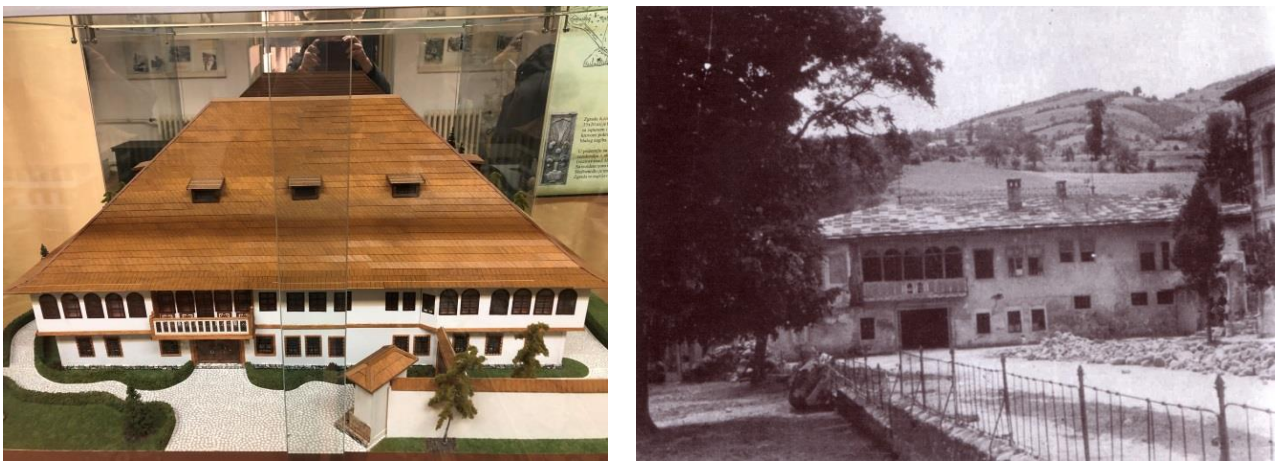


Figure 1: *Left*: Reconstruction model of the *konak* building in Travnik under Ottoman rule, with the traditional Bosnian steep roof silhouette, wooden roof-cover and hatches for the smoke (*photo Jaeger-Klein, May 2019*); *Right:* The building in 1950 with the gently-sloped roof, the fire-proof brick covering and chimneys according to the regulations of Austro-Hungarian administration (*photo from Sujoldžić, Stari Vodovodi, 2012, p.94*)

A set of plans, which survived and are located in Travnik Canton's district archive, give us some hints about this adaptation process. From 1882 to 1886, the existing building, including its steep traditional Bosnian roof structure, gained a new brick-tile covering. This was implemented in several phases. Additionally, a new heating system with fireproof chimneys was installed, maybe partially already under Ottoman rule. Noticeable in particular is the roof-plan, which details the replacement

of the traditional wooden roof-cover by brick-tiles, as the contemporary black-and-white photo shows. Obviously, the government could not afford to change the cover into brick within one budget-year. The plan gives evidence that it was done over four periods: 1882 first in dark red, and then from 1884 to 1886 once a year another part, and finally for the last phase, marked in very pale red, the figure of 177 m2 in total is given. Also visible are the new chimneys, which replaced the hatches for smoke.

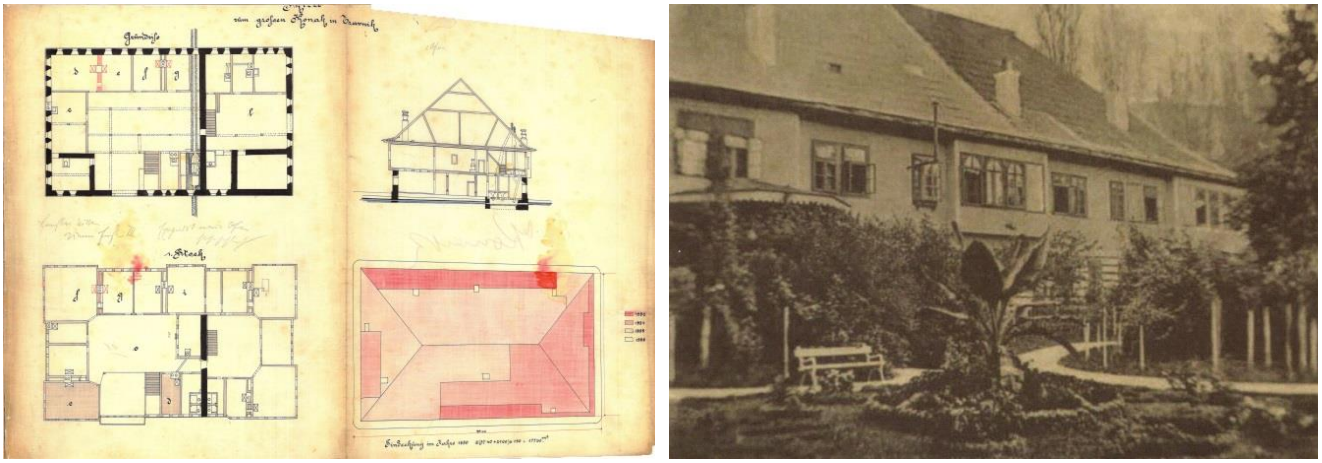


Figure 2: *Left:* The first adaptation phase (1882-86) of the 'great *konak* building' in Travnik under Austro-Hungarian rule; the roof-cover was switched to burnt brick material in four stages (*scan from the district archive of the Travnik Canton*); *Right:* A contemporary photograph shows the freshly brick-covered *konak* from the rear (*photo from Sujoldžić, Stari Vodovodi, 2012, p.9*)

In 1895, the plan documentation of the great *konak*'s existing structure seemed to show the first phase of remodeling as finished. In the ground plans, someone noted in pencil the use of the re-configured rooms, and the option for reducing the roof's height. In 1906, a detailed construction plan fixes this proposed height reduction and replacement of the traditional Ottoman-era roof-structure. The photos from 1950, when the *konak* was destroyed, still document the results of that last adaptation phase. This series of plans matches the reports by Stix (1887) and Schmid (1914), who testify that during the new administration's early years existing structures were adapted to administrative purposes. For financial reasons, they were equipped according to the new building-code standards of Austro-Hungary, with minimal effort.

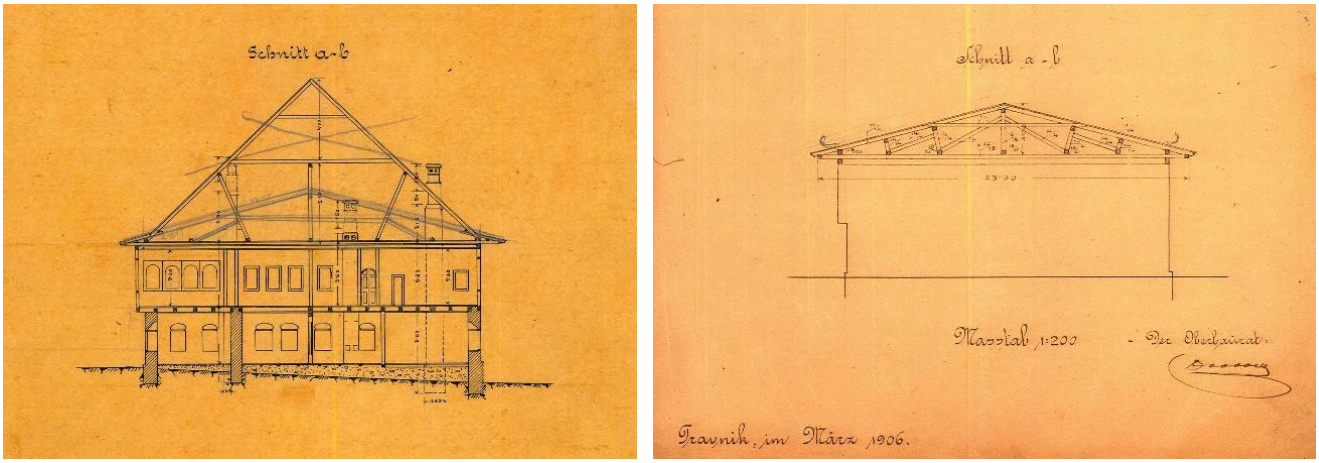


Figure 3: Some early considerations about the modified roof-structure, from the documentation plans of 1895 (*left*) and the final solution from March 1906 (*right); both scans from the district archive of Travnik Canton*

3.2 The great fire of Travnik in 1903

In September 1903, Travnik suffered a major fire. It started on September 3 as a result of a large spark from a passing locomotive, igniting the hay in a building around the Hasanpašić Tower, in the Šumeće *mahala*, at the eastern end of town. A precise plan, drawn by Austro-Hungarian clerks immediately after the fire, shows in detail how the fire spread and was rapidly transmitted from one place to another due to strong winds. Firefighting teams consisting of volunteers from Jajce, Zenica and Sarajevo had little success in extinguishing the fire, mainly due to a lack of sufficient equipment but also due to the fast burning of densely packed wooden buildings. The wooden mosques, including the surrounding porches of wood and their wooden minarets directly attached to the steep-hipped roofs, burned particularly well. The different firefighting lines, which the authorities documented well in the mentioned plan, did not work well enough. Only the barrier of the railway managed to keep the fire out of the town's southern part.

There was, however, another fire, which started on September 10 of the same year. It spread across the railway tracks and into the central parts of town. According to the various reports, half of the population lost their homes and their income, since in addition to the 582 destroyed houses, 60 shops and warehouses as well as 337 commercial buildings were lost or heavily damaged. The Austro-Hungarian government reacted quickly by investing in the town's rebuilding. Building material like timber, stone and sand were provided for free and, as after the 1879 fire in Sarajevo, taxes for the newly built houses were exempted for ten years, for poorer citizens even twenty years [17].



Figure 4: The results of the 1903 Travnik fires in a photograph *(Source: Sujoldžić, Sjećanje, 2019, p.135)*

3.3 The reconstruction of Travnik's mosques under Austro-Hungarian administration

In the great fire of 1903 nine mosques were damaged. The state government *(Landesregierung)* supported the reconstruction of three *mahale*-mosques in the Šumećka, Kahvica and Zulići neighborhoods. Two other mosques of this type from the east end of town, Varoška and Lončarica, were rebuilt with private local donations. For Lukačka mosque, prominently located on the main street, the Austro-Hungarian governor Stephan Burián personally financed its reconstruction. At first glance, it is obvious that four mosques – Šumećka, Kahvica, Zulići and Lončarica – were built on the base of a fixed model. So far, the ERC research team could locate only one plan set in Bosnian archives, the blue-print of Kahvica mosque's design.

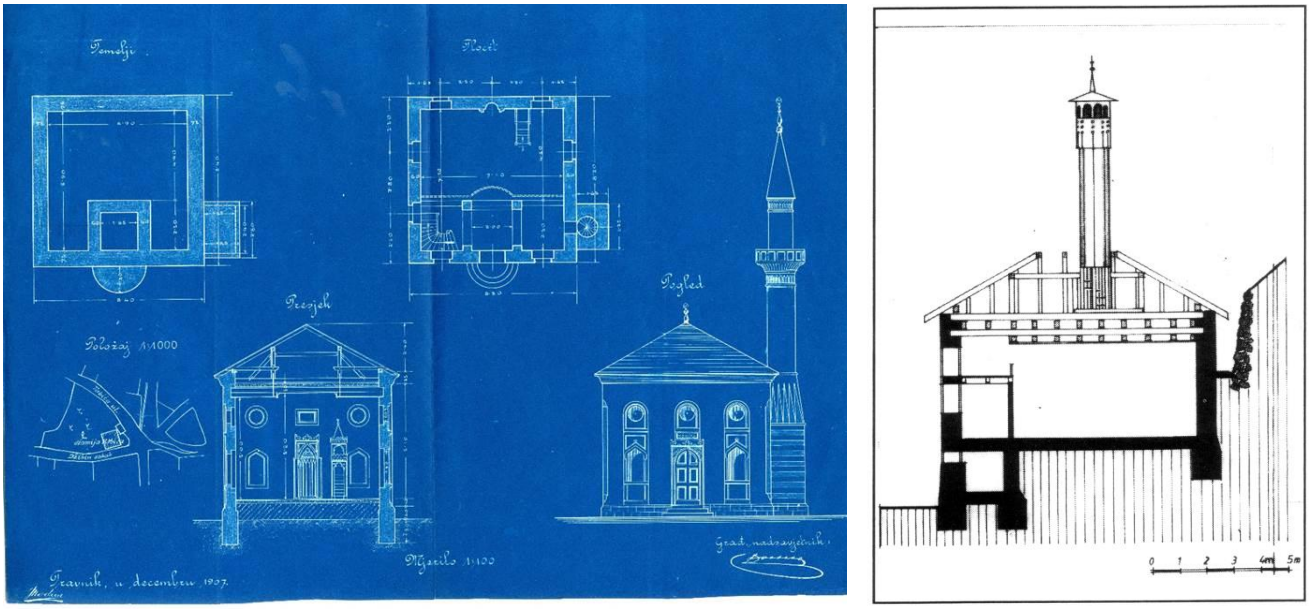


Figure 5: *Left*: Blue-print of the new Austro-Hungarian model-plan design for Kahvica Mosque (*from Archive of Bosnia and Hercegovina, GDZVS, 1878-1918, Box 64b, obj 65*), dated December 1907*; Right:* Section through a typical traditional wooden mosque of Travnik *(plan of Osoje mahale mosque from Sujoldžić, Džamije, 2013, p.111)*. Kahvica Mosque was one such typical wooden neighborhood mosque before the great fire of 1903 destroyed it.

At the end of the nineteenth century, the Austro-Hungarian government of Bosnia had popularized an Orientalizing style through its architectural projects. This style mostly drew upon the Islamic artistic heritages of Andalusia and Egypt. The Kahvica mosque's blueprint reveals that the administration's architects, trained in the universities and academies of the monarchy, could design in the 'Oriental aesthetic'. To implement it constructively, they stayed within their Austrian-based knowledge and experience. Their Western training probably led to a smooth use of type planning, which could come in handy for situations like the one in Travnik after the great fire. For many building types, such as school-buildings, train stations and administrative structures, the central building administration of Sarajevo province seemed to have developed model-plans that district engineers could quickly modify according to local circumstances. The freshly rebuilt Lončarica, Zulići, Kahvica and Šumećka mosques seem to follow such a model-plan. A group of master-students from Vienna University of Technology went to Travnik in May 2019 to survey the mosques *in situ*.



Figure 6: Mosques built according to one model-plan in Travnik after the great fire: *From the left:* Lončarica, Zulići, Šumećka and Kahvica *(all photos by Jaeger-Klein in May 2019)*

As preliminary results, the following can be stated: the footprint of the mosques and their size accords with the lost wooden mosques that they replaced. Their facades all follow a 3x2 module with two levels of windows, but variations in ornament. For those ornaments, the local Austro-Hungarian technicians developed a variation on motifs from the great representative structures like the Elči Ibrahim-paša medresa; that structure was built in the distinct Austro-Hungarian Orientalizing style in 1895 after designs by Ćiril Iveković (1844-1933), one of the prestigious architects employed by the provincial government. The challenge was to fit the motifs into the ensemble, in size, volume and decoration. Sitting at one flank of the entrance façade, the minarets no longer extend out of the roof, and make the women's gallery accessible through their winded staircase within the shaft. Stylistically, they now match the typical pencil-minarets of Ottoman architecture, but not the local wooden minarets. The steep, tent-hipped roof covered with wooden shingles is replaced by a lower, brick-covered, but still tent-hipped roof. Finally, all the materials as well as the construction techniques correspond with the modern building regulations.

Two of the reconstructed mosques certainly do not follow this model and were individually planned. Varoška mosque, before the great fire of 1903 certainly a typical *mahala*-mosque constructed from cedar wood with a traditional Bosnian roof, was 'upgraded' to a mosque with a, for Bosnia, highly unusual onion-shaped cupola and extremely high minaret [18]. The reason for this upgrade is unknown. Maybe this is a tribute to the specific history of the Varoška mosque. It was Travnik's first mosque built in the suburb (*Varoš*) outside of the medieval castle's defense-walls. With the generous donation of a local lady, Ziba Hanuma Arnautović-Kopčić, the mosque was realized quickly in 1906, according to Sujoldžić after plans by the architect Miloš Milosević [19], who is not listed as one of the local Austro-Hungarian administration's technicians. Varoška mosque's new configuration clearly represents the Orientalizing style, which Austro-Hungary used as a kind of corporate identity. Distinct ochre-red horizontal stripes cover its façade. The entrance is marked by a monumentalized double-story porch, which reveals the Austro-Hungarian interpretation of in general oriental, but certainly not local elements of architecture.

The second mosque, the shape and aesthetic of which does not correspond to the four type-planned ones, is the Lukačka mosque. Located on the main-street of Travnik, this mosque needed only partial reconstruction after the second great fire of September 1903. The 1821 configuration of this early seventeenth-century mosque is described as a rectangular volume with a lower four-hipped roof and a porch of six stone pillars that reached to the height of the eves.

Its walls already consisted of a massive structure, with a brick-tiled roof and a minaret made of stone, enabling the mosque to survive the conflagration. The Austro-Hungarian governor Stephan Burián, who visited Travnik after the fire, privately financed its necessary retrofitting [20]. The porch was lowered, and gained an Egyptian-Mameluke-inspired crenellation and extraordinarily slim columns. Their shafts were from cast-iron, while bases and heads were from gypsum-mortar in *muqarnas*-décor. The whole exterior was whitewashed, and some of the former colored, figurative murals survived in the roof-structure of the new porch [21].

This illustrates the wide spectrum within the Orientalizing style, reinterpreted by the Austro-Hungarian architects and engineers. Lukačka mosque did not use any color other than white for its facade. The materials used make for an interesting observation: apparently, all of the porch columns were made of industrially produced rounded iron-profiles, which could have been used for railway platform shelters. Other European architects working in the Near East, like Carl von Diebitsch (1819-1869), used to pre-order iron casts or pillars for their constructions in Orientalizing styles and assembled them *in situ*, which may explain why cast-iron columns were also used in Travnik.

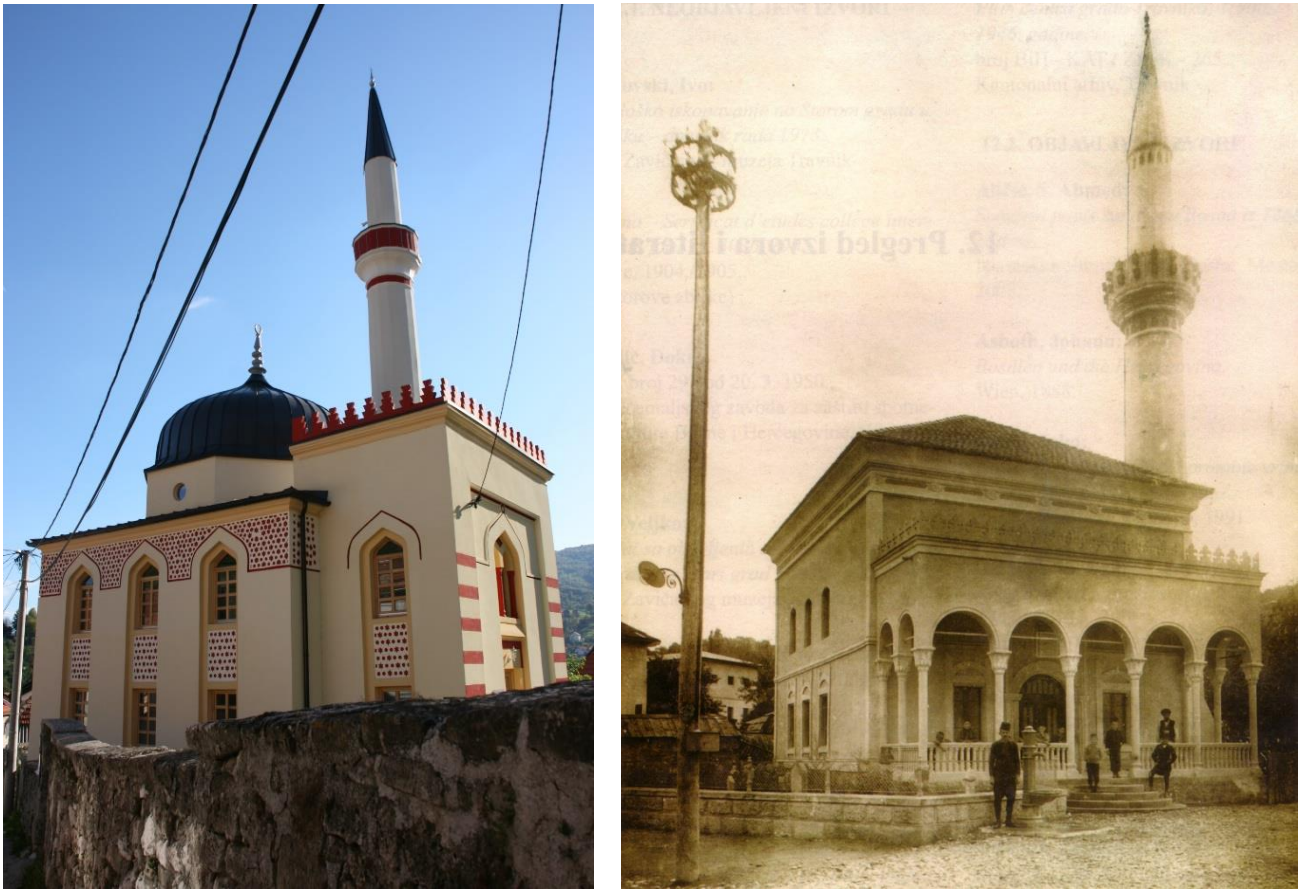


Figure 7: Reconstruction of mosques in the style promoted by the regional government: *Left:* Varoška mosque in Travnik: Monumentalized replacement of the former wooden, modest mosque (*photo Jaeger-Klein, September 2018*); *Right*: Lukačka mosque in Travnik with its new porch replacing the former double-floor height one (*historic photo from Sujoldžić, Sjećanje, 2019, p.167*)

4 MAINTAINING THE TRADITIONAL CITY SCAPE AFTER DESCTRUCTION

The measures undertaken by the government to avoid fire tragedies of this scale were rather effective, if we consider that the Austro-Hungarian building stock remained pretty much intact into the twenty-first century. Nevertheless, contemporary critique arose quickly even under the Austro-Hungarian officials. Edmund Stix, head of the Bosnian building department in Sarajevo, stated critically in 1887 that the picturesque "oriental character" of the towns was already fading [22]. Even though the newly erected or renovated buildings followed the new building protocols, they lost authenticity. Later, in Travnik, the new buildings were not designed thoughtlessly. The *mahale*-mosques, for example, kept their architectural footprint as well as their traditional scale. The big *konak* of the Ottoman viziers, which Austro-Hungarian technicians upgraded to their structural standards, stood in place until 1950, when it was demolished by the authorities with the goal of creating a new city center in the global language of Yugoslav architecture [23].

CONCLUSIONS

- When the Austro-Hungarian administration took over rule of Bosnia and Herzegovina, it already had long-term experience in fire-prevention from Vienna by means of building regulations and the rigid supervision of proper implementation.
- The disastrous Sarajevo fire in 1879 led the authorities to take immediate action by implementing a modern Building Code for Sarajevo and other selected Bosnian towns. They supervised especially its proper implementation, but encouraged citizens to rebuild quickly according to the new standards through means of tax relief and tax exemption.
- The 1903 fire-catastrophe in Travnik proved that buildings retrofitted according to modern regulations, like the renovated Ottoman *konak,* survived even such destructive events.
- Replacing the steep wooden roofs of traditional Bosnian architecture as well as rebuilding wooden mosques with fireproof material was an effective measure against fire disasters but it interfered heavily with the traditional cityscape.
- To counterbalance this loss of cultural identity, the new authorities promoted an Orientalizing style.

Acknowledgements. We would like to extend our sincere thanks to the director of the Local Museum Travnik, Mrs. Fatima Maslić and her team for their overwhelming support and assistance. Especially helpful were the talks we had with Mr. Enver Sujoldžić, a passionate researcher of the local architectural history. He measured and documented the majority of local mosques before and during the Bosnian war (1992-1995) and therefore preserved at least some reliable information on the buildings, which are lost to us today. Thanks to him, Mrs. Maslić, her team and the staff of the district archive of the Travnik Canton, a surprisingly intact legacy of the Austro-Hungarian administration came to our attention. Finally, our warm thanks additionally go to Mr. Salih Effendi Indžić and the team of the Travnik Medžlis, who gave us unlimited access to the mosques for conducting our research, even during Ramadan.

REFERENCES

[1] Hartmuth, M., Amtssprache Maurisch? Zum Problem der Interpretation des orientalisierenden Baustils im habsburgischen Bosnien-Herzegowina. In: *Bosnien-Herzegowina und Österreich-Ungarn, 1878–1918: Annäherungen an eine Kolonie.* Eds. Clemens Ruthner & Tamara Scheer. Tübingen 2018, p.251-268.

[2] *Hauptresultate der Volkszählung in Bosnien und der Hercegovina vom 22. April 1895*, Sarajevo 1896, p.XCIV.

[3] Donia, R. J., *Islam under the Double Eagle: The Muslims of Bosnia and the Hercegovina, 1878-1914*, Boulder, New York (1981), p.11.

[4] Donia, R. J., *Islam under the Double Eagle: The Muslims of Bosnia and the Hercegovina, 1878-1914*, Boulder, New York (1981), p.14.

[5] Enzersdorfer, A., *Gebäude versus Paragraf*, unpublished diploma-thesis Vienna University of Technology (2018), p.13.

[6] Enzersdorfer, A., *Gebäude versus Paragraf,* unpublished diploma-thesis Vienna University of Technology (2018), p.17.

[7] *Circulare der k.k. Landesregierung im Erzherzogthume Oesterreich unter der Enns*. Wien 1829, reprint Vienna (1840), p.1.

[8] Bertram, C., *Ottoman Sarajevo. The Urban History of Sarajevo in the Ottoman Period and Into the Period of the Dual Monarchy*: http://www.friends-partners.org/bosnia/cb1.html.

[9] Prstojević, M., *Forgotten Sarajevo*, Wien (2010), p.67.

[10] Österreichische Nationalbibliothek, ALEX – Historische Rechts- und Gesetzestexte online, *Sammlung der Gesetze und Verordnungen für Bosnien und Hercegovina 1878-1880*, p.180-283: http://alex.onb.ac.at/tab_lbh.htm.

[11] Österreichische Nationalbibliothek, ALEX – Historische Rechts- und Gesetzestexte online, *Sammlung der Gesetze und Verordnungen für Bosnien und Hercegovina, Bauordnung für die Landeshauptstadt Sarajevo 1893*, p.410-435: http://alex.onb.ac.at/tab_lbh.htm.

[12] Schmid, F., *Bosnien und die Herzegovina unter der Verwaltung Österreich-Ungarns,* Leipzig (1914), p. 525.

[13] Stix, E., *Das Bauwesen in Bosnien und der Hercegovina von Beginn der Occupation durch die österr.-ung. Monarchie bis in das Jahr 1887*. Wien (1887), p.103.

[14] Österreichische Nationalbibliothek, ALEX – Historische Rechts- und Gesetzestexte online, Sammlung der Gesetze und Verordnungen für Bosnien und Hercegovina 1878-1880, p.271f..; http://alex.onb.ac.at/tab_lbh.htm.

[15] Schmid, F., *Bosnien und die Herzegovina unter der Verwaltung Österreich-Ungarns*, 1914 p.525f.

[16] Hodnik, Z., Maslić, F., *Travnik Vezir Konaği Maketi*, Travnik (2012), p.16.

[17] Sujoldžic, E., *Sjećanje na Travnik*, Travnik (2019), p.132-136.

[18] Sujoldžic, E., *Džamije Travnika*, Travnik (2013), p.17-19.

[19] Sujoldžic, E., *Džamije Travnika*, Travnik (2013), p.18.

[20] Sujoldžic, E., *Džamije Travnika*, Travnik (2013), p.48.

[21] Sujoldžic, E., *Džamije Travnika*, Travnik (2013), p.47-53.

[22] Stix, E., *Das Bauwesen in Bosnien und der Hercegovina von Beginn der Occupation durch die österr.-ung. Monarchie bis in das Jahr 1887*. Wien (1887), p.103.

[23] Sujoldžic, E., *Sjećanje na Travnik*, Travnik (2019), p.88.

12th International Conference on Structural Analysis of Historical Constructions
SAHC 2020
P. Roca, L. Pelà and C. Molins (Eds.)

LANDSLIDE HAZARD AFFECTING HISTORICAL BUILDINGS: SANTA SCOLASTICA MONASTERY IN SUBIACO

MARIALUIGIA SANGIRARDI[1*], ANGELO AMOROSI[2] AND GIANMARCO de FELICE[1]

[1]Department of Engineering, Roma Tre University
Via Vito Volterra 62, 00146, Rome, Italy.
e-mail: {marialuigia.sangirardi, gianmarco.defelice}@uniroma3.it https://www.romatrestrutture.eu/

[2] Department of Structural and Geotechnical Engineering, Sapienza University of Rome
Via Eudossiana 18, 00184, Rome, Italy.
Email: angelo.amorosi@uniroma1.it, https://web.uniroma1.it/disg/

Keywords: Masonry, Finite Elements, Landslides, Jointed Masonry Model

Abstract. *Every year landslides occur as a consequence of ground conditions, geomorphological, physical or man-made processes, often triggered by heavy rainfalls or earthquakes. They affect buildings and infrastructures, causing economic and life losses. On the Italian territory, more than 14,000 heritage sites interact with potentially unstable slopes.*

This work investigates the effects of a landslide, occurred on the 26th of November 2018, on the Monastry of Santa Scolastica in Subiaco (Rome), one of the most ancient and well-preserved examples of medieval architecture in Central Italy. The geometry of the slope was reconstructed based on aerial photographic survey and point-cloud processing, obtaining meshed surfaces and extracting relevant sections.

The mechanical parameters and the specific hydraulic conditions triggering the failure mechanism were first recognised by traditional limit equilibrium back-analyses and then implemented in a 3D non-linear finite element (FE) model, which included both the slope and the interacting portion of the ancient structure. Elastic-perfectly plastic constitutive assumptions were adopted for the soil, while the structure was modelled by a three-dimensional anisotropic elastic-perfectly plastic constitutive model, specifically conceived for masonry, accounting for block dimensions and staggering joints effects.

Finite element approach proves to be very effective in the analysis of such a coupled interaction problem, leading to a realistic representation of the interplay between the soil displacements and their deformative effects within the structure. The numerical results have been interpreted to highlight the structural response in terms of crack pattern and stress distribution as induced by the interaction with the deforming slope, leading to a quantitative evaluation of the landslide-induced damage. Several scenarios were simulated: first, the pre-landslide existing crack pattern was reproduced, then the event was modelled as it occurred, evaluating its consequences on the structure.

1 INTRODUCTION

The evaluation of the impact of natural hazards on world's architectural heritage is a complex, though intriguing, task for the scientific community, which necessarily requires interdisciplinary approaches to be analysed and solved.

Together with earthquakes, landslides are one of the most destructive geotechnical hazards affecting constructions, economy and, more in general, the quality of life of the communities populating the hit areas. In fact, though most of the landslides usually occur in rural districts, they can cause significant damage to infrastructures [1] and have not rarely caused severe damage to monuments.

Slope movements are essentially related to the instability conditions occurring once the overall mobilised shear stresses along a slip surface equal the available shear strength. Such conditions can be triggered by various phenomena, including modifications of the morphology of the slope, groundwater effects leading to increased pore-water pressures or static and/or dynamic actions affecting the soil mass. In some cases risk is increased by some predisposing factors, such as land urbanization of the hill-sides.

Some well-known examples of UNESCO Sites subjected to landslides hazard or effects are, among others, the right coast of the river Moskow (Russia), Machu Picchu (Peru) cultural heritage site or some villages in Italy like Orvieto and Rocca Ripesena [2].

Italy, with reference to landslide hazard, is recognized as a very vulnerable country: 620,808 landslides have been identified on the national territory, constituting around the 80% of the total number of landsides in Europe. In particular, Lazio and Umbria regions are the most affected [3].

A number of studies deal with the definition or fragility curves at the urban scale, with particular reference to slow moving landslides [4,5], while analyses at the scale of the building have also been performed for both reinforced concrete [6] or masonry structures [7].

The Monastery of Santa Scolastica in Subiaco is a very well-preserved example of medieval architecture and is the most ancient Benedict's monastery in the world. It is located in a landslide prone area and, due to exceptionally heavy rainfalls, a landslide occurred on the 25th of November 2018 in the vicinity of the structure, causing fear and temporary closing of the buildings where a monastic community is still settled. The event can be classified as a flow-type landslide, a fast phenomenon, typically triggered by altered hydraulic conditions, as in the case under study, or earthquakes impulsive actions. Damage patterns had already been detected in some portions of the structure well before the landslide: as such, it was essential to assess whether or not the event had further compromised the safety conditions of the monastery.

As a first step, it was necessary to acquire an updated and well-defined sketch of both the slopes and the structure geometries: this was achieved by modern geometrical laser-scanner survey techniques. A classical decoupled approach was then adopted to back-analyse the landslide, by means of two dimensional (2D) limit equilibrium methods. The results of these calculations were then used to define the three dimensional (3D) finite element (FE) model, which not only included the geotechnical details of the soil deposits surrounding and below the monastery but also a fairly realistic representation of the structure. This mixed geotechnical and structural model was used to investigate the whole interaction processes that occurred between the monastery and the soil, including those related to the construction stages of the structure and the ones induced by the landslide.

In particular, the aims of the study are the following: first to identify and reproduce the detected damage of the structure as induced during and after the construction stages, then to analyse the effects of the subsequent landslide, thus assessing its role on the current safety conditions of the building.

2 PROBLEM STATEMENT

The use of numerical methods (finite-element or finite-difference methods) in structural and geotechnical applications is nowadays common, though their effectiveness strongly depends on geometrical discretisation, initial conditions, correct representation of the construction stages, constitutive hypotheses and numerical techniques (e.g.: [8]).

The adoption of elasto-plastic constitutive hypotheses within FE models can be considered as a well-established approach to analyse slope stability problems, though the use of more traditional methods, as those based on limit equilibrium, is still often preferred. This should be ascribed to the aim of the analysis, which typically focuses mainly on failure conditions, thus justifying the use of rather simple limit equilibrium reference conditions and related rigid plastic constitutive assumptions. When used at this scope, the complexity of non-linear FE analyses does not often lead to a gain in terms of accuracy of the solution. On the other hand, when the focus is on the deformation behaviour, either in the pre-landslide stage or in relation to this event, possibly including the interaction with an adjacent structure, FE models provide a far more realistic representation of the phenomena. In fact, they not only satisfy local and global equilibrium conditions up to failure, but also compatibility and constitutive assumptions, as such reproducing the deformation patterns of any element in the domain, provided appropriate constitutive assumptions are adopted based on carefully identified parameters.

2.1 Landslide modelling

As mentioned above, the modelled landslide has first been back-analysed by limit equilibrium approach, to identify the combination of shear strength soil parameters and hydraulic conditions, in terms of phreatic level, leading to failure. In the 3D FE analysis the geometry and failure plane of the slope has been reconstructed in light of the survey data and the results of the 2D back-analysis. This latter has also allowed the evaluation of the mobilised strength parameters. The landslide was triggered in the 3D numerical model by imposing a variation of the water table height, as possibly occurred at the time of the event due to heavy rainfalls. In detail, the stages of the analysis are the following: model stress initialization, structure construction and related interaction with the foundation soil, strength parameters degradation of a thin soil layer located at the pre-defined failure slip surface, positive variation of the water table level along the slopes to finally trigger the sliding. In the analyses here discussed, the non-convergence of the solution was considered as a suitable indicator of failure, as discussed in [9,10]. When the algorithm cannot converge within a specified maximum number of iterations, no stress distribution can be found that is simultaneously able to satisfy both the Mohr-Coulomb failure criterion and global equilibrium. Under these conditions, failure is assumed to have occurred and it is accompanied by a dramatic increase in the nodal displacements within the mesh.

2.2 Constitutive models for soil and masonry

The constitutive models adopted for the soil and the structure are both formulated according to classic rate-independent plasticity. The soil behaviour is modelled by a linear elastic-perfectly plastic constitutive model, characterised by a no-traction Mohr-Coulomb yield criterion and a null dilatancy angle. This is a relatively simple assumption, nonetheless it allows to realistically estimate the main phenomena involving the soil in the slope movement, while also reproducing with reasonable accuracy the interactions between the soil and the structure throughout the whole construction sequence and landsliding processes simulated numerically. In the analyses the bedrock stratum is assumed as rigid, thus not exhibiting any deformation or collapse.

The constitutive model adopted for masonry is a three-dimensional anisotropic elastic-perfectly plastic one [11], in which block aspect ratio and staggering joints effects are considered. Macroscopic elastic properties are derived in the framework of homogenisation theory of periodic media, while yielding is characterized by the intrinsic material anisotropy. A set of (maximum) three sliding directions, on which failure is meant to occur, is defined in the *xyz* space and described by means of dip and strike angles, representing, for each plane, the positive rotation along the *x*-axis and the negative rotation along the *z*-axis, respectively [12]. In the analyses only two planes (head and bed joints) are activated. Yield functions are defined, for each orientation, in terms of local stress components according to Coulomb's and tensile criterion as follows:

$$f_i^c = \left|\tau_i\right| + \sigma_{n,i} \tan\phi_i - c_i \tag{1}$$

$$f_i^t = \sigma_{n,i} - \sigma_{t,i} \tag{2}$$

where i = 1,2,3 is the plane id, $\sigma_{n,i}$ and τ_i are the normal and the shear stress along each orientation, ϕ_i is the friction angle, c_i is the cohesion and $\sigma_{t,i}$ is the tensile strength along the joints. The interlocking effect is accounted by modifying the strength parameters on the head-joints plane, stemming from equilibrium conditions and considering the aspect ratio of the blocks (being b and a their width and height respectively) their through the parameter β, which depends on the friction angle of the bed joints:

$$\beta = \tan\phi_2 \frac{b}{2a} \tag{3}$$

Tensile strength and cohesion on the head joints are hence calculated according to the following expressions:

$$\sigma_{t,1} = \sigma_{t0,1} - \beta\,\sigma_{n,2} + c_{0,2} \frac{\beta}{\tan\phi_2} \tag{4}$$

$$c_1 = c_{0,1} - \left(\beta\,\sigma_{n,2} - c_{0,2} \frac{\beta}{\tan\phi_2} \right) \tan\phi_1 \tag{5}$$

3 CASE STUDY

The Monastery of Santa Scolastica is the most ancient Benedict's monastery in the world. It is located in the Aniene river valley (Lazio, Italy), recognized as the cradle of the Benedict's community. It is an aggregate, developing around three cloisters, a church, a hostel for pilgrims

and a library. Even if the first settlement dates back to the VI-VII Centuries, the structure has undergone deep modifications during time, and the original configuration was outlined only during the Sixties, thanks to the findings of an archaeological campaign.

In the following, the adopted strategy to reconstruct the geometry of the slope and the structure, the back analysis performed on the slope and the mechanical characterization of the structure are briefly outlined.

3.1 Geometrical reconstruction of the slope and the structure

Terrestrial laser scanner or closed range photogrammetry are modern and efficient tools to reconstruct complex geometries; in some recent applications [13], they have also been adopted to directly obtain three-dimensional finite element meshes through a semi-automatic processing of the points-cloud.

In this study, a complete photogrammetric survey of the Monastery and the close surroundings was performed. The points-cloud has been post-processed to determine the detailed geometrical configuration of the structure, the slopes and of the area affected by the earth sliding, all then introduced into the numerical 3D model used to study the interaction between the landslide and the structure.

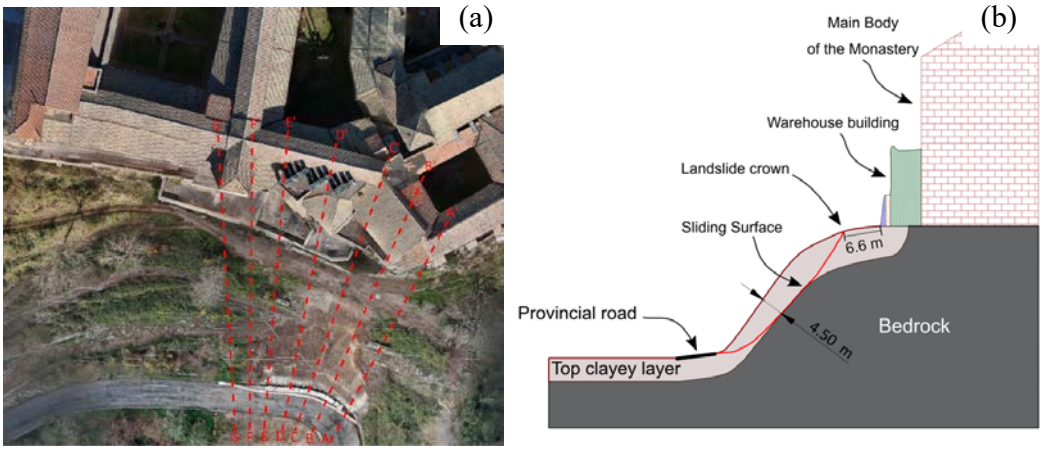


Figure 1: Aerial view of the selected sections of the points cloud (a) and result of the 2D post-processing of the pre-event geometry (b)

The aerial view reported in Figure 1a shows the position of the selected sections, chosen based on the following criteria: sections BB', CC', DD' and EE' have been used to determine the landslide failure surface, while sections FF' and GG', which lie outside the landslide, have been superposed to the others to reconstruct the morphology of the top soil layer prior to the slope instability. Section AA' was also considered in the 3D definition of the model as located close to the borehole used to define the local stratigraphy. The resulting volume of the landslide mass, equal to about 2000 m^3 when estimated through the geometrical reconstruction described above (Figure 1b), is in good agreement with the data reported by local authorities.

The points cloud model has also been adopted to build the structural model, for which volumes have been extruded from horizontal sections, at different heights.

3.2 Back-analyses of the slope

Two boreholes have been drilled in the vicinity of the Monastery, both indicating the presence of a top layer of clayey soil, 4 to 5 m thick, overlaying the calcareous bedrock. A limited number of laboratory tests were available, all referred to the intact state of the soil stratum, while those acting along the failure surface have been deduced through a back-analysis of the slope stability conditions. At this scope, 2D analyses were performed under the hypothesis of plain strain conditions and referring to an equivalent simplified geometry, adopting for the limit equilibrium approach the one proposed by Morgenstern & Price [14].

The laboratory investigations and the back-analysis lead to the definition of set of parameters reported in Table 1; the 2D back-analysis also shows that the triggering hydraulic conditions correspond to a water table located 4.0 m below the ground level and about parallel to it.

Table 1: Soil parameters

γ	E'	ν'	c'	ϕ'
kN/m^3	MPa		kPa	°
19	50	0.15	25	24

3.3 Structural damage and material characterization

The structures of the Monastery are in good preservation state, they have undergone several maintenance interventions and some parts are currently under restoration. Only one portion of the structure shows clear signs of damage, that is the front one, only recently constructed, during the Seventies, and originally conceived as a warehouse, which has apparently never been used at the scope.

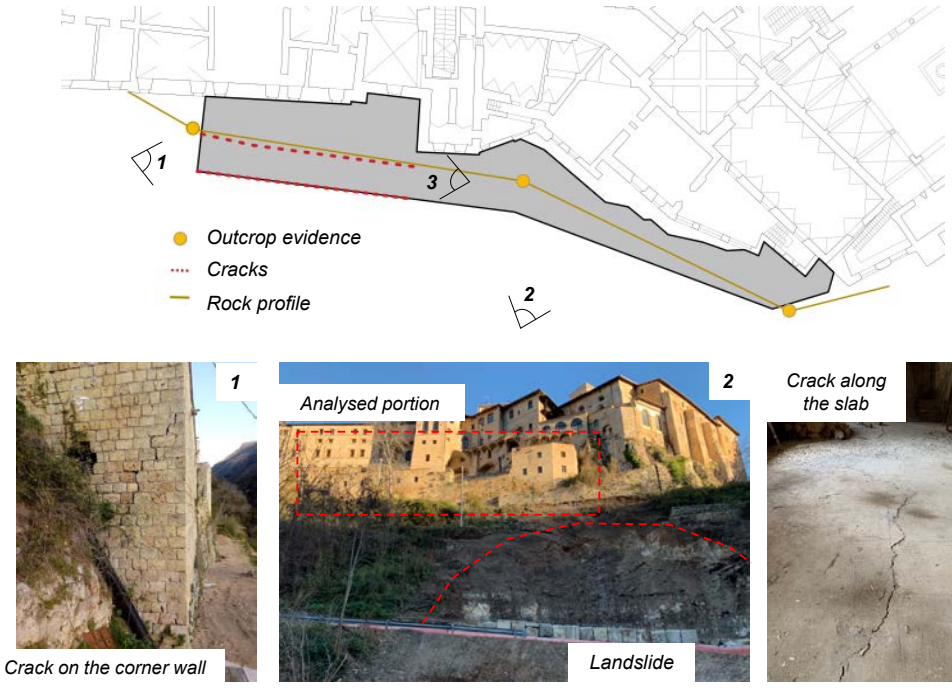


Figure 2: Visual inspection in the warehouse building

Thanks to a visual inspection of the structure, the main evidences of damage were located, rock outcrop profile directly interacting with the structure was obtained through interpolation of some outcrop points and masonry typology was identified in some parts of the building (Figure 2). The structure has been constructed with poor-quality masonry with irregular stones, covered by an external facing of regularly bonded calcareous stones.

Mechanical properties assigned to the masonry are reported in Table 2 and refer to the Jointed Masonry model described in the previous section. In this case, an isotropic elastic behaviour is assumed, and the strength parameters are assigned according to the identified masonry typology (disordered rough stone masonry) and current code prescriptions [15].

Table 2: Masonry parameters

$c_{0,i}$	$\sigma_{t0,i}$	ϕ_i	β	G	γ
kPa	kPa	°	-	MPa	kN/m^3
20	20	31	0.3	350	19

4 NUMERICAL MODELLING

The three-dimensional model adopted to analyse the interaction problem has been constructed in the software *PLAXIS 3D* and is made out of 63381 solid 10-noded elements. Only the most recent part of the structure was included in the model, as the only one affected by damage. In fact, the analysed portion of the Monastery is considered structurally independent from the rest of the aggregate, since its construction dates back to 1970, and joint-sections are clearly visible. The analyses were performed aiming first at identifying the causes of the detected damage on the structure, then at understanding possible interaction phenomena during the landslide event, which could have possibly worsened the pre-existing damage pattern.

4.1 Settlements induced damage and landslide scenario

The first analysed scenario does not consider the landslide occurrence but focuses on the effects of the heterogeneous soil foundation conditions on the structure. In particular, the model accounts for the fact that the building is partly founded on the stiff bedrock and partly on the softer silty deposit; this condition is responsible of both the cracking of the first-floor slab and the damage on the corner external wall, as indicated by the results summarized in Figure 3. This crack pattern is expressed in terms of maximum tensile strain and plastic points distribution on the horizontal slab and on the western wall respectively.

The landslide is then simulated according to the procedure described in Section 2, while monitoring the configuration of the structure at the end of each stage. It is shown that no sensitive change in tensile strain and plastic points distribution can be related to the occurrence of the landslide.

The results are in line with the vertical displacement graph plotted on the monitored line section, which has been chosen as running parallel to the floor on the most damaged wall. Figure 4a) reports the displacement measured on the section highlighted in bold in Figure 4b). The pre- and post-event scenarios are plotted together with a solid black line, outlining the correspondent

quantities in the ideal case of rigidly supported foundations. This line shows that, albeit negligible, a vertical displacement could be ascribed to masonry deformability.

These information allowed to conclude that a significant interaction between the structure and the soil only took place during the construction stages, leading to the observed damage pattern, while no further displacements occurred at the control points during and after the landslide.

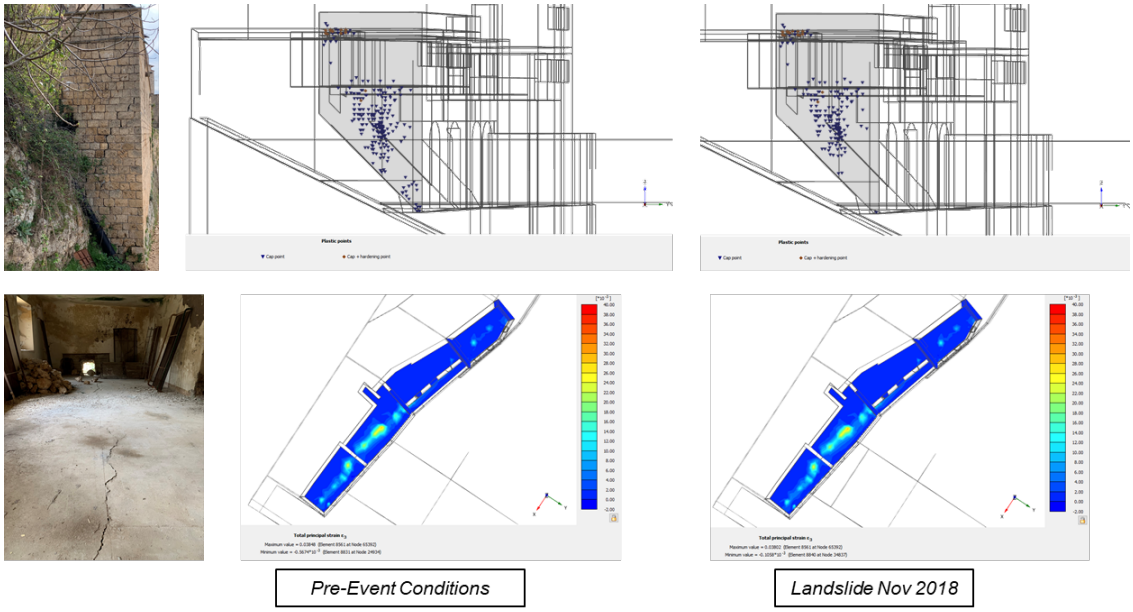


Figure 3: Results at the end of the construction of the structure

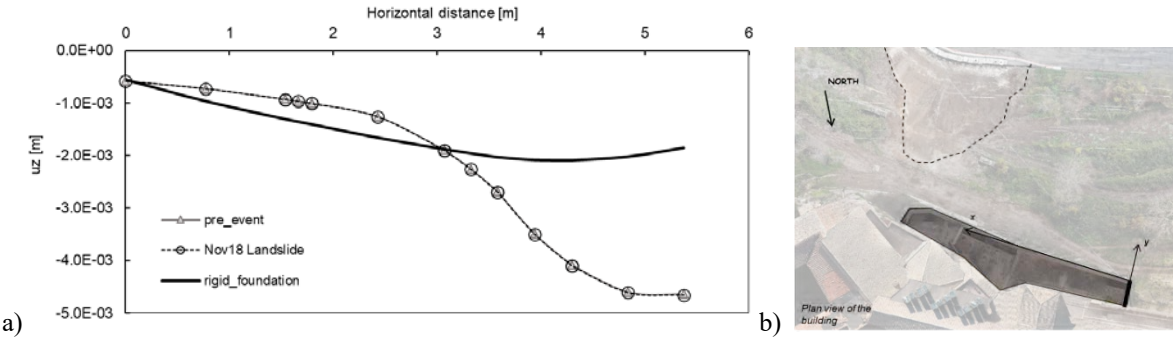


Figure 4: Vertical displacement in the three scenarios

5 CONCLUSIONS

In this work a fully coupled soil-structure interaction analysis was performed, in order to determine possible effects of a landslide occurred near a monumental building. During post-event surveys some damage was identified and possible interaction with the slope, that might have worsened the safety conditions of the structure, had to be evaluated and/or excluded.

A semi-automatic procedure, stemming from laser scanner survey, allowed to build a three dimensional model in which the geometrical complexity of the structure and the interacting

rock and soil strata was preserved and reproduced. A series of preliminary back analyses were performed to get an *a-posteriori* definition of the mechanical properties of the soil and of the triggering condition of the event. A fully coupled geotechnical and structural finite element analysis was then performed in order to have an insight into the possible evolution of damage to identify its causes. The analysis was carried out considering the different stages that characterise the evolution of the site, from the construction of the structure to the occurrence of the landslide. The results show that the structural damage detected in the survey should be ascribed to foundation differential settlements occurred at the construction stages, due to some remarkable heterogeneity of the local subsoil, thus excluding any landslide-related worsening effect.

Acknowledgements. This research has been funded by the Regione Lazio SiCura 2018-2020 (Tecnologie sostenibili per la protezione SIsmica del patrimonio Culturale).

REFERENCES

[1] Puzrin, A. M., Alonso, E. E. and Pinyol, N. M. *Geomechanics of failures*. Springer Science & Business Media, (2010).

[2] Canuti P., Margottini C., Fanti R. and Bromhead E.N. Cultural Heritage and Landslides: Research for Risk Prevention and Conservation. In: Sassa K., Canuti P. (eds) Landslides – Disaster Risk Reduction. Springer, Berlin, Heidelberg (2009).

[3] ISPRA. Landslides in Italy. Special Report 2008; ISPRA: Roma, Italy, 2008; ISBN 978-88-448-0355-1.

[4] Negulescu, C., Ulrich, T., Baills, A., and Seyedi, D. M. Fragility curves for masonry structures submitted to permanent ground displacements and earthquakes. *Natural hazards* (2014) **74**(3): 1461-1474.

[5] Palmisano, F., Vitone, C., and Cotecchia, F. Assessment of landslide damage to buildings at the urban scale. *Journal of Performance of Constructed Facilities* (2018) **32**(4):04018055.

[6] Parisi, F., Galasso, C., and Sabella, G. Fragility of reinforced concrete framed structures to flow-type landslides. In: *12th International Conference on Applications of Statistics and Probability in Civil Engineering (ICASP12)* (2015).

[7] Ferlisi, S., Nicodemo, G., Peduto, D., Negulescu, C., and Grandjean, G. Deterministic and probabilistic analyses of the 3D response of masonry buildings to imposed settlement troughs. *Georisk: Assessment and Management of Risk for Engineered Systems and Geohazards*, (2019), 1-20.

[8] Fargnoli, V., Boldini, D., and Amorosi, A. Twin tunnel excavation in coarse grained soils: observations and numerical back-predictions under free field conditions and in presence of a surface structure. *Tunnelling and Underground Space Technology* (2015) **49**: 454-469.

[9] Zienkiewicz, O.C. and Taylor, R.L. *The finite element method*. McGraw Hill, Vol. I., (1989), Vol. II, (1991).

[10] Griffiths, D. V. and Lane, P. A. Slope stability analysis by finite elements. *Geotechnique* (1999) **49**(3), 387-403.

[11] Lasciarrea, W. G., Amorosi, A., Boldini, D., de Felice, G., and Malena, M. Jointed Masonry Model: A constitutive law for 3D soil-structure interaction

analysis. *Engineering Structures* (2019), **201**: 109803.
[12] Sangirardi, M., Malena, M., and de Felice, G. (2019) Settlement-induced crack pattern prediction through the jointed masonry model. In: *AIMETA 2019 XXIV conference. The Italian Association of Theoretical and Applied Mechanics, Rome, Italy* (2019).
[13] Castellazzi, G., D'Altri, A. M., de Miranda, S., and Ubertini, F. An innovative numerical modeling strategy for the structural analysis of historical monumental buildings. *Engineering Structures* (2017) **132**: 229-248.
[14] Morgenstern, N.U. and Price, V.E. The analysis of the stability of general slip surfaces. *Géotechnique* (1965) **15**(1): 79-93.
[15] NTC, 2018. Ministero Infrastrutture e Trasporti (MIT). D.M. 17.01.2018. Norme Tecniche per le Costruzioni. Rome, Italy.

12th International Conference on Structural Analysis of Historical Constructions
SAHC 2020
P. Roca, L. Pelà and C. Molins (Eds.)

POST - EARTHQUAKE RECONSTRUCTION OF THE HISTORIC CITY CENTRE OF L'AQUILA: A PROPOSAL CONCERNING THE RUBBLE TRANSPORTATION PROBLEM

S. DI MARCO [1], M. A. BRAGADIN [*2]

[1] Department of Architecture
Alma Mater Studiorum University of Bologna
Viale Risorgimento 2, 40136 Bologna, Italy
e-mail: serena.dimarco@studio.unibo.it, www.unibo.it

[2] Department of Architecture
Alma Mater Studiorum University of Bologna
Viale Risorgimento 2, 40136 Bologna, Italy
e-mail: marcoalvise.bragadin@unibo.it, www.unibo.it (*corresponding author)

Keywords: Historical city, Earthquake, re-construction, demolition, L'Aquila

Abstract. *Post -earthquake reconstruction of the historic city Centre of L'Aquila, Italy, can be considered as the largest building site now under operation in Europe. The earthquake that hit the city of L'Aquila on the 6th April 2009 generated a so-called seismic crater that comprises 56 municipalities and concerns an area of almost 2.400 Km2. The earthquake of 2009 destroyed or severely damaged all historic buildings of the city Centre. Nowadays, in 2020 there are more than 8.000 completed construction projects that produced almost 4.000.000 t of removed rubble. The reconstruction process of L'Aquila has been soon defined as "the biggest construction site of Europe". This experience of managing a huge number of construction projects in the same town highlighted the need of a multi-project coordination of the re-construction activities, and a central co-ordination office has been created. Problems concerning the co-ordination of many construction sites that are located very close to each-other are many and are related to the organization and sharing of different resources: space for tower cranes, access routes for vehicles, space for temporary scaffoldings and space for debris storage and disposal. The programme management of these production resources needs to be based on a General Management plan that is proposed. In particular, the problem of rubble production, transport and storage has been addressed in the plan proposition. In fact, the production, transportation and storage of rubble produced by construction operations can be considered one of the main criteria of the multi-project optimization process needed for the co-ordination of the city reconstruction. As a pilot study, a simulation of project co-ordination of an urban area that includes eleven building blocks under re-construction has been performed with the traditional resource levelling procedure. Therefore, the reconstruction programme schedule of the area has been optimized considering the process constraints due to quantitative limits of rubble transportation and disposal.*

1 INTRODUCTION

Reconstruction following a destructive natural hazard is of paramount importance for human

life and built environment. The post - earthquake reconstruction of the historic city Centre of L'Aquila, Italy, can be considered as the largest building site now under operation in Europe. The earthquake that hit the city of L'Aquila on 6th April 2009 generated a so-called seismic crater that comprises 56 municipalities and concerns an area of almost 2.400 Km2. The earthquake of 2009 destroyed or severely damaged all historic buildings of the city Centre. After the seismic event of 2009 the reconstruction phase took place in two times. Firstly, soon after the earthquake, the reconstruction focused on timely interventions of safety works to prevent additional collapses of damaged buildings. After this, in 2010 started the reconstruction process concerning the renovation or reconstruction of damaged and collapsed buildings. Nowadays, in 2020 there are more than 8.000 completed construction projects that caused the removal of almost 4.000.000 t of rubble. The reconstruction process of L'Aquila has been soon defined as "the biggest construction site of Europe" [1]. This experience of co-ordination of a huge number of building project in the same urban area highlighted the need of multi-project coordination of the reconstruction activities and a municipality project co-ordination office has been created [2][3][4]. Therefore, a general construction site plan has been proposed, with the aim of the co-ordination of the thousands of contemporary construction sites under operation [1]. The co-ordination of many construction projects that are located in the same town and near to each-other is needed to manage and share different and scarce resources: space for tower cranes, access routes for vehicles, space for temporary scaffoldings and space for debris storage, transportation and disposal. In particular, the problem of rubble productions, storage and transportation has been addressed in the presented pilot study. A simulation of project co-ordination in an urban area (termed compartment by the municipality project coordination office), composed by eleven building blocks under re-construction has been addressed. The debris production, storage and transportation process has been optimized by application of the traditional multi-project resource allocation process. Considering a specific time frame, the rubble production process can be planned for each construction site. Then the multi-project schedule is optimized considering the quantitative constraints of on-site rubble storage and transportation to the sanitary landfill.

2 THE RECONSTRUCTION OF THE HISTORIC CITY CENTRE OF L'AQUILA

The approach adopted by the Municipality of L'Aquila for the reconstruction of the historic city Centre after the earthquake of 2009 was based on extraordinary regulations that introduced the Reconstruction Plan as an urban planning tool by establishing objectives such as: the socio-economic recovery of the city, the redevelopment of the town and the return of the population to homes damaged by the earthquake [3]. The Reconstruction Plan was defined as a technical tool in order to establish some procedures for the reconstruction. The chosen strategy for the reconstruction of the historic city centre and of the surrounding hamlets, entailed as a first step the definition of the perimeter of the historic city of L'Aquila and of the surroundings. Therefore, various reconstruction areas have been identified. The idea was of favoring the direct and free action of restauration and building rehabilitation of single private owners, without limiting their actions in the framework of the national and local building regulations. The complete overview of the planned and in-progress construction projects of the city was provided by a local project coordination office of the municipality, termed "Supercantieri" [3], [4], [5], [6].

The observation of the complicated development of the reconstruction process of the historic City Centre of L'Aquila [1], has highlighted the need of a General Reconstruction Plan like the one presented by the Municipality of Villa Sant'Angelo, a small town nearby L'Aquila. The General Construction Plan of Villa Sant'Angelo [7] was developed with the aim of satisfying the needs of the owners and of the construction companies that are operating simultaneously for the town reconstruction. A need of coordination, indeed, arises when there are many construction projects operating on nearby sites or in a single building block. For instance, the operating area of tower cranes needs to be planned to avoid clashes and hazards in the interfering areas of the lifting machines. Another case concerns the incorrect positioning of a tower crane in a construction site that can hinder the installation of other construction equipment in the adjacent construction sites.

The proposed general construction plan provides for a series of graphic layouts concerning [7]:

- division of the town into transit areas with the aim of better organizing the layout of construction spaces;
- identification of the entries to the historic center and of the main driveways, with the indication of the minimum roadway dimensions;
- identification of the active construction sites;
- indication of the spaces to be allocated to individual construction sites and their equipment and temporary facilities (cranes, storage areas, scaffolding);
- preparation of a plan for emergencies;
- detailed assessment concerning the dimensions of the roads and the consequent maximum size of the scaffolding that can be installed to allow the passage of vehicles.

Actually, without a detailed general construction plan the post-earthquake reconstruction of L'Aquila was developed not without difficulties. The effect of this was that the choices of the construction projects that first received the state funding and the notice to proceed, may have hindered the process organization of the adjacent construction projects, therefore delaying the execution of the other works.

3 THE GENERAL CONSTRUCTION PLAN OF RECONSTRUCTION: A PROPOSAL

In the research work under this paper, the development of a General Construction Plan for the reconstruction of the historic city centre of L'Aquila is proposed [1]. The aim is to develop an approach and a tool that can give to construction companies and consulting professional the fundamental technical indications to install and operate more efficient and more safe construction projects.

A sector of the central axis of the historic center of the city has been chosen for the proposed pilot application and study. The central axis is an area in the historic city centre of L'Aquila which extends along the main street of the city (Corso Vittorio Emanuele). This is the fulcrum of the city but at the same time the most problematic area, presenting almost all the characteristics of all the historic city centres: narrow streets, structural units of buildings belonging to different historical periods, different construction techniques etc. Then, new earthquake – related characteristics have been added to this: the installation of general safety

provisions as large shoring and scaffoldings, the presence of dangerous buildings, of ruins on the ground and in the streets, of hazardous and forbidden areas. In addition to this, the contemporary presence of a multitude of activities and different operators (Fire Brigade and Army forces, private citizens, professionals, a large number of workers, etc.). In order to better manage the reconstruction of the central axis, the Municipality has provided for the subdivision of this area into the so called "compartments", each of which has different dimensions and characteristics [3]. The presented pilot study considers only one compartment (the A9) of the ten of the urban sector (fig.1).

The proposed general construction site plan develops in two parts: a cognitive section and an operational section.

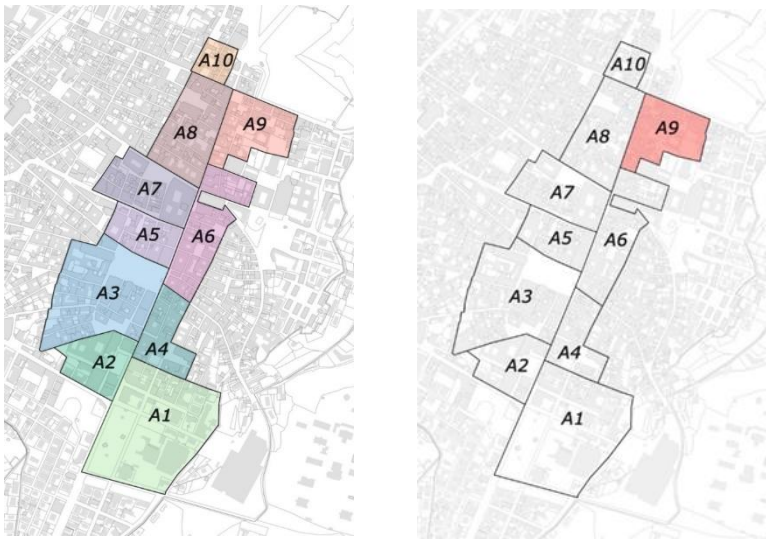


Figure 1: compartments of the old town of L'Aquila [3] [5]

A) Cognitive section. The first step of the cognitive phase involves the identification of the sector within the urban area of the historic city, the mapping of the building aggregates that are inside it and their compliance to building safety standards. After this, the following features are identified: the possible entries to the sector; the direction of travel and the driveways (of which the minimum size is reported). In this way it is possible to establish which roads should be closed because of construction works and which type of vehicles can circulate (fig.2). In analyzing the urban viability, the plan detects the areas that can be used as operational logistic centers for the construction sites of the sector due to their size and accessibility. The same study includes all those areas of reduced dimensions such as internal courtyards, open spaces, small squares that can be used for the installation of any construction equipment and temporary infrastructure. The aim is to produce a complete knowledge of the construction – related characteristics of the urban sector.

B) Operational section. The operational section indicates the provisions relating to the construction sites of the building aggregates. Firstly, the hypothetical positions of the tower cranes of each building aggregate are defined, considering they are all simultaneously operating. The interferences between the cranes are then evaluated: if these are such as not to allow the activities to be carried out simultaneously, a priority of

intervention between the construction projects needs to be assessed, eventually indicating which project can start as first the project operations and which has to remain idle or can only start after the completion of the preceding one. Therefore, a sequence of construction operations can be defined because of the priority of installation of lifting equipment, usually indicating two phases of construction: in the first step the predecessor construction projects are executed, in the second step the successor projects starts the operations (figure 3).

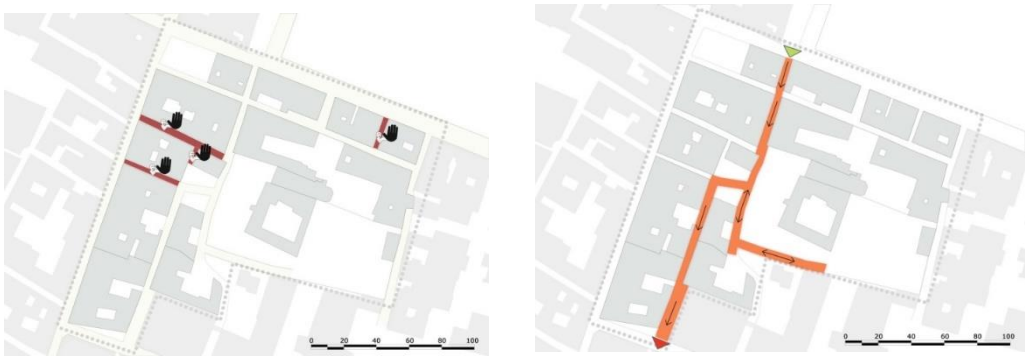


Figure 2: Sample of street categorization inside compartment no. A9



Figure 3: Compartment A9. Tower cranes general plan – phase 1

In the Cognitive section, the definition of the types of scaffolding is of capital importance to allow easy and safe traffic to and from construction sites and to permit the passage of emergency vehicles. Due to the presence of narrow roads, scaffoldings with a short span between the struts at the basis are preferred. The contractors must therefore install scaffoldings that fit the maximum overall basis dimension indicated in the general plan.

When the plan has set the admissible type of scaffolding for each building, the actual width of the roads can be measured considering the space occupied by the temporary provisions. Therefore, the type and size of the vehicles that can transit need be described in the plan. This

is very important because the type of roll-off or site boxes for temporary containment of rubble is planned based on the access roadways to the construction site and on the available space on site.

An estimation of the quantity of debris produced by each building block is needed. The quantity of debris produced by construction operations in each building block is of difficult estimation. As a first estimate, it is possible to quantify the rubble produced by each building block depending on the level of damage caused by the earthquake. A research by the "Istituto per le Tecnologie della Costruzione" and the Italian national "Fire Brigades Corps" [8] found that the quantity of debris caused by the Abruzzo earthquake of 2009 can be computed as a percentage of the gross volume of the building depending on the level of damage. As the complete data concerning the level of damage of each building as detected in the survey performed after the seismic event with the AeDES data sheets [9] were not available for the authors, an estimation of the maximum percentage of debris for each condemned building was used based on the results of the Fire Brigades research [8]. Following the procedure proposed by the Fire Brigades, the quantity of rubble produced by each condemned building having the maximum level of damage (L5), is a rate of 1% of the gross volume of the building itself. Therefore, after the having evaluated the gross volume of each building of the block, the quantity of the rubble produced by each construction project can be quantified (table1). Note that it is assumed that the rubble considered is completely produced by the construction project instead of being produced by the seismic event.

Therefore, an evaluation of the space needed for debris storage on site is detected. The number, the size and available dimensions of debris containers (roll-offs) that can be placed on site is then detected, and then the maximum quantity of debris that can be stored before the transportation to the disposal point can be assessed. The number and size of containers depends on the available space on site, on the size of access roadways. The obstruction of roads due to scaffoldings and shoring of buildings and the availability of maneuver area for trucks should be also taken into account.



Figure 4: Building Block A9. Tower cranes general plan – phase 2

With these assumptions and data it is possible to estimate the maximum amount of rubble produced by each building block. Based on these results, it is possible to estimate the size and number of roll-offs required.

4 THE TRANSPORT PLAN FOR RUBBLE DISPOSAL – PROPOSED APPROACH

One of the main problems in the management of post-earthquake re-construction is the disposal of huge quantity of rubble. As before mentioned, L'Aquila had the greatest damage in terms of volume of rubble compared to all the other municipalities of the seismic crater. Approximately, a grand total of 1,500,000 m3 of rubble have been estimated. Two different stages can be identified for the removal of rubble. The first one concerns rubble deriving from earthquake collapses, or safety provisions and demolition of unstable buildings. In this phase the rubble disposal is managed by state-owned agencies, Army – Corps of Engineers etc. The second one entails the disposal of rubble produced by the renovation and rehabilitation projects of private owned buildings, managed by contractors [10]. In the L'Aquila experience of 2009 and after that, in the experience of the seismic events that affected central Italy in 2016, both phases required long waiting times, consequently slowing down the commencement and the duration of re-construction projects. The causes can be found in bureaucratic issues and in the long time needed to find the locations for rubble storage centers. In the L'Aquila case, the rubble deriving from the reconstruction projects of private owned buildings was delivered to 90 collection points of which only 41 were located in the province of L'Aquila. The other ones were located faraway in the Abruzzo region. The distance of the rubble collection points from the historic city is one of the causes of the increase of time needed for reconstruction, and at the same time caused a vehicular overload of roads [6] [7]. On the other hand, the management of the rubble disposal caused by the 2012 earthquake in the Emilia region was considered a success. Only one year after the Emilia main seismic event, 90% of the rubble had been removed. This was possible because the Municipalities had prepared a plan with a precise sequence of operating phases: with a "request to remove rubble" the owners of the buildings were able to report to their municipal administration the presence of rubble; therefore, following an inspection on site by officers, the waste service manager and the municipal administration assessed the quantity and quality of the waste to be removed and planned the specific removal operations, writing them down in a numbered list, so as to establish priorities [11].

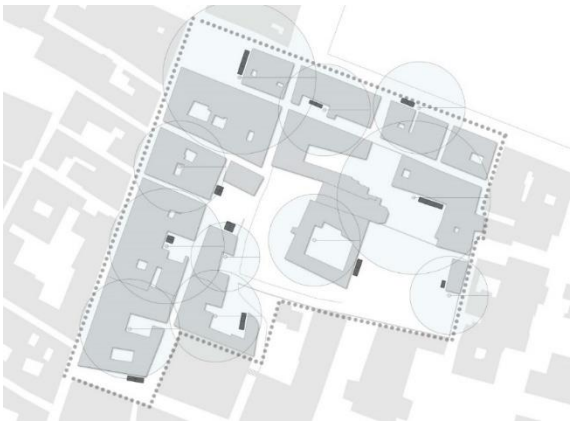


Figure 5: compartment A9. Roll-offs locations

Therefore, it is proposed to apply a new approach to the L'Aquila management method, to be simulated in the case study of the historic city center of L'Aquila. The method is based on

the development of the following three strategic choices.

Table 1: rubble quantities evaluation and available storage on site

building block	*gross building area* (m2)	*mean building height* (m)	*gross building volume* (m3)	*rubble quantity* (m3)	*skip dimensions*	*skip capacity* (m3)	*skip number*	*total quantity of rubble storage on site*
1	1556	8	12448	125	2,30 x 4,30	6	2	12
2	1753	9	15777	158	1,70 x 3,50	2	2	4
3	866	9	7794	78	2,25 x 3,50	4	2	8
5	1684	9	15156	152	2,30 x 4,30	6	3	18
7	743	9	6687	67	1,70 x 3,50	2	2	4
8	562	9	5058	51	2,25 x 3,50	4	2	8
10	1143	9	10287	103	2,30 x 4,30	6	3	18
11	135	9	1215	12	2,25 x 3,50	4	1	4
12	722	6	4332	43	2,30 x 4,30	6	2	12
13	427	9	3843	38	2,30 x 4,30	6	2	12
14	729	9	6561	66	2,30 x 4,30	6	2	12

4.1 Rubble transfer points

In order to limit as much as possible the vehicles overload of roads, it is proposed to identify a set of temporary transfer points of rubble near the historic center. Each transfer point can collect the rubble coming from a certain number of sectors. In these collecting points rubble from the private owned construction projects will be stored and then transported by larger vehicles to the local collection points identified by the Municipality. The central axis of L'Aquila can be divided into transit areas and for each area a temporary storage site is indicated in the plan. The plan introduces also a transport organization of the travelling paths of each single vehicle that maintains the existing one-way streets and travelling directions that operate before the seismic event. The size and the boundaries of the urban areas have been identified in the plan based on a balance of the distribution of the quantities of rubble of each transfer point. After the identification of the travel paths of vehicles, a traffic analysis of the compartment no. 9, included in transit zone 1 is performed. Therefore, the driveways that connect the compartment with the temporary transfer point are studied. Two different paths are identified based on the positioning of building blocks. The two path are the only possible routes for vehicles used for the rubble disposal.

4.2 Rubble transport organization

The second strategic choice concerns the transport organization: only one vehicle is allowed for each construction site. This provision helps surely the reduction of the environmental impact caused by the traffic of construction vehicles for the reconstruction, but also the following objectives related to the negative aspects of the traffic of construction vehicles in urban areas: a) traffic congestion; b) noise and air pollution; c) car accidents. It should be observed that only in sector 9 the plan indicates the contemporary presence of 11 construction projects in the first phase, and approximately a similar number of projects can be forecasted for all other sectors of the central axis. Therefore, it is clear that the issue of the rubble transport must be addressed with the aim of limiting the traffic in order to manage the rubble removal in a better and safer way. The proposed optimized schedule can be performed with only one vehicle per

compartment.

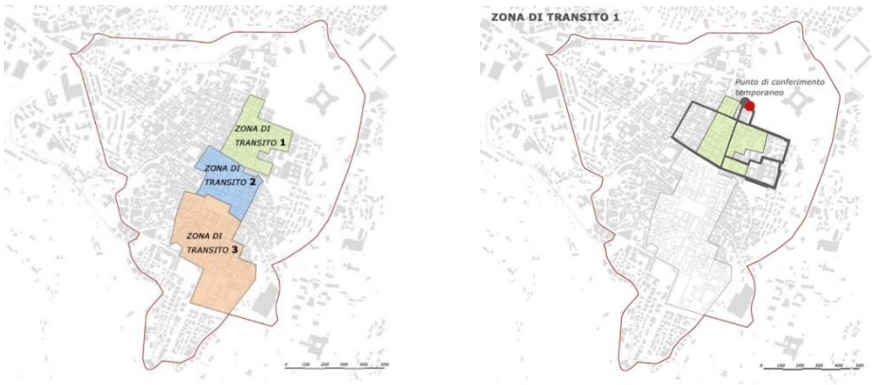


Figure 6: Compartment A9. Transit zone no.1

4.3 Demolition and construction processes management

Finally, the project choices concerning the production of rubble on site is strictly connected to the constraints and decisions previously mentioned. The provision concerning the possibility of using only one vehicle per site, and the available size and number of roll-offs for the rubble storage on site, indicates that a storage limit of debris needs to be set for each construction site as a process constraint. Note that Italian law D.lgs. no. 152/2006 concerning waste management allows a max quantity of 30 cubic metres of waste to be stored on site for a max duration of one year. Therefore, the demolition and construction processes that produce rubble should be optimized for each project, and the number of working crews and their productivity should be planned and scheduled for each working day. This optimization process can be performed with the following steps. Firstly, the type of vehicle and its load carrying capacity needs to be set for each construction project. Then, the lengths of the routes from the site to the rubble transfer point and back to the site should be assessed. The time taken to load / unload the rubble should be estimated, together with the available storing capacity on site. With these assumptions it is possible to determine the maximum amount of rubble that can be produced, stored and transported on each working day and consequently, a multi-project schedule of the demolition phase can be developed.

5 PILOT STUDY

The pilot study considers a simulation of a project coordination activity in the historic city centre of L'Aquila. A compartment that includes eleven building blocks has been considered and a proposed multi-project schedule has been developed with the aim of optimizing the re-construction and demolition processes. The programme schedule, or multi-project schedule, has been developed by optimizing the co-ordination of the single building blocks activities with the traditional resource levelling technique [12]. Therefore, the storage and transportation of rubble that needs to be removed or that is produced on site can be considered a basic criterion for the multi-project optimization process.

Firstly, the programme constraints have been identified for each building block and for each urban area (compartment). The maximum rubble quantity that can be stored on site can be

computed by the analysis of the space availability for skips or open-top roll-offs or dumpsters. Therefore, the size and quantity of skips for each size can be assessed (table 1). The project constraints concerning the rubble transportation are then identified. The type of vehicle and their load carrying capacity is indicated in the plan. Therefore, the number of trips per day needed to haul the rubble stored on site can be computed (table 2). Those data indicate the maximum productivity level that can be achieved by each re-construction project.



Figure 7: Compartment A9. Travel paths A and B

Table 2: Programme constraints

Constraints per area		**area A9**										
max limit of rubble transportation	*for each area*	*Area A9*										
number of trips	for each area per day	25										
quantity limit per working day	for each area	100										
	building block		***1***	***2***	***3***	***5***	***7***	***8***	***10***	***11***	***12***	***13***	***14***
max storage	*for each building block*												
roll-offs size and quantity	for each building block		12	4	8	12	4	8	12	4	12	12	12
max limit of rubble transportation	*for each building block*												
type of vehicle and load carrying capacity	for each building block		4,7	4,7	4,7	4,7	4,7	4,7	4,7	4,7	4,7	4,7	4,7
number of trips	for each building block		3	1	2	3	1	2	3	1	3	3	3
max quantity per working day	for each building block		*14*	*4,7*	*9,4*	*14*	*4,7*	*9,4*	*14*	*4,7*	*14*	*14*	*14*

Secondly, the duration of project activities can be evaluated. It is assumed that all the rubble to be transported is produced by the demolition of masonry structures for the reconstruction and rehabilitation of building structures. The labor-days needed to complete each demolition activity can be easily estimated. The number of masons allocated to each demolition activity is set depending on the amount of work to be performed. Therefore, the duration of each activity of the project can be evaluated. At the same time, the rubble produced in each working day by each project activity can be estimated (table 3).

The optimization process can be performed with the traditional project resource levelling procedure [12]. The multi-project optimization can be easily solved with the eleven contemporary activities initially performed starting at the same time. The activity network computations produce an output of 46 days to complete the programme, that is the duration of the longest activity (B2) and the critical path (figure 8). The quantity limit of rubble that can be produced per day by the entire multi-project programme can be set by assuming a maximum number of 5 trips of load carrying vehicles. As each small truck can haul 4,7 m3 of rubble, the max quantity per day is 23.5 m3. Then, by shifting non-critical activities with the priority criterion of the max rubble quantity per day the programme levelling can be performed. After

only 7 iterations the result is displayed in figure 8. The optimization process levelled the peaks of rubble removal, achieving an even distribution of demolition works always under the max limit of 5 trips per day per compartiment, causing no delays to the total multi-project duration of 46 days.

Table 3: Activity durations and rubble production

Activity number	Activity id.	activity description	measure unit	Rubble quantity	unit price €	sum total €	labor percentage %	labor cost	labor cost per day	men-days	number of workers	activity duration	rubble quantity per day
1	B1	**Building Block 1**	m3	125,00	146,63 €	€ 18.328,75	79%	€ 14.479,71	€ 200,00	72,4	3	**25**	5,00
2	B2	**Building Block 2**	m4	158,00	146,63 €	€ 23.167,54	79%	€ 18.302,36	€ 200,00	91,5	2	**46**	3,43
3	B3	**Building Block 3**	m5	78,00	146,63 €	€ 11.437,14	79%	€ 9.035,34	€ 200,00	45,2	2	**23**	3,39
4	B5	**Building Block 5**	m6	152,00	146,63 €	€ 22.287,76	79%	€ 17.607,33	€ 200,00	88,0	3	**30**	5,07
5	B7	**Building Block 7**	m7	67,00	146,63 €	€ 9.824,21	79%	€ 7.761,13	€ 200,00	38,8	1	**39**	1,72
6	B8	**Building Block 8**	m8	51,00	146,63 €	€ 7.478,13	79%	€ 5.907,72	€ 200,00	29,5	2	**15**	3,40
7	B10	**Building Block 10**	m9	103,00	146,63 €	€ 15.102,89	79%	€ 11.931,28	€ 200,00	59,7	3	**20**	5,15
8	B11	**Building Block 11**	m10	12,00	146,63 €	€ 1.759,56	79%	€ 1.390,05	€ 200,00	7,0	1	**7**	1,71
9	B12	**Building Block 12**	m11	43,00	146,63 €	€ 6.305,09	79%	€ 4.981,02	€ 200,00	24,9	3	**9**	4,78
10	B13	**Building Block 13**	m12	38,00	146,63 €	€ 5.571,94	79%	€ 4.401,83	€ 200,00	22,0	3	**8**	4,75
11	B14	**Building Block 14**	m13	66,00	146,63 €	€ 9.677,58	79%	€ 7.645,29	€ 200,00	38,2	3	**13**	5,08

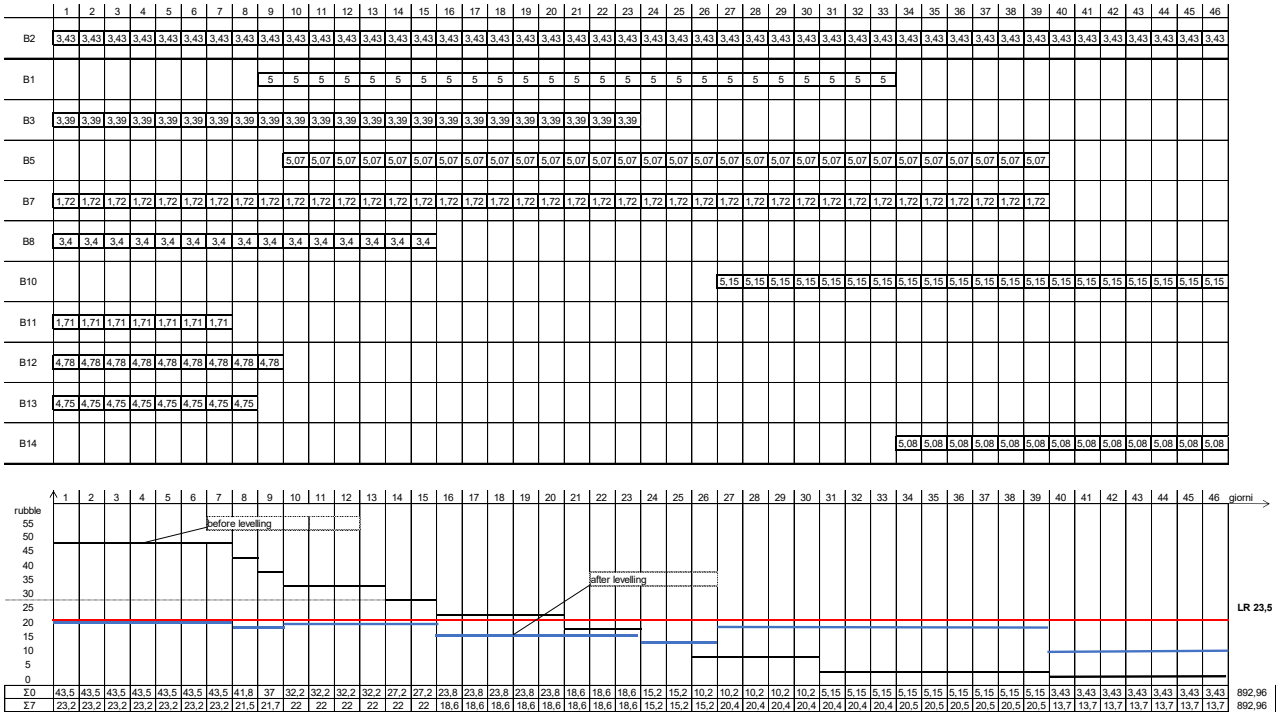


Figure 8: Compartment A9. Schedule optimization procedure

6 CONCLUSIONS

The lesson learned from the re-construction of the historic city centre of L'Aquila has been studied, focusing on the problem of managing a huge number of contemporary building sites in the same location. The study highlighted the need of a multi-project coordination approach of

the reconstruction activities that has been implemented by a municipal project coordination office. Anyway, as the co-ordination of many construction sites that are located very close to each-other needs the managing and sharing of different scarce resources: space for tower cranes, access routes for vehicles, space for temporary scaffoldings, space for rubble storage and transportation, a more detailed General Plan is proposed. In particular, the General Plan could address the problem of rubble production, storage and transportation, as a set of basic criteria for the multi-project optimization process. A simulation of project coordination of an urban area that includes eleven contemporary construction projects has been performed with the traditional resource levelling procedure. Therefore, the reconstruction multi-project schedule of the area can be optimized considering the constraint due to quantitative limits of rubble transportation and disposal processes.

REFERENCES

[1] S. Di Marco, "Construction Site Planning for the Reconstruction of a Historic Earthquake City: the Case Study of L'aquila", IN_BO, Vol. 13, pp. 82-93, (2018).
[2] L. Bosher, J. Meding, C. Johnson, F. Farmaz, K. Chmutina, Y. Chang-Richards, "Disasters and the Built Environment" 1st Edition, CIB Publication 410 (2016).
[3] Assessorato alla Ricostruzione e Pianificazione, Settore Pianificazione e Ripianificazione del territorio, Comune di L‟Aquila, Il Piano di Ricostruzione dei centri storici di L‟Aquila e Frazioni, L‟Aquila, 2011
[4] Angeletti P., Cherubini A., Cifani G., De Marco R., Ferrini M., Fish G., Iacovone D., Lemme A., Petrini V., Fabrizi V., Santoro C., Miozzi C., La Ricostruzione dei centri storici di L'Aquila e delle sue frazioni, L‟Aquila, 2013
[5] Criteri operativi per la programmazione della ricostruzione privata nei centri storici del comune di L‟Aquila, a cura dell‟Assessore Pietro Di Stefano, L‟Aquila, 2013.
[6] Protocollo di intesa Emergenza sisma Abruzzo 2009: ottimizzazione delle attività relative alle misure per la salute e sicurezza nei cantieri temporanei o mobili, L‟Aquila, 30 novembre 2009
[7] Libro bianco sulla ricostruzione privata fuori dai centri storici nei comuni colpiti dal sisma dell‟Abruzzo del 6 aprile 2009, a cura di Cineas, Fintecna e ReLUIS, L‟Aquila
[8] SISMA ABRUZZO 2009 – messa in sicurezza degli edifici monumentali: percorso metodologia e tecniche di intervento, atto di convegno, XIV Convegno ANIDIS: L‟ingegneria sismica in Italia, L‟Aquila, 2011.
[9] Linee guida per il rilievo, l'analisi e il progetto di intervento di riparazione e rafforzamento/miglioramento di edifici in aggregato, a cura di ReLUIS, L‟Aquila, 2010.
[10] Manuale Istruzioni – allegati Scheda di accompagnamento al progetto esecutivo ricostruzione per L‟Aquila, a cura dell‟Ufficio Speciale per la Ricostruzione di L‟Aquila, L‟Aquila, marzo 2013.
[11] Soluzioni logistiche e sostenibilità nella costruzione di grandi infrastrutture nei centri urbani: focus sulle esperienze in Emilia-Romagna, a cura di Giarandoni A, Atto di convegno, Bologna, 20 settembre 2017.
[12] Harris R. B. (1978) Precedence and Arrow Networking Techniques for Construction Wiley, New York U.S.

POST-QUAKE SMALL ITALIAN HISTORICAL CENTRES: URBAN RESILIENCE BETWEEN RHETORICS AND REALITY. THE CASE STUDY OF NOCERA UMBRA AFTER THE 1997 UMBRIA-MARCHE EARTHQUAKES

E. CIANCI[1*], C. FONTANA[1], G. OCCHIPINTI[1] AND G. ROMAGNOLI[1]

[1]Institute of Environmental Geology and Geoengineering (IGAG),
Italian National Research Council (CNR) Rome, Italy
e-mail: {eleonora.cianci, cora.fontana, gino.romagnoli, giuseppe.occhipinti}@igag.cnr.it ,
(*corresponding author)

Keywords: Resilient urban planning, Building heritage, Site effects, Post-earthquake reconstruction

Abstract. *The small and medium Italian historical centres are characterized, among other things, by reconstruction that have occurred over the centuries after earthquakes. While earthquakes determine structural damages, human losses and loss of the functionality of an urban system above all, they may create, at the same time, new opportunities if the urban and socio-economical structures are improved during the reconstruction processes as a whole. These processes and the optimal implementation of planning models within them is not straightforward [1], due to that several issues emerge as a challenge of the reconstruction programmes (decision-making processes, general vision for the entire urban system for instance). According to the literature, although a unique definition has not still been coined, resilience can be defined as the capacity of a system (a city) to withstand and restore after a shocking episode (an earthquake). Mainly in the context of cities [2], some approaches have been framed and experimented by other authors [3, 4, 5]. Starting from a short literature review, focuses on theories and methodological approaches to evaluate urban resilience, this work analyses – through an interdisciplinary approach – the case study of Nocera Umbra twenty years after two devastating earthquakes occurred in 1997. The research represents a first attempt that aims at analysing if the implemented reconstruction strategies have made the urban system more resilient with respect to both the built and the socio-economic environment.*

1 INTRODUCTION

Almost all the Italian peninsula is a seismic prone area where one third of the population live into 5.4 million vulnerable buildings [6]. Controversially, an urban or territorial planning project specifically oriented to seismic risk mitigation has not been yet consolidated in Italy. The authors observed that interruption of the urban system functionality due to severe structural damages is one of the most evident aspects in all the main Italian earthquakes [6]. Among the causes, the seismic vulnerability of existing buildings, the lack of risk mitigation policies at the urban scale and the absence of a clear and robust recovery framework, affected all the events. The authors believe that a good reconstruction programme depends not only on improvements at single building scale, despite the common public and private trends, but also on the recovery of the functionality of the urban system as a whole [7]. The relationship between resilience and post-quake recovery is evident if resilience is assumed as the capacity of a system to withstand shocks in terms of recovery or improvement of pre-event conditions and of adaptation and reorganization of the new post-event configuration. Based on that, a simple concept can be coined: as much the system responds positively to the shock as more resilient that system is. On the base of this assumption, the knowledge of the pre-event conditions, in terms of hazard, vulnerability and exposure, is fundamental to assess the response capacity of the urban system after the seismic event. The town of Nocera Umbra, that was hit by two destructive earthquakes the 26th September 1997, has been chosen as case study for this research, that aims, through an interdisciplinary approach among urban planning, engineering and geology, to explore two of the main aspects that contribute to defining urban resilience: disaster's severity (damage condition) and exogenous factors (planning framework, reconstruction strategy and governance) [4].

2 LITERATURE REVIEW - FRAMING RESILIENCE

As a unique and shared definition of resilience is not yet coined, especially in the context of spatial planning and engineering [2], a review of literature on the subject is needed. The concept of resilience has been already developed in different disciplines (psychology, ecology, social science, economics and engineering) since the 70's. Due to the multidisciplinary nature of resilience, mostly fragmented literature focused on natural risks has been produced [4].

Resilience was initially used to define a measure of the persistence of systems and the ability of a system to absorb change and disturbance and still maintain the same relationships between population or state variables [8]. Later, it was defined as the ability of a system to return to its optimal condition in a short period of time [9] or reach advancements [10], after the shock. In the constellation of existing literature is possible to assert that the main difference defining resilience emerges between the engineering approach and the ecological one [3, 4]. The first perspective considers resilience as the ability of a system to recover towards a previous or an improved stable state [11]; while the second perspective as a given ecosystem capacity to reorganize and manage changes in order to maintain the same structure and functions [12]. About this second perspective, an ambitious theoretical perspective was framed by Holling [12] and Gunderson et al. [13], the adaptive cycle: a hierarchical cross-scale structure where natural and human systems are linked in a continuous adaptive cycle of growth (exploitation), accumulation (conservation), release (collapse) and renewal

(reorganization). In their view resilience potentially depends on these four different phases. What is interesting about the concept of the adaptive cycle, is the relation between space and time scale, considering that in all systems adaptation and transformations occur as multi-scalar (spatial and temporal) process [2].

However, in the hazard arena most of the resilience models involved engineered systems [4] that consider robustness, redundancy, resourcefulness, rapidity as fundamental characteristics that define the failure behaviour [11]. As claimed by Cutter et al. [4], these frameworks often fail in capturing pre-event conditions that occur at the local level or to account for the vulnerability or resilience of the environment. This work analyses the two different approaches as separated but often linked theoretical perspectives. Sharing the assumption that resilience has two different qualities: inherent (positive behaviour during non-crisis period) and adaptive (flexibility in response during seismic events) [4], the authors considers resilience as a dynamic process dependent on: 1) pre-event conditions, 2) disaster's severity (damage condition) 3) time(s), the temporal scale from the emergency response and the long-term recovery phase, 4) influences from exogenous factors (planning framework, governance and organizational capacity) during the temporal scale of interest.

3 THE CASE STUDY: NOCERA UMBRA

Nocera Umbra is a small historical town located within the province of Perugia (Umbria Region), Italy. Within the municipality boundaries, an historical centre surrounded by recent periphery and several little hamlets can be identified. This urban setting is typical of the Apennine municipalities of central Italy. On 26th September, 1997, the area between Umbria and Marche (two Italian regions) was hit by two strong earthquakes (MW = 5.7, at 00:33 GMT and MW = 6.0 at 09:40 GMT). In the Umbria region 76 municipalities were considerably damaged. Nocera Umbra was one of the most affected towns (Figure 1).



Figure 1: Umbria Region in Italian territory and epicentral area of 1997-1998 Umbria – Marche seismic sequence. The red circle represents the location of Nocera Umbra. [15]

During the decades before the earthquake, the municipality of Nocera Umbra, as well as other small towns in that region and along the Apennines, was experiencing some socio economics processes: the switch from an agricultural based economy until the '70s to the current more

industrial and tertiary (non-market services) economic profile. By analysing the variation before and after the two seismic events, while the industrial sector did not experience a significant variation, the agriculture sector decreased from 12,9% to 4%, while on the opposite, the market service sector has incremented from 11,8% to 18,3%.
Nocera Umbra municipality has been affected by a depopulation process over decades. An amount of 8.853 inhabitants in 1951 decreased up to the current number of 5.680 inhabitants that corresponds to the population density of 36 inhabitants per square kilometre even if this trend can be considered stable since 1971.

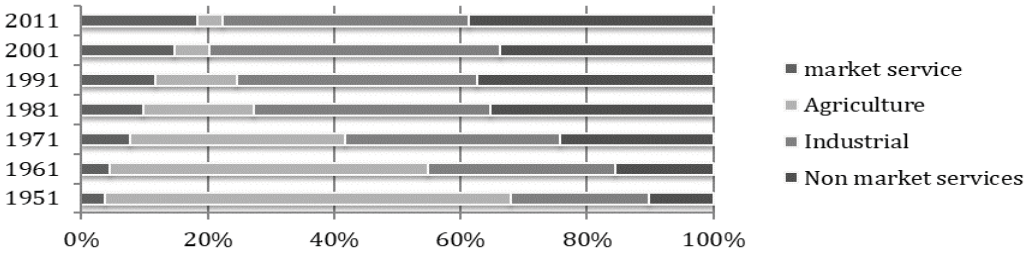


Figure 2 Prevalent economic sectors 1951-2011.

3.1 THE DAMAGE CONDITION

The so-called Umbrian-Marchigiana sequence hit the Central Italy area between September 1997 and April 1998. The reconstructed macroseismic field evidences peaks equal to the IX degree of the MCS scale (Mercalli-Cancani-Sieberg), related to the two earthquakes of 26th September 1997 (MW = 5.7, at 00:33 GMT, and MW = 6.0 at 09:40 GMT). Despite of the relatively modest magnitude of the two seismic events and a more than 10 km distance from two epicentres (13,2 km and 10,9 km respectively [15]), high values of PGA (Table 1) were recorded close to Nocera Umbra as consequence of local seismic site amplifications due to local geological conditions of the area.

Table 1: Main shocks records on 26th September 1997 [15]

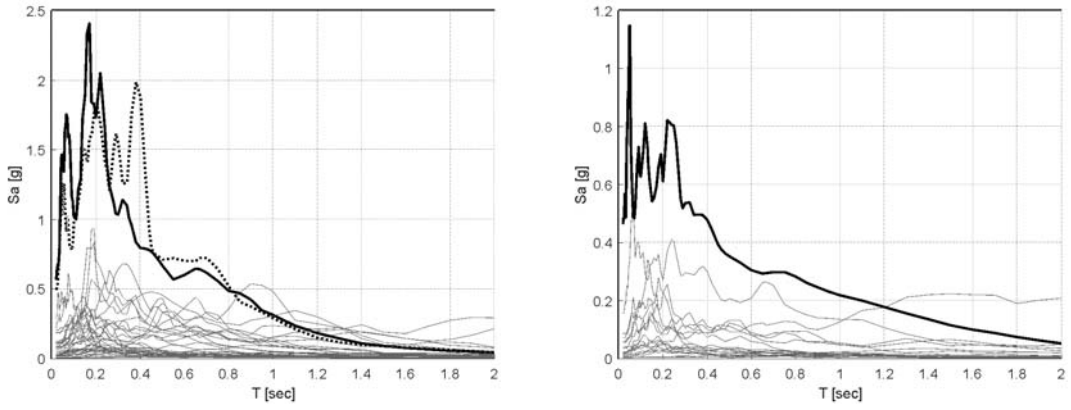
Event		1ST	2ND
ID ITACA		IT-1997-0004	IT-1997-0006
Data		1997-09-26 00:33:11	1997-09-26 09:40:24
Lat.		43.02300	43.03100
Long.		12.89200	12.86200
Deep	[Km]	5.7	5.7
ML		5.6	5.8
MW		5.7	6
Station		NCR	NCR
Soil Class EC8		E	E
Epicenter Distance	[km]	13.2	10.9
Azimuth	[°]	138.3	144.8
PGA	[cm/s2]	387.399	492.165
PGV	[cm/s]	12.676	32.574
PGD	[cm]	1.893	2.601

Table 1 reports some of the properties of the two events. It is worth noting that the two Seismic Stations are placed on Soil Class E (EuroCode8). The linear distance between the

epicentre and the seismic station is expressed in km. The azimuth defines the strike of seismogenic fault planes and it is expressed in decimal degrees. Lastly, the peak ground acceleration (PGA), velocity (PGV) and displacements (PGD) are expressed in centimetres and seconds.

Considering the map of the damages of Nocera Umbra and other close villages [17], a not uniform damage distribution in the area is noticed. Moreover, the site amplification effects, depending on the heterogeneous subsurface geological model structure, must be considered in the damage analysis [16].

The seismic amplifications were estimated by seismic microzonation studies carried out in Nocera Umbra [17, 18]. According to the data, relevant local seismic site amplifications affected extended areas. As an effect of unfavourable geological conditions related to alluvial and colluvial cover terrain, several buildings were heavily damaged or completely destroyed (e.g. the Isola and Nocera Scalo hamlets). On the contrary, despite the historical centre of Nocera Umbra was characterized by a high vulnerability of the buildings, no collapses occurred, probably as a consequence of the discrete condition of the geological substratum. Around the historical city centre collapses and damages affected historical structures and modern buildings that were designed according to the seismic code of that period. The high values of PGA registered by the NCR stations were caused by the amplification of ground motion due to adverse geological conditions related to contact (about 7 m deep) between alluvial cover deposits and weathered geological substratum on geological bedrock [19]. The high damage levels of Nocera Scalo area, an inhabited centre severely struck by the seismic sequence of 1997, is correlated also to liquefaction phenomena related to local geological conditions consisting of recent alluvial sands, containing a shallow ground water table [20]. This data suggest a great influence of site effect on damage patterns, as evidence in other geological context [30] In Figure 3 the earthquakes that affected the municipality of Nocera Umbra are expressed in terms of pseudo-acceleration spectrum in the two components (black continuous line HNN direction and dots line HNE) in comparison to those obtained by all the other stations. As the figures show, even in vertical components, the area was affected by extremely high pseudo acceleration values in range between 0 and 0,2 seconds that generally mark small masonry buildings widely spread in all the Italian territory.



a) **b)**

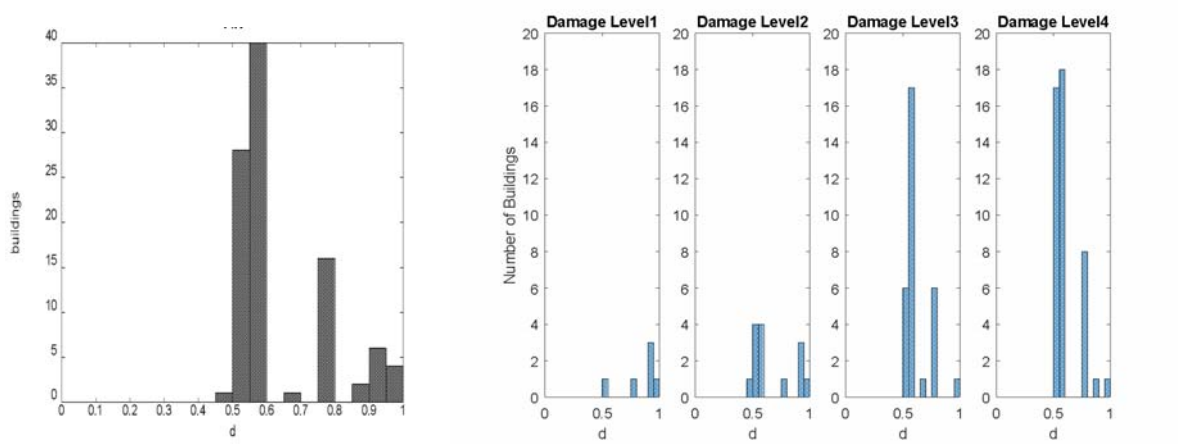
Figure 3: Main shock (**2nd**) response spectra in a) horizontal and b) vertical components

Other authors carried out research on the damaged structures that were struck by the two earthquakes [21]. The authors are aware that the seismic response of masonry structures cannot be described by single structural detail but by the interdependency of all the structural details. In this paper a novel approach is proposed. Each structure is considered in terms of discrepancy from a structural prototype. The prototype is an ideal building characterised by optimal properties that play a fundamental role in the seismic behaviour and can define, ideally, small or neglectable seismic vulnerability. The surveys [22] that were carried out in post-event condition identified the structural characteristics and damages by means of a fast procedure. The procedure was based on a form that assigned different weights to all the possible structural properties of the buildings. Some of these properties have been considered as fundamental in this work and adopted in the next equation. The authors, inspired by basic concepts of nature, namely genes and chromosomes, adopted the above mentioned terms for defining an "optimal gene" that may represent a low vulnerable masonry building [23, 24]. On the other hand, on the base of the same "chromosomes", each building can be defined by its own genes. The aim is to establish a "discrepancy index" that can globally describe the structures and their propensity to damage.

$$d_j = \frac{\overline{\mathbf{g}} \cdot \mathbf{g}_j^T}{\sqrt{\left(\overline{\mathbf{g}} \cdot \overline{\mathbf{g}}^T\right)\left(\mathbf{g}_j \cdot \mathbf{g}_j^T\right)}}$$

In the previous equation the symbols $\overline{\mathbf{g}}$ and $\mathbf{g}_j$ are the "optimal gene" and the j-th "building gene", respectively. The index, that is part of an ongoing research, does not consider different weights for each structural property. The aim is to understand if, globally, all the elements can contribute to the level of damage and if the propension to damage can be expressed without a-priori weights. The presence, or absence, of the following characteristics has been considered: foundations, masonry typology, mortar quality, presence/absence of i) edge beams at floor or roof levels, ii) corners , iii) connections between floors and walls, iv) steel tie-rods at floor or roof levels, v) horizontal loadings, vi) masonry quality, vii) walls geometry, viii) irregular walls distribution, ix) uniformity of the structural typology, x) relevant structural defects. With regard to the buildings that were included in IRP acronym for Integrated Recovery Programmes IRP (L. n. 61/98, L.R. n.15/9) project and on the base of surveys [22] the following histograms show how the structures that were hit by the two earthquakes were majorly marked by low discrepancy indices that represent structures with non-optimal structural properties. The Damage Levels can be synthetized as in the following. Level 1 or Significant Damage. This is defined by cracks and crushes that involve the 30% of structural elements at least. Level 2 or Heavy Damage. Shear cracks in the 30% of structural elements, compressive crushes in 5% of the structural elements, collapse of 5% of the entire building area, out-of-plane displacements up to 5 cm, foundation failures, hydrogeological issues. Level 3 or Extremely Heavy Damage. Shear cracks in the 30% of structural elements of 10 mm, compressive crushes in 10% of the structural elements, collapse of 20% of the entire building area, out-of-plane displacements up to 10cm, foundation failures, hydrogeological issues. Level 4 or Collapse Damage. Collapse of more than 30% of the building. All the analysed structures reported heavy structural deficiencies that probably determined the collapses or damages even in case of unitary discrepancy index, as in Figure 4.b is evident in case of Damage Levels 1 and 2. All the structures that were part of the IRP project were affected by heavy structural deficiencies. The index is part of an on-going

research and the authors are aware that additional comparisons with other real cases are necessary.



a) **b)**

Figure 4: Discrepancy indices of the a) IRP buildings and b) divided in order to the reached damage levels

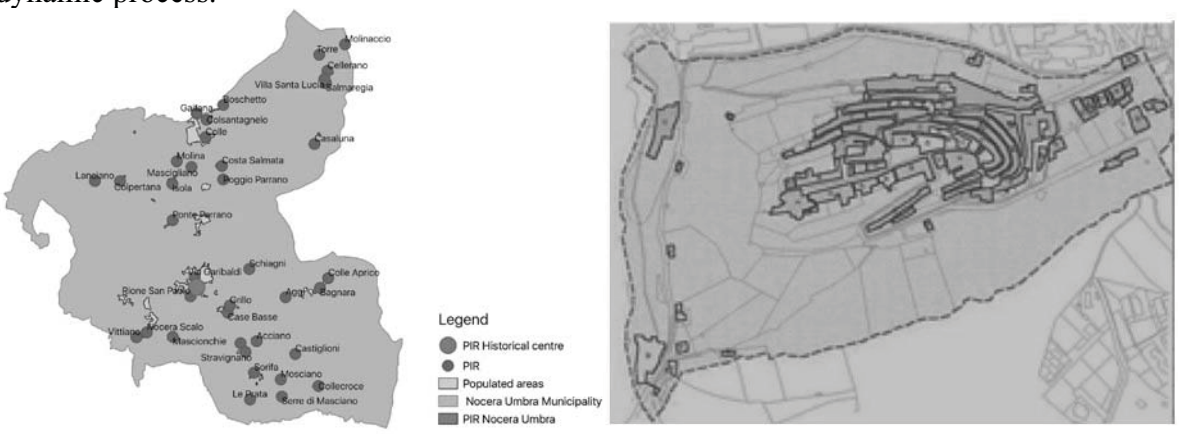
3.2 THE RECONSTRUCTION FRAMEWORK

Although some buildings collapsed as a consequence of the two earthquakes, there were no casualties. Nevertheless, 80% of the population (4,499 inhabitants) was evacuated.

Immediately after the earthquakes, Umbria Region claimed that the reconstruction should have been an opportunity to foster the recovery of the economic activities, improve the quality of the urban fabrics and the connection among the settlements, and reduce the social vulnerability of local communities [25]. After the 1997 earthquakes, the actors in charge of the decision-making process have developed the reconstruction model around three main ambitious goals [26]: 1) subsidiarity governance, 2) transparency and accountability, 3) quality of the reconstruction. While the first two goals are linked to political and governance issues, the third one is strictly related to spatial and physical reconstruction. Through this goal the actors in charge of the reconstruction process aimed from the beginning at preserving the urban legacy of the damaged settlements, together with the cultural and social identity of their communities [26]. The paradigm was 'how it was, where it was'. The reconstruction strategies were based on three macro categories: i) Light reconstruction (OCD n.61, 1997) (i.e. restoration of buildings that were relatively not massively damaged); ii) Heavy reconstruction (L. n.61/98, LR n.30/98, DGR n.5180/98) (i.e. reconstruction of severely damaged isolated buildings, limited to those located outside the integrated recovery programmes); iii) Integrated reconstruction (L. n. 61/98) (i.e. restoration of the historical cores, in terms of architectural and landscape heritage, and socio-economic conditions). The latter represents the most interesting experience and involved more than 40% of the building stock. The integrated reconstruction was implemented through the Integrated Recovery Programmes (IRP). The IRP are planned as tools for programmatic and financial coordination with two purposes: 1) ensure the unitary and coordinated implementation of intervention on private and public buildings, the infrastructural setting and the public spaces; 2) prevent the most affected areas, mainly inner areas or depopulated villages, from becoming abandoned

and vacant. The Reconstruction Observatory that was established for monitoring all the reconstruction process claimed that even though IRP programmes cannot be considered directly as instruments for economic and social development, they can actually act as flywheel to revitalize the villages towards a new economic recovery and re-settlement [14]. From these premise, Umbria Region activated 185 IRP in 22 municipalities of which 41 in the municipality of Nocera Umbra (Figure 5.a). One of the IRP corresponded to the perimeter of the entire historical centre (Figure 5.b).

In order to define the IRP perimeter, the area, any historical urban or rural core or village, should have had at least one of three main features: i) historical and monumental value; ii) landscape or environmental value; iii) socio-economic issues related to post-earthquake needs. Every IRP projects area were composed of both private and public buildings and infrastructures that hosted different urban functions: housing, public services and public spaces, economic activities, social and cultural places and buildings. The interventions on public, private or mixed properties, included within the perimeter area, were organized in Minimum Intervention Units, whose sizing took into account the unitary needs of the organization of interventions under the structural, technical, economic, architectural and urban profile [14]. The innovative aspect of IRP programmes was the aggregation of single buildings towards a systemic urban vision and the definition of recovery mechanism as a dynamic process.



a) b)

Figure 5: Spatial distribution of IRP within a) the boundaries of Nocera Umbra municipalities and b Nocera Umbra Historical centre). (Reconstruction Observatory. Last access, January 2020. Modified)

4 NOCERA UMBRA TWENTY YEARS AFTER

After more than twenty year, some considerations on the reconstruction model and its implementation can be framed: 623 interventions of heavy reconstruction (97%) and 220 of the light (100%) have been concluded. According to the Reconstruction Observatory, 41 IRP have been activated until july 2018, in the Municipality of Nocera Umbra, with an amount of 387 interventions activated, 429 started and 388 concluded (90%). In terms of public buildings 20 upon 25 interventions (80%) have been concluded. While for the cultural heritage the 11% still have to be activated (Figure 7). Generally, even some buildings have to be still reconstructed, the process seems characterized by a satisfactory equilibrium between quality and velocity of the reconstruction [25]. The paradigm “how it was, where it was” has prevented, mainly in the sprawled environment and in the little villages, the triggering of

further process of abandonment, in a territory already heavily affected by depopulation issues [27]. The IRP programme, that was essentially a financial and programmatic project that did not take directly into consideration spatial planning considerations, has represented one of the most innovative reconstruction instruments.

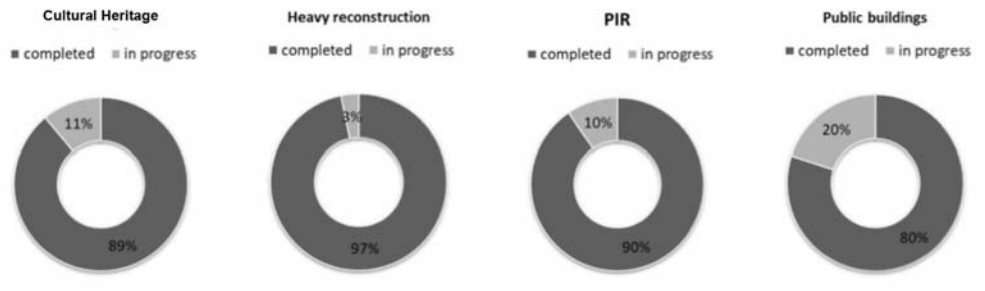


Figure 7: State of the reconstruction. Elaboration by the authors on Reconstruction Observatory data

The Umbria reconstruction strategy produced a complex but coordinated series of interventions, both on private and public building, having also considered the infrastructural and public space systems. Moreover, for the first time after a major earthquake in Italy, the complexity of the post-quake reconstruction of historical centres was recognized, understanding that all the recovery operations should have been planned in an integrated way, through the involvement of different aspects: private and public buildings, cultural heritage, infrastructural systems, and geo instabilities [28]. In this sense the IRP experience could be considered a valid effort in terms of reinforcing urban resilience and testing the response capacity of the local actors involved in the reconstruction process. It is evident that the coordination of IRP projects have functioned in a context made of small towns and villages; moving the scale on a more complex and large urban system, the same structure could not guarantee the same conditions. Additionally, even in the same region, in some municipalities the IRP programmes have been recognized as best practices, while in some others, such as Nocera Umbra, they could be considered not such a successful experience. Immediately after the earthquake the historical centre was closed off to the population for two years, causing the abandon of the old town. The main facilities were dislocated in the outskirts, where people were temporarily living. The reconstruction of Nocera Umbra followed the same strategy of all the other municipalities but experienced several delays due to different factors, such as the lack of IRP coordination and the slow restoration of the historical centre that has been concluded 15 years after only. The historical centre was totally renewed, but depopulated [29]. According to other authors [26] several critical aspects influenced the reconstruction of Nocera Umbra negatively: 1) the structural complexity of the interconnected buildings in the historical centre, that increased the difficulty in establishing the owners unions required for the constitution of the IRP perimeters; 2) the issue of private property owners, because many of the building owners did not dwell in the Municipality of Nocera Umbra, so were not able to follow closely the process; 3) the general lack of institutional capacity of the actors involved in the processes.

5 CONCLUSION

The paper analyses the case study of Nocera Umbra that was hit by devastating earthquakes in 1997 in order to provide a first assessment of the post- earthquake

reconstruction considering two scale of analysis: the single building scale and the broader urban one. Resilience offers a significant paradigm to gain a better understanding in reading the capacity of a system to respond to shocks, mainly in terms of analysis of the damage conditions and the exogenous factors (such as the reconstruction planning framework and the reconstruction governance). Authors focused mainly on the analysis of the reconstruction process and strategies, and their effects on the urban system. In terms of vulnerability of the building heritage, the authors proposed a speditive vulnerability index. The idea is to compare each building with a less vulnerable prototype by means of key features establishing a discrepancy value. This is part of an on-going research and more data and validation are needed. On the other hand, the index can be easily adapted and more terms can be considered in view of geological effects on structures or, more generally, resilience porpoises. Since the research is still ongoing, it is possible to outline only preliminary conclusions, and authors are aware that additional data research, analysis and comparisons with other real cases are needed. About data analysis, one of the issues is the poor quality and the absence in many cases of data before 1997. The consequence is the difficulty to compare the pre- and post-phase, both in terms of physical-spatial and socio-economic outcomes. Nevertheless, is anyway possible to go to some preliminarily conclusive points. Nocera Umbra constitutes an interesting case study that is worth observing. Beside the critical aspects that influenced negatively the reconstruction of Nocera Umbra, the Umbria reconstruction experience was important for post-earthquake Italian cases. It aroused attention to prevention and mitigation seismic risk, in terms of urban and regional planning. For instance, the Regional Law n.11/2005 obliges all the municipalities to enclose the SUM (Acronym for Minimum Urban Structure) in the general regulatory planning tool [25]. This disposal derives from the IRP programmes and, on one hand, facilitates the local governments to cope with seismic risk mitigation issues and, on the other hand, on resilience in terms of relationship between seismic risk mitigation and territorial planning. The obtained results encourage the authors to consider critical the analysis of real cases as useful tool for the development of effective resilience strategies that hopefully can be applied to entire urban areas for seismic mitigation purposes.

Acknowledgments

This research was supported by the Italian Department for Civil Protection (DPC) within the "PON Governance 2014-2020 project on the reduction of seismic, volcanic and hydrogeological risk for civil protection purposes - CIG 6980737E65 - CUP J59G16000160006" (Scientific coordinator for CNR, Massimiliano Moscatelli). Authors would like to thank Fabrizio Bramerini, Sergio Castenetto, Antonella Gorini, Giuseppe Naso, and Daniele Spina (all of them from DPC; F.B. coordinator) for the useful discussions.

REFERENCES

[1] E. Quarantelli, “Converting disaster scholarship into effective disaster planning and managing: possibilities and limitations,” *International Journal of Mass Emergencies and Disasters,* vol. 11, pp. 15-39, 1993.

[2] L. Chelleri, J. Waters, M. Olazabal and G. Minucci, “Resilience trade-offs: addressing multiple scales and temporal aspects of urban resilience,” *Environment and*

Urbanization, vol. 27, no. 1, pp. 181-198, 2015.

[3] G. Cimellaro, C. Renschler, A. Reinhorn and L. Arendt, "PEOPLES: A framework for evaluating resilience.," *Journal of Structural Engineering,* vol. 142, no. 10, 2016.

[4] S. Cutter, L. Barens, M. Berry, C. Burton, E. Evans, E. Tate and J. Webb, "A place-based model for understanding community resilience to natural disasters," *Global environmental change,* vol. 18, no. 4, pp. 598-606, 2008.

[5] O. Kammouh, A. Zamani Noori, G. Cimellaro and S. Mahin, "Resilience Assessment of Urban Communities," *SCE-ASME Journal of Risk Uncertainty Engineering System, Part A: Civ. Eng.,,* vol. 5, no. 1, 2019.

[6] CRESME, "Rapporto sullo stato di rischio del territorio italiano," Rome, 2017.

[7] A. Fiore, C. Suplizio, C. Demartino, I. Vanzi, S. Biondi and V. Fabietti, "Seismic vulnerability assessment of historical centers at urban scale," *International Journal of Architectural Heritage. Conservation, Analysis and Restoration,* vol. 12, no. 2, pp. 257-269, 2018.

[8] C. Holling, "Resilience and stability of ecological systems," *Annual Review of Ecology, Evolution and Systematics,* vol. 4, no. 1, p. 1–23, 1973.

[9] Y. Haimes, "On the definition of resilience in systems," *Risk Analysis,* vol. 29, no. 4, pp. 498-501, 2009.

[10] C. Folke, "Resilience: the emergence of a perspective for social-ecological systems analysis," *Global Environmental Change,* vol. 16, no. 3, pp. 253-267, 2006.

[11] M. Bruneau, S. Chang, R. Eguchi, G. Lee, T. O'Rourke, A. Reinhorn, M. Shinozuka, K. Tierney, W. Wallace and D. von Winterfeldt, "A framework to quantitatively assess and enhance the seismic resilience of communities," *Earthquake Spectra,* vol. 19, no. 4, pp. 733-752, 2003.

[12] C. Holling, "Understanding the Complexity of Economic, Ecological, and Social Systems.," *Ecosystems,* vol. 4, pp. 390-405, 2001.

[13] C. Gunderson, J. Holling, G. Pritchard and L. Peterson, Resilience of large-scale resource systems, Washington, DC: Island Press, 2002.

[14] Osservatorio sulla ricostruzione, "Osservatorio sulla ricostruzione," [Online]. Available: http://www.osservatorioricostruzione.regione.umbria.it. [Accessed 12 February 2020].

[15] INGV, "ITACA - Italian Accelerometric Archive," [Online]. Available: itaca.mi.ingv.it.

[16] S. Catalano, S. Grassi, S. Imposa, G. Tortorici, G. Cavuoto, V. Di Fiore, G. Alleanza, A. Chiaradonna, F. de Silva, A. d'Onofrio, F. Silvestri and G. Romagnoli, "The subsoil model for seismic microzonation study: the interplay between geology, geophysics and geotechnical engineering.," *Geotechnical Engineering for Protection and Development of Environment and Constructions,* 2019.

[17] M. A., "Microzonazione sismica di Nocera Umbra. Rapporto UMSEG,," 1998.

[18] F. Bozzano, F. Parroni, P. Traversa and G. Valentini, Geological engineering input data for microzonation of Nocera Umbra Commune, Vols. RIG, Special Issue on Umbria Marches Earthquakes of 1997, 2000.

[19] T. Crespellani, C. Madiai, G. Simoni and G. Vannucchi, "Dynamic geotechnical testing and seismic response analysis in two sites of the Commune of Nocera Umbra, Italy.," *Rivista Italiana di Geotecnica,* vol. 4, 2001.

[20] T. Crespellani, C. Madiai and G. Vannucchi, “Liquefaction risk analysis during earthquakes at Nocera Scalo, Italy, Part I: Assessment of liquefaction potential using simplified procedures.,” *Italian Geotechnical Journal,* no. 4, pp. 24-45, 2002.

[21] P. Angeletti, F. Baciucco, M. Barluzzi, P. Battisti, P. Macaluso, P. Materazzi and R. Panella, “Confronto fra danni, vulnerabilità ed interventi di consolidamento.Il caso dell’Umbria negli eventi sismici del 1997-1998,” in *ANIDIS*.

[22] Regione Umbria, “Comitato Tecnico Scientifico (istituito con Ordinanza n.2669/97) Interventi di ricostruzione degli edifici distrutti e di ripristino con miglioramento sismico SCHEDE TECNICHE DI ACCOMPAGNAMENTO AL PROGETTO,” 1997.

[23] E. César Javier Chácara, C. Francesco, C. Francesco, P. Bartolomeo and L. Paulo B., “Seismic vulnerability of URM structures based on a Discrete Macro-Element Modeling (DMEM) approach,” *Engineering Structures,* vol. 201, September 2019.

[24] A. Greco, G. Lombardo, B. Pantò and A. Famà, “Seismic Vulnerability of Historical Masonry Aggregate Buildings in Oriental Sicily,” *International Journal of Architectural Heritage,* December 2018.

[25] G. Nigro, “La ricostruzione dopo il terremoto,” *Urbanistica Informazioni,* vol. 226, pp. 22-24, 2009.

[26] R. Segatori, “La ricostruzione post-sismica in Umbria come modello di governance,” *Oltre la ricostruzione,* vol. 5, 2007.

[27] M. Sartore, “Umbria 1997. Ricostruire "dov'era, com'era". Ma basta?,” *Lente d'ingrandimento,* 2009.

[28] S. Bosi and A. Moretti, “Programmazione e strumentazione urbanistica,” *Urbanistica Informazioni,* vol. 226, pp. 24-26, 2009.

[29] G. Bicchieri, Pianificare la temporaneità. Storie di gestione e autogestione nel post sisma del centro Italia, Torino: Tesi di laurea, Politecnico di Torino, Laurea Magistrale in Pianificazione territoriale urbanistica e paesaggio ambientale, AA 2017/2018.

[30] F. Panzera, G. Lombardo, S. Imposa, S. Grassi, S. Gresta, S. Catalano, G. Romagnoli, G. Tortorici, F. Patti, E. Di Maio, “Correlation between earthquake damage and seismic site effects: the study case of Lentini and Carlentini, Italy”. Eng. Geol. 240, 149–162. 2018

12th International Conference on Structural Analysis of Historical Constructions
SAHC 2020
P. Roca, L. Pelà and C. Molins (Eds.)

PRELIMINARY APPROACH FOR A PROTOTYPE OF SUSTAINABLE ANTISEISMIC DWELLING IN NEPAL BASED ON THE HISTORIC VERNACULAR TRADITION

FERNANDO VEGAS LÓPEZ-MANZANARES [1*], CAMILLA MILETO[1], WALTER PISARRA[1] AND FRANCESCA TRIZIO[1]

[1]Universitat Politècnica de València (UPV)

IRP, Camino de Vera s/n, 46022 Valencia, Spain

e-mail: fvegas@cpa.upv.es[*] ; cami2@cpa.upv.es; walter.pisarra@gmail, fratri@upvnet.upv.es

Keywords: Vernacular architecture, Rammed Earth, Pendentive dome, Antiseismic Structure

Abstract. *The effects of the 2015 Gorkha earthquake in Nepal revealed deficiencies in the most recent vernacular architecture, which no longer uses wooden reinforcements due to national anti-deforestation laws. It also highlighted the shortcomings found in reinforced concrete architecture, which is generally scanty and poorly reinforced due to the high import cost of construction steel. The geography of Nepal has led to the development of a wide variety of vernacular architecture using local materials such as stone, brick or earth in the form of rammed earth and adobe walls [1]. Moreover, although its tradition in the construction of vaults is not as prominent as in neighbouring regions of India, Nepal has developed its own tradition in the construction of vaults and domes, which are generally self-supporting and made of brick or adobe with lime mortar. The design of a prototype of seismic house in Nepal aims to use a modular housing unit with rammed earth walls and/or walls made of materials recycled from previous earthquakes, as well as tile vaults with bamboo sleepers, and possibly vegetable fibre grids. These avoid the use of imported materials, favouring km0 and sustainable materials while following local tradition. Several potential housing units have undergone linear seismic analysis on finite element models, with variations in planimetric layout and the types of tile vault, from the simpler barrel vault to the sail vault. Both are analysed searching for the best shape in terms of seismic efficiency, evaluating stress and strain state. The results obtained from this preliminary study clearly show that, under seismic actions, the response from the construction system using depressed sail vaults and rammed earth walls with bamboo reinforcements is more efficient and homogeneous in terms of tension and deformation. This is due to the geometric symmetry which determines the same response in several directions, unlike vaults with a characteristically strong directionality (barrel vault). The seismic response of the prototype described is examined by assessing the influence in terms of thrust and deformation of bamboo reinforcements inside the walls. For this, laboratory tests are used to identify the mechanical characteristics of bamboo to be employed in the finite element modelling and calculation, as the values found in the literature vary depending on the physical and chemical characteristics of the material. This study therefore proposes a more sustainable architectural model with greater antiseismic resistance, always in keeping with local constructive tradition.*

1 INTRODUCTION

The project of an antiseismic dwelling in Nepal aims to merge the characteristics and needs of an antiseismic structure with the architectural tradition of Nepal. The damage caused by the earthquake has steered design towards a modernization of the vernacular architecture, reproducing Western architecture and using reinforced concrete structures. However, these are unsustainable both in environmental and economic terms, given high construction costs. The design of a housing unit prototype is proposed in order to return to the language of vernacular architecture using local materials, but avoiding wood which has become considerably more expensive following the implementation of anti-deforestation legislation. Therefore, a prototype of a dwelling with rammed-earth walls and bamboo reinforcements has been studied. The rammed earth technique, which compacts the soil in formwork using a rammer, is a highly sustainable practice already widespread in Nepal. This technique has been largely researched in the last two decades due to its properties, including good hygrothermal behaviour and low embodied energy. Numerous studies have been carried out on its mechanical characteristics [2-9], seismic assessment [10-12] and energy efficiency [13,14]. The use of structural elements in bamboo (*Bambusa Balcooa*), plentiful in the region, was decided in order to overcome the shortage of wood. Different studies have also been carried out on the physical and mechanical properties of bamboo [16-23] and its application in rammed earth structures [24,25]. The slabs are to be made of tile vaults, which are increasingly gaining international recognition for their durability, economy and ease of construction, as they require no centring [17-19]. Finite element models were created and analysed before the prototype was built in order to identify the type of vaulted dwelling with no fibre grid reinforcement in the type of vault most resistant to seismic stress. This paper reflects this first study. In a second step, this project will focus on the potential improvement of this vault with the insertion of a fibre grid reinforcement, in a departure from previous experiences in the field [30,31].

2 BAMBOO CHARACTERISTICS

In Nepal, bamboo is the natural material most widely used for different purposes, such as the production of tools or the manufacturing of construction elements. As a construction material, bamboo offers many advantages, as it is sustainable and easily renewable, with mechanical properties comparable to timber. One of the main advantages to bamboo is its rapid growth, which means it can also be widely used in areas where there is a shortage of wood for construction, as in Nepal, where the exploitation of forests has been restricted to prevent deforestation [24]. Furthermore, although bamboo is a type of woody grass and not a tree, bamboo forests display similar characteristics to tree forests in terms of their contribution to the carbon cycle, as bamboo retains carbon in its fibres and soil through photosynthesis [25]. Bamboo is part of the *Bambusoideae* grass family and its cellulose fibres, about 2 mm long with an average diameter of 20 μm, are immersed in a wooden matrix. The number of bundles of fibres and their scattering inside the bamboo culm affect the hardness of the bamboo [26]. In order to evaluate the potential use of bamboo ties in the prototype walls, the tensile strength of the bamboo (*Bambusa Balcooa*) samples taken in situ was assessed through laboratory tests.

Given the limited availability of specimens due to the distance from the site, these tests were conducted to compare the tensile strength of the specimens with the values found in literature [21-23], thus selecting proper values for the analysis.

Laboratory tests were carried out on three specimens from a bamboo culm from the *Bambusa Balcooa* species obtained in situ (Fig. 1). Three specimens of different widths and 9.5 mm thick were obtained eliminating the outer skin of the culm to obtain a smooth regular surface (Fig. 2). The first standard specimen [27] has a 20x9.5mm shaped section in the useful segment; the second has a rectangular section of 25x9.5mm, and the third a rectangular section of 50x9.5mm.



Figure 1. Bamboo culm.



Figure 2. Bamboo samples.

The first specimen, with a section shaped like a bowtie, was subjected to a direct tension test at a velocity of 0.5KN/sec (Fig. 3).

In the test the fibres slid and broke due to shear (Fig. 4). At breaking point a tension of 20.34 KN had been reached, with a tensile strength of 107.2 Mpa.

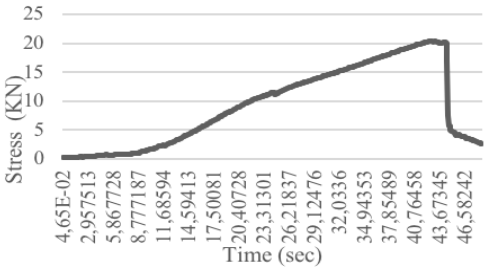


Figure 3. Traction equipment.



Figure 4. First specimen after the break.

Table 1. Stress trend. First specimen

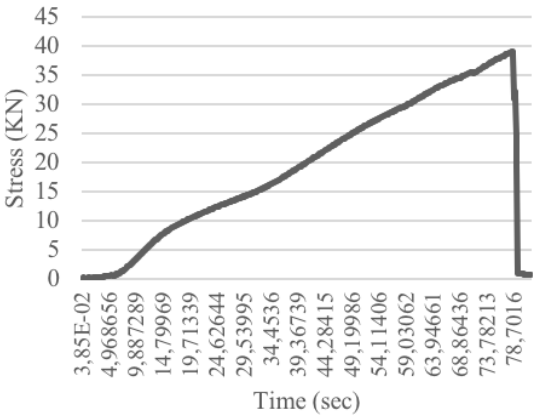


The second direct tension test was carried out on the specimen with a 50x9.5mm rectangular section. Under the same tensile velocity as that of the first test a break was also observed due to the compression of the ties at the end (Fig. 5). The tension recorded at breaking point was 39.10 KN and tensile strength was 82 Mpa.



Figure 5. Second specimen

Table 2. Stress trend. Second specimen



Finally, a bending test was carried out on the specimen with the 25x9.5mm rectangular section in order to indirectly obtain the tensile value which caused the inner fibres to break during the test. The specimen was subjected to continuous compression at a velocity of 4 mm/min, until the inner fibres broke due to tension (Fig. 6). Bending strength at breaking point was 118.9 MPa and, considering that the fibres under the neutral fibre reach breaking point due to tension when the section is subjected to bending, this value was considered equal to the tensile strength of the specimen.

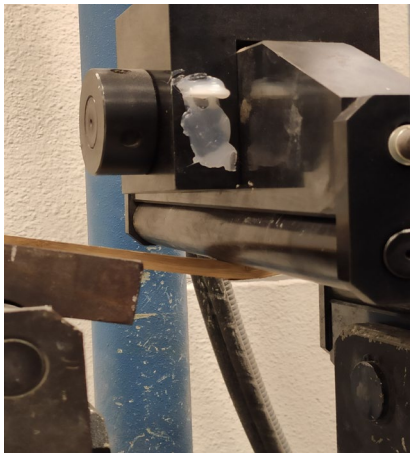


Figure 6. Rupture of the fibres of the third specimen.

Table 3: Stress-strain trend – Third specimen



The mean tensile strength value is 102.7 Mpa. This value should be considered a minimum tensile strength value as not all specimens broke due to the tension of fibres, but because of shear or the pressure of the ties.

Given the difficulties in accessing the location to obtain specimens the number of tests carried out may not be enough to obtain a population of values to define the characteristic tensile strength value. Thanks to the tests carried it was verified that the values obtained are within the range of values found in specialist literature [21-23]. Therefore, it was considered necessary to use the characteristic tensile strength values and other mechanical characteristics of bamboo as detailed by Kaminski et al. (2016), considered valid for all the species in the scheme design phase for buildings with smaller floor plans and elevations.

3 CONCEPTUAL DESIGN OF THE PROTOTYPE

Preliminary analysis with the finite element method was crucial to the definition of the type and shape of the vault to be used, given the extreme vulnerability of vaulted structures to drift. When executing a finite element analysis, the materials must be exactly defined. In this case, given the lack of experimental data, the mechanical properties considered for simple rammed earth are those found in the literature [4-9], reported in Table 4.

Table 4. Rammed earth mechanical properties in the literature

Author	Density [kg/m^3]	Compression [MPa]	Tensile [MPa]	Shear [MPa]	E [MPa]	G [MPa]	Poisson *v*	Specimen [cm]
Lilley [6]	1870-2170	1.80-2.00	-	-	-	-	-	cube 15
Jaquin [7]	-	0.60-0.70	-	-	60	-	-	10x10x30
Novamooz [9]	2000	-	-	-	-	-	0.33	cylinder d=7 h=2
Bui [4]	2000	-	-	-	100-500	41-180	0.22-0.40	40x40x65
Gomes [5]	1900	0.67	0.13	0.08	200	74	0.35	NZ4297 [15]

The mechanical properties for rammed earth and bamboo used for FE analysis are shown in Table 5 and Table 6.

Table 5. Rammed earth mechanical properties used for the models.

E [MPa]	Compression [Mpa]	Tensile [Mpa]	Density [kg/m^3]
250	2.00	0.20	2000

ºTable 6. Bamboo mechanical properties used for the models.

Author	E [MPa]	Compression [Mpa]	Tensile [Mpa]	Flexure [Mpa]	Shear [Mpa]
Kaminski et al. [21]	17000	20	40	30	2

Linear seismic analysis on finite element models was carried out on several prototypes of housing units with different plans and tile vault types, from simple barrel vaults (Fig. 7) to pendentive domes or sail vaults (Fig. 8). This assumed different values for the height of the springer, rise and thickness, evaluating the tensile and deformative state, in order to establish the best overall shape in terms of seismic efficiency. Since this is a preliminary analysis, no non-linear analysis was carried out due to the highly variable data and computational difficulty.

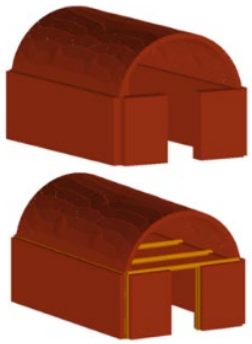


Figure 7. Models with barrel vault.

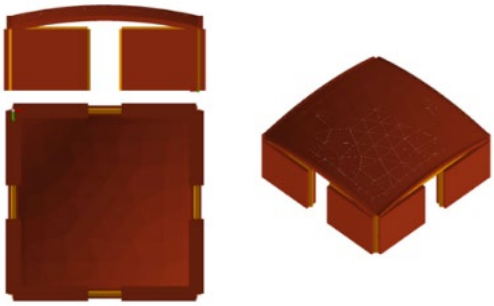


Figure 8. Model with pendentive dome.

Rammed earth walls (45 cm thick) and the tile vault were modelled as shell elements defined by three and four nodes in space and five DOF (degrees of freedom) consisting of three components of translation and two components of rotation in the plane of the element.

In addition, bamboo elements were modelled as beam elements defined by six DOF consisting of three translation components and three rotation components, with a hollow section with a 7.5 cm external radius and 6 cm internal radius.

The analyses were carried out by varying the thickness of the tile vault, from a minimum of 7.5 cm to a maximum of 10 cm. Based on the incidence of bamboo reinforcements assessed for the individual models it can be stated that, regardless of the shape considered, the value of displacements significantly decreased when ties were used, improving seismic response (Fig. 10).

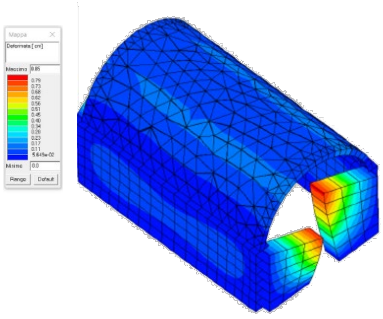


Figure 9. Deformation. Fifth mode. Unreinforced model.

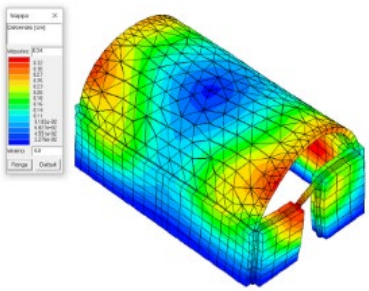
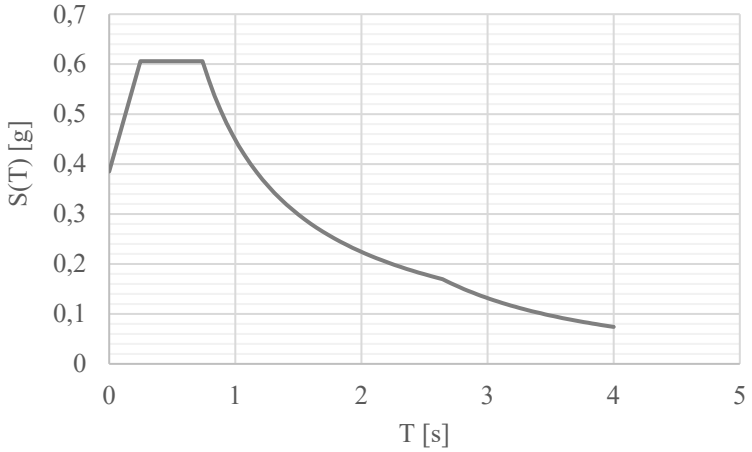


Figure 10. Deformation. Fifth mode. Reinforced model.

The 2015 Gorkha earthquake had a magnitude Mw of 7.8, 15 km deep, the recorded maximum PGA was ~ 0.25 *g*. The design PGA recommended by the Nepal building codes is 0.36 *g* (NBC-105, 1994). Based on the previous data, the acceleration response spectrum shown in Table 7 was considered.

Table 7. Design acceleration response spectrum



Tables 8 and 9 show the period and frequency values corresponding to the first 10 modes of vibration.

Table 8. Modal analysis results-barrel vault model

Modes	Frequency	Period
1	6.81	0.15
2	15.63	0.06
3	15.98	0.06
4	16.42	0.06
5	20.02	0.05
6	21.22	0.05
7	21.66	0.05
8	25.58	0.04
9	25.70	0.04
10	28.36	0.04

Table 9. Modal analysis results-pendentive dome model

Modes	Frequency	Period
1	7.32	0.14
2	8.77	0.11
3	8.77	0.11
4	9.02	0.11
5	9.43	0.11
6	9.91	0.10
7	11.14	0.09
8	11.16	0.09
9	14.02	0.07
10	14.10	0.07

To better understand the seismic behaviour of the models, it is useful to observe the major difference in behaviour between a simpler vault such as the barrel vault and the pendentive dome. The seismic response of the barrel vault model is poorer than that of the model with a pendentive dome. In fact, the deformation and the tensional state of a barrel vault are

noticeably influenced in the direction of the earthquake, giving rise to greater deformation if orthogonal to the direction of the axis. In addition, tensile stresses appear in the entire structure which could lead to collapse. In Fig. 13 and Fig. 14, only tensions are highlighted, in order to reflect the peak reached when the seism is orthogonal to the axis, with a maximum value of 6.95 daN/cm^2. In contrast, the response of the model with a pendentive vault is not significantly affected by the direction of the earthquake, and the final deformation appears more homogeneous. Likewise, the tensional state of this model is less critical, considering the decrease of the tensile stresses, with a maximum of 2.12 daN/cm^2.

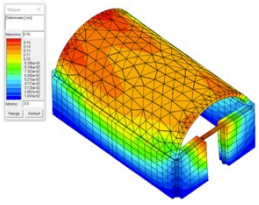


Figure 11. Barrel vault. Strain analysis. Seism: 30%X – 100%Y.

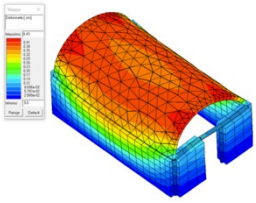


Figure 12. Barrel vault. Strain analysis. Seism: 100%X – 30%Y.

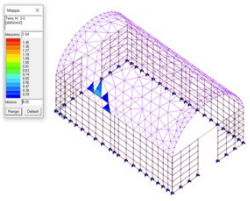


Figure 13. Barrel vault. Tension analysis. Seism: 30%X – 100%Y.

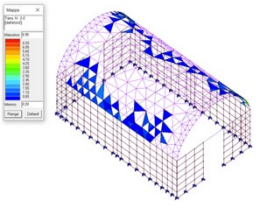


Figure 14. Barrel vault. Tension analysis. Seism: 100%X – 30%Y.

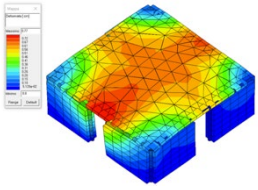


Figure 15. Pendentive vault. Strain analysis. Seism: 30%X -100%Y.

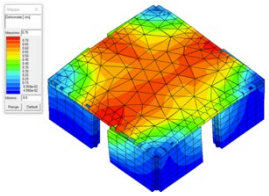


Figure 16. Pendentive vault. Strain analysis. Seism: 100%X – 30%Y.

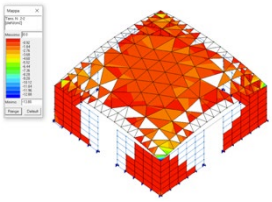


Figure 17. Pendentive vault. Compression. Seism: 30%X – 100%Y.

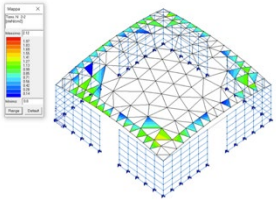


Figure 18. Pendentive vault. Tensile strength. Seism: 100%X – 30%Y.

4 CONCLUSIONS

Preliminary analysis of the models made it possible to identify the advantages and weaknesses of the recovered construction system, in order to move forward with a design which preserves traditional construction techniques while resisting seismic events, through the use of ties. Bamboo ties were inserted in order to ensure maximum sustainability for the project. It should be noted that tensile rupture of the test piece was not reached in any of the cases, and therefore the resistance values obtained should be considered to be minimum. Finally, the HouSe-Nepal project is imbued with the general spirit of the project of an antiseismic housing module born from the reinterpretation of vernacular architecture, better adapted to the environment both in terms of architecture and materials, and in terms of social and economic impact. The dwelling modules and the construction techniques presented in this paper are preliminary approaches to the design of a sustainable antiseismic dwelling in Nepal trying to provide an alternative for Nepalese dwellings which are currently being built with industrial materials such as cement blocks and metal sheets, which often generate unhealthy spaces.

Acknowledgements. This work is part of the research project "HouSe-Nepal. Prototype for a sustainable anti-Seismic dwelling in Nepal", funded by the Centre for the Cooperation to Sustainability of the Universitat Politècnica de València (main researcher: Fernando Vegas López-Manzanares).

REFERENCES

[1] CBS 2014, *Annual household survey*. Gov.Nepal. Katmandú (2014).
[2] Bui, T.T., Bui, Q.B., Limam, A., Maximilien, S. Failure of rammed earth walls: From observations to quantifications. *Constr. and Building Materials* (2014) **51:** 295–302.
[3] Bui, T.T., Bui, Q.B., Limam, A., Morel, J.C. Modeling rammed earth wall using discrete element method. *Continuum Mech. Thermodyn.* (2016) **28**:523–538.
[4] Bui, Q. B., Morel, J., Hans, S., Meunier, N. Compression behaviour of non-industrial materials in civil engineering by three scale experiments: The case of rammed earth. *Materials and Structures/Materiaux et Constructions* (2009) **42(8):** 1101-1116.
[5] Gomes, M.I., Lopes, M. And De Brito, J. Seismic resistance of earth construction in Portugal. *Engineering Structures* (2011) **33(3)**: 932-941.
[6] Lilley D.M., Robinson J. Ultimate strength of rammed earth walls with openings. In: *Proceedings of the Inst. of Civil Eng. – Struc. and Buildings* (1995) **110(3)**: 278 – 287.
[7] Jaquin P. A., Augarde C.E., Gerrard C.M. Analysis of historic rammed earth construction. In: *Structural analysis of historical constructions,* New Delhi (2006).
[8] Miccoli, L., Drougkas, A., Müller, U. In-plane behavior of rammed earth under cyclic loading: Experimental testing and finite element modelling. *Eng. Struct.* (2016) **125**: 144–152.
[9] Nowamooz, H., Chazallon, C. Finite element modelling of a rammed earth wall. *Construction and Building Materials* (2010) **25(4)**: 2112-2121.
[10] Bui, Q.B.; Bui, T.T.; Limam, A. Assessing the seismic performance of rammed earth walls by using discrete elements. *Cogent Eng.* 2016, 3, 1200835.
[11] Liu K, Wang YA, Wang M. Experimental and numerical study of enhancing the seismic behavior of rammed earth buildings. In: *Advanced Materials Research* Vols 919-921 (2014) pp. 925-931.
[12] El-Nabouch R., Bui Q.B., Plé O., Perrotin P. Assessing the in-plane seismic performance of rammed earth walls by using horizontal loading tests, *Engineering Structures,* (2017) **145**: 153-161.
[13] Allinson, D., Hall, M. Hygrothermal analysis of a stabilized rammed earth test building in the UK. *Energy and Buildings* (2010) **42**: 845–852.
[14] Soudani, L., Fabbri, A. Morel, J.C. Assessment of the validity of some common assumptions in hygrothermal modelling of earth-based materials. *Energy and Building* (2016) **116**: 498–511.
[15] NZ 4297. 1998 Engineering design of earth buildings. New Zealand: Earth Building. Association of New Zealand.
[16] Maldonado Ramos, L., Castilla Pascual F. J., Vela Cossio F. La técnica del tapial en la Comunidad Autónoma de Madrid. Aplicación de nuevos materiales para la consolidación de muros de tapia. *Informes de la construcción* (1997) Vol. 49 **452**: 27-37.

[17] Ramage, M., Ochsendorf, J., Rich, P. Sustainable shells: New African vaults built with soil-cement tiles. *Journal of the IASS* (2010, December) Vol. 51(4): 255-261.
[18] Block, P., DeJong, M., Davis, L., Ochsendorf, J. Tile vaulted systems for low-cost construction in Africa. *Journal of the African Technology Development Forum (ATDF) – Special Issue on Architecture for Development* (2010) **7**: 4-13.
[19] Block, P., Van Mele, T., & Rippmann, M. Structural Stone Surfaces: New Compression Shells Inspired by the Past. *Architectural Design* (2015) **85**(5): 74–79.
[20] Bhattacharya, S., Ghosh, J.S., Sahoo, D. K., Dey N., Pal A. Screening of superior fiber-quality-traits among wild accessions of Bambusa balcooa: efficient and non-invasive evaluation of fiber developmental stages. *Annals of Forest Science*, Springer Verlag/EDP Sciences (2010) **67** (6).
[21] Kaminski, S., Lawrence, A., Trujillo, D., Feltham, I., Lopez, L.F. Structural use of bamboo. Part 3: Design values. *Structural Engineer* (2016) **94** (12).
[22] Sanchez Vivas, L., Mullins, G., Cunningham, J. A., Mihelcic, J. R. Mechanical properties of bamboo: a research synthesis of strength values and the factors influencing them. *Journal of American Bamboo Society* (2019, October) **29(7)**: 1-22.
[23] Awalluddin, D., Ariffin, M. A., Osman, M., Hussin, M., Ismail, M., Lee, H., Abdul S. L., Nor H. Mechanical properties of different bamboo species. *MATEC Web of Conferences* (2017) **138**: 01024.
[24] Sharma, B., Gatóo, A., Bock, M. and Ramage, M. Engineered bamboo for structural applications. In: *Construction and Building Materials* (2015) **81:** 66–73.
[25] Yiping, L., Yanxia, L., Buckingham, K., Henley, G., Guomo, Z. *Bamboo and Climate Change Mitigation*. (2010).
[26] Seema Jain, R. K., Jindal, U. C. Mechanical behavior of bamboo and bamboo composite. In: *Journal of Materials Science* **27** (1992) 4598-4604.
[27] Aiping, Z., Dongsheng, H., Haitao, L. and Yi, S. Hybrid approach to determine the mechanical parameters of fibers and matrixes of bamboo. *Construction and Building Materials* (2012) **35:** 191–196.
[28] Tripura, D.D., Singh, K.D. Axial Load-Capacity of Bamboo-Steel Reinforced Cement Stabilised Rammed Earth Columns. *Struc. Engineering International*. (2016) **29** (10).
[29] Tripura, D.D, Singh, K.D. Mechanical behaviour of rammed earth column: a comparison between unreinforced, steel and bamboo reinforced columns. *Materiales de Construcción* (2018) **68** (332) 174.
[30] DeJong, M.J., Ramage, M.H., Travers, B., Terry, S. Testing and analysis of geogrid-reinforced thin-shell masonry. In *Proceedings of the IABSE-IASS Symposium*, London (2011, September).
[31] Ramage, M.H., DeJong, M.J. Design and construction of geogrid-reinforced thin-shell masonry. In *Proceedings of the IABSE-IASS Symposium*, London (2011, September).
[32] Nepal Building Codes (NBC-105). Seismic design of buildings in Nepal. Dep. of Urban Dev. and Buil. Constr. Min. of Housing and Physical Planning, Gov. of Nepal (1994).

12th International Conference on Structural Analysis of Historical Constructions
SAHC 2020
P. Roca, L. Pelà and C. Molins (Eds.)

RESILIENCE AND VULNERABILITY OF HISTORICAL CENTERS: THE CASE OF THE DISTRICT OF CAMERINO IN THE MARCHE REGION

E. PETRUCCI[1], L. BARCHETTA[2 *] AND D. LAPUCCI[2]

[1] University of Camerino, School of Architecture and Design
Viale della Rimembranza, 63100 Ascoli Piceno, Italy
e-mail: enrica.petrucci@unicam.it

[2] University of Camerino, School of Architecture and Design
Viale della Rimembranza, 63100 Ascoli Piceno, Italy
e-mail: lucia.barchetta@unicam.it (*corresponding author)
diana.lapucci@unicam.it

Keywords: Historical Centers, Masonry, Earthquake, Resilience

Abstract. *The seismic events that hit central Italy in 2016, causing extensive damage to cultural heritage and the loss of entire villages, showed the extreme fragility of the Marche territorial system with strong repercussions on the economic and social development. In the historic villages, the high inherent seismic vulnerability of the building makes it difficult to apply regulations oriented to the protection and preservation of historical and cultural values: strategies for the recovery of the buildings seem very complex. The historical building is generally characterized by a high building density, a scarcity of urban voids and an articulated accessibility system. In recent years the Marche region has developed, due to the intensification of earthquakes, a particular susceptibility to seismic risk. The historic centres have shown a scarce capability to adaptation and difficulties in hypothesizing new scenarios after the damage. In this context, we want to define an analytical method of the systemic vulnerability in the historical centres; this vulnerability is considered as a result of the complex interaction of individual structural units, aggregates and urban spaces. The aim is to compare this vulnerability with the effects that the earthquake really had on the buildings: the knowledge of the real behaviour in the historic centres will guide the research towards the definition of actions aimed at the mitigation of the seismic risk through the reduction of intrinsic vulnerabilities in the building and the implementation of the capability to face the earthquake, in order to develop a "new resilience". The district of Camerino is taken as a case study; it's a territorial hub of services and activities as well as being one of the largest inhabited centres affected by the 2016-2017 earthquake.*

1 INTRODUCTION

The concept of resilience is used more and more frequently in the debate around risk reduction and in processes of transformation, regeneration, development of the territory that disasters force to apply efficiently.

The term *resilience* refers to the change of approach deemed necessary to continue guaranteeing sustainability prospects related to changes. In research aimed at mitigating territorial risks, the concept of resilience assumes a central role in the construction of strategies aimed at disaster risk reduction with a plurality of objectives related to territorial quality. In the urban context, it seems impossible to talk about resilience without investigating the aspect of vulnerability [1]. The city, in particular the historical one, is an asset exposed to risk, weak and vulnerable: the aim is the reduction of urban vulnerability through risk control and management considered as the improvement of urban resilience as the ability to respond and adapt to the phenomenon suffered by the urban system itself [2].

The earthquake that recently hit the regions of central Italy and in particular the Marche hinterland requires the development of new observations. The enormous loss of human lives, the seriousness of the destruction, the vastness of the affected area and the need for a rapid reconstruction require reconsidering issues such in the process of the abandonment of the internal area, already started before the earthquake. Although we are looking for references in history, we are unable to trace a reconstructive model especially as regards the intervention in historic centres which are generally more damaged by seismic events [3]. The main aim of the research is, therefore, to identify an effective method aimed at strengthening the resilience capacities of the historical centres of the Marche region, which are currently extremely fragile and vulnerable, without a specific codification of the peculiar characteristics that should be preserved and valued. An expeditious method is identified for the analysis and evaluation of the typical and specific vulnerabilities of the historic centres starting from the estimate of the damage actually immediately after the last earthquake, which allows us to have real feedback on which to base forecasts and methodologies of intervention.

2 THE HISTORICAL CENTRES OF THE MARCHE REGION

The historical centres of the Marche region, like most of the Italian centres, are born with typical structural concepts of the time of construction, however, they evolve over time according to growth and transformation processes that change their original shape. These evolutions often involve the presence of different construction materials and technologies. These factors determine a certain difficulty in identifying the "assembly" processes of multiple structural units interacting with each other. In fact, a *building cluster* is made up of multiple parts that are the result of an articulated and non-unitary genesis, due to different factors (construction sequence, change of materials, changed needs, changes of owners, etc.) [4]. Analyzing a building belonging to a cluster; therefore, it is necessary to take into account the possible interactions deriving from the structural contiguity with the adjacent buildings, connected or in adherence to it. This complexity makes the correct knowledge of the structural system that composes it difficult, but necessary. As part of the research on the historic centres of the Marche region, it is essential to deepen the issues concerning urban morphology considered in its historical evolution. The absence of a recognized cognitive approach,

unfortunately, makes the dissertation uncertain: an attempt has therefore been made to characterize the historic centres of the Marche as far as possible. The identification of a territorial type, intended as the recurrence of physical elements but also of culture and language that link the settlements present in a given geographical context, arouses some interest. They have the essential prerogative to have been built within the perimeter walls delimiting the urban core which often had a natural defensive function [5]. In almost all cases, historical centres in the Marche region can be differentiated into two main types:

1) Urban cores with pre-medieval phases:
   - Pre-existence of an organized form of the current urban centre dating back to remote ages (Roman or previous classicism);
   - Subsequent urban development of the late ancient or early medieval period.
2) Urban cores with a new medieval foundation:
   - Closely related to the morphology of the territory;
   - Articulated morphological schemes;
   - A propensity to use masonry cells organized in compact blocks.

The Marche Region is characterized by a territory that is divided into three bands parallel to the Adriatic Sea. The inland areas are the most fragile. As a matter of fact. even before the seismic events, the historic centres located in the hinterland had had to face a series of difficulties, related to the phenomenon of abandonment, of depopulation of young people with low generational turnover. These phenomena were also accentuated hydrogeological instabilities and the presence of weak infrastructures. Three years after the earthquake, the most affected historical centres, when not completely destroyed, are impossible to access, most of the people who used to live there moved mostly along the coast where services and infrastructures are more efficient; commercial activities are located and concentrated in temporary structures, with an exponential acceleration of the depopulation processes that were already underway. In this research, the historical centre of Camerino is analyzed, a city heavily affected by the earthquake in Central Italy 2016.

3 BRIEF HISTORY AND SEISMICITY OF CAMERINO

The toponym *Camerinum* is attested by classical and medieval sources but some recent studies have delineated its most ancient phases, identifiable in prehistoric and protohistoric times, according to typical settlement models, entirely analogous to the nearby plestine context. The hill where the historic centre of the city of Camerino rises, which dominates the surrounding area, has been inhabited without interruption until today, creating a settlement stratification; this, if on the one hand severely compromised the full understanding of the previous phases, proves the favourable location of the site. Here the discoveries of prehistoric and protohistoric age are rare, while more frequent are the discoveries that attest to proto-urban forms starting from the fourth century. BC. Around the end of the 1st century BC a.C., perhaps in conjunction with the territorial reorganization of the Augustan age, this urban area also seems to have undergone a significant transformation with the construction of large *domus*, which remain until the late ancient era. In the Roman age, Camerino assumed an important role, as evidenced by the alliance agreement (*aequum foedus*) stipulated with Rome in 309 BC. The religious tradition preserved the memory of the siege that Alaric placed in the city in 409. After the defeat the Goths in 553, it became part of the Byzantine exarchate and in 592, with the

Lombard conquest, Camerino gave the name to a duchy incorporated into the one of Spoleto (VI-VIII century). It was already a bishopric in 465 and it had a vast ecclesiastical jurisdiction for over a millennium. Carlomagno elected Camerino as the capital of the homonymous *marca*, which extended from the Apennines to the Adriatic. After 1198 it became part of the domains of the Church, maintaining its autonomy. During the first half of the century XIII fiercely defended the Guelph side against the Swabians. It was destroyed by Manfredi's troops (1259). After a short period of abandonment, the area was recovered with new urban arrangements. Under the Lordship of the Da Varano family, which lasted until the mid-sixteenth century, Camerino knows a period of intense political and cultural vitality and economic prosperity with a significant population increase. These positive factors, combined with a significant urban transformation, changed the layout of medieval townhouses. From 1545 the city returned under the direct dominion of the Church with the function of the capital of the Apostolic Delegation. Thus, began a long phase of political and social stability, but also of silent decline. The bishops, in the last decades of the sixteenth century, built their palace, facing the ducal one. Until the French invasion, history was free of significant events. The history of the 1600s was articulated with the multiplicity of particular statutes.



Figure 1: Anonimous artist, *View of the city and the state of dressing room towards tramontana,* painting from around 1600 (Sala dei Priori, Palazzo Comunale in Camerino)

The state was divided into more than 100 communities, run by 3 vicariates. In the eighteenth century, Camerino was reduced to a large agricultural village with a limited economy and some industry in the area. During the French occupation, Camerino was aggregated to the *Tronto* department. In 1799, due to the reaction of the insurgents, the city was at the centre of various struggles, until on July 28, 1799, it was devastated by a serious earthquake that caused death and destruction. In 1809, during the Napoleonic era, the city was incorporated with the other marches of Fermo and Ancona, becoming the district capital. The Austrian invasion that followed the Napoleonic government desolated the territory even more. The Return of the Papal States was therefore welcomed with sincere enthusiasm; it gave Camerino a period of tranquillity and order but was unable to recover the city from its decline. Famine followed (1816-1817). In 1860 it was annexed to the Kingdom of Italy [6].

The historical events are intertwined with the changes in the urban layout of the city, starting from the early Middle Ages, with evident medieval and Renaissance transformations; these are works that go up to the modern age, also characterized by reconstructions following some disastrous seismic events: this makes the identification of recurrent constructive methods more

complex. The knowledge of the local seismic history is known only from 1279; there are numerous events which confirm that the high seismic susceptibility of the area, which was also affected by earthquakes with epicentres in the central and central-southern Apennines.

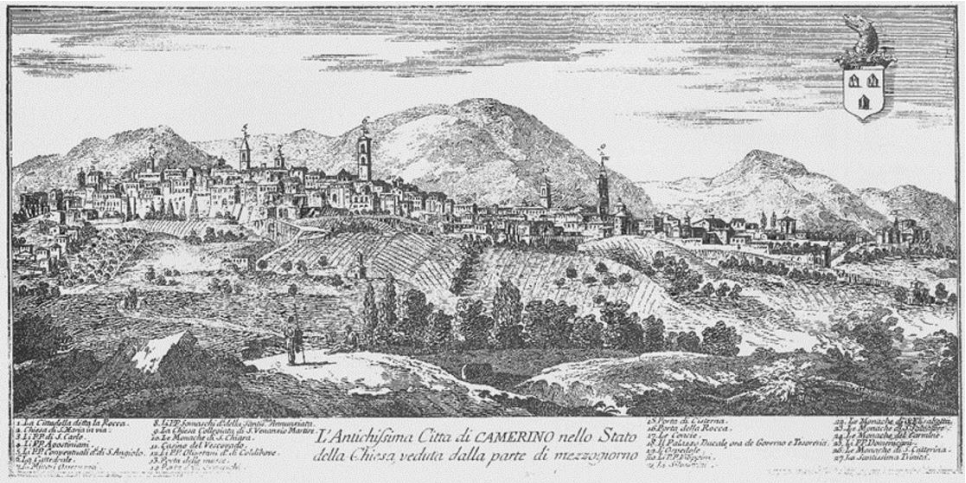


Figure 2: Salmon T., *The Ancient City of Camerino in the State of the Church seen from the south side,* engraving from around 1750.

Figure 3 shows the most important events that affected the municipal area. The most significant events, excluding the most recent, are those of 1279, recorded in the Umbrian-Marche Appennines, the one of 1328 and 1703 in Valnerina, then the1799 earthquake with an epicentre in the Camerino area, one in 1873 always in the Appennines, in 1979 in Valnerina and finally the one in 1997 which once again struck the Umbria-Marche Appennines.

Most of the oldest buildings in the area and the infrastructures were seriously damaged by the seismic events of 1997-98, with rare collapse phenomena of some more vulnerable buildings.

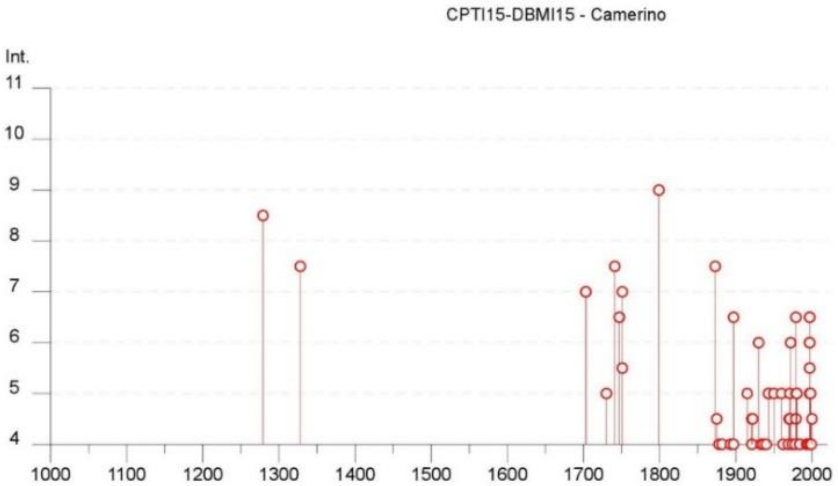


Figure 3: List of historical Earthquakes by INGV site *http://www.mi.ingv.it/terremoti-storici/* [view on 28.01.2020]

Starting from the historical sequence of the earthquakes that affected the territory of Camerino, three events have been identified that caused significant damage; on them, it is possible to perform a damage analysis, in order to have a map of the effects that every single event had on the historical buildings. These are the earthquake of 1799, the one of 1997/98 and the last one in 2016-2017. As regards the earthquake of 1799, historical research has been done at the state archive of Camerino. The documents available refer to the reports drawn up by the architect Andrea Vici in 1800, who compiles a careful description of the damage and interventions to be performed on buildings of particular importance; in addition, associated the evaluation of the costs related to the repairs of the damages occurred in the whole historical centre. This information is also reported in the recovery plan drawn up for the city of Camerino after the earthquake of 1997-98. The latter reports a precise mapping of the damages found and an assessment of the specific vulnerabilities.

After the 2016 earthquake, all the Cultural Heritage was highly damaged and, in some cases, collapsed with consequent loss of the building. The historic centre is seriously damaged so as to make it inaccessible to citizens. The first shock, which occurred on the night of August 24th, 2016 with magnitude 6.0 and Accumoli epicentre (about 51 km from Camerino), caused about 300 victims in Lazio and Marche regions, devastating the inhabited centres of Amatrice, Accumoli, Pescara del Tronto and Arquata del Tronto. In Camerino there were no victims and, with the first shock, the damages were almost zero except for some injury or slight collapse of some historic buildings such as the cathedral. On October 26th, two big shocks were detected, both with an epicentre in Castelsantangelo sul Nera (about 28 km from Camerino): the first at 19:10 of magnitude 5.4, the second at 21:18 of magnitude 5.9. Fortunately, the first shock led the inhabitants of the historic centre to abandon their homes, as the second shock, of greater intensity, led to the collapse of various parts of the buildings of the historic centre, such as the bell tower of the church of Santa Maria in Via, ruinously fallen on a building inhabited by some families fortunately outside because of fear. Such shocks, like the previous one, did not cause victims, but the intensity of the damage could not be recorded due to a further shock that occurred after only 4 days. At 7.40 on 30 October 2016, in fact, there was a shock with a magnitude of 6.5 with the epicentre between the hamlet of Campi di Norcia and Norcia itself (about 28 km away from Camerino). This, fortunately, like the previous ones, did not cause any victims, as the historic centre was almost empty and because the most important damages had already been recorded in the previous days. A further earthquake seismic swarm hit the town on January 18th, 2017, with its epicentre in Capitignano, in the province of L'Aquila, about 72 km from Camerino, causing a slight aggravation of the crack picture of some buildings in the historic centre, also due to the considerable distance from the epicentre.

4 SPEDITIVE ANALYSIS OF DAMAGES IN THE HISTORICAL CENTER OF CAMERINO

The first part of this work includes an analysis carried out through a rapid survey based on visual investigations of the damage following the 2016 earthquake. These were then compared with the data from the AeDES forms, the 1st level forms for compliance with safety standards an detection of damages during the seismic emergency used for a quick detection of damages, definition of prompt intervention measures and evaluation of the post-seismic safety of

buildings with ordinary structural typology (masonry, reinforced concrete or steel or wood). An inspection campaign was carried out in which 249 buildings were analyzed. The investigations were carried out by completing a revised version of the STAP form used in the 1997 earthquake in order to be able to compare it with the data relating to the damage levels detected in the previous earthquake. For the types of damage and for the classification of the same, reference was made to paragraph 2.2 of Annex B to the D.G.R. Marche region n. 2153 of 09/14/1998.

The observed damages can be classified into [7]:

- Damage to masonry
- Detachment between the structural elements
- Floors, arches and lintels collapses
- Foundation settlements
- Hammering
- Collapse, even partial, of the structural elements

For the definition of the damage levels, reference was made to the following table (Figure 4):

DANNO (**F** = crollo, **E** = gravissimo, **D** = grave, **C** = medio, **B** = leggero, **A** = nullo)

MURATURA O MISTO Tipologie di danno (par 2.2 e 5 alla D.G.R. delle Marche n. 2153 del 14.09.98 "Modalità e procedure per la concessione dei contributi previsti dall'art.4 della L.N. 61/98)	**DANNI RIPORTATI**						Dovuti al sisma	Preesistenti
	F	E	D	C	B	A		
Danni ai maschi murari	☐	☐	☐	☐	☐	☐	☐	☐
Lesioni di distacco fra gli elementi strutturali	☐	☐	☐	☐	☐	☐	☐	☐
Dissesti negli orizzontamenti, archi e architravi	☐	☐	☐	☐	☐	☐	☐	☐
Cedimenti	☐	☐	☐	☐	☐	☐	☐	☐
Martellamenti	☐	☐	☐	☐	☐	☐	☐	☐
Crolli, anche parziali, degli elementi strutturali	☐	☐	☐	☐	☐	☐	☐	☐
Altro da specificare	☐	☐	☐	☐	☐	☐	☐	☐
Edificio in muratura: si sono verificati cedimenti?							SI ☐	NO ☐
Edifico in muratura: si sono verificati martellamenti con edifici adiacenti?							SI ☐	NO ☐

Figure 4: STAP form for the evaluation of the damage level

The damage levels are detected through the archiving method and provide a classification based on 5 degrees from the most serious (total collapse) to the lowest (zero damage). All visible damages were assessed - building by building - and classified according to each damage level which is represented with a different colors. The mapping of the damage levels (Figure 5) shows a difference in behaviour between the various areas of the historic centre: most of the buildings (70%) are classified in the worst categories (serious and very serious damage with partial collapse). These levels of damage justify the extent of the red zone also following certain safety measures.

Some building clusters in the central area already restored following the 1997 seismic events, resisted better than other clusters in which the consolidation interventions had not been carried out or the works had been partially carried out. Furthermore, the most damaged

buildings, as also occurred in other historic centres, such as in Norcia, the most damaged buildings are special buildings, churches, monasteries and large historic buildings, such as Ducal Palace, headquarters of the University. Specialist buildings have a particular performance to seismic actions which can be described using studies that highlight typical and specific vulnerabilities, recurring the abacus of damage mechanisms for non-ordinary construction types, such as such as churches, fortifications or palaces [8].



Figure 5: Representation of the levels of damage detected through the filing method (elaboration from QGis Platform, 2019)

5 PILOT STUDY OF A BUILDING CLUSTER

The second phase of the research proposes a different method of analyzing the damage referred to the historical centre. In fact, starting from the assumption that it was not possible to access the single structural units, the AeDES forms were used. They are first damage detection forms made by professionals in charge who carried out an inspection to estimate the extent of the damage and the safety of the buildings.

A pilot building cluster was identified in which enough information was available to be able to compare it with the damage map previously shown. In order to compare them, each structural unit was evaluated on the severity of damage and the results of the AeDES forms. Specifically, the results reported in the sheets are as follows:

A - safe building

B - building temporarily unusable (in whole or in part) but accessible with emergency measures

C - partially unusable building

D - temporarily unusable building to be reviewed in-depth

E - unusable building

F - building unusable due to external risk

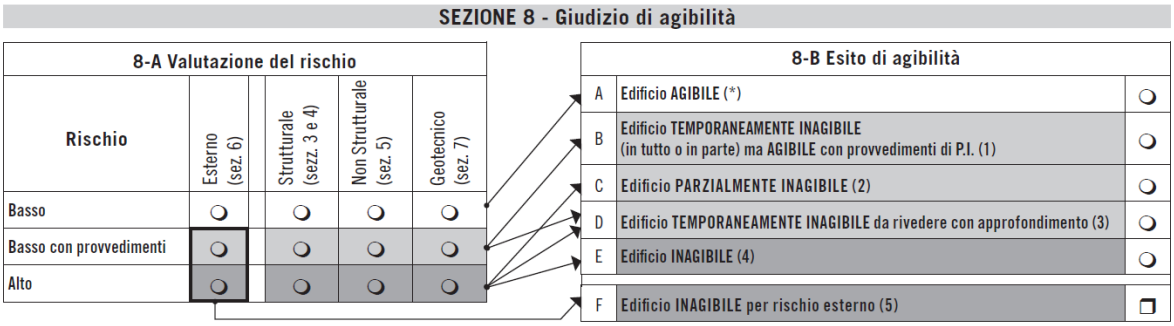


Figure 6: AeDES forms. Results.

Buildings with outcome A were assigned the "no damage" rating (figure 5 – grey), while for buildings that reported B/C/D as a result, a "minor" damage level was generally assigned (figure 5 – light blue). With regard to outcome E, on the other hand, the level of damage was divided into two: "significant" (figure 5 – yellow) and "serious" (figure 5 – orange), depending on what is reported in the specific table regarding the damage identified.

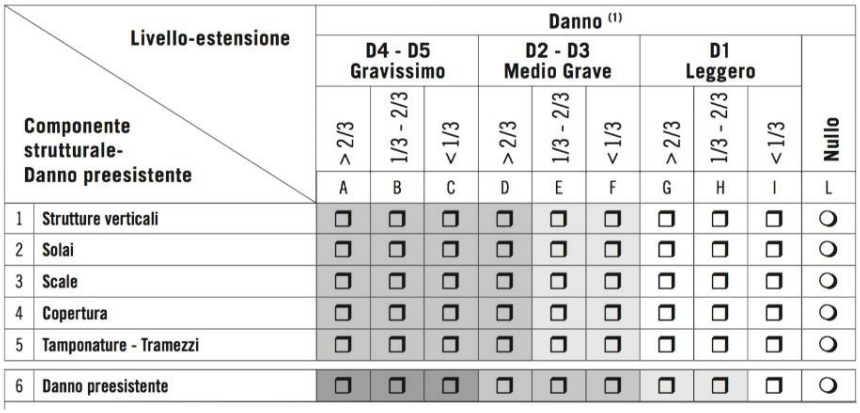


Figure 7: AeDES forms. Evaluation of damages.

The identification of the damage is shown below, comparing it with the system used in the previous paragraph with the pilot cluster. As can be seen from figure 8, the results obtained from the two types of expeditious analyzes are consistent in the presence of the damage, but, as

we can see, in the map on the upper right corner (the one relating to the global survey carried out through external inspections) the damage appears to be underestimated. Specifically, there are buildings that apparently have not suffered any damage outside, however, they are unusable.

From the investigations carried out on the whole historical centre of Camerino, this inhomogeneity of the damage between inside and outside is due to the great inhomogeneity of the elements constituting the masonry (mortar and brick). The walls are, in fact, mainly double leaves walls, which cannot be analyzed as a monolithic wall as it is made up of three distinct parts (the two leaves and the internal core generally made up of inconsistent material). The two vestments, moreover, are often not connected to each other and this generates a different behaviour between inside and outside. In clusters, moreover, the connection between the walls is often non-existent or weak.



Figure 8: Comparison of the results of the two expeditious investigations. The global survey in the upper right corner and AeDES forms analysis in the lower right corner.

All these changes over time are reflected in the various types of masonry. They have been classified, following what established by the Ministerial Circular n.7/2019 (*Instructions for the application of the technical standards for buildings update*).

The masonry works are listed according to 8 typologies, some well-built others with limited respect for the "regola dell'arte" and therefore with a low Masonry Quality Index (IQM) [9]:

a. Chaotic stone masonry (pebbles, erratic and irregular stones);
b. Brickwork with rough-hewn segments, with uneven wall thickness;
c. Split stone masonry with good texture;

d. Uneven soft stone masonry (tuff, calcarenite, etc.);
e. Smooth-block masonry of soft stone (tuff, calcarenite, etc.);
f. Squared stone block masonry;
g. Solid brick masonry and lime mortar;
h. Semi-solid brick masonry with cement mortar.

Each of them, recurring throughout the historic centre, systematically presents modifications, fillings, changes of material, the result of the various interventions carried out over the centuries.



Figure 9: The most common types of masonry in Camerino: 1 - f) Masonry with square stone blocks; 2- e) Regular-block masonry of soft stone (tuff, calcarenite, etc.); 3 - c) Split stone masonry with good texture; 4 - g) Solid brick masonry and lime mortar.

The masonry analyses are particularly complex and further interpolations are needed to compare the data collected with the expeditious method for the recognition of the damage which may not be sufficient to give a real response to quantify the seismic vulnerability in an urban context, such Camerino historical centre.

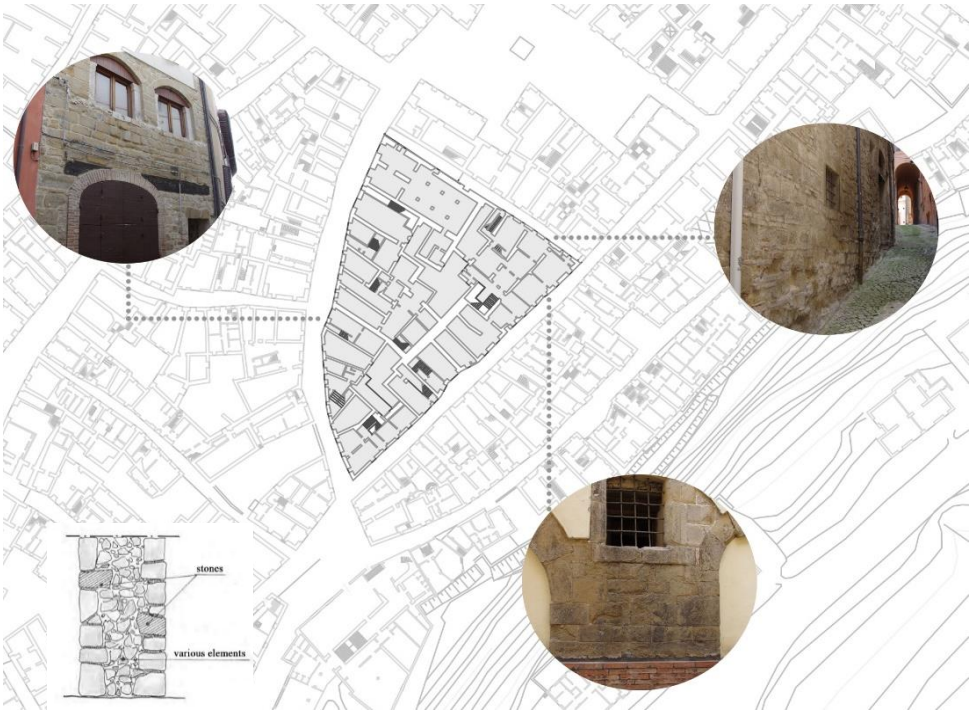


Figure 10: Characteristic walls of the pilot cluster, consisting of terraced typological units, in some cases recast into more complex buildings that show evident signs of transformations (Elaboration Barchetta, 2019).

6 CONCLUSIONS

Starting from what is observed in this article, the analysis of local vulnerabilities should be divided into three in-depth phases: knowledge, analysis and evaluation [10]. The assessment of the damage suffered by the historic centre of Camerino after the aftershocks of the 2016-2017 seismic sequence is a good starting point for identifying the recurrent mechanisms. The expeditious analysis of the damage that is proposed here is a good basic method but the actual extent of the same is underestimated and therefore the results do not fully agree with what emerges from direct observation. For an optimal response, however, the cross-reading of the different information from various sources can allow a more precise assessment, to be put in relation with the actions aimed at ensuring the development of a new resilience for the reduction of vulnerability in historic centres, taking into account typical and specific peculiarities that represent the identity value that characterizes the internal areas of the Marche, of which Camerino is one of the most emblematic cases.

REFERENCES

[1] Galderisi A., Ceudech A., Resilienza e vulnerabilità dei sistemi urbani. una proposta di metodo per la mitigazione del rischio sismico. In XXIV Conferenza Italiana di Scienze regionali, Perugia 8-10 Ottobre 2003, 1-24.

[2] D'Amico A., Currà E., Urban Resilience in the Historical Centres of Italian Cities and Towns. Strategies of Preventative Planning. *TECHNE - Journal of Technology for Architecture and Environment*, 15, 2018, 257-268.

[3] Petrucci E., *Le alterazioni del linguaggio nell'emergenza post-sisma. Ricostruzione o abbandono*. In E. Petrucci, L. Romagni (Eds), *Alterazioni. Osservazioni sul conflitto tra antico e nuovo*, Quodlibet, (2018), 45-73.

[4] Lombardo G., Greco A., Caddemi S., *La vulnerabilità sismica degli edifici storici in aggregato. Nuove metodologie negli approcci speditivi e di modellazione strutturale,* Edizioni Efesto, (2018), 9-14.

[5] Mochi G., Predari G., *La vulnerabilità sismica degli aggregati edilizi: una proposta per il costruito storico*, Edicom (2016)

[6] Savini P., *Storia della città di Camerino*, Tipografia Savini, II ed.,1895, 34-42.

[7] De Felice G., Pugliano A., *Il lessico costruttivo dell'edilizia storica. In A. Giuffre (Ed.), Sicurezza e conservazione dei centri storici. Il caso di Ortigia*, Editori Laterza, (1993), 69-99.

[8] Ferrigni F., et al., *Ancient buildings and earthquakes The local Seismic Culture approach: principles, methods, potentialities*, Edipuglia, (2005).

[9] Borri A., De Maria A., 2019. Qualità muraria secondo il metodo IQM: aggiornamento alla Circolare esplicativa n.7 del 2019. *Structural. Building Engineering+ Structural Design*, 222, marzo-aprile 2019, 1-21, *https://doi.org/10.12917/STRU222.07.*

[10] Agostiano M., Concas D., La conoscenza del patrimonio culturale fondamentale per la conservazione in sicurezza: la verifica di vulnerabilità sismica. In: A. Aveta (Ed.), *RICerca/REStauro, Sez. 3B: Progetto e cantiere: problematiche strutturali*, Edizioni Quasar, (2017), 782-792.

12th International Conference on Structural Analysis of Historical Constructions
SAHC 2020
P. Roca, L. Pelà and C. Molins (Eds.)

RESILIENCE OF HISTORIC RESIDENTIAL AREAS SUBJECTED TO NATURAL DISASTERS

M. DRDÁCKÝ[1*], R. CACCIOTTI[2] AND T. DRDÁCKÝ[1]

[1]Institute of Theoretical and Applied Mechanics of the Czech Academy of Sciences
Department of Heritage Science
Prosecká 76, 190 00 Praha 9, Czech Republic
e-mail: drdacky@itam.cas.cz, drdackyt@itam.cas.cz, www.itam.cas.cz (*corresponding author)

[2] Institute of Theoretical and Applied Mechanics of the Czech Academy of Sciences
Department of Diagnostics and Conservation of Monuments
Prosecká 76, 190 00 Praha 9, Czech Republic
email: cacciotti@itam.cas.cz, www.itam.cas.cz

Keywords: historic city, risk mitigation, resilience, decision support tool

Abstract. *The paper presents decision support tools developed for municipalities and historic city managers. These exploit the categorization of cultural heritage assets according to their vulnerability in disaster situations. A manual guiding individual cultural heritage owners, users and other citizens of historic areas provides advices on how to prevent or reduce damage and loss to cultural heritage. The recommendations cover pre-disaster, during as well as post-disaster situations and concern both built and moveable heritage. All measures are illustrated with examples taken during real disaster situations. The methodology has been tested during the international research project "ProteCHt2save" supported under the Interreg CE program.*

1 INTRODUCTION

The concept of urban resilience indicates the ability of a city to withstand shocks to its survival. There exist various general definitions of resilience, such as the one by C. E. Cloete [1]: resilience represents "the ability of a system to absorb changes without a transition to a different state". This can be expressed in other words as "the capacity of a system or object to absorb disturbances and reorganize while undergoing change so as to retain essentially the same function, structure, identity, and feedbacks" [2]. The concept of resilience has been further developed within a network supported by the Rockfeller Foundation, in 100 large cities. In this project, the urban resilience is defined as the capacity of individuals, communities, institutions, businesses and systems within a city to survive, adapt and grow no matter what kinds of chronic stresses and acute shocks they experience [3].

The resilience of residential areas exploits, for the study of its behaviour and change, an approach of so called complex adaptive systems [4,5,6]. Complex adaptive systems have various characteristics which are focused on the important properties related to change and the ability of a system to deal with change. First of all, the complex adaptive systems have histories allowing learning from experience, which is decisive for adaptability as well as

resilience of a system.

The complex adaptive systems are alternatively also denoted multi-agent systems with its components called agents [7]. Agents are autonomous individual components with a capacity to play specific roles and an ability to interact with the others. Such interactions may result in effects of an emergent nature with important resilience impacts.

Residential areas with cultural heritage assets, referred to as historic residential areas, are considered as complex adaptive systems with specific characteristics. The resilience of built heritage, intended as a substance or a set of elements of a historic city, takes into account resilience of individual cultural heritage objects together with their interactive, dynamic, emergent and adaptive roles. Therefore, the resilience-building approach envisaged in the ProteCHt2Save project involves cultural heritage stakeholders into the development and materialization of measures reducing possible damage from natural hazards and climate change harming actions. It is based on the identification of controllable criticalities decisive for improved resilience of cultural heritage affected by natural hazard risks and the associated measures.

2 DIMENSIONS OF RESILIENCE MEASURES

The understanding of the multifaceted nature of the impact of disasters is an essential prerequisite for an adequate assessment of vulnerabilities of cultural heritage assets as well as for the design and implementation of effective risk reduction strategies in different hazard scenarios. Resilience measures, in fact, present also a multidimensional characteristic which needs to be carefully explored and evaluated. The most relevant dimensions can be summarised as follows: 1) informational dimension; 2) managerial dimension including decision making and actions; 3) physical dimension with socio-cultural, emotional and economic aspects. These dimensions are presented in the next paragraphs.

2.1 Informational dimension

The informational dimension is a crucial one as it refers to data gathering and processing activities and to the availability of risk related information enabling to determine the distribution and magnitude of hazards and vulnerabilities of cultural heritage systems. Reliable and solid data create the basis for planning and coordinating preventive measures, rescue actions as well as post-disaster activities. Typical examples are constituted by inundation maps which were introduced a decade ago as obligatory in all EU countries and still exhibit serious deficiencies from the cultural heritage point of view. They are mostly developed only for the river flood situations and typically do not contain information on the location of heritage assets and especially on the condition of such assets, which may affect approach to the resilience measures. Flash floods on small rivers and creeks due to heavy rains and storms are partly predictable using interactive maps which are available in some countries. Maps of flash flood inundation in plain like historic districts are mostly missing even though their occurrence is more frequent in the recent time. This is a challenge for development of future resilience methodologies. The problem has been recently identified as important after an assessment of the impact of heavy storms on some American cities [8] and it is also linked to information on a condition of infrastructure, namely rainwater drainage systems and channels.

Maps have a strong potential for emergent response of communities in the historic residential areas. Even though remote sensing systems enable to a certain extent to include time effect and thus to slightly upgrade the 2D character of the hazard maps, there is still missing important information transforming visual data into 3D object or even 4D data suitable and necessary for temporary preventive measures, rescue as well as post disaster interventions and their evaluation. The authors believe that such a transformation can be achieved by a larger involvement of the human community potential. The following paragraphs present a possible approach focused mainly on the physical dimension of the resilience measures.

2.2 Managerial dimension

The managerial dimension includes those decision making processes and actions which dictate the major centrally managed resilience focused measures. However, any disaster´s impact is usually unevenly distributed across the historic residential area territory. On the other hand in some situations an adoption of mitigating measures can also be effectively applied in a selective way. Therefore, a reasonable balance between centralized and individual resilience improving actions is desirable. In the ProteCHt2Save project, selected elements of cultural heritage have been categorized and ranked according to their vulnerability in hazard situations [9]. These are denoted as serious criticalities and exhibit a capacity to be controllable. A critical element can be defined as a factor or aspect of a CH system, intended as the ensemble of its physical and managerial characteristics, which proves to be crucial for the determination of its resilience to natural disasters and climate change actions.

Managerial critical elements relate to those aspects of a CH system which are not connected to the physicality of the asset but rather to its operation, administration and care. Managerial critical elements therefore include how CH environments are used and protected involving social and economic as well as policy and regulation issues.

From the main findings of the project, transnational examples of managerial critical elements include the lack of knowledge or information, negligence (lack of maintenance), inadequate decision making, poorly designed emergency or post-disaster plans, missing funds etc. [10]. All these represent fundamental controllable features of a CH system which can be modified and adjusted by adopting appropriate management actions and measures. Each managerial critical element is strongly context-specific and requires an accurate assessment and thoughtful prioritisation in order to reduce the risks related to natural hazards and climate change and improve the resilience of the overall CH system.

2.3 Physical dimensions

The physical dimension of the measures relates to those aspects of a CH system involving its actual material composition and structural conditions. The sensitivity of historic structures and structural elements to weather and disasters is influenced by material and structural capability to resist exceptional loads and environments during disastrous situation. As mentioned for the previous dimension, also physical critical elements are significantly context-specific and require a thorough investigation of material characteristics and the general environmental situation (e.g. hydrogeological conditions) before being adequately evaluated. In some cases, in fact, it is not the historic structure itself that is sensitive to

climatic conditions, but the surroundings and the supporting structure can also be affected. It should be emphasised that it exists a wide range of historic structures and materials, and also a wide range of types of damage. This makes it difficult to design widely applicable measures and unified methods. In this research, physical critical elements are analysed considering a ranking of historic structures, elements and situations according to their sensitivity to the effects of weather and natural disasters. In order to facilitate preventive protection and adaptation measures the authors suggested ranking of immovable heritage into five categories according to their vulnerability during individual natural disasters [11,12]. The ranking helps to identify the best practice and design decision making support tool. Criticalities are hence categorised as follows: a) flood, b) fire due to drought, 3) wind and 4) heavy rain group.

3 RESILIENCE-BUILDING DECISION SUPPORT TOOLS

The number of historic structures in historic residential areas endangered by natural or anthropogenic hazards is enormous and it is practically impossible to apply ideal permanent measures to upgrade all historic structures to a level corresponding contemporary knowledge and standards pertaining to the risks generated by earthquake, very strong windstorms, landslides or floods. Most historic structures that collapse fatally during natural disasters do so due to structural deficiencies, an inappropriate repair of minor faults or harmful structural modifications. Neglectful or inadequate maintenance of historic structures is a frequent phenomenon, to a large extent caused by the ignorance of the heritage owners or users [13,14]. Even on the central level, knowing the threats applying to a specific context and the related preventive measures necessary can be basically useless unless the actual measures are implemented. Therefore, in the ProteCHt2Save project an innovative approach has been tested transnationally among the users in Austria, Hungary, Croatia, Italy, Poland and Slovenia in a simplified version with an aim to mobilize stakeholders and public for involvement in the community resilience process.

The novelty takes advantage of a combined non-centralized and centralized approach to the protection and use of cultural heritage. It is well known that CH sustainability is strongly dependent on its condition as well as a mode of use. The both aspects are better controllable by the stakeholders, namely owners, managers and users, than by centralized authorities.

The condition diagnostics of built heritage or the built environment is frequently compared to the medical health investigations. The presented approach learns from the success in the medicine in the recent decades when in relation to some diseases a self-investigation plays an important role in preventive treatment and mitigation of fatal cases. Therefore, the approach aims at development of tools for and a rise of awareness in a wide public concerning methods of indication of critical conditions or even defects which endanger heritage objects and decrease their sustainability and resilience in case of disasters.

The involvement of the “basic level” stakeholders has limitations in the necessary level of their knowledge. The developed tools increase substantially this level, however, in some situations a further step is necessary and then a more centralized approach is introduced. The approach thus develops a hierarchy of steps which significantly increase the scope of protection and resilience of heritage assets at reasonable costs, however, with a higher quality and longer sustainability. There is no limitation for the type of tangible cultural heritage in concern including intangible context when applicable. Moreover the full breadth of the

"institutionalized" heritage is widened with a category of "family" heritage, i.e. the cultural heritage of mostly regional or local importance, which is the most endangered group during disaster situations and at the same time the category significantly influencing social strength and resilience capacity of communities. The family heritage involvement approach further increases a potential for safeguarding vanishing heritage, especially oral or unofficially stored on fragile media, e.g. mg tapes. It also substantially contributes to the complexity of a spatial scale of the resilience measures. The focus on resilience enhancement naturally supports the temporal scale of approaching the protection and conservation of cultural heritage. According to the modern resilience theories presented in the introduction only the communities with history can represent complex adaptive systems ready for successful resilience after disastrous events. The tools, briefly presented in the paragraphs below, are built as open to all forms of cultural heritage expressions as well as to the plurality of values attached to heritage. It has been explained above that one of the main principle accepts decentralization where possible and centralization where necessary or beneficial for the protection and conservation of cultural heritage.

3.1 Manual of good and bad practices for managers

The physical resilience of complex adaptive systems with cultural heritage assets to the impact of natural and man-made disasters can be improved by means of four basic approaches: i) preventive protection, ii) adaptation, iii) evacuation and iv) resilience preparedness and their combinations.



Figure 1: Left: unprotected historic Troja district (Prague, Czech Republic) during flood in the year 2002; right: the same area protected with a combined permanent and temporary wall during flood in the year 2013.

Preventive protection is cost demanding, not always feasible and it can sometimes lead only to partial benefits, such as for example in the case of threat of landslides. As far as the

scale is concerned, preventive protection can be designed and implemented at territorial, building and material levels. Territorial protection, like barriers against flooding for example, could beneficially influence the resilience capacity of a CH system; however, at the same time, it should be considered that such large scale protection approach might induce a rather significant impact on values of the area with heritage assets, in case when stable structural measures are applied. It concerns namely landscape, visual and contextual values.

As an example let us present a case of a historic district in Prague Troja which was affected seriously during the flood in the year 2002 when water depth reached some eight meters. The so called historic "fishermen village" and an adjacent Baroque chateau were damaged, Fig. 1 left. Then the area has been protected by a combination of the permanent and temporary walls which effectively prevented inundation of the historic district during a later flood in the year 2013, Fig. 1 right. However, the natural contact and context between the village and the river was lost, Fig. 2. Fortunately, in this specific case the space between barriers and river is sufficiently large and could be developed for recreational activities substituting the historic attractions (sports, galleries, bars) less vulnerable to the impact of present threats.



Figure 2: Construction phase of the combined earth levee, permanent reinforced concrete wall with columns prepared for temporary metal barriers.

Preventive protection of buildings and complexes of buildings presents greater advantages when implemented using temporary measures, which are removable after the event. On the other hand, material protection is almost always irreversible, however for individual immovable artefacts or buildings could be very effective.

Adaptation is also cost demanding and can influence negatively the cultural heritage context and values. This approach is usually adopted in relation to climate induced risks or similar largely distributed threats and it needs wider campaigns and appropriate largely adopted financing.

Evacuation is the best protective measure suitable and applicable for moveable heritage. However, it needs planning, fast action and a safe space for temporary storage of the replaced artefacts. In the above mentioned case the river bank accommodates several objects with artefacts of cultural heritage value. One of them is so called "Troja Horse gallery" and Fig. 3 presents a schematic logistics for its evacuation.

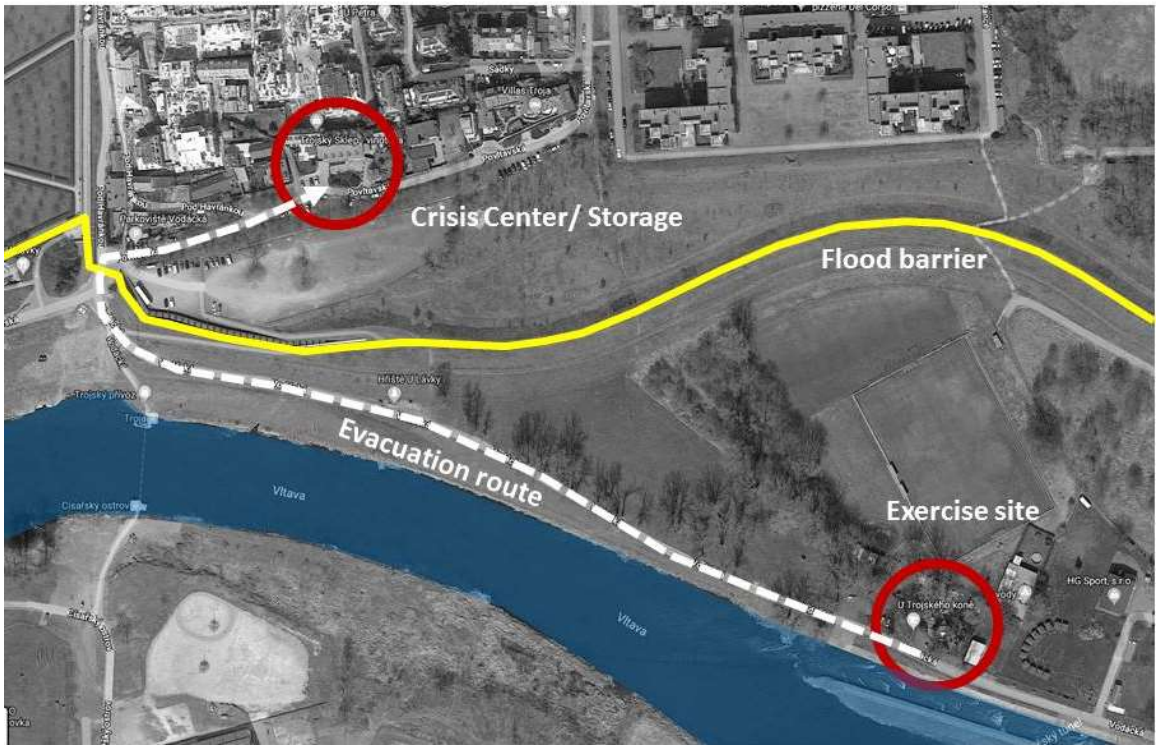


Figure 3: Situation of the gallery to be evacuated, the evacuation road, protected crisis centre and storage space



Figure 4: Evacuation of sculptures and paintings from the Troja Horse gallery – a training exercise

The effective application needs appropriate learning of local stakeholders and a regular training of the involved parties, Fig. 4. Resilience preparedness combines the all above mentioned approaches, involving to a larger extent the public and proving to be effective in complex situations such as in the protection of cultural heritage systems. Such resilience-based approach is a core strategy for the INTERREG CE ProteCHt2save project, presenting a clear potential to be cost effective at ensuring high benefits [9].

3.2 Handbook for owners

The suggested centralised/non-centralised approach to resilience building, foresees the participation of non-technical stakeholders to preventive and rescue activities. Fur such reason a simple manual has been provided in order to help cultural heritage owners to identify controllable criticalities in their neighbourhood. Fig. 5 presents a typical page of the manual.

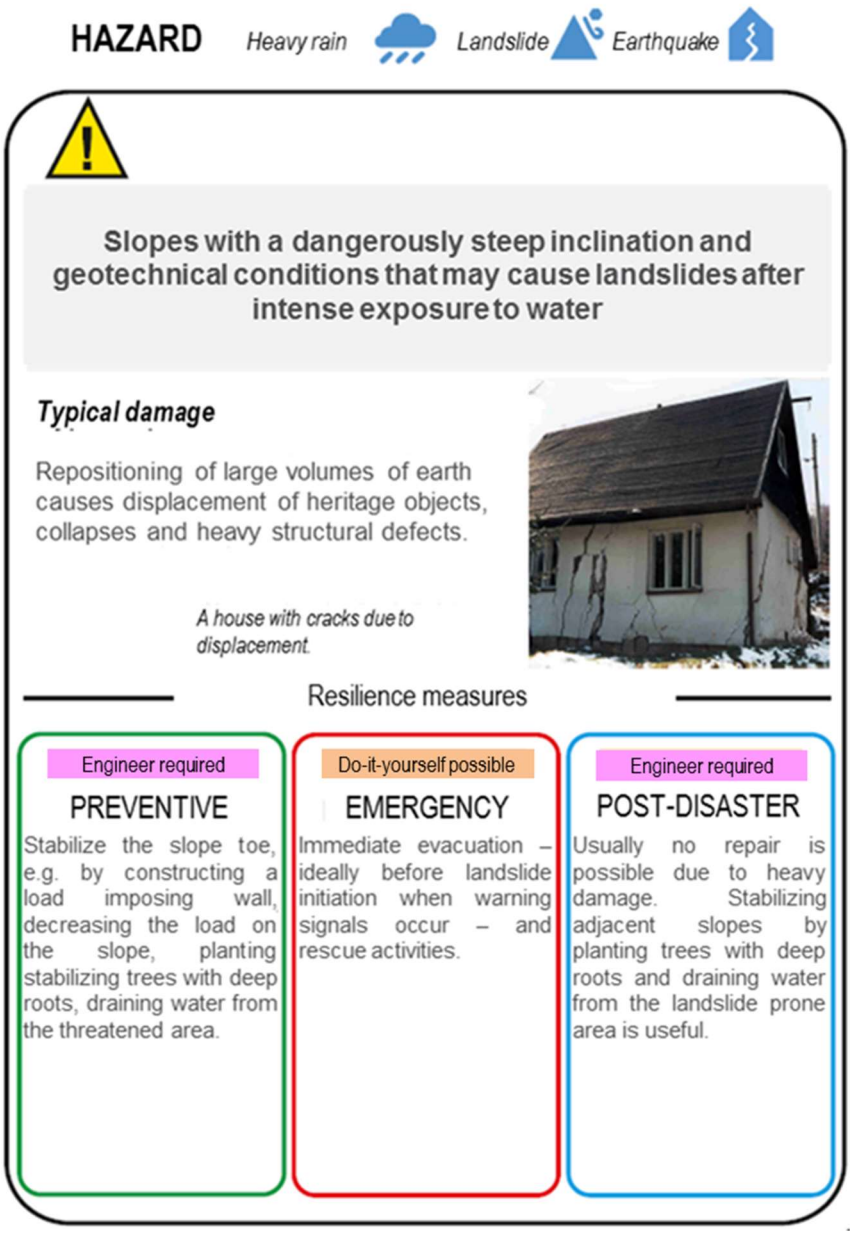


Figure 5: Example of one page of the manual

The page informs about one critical feature called “criticality” of a structure, building or object, which is observable by visual inspection. It is further illustrated with a typical damage or defect which the criticality can initiate or intensify. Then possible typical resilience

supporting measures are suggested following the time periods of a disaster – preventive measures before the disaster starts, emergency actions during the disaster and post-disaster measures reducing damage due to mostly ignorance and negligence. Additionally, it is indicated which measures can be done by the owners or other stakeholders and which ones need skilled craftsmen and specialized professional in engineering or conservation. The pilot manual contains 40 pages of such guiding sets and covers problems typical for floods, windstorms, landslides, harsh weather situations. Use of the manual needs a short training and it is supported by consulting services, phone applications and an information system on damage of cultural heritage – MONDIS [15].

4 CONCLUSIONS

The approach outlined in this paper considers the resilience of the historic city as that of individual cultural heritage objects together with their interactive, dynamic, emergent and adaptive roles. It endorses the engagement of cultural heritage stakeholders into the development and materialization of measures reducing possible damage from natural hazards and climate change harming actions. This is based on the identification of controllable criticalities decisive for improved resilience of cultural heritage affected by natural hazard risks and the associated measures.

The understanding of the multifaceted nature of the impact of disasters is an essential prerequisite for an adequate assessment of vulnerabilities of cultural heritage assets. It helps designing and implementing correct risk reduction strategies for different hazard scenarios. In this perspective, the research individuates the most relevant dimensions of resilience measures as well present a multidimensional characteristic which needs to be carefully explored and evaluated, namely: 1) informational dimension; 2) managerial dimension including decision making and actions; 3) physical dimension with socio-cultural, emotional and economic aspects. The resilience-building decision support tools presented in this paper, available on the ProteCHt2Save project website [9], include: the manual of good and bad practice and the handbook for owners. These aim at strengthening the resilience of cultural heritage assets as well as at enabling the participation of those users which are commonly excluded from the decision making processes, such as owners for the sake of determining a beneficial balance between centrally and non-centrally managed resilience measures.

Acknowledgements. This paper is based on the results of the research supported by the Interreg CE 1127 ProteCHt2save project (Risk assessment and sustainable protection of Cultural Heritage in changing environment) and the institutional project RVO 68378297.

REFERENCES

[1] Cloete, C.E. Assessing urban resilience. *WIT Transactions on Information and Communication Technologies*, Vol 44 (2012), W IT Press, www.witpress.com, ISSN 1743-3517 (on-line).

[2] Vale, L.J. and Campanella. T.J. *The Resilient City*. Oxford, University Press: New York, (2005).

[3] Rockefeller Foundation. *100 Resilient Cities*. www.100resilientcities.org

[4] Cilliers, P. *Complexity and Post-modernism: Understanding complex systems*. Routledge: London, (2008), p.45,.
[5] Nel, D. Exploring a complex adaptive system approach to the study of urban change. *Thesis University of Pretoria*, December 2015 https://repository.up.ac.za/handle/2263/56093.
[6] Wohl, Sh. Complex Adaptive Systems and Urban Morphogenesis: Analyzing and designing urban fabric informed by CAS dynamics. *Thesis TU Delft*, 2018 https://doi.org/10.7480/abe.2018.10.2397.
[7] Heylighen F., Cilliers, P. and Gershenson, C. Complexity and Philosophy. In: Jan Bogg and Robert Geyer (eds.): *Complexity, Science and Society*, Radcliffe Publishing: Oxford, (2007).
[8] National Academies of Sciences, Engineering, and Medicine 2019. *Framing the Challenge of Urban Flooding in the United States.* Washington, DC: The National Academies Press. https://doi.org/10.17226/25381.
[9] www.interreg-central.eu/Content.Node/ProteCHt2save.html
[10] Bonazza, A., Maxwell, I., Drdácký, M., Vintzileou, E., Hanus, Ch.: Safeguarding Cultural Heritage from Natural and Man-Made Disasters – A comparative analysis of risk management in the EU (with substantial contribution of Ch. Ciantelli, P. De Nuntiis, E. Oikonomopoulou, V. Nikolopoulou, S. Pospíšil, C. Sabbioni, P. Strasser). Luxembourg: Publications Office of the European Union, 2018, 187 p., ISBN 978-92-79-73945-3 DOI:10.2766/224310 (catalogue) NC-05-17-059-EN-N.
[11] Sabbioni, C., Bonazza, A., Messina, P., Cassar, M., Biddulph, Ph., Blades, N., Brimblecombe, P., Grossi, C.M., Harris, I., Tidblad, J., Kozlowski, R., Bratasz, L., Jakiela, S., Drdácký, M., Bláha, J., Herle, I., Lesák, J., Mašín, D., Pospíšil, S., Slížková, Z., Saiz-Jimenez, C., Grøntoft, T., Svenningsen, G., Wainwright, I., Hawkings, Ch., Gomea-Bolez, A., Ariño Vila, X., Llop, E. The Atlas of Climate Change Impact on European Cultural Heritage - Scientific analysis and management strategies, ISBN-13: 978 1 84331 798 2 (Hbk), ISBN-10: 1 84331 798 2 (Hbk), ISBN-13: 978 1 84331 861 3 (eBook), ISBN-10: 1 84331 861 X (eBook), Anthem Press, London/New York, 146 p., 2010
[12] Drdácký, M., Slížková, Z. Structural strategies and measures reducing flood action on architectural heritage. In "Risk Analysis VIII" (C.A. Brebbia - ed.), WIT Transactions on Information and Communication Technologies, Vol 44, WIT Press, Ashurst, Southampton, UK, 2012, pp. 249-259, doi:10.2495/RISK120221.
[13] Drdácký, M., Herle, I., Pospíšil, S., Slížková, Z. Protecting cultural heritage against natural hazards, in Keynote Papers "Seismic protection of cultural heritage", Proc. of the 2nd WCCE-ECCE-TCCE Joint Conference, Antalya, ISBN 978-605-01-0188-1, Turkish Chamber of Civil Engineers, Ankara, 2011, pp. 103-122
[14] Drdácký, M.: The vulnerability and resilience of historic structures. Transsylvania Nostra. (2017) **11**: 8-12.
[15] Cacciotti, R., Blaško, M., Valach, J. A diagnostic ontological model for damages to historical constructions, J. Cult Her (2015) **16**: 40-48.

12th International Conference on Structural Analysis of Historical Constructions
SAHC 2020
P. Roca, L. Pelà and C. Molins (Eds.)

AN INTEGRATED MODELING APPROACH THAT COMBINES ELASTIC AMPLIFICATION AND ROCKING ANALYSIS FOR SEISMIC ASSESSMENT OF A MASONRY TOWER

ANJALI MEHROTRA[1*], ANDREW LIEW[2], PHILIPPE BLOCK[3] AND MATTHEW J. DEJONG[4]

[1] Institute for Sustainability and Innovation in Structural Engineering
University of Minho, Portugal
e-mail: anjali.a.mehrotra@gmail.com (*corresponding author)

[2] Department of Civil and Structural Engineering
University of Sheffield, UK
email: a.liew@sheffield.ac.uk

[3] Block Research Group – Institute for Technology in Architecture
ETH Zurich, Switzerland
email: block@arch.ethz.ch

[4] Department of Civil and Environmental Engineering
University of California – Berkeley, USA
e-mail: dejong@berkeley.edu

Keywords: Masonry, Rocking Dynamics, Finite Element Modeling, Amplification Effects, Computational Tools

Abstract. *Failure of masonry structures during earthquakes often occurs via specific, well-documented collapse mechanisms, many of which involve partial collapse of the structure well above ground level. Consequently, the elastic response of the structure needs to be considered, which in the case of historic structures such as bell towers and churches often requires modal analysis using finite element models - the generation of which can be labour-intensive and time-consuming. This paper presents a new integrated modeling approach which combines finite element analysis with rocking dynamics in order to model the seismic response of complex structural geometries in a computationally-efficient manner. The modeling strategy is implemented within COMPAS - an open-source computational framework that provides geometry processing independent of CAD software, and is incorporated within the broader framework of a tool being developed for the seismic collapse assessment of masonry structures. The framework of this new tool is first outlined, and the utility of the new modeling approach then demonstrated through application to the seismic assessment of a historic masonry tower in North-Eastern Italy. The analysis results indicate that for the level of seismic hazard expected on site, failure of the tower is most likely to occur via overturning collapse of one of the rampart elements. The importance of accounting for elastic amplification effects, as well as the influence of varying boundary conditions on the dynamic response, is also demonstrated.*

1 INTRODUCTION

Masonry structures are susceptible to collapse under the influence of seismic action. When such structures fail, they often do so via specific, well-documented collapse mechanisms ([1], [2]) – analysis of which can be conducted using either simplified analytical procedures (as implemented in many building codes) or through the use of more complex numerical modeling strategies (such as finite element analyses or discrete element methods). While the former can be over-conservative, often underestimating dynamic capacity and leading to expensive - and at times unnecessary - retrofitting solutions, the latter can be fairly computationally-expensive and time-consuming, especially when trying to model collapse. As an alternative analysis approach, rocking dynamics, whereby equations of motion describing different collapse mechanisms are directly derived and solved, can be used instead ([3]–[6]). Such an approach has the advantage of being less computationally-demanding than most numerical models, while providing more accurate predictions than most simplified analytical methods.

However, assessment of real structures often requires consideration of numerous different collapse mechanisms, many of which involve partial collapse of the structure well above ground level. Thus amplification and filtering of the ground motion by the building – which depends in turn on the natural frequency of the structure, also needs to be taken into account [7]. While the natural frequency and modes of simple, regular structures can be determined analytically, for many historic structures (e.g. bell towers, churches) consideration of the elastic response requires modal analysis using finite element models ([8]–[10]), the generation of which can be labour-intensive and time-consuming.

In this paper, a new integrated modeling approach - which requires only a 3D CAD model of the structure as input - is presented, which combines finite element analysis with rocking dynamics to model the seismic response of complex geometries in a computationally-efficient manner. The modeling strategy is implemented within COMPAS - an open-source computational framework that provides geometry processing independent of CAD software [11], and is incorporated within the broader framework of a tool being developed for the seismic collapse assessment of masonry structures [12]. To keep the solving strategy open-source, modal analyses are conducted using the *compas_fea* package [13], which directly constructs the FE model from the input geometry, and analyses it using the open-source finite element solver *OpenSees* [14]. The results of the modal analysis are subsequently used to define an equivalent single-degree-of-freedom (SDF) oscillator, which is subjected to different ground motion records. The response of the oscillator is then scaled appropriately, with the scaled response serving as the input signal at the base of the rocking mechanism. The procedure can be repeated for a wide range of potential collapse mechanisms within a structure, to determine the most vulnerable mechanisms for a given suite of ground motions. The utility of this new modeling approach is finally demonstrated by applying it to the seismic assessment of a historic clock tower in Lendinara, Italy.

2 METHODOLOGY

A flowchart outlining the functioning of this proposed tool can be found in Figure 1.

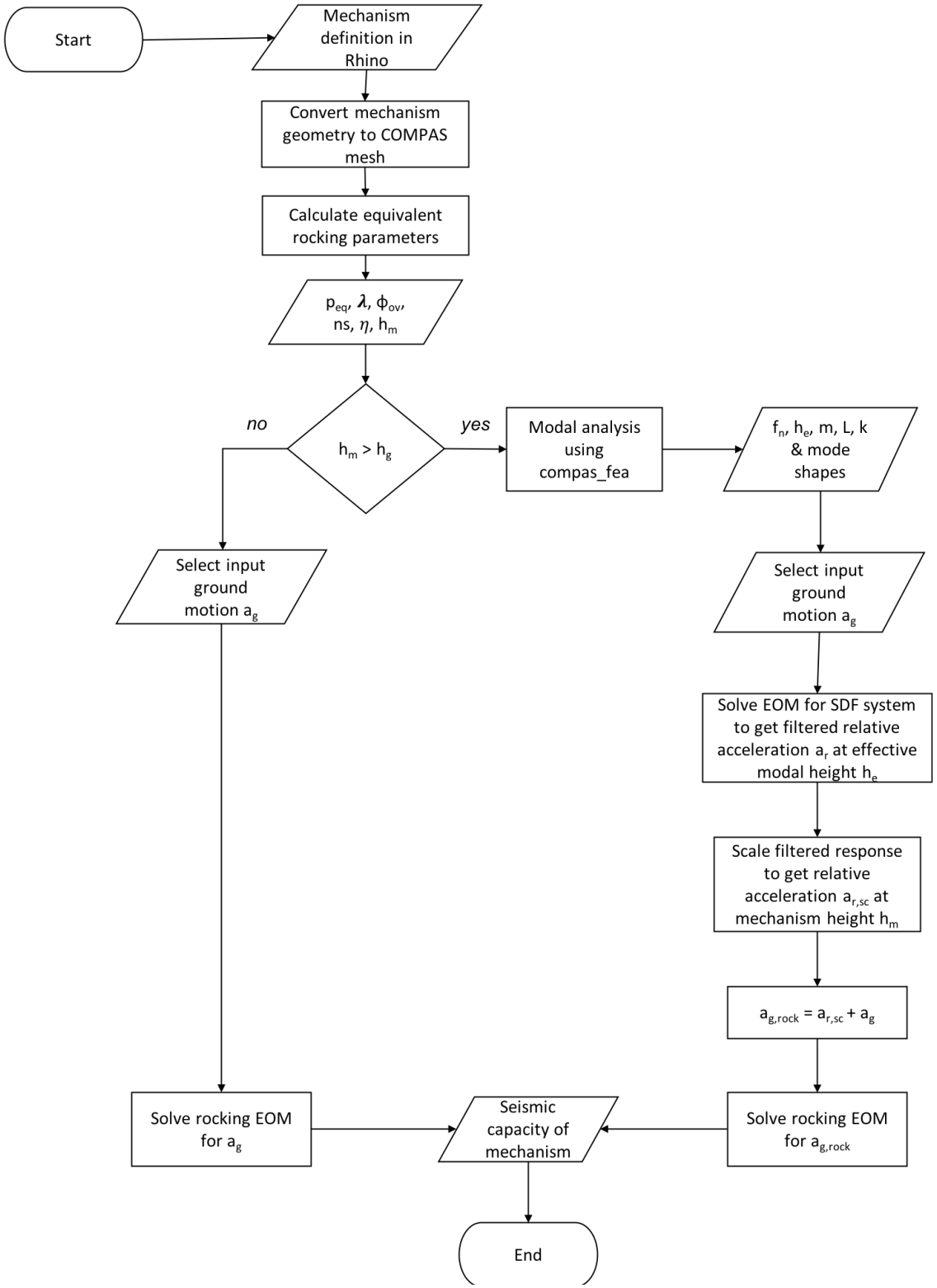


Figure 1: Flowchart illustrating the functioning of the proposed computational tool/modeling approach

2.1 Geometry and mechanism definition in the CAD interface

As stated in the introduction, the proposed modeling strategy only requires a 3D CAD model of the structure as input. However, as this strategy is implemented within COMPAS, which is a Python-based framework, it is crucial that the CAD program used is capable of editing and executing Python-based scripts. To that end, the CAD program Rhino [15] was selected as the preliminary interface for this tool, as it not only comes with its own Python interpreter, but also works on both Windows and Mac computers.

Once the geometry of the whole structure has been defined in Rhino, the portion of the structure involved in the collapse mechanism needs to be demarcated. The mechanism geometry is then meshed in Rhino, and the *compas_rhino.helpers* package is subsequently used to convert this Rhino mesh into its COMPAS counterpart – essentially converting the 3D solid into a datastructure defined by a set of vertices and faces. The axis of rotation as defined by the user is also saved as an attribute of this mesh so that it can be easily accessed in the next stage of analysis. If the mechanism takes place above ground level, a second mesh comprising the entire structure is also created and converted into its COMPAS counterpart. Attention must be paid to the density of this second mesh as it serves as the basis of the finite element model used for the modal analysis.

However, as the mesh datastructures as exported from Rhino comprises only 2D face meshes, i.e. only the external faces of the solids are meshed, the meshes first need to be converted into 3D tetrahedral meshes (i.e. internally meshed) before any operations can be performed on it within the COMPAS framework. This is done using the package MeshPy [16], which in turn provides a Python interface to program TetGen [17].

2.2 Calculation of equivalent rocking parameters

Once the mechanism geometry has been converted to the 3D mesh datastructure, geometric operations can be directly performed on it within the COMPAS environment. These include extraction of the various geometric properties (such as moment of inertia, volume and centre of mass) that are used to define the rocking equation of motion, which assumes the following general linearized form [4]:

$$\tilde{I}\ddot{\phi} - \tilde{K}\left(\phi - \phi_{cr}\right) = -\tilde{B}\ddot{u}_g \quad +\tilde{M} \tag{1}$$

where $\tilde{I}$, is the moment of inertia of collapsed portion of the structure about the axis of rotation, $\tilde{M}$ is the moment caused by the external static forces, ϕ_{cr} is the critical rotation, $\tilde{K}$ is the rotational stiffness of the system, and $\tilde{B}\ddot{u}_g$ is the moment provided by the ground motion applied to the structure. Note that the linearization here has occurred about the point of unstable equilibrium (i.e. $\phi = \phi_{cr}$) in order to obtain local dynamic equivalence with the single rocking block. This single equation of motion can then be used to describe a variety of different mechanisms, ranging from the overturning of a single rocking block to the dynamic behaviour of more complex two and three block mechanisms.

By using the following transformation of variables:

$$\theta = \phi \frac{\tilde{K}}{g\tilde{B}} \tag{2}$$

Equation (1) can be rewritten as:

$$\ddot{\theta} = p_{eq}^2 \left(\theta - \lambda - \frac{\ddot{u_g}}{g} \right) \tag{3}$$

where p_{eq} is the rocking frequency parameter and λ is an approximation of the static load multiplier that activates the mechanism. Both these terms depend on the kinematic constants $\tilde{I}$, $\tilde{K}$, $\tilde{B}$, $\tilde{M}$ and ϕ_{cr}, which in turn depend on both the geometry of the structure as well as the type of collapse mechanism; more detailed expressions for which can be found in [12].

Additionally, the overturning rotation ϕ_{ov}, that is, the rotation upon the exceedance of which the structure will overturn and collapse, can also be calculated using the aforementioned kinematic constants as shown below:

$$\phi_{ov} = \phi_{cr} - \frac{\tilde{M}}{\tilde{K}} \tag{4}$$

Moreover, in the case of impact, energy dissipation by the block(s) is accounted for through the coefficient of restitution η, which depends not only on the geometry of the blocks but also on the type of rocking, i.e. one or two-sided – indicated in this paper by the term *ns*. For more detailed expressions for the coefficient of restitution, please refer to [12]. Finally, the height h_m at which the mechanism occurs is determined by taking the average of the heights of the two points defining the axis of rotation, previously saved as an attribute of the mesh.

2.3 Modal analysis using *compas_fea*

In the case of mechanisms that take place above ground level (i.e. $h_m > h_g$) modal analyses need to be conducted to define an equivalent single-degree-of-freedom elastic oscillator, which in turn is used to account for the amplification and filtering of the ground motion by the structure.

Using the tetrahedral mesh of the entire structure as generated in Section 2.1, the *compas_fea* package is utilized for the construction of the corresponding finite element model. To do this, a *Structure* object is first created, with nodes corresponding to each of the points of the tetrahedral mesh and elements corresponding to each of the tetrahedral elements. Material properties are set through the assignment of a material type (for the purpose of this analysis, elastic isotropic) which in turn is characterized by a user-defined Young's modulus, Poisson's ratio and density. Boundary conditions are specified through the assignment of pinned displacements to predefined node sets, which are applied through the addition of a *Step* object. A second *Step* object, in this case *ModalStep*, is then added to instruct the finite element solver to conduct a modal analysis, specifying the number of modes to be analysed.

After the *Structure* object has been constructed, it is written to a .tcl input file which is subsequently sent to *OpenSees* for analysis. The analysis is conducted in the background and once completed, the results - such as modal frequencies f_n and nodal displacements u for each mode - are returned. Post-processing of this data results in the structure being transformed into an equivalent single-degree-of-freedom elastic oscillator, defined by the following equation of motion:

$$\tilde{m}\ddot{z} + 2\tilde{m}\xi\omega_n\dot{z} + \tilde{k}z = -\tilde{L}\ddot{u_g} \tag{5}$$

where:

$$\tilde{m} = \sum_{i=1}^{N} m_i u_i^2 ; \quad \tilde{L} = \sum_{i=1}^{N} m_i u_i ; \quad \omega_n = 2\pi f_n \quad and \quad \tilde{k} = \tilde{m}\omega_n^2 \tag{6-9}$$

where m_i is the mass lumped into each of the nodes of the model and u_i their corresponding displacements. System damping is specified through the term ξ, and is set to 5% for the analyses conducted in this paper. Solving Equation (5) gives the response of the oscillator at the effective modal height h_e, which is determined using the following expression:

$$h_e = \frac{\sum_{i=1}^{N} m_i u_i h_i}{\sum_{i=1}^{N} m_i u_i} \tag{10}$$

where h_i is the height of each node. However, for mechanisms that occur at a height above or below h_e (i.e. $h_m \neq h_e$), the response needs to be scaled using the mode shapes, which are extracted using the nodal displacements u. This is illustrated by Figure 2 for a sample tower with varying boundary conditions, including the isolated case, that is, only base nodes pinned and the "fixed" case, that is, nodes on either side of the structure also pinned up to a certain height, to simulate the connectivity of the tower to adjacent buildings.

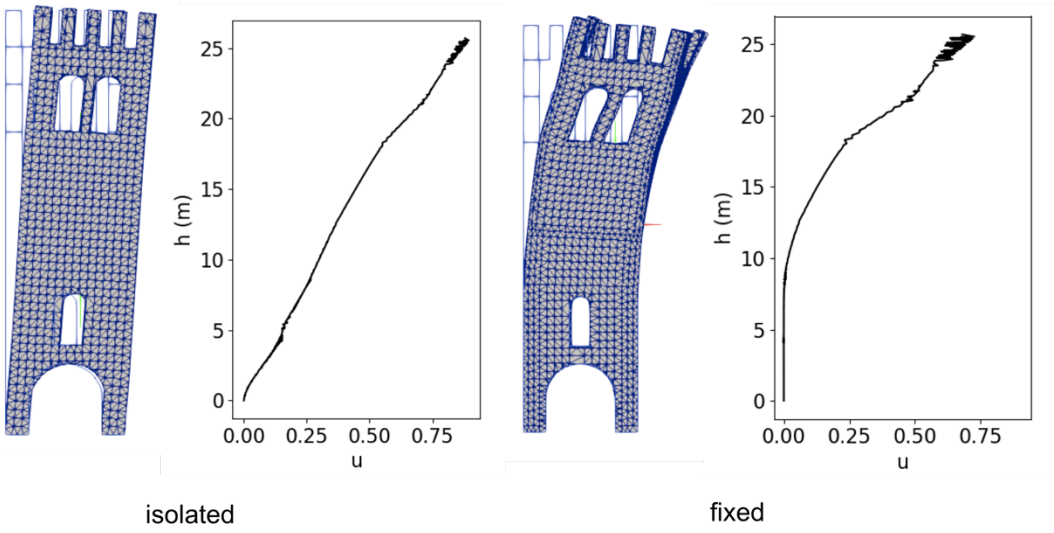


Figure 2: First mode shapes extracted by the tool for a sample tower, for both the isolated case as well as the case where the tower is connected to the adjacent buildings ("fixed" case)

2.4 Full time-history analysis

In the case of full time-history analyses, Equation (5) is first solved for the unscaled input ground acceleration a_g (i.e. $\ddot{u}_g = a_g$, Figure 3a). The solution to the equation of motion yields the filtered response of the structure a_r – relative to the ground - at the effective modal height h_e (Figure 3b). For mechanisms that occur at a height other than h_e ($h_m \neq h_e$), a_r then needs to be scaled using the mode shapes (Figure 2), to get the filtered and scaled response $a_{r,sc}$ at the mechanism height h_m (Figure 3c), as shown below:

$$a_{r,sc} = \frac{u(h_m)}{u(h_e)} a_r \tag{11}$$

However, $a_{r,sc}$ is only the scaled and filtered response of the structure relative to the ground. Thus to get the total acceleration experienced by the structure at the base of the rocking mechanism, this acceleration $a_{r,sc}$ is added to the original input ground acceleration a_g and the final combined acceleration is illustrated by Figure 3d. This acceleration $a_{g,rock}$ serves as the

final input signal for the rocking equation of motion (Equation (3), $\ddot{u}_g = a_{g,rock}$), which is then solved to predict the response of the rocking mechanism in terms of rotation ϕ over time.

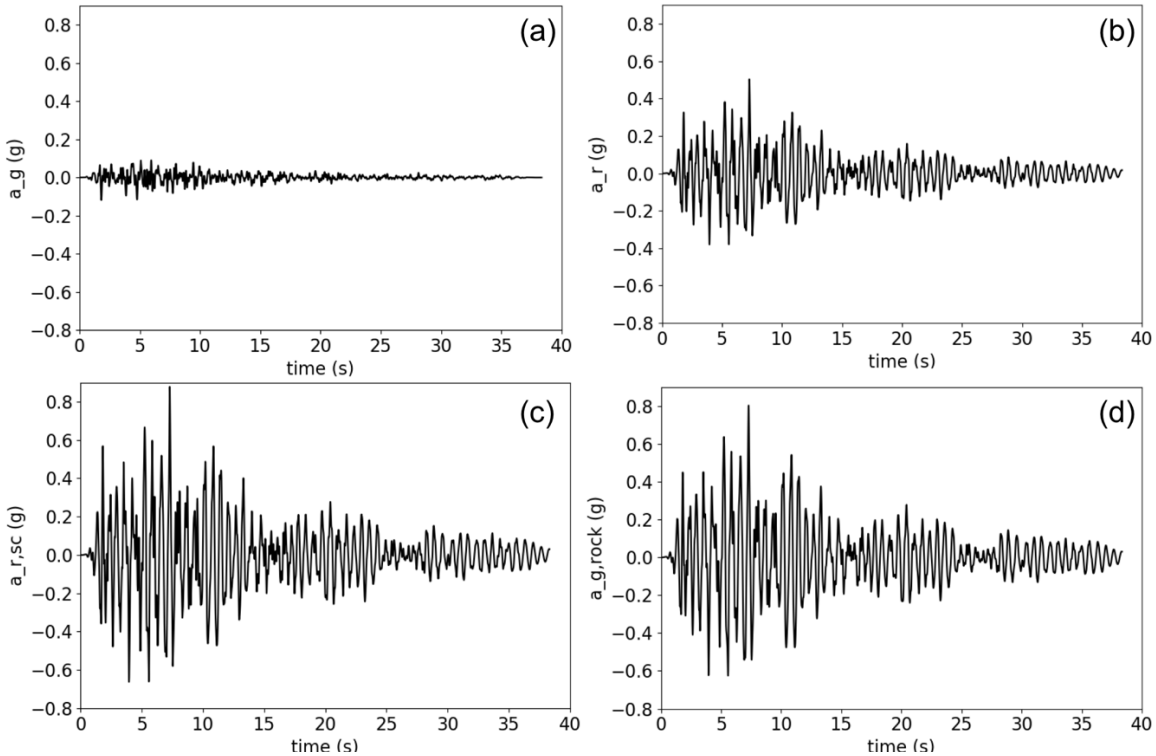


Figure 3: Procedure for filtering and scaling of the input ground motion: (a) unscaled input ground acceleration a_g, (b) filtered relative acceleration a_r at the effective modal height h_e, (c) scaled and filtered relative acceleration $a_{r,sc}$ at the mechanism height h_m and (d) final input signal at base of rocking mechanism $a_{g,rock}$

3 CASE STUDY: CLOCK TOWER IN LENDINARA

To demonstrate this new integrated modeling approach, a clock tower in the city of Lendinara, Italy was chosen as a case study. Full time-history analyses were conducted for a predefined set of collapse mechanisms, and the results compared to the expected seismic hazard in the region.

3.1 Geometry of the tower and seismic hazard of the area

The clock tower chosen for analysis is approximately square in plan and constructed entirely in brick, with a height of 25.7 m and base dimensions of 7.2 × 8.0 m [18]. The walls are roughly 100 cm thick for the bottom 12.6 m, with this thickness reducing to 50 cm near the top [18]. Two large arches are present on the eastern and western façades at the bottom of the structure, which enable the tower to connect the two small squares that it borders, while all four façades have large double openings at the upper level of the structure, with merlon (rampart) elements present at the very top [18].

The tower is located in North-Eastern Italy in a zone of low seismicity, with a maximum PGA of 0.075 – 0.100g expected with a 10% probability of exceedance in 50 years. In this analysis, the ground motion applied to the tower will thus be scaled to PGA = 0.1g (or some

factor thereof) to gauge the vulnerability of the structure to collapse.

3.2 Mechanisms selected for analysis

As illustrated by Figure 4, three different collapse mechanisms were selected for analysis, all of which occur high enough up so that amplification effects will not be negligible. These include the overturning of one of the merlon/rampart elements at the very top of the tower (Mechanism a1), as well as corner failure with cracks originating at the large double openings. In the case of the corner mechanisms, the crack angles were chosen to represent both an average value ($\alpha_c = 45°$, Mechanism b1) as well as an upper limit ($\alpha_c = 70°$, Mechanism b2) for a range of different brick aspect ratios and bonding patterns.

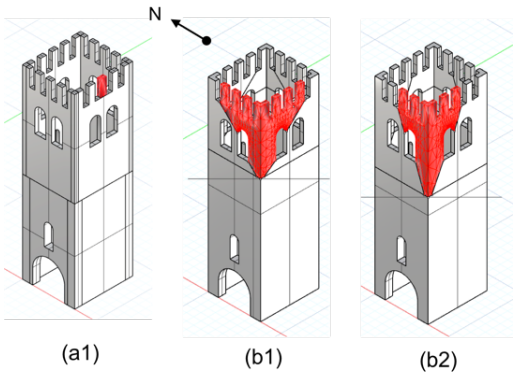


Figure 4: Collapse mechanisms selected for analysis: (a1) single-block rampart overturning, (b1) corner failure with a crack angle $\alpha_c = 45°$ and (b2) corner failure with a crack angle $\alpha_c = 70°$

The meshed mechanism geometries were then exported to COMPAS to calculate their equivalent rocking parameters, as listed in Table 1 for each of the different mechanisms. Note that the coefficient of restitution η is negative for Mechanisms b1 and b2 as both undergo one-sided rocking, that is, they rebound against the rest of the tower.

Table 1: Equivalent rocking parameters for the different mechanisms

	a1	**b1**	**b2**
p_{eq} **(s^{-1})**	2.55	1.22	1.12
λ **(rad)**	0.22	0.33	0.20
ϕ_{ov} **(rad)**	0.22	0.33	0.20
ns	2	1	1
η	0.93	-0.35	-0.56
h_m **(m)**	23.5	17.1	15.0

3.3 Modal analyses

As all three mechanisms take place at a height above ground level ($h_m > h_g$), modal analyses were conducted using *compas_fea*. Note that as the mechanisms all occur in the same tower, only one meshed model of the full structure was exported to COMPAS.

The bottom 8.55 m of the tower is connected to the adjacent buildings on its northern and southern façades, but limited information is available about the type/level of connectivity.

Therefore, two different boundary conditions were considered to provide a lower and upper bound for this parameter. These are the isolated case (zero connectivity to the adjacent structures) and the fixed case (tower completely restrained, i.e. pinned, to the adjacent structures). The material properties assumed for both models were that of an elastic isotropic material characterized by a Young's modulus $E = 0.84$ GPa, a Poisson's ratio $\nu = 0.2$ and density $\rho = 2000$ kg/m^3.

The results of the modal analyses were then used to define two SDF elastic oscillators, characterized by average frequencies of 1.55 Hz and 2.74 Hz for the isolated and fixed cases respectively, and first mode shapes as illustrated by Figure 2.

3.4 Full time-history analyses

Full time-history analyses were subsequently conducted for the three different collapse mechanisms for a suite of earthquake ground motions. Using the PEER NGA-West2 ground motion database, fifteen different ground motions were selected for this analysis, scaled to the site-specific response spectrum as defined in Eurocode 8, assuming soil type C, and as illustrated by Figure 5.

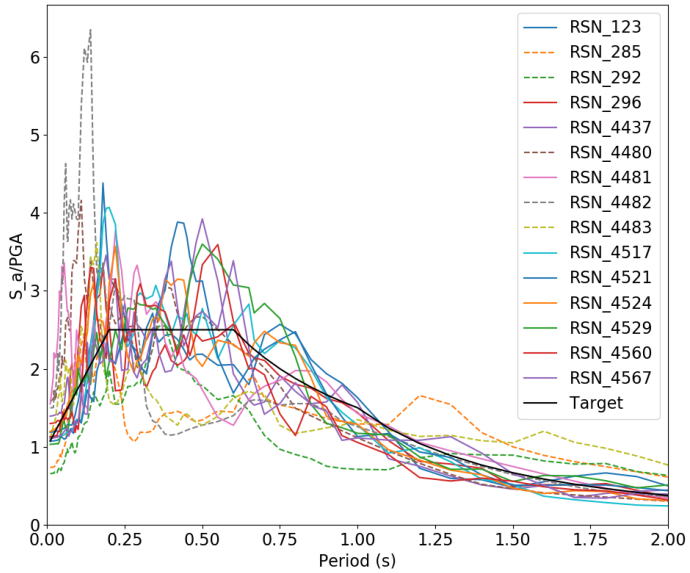


Figure 5: Elastic acceleration spectra (normalized by PGA) of the ground motions selected for analysis. Note that the site-specific target spectrum is shown in black.

Equation (5) was then solved for the two SDF elastic oscillators (for the isolated and fixed cases) for each of the ground motions, and the response scaled to get the final input signals at the base of the three rocking mechanisms. The filtered and scaled input signals were then substituted into Equation (3), which was solved to predict the response of each of the rocking mechanisms to the different ground motions, for both the isolated ("iso") and fixed cases, with the predictions expressed in terms of rotation ϕ over time. For each mechanism, the maximum predicted rotation ϕ_{max} normalized by the overturning rotation ϕ_{ov}, was then compared for each of the different ground motion records, for both connectivity cases ("iso" and "fixed"), as illustrated by Figure 6 for Mechanism a1 (scaled to a PGA = 0.1g).

As Figure 6 illustrates, for the isolated case, the tower fails via Mechanism a1 for 4 out of 15 of the earthquake records when the ground motion is scaled to PGA = 0.1g. Failure in this case is defined as overturning collapse, with overturning taking place when $\phi_{max}/\phi_{ov} = 1$, although failure would occur at lower rotations in reality. For the full suite of earthquake ground motions, ϕ_{max}/ϕ_{ov} had a median value of 0.71. For the fixed case, i.e. for the tower connected to the adjacent structures, the predictions of the rocking equation of motion are consistently lower than for the isolated case (with the exception of RSN 4437 where the two predictions are equal), with a median value of 0.30 for ϕ_{max}/ϕ_{ov} for the entire suite of ground motion records.

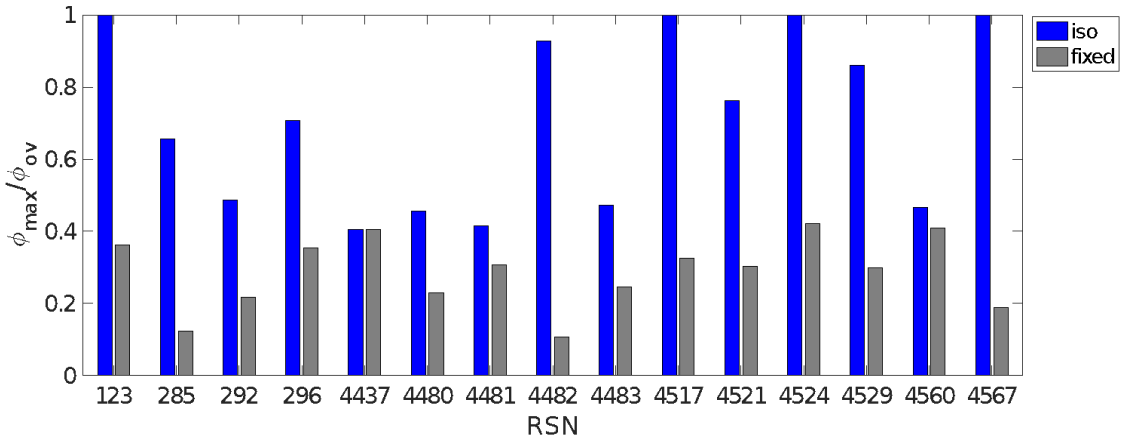


Figure 6: Mechanism a1: maximum rotation ϕ_{max} (normalized by overturning rotation ϕ_{ov}) recorded for each of the different ground motion records, for both the isolated and fixed cases (PGA = 0.1g)

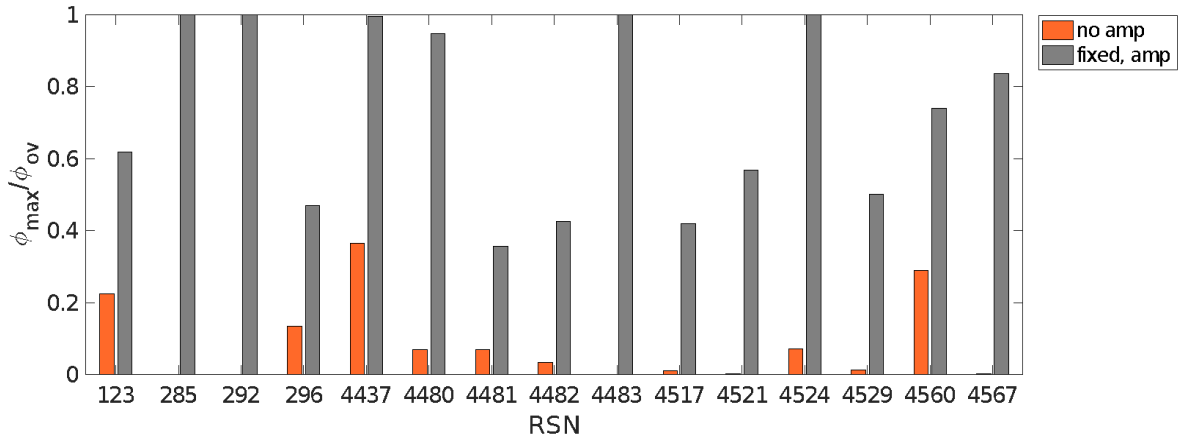


Figure 7: Mechanism a1: maximum rotation ϕ_{max} (normalized by overturning rotation ϕ_{ov}) recorded for each of the different ground motion records, for both the case without amplification and with amplification (fixed case) (PGA = 0.25g)

To demonstrate the importance of accounting for amplification effects, another set of analyses were conducted on Mechanism a1, now including the case where amplification effects were neglected, that is, the input ground motion $\ddot{u}_g$ for Equation (3) was set equal to the original ground motion a_g. For rocking to initiate in this case, the ground motion records were now scaled to a PGA of 0.25g and the results of these analyses are presented in Figure 7. Note that

only the fixed case results are provided for comparison here, as the isolated case resulted in overturning failure for all considered ground motion records. As Figure 7 illustrates, this level of scaling of the ground motion results in collapse of the mechanism for the fixed case (i.e. with amplification) for 5 out of 15 of the selected earthquake records, with a median value of 0.74 for ϕ_{max}/ϕ_{ov} for the entire suite. Neglecting amplification effects ("no amp") on the other hand results in comparatively smaller rotations being predicted for the structure, with a median value of 0.03 for ϕ_{max}/ϕ_{ov} for the entire suite.

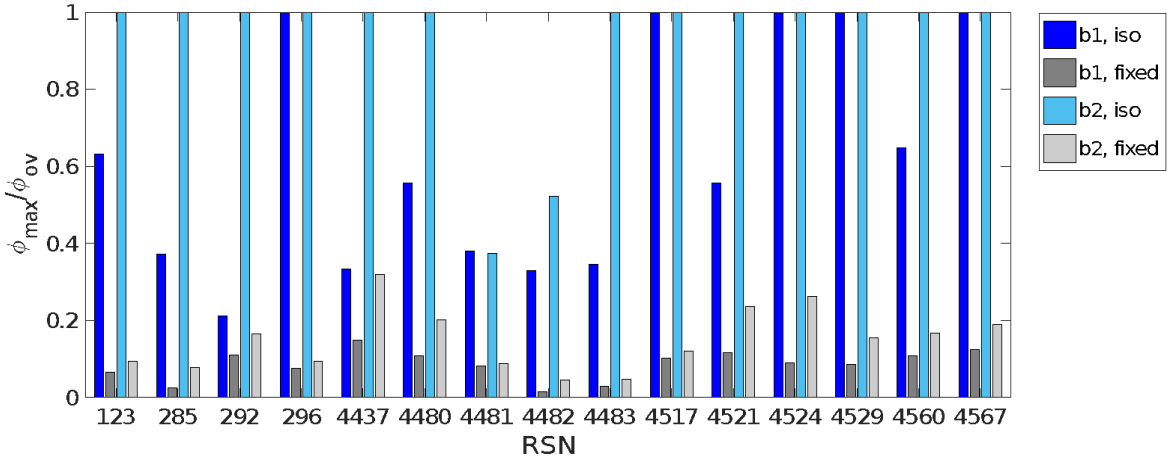


Figure 8: Mechanisms b1 and b2: maximum rotations ϕ_{max} (normalized by overturning rotation ϕ_{ov}) recorded for each of the different ground motion records, for both the isolated and fixed cases (PGA = 0.5g)

The final set of time-history analyses were conducted on Mechanisms b1 and b2, with the ground motion now scaled to a PGA = 0.5g to initiate rocking for the relatively stockier Mechanism b1. The results of these analyses are presented in Figure 8 for both the isolated and fixed cases. As Figure 8 illustrates, this level of ground motion scaling results in failure via Mechanism b1 for 5 out of 15 and failure via Mechanism b2 for 13 out of 15 of the earthquake records for the isolated case, with median ϕ_{max}/ϕ_{ov} values of 0.56 and 1.00 respectively. It is clear that in this case the slenderness of b2 ($\lambda = 0.20$, as opposed to $\lambda = 0.33$ for b1) controls the response, resulting in the overturning of b2 more frequently than b1 – despite the fact that both mechanisms are of similar scale, with b1 also occurring slightly higher up than b2 and consequently experiencing a greater degree of amplification. Similarly, for the fixed case, Mechanism b1 records smaller median ϕ_{max}/ϕ_{ov} values than Mechanism b2 (0.09 and 0.16 respectively). As in the case of Mechanism a1, the predictions for the fixed case are also considerably less conservative than their isolated counterparts.

4 CONCLUSIONS

In this paper, a new modeling approach for the seismic collapse assessment of masonry structures is presented, which integrates finite element analysis with rocking dynamics to model the dynamic response of complex structural geometries in a computationally efficient manner. This new modeling strategy, implemented using the COMPAS framework, is first described, following which it is applied to the seismic assessment of a historic masonry tower in North-Eastern Italy.

For the level of seismic hazard expected on site, failure of the tower is most likely to occur via overturning of one of the merlon/rampart elements. The results also illustrated the importance of accounting for ground motion amplification effects, as well as the influence of varying boundary conditions (isolated vs fixed) on the dynamic response.

REFERENCES

[1] D'Ayala, D. and Speranza, E. An Integrated Procedure for the Assessment of Seismic Vulnerability of Historic Buildings. In: *Proceedings of the 12th European Conference on Earthquake Engineering*, (2002).

[2] PCM-DPC MiBAC. *Model A-DC Scheda per il rilievo del danno ai beni culturali - Chiese*. (2006).

[3] Housner, G.W. The Behavior of Inverted Pendulum Structures during Earthquakes. *Bull. Seismol. Soc. Am.* (1963) **53**: 403–417.

[4] Mauro, A., de Felice, G. and DeJong, M.J. The relative dynamic resilience of masonry collapse mechanisms. *Eng. Struct.* (2015) **85**:182–194.

[5] DeJong, M.J. and Dimitrakopoulos, E.G. Dynamically equivalent rocking structures. *Earthq. Eng. Struct. Dyn.* (2014) **43**:1543–1563.

[6] Makris, N. and Vassiliou, M.F. Planar rocking response and stability analysis of an array of free-standing columns capped with a freely supported rigid beam. *Earthq. Eng. Struct. Dyn.* (2013) **42**:431–449.

[7] Priestley, M.J.N. Seismic behaviour of unreinforced masonry walls. *Bull. New Zeal. Soc. Earthq. Eng.* (1985) **18**:191–205.

[8] Casarin, F. and Modena, C. Seismic Assessment of Complex Historical Buildings: Application to Reggio Emilia Cathedral, Italy. *Int. J. Archit. Herit.* (2008) **2**:304–327.

[9] Castellazzi, G., Gentilini, C. and Nobile, L. Seismic Vulnerability Assessment of a Historical Church: Limit Analysis and Nonlinear Finite Element Analysis. *Adv. Civ. Eng.* (2013) **2013**:1-12.

[10] de Felice, G., Genoese, A., Genoese, A. and Malena, M. Seismic Vulnerability Assessment of the Casamari Gothic Church. In: *Proceedings of the 15th International Conference on Civil, Structural and Environmental Engineering Computing*, (2015).

[11] Van Mele, T. et al. *COMPAS: A framework for computational research in architecture and structures.* (2017-2020).

[12] Mehrotra, A. and DeJong, M.J. A CAD-interfaced dynamics-based tool for analysis of masonry collapse mechanisms. *Eng. Struct.* (2018) **172**: 833–849.

[13] Liew, A. and Mendez Echenagucia, T. *compas_fea: Finite Element Analysis package for the COMPAS framework*. (2017).

[14] McKenna, F., Fenves, G.L., Scott, M.H. and Jeremic, B. *Open system for earthquake engineering simulation (OpenSees)*. (2000).

[15] Robert McNeel & Associates. *Rhinoceros 5.* (2014).

[16] Klöckner, A. *MeshPy.* (2008).

[17] Si, H. TetGen, a Delaunay-Based Quality Tetrahedral Mesh Generator. *ACM Trans. Math. Softw.* (2015) **41**: Article 11.

[18] Valente, M. and Milani, G. Seismic assessment of historical masonry towers by means of simplified approaches and standard FEM. *Constr. Build. Mater.* (2016) **108**:74–104.

12th International Conference on Structural Analysis of Historical Constructions
SAHC 2020
P. Roca, L. Pelà and C. Molins (Eds.)

ASSESSMENT OF THE SEISMIC RETROFITTING OF A HISTORICAL MASONRY MOSQUE BY MEANS OF NONLINEAR DYNAMIC ANALYSIS

ABİDE AŞIKOĞLU[1*], LUIS C. SILVA[1], ÖZGÜR AVŞAR[2], AND PAULO B. LOURENÇO[1]

[1] Institute for Sustainability and Innovation in Structural Engineering (ISISE)
University of Minho
Azurém, 4800-058 Guimarães, Portugal
e-mail: abideasikoglu@hotmail.com, luisilva.civil@gmail.com, pbl@civil.uminho.pt - http://isise.net
(*corresponding author)

[2] Department of Civil Engineering, Eskisehir Technical University
26555 Eskişehir, Turkey
e-mail: ozguravsar@eskisehir.edu.tr - http://insaat.eskisehir.edu.tr

Keywords: Historical Masonry, Seismic retrofitting, Finite Element Method, Nonlinear dynamic analysis

Abstract. *Seismic actions have been a great challenge for structures in the structural engineering community, and the need for further developments has been approved by catastrophic seismic events at each time. Reproducing the dynamic behavior of structures with an acceptable level of accuracy is a complex task due to uncertainties related to the geometrical, material and physical structural system, more particularly, in the case of existing historical masonry structures. The use of dynamic analysis is a better choice than the use of static or quasi-static approaches since it is a better representation of the dynamic response of a structure by taking account of its energy dissipation capacity. The scope of the present paper is focused on a seismic assessment of a historical masonry structure, Kütahya Kurşunlu Mosque located in Turkey, before and after it has been retrofitted. The historical mosque is located in a seismic prone zone where it is crucial to ensure seismic safety of structures and the local community. Based on the condition of the structure reported from the site inspections, a seismic retrofitting by using steel girder elements was implemented on the structural load-bearing walls. The effectiveness of the seismic retrofitting to the seismic response of the mosque was investigated by means of the finite element method. Three bi-directional nonlinear dynamic analyses were performed by using real ground motion records aiming at the validation of the nonlinear dynamic response of the numerical model in terms of damage patterns, and demonstration of the contribution of the seismic retrofitting by comparing the representative model with its retrofitted counterpart. The comparison has been carried out in terms of peak displacement and damage patterns. It is found that the contribution of the seismic retrofitting is considerable for the out-of-plane displacements of the load-bearing walls. Furthermore, a good correlation between existing damage and the numerical damage is achieved, and, therefore, the validation of the nonlinear response of the representative model is attained.*

1 INTRODUCTION

Throughout the history, national and cultural identity of society has been declared by means of tangible and intangible cultural heritage. The Nara Document (1994) emphasizes that "The protection and enhancement of cultural heritage and heritage diversity in our world should be actively promoted as an essential aspect of human development". Architectural heritage, i.e. tangible cultural heritage, is the most concrete example of a culture that defines identity to the community where it belongs, and, also, its legacy shares a particular creative quality, uniqueness, originality, and authenticity that makes it a universal heritage of humankind (Jokilehto, 1999). Furthermore, historic areas have been a catalyst for the regeneration of their environment and contribute to the economy of cities (Orbaşlı, 2007). Therefore, conservation of historical structures is significant to be conducted according to the principle of minimum intervention, as admitted in ICOMOS (2013). Ancient structures have unique architectural, material and structural properties owing to their complex geometry, variety in construction materials, and, changes due to repair works, long-term effects, or damage (Roca (2006)). In this sense, case-based solutions need to be developed for conservation, strengthening, and retrofitting of heritage structures. Moreover, the seismic performance of such buildings is highly dependent on its heterogeneous material distribution, sophisticated geometric features, limited information regarding the connections between structural components, building condition under long-term effects, and absence of global structural behavior (Lourenço et al., 2011). The present study investigates a historical masonry mosque located in Turkey which is situated in the Alpine-Himalayan Seismic Belt. There are destructive major fault lines such as North Anatolian Fault (NAF), East Anatolian Fault (EAF), and Aegean Graben. Although the prediction of an earthquake by day and time is impossible, past seismic events provide significant information. For instance, NAF is experiencing a westward migrating earthquake sequence as shown in Figure 1. The sequence has begun with 1939 Erzincan Earthquake resulting in 360 km-length surface rupture and right-lateral displacements up to 10 m. Following events happened in 1942 (M7.1, with 50 km rupture), 1943 (M7.7, with 280 km rupture), 1944 (M7.4, 165 km rupture), 1951 (M6.8, 30 km rupture), 1957 (M7, rupture ranging between 30 – 50 km), 1967 (M7.2, 80 km rupture), and finally, two earthquakes happened in 1999 (M7.5, 130 km rupture and M7.1, with 50 km of rupture)[4]. Consequently, approximately 1,000 km fault unzipped starting from Erzincan nearly to the Marmara Sea [4]. Rockwell (2013) [4] states that a similar earthquake sequence happened a century ago was concluded regarding the paleo-seismic site works and it is found that the current sequence, which has started in 1939, has not completed yet. Therefore, another destructive earthquake is expected in the Marmara Sea close to İstanbul in which 15 million people live. In addition, the western part of the country is expected to be affected.

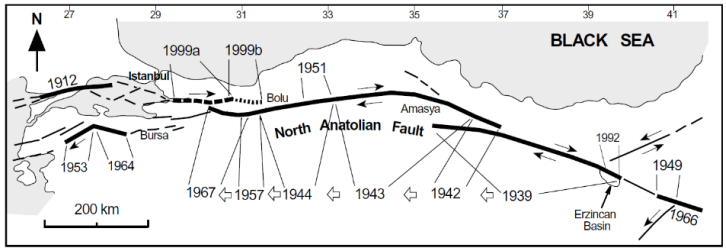


Figure 1. The westward migrating earthquake sequence along the NAF starting from 1939 [5]

It is obvious that it is crucial to minimize the effects of earthquakes on the structures in order to ensure the social and economic concerns of the society. However, the protection of heritage structures still requires significant developments and collapse or severe damage of any structure which promotes value for the society that should be prevented against earthquake actions. Turkey has been home to many civilizations throughout history and consequently, the culture of the country has been influenced and shaped by those periods of time. Therefore, there is a wide range of cultural and built heritage belonging to different eras of time which forms Turkey's outstanding legacy of heritage. For instance, Turkey has 17 properties inscribed on the UNESCO World Heritage List, and, additionally, 71 historical sites have been nominated in the Tentative List of UNESCO World Heritage. In fact, the General Directorate of Cultural Heritage and Museums of the Republic of Turkey Ministry of Culture and Tourism stresses that there is approximately 107,000 immovable cultural property that requires preservation and protection all around the country. Immovable heritage properties are defined according to their service whereas types of the built heritage have been specified as a sample of civil architecture, religious, cultural, governmental, military, industrial, commercial structures, cemeteries, ruins, memorials and monuments, and, protected streets. Several cities with a high number of immovable built heritage are listed in Table 1. The vast majority of the heritage construction has been recorded in İstanbul, with nearly 31,000, followed by İzmir, Bursa, Ankara, and Kütahya. It is emphasized that the given cities are only some that have high seismic activity. Obviously, the majority of the architectural heritage is under seismic risk.

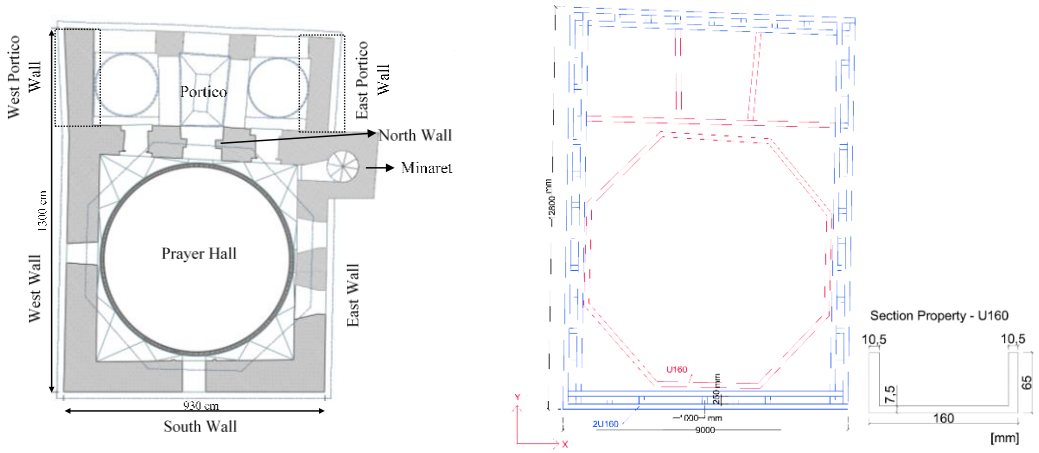
Table 1. Number of immovable cultural property in Turkey and selected cities in Turkey (Aşıkoğlu, 2018)

Type	Number of immovable cultural properties need to be conserved					
	Turkey	İstanbul	İzmir	Bursa	Ankara	Kütahya
Civil architecture	68114	25026	4623	3164	1215	1056
Religious structures	9876	1232	435	420	228	223
Cultural structures	12118	2308	587	308	199	174
Governmental structures	2889	521	227	86	187	29
Military structures	1225	107	27	49	9	2
Industrial and commercial	3992	532	708	49	90	27
Cemeteries	5168	690	174	167	146	54
Memorials and monuments	356	74	28	13	34	6
Ruins	2552	691	94	72	19	13
Protected streets	69	10	6	1	-	-
Total	**106359**	31191	6909	4329	2127	1584

2 HISTORICAL KÜTAHYA KURŞUNLU MOSQUE

Construction of Kütahya Kurşunlu Mosque dates back to 1377-1378, using ruins of a pre-existing building, and the Mosque suffered several conservation and restoration interventions between the 13th and 19th centuries. Although the mosque is standing for centuries, it is inevitable that the structure has experienced human and natural originated damage during its life span. In 2013, the Directorate General of Foundations of Turkey started restoration works and seismic retrofitting actions on the Mosque to address architectural and structural concerns. Thus, the present work examines the seismic behavior of the Mosque—located in Kütahya province with a high seismic exposition—before and after it has been retrofitted.

Kütahya Kurşunlu Mosque is located in the residential area of the city and being detached. The Mosque has a rectangular plan with a length of 13.0 m and a width of 9.3 m (Figure 2). The highest element of the Mosque is the minaret, with a height of 28.0 m, and it has a rectangular base with a polygonal transition section to a circular body. In the main body, the height of the load-bearing walls, which were constructed as three-leaf masonry, and the top point of the dome are 7.8 m and 11.0 m, respectively. The construction material of the Mosque is cut stone and brick, and the outer layer of the walls was built with cut stone, whereas rubble stone was used for the inner layer and core of the load-bearing walls. The dome, which is restrained by an octagonal drum, the vaults, pendentives, and octagonal drum were constructed using brick. The minaret base and circular body are constituted with cut stone and brick, respectively.



(a) (b)

Figure 2. Structural description, (a) architectural plan, (b) steel girder application plan

Deterioration and cracks were noticed during the site investigations, as illustrated in Figure 3. Some of the timber elements, which were obliged to prevent the development of thrust at the arch elements, were deteriorated and some of them were missing. Additionally, loss of wooden tie beams, that was supposed to be located inside the load-bearing walls along the length, was reported. Various moderate vertical cracks were noticed mainly around the window openings and at the intersection of two perpendicular walls. Moreover, moderate damage was observed on the octagonal drum and the dome, both at the interior and exterior surfaces. It is possible to say that the response of the structure and, also the dome seem to be dominated by out-of-plane mechanisms and expansion of the octagonal drum due to lack of global structural behavior. Based on the observed damage on the Mosque, it was decided to implement steel girder retrofitting having a cross-section of U160, at the top level of the load-bearing walls to achieve a better interaction between the walls (Figure 4). The connection between the steel elements and the masonry walls were provided by steel anchor. Additionally, steel elements were also inserted to the base section and top of the drum walls whereas timber elements were used to be found. In this part, the steel elements were placed, welded, and then, the gap between the elements and the masonry was filled with hydraulic lime-based mortar.

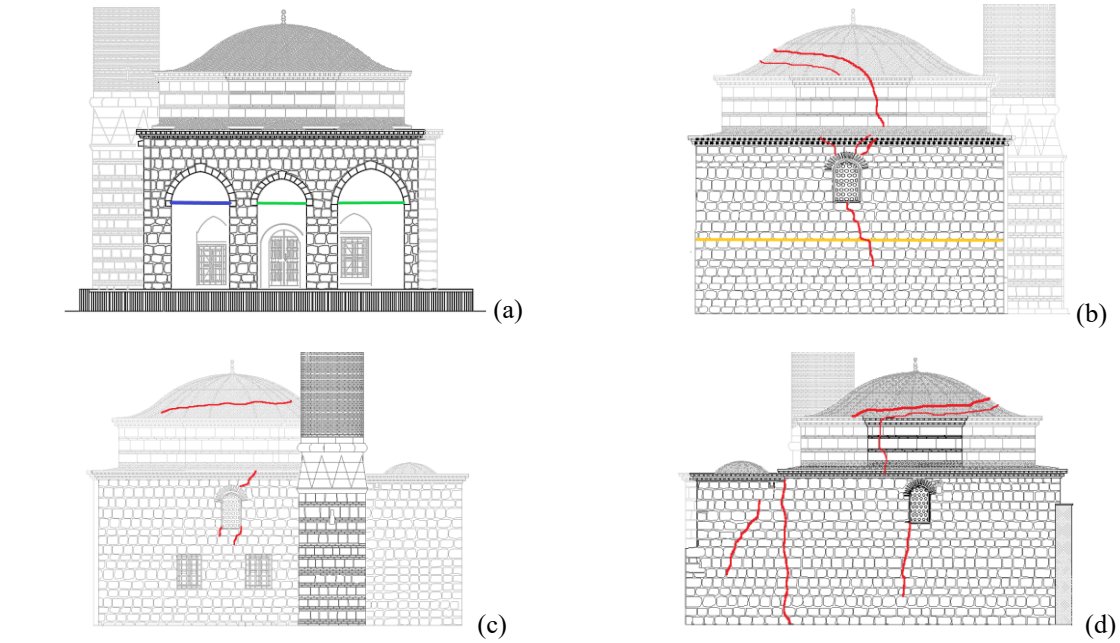


Figure 3. Damage map, (a) north elevation (b) south elevation, (c) east elevation, (d) west elevation



Figure 4. Application of single steel girder (U160) at the top and bottom of the drum, and double steel girder (2U160) on the load-bearing walls

4 REPRESENTATIVE NUMERICAL MODEL

An optimized numerical model of the Mosque was prepared by using FX+ for DIANA [6]. The representative model was constructed as a continuum element model assuming homogenous material behavior throughout the structure [7]. The finite element model created using beam, shell, and solid elements. Steel girder elements in the retrofitted model are represented by a set of beam elements (L13BE) while shell elements (triangular T15SH) are used to model the load-bearing walls, arcades, dome, and drum. On the other hand, a tetrahedron (TE12L) solid elements were used to model the pendentives since they have a complex volume. The continuum model of the retrofitted Mosque has 27,250 elements, having 428 beam, 22,978 shell, and 3844 solid elements, with a total number of 12,892 nodes and 72,950 degrees of

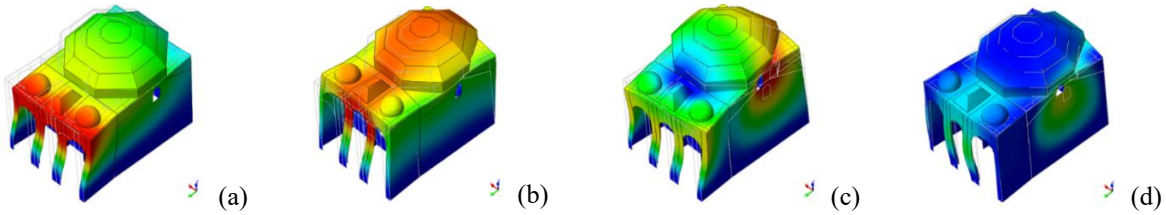
freedom. The degrees of freedom located at the foundation of the structural system was assumed as fully fixed. A detailed description of the numerical model is given in [8]. The constitutive model of the masonry material was assigned as a total strain fixed crack model that has been applied in several studies, such as [9] and [10]. The tensile behavior is defined by exponential stress-strain relation in the post-peak regime while compressive behavior is assumed to be parabolic for both pre- and post-peak response [11]. The material properties are listed in Table 2. The detailed description of the material properties is given in [8]. Accordingly, calibration of the continuum model was carried out by changing the Young's modulus of masonry material considering the results obtained from Operational Modal Analysis. Thus, the modal response of the representative model is given in Figure 5.

Table 2. Mechanical properties of the materials

Material	γ (t/m^3)	E (MPa)	υ (Poisson ratio)	Compressive strength (f_c) [MPa]	Tensile strength (f_t) [MPa]	Compressive fracture energy (G_c) [N/mm]	Tensile fracture energy (G_t) [N/mm]
Cut Stone	2.1	1500*	0.2	2.6	0.1	4.2	0.012
Brick	2.0	2500*	0.2	6.0	0.1	9.6	0.012
Timber	0.7	11000	0.3	-	-	-	-
Steel	7.85	200000	0.3	235	235	-	-

*Obtained from dynamic identification

It is important to mention that the non-retrofitted model, in terms of geometrical and material properties, is the same as the retrofitted model, the only difference being the existence of the steel girders on the latter model. In fact, frequencies, mode shapes, and cumulative mass participation ratios of the non-retrofitted model are quite similar to the retrofitted finite element model, and there is no significant change in modal response, as expected. Therefore, the non-retrofitted model was used to represent the nonlinear response of the non-retrofitted condition of the Mosque before the damage. The damage was not considered in the numerical model due to the limited information about the internal damage and the lack of representativeness.



(a) f_{num} = 5.77 Hz, Sum_Mx (%) = 60.72, Sum_My (%) = 0.00

(b) f_{num} = 7.87 Hz, Sum_Mx (%) = 61.13, Sum_My (%) = 66.95

(c) f_{num} = 9.77 Hz, Sum_Mx (%) = 70.80, Sum_My (%) = 67.27

(d) f_{num} = 11.32 Hz, Sum_Mx (%) = 70.83, Sum_My (%) = 67.28

Figure 5. The modal response of the first four modes, (a) 1st mode, (b) 2nd mode, (c) 3rd mode, (d) 4th mode

5 NONLINEAR DYNAMIC ANALYSIS

In order to perform the dynamic analyses, three ground motions recorded from past earthquakes occurred in Turkey were used. The location of the epicenter of each selected earthquake and its ground motions' seismological properties are given in Table 3. The vertical component of the earthquakes was disregarded, and both horizontal components of each input motions were applied orthogonally to the global coordinate axes of the mosque. The transverse components of Erzincan and Bolu records and longitudinal component of Bingöl record were

performed in the transversal direction (+X) of the mosque while the rest of the input were acted in the longitudinal direction (+Y) (Figure 6). The application of the orthogonal components was decided through the weaker axis according to the spectral acceleration values for the first mode of vibration period. The response spectra of the input motions and the elastic design spectra defined in TEC 2007 are given in Figure 7. The viscous damping ratio required for the Rayleigh damping strategy was assumed as 3%. Due to the fact that nonlinear time history analyses require high computational effort, only a part of the strong ground motions was considered in order to reduce the computation time. Thus, the duration of each record was shortened according to the cumulative energy duration [13] and only the first 20 s of each acceleration – time series were considered. The seismic performance of the retrofitted and non-retrofitted mosque was studied by means of bidirectional nonlinear time history analyses using the Hilber-Hughes-Taylor method (α-method). The numerical procedure was carried out using the secant method and energy norm convergence criteria with a tolerance value of 0.001 to solve dynamic equilibrium solution at each iteration. Accordingly, the effectiveness of the seismic retrofitting was investigated and presented in terms of out-of-plane displacements and principal tensile strain distribution on the structure.

Table 3. Seismological properties of selected ground motions (TR-NSMN)

Earthquake	March 13, 1992 Erzincan	November 12, 1999 Düzce	May 1, 2003 Bingöl
Depth (km)	23	11	6
Mw	6.6	7.1	6.3
Longitudinal PGA (g)	0.413	0.754	0.556
Transverse PGA (g)	0.480	0.821	0.282

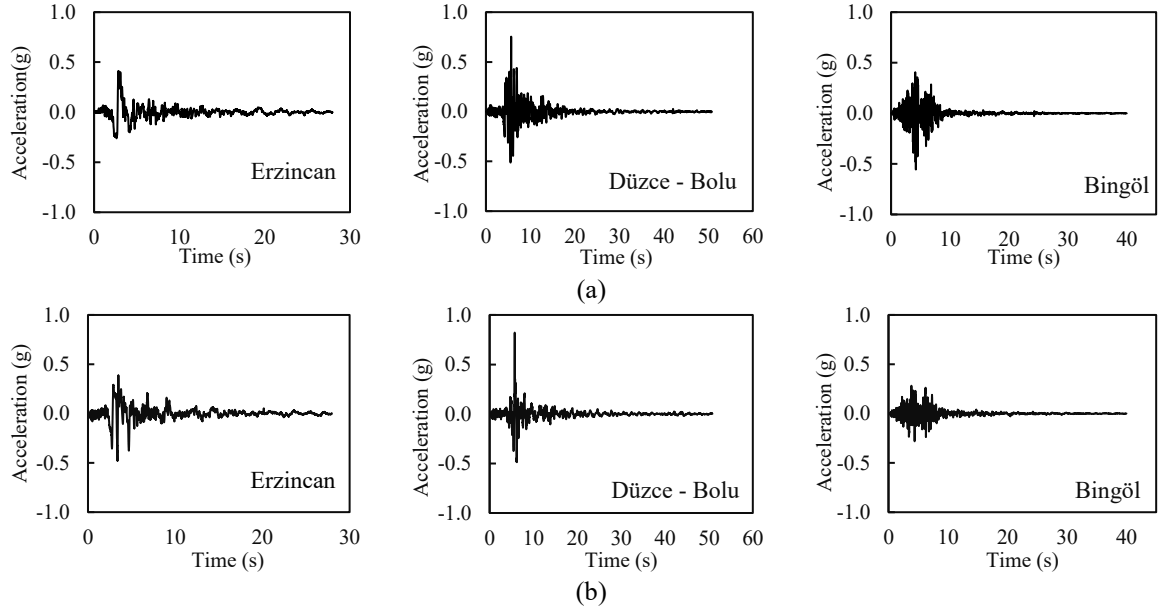


Figure 6. Acceleration-time series (TR-NSMN), (a) longitudinal (N-S), (b) transversal component (E-W)

Displacement response of the non-retrofitted and retrofitted model is given in Figure 8 and Figure 9 for the out-of-plane direction of the investigated structural walls, transversal (X) direction for East and West wall, longitudinal (Y) direction for South and North wall. It is found that two nodes located on the parallel walls have similar trends, but residual displacements are

in the opposite direction from their origin. Notwithstanding, the results obtained from the retrofitted model exhibit that improvement in the global structural behavior is achieved due to the fact that the residual displacement is considerably reduced. Indeed, the steel girder retrofitting contributes to the seismic response. In general, a considerable decrease in the peak displacement was observed in the Erzincan and Bingöl Earthquake cases. However, it is important to notice that although there is a reduction in the peak displacement, for instance as a result of the Düzce-Bolu Earthquake, the imposed displacement values are still high and might be an indication of structural damage. Reduction in the out-of-plane displacements on the East and West walls is nearly up to 55% while the difference in the South and North Wall reach 86% and 66%, respectively. Above all, the expansion of the dome is reduced significantly by implementing the seismic retrofitting, as shown in Figure 10.

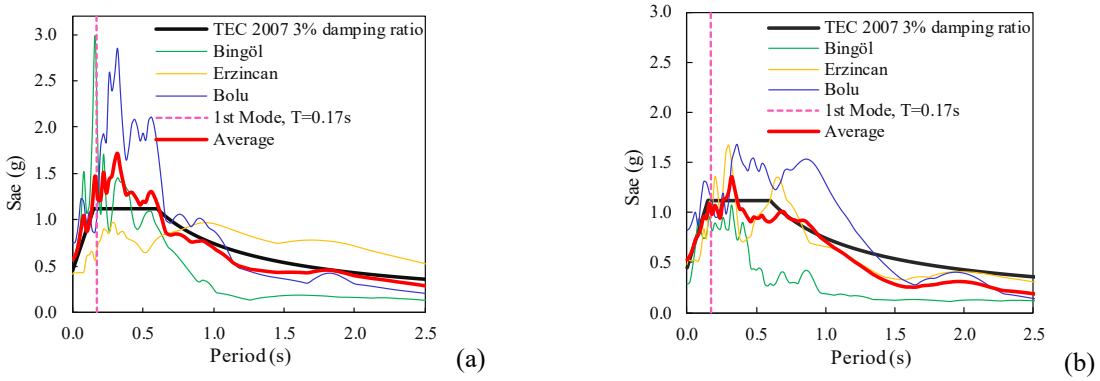


Figure 7. Elastic response spectra for Z3 soil condition, (a) longitudinal (N-S), (b) transverse component (E-W)

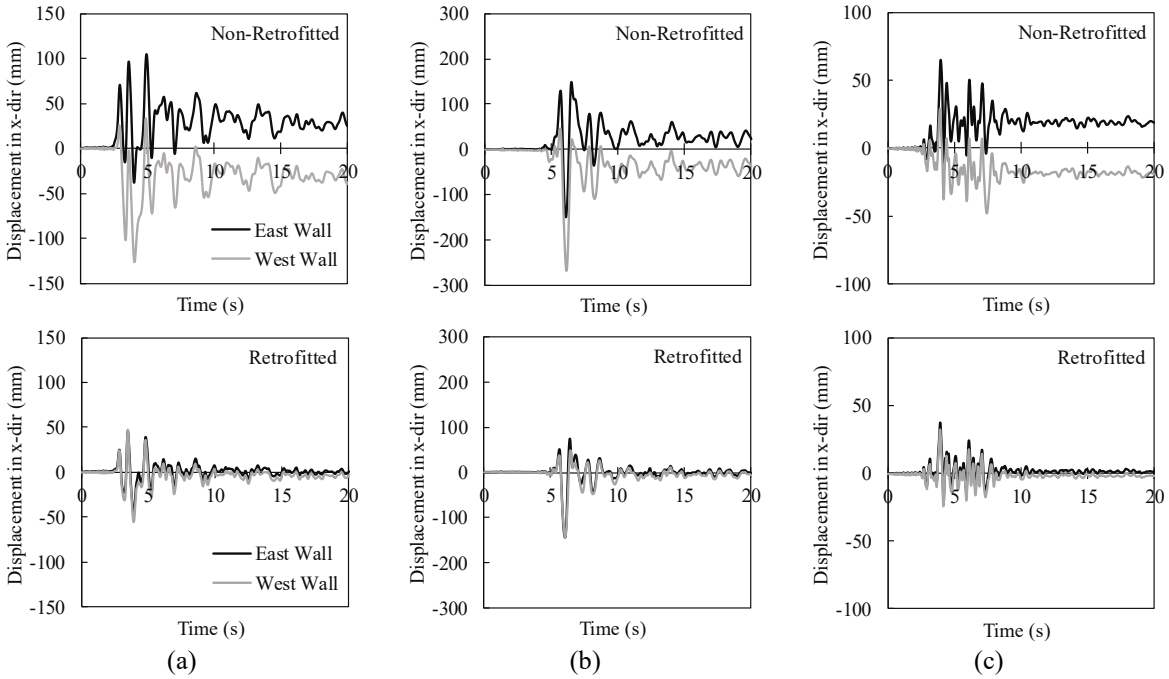


Figure 8. Displacement response at east and west walls in the x-direction, (a) Erzincan, (b) Düzce, (c) Bingöl

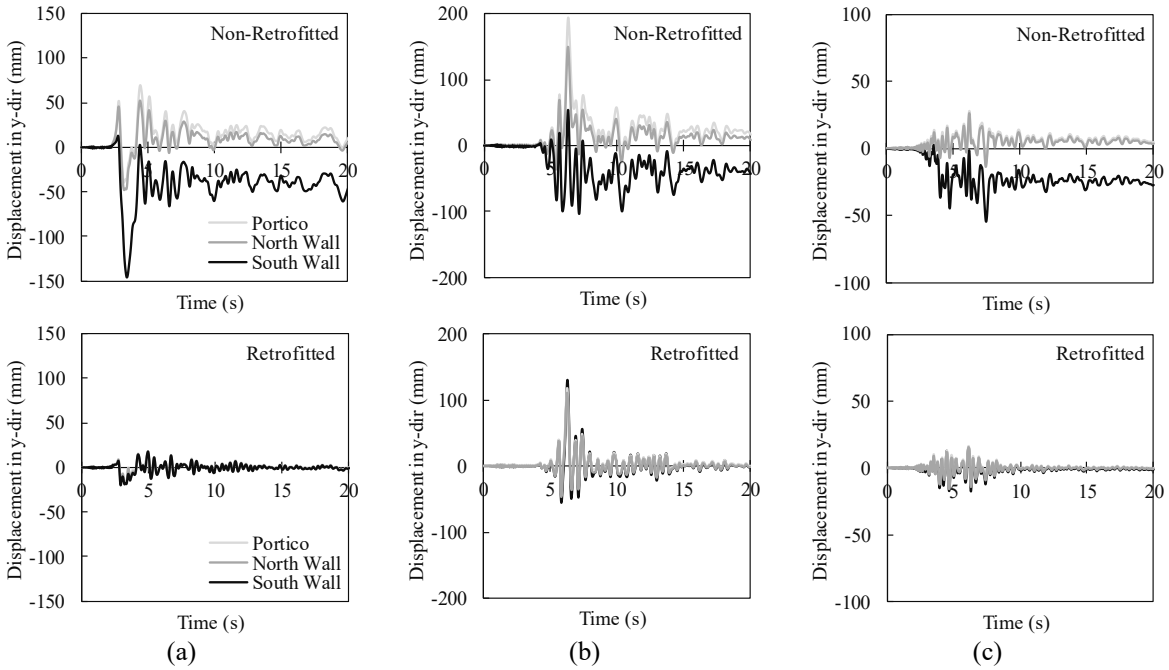


Figure 9. Displacement response at north and south walls and portico in the y-direction, (a) Erzincan, (b) Düzce, (c) Bingöl

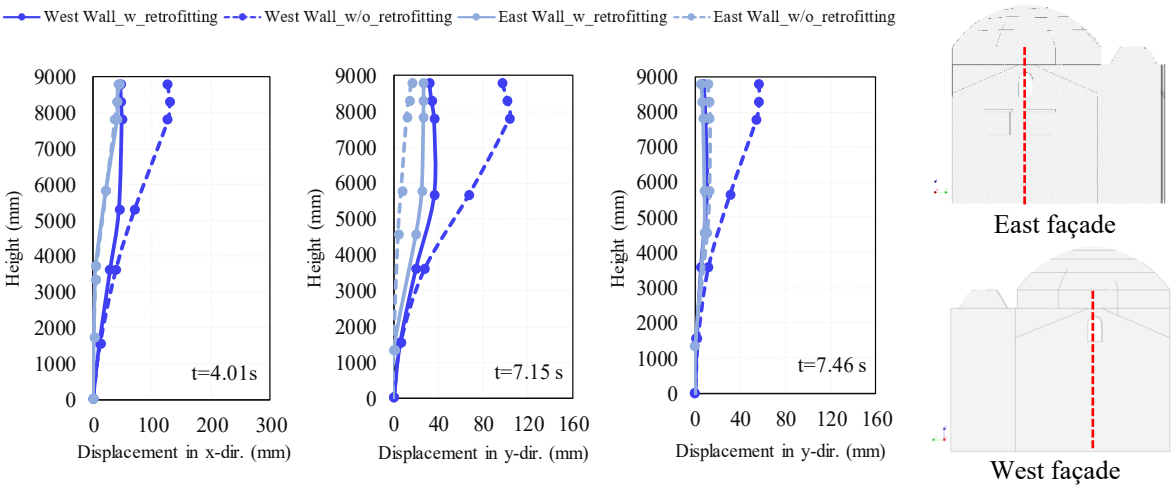


Figure 10. Change in absolute displacement in the out-of-plane direction, at time-step when the west wall has peak displacement, (a) Erzincan, (b) Düzce - Bolu, (c) Bingöl, (d) location of the section cuts

According to [15], the principal tensile strain distribution is a good qualitative damage indicator. A fictitious homogenous material is adopted and, therefore, the strain values observed on the numerical model does not correspond to the values that are expected on the real structure. In this regard, strain distribution of the structural response was analyzed at the time step in which the peak displacement was achieved on each structural component (see [16]). In the present paper, the most critical plots are presented in Figure 11, Figure 12, and Figure 13. Numerical simulation satisfactorily reproduced a crack pattern similar to the existing one. In

particular, the numerical damage observed on the South Wall and the dome are compatible with the moderate crack found on the real structure. According to the difference in strain distributions of two models, the effect of steel girder retrofitting on seismic response is observed. The non-retrofitted structure is dominantly subjected to vertical cracks, i.e. out-of-plane behavior, resulting in high tensile stresses on the significant portion of the structure. Nevertheless, change in damage patterns is noticed and can be an indication of the limitation of out-of-plane response. Still, even with the retrofitting, the structure experiences damage depending on the dynamic input.

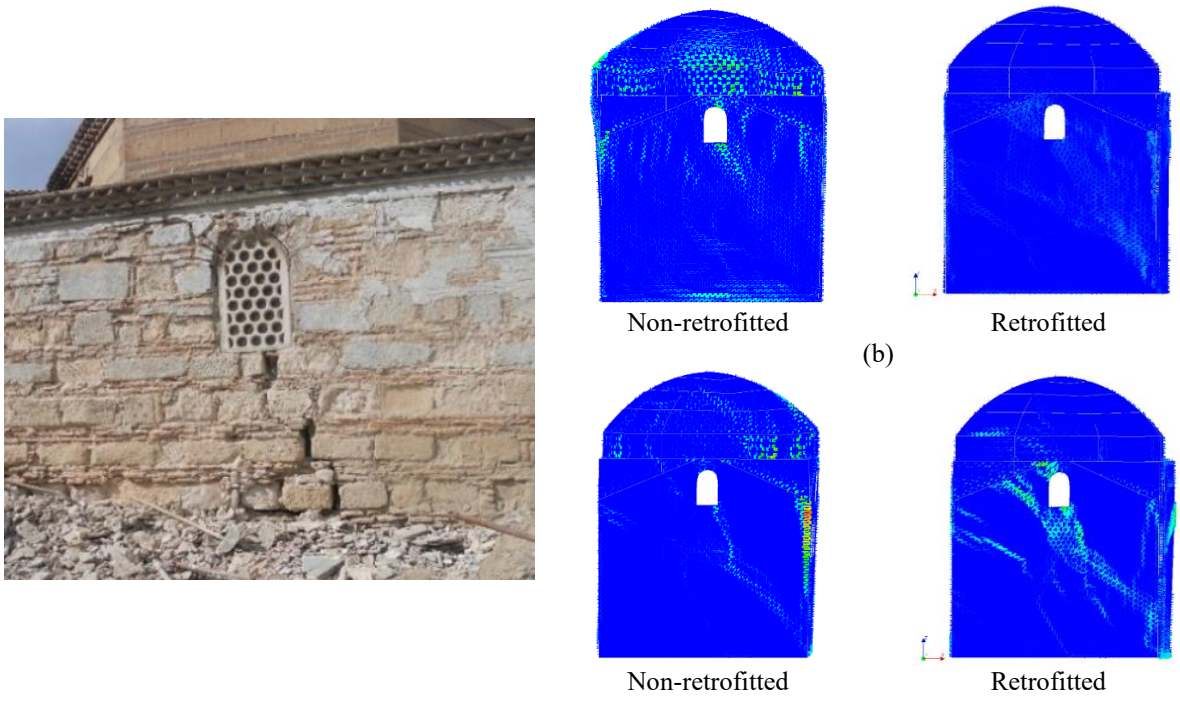


Figure 11. Correlation of (a) real damage; and total principal tensile strain distribution on the south façade, (b) Erzincan Earthquake at time-step 3.43s, (c) Bingöl Earthquake at time-step 3.99s

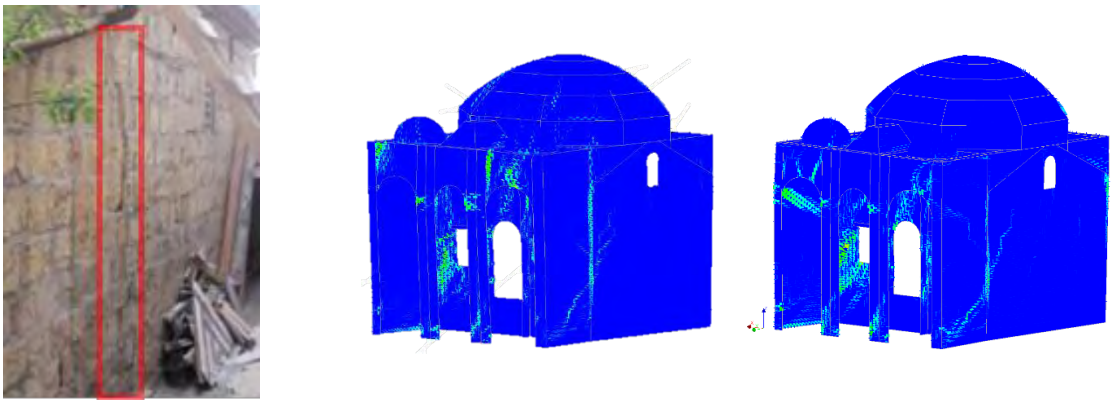


Figure 12. Correlation of (a) real damage, and total principal tensile strain distribution on the west façade subjected to the Bingöl Earthquake, at time-step 3.99s, (b) non-retrofitted, (c) retrofitted

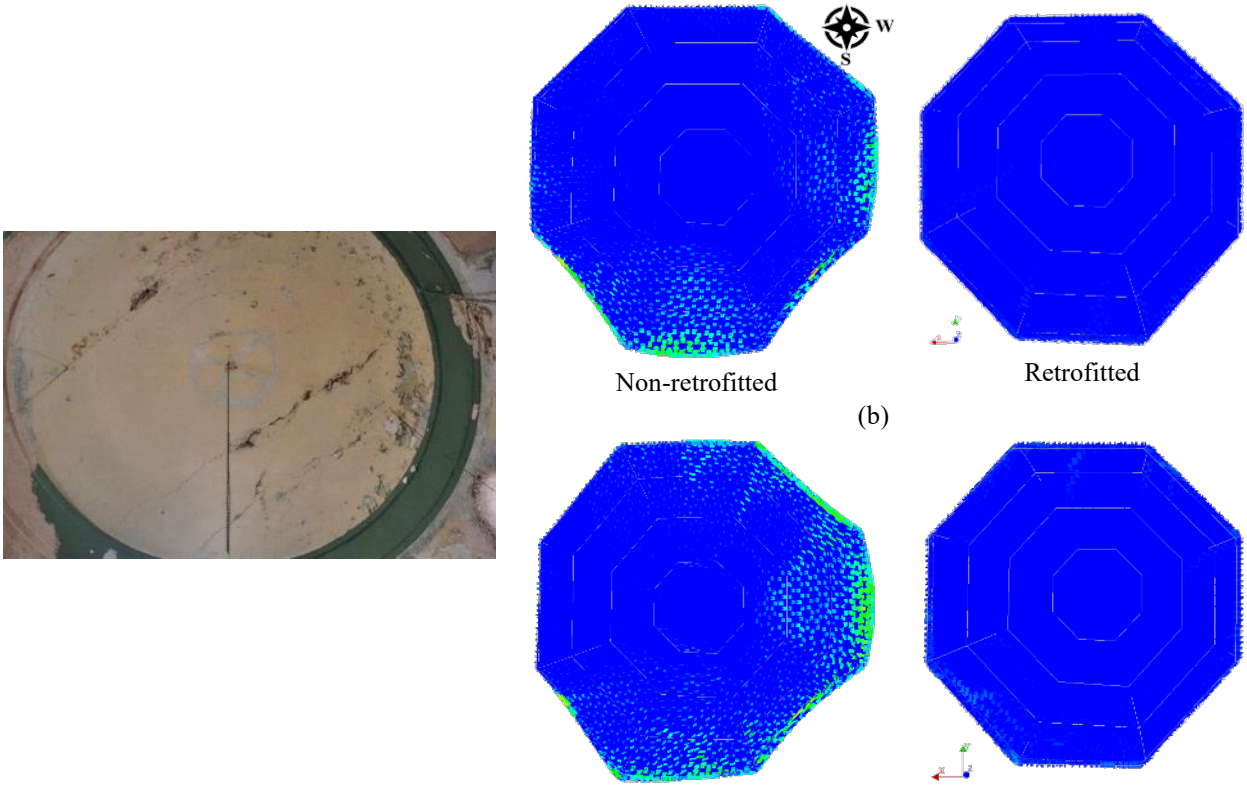


Figure 13. Correlation of the crack patterns, (a) real damage; total principal tensile strain distribution on the dome (b) the Erzincan Earthquake at time-step 3.43s, (c) the Bolu Earthquake at time-step 6.12s

6 CONCLUSIONS

In the present study, a historical masonry mosque, namely Kütahya Kurşunlu Mosque was investigated. Severe damage was observed on the mosque and several interventions and retrofitting actions were carried out. Regarding the site observations, severe damage can be attributed to the lack of connections and integrity of the overall system. Within this context, steel girder elements were introduced to the structure and anchored at the top of the load-bearing walls, and, bottom and top level of the octagonal drum (dome support). In order to study the effectiveness of the introduced retrofitting technique, the finite element method was used. The nonlinear dynamic analysis was conducted by using three different real ground motions in which both horizontal components of the accelerograms were used. According to the analysis results, the model without the retrofitting experiences high residual displacements whereas, in the retrofitted model, the imposed residual displacements are limited. Thus, the steel girders are effective in what concerns the out-of-plane behavior providing the so-called box behavior for the historical structure. The validation of the performed analysis can be made by considering the non-retrofitted model. Once the damage is known for this case, numerical damage verifies the constituted hypotheses. Therefore, the response of the retrofitted case obtained from the numerical analysis is assumed to be representative of the actual response.

REFERENCES

[1] ICOMOS, "ICOMOS Turkey Architectural Heritage Conservation Charter," 2013.

[2] P. Roca, "The study and restoration of historical structures: From principles to practice," in *Structural Analysis of Historical Constructions*, 2006, pp. 9–24.

[3] P. B. Lourenço, N. Mendes, L. F. Ramos, and D. V. Oliveira, "Analysis of masonry structures without box behavior," *Int. J. Archit. Herit.*, vol. 5, no. 4–5, pp. 369–382, 2011.

[4] T. Rockwell, "North Anatolian Fault," in *Encyclopedia of Natural Hazards*, P. T. Bobrowsky, Ed. Springer, 2013, pp. 738–739.

[5] H. . Akyüz *et al.*, "Surface Rupture and Slip Distribution of the 12 November 1999 Düzce Earthquake (M 7.1), North Anatolian Fault, Bolu, Turkey," *Bull. Seismol. Soc. Am.*, vol. 91, no. 1, pp. 61–66, 2002.

[6] FX+ for DIANA, "Midas FX+ for DIANA, Customized Pre/Post-processor for DIANA." MIDAS Information Technology Co., Ltd., 2013.

[7] P. B. Lourenço, "Computations on historic masonry structures," *Prog. Struct. Eng. Mater.*, vol. 4, no. 3, pp. 301–319, 2002.

[8] A. Aşıkoğlu, Ö. Avşar, P. B. Lourenço, and L. C. Silva, "Effectiveness of seismic retrofitting of a historical masonry structure: Kütahya Kurşunlu Mosque, Turkey," *Bull. Earthq. Eng.*, vol. 17, no. 6, pp. 3365–3395, 2019.

[9] L. C. Silva, N. Mendes, P. B. Lourenço, and J. Ingham, "Seismic Structural Assessment of the Christchurch Catholic Basilica, New Zealand," *Structures*, vol. 15, pp. 115–130, 2018.

[10] N. Mendes and P. B. Lourenço, "Sensitivity analysis of the seismic performance of ancient masonry buildings," *Eng. Struct.*, vol. 80, pp. 137–146, 2014.

[11] DIANA FEA, "User's Manual Release 10.2." The Netherlands, 2017.

[12] TEC, "Turkish Earthquake Code: Specifications for the Buildings to be Constructured in Disaster Areas," in *Official Gazette No 26454*, 2007.

[13] M. D. Trifunac and A. G. Brady, "A study on the duration of strong earthquake ground motion," *Bull. Seismol. Soc. Am.*, vol. 65, no. 3, pp. 581–626, 1975.

[14] TR-NSMN, "Strong Motion Database," *AFAD*. [Online]. Available: kyhdata.deprem.gov.tr.

[15] N. Mendes, "Seismic Assessment of Ancient Masonry Buildings : Shaking Table Tests and Numerical Analysis," PhD Thesis, University of Minho, 2012.

[16] A. Aşıkoğlu, "Numerical Investigation on the Effectiveness of Seismic Retrofitting of a Historical Masonry Mosque," MSc Thesis, Anadolu University, 2018.

12th International Conference on Structural Analysis of Historical Constructions
SAHC 2020
P. Roca, L. Pelà and C. Molins (Eds.)

COMPARISON OF TWO DIFFERENT APPROACHES FOR THE SEISMIC EVALUATION OF THE BONET BUILDING OF THE NATIONAL PALACE OF SINTRA, PORTUGAL

M. PONTE[1*], M. MALCATA[1], AND R. BENTO[1]

[1]Civil Engineering Research and Innovation for Sustainability (CERIS)
Instituto Superior Técnico (IST), Universidade de Lisboa
Av. Rovisco Pais, 1049-001 Lisboa, Portugal
e-mail: {madalenaponte, madalena.malcata, rita.bento}@tecnico.ulisboa.pt

Keywords: Seismic Assessment, Cultural Heritage, Equivalent Frame Method, Finite Element Model

Abstract. *Complex masonry monuments represent an important part of the built cultural heritage and most of them are vulnerable to seismic actions. Their large scale, irregularity, and heterogeneity makes it challenging to characterize their structural behaviour.*

This work addresses the state of conservation as well as the structural behaviour and seismic vulnerability of the most ancient body of the National Palace of Sintra, Portugal: the Bonet building. This body was built on top of Arabic foundations during the reign of King Dinis, around the year 1281, and since then few alterations were made to the building.

In order to minimize the multiple uncertainties usually existing in complex masonry buildings, whether related to geometry or masonry mechanical properties, a detailed structural survey was conducted together with different in-situ experimental tests. All the tests performed were important to the adequate characterization of the building and the calibration of the numerical models. The final values adopted for the mechanical properties of the rubble stone masonry are presented and can be used as a reference for future works in ancient Portuguese monuments of the same period.

Afterwards, nonlinear static analyses were performed in two different software (3MURI and ABAQUS). Comparisons and discussion of the results are made. The differences in modelling strategies and characterization of materials between the two software are considered with regard to their realism, computational effort, data availability and applicability to large scale structures. Efforts to calibrate and obtain the same behaviour of the building for the different software were made, involving geometry, boundary conditions and characterization of the material constitutive laws.

1 INTRODUCTION

This work is part of a research project which aims to evaluate the seismic safety of the National Palace of Sintra, by identifying possible structural anomalies and vulnerability factors. This project was developed by Instituto Superior Técnico, University of Lisbon and promoted by Parques de Sintra – Monte da Lua, S.A. (PSML). The palace is an agglomerate of buildings

of different volumes and styles added over time that presents a beautiful and harmonious unity, characterized by its iconic chimneys, as can be seen in Figure 1.



Figure 1: On the left: North-facing top picture of the National Palace of Sintra. On the right: Northeast view of the palace with the identification of the Bonet Building and the chapel (images captured by the drone of the IST)

This study aims at the structural safety verification of the Bonet Building, one of the oldest structures from the National Palace of Sintra, built over the foundations of an ancient Arab palace. At the request of King D. Dinis, whose reign took place between 1261 and 1326, the Bonet Building was expanded, and the adjacent Palatine Chapel building was built from scratch, both identified in Figure 1 (right).

The palace is located in Sintra, a town of the Lisbon district, which is a zone of Portugal mainland characterized by high seismic risk. The seismic assessment of complex masonry structures such as this palace, in which the Bonet building is included, presents several difficulties. One of them is the definition of the best numerical modelling option, where one needs to choose between a rational computational effort and assuring a reliable structural assessment able to characterize the building's correct behaviour. Other adversity is the lack of tools and consistent procedures to perform the seismic analysis and verification of such complex masonry structures ([1], [2]).

For the complete characterization of the Bonet building, an experimental campaign was carried out including *in-situ* experimental tests aiming for the mechanical characterization of materials and/or structural elements, and the geometric and dynamic identification of the structure [3]. A detailed geometric inspection was performed using a laser scanner that allowed to obtain data with an accuracy of up to $1x10^{-6}$ m, thus constituting a suitable methodology for cases of complex geometry. The data collection was aided by a UAV equipped with a Sony 7R digital camera so that it was possible to obtain full information of the outside of the palace. The set of data obtained gave rise to a three-dimensional point cloud (Figure 2, left), later treated and used in Revit software for the development of an H-BIM model (Figure 2, right).

The GPR (Ground Penetrating Radar) test, a non-destructive method, aims to characterize the masonry by detecting types of materials and anomalies (voids, cracks, water), using different frequencies' antennas. With this test, two major conclusions were obtained: i) "the majority of the walls are composed of two interior-filled masonry leaves, and usually the outer leaf is approximately 0.30m thick" [4]; and ii) the walls built around the rock are directly in contact with it, without empty spaces in between.



Figure 2: Bonet Building, North Facade: Point clouds (on the left) and Revit Model (on the right)

Flat-jack tests, considered to be semi-destructive, aim to characterize the mechanical capacity of structural masonry walls. The fact that Bonet is a historical building increases the difficulty of locating the experimental tests. Despite this, the wall to be tested should accomplish still the following conditions: to present a certain level of compression and not be located near doors, windows, or another singularity that can alter the stress field. With this in mind, two locations were defined, one on the north facade of the building and the other on the south. The results of the single test indicate that the Bonet structure is poorly compressed in the tested areas, although the results may be considered with caution due to their punctual character and the physical characteristics of the walls, which present high thicknesses. From the double tests, the stress-strain curves were obtained and then the stiffness, maximum stress, and Poisson's ratio were determined. Young's Modulus values are high, justified by the boundary conditions of the walls examined, which are built against the bedrock (the only possible locations on the building to perform these tests). Therefore, this parameter obtained was taken into account only as an upper limit value during the numerical model calibration.

In addition, samples were collected in the form of cores (semi-destructive test) near to the locations were the flat-jack tests were carried out, in order to characterize the material and its constituents. However, due to the heterogeneity of the masonry, the samples can only represent the material locally. From this type of test, qualitative results were obtained, concluding that the state of degradation of the masonry in the Bonet building is quite high, even one of the worst of the entire palace [3].

The ambient vibration tests are non-destructive and suitable for the seismic assessment of existing buildings, especially for historic and heritage buildings. By measuring the structure vibrations subjected to external environmental inputs, it is possible to identify the modal dynamic characterization parameters. The dynamic characterization of the structure is crucial for the calibration of its numerical model. The processing of the obtained data was performed with the ARTeMIS Modal Pro software [5] that allowed to obtain the fundamental frequencies and the vibration modes of the structure. Results reached are available further on in Table 1 and Figure 4.

3 NUMERICAL MODEL

The Bonet Building was modelled in parallel using two software, 3Muri [6] and ABAQUS [7]. For both models, it was ensured that the structure geometry is identical, even with the required simplifications, and consistent with the data collected by the Laser Scanner.

Both ABAQUS and 3Muri models were defined based on the BIM model. It was decided to export the Revit model [8] and to import it into ABAQUS, saving time and significant manual effort. In 3Muri, this specific option is not possible. Nevertheless, one should be aware of the usual excessive detailing in BIM models for the purposes of numerical modelling, with all the architectural ornamentation, that cannot be directly used in FE software. Thus, as explained in [9], in order to achieve an adequate FE model, several manual simplifications are required to guarantee mesh compatibility, to avoid mesh local distortions or small elements, and to model complex architectural objects. With that in mind, some geometric simplifications were adopted, namely the use of the mean value of thickness in walls of variable thicknesses.

For the ABAQUS model, in solid FE elements, a 10-node tetrahedral finite element mesh with a maximum size of 700mm was defined (Figure 3, left), thus ensuring for each thickness the existence of three nodes. As presented in Figure 3 (right), the EF method is adopted in 3Muri [3], defining the walls in macroelements that consist of piers (represented in orange), spandrels (in green), and rigid nodes (in light blue).

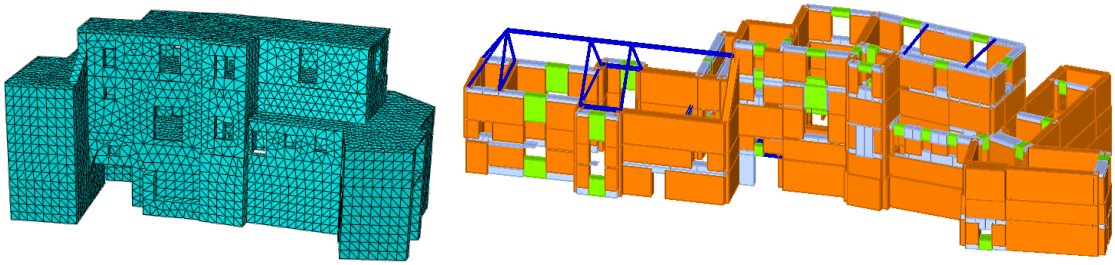


Figure 3: Bonet Building (view of the North facade): on the left, ABAQUS Model with FE Discretization; on the right, 3Muri model with macroelements discretization

One of the most difficult challenges when modelling complex structures is the definition of the boundary conditions. Therefore, the necessary parts of the adjacent buildings were modelled to account for the interactions and impact they have on the overall behaviour of the Bonet Building.

3.1 Calibration

The calibration of the numerical models, in ABAQUS and 3Muri, is an important step and fundamental to reach reliable results. In this phase, an iterative process was followed, in which the values obtained in the experimental campaign [3] were considered as reference and in each step special attention was taken to the:

- definition of the boundary conditions, considering the adjacent buildings;
- type of boundary conditions when modelling the structural walls in contact with the bedrock;
- values adopted for the definition of the masses;
- values adopted for Young's modulus (E) of the materials, in particular to the masonry walls (significantly cracked on the top floor and not cracked on the other floors).

Table 1 illustrates the fundamental frequencies for the first three vibration modes obtained experimentally (ARTeMIS) and numerically (ABAQUS and 3Muri), as well the relative error obtained when comparing the numerical to the experimental results, in percentage. Figure 4

presents the corresponding vibration modes: the first and second mode represent the translational modes in the north-south direction (Y - transversal), and the third mode corresponds to the vibration in the east-west direction (X - longitudinal). It is worth noting the close similarity between the frequency values and deformed shapes obtained in the numerical models and the experimental results.

Table 1: Frequencies of first vibration modes, Relative Errors of models in ABAQUS and 3Muri (numerically) in comparison to the model in ARTeMIS (experimentally)

	ARTeMIS	ABAQUS		3Muri	
Mode:	**f (Hz)**	**f (Hz)**	**Difference (%)**	**f (Hz)**	**Difference (%)**
1st Y	5.00	5.05	0.96	4.98	-0.40
2nd Y	5.18	6.17	19.11	5.55	7.14
1st X	8.20	7.27	-11.34	7.03	-14.27

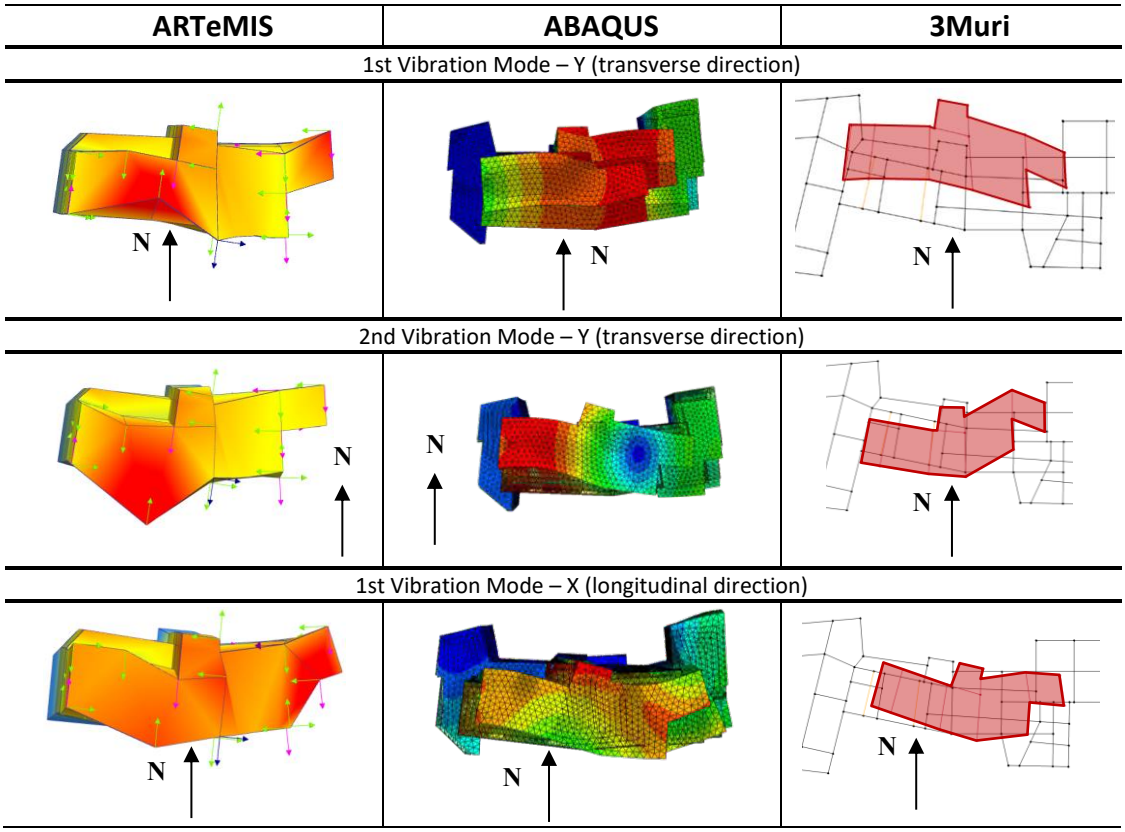


Figure 4 - Deformed shapes of the main vibration modes obtained experimentally (ARTeMIS) and numerically (ABAQUS and 3Muri) – plan view

For the verification of the seismic safety of the structure, nonlinear static analyses were performed. Different approaches were followed to model the nonlinear behaviour of the masonry panels.

For the Equivalent Frame (EF) models (3Muri program), the masonry panels were modelled as nonlinear beams with lumped plasticity and a piecewise-linear behaviour, that are able to describe the nonlinear response until very severe damage levels through progressive strength decay in correspondence with assigned values of drift [10]. In the EF models, according to the failure modes which can occur, it is possible to use specific failure criteria for the masonry panels. It is highlighted that with this modelling technique only the in-plane behaviour of the walls is considered, assessing the walls' response in terms of global stiffness, strength and ultimate displacement capacity by assuming a proper shear-drift relationship [6]. This relationship depends on the different failure modes, which in turn depend on several parameters: the geometry of the element, the boundary conditions, the axial load, and the mechanical characteristics of the masonry constituents (e.g. mortar and units).

Regarding the FE model (ABAQUS), the masonry walls have been simulated by using the Concrete Damage Plasticity Model (CDPM) and the stress-strain relationships defined separately for compression and tension. The CDPM was designed to define the plastic properties of concrete or quasi-brittle materials developed by Lee & Fenves [11]. This model uses the concepts of damaged elastic isotropic material in conjunction with the compressive and tensile plastic stress of isotropic material to represent the non-elastic behaviour of masonry, as explored in the ABAQUS Theory Manual [12]. Therefore, it is recommended to be used in masonry materials, despite being developed for concrete. The plastic model assumes that the two main collapse mechanisms are tensile diagonal cracking and compressive crushing. The evolution of the yield surface is controlled by the tensile and compressive strain, considering different types of behaviour related to the failure mechanisms under load, as explained in the ABAQUS Theory Manual. In this study, simplified constitutive laws for compressive and tensile behaviour were based on [13] and [14], respectively.

The value assumed for the masonry compressive strength was defined proportional to the calibrated Young's modulus (E), according to MIT [15] reference intervals. The value adopted for the tensile strength was defined as 3/2 of the value of cohesion. The mechanical parameters, assumed in both software, ABAQUS and 3Muri, for rubble stone masonry of the Bonet and adjacent buildings are presented in Table 2. In this table, E stands for the Young modulus, G for shear modulus, f_t for tensile strength, f_c for compressive strength, and w for the specific weight of the material.

Table 2: Rubble stone masonry mechanical properties

	E (GPa)	G (GPa)	f_t (MPa)	f_c (MPa)	w (kN/m^3)
Disorganized irregular stone masonry					
MIT (2009)	0.69 – 1.05	0.23 – 0.35	0.030 – 0.048	1.00 – 1.80	19
Bonet Building (Last Floor) Cracked	0.40	0.13	0.018	0.62	18
Bonet Building	0.80	0.26	0.036	1.24	18
Irregular stone masonry with two external leaves and internal core					
MIT (2009)	1.02 – 1.44	0.34 – 0.48	0.053 – 0.077	2.00 – 3.00	20
Chapel	1.44	0.48	0.080	3.00	19
Brasões Room	1.20	0.40	0.063	2.43	18

In ABAQUS, damage variables for the compression and tension of each material are necessary to define to control the loss of stiffness and resistance of the material that occurs upon entering the plastic regime, increasing progressively with the stress decay. The damage variables are fundamental to represent the real behaviour of the material during the nonlinear analysis since the damaged masonry presents significant stiffness reductions. A linear progression was adopted since entering the plastic regime until the maximum strain of decay, when it was assigned the maximum damage value of 0.9.

To define the CDPM in ABAQUS, the values of the following parameters are assumed as being the typical ones for masonry, as explained in [2]: (i) the dilation angle, equal to 10°; (ii) the flow potential eccentricity, set equal to 0.1; (iii) the ratio between the initial biaxial compressive yield stress and the initial uniaxial compressive yield stress, set equal to 1.16; (iv) the ratio of the second stress invariant on the tensile meridian and the same on the compressive meridian, set equal to 0.666; (v) the viscosity parameter, which defines visco-plastic regularization, equal to 0.002.

5 NONLINEAR STATIC ANALYSES

5.1 Pushover curves

In this work, two distributions of lateral loads were considered: uniform – proportional to the mass, and inverse-triangular (named triangular for simplicity) – proportional to the product between the mass and the height of the building. The analyses are performed for the two main directions of the building (longitudinal, X, and transversal, Y), including negative and positive orientation.

Figure 5 presents the final pushover curves obtained with 3Muri and ABAQUS in terms of base acceleration, and displacement divided by global height. The last point of the capacity curves corresponds to the ultimate displacement divided by the global height. As expected, for the initial phase, similar values of initial stiffness in pushover curves were obtained for both software, since the dynamic characteristics obtained in the modal analysis were also very similar.

On the other hand, some differences in terms of maximum base acceleration exist for the curves in the X direction. For this direction, the curves in 3Muri present less acceleration, that is translated into less strength capacity. This result can be related to the different constitutive laws considered in each software; however, the most likely justification is the fact that in 3Muri the entirely of the adjacent buildings were modelled, while in ABAQUS only small parts with constraints at its extremities were modelled. The constraints do not allow to consider the damages or even the collapse of the adjacent buildings suffered during the pushover analyses, increasing the strength of the ABAQUS model. This modelling option was made taking into account the computational capacity required to model the entire adjacent buildings in ABAQUS software and the calibration of the model.

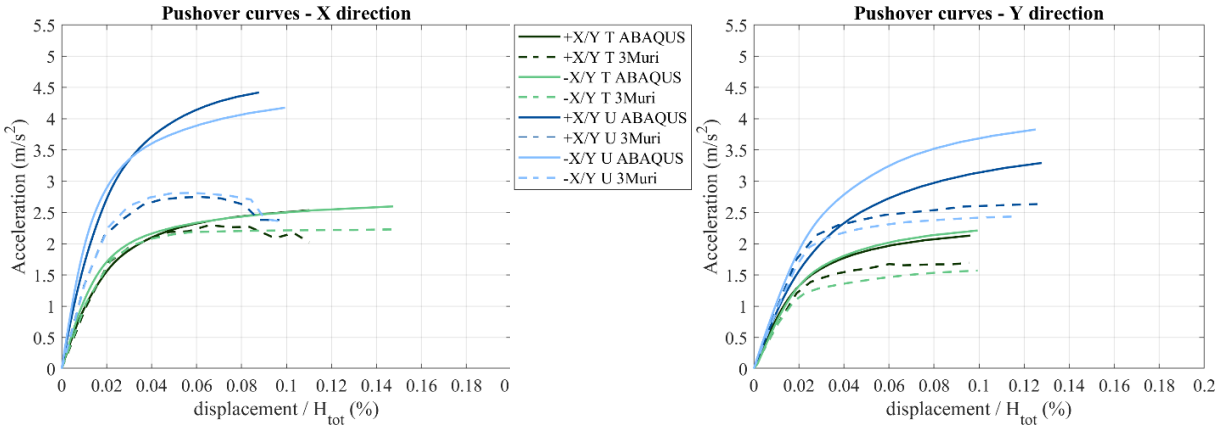


Figure 5: Final Pushover Curves, X direction (left) and Y direction (right), ABAQUS and 3Muri

5.2 Ultimate displacement definition

The ultimate displacements of the pushover curves obtained in 3Muri were calculated based on two-level multiscale approach: global damage, measured when achieving a decay of 20% of the base shear force on the pushover curve; and local damage, defined when a collapse mechanism occurs.

The CDPM implies that for each time increment the applied load is also increasing and, regardless of the damage variables defined, the total strength of the structure does not decrease. Thus, with the ABAQUS software, there is a difficulty in determining the ultimate displacement, becoming necessary to define a criterion for its definition.

Since one of the main objectives of the ABAQUS model is to compare the results with the 3Muri model, in addition to performing the seismic evaluation of Bonet building, the ultimate displacement calculated in 3Muri was used in the corresponding curves obtained in ABAQUS. Subsequently, the ultimate displacement was verified using the Italian Standard [16] criterion - the ratio between the ultimate displacement value and the yield displacement must be between 3 and 6 - and, if necessary, a correction was implemented.

5.3 Safety verification – N2 method

Safety is verified using the N2 method, as suggested in Part 3 of Eurocode 8 [17] and defined in its Part 1 [18]. In this study, for the safety verification, the ratio of the maximum acceleration compatible with the fulfilment of each limit state ($a_{g,max}$) and the reference ground acceleration (a_{gR}) is evaluated and analysed. The ration between the ultimate displacement and the target displacement was not analysed for the safety verification, since the definition of the ultimate displacement is one of ABAQUS limitations. For the definition of the equivalent single degree of the system (SDOF), a transformation factor needs to be evaluated; as opposed to 3Muri, ABAQUS does not automatically calculate the transformation factor, for this reason, it was obtained manually for each direction, which is a demanding process for complex structures such as the Bonet Building. The degrees of freedom were considered at the floor levels of the structure that are not restrained by the bedrock. The mass associated with each degree of

freedom was calculated considering the displacements of each floor associated with the vibration modes.

The seismic action was defined according to EC8-1 [18], complemented by the Portuguese Annex. According to EC8-3, three limit states should be considered for the seismic safety verification: Limit Damage (LD), Severe Damage (SD), and Near Collapse (NC).

Safety is verified when the ratio is greater than 1. Figure 6 shows the safety verifications for the type 1 earthquake, the most demanding one, and the near collapse limit state (the one with the highest requirements) of the equivalent SDOF system in ABAQUS and 3Muri. It is then possible to state that safety is not verified for the Bonet Building, with Y direction being the most vulnerable for both models. It should be added that, due to the restrictions of ABAQUS when defining the ultimate displacement, it is more useful and interesting to compare the results of both software in terms of damage patterns, as will be commented below.

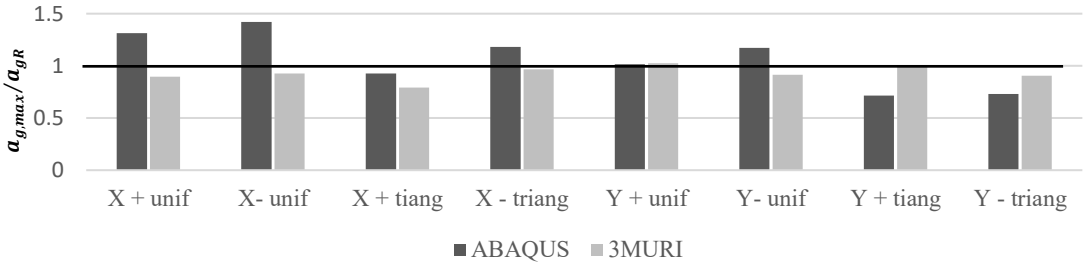


Figure 6: Safety Verification, NC, Earthquake Type 1

5.4 Damage pattern

A comparison is made between the damage patterns results obtainable from the FE model developed in ABAQUS, and those obtainable from the Equivalent Frame approach, by using the 3Muri software. Here only the most demanding case is presented: + Y, triangular lateral load distribution (Figure 7 and Figure 8). The damage patterns depicted correspond to the ultimate displacement.

According to the 3Muri results presented in Figure 7, it is possible to identify in the Bonet building a concentration of damaged elements at the top floor, even with a pier collapsed due to shear on the western sidewall. The walls of the top floors along the Y direction present damage mainly due to shear behaviour. As expected, the type of collapse is severely influenced by the height/length ratio; walls with lower values are controlled by shear, while walls with higher ratio values tend to present flexural damage.

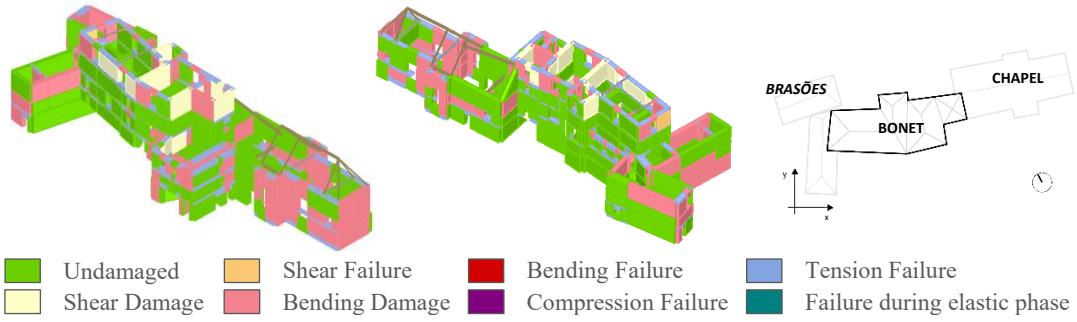


Figure 7: Damage Pattern, 3Muri (+Y, triangular distribution) – damage in Equivalent Frame Model

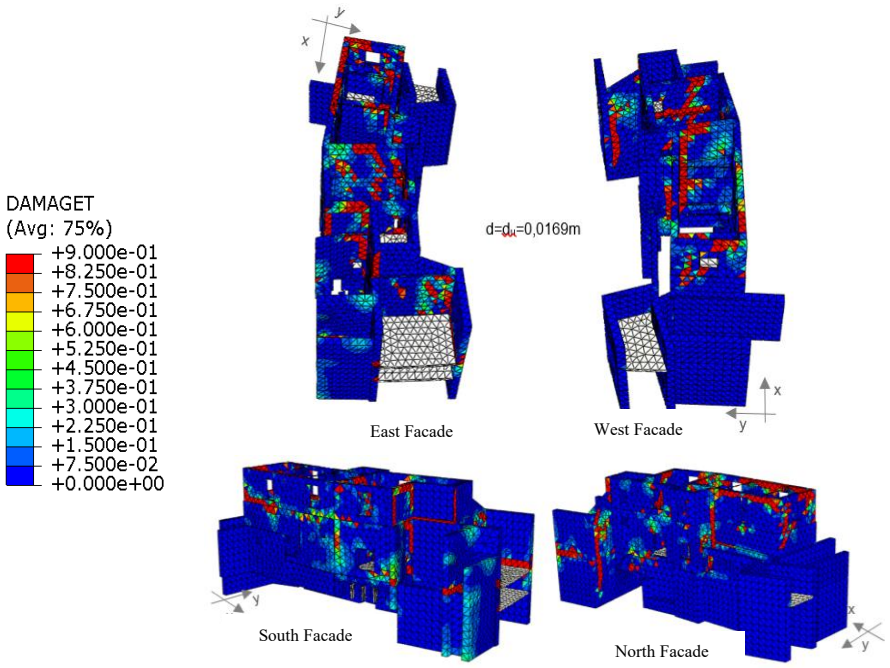


Figure 8: Damage Pattern, principal inelastic Tensile strains, ABAQUS (+Y, triangular distribution)

Finite element analysis in the ABAQUS model allows studying the local evolution of the damage in detail in terms of strains, which can be increased if necessary, with mesh refinement. On the other side, refining the mesh will require more computational effort and time, which for complex structures of this size can be unportable. Moreover, it is worth noting that ABAQUS does not identify the type of damage or collapse the walls suffer as in 3Muri, making the analysis less user-friendly. This program presents the damage through the separate interpretation of the damage caused by tension or compression. Analysing the damage parameter in ABAQUS for the tensile strains (Figure 8), it can be concluded that most of the damage is also concentrated on the walls of the top floor. The diagonal inclination of the cracks at the top floor walls along the Y direction clearly indicates the activation (or close to the activation) of shear failure, as seen in 3Muri damage patterns. It is worth mentioning that the maximum tensile damage is presented in the upper spandrels of the last floor walls, in both facades, where the tie rods are located. This effect cannot be identified in 3Muri since a global analysis is performed, without considering the out-of-plan behaviour.

In the past, some numerical comparisons have already been carried out for masonry walls ([19], [20]) and the results have shown generally good agreement in terms of damage pattern. This is in accordance with the observed in the Bonet building analyses for FE and EF models.

6 CONCLUSIONS

Regardless of the numerical software used, the point cloud based on the laser scanner survey is essential for the correct geometric characterization of a complex building. As the construction of complex structures in ABAQUS is very difficult, it is suggested, whenever possible, to import a BIM model of the structure directly into the software. Otherwise, it may not be

advisable to use ABAQUS to assess this type of structures, as the effort of building the numerical model will not be worthwhile. Moreover, the BIM model has to be architecturally simplified and built in order not to create distorted finite elements when generating the mesh in the FEM software. On the other hand, 3Muri is a program developed for masonry building modeling and analysis, leading to a simplified process of construction and alteration of the geometric characteristics of the structure.

In general, good correspondence is observed between the predictions of the two numerical models considered. Note that ABAQUS presents a high graphical ability to observe the results. In the modal analysis, it is possible to rigorously study the deformed structure for the various vibration modes. The same conclusion can be drawn when interpreting the damage pattern since one can observe the damage evolution for each finite element node, while 3Muri presents the damage evolution for each macroelement. However, 3Muri designates the type of damage or collapse in each element, which is very useful to the user.

In addition, 3Muri is a more suitable program for performing pushover analysis and subsequent security verifications. The program proposes for each analysis an ultimate displacement and automatically calculates the transformation factor of the models from MDOF to SDOF. These two points are of high difficulty in ABAQUS, involving a complex calculation, especially for complex buildings. On the other hand, in ABAQUS, non-linear analyses performed with refined FE discretizations of the critical regions and with more sophisticated material models, are useful to deepen the knowledge of the behaviour of complex structures under seismic actions.

Lastly, 3Muri does not require the large computational effort and time that ABAQUS requires, which is a very important aspect to take into account when dealing with very large and complex structures. In the end, it will be necessary for the user to choose between more geometry accuracy and detail with ABAQUS or less computational effort with 3Muri.

Acknowledgements. The authors wish to thank the IST and PSML teams involved in the project. In addition, the first author would like to acknowledge the financial support of the Portuguese Foundation for Science and Technology (Ministry of Science and Technology of the Republic of Portugal) through a PhD scholarship [grant number SFRH/BD/145571/2019]. The authors also thank Simone Tiberti and Gabriele Milani from Politecnico di Milano, who provided insight and expertise that greatly assisted the development of the model in ABAQUS.

REFERENCES

[1] Sarhosis, V., Milani, G., Formisano, A. and Fabbrocino, F. Evaluation of different approaches for the estimation of the seismic vulnerability of masonry towers. *Bull. Earthq. Eng.* (2017) **16**(3):1511–45.

[2] Degli Abbati, S., D'Altri, A.M., Ottonelli, D., Castellazzi, G., Cattari, S., de Miranda, S. and Lagomarsino, S. Seismic assessment of interacting structural units in complex historic masonry constructions by nonlinear static analyses. *Computers and Structures* (2019) **213**:72-81. https://doi.org/10.1016/j.compstruc.2018.12.001

[3] Ponte, M., Bento, R., Silva, D.V. A multi-disciplinary approach to the seismic assessment of the National Palace of Sintra. *International Journal of Architectural Heritage* (2019). https://doi.org/10.1080/15583058.2019.1648587

[4] Bento, R. An interdisciplinary approach to the seismic assessment of built cultural heritage: Case studies in Lisbon and outskirts. In: R. Aguilar et al. (Eds.): *Structural Analysis of Historical Constructions*, RILEM Bookseries 18 (2019), pp. 3–18. Cham: Springer. 10.1007/978-3-319-99441-3_1.
[5] ARTeMIS Modal Pro (version 3.0). 2013. Aalborg: Structural Vibration Solutions A/S.
[6] 3Muri (version 11.4.0). 2018. S.T.A. DATA.
[7] ABAQUS CAE (version 16.14-1). Complete Solutions for Realistic Simulation (2014).
[8] Querido, J. O *Edifício Bonet do Palácio Nacional de Sintra: Caracterização e avaliação do desempenho estrutural*. MSc thesis, Instituto Superior Técnico, Universidade de Lisboa (2018). Lisboa. (in Portuguese)
[9] Castellazzi, G., D'Altri, A.M., Bitelli, G., Selvaggi, I., and Lambertini, A. From laser scanning to finite element analysis of complex buildings by using a semi-automatic procedure. *Sensors* (2015) **15**(8): 18360–18380. https://doi.org/10.3390/s150818360
[10] Lagomarsino, S., Penna, A., Galasco, A., and Cattari, S. TREMURI program: An equivalent frame model for the nonlinear seismic analysis of masonry buildings. *Engineering Structures* (2013) **56**: 1787-1799. http://dx.doi.org/10.1016/j.engstruct.2013.08.00
[11] Lee, J. and Fenves, G.L. Plastic-Damage Model for Cyclic Loading of Concrete Structures. *Journal of Engineering Mechanics* (1998) **124**(8): 892–900. https://doi.org/10.1061/(ASCE)0733-9399(1998)124:8(892)
[12] Simulia. ABAQUS Theory Manual. Version 6.6. (2014)
[13] Kaushik, H.B., Rai, D.C., and Jain, S.K. Uniaxial compressive stress-strain model for clay brick masonry. *Current Science* (2007) **92**: 497–501.
[14] Dhanasekar, M., and Haider, W. Explicit finite element analysis of lightly reinforced masonry shear walls. *Computer and Structures* (2008) **86**: 15–26. https://doi.org/10.1016/j.compstruc.2007.06.006
[15] MIT. Circolare n. 617 del 2 Febbraio 2009. Istruzioni per l'Applicazione Nuove Norme Tecniche Costruzioni di cui al Decreto Ministeriale 14 Gennaio 2008 (2009). (in Italian).
[16] NTC. Norme Tecniche per la Construzioni (NTC). Decreto Ministeriale 17/01/2018, Official Gazette (2018). Roma (in Italian).
[17] CEN. NP EN 1998-3: Eurocódigo 8 – Projecto de estruturas para resistência ao sismo. Parte 3: Avaliação e Reabilitação de edifícios. Instituto Português da Qualidade. European Committee for Standardization, (2017). Retrieved from http://www.iso.org/iso/foreword.html (in Portuguese)
[18] CEN. NP EN 1998-1: Eurocódigo 8 – Projecto de Estruturas para resistência aos sismos. Parte 1: Regras gerais, acções sísmicas e regras para edifícios. Instituto Português da Qualidade. European Committee for Standardization, (2009). (in Portuguese)
[19] Calderini, C., Cattari, S., Lagomarsino, S. In-plane seismic response of unreinforced masonry walls: comparison between detailed and equivalent frame models. In: *Proc. of Int. Conf. on Computational Methods in Structural Dynamics and Earthquake Engineering* (COMPDYN 2009), Rhodes, Greece, (2009).
[20] Camilletti, D., Cattari, S., Lagomarsino, S. (2018). In plane seismic response of irregular URM walls through equivalent frame and finite element models. In: *16th European Conference on Earthquake engineering* (16ECEE), Thessaloniki, Greece, (2018).

DAMAGES PATTERNS IN HISTORICAL TEMPLES OF PUEBLA, MORELOS AND OAXACA AFTER SEPTEMBER 2017 MEXICO EARTHQUAKES

MARCOS M. CHÁVEZ[1*], FERNANDO PEÑA [1], NATALIA GARCÍA[2] AND DANIEL DURÁN[1]

[1] Instituto de Ingeniería
Universidad Nacional Autónoma de México (UNAM)
Av. Universidad 3000, 04510 Mexico City, Mexico
e-mail: mchavezc@iingen.unam.mx (*corresponding author) fpem@pumas.iingen.unam.mx, ddurans@iingen.unam.mx, www.ii.unam.mx

[2] Faculty of Architecture
Universidad Autónoma del Estado de Morelos (UAEM)
Av. Universidad 1001, 62209 Morelos, Mexico
e-mail: natalia.garcia@uaem.mx

Keywords: Stone Masonry, Damage Assessment, Architectural Heritage Buildings, Seismic Behavior

Abstract. *A brief description of the damages observed after the occurrence of the September 2017 earthquakes in some temples located in the states of Oaxaca, Puebla and Morelos is presented. A total of 48 temples were visited where we observed partial or total collapses of structural elements as: towers, roofs, buttresses, walls and arches in the temples. In some cases, the level of the damage was so severe that compromised the stability of the temples.*

1 INTRODUCTION

During September 2017, two high intensity earthquakes hit the central and southern region of Mexico. At 23:49:17 local time on September 7, 2017, an earthquake of magnitude Mw 8.2 occurred in the Gulf of Tehuantepec, 133 km southwest of Pijijiapan, Chiapas and 700 km from Mexico City. According to the National Seismological Service (SSN), this earthquake was catalogued as a normal fault [1]. The maximum acceleration recorded near to the epicenter (PGA) was over 2.28 m/s^2 [2]. Serious damage was reported in the states of Oaxaca, Chiapas and Tabasco; mainly to housing, ancient buildings and some infrastructure facilities.

On September 19, a second strong earthquake with a magnitude Mw 7.1 was felt at 13:14:40 local time. The epicenter was located between Puebla and Morelos states, 12 km southeast of Axochiapan, Morelos and 120 km from Mexico City. According to the SSN [3], the earthquake was a normal fault intraplate with a maximum acceleration recorded over 2.20 m/s^2, measured near to the epicenter area [4].

According to Meli [5], 2,340 historical buildings suffered some kind of damage, due to the occurrence of the September earthquakes. Table 1 shows the number of heritage buildings damaged in the different states by both September earthquakes, as well as the level of damage reported by the National Institute of Anthropology and History, INAH [6]. INAH established three levels of damage: minor, moderate and severe. In general, minor damage refers to damage without effect in structural elements; moderate damage is when the damage is present in some structural elements but without represent a risk to structural safety of the buildings; the severe damage is when the damage affects the structural safety of part or all of building.

Table 1: Number of heritage buildings damaged by the earthquakes [5]

City	Type of damage			Total damaged buildings	Percentage of damaged buildings compared to the total
	Severe	Moderate	Minor		
Chiapas*	21	29	64	114	4.9
Ciudad de México	51	65	81	197	8.4
Guerrero	11	41	43	95	4.1
Hidalgo	2	6	5	13	0.6
Estado de México	52	135	92	279	11.9
Morelos	122	84	53	259	11.1
Oaxaca	34	308	245	587	25.1
Puebla	125	335	161	621	26.5
Tabasco	1	2	24	27	1.2
Tlaxcala	11	12	111	134	5.7
Veracruz	1	2	11	14	0.6
Total	431	1019	890	2340	100

**Note. The building damages only corresponds to the earthquake of September 7*

Only three entities: Oaxaca, Puebla and Morelos concentrated 62.7% of the total damages. Of these, Oaxaca and Puebla represented just over half of the damages (51.6%). For this reason, a campaign of reconnaissance of damages was performed in order to assessment the damage in historical temples in these states. A total of 48 temples were visited (Fig. 1): 22 in Oaxaca, around of the *Mixteca Alta* and Tehuantepec regions; 11 inside of the *Mixteca* region, Puebla; 15 in Morelos, along of the route called *Ruta de los Conventos*. Some of them are included on the World Heritage List of the UNESCO, as "Earliest 16th Century monasteries on the slopes of Popocatepetl". The damage observed is describe in this paper; according to the type of structural element of the temple. For this purpose, the temples were divided into: façades and bell towers; domes and vaults; side walls and apse.



Figure 1: Location of the temples visited after the earthquake of September 19, 2017

2 FACADES AND BELL TOWERS

The damages observed into the façades were produced mainly due to higher levels of shear stresses into the plane of this element. These damages were displayed with the formation of diagonal cracks and/or with the separation of the main body of the facade or the separation of the side walls. However, some damages were associated with an out-of-plane behavior. Mainly, due to the overturning of the frontispiece and belfries. The bell towers were one of the most damaged elements. In most cases, partial or total collapse of the bell tower bodies was observed.

Some examples are showed in figure 2. The façade of Tlaquiltenango temple, in Morelos, present a separation between the façade and sidewalls; as well as, a diagonal crack in the middle of this element (Fig. 2a). In Tlayacapan, some diagonal cracks were located over the façade, near to the door and windows. The bell gable showed a partial collapse due to the out of plane behavior of this element (Fig. 2b). A similar behavior was observed in the *Sagrario* temple, in Huajuapan de León, Oaxaca (Fig. 2c). The façade of Chila de la Sal chapel showed some cracks between the side walls, in the middle, and the towers (Fig. 2d).



Figure 2: Damages patterns in façades: a) Tlaquiltenago, Morelos; b) Tlayacapan, Morelos; c) Huajuapan de León, Oaxaca and d) Chila de la Sal, Puebla

The towers were the structural element that more damages presented in temples located, mainly, in Puebla and Morelos. In San Andrés de la Cal chapel, Morelos, the arches of the lower body of the bell tower collapsed and horizontal cracks appeared in the upper and base of the pilasters (Fig. 3a). Similar behavior was observed in the pilasters of the bell towers of Santa Ana Jolalpan (Fig. 3b) and Pilcaya, (Fig. 3c) Puebla.

a)  b)  c) 

Figure 3: Damages patterns in bell towers: a) San Andrés de la Cal, Morelos; b) Santa Ana Jolalpan, Puebla c) Pilcaya, Puebla

The temples Hueyapan, Jiutepec and Ocuituco located into the *Ruta de los Conventos,* in Morelos, they have only a one bell tower. In all cases, this element presented a different level of damage, from only cracks until partial or total collapse (Fig. 4). Hueyapan tower shown cracks upper and the base of the pilasters of the first body of the belfry. This is because the upper body, being more rigid and smaller, worked mainly as a rigid body with a considerable mass, where the seismic shear was concentrated (Fig. 4a). The temples of Jiutepec and Ocuituco presented collapses of the bell towers, while the main walls of the facades had slight damage, which was concentrated in the opening of the window of the choir (Figs. 4b and 4c).

a)  b)  c) 

Figure 4: Damage to facades of temples in Morelos: a) Hueyapan; b) Jiutepec; c) Ocuituco

Although most of the temples in Mexico have a vaulted roof, as stone o brick masonry, some façades were damages due to presence of the out of plane behavior. For example, in Pilcaya (Fig. 5), the facade was separated from the vault because a deficient anchoring of the roof to the facade wall. Likewise, the frontispiece collapsed due to movement out of plane. In Tlayacapan (Fig. 6) vertical cracking are showed between the façade and the side walls of the nave, due to an out-of-plane behavior.

a)  b) 

Figure 5: Temple of Pilcaya, Puebla: a) turning of the frontispiece; b) separation of the facade from the body of the nave

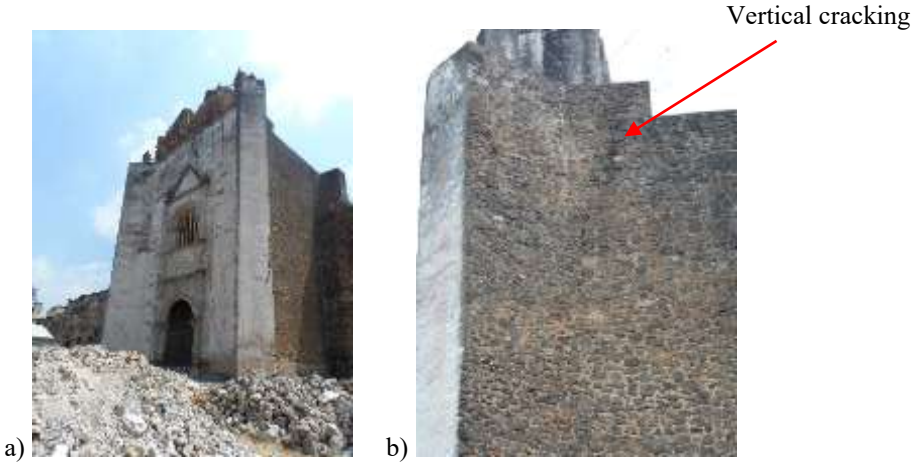


Figure 6: Facade of the Tlayacapan temple, Morelos: a) General view; b) Vertical cracking between the facade and the wall of the nave

3 ROOFING SYSTEM

The roofing system of this kind of temples is mainly made by domes and vaults. The most common are the barrel vaults without or with lunettes. Many cases of damages in this system was observed, from longitudinal and transversal cracks until partial or total collapses. Figure 7 shows the typical cracking of continuous barrel vaults, where longitudinal cracks are present along the vault. Usually a crack appears at the top of the vault, in the intrados and extrados, ridding the fillings that commonly cover the kidneys of the vault in the extrados (Fig. 7). In some cases, the cracks were large enough to cause the collapse of the vault and arches.

a)  b) 

Figure 7: Damage in vaults: a) Tlayacapan, Morelos and; b) Tlaquiltenango, Morelos

About of the domes, typical damages were observed: radial cracks at the base of the dome and meridians on the body of the dome (Fig. 8). In some cases, the damages were located only in the drums. In others, the dome collapsed and the drum remained standing, apparently undamaged (Fig. 9).



Figure 8: Radial and meridian cracks in the dome of the Jiutepec temple, Morelos

a)  b) 

Figure 9: Damage to the main dome in temples in Morelos: a) Totolapan (sail vault); b) Zacualpan

4 SIDE WALLS AND APSE

The temples are massive structures. The weight of their structural elements contributes to the stability. The walls usually are robust and can hardly collapse. However, damage may occur mainly by shear forces that the masonry cannot resist as shown in figure 10.

a)  b) 

Figure 10: Damage in side walls: a) El Calvario temple, Huajuapan, Oaxaca; b) Ayoxutla, Puebla

In some cases, the side walls have horizontal cracks that cross the thickness of the wall and generally are located below the windows (Fig. 11). This type of cracking is due to bending moments outside the plane of the wall; which occur mainly in churches that have other bodies attached to the side wall, such as convents, chapels or parish offices. These attached bodies function as struts on the side walls.



Figure 11: Horizontal wall cracks in the temple of Tlayacapan, Morelos

Buttresses with added sections at different stages of construction collapsed by separating mainly in areas with old cracks that had been repaired in previous works. In flying buttresses, shear cracks occurred even when their arches had been bricked up, in addition to the separation of the walls (Fig. 12).



Figure 12: Typical damage to buttresses in Morelos: a) Tlayecac; b) Tlayacapan and c) Totolapan

5 CONVENT BUILDINGS

The convents buildings visited have a central quadrangular cloister, with one or two levels, surrounded by arcades with or without buttresses, and halls covered by masonry vaults or wooden roofs. They were built during the 16th century. The damages were located in the cloister arches and the roofs of the halls, as well as the walls and vaults of the rooms.

The barrel vaults in the corridors showed longitudinal cracks, located at the top and in the kidneys of the roof; in a few cases they were located in the bases of the vault, as in the Totolapan convent (Fig.13a). These cracks are located frequently next to the cloister, because in this side, the structural elements are insufficient to contain the thrust of the vault, compared to the opposite side, that contain the walls of the rooms, which are more rigid (Figs. 13a and 13b).

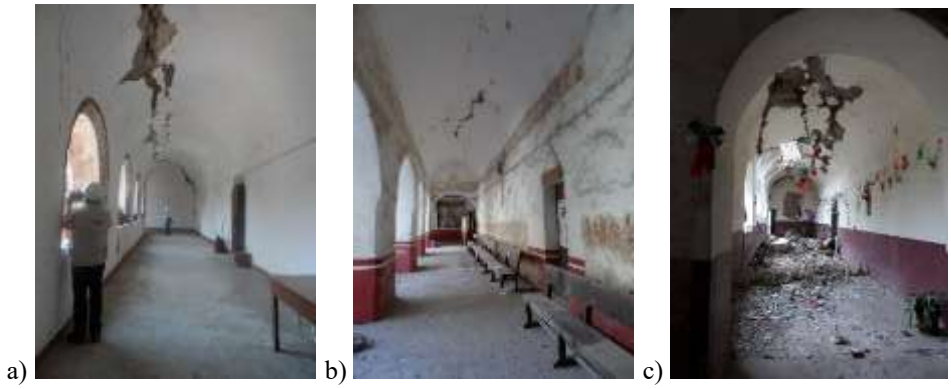


Figure 13: Typical damages in Morelos convents: a) Ocuituco; b) Jiutepec; c) Totlolapan

In some convents, the arches of the upper cloister collapse because they have an important opening and the poor quality of the material building. In particular, the convents of Jiutepec and Totolapan, located in Morelos, were the most affected. In the first, the roof of the high cloister was formed by wooden and tiles, with thickness arcades and without buttresses (Fig. 14a). In Totolapan, the damage was associated to the poor quality of the masonry, maybe for a lack of maintenance. The low cohesion between the mortar and the stone induce the crumbling of the masonry, which caused the collapse of the buttressed arch and the barrel vault in the gallery of the high cloister, due to movement out of plane (Figure 14b).

a)  b) 

Figure 14: Damage to the upper cloister of Morelos convents: a) Jiutepec; b) Totolapan

The convent of Jantetelco presented severe damage due to the low resistance of the masonry used for its construction; since it is made mostly of large pebbles and a low quality mortar, causing an inadequate adherence between the mortar and the stone as well as for the poor interlocking between the stones. Due to this, when the action of the earthquake induced high levels of stresses on the convent, the masonry crumbling. Figure 15 shows the cloister with debris of the masonry.



Figure 15: Damage to the cloister of the convent of Jantetelco, Morelos

6 BEHAVIOR OBSERVED IN PREVIOUSLY REINFORCED TEMPLES

Actually, it is difficult to find a temple without any process of intervention realized. In some cases, these interventions are visible and others are hidden. When the intervention is associated to improve the structural response of the temple, the earthquakes are the best test to evaluate the effectiveness of the intervention. During the visits of recognition of damages, some temples structurally intervened were find. Regardless if the intervention was made according to the criteria of conservation of Heritage buildings or not, some cases are presents.

In Oaxaca are located some temples intervened with massive reinforced concrete elements, because they were severely damaged for previous earthquakes. Figure 17 shows two cases: Santiago Cacaloxtepec and San Andrés Dinicuiti, both with reinforced concrete elements embedded in the walls and the vault (Figure 16 and 17). In San Andrés Dinicuiti, the original vault was replaced totally by a reinforced concrete slab (Figure 17b). In both temples, not damages by the earthquake of the September 19 were detected.

a)  b) 

Figure 16: Temple of Santiago Cacaloxtepec reinforced with concrete element: a) walls and b) vault

a)  b) 

Figure 17: Temples of San Andrés Dinicuiti reinforced with concrete elements: a) walls and b) vault

Other cases were found where only the interventions of reinforcement were applied locally in specific structural element, without intervening adjacent elements. Causing that the damages were transferred to weakest regions that probably before the intervention had not been damages. For example, Figure 18 shows the damage in the drum of the Huajuapan Cathedral. In this case, the dome was rebuilt previously with reinforced concrete. Another example is when reinforced concrete or steel elements are incorporated as structural reinforcement. However, due to incompatibility of materials or an inadequate anchorage with around structural elements, some damages were produced as show in Figure 19.



Figure 18: Damage in the dome of Huajuapan Cathedral, Oaxaca due to interventions before to the 2017 earthquakes

a)  b) 

Figure 19: Wall collapses due to interventions with concrete slabs in the convent of Jiutepec, Morelos: a) Slab supported directly on the wall; b) Beams supported on the walls

7 CONCLUSIONS

The damages reported in this paper correspond to the observed in historical temples of Oaxaca, Puebla and Morelos states due to the earthquakes of September 2017. The damage patterns and mechanisms of collapse described are the same like observed in previous earthquakes. The bell towers, vaults and domes still remain as the most vulnerable elements. Lack of maintenance, poor quality of the masonry, structural modifications and inadequate previous interventions are the main causes of the damages observed in this kind of structures.

Continuous and correct maintenance of the structure is indispensable to reduce the possible damages due to earthquakes. A detailed structural assessment of the temples always is necessary to performance an adequate intervention program according to the criteria of restauration of Heritage Buildings.

Acknowledgements. Authors acknowledge to Instituto Nacional de Antropología e Historia for the support provided for visiting damaged buildings. In particular, to the regional centers of Morelos, Puebla, and Oaxaca, through to the Dra. María Isabel Campos Goenaga, Dra Laura Ledesma; Arch. Rutilia Amigón, and the Arch. Gustavo Donnadieu, respectively. To the students: Martín Daniel Zúñiga Ontiveros, Gustavo Monroy Guzmán, and Andrés Morales Morales.

REFERENCES

[1] Servicio Sismológico Nacional, Sismo de Tehuantepec (2017-09-07 23:49 Mw8.2), Reporte Especial, México (2017).

[2] Chávez, M. M., Arnau, O., Guerrero-Bobadilla, H., Jaimes-Téllez, M. A., and Pozos, A. Observations of damages in some locations of Oaxaca due to the Tehuantepec Mw 8.2 earthquake, 6th Structural Engineers World Congress, Cancún, Mexico, (2017).

[3] Servicio Sismológico Nacional, Sismo del día 19 de septiembre de 2017, Puebla-Morelos (M7.1), Reporte Especial, México (2017).

[4] Jaimes-Téllez, M. A. (2017). Sismo del 19 de septiembre de 2017, Mw7.1, Puebla-Morelos, Reporte, Instituto de Ingeniería, UNAM, México.

http://www.iingen.unam.mx/esmx/Investigacion/Proyectos/Paginas/Sismo19sept2017.aspx., visitada el 30 de agosto de 2018.

[5] Meli, R. (2018). La ingeniería civil ante los efectos de los sismos de 2017 en los edificios patrimoniales (el equilibrio entre la autenticidad y la seguridad). En: Sismos y patrimonio cultural. Testimonios, enseñanza y desafíos, 2017 y 2018, Secretaría de Cultura, México, 62-81.

[6] INAH (2017). Censo de daños al patrimonio por el sismo del pasado jueves 7 de septiembre, Boletín N° 324 – 14 de septiembre de 2017, Instituto Nacional de Antropología e Historia.

12th International Conference on Structural Analysis of Historical Constructions
SAHC 2020
P. Roca, L. Pelà and C. Molins (Eds.)

DESIGN OF SHAKE TABLE TESTS OF MULTI-LEAF MASONRY WALLS BEFORE AND AFTER RETROFITTING

STEFANO DE SANTIS[1,*], OMAR ALSHAWA[2], GERARDO DE CANIO[3], SARA FORLITI[3], DOMENICO LIBERATORE[2], PIETRO MERIGGI[1], IVAN ROSELLI[3], LUIGI SORRENTINO[2], AND GIANMARCO DE FELICE[1]

[1] Department of Engineering, Roma Tre University
Via Vito Volterra 62, 00146 Rome, Italy
Email: { stefano.desantis, pietro.meriggi, gianmarco.defelice} @uniroma3.it
Web page: www.romatrestrutture.eu (*corresponding author)

[2] Department of Structural and Geotechnical Engineering, Sapienza University of Rome
Via Antonio Gramsci 53, 00197 Rome, Italy
e-mail: {omar.alshawa, domenico.liberatore, luigi.sorrentino} @uniroma1.it
Web page: www.disg.uniroma1.it

[3] Laboratorio Tecnologie per la Dinamica delle Strutture e la Prevenzione del rischio sismico e idrogeologico, ENEA Centro Ricerche Casaccia
Via Anguillarese 301, 00123 Santa Maria di Galeria (Rome), Italy
Email: {gerardo.decanio, sara.forliti, ivan.roselli} @enea.it - Web page: www.enea.it

Keywords: 2016-2017 Central Italy Earthquake, 3DVision, Composite materials, Natural accelerogram, Seismic retrofitting.

Abstract. *A significant proportion of the built heritage in historic centres is constituted by rubble stone masonry structures. Collapses by leaf separation and disaggregation observed after earthquakes highlight their dramatic vulnerability, especially under out-of-plane loads. Nevertheless, their dynamic response still needs to be fully investigated and their capacity may be overestimated by assessment approaches based on rigid-body mechanics. Effective retrofitting solutions are also needed to protect human lives and safeguard the built heritage, while ensuring the conservation of its architectural value. This paper describes the design of a shake table investigation on stone masonry walls, whose materials and arrangement reproduce those surveyed in the villages of central Italy struck by the 2016-2017 earthquake sequence. The test setup was conceived to induce out-of-plane vertical bending under earthquake base motion and investigate the dynamic response of multi-leaf rubble stone masonry and the gain in seismic capacity that can be achieved with mortar-based composite reinforcements, designed to prevent the leaf separation and disaggregation of the wall without compromising its fair face.*

1 INTRODUCTION

A seismic sequence activated in central Italy in Summer 2016 and struck a number of historic centres located in four regions (Lazio, Marche, Umbria and Abruzzo). The first event occurred

on August 24th 2016, had a magnitude of M_W 6.0 and its epicentre was in Accumoli (RI, Lazio). Other events followed, the strongest ones being on October 26th 2016 (M_W 5.9, Castelsantangelo sul Nera, MC, Marche), October 30th 2016 (M_W 6.5, Norcia, PG, Umbria) and January 18th 2017 (M_W 5.5, Capitignano, AQ, Abruzzo) [1]. In addition to the 299 fatalities and almost one thousand people injured, several collapses occurred (the centres of Amatrice, Accumoli and Arquata del Tronto were almost destroyed) and severe damages were surveyed [2]. Such scenario is associated with the building stock of the areas struck by the earthquake, mainly constituted by old structures in rubble stone masonry (Figure 1) and ordinary reinforced concrete buildings, including churches and palaces of architectural value [3].

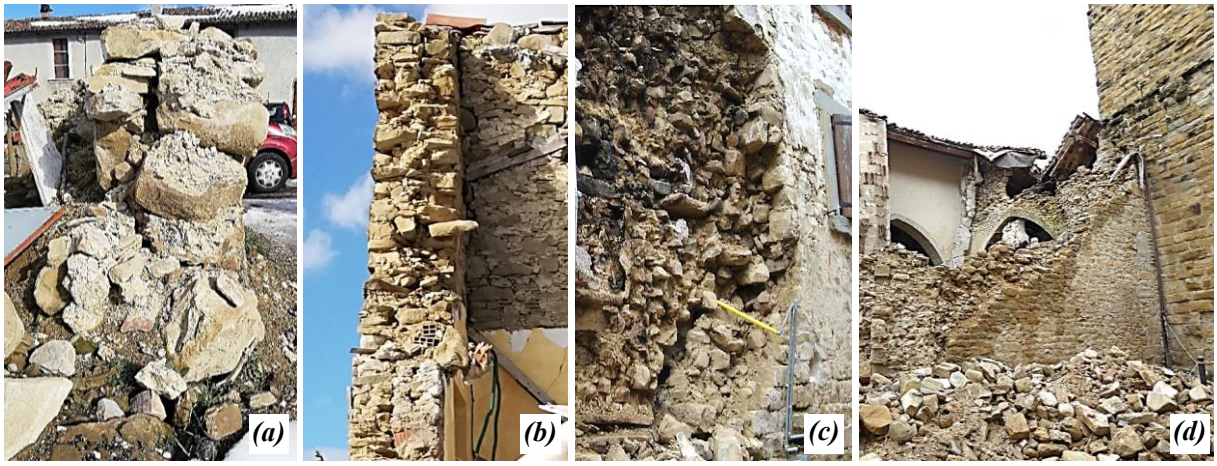


Figure 1: Survey of masonry typologies in the centres struck by the 2016-2017 earthquake sequence

The 2016-2017 earthquake fostered a new boost to the scientific and technological research devoted to the seismic assessment and protection of the building stock in earthquake prone areas, with specific reference to historic structures and architectural heritage. Two research projects have been recently funded by Lazio Region. SISMI (Technologies for the improvement of the seismic safety and the restoration of historical centres) gathers the main research institutions in the Region in a wide range of activities, including architectural survey of the built heritage of the earthquake prone areas of the Region, seismological characterization of the territory, structural assessment tools, smart materials for retrofitting, full-scale tests, and monitoring. SICURA (Sustainable technologies for the seismic protection of the cultural heritage) is coordinated by Roma Tre University and involves suppliers of reinforcement systems, software houses, design companies and contractors. The project aims at developing an advanced knowledge on the seismic retrofitting of architectural heritage with mortar-based composites and includes experiments on small-scale specimens and on full-scale retrofitted structures, and the development of advanced software tools and expeditious analytical methods for the reinforcement design and the assessment of retrofitted structures. Both the projects include shake table tests on full-scale structural members for investigating the seismic response of historic masonry, validating numerical models and demonstrating the effectiveness of strengthening technologies. This paper presents the design of this table test, starting from the identification of the problems under study and including the collection of the materials, the design of the setup, the selection of the inputs, and the development of retrofitting solutions.

2 PROBLEM STATEMENT AND GOALS OF THE STUDY

Rubble stone masonry structures proved extremely vulnerable against seismic actions. Due to their the irregular arrangement (Figure 1a,b), poor quality of the mortars, and weak connection with orthogonal walls and horizontal structures (floor, roof), the perimeter walls tend to separate from the rest of the construction and collapse out of their plane [4]. Not only this, but also such type masonry generally fails by leaf separation (Figure 1c) and disaggregation (Figure 1d), such that, on the one hand, tie-bars and crowning beams (possibly installed after past earthquakes) do not effectively prevent collapse and, on the other hand, their seismic capacity may be overestimated by the assessment approaches based on rigid-body mechanics [5]. The surveys carried out after the events of the 2016-2017 earthquakes confirmed such feature, highlighting the dramatic fragility of the territories struck by the seismic sequence. Nonetheless, the dynamic response of this type of masonry still needs to be deeply investigated to develop adequate assessment tools and effective retrofitting solutions. With these purposes, a shake table test investigation was designed on four full-scale wall specimens, built with the stones collected in a small village struck by the earthquake and a mortar developed on the basis of the samples taken in the field. The programme includes a first test on one unreinforced wall, followed by the tests on three walls retrofitted with different strengthening solutions. Each specimen will be subjected to a sequence of seismic inputs at the base, along the horizontal direction (out of the plane of the wall) and along the vertical direction, which will be progressively scaled up to collapse. This allows following the development of damage, although the test sequence is expected to affect the results and it is difficult to identify one single input signal that corresponds to the whole sequence. The experimental setup was designed to constrain the top horizontal displacement and leave vertical displacement and rotation free, to induce vertical bending under earthquake base motion.

This experimental study requires important efforts for the construction of the specimens and the setup, the implementation in the laboratory, the design and installation of the reinforcements, and the acquisition, analysis and interpretation of test data. On the other hand, it allows overcoming the drawbacks of simpler experimental methods and achieving results that would be unavailable otherwise. First, the investigation of full-scale specimens makes it possible to build the walls and apply the seismic inputs without scale effects. The use of original materials makes it possible to represent the masonry types surveyed in the field, which is essential to investigate their behaviour, replicate their failure modes and assess the effectiveness of retrofitting strategies [6]. Placing full-scale walls in vertical (with the addition of masses on top) makes it possible to apply a vertical compression in addition to the out-of-plane loads, thus replicating the stress state experienced by masonry walls in the field, which is unfeasible when medium-scale wall panels are tested with a three/four point bending test configuration [7]. Second, the careful design of the constraint that prevents the horizontal displacement of the top of the wall (simulating the effect of a tie-bar or of a crowning beam) while leaving the vertical displacement and the rotation free, aims at reproducing the actual boundary conditions of a façade at the highest storey of a building. Indeed, it has been observed that the dynamic behaviour of a masonry wall under out-of-plane bending is highly affected by the boundary conditions and especially by the restraint imposed to the top vertical displacement [8]. Finally, the use of a shake table infrastructure allows the application of acceleration time histories at the base of the specimens, thus reproducing the actual distribution of inertial forces experimented

by the wall under earthquake base motion, including their dynamic amplification and rapid variation and reversal, which cannot be simulated in quasi-static tests [9]. Moreover, the application of the vertical component of the seismic inputs makes it possible to take into account its effects on the dynamic response, which cannot be neglected when unreinforced masonry is under investigation [10].

With these premises, this shake table investigation aims to:

(i) develop a deeper understanding of the seismic behaviour of historic multi-leaf rubble stone masonry walls under out-of-plane loads, with specific reference to boundary conditions that prevent the onset of overturning such that disaggregation, possibly combined with leaf separation, is the expected failure mode;

(ii) contribute to the development of seismic assessment methods that account for the arrangement of masonry and its effect on the dynamic response and failure mode under out-of-plane loads, overcoming the approaches based on rigid-body mechanics recommended by standard codes [5], which may be unconservative if collapse occurs by disaggregation;

(iii) investigate the effectiveness of innovative mortar-based composites for the seismic retrofitting of architectural heritage and promote the development and the confident use in rehabilitation practice of strengthening solutions that combine structural effectiveness and fulfilment of conservation principles;

(iv) foster the fruitful cooperation between academia, industrial partners, institutions and practitioners for the transfer of knowledge from the scientific community to engineers and decision makers, as well as the involvement of citizens and local administrators in the whole process of post-earthquake reconstruction.

3 WALL SPECIMENS UNDER INVESTIGATION

Four wall specimens, with a thickness of 0.50m, a width of 1.70m and a height of 3.70m, will be tested on the shake table (Figure 2). The walls will be built using rubble limestone units collected in Collespada, a village in the municipality of Accumoli (RI), where several buildings collapsed after the event of October 26th 2016. A mortar with natural aerial lime and siliceous aggregates will be used, having 1:9 binder:aggregate weight ratio and 0÷2mm grain size range, according to the physical and chemical analyses on mortar samples taken in the field [11]. To the purpose of reproducing the arrangement of the masonries surveyed in the historic constructions of central Italy, the walls will have two leaves without transversal connection, small and irregular stones and mortar joints with irregular layout and thickness. Each wall will be built on a reinforced concrete foundation beam, in order to be moved in the laboratory hall and fixed to the shake table (Figure 2a). The first layer of masonry will be partially laid in the foundation to prevent sliding. On top of each wall, a 0.30m high top beam will be built in reinforced brickwork. Glass fibre meshes will be placed in the bed joints during construction to provide the top beams with tensile and bending strength. Vertical connectors, inserted in drilled holes injected with a lime-based grout, will ensure the connection with the stone masonry. The top beams will represent a crowning beam built to contribute to their horizontal bending capacity and improve their connection with other orthogonal walls, preventing the onset of out-of-plane overturning mechanisms and providing the structure with a box type behaviour. Finally, a 15 kN weight will be applied on top to simulate the axial load of a floor or a roof.

4 EXPERIMENTAL SETUP AND SEISMIC INPUTS

Steel frame and setup details

A steel frame structure will be fixed to the shake table, which is comprised of two braced frames, placed at the two sides of the specimen, and two I-girders, bolted on top of the frames, one on the front side and one on the back side (Figure 2b). Rubber rollers, fixed to the I-girders, will be put in contrast with the top beam in order to constrain its horizontal displacement, while leaving its upward displacement and its rotation free. This setup has already proved effective in a recent experimental investigation [7]. The steel structure is designed to minimize the relative displacements between the top beams and the reinforced concrete foundation even if it should be noted that, due to the dynamic amplification of the seismic input over the height of a construction, the dynamic actions at the base and on top are not expected to be identical.

Natural accelerograms selected for the shake table tests

The acceleration time histories of the main events of the 2016-2017 earthquake sequence will be used in shake table tests. Input signals will be applied along horizontal and vertical directions and progressively scaled up to collapse. The use of different accelerograms will make it possible to investigate the correlation between the response of the wall and several intensity parameters, including peak ground acceleration (PGA), velocity (PGV) and displacement (PGD), Housner intensity, mean incremental velocity (MIV) and spectral acceleration. Data acquisition will be continued for 20 seconds after the end of the input to record displacements and accelerations under free oscillations and collect data for dynamic identification. For the same reason, tests under white noise will be carried out before the beginning of the tests and after each sequence of tests with the same scale factor. Clearly, the test sequence performed on the unreinforced specimen will be repeated on the retrofitted specimens for comparisons.

Instrumentation

The tests will be carried out at ENEA Casaccia Research Centre (Rome) using a 4m×4m shake table with six degrees of freedom. The accelerations will be recorded by piezoelectric accelerometers placed on the table, on the reinforced concrete foundation, on the wall specimen and on the top beam, in order to detect the actual base input experienced by the walls and their response, including the dynamic amplification throughout the height. A high-resolution optical system named 3DVision will be also used to record the spatial displacements of several measurement points [12]. Near infrared digital cameras will be placed around the specimen. LEDs will illuminate wireless retro-reflecting spherical markers and the reflected radiation will be captured by the sensors of the cameras and processed. Displacement data will be filtered to remove noise and analyzed to derive acceleration time histories [13] and calculate fundamental frequencies and modal shapes through Multi-Input/Multi-Output (MIMO) experimental modal analyses [7]. Data provided by accelerometers and 3DVision will be compared for mutual validation and for calibrating filter parameters and will integrate each other for a comprehensive detection and representation of test results. 3DVision offers the advantage that the spatial displacement of a large amount of points can be measured during tests, overcoming the limitations of traditional devices associated with encumbrance, range, cables, need of stiff reference structures, and risk of damage to expensive instrumentation.

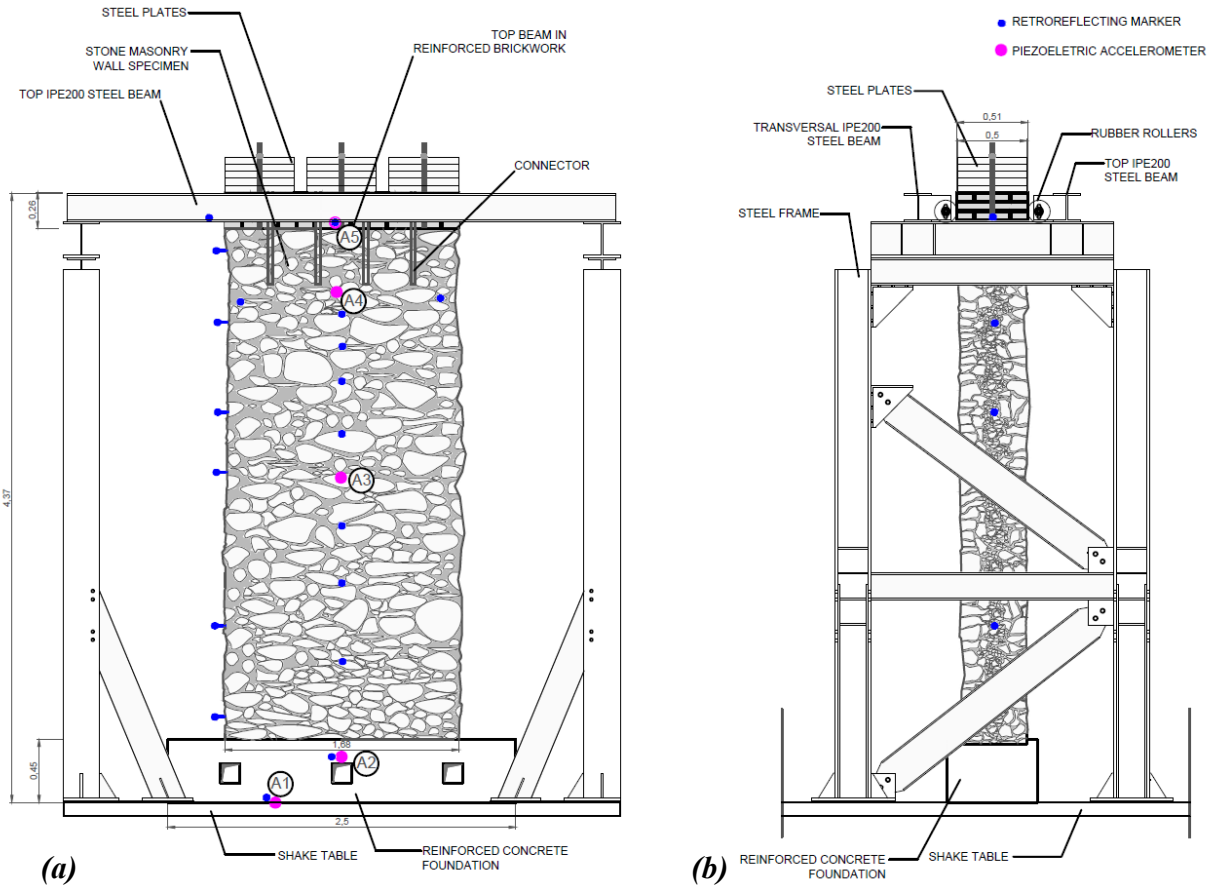


Figure 2: Wall specimens under investigation an experimental setup.

5 RETROFITTING DESIGN WITH MORTAR BASED COMPOSITES

Different retrofitting solutions will be applied to three wall specimens, using mortar-based composites, such as fabric reinforced cementitious matrix (FRCM) [7,14,15] and composite reinforced mortar (CRM) [16,17]. These systems, which have been developed and introduced in the market in the last decade, are comprised of an open mesh applied to the outer surface of the wall with a mortar matrix. They can be seen either as an evolution of ferrocement [18], an overlay of cement plaster applied over one or more layers of a thin steel net, or of Textile Reinforced Concrete (TRC) [19], in which glass or carbon fabrics were used instead of steel nets, to precast thin structural elements. Nevertheless, ferrocement and TRC have been mainly developed for load-bearing new structural members, whereas FRCM and CRM systems are conceived for the external reinforcement of existing structures. They proved effective for enhancing the ultimate capacity of structural members with no increase of mass to the original structure, by the virtue of their high strength-to-weight ratio. The installation is relatively fast and easy, even on uneven or wet substrates, and they can adapt to a broad range of shapes and layouts. When lime-based mortars are used, the retrofitting complies with the principles of conservation as it ensures vapour permeability and physical/chemical compatibility with masonry substrates. In this case, additional challenges are posed by the arrangement of the masonry and its expected failure mode by disaggregation, as well as by the need of preserving its fair face on one side, in order

to preserve the architectural value of the façade. For these purposes, a hybrid system will be tested, which comprises an FRCM or a CRM overlay installed on one side (the interior one), whereas, on the other side (the façade), mortar joints will be repointed with high strength stainless steel wires [20]. On both sides, the retrofitting system will be installed over the whole surface of the wall in order to prevent disaggregation and provide a distributed bending strength. Transversal connectors will be also installed to contrast leaf separation and contribute to the substrate-to-reinforcement load transfer mechanism. The reinforcements are designed in accordance with the guidelines developed by the RILEM Technical Committee 250-CSM jointly with the ACI (American Concrete Institute) 549 Committee [21]. The formulation is based on a cross-sectional analysis and assumes ultimate strain values for the materials derived from an acceptance procedure that combines direct tensile and shear bond tests. Tuning coefficients and safety factors are calibrated on experimental databases, as recommended by Eurocodes [22].

6 FURTHER STEPS AND EXPECTED OUTCOMES

The outcomes of this investigation will contribute to the development of an improved understanding of the seismic response of historic structures, built in irregular rubble multi-leaf masonry, which, despite their architectural and cultural value, represent a dramatic element of vulnerability in earthquake prone areas. The enhancement of tools for structural assessment as well as of seismic retrofitting technologies will contribute to an improved approach to the seismic protection of the building stock. The transfer of the scientific knowledge developed within this project to engineers, private and public stakeholders, with the active involvement of general public will foster the implementation of proper structural rehabilitation practices.

Acknowledgements. This work was carried out within the Research Projects "SICURA Sustainable technologies for the seismic protection of the cultural heritage" (2018-2020) and "SISMI Technologies for the improvement of the seismic safety and the restoration of historical centres" (2018-2019) funded by Lazio Region. SDS, PM and GdF acknowledge funding from the Italian Ministry of Education, University and Research (MIUR), attributed to the Department of Engineering of Roma Tre University, in the frame of the Departments of Excellence Initiative (2018-2022).

REFERENCES

[1] Mollaioli, F., AlShawa, O., Liberatore, L., Liberatore, D. and Sorrentino, L. Seismic demand of the 2016–2017 Central Italy earthquakes. *Bull. Earthq. Eng.* (2019) 17(10):5399-5427.

[2] Sorrentino, L., Cattari, S. Da Porto, F., Magenes, G. and Penna, A. Seismic behaviour of ordinary masonry buildings during the 2016 central Italy earthquakes. *Bull. Earthq. Eng.* (2018) 17(10):5583-5607.

[3] AlShawa, O., De Canio, G., de Felice, G., De Santis, S., Forliti, S., Liberatore, D., Mirabile Gattia, D., Perobelli, S., Persia, F. and Sorrentino, L. Investigation of rubble-masonry wall construction practice in Latium, Central Italy. In: Proceedings of SAHC 2020 Conference.

[4] Lourenço, P.B., Mendes, N., Ramos, L.F. and Oliveira, D.V. Analysis of masonry structures without box behaviour. *Int. J. Archit. Herit.* (2011) 5(4-5):369-382.

[5] Sorrentino, L., D'Ayala, D., de Felice, G., Griffith, M., Lagomarsino, S. and Magenes, G. Review of out-of-plane seismic assessment techniques applied to existing masonry

buildings. *Int. J. Archit. Herit.* (2017) 11(1):2-21.
[6] Giaretton, M., Valluzzi, M.R., Mazzon, N. and Modena, C. Out-of-plane shake-table tests of strengthened multi-leaf stone masonry walls. *Bull. Earthq. Eng.* (2017) 15:4299-4317.
[7] De Santis, S., De Canio, G., de Felice, G., Meriggi, P. and Roselli I. Out-of-plane seismic retrofitting of masonry walls with Textile Reinforced Mortar composites. *Bull. Earthq. Eng*. (2019a) 17(11):6265-6300.
[8] Graziotti, F., Tomassetti, U., Penna, A. and Magenes, G. Out-of-plane shaking table tests on URM single leaf and cavity walls. *Eng. Struct.* (2016) 125:455-470.
[9] Costa, A.A., Arêde, A., Costa, A. and Oliveira C.S. Out-of-plane behaviour of existing stone masonry buildings: experimental evaluation. *Bull. Earthq. Eng.* (2012) 10(1):93-111.
[10] Derakhshan, H., Griffith, M.C. and Ingham, J.M. Airbag testing of multi-leaf unreinforced masonry walls subjected to one-way bending. *Eng. Struct.* (2013) 57:512-522.
[11] Roselli, G., Mirabile Gattia, D., AlShawa, O., Cinaglia, P., Di Girolami, G., Francola, C., Persia, F., Petrucci, E., Piloni, R., Scognamiglio, F., Sorrentino, L., Zamponi S. and Liberatore, D. Mortar analysis of historic buildings damaged by recent earthquakes in Italy *Eur. Phys. J. Plus* (2019) 134:540.
[12] De Canio, G., de Felice, G., De Santis, S., Giocoli, A., Mongelli, M., Paolacci, F. and Roselli, I. Passive 3D motion optical data in shaking table tests of a SRG-reinforced masonry wall. *Earthq. Struct.* (2016) 10(1):53-71.
[13] Mongelli, M., Roselli, I., De Canio, G., and Ambrosino, F. Quasi real-time FEM calibration by 3D displacement measurements of large shaking table tests using HPC resources. *Adv. Eng. Softw.* (2016) 120:14-25.
[14] Papanicolaou, C.G., Triantafillou, T.C. and Lekka, M. Externally bonded grids as strengthening and seismic retrofitting materials of masonry panels. *Constr. Build. Mater.* (2011) 25(2):504-515.
[15] Babaeidarabad, S., De Caso, F. and Nanni A. (2014) Out-of-Plane Behavior of URM Walls Strengthened with Fabric-Reinforced Cementitious Matrix Composite. *J. Compos. Constr.* (2014) 18(4):04013057.
[16] Gattesco, N. and Boem, I. Out-of-plane behavior of reinforced masonry walls: Experimental and numerical study. (2017) *Compos. Part B Eng.* (2017) 128:39-52.
[17] De Santis, S., de Felice, G., Di Noia, G., Meriggi, P. and Volpe, M. Shake table tests on a masonry structure retrofitted with composite reinforced mortar. *Key Eng. Mater.* (2019b) 817:342-349.
[18] ACI 549R-97 State-of-the-art Report on Ferrocement. Farmington Hills, US (1997).
[19] Brameshuber, W. Textile reinforced concrete. State-of-the-art report of RILEM Technical Committee 201-TRC. Report 36, Bagneux, RILEM (2006).
[20] Corradi, M., Borri, A., Castori, G. and Sisti, R. The Reticulatus method for shear strengthening of fair-faced masonry *Bull. Earthq. Eng.* (2016) 14(12):3547-3571.
[21] ACI 549 0L – RILEM TC 250-CSM: Guide to Design and Construction of Externally Bonded Fabric-Reinforced Cementitious Matrix (FRCM) and Steel-Reinforced Grout (SRG) Systems for Repair and Strengthening Masonry Structures (2020).
[22] Meriggi, P., de Felice, G. and De Santis, S. Design of the out-of-plane strengthening of masonry walls with fabric reinforced cementitious matrix composites. *Constr. Build. Mater.* (2019) DOI: 10.1016/j.conbuildmat.2019.117946.

12th International Conference on Structural Analysis of Historical Constructions
SAHC 2020
P. Roca, L. Pelà and C. Molins (Eds.)

EFFECT OF HISTORIC TIMBER ROOF STRUCTURES ON THE STRUCTURAL BEHAVIOUR OF MASONRY BUILDINGS DURING SEISMIC EVENTS

ALEXANDRA I. KELLER[1,2*], MARIUS MOSOARCA[1,2]

[1]Politehnica University of Timisoara, Faculty of Architecture and Urban Planning
2/A Traian Lalescu, Zip code 300223, Timișoara, Romania
e-mail: alexandra.keller@upt.ro (*corresponding author), marius.mosoarca@upt.ro

[2] Politehnica University of Timisoara, Urban Planning and Architecture research centre
2/A Traian Lalescu, Zip code 300223, Timișoara, Romania

Keywords: Historic timber roof structure, Historic masonry structure, seismic events

Abstract. *Roofs are complex elements of heritage structures which are not only meant to protect the building from exterior methodological factors but are also defining the skyline of a city while highlighting the importance and aesthetics of the building they belong to. However, in seismic areas, roof structures prove out to either trigger the out-of-plane behaviour of historic masonry buildings [1] or reduce the horizontal displacement, depending on their type and their connection to the masonry walls [2]. The study is therefore aiming do highlight the effect of common roof structure types from Timisoara, a city placed in the western part of Romania, subjected to shallow earthquakes, on the seismic behaviour of a local type of masonry structure, with a ground-floor and 2 upper floors, from the 18th century.*

Throughout the study, three different types of roof structures were placed on the same masonry building and the out-of-plane horizontal displacement, inter-story drift, damage level and internal forces were assessed. The main scope of the study is to highlight how the chosen roof structures from the 18th, 19th and 20th century, would influence the behaviour of a masonry building during seismic events. Detailed numerical simulations using finite element models of the building and the three roof structures were performed in order to obtain the four assessed parameters, which prove that, depending on the connection to the masonry walls and the state of conservation of the timber elements, roof structures would significantly improve the seismic behaviour of historic masonry buildings in this area.

1 INTRODUCTION

Heritage buildings were built considering the local environmental factors, by taking all the risks into consideration and adapting the structural features of the building in order to ensure good structural behaviour during extreme events. This can strongly be observed in earthquake-prone areas, where various solutions were found in order to reduce the seismic vulnerability of the heritage structures which are able to preserve the integrity of the building and ultimately save the life of their inhabitants [3,4]. More recent studies also confirm that roof structures can

influence the seismic behaviour of historic masonry buildings. More than that, they also highlight that the connection between the roof structure and the state of conservation of the timber joints is also significantly influencing the behaviour of the roof structure and ultimately that of the masonry building during that seismic event [5,6]. It can, therefore, be stated that timber structures can enhance the seismic behaviour of historic masonry building [7,8] but also in a bad state of conservation trigger significant damage [9,10].

Considering this observations, a study has been performed in Timisoara, concerning the effect of three representative roof structure types on the seismic behaviour of a characteristic historic masonry building from the 18th century by evaluating the out of plane displacement of the walls, their damage level and the internal forces by also highlighting the effect of the decay of the timber elements on this behaviour [11].

2 NUMERICAL MODELING OF THE BUILDING AND ROOF STRUCTURES

Finite element numerical simulations have been performed using the structural analysis software SCIA engineer [12]. By using the equivalent lateral forces method, the software is performing a static seismic behaviour analysis of the model, based also on dynamic analysis data like the defined seismic response spectrum and the distribution of the masses on each floor of the building. Thus, for the numerical simulation, the local characteristics of the earthquake were taken into consideration. The western part of Romania is the second seismic area of the country regarding the seismic intensity [13] but is mainly influenced by rather shallow earthquakes, which are only producing significant damage starting with 8 kilometres around the epicentre [14]. 94 seismic events with a seismic intensity between V and VIII on the Mercalli scale were recorded in the region [15,16].

2.1 Characteristics of the building

For the numerical simulations, a characteristic building from the historic part of the city was chosen, which includes all the specific features of 18th century buildings (Figure 1).

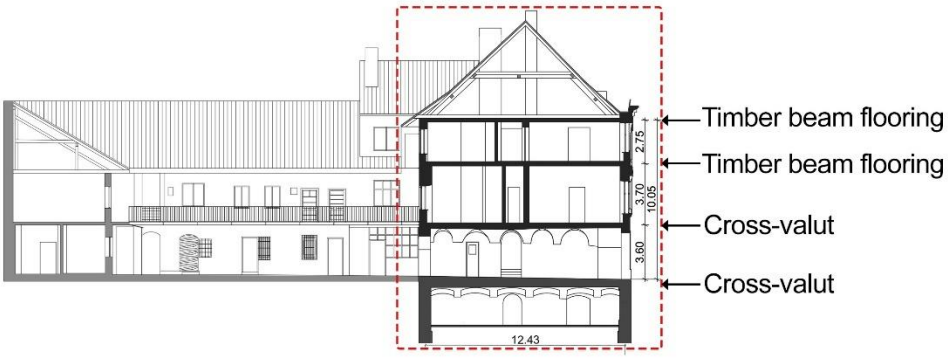


Figure 1: Section of the 18th century building – marked area which was considered for the study

The building has an L shaped plan, with the main building placed parallel to the street and a secondary wing placed towards the courtyard, perpendicular to the street. Therefore, for the study, only the main building was considered. It has one underground floor and three levels above ground each of them presenting a different functional purpose. Therefore, the ground

floor was used for commercial purposes while the two upper floors where residential. The structure is also changing with the height of the building, the width of the historic masonry walls decreasing from 90 centimetres at the ground floor down to 45 at the top of the building, while the floor structure is changing from cross vaults used for the ground floor to timber beam flooring at the upper floors.

Unfortunately, due to low maintenance the building was partially demolished and an up to date hotel is planned to be built instead.

2.2 Characteristics of the roof structures

The three chosen structures are not only the main roof structure types which can be found in the city, until the beginning of the 20th century, they are also specific for the period in which they were built. This is why a characteristic roof structure from the 18th, 19th and beginning of the 20th century was chosen for the study (Figure 2). The three structures are all purlin roof structures composed of main and secondary trusses, but they present completely different approaches regarding the used structural elements, their cross-section and their position, therefore influencing the seismic behaviour of the building in different ways.

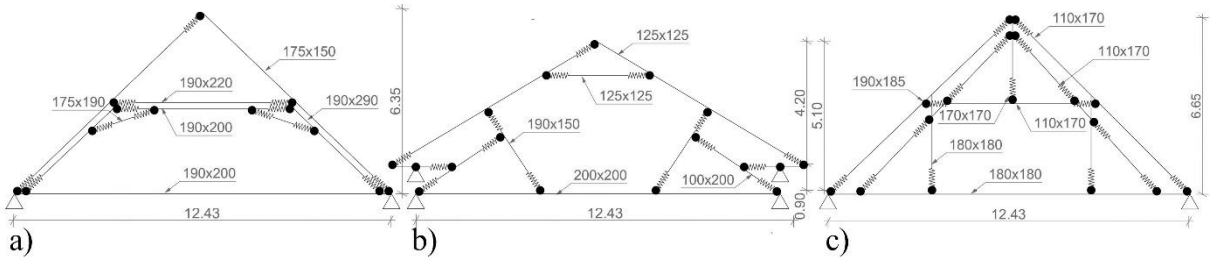


Figure 2: Considered roof structure types (a) 18th century; b) 19th century; c) 20th century)

The 18th-century roof structure (Figure 2a) is presenting a complex strutting device, specific for structures built in this period, which is composed of a tie beam, a straining beam and two compound rafters. Additionally, a second layer of structural elements was placed on the exterior of the strutting device, composed of a collar beam and the two rafters meant to compose the support of the roof envelope. At the same time, the roof structure is also presenting a complex system of diagonal elements placed between the rafters meant to also increase its rigidity in the longitudinal direction. The connection to the wall is made by a wall plate, partially inserted in the historic masonry wall and connected to the tie beam through a traditional crafted lap joint.

The 19th century roof structure (Figure 2b) is rather peculiar since it is a queen-post structure with inclined post and without a collar beam connecting the top part of the posts. Still, an angle brace was placed in the upper part of the structure, connecting only the rafters. This roof structure is also presenting a different type of longitudinal rigidity enhancing system, which is composed of heathers and trimmers and placed above the masonry wall.

The beginning of the 20th century roof structure type (Figure 2c) is a typical queen and king post structure with two queen posts placed in the inferior part of the structure and one king post placed above the collar beam meant to increase the height of the roof. In this case, no additional rigidity enhancing system was observed in the longitudinal direction.

For the 19th and 20th century roof structures passing braces were used to connect the posts to

the tie-beam. At the same time, it was observed that the used cross-section of the timber elements is lower than in the 18th century roof structure case. Except for the tie beam to wall plate joint which is a lap joint, all the other joints are tenon and mortise joints with or without additional wooden and steels pegs, depending on their position.

2.3 Characteristics of the models

Due to the significant height of the roof structures, it was impossible to assess their behaviour in a laboratory and numerical simulations were performed by placing each of the three chosen roof structures on the characteristic 18th century historic masonry building in SCIA Engineer. For both the building and the roof structure, the surveyed geometric characteristics of the structural elements were used in the models. For the models, the timber elements of the roof structures were modelled 1D members and the masonry walls as orthotropic 2D elements. Concerning the material properties, it was decided to use code-based mechanical properties for the timber (D18) and the historic masonry [11], since only few laboratory tests have been performed on historic timber and brick in Timisoara.

Previously performed studies concerning the behaviour of historic timber roof structures and their effect on masonry structures are highlighting the importance of properly considering the connection between the roof and the wall but also the significant effect of the joint axial stiffness on the general behaviour of the roof structure. Therefore, during the study, three different support types were taken into consideration: rigid, sliding and hinged and sliding, while the joins were modelled using five principles: first using a more conservative approach and modelling them as rigid and hinged and secondly considering their semi-rigid behaviour and using three different methods: the component method [17,18], the Heimeshoff and Köhler method [19,20] and the Hölzer method [21,22], thus resulting 15 different scenarios for each roof structure model.

3 RESULTS

After modelling the building and placing the three roof structures, the behaviour of the masonry building during local seismic events was analysed by comparing five parameters, which could highlight if the roof structures are actually improving the seismic behaviour of the chosen historic masonry building and which one is presenting the best effect (Figure 3).

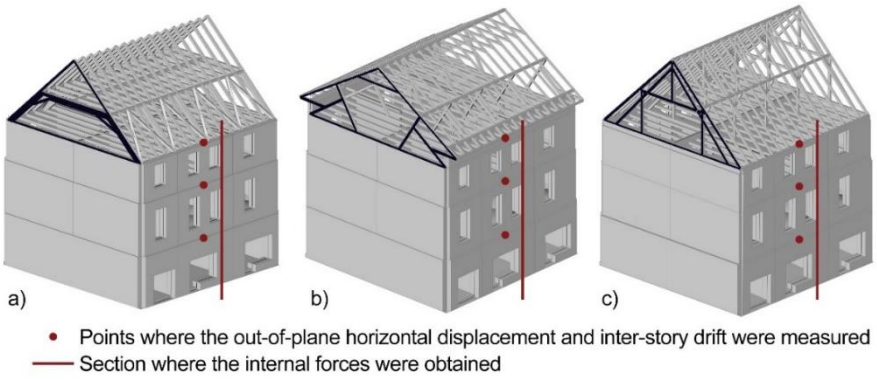


Figure 3: The three models with roof structures (a) 18th century; b) 19th century; c) 20th century) (after [11])

Therefore the horizontal out-of-plane displacement and inter-story drift of a selection of points, placed on a longitudinal exterior wall in the area of each slab, but also the deformed shape of the building, the damage level of the masonry wall on each floor and the internal forces were considered.

3.1 Out-of-plane displacement

First in order to observe the effect of the roof structures on the seismic behaviour of the masonry building the out-of-plane displacement of the building without roof structure was compared with the results obtained for the same building with the three chosen roof structures.

While comparing the results, it was observed that the out-of-plane displacement is approximately similar on the first floor of the building with variations reaching up to 10% compared to the no roof structure building. The presence of the 20th century roof structure is causing the most peculiar behaviour of the building since it presents the lowest horizontal displacement at the first and second floor but the highest displacement at the top, decreasing it with only 20% compared to the no roof structure case. Compared to this, the presence of the 18th century roof is presenting the most significant improvement of the top out-of-plane displacement, reducing the displacement with about 50%, while the 19th century roof structure is reducing it with around 40%. Still, in all the three cases, a difference between the obtained displacements was observed influenced by the considered scenarios (Table 1, Figure 4).

Table 1: Mean displacement of the building without a roof and with the three roof structures without decay

		No roof	With roof structure		
			18th century	19th century	20th century
1st floor	Displacement [mm]	2.18	2.08	2.29	1.95
	Compared to no roof		-5%	+5%	-10%
2nd floor	Displacement [mm]	7.28	6.55	7.77	6.32
	Compared to no roof		-10%	+5%	-15%
3rd floor	Displacement [mm]	19.86	10.22	11.44	15.71
	Compared to no roof		-50%	-40%	-20%

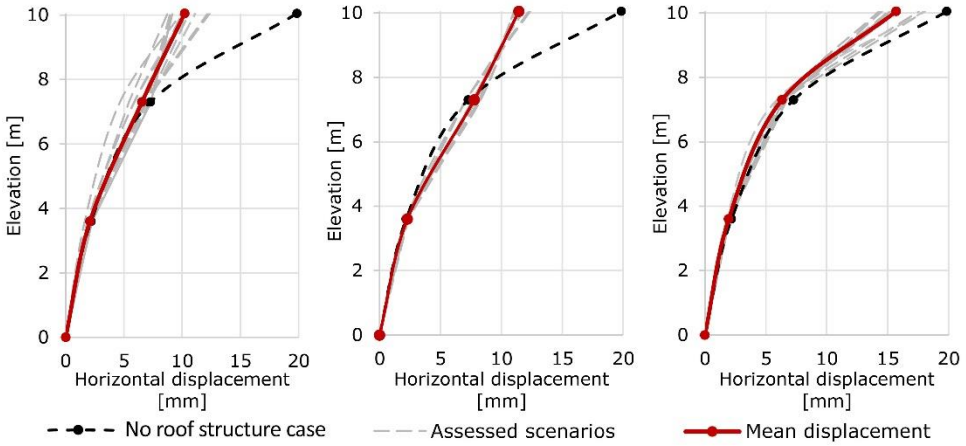


Figure 4: Horizontal out-of-plane displacement of the building without and with roof structures (a) 18th century; b) 19th century; c) 20th century) without decay

If, however, the timber elements are decayed, the numerical simulations highlight that the effect of the roof structures is different (Table 2, Figure 5). It can be observed that the presence of the 20th century roof structure is causing a slight increase of the horizontal displacement at the first and second floor but still reducing the top horizontal displacement with about 30%, more than is the case with the same roof structure in a good state of conservation. At the same time, it could be observed that the 19th century structure is also increasing the horizontal displacement on the first floors while significantly reducing the top horizontal displacement with up to 40%. The 18th century rood structure, on the other hand, is still presenting a reduction of the horizontal displacement at the first and second floor, but only a 40% reduction at the top. Still, compared to the displacement recorded for the 19th and 20th century roof structure, where the differences between the assessed scenarios are rather low, in the case of the 18th century roof, a clear variation depending on the chosen to support and joined axial stiffness was observed reaching up to 25%.

Table 2: Mean displacement of the building without a roof and with the three roof structures with 20% decayed timber elements

		No roof	With roof structure		
			18th century	19th century	20th century
1st floor	Displacement [mm]	2.18	2.15	2.42	1.20
	Compared to no roof		0%	+10%	0%
2nd floor	Displacement [mm]	7.28	7.05	8.69	7.62
	Compared to no roof		-5%	+20%	4%
3rd floor	Displacement [mm]	19.86	11.81	11.33	14.44
	Compared to no roof		-40%	-45%	-30%

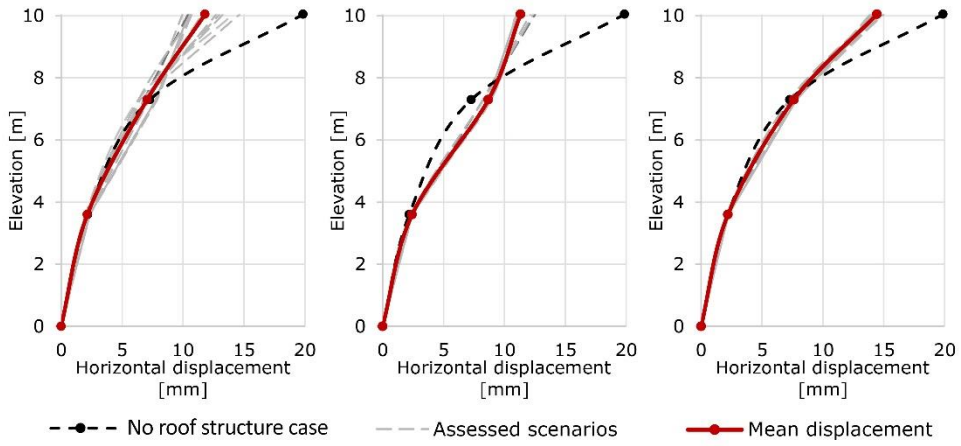


Figure 5: Horizontal out-of-plane displacement of the building without and with roof structure (a) 18th century; b) 19th century; c) 20th century) with 20% decayed timber elements

3.2 Out-of-plane inter-story drift

The analysis of the out of plane inter-story drift is once again highlighting the different effect of each roof structure on the seismic behaviour of the building. The analysis clearly shows that the 18th and 19th century roof structures are presenting a clear decrease of the inter-story drift on the third floor of the building, the 19th century roof structure presenting a clear decrease

between the 2nd and 3rd floor of 35%. The 20th century roof structure, on that other hand, is presenting a steady increase of the inter-story drift starting with the first floor with a significant increase at the last floor of 55% (Table 3).

Table 3: Mean inter-story drift of the building without a roof and with the three roof structures without decay

		No roof	With roof structure		
			18th century	19th century	20th century
1st floor	Interstory drift [mm]	2.18	2.08	2.29	1.95
	Interstory drift ratio [%]	0.06	0.06	0.06	0.05
	Compared to no roof		-4.72%	4.60%	-10.68%
2nd floor	Interstory drift [mm]	5.10	4.47	5.48	4.37
	Interstory drift ratio [%]	0.14	0.12	0.15	0.12
	Compared to no roof		-12.41%	7.56%	-14.34%
3rd floor	Interstory drift [mm]	12.58	3.67	3.67	9.39
	Interstory drift ratio [%]	0.46	0.10	0.10	0.26
	Compared to no roof		-70.82%	-70.80%	-25.37%

The decay of the timber elements is emphasizing these changes. The presence of the 19th century roof structure is decreasing the top out-of-plane inter-story drift with 60% compared to the second floor, while the presence of the 20th century structure is increasing it with only 20%, compared to the previous 55%. The effect of the 18th century roof structure is not as visible at the top of the building (Table 4).

Table 4: Mean inter-story drift of the building without a roof and with the three roof structures with 20% decayed timber elements

		No roof	With roof structure		
			18th century	19th century	20th century
1st floor	Interstory drift [mm]	2.18	2.15	2.42	2.20
	Interstory drift ratio [%]	0.06	0.06	0.07	0.06
	Compared to no roof		-1.57%	10.96%	0.85%
2nd floor	Interstory drift [mm]	5.10	4.90	6.27	5.42
	Interstory drift ratio [%]	0.14	0.14	0.17	0.15
	Compared to no roof		-3.80%	22.88%	6.24%
3rd floor	Interstory drift [mm]	12.58	4.75	2.64	6.82
	Interstory drift ratio [%]	0.46	0.13	0.07	0.19
	Compared to no roof		-62.20%	-79.00%	-45.82

3.3 Deformed shape

As could be observed in the displacement and inter-story drift analysis, each roof structure is causing a different type of deformation of the historic masonry building. While the building without roof structure is clearly presenting a flexural deformation, the presence of the 18th and 19th century roof structure is causing a change to shear deformation for more than half of the considered scenarios, while the other scenarios are still presenting flexural deformation. If however, the timber elements are decayed, more scenarios are causing a flexural deformation of the building. The presence of the 20th century roof structure, on the other hand, is presenting

for both roof structure in a good state of conservation and 20% decayed timber elements, a clear flexural deformation.

3.4 Damage level

Further, in order to better understand the effect of the roof structure on the seismic behaviour of the building, the damage level, which would be recorded on the masonry walls was analysed (Table 5). Three different limit state were taken into consideration, according to the Eurocode, the Failure Mechanism Identification and Vulnerability Evaluation procedure (FaMIVE) and based on previously performed experimental campaigns [23].

Since the building without any roof structure is presenting significant damage both in-plane and out-of-plane but also considering the combined behaviour, the results show once again an improvement of the behaviour of the building due to the presence of the roof structures. It was observed that the presence of the 18th century roof structure, in a good state of conservation, is presenting limited damage for almost all the limited states, both in-plane and out-of-plane. Still, if the roof structure is decayed, significant damages tend to also appear in-plane at the second and third floor of the building according to the FaMIVE limit state and at the third floor considering the combined prevalent behaviour.

The 19th century roof structure is presenting a rather peculiar effect, since the presence of the roof structure in a good state of conservation is causing significant damage on the second and third floor of the building, considering the in-plane prevent behaviour but only on the third floor if the timber elements are decayed. At the same time, the combined prevalent behaviour for the decayed roof structure is presenting significant damage not on the third but on the second floor. The 20th century roof structure, on the other hand, is presenting only a slight improvement of the damage level, still presenting significant damage on the third floor of the building, but not for all the limit state like in the case of the building without a roof. Once again, the decay of the roof structure is leading to limited out-of-plane damage, and significant damage also on the second floor considering the in-plane prevalent behaviour.

Table 5: Damage level of the building without and with roof considering the mean inter-story drift ratio

			Without roof	With roof					
				Roof 1		Roof 2		Roof 3	
				100%	-20%	100%	-20%	100%	-20%
In-plane	EC8 Part3	2nd floor	D.l.	D.l.	D.l.	D.l.	D.l.	D.l.	D.l.
		3rd floor	S.d.	D.l.	D.l.	D.l.	D.l.	D.l.	D.l.
	FaMIVE	2nd floor	S.d.	D.l.	S.d.	S.d.	S.d.	D.l.	S.d.
		3rd floor	S.d.	S.d.	S.d.	S.d.	D.l.	S.d.	S.d.
	Experimental	2nd floor	D.l.	D.l.	D.l.	D.l.	D.l.	D.l.	D.l.
		3rd floor	S.d.	D.l.	D.l.	D.l.	D.l.	S.d.	S.d.
Out-of-plane	EC8 Part 3	3rd floor	D.l.	D.l.	D.l.	D.l.	D.l.	D.l.	D.l.
	FaMIVE	3rd floor	S.d.	D.l.	D.l.	D.l.	D.l.	D.l.	D.l.
	Experimental	3rd floor	D.l.	D.l.	D.l.	D.l.	D.l.	S.d.	D.l.
Combined		2nd floor	D.l.	D.l.	D.l.	D.l.	S.d.	D.l.	D.l.
		3rd floor	S.d.	D.l.	S.d.	D.l.	D.l.	S.d.	S.d.

3.5 Internal forces

Ultimately, the internal forces were analysed, along the wall facing the street (Figure 3) by comparing the vertical axial forces (N_x), the shear forces perpendicular to the walls (V_z) and the out-of-plane bending moments (M_y) and the differences between the building without roof structure and with the three roof.

For the roof structures in a good state of conservation (Figure 6), it was observed that the vertical axial forces are presenting only little changes on the first and second floor of the building. The main differences are highly visible on top of the third floor, where the first and third roof structure are presenting tensile axial forces and the presence of the second roof structure is causing higher compressive forces than in the case of the building without a roof.

The shear forces perpendicular to the wall present the same trend, with clear changes rather visible on the third floor where the 18th century roof structure is presenting a 45% increase of the shear forces, the 19th century a 4 times increase and the 20th century an 40% increase. Remarkable is the influence of the cross-vault on the recorded shear forces since in all the three cases the forces are in the opposite direction compared to all the other floors.

The out-of-plane bending moment differences between the assessed cases, start to be visible above the top part of the second floor. It can be observed that the bending moments are high at the top part of the second floor, decrease at the base of the third and rise once again towards the top of the building. At the same time, it can also be observed that the presence of the 20th century roof structure is causing the highest bending moment at the top of the second floor and the minimum at the top of the building while the 19th century roof structure is causing the highest bending moment at the top of the building. The 18th century roof, on the other hand, is presenting lower bending moments than the no roof structure case until the base of the third floor, and slightly higher values at the top of the building.

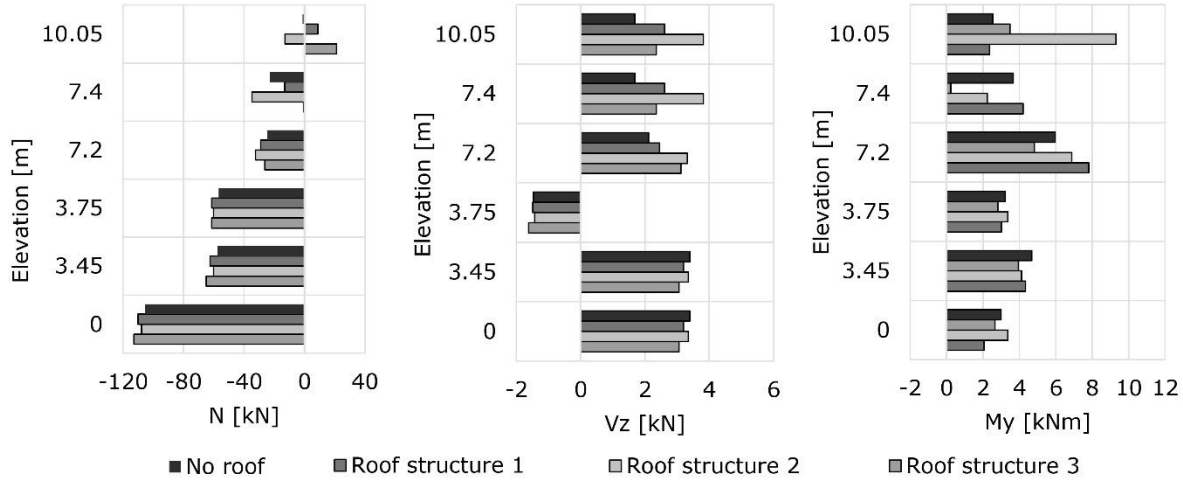


Figure 6: Internal force diagrams of the building without and with roof structures (a) 18th century; b) 19th century; c) 20th century)

The decay of the roof structures is also changing the recorded internal forces (Figure 7). The axial forces are like in the case of the roof structures in a good state of conservation, approximately similar until the top of the second floor. Above this, the effect of the three roof

structures is clearly visible. Therefore, it could be observed that the 18th and 19th century roof structures are causing tensile forces only at the top of the building, while the presence of the 20th century roof structure is causing tensile forces also at the base of the third floor.

The shear forces perpendicular to the wall also present similar values until the base of the second floor, for all the four considered cases, but above this level, the effect of the roof structures is visible. Therefore, it could be observed that all the roof structures are causing an increase of the shear forces, of up to 30% for the 18th century roof structure, up to 40% for the 20th century roof and almost 2.5 times higher in the case of the 19th century roof structure. As in the not decayed roof structure case, the presence of the cross-vault is still causing shear forces in the opposite direction.

The bending moments are also similar until the base of the second floor. Above this level, each roof structure is influencing the bending moments differently. The 18th century and 19th century roof structures are presenting lower values than the no roof structure case at the top of the second floor and base of the third. At the top of the building, the bending moments caused by the 18th century roof is only slightly higher than the no roof structure ones, while the 19th century ones are the highest when comparing all the four cases. The 20th century roof structure, on the other hand, is presenting maximum bending moments at the top of the second floor and only slightly higher bending moments than the ones recorded for the no roof structure case on the top of the building.

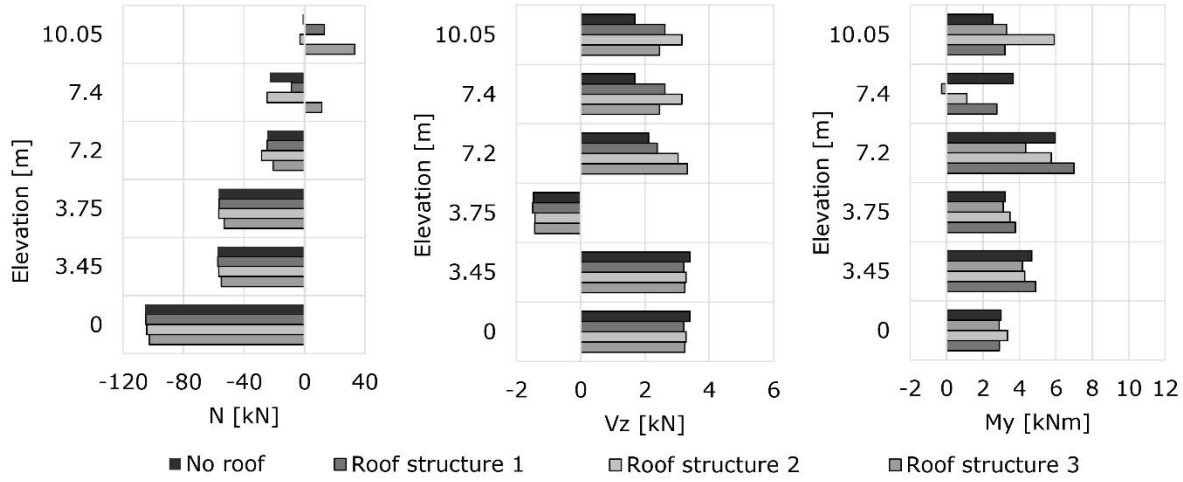


Figure 7: Internal force diagrams of the building without and with roof structures (a) 18th century; b) 19th century; c) 20th century) with 20% decayed timber elements

In both cases, for the roof structures in a good state of conservation or decayed, the obtained axial forces presented significant variations influenced by the chosen support type and joint stiffness.

4 CONCLUSIONS

The presented study is trying to bring forward that heritage buildings have to be regarded as a whole when addressing their seismic vulnerability and that roof structures are playing an important role.

The numerical simulations performed on the 18th century masonry building has brought forward that depending on the roof structure type, its state of conservation and the considered properties of the supports and joints:

1. The out-of-plane displacement can be reduced with 10 up to 55%;
2. The inter-story drift can be reduced with up to 85%;
3. The deformation of the historic masonry building can be changed from flexural to shear;
4. The damage level of the building after the seismic event can be improved;
5. Tensile vertical forces can appear at the top of the building;
6. Shear forces perpendicular to the wall and out-of-plane bending moments can suffer an increase at the top of the building.
7. Out-of-plane bending moments present a clear increase at the top of the building but lower values at the base of the last floor.

At the same time, the effect of the cross-vaults on the shear forces perpendicular to the wall was also observed, changing the direction of the forces.

Since roof structure types are diverse and highly influenced by local structural features, further studies, both laboratory and numerical are needed to be able to properly determine how various roof structure types are influencing the seismic behaviour of heritage buildings. In the same time, it is important to how interlinked these two parts of buildings are and introduce these new data in seismic vulnerability assessment methodologies developed for heritage buildings.

REFERENCES

[1] Parisi, M.A. and Chesi, C. Seismic vulnerability of traditional buildings: the effect of roof-masonry walls interaction. In: *Tenth U.S. National Conference on Earthquake Engineering Frontiers of Earthquake Engineering*.Anchorage, Alaska (2014).

[2] Keller, A. Chieffo, N. and Mosoarca, M. Influence of roof structures on seismic behavior of historic buildings. In: Mazzolani F (eds.). *3rd International Conference on Protection Of Historical Constructions, PROHITECH'17* (2017).

[3] Touliatos, P. Traditional aseismic techniques in Greece. In: Mendés V (eds.). *Proceedings of the Interantional Workshop Les sytèmes nationaux faces aux seismes majeurs*. Lisbon, Portugal, (1993), pp. 110–124.

[4] Ortega, J. Vasconcelos, G. Rodrigues, H. and Correia, M. Local seismic cultures: The use of timber frame structures in the south of Portugal. In: Cruz H (eds.). *Historical Earthquake-Resistant Timber Framing in the Mediterranean Area*. Springer, (2016), pp. 101–111.

[5] Parisi, M.A. and Piazza, M. Seismic behavior and retrofitting of joints in traditional timber roof structures. *Soil Dyn Earthq Eng* (2002) **22**(9–12):1183–1191.

[6] Parisi, M.A. Chesi, C. Tardini, C. and Piazza, M. Seismic vulnerability and preservation of timber roof structures. In: Dina D (eds.). *Structural Analysis of Historic Construction*.Bath, United Kingdom, (2008), pp. 1253–1260.

[7] Touliatos, P. The box framed entity and function of the structures: the importance of wood's role. In: *Conservation of historic wooden structures: proceedings of the international conference*. Florence, Italy, (2005), pp. 52–64.

[8] Giongo, I. Dizhur, D. Tomasi, R. and Ingham, J.M. In-plane assessment of existing timber diaphragms in URM buildings via quasi-static and dynamic in-situ tests. In:

Advanced Materials Research. (2013), pp. 495–502.
[9] Parisi, M.A. Chesi, C. and Tardini, C. The role of timber roof structures in the seismic response of traditional buildings. In: *15th World Conference on Earthquake Engineering*.Lisbon, Portugal, (2012).
[10] Parisi, M.A. Chesi, C. Tardini, C. and Piazza, M. Seismic vulnerability assessment for timber roof structures. In: *The 14th World Conference on Earthquake Engineering*.Beijing, China, (2008), pp. 12–17.
[11] Keller, A. Parisi, M.A. Tsakanika, E. and Mosoarca, M. Influence of historic roof structures on the seismic behaviour of masonry structures. *Proc Inst Civ Eng - Struct Build* (2019):1–27.
[12] Nemetschek. *SCIA Engineer User Manual*. (2013).
[13] Marin, M. Roman, L. and Roman, O. Earthquakes in the Banat area - Timisoara (in Romanian). *Bul AGIR* (2011) **2**:23–27.
[14] Oros, E. *Earthquakes in the Banat plain (in Romanian)*. Graffiti, Timisoara, Romania, (1991).
[15] Oros, E. and Diaconescu, M. Recent vs. historical seismicity analysis for Banat seismic region (western part of Romania). In: Vacareanu R (eds.). *Proceedings of the 5th National Conference on Earthquake Engineering and 1st National Conference on Earthquake Engineering and Seismology*. CONSPRESS, (2014)
[16] Oros, E. Popa, M. and Moldovan, I.A. Seismological database for Banat seismic region (Romania)-part 1: the parametric earthquake catalogue. *Rom J Phys* (2008) **53**(7–8):955–964.
[17] Descamps, T. and Lemlyn, P. Effects of the rotational, axial and transversal stiffness of the joints on the static response of old timber framings. In: Mazzolani F (eds.). *Protection of Historical Buildings, PROHITECH 09*. CRC Press, Taylor & Francis Group, Rome, Itlay, (2009), pp. 291–286.
[18] Branco, J.M. and Descamps, T. Analysis and strengthening of carpentry joints. *Constr Build Mater* (2015) **97**:34–47.
[19] Heimeshoff, B. and Kohler, N. Assessment of the structural behaviour of timber joints (in german). Munchen, (1989).
[20] Meisel, A. *Historische Dachwerke Beurteilung, realitätsnahe statische Analyse und Instandsetzung*. Monographi. Verlag der Technischen Universität Graz, Graz, (2015).
[21] Holzer, S.M. *Statische Beurteilung historischer Tragwerke. Band 2, Holzkonstruktionen*. Wiley-VCH Verlag GmbH & Co. KGaA, Weinheim, Germany, (2015).
[22] Holzer, S.M. Analysis of historical timber structures. In: Van Balen & Verstrynge (eds.). *Structural Analysis of Historical Constructions – Anamnesis, diagnosis, therapy, controls*.Taylor & Francis Group, Leuven, Belgium, (2016), pp. 1203–1210.
[23] Vicente, R. D'Ayala, D. Ferreira, T.M. Varum, H. Costa, A. da Silva, M. et al. Seismic vulnerability and risk assessment of historic masonry buildings. In: *Structural Rehabilitation of Old Buildings*. (2014), pp. 307–348.

12th International Conference on Structural Analysis of Historical Constructions
SAHC 2020
P. Roca, L. Pelà and C. Molins (Eds.)

EVOLUTION OF LATERAL DESIGN IN THE UNITED STATES

NATHAN A. HICKS[1] PE, SE AND EDMUND P. MEADE[2] PE, FAPT

[1]Silman - 1053 31st Street, NW - Washington, DC 20003 – United States
e-mail: hicks@silman.com, www.silman.com

[2]Silman – 32 Old Slip, 10th Floor – New York, NY 10005 – United States
email: meade@silman.com, www.silman.com

Keywords: Lateral, Seismic, Wind, Earthquake

Abstract. *This paper explores the design profession's evolving understanding of lateral design. It shows how the United States building codes' handling of seismic and wind forces has changed over time, often in response to extreme events or technological developments. Prior to the early 1900s most buildings were designed without an explicitly defined lateral force resisting system. Up to that time period earthquakes and strong wind events produced little in the way of code requirements to address lateral forces. It was the advent of steel and high-rise construction in the late 19th Century that triggered a need to consider lateral loads. During the early 20th Century little consensus existed regarding the lateral forces that needed to be resisted. Wind loading provisions began appearing in the codes of large cities in the early 1900s, but it would not be until the 1930s that seismic provisions started to be codified, and then only in California. Throughout the 20th Century significant lateral events have continued to expose vulnerabilities that have been subsequently addressed with changes in construction detailing and code restrictions. In the mid-1900s regional building codes developed, focusing on the lateral hazards present in their locality. By 2000 these regional codes were replaced by a national code, and lateral design has now started to shift from prescriptive requirements towards performance-based design. This paper will help structural engineers better understand the historic building stock by exploring how lateral design has evolved in the US over the last hundred years.*

INTRODUCTION

Lateral design of buildings is a relatively new field within structural engineering. Until recently, building codes in the United States and throughout the world included few, if any, requirements for wind and seismic. In the early 1900s the education of engineering students included little on the effect of wind on structures, and knowledge about earthquakes was very limited. When looking at earthquakes and extreme wind events, it is interesting to examine why lateral design took so long to evolve. Part of the reason is the perceived risk, which is tied to the fact that such events occur infrequently. While gravity loads are always present, a significant lateral load event might have a mean return period of over a hundred years. The longer return interval means a large hazard database does not exist, and lessons learned were often forgotten. "Gravity was always available to test construction and did so whether the builders wanted their structures tested or not as they assembled their pieces.

Refinements…incrementally proceeded as an applied research by-product of construction. Even if one way of arranging material was a little more earthquake resistant than another there was usually no feedback for the building, only an earthquake test that might happen a few hundred years later." [1]

Unraveling the history of lateral design is a complex task – it comes to us as a web of events, technological advances and contributions from across the engineering community. Although the understanding of wind and earthquakes relies on contributions from individuals around the world, this paper is focused on its evolution in the United States. The purpose of this paper is to examine how lateral design for buildings has changed over time and give examples from our own work on existing buildings.

EARLY HISTORY

Before the mid-1800s attempts to understand the source and nature of lateral loading were limited. Regardless of the designer's intent, gravity systems served to resist lateral forces. While it is tempting to give credit to past engineers for development of lateral resistant designs, it was often an unknown benefit of common construction practices. As an example, Fort Point in San Francisco survived the 1906 Earthquake with little damage. This was a secondary benefit of the extremely thick masonry walls common to fort construction. The Fort was designed to provide protection against attack, not protection against earthquakes.[2]

18th Century European Developments

Many point to Europe for early developments of lateral design for buildings. "Portugal and Italy are the first two countries where one can definitely point to evidence that earthquake resistance was intentionally incorporated into traditional building construction practices, and in both cases, it happened in the aftermath of earthquake disasters." [3] The advances in Italy were largely in response to the 1694 Melfi and 1783 Calabria Earthquakes, and in Portugal to the 1755 Lisbon Earthquake. As the cities rebuilt, regulations were issued to address vulnerabilities in unreinforced masonry construction. The use of iron tie-rods became a recommended practice to restrain out-of-plane failure of masonry walls and building height restrictions were passed. In both regions a construction system using heavy timber frames with masonry infill was introduced. The construction was called "casa baraccata" in Italy and "gaiola" in Portugal.[4] In our work in the US, we often come across similar wood frame and masonry infill construction from the 17th and 18th Centuries, which is known as brick noggin. What makes Italy and Portugal unique is that the wood frame was clearly intended as a seismic retrofit, whereas in the US, the system appears to have developed with less consideration of lateral loads.

1811 New Madrid Earthquakes

In the winter of 1811 and 1812, a series of three earthquakes were centered around New Madrid in what is now Missouri. Prior to the 20th Century these events were the most powerful earthquakes in recorded US history. The entire town of New Madrid was destroyed, but the effects were felt wider, as chimneys collapsed as far away as Cincinnati, and ground shaking could be felt in Boston.[5] While New Madrid was an incredibly powerful earthquake, it had little impact on advancing earthquake engineering in the US. Its epicenter was in a

relatively undeveloped region of the young nation, so it is not surprising that no building regulations came about as a result.

Early US Building Codes

Building regulations, in modern form, did not exist prior to the mid-1850s in the US. When major cities started to establish building codes, they were focused on the frequent hazard of fires and silent on the infrequent hazard of lateral events. "Loss of life and property in several fires led to widespread support for development and enforcement of building standards. The earliest building controls were enacted at the local level…urged by insurance companies as a way of controlling financial loss." [6] In the US, some of the first building regulations arose in cities like Baltimore in 1859, New York with the 1867 Tenement House Act, and in 1875 in Chicago following the 1871 Great Chicago Fire.[7]

LATE 19TH CENTURY

At the beginning of the 1800s, timber framing and unreinforced masonry comprised almost all structures in the US. In the mid-1800s wrought iron and cast iron slowly started to gain use in buildings as they became more economical. It was at this same time that reinforced concrete construction also started to develop. Finally, in the late 1800s mild steel started to take the place of iron, ushering in a new era of construction.[8]

Steel Frame Construction

The Home Insurance Building in Chicago was built in 1885 and is often regarded as the first skyscraper – the beginning of a transition to high rise construction in Chicago, New York and other cities. Steel along with the advent of the elevator were the technological breakthroughs that allowed for greater efficiency and taller buildings in the 1890s. "The ultimate step in the creation of the modern skyscraper came with the construction of the second Rand McNally Building in Chicago between 1889 and 1890. Here the frame of the high office building was wholly freed from its masonry adjuncts and built entirely of steel." [9] Global annual output of steel output grew exponentially between 1870 and 1900, from 0.5 to 28 million tons.[10] As buildings in the US abandoned their thick masonry walls and grew taller, engineers realized they could no longer ignore the need to rationally respond to wind and seismic lateral loads.

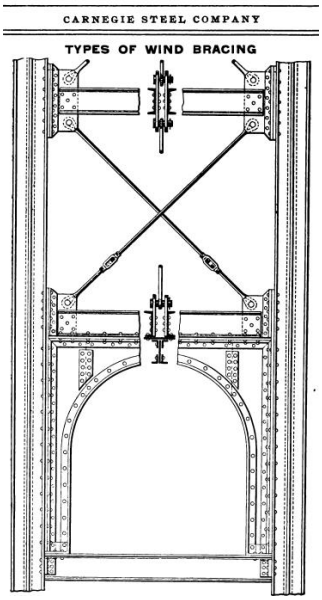
Beginning of Wind Design

Builder handbooks from the time period note that "when office and other building of six to ten stories were built with solid masonry walls no attention was paid to the lateral strains due to wind pressure, except, perhaps, to make the walls and partitions a little heavier. And as such buildings were seldom built of a less width than 50 feet, no other precautions were really necessary, for whenever buildings of ordinary construction have been blown down, it has generally been due more to a poor quality of work…rather than to faulty design." [11] The consideration of wind loads was so foreign in these early years that a view persisted through the early 1890s that high-rise buildings with "sufficient" plan dimensions relative to their height did not need an explicit lateral force resisting system. Many early high-rises were

designed without wind bracing, and our office has worked on several such buildings throughout the Midwest and Northeast. Luckily, the early skeleton frame structures often still had infill masonry between frames that stiffened the structure and improved lateral performance.[12]

Finally, in the late 19th Century there was an acknowledgement that high-rise structures needed to consider wind loading. A guidebook from the turn of the century puts it well, "the modern steel buildings are built to such great heights, especially in proportion to their width, and are so destitute of ordinary means of resisting wind pressures, such as solid walls and partitions, that some efficient means of bracing the steel frame would seem to be a matter of necessity. As a matter of fact, few if any skeleton steel buildings are now being erected without some provisions for bracing the steel frame independent of the partitions. In some buildings these provisions consist merely in using girders built of angles and plates of good depth and use of riveted connections…while in others heavy sway-bracing, knee or portal bracing, or both combined have been employed."[13]

Steel manufacturers started to publish recommended wind bracing details, and common builder guidebooks printed tables correlating wind velocity to pressures (see Figure 1). Much of the early research into wind design was taken from the railroad industry and the field of bridge design. While there was a diversity in practice for buildings, bridge engineers were designing their structures to resist wind loads on the order of 30 to 60 psf.[14]



FORCE OF THE WIND.

(Builders' Guide and Price Book.)

Miles per Hour.	Feet per minute.	Feet per second.	Force, in lbs., per square foot.	Description.
1	88	1.47	0.005	Hardly perceptible.
2	176	2.93	0.020	Just perceptible.
3	264	4.4	0.044	
4	352	5.87	0.079	Gentle breeze.
5	440	7.33	0.123	
10	880	14.67	0.492	Pleasant breeze.
15	1320	22	1.107	
20	1760	29.3	1.970	Brisk gale.
25	2200	26.6	3.067	
30	2640	44	4.429	High wind.
35	3080	51.3	6.027	
40	3520	58.6	7.870	Very high wind.
45	3960	66	9.900	
50	4400	73.3	12.304	Storm.
60	5280	88	17.733	Great storm.
70	6160	102.7	24.153	
80	7040	117.3	31.490	Hurricane.
100	8800	146.6	49.200	

Figure 1: Typical Wind Bracing Details *(left)* and Wind Table *(right)*[15]

The West Coast

In most of the country, high-rise construction focused on wind, but on the West Coast earthquakes presented a far greater risk. While earthquakes were known to occur in California, they did little damage given the sparse population. While seismic concerns had caused investors to initially balk at high-rises, several were built in San Francisco by the late

1890s. “An earthquake shock which disturbed that locality in the spring of 1898 was reported to have caused the buildings to rock and sway but to have left them practically uninjured.” [16] Small steps were made to improve lateral seismic loading resistance of buildings in the later part of the 19th Century. For instance, following the 1868 Hayward California Earthquake, changes were instituted to load-bearing masonry walls (built prior to the introduction of steel and concrete frame buildings). Some of these buildings performed well during the 1906 San Francisco Earthquake.[17]

1886 Charleston Earthquake

The most notable seismic event in the US from the latter half of the 19th Century was the 1886 Charleston Earthquake in South Carolina, which is still the largest record seismic event for the Eastern US. Over 100 buildings were destroyed, and 90 percent of the buildings in the city were damaged. Nearly every chimney in the city collapsed and ground shaking was felt as far away as St. Louis, Chicago and Boston.[18] The Charleston Earthquake represented the first well studied earthquake in US history. The insurance industry went building by building documenting observed damage, and Clarence Dutton of the US Geological Survey produced a detailed report on typical failure mechanisms. Unfortunately, the Charleston Earthquake and Dutton’s work did little to drive change in the US or advance earthquake engineering.[19]

EARLY 20TH CENTURY

At the beginning of the 1900s lateral design was still a relatively new concept, and designers had a variety of approaches. Over the ensuing decades various jurisdictions attempted to bring order by establishing building code provisions for wind and earthquakes.

Case Study

Our office recently completed the structural engineering design for the exterior restoration of an early 20th Century office building. This building consisted of a riveted steel frame substantially braced by its exterior load-bearing masonry walls. Based on our review of existing drawings and investigations, we determined that the steel frame provided limited lateral resistance due to the modest steel connections. No braced frames were present and while the connections were well detailed, they had limited ability to act as a moment frame. The building is surrounded by an exterior masonry wall that consists of exterior architectural terra cotta, six to seven wythes of brick, and interior architectural terra cotta infill. Compared to the stiffness of the masonry walls, the stiffness of the steel frame is almost negligible.

We evaluated the condition of the masonry walls by performing selective probes and non-destructive testing techniques. We used site-specific seismic force coefficients developed by geotechnical engineers and the known characteristics of the building to begin our analysis. Using code-prescribed formulas, we evaluated the effect of the removal of four to eight inches of exterior terra cotta on the shear capacity of the walls. Our structural evaluation revealed that with removal of the selective amounts of exterior terra cotta there would be a nominal, acceptable increase in the maximum stresses within the masonry wall. Seismic loading controlled over wind loading due to the weight of the building. Based on these findings, no temporary or permanent seismic reinforcement was required to accommodate the proposed alterations to the exterior masonry walls. The removal and restoration of the architectural

exterior terra cotta proceeded without concern on the lateral load carrying capacity of the structure. See Figure 2 for a depiction of a typical cross section through the exterior wall and steel frame, and a view of the tightly integrated exterior terra cotta and backup brick masonry.

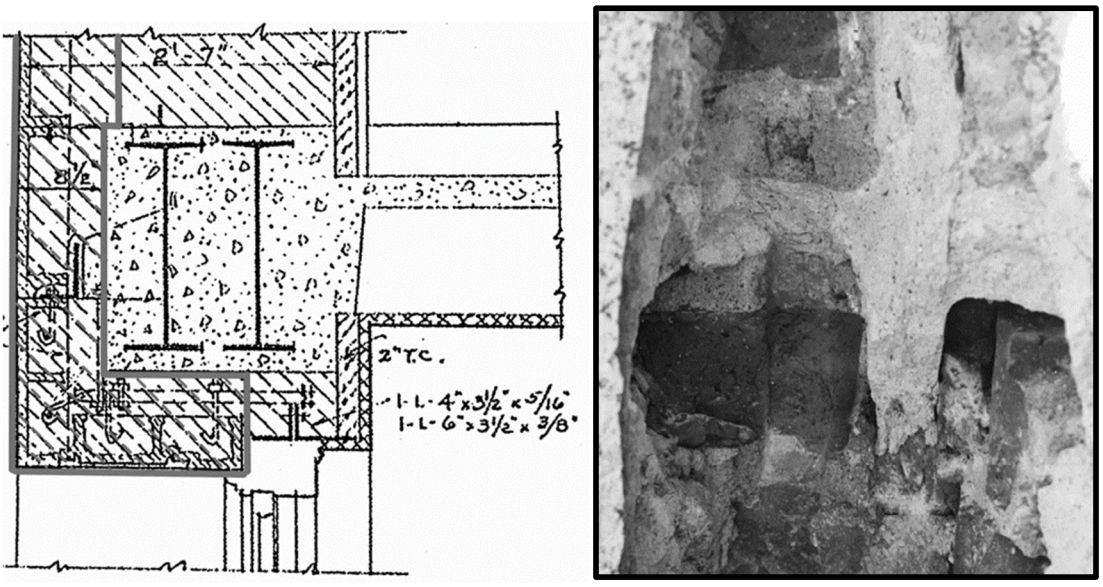


Figure 2: Typical Cross Section *(left)* and Probe into Exterior Wall *(right)*

1906 San Francisco Earthquake

In 1906 San Francisco was one of the largest cities in the US, and by far the largest on the West Coast. On April 18th an earthquake hit the city and caused significant damage. The initial shock was followed by an even more devastating fire killing over 700 people. The portions of San Francisco built over landfill sustained the greatest damage from the ground shaking.[20] The earthquake was one of the first lateral load tests for skyscrapers. In 1906 there were over two dozen steel frame buildings in San Francisco, and none collapsed. There was damage at the exterior infill masonry walls and interior masonry partitions, but overall, the steel frames performed relatively well. The performance led to a long-held belief these systems were earthquake resistant.[21] With these early high rises, San Francisco engineers had put thought into how to resist seismic loads. The beam-column joints were heavily riveted and many of the wind bracing techniques used in Chicago and New York were adapted for San Francisco. While there were no mandatory seismic provisions at the time, most engineers in the area used a high wind loading of 30 psf as a substitute for seismic loads.[22]

Although the 1906 Earthquake is still perhaps the most notable seismic event in US history, its immediate impact on structural engineering was minimal. On the national scale, earthquakes were viewed as a California problem. Even on the local scale, seismic loading recommendations were lowered from 30 to 15 psf to permit quick reconstruction. Unreinforced masonry construction, which had fared poorly, became even more prevalent across the city.[23] A couple decades later "some buildings in San Francisco were designed with a seismic coefficient of 10%...however, one contemporary of that time estimates that in the 1920s a minority of engineers there computed any earthquake forces."[24]

Code Provisions for Wind

At the turn of the century, building ordinances in larger cities started to bring uniformity to wind design. To illustrate the earlier diversity, an engineer from the time mentions a 17-story building in New York with a lateral force resisting system that relied on interior terra cotta partitions, whereas a similar 17-story building a couple blocks away was built at the same time with significant steel sway bracing.[25] By the early 1900s both Chicago and New York building codes required a wind pressure of 30 psf for buildings of skeleton construction. Provisions also required the engineer to ensure the overturning moment due to wind did not exceed 75% of the resisting moment due to dead load.[26] Baltimore and Philadelphia passed similar laws shortly thereafter. By the 1920s most major US cities had wind ordinances and where they did not wind pressures of 20 to 30 psf were generally considered adequate.[27]

1927 Uniform Building Code

In 1927 the Pacific Coast Building Officials adopted the Uniform Building Code (UBC). It quickly became the accepted standard throughout California and eventually the West. The first edition had seismic provisions, but these were optional and included as an appendix. The appendix was unique in that it applied a seismic coefficient rather than using wind pressures as a pseudo-seismic force. Engineers at the time argued that the "force of an earthquake shock depends on the mass of the building and its contents" [28] and pointed to the use of seismic coefficients of 10% of gravity in Japan as an example. The 1927 UBC recommended a seismic coefficient of 7.5% of the building's weight, which varied slightly based on the site's soil type. It is deceptive to compare modern coefficients with these earlier ones as the weight included significant live load. The appendix represented a shift to an equivalent lateral force approach, which is still common in the US today.[29]

1933 Long Beach Earthquake

In March 1933 an earthquake hit Long Beach, California. Although much less powerful than the 1906 San Francisco Earthquake, it proved to be a catalyst for change. California was finally ready to implement seismic regulations. The Los Angeles Chamber of Commerce spearheaded an effort to ensure that earthquake resistant construction became the standard in California with new code requirements and limitations on unreinforced masonry construction.[30] The 1933 Long Beach Earthquake eventually led to the Field and Riley Acts. These were statewide laws that applied to most structures other than single family residences. Like the 1927 UBC, these acts applied seismic coefficients of between 2% and 10% as a lateral load. They were the first codified examples in the US of varying lateral loads based on the site's soil type and the importance of the building occupancy.[31]

MID 20TH CENTURY

It was during the mid-20th Century that development of codes began to shift away from cities to model building codes for specific regions. In the West, the International Conference of Building Officials (ICBO) developed the UBC. In 1950 the Building Officials and Codes Administrators (BOCA) published a model code to serve the Midwest and New England regions. In the South, the Southern Building Code Congress International (SBCCI) published

the Standard Building Code (SBC) in 1945. From a structural perspective, each of these model codes primarily focused on the hazards and lateral loads most common to their geographic area. The UBC emphasized earthquakes, and the SBC and BOCA emphasized wind.[32]

In 1945 the first national standard for *Minimum Design Loads in Buildings and Other Structures (ANSI 58.1)* was developed. The standard was the precursor to the ASCE 7, which is still referenced for lateral loadings in the US today. The standard introduced several new concepts – wind pressure on a building surface increased with height, maps were included with recommended design wind velocities, and a minimum seismic force of 5 percent of dead load was recommended for all buildings (see Figure 3). [33]

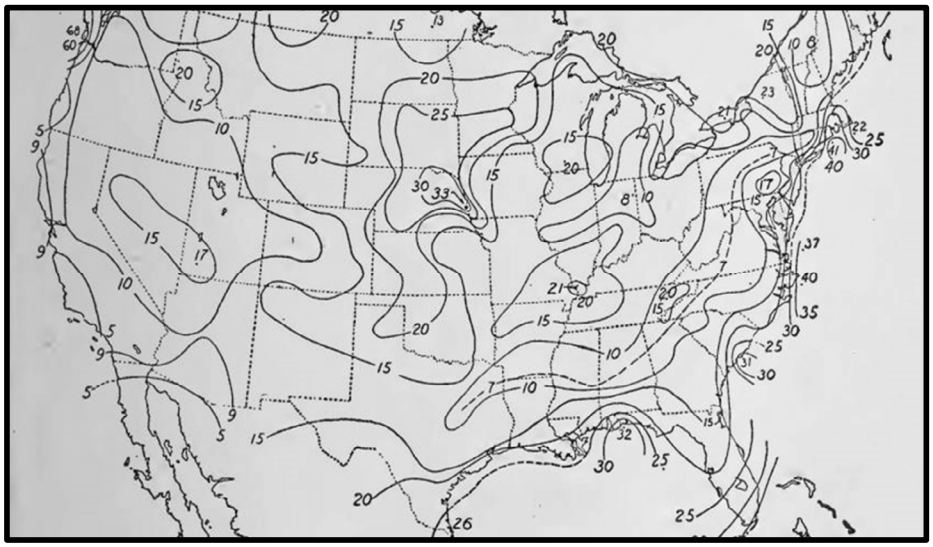


Figure 3: Map from 1945 ANSI 58.1 Showing Design Wind Pressures Across US

Jurisdictions had the freedom to adopt as much, or as little, of the model building codes as they felt to be appropriate. As a result of this freedom, large differences began to emerge in between the seismic provisions of Northern and Southern California. Many of the changes were quite forward thinking, but not universally adopted. The 1943 Los Angeles code lowered base shear as the height of a building increased, associating longer period structures with smaller seismic forces. In the 1949 many cities removed live loads from the effective seismic weight and started to use an inverted triangle to distribute seismic loads up the height of a building. In the 1950s certain jurisdiction required retrofit of unreinforced masonry buildings. These are a few of the examples, which eventually led the Structural Engineers Association of California (SEAOC) to develop the *Recommended Lateral Force Requirements and Commentary*, more commonly known as the Blue Book. For several decades this Blue Book would serve as the basis for seismic building codes across the US.[34]

Florida Wind Standards

As building codes in California led the way in seismic design, Florida building codes started to lead the way in wind. Between 1940 and 1970 several hurricanes, coupled with

booming population growth in the state led to increased wind requirements. In most parts of the state the wind provisions were taken from the SBC, but in Dade and Broward counties, the South Florida Building Code developed with additional wind provisions to cover the higher risk. Florida codes were reactive and based on observed failures after hurricanes with requirements focused on the main wind force resisting system.[35]

1964 Alaska Earthquake

The 1964 Alaska Earthquake is one of the most powerful earthquakes ever recorded. It hit a relatively undeveloped region but still caused substantial damage. The earthquake exposed previously unknown vulnerabilities with concrete construction. Specifically, it showed the need to strengthen connections at tilt-up construction and reinforcement detailing at concrete frames. The 1971 San Fernando Earthquake, while a much smaller at magnitude, highlighted similar lessons with concrete construction.[36]

By the 1960s and 70s ground motion records had started to accumulate. While codes at the time implied seismic accelerations on the order of 5%-20% g, instrumentation showed accelerations over 100% g. The 1974 Blue Book stated that "design forces...are not to be implied as the actual forces to be expected during an earthquake. The actual motion generated by an earthquake may be expected to be significantly greater than the motions used to generate the prescribed minimum design forces."[37] The code was in effect relying on the dissipation of energy through inelasticity. This represented a large shift in thinking for engineers. For other loadings, a structure is designed to remain elastic, but for a design level earthquake, this is impractical. Over the 1970s and 80s the concept of ductility was slowly introduced through an 'R' (or response modification) factor. The R factor was a way to rationalize the reduction of ground motion accelerations based on the ductility of the building's seismic force resisting system.[38]

RECENT HISTORY

The two most prominent earthquakes in recent US history were the 1989 Loma Prieta and the 1994 Northridge Earthquakes in California. These were the first significant tests of US seismic engineering in major metropolitan areas. While there were failures, the loss of life and structural damage were minor given the magnitude of ground motions. These earthquakes showed that when strong engineering measures are in place, it can mitigate much of the risk for extreme lateral events. Despite the relatively good performance of most structures, there were still some critical lessons learned that have been incorporated into the code. Specifically, during the 1994 Northridge Earthquake fractures were observed in several beam to column connections for steel moment frames. Subsequent research showed the need to improve detailing to ensure a strong column/weak beam response for moment frames. By forcing the yielding of the connection in the beam member, the overall system's ductility is improved, which has now become standard in high seismic regions.[39]

Hurricanes

Over the last 30 years hurricanes in Florida and the Gulf Coast provided valuable lessons for wind design. In 1992 Hurricane Andrew was the first major test for Florida following the 1970s population boom. Buildings did not perform as well as might have been expected.

There were failures at gable end roofs, rooftop equipment, wood frames racking, and roof to wall, and wall to foundation connection issues.[40] The storm also highlighted the vulnerability of building envelopes to wind-borne debris. Prior to the storm, there were no requirements for storm shutters protecting glazing, which contributed to the high cost of the hurricane. The poor performance led to the first statewide building code and significant changes in loading and detailing requirements for wind.[41]

Between 2004 and 2005 a series of powerful hurricanes, including Charley, Frances, Jeanne, Katrina and Wilma, all made landfall in the Southeast. Much construction had taken place under codes written in the 1990s, so this increased storm activity gave engineers an opportunity of evaluating the effectiveness of new code requirements. The storms highlighted the need for additional mitigation measures to address building envelopes, roof soffits, and the performance of essential facilities.[42]

Moving Forward

For much of the 20th Century there were three predominant model building codes in the US. Beginning in the 1980s efforts were made to start improving the consistency between the UBC, BOCA and SBC. Finally, in 2000 the International Code Council (ICC) published the International Building Code (IBC), which has since been updated every three years. The IBC represented the first national building code and brought a uniformity to lateral load design that had been lacking with the regional codes.[43] No longer could the West Coast engineer only consider seismic and the East Coast engineer only consider wind.

With the IBC came the International Existing Building Code (IEBC), which covered lateral loads applied to the existing building stock. Traditionally, existing buildings can remain and continue to be used, with mandated changes only triggered by renovations or changes in occupancy. This reflects the concept of nonconforming rights, which establishes that while an existing building may not meet current code requirements, the increased risk has been deemed acceptable. Occasionally, when a jurisdiction believes that the hazard is too high, building laws are applied retroactively, but this is rare.[44] An example of this is the California requirements to retrofit unreinforced masonry structures.

Advances in computing technology have started to change the way existing buildings, and all structures, are analyzed for lateral loads. We are now able to capture nonlinear behavior of building materials, create finite element models, and apply dynamic loadings, such as earthquake time histories. As a result, the industry has started to slowly shift away from prescriptive requirements to performance-based design. For lateral loads, the idea is to pair an established hazard level (based on a recurrence interval) with the desired performance following the hazard (collapse prevention, life safety, immediate occupancy, etc.). This permits the design of new buildings or reinforcement of existing buildings with an understanding of the risk of casualties, occupancy interruption, and economic loss that may occur as a result of a design-level wind or seismic event.[45]

The benefits of performance-based design were highlighted following the 2011 Mineral Earthquake centered in Virginia near the nation's capital. The seismic event was felt throughout East Coast, and while not as large as other events highlighted herein, hit a region unaccustomed to seismic events with far more historic unreinforced masonry structures. Our firm studied numerous parapet and chimney collapses, along with several instances of failed

facades due to poor connections with the backup structure. Some of the most notable damage included tall, slender unreinforced structures such as the spires and towers on the Smithsonian Castle. Significant damage was documented in the decorative plaster ceilings at Washington Union Station. While little damage was reported to global seismic force resisting systems, the Mineral Earthquake highlighted the vulnerabilities of non-structural components, which in low to moderate seismic regions are often left unchecked by prescriptive codes.

CONCLUSION

Even today the profession learns something new after each major event; strong evidence that the field has yet to stabilize upon a singular, broadly recognized approach towards lateral design and construction standards. Our understanding of lateral loads and how to resist these extreme events in our building design continues to evolve. As structural engineer George Housner once stated, engineering for lateral loads "is a 20th Century development, so recent that it is yet premature to attempt to write its history.[46] While perhaps too soon, the hope is that this short history has helped to explain how lateral design has evolved in the US, and that by understanding that history, we can make more informed decisions about how to move forward and how to address the past.

REFERENCES

[1] Reitherman, Robert K. *Earthquakes and Engineers: An International History.* ASCE Press, Reston (2012) p 46.
[2] Reitherman. *Earthquakes and Engineers.* p 47.
[3] Reitherman. *Earthquakes and Engineers.* p 85.
[4] Reitherman. *Earthquakes and Engineers.* p 85-93.
[5] *American Standard Building Code Requirements for Minimum Design Loads in Buildings and Other Structures (A58).* National Bureau of Standards. United States Government Printing Office, Washington (1945) p 30.
[6] Green, Melvyn. *Building Codes for Existing and Historic Buildings.* John Wiley & Sons, Inc., Hoboken (2012).
[7] Rossber, Jim and Leon, Roberto T. *Evolution of Codes in the USA*. National Earthquake Hazards Reduction Program (2013).
[8] Friedman, Donald. *Historical Building Construction: Design, Materials & Technology.* W.W. Norton & Company Inc., New York (2010).
[9] Reitherman. *Earthquakes and Engineers.* p 147-151.
[10] Derry, T.K. and Williams, T.I. *A Short History of Technology from the Earliest Times to A.D. 1900*. Dover Publications, New York, NY (1993) p 481-486.
[11] Kidder, Frank E. *The Architect's and Builder's Pocket-Book.* John Wiley & Sons, New York (1908) p 1082.
[12] Reitherman. *Earthquakes and Engineers.* p 147-151.
[13] Kidder. *The Architect's and Builder's Pocket-Book.* p 1082.
[14] Trautwine, John C. *The Civil Engineer's Pocket-Book.* Renouf Publishing Co., Wallingford (1872).

[15] *Pocket Companion Containing Useful Information and Tables Appertaining to the Use of Steel*. Carnegie Steel Company. Pittsburg (1903) p 58.
[16] Freitag, Joseph Kendall. *Architectural Engineering with Especial Reference to High Building Construction.* John Wiley & Sons, New York (1909) p 282.
[17] Tobriner, Stephen. *Bracing for Disaster: Earthquake-Resistant Architecture and Engineering in San Francisco, 1838-1933*. Heyday Books, Berkeley (2006) p 166.
[18] *Minimum Design Loads in Buildings and Other Structures (A58)* p 30-32.
[19] Reitherman. *Earthquakes and Engineers.* p 109 & 648.
[20] *Minimum Design Loads in Buildings and Other Structures* (A58) p 30-32.
[21] Reitherman. *Earthquakes and Engineers.* p 147-151.
[22] Reitherman. *Earthquakes and Engineers.* p 650.
[23] Reitherman. *Earthquakes and Engineers.* p 200.
[24] Pregnoff, M.V. *Connections: EERI Oral History Series, Michael Pregnoff and John Rinner.* Earthquake Engineering Institute, Oakland (1996) p.14-17.
[25] Freitag. *Architectural Engineering*. p 249.
[26] Kidder. *The Architect's and Builder's Pocket-Book.* p 1082-1083.
[27] Kidder, Frank E. and Nolan, Thomas. *The Architects' and Builders' Handbook.* John Wiley & Sons, New York (1921) p 1171-1193.
[28] Freeman, John R. *Earthquake Damage and Earthquake Insurance*. McGraw-Hill Book Company, New York (1932) p. 172.
[29] Reitherman. *Earthquakes and Engineers.* p 200.
[30] Reitherman. *Earthquakes and Engineers.* p 223.
[31] Reitherman. *Earthquakes and Engineers.* p 161, 222
[32] Rossber. *Evolution of Codes in the USA.*
[33] *Minimum Design Loads in Buildings and Other Structures* (A58).
[34] Reitherman. *Earthquakes and Engineers.* p 33, 288.
[35] Dixon, Rick. *The Florida Building Code – Florida's Response to Hurricane Risk*. Presentation by Florida Building Commision (2009).
[36] Reitherman. *Earthquakes and Engineers.* p 272, 476
[37] SEAOC Seismology Committee. *Recommended Lateral Force Requirements and Commentary.* Structural Engineers Association of California (1974), p-7C.
[38] Reitherman. *Earthquakes and Engineers.* p 585.
[39] Reitherman. *Earthquakes and Engineers.* p 371.
[40] Dixon, Rick. *The Florida Building Code – Florida's Response to Hurricane Risk.*
[41] Knezevich, John W. *Hurricane-Driven Building Code Enhancements.* Structure Magazine (July 2017).
[42] FEMA. *Hurricanes' Impact on Florida's Building Codes & Standards.* FEMA Mitigation Section Technical Services Branch (2005).
[43] Reitherman. *Earthquakes and Engineers.* p 585.
[44] Green. *Building Codes for Existing and Historic Buildings.*
[45] Rossber. *Evolution of Codes in the USA*.
[46] Housner, G.W. *Historical View of Earthquake Engineering*, Proceedings of the Eighth World Conference on Earthquake Engineering, San Francisco (1984).

12th International Conference on Structural Analysis of Historical Constructions
SAHC 2020
P. Roca, L. Pelà and C. Molins (Eds.)

EXTRADOS STRENGTHENING OF SINGLE-LEAF VAULTS AGAINST SEISMIC ACTIONS

S. COMINELLI[1], C. PASSONI[2*], A. MARINI[2] A. BELLERI[2], AND E. GIURIANI[1]

[1] Dipartimento di Ingegneria Civile, Architettura, Territorio Ambiente e Matematica (DICATAM)
Università degli Studi di Brescia
Via Branze 43, 25123, Brescia (BS), Italy
e-mail: {stefania.cominelli, ezio.giuriani}@unibs.it, http://www.unibs.it

[2] Dipartimento di Ingegneria e Scienze Applicate (DISA)
Università degli Studi di Bergamo
Viale Marconi 5, 24044, Dalmine (BG), Italy
e-mail: {chiara.passoni, alessandra.marini, andrea.belleri}@unibg.it, http://www.unibg.it
(*corresponding author)

Keywords: single-leaf vaults, seismic strengthening, direct bending, extrados techniques, plywood centering, FRP laminates

Abstract. *Single-leaf vaults are acknowledged among the most vulnerable components of historical masonry constructions with respect to earthquake loads, particularly when featuring large span to thickness ratios, as in the case of single leaf covering the main nave of churches. These elements often require structural strengthening against seismic actions. In this paper, two different extrados techniques are tested: lightweight plywood restraining elements and FRP laminates embedded in a lime mortar layer. The techniques are tested on single leaf vaults having a very unfavorable span to thickness ratio.*

A previous study on less slender vaults, showed that lightweight plywood centerings, applying passive confinement to the vault extrados, inhibit the onset of the typical four-hinges failure mechanism. This lightweight, dry solution can be easily prefabricated, transferred and assembled at the construction site. The technique is reversible and fully compliant with the major preservation principles. FRP is also effective against the onset of the failure mechanism but entails larger deformations of the retrofitted vault, which may be detrimental in the case of possible decorations. The solution requires special man labor to ensure correct smoothening and cleaning of the vault extrados and to trigger effective bond between the mortar and the vault extrados. Both solutions are shown to enable small relative displacements of the vault springing, which may follow the deformation of possible internal ties.

The effectiveness of these retrofit techniques was comparatively verified through experimental tests on single-leaf barrel vault stripes at 1:2 scale subjected to cyclic distributed unsymmetrical loads and through comparison with the seismic response of a reference unreinforced single-leaf vault.

1 INTRODUCTION

Single leaf vaults are thin vaults (about 50 mm thick) adopted in churches and historical buildings all over the European territory [1-3] as lightweight false ceilings, typically decorated with stuccos and frescoes. These elements, which are made of a single layer of bricks laid flat and usually lacking any extrados backfilling material and lunettes, are acknowledged among the most vulnerable components of historical masonry buildings with respect to earthquake loads, particularly when featuring quite large span to thickness ratios. Single leaf vaults may bridge spans ranging between 3 and 6m in residential historical buildings and between 6 to 10m in the main naves of churches.

Considering single-leaf barrel vaults lacking backfill material, equilibrium is guaranteed as long as the thrust line, associated with both static and seismic loads, develops within the vault thickness [4-8]. Unsymmetrical load distributions may be detrimental for these structures provided that the ideal resisting arch has a reduced possibility to shift and modify within such a reduced thickness. This problem could be emphasized in the case the vault has not a catenary geometry, but rather a circular geometry, in which case the thrust line in static conditions does not overlap the centroid axis. As a result, these structures are particularly vulnerable even for low-intensity earthquakes, as confirmed by the collapses observed after recent earthquakes [9].

As stated in [9-10], 3 mechanisms may be experienced by thin single-leaf vaults in the case of a seismic event: (a) indirect differential bending of the vault crown caused by the rotation of the vault springing due to the unconstrained rocking motion of the supporting wall (Fig. 1a); (b) severe shear distortion stresses and distortions due to the onset of the differential rocking mechanism along the nave ends – usually as a result of the different stiffness of the façade and the transverse arches (Fig. 1b); and (c) direct differential bending with the onset of a four hinge mechanism due to the distributed seismic actions associated to the vault mass (Fig. 1c).

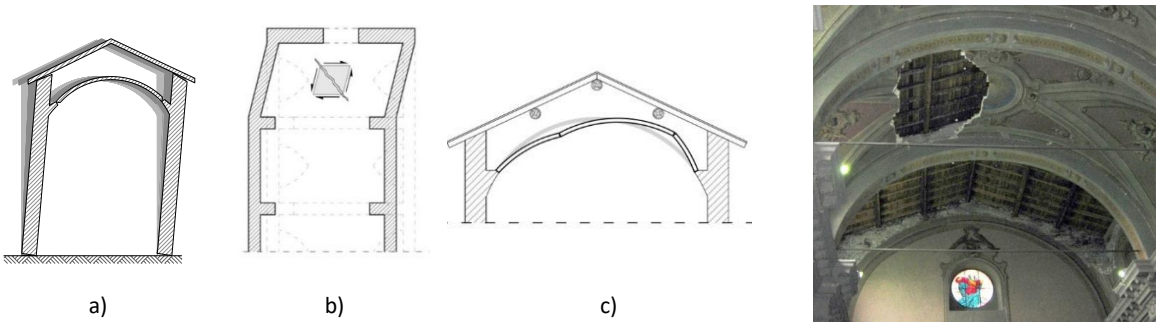


Figure 1: Main seismic vulnerabilities of single-leaf vaults: (a) indirect bending following rocking of the abutments; (b) shear distortion following differential rocking; (c) direct bending of the vault due to its own mass (from [17]). On the right: total collapse of the first bay (due to mechanism b) and partial collapse of the second bay (due to mechanism c) of the main nave of S.Pietro Church, Vobarno, Italy, after Salò earthquake, 2004 [9].

The two former mechanisms can be limited or inhibited through global interventions, such as either perimeter ties (mechanism a), or roof and floor diaphragms (mechanism a and b), which reduce the vault impost rotation and relative displacement [11]. On the contrary, the direct differential bending (mechanism c) cannot be inhibited, unless special targeted interventions are carried out on the structural element. Possible collapse induced by direct differential bending was addressed in a research carried out at the University of Brescia, in

which a series of strengthening solutions were proposed and tested on full scale single-leaf vaults having 1/100 thickness to span ratio and a span of 5m [12-17].

In the present paper, the study was extended to assess the effectiveness of some strengthening solutions in the case of thinner single-leaf vaults, with 1/200 thickness-to-span ratio, thus bridging larger spans up to 10m. Two different extrados techniques were proposed, namely: lightweight plywood restraining elements, and FRP laminates embedded in a lime mortar layer. To this end, 1:2 scaled single-leaf barrel vault stripes subjected to cyclic distributed unsymmetrical loads were tested. Results were compared with the seismic response of a reference unreinforced single-leaf vault.

2 STRENGTHENING TECHNIQUES INHIBITING DIRECT DIFFERENTIAL BENDING MECHANISM

The strengthening of single leaf barrel vaults with respect to direct differential bending mechanism usually adopts techniques derived from the traditional strengthening of masonry vaults, selecting those which do not increase the vault mass and avoiding unsymmetrical load sets [12]. The most common techniques entail the adoption of masonry spandrel walls [18] [10] [12-13], RC extrados slabs, or high-performance lime mortar extrados slabs strengthened with fiber mesh [12-13]. The former solution constrains the deformation of the vault crown and allows the thrust line to migrate within the spandrel wall height. The latter techniques enforce a composite structure behavior, allowing the ideal resisting arch to adjust within a higher thickness, but increases the mass of the vault and, more importantly, in seismic conditions, the migration of the thrust line may lead to a decompression of the vault crown, entailing the risk of debonding and unthreading of bricks from the existing structure [17]. Innovative lightweight ribs overlaying the vault extrados profile, made of lime mortar reinforced with inorganic matrix grids and of an inner polystyrene core, were also proposed [14].

Extrados stiff lightweight plywood retaining structures (also referred to as ‘centerings’) simply overlaying and not connected to the existing vault were also proposed [16-17]. The adoption of extrados centerings is a passive solution, which is conceived to maintain the structural role of the vault in static conditions and to provide the necessary passive confinement in seismic conditions (Fig. 2 left). The system is designed as a 3-hinged arch overlaying the existing vault extrados, hinged at the abutments and with an internal hinge at the vault key section (Fig. 2 right). Connections along the centering-to-vault interface are avoided as to prevent the decompression of the vault. This is a lightweight, dry and cost-effective solution, fully reversible, minimally impairing, and not requiring any special man labor. The effectiveness of the system against direct differential bending was verified on single-leaf vaults having 1/100 thickness-to-span ratio [16-17]; in the tests, the collapse mechanism was inhibited for accelerations up to 4 times those causing the collapse of the unreinforced vault, and the stiffness of the vault was increased.

The use of fiber-reinforced polymer (FRP) strips is another efficient solution [19]. In this case, failure of the strengthened structure may arise due to possible shear failure close to the springing, as the technique enhances the sole bending capacity, or due to delamination of the FRP strips, triggered either by the uneven surface of the vault or by failure of the bond between the vault and the laminate. In order to solve durability issues and decay processes due to loss of transpiration potential, steel-reinforced grouts (SRG) [20], or inorganic matrix grids (IMG)

embedded in lime-based mortar are alternative techniques [21-22]. In the present study, FRP laminates embedded in a lime mortar layer were considered.

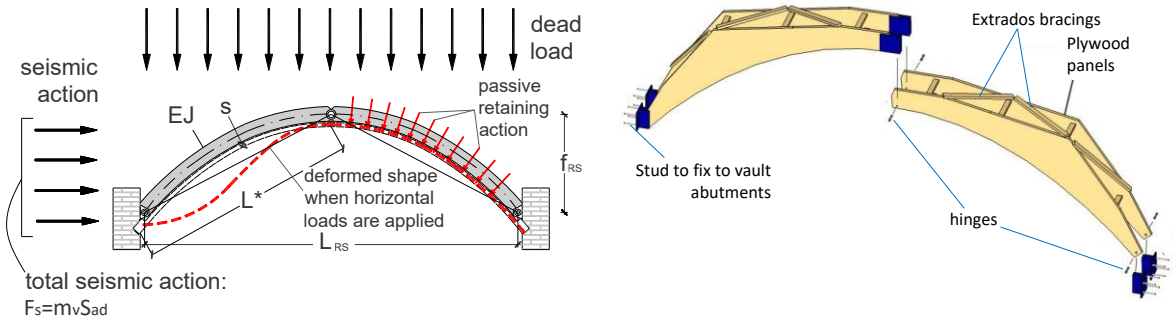


Figure 2: Confining action of the plywood centering in case of earthquake (left) and details of the centering components and of the hinge location (right) [17]

3 EXPERIMENTAL TESTS

The experimental campaign was aimed at assessing the effectiveness of lightweight plywood centerings and FRP laminates for single-leaf vaults with very unfavorable thickness-to-span ratio (1/200) and was inspired by the campaign carried out at the University of Brescia on medium-span single-leaf vaults (1/100) [15-17]. The same testing bench was adopted, and the thickness of the vault was reduced to resemble a 50mm vault bridging about 10m span.

3.1 Modelling hypothesis

According to the previous studies [15-17], the single-leaf vault was modelled as a series of transversal adjoining vault stripes, thus disregarding the possible tridimensional confining effects due the longitudinal arches developing between the head walls or transverse arches, which is a conservative assumption.

In addition, it was assumed that both indirect differential bending and shear distortion (mechanism a and b of Fig. 1) are inhibited through global interventions; so, it is considered that the vault is affected by the sole direct differential bending (mechanism c of Fig. 1).

Based on these two assumptions, a single barrel vault stripe of unit width was modelled in the experimental specimen, and the vault springing were assumed as fixed to the testing bench.

3.2 Description of the unreinforced experimental specimen

The experimental masonry vault specimen is a basic single-leaf barrel vault stripe of unit width at a scale 1:2 with a polycentric profile (span L=5m, rise f=1.42m, thickness t=27mm) (Fig. 3), thus representing a real vault of span L=10m, rise f=2.84m and thickness t=54mm.

A flat brick arrangement with a running bond masonry texture was adopted; the ultimate capacity of possible plastic hinges is thus associated with the tensile resistance of the joints. The vault stripe is embedded at the springing and pre-stressing clamps and anchoring bars were installed to fix the vault abutments to the testing bench.

Mechanical properties of the adopted bricks and mortar (7.5% NHL 3.5, 8.5% lime putty, 34% 1.5mm aggregates, 34% 3.0mm aggregates, 16% H_2O) are reported in Table 1.

Table 1: Average mechanical properties of bricks and mortar

Solid Clay Bricks (27x120x250mm)	Mortar (bed joints 7-8mm)
Compressive strength: 2.245 MPa	Compressive strength: 0.337 MPa
Flexural strength: 4.79 MPa	Flexural strength: 0.180 MPa
Young's modulus: 10883.26 MPa	Flexural strength (joint): 0.328 MPa

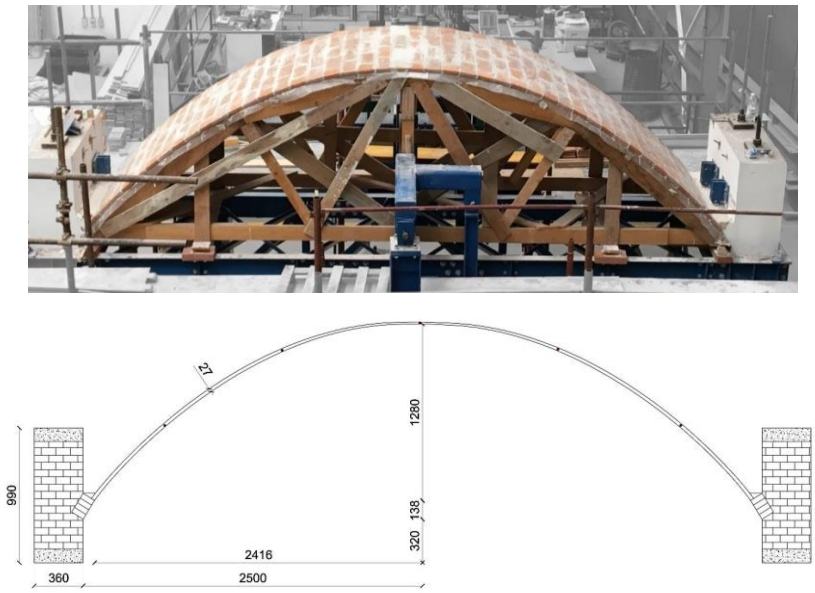


Figure 3: Side view (top) and geometry (bottom) of the unreinforced vault stripe layout (depth = 970mm)

3.3 Description of the experimental specimen reinforced with plywood centering

The single leaf vault specimen is strengthened by means of two extrados lightweight 3-hinge wooden centerings, made of 30mm thick plywood panels, braced along the extrados edge to avoid buckling (Fig. 4). The extrados reinforcement is designed as a 3-hinged arch. Such a structural scheme enables small relative displacements of the vault springing, which may follow the deformation of the possible internal ties or of the roof box structure. The effectiveness of the system, both in the case of fixed supports and of a possible horizontal settlement of the vault abutments, was studied in a previous research [17].

The centering physical hinges at the springing and at the vault key are located as close as possible to the centering-to-vault extrados interface, as to reduce the offset of the vault centroid axis with respect to the centering. This reduces the relative displacements of the two structures both in the case of unsymmetrical load conditions (such as in the case of an earthquake) and in the case of spreading supports. No shear transfer is allowed along the vault-to-centering interface, whilst initial contact between the centering and the vault is enforced through thin wooden wedges. More about the design of the strengthening intervention in terms of flexural stiffness of the plywood centering may be found in [17].

Two tests were carried out on this specimen. In the first test, the wooden wedges were positioned between the vault and the centering and were simply glued to the vault, to enable a passive confining action; in the second test, the wedges were forced in correspondence of the

vault-to-centering interface and were fixed in that position, thus leading to an active confining intervention. The results of both the tests are reported and commented in the following.

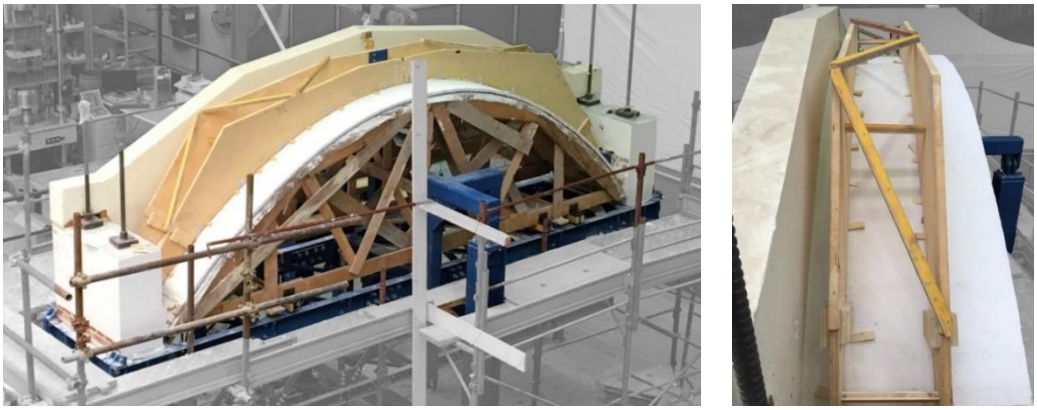


Figure 4: Side and top view of the vault stripe reinforced with the plywood centering

3.4 Description of the experimental specimen reinforced with FRP laminates

The single leaf vault specimen is strengthened by means of FRP laminates embedded in a pozzolanic hydraulic lime mortar layer (Fig. 5 left). The choice of an inorganic matrix was aimed at improving the transpiration potential of the retrofit intervention with respect to a polymer matrix, for the sake of durability.

A first layer of 3-4mm thickness was laid on the bare vault extrados and on the abutments, the carbon fiber mesh was embedded and then covered with a second layer of mortar with equal thickness (Fig. 5 right). The mechanical properties of the mesh and of the mortar are reported in Table 2.



Figure 5: Side view of the vault stripe reinforced with the FRP laminates before the test (left) and top view of the vault during the strengthening operations (right)

Table 2: Average mechanical properties of carbon fiber grid and mortar

Carbon fiber mesh	Mortar matrix
Ultimate tensile strength: 4830 MPa	Compressive strength: 20.98 MPa
Elongation at break: 1.9%	Flexural strength: 4.83 MPa
Young's modulus: 240000 MPa	Young's modulus: 10633 MPa

3.5 Test set-up

The same test set-up proposed in [15-17] was adopted. The single leaf vault strip was assembled on a special swinging steel frame (Fig. 6a). By swinging the testing frame, increasing uniformly distributed inertia forces are applied along the vault crown. Rotation, and thus inertia forces, can be increased either up to failure of the specimen or up to the maximum rotation capacity of the testing bench. Dynamic effects cannot be considered.

The testing bench is composed by a rigid steel deck rotating both clockwise and counter-clockwise about a pivot point A on a vertical frame fixed to the ground. The deck rotation is applied through a mechanical transmission system, actuated by an electromechanical jack (Fig. 6a).

By assuming local reference fixed to the deck, the rotation of the specimen due to the swinging of the testing bench causes the gravity acceleration to decompose into one component parallel (horizontal, $a_x(\theta)$) and into a component orthogonal (vertical, $a_y(\theta)$) to the deck. For increasing the tilting angle (θ) from 0 to 30°, $a_x(\theta)$ increases, simulating earthquakes of increasing intensity; on the other hand, $a_y(\theta)$ slightly reduces, thus simulating a reduction of the vertical load in static conditions ranging between 0 and 13.4%. The horizontal-to-vertical spectral ratio $\alpha(\theta)=a_x(\theta)/a_y(\theta)$ can be easily determined (box in Fig. 6).

During all tests, the vault ring differential deflection was monitored in five points through vertical and horizontal displacement transducers, pinned to the vault mid axis and to a rigid polystyrene arch fixed to the abutments (Fig. 6b). The deck tilting angle was monitored by two one-direction accelerometers fixed to the specimen abutments and directed as the local reference horizontal axis x. Further details may be found in [15-17].

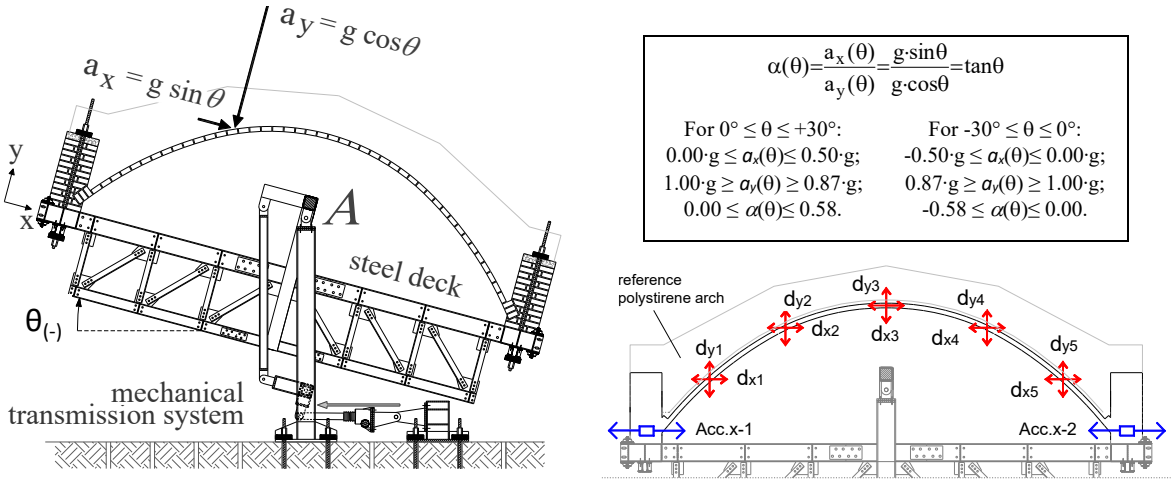


Figure 6: a) Side view of the swinging testing frame in the tilted position (in the box: clockwise and counter-clockwise maximum rotations and corresponding extreme values of relative accelerations and horizontal-to-vertical acceleration ratio); b) instruments set-up: red arrows represent displacement transducers (d_x, d_y) and blue arrows represent accelerometers (Acc.x) [17].

4 EXPERIMENTAL TEST RESULTS AND DISCUSSION

Four experimental tests were carried out. In the first test (Test 0), the tilting angles corresponding to the first cracking and to the collapse of the unreinforced vault were determined as reference values. Only counter-clockwise rotations were imposed to the specimen in order to avoid damage on both sides of the vault crown. The test was stopped at the tilting angle corresponding to the collapse of the vault (Fig 7a). Three tests on the reinforced vault were then carried out: two tests on the vault reinforced by means of plywood centerings with unforced (Test 1a) and forced (Test 1b) wooden wedges; and a test on the vault strengthened with FRP laminates (Test 2). Applied rotation cycles are shown in Fig. 7. All tests were interrupted for overcoming the rotation capacity of the testing frame (θ=30°), corresponding to an $a_x(\theta)$ of about 0.50g and α(θ) of about 0.58.

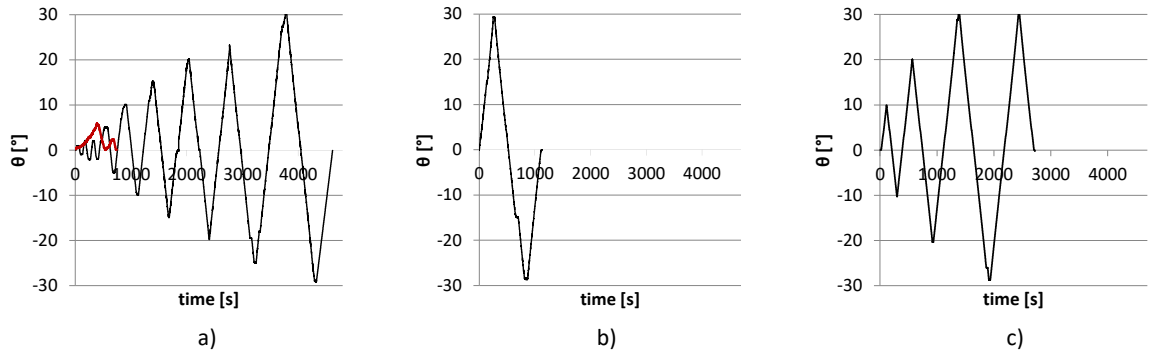


Figure 7: Applied rotation cycles in the case of: a) the unreinforced vault (Test 0) (bold red line) and of the vault reinforced with plywood centering with unforced wedges (Test 1a) (black line); b) vault reinforced with plywood centering with forced wedges (Test 1b); c) vault reinforced with FRP laminates (Test 2).

In Test 0, the unreinforced specimen was rotated up to the onset of the first crack. For a tilting angle θ=5.8° (corresponding to α=0.105), the windward vault segment collapsed leaning against the construction framework kept beneath the specimen (Fig. 8). The testing bench was then brought back to the horizontal position, and the vault restored the initial uncracked configuration. In a second cycle, the tilting angle was increased up to a second collapse of the vault. This time, the unreinforced vault collapsed for a tilting angle θ=2.4°, lower than that experienced in the previous cycle, since the specimen was already damaged. The ultimate horizontal-to-vertical spectral ratio was thus considered α =0.044 for the damaged vault.



Figure 8: Side view of the vault for a counter-clockwise rotation θ=5.8°, corresponding to the first collapse. The red arrow and the figure on the right show the vault leaning against the construction framework.

In the second phase of the experimental campaign, the vault was reinforced without repairing the cracking triggered during Test 0, so as to be representative of a damaged existing vault.

The vault was first reinforced by means of plywood centerings with unforced wooden wedges ensuring contact at the vault-to-centering interface. In this first test (Test 1a), the vault did not collapse even for tilting angles up to ±30° (Fig. 9 left); however, deformations higher than expected were recorded. Two corrective measures were thus applied as to reduce the vault deformations (Test 1b): the wooden wedges at the vault-to-centering interface were forced as to simulate an active strengthening intervention, and an additional restraint was positioned at the centering ends as to limit possible vertical movements of the hinges. In this case, substantially smaller vertical displacements of the reinforced vaults were observed (Fig. 10). In both cases, the effectiveness of the plywood centerings in constraining the upward vertical displacement was verified.

Finally, the vault was reinforced by means of FRP laminates embedded in the lime mortar layer (Test 2). In this case, a crack opened in correspondence of the measuring point 2 (Fig. 6b) for a tilting angle θ=25.9°; however, collapse of the vault was not triggered even for tilting angles up to the testing bench capacity ±30°.

A side view of the vault strengthened with plywood centerings and FRP laminates in correspondence of a counter-clockwise rotation equal to 30° is shown in Fig. 9.

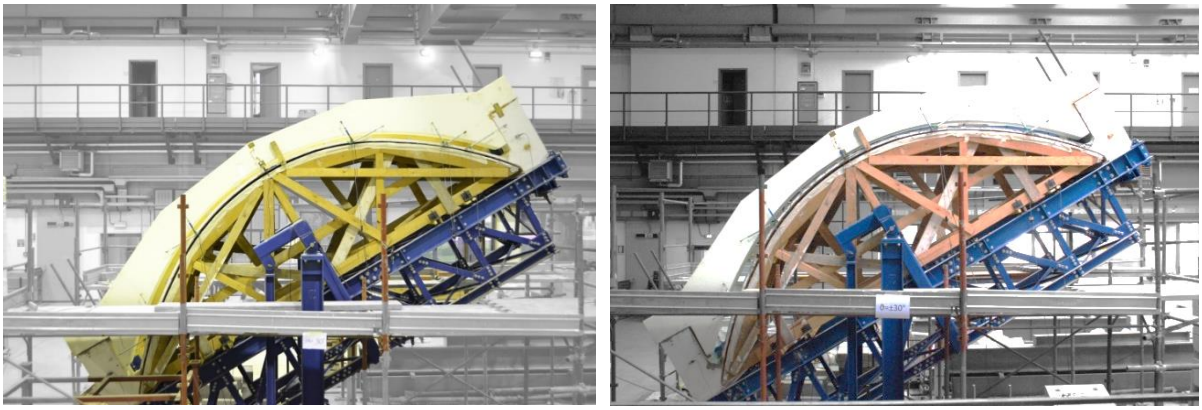


Figure 9: Side view of the vault for a counter-clockwise rotation θ=30°, corresponding to the rotation capacity of testing bench, for the vault strengthened with plywood centerings (left) and FRP laminates (right)

The deformed shape of the vault in the unreinforced condition is compared to the deformed shape for a counter-clockwise rotation of 30° in Figure 10a. Figure 10b shows the comparison of the deformed shapes of the vaults retrofitted with the three different strengthening solutions for a tilting angle equal to a counter-clockwise rotation of 30°. Deformations are magnified by a factor of 20. It should be noted that in Test 1b, the undeformed shape of the vault shown in the figure is not representative of the actual initial shape of the vault since the forcing operation of the wooding wedges was neither perfectly homogeneous nor symmetric along the vault extrados.

In all tests, for increasing rotation, the leeward part of the vault moves upward whereas the windward part moves downward. In case of centering strengthening, the leeward part of the vault pushes on the centering whereas the windward part may detach from it, thus leading to higher displacements in the windward part with respect to the leeward one. Displacements of

the retrofitted vault are quite small even in correspondence of tilting angles approaching the rotation capacity of the testing frame. In the case of FRP strengthening, the behavior is similar meaning that the deformed shape shows the windward vault segment moving downwards, and the leeward segment moving upwards, but, in this case, larger displacements are observed with respect to the case of centering strengthening.

All the proposed techniques are proved to be effective solutions in improving the seismic response of the single leaf vault. However, the compatibility of the higher deformations exhibited by the vault strengthened with FRP laminates with the conservation of possible frescoes or stuccos on the vault intrados needs to be verified.

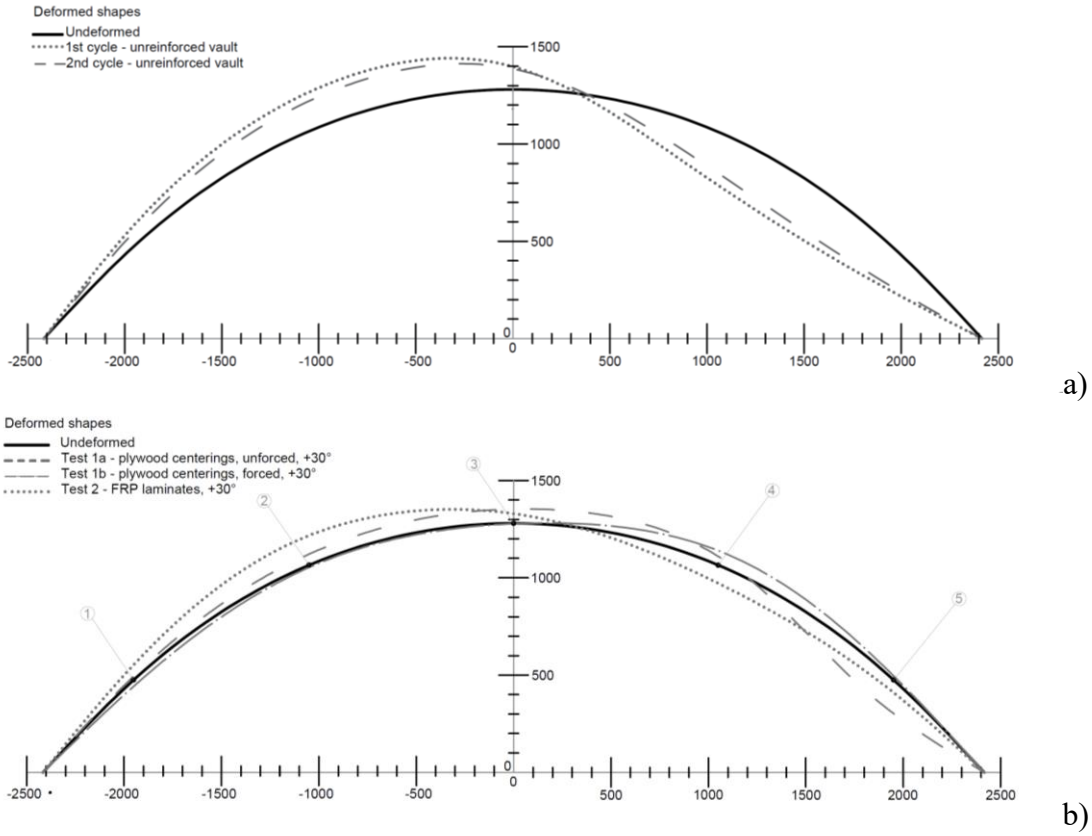


Figure 10: Deformed shape of the unreinforced vault (a) and comparison of the deformed shapes of the vaults retrofitted with the three different strengthening solutions (b) for counter-clockwise rotation of 30°

5 CONCLUDING REMARKS

In this paper the seismic strengthening of barrel single-leaf masonry vaults with large span to thickness ratios, lacking lunettes and backfill material, is addressed. Such a typology is quite frequently found in churches, where single leaf vaults cover the main naves. The three major failure mechanisms of single leaf vaults subjected to earthquake were addressed, and focus was made on the strengthening against direct differential bending, which was acknowledged as the mechanism that cannot be inhibited by means of global seismic retrofit techniques (such as perimeter ties and roof or floor diaphragms) but rather requires specific strengthening of the vault. In particular, focus was made on vaults with large span-to-thickness ratios.

An overview of possible strengthening techniques against direct bending mechanism was presented, and two different extrados solutions were proposed and tested: lightweight plywood restraining elements and FRP laminates embedded in a lime mortar layer.

Plywood centerings apply passive confinement to the vault extrados. The reinforcement is designed as a 3-hinged arch to allow accommodating possible small relative displacements of the vault springing, which may follow the deformation of internal ties or roof box structure. The solution may be conceived as passive or slightly active, in the latter case wooden wedges are forced along the vault-to-centering interface. FRP strengthening consists in embedding a carbon fiber grid into an inorganic pozzolanic lime mortar matrix.

The effectiveness of the retrofit techniques was verified through experimental tests on single-leaf barrel vault stripes at 1:2 scale, subjected to cyclic distributed unsymmetrical loads and through comparison with the seismic response of a reference unreinforced vault.

Lightweight plywood centerings were shown to inhibit the onset of the typical four-hinges failure mechanism. This lightweight, dry solution can be easily prefabricated, transferred and assembled at the construction site. The technique is reversible and fully compliant with the major preservation principles. FRP is also effective against the onset of the failure mechanism but entails larger deformations of the retrofitted vault, which may be detrimental in the case of possible decorations. The solution requires special man labor to ensure correct smoothening and cleaning of the vault extrados and to trigger effective bond between the mortar and the vault extrados. Both solutions are shown to enable small relative displacements of the vault springing, which may follow the deformation of possible internal ties.

Acknowledgements. This work was partly financed and developed within the research project DPC-ReLUIS 2014-2016 – Research line n.1. The authors thankfully acknowledge Marco Leali and Federico Carollo for carrying out the experimental tests and express their appreciation to the technical staff of the Structural Testing Facility at the University of Brescia for their assistance in the test program.

REFERENCES

[1] Gulli, R., 1993, Le volte in folio portanti: tecnica costruttiva ed impiego nell'edilizia storica e moderna", in: *Proceedings of "I° Convegno Nazionale Manutenzione e Recupero nella città storica"*, Rome. ARCO.

[2] Gulli, R. & Mochi G., 1995, "Bóvedas tabicadas: architettura e construzione", in: "*Il modo di costruire*", CDP editrice.

[3] Ochsendorf, J. & Freeman, M. (photographs), 2010, "Guastavino vaulting: the art of structural tile", New York: Princeton Architectural Press.

[4] Heyman, 1966, "The stone skeleton", *International Journal of Solids and Structures* 2, 249-279.

[5] O'Dwyer, D., 1999, "Funicular analyses of masonry vaults", *Computer & Structures*, 73: 187-197.

[6] Ramage, M., Ochsendorf, J., Block, P. & Rich, P., 2008, "Advanced Geometry, Rudimentary Construction: Structural Form Finding for Unreinforced Thin-shell Masonry Vaults" in *Advances in Architectural Geometry* 2008, Vienna, Austria

[7] Block, P., DeJong, M. & Ochsendorf, J., 2006, "As hangs the flexible line: Equilibrium of masonry arches". *The Nexus Network Journal* 8 (2), pp. 13-24.

[8] D'Ayala, D. and Tomasoni, E. 2008. The structural behaviour of masonry vaults: Limit state analysis with finite friction. *Proceedings of the VI International Conference on Structural Analysis of Historical Constructions SAHC*. 2-4 July, Bath, England. pp. 47-71. Ed. Taylor and Francis, London, UK.

[9] Giuriani, E. & Marini, A., 2008 "Experiences from the Northern Italy 2004 earthquake: vulnerability assessment and strengthening of historic churches", *Proceedings of the VI International Conference on Structural Analysis of Historical Constructions SAHC*. 2-4 July, Bath, England. pp. 13-24. Ed. Taylor and Francis, London, UK.

[10] Giuriani, E., Marini, A., Porteri, C. & Preti, M., 2009 "Seismic vulnerability of churches associated to transverse arch rocking", *International Journal of Architectural Heritage*, 3: 1–24, 2009. Ed. Taylor & Francis Group, LLC.

[11] Giuriani, E. & Marini, A., 2008, "Wooden roof box structure for the anti-seismic strengthening of historic buildings", *Journal of Architectural Heritage: Conservation, Analysis and Restoration*, Vol.2(3) pp. 226-246.

[12] Ferrario, L., Marini, A., Riva, P. & Giuriani, E., 2009, "Traditional and Innovative Techniques for the Seismic Strengthening of Barrel Vaulted Structures Subjected to Rocking of the Abutments", *Proceedings of ATC-SEI Conference on Improving the Seismic Performance of Existing Buildings and Other Structures*. San Francisco, California, December 9 -11.

[13] Ferrario, L., Marini, A., Riva, P. & Giuriani, E., 2010, "Proportioning criteria for traditional and innovative Extrados techniques for the strengthening of barrel vaulted structures subjected to rocking of the abutments", *Journal of Civil Engineering and Architecture*, David Publishing Company, USA, pp.1-15. Vol. 4, N.5.

[14] Ferrario, L., Marchina, E., Marini., A., Preti, M. & Giuriani, E., 2010, "Lightweight ribs for the strengthening of single-leaf vaults undergoing seismic actions", *Proceedings of the VIII International Conference on Structural Analysis of Historical Constructions*, Published in Advanced Materials Research, Vol.133-134, pp.923-928. Ed. Xianglin Gu and Xiaobin Song, China.

[15] Ferrario, L., 2013, "*Masonry single-leaf barrel vaults: from the seismic vulnerability assessment to the proposal of an innovative retrofitting approach*", Ph.D. Thesis, University of Brescia.

[16] Marini, A., Giuriani, E., Belleri, A., Preti, M., Ferrario, L., 2016, "Plywood extrados retaining structures for the retrofit of single leaf vaults", in: *Proc. Of 16th International Brick and Block Masonry Conference "Masonry in a world of challenges"*, June 26 - 30, Padova, Italy

[17] Marini, A., Belleri, A., Preti, M., Riva, P., Giuriani, E., 2017, "Lightweight extrados restraining elements for the anti-seismic retrofit of single leaf vaults", *Engineering Structures*, 141, 543-554

[18] Tomasoni, E., 2008, "*Le volte in muratura negli edifici storici, Tecniche costruttive e comportamento strutturale*", Ph.D dissertation, University of Trento.

[19] Valluzzi, M., Valdemarca, M. & Modena, C., 2001, "Behavior of Brick Masonry Vaults Strengthened by FRP Laminates." *Journal on Composite Construction*, 10.1061/(ASCE)1090-0268(2001)5:3(163), 163-169.

[20] Girardello, P., Pappas A., da porto F., Valluzzi, M.R., 2013, "Experimental testing and numerical modelling of masonry vaults". *International Conference on Rehabilitation and Restoration of Structures, Chennai, 13-16 February 2013*

[21] Giamundo, V., Lignola, G. P., Maddaloni G., Da Porto, F., Prota, A., Manfredi, G., 2016, "Shaking table tests on a full-scale unreinforced and IMG retrofitted clay brick masonry barrel vault", *Bull Earthquake Eng* 14:1663–1693

[22] Giamundo V., Lignola G.P., Maddaloni G., Manfredi G., 2015, "Experimental investigation of the seismic performances of IMG reinforcement on curved masonry elements". *Compos Part B*, Eng 70:53–63.

12th International Conference on Structural Analysis of Historical Constructions
SAHC 2020
P. Roca, L. Pelà and C. Molins (Eds.)

INADEQUATE CASES OF INTERVENTION IN ARCHITECTURAL HERITAGE BUILDINGS IN MEXICO AFTER THE SEPTEMBER 2017 EARTHQUAKES

FERNANDO PEÑA[1*] AND MARCOS M. CHÁVEZ[1]

[1]Instituto de Ingeniería
Universidad Nacional Autónoma de México
Ciudad Universitaria, 04510 Mexico City, Mexico
e-mail: fpem@pumas.iingen.unam.mx, mchavezc@iingen.unam.mx, www.iingen.unam.mx

Keywords: Historical Structure, Architectural Heritage, Structural Intervention, Earthquake

Abstract. *The two large-scale earthquakes that occurred on September 7 (Mw 8.2) and 19 (Mw 7.1), 2017 in Mexico left 2,340 damaged architectural heritage buildings throughout the country. Due to the large amount of architectural heritage buildings damaged, the government department responsible for protecting the architectural heritage and the practitioners specialized in conservation was overwhelmed. Therefore, it was necessary to incorporate practitioners who are not specialized in conservation, first to attend the emergency works and later into structural intervention works. In this way, this paper presents some examples of emergency work, as well as intervention proposals that have been inadequate. The common errors observed in emergency works are discussed, as well as the application of erroneous or inadequate concepts in intervention proposals. Comparison with correct intervention works are also presented.*

1 INTRODUCTION

The architectural heritage in Mexico is wide, rich and varied. It has more than 50,000 archaeological sites and 110,000 buildings built between 16th and 19th centuries; as well as 35 sites inscribed on the UNESCO World Heritage List. The two large-scale earthquakes that occurred on September 7 (Mw 8.2) and 19 (Mw 7.1), 2017 in Mexico left 2,340 damaged architectural heritage buildings throughout the country; which corresponds around 6% of the total of architectural heritage buildings located in the affected area.

The earthquake of September 7, with a magnitude Mw 8.2, occurred at 23:49:17 local time. The epicenter was located in the Gulf of Tehuantepec, 133 km southwest of Pijijiapan, Chiapas and 700 km from Mexico City. This event was cataloged by the National Seismological Service (SSN) as normal failure and is the largest recorded in the country. The maximum accelerations recorded in the field were higher than 228 Gal [1]. On the other hand, the earthquake of September 19 occurred at 13:14:40 local time, with a magnitude Mw 7.1. The epicenter was located on the border between the states of Puebla and Morelos, 12 km southeast of Axochiapan, Morelos and 120 km from Mexico City. According to the SSN, it was an intraplate earthquake of normal failure. According to official records, the maximum accelerations recorded in the field were greater than 220 Gal, in the epicentral zone [2].

Due to the large amount of architectural heritage buildings damaged, the government department responsible for protecting the architectural heritage and the practitioners specialized in conservation were overwhelmed. Therefore, it was necessary to incorporate practitioners who are not specialized in conservation, as well as volunteers from communities with little or no supervision of engineers or architects, first to attend the emergency works and later into structural intervention works. In this way, this paper presents some examples of emergency work, as well as intervention proposals that have been inadequate. The common errors observed in emergency works are discussed, as well as the application of erroneous or inadequate concepts in intervention proposals. Comparison with correct intervention works are also presented.

2 EMERGENCY WORKS

One of the first activities in a structure damaged by an earthquake is to carry out emergency works, to avoid collapse of the damaged areas. The objective of emergency works are to improve the stability conditions of the damaged structure, to resist, not only the own weight of the structure, but also accidental loads that may occur before or during the restoration works, such as the aftershocks [3-6]. For example, figure 1a shows the damage tower of the temple of Pilcaya, Puebla after the earthquake. It can be observed that although the tower had severe damage, it did not collapse. Few days later, before the emergency works began, the tower collapsed, standing only part of the first body of the tower (figure 1b). It seems that the cause of the collapse was the vibration inducing by passing trucks and vehicles on the streets adjacent to the temple.

a)  b) 

Figure 1: Damaged tower of temple of Pilcaya, Puebla: a) after earthquake; b) few days after the seismic event

Due to the urgency of keeping damaged structures standing, emergency work is often carried out by volunteers from communities with little or no supervision of engineers or architects. Because of this, solutions that do not increase the structural capacity of the building are often implemented. In most of these cases, it is believed that emergency works only serves to support the weak parts of the structure that are in danger of collapse.

Figure 2 shows the Municipal Palace of Hueyapan, Morelos after the earthquake. The building was made with unreinforced brick masonry. The loss of the lower archway is observed, which puts the stability of the balcony at risk. In the upper part, diagonal shear cracks are observed. It is noted that the balcony shoring system is not adequate, as the struts will not be able to withstand lateral forces in case of an aftershock. In this particular case, the shoring system was thought only for vertical forces.



Figure 2: Municipal Palace of Hueyapan, Morelos

When the building has two or more levels and the damage are located in superior levels, it is necessary to ensure that the transmission of shoring system loads from the upper levels to the foundation is carried out properly. This is particularly important when the shoring of the upper levels rests directly on the slab, arches or beams of the lower level. In order to avoid overloading and damage of the supporting structural elements, a shoring must be placed in the lower levels in order to have a correct transmission of the loads. For example, figure 3 shows an example where a shoring in the ground floor was set in order to take the loads of the upper shore.



Figure 3: Example of a correct transmission of shoring system loads of higher than lower levels

The shoring system is a temporary system that must be removed when the intervention works are finished. Wood is the most common material used for shoring system due its versatility, manageability, ease of construction and cheap. However, good quality wood must be used; as well as particular attention to the connections must be paid. The quality of the wood is with regard to: material (use of structural wood), element (no slender elements or buckling elements) and structural system (strength capacity). In the case of wooden elements, the most common practice is to build a wooden truss support (figure 4a). In other cases, especially when the height of building is considerable, as in churches, a steel shoring system (fig. 4b) or mixed system of steel and wood are used (fig. 4c).

a)  b)  c) 

Figure 4: Examples of shoring systems: a) wood; b) steel; c) mixed

a)  b) 

Figure 5: Example of bad quality wooden elements: a) buckled element; b) slender elements

Figure 5 shows two example of a bad quality of wooden systems. In figure 5a, it can see that one of the vertical element is buckling, reducing its structural capacity. Additionally, vertical elements are not high enough, so brick pieces were used at the base, to increase their height.

Figure 5b shows an example of a scarce shoring system, where slender elements are used. It is clear that this system is unable to take lateral and vertical forces.

Due to the lack of experience and non-engineering criteria, there are cases in which there is a waste of economic and material resources, as well as workmanship, which can be used in other damage buildings. For example, there are cases with an excessive shoring, preventing people from entering the building. In these cases, part of the scaffolding must be dismantled before an intervention process, in order to have space to start the intervention works. There are also cases, in which the shoring is placed directly over a crack, so it will be necessary to remove it in case of an intervention (fig. 6). For this reason, it is important to make a preliminary structural analysis to determine the characteristics of the shoring system and as far as possible, place it so that it does not interfere with the intervention works.

a)  b) 

Figure 6: Example of bad criteria of emergency works: a) excessive shoring; b) shoring over a crack

3 INTERVENTION PROPOSALS

As previously mentioned, due to the large amount of heritage buildings damaged, the government and the practitioners specialized in conservation were overwhelmed. Therefore, it was necessary to incorporate practitioners who are not specialized in conservation. This has caused that some intervention proposal do not comply with the internationally accepted conservation principles. In general, non-specialized professionals believe that heritage buildings have a structural behavior similar to modern masonry or reinforced concrete structures. In some cases, this has generated intervention proposals that are not compatible, both structurally and conservation.

For example, some proposals to rebuild the belfry and to strengthen the bell tower of the church shown in figure 1. One of the proposals consisted to rebuild the belfry with reinforced concrete and strength the body of the tower with reinforced concrete walls (fig. 7). But this solution is invasive and irreversible; as well as, change the structural authenticity. In addition, there is incompatibility between the new and old elements. It is not clear how the union between the elements of reinforced concrete and the original elements of stone masonry will be made. The concrete walls do not reach the foundation, which will cause a concentration of stresses in the non-reinforced elements.

Other proposal was to rebuild the belfry with perforated steel plates (fig. 8). In this solution, there is mechanical incompatibility between the steel elements and stone masonry, as well as difficulty of guaranteeing a good anchoring of the metallic elements. High possibility of failure

of the masonry can occur in the part where the reinforcement ends, due to a local concentrations of stresses in this region. There is a loss of the cultural, artistic and historical values of the church.

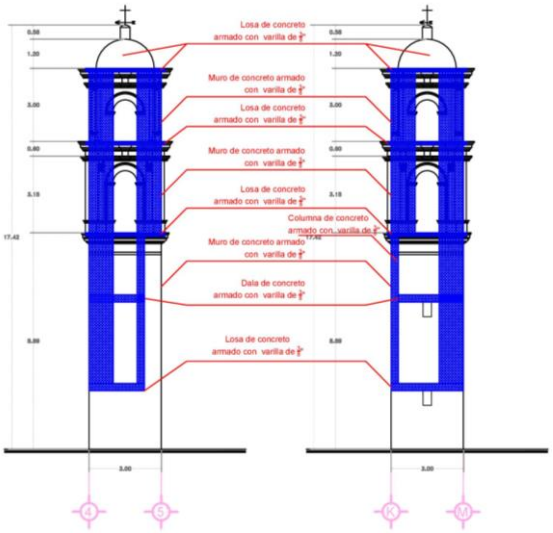
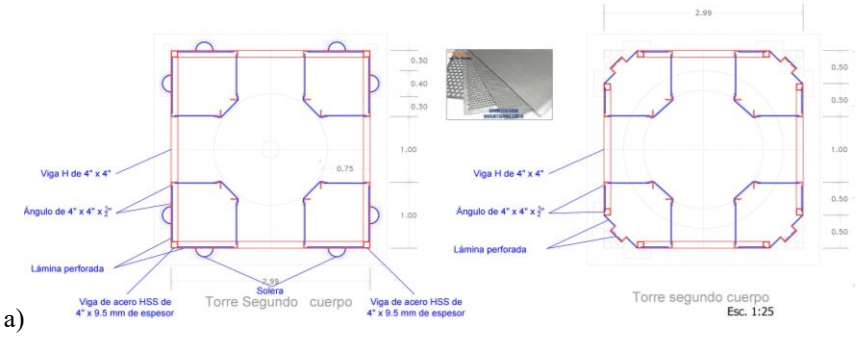
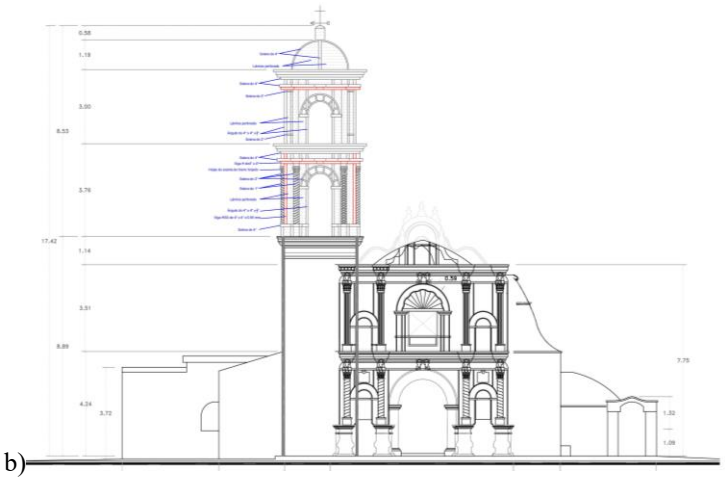


Figure 7: Reinforcement of a bell tower with concrete walls



a)



b)

Figure 8: Reconstruction of the belfry with perforated steel plates: a) plan view; b) frontal view

Finally, the belfry was reconstructed with similar materials (stone masonry) and geometry (two bodies) as the original one. In this case, the cultural, artistic and historic values of the church were conserved. However, as the belfry was reconstructed equal as the original, without any structural upgrade (increase of the structural strength or reduce of seismic forces), it is a high probability to have similar damages in future seismic events.

Another example is the intervention in a cloister of a convent. The cloister is a rectangular two-level floor, attached to the west side of the temple. The vaults of the corridors showed longitudinal cracks. Additionally, significant cracking occurred on the walls (fig. 9a), mainly because the masonry have a poor quality. Rounded stones (pebbles) joined with a lime – sand – soil mortar compose the masonry. These type of stones offer a very low bond with the mortar.

The consolidation of the cracks were realized by injection and the cusci-scusci technique was used (fig. 9b). Similar stones (pebbles) and mortar (lime-sand-soil) was used. Thus, the structural capacity was not upgrade. Furthermore, only the visible cracks due to earthquake damage were repaired. The intervention only aimed to return the structure to its original state regardless of the quality of the material, without improve the structural behavior of the building.

a)  b) 

Figure 9: Damage on walls of a cloister: a) cracks; b) consolidation of the cracks

4 FINAL REMARKS

- Two large-scale earthquakes hit Mexico on September 7 (Mw 8.2) and 19 (Mw 7.1), 2017 and both left 2,340 damaged architectural heritage buildings throughout the country.
- Due to the large number of damaged heritage buildings, it was necessary to incorporate practitioners who are not specialized in conservation, as well as volunteers from communities with little or no supervision of engineers or architects, first to attend the emergency works and later into structural intervention works.
- There were three main and common errors observed in emergency works were: solutions that do not increase the structural capacity of the building; bad quality of wooden elements, as seen by use of slender vertical elements and/or buckling of these elements; and scarce or excessive shoring system.
- Wood was the most commonly used material in the emergency works, due to its

versatility, manageability and ease of construction. Steel shoring system or mixed system of steel and wood are also used.
- Scarce shoring system were found on isolated communities and excessive shoring system were found on richer communities.
- It has been detected that the economy of the community has a significant influence on emergency works. In low-income populations, they seek savings in materials that generally lead to poor shoring systems. On the other hand, in richer populations, there may be excessive use of materials.
- In the case of intervention proposals, three common errors were detected: take the same reinforcement considerations as for modern buildings, use of concrete and/or steel elements in order to increase the structural capacity, and reconstruct with the same materials and characteristics as the original structure without increasing its structural capacity.
- If the structure is rebuilt with the same materials and characteristics, without increasing its structural capacity, it will have the same weaknesses and problems. Therefore, it will be expected that in future earthquakes there will be the same damages that have occurred in the past.
- Therefore, it is necessary to increase the structural capacity of the structure or seek to reduce its seismic demand, in order to avoid future damages.

Acknowledgements. Authors acknowledge to Instituto Nacional de Antropología e Historia for the support provided for visiting damaged buildings. In particular to the regional centers of Puebla and Morelos, through the Arch. Rutilia Amigón and Dra. María Isabel Campos Goenaga, respectively.

REFERENCES

[1] Servicio Sismológico Nacional. *Sismo de Tehuantepec (217-09-07 23:49 Mw 8.2)*. Special Report, Servicio Sismológico Nacional (2017). Available on: http://www.ssn.unam.mx/sismicidad/reportes-especiales/2017/SSNMX_rep_esp_20170907_Tehuantepec_M82.pdf

[2] Servicio Sismológico Nacional. *Sismo del día 19 de Septiembre de 2017(Mw 7.1)*. Special Report, Servicio Sismológico Nacional (2017). Available on: http://www.ssn.unam.mx/sismicidad/reportes-especiales/2017/SSNMX_rep_esp_20170919_Puebla-Morelos_M71.pdf

[3] Barker, M., Stone, H., Hammond, D. and O'Connell, J. *Field guide for building stabilization and shoring techniques*. Department of Homeland Security, USA (2011).

[4] FEMA. *Shoring Operations Guide*. U.S. Army Corps of Engineers, 2nd Edition, USA (2009).

[5] Corpo Nazionale dei Vigili dei Fuoco. *Vademecum STOP. Schede tecniche delle opere provvisionali per la messa in sicurezza post-sisma da parte dei Vigili del Fuoco*. Corpo Nazionale dei Vigili del Fuoco – Ministero dell'Interno, Roma (2010).

[6] Grimaz, S. Management of urban shoring during a seismic emergency: advances from the 2009 L'Aquila (Italy) earthquake experience. *Bolletino di Geofisica Teorica ed Applicata* (2011) **52**(2):341-355.

12th International Conference on Structural Analysis of Historical Constructions
SAHC 2020
P. Roca, L. Pelà and C. Molins (Eds.)

MACROELEMENT NUMERICAL SIMULATION OF THE SEISMIC RESPONSE OF A TIMBER-RETROFITTED MASONRY PIER

M. MIGLIETTA[1*], N. DAMIANI[1], S. BRACCHI[2], G. GUERRINI[2,3], F. GRAZIOTTI[2,3] AND A. PENNA[2,3]

[1] Understanding and Managing Extremes (UME) Graduate School
Istituto Universitario degli Studi Superiori di Pavia (IUSS Pavia)
Piazza della Vittoria 15, 27100 Pavia, Italy
Email: marco.miglietta@iusspavia.it - nicolo.damiani@iusspavia.it
Web page: http://www.iusspavia.it

[2] Dept. of Civil Engineering and Architecture (DICAr)
University of Pavia, via Ferrata 3, 27100 Pavia, Italy
Email: stefano.bracchi@unipv.it - gabriele.guerrini@unipv.it - francesco.graziotti@unipv.it - andrea.penna@unipv.it - Web page: http://dicar.unipv.it/

[3] European Centre for Training and Research in Earthquake Engineering (EUCENTRE)
Via Ferrata 1, 27100 Pavia, Italy
Email: gabriele.guerrini@eucentre.it - francesco.graziotti@eucentre.it - andrea.penna@eucentre.it
Web page: https://www.eucentre.it/

Keywords: Failure modes, in-plane shear-compression tests, nonlinear macroelement, numerical simulation, timber retrofit, unreinforced masonry.

Abstract. *In the North-East part of The Netherlands, induced seismicity due to gas extraction is affecting a local building stock consisting mainly of unreinforced masonry (URM) houses not designed for earthquake resistance. Experimental and numerical studies conducted at EUCENTRE, Pavia (Italy), have demonstrated that buildings with URM cavity-walls structural systems are among the most vulnerable existing Dutch construction typologies. A light and reversible retrofit system made of timber frames and oriented-strands boards was then designed and tested to increase the in-plane and out-of-plane capacities of masonry piers and to enhance their connections with the floor diaphragms. The development of modelling approaches able to simulate the influence of the retrofit system is of fundamental importance for future applications to real-case existing buildings and for vulnerability studies on different building stocks. Based on two quasi-static in-plane shear-compression tests on two full-scale masonry piers, one in bare and one in retrofitted configuration, a specific macroelement was calibrated to simulate the bare pier lateral response and the effects of the retrofit on the in-plane flexural and shear capacities. This paper discusses the adopted modelling strategies and the comparison between numerical and experimental results.*

1 INTRODUCTION

In recent years, human activities or natural phenomena (e.g. gas extraction [1,2,3] or slip of unknown faults [4]) have demonstrated the possibility that areas historically considered not

prone to seismic events can be subjected to earthquakes. Due to the unexpected nature of such occurrences, they usually hit regions where buildings do not typically incorporate seismic details, and therefore are highly vulnerable to lateral loads. Unreinforced masonry (URM) buildings constitute one of the most sensitive structural typologies in these areas; moreover, they usually include cultural heritage buildings and thus deserve particular attention.
Aiming at preserving these structures, several retrofit techniques have been developed for URM buildings in seismic regions. Some of them are based on the application of an additional material layer to the masonry [5,6], other ones on the application of steel profiles or of post-tensioning [7]. Furthermore, the seismic behavior of URM buildings can be effectively improved by enhancing the connections between masonry walls and floor systems[8,9]. However, structural strengthening in low-seismicity areas needs to be sustainable, light, reversible, and cost-effective.
A new retrofit system consisting of timber frames and oriented strand boards (OSB) was proposed and investigated through quasi-static in-plane shear-compression tests on two identical calcium-silicate (CS) masonry piers, one bare and one strengthened [10]. The experimental lateral responses of the specimens were then simulated with the software TREMURI by means of nonlinear macroelements. This paper focuses on the basic assumptions behind the nonlinear models and discusses the simulation of the response of the two piers. This study is part of a comprehensive experimental campaign aiming at the assessment and mitigation of the seismic vulnerability of URM buildings in the Groningen region of The Netherlands [11], recently interested by induced seismicity.

2 QUASI-STATIC IN-PLANE SHEAR-COMPRESSION TESTS

Two CS masonry piers with equal geometrical and mechanical properties, one in bare and one in retrofitted configuration, were subjected to quasi-static in-plane shear-compression tests at the EUCENTRE laboratories in Pavia (Italy), under the same vertical stress σ_v = 0.5 MPa and double-fixed boundary conditions. A detailed discussion on the strengthening intervention and on experimental results can be found in [10]. The tests allowed investigating the influence of the newly proposed timber retrofit system on the lateral capacity of the bare masonry pier. The campaign was complemented by mechanical characterization tests on masonry, bricks, and mortar.

2.1 Overview of the specimens and material properties

The specimens represented a first-storey loadbearing pier from the prototype of a URM Dutch terraced-house end-unit tested at the EUCENTRE facilities [11]. The building prototype consisted of URM cavity-walls, with a single-wythe internal loadbearing CS leaf and a single-wythe external clay veneer with no structural function. The specimens consisted of 33 courses of CS bricks, with average dimensions of 210 x 100 x 70 mm, and 10-mm-thick mortar joints, resulting in height H = 2.70 m, length L = 2.00 m, and thickness t = 0.10 m (Figure 1). The clay outer-leaf was not included because irrelevant for the seismic capacity of the specimens. The walls were built simultaneously and matured under the same environmental conditions, after which, on one of the two was strengthened.
The retrofit system consisted of a timber frame made of vertical posts and horizontal blockings, fastened to the masonry (Figure 1b, c and d). Horizontal top and bottom sill plates allowed

connecting the frame to reinforced concrete (RC) footing and top beam. All timber elements had a section of 60 x 80 mm, where the 60-mm dimension was oriented perpendicular to the wall. Steel tie-down connections were provided between posts and RC top and bottom elements through the sill plates, to ensure in-plane flexural and sliding resistance. 18-mm-thick OSB were nailed to the timber frame to enhance the pier shear capacity.
The masonry mechanical parameters of interest, obtained from characterization tests, are reported in Table 1. The timber was red solid fir (Picea-abies) of class S10/C24 [12] with a density of 517 kg/m^3, mean Young modulus $E_{0,mean}$ = 11000 MPa and shear modulus $G_{0,mean}$ = 690 MPa, and characteristic tensile strength parallel to the fibers $f_{t,0}$ = 14 MPa. The OSB were classified as OSB/3 [13] with a density of 572 kg/m3. Tie-down connectors had a characteristic tensile strength of 11.6 kN [14].

2.2 Experimental results

The unstrengthened specimen exhibited a hybrid flexural and shear-sliding response (Figure 2a). The development of a full-length crack between the 32nd and 33rd brick courses at a drift ratio (top displacement divided by *H*) of 0.20 % determined the transition from flexural rocking to shear sliding. The lateral strength reached its peak of 78 kN at this drift ratio, then it decreased to a residual value of about 65 kN. The test was interrupted when the specimen lost its vertical load-bearing capacity at an ultimate drift of 0.75%.

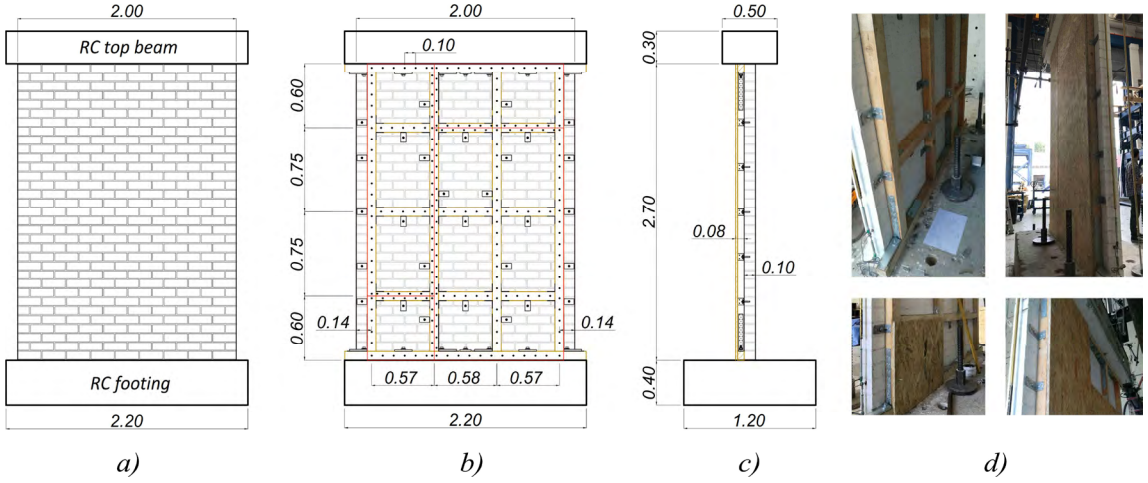


Figure 1: Specimen geometries and details: a) bare pier; b, c, d) retrofitted pier.

Table 1: Masonry mechanical properties.

	Mean	C.o.V.
Density (ρ)	1836 kg/m^3	0.01
Compressive strength (f_m)	10 MPa	0.06
Young modulus (E_m)	6593 MPa	0.09
Initial shear strength (f_{v0})	0.62 MPa	-
Shear friction coefficient (μ)	0.71	-

The retrofitted specimen exhibited 35%-higher strength and 166%-higher displacement capacity compared to the bare pier. The maximum lateral force of 105 kN was reached at a drift ratio of 0.8%. The retrofit prevented shear sliding and forced a flexural rocking response up to 1.0% drift ratio. The pier strength decreased during the last two sets of cycles upon diagonal shear cracking of the masonry. The test was terminated at a drift of 2.0% when the timber system was supporting most of the applied vertical load. It is worth noting that both specimens exhibited a first cracking drift ratio of 0.075%: the strengthening system did not have any effect on the first cracking due to its lower stiffness compared to the masonry.

3 NUMERICAL SIMULATION OF THE TESTS

The assessment of the seismic vulnerability of buildings requires reliable numerical models capable to capture the main features of the actual structural response. For this reason, two-dimensional numerical models of the tested piers were built and validated against the experimental results using the software TREMURI [15], which employs nonlinear macroelements [16]. Each pier was discretized in a series of macroelements of equal length, as proposed by [17] to model reinforced masonry. This strategy was adopted to capture the effect of the timber posts (Figure 1) on the axial-flexural response of the pier: in fact, they act as longitudinal reinforcement bridging cracks. The rotations of top and bottom nodes were restrained to impose double-fixed boundary conditions.

3.1 Nonlinear macroelement

The macroelement implemented in TREMURI is capable to reproduce shear and flexural failure modes, as well as the transition from one mode to the other one due to axial force variations. The numerical flexural behavior relies on a nonlinear degrading model for rocking damage, allowing consideration of finite masonry compressive strength and stiffness degradation due to toe-crushing (Figure 3a).

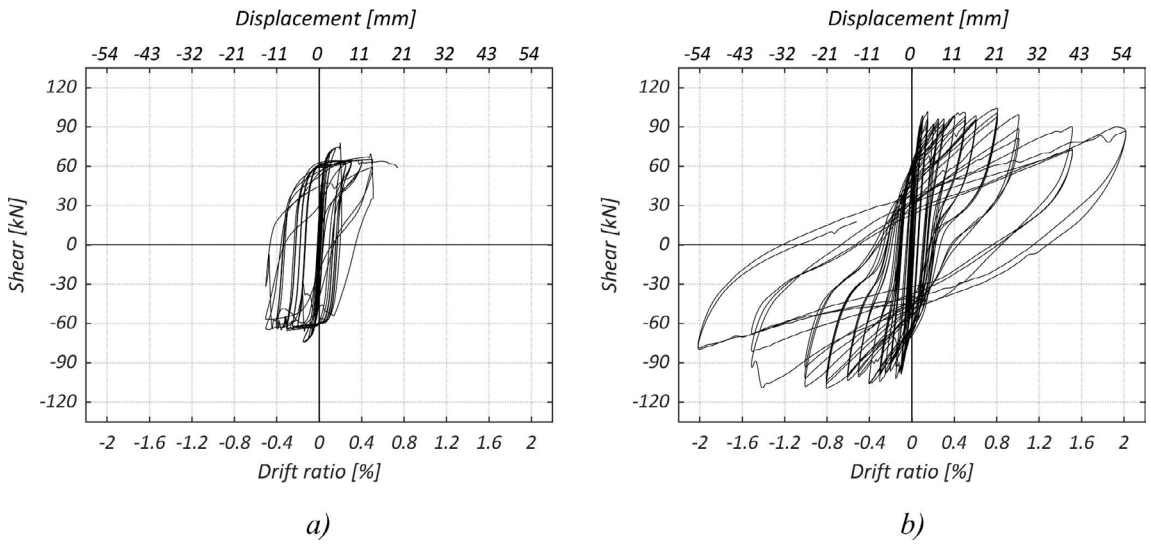


Figure 2: Experimental hysteretic responses: a) bare pier; b) retrofitted pier.

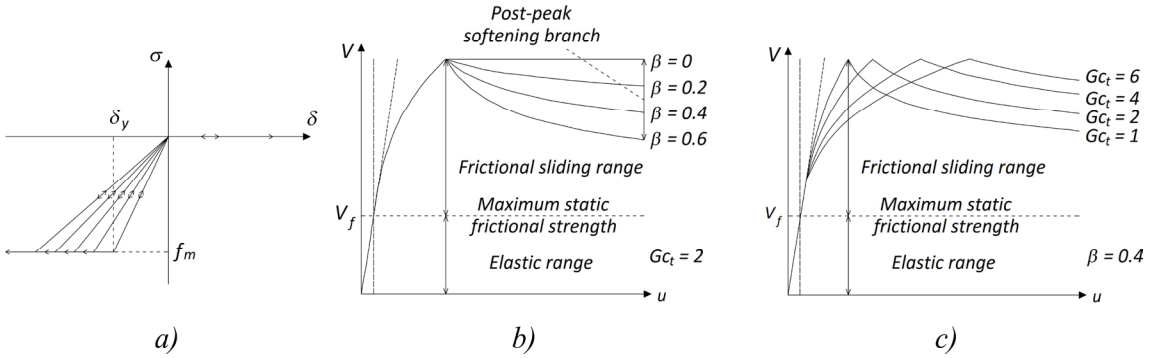


Figure 3: Nonlinear macroelement behavior: a) nonlinear flexural degrading model; b) role of parameter β on the shear model; c) role of parameter Gc_t on the shear model.

The shear model is characterized by elastic, inelastic, and sliding ranges, with a post-peak softening branch that tends asymptotically to a residual static frictional strength. Parameters β (softening parameter, Figure 3b) and Gc_t, (nonlinear deformability parameter, Figure 3c) control the transition from peak to residual shear strength and the displacement at peak strength, respectively. For all shear failure criteria presented in the following paragraph, β and Gc_t were kept constant as 0.5 and 1.1, respectively.

3.2 Bare pier numerical model

The values of masonry mean elastic modulus (E_m = 6593 MPa) and compressive strength (f_m = 10 MPa) obtained from material characterization tests were assigned directly to the macrolement. The shear modulus was conventionally taken as G_m = 0.35 E_m [10]. The masonry shear resistance is implemented as a Coulomb failure criterion in TREMURI:

$$V_{Rd} = L \cdot t \cdot (\tilde{f}_{v0,mas} + \tilde{\mu}_{mas} \cdot \sigma_v) \tag{3.1}$$

where L and t are the length and thickness of the pier; $\tilde{f}_{v0,mas}$ is the equivalent initial shear strength parameter; $\tilde{\mu}_{mas}$ is the equivalent friction coefficient; and σ_v is the mean compression stress applied on the pier.

Four different strategies were followed to calculate the equivalent parameters $\tilde{f}_{v0,mas}$ and $\tilde{\mu}_{mas}$. The first two cases were obtained by computing them from the diagonal shear failure criterion for regular masonry, according to the Italian building code [18]:

$$V_{Rd} = \frac{L \cdot t}{b} \cdot \left(\frac{f_{v0}}{1 + \mu \cdot \Phi} + \frac{\mu}{1 + \mu \cdot \Phi} \cdot \sigma_v \right) \tag{3.2}$$

where b is a coefficient depending on the pier slenderness, which can by assumed equal to 1.5; t is thickness of the pier; f_{v0} is the initial shear strength of the masonry material; and μ is the shear friction coefficient of the masonry material. Parameter Φ is the average slope of a stair-stepped crack computed as:

$$\Phi = \frac{2h_{brick}}{b_{brick}} \tag{3.3}$$

where b_{brick} and h_{brick} are the length and height of a brick in the shear plane. Equivalent initial shear strength and equivalent friction coefficient are then defined as:

$$\tilde{f}_{v0,mas} = \frac{f_{v0}}{b \cdot (1 + \mu \cdot \Phi)} \tag{3.4}$$

$$\tilde{\mu}_{mas} = \frac{\mu}{b \cdot (1 + \mu \cdot \Phi)} \tag{3.5}$$

Two cases stemmed from this approach, using either the standard mechanical properties suggested by the code or the actual values obtained through material characterization tests (Table 1). Substituting the experimental masonry mechanical properties (Table 1) into equations 3.4 and 3.5, values $\tilde{f}_{v0,mas}$ = 0.28 MPa and $\tilde{\mu}_{mas}$ = 0.32 were obtained. In the second case, the friction coefficient μ = 0.577 suggested by the Italian code [18] was adopted, while keeping the experimental value f_{v0} = 0.61 MPa; this resulted in equivalent parameters $\tilde{f}_{v0,mas}$ = 0.3 MPa and $\tilde{\mu}_{mas}$ = 0.28.
Similarly, two other cases were derived based on the shear-sliding failure criterion, defined as [19,20]:

$$V_{Rd} = V_{R,fvo} + V_{R,\mu} = L \cdot t \cdot \left(\frac{f_{v0} \cdot L_c}{L} + \mu \cdot \sigma_v\right) \tag{3.6}$$

where L is the pier length and L_c the compressed length of the cracked cross-section. The latter can be computed neglecting the tensile strength of bed-joints and assuming a simplified distribution of stresses, with upper bound given by the entire pier length and lower bound by the neutral-axis depth at ultimate flexural conditions [19]:

$$L\ \frac{\sigma_v}{\eta \cdot \lambda \cdot f_m} \leq L_c = 1.5 \cdot L \cdot \left(1 - \alpha_v \frac{3 \cdot f_{v0} + 2 \cdot \mu \cdot \sigma_v}{\sigma_v\ + 3 \cdot f_{v0} \cdot \alpha_v}\right) \leq\ L \tag{3.7}$$

where $\alpha_v = M/(V \cdot L)$ is the shear-span ratio, assumed equal to 0.67; and η and λ are the stress-block intensity and depth parameters, respectively equal to 0.85 and 0.80.
The equivalent friction coefficient ($\tilde{\mu}_{mas}$) in this case coincides with the material one, while the equivalent initial shear strength can be obtained as:

$$\tilde{f}_{v0,mas} = \frac{f_{v0} \cdot L_c}{L} \tag{3.8}$$

In one case, substituting the experimental initial shear strength (Table 1) in equation 3.8, a value $\tilde{f}_{v0,mas}$ = 0.045 MPa was calculated, to be used in combination with experimental $\tilde{\mu}_{mas} = \mu$ = 0.71. In the other case, the equivalent initial shear strength was still derived from experimental properties as $\tilde{f}_{v0,mas}$ = 0.045 MPa, while the equivalent friction coefficient $\tilde{\mu}_{mas} = \mu$ = 0.4 was taken according to the Italian building code [18].

3.3 Retrofitted pier numerical model

Starting from the outcomes of the bare pier calibrated model, the simulation of the retrofitted specimen experimental response required additional considerations. The connections between masonry and timber grant deformation compatibility, with the actual mechanism controlled by

the lower total strength of the combined masonry/timber system. Furthermore, the flexural and shear strength contributions of the timber system need to be modelled separately since they are provided by different components. While the former is governed by yielding of tie-down connections between vertical posts and RC top beam and footing, the latter is given only by the nailed OSB.

In light of these considerations, the vertical posts were modelled by nonlinear beam elements, discretized in segments of equal length and connected to the same top, bottom, and intermediate nodes as the discretized macroelements (Figure 4). The intermediate segments of each post were assigned the timber member properties: mean elastic moduli ($E_{0,mean}$ = 11000 MPa and $G_{0,mean}$ = 690 MPa), characteristic tensile strength ($f_{t,0}$ = 14 MPa), and cross-sectional area and moment of inertia (A_p = 4800 mm^2 and I_p = 2.56x10^6 mm^4). Instead, the top and bottom end-segments were modelled with equivalent elastic moduli (E_{eq} = 11732 Mpa and G_{eq} = 4106 MPa) and strength ($f_{y,eq}$ = 2.66 MPa), computed to restitute the actual axial force-displacement relationship of the tie-down connector over its free length between fasteners, assigning cross-sectional area A_p as for the timber members and zero moment of inertia. The equivalence on the material properties was required by the different end-segment lenght and cross-sectional area, compared to the actual free length and resisting area of the steel connector. Before calculating $f_{y,eq}$, a factor 1.1 was applied to the characteristic yield strength of the connector to estimate its expected value [21].

The contribution of the OSB to the shear resistance was accounted through an equivalent friction coefficient ($\tilde{\mu}_{tot}$). Knowing the axial compression acting at mid-height of the pier ($N_{Ed,mid}$) and the shear resistance offered by the panels ($V_{Rd,tim,s}$), the equivalent friction coefficient can be found by adding the contribution of the timber retrofit ($\tilde{\mu}_{tim}$) to the one calibrated for the bare pier ($\tilde{\mu}_{mas}$ from section 3.2):

$$\tilde{\mu}_{tim} = \frac{V_{Rd,tim,s}}{N_{Ed,mid}} \tag{3.9}$$

$$\tilde{\mu}_{tot} = \tilde{\mu}_{mas} + \tilde{\mu}_{tim} \tag{3.10}$$

Given the axial compression $N_{Ed,mid}$ = 106 kN and the expected panel shear strength $V_{Rd,tim,s}$ =45 kN [10,21,22], equation 3.9 resulted in $\tilde{\mu}_{tim}$ = 0.42.

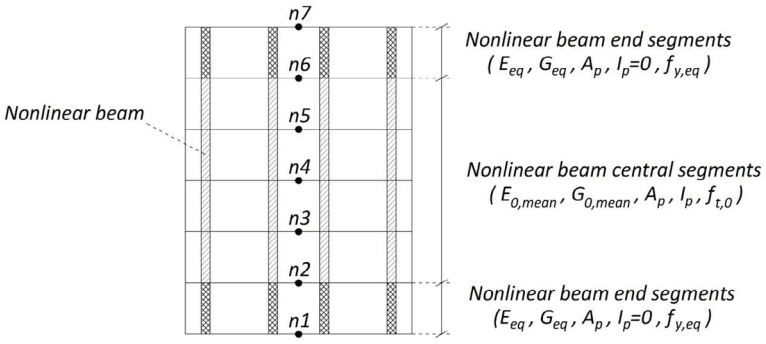


Figure 4: Retrofitted pier model.

3.4 Calibration of the models

The results of both simulations based on the diagonal shear failure criterion showed very similar numerical responses, initially governed by a flexural behavior followed by a shear-sliding one (Figure 5a and b). While the flexural part approximates well the experimental response, the transition to shear-sliding was predicted at an earlier drift ratio than in reality. Moreover, the predicted residual shear strength was lower than the experimental one, and the strength drop from rocking to sliding behavior appeared overestimated, denoting an excessive influence of the cohesive contribution to the total strength of the pier.

Looking at the numerical results of the two models based on the shear-sliding failure criterion, two essentially different outcomes were obtained. The use of the friction coefficient from material characterization tests induced a flexure-only response (Figure 5c), denoting that the model was overestimating the shear-sliding resistance. On the other hand, the use of the equivalent friction coefficient suggested by the Italian code [18] led to a shear-only response, due to a significant underestimation of the specimen shear strength (Figure 5d): the flexural mechanism could not be activated in this case, since the shear-sliding resistance was too low and governed the response from the very beginning. However, comparing all numerical results, the models based on the shear-sliding failure criterion were deemed to be more appropriate since the real behavior of the bare pier was hybrid, with a transition from rocking to sliding, and no diagonal shear failure was triggered.

The experimental bare pier behavior was initially very similar to the numerical flexural response of Figure 5c, then it switched to a sliding-shear behavior similar to the numerical one of Figure 5d, but with higher residual strength. Accordingly, the equivalent friction coefficient was selected to obtain the experimental residual shear-sliding strength: the ratio between the residual strength (65 kN) and the applied vertical load at mid-height of the pier (106 kN) resulted in an equivalent friction coefficient $\tilde{\mu}_{mas}$ = 0.60, which is 15% smaller than the one obtained from material characterization tests. The initial shear strength $\tilde{f}_{v0,mas}$ = 0.12 MPa was then calibrated to match the switch of governing behavior at 0.20% of drift ratio. The final outcome of the procedure is showed in Figure 6a. Negligible errors, less than 1% and 3%, were obtained in terms of simulated maximum and residual strengths, respectively.

Figure 6b compares the numerical response of the retrofitted pier model with the experimental one. The strategy adopted to simulate the influence of the retrofit system on the bare pier capacity captured the experimental behavior with good approximation and did not require any calibration or iteration. Negligible errors, less than 4%, were obtained in terms of specimen strength. Combining the elastoplastic hysteresis of the beam segments simulating tie-down connections, with the nonlinear elastic rocking response of the masonry pier, resulted in a flag-shaped overall hysteretic behavior, which approached the actual dissipative response of the retrofitted pier. Minor discrepancies were observed because the additional energy dissipated by friction at crack interfaces and connections was not captured, as well as the initial accumulation of small residual displacements. Furthermore, the model was not able to reproduce the development of diagonal shear cracking beyond 1.0% drift ratio, which ultimately led to failure of the retrofitted specimen. Overall, despite these small discrepancies, the simulation successfully reproduced the experimental behaviour of the retrofitted pier.

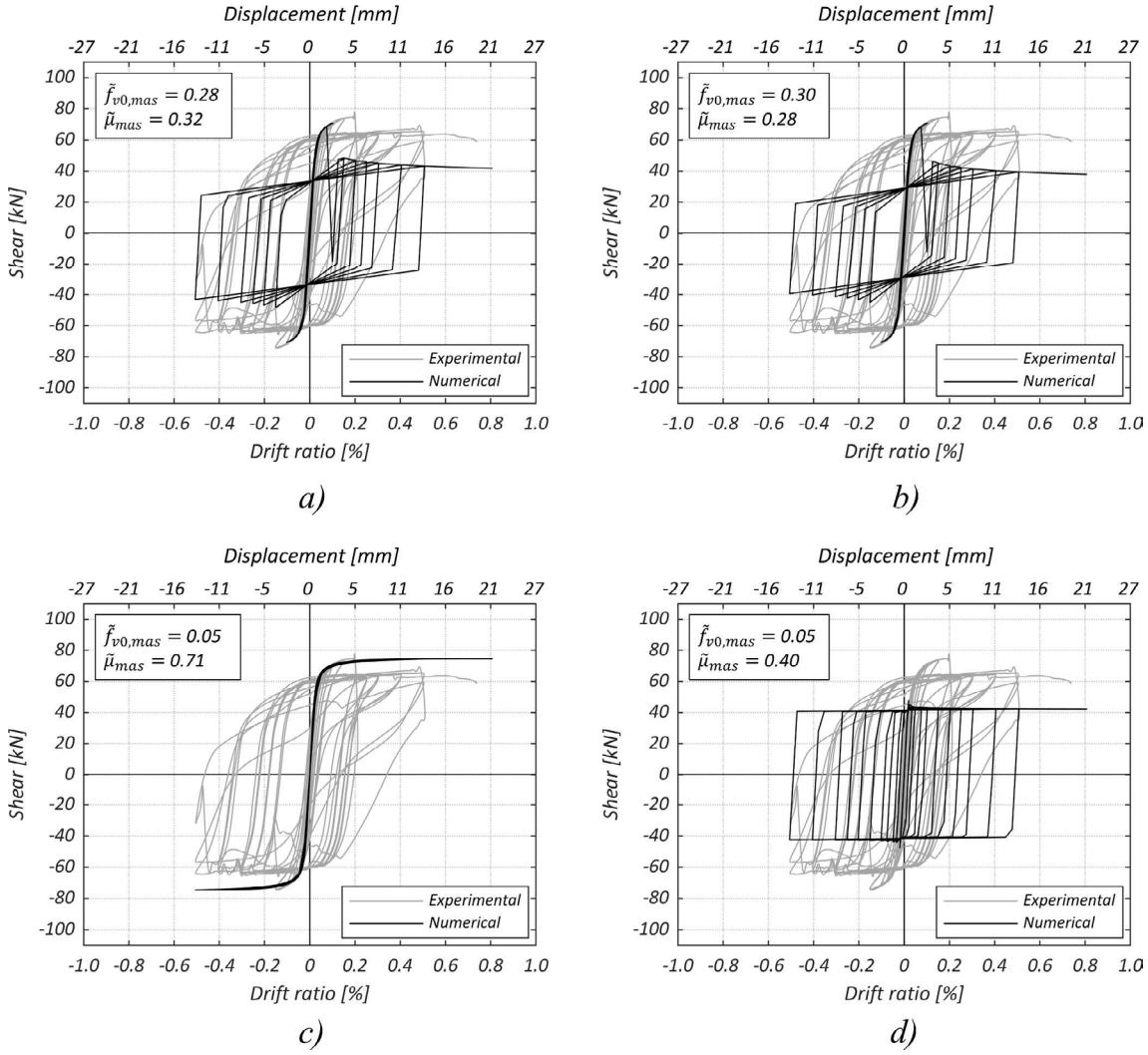


Figure 5: Bare pier numerical and experimental responses: a) diagonal shear failure criterion with friction coefficient from material characterization; b) diagonal shear failure criterion with friction coefficient suggested by [18]; c) shear-sliding failure criterion with friction coefficient from material characterization; d) shear-sliding failure criterion with friction coefficient suggested by [18].

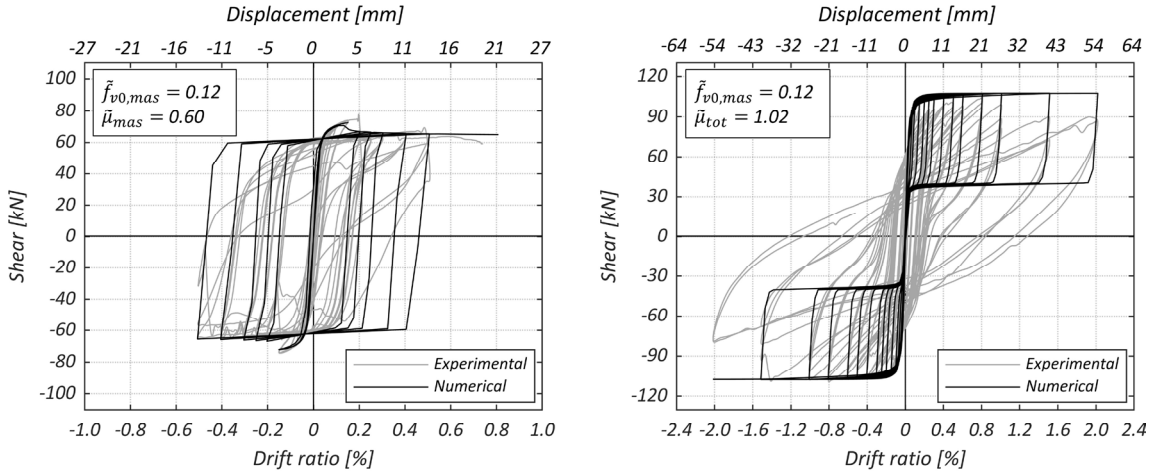


Figure 6: Numerical and experimental responses after model calibration: a) bare pier; b) retrofitted pier.

4 CONCLUSIONS

This paper discussed the numerical simulation of two in-plane shear-compression tests performed on two identical calcium-silicate masonry piers, one in bare conditions and one retrofitted with a newly proposed timber system. The retrofit consisted of timber frames, mechanically connected to the masonry and to top and bottom RC elements to increase the pier flexural capacity, and OSB panels nailed to the timber frame to enhance also the shear strength. The software TREMURI was used to simulate the experimental response, with discretized nonlinear macroelements constituting the piers and nonlinear beam elements modeling the timber frames and their connections to RC footing and top beam.

First, the macroelement properties were calibrated to reproduce the bare masonry pier performance, starting from mechanical material properties and common failure criteria and applying some corrections. Recognizing a hybrid failure mode which transitioned from flexural rocking to sliding-shear, an equivalent friction coefficient was adopted based on the experimental residual lateral strength and applied axial compression. Then, the equivalent initial shear strength was calibrated to force the transition from rocking to sliding mode at 2.0% drift ratio, as recorded in the experiment. The masonry elastic modulus and compressive strength from material characterization did not require any adjustment. The peak and residual lateral strength of the bare pier were then captured with errors of less than 1% and 3%, respectively.

After calibration of the bare masonry pier, additional considerations were necessary to reproduce the behavior of the retrofitted one. Vertical posts were explicitly modelled as nonlinear beam elements, discretized in segments and connected to the same top, bottom, and intermediate nodes as the discretized macroelements. The contribution to the shear resistance of the specimen, provided by the nailed OSB, was simulated instead by increasing the friction coefficient of the masonry macroelements. The numerical strength approached the experimental one with an error of less than 4%, without any calibration or iteration, and reproduced with good approximation the flag-shaped hysteretic cycles. However, the model did not capture the

development of diagonal shear cracking beyond 1.0% drift ratio, which ultimately led to failure of the retrofitted specimen.

Acknowledgements. This work is part of the EUCENTRE project "Study of the vulnerability of masonry buildings in Groningen", within the research programme framework on hazard and risk of induced seismicity in the Groningen province, sponsored by the Nederlandse Aardolie Maatschappij BV (NAM). The modelling activity was funded by the DPC-ReLUIS within the framework of the Work-Package-5 2019-2021: "Interventi di rapida esecuzione a basso impatto ed integrati". The authors would like to thank all parties involved in this project: the DICAr Laboratory of the University of Pavia and the EUCENTRE Laboratory, which performed the tests, the DPC-ReLUIS and the partner NAM.

REFERENCES

[1] Bourne, S.J., Oates, S.J., Bommer, J.J., Dost, B., van Elk, J., & Doornhof, D. A Monte Carlo method for probabilistic hazard assessment of induced seismicity due to conventional natural gas production. *Bulletin of the Seismological Society of America* (2015) **105(3)**: 1721-1738.

[2] Crowley, H., Pinho, R., van Elk, J., & Uilenreef, J. Probabilistic damage assessment of buildings due to induced seismicity. *Bulletin of Earthquake Engineering* (2019) **17(8)**: 4495-4516.

[3] Graziotti, F., Penna, A., & Magenes, G. A comprehensive in situ and laboratory testing programme supporting seismic risk analysis of URM buildings subjected to induced earthquakes. *Bulletin of Earthquake Engineering* (2018) **17(8)**: 4575-4599.

[4] Horton Jr., J.W. & Williams, R.A. The 2011 Virginia earthquake: What are scientists learning? *Eos, Transactions American Geophysical Union* (2012) **93(33)**: 317-318.

[5] Babaeidarabad, S., Arboleda, D., Loreto, G., & Nanni, A. Shear strengthening of un-reinforced concrete masonry walls with fabric-reinforced-cementitious-matrix. *Construction and Building Materials* (2014) **65**: 243-253.

[6] Giaretton, M., Dizhur, D., Garbin, E., Ingham, J. M., & da Porto, F. In-plane strengthening of clay brick and block masonry walls using textile-reinforced mortar. *Journal of Composites for Construction* (2018) **22(5)**: 04018028.

[7] Ma, R., Jiang, L., He, M., Fang, C., & Liang, F. Experimental investigations on masonry structures using external prestressing techniques for improving seismic performance. *Engineering Structures* (2012) **42**: 297-307.

[8] Podestà, S., & Scandolo, L. Earthquakes and Tie-Rods: Assessment, Design, and Ductility Issues. *International Journal of Architectural Heritage* (2019) **13(3)**, 329-339.

[9] Senaldi, I. E., Guerrini, G., Comini, P., Graziotti, F., Penna, A., Beyer, K., & Magenes, G. Experimental seismic performance of a half-scale stone masonry building aggregate. *Bulletin of Earthquake Engineering* (2019) 1-35.

[10] Guerrini, G., Damiani, N., Miglietta, M. & Graziotti, F. Cyclic response of masonry retrofitted with timber frames and boards. *Structures and buildings* (2020) in press. DOI: 10.1680/jstbu.19.00134.

[11] Damiani, N., Miglietta, M., Mazzella, L., Grottoli, L., Guerrini, G., & Graziotti, F. *Full-scale shaking table test on a Dutch URM cavity-wall terraced-house end unit – A retrofit solution with strong-backs and OSB boards – EUCBUILD-7*. Research report

EUC052/2019U, (2019) EUCENTRE Pavia, Italy.
[12] European Committee for Standardization (CEN). EN 14081-1: Timber Structures. Strength graded structural timber with rectangular cross section. Part I: General requirements. European Committee for Standardization (2016), Brussels, Belgium.
[13] European Committee for Standardization (CEN). EN 300: Oriented Strand Boards (OSB). Definitions, classification and specifications (2006), Brussels, Belgium.
[14] Rothoblaas. Wood connectors and timber plates (2015). https://www.rothoblaas.com/catalogues-rothoblaas.
[15] Lagomarsino, S., Penna, A., Galasco, A., & Cattari, S. TREMURI program: an equivalent frame model for the nonlinear seismic analysis of masonry buildings. *Engineering structures* (2013) **56**: 1787-1799.
[16] Penna, A., Lagomarsino, S., & Galasco, A. A nonlinear macroelement model for the seismic analysis of masonry buildings. *Earthquake Engineering & Structural Dynamics* (2014) **43(2)**: 159-179.
[17] Bracchi, S., Mandirola, M., Rota, M. & Penna, A. A new macroelement-based strategy for modelling reinforced masonry piers. *17th International Brick and Block Masonry Conference* (2020).
[18] Ministero delle infrastrutture e dei trasporti. Aggiornamento delle Norme tecniche per le costruzioni. Gazzetta Ufficiale (2018). Rome, Italy.
[19] Magenes, G., & Calvi, G. M. In-plane seismic response of brick masonry walls. *Earthquake engineering & structural dynamics* (1997) **26(11)**: 1091-1112.
[20] Eurocode 6. Design of masonry structures. Part 1-1: General rules for buildings. Rules for reinforced and unreinforced masonry (2005). British Standard Institution, London.
[21] American Society of Civil Engineers (ASCE). ASCE/SEI 41-17: Seismic evaluation and retrofit of existing buildings (2017). Reston, Virginia, USA.
[22] American Wood Council (AWC). ANSI/AF&PA SDPWS-2008: Special design provisions for wind and seismic (2018). Washington, DC.

12th International Conference on Structural Analysis of Historical Constructions
SAHC 2020
P. Roca, L. Pelà and C. Molins (Eds.)

MECHANICAL CHARACTERIZATION OF ENERGY DISSIPATION DEVICES IN RETROFIT SOLUTION OF REINFORCED CONCRETE FRAMES COUPLED WITH SOLID WOOD PANELS

CAROLA TARDO[1*], FRANCESCO BOGGIAN[2], MAGNUS HATLETVEIT[3], EDOARDO M. MARINO[1], GIUSEPPE MARGANI[1], AND ROBERTO TOMASI[3]

[1]Department of Civil Engineering and Architecture (DICAr), University of Catania
via S. Sofia 64, 95123 Catania, Italy
e-mail: carola.tardo@unict.it (*corresponding author)

[2] Department of Civil, Environmental and Mechanical engineering, University of Trento
via Mesiano 77, 38123 Trento, Italy

[3] Faculty of Science and Technology, Norwegian University of Life Sciences
Drøbakveien 31, 1430 Ås, Norway

Keywords: Seismic renovation, Reinforcement, RC frame, CLT, Steel Dissipation device

Abstract. *Deep renovation interventions on existing buildings remain currently unattractive due to technical, financial and cultural/social barriers. Now that the European Union 2018 Energy Performance Directive aims to "reach the long-term greenhouse gas emission goal and decarbonize the building stock", Member States may use their long-term renovation strategies to address risks also related to fire hazards and seismic loads in addition to energy renovation. This opens a wider market for innovative approaches in retrofit of existing buildings.*

The current paper illustrates the primary outcomes of an ongoing multidisciplinary Horizon 2020 research project (called e-SAFE), tackling the integration of energy, seismic and architectural renovation interventions through an innovative and combinable technological solution, applicable to non-historic RC framed buildings (i.e. built after 1950) and easily adaptable to specific climatic conditions, seismicity levels and other boundary conditions. Hence, the proposed solution will contribute to the de-carbonization of the EU building stock, reducing the occurrence of natural hazards related to climate changes, and, at the same time, to the improvement of the social resilience against earthquakes and to the enhancement of buildings architectural image.

The seismic retrofit technology consists in the external application of modular prefabricated Cross Laminated Timber (CLT) panels on the existing perimetral walls. These panels are connected to the beams of two consecutive floors by means of friction dampers and provide additional lateral stiffness and strength to the existing structure, thus reducing the storey drift demand in case of earthquake. The friction dampers cut the force transmitted by the CLT panel to the structure and dissipate energy, which further reduce the drift demand. Strength, stiffness and dissipation capacity provided by the system are controlled by modulating the thickness and the number of CLT panels, as well as the friction dampers size.

In this research phase, friction damper prototypes have been designed in order to optimize

both mechanical performance and production process. Detailed numerical models allowed to investigate the stress distribution in the dissipative connections. The results of the preliminary testing campaign will be presented and discussed in this paper, also in relation with the findings of the numerical analysis and future tests.

1 INTRODUCTION

A recent issue in the building renovation sector is the need of innovative and holistic design approaches, which combine both energy-efficient and anti-seismic interventions in order to meet the current Energy Performance of Buildings Directive (EPBD) [1], meanwhile improve the social resilience against earthquakes. In fact, in European seismic countries, most of the existing buildings (around 50% of the residential stock) were built between the 1950s and 1990s, before the enforcement of the most recent energy and seismic codes [2]. Therefore, these buildings are highly energy-intensive, thus contributing to the increase in greenhouse gas (GHG) emissions and, consequently, to the climate changes and related natural hazards (e.g. floods, hurricanes, torrential rainfall, windstorms). At the same time, they are extremely vulnerable to seismic excitation, since only gravity loads were considered at the design stage, according to the old standards. Typically, these buildings are multi-storey and have a reinforced concrete (RC) frame structure with infill walls made of brittle hollow clay bricks. RC frames are often oriented along one-direction and poor structural details usually characterize members and joints, resulting in low strength, stiffness and deformation capacity of the structure in relation to lateral actions. In the event of a severe earthquake, extensive damages or collapse of these buildings are likely to occur causing considerable human and economic losses, as well as environmental harm. For instance, in Italy, in the last two centuries, earthquakes have caused about 160.000 deaths and, in the last 50 years, over €180 billion monetary losses [3] .

Combining energy-efficient retrofitting with seismic upgrading is then required in order to reduce the seismic risk in the European territory, also contributing to improve the attractiveness of deep renovation strategies on the existing buildings.

However, current techniques for seismic retrofitting of RC framed buildings are often very expensive, time-consuming, invasive and not reversible. Furthermore, they also are highly waste producers, resulting poorly accessible and low environmentally friendly, especially in view of a renovation that should involve most of the existing building stock. These techniques aim at increasing the strength, stiffness and deformation capacity of the structure or reducing the seismic demand. They include the jacketing of the existing structural elements with steel, RC, fibre-reinforced polymer (FRP) or textile-reinforced mortar (TRM) [4-7], the addition of new RC shear walls or steel-braced frames, located inside or outside of the existing building [8], and the installation of energy dissipation devices or base isolators [9-10].

Recently, several researches have proposed innovative integrated seismic and energy renovation solutions based on external-dry installation and on the use of low-carbon recycled or recyclable materials such as solid wood panels, e.g. Cross Laminated Timber Panels (CLT) [11]. CLT panels coupled with an insulation layer and finishing materials have been investigated in replacement of the existing masonry infill walls of RC framed buildings [12] or in addition to the external walls [13], with the main purpose of increasing the overall lateral stiffness of the structure. Special dissipative connections between CLT panels and building RC frame have also been preliminarily examined in order to provide the existing structure with

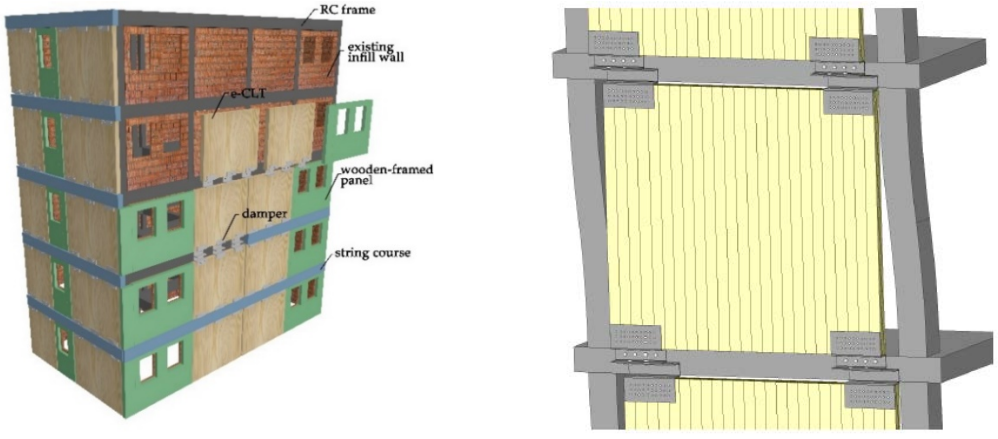
additional seismic energy dissipation capacity [13], but more comprehensive investigations on new potential dissipative devices are required in order to optimize their structural efficiency, durability and industrial replicability.

In this framework, the paper illustrates the first outcomes of an ongoing multidisciplinary Horizon 2020 project, called e-SAFE (energy and Seismic AFfordable rEnovation solutions), aimed at investigating innovative and combinable integrated retrofitting interventions. The seismic technology (named e-CLT) that drives this intervention is based on the use of modular prefabricated CLT panels equipped with innovative energy dissipation devices.

2 e-CLT SYSTEM

The e-CLT technology consists in the external application of prefabricated CLT structural panels on the outer walls of the existing building, by connecting them to the RC beams through innovative friction dampers (Figure 1a). In occurrence of moderate ground motions, the dampers rigidly connect CLT panels to the RC structure, thus making available additional lateral stiffness and strength. Conversely, friction dampers activate in occurrence of strong ground motions, thus dissipating part of the input seismic energy (Figure 1b). These two features of the e-CLT system reduce the storey drift demand of the structure and, consequently, the damage to non-structural and structural components. Strength, stiffness and dissipation capacity provided by the proposed system are controlled by modulating the thickness and the number of CLT panels, as well as the damper size.

The integrated retrofitting intervention under investigation aims to combine the e-CLT technology with non-structural pre-assembled panels made of wooden frames and provided with high-performing windows that will replace the existing ones. Both structural and non-structural panels integrate bio-based insulation materials and the desired finishing layer, in order to improve also the energy performance and the architectural image of the renovated building [14]. Cladding solutions integrated to both panels or separated string courses allow to cover the RC beams and protect the dampers, while providing the building with architectural uniformity. One important feature of the proposed system is that is can be applied from the outside of the building, thus limiting the discomfort for internal users.



(a) (b)

Figure 1: (a) Components of the integrated retrofitting system and (b) e-CLT technology under seismic loads

3 PROPOSED FRICTION DAMPERS

Currently, the friction damper is under study with the main purpose of optimizing its shape to meet the needs of structural, technological and industrial efficiency. Specifically, four configurations of the proposed friction damper have been here investigated, in order to identify potential limits and advantages for each one (Figure 2a-d).

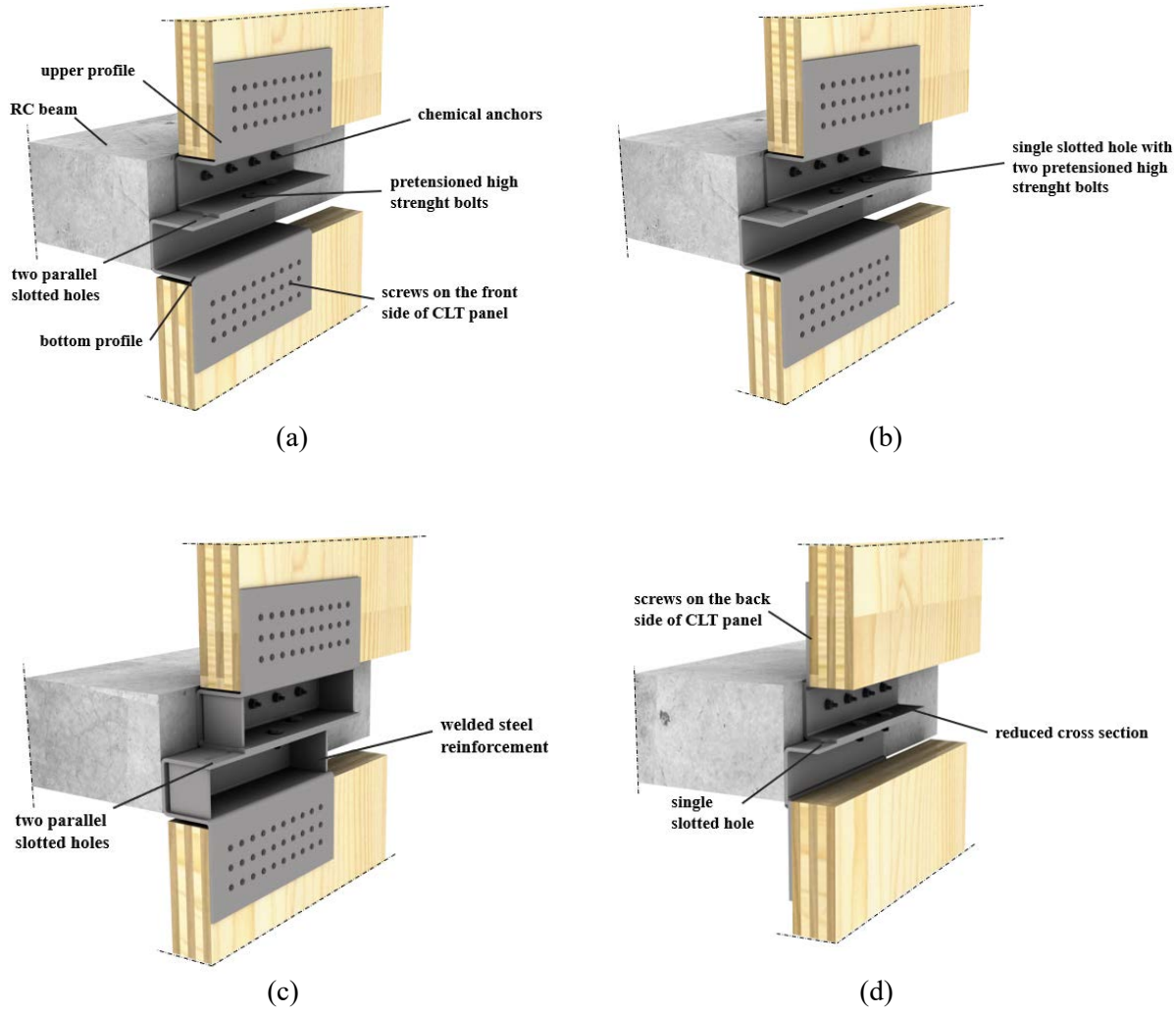


Figure 2: Friction damper configurations under study: (a) STD, (b) STD-1H, (c) STD-R; (d) ALT. (Abbreviations: STD=Standard; R=Reinforcement; H=Hole; ALT= Alternative)

In all the analysed configurations the damper consists of two cold bent steel profiles that connect the CLT panels of two consecutive storeys with the existing interposed RC beam. The upper profile is connected to the RC beam by anchor bolts. The bottom profile is provided with slotted holes and is connected to the upper one by pretensioned high strength bolts. Common timber screws connect both the upper and bottom profile to the CLT panels. The shear force is transmitted between the two profiles by means of the friction exerted in the contact surface.

During earthquake, when the force transmitted by the damper attains the value of the friction force, the upper profile slides on the other one and dissipates seismic energy. The activation of the sliding movement between the two profiles by a predefined force allows to control the internal forces on both the damper components (steel profiles and fasteners) and CLT panels, thus properly dimensioning them and limiting or avoiding damage of these elements and the need of their replacement after the seismic event.

Specifically, in the standard configuration (damper STD in Figure 2a) the friction connection consists of two pretensioned bolts located in parallel slotted holes and the CLT/steel connections are on the front side of the CLT panels. The standard design has also been investigated in two slightly modified additional configurations: with the two pretensioned bolts located in a single centred slotted hole (damper STD-1H in Figure 2b), and with additional welded steel reinforcements at the outer edges of the bent sections of both profiles (damper STD-R in Figure 2c).

Instead, in the alternative configuration (damper ALT in Figure 2d) the CLT-steel connections are on the back side of the CLT elements, the profiles cross section is reduced and the two pretensioned bolts are in the same centred slotted hole, located closer to the vertical edge of the upper profile, in order to decrease the eccentricity of the connection. For this design, both the upper and bottom profile consists of two separate plates, welded together with a small overlap to create a gap to fit the screw heads without risking rubbing between the profiles and the RC beams. Countersunk holes in the steel plates for the screw heads have been avoided because they make industrial production more complex.

In this work, the prototypes are 450 mm wide, 8 mm thick and are made of S235 steel.

Concrete/steel connection consists of four M14 concrete anchors with 90 mm spacing, while the friction connection is provided by two M14 high strength pretensioned bolts.

The slotted holes are 240 mm long in the two-holes configurations and 370 mm in the single-hole one, assuming a building storey drift equal to 3% of the common RC building storey height, i.e. 3 m, and additional 20 mm tolerance in both sliding directions. Furthermore, the CLT-connections consist of 30 screws (8x80 mm) arranged on three rows of 10 screws each. The spacing and edge distance of bolts and screws are in accordance with EN 1993-1-8:2005 and ETA-11/0030, respectively.

On an industrial scale, the innovative design of the proposed friction damper enables an easy and efficient manufacturing process, since the upper and bottom steel profiles have the same development in size and are produced by cold bending and welding of steel sheets.

The damper is also designed to allow a fast and simple external installation of the proposed e-CLT technology, and to make it well adaptable to the most common RC framed buildings. For instance, in buildings with external RC flat beams and balconies, the upper profile could be directly fixed to the above overhang.

The damper configurations STD, STD-1H and STD-R allow to pre-assemble the CLT panels off-site with only the upper profiles, while the bottom profiles are fixed on site during installation in order to properly align and connect the friction surfaces of the two profiles. On the other hand, the back fitting of the CLT-steel connections in the alternative configuration ALT requires to pre-assemble the CLT panels off-site with both the profiles at the edges, and then connect them to each other and to the RC beams on site. However, in this case high precision in the damper production is required, since the adjustment of the friction surfaces alignment cannot be guaranteed on site. Another main difference between the proposed designs

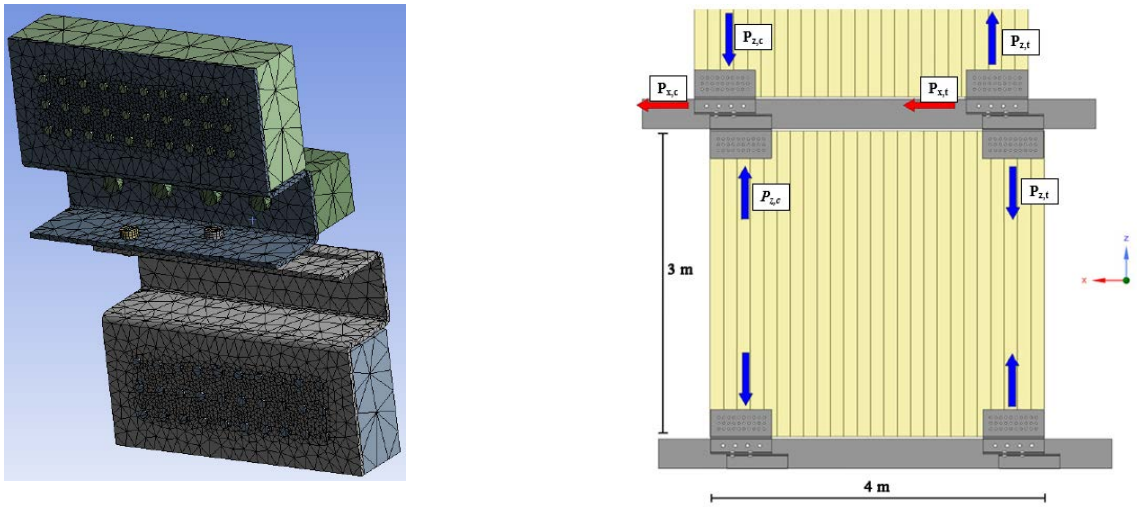
regards the inspection and replacement of the dampers after a seismic event: a swift and uncomplicated process in the first three designs, a bit more complex and time consuming in the last case.

4 MATERIALS AND METHODS

4.1 Numerical modelling

FEM analyses have been performed for each damper design in Ansys® *Academic Research Mechanical, Release 19.2*. Automatic meshing was used for the models, resulting in tetrahedron meshing for all damper components, except the pretensioned bolts, where hex dominant meshing was used, as shown in Figure 3a. Local mesh refinements were applied to the edge of slotted holes.

The CLT elements and RC beam have been modelled with an area equal to the adjacent steel plate one and a thickness of 100 mm, while pretensioned bolts and screws have the same diameters as holes. A perfectly elastic material with modulus of elasticity of 210 GPa and Poisson's ratio of 0.3 was assigned to both the profiles and pretensioned bolts. A single elastic modulus was estimated for the CLT-steel connections. Specifically, this simplified approach is achieved by assuming the characteristic axial and shear screw strain equal to the characteristic compressive CLT strain, perpendicular and parallel to the grain, respectively. The same modulus of elasticity of 200 GPa was also used for the concrete-steel connection, as suggested from the ETAG 001. Elastic analyses have been conducted on each numerical model in order to preliminarily analyse the damper loading response. Damper loading consists of a shear load Px of 30 kN, value chosen according to other testing campaigns of similar devices [15], and vertical compressive or tension loads Pz resulting from the moment obtained by considering a one-bay RC frame with a CLT panel 3 m tall and 4 m wide, as reported in Fig. 3b. This results in two loading cases for each damper design. More details can be found in [16].

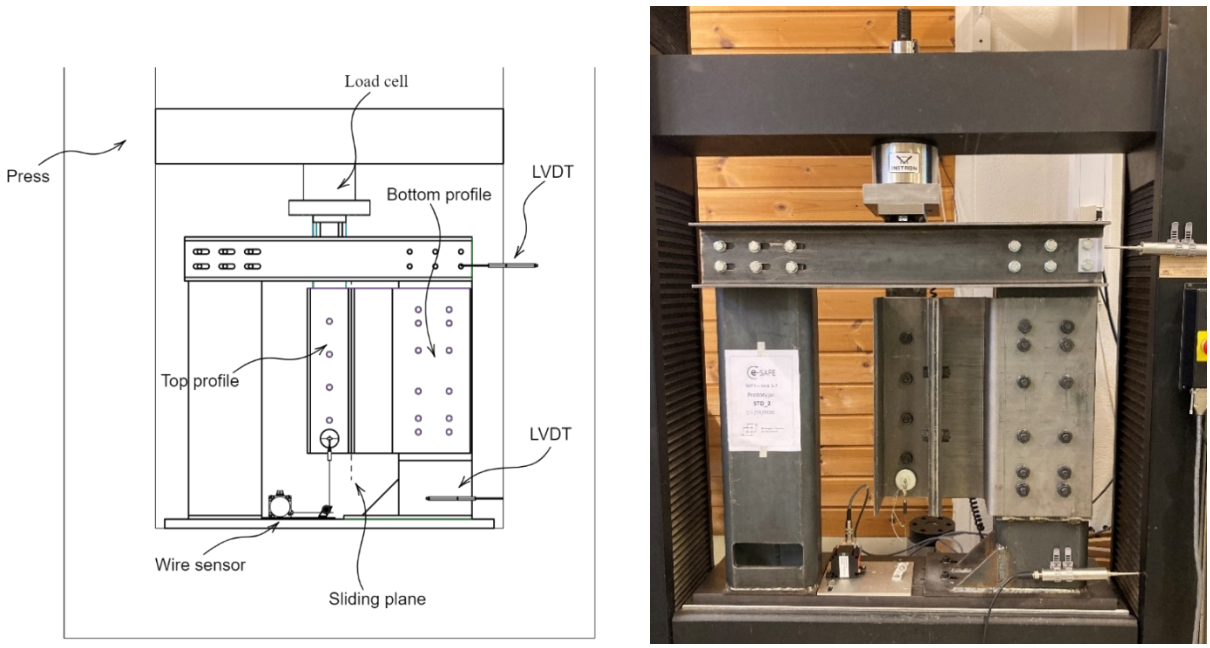


(a) (b)

Figure 3: (a) Meshing of the STD damper model and (b) acting forces in the concept of e-CLT system (Images used courtesy of ANSYS, Inc.)

4.2 Test campaign

A preliminary testing campaign is currently ongoing, with the goal being the study of the behaviour of the proposed friction connection. A specific setup was designed and built, in order to include only the dampers and no CLT elements (Figure 4 a-b). The setup consists of a rigid steel frame, namely the columns have a 12.5mm thickness and 100x200mm rectangular section, the bottom profile of the specimen is attached to the right column, while the top profile is in the central part of the frame and is free to slide, being connected to the actuator of the press. An additional steel cap plate and two aluminium shim layers were inserted between the profiles, in order to obtain an asymmetrical friction connection, as described by [17]. In this configuration the top profile is moved up and down by the press machine, to simulate the movement applied by the RC beam in a real building, and the bottom profile is fixed to the column, as it would be fixed to the CLT panel in reality.



(a) (b)

Figure 4: (a) Components of the testing setup and (b) testing setup

The damper designs considered for the test are four: the base configuration STD and STD-1H (with two or one slotted holes for sliding respectively), the reinforced configuration STD-R and the alternative configuration ALT. Each specimen presents minor modifications in respect to the real configurations described in the previous sections, in order to fit the setup. Namely the bottom profile was fixed to the column with bolts, and the top profile was simplified to a C-shape, since its role in testing was only to transfer the load from the press.

The loading protocol is cyclic, adapted from ISO16670 and EN151229, which express the protocol as a function of the ultimate displacement. In this case an ultimate displacement vu=100mm was assumed, estimated as 3% of the interstorey drift of a common RC frame building. The tests are conducted in displacement control. The load is measured by the load cell

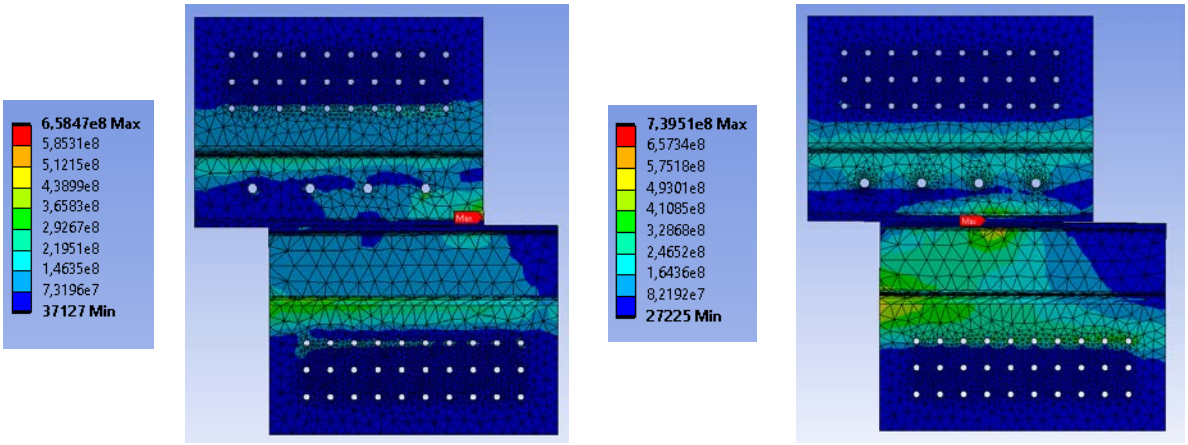
of the press, while the displacement of the top profile is recorded both by the press and by and additional wire sensor. Two horizontal LVDTs were used to acquire measures of displacement at the top and bottom of the right column, in order to verify the sufficient stiffness of the setup.

5 RESULTS AND DISCUSSION

5.1 Numerical modelling

Figures 5-7 show the results of the numerical analyses in terms of profiles stress distribution. Regarding damper STD in compression load case, the results show a maximum equivalent von-Mises stress of 658 MPa in the upper profile, specifically at the right edge of the friction connection (Figure 5a). This stress is 2.8 times the characteristic yield capacity of the S235 steel. Stress concentrations in the innermost row of screws on both the upper and bottom profiles are also observed. The second most critical stress is located at the left edge of the outer bend of the bottom profile, with a critical stress of 469 MPa. This stress is likely the result of a moment Mx.c of 1.7 kNm resulting from the high eccentricity of the vertical force acting in the friction connection, as well as a torsion effect resulting from a large moment My,c of 4.4 kNm.

The bending and torsion effects also persist in the plate bends of damper STD in tension load case (Figure 5b). In addition, higher tension reaction force is observed in the inner pretensioned bolt compared to the outer one, resulting in a large vertical stress concentration of 687 MPa at the vertical side of both the bends of friction connection. This could be a result of the inner bolt being located closer to the vertical bend of the plate, resulting in greater stiffness compared to the outer bolt.



(a) (b)

Figure 5: Equivalent von-Mises stress [N m^{-2}] on damper STD in compression (a) and tension (b) (Images used courtesy of ANSYS, Inc.)

In damper STD-R lower stresses act on the bends of both profiles, compared to damper STD, since they are concentrated in the steel welded reinforcements, as a result of the local stiffness increase (Figure 6a). In particular, a critical stress of around 450 MPa is located above the left reinforcement of the bottom profile in case of damper compression, while a critical stress of 628 MPa is on the bend below the same reinforcement in tension (Figure 6b).

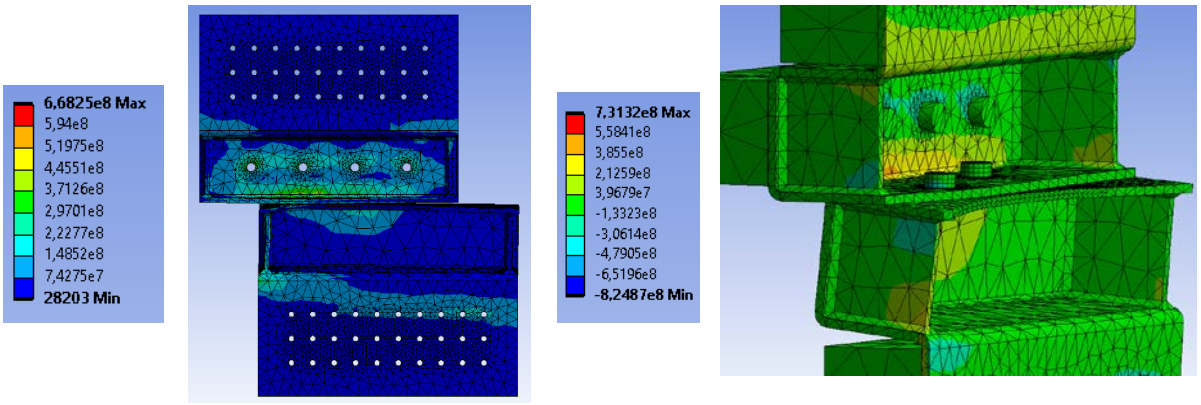


Figure 6: Equivalent von-Mises stress (a) and equivalent stress along Z-axis (b) [N m^{-2}] on damper STD-R (Images used courtesy of ANSYS, Inc.)

The design of damper ALT is the result of the above-mentioned preliminary numerical outcomes. Lower stresses and a more even distribution are here observed, indicating a more rigid behaviour of the connection plates (Figure 7). In this configuration, the lower eccentricity of both friction and CLT-steel connections, compared to the other design, results in lower values of bending moments Mx and Mz, which never exceed 0.4 and 0.7 kNm in compression and tension, respectively. As a result, the stresses on the damper are always smaller than 150 MPa for both load cases, except for local stress concentrations around the edges of the elongated hole, where the stress is equal to 281 and 460 MPa for compression and tension load case, respectively (Figure 7a-b).

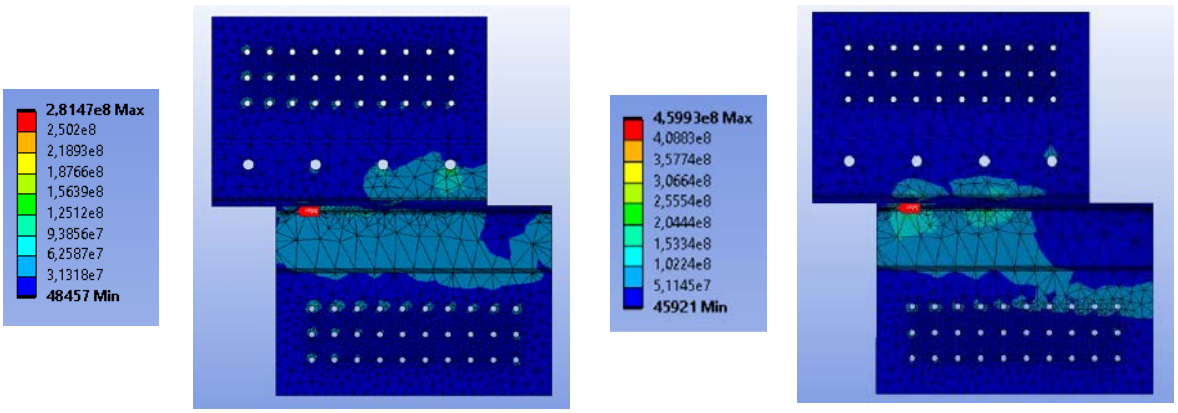


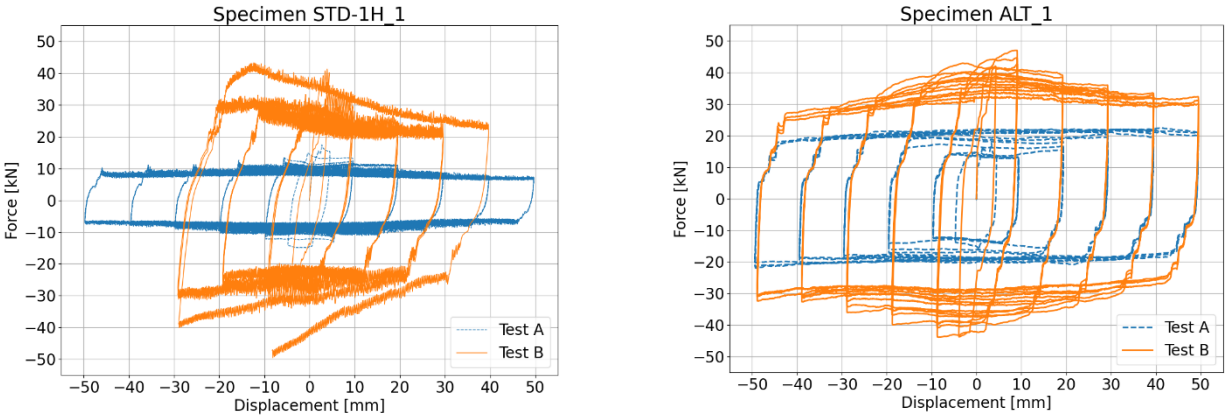
Figure 7: Equivalent von-Mises stress [N m^{-2}] on damper ALT in compression (a) and tension (b) (Images used courtesy of ANSYS, Inc.)

5.2 Experimental campaign

The preliminary results of the testing campaign are presented for STD-1H and ALT damper design, since STD and STD-R suffered from big deformations, as expected from the high

stresses found in the numerical analyses, so more investigations are required. The load protocol was applied with a speed of 0.5 mm/s, and after one initial cycle of 5mm amplitude then 3 cycles for 10-20-30-40-50 mm were applied. It is important to note that this was one of the initial tests, directed at understanding the behaviour of the prototypes, and thus the input protocol was set till 50% of the ultimate displacement capacity of the specimen.

Two tests were performed on both dampers: test A with a bolt preload of 24kN, and test B with a higher preload evaluated from the results of test A, with the goal of reaching a friction value of 30kN. This then translated in a preload of 45kN and 36kN during test B, for specimen STD-1H and ALT, respectively. As seen from Figure 8, the graphs of test A exhibit a behaviour that can be considered plastic, with a good stability of the hysteresis loops. Some corner chipping is present in the loops, which is common for asymmetrical friction connections, probably because of "dragging" phenomena of the cap plate not fixed to anything. Conversely, test B highlights strong differences in the behaviour of the two specimens. Damper STD-1H was subjected to big deformations in the bend of the bottom profile close to the column, which were likely the cause of big spikes in measured force and brought the test to an end before finishing all the cycles. Damper ALT exhibited better behaviour, reaching the designed 30kN value for friction. In this case though the loops present a moderate level of stability, which is worse than the case of test A with lower preload. This is in accordance with the findings of [17], since a material with low hardness like aluminium was used as shim layer.



(a) (b)

Figure 8: Force-displacement graphs for dampers (a) STD-1H and (b) ALT

7 CONCLUSIONS AND FUTURE WORK

This paper illustrates the first outcomes of an ongoing H2020 project aimed at investigating the e-CLT technology, a new seismic retrofit solution for RC framed buildings. This solution is part of an innovative and integrated renovation intervention also aimed at improving energy performance and architectural features of the building.

The e-CLT technology consists in the external application of prefabricated CLT structural panels on the existing outer walls, by connecting them to the RC beams through innovative friction dampers. Specifically, four configurations of the proposed friction damper have been

investigated, in order to identify potential limits and advantages for each one and, consequently, to optimize both the mechanical performance and production process.

The four distinctive designs are: STD, the standard configuration; STD-1H, which has only one elongated hole instead of two; STD-R, which presents additional reinforcements in respect to the standard configuration and ALT, an alternative configuration with a different geometry and mounting procedure.

3D FEM analyses were performed in Ansys® *Academic Research Mechanical, Release 19.2*, which pointed out the presence of great stress concentrations in all the STD configurations, likely due to the eccentricity between the friction connection and the CLT-steel one. Design ALT was then conceived and simulated to see the effect of reduced eccentricity, and the stresses were lower than the previous cases.

A testing campaign is ongoing on the four dampers, which in part confirms what was revealed by the FEM analyses. Specimens STD and STD-R suffered major deformations, particularly in the outer bend of the bottom profile, while dampers STD-1H and ALT offered more promising results. In particular, damper STD-1H provided satisfactory hysteretic behaviour for low level of bolts preload, but experienced high deformations and loop instability at higher level of bolts preload. Specimen ALT performed well in both cases of bolts preload, with good and moderate loop stability, respectively.

New prototypes will be produced, with new geometry devised from the results illustrated in this paper and from considerations regarding the need of easy installation and maintenance of the e-CLT technology. The testing campaign will also be extended, by testing new materials as shim layers.

Acknowledgements

This project has received funding from the European Union's Horizon 2020 Innovation action under grant agreement No. 893135.

The authors would like to thank: Alberto Moretti and the Italian company Adveco s.r.l. for their relevant and continuous support during the dampers prototyping stage and for providing the dampers for the testing campaign; the master student Mathilde Marthinsen for her precious contribution during the testing campaign and the head engineer Øyvind Hansen of NMBU for his continuous support regarding the design and production of the test setup.

REFERENCES

[1] Directive 2010/31/EC. Energy performance of buildings, directive of the European parliament and of the council of 19 May 2010 on the energy performance of buildings (recast)European parliament. 2016

[2] La Greca, P.; Margani, G. Seismic and Energy Renovation Measures for Sustainable Cities: A Critical Analysis of the Italian Scenario. *Sustainability* 2018, 10(1), 254.

[3] Presidency of the Council of Ministers Italian Civil Protection Department. National risk assessment. Overview of the potential major disasters in Italy: seismic, volcanic, tsunami, hydro-geological/hydraulic and extreme weather, droughts and forest fire risks. 2018

[4] Chandrakar, J.; Singh, A.K. Study of Various Local and Global Seismic Retrofitting Strategies – A review. *International Journal of Engineering Research & Technology*

2017, 6(06), 824-831.
[5] Bournas, D. Innovative Materials for Seismic and Energy Retrofitting of the Existing EU Buildings; EUR 29184 EN, Publications Office of the European Union: Luxembourg, 2018.
[6] Lau, D.; Qiu, Q.; Zhou, A.; Lun, C. Long term performance and fire safety aspect of FRP composites used in building structures. *Constr. Build. Mater.* 2016, 126, 573–585.
[7] Tetta, Z.C.; Koutas, L.N.; Bournas, D.A. Textile-reinforced mortar (TRM) versus fiber reinforced polymers (FRP) in shear strengthening of concrete beams. *Compos. Part B* 2015, 77, 338-348.
[8] Rahimi, A.; Maheri, M. R. The effects of steel X-brace retrofitting of RC frames on the seismic performance of frames and their elements. *Eng. Struct.* **2019**, *206.*
[9] Barbagallo F., Bosco M., Marino E.M., Rossi P.P., Stramondo P.R. A multi-performance design method for seismic upgrading of existing RC frames by BRBs; *Earthq. Eng. Struct. D.* 46 (2017) 1099–1119.
[10] Mazza, F.; Pucci, D. Static vulnerability of an existing r.c. structure and seismic retrofitting by CFRP and base-isolation: A case study. *Soil. Dyn. Earthq. Eng.* 2016, 84, 1-12.
[11] Bjo¨rnfot A, Boggian F, Steinsvik Nyga˚rd A, Tomasi R (2017) Strengthening of traditional buildings with slim panels of cross-laminated timber (CLT). In: Proceedings of the 4th international conference on structural health assessment of timber structures (SHATIS'17), Istanbul, 20–22 September
[12] Stazi, F.; Serpilli, M.; Maracchini, G.; Pavone, A. An experimental and numerical study on CLT panels used as infill shear walls for RC buildings retrofit. *Constr. Build. Mater.* 2019, 211, 605-616.
[13] Sustersic, I.; Dujic, B. Seismic shaking table testing of a reinforced concrete frame with masonry infill strenghtened with cross laminated timber panels. World Conference on Timber Engineering, Quebec City, Canada, August 10-14, 2014.
[14] Margani, G.; Evola, G.; Tardo, C.; Marino, E.M. Energy, Seismic and Architectural Renovation of RC Framed Buildings with Prefabricated Timber Panels. *Sustainability* 2020, *12*(12), 4845.
[15] Zheng L., Hanlin D., Xijun W., Minjuan H. Experimental and numerical investigations into seismic performance of timber-steel hybrid structure with supplemental dampers. Engineering Structures 151 (2017) 33–43
[16] Hatletveit M. Mechanical assessment of a steel dissipating system for RC buildings retrofitting with CLT panels. Master thesis, 2020. Norwegian University of Life Sciences
[17] Golondrino JC, MacRae GA, Chase JG, Rodgers GW. Behaviour of Asymmetrical Friction Connections using different shim materials. In: 2012 NZSEE Conf.; 2012. p. 1–7.

12th International Conference on Structural Analysis of Historical Constructions
SAHC 2020
P. Roca, L. Pelà and C. Molins (Eds.)

NUMERICAL INVESTIGATION OF THE RETROFITTING INTERVENTIONS OF THE SAN BENEDETTO CHURCH COMPLEX IN FERRARA (ITALY) FROM A SEISMIC VULNERABILITY PERSPECTIVE

RAFAEL SHEHU[1*]

[1]Department of Civil and Environmental Engineering (DICA)
Politecnico Di Milano,
Piazza Leonardo Da Vinci 32, 22133, Milan, Italy
e-mail: rafael.shehu@polimi.it

Abstract. *The San Benedetto church complex is an iconic architectural heritage asset of Ferrara, an attractive small city in the North of Italy. This paper investigates two separate parts from the complex, respectively the church, and the bell tower. The construction of the church dates back in the XV century, and many modifications were carried through years. During the second world war the church was severely damaged and then was fully restored to the original design. The bell tower instead is a typical tower of northern Italy, notably inclined by 3°. In the last decade, severe earthquake sequences occurred in the nearby areas, and the occupancy and safety of the structures were compromised. Several observed damages impelled upgrading measures, and consequently, many different retrofitting interventions got executed. Advanced numerical simulations are conducted in order to estimate the seismic vulnerability of each structure, by means of non-linear dynamic analysis. A critical historical evolution of the structure is considered, and two models for each structure are conceived respectively. The church models consist of 1) post-war reconstruction modeled with two distinct materials; 2) post-earthquake intervention with repointing technique and composites. The bell towers models consist of 1) the non-retrofitted tower; 2) the model with steel hooping bars. A comparative analysis is carried out based on the numerical results highlighting the pros and cons of each modeling technique and the efficiency of each intervention. Structural stiffening incorporated with a non-uniform distribution of the resisting capacities of the load-bearing elements highlights the seismic vulnerabilities. The necessity for the advanced numerical simulation emerges by the evidenced vulnerabilities in the performed simulations concerning the overall structural safety.*

Keywords: Masonry Structures, Seismic Vulnerability, Seismic Analysis, Retrofitting

1 INTRODUCTION

The conservation and preservation of cultural heritage are a topic of great interest in seismic-prone regions, such as Italy [1–4]. Recent earthquakes in the Italian territory (Umbria-Marche 1997, L'Aquila 2009, Emilia 2012, Central Italy 2016) highlighted the vulnerability of old masonry constructions to seismic excitations [5,6]. In particular, historical masonry churches

proved to be highly vulnerable against horizontal loads [7–9]. Post-earthquake damage surveys carried out after past seismic events highlighted that one of the main causes of vulnerability for such structures is associated with local failure modes, mainly due to the out-of-plane response of macro-elements [10,11].

It is a prevailing opinion, based upon vast research on their structural performance, that the masonry towers are relatively very vulnerable against seismic loads, [12,13]. The low tensile strength characterizes the masonry material and it is a paramount aspect that causes severe damages to occur. However, the mechanical properties are only one aspect of their vulnerability. Indeed, peculiar geometrical configurations, confinement with other constructions, the soil-structure interaction, or the inclination plays a relevant role in their performance [14–16].

This study is conceived as a comparative study between two different models of the church and the bell tower of the San Benedetto Complex. As will be detailed in the following paragraph, the studied structures represent complex futures, of geometry, materials and restoration interventions. All these aspects influence the seismic vulnerability thenceforth a detailed investigation is a step toward the knowledge of their actual safety level. Two models have been conceived in this study, corresponding to the state before and after the carried-out interventions. Non-linear dynamic analysis is the implemented numerical strategy to compare the seismic performance of the structures in terms of the induced damages. This study is a preliminary estimation of the efficiency of structural strengthening.

2 GENERAL DESCRIPTION OF THE SAN BENEDETTO COMPLEX

The San Benedetto church complex is an iconic structure belonging to the cultural and architectural heritage of Ferrara, an attractive small city in the North of Italy. This paper investigates two separate parts from the complex, which are respectively the church and the bell tower. The construction of the church dates back in the XV century, and many modifications to the original structure were carried through years.

2.1 San Benedetto Church

San Benedetto Abate Church in Ferrara was built between 1496 and 1553. During the Second War World, the church was severely damaged and partially destroyed, see Figure 1. A reconstruction process was performed according to the original drawings, and the works were completed in 1954. The overall length of the church is about 60m and the height is almost 28 m. The façade, which is subdivided into three parts by decorative pilasters and has a large rose window in the upper part. The church has the plan layout of a typical regular Latin cross with three naves. The naves are separated by two rows of columns, and along the aisles, there are six chapels in both sides symmetrically. The nave walls are approximately 18m high and present a circular opening of diameter equal to 2.4m at about mid-length. The aisles' walls are 11m high, while each side chapel is 8m high and presents high window openings. The transept of the church is almost 45m long and 18m high similar to the nave. The nave and the transept are covered with barrel vaults reinforced with ribs. The end part of the church consists of a semi-circular apse and two small side apses, which have the same dimensions as the side chapels of the naves. The apses and the transept have a radius of almost 6m, two elongated windows at the end and two infilled circular windows aside.

2.2 San Benedetto Bell Tower

The bell tower of San Benedetto Church as construction is newer compared to the church. It was built in 1621 according to a design by Giovani Battista Aleotti. The main future is the slenderness and the inclination. The last one is typical for all the towers in Ferrara, but this tower is the highest and the most inclined one. The height of the tower is 54m, and the base width is 7.1m. The tower is highly irregular in the upper part. It is composed of a regular tube (30m) in the lower zone, and two blocks in the belfry zone. The wall thickness varies from 130cm at the base to 30cm at the top. The present inclination is 3.0° towards the West and 0.5° towards the North. The inclination influence and the last earthquake has caused vertical cracks passing through the openings. An intervention consisting of horizontal steel bars placed for hooking effect along the height was carried out after the earthquake in 2012.



Figure 1: San Benedetto church after World War II (left image) actual state (right image)

3 NUMERICAL SIMULATION STRATEGY

3.1 FE models

The main focus of the research, to investigate the seismically induced damages, impose the utilization of advanced numerical models. The literature offers different approaches towards the modeling of masonry structures where its heterogeneity is emphasized and crucial aspect, i.e. [10,17–19]. In order to mimic the non-linear behavior of the masonry material under seismic cyclic loads and characterizing the damage of the material, the Abaqus CAE software is used [20]. The constitutive modeling of masonry in the non-linear phase is approached according to a Concrete Damage Plasticity material model distinct damage parameter for compression and tension, [20]. The numerical models are discretized by means of tetrahedron elements that suit best for meshing any irregular shape. The characteristic length of the element is lower than 28cm in all cases. Abaqus CAE automatically regularizes the fracture energy for each element based on its corresponding h parameter, [20]. As mentioned in the previous paragraph, both structures have undergone different retrofitting interventions. Herein, two different models are conceived, respectively representing the state before and after retrofitting. As depicted in Figure 1, the church was rebuilt in approximately half of it. A simplified model, considering the old masonry material and the newly replaced one is implemented as depicted in Figure 3. In the absence of a detailed investigation of the material properties, a first investigation is made upon recommended parameters. For masonry constructions built with regular bricks and lime mortar,

the Italian code recommends some reference values to be utilized during the analysis, provided in Table C8A.2.1, [21], while for the retrofitted material, by repointing or the undo-redo technique, the data of Table C8A.2.2 are combined with Table C8A.2.1 in order to obtain the mechanical properties. The Italian guideline CNR-DT215 [22], provides a reliable framework on how to design the retrofitting of existing structures using high-performance materials. According to those specifics, it is modeled the intervention of the vaults and dome with TRCM (textile reinforced cementitious matrix). While the vaults built with hollowed bricks are not modeled, A representative section of the structural elements is provided in Figure 2.

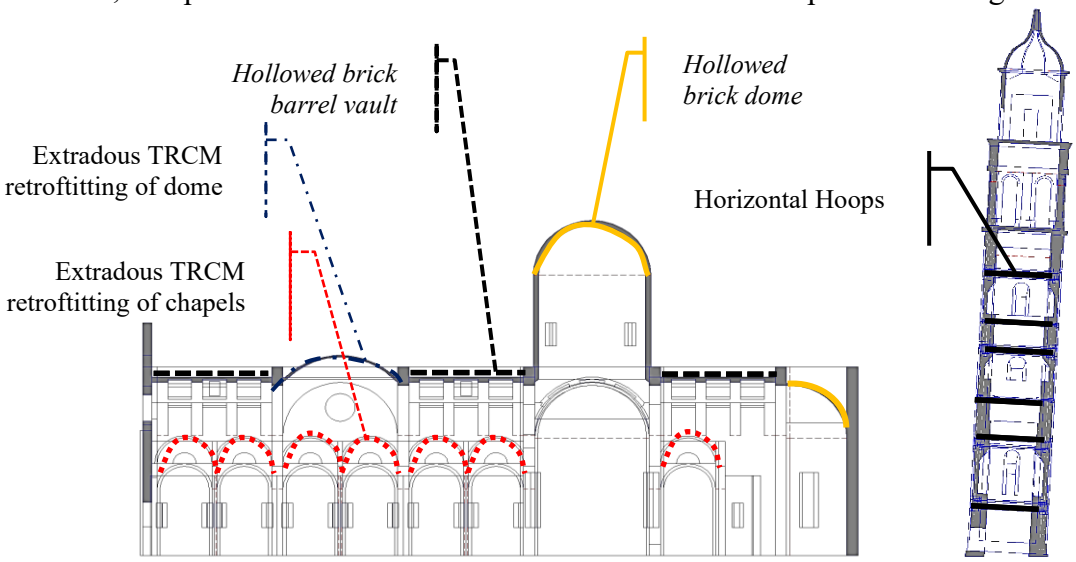


Figure 2: Section view of the San Benedetto Complex.

The masonry tower is modeled inclined, for both cases. In the retrofitted model, horizontal steel bars are modeled with an applied pretension force, equivalent to compression stress in the masonry of $0.2f_{cm}$. These bars were placed for closing the vertical cracks passing through the opening of the north and south façade. A correct model of a tower should also consider the soil-structure interaction [23]. However, the reinforced concrete piles imply a rigid foundation approach as a reliable one for the present case.

3.2 Seismic analysis approach

In the common practice of earthquake engineering, there are many strategies to address the verification of the limit states for any structure. Still, the highest accuracy is achievable by utilizing the non-linear dynamic analyses. Three real accelerograms are used instead, see Figure 4. Three real accelerograms obtained from Berkeley World Earthquakes Database (//ngawest2.berkeley.edu/), by inserting the characteristic response spectrums of Ferrara, are used. According to the Italian Code, the minimal number of pairs accelerograms to perform a seismic performance estimation is equal to three, and the worst output is taken as a referential response. The importance of the subjects imposes to verify the ultimate limit state of life safety with earthquakes compatible with a return period spectrum of 715 years. Such demand results to be very severe for masonry structures, thence, aiming to investigate the seismic vulnerability primary to a structural safety estimation, a return period of 475 years is chosen in this study.

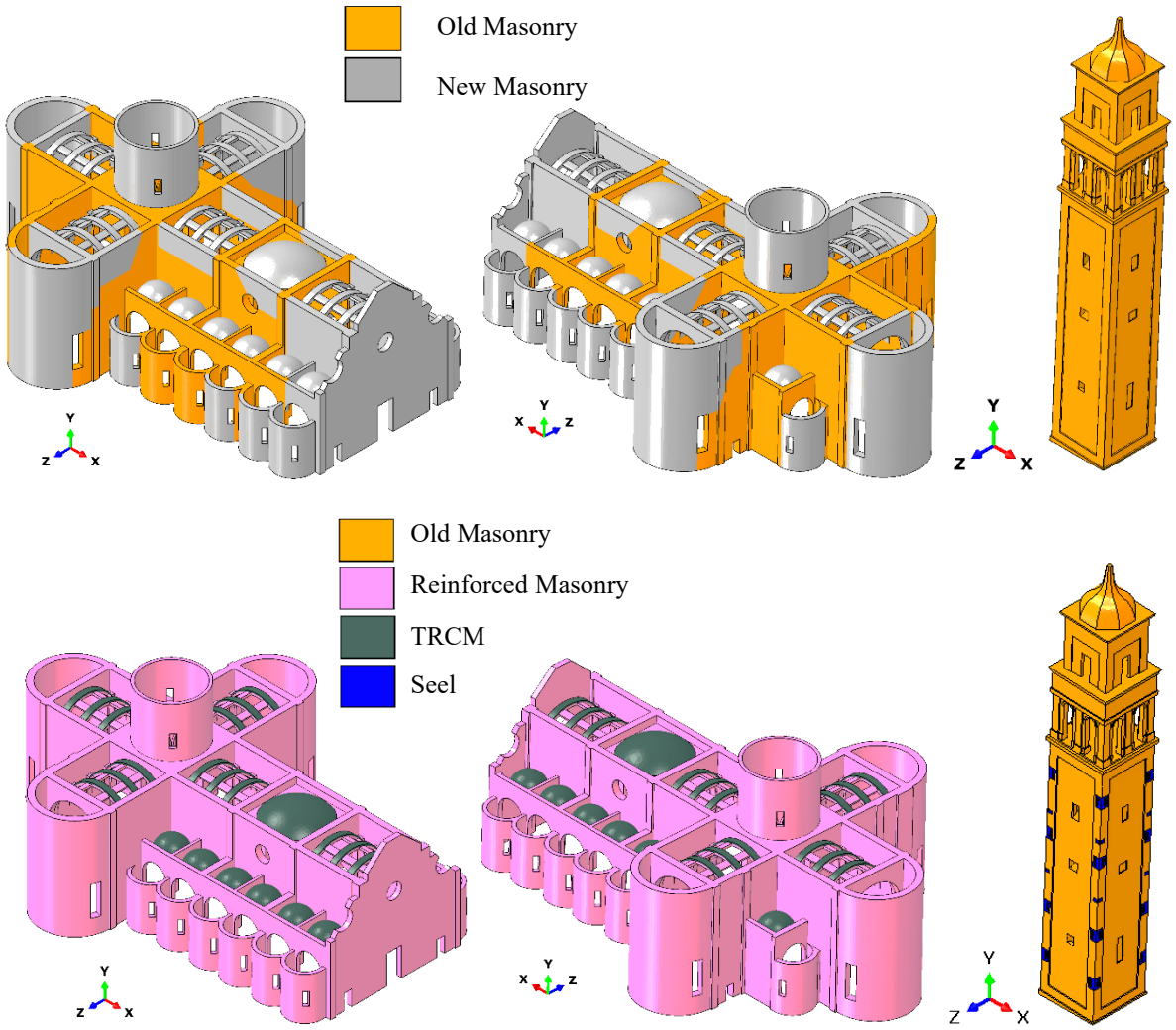


Figure 3: 3D view of the models:-before intervention (upper image);-after interventions (lower images)

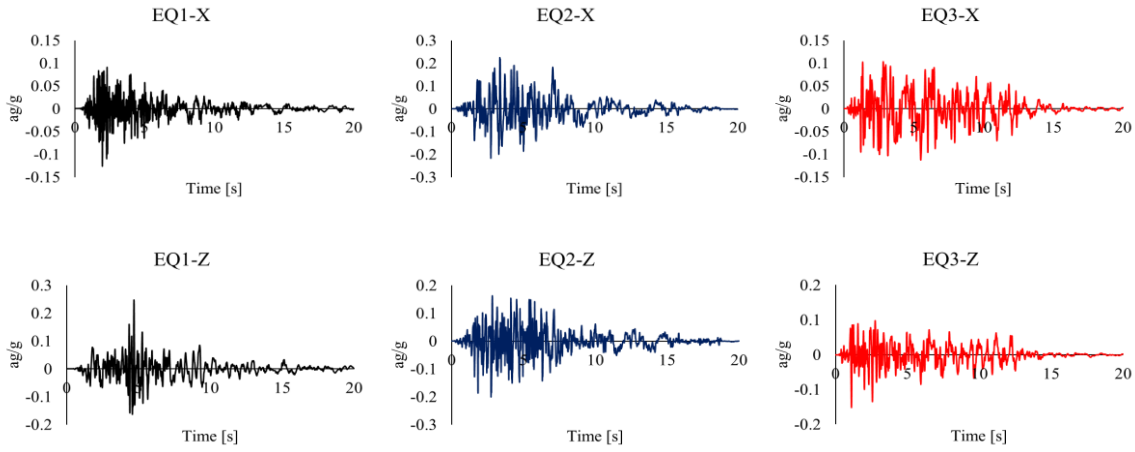


Figure 4: Horizontal components of the utilized accelerograms.

4 RESULTS

In the followings images are depicted the induced seismic damage at the end of the seismic accelerograms prolonged for 30 seconds, as suggested by Eurocode 8, [24]. The damage parameter in tension is visualized. This parameter is an adequate approach for showing the initiation and the crack growth location for the concrete damage material. A relatively low value of the "h" parameter on the element's dimensions ensures a reliable result. Due to the acknowledged uncertainties and the role of accelerograms selection in the output results, the comparison among the models is made primarily in terms of qualitative results than quantitative ones. Also, it is well-known that the behavior of macroelements rules the vulnerability of masonry structures.

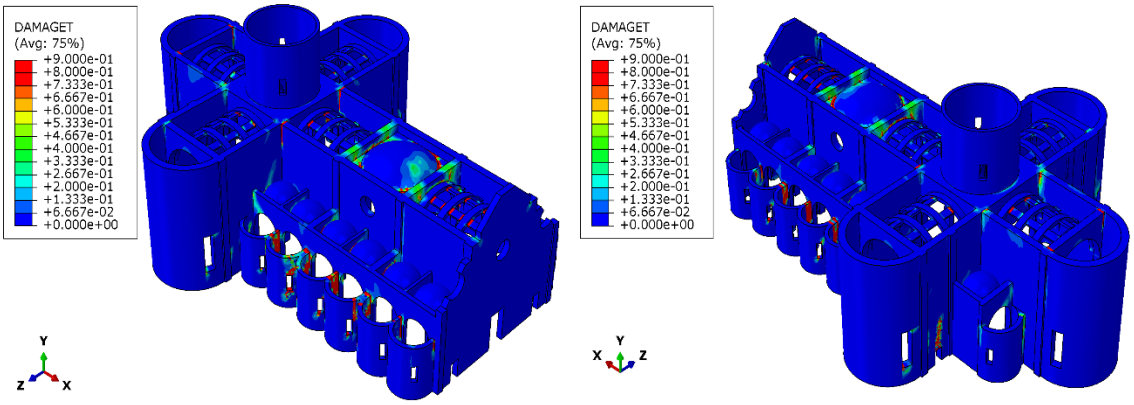
Figure 5 depicts the damage pattern for the church before the retrofitting. The diffusion of crack highlights some vulnerabilities, like severe damage of the interlocking between the chapels and the church, in the arches, or the intersection of the nave with the transept. It is worth noting that the traces of some damages follow the interface between the old masonry and the new texture. It highlights the relevance of the mechanical properties and the lack of homogeneity which brings to predefined failure surfaces which should be cured with special attention. The vault ribs result to be very vulnerable. Even though their structural relevance is negligible, its role in the operationality of the church and the aesthetic aspects is crucial.

The retrofitted church represents a lower level of seismic damage severity compared to the non-retrofitted church, as depicted in Figure 6. The vaults ribs are still prone to be damaged even they are retrofitted, an expected result due to their geometrical futures, [25]. To be highlighted is the scarce interlocking between the chapels and the church, which heralds the presence of this vulnerable joint. Careful observation should be paid to the façade system. Although substantial damage is not registered for the conducted simulations, the retrofitted one represents a similar level of damage which warns for earthquakes that might activate the rocking of the façade due to a detachment.

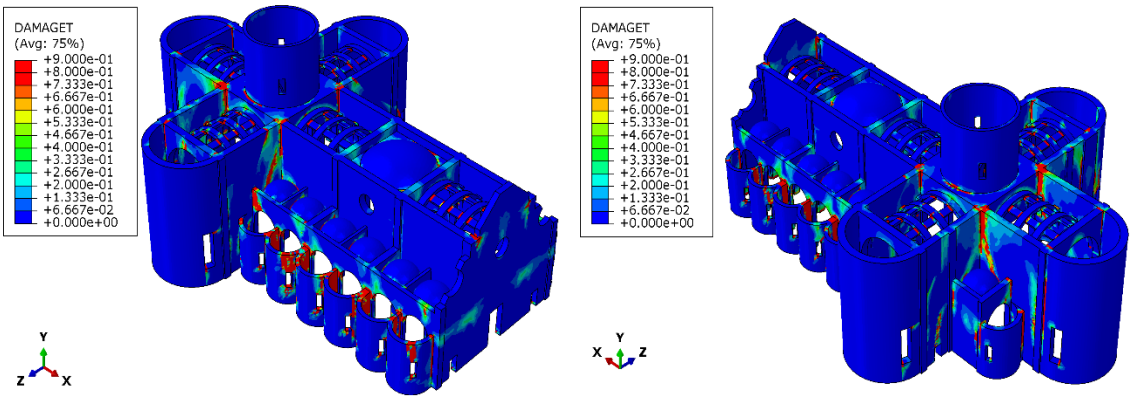
From a critical point of view, retrofitting has improved the seismic performance of the church. However, some drawbacks are worthy of being addressed. In such cases, other strengthening strategies like tie rods could help transform the structural system into a safer one. It could be a good motivation to investigate if such elements would not result in efficient ones, as likely occurred to be those applied to the tower.

Figure 7 and Figure 8 summarizes the registered damages for the non-retrofitted and retrofitted tower, respectively. At first glance, they represent the same picture, and it can be concluded that in terms of vulnerability, the present retrofitting does not provide a relevant contribution. The role of hooping steel rods into the incremented towers' capacity to withstand horizontal loads is not reflected.

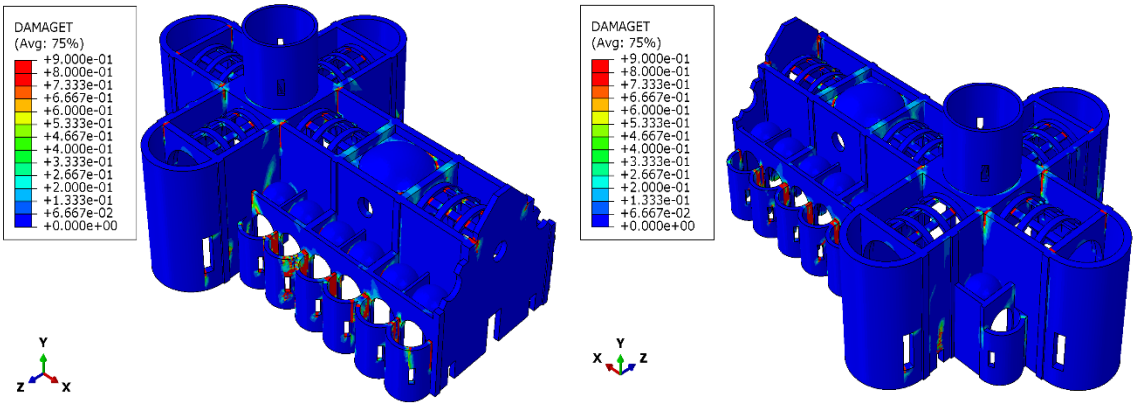
Due to the slenderness and the inclination, the base of the structure and the belfry are very exposed to possible damages. The inclination has imposed the damage formation only on the tension side of the tower.



Earthquake 1

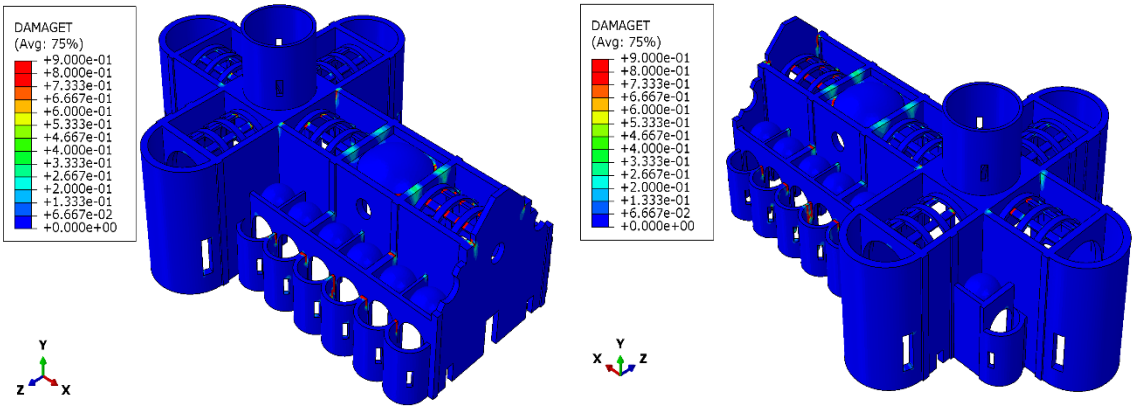


Earthquake 2

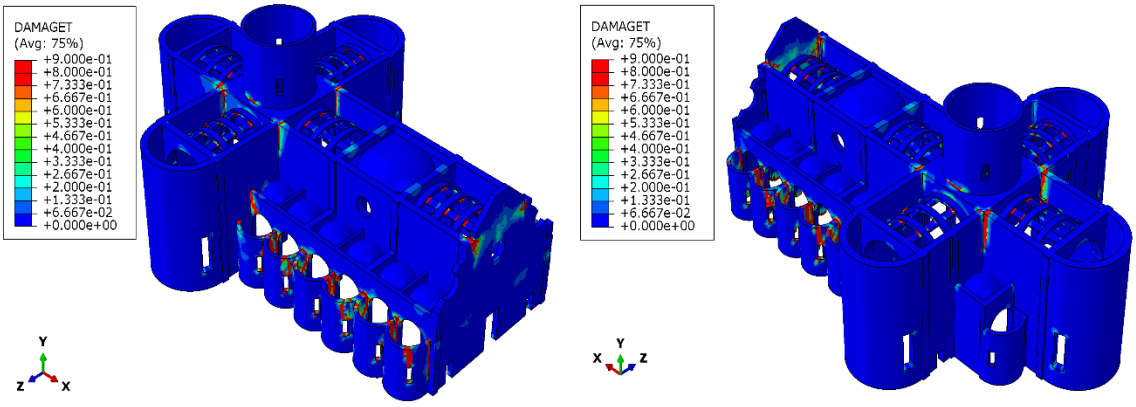


Earthquake 3

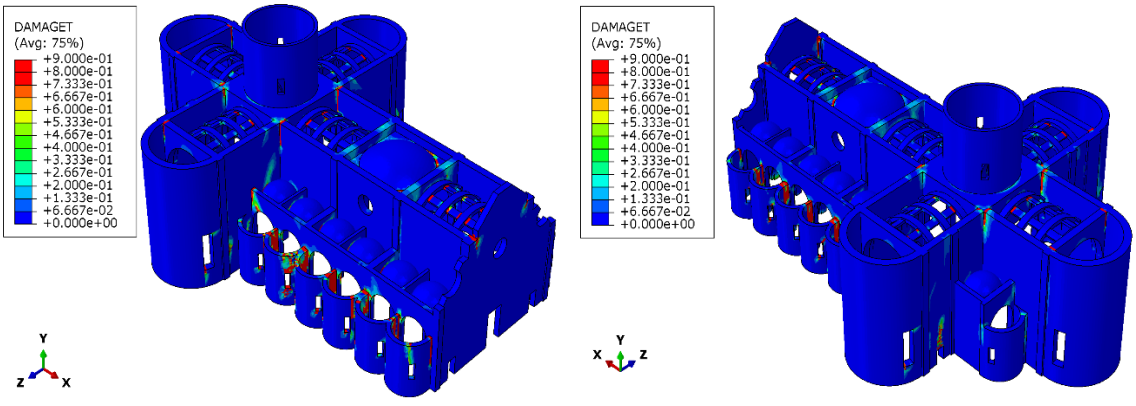
Figure 5: Seismically induced cracks in the church before retrofitting.



Earthquake 1

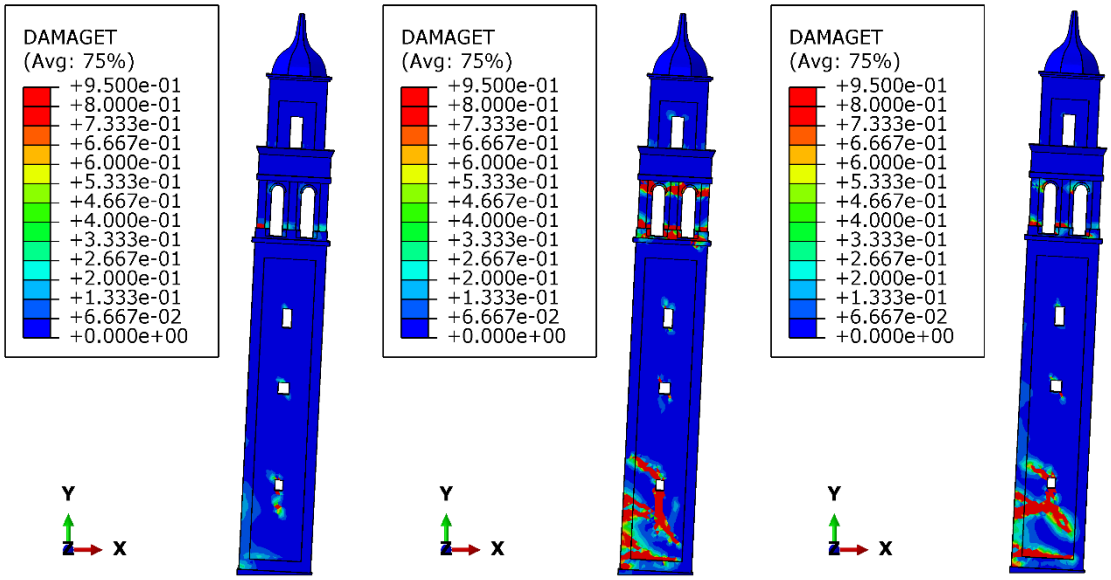


Earthquake 2



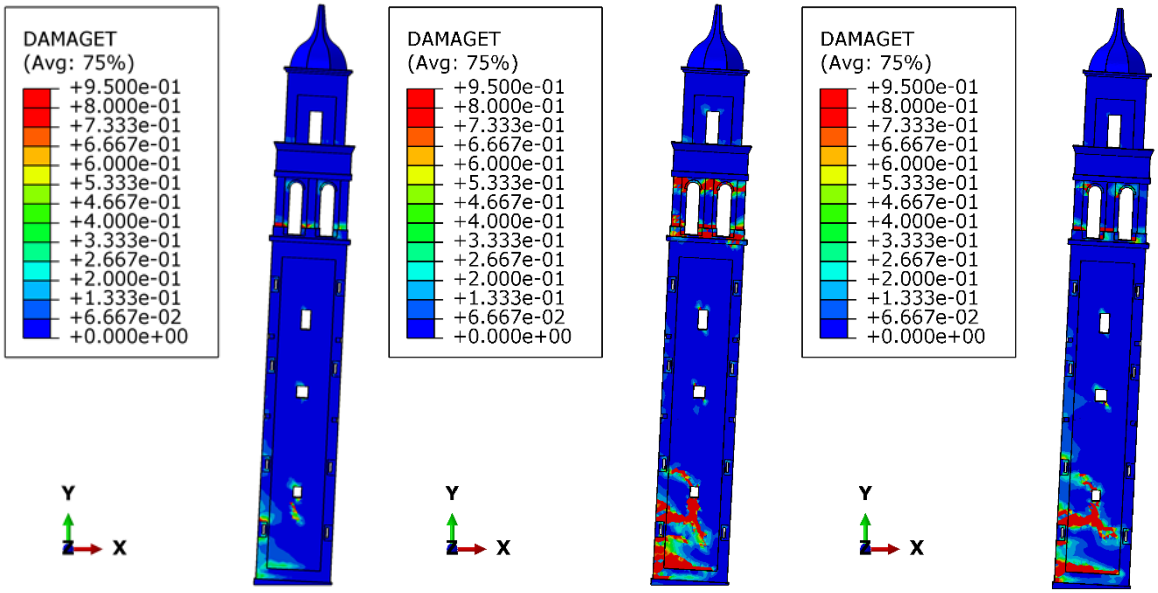
Earthquake 3

Figure 6: Seismically induced cracks in the church after retrofitting.



Earthquake 1 Earthquake 2 Earthquake 3

Figure 7: Seismically induced cracks in the tower before retrofitting.



Earthquake 1 Earthquake 2 Earthquake 3

Figure 8: Seismically induced cracks in the tower after retrofitting.

5 CONCLUSIONS

This study provides a numerical insight into the seismic vulnerability and the effectiveness of retrofitting interventions for the San Benedetto's church and bell tower located in the

province of Ferrara, Italy. The structures were retrofitted, by means of a post-seismic repairing of the damaged parts. Two different models were investigated and compared in terms of seismic performance and the role of retrofitting for each structure. Both structures were tested under the same level of seismic intensity. The bell tower, very slender and inclined, resulted to be more vulnerable compared to the church, a massive construction with high wall thicknesses.

The results showed some present challenges on the efficiency of retrofitting solutions. The bell tower was strengthened by horizontal steel bars which improved the interlocking of the walls and compacting the shaft; however the rocking at the base and the flexible belfry remain to be addressed in the future. The improved mechanical properties of the masonry for the church resulted in being quite effective. Despite that two issues should be faced. The first one is related to the quality of the intervention and the reliability of achieving such performance. The second one is related to the upgrade of the structural towards a less vulnerable one.

REFERENCES

[1] L. Binda, C. Modena, F. Casarin, F. Lorenzoni, L. Cantini, S. Munda, Emergency actions and investigations on cultural heritage after the L'Aquila earthquake: The case of the Spanish Fortress, Bull. Earthq. Eng. (2011). doi:10.1007/s10518-010-9217-3.

[2] A. Borri, M. Corradi, G. Castori, A. De Maria, A method for the analysis and classification of historic masonry, Bull. Earthq. Eng. 13 (2015) 2647–2665. doi:10.1007/s10518-015-9731-4.

[3] A.B. Habieb, M. Valente, G. Milani, Hybrid seismic base isolation of a historical masonry church using unbonded fiber reinforced elastomeric isolators and shape memory alloy wires, Eng. Struct. (2019). doi:10.1016/j.engstruct.2019.109281.

[4] G. Milani, R. Shehu, M. Valente, Seismic Upgrading of a Masonry Church with FRP Composites, Mater. Sci. Forum. 866 (2016) 119–123. doi:10.4028/www.scientific.net/MSF.866.119.

[5] F. Mollaioli, O. AlShawa, L. Liberatore, D. Liberatore, L. Sorrentino, Seismic demand of the 2016–2017 Central Italy earthquakes, Bull. Earthq. Eng. (2018). doi:10.1007/s10518-018-0449-y.

[6] M. Acito, E. Magrinelli, G. Milani, S. Tiberti, Seismic vulnerability of masonry buildings : Numerical insight on damage, J. Build. Eng. (2019) 101081. doi:10.1016/j.jobe.2019.101081.

[7] M. Valente, G. Milani, Seismic response and damage patterns of masonry churches: Seven case studies in Ferrara, Italy, Eng. Struct. 177 (2018) 809–835. doi:10.1016/j.engstruct.2018.08.071.

[8] A. Aşıkoğlu, Ö. Avşar, P.B. Lourenço, L.C. Silva, Effectiveness of seismic retrofitting of a historical masonry structure: Kütahya Kurşunlu Mosque, Turkey, Bull. Earthq. Eng. (2019). doi:10.1007/s10518-019-00603-6.

[9] L. Sorrentino, L. Liberatore, L.D. Decanini, D. Liberatore, The performance of churches in the 2012 Emilia earthquakes, Bull. Earthq. Eng. 12 (2014) 2299–2331. doi:10.1007/s10518-013-9519-3.

[10] P. Roca, M. Cervera, G. Gariup, L. Pela, Structural analysis of masonry historical constructions. Classical and advanced approaches, Arch. Comput. Methods Eng. 17 (2010) 299–325. doi:10.1007/s11831-010-9046-1.

[11] S. Casolo, S. Neumair, M.A. Parisi, V. Petrini, Analysis of seismic damage patterns in old masonry church facades, Earthq. Spectra. 16 (2000) 757–773. doi:10.1193/1.1586138.
[12] V. Sarhosis, G. Milani, A. Formisano, F. Fabbrocino, Evaluation of different approaches for the estimation of the seismic vulnerability of masonry towers, Bull. Earthq. Eng. (2017). doi:10.1007/s10518-017-0258-8.
[13] M. Shakya, H. Varum, R. Vicente, A. Costa, Seismic vulnerability assessment methodology for slender masonry structures, Int. J. Archit. Herit. 00 (2018) 1–30. doi:10.1080/15583058.2018.1503368.
[14] M. Valente, G. Milani, Effects of Geometrical Features on the Seismic Response of Historical Masonry Towers, J. Earthq. Eng. (2017) 1–33. doi:10.1080/13632469.2016.1277438.
[15] G. Milani, R. Shehu, M. Valente, Seismic vulnerability of leaning masonry towers located in Emilia-Romagna region, Italy:FE analyses of four case studies, AIP Conf. Proc. 1790 (2016) 130002. doi:10.1063/1.4968720.
[16] G. Milani, R. Shehu, M. Valente, Seismic Assessment of Masonry Towers by Means of Non-linear Static Procedures, Procedia Eng. 199 (2017) 266–271. doi:10.1016/j.proeng.2017.09.022.
[17] P.B. Lourénço, R. De Borst, J.G. Rots, A plane stress softening plasticity model for orthotropic materials, Int. J. Numer. Methods Eng. 40 (1997) 4033–4057. doi:10.1002/(SICI)1097-0207(19971115)40:21<4033::AID-NME248>3.0.CO;2-0.
[18] L. Gambarotta, S. Lagomarsino, Damage Models for the Seismic Response of Brick Masonry Shear Walls. Part II: the Continuum Model and Its Applications, Earthq. Eng. Struct. Dyn. 26 (1997) 441–462. doi:10.1002/(SICI)1096-9845(199704)26:4<441::AID-EQE651>3.0.CO;2-0.
[19] S. Lagomarsino, A. Penna, A. Galasco, S. Cattari, TREMURI program: An equivalent frame model for the non-linear seismic analysis of masonry buildings, Eng. Struct. 56 (2013) 1787–1799. doi:10.1016/j.engstruct.2013.08.002.
[20] D.S. Simulia, Abaqus 6.14 documentation, (2014).
[21] NTC, Aggiornamento delle “Norme Tecniche per le Costruzioni” - NTC 2018, Italy, 2018.
[22] CNR-DT 215, Istruzioni per la Progettazione, l’Esecuzione ed il Controllo di Interventi di Consolidamento Statico mediante l’utilizo do Compositi Fibrorinforzati a Matrice Inorganica, 2018.
[23] S. Casolo, V. Diana, G. Uva, Influence of soil deformability on the seismic response of a masonry tower, Bull. Earthq. Eng. 15 (2017) 1991–2014. doi:10.1007/s10518-016-0061-y.
[24] EC-8-P-1, Eurocode 8 : Design of structures for earthquake resistance - Part 1, 2014.
[25] G.L. Stockdale, V. Sarhosis, G. Milani, Seismic capacity and multi-mechanism analysis for dry-stack masonry arches subjected to hinge control, Bull. Earthq. Eng. (2020). doi:10.1007/s10518-019-00583-7.

12th International Conference on Structural Analysis of Historical Constructions
SAHC 2020
P. Roca, L. Pelà and C. Molins (Eds.)

NUMERICAL INVESTIGATIONS FOR ASSESSING THE SEISMIC PERFORMANCE OF MULTI-TIERED NEPALESE TEMPLES

MIRKO PEJATOVIC[3], VASILIS SARHOSIS[2], GABRIELE MILANI[1]

[1] Department ABC, Technical University of Milan
Piazza Leonardo da Vinci 32, Milan 20133, Italy, gabriele.milani@polimi.it

[2] School of Civil Engineering, University of Leeds
LS2 9JT, Leeds, UK, v.sarhosis@leeds.ac.uk

[3] Department of Architecture, Built Environment and Construction Engineering,
Technical University of Milan
Piazza Leonardo da Vinci 32, Milan 20133, Italy, mirko.pejatovic@polimi.it

Keywords: Nepal earthquake, Cultural heritage buildings, Seismic damage, Masonry, Finite element method, Numerical modelling

Abstract. *In this study, the seismic performance of old multi-tiered temples in Nepal has been addressed using three different computational approaches, including a) linear elastic; b) nonlinear static; and c) nonlinear dynamic analyses. Also, a sensitivity study was undertaken to understand the influence of wall thickness and height of Nepalese temples on their seismic behavior. Vertical oscillating modes using the elastic response spectrum of the Nepalese Building Code were obtained using linear analysis. Nonlinear static analysis (NLSA) were implemented to obtain the load carrying capacities of different in geometry temples e.g. different thickness of central core walls and number of tiers. Additionally, nonlinear dynamic analysis (NLDA) using the Finite Element Method (FEM) were performed to evaluate the characteristic tensile damage patterns. The results comparatively indicate the weakest zones depending on wall thickness, central core slenderness, opening distribution, box-like confinement, vertical misalignment of walls and so forth. Also, the results of the NLDA affirm high vulnerability of the multi-tiered temples showing extensive cracks at relatively low peak ground accelerations. It is anticipated that outcomes of this study can help practicing engineers to understand how these structures behave when subjected to seismic loads and provide insights towards their strengthening and retrofitting.*

1. INTRODUCTION

The preservation of cultural heritage is a crucial issue all over the world, such as Nepal, whose territory is characterized by both significant seismicity and presence of a large amount of monumental masonry constructions of major historical importance, such as temples. Despite the importance of such kind of structures, research has recently been more focused on

architectural heritage buildings belonging to Mediterranean countries (industrially developed but at the same time in high seismicity regions), and hence on masonry churches (e.g. [1], towers [2, 3], etc. The lessons learnt from previous earthquakes together with deep study of structural weaknesses of monumental buildings lead to proper intervention design and their conservation [4].

Multi-tiered temples (See Figure 1) built in Nepal are traditional and monumental structures which apart from their architectural significance, present both valuable historic and archaeological importance. However, the 2015 Gorkha Earthquake and its related aftershocks dramatically altered the iconic historic structures in Nepal. According to Nepal's Department of Archaeology, around 750 heritage structures of significant cultural and religious value (e.g. temples and shrines) were affected. Discussions to place it on UNESCO's List of "World Heritage in Danger" are already underway.

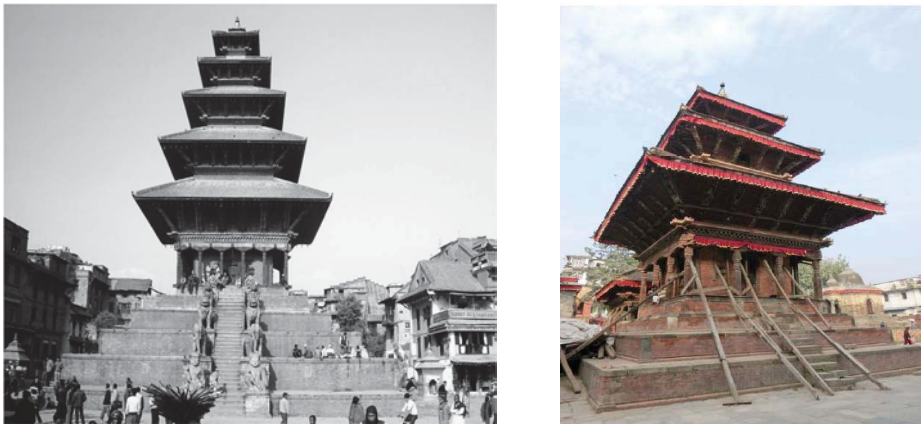


Figure 1 – Multi-tiered temples: Nyatopol temple (left) [5] and Gopinath temple (right) [6].

In particular, Nepalese multi-tiered temples are characterized by a combination of brickwork constructed with mud mortar. These structures are characterized by: a) geometric symmetry; b) asymmetry in mass distribution along the height of the structure i.e. the mass of the structure increases from top to bottom; and c) the temples are resting on a huge and massive plinth (or exposed foundation) [7].

Modelling multi-tiered Nepalese temples is a very complex task due to numerous uncertainties and lack of accurate material characterization. Aligned with the UN Sustainable Development Goal 11.4 "Strengthen efforts to protect and safeguard the world's cultural and natural heritage" and Nepal's national strategy for disaster risk management (2009) the research presented herein aims to assess seismic performance of old multi-tiered temples in Nepal using different computational approaches, including: a) linear elastic; b) nonlinear static; and c) nonlinear dynamic analyses. A sensitivity study is also undertaken to understand the influence of wall thickness and height of Nepalese temples on their seismic behavior.

2. NUMERICAL MODELING OF MULTI-TIERED TEMPLES

Initially, elastic models of the Gopinath and Nyatopol temples were developed and modal analysis were undertaken in order to verify the dynamic properties of the structures. Eccentric effects of the walls and the top of the temples were considered. Numerical models based on the macro-modelling approach have been developed in which masonry is represented using the Concrete Damaged Plasticity law (CDP), available in ABAQUS software. In addition, for the development of the numerical models it was assumed that: a) the plinth is rigid; b) the floors are rigid, since timber beams are attached to walls; c) the roof is considered as non-structural element; and d) the weight of the wooden pinnacle is neglected at the very top since its weight is small relatively to the other parts of the structure.

2.1 Dynamic identification of the multi-tiered temples

Initially, the mechanical properties of the masonry material to be inputted into the numerical model calibrated. Material calibration was performed by dividing the structure into three regions. A different modulus of elasticity has been selected for each case (see Figure 2).

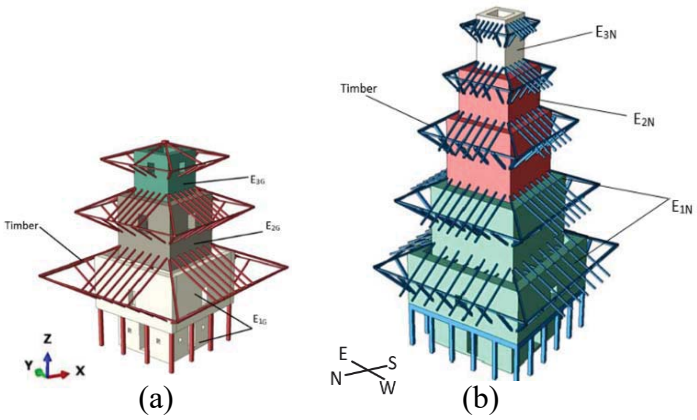


Figure 2 – Three dimensional FE models of: (a) Gopinath and (b) Nyatopol temples. Different colors represent the different modulus of elasticity assigned to the models (see also Tables 2 and 3)

The numerical frequencies obtained from the numerical model are less than 5% different to the ones obtained experimentally. Calibrated modes for both temples are the first three main flexural modes in one of the principal directions (see Table 1 and

Table 2).

Table 1 – Calibration of parameters for Gopinath temple– E_1=140MPa; E_2=141MPa; E_3=140MPa

Mode	Direction	Numerical freq. (Hz) [6]	Error (%)
Mode 1	Horizontal	1.90	-5.00
Mode 4	Horizontal	4.37	-2.88
Mode 8	Horizontal	7.77	5.00

Table 2 – Calibration of parameters for Nyatopol temple –E_1=265MPa; E_2=245MPa; E_3=245MPa

Mode	Direction	Numerical freq. (Hz) [5]	Error (%)
Mode 1	Horizontal	1.60	-4.59
Mode 4	Horizontal	3.91	-0.98
Mode 7	Horizontal	6.67	4.90

3. LINEAR ANALYSES

Linear analysis of the temples were undertaken to understand the local dynamic response and identify the possible local failure mechanisms that can occur before their global collapse. In the case when the timber links were not present (non-existing as structural elements or broken due to excess of load carrying capacity), the external walls were not restrained along the upper edge and unable to resist lateral loads alone. This may lead to overturning as a result of out-of-plane failure associated with extensive cracking pattern in the vertical direction at the corners.

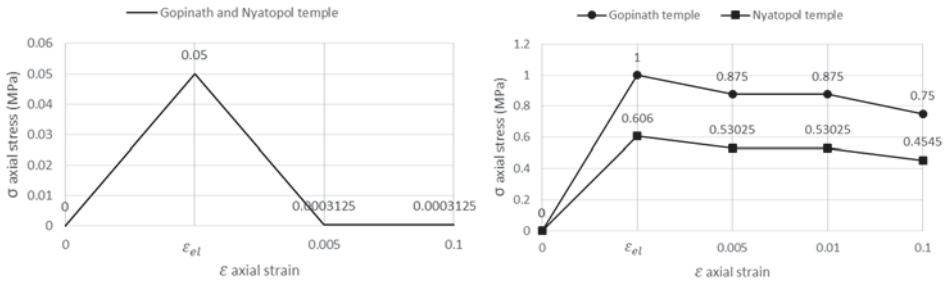
Global dynamic response of the temple is significantly influenced by oscillations in Z direction that have more or less substantial effective mass and fall at the plateau of the elastic response spectrum. This is due to the fact that the top tower is supported by timber beams, thus being eccentrically positioned with respect to the central masonry core. It is the eccentricity of the masonry walls which produce discontinuity in vertical stress transmission. Consequently, static and dynamic effects coming from the structure above are concentrically transmitted to the masonry core being applied as patch loads before being smeared through disturbed region. This effect can cause local crushing of masonry material at the points of stress concentration. Crushing of masonry at the contact between timber links and external masonry wall can be observed from the outcomes of the pushover analysis performed. The results indicate crack pattern due to excess stress concentrations.

4. PUSHOVER ANALYSIS

A macro-element model has been developed and the concrete damage plasticity model (CDPM) [8] implemented in ABAQUS has been used. Figure 3 shows actual non-linear behavior of masonry in both tension and compression.

Comparative pushover analyses have been performed on Gopinath and Nyatopol temples by varying their height and wall thicknesses. The geometric parametric configuration used as part of this study is shown in Figure 4.

Figure 4 shows the different geometrical configurations of temples obtained by the variation of two main parameters: (a) the total height (H) of temple; and (b) the thickness of the wall (d) at the central masonry core at the ground level.



(a) (b)

Figure 3 - Non-linear uniaxial stress-strain actual behavior of masonry ((a) in tension; (b) in compression) [9].

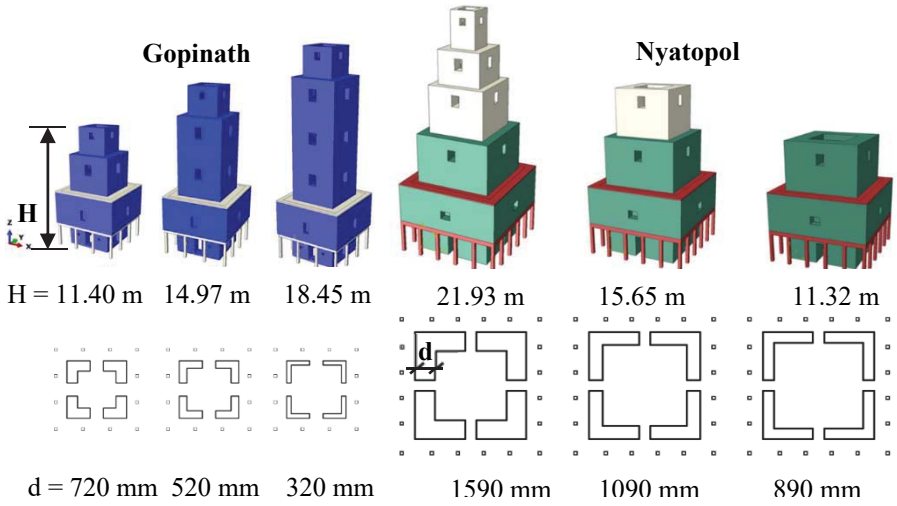


Figure 4 - Gopinath and Nyatopol temples: Different heights (H) and thicknesses (d) of masonry walls

Figure 5 and Figure 6 show the capacity curve diagrams and tensile damage patterns of the corresponding structures in three-dimensional view. Capacity curves give information about variation of ultimate base shear in X direction limited by black circles at the position of ultimate displacements, which are evaluated according to the Italian Guideline for Built Cultural heritage as six times the displacements at elastic limit [10].

Tensile damage patterns consist of cracks at the beginning of each floor (see Figure 5). This is evident for the Nyatopol temple (see Figure 6) which possesses characteristic pyramidal configuration and abrupt change of stiffness at each tier with vertical misalignments of walls of central masonry core. Taller structures behave similarly to towers forming plastic hinges at its bases accompanied with horizontal and diagonal cracks. Figure 5 shows that stocky temples experience shear failure, while in the case of slender temples flexural failure with formation of plastic hinge at the level of second floor was observed. The intermediate cases which were investigated found to undergo a combination of shear and flexural behavior at collapse.

Figure 6 shows that Nyatopol temples with varied geometrical parameters show similar cracking trends. Finally, in both groups of temples progressive change of failure mechanism is

evident, passing from shear failure for stocky to flexural failure for slender temples. Conveniently established failure mechanisms for certain typology of structures are crucial step towards simplified analysis using pre-assigned failure modes, which must be justified by nonlinear dynamic analysis.

The ultimate base shear decreases as the thickness of walls of central masonry core decreases, but particularly decreases in the case of increase of the total height. In particular, for the case of the Gopinath temple with fixed values of thickness at the ground floor, the total base shear at ultimate decreases from 43% to 48% when one floor was added and from 63% to 68% when two floors were added. In addition, in the case of temples with fixed heights, the base shear drop ranges between 9% and 13% when the thickness of the walls was reduced by 200 mm and from 21% to 32% when the reduction was 400 mm. The blue color stands for undamaged structural regions while the red color indicates fully damage regions. Control points are denoted at each structure.

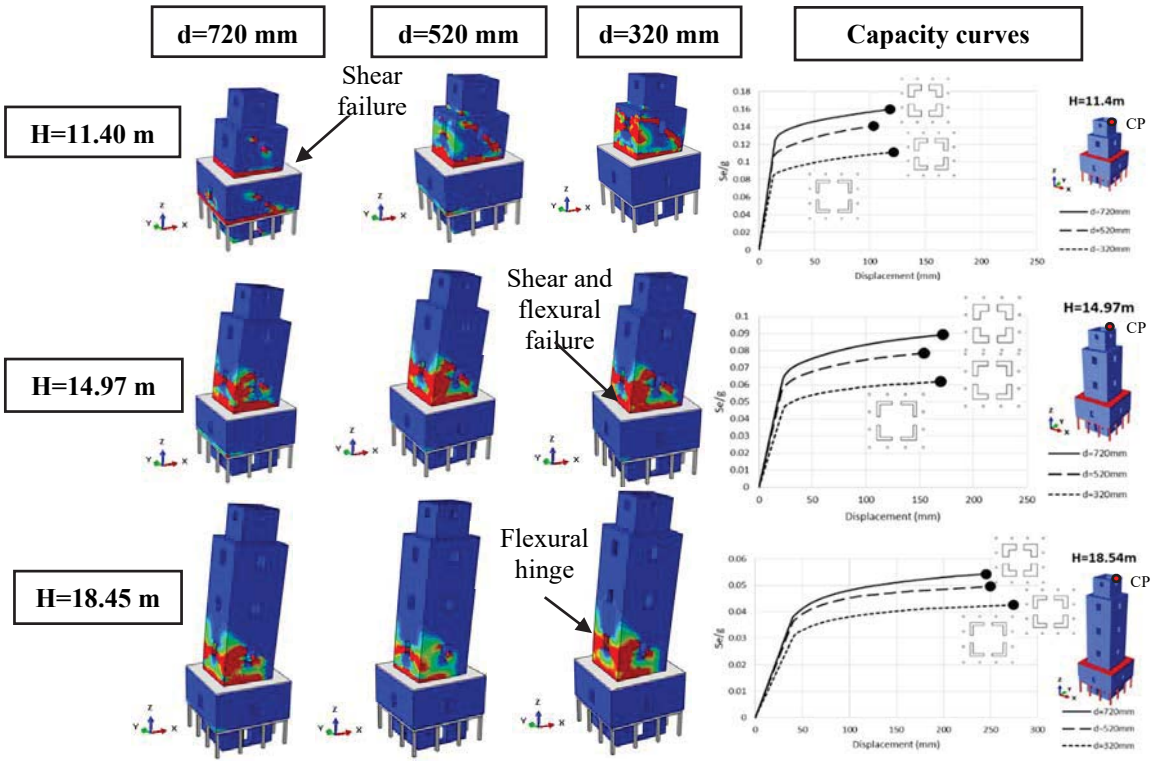


Figure 5 – Tensile damage patterns and capacity curves for Gopinath temple with varied thickness at the ground floor d=720 mm, d=520 mm and d=320 mm and varied heights H=11.40 m, H= 14.97 m and H=18.54 m

Regarding variation of the total height, similar trend can be observed in Nyatopol temples, but oppositely with respect to the first group of temples (if the height is reduced then the ultimate base shear increases). However, for the second group of temples, thickness reduction has beneficiary effect on the ultimate base shear expressed as a function of gravity acceleration

(g). The reason is that structural weight becomes strongly reduced which has a more dominant influence on the growth of the ratio V/W.

Regarding Nyatopol temple with fixed values of wall thickness at the ground floor, the total base shear at ultimate increases from 26% to 103%, if the two last floors were removed. Also, when three floors removed then the total base shear at ultimate increases from 72% to 161%. If the heights were kept constant and the thickness of the wall is equal to 500 mm, then the total base shear at ultimate ranges from 4% to 12%, while when the wall thickness is equal to 700 mm, the total base shear decreases from 12% to 26%.

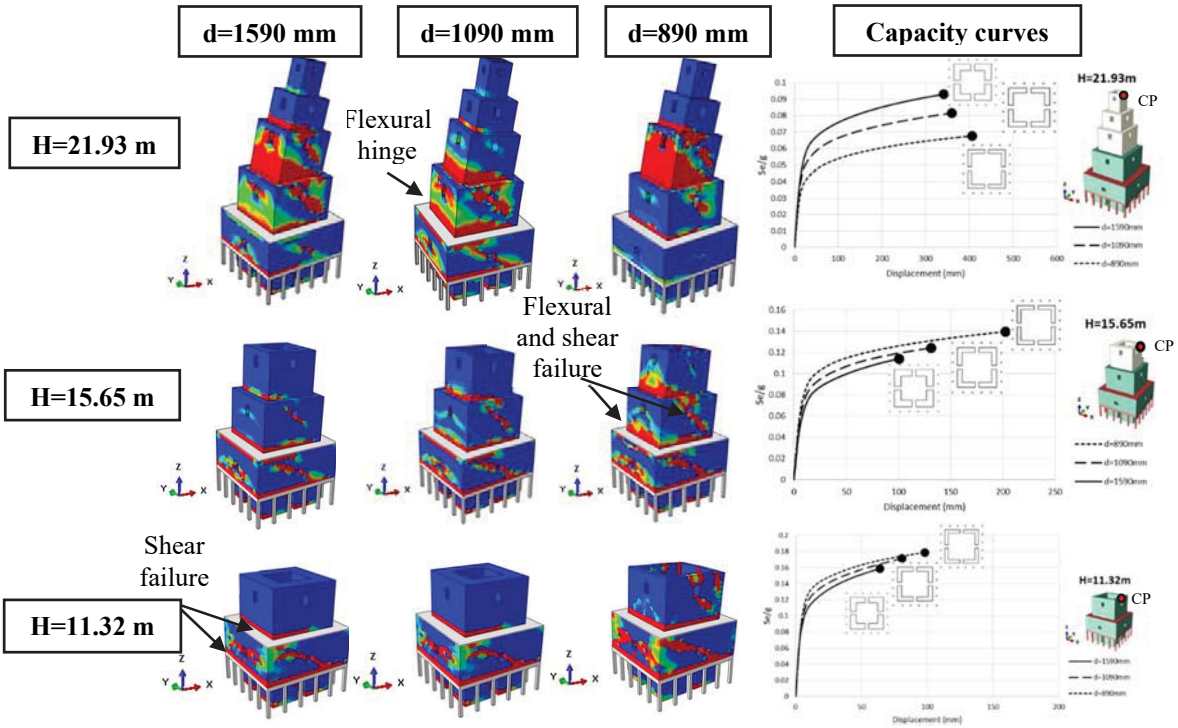


Figure 6 – Tensile damage patterns and capacity curves for Nyatopol temple with varied thickness at the ground floor d=1590 mm, d=1090 mm and d=890 mm and varied heights H=21.93 m, H= 15.65 m and H=11.32 m

5. NONLINEAR DYNAMIC ANALYSIS (NLDA)

Time-history nonlinear analyses were performed using spectrum compatible for the location of Kathmandu Valley accelerogram as shown in Figure 7. This spectrum compatible accelerogram was used mainly for comparative reasons and to assess the damage and preliminary load carrying capacity evaluation of the temples under consideration.

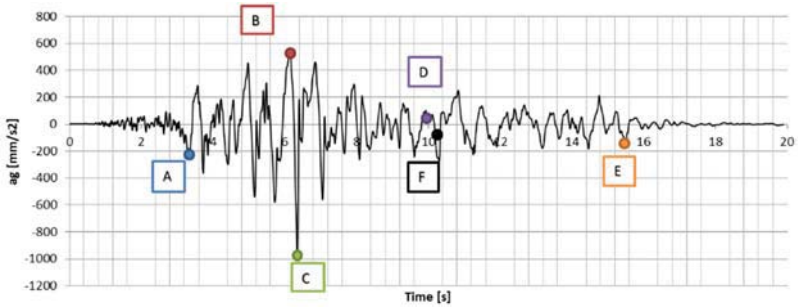


Figure 7 –Spectrum compatible accelerogram PGA=0.1 g

In the NLDA, the peak ground acceleration has been take as 0.1g for all 18 structures in each group of temples in order to compare tensile damages. In other words, the analysis was related to comparative damage analysis of two groups of temples with different dynamic responses under the uniform seismic recording applied in X direction for each temple.

Figure 8 shows the tensile damage patterns and time history of relative drift for the first group of temples. Relative drift has been defined as the displacement normalized with the total height, expressed in percentages. When drift at the top of the structure is greater than 0.8 %, the structure fails. From Figure 8, it can be observed that for the original height which is equal to 11.40 m, damages are dominantly concentrated along the perimeter of the central masonry core at the level of the second floor, independently of the thickness of the walls.

For the structures with the height equal to 14.97 m, or in other words when one floor was added in the original geometry of the temple, damage patterns are to the great extent similar to the ones observed in the group of structures with the height equal to 11.40 m. Besides these, there are inclined damages in the case with the thickness of 320 mm which corresponds to transition from shear failure to flexural failure modes.

In the case when the height of the temple was equal to 18.54 m, damages migrate at the level of the lowest window openings. Cracks start from the end of the window openings and propagate to the top, allowing the upper part of the temple to overturn. The two temples with 18.54 m height experience incipient collapse (drift surpasses 0.8 % of the total height) with overturning of the tower-like upper part, which can be observed in the final row of Figure 8. Evidently, NLDA shows that plastic hinges for the most slender Gopinath temples occur at the level of the lowest set of window openings, while in pushover analysis overturning takes place around the hinge at the level of second floor.

Figure 9 shows that in stockier structures of the second group of temples, various damage patterns that precede shear failures of entire structural parts (exterior walls and walls of central masonry core) are visible. However, Nyatopol temple with original height which is equal to 21.93 m is characterized by vertical misalignments and thickness reduction of walls of central masonry core at each floor. These are the reasons for these zones to be the weakest in the structure, which can be justified observing concentration of damages (see the first row of Figure 9). However, certain closed crack patterns in the shape of ellipse are visible from the side perpendicular to ground motion direction. That is the consequence of oscillations of the wall free surface which is far from its constraint zones. These cracks are particularly pronounced in

the case of the smallest thickness of the base wall which equals 890 mm. This is in opposition with the damage maps obtained by pushover analysis, which forces flexural failure at each level. The reason is irregular pyramidal configuration of the structures with progressive reduction of cross section along the height. Such irregular configuration induces more shear resistance in its behavior than regular slender configuration leading to shear failures of certain structural parts.

Consequently, unlike towers with simple and regular geometry, seismic performance assessment of Nepalese temples with numerous irregularities cannot be evaluated by applying pushover analysis, hence more accurate NLDA is necessary for the evaluation of the dynamic behavior of such temples. This comparative damage analysis shows that one has to be particularly careful while choosing analysis method in order to obtain convenient results. Finally, reliable results are of the utmost importance for implementing intervention strategies which are essential for the preservation of such invaluable built cultural heritage.

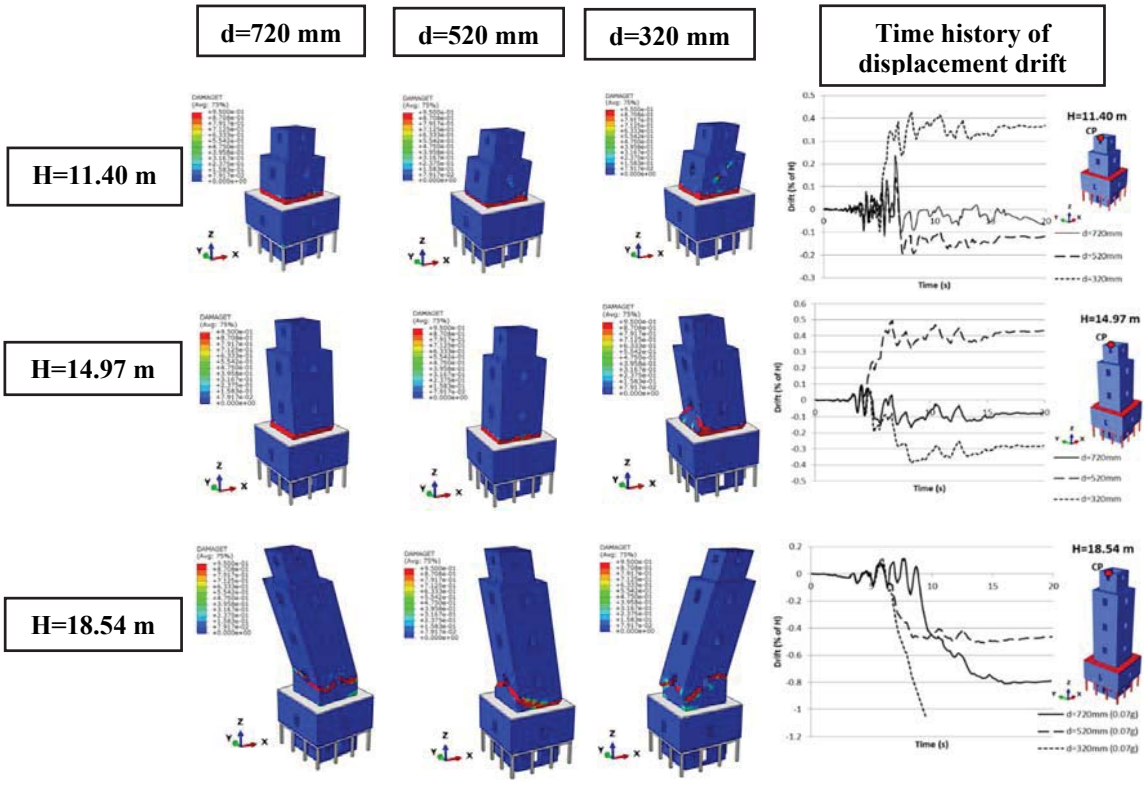


Figure 8 – Final tensile damage patterns and time history of displacement drift of the control points for Gopinath temple with varied thickness d=720 mm, d=520 mm and d=320 mm at the ground floor and varied height H=11.40 m, H= 14.97 m and H=18.54 m

A comparative analysis was performed assuming stiff and flexible floors at second floor. Two extreme examples in terms of global structural slenderness investigated: a) Gopinath temple with height equal to 18.54 m; and b) Nyatopol temple with 11.32 m of the height with

varied thickness. The main goal was to prove that failure mechanism which occurs in slender temples does not depend on the aforementioned assumption. The reason is the fact that tensile damages are concentrated at the section which is weakened by the window openings and that the structure has characteristic flexural failure mechanism.

For the temples with height equal to 18.54 m, damages were dominantly concentrated along the perimeter of the central masonry core, forming a flexural failure mechanism for all three different thicknesses investigated. Additionally, incipient collapse situation was reached, which was visible by looking at the amount of drift at the control point at the top of the temples.

For the temples with thickness of the walls (d) equal to 720 mm, cracks initiated at the lowest set of window openings, while at the second floor there was a slight indication of damage. Low-intensity damages can be observed at re-entrant corners of the lowest windows. In the case of wall thickness equal to 520 mm, crack pattern was partially flat over the second floor onset and started to be inclined towards the corners of the window opening.

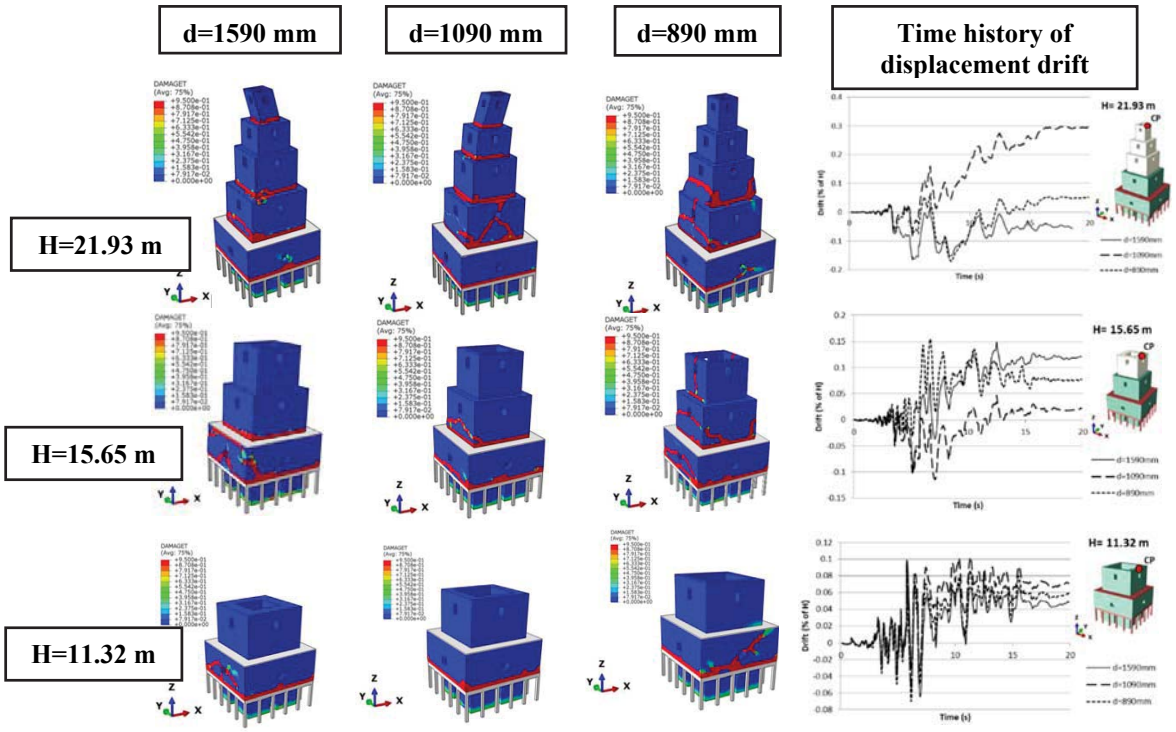


Figure 9 – Final tensile damage patterns and time history of displacement drift of the control points for Nyatopol temple with varied thickness d=1590 mm, d=1090 mm and d=890 mm at the ground floor and varied height H=21.93 m, H= 15.65 m and H=11.3 m

If strengthening measures are not already applied, the assumption of box-like behavior including metal plates at the top of corners of external walls cannot be presupposed.

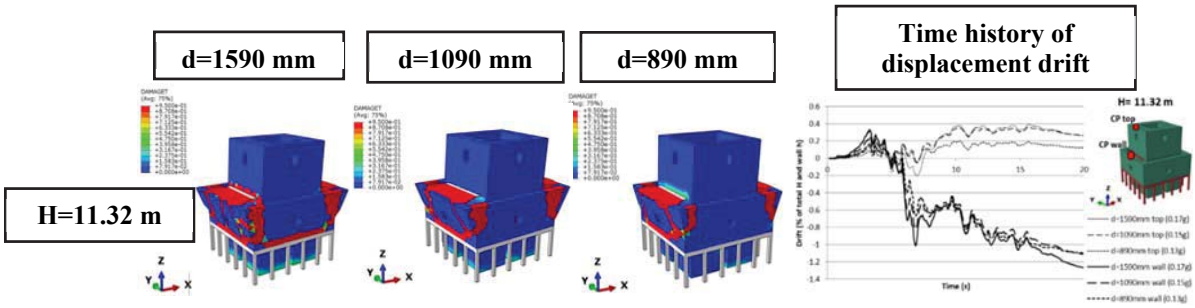


Figure 10 - Final tensile damage patterns and time history of relative drift of the control points for Nyatopol temple with H= 11.32 m with flexible floor assumption

In that case, another modeling approach was applied, which rendered out-of-plane overturning of external walls, especially when stocky structures were at stake. In other words, when slenderness was higher (e.g. Gopinath temple with H=18.54 m) the structure behaved similarly to towers (flexural hinge occurs), while when the slenderness was smaller (e.g. Nyatopol temple with H=11.32 m) collapse mechanisms include out-of-plane overturning of external walls perpendicular to ground motion actions and the loss of interlocking between perpendicular walls was evident at both (see Figure 10).

6. CONCLUSIONS

In this study, the seismic performance of old multi-tiered temples in Nepal were assessed using different computational approaches including: a) linear; b) nonlinear static; and c) nonlinear dynamic analyses. A sensitivity study was also undertaken to investigate the influence of wall thickness and height of Nepalese temples on their seismic behavior. A series of macro-models based on the finite element method of analysis were developed. Masonry has been modeled based on the Concrete Damaged Plasticity Model (CDPM) available in ABAQUS.

Comparative damage analysis shows that the selection of the suitable approach for modelling such structures is critical to avoid misleading information about their seismic performance. NLDA shows that pyramidal configuration with progressive reduction of cross section at each floor activates more shear resistance in its behavior than the flexural one. Application of nonlinear static analysis thus is not justified since its results are in principle more oriented to flexural than to shear behavior, which is not in correspondence with the most accurate NLDA for this type of structures. Correct assessment of failure modes is essential for proper design of intervention strategy which is necessary to be done for many temples.

Under the assumption of stiff floor, failure mechanisms do not change in the case of the most slender temples among all investigated (Gopinath temples with H=18.54 m with varied thickness) comparing to the case of flexible floor. In the case of the stockiest temples (Nyatopol temples with H=11.32 m) the failure mechanism is reached only when flexible floor is assumed. Being closer to reality, it is evident that overturning of the external walls takes place. In order to avoid this proper strengthening measures are necessary to be applied.

Acknowledgement. The authors would like to acknowledge the funding received from British Academy's Global Challenges Research Fund: Cities and Infrastructure Program to carry out the research titled 'Reducing Disaster Risk to Life and Livelihoods by Evaluating the Seismic Safety of Kathmandu's Historic Urban Infrastructure' (CI70241) and the generous logistical support offered by the Pashupati Area Development Trust and the Department of Archaeology, Government of Nepal.

REFERENCES

[1] M. Betti, A. Borghini, S. Boschi, A. Ciavattone and A. Vignoli, "Comparative Seismic Risk Assessment of Basilica-type Churches," *Journal of Earthquake Engineering, 22:sup1, 62-95, DOI: 10.1080/13632469.2017.1309602,* 2018.

[2] V. Sarhosis, G. Milani, A. Formisano and F. Fabbrocino, "Evaluation of different approaches for the estimation of the seismic vulnerability of masonry towers," *Bull Earthquake Eng (2018) 16:1511–1545.*

[3] M. Valente and G. Milani, "Effects of Geometrical Features on the Seismic Response of Historical Masonry Towers," *Journal of Earthquake Engineering, 22:sup1, 2-34, DOI: 10.1080/13632469.2016.1277438,* 2018.

[4] A. M. D'Altri, G. Castellazzi and S. Miranda, "Collapse investigation of the Arquata del Tronto medieval fortress after the 2016 Central Italy seismic sequence," *Journal of Building Engineering 18 (2018) 245–251.*

[5] J. Bijaya, R. Wei-Xin, Z. Zhou-Hong and M. Prem Nath, "Dynamic and seismic performance of old multi-tiered temples in Nepal," *Engineering Structures 25 (2003) 1827–1839,* 11 August 2003.

[6] A. Arce, P. Awal and A. Tamrakar, "Structural analysis and strengthening proposals for the Gopinath temple in Kathamndu Durbar Square," January 2018.

[7] D. Sonda, D. Bothara, C. Chesi, V. Sumini and e. al, "ANALYSIS OF THE SEISMIC PERFORMANCE OF A STRENGTHENED PAGODA TEMPLE DURING GORKHA EARTHQUAKE," in *16th World Conference on Earthquake, 16WCEE 2017*, Santiago Chile, January 9th to 13th 2017.

[8] P. Grassl, D. Xenos, U. Nystrom, R. Rempling and K. Gylltoft, "CDPM2: A damage-plasticity approach to modelling the failure of concrete," 26 Jul 2013.

[9] G. Milani and M. Valente, "Failure analysis of seven masonry churches severely damaged during the 2012 Emilia-Romagna (Italy) earthquake: Non-linear dynamic analyses vs conventional static approaches," *Engineering Failure Analysis 54 (2015) 13–56,* 31 March 2015.

[10] " Direttiva del Presidente del Consiglio dei Ministri - Valutazione e riduzione del rischio sismico del patrimonio culturale con riferimento alle Norme techice per le construzioni di cui al D.M. 14/01/2018," p. 29, 9 Febbraio 2011.

12th International Conference on Structural Analysis of Historical Constructions
SAHC 2020
P. Roca, L. Pelà and C. Molins (Eds.)

NUMERICAL SIMULATION ON SEISMIC PERFORMANCE OF RETROFITTED MASONRY WALL IN HISTORICAL BUILDINGS DAMAGED IN EARTHQUAKE

BIYE WU [1], JUNWU DAI [1*] AND WEN BAI [1]

[1] Key Laboratory of Earthquake Engineering and Engineering Vibration,
Institute of Engineering Mechanics, China Earthquake Administration
29# Xuefu Road, Harbin, Heilongjiang, China, 150080
e-mail: { hit-wby@163.com , jwdai@iem.cn (*corresponding author),
781090853@qq.com },www.iem.ac.cn

Keywords: Earthquake Damaged Wall, Seismic Performance Assessment, External Mortar Layer, External Fibre Layer, Hysteretic Curve.

Abstract. *Due to the characteristics of lower strength, anisotropy, heterogeneity and poor ductility, historical masonry structures usually show poor seismic performance. During earthquakes, the damage severity of masonry structural members varies with their real capacity mostly. To avoid waste and save resources, the following retrofitting strategies would be determined in comply with the cost-effective principles corresponding to the severity level of the damaged buildings. The mechanical properties as to the seismic performance of the critical load bearing walls in the damaged buildings could be improved by retrofitting and repairing. However, how to reasonably and effectively estimate the seismic performance of the retrofitted wall with some level of damage could be the most critical and challengeable point. Based on the finite element analyses, simulation method for the seismic performance of retrofitted masonry wall with damage in earthquake is developed in this paper. The stress and strain hysteretic model for the retrofitted wall element is proposed to consider the three stage effects: original damage, retrofitting or repair, and reloading. According to relevant codes and research results, the damage level of components is classified in terms of the loss level of the axial and shear capacity as well as the deformability. Damage patterns, hysteretic relationships among different retrofitting methods in terms of the external single side of reinforced mortar layer and external single side of fibre reinforced lime mortar layer are compared and analyzed. The seismic capacity and hysteretic skeleton curve of retrofitted masonry wall specimens with different damage levels are developed and discussed. The operational cost-effective retrofitting schemes for masonry walls with different damage levels are proposed.*

1 INTRODUCTION

Historical buildings experienced many destructive uncertainties in their long histories. This results in different degrees of damage and reduced bearing capacity to masonry structures, which makes it difficult to continue to maintain the functionality. The long life of historical architecture makes it have rich cultural mark, which is the mark of architectural history and

cultural development history. The strength of masonry mortar in most brick masonry historical buildings is relatively low, and the compressive strength of masonry mortar in most brick masonry historical buildings is less than 1.0MPa or even close to 0.1MPa. At the same time, due to the construction of brick masonry structure and the improper use of lots of reasons historical buildings tend to demonstrate different kind of damage pattern (crisp, mortar pulverization, wall cracks, wall moisture, etc.). These adverse factors weaken the masonry strength and the deformability, thus the structural seismic performance is also decreased.

The painful lessons learned from the Tangshan earthquake in 1976 made Chinese scholars [1-3] paid much attention on the seismic reinforcement of the masonry structures and took a lot of researches on the seismic reinforcement of masonry structures with reinforced (steel mesh) mortar or concrete.

Traditional materials used in masonry structures are mostly brittle with little ductility to resist natural disasters. Based on this point, scholars [4-6] started to study how to reinforce the masonry structures with fibre reinforced materials in lab tests. Carbon fibre and basalt fibre are the most typical fibre reinforced materials in most studies. Strengthening patterns are given priority to use paste fibre cloth. The factors affecting seismic shear bearing capacity of the wall after reinforcement include fibre material properties, paste form, the elastic modulus and compatibility of fibre material, the consolidation time, etc. The results show that the cracking load and ultimate bearing capacity as well as the seismic energy dissipation capacity of the walls are increased to different degrees with factors change.

The height of historical buildings is generally short, so the vertical pressure on the walls is relatively low. The reinforcement of brick masonry walls under low pressure usually adopts the method of sticking fibre reinforcement or steel meshed mortar layer reinforcement. Sticking the fibre can improve the ductility of the wall, and the external steel meshed mortar layer can greatly improve the bearing capacity of the wall. Both methods are widely used in engineering practice, but they are mostly not allowed to use for the brick masonry historical buildings. For the wall has been broken seriously with uneven surface, it is difficult to paste fibre cloth. At the same time, the fibre cloth and the original brick wall has a large visual difference, it is difficult to accept by the architect. After reinforcement with steel meshed mortar layer, the wall stiffness increases, but the wall ductility enhancement effect is not significant. In fact, the original wall is disturbed greatly during construction, and the facade effect is changed after reinforcement, these aspects are all shortcomings for historical masonry structural buildings.

In order to reinforce the brick masonry historic buildings with low strength mortar under low pressure, this paper proposes the method of replacing the steel mesh with natural linen fibre bundles embedded in the external mortar layer. During construction, the cracked wall is firstly repaired with mortar pressure grouting, then pasted with fibre cloth, and finally coated with mortar, the effect is equal to the reinforcement method of the external steel mesh mortar layer. In order to study the adaptability of the traditional mortar strengthening methods to the earthquake damaged brick masonry structure, to determine the usable strength range of masonry mortar for providing sufficient seismic shear bearing capacity after retrofitting, this paper conducted series of numerical analyses about the seismic bearing capacity of damaged low strength masonry walls retrofitted with masonry mortar with strength of 0.4 MPa under axial pressure of 0.3 MPa as example.

2. NUMERICAL SPECIMEN MODEL

2.1 Specimen design

Historical buildings have experienced the aging effect of many natural factors such as man-made damage, earthquake damage, differential settlement deformation and freeze-thaw deterioration or temperature deformation etc. during their long service period. Before strengthening the walls of masonry structure historical buildings, it is necessary to investigate the existing damages of the buildings in detail, conduct sample extraction to detect the degradation of materials and evaluate the strength. At the same time, based on the existing degradation status of the buildings and the following usage purpose, appropriate reinforcement methods should be selected based on the principle of repairing the old as old. In this paper, brick walls are divided into five grades: undamaged, slightly damaged, moderately damaged, severely damaged and nearly collapsed according to the degree of bearing capacity loss of the existing buildings. The classification method is shown in Table 1.

Table 1: Damage grade of original brick wall

Grade of damage	Embody			
	Lateral bearing capacity loss	Lateral displacement at the wall top	Story drift	Performance of the wall
Undamaged (d0)	No loss	-	-	-
Slight damaged (d1)	loss<10%	3.5 mm	1/300	very slight
Moderate damaged(d2)	10% < loss< 20%	4.8 mm	1/220	Visible cracks
Serious damaged(d3)	20% < loss< 40%	6.0 mm	1/180	More fractures
Close to collapse(d4)	loss> 40%	7.0 mm	1/150	Penetrating

Note: The results of wall state refer to the experimental results of some scholars [1-3]. Story drift is the lateral displacement at the wall top to the wall height 1061mm.

Table 2: Specimen parameters

Group	Specimen number	A/mm	T/mm	Mortar grade	Damage	σ_v/MPa
Ⅰ	Ud-test	-	240	M0.4	d0	0.3
	Ud-simulation	-				
Ⅱ	EW-0.4-d1-0.3-0-WJG	-	240	M0.4	d1	0.3
	EW-0.4-d1-0.3-S20-M**	20				
	EW-0.4-d1-0.3-BFS40-M**	40				
	EW-0.4-d1-0.3-SMS40-M**	40				
Ⅲ	EW-0.4-d2-0.3-0-WJG	-	240	M0.4	d2	0.3
	EW-0.4-d2-0.3-S20-M**	20				
	EW-0.4-d2-0.3-BFS40-M**	40				
	EW-0.4-d2-0.3-SMS40-M**	40				
Ⅳ	EW-0.4-d3-0.3-0-WJG	-	240	M0.4	d3	0.3
	EW-0.4-d3-0.3-S20-M**	20				
	EW-0.4-d3-0.3-BFS40-M**	40				
	EW-0.4-d3-0.3-SMS40-M**	40				
Ⅴ	EW-0.4-d4-0.3-0-WJG	-	240	M0.4	d4	0.3
	EW-0.4-d4-0.3-S20-M**	20				
	EW-0.4-d4-0.3-BFS40-M**	40				
	EW-0.4-d4-0.3-SMS40-M**	40				

Note: Ud-un damaged wall; T is wall thickness; σv is the vertical pressure at the wall top; A is the thickness of side reinforcement surface layer; S20 is single side 20 mm lime mortar layer; S40 is single side 40 mm lime

mortar layer; BF is the surface layer of fibre bundle mortar; SM is the surface layer of steel mesh mortar; M** is the strength grade of surface mortar, classified as M2.5, M5, M7.5 and M10.

For studying of the reinforcement effect of surface strengthening methods to low strength brick walls in different seismic damage degree and the effect of material degradation caused by the aging and permanent deformation, five groups of 53 specimens of wall are designed in this paper, including one piece of benchmark wall without any damage or any reinforcement, 4 pieces of damaged wall, 16 pieces of single side lime mortar reinforced damaged wall, 16 pieces of single side fibre bundle lime mortar reinforced damaged wall, 16 pieces of single side steel mesh mortar reinforced damaged wall, The parameters of each specimen are shown in Table 2.

In the following study, the specimen size, numerical simulation parameters are same with reference [7], see Fig.1. In the numerical simulation, specimens are strengthened with 20 mm thick of plain lime mortar surface layer, 40 mm of reinforced surface layer with D=6mm@300mm steel mesh and same spacing fibre bundles respectively. The fibre bundle area shall be equivalent to the fibre cloth area. The relevant parameters of the reinforcement and fibre bundle materials are shown in Table 3. The strength grade of bricks is MU10 for all specimens, the masonry mortar grade is M0.4 mortar mixed with water, cement and lime, and the external strengthen mortar is M2.5, M5, M7.5 and M10 lime mortar respectively. The strength of materials used in all specimens is shown in Table 3.

Table 3: Strengthening material parameters

Type	Density	elastic modulus	Poisson's ratio	Yield strength	Ultimate strength	Cross-sectional area
Rebar	7850	206GPa	0.3	335MPa	499MPa	28.3 mm^2
Fibre	2820	105GPa	0.2	2303MPa	-	3.63 mm^2

Note: The steel reinforcement adopts HRB335 class ribbed steel bar with diameter of 6mm; the fibre bundle is 0.121mm thick and 30mm wide with equivalent area of basalt fibre belt.

The size of all specimens is the same height1061mm×wideth1645mm×thickness240mm with aspect ratio 0.66. The test specimens are set between the base concrete beam and the top loading beam cast in-situ with C30 concrete. In the numerical simulation, the top beam is set in the model to facilitate load application, and the wall bottom is restrained. The bottom beam is assumed to be the fixed boundary, see Fig. 2.

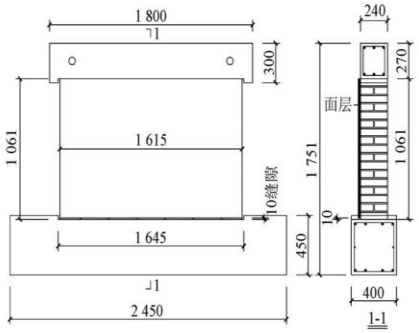


Fig.1. Geometry dimension of the test specimen [7].

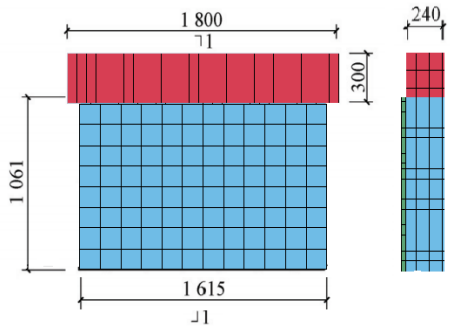


Fig.2. Specimen in numerical simulation

2.2 Establishment of numerical model

In this paper, a numerical model is used to study the large deformation behavior of brick masonry walls by using the explicit integration algorithm, and the general large finite element

software LS-DYNA is used to analyze the bearing capacity and deformation capacity of the unreinforced and reinforced walls. When the numerical model is established, solid elements are used to simulate the brick wall and external mortar layer, while beam elements are used to simulate the fibre bundle and steel mesh. The loading beam and the brick wall are connected by tie elements among surfaces, while the brick wall and the surface mortar are connected by tied nodes.

In the modeling of brick wall materials, mortar and brick blocks are not distinguished and assumed as homogeneous material. The material constitutive model is a double-scalar three-axis damage constitutive model developed based on the plastic damage mechanics theory in literature [8]. At the same time, the maximum tensile stress theory Rankine (1876) was taken into account in the model, enabling the model to consider permanent deformation in the tensile state. Totally 12 parameters in the constitutive model needs to be determined respectively, including the density R_0, elastic modulus E_0, Poisson's ratio P_R, the ratio of biaxial compression strength to uniaxial compression strength RATIO, tensile strength F_{0t}, compressive yield strength F_{0c}, plastic flow constant Beta, fracture energy G_F, compression damage evolution equation model parameters A_c and B_c, tensile damage evolution equation model parameters A_t, same with references [8-11], shown in Table 4. When the maximum tensile stress of the element exceeds F_{0t} or the maximum compressive strain exceeds 0.0023, the element is considered to be failed.

Table 4: Constitutive model parameters of brick block materials

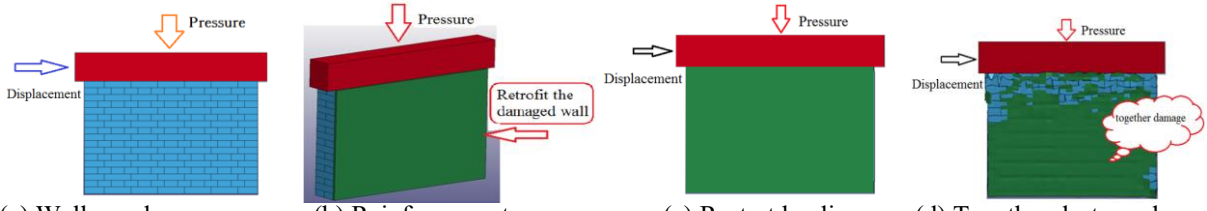
Type	R_0	E_0	P_R	RATIO	F_{0t}	F_{0c}
Value	2000	0.8GPa	0.2	1.0	0.056MPa	0.91MPa
Type	Beta	G_F	A_c	B_c	A_t	
Value	1.09	240J	1.1	0.60	0.01	

In this paper, *MAT_PLASTIC_KINEMATIC is used to simulate the reinforcement and fibre bundle material. The parameters were defined in Table 3. The*MAT_CONCRETE_DAMAGE_REL3 material in the finite element software library is used to simulate the mortar layer material, while the hardening elastic modulus is not taken into account. When the maximum compressive strain of the element reaches 0.0033 or the main tensile stress, it is considered to be invalid, in which the main tensile stress is 1/10 of the compressive strength of the mortar.

2.3 Establishment of damage mechanism and loading system

Masonry is one kind of the most important structural materials in construction of historical buildings. In fact, structural masonry walls in historical buildings usually experience a long term deterioration in strength, stiffness as well as bearing capacity caused by aging, erosion or even kinds of natural or mankind damages. As matter of fact, existing stress and strain usually remains at a certain level in the original parts of the retrofitted wall, while the latterly attached new parts especially the externally reinforced mortar layer in retrofitting usually can’t share vertical loads with the original wall together immediately after the retrofitting construction if there were no new deformation or loading condition change of the retrofitted structure. Using full restart analysis function in the finite element analyses, the above concern could be solved. Full restart analysis is a continuation of the previous analysis. When restarted, latterly attached parts could be added correspondingly. In the full restart analysis, the first step is to

load damage to the wall, the second step is to retrofit the damaged wall, and then to restart analysis, the original part of the model to read the results of the first step for stress initialization. The entire analysis process is shown in the Fig.3.



(a) Wall pre-damage (b) Reinforcement (c) Restart loading (d) Together destroyed

Fig.3. Reinforcement analysis procedure with completely restart in numerical simulation.

In the numerical simulation, the "displacement loading" protocol is used to for all specimens. As well, a 0.3MPa constant vertical pressure is applied on the beam top of the wall, and simultaneously a horizontal low cycle concentrated load is applied to the load beam on top of the wall specimen. Starting from the first stage of cyclic load with displacement of ± 1mm, each cycle increases by 1mm step by step, and the load of each stage repeats once. The displacement load protocol is shown in Fig.4, where 0-6 seconds is the pre-damage loading duration, and 6-16 seconds is the loading duration of the reinforcement. Completely restart at the 6.0th seconds, the external mortar layer begins to participate with the same stress.

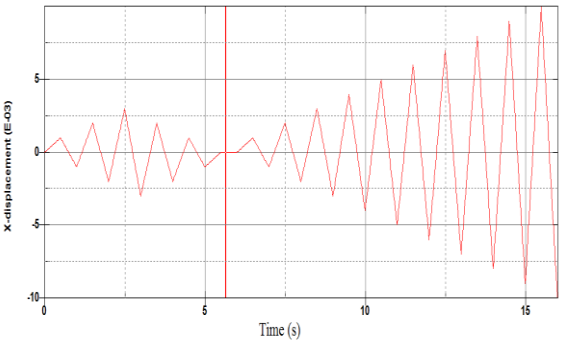
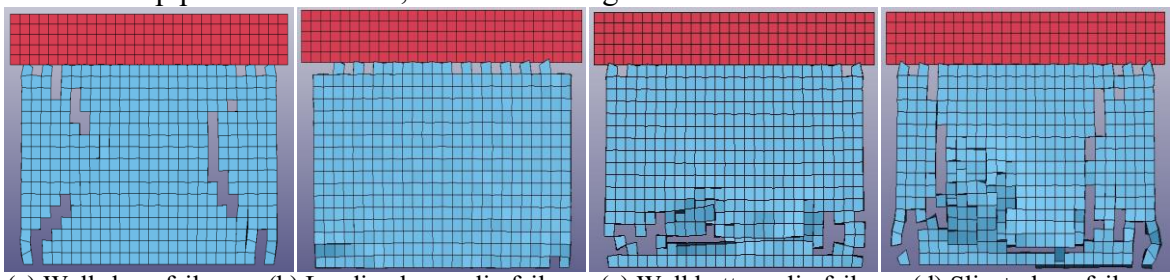


Fig.4. Displacement load - time curve of loaded beam

3. NUMERICAL MODEL ANALYSIS RESULTS

In the numerical simulation, the top loading beam and the wall are tied surface to surface while the bottom node of the wall is directly restrained with fixed boundary. Shear failure is the main pattern of all wall specimens together with loading beam slip, wall bottom slip failure and slip plus shear failure, as shown in Fig. 5.



(a) Wall shear failure (b) Loading beam slip failure (c) Wall bottom slip failure (d) Slip + shear failure

Fig.5. Failure pattern of wall specimen

The analysis results of 53 wall reinforcement specimens show that the damage of the internal original part of brick wall is still the main failure pattern, and most specimens can sustain the load bearing capacity even when the external mortar layer collapse, only partial spalling or severe cracks. Brick wall damage mainly demonstrates as above four patterns shown in fig.5, the only difference is the shape and size of cracks.

3.1 Single side reinforcement with 20 mm lime mortar layer

In the numerical simulation, equivalent material grade M0.4 is used to simulate the original masonry wall. All models are preloaded to form the initial conditions corresponding to different damage levels, and then strengthened with the single side of 20mm lime mortar layer in four strength levels of M2.5, M5, M7.5 and M10. The test results are shown in Table 4.Due to the paper space limitation, only failure patterns are demonstrated here, as shown in Fig.6. It can be seen that the X-type shear failure is the main pattern for the original wall both in lab experiment and numerical simulation.

Results in Table 4 shows that: For wall with strength grade of M0.4, in case of the single side of 20 mm lime mortar layer is used for reinforcement, the deformability of the original wall is enhanced by about 20% at the slight damage level, while the horizontal ultimate bearing capacity of the wall is not increased. Considering the perspective of residual bearing capacity, M5 is the best. Compared with the unreinforced damaged wall, the deformability of M5 wall used for the external mortar layer is enhanced by about 20% corresponding to the moderate damage level of the original wall, and the residual bearing capacity before collapse is higher. Corresponding to the severe damage level of the original wall, the mortar layer with various strengths all can enhance the deformability by about 25%-30%. The residual bearing capacity of the external mortar layer before M5 collapse is relatively high. When the original wall is close to collapse, the effect of the external mortar layer reinforcement on the deformability and horizontal ultimate bearing capacity of the wall is not obvious.

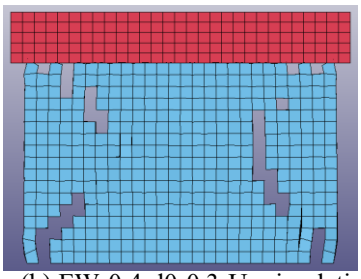
Table 4: EW-0.4-**-0.3-S20-M** numerical analysis results

Damage level	Specimen number	Value				Failure pattern
		F_P (KN)	$\triangle_P$ (mm)	$\triangle_u$ (mm)	F_R (KN)	
d0	Ud-test	+105.8/-89.2	+2.75/-1.96	-	-	shear failure
	Ud-	+103.6/-94.5	+2.94/-2.90	+6.0/-6.0	+62.8/-69.4	shear failure
d1	0-WJG	+97.2/-91.1	+4.0/-3.92	+6.0/-5.0	+65.6/-52.8	shear failure
	S20-M2.5	+97.6/-95.8	+3.9/-3.95	+6.2/-5.7	+74.1/-43.8	shear failure
	S20-M5	+98.5/-96.1	+3.9/-3.96	+6.2/-6.0	+28.8/-58.8	shear failure
	S20-M7.5	+97.4/-96.3	+3.9/-3.96	+6.1/-6.0	+14.7/-52.6	shear failure
	S20-M10	+98.7/-97.2	+3.0/-3.98	+6.2/-6.0	+31.2/-59.4	shear failure
d2	0-WJG	+90.3/-85.5	+3.0/-3.93	+6.0/-5.0	+59.1/-36.9	shear failure
	S20-M2.5	+93.0/-85.7	+3.0/-3.98	+6.0/-5.8	+60.8/-40.2	shear failure
	S20-M5	+94.6/-89.7	+3.0/-3.98	+6.0/-6.0	+71.6/-49.5	shear failure
	S20-M7.5	+94.9/-84.8	+3.0/-3.90	+6.0/-6.0	+66.9/-56.8	shear failure
	S20-M10	+95.3/-89.1	+3.0/-3.99	+6.0/-6.0	+66.4/-49.2	shear failure
d3	0-WJG	+71.0/-64.4	+2.9/-3.0	+5.0/-5.0	+64.8/-60.3	shear failure
	S20-M2.5	+76.5/-71.1	+3.9/-3.95	+5.0/-5.0	+62.6/-42.3	shear failure
	S20-M5	+76.4/-73.6	+3.0/-3.94	+5.0/-5.0	+63.6/-42.2	shear failure
	S20-M7.5	+76.6/-74.2	+3.0/-3.99	+5.2/-5.0	+27.8/-41.1	shear failure
	S20-M10	+76.8/-75.8	+3.9/-3.7	+5.2/-5.0	+39.3/-46.8	shear failure
d4	0-WJG	+60.0/-55.4	+2.9/-3.90	+4.0/-4.0	+41.0/-50.1	shear failure
	S20-M2.5	+61.3/-52.4	+3.0/-3.94	+4.3/-4.0	+32.2/-51.2	shear failure
	S20-M5	+61.1/-54.3	+3.0/-3.99	+4.3/-4.0	+32.5/-53.3	shear failure
	S20-M7.5	+65.3/-52.3	+3.0/-4.0	+4.6/-4.0	+38.7/-49.6	shear failure
	S20-M10	+63.2/-56.8	+3.0/-3.94	+5.0/-4.2	+41.2/-20.6	shear failure

Note: Ud-un damaged wall, FP - horizontal ultimate bearing capacity of wall, △P- displacement corresponding to the horizontal ultimate bearing capacity, △u- refers to the wall's ultimate displacement value, FR-wall residual bearing capacity, that is the peak bearing capacity before the ultimate displacement of the wall.



(a) EW-0.4-d0-0.3-U_d-test [7]



(b) EW-0.4-d0-0.3-U_d-simulation

Fig.6. The failure pattern in numerical simulation and failure pattern lab test

For brick walls with masonry mortar grade of M0.4 and top pressure of 0.3MPa, when a single side of 20 mm lime mortar layer is used for reinforcement, the attached mortar layer has little effect on the horizontal ultimate bearing capacity of the wall, but it can improve the deformability of the wall obviously. When the damage level is d1-d3, the most compatible mortar strength grade is M5. When the damage level is d4, the effect of strengthening with a single side of 20 mm lime mortar layer on the deformability is very weak, so the single side of 20 mm mortar layer reinforcement method is not recommended for this damage level.

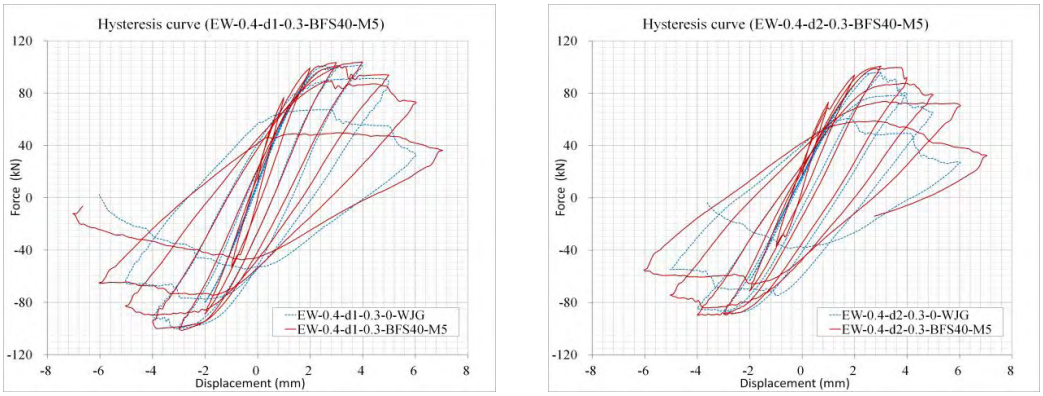
3.2 Single side of 40 mm fibre bundle lime mortar layer reinforcement

The brick wall specimens with M0.4 masonry mortar reinforced with single side of 40 mm fibre bundle lime mortar layer are numerically simulated in this part. The mortar strength is set with grades of M2.5, M5, M7.5 and M10 respectively. The analysis results are shown in Table 5, the load-displacement hysteretic curve is shown in Fig.7, and the comparison with the skeleton curve of the undamaged wall is shown in Fig.8.

Table 5: EW-0.4-**-0.3-BFS40-M** numerical analysis results

Damage level	Specimen number	Value				Failure pattern
		F_P (KN)	$\triangle_P$ (mm)	$\triangle_u$ (mm)	F_R (KN)	
d0	U_d-test	+105.8/-89.2	+2.75/-1.96	-	-	shear failure
	U_d-	+103.6/-94.5	+2.94/-2.90	+6.0/-6.0	+62.8/-69.4	shear failure
d1	0-WJG	+97.2/-91.1	+4.0/-3.92	+6.0/-5.0	+65.6/-52.8	shear failure
	BFS40-M2.5	+104.1/-101	+3.2/-3.7	+7.0/-7.0	+59.2/-21.3	shear failure
	BFS40-M5	+104.3/-101	+4.0/-2.9	+7.0/-7.0	+48.8/-45.6	shear failure
	BFS40-M7.5	+104.3/-103	+2.9/-3.4	+8.0/-7.0	+24.6/-51.6	shear failure
	BFS40-M10	+103/-111	+2.0/-3.5	+8.0/-7.0	+47.2/-70.1	shear failure
d2	0-WJG	+90.3/-85.5	+3.0/-3.93	+6.0/-5.0	+59.1/-36.9	shear failure
	BFS40-M2.5	+97.3/-89.3	+3.0/-4.0	+7.0/-6.0	+33.1/-65.4	shear failure
	BFS40-M5	+101/-89.9	+3.0/-3.7	+7.0/-7.0	+54.4/-16.1	shear failure
	BFS40-M7.5	+102/-91.6	+3.6/-4.0	+7.0/-7.0	+55.1/-27.1	shear failure
	BFS40-M10	+103/-98.2	+3.0/-3.7	+7.0/-7.0	+50.2/-31.6	shear failure
d3	0-WJG	+71.0/-64.4	+2.9/-3.0	+5.0/-5.0	+64.8/-60.3	shear failure
	BFS40-M2.5	+78.5/-76.2	+3.0/-3.0	+6.0/-6.0	+41.7/-20.1	shear failure
	BFS40-M5	+80.0/-80.3	+3.3/-3.0	+6.0/-6.0	+58.6/-43.9	shear failure
	BFS40-M7.5	+81.4/-80.0	+3.0/-3.0	+6.0/-6.0	+57.7/-50.2	shear failure
	BFS40-M10	+81.5/-80.0	+3.0/-3.1	+6.0/-6.0	+58.4/-43.9	shear failure
d4	0-WJG	+60.0/-55.4	+2.9/-3.90	+4.0/-4.0	+41.0/-50.1	shear failure
	BFS40-M2.5	+7.9/-66.8	+2.9/-3.7	+6.0/-5.0	+21.5/-47.6	shear failure
	BFS40-M5	+70.7/-60.5	+3.0/-3.4	+6.0/-5.0	+45.0/-54.9	shear failure
	BFS40-M7.5	+69.1/-53.8	+2.9/-3.2	+6.0/-5.0	+42.7/-22.5	shear failure
	BFS40-M10	+74.7/-63.6	+3.0/-3.5	+6.0/-5.0	+34.9/-56.6	shear failure

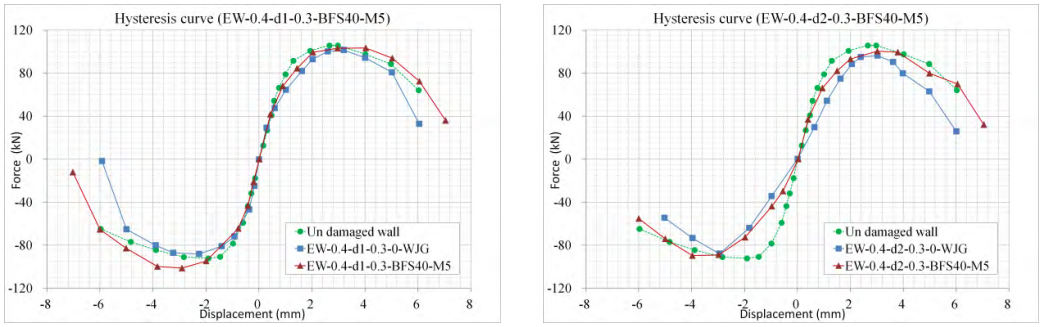
The analysis results in Table 5 show that for brick walls with masonry mortar strength level of 0.4MPa, the failure mode of all wall specimens remains unchanged and remains shear failure even reinforced with single side of 40 mm fibre bundle lime mortar layer. In a variety of damage states, the bearing capacity and deformability of the wall are enhanced after reinforcement, but not significantly increased with the mortar strength increasing. Also, the M5 grade lime mortar can be considered for reinforcement.



(a) BFS40 compared with WJG at d1 level (b) BFS40 compared with WJG at d2 level

Fig.7. Load-displacement hysteretic curve of single side of 40mm fibre bundle lime mortar reinforcement

Fig.7 shows the strengthening effect of single 40 mm fibre bundle lime mortar layer reinforcement. Compared with the unreinforced damaged wall, the deformability of the original wall strengthened by M5 lime mortar was increased by about 15% and the horizontal ultimate bearing capacity of the wall increased by about 7% at the slight damage level. While at the moderate damage level of the original wall, the deformability of the wall strengthened by M5 lime mortar increased by about 15-40%, and the horizontal ultimate bearing capacity of the wall increased by about 14%.



(a) BFS40 compared with WJG at d1 level (b) BFS40 compared with WJG at d2 level

Fig.8. Skeleton curve of single side of 40mm fibre bundle lime mortar reinforcement

As can be seen from Fig.8, for the damaged wall strengthened by the external layer of single side of 40mm fibre bundles lime mortar, if the original wall is slightly damaged and generally damaged, M5 lime mortar is adopted to reinforce the wall, the horizontal ultimate bearing capacity and deformability of the wall can be restored to the level before the damage.

3.3 Single side of 40 mm steel mesh lime mortar layer reinforcement

Similarly, in this part the brick wall specimens are all set with M0.4 masonry mortar and

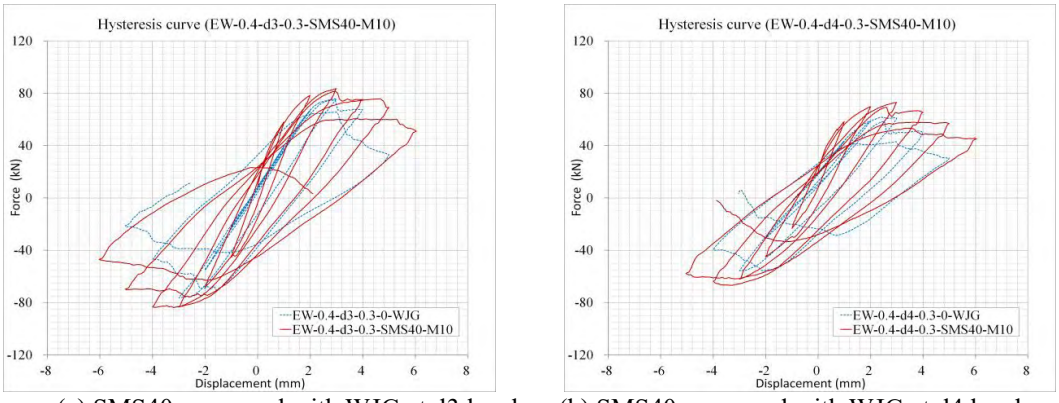
strengthened with external single side of 40 mm steel mesh lime mortar layer. The mortar grades also uses grade of M2.5, M5, M7.5 and M10 respectively. The corresponding analytical results are shown in Table 6, the comparison with the skeleton curve of the undamaged wall is shown in Fig.9.

Table 6: EW-0.4-**-0.3-SMS40-M** numerical analysis results

Damage level	Specimen number	Value				Failure pattern
		F_P (KN)	△P (mm)	△u (mm)	F_R (KN)	
d0	Ud-test	+105.8/-89.2	+2.75/-1.96	-	-	shear failure
	Ud-simulation	+103.6/-94.5	+2.94/-2.90	+6.0/-6.0	+62.8/-69.4	shear failure
d1	0-WJG	+97.2/-91.1	+4.0/-3.92	+6.0/-5.0	+65.6/-52.8	shear failure
	SMS40-M2.5	+105/-103	+3.7/-2.8	+7.0/-7.0	+58.7/-30.9	shear failure
	SMS40-M5	+105.3/-	+3.9/-3.0	+7.0/-7.0	+57.3/-68.2	shear failure
	SMS40-M7.5	+107/-105	+4.0/-3.0	+7.0/-7.0	+41.6/-65.8	shear failure
	SMS40-M10	+112.2/-110	+4.0/-3.7	+7.0/-7.0	+46.2/-68.0	shear failure
d2	0-WJG	+90.3/-85.5	+3.0/-3.93	+6.0/-5.0	+59.1/-36.9	shear failure
	SMS40-M2.5	+98.7/-92.3	+3.0/-3.0	+7.0/-7.0	+60.8/-21.9	shear failure
	SMS40-M5	+101.4/-93.0	+2.9/-3.0	+7.0/-7.0	+74.5/-44.4	shear failure
	SMS40-M7.5	+104/-95.7	+3.0/-4.0	+7.0/-7.0	+71.5/-54.7	shear failure
	SMS40-M10	+106/-96.4	+3.0/-4.0	+7.0/-7.0	+66.6/-53.5	shear failure
d3	0-WJG	+71.0/-64.4	+2.9/-3.0	+5.0/-5.0	+64.8/-60.3	shear failure
	SMS40-M2.5	+78.9/-75.2	+3.0/-3.0	+6.0/-6.0	+57.2/-35.1	shear failure
	SMS40-M5	+82.7/-87.4	+3.3/-4.0	+6.0/-6.0	+36.9/-62.9	shear failure
	SMS40-M7.5	+82.5/-82.1	+3.0/-3.0	+6.0/-6.0	+66.6/-52.6	shear failure
	SMS40-M10	+83.6/-82.1	+3.0/-3.2	+6.0/-6.0	+60.3/-61.6	shear failure
d4	0-WJG	+60.0/-55.4	+2.9/-3.90	+4.0/-4.0	+41.0/-50.1	shear failure
	SMS40-M2.5	+69.0/-62.1	+3.0/-3.2	+5.0/-5.0	+58.3/-53.7	shear failure
	SMS40-M5	+71.0/-61.4	+3.0/-3.8	+6.0/-5.0	+41.2/-55.7	shear failure
	SMS40-M7.5	+72.3/-65.3	+3.0/-4.0	+6.0/-6.0	+45.9/-47.6	shear failure
	SMS40-M10	+73.0/-66.8	+3.0/-3.4	+6.0/-6.0	-51.9/-32.8	shear failure

Note: The related variables in the table have the same meaning as in Table 4.

The analysis results in Table 9 show that for brick walls with masonry mortar strength level of 0.4MPa, the failure mode remains unchanged as shear failure after reinforcement with single side of 40 mm steel mesh lime mortar layer. At all damage level, the bearing capacity and deformability of the wall are enhanced. The higher the strength of the mortar used in wall reinforcement, the more significant the growth of the deformability and the bearing capacity.

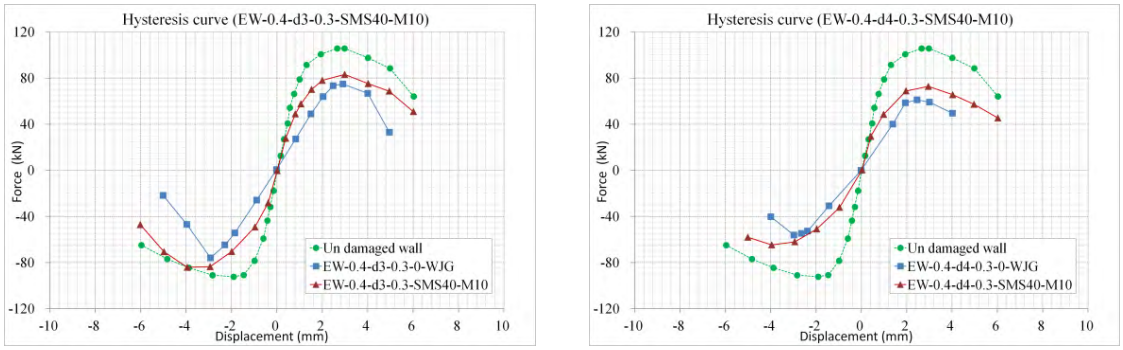


(a) SMS40 compared with WJG at d3 level (b) SMS40 compared with WJG at d4 level

Fig.9. Load-displacement hysteretic curve of single side of 40 mm steel mesh lime mortar reinforcement

Fig.10 shows the strengthening effect of single side of 40 mm steel mesh lime mortar reinforcement. Compared with the unreinforced damaged wall, When the original wall was seriously damaged, the deformability of the wall was strengthened with M10 lime mortar increased by about 20%, and the horizontal ultimate bearing capacity increased by about 27.5%. When the original wall was close to collapse, the deformability of the wall strengthened by M10 lime mortar increased by nearly 50%, and the horizontal ultimate bearing capacity increased by about 21.7%.

It can be concluded from the comparative analysis in Fig.10 that for the damaged wall strengthened by the external single 40mm steel mesh mortar layer, when the strength of mortar is M10, the bearing capacity can reach or even exceed the bearing capacity of the wall before the damage, and the deformability can be increased by about 15%. Under the condition of severe damage or close to collapse, the horizontal ultimate bearing capacity of the reinforced wall can reach 70-80% of the horizontal ultimate bearing capacity of the wall before the damage, and the deformability can reach that of the wall before the damage.



(a) SMS40 compared with WJG at d3 level (b) SMS40 compared with WJG at d4 level

Fig.10. Skeleton curve of single side of 40mm steel mesh lime mortar reinforcement

4. CONCLUSIONS

The brick masonry historical buildings are usually experience unexpected degradation and conditions of the critical load bearing walls are complex. When choosing proper reinforcement method, extensive investigations and tests should be conducted in considering of the history and current situation of the building, so as to clarify the damage state of the walls, and appropriate reinforcement methods should be selected in combination with the architectural features.

From above studies, it can be seen that for the brick masonry historic buildings with weathered and damaged surface, its deformability can be improved using the single side of 20 mm M5 lime mortar.

For the brick masonry walls with slight damage and moderate damage in historical buildings, the single side of 40 mm lime mortar layer can be used for reinforcement, and the reinforcement materials inside the mortar can be fibre bundle or steel mesh. When the fibre bundle is used as the reinforcement material, the mortar strength should be selected as M5, and the horizontal ultimate bearing capacity and deformability of the wall can be restored to the pre-damage level with the reinforcement. When steel mesh is used as reinforcement material, the strength grade of mortar can be selected as M10, the horizontal ultimate bearing

capacity of the wall can exceed the bearing capacity of the wall before damage, and the deformability can be enhanced by about 10%.

In the reinforcement and repair of historical buildings, for walls with serious damage or is close to collapse, the effect of strengthening the bearing capacity and deformation capacity of the wall by fiber bundle is not significant. When reinforced steel mesh is used as the reinforcement material, for the wall with severe damage, the bearing capacity of the reinforced wall can reach 81% that of the intact wall. The deformability can reach 100% that of the intact wall. For a severe damaged wall which is close to collapse, the bearing capacity of the reinforced wall can reach 70% that of the intact wall. The deformability can reach 100% that of the intact wall.

Acknowledgements. This work is supported by the national key research and development plan "major natural disasters monitoring, early warning and prevention" special project of 2018 (2018YFC1504400).

REFERENCES

[1] Zhu Bolong, Wu Mingshun, Jiang Zhixian. A study on seismic capacity of brick wall strengthened with cement mortar reinforced with steel mesh [J]. Earthquake Engineering and Engineering Vibration, 1984, 4(1):70-81.

[2] Huang Zhongbang. The study on adopting the cover with cement mortar and the cover with reinforced cement mortar to strengthen brick masonry [J]. Journal of Tianjin University, 1994, 27(6):764-770.

[3] Liming, Wang Zhihao. Experimental research on masonry wall with low-strength mortar strengthened with steel-mesh cement mortar [J]. Building Structures, 2003, 33(10):34-36.

[4] Triantafillou T C, Fardis M N. Strengthening of historic masonry structures with composite materials [J]. Materials and Structures, 1997, 30(8):486-496.

[5] Kuzik M D, Elwi A E, Cheng J J R. Cyclic Flexure Tests of Masonry Walls Reinforced with Glass Fibre Reinforced Polymer Sheets [J]. Journal of Composites for Construction, 2003, 7(1):20-30.

[6] Jing M, Raongjant W. Experimental Study on Historic Masonry Walls Retrofitted with GFRP Sheets in Different Patterns [J]. Applied Mechanics and Materials, 2015, 723:377-381.

[7] Tang Caoming, Luo Rui, Cheng Shaoge, Huang Baodong. Experimental study of seismic performance of low strength masonry walls reinforced with one-side cement mortar splint [J]. Journal of Building Structures, 2017, 38(10):157-167.

[8] R. Faria, J. Oliver, M. Cervera. A strain-based plastic viscous-damage model for massive concrete structures [J]. International Journal of Solids & Structures, 1998, 35(14):1533-1558.

[9] J. Lee, G. L. Fenves and ASCE. Plastic damage model for cyclic loading of concrete structures. Journal of Engineering Mechanic, 1998, 124(8): 892-900.

[10] LI Zheng, LI Zhong-xian. A modified elastic damage constitutive model of concrete and its application [J]. Engineering mechanics 2011, 28(8):146-150.

[11] Mortezaei A, Kheyroddin A, Ronagh H R. Finite element analysis and seismic rehabilitation of a 1000-year-old heritage listed tall masonry mosque [J]. The Structural Design of Tall and Special Buildings, 2012, 21(5):334-353.

12th International Conference on Structural Analysis of Historical Constructions
SAHC 2020
P. Roca, L. Pelà and C. Molins (Eds.)

REPAIR AND RETROFIT OF A ROMAN BRIDGE IN TURKEY

H. SESIGUR[1*] AND M. ALABOZ[2]

[1]Istanbul Technical University Faculty of Architecture Division of Theory of Structures
Taskisla, Taksim, 34437, İstanbul, Turkey
e-mail: haluk@itu.edu.tr, www.itu.edu.tr (*corresponding author)

[2] ARKE Project Design Company, İstanbul, Turkey
email: alaboz.murat@gmail.com

Keywords: Historical Structure, Masonry, Roman Bridge, Retrofit

Abstract. *This study assesses the earthquake performance of a historical masonry arch bridge in Aizanoi ancient city, which is located in the mid part of Turkey near Kütahya. Aizanoi was the capital of the territory called Aizanitis, located in the area of Phrygia. Historians agreed that Roman settlement in this area started in 3rd millenium BC. The structure is made of stone and has five arches of 5.40m, 6.70m, 7.30m spans. Rise of the arches are varying from 2.70m to 3.65m. Restoration works have completed in 2018. Before the restoration works have been started the bridge was used for vehicles, even for heavy trucks. Today the bridge is using only for pedestrians. After a detailed site investigation, material characterisation and soil tests were performed, ambient vibration test was carried out on site, by placing accelerometers at several points on bridge span to capture dynamic properties of the structure. Different methods such as Frequency Domain Decomposition, SSI were used to extract the experimental natural frequencies, mode shapes, and damping ratios from these measurements. Experimental results were compared with those obtained by the linear finite element analysis of the bridge. Good agreement between mode shapes was observed in comparison, though natural frequencies disagree by 8-10%. The boundary conditions of the linear finite element model of the bridge were adjusted such that the analytical predictions agree with the ambient vibration test results. According to the total strain crack material model, the calibrated linear FE model was extended into a nonlinear model then Nonlinear Static Pushover analyses of the bridge along longitudinal and transversal directions were performed. Obtained results are in good agreement with previous case studies' results. In order to compare collapse load of the bridge with pushover analysis results, kinematic limit analysis procedure is used to assess longitudinal and transverse seismic capacities. The capacity curves are obtained by means of limit analysis approach. The study is aimed to identify on one hand the horizontal load multiplier that activates the kinematic mechanism, on the other hand the collapse displacement. The numerical results of the structural capacity so found have been compared with the results available in literature and acceptable agreement of the results have been obtained.*

1 INTRODUCTION

The assessment of the condition of historical bridges is an important issue in recent years. This task is particularly difficult when dealing with historical masonry arch bridges due to their

specificities as use of natural materials, lack of knowledge related to mechanical properties of materials and their large variability, existing damage caused by increasing traffic loads, aging and environmental factors and lack of maintenance. A very important approach is the use of numerical models able to reproduce the structural response, both at serviceability and ultimate limit states. In order to solve this problem several methods and computational tools are available. Different types of constitutive models originate a sequence of models, which allow the analysis to include more complex response effects. The most common idealizations of material behaviour are elastic behaviour, plastic behaviour and nonlinear behaviour. In general linear elastic analyses might not appropriate for masonry structures, namely masonry arch bridges, however, in a first stage of analysis, the hypothesis of linear elastic behaviour can be of great help. A linear analysis requires few input data, being less demanding, in terms of computer resources and engineering time used, when compared with nonlinear methods. Moreover, for materials with low tensile strength, linear analysis can provide a reasonable description of the process leading to the crack pattern.

Plastic analysis, or limit analysis, is concerned with the evaluation of the maximum load that a structure can sustain. The assumption of plastic behaviour implies that, on one hand, the maximum load is obtained at failure and, on the other hand, the material should possess a ductile behaviour. Apparently, this last requirement seems to be unrealizable since the plastic deformations may exceed the ductility of the masonry. However, the limited ductility in compression does not play a relevant role as collapses are generally related to the low tensile strength. Thus, the assumption of a zero tensile strength renders the method of plastic analysis adequate for the analysis of masonry arch bridges. Finally, nonlinear analysis is the most powerful method of analysis, the only one able to trace the complete structural response of a structure from the elastic range, through cracking and crushing, up to failure.

Several procedures have been formulated in last decades in order to predict the behaviour of masonry arch structures: the difficulty in representing the behaviour of the material and the resistant skeleton requires the use of simplified but effective structural models. In particular the assessment could be based commonly on limit analysis [1,2,3] or nonlinear incremental techniques [4,5,6]. The kinematic method, based on an adaptation of limit design for masonry structures, has proved to be a conceptually simple and robust procedure to verify the safety of masonry arch bridges under vertical loads. The method can also be applied for seismic assessment, providing a limit of bridge capacity under horizontal loads. Since [7] noted that the plastic theory, initially formulated for steel structures, could also be applied to masonry structures, many studies have focused on limit analysis to assess the vertical load-bearing capacity of single and multi-span masonry arches [1,8] adopted some simplifying assumptions to perform aforementioned analyses: absence of sliding between voussoirs: infinite compressive strength and no tensile resistance of masonry.

With these hypotheses, arch failure occurs when a thrust line can be found, lying wholly within the masonry and representing an equilibrium state for the structure under acting loads, which allows the formation of a sufficient number of plastic hinges to transform the structure into a mechanism. Following Heyman's assumptions, iterative methods to find the geometric safety factor, related to minimum arch thickness under dead and live loads, were proposed by [9]. Several authors have incorporated crushing of masonry, which cannot sustain infinite

compressive stresses [9,10,11]. Sliding between adjacent blocks was introduced and evaluated by [12], who successfully modelled multi-span brickwork arch bridges. Recent research has been carried out on the application of limit analysis for assessing masonry arches under horizontal (seismic) loads. In particular, research has focused on the longitudinal behaviour of arched structures. Some papers [13] have studied the dynamic response of a single masonry arch under base motion, providing the horizontal acceleration factor. [14] used discrete element modelling to predict the combinations of impulse magnitudes and durations which lead unreinforced masonry arches to collapse, and analysed the impact of rigid blocks over several cycles of motion. [15] examined the activation of semi-global and global mechanisms involving not only local arch failure but also the simultaneous formation of hinges in the arch and at the base of abutments.

2 STRUCTURAL DEFINITION OF THE BRIDGE

This study assesses the earthquake performance of a historical masonry arch bridge in Aizanoi ancient city, which is located in the mid part of Turkey near Kütahya. Aizanoi was the capital of the territory called Aizanitis, located in the area of Phrygia. Historians agreed that Roman settlement in this area started in 3rd millenium BC. The structure is made of stone and has five arches of 5.40m, 6.70m, 7.30m spans. Rise of the arches are varying from 2.70m to 3.65m.



Figure 1. Pictures taken from during the restoration works

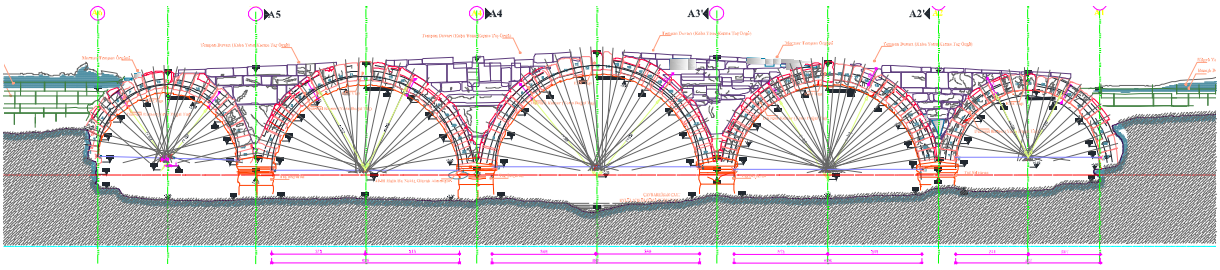


Figure 2. Elevation of the bridge

3 ASSESSMENT OF THE STRUCTURAL SYSTEM

3.1.Damage mapping

After surveying studies were completed on site investigation was carried out. During the site visit some damages were observed such as visible cracks on the surface of the abutments, material losses, deterioration and also some detachment of joints.



Figure 3. Material losses and joint damages



Figure 4. Some damages on joints

3.2.Structural analysis

In order to assess the existing vertical and lateral load capacity of the structure and to give possible intervention proposals, the structural and geometrical configurations defined have been modelled using the software DIANA: for masonry structures, the best modelling technique is usually chosen in function of the analysis objective between different modelling strategies and modelling levels such as micro-modelling or macro-modelling. 3D models implementing a macro-modelling approach have been adopted for finite element discretization, where masonry

was modelled as an homogeneous continuum using six- and eigth-node elements, Figure 5.

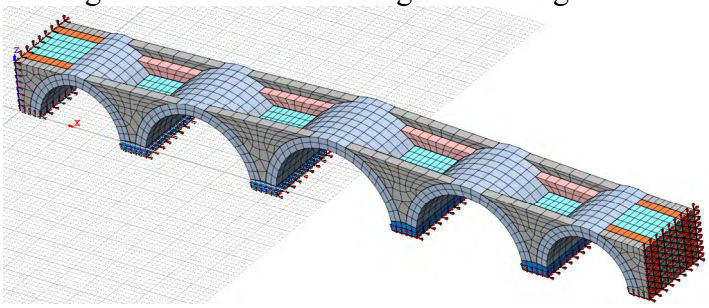


Figure 5. 3D model of the bridge

The Total Strain Crack Model implemented in DIANA was used as constitutive law of masonry. The masonry material exhibits isotropic properties prior to cracking and anisotropic properties after cracking, the cracks being orthogonal to the directions of the main strains. The main materials' mechanical characteristics have been assumed according to literature, considering masonry compressive strength f_c equal to 5MPa, masonry tensile strength f_t equal to 0.3MPa and elastic modulus EM equal to 5000MPa. The filling material has been modelled considering Drucker-Prager constitutive law with an elastic modulus EF equal to 500MPa, internal friction ϕ=37° and cohesion c=10kPa [16]. For both materials (masonry and filling material) a specific weight ρ of the stone equal to 26.5 kN/m^3 weight of the infill equal to 18kN/m^3 and a Poisson ratio ν equal to 0.2 have been assumed. The constitutive model used for masonry has been considered elasto-plastic in compression and elastic with linear softening in traction. Mode I fracture energy is taken as 50N/m. This constitutive model allowed to well represent the arches' failure mode where the typical four cracking hinges that arise in masonry arches subjected to longitudinal seismic actions can be clearly observed.

3.3.System identification

System identification test was carried on under ambient vibration on the bridge to check if the integrity of the structure is satisfied as defined in FEM model as a homogeneous modelling technique. In the process, 4 high accuracies, low noise, 3 axial accelerometers were used. In 100 Hz, 10-20 min records were collected in setups by placing the sensors at 6 locations at top of the bridge, Fig. 6.

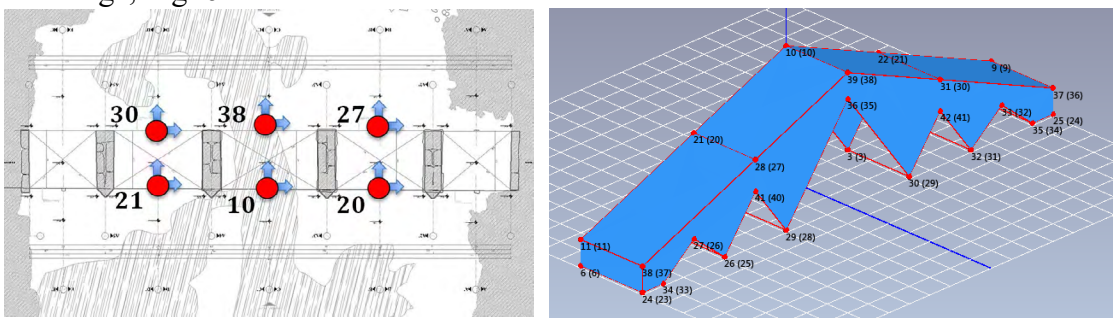


Figure 6. Sensor locations on the bridge

Natural frequencies were obtained and mode shapes of the bridge, the consistency of the mathematical model was checked. Considering the frequency values, lower frequency in system identification test might be the result of a lower modulus of elasticity. However, the differences are in an acceptable range to rely on FEM model and assumptions to carry on further analysis (Table 1). When the model shapes are compared, the amplitudes of modal displacements obtained by system identification exhibits higher values then FEM model. Peaks in different channels in spectral density graph might be referred to some local discontinuities or irregularities at the inner sections, Fig.7. Mode shapes are depicted in Fig.8.

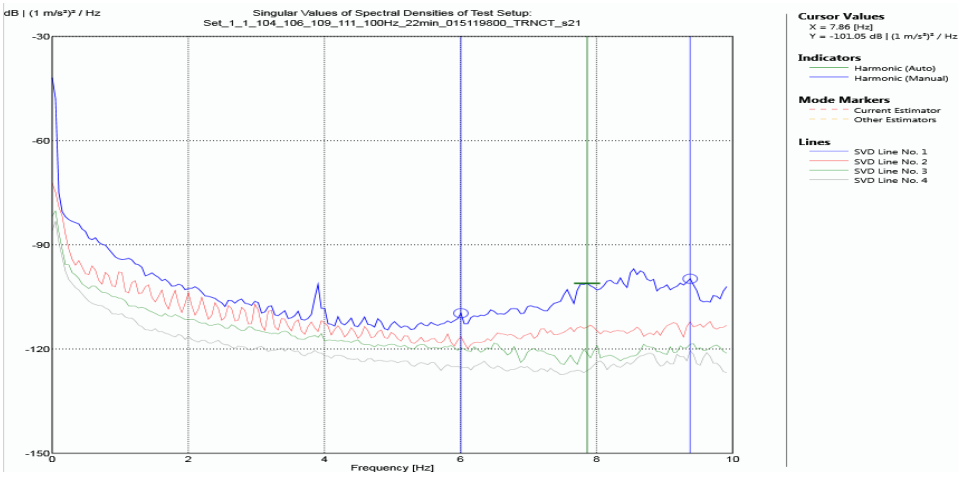
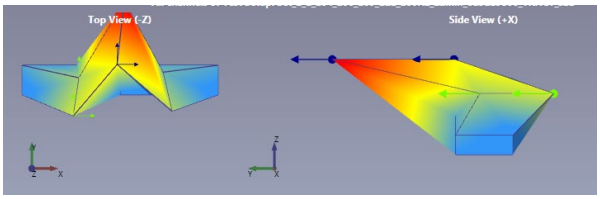


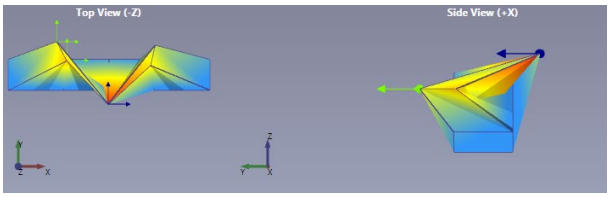
Figure 7. Spectral density diagram

Table 1. Comparison of the frequencies.

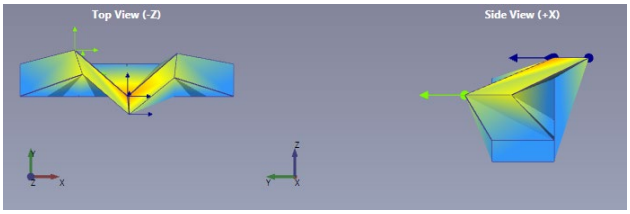
OMA	FEM	Difference %
6.006	6.806	13.32
7.861	7.284	7.34
9.375	8.229	12.22



Mode 1. 6.006Hz



Mode 2. 7.861 Hz



Mode 3. 9.375 Hz

Figure 8. Mode shapes of the bridge

3.4.Nonlinear static analyses

Pushover analyses performed on 3D models have led to the assessment of peak ground acceleration (PGA) which turn the structure into global and local failure mechanisms and to the construction of the relative capacity curves. The results obtained from the analyses carried out on the finite element models in longitudinal and transversal directions have been plotted in terms of ratios between peak ground acceleration corresponding to the occurrence of a local failure mechanism for the arch and PGA values related to the creation of a global mechanism, Fig. 9,10. PGA values have been obtained with N2 method [17] and the spectra type adopted in this work according to Turkish Earthquake Code (2007) for the ultimate limit state (10% exceedance probability during 50 years). The failure mechanism substantially depends from the height to width (H/B) and rise to span (f/L) ratios, and quite apart from the geometrical dimensions: in some studies, it has been observed that masonry arches with higher f/L values are more vulnerable than others characterized by lower f/L ratios. For semi-circular masonry arch bridges, also in the case of slender piers, the four plastic hinges that define the collapse mechanism are generally localized in the arches involving a local failure mode; masonry piers characterized by low H/B values are instead substantially less vulnerable than the slender ones. In transversal direction, failure mechanisms have been identified on the basis of a critical evaluation of the results obtained from the pushover analyses. Capacity curves have been expressed in the ADRS (Acceleration Displacement Response Spectrum) plane and interpolated with an elasto-plastic curve, defined by the yielding displacement d_y and the ultimate displacement point represented by the displacement value d_u and the maximum peak ground acceleration PGA, in both longitudinal and transversal directions.

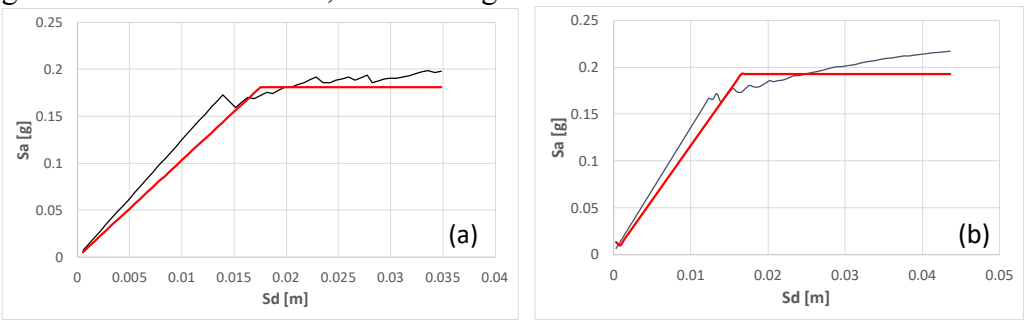


Figure 9. Capacity curve of existing bridge in a) longitudinal direction b)transversal direction

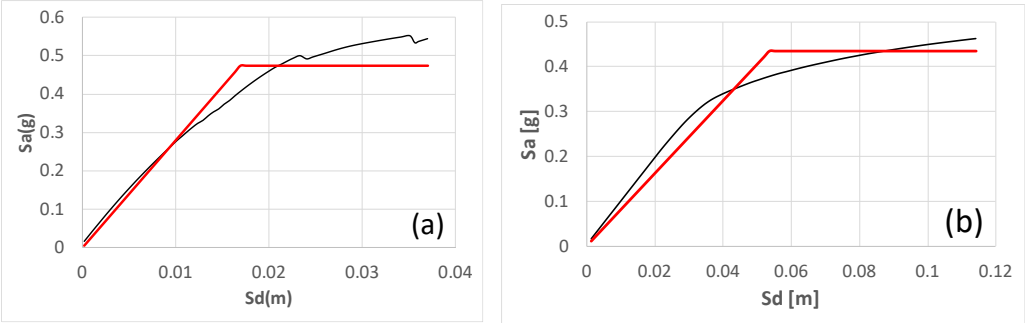


Figure 10. Capacity curve of restorated bridge in a)longitudinal direction b)transversal direction

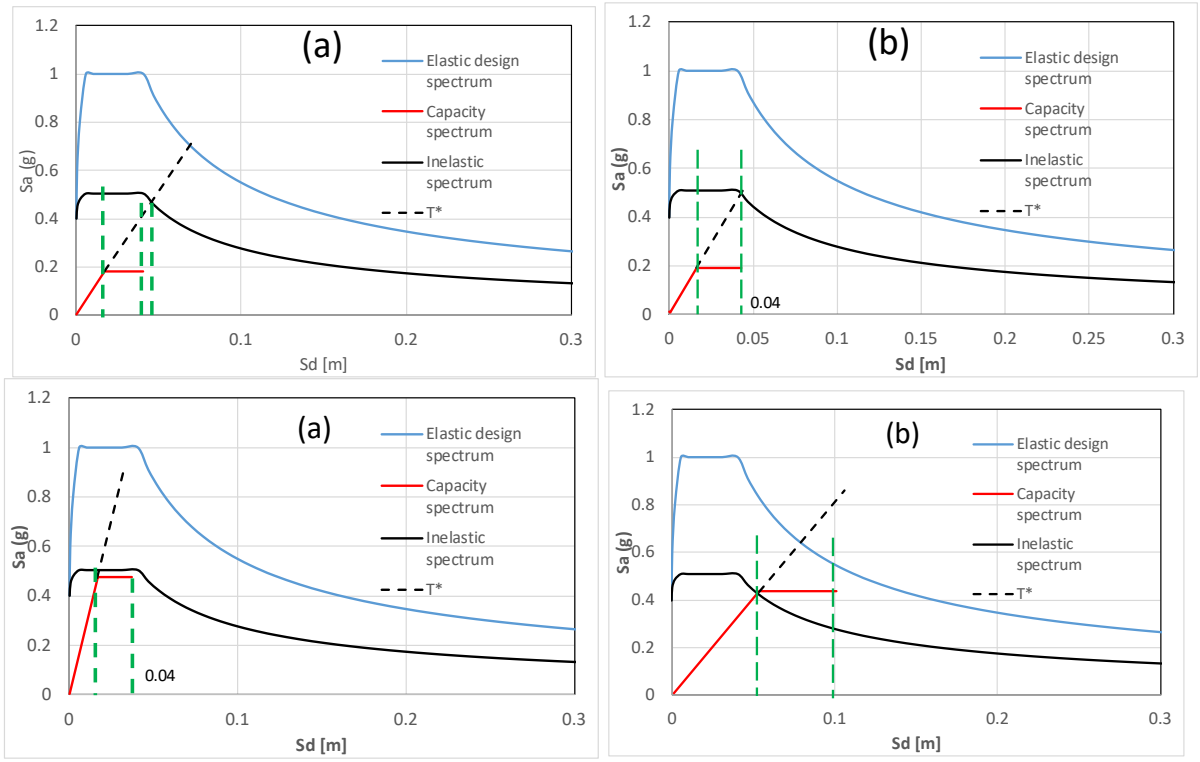


Figure 11. Performance points of existing and renovated bridge along longitudinal (a) and transversal (b) directions

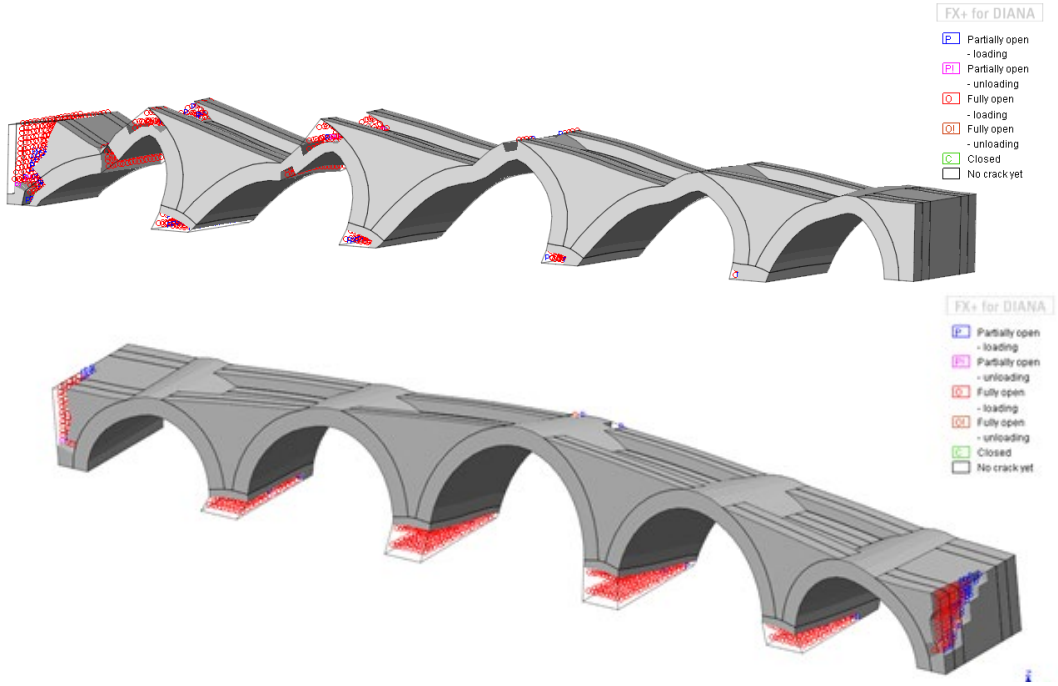


Figure 12. Collapse mechanisms along longitudinal and transversal directions

3.5.Limit analysis

Various specialized analysis programs which rely on the theorems of limit analysis have been developed over years. Currently available tools include ArchieM (Obvis 2007) and ring 2.0 (LimitState 2007b). ArchieM is based on a lower bound line of thrust methodology. The program displays graphically a potential thrust-line for any given load. If a thrust-line cannot be found which lies entirely within the masonry, then the bridge can be considered potentially unsafe. In contrast ring 2.0 uses mathematical optimization to directly identify the collapse state, computing the load factor which, when applied to the specific live load, will lead to collapse.

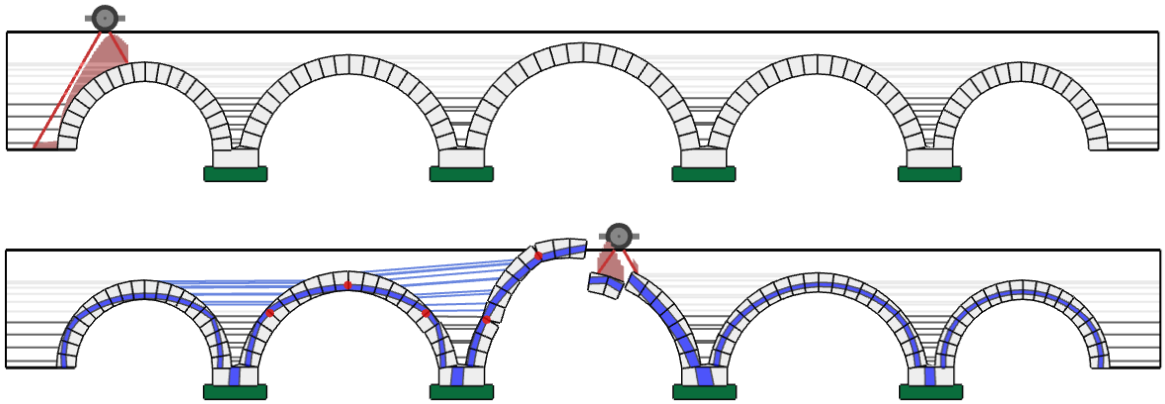


Figure 13. Modelling of the bridge with ring software

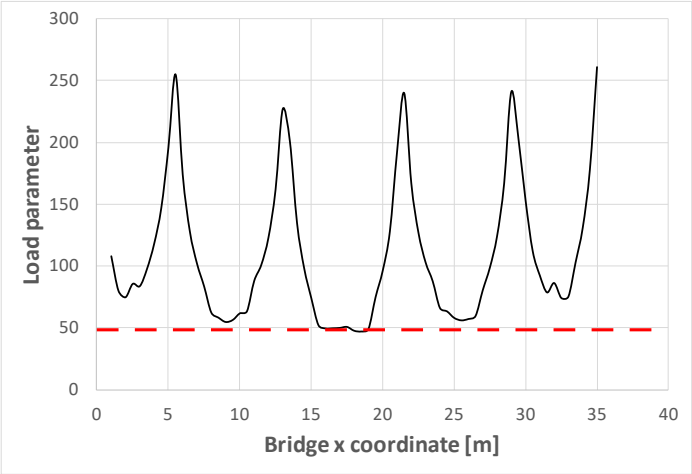


Figure 14. Collapse load of the bridge

Limit analysis with ring software is carried out and the result is obtained as 50kN for live load which can be determined from Fig. 14.

4 CONCLUSIONS

In this study the earthquake performance of a historical masonry arch bridge is assessed in Aizanoi ancient city, which is located in the mid part of Turkey near Kütahya. Before the restoration works have been started the bridge was used for vehicles, even for heavy trucks. Today the bridge is using only for pedestrians. After a detailed site investigation, material characterisation and soil tests were performed, ambient vibration test was carried out on site, by placing accelerometers at several points on bridge span to capture dynamic properties of the structure. Different methods such as Frequency Domain Decomposition, SSI were used to extract the experimental natural frequencies, mode shapes, and damping ratios from these measurements. Experimental results were compared with those obtained by the linear finite element analysis of the bridge. Nonlinear Static Pushover analyses of the bridge along longitudinal and transversal directions were performed. Obtained results are in good agreement with previous case studies' results. In order to compare collapse load of the bridge with pushover analysis results, kinematic limit analysis procedure is used to assess longitudinal and transverse seismic capacities with a software of ring. The numerical results of the structural capacity so found have been compared with the results available in literature and acceptable agreement of the results have been obtained.

REFERENCES

[1] Heyman, J. *The masonry arch*. Ellis Horwood, Chicester (1982).
[2] Gilbert, M. and Melbourne C., Rigid block analysis to masonry arch bridges. *Struct. Eng.* (1994) 72:pp.356-361.
[3] Boothby, T., Collapse modes of masonry arch bridges, *Journal of Bridge Masonry Society* (1995) 9 (2): pp. 62–69.
[4] Audenaert et al. 2D analysis of arch bridges using an elasto-plastic material model. *Engineering Structures* (2008) 30: pp.845-855.
[5] Brencich, A. and De Francesco, U. Assessment of multi-span masonry arch bridges. Part I: a simplified approach. Part II:examples and applications. *Journal of Bridge Engineering ASCE* (2004) 9 (6): pp.582-598.
[6] Molins, C. and Roca, P. Capacity of masonry arches and spatial frames. *Journal of Structural Engineering* (1998) 124:pp.653-663.
[7] Heyman, J. The Stone Skeleton. *International Journal of Solids and Structures* (1966) 2:pp.249-279.
[8] Gilbert, M. Limit analysis applied to masonry arch bridge: state of the art and recent developments. *Proc. 6th international conference on arch bridges, ARCH'07* (2007).
[9] Clemente et al. Limit behavior of stone arch bridges. *Journal of Structural Engineering ASCE* (1995) 121 (7): pp.1045-1050.
[10] Gilbert, M. On the analysis of multi-ring brickwork arch bridges. *Proc. 2nd International conference on arch bridges.* (1998).
[11] Clemente et al. Application of limit analysis to stone arch bridges. *Proc. 6th International conference on arch bridges ARCH'010.* (2010).

[12] Gilbert, M. and Melbourne, C. Rigid-block analysis to masonry arch bridges. *Struct. Eng.* (1994) 72: pp.356-361.
[13] Clemente, P. Introduction to dynamics of stone arches. *Earthquake Engineering and Structural Dynamics* (1998) 27:pp.513-522.
[14] De Lorenzis et al. Failure of masonry arches under impulse base motion. *Earthquake Engineering and Structural Dynamics.* (2007) 6:pp.2119-2136.
[15] De Luca et al. A simplified procedure for assessing the seismic capacity of masonry arches. *Engineering Structures* (2004) 26:pp.1915-1929.
[16] Cavicchi, A. and Gambarotta, L. Collapse analysis of masonry bridges taking into account arch-fill interaction. *Engineering Structures.* (2005) 27:pp.605-615.
[17] Fajfar, P. and Gaspersic, P. The N2 method for the seismic damage analysis of RC buildings. *Earthquake Engineering and Structural Dynamics.* (1996) 25:pp.23-67.

12th International Conference on Structural Analysis of Historical Constructions
SAHC 2020
P. Roca, L. Pelà and C. Molins (Eds.)

SEISMIC ASSESSMENT AND STRENGTHENING INTERVENTIONS OF ATOP SINGLE-BLOCK ROCKING ELEMENTS IN MONUMENTAL BUILDINGS: THE CASE STUDY OF THE SAN FELICE SUL PANARO FORTRESS

S. DEGLI ABBATI[1*], S. CATTARI[2], S. LAGOMARSINO[2] AND D. OTTONELLI[2]

[1]Department of Civil, Chemical and Environmental Engineering
University of Genova
Via Montallegro 1, 16145 Genova, Italy
e-mail: stefania.degliabbati@unige.it (*corresponding author)

[2] Department of Civil, Chemical and Environmental Engineering
University of Genova
Via Montallegro 1, 16145 Genova, Italy
email: {serena.cattari, sergio.lagomarsino, daria.ottonelli}@unige.it

Keywords: Masonry, Merlons, Kinematic analyses, Macro-block models

Abstract. *The paper describes the seismic assessment of the San Felice sul Panaro Fortress (Italy), focusing the attention on the activation of the out-of-plane response of the North walkway, characterized by the presence of an apparatus of merlons which highlighted a significant damage after the Emilia earthquake (2012). Nonlinear kinematic analyses have been performed, referring to a macro-block model and considering both the original configuration and two different possible strengthened strategies. For the definition of the seismic input in terms of floor spectra, the analyses also benefitted from the results obtained for the global response through a detailed 3D model of the whole fortress. The results were coherent with the observed damage after the seismic event, highlighting in this way the reliability of the adopted modelling strategies and analysis method, and allowed to outline possible strengthening solutions targeted to minimize the impact on the monument and guarantee its preservation.*

1 INTRODUCTION

The seismic assessment and the protection of historical fortified buildings represent a very challenging issue: firstly, because of their significant vulnerability, as testified by past seismic events ([1], [2]); and secondly, due to the necessity to combine the need of safety with the conservation aims. In particular, their complex configurations make them particularly susceptible to the activation of local mechanisms, involving the out-of-plane response of singular walls or protruding elements (called merlons), that are the solid standing part of battlements or crenelated parapets, typical of these kinds of structures. The collection and cataloguing of seismic damages on fortified architectures ([1],[2]) highlighted that merlons are frequently damaged, even for quite low accelerations.

Within this context, the paper illustrates the results obtained from nonlinear analyses performed on the San Felice sul Panaro Fortress (Italy), focusing the attention only on the activation of the out-of-plane response of the North masonry walkway, that is characterized by the presence of an apparatus of merlons placed at its top, which resulted significantly hit by the Emilian earthquake (2012).

In particular, nonlinear kinematic analyses have been performed referring to a Macro-Block Model (MBM). For the definition of the seismic input, and in particular for the computation of the floor spectra, the analyses also benefitted from the results obtained for the global response through a detailed 3D model of the whole fortress, as already illustrated in [3]. Both the original configuration and some possible strengthened states have been analysed in order to: firstly, validate the modelling strategy and the method of analysis adopted through the comparison with the observed damage; secondly, verify the effectiveness of possible mitigation strategies.

2 CASE-STUDY DESCRIPTION: THE SAN FELICE SUL PANARO FORTRESS

The San Felice sul Panaro Fortress ([4],[5]) is a medieval historical building dating back to the 14th-15th century and located near the city of Modena in San Felice sul Panaro (Italy). This fortress represents a typical example of Emilian fortified medieval architecture, composed by a very massive main structure, characterized by a compact quadrilateral plan with an inner yard and five towers: four of them are localized at the corners, while the other one is placed on the north fortress façade (Figure 1a e b).



a. b. c. d. e.

Figure 1: Schematic floor plan (a) and general view (b); examples of collapse mechanisms exhibited by the fortress: collapse of a minor tower's roof (c), damage pattern in the Mastio (d) and collapse in the north tower (e)

The fortress was seriously damaged by the Emilian earthquake of May 2012 [1], which induced: the collapse of the four minor towers roofs (Figure 1c); shear cracks on the main body of the Mastio (Figure 1d) and of the other towers; and extensive collapse in the north tower (Figure 1e), also promoted by some heavy interventions realized in the past [1]. Furthermore, a significant damage was concentrated in the merlons that exhibited different failure mechanisms and different levels of damage, as a function of their position on the fortress. In particular, some of them exhibited horizontal cracks at their base, others shear cracks, while most of them were interested by an out-of-plane mechanism which even induced in some cases the overturning of some elements. Figure 2 shows some pictures of the occurred damage, mainly concentrated in the North walkway connecting two towers (identified in Figure 2a).



a. b. c.

Figure 2: Damage pattern after the Emilian earthquake (2012) in the apparatus of merlons

3 SEISMIC OUT-OF-PLANE ASSESSMENT OF MERLONS

3.1 Adopted procedure

Non-linear kinematic analyses have been performed, by adopting a Macro-Block Model (MBM) and using the software MB-Perpetuate, developed in the framework of the Perpetuate Project [6]. The criteria adopted for the seismic out-of-plane assessment of the San Felice sul Panaro Fortress are defined on the basis of the analyses illustrated in [7] and [8], regarding the evaluation of the capacity curve, the definition of the assumed Limit States (LSs) and the criteria adopted to provide the comparison with the seismic input. Regarding the first aspect, Figure 3a shows the system capacity curve on which progressing Damage Levels (DLs) are identified. These latter are then correlated to corresponding LSs. As it is possible to observe, the curve is different from the ideal one of the rigid block, in order to consider a behaviour characterized by a bi-linear trend, more coherent with the one exhibited by real structures [8] and characterized by a first elastic branch defined by an initial elastic period T_e.

The seismic assessment has been performed, considering the following correspondence between DLs and LSs:

- DL2 assimilated to the Damage Limit State (SLD), corresponding to the mechanism activation;
- DL4 assimilated to the Safeguard Life Limit State (SLV), corresponding to the displacement $d_{SLV}=0.4d_0$, where d_0 is the value corresponding to the load multiplier $\alpha=0$ (representative - under static condition - to the collapse for overturning).

Once defined the capacity curve and the LSs of the system, the capacity curve has been compared with the spectrum in order to complete the seismic assessment (Figure 3b). In particular, in the case of local mechanisms involving macroelements placed in the upper part of the building, it has to be considered a proper modified response spectrum (floor spectrum) aimed to take into account the filtering effect provided by the main structure. For the latter, in this paper, the analytical expression recently proposed in [9] has been used, which allows evaluating the floor spectra in different points of the building and at different levels by considering the contribution of the more relevant modes, properly combined. It gives the acceleration floor spectra at the level Z of the main structure (where the element to be verified of period T and damping ξ is placed) as:

$$S_{aZ}(T,\xi)=\sqrt{\sum_{k=1}^{N}S_{aZ,k}^{2}(T,\xi)} \quad \left(\geq S_a(T)\,\eta(\xi) \quad for\ T>T_1 \right) \tag{1}$$

where: $S_a(T)$ is the acceleration response spectrum of the ground motion; N is the number of considered modes, selected since they activate the out-of-plane response of the examined element; $S_{aZ,k}(T,z)$ is the contribution of mode k^{th} that is given by:

$$S_{aZ,k}(T,\xi)=\begin{cases}\dfrac{AMP_k\ PFA_{Z,k}}{1+\left[AMP_k-1\right]\left(1-\dfrac{T}{T_k}\right)^{1.6}} & T\le T_k\\ \dfrac{AMP_k\ PFA_{Z,k}}{1+\left[AMP_k-1\right]\left(\dfrac{T}{T_k}-1\right)^{1.2}} & T>T_k\end{cases} \tag{2}$$

where:

- $PFA_{Z,k}$ is k^{th} Peak Floor Acceleration that depends on the modal parameters of the main structure in terms of natural periods (T_k), modal participation coefficients (γ_k) and modal shapes (ψ_k (x y z)) and its viscous damping ξ_k. Furthermore, it depends on the ground spectrum $S_a(T_k)$ calculated in correspondence of the structure natural period T_k and properly reduced through the damping correction factor $\eta(\xi_k)$ (which can be calculated for example as proposed in [10]):

$$PFA_{Z,k}=S_a(T_k)\,\eta(\xi_k)\,\left|\gamma_k\,\psi_k(x,y,z)\right|\sqrt{1+4\xi_k^2} \tag{3}$$

- AMP_k is an amplification factor of the $PFA_{Z,k,}$ defined by two contributions: f_k that depends only on the viscous damping of the main structure, and f_s that depends only on that of the secondary element. The expressions proposed to calculate these latter are:

$$f_k=\xi_k^{-0.6} \tag{4}$$

$$f_s=\eta\left(\xi\right)=\sqrt{\frac{0.1}{0.05+\xi}}\ge 0.55 \tag{5}$$

In the examined case, the floor spectra have been determined taking into account the contributions of the modes selected since considered relevant for the out-of-plane response of the merlons. The definition of such dynamic parameters takes advantage of the results of the modal analysis performed on a 3D Finite Element (FE) model of the entire structure (§3.3). Moreover, the definition of the damping value ξ_k has been obtained by the non-linear analyses previously performed on this global model that allowed taking into account the interactions between the different towers (as already illustrated in [3]).

The final step of the procedure was the comparison between the bi-linear capacity curve and the floor spectrum. According to [7], this latter has been made smooth in order to remove all the indentations (see the dotted graph in Figure 3b), thus implicitly taking into account the peaks present in the response spectra, which could affect the dynamic response of rocking systems. From this comparison, it was possible to evaluate the values of the maximum peak

ground accelerations (selected as the Intensity Measure -IM- aimed to describe the seismic demand) compatible with the achievement of the above-defined LSs.

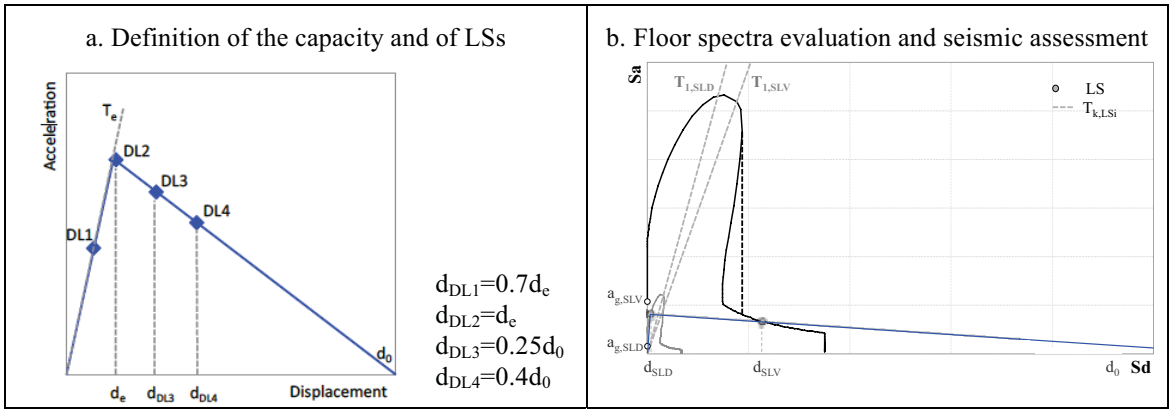


Figure 3: Out-of-plane seismic assessment: sketch of the adopted criteria (compatible with the procedure outlined in [7])

3.2 Considered MBM models

The analysis of the damage pattern occurred in the North walkway after the Emilian earthquake (2012) mainly highlighted the activation of two kinds of mechanisms: the rocking of single merlons - Figure 2b and the out-of-plane behaviour of the entire walkway - Figure 2c. Thus, two different models have been considered in the analyses (Figure 4):

- the first one (named hereafter *"Macroelement 1"*), representative of the rocking response of single independent merlons starting from the level of the walkway parapet (Figure 4b);
- the second one (named hereafter *"Macroelement 2"*) representative of the out-of-plane behaviour of the entire walkway and then characterized by the presence of two blocks (one representative of the internal apparatus of merlons and the other representative of the external one) connected through a timber beam of the roof (Figure 4c). It is localized in blue in the plan presented in Figure 4a.

Figure 4 illustrates the two models considered in the analyses (the hinges are identified in yellow). For both of them, the roof has been modelled as an external force P_C, resulting from the performed loads analysis, while W_M is the gravity load of each masonry elements (calculated as the product between the volume of each block and the masonry density equal to 18 kN/m^3, representative of a masonry built with bricks and lime mortar).

Concerning the "*Macroelement 1"*, two different merlons have been considered (n.1 and n.2 in Figure 4a). This choice is due to the occurred damage, which highlighted a different damage pattern as function of the merlons position in plan along the walkway. In fact, while the central merlon (n.1 in Figure 4a) collapsed, the merlons close to the walkway extremity (n.2) did not overturn even if completely cut at the base (Figure 2b). This is coherent with the flexural behaviour exhibited by the North walkway, as highlighted by the analysis of the modal shapes on the 3D model of the entire fortress (see §3.3, Figure 5a) and it is probably due also to a different punctual effectiveness of the roof connection, which in some cases prevented the incipient overturning of merlons.

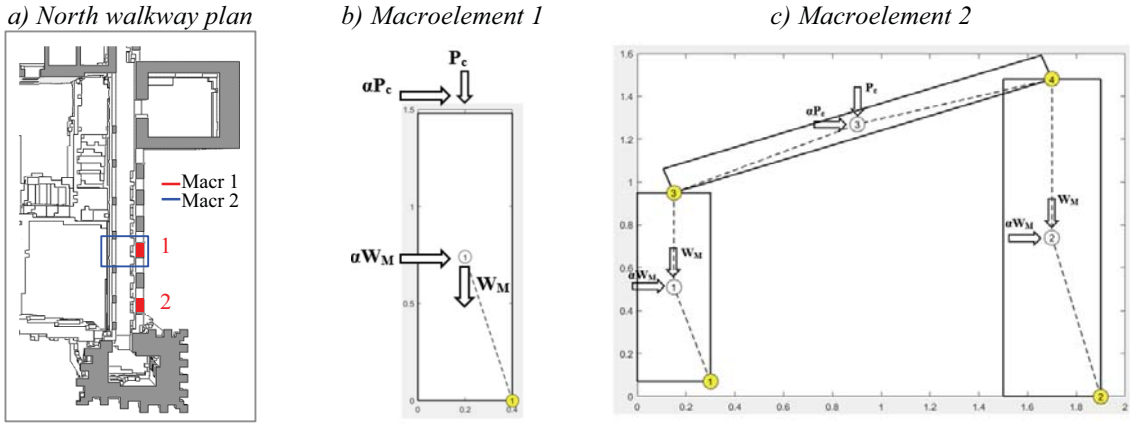


Figure 4: Macroelements considered in the analyses

3.3 Floor spectra definition

The San Felice sul Panaro Fortress is a complex monumental building, characterized by different interacting units and flexible diaphragms; thus, it is characterized by many relevant modes, which can be also close one each other and characterized by modal participation coefficients which can be low, since they involve the response of limited parts of the entire structure. This feature highlights the importance of the higher modes. For this reason, in order to calculate the dynamic parameters for the floor spectra computation, it was firstly necessary to perform a modal analysis of the entire structure. This latter has been realized by the University of Bologna, developed by means of a non-standard mesh generation procedure called CLOUD2FEM ([11], [12]). Once performed the modal analysis [3], only the relevant modes – i.e. those activating the out-of-plane response of the considered mechanisms - have been selected. Among them, in order to understand the ones characterized by a more significant contribution in terms of PFA (thus, in terms also of spectral peak), it has been sufficient to check the product $|\gamma_k \, \psi_k(x,y,z)|$ and, as a function of them, identify the modes that can be significant for the localization of the considered merlons. Figure 5a shows the deformed shapes in plan of some modes that interested the out-of-plane response of the examined mechanisms and with the most significant contribution. Figure 5b illustrates (for sake of example for the SLV LS) the comparison between: the floor spectrum evaluated for the "*Macroelement 1"*(merlon n.1) and "*Macroelement 2"* (black curve), respectively; the one evaluated for the "*Macroelement 1"* (merlon n.2). They have been obtained combining the contribution of the more significant modes through the SRSS modal combination.

Furthermore, it has to be specified that they have been calculated assuming a damping for the main structure equal to ξ_k=15%, consistently with the post-earthquake damage pattern which highlighted as the fortress was fully in a nonlinear phase. Concerning the damping of the merlons apparatus, it has been assumed equal to ξ=5%. The input response spectrum has been defined consistently with what prescribed by NTC 2018 [13] for the site of San Felice sul Panaro. As one can see from Figure 5b, as function of the mechanisms position along the fortress walkway and of its dynamic response (Figure 5a): the floor spectrum of *"Macroelement 1"* (merlon n.1) is the same of *"Macroelement 2"*, since the position of these

latter coincides (see Figure 2a); the floor spectrum of *"Macroelement 1"* (merlon n.1) is higher than the one of *"Macroelement 1"* (merlon n.2). This is due to the fact that, while the first one is placed in the central part of the walkway (where there is the maximum deformed shape of the different modes), the second one, placed at the edges, can benefit of the restraint action guaranteed by the perimeter walls of the tower. This result is also coherent with the observed damage after the Emilian earthquake (2012) as already described (Figure 2b).

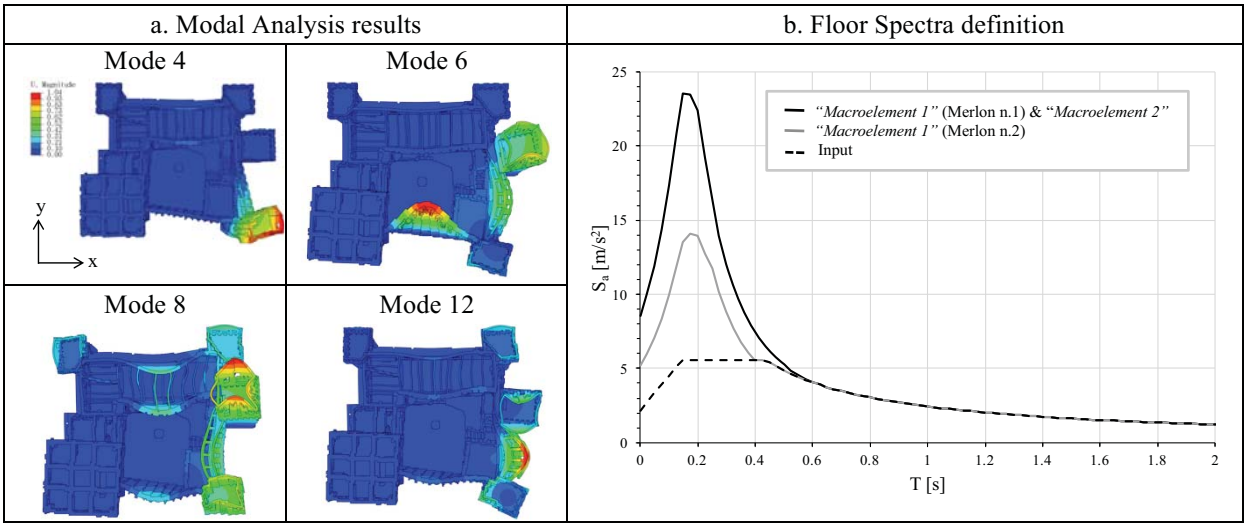


Figure 5: a) Deformed shapes in plan of some modes which interested the out-of-plane response of the examined mechanisms; b) Floor spectra definition

3.4 Results

As above mentioned, kinematic non-linear analyses have been performed by using the software MB-Perpetuate. In particular, the value of the maximum peak ground acceleration compatible with the fulfilment of a given DL has been compared with the one obtained by the design spectrum. Table 1 illustrates the results obtained in terms of: peak ground acceleration corresponding to the fulfilment of the damage level DL2 (a_g^{SLD}) and DL4 (a_g^{SLV}); peak ground acceleration of San Felice sul Panaro for the same DLs ($a_g^{site,SLD}$; $a_g^{site,SLV}$); corresponding safety factors $\alpha_{SLD}= a_g^{SLD}/ a_g^{site,SLD}$ and $\alpha_{SLV}= a_g^{SLV}/ a_g^{site,SLV}$. Safety factors lower than 1 indicate that the seismic verification is not satisfied.

Table 1: Results for the examined mechanisms

	a_g^{SLD} [m/s^2]	a_g^{SLV} [m/s^2]	$a_g^{site,SLD}$ [m/s^2]	$a_g^{site,SLV}$ [m/s^2]	α_{SLD}	α_{SLV}
"Macrolement 1" (merlon n1)	0.435	2.781	0.75	2.159	0.58	1.288
"Macroelement 2"	0.330	2.736			0.44	1.267

In particular, the table shows only the results of the mechanisms named *"Macroelement 1"* – merlon n.1 and *"Macroelement 2"*, which are the ones turned out to be the most vulnerable

with respect to the SLV LS. As one can see, while the verifications are satisfied with respect to the SLV, they are not satisfied with respect to the SLD, highlighting the vulnerability concerning the mechanisms activation.

4 PROPOSAL OF POSSIBLE STRENGTHENING INTERVENTIONS

4.1 Intervention description

The results presented in Table 1 highlight the necessity to define a strengthening intervention for the North walkway. Two different proposals have been elaborated:

a) A more traditional intervention with two vertical tie-rods (Φ10, S275 steel and prestress force equal to 10 kN);
b) A more innovative one realized with the insertion of the two vertical tie-rods coupled in series to a device formed by springs and fixed at the top of each merlon (Figure 6). This device aims to protect the tie-rods, in order to avoid its premature plasticization. In particular, it has been designed in order to bear a maximum load equal to the tie-rods yielding force and with stiffness equal to $1.18 \cdot 10^6$ N/m. The use of an elastic device in the tie-rods has been recently proposed by [14], but in this paper the Authors have specifically proposed its application to vertical tie-rods.

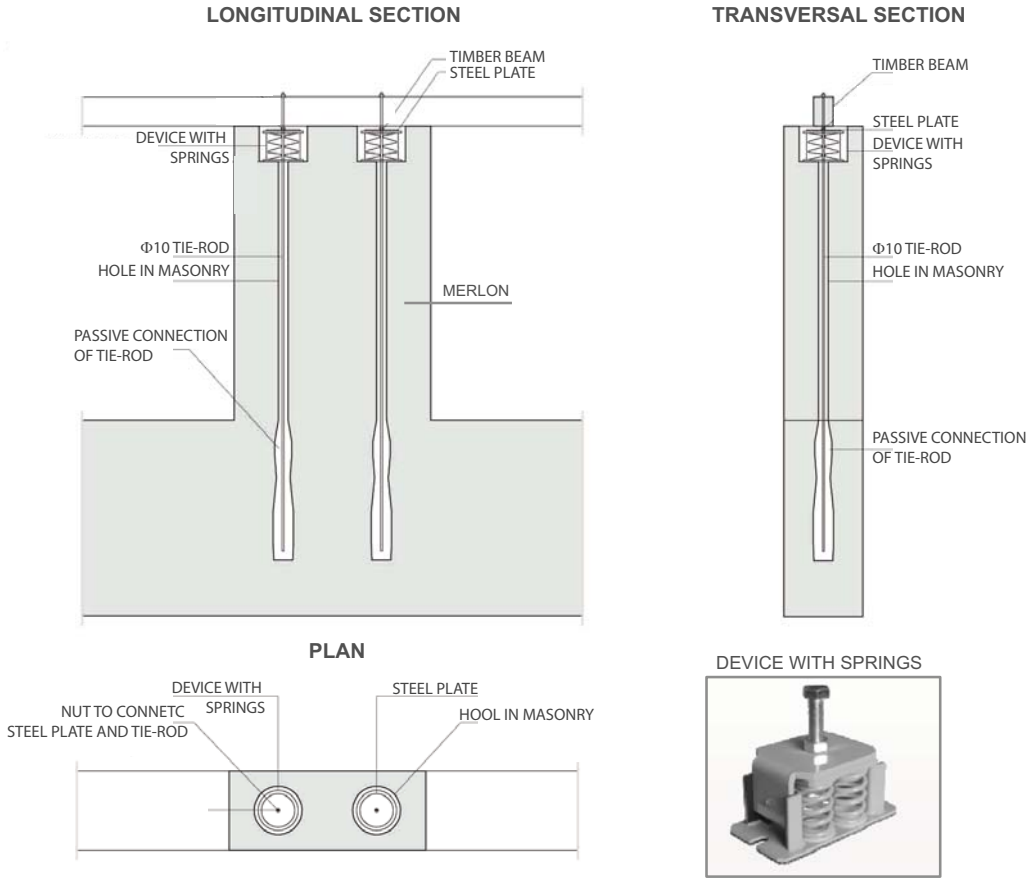


Figure 6: Sketch of the strengthening intervention provided for the merlons

Furthermore, a proper connection between roof and battlements has to be guaranteed. In fact, the post-earthquake damage clearly showed that, sometimes, despite the high damage occurred in some merlons, they did not collapse thanks to the restraint action of the roof. The connection with the roof can be realized by means of the vertical tie-rods that strengthen the merlons: in this way, merlons and roof creates an actual "rocking frame". According to this solution, the longitudinal timber beam at the top of each merlon has to be linked to the tie-rods, which are longer than the merlons height and cross the timber beam. Internally, a small break has to be guaranteed in order to periodically restore the pre-stress in the bars. Finally, since the modal shapes in this area highlighted a quite pronounced flexural behaviour of the whole walkway, a double timber boarding at the roof level could be inserted, with the aim to increase the flexural stiffness of the entire walkway.

4.2 Seismic assessment in the proposed design states

In order to quantify the effectiveness of the two alternative possible interventions, the return periods (T_R) inducing the Damage Limit State (SLD) and Safeguard Life Limit State (SLV) have been computed. In the analyses, the two mechanisms already presented in Table 1 have been considered. In particular, tie-rods were modelled, according to the principles of the nonlinear (incremental) kinematic analysis, as equivalent external forces, whose value is function of: initial force in the tie-rod, tie-rod's area, tie-rod's stiffness, tie-rod's yielding stress, ultimate strain. It has to be pointed out that, for the strengthening intervention b), the vertical tie-rods coupled in series with the device have been considered as an equivalent tie-rod with an equivalent stiffness. Table 2 presents the results of the design state. It has to be underlined that the SLD LS is verified when T_R is higher than 50 years, while SLV LS is verified when T_R is higher than 475 years.

Table 2: Results in the design state for the two alternative strengthening solutions

	State	SLD – DL2	SLV – DL4	I_{SSLV}
"Macroelement 1" (merlon n1)	Actual state	$T_R < 30$ years	$T_R = 743$ years	1.29
	Design state – sol. a)	$T_R = 127$ years	$T_R > 2475$ years	3.44
	Design state – sol. b)	$T_R = 113$ years	$T_R > 2475$ years	4.19
"Macroelement 2"	Actual state	$T_R < 30$ years	$T_R = 519$ years	1.27
	Design state – sol. a)	$T_R = 204$ years	$T_R > 2475$ years	2.77
	Design state – sol. b)	$T_R = 175$ years	$T_R > 2475$ years	5.03

As one can see from Table 2, with both the strengthening interventions, both the LSs are satisfied. However, the best choice seems to be the solution b), since it allows protecting the tie-rod from a premature plasticization, as one can see from the comparison in terms of capacity curves (Figure 7). In fact, while with the traditional solution (a) the DL4 occurs when the tie-rod is already collapsed, with the more innovative one (b) this DL occurs when the tie-rod is just yielded.

Furthermore, the higher effectiveness of the solution b) is also highlighted by computing the value of the peak ground acceleration corresponding to the beginning of the yielding

(Table 3), from which one can see that with the SLV response spectrum (characterized by a PGA equal to 2.16 m/s^2), the traditional tie-rod (and not the tie-rod coupled in series to the device with springs) would be already yielded imposing its replacing after the potential occurrence of such a seismic event.

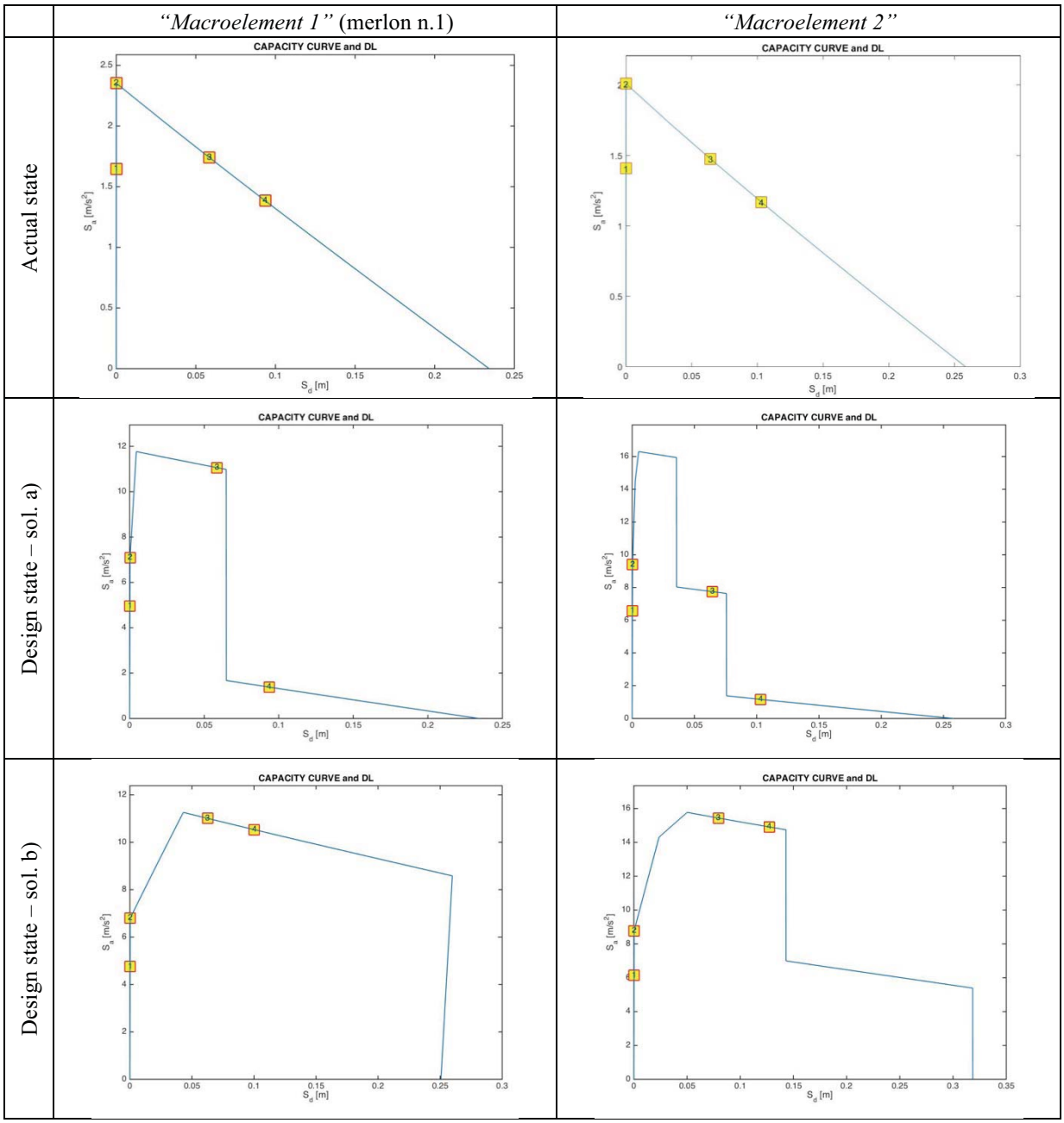


Figure 7: Capacity curves in the actual and design states

Table 3: Values of PGA corresponding to the yielding in the two solutions of intervention

	Sol. a)	Sol. b)
$PGA_{yielding}$ [m/s^2]	1.75	5.26
PGA_{SLV} [m/s^2]	2.16	

5 FINAL REMARKS

The paper pointed out that a reliable seismic assessment of atop single-block rocking elements (that are the merlons in the examined case) needs the proper evaluation of the filtering effect provided by the main structure. The analyses of the merlons n.1 and n.2 highlighted that it is important not only to properly quantify the seismic amplification, but also its variation depending on the mechanism position as a consequence of the modal shapes of the main structure.

The results obtained were coherent with the observed damage after the Emilian earthquake (2012), demonstrating in this way the reliability of the assumed model and the analytical expressions adopted for the computation of the seismic input.

Then, the different strengthening intervention strategies discussed in the paper clearly pointed out that it is important not only to design in terms of strength (in order to prevent the mechanism's activation), but also in terms of stiffness and ductility of the inserted tie-rod, in order to protect it from a premature plasticization and then avoid its replacing in the post-earthquake phase. This strategy is compatible with the conservation needs and the criteria of easy repairability that are concepts always more frequently highlighted by the recent Italian earthquakes, also in terms of repercussions on the economic loss.

Finally, the two different presented hypotheses on the possible strengthening interventions allowed outlining the most effective solution, able to minimize the impact on the construction and guarantee its preservation.

Acknowledgements. The activities have been originally developed in the framework of the research agreement for the seismic assessment of the San Felice sul Panaro Fortress after the Emilian earthquake (2012), financed in the 2016 by the municipality of San Felice sul Panaro. Moreover, the research is still ongoing within the national research project ReLUIS 2019-2021 (WP5 - Task 5.3) founded by the Italian Civil Protection Agency.

REFERENCES

[1] Cattari, S., Degli Abbati, S., Ferretti, D., Lagomarsino, S., Ottonelli, D., Tralli, A. Damage assessment of fortresses after the 2012 Emilia. *Bulletin of Earthquake Engineering* (2014) **12**(5):2333-2365.

[2] Coïsson, E., Ferretti, D., Lenticchia, E. Analysis of damage mechanisms suffered by Italian fortified buildings hit by earthquakes in the last 40 years. *Bulletin of Earthquake Engineering* (2017) **15**(12):5139–5166.

[3] Degli Abbati, S., D'Altri, A.M., Ottonelli, D., Castellazzi, G., Cattari, S., de Miranda, S., Lagomarsino, S. Seismic assessment of interacting structural units in complex historic

masonry constructions by nonlinear static analyses. *Computers and Structures* (2019) **213**:51-71.

[4] Orlando, A. Estense fortress at San Felice sul Panaro: modelling and seismic assessment. Master thesis (2014), University of Genova.

[5] Ferrari, L., Goldoni, G. Behind the sign. Inside and outside the San Felice sul Panaro fortress restoration work. Master thesis (2014), University of Parma.

[6] Lagomarsino, S., Ottonelli, D. A Macro-Block program for the seismic assessment (MB-PERPETUATE). PERPETUATE - EC-FP7 project (2012), Deliverable D29, www.perpetuate.eu.

[7] Lagomarsino, S. Seismic assessment of rocking masonry structures. *Bulletin of Earthquake Engineering* (2015) **13**(1):97-128.

[8] Degli Abbati, S., Lagomarsino, S. Out-of-plane static and dynamic response of masonry panels. *Engineering Structures* (2017) **150**:803-820.

[9] Degli Abbati, S., Cattari, S., Lagomarsino, S. Theoretically-based and practice-oriented formulations for the floor spectra evaluation. *Earthquake and Structures* (2018) **15**(5):565-581.

[10] CEN (2004), Eurocode 8: Design of Structures for Earthquake Resistance Part 1: General Rules, Seismic Actions and Rules for Buildings, European Code EN 1998 1, European Committee for Standardization, Brussels.

[11] Castellazzi, G., D'Altri, A.M., Bitelli, G., Selvaggi, I., Lambertini, A. From laser scanning to finite element analysis of complex buildings by using a semi-automatic procedure. *Sensors* (2015) **15**(8):18360–80.

[12] Castellazzi, G., D'Altri, A.M., de Miranda, S., Ubertini, F. An innovative numerical modeling strategy for the structural analysis of historical monumental buildings. *Engineering Structures* (2017) **132**:229–48.

[13] NTC 2018. Italian Technical Code, Decreto Ministeriale 17/1/2018. "Aggiornamento delle Norme tecniche per le costruzioni". Ministry of Infrastructures and Transportation, G.U. n.42 of 20/2/2018 (In Italian).

[14] Melatti, V., D'Ayala, D., Modolo, E. Computational validation of dissipative device for the seismic upgrade of historic buildings. *Proc. of 7th International Conference on Computational Methods in Structural Dynamics and Earthquake Engineering - Compdyn* (2019), 24-26 June, Crete (Greece).

12th International Conference on Structural Analysis of Historical Constructions
SAHC 2020
P. Roca, L. Pelà and C. Molins (Eds.)

SEISMIC ASSESSMENT OF DUTCH URM BUILDINGS ACCORDING TO NPR9998:2018 CODE WITH AN EQUIVALENT-FRAME APPROACH

STEFANO BRACCHI[1*], FRANCESCO GRAZIOTTI[1], FRANCESCO MESSALI[2] AND ANDREA PENNA[1]

[1]Department of Civil Engineering and Architecture (DICAr)
University of Pavia
Via Ferrata 3, 27100 Pavia, Italy
e-mail: stefano.bracchi@unipv.it (*corresponding author), francesco.graziotti@unipv.it, andrea.penna@unipv.it, http://dicar.unipv.it/

[2]Department of Materials, Mechanics, Management & Design
Technical University of Delft
Stevinweg 1, Delft, Netherlands
e-mail: f.messali@tudelft.nl, http://www.tudelft.nl/en/ceg/about-faculty/departments/materials-mechanics-management-design-3md/

Keywords: Equivalent-Frame, Seismic Assessment, Induced Seismicity, Pushover Analysis, Numerical Modelling

Abstract. *In the last two decades, the province of Groningen, located in the North-East of the Netherlands, has been subjected to an increasing number of earthquakes induced by gas extractions. The existing building stock is mainly composed by unreinforced masonry (URM) buildings not conceived to resist seismic loads. The need of reducing the vulnerability of these buildings by means of retrofit interventions, led to the development and adoption of a new guideline (NPR9998:2018). As regards the seismic assessment of URM buildings using nonlinear static analysis, the guideline includes significant differences with respect to Eurocode 8, which is adopted in other European countries. The more significant differences lay in the description of failure mechanisms and constitutive laws of piers and spandrels, in the identification of limit states and in the calculation of seismic demand. In the last years, the assessment and retrofit in the region has been carried out using software based on an equivalent-frame strategy: among these, the 3Muri software has been widely adopted. The solver of this program is the research software TREMURI. In this work, a new version of the solver adopted by the software 3Muri, complying with the requirements of the new Dutch guideline, was developed; the tool was then validated with simple examples. To illustrate the specificities of the new guideline, the seismic assessment of a building representative of one of the most widely diffused URM building typologies in the area was performed.*

1. INTRODUCTION

In the last decades the province of Groningen, located in the North-East Netherlands, has been subjected to earthquakes induced by reservoir depletion due to gas extraction. The

existing building stock is not designed to resist seismic loads and it is mainly composed by unreinforced masonry (URM) buildings. To study the seismic response of construction typologies similar to those of the Dutch practice, an experimental campaign has been recently carried out. Among the various tests, a significant number of shake-table tests were performed at the EUCENTRE laboratory on buildings representative of the most vulnerable and diffused URM building typologies of the area [1].

In the meantime, Dutch engineering companies have been performing the seismic assessment of residential buildings in the Groningen area. For the weaker structures, they have also been performing structural retrofit to improve the seismic performance. To this aim, several guidelines were developed by the regulator, starting from the guideline NPR9998:2015 [2], followed by NPR9998:2017 [3], up to the most recent NPR9998:2018 [4]. The last two codes were written accounting for the results of recent research in the field of seismic assessment of buildings; prescriptions regarding the global and local assessment are described in Annex G and H, respectively. The various documents contain significant differences with respect to the official European seismic code Eurocode 8-Part 1 [5] and 3 [6].

To perform the assessment, the engineers mainly use nonlinear static analyses carried out with models based on an equivalent-frame discretization of the building, which is a widely adopted technique for URM ([7],[8],[9]). The opportunity of performing the seismic assessment of URM buildings with pushover analysis was considered in the first guideline NPR9998:2015, but no specific recommendations were provided, and the analyst had to refer to Eurocode 8–Part 1. On the opposite, the last version NPR9998:2018 contains specific recommendations for the assessment by means of nonlinear static analysis. One of the software used by the engineers is 3Muri [10], which was developed to fulfil the recommendations included in Eurocode 8. It was therefore suitable to be used with NPR9998:2015, whereas it needs some changes to fulfil NPR9998:2018.

This paper firstly identifies the specificities of the guideline NPR9998:2018 (called NPR 2018 in the followings). Then, a new version of the TREMURI research program [11] was developed and validated. This represents the solver of the commercial software 3Muri. Finally, the seismic assessment of a case study building was performed according to NPR 2018. This work focuses on global analysis only, i.e. local verifications are not considered.

2. SPECIFICITIES OF THE DUTCH PRACTICE GUIDELINE NPR9998:2018

As a first step, the differences between NPR 2018 and Eurocode 8 were identified, limiting the study to the aspects relevant for the assessment of URM building by means of nonlinear static analysis using equivalent-frame models. The main differences regard the constitutive laws of the structural elements and the identification of displacement demand and capacity.

2.1. Constitutive laws of the structural elements

As regards piers, NPR 2018 defines three mechanisms: flexural and shear associated with failure of masonry or with sliding along a damp proof course membrane DPCM. The strength associated with the flexural mechanism V_p is:

$$V_p = F\frac{l_{penant}}{2h_0}\left(1-1.15\frac{\sigma_y}{f_{ma;m}}\right) \tag{1}$$

where F is the axial load acting on the critical cross-section, l_{penant} is the length of the pier, h_0 is the distance between the section where the flexural strength is reached and the inflection point, σ_y is the average compressive stress on the full cross-section and $f_{ma;m}$ is the compressive strength of masonry. The strength of the pier is the minimum between the one calculated at the top and bottom section of the pier.

The rocking of a pier is limited by the crushing failure of masonry attained at the toes. This mechanism is taken into account limiting the displacement capacity of the flexural mechanism. In particular, the drift limit for the near collapse (NC) limit state θ_{NC} is:

$$\theta_{NC} = 0.0135\left(1 - 2.6\frac{\sigma_y}{f_{ma;m}}\right)\frac{h_{ref}}{h_{penant}}\sqrt{\frac{h_{penant}}{l_{penant}}} \tag{2}$$

where σ_y is the average compressive stress at the base of the pier on the full cross-section, h_{penant} is the height of the pier (in m) and h_{ref} is the reference height (2.4 m). No indication is given in NPR 2018 for the severe damage (SD) limit state; for consistency with the previous guideline, the drift capacity is assumed to be equal to 75% of the drift capacity at NC.

The constitutive force/drift law is bilinear with an elastic branch up to the yielding drift θ_y followed by a constant branch up to the drift corresponding to NC (Figure 1).

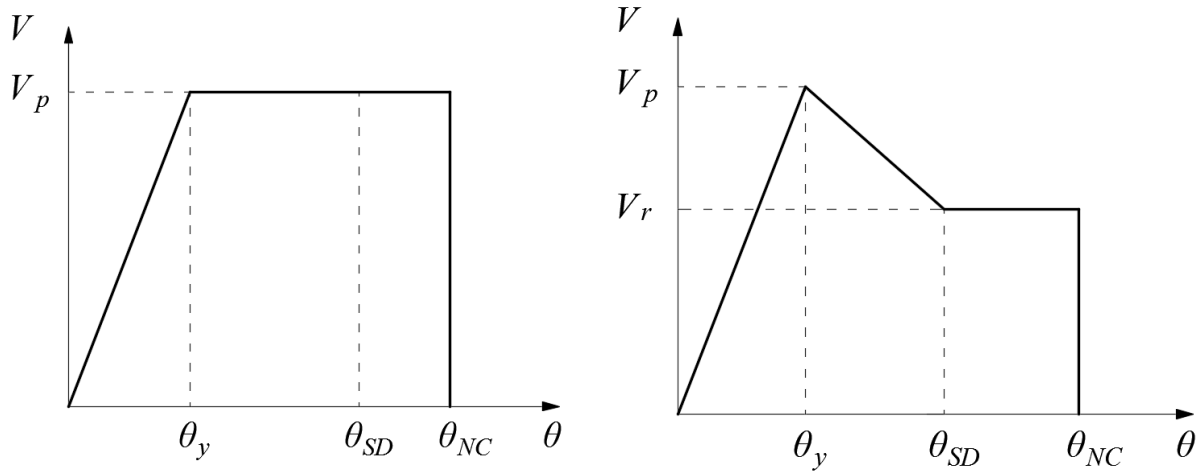


Figure 1: Capacity curve of a pier: flexural (left) and shear for failure of masonry (right) mechanism

The constitutive force/drift law associated with the shear mechanism of failure of masonry is piece-wise linear, with a peak strength followed by a linear decay up to the residual strength (Figure 1). The peak strength V_p is the minimum of the shear strength calculated at the two ends of the element, each one with its axial load. At each end, the strength is given by:

$$V_p = \min\left\{V_{p,1}, V_{p,2}\right\} \tag{3}$$

where

$$V_{p,1} = l_C t_{penant}\left(f_{ma;v;0;m} + \mu_{ma;m}\sigma_y\right) \tag{4}$$

$$V_{p,2} = 0.1 f_b l_C t_{penant} \tag{5}$$

where l_C is the length of the compressed part of the section, $f_{ma;v;0;m}$ is the initial average shear strength of masonry, $\mu_{ma;m}$ is the average friction coefficient, σ_y is the average compressive stress in the compressed part of the section, f_b is the normalized average compressive strength of bricks in the load direction and t_{penant} is the thickness of the pier. Eq. (4) is associated with stepped cracks through the mortar joints, whereas Eq. (5) with cracks through the bricks. Moreover, the length of the compressed part of the section cannot exceed a maximum value equal to the length of the section, and a minimum value corresponding to a rectangular stress block idealization of the compressive stress profile. For solid clay bricks NPR 2018 suggests that the value of f_b is generally at least 20 MPa. In case of calcium-silicate bricks and blocks, the value of f_b is at least 12 MPa, whereas for calcium-silicate elements f_b is at least equal to 15 MPa.

The residual shear strength is equal to:

$$V_r = \min\left\{l_C t_{penant} \mu_{ma;m} \sigma_y ; 0.1 f_b l_C t_{penant}\right\} \tag{6}$$

The drift capacity at NC θ_{NC} is equal to 0.75% in case Eq. (4) governs and to the θ_{NC} of flexural mechanism (Eq. (2)) in case Eq. (5) governs. The drift capacity at SD θ_{SD} is equal to 0.3% in case Eq. (4) governs and to 75% of θ_{NC} in case Eq. (5) governs, in analogy with the flexural failure mode (even if NPR 2018 does not give indications for this last case).

In case a damp proof course membrane is present, it forms a potential slip surface that can limit the shear strength of a pier. The strength associated with this slip-plane failure mechanism is:

$$V_p = l_C t_{penant} \mu_{dpc} \sigma_y \tag{7}$$

The axial stress at the base of the element (i.e. where the membrane is usually located) has to be considered, whereas the NC and SD drift limits are the same as the one for shear mechanism of masonry in case of stepped cracks. The constitutive force/drift law is again bilinear (Figure 2). The shear mechanism is attributed to the pier based on the minimum peak shear strength associated with the failure of masonry or the slip-plane failure.

As regards spandrels, NPR 2018 defines two mechanisms: flexural and shear mechanism. In both the cases, the constitutive force/drift law is piece-wise linear, characterized by a peak and a residual strength (Figure 2).

The peak flexural capacity of spandrels V_p is given by:

$$V_p = \left(f_t + \sigma_{borstw}\right) \frac{h_{borstw}^2 b_{borstw}}{3 l_{borstw}} \tag{8}$$

where f_t is the equivalent tensile strength of the spandrel, σ_{borstw} is the axial stress in the spandrel assuming a uniform stress distribution, h_{borstw} is the height, b_{borstw} is the thickness and l_{borstw} is the length of the spandrel. Unless the spandrel is pretensioned, it is assumed that the axial load in the spandrel is negligible when determining the peak shear strength. The equivalent tensile strength of the spandrel f_t is calculated as:

$$f_t = 1.3\left(f_{ma;b;per} + 0.5\mu_{ma;m} \frac{\sigma_{p,left} + \sigma_{p,right}}{2}\right) + \frac{f_{ma;b;per}}{2\mu_{ma;m}} \tag{9}$$

where $f_{ma;b;per}$ is the bonding strength of the joint of masonry (equal to the cohesion $f_{ma;v;0;m}$, as

specified in NPR 2018), $\mu_{ma;m}$ is the average friction coefficient of masonry, $\sigma_{p,left/right}$ is the axial stress in the left/right pier adjacent to the spandrel.

When lintels are sufficiently anchored into the piers, the lintel contribution to the residual flexural capacity of the spandrel should be considered. The residual flexural strength V_r can be estimated as:

$$V_r = \frac{\sigma_{borstw} h_{borstw}^2 b_{borstw}}{l_{borstw}} \left(1 - \frac{\sigma_{borstw}}{0.85 f_{h;m}}\right) \leq V_p \tag{10}$$

where $f_{h;m}$ is the compressive strength of masonry in the horizontal direction (equal to 0.5 $f_{ma;m}$) and V_p is the minimum between the peak flexural and shear strength of the spandrel. The axial stress in the spandrel should be taken into account when calculating the residual strength; an upper bound estimate of the axial stress σ_{borstw} in a restrained spandrel can be determined as:

$$\sigma_{borstw} = (1 + \beta_{borstw}) f_{ma;dt;m} \frac{l_{borstw}}{\sqrt{l_{borstw}^2 + h_{borstw}^2}} \tag{11}$$

where β_{borstw} is the shear stress factor depending on the geometry of the spandrel and $f_{ma;dt;m}$ is the diagonal strength of masonry.

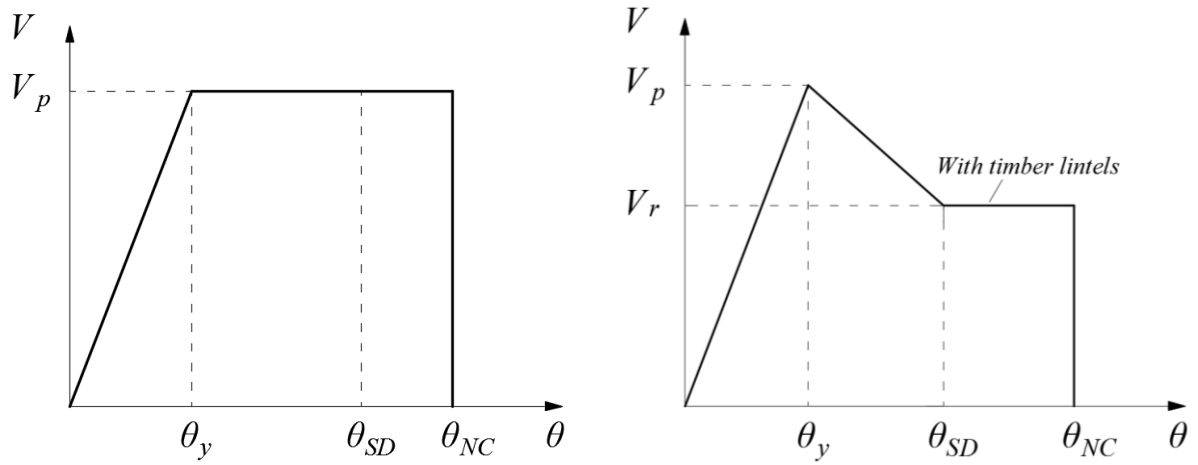


Figure 2: Capacity curve of a pier with slip-plane failure mechanism (left) and capacity curve of a spandrel with flexural and shear mechanism (right)

The peak shear strength of a spandrel V_p can be estimated as the minimum between the ones associated with two mechanisms: formation of cracks through head- and bed-joints over almost the entire height of the spandrel (Eq. (12)) and cracks in the bricks (Eq. (13)). The first mechanism takes place when mortar is weaker than bricks, whereas the second one corresponds to the case of weaker bricks. Timber lintels do not give a significant contribution to the peak shear capacity of URM spandrels and therefore they can be ignored.

$$V_p = \frac{2}{3} (f_{ma;b;per} + \mu_{ma;m} \sigma_{borstw}) h_{borstw} b_{borstw} \tag{12}$$

$$V_p = f_{ma;dt;m}\beta_{borstw}\sqrt{1+\frac{\sigma_{borstw}}{f_{ma;dt;m}}}h_{borstw}b_{borstw} \tag{13}$$

When lintels are sufficiently anchored into the piers, the lintel contribution to the residual shear capacity of the spandrel should be considered and the residual shear strength is calculated with Eq. (10).

The drift limits for spandrels are common for both flexural and shear mechanism. The drift capacity at NC is equal to $4\theta_y$, where θ_y is the yielding drift, whereas the drift capacity at SD is equal to $3\theta_y$.

2.2. Global displacement demand and capacity

As regards the definition of displacement capacity and demand of the global analysis, the new aspects of NPR 2018 consist in the definition of the equivalent single degree of freedom (SDOF) system, of the equivalent bilinear curve and the adoption of the capacity spectrum method to compute the displacement demand. In particular, the single degree of freedom (SDOF) system equivalent to the building is defined as:

$$S_a = \begin{cases} \dfrac{V_{cap,base}}{m^*} & n \le 2 \\ \dfrac{V_{cap,base}}{\Gamma m^*} & n > 2 \end{cases} \qquad S_d = \begin{cases} u_{roof,cap} & n \le 2 \\ \dfrac{u_{roof,cap}}{\Gamma} & n > 2 \end{cases} \tag{14}$$

where S_a, S_d and m^* are the acceleration, displacement and mass of the SDOF system, $V_{cap,base}$ is the base shear of the building, Γ is the modal participation factor, $u_{roof,cap}$ is the displacement of the highest level of the building and n is the number of storeys.

The bilinear curve equivalent to the capacity curve of the SDOF system is calculated with a standard approach based on equivalence of areas. However, although the equivalence of area is performed up to the displacement corresponding to the 20% decay of the base strength, the plateau of the bilinear is extended up to the displacement corresponding to the 50% decay of the base shear, which represents the global displacement capacity at NC. To account for soil-structure interaction, NPR 2018 suggests to increase the displacement of the SDOF system (obtained from an analysis with fixed foundations), as a function of the acceleration of the SDOF system.

As regards the calculation of the displacement demand, NPR 2018 suggests the use of an iterative capacity spectrum method with over-damped spectra, discouraging, although not precluding, other methods (e.g. N2 [12]). The iterative capacity spectrum method of NPR 2018 consists of firstly determining the global ductility of the equivalent SDOF system, μ_{sys}, calculated as $u_{duct,sys}/u_{y;sys}$, where $u_{duct,sys}$ is the minimum between the displacement capacity ($u_{cap;sys}$) and the displacement corresponding to the intersection of the bilinear capacity curve and the spectrum in S_a vs. S_d format and $u_{y;sys}$ is the yield displacement of the SDOF system.

Secondly, the hysteretic damping of the system ξ_{hys} has to be calculated as:

$$\xi_{hys} = 0.42\left(1-\frac{0.9}{\sqrt{\mu_{sys}}}-0.1\sqrt{\mu_{sys}}\right) \le 0.15 \tag{15}$$

where $\xi_{hys} = 0.15$ for $\mu_{sys} > 4$, followed by the determination of the total damping ($\xi_{sys} =$

$\xi_0+\xi_{hys}+\beta_0 \leq 0.4$), where β_0 is the contribution due to the soil. The reduction factor of the spectrum can then be obtained as:

$$\eta_\xi = \sqrt{\frac{7}{2+\xi_{sys}}} \geq 0.55 \tag{16}$$

With the new ductility μ_{sys}, iterations can be performed until the initial and final ductilities are similar. The displacement demand is the intersection between the bilinear and the reduced spectrum. Figure 3 shows the application of the iterative capacity spectrum method.

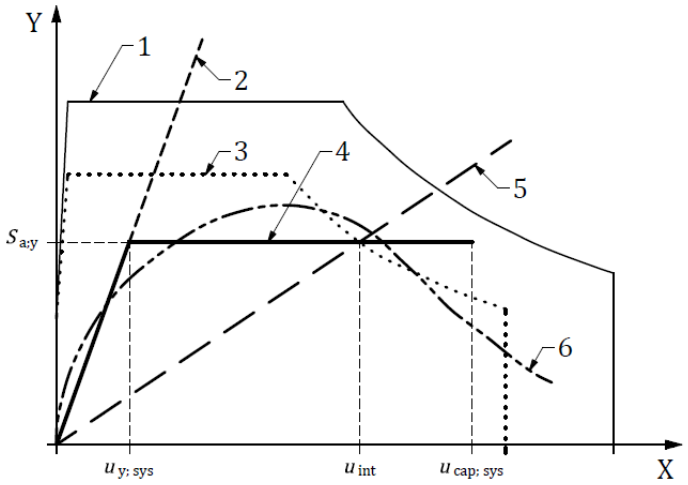


Figure 3: Iterative capacity spectrum method of NPR 2018 [4]

3. DEVELOPMENT OF TREMURI NPR9998:2018 VERSION

A new macroelement, featuring the constitutive laws previously described for piers and spandrels was developed and implemented in the TREMURI software. To test the efficiency of the new element in reproducing the code force/drift laws, a series of nonlinear analyses in displacement control were performed. In the case of single piers, a monotonically increasing horizontal displacement was applied to the top of the element, whereas in the case of single spandrels a vertical displacement was applied. Figure 4 and Figure 5 show the results of the analyses in terms of force vs. drift curves and damage patterns for piers and spandrels, respectively. In the damage pattern representation, different colors indicate different damage mechanisms, whereas different markers identifies the level of damage (plastic, SD, NC) of the element.

The new element was also implemented in the commercial software 3Muri [10], together with the automatic calculation of displacement demand and capacity as described in the previous section. This would allow engineers to perform the seismic assessment and retrofit according to the considered guideline.

In the following, the seismic assessment was performed obtaining the global pushover curve using the software TREMURI and calculating the seismic demand and capacity according to NPR 2018 using properly developed tools external to TREMURI and 3Muri.

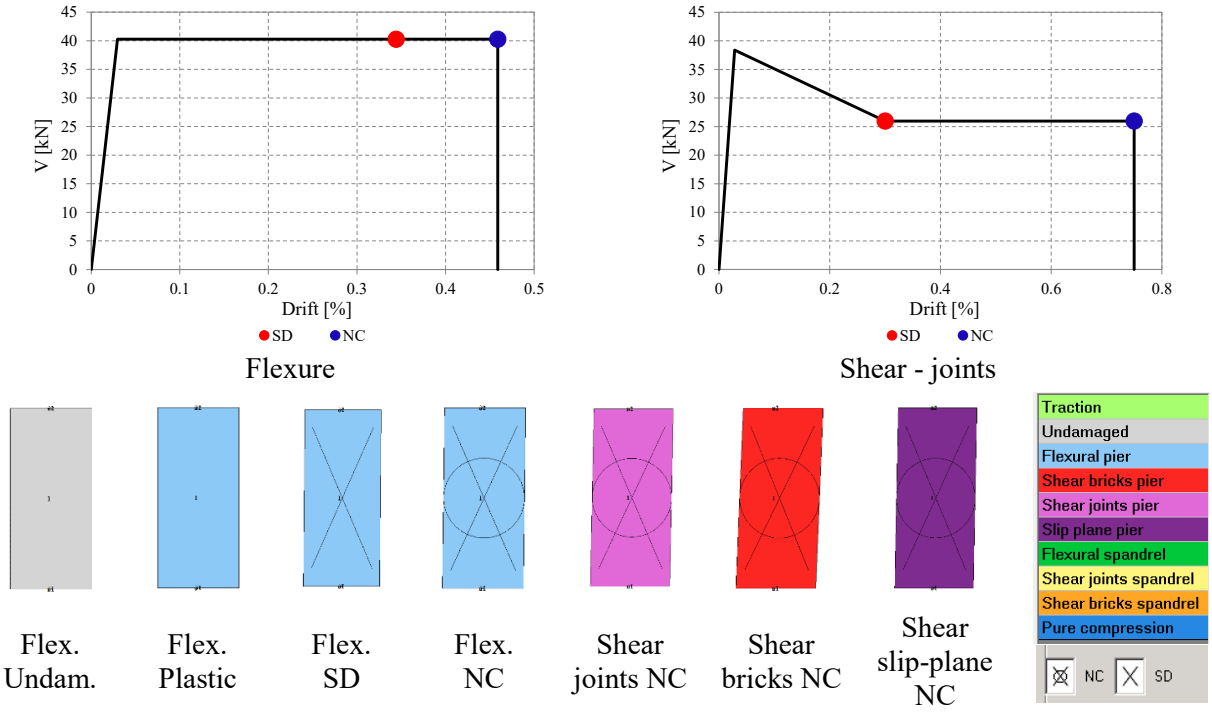


Figure 4: Force vs. drift curves of single piers and damage patterns with the indication of the different mechanisms and extent of damage

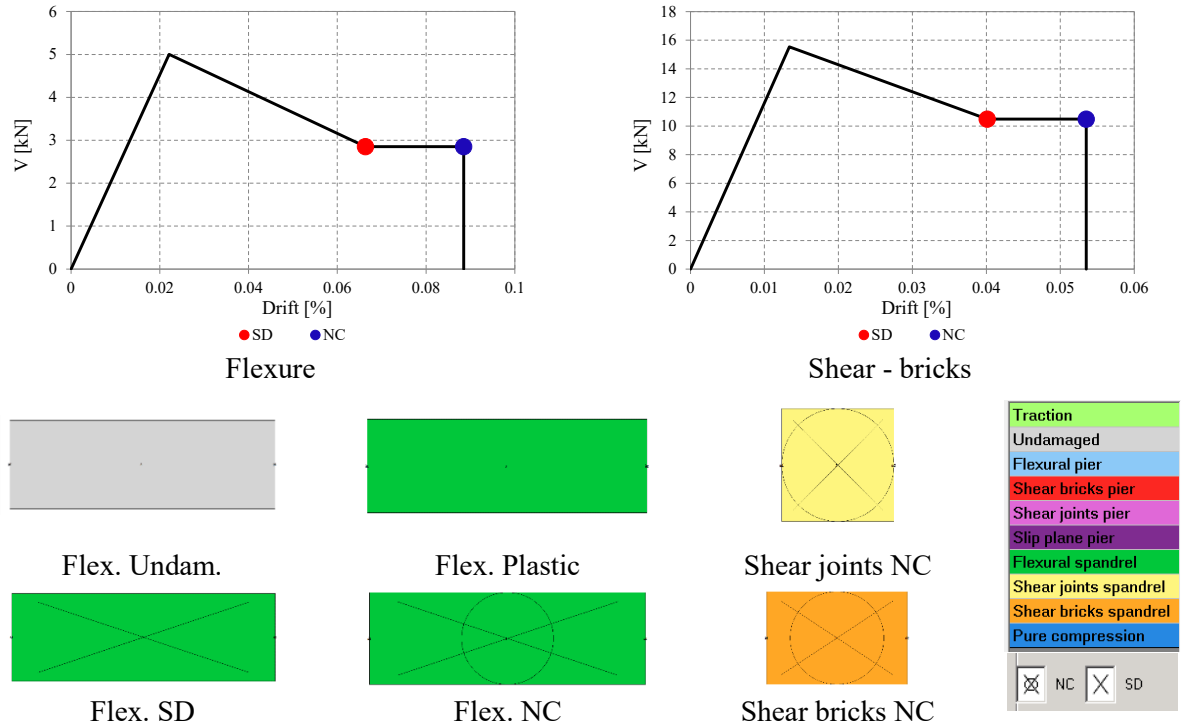


Figure 5: Force vs. drift curves of single spandrels and damage patterns with the indication of the different mechanisms and extent of damage

4. EXAMPLE OF GLOBAL SEISMIC ASSESSMENT ACCORDING TO NPR9998:2018

A simple case study building representative of one of the typologies of the building stock of the Groningen area was selected (Figure 6). The specimen tested by [13] on the shake-table of the EUCENTRE laboratory was considered: it is the end-unit of a terraced house building with cavity walls, which is one of the most vulnerable building typologies of the area. The structure is characterized by a weak direction (the one parallel to the openings) and a strong direction characterized by no openings. In developing the TREMURI model of the case study, a series of simplifying assumptions were performed in order to simulate the model built by a professional engineer in charge of the assessment (e.g. roof and external leaves of cavity walls modelled as additional masses only).



Figure 6: Case study building: North-West (left) and South-West (centre) view (adapted from [13]) and TREMURI model (right)

As regards the mechanical properties, the typology "Calcium silicate brickwork with general purpose mortar (1960-present)" described in NPR 2018 was considered. Material properties of the clay leaf were not considered, since this was modelled as additional mass only. The elastic moduli E and G were reduced by a factor 2 to account for cracked stiffness.

Table 1 reports the values of mechanical properties used in this study. Moreover, damp proof courses were assumed not to be present; therefore, the slip-plane failure mechanism was not considered. Floors were assumed to be rigid, with 100% of the acting load assigned to the walls orthogonal to the spanning direction and 0% to the walls parallel to it.

Table 1: Values of mechanical properties

E [MPa]	G [MPa]	ρ [kg/m^3]	f_m [MPa]	f_{v0} [MPa]	μ [-]	f_b [MPa]
2000	825	1834	7	0.25	0.6	12

When performing the assessment, soil-structure interaction was considered, whereas the soil damping was neglected. The demand was maintained fixed and corresponded to the spectrum of the village of Loppersum, obtained from [14] for a return period of 2475 years,

corresponding to near collapse limit state (with a_gS = 0.1976 g, p = 1.919, T_b = 0.154 s, T_c = 0.664 s, T_d = 0.909 s, η_{el} = 1). A more detailed study on the demand is reported in [15].

Figure 7 shows the pushover curve and damage patterns obtained with the TREMURI element consistent with NPR 2018 for a selected analysis in the weak direction, compared to the ones obtained with the Eurocode 8 element. From the damage patterns, it can be noticed that NPR 2018 is predicting a shear behavior (attainment of shear strength of bricks) in some elements with damage concentrated in the piers at the ground level. On the contrary, Eurocode 8 predicts a flexural mechanism, again with damage concentrated in the piers at the ground level. However, the displacement capacity obtained according to NPR 2018 tends to be higher, due to the formulation adopted for the element drift limit at near collapse (NC) limit state.

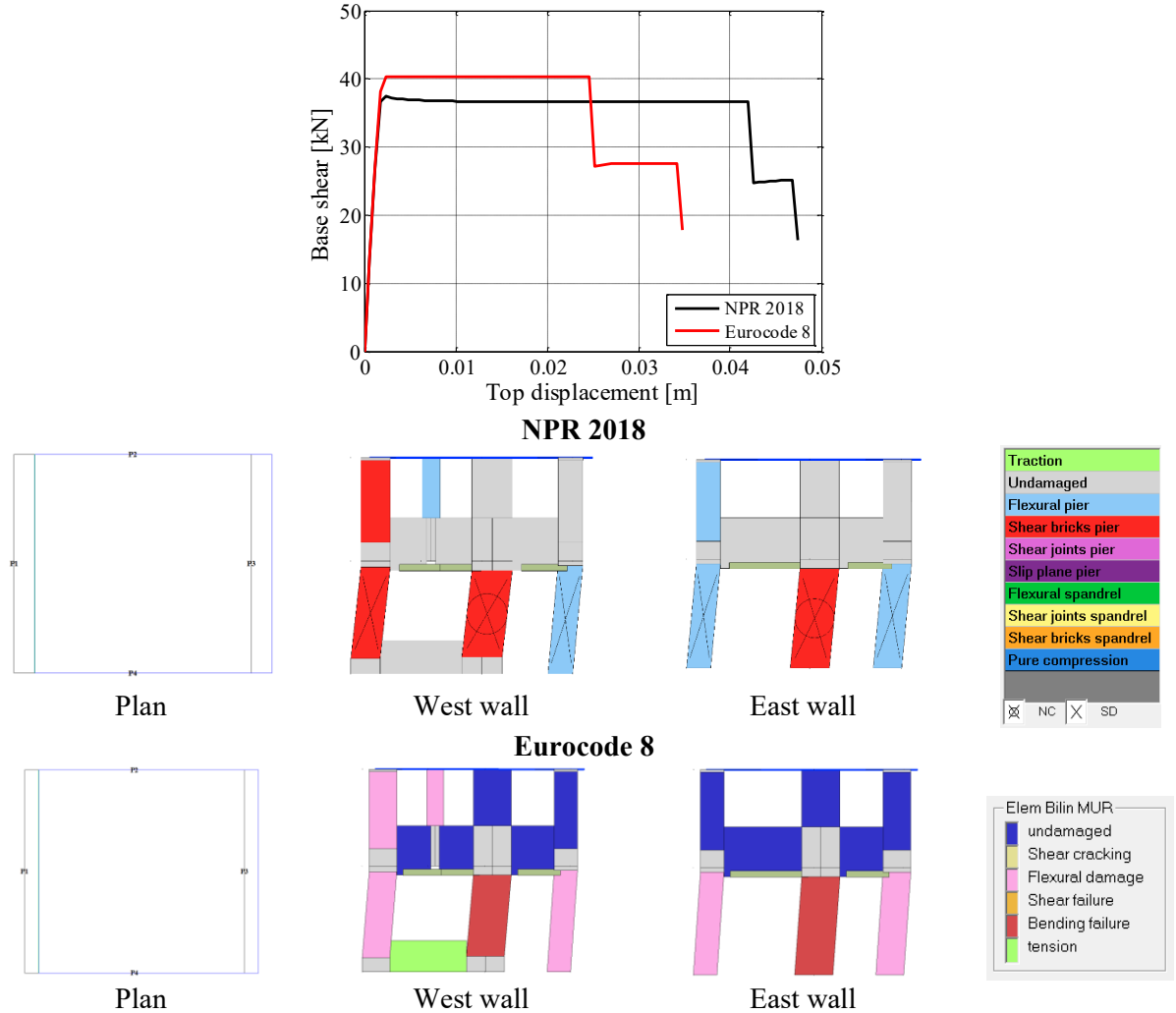


Figure 7: Pushover curve, plan deformed shape and damage patterns according to NPR 2018 and Eurocode 8 in the weak direction - inverse triangular distribution of forces, positive verse, no eccentricity

Figure 8 shows the results of the assessment according to NPR 2018 for the considered direction with reference to the critical analysis (i.e. the one with a mass proportional

distribution of forces, applied in the negative direction and with positive eccentricity). The building is verified, although in the nonlinear branch of the bilinear curve, as also confirmed by the large amount of reduction of the demand spectrum in the capacity spectrum method.

d_{dem}/d_{cap} = 0.68
$d_{SDOF,dem}$ = 32 mm
Safety check: verified

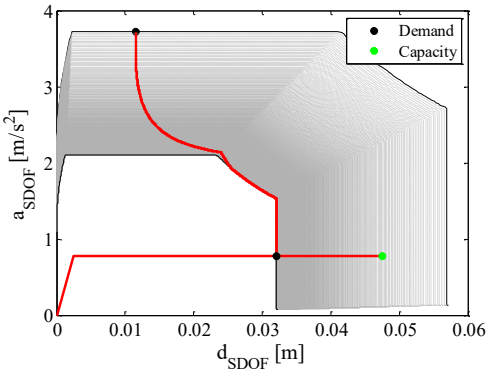


Figure 8: Results of the safety check according to NPR 2018 in the weak direction for the critical analysis

5. CONCLUSIONS

This paper presents the results of the seismic assessment of URM buildings performed according to the Dutch practice guideline NPR9998:2018 by means of nonlinear static analysis with an equivalent-frame model. Firstly, the main new aspects of the guideline with respect to Eurocode 8 were identified: these consist in the constitutive laws of the single elements (piers and spandrels), in the definition of the equivalent SDOF system and in the adoption of the capacity spectrum method in the calculation of the seismic demand. Secondly, a new macroelement including all the constitutive laws depending on the various failure mechanisms was developed and implemented in the TREMURI research software. This allows the performance of nonlinear static analyses according to the considered guideline. Finally, the seismic assessment of a case study building was performed. After the calculation of the capacity curve, the seismic demand and capacities were calculated according to NPR 2018, adopting a seismic action consistent with the seismicity of the area.

The whole assessment procedure, from the definition of the capacity curve to the calculation of displacement capacity and demand by means of the capacity spectrum method was then implemented in the commercial software 3Muri. The goal of the work is to provide engineers with a simple software fully compliant with the adopted guideline to perform the seismic assessment and retrofit of URM buildings.

Acknowledgements. The work presented in this paper was carried out within the activities of two TU Delft-University of Pavia 2018-2019 projects, funded by Nationaal Coordinator Groningen NCG, Centrum Veiling Wonen CVW and Econstruct BV. However, opinions and conclusions do not necessarily reflect those of the funding entities. The authors would like to particularly thank Wim Meilink for his help and suggestions in the various phases of the projects.

REFERENCES

[1] Graziotti, F., Penna, A. and Magenes, G. A comprehensive in situ and laboratory testing

programme supporting seismic risk analysis of URM buildings subjected to induced earthquakes. *Bull. Earthq. Eng.* (2019) **17**:4575-4599.
[2] Nederlands Normalisatie Instituut (NEN), NPR 9998:2015. Beoordeling van de constructieve veiligheid van een gebouw bij nieuwbouw, verbouw en afkeuren - Grondslagen voor aardbevingsbelastingen: geïnduceerde aardbevingen. Assessment of buildings in case of erection, reconstruction and disapproval - Basic rules for seismic actions: induced earthquakes (2015) (in Dutch).
[3] Nederlands Normalisatie Instituut (NEN), NPR 9998:2017. Beoordeling van de constructieve veiligheid van een gebouw bij nieuwbouw, verbouw en afkeuren - Grondslagen voor aardbevingsbelastingen: geïnduceerde aardbevingen. Assessment of structural safety of buildings in case of erection, reconstruction and disapproval - Basic rules for seismic actions: induced earthquakes (2017) (partially in Dutch).
[4] Nederlands Normalisatie Instituut (NEN), NPR 9998:2018. Beoordeling van de constructieve veiligheid van een gebouw bij nieuwbouw, verbouw enafkeuren - Geïnduceerde aardbevingen - Grondslagen, belastingen en weerstanden. Assessment of structural safety of buildings in case of erection, reconstruction and disapproval - Induced earthquakes - Basis of design, actions and resistances (2018) (in Dutch).
[5] CEN, European Committee for Standardisation, Eurocode 8: Design of structures for earthquake resistance – Part 1: General rules, seismic actions and rules for buildings, Design Code EN 1998-1, Brussels, Belgium (2004).
[6] CEN, European Committee for Standardisation, Eurocode 8: Design of structures for earthquake resistance – Part 3: Strengthening and repair of buildings, Design Code EN 1998-3, Brussels, Belgium (2005).
[7] Bracchi, S., Rota, M., Penna, A. and Magenes, G. Consideration of modelling uncertainties in the seismic assessment of masonry buildings by equivalent-frame approach. *Bull. Earthq. Eng.* (2015) **13**:3423-3448.
[8] Bracchi, S., Rota, M., Magenes, G. and Penna, A. Seismic assessment of masonry buildings accounting for limited knowledge on materials by Bayesian updating. *Bull. Earthq. Eng.* (2016) **14**:2273-2297.
[9] Cattari, S., Camilletti, D., Lagomarsino, S., Bracchi, S., Rota, M. and Penna, A. Masonry Italian code-conforming buildings. Part 2: nonlinear modelling and time-history analysis. *J. Earthq. Eng.* (2018) **22**:2010-2040.
[10] STADATA, "3Muri User manual. Version: 11.4.0", [www.stadata.com].
[11] Lagomarsino, S., Penna, A., Galasco, A. and Cattari, S. TREMURI program: an equivalent frame model for the nonlinear seismic analysis of masonry buildings. *Eng. Struct.* (2013) **56**:1787-1799.
[12] Fajfar, P. A nonlinear analysis method for performance-based seismic design. *Earthq. Spectra* (2000) **16**:573–592.
[13] Graziotti, F., Tomassetti, U., Kallioras, S., Penna, A. and Magenes, G. Shaking table test on a full scale URM cavity wall building. *Bull. Earthq. Eng.* (2017) **15**:5329-5364.
[14] http://seismischekrachten.nen.nl/webtool.php.
[15] Kallioras, S., Guerrini, G., Bracchi, S., Penna, A. and Graziotti, F. Displacement demand equations for the non-linear static analysis of short-period masonry structures. *13th North American Masonry Conference*, Salt Lake City, USA (2019).

12th International Conference on Structural Analysis of Historical Constructions
SAHC 2020
P. Roca, L. Pelà and C. Molins (Eds.)

SEISMIC ASSESSMENT OF HERITAGE BUILDINGS IN BULGARIA

MARINA D. TRAYKOVA[1*], ALEXANDER V. TRAYKOV[2]

[1]University of Architecture, Civil Engineering and Geodesy (UACEG)
Faculty of Structural Engineering
1, Hristo Smirnenski Blvd., 1046 Sofia, Bulgaria
e-mail: marina5261@abv.bg, www.uacg.bg (*corresponding author)

[2] University of Architecture, Civil Engineering and Geodesy (UACEG)
Faculty of Structural Engineering
1, Hristo Smirnenski Blvd., 1046 Sofia, Bulgaria
e-mail: traykovalexander@gmail.com, www.uacg.bg

Keywords: Historical Structure, Seismic Assessment, Computer Modelling

Abstract. *Earthquakes are some of the most serious causes of degradation and destruction of the heritage buildings. The earthquake can cause different damages, directly and indirectly to the historical buildings and their elements. The biggest part of the heritage buildings was built essentially following empirical rules, refining the proportions of structural elements by an intuitive perception of the structural behaviour. In most cases, this trial took only static actions into consideration, so, since seismic horizontal actions modify the behaviour in a significant way, an earthquake may frequently produce cracks and local collapses. Seismic assessment of heritage buildings is relevant for any preservation project. Using specific investigations and checks, the best retrofit method can be chosen. Based on different case studies, the aim of the paper is to recommend useful framework and easy applicable assumptions for practicing engineers to evaluate the vulnerability of the historic structures and the possibilities of further steps in their development. Seismic assessment of historic buildings remains a challenging task. There is a high level of complexity compared with the assessment of standard buildings. The assessment and the diagnosis of heritage buildings in seismic areas require an extensive knowledge on the structural typologies and behaviour of heritage buildings. The investigation on previous damages from earthquakes is very important. Adequate and realistic computer modelling of complicated historic structures requires significant designers' expertise. It is probably best to start with the simplest realistic model and then, if necessary, develop a model that reflects more structural features and complexity. The presented paper investigates the challenges posed by, and solutions needed, to ensure the structural longevity of historic structures. Finding the potential for future development of heritage buildings is an important task of the contemporary construction sector. The paper presents only 3 specific case studies but based on the results it is possible to produce some more general recommendations concerning the seismic assessment, the possibility to identify the vulnerability of historic structures and to give the recommendations for extending the service life of Heritage buildings.*

1 INTRODUCTION

Buildings and structures may be classified as historic for three main reasons: they are associated with acts of historical importance, they are old and a long time has passed since their construction, and they are monumental and irreplaceable. What makes it an edifice that must be preserved for future generations are one or more of its cultural, architectural, symbolic, social or historic attributes. Studies of the seismic vulnerability of historic buildings and attempts to mitigate the associated hazards [whether by retrofitting or other procedures] and improve both the load resisting capacity and the longevity of such structures are therefore of great interest.

The assessment and the diagnosis of heritage buildings in seismic areas require an extensive knowledge on the structural typologies and behaviour of heritage buildings. The investigation on previous damages from earthquakes is very important. The presented paper investigates the challenges posed by, and solutions needed, to ensure the structural longevity of historic structures.

The main cause of the inappropriate choices of intervention techniques is due to the lack of knowledge on the material and the behaviour of the peculiar type of structure. To provide the best assessment and to collect properly the data, it is necessary to have enough information concerning: 1) the geometrical, technological and constructive characteristics of the surveyed structure; 2) the material properties; 3) past interventions; 4) the damage state, the possible collapse mechanisms. The information above is possible to be collected after a special on site investigation.

The survey on the site should identify the following details: 1) Age of the building; 2) Structural symmetry; 3) Number of stories; 4) Total height of the building: 5) Foundations (type and material); 6) Structural elements –walls, columns, floors; 7) Size and cross sections of the structural elements; 8) Lateral resisting structural elements; 8) Materials, used for the structure, characteristics; 9) Damages and interventions.

The steps to be followed for the assessment may therefore be summarized as follows:

- Identify the structural characteristics of the structure under consideration, that is, the way in which it responds to the seismic excitation, and what its capacity might be.
- Diagnose the evidence of present structural condition, both visible and concealed. Do the necessary investigations for this diagnosis, including assessment of foundation conditions.
- Make complementary assessment of the local seismic hazard.
- Decide whether temporary shoring is needed to safeguard a damaged structure before, during and after rehabilitation.
- Propose and justify schemes for final repair and strengthening. Prepare the necessary documentation for the selected scheme, in cooperation with other experts if necessary.

During the above architectural/structural survey, a detailed analysis of structural failures, local or otherwise, a thorough study of cracks, the nature of the soil, faults in the original structure, defects of construction, shifting of the foundations, signs of excessive stresses, defective components, etc. should be carefully investigated. For most important edifices, a photogrammetric survey utilizing laser technology may be appropriate.

2 SEISMIC RISK IN BULGARIA

Seismic hazard [1] represents the probability of seismic earth movements to exceed a given seismic level over a certain period of time. The seismic hazard is presented through maps with

expected seismic impacts for a different period of occurrence.

Seismic risk [1] is the probability of occurrence of given losses over a given period of time for a given location as a result of an earthquake.

The assessment of the seismic risk establishes:

- the expected losses according to the seismic impact;
- whether sufficient preventive measures have been taken to reduce the impact of the seismic actions.

Bulgaria is located in the central part of the Balkan Peninsula, which from the tectonic point of view is an element of the Eurasian continental border. The earthquake activity on the territory of the country and its surroundings is one of the most prominent manifestations of modern regional geodynamics.

The seismic situation of the Balkans has some specific aspects. The origin of most of the earthquakes that affect Bulgarian territory are shallow with focus that is less than 60 km in depth. That fact significantly increases the effects of the earthquakes on surface.

According to the 1987 standard map of Bulgaria, 98% of the territory of Bulgaria can be subjected to seismic impact with a magnitude of 7 and higher, of which magnitude 7 - 51%, 8 - 28%, 9 and higher - 19%. Maps of the seismic hazard in Bulgaria are generated at maximum acceleration, soil type A (according to the EC8 classification) for two occurrence periods of 95 and 475 years. The seismic hazard of Bulgaria (for both periods of occurrence) was determined mainly by seismic sources identified on the territory of the country and source Vrancea (Romania).

The most significant earthquakes in Bulgaria after 1900 are: Shabla (31.03.1901, magnitude 7,2), Struma (04.04.1904, magnitude 7,8), Gorna Oriahovica (14.04.1913, magnitude 7,0), Chirpan (14.04.1928, magnitude 6,8), Shabla (30.06.1956, magnitude 5,5), Strajica (07.12.1986, magnitude 5,7), Pernik (22.05.2012, magnitude 5,6).

Seismic design of buildings and facilities in Bulgaria over the years is regulated as follows:

1) Until the beginning of 1957, the buildings (including different categories of the Bulgarian cultural heritage on the territory of the country) are not secured against earthquake effects;

2) 1957 –The "Regulations for the Design and Construction of Buildings and Engineering Facilities in Seismic Areas" started, based on a seismostatistic zoning map, reflecting the observed intensities of the documented previous earthquakes;

3) 1961 and 1964- The map has a new edition concerning the reducing of the areas of the zones with intensity VII, VIII and IX;

4) 1977 - After the earthquake in Vrancea (Romania), new areas of VII and VIII intensity were added in the Danube area of Northern Bulgaria;

5) 1987 – A new seismic zoning of Bulgaria has been introduced;

6) January 2012 - A seismic zoning of Bulgaria is introduced based on the reference maximum acceleration.

It is possible to define five groups that account the year of design of the structure [2]:

- Very old (before 1919)
- Pre-code period (before 1920-1945)
- Low-code period (1946- 1964)
- Moderate-code period (1964- 1987)
- Moderate to High-code period (after 1987)

In analyzing the conditions of Bulgaria to face a strong earthquake, we must note the

following serious problems: 1) A large percentage of the available building stock was (including heritage buildings) designed and built before the new anti-earthquake standards of 1987, for very low levels of seismic provision; 2) There are no preventive measures taken for the preservation of discovered, preserved and restored archaeological structures, buildings and ensembles of national importance for the preservation of the movable historical and cultural heritage from the impact of the risk factors in general (earthquakes, floods, wind, temperature, etc); 3) Work is not being done to reduce or to stop the degradation of the existing building stock.

3 SEISMIC PROTECTION AND STRUCTURAL INTERVENTIONS ON BULGARIAN HERITAGE BUILDINGS

The paper is mainly dedicated to two groups of Heritage buildings: with masonry structure and with reinforced concrete structure.

The buildings with masonry structure are typical representative of the building typology from the end of 19th century and beginning of 20th century in the big cities of Bulgaria. Usually the masonry buildings have: 1) Deformable floor: timber floor and "Prussian vault" (steel structure) or 2) Reinforced Concrete floor. The first type has usually 1-4 storeys, the second type- 1-5 storeys. Later, in the group of the Heritage buildings in the big cities, the reinforced concrete structures appeared. These buildings are mainly with frame structure and masonry infills.

As noted in [3] with regard to bridge renovation, two main types of interventions have to be distinguished: rehabilitation and modification. In rehabilitation, the goal is to provide the bearing capacity and the operational suitability of the building or the facility in the absence of a change of function. These activities are related to the continuous maintenance and change of insulation, joinery, flooring, plastering and other different secondary non-structural elements. In rehabilitation, intervention on structural elements should be minimal and should be summarized in the reconstruction of damages resulting from aging, cracks, spalling of concrete, missing concrete cover, etc. In the case of modification, the structure is modified so that it meets or performs the new load-bearing function. In this regard, it should be explicitly noted that this approach encounters significant difficulties in providing the renovated structures with the requirements of contemporary seismic standards. The requirements of the Bulgarian regulations now set the conditions for the strengthened structure to meet the current standards. In practice, this often leads to the need for costly structural intervention that in fact underestimates the strengthening process and hence the maintenance of the existing building or facility.

4 EXAMPLES FROM THE BULGARIAN PRACTICE

The principles of the seismic assessment, outlined in the introduction of the paper, are illustrated by the following examples of procedures and recommendations dedicated to the extension of the service life of 3 Heritage buildings in Bulgaria. A very interesting example of the investigation and choosing the most appropriate method for rehabilitation of an industrial building structure is discussed in [4].

4.1 Hotel “Lege Palace”, Sofia, Bulgaria

The first case study is dedicated to one of the emblematic buildings of Sofia –Lege Palace (Figure 1.).



Figure 1: “Lege Palace” – actual view [11]

The analysed building is constructed in the period 1910-1914. The architectural design is realized by three famous Bulgarian architects: Georgi Fingov, Dimo Nichev and Nikola Uroukov.

The structure of the building has a typical masonry structure. The floors are constructed according to the system “Prussian vault”: the main element is a steel double T flanged beam. The concept of the system “Prussian vault” is to arrange beams (usually steel beams) and to fill the space between them with bricks shaped as vault. Very often, just to provide the horizontal stability of the structure, one part of the main beams is anchored in the wall with steel “anchors” or if the support is an other steel beam, the connection is provided by steel profiles and rivets. Figure 2 presents the architectural plan of the ground floor.

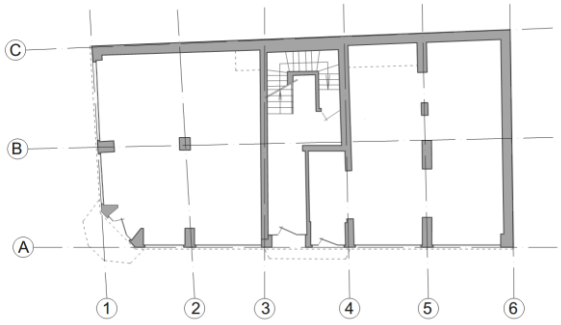


Figure 2: Plan of the ground floor (Lege Palace) [10]

The numerical analysis of the structure is provided by the program SAP2000 [5] based on FEM and a 3D model is defined (Figure 3.). The first step in the modeling is the definition of the characteristics of the materials. EC 6 [6] is the standard for the masonry structures and all the characteristics of the bricks are adopted according to the prescriptions of the standard.

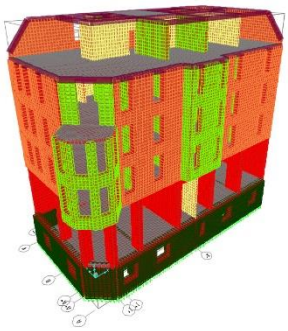


Figure 3: Numerical model in SAP2000 (Lege Palace) [5]

The next step in the numerical analysis is the definition of the loads EC 1 [7]. Three main types of loading are included: permanent loads G, variable loads Q, snow S and seismic load E. Two basic combinations are considered: the fundamental and the seismic.

Concerning the model, shell elements are used for the definition of the computational model. The contact of the structure with the foundations is assumed stiff. The thickness of the walls and the size of the structural elements are adopted according to the available drawings and the information from the site investigation. The floors are not a subject of the presented assessment and for that reason they are involved in the model in order to account for better distribution of the loading between the vertical elements and because of their specific behaviour in the performance of the structure. The floors are modeled as diaphragms.

The main results obtained from the analysis are: 1) Modal periods (Table.1); 2) Normal forces in the vertical elements; 3) Displacements from the seismic combination in the main directions and axes.

Table 1: Modal periods and frequencies [5]

TABLE: Modal Periods And Frequencies						
OutputCase	**StepType**	**StepNum**	**Period**	**Frequency**	**CircFreq**	**Eigenvalue**
Text	Text	Unitless	Sec	Cyc/sec	rad/sec	rad2/sec2
MODAL	Mode	1	0,9181	1,089	6,843	46,833
MODAL	Mode	2	0,7910	1,264	7,944	63,103
MODAL	Mode	3	0,5687	1,759	11,049	122,087
MODAL	Mode	4	0,3626	2,758	17,328	300,252
MODAL	Mode	5	0,2952	3,387	21,283	452,946
MODAL	Mode	6	0,2791	3,583	22,510	506,697
MODAL	Mode	7	0,2621	3,814	23,966	574,357
MODAL	Mode	8	0,2402	4,163	26,157	684,178
MODAL	Mode	9	0,2337	4,280	26,891	723,118
MODAL	Mode	10	0,2261	4,424	27,795	772,543
MODAL	Mode	11	0,2057	4,860	30,538	932,575
MODAL	Mode	12	0,2008	4,980	31,291	979,112

According to the standards in use, the checks for the displacements are basic for the assessment of the structural behaviour. Usually, for existing structures, the control of the damages as a result from excessive displacement are definitive for the behaviour. The results show that the displacements for the biggest part of the vertical elements (for the seismic combination) are not in the limits given in the standard. Analyzing the normal forces in the elements, it was found that the real value of the normal forces in the vertical elements also exceeds the maximum capacity of the elements.

In addition, analysis according to the actual Bulgarian regulations [8] is done. The same elements are checked. The results are similar but the safety according to EC8 [9] is lower than the safety according to the Bulgarian regulations [8]. The difference in the value of the modulus of elasticity of the bricks, defined in the two standards, leads to different stiffness of the walls. The ground floor has some previous interventions and after the site investigation was clear that some of the walls are removed in the past. This fact is related to the decreasing of the global stiffness of the structure. All changes in the first floor (produced on site without any specific design), representing removal of some brick walls, has unfavorable influence on the global seismic performance of the building. The actual conditions of the vertical elements after the on-site inspection shows that there are cracks and damages in them and they need special measures for strengthening.

The provided checks show that the building needs remedial measures for the damaged elements but any future changes in the structure will affect significantly the safety. It is not recommended to make any interventions without a special design for the strengthening. Special care is necessary for the foundations. The observed high level of moisture in the basement requires the execution of waterproofing insulation.

The results of the seismic assessment show that the bearing capacity of the vertical structural elements is reached and for some elements even exceed the limit. The displacements of the biggest part of the vertical elements are bigger than the prescribed limit value. That is the reason to recommend to the Investors to keep the structure without further changes and to strengthen the original structure using the results of the analysis.

4.2 Marine Station, Varna, Bulgaria

The Marine Station in Varna is the biggest on the Black Sea cost in Bulgaria (Figure 4). The original design started in 1965. The construction of the building lasted from August 1966 until the end of 1968. The structure of the building is a classic monolithic reinforced concrete frame structure. The frames are designed in transverse direction. The distance between the frames is 9,00 m. In the longitudinal direction the frames are connected with beams. According to the specific soil conditions, the foundation is realized with 150 driven piles. The length of the piles is 15 m and their cross section is 35/35 cm.



Figure 4: Marine Station, Varna - actual view [11]

For the structural seismic assessment a few numerical models in SAP2000 (Figure 5) are analyzed, using finite elements. The first 3 modal periods according to EC8 and the Bulgarian standards are practically the same. The elastic story drifts exceed the prescribed limits. The comparison is done according to EC8 [9] and according to the actual Bulgarian regulations [8].

The main checks for the structural elements – columns, beams, slabs, etc. show that the available reinforcement in some sections is not according to the contemporary standard requirements. The detailing of the structure is also not according to the standards.

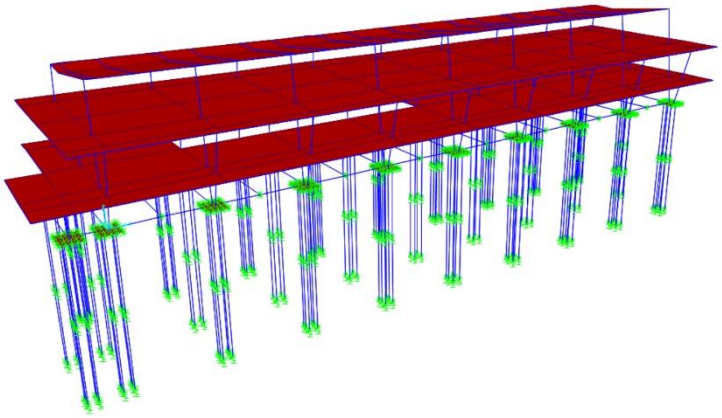


Figure 5: Numerical model in SAP2000 (Marine Station) [5]

Despite the overall relatively good condition of the building, the structure is seriously endangered because of the very active processes of carbonization of the concrete and the reinforcement (Figures 6). The high level of carbonization results from the high humidity and the aerosol impact of seawater.

It is believed, that the building has exhausted its bearing capacity on the basis of the currently applicable regulations for the design of reinforced concrete structures and future functional changes are possible after strengthening of the existing structure.



Figure 6: Actual condition of some structural elements [11]

It is believed, that the building has exhausted its bearing capacity on the basis of the currently applicable regulations for the design of reinforced concrete structures and future functional changes are possible after strengthening of the existing structure.

Adjusting the building structure according to the contemporary standards is not possible for the following reasons: 1) Actual condition of the construction materials; 2) Lack of precise information for the detailing; 3) The parameters of the seismic performance- modal periods, story displacements, are not in accordance to the prescribed recommendations and limits; 4) The numerical checks show that serious number of structural elements are at the limit of the load-bearing capacity determined by the standards or even exceed it by the effect of the various load effects and their combinations. Here, it is important to add that the assessment of the physical condition of the construction materials and the actual condition of the elements limits the future activities. The intention of investment should be based on the provided assessment.

4.3 Serdica building in Sofia, Bulgaria

The Serdica building (Figure 7) is situated in the historical center of Sofia. The building is built in the 20ies of the 20th century. It is a typical brick masonry structure. The floors are constructed according to the system of "Prussian vault" (Figure 8). The roof structure is a timber structure. The foundation is a dry stone masonry.



Figure 7: Serdica Building- main façade [10]

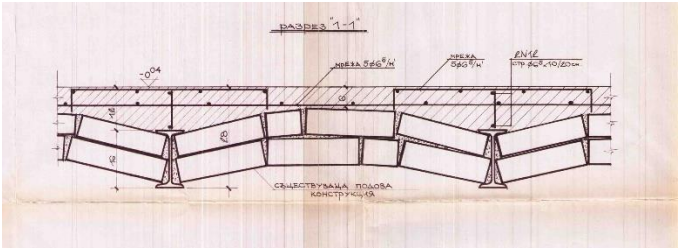


Figure 8: Strengthen floor structure "Prussian vault" (Serdica Building) [10]

After the visual inspection and according to the design documentation, the following conclusion can be drawn: many changes are realized in the long life of the structure. The seismic safety of the building is significantly deteriorated compared to the same at the time of construction.

This is to a lesser extent due to a deterioration in the characteristics of building materials as a result of aging and to greater changes, mainly in: 1) Increased weight of the structure, leading to increasing of seismic forces (new internal changes and additional intermediate level); 3) Contact between the new intermediate level with the existing structure; 3) Reduced stiffness after reduced length of the brick walls (in comparison of the original design), additional openings in the internal and external brick walls; 4) Unfavorable influence of the irregularity in the geometry and the distribution of the stiffness.

Similar to the previous cases, the future intentions of the Investor are limited and need a serious revision according to the provided assessment.

5 CONCLUSIONS AND RECOMMENDATIONS

The paper is presenting only 3 specific case studies, but based on the results it is possible to produce some more general recommendations concerning the seismic assessment, the possibility to identify the vulnerability of historic structures and to give the recommendations for extending the service life of the Heritage buildings:

- A greater problem lies in the fact that the vast stock of heritage buildings in the world does not conform to the requirements stipulated by current knowledge as necessary for seismic safety. The seismic upgrading of historic structures differs from that of more modern structures in that historic buildings do not have to conform to design codes and specifications which, thereby, are not applicable to such structures. More importantly, all seismic retrofitting must be reversible. A considerable difficulty in the practical application of the methodology for renovation of existing buildings and facilities of historical importance in Bulgaria is the lack of specially developed regulations for solving such problems. Some exceptions are the recommendations in Part 8.3 of the EC 8, which however are of a general nature and do not treat historical buildings. This complicates the work of structural engineers and forces them to apply existing rules designed for new buildings in solving the specific task described. As a general rule, the results are inadequate in relation to the intended purpose and the factual situation. It is necessary to develop specific national methodologies that distinguish between the design of new and the strengthening of existing buildings of historical importance.
- Historic structures have generally been constructed with basic building materials such as rock and stone, brick masonry and, in some cases, adobe or wood. The buildings

made from these traditional materials usually possess strength but lack ductility, i.e. the capacity to undergo deformation without collapsing. Historic buildings tend to be massive and stiff structures made of brittle material.

- For some old structures, or buildings that may not allow major intervention, the possibility of providing base isolation may be envisaged. For historic structures which are not base-isolated, the necessity and economic feasibility of retrofitting (providing additional strength by using pre-stressed tie-rods, thin plates, buttresses, etc.) for seismic protection and risk reduction needs to be investigated.
- Any structural intervention must not, if possible at all, create aesthetic conflict. An unstated rule is that the retrofitting of historic structures be almost invisible.
- Material properties from the structure to be protected need to be assessed on the basis of accurate experiments. Sometimes for the initial assessment, it is possible to use some practical recommendations for the characteristics of the construction materials given in the standards.
- Adequate and realistic computer modelling of complicated historic structures requires significant designers' expertise. It is probably best to start with the simplest realistic model and then, if necessary, develop a model that reflects more structural features and complexity. Important aspects and considerations about the process of numerical modelling of structures that will be rehabilitated are presented in [12], despite that the example is not a historic structure.
- Seismic assessment of historic buildings remains a challenging task. There is a high level of complexity compared with the assessment of standard buildings. The heritage buildings are prone to collapse from seismic actions due to different types of seismic vulnerabilities. It is very important to find these vulnerabilities for the different types of structures and to find the specific mechanisms of failure.

REFERENCES

[1] Solakov D. *Seismic mapping of Bulgaria according to Eurocode 8 with reporting the seismic hazard on the territory of the country* , (2009)

[2] Kostov M., Kaneva A., Vaseva E., Stefanov D., Varbanov G., Koleva N. An advanced approach to earthquake risk scenarios of Sofia, *International Conference on Civil Engineering Design and Construction, Varna, Bulgaria*, pp. 245-251, (2006)

[3] Bruhwiler E. Extending the service life of Swiss bridges of cultural value. *Engineering History and Heritage*, Vol.165, issue EH4, pp. 235-240, (2012)

[4] Traykov A. contributor Rehabilitation of the Complex Reinforced Concrete Shell Roof Structure of an Industrial Building, Pelke E., Bruhwiler E. IABSE Structural Engineering Documents SED15: *Engineering History and Heritage Structures – Viewpoints and Approaches*, IABSE 2017, Zurich, Switzerland, pp.67-70, (2017)

[5] Sap 2000 – Computational program

[6] BDS EN 1996-1-1: Design of masonry structures – Part 1-1: General rules for reinforced and unreinforced masonry structures (EC 6)

[7] BDS EN 1991-1-1/NA: Actions on structures- Part 1-1: General actions -Densities, self-weight, imposed loads for buildings (EC 1)

[8] Ordinance № РД-02-20-2/ 12.01.2012 and revised edition 2014 for the design in seismic regions
[9] BDS EN 1998-1: Design of structures for earthquake resistance- Part 1: General rules, seismic actions and rules for buildings (EC 8)
[10] Technical archives of Sofia Municipality – As built drawings
[11] Personal photo archive
[12] Traykova M., Boiadjieva R. Assessment and rehabilitation of the structure of existing reinforced concrete tank, *37th IABSE Symposium, Madrid, Spain*, pp. 543-549, (2014)

12th International Conference on Structural Analysis of Historical Constructions
SAHC 2020
P. Roca, L. Pelà and C. Molins (Eds.)

SEISMIC BEHAVIOUR OF LA MERCED TEMPLE IN MORELIA, MEXICO

LIDIA MEJIA[1], GUILLERMO MARTINEZ[1*], BERTHA OLMOS[1] AND JOSE MANUEL JARA[1]

[1]Civil Engineering Department
Universidad Michoacana de San Nicolás de Hidalgo (UMSNH)
Av. Gral. Francisco J. Mújica S/N, Felcitas del Río, 58004 Morelia, Mich., Mexico
e-mail: guillermo.martinez@umich.mx (*corresponding author)

email: {lidiamejiaolmos, ba.olmos, jmjara70}@gmail.com

Keywords: Macroelement, Earthquake, Nonlinear Analyses, Masonry

Abstract. *This paper studies the seismic behaviour of La Merced temple, dating from the beginning of s. XVII and is located in the historic center of the city of Morelia considering a set of 9 real September 19, 2017, earthquake acceleration records obtained in seismic stations located near the epicenter, which were used without any scaling factor and then applying a scaling factor to reach the site maximum expected peak ground accelerations for probabilistic return periods of 475 years and 975 years.*

1 INTRODUCTION

The temple of La Merced in the historic center of the city of Morelia, Mexico, is located with coordinates 19 ° 42'10``N, 101 ° 1149"W, Figure 1a, which, as seen in Figure 1b, adjoins to the David G. Berlanga elementary school, which was formerly part of the conventual structure. At the end of the 16th century the Order of Nuestra Señora de la Merced settled in New Spain, which throughout the first century of colonial life had stood out in a remarkable way due to the fact that its friars were part, by generally, of the army of conquerors, in which they normally functioned as chaplains [1]. In 1604, Mercedarian friars Pedro de Burgos and Álvaro García obtained a license from Viceroy Luis de Velasco and Bishop Juan Fernández Rosillo to found a convent in the city of Valladolid, now Morelia, for which they acquired a house owned by Melchor Pardo and his wife María Ortega, to which they later added two adjacent pieces of land donated by the City Council. The founding friar of the convent, Felipe Gutiérrez, began the work of the church and convent with the alms of the neighbors. However, in 1606, at the death of Bishop Fernández Rosillo, the vacant headquarters council issued a suspension order of the work trying to avoid the convent foundation. The mercedarios went for their defense before the viceroy and subsequently obtained the support of the new bishop Friar Baltazar de Covarrubias, who endorsed the respective license and suspended the Cabildo's order; the work resumed around 1608-1609, under the direction of the new prior of the convent Friar Andrés de la Fuente

[1]. The religious order of La Merced was the one that suffered the most economic difficulties in the city, the most difficult situation for which the temple was concluded in 1736 with the construction of its east or main façade, which at the day, retains its original door.



Figure 1: a) La Merced church. b) old convent cloister today David G. Berlanga elementary school

2 ARCHITECTONIC CHARACTERISTICS

The church has two façades as shown in Figure 1a, the main façade facing east was built in the 18th century and the north or longitudinal façade, was built in the 17th century and is stiffened by two buttresses with different heights. The bell tower, Figure 2a, has 31.33m height and is attached to the main façade while the dome was added in the 18th century, Figure 2b, and rests on an octagonal drum with baroque elements that is located on the false transept of the nave which has a length of 35.39m with a height of 13.04m and an-interior 6.69m span as can be seen in Figure 3. Figure 4 shows the vaults that are of lunettes between masonry rib arches

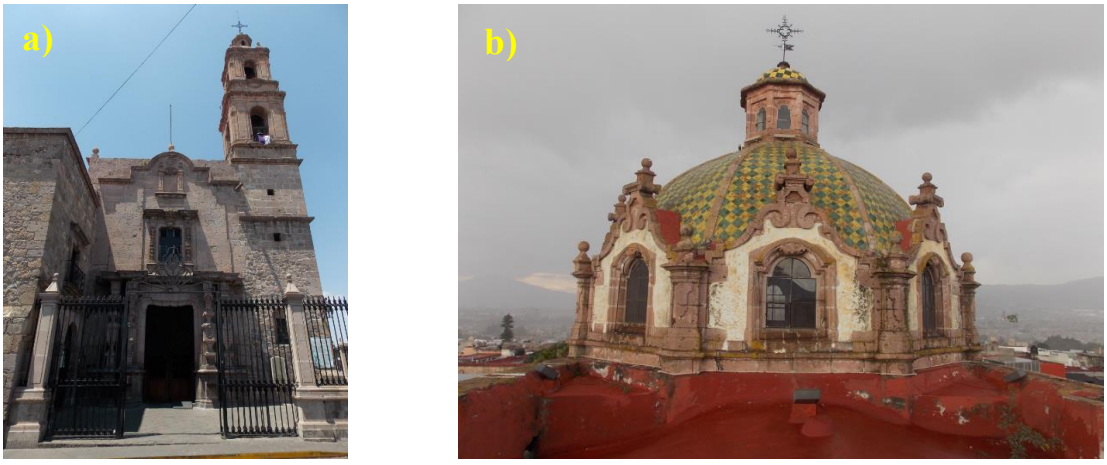


Figure 2: a) Bell tower and east façade, b) XVIII century dome.

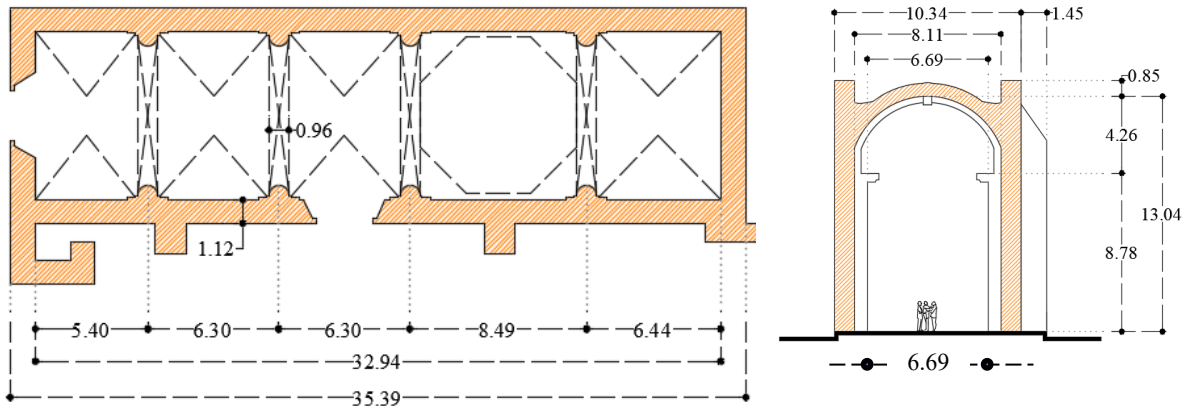


Figure 3: Nave plan view and transversal section

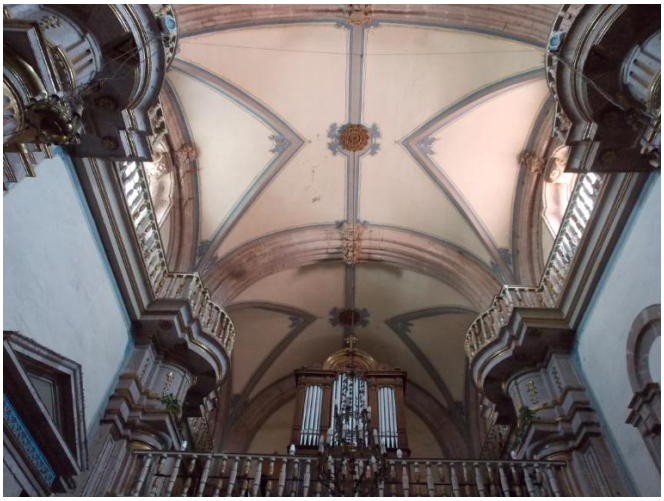


Figure 4: Nave chorus and lunette vaults stiffened with rib arches

3 EXISTING DAMAGE

The church of La Merced presents different damages, which, qualitatively, can be related more to seismic action than to another type of action, since the building was built on a stiff clay which reduces the risk of ground settlement, situation which is verified in neighboring buildings, which also do not present problems due to the service limit state.

3.1 East façade damage

It presents slight damage composed by a shear crack caused by the interaction of the facade with the bell tower, which starts from the upper corner of the coral window and extends vertically as shown in Figure 6.

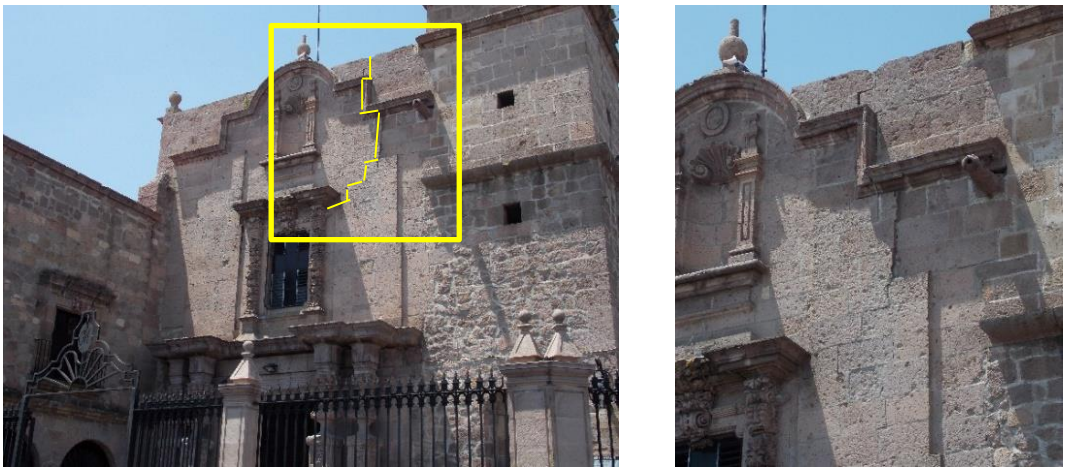


Figure 6: Main façade damage

3.2 Ribbed dome damage

The dome has cracks in each of its eight shells between ribs as shown in Figure 7. The cracks reach the lantern ring, damage that can also be attributed to past seismic actions. On the outside, the rocking effect of the pinnacles that are located on the drum ornamentation is evident, some of which have failed due to shear as indicated in Figure 8. Without any doubt, the pinnacles damages has been caused by historical earthquakes.



Figure 7: Cracks on the masonry dome



Figure 8: Pinacles rocking and shear base damages

3.3 Nave vault damages

The lunette nave vaults have Sabouret cracks, Figure 9, as well as shear cracks that have practically been connected to each other in such a way that they can form rigid blocks that could become unstable in future seismic events of importance as seen in the Figure 10. It is also clear that such damage patterns can be associated without major error to the seismic action of the past.



Figure 9: Vault Sabouret crack



Figure 10: Main nave vault cracks

3.4 Rib arches damage

These arches are 0.96m wide and 0.40m height. One of these arches shows damage to the intrados of one of it´s kidneys as shown in Figure 11a, so a safety mesh has been placed to prevent damage to people who come to church every day. These arches have also lost their mortar joints between dowels and in recent years mortar injections have been made to consolidate them as shown in Figure 11b. Subjectively, it is not clear whether the damages observed could have been caused by seismic action.



Figure 11: a) Daños en arco fajón and b) mortar injection nozzles

4 SEISMIC DEMAND

In order to better understand the seismic behavior for the Merced church, a seismic demand composed by nine acceleration records obtained near to the most damaged zones in the Morelos and Puebla States for the september 19, 2017 earthquake (Ms 7.2) were used. This records were obtained in seismic stations located between 85 to 100km distance from the epicenter. The normal focal mechanism of this seismic event produced spectral amplifications in a range of periods of 0.18 to 0.54 seconds, reaching a maximum pseudoacceleration value of 1.01g for a 0.44 seconds vibration period, Figure 12.

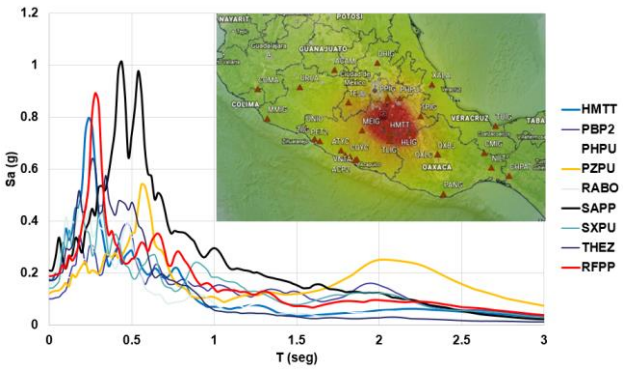


Figure 12: Response spectra of the nine highest peak ground accelerations (Seismic stations Map from the UNAM Engineering Institute)

5 SEISMIC BEHAVIOUR

Two-dimensional Rigid Element macroelements were analyzed [2] for which the horizontal ground seismic shaking component was considered in a first stage, and in a second stage, the horizontal component acting simultaneously with the vertical component of the seismic record were applied, both in the transverse and longitudinal directions of the nave. The seismic demand was introduced with its original acceleration amplitudes and then scaling these amplitudes to the maximum probabilistic 475 and 975 year recurrence peak ground accelerations, that is, for 96.9 and 139.24gals.

5.1 Macroelement definition

Figure 13 shows the macroelements considered in the analysis; in the longitudinal direction is the located over the nave south wall and in the transverse direction the one corresponding to the nave connected to an existing flying arch, which, at the moment is inserted in the two old cloister levels of the David G. Berlanga elementary school. This macroelement was considered due to it has a high stiffness wich can concentrate major damages.

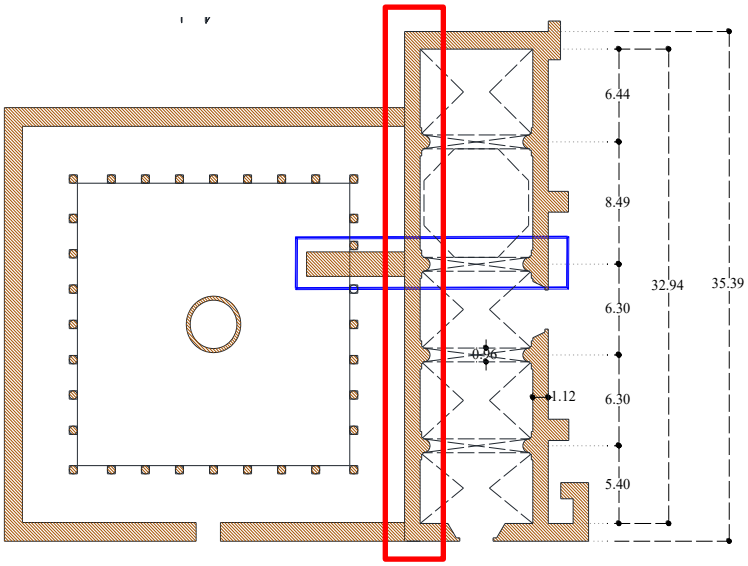


Figure 13: Macroelement definition. Transversal macroelement (blue) and longitudinal macroelement (red)

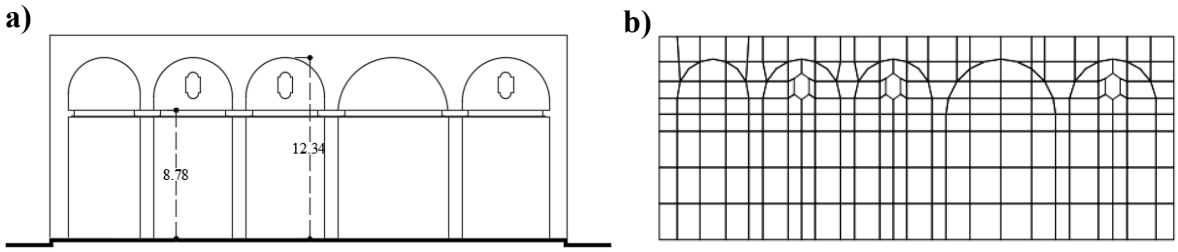


Figure 14: a) Longitudinal macroelement and b) Rigid element mesh

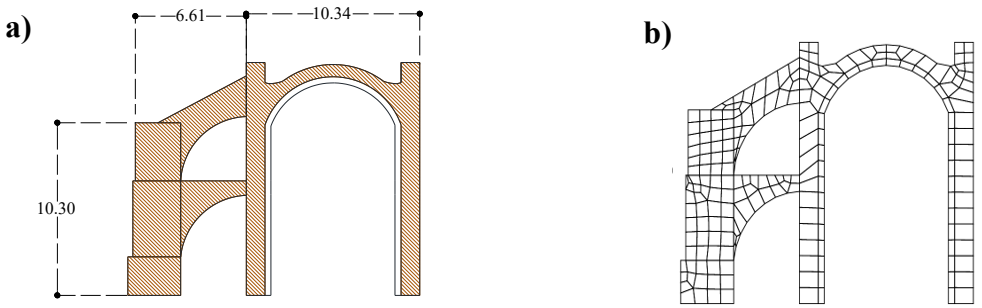
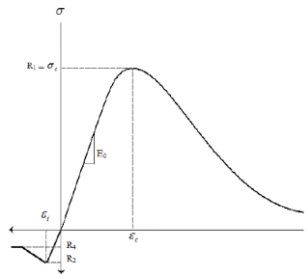


Figure 14: a) Longitudinal macroelement and b) Rigid element mesh

5.2 Constituve model

An exponential constitutive model was used for nonlinear analysis [3], in which the compression behavior is defined only by the initial stiffness of the material and the maximum compression strength as indicated in Table 1.

Table 1: Constitutive model parameters



Material	R1 (Mpa)	R2 (Mpa)	R3 (Mpa)	R4 (Mpa)	Young Modulus (Mpa)	Poisson Modulus	Density (Kg/m3)
Masonry	10.8	-1.08	6.963	-0.32	1000	0.2	1800
Vault infill	4.904	-0.49	0.314	-0.15	500	0.2	1600

5.3 Longitudinal macroelement

The longitudinal macroelement has a high resistance and a high lateral stiffness as shown in Figure 15, and for the whole seismic demand no damages were obtained, so that the considered seismic demand does not cause any traction, compression or shear damages.

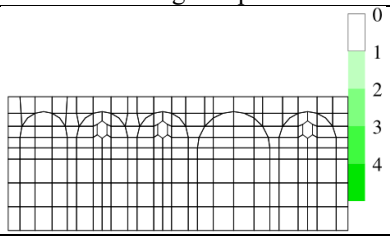
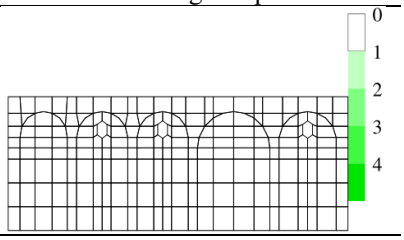
Seismic record	Traction damage degree H shaking component	Traction damage degree H+V shaking component
SAPP1709		

Figure 15: Longitudinal macroelement traction damage for one of the seismic records

5.4 Transversal macroelement

In the nave transverse direction, the structural behavior was similar for all the considered seismic demand in terms of damage distribution, with moderate to extensive damage degrees at the key and springers of the vaults and arches. Such damages can be associated to the crack pattern observed in the vaults, and it is appreciated that the damage pattern does not change significantly when the earthquake vertical component is involved in the analyses, attributing such a situation to the reduced span of the nave of only 6.69m.

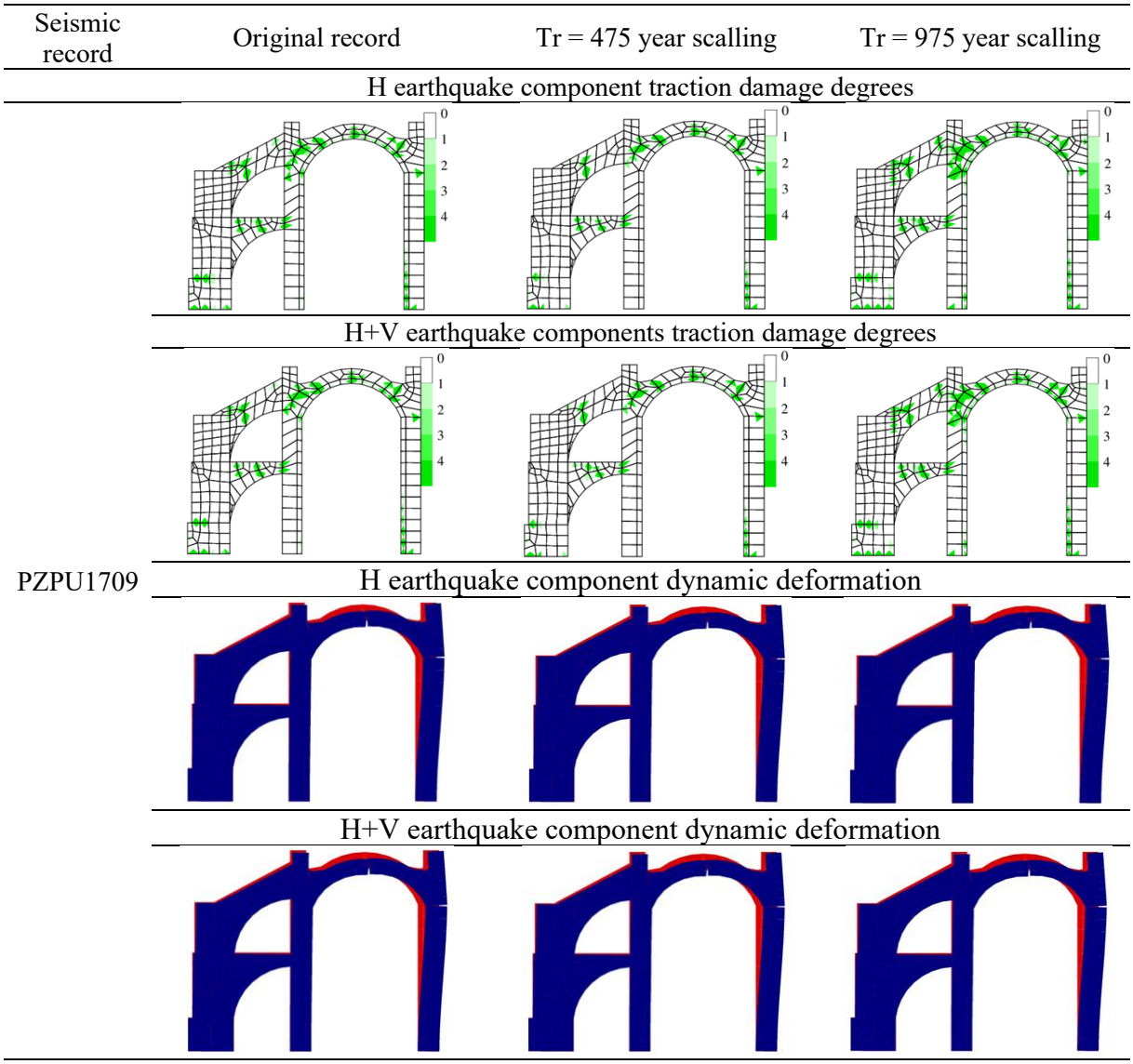


Figure 16: Transversal macroelement traction damages and dynamic deformations

The maximum lateral displacements are indicated in Table 2 for the considered seismic demand, finding that the greatest differences between introducing only one or two components

of the earthquake ground shaking were only 13% of surplus and 7% in the opposite case. Therefore, for this particular church, the vertical component was favorable in introduce earthquake compression loads on the elements, which tended to close the produced cracks. For the Rigid program, values with zero displacement equal compression failure in some zone of the structure, which indicates that the maximum displacement that the temple vault can tolerate is less than or equal to 0.663cm.

Table 2: Transversal macroelement lateral displacements

Seismic Record	Original record (cm)		Tr = 475 year scalling (cm)		Tr = 975 year scalling (cm)	
	H	H+V	H	H+V	H	H+V
HMTT1709	0.274	0.255	0.163	0.158	0.234	0.233
PBP21709	0.240	0.257	0.463	0.491	0.000	0.000
PHPU1709	0.506	0.503	0.319	0.318	0.000	0.000
PZPU1709	0.438	0.424	0.265	0.265	0.604	0.601
RABO1709	0.282	0.278	0.178	0.207	0.261	0.000
RFPP1709	0.429	0.380	0.206	0.205	0.274	0.275
SAPP1709	0.663	0.658	0.572	0.559	0.000	0.000
SXPU1709	0.168	0.172	0.151	0.161	0.233	0.221
THEZ1709	0.476	0.489	0.379	0.389	0.468	0.000

Regarding the dissipated hysterical energy in the structure for the seismic demand without scaling and with scaling, Table 3 shows a small variation between the horizontal component exclusively and the combination of the horizontal with the vertical shaking. The greatest differences were found for the scaled 475 year recurrence with an 8.88% value, so it is verified that the dissipated hysterical energy differences were small. The zero value again implies compression failure in some macroelement area.

Table 3: Transversal macroelement histeretic disipated energy

Seismic Record	Original record (J)		Tr = 475 year scalling (J)		Tr = 975 year scalling (J)	
	H	H+V	H	H+V	H	H+V
HMTT1709	4.16E+05	4.19E+05	1.45E+05	1.67E+05	2.93E+05	3.19E+05
PBP21709	8.06E+05	8.66E+05	1.35E+06	1.47E+06	0.00E+00	0.00E+00
PHPU1709	5.55E+05	5.27E+05	3.08E+05	2.98E+05	0.00E+00	0.00E+00
PZPU1709	1.17E+06	1.15E+06	6.79E+05	6.85E+05	1.79E+06	1.78E+06
RABO1709	7.58E+05	7.07E+05	3.04E+05	3.73E+05	6.28E+05	0.00E+00
RFPP1709	7.39E+05	6.22E+05	3.24E+05	3.25E+05	5.06E+05	5.07E+05
SAPP1709	8.59E+05	8.51E+05	6.58E+05	6.54E+05	0.00E+00	0.00E+00
SXPU1709	1.85E+05	2.07E+05	1.76E+05	1.85E+05	2.74E+05	2.94E+05
THEZ1709	6.68E+05	5.32E+05	3.77E+05	3.78E+05	7.18E+05	0.00E+00

To have a better damage degree indicator in the transverse direction of the nave, Table 4 shows the damage index (D) for the considered seismic demand without scaling and with scaling, which were calculated using the Park, Ang and Wen [4] formulation for masonry structures:

$$D = \frac{U_m}{U_f} + \frac{\varepsilon}{q_u * U_f} \int dE \tag{1}$$

Where: U_m is the maximum response deformation, $\int dE$ the incremental dissipated hysteretic energy, U_f is the ultimate deformation capacity under monotonic loading, q_u the yield strenght and ε a non-negative experimental constant equal to 0.075. The damage index is a normalized amount, whose value is, by definition, between 0 and 1. The value of D equal to zero denotes an undamaged structure, that is, the linear elastic behavior of the structure during the earthquake, while a value greater than or equal to 1 denotes the failure of the structure, that is, local or general collapse of the structure.

Table 4: Damage Index (D) for the transversal macroelement

Seismic	Original record		Tr = 475 year scalling		Tr = 975 year scalling	
Record	H	H+V	H	H+V	H	H+V
HMTT1709	1.90	1.78	1.07	1.05	1.59	1.59
PBP21709	1.91	2.05	3.57	3.81	1.00	1.00
PHPU1709	3.38	3.35	2.11	2.10	1.00	1.00
PZPU1709	3.32	3.22	1.99	2.00	4.68	4.65
RABO1709	2.14	2.08	1.25	1.47	1.94	1.00
RFPP1709	3.02	2.66	1.44	1.43	1.95	1.96
SAPP1709	4.51	4.47	3.84	3.39	1.00	1.00
SXPU1709	1.12	1.16	1.02	1.08	1.57	1.51
THEZ1709	3.27	3.26	2.51	2.57	3.24	1.00

7 CONCLUSIONS

La Merced church in Morelia city, Mexico, has a high strength and stiffness in their longitudinal walls and did not show any damage against the seismic demand produced by the September 19, 2017 earthquake, however, in its transverse direction, the nave would suffer local or global collapse before this seismic demand with and without scaling factors, which derives in a critical scenario for the building in the future since there are currently slight damages that would undoubtedly increase. With the above, it is essential to take urgent structural measures for the church, in order to achieve an adequate future seismic performance of this structure listed as a World Heritage Site since 1991 by UNESCO and thus avoid any social or cultural loss.

REFERENCES

[1] León, R. *Los orígenes del clero y la iglesia en Michoacán, 1525-1640*. Colección Histórica Nuestra No. 16, Instituto de Investigaciones Históricas, Universidad Michoacana de San Nicolás de Hidalgo, *in Spanish*, (1997).

[2] Casolo S. and Peña F. Rigid element model for in-plane dynamics of masonry walls considering hysteretic behaviour and damage, *Earthquake Engineering and Structural Dynamics* (2007), **36**: 1029-1048.

[3] Peña, F. RIGID (v.0.4.1) *Programa de Elementos Rígidos para en Análisis Dinámico no Lineal de Estructuras de Mampostería*, Instituto de Ingeniería, Universidad Nacional Autónoma de México, México (2010).

[4] Y. J. Park, Y.J., A. H-S. Ang, A. H-S., and Wen, Y.K. Damage-Limiting Aseismic Design of Buildings. *Earthquake Spectra* (1987), **3**:1, 1-26.

12th International Conference on Structural Analysis of Historical Constructions
SAHC 2020
P. Roca, L. Pelà and C. Molins (Eds.)

SEISMIC DAMAGE MECHANISMS FOR CHURCHES AND DAMAGE SEQUENCE: CONSIDERATIONS FROM A CASE STUDY

MARIA A. PARISI[1]*, YLENIA ANZILOTTI[1], GRACE I. FUENTES RIVERA[1], GESSICA SFERRAZZA PAPA[1], STEFANO BARBÒ[1]

[1]Department of Architecture, Built Environment and Construction Engineering (ABC)
Politecnico di Milano
Piazza Leonardo da Vinci, 32, 20133 Milano, Italy
*e-mail: maria.parisi@polimi.it

Keywords: Churches, Masonry, Seismic damage, Damage mechanism, Progressive failure

Abstract. *Several high-intensity earthquakes have occurred in Italy in the last decades, causing considerable damage to architectural heritage and pointing out the particularly high seismic vulnerability of masonry churches. A significant research effort has been devoted to develop specific methods for the damage analysis and the seismic vulnerability assessment of these assets. An abacus of damage mechanisms recurring in the church structural components has been developed and has become an important reference in rapid assessment procedures as well as in more detailed analyses. In this perspective, the damage occurred to a church during the Pianura Padana Emiliana (Emilia) Earthquake of 2012 is analyzed here. The damage pattern reproduced, indeed, situations listed in the abacus of mechanisms. The seismic response of the church has been analyzed with different numerical approaches, with complete and with partial models that have allowed an appreciable understanding of the global behavior and of the modality of damage progressing into the mechanisms. The use of vector graphics software tools for 3D modelling that have become available in recent times has allowed to thoroughly understand the constructional complexity of the asset and, consequently, to develop simpler but structurally significant models for numerical analysis.*

1 INTRODUCTION

The numerous high-intensity earthquakes that have occurred in Italy in the last decades have caused considerable damage and losses to the architectural heritage. The damage toll taken by earthquakes has been particularly heavy on historic masonry churches, which are especially vulnerable to seismic action due to their structural characteristics. These circumstances have conveyed a significant research effort into studying specific methods for

-analysing the damage to churches,
-in a prevention phase, assessing their seismic vulnerability [e.g. 1],
-assessing the validity of interventions for damage repair and for structural improvement.

The method of limit equilibrium has proven to be a powerful tool for both damage and vulnerability analyses. An abacus of possible limit mechanisms that recur in the church structural components, or macro-elements, has been developed. It is founded on a very ample

base of observational data derived from different earthquakes and in different regions, thus covering differences in constructional traditions and typologies, and it has become a widely used reference in rapid assessment procedures as well as in more detailed analyses. Specifically, a survey form is used to collect information on what damage mechanisms have developed; for each mechanism, damage is graded referring to a scale from 1 to 5, where 5 is the collapse state [2]. Extensive use of this reference in recent earthquakes has proven its general validity, but also indicated possible further developments. These may regard consideration of additional damage cases as well as a deeper understanding of the progression of mechanism development. To this purpose, the post-earthquake observation and analysis of damage cases remains a fundamental step for improving this additive knowledge.

Within this context, the damage occurred to a church during the Pianura Padana Emiliana Earthquake of 2012 that produced extended damage to these assets [3] is interpreted here. The church, built in the 18th century and located in a village in the province of Mantova, presented severe damage in different areas, especially in the vaults covering the three naves. For these elements, the damage pattern reproduced situations listed in the abacus of mechanisms. The church façade, with an imposing tympanum according to the style of the time, instead, reported only initial damage from an out-of-plane rotation of the tympanum, and some more extended damage from a rotation of the entire façade, an unusual situation crossing two different mechanisms.

In order to investigate this case, a meaningful representation of the original ground motion is necessary. Earthquake recordings taken in the vicinity of the church for the two major shocks satisfied this requirement.

A different but equally important need for these structures is the possibility of their accurate representation, both for a thorough understanding of their constructional complexity and for the subsequent step, that is, to develop simpler but structurally significant models for numerical analysis [4]. The recent development of high-power software tools for 3D modelling allows to visualize the shape of the asset but also to understand in detail its geometry and its building process to a level not easily reachable before. On this basis, the seismic response of the church has been analyzed with different approaches, with complete and with partial models that have allowed an appreciable understanding of the global behavior and of the modality of damage development, as described in the following sections.

2 REFERENCE DAMAGE MECHANISMS FOR CHURCHES

One of the most frequent damage modes in churches concerns the façade, which may fail in different and typical ways depending principally on its geometry, on the quality of its connection with side walls, on the presence of thrusts from the roof or other elements behind, and the main direction of motion. Figure 1 reports typical façade mechanisms, taken from the abacus mentioned above, with out-of-plane rotation of the entire façade wall or of the tympanum. These mechanisms will be found in the case study analyzed. In-plane shear modes may also occur in the façade element.

Another dominant failure mode associated to the transversal response of the building is the out-of-plane failure of the nave walls, summarized also in fig.1. This mode occurs particularly in those architectural styles where the walls of the central nave of three-nave churches are

particularly slender, possibly with the presence of a clerestory. This failure mode may be the result of interaction with heavy roof trusses or be triggered by non-restrained thrusts from the arches and vault covering the central nave. It is particularly critical, as collapse of the top of the wall most often causes the collapse of the vault or deprives the roof trusses of support, resulting in their fall.

Vaults, which are structural elements particularly suitable to carry vertical loads, are particularly sensitive to lateral forces from seismic action: they develop crack patterns depending on the vault geometry.

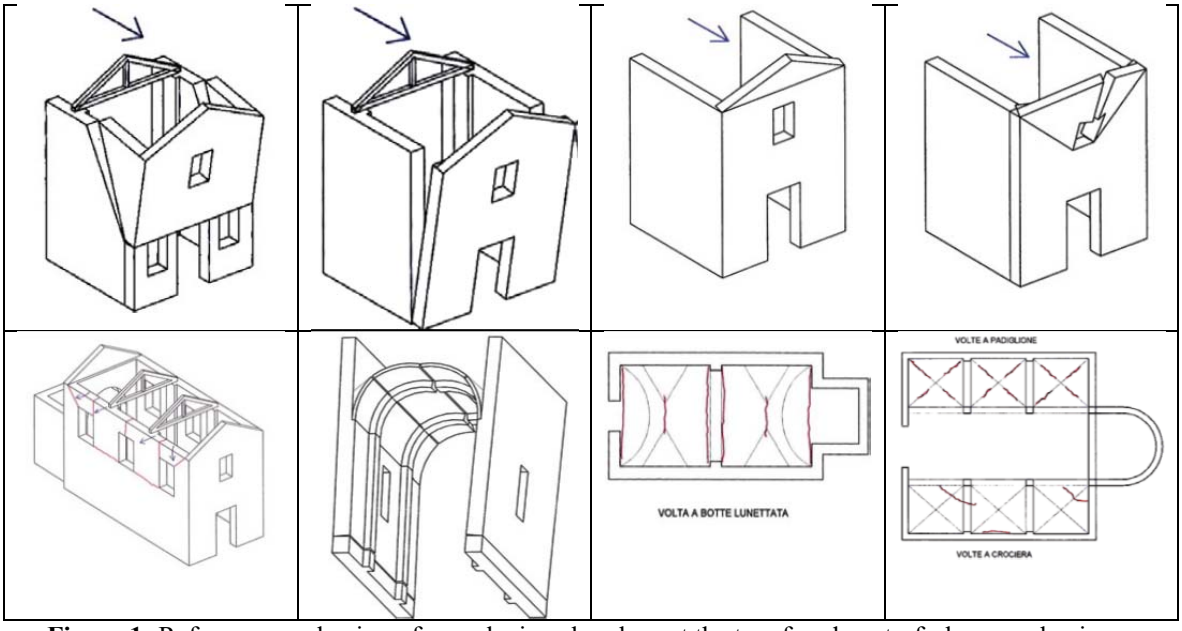


Figure 1: Reference mechanisms for analyzing churches; at the top, façade out-of-plane mechanisms; at the figure bottom, nave wall mechanisms (left) and crack patterns for vaults (right)

3. THE EMILIA EARTHQUAKE OF 2012 IN THE PROVINCE OF MANTOVA

In the month of May 2012, the territory of Emilia Romagna and nearby regions in northern Italy were hit by an earthquake sequence, with seven main shocks having a moment magnitude M_w higher than 5. Five of them occurred between May 20 and May 29, 2012.
The region stricken by this earthquake had no history of frequent or strong earthquakes. The most significant one dated back to 1570 in Ferrara, in the eastern part of the area, and was estimated as of M_w 5.46. The seismic hazard of the region had been classified at a low-to-moderate level only since 2003, when seismic design of buildings was enforced. Thus, until recently also the new buildings were not designed according to seismic requirements. Lack of awareness of seismic risk seems to have affected the traditional constructional practice that did not include provisions adopted in other parts of the country. This situation caused extended damage to new and old buildings in the Emilia region as well in the adjacent provinces of Mantova and Cremona, in Lombardy, where a signicant number of cultural heritage buildings and churches was damaged.

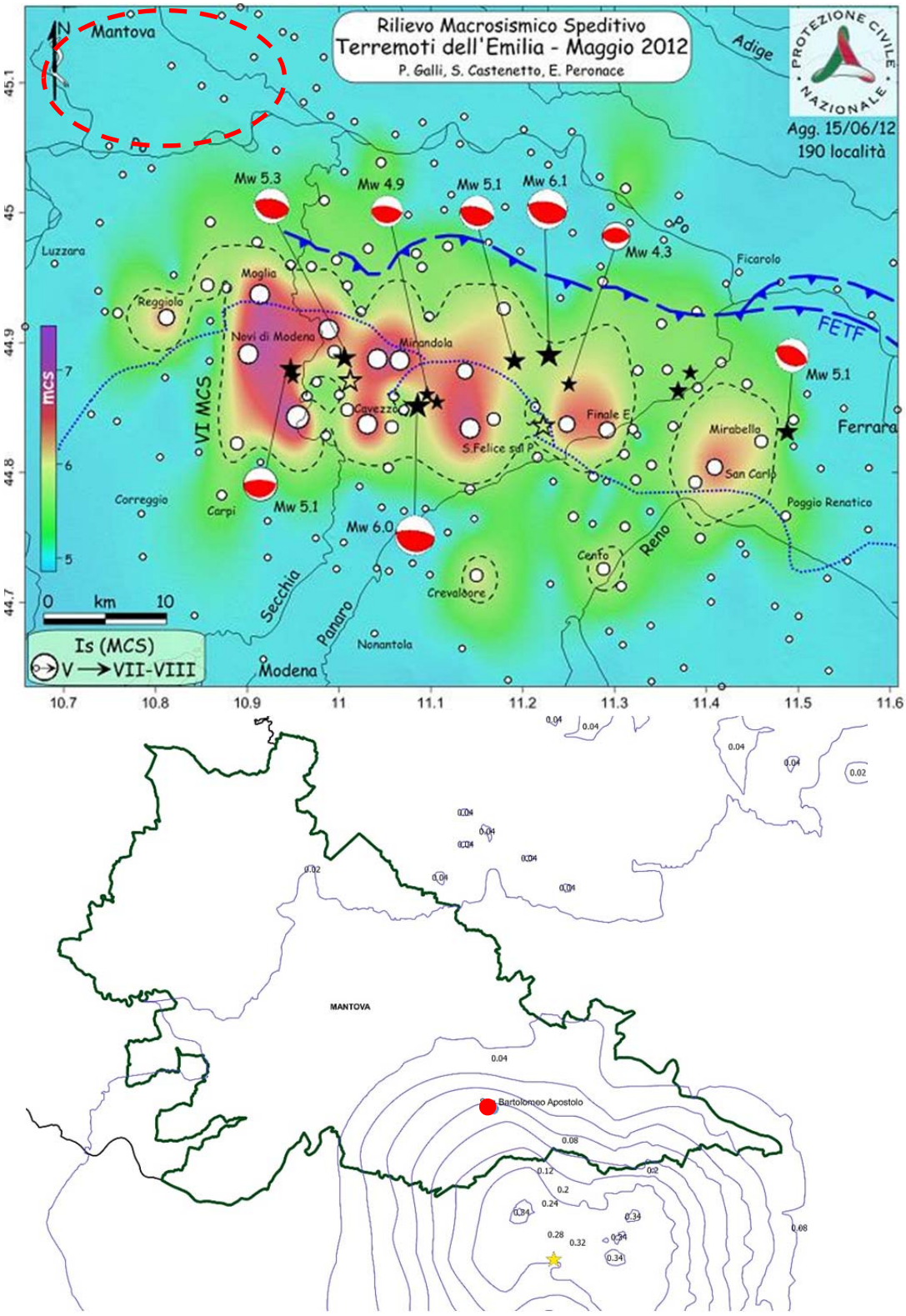


Figure 2: Map of the major events in the 2012 Emilia earthquake (top) and the isoseism map in the area of Mantova in the event of May 29 (bottom); the church of this case study is shown with a red dot

With reference to fig. 2, top, showing the major events in the sequence, the province of Mantova is located NW. Here, the most damaging shocks have been those of May 29, which had a closer epicenter and which found a building stock already weakened by the previous events.
Several churches in the area were built in the local expression of the baroque style, having elements and proportions that made them particularly exposed to seismic damage. The church investigated here is representative of this typology. Its location is shown in fig.2, within the isoseism map of the May 29, 9:00 02 a.m. event.

4. DAMAGE STUDY

The earthquake series of 2012 severely damaged 129 churches of the diocese of Mantova, amounting to 42 percent of the total. Damage surveys that were carried out in the immediate post-earthquake period to assess the situation over the territory made reference to the abacus of possible mechanisms. While this reference has allowed homogeneity in treating and comparing the many cases examined, some situations that were difficult to interpret have suggested to investigate in more detail the damage occurred and the modality in which it developed.

4.1 The church of San Bartolomeo at Quistello

The church of San Bartolomeo at Quistello has been chosen for a study because it is representative of many similar assets both in terms of architectural characteristics and of extension and type of suffered damage. The façade before the earthquake is shown in fig. 3. Each space defined in the plan is covered by vaults, separated by arches, and by a dome at the midplan, in a complex pattern shown in fig. 4.
Reports on the historical documentation was available and could be consulted for this church, which permitted to retrace interventions and modifications carried out at different times. A recent detailed study by diagnostic testing evidenced a good quality of brick masonry.
During the earthquakes of 2012, the many seismic shocks that occurred from the 20th and particularly on 29th of May heavily damaged the church that reported collapses of the vaults and wide cracks on many bearing walls of the central nave, as well as the collapse of the roof behind the façade. The event of the 20th of May caused out of plane, overturning cracks on the façade in the proximity of the gable and the overturning toward the interior of the marble element supporting the cross, at the top of the façade, that collapsed into the roof. The fall of such non-structural element caused damage to the roof behind the façade and to the counter-façade vault underneath. This kind of damage was observed in other churches in the area.
The second important shock of the 29th of May, at 9:00 a.m., deteriorated further the situation. Many of the vaults collapsed, causing additional damage to decorations and other art elements below. The damaged vault behind the façade fell, entailing the collapse of the organ, see fig. 5.
Other elements and parts of the church were also severely damaged. Important cracks opened in the entablature above the arches along the central nave as well as in those between the chapels. In many cases they reached the vaults above, as in fig. 6. The apse developed numerous inclined cracks, which are frequently found in such element: a situation that has been listed in the abacus of typical mechanisms.



Figure 3: The church of San Bartolomeo Apostolo at Quistello

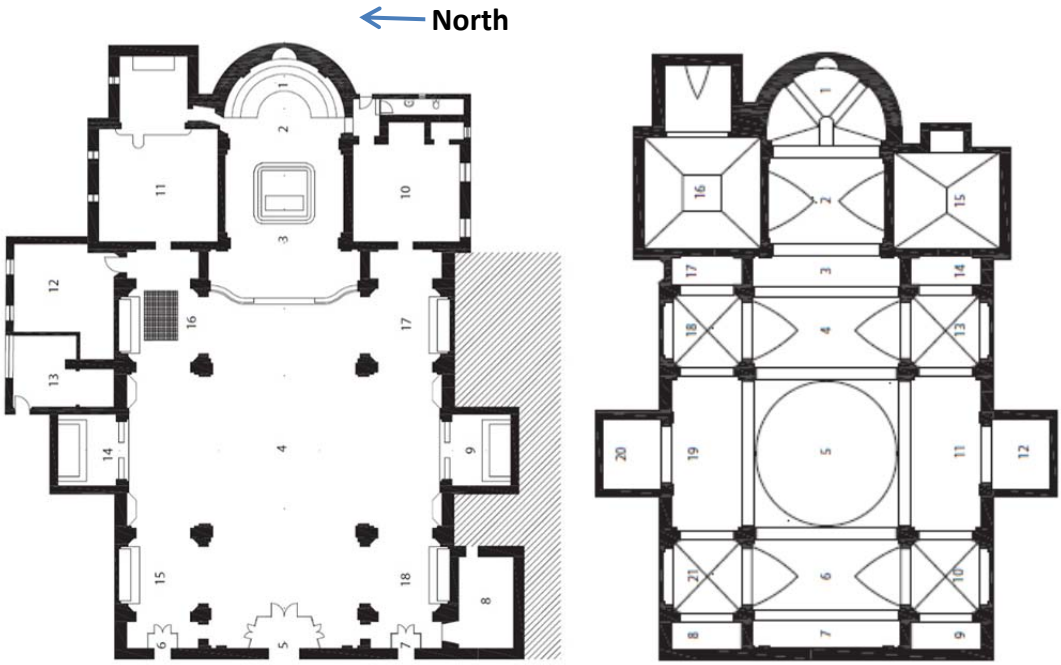


Figure 4: The plan and the vault system

The façade usually suffers severe damage, either locally due to overhanging parts and little restrained areas, or globally, when the façade is badly connected to the nave walls. This situation is frequent for architectural and construction reasons and usually evolves into the

detachment and out-of-plane rotation of the entire façade wall [e.g. 5, 6]. Façade damage modes, for their importance, are the first indicated in the abacus of mechanisms. Here they are shown in fig. 1. Yet, in San Bartolomeo only some limited damage to the gable top was found, together with an initial global rotation of the façade, that is, two façade mechanisms seemed to have developed but the first only to a small extension. In order to investigate the structural behavior of the church and follow the development of its seismic response that brought to the observed damage, a series of numerical analyses were planned. A detailed geometric model and different numerical ones were developed to this purpose.



Figure 5: Collapse of the vault behind the façade



Figure 6: Cracks in the arches along the nave and transversal to it.

5 THE MODELS

The information available on the building was basically in traditional two-dimensional formats. The creation of a three-dimesional (3D) model by vector graphics software [7] was a fundamental step toward a thorough understanding of the church in its construction process, its composition, as well as its present state. The correct representation of the vault system requires particular effort, yet this process brings to a deep understanding of the system in its complexity. In the development of the architectural model, attention was paid to select options that would facilitate the subsequent translation to a numerical model for finite element structural analysis. Figures 7 and 8 show global renderings of the architectural model and the finite element model, which was formed with over 103000 nodes and 57100 elements. Shell elements were used for vaults and solid elements for the other parts. The final model included the roof structure, following damage observations that indicated its positive interaction with walls in the response, [e.g. 8].

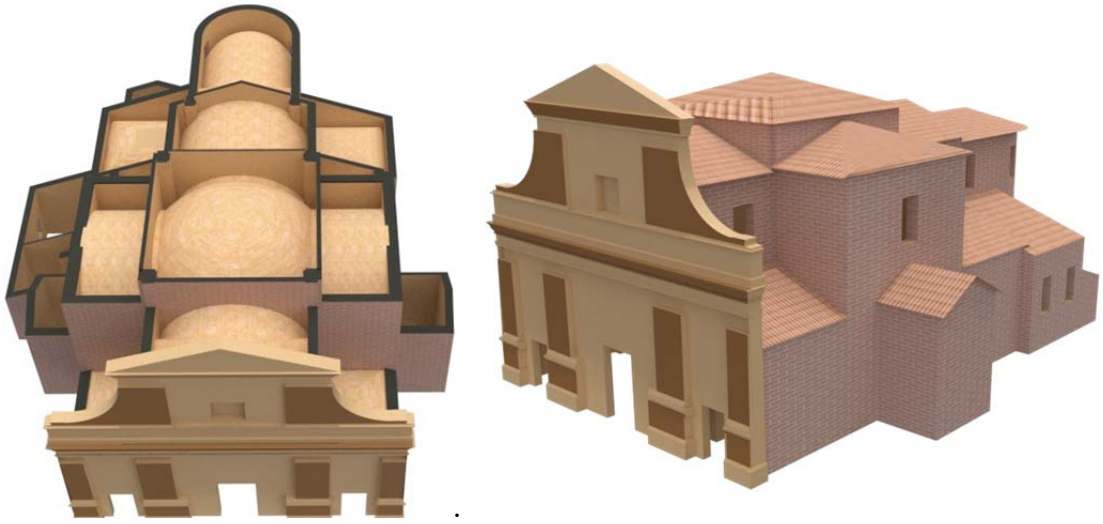


Figure 7: the vault system and a general view of the church model

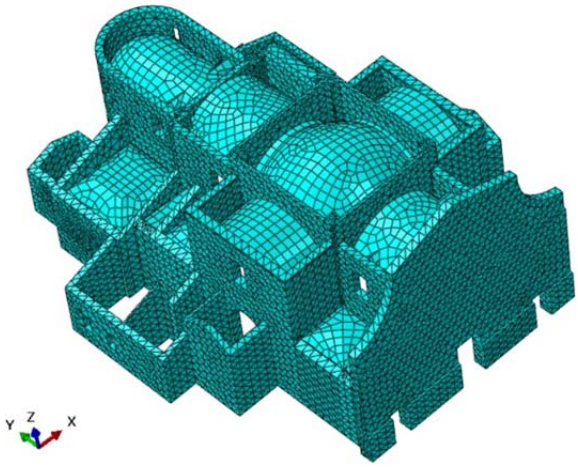


Figure 8: the finite element mesh

5. NUMERICAL ANALYSES

Different types of analysis were carried out on the model for an in-depth view of the structural behaviour. In the elastic field, after a *static analysis* to assess the general stress levels and distribution in normal loading conditions, a *modal analysis* was performed to investigate the characteristics of the dynamic response. The first periods are around 0.3 seconds, a reasonable value for these structures. The first three modes are in fig. 9. While the second mode is transversal and involves the main body of the church including the vault system, the main mode and the third both concentrate mainly on the façade. Their modal shapes resemble the corresponding damage mechanisms. The modes indicate, thus, an enhanced out-of-plane deformability of the gable that could possibly evolve into the corresponding damage pattern, which is somewhat inconsistent with the actual outcome that saw little damage to this part. This question has been the particular focus of further analyses.

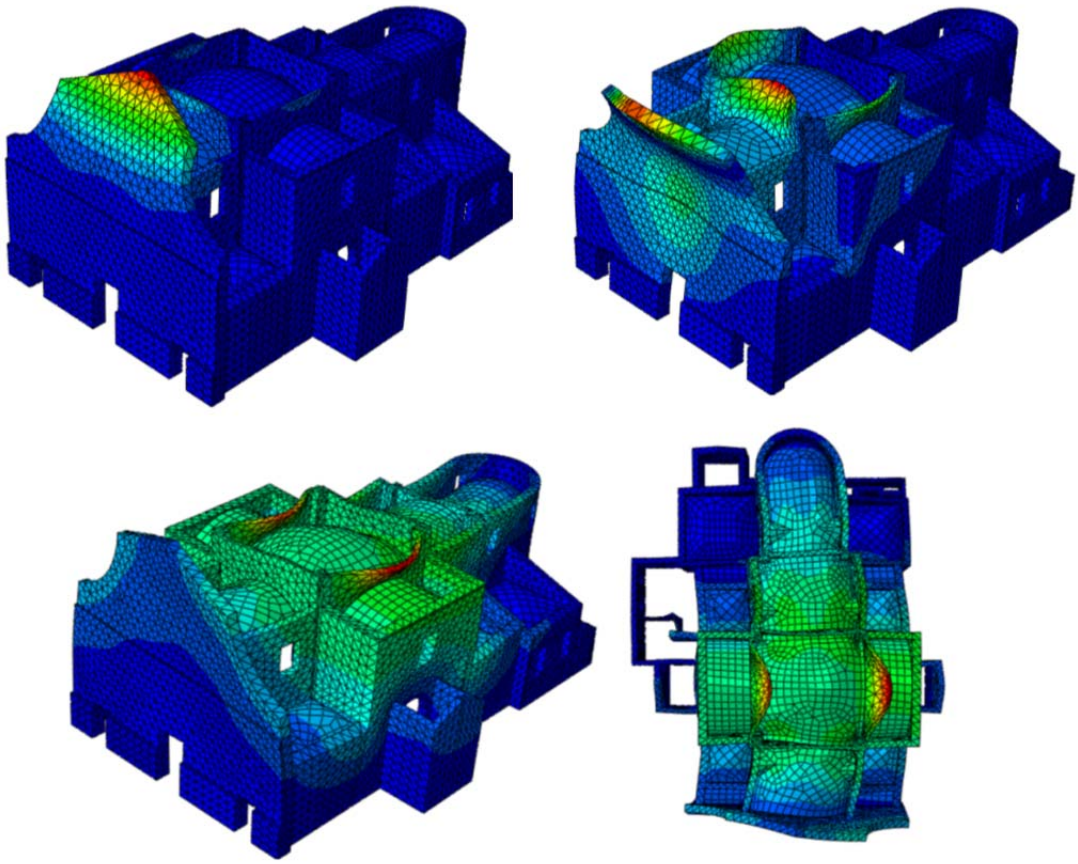


Figure 9: first and third modal shape (top) and second modal shape with two views (bottom)

In order to perform seismic analyses, reference has been made to recordings from the station of Poggio Rusco, the closest to the area, in the EW direction, making reference to the event of May 29 at 9: 00 02 a.m., which had been the most damaging. The response spectrum

derived from the recording is shown in fig. 10, together with the elastic design spectrum with return period of 475 years given by the Italian Design Code at the church coordinates.

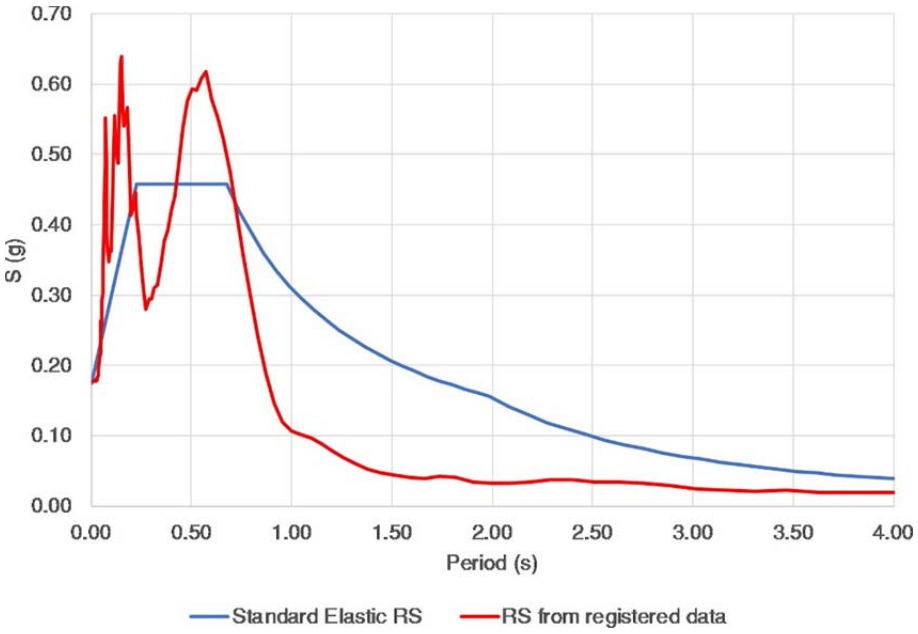


Figure 10: response spectrum

The aim of a *response spectrum analysis* was to find the general distribution of stresses and the most solicited elements, until damage would become significant. Once more, the façade top appeared to concentrate the highest stress levels clearly showing out-of-plane bending, as in fig. 11. Vaults and arches, especially those close to the façade, also appeared in critical conditions.
In order to clarify the behavior of the façade, a *limit equilibrium analysis* modeling the overturning of the gable was performed with non-linear kinematic approach. The acceleration activating the mechanism resulted lower than the peak ground acceleration and the spectral acceleration occurred during the earthquake, once more indicating failure of this element.

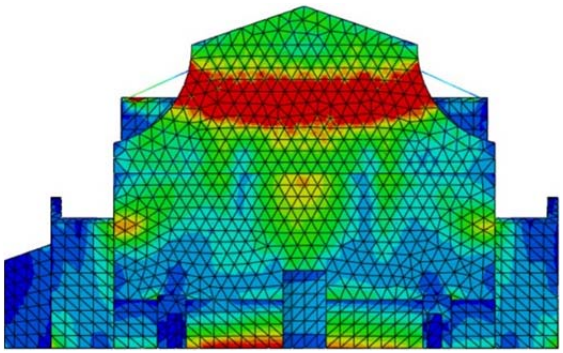


Figure 11: tensile stress distributions, where blue is null and red the maximum value

The analyses discussed so far could not consider the effect of duration of the earthquake, and of possible variations in the structural behavior with time. In order to shed light on this point, a *nonlinear time-history analysis* was performed. The nonlinearity of the material was modeled through a concrete plasticity model available in Abaqus [9] and calibrated for masonry, as several cases found in the literature suggested. Nonlinearity and the size of the full model would require an unreachable computational effort. Since the focus of this analysis was the front area, only this part has been studied, with reference to the significant duration of motion [10].

In order to adopt a reduced but significant model, extension and boundary conditions of the reduced models have been based on a calibration comparing periods and modes of the reduced part with the full model. The final simplified model, shown in fig. 12, had 31336 finite elements, which made computations still demanding but feasible on a high capacity computer.

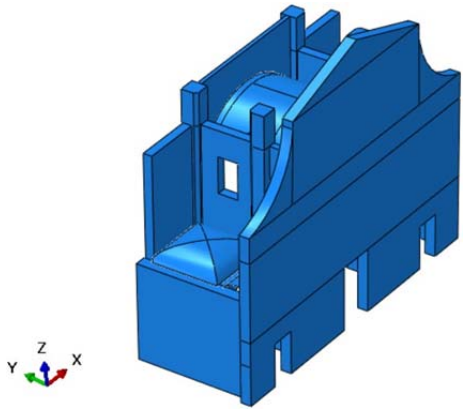


Figure 12: reduced model for nonlinear analysis

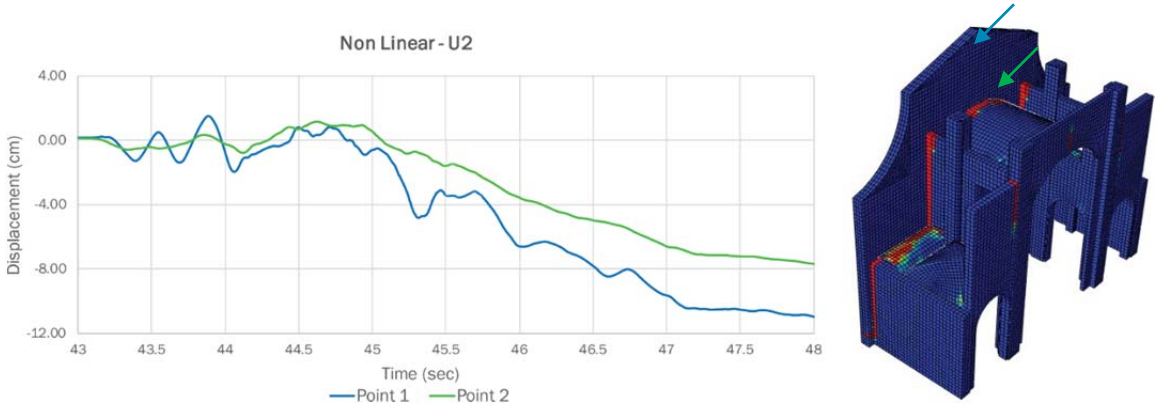


Figure 13: development of displacements at the vertex (blue, dark line) and at the connection of façade and vault (green, light line), see arrows, and model in damaged conditions along the red line

Results may be summarized making reference to fig. 13. An initial oscillation occurs at the top, until the connection of the façade with the back part deteriorates; at this time, the entire façade is weakly restrained and a trend toward a full façade rotation sets in.

Meanwhile, larger displacements occur at the vault, now separated from the façade, bringing to its collapse. A switch from an initial gable mechanism to a façade overtopping one has avoided further development of the first; damage in the second has also developed partially. The situation could not be described without a time history analysis, but the reference to codified damage mechanisms has helped in pointing out this particular situation.

7 CONCLUSIONS

- The usefulness of making reference to a classification by mechanisms for damage description has once more been confirmed.
- For the façade, response spectrum and limit equilibrium analyses had indicated the out-of-plane failure of the tympanum as the first mechanism likely to develop. The real damage was better interpreted by a non-linear time-history analysis showing the initial involvement of the tympanum subsequently controlled by the establishing of a global façade mechanism.
- Recent possibilities of geometric representation of 3D models with vector graphics proved to be a step forward in the understanding of complex existing structures.

Acknowledgements. Research partially funded by Reluis-DPC Project 2019-21. The authors wish to thank Arch. Anna Maria Basso Bert, Soprintendenza Archeologia, Belle Arti e Paesaggio per le province di Bergamo e Brescia, for making this study possible, giving access to documental material and damage data.

REFERENCES

[1] Lagomarsino, S. and Podestà, S. Seismic vulnerability of ancient churches: part 1. Damage assessment and emergency planning, *Earthq. Spectra* (2004) **20**(2): 377-394.
[2] MiBAC, (2006). Scheda per il rilievo del danno ai beni culturali – Chiese, modello A-DC.
[3] Sorrentino, L., Liberatore, L., Decanini, D. and Liberatore, D. The performance of churches in the 2012 Emilia earthquakes, *Bull. of Earthq. Eng.* (2014), **12:** 2299–2331.
[4] Parisi, M.A. and Chesi, C. (2019) Structural characterization for the seismic protection of heritage churches, In: R. Aguilar et al. (Eds.): *Structural Analysis of Historical Constructions*, RILEM Bookseries **18**: 1392-1400.
[5] Binda, L., Chesi, C. and Parisi, M.A. (2010) Seismic Damage to Churches: Observations from the L'Aquila, Italy, Earthquake and Considerations on a Case-study, *Adv. Mat. Res.,* **133-134***:* 641-646.
[6] Sferrazza Papa G, Silva B (2018) Assessment of Post-Earthquake Damage: St. Salvatore Church in Acquapagana, Central Italy. *Buildings* **8:** 45
[7] Rhinoceros (2019). User manual, version 6.0, Robert McNeel & Associates.
[8] Parisi M.A. and Chesi C. (2014) Seismic vulnerability of traditional buildings: the effect of roof-masonry walls interaction. In: *Proceedings 10th U.S. NCEE*, Anchorage, Alaska.
[9] Abaqus. (2016). Theory manual, version 2016.
[10] Trifunac, M.D. and Brady, A.G. (1975). A study on the duration of strong earthquake ground motion. *Bulletin of the Seismological Society of America*, **65(3):**581

12th International Conference on Structural Analysis of Historical Constructions
SAHC 2020
P. Roca, L. Pelà and C. Molins (Eds.)

SEISMIC FRAGILITY ANALYSES OF THE CABINET STORED ARTEFACTS WITH AND WITHOUT DAMPING METHOD

BAI WEN*, DAI JUNWU, YANG YONGQIANG

Key Laboratory of Earthquake Engineering and Engineering Vibration, Institute of Engineering Mechanics, China Earthquake Administration
Harbin 150080, China
e-mail: 781090853@qq.com(*corresponding author)

Keywords: Historical Structure, Masonry, Monitoring, Non-Destructive Inspection

Abstract. *The Forbidden City, the former Chinese imperial palace, now houses the Palace Museum. It is not only famous for its splendid wooden palace complex, but also prestigious for the millions of precious artefacts stored. The Forbidden City is located in the center of Beijing, which is a high seismic hazard zone. Wooden structures usually perform well during earthquakes because of their large deformation and damping capacities. Meanwhile, most artefacts are fragile due to their delicate shapes and aging issues, and also due to their unanchored place form. Only a few of those artefacts are on exhibit, while most of the others are placed in cabinets and stored in warehouses. This paper focuses on seismic protection of these cabinet stored artefacts. Considering the tremendous amount and the rigorous requirements for moving the artefacts, base isolation is not a favored method. Using base isolation requires lifting the artefacts or cabinets while installing isolation bearings and this is very time consuming because of the rigorous requirements for moving artefacts. Also, artefact damage might happen during this process. Thirdly, much more spaces are required to accommodate the potential isolation deformation. Considering all these adverse aspects, this paper tries to use dampers to connect all adjacent cabinets to enhance the integrity and increase the damping ratio and thus protect the stored artefacts. This method is applicable for both new and existing cabinets. No artefact movement and extra space are required. All the dampers are installed with mechanical buckles and the whole installation is reversible. In order to validate the effectiveness of this method, shake table tests and finite element analyses based on practical cabinet layout with and without this damping method are designed and conducted. Ten ground motions are chosen and used to conduct fragility analyses. The cabinet sliding displacements are chosen as the damage index. Seismic fragility curves of the cabinets with and without dampers are plotted and compared. Results demonstrate the effectiveness of the proposed damping method.*

1 INTRODUCTION

The Forbidden City, the former Chinese imperial palace, now houses the Palace Museum. Currently, more than 1.80 million pieces of artefacts are stored here. Dedicate shapes, brittle materials and aging issues are the major reasons why many of the artefacts are fragile. Meanwhile, Beijing, where the Forbidden City seats, is an earthquake prone area and thus the seismic damage risks of these invaluable treasures are high. Past earthquakes have

demonstrated that tremendous damage to artefacts might be caused due to earthquakes. For example, during the 2008 Wenchuan earthquake, 4379 pieces of artefacts damaged, including 208 pieces of high value [1].

In order to reduce the potential adverse consequences caused by earthquakes, the dynamic response characteristics of artefacts and related floating items under earthquakes have been researched [2-11]. Many methods, both traditional and innovative, have been proposed and used [12-20]. As illustrated in Figure 1, nylon lines are used to offer extra constrains. Side support are added at the horse leg. Clamps are used to fix the vase and prevent the vase overturn. Meanwhile, modern methods like base isolation have also been used. The acceleration responses of the floating items could be significantly reduced.



(1) Nylon lines (2) Side support (3) Base fixation

Figure 1: Traditional methods used to protect artefacts

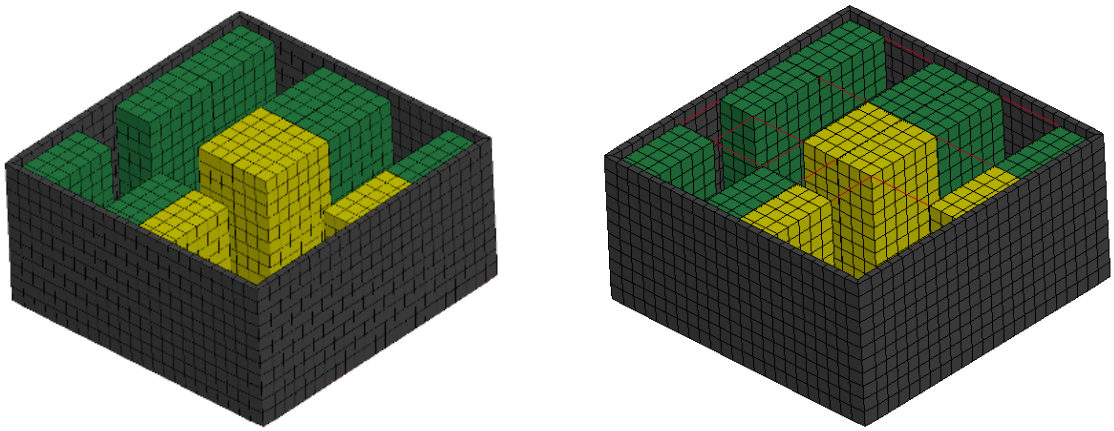
Both traditional and innovative methods have been demonstrated effective. The problem is the awareness of taking seismic measures. The vast majority are just left there without any seismic protections. As for the numerous treasures in the Palace Museum, most of them have not been properly seismic protected. Another factor needs to be considered is that only a few of these artefacts are exhibited while most of the others are stored in the warehouse. It is not practical to take measure like nylon lines to protect each artefact because there is too much work, and this will cost years to complete. Besides, there are the risks that damage might be caused during the seismic protection process instead of earthquake itself. Base isolation has the same issues. The artefacts need to be moved during the application.

To protect these artefacts while avoiding unnecessary movement of these artefacts, a compromise method is advocated. Since most of the artefacts are placed in the cabinets and are stored in warehouses, silicon dampers are used to connect these cabinets to increase the system damping and integrity during earthquakes. The dynamic responses of the cabinets are expected to be decreased and those cabinet stored relics are to be protected. Numerical simulations and shake table tests are used to validate this method.

The numerical simulations are first presented and the shake table test results are then discussed.

2 NUMERICAL SIMULATIONS

In the numerical simulation, the cabinets are established with SHELL element. The dampers are established with two-node combination damper element. The static friction coefficient is set as 0.2 and related dynamic friction coefficient is set as 0.16. The models with and without dampers are shown in Figure 2. The plane layout is plotted in Figure 3. The size of the cabinets is 1200 mm × 600 mm × 2000 mm (height). There are two types of cabinets with different masses, which are 200 kg and 400 kg, respectively. As for the damper parameters, the velocity exponent θ is 0.25. The damping coefficient is set as 5.0 kN(s/m)$^{\theta}$.



(1) Without dampers (2) With dampers

Figure 2: Numerical models with and without dampers

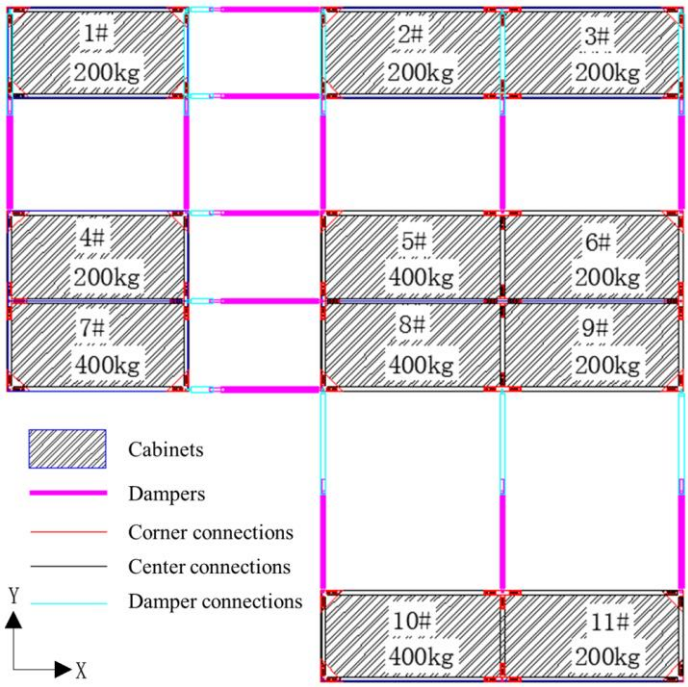


Figure 3: Plane layout of the cabinets

Ten ground motions are chosen and used to conduct the fragility analyses. The information is listed in Table 1. Related acceleration spectra at X direction are plotted in Figure 4.

Table 1: Ground motions in the numerical analyses

No.	Earthquake name	Year	Station	Magnitude	Focal distance
01	'Mammoth Lakes-01'	1980	'Long Valley Dam (Upr L Abut)'	6.06	15.52
02	'Chi-Chi, Taiwan'	1999	'CHY036'	7.62	44.74
03	'Cape Mendocino'	1992	'Rio Dell Overpass - FF'	7.01	24.55
04	'Imperial Valley-06'	1979	'Delta'	6.53	35.17
05	'Kocaeli, Turkey'	1999	'Yarimca'	7.51	25.07
06	'Imperial Valley-06'	1979	'Calipatria Fire Station'	6.53	58
07	'Chi-Chi, Taiwan'	1999	'CHY034'	7.62	46.82
08	'Chi-Chi, Taiwan'	1999	'NST'	7.62	89.2
09	'Kocaeli, Turkey'	1999	'Duzce'	7.51	99.52
10	'Trinidad'	1980	'Rio Dell Overpass, E Ground'	7.2	78.22

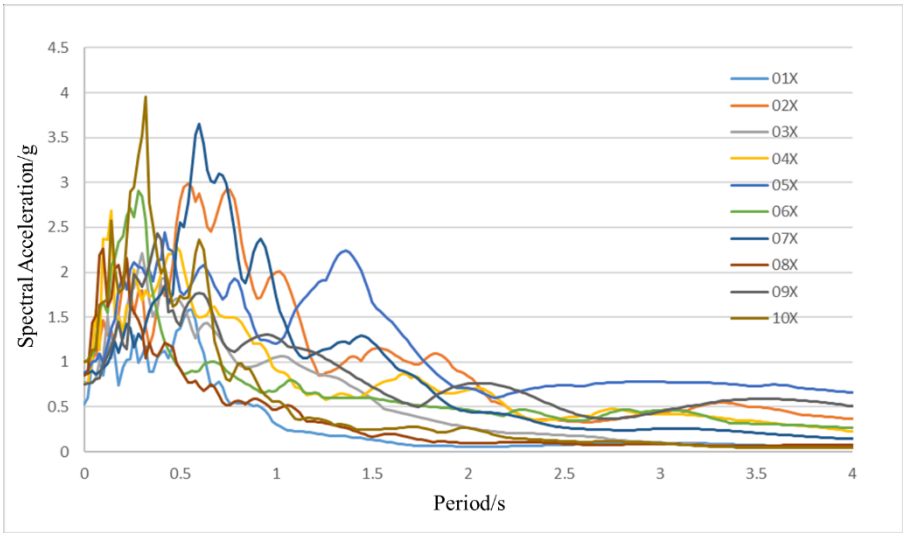


Figure 4: Acceleration spectra of the 10 input ground motions at X direction

Table 2: Damage states

Damage State	Description	Residual lateral dispalcement (mm)
DS0	Intact	(0,10]
DS1	Slight	(10,100]
DS2	Moderate	(100,200]
DS3	Severe	(200,above)

In the numerical simulations, IDA analyses are conducted. The resolution of the PGA increment is 0.1 g. The residual lateral displacement is chosen as the damage state (DS). Four DSs are defined and listed in Table 2. The numerical fragility results are listed in Table 3. In the table, results at different DSs with and without the damping systems are listed,

corresponding fragility curves are plotted in Figure 5.

It can be seen from the results that dampers are effective. The sliding distances are reduced with the use of dampers. As the PGA increases, the effectiveness also increases.

Table 3: Fragility results of the cabinets

PGA/g	Damage probability without dampers			PGA/g	Damage probability with dampers		
	DS1	DS2	DS3		DS1	DS2	DS3
0.1	27.84%	0.00%	0.00%	0.1	20.25%	0.00%	0.00%
0.2	62.54%	0.01%	0.00%	0.2	54.42%	0.00%	0.00%
0.3	80.24%	1.02%	0.28%	0.3	74.63%	0.48%	0.12%
0.4	89.01%	8.87%	2.92%	0.4	85.42%	5.10%	1.42%
0.5	93.56%	27.53%	11.26%	0.5	91.28%	18.53%	6.26%
0.6	96.06%	50.69%	25.56%	0.6	94.59%	38.56%	15.98%
0.7	97.50%	70.42%	42.59%	0.7	96.54%	58.72%	29.44%
0.8	98.36%	83.80%	58.72%	0.8	97.72%	74.64%	44.17%
0.9	98.89%	91.67%	71.89%	0.9	98.46%	85.40%	57.95%
1.0	99.24%	95.89%	81.61%	1.0	98.93%	91.97%	69.55%
1.1	99.46%	98.02%	88.32%	1.1	99.25%	95.72%	78.60%
1.2	99.61%	99.07%	92.74%	1.2	99.46%	97.77%	85.30%
1.3	99.72%	99.56%	95.55%	1.3	99.61%	98.85%	90.06%
1.4	99.79%	99.80%	97.30%	1.4	99.71%	99.41%	93.37%
1.5	99.84%	99.90%	98.37%	1.5	99.78%	99.70%	95.61%
1.6	99.88%	99.96%	99.02%	1.6	99.84%	99.85%	97.11%
1.7	99.91%	99.98%	99.41%	1.7	99.88%	99.92%	98.11%
1.8	99.93%	99.99%	99.65%	1.8	99.90%	99.96%	98.76%
1.9	99.95%	100.00%	99.79%	1.9	99.93%	99.98%	99.19%
2.0	99.96%	100.00%	99.87%	2.0	99.94%	99.99%	99.47%
0.1	27.84%	0.00%	0.00%	0.1	20.25%	0.00%	0.00%
0.2	62.54%	0.01%	0.00%	0.2	54.42%	0.00%	0.00%
0.3	80.24%	1.02%	0.28%	0.3	74.63%	0.48%	0.12%
0.4	89.01%	8.87%	2.92%	0.4	85.42%	5.10%	1.42%
0.5	93.56%	27.53%	11.26%	0.5	91.28%	18.53%	6.26%
0.6	96.06%	50.69%	25.56%	0.6	94.59%	38.56%	15.98%
0.7	97.50%	70.42%	42.59%	0.7	96.54%	58.72%	29.44%
0.8	98.36%	83.80%	58.72%	0.8	97.72%	74.64%	44.17%
0.9	98.89%	91.67%	71.89%	0.9	98.46%	85.40%	57.95%
1.0	99.24%	95.89%	81.61%	1.0	98.93%	91.97%	69.55%
1.1	99.46%	98.02%	88.32%	1.1	99.25%	95.72%	78.60%
1.2	99.61%	99.07%	92.74%	1.2	99.46%	97.77%	85.30%
1.3	99.72%	99.56%	95.55%	1.3	99.61%	98.85%	90.06%
1.4	99.79%	99.80%	97.30%	1.4	99.71%	99.41%	93.37%
1.5	99.84%	99.90%	98.37%	1.5	99.78%	99.70%	95.61%
1.6	99.88%	99.96%	99.02%	1.6	99.84%	99.85%	97.11%
1.7	99.91%	99.98%	99.41%	1.7	99.88%	99.92%	98.11%
1.8	99.93%	99.99%	99.65%	1.8	99.90%	99.96%	98.76%
1.9	99.95%	100.00%	99.79%	1.9	99.93%	99.98%	99.19%
2.0	99.96%	100.00%	99.87%	2.0	99.94%	99.99%	99.47%

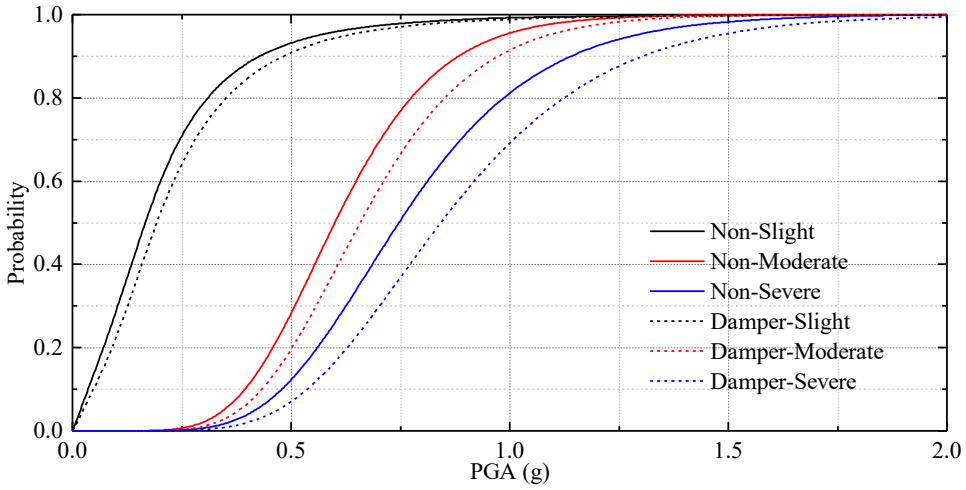
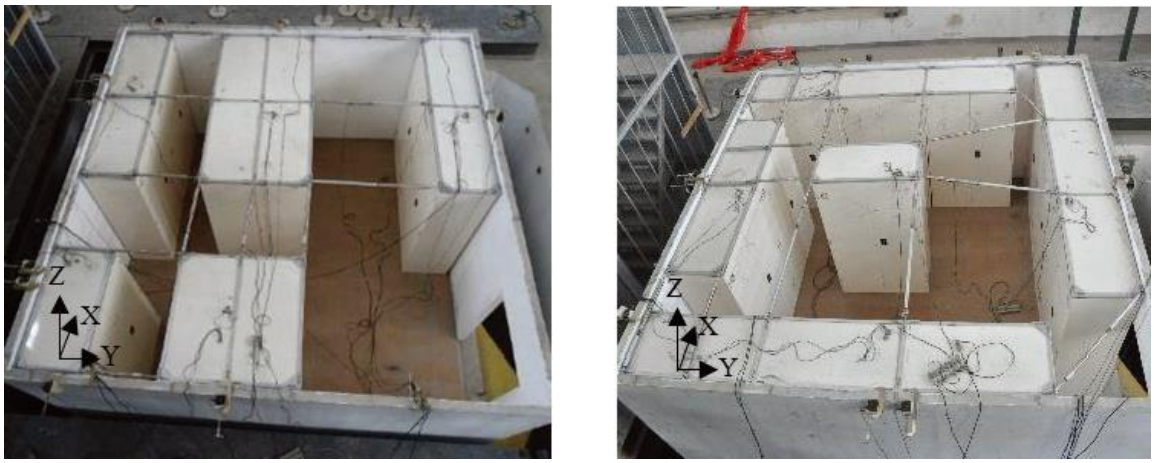


Figure 5: Fragility curves of the cabinets with and without dampers

3 SHAKE TABLE TESTS

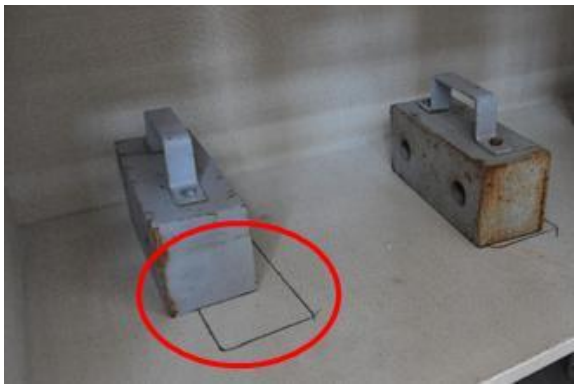
Shake table tests are also conducted to validate the effectiveness of this method. Two types of cabinet layout are tested and shown in Figure 6. Three sets of three-dimensional ground motions at three different PGA levels are input. The PGA at 0.20 g, 0.40 g and 0.62 g are tested [21]. The acceleration amplitude at three directions are set as X: Y: Z= 1.00: 0.85:0.65. Iron blocks are placed in the cabinets to simulate the floating relics. The test phenomenon are presented in Figure 7. The acceleration and relative displacement responses of the cabinets are plotted in Figure 8.

It can be seen from the phenomenon that (1) the sliding distances of the floating brick are smaller with dampers than without dampers. (2) The sliding distances of the cabinets are also smaller with dampers than without dampers. (3) Less cabinet doors opened during earthquake with dampers. Meanwhile, the response histories shows that both acceleration and relative displacements can be reduced. The relative displacement is significantly reduced.



(1) Layout A (2) Layout A

Figure 6: The shake table test layouts



(1) Without dampers, Layout A, PGA 0.20 g



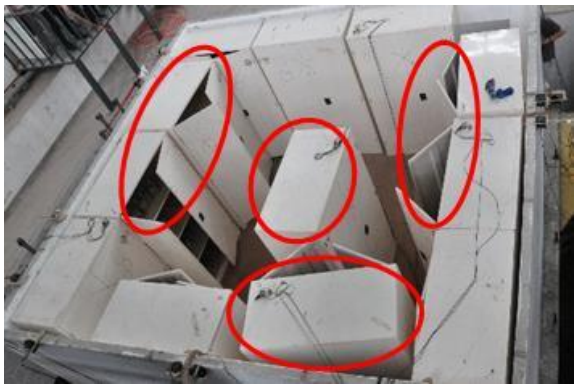
(2) With dampers, Layout A, PGA 0.20 g



(3) Without dampers, Layout A, PGA 0.40 g



(4) With dampers, Layout A, PGA 0.40 g

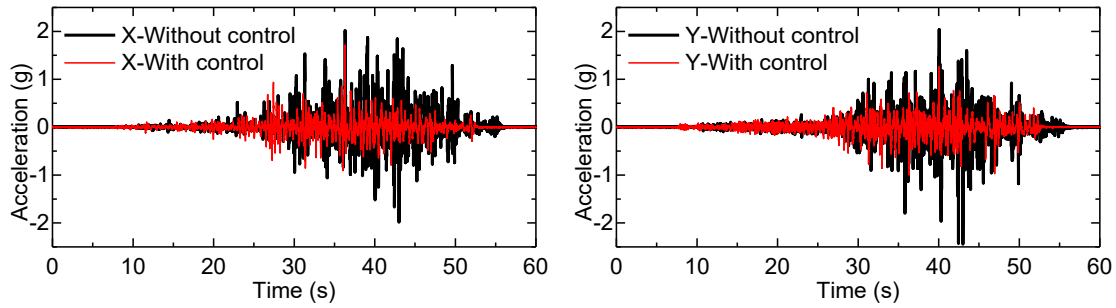


(5) Without dampers, Layout B, PGA 0.62 g



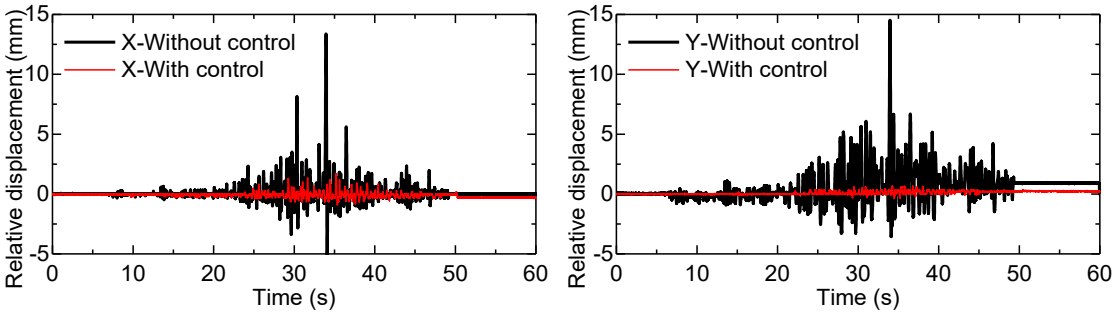
(6) With dampers, Layout B, PGA 0.62 g

Figure 7: Traditional methods used to protect artefacts



(1) X direction (2) Y direction

Figure 8: Acceleration comparison at Layout A, 4# cabinet, PGA=0.62 g under Tangshan earthquake



(1) X direction (2) Y direction

Figure 9: Relative displacement comparison at Layout B, 12# cabinet, PGA=0.20 g under Tangshan earthquake

4 CONCLUSIONS

Floating artefacts, as treasures to the whole society, have not been fully seismically protected. With the increasing awareness of seismic protection, measures are expected to be taken. Considering the potential work amount and the risk of artefact damage during the seismic protection application, a compromise measure is proposed and researched for the cabinet stored relics. The cabinets are connected with dampers to increase the system integrity and damping. The stored relics are not directly touched or moved. Numerical simulation and shake table tests are conducted to validate the effectiveness of this method. Fragility curves of the cabinets are plotted. Results shows that the acceleration responses and lateral sliding distances of the cabinets can be reduced. As the PGA of the input ground motion increases, the effectiveness increases.

Acknowledgements. This work is supported by Earthquake Research Fund of CEA (2019B01, 2019C09), Heilongjiang Provincial Natural Science Foundation of China (LH2019E094), Program for Innovative Research Team in China Earthquake Administration.

REFERENCES

[1] M.-T. Gong, Q. Wei, P.-L. Feng, Z.-J. Zhang, and J. Yang,“Survey on the damaged levels

of the movable cultural relics and buildings during the 5.12 Wenchuan earthquake in Sichuan province," *Sciences of Conservation and Archaeology*, vol. 28, no. 4, pp. 40–47, 2016 (in Chinese).

[2] E. Cosenza, L. Di Sarno, G.Maddaloni, G.Magliulo, C. Petrone, and A. Prota, "Shake table tests for the seismic fragility evaluation of hospital rooms," *Earthquake Engineering & Structural Dynamics*, vol. 44, no. 1, pp. 23–40, 2015.

[3] L. Di Sarno, C. Petrone, G. Magliulo, and G. Manfredi, "Dynamic properties of typical consultation room medical components," *Engineering Structures*, vol. 100, pp. 442–454, 2015.

[4] C. Petrone, L. Di Sarno, G. Magliulo, and E. Cosenza, "Numerical modelling and fragility assessment of typical freestanding building contents," *Bulletin of Earthquake Engineering*, vol. 15, no. 4, pp. 1609–1633, 2017.

[5] C. C. Spyrakos, C. A.Maniatakis, and I.M. Taflampas, "Application of predictive models to assess failure of museum artifacts under seismic loads," *Journal of Cultural Heritage*, vol. 23, pp. 11–21, 2017.

[6] T. Neurohr and G. McClure, "Shake table testing of museum display cases," *Canadian Journal of Civil Engineering*, vol. 35, no. 12, pp. 1353–1364, 2008

[7] Q. Zhou, W. M. Yan, and J. B. Ji, "Experimental study on aseismic behaviors of a free-standing cultural relic supported by traditional methods," *Sciences of Conservation and Archaeology*, vol. 27, no. 2, pp. 63–72, 2015 (in Chinese).

[8] FEMA, FEMA E-74: Reducing the Risks of Nonstructural Earthquake Damage - A Practical Guide, 2012.

[9] D. Konstantinidis and N.Makris, "Experimental and analytical studies on the response of freestanding laboratory equipment to earthquake shaking," *Earthquake Engineering & Structural Dynamics*, vol. 38, no. 6, pp. 827–848, 2009.

[10] C. E. Wittich and T. C. Hutchinson, "Shake table tests of unattached, asymmetric, dual-body systems," *Earthquake Engineering& Structural Dynamics*, vol. 46, no. 9, pp. 1391–1410, 2017.

[11] M. P. Singh and L. M. Moreschi, "Optimal placement of dampers for passive response control," *Earthquake Engineering & Structural Dynamics*, vol. 31, no. 4, pp. 955–976, 2002.

[12] Xiaoqing, Ning , et al. "Seismic Protection of Cabinet Stored Cultural Relics with Silicone Dampers." *Shock and Vibration* 2018(2018):1-15.

[13] L. M. Zhu, Seismic Control and Optimization Design of Large-Span Space Structures with Viscous Dampers, *China Academy of Building Research*, 2007.

[14] Z.-D. Xu, Y.-P. Shen, and H.-T. Zhao, "A synthetic optimization analysis method on structures with viscoelastic dampers," *Soil Dynamics and Earthquake Engineering*, vol. 23, no. 8, pp. 683– 689, 2003.

[15] D. L. Garc´ıa, "A simple method for the design of optimal damper configurations in MDOF structures," *Earthquake Spectra*, vol. 17, no. 3, pp. 387–398, 2001.

[16] K. Yusuke, I. Kazuyuki, and T. Kenzo, "Use of adhesive mats to protect cultural properties from fall down during earthquakes," *Proc of Urban Cultural Heritage Disaster Mitigation*, vol. 2, pp. 85–90, 2008.

[17] B. Myslimaj, S. Gamble, D. Chin-Quee et al., "Base isolation technologies for seismic protection of museum artifacts," Quee, 2003.

[18] I. Cali`o and M.Marletta, “Passive control of the seismic rocking response of art objects,” *Engineering Structures*, vol. 25,no. 8, pp. 1009–1018, 2003.
[19] L. Berto, T. Favaretto, and A. Saetta, “Seismic risk mitigation technique for art objects: Experimental evaluation and numerical modelling of double concave curved surface sliders,” *Bulletin of Earthquake Engineering*, vol. 11, no. 5, pp. 1817–1840, 2013.
[20] J. Podany, “An overview of seismic damage mitigation for museums,” in Proceedings of the International Symposium on Advances of Protection Devices for Museum Exhibits, Beijing, China, 2015.
[21] GB50011-2010, Code for Seismic Design of Buildings, 2010 (in Chinese).

12th International Conference on Structural Analysis of Historical Constructions
SAHC 2020
P. Roca, L. Pelà and C. Molins (Eds.)

SEISMIC PERFORMANCE EVALUATION OF BOX-SHAPED WALL STRUCTURES BUILT WITH THICK EARTHEN WALLS

HAJIME YOKOUCHI[1*], YOSHIMITSU OHASHI[2]

[1] Architecture Course, School of Science and Technology
Kokushikan University
4-28-1, Setagaya, Setagaya-ku, Tokyo, Japan
e-mail: yokouchi@kokushikan.ac.jp, web page: https://kokushikan-arch.net/yokouchi-lab/

[2] Department of Architecture, Faculty of Engineering
Tokyo City University
1-28-1, Tamazutsumi, Setagaya-ku, Tokyo, Japan
e-mail: ohashi-y@tcu.ac.jp

Keywords: Traditional Japanese Structure, Mud Wall, Loading Test, Response Spectrum Method

Abstract. *A "dozo-dukuri" is a type of traditional Japanese building characterized by a box-shaped wall structure built with thick earthen walls. This structure is referred to as the dozo structure in this paper. However, very little information on the seismic performance of dozo structures have been provided in the literature. Therefore, we performed a horizontal loading test on full-scale walls produced based on survey results and specifications of earthen walls around the northern Kanto region to determine the walls' structural performance when receiving a horizontal force (e.g., an earthquake). As a case study, the seismic performance of an existing building was evaluated using the test results. The case study results indicate that if the maximum response deformation angle is equal to that in the calculation result or less, the possibility of a building collapse due to the assumed ground motion is low.*

1 INTRODUCTION

Methods of mixing soil with organic fibers, such as straw, and fixing soil on a substrate knitted with bamboo or wood have been used for construction worldwide [1–7]. Earthen walls have also been used in Japan since a long time ago. A type of traditional Japanese building is the "dozo-dukuri," which is a box-shaped wall structure built with thick earthen walls. The structure is referred to herein as the dozo structure. Figure 1 shows examples of dozo structures, including "misegura," which are dozo townhouses intended to be multiuse shops or dwellings, and storehouses, called "dozo." The northern Kanto region and their surroundings form a distinctive historical townscape because these traditional Japanese buildings built from the end of the Edo Period to the early Showa Period (approximately 70–180 years ago) were constructed in rows and clusters. Dozo structures have earthen walls that are 200–300 mm thick at their outer circumference for protection against fire. Although originally used as warehouses, these structures came to be used as stores, parlors, and other kinds of buildings in modern times.

The traditional townscapes and dozo structures of the Kanto region were seriously damaged in the 2011 Tohoku Region Pacific Offshore earthquake [8,9]. The Kumamoto and Tottori

earthquakes that occurred in 2016 also caused significant damage to the shear walls of the dozo structures, and their restoration is still ongoing. Damage to historical structures not only creates a safety hazard for people in and around them, but also strikes a blow to the vitality of a community. Therefore, their seismic performance must be understood, and measures for damage reduction must be taken. However, there is little information on the seismic performance of dozo structures. Therefore, we must create an evaluation method of the seismic performance of these traditional and existing houses and buildings.

This study performs a horizontal loading test on full-scale walls produced based on the specifications of the earthen walls around the northern Kanto region to determine the walls' structural performance when experiencing horizontal force (e.g., an earthquake). As a case study, the seismic performance of the existing building is then evaluated using the test results.



(a) Misegura (b) Dozo

Figure 1: Examples of dozo structures

2 SPECIFICATIONS OF THE EARTHEN WALLS USED IN DOZO STRUCTURES

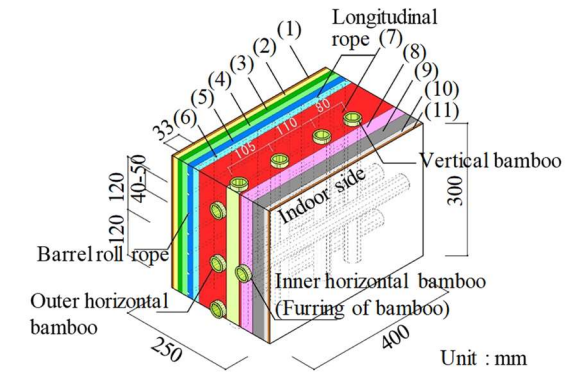
Figure 2 shows a detailed view of the inner earthen wall after the sampling survey. Figure 3 depicts a detailed cross-sectional view around a pillar. Table 1 presents the specifications of the earthen walls around the northern Kanto region observed from the surveys. The following procedure was used to identify the details and processes of the walls. (1) We interviewed skilled technicians (carpenters and plasterers); (2) conduct a field survey to measure features such as the size and placement of the bamboo and penetrating tie beam inside the earthen wall from walls where the mud had peeled off; and (3) cut out the wall of a storehouse to be demolished.

Two types of mud, namely, rough wall mud and intermediate coating mud, were used in the earthen walls. The rough wall mud was clay mixed with straw that was approximately 50 mm long and kneaded with water. The intermediate coating mud was clay mixed with sand and fibrous straw that was approximately 20–30 mm long and kneaded with water.

Traditional Japanese wooden structures feature walls constructed with exposed timber pillars, but in dozo structures, thick earthen walls were used to cover the outside pillar. Therefore, the base layer bamboo was not split, and round bamboo was used. First, an inner horizontal bamboo was hung between the pillars on both sides in a frame, and a vertical bamboo was installed on the outside. An outer horizontal bamboo was placed into a sawblade-shaped bracket cut out of the pillar, such that the weight of the mud was transferred from the outer horizontal bamboo to

the pillars. The bamboo intersections were tightly tied with a straw rope to produce a solid substrate.

In constructing parts of the wall, where the cross-section became smaller due to the timber frame, the rough wall, longitudinal rope, barrel roll, and straw rope were densely arranged to maintain mud integrity. Furthermore, when increasing the wall thickness, rough wall mud was used with intermediate coating mud thinly plastered to reinforce the fixing of the rough wall mud and smoothen the wall surface. Then, the walls were retouched, and the finishing materials were plastered.



(1) Stucco 5 mm
(2) Undercoating 11 mm
(3) Intermediate coating (ICM) 13 mm
(4) Retouch (ICM) 15 mm
(5) Barrel roll and Rope hiding (RWM) 15 mm
(6) Longitudinal rope and Rope hiding (RWM) 15 mm
(7) Rough wall (RWM) 100-110 mm
(8) Backing (RWM) 20-30 mm
(9) Rammed earth 30-50 mm
(10) Undercoating 10 mm
(11) Stucco 5 mm

RWM: Rough wall mud ICM: Intermediate coating mud

Figure 2: Details of the dugout wall interior

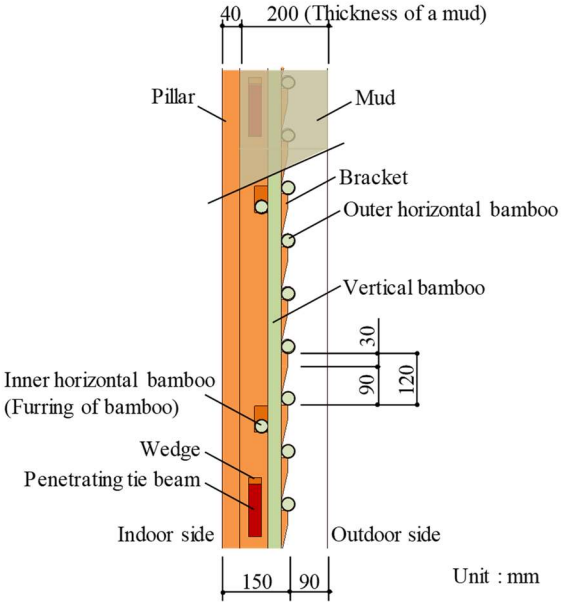


Figure 3: Detailed cross-sectional view

Table 1: Specifications of the earthen walls around the northern Kanto region

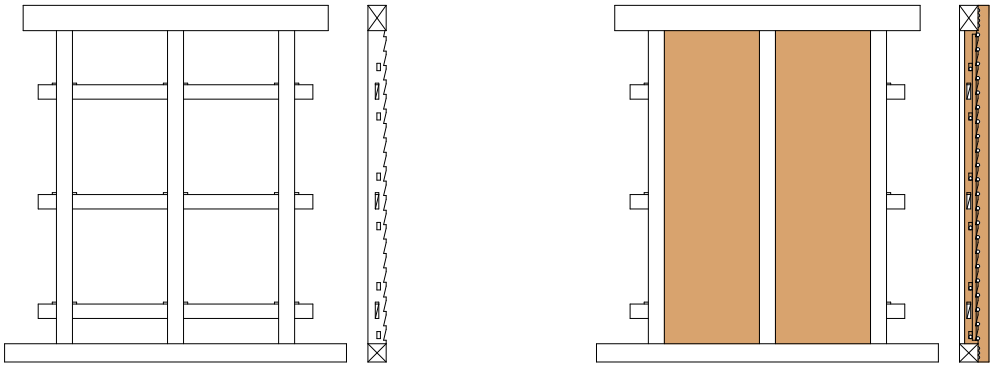
Materials	Specifications	
Penetrating tie beam	Size	Thickness: 30 mm Height: 120 mm
	Pitch	909 mm
Inner horizontal bamboo (Furring of bamboo) Outer horizontal bamboo Vertical bamboo	Size	Diameter: about 25-30 mm
	Shape	Round bamboo
	Pitch	Inner horizontal bamboo: 2 (Between the upper and lower penetrating tie beams) Outer horizontal bamboo: about 100 mm Vertical bamboo: about 120 mm
Mud	Thickness	about 150-250 mm (The wall thickness changes according to the needs of the owner.)

3 STRUCTURAL PERFORMANCE EVALUATION OF THE EARTHEN WALLS

3.1 Specimen overview

This research included the construction and load testing of two specimen types, as described in Figure 4. The Type A specimen, which was of the framework only, was used to confirm the

effect of the penetrating tie beams. Meanwhile, the Type B specimen was used to clarify the strength, deformation performance, and damage state of the original earthen wall of a dozo



(a) Type A (b) Type B

Figure 4: Schematic of the specimens

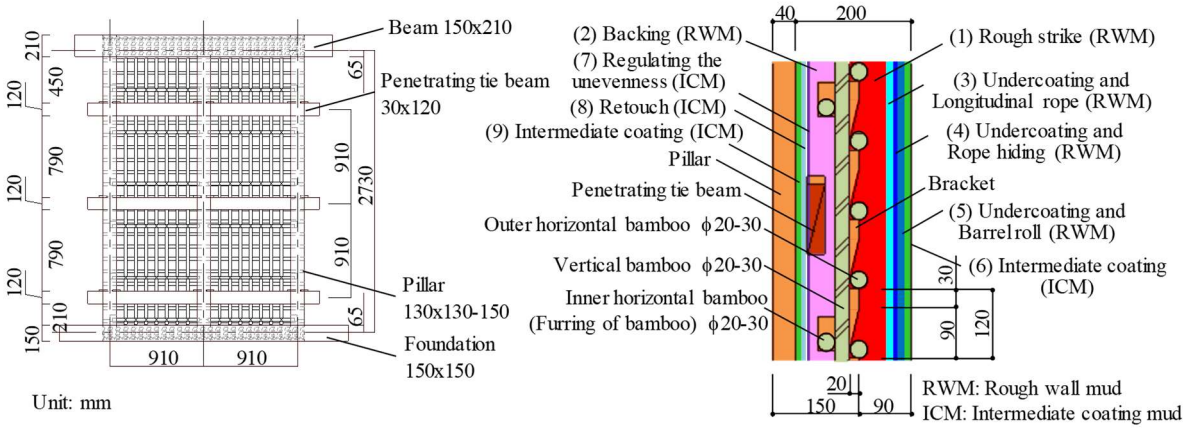


Figure 5: Shapes and dimensions of the Type B specimen

Table 2: Outline of elements and specifications

Elements			Specifications
Type A Type B	Pillar	Material	Japanese cedar
		Size	Width 130mm x Depth 130-150mm (Bracket 20mm)
	Foundation	Material	White cedar
		Size	150mm x 150mm
	Beam	Material	White cedar
		Size	Width 150mm x Depth 210mm
	Penetrating tie beam	Material	Japanese cedar
		Size	Width 30mm x Depth 120mm
	Wedge	Material	White cedar
Type B	Surface protection of penetrating tie beam	Material	Rush (Ryukyu) L=250mm
	Bamboo	Material	Long-jointed bamboo (Madake)
		Size	Diameter: 20-30mm
	Mud wall	Thickness	Plan: 200mm Product: 204mm

structure. The Type B specimen was constructed based on the specifications clarified in the earlier survey, such as including bamboo fitting in the wall, production process, and preparation of the wall mud plaster (i.e., rough wall mud and intermediate coating mud).

Figure 5 shows the shapes and dimensions of the Type B specimen. Table 2 presents the materials and specifications used. The specimen shapes and dimensions and the materials used were basically the same (i.e., width: two 910 mm spans and height: 2730 mm). The joint between the pillar and the horizontal frame was shaped such that the pillar end did not touch the horizontal frame, even in the case of a significant deformation. By doing so, we ignored the resistance caused by the pillar sinking into the horizontal frame; hence, we could observe only the wall panel performance.

Table 3 lists the composition of the rough wall mud and the intermediate coating mud used in the test specimens. Figure 6 illustrates the compression strength tests for the two types of mud performed according to the method developed by the Japanese Housing and Wood Technology Center [10]. Table 4 presents the compression strength test results. Figure 7 shows the stress–strain curves with an average of six samples.

Table 3: Mud type and preparation

Rough wall mud	About 60-70 kg of straw per cubic meter of cray
Intermediate coating mud	Cray: 10kg, sand: 15kg, Fibrous straw: 300g, Water: 7-8L

Table 4: Compression strength test results of the mud

Sample	Thickness [mm]	Number of samples	Age [day]	Maximum compression strength [N/mm^2]			Density [g/cm^3]
				Min.	Max.	Average	
Rough wall mud	70	6	43	0.371	0.391	0.378	1.30
Intermediate coating mud	70	6	41	0.700	0.801	0.758	1.62



Figure 6: Situation of the material tests

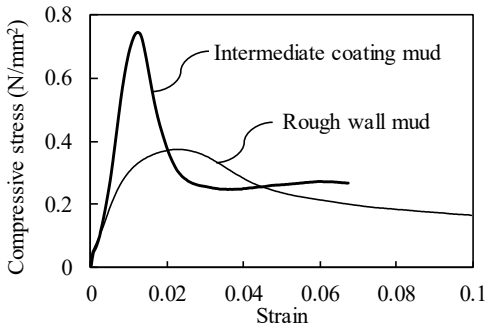


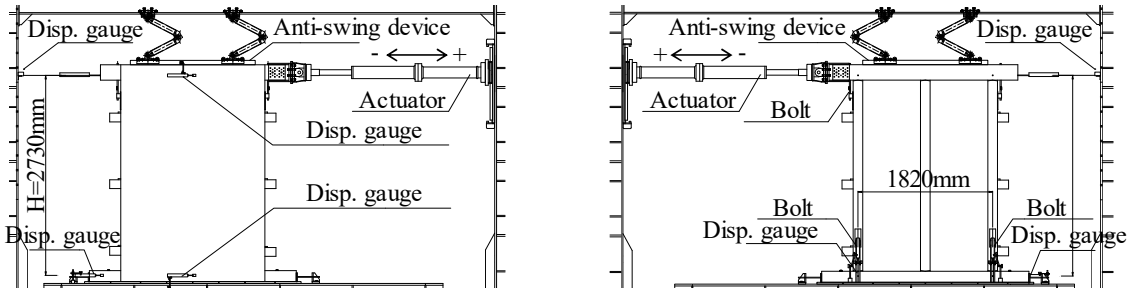
Figure 7: Stress–strain curves with an average of six samples

3.2 Load-measuring method

Measurement and loading were performed using the method in Figure 8. Positive and negative alternating loading by displacement control was performed. The loading schedule of gradually increasing the shear deformation angle to 1/600 rad, 1/450 rad, 1/300 rad, 1/200 rad, 1/150 rad, 1/100 rad, 1/75 rad, 1/60 rad, 1/50 rad, 1/40 rad, and 1/30 rad in three cycles was

followed by one cycle of 1/20 rad loading. Finally, we applied loading (deformation angle: approximately 1/7 rad) to pull up to the allowable jack stroke.

The measurement items common to all the specimens were horizontal load, horizontal displacement of the beam and foundation, lifting displacement of pillar bases, and axial strain of the pillar top/base fixing bolts. In the Type B specimen, we regarded the crack occurrence and the main crack width when each controlled deformation was reached.



(a) Outdoor side (b) Indoor side

Figure 8: Methods of measurement and loading

3.3 Test results

Figure 9 displays the relationship between the horizontal load and the shear deformation angle of the type A and B specimens as obtained from the loading tests. The strength of the Type A wall was significantly less than that of the Type B specimen. However, as the deformation increased, the proof strength, which continued to increase with the deformation, was confirmed even if the deformation reached 1/7 rad or more because the resistance caused by the penetrating tie beams sinking into the pillars became larger. The maximum proof strength of the Type B specimen was 37.1 kN. The deformation angle at that time was 1/30 rad.

Figure 10 shows the skeleton curves during the positive loading of the type A and B specimens and the restoring force of only the mud wall panel subtracting the Type A specimen from Type B at the same deformation. After the maximum proof strength was obtained, the resistance strength of the mud wall panel decreased; however, with Type A, the resistance strength of the penetrating tie beams increased with the horizontal deformation. We confirmed

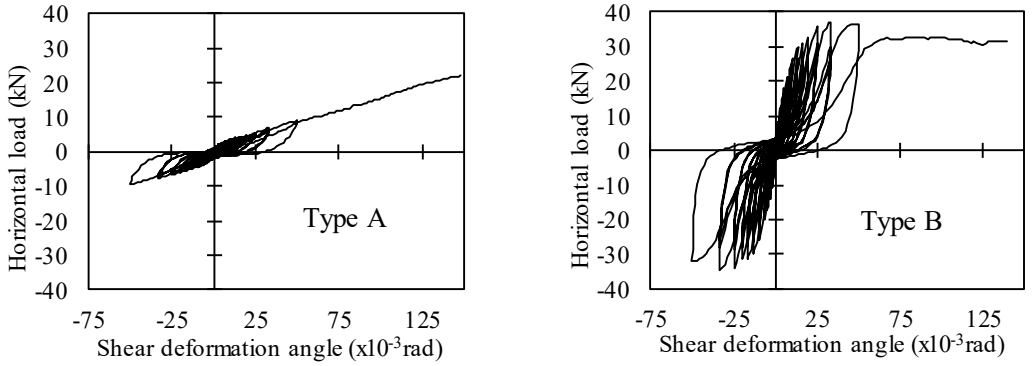


Figure 9: Relationship between the horizontal load and the shear deformation angle

the toughness of the thick earthen walls by maintaining a proof strength of 84% or higher of the maximum up to the final deformation by balancing the mud wall panel resistance and the penetrating tie beam resistance.

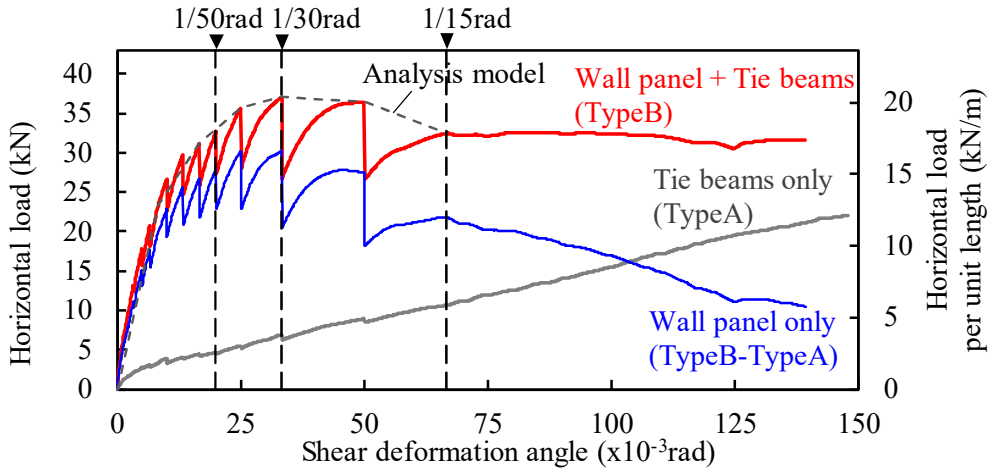


Figure 10: Skeleton curve comparison during positive loading

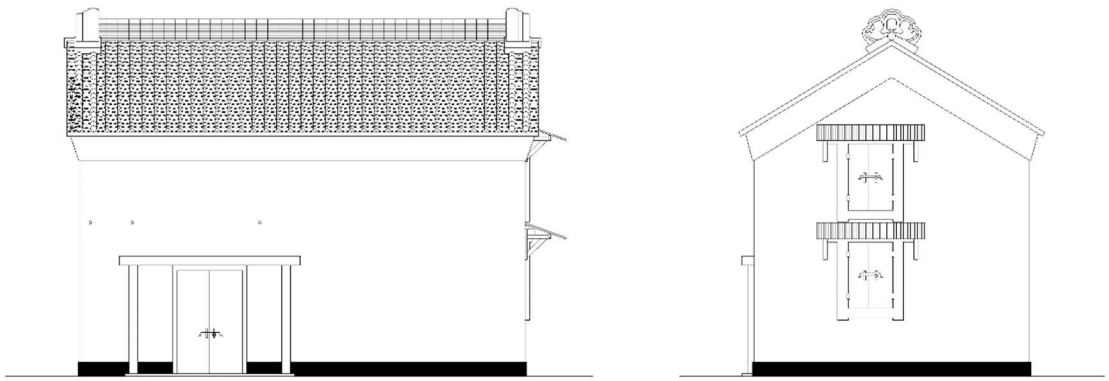
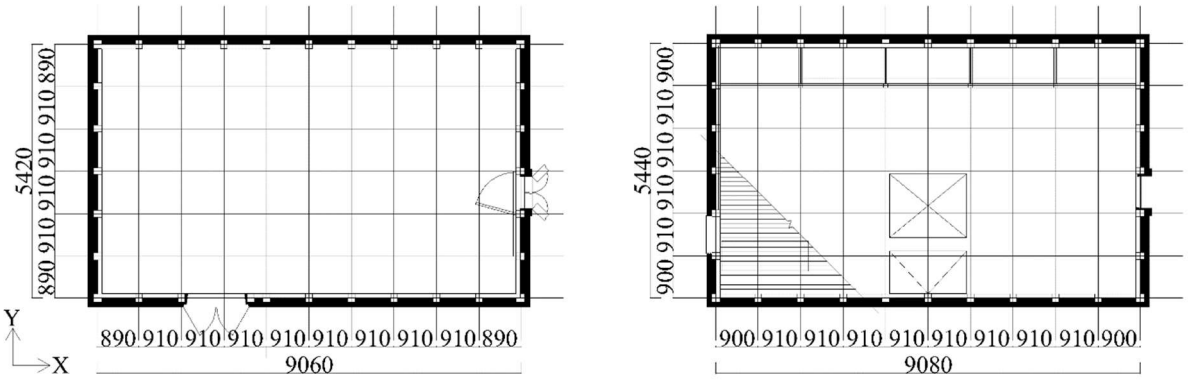


Figure 11: Elevation view of the target building



(a) 1st floor (b) 2nd floor

Figure 12: Plan view of the target building

4 CASE STUDY ON THE SEISMIC PERFORMANCE OF THE EXISTING BUILDING

4.1 Target building overview

The building is a two-story dozo structure located in a city in Tochigi Prefecture. It has 10 spans in the X direction and six spans in the Y direction and was constructed more than 150 years ago. Figures 11–12 show the elevation and plan views of the building used as a case study model, respectively. The building weight was evaluated using the weight per unit area shown in Table 5. The weight of the first story is 279.1 kN, while that of the second story is 167.2 kN.

Table 5: Weight per unit area for the building weight evaluation

Elements		Weight per unit area	
Roof	Tile-roofing	Per roof area	600N/m^2
	Roof truss		250N/m^2
Outer wall	Earthen wall	Per wall area	3204N/m^2
	Framework		150N/m^2
	Weather-board		100N/m^2
2nd floor	Cross member	Per floor area	170N/m^2
	Floor board		150N/m^2
2nd floor fittings		Per elevation surface	200N/m^2
Live load	(Evaluation only on the second floor)	Per floor area	600N/m^2

4.2 Evaluation method of the seismic performance

We verified the seismic performance against extremely rare earthquakes (large earthquakes) of the Japanese seismic design standard by calculating the response and the limit strength. the evaluation of seismic performance by calculating the limit strength was performed following the manual of the Japan Structural Consultants Association as a reference [11].

The acceleration response spectrum used for the seismic evaluation is a spectrum for an extremely rare earthquake defined in the Japanese seismic design standard. Here, the ground surface amplification was evaluated according to the simplified method of the Japanese seismic

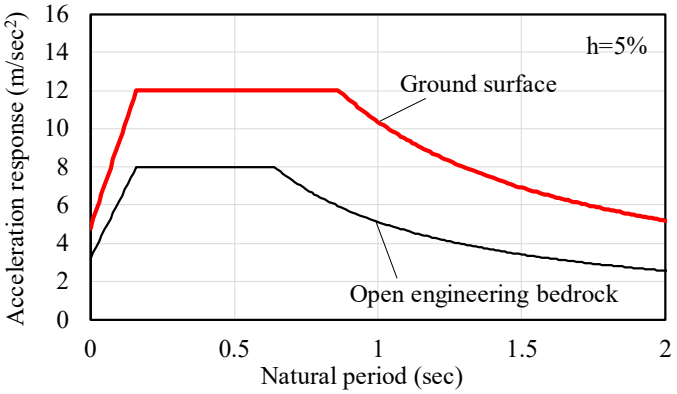
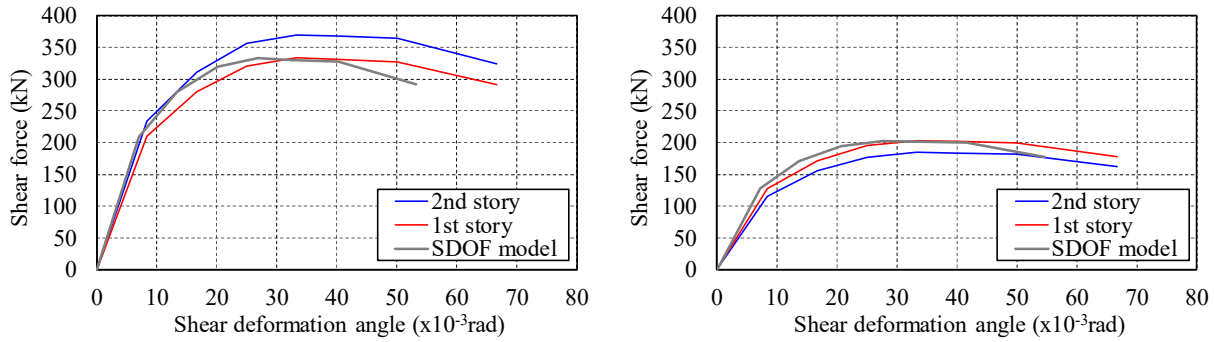


Figure 13: Acceleration response spectra (h = 5%)

design standard. Figure 13 shows the acceleration response spectra (h = 5%) at the open engineering bedrock and the ground surface amplification.

All the horizontal strength resistance elements must be added to accurately evaluate the restoring strength characteristics of a building. Examples of the horizontal strength resistance element of the target building included the earthen and hanging walls and bearing of penetrating beam and timber connection, among others. However, the contribution of the strength of the full surface earthen walls arranged to surround the outer periphery of the building was very dominant; hence, the restoring strength characteristic of the building was simply evaluated herein considering only the full surface walls. Figure 10 shows the skeleton curve used for the calculation in comparison with the horizontal loading test results. The restoring strength characteristic of the target building was evaluated by multiplying the horizontal strength per unit length, which was calculated by dividing the horizontal strength of the test result by the specimen width of 1.82 m, by the wall length for each floor and direction. Figure 14 illustrates the restoring strength characteristics of each story and the equivalent single degree of freedom (SDOF) model in each direction. The base shear coefficients at the maximum proof strength were 0.75 and 0.46 in the X and Y directions, respectively.



(a) X direction (b) Y direction

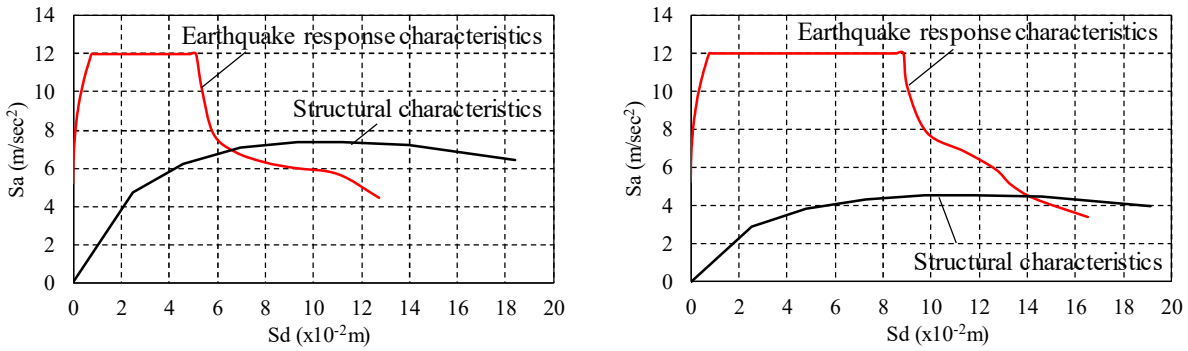
Figure 14: Restoring force characteristics

4.2 Seismic performance evaluation results

Figure 15 shows the structural characteristic curves (Sa–Sd spectra) of the SDOF model. Table 6 presents the maximum response deformation angle and the base shear coefficient at that deformation. The maximum response deformation angles of the first story (i.e., 1/42 rad in the X direction) were larger than those of the second story (i.e., 1/21 rad in the Y direction) in each direction. The base shear coefficients at that deformation were 0.71 and 0.45 in the X and Y directions, respectively.

Traditional timber frame structures in Japan can often be judged to have sufficient deformation capacity up to the story deformation angle of approximately 1/15 rad. In addition, the earthen wall performance confirmed in the test was observed at a certain strength level even at a large deformation of 1/15 rad or more without brittle fracture. Furthermore, the planar shape of the target building was rectangular, and the torsional vibration influence was small. Considering these things, if the maximum response deformation angle is similar to that in the

calculation results or less, then the possibility of a building collapse due to the assumed ground motion is low. However, the response deformation exceeds the maximum proof strength, and seismic reinforcement is deemed desirable for controlling the response deformation when emphasizing restorability and continuity of use.



(a) X direction (b) Y direction

Figure 15: Structural characteristic curves (Sa–Sd spectra) of the SDOF model

Table 6: Maximum response deformation angle

		X-dir.	Y-dir.
Maximum response deformation angle (rad)	2nd story	1/187	1/55
	1st story	1/42	1/21
Base shear coefficient at the maximum response deformation		0.71	0.45

5 CONCLUSIONS

The following conclusions are drawn from this study:

- We performed a horizontal loading test on full-scale walls produced based on the survey results and the specifications of the earthen walls around the northern Kanto region to determine the walls' structural performance when receiving a horizontal force, such as an earthquake. The maximum proof strength of an earthen wall was 37.1 KN. The deformation angle at that time was 1/30 rad. We confirmed the toughness of the thick earthen walls through maintaining a proof strength of 84% or higher of the maximum up to the final deformation by balancing the mud wall panel resistance and the penetrating tie beams resistance.
- We conducted a case study on the seismic performance of the existing building using full-scale wall test results. The maximum response deformation angles of the first story (i.e., 1/42 rad in the X direction) were larger than those of the second story (i.e., 1/21 rad in the Y direction) in each direction. According to the case study results, if the maximum response deformation angle is similar to that in the calculation result or less, then the possibility of a building collapse due to the assumed ground motion is low.
- Methods of mixing soil with organic fibers (e.g., straw) and fixing soil on a substrate knitted with bamboo or wood similar to a Japanese dozo structure are used for

construction worldwide. This study will be useful not only for Japanese dozo structures, but also for the seismic evaluation of similar buildings outside Japan.

REFERENCES

[1] E. Fodde. *Traditional earthen building techniques in Central Asia.* International Journal of Architectural Heritage, Vol. 3:2, (2009), pp. 145–168.

[2] Natalie Quinn, Dina D'Ayala & Thierry Descamps. *Structural characterization and numerical modeling of historic quincha walls*. International Journal of Architectural Heritage, Vol. 10:2–3, (2016), pp. 300–331.

[3] M. Blondet, J. Vargas-Neumann, N. Tarque, J. Soto, C. Sosa & J. Sarmiento. *Seismic protection of earthen vernacular and historical constructions.* Proceedings of the 10th International Conference on Structural Analysis of Historical Constructions, Leuven, Belgium, (2016), pp. 3–14.

[4] M. Maheri, A. Maheri, S. Pourfallah, R. Azarm & A. Hadjipour. *Improving the durability of straw-reinforced clay plaster cladding for earthen buildings*. International Journal of Architectural Heritage, Vol. 5:3, (2011), pp. 349–366.

[5] Q. Ali, N. Ahmad, M. Ashraf, M. Rashid & T. Schacher. *Shake table tests on single-story Dhajji Dewari traditional buildings*. International Journal of Architectural Heritage, Vol.11:7, (2017), pp. 1046–1059.

[6] C. Kawashima. *Design of private houses, Overseas version (in Japanese)*. Suiyosha Publishing Inc. (2016), pp. 67–96.

[7] K. Ohta. *Wooden building in Eastern Europe (in Japanese)*. Sagami-Syobo (1988), pp. 39–48.

[8] H. Yokouchi, Y. Ohashi. *Earthquake resistance evaluations and seismic damage assessment of Japanese traditional building in Tochigi*. Proceedings of the 15th World Conference on Earthquake Engineering, Lisbon, Portugal, (2012), No. 1272.

[9] Joint Editorial Committee for the Report on the Great East Japan Earthquake Disaster. *Report on the Great East Japan Earthquake Disaster (in Japanese)*. Building Series Volume 4, Damage of Historic Buildings, Architectural Institute of Japan (2015).

[10] National Institute for Land and Infrastructure Management. *Technical manual on the shear wall factor of mud wall, surface lattice wall and inserted wooden siding wall (in Japanese)*. Japanese Housing and Wood Technology Center (2004), pp. 144–147.

[11] Kansai Office of Japan Structural Consultants Association. *Seismic performance evaluation and seismic retrofitting manual for wooden house and building mainly using traditional timber frame construction (in Japanese)*, Second Edition (2014).

12th International Conference on Structural Analysis of Historical Constructions
SAHC 2020
P. Roca, L. Pelà and C. Molins (Eds.)

SEISMIC PERFORMANCE OF MASONRY CROSS VAULTS THROUGH SHAKING TABLE TESTING ON A SCALED MODEL

N.BIANCHINI[1*], N. MENDES[1], P. CANDEIAS[2], M. ROSSI[3] , C. CALDERINI[3], P.B. LOURENÇO[1] AND A. CAMPOS COSTA[2]

[1] Institute for Sustainability and Innovation in Structural Engineering (ISISE)
University of Minho
Department of Civil Engineering, Campus de Azurém, 4800-058 Guimarães, Portugal
e-mail: nicoletta.bianchini@gmail.com, {nunomendes, pbl}@civil.uminho.pt; webpage: www.isise.net (*corresponding author)

[2] National Laboratory for Civil Engineering (LNEC) Department of Structures,
Avenida do Brasil, 101, 1700-066, Lisbon, Portugal
e-mail: : pcandeias@lnec.pt; webpage: http://www.lnec.pt

[3] Department of Civil, Chemical and Environmental Engineering (DICCA)
University of Genoa
Via Montallegro 1, 16145 Genoa, Italy
email: {chiara.calderini, michela.rossi}@dicca.unige.it - web page: www.dicca.unige.it

Keywords: Masonry cross vault, Shake table tests, Shear failure, Seismic motions

Abstract. *Masonry cross vaults are among the most widely used typologies of horizontal structural elements for covering spaces of both ordinary and monumental buildings in the European countries. Their seismic vulnerability has been proved by systematic damages and collapses surveyed throughout the centuries. Therefore, the assessment of their structural safety is a crucial issue for the conservation and preservation of historical buildings. Although various methods have been developed and used to analyse both the stability (e.g. equilibrium method) and the dynamic behaviour (e.g. finite and discrete element approaches) of vaulted structures, experimental studies are constantly needed to validate and calibrate models. In this regard, limited experimental studies to understand the dynamic response of vaults have been done. The present paper describes the results of shake table tests on a 1:5 scaled cross vault model made of 3D printed blocks assembled with dry joints, carried out at the 3D LNEC shake table (Portugal). The main aim of the tests is to investigate one of the most typical seismic damage for cross vaults: the shear failure. This type of mechanism frequently affects vaults of lateral aisles and it is mainly caused by a significant difference in stiffness of vaults' supports. Indeed, the lower stiffness of the central nave colonnade compared to the external wall may induce an in-plane shear distortion of the vault caused by a differential longitudinal displacement of its opposite sides. Incremental seismic motions are conducted up to collapse using Emilia Romagna earthquake. The results are analysed in terms crack pattern and damage mechanisms.*

1. INTRODUCTION

Masonry vaults represent one of the most widespread horizontal structural elements in historical buildings. Systematic post-earthquake damage surveys in churches and historical constructions have proved the vulnerability of vaults towards dynamic actions. Although understanding the 3D seismic behaviour of vaults is of primary importance for preserving the cultural heritage, the research in this field is still limited. Most of the works in literature were focused on the 2D analysis of vaults modelled as a sequence of arches, under both static and dynamic actions. Few researchers analysed the 3D behaviour of vaults by simulating seismic actions as differential displacements applied to supports using both numerical and experimental approaches [1]–[3]. The main aim of this paper is to investigate the seismic behaviour of a groin vault with asymmetric boundary conditions, a typical configuration found for example in vaults covering the lateral aisles of the churches or the loggias and porches of palaces [4][5]. During seismic events, especially when the action is mainly acting along the longitudinal direction, the lower stiffness of the central nave's colonnade, compared to the external walls, can lead to differential displacements along the longitudinal direction and, consequently, to the development of a shear damage mechanism in the horizontal structural elements (Figure 1). This failure is mainly identified by typical diagonal crack occurrence, as shown in Figure 1(a) that is recurrently observed during post-earthquake surveys. This is due to the lower stiffness of the central nave's colonnade compared to the external walls can lead to differential displacements along the longitudinal direction and, consequently, the development of a shear mechanism in the horizontal structural elements [6]. This paper describes the experimental campaign on 1:5 scale model of a groin vault tested on the shake table at the LNEC (National Laboratory for Civil Engineering, Lisbon, Portugal) within SERA-(Seismology and Earthquake Engineering Research Infrastructure Alliance for Europe) Transnational Access Project. The mock-up's geometry and boundary conditions can be representative of a central bay located in the lateral nave of a three-nave church (in grey in Figure 1(a) and (b)).

The shake table tests' results are compared with the results of the quasi-static tests carried out by Rossi *et al*. [6], where the in-plane shear response of the small-scale model was investigated by applying differential displacements on the abutments (Figure 1(b)).

During the shake table tests, the response of the mock-ups was evaluated as function of an increasing intensity earthquake testing protocol, in which a pre-processed strong ground motion component of the *Mirandola* station (MRN) was used, recorded on May 29, 2012 (Emilia Romagna earthquake).

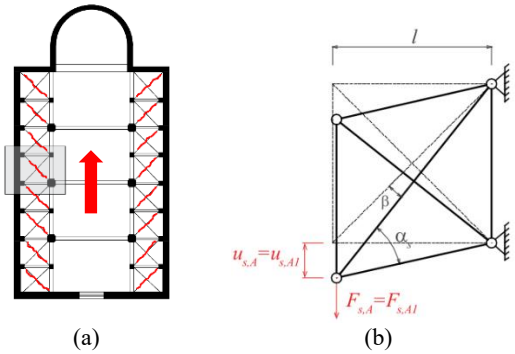


Figure 1. (a) Typical crack pattern of lateral naves vaults due to the shear mechanism caused by the longitudinal seismic action (red arrow) [7]; (b) simple shear setting studied in [7] and [4].

2. EXPERIMENTAL TESTS

2.1 Physical model: geometry of the specimen and material

The tests were performed on a 1:5 scale model made by 3D printed plastic blocks with dry joints. The same mock-up was already tested under static condition by Rossi *et al*. [6]. The blocks were 3D printed with the SLS (Selective Laser Sintering) technology: an efficient method to generate small-scale models with high geometrical accuracy (0.1 mm), low cost and short time of production. Moreover, it allows for the production of blocks with high stiffness (to take into account rigid block assumption and to guarantee the repeatability of the tests by minimizing the damage due to impacts) and high friction (to inhibit sliding between blocks).

The shape and the geometry of the scaled model derived from the intersection of two semi-circular barrel vaults, generating a squared base groin vault with a net span of 0.620 m and a rise of 0.225 m. The model is made up of 1132 blocks (Figure 2a). The standard blocks (red blocks in Figure 2a) were designed considering the typical dimensions of clay bricks, which are $0.06 \times 0.12 \times 0.24$ m^3 in order to keep a classic bond stereotomy of medieval groin vaults. Blocks of other different dimensions are placed along the outer edges of the webs to guarantee the offset of the joints. Blocks shape is slightly trapezoidal in order to compensate for the absence of mortar between them. Special care was taken to design the stereotomy of the elements located along the diagonals (Figure 2b) to guarantee the correct interlocking between adjacent webs. Each block was identified by a numeric code, in order to easily rebuild the model after each test.

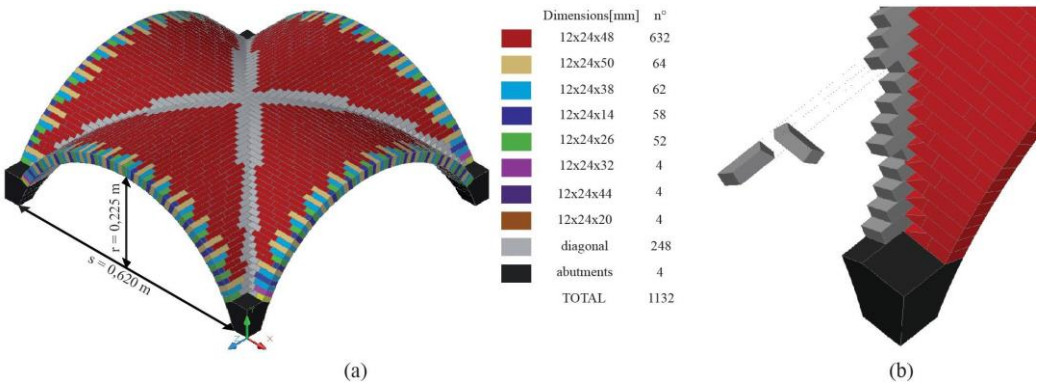


Figure 2. Geometry of the small-scale vault and blocks (a); stereotomy of the diagonal blocks (b). [6]

Regarding the stereotomy of masonry brick vaults, the arrangement of the bricks can be varied, as described in Figure 3 [8]. The selected arrangement corresponds to the easiest one to be assembled [4] (Figure 3e). This configuration is called “orthogonal weaving”. It directly transfers the thrusts to the supports and it is characteristics of medium and large vaults. However, it needs a temporary timber structure to build the shell of the vault. Therefore, in order to build the model, a temporary supporting structure (scaffolding), made of plywood, has been designed. It consists of four pieces corresponding to the vault webs. Once the model is built, the scaffolding is removed by let the pieces sliding on proper inclined rails, as illustrated in Figure 4.

The vault's abutments can move freely on a flat surface thanks to four steel plates equipped with some spherical wheels at their extrados. As an alternative, the plate can be anchored to the flat surface by using bolts. The plates are linked to each other by aluminium rods hinged at both ends with uniball joints.

The material density $\rho = 0.55 \pm 0.02$ g/cm^3 and the friction angle $\mu = 39 \pm 2.46°$ of the blocks have been determined by testing 12 samples. Since the quite low density of the material could compromise the model stability under accidental actions, the weight of blocks was increased by inserting a steel plate within each of block (Figure 5). The final weight of the whole structure is about 43 kg.

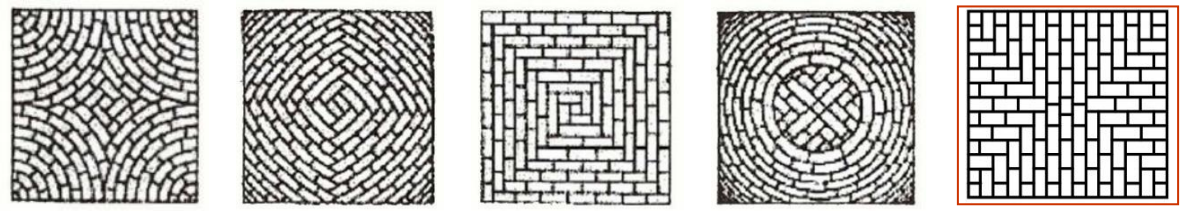


Figure 3. Most common arrangements for masonry cross vaults [8].

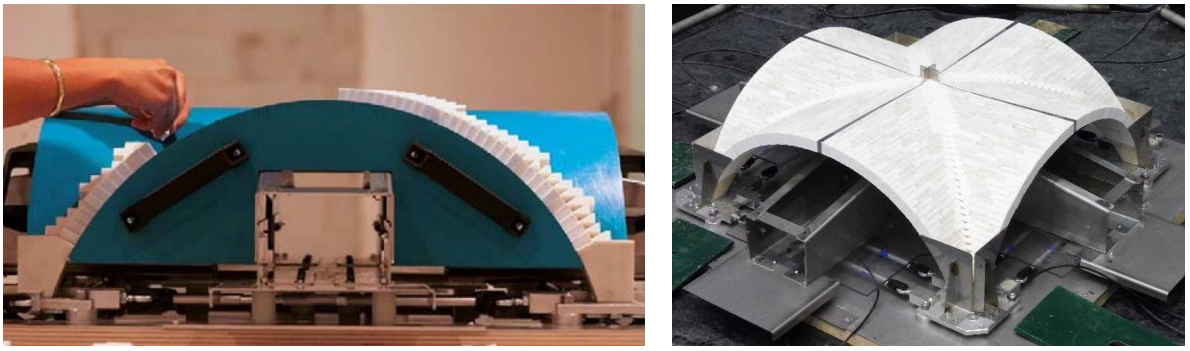


Figure 4. (a) Details of the construction on the plywood scaffolding and (b) the end of the construction [6].

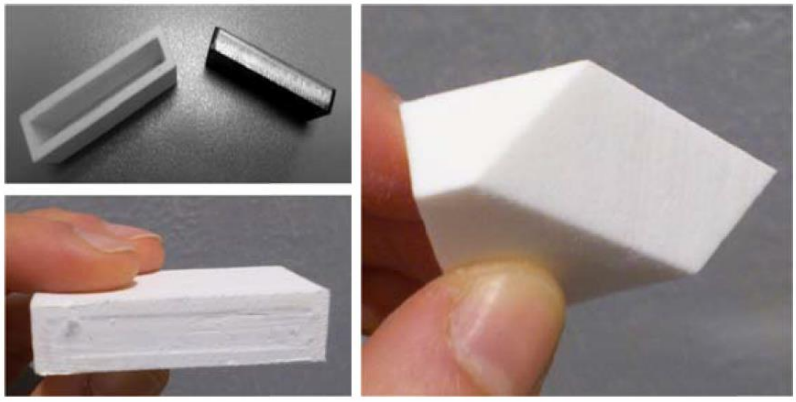
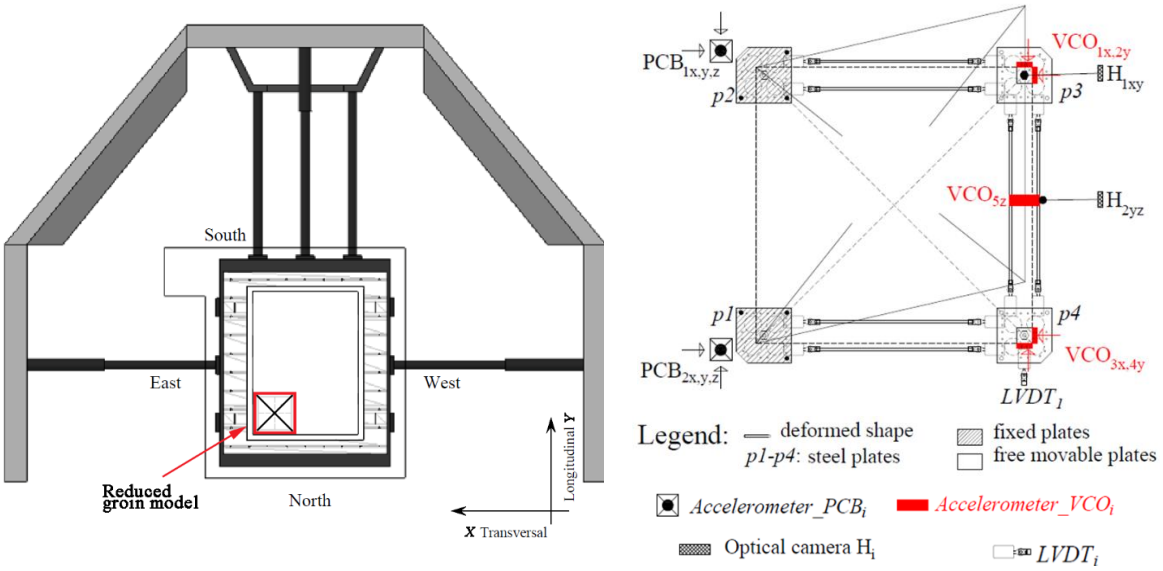


Figure 5. Details of the blocks and of the elements of the diagonals.

2.2 Shake table test setup

The tests were performed at the National laboratory of Civil Engineering in Lisbon (LNEC), which owns a large-scale experimental facility for seismic testing of structures, namely a three axial shake table (Figure 6a). The setup was carefully designed in order to get the most important outputs derived from the induced shear failure on the mock-up, with similar conditions to the real prototypes and measure the relevant effects, which are necessary for the performance assessment (Figure 6b). The abutments *p1* and *p2* were anchored to the ground with bolts, while *p3* and *p4* were let free to move on the flat surface.



(a) (b)

Figure 6. Shaking table: (a) plan with the location of the model in red; (b) Instrumentation setup: Top view.

The instrumentation of the small-scale groin vault was defined according to the expected behaviour of this kind of mock-up under seismic actions. Therefore, the bases, the movable plates and the lateral arch (west side) are of interest. Due to the reduced geometrical dimensions of the model, specific equipment was implemented, as referred in Figure 6. One linear variable displacement transducer ($LDVT_1$), located at the N-W corner, measuring the relative longitudinal displacement of the movable piers. Six piezoelectric accelerometers (named PCB_{1x}, PCB_{1y}, PCB_{1z}, PCB_{2x}, PCB_{2y}, PCB_{2z} in Figure 6b) were placed at the bottom of the vault to evaluate the response of the fixed plated, while five variable capacitance unidirectional accelerometers (VCO_{1x}, VCO_{2y}, VCO_{3x}, VCO_{4y}, VCO_{5z}) were placed on the vault itself, mainly due to the fact that their dimensions and weight are compatible with the dimension of the blocks. Moreover, two optical cameras were used to record the response of the key of the western arch and of the movable piers respectively along the plane *xy* (H_{1xy}) and *yz* (H_{2yz}).

Two video cameras were placed to record the tests, one exactly at the top of the model using the scaffolding pipes and one located in front of the East façade on a tripod outside of the shake table. From those cameras, the collapse mechanism was evaluated (Section 3).

2.3 Dynamic identification tests

Dynamic identification tests are useful to depict the modal properties of the structure. Dynamic identification techniques can be divided in three main groups: (a) input/output vibration tests, where the excitation applied on the structure and the vibration response are measured; (b) output only vibration tests, where only the vibration response is measured during the service conditions of the structure; (c) free vibration tests, where the structure is forced to an initial deformation and is then quickly released [9]. In this work, only input/output vibration tests were performed.

In the dynamic identification tests, a "pink noise" signal, with large frequency range and low amplitude, was used, aiming at determining the modal parameters for the undamaged and damaged configurations. The duration of this signal is 165 s, with an intense phase of about 60 s. The amplitudes of the inputs were increased, aiming at evaluating the influence of the amplitude of the signal on the dynamic properties. The amplitude of the signals is here defined in terms of nominal displacement. From Figure 7 it is possible to notice that the frequencies range from 3.22 Hz to 4.5 Hz for a variation of the amplitude of the signal between 8 mm and 3 mm, respectively. As expected, the increase of the signal amplitude (nominal displacement) causes a decrease in the frequency of the mock-up. Furthermore, the dynamic identification tests carried out in different days and after different rebuilds of the mock-up present similar frequencies for the same signal amplitude (5 mm), leading to the conclusion that the mock-up keeps constant the modal frequencies, despite different construction processes or conditions. Therefore, its replicability is a powerful tool that assure consistency in the interpretation of the results.

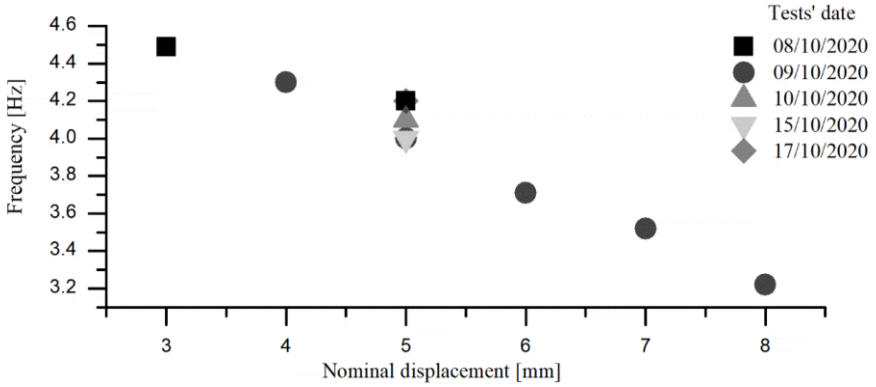


Figure 7. Frequencies as function of the amplitude of signal of the dynamic identification tests.

2.4 Seismic tests: Emilia earthquake (Mirandola station)

The Emilia's earthquake was selected for the seismic action, mainly due to the significant presence of masonry groin vaults in the Emilia's Region. In the post-earthquake survey occurred in this region, several cases of shear failures on churches and palaces were observed. Mirandola seismic station (MRN), located 4 km far from the epicentre, was adopted. It recorded a macro seismic intensity of 7-8 EMS and PGA between 0.27-0.30 g in the North-South direction (recorded during the main shocks; May 20th and May 29th, 2012) (Figure 8) [10]. The seismic ground motion, whose entire duration is equal to 30 s, was cut in its intense phase and then filtered, including a baseline correction.

Figure 8 presents the peak ground-motion parameters, namely the PGA, the peak ground velocity (PGV) and the peak ground displacement (PGD), for each component recorded at the MRN station.

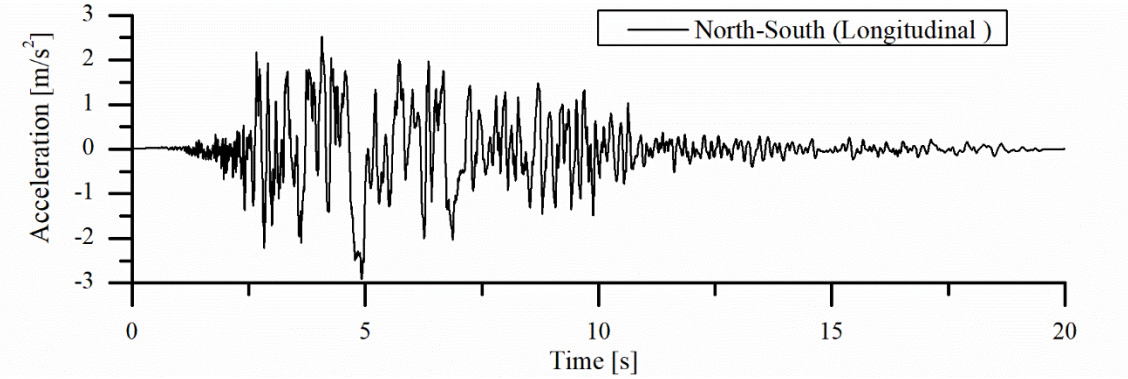


Figure 8. Acceleration time history recorded by Mirandola seismic station along the longitudinal (May 29th).

Table 1: Peak ground-motion parameters for each component recorded at the MRN station (May 29th) [11].

	PGA [m/s²]	PGV[m/s]	PGD [m]
East-West (Transversal)	0.224	0.300	0.081
North-South (Longitudinal)	**0.295**	**0.463**	**0.105**
Vertical	0.900	0.059	0.018

In the shake table tests, the proper scale factor for the input signals was considered. Thus, the total duration of 20 s was reduced using a factor equal to the square root of 5, resulting in total duration of about 9 s.

Table 2 lists the sequence of shake table tests performed on the mock-up with the modal frequency obtained from input/output dynamic identification tests (DIT), performed before and after every percentage of seismic motion and a brief description of the damage. Here, the signal with amplitude equal to 5 mm was adopted for all the tests. The results shows a maximum frequency reduction, in the last dynamic identification test, of about 21% (3.22 Hz), with respect to the initial frequency (4.10 Hz).

For the seismic tests, the spectral acceleration associated to the first period of the reduced scale vault was calculated. The period varies between 0.24-0.25 s, which was obtained from the frequencies obtained by the dynamic identification tests (Table 2).

Table 2. Sequence and brief description of the shake table tests with the reduction of the frequencies.

Date	Type of test	Frequency [Hz]	Description of the damage
14/01/20	DIT	4.10	Undamaged configuration
	Seismic: 10%		Middle blocks felt down (n°2)
15/01/20	DIT	4.10	Middle blocks felt down (n°3) and 1 central steel plate
	Seismic: 25%		No damage
	DIT	4.00	Middle blocks felt down (n°3) and 2 central steel plates
	Seismic: 50%		Diagonal /shear failure. Sliding in the corners (fixed piers East facade)
	DIT	3.91	Middle blocks felt down and two central steel plates

	Seismic: 75%		**Collapse**
17/01/20	DIT	4.00	Undamaged configuration
	Seismic: 55%		Collapse of the centre and sliding of the corner
	DIT	3.42	No additional damage
	Seismic: 25-Aftershock$_1$		East side more damaged
	DIT	3.22	East side more damaged
	Seismic: 35-Aftershock$_2$		**Collapse**

Figure 9 presents the spectral acceleration for each seismic action applied during the sequence of tests (Table 2). In comparison with the quasi static tests performed by Rossi *et.al* [6] and also with the numerical analyses carried out by Gaetani *et al*. [12] (dot line in Figure 9), the results obtained from the shake table tests show that the same model can resist about 1.5 times more under dynamic actions than static ones.

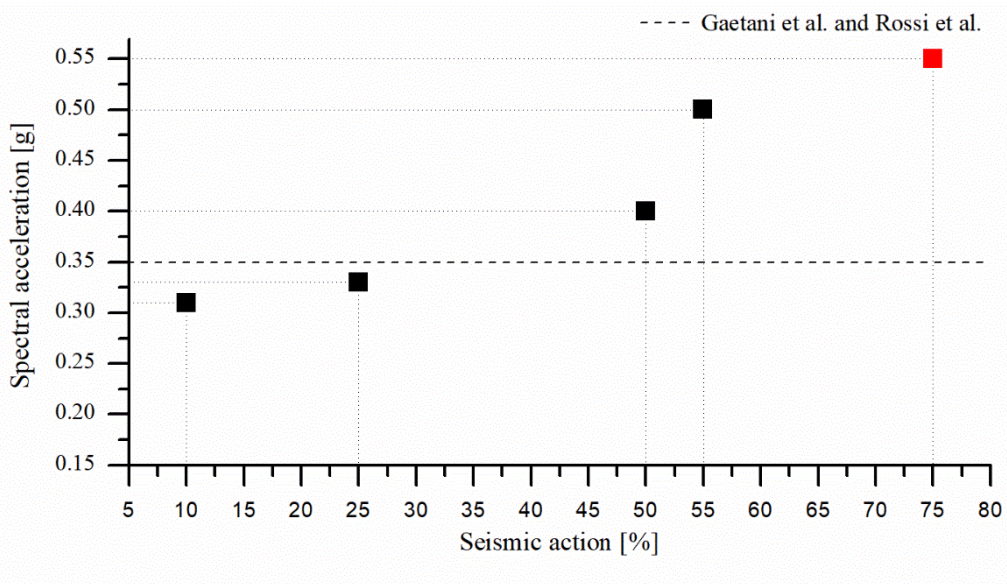


Figure 9. Spectral acceleration as function of seismic actions (no-aftershocks). (Red color corresponds to the collapse).

3. EVALUATION OF THE COLLAPSE MECHANISM

As previously mentioned, the shake table tests involved several seismic tests with different amplitude. In this Section, the collapse mechanism obtained for the 75% of the Mirandola earthquake applied in the longitudinal direction (from North to South, Figure 6) is evaluated. The collapse mechanism is discussed using a sequence of photos, where the number and locations of the hinges is also evaluated. Figure 10 presents the more intense phase before the collapse of the vault, recording five frames per second, with the camera placed at the top of the central key of the model.

The centre of the vault is the first to collapse, due to geometrical configuration. The fall of the blocks at centre of the vault do not interfere with the shear failure, which is the first to occur at 2 s while the hinges are starting to appear. The external edges (North and West side) continue to stand, even when the other sides already felt down. The location of the hinges was observed

from the East façade, where it is possible to notice the similarities with the quasi-static tests (Figure 11).

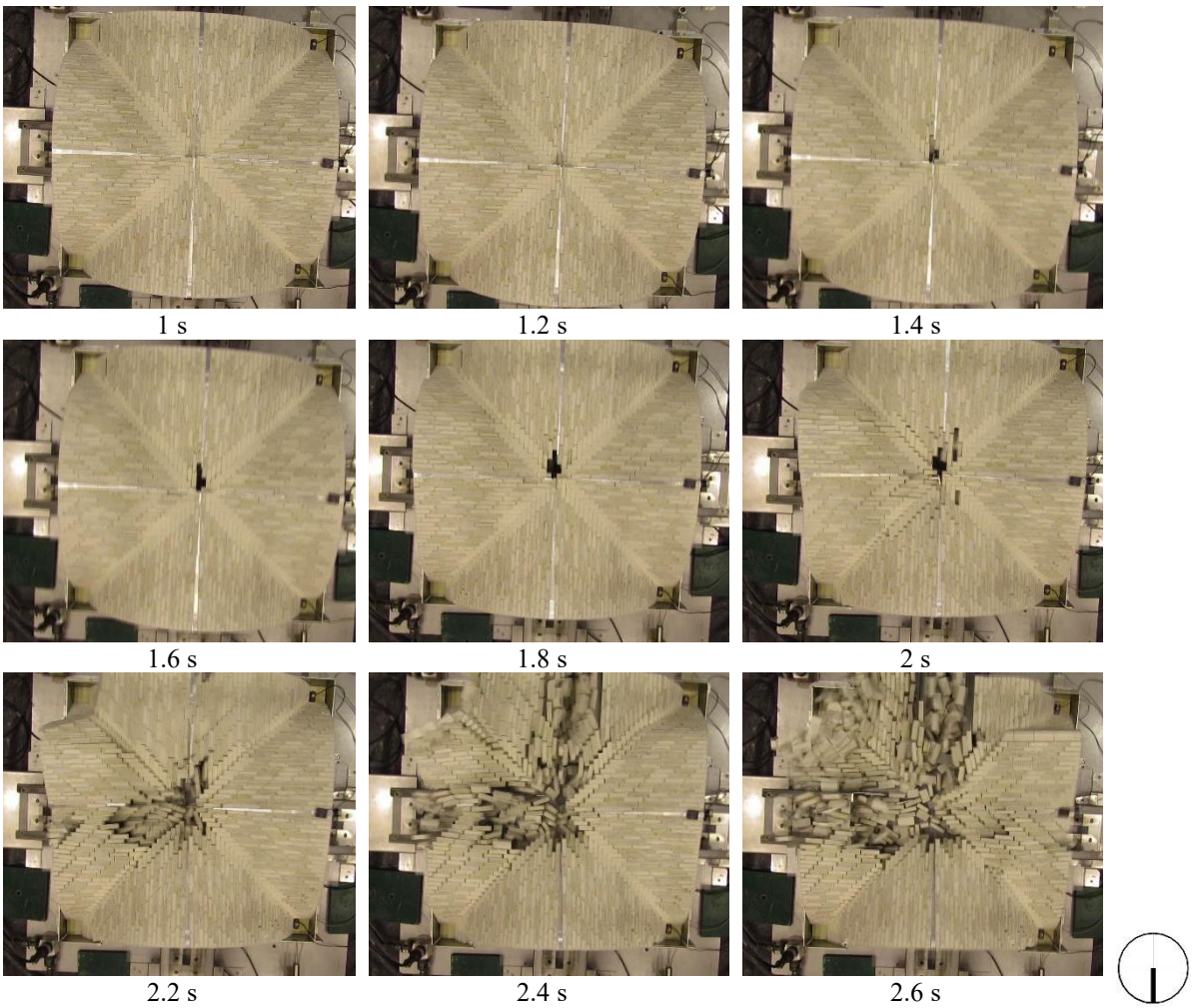
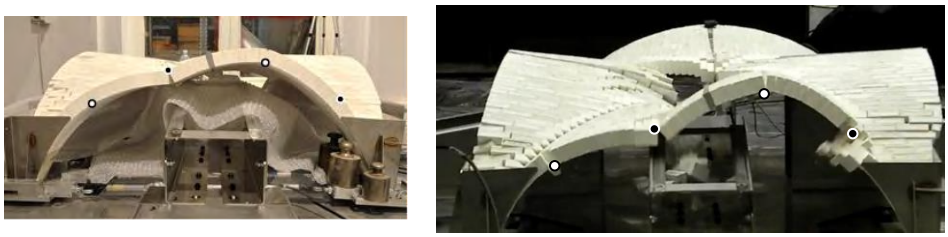


Figure 10. Damage progression of the mock-up during the intense phase of the seismic input 75% (5 frames/s). (Left side: fixed supports; right side: movable supports).

The steel plates at the corners make the boundaries of the shell of the vault stiffer and, therefore, two hinges take location where the steel plates do not act anymore. This is in agreement with the prediction of Oppenheim and De Lorenzis *et al*. [13], [14], based on the minimum energy formulations. The arch mechanism is clear (four hinges) and it is mainly associated to the edge side where the supports are fixed and the response is more rigid (Figure 11).



(a) (b)

Figure 11. Comparison between the quasi-static [6] (a) and the shake table tests (b).

4. CONCLUSIONS

This paper presents the first study on the behaviour of a brick masonry groin vault, namely the first set of shake table tests. The tests aim at evaluating the shear failure of a vault composed by 3D printed blocks and built at 1:5 scaled model with dry joints, previously used also in quasi-static tests. The shake table tests involved dynamic identification tests and seismic tests, where the 2012 Emila's Earthquake recorded in Mirandola station was adopted.

The dynamic identification tests allowed to evaluate the variations on modal properties of the model as function of the construction process and amplitude of the seismic action. The results of the shake table tests were evaluated and compared with the quasi-static tests, leading to the following conclusions: (a) the location of the hinges is similar and there are more clear from the side where the structure is more rigid (East side); (b) the shear failure was obtained showing, as expected, the main concentrations of damage along the rib of the vault; (c) the capacity of the structure is higher than the capacity obtained from the quasi-static tests, namely about 1.5 times, showing a spectral amplitude at the collapse equal to 0.55 g. It is noted that this value corresponds to the base of the vault and does not take into account the amplification in elevation on the structure.

Further investigations should carried out, namely for other types of seismic motions, such as artificial earthquakes and sine-pulse motions. Furthermore, a numerical work should be performed, aiming at validating the results obtained in the tests and evaluating the response of brick masonry groin vault taking into account the dispersion on their features.

Acknowledgements. The authors are grateful to the National Laboratory of Civil Engineering for providing the experimental data for the shaking table tests. This work was partly financed by FCT – Foundation for Science and Technology within the scope of the project "Seismic Response of Masonry Cross Vaults: Shaking table tests and numerical validations" and the PhD grant SFRH/BD/136831/2018.

REFERENCES

[1] P. Block, T. Ciblac, and J. A. Ochsendorf, 'Real-time limit analysis of vaulted masonry buildings', *Comput. Struct.*, vol. 84, no. 29–30, pp. 1841–1852, Nov. 2006.

[2] G. Milani and A. Tralli, 'A simple meso-macro model based on SQP for the non-linear analysis of masonry double curvature structures', *International Journal of Solids and Structures*, vol. 49, no. 5. pp. 808–834, 2012.

[3] B. Torres, E. Bertolesi, J. J. Moragues, P. A. Calderón, and J. M. Adam, 'Experimental investigation of a full-scale timbrel masonry cross vault subjected to vertical settlement', *Constr. Build. Mater.*, vol. 221, pp. 421–432, 2019.
[4] M. Rossi, 'Evaluation of the Seismic Response of Masonry Cross Vaults', Università degli Studi di Genova, 2015.
[5] F. Giovanetti, *Manuale del recupero del Comune di Città di Castello*. Rome (in Italian): DEI, 2000.
[6] M. Rossi, C. Calderini, and S. Lagomarsino, 'Experimental testing of the seismic in-plane displacement capacity of masonry cross vaults through a scale model', *Bull. Earthq. Eng.*, vol. 14, no. 1, pp. 261–281, 2016.
[7] N. Bianchini, N. Mendes, P. B. Lourenço, C. Calderini, and M. Rossi, 'Seismic assessment of masonry cross vaults through numerical nonlinear static and dynamic analysis', in *COMPDYN 2019 7th ECCOMAS Thematic Conference on Computational Methods in Structural Dynamics and Earthquake Engineering*, 2019, no. I, pp. 600–612.
[8] A. Raimondi, 'La chiesa di Santa Maria in Scaria. Gestire la complessità: dal rilievo al BHIM.', 2013.
[9] L. F. Ramos, 'Damage Identification on Masonry Structures Based on Vibration Signatures', Universidade do Minho, 2007.
[10] A. Penna, P. Morandi, M. Rota, C. Filippo, and P. Guido, 'Performance of masonry buildings during the Emilia 2012 earthquake', *Bull. Earthq. Eng.*, pp. 2255–2273, 2014.
[11] F. Bozzoni, C. G. Lai, and L. Scandella, 'Preliminary results of ground-motion characteristics', *Ann. Geophys.*, vol. 55, no. 4, pp. 609–614, 2012.
[12] A. Gaetani, N. Bianchini, and P. B. Lourenço, 'Simplified micro-modelling of masonry cross vaults: stereotomy and interface issues', *Int. J. Mason. Res. Innov.*, p. Accepted manuscript, 2019.
[13] I. J. Oppenheim, 'The masonry arch as a four-link mechanism under base motion', *Earthq. Eng. Struct. Dyn.*, vol. 21, no. 11, pp. 1005–1017, 1992.
[14] L. De Lorenzis, M. J. Dejong, and J. A. Ochsendorf, 'Failure of masonry arches under impulse base motion', *Earthq. Eng. Struct. Dyn.*, vol. 36, no. 14, pp. 2119–2136, Nov. 2007.

12th International Conference on Structural Analysis of Historical Constructions
SAHC 2020
P. Roca, L. Pelà and C. Molins (Eds.)

SEISMIC RESPONSE OF HAGIA SOPHIA CHURCH IN THESSALONIKI INCLUDING SOIL-FOUNDATION-STRUCTURE INTERACTION

A. CHOUNTA[1], C. MALAKOUDI[2], C. PETRIDIS[3] AND D. PITILAKIS[4]

[1]Civil engineer, Aristotle University of Thessaloniki
e-mail: nasiachounta@yahoo.gr
[2]Civil engineer, Aristotle University of Thessaloniki
e-mail: malakoudichristina@gmail.com
[3]Civil Engineer, MSc, PhD Candidate , Aristotle University of Thessaloniki
e-mail: cpetridi@civil.auth.gr
[4]Associate Professor , Aristotle University of Thessaloniki
e-mail: dpitilakis@civil.auth.gr

Keywords: Historical Structure, Masonry, Monitoring, Non-Destructive Inspection

Abstract. *This study investigates the behavior of "Hagia Sophia" church in Thessaloniki under seismic loading. It is one of the greatest Byzantine churches in the city and it is inscribed on the World Heritage List. The main scope of this work is to estimate the seismic response of the historic structure accounting for the actual foundation and soil flexibility at its base, to find the locations in need for retrofit and finally, to propose possible intervention methods. We simulate numerically the soil - foundation - structure system, and for the properties of the building materials we estimate their strengths with the use of two codes; the EC6 and the Greek Regulation for the structural intervention of masonry (KADET). We simulate soil-foundation flexibility using impedance functions under the foundation according to NIST (2012) provisions. The influence of soil–foundation-structure interaction is investigated. As a reference case, we also consider a fixed-base model to compare the output of the two analyses and highlight the influence of the soil and masonry foundation flexibility on the dynamic response of the church. Finally, we further analyze the intervention method of micropiles as a possible method of enhancement for the foundation of the monument.*

1 INTRODUCTION

Hagia Sophia of Thessaloniki is one of the oldest Byzantine temples in the city of Thessaloniki, Greece [1]. Situated in the center of Thessaloniki, it still operates as the Cathedral of the City. It was built in the middle of the 7th century A.D., on the wreckage of a Christian basilica that was probably destroyed by an earthquake at the beginning of that century. During the 4th Crusade, in 1205, the building was used as a cathedral and during the Ottoman period, Hagia Sophia was converted into a mosque in 1430. It was reconverted to a church upon the liberation of Thessaloniki in 1912. Four years later, in 1917, the church suffered extensive damage due to the great fire and was gradually restored. The dome's restoration wasn't

completed before 1980 [2].

In this paper, ETABS is used to model and analyze a 3D model of the church of Hagia Sophia accounting for the soil-structure interaction, using geotechnical data available from boreholes. Pitilakis and Karatzetzou (2015) concluded that SSI is important for heavy historical masonry structures [3] Two different types of springs are considered in order to compare the output of the two analyses and examine the importance of considering the influence of the soil and masonry foundation flexibility. The model is created in a simplified, yet accurate in terms of the dynamic characteristics, manner.

2 DESCRIPTION OF THE STRUCTURE, BUILDING MATERIALS, AND SUBSURFACE OF THE CHURCH.

Hagia Sophia is a heavy cubic building with internal dimensions 30.92m width and 28.90m length. To the east of the temple stands the chancel. In some parts of the temple, its foundations lay on arches, connected to the foundations of the pre-existing Christian basilica, on which it was built (9th Ephorate of Antiquities of Thessaloniki City, personal communication, 2018). The construction of the church is divided into 5 phases; 4 phases of the building and one of the later subsequent interventions (Fig. 1). The first three chronological phases are analyzed below, as they are present in the structural majority of the temple.



Figure 1: West view of "Hagia Sophia" church. [1]

Phase A: The foundations were made of stone known as gneiss, a green rock quarried from the surrounding hills. The masonry was composed of bricks and stones. The rough carving stones used were a mixture of limestone and sandstone in small proportion with a high content of shellfish fossils. This rock is not considered as a good building material because of its organic impurities. However, it's a material quite soft and easy to extract and carve. It is believed that it was imported from Chalkidiki, so it was a local material. This probably led to the use of this rock, despite its poor quality.

The bricks used were of good quality, with several aggregate impurities in the clay mass.

Their dimensions were usually 40-by-30÷32-by-4.5÷5cm. The mortar used for the construction is kurashani, a strong pink mortar. The use of crushed tile was also significant, both for the composition of cement in the form of brick powder and for the composition of aggregates, which exhibited continuous grading gradient, ranging in size from coarse sand to grains 1÷2 cm in diameter.

Phase B: It is characterized by masonry that also forms brick and stone zones, but in this case, the red brick zones are less uniform. The stone used was schist and the building's mortar was similar to the first phase but sometimes less robust.

Phase C: The masonry consisted of irregular stones with joints filled with smaller stones and pieces of brick in horizontal layers. The exterior of the masonry had a rough appearance [1]. The following table shows the mechanical properties (modulus of elasticity E, specific weight γ, density ρ, Poisson's ratio ν, strength of material f_b and of mortar f_m) of the materials used in the temple (Table 1).

Following geotechnical research in the surrounding area of the temple, the following soil layers (Fig. 2) can be distinguished under the location of the temple [G.Penelis, personal communication, 2018].

From the results of the NSPT test and the Pitilakis et. al (1992) [4] equation, the velocity of shear waves is calculated from the relation: Vs = 132 (N60)•0.2271 (N60 is the corrected value of N). Thus, the shear wave velocity for the first layer is V_{s1}=231,91 m/s for the second layer is V_{s2}=274,98 m/s and finally for the third layer is V_{s3}=358,70 m/s. Finally, the mean V_s = 280 m / s is obtained for the foundation soil. The shear modulus G is calculated from the equation $G = \rho \bullet V_{s2}$.

Table 1. Mechanical properties of the building materials.

	E (Gpa)	**γ** (KN/m^3)	**ρ** (t/m^3)	**ν** (%)	**f_b** (Mpa)	**f_m** (Mpa)
Foundation						
Gneiss	30	27	2,25	15	40	
Kurashani	5		1,5	30		2
Masonry – Phase A						
Limestone	30	18.7 ÷ 26.9	1,8	15	40	
Sandstone	20	22.0 ÷ 27.0			30	
Brick		20	1,5	16	40	
Kurashani	5					2
Masonry – Phase B						
Schist	50	28		20	60	
Brick	40	20	1,5	16	30	
Kurashani	5					2
Internal column						
Marble	80	26.4 ÷ 28.6	2,7	20	80	

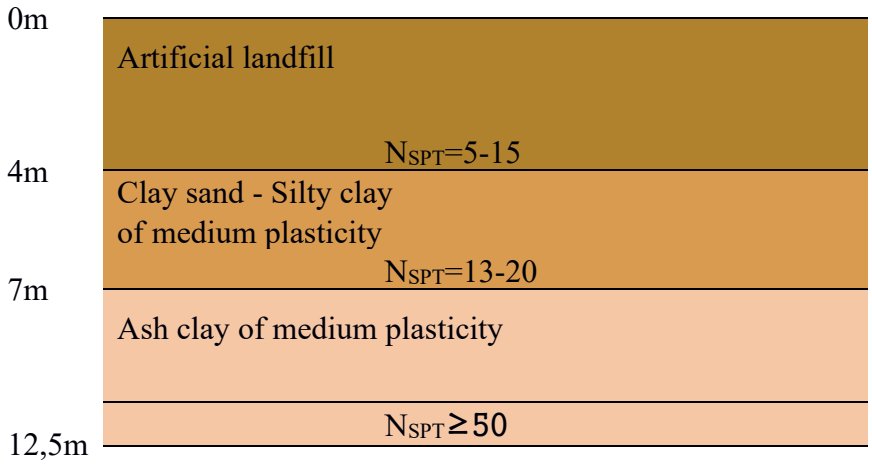


Figure 2. Territorial section of the subsurface, from the surrounding area of the temple. (Nspt is the value of standard penetration resistance)

3 3D NUMERICAL MODELING OF THE TEMPLE

The strengths of the building materials were impaired with the use of the Greek Regulation of the structural intervention of masonry (KADET) [5]. The purpose of the Regulation is to establish criteria for assessing the bearing capacity of existing load-bearing masonry structures formed by mortar-bonded stones for their anti-seismic design as well as for any interventions, repairs or reinforcements.

Its purpose is to:

1. Provide criteria for evaluating the seismic behavior of existing individual buildings.
2. Describe the approach for selecting the necessary corrective measures.
3. Set criteria for the design of intervention measures

Regarding the church of Hagia Sophia, the masonry is unreinforced, meaning that it is composed exclusively of stones and mortar. It's also a three-layer masonry (see Fig. 3), which means that there is a gap area between the two outer walls of the masonry consisting of filler material. The filler consists of pieces of stone and/or mortar mixed with mortar (usually the same as construction mortar) and spaced at intervals in height, without condensation. Thus, it is usually a relatively loose material with a large percentage of gaps and very poor mechanical properties.

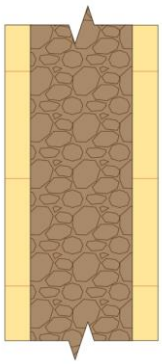


Figure 3. Sketch of the three-layer masonry.

The compressive strength of three-layer masonry can be estimated by the following relation:

$$f_{wc} = \frac{1}{\gamma Rd} \frac{2\lambda_e \delta f_{c,e} + \lambda_i f_{c,i}}{1 + 2\delta} \quad (1)$$

where, δ, is the ratio of the thickness of the outer side to the thickness of the filler, $f_{c,e}$, and f_c, are the compressive strength of the outer walls and the filler respectively, λ_e (<1,00) and λ_i (> 1,00) are empirical coefficients, which take into consideration the interaction of outer layers and filler material, γ_{Rd}, is an uncertainty index, which can be taken equal to 1.50. The uncertainty ratio is taken as 1.25. The compressive strength of the filler is obtained equal to the 2/3 of the compressive strength of the outer walls [C. Ignatakis, personal communication, 2018].

The characteristic compressive strength of three-walled masonry is calculated by the equation: $f_{wc}^k = f_{wc}$-1,645, and the specific modulus is 1000 times the characteristic compressive strength of each wall. Finally, the introduced specific modulus in the program is equal to half of the calculated (loss of material strength due to the age of construction) [5].

The table below (Table 2) shows the calculation that led to the values of comprehensive strength f_{wc} and modulus of elasticity E_{wc} of the masonry, which were input into the program. The parameters shown on the equations are the following: f_{bc} and f_{mc} the compressive strength of lithosomes and mortar respectively, γ_{Rd} an uncertainty index, outer wall $f_{c,e}$ and filler material f_{ci} comprehensive strength, the empirical factor ξ which takes into account the adverse effect of the mortar joints' thickness, coefficient λ which takes into consideration the interaction of outer layers and filler material, the ratio δ of the thickness of the outer side to the thickness of the filler and coefficient f_o which takes into account the degree stone carving.

The first model examined does not take into account the soil-foundation interaction, so it is a model fixed in the entire height and length of the foundation. In the second model created, the foundation substrate was simulated by vertical and horizontal springs applied around the length and height of the foundations of the construction. For the calculation of the spring constants, the properties of the soil under the foundation were used.

The soil-foundation flexibility was simulated using impedance functions under the foundation, according to NIST 2012 provisions [6]. The term "soil-structure interaction" describes the differentiation in the dynamic response of construction when taking into account the finite stiffness of the foundation and the underlying soil. More specifically there is:

- Modified movement at the base of the construction.
- Different dynamic oscillation characteristics of the building due to foundation flexibility.
- The oscillation of the structure imposes additional stresses and deformations on the base resulting in increased damping of the system.

The model was made by making some simplifying assumptions. The assumptions and simplifications lead to a rougher description of the church, however reliable enough to exclude significant errors in its analysis. These assumptions were:

1. Not modeling the dome, whose loads were calculated and imposed on the perimeter walls of the temple.

2. Not modeling the upper floor whose impact is simulated by a diaphragm.
3. The curved surfaces of some elements, e.g. of the three-sided chancel and the arched openings, were simulated with polygonal surfaces.
4. Ignoring the arched connection of the foundations of Hagia Sophia with foundations of earlier periods.
5. Due to the large volume of the monument and its corresponding weight, the live loads are considered negligible and are not taken into account in the solution.
6. Due to the similar mechanical characteristics of the masonry materials in the first and second phase, it is assumed that the masonry up to the height of the masonry belongs to one phase.
7. Firstly, five masonry sections were created, with different dimensions each one, to simulate different thicknesses in each side of the temple and one frame section for the simulation of the marble columns.
8. The model was created in 3 stages, first the foundation, after the first level until the height of the upper room, and finally the second level until the height of the roof. Thereafter, the model was discretized (meshed), in every 0,5m, and all the openings have been designed (Fig.4). The influence of the upper room and the dome was simulated by the entrance of two diaphragms, one at the end of the first and one at the end of the second level, respectively.

Table 2. Mechanical characteristics of masonry.

	Outer walls compressive strength	Filler material compressive strength	Masonry compressive strength (average value)
	$f_{wc}=\xi\cdot[\{\frac{2}{3} f_{bc}^{0,5}-f_o\}+\lambda\cdot f_{mc}]$(Mpa)	f_{ci} (Mpa)	$f_{wc}=\frac{1}{\gamma Rd}\cdot\frac{2\lambda e\delta fc,e+\lambda ifc,i}{1+2\delta}$ (Mpa)
Foundation	2,966370214	1,98	1,90
Masonry A,B	2,694053189	1,80	1,72
Masonry C	1,73142397	1,15	1,11

	Masonry compressive strength	Modulus (EC6)	Modulus (final)
	$0,67\cdot f_{wc}$ (Mpa)	$E_{wc}=1000\cdot f_{wc}$ (Mpa)	$E_{wc}'=1/2\cdot E_{wc}$ (Mpa)
Foundation	1,27	1271,98	635,99
Masonry A,B	1,16	1155,21	577,61
Masonry C	0,74	742,43	371,22

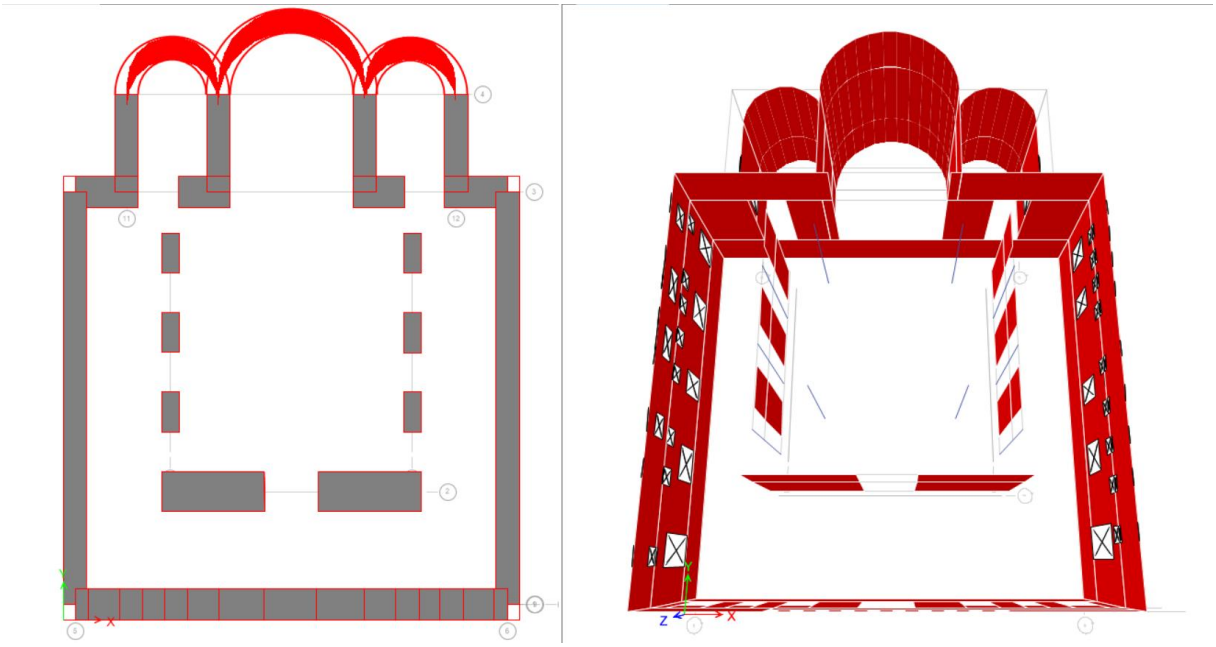


Figure 4. Plan view of the ground floor and 3D model design before the change of the three-sided chancel into polygonal surfaces.

For the calculation of the spring constants, the properties of the subsoil according to the geotechnical research in the surrounding area of the temple were used. Using the equations of dynamic soil-superstructure interaction and soil parameters, according to NIST 2012, the spring constants are calculated on the x, y, z axes.

Stiffness is denoted k_j, and is a function of foundation dimensions (B, L), soil shear modulus, G, Poisson's ratio of the soil, ν, dynamic stiffness modifiers, a_j, and embedment modifiers, η_j.

$$k_j = K_j \cdot a_j \cdot \eta_j \quad (9)$$

, where K_j is the static foundation stiffness at zero frequency for mode j. The equations used for the calculations of the spring's components are presented on the following Table (Table 3). [4]

The behavior of the soil has been simulated by modeling the same with a set of linear elastic springs. Three translational springs along mutually perpendicular global axes are assigned to all the nodes that are perpendicularly along the length and height of the foundations of the structure. Indicatively on the foundation of the south wall, the stiffness calculated respectively for z direction, y direction and x direction were k_z=11228225N/m, k_y=12226456N/m and k_x=9796668N/m. These values were divided by the nodes corresponding to each direction and applied to the model as linear elastic springs. The same procedure was followed for all parts of the church foundations. In addition, a fixed-base model was created to compare the results of the two analyzes in order to better understand the effect of the soil on the dynamic response of the model.

Table 3. Pais and Kausel (1988) [7] equations, used for the calculations of the foundation springs

	Static stiffness	Embedment corrector for static stiffness	Dynamic stiffness modifiers
Direction z	$K_z=\frac{G\cdot B}{1-\nu}\cdot[3{,}1\cdot(\frac{L}{B})^{0{,}75}+1{,}6]$ (10)	$\eta_z=1{,}0+(0{,}25+\frac{0.25}{(L/B)})\cdot(\frac{D}{B})^{0{,}8}$ (11)	$\alpha_z=\left(\frac{\left(0{,}4+\frac{0{,}2}{\frac{L}{B}}\right)\cdot\alpha o^2}{\left(\frac{10}{1+3\left(\frac{L}{B}-1\right)}\right)+\alpha o^2}\right)$ (12)
Direction y	$K_y=\frac{G\cdot B}{2-\nu}\cdot[6{,}8\cdot(\frac{L}{B})^{0{,}65}+0{,}8\cdot(\frac{L}{B})$ +1,6] (13)	$\eta_y=1{,}0+(0{,}33+\frac{1{,}34}{1+(L/B)})\cdot(\frac{D}{B})^{0{,}8}$ (14)	$\alpha_y=1$
Direction x	$K_x=\frac{G\cdot B}{2-\nu}\left[6{,}8\cdot\left(\frac{L}{B}\right)^{0{,}65}+2{,}4\right]$ (15)	$\eta_x\approx\eta_y$ (16)	$\alpha_x=1$

4 DYNAMIC RESPONSE UNDER SEISMIC LOADING

Two loading cases have been imposed, static and dynamic ones. The static loads are coming from the self weight of the roof and the dome, as well as from the weight of the masonry. These loads have been calculated and applied to the perimeter of the masonry, as vertical forces. The loads imported to the temple by the perimeter and the interior walls are automatically calculated by the program and are evenly distributed over the entire surface of each wall.

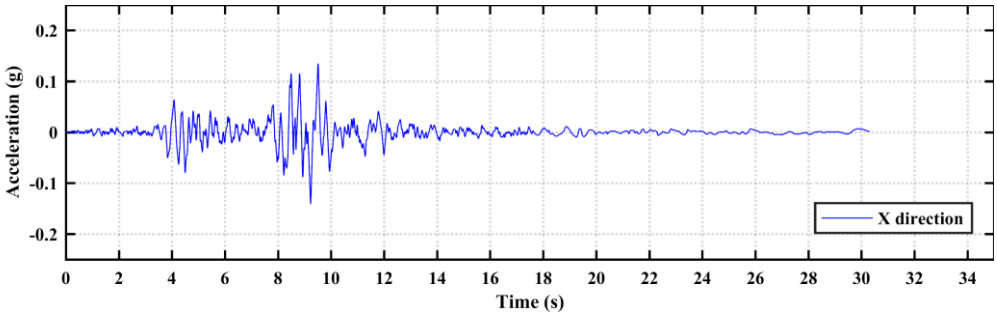


Figure 5. Time history on x direction

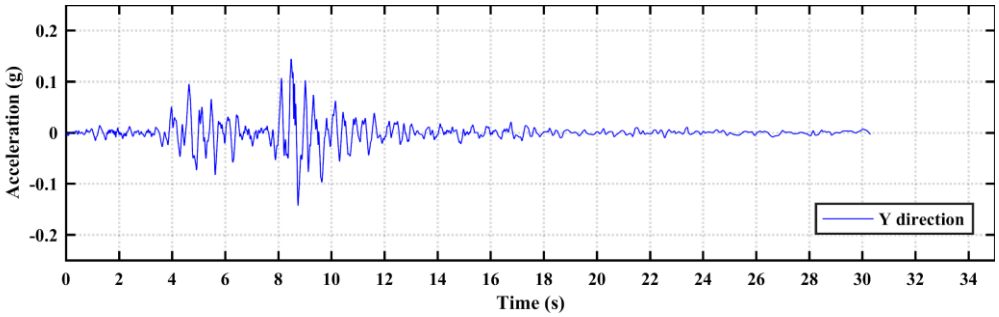


Figure 6. Time history on y direction

Model dynamic loading: The analysis is carried out first for the charge status of the self weights, as the mobile loads are ignored, and then the seismic action is added. The simulation of the seismic activity was carried out by the introduction of accelerometers recorded during the Thessaloniki earthquake on June 20, 1978 at the CITY Hotel. It is chosen to simulate the seismic motion in terms of time-acceleration time histories. The following figures illustrate the time histories of the charge states in the x (Fig.5) and y (Fig.6) directions. A time step of 0.01s resolutions is set and 3000 consecutive steps are selected in total.

The results of the seismic response of the model are presented through diagrams of maximum movements, at non-simultaneous times. Therefore, the distribution of the growing stresses of the south wall of the temple are presented.

The maximum displacements at non-simultaneous moments, in the fixed-base model (Fig. 7) and in the model with salable soil (Fig.7), under seismic loading, are represented in the following figure. The horizontal axis shows the value of the displacements (in millimeters) and the vertical is the height of the construction at which they appeared. In the fixed-based model, displacements are zero, throughout the foundation while on the contrary, on the flexible base model, small-value displacements are developed at its foundation. In both models, displacements are increasing as we approach the height of the first floor and after decreasing slightly.

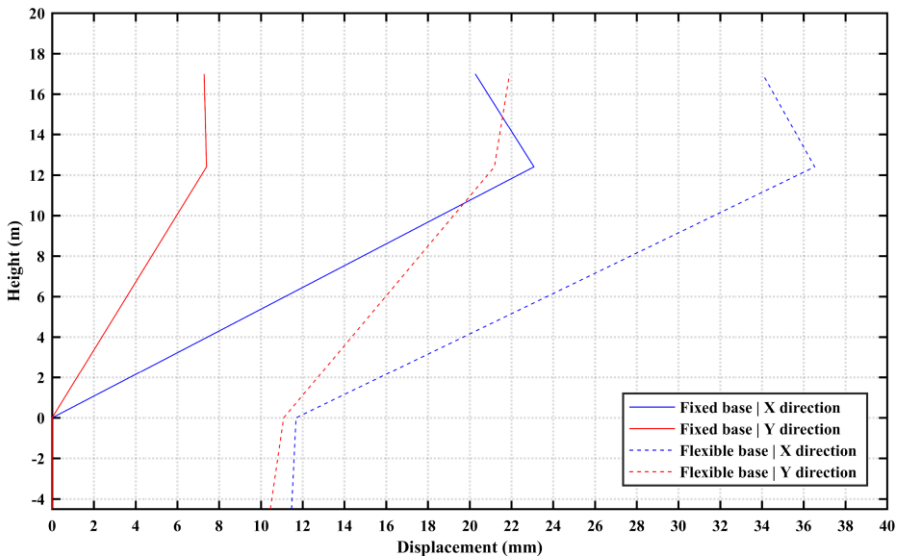


Figure 7. Displacements on fixed and on the flexible base model.

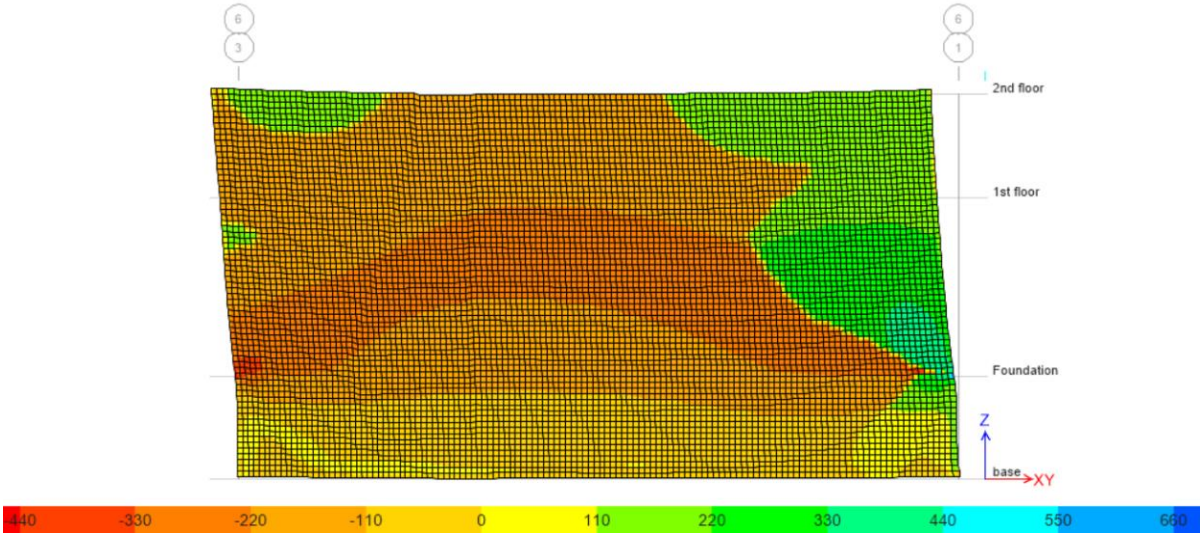


Figure 8. Distribution of shear stresses on the south wall of the temple. (model with springs) The horizontal axis at the bottom of the figures shows quantitative (color-based) stresses in the temple in MPa.

Figure 8 shows the distributed shear stresses at non-simultaneous times on the south wall of the temple as recorded in the ETABS program. The horizontal axis at the bottom of the image shows quantitative (color-based) stresses in the wall in MPa. On the south wall, negative stresses (orange) are observed, which are increasing at an absolute value in its center. Positive stresses (green) are developed on the right side of the wall. In the case of wall connections with adjacent walls, which are sensitive areas of a building, high tensile stresses have been observed. This indicates a greater risk of failure.

5 REHABILITATION METHOD

The building considered, belongs to the category of the preserved masonry buildings. This particularity greatly limits the possible ways of intervention. It is important to avoid interference on the frame of the church. The main purpose is the measure to be as painless as possible, to not damage the cultural heritage. The proposed method is deep subjection using micropiles. This technique is designed to succeed in both soil and bearing capacity of foundations improvement. Micropiles have a quick application, and they can gradually receive loads and lead to the stabilization of the displacements. For a succeeding application of the technique, the cost might be relatively high.

In order to simulate the micropiles in the model, the values of the spring constants were increased. This is achieved by increasing G by 50%. Thus, the spring constants resulting from this modification indicative for the south wall, that was previously analyzed, were Kz = 16842338N/m, Ky = 18339684N/m and Kx = 14695002N/m. These spring values were then applied to the model in the same way as discussed above. The results of displacements in relation to displacements with non-reinforced springs are shown in Fig. 10.

From the results of the analysis of the model after reinforcement, there is an increase in the stiffness of the construction and decrease on the displacements, a 5% decrease in the x direction and a 30% decrease in the y direction, compared to the original spring model. Therefore, it seems that micropiles could be a valuable solution to the reinforcement of the foundation.

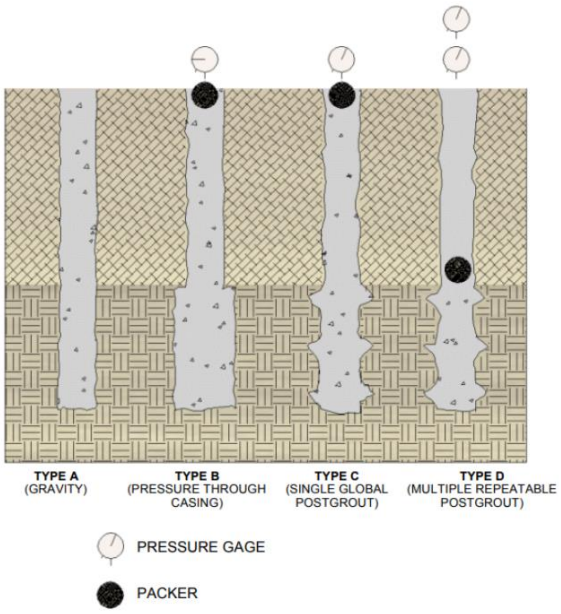


Figure 9. Type of micropiles used in practice, according to [8] .

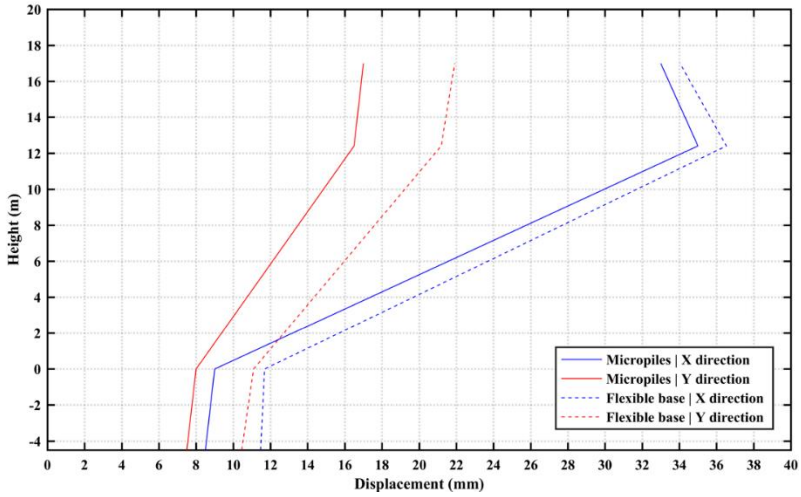


Figure 10. Displacements on the flexible base model and on model with micropiles.

6 CONCLUSION

Comparing the two models (fixed base model and model with no reinforcement springs) , there is an increase in the idle period as well as an increase in the total and relative drift of the construction to the model with the springs relative to the fixed model. The maximum displacement does not occur at any of the corners of each wall. For the spring model, it is 35.9 mm in x-direction and 21.1 mm in y-direction, while for the spring model it is 22.3mm and 8.0mm in the x- and y-directions respectively. The maximum off-plane movements are observed in the middle of each wall and this is because there is their free section (we have off-plane commitments at the endpoints of the wall). It is therefore observed that due to the

introduction of the springs the translations at the checkpoints are increased by 60% in the x-direction and 175% in the y-direction.

As shown in the workflow and results of the work, the influence of the dynamic soil-superstructure interaction plays an important role in the construction response, so a proper foundation simulation cannot be based on a flexibility-ignorant model. It is necessary to consider the soil-structure interaction in assessing the vulnerability of heavy structures and in managing seismic risk. Finally, an important conclusion is that the reliability of the results is largely based on assumptions and simplifications made by the user during modeling. Thus, experience and knowledge of the behavior of the construction against past earthquake events play a crucial role.

In cases where monuments renovation, in which an intervention is to be performed, its effectiveness should be studied in detail. As shown in the results after the simulation of the micropiles the decrease of the displacements were not as large as those of the model with the non-reinforced springs, so it would be incorrect to rely on this study for possible intervention, given the high cost of their construction. The present paper uses linear analysis as a reliable method to evaluate the effectiveness of various building reinforcement interventions before they are implemented. However, nonlinear analysis could be a more accurate method.

ACKNOWLEDGMENTS

We acknowledge support by the project “HELPOS - Hellenic Plate Observing System” (MIS 5002697) which is implemented under the Action “Reinforcement of the Research and Innovation Infrastructure”, funded by the Operational Programme "Competitiveness, Entrepreneurship and Innovation" (NSRF 2014-2020) and co-financed by Greece and the European Union (European Regional Development Fund).

REFERENCES

[1] Theocharidou K. *The architecture of Hagia Sophia, Thessaloniki*. Publish of The Archaeological Receipts and Expropriations Fund, (1994).

[2] *Hagia Sophia, Thessaloniki*. Wikipedia, viewed 15 July 2019.

[3] Pitilakis D., Karatzetzou A. Dynamic stiffness of monumental flexible masonry foundations. Bulletin of Earthquake Engineering. 13(1):67-82 (2015).

[4] Pitilakis K., Anastasiadis A. and Raptakis D. Field and laboratory determination of dynamic properties of natural soil deposits. *Proceedings of the10th world conference on earthquake engineering*, (1992).

[5] *Greek Regulation of the structural intervention of masonry (KADET)*. (1rst plan 2019), Athens, (2019).

[6] NIST, 2012. *Soil-Structure Interaction for Building Structures*. Tech. Rep. (2019).

[7] Pais, A. and Kausel, E. Approximate formulas for dynamic stiffnesses of rigid foundations. *Soil Dynamics and Earthquake Engineering* (1988) **7(4)**: 213-227.

[8] Antunes, T. *Rehabilitation of foundation of old buildings using micropiles.* (extended abstract). Técnico Lisboa, Lisbon, Portugal, (2012).

12th International Conference on Structural Analysis of Historical Constructions
SAHC 2020
P. Roca, L. Pelà and C. Molins (Eds.)

SEISMIC RETROFITTING OF HISTORICAL MASONRY HERITAGE STRUCTURES: A CASE STUDY OF AN ADOBE MASONRY BUILDING IN LIMA, PERU

TIAGO MARTINS[1*], JULIA GARCÍA[1], ALEJANDRO FERRÁNDEZ[1], NICOLA TARQUE[2] AND JAIME FERNÁNDEZ[1]

[1]Escuela Técnica Superior de Ingenieros de Caminos, Canales y Puertos
Universidad Politécnica de Madrid
Campus Ciudad Universitaria, 28040 Madrid, España
e-mail: tiago.martins@upm.es, web page: http://www.caminos.upm.es

[2]Departamento de Ingeniería - Sección Ing. Civil, Pontificia Universidad Católica del Perú (PUCP)
Campus principal, Av. Universitaria 1801, San Miguel
Lima 32, Perú
e-mail: sntarque@pucp.edu.pe - web page: https://www.pucp.edu.pe/

Keywords: Adobe masonry, Seismic behaviour, Seismic retrofitting

Abstract. *The need for seismic retrofitting on a historical masonry heritage structure raises questions that go beyond the improvement of its seismic behaviour after the intervention. Indeed, principles as minimum intervention or reversibility must be considered before a consensus decision can be reached, especially when this process is just a part of a broader and deeper intervention on this kind of building.*

Moreover, the complexity to perform in-situ experimental tests results in the uncertainty on the masonry mechanical properties, which are typically assumed as a homogeneous and isotropic material. All these uncertainties, among others, result in the difficulty to predict the different possible failure mechanisms of the complete structure and its structural behaviour.

Through the analysis of different possible seismic strengthening solutions for a 19th century historical masonry heritage building these issues are tackled. The selected case study is the fort of Santa Catalina, an adobe masonry load-bearing wall building located in Lima, Peru, on which it has been decided to carry out its seismic retrofitting among the complete rehabilitation of the building. The Peruvian coast is classified as a high seismic activity zone, where an 8.0 Mw is expected to occur according to recent studies performed by the Geophysical Institute of Peru.

In this context, this work presents the results of a preliminary characterization of the selected adobe masonry building and the subsequent evaluation of its seismic vulnerability in order to define the fitting solution.

Thus, the ongoing research allows to define an effective seismic retrofit solution and respectful to the building's historic significance.

1. INTRODUCTION

For centuries, the use of unreinforced masonry was common in Central and South America, Eastern Europe, the Himalayan region, Indian subcontinent and other parts of Asia [1]. Taking as an example the case of Peru, statistics show that adobe o rammed earth, still represent currently 30% of the predominant material of the houses' outer walls [2]. Many of those buildings, such as the mentioned case of Peru, were built on high seismic activity zones and, due to that, different seismic events have shown poor seismic performance of existing masonry structures [3]. It is noted that the Peruvian coast is classified as a high seismic activity zone, where an 8.0 Mw is expected to occur according to recent studies performed by the Geophysical Institute of Peru [4, 5]. In this context, seismic retrofitting of those masonry constructions is required for reducing their seismic vulnerability.

Different solutions, such as confinement, mesh reinforcement or junction strengthening, have been developed and implemented with the aim of improving seismic behaviour of masonry structures, and so reduce their future seismic vulnerability [1, 3, 6–9]. Nevertheless, in the case of historical masonry heritage buildings, in the decision process of their seismic retrofitting solution frequently intervene different factors, related with preservation principles or even with economical questions, that go beyond the strict improvement of the seismic behaviour of those buildings after the intervention. This may cause, in some cases, that the solution adopted is not the most effective from the point of view of seismic strengthening.

Through the analysis of a 19th century historical masonry heritage building case study these issues are tackled. The selected construction is the fort of Santa Catalina, an adobe masonry load-bearing wall building located in Lima, Peru, on which it has been decided to carry out its seismic retrofitting among the complete rehabilitation of the building.

For this purpose, and taking into account that, in order to support correct pre-evaluation decisions regarding strengthening or retrofitting, the first step of any rehabilitation process must be the understanding of building's construction system and its so far performance [8], it was initially performed a building survey to characterize the structural and constructive solutions adopted, as well as a damage inspection of the building. The information obtained from the construction survey accomplished and the available literature on this topic, allowed the subsequent evaluation of its seismic vulnerability with the purpose of defining a suitable retrofitting solution. Hence, the paper presents the results of the analyses carried out and the seismic retrofit solution achieved for the case study building.

2. CONSTRUCTION SURVEY

In order to characterize structural and constructive solutions adopted on the case study building, as well as to collect data of building's seismic vulnerability, an extensive inspection campaign was carried out, whose results are described in this section. This allowed to complete the historical information of the building, create advanced 3D models and plans. In addition, a complete building damage inventory was also conducted with the purpose of evaluate the construction conservation condition and current damage grade.

The analysis is narrowed to one of the buildings of the complex, called the “Cuadra”. The structure was built in the XIX century by the Spanish during the colonial period. This unique building comprises all the features to be considered as highly valued and therefore make it worth of an intervention. Its past uses, reconstructions, the employed materials and building techniques make it a living witness of the history of Lima.



Figure 1. Aerial view of the fort of Santa Catalina.

2.1. Structural behaviour

The “Cuadra” is a two-story adobe masonry building. The first floor is made up of 5-meter-high adobe walls while the second floor is built in wood and quincha with a height of 3,6 meters. The benefit of the difference in rigidity of the adobe-quincha system is that the structure supports fewer shear strengths and the relative displacements presented by the first adobe floor are less. The second floor presents greater displacements; however, the quincha is composed of wood which is a flexible material that can support large displacements without collapsing [11].

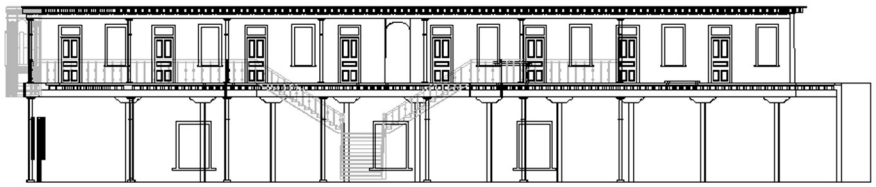


Figure 2. Front view of the building (Source: Escuela Taller de Lima, 2007).

The roofs lay on wooden girders sustained by quincha walls, a construction methodology consisting of wooden posts, wooden beams at the bottom and top and a combination of woven cane and clay as filler, which also partition the space into sixteen small rooms (Figure 3).

The loads from the second floor are transmitted to the masonry bearing walls and to a main wooden beam in the middle of the first story space, using wooden girders that lay directly on the central beam and are embedded in the adobe walls which constitute the enclosure of the first floor. On this level there are also two spaces separated from the main room by other adobe

walls, as it can be seen in Figure 4.

The wooden beam is supported by various wooden pillars along its length, represented by the circles in the middle of the main space in Figure 4 . The two lateral alignments of circles represent the struts that were added afterwards to avoid collapsing.

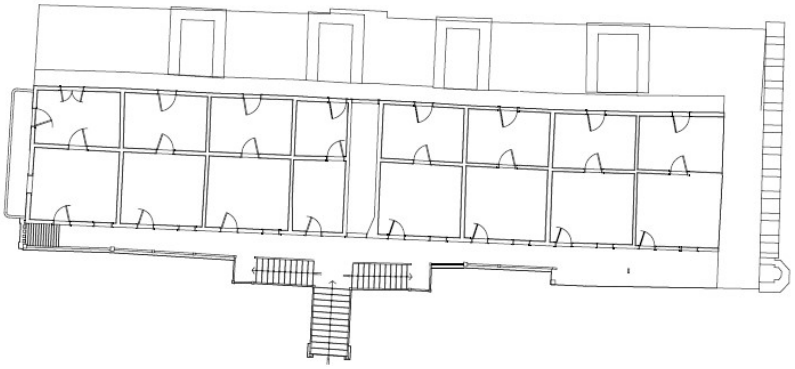


Figure 3. Second floor (Source: Escuela Taller de Lima, 2007).

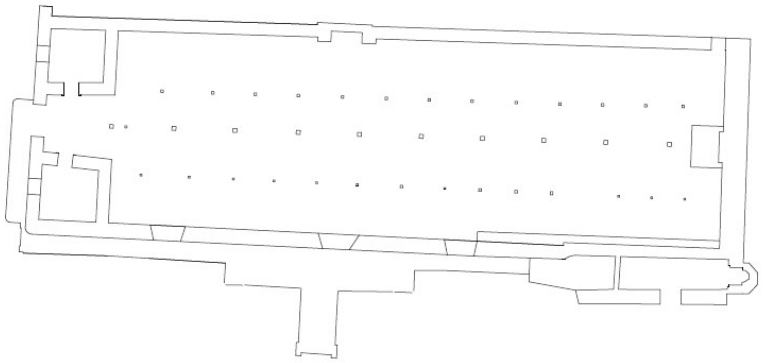


Figure 4. First floor (Source: Escuela Taller de Lima, 2007).

The transmission of loads from the masonry walls to the ground is done through the foundation, built as was traditional in the period of construction of the fort. The walls are prolonged and embedded in the soil, with two layers: the upper one is made up of fifteen centimetres of brick with lime and sand mortar while the lower layer is made up of forty-five centimetres of round pebbles with soil mortar.

2.2. Methodology

The surveying campaign comprised a thorough identification of the materials involved in the structural behaviour of the building, as well as its aesthetics. However, the essential set of in situ tests required to characterize their mechanical properties could not be performed for the time being, nor the collection of samples to be tested in the lab. Since the fort is strongly

protected by the Peruvian Government for being of high historical value, the permits could not be delivered for a research project like this.

Hence, a different approach was needed. The characterization of the materials was estimated employing the test results and properties from the same materials used in a nearby manor house project [19]. Since the house was built during the same period, in the same area and employing identical building techniques and materials, the resemblance allows to use the results for the ongoing research project.

2.3. Damage survey

The fort was last used as headquarters for the "Escuela Taller de Lima". Its administrators performed different projects for refurbishing and damage repair. However, the school closed, and the building changed hands, being now of the jurisdiction of the Ministry of Culture. After that, it was left almost abandoned. Thus, the level of damage in the building at the time of the survey was huge. These damages not only compromise the aesthetics of the structures but also affect their structural capacity, which is why it is necessary to carry out an in-situ data recompilation. The results are summarized in the following lines by means of photographs, as a previous step to define what type of reinforcement will be carried out in it.

Beginning with the first floor, the most notable damage to the facades are multiple fractures generally followed by detachment of the exterior cladding and partial demolition of parts of the masonry walls, with material expulsion. The latter happening specially in the vicinity of the openings that serve as windows (Figure 5: a) and at the joints of the first and second floor walls, as well as at the corners (Figure 5: b.).

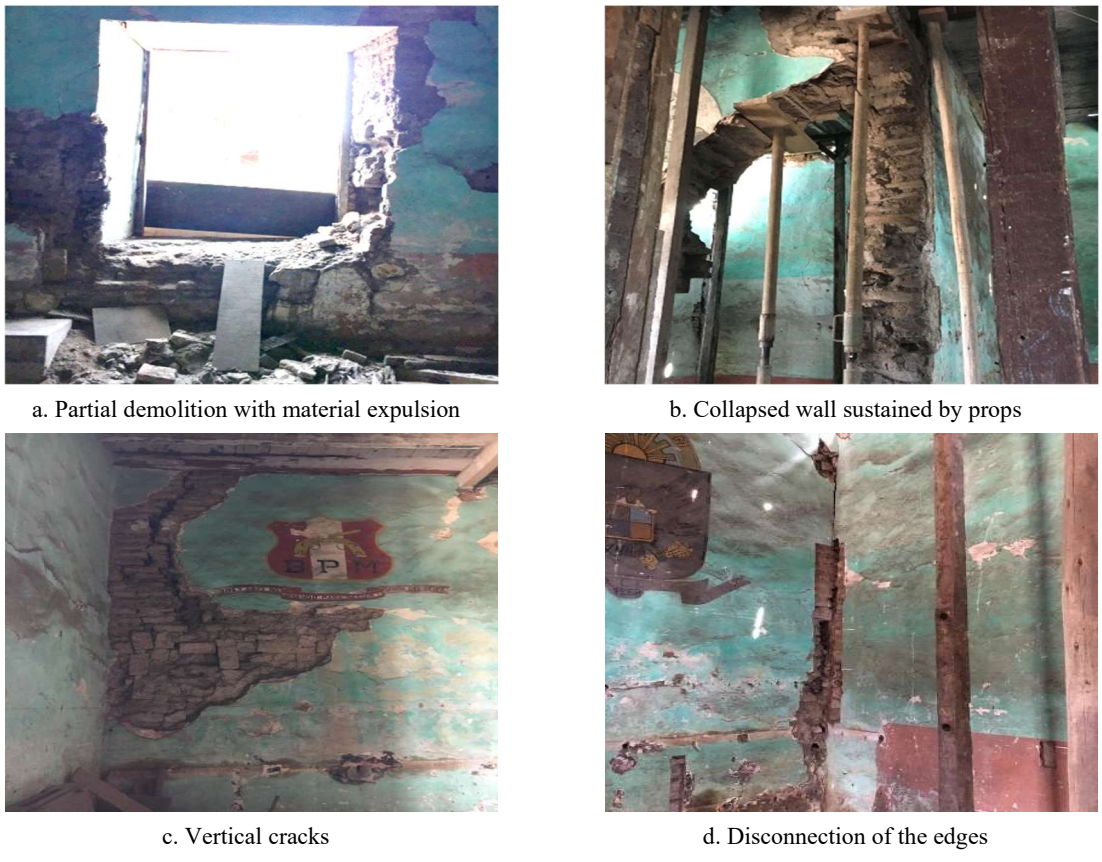


a. Cracks, cladding detachment and partial of walls b. Partial demolition with material expulsion in corner

Figure 5. External facade of the first floor.

Inside this level, it also takes place detachments of material on the walls (Figure 6: a.). One of them, which served to separate a small room from the main one, has collapsed (Figure 6: b.). In addition, the presence of vertical cracks extends throughout all the load-bearing walls (Figure 6: c.), causing disconnection of all the edges between adobe masonry walls, making them work separately and not allowing a box effect (Figure 6: d.). Other important damages are those related

to the beams, highlighting the multiple fractures in the main beam supporting the girders and the deterioration of the girders that separate both levels.



a. Partial demolition with material expulsion

b. Collapsed wall sustained by props

c. Vertical cracks

d. Disconnection of the edges

Figure 6. First floor damages.

The analysis continues on the second floor. The only access to it is by a wooden stairway in a high state of deterioration. The quincha walls used as separation elements for the sixteen departments that conform the second floor have damages generated by the attack of xylophages. This causes the need to rebuild the quincha walls (Figure 7: a.) and the girders from the wooden slab as well because of their high deterioration. Finally, it can be seen how the walls of the rear facade, are inclined, making it necessary to support them with braces (Figure 7: b.).

In its current state the building can only stand thanks to a series of wooden and steel braces all around the main space, which support the main and secondary girders and avoid imminent collapse. Therefore, the retrofitting must begin with a reconstruction to provide the building its original mechanical properties.



a. Damaged quincha walls b. Inclined rear facade

Figure 7. Second floor damages.

2.4. Seismic vulnerability assessment

After an exposition of the mechanisms that govern the structural behaviour of the building, the materials' characteristics and the damages present in the structure, an assessment of its seismic performance must be done. For this purpose, the Peruvian Standard for seismic design of structures [12] is to be followed. In the case of earth structures, a special standard is employed [13].

Lima is located in Zone 4, the area with the highest seismicity in Peru. The main effect of a seism is a ground acceleration that translates into horizontal forces in our structure. In the case of Fort of Santa Catalina, it is founded in a relatively high capacity soil of compacted gravel and a sandy matrix, with a bearing capacity of around $11.08\ MPa$ [14]. According to the standard, for this area, soil factor and use factor, the horizontal forces for design are 0.35 times the weight of the building.

It can be noted that this factor is used for new construction, where special criteria for the materials and the design are to be followed. However, for the reinforcement of the "Cuadra" there is no appliable standard or guidelines to follow, so a different approach oriented to literature and state of the art practices must be considered. What is more, the building has features that affect positively or negatively to its seismic performance and differ from today's design guidelines. Beginning with details from the original design, the ground plan configuration is inadequately asymmetrical and with a much longer dimension than the other. These long spans are not reinforced nor confined intermediately, causing out-of-the-plane stresses induced by the earthquake to be inacceptable. What is more, the vertical loads from the second floor are not transmitted straight to the adobe bearing walls but with a certain gap, inducing moments in the walls. Lastly, the enormous damages existing in the structure barely allow it to resist its own weight, much less the effects of an earthquake, with all the adobe walls working separately due to the disconnected corners.

On the other hand, the combination of a stiff first floor with a flexible quincha second floor, as mentioned in chapter *2.1*, presents a good seismic performance. This combination of building materials was settled by the Spanish through a Royal Order, after the huge earthquake in 1756 [18]. This combination, together with the good quality of the soil and the foundation, is probably

the reason why the building remains standing and has not already collapsed in previous earthquakes.

Finally, it must be noted that the most likely outcome (without an intervention) in the event of a seism is the collapse of the building. However, a complete seismic vulnerability assessment is still needed, for which material testing will become vital. The retrofitting alternatives, consequently, must be designed to avoid the main failure modes under cyclic loads for this particular building.

3. ANALYSIS OF RETROFITTING ALTERNATIVES

Given the seismic vulnerability of the building achieved from the construction survey data assessment carried out, a range of possible retrofitting alternatives were evaluated in order to improve the seismic behaviour of this construction. Based on the information obtained from the field work research and the available reference literature on this topic, the retrofitting solutions were analysed according to different criteria, such as seismic response, conservation principles, material and installation costs, installation feasibility and compatibility. Table 1 presents an evaluation of the common retrofitting solutions. In this line, some of them are immediately discarded for being too invasive and incompatible with the original building materials.

According to the analysis carried out and considering the existing level of damage that the structure presents currently, it was decided that the adequate solution to be adopted was a combination of actions to reinforce the walls structurally, allowing them to resist seismic actions and weather variations, as well as those inherent to the weight of the structure, to be assumed by its walls, without them suffering cracks and subsequent overturning.

Table 1. Summary of the evaluation of the most common retrofitting solutions

Vertical confinement with reinforced concrete tie columns	
Seismic response	The confinement prevents disintegration and improves ductility and energy dissipation of unreinforced masonry buildings but has limited effect on the ultimate load resistance [16]. Actually, the masonry being confined by reinforced concrete frame may behave effectively as a diagonal compressive strut under lateral loading and may improve the behaviour considerably as compared to what is observed in case of a bare frame (frame containing concrete columns and beams only) [1].
Conservation values criteria	It is an invasive and destructive procedure, much more intrusive than permitted by conservation standards [6].
Costs and feasibility	This type of seismic retrofit is expensive [6]. Indeed, requires demolition and reconstruction of wall sections making it uneconomical [1].
Compatibility	The combination of concrete and adobe may result in problems of material compatibility that will be realized only years after the original retrofit [6]
Horizontal superior confinement with concrete bond beams placed at the tops of walls below the roof	
Seismic response	Provides out-of-plane strength and stiffness. Also, lateral support and continuity enough to transmit the loading from the out-of-plane walls to the in-plane walls. However, bond beam when used without other retrofit measures is not enough to restrain the movements of the cracked block sections of the walls [6]
Conservation values criteria	It's an invasive and destructive procedure [6] much more intrusive than permitted by conservation standards [6].

Costs and feasibility	This type of seismic retrofit is expensive and requires the removal of the roof system [6].
Compatibility	The combination of reinforced concrete and adobe may result in problems of material compatibility that will be realized only years after the original retrofit [6].
External polymer mesh (industrial geogrid and construction site "soft" fence)	
Seismic response	Increases the stiffness, strength and deformation capacity of the adobe walls [15]. Prevents partial or total collapse of adobe buildings [7]. Placing the mesh in critical locations can be enough to avoid collapse [7]. The mud plaster over the external reinforcement increases the initial shear strength and the stiffness of the walls [7].
Conservation values criteria	It is not reversible and cannot be applied on surfaces that must be preserved in their original form (wall paintings, frescoes, adornments, etc.) [17].
Costs and feasibility	Should be placed on both sides of the walls, and tightly connected through the walls [7]. It is convenient to cover the reinforcement mesh with mud plaster, but it is not necessary to completely cover the walls with the polymer mesh [7]. It's an economical solution [7].
Compatibility	The mesh works well together with the adobe walls even for high levels of seismic intensity [7].

3.1. Wooden porticos

Although reinforced concrete would be a more efficient solution by cost and seismic response, according to Table 1 the high incompatibility of concrete with the original materials makes its use unadvisable.

This solution consists in the insertion of wooden profiles in the walls that make up the building's facades. They shall be arranged at the corners and along the length of the same, embedded in its section. They shall be linked by another wooden beam, arranged horizontally, at the intersection between the two levels in the form of porticos that receive the loads from the upper floor and distribute them to the ground.

3.2. Repair of the adobe walls

Adobe walls will be reconstructed (for those which already collapsed) or repaired. The damaged sections of the walls will be torn down and rebuilt employing similar adobe bricks to the original ones.

3.3. Geogrid retrofit

In order to prevent partial or total collapse of building's adobe walls as well as to increase their stiffness, strength and deformation capacity, a state-of-the-art polymer mesh of industrial geogrid is going to be applied for the seismic retrofit of the building. This intervention will be completed with a cover of the reinforcement mesh made of mud plaster.

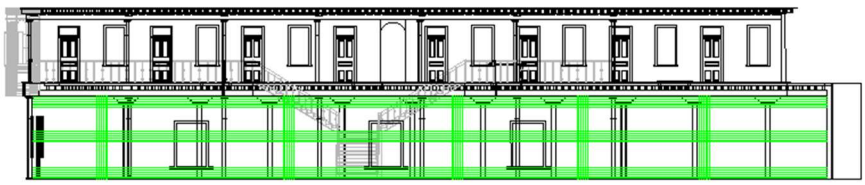


Figure 8. Frontal view of the building with the geogrid applied.

3.4. Lime and earth mortar

Once again, the more efficient solution of application of shotcrete cannot be performed due to the high incompatibility and lack of "breathing" for the adobe wall. In this line, plaster will be made with a mortar composed of lime and earth, both natural materials, constituting a much less invasive solution.

3.5. Replacement of the central beam, pillars and slab girders

The damaged wood beam shall be removed, and the wooden girders repaired or replaced in order to allow a central open space without the multiple struts currently present in the structure.

The already mentioned inclusion of porticos will reduce the number of pillars needed for the central beam, giving the interior more usefulness.

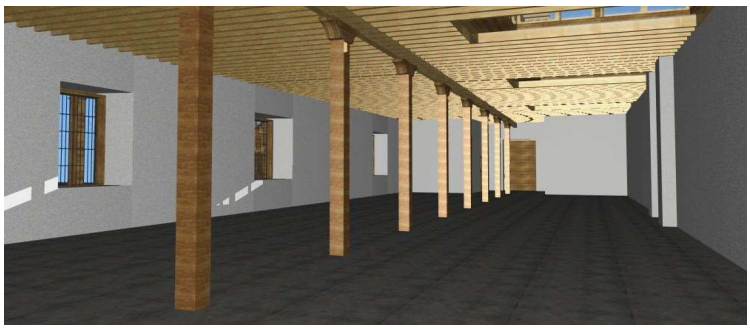


Figure 9. 3D simulation of the main space (Source: Escuela Taller de Lima, 2007).

3.6. Reconstruction of the second level

This action will be done maintaining its constructive nature, that is, the reconstruction will be in quincha panels between wooden columns that constitute the different divisions in the original plans. In addition, the wooden slab, on which the upper level rests, will be rebuilt consisting of wooden beams that will distribute the loads they receive towards the bearing walls of the lower level.



Figure 10. 3D simulation of the main facade (Source: Escuela Taller de Lima, 2007).

4 CONCLUSIONS

The results achieved in the analysis of the case study building permitted to accomplish relevant information about the possible structural and constructive solutions to be adopted, along with its current damage level.

This knowledge allowed the preliminary evaluation of its seismic vulnerability and a proposal of an appropriate retrofitting solution for the building.

A future research based on materials characterization and a numerical modelling structural assessment of building's seismic performance, with and without the retrofitting measures, should be conducted in order to confirm the obtained results on the seismic vulnerability of the construction and the suitability of the retrofitting solutions proposed.

One conclusion is clear: the high value of the building and the excellent retrofitting results that can derive from the intervention make it worth it to be restored.

This paper contributes also to the knowledge of this kind of adobe masonry historical heritage buildings, especially the Peruvian ones, as well as to a possible approach to its assessment, and the information obtained can be used as a reference for future case studies.

ACKNOWLEDGMENTS

The authors are greatly acknowledged for the contribution of Leslie Quiroz, Luiggi Vargas, Edwards Gonzales, Jaffet Villena and the personnel of the Laboratory of Structures of Pontificia Universidad Católica del Perú in this project.

A special recognition for the architect Jorge Larrea for his contributions and support for the realization of this work; and to Escuela Taller de Lima for the access to their files and previous works about the fort of Santa Catalina.

REFERENCES

[1] Bhattacharya, S., Nayak, S. and Chandra, S. A critical review of retrofitting methods for unreinforced masonry structures, *Int. J. Disast. Risk Reduct.*, 7 (2014), pp. 51-67.
[2] Instituto Nacional de Estadística e Informática (INEI) – PERÚ, *Características de las viviendas particulares y los hogares*. Censos Nacionales de Población y Vivienda (2017).
[3] Tarque, N., Salsavilca, J., Yacila, J. and Camata, G. Multi-criteria analysis of five reinforcement options for Peruvian confined masonry walls. *Earthquake Struct* 17(2) (2019), pp. 205–219.
[4] Tavera, H. Escenario de Sismo y Tsunami en el borde occidental de la región central del Perú, *Dirección de Sismología, Instituto Geofísico del Perú*, Lima- Perú. 30 pp. (2014).
[5] Tavera, H. Actualización del escenario por sismo, tsunami y exposición en la región central del Perú, *Dirección de Sismología, Instituto Geofísico del Perú*, Lima- Perú. 24 pp. (2017).
[6] Tolles, L., Kimbro, E., Webster, F. and Ginell, W. Seismic Stabilization of Historic Adobe

Structures, *Final Report of the Getty Seismic Adobe Project*, The Getty Conservation Institute, Los Angeles (2000).

[7] Blondet, M., Torrealva, D., Vargas, J., Velasquez, J. and Tarque, N. Seismic reinforcement of adobe houses using external polymer mesh. *First European Conference on Earthquake Engineering and Seismology*, Geneva, Switzerland (2006).

[8] Rouhi, J., and Hejazirad, F. A Review on the Large-Scale Modeling for Seismic Strengthening of Adobe-Mud Brick Structures, *International Conference on Civil Engineering, Architecture and Urban Management in Iran*, Tehran University (2018).

[9] Yacila, J., Salsavilca, J., Tarque, N. and Camata, G. Experimental assessment of confined masonry walls retrofitted with SRG under lateral cyclic loads, *Engineering Structures*, 199 (2019) 109555.

[10] Tavares A., D'Ayala D., Costa A. and Varum H. Construction Systems. In: Costa A., Guedes J., Varum H. (eds) *Structural Rehabilitation of Old Buildings. Building Pathology and Rehabilitation*, vol 2. Springer, Berlin, Heidelberg (2014).

[11] Santa María, A.E. and Torrealva, D.E. Comportamiento dinámico de una estructura mixta de dos pisos compuesta por adobe y quincha, *Pontificia Universidad Católica del Perú: Facultad de ciencias e ingeniería.* Lima, Perú (2018).

[12] MVCS. Norma Técnica E.030 Diseño Sismorresistente. *Ministerio de Vivienda, Construcción y Saneamiento.* Perú (2018).

[13] MVCS. Norma E.080 Diseño y Construcción con Tierra Reforzada. *Ministerio de Vivienda, Construcción y Saneamiento.* Perú (2017).

[14] Tavera, H., Bernal, I. and Gómez, J.C. Zonificación sísmico-geotécnica para el centro histórico de Lima, *Sistema de Información para la Gestión del Riesgo de Desastre, Centro Nacional de Estimación, Prevención y Reducción del Riesgo de Desastres* (2010).

[15] Blondet, M., Villa Garcia, G., Brzev S. and Rubiños, A. *Earthquake-resistant construction of adobe buildings: A tutorial.* Oakland: 2010 Earthquake Engineering Research Institute (2011).

[16] Elgawady, M., Lestuzzi, P., and Badoux, M. A Review of Conventional Seismic Retrofitting Techniques for URM. *13th international brick and block masonry conference*. Amsterdam, Netherlands (2004).

[17] Peña, F. and Lourenço, P. Criterios para el refuerzo antisísmico de estructuras históricas. *Revista de Ingeniería Sísmica*. 87 (2012) pp. 47-66 Sociedad Mexicana de Ingeniería Sísmica Distrito Federal, México (2012).

[18] Blondet, M., Vargas, J., Tarque, N. and Iwaki, C. Seismic resistant earthen Construction: the contemporary experience at the Pontificia Universidad Católica del Perú. *Informes de la Construcción Vol. 63, 523, 41-50.* Julio-septiembre 2011.

[19] Cancino, C., Lardinois, S., D'Ayala, D., Fonseca, C., Torrealva, D., Vicente, E. and Villacorta, L. Proyecto de Estabilización Sismorresistente: Estudio de edificaciones tipológicas, Vol. 1. *The Getty Conservation Institute*. Los Angeles (2012).

12th International Conference on Structural Analysis of Historical Constructions
SAHC 2020
P. Roca, L. Pelà and C. Molins (Eds.)

SEISMIC STABILITY ANALYSIS OF INCA EARTHEN WALLS

ARTURO TORRES[1*], MARCIAL BLONDET[2] AND SANDRA SANTA CRUZ[2]

[1]e-mail: arturo.torres@pucp.pe

[2] Departamento de Ingeniería
Sección Ingeniería Civil, Pontificia Universidad Católica del Perú (PUCP)
Avenida Universitaria 1801, San Miguel 15088, Lima, Perú
email: {mblondet, ssantacruz}@pucp.edu.pe, www.pucp.pe

Keywords: Inca walls, Rocking, Adobe, Tapial

Abstract. *In many places around the world there still exist statues, walls and columns which, despite being located in areas of high seismicity, are still standing and in good conditions after several hundred years. Although Peru is located on a zone of high seismicity, some preColumbian walls are still standing after having withstood many intense earthquakes. The remarkably stable dynamic response of these structures when rocking freely due to horizontal ground motions has been extensively studied [1] [2]. The aim of the project presented in this article is to evaluate the probability of seismic overturning of Inca monuments (XVth century CE) during future strong earthquakes. The Wiracocha temple walls located near Cusco and the Inca trail walls that cross the PUCP campus in Lima were selected for this study. Both earthen walls were modelled as free-standing rigid blocks which could rotate around the corners at their base. A set of synthetic ground acceleration signals were then generated according to the seismicity and ground conditions of both sites. The artificial ground acceleration records were scaled to the uniform hazard spectrum of Peru for return periods of 500, 1000 and 2500 years and different moment magnitudes [3] [4]. The rocking time history response of each wall due to these ground motions was then numerically computed and plotted in order to assess the seismic risk due to overturning of these important earthen monuments.*
The main conclusion is that these walls will most probably remain standing for many more centuries.

1 INTRODUCTION

In many areas of high seismicity across the world you can visit historical monuments that are simply supported and are still standing and in good condition many centuries after being built. In Peru, for example, some pre-Columbian walls have survived several intense earthquakes, while other similar structures have collapsed. This work aims to give some explanations for this phenomenon by analyzing the seismic rocking response of rigid blocks.

The rocking of rigid blocks subjected to horizontal base motions has been extensively studied ever since Housner published a seminal article on the topic [1]. Since then, many researchers have expanded significantly on the theory (see, for example, [2]) and developed analytical, numerical and experimental studies to better understand this interesting and

complex phenomenon.

This article briefly presents the analytical formulation and a numerical method to estimate the rocking response of rectangular rigid walls caused by horizontal seismic excitation at the base. The mathematical expressions presented were then used to evaluate the seismic safety of two Peruvian pre-Hispanic monuments. For this study, a portion of the wall of the temple of the god Huiracocha in Raqchi, near Cusco, and a portion of the border wall of the Inca trail that crosses the PUCP campus (in Lima) were selected. Both earthen walls were built in the Inca period, during the 15th century AD. Ground shaking was characterized by a set of synthetic horizontal acceleration signals, generated according to the local seismicity and soil conditions of both locations. For each site, synthetic accelerograms were generated corresponding to return periods of 500 years (rare earthquake), 1000 years (very rare earthquake) and 2500 years (extraordinary earthquake), and for moment magnitudes consistent with the local seismicity [3][4]. The time history rocking response of each wall was calculated numerically and then the overturning seismic risk of these important earthen monuments was then evaluated.

The main conclusion of the study is that the Inca wall at PUCP will probably collapse during a future earthquake, while the Huiracocha wall in Raqchi will remain standing for many more centuries.

2 SEISMIC ANALYSIS OF RIGID BLOCKS

In 1963 Caltech professor George Housner published an article on rigid block vibrations, where he presented the equation describing the movement of a block that wobbles around its lower corners due to the movement of its base. There is extensive literature on the rocking response of rigid solids subjected to earthquakes, as well as a large number of analytical, numerical and experimental investigations on that subject. Figure 1 presents the geometric parameters of the generic rigid block studied in this article. The block size is characterized by the radius R and the slenderness is described by the characteristic angle α = atan(b⁄h). The rocking response of the block around its base corners is described by the variation in time of the rotation angle θ.

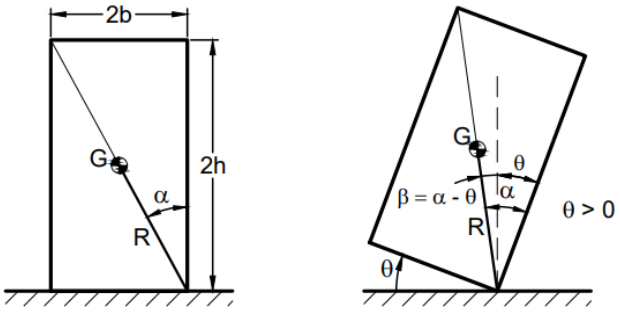


Figure 1 Geometric parameters of the rigid block

If a rigid block is subjected to an acceleration at its base $\ddot{u}_g(t)$, it will move together with the ground as long as $\ddot{u}_g < \mu g$ where μ is the coefficient of static friction between the block and the ground and g is the acceleration of gravity.

The condition for no slip in the base is then

$$|\ddot{u}_g| < \mu g \tag{1}$$

the block will not uplift as long as the moment of the inertia forces is less than the resistant moment due to the weight, that is if $m\ddot{u}_g h < mgb$. Therefore, the condition for the block to start rotating around a lower corner is

$$|\ddot{u}_g| \geq gb/h \tag{2}$$

2.1 Rocking equation of motion

The equations of motions developed by Housner (1963) are presented here. Rocking response of a rectangular block was expanded on and discussed in detail by Makris and Roussos (2000) [5]. It is assumed that the block is perfectly rigid and that impact with the ground is produced by a concentrated force acting in a lower corner. The rocking equations of motion are the following,

When the angle of rotation is positive,

$$I_0\ddot{\theta} + mgRsen(\alpha - \theta) = -m\ddot{u}_g Rcos(\alpha - \theta), \ \theta > 0 \tag{3a}$$

Meanwhile, when the angle of rotation is negative,

$$I_0\ddot{\theta} + mgRsen(-\alpha - \theta) = -m\ddot{u}_g Rcos(-\alpha - \theta), \ \theta < 0 \tag{3b}$$

For rectangular blocks, $I_0 = (4/3)\, mR^2$, and the equations (3) are expressed as

$$\ddot{\theta}(t) = -p^2\, I_0(sen(-\alpha - \theta(t)) + \tfrac{\ddot{u_g}}{g}\, cos(-\alpha - \theta(t)), \ \theta < 0 \tag{4a}$$

$$\ddot{\theta}(t) = -p^2\, I_0(sen(+\alpha - \theta(t)) + \tfrac{\ddot{u_g}}{g}\, cos(+\alpha - \theta(t)), \ \theta < 0 \tag{4b}$$

Where $p = \sqrt{3g/4R}$ it is a parameter with angular frequency units (called "frequency parameter" although it is not proportional to the angular natural frequency ω_n).

The principle of conservation of angular momentum implies that the block loses energy every time the pivot moves from one corner to the other at each swing. If the coefficient of restitution r is defined as the ratio between kinetic energies after and before impact, that is $\sqrt{r} = \frac{\dot{\theta}_1}{\dot{\theta}_2}$, the equation published by Makris and Zhang (2001) [2] is obtained:

$$r = \left(1 - \frac{3}{2} sen^2\alpha\right)^2 \tag{5}$$

2.2 Numerical integration methods

A rigid block subjected to excitation at its base will begin to oscillate around a lower corner if $\ddot{u}_g > g\, b/h$ (equation 2) and, while the oscillations last, its movement will be governed by equations (3a) and (3b). There are several numerical methods to solve these equations and calculate the response of slender rigid blocks subjected to seismic excitation. This work uses the method presented by Santa Cruz (2000) [6], which is based on the method of interpolation of the excitation published by Chopra (2014) [7] to study the seismic response of viscoelastic oscillators.

The acceleration of the ground $\ddot{u}(t)$ must be discretized at equal intervals of duration Δt. If for the instant t_i, the angle of rotation θ_i, the angular velocity $\dot{\theta}_i$ and angular acceleration $\ddot{\theta}_i$, are known, we want to calculate these values for the next instant $t_{i+1} = t_i + \Delta t$.

The following expressions, in which $pt = p\ \Delta t$, $sh = senh\ pt$, and $ch = cosh\ pt$, are sufficient to calculate the rotation θ_{i+1} and angular velocity $\dot{\theta}_{i+1}$ at the end of the interval.

$$\theta_{i+1} = A\dot{\theta}_i + B\theta_i + C\ddot{u}_{i+1} + D\ddot{u}_i + K \tag{6a}$$

$$\dot{\theta}_{i+1} = A'\dot{\theta}_i + B'\theta_i + C'\ddot{u}_{i+1} + D'\ddot{u}_i + K' \tag{6b}$$

Where

$$A = sh/p \qquad A' = ch$$
$$B = ch \qquad B' = p.sh$$
$$C = (1 - sh/pt)\ /\ g \qquad C' = (1 - ch)\ /\ g\Delta t$$
$$D = (sh/pt - ch)\ /\ g \qquad D' = (ch - pt.sh - 1)\ /\ (g\Delta t)$$
$$K = \alpha(1 - ch)sgn(\theta_i) \qquad K' = -\alpha p.sh.sgn(\theta_i)$$

Finally, the angular acceleration of the block at the end of the interval $\ddot{\theta}_{i+1}$ is obtained from the equations of motion (3a and 3b).

2.3 Response to harmonic excitation

Manos and Demosthenous (1995) [8] studied the response of truncated cones subjected to harmonic displacements of amplitude A and circular frequency Ω. To interpret the results obtained, they produced a two-dimensional graph containing coordinate points (A, Ω) identified with the letter O if the block is overturned (Overturn), R if it rocks (Rocking), or N if It does not rock. In this work, an analogous graph was created for rectangular rigid blocks subjected to harmonic acceleration (Figure 2) where the type of response is represented by a symbol and the harmonic excitation is defined by the dimensionless amplitude $a_{gm}/g\alpha$ (a_{gm} is the peak acceleration, g is the acceleration of gravity and α is the characteristic angle of the block) and the frequency ratio ω_g/p.

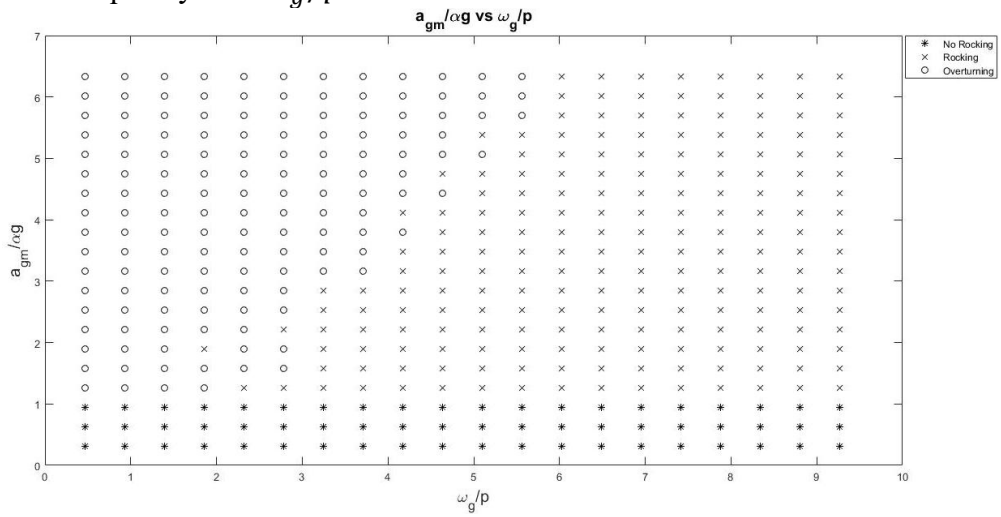


Figure 2 Response to harmonic excitation of the sinusoidal type

It is observed that, in the entire frequency range studied, if the amplitude of the harmonic movement is small, the blocks translate with the ground and that there is a well defined amplitude of the ground motion from which the blocks oscillate. For low frequencies, the blocks overturn, while for high frequencies the blocks oscillate, and only overturn when the intensity of the movement increases. As the intensity of the base motion increases, the frequency zone in which the blocks are turned widens, but the threshold that defines whether a block turns over is not clearly defined.

In order to visualize the dynamic behavior of the block subjected to harmonic excitation as a function of time, a three-dimensional response spectrum was drawn up, in which the variation of the dimensionless rotation response amplitude θ(t)/α is plotted as a function of time (in absolute value) for a series of rigid blocks with different frequency ratios ω_g/p. The intensity of the excitation is characterized by the dimensionless ratio PGA / g tan α. To calculate the response of rotation of each block, the ground acceleration record was smoothed by means of a Blackman-Harris window [9] so that the movement of the soil begins and ends smoothly. The 3D response spectrum is then a surface on the plane ω_g/p vs time, whose height is the dimensionless rotation response θ / α.

Figure 3 shows the 3D spectrum corresponding to an intensity PGA / g tan α = 4. The amplitude of the rotation at each moment is measured by the height of the surface above the base plane (θ = 0) and can be better visualized by the color, which varies from dark blue for small oscillations to yellow for large oscillations. The blocks are considered to overturn when the inclination of their diagonal exceeds the vertical, that is when | θ | > α. The black zone then represents the rotation response of the blocks that would have collapsed. The onset of collapse can be visualized as the intersection between the response surface and the horizontal plane θ / α = 1.

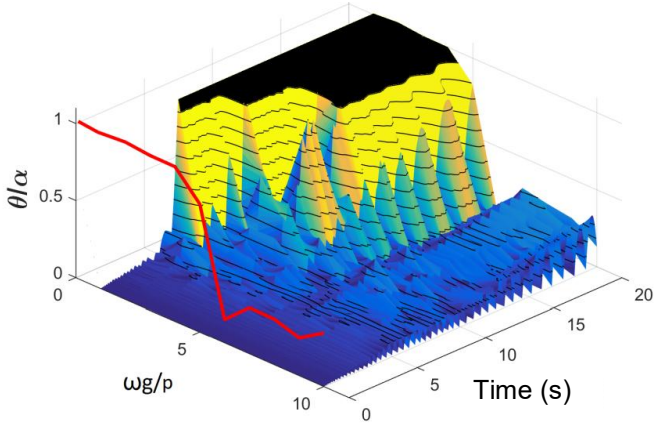


Figure 3 3D response spectrum of block rotation response to harmonic excitations

It is interesting to note that the projection of the 3D surfaces on the plane at t = 0 (the red line in Figure 3) represents the traditional 2D response spectrum, in which the maximum amplitude of the rotation response θ/α is plotted versus the frequency ratio ω_g/p.

To study the influence of the intensity of the harmonic excitation on the rigid block rotation response, the maximum rotation response for several intensity levels was calculated, and Figure 4 shows the results obtained.

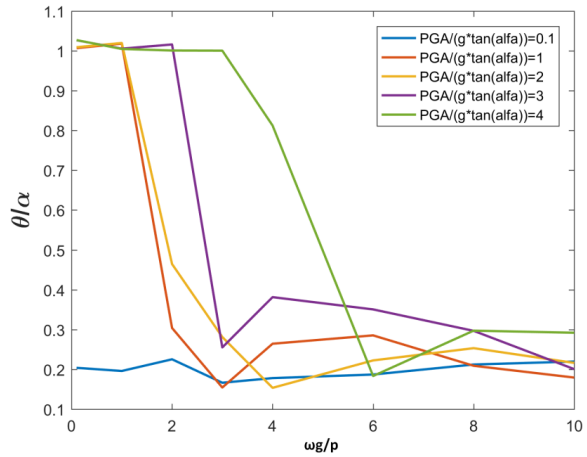


Figure 4 Block rotation response spectra for harmonic excitations

It is observed that for very low excitation levels (PGA ≤ 0.1 g tan α), the rotational response is also low, with θmax ≈ 0.2α and no overturning. For high intensities (PGA ≥ g tan α) and low frequencies some blocks tend to tip over a range of frequencies that increase as the intensity increases. A transition zone is noted between the overturning frequency range and the frequency range with low amplitude oscillations. Makris (2014) [10] and Bachmann et al. (2018) [11] also studied this phenomenon in great detail and produced graphs that show the complex relationship between the rocking response and the intensity and frequency characteristics of sinusoidal pulses. The authors of this paper generated Figure 5, which shows a 2D graph of rotational amplitude θ/α vs frequency ratio ω_g/p for ground shaking intensity PGA / g tan α = 5, in which the overturning black zone (θ/α = 1) is consistent with the Bachmann and Makris graphs.

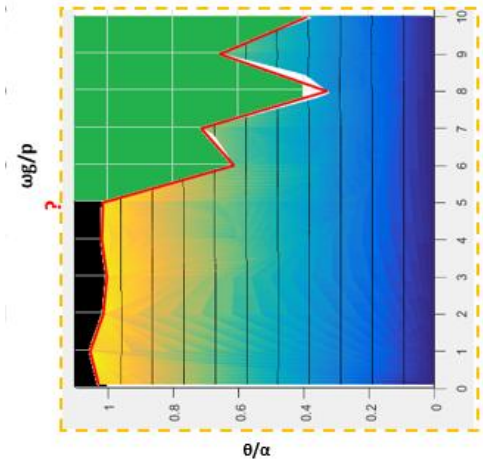


Figure 5 Rocking spectra

3 SEISMIC ANALYSIS OF THE INCA WALLS

The Huiracocha temple (Figure 6a) is located in the town of Raqchi, 118 kilometers from the city of Cusco. Legend says that Raqchi's citizens had stopped worshiping the god Huiracocha, and he, to punish them, sent a rain of fire. That is why after the punishment, the

people of Raqchi built this temple for his worship. Since the walls of the Huiracocha temple are damaged, the residents of Raqchi have decided to reinforce them as shown in Figure 6a.

Some walls of the Inca Trail (Figure 6b) are located within the PUCP university campus in the city of Lima, on the central coast of Peru. The Inca Trail (Qhapaq Ñan) is a walled road that in ancient times connected important sites of the Inca empire. Many sections of the trail were destroyed for the construction of the University Avenue road in Lima. The 467 meters of the Inca Trail that are inside the PUCP campus are conserved with great care by the university community.



a) Huiracocha Temple in Cusco



b) Inca Trail PUCP in Lima

Figure 6 pre-Hispanic earthen walls studied

The risk of seismic overturning of the Huiracocha Temple and the Inca Trail walls was evaluated by analyzing their rocking response to simulated earthquake motion. Ground shaking was specified via synthetic accelerograms corresponding to earthquakes with return periods of 500, 1000 and 2500 years. Each wall was modelled as a rigid rectangular solid with uniform density subjected only to horizontal seismic excitation at the base. The dimensions of each wall were measured in situ and the density of each material was estimated from known values. With these data, the geometric (b and h) and inertial (m and I_O) properties of the mathematical models of each wall were estimated. Then the rotational response of each wall to the ground motions earthquakes generated for each site was calculated. Finally, the seismic risk of each wall was characterized by the period of return of the earthquake capable of producing wall failure due to overturning.

To assess the vulnerability of historical monuments, it is necessary to estimate with confidence the seismic hazard of the region where they are located, for which it is required to have a large database of seismic records over time. In Peru, unfortunately, these records are still scarce and the use of synthetic accelerograms is required to perform seismic risk studies of important buildings such as historical monuments.

Synthetic signals appropriate to the sites studied were generated as follows: first, the distance to the nearest seismogenic source and the soil stiffness characteristics of each site were estimated. With this information, uniform hazard spectra were generated, and scaled to the spectral form of document FEMA 356 [12]. Finally, appropriate attenuation curves were applied in order to obtain acceleration spectra corresponding to earthquakes with return periods of 500 years (rare earthquakes), 1000 years (very rare earthquakes) and 2500 years (extraordinary earthquakes), respectively.

Peru is located in an area of high seismic activity due to the subduction process of the

Nazca plate below the South American plate. Figure 7 [3] shows the seismogenic sources corresponding to the capital city of Lima and the imperial city of Cusco. To generate the synthetic accelerograms used in this study for each of these cities, it was decided to use the SeismoArtif 2018 software.

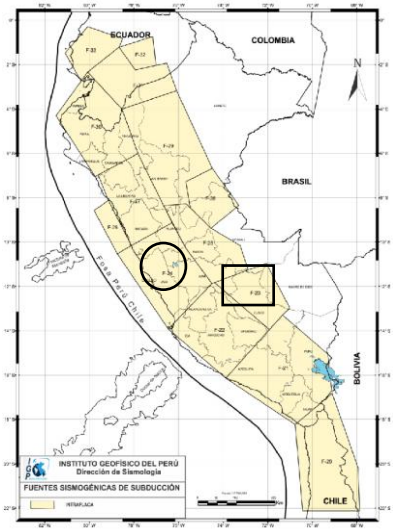


Figure 7 Map of seismogenic foci of Peru and location of Lima and Cusco

3.1 Accelerograms for Cusco

The seismogenic sources for Cusco come from cortical deformation processes (F-19 in Figure 7) and geometric effects of the Nazca plate under the continent (F-21, F-22 and F-23). Only the F-23 source was considered, being the closest to Cusco. The response spectra shown in Figure 8 were generated for return periods Tr of 475, 1000 and 2500 years and a rupture length of 10 km. The 475-year earthquake (usually referred to as the 500-year earthquake) corresponds to the design earthquake specified in the Peruvian Seismic Standard.

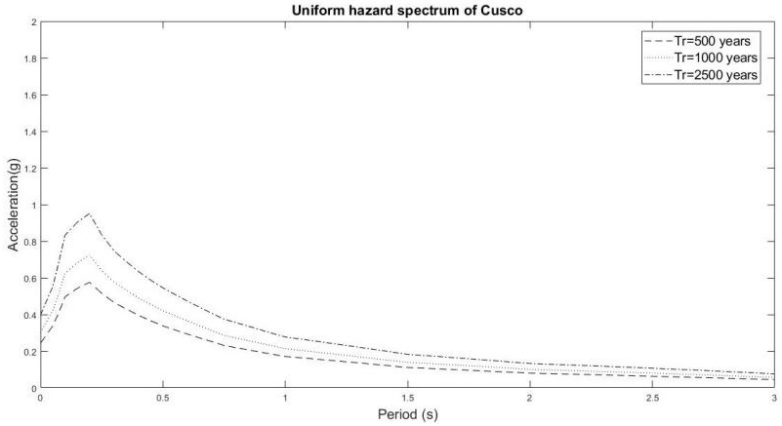


Figure 8 Spectra of synthetic earthquakes generated for Cusco

Figure 9 shows a set of synthetic accelerograms for the city of Cusco, compatible with the generated spectra.

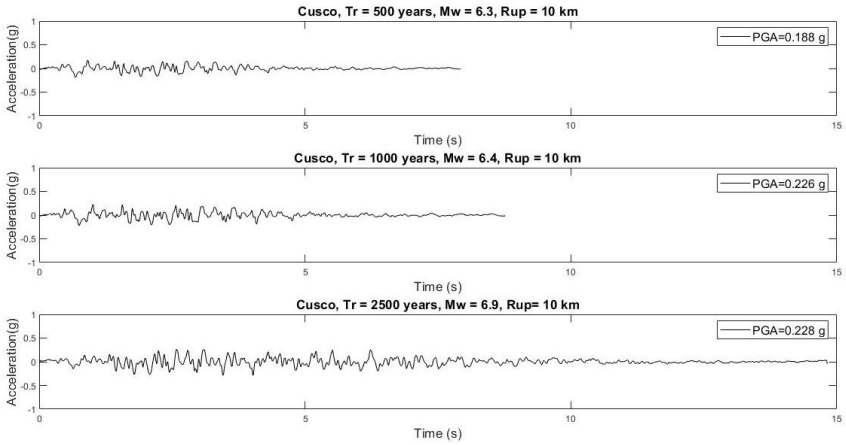


Figure 9 Synthetic accelerograms for Cusco

3.2 Accelerograms for Lima

The seismogenic sources for Lima shown in Figure 7 come from subduction (F-24) and interface (F-4) processes. Only the F-24 source was considered, as being the closest to Lima, with a rupture length of 25 km. The spectra generated for Lima appear in Figure 10 and a compatible set of accelerograms is shown in Figure 11.

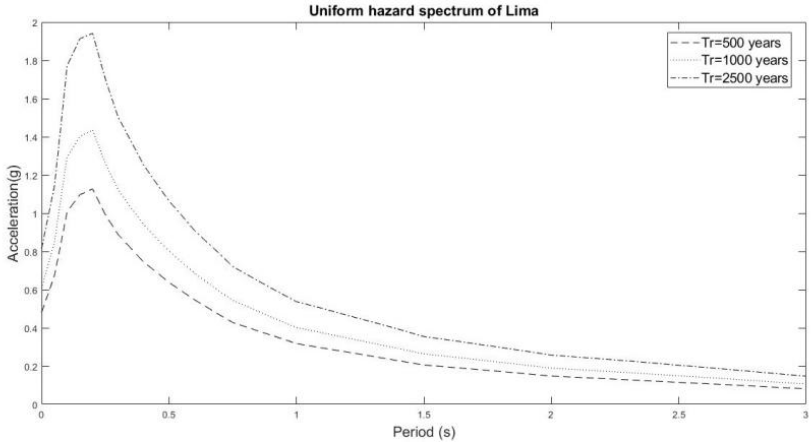


Figure 10 FEMA 356 Design Spectrum for Tr = 475 years, 1000 and 2500 years, (Barreto 2019)

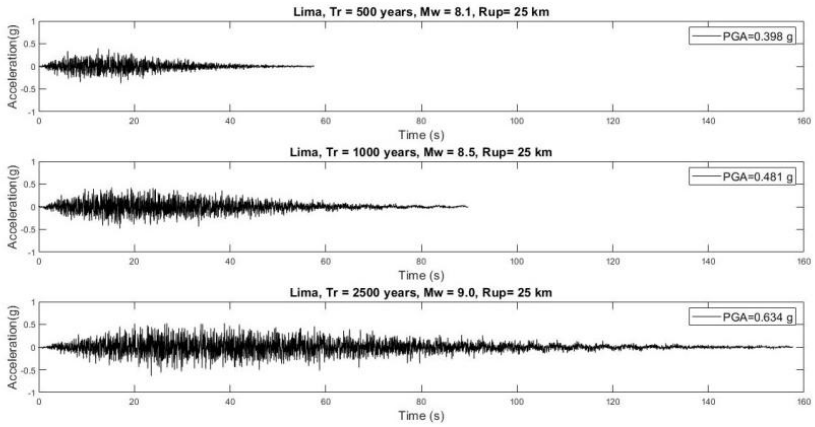
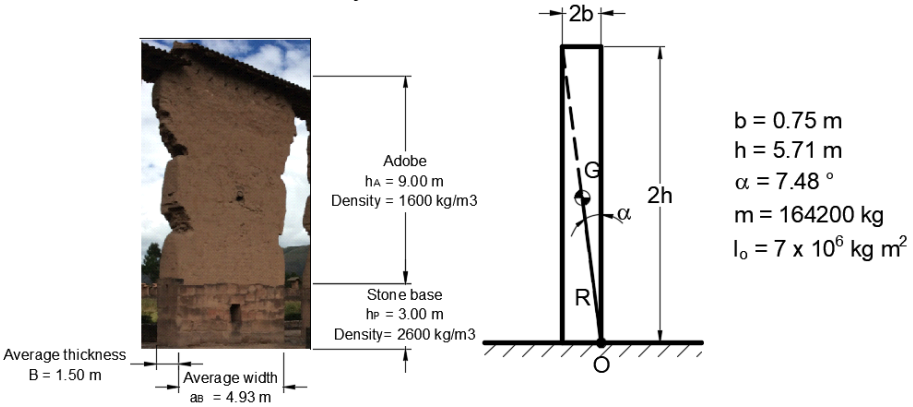


Figure 11 Synthetic accelerograms for Lima

3.3 Seismic analysis of the Huiracocha temple

The wall is composed of a stone base of total height H_P = 3 m and mass m_P = 57,700 kg, on which an adobe wall of height H_A = 9 m and mass m_A = 106,500 kg rests. The average wall thickness is 1.5 m and the average width is 5 m. The average density of the stone wall was considered to be 2600 kg/m^3 and the average density of the adobe wall is 1600 kg/m^3.

To perform the seismic analysis, the wall was modeled as a rigid rectangular solid of uniform material, with total mass $m = m_A + m_P$ = 164,200 kg, total height $2h$ = 11.42 m and base $2b$ = 1.50 m, so that the mathematical model has the same moment of rotational inertia I_o = 7.0x10^6 as the real wall. Figure 12 shows a photo of the wall and a drawing of the mathematical model used in seismic analysis.



a) Real wall b) Mathematical model

Figure 12 Portion studied from the wall of the Huiracocha temple

None of the generated ground motions was strong enough to cause wall overturning. The maximum rotation that the wall would experience due to the 2500-year earthquake would be around 1°, much smaller than the angle required to cause overturning (α = 7.48 °), as shown in Figure 12. Therefore, the wall of the Huiracocha temple is safe against overturning even with the most intense earthquake possible in Raqchi.

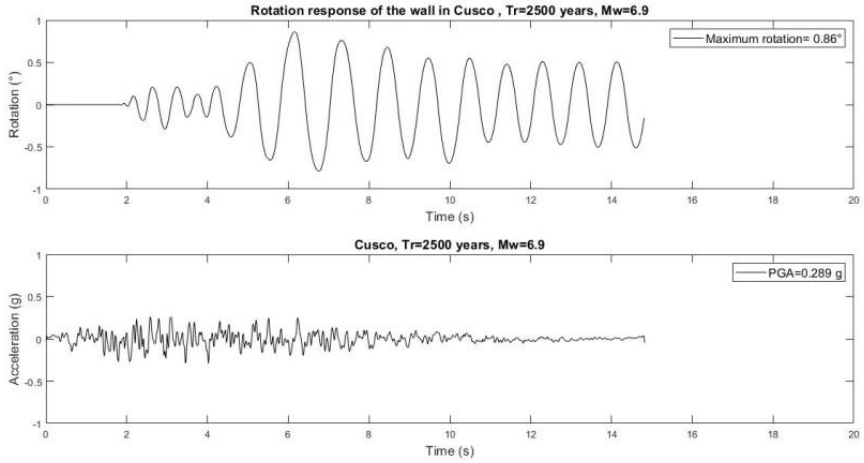
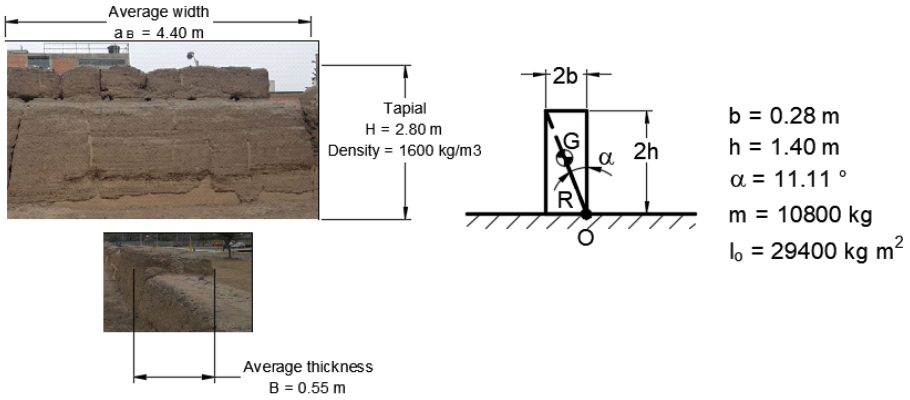


Figure 13 Rotation response of the Huiracocha temple wall for a synthetic signal of Tr = 2500 years and Mw = 6.9

3.4 Seismic analysis of the PUCP Inca Trail in Lima

The out-of-plane seismic response of the wall portion shown in Figure 14a was studied. The wall is made of *tapial* and has a total height *2h* of 2.80 m and a total mass *m* of approximately 10,800 kg. The average wall thickness is 0.55 m and the average width is 4.40 m. The average density of the material was considered to be 1,600 kg/m^3.



a) Real wall b) Mathematical model

Figure 14 Portion studied of the wall

Dynamic analysis of the wall reveals that this wall would rock without overturning during the 500-year earthquake, but that it would overturn due to the 1000-year earthquake, as shown in Figure 15.

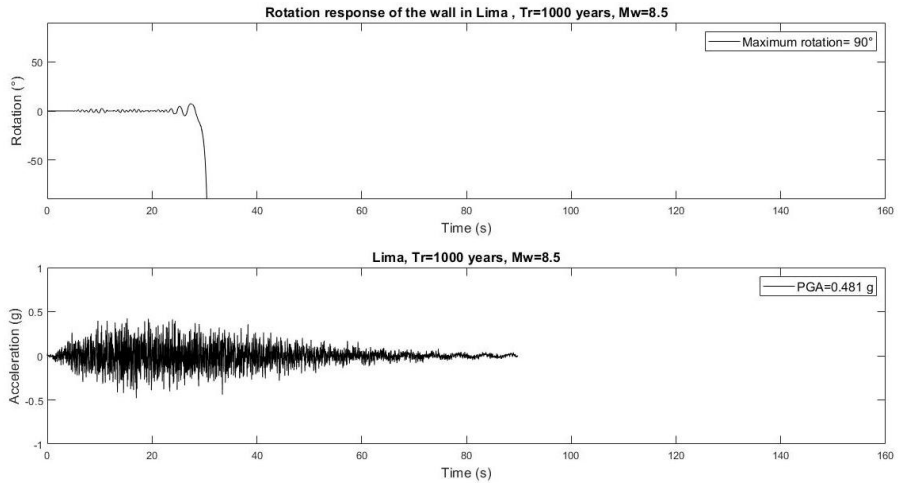


Figure 15 Response of the PUCP Inca Trail wall to a synthetic ground motion with Tr = 1000 years and Mw = 8.5

4 CONCLUSIONS

In several highly seismic areas of the world there are independent, simply supported historical monuments that have survived intact for many centuries, while nearby buildings have collapsed. This information is surprising and motivating to study the seismic response of rigid solids that respond by rocking under base movements.

Although the oscillating movement of rigid blocks subjected to excitation at the base is

complex, it is possible to develop reasonable equations of motion assuming perfectly elastic impact forces concentrated in the corners. These equations can be solved numerically with acceptable precision by methods widely available in the literature. In particular, the method of excitation interpolation has yielded seemingly reliable results to study the response of the pre-Hispanic walls of Raqchi and the Inca Trail.

The 3D response spectra allow visualization of the evolution of the dynamic response of rigid blocks with different physical characteristics subjected to harmonic excitation in the base, and seem useful to describe the complex phenomenon of the rocking response of structures that can be modeled as rigid blocks.

The return period of the earthquakes that would cause the walls to overturn is a useful piece of information to make decisions on the seismic protection for these valuable structures. For example, consideration should be given to adopting measures to improve the seismic protection of the walls of the Inca Trail. The methodology used in this work could be extended to evaluate a greater number of monuments and thus contribute to the improvement of the conservation and protection policies of historical monuments in seismic areas of the world.

REFERENCES

[1] Housner, G. W. (1963). The behavior of inverted pendulum structures during earthquakes. *Bulletin of the Seismological Society of America*, 53:2, 403–417.

[2] Zhang, J., & Makris, N. (2001). Rocking Response of Free-Standing Blocks Under Cycloidal Pulses. *Journal of Engineering Mechanics*, 127(May), 473–483.

[3] Tavera, H. (2014). Re-evaluación del peligro sísmico probabilístico para el Perú, IGP.

[4] Roncal, M. (2017). Determinación del peligro sísmico en el territorio nacional y elaboración de aplicativo web.

[5] Makris, N., & Roussos, Y. S. (2000). Rocking response of rigid blocks under near-source ground motions. *Geotechnique*, 50:3, 243–262.

[6] Santa Cruz,S.,Ordaze,M.,Guerrero del Ángel,R. (2017). Estimación de pérdidas en contenidos ubicados dentro de naves industriales debido a sismos. *Sociedad Mexicana de Ingeniería Estructural.*

[7] Chopra, A. (2014). Dinámica de Estructuras. *Pearson Educación de México*.

[8] Manos, G. C., & Demosthenous, M. (1995). Models of Ancient Columns and Colonnades Subjected to Horizontal Base Motions-Study of their Dynamic and Earthquake Behaviour. Transactions on the Built Environment, 8, 1–3.

[9] Harris, F. (1978). On the use of Windows for Harmonic Analysis with the Discrete Fourier Transform.

[10] Makris, N. (2014). A half-century of rocking isolation. *Earthquake and Structures*, 7:6, 1187–1221.

[11] Bachmann, J. A., Strand, M., Vassiliou, M. F., Broccardo, M., & Stojadinović, B. (2018). Is rocking motion predictable? *Earthquake Engineering and Structural Dynamics*, 47:2, 535–552.

[12] Federal Emergency Management Agency (FEMA), & (ASCE), A. S. of C. E. (2000). Prestandard and commentary for the seismic rehabilitation of buildings. *Federal Emergency Management Agency.*

12th International Conference on Structural Analysis of Historical Constructions
SAHC 2020
P. Roca, L. Pelà and C. Molins (Eds.)

SIMPLIFIED METHOD FOR THE LATERAL STRENGTHENING OF EARTHEN CHURCHES

ROSSEMARY ENCISO[1*], MARÍA N. NOEL[1] AND RAFAEL AGUILAR[1]

[1]Engineering Department, Civil Engineering Division
Pontificia Universidad Católica del Perú
Av. Universitaria 1801, Lima, Perú
e-mail: {rossemary.enciso, mariaf.noel, raguilar}@pucp.pe

Keywords: Limit analysis, buttress design, Andean colonial churches

Abstract. *The evaluation of the seismic safety of Andean colonial churches is of high importance as those buildings represent part of the identity of the society and are historical emblems for the communities. Most of these buildings are composed of elongated naves with adobe masonry walls with flexible (or nonexistent) horizontal diaphragms, which generates potential of out-of-plane failures. In the last decades, different methodologies using advanced numerical analyses have been developed that allow evaluating the structural behavior of historical constructions at the expense of an arduous computational effort. In the present paper, a simplified tool is proposed for the design of walls lateral reinforcement using buttresses. The tool uses limit analysis and provides an adequate buttress design according to the configuration of the wall and seismicity of the area where the church is located. The results of the application of the methodology showed that the developed tool provides fast and accurate alternatives for the seismic strengthening of Andean adobe churches. The use of buttresses as structural reinforcement control the development of out-of-plane failure mechanisms, and provide lateral stability and resistance to the structure.*

1 INTRODUCTION

Unreinforced masonry constructions are a significant percentage in different urban areas around the world, with heritage buildings being the most representative. However, in the case of seismic events these buildings do not behave satisfactorily due to their lack of structural capacity, which is why they are known as the most vulnerable constructions to suffer irreparable damage [1-2]. In recent decades, there has been an increase in interest in the conservation of heritage buildings as a way of preserving the history of a region. Currently, there are numerous methods of analysis and computational tools available for the evaluation of the mechanical behavior of historic structures that can be successfully used in the study of masonry structures [2-3]. However, despite the great progress made in the study of historical masonry structures, important challenges still have to be faced, such as the characterization of generally complex geometries, the difficulty of developing a good analysis and the high computational effort [4]. The limit analysis is a simplified, fast and effective method that allows the analysis of the seismic behavior of heritage buildings from the study of the possible failure mechanisms that may occur. In case of the buildings with flexible diaphragms the most critical mechanisms are the ones associated to the out-of-plane overturning of walls [1-5]. The guidelines for the

development of the limit analysis are detailed in the Italian construction standard, which considers certain essential principles for its application in existing non-reinforced constructions [6-7]. In the present study, a first stage of the methodology based on the use of limit analysis was apply to understand the seismic vulnerability of the church of Sacsamarca located in Ayacucho, Southern Peru. A second stage of the methodology was then applied for dimensioning the buttress solution which was adopted to increase the lateral stability of the nave walls.

2 METHODOLOGY FOR THE EVALUATION SEISMIC CAPACITY AND DIMENSIONING OF BUTTRESSES

The methodology proposed for the design of buttresses consists of two phases described in Figure 1. As a first step, the structural capacity of the longitudinal wall is calculated using limit analysis, for which it is necessary to know certain data such as the materials, loads, geometry of the wall, and seismic parameters of the site. If the structural capacity does not exceed the seismic demand, the wall must be reinforced by adding buttresses. Phase 2 is the design of the buttresses considering a series of possible design configurations that were defined based on the guidelines proposed by the Indian [8] and Peruvian [9] standards. The structural capacity of the reinforced system is calculated, taking into account the configurations established in order to determine those that offer greater lateral stability to the wall.

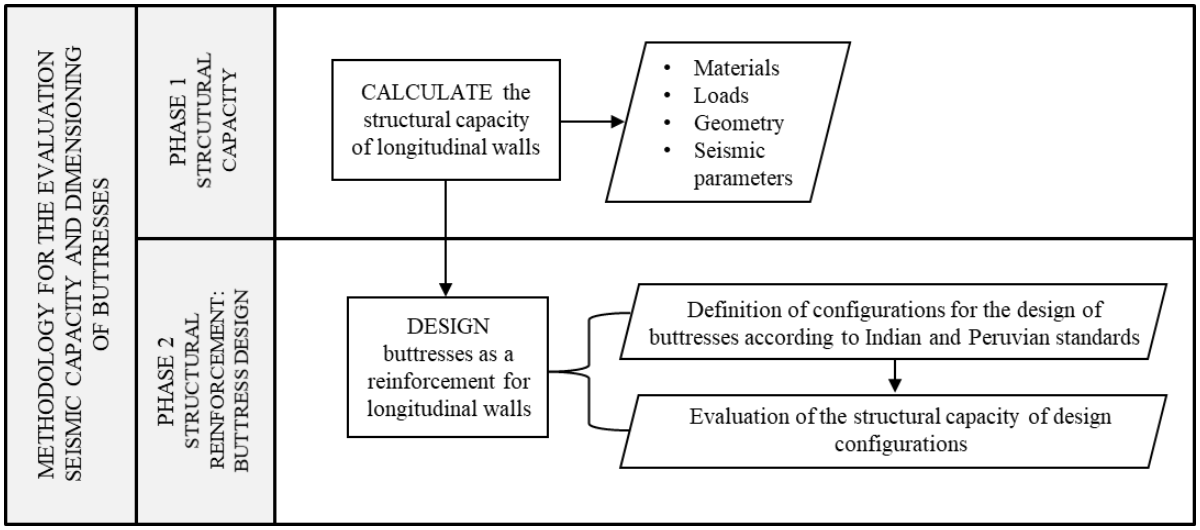


Figure 1: Methodology of analysis and design of buttresses for Andean colonial churches

3 EVALUATE THE SEISMIC SAFETY OF THE LONGITUDINAL WALLS OF THE SACSAMARCA CHURCH

3.1 Description of the case study

The church of the Virgin of the Assumption of Sacsamarca is located in the department of Ayacucho and its construction began during the last decades of the sixteenth century. It has adobe walls, stone foundations, and a wooden roofing system (Figure 2-a and 2-b). The church

has a central nave that is 50 m long and approximately 12 m wide. The longitudinal walls have "arrimos" which are elements made of unconsolidated stone masonry and are a type of buttress whose function is to provide stability to the walls (Figure 2-c). The walls are made of adobe with a thickness of 1.5 m and a height of approximately 9.0 m. It has a roofing system known as "pair and knuckle" (Figure 2-d).

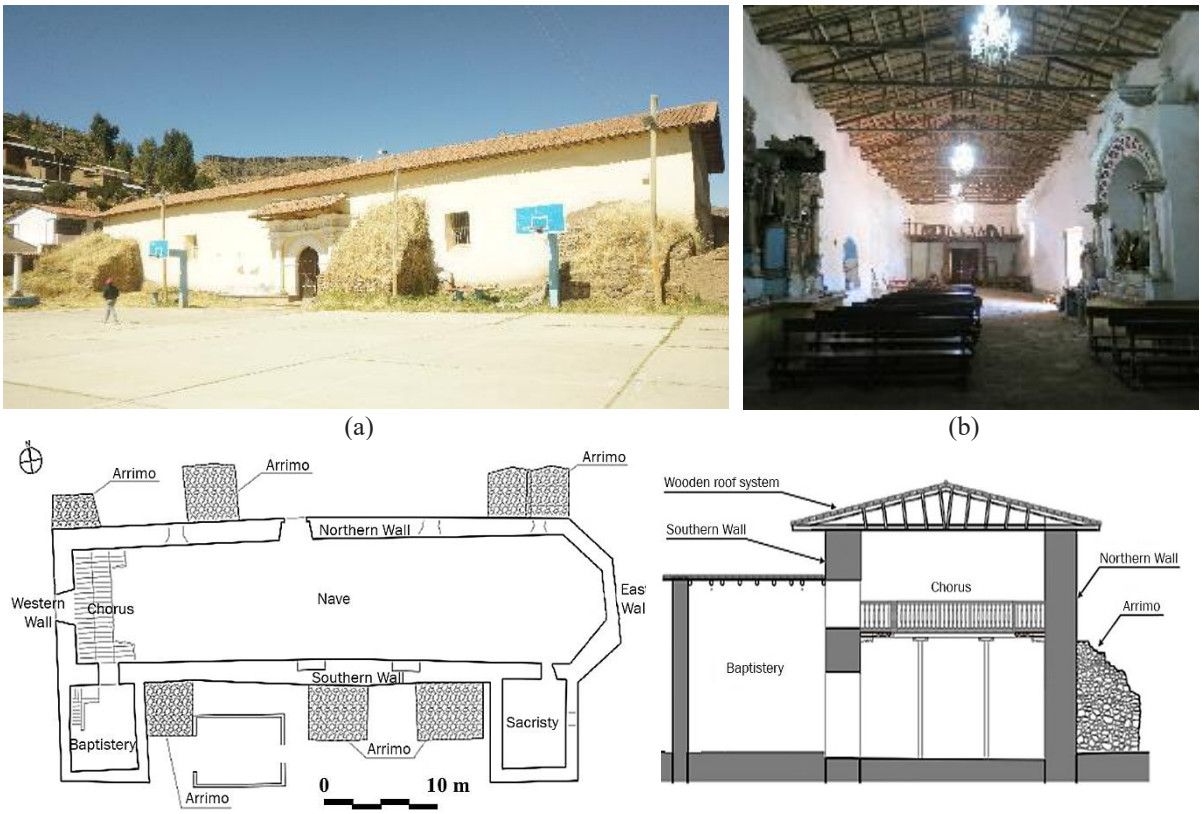
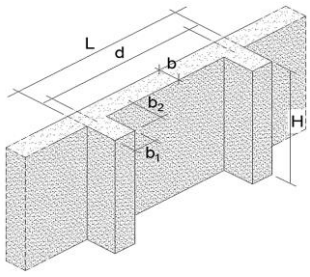


Figure 2: General views of the Sacsamarca church: (a) exterior view, (b) interior view and architectural plans: (c) plan view of the height of the base of the wall and (d) cross section

3.2 Dimensioning of the buttress

Based on the design guidelines suggested by the Indian [8] and Peruvian [9] standards for the reinforcement of walls using buttresses, a set of configurations was determined, grouped into cases I and II. It should be noted that the variable parameters are in function of b and H, which are the thickness and height of the reinforced wall. The variables b_1 and b_2 are the dimensions of the buttresses (thickness and depth) and d the distance between the reinforcements (see Table 1). The property has a stone overhang of 1.3 m and an adobe wall height of 6.6 m, however, the wall section was considered to be made only of adobe in its entire height since it is the most predominant material compared to stone, therefore, the total height of the wall was considered to be 9.0 m.

Table 1: Section values of the buttressed wall for Case I and Case II



Case I b_1=b, b_2=1.5b y d=[3-13]b				Case II b_1=b, b_2=2.0b y d=[3-13]b			
b (m)	b_1	b_2	d	b (m)	b_1	b_2	d
1.5	1.5	2.25	4.5	1.5	1.5	3.0	4.5
1.5	1.5	2.25	6.0	1.5	1.5	3.0	6.0
1.5	1.5	2.25	7.5	1.5	1.5	3.0	7.5
1.5	1.5	2.25	9.0	1.5	1.5	3.0	9.0
1.5	1.5	2.25	10.5	1.5	1.5	3.0	10.5
1.5	1.5	2.25	12.0	1.5	1.5	3.0	12.0
1.5	1.5	2.25	13.5	1.5	1.5	3.0	13.5
1.5	1.5	2.25	15.0	1.5	1.5	3.0	15.0

In addition, for the development of the limit analysis methodology, a geometric conversion was performed from the original section (wall plus buttresses) called type C section (Figure 4-a) to an element of constant thickness b_{eq} (Figure 4-b). This proposed methodology for section conversion is intended to perform in a simpler and faster manner the calculation of the factor that activates the tipping failure mechanism in the limit analysis from the system load equilibrium. To calculate the equivalent thickness, a non-linear static pushover analysis using DIANA-FX software was used to evaluate the conversion of sections by generating models with displacement and rotation restrictions at the base. A horizontal force was applied to the highest node of the element to obtain the maximum displacement. The equivalent section was modeled repeatedly until obtaining a similar stiffness value to the C-type wall, applying the same force and obtaining the same displacement for both walls.

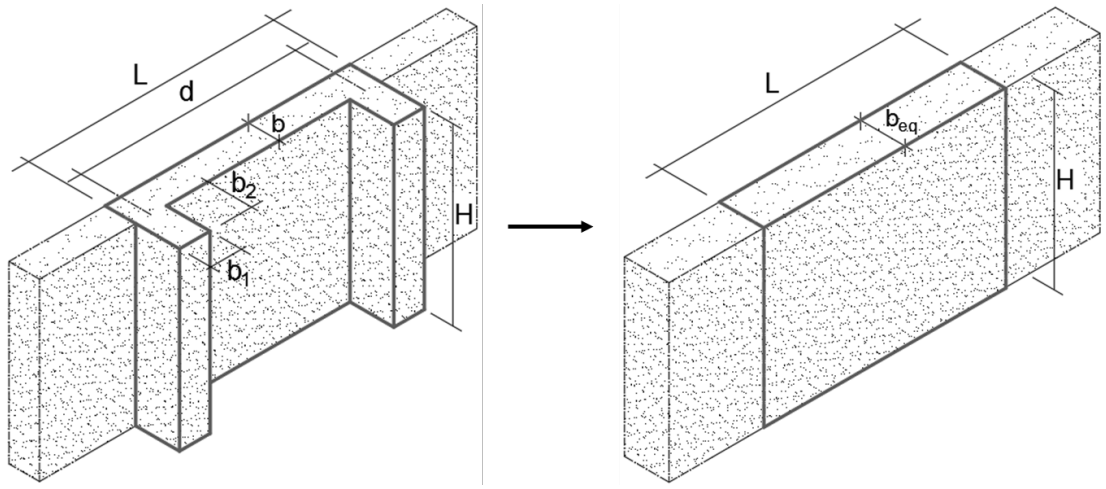


Figure 4: Diagram of the reinforced wall section and conversion of (a) a type C wall to a typology of (b) wall with equivalent thickness

From the results obtained from the modeling of the two types of walls for each configuration, an equation was constructed that allows the value of the equivalent thickness to be obtained.

This equation (Eq. 1) is based on the relationship between the cross-sectional areas of type C sections and equivalent sections, considering a parameter K that represents the stiffness contribution of the buttresses to the walls. Since in cases I and II there are different dimensions for the buttresses, the values of parameter K vary resulting in K=1.8 for Case I and K=1.5 for Case II.

$$b_{eq} = b_{muro} + \mathrm{K}\frac{(2 * b1 * b2)}{d + b1} \quad (1)$$

3.3 Verification of the structural contribution of the buttress system using numerical analisis

According to the proposed methodology, for phase 1 the structural capacity of the longitudinal walls with a tendency to develop an out-of-plane tipping fault mechanism must be calculated from the development of the limit analysis. The guidelines of the Italian standard and its derivatives [6-10] for limit analysis were adopted, and the limit state relating to safety of life (SLV) was applied. Additionally, it was necessary to know the zoning and soil type parameters of the area to calculate the seismic demand. These parameters are extracted from the Peruvian seismic-resistant standard [11] and are detailed in Table 2.

Table 2: Zoning and soil type parameters for the case study

Description	Code	Value	
Maximum horizontal site acceleration: Z3	NTE 030	a_g	0.35g
Category coefficient of the subsoil and topographic conditions: Considered a bad soil in the absence of specific information	NTE 030	S	1.20
Period corresponding to the beginning of the section at constant speed of the spectrum: Tc = Tp	NTE 030	T_P	1.0 s
Period corresponding to the beginning of the section at constant spectrum shift: $T_D = T_L$	NTE 030	T_L	1.6 s

The mechanical properties of the materials were taken from the structural survey report of the Sacsamarca church [12], where the average specific weight of the masonry is 2130 kg/m3, modulus of elasticity E=271x106 N/m2 and a ductility of 1.6 mm. Table 3 details the structural parameters required for the linear and non-linear verifications of the limit analysis of the case study. The partial safety coefficient to be used for the seismic design of masonry structures q_e is equal to two according to the Italian standard (chapter 7.8) [6]. On the other hand, the Italian standard recommends the use of a factor q for the confidence level of the structure from the determination of the level of knowledge of the property. In this study, it was decided to consider conservative values and for this reason a knowledge level LC2 was chosen, related to a factor $q = 1.2$, because previous studies were carried out on the properties of the building materials [6].

Table 3: Structural parameters to calculate the accelerations and spectral displacements

Description	Value	
q_e: Structure factor	2	-
Z': Height at which the center of masses is located	4.5	m

H: Total height of the wall	9.0	m
Ψ(Z'): First form of vibration in the direction of analysis: Z'/H	0.5	-
N: Number of levels in the structure	1	-
γ: Modal participation coefficient: 3N/(2N+1)	1	-

In addition, the virtual working principle was used to calculate the factor of the turning fault (α_0). The linear safety check in terms of acceleration (Eq-2) is performed to ensure safety in the damage limit state (SLD) and the ultimate limit state (SLU). This equation makes it possible to calculate the spectral acceleration demand of the earthquake according to the Peruvian earthquake-resistant standard [11]. On the other hand, for the verification of the SLU state, the properties of the structure and the soil are used, and the structural capacity expressed in terms of acceleration (Eq-3) is calculated. The factor S is the soil amplification factor, Z is the zoning coefficient whose values are shown in Table 2, while the factor q governs the behavior of the structure and is indicated in Table 3 [6].

$$a_0^* \geq \frac{Z \cdot S \cdot g}{q} \tag{2}$$

$$a_0^* \geq \frac{Z}{q} \cdot \min\left(2.5\frac{Tp}{T1}, 2.5\right) \cdot S \cdot g \cdot \varphi(z) \cdot \gamma \tag{3}$$

The factor T_p is the period corresponding to the final part of the plateau (constant zone) in the elastic acceleration response spectrum and T_1 is the period of fundamental vibration of the structure. The factor $\varphi(z)$ is the first normalized vibration mode of the structure and is estimated as the ratio of the point of the center of masses relative to the ground and the total height of the element relative to the ground Z'/H. Finally, γ is the modal participation factor which is calculated as $3N/(2N+1)$, where N is the number of levels of the structure [4-13].

Furthermore, it is necessary to verify the system by means of a non-linear analysis in terms of the displacements. The ultimate spectral displacement ${d_u}^*$ corresponds to the limit state of the structure's service and is equivalent to $0.4\,{d_0}^*$. It is compared ${d_u}^*$ with the demand of spectral displacement ${\Delta_d}^*$ which is calculated from the secant period T_s defined for the system of a degree of freedom [6-14]. The seismic displacement demand $\Delta_d^*(Ts)$ is calculated from equations Eq-4, Eq-5 or Eq-6. Finally, the safety verification for the ultimate limit state is guaranteed when the ultimate displacement satisfies the following relation: $\Delta_d \leq d_u^*$ [13].

$$Ts < 1.5T_1 \qquad \Delta_d^*(Ts) = a_g S \frac{T_s^2}{4\pi^2}\left(\frac{3(1+Z'/H)}{1+(1-Ts/T1)^2} - 0.5\right) \tag{4}$$

$$1.5Ts \leq Ts < T_D \qquad \Delta_d^*(Ts) = a_g S \frac{1.5T1Ts}{4\pi^2}\left(1.9 + 2.4\frac{Z'}{H}\right) \tag{5}$$

$$T_D \leq T_s \qquad \Delta_d^*(Ts) = a_g S \frac{1.5T1T_D}{4\pi^2}\left(1.9 + 2.4\frac{Z'}{H}\right) \tag{6}$$

With the detailed information on the development of the limit analysis, the seismic safety of one of the longitudinal walls of the case study was evaluated. The geometry of the wall according to the architectural plans consists of a thickness of 1.5 m, a height of 9.0 m and a length of 43.3 m. Table 4 shows the results obtained for the structural capacity of the wall,

resulting in a value of 0.139g compared to a seismic demand of 0.263g. Although the non-linear verification by displacement is satisfactorily fulfilled, it is necessary to propose a reinforcement to the wall until both verifications of the limit analysis are satisfied.

Table 4: Structural capacity of the longitudinal wall of the case study

Structural capacity			Seismic Demand		SF_a (g/g)	SF_d (mm/mm)	Safety
α_0	a_0*	d_u*	a_d*	Δ_d*			
0.167	0.139	296	0.263	21	0.53	14.10	Unsafe

For Phase 2 of the methodology, the reinforcement of the wall from the design of the buttresses is evaluated using the methodology of the limit analysis, the configurations set out in Table 1 and equation Eq-1 for section conversion. Table 5 shows the results of the verifications of the limit analysis for cases I and II. A comparison between the values of structural capacity and seismic demand gives the safety factors (SF) as a function of accelerations (g) and displacements (mm). If for a configuration both factors are greater than the unit, the structure is considered to be safe, otherwise it is sufficient that one factor does not satisfy the requirement to be considered an unsafe structure that does not verify the safety of the damage limit state (SLD).

Table 5: Linear and non-linear checks of the limit analysis in cases I and II

Case	Config. "d"	Structural capacity			Seismic Demand		SF_a (g/g)	SF_d (mm/mm)	Safety
		α_0	a_0*	d_u*	a_d*	Δ_d*			
I	3b	0.392	0.326	656	0.263	21	1.24	31.24	Safe
	4b	0.347	0.289	590	0.263	21	1.10	28.10	Safe
	5b	0.317	0.264	543	0.263	21	1.00	25.86	Safe
	6b	0.295	0.246	510	0.263	21	0.94	24.29	Unsafe
	7b	0.279	0.233	484	0.263	21	0.89	23.05	Unsafe
	8b	0.267	0.222	464	0.263	21	0.84	22.10	Unsafe
	9b	0.257	0.214	447	0.263	21	0.81	21.29	Unsafe
	10b	0.248	0.207	434	0.263	21	0.79	20.67	Unsafe
II	3b	0.417	0.347	692	0.263	21	1.32	32.95	Safe
	4b	0.367	0.306	620	0.263	21	1.16	29.52	Safe
	5b	0.333	0.278	569	0.263	21	1.06	27.10	Safe
	6b	0.310	0.258	532	0.263	21	0.98	25.33	Unsafe
	7b	0.292	0.243	504	0.263	21	0.92	24.00	Unsafe
	8b	0.278	0.231	482	0.263	21	0.88	22.95	Unsafe
	9b	0.267	0.222	464	0.263	21	0.84	22.10	Unsafe
	10b	0.258	0.215	449	0.263	21	0.82	21.38	Unsafe

It should be noted that the structural capacity of the original longitudinal wall is 0.139g, so adding buttresses as a reinforcement system improves the stability of the wall and can increase lateral resistance by more than 50%.

For the validation of the limit analysis methodology developed, the results obtained for the design of buttresses were compared with the results of applying the pushover analysis in the same configurations. The model of the section in study is built with finite elements (FEM) using tetrahedral elements (TE12L) with an average size of 0.5 m. The numerical model was obtained using the software DIANA-FX. The vertical forces were considered to be loads from the own weight and the seismic forces as horizontal thrust forces whose direction of analysis was +Y axis. The iteration method used to analyze gravity and seismic loads was the Modified Newton-Raphson method combined with the arc length method ARC LENGHT [4], only in the cases of seismic load analysis. The control points in each configuration were located in the highest part of the reinforced walls in order to quantify the maximum displacement [15]. Convergence was controlled from the energy parameter using a tolerance of 0.001. According to [16], a non-linear behaviour for masonry should be considered by means of a constitutive model based on total deformation (Total Strain Crack Model), since this model provides good stability in crack opening control. In addition, a crack model called the Rotating Crack Model was used and the condition of embedding in the base was absolute (FIXED).

According to the study by [17], the behaviour developed by the masonry in traction follows a model of post-peak exponential softening, while in compression it adopts parabolic hardening, followed by post-peak parabolic softening [17,18,19]. The elastic and non-linear properties of Table 6 were used to perform the pushover analysis.

Table 6: Elastic and non-linear properties of adobe material

Tensile modulus (E)	Specific weight (γ)	Compressive strength (fm)	Tensile strength (ft)	Compression fracture energy (Gm)	Tensile fracture energy (Gt)	Coefficient of ductility (μ)	Poisson Module (ν)
MPa	kg/m^3	MPa	MPa	N/m	N/m	mm	-
271	2130	0.6775	0.06775	1084	10	1.6	0.24

After performing the pushover analysis, Table 7 shows the structural capacity values which are compared to the seismic demand of the area.

Table 7: Results of the maximum structural capacity as a function of acceleration

a_0* (g)	Design configurations							
	3b	4b	5b	6b	7b	8b	9b	10b
Case 1	0.333	0.298	0.275	0.257	0.244	0.229	0.218	0.215
Case II	0.360	0.311	0.291	0.267	0.254	0.234	0.228	0.221

The comparison of the structural capacity results of the configurations for both methods of analysis is shown in Figure 5-a and Figure 5-b for cases I and II, respectively. From the graphics it can be seen that the limit analysis gives clearly similar values to those obtained from the pushover analysis with an error between the results not exceeding 5% with respect to the results

of the pushover analysis. It is demonstrated that using limit analysis to calculate the structural capacity of existing masonry constructions, in this case Andean colonial churches, in the face of the occurrence of seismic phenomena provides reliable results that are significantly close to the real behavior of these buildings.

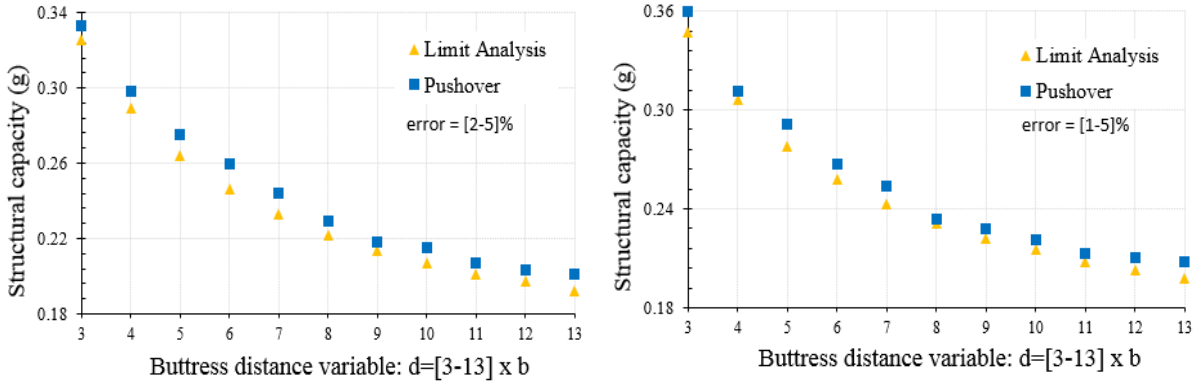


Figure 5: Comparison of results between limit and pushover analysis for cases (a) I and (b) II

4 PROPOSAL OF A SIMPLIFIED METHODOLOGY FOR THE DESIGN OF BUTTRESSES IN ADOBE CHURCHES

A proposal was elaborated to design buttresses to reinforce the longitudinal walls of Andean colonial churches through the creation of a computer program using MatLab software. The program implicitly develops the limit analysis and verifications for each of the proposed configurations. The objective is to obtain reinforcement designs that provide additional resistance to the wall and thus overcome the seismic demand of the area. On the other hand, the architecture of Andean colonial churches has a common pattern for such structures. They have one or more bell towers, apse, chapels, longitudinal walls on which the roof, facade and in some cases buttresses or "arrimos". It must be taken into account that these constructions have longitudinal walls whose dimensions vary from one church to another. However, it is possible to consider typical ranges for the dimensions of the wall. In addition, because the presence of seismic events generates a variety of fault mechanisms, in the case of churches the prevailing fault is that of out-of-plane turning due to their extensive walls [20]. Table 8 shows a group of Andean colonial churches considered to be the most representative for this study.

Table 8: Dimensions of longitudinal walls in the most representative Andean colonial churches

Name	Location	Thickness (m)	Height (m)
San Juan Bautista of Huaro Church	Cusco	1.6	11
San Pedro Apóstol of Andahuaylillas Church	Cusco	1.8 - 2.0	10
Canincunca Chapel	Cusco	1.3	8
San Blas Church	Cusco	1.5	11
Temple of San Sebastián	Cusco	1.5 - 2.0	12
Kuño Tambo Church	Cusco	1.6 - 1.9	8
Sacsamarca Church	Ayacucho	1.5	9

Design configurations were generated taking as reference the Indian standard [8] and the Peruvian adobe standard [9] for masonry wall reinforcement. Table 9 shows the ranges of values to be considered for the dimensions and distances of the buttresses.

Table 9: Configurations for the design of buttresses that the program evaluates

Wall thickness b (m)	Wall height H (m)	Distance between buttresses d (m)	Buttress thickness b_1 (m)	buttress length b_2 (m)
1.0, 1.5 and 2.0	[8-12]	[3b-10b]	Equal to b	1.5b and 2b

Equation Eq-1 is also used to calculate the coefficient K with which the equivalent thickness (b_{eq}) can be determined in each of the configurations (see Table 10). In total, the program must analyze 240 design configurations by applying limit analyses and evaluating conformity to safety checks where the input parameters are the dimensions of the wall (thickness and height), the soil parameters and zoning of the site according to the Peruvian seismic-resistant standard [11].

Table 10: Values for the coefficient K to find the equivalent thickness

K	$1.0 \leq b \leq 1.2$	$1.2 < b \leq 1.5$	$1.5 < b \leq 2.0$
$b_2=1.5b$	2.1	1.8	1.6
$b_2=2b$	1.9	1.5	1.4

The program executes the limit analysis for each design configuration of buttresses in order to calculate the structural capacity of the reinforced system. Each of these results is compared to the seismic demand of the zone and then the program shows those configurations that comply satisfactorily with the linear and non-linear verifications of the limit analysis. If the program shows more than one design configuration, the professional in charge must choose the one that best matches the geometry of the church.

4 CONCLUSIONS

This work proposes a methodology for the design of buttresses with the aim of strengthening those Andean colonial churches that are vulnerable to earthquakes. Likewise, this study contributes substantially to the field of conservation and reinforcement of Andean colonial churches in Peru since, to date, there is no known simplified, fast and effective methodology based on the limit analysis that allows to verify whether or not the seismic demand of the area is exceeded. In the case that more than one design configuration is presented, the responsible professional (PR) should consider that the churches have an architecture with openings in the walls (windows and doors), as well as the presence of chapels that somehow provide stability to the walls. This means that the PR must choose the configuration that can satisfy the seismic demand of the area and that, additionally, is compatible with the architectural distribution of the building. Finally, it was possible to prove that limit analysis can be a powerful tool to evaluate the seismic vulnerability of historical adobe masonry structures.

Acknowledgements. This research was carried out thanks to the support of the Engineering and Heritage research group of the PUCP.

REFERENCES

[1] Lourenço, P., Mendes, N., Ramos, L. & Oliveira, D. (2011). Analysis of masonry structures without box behavior. International Journal of Architectural Heritage: Conservation, Analysis, and Restoration, 5(4-5), 369-382.

[2] Araujo, A., Lourenço, P., Oliveira, D. y Leite, J. (2012). Post-earthquake numerical assessment and reinforcement of St James Church, New Zealand. Conferencia 15th World Conference on Earthquake Engineering 2012 (15WCEE), Lisboa, Portugal.

[3] Krawinkler, H., & Seneviratna, G. (1998). Pros and cons of a pushover analysis of seismic performance evaluation. Jounal: Engineering Structures, 20(4-6), 452–464.

[4] Aguilar, R., Noel, M. & Ramos, L. (2019). Integration of reverse engineering and non-linear numerical analysis for the seismic assessment of historical adobe buildings. Journal: Automation in Construction, 98, 1-15.

[5] Tolles, E., Kimbro, E. & Ginell, W. (2003). Planning and engineering guidelines for the seismic retrofitting of historic adobe structures. The Getty Conservation Institute (GCI).

[6] NTC (2018). Normas Técnicas para las Construcciones. Italia.

[7] Rivera J. & Muñoz E. (2005). Caracterización estructural de materiales de sistemas constructivos en tierra: el adobe. Revista de Desastres Naturales, Accidentes e Infraestructura Civil, 5(2), 135-148.

[8] National Building Code of India (2016). Bureau of Indian standards (IBC). India.

[9] Norma E080 (2017). Diseño y construcción con tierra reforzada. Lima, Perú.

[10] OPCM (2003). Ordenanza del Presidente del Consejo de Ministros N° 3274. Roma, Italia

[11] Norma E030 (2016). Norma Técnica Diseño Sismorresistente: Reglamento Nacional de Construcciones. Lima, Perú.

[12] Aguilar, R. (2018). Informe Peritaje Estructural: Iglesia Virgen de la Asunción de Sacsamarca. Engineering & Heritage (PUCP).

[13] Aguilar, R., Marques, R., Sovero, K., Martel, C., Trujillano, F. y Boroschek, R. (2015). Investigations on the structural behaviour of archaeological heritage in Peru: From survey to seismic assessment. Engineering Structures, 95, 94-111.

[14] Faccio, P. (2012). Consolidamento degli edifice storici (Lezione N°7): Meccanismi di collasso. Venezia, Italia.

[15] Conde, C. & Schiavi, E. (2009). Métodos numéricos de resolución de ecuaciones no lineales. Universidad Politécnica de Madrid y Rey Juan Carlos, Madrid, España.

[16] Lourenço, P., Trujillo, A., Mendes, N. & Ramos, L. (2012). Seismic performance of the St. George of the Latins church: Lessons learned from studying masonry ruins. *Journal: Engineering Structures*, *40*(2012), 501-518.

[17] Angelillo, M. (2014). Mechanics of Masonry Structures. New York, US: Springer.

[18] Lourenço, P & Roca, P. (2001). Analysis of historical constructions: From thrust-lines to advanced simulations. Historical Constructions, 91-116.

[19] Lourenço, P. (2009). Recent advances in masonry structures: Micromodelling and homogenization. Multiscale Modeling in Solid Mechanics: Computational Approaches, 251-294.

[20] Karanikoloudis, G. & Lourenço, P. (2018). Structural assessment and seismic vulnerability of earthen historic structures. Application of sophisticated numerical and simple analytical models. Journal: Engineering Structures, 160, 488–509.

12th International Conference on Structural Analysis of Historical Constructions
SAHC 2020
P. Roca, L. Pelà and C. Molins (Eds.)

STRUCTURAL ANALYSIS OF A RESTORED BYZANTINE MONASTERY: EFFECTIVENESS OF THE INTERVENTIONS

PAOLA CONDOLEO[1] AND ALBERTO TALIERCIO[1*]

[1]Department of Civil and Environmental Engineering
Politecnico di Milano
Piazza Leonardo da Vinci 32, 20133 Milan, Italy
e-mail: {paola.condoleo, alberto.taliercio}@polimi.it (*corresponding author)

Keywords: Byzantine Monastery, Masonry, Restoration, Finite Elements, Seismic Analysis

Abstract. *The effectiveness of the restoration interventions carried out on the Byzantine monastery of St. Nicholas at Mesopotam, Albania, is discussed. The interventions aimed at consolidating the church, while bringing it back to its original conditions. Two finite element models were developed: one describing the church as it was until 2009, and one after the planned intervention. The models try to reproduce as accurately as possible the main geometric details of the building, and take into account the macroscopically orthotropic behaviour of masonry and the main cracks. Linear elastic analyses of both models were carried out considering gravity loads and lateral loads equivalent to seismic actions according to the Italian standards. The numerical results show that, in the occurrence of an earthquake, the stress in the building would considerably increase after the restoration interventions. In particular, removal of a buttress turns out to be an operation controversial, not to say detrimental.*

1 INTRODUCTION

The restoration of the Byzantine monastery of St. Nicholas in Mesopotam is part of a vast project, launched in 2006 and supported by UNESCO, aimed at preserving and exploit the rich cultural heritage of Albania. Started as a joint project involving Albanian professionals and researchers from several Italian universities, including the Technical University (Politecnico) of Milan, the project was eventually entrusted only to Albanian experts, following an interruption as abrupt as unmotivated of the cooperation with the Italian research team.

Mesopotam is one of the most interesting archaeological sites in southern Albania, both from an artistic point of view, because of the originality and richness of the frescoes decorating the interior of the church, and from an engineering point of view. The church of St. Nicholas was probably built around the XIII century [1], but the building was heavily modified over time because of the damages induced by seismic events, as numerous as detrimental, that hit the region of Delvina, where the church is located, especially during the XVI and XVIII century. Many interventions were carried out, mainly in the XVIII century, to improve the safety of the building [2][3]: a buttress was added on the south side; the central

column was embedded within a massive, rectangular pillar; another pillar was added to support the central arch of the western colonnade.

The ambitious restoration intervention, which started in 2009 and ended in 2011, aimed to preserve the stability of the building whilst bringing it back to its original condition, i.e. prior to the XVIII century. Some parts were removed or replaced, and some external ties were added.

This paper focuses on the structural effectiveness of the intervention. Finite Element models of the building as it was until 2009 and after the restoration were developed. Although conceived for simple linear elastic analyses, the models try to capture as accurately as possible the main characteristics of the building, by taking into account both the heterogeneous and anisotropic nature of the materials, and the crack pattern. The two models were submitted to gravity loads and statically equivalent seismic loads, of an intensity defined by the current Italian standards. The main results of the FE analyses are presented hereafter, and the consequences of the restoration interventions on the static behaviour of the church are critically discussed.

2 DESCRIPTION OF THE BUILDING

The church of St. Nicholas stands isolated within large defensive walls and, apart from some archaeological remains, it is the only building of the former monastery that has survived to this day (Figure 1(a)).

The church has a rectangular plan (Figure 1(b)), and is internally divided into three areas: the central nave (or *naòs*), the narthex and the apse (or *bema*) at the ends. The *naòs* is covered by four domes of irregular geometry, resting on drums pierced by eight windows each; most of the windows are currently walled up. The drums are connected to the perimeter arches by pendentives. The arches, in turn, are supported by pilasters and a central columns (Figure 1(c)). The narthex and the *bema* are separated from the central area by two colonnades of four arches and covered by sail vaults.

The building was seriously affected by a major earthquake that hit Delvina region in 1745, during which the two apses - a peculiar feature of the church - collapsed. Later on, in the XVIII century, the following consolidation interventions were carried out (see Figure 1(b)):

- a massive buttress was added on the southern front of the church;
- one of the apses was completely rebuilt, in the shape of a four-sided polygon;
- the former central column supporting the domes was embedded within a massive pillar with a rectangular section;
- a second rectangular section pillar was added, to support the central arch of the colonnade which divides the *naòs* from the narthex.

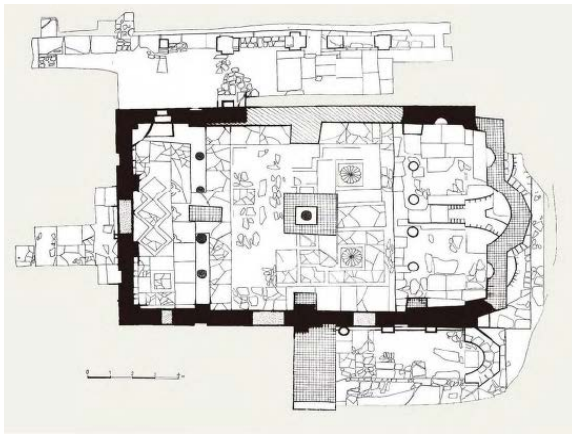
The widespread crack pattern visible in the church (see e.g. Figure 1(c)) shows that the eighteenth-century interventions and the closure of several openings have preserved the building from further serious damages that might have developed following the seismic events that occurred later and up to the present day.

A survey campaign was carried out from 2006 to 2008 to assess the state of preservation of the church and the main failures. The crack pattern was surveyed, a monitoring system was installed, and the occurring damage mechanisms were identified accordingly. By perusing the diagrams showing the time evolution of the cracks, and by comparing them with the off-

plumb of the walls [4], it was possible to highlight the tendency of the façade and the apse to tilt (Figure 2).



(a)



(b)



(c)

Figure 1: (a) Plan of the church of St. Nicholas: the construction phases are outlined; dashed areas: interventions of the XVIII century [2]. (b) External view of the church [4]. (c) View of one of the domes

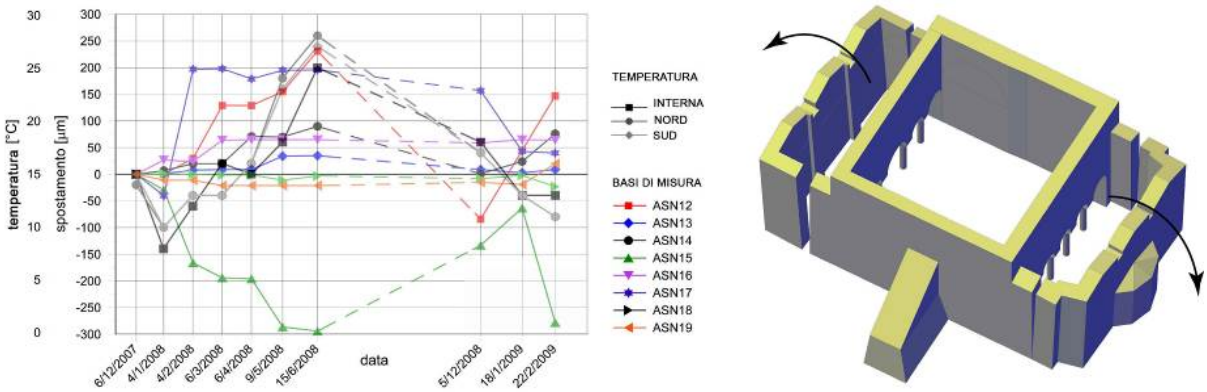


Figure 2: Left: time evolution of selected cracks (dashed lines correspond to months in which no measurement was taken). Unstable cracks are labelled ASN15, ASN16, ASN17. Right: schematic failure modes

The restoration interventions started in 2009 and involved the demolition of the buttress, which was a source of asymmetry and anomalous loads according to the designer, especially in the event of an earthquake. The buttress was replaced, at least provisionally, by two steel bracings (Figures 3(a,b)).

The massive central pillar in the *naòs* was demolished up to a height of about 2.5 m, and the original column was brought back to light. The remaining, upper part of the pillar was supported by a steel frame. Similarly, the lower part of the pillar supporting the central arch of the narthex colonnade was partially demolished, for a height of 2.5 m, and replaced by a steel frame.

The rotational movements of the façade and the apse can be prevented from progressing by suitable connections. The designer added an external double steel tie at about 2/3 of the height (Figure 3(c)) to hoop the building. Additionally, C-section steel beams were fit into the perimeter walls at about 1/3 of their height, where heavily damaged timber ties existed previously. These beams, however, are missing at the apse because of the difficulties encountered during installation. Contrary to the original retrofitting project, steel ties at 1/2 and 2/3 of the height of the walls were not inserted.

The domes were hooped both individually and collectively by polyester strips, which can be manually adjusted by ratchets.

On the western front of the church, the main entrance door and the side windows were reopened, so as to “lighten” the facade.



(a) (b) (c)

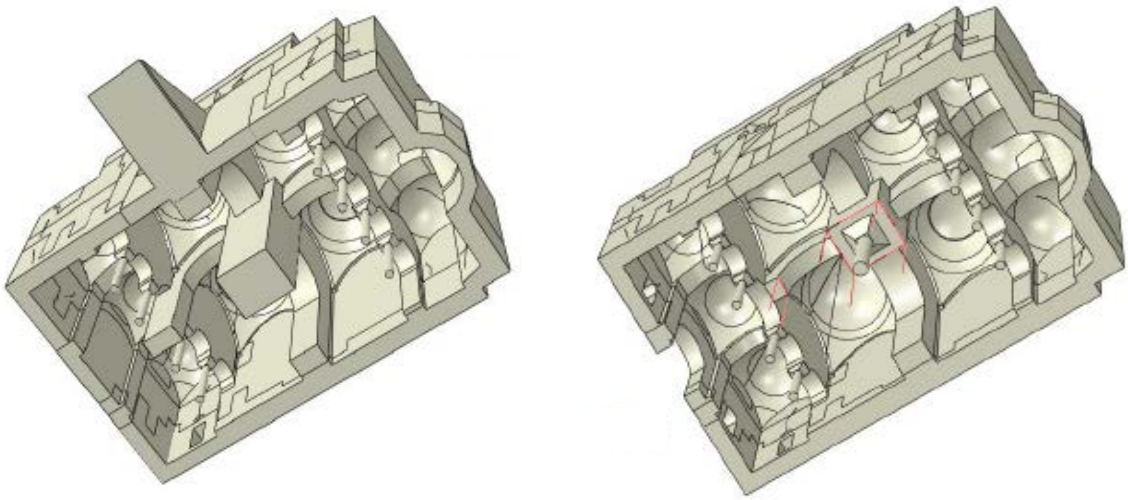
Figure 3: (a) Partial demolition of the buttress. (b) Detail of the steel bracing. (c) Double external steel tie hooping the church

3 MODEL OF THE BUILDING

3.1 Geometrical model

Thanks to the extensive database collected during the survey campaign of 2007-08 by a research group of Milan Technical University (Brumana et al., 2014), a 3D geometrical model of the building was developed in the AutoCAD® environment. The model is sufficiently simple to avoid excessively heavy numerical analyses, but, at the same time, accurate enough to capture the salient features of the building.

The model of the building as it was before the recent interventions described in Sec. 2 is shown in Figure 4(a), whereas that of the building in the presumed current conditions is shown in Figure 4(b). The steel frames are represented by red lines.



(a) (b)

Figure 4: Geometrical model of the church (a) before and (b) after the restoration works carried out from 2009 to 2011

3.2 Materials

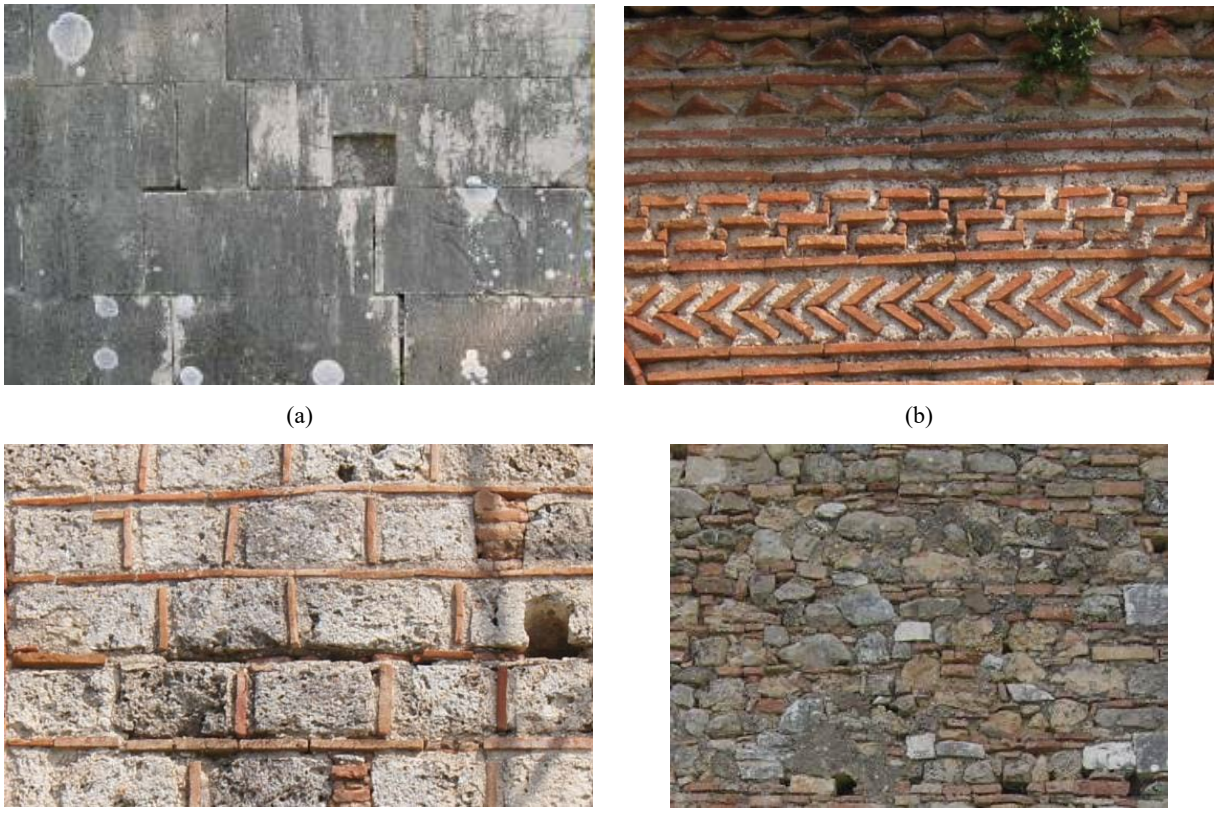
The church of St. Nicholas in Mesopotam exhibits a wide variety of masonry, including different types of brick- and stonework. On the one hand, this is related to the construction techniques typical of the local architecture, which has the formal characteristics of Byzantine models. On the other, historical and natural events that have profoundly marked the formal and structural aspect of this artifact over time.

The classification of the materials used in the construction of the building is based on the analysis of the monastery walls carried out by Triggiani [5]. Over the centuries, new materials have been added to the original ones. Nowadays, four predominant types of materials can be identified:

- Ashlar masonry (Figure 5(a)). It is the material of which the lower part of the load-bearing walls of is made (in red, in Figure 6). It mostly consists of fairly regular medium grained limestone blocks. Similar materials were used for the buttress on the south façade, added

after the earthquake of 1510, the pillar that incorporated the central column, and the pillar that supported the central arch of the eastern diaphragm, both added in 1793.

- Brick masonry (Figure 5(b)). Masonry made of bricks of different size, mostly 160 and 260 mm thick, arranged and laid with a considerable amount of mortar (30 to 60 mm thick). Most of the perimeter walls are made of brickwork (in blue, in Figure 6), and so are the intrados of the pendentives and the domes. Brickwork combines structural performances with aesthetic rendering.
- Mixed masonry (Figure 5(c)). Masonry consisting of limestone blocks framed by bricks. It forms most of the top of the perimeter walls (in gray, in Figure 6).
- Stone masonry (Figure 5(d)). Masonry made up of irregular elements, of variable shape and size, bonded with mortar. It can be found in the regions shown in beige, in Figure 6.



(a) (b)

(c) (d)

Figure 5: Main masonry typologies in the church. (a) Ashlar masonry. (b) Brick masonry. (c) Mixed masonry. (d) Stone masonry

The nine columns inside the church are of made of a having medium-to-fine grained sandstone, also known as “pietra serena” (in pink, in Figure 6).

Except for sandstone and stone masonry, the other types of materials of which the building is made are macroscopically orthotropic. Table 1 summarizes the elastic properties that have been assigned to materials in numerical analyses, in addition to density ρ. Subscript 1 refers to

an axis parallel to the bed joints, 2 to an axis parallel to the head joints, and 3 to an axis along the wall thickness.

In the restoration works, steel beams and tie-rods were used, together with polyester strips. As accurate data are not available, according to the photographic documentation collected during the survey the following assumptions were made regarding the reinforcing elements:

- polyester strips hooping the domes: cross-section = 50×2 mm^2, elastic modulus E = 5 GPa;
- steel ties externally hooping the perimeter walls: diameter = 20 mm;
- UPN C-section steel beams internally hooping the perimeter walls + steel frames inside the church: height = 100 mm, width = 50 mm, thickness = 6 mm.

The properties of the steel elements are also listed in Table 1.

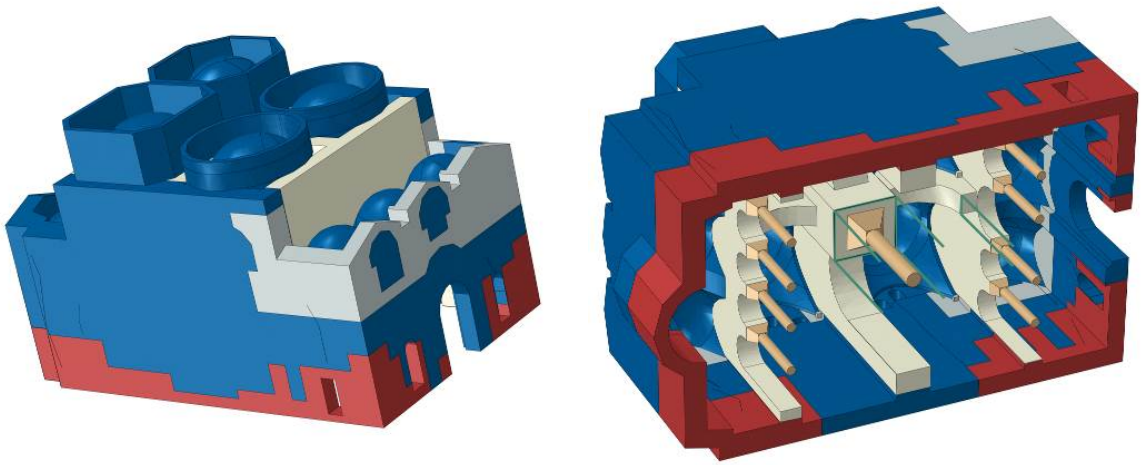


Figure 6: Subdivision of the geometrical model according to the material type. Red: ashlar masonry. Blue: brick masonry. Gray: mixed masonry. Beige: stone masonry. Pink: sandstone

Table 1: Mechanical properties of the materials used in the numerical analyses

	Sandstone	Ashlar masonry	Brick masonry	Mixed masonry	Stone masonry	Steel
ρ [kg/m^3]	2500	2200	1800	2100	1800	7800
E_1 [MPa]	18000	2800	1600	1950	1200	210000
E_2 [MPa]		2300	1100	1350		
E_3 [MPa]		2100	900	1200		
G_{12} [MPa]	7500	1300	790	930	540	80770
G_{23} [MPa]		880	440	580		
G_{13} [MPa]		820	390	470		
ν_{12}	0.2	0.23	0.13	0.16	0.11	0.3
ν_{23}		0.19	0.11	0.13		
ν_{13}		0.18	0.10	0.12		

3.3 Loads

Both in pre- and post-intervention conditions, the church was analyzed under the effect of gravity loads and horizontal loads equivalent to an earthquake according to the current Italian standards.

From a rough analysis of the loads, the weight of the roofs was assumed to be equivalent to a vertical pressure of 3.5 kN/m^2 uniformly distributed on the top of the drums and the perimeter walls of the narthex and the apse.

As for the earthquake, the region of Mesopotam region was assumed to be seismically similar to "zone 2" of the Italian standards legislation. Accordingly, the maximum value of the horizontal acceleration, a_g, was assumed to be 0.25g. The structural factor, $q = 2.0 \times \alpha_u/\alpha_1$, was taken equal to 2.8, being $\alpha_u/\alpha_1 = 1.4$ for one-storey ordinary masonry buildings. Finally, the S-factor that takes into account the stratigraphic profile of the soil on which the building stands was taken equal to 1.25: as the monastery is located in a gently sloping alluvial plain, this value corresponds to a soil class intermediate between B and C according to the Italian standards.

In conclusion, the value of the design spectral acceleration is

$$S_d(T) = a_g \cdot S \cdot \frac{2.5}{q} = 2.7372 \text{ m/s}^2 \tag{1}$$

for 0.15s ≤ T ≤ 0.5s. This value is in line with that of the PGA (Peak Ground Acceleration) in the area of Mesopotam, inferable from the Global Seismic Hazard Assessment Program yearbook and issued by the National Institute of Geophysics [6], according to which PGA ≈ 2.4 m/s^2.

The equivalent static lateral load is assumed to act along the weak direction of the building (short side), either in the N-S or in the S-N direction.

3.4 Finite Element model

The three-dimensional model of the church before and after the restoration works, including the main crack pattern, was exported to the ABAQUS® FE code to estimate the stress and displacement fields with a good degree of approximation.

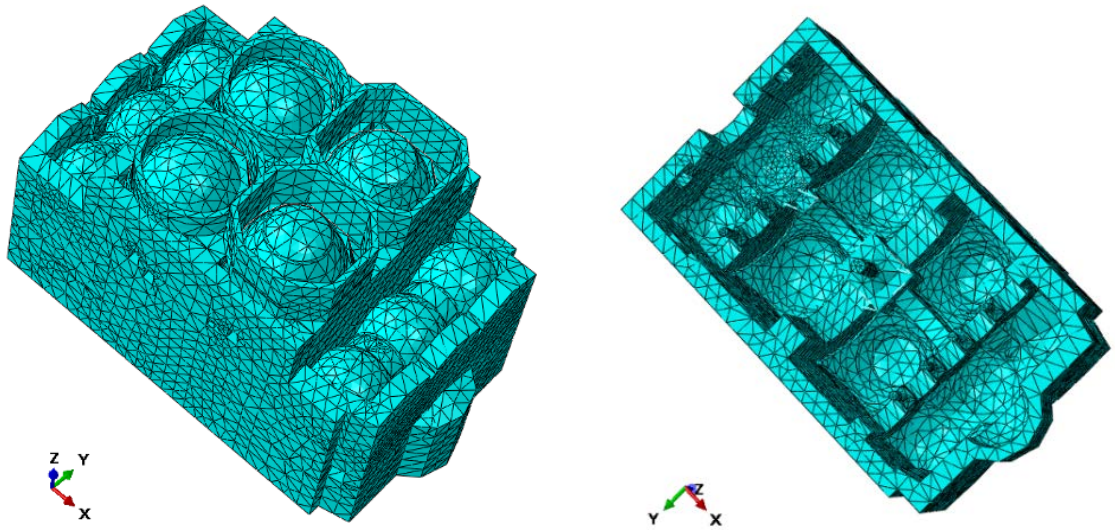
The polyester strips around the domes, the external steel tie-rods and the UPN beams fit inside the masonry walls were modelled by means of spring elements, characterized by a stiffness constant $k = EA/L$. The steel frames supporting the pillars were modelled by beam elements, the section and mechanical properties of which were defined in Par. 3.2.

The FE mesh consists of 10-node tetrahedral elements with quadratic modelling of the displacement field, having sides of length equal on average to 400 mm. Figure 7 shows views from above (a) and from below (b) of the FE model of the post-restoration church.

4 NUMERICAL ANALYSES

The numerical models described in Par. 3.4 were subjected to linear elastic static analyses. In the following paragraphs, the results obtained on the pre- and post-intervention model are discussed and compared under gravity loads only (Par. 4.1), or under combined gravity loads and equivalent lateral loads acting along the short side of the building (Par. 4.2). Principal

tensile stresses greater than 0.2 MPa are considered to be dangerous, being able to originate further cracks.



(a) (b)

Figure 7: Views from above (a) and from below (b) of the Finite Element model of the church after the restoration works

4.1 Gravity loads

The stress state in the structure under service loads (i.e. gravity loads) is first analyzed. In Figure 8(a) (respectively, in Figure 8(b)) the contours of the maximum (tensile) principal stress are reported in the pre-restoration (resp. post-restoration) condition. In Figure 8(b), note the spring elements that simulate reinforcements.

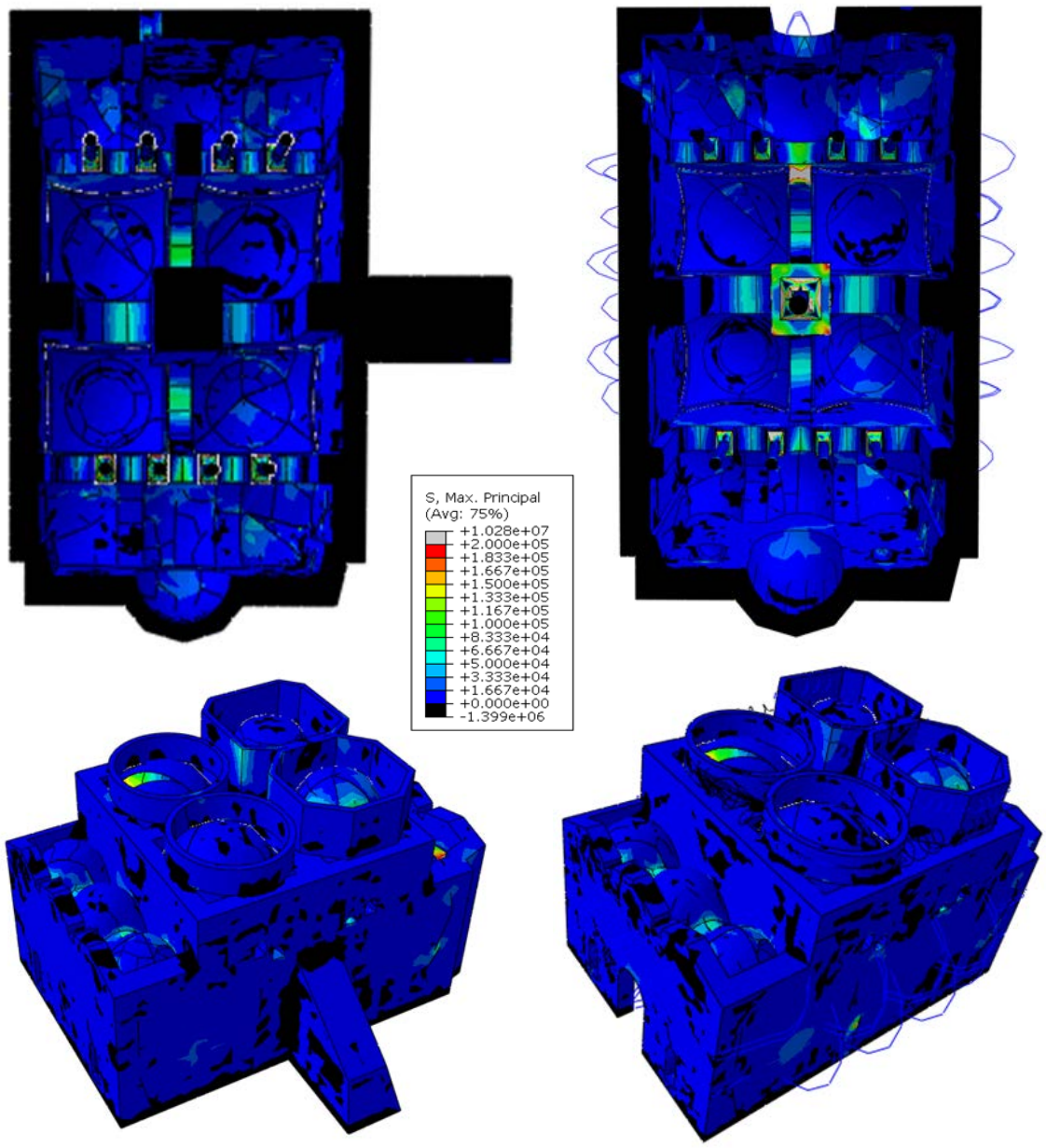
By comparing Figures 8(a) and 8(b), it can be noted that the restoration intervention has not significantly changed the stress in the external walls, in which tensile stresses are negligible. Conversely, high tensile stresses occur near the removed pillars, both in the central column and in the western vault supported by the steel frame.

In both models, stress peaks are also recorded at the extrados of one of the domes and in the arches, which are the most stressed elements.

4.2 Combined gravity and seismic loads

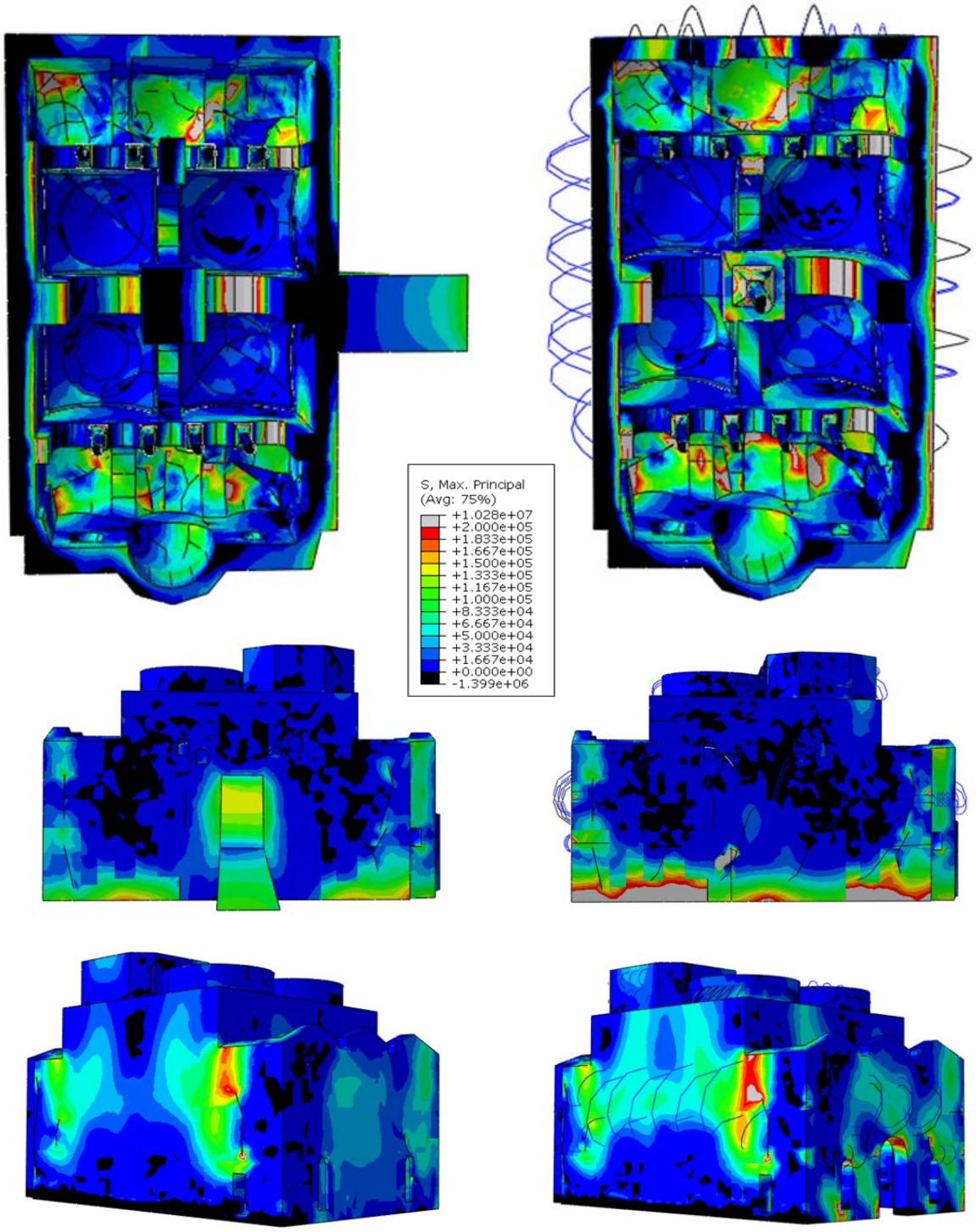
The stress in the building induced by seismic loads is now evaluated. This is the most interesting load condition, as it allows the effectiveness of the design choices that underlie the restoration works to be assessed, with special attention to the demolition of the buttress and the replacement of the pillars with steel frames.

The presence of the buttress means that the median axis of the church was not an axis of symmetry for the building before restoration: accordingly, it is necessary to separately study the effects of an earthquake acting along the short side of the church in one direction or in the opposite one.



(a) (b)

Figure 8: Contours of the maximum principal stress in the church (a) before and (b) after the restoration works under gravity loads



(a) (b)

Figure 9: Contours of the maximum principal stress in the church (a) before and (b) after the restoration works under gravity loads and equivalent lateral loads acting along the S-N direction. Top: view from below; center: view from the south side; bottom: view of the N and W sides

Figure 9 shows the contours of the maximum principal stress assuming the earthquake to act in the S-N direction. Compared to the pre-restoration conditions, there is an increase in tensile stress in the domes above the narthex and the apse. Moreover, if on the one hand the stress in the left arch is reduced by the removal of the central pillar, on the other hand the stress is considerably increased in the right arch. Also, the central column which was originally embedded in the pillar experiences high stresses, despite the presence of the metal frame.

The southern front of the building from which the buttress was removed deserves particular attention. From the stress contours in Figure 9 there is a dramatic increase in tensile stress with respect to the pre-intervention model, which can be explained by the removal of the element that carried most of the lateral load. The choice of removing the buttress could therefore weaken the structure and endanger the stability of the building in the event of an earthquake. It must also be acknowledged that an earthquake acting in the S-N direction is likely to cause debonding of the main body from the buttress, which would therefore be ineffective.

Similar considerations apply in the case of an earthquake acting in the N-S direction. Also in this case it is found that the modifications aggravate the stress state in some elements: in addition to the arches on the north side of the building (in which the highest tensile stress occurs), several parts of the outer domes experience stresses well above the presumed tensile strength. On the south front, the demolition of the buttress increases the tensile stress in the areas between the central body and the lateral elements. Finally, the seismic load causes a significant increase in tension at the base of the walls on the north side and in the façade of the church deprived of the buttress.

5 CONCLUDING REMARKS

The main objective of the restoration works carried out on the church of St. Nicholas in Mesopotam was to avoid further propagation of the crack pattern, while bringing back the church to its original conditions, before the XVIII century. The effectiveness of the conservative intervention was assessed by analyzing the structure by finite elements under different load conditions.

According to the numerical results, the stress state in the building has mostly worsened after restoration because of some questionable design choices. The will to restore the “original” conditions of the building proved to be too ambitious from the structural point of view in the face of the retrofitting intervention.

As for the restoration of the interior of the church, the idea of rearranging the space by demolishing two massive pillars dating back to the XVIII century, which negatively affected the appearance of the internal space, can be considered appropriate in principle. The way this idea has been implemented, however, is unsuitable. As the central pillar was only partially demolished, the remaining block behaves like an anomalous load for the underlying column, which experiences a dramatic increase in stress despite the addition of a steel frame.

As for the exterior of the church, the most controversial change is the removal of the buttress on the southern side. The results provided by a static linear analysis show that, in the event of seismic actions acting along the short side of the building, the tensile stresses increase in several parts of the walls significantly and exceed the admissible values.

Finally, hooping domes with polyester strips proves to be ineffective, as the stress is virtually equivalent to that in the unreinforced domes. Using strips made of stiffer materials is likely to be a smarter choice.

In the continuation of the research, nonlinear dynamic analyses will be carried out to estimate the stress induced in the building by an earthquake more accurately. Alternative retrofitting solutions will be also proposed.

REFERENCES

[1] Macchiarella, G. Un caso a sé: San Nicola di Mesopotam (Albania). In: C. Gelao & L. Derosa (eds.): *Tempi e forme dell'arte. Miscellanea di Studi offerti a Pina Belli D'Elia*, Claudio Grenzi, Foggia, Italy (2011), pp. 123-135.

[2] Meksi, A. Arkitektura e kishës së Mesopotamit. *Monumentet* (1972) **3**:75-94.

[3] Meksi, A. Arkitektura e kishave të Shqipërisë (Shekujt VII-XV). *Shtepia Botuese Uegen*, Tirana (2004).

[4] Brumana, R., Oreni D., Cuca B., Binda L., Condoleo P. and Triggiani M. Strategy for integrated surveying techniques finalized to interpretive models in a Byzantine church, Mesopotam, Albania. *Int. J. Arch. Herit.* (2014) **8**:886-924.

[5] Triggiani, M. San Nicola di Mesopotam: Correnti culturali adriatiche. In: M. Guidetti & S. Mondini (eds.): *A mari usque ad mare – Cultura visuale e materiale dall'Adriatico all'India*, Ca' Foscari, Venice (2016).

[6] Italian National Institute of Geophysics: Global seismic hazard assessment program, June-July 1993.

12th International Conference on Structural Analysis of Historical Constructions
SAHC 2020
P. Roca, L. Pelà and C. Molins (Eds.)

STRUCTURAL ASSESSMENT OF THE 13TH CENTURY GREAT MOSQUE AND HOSPITAL OF DIVRIGI: A WORLD HERITAGE LISTED STRUCTURE

CEM DEMIR*†, OMER FARUK HALICI††, ALI NAKI SANVER†††, MUSTAFA COMERT†††, FIKRET KURAN††††, NICOLA BERLUCCHI†††††, ALI HURATA†††† AND ALPER ILKI†

† Istanbul Technical University, Civil Engineering Faculty

Ayazaga Campus, 34750, Sariyer, Istanbul, Turkey
E-mail: demirce@itu.edu.tr*, ailki@itu.edu.tr - Web page: http://www.itu.edu.tr

†† MEF University, Department of Civil Engineering

Ayazaga Caddesi, No: 4, 34396, Sariyer, Istanbul, Turkey
E-mail: halicio@mef.edu.tr - Web page: http://www.mef.edu.tr

††† RISE Engineering & Consultancy

Eclipse Maslak C15, Maslak, Sariyer, Istanbul, Turkey
E-mail: alinaki@rise.ist, mustafa@rise.ist - Web page: http://www.rise.ist

†††† Directorate General of Foundations

Milli Müdafaa Caddesi, No: 20, Kızılay , Çankaya, Ankara, Turkey
E-mail: f.kuran@vgm.gov.tr, a.hurata@vgm.gov.tr - Web page: http://www.vgm.gov.tr

††††† Studio Berlucchi S.r.l

Contrada Soncin Rotto, 4, Brescia, Italy
E-Mail: nicolaberlucchi@studioberlucchi.it - Web page: http://www. studioberlucchi.it

Keywords: Assessment, Masonry, Mosque, Seismic, Retrofit, World Heritage

Abstract. *The Great Mosque and Hospital of Divrigi is located in the central eastern part of Turkey, in Divrigi, Sivas. The historical facility consists of a monumental mosque and a two-story hospital, which are adjacent to each other. The structure dates back to 13th century Mengujekids period and has been listed by the UNESCO as a World Heritage since 1985. Great Mosque and Hospital of Divrigi is particularly notable for its monumental stone portals that are decorated with three-dimensional ornaments carved from stone. The structural system of the monument consists of multi-leaf stone masonry walls and stone piers that support the roof structure which consists of stone and brick arches and vaults. The structure is located about 90 km away from the North Anatolian Fault Line, that has been causing several destructive earthquakes. Consequently, the structure is prone to destructive seismic activities. In this study, after a brief introduction on the structural system and current condition of the structure, the structural performance of the Great Mosque and Hospital of Divrigi is investigated through site observations and structural analyses. For this purpose, linear and nonlinear 3D finite element models of the structure are developed and the structure is examined under the effects of vertical loads and seismic actions. In the light of the analyses results, recommendations for potential interventions are outlined for further preservation of the structure.*

1 INTRODUCTION

The Great Mosque and Hospital of Divrigi (Figure 1), an UNESCO World Heritage listed structure since the year 1985, dates back to the Mengujekids period (13th century). The structure, located in the central eastern part of Turkey (today Divrigi, Sivas), is constructed on a sloped hill. Great Mosque and Hospital of Divrigi is particularly notable for its monumental stone portals and vaults that are decorated with three-dimensional ornaments carved from stone (Figures 2 and 3). The structure is a unique piece of civil architecture of its period and several restoration works had been performed in the past. However, the monument still needs further attempts for enhancement of the structural system, repair of damages, removal of the traces of past malpractice and conservation of its exceptional architectural features. For this purpose, Ministry of Culture and Tourism and General Directorate of Foundations of Turkey have recently launched an extensive restoration campaign, which is being carried out by a group of experts from various disciplines. The structural analyses presented in this study is a short summary of several efforts spent in the scope of this project.

In this study, after a brief introduction of the structural system and current condition of the monument, the structural performance of the Great Mosque and Hospital of Divrigi is investigated through site observations, historical records and structural analyses. For this purpose, a 3D finite element model of the structure is developed and examined under the effects of vertical loads and seismic actions. For realization of the linear and nonlinear structural analyses, the recommendations given in the Guidelines for Management of Seismic Risks for Historical Constructions document are followed [1]. In the light of the analyses results, the potential reasons for existing damages and previous interventions are investigated and recommendations for potential interventions are outlined for further preservation of the structure. It should be noted that the intervention proposal reported here is not yet officially approved and applied. So, they should be accepted as draft proposals.



Figure 1: Exterior and interior views of the structure



Figure 2: Decorated monumental stone portals



Figure 3: Stone vaults with ornaments

2 STRUCTURAL FEATURES OF THE GREAT MOSQUE AND HOSPITAL OF DIVRIGI

The complex compromises of a monumental mosque and a two-story hospital, which are adjacent to each other (Figure 4). The mosque and the hospital parts are structurally connected to each other and the southern kiblah wall of the mosque partitions these two spaces. The structural system of the Great Mosque and Hospital of Divrigi consists of stone masonry walls and stone piers that support the vaulted roof structure. The dimensions of the structure are approximately 73 m × 32 m in plan and the average height for façades is about 12 m. The façade views can be seen in Figure 2.

The walls are approximately 1.4 m thick multi-leaf walls with cut-stone outer leaves and a rubble masonry infill. The roof structure consists of stone arches and vaults. The only exception to this use of stone masonry is the brick masonry vaults (Figure 5) covering the areas adjacent to the western façade that are known to be damaged/collapsed and rebuilt together with stone buttresses adjoining with the western façade main wall. Another surviving trace of this incident is the significant out-of-plumb top displacement (almost 60 cm) of the mosque section western façade wall and portal (Figure 6).

Located at about 90 km away from the North Anatolian Fault Line, that is known to have created M_w>7.0 earthquakes in the past, the structure is prone to destructive seismic activities. Being in such an active seismic region, the structure underwent several extensive repair and intervention works not only during the Ottoman, but also during the Republic periods. Although at its current state the structure is intact, several structural deformations in the form of cracks,

material losses and dislocations can be observed over the walls, piers and vaults (Figure 7). Additionally, material deteriorations and traces of malpractices of past restoration works (i.e.. poor workmanship, use of unsuitable materials like cement, interventions structurally and architecturally not coherent with the original techniques) can also be widely observed.

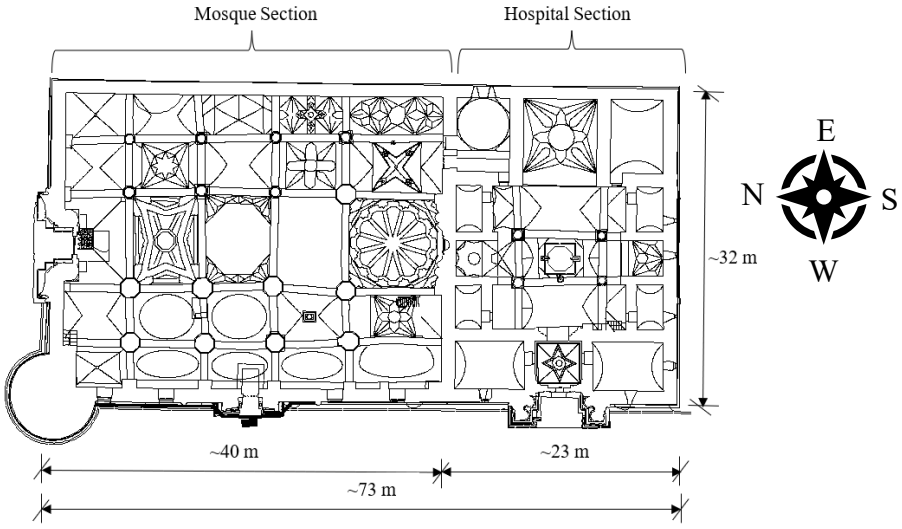


Figure 4: Plan view of the structure



Figure 5: Brick vaults adjacent to the western façade of the mosque section



Figure 6: Out-of-plumb deformation of the western façade mosque portal



Figure 7: Typical damages on structural members

3 STRUCTURAL ANALYSES

This section presents the safety and structural performance evaluations of the monumental structure which are investigated through finite element analyses. Three-dimensional Finite Element (FE) models representing the present condition and deficiencies of the structure were developed based on available drawings, in situ measurements and visual observations. Two 3D FE models were created to evaluate the behavior of the structure under vertical loads and representative seismic actions. The first FE model was formed with linear elastic approach to assess the global response, stress distributions, and safety of the structure. While the second FE model was constructed to specifically investigate the safety status of the western façade wall, which has tilted nearly 4° thought to have occurred during past earthquakes. A nonlinear approach in terms of material and geometry was adopted in the second FE model.

The general modeling assumptions and the brief results obtained from these two FE models are presented in the following subsections.

3.1 Linear Elastic Analysis Investigating the Global Response of the Structure

The first model was established using SAP2000 v20 structural analysis program [2]. Structural components such as walls, vaults, and domes were modeled with 2D four-node shell elements with three translational degree of freedoms at each node. While components including stone piers and arches were modeled with two-node beam elements. General views of the structural model are presented in Figure 8. Structural safety was evaluated based on the implications stated in Guidelines for Management of Seismic Risks for Historical Constructions

[1], where the components of the structures having world-wide importance are proposed to have sufficient capacity against the effects of vertical loads and earthquake actions with 2475-year return period considering a seismic load reduction factor (R) of 3 (indicated as Controlled Damage performance level in [1]). For this purpose, site-specific earthquake spectra were developed for the earthquakes with return periods of 72, 475 and 2475 years. Among these ground motions 72 years was used for design of the temporary shoring structures to be used during the restoration works and 475 years to check the western façade wall out-of-plane performance. In the determination of such spectra, the attenuation relationship developed by Campbell and Bozorgnia [3] was benefited considering the seismic faults near the area.

The mechanical properties of the structural materials were taken from [1] based on the site observations and masonry quality. Accordingly, the modulus of elasticity values for the stone masonry and brick masonry were taken as 1750 MPa and 2100 MPa, respectively. Similarly, the compressive and tensile strengths of stone masonry were considered as 1.80 MPa and 0.20 MPa, respectively. While they were 2.20 MPa and 0.20 MPa and for brick masonry, respectively. Also, the initial shear strength values were 0.065 MPa and 0.075 MPa for stone and brick masonry. The results of the structural analyses indicated that under gravitational loads and 2475-year return period seismic action, the obtained compressive stress values did not exceed the compressive strength values defined for the brick and stone masonry. However, the tensile stress values obtained at the critical sections of the vaults and the domes were generally greater than the assumed tensile strength values. Figure 9 shows the tensile stress distribution obtained for the roof structure.

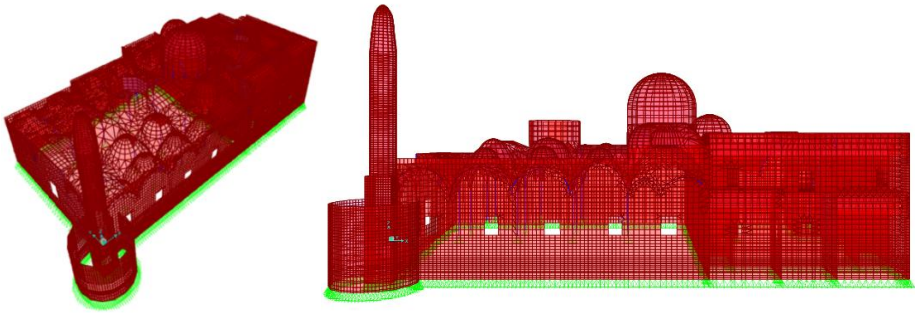


Figure 8: General views of the first FE model

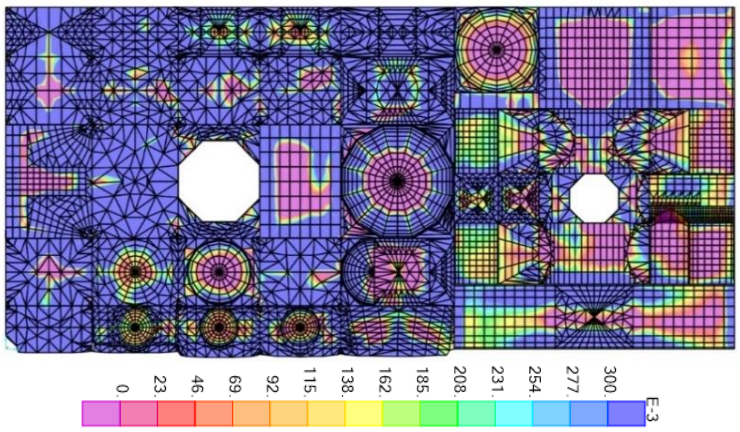


Figure 9: Tensile stress distribution for the roof structure [MPa]

The shear stress values obtained for the masonry walls were compared with the calculated shear strengths of the materials. The shear strength (τ) at the critical sections was calculated using Equation 1, where τ_0 is the initial shear strength and σ is the compressive stress at the corresponding section. Shear stress distribution obtained for the western wall is shown in Figure 10.

$$\tau = \tau_0 + 0.4\sigma \quad (1)$$

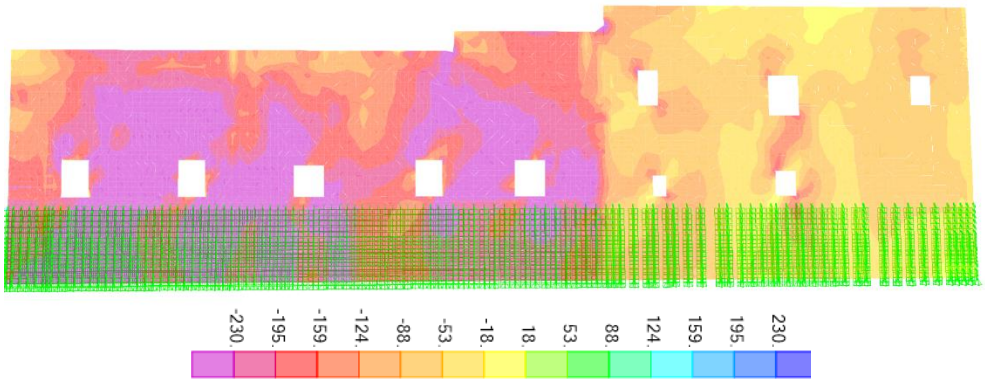


Figure 10: Shear stress distribution on the western wall (unit: kPa)

On the whole, the obtained internal forces for shear, tension and out-of-plane (OOP) bending moment were greater than the calculated capacities of the many structural components. Hence, it was concluded that with its present condition, the structure does not satisfy the Controlled Damage performance level for 2475 years return period ground motion predefined in Guidelines for Management of Seismic Risks for Historical Constructions [1]. However, when the analyses were repeated for a 475 years period ground motion for Controlled Damage state (with R=3), it has been observed that the capacities of main walls and piers were found to be acceptable except for the out-of-plane behavior of the main façade walls of the mosque section. This observation was also compared and confirmed with simple mechanism-based calculations for overturning of these main walls.

3.2 Nonlinear Analysis Investigating the Response of the Western Wall

The second FE model was developed by using Abaqus 2019 FE software [4]. As the main purpose of this FE model was to investigate the safety of the tilted part of the western façade wall, the wall and the supporting buttresses (which were added to the inner face of the western façade wall during past interventions) were modeled in detail using eight-node 3D solid elements with simplified micro modeling approach. Material and geometric nonlinearity approaches were adopted in the modeling of the western wall. All other structural components were modeled as in the first FE model described in Section 3.1. Besides the tilted part of the western wall, other components of the structure were included in the model in order to represent the wall boundary conditions realistically. General views of the model are shown in Figure 11. Due to different modeling approaches and the tilted geometry of the western wall, gaps between the western wall and the adjacent walls were present in the model. Nonetheless, kinematic constraints were defined in those regions to provide connection between structural elements.

The multi-leaf masonry wall is made of two cut stone masonry units at the exterior and interior faces which are separated by rubble stone masonry units in the middle. Further information on the behavior multi-leaf walls can be found in [5-7]. The dimensions of the examined part of the western wall are 33 meters in length, 12 meters in height. The thickness of the wall is 1.4 meter. The rubble stone masonry was modeled as one solid part, while the cut stone masonry units were modeled as separated micro elements. In order to represent the randomness of the stone unit configuration, different cut stone unit dimensions were assembled in the model. The length of the cut stone units was ranging between 0.40 and 0.80 meter, whereas the thickness of the units was either 0.30 or 0.45 meter. The assembled wall configuration is presented in Figure 12.

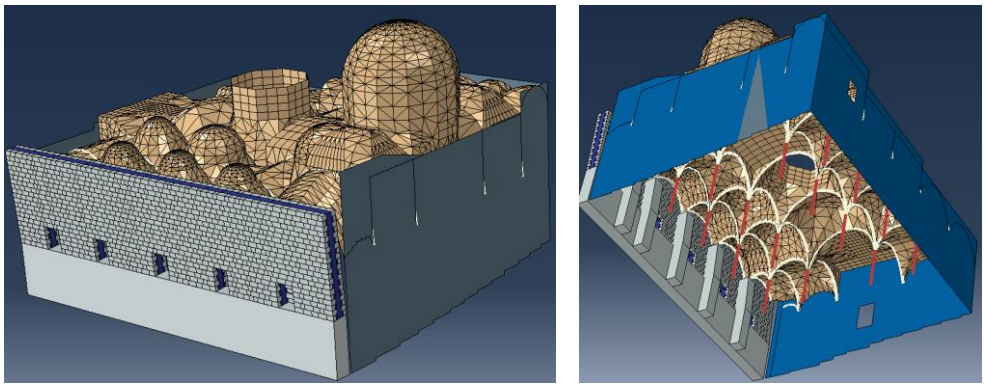


Figure 11: General views of the second FE model

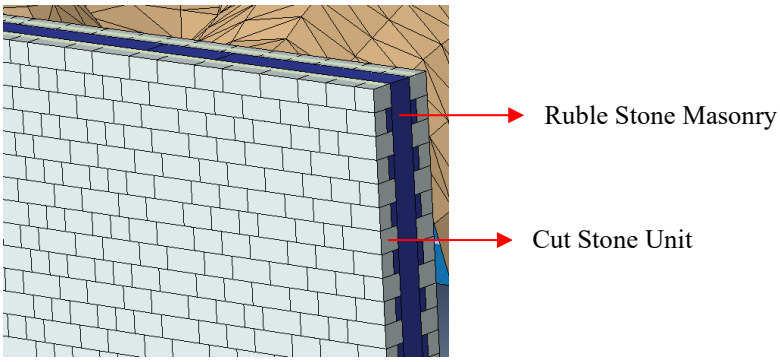


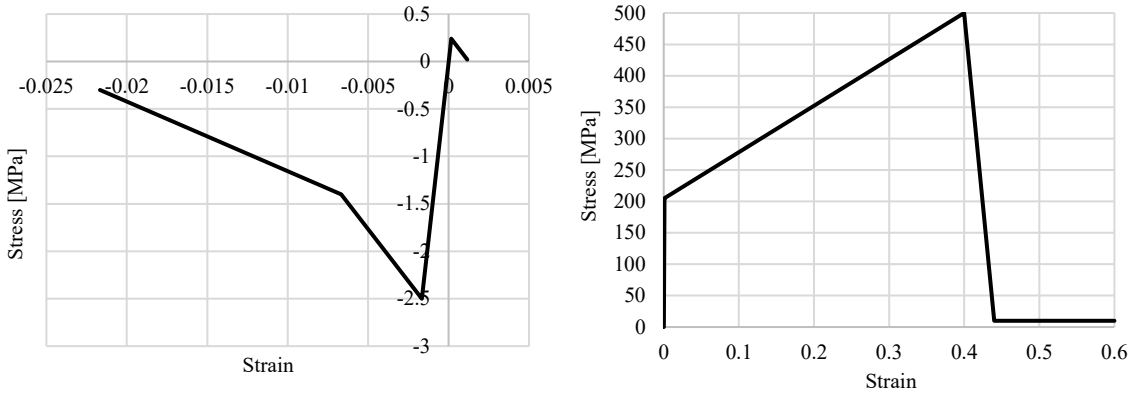
Figure 12: Wall configuration with different wall unit geometries

The nonlinear stress-strain relationship for the rubble masonry wall is presented in Figure 13a. The cut stone masonry units were modeled with linear elastic material properties with a Young's Modulus of 2500 MPa. The interface behavior between rubble stone and cut stone units were modeled with nonlinear cohesive-frictional interaction properties. Hard contact was defined between all surfaces in contact. The cohesive-frictional interfaces remain elastic until the normal stress and/or shear stress values at the interfaces reach the specified strength values (f_{ti} for interface tensile strength, τ_{oi} for interface initial shear strength in Table 1). Then, the interactions continue to transfer shear forces with respect to the friction coefficient (μ) and the normal stress (σ) acting on the surface. Conversely, the interfaces between cut stones were modeled without cohesion and tensile strength as no grout between

stone units was observed during site visits. The selected interaction properties at different interfaces are outlined in Table 1.

Table 1: Interaction properties at the interfaces

Interface	f_{ti} [MPa]	τ_{oi} [MPa]	μ
Rubble Stone – Cut Stone	0.10	0.20	0.50
Buttress – Cut Stone	0.10	0.20	0.50
Cut Stone – Cut Stone	-	-	0.50



(a) (b)

Figure 13: Nonlinear material properties: (a) Rubble stone; (b) AISI 316

Site-specific response spectrum with 475-year return period was used to investigate the safety status of the western wall against seismic actions with its current condition. As a case study, an acceleration time history record was provided from PEER Ground Motion Database [8]. H1 component of 'RSN1161' Kocaeli earthquake record (1999) was selected and scaled by 1.185 to match the site-specific response spectra (Figure 14). The acceleration time history was applied in the out-of-plane (OOP) direction of the western wall. In the time-history analysis, the wall exhibited large OOP displacements which eventually initiated the instability and resulted with the collapse of the wall (Figure 15).

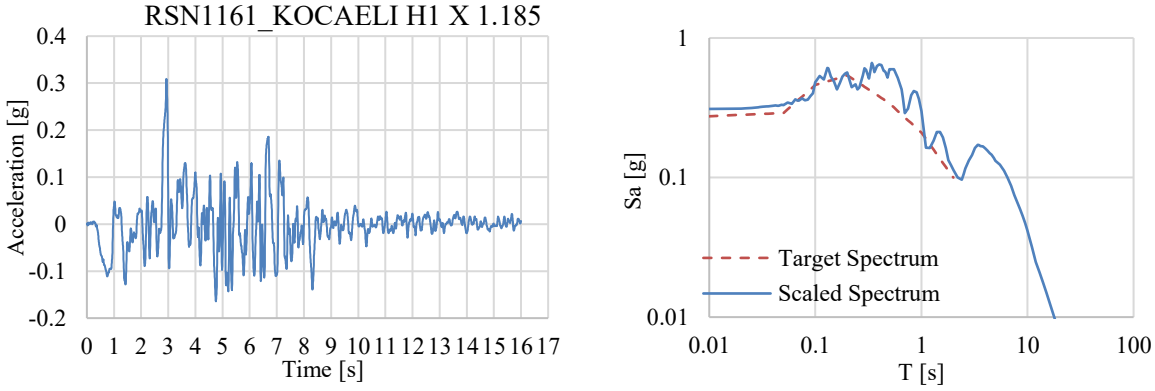


Figure 14: (a) Selected acceleration record, (b) target and obtained response spectra

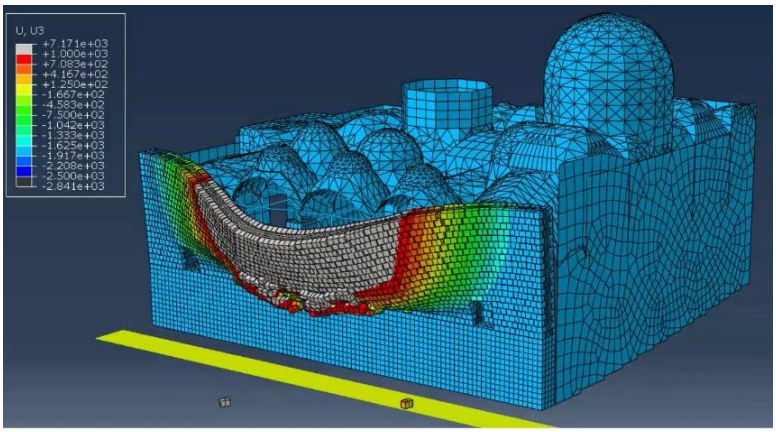
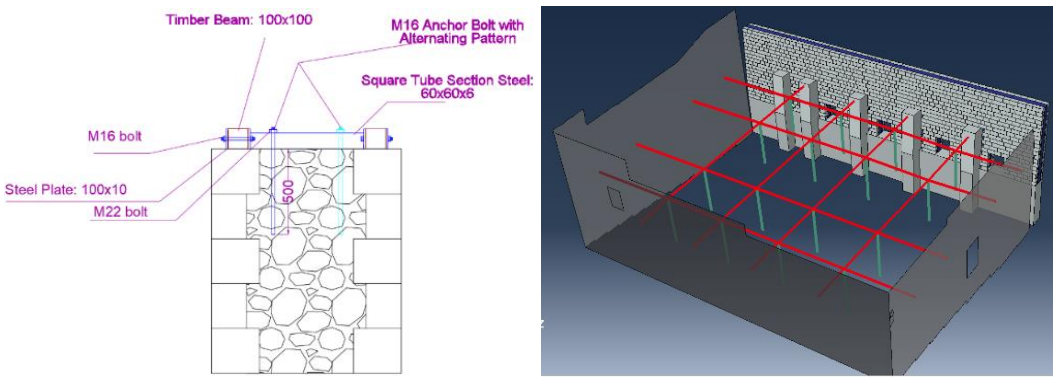


Figure 15: Out-of-plane collapse of the western façade wall observed during the time-history analysis (horizontal displacement contour in mm unit)

4 REHABILITATION METHODOLOGY PROPOSAL

Linear and nonlinear structural performance analyses showed insufficient capacity of the structure against the combination of gravitational and seismic load effects. The internal forces within the walls, such as shear, tension and moment exceeded the relevant capacities of the load bearing members. Based on these analyses results and site observations, a series of structural interventions was proposed to enhance the behavior of the structure against future earthquakes.

In order to enhance the structural integrity and increase the OOP bending moment capacity, steel-timber composite bonding beams were proposed to be placed above the main walls. The projected system includes two timber beams having 100 x 100 mm x mm cross-section dimensions with two steel plates attached on both sides of each timber frame. The attached steel plates have 10 x 100 mm x mm cross-section dimensions. In plan, the two composite beams are connected together by steel cross ties at each 750 mm distance. The cross ties have square tube cross-sections with 60 mm of edge length and 6 mm of wall thickness. The view of a typical wall section with the top bonding beam is presented in Figure 16a.



(a) (b)

Figure 16: (a) Cross-section of wall with composite bonding beam (units mm), (b) layout of ties between piers and walls

The second recommended rehabilitation methodology to improve the structural performance was bracing the piers and the walls with stainless steel ties. It should be noted that, in the current state, only the naives close to the western façade are reinforced with timber ties. In order to

provide ties to whole structure, 50-mm-diameter tension rods with AISI 316 steel class were proposed to connect the vertical components of the structure. The stress-strain relationship of AISI 316 and a view of the planned layout of the steel ties are shown in Figure 13b and Figure 16b, respectively.

The described rehabilitation methodologies above were then defined in the nonlinear FE model and the time-history analysis was repeated under the same earthquake excitation. The rehabilitated wall did not exhibit instability and managed to withstand the seismic excitations until the end of the analysis. Displacement time histories measured at the top of the wall are presented in Figure 17 for both cases. It was concluded that, with the application of the proposed rehabilitation methods, the OOP displacement of the western wall can be reduced to nearly 25% of the same displacement obtained with the present condition of the wall.

In addition to the above mentioned reinforcing methodologies, other structural interventions such as lime grout injection to walls and cracks, local repairs, replacement of heavily damaged/decayed masonry units, retrofitting of vaults with textile reinforced mortar (TRM) and bracing of cracked piers/pier caps are also planned.

In order to protect the structure from harsh weather conditions of the region during the extensive restoration works; a temporary roof structure has been designed and constructed as can be seen in Figure 18. The light roof system formed with steel and aluminum members has a single span in the transverse direction (approximately 40 m long) and has the ability to melt the snow during the winter season by the help of a heater system.

It should be also noted that an extensive structural health monitoring (SHM) system with more than 70 channels has been activated for continuously observing the structure electronically before, during and after the restoration works which is still under operation.

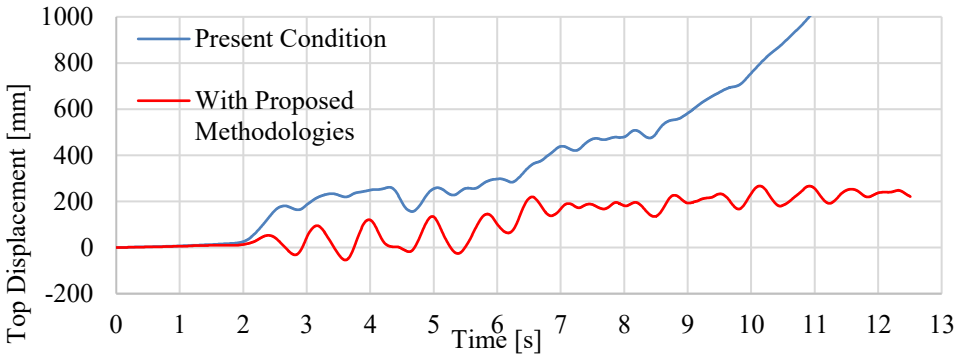


Figure 17: Wall out-of-plane displacement at the top (measured relative to the ground)



Figure 18: Temporary roof structure for protecting the structure during the restoration works

5 CONCLUSIONS

In this study, the seismic performance of the Great Mosque and Hospital of Divrigi located in eastern Turkey was investigated through site observations and structural analyses. The linear and nonlinear finite element models of the 13th century UNESCO World Heritage structure was constructed, and the seismic performance of the monument was assessed for the combined actions of vertical and seismic loads. The analyses results indicated that the structural performance of the Great Mosque and Hospital of Divrigi may have some flaws particularly for the out-of-plane behavior of 12 m high western wall. Consequently, a rehabilitation scheme including the introduction of stainless steel ties and wall-top bonding beams has been proposed for enhancing the seismic performance of the structure. The nonlinear finite element analyses results show that with the proposed interventions, the integrity of the structural system can be significantly enhanced, and the seismic capacity can be considerably improved.

Acknowledgements. The authors would like to express their sincere gratitude to Directorate General of Foundations and Ministry of Culture and Tourism of Turkey for their generous supports during the study. Contractors of the restoration project, Kadioglu Construction and Dor Yapi Construction companies are also acknowledged.

REFERENCES

[1] Guidelines for Management of Seismic Risks for Historical Constructions, Directorate General of Foundations, Ankara, Turkey (Online in Turkish: https://www.ipkb.gov.tr/tr/yayinlar), (2017).

[2] Computers and Structures. SAP2000 v20 Integrated finite element analysis and design of structures basic analysis reference manual. Computers and Structures, Inc., Berkeley, California, USA, (2018).

[3] Campbell, K.W. and Bozorgnia, Y. NGA Ground Motion Model for the Geometric Mean Horizontal Component of PGA, PGV, PGD and 5% Damped Linear Elastic Response Spectra for Periods Ranging from 0.01 to 10 s. *Earthquake Spectra, 24*(1), 139-171, (2008).

[4] Abaqus F.E.A. "Analysis User's Manual" Dassault Systemes Simulia Corp., Providence, RI, (2019).

[5] Demir, C. and Ilki, A. Characterization of the materials used in the multi-leaf masonry walls of monumental structures in Istanbul, Turkey. *Construction and Building Materials*, 64, 398-413, (2014).

[6] Demir, C., Dogu, E., Ispir, M. and Ilki, A. Seismic Behavior of Ottoman Empire Classical Period Stone Masonry Walls. In: *10th International Conference on Urban Earthquake Engineering (10CUEE)*, Tokyo Institute of Technology, (2019).

[7] AlGohi, B.H., Baluch, M.H., Rahman, M.K., Al-Gadhib, A.H. and Demir, C. Plastic-Damage Modeling of Unreinforced Masonry Walls (URM) Subject to Lateral Loading. *Arabian Journal for Science and Engineering* (2017) 42(9), 4201-4220.

[8] Chiou, B., Darragh, R., Gregor, N. and Silva, W. NGA Project Strong-Motion Database. *Earthquake Spectra* (2008) 24(1), 23-44.

12th International Conference on Structural Analysis of Historical Constructions
SAHC 2020
P. Roca, L. Pelà and C. Molins (Eds.)

THE FLOOR STIFFNESS EFFECT ON VULNERABILITY ASSESSMENTS AND INTERVENTION DESIGNS OF HISTORIC BUILDINGS: THE CASE STUDY OF THE "PROCURATIE VECCHIE" IN VENICE, ITALY

IRENE ROCCA[1]*, LUISA BERTO[1], SONIA BELLIN[2], BEAUDIN F. DONGMO[3], ANNA SAETTA[1], RENATO VITALIANI[4]

[1] DCP - University IUAV of Venice
Campus Terese, Dorsoduro 2206- 30123 Venice - Italy
e-mail: irocca@iuav.it; lberto@iuav.it; saetta@iuav.it

[2] Structural engineer
e-mail: soniabellin93@gmail.com

[3] Structural engineer
e-mail: fdongmo@yahoo.fr

[4]DICEA - University of Padua,
Via Francesco Marzolo 9, 35131 Padova – Italy
e-mail: renato.vitaliani@unipd.it

Keywords: Historical Structure, Masonry, Floor in-plane stiffness

Abstract. *In the Italian seismic scenario, and beyond, interventions on existing buildings focused on the evaluation and reduction of seismic risk of cultural heritage have gained more and more importance in the engineering field.*

Therefore, for the designer it becomes increasingly useful to have a methodology that allows to carry out, in the study of an existing structure behavior, the vulnerability assessment of both the actual state and the design state, evaluating the adequacy of potential intervention of seismic improvement.

In this paper some phases of this methodology are presented in the context of the restoration work started in November 2017, and currently in progress, of the historical building of Procuratie Vecchie in Piazza San Marco in Venice, with particular focus on the consolidation intervention of the timber floors which satisfy the conservation requirements imposed by the Superintendence of Venice. Actually, the influence of floor diaphragms on structural behavior of existing masonry building subjected to seismic action is critically discussed with particular reference to the effects of in-plane stiffness of floors on the seismic distribution of forces on lateral walls and on the out–of–plane mechanism of the walls.

1 INTRODUCTION

The damage caused by recent and past earthquakes in Italy and in the Mediterranean area has shown the high seismic vulnerability of the cultural heritage. Therefore it is mandatory to invest in interventions on historical constructions, aimed to the reduction of their seismic risk. In this field, one relevant case study is represented by the restoration work currently in progress in the Procuratie Vecchie in Piazza San Marco in Venice.

Some aspects of this work are described in the present paper, focusing to the timber floors consolidation intervention and its effect on the seismic response of the building. Starting from the design restrictions of complete reversibility of the intervention and low degree of invasiveness on the historic building, an effective and non-invasive solution was proposed for the consolidation of timber floors based on the insertion of steel ring beam (i.e. a steel perimeter chord) and a doubly diagonal mesh of flat steel ties anchored to the beams and to the perimeter walls. The proposed intervention guarantees proper resistance and stiffness to the floor, without significant modifications of the global dynamic behavior of the structure.

It is worth noting that this type of floor does not behave as an infinitely rigid diaphragm, and this consolidation intervention can be considered classifiable as limited stiffening. In order to study the relation between floor stiffness and the earthquake resistant structures behavior (i.e. the masonry walls), and to establish the proper interventions, the results of four different models of a portion of Procuratie Vecchie are critically discussed. The selected portion of the building is representative of a "module" between two subsequent masonry wall alignments. The four models simulate four different hypotheses of the floors behavior, in order to capture the progressive effect of increasing floor stiffness due to the introduction of the various structural components.

2 THE "PROCURATIE VECCHIE" IN VENICE: KNOWLEDGE PATH

The "Procuratie Vecchie", that overlooks south Piazza San Marco in Venice, is part of the complex of Procuratie, which is divided into three buildings: the Procuratie Vecchie, the Procuratie Nuove, dating back to the 14th century, and the Procuratie Nuovissime, or Ala Napoleonica, built by Napoleone Bonaparte in the early 19th century (Figure 1 and Figure 2).

The Procuratie Vecchie building was erected in the 12th century, at will of Doge Sebastiano Ziani in order to host the accommodation of the Procurators of Venice. There is no evidence of the original internal distribution, due to the scarcity of sources related to the building in medieval times.

After the destruction caused by fire on February 1st 1512, great reconstruction works took place, which were well documented through iconography, even if the actual design authorship of the reconstruction work is not completely certain. There is certainty that between 1519 and 1529 the Procuratie Vecchie construction site was directed by Bartolomeo Bon (at least for the *Clock Tower* up to the *Sottoportico dei Dai*), while from the *Sottoportico dei Dai* to the *San Geminiano Church* the project is certainly attributable to Jacopo Sansovino. Later in 1909, the substantial restoration of the building, especially in terms of internal distribution, was entrusted to engineer Fano. He made substantial modifications to the building, especially in terms of internal distribution, as the new client's intention was to transform the traditional residential function maintained by the Procuratie Vecchie up to that time into office functions.



Figure 1: Indication of Procuratie Vecchie in the: (a) Aereal view of Piazza San Marco; (b) Procuratie complex



Figure 2: Façade of Procuratie Vecchie

The Procuratie Vecchie have a load-bearing brick masonry structure with a roughly rectangular and rather elongated shape, with a greater side of 152m oriented along the East-West axis and a smaller side of 25m along the North-South axis. The building has eight storeys above ground (four noble storeys, three mezzanine storeys and an attic storey), all characterized by the same overall plan extension, except for the attic.

Regarding the inter-storey height, the floor of the mezzanine level, originally placed over the entire storey plan extension, were largely demolished during the restoration works that affected the building in the twentieth century, increasing the inter-storey height in such positions. The building has a top height of 21.4m in the western part (for the whole extension of the attic storey), and a lower height of 19.0m at the top for the remaining portion. The monumental façade on San Marco Square is 16.7m high and is entirely made of white Istrian stone.

All the information about the dimensions and geometry of the entire Procuratie Vecchie building in its actual state was provided by the geometric survey, carried out with an integrated methodology of direct-and-instrumental survey.

Then an accurate material-constructive survey was carried out in order to acquire knowledge about the materials and their state of conservation, as well as the technique used to construct the building, the relationships between the parts, and the quality of the building itself (e.g. the accordance with the best constructive practices, the so called "rules of thumb"). To this aim, many visual inspections were carried out together with a limited number of weakly destructive tests for the material characterization (e.g. for masonry: single and double flat jacks tests, Shove test, petrographic characterization of mortar) according to Italian Regulation D.P.C.M. 9/02/2011 [1] and Commentary of Italian Technical Standards NTC08 (2009) [2] in order to obtain a knowledge level equal to LC2 (which corresponds to KL2, Normal Knowledge in Eurocode 8-part 3 [3]).

The masonry of vertical elements was classified as solid brick masonry with lime or cement-lime mortar joints with regular texture. The only exception is represented by the façade facing Piazza San Marco that, as previously stated, is made of white Istrian stone.

The orthogonal walls are well connected, while, with regard to the connection between walls and floors, several critical points were highlighted, requiring restoration interventions.

Besides, seventy visual inspections were carried out for characterizing the floor system. Two prevalent floor types have been identified:

1. one–way timber floor with beams and simple plank;
2. one–way hollow bricks and concrete floor with joists cast on site

For both of them different variants are present in terms of layers' thickness, geometrical dimension, spacing of timber beams, etc.

3 OVERVIEW OF THE SEISMIC VULNERABILITY ASSESSMENT OF THE ENTIRE BUILDING

3.1 Seismic action

The seismic action has been assessed according to NTC2018 [4] and the probabilistic seismic hazard maps of Italian territory (MPS04) published by INGV. A soil type E and a topographic category T1 were assumed. For the building, a reference period V_R equal to 75 years was assumed, which corresponds to a return period T_R of the seismic action at Life-Safety Limit State equal to 712 years, with a PGA value equal to 0.128g. A behavior factor q equal to 2.25 was adopted.

3.2 Seismic analyses

Historic masonry buildings, like Procuratie Vecchie, are complex for their typology and construction techniques. Therefore the analysis of their structural behaviour and their seismic assessment are conditioned by significant uncertainties in defining the mechanical properties of the materials and the connection conditions of the various elements, which can make the results of the numerical analysis on the whole building not reliable enough. In particular, the activation of local collapse mechanisms does not allow the structure to behave as a whole, and then these activations have to be checked.

Firstly, preliminary evaluations of seismic safety were performed according to the Evaluation Level 1 (LV1) introduced in [1], by means of the simplified mechanical model defined for "Buildings, villas and other structures with bearing walls and horizontal

diaphragms".

Then local collapse mechanisms of single portions of the building were evaluated according to the Evaluation Level 2 (LV2), that is based on the evaluation of individual macro elements. Among others, the simple overturning of the façade facing San Marco's Square, the overturning of the corner on San Marco's Square and the horizontal confined wall deflection on the Bacino Orseolo side are analyzed.

Then, starting from the information collected by the geometric and material constructive survey of the building, a global FE model of the building was created in order to study its dynamic behavior, Figure 3. The numerical analyses were performed with the FE program Midas Gen [5]. The types of element used are:

- 3 or 4 node Shell elements, with both flexural and membranal stiffness, for the walls;
- Truss elements for the columns of the porticoes and the columns of the arches characterizing the facade of San Marco's Square, as well as for the tie rods at the various floors;
- Beam elements for the floor beams. It is worth noting that, in this global model, the timber floors are modelled with equivalent beams which guarantee the same stiffness of the actual timber floor.

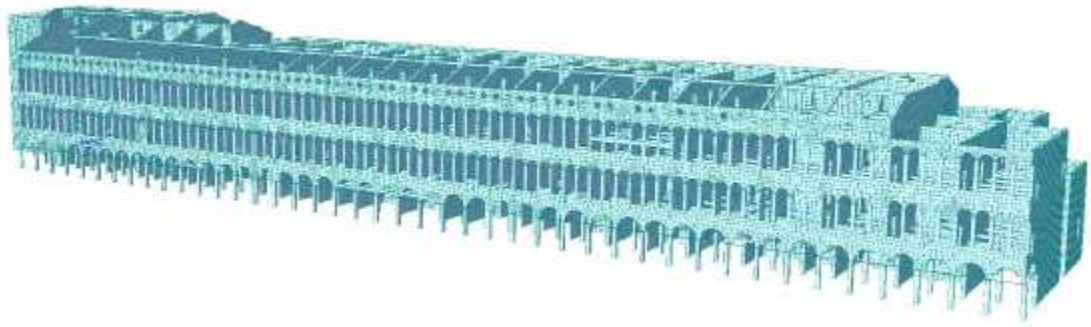


Figure 3: Global FEM of Procuratie Vecchie building in Piazza San Marco, Venice. (Midas Gen)

The model of the structure has been fixed at the base and the interaction with the adjacent buildings has been neglected considering also that they were constructed in successive periods. All the details about geometrical characteristics, material properties and acting loads can be found in [6].

Masonry has been modelled as isotropic linear elastic material. Lateral force method of analysis and modal response spectrum analysis were carried out. The choice to perform linear elastic analysis is mainly motivated by the scarcity of available data on the materials, due to the conservation restrictions imposed by Superintendence and by the private ownerships, which did not allowed to reach a knowledge level sufficient to carry out reliable non-linear analyses. Secondly, the linear analysis allows to have a reasonable description of the process leading to a possible crack pattern and to maintain a good control on the results.

3.3 Vulnerabilities and consolidation interventions

The static and seismic verifications carried out on wall alignments have identified some

vulnerabilities, which can be solved with consolidation interventions of the masonry structure, elimination of the local mechanisms of collapse and consolidation of timber floors, both from the point of view of stiffness and resistance. This last intervention improves the floor behavior making the floor capable of resisting the greater imposed load due to the change in functional destination of the building and at the same time of transferring the seismic actions to masonry bracing walls and of limiting the out of plane deformation of the walls.

Focusing on the timber floor intervention, in order to comply with both structural safety issues and conservation requirements (e.g. complete reversibility and low degree of invasiveness on the existing building), an effective and non-invasive solution has been proposed for the consolidation of timber floors. It consists of reuse of the main existing timber beams; replacement of the existing timber floor with a new one, with improved mechanical characteristics (3cm thick); insertion of steel ring beam (i.e. a steel perimeter chord) with an L-shaped section 75x75x8, connected to masonry walls by proper anchors; insertion of a doubly diagonal layer of steel band (width 80mm and thickness 1.5mm) anchored to the beams and to the perimeter walls, as well as to the timber floor by means of mechanical nail connectors, in order to guarantee an overall floor diaphragm behavior (Figure 4).

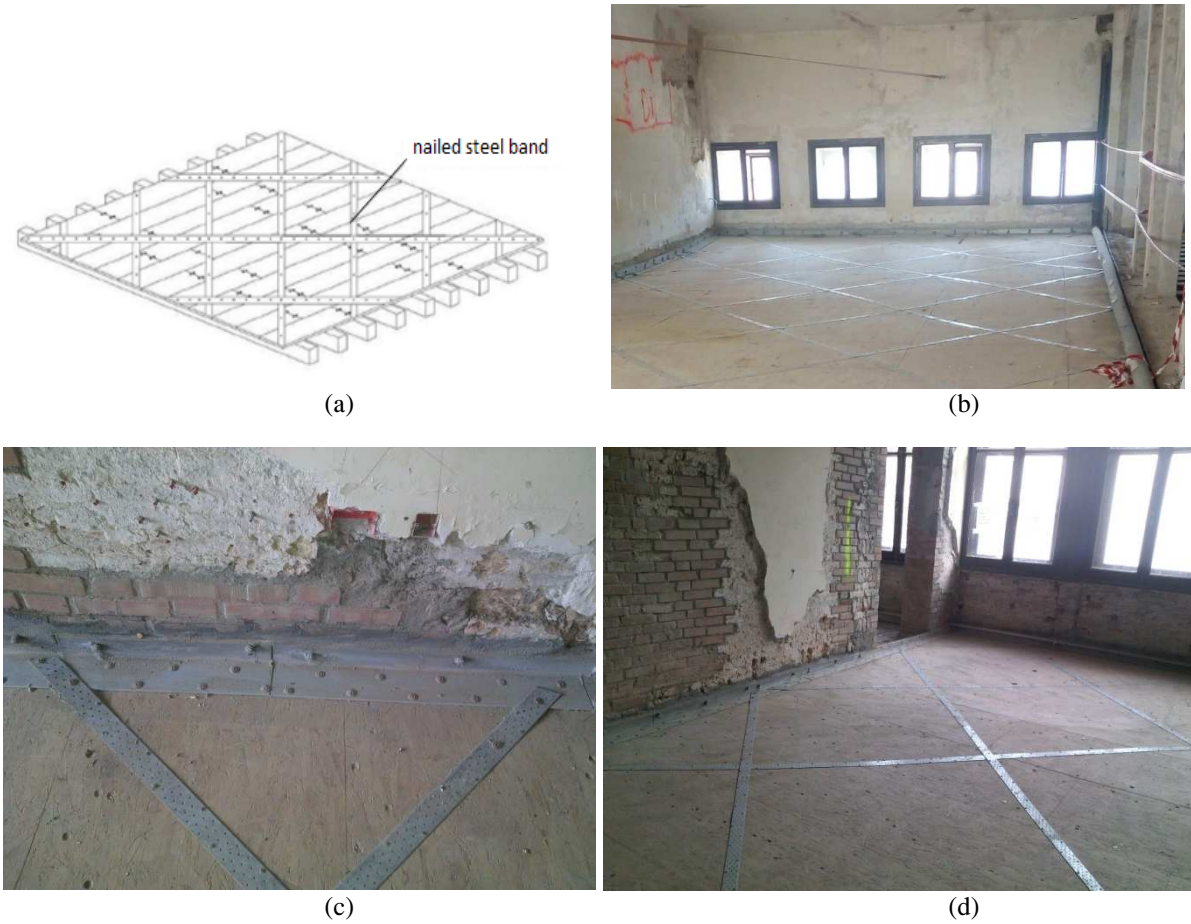


Figure 4: Reinforcement intervention of timber floors: (a) schematic representation; (b)-(c)-(d) views of the intervention.

This kind of intervention is simple and has the advantages of the dry strengthening techniques. It ensures an improvement of wooden floor behavior, increasing its strength and in-plane stiffness minimizing the additional load on the existing structure and without significantly modifying the structural dynamic behavior. In the following, it is shown that this type of floor does not behave like an infinitely rigid diaphragm, instead it can be classified as a "limited stiffening" (see Commentary of NTC 2018 [7]). This type of reinforcing intervention has been successfully adopted in the restoration works on the 'La Fenice' Theatre in Venice, described in [8], destroyed by fire in 1996. Since then it has been used in many other cases for the restoration of monumental building floors.

4 THE ROLE OF IN-PLANE FLOOR STIFFNESS IN THE SEISMIC BEHAVIOUR OF THE BUILDING

4.1 Sub-structure FE models

In order to study the influence of floor diaphragms on structural behavior and the effects of floor stiffness, a portion of the Procuratie Vecchie - with plan dimensions about 6.2x24.0m - between two subsequent masonry wall alignments is considered. Therefore, the model represented in Figure 5 was analysed considering different hypotheses for floor models characterized by increasing stiffness.

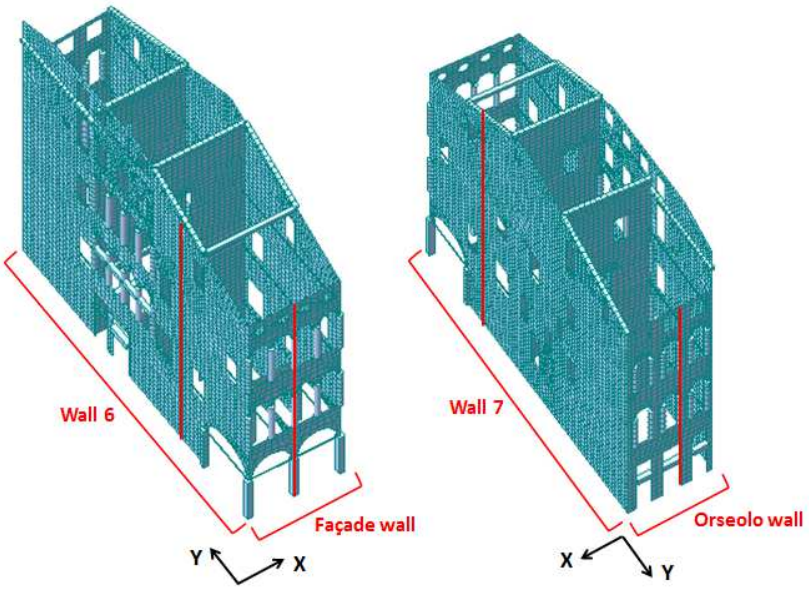


Figure 5: Sub-structure FE model with identification of the wall alignments considered

Masonry walls, columns and all the other structural elements were modelled as in the global model described in §3 and the building was assumed fixed at the base and the walls perfectly connected to each other. Regarding floor modelling, four different models are considered in order to capture the progressive effect of increasing floor stiffness:

- Model 1: floors modelled only with beam elements of rectangular section with spacing 38 cm (simulating the actual timber beams – 15x20cm).

- Model 2: representative of the actual condition. Floors modelled with beam elements and 4-nodes plate elements, 3cm thick, respectively representing the timber beams and the over placed timber plank. These 1D and 2D elements were connected by elastic springs of lateral translational stiffness estimated considering Eurocode 5 [9] formula for the case of nailed connection. This Standard provides a value of stiffness for each single connection element K_{ser} (instantaneous sliding module), that for timber-timber joints and for nail with pre-drilling connector in absence of more accurate determinations can be assumed as:

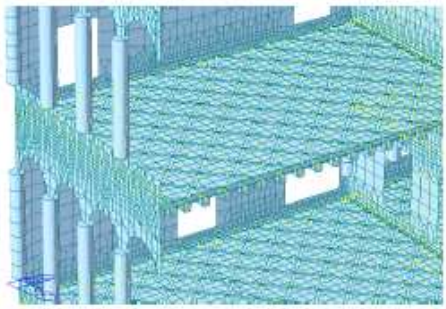
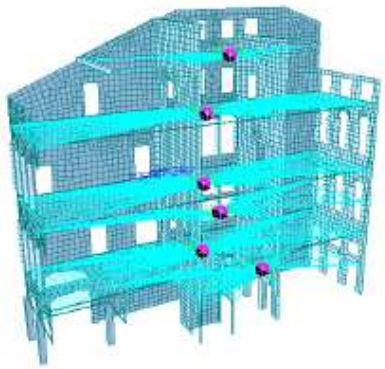
$$K_{ser} = {\rho_k}^{1.5} \frac{d}{20} \left[\frac{N}{mm}\right] \quad (1)$$

  where d represents the nail diameter in *mm* and ρ_k the characteristic value of timber density expressed in kg/m^3.
- Model 3: representative of the proposed intervention. The floor model is obtained starting from the actual state model (i.e. Model 2), in addition using beam elements with L-section all around the walls, connected through *Rigid Links* to the masonry elements (supposing rigid connection), and truss elements of *Tension Only* type, to model the doubly diagonal steel band on the surface of the timber floors. These strips are linked in continuity with the Beam elements, while to the underlying plank with *Rigid Links*.
- Model 4: (limit condition) floors modelled with the conventional schematization of in plane infinitely rigid diaphragm, often used in the professional practice. It is realized by a *Master Node* (i.e. floor center of mass) and *Rigid Links* connected to all the nodes of the masonry elements at the respective floor level.

In Models 1-2-3 the beam elements representing the joints are not horizontally connected to the masonry nodes since the restrain effect due the friction force cannot be considered in case of seismic action.

The seismic action was applied as nodal forces acting at masonry at the floor level. The values of these forces at each level were obtained dividing the floor force resulting by the equivalent static analysis on the global model (Figure 3), by the number of masonry nodes at the related level since the inertial force is primarily due to the mass of the walls, which are much heavier than the floors. The magnitude of floor force applied at each level is equal for all the four models. The permanent and accidental loads were applied in the models as summarized in Table 1.

Table 1: Different floor models considered in the study

Model	FE model of floors
 **Model 1**	Floors modelled with beam elements; Permanent and Accidental load applied as line loads on the beam elements.
 **Model 2**	Floors modelled with beam elements and 4-nodes plate elements; Permanent load applied assigning material density; accidental load applied as pressure load on Plate elements.
 **Model 3**	Floor modelled as Model 2, in addition: truss elements (*Tension Only)* to model the doubly diagonal steel bands and beam elements all around the walls; Permanent and Accidental load applied as in Model 2.
 **Model 4**	Rigid floor (master/slave); Permanent and accidental loads applied as Floor Load in the area where the floors are present.

4.2 Floor stiffness effect on vulnerability assessments

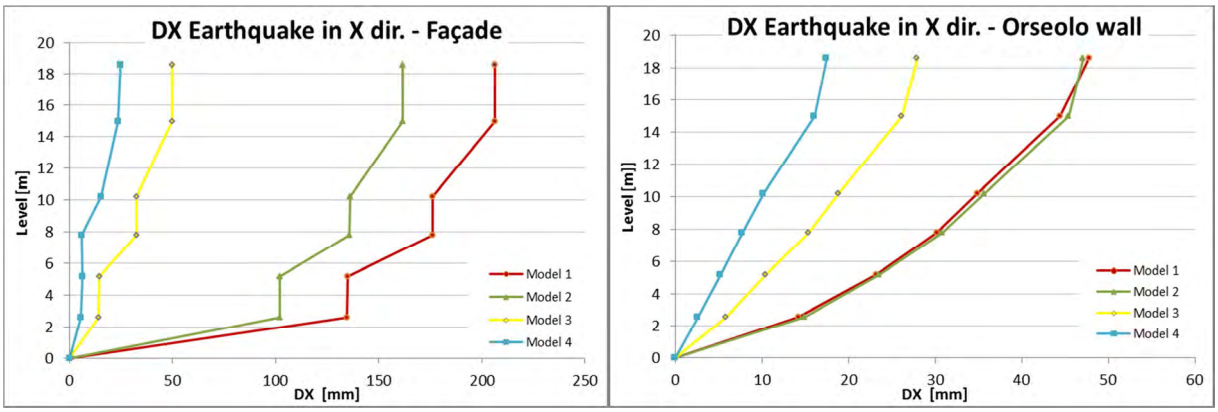
In order to evaluate the effect of in-plane stiffness of floors on the seismic distribution of forces on lateral walls and on the out–of–plane mechanism of the walls, the horizontal displacements obtained by the numerical analyses for seismic actions acting alternately in X and Y plan directions are considered.

In Figure 6 and Figure 7, for example, the profiles of the horizontal displacement obtained for action in X direction are reported in correspondence of the four vertical sections of the walls, identified in Figure 5, in order to investigate the in-plane and out-of-plane behaviour of the walls, respectively for Façade and Orseolo walls and for 6 and 7 walls.

As observable, the displacement decreases significantly with the increase of the floor in-plane stiffness. The Façade wall in Model 1 (which substantially corresponds to the absence of floor diaphragm action) shows a very high horizontal displacement, with a high drift at the 1st level (height 2.6m) due to the presence of pillars at ground floor (Figure 5). In design conditions (Model 3) these displacements decrease a lot, remaining nonetheless greater than those obtained with Model 4 (which corresponds to the case of infinitely rigid floor). Orseolo wall (which is an almost full masonry from ground to roof), due to its higher horizontal stiffness, shows a horizontal displacement in the actual condition (Model 2) equal to about one third of the corresponding value on the Façade. On the other hand the design condition (Model 3) ensures greater homogeneity of displacements between the different walls, including the façade wall, greatly reducing the maximum displacement values (both in-plane and out-of-plane) without reaching the case of the infinitely rigid floor model.

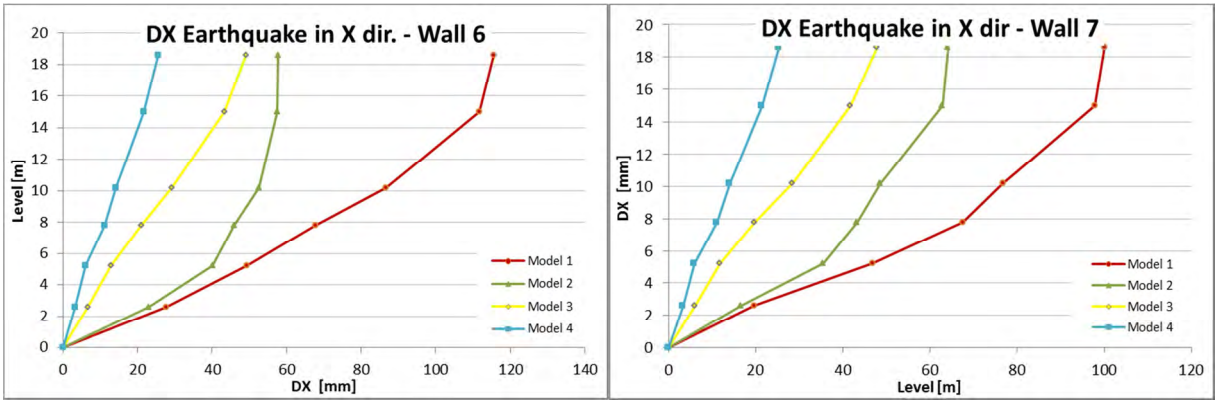
The effect of seismic forces redistribution on the lateral walls due to the floor consolidation intervention are appreciable comparing the design state (Model 3) with the actual state (Model 2) in terms of displacements, both in-plane (Façade and Orseolo walls) and out-of-plane (wall 6 and 7). In particular, the decrease in terms of displacement, averaged among floors, corresponds to about 68% for Façade and 50% for Orseolo wall, and to about 45% for walls 6 and 7.

The increase of floor in-plane stiffness between the actual state (Model 2) and the design state (Model 3) for both X and Y directions can be observed from Figure 8, where, for each level, the ratio between the maximum horizontal displacement of the floor and the corresponding one in case of rigid diaphragm assumption (Model 4) is displayed. In design state (Model 3), the maximum displacement settles at values that are approximately double the one of rigid floor hypothesis (Model 4), for both seismic forces directions. The effect of floor consolidation intervention (i.e. from actual state to design state) is more felt in X direction than in Y direction since the presence of multiple walls in this direction makes the hyperstatic force distribution more affected by the diaphragm in-plane stiffness.



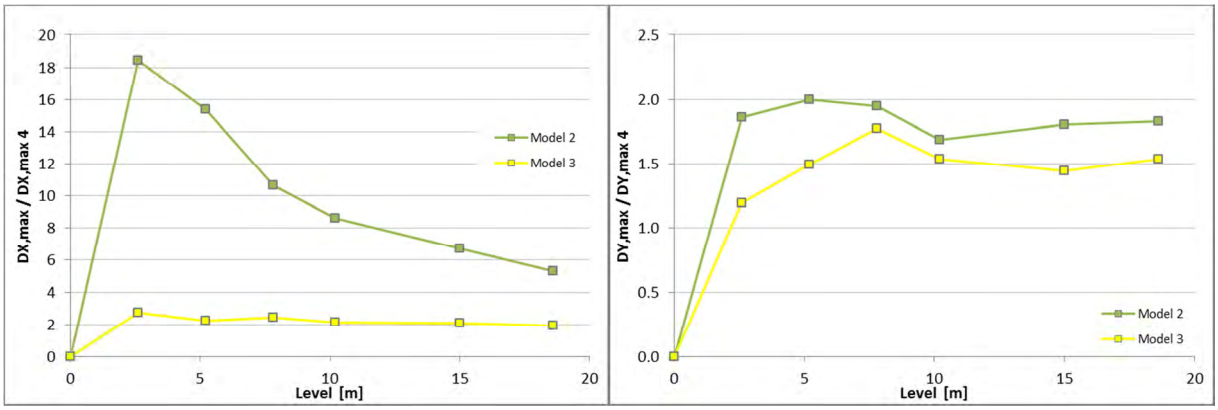
(a) (b)

Figure 6: Seismic action along X direction: in-plane effect. DX displacements profile along the height in correspondence of the middle vertical section for: (a) Façade wall; (b) Orseolo wall



(a) (b)

Figure 7: Seismic action along X direction: out-of-plane effect. DX displacements profile along the height in correspondence of the vertical section South for: (a) Wall 6; (b) Wall 7



(a) (b)

Figure 8: Ratio between the maximum horizontal displacement of the floor and the corresponding one in case of rigid diaphragm assumption: (a) Displacements in X direction for seismic input in X direction, (b) Displacements in Y direction for seismic input in Y direction

12 CONCLUSIONS

The proposed case study, the Procuratie Vecchie in Piazza San Marco in Venice, is an example of historical buildings that can be highly vulnerable to seismic actions if in-plane strength and stiffness of floors are not enough to limit out-of-plane mechanisms of walls and to distribute effectively the seismic forces among lateral walls.

The proposed consolidation intervention for the timber floors is investigated and compared to the actual condition and to the infinitely rigid diaphragm case. It is demonstrated that the proposed consolidation intervention can be considered as of "limited stiffening", being able to increase the strength and stiffness of the traditional flexible floor, but not so much to make it an infinitely rigid diaphragm. In this way the building behaviour is improved, allowing the redistribution of horizontal forces and preventing the collapse of the most vulnerable walls. Moreover, the design restrictions of complete reversibility of the intervention and low degree of invasiveness are also respected, necessary in a building belonging to the national historical and cultural heritage.

REFERENCES

[1] DPCM 2011: Direttiva P.C.M. 12 ottobre 2007 per la valutazione e riduzione del rischio sismico del patrimonio culturale tutelato, S.O. n. 25 alla G.U. n. 24 del 29 gennaio 2008, update 9 febbraio 2011, (GU n. 47 del 26.02.11), (in Italian)

[2] CSLLPP. Circolare 02 febbraio 2009 n. 617 Istruzioni per l'applicazione delle "Nuove norme tecniche per le costruzioni" di cui al DM 14 gennaio 2008. Gazzetta Ufficiale della Repubblica Italiana n. 47, Supplemento Ordinario n. 27. (In Italian)

[3] EC8: EN 1998-3:2005 Eurocode 8: Design of structures for earthquake resistance. Part 3-Assessment and retrofitting of buildings

[4] MIT - Ministro delle infrastrutture e dei trasporti, G.U. S.O. n 42, 20 February 2018. NTC (2018) Aggiornamento delle «Norme tecniche per le costruzioni», decree on 17 January 2008; 2018. (in Italian)

[5] Midas Gen 2020 User's guide, getting started & tutorials

[6] Bellin, S. Il caso studio delle Procuratie Vecchie di Venezia: un esempio di recupero di un bene architettonico vincolato con valutazioni sulla rigidezza di piano, Master Thesis, University of Padova, Civil, Environmental and Architectural Engineering Department, Academic year 2017-2018

[7] MIT - Ministro delle infrastrutture e dei trasporti Circ. C.S.Ll. 21 gennaio 2019 n. 7. Istruzioni per l'applicazione dell'≪Aggiornamento delle "Norme tecniche per le costruzioni"≫ di cui al decreto ministeriale 17 gennaio 2018; 2019. (in Italian)

[8] Gasparini, A., Serafini, G., Scotta, R., Vitaliani, R., Saetta, A. Retrofitting of 'La Fenice' Theatre for Seismic Loads. ConMat'05 3rd Int. Conf. on Construction Materials: Performance, Innovations and Structural Implications, Vancouver, Canada, August 22-24, 2005

[9] EN 1995-1-1:2004 (2004) Eurocode 5: Design of timber structures - Part 1-1: General - Common rules and rules for buildings

12th International Conference on Structural Analysis of Historical Constructions
SAHC 2020
P. Roca, L. Pelà and C. Molins (Eds.)

UNDERSTANDING TRADITIONAL ANTI-SEISMIC STRATEGIES BEYOND THEIR DISAPPEARANCE AND DISTORTIONS: YAZD QAJAR ARCHITECTURE CASE STUDY

EUGÉNIE CRÉTÉ[1*], SANTOSH YADAV[2], NARIMAN FARAHZA[3], LUIS ARLEO[1], MAJID HAJMIRBABA[1] , YANNICK SIEFFERT[2] AND PHILIPPE GARNIER[1]

[1]CRAterre laboratory, Architecture, Environnement et Cultures Constructives research unit
Ecole Nationale Supérieure d'Architecture de Grenoble
60 av. de Constrantine, 38000 Grenoble, France
e-mail: crete.eugenie@gmail.com
(*corresponding author)
[2] Univ. Grenoble Alpes, CNRS, Grenoble INP, 3SR, 38000 Grenoble, France
[3] Earthen Architecture department of the Vernacular Architecture Research Center (VARC), Art and Architecture Faculty, Yazd university, Iran

Keywords: traditional seismic strategies, Qajar architecture, earthen heritage, Yazd, Iran

Abstract. *Understanding traditional seismic strategies is necessary to conduct appropriate restoration of historic buildings and city centers located in earthquake-prone areas. But, the fast disappearance of vernacular built heritage and of the associated popular knowledge and know-how, along with the spread of inappropriate maintenance works, make it very difficult. To overcome these obstacles, it is suggested to broaden the scope of observations by including both larger geographical areas and elements that do not appear as seismic features at first consideration. This paper illustrates the relevance and the limits of this approach by applying it to the case study of Yazd historic city center. Yazd is located in a moderate seismic area and is famous for its well-preserved historic city center, with a high number of Qajar adobe buildings in various conditions. The authors combined literature review, direct observation of numerous buildings and a deeper study of four Qajar houses to conduct the first part of their research. The data collected mainly relates to the geometrical features, the materials used and the interconnections between elements at different scales. Their analyses led to the elaboration of several assumptions on the seismic behaviour of the studied adobe buildings and vaults and on the distortions some features may have suffered. To validate these assumptions, two methodologies were used. Both are illustrated in this paper through the study of the insertion of baked bricks in adobe vaults. The first one is based on observation campaigns on damaged houses. The second one is based on experimental works, with tests conducted on the shear strengths of masonry made with mud mortars and adobes or baked bricks to better understand how builders benefited from mixing these materials in an adobe vault. Finally, the authors discuss the limits of the method and the extent to which restoration projects can benefit from it.*

1 INTRODUCTION

Earthen historic buildings are usually associated to features improving their behaviour in case of dynamic solicitations, amongst others in case of earthquakes. Most of them are not endorsed by official seismic codes that currently apply in numerous countries. Those codes are based on the technical knowledge that was recognized at the time of their redactions – which is mostly after the Second World War. At that time, engineers and institutions were focusing on modern materials such as steel and concrete and the strategies associated with them. The absence of research on traditional technics and materials, and more particularly on their aspects related to seismic engineering, induced a lack of academic knowledge that makes their efficiency difficult to calculate or digitally assess. Yet, the precision and the amount of recognized information related to a technic often take precedence over its effective performance when judging it [1]. The efficiency of a traditional technic can be assessed by post-earthquake observation. This kind of analyses and learning processes were part of builders capacity building in most seismic areas until the end of 19th century [1] but was neglected ever since in favor of calculation and digital analysis. Post-earthquake observations and empirical assessments are nowadays facing three main interlocked hindrances: post-earthquake quick destruction of vernacular heritage by the institutions in charge of rebuilding, the distortion of traditional technics induced by previous loss of knowledge, and the destructions due to unsuitable previous maintenance of built heritage [2,3]. Hence, the characterizations of traditional seismic strategies are often long and complex, which turns out to be a major issue as it is often a necessary step to conduct an appropriate maintenance and restoration of historic buildings.

To what extent can researchers overcome these disappearances and distortions? Is the extension of observations to broader geographical areas, not restricted to highly seismic ones, helping? And what about including in the characterization researches elements that do not appear as anti-seismic features at first consideration? To what extent can this two-fold broadening feed the elaboration of technical assumptions that can later be assessed by observation campaigns or experimental ones? This paper discusses the accuracy of this approach by applying it to the case study of Yazd city center and more specifically to the insertion of baked bricks in adobe vaults.

Yazd is a city in the desert part of Iran that is famous for its well preserved historic city center. Most of its historic buildings were heavily modified during its latest prosperous period (18th century) and until the middle of the 19th century (Qajar period) [4]. Yazd historic city center is a dense area where traditional buildings are mainly made out of adobes [5]. They are closely interlocked: Lateral thrusts that result from vaults and domes are balanced on scales that range from inside a single house to inside an urban block and up to in-between blocks, thanks to arches and vaults crossing the streets. Traditional buildings usually have one or two levels above the ground and up to three underground levels. Iran is located in a highly seismic zone, and earthquakes in Yazd are numerous and of low magnitudes. An acceleration of 0.25g (associated to a return time of 475 years) is to be taken into account when building in Yazd, according to Iranian seismic design code [6].

2 METHODOLOGY

In order to overcome the difficulties linked to the understanding of traditional anti-seismic

strategies through direct post-earthquake observations, the authors suggest a two-step methodology that is detailed below. First step consists in developping technical assumptions on traditional anti-seismic features by broadenning the scope of observations at two levels: first, a geographical broadening, and second, a technical broadening. Then, the technical assumptions resulting from these observations are assessed through different methods designed on a case-by-case basis. This methodology was applied to study traditional seismic technics related to Qajar architecture, as illustrated in this paper.

2.1 Geographical broadening

The suggested geographical broadening consists in studying anti-seismic architectural features without restricting the observations to highly seismic areas. This is based on the following argumentation: A local seismic building culture is likely to develop in locations where earthquakes are frequent enough with intensities that are medium enough to allow for feedbacks [3]. These local seismic cultures then often spread into less seismic areas, facing more or less distortions [1]. Earthquakes in Yazd are numerous but of too low intensities to stir up the development of a specific seismic culture. But building cultures in Yazd were fed by those of the surrounding areas – that face earthquakes of higher intensities – with possibilities of distortions that must be kept in mind while conducting the analyses.

Yazd historic city center is very instructive thanks to its high number of Qajar buildings and their various conditions. Though many houses are built inwards, around a central courtyard, the collapsing of numerous external walls makes it easy to have an understanding of several architectural features by walking into this 800ha area. The authors could complement these theme-based walks by deeper visits of 4 houses owned by the Faculty of Architecture of Yazd and whose plans were available, named: *Shamsaei*, *Shafipour*, *Mortaz* and *Nikbin* houses. The data collected mainly relates to the elements geometrical features, the materials used and the interconnections between elements, on three different scales: The largest one relates to the house itself and its block; the second one to the walls; and the smallest one to the materials used and their layouts. These field visits were conducted in December 2015 and January 2016.

2.2 Technical broadening

Numerical modellings usually are of low accuracy to conduct seismic assessments of adobe historic buildings as they do not assess properly traditional materials and connections – especially when subject to dynamic solicitations – by lack of knowledge or to avoid unmanageable complexity induced by advanced nonlinear analyses [1,7,8]. Though innovative modelling may help in better understanding adobe buildings behaviour [9], geometrical considerations still are of major interest to conduct a first assessment. An analysis of Qajar buildings was conducted considering usual earthquake-resistant guidelines of masonry buildings, a simplified method for the estimation of the resonant period of buildings [10], and several indexes proposed by Lourenço et al [11] and used by Sadeghi et al [8] to assess numerous Yazdi buildings. Moreover, the analysis included studies on the stiffness of the different elements and their connections [12], on the collapsing mechanisms of vaults [13], and on the energy dissipation due to friction in the connections between structural elements [14]. Besides, research works conducted on earthen building materials helped

understanding mud mortars characteristics and the importance of friction in the seismic behaviour of adobe buildings [15,16].

The technical broadening suggested as part of the methodology was conducted after this first analysis of Qajar buildings seismic behaviour based on usual technical considerations. It consists in a second analysis including elements of Qajar architecture that did not appear as anti-seismic at first consideration. Indeed, the loss of knowledge and the distortion of some traditional anti-seismic strategies that inexorably results from it prevent from identifying (and understanding) them easily. The main challenge is then to identify if they could be the remains of any forgotten anti-seismic strategy and to what extent they have been distorted. To conduct this technical broadening, it is necessary to get familiar with the wide scope of traditional anti-seismic technics and practices that developed in various locations. A collection of examples resulting from 10 years of field observations by CRAterre and its partners helps in getting this wider understanding of seismic strategies through the study of traditional monumental and vernacular architecture [17]. Applying this method on Yazdi built heritage requires a global knowledge of Qajar architecture beyond structural features [18] and of its assumed vulnerability [5,8,19] in relation with Yazd seismic activity [6].

2.3 Consolidating the induced technical assumptions

In order to illustrate the second step of the methodology – the consolidation of the technical assumptions resulting from step 1 – the authors selected one of their technical assumptions and consolidated it thanks to two different methods. First, by observations conducted on collapsing structures, whether indirect observations of damage resulting from seismic solicitations of similar houses thanks to studies conducted in Bam [20,21,22], or direct observations of collapsing houses in Yazd. Second, by an experimental campaign: In this case study, the authors tested different brick-mortar-brick sandwiches to compare the shear resistances provided by cohesive bonding between mortar and brick.

3 RESULTS

3.1 The elaboration of technical assumptions related to traditional anti-seismic features of Yazdi Qajar architecture

Yazdi Qajar architecture presents a lot of strengths regarding its seismic behaviour. The global shape, mass and rigidity of most Qajar houses in Yazd reduce the risks of resonance between the building and the ground in case of an earthquake: buildings resonant period was estimated to 0.1s using the equation developped in the Argentinian seismic code [10]. This equation results in a rough approximation as it relies on a basic oscillator model and do not take into account several influencing elements (including the foundations type, the number and spacing of the building levels, the ground nature and the mechanical coupling of the building and the ground), which could result in an error of up to 50% [10]. It is to compare with Yazd ground periods that was estimated between 0.2s and 0.5s thanks to Eurocode 8 and local geological data [23]. Moreover, most Qajar houses include one or several courtyards. These are typical local open spaces that are often used as a living space during seismic episode in different cultures, with testimonies of this practice in Northern Iran [19]. Yazdi houses are built inside a boundary wall with an almost rectangular shape and very few

openings. Inside this surrounding wall, rooms are built with a highly symmetrical pattern. Besides, an important part of the rooms are built underground and around a massive soil core that is the ground under the courtyard: the basement stiffness is thus so high that the ground motions are transferred to the first floor without amplification. Those three points result in a stiffness distribution of the construction that greatly reduces risks of walls distortion in case of an earthquake.

Focusing on *Nikbin* house, the authors calculated different indexes that can help in assessing the sizing of the walls. First, the load analysis resulted in an estimation of static loads of 0.15 MPa, that is more than ten time lower than the estimated ultimate compression resistance of the adobe masonry [24]. This oversizing is usual in traditional masonry structures and allows for important dynamic load to apply without endangering the structure [3]. Moreover, the authors estimated the area of walls that would resist shear stresses in case of a quake by calculating its density value, that is defined as the ratio between the total shear walls sectional area and the floor area. Eurocode 8 recommends a minimum density value of 10% in seismic zones where predictable ground acceleration is above 0.2g, which is the case in Yazd [6]. This value has been estimated to 15% in both principal directions. Moreover, it is interesting to compare the shear walls sectional area – that is related to their resistance to shear stress – to the building weight – that is related to the shear stress the whole building will have to resist. This indicator was estimated to $5m^2/MN$, which is one more time far above the minimum recommended value in highly seismic zone ($2.5m^2/MN$) [11]. This means that its walls should theoretically resist the compression and shear stresses that would be induced by an earthquake before collapsing, with a high safety margin.

Going beyond these general considerations, several technical assumptions were elaborated relating to the seismic behaviour of different architectural items thanks to the observation campaigns conducted on Yazdi Qajar houses.

A first assumption relates to the smaller vaults that are built above the haunches of many vaults. A vault stability is compromised mainly by the inertial forces due to its own materials, if precluding any differential shift of its supports. These forces induce deformations that are efficiently reduced thanks to the fillings that are above the haunches of the vault [13], but these fillings increase the weight of the roofing. In Yazdi architecture, the haunches of the vaults are often not strengthened by fillings but by smaller vaults named *kane poush*, that are either perpendicular to or with the same axis as the main one (Figure 1). These smaller vaults are usually explained by their thermal and execution efficiency, but they are also probably of high importance to increase the resistance of the main vault without burdening it.



Figure 1: An example of *kane poush* filling the haunches of a collapsed vault, Yazd (Créte, 2015)

A second example relates to the wooden and glass façade that often closes winter living spaces in traditional Qajar houses. Gable-end walls are often the first to collapse in case of an earthquake: they are usually slightly linked to the rest of the structure and have a high slenderness ratio. Gable-end walls that were not rigid enough have turned disastrous during Bam earthquake [20]. Closing those spaces with a light and flexible item is not only allowing for large amount of light to enter, it also contributes to avoiding the collapse of heavy walls in case of out-of-plan quake.

A third example relates to the layout of masonry infill panels and seems to be a variation of a well-known seismic principle of framed structure: masonry infill walls should be weaker than the load-bearing structure as it should fail first in case of too high solicitations [12]. In Yazd, most infill panels are built with specific layouts that have an obvious aesthetic aim. But they are also probably less rigid than common masonry layout. Moreover, cracks can propagate easily through the pattern but by dividing the panel in elements that keep interlocked thanks to their geometry (Figure 2). From a structural point of view, it is hence probably very interesting to use them as infill of load-bearing structures.



Figure 2: Masonry cracks in an infill masonry panel, Yazd (Créte, 2015)

The last example relates to rows of baked bricks that are inserted into *zarbi* adobe vaults (barrel vaulting), approximately every 50 cm, and that may be part of a strategy to improve the global stability of adobe vaults. In case of heterogeneous composition of masonry structure, the mortar joint acts as a weak plane from where the failure occurs [25]. In case the interface between the baked brick and the mud mortar is weaker than the one between the adobe and the mud mortar, this technic can be understood as a way to create fuse interfaces and facilitate the creation of sectional cracks during a quake (thus preventing diagonal cracks that would endanger the structure). The formation of cracks and the local shifts that occur at those interfaces are often very efficient to dissipate the energy the building caught during the quake [14].

Finally, it may happen that traditional seismic features have face such distortions that they do not contribute anymore to improving the building's earthquake behaviour. For example, alcoves are a major aesthetical element of Yazdi traditional architecture (Figure 3) [18]. But they should not be reduced to their aesthetical function in a seismic context: First, because they can allow for storing items without risking cupboard overturning. Second, because they are the negative of buttresses that increase the wall stability with a limited amount of material. But the size of many alcoves and the way they were built make it difficult to keep in mind

those technical advantages, as they have often been reduced to a dozen cm deep and made out of plasters, or are no longer structurally linked to the walls.



Figure 3: Different kind of alcoves in *Shafipour* house, Yazd (Créte, 2015)

3.2 A deeper study of the baked brick insertions in adobe vaults

The broadening of observations enabled the authors to elaborate several technical assumptions regarding architectural features typical of Qajar architecture that were probably developed as part of a local seismic culture. The authors selected one of them for a deeper study, that is the insertion of baked bricks in adobe vaults. In order to consolidate the hypotheses resulting from their first analyses, the authors based their works on two research campaigns: an observation campaign of collapsing houses and an experimental campaign in a laboratory.

The insertion of baked bricks in adobe vaults is hardly visible as the vaults are plastered. Nevertheless, the authors observed it in three Qajar houses in Yazd historic city center, where plaster was partially removed: *Dar Houkouma*, *Nikbin* and *Shamsaei*. The observation campaign mainly focused on *Shamsaei* house as its condition allowed for a deeper understanding of the formation of cracks in these vaults. This Qajar house suffered from improper maintenance, amongst others related to its roofing plaster, and had been abandonned for a dozen years at the time of the campaign (2016). It was especially interesting as it includes five collapsing or badly cracked vaults built using both adobes and baked bricks. One or two rows of baked bricks were regularly inserted in the barrel adobe vaults, at a distance ranging from 30cm to 1m. Wherever visible, it was noticed that main cracks and partial collapses systematically occurred at the baked bricks rows locations (Figure 4).



Figure 4: Baked bricks rows in an adobe vault and the creation of sectional cracks, the example of *Shamsaei* house, Yazd (Créte, 2015)

This observation campaign confirmed the frequent propagation of cracks at the interface between baked bricks and adobe bricks. An experimental campaign based on the shear strength assessment of brick masonry [25,26,27] was then conducted at 3SR laboratory in order to better understand this phenomenon. The authors first had to determine a composition for the mud mortar they would use for the campaign. They tested several compositions based on clay, sand and fibers. They selected 4 formulas out of 7 thanks to qualitative observations. They then performed shear tests on 8 sandwiches made out of adobe and 4 kinds of mud mortars after complete drying (1 month): clay with 20% fiber by volume of clay (OC20F), clay with 20% fiber and 10% sand (OC20F10S), clay with 10% fiber and 10% sand (OC10F10S) and clay with 20% fiber and 20% sand (OC20F20S). The experimental setup using Schenck press in shown in Figure 5. The average shear stress value ranged from 0.032Mpa for the OC20F20S mortar to 0.059Mpa for the OC20F10S mortar, which was chosen to perform the next tests.



Figure 5: The shear stress value of a sandwich sample made out of two adobes and mud mortar is tested with a Schenck press

Once the composition of the mud mortar defined, six sandwich samples were produced to assess their shear stress value: Three samples were made out of baked bricks (samples A, B and C), three out of adobe bricks (samples 1,2 and 3). A main factor of influence on the bond development being the water content of the bricks before mortar laying [28], two samples of each type were prepared by wetting the bricks before applying the mortar (samples A,B, 1 and 2), and one was prepared without wetting the bricks (samples C and 3). The following average shear stresses were measured:

Adobe	Wet (samples 1, 2)	0.86 MPa ; 0.130 MPa
	Dry (sample 3)	0.008 MPa
Baked bricks	Wet (samples A, B)	0.84 MPa ; 0.145 MPa
	Dry (sample C)	0.055 MPa

Table 1: The shear stress values (Mpa) of adobe and baked bricks sandwiches samples

When wet before mortar application, the shear stress values for both baked and adobe bricks are comparable. They are respectively two times and ten times higher than when samples were prepared without wetting the bricks before the application of mortar. This important decrease in shear resistance may be explained by an improper bond development due to a too fast moisture flow between the bricks and mortars, inducing important shrinkage in the mud mortar as can be seen in Figure 6. This phenomenon could also explain the gap between samples 3 and C, as adobe bricks have higher absorption rate than baked bricks.



Figure 6: The joint failure in case of samples prepared with wet brick surface (left) and with dry brick surface (right)

5 CONCLUSION

In earthquake-prone areas, seismic practices developed as part of the local building cultures. Earthen historic constructions are usually associated to features improving their behaviour in case of earthquakes, but that suffered such distortions or improper maintenance that they may not be efficient anymore, which makes them even more difficult to identify and analyse, triggering a vicious circle. The methodology illustrated by Yazdi Qajar architecture study in this paper helped in identifying several features that may be of importance regarding the seismic behaviour of Qajar buildings, amongst other the insertion of baked bricks in adobe vaults. The observation campaign showed that major cracks frequently occurred at the interface between baked bricks and mud mortar in adobe vaults. Further observation campaigns on collapsing Qajar houses in other cities were Qajar architecture is found would confirm if this observation is wide-spread or local. The experimental campaign showed that for the same composition of mud mortar, the shear strength value is similar with baked brick or adobe brick which are prepared by wetting the brick before application of mortar, but that this shear resistance is two times lower if bricks are not wet. Could this be a technic used by traditional masons to create fuse surface that would crack first, thus dissipating energy without endangering the vault stability? To further consolidate this technical assumption, it would be interesting to conduct the same experimental campaign on samples prepared with Yazdi traditional adobes, baked bricks and mud mortar. This could highlight other factors explaining lower bond strengths between baked bricks and mud mortars.

The suggested methodology helped in identifying architectural features that may have developed as part of a local seismic culture but that suffered from distortions or forgetfulness.

But once these elements identified and understood, complementary research must help understanding why these distortions happened and especially if they were intentional or not. This must be understood before restoration works to decide whether the distorted element should be kept in its adapted version or if it must be corrected to improve the building behaviour in case of seismic solicitations. Intentional distortion may result from an adaptation of the technic to lower seismic areas because another stake was given priority, as noticed for example by Hofmann [1] in relation with the spacing between timber seismic bands in Turkey. In Iran, the reduction of buttresses and the turning of many alcoves into merely aesthetic elements may be an intentional distortion. Further research in more seismic areas where Qajar architecture disseminated would help validating this hypothesis. The unintentional distortions, out of forgetfulness or misunderstanding of the seismic interest of a practice, is closely related to the disruption of traditional knowledge transfer processes that happened mainly from the end of 19th century [1]. Could a datation of the distortion help in sorting out if it is an intentional one or not? And to what extent should we consider that the highest stakes at the time of the construction (for example economical ones), that may have induced intentional distortions, are still consistent nowadays? Keeping in mind that the preservation of cultural heritage falls increasingly into a narrative of continuous evolution and adaptation to current stakes, an approach that may help in building cultural resilience [29].

Whether distorted or not, a deep understanding of these features is of major importance to develop proper maintenance of historic buildings. The loss of knowledge and understanding can induce adverse consequences when they result in the replacement of traditionally used materials by others with different properties. In Yazd, several maintenance issues that endanger vernacular built heritage can be observed. Many earthen walls are partially rebuilt with inconsistent materials from both mechanical and hygrometric points of view. It may entail an acceleration of degradation of the earthen parts of the wall due to crushing, water runoff concentration, excessive water vapor condensation, concentration of capillary rises in specific zones, salts migration… These modifications often turn disastrous in case of an earthquake, because of the lack of connections between load-bearing elements and because of the burdening of traditional structures. Based on the hypotheses detailed in this paper regarding several seismic features of Qajar architecture, several other examples of improper maintenance should be highlighted: for example when changing the traditional mortar by a stronger one in panels whose relative weakness is important. Or in case the mortar is stronger than the bricks, resulting in a propagation of cracks inside bricks and not only inside mortar which no longer induce a delimitation of interlocked blocks. Besides, baked bricks walls are often used to obstruct historic access. These panels may induce severe damage in case of an earthquake because of their relatively high stiffness and because of the lack of good connections with original walls. This discussion on the improper maintenance that can be observed regarding Yazd city center highlights the importance of identifying and understanding these traditional seismic practices.

Moreover, further research is needed to get a deeper understanding of the practices exposed in this paper and further consolidate the assumptions the authors could elaborate, especially regarding the different masonry patterns. Besides, other practices were noticed by the authors, without them being able to conduct further work to develop assumptions about their interest from a seismic point of view. One relates to the high occurrence of empty vertical joints in adobe masonry: Is it mere faulty works, or could it be a way to keep strains

localized under lateral stresses? A second one relates to *muqarnas*, that may have developed as a friction damper timber capital (a practice documented in Nepal and Pakistan [17]) when built out of several wooden pieces and not out of a single one as is mostly done nowadays. Finally, the authors would recommend further research regarding the mix of adobes and baked bricks when building windcatchers along with research on their structural behaviour, as the very function of those items induces a need for structural strategies to cope with the vibrations and lateral forces due to winds.

Acknowledgements. This work was conducted in the framework of the LABEX AE&CC and the IDEX CDP Risk@Univ. Grenoble Alpes as part of the program ‘‘Investissements d’Avenir” overseen by the French National Research Agency (reference: ANR-15-IDEX-02).

REFERENCES

[1] Hofmann, M. *Le facteur séisme dans l’architecture vernaculaire. Un décryptage entre déterminants culturels, types de structures et ressources cognitives parasismiques*. PhD thesis. EPFL : EPFL – ENSAG (2015)

[2] Feilden, B.M. *Between two earthquakes: cultural property in seismic zones*. Rome : Marina del Rey, Calif., USA : ICCROM ; Getty Conservation Institute. (1987) 103 p. ISBN 978-0-89236-128-1

[3] Ferrigni, F., European University Centre For The Cultural Heritage (dir.). *Ancient buildings and earthquakes: reducing the vulnerability of historical built- up environment by recovering the local seismic culture ; principles, methods, potentialities*. Bari : Edipuglia. (2005) 360 p. ISBN 978-88-7228-403-2

[4] Modarres, A. *Modernizing Yazd: selective historical memory and the fate of vernacular architecture*. Costa Mesa, Calif : Mazda Publishers. (2006) 199p. ISBN 978-1-56859-140-7

[5] Fallah Aliabadi, S., Sarsangi, A., Modiri, E. « The social and physical vulnerability assessment of old texture against earthquake (case study: Fahadan district in Yazd City) ». In : *Arabian Journal of Geosciences* [en ligne]. (2015). DOI 10.1007/s12517-015-1939-8. Disponible sur : < http://link.springer.com/10.1007/s12517-015-1939-8 > (last accessed on 30 september 2015).

[6] BHRC, *Iranian code of practice for seismic resistant design of buildings (Standard No. 2800). Fourth Revision*. Tehran, Iran: Building and Housing Research Center, Iran (2015) (in Persian).

[7] Lourenço, P.B., Oliveira D.V., et al. "Simplified indexes for the seismic assessment of masonry buildings: International database and validation". In: *Engineering Failure Analysis*. (2013) 34:585-605. DOI: 10.1016/j.engfailanal.2013.02.014

[8] Sadeghi, N.H., Oliveira D.V. et al. "Seismic performance of historical vaulted adobe constructions: a numerical case study from Yazd, Iran". In : *International Journal of Architectural Heritage* (2017). DOI: 10.1080/15583058.2017.1422573

[9] Lourenço, P.B., Greco, F.,et al. *Seismic Retrofitting Project - Modeling of Prototype Buildings*. Getty Conservation Institute : Los Angeles. (2019) ISBN: 978-1-937433-63-5

[10] Jarpa, T.R. *Détermination de la période fondamentale des bâtiments. Proposition d’un outil simplifié à l’usage des architectes*. Paris : ENSAPB. (2014)

[11] Lourenço, P.B., Roque, J.A. « Simplified indexes for the seismic vulnerability of ancient masonry buildings ». In : *Construction and Building Materials*. (2006). Vol. 20, n° 4, p. 200-208. DOI 10.1016/j.conbuildmat.2005.08.027

[12] Billard, A. *Risque sismique et patrimoine bâti: réduction de la vulnérabilité : savoirs et savoir-faire*. Paris; La Plaine Saint-Denis : Eyrolles ; AFNOR. (2014) ISBN 978-2-212-13613-5.

[13] Gelfi, P. "Role of horizontal backfill pressure on the stability of masonry vaults". In: *Internationale Zeitschrift fur Bauinstandsetzen und Baudenkmalpflege*. (2002) 8. Jahrang, Heft 6, 573-590

[14] Peyret, N. *Dissipation de l'énergie mécanique dans les assemblages : effet du frottement en sollicitation dynamique*. PhD Thesis. Paris : Université Paris-Est (2012)

[15] Crete, E., Yadav S. et al. "Timber seismic bands: correlating their characteristics with local seismic activities and understanding their effects under seismic loads". In : *Anti-Seismic Vernacular Heritage of Anatolia and Beyond*. Istanbul : ICOMOS ISCARSAH Turkey. (2018) ISBN: 978-605-245-789-4

[16] Yadav, S., Sieffert, Y., Crete, E., Vieux-Champagne, F., Garnier, P. "Mechanical behaviour of different type of shear band connections being used in reconstruction housing in Nepal". In : *Construction and Building Materials*, Elsevier, (2018) 174, pp.701-712. ⟨10.1016/j.conbuildmat.2018.04.121⟩. ⟨hal-01780074⟩

[17] Caimi, A., Moles, O., Crete, E. *Local building cultures for resilience and development - Examples of local good practices and technical solutions*. Villefontaine : CRAterre. (2017) ISBN 979-10-96446-13-1

[18] Shakouri, R. *Habitat résidentiel durable en Iran - savoirs-faire traditionnels et technologies nouvelles à Yazd*. PhD thesis. Grenoble : Pierre Mendes France. (2008)

[19] Arbabian, H. « *Architectural Issues in Earthquake Rehabilitation of the Iranian Cultural Heritage | CICOP Italia* ». In : [on line] < https://www.cicop.it/wordpress/en/pubblications-articles/architectural-issues/> (2002) (last accessed on 20 December 2019).

[20] Maini, S. *Diagnostic of damages to vaulted structures Arg-e-Bam and Bam area, Iran*. Auroville : Auroville Earth Institute (2004)

[21] Joffroy, T., Moriset, S., Hajmirbaba, M., Gandreau, D. Bam, *Iran - Final report*. (2006)

[22] Bolorizadeh, M. *The Secrets to Earthquake Resistance of Mud-brick Structures in Bam, After 2004 Earthquake, with a Methodological Approach*. Yazd : Faculté d'Architecture de Yazd (2015)

[23] Deghan, M., *Laboratoty analysis of Yazd clay based on swelling potential and mineral components*. Tehran : Faculty of civil engineering, University Amir Kebir (2003) (in Persian)

[24] Hejazi, M., Saradj, F. M. *Persian Architectural Heritage: Architecture, Structure and Conservation*. Southampton : WIT Press. (2014) 527 p. ISBN 978-1-78466-070-3.

[25] Dhanasekar, M., Kleeman, P. W., Page, A. W.: Biaxial Stress-strain Relations for Brick Masonry. In: *Journal of Structural Engineering* (ASCE), v. 111, n. 5 (1985). https://doi.org/10.1061/(asce)0733-9445(1985)111:5(1085)

[26] Alecci, V., Fagone, M., Rotunno, T., & De Stefano, M.. Shear strength of brick masonry walls assembled with different types of mortar. *Construction and Building Materials*, 40, 1038–1045. https://doi.org/10.1016/j.conbuildmat.2012.11.107 (2013)

[27] Ali, Q., Badrashi, Y. I., Ahmad, N., Alam, B., Rehman, S., & Banori, F. A. S.. Experimental investigation on the characterization of solid clay brick masonry for lateral shear strength evaluation. *International Journal of Earth Sciences and Engineering*, 05(04). (2012)

[28] Groot, C. J. W. P., *Effects of water on mortar brick bond*. PhD thesis, University of Delft, Delft, The Netherlands (1993)

[29] Holtorf, C., Enhancing cultural resilience by learning to appreciate change and transformation, in: *Humanistic futures of learning - Perspectives from UNESCO Chairs and UNITWIN Networks*. Paris: UNESCO (2020). ISBN 978-92-3-100369-1

12th International Conference on Structural Analysis of Historical Constructions
SAHC 2020
P. Roca, L. Pelà and C. Molins (Eds.)

ASSESSMENT AND MONITORING OF HISTORICAL TIMBER CONSTRUCTION: AVAILABLE TOOLS TO SUPPORT DECISION-MAKING PROCESSES.

MARIAPAOLA RIGGIO[1*]

[1] Wood Science and Engineering Department, College of Forestry, Oregon State University.

Richardson Hall 119, Corvallis, 97331 OR, United States
e-mail: mariapaola.riggio@oregonstate.edu

Keywords: Historical Timber Structures, Monitoring, Assessment, Decision-making tools.

Abstract. *Timber structures represent a rich although still underestimated portion of the historical built asset worldwide documenting a tradition of sustainable practices and craftsmanship. Assessment of their condition is a fundamental step towards their conservation. While some overarching approaches for the assessment of timber structures are not dissimilar to those used for other types of structures, there are some specific factors affecting timber structures behavior that should be taken into consideration. Such factors are especially related to the organic nature of wood, which makes timber's properties largely variable and influenced by the environment. Successful conservation of historical timber structures requires combination of many different disciplinary contributions, from wood science and technology, to structural engineering, building physics, architecture, art history and environmental science, among others. This contribution aims to present an overview of tools supporting decision-making processes for the assessment and conservation of existing timber structures, including both methodological frameworks and technical approaches for data collection and analysis. These tools are reviewed according to the scope of the assessment and considering multiple levels at which timber structures are studied, at the material, system and building scale. Additionally, emerging approaches and challenges for holistic assessment of historical timber structures are discussed.*

1. INTRODUCTION

In the last decades, institutions, authorities and various stakeholders have recognized the urgent need to maintain and preserve a rich and diverse cultural asset, represented by traditional timber structures. Ad hoc international and national technical committees, such as ICOMOS's IWC (International Wood Committee) and ISCARSAH (International Scientific Committee on the Analysis and Restoration of Structures of Architectural Heritage), RILEM TC 215 AST (in situ assessment of timber), RILEM TC RTE (Reinforcement of Timber Elements in Existing Structures), and the Working Group 10 of the CEN TC 346 " Conservation of cultural property", have been created to evaluate and develop decision-making tools for the assessment and conservation of (timber) structures of historical and cultural interest.

Information on traditional timber structures, acquired by means of structural health monitoring (SHM) and assessment methods, is fundamental to support decision-making

processes. The discipline of structural health assessment and monitoring of timber structures is nowadays critical to the success of many conservation projects, and requires increasingly articulated and multidisciplinary skills. For these reasons, an interdisciplinary, multiscale approach (from the material to the building and context) is required for the assessment of timber structures.

This contribution aims to discuss the state-of-the-art by providing an overview of tools supporting decision-making processes for the assessment and conservation of existing timber structures. Methodological frameworks and technical approaches for data collection and analysis are reviewed according to the scope of the assessment and considering multiple levels at which timber structures are studied, at the material, system and building scale. Additionally, emerging approaches and challenges for holistic assessment of historical timber structures are discussed.

1.1. The decision-making process

Decision-making processes related to the management of heritage buildings is a challenging task due to conflicting priorities pursued by multiple stakeholders. As an example, intervention to complying with code requirements, such as those addressing seismic or energy performance, may conflict with the need of safeguarding the historical value and authenticity of a traditional timber system, without altering the original static scheme and, in some cases, maintaining the original features of a building enclosure. [1] describe, for instance, issues arisen with the seismic retrofitting of masonry buildings in Italy, as an application of building codes in force in the 1980s and 1990s, which caused the frequent replacement of existing timber floors and roofs with solid or hollow-core concrete diaphragms. Besides the loss of a vast historical built asset, these interventions proved to be ineffective and even detrimental, leading to failures during seismic episodes, due to increased loads, punching shear action of the new rigid slabs and overturning mechanism of the external walls [1].

Considering the complexity of choices associated with the assessment and conservation of historical timber structures, Multi-criteria Decision Analysis (MCDA) can support decision making processes, helping evaluation of a variety of conflicting and non-homogeneous criteria. A review on different approaches in the use of MCDA models for the preservation of historical built asset has been proposed in [2]. An example of application of a decision-making tool to assess energy efficiency and overall carbon footprint during maintenance and adaptive interventions of historical wooden façades is reported in [3].

The aim of the assessment is to facilitate the decision-making process, support a more sensible approach to the preservation and reduce the costs of the required interventions. As a matter of fact, the “cost of information” should offset the cost of intervention, and possibly have additional non-economic benefits. Diverse procedures and tools can assist experts in the assessment of timber structures. However, the value of historic buildings may justify greater expenses in sophisticated survey procedures and use of multiple methodologies for the diagnosis and assessment of timber structures.

Recent advances of sensing technologies have allowed for development of Structural Health Monitoring (SHM) systems, which provide information on the condition of a system and evaluate time-dependent phenomena which can affect a building performance. Monitoring systems may therefore serve for supporting decisions pertaining to the planning of appropriate

inspection and maintenance actions in case of (or to avoid) damage or deterioration, as well to evaluate the effectiveness and long-term performance of an intervention.

Structural health monitoring of timber structures is generally categorized in two main areas: hygrothermal and structural monitoring, depending on the type of action, environmental or mechanical, respectively. The hygrothermal behaviour of wooden assemblies has significant influence on the durability and service life of timber buildings. Environmental factors are generally considered also in structural monitoring, as they have an impact on how reliably a timber structure can carry current or future loads. Therefore, multiple data are typically acquired in a SHM program. SHM strategies may be optimized considering the Value of Information (VoI) from the SHM systems [4]. Accordingly, the placement of sensing devices can limited to the minimal amount required for the control (and possibly correlation) of the identified key parameters affecting a timber structure performance, with the goal to holistically identify potential deterioration processes and even prevent damage to occur.

A literature review [5] found that on a total of 193 timber structures monitored from 1980 to 2019, 86 were existing buildings and 42 of them were historic timber structures, which were monitored to assess their safety and serviceability or to develop maintenance plans. The survey also found that, while in the past most SHM projects were aimed at the conservation of existing/historical timber structures (with a principal geographic concentration in Europe), more recently the focus has been shifting to new timber construction [5]. Some open questions are: what has been the use and value of information from previous SHM programs of historical timber structures? Can we increase the VoI from on-going and future SHM of historical timber structures?

1.2. Workflows: data production and interoperability

Assessment of historical timber structures encompasses different types and levels of analysis to consider technological, structural, material and architectonic features at the different scales of a structure, as well as inter-dependences between those features. Consequently, data should be collected in a way that allows various experts involved in the assessment to easily communicate and process information. [6] review available standards, guidelines and other practice-oriented documents supporting the assessment of historical timber structures. Reviewed documents are discussed in light of their use for specific assessment purposes, namely for a) the documentation of the building for conservation/preservation purposes, b) vulnerability and damage assessment, with a specific focus on seismic performance, and c) analytical assessment for serviceability and safety evaluation [6].

Categories of data which are collected in various stages, and for different assessment scopes, encompass: environmental data and wood moisture content (see section 2.1 of this paper); data for the mechanical characterization of the timber structural elements (section 2.2); data descriptive of alterations to the original structural systems and individual timber members (section 2.3) and geometrical data (section 2.4). As a result, different data types and formats are collected at multiple scales and by using various procedures, thus leading to issues of interoperability as well as of physical, spatial and statistical correlation.

The Swiss standard SIA 265/5:2011 [7], and the guidelines developed within the COST Action IE0601 [8] and further implemented in the prEN 1712 by the Working Group 10 of the CEN TC 346 [9], are to date the only available documents that consider the different levels of

the investigations at the various hierarchical levels of a timber structure.

[8] describe stages and tasks for the assessment of historical timber structures, with a particular emphasis on technological aspects. The procedure consists in three different stages of analysis. The preliminary assessment entails historical survey, preliminary visual survey, measured survey (geometry, technology, damage), and preliminary structural analysis. A detailed survey of timbers aims to identify wooden species, estimate wood moisture content and mechanical parameters, and assess biological damage. A visual strength grading procedure adapted for grading timbers on site and originally developed in the Italian UNI 11119:2004 [10]is referred in [8]. The third stage of the assessment process is a technological survey of timber joints.

Visual inspection is a fundamental first step for all different scopes and levels of assessment. [6] and [11] present a digital template to collect information during visual inspection, by considering the different hierarchical levels of a timber structure: from the building as a whole, the structural complex and system/s, the timber elements and the connecting joints. Following this multi-scale approach, the template includes a section for damage assessment [11]. While the template is designed to be adapted to different construction types, its implementation and initial use have been limited so far only to timber roof systems typical of the Western construction tradition.

Other forms of assessment templates are available, and mainly target a specific scope of the assessment. These tools are generally meant to enable a standardized and rapid visual screening and data collection on site. Among them, it is worth mentioning the AeDES form to assess seismic damage [12], forms to assess causes of failures in engineered timber roof structures [13], [14], [15], and forms to assess the seismic vulnerability of traditional Italian timber roof structures [16]. It is worth mentioning that the latter is the only one, among the three cases above, specifically addressing historical timber systems.

Traditional paper forms have been increasingly replaced with digitally-supported tools to be used on mobile devices, thus expediting the inspection activities and enabling almost real-time data sharing. The use of digital platforms for data collection can be two-fold: to facilitate and standardize data collection, storage and sharing; and to allow for automatic or semi-automatic analysis in decision making processes.

Periodic inspection is one application where the first type of platform can be particularly useful. For instance, a bridge inspection procedure based on a software tool has been extensively used to inspect and monitor timber bridges in Slovenia [17][18].

The second approach requires structured data acquisition so that data can be exploited by automated reasoning systems. In the MONDIS Project [19] a knowledge-based system has been developed to support damage assessment of historical buildings. The main scope of the developed “Monument Damage Ontology” is to enable collaboration and data-sharing within the expert community, as well as to integrate existing data from different sources [19]. On line, expert-trained systems accessible from mobile devices have been developed to support time-sensitive, decision-making processes during assessment of damaged structures (for instance, planning shoring and repairs to avoid imminent collapse) (see for instance, [20]. The FaMIVE (Failure Mechanism Identification and Vulnerability Evaluation) [21], has been designed to be a flexible data collection platform for vulnerability assessment of historical structures, including traditional timber roofs and floors. More recently, this platform has been further developed to rapidly assess seismic and wind response of timber roofs [22]. It is worth noting,

that most of the available documents for vulnerability/damage assessment refer to specific structural types or class of buildings. Therefore, many heritage timber structures, which do not fall in the covered categories, cannot be assessed with the codified criteria. The reader can find a more exhaustive review of inspection and assessment formats in [6].

Following visual inspection, further stages of the assessment pose additional challenges for data interoperability. While integration and spatial/physical correlation of non-destructive (NDT) and semi-destructive (SDT) testing data in a holistic assessment platform is becoming an increasing need, use of non-destructive (NDT) and semi-destructive (SDT) testing techniques for the assessment of timber structures is far from being a standardized procedure [23][24][25]. In sections 2.2 and 2.3, some studies focusing on data mining and multivariate analysis approaches of multi-sensor data to support decision making process are cited.

In the last two decades, multiple strategies have been developed for range- and image-based modelling techniques for buildings surveys. Seamless integration of 3D geometric data from 3D scanning or photogrammetry, building information modelling (BIM) and finite element modelling (FEM) is one of the emerging research topics in the field of cultural heritage management and structural health assessment and monitoring, which has seen some promising applications on heritage timber structures. In section 2.4, metric and non-metric data flow and interoperability among different tools supporting modelling tasks are discussed.

2. STATE OF THE ART AND EMERGING APPROACHES IN THE ASSESSMENT AND MONITORING OF HISTORICAL TIMBER STRUCTURES

In the following sections, different operational categories involved in the assessment of timber structures are introduced; state of the art tools and emerging approaches for the acquisition and analysis of data are then discussed for each category. Information acquired can be used for the assessment of both load-bearing and non-load-bearing timber elements, or applied just to the former category, when related to mechanical and structural performance.

2.1. Environmental and hygrothermal conditions

Type, magnitude, duration and frequency of environmental loads acting on a building should be evaluated in the structural assessment process, as they can greatly affect the performance of timber structures. As a hygroscopic material, wood exchanges moisture with the surrounding environment. Moisture content (MC) changes in the hygroscopic range (0-28%) affect wood physical and mechanical property. Therefore, MC measurement is important for correct strength grading (see section 2.2) and calibration of non-destructive (NDT) and semi-destructive (SDT) measurements [23]. Long-term, load-bearing behaviour of timber members (i.e., creep) can be negatively influenced by prolonged or recurrent exposure to a humid microclimate [26]. Additionally, MC changes in the hygroscopic range induce dimensional movement of the elements in service, with possible deformations, disconnections or occurrence of internal stresses due to constrained swelling or shrinkage [27].

In conditioned indoor climates, wood moisture content typically ranges between 8-12%. However, damage or defects of the building enclosure can expose wood to bulk liquid (e.g., a leak) or condensation, resulting in undesirable moisture gains which can reach the fiber saturation point (FSP, ~28%). This condition makes wood more susceptible to fungal attack that ultimately reduces the material structural integrity. Therefore, detection of moist areas is

important as those areas are at risk of bio-deterioration.

Electrical and hygrothermal methods are the most common approaches to estimate and monitor MC in timber members. [23] and [28] review methodological criteria for MC estimation and monitoring using these non-destructive techniques. It is worth mentioning that large structural timbers are often characterised by non-uniform moisture distribution, which can vary along a member length and cross section. As moisture content estimates from resistance or capacitance data only depict local conditions, challenges in terms of data sampling are implicit with these methods, and require careful evaluation of potential vulnerable/more exposed areas, where moisture can reach higher values. These challenges are common to both historical and modern timber construction, and some sampling criteria to monitor wood moisture content in modern mass timber buildings are discussed in [29].

Long-term moisture content monitoring has proven to be effective to support decision-making processes in the conservation of historical timber structures [5]. Some authors highlight the importance of data processing of continuous moisture content data to support decision making processes related to the service life management of the monitored structure. Post-processing techniques such as moving average and erroneous data omission [29] have been proposed to improve data readability and automatize some analytical procedures.

Wave-based NDT imaging of wood has a great potential as preliminary non-contact screening procedure to detected moist areas along a timber member. Active thermography, for instance, can be used with some success to localize surface areas with high moisture content [30], [31]. Microwave reflectometry (MWR) can be used for detection of high moisture content in wood [32]. However, since MWR is affected by water, but also by decay and defects in wood, the simultaneous presence of many heterogeneities can be masked in MWR maps [32].

2.2. Mechanical characterization of timber members

Structural timber members present a high variability of properties (within and among members) which are affected by material and environmental factors, such as wood species, density, naturally occurring heterogeneities and moisture content. Some of these factors, such as the presence of knots, have a different impact on the mechanical behaviour of a timber member, depending on a member's structural use in a system (for instance, as a flexural or compressive element). Therefore, timber capacity assessed by applying standard visual strength grading (VSG) procedures intended to be used in the sawmill have some limitations for the prediction of mechanical characteristics of timber load-bearing members on site and their results are generally over conservative, thus leading often to unnecessary demolitions. Adaptation of visual strength grading procedures for on-site assessment first introduced by UNI 11119:2004 standard [10] is discussed in several studies (e.g., [33]) and harmonization documents (e.g., [8]).

Except for proof-loading, which is a direct measure of stiffness, other on-site testing techniques indirectly estimate mechanical parameters. NDT parameters used to characterize structural timbers are mainly based on elastic-wave transmission/vibrational methods, with the NDT variables being the time of flight (TOF)[25] or the natural frequency [34]. TOF measurements are affected by a number of conditions such as the direction of the signal transmission with respect to the wood anatomical directions, and the wood MC [25]. Determination of the dynamic Elastic modulus from the natural frequency relies on a series of

simplistic assumptions, such as geometric (prismatic) regularity of a timber member, approximation of its weight and of its boundary conditions. For accessibility reasons, transverse vibration tests are generally preferred (for instance, [34]).

A number of SDT techniques have been proposed for the estimation of mechanical parameters of timber members (see for instance, [24][35]). These techniques either quantify the local resistance of the material against the action of specific probes or directly measure local properties of extracted samples. Major limitations of SDT for the mechanical characterization of timbers are: the lack of standardized procedures and, in many cases, of commercial equipment; sampling criteria, which should consider the local validity of the measurements and the inherent variability of the material; related to the previous point, the necessity of correction factors to apply estimated clear wood properties to full-size structural timbers; reliability of uni- or multivariate empirical models (e.g. regression analysis) linking indirect measurements to inferred properties; and, other factors affecting the relationship between NDT parameter and inferred property (for indirect methods).

[36] propose modification factors for the standardization of non-destructive variables (i.e., TOF, natural frequency, penetration depth, pull-out resistance and drill resistance) taking into account affecting variables such as moisture content, temperature, size/length, and probe position with respect to grain direction.

While most NDT methods are global (involving a large volume of the element), SDT are local measurements. Combination of information provided by two or more independent methods, for instance of a global and a local testing data, in one single model can lead to a more reliable prediction of the property of interest. For instance, [37] suggests combining density data from wood core to improve prediction of dynamic modulus of elasticity (Edyn) using stress wave tests (REF). Additionally, integration of information from visual inspection and NDT/SDT data are proposed to support decision-making processes, for instance using Bayesian methods [38].

2.3.Characterization of decay and damage

Due to wood biological nature, timber artefacts can undergo to biodegradation during their service life. An early evaluation of the degrading phenomena is crucial to plan remedial actions and reduce the impact of invasive intervention. Investigations of biodegradation mechanisms, and the influence of changes of wood chemical/physical properties on mechanical characteristics have been subjects of intensive research [39].

During assessment of timber artefacts, evaluation of the occurrence, severity, and nature of decay and damage is a fundamental task that generally starts with visual inspection. Visual inspection enables the detection of wood decay visible on an element surface, however, decay can occur in many hidden segments of timber, such as beam ends buried into masonry. Additionally, early decay is virtually impossible to be detected visually. For these reasons, a series of instrumental techniques can be used to complement visual inspection and more comprehensively characterize decay and damage in timber members.

Also NDT and SDT methods for characterization of decay and damage can be global or local, and result in different levels of resolution [40]. Measurement of drilling resistance is probably the most common and validated technique to detect the presence and extent of decay within timber members, providing high-resolution (typically 0.1 mm) profiles correlated with

density variations within the material. In [32] drill-resistance data are mapped within a measuring grid to compare results with stress-wave TOF tomograms to estimate residual cross-sections in decayed timber members [32].

Among the electromagnetic wave-based NDT imaging techniques, digital radiography is readily available, as nowadays various manufacturers produce portable digital X-ray systems. Digital radioscopy has proven to be effective in detecting internal decay and insect attack in timber members, as well identifying construction defects and damage [23][31].

Probably, the most important information to collect for the characterization of decay in timber members are about the triggering and influencing factors (i.e., environmental, constructive, etc.), the type of decaying agents, and if the observed phenomena are active or not. In case of active phenomena or presence of conditions affecting those phenomena, decision should be made, based on prediction of the behaviour of the structure within a specified time frame. Near-infrared spectroscopy and multivariate analysis based on partial least-squares (PLS) has been used to evaluate type of degrading agents and develop prediction models to characterize and monitor decay in timber members [41] and wood surface weathering [42].

2.4. From geometrical characterization to structural analysis and monitoring (and closing the loop)

Geometric data is instrumental in supporting various decision-making processes; critical to documentation, preventive conservation and maintenance programs, essential for diagnostic investigation, structural analysis and design of interventions. A thorough representation of the configuration of the structural system aimed at understanding the behavior and the structural role of each component and of the joints is instrumental to the static analysis of a structure, help defining the load paths in timber frameworks and determine critical structural units and elements subjected to greater static demands. Analysis of the geometric data is also fundamental to identify alterations in the structure, such as rigid movements or deformation.

3D geometric data acquisition may be accomplished either through image-based or range-based methods. Availability of 3D data can enhance the production of 3D models and support metrical, structural and technological analysis at different levels of a building and timber structure. This rich 3D datasets can encompass various levels of details, for instance including non-rectangular and varying sections, non-linear beams, out of the plane elements and individual variations of carpentry joints.

NDT imaging methods with different resolution and penetration capabilities, such as radiography [31], GPR [43] , and IR thermography [44], have been successfully used to acquire geometric data of hidden features, such as reinforcements and connections in timber members [31] or timbers concealed by other systems [43][44]. Local SDT, such as drill resistance tests, can provide enriched data on irregular timber cross-sections [45].

The need to develop and use a uniform data model and an exchangeable format to process and communicate metric, non-metric and semantic data is becoming increasingly important. Building Information Models (BIM) and use of Industry Foundation Classes (IFC) as open standard for data exchange are transforming the way geometric data are used in the construction industry, and also in the cultural heritage industry [46]. For the latter, heritage BIM library projects, such as HBIM, provide solutions to integrate and update information from different survey and test methods and use the resulting model as a platform for collaborative data

management among different cultural heritage stakeholders [46].

Emerging applications of HBIM systems in heritage management are to support advanced data query off-site and onsite. For instance Virtual Reality (VR) and Augmented Reality (AR) technologies have been applied to the HBIM system to augment expert's access to a building information during on-site risk management, including advanced data query of traditional wooden connections [47].

Advantages of using HBIM platforms for comprehensive structural analysis of traditional timber systems is discussed by [48]. A comparison of structural analysis of traditional timber roof performed with conventional wire-frame models and more complex parametric models showed that the differences in geometry, captured by the parametric model, have a significant impact on the simulation results and are crucial to inform the preservation process [48].

The structural evaluation of existing timber structures presents a challenge due to the necessity to assess the mechanical behavior of timber members and joints, as well as taking into consideration time-dependent variables (creep and load-duration) and biological deterioration. HBIM models can be used as updateable digital replicas of a building or system. While BIM relies mostly on manual update of the model by the users, integration of sensor data into HBIM models can automatize and streamline model update. Implementation of so-called Digital Twin (DT) resulting from the integration of digital models and sensor data holds huge potential for structural assessment and monitoring of historical (as well as new) timber structures. In addition to short-term benefits, such as the possibility to set early-warning, hazard and damage detection systems, long-term advantages include a better understanding of interferences between timber buildings and their environment, and can help buildings' managers evaluating the impact of each implemented technical solution.

3. CONCLUSIONS

Holistic assessment methodologies are required to capture the complexity of traditional timber structures, their morphological, technological, material and mechanical variability, and their interaction with the environment. Some of the challenges to effective assessment and monitoring of historical timber structures are due to the scarcity of relevant standards and the lack of a commonly accepted ontological approach, relating scope of the assessment, information required and necessary procedures.

Although seamless data integration and information exchange are key factors for effective assessment and management of historical timber structures, current practice generally follows segmented approaches for each assessment scope and phase, as well as traditional data processing applications, which may not be able to capture the relationships among all the variables affecting the behavior of existing timber structures. This may limit the possibility to turn data into valuable, actionable information.

Multi-criteria tools, data integration and sharing through platforms such as HBIM and digital twins represent promising approaches to support decision-making processes for the assessment and conservation of historical timber structures.

REFERENCES

[1] Borri, A, Corradi, M. (2019). Architectural Heritage: A Discussion on Conservation and Safety. Heritage 2019, 2, 631–647; doi:10.3390/heritage2010041

[2] Morkunaite, Z, Kalibatas, D, Kalibatiene, D. (2019). A bibliometric data analysis of multi-criteria decision making methods in heritage buildings. Journal of Civil Engineering and Management. 25. 76-99. 10.3846/jcem.2019.8315.
[3] Bertolin, C, Loli, A. (2018). Sustainable interventions in historic buildings: a developing decision making tool. Journal of Cultural Heritage 34 (2018) 291–302.
[4] Pozzi, M, Kiureghian, A.D. 2011. Assessing the Value of Information for long-term structural health monitoring. Health Monitoring of Structural and Biological Systems 2011. 7984, (2011).
[5] Riggio, M, Dilmaghani, M. (2019) Structural health monitoring of timber buildings: A review of monitoring projects and lessons learned". Building Research & Information. https://doi.org/10.1080/09613218.2019.1681253
[6] Riggio, M, D'Ayala, D, Parisi, MA, Tardini, C. (2018). Assessment of heritage timber structures: Review of standards, guidelines and procedures. Journal of Cultural Heritage 31, 220-235.
[7] SIA 269/5:2011, Existing Structures – Timber Structures, Schweizer Norm,Swiss Society of Engineers and Architects, Zurich, Switzerland, 2011.
[8] Cruz, H, Yeomans, D, Tsakanika, E, Macchioni, N, Jorissen, A, Touza, M, Mannucci, M, Lourenço, PB. (2015). Guidelines for on-site assessment of historic timber structures, Int. J. Architect. Herit. 9 (3): 277–289.
[9] Macchioni, N., Feio, A. Ruisinger, U., Saporiti, J., Tsakanika, E., Yeomans, D. (2019). The prEN 17121: Historic Timber Structures – Guidelines for the on-site assessment of load-bearing timber structures. SHATIS'2019. 25-27 September 2019, Guimarães, Portugal.
[10] UNI 11119:2004, Cultural Heritage – Wooden Artefacts – Load Bearing Structures of Buildings. Criteria for the Preliminary Evaluation, Design and Execution Works, UNI (Ente nazionale italiano di unificazione), 2004 (in Italian).
[11] Serafini, A., Riggio, M., González-Longo, C. (2017). A Database Model for the Analysis and Assessment of Historic Timber Roof Structures. International Wood Products Journal. Assessment, Reinforcement and Monitoring of Timber Structures: Research outputs from the COST ACTION FP1101. 8 (1): 3-8.
[12] Baggio, C., et al. 2007. Field Manual for post-earthquake damage and safety assessment and short term countermeasures (AeDES). European Commission, Joint Research Centre, Institute for the Protection and Security of the Citizen.
[13] Frese, M., Blas, H. J., 2011. Statistics of damages to timber structures in Germany, Engineering Structures, 33, 2969-2977.
[14] Toratti, T. 2011. Proposal for a failure assessment template. Engineering Structures. 33: 2958–2961.
[15] Hansson, E. F. 2011. Analysis of structural failures in timber structures: typical causes for failure and failure modes. Engineering Structures. 33: 2978–2982.
[16] Parisi, M. A., Chesi, C. and Tardini, C. 2013. Seismic vulnerability of timber roof structures: classification criteria. Advanced Materials Research. 778: 1088–1095.
[17] Žnidarič ,A. (2013) e-bridge – Bridge Inspection Software, Technical Background, V0.5, Slovenian National Building And Civil Engineering Institute.
[18] Pazlar, T., Kramar, M. (2014) Assessment of Timber Bridges in Slovenia. Proceedings of the COST Timber Bridge Conference - CTBC 2014. 25–26 September 2014. Bern University of Applied Sciences. Biel, Switzerland

[19] Cacciotti, R., Blaško, M., Valach, J. (2015) A diagnostic ontological model fordamages to historical constructions. Journal of Cultural Heritage. 16 (1): 40-48.
[20] Novelli, VI, and D'Ayala D. (2015). LOG-IDEAH: LOGic trees for identification of damage due to earthquakes for architectural heritage, Bull. Earthquake Eng. 13 (1) 153-176.
[21] D'Ayala, D, Speranza, E. (2003). Definition of collapse mechanisms and seismic vulnerability of historic masonry buildings, Earthquake Spectra 19 (3) 479–509.
[22] D'Ayala, D, Galasso, C, Putrino, V, Fanciullacci, D, Barucco, P, Fanciullacci, V, Bronzino, C, Zerrudo, E, Manalo, M, Fradiquela, C, Regalado, J. (2016). Assessment of the Multi-Hazard Vulnerability of Priority Cultural Heritage Structures in the Philippines, in: ICONHIC 2016, Chania, Crete.
[23] Riggio, M, Anthony, RW, Augelli, F, Kasal, B, Lechner, T, Muller, W, Tannert, T. (2014). In situ assessment of structural timber using non-destructive techniques. Materials and Structures 47(5), 749-766.
[24] Tannert, T, Anthony, RW, Kasal, B, Kloiber, M, Piazza, M, Riggio, M, Rinn, F, Widmann, R, Yamaguchi, N. (2014). In situ assessment of structural timber using semi-destructive techniques. Materials and Structures 47(5), 767-785.
[25] Dackermann, U, Crews, K, Kasal, B, Li, J, Riggio, M, Rinn, F, Tannert, T (2014). In situ assessment of structural timber using stress-wave measurements. Materials and Structures, 47(5), 787-803.
[26] Fridley, KJ, Tang, RC, Soltis, LA, Yoo, CH (1992) Hygrothermal effects on load-duration behavior of structural lumber, J. Struct. Eng. 118 (4): 1023–1038.
[27] Fragiacomo, M, Fortino, S, Tononi, D, Usardi, I, Toratti, T. (2011). Moisture-induced stresses perpendicular to grain in cross-sections of timber members exposed to different climates, Engineering Structures 33 (2011) 3071–3078.
[28] Dietsch, P, Franke, S, Franke, B, Gamper, A, Winter, S. (2014). Methods to determine wood moisture content and their applicability in monitoring concepts. Journal of Civil Structural Health Monitoring, 5(2):115–127
[29] Schmidt, E, Riggio, M. (2019). Monitoring Moisture Performance of Cross-Laminated Timber Building Elements during Construction. Buildings, 9, 144
[30] Ludwig, N, Redaelli, V, Rosina, E, Augelli, F. (2004). Moisture detection in wood and plater by IR thermography. Infrared Physics & Technology. 46 (1-2): 161-166
[31] Riggio, M, Sandak, J, Franke, S. (2015). Application of imaging techniques for detection of defects, damage and decay in timber structures on-site. Constr. Build. Mater., 101, 1241– 1252.
[32] Riggio, M, Macchioni, N, Riminesi, C. (2017). Structural health assessment of historical timber structures combining non-destructive techniques: The roof of Giotto's bell tower in Florence. Struct. Control Health Monit.,. 24 (7)
[33] Riggio, M, Piazza, M. (2011). Hardness Test. In Situ Assessment of Structural Timber: Discussion of Classical and Modern Non-Destructive and Semi-Destructive Methods for the Evaluation of Wood Structures. 7: 85-95.
[34] Hunt, MO, Ross, RJ, Wang. W, Soltis, LA. (2007). Assessment of in-place wood floor systems. Journal of Architectural Engineering, 13 (1) 30-35
[35] Kloiber, M, Drdacky´, M, Machado, JS, Piazza, M, Yamaguchi, N. (2015). Prediction of mechanical properties by means of semi-destructive methods: A review. Constr. Build.

Mater. 101 (2): 215–1234.
[36] Íñiguez-González, G, Arriaga, F, Esteban, M, Llana, DL. (2015). Reference conditions and modification factors for the standardization of nondestructive variables used in the evaluation of existing timber structures. . Constr. Build. Mater. 101 (2015) 1166–1171
[37] Morales-Conde MJ, Machado, JS. (2017). Evaluation of cross-sectional variation of timber bending modulus of elasticity by stress waves. Constr. Build. Mater. 134 (1): 617-625
[38] Feio, A, Machado, JS. (2015). In-situ assessment of timber structural members: Combining information from visual strength grading and NDT/SDT methods–A review. Constr. Build. Mater. 101 (2) 1157-1165
[39] Curling, S, Clausen, C, Winandy, J. (2002). Relationships between mechanical properties, weight loss, and chemical composition of wood during incipient brown-rot decay. Forest products journal, 52, 34.
[40] Machado, JS, Riggio, M, D'Ayala, D. (2015). Assessment of structural timber members by non-and semi-destructive methods. Constr. Build. Mater. (101), 1155–1156.
[41] Sandak, A, Sandak, J, Riggio, M. (2016) Assessment of wood structural members degradation by means of infrared spectroscopy: an overview. Struct. Control Health Monit., 23 (3)
[42] Sandak, J, Sandak, A, Riggio, M. (2015). Characterization and monitoring of surface weathering on exposed timber structures with a multi-sensor approach. Int. J. Architect. Herit., 9(6), 674–688.
[43] Fontul, S, SOll, M, Cruz, H, Machado, JS, Pajewski, L. (2018). Ground penetrating radar investigations in the Noble Hall of São Carlos Theater in Lisbon, Portugal. Survey in Geophysics 39 (6), 1125-1147.
[44] Cantini, L, Tedeschi, C, Tiraboschi, C, Binda, L. (2012).Use of thermovision for the survey of a timber vault in Torino, in: O. Büyüköztürk et al. (Eds.), Nondestructive Testing of Materials and Structures, RILEM Book series 6, pp.1203–1208. RILEM 2012.
[45] Cabaleiro, M, Branco JM, Sousa HS, Conde B (2018). First results on the combination of laser scanner and drilling resistance tests for the assessment of the geometrical condition of irregular cross-sections of timber beams. Materials and Structures, 51 (99)
[46] Logothestis, S., Delinasiou, A., Stylianidis, E. (2015). Building information modelling for cultural heritage: a review. ISPRS Annals of the Photogrammetry, Remote Sensing and Spatial Information Sciences, Volume II-5/W3, 2015
[47] Lee, J, Kim, J, Ahn, J, Woo, W. (2018). Mobile Risk Management for Wooden Architectural Heritage in Korea using HBIM and VR. (DigitalHERITAGE 2018) & (VSMM 2018), 26-30 Oct. 2018, San Francisco, CA, USA.
[48] Bassier, M, Hadjidemetriou, G, Vergauwen, M, Van Roy, N, Verstrynge E. (2016). Implementation of Scan-to-BIM and FEM for the Documentation and Analysis of Heritage Timber Roof Structures. EuroMed 2016, Part I, LNCS 10058; 79–90.

12th International Conference on Structural Analysis of Historical Constructions
SAHC 2020
P. Roca, L. Pelà and C. Molins (Eds.)

CONTINUOUS STRUCTURAL MONITORING OF ADOBE BUILDINGS: SUMMARY OF A THREE YEARS EXPERIENCE IN PERU

GIACOMO ZONNO[1], RAFAEL AGUILAR[1*], RUBÉN BOROSCHEK[2] AND PAULO B. LOURENÇO[3]

[1] Department of Engineering, Pontificia Universidad Católica del Perú - PUCP,
Av. Universitaria 1801, San Miguel, Lima 32, Peru
e-mail: g.zonno@pucp.edu.pe, raguilar@pucp.pe (*corresponding author)

[2] University of Chile, Department of Civil Engineering,
Av. Blanco Encalada 2002, Santiago, Región Metropolitana, Chile
e-mail: rborosch@ing.uchile.cl

[3] University of Minho, ISISE, Department of Civil Engineering,
Campus de Azurém 4800 - 058 Guimarães, Portugal
e-mail: pbl@civil.uminho.pt

Keywords: Historic Structure, Andean Church, Structural Monitoring, Environmental Monitoring, Correlation Analysis

Abstract. *The paper describes in detail the application of a vibration-based structural health monitoring system installed in the "San Pedro Apostol" church of Andahuaylillas located in Cusco (Peru), a 16th century adobe church considered a representative example of South America baroque architecture. The results of three years of long-term vibration and temperature and humidity monitoring program are reported in detail in the paper, with a focus on the long-term and short-term correlations between natural frequencies and environmental parameters. The results demonstrate that an accurate estimation of the first eight frequencies in the range 2-6 Hz is possible in the case of complex adobe structure and the existence of an annual cyclical behavior of the natural frequencies with a clear correspondence with the changes in environmental conditions due to seasonal influences. The performed correlations of ambient conditions and structural parameters confirmed the presence of different timescales and their not negligible influence in the case of a vibration-based structural health monitoring assessment of adobe systems with large thermal inertia large thermal inertia.*

1 INTRODUCTION

Adobe has a very significant place in the field of civil construction materials. Different types of structures were made over the centuries and in various parts of the World with this material due to its attractive characteristics such as low cost, local availability, the possibility to be self/owner-made, good thermal insulation and acoustic properties [1]. The use of sun-dried

blocks dates bakes to 8000 BCE and, in more recent times, it was estimated that around 30% of the world population lives in earthen constructions [2]. Nowadays, a wide range of earth buildings can be found in Europe, Asia, Middle East, Africa and America. In particular, adobe buildings are extensively diffused in Latin America, and in Peru where cultural heritage and archaeological sites made of this material are a fundamental part of its intellectual richness and cultural diversity. The sacred city of Caral (2000 BCE), the complexes of "Huaca del Sol" and "Huaca de la Luna" (100-800 CE), the pre-Colombian city of Chan-Chan (850-1476 CE) are some of the numerous examples of Peruvian earthen monuments [3].

Unfortunately, these structures require a special attention and investigation due to the high vulnerability of the adobe heritage buildings affected by anthropological factors (such as lack of maintenance, inappropriate use and traffic vibrations), natural factors (such as earthquakes, tsunami and environment conditions) and intrinsic factors (such as aging of the materials and the low tensile strength and brittle behaviour of the adobe) [4]. Modern tools were developed to assess existing buildings and reduce their vulnerability. Within the available tools, vibration-based structural health monitoring (vSHM) is finding an increasing use in the preservation and conservation of historical constructions such as bell towers [5], stone masonry churches [6] and buildings [7] due to its low invasiveness, the possibility to increase of the level of knowledge of structural system with high accuracy and the possibility of check the health state of the structures [8]. The structural health assessment of existing buildings by vibration-based monitoring systems is a challenge task because the influence of the environmental parameters (mainly temperature and humidity) can lead a variation of the boundary conditions [9], in the system stiffness [10] and others, masking variations due to structural damages. In the case of earthen existing buildings, the authors show in [11-12] how thermohygrometric variations can produce significative changes in natural frequencies at long and short scales because the environmental parameters are time-dependent and non-uniform quantities.

The paper reports the results obtained with the three years of vSHM of a masterpiece of the Peruvian cultural heritage earthen building, the "San Pedro Apostol" church of the Andahuaylillas, located in Cusco (Peru). The monitoring system was installed on March 2017 and continuously records the dynamic response of the church by four force-balances accelerometers and the environmental conditions by temperature and humidity sensors. The paper in Section 2 describes the cases study and the carried-out monitoring systems, in Section 3 describes the obtained results and Section 4 concludes the paper.

2 THE "SAN PEDRO APOSTOL" CHURCH OF ANDAHUAYLILLAS

2.1. Description of the case study

The "San Pedro Apostol" church is located in the main square of the Andahuaylillas, a village close to the Cusco city, in southeastern Peru, in the Andean region and it is considered the most emblematic colonial adobe church of South America (Fig. 1a). The church was built by Jesuit in the 16th century and is known as the "Sistine Chapel of Latin America" for its inestimable mural painting (Fig. 1b). The church covers an area of 61 x 27 m (Fig. 1c), with a main nave of 58 x 12 m and a height of 10 m, and it is connected directly to the baptistery, the bell tower, two later chapels and, by a triumphal arch, to the presbytery (Fig. 1d). The adobe walls have a variable thickness from 1.10 m to 2.00 m and a stone masonry foundation with a height of 1.5 m. The longitudinal walls of the nave are connected by wooden tie-beams and

steel tie-rods and the roofing system is composed by a "A-shape" trusses of timber elements [13].



Figure 1: "San Pedro Apostol" church of Andahuaylillas: (a) exterior view, (b) interior view, (c) 3D reconstruction, and (d) plan view at the height of the base.

2.2. Description of the monitoring system

For the importance of the building and to increase the knowledge about the dynamic and thermohygrometric behaviour of the structure, a remote and continuous dynamic monitoring system and an environmental monitoring system were installed on the church on March 2017. The implemented monitoring systems are summarized in Fig. 2, and consist: (i) local acquisition and storage of the raw data (dynamic and environmental data), (ii) transmission of the raw data by a 4g data plan to the central monitoring station, (iii) reception and storage of data, (iv) processing of raw data, and (v) publishing the results in a web platform using a cloud engine. For the processing of the dynamic raw data (stage iv of the monitoring system), an automatic processing tool was developed and tested in [14]. In particular, the developed tool is able to identify automatically the frequencies, mode shapes and damping values of the structure through four main steps: (a) digital signal pre-processing of the dynamic data; (b) application of the SSI-Data method to obtain the stabilization diagram; (c) filtering of the stabilization diagram with the application of hard and soft validation criteria; (c) automatic detection of the modal parameters using hierarchical clustering approach and automatic thresholds; and (d) the

application of an adaptive modal tracking for a final cleaning of the dynamic results (see more details in [14]).

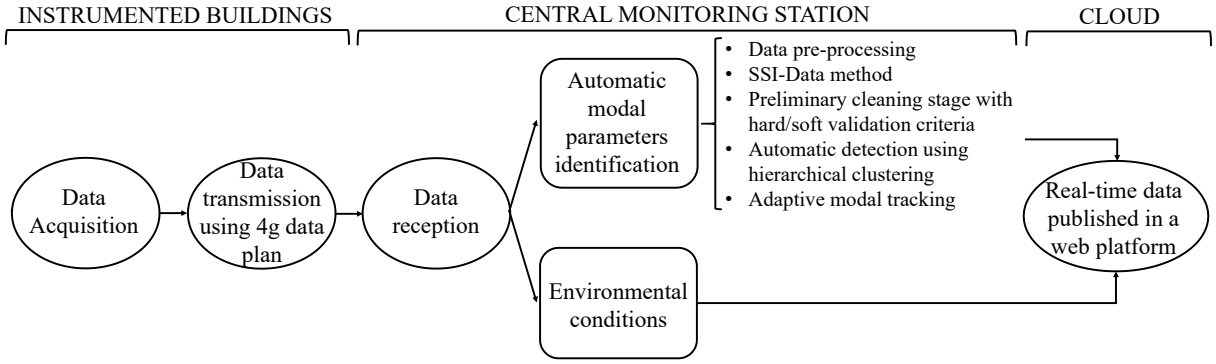


Figure 2: Overview of the structural monitoring system implemented in the "San Pedro Apostol" church.

Within this context, the implemented dynamic monitoring system consists of a Kinemetrics Obsidian 8x [15], a data acquisition unit with a capacity of 8-channels and 24 bits of resolution (Fig. 3f) and four uniaxial force balance accelerometers Episensor ES-U2 [16] with a bandwidth range from DC to 200 Hz, a dynamic range of 155 dB+, a sensitivity of 10 V/g, and an operating temperature range from −20 °C to 70 °C (Fig. 3c). To generate a stable power supply, an external battery (Fig. 3h) with a voltage regulator (Fig. 3i), and a battery charging-maintainer (Fig. 3g) are incorporated. The accelerometers are located at the top height of the north and south nave walls (see Fig. 3c) to record the horizontal (out of plane) movements of the main nave. The data acquisition parameters are set at a sampling rate of 200 Hz, at a sampling time of 900 s for each event and with a time recurrence of one hour.

The environmental monitoring system used to perform the remote and real-time monitoring of the external and internal temperature and humidity is composed by a HOBO RX-3000 Data Logger [17] (Fig. 3l) and two S-THB-M008 environmental sensors [18] (Fig. 3m). The S-THB-M008 sensors have a temperature resolution of 0.02 °C, a humidity resolution of 0.1%, a temperature measurement range between −40 °C and 75 °C, and a humidity measurement range between 0 and 100%. The environmental sensors are placed outside (T_{ext} and H_{ext} in Fig. 3a) and near the entrance of the church (T_{int} and H_{int} in Fig. 3a) to record the internal and external temperature and humidity. The environmental parameters are recorded with a time recurrence of one hour. For remote communication, the Obsidian 8x, and the HOBO RX-3000 Data Logger were connected by Ethernet cables to a TP-Link modem with a phone data plan (Fig. 3d) to automatically send the recorded information to the central monitoring station using a safe File Transfer Protocol (FTP). During the entire monitoring period more than 23000 raw data was sent from the instrumented building to the central station.

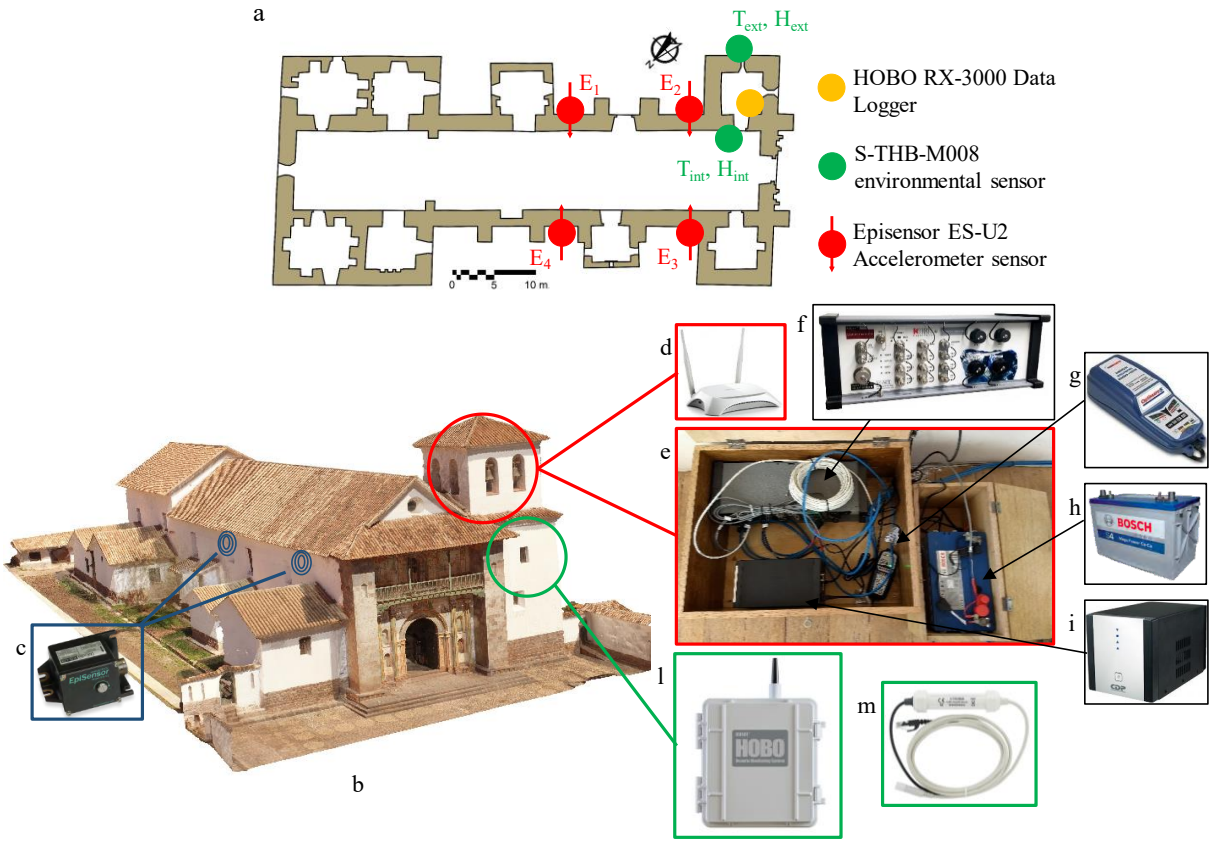


Figure 3: Dynamic and environmental monitoring systems: (a) location of the dynamic and environmental sensors, (b) 3D reconstruction of the church with the device locations, (c) EpiSensor ES-U2 accelerometer sensor, (d) TP-Link modem, (e) data acquisition station, (f) Obsidian 8x acquisition system, (g) battery charging-maintainer, (h) external battery, (i) voltage regulator, (l) HOBO RX-3000 Data Logger, and (m) S-THB-M008 temperature/ humidity sensor.

3 MONITORING SYSTEMS RESULTS

The analysis of the recorded ambient vibration data was performed, and the results are presented in Fig. 4. As shown, the first eight frequencies of the adobe church were clearly detected in the range 2 Hz and 7 Hz. As shown, the results indicate a seasonal influence during the monitoring period. Lower frequency values were reached during colder months (between June and September), while higher values in the summer months (between December and March). An irregular behavior was detected close to November 2018 with a local decrease of all the identified frequencies.

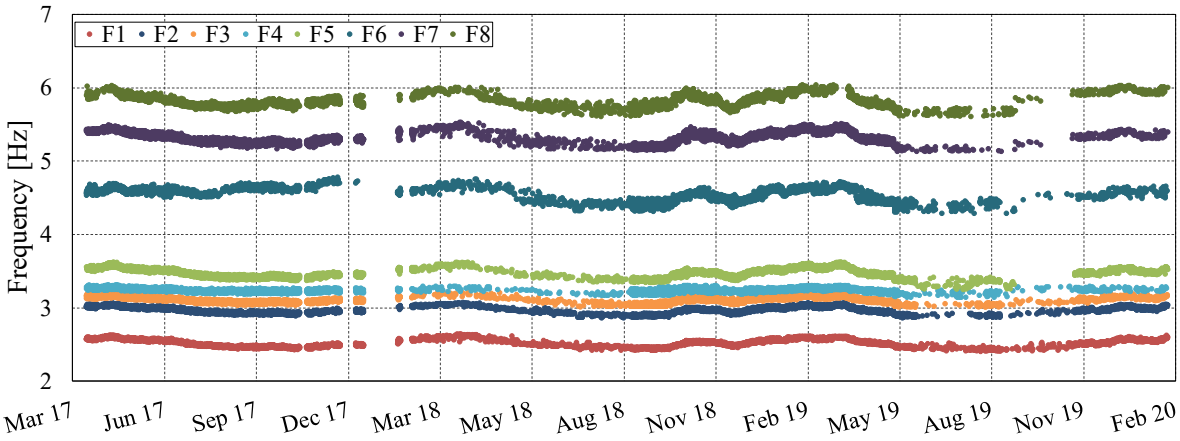


Figure 4: Time evolution of the first eight natural frequencies of the "San Pedro Apostol" church from March 2017 to November 2019.

The results of the ambient temperature and relative humidity evolution are shown in Fig. 5. The external ambient temperature (T_{ext}) exhibits a not clear seasonal trend of the data with higher daily variations in the summer period and lower in the winter one (Fig. 5a), reaching a maximum value of 28°C and a minimum value of 5°C during the monitoring period. On the contrary, the internal ambient temperature records (T_{int}) shows clear seasonal trends, with an increase of the values during the summer period and a decrease in the winter one (Fig. 5a). An attenuation phenomenon of the daily thermal variation compared to the external ambient records, reaching a maximum value of 21°C in winter and a minimum value of 11°C in summer. Similar attenuation between external and internal measurements was recorded in the case of relative humidity (see the external relative humidity, H_{ext} and the internal relative humidity, H_{int} of Fig. 5b). The values of the external relative humidity range between 82% and 7%, in comparison with the values of the internal relative humidity that range between 71% and 12%. Clear seasonal trends were also detected with a humidity drop in the winter period (between June and September) in both external and internal values.

Aiming at developing a single variable that integrates information of ambient temperature and relative humidity, the external and internal absolute humidity ($AbsH_{ext}$ and $AbsH_{int}$, respectively) were calculated to achieve a better understanding of the effects of thermohygrometric parameters on the natural frequencies of the adobe church (see more details of how this variable is calculated in [13]). In particular, $AbsH_{ext}$ and $AbsH_{int}$ were calculated using the recorded data of T_{ext}/H_{ext}, and T_{int}/H_{int} sensors, respectively, and they represent the amount of water vapor in the external and internal air of the church. The results of the calculated absolute humidity values in the entire monitoring period are showed in Fig. 5c. A clear seasonal decrease (from 10 g/m^3 to 2 g/m^3) was recorded for both parameters in the winter period, with an irregular behavior detected close to November 2018, with a clear similarity of the time evolution of the identified frequencies. Furthermore, high capacity to reduce the variation between the external and internal measurements is shown by this calculated parameter.

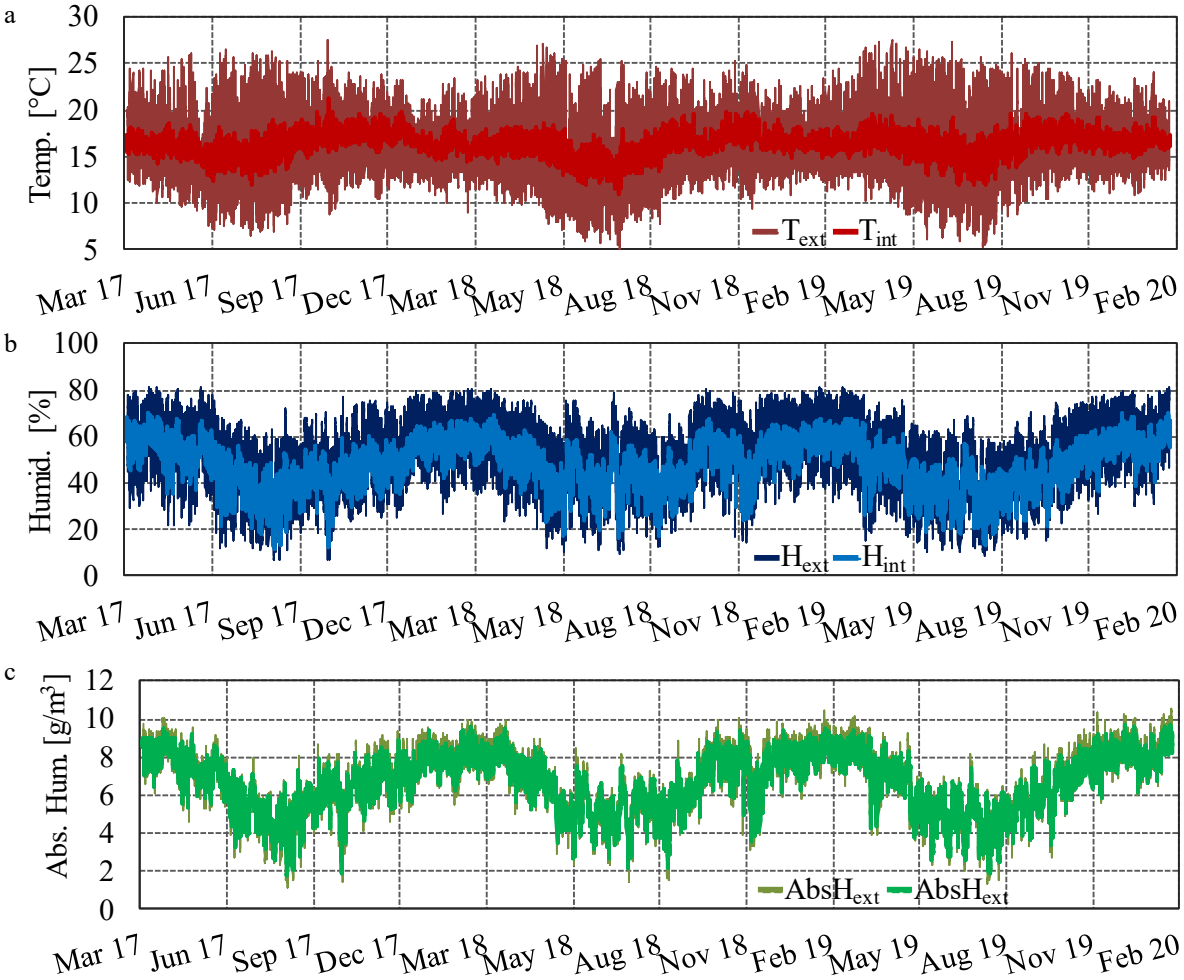


Figure 5: Time evolution of the church's ambient temperature and humidity: (a) external and internal ambient temperatures T_{ext} and T_{int}, (b) external and internal relative humidity H_{ext} and H_{int}, and (c) external and internal absolute humidity $AbsH_{ext}$ and $AbsH_{int}$.

4 ANALYSIS OF THE INFLUENCE OF AMBIENT CONDITIONS IN THE DYNAMIC STRUCTURAL BEHAVIOUR

A detailed study was performed between the first frequency of the "San Pedro Apostol" church and the external ambient humidity. The external ambient humidity was selected as parameter for comparison due to:

(a) the absolute humidity has demonstrated to be an effective parameter for performing correlation analyses [12];

(b) t absolute humidity is less affected by the thermal inertia of the adobe, demonstrated by a higher correlation between external and internal environmental measurements;

(c) in most structural monitoring, the external environmental parameters are easier to obtain.

Furthermore, in sake of brevity, in the present paper only the results of the first frequency will be described in detail.

Fig. 6 shows the correlation distributions of the first frequency with the external absolute

humidity corresponding to the entire monitoring period. Aiming at analyzing the influence of the environmental parameters on the frequency with different timescales, the raw data was filtered by averages with different timescale. In particular, Fig. 6a shows the correlation distribution obtained by the raw data. Fig. 6b shows the correlation distribution obtained by filtering the raw data with a daily average (the mathematical average was carried out with the 24 data recorded in one day). Finally, Fig. 6c, Fig. 6d, and Fig. 6e show the correlation distribution obtained by filtering the raw data by averaging the data of 7 days, 15 days and 30 days, respectively.

The results show that the correlation coefficients between the raw data of the first frequency and external ambient humidity are almost good (R^2=0.35) with a positive trend. The results of the correlation distribution with the daily average filtered data show a higher value of correlation coefficient (R^2=0.47) with a clearer positive trend. The results improve with the 7 days average filter, reaching a correlation coefficient of 0.58. Finally, with the 15 days average filter and the 30 days average filter, there is a slight improvement of the results, reaching a correlation coefficient of 0.65.

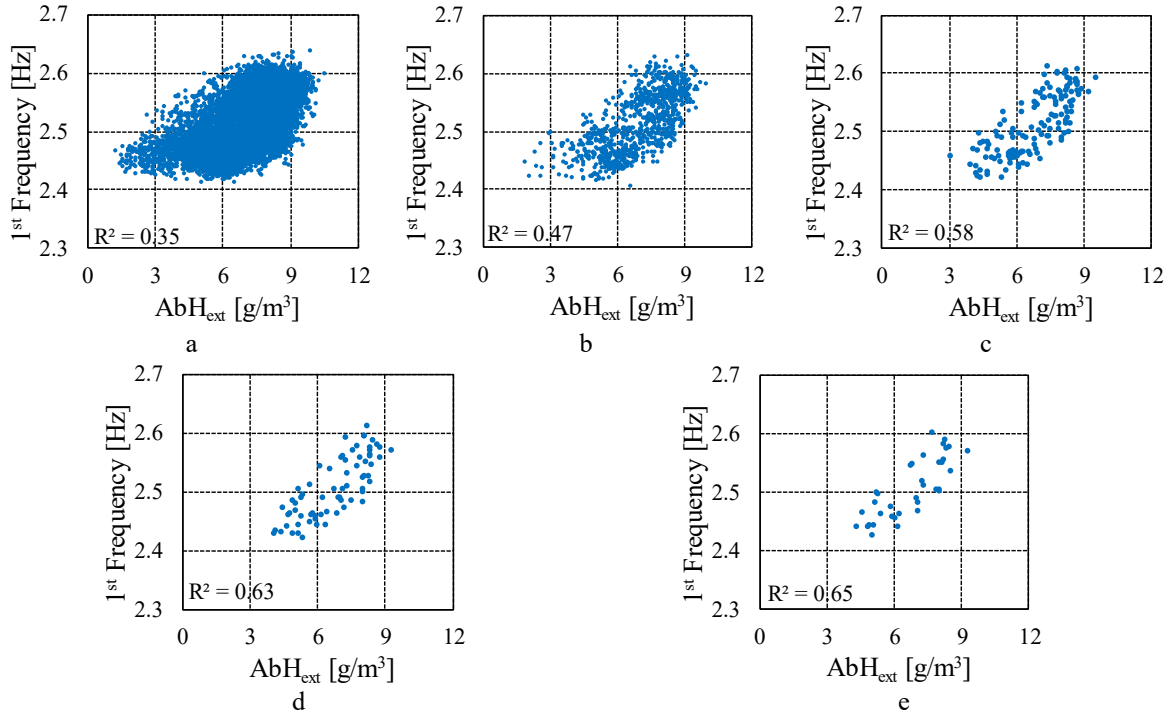


Figure 6: Correlation coefficients distribution between the first natural frequency and external absolute humidity: (a) raw data, (b) data filtered by a daily average, (c) data filtered by a 7 days average, (d) data filtered by a 15 days average, and (e) data filtered by a 30 days average.

5 CONCLUSIONS

The paper reports the results of almost three years of environmental and dynamic monitoring of the emblematic "San Pedro Apostol" adobe church of Andahuaylillas, Cusco (Peru). The results show on one side the influence of the adobe structure on the diffusion of temperature and humidity inside the church, and on the other side, the influence of the environmental

parameters on the dynamic response of the same structure.

The comparison between the evolution of the internal and external environmental conditions shows a clear attenuation of the internal measurements, confirming the influence of the thermal inertia of this type of buildings, mitigating the extreme ambient climatic conditions recorded outside the church.

The analysis of the influence of the environmental parameters on the dynamic response of the structure show an annual cyclical behavior in the time evolution of the first eight frequencies of the church, with a clear similarity with the time evolution of the environmental parameters (long-term analysis). Furthermore, a medium-term and a short-term analyses were performed with the calculated external absolute humidity, and improved results were attained when the daily variation, the 7 days variation, the 15 days variation and the 30 day variation were removed from the original raw data of natural frequencies and environmental parameters

The successful implementation of an environmental and dynamic monitoring system in a 16th century historical adobe church and the obtained results about the relevant role of the environmental parameters at different time scales in the dynamic response of adobe systems make the vibration-based structural health monitoring system a useful tool for the conservation and protection of the cultural heritage buildings.

REFERENCES

[1] Varum, H., Tarque, N., Silveira, D., Camata, G., Lobo, B., Blondet, M., et al. Structural behaviour and retrofitting of adobe masonry buildings. *Structural rehabilitation of old buildings*. Springer, Berlin, Heidelberg. (2014). pp. 37-75.

[2] Houben, H., Guillard, H. *Earth Construction: A Comprehensive Guide*. Practical Action, London. (1994).

[3] Ciocci, M. P., Sharma, S., and Lourenço, P. B. Engineering simulations of a super-complex cultural heritage building: Ica Cathedral in Peru. *Meccanica*. (2018). **53**(7): 1931-1958.

[4] Karanikoloudis, G., and Lourenço, P. B. Structural assessment and seismic vulnerability of earthen historic structures. Application of sophisticated numerical and simple analytical models. *Eng. Struc.* (2018). **160**: 488-509.

[5] Saisi, A., C. Gentile, and A. Ruccolo. Continuous monitoring of a challenging heritage tower in Monza, Italy. *J. Civ. Struct. Health Monit.* (2018). **8**(1): 77–90.

[6] Elyamani, A., O. Caselles, P. Roca, and J. Clapes. Dynamic investigation of a large historical cathedral. *Struct. Control Hlth* (2017). **24**(3): e1885.

[7] Lorenzoni, F., F. Casarin, M. Caldon, K. Islami, and C. Modena. Uncertainty quantification in structural health monitoring: Applications on cultural heritage buildings. *Mech. Syst. Signal Pr*. (2016). **66**:268–81.

[8] Ramos, L., Marques, L., Lourenço, P. B., De Roeck, G., Campos-Costa, A., Roque, J. Monitoring historical masonry structures with operational modal analysis: two case studies. *Mech. Syst. Signal Pr*. (2010), **24**: 1291–1305.

[9] Ubertini, F., C. Gentile, and A. L. Materazzi. Automated modal identification in operational conditions and its application to bridges. *Eng. Struc.* (2013). **46**:264–78.

[10] Maeck, J., B. Peeters, and G. De Roeck. Damage identification on the Z24 bridge using vibration monitoring. *Smart Mater. Struct.* (2001). **10**(3):512.

[11] Zonno, G., R. Aguilar, R. Boroschek, and P. B. Lourenço. Experimental analysis of the thermohygrometric effects on the dynamic behavior of adobe systems. *Constr. Build. Mater*. (2019). **208**:158–74.
[12] Zonno, G., Aguilar, R., Boroschek, R., and Lourenço, P. B. Environmental and ambient vibration monitoring of historical adobe buildings: applications in emblematic Andean churches. *Int. J. Archit. Herit.* (2019). https://doi.org/10.1080/15583058.2019.1653402
[13] Zonno, G., Aguilar, R., Boroschek, R., and Lourenço, P. B. Analysis of the long and short-term effects of temperature and humidity on the structural properties of adobe buildings using continuous monitoring. *Eng. Struc.* (2019). **196**: 109299.
[14] Zonno, G., Aguilar, R., Boroschek, R., and Lourenço, P. B. Automated long-term dynamic monitoring using hierarchical clustering and adaptive modal tracking: validation and applications. *J. Civ. Struct. Health Monit.* (2018). **8**(5): 791-808.
[15] KINEMETRICS. (2019). Obsidian 8x multichannel seismic recorder. https://kinemetrics.com.
[16] KINEMETRICS. (2019). EpiSensor ES-U2 uniaxial episensor accelerometer. https://kinemetrics.com.
[17] ONSET. (2019). HOBO RX3000 remote monitoring station data logger. http://www.onsetcomp.com.
[18] ONSET. (2019). S-THB-M008 temperature/relative humidity smart sensor. http://www.onsetcomp.com.

12th International Conference on Structural Analysis of Historical Constructions
SAHC 2020
P. Roca, L. Pelà and C. Molins (Eds.)

DATA ANALYSIS USING ARX MODELS APPLIED TO STATIC STRUCTURAL HEALTH MONITORING OF THE MONASTERY OF SANT CUGAT

N. MAKOOND[1*], L. PELÀ[1], C. MOLINS[1] AND P. ROCA[1]

[1]Department of Civil and Environmental Engineering
Universitat Politècnica de Catalunya (UPC-BarcelonaTech)
Jordi Girona 1-3, 08034 Barcelona, Spain
e-mail: nirvan.makoond@upc.edu, luca.pela@upc.edu, climent.molins@upc.edu,
pere.roca.fabregat@upc.edu

Keywords: Masonry, environmental effects, dynamic regression models, diagnosis

Abstract. *The church of the monastery of Sant Cugat close to Barcelona is a medieval construction characterized by a complex structural behaviour stemming from the interaction among various structural elements built over different periods. Despite having survived for several centuries, such structures are often affected by slow irreversible deterioration mechanisms that can jeopardise their stability in the future. In order to identify such mechanisms at an early stage, and to better understand the cause of visible pathologies, a static structural health monitoring (SHM) system was installed in the church since 2017. Although this monitoring strategy, aimed at the continuous measurement of key slow-varying parameters, has been used successfully in the past to facilitate the diagnosis of this structural typology, the interpretation of data collected by such systems remains a challenging task. One of the main reasons for this is the fact that many monitored damage and deformation features are sensitive to changes caused by environmental conditions. To address this issue, this paper presents the application of a fully automated data analysis procedure to the records collected from the SHM system installed in the church of the monastery of Sant Cugat. The procedure consists of two parts. The first relies on the identification of models that comprehend an Auto-Regressive output and an eXogenous input (ARX) to represent the dynamics of each monitored response using suitable environmental parameters as predictors. The identified models are then used to estimate filtered evolution rates. The second part of the procedure involves classifying each monitored response into pre-defined evolution states based on outcomes from the first part. The main results from the application to the case of the church of the monastery of Sant Cugat are presented and the implications for the diagnosis of the structure are discussed.*

1 INTRODUCTION

The monastery of Sant Cugat is located near Barcelona in Catalonia, Spain. The masonry structure at the site today consists of different parts built over different time-periods mostly from the mid-12th century to the 15th century. The monastery is composed of a cloister and a church, with the latter being the main focus of this study. The church exhibits several pathologies notably in the form of cracks and inclinations. Hypotheses have been developed

regarding the possible causes of these pathologies and an extensive restoration and strengthening campaign was even completed in 1996. However, the true cause of many pathologies, as well as the current evolutionary condition of possible deterioration mechanisms, remain unknown. Since identifying active mechanisms is crucial for a complete diagnosis of the church's current structural condition, a long-term static structural health monitoring (SHM) system was installed in the structure in March 2017.

The initial interpretation task in the case of static SHM involves the identification of either a stationary or an evolutionary condition from the recorded data of each monitored response. However, since monitored features are often sensitive to both damage and environmental changes, there usually exists no clear distinction between irreversible changes linked to active deterioration mechanisms and reversible ones caused by daily and seasonal environmental fluctuations. This, together with the complex interaction among structural elements, can make the interpretation of static SHM data very challenging in actual practice.

Nevertheless, in spite of these difficulties, there exist many examples of successful applications of static SHM for the diagnosis of masonry heritage structures. Many of these have relied on directly fitting linear or periodic models to the recorded time series of the monitored responses. Others have explicitly taken measured environmental parameters such as temperature into consideration by using a simple linear model to predict and filter out the estimated change of the monitored structural response caused by environmental changes.

Because the most common monitored structural responses in the case of masonry structures (cracks and inclinations) frequently show a predominantly linear dependence to the most influential monitored environmental parameter (temperature), the above-mentioned filtering method often leads to accurate estimates of underlying evolution rates. However, it is not very robust because the linear model is certainly an over-simplification of the true nature of the relationship. Notably, in the case of the relationship between temperature and structural parameters, a linear model is not able to consider effects caused by the thermal inertia of the material or by thermal gradients between interior and exterior temperature.

Dynamic linear regression models that comprehend an Auto-Regressive output and an eXogenous input (ARX) appear to be an appealing alternative since they can account for more of the dynamics of relationships between environmental and structural parameters. As their name suggests, these black box models can exploit a large number of observations to reconstruct linear dependencies of monitored responses on their own rate of change, on the rate of change of selected predictors and on the present value of predictors. The first step of such a filtering procedure involves selecting which measured environmental variables will be used as predictors in the ARX model. Before the parameters of ARX models can be estimated, it is also very important to define the number of past response and predictor samples that will be used to describe the system. These are referred to as the model orders. Although there exist some examples of successful applications of ARX models to filter out environmental effects from dynamic SHM data [1,2], the application to static SHM data has been very limited [3]. As a result, there is very little guidance available on how to select appropriate model orders and there is a clear lack of tools for the interpretation of results from the identified ARX models.

In order to address this issue, a fully automated data analysis procedure incorporating ARX models has recently been proposed [4]. The entire process includes a method to select optimal model orders from a pre-defined range as well as a procedure to classify each monitored

response according to their estimated evolutionary state. This paper presents the application of this fully automated procedure for the diagnosis of the church of the monastery of Sant Cugat.

Firstly, the SHM system currently installed in the monastery is briefly described. Some methods that attempt to filter out environmental effects from monitored responses are then described. The classification procedure that utilises results from all the filtering methods is then presented. Finally, the estimated evolutionary conditions and their corresponding rates are presented before discussing their implications for the diagnosis of the structure.

2 STRUCTURAL HEALTH MONITORING SYSTEM

The SHM system installed in the church of the monastery of Sant Cugat consists of 14 crackmeters, 2 inclinometers, 3 thermistors and 3 humidity sensors, as shown in Figure 1. The cracks and inclinations to be monitored were chosen following a comprehensive damage survey and analysis. Of the 22 sensors, only 3 were placed on the exterior of the structure. Crackmeter FS 3-15 was fixed on the exterior wall of the central nave adjacent to the cimborio while the temperature and humidity sensors, TEMP-2.4 and HUMI-2.4, were installed on the exterior wall of the bell tower facing the cimborio (see Figure 1). Most of the sensors have been installed since March 2017. The two crackmeters placed on cracks beneath the rose window (FS-3.19 and FS-3.20) were installed in December 2017 and the one placed in the lintel of the main entrance (FS-3.21) was installed in April 2018. All the methods presented in this paper make use of data collected up to 02/02/2020. This constitutes 2.9 years of data for most sensors, 2.1 years for FS-3.19 and FS-3.20 and 1.8 years for FS-3.21.

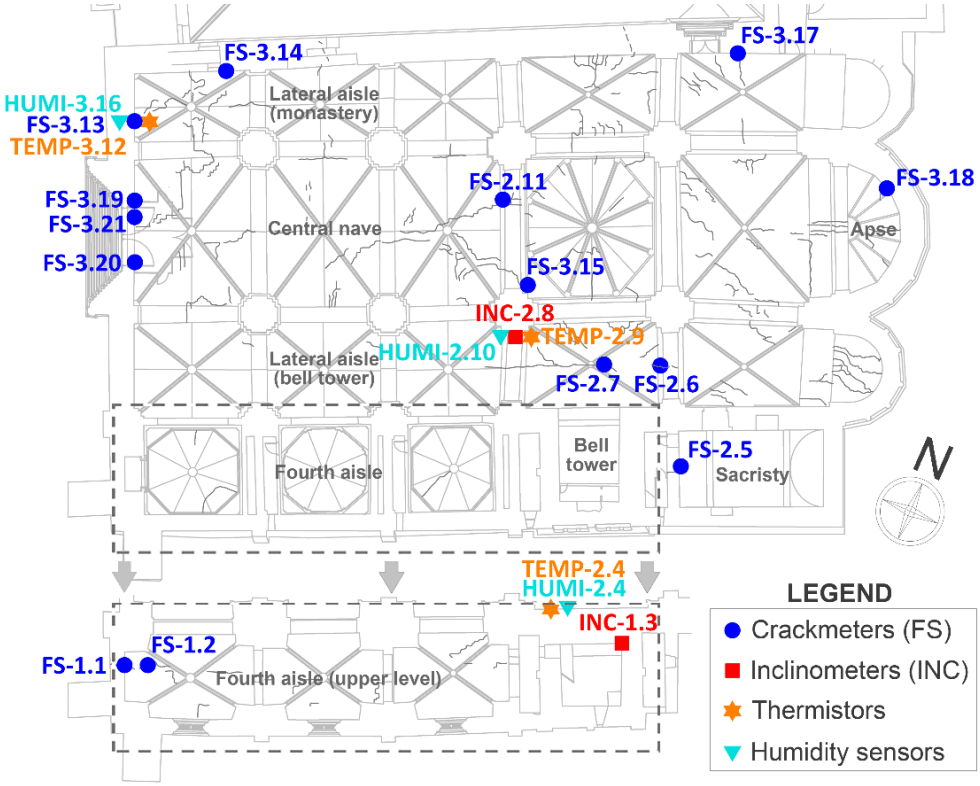


Figure 1: Plan view showing layout of the SHM system installed in Sant Cugat monastery.

3 METHODS FILTERING OUT EFFECT OF TEMPERATURE

The simplest analysis methods that have been applied to static SHM data consist of estimating underlying evolution rates by directly fitting the time series of each monitored structural response to a linear or to a nonlinear periodic model. Although there exist several successful examples of such applications, particularly when long monitoring periods are available, estimates from these types of analyses can easily be biased by underlying trends or irregular changes in environmental parameters.

Many of the shortcomings of the above-mentioned methods can be addressed by taking advantage of environmental parameters monitored on site to better characterise their effect on monitored responses. As such, the SHM system installed in the monastery of Sant Cugat included sensors to measure two of the most relevant environmental parameters, i.e. temperature and relative humidity (see Figure 1). Although the methods presented in this section can be applied to any monitored environmental parameter, only the effect of temperature will be discussed in the case of Sant Cugat because a preliminary evaluation clearly revealed that the monitored responses are generally significantly more strongly correlated to temperature than to relative humidity.

3.1 Preliminary evaluation of correlation

Before identifying the parameters of any model to represent the dependence of a structural response on environmental parameters, it is important to identify which environmental parameters are more suitable to be used as predictors in the model. This can be achieved by computing the Pearson correlation coefficient (R) between measured environmental and structural parameters [4]. This coefficient can vary between -1 and +1 with absolute values closer to unity indicating a stronger linear correlation. The sign of the coefficient reveals the type of correlation. A negative sign implies that an increase of a parameter leads to a decrease of the other and vice-versa.

The R-values between temperature and each structural response monitored in the monastery of Sant Cugat are shown in Figure 2. For each response, the preliminary evaluation of correlation was carried out with exterior temperatures recorded by the thermistor placed outside the structure, as well as with interior temperatures recorded by the nearest thermistor placed inside the structure.

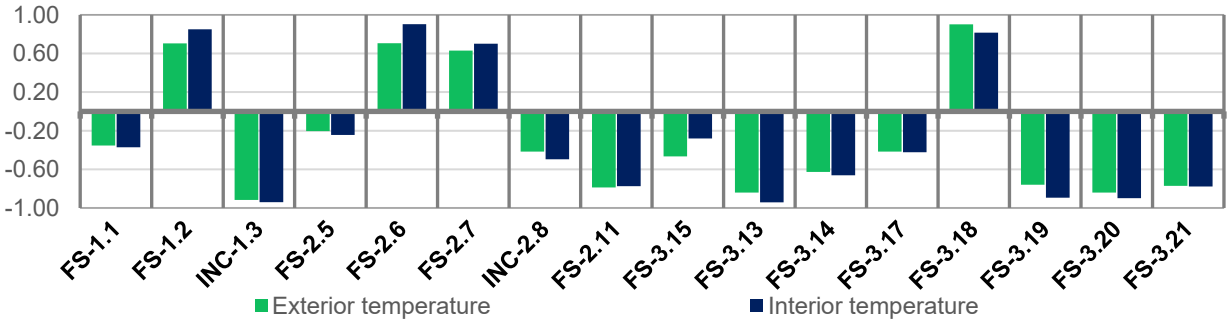


Figure 2: Correlation coefficients of monitored structural parameters with temperature computed over the entire monitoring period.

Both inclinometers have a strong negative correlation with temperature. This indicates that

both the bell tower and the pillar at the southwest corner of the cimborio tend to incline towards the south when temperatures increase.

As expected, most monitored crack widths exhibit a negative correlation with temperature. This is the expected behaviour since increasing temperatures cause materials to expand thus reducing crack widths and vice versa. However, four of the monitored cracks show a positive correlation with temperature. It is possible that the unexpected thermal response of some of these cracks is linked to the structural intervention that was completed in 1996 [5]. This activity involved inserting several tie rods in the southern part of the church, as shown in Figure 3. If these elements were actively working, an increase in temperature would cause an expansion of the tie rod and a subsequent loss in tension, which could induce the opening of cracks. This type of response has been observed previously in a masonry tower as reported in [6].

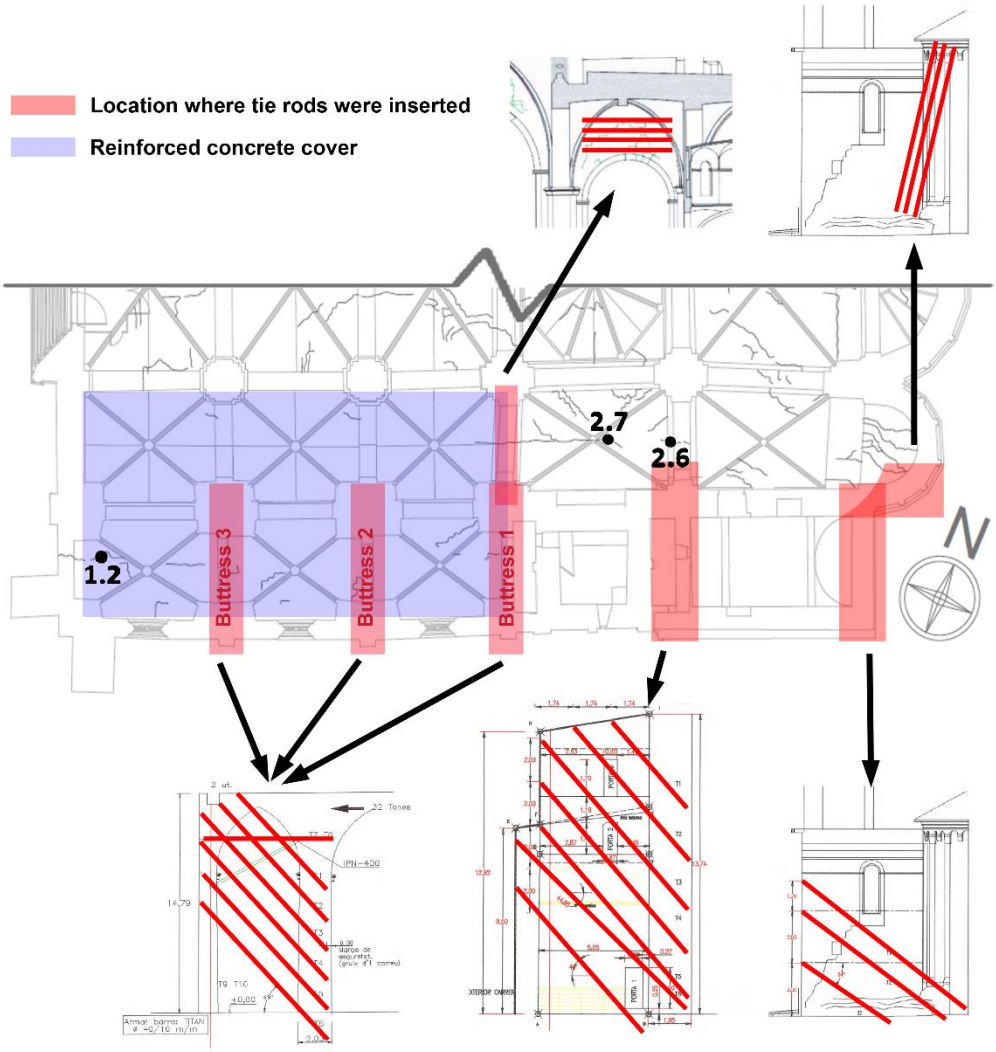


Figure 3: Structural interventions completed in 1996 in the southern part of the church, with the position of some sensors monitoring cracks which exhibit a positive correlation with temperature.

In addition to the insertion of tie rods, the structural intervention of 1995-1996 also involved

consolidation with a heavily reinforced concrete overlay of the gothic vaults of the fourth and lateral aisle on the side of the bell tower (see Figure 3). The expansion of the reinforcement during increasing temperatures can exert a force on the concrete and subsequently on the masonry. This effect can also contribute to the positive correlation observed between temperatures and the crack widths monitored by FS-1.2, FS-2.6 and FS-2.7.

3.2 Filtering environmental effects through linear models

The simplest method to characterise explicitly the direct effect of temperature uses a linear model between measurements of temperature and each structural parameter, as shown in Figure 4. Since only a single predictor can be used for such a model, only the interior or exterior temperature is used for each response depending on which one has the greatest correlation coefficient.

Due to the simplicity of this model, it can be said that effects caused by structural mechanisms of interest are less likely to influence the identified models if data from only a single seasonal cycle is used for the estimation of model parameters. When this practice is carried out, the first year of monitoring is usually used for the estimation of model parameters, and is referred to as the estimation phase. However, it can be argued that using data from the entire monitoring period would allow the model to better capture the changing nature of the relationship in some cases. Therefore, as recommended in [4], both operations listed below were carried out for each response variable and the results from both methods were compared:

1. **Linear filter (i):** Linear regression between selected predictor and response variable, using data from the entire monitoring period.
2. **Linear filter (ii):** Linear regression between selected predictor and response variable, using data only from the first complete year of monitoring (estimation phase).

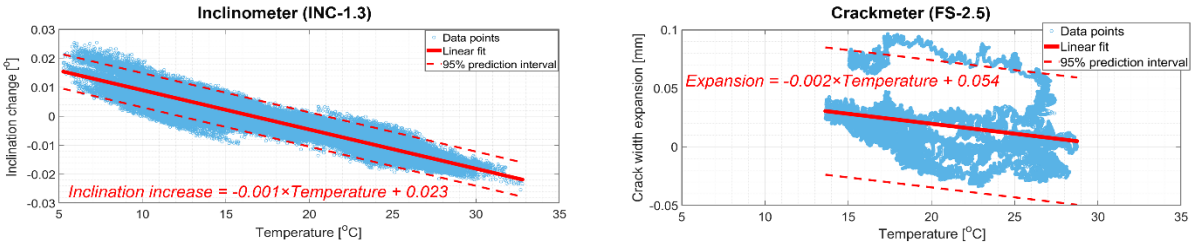


Figure 4: Examples of linear regression between monitored structural parameters and temperature over the entire monitoring period.

Once the regression procedure has been completed, measured values of each predictor can be substituted into the identified linear models to simulate changes of the structural parameter that have been caused by changes in temperature. Actual measurements of the structural response are then filtered by simply subtracting the simulated temperature effect, as shown in Figure 5. Estimates of the underlying evolution rates ($ER_{lin(i)}$ and $ER_{lin(ii)}$) can then be obtained by carrying out a regression of the filtered residuals.

A significant advantage of this method is that it enables the assessment of how well each linear model can predict the relationship between temperature and every structural parameter. If we assume that residuals are normally distributed when no significant structural mechanism is present, a prediction interval representing a specific level of confidence can be obtained based

on the standard error of the estimate (σ_e), computed using the differences between predicted and measured values. Figure 5 shows the plot of the 95% prediction interval.

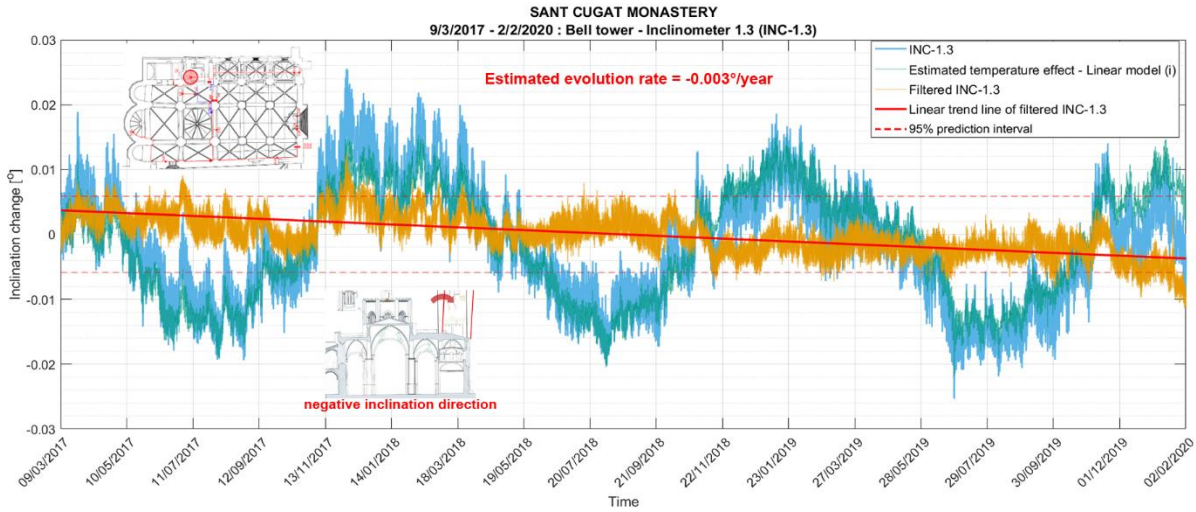


Figure 5: Filtering of temperature effect based on identified general linear trend and estimation of evolution of INC-1.3 from filtered residuals.

3.3 Filtering environmental effects using ARX models

It is clear that the relationship between temperature and structural parameters can often be sufficiently well represented by a linear model. However, it can fail to do so in many cases since it cannot account for certain effects influencing the system it aims to describe, such as those due to thermal inertia or caused by thermal gradients. Auto-Regressive models incorporating an eXogenous input (ARX) are better equipped to deal with such effects because they utilise measured values of past responses together with those of past and current or delayed predictors to describe the dynamics of a system. In this case, only measurements collected during an estimation phase are used to estimate the parameters of the models. As was the case for *Linear filter (ii)*, this estimation phase should span a full year to capture most of the reversible components caused by environmental effects during a complete seasonal cycle. The identified models are then used together with data collected over the entire monitoring period (simulation phase) to simulate responses based on measured predictors.

For each structural response monitored in the monastery of Sant Cugat, a single-input single output (SISO) ARX model was first employed using the same predictor as was used for the linear filters. Multiple-input single output (MISO) ARX models incorporating both interior and exterior temperatures as predictors were then implemented to allow the model to consider effects caused by thermal gradients. The complete procedure incorporating ARX models that was used for the analysis of data from the static SHM system is described in [4] and will not be reiterated in this article. Besides the measurements of the response and of selected predictors, the only other required input to the procedure is the range of model orders to be tested.

The final quality of ARX models depend strongly on the model orders which define the number of past response and predictor samples used to describe the system. Although the procedure described in [4] suffers from the disadvantage of being more computationally expensive than using fixed model orders, if an adequate range is defined, it ensures an optimal

choice of model orders for each response based on the characteristics of the data itself. This in turn ensures that a sufficiently accurate ARX model will be obtained. Several ranges were tested as part of this research and for medieval masonry structures such as the church of the monastery of Sant Cugat, it is recommended to set the lower limit of the range to one corresponding to at least 4 days while it is recommended to set an upper limit corresponding to at least 10 days [4]. Naturally, the final range selected is largely dependent on the computational expense that can be spared. For the case study forming part of this research, a range corresponding to a duration from 5 to 25 days was specified for the SISO ARX models, and one corresponding to a duration from 4 to 10 days was specified for the MISO ARX models.

Once the effect of measured environmental parameters has been simulated with ARX models, the filtered evolution rate ($ER_{SISO\text{-}ARX}$ or $ER_{MISO\text{-}ARX}$) of each response can be computed in the same way as it was with the linear filters described in Section 3.2.

Several error metrics were used to assess the accuracy of the different models used to characterise the relationship between temperature and monitored responses. However, the standard error of the estimate (σ_e) is probably the one that is most easily interpreted since it is a measure of the dispersion of simulated values from measured ones expressed in the same units as the measurements. Figure 6 shows the values of σ_e for each monitored response using all the filtering procedures applied.

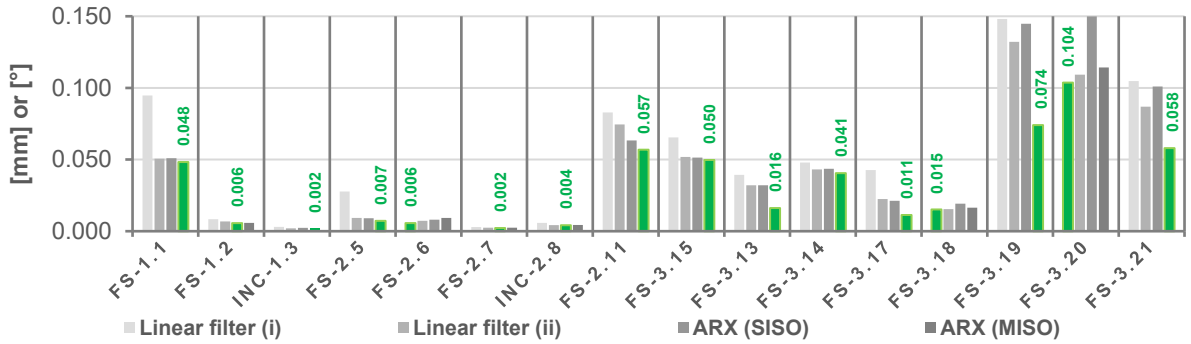


Figure 6: Standard error of the estimate (σ_e) computed from residuals between measured and simulated responses using different models over estimation phase.

It is clear to see that the ARX models are better suited to model the environmental variation since their residuals have a smaller dispersion than those of the linear models for 13 out of 16 monitored responses. Moreover, the added benefit of using both interior and exterior temperature as predictors is also apparent since the MISO models outperform the SISO ones for 10 of these 13 responses even if they have lower model orders.

4 AUTOMATED CLASSIFICATION PROCEDURE

Although using SISO and MISO ARX models to filter out the effect of environmental parameters can greatly improve the accuracy of the estimated filtered evolution rates, it is still important to consider the uncertainties and errors associated to modelling the effect of temperature. As a result, the interpretation of results can still be challenging. Utilising the automated classification procedure elaborated in [4] can greatly facilitate this task. This multi-step classification procedure involves 5 tests.

All of these tests rely on comparisons between the estimated filtered evolution rate computed

using the most sophisticated ARX model employed (ER_{ARX}) and the standard error of the estimate computed over the estimation phase from residuals associated to the same model ($\sigma_{e\text{-}ARX}$). Note that in the case of the analysis carried out for the SHM data collected in the monastery of Sant Cugat, the most sophisticated ARX models employed refers to the MISO models. Some tests also consider the normality of the residuals, the magnitude of daily fluctuations and results from all the procedures described in Section 3. A detailed description of each test is not given here but can be found in [4].

Based on the outcomes of the tests, each response is classified in one of the following 5 categories.

1. **Stationary:** Responses showing a clear stationary trend outside reversible variations caused by environmental parameters.
2. **Evolutionary:** Responses showing a clear evolutionary trend outside reversible variations caused by environmental parameters.
3. **Apparently stationary:** Responses showing a stationary trend but for which there is still a relatively large uncertainty associated to the estimation of the trend.
4. **Apparently evolutionary:** Responses showing an evolutionary trend but for which there is still a relatively large uncertainty associated to the estimation of the trend.
5. **Inconclusive:** Monitored parameters for which no clear conclusion can be made on its evolutionary state from the available monitoring data alone.

5 RESULTS AND DISCUSSION

The estimated filtered evolution rates from all the methods described in Sections 3.2 and 3.3 are summarised in Table 1, together with the evolution state estimated from the classification procedure presented in Section 4.

Table 1: Comparison of estimated evolution rates for monitored structural parameters of Sant Cugat monastery from methods filtering out the simulated effect of measured environmental parameters.

Sensor	Units	Estimate of annual evolution rate [unit/year]				Estimated condition
		Linear filter (i)	Linear filter (ii)	SISO ARX filter	MISO ARX filter	
FS-1.1	mm	0.102	0.102	0.100	0.100	App. Evolutionary
FS-1.2	mm	0.003	0.003	0.003	0.003	App. Evolutionary
INC-1.3	°	-0.003	-0.003	-0.003	-0.003	**Evolutionary**
FS-2.5	mm	0.029	0.029	0.025	0.026	**Evolutionary**
FS-2.6	mm	0.001	0.001	0.000	0.001	App. Stationary
FS-2.7	mm	0.001	0.001	0.001	0.001	**Stationary**
INC-2.8	°	-0.006	-0.006	-0.007	-0.007	**Evolutionary**
FS-2.11	mm	0.068	0.067	0.072	0.070	App. Evolutionary
FS-3.15	mm	0.002	0.001	0.001	0.000	Inconclusive
FS-3.13	mm	-0.003	-0.002	-0.004	-0.009	App. Evolutionary
FS-3.14	mm	-0.013	-0.014	-0.013	-0.014	Inconclusive
FS-3.17	mm	-0.041	-0.042	-0.042	-0.047	App. Evolutionary
FS-3.18	mm	0.001	0.001	-0.002	0.002	App. Stationary
FS-3.19	mm	-0.060	-0.063	-0.081	-0.060	App. Evolutionary
FS-3.20	mm	-0.023	-0.017	-0.040	-0.014	Inconclusive
FS-3.21	mm	0.138	0.135	0.170	0.126	App. Evolutionary

The results reveal that 3 of the monitored responses are experiencing significant evolutionary trends outside of cyclic seasonal fluctuations: the southward inclination of the bell tower (INC-1.3) and of the pillar in the southwest corner of the cimborio (INC-2.8) and the opening of the crack in the Sacristy (FS-2.5). The estimated evolution rates from all methods are in very good agreement for these responses. Given the nature of the observed trends and the relative position of the sensors capturing these movements, it is highly likely that the 3 trends identified as evolutionary are being caused by the same deterioration mechanism linked to an outward leaning of the bell tower towards the south (see Figure 8).

Since the western wall of the sacristy is intrinsically tied to the bell tower, the opening trend observed there could be an indication that the outward rotation of the bell tower is starting from a considerably low point of the structure. These observations are consistent with the construction history of the structure since most of it was built in the 14th century but the bell tower was only completed in the 18th century, when an arch joining the then incomplete tower and the cimborio was dismantled. It seems that the addition of this part of the structure is having an effect even today. Since the bell tower has a total height of approximately 40 m, the estimated evolutionary trend of 0.003°/year corresponds to an outward leaning of approximately 2 cm every 10 years assuming rigid block motion. In fact, recent topographic and laser scan surveys of the bell tower's geometry reveal that its southern and eastern walls have inclinations of up to 1.5% with a net displacement of 52 cm from the vertical position at the top of the main body of the tower. This strengthens the findings from the SHM analysis and suggests that a structural intervention addressing this mechanism could be required in the future.

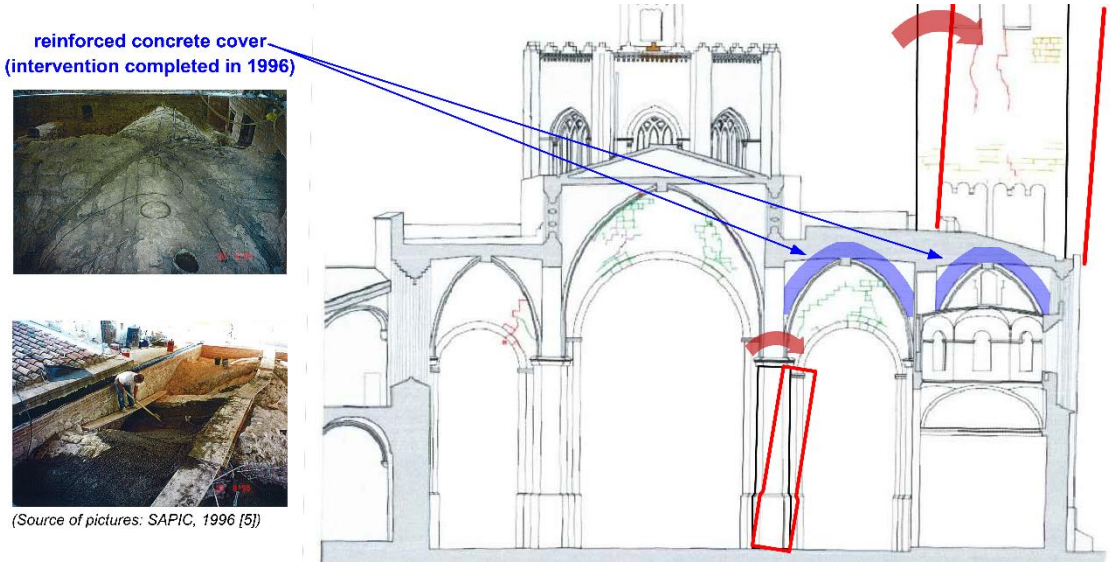


Figure 7: Observed inclination trends and location of reinforced concrete cover added in 1995-1996.

Another observation that can be made is that the monitored crack across the vault on the lateral aisle (FS-2.7) appears to be stationary outside seasonal fluctuations. This can probably be partially attributed to the flexibility of vaults as structural members, giving them an increased ability to deform without suffering irreversible damage in comparison to stiffer members. However, this could also be linked to some of the strengthening measures implemented during

the restoration campaign completed in 1996. The monitored crack goes through the arch immediately west of the sensor location. This arch was strengthened with 4 hollow metallic bars that were injected with cement grout. In addition, all gothic vaults of the lateral and fourth aisle west of this arch were stiffened considerably with a reinforced concrete cover, as shown in Figure 7. In fact, it is interesting to note that strengthening measures were carried out during the same campaign in the vicinity of the other 2 monitored cracks classified as apparently stationary (FS-2.6 and FS-3.18).

It is also worth mentioning that the greatest estimated crack opening rates are associated to two vertical cracks in the western wall: one in the fourth aisle (FS-1.1) and one above the main entrance (FS-3.21). Although the opening trend is clearer for the crack in the fourth aisle, the magnitude of cyclic variations experienced by both cracks are relatively large. As such, a longer monitoring period will provide an improved understanding of the actual extent of the underlying trends.

6 CONCLUSIONS

The application of the analysis method described in this paper has demonstrated the suitability of using dynamic linear regression models that comprehend an Auto-Regressive output and an eXogenous input (ARX) for filtering out the environmental effect from responses monitored in static structural health monitoring (SHM) systems. Moreover, it is clear that the fully automated robust analysis methodology employed can help facilitate the task of interpreting data collected by static SHM systems for the diagnosis of masonry heritage structures and avoid misinterpretation.

With respect to the church of the monastery of Sant Cugat, the outcomes of the analysis reveal that some parts of the structure are being affected by an ongoing deterioration mechanism linked to the outward leaning of the bell tower towards the south. Although there is evidence that some of the strengthening measures completed in 1996 could have reduced the effects related to some mechanisms in localised parts of the structure, it is clear that the measures have not been successful in completely containing the outward leaning of the bell tower and its related impacts.

Acknowledgements. This research has received financial support from the City Council of Sant Cugat (Ajuntament de Sant Cugat) through a project aimed at monitoring the structure of the church of the monastery of Sant Cugat (ref. num. C-10764). The authors also gratefully acknowledge the financial support from the Ministry of Science, Innovation and Universities of the Spanish Government (MCIU), the State Agency of Research (AEI), as well as the ERDF (European Regional Development Fund), through the SEVERUS project (Multilevel evaluation of seismic vulnerability and risk mitigation of masonry buildings in resilient historical urban centres, ref. num. RTI2018-099589-B-I00). Support from the AGAUR agency of the Generalitat de Catalunya and the European Social Fund, in the form of a pre-doctoral grant awarded to the corresponding author is also gratefully acknowledged.

REFERENCES

[1] L.F. Ramos, L. Marques, P.B. Lourenço, G. De Roeck, A. Campos-Costa, J. Roque, Monitoring historical masonry structures with operational modal analysis: Two case

studies, Mech. Syst. Signal Process. 24 (2010) 1291–1305.

[2] A. Kita, N. Cavalagli, F. Ubertini, Temperature effects on static and dynamic behavior of Consoli Palace in Gubbio, Italy, Mech. Syst. Signal Process. 120 (2019) 180–202.

[3] F. Lorenzoni, F. Casarin, M. Caldon, K. Islami, C. Modena, Uncertainty quantification in structural health monitoring: Applications on cultural heritage buildings, Mech. Syst. Signal Process. 66–67 (2016) 268–281.

[4] N. Makoond, L. Pelà, C. Molins, P. Roca, Automated data analysis for static structural health monitoring of masonry heritage structures, ***Manuscript submitted for publication*** (2019).

[5] SAPIC, Works to consolidate Baroque chapels and restore the south facade of the church of the monastery of Sant Cugat dels Vallès (Obres de consolidació de les capelles barroques i restauració de la façana sud de l'església del monestir de Sant Cugat dels Vallès, 1996.

[6] A. Saisi, C. Gentile, A. Ruccolo, Pre-diagnostic prompt investigation and static monitoring of a historic bell-tower, Constr. Build. Mater. 122 (2016) 833–844.

12th International Conference on Structural Analysis of Historical Constructions
SAHC 2020
P. Roca, L. Pelà and C. Molins (Eds.)

DEVELOPMENT OF A WIRELESS ACCELERATION MEASUREMENT SYSTEM

TAKAHIRO YAMASAKI[1*], KANA OTA[2], MITSUHIRO MIYAMOTO[2], YUICHIRO AMANO[3], MASATOSHI OKADA[3], AND TOMOYUKI KIDO[3]

[1]Shikoku Research Institute Inc
Civil Engineering Department
2109-8, Yashimanishimachi, Takamatu City, Kagawa Prefecture, Japan
e-mail: t-yamasaki@ssken.co.jp, web page: http://www.ssken.co.jp

[2]Kagawa University
Faculty of Engineering/And Design
2217-20, Hayashicho, Takamatsu City, Kagawa Prefecture, Japan
Web page: https://www.kagawa-u.ac.jp

[3]Shikoku Electric Power Company, Inc.
Civil & Architectural Engineering Department
2-5, Marunouchi, Takamatsu City, Kagawa prefecture, Japan
Web page: https://www.yonden.co.jp

Keywords: Acceleration Monitoring, Wireless sensor, 920MHz, Multipoint synchronization

Abstract. *The newly developed low-cost micro-electro-mechanical system (MEMS)-based acceleration sensors exhibit sufficient accuracy and stability to monitor the shaking of structures caused by an earthquake. We have developed a practical shaking-monitoring system using MEMS-based acceleration sensors and a 920 MHz multi-hop radio communication method that offers reliable radio wave communication, even within buildings. In this system, the base clock of each sensor unit must be closely synchronized to the master clock to minimize acceleration-induced phase synchronization error. In the proposed system, this error can be limited to three milliseconds in a system of multiple sensor units.*

1 INTRODUCTION

In the 1995 Hyogo-Ken Nanbu earthquake, many wood-framed residential structures and other traditionally built Japanese structures were damaged. Following the earthquake, interest in the study of earthquake resistance of historical buildings such as traditional wooden buildings has grown. The 1999 publication of Japanese guidelines for the seismic diagnosis of historical buildings[1] led to widespread quantitative evaluation of the seismic performance of historical buildings and routine seismic reinforcement.

In the seismic diagnosis of historical buildings, it is important to understand the characteristics of building vibrations, using seismic measurement. However, such measurements must be conducted nondestructively to prevent damage to the structure, using a wireless acceleration measurement system that can be easily installed without wiring.

Many wireless acceleration measurement systems built with the inexpensive and highly

accurate micro-electro-mechanical system (MEMS) acceleration sensor are in current use. Generally, in acceleration measurement systems that work at multiple points simultaneously, time synchronization between sensors is important. Many such systems adopt highly accurate time synchronization methods using the Global Positioning System (GPS). Furthermore, in relation to the operation of acceleration measurement systems in buildings, it is necessary to establish stable and highly accurate time synchronization methods, even where GPS radio waves do not reach. In the time synchronization operations of wireless acceleration measurement systems intended for indoor use, the use of broadcast time stamps[2][3] has been proposed.

Many of the wireless acceleration measurement systems currently in use employ radio waves in high-frequency bands such as the 2.4 GHz band. Large amounts of data can be transmitted easily by radio waves in this band. However, in the context of indoor use, these systems may not provide reliable communication, failing due to the interference of walls, other devices using the 2.4 GHz band, and walls. Therefore, we considered it desirable for wireless accelerometer systems used in buildings to employ radio waves in the 920 MHz band that enables stable communication even in buildings with much interference.

However, there are few wireless acceleration measurement systems that use 920 MHz band radio waves with highly accurate time synchronization in buildings and structures. The purpose of this study is to develop a wireless acceleration measurement system for use in buildings and constructions that can easily be installed.

This paper presents this system, which shows high time synchronization accuracy and stable communication performance.

2 A WIRELESS ACCELERATION MEASUREMENT SYSTEM

2.1 System overview

The newly developed wireless acceleration measurement system SwingMinder uses openATOMS communication technology, a wireless on-demand monitoring system developed by Y. Nakanishi.[4] Many wireless sensors have been developed that use 2.4 GHz band radio waves, but SwingMinder uses 920 MHz radio waves, which enable long-distance communication of up to 1000 m per hop, with a radio wave output of 20 mW outdoors. This enables wireless communication paths that can transmit radio waves through concrete slabs in buildings.

SwingMinder includes a data-collection unit called the network computer (NC) and multiple acceleration sensor units called networked intelligent cells (NICEs). Figure 1 shows an NC and an NICE, and Figure 2 presents the system configuration of SwingMinder. The acceleration time history data recorded by each NICE are collected by the NC and are transmitted to external remote-monitoring devices through an internet network such as 3G/LTE. The transmitted data can be converted into a csv format, confirmed, and analyzed remotely.

Each NICE is equipped with a 32-bit micro controller unit (MCU) that is capable of performing real-time fast Fourier transform (FFT) processing while measuring acceleration time history data and saving them sequentially in a recording medium. By placing data-analytical capabilities in the NICE units, which then transmit only important data, we resolved the issue of communication limitations that can be present when 920 MHz band

radio waves are used. Additionally, because the trigger for starting acceleration measurement in placed within each NICE unit, only important data are recorded, and reducing the amount of data that must be transmitted.

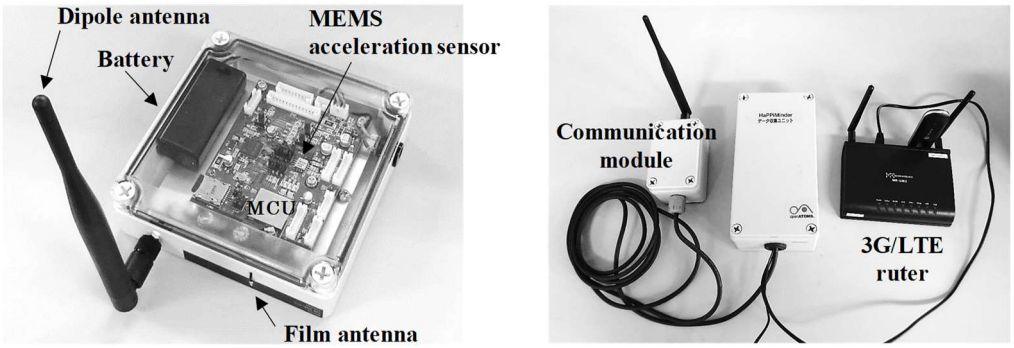


Figure 1. SwingMinder (left, NICE; right, NC)

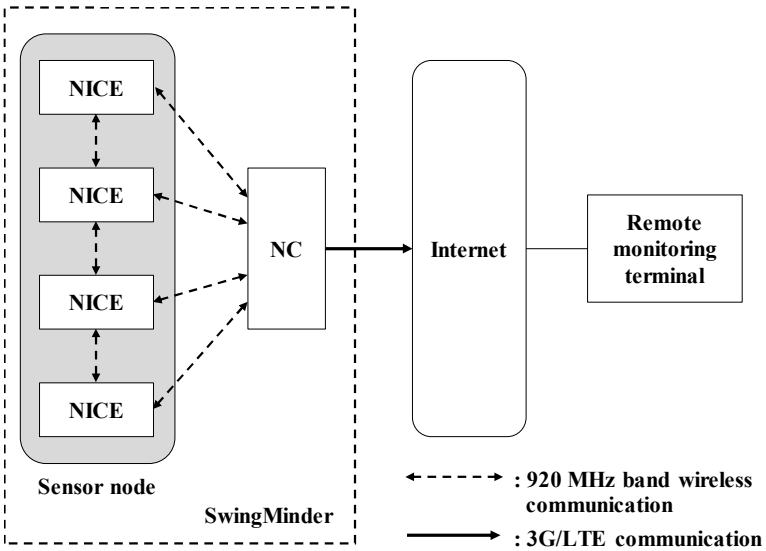


Figure 2. System configuration of SwingMinder

Long-term power outages can be predicted in earthquakes. The emergency power supply in each NICE is two lithium AAA batteries that deteriorate slowly, and these supplement the regular electrical power supply. They will enable each NICE unit to run for about 30 hours in conditions of power outage.

NICE uses ADXL355, a three-axis MEMS accelerometer built by Analog Devices, for its acceleration sensor. The ADXL335 can measure acceleration from 0.1 Gal to 8,000 Gal and registers tilt angles at 0.01° increments. To measure the primary wave, acceleration 10 seconds before the trigger is activated can be also measured. In addition, any acceleration at any time after trigger is released is also measured. The measurement specification of the NICE unit can easily be changed by rewriting the contents of the setting file that is saved on the memory card. The out shape of the NICE's resin case, which contains an MEMS

accelerometer, an MCU, and two lithium AAA batteries, is 125 × 125 × 35 mm and can be installed in narrow space. Table 1 shows the main specifications and performance of the SwingMinder. The acceleration measurement range can be set at ±2 G, ±4 G, or ±8 G, and the sampling frequency can be set at 100 Hz, 200 Hz, or 400Hz. NICEs are powered by 3.3V DC power, converted from power provided by 100 V outlets with an AC adapter.

Table 1. Performance specifications of SwingMinder

Wireless communication module	920 MHz multi-hop method Communication distance: 1000 m Communication speed: A few kbps to about 100kbps
Acceleration sensor	ADXL355 (analog device)
Acceleration measurement range	Set at ±2 G, ±4 G, or ±8 G
Sampling frequency	Set at 100 Hz, 200 Hz, or 400 Hz
Power supply	With AC adapter (DC 3.3 V)
Operating time under conditions of power failure	About 30 hours (on backup built-in AAA lithium battery power source)

2.2 Time Synchronization between NICEs

When each NICE was tested with synchronization provided by the RC transmitter that is standard in an MEMS accelerometer, synchronization error between the NICEs was on the order of 100 milliseconds. Thus, the NICEs could not be synchronized within 5 milliseconds, as is required for simultaneous measurement at multiple points. Therefore, we equipped NICEs with high-precision programmable MEMS transmitters (with an error of 0.002% or less) to allow times to be accurately recorded at arbitrary intervals. In addition, between the NC and each NICE, the time was set at with accurate timing check at every 10 seconds, using the MCU internal time, which was maintained with high accuracy. Thus, the NICEs were designed to be able to synchronize times within ±3 milliseconds, which was below the necessary time increment for acceleration measurement to be performed at a sampling frequency of 200 Hz.

2.3 Data transmission method between NICEs

Using 920 MHz band radio waves, SwingMinder can secure stable communication in buildings. However, because the communication speeds enabled by 920 MHz band radio waves is low, they would require long transmission times for communicating the large amount of data necessary to interpret the variable acceleration time history data for each floor of a building in an earthquake.

To solve this problem, SwingMinder creates acceleration time history data every 10 seconds and transmits them sequentially after acceleration is measured that exceeds the threshold. This evades the disadvantage of the slow communication speeds on the 920 MHz band and enables acceleration time history data to be collected quickly after an earthquake.

2.4 Calibration of NICEs

The MEMS accelerometer used in SwingMinder calculates acceleration by electrically measuring the distance that the weight and silicon springs installed inside the accelerometer move. Because there is a known inherent error of the silicon springs in the accelerometer, an initial calibration of the accelerometer is required for accurate measurement.

We measured gravitational acceleration with 65 MEMS accelerometers without initial calibration and compared them to standard gravity values; this indicated that the maximum error between measured acceleration and standard gravity was about 4.0% in the x-axis, 4.5% in the y-axis, and 13.8% in the z-axis. This showed that unacceptable measurement error is possible if the NICE units are not properly calibrated.

An important factor in measurement error is sensitivity error, which refers to the variation in the slope of the input and output of the transfer function measured at +1 g and −1 g. Another factor is the initial absolute offset, which was measured immediately after manufacture. We calibrated these errors using the two-point calibration method.[5]

With equations (2) and (3), the correction coefficients for the initial absolute offset and sensitivity errors were calculated. Then, using following equation (1), measurement acceleration was corrected. The accelerometer was calibrated using the same method for the y-axis and the z-axis.

$$X = (AX_1 \cdot a/g \cdot b)(X_0 + a \cdot AX_0) \quad (1)$$

$$AX_0 = -(X_1 + X_2)/(2a) \quad (2)$$

$$\mathrm{A}X_1 = 2g/(X_1 - X_2)b \quad (3)$$

X: Measured acceleration after calibration(m/s^2)
X_0: Measured acceleration before calibration(m/s^2)
AX_0: Correction coefficient of initial absolute offset
AX_1: Correction coefficient of sensitivity error
X_1: Measured acceleration upward along the x-axis
X_2: Measurement acceleration downward along the x-axis
a: Measurement resolution of acceleration
b: Integer actor
g: Standard gravity

3 EXPERIMENT TO EVALUTE TIME SYNCHRONIZATION ACCURACY BETWEEN NICE UNITS

3.1 Experimental method

To evaluate the time synchronization accuracy between the NICEs, a simultaneous excitation experiment of 10 units was conducted using a two-axis shaking table. Figure 3 shows the experimental setup. First, 10 NICE (NICE00 to NICE09) were fixed to a wooden board with screws. Next, the wooden board was fastened to the shaking table with bolts, so that the NICEs and the shaking table could be vibrated together. Then, the table was vibrated using the input waves shown in Table 2, and the acceleration of the shaking table was measured by the units. The excitation was conducted in the direction shown in Figure 3, set to the x and y directions. The sampling frequency of the NICE was set to 200 Hz, which is generally used for observation of seismic motion.

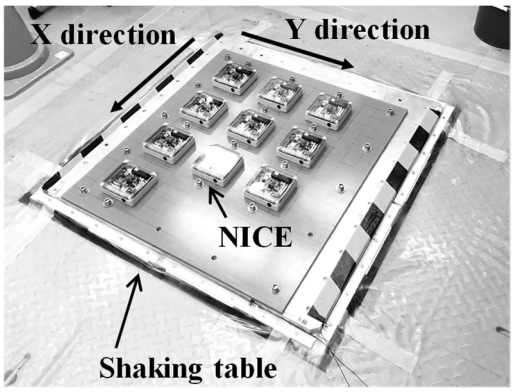


Figure 3. Experimental situation

Table 2. Excitation case

case	Input wave	Direction	Amplitude (mm)	Frequency (Hz)	Number of data
1-1	Sine wave	X	10.1	2	1024
1-2	Sine wave	X	10.1	5	1024
1-3	Sine wave	Y	10.1	2	1024
1-4	Sine wave	Y	10.1	5	1024
1-5	Sweep wave	X	2	0.1 - 20	4096
1-6	Sweep wave	X	2	20 - 0.1	4096
1-7	Sweep wave	Y	2	0.1 - 20	4096
1-8	Sweep wave	Y	2	20 - 0.1	4096

3.2 Results of the experiment

In cases 1-1 to 1-4, the time synchronization accuracy was evaluated using 1024 pieces of data where the sine wave was in a steady state for the time history data of each case. In cases 1-5 to 1-8, the time synchronization accuracy was evaluated using 4096 data, where clear sweep vibration was measured in the time history data of each case. Table 2 shows the number of data used for analysis in each case.

To quantitatively evaluate the time synchronization accuracy between each NICE, the time lag of the measurement acceleration was calculated for each frequency. The time lag between the NICE units can be evaluated by calculating the phase differences of the transfer functions of each NICE, relative to the reference NICE, using FFT. Equation (4) shows the relationship between the frequency and the period. Equation (5) shows the relationship between the phase differences and the time lag, such that by combining equations (4) and (5), we obtain equation (6), which shows that if there is a time lag between NICE, the phase difference changes with the frequency. Here, the phase difference is calculated by passing a straight line through the origin and assigning to each frequency slope of the time lag times 360. If there is no time lag, the phase difference is 0°.

$$f = 1/T \tag{4}$$

$$\theta = t_d/T \cdot 360 \tag{5}$$

$$\theta = 360 \cdot t_d \cdot f \tag{6}$$

f: Frequency (Hz)
T: Period (second)
θ: Phase difference (degree)
t_d: Time lag (second)

Figure 4 shows a representative analytical result for all excitation cases, with the amplitude and phase difference of the transfer functions of the acceleration measured by NICE09, relative to the one measured by NICE00. The horizontal axes of the graphs in Figure 4 show frequency, and the vertical axes show amplitude and phase differences. The results are shown up to the frequency of 20 Hz, the target for seismic response evaluation of buildings. In the graphs, the phase differences for time lags of ±3 milliseconds are shown with dotted lines. The time lag is found to be within the ±3 milliseconds set as the performance target because the phase difference is generally within the dotted lines in all excitation cases. Additionally, the same acceleration can be measured by each NICE unit because the amplitude of the

transfer function is approximately 1.0. The results of these tests suggest that each NICE unit produces highly accurate time synchronization.

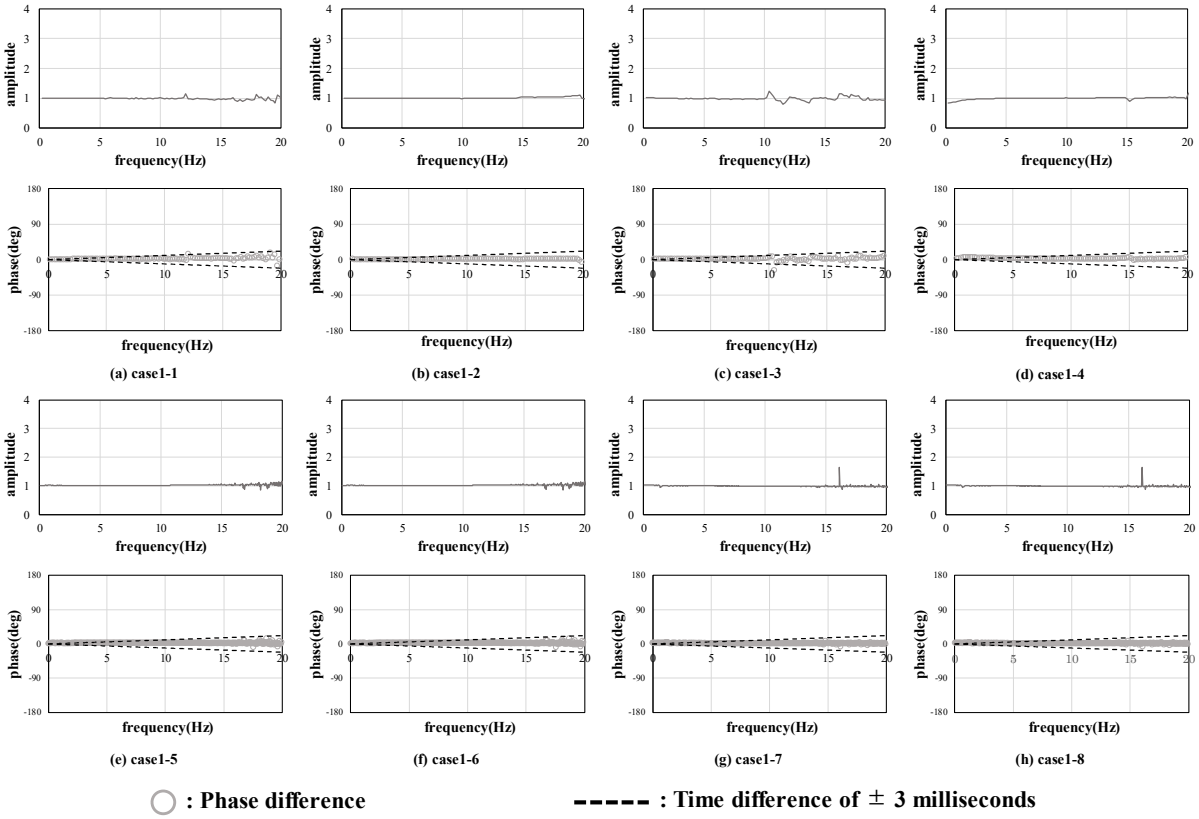


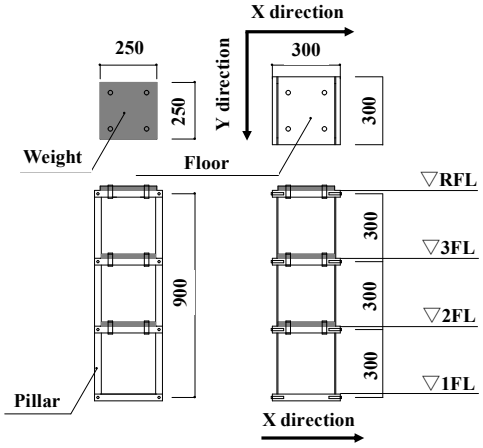
Figure 4. Transfer function between NICE00 and NICE09 (top: amplitude bottom: phase difference)

4 EXPERIMENT TO EVALUTE ACCELERATION MEASUREMENT ACCURACY OF NICE

4.1 Method of experiment

This chapter describes the contents and results of the excitation experiment used to simulate building motion in a simple three-layer model, conducted to evaluate the acceleration measurement accuracy of SwingMinder in structures. We created the three-layer model shown in Figure 5, which consisted of four square floors, with a length of 300 mm and a thickness of 30 mm, and four pillars, with a width of 30 mm, a thickness of 4.5 mm, and a height of 930 mm. The floors and pillars were made of aluminum, and each floor was equipped with an iron weight with a length of 250 mm, and a thickness of 18 mm to change the model weight. Four NICE units were installed on each floor of the model, which was placed on the shaking table, and one NICE was installed on table itself. Then, the table was vibrated, and the response acceleration on each floor was measured using the NICEs. Additionally, to provide the reference values for the measured acceleration, calibrated reference accelerometers were also installed on each floor, and the response acceleration was measured with the reference accelerometer. The measurement accuracy of the NICEs was

evaluated by comparing their results with acceleration measured by the reference accelerometer. The reference accelerometer measured acceleration at a sampling frequency of 240 Hz, and the NICE measured at a frequency of 200 Hz. Table 3 shows the excitation cases, and input waves were input in the x direction, as shown in Figure 5.



Total height (mm)	930
Total weight (kg)	58.6
Fundamental natural period (s)	0.299
Member material	Aluminum
Weight material	Steel

Figure 5. Outline drawing of the experimental model

Table 3. Excitation case

Case	Input wave	Amplitude (mm)	Frequency (Hz)	Duration (s)
2-1	Sweep wave	0.5	0.1–10	40
2-2	Sweep wave	0.5	10–0.1	40

4.2 Results of experiment

The sampling frequency of the acceleration measured by the reference accelerometers was converted from 240 Hz to 200 Hz and compared with to that measured by the NICEs. To confirm the effects of the conversion of the sampling frequency on the results, the difference between the maximum measured acceleration before and after conversion was compared. The maximum difference was 0.11 m/s^2, and the ratio of the maximum difference divided by the maximum acceleration before the conversion was 0.8%. These results suggest that the conversion of the sampling frequency had little effect on the comparison results.

Figure 6 shows the acceleration of each floor for each excitation case, measured simultaneously by a NICE and the reference accelerometer. The horizontal axis for each graph in Figure 6 shows the acceleration measured by a NICE, and the vertical axis shows the acceleration measured by the reference accelerometer. The solid line in each graph is a reference line representing the coincidence of acceleration. In each excitation case, the accelerations measured by the NICE and the reference accelerometer are plotted near the reference line. This finding suggests that the accelerations measured by the NICE and the reference acceleration are approximately equal. When SwingMinder is used as the acceleration measurement system in buildings, it is essential that it accurately measures the maximum acceleration in the building to enable proper seismic analysis.

Figure 7 gives a comparison of the maximum acceleration of each floor, as measured by

NICE and the reference accelerometer. The difference between the measurements was 0.41 m/s^2 on the rooftop. The difference between the results, divided by the maximum acceleration measured by the NICEs, was 2.97%. This shows that the difference is small compared with the measured value, and that the measurement accuracy of SwingMinder is equivalent to that of a wired accelerometer.

This suggests that SwingMinder has sufficient measurement accuracy to be used as an acceleration measurement system in buildings.

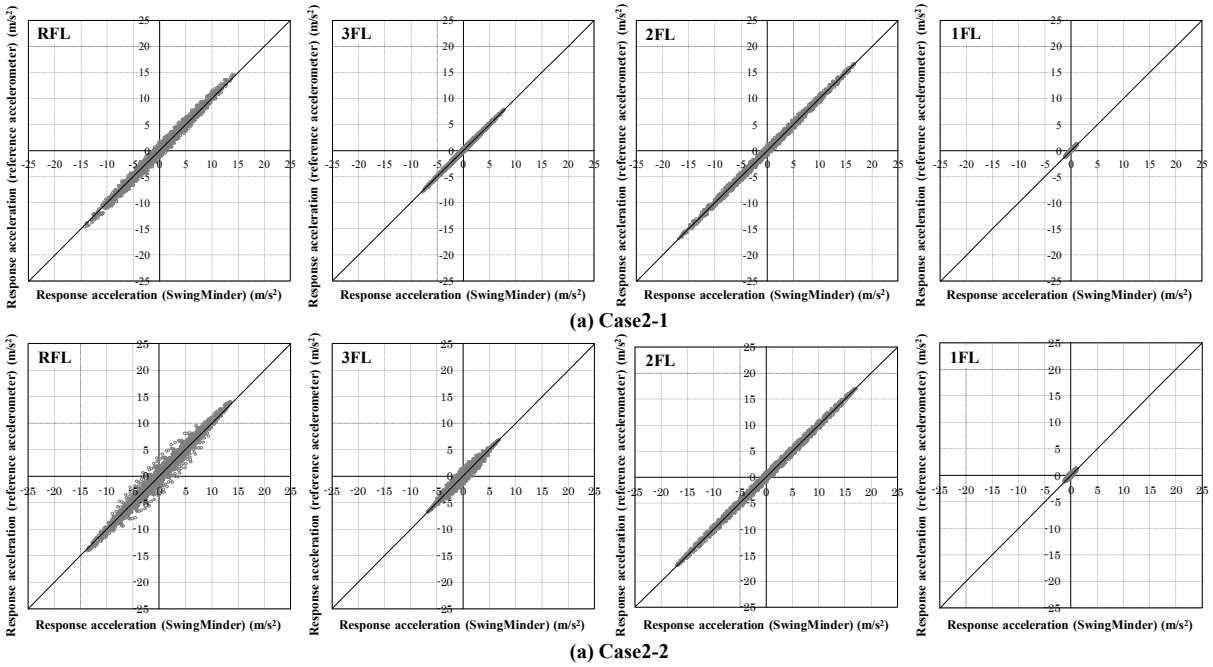


Figure 6. Comparison of response acceleration between NICE and reference accelerometer

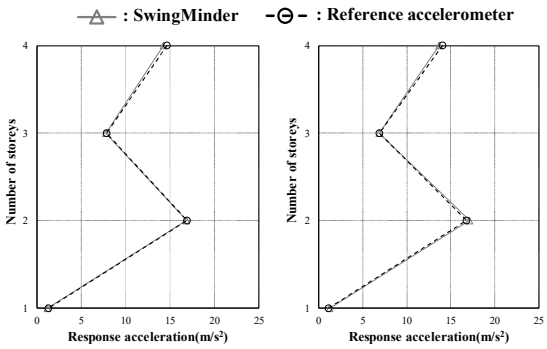


Figure 7. Comparison of maximum response acceleration (left, case 2-1; right, case 2-2)

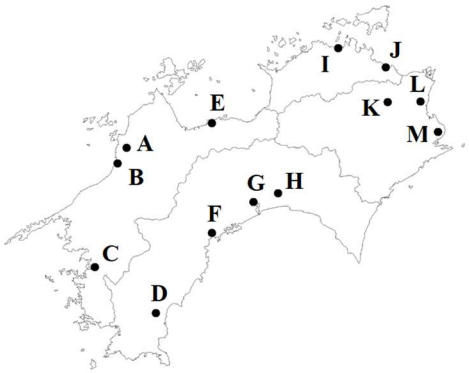
5 VERIFICATION OF USABILITY IN ACTUAL BUILDINGS

5.1 Verification method

The experiments reported above showed that SwingMinder can be used as a wireless

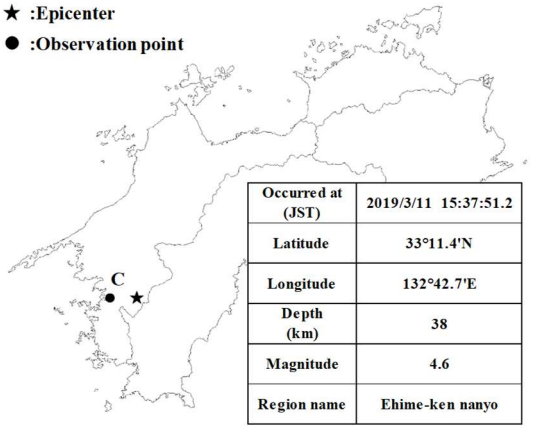
acceleration measurement system. We also confirmed the usability of the SwingMinder system in actual buildings by installing it in 13 office buildings in the Shikoku region of Japan conducting earthquake observation. Figure 8 shows the specifications and locations of 13 buildings where seismic observation was conducted. NICEs were installed on each floor, and seismic observation was conducted after the communication between the NICE and NC began. The sampling frequency of the NICE was 200 Hz, and the threshold for beginning the acceleration recording was 0.05 m/s^2.

The acceleration data were recorded in some buildings shown in Figure 8 where earthquakes occurred in the Shikoku region during the observations. For example, an earthquake was observed at 15:37 on March 11 in Nanyo, Ehime Prefecture. The record was measured at Building C, and Figure 9 shows the earthquake information and the positional relationships between the epicenter and Building C. Building C is a seven-story reinforced concrete building, and NICEs were installed on each floor, with the NC installed on the rooftop.



Building name	Number of storeys	Structure
A	9	Reinforced concrete building
B	3	Reinforced concrete building
C	7	Steel reinforced concrete building
D	7	Steel building
E	6	Reinforced concrete building
F	2	Steel building
G	8	Steel reinforced concrete building
H	2	Steel building
I	7	Steel building
J	3	Reinforced concrete building
K	2	Reinforced concrete building
L	10	Steel reinforced concrete building
M	3	Steel building

Figure 8. Target buildings used for verification



Occurred at (JST)	2019/3/11 15:37:51.2
Latitude	33°11.4'N
Longitude	132°42.7'E
Depth (km)	38
Magnitude	4.6
Region name	Ehime-ken nanyo

Figure 9. Epicenter information and observation points

5.2 Verification results

After SwingMinder was installed in Building C, we confirmed that the communication path between the NC and NICE units was open. In the time synchronization program of

SwingMinder, the time synchronization accuracy, as shown in section 3, was ensured by checking the status of the time synchronization using feedback signals between the NC and NICEs at regular intervals. Here, where the communication path between NC and NICE was open, we determined that time synchronization accuracy within ±3 milliseconds was secured in Building C. Figure 10 shows the observation records for this building.

In Figure 10, the acceleration data for the x (east–west), y (north–south), and z (vertical) directions are shown, as measured without loss from all NICEs, from the first floor to the rooftop. Additionally, it was confirmed that the absolute value of the maximum acceleration increased progressively from lower to upper floors. In the case of the given earthquake, all the observation records were collected via the Internet from Kagawa Prefecture, which is remote from the building in Ehime Prefecture, approximately 10 minutes after the earthquake. The acceleration measurement accuracy of SwingMinder is founded on the accuracy of the MEMS accelerometer. Therefore, where NICEs are operating normally and acceleration measurement is possible, as in this verification, measurement records were collected with the acceleration measurement accuracy shown in section 5.

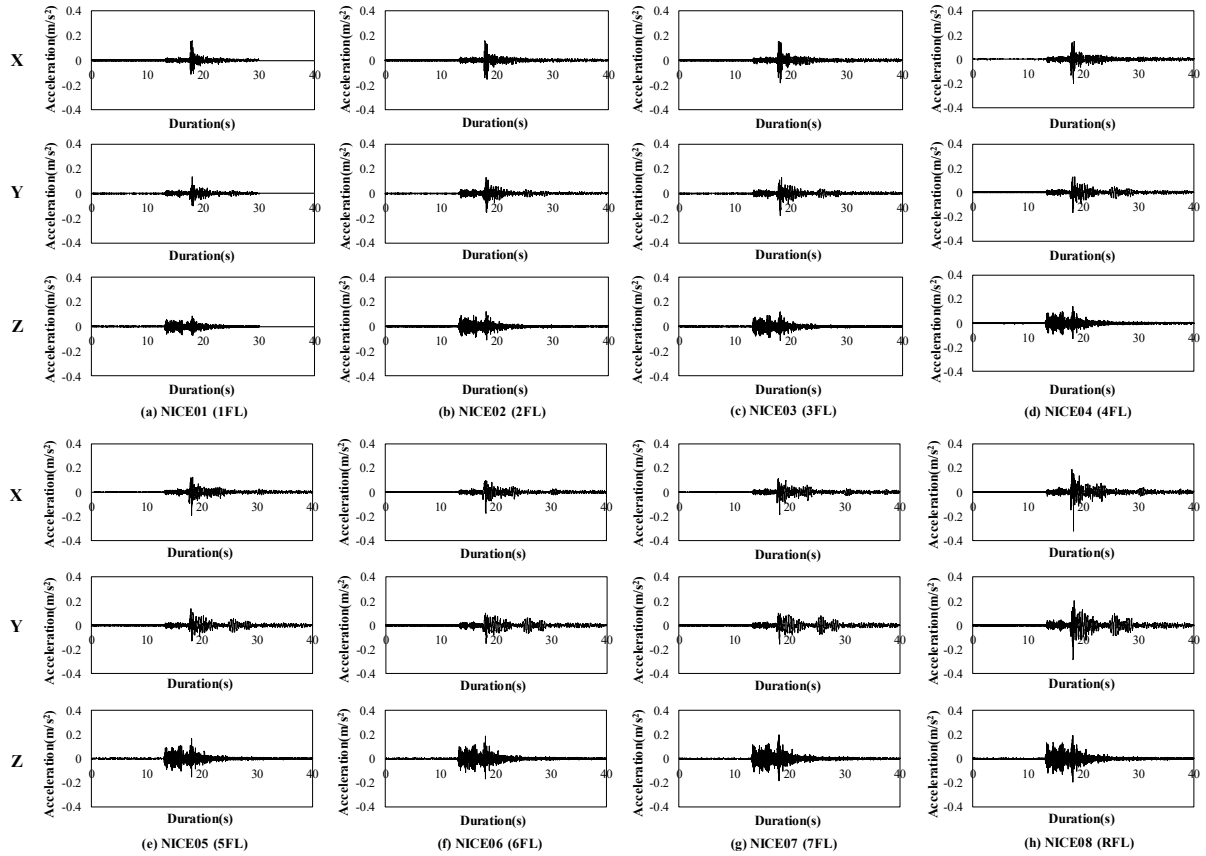


Figure 10. Observed acceleration time history for each floor in Building C

These results show SwingMinder is usable as an acceleration measurement system in actual buildings.

6 CONCLUSIONS

This study developed a commercial wireless acceleration measurement system with high time synchronization accuracy and stable communication capabilities within buildings, called SwingMinder. Verification tests were conducted on its synchronization and measurement accuracy and its usability in actual buildings, and the results are presented here. The following findings were obtained.

- SwingMinder has high time synchronization accuracy, with a time lag of each NICE within ±3 milliseconds.
- The maximum measurement error between SwingMinder and the wired accelerometer was 2.97%, indicating that SwingMinder's measurement accuracy matched that of the wired accelerometer.
- The usability of the acceleration measurement system in actual buildings was verified, and the measured acceleration of the buildings was collected in a location that is remote from where the earthquake occurred.

These findings indicate that SwingMinder can be used as a wireless acceleration measurement system in actual reinforced concrete or steel buildings.

SwingMinder is also installed in traditional Japanese traditional buildings, and seismic observations have been carried out for the purpose of structural analysis. In the future, SwingMinder is expected to be used in more traditional Japanese buildings and other structures to provide seismic analysis and monitoring of structural health.

Acknowledgments. We are grateful to Y. Nakanishi for the development of SwingMinder. We are also grateful to N. Kotake and R. Fukuda for their assistance in the excitation experiments.

REFERENCES

[1] Cultural Properties Protection Department, *Guideline for Assessing Seismic Resistance of Important Cultural Properties (Buildings)*, (2012).

[2] Nagai, N., Mita, A., Yakoh, T. and Sato, T.: *Wireless Sensor for Structural Health Monitoring,* Journal of Japan Association for Earthquake Engineering, Vol.3, No.4 (2003), pp.1-13.

[3] Sawada, M., Shiba, Y. and Oguni, K.: *Development of robust time synchronization method for wireless sensor network*, Journal of Japan Society of Civil Engineers A1 (Structural Engineering & Earthquake Engineering), Vol.65, No.1 (2009), pp.30-37.

[4] Nakannishi, Y.: *Development and operation of the practical field monitoring systems based on openATOMS*, Proceedings of Annual Conference of Electronics, Information and Systems Society (2011), pp.724-727.

[5] Allen Fan: *How to Improve the Accuracy of Inclination Measurement Using An accelerometer*, AnalogDialogue, Vol.52 (2018), Analog Devices.

[6] Takahiro Yamasaki, Yuichiro Amano, Kana Ota, Mitsuhiro Miyamoto and Masatoshi Okada: *Development of wireless acceleration measurement system applied to structural health monitoring – Consideration for introduction to existing buildings* -, Journal of Structural and Construction Engineering (Transactions of AIJ), Vol.84, No.765, pp.1389-1399. (2019.11)

12th International Conference on Structural Analysis of Historical Constructions
SAHC 2020
P. Roca, L. Pelà and C. Molins (Eds.)

DYNAMIC IDENTIFICATION OF THE SO-CALLED TEMPLE OF MINERVA MEDICA: COMPARISON OF DIFFERENT INSTRUMENTATIONS AND METHODS FOR MUTUAL VALIDATION OF THE RESULTS

C. BAGGIO[1], V. SABBATINI[1*], S. SANTINI[1], C. SEBASTIANI [1]

V. FIORITI[2], I. ROSELLI[2], A. COLUCCI[2], F. SAITTA[2], S. FORLITI[2]

[1]Roma Tre University, Department of Architecture
Largo Giovanni Battista Marzi 10, 00153, Rome, Italy
Email: valerio.sabbatini@uniroma3.it (*corresponding author)

[2]ENEA
Casaccia Research Center,
Via Anguillarese 301, Rome, Italy

Keywords: Historical Structure, Masonry, Operational Modal Analysis, Dynamic Identification, Non-Destructive Inspection, Accelerometer vs Velocimeter

Abstract. *Dynamic monitoring is a well-established technique used to gain information on the global health of constructions. In particular, ambient vibration tests have achieved important results in the dynamic characterization of modal parameters. Several techniques and instrumentations are currently available, however the accuracy of these results is often unquestioned. The mutual validation between different modal analysis techniques is an important procedure to assess the reliability of the results. In the present paper the ambient vibration tests performed on the so-called 'Temple of Minerva Medica' in Rome considering different techniques and instrumentations will be described and compared. While it is referred to as the Temple of Minerva Medica, the structure is actually a ruined decagonal nymphaeum in opus latericium that dates to the 4th century AD. Today, the construction is located between the main central train station (Roma Termini) and the local tram way. Ambient vibration data were acquired during different campaigns [1] to characterize the effects of the vibrations and the modal parameters of the structure. This work deals with the data collected on the 11th of July 2019 within the project "Tecnologie per il miglioramento della Sicurezza e la ricostruzione dei centri Storici in area sismica" coordinated by DTC Lazio (Distretto Tecnologico beni e attività culturali). The instrumentation comprised of several seismographs equipped with triaxial velocimeters and piezoelectric accelerometers. A variety of techniques were applied to process the acquired vibration data in order to extract the modal parameters of the studied structure including PolyMAX, FDD, EFDD, CC-SSI, HVSR and FRF. Comparison of the modal parameters obtained by each different technique was considered to provide indications on the reliability of the instruments.*

1 INTRODUCTION

The accurate and reliable characterization of structures and materials provides crucial information in the restoration and conservation of historic constructions. In recent years, Structural Health Monitoring has had extraordinary success due to the sustainability of its techniques and the relevance of its results. Dynamic identification is a well-established technique; its results play a significant role in the prediction of the seismic response of the construction and they are commonly used as reference to update material properties and boundary conditions of complex numerical models [2]. However, the reliability of the results is subject to several uncertainties related to the acquisition and processing of data.

In the present paper through the case study of the so-called Temple of Minerva Medica located in Rome, different dynamic identification techniques and instruments are presented and compared in order to evaluate the accuracy and efficacy of the results.

2 THE SO-CALLED TEMPLE OF MINERVA MEDICA IN ROME

The construction, built in the early 4th century, was originally a *nymphaeum* in the *Horti Liciniani*. The name "Temple of Minerva Medica" dates back to the 16th century and it originated as an incorrect interpretation by Pirro Ligorio following the discovery of a statue of "*Minerva con dracone*" in the surrounding area [3]. The main hall of the complex has a decagonal polylobate plan with a diameter of 25 m and two orders of arcades with an overall height of 32 m, today reduced to 24 m after the partial collapse of the dome in 1828 [4].

The structure was initially constructed with *opus latericium*; interventions in *opus mixtum* of tuff and Roman bricks were carried out over the centuries; in particular, the openings in the niches were closed and two buttresses were added on the southeast side (Figure 1). In 1846, the lower arcade of the southeast side was reconstructed, while the upper arcade was completed in 2013 [5].

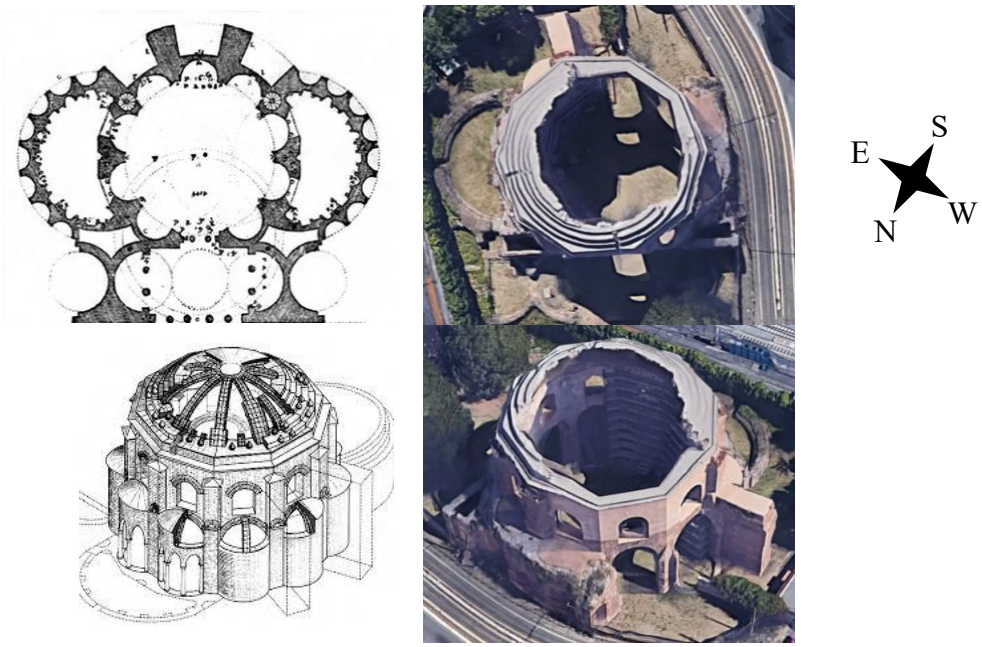


Figure 1: Possible original configuration [6] (left) and current condition (right) of the so-called Temple of Minerva Medica plan view (top) and perspective view from South (bottom)

3 THE EXPERIMENTAL CAMPAIGN

While several experimental campaigns were carried out on the Temple of Minerva Medica [7] [8] [9], this work deals with the data collected on the 11th of July 2019 within the project "Tecnologie per il miglioramento della Sicurezza e la ricostruzione dei centri Storici in area sismica" coordinated by DTC Lazio (Distretto Tecnologico beni e attività culturali).
Different sets of data were recorded considering two different types of instrumentations as shown in Figure 2.

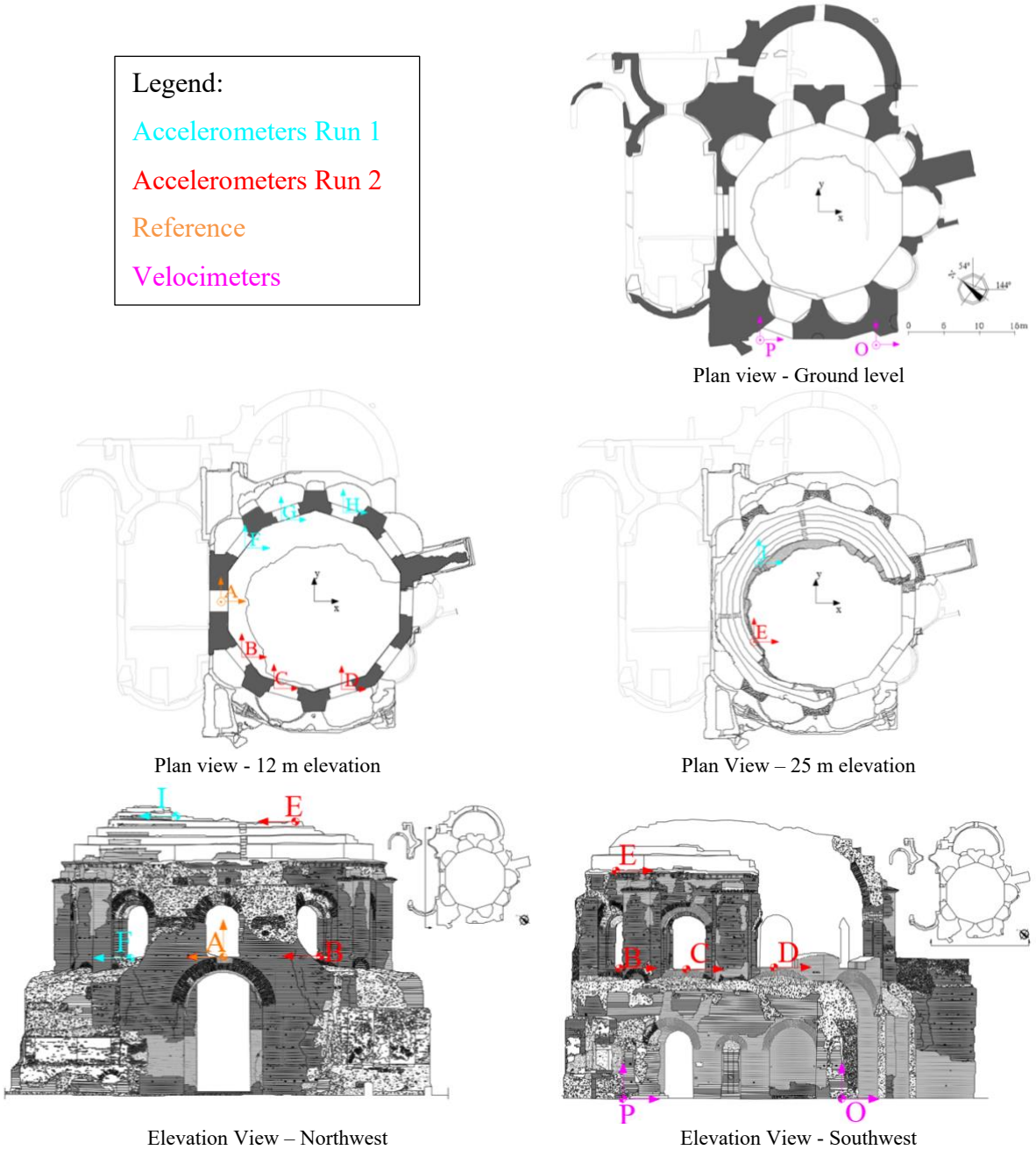


Figure 2: Sensors positions and directions, both triaxial accelerometer and velocimeter were located in the reference position A

3.1 Accelerometers

Twelve ICP piezoelectric monoaxial accelerometers (10 V/g sensitivity, measure range ± 0.5g, frequency range from 0.15 to 1000 Hz and 8μg rms resolution) were positioned on 5 different locations per run, cubical metal supports were used to orient the sensors according to a global reference system (Y-axis oriented 54° clockwise from North). Two runs of accelerations were recorded, each one for a period of approximately 45 minutes, only one location was kept unvaried (A) as reference for the merging process. Data were acquired from approximately 10:00 AM to 4:00 PM (local time).

3.2 Velocimeters

Three seismometers were located in positions A, P and O. They are SL06 SARA Instruments digital recorders equipped with SS02 triaxial velocimeters. Each seismograph is independent and provided with battery for the energy supply and with a GPS antenna for synchronization to the U.T.C. time so that data from different instruments can be compared in the time domain. This instrumentation is generally used for measuring very low vibrations, such as seismic monitoring for the characterization of soil amplification and microzonation applications. It has sensitivity of 400 V/m/s and frequency range from 0.2 to 50 Hz. In the present work sampling frequency was set at 200 Hz. Data were acquired from 9:50 a.m. to 12:50 a.m. (local time). The seismographs were oriented with the same X, Y, Z directions as the accelerometers (see previous sub-section 3.1) in order to make data comparison easier.

3.3 Air temperature and humidity

In order to take account of the effect of the environmental conditions that might affect the dynamic behavior of the studied structure, also micro-climatic parameters were measured. In particular, air temperature and relative humidity were recorded through two data-loggers, equipped with thermometer and humidity sensor, positioned at the Northeast and Southwest sides of the monument. The effect of wind was neglected, as, according to local meteorological station, average wind speed was 10 km/h corresponding to light breeze, as defined by Beaufort scale (or Beaufort number 2), during ambient vibration acquisition.

4 PROCESSING AND RESULTS

4.1 Multi-run Operational Modal Analysis (accelerometers)

The Temple of Minerva Medica is strongly affected by the vibrations caused by the local tram, the nearby train railway, and the vehicular traffic [9]. Moreover, the wind action, whose intensity was mostly constant during the acquisition, allows the assumption of zero Mean Gaussian white noise excitations, suitable for output only modal analysis [10].

The accelerometer measurements were recorded with a sampling frequency of 441Hz and subsequently resampled to 60Hz according to the significant frequency band of the building, the data was filtered with low cut frequency of 0.2 Hz and high cut of 30 Hz and then the Cross-spectra were calculated with 1024 time lags and 1% windowing.

Modal parameters were extracted through PolyMAX algorithm implemented in the software Simcenter Testlab [11]. PolyMAX is based on a common-denominator transfer function model,

the Cross-spectra are processed in a complex polynomial rational function, whose grade represents the order of the model and the zeros of the denominator the poles that identify the modes of vibration of the system [12].

The extracted modal frequencies from the two sets of accelerations are reported in Table 1.

Table 1 Modal frequencies from the acceleration measurements

Run 1		Run 2	
Frequency [Hz]	Damping [%]	Frequency [Hz]	Damping [%]
2.064	0.93	2.054	0.36
2.455	1.44	-	-
2.579	1.31	-	-
2.780	1.98	2.765	1.01
3.598	1.49	3.601	0.89

The last step is to combine and scale the extracted modes to obtain the global modal parameters of the construction. The target modes were selected based on the optimum validation parameters (Modal Assurance Criterion, Modal Phase Collinearity, Mean Phase Deviation) [13]. The merging process is performed in accordance with MAC correspondence in band; the mapping between the target and the merged modes considers MAC correspondence according to the three common DOF (Reference node A). Finally, the modes were scaled considering (1).

$$Scale\ Factor = \sum_i \frac{\varphi_t(i)^* \cdot \varphi(i)}{\varphi_t(i)^* \cdot \varphi_t(i)} \quad (1)$$

$\varphi_t(i)$: ith common mode shape value of the target mode
$\varphi(i)$: ith common mode shape value of the mode to be merged
* denotes the conjugated value

The recorded data of Run 1 returned more accurate validation parameters, for this reason the modal frequencies and damping of Run1 were identified as final quantities, however the merging and scaling process of the modal shapes combined both the acquisitions with the following results.

The 1st mode expresses a global translational in the NW-SE direction.

The 2nd and 3rd modes identify the northwestern and the northeastern portion of the temple due to the only reliability of Run 1: the 2nd mode expresses a translational mode in the North direction coupled with a slight II order bending mode in the NW-SE direction, the 3rd mode expresses a main translational mode in the NE-SW direction with a small vertical component for the top of the construction.

The 4th mode expresses two coupled bending modes in the NW-SE and NE-SW direction basically a torsional mode.

The 5th mode is mostly translational in the NW-SE direction with II order bending component in the NE-SW direction for the northern portion of the temple.

The modal parameters and its main features are summarized in Figure 3.

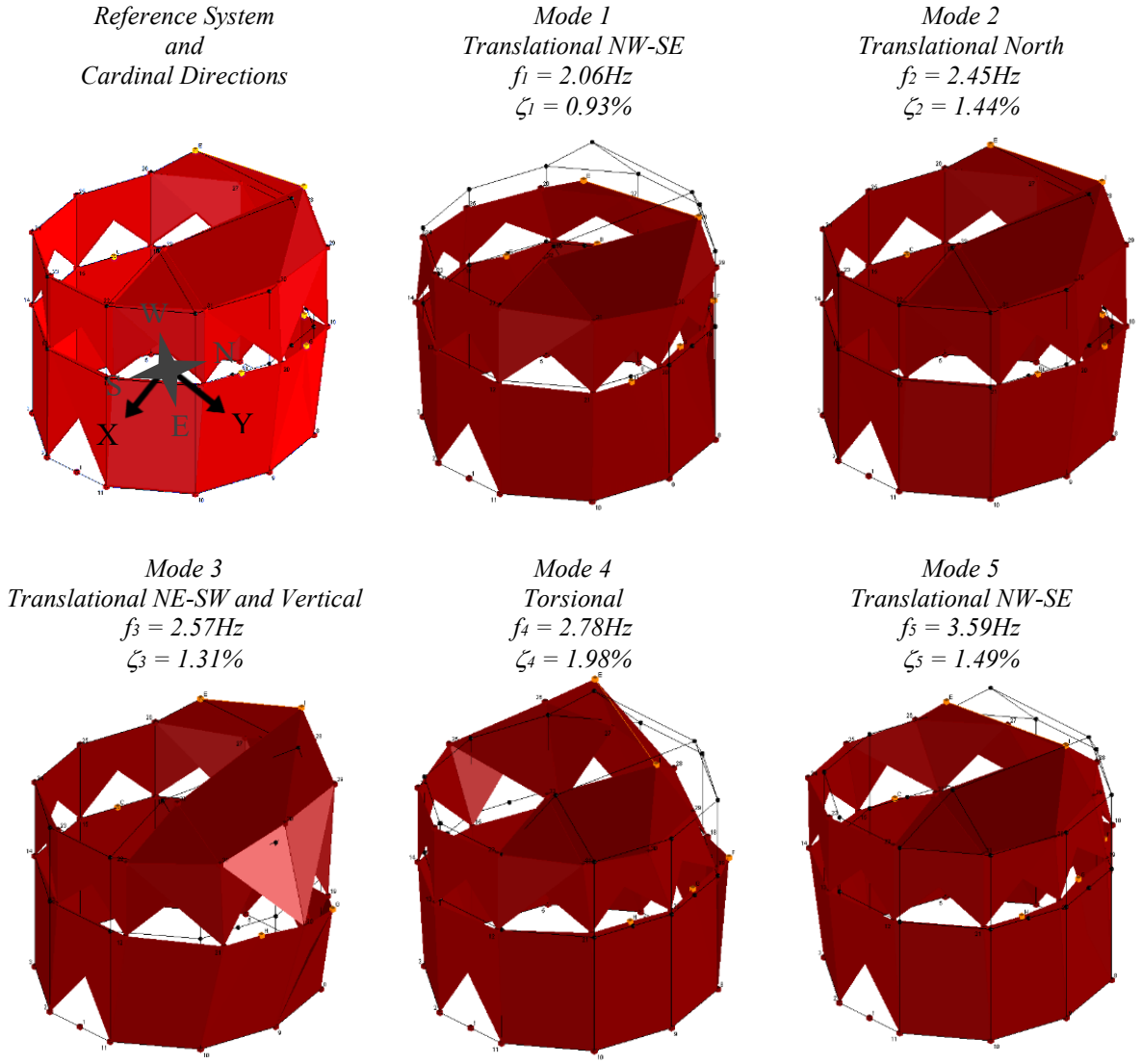


Figure 3: Extracted Modal Parameters

4.2 Experimental and Operational Modal Analysis (velocimeters)

Only velocimeters data acquired in late morning (after 12:00 a.m.) were considered in order to obtain results at environmental conditions comparable with the ones from accelerometers, which were acquired in the early afternoon. The measured air temperature at midday was 27-28° C, while the peak temperature in the afternoon was 29° C.

The pre-processing procedure already applies low-pass filtering of data and conversion to velocity values. However, as the velocimeters mounted on the utilized seismographs provide affordable measurements for vibration frequencies higher than 0.2 Hz, a high-pass band filter at 0.3 Hz was also applied.

The data were then processed with a variety of modal analysis methods. In particular, the Frequency Response Function (FRF) of position A (output signal on the elevated structure) with respect to positions P and O (input signal at ground level) was obtained (Figure 7). FRF

was computed through an algorithm based on the H_1 transmissibility function, which considers the cross-correlation of input and output signals at the numerator [14].

The triaxial signals of position A were processed to provide also the Horizontal-to-Vertical Spectral Ratio (HVSR) [15]. This was obtained by computing the ratio between the Power Spectral Density (PSD) of the horizontal components of the signals with respect to the vertical component (Figure 7).

Several output-only (OMA) techniques were applied. In particular, the Frequency Domain Decomposition (FDD), Enhanced Frequency Domain Decomposition (EFDD) and Crystal Clear Stochastic Subspace Identification (CC-SSI). As OMA methods assume that data provide white-noise low-intensity signals coming from random ambient vibration, the recordings were pre-treated in order to exclude the signal during tram passages, which induced strong vibration and might not be assumed as white-noise. Some examples of OMA analyses are shown in Figure 8.

The above analyses focused on detecting the first 5 modes of the monument.

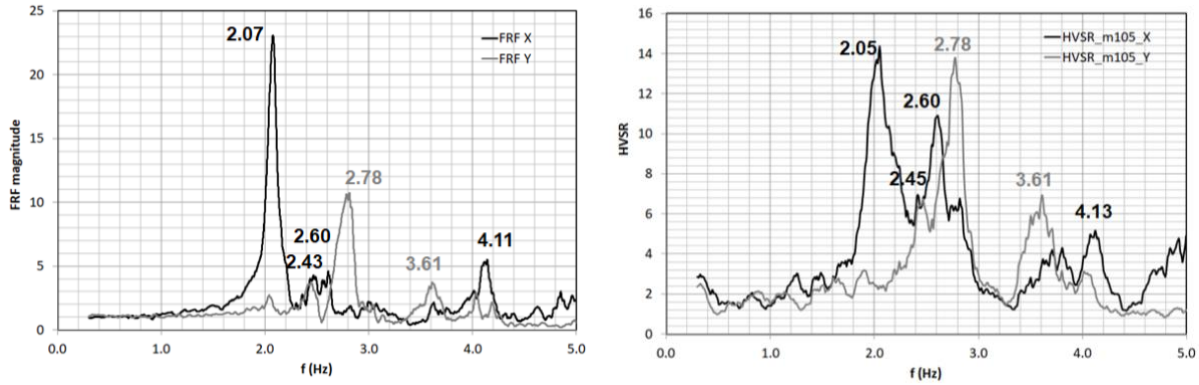


Figure 7: Identification of the modal frequencies by detecting the peaks in the FRF (left) and HVSR functions (right) in both X (black line) and Y (grey line) directions.

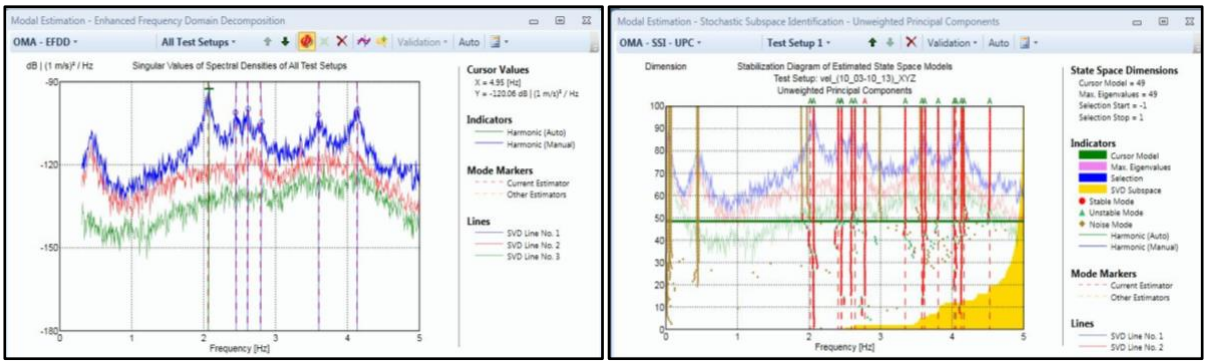


Figure 8: Identification of the modal frequencies by EFDD (left) and CC-SSI (right) techniques.

5 DISCUSSION

5.1 Finite element model

An additional comparison of the experimental results was accounted by considering a finite element model (FEM) using the commercial software Midas Gen [16].

A fixed based model with a total number of 72980 solid elements and 19457 nodes have been adopted; the material has been modeled as homogeneous and isotropic with the following parameters: unit weight of 18 kN/m3, Poisson ratio of 0.2 and 744 MPa of Young modulus.

The presented model was obtained by updating the initial value of the masonry (starting from the reference values of the Italian Code [17]), in order to achieve a sufficient match with the experimental frequencies. The results in terms of frequency and vibration modes are reported in Figure 4.

Mode	Frequencies [Hz]
1	2.070
2	2.392
3	2.466
4	2.628
5	3.494

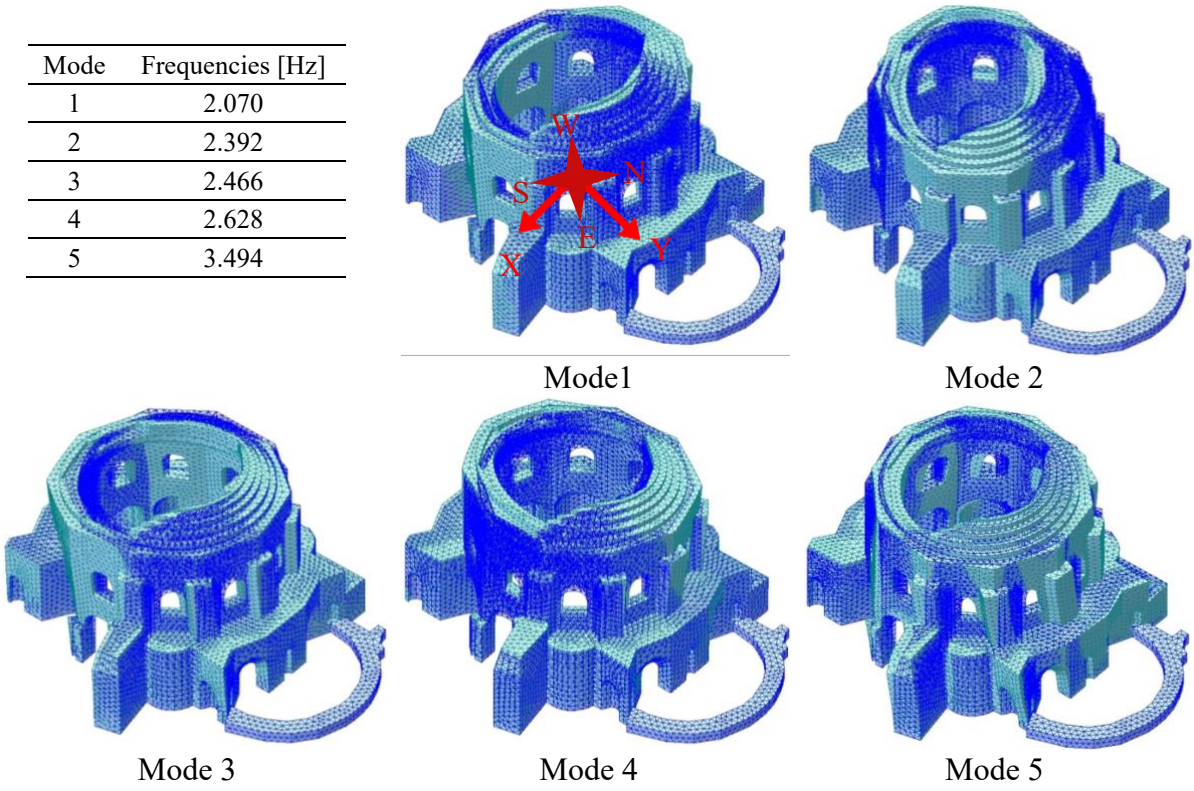


Figure 4 Numerical Vibration Modes

5.2 Comparison

The results from both the instrumentations and the different processing methods show an accurate correspondence of the modal frequencies with extremely small coefficient of variation and stable deviation standard between 0.009 and 0.012 Hz as reported in Table 2.

Table 2 Modal Frequencies comparison

	Experimental									Numerical
	Frequency [Hz]						Statistics			Frequency
Mode	PolyMAX	FDD	EFDD	CC-SSI	HVSR	FRF	Average [Hz]	Standard Dev. [Hz]	Coefficient Variation	MidasGen
1	2.064	2.080	2.060	2.060	2.050	2.070	2.064	0.010	0.494 %	2.070
2	2.455	2.440	2.450	2.450	2.450	2.430	2.446	0.009	0.375 %	2.392
3	2.579	2.610	2.610	2.590	2.600	2.600	2.598	0.012	0.462 %	2.466
4	2.780	2.810	2.790	2.780	2.780	2.780	2.787	0.012	0.435 %	2.628
5	3.598	3.590	3.600	3.580	3.610	3.610	3.598	0.012	0.324 %	3.494

By considering the average experimental frequencies as reference, the EFDD method return the most accurate results with an average frequency error of 0.20%, followed by PolyMAX (0.27%), CC-SSI (0.28%), HVSR (0.30%), FRF (0.32%) and FDD (0.51%). However, if the errors of mode 2 and 3 are excluded from the calculation, the average error of PolyMAX lows to 0.08% followed by EFDD with 0.12%; this analysis confirms the small discrepancy of 2nd and 3rd mode of vibrations identified by PolyMAX, this could be related to the difficulties in the validation of these frequencies in Run 2. In terms of frequency, the numerical model returned a sufficient correspondence with the experimental values, as a consequence, it can be performed a qualitative comparison with the experimental values in terms of modal displacements.

A rigorous comparison between the modal shapes of the different methods and instrumentations was not possible since the accelerometers spatial configuration provided a much more accurate description of the overall modal displacements; however, the normalized modal displacements of the common reference position “A” was considered to relate the different results.

A simple statistical analysis was performed to compare the modal displacements resulted from the different processing of the velocimeter acquisition (Table 3). The velocimeter modal displacements returned more dispersed values than its frequency results as expressed by the coefficients of variation in Table 4; its average was considered enough representative to compare the displacements with the accelerometer and FEM values.

Table 3 Different processing of velocimeter modal displacements

	FDD		EFDD		CC-SSI		HVSR		FRF	
Modes	X	Y	X	Y	X	Y	X	Y	X	Y
1	84%	16%	82%	18%	90%	10%	86%	14%	90%	10%
2	46%	-54%	49%	-51%	46%	-54%	52%	-48%	53%	-47%
3	53%	47%	51%	49%	41%	59%	62%	38%	68%	32%
4	24%	76%	33%	67%	25%	75%	31%	69%	16%	84%
5	-27%	73%	-27%	73%	-32%	68%	-35%	65%	-40%	60%

Table 4 Different instruments modal displacements

	FEM		Accelerometer		Velocimeter					
	MidasGen		PolyMAX		Average		Standard Deviation		Coefficient Variation	
Modes	X	Y	X	Y	X	Y	X	Y	X	Y
1	97.6%	-2.4%	96.2%	-3.8%	86.4%	13.6%	3.6%		4.1%	26.3%
2	-3.6%	-96.4%	-8.9%	-91.1%	49.2%	-50.8%	3.3%		6.6%	6.4%
3	-77.4%	-22.6%	-7.9%	-92.1%	55.0%	45.0%	10.4%		18.9%	23.1%
4	37.3%	-62.7%	50.6%	49.4%	25.8%	74.2%	6.7%		25.9%	9.0%
5	5.1%	94.9%	0.4%	99.6%	-32.2%	67.8%	5.5%		17.2%	8.2%

MAC [13] was calculated to evaluate the agreement of each mode (Table 5); the 1st mode is perfectly represented by all the measurements as a MAC higher than 90% expresses a satisfactory match of the displacements. The rest of the modes present some similarities, the FEM and accelerometer results agree on the modal displacement of 2nd and 5th mode while the 3rd mode is well expressed by the modal displacement of the velocimeter and numerical model. All the results disagree on the 4th mode behaviour. The coefficient of correlation was also evaluated to have a qualitative global likeliness of the measurements (Table 5), the FEM and the accelerometer return the most correlated results.

Table 5 Comparison of the measurements

	MAC		
Modes	Numerical Accelerometer	Accelerometer Velocimeter	Numerical Velocimeter
1	100.0%	96.2%	99.9%
2	99.6%	41.9%	0.1%
3	13.0%	48.6%	92.1%
4	5.5%	80.0%	26.1%
5	99.8%	81.3%	0.3%
Coeff. Correlation	0.74	0.61	0.42

6 CONCLUSIONS

Dynamic identification proved to be a reliable test for a historical masonry building located in an extremely disturbed urban area.

In general, seismometers are designed to be very sensitive for detecting weak signals of ground motion, as such, the instruments used in the present work have a frequency band from 0.2 to 50 Hz and sensitivity of 400 V/m/s. However, the signal can saturate easily and the differentiation from velocity to acceleration introduce small numerical errors. On the other

hand, piezoelectric accelerometers are generally used to record the response acceleration of structures to strong motion, however the instruments used have high sensitivity (10 V/g), frequency band from 0.15 to 1000 Hz and range of ±0.5g, which limits the possibility of overloads.

Despite the complex dynamic behavior of the so-called temple of Minerva Medica, both instrumentations returned extremely similar results in terms of frequency with remarkably contained coefficient of variation.

The extracted modal displacements yielded to sparse values, only the 1st mode was accurately identified by all the instrumentations while the rest of the modes have partial agreements, in particular, the results from the accelerometers returned the highest correlation with the other values.

Dynamic monitoring of the so-called Temple of Minerva Medica identified irregular and partially coupled vibration modes, as a consequence, the modal displacements of the Northern and Western sides of the temple expressed wider amplitudes then the Eastern side where less sensors where located and the presence of the buttress partially retained the movements.

Regardless the complicated application, dynamic identification with different instrumentations and processing methods allowed a mutual validation of the results and highlighted the resilience of each approach.

The possibility to refer to multiple data and processing improves the reliability of the results and allows the confirmation or the repetition of the measurements.

BIBLIOGRAPHY

[1] I. Roselli, V. Fioriti, M. Mongelli, I. Bellagamba and G. De Canio, "Mutual Validation between different Modal Analysis Techniques for Dynamic Identification of the so-called Temple of Minerva Medica," in *IOP Conf. Series: Materials Science and Engineering*, Rome, 2018.

[2] C. Baggio, V. Sabbatini and S. Santini, "Model Updating of a Masonry Historical Church based on Operational Modal Analysis: the case study of San Filippo Neri in Macerata," in *7th International Conference on Computational Methods in Structural Dynamics and Earthquake Engineering*, Crete, Greece, 24–26 June 2019.

[3] M. Barbera and M. Magnani Cianetti, Minerva Medica. Ricerche, scavi e restauri, Milano, Rome: Electra, 2019.

[4] M. Barbera, S. Di Pasquale and P. Palazzo, "Roma, studi e indagini sul cd. Tempio di Minerva Medica," *The Journal of Fasti Online,* 2007.

[5] M. Barbera, M. Magnani Cianetti and S. Barrano, Da Massenzio a Costantino: le indagini in corso nel c.d. Tempio di Minerva Medica, Bari: Edipuglia, 2014.

[6] RomanoImpero, "romanoimpero.com," 2015. [Online]. Available: https://www.romanoimpero.com/2015/02/tempio-di-minerva-medica.html.

[7] I. Roselli, A. Tatì, V. Fioriti, I. Bellagamba, M. Mongelli, R. Romano, G. De Canio, M. Barbera and M. Magnani Cianetti, "Integrated approach to structural diagnosis by non-destructive techniques: the case of the Temple of Minerva Medica," *Acta IMEKO,* vol. 7, no. 3, 2018.

[8] V. Fioriti, I. Roselli, A. Tatì, R. Romano and G. De Canio, "Motion Magnification Analysis for structural monitoring of ancient constructions," *Measurement,* vol. 129, pp. 375-380 , 2018.

[9] I. Roselli, V. Fioriti, I. Bellagamba, M. Mongelli, A. Tatì, M. Barbera, M. Magnani Cianetti and G. De Canio, "Impact of traffic vibration on the Temple of Minerva Medica, Rome: preliminary study within the CO.B.RA. Project," *International Journal of Heritage Architecture,* vol. 2, no. 1, pp. 102-114, 2018.

[10] C. Rainieri, Operational Modal Analysis for Seismic Protection of Structures, Napoli: University of Naples "Federico II", PhD Thesis, 2008.

[11] Siemens, "Simcenter Testlab 18.0," 2018.

[12] Siemens, "Modal Analysis," in *LMS Test.Lab Manual*, pp. Section 1.3.3, Polymax pg. 30 – Section 6.2, MAC, MPC e MPD pg. 228 - Section 8.20, The Multi-Run Modal Analysis pg. 464.

[13] B. D. Allemang, "A correlation coefficient for modal vector analysis," in *1st international modal analysis conference*, Orlando, 1982.

[14] J. S. Bendat and A. G. Piersol, "Engineering applications of correlation and spectral analysis," New York, Wiley-Interscience, 1980.

[15] M. R. Gallipoli, M. Mucciarelli and M. Vona, "Empirical estimate of fundamental frequencies and damping for Italian buildings," *Earthquake Engineering and Structural Dynamics,* vol. 8, no. 38, pp. 973-988, 2009.

[16] Midas IT, "Midas Gen v 1.1," Midasoft Inc., 2019.

[17] Ministero delle Infrastrutture e dei Trasporti, "Circolare n. 617," in *Istruzioni per l'applicazione delle "Nuove noerme techniche per le costruzioni" di cui al decreto ministeriale 14 gennaio 2008 (GI n. 47 del 26-2-2009, Suppl. Ordinario n. 27)*, Roma, Gazzetta Ufficiale, 2009, p. 447.

[18] R. Bricker and C. E. Ventura, "Introduction to Operational Modal Analysis," *Wiley Online Library,* 2015.

[19] K. V. Yuen and L. S. Katafygiotis, "Bayesian time-domain approach for modal updating using ambient data," *Probabilistic Engineering Mechanics,* vol. 3, no. 16, pp. 219-231, 2001.

[20] N. Møller, H. Herlufsen and S. Gade, "Stochastic Subspace Identification Techniques in Operational Modal Analysis," in *Proc. 1st Int. Operational Modal Analysis Conference*, Copenhagen, Denmark, 2005.

12th International Conference on Structural Analysis of Historical Constructions
SAHC 2020
P. Roca, L. Pelà and C. Molins (Eds.)

HEALTH MONITORING TESTS OF HERITAGE STRUCTURES: APPLICATION OF MEMS ACCELEROMETERS TO TWO MULTI TIER PAGODAS

YOHEI ENDO[1*] AND YASUSHI NIITSU[2]

[1]Shinshu University, 4-17-1, Wakasato, Nagano City 380-8553, Japan
e-mail: endii@shinshu-u.ac.jp (*corresponding author)

[2]Tokyo Denki University, 2-1200 Muzai Gakuendai Inzai, Chiba, 270-1382 Japan
e-mail: yniitsu@cck.dendai.ac.jp

Keywords: Health monitoring test, Historical structures, MEMS accelerometers, Multi-tier pagodas

Abstract. *The paper introduces a health monitoring system based on MEMS (micro-electromechanical systems) accelerometers. The used MEMS accelerometers were recently developed by one of the authors. They excel in cost efficiency, calibration accuracy and robustness. The health monitoring system was installed in two multi-tiered pagodas. They were a two-tiered pagoda, Pashupatinath temple and a five-tiered pagoda, Nyatapola temple for four months. Both pagodas are located in Nepal. In both cases, a number of earthquakes were captured by the installed accelerometers, as it permitted estimation of the fundamental mode of the tested pagodas.*
The paper deals with two tasks. The first task introduces the used MEMS accelerometers. The features of the accelerometers are discussed. The second task discusses the dynamic behaviour of the pagodas identified by the installed monitoring system. The paper presents adequacy of the developed MEMS accelerometers for health monitoring test of heritage structures.

1 INTRODUCTION

Micro-electromechanical systems (MEMS) were commonly used in the automotive and mobile technologies [1]. Recently, the MEMS are used also in the civil and structural engineering field. The MEMS permits the monitoring in the wireless environment. This is convenient especially for heritage structures since the installation of sensors can be restricted due to the access limitation in some structures. Thanks to the development in the MEMS technology, today MEMS can perform much higher resolution monitoring than decades ago [2]. However, still further investigations are necessary for reliable monitoring of historical structures by means of the MEMS. For instance, MEMS accelerometers may not capture higher modes as clearly as piezoelectric accelerometers when the structure is not sufficiently excited [3].

The paper discusses health monitoring tests perfected on two multi-tier pagodas in Nepal by means of MEMS accelerometers. They were a two-tiered pagoda, Pashupatinath temple and a five-tiered pagoda, Nyatapola temple for four months. During the monitoring period, the adopted systems captured a number of vibrations caused by earthquakes. This helped detecting eigenvalues and eigenvectors of the tested structures. The present research provides insights on efficient strategies for monitoring of heritage structures by means of MEMS accelerometers.

2 DESCRIPTION OF THE DEVICE

The developed MEMS accelerometers are composed of an acceleration sensor, micro-processing unit (MPU) board, real time clock (RTC), 1-GB flash memory and USB interface (figure 1 a,b). The installed acceleration sensor is ADXL-355 [4]. Table 1 shows specifications. The accelerometers are tri-axial with signal-conditioned voltage outputs and 20-bit resolution digital outputs. It is possible to download the stored acceleration data and also to transfer the data directly to a personal computer in real time. The former is called offline mode in this paper while the latter real-time mode. The power consumption of the accelerometers is sufficiently small. The sensor functions for about three weeks with three AA alkaline batteries in continuous-monitoring mode.

Table 1 Specifications of the developed MEMS accelerometer

Parameter	Value / Conditions
Resolution	0.005 gal/LSB (± 2 G full-scale) 0.25gal/LSB (± 8 G full-scale)
Noise density	25 microG / √Hz
Operation Temp.	-20 to 60 °C
Sampling rates	10, 20, 50, 100, 200、256 /s
Storage memory	1 GB
Interface	USB 1.1 (160kByte/s)
Power supply	3.6 to 12 V (7.8mA)
Size	69 x 64 x 16 mm
Weight	45 g

(a) 

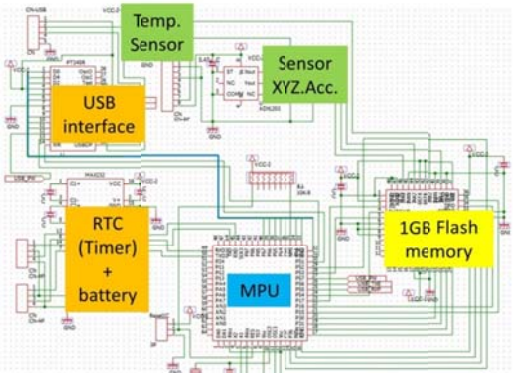
(b) 

Figure 1: Developed accelerometer: (a) top view and (b) block diagram.

The accelerometer has a 10-pin connector. Sensors are coupled by the connector, as it enables to operate multiple sensors and to supply power simultaneously. One accelerometer is assigned as a master and the others as slaves. The time is synchronised in accordance with the master. The acceleration data rate can be chosen among 10, 20, 50, 100, 200, 256 samples/second. It is noted that the rate of 256 samples/ second is available only in the real-time mode. The mode of data collection can be chosen between continuous monitoring and triggered monitoring. The continuous monitoring signifies MEMS record acceleration data in accordance with the predefined sample rate. In case of the continuous monitoring with 100 samples/ second, the 1-GB memory becomes full around in 22 days. The triggered monitoring collects acceleration data every second. However, in case the amplitude of the acceleration for each second is smaller than the specified offset value, only the average value or maximum and minimum values are stored. In case the amplitude is larger than the specified value, the data is stored according to the specified sample rate. The 1-GB memory can store data for one year at maximum with the trigger monitoring of 100 samples/ second in case the amplitude does not exceed the predefined offset values during the monitoring period. The accelerometers contain a RTC. Since the RTC does not output sub-second, the RTC time is read at the beginning, the middle, and the last of every second. When the displayed time of an accelerometer deviates from the RTC, it is corrected by 1/400 second. The operation permits matching the displayed time to RTC without changing the number of samples per second.

The operation permits matching the displayed time to RTC without changing the number of samples per second. The master accelerometer sends a pulse to slave accelerometers to match them with RTC of the master. The pulse is sent every two minutes and 1/50 seconds at the beginning of the minute. The slave accelerometers examine the pulse every 1/400 seconds. When they receive the pulse, they change the RTC to the beginning of minute. As a result, if the RTC of plural accelerometers are adjusted within 30 seconds in the initial state, the RTC of the slave accelerometers is set to the RTC of the master in two minutes after the start of the measurement. Since the displayed time of each accelerometer is matched to RTC, the displayed time of all the accelerometers are synchronised.

The MEMS accelerometers and servo accelerometers were compared. The compared servo accelerometers were capable of measuring ± 20 m/s^2. The noise density was 1 μG/√Hz. A MEMS accelerometer and servo accelerometer were located on a floor. Arbitrary vibrations were given by hitting the floor by foot. The sampling rate of both accelerometers was set as 256 samples/ second. Figure 2a shows vertical vibrations calibrated by the two accelerometers in the vertical direction. In the present paper, the X and Y axis denote horizontal vibrations while the Z axis vertical vibration. The vertical axis indicates the amplitude of the frequency component. It is noted that both accelerometers show the noise equal to about 1/2500g in Figure 2a due to the lack of a low pass filter. Figure 2b-d present the comparison of frequency power spectra between MEMS accelerometer and servo accelerometers in X, Y, Z axis. The frequency power spectra were calculated as the level of vibrations (L_v) according to the equation (1)

$$L_v = 20 \log \frac{a}{a_0} (\text{dB}) \tag{1}$$

where:
a is acceleration,
a_0 is equal to 10^{-5} m/s^2.

When the acceleration was over 30 dB, both accelerometers showed good agreement especially in the X and Z axis (see, Figure 2b,d). On the other hand, the MEMS accelerometer showed different values from the servo accelerometer when the acceleration was over 30 dB. However, the value (30 dB) is nearly equal to 3.1/10000g. It is a very small value compared to expected acceleration in heritage structures during health monitoring tests. Considering The tested MEMS accelerometers are much more cost efficient, light and robust than servo accelerometers, in spite of the dissimilarities of measurement results below 30 dB, they are considered suitable for health monitoring tests of heritage structures.

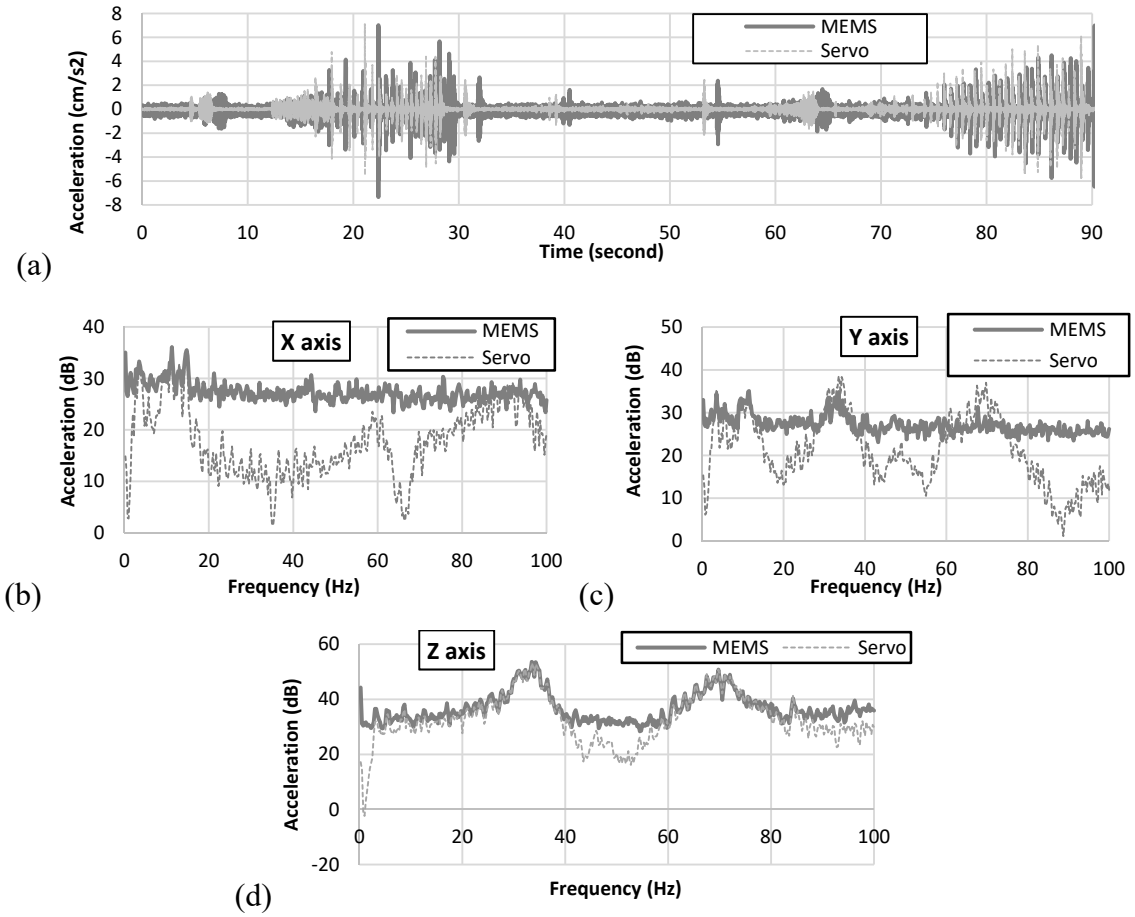


Figure 2: A comparison of the measurement results of MEMS accelerometer and servo accelerometer: (a) acceleration time history in the Z axis and (b-d) frequency power spectra in X, Y, Z axis.

3 HEALTH MONITORING TESTS

3.1 Description of the case study objectives

The monitoring tests were performed on a two-tier pagoda and five-tier pagoda. The Pashupatinath temple is a two-tier pagoda located in the historic centre of Bhaktapur (Figure 3a). It is also known as Yaksheshvara Mahadev temple. It is a replica of the same name temple built in Bagmati, Kathmandu [5]. The original structure was built by King Yaksha Malla in the 15th century [6]. It was reconstructed twice: in 1692 and after an earthquake of 1934.

The Nyatapola temple is a five-tier pagoda situated in the Taumadh square, Bhaktapur (Figure 3b). The temple was constructed by King Bhupatindra Malla in 1702 [7]. The top tier was collapsed during the earthquake of 1934 and later it was reconstructed [6]. Minor repair was conducted in 1962 and the roofs were reconstructed between 1998 and 1999. It is one of the two surviving five-tier pagodas in the Kathmandu valley.

(a)  (b) 

Figure 3: Tested pagodas: (a) Pashupatinath temple and (b) Nyatapola temple.

3.2 Monitoring setup

Three sensors (P1-3) were installed to the Pashupatinath temple as shown in Figure 4a. The P1 sensor was put on the plinth surface. Two sensors (P2-3) were put at the height of the ceiling level of the ground tier. The P2 sensor was attached to a pillar while the P3 to a wall. The two sensors were attached to a masonry wall. The triggered monitoring was applied. The trigger level was set as 1/1000g. In case the difference between the maximum and the minimum value within one second exceeded 1/1000g, the data was recorded at the rate of 100 samples/ second. In case the difference between the maximum and the minimum value was less than 1/1000g, only the maximum and minimum values were recorded. The monitoring was continued for three months (from December, 2016 to March, 2017).

Three MEMS accelerometers (N1-3) were installed to Nyatapola temple (Figure 4b). The N1 sensor was located at the plinth surface, the N2 sensor at the ceiling level of first tier, and the N3 sensor at the ceiling of the third tier. N2 and N3 sensors were attached to timber beams. The triggered monitoring was adopted. The trigger level was set as 1/1000g. The monitoring

was continued for four months (from August, 2017 to December, 2017). Both tests were conducted in offline mode.

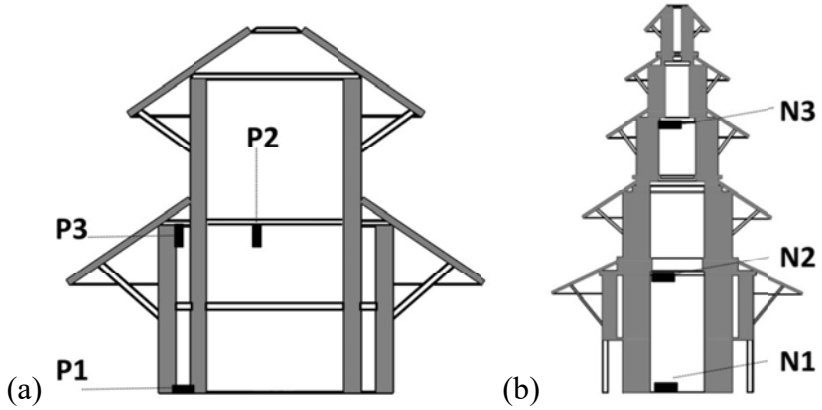


Figure 4: Sensor locations: (a) Pashupatinath temple and (b) Nyatapola temple.

3.3 Results of monitoring

Five earthquakes were detected by sensors during the monitoring period. In fact, number of earthquakes occurred around Nepal during the period but they were not captured by the sensors. This is presumably derived from the assigned trigger condition (1/1000g). The value was possibly too low for minor and/or distant earthquakes. Among five earthquakes detected by sensors, the three sensors detected two earthquakes which struck Nepal on February 27, 2017. One of them, a M4.7 earthquake occurred about 350 km west to Bhaktapur [8]. The recorded waveforms permitted estimation of natural frequencies of the tested pagoda. The captured waveforms were decomposed by Fourier transforms (Figures 5). P2 sensor calibrated 1.9 Hz as the fundamental natural frequency while P3 sensor 2.1 Hz.

During the monitoring of the Nyatapola temple, 10 earthquakes (>M2.5) unleashed around Nepal. Among them, two earthquakes were detected by the three sensors. They are a M4.5 earthquake on August 21, 2017 (named earthquake-A in this paper) and M5.0 earthquake on December 8, 2017 (earthquake-B) [8]. For the earthquake-A, N3 sensor recorded the maximum amplitude equal to 0.003g. As for the earthquake-B, the N3 sensor recorded maximum amplitude close to 0.009g. From the earthquake-A, a natural frequency equal to 1.60 Hz was detected and from the earthquake-B a natural frequency equal to 1.48 Hz (Figure 6 a-c). In fact a M6.9 earthquake hit Mainling, Tibet on November 18, 2017. The epicentre was about 1,000 km east of Bhaktapur. As for this earthquake, waveforms were recorded by N2 and N3 sensors although they did not permit estimation of natural frequencies of the pagoda due to the lack of sufficient amount of data.

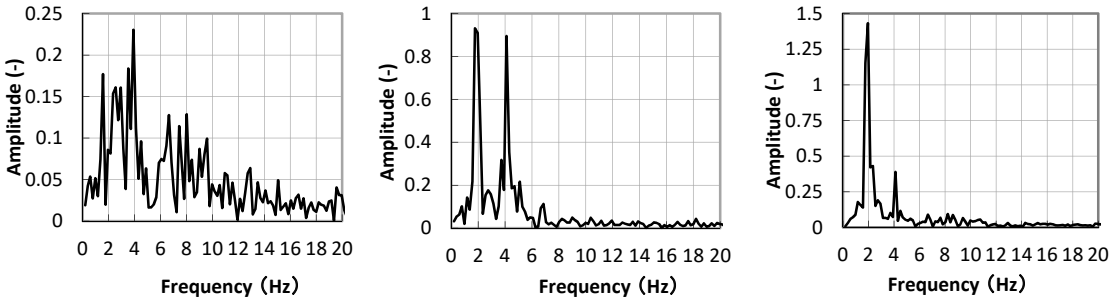


Figure 5: Fourier transforms in X axis of a M4.7 earthquake February 27, 2017, which hit Pashupatinath temple: (a) P1 sensor, (b) P2 sensor and (c) P3 sensor.

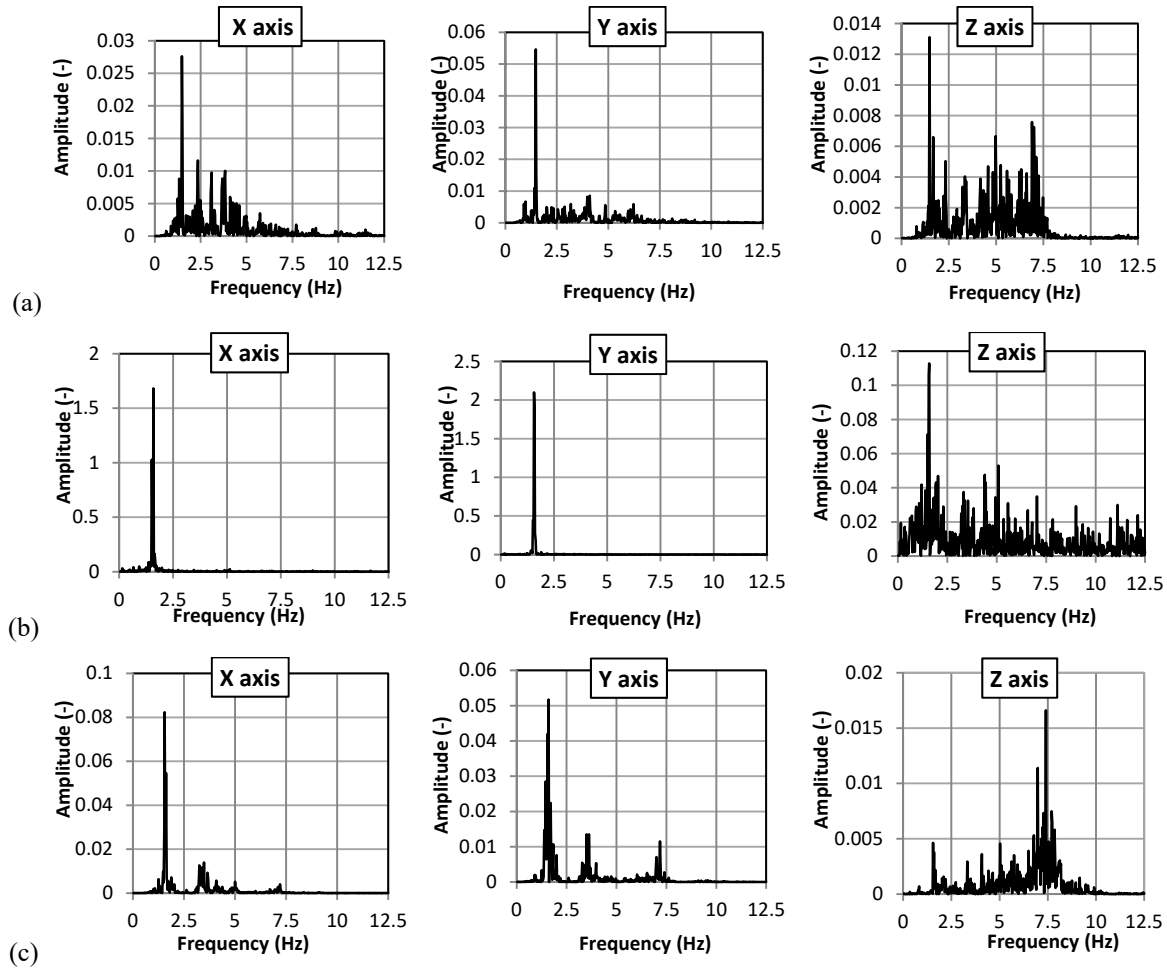


Figure 6: Fourier transforms of a M5.0 earthquake on December 8, 2017, which hit Nyatapola temple: (a) N1 sensor, (b) N2 sensor and (c) N3 sensor.

4 CONCLUSIONS

The paper introduced newly developed MEMS accelerometers. Health monitoring tests were performed on two multi-tier pagodas. They measure acceleration tri-axially under the conditions set by an internal MPU. The noise level is less than 1/5000g and to an inclination of 0.01 degree. They can be controlled by the trigger criterion. It allows the accelerometers to record detailed data of only strong vibrations, saving the battery and disk space. Theoretically, the monitoring for two years at maximum is possible without changing the battery or downloading/removing the stored data.

Health monitoring tests were performed on two multi-tier pagodas using the developed MEMS accelerometers. In both tests, the accelerometers detected multiple earthquakes, as it permitted estimation of the fundamental frequency. It is added that the used MEMS accelerometers are still under development. They will be improved in terms of data collection. Currently cable connections are necessary for the MEMS accelerometers to send data to a server PC. Using network connections, the MEMS will send data to a server PC.

Acknowledgements. The research is being supported by the funding of Grant-in-Aid for scientific research (A) provided by the Japan Society for the Promotion of the Science (Grant number: 16H01825). The authors show appreciation to Dr. Manjip Shakya for his assistance in conducting the laboratory tests at KHWOPA engineering college, Nepal.

REFERENCES

[1] Tadigadapa, S. and Mateti, K. "Piezoelectric MEMS sensors: state-of-the-art and perspectives." *Measurement Science and technology* 20, no. 9 (2009): 092001.

[2] Sabato, A., Niezrecki, C. and Fortino, G. "Wireless MEMS-based accelerometer sensor boards for structural vibration monitoring: a review." *IEEE Sensors Journal* 17, no. 2 (2016): 226-235.

[3] Bassoli, E., Vincenzi, L., Bovo, M. and Mazzotti, C. "Dynamic identification of an ancient masonry bell tower using a MEMS-based acquisition system." *In 2015 IEEE Workshop on Environmental, Energy, and Structural Monitoring Systems (EESMS) Proceedings*, pp. 226-231. IEEE, (2015).

[4] "Analog device *Data Sheet ADXL354/ADXL355 (2018) "*. https://www.analog.com/media/en/technical-documentation/data-sheets/adxl354_355.pdf.

[5] Wiesner, U. *Nepalese temple architecture: its characteristics and its relations to Indian development.* Vol. 8. Brill, (1978).

[6] Amātya, S. *Monument conservation in Nepal: My experience with the world heritage sites of Kathmandu valley*. Vajra Publications, (2007).

[7] Shrestha, D.B. and Singh, C.E. *The History of Ancient and Medieval Nepal in a Nutshell: With Some Comparative Traces of Foreign History.* Vol. 1. (1972).

[8] USGS, *" Earthquake hazards" (*2019). https://www.usgs.gov/natural-hazards/earthquake-hazards/earthquakes

12th International Conference on Structural Analysis of Historical Constructions
SAHC 2020
P. Roca, L. Pelà and C. Molins (Eds.)

LONG-TERM STRUCTURAL HEALTH MONITORING OF THE FORTEZZA FORTRESS: APPLICATION OF DAMAGE DETECTION TECHNIQUES ON EXISTING CRACKS

MYRONAS DRYGIANNAKIS[1], GEORGIOS VLACHAKIS[2*] AND ANASTASIA TZIGOUNAKI[3]

[1]Freelancer Civil / Structural Engineer
Rethymnon - Crete, Greece
e-mail: myronasdr@gmail.com

[2] ISISE - University of Minho, Department of Civil Engineering
Campus de Azurém, 4800-058, Guimarães, Portugal
email: giorgovlachaki@gmail.com, (*corresponding author)

[3] Director of the Ephorate of Antiquities of Rethymno, Hellenic Ministry of Culture and Sports
Arkadiou 214, P.C. 74100, Rethymno - Crete, Greece
email: atzigounaki@culture.gr

Keywords: Masonry Cracks, Diagnosis, STORM-project, Climate Change

Abstract. *Structural Health Monitoring (SHM) consists of an elaborated technique, assisting the assessment of existing structures through the detection of active or sudden damages, as well as the diagnosis of possible causes for them. Within the STORM-project [1], the SHM strategy selected for the assessment of the Venetian fortress of Fortezza in Rethymno, Greece was the continuous crack monitoring of four different existing cracks of the structure, due to their relatively large width, located at the Bastion of St. Paul's, Prophet Elias' and St. Luke's as well as the Episcopal mansion.*

Besides the crack displacement measurements, several other environmental quantities were monitored at the weather stations, which are known to have a strong influence on the crack width. Considering the fact that most weather fluctuations have reversible effects on structural integrity, it is of great importance to recognize the environmental and operational variation of the structure, and subsequently identify any separate structural change caused by damage [2], [3]. This was achieved by employing a statistical ARX model (Auto-Regressive model with eXogenous input) [4], calibrated for each case after several months. Once this process was completed it was possible to detect possible active damage on the examined structures and estimate possible causes for them.

The successful application of the methodology at the four monitored cracks provided important information about their state of damage, possible causes and early warnings in case of hazard. Over the evaluated period, it appears that the bastion of Prophet Elias is in stable condition, while the bastion of St. Luke and St. Paul are vulnerable to heavy precipitation. Moreover, the Episcopal mansion showed a destabilization response during the rainfall period, which is possible to result in the activation of an overturning mechanism.

1 INTRODUCTION

Cultural heritage constructions are critically endangered by natural hazards, while their significance has resulted in serious societal efforts to protect and preserve their integrity [5]. Structural Health Monitoring (SHM) has proven to be a valuable assistance in the diagnosis and control process of heritage structures [6]–[10], presenting promising characteristics and potentials. Important aspects of a SHM application include the planning of type and layout of the sensors, and the employment of a damage detection methodology to process the data and derive meaningful conclusions [11].

The present paper illustrates a case study application of a SHM campaign at the Venetian fortress of Fortezza, the foremost landmark in the city of Rethymno, on the island of Crete. The masonry constructions of the monument are exposed to several natural hazards that could hinder their integrity [12]. More specifically, the area of Rethymno is characterized by high seismicity, as well as environmental conditions, intensified by the climate change. Just to mention, partial collapses of the Rampart of Lando Bastion of Chania Venetian Fortifications, in 26 and 28 February 2017 and in 11 and 14 February 2019, due to great storms that hit Crete in winters 2017 and 2019. Herein, it is attempted to estimate the condition of four cracks located in the Fortezza fortress, taking into account the influence of the environmental conditions.

2 DESCRIPTION OF THE CASE STUDY

2.1 The Fortezza fortress

In the north-west part of the Historical Centre of Rethymno stands the Fortezza fortress. It consist the foremost landmark and largest monument of the city of Rethymno, built on the natural hill of the city's cape. Archeological findings trace back the human presence in the area during Neolithic period, while it has been constantly occupied at least since the Hellenistic period up to present. The fortress was built by the Venetian Republic at the end of the 16th century and is a representative specimen of the Venetian fortification architecture.

The layout of the fortification is composed by four bastions: two at the south (Prophet Elias and St. Luke) and two at the east (St. Nicolas and St. Paul), while the north and west part of the fortress is next to the sea and has three peaks (the Holy Spirit, the St. Ioustine and the St. Sozon). The total length of the fortification walls counts approximately 1370 m, and their height varies from 6 m to 13 m.

Despite the fact that the fortress used to enclose many buildings, the vast majority have been destroyed, and only a few there still exist, such as the mosque of Sultan Ibrahim Han, the armory, the Episcopal mansion, the Rector's house, the Chancellor's house etc. Nevertheless, those constructions reflect the different historical phases of the fortress and nowadays host many exhibitions, concerts and cultural events.

2.2 Structural health monitoring campaign

In the last decades, the Ephorate of Antiquities of Rethymno (EFARETH) has given a huge effort to protect the monument by carrying out restoration works. As part of this effort, the fortress has been selected and included in the STORM project, with the aim to assist

EFARETH in assessing and managing risks associated with natural hazards. More specifically, the local partners of the project EFARETH and the Geophysical-Satellite Remote Sensing and Archaeoenvironment Lab of the Institute for Mediterranean Studies – Foundation for Research and Technology, in collaboration with the European partners, conducted hazard studies [12], non-destructive investigation works [13] and developed a methodology and associated supporting tools for early warning and decision making for risk mitigation [1].

Among the works of the STORM project, four cracks have been chosen to be monitored in a long-term basis, due to their relatively large width and their structural significance. The positions of the cracks monitored are displayed in Figure 1 and are located on the fortress' walls at the bastion of Prophet Elias, St. Luke, St. Paul and the west part of the north façade of the Episcopal mansion. The crack at the bastion of Prophet Elias is located at the intruding connection of the bastion with the rest of the wall and propagates vertically. Concerning the crack at St. Luke's bastion, it appears to start from the *parapetto* and extends downwards to an area reconstructed by the Ottoman's in the late 17th cent. St. Paul bastion's crack appears at the east part of the bastion's corner and expands vertically down to the ground. Finally, the monitored crack at the Episcopal mansion crosses the vault in the longitudinal direction of the west portion of the building aggregate and propagates vertically both at the north and south façades. In each location, a rectilinear displacement transducer (LVDT) has been installed in order to measure the relative displacement movement of the cracks. A sampling period of four hours was chosen as adequate of replicating the daily fluctuation, after an initial test of one hour sampling.

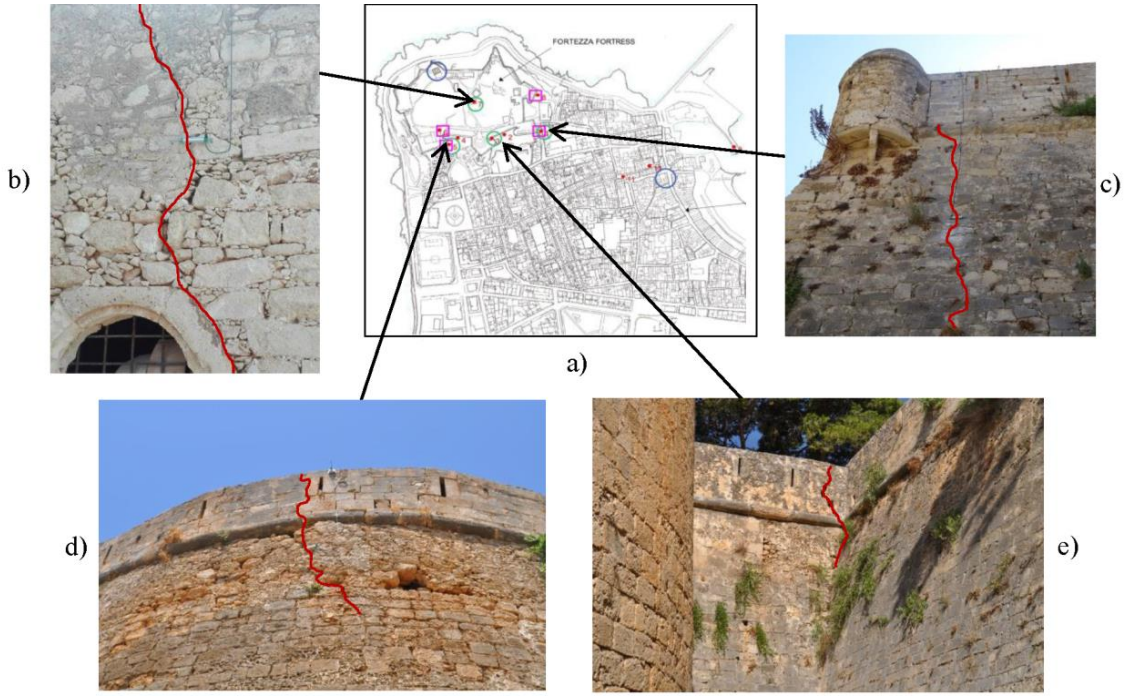


Figure 1: a) Map of the historical center of Rethymno and the Fortezza fortress; including the locations of: b) the Episcopal mansión, c) the bastion of St. Paul, d) the bastion of St. Luke, and e) the bastion of Prophet Elias. The positions and patterns of the monitored cracks are highlighted.

It is well known that environmental conditions affect the structural state of constructions [2], [3], [14], especially in case of cracks [15]–[17]. Therefore, besides the crack displacement measurement, several other environmental quantities were monitored by a weather station installed on the fortress. These included external temperature, relative humidity, precipitation and wind speed and direction. Moreover, the board temperature of each crackmeter was also measured.

The present paper presents results of each crack for the periods shown in Table 1. For the case of St. Paul only a few months of measurements were available due to technical issues.

Table 1: Periods of available measurements of the crack monitoring campaign

Bastion of Prophet Elias	24/05/2018 – 10/10/2019
Bastion of St. Luke	31/05/2018 – 10/10/2019
Bastion of St. Paul	13/07/2017 – 06/02/2018
Episcopal mansion	24/05/2018 – 10/10/2019

3 DAMAGE DETECTION METHODOLOGY

3.1 Strategy of the adopted methodology

The main task of SHM is to identify the presence or not of an active damage process on the structure, by employing a damage detection methodology. The main challenge of such a methodology is to be able to describe the environmental and operational variation of the structure, and subsequently identify any separate structural change caused by damage. This is of major importance, as has been pointed out by [18], because changes to monitored parameters induced by environmental effects can be larger than changes due to significant damage. In this study, the dynamic AutoRegressive model with eXogenous inputs (ARX model) has been employed, previously proposed and used by [11], [17], [19], among others.

Initially, a calibration phase is required to create the statistical ARX model, which includes, ideally, a complete environmental cycle, i.e. a year. Then, after the model has been created, the prediction phase starts, during which the model's prediction is compared with the actual measurements. This comparison, which can be done by a residual analysis, is the key point of the methodology, since it should provide a removal of the effect of the environmental conditions on the signal. In other words, if the real measurements diverge significantly from the predicted values, then another separate process is acting on the structure, which was not taken into account by the statistical model. This indicates a change of the response which might be irreversible (active damage).

3.2 Brief description of the ARX model

The basic advantage of the statistical ARX model is its ability to relate the present outputs to past inputs and outputs. This feature, in contrast with static linear or non-linear regression models, makes it ideal for representing monitored parameters that depend on the rate of change or trend of an environmental parameter. This is a key aspect for huge and complex structures, which are characterized by e.g. thermal inertia, such as the Fortezza fortress examined herein.

The mathematical expression of the multivariable ARX model with n inputs x and one

output y is presented by:

$$\hat{y}_k + a_1 y_{k-1} + \cdots + a_{na} y_{k-na} = b_1 x^{env}_{k-nk} + b_2 x^{env}_{k-nk-1} + \cdots + b_{nb} x^{env}_{k-nk-nb+1} + e_k \quad (1)$$

Where y_k is the monitored response (actual measurement) in the instant k, $\hat{y}_k$ is the estimated response, x^{env} is the input environmental parameter (e.g. the temperature), a_i and b_i are coefficients for the autoregressive and exogenous part, respectively, n_a is the autoregressive order, n_b the exogenous order, n_k is the number of delays from input to output and $e_k = y_k - \hat{y}_k$ is the unknown residual that can be assumed Gaussian. The coefficients of the polynomials a_i and b_i can be estimated using the simple linear least square method. In this work, the SISO form of the ARX model is employed; yet it could be expanded to include multiple input variables i.e. having a MISO form [18]. In that case, eq. (1) is still valid but x^{env} is a column vector, the b_i coefficients are row vectors and a distinct order n_b and n_k characterizes each input variable.

The choice of the appropriate AR model order is done with the assistance of the quality criteria proposed by [18]–[20]. These criteria include: a) the value of the loss function V, b) the Akaike's Final Prediction Error FPE, c) the coefficient of determination R^2, and d) the autocorrelation function λ_i. Firstly, the loss function is defined as: $V = \frac{1}{N}\sum_{k=1}^{N} e_k^2$, where e_k is the residual error, and its value represents a finer model as it tends to zero. Secondly, the Final Prediction Error is defined as: $= V\frac{1+d/N}{1-d/N}$, where V is the loss function and d is the number of estimated parameters. Once more, a value of FPE closer to zero indicates a preferable model. The coefficient of determination is defined as the ratio between the variances of the fitted values of the model ($\hat{y}_k$) and the measured values of the dependent variable (y_k): $R^2 = \frac{\sum(\hat{y}_k - \bar{y})^2}{\sum(y_k - \bar{y})^2}$. A higher value of R^2 is preferred. Finally, the auto-correlation function of the prediction error, defined as $\lambda_i = \frac{1}{N}\sum_{k=1}^{N} e_{k+i} e_k$, should be zero-mean white noise in the case that a good ARX model is obtained.

During the prediction phase, the residual analysis is performed by quantifying the simulation error $e_k = y_k - \hat{y}_k$. Confidence intervals can be established based on the statistics of the prediction, in order to judge whether the simulation error is statistically significant or not. If $\hat{y}$ is the predicted output and $\hat{\sigma}_y$ the estimated standard deviation on a new observation, the $(100 - a)\%$ confidence interval on $\hat{y}$ is given by:

$$\left[\hat{y} - t_{a/2,v}\hat{\sigma}_y\,, \quad \hat{y} + t_{a/2,v}\hat{\sigma}_y\right] \quad (2)$$

where the value $t_{a/2,v}$ is found from a statistical table of the t-Student distribution. The established confidence intervals can be considered as warning thresholds for possible damage detection in real time, and thus provide an instant alert in case of sudden-onset hazard.

The workflow of the aforementioned methodology is presented in the following Table 2.

Table 2: Workflow of damage detection methodology

1.	Read and filter data at specified sampling period
2.	Calculate basic statistical characteristics of data
3.	Decide environmental parameters to consider in the ARX model

4.	Check V and FPE for different n_k, by temporary assuming high values of n_a and n_b
5.	Decide n_k
6.	Check V, FPE and R^2 for different combinations of n_a and n_b
7.	Decide n_a and n_b
8.	Calculate polynomial coefficients and construct ARX model
9.	Calculate residual errors and λ_i
10.	Calculate confidence intervals
11.	Compare λ_i with confidence intervals. If λ_i is not included within the confidence intervals go to step 7 and reconsider n_a and n_b
12.	Continue with simulation of expected response of the prediction phase with the established confidence intervals
13.	Compare simulation error with confidence intervals (thresholds) to detect possible damage

4 RESULTS AND DISCUSSION

The results after the application of the aforementioned methodology are presented in Figure 2 - Figure 5. More specifically, Figure 2 shows the evolution in time of the four monitored cracks and the corresponding board temperatures. Figure 3 shows the correlation of the same measurements, while highlighting the time evolution through a color scale (blue to yellow). Figure 4 demonstrates the fitting achieved using the proposed ARX model for all the crackmeters, also indicating the date of calibration. Finally, Figure 5 illustrates the results of the residual analyses of the actual measurements and the statistical model, including the derived thresholds. In the same graph, the corresponding precipitation is shown, except for the bastion of St. Paul due to the lack of weather data at that period.

In all cases, both a daily and seasonal crack fluctuation has been observed. After examining the correlation of the crack displacements with all the rest monitored environmental parameters, the best correlation is obtained with the board temperature for all cases, and therefore is adopted as the exogenous parameter employed further on. Except the bastion of Prophet Elias, this correlation is generally negative (Figure 3), as expected [15], [17], and this can be explained by the physical phenomenon of temperature expansion and contraction: as the temperature rises, the stones at the two sides of the crack expand causing a crack closure, and vice-versa for contraction.

In the case of the bastion of Prophet Elias, a negative correlation is observed only in a daily basis, while when considering the complete seasonal response, a positive correlation is obtained. An explanation to this phenomenological paradox could resort to any or a combination of the following: a) the highly statically indeterminate nature of the structure, b) the complex boundary conditions affecting the fortress walls, or even c) the closely presence of other cracks. It is interesting to note that this positive correlation is shown in Figure 2a to have a delay of about two months. This is also observed in Figure 3a by the circular path tracing the response (from blue to yellow), instead of a simple linear. This delay peculiarity indicates that thermal inertia is guiding the global response: probably the thermal inertia of the whole bastion. Nevertheless, a good fit is obtained by the ARX model, while no significant excess of the confidence intervals is shown in Figure 5a, underlining a stable condition of the crack.

The crack at the bastion of St. Luke is characterized by several response peaks at specific dates. Those peaks appear in most cases at low temperatures (Figure 3b), while after a closer

look at Figure 5b it is clear that they coincide with rainfall events. Interestingly, not all rainfall events cause a destabilization. Yet, despite these peaks of relative displacement, the crack opening appears to recover after the specific events, without retaining a residual displacement (Figure 3b). The aforementioned characteristics indicate that this vulnerability is possibly arising by the saturation and in turn expansion of the backfill soil of the fortress wall. This finding is in line with [1], where the presence of water flows and moisture in the filling material was identified using the Electrical Resistivity Tomography (ERT) method.

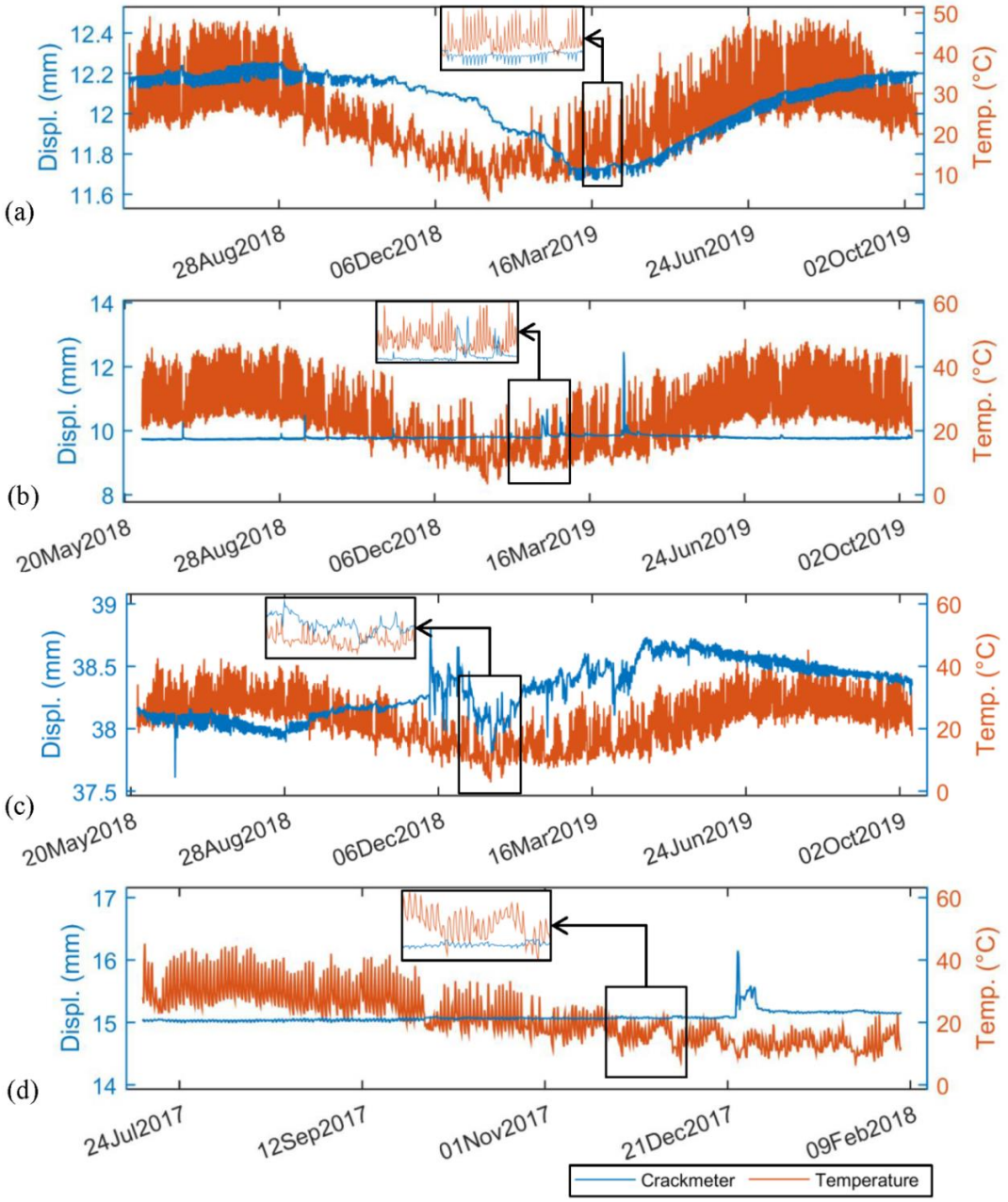


Figure 2: Time history of monitored crack displacement and board temperature for: a) the bastion of Prophet Elias, b) the bastion of St. Luke, c) the Episcopal mansión, and d) the bastion of St. Paul

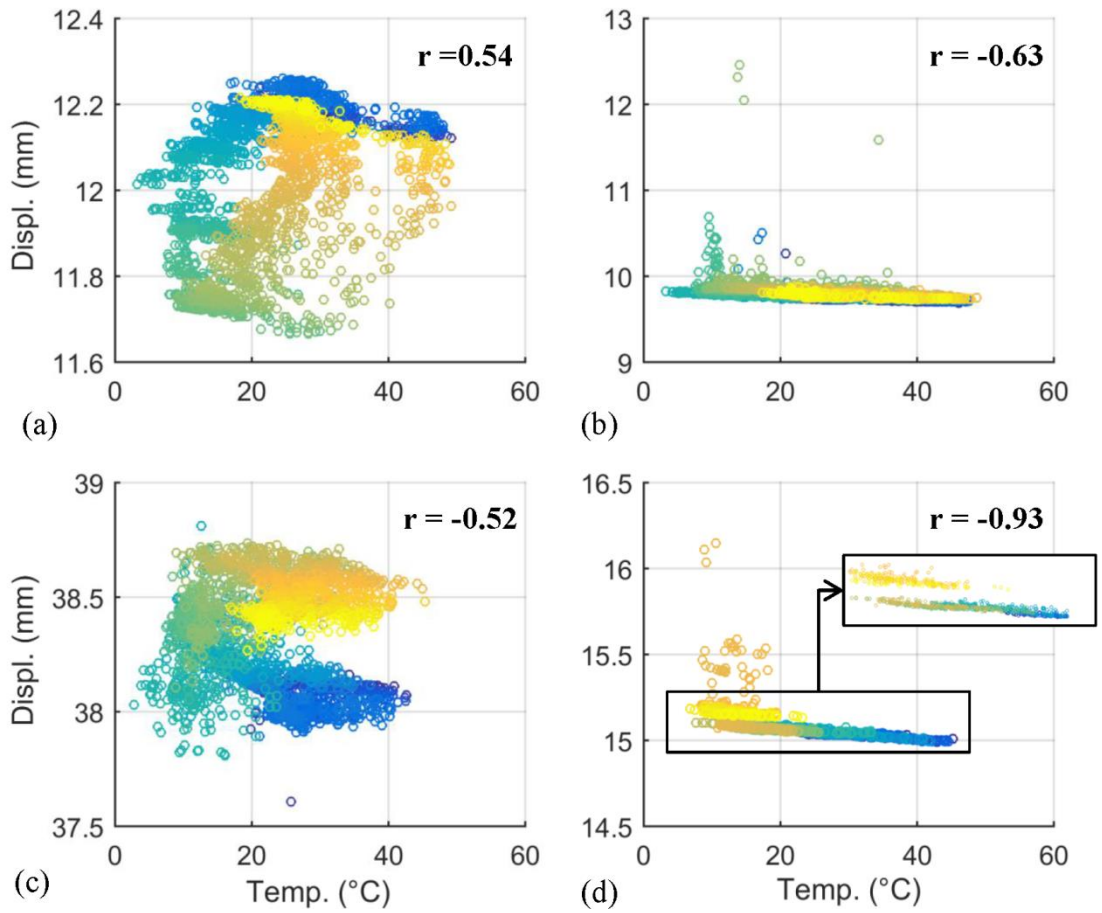


Figure 3: Correlation of monitored crack displacement and board temperature for: a) the bastion of Prophet Elias, b) the bastion of St. Luke, c) the Episcopal mansión, and d) the bastion of St. Paul. The color scale indicates the time evolution: blue to yellow correspond at early to late records, respectively

The Episcopal mansion's crack shows an unstable response during the winter (Dec. 2018 – April 2019), coinciding with high rainfalls (Figure 5c). More specifically, high variations of the crack opening are observed, when compared with other periods of the year. After this period, the crack appears to be stable again, although around a new equilibrium position, with a gain of around 0.5 mm. This is clearly shown in Figure 3c, where the blue points represent the equilibrium position before the winter, the green points the high fluctuation of the winter and the yellow points the new equilibrium position right after, having an offset from the initial. In contrast with the instabilities of the bastions of St. Luke and Paul where only a crack widening is observed, the variation in this case appear both positive and negative, as this is not a retaining structure. Therefore, a possible cause could be a foundation soil settlement due to intense rainfalls, or an intense evolution of the deterioration process due to the harsh weather conditions.

As already mentioned, for the bastion of St. Paul only a few measurements are available, and therefore the following outcomes might not be fully representative of the complete response of the crack. A normal response is observed until the end of December 2017. Then, the crack shows a destabilization for several days, and thereafter it stabilizes again but with a

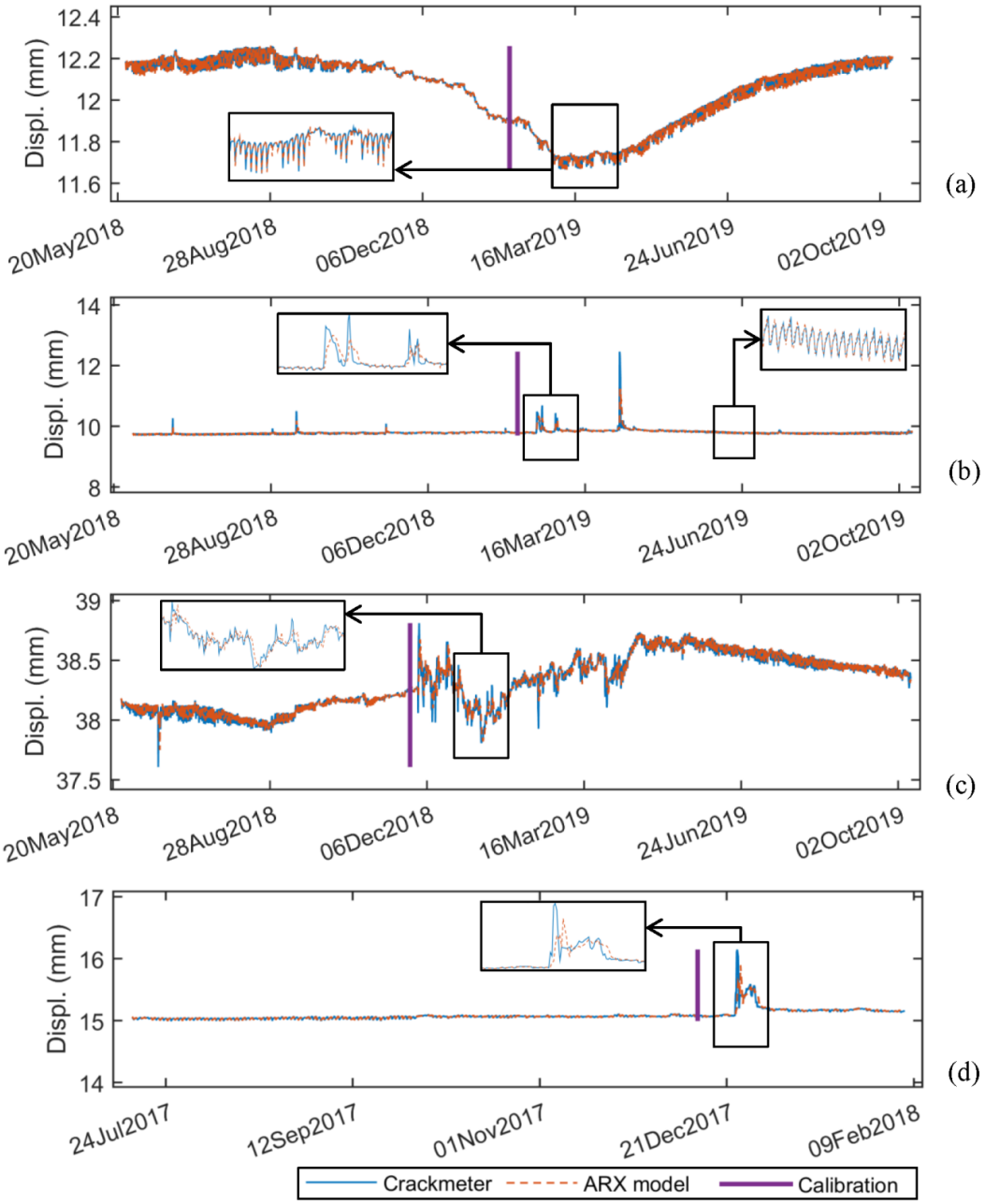


Figure 4: Time history of monitored crack displacement and the corresponding prediction of the ARX model for: a) the bastion of Prophet Elias, b) the bastion of St. Luke, c) the Episcopal mansión, and d) the bastion of St. Paul

retained displacement. This is clearly illustrated in Figure 3d, where an offset appears between the blue and yellow points, yet with a small gain of around 0.1 mm. In the same figure it can also be appreciated that those peaks always appear during low temperatures, as possible cause a rainfall event. Moreover, similarly with St. Luke, [1] have pointed out that

the filling material retains moisture due to water flow. Although precipitation measurements are not available for this period to derive a quantitative correlation, by looking the local daily weather data available online by the National Observatory of Athens, rainfall events occurred the same days of destabilization.

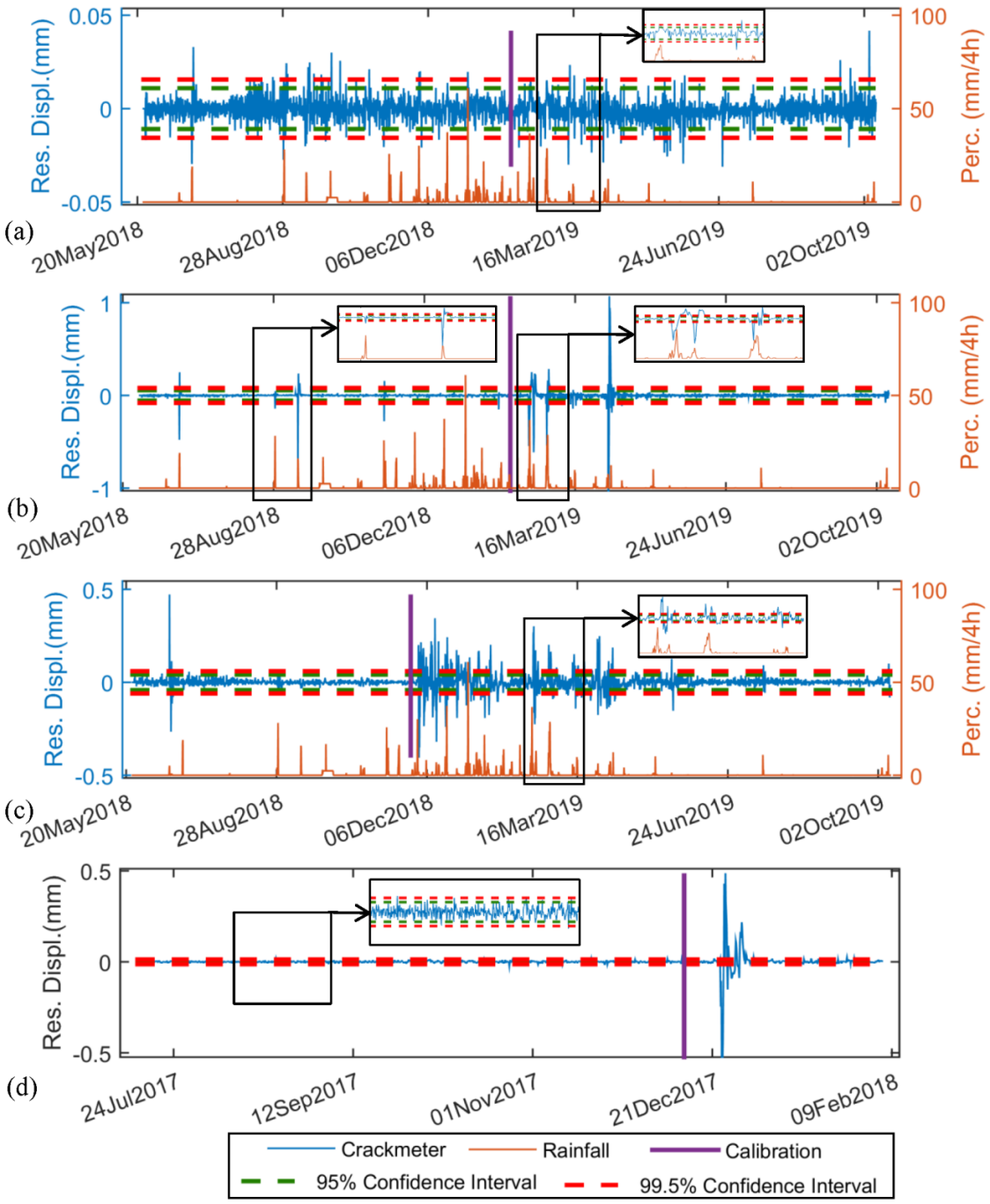


Figure 5: Time history of the residual analyses of the monitored crack displacement and the corresponding prediction of the ARX model, including percipitation and confidence interval thresholds for: a) the bastion of Prophet Elias, b) the bastion of St. Luke, c) the Episcopal mansión, and d) the bastion of St. Paul.

5 CONCLUSIONS

This study presents the application of a long-term SHM campaign on four cracks of the Fortezza fortress in the city of Rethymno, in Greece. Being part of the STORM project, the aim of the application is to develop an appropriate methodology and associated supporting tools and services to assess and manage risks associated with natural hazards.

A weather station was also installed, in order to assess the influence that the environmental conditions have on the cracks. A statistical ARX model is employed to describe the cyclic environmental operational variation of the cracks, and therefore detect any separate acting damage on the structure.

The crack at the bastion of Prophet Elias illustrates a stable condition, during the examined period. In the case of St. Luke, the crack shows a widening during rainfalls, yet followed by a full recovery. The Episcopal mansion's crack appears to be unstable during winter and intense rainfalls. An increase of the crack-width is retained after such events, which could compromise its safety. Finally, not enough measurements are yet available in order to conclude with certain about the bastion of St. Paul. However, the present results indicate vulnerability in rainfalls, once more, so EFARETH proceeded to urgent structural stabilization of the bastion's watchtower.

Considering the outcomes of the present work, future developments could attempt to include the influence of precipitation and humidity data in the ARX model. To this end, the MISO form of the model could be employed.

Acknowledgements. This article is based on the STORM (Safeguarding Cultural Heritage through Technical and Organisational Resources Management) Project, funded by the European Union's Horizon 2020 research and innovation program under Grant agreement No. 700191.

REFERENCES

[1] V. Resta, A. B. Utkin, F. M. Neto, and C. Z. Patrikakis, *Cultural Heritage Resilience Against Climate Change and Natural Hazards*. Pisa University Press, 2019.

[2] H. Sohn, "Effects of environmental and operational variability on structural health monitoring," *Philos. Trans. R. Soc. A Math. Phys. Eng. Sci.*, vol. 365, no. 1851, pp. 539–560, 2007.

[3] G. Zonno, R. Aguilar, R. Boroschek, and P. B. Lourenço, "Analysis of the long and short-term effects of temperature and humidity on the structural properties of adobe buildings using continuous monitoring," *Eng. Struct.*, vol. 196, no. December 2018, p. 109299, 2019.

[4] C. Modena, F. Lorenzoni, M. Caldon, and F. da Porto, "Structural health monitoring: a tool for managing risks in sub-standard conditions," *J. Civ. Struct. Heal. Monit.*, vol. 6, no. 3, pp. 365–375, 2016.

[5] P. Roca, P. B. Lourenço, and A. Gaetani, *Historic Construction and Conservation*. New York: Routledge, 2019.

[6] M. G. Masciotta, L. F. Ramos, and P. B. Lourenço, "The importance of structural monitoring as a diagnosis and control tool in the restoration process of heritage structures: A case study in Portugal," *J. Cult. Herit.*, vol. 27, pp. 36–47, 2017.

[7] A. Dal Cin and S. Russo, "Evaluation of static and dynamic long-term structural monitoring for monumental masonry structure," *J. Civ. Struct. Heal. Monit.*, vol. 9, no. 2, pp. 169–182, 2019.
[8] P. Roca, C. Blasi, and F. Ottoni, "Editorial," *Int. J. Archit. Herit.*, vol. 9, no. 1, p. 1, 2015.
[9] M. G. Masciotta, J. C. A. Roque, L. F. Ramos, and P. B. Lourenço, "A multidisciplinary approach to assess the health state of heritage structures: The case study of the Church of Monastery of Jerónimos in Lisbon," *Constr. Build. Mater.*, vol. 116, pp. 169–187, 2016.
[10] F. Lorenzoni, F. Casarin, C. Modena, M. Caldon, K. Islami, and F. da Porto, "Structural health monitoring of the Roman Arena of Verona, Italy," *J. Civ. Struct. Heal. Monit.*, vol. 3, no. 4, pp. 227–246, 2013.
[11] F. Lorenzoni, F. Casarin, M. Caldon, K. Islami, and C. Modena, "Uncertainty quantification in structural health monitoring: Applications on cultural heritage buildings," *Mech. Syst. Signal Process.*, vol. 66–67, pp. 268–281, 2016.
[12] M. Ravankhah *et al.*, "Integrated Assessment of Natural Hazards, Including Climate Change's Influences, for Cultural Heritage Sites: The Case of the Historic Centre of Rethymno in Greece," *Int. J. Disaster Risk Sci.*, vol. 10, no. 3, pp. 343–361, 2019.
[13] M. Manataki, A. Sarris, D. Oikonomou, K. Simirdanis, G. Strapazzon, and P. T. Fernández, "Contribution of GPR method in monitoring and evaluating the conservation state of Fortezza, Rethymno, Greece," *2018 17th Int. Conf. Gr. Penetrating Radar, GPR 2018*, 2018.
[14] F. Ubertini, G. Comanducci, N. Cavalagli, A. Laura Pisello, A. Luigi Materazzi, and F. Cotana, "Environmental effects on natural frequencies of the San Pietro bell tower in Perugia, Italy, and their removal for structural performance assessment," *Mech. Syst. Signal Process.*, vol. 82, pp. 307–322, 2017.
[15] A. Kita, N. Cavalagli, and F. Ubertini, "Temperature effects on static and dynamic behavior of Consoli Palace in Gubbio, Italy," *Mech. Syst. Signal Process.*, vol. 120, pp. 180–202, 2019.
[16] R. Ceravolo, A. De Marinis, M. L. Pecorelli, and L. Zanotti Fragonara, "Monitoring of masonry historical constructions: 10 years of static monitoring of the world's largest oval dome," *Struct. Control Heal. Monit.*, vol. 24, no. 10, pp. 1–11, 2017.
[17] F. Casarin, F. Porto, C. Modena, P. Girardello, and I. Kleidi, "Optical Structural Health Monitoring of the Frescoes in the Conegliano Cathedral , Italy," in *SAHC2014 - 9th International Conference on Structural Analysis of Historical Constructions*, no. October, F. Pena and M. Chavez, Eds. 2014.
[18] B. Peeters, "System identification and damage detection in civil engineering, PhD Dissertation," Katholieke Universiteit Leuven, 2000.
[19] L. F. Ramos, "Damage identification on masonry structures based on vibration signatures," *PhD Thesis*, 2007.
[20] F. Lorenzoni, "Integrated methodologies based on Structural Health Monitoring for the protection of Cutural Heritage buildings. PhD Thesis," University of Trento, 2013.

SAHC 2020
P. Roca, L. Pelà and C. Molins (Eds.)

MONITORING OF INDOOR ENVIRONMENTAL CONDITIONS OF THE KVERNES (NORWAY) STAVE CHURCH

CHIARA BERTOLIN[1*], LAVINIA DE FERRI[1], TONE MARIE OLSTAD[2]

[1]Department of Mechanical and Industrial Engineering, Norwegian University of Science and Technology, Trondheim, Norway.
e-mail: chiara.bertolin@ntnu.no, https://www.ntnu.edu/employees/chiara.bertolin (*corresponding author); lavinia.de.ferri@ntnu.no

[2] Norsk institutt for kulturminneforskning, Storgata 2, 0155 Oslo, Norway e-mail: tone.olstad@niku.no; web page: https://www.niku.no/en/ansatt/tone-marie-olstad/

Keywords: Risk assessment, Stave churches, wood, indoor monitoring

Abstract.

The proposed study deals with environmental data collected in the Kvernes stave church, belonging to the Møre type. The nave and the chancel belonging to the original structure, probably dated back to early 1600, are one of the few cases – among the 28 existing Stave Churches - still maintaining the internal wall painting, realized with a tempera technique in 1633. Due to its geographical position, the Kvernes church is particularly exposed to weather and consequently maintenance interventions have been carried out in 2015 (Stave Church Preservation Programme) to preserve the building. Previously in 2011 and 2012, 4 data loggers were installed to monitor indoor microclimatic variations basically referable to climatic external conditions, the performance of liturgical functions, and to the presence of visitors (depending on the periods of the year), since none active heating system has never been installed in the church.

In the frame of the international research project SyMBoL (Sustainable Management of Heritage Buildings in a Long-term perspective) such environmental data were elaborated. They represent the firsts internationally published information from long-term monitoring campaigns in stave churches.

1 INTRODUCTION

The monitoring of internal conditions of historical buildings is an issue receiving growing attention in the last decades even if not everywhere. Data from long- and short-term indoor monitoring campaigns are still not easily available for the northern Europe Cultural Heritage, particularly rich in stone-based monuments or in peculiar wooden-based structures of Medieval epoch such as most of the Stave Churches. Most of existing data are still unpublished at international level, being generally part of internal reports created by the Norwegian Directorate of Cultural Heritage (Riksantikvaren) [1], and conservation reports by the Norwegian Institute for Cultural Heritage Research (NIKU). Exceptions are represented by few papers as BylundMelins thesis from 2017, an important contribution to the correlation between climatic stress and painted wood [2], and the recent contribution of Napp et al. [3] studying a stonebased medieval church in Sweden and assessing an adaptive ventilation system for reducing internal Relative Humidity (RH) conditions. Alternatively, only a couple of other scientific articles

discuss such problem, focusing on wooden architectural heritage. In 1994 Olstad reports about the results of a project started in 1986 with the aim of improving the conditions for painted wooden objects in wooden churches in Norway and involving the recording of Temperature (T) and RH values in two unheated and three heated churches [4]. About 18 years later, in 2012, relative humidity variations induced by the heating system were studied in the Hedalen Stave church by Lasyk et al. [5]: in that case internal temperature was continuously maintained at 7°C and increased up to 18-19° C when the church was used. As the authors report, the heating episodes lead to periodic fluctuations of RH and they refer to data of monitoring campaigns acquired in three main intervals: from 1986 to 1994, from 2001 to 2003 and from 2008 to 2009. The maximum fluctuation (38% in 36 h) was found for winter 2008/2009, whereas absolute minimum and maximum reached values were 21 and 72% respectively [5]. Very recently a paper mainly focusing on alteration products observed on the Hopperstad stave church also reported average T and RH data recorded from December to June 2017 [6].

Efforts are currently ongoing to fill this gap thanks to active programs such as the SyMBoL (Sustainable Management of heritage Buildings in a Long-term perspective) coordinated by the Norwegian University of Science and Technology (NTNU), and the MOV Projects coordinated by NIKU. The first foresees the acquisition of microclimatic data in Heddal and Ringebu stave churches for ca. 24 months since March 2019. Parallel, the MOV Project plans to cover a period of 50 years. The first part however is for the period 2017-2026 monitoring a total of 35 medieval wood and stone-based buildings.

A stave church is a frame construction resting on stone foundations consisting of horizontal and vertical wooden elements co-jointed to the staves placed in the corners. In most cases, they had a raftered roof, while corners and angles joints were strengthened thanks to brackets obtained by the wood from the transition zone between the roots and the trunk; strong construction elements due to the fiber-direction of the wood [7]. Norway totally still has 28 stave churches groupable into 4 main typologies of structures: i) simple; ii) Møre; iii) center post; iv) churches with an elevated section in the nave and in the chancel [7].

The Kvernes stave church, object of the presented study, is a single-nave church (16x 7.5 m; capacity = 200 people) dated back to the beginning of 1600. It is located in Møre and Romsdal county on the west coast of Norway and is exposed to wind, high RH conditions through the year, and mild winters due to the proximity of the sea.

Internally the church displays a rich decorative apparatus being walls, the ceiling in the chancel, the nave, as well as the baptistery in the western end of the nave totally covered by distemper paintings dated back to 1630s. Additionally a carved and painted polychrome epitaph dated to 1671 is positioned on northern wall, while a wooden painted altar carries an altarpiece with the corpus of a triptych (the wings are lost) referable to the late mediaeval period inserted into a carved and painted altarpiece in realized in 1695.

Contrarily to what happened in many historical churches in the 20th century, the Kvernes stave church never underwent the installation of a heating system due to the construction of a new second church in its proximity. For this reason, microclimatic fluctuations in the medieval church are basically referable to climatic external conditions, the performance of liturgical functions and to the presence or absence of visitors.

The research presented in this paper focuses on microclimatic data acquired through the installation of data loggers in 2011 during the Stave Church Preservation Programme for the monitoring of the Kvernes church over a 1-year period. Such data have been elaborated and represent the first real effort to scientifically investigate the internal microclimatic conditions achievable by monitoring campaigns in Stave Churches.

2 MATERIALS AND METHODS

Four Tinytag data loggers (Gemini Data Loggers Ltd, Chichester, UK) were placed in the east side of the Kvernes church as shown in Figure 1. The high of the four loggers was slightly different. Log named 1 and 2 were placed at a height of approx. 2 meters, while log named 4 and 5 were at about 3 meters above the floor.

T and RH data were collected from 20/06/2011 to 13/06/2012. Since logger 1-4 collected data every hour while log 5 every two hours, this last acquisition interval was selected in order to obtain comparable data series [8]. Outdoor data was collected from weather stations in proximity of the church site (63.0° N, 7.7° E). Two weather stations were selected: i) Kristiansund Lufthavn (63.1° N, 7.8° E, being associated to the Kristiansund Airport), recording from June 1970, to compare data acquired by loggers and ii) Kristiansund N, recording between March 1946 and December 1975, used to investigate a homogeneous climate normal period.



Figure 1: Images showing the location of the four data loggers in Kvernes stave church. Photo: NIKU © 2011. a) loggers 1 and 2; b) loggers 4 and 5.

It is the average value of meteorological data over several decades and normally a 30 years period is considered, as required by the United Nations World Meteorological Organization (WMO), with the most used being the 1961-1990. However, in the case of weather stations in proximity of Kvernes, it has been not possible to find RH (%) values over such normal period, for this reason a different time-window has been designated as reference period for our study. The utilized normal climate/ reference period is the 1957-1975 window, available from the weather station Kristiansund N and it allowed comparing the conditions of these 28 years with the monitored period 2011-2012 to assess the climate anomaly or variability during the monitoring campaign.

3 DISCUSSION OF THE RESULTS

The analysed 2011-2012 indoor data present the microclimatic situation of a typical unheated stave church in a coastal climate in Norway, which can be interestingly compared with available results from previous microclimatic monitoring campaign conducted in Medieval churches in Scandinavia.

3.1. The comparision within Scandinavian Medieval Churches

Elaborations showed how information form LOG 1,2 and 4 resulted almost equivalent; consequently LOG 4 has been chosen as representative for the group of loggers. On the other hand, LOG 5 that was opportunely positioned in a location constantly hit by sun radiation, is representative of the radiation effect inside the church. Table 1 resumes results obtained in

Kvernes and shows how the most significant differences among the two loggers concern RH values. Values collected by LOG5 are, in fact, generally lower, especially in summer (JJA). Obtained values can be compared with those more recently acquired (2017-2018) in the UNESCO World Heritage Site of the Urnes stave church (Table 2) and with those published by Napp et al [3] for Hangvar church, a Swedish medieval stone-based church in the northern part of the Gotland island in the Baltic sea (Table 3), and collected between 2010 and 2013. Values, seem to be comparable between the Kvernes and the Hangvar churches, even if the two structures have been realized using different materials. When comparing data with those acquired in Urnes, stronger variations emerge. In particular the average winter (DJF) temperature stays below 0°C, probably because of the different climatic conditions in the area surrounding the Urnes church with respect to those of Kvernes located on the north west Norwegian sea-shore. Urnes is in the Sogn og Fjordane Region in the west, close to the shore of the innermost branch of a fiord.

Table 1: Results from the microclimatic monitoring campaign in Kvernes (Norway) in 2011-2012. Av T= Average Temperature (Av T); Av RH =Average Relative Humidity; Max RH= Maximum Relative Humidity; Min RH= Minimum Relative Humidity; %RH>70%= % of values exceeding 70% RH; % of values exceeding the limit indicated by the EN15757:2016 [9]. SON= September-October-November; DJF= DecemberJanuaryFebruary; MAM= March-April-May; JJA= June-July-August.

LOG4	**Av T (°C)**	**Av RH (%)**	**Max RH (%)**	**Min RH (%)**	**% RH>70**	**% RH_{lim}**
SON	6.76	77.37	98.68	52.53	76.3	16.5
DJF	3.15	77.26	100	46.45	80	28
MAM	10.06	80.47	92.39	48.15	93	5.1
JJA	14.48	80.85	92.66	52.28	95	1.7
LOG5						
SON	6.83	74.48	98.88	42.32	60	20
DJF	2.88	77.28	100	46.3	78	23
MAM	9.90	79.31	93.23	47.2	90	6
JJA	10.96	77.89	87.72	45.86	84	2

Table 2: Results from the microclimatic monitoring campaign in Urnes (Norway) in 2017-2018. Av T= Average Temperature (Av T); Av RH =Average Relative Humidity; Max RH= Maximum Relative Humidity; Min RH= Minimum Relative Humidity; %RH > 70%= % of values exceeding 70% RH; % of values exceeding the limit indicated by the EN15757:2016 [9]. SON= September-October-November; DJF= December-January-February; MAM= March-April-May; JJA= June-July-August.

Urnes SON	**Av T (°C)**	**Av RH (%)**	**Max RH (%)**	**Min RH (%)**	**% RH>70**	**% RH_{lim}**
	7.40	77.51	96.1	45.3	77	10
DJF	-0.63	80.72	97.1	32.9	87	9.9
MAM	7.418	60.16	90	29.6	27	27

JJA	15.65	66.04	87.7	25.6	32	12

Table 3: Results from the microclimatic monitoring campaign in Hangvar (Sweden) in 2010-2013 (adapted from [3]). Av T= Average Temperature (Av T); Av RH =Average Relative Humidity; Max RH= Maximum Relative Humidity; Min RH= Minimum Relative Humidity; %RH>70%= % of values exceeding 70% RH; % of values exceeding the limit indicated by the EN15757:2016 [9]. SON= September-October-November; DJF= DecemberJanuary-February; MAM= March-April-May; JJA= June-July-August.

Hangvar	Av T (°C)	Av RH (%)	Max RH (%)			
				Min RH (%)		
SON	11.3	77	90		% RH>70	% RH_{lim}
DJF	3.3	75	96	63	89	19
				54	78	0
MAM	6.8	80	90	63	100	0
JJA	9.6	81	96	63	98	31

3.2. Analysis of T and RH variations in the Kvernes Stave Church.

Elaborations of data collected in Kvernes are shown in Figure 2 in term of T and RH differences between indoors values at different daily time (i.e. at 8 a.m., 2 p.m. and 9 p.m.) and the outdoor minima, maxima and average values from the Kristiansund Lufthavn Station. A quite strong day-night variability is observable as well as differences due to the seasonal cycles caused by the synergistic effect of the building envelope, the use of the church (e.g. weekly religious offices and visitors presence in summer), and the distance between the church and the weather station location (ca. 10 km). This effect changes during daytime along the year.

Morning: during all the year the indoor temperature at 8 a.m. (blue line, Figure 2) is warmer of ca. 2 °C respect to the outdoor daily minima. As already stated in Camuffo et al. 2016 [10], readings collected indoors at this time are not representative of the outdoor daily minima especially in Scandinavian countries where the time lag after sunrise changes quite a lot during the calendar year. In Kvernes at 8 a.m, LOG 4 is never hit by solar radiation and therefore is representative of a stable situation. On the contrary, LOG5 fluctuates more: during equinoxes the sensor is hit (NE direction, ca. at 8 a.m.) by direct solar radiation with an increase of ca. 2 °C (Figure 2b, blue line) on the mean ΔT; during summer solstice it is also hit but with the maximum direct solar radiation occurred earlier in the morning; finally in the winter solstice LOG5 is not reached by radiation.

Afternoon: the indoor T measured at 2 p.m. (red line, Figure 2) can be representative of the outdoor daily maxima. During the whole year period, LOG 4 is hit by solar radiation: during summer solstice and equinoxes, the maxima of radiation impinging LOG4 (SW direction) occur respectively at ca. 3 p.m. and 2 p.m. while in winter solstice such maxima are extinguished some minutes earlier. For this reason, the indoor T is lower than outdoor maxima of ca. 2 °C, fluctuating around or slightly exceeding this value from April to October (red line, Figure 2). LOG5, (NE corner direction) shows a similar situation, but being nor directly heated by solar radiation in the afternoon, it has a constant slightly lower indoor temperature.

Evening-Night: the ΔT obtained by the indoor T - measured at 9 p.m.- minus the mean outdoor daily T, is reported as black line in Figure 2. Black line fluctuates between 0 °C and 2 °C along the year, highlighting how the indoor reading at 9 p.m. is representative of the 24 hours outdoor daily mean [11]. This is especially true at equinoxes with a certain level of departure mainly during the summer solstice when LOG4, being hit for longer time in the afternoon and evening by solar radiation, records a departure of ca. 2°C.

Similarly, also RH values detected indoors and outdoors and by the two loggers look quite different. An average situation, highlighted by the black line in Figure 2c and 2d demonstrated that there is almost no difference between the RH measured at 9 p.m. inside

Kvernes and the outdoor daily mean, except in summer, when due to the larger difference T and mixing ratio (MR) between the indoors and the outdoors, the RH values are lower inside of almost 7%. Different are the situations induced by T and MR in the morning - that sees indoor RH fluctuating around a level 15% higher than the minimum RH measured outdoors – or in the afternoon, at 2 p.m. that sees indoor RH fluctuating around a level 15% lower than the maxima RH measured outdoors, showing a slight damping of the fluctuations of RH compared with the external ones. The most evident difference between LOG5 and 4 being the T effect at 2 p.m. which induced a drop in the measured RH.

In order to deeper investigate the internal microclimatic conditions of the Kvernes stave church, a detailed analysis of the central months of each season was performed for LOG4 and LOG5. Elaborations proposed in Figures 3 and 4 show vertical windows individuating the daily light durations as indicated by data available at [12], superimposed to T, RH and Mixing Ratio (MR) trends. Since the Kvernes church has never been heated, the indoor climate follows the outdoor one except when people visit church (summer): in these cases, the presence of numerous visitors can strongly modify the indoor climate. Kvernes is, in fact, a museum church, housing special events and open for tourists (ca. 10 000 visitors per year) in the summer season. While the impact of visitors is embedded in the microclimate reported in Figure 2 (period: end of June to mid-September), the observed environmental variations in Figures 3 and 4 cannot be imputed to these activities but rather at the standard condition of use of the church with its weekly religious service only. Internal data acquired by loggers can indeed be related to variations in T and RH of the external climate, which are shown in Figure 5. The analysis of outdoor temperature evolution indicates an overall high temperature period, as expectable, between the end of June and the end of September 2011, with two additional maxima in October 2011 and half of March 2012 (Figure 5a). The anomaly (Figure 5b green line) has highlighted two spells of drier period in October 2011 and in January 2012, just before the peak of temperature anomalies (Figure 5a, green line). While, as opposite a more humid period outside has been detected in March 2012 before the negative anomaly in temperature (Figure 5a, green line). These climate conditions outdoors show an enrichment of grams of water vapor over one kg of dry air in average of 1 gr/kg (Figure 5c) although spells of depletion of water vapor exist in conjunction with the drops in RH. Analyzing the microclimatic condition indoors for a representative week in summer, Figures 3 and 4 shows wider daily T and RH cycles with indoor RH changes ca. 10% lower than outdoor conditions and following its seasonal cycle.

Daily T and RH minima and maxima fall within the daylight cycles. In this season, as reported in Table 3, the higher risk for the conservation of the decorated wooden elements in Kvernes is represented by the RH and T conditions which may trigger biological decay (i.e. T >14°C and RH >70%) that occur in the 95% of the time.

In the same season, Urnes stave church appears having lower risk of biological decay due to the generally lower indoor RH values (Table 2) [13]; while the appearance of fungi infestation in Hangvar with very high indoor RH may be naturally controlled in this season thanks to the still lower indoor T. However, biological decay- mould- is observed on the unpainted as well as the painted walls in Urnes, but not in Kvernes. In the representative week in autumn, indoor RH is usually higher than outdoor ones, the daily T and RH cycle is less evident (more evident from LOG4 readings than LOG5), in such microclimatic conditions in Kvernes, a certain risk of RHinduced mechanical decay can be recorded i.e. when indoor RH variability exceeds the safe limit of the target range of RH fluctuation, as defined by the EN15757:2010 [9] standard, and determined as the 7th and 93rd percentile of the fluctuations recorded in the monitoring period respect to the moving average [9] (Table 1).

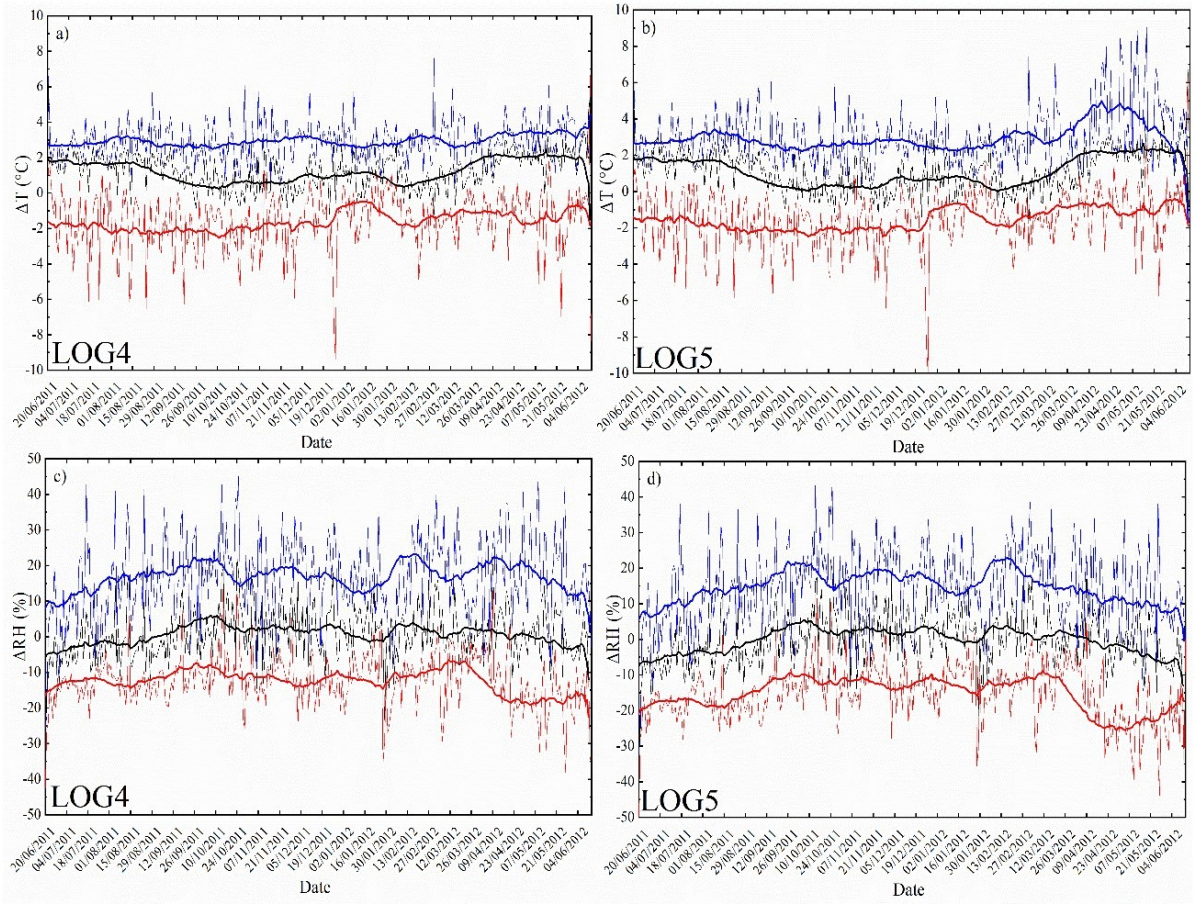


Figure 2: a, b) Differences between indoor temperature values at 8 a.m. (blue lines), 2 p.m. (red lines) and 9 p.m (black lines) measured by LOG4 and 5 and the outdoor daily minima, maxima and mean values as measured at the Kristiansund Lufth. Station. Thicker lines represent running averages of every series of data. c, d) Differences between indoor Relative Humidity values measured at 8 a.m. (blue lines), 2 p.m. (red lines) and 9 p.m (black lines) by LOG4 and 5 and the outdoor minima, maxima and mean values measured at the Kristiansund Lufth. Station. Thicker lines represent running averages of every series of data.

More in detail, the 7th or 93rd percentiles are obtained by ordering the fluctuations from the lowest negative value to the highest positive one and selecting the values below which 7th or 93rd percent of observations are found, respectively. In this way 14 % of the largest, most risky fluctuations are excluded, the cuts being equally applied to peaks and drops in RH, yielding excessively moist or dry environments. In Kvernes, such risk of mechanical decay is at its maximum in winter when it can be further exacerbated by T-induced mechanical decay conditions of the winter season in Scandinavian countries last for longer time, often the spring due to freezing/thawing cycles. In a representative week in winter the daily T and RH cycle is smoothed out and the indoor RH becomes comparable with the outdoor ones. As the climatic season (MAM) resembles the winter in term of indoor microclimatic conditions. This is evident in the Urnes stave church (Table 2) that shows the higher risk of RH-induced mechanical decay

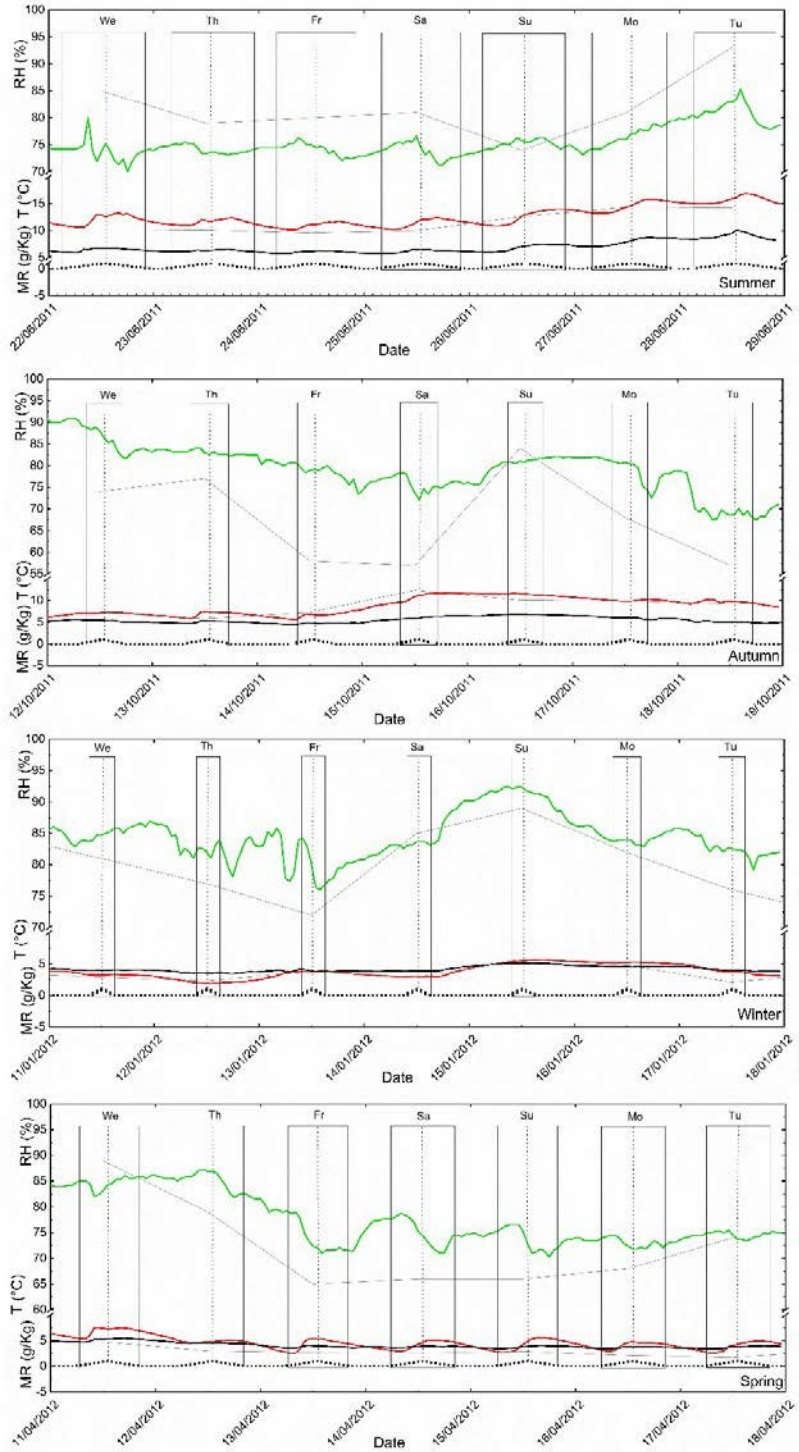


Figure 3: Indoor RH (%)-green line, T (°C)- red line, MR (g/Kg)-black line values for a representative week in four seasons as measured by LOG 4. a) Summer 22/06/2011 and 28/06/2011; b) Autumn 12/10/2011 and 18/10/2011; Winter c) 11/01/2012 and 17/01/2012; d) Spring 11/04/2012 and 17/04/2012. The grey line refers to outdoor RH values collected by the Kristiansund Lufthavn meteorological station.

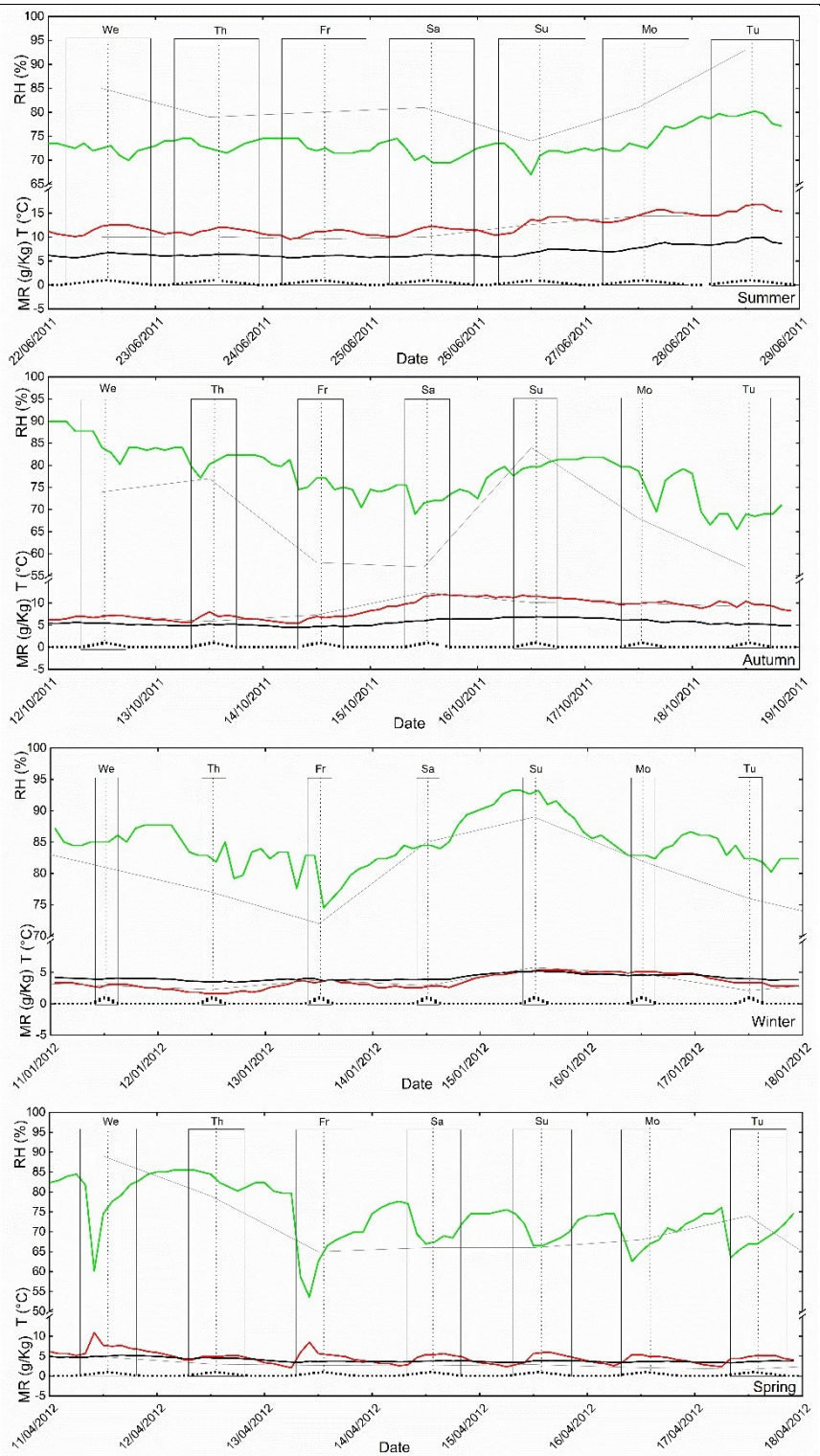


Figure 4: Indoor RH (%)-green line, T (°C)- red line, MR (g/Kg)-black line values for a representative week in four seasons as measured by LOG 5. a) Summer 22/06/2011 and 28/06/2011; b) Autumn 12/10/2011 and 18/10/2011; Winter c) 11/01/2012 and 17/01/2012; d) Spring 11/04/2012 and 17/04/2012. The grey line refers to outdoor RH values collected by the Kristiansund lufthavn meteorological station.

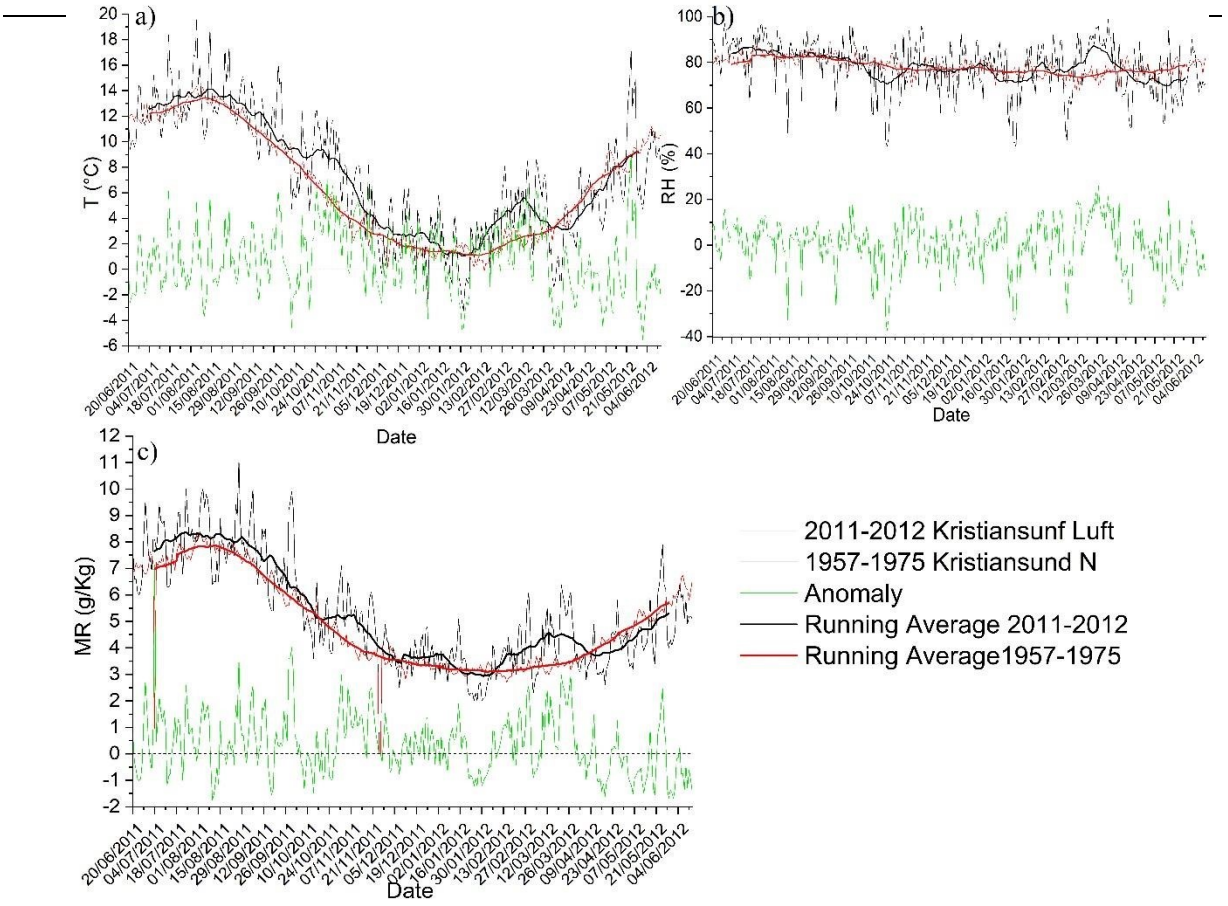


Figure 5: a) Daily outdoor temperature (°C) from the Kristiansund Lufthavn station between 20/06/2011 and 13/06/2012 and at the Kristiansund N. station for the normal period 1957-1975. T Anomaly (°C) between data recorded in 2011-2012 and in 1957-1975. b) Daily outdoor Relative Humidity (%) from the Kristiansund Lufthavn station between 20/06/2011 and 13/06/2012 and at the Kristiansund N. station for the normal period 1957-1975. Relative Humidity Anomaly (%) between data recorded in 2011-2012 and in 1957-1975; c) Daily outdoor Mixing Ratio (g/Kg) from the Kristiansund Lufthavn station between 20/06/2011 and 13/06/2012 and at the Kristiansund N. station for the normal period 1957-1975. Mixing Ratio Anomaly (g/Kg) between the data recorded in 2011-2012 and in1957-1975.

in this period, while Hangvar medieval stone church may encounter higher risk of mould infestation or condensation (Table 3).

4 CONCLUSIONS

The SyMBoL project is currently carrying out long-term (more than 2 years) monitoring campaigns in two stave churches in different climatic sites and under different in-use conditions (Heddal and Ringebu) to improve understanding of the "historic climate" [9]. Being most of existing data on microclimatic conditions in Scandinavian Medieval churches still unpublished at international level, this contribution was aimed on elaborating and presenting all the available data (i.e. with not restricted access) obtained by the monitoring campaigns conducted inside the Kvernes (Norway) Stave Church in 2011-2012. Being the church still unheated, variations in term of T, RH and MR are completely imputable to external climate modifications or to the presence of visitors in the summer opening and for special religious services. The effect of the church geographical position on its internal microclimate was assessed by comparison with data available from Urnes, located in a more internal area, not so affected by the sea influence (the Golf stream). Furthermore, the detailed analysis of indoor and outdoor conditions evidenced the relevance in loggers positioning in order to obtain complementary information permitting to depict a complete picture of the site internal conditions.

This study will be very beneficial as knowledge background for the MOV research project in Norway that, beside SyMBoL, is a long-term monitoring (planned for 50 years) project which aims to collect indoor and outdoor data on a similar category of historical buildings over a period of time comparable with that of climate norm.

The microclimatic analysis of the presented study highlights similarities in indoor climate conditions in unheated stave churches - located in different regions in Norway – and in a medieval stone church in Sweden. Such natural condition which the unheated church gives, may be ideal for the preservation of the distemper paints as these artworks remained in quite good conditions over centuries up to nowadays. In addition, the comparison with a stone-based medieval church located in a similar climate indicated no substantial differences within the two structures. This constitutes an additional important information for heritage managers and church owners, often dealing with the identification of risks situations and discrimination among the possible typologies of decay. The presented paper also provides reliable information for supporting risk management and climate change adaptation plans for the preservation of Medieval churches in Scandinavian countries because it makes available the actual or recent past or the zero level.

Funding: This study was funded by the Norwegian Research Council within the framework of the "SyMBoL – Sustainable Management of Heritage Building in a Long-term Perspective" Project (Project No. 274749). The authors are grateful to Else Marie Bae for her kind support during the monitoring campaign and to Kjersti Marie Ellewsen for sharing the data of her Master-thesis on the monitoring campaign conducted in Urnes Stave Church. The authors declare no conflict of interest.

References

[1] Cultural Heritage Act of June 9, 1978. https://www.regjeringen.no/no/dokumenter/kulturminneloven/id173106/ (accessed on 08/01/2020)

[2] Bylund Melin, C. Wooden objects in historic buildings: Effects of dynamic relative humidity and temperature. PhD thesis. Department of Conservation; Göteborgs universitet. Naturvetenskapliga fakulteten, 2017.

[3] Napp,M., Wessberg, M., Kalamees, T., Brostrom, T. Adaptive ventilation for climate control in a medieval church in cold climate, *Int. J. Vent*. (2016) **15**: 1-14.

[4] Olstad, T.M. Mediaeval wooden churches in a cold climate—parish churches or museums? *Stud. Conserv.* (1994) **39**: 99-103.

[5] Lasyk, Ł., Łukomski, M., Olstad, T. M., Haugen, A. Digital speckle pattern interferometry for the condition surveys of painted wood: Monitoring the altarpiece in the church in Hedalen, Norway, *J. Cult. Herit.* (2012) **13S**: S102-S108.

[6] Lehne, M., Mantellato, S., Aguilar Sanchez, A. M., Caruso, F. Conservation issues and chemical study of the causes of alteration of a part of the Stave Church in Hopperstad (Norway), *Herit. Sci.* (2019) **7**:80.

[7] Anker, L. What is a Stave Church. In: K. Bakken (Ed): *Preserving the Stave Churches, Craftsmanship and Research*, Print Best OU, Estonia, (2016), pp.17-22.

[8] Olstad, T. M. Klimaregistreringer i Kvernes stavkirke 2011-2012. Averøy kommune, Averøya. NIKU Report 24/2013. Unpublished. 2013.

[9] EN 15757:2010. Conservation of Cultural Property – Specifications for Temperature and Relative Humidity to Limit Climate-Induced Mechanical Damage in Organic Hygroscopic Materials, European Committee for Standardization, Brussels.

[10] Camuffo, D., della Valle, A., Bertolin C., Santorelli, E. The Stancari air thermometer and the 1715-1737 record in Bologna, Italy. *Climatic Change* (2016) **139**: 623-636.

[11] Camuffo, D., della Valle, A., Bertolin, C., Santorelli, E. Temperature observations in Bologna, Italy, from 1715 to 1815: a comparison with other contemporary series and an overview of three centuries of changing climate. *Climatic Change* (2017) **142**: 7-22.

[12]http://sharki.oslo.dnmi.no/portal/page?_pageid=73,39035,73_39049&_dad=portal&_schema=PORTA L (accessed 08/01/2020)

[13] Olstad, T. M., Ørnhøi, A. A., Kjølsen Jernæs, N., de Ferri, L., Freeman, A., Bertolin, C. Investigation, monitoring, risk assessment and decision making for the preservation of distemper paintings in Kvernes Stave Church, *Climate*, Submitted.

12th International Conference on Structural Analysis of Historical Constructions
SAHC 2020
P. Roca, L. Pelà and C. Molins (Eds.)

MULTI-MODAL ANALYSIS OF VIBTATION AND METEOROLOGICAL DATA FOR STRUCTURES ON THE WORLD HERITAGE SITE "BATTLESHIP ISLAND"

NARITO KURATA[1*], KAZUKI TAKAI[2], AKIHIRO TOMIOKA[2], TAKUYA DAIGO[2], SHUNSUKE SARUWATARI[3] AND TAKUJI HAMAMOTO[4]

[1] Graduate School of Technology and Science
Tsukuba University of Technology (NTUT)
3-4-15 Amakubo, Tsukuba city, Ibaraki 305-8520, Japan
e-mail: kurata@home.email.ne.jp, www.tsukuba-tech.ac.jp/english

[2] Akishima Plant
Japan Aviation Electronics Industry, Ltd. (JAE)
3-1-1 Musashino, Akishima city, Tokyo, 196-8555, Japan
email: { takaikz, tomiokaa, daigot }@ jae.co.jp, www.jae.com/en

[3] Graduate School of Information Science and Technology
Osaka University
1-5 Yamadaoka, Suita, Osaka, 565-0871, Japan
email: saru@ist.osaka-u.ac.jp, www.osaka-u.ac.jp/en

[4] Tokyo City University (TCU)
1-28-1 Tamazutsumi, Setagaya-ku, Tokyo, 158-8557, Japan
email: hamamoto325@gmail.com, www.tcu.ac.jp/english

Keywords: Structural Health Monitoring, Vibration Measurement, Meteorological Observation, Accelerometer

Abstract. *This paper reports the results of vibration and meteorological observations of a buildng built on Hashima, Nagasaki, southern part of Japan, which was registered as a World Heritage Site in 2015 [1], and analyzes its dynamic characteristics. Hashima is called "Battleship Island" because its appearance resembles a battleship due to the many buildings standing upon it. The structure contributing most to the battleship appearance is No. 3 Building. An accelerometer and a weather sensor have been installed in No. 3 Building for long-term measurements. Multi-modal analysis of vibration and meteorological data was performed for 5 months, and the dynamic characteristics of No. 3 Building were examined.*

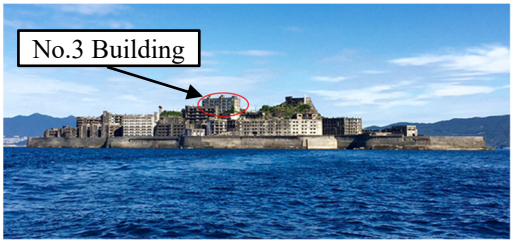
1 INTRODUCTION

Hashima Island in Nagasaki City in the south of Japan was registered as a World Cultural Heritage in 2015 [1]. The island was an offshore city that prospered as an undersea coal mine from the 1800s, and had a population density higher than that of Tokyo. The shape of the island resembles that of a battleship, so it is also referred to as "Battleship Island" (or Gunkanjima).

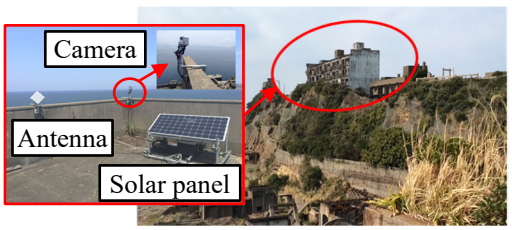
As a result of the effect of the energy policy from the 1970s onwards the mine closed on 15th January 1974. Thereafter Battleship Island became unoccupied, but a group of building structures that are degrading with time under the severe natural environment remain. The authors have installed various types of sensors on the group of structures on Battleship Island, and are performing monitoring [2]. Building No. 3 contributes most to the resemblance of the silhouette of this island to a battleship. It is the most important among the structures of Battleship Island and must be preserved. A new vibration monitoring system was installed on Building No.3 in May 2019. Building No. 3 is a 4-story reinforced concrete structure; a total of ten accelerometers were installed on each floor on both sides of the rectangular plan, and vibration measurements for the structural health monitoring [3] have been carried out over several months. Every two hours microtremor measurements are performed for 10 minutes, and in addition when vibrations exceeding a certain level occur such as during typhoons and earthquakes, vibration measurements are taken. On the other hand, meteorological sensors were installed on the rooftop of Building No. 3 in October 2017, measuring items such as air temperature, humidity, atmospheric pressure, wind direction, wind velocity, sunlight intensity, and rainfall. This paper presents the results of analysis of the dynamic properties of Building No. 3, obtained from a multi-modal analysis of the vibration data and the meteorological data.

2 NO.3 BUILDING, THE SYMBOL OF BATTLESHIP ISLAND

No. 3 Building on Battleship Island, shown in Fig. 1, is a 4-story reinforced concrete housing complex constructed in 1959. It is located at the highest point on Battleship Island, and is a symbolic building that has a silhouette similar to that of a battleship. The building is relatively new on the island, with little sign of aging and damage. On the rooftop of No.3 Building, a wireless antenna for maritime radio communication with the Battleship Island Museum on the opposite shore, a solar panel, a storage battery, and cameras that capture images of the surrounding area are installed. These serve as communication bases for the monitoring system.



(a) Panoramic View



(b) Camera, Energy and Network System



(c) Plan View

Figure 1: No.3 Building

3 VIBRATION MEASUREMENT SYSTEM

Fig. 2 shows the locations of the accelerometers in No. 3 Building [4]. No. 3 Building has a flat, rectangular shape, with a total of 10 acceleration sensors installed on both sides of each floor. Fig. 3 and Table 1 show the system configuration and the specifications of the acceleration sensors [5]. The accelerometers used are JA-70SA manufactured by Japan Aviation Electronics Industry. This accelerometer can measure a wide range of vibrations from microtremors, to strong vibrations during a typhoon or large earthquake. For vibration measurement, a data acquisition device (referred to as a DAQ) having a 16-channel A/D conversion module is used, and synchronization is performed to within 5 μsec by a multiplexer at the preceding stage. Time synchronization is performed by GPS, and the sampling frequency is set to 100Hz. A continuous measurement function that saves 10 minutes of measurement data every 2 hours and a trigger function that stores measurement data when more than a certain level of vibration occurs due to a typhoon or an earthquake are installed. The data stored in the data recorder is transmitted to a data server in the Battleship Island Museum on the opposite shore by a maritime radio communications antenna (see Fig. 1) installed on the rooftop. This data server is accessible via the Internet. Solar panels and storage batteries are installed on the rooftop of the structure to serve as a power source for the vibration measurement system. PCs, the DAQ and accelerometers consume higher power, but they use system power efficiently to provide constant remote monitoring and continuous measurement.

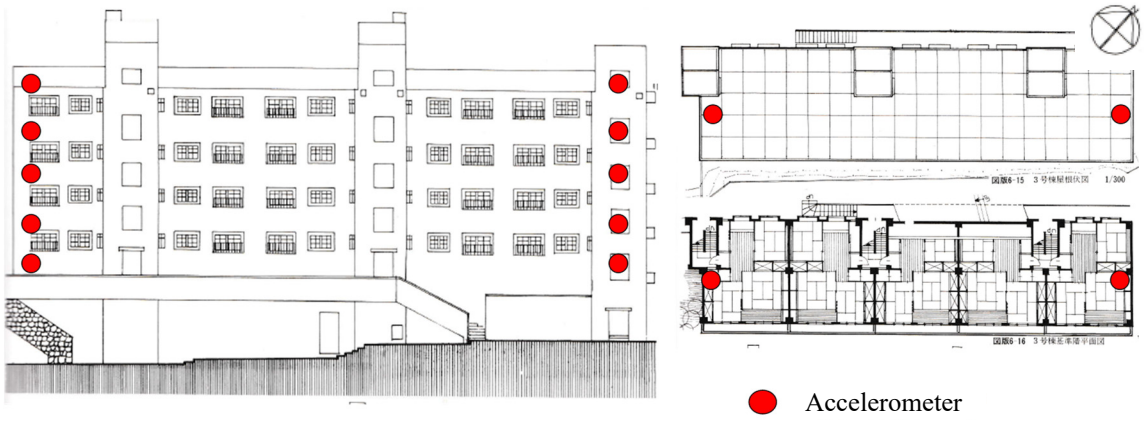


Figure 2: Sensor Location

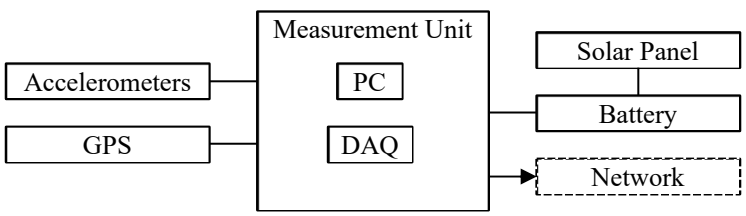


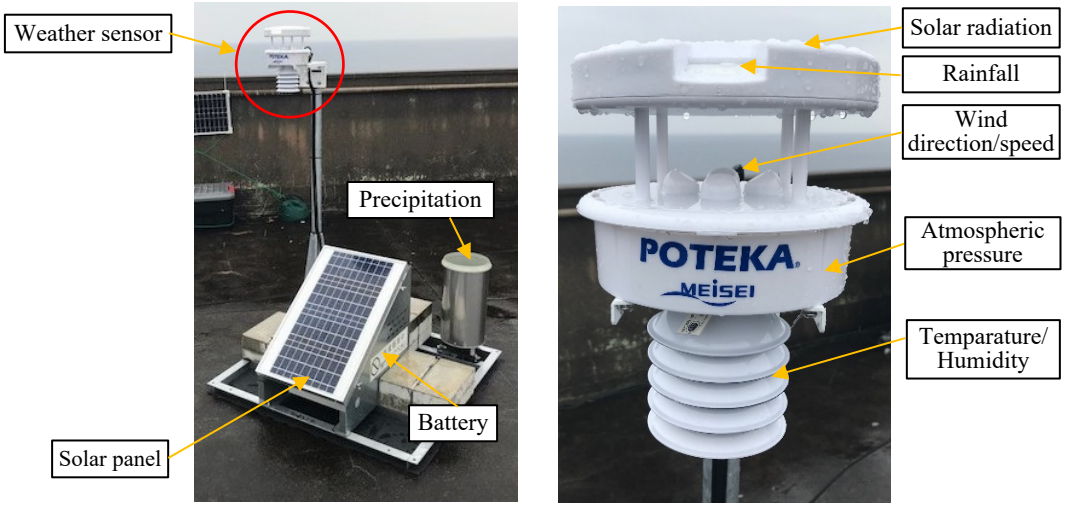
Figure 3: Vibration Measurement System

Table 1: Specifications of Accelerometer

Item		Units	JA-70SA
Measurement range		$\pm m/s^2$ [±G]	X,Y axes: ±19.6 or higher [±2] Z axis: -9.8 - +29.4 [-1~+3]
Voltage sensitivity (Note 1)		$V/(m/s^2)$ [V/G]	0.2039±5% [2.000±5%]
Zero point imbalance (Note 2)		m/s^2 [mG]	X,Y axes: within ±0.98 [±100] Z axis: 9.81±0.98 [-1000±100]
Case alignment		mrad	within ±20
Linearity		%FS	within ±2
Self-noise (@1~30Hz)		(m/s^2) rms/√Hz [Grms/√Hz]	$9.8x10^{-6}$ $[1x10^{-6}]$
Frequency response		Hz(±3dB)	≥200
Voltage sensitivity:temperature coefficient		ppm/°C	within ±200
Zero point imbalance: temperature coefficient		$\mu(m/s^2)$/°C [μG/°C]	±1961[±200]
Environmental resistance	Operating temperature	°C	-25~+70
	Non-operating temperature	°C	-40~+80
	Humidity	%RH	20~80
	Vibration resistance JIS C60068-2-6	10-60Hz 0.75mm, 60-500Hz 100m/s^2 [10G} Sinusoidal vibration 10 times for each axis 2H/time	
	Impact resistance JIS C60068-2-27	9800m/s^2 [100G] 6ms Half-sin 3 times for each axis、±direction	
Electrical properties	Power supply voltage	V(DC)	±5±0.5
	Consumption current	mA	<17
	Output impedance	Ω	47typ.
External dimensions	Width	mm	38.6
	Depth	mm	41.0
	Height	mm	24.8
Mass		g	≤100

4 AUTONOMOUS METEOROLOGICAL OBSERVATION SYSTEM

An autonomous meteorological observation system (Meisei Electric, POTEKA) is installed on the rooftop of No. 3 Building (see Fig. 4) [6]. As shown in Fig. 4(a), the system includes solar panels, storage batteries, a radio communication unit, a weather sensor station, rain gauges, and a base for fixing these devices. The weather sensor station comprises 7 types of sensors (temperature, pressure, humidity, solar radiation, wind direction, wind speed, and precipitation) as shown in Fig. 4(b). Because observation data is updated every minute, it is possible to capture changes in weather conditions in real-time. The weather data is transmitted to the server in real-time via a mobile phone network. Table 2 shows the specifications of the autonomous meteorological observation system, and Table 3 shows the specifications of the weather sensors.



(a) System View (b) Weather Sensor

Figure 4: Meteorological Observation System

Table 2: Specifications of Meteorological Observation System

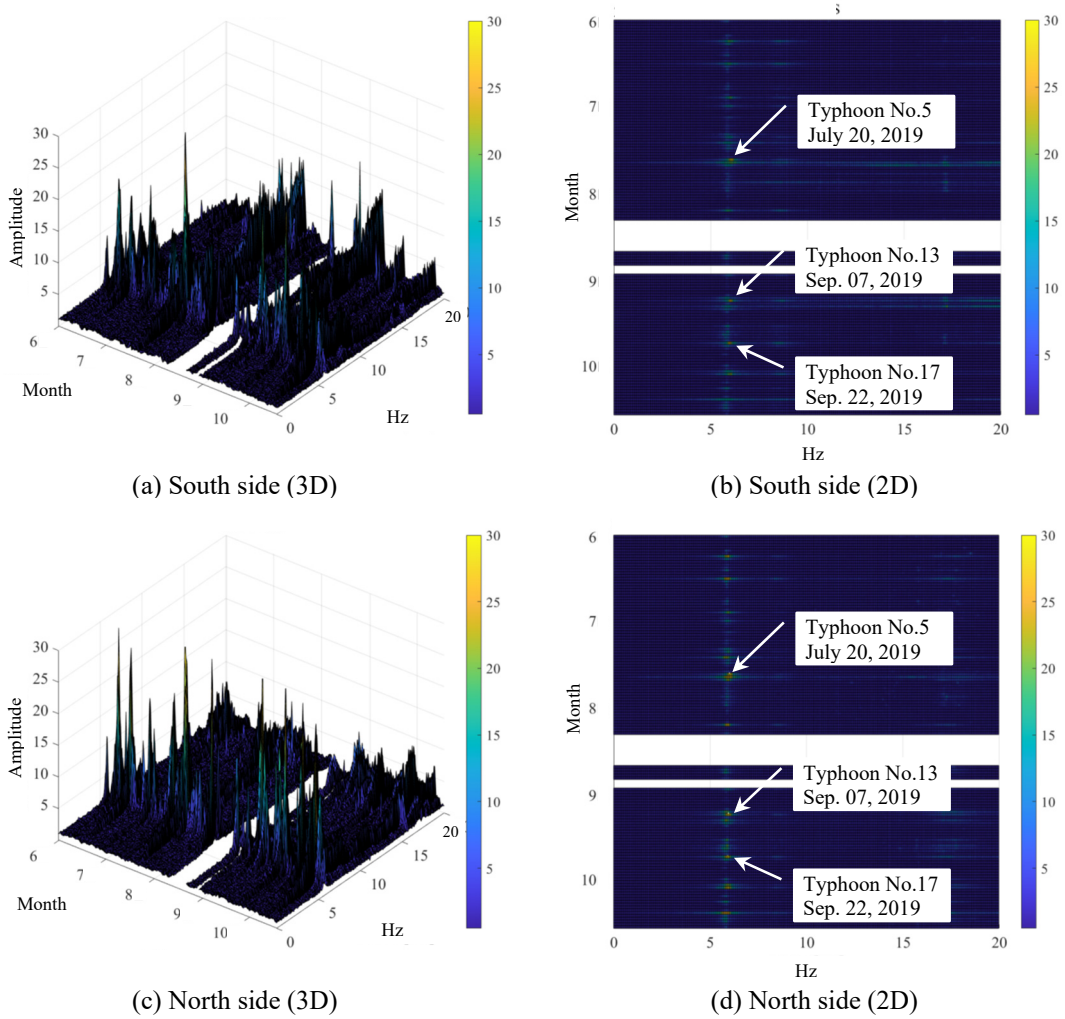
Observation element of weather sensor	Air temperature, atmospheric pressure, humidity, solar radiation, wind direction, wind speed, rainfall, precipitation
Sampling period	1 second
Statistical interval (output values)	1 min average
Communication interval	60 sec (variable from 10~999 sec)
Data storage	14 days
Solar battery capacity	30 W
Storage cell capacity	18 Ah
Built-in cell	Nickel-hydrogen cell 700mAh
Power interruption backup time	More than 6 hrs.
Operating temperature range	-10°C~+60°C
Wind speed resistance	Average wind speed 60m/s
Communications circuit	3G circuit

Table 3: Specifications of Weather Sensor

Element	Measurement method	Observation range	Precision
Air temperature	Platinum resistor	-50.0~+50.0°C	±0.3°C
Humidity	Capacitive type	0.0~100.0%RH	±5%
Atmospheric pressure	Capacitive type	870.0~1050.0hPa	±0.7hPa
Wind direction	Ultrasonic	0~360°	±10°
Wind speed	Ultrasonic	0.0~30.0m/s	±0.3m/s (0~10m/s) ±5% (10~30m/s)
Solar radiation	Photodiode	0~1400W/m^2	±10%
Rainfall	Capacitive type	0/1	-
Precipitation	Tipping bucket type	Below 200mm/h	±0.5mm (below 20mm) ±3% (above 20mm)

5 ANALYSIS OF VIBRATION AND METEOROLOGICAL DATA

Figs. 5 and 6 show amplitude ratios of Fourier acceleration spectra on the rooftop and the first floor calculated from acceleration data measured for 10 minutes from 12:00 every day, from June 1 to October 18, 2019. As can be seen from the figures, some parts of the data from August 12 to 19 and August 27 to 28 during the measurement period are missing. In each figure, the measurement dates, frequencies, and ratios of Fourier spectra are displayed in 3D and 2D. In addition, the dates of occurrence of three typhoons that caused strong vibrations in No. 3 Building during the measurement period are shown. Fig. 5 shows the analysis results of the long-side components of the sensors installed on the south and north sides of No. 3 Building. From these figures, it can be seen that the first characteristic frequency clearly appears around 6 Hz during strong winds or a typhoon. In addition, characteristic frequencies of higher-order modes can be observed near 17 Hz. Further, if vibration of the building increases due to strong winds or a typhoon, vibration in the high frequency region of 10 Hz or more increases on the south side.

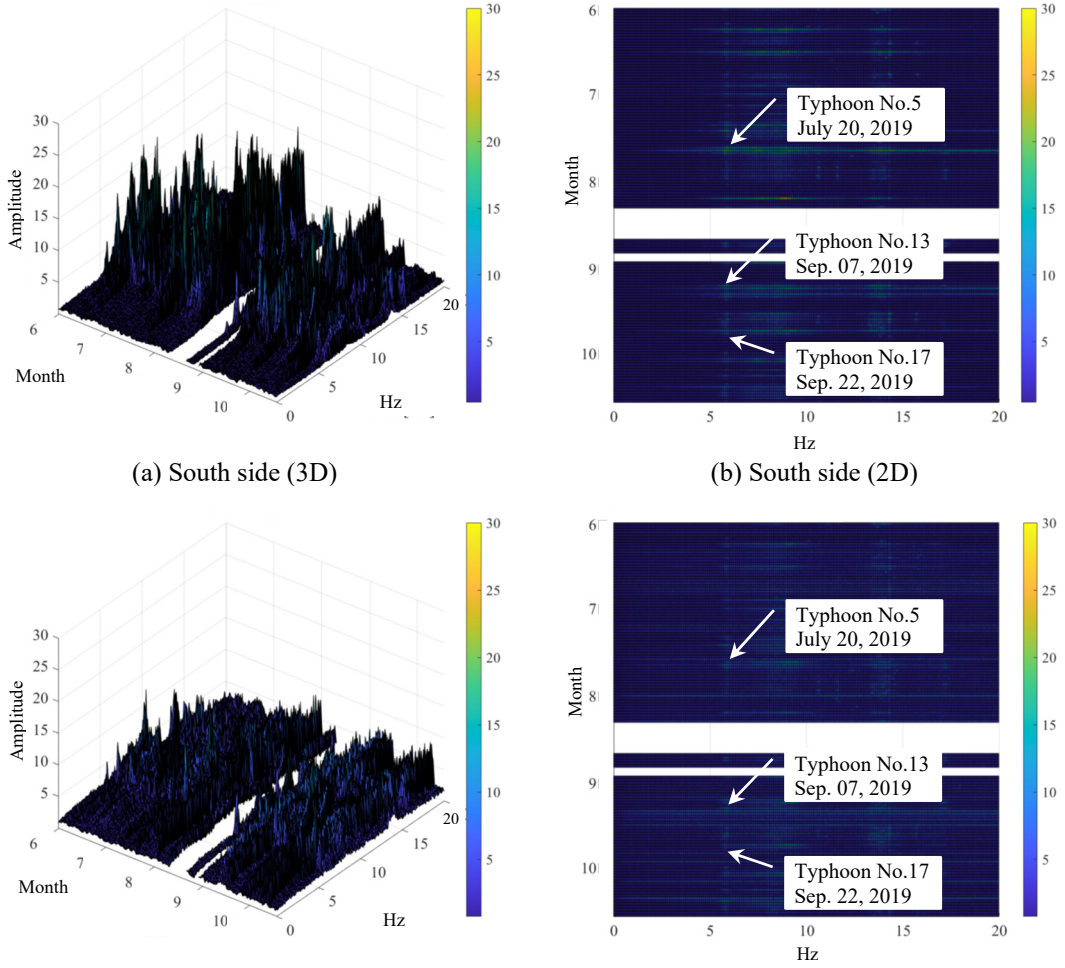


(a) South side (3D) (b) South side (2D)

(c) North side (3D) (d) North side (2D)

Figure 5: Fourier amplitude spectrum ratios of the acceleration data (Long-side component)

Fig. 6 shows the analysis results of the short-side components of the sensors installed on the south and north sides of No. 3 Building. From these figures, it can be seen that characteristic frequencies appear at around 9 Hz and 14 Hz in addition to 6 Hz during strong winds or a typhoon. Further, when vibration of the building increases due to strong winds or a typhoon, the vibration on the south side is larger than that on the north side, and on the south side, vibration in the high frequency region of 10 Hz or more increases.



(a) South side (3D) (b) South side (2D)

(c) North side (3D) (d) North side (2D)

Figure 6: Fourier amplitude spectrum ratios of the acceleration data (Short-side component)

Fig. 7 shows the average air temperature and the maximum instantaneous wind speed every 10 minutes, measured from June 1, 2019 to October 18, 2019. This figure also shows the dates of three typhoons that caused large vibrations in No. 3 Building during the measurement period. When the wind speed increases due to a typhoon, the vibration of the building increases, but in No. 3 Building, vibrations other than the characteristic frequencies are excited. As an example, Fig. 8 shows Fourier acceleration spectrum ratio of the roof and first floor in the short-side direction on the south side of the building calculated from acceleration data measured during

Typhoon No. 5. The figure shows the analysis results of data measured for 10 minutes every 2 hours, for 48 hours from 12:00 on July 19 until 12:00 on July 21, or from when Typhoon No. 5 approached until it passed. In the figure, the time zone where the wind speed is high is clearly indicated by the red frame. As the wind speed increases due to the typhoon, the vibration of the building increases, and it can be seen that on the south side of the building, vibrations in the high frequency region of 10 Hz or more are excited.

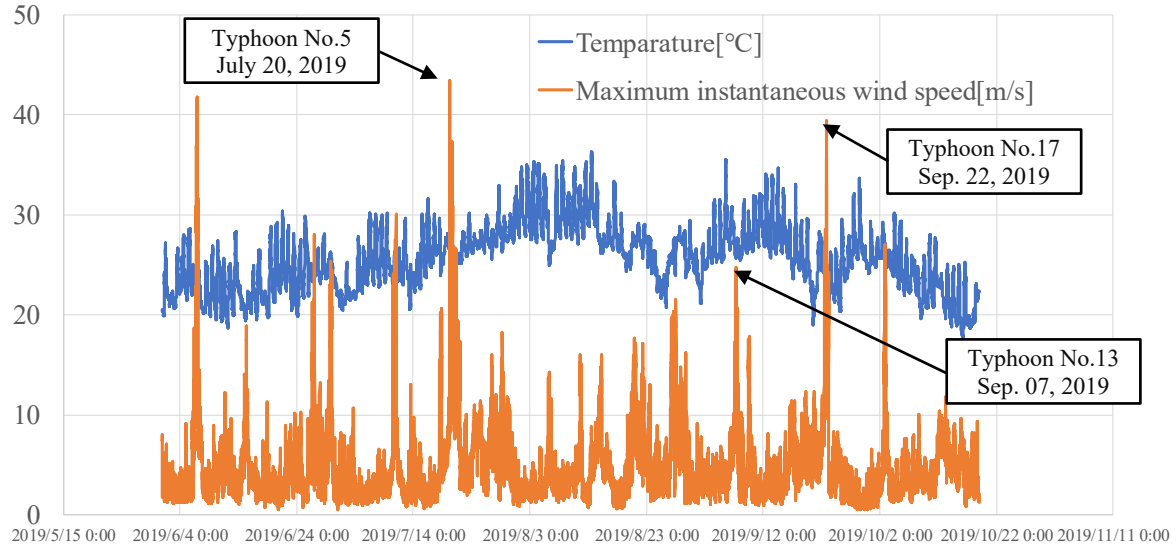


Figure 7: Average air temperature and the maximum instantaneous wind speed

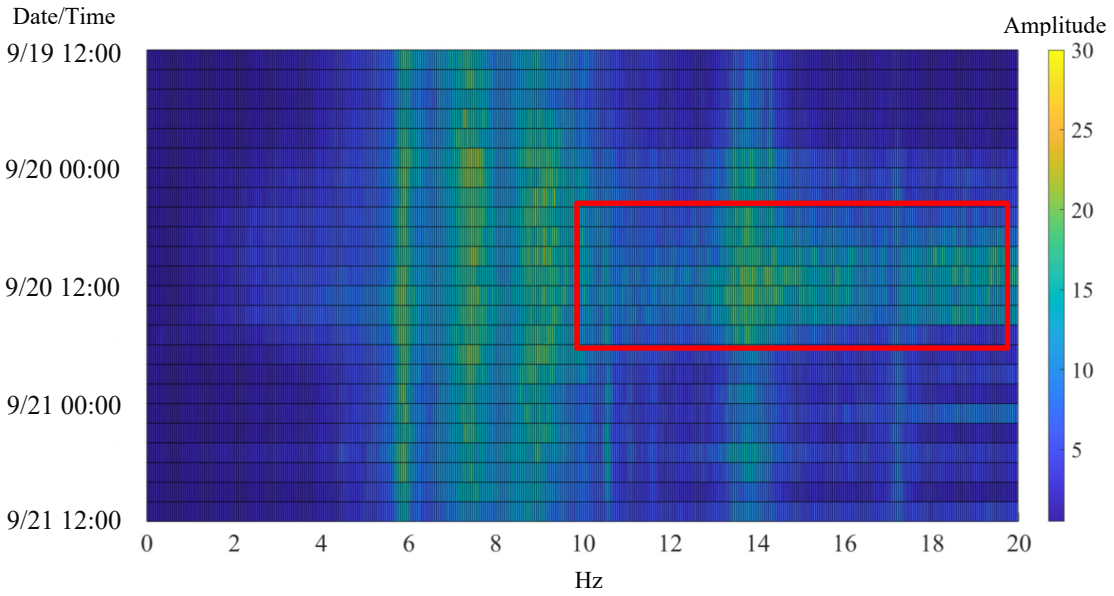


Figure 8: Fourier amplitude spectrum ratios of the acceleration data (Short-side component)

6 CONCLUSIONS

In this paper, vibration measurements and meteorological observations were made on the building of Battleship Island, which is registered as a World Cultural Heritage site, and their dynamic characteristics were analyzed. In the target, No. 3 Building, no change in low-order mode dynamic characteristics due to temperature changes from spring to autumn was observed. It was found that when vibration of the building increased due to strong winds or a typhoon, vibration on the south side was larger than that on the north side, and vibration in the high frequency region was also larger. This suggested that, by observing the fluctuations of low frequency region on the south side after large vibrations occur due to strong winds, a typhoon or an earthquake, it is possible to detect loss of structural stability of the building. In the future, it is planned to continue vibration measurements and meteorological observations for No. 3 Building, and compare the measurement results on a yearly basis including winter.

Acknowledgements. This work was supported by JSPS KAKENHI JP17KT0042 and JP26289194. Nagasaki City cooperated with the installation and measurement on the island. The photos were taken with the special permission of Nagasaki City.

REFERENCES

[1] World Heritage Committee. Decisions adopted by the World Heritage Committee at its 39th session (Bonn, 2015). United Nations Educational, Scientific and Cultural Organization, (2015).

[2] Hamamoto, T., Kurata, N., Saruwatari, S., Kawamoto, K., Tomioka, A. and Daigo, T. Field Test of Change Detection System of Building Group in Preparation for Unexpected Events in GUNKANJIMA. *AIJ J. Technol. Des.* (2018) **24** (57):553-558. in Japanese.

[3] Boller, C., Chang, F-K. and Fujino. Y. (EDS): *Encyclopedia of Structural Health Monitoring*, John Wiley & Sons, 2009.

[4] Akui, Y. and Shiga, H. *Gunkanjima Survey Data Collection (Supplementary Edition)*, Tokyo Denki University Press, 2005. in Japanese.

[5] Tomioka, A., Hamamoto, T., Kurata, N. and Saruwatri, S. Gunkanjima Monitoring Project Part 10: Configuration of MEMS Accelerometer Network. *Summaries of technical papers of annual meeting, Architectural Institute of Japan* (2018), pp. 151-152. in Japanese.

[6] Kurata, N., Sasaki, K., Saruwatari, S., Hamamoto, T. and Tomioka, A. Gunkanjima Monitoring Project Part 11: Autonomous Weather Sensor System installed at the No.3 Building. *Summaries of technical papers of annual meeting, Architectural Institute of Japan* (2018), pp. 83-84. in Japanese.

12th International Conference on Structural Analysis of Historical Constructions
SAHC 2020
P. Roca, L. Pelà and C. Molins (Eds.)

ONE YEAR STATIC MONITORING OF THE MILAN CATHEDRAL

ANTONELLA SAISI[1], ANTONELLO RUCCOLO[1] AND CARMELO GENTILE[1*]

[1]Department of Architecture, Built environment and Construction engineering (DABC)
Politecnico di Milano
P.za Leonardo da Vinci 32, 20133 Milan, Italy
e-mail: {antonella.saisi, antonello.ruccolo, carmelo.gentile}@polimi.it (*corresponding author)

Keywords: Historic Cathedral, Environmental Effects, Long-term Monitoring, Strain, Tilt

Abstract. *The paper focuses on the long-term monitoring of the Milan Cathedral. After a concise historic background on the monument and the description of the sensing devices installed in the church, selected results obtained during the first year of static monitoring are summarized as well as the lessons learned in view of the Structural Health Monitoring (SHM) of the Cathedral. In more details, the time evolution of different static features (i.e. strain of metallic tie-rods and tilt of columns) is presented, along with the correlation between those features and the environmental parameters and the possible minimization/removal of the environmental effects with SHM purposes.*

1 INTRODUCTION

The Milan Cathedral is the most iconic symbol of Milan and is world-wide known for being one of the largest Heritage monuments ever built. The construction of the cathedral took more than 4 centuries, from the apse erection in 1386 until the façade finalization in 1814 [1]; subsequently, architectural and maintenance works were carried out for a long period, so that the installation of the last iron gate in the façade (on January 6th, 1965) is usually indicated as the official building completion.

Since 1387 all operational aspects related to the construction, maintenance and restoration of the Milan Cathedral are managed by the historic Institution named *Veneranda Fabbrica del Duomo di Milano* [2] and denoted as *Fabbrica* in the following. After the completion of the church structures, the *Fabbrica* main mission moved to continuous inspection, maintenance and architectural restoration of the monument, with those activities being especially related to surfaces, decorations and statues in Candoglia marble. In the last decades, the traditional inspections have been often coupled with the installation of different sensing devices, aimed at monitoring local strengthening interventions (see e.g. [3]) or investigating the evolution of possible structural issues. Remarkable examples of sensing systems operating in the past includes: (a) the inverted pendulum installed in the main spire on late September 1904 to measure the horizontal displacements induced by strong winds [4]; (b) the traditional monitoring system, based on geometric levelling and established to measure the horizontal deflection of the piers in the late sixties. Although the latter system is not computer based, it has been active in measuring the piers deformation at pre-selected intervals (May and November) for more than 50 years and is still fully operating.

During the recent assessment of the state of preservation and the tensile force of the metallic tie-rods of the Cathedral [5], the idea of implementing a Structural Health Monitoring (SHM) strategy has been taking shape and a monitoring system was designed [6] and implemented with the two-fold objective of providing the information needed for the condition-based structural maintenance and the creation of a large archive of experimental data useful to improve the knowledge of the monument.

The long-term monitoring system [6], fully computer based and with efficient transmission of the collected data, includes static and dynamic measurements. The static monitoring system consists of: (a) bi-axial tilt-meters installed at the top of selected piers and at 3 levels of the main spire; (b) vibrating wire extensometers mounted on the iron tie-rods which are characterized by the higher tensile stress; (c) temperature and humidity sensors for the measurement of internal and external environmental parameters. The dynamic monitoring is performed through seismometers (electro-dynamic velocity sensors) installed at the top of 14 selected piers and at 3 levels of the main spire.

After a brief description of the Milan Cathedral, the paper is mainly aimed at describing the monitoring system installed in the church with emphasis on the static (i.e. tilt of columns and strain of metallic tie-rods) and environmental (temperature and humidity) measurements collected in the first year of continuous monitoring. Selected results are presented on the evolution in time of the environmental and static parameters and extensive comments are given on the removal/minimization of the environmental effects with SHM purposes.

2 THE MILAN CATHEDRAL

The Milan Cathedral (Figs. 1-2), spreading over an area of more than 10400 m^2 and with a volume of about 300000 m^3, is the second largest Gothic cathedral in the world by volume and area. Moreover, the church exhibits the second tallest main nave among Gothic cathedrals, with the height of the vault intrados of the main nave being at about 45 m from the ground (Fig. 3a).

A longitudinal section of the Cathedral is shown in Fig. 2, along with an essential chronology of the construction phases.

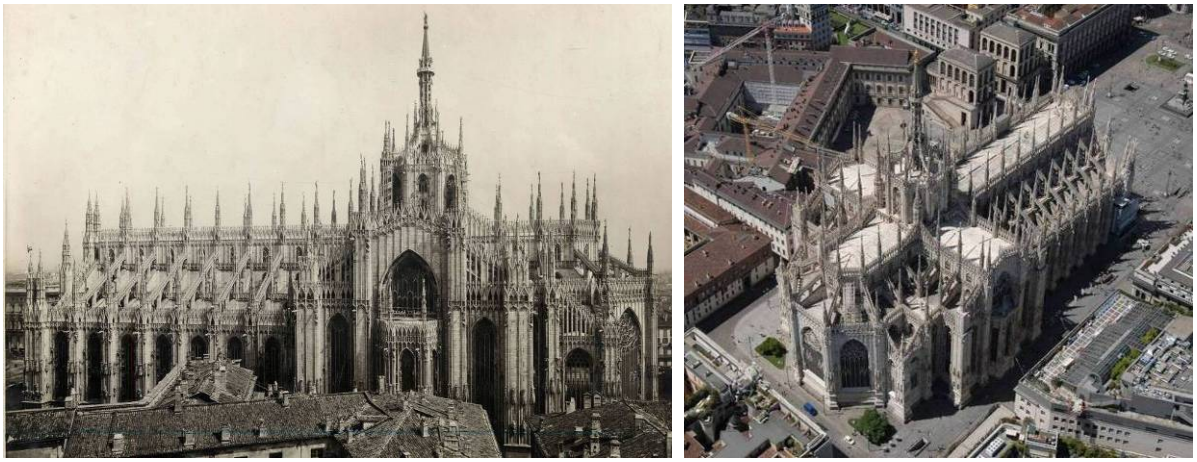


Figure 1: Views of the Milan Cathedral (courtesy of *Veneranda Fabbrica del Duomo di Milano*)

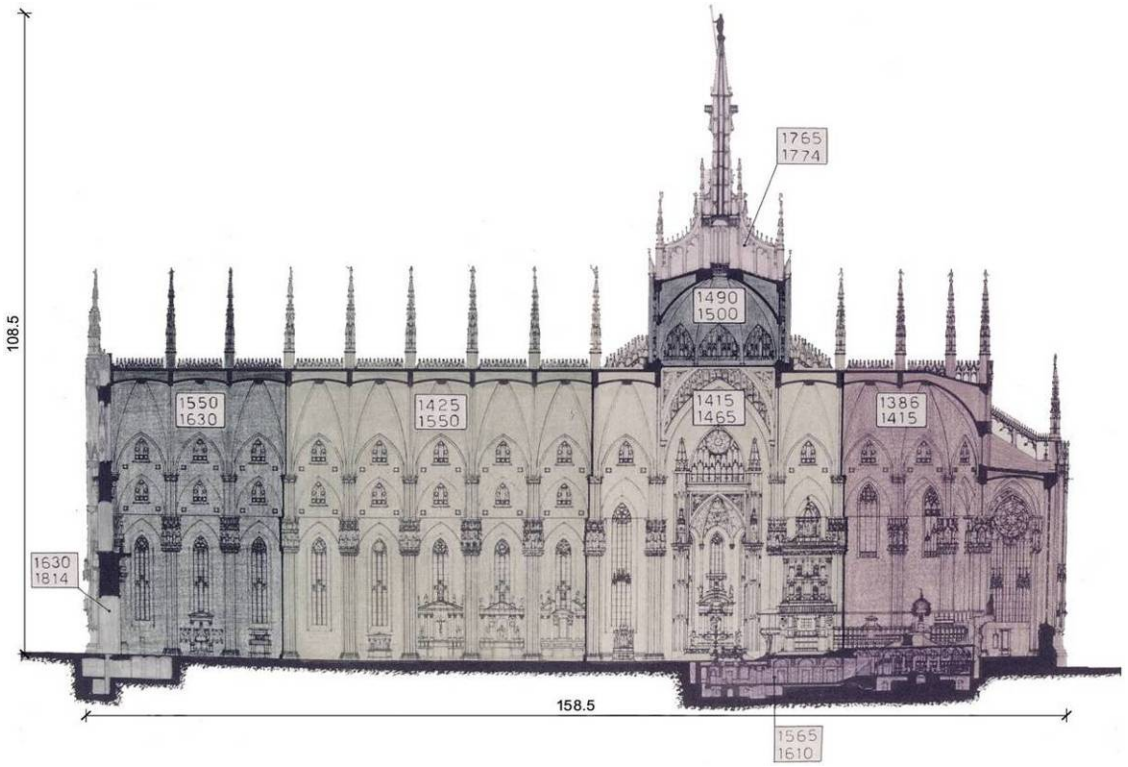


Figure 2: Views of the Milan Cathedral (courtesy of *Veneranda Fabbrica del Duomo di Milano*)

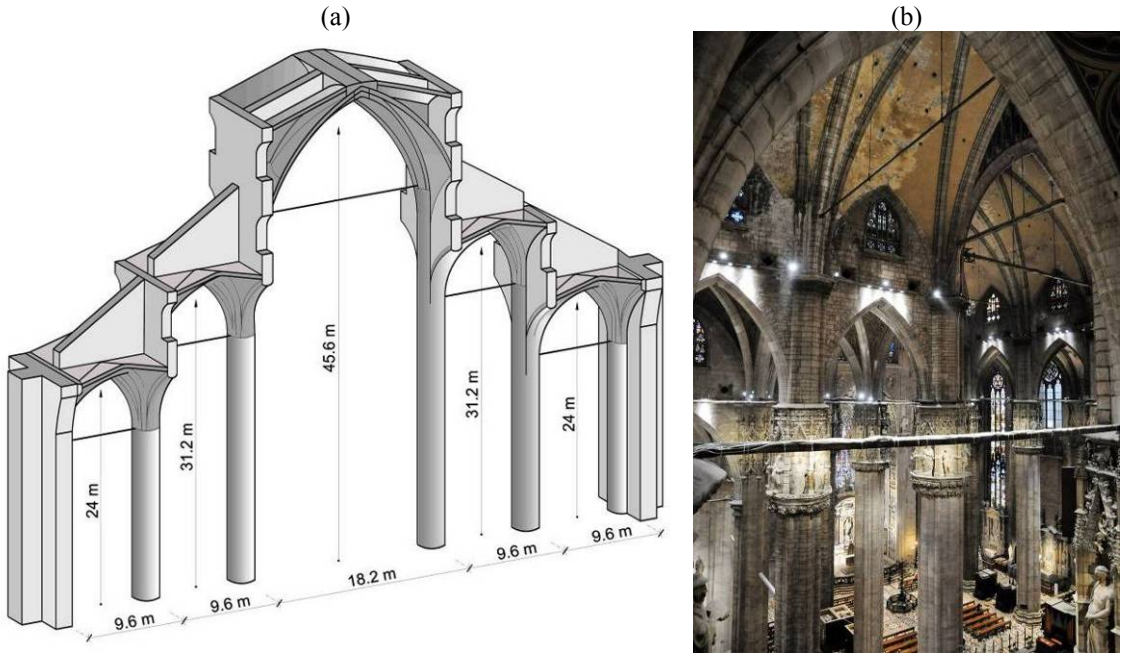


Figure 3: (a) Schematic of the structural arrangement exemplified on one bay of the Milan Cathedral; (b) Inside view of arches, vaults and iron tie-rods

The church construction started in 1386 from the half-octagonal apse and East choir, and proceeded with the transept, the main dome, the *tiburio* (i.e., the prismatic structure with octagonal base, which is built around the main dome); subsequently, the five-nave structure over eight bays was built, whereas the main spire and the neo-Gothic façade dates back to 1774 and 1814, respectively.

The structural arrangement of the main limb is exemplified in Fig. 3a, illustrating the distinctive elements of the structural schematic, such as double masonry vaults (i.e., cross vaults and barrel vaults) and permanent metallic tie-rods (Fig. 3b) placed under each arch. It is worth mentioning that the adoption of 122 iron tie-rods, still exerting an active role in resisting the lateral thrusts [5], is one of the main characteristics of the Milan Cathedral: the construction Masters decided to connect the capitals of all adjacent piers by means of metallic elements to reduce the thrust on the slender lateral buttresses and in response to the critical comments raised by the French Architect Jean de Mignot [1]. This peculiar structural arrangement is unique in Gothic cathedrals, where wooden or metallic ties were used as provisional elements and removed at the end of the construction.

The Cathedral has a Latin cross shape in plan (Fig. 4a), with the overall dimensions being about 66 m × 158 m; it should be noticed that the longitudinal limb points the East-West direction, whereas the transversal transept is oriented in the North-South direction.

3 DESCRIPTION OF THE MONITORING SYSTEM

The knowledge of the monument, along with targeted documentary research in the archives of the *Fabbrica* and recent experimental tests [5], allowed to identify the sub-structures to be initially involved in the monitoring: (a) the structural elements subjected to past important strengthening interventions, such as the main spire [7] and the 4 piers [3] supporting the *tiburio*; (b) the piers of the apse (as those elements are not stiffened by buttresses in Gothic cathedrals); (c) selected piers, which are placed in key areas of the church (i.e., transepts, main naves and façade) and (d) selected tie-rods, exhibiting tensile stress of the order of 100 MPa or higher [5].

Since the monitoring system includes a relatively high number of different sensors and the sensing devices are widespread over a large area, a distributed sensor network was implemented to minimize wiring inside the church, with the network being fully computer based and allowing on-site data acquisition and real-time data transfer to remote site. In short, the sensor network inside the Milan Cathedral [6] includes: (a) 12 bi-axial tilt-meters on the capital of selected piers, each with integrated temperature sensor; (b) 12 extensometers on selected tie-rods; (c) 12 hygrometers inside the church; (d) 27 seismometers. Furthermore, one weather station, 3 bi-axial tilt-meters (with integrated temperature sensors) and 9 seismometers are installed in the main spire [6].

Data acquisition (and data analysis) is continuous, even if different sampling rates are adopted for quasi-static and dynamic time series: strains, rotations and environmental data are collected at a rate of two samples per hour, whereas the dynamic monitoring is performed at a sampling frequency of 100 Hz.

A complete description of the static and dynamic monitoring systems can be found in [6], whereas only a brief overview of the static monitoring devices is herein presented. A schematic of the extensometers and tilt-meters installed in the Cathedral is shown in Fig. 4.

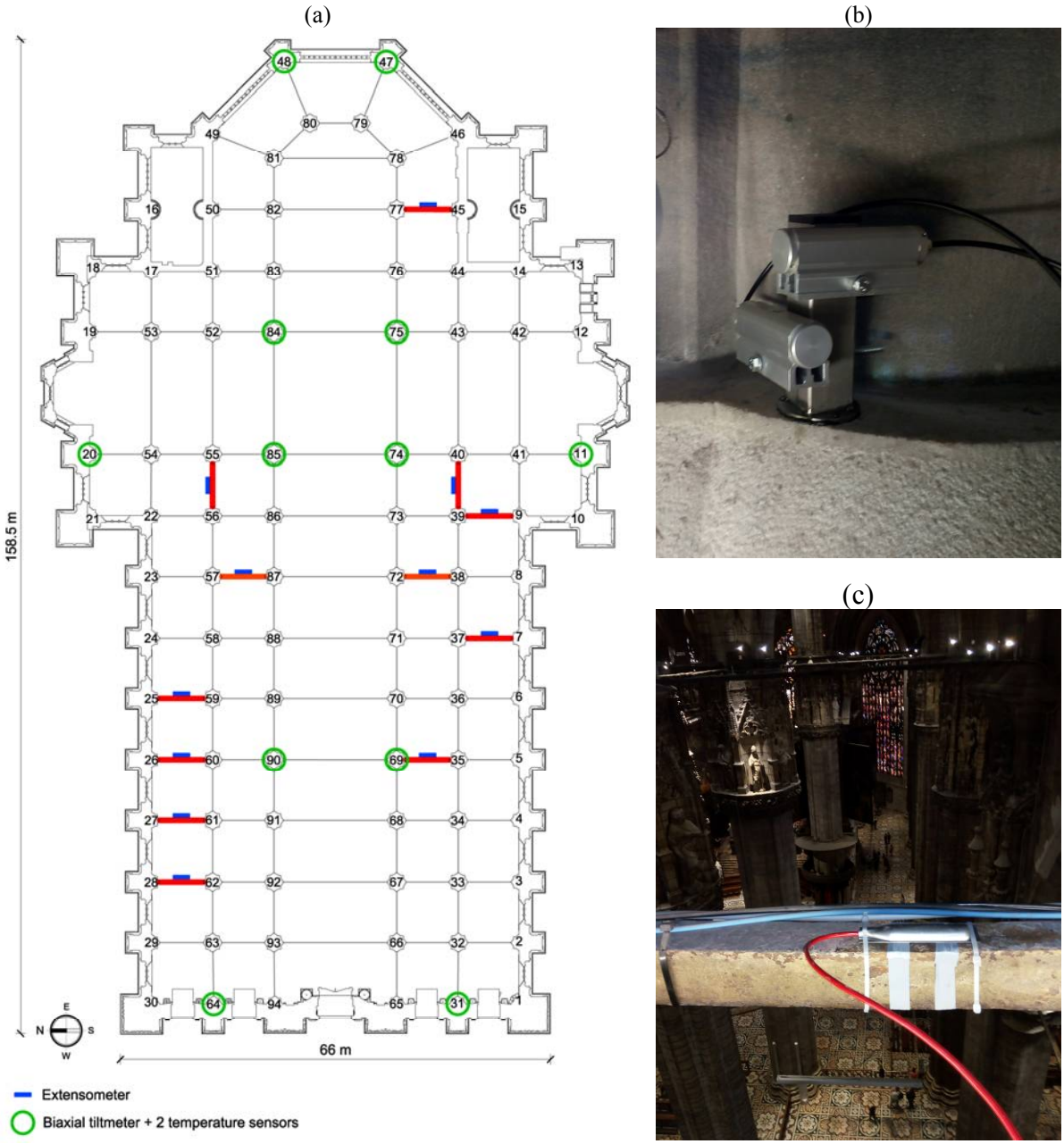


Figure 4: (a) General layout of the static monitoring system installed in the Cathedral (dimensions in m); (b) Bi-axial tilt meter mounted on one capital; (c) Extensometer installed on one tie-rod

In more details: (a) the bi-axial tilt-meters (Fig. 4b, measurement range of ±0.5º and resolution of ±0.5 mm/m) are placed on the capital of piers 31 and 64 (façade), 69 and 90, 11 and 20 (transept), 74-75 and 84-85 (*tiburio*), and 47-48 (apse); (b) the vibrating wire extensometers (Fig. 4c, measurement range of ±3000 με and resolution of 1 με) measure the axial strain of metallic tie-rods with high tensile stress (marked in red in Fig. 4a) or affected by slight damage (marked in orange in Fig. 4a) [5].

As previously pointed out, the indoor and outdoor environmental conditions are extensively measured also to evaluate the risks for the conservation of the main artifacts present in the church [8] and not only for establishing correlations with the structural parameters changes. The indoor and outdoor temperature sensors, with temperature range being between –20 °C and +60 °C and resolution of 0.2 °C, are integrated with each tilt-meter (Fig. 4a); the hygrometers, with measurement range 0-100% and resolution of 1%, are mounted in the neighborhood of the extensometers.

The data transfer of the static devices inside the Cathedral is wireless and each sensor is wired to high capacity batteries, which are placed in walkways over the vaults, quite easy to access for maintenance and substitution. Static and environmental sensors are grouped together (with the number of the sensors in each group being dependent on the relative distances) and are managed by local nodes. The data collected by neighboring nodes are transmitted to routers and those routers, in turn, transmit the information to a local workstation managed by the *Fabbrica* technical staff. The local workstation is equipped with appropriate software codes aimed at the remote management of the different devices, the transformation of raw data and the storage in digital archives. Furthermore, through the Internet, the data might be post-processed by authorized users (such as Politecnico di Milano) and results come back to the *Fabbrica* workstation for being included in digital archives. Typical post-processing includes the removal of environmental effects, which will be exemplified in the forthcoming sections.

4 SELECTED RESULTS FROM THE CONTINUOUS STATIC MONITORING

The static monitoring of the Milan Cathedral is fully active since October 19th, 2018. This section summarizes selected results from the static monitoring over the first year of monitoring (from 19/10/2018 to 18/10/2019) and, for the sake of consistency, only the experimental results collected in the Cathedral are presented and discussed (with no comments being provided on the data measured on the main spire).

As usual for masonry buildings, the evolution in time of environmental parameters is firstly presented in order to understand the effects of changing environment on the variations observed in the quasi-static measurements (strain of the tie-rods and tilt of the columns).

4.1 Environmental parameters

As previously pointed out, a quite extended grid of temperature sensors and hygrometers has been installed inside the church, with the objective of supporting both the SHM program and the preservation of statues, paintings and decorative elements, which are kept inside the monument. The variation in time of the average indoor temperature and the outdoor temperature (measured by the weather station) is shown in Fig. 5a, whereas Fig. 5b refers to the average indoor humidity.

The orange line in Fig. 5a presents the evolution of the outdoor temperature and highlights changes between −1.7°C and +35.4°C, with remarkable daily variations in sunny days. The corresponding variation of the average indoor temperature is represented by the red line in Fig. 5a and ranges between +8.8°C and +30.6°C: it is further noticed that the availability of a large number of temperature sensors in the church allows to verify [6] a low temperature gradient in space, with the difference between the extreme values not exceeding 0.5°C.

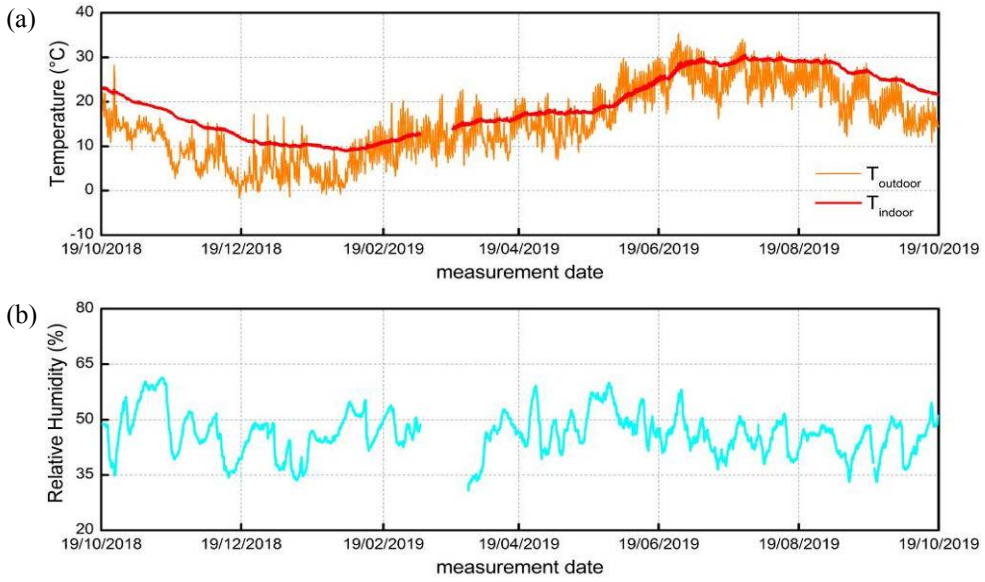


Figure 5: Evolution in time of: (a) average indoor temperature and outdoor temperature; (b) average indoor relative humidity.

Consequently, the low temperature gradient and the correlation coefficients (always larger than 0.99) between the measured temperatures allow to assume the average indoor temperature (Fig. 5a) as a representative quantity for the SHM correlations. A similar conclusion is drawn for the relative humidity, whose time series are highly correlated [6], [8] and exhibit correlation coefficients of the order of 0.90 or larger.

4.2 Static behavior and environmental effects

The time series of measured strain on tie-rods 28-62, 39-09 and 39-40 are plotted in Figs. 6a, 7a and 8a, with a sampling time of 60 min. It should be observed that, although the tension bars 28-62, 39-09 and 39-40are located in the north and south side aisle of the limb (Fig. 4a), the strain variation trend is very similar. The inspection of Figs. 6a, 7a and 8a shows that: (a) the tensile strain increases in winter and the maximum increment is attained on all tie-rods on February 2019, in correspondence with the minimum values of both outdoor and indoor temperature; (b) the strain condition at the beginning of the monitoring (i.e., zero strain increase) is recovered almost simultaneously in all instrumented ties at the end of June 2019 and approximately at the end of the first year of monitoring (Figs. 6a, 7a and 8a).

Figures 6b, 7b and 8b reveals a high correlation between measured strains and (average) indoor temperature, with the coefficient of determination R^2 being larger than 0.90 for tie-rods 28-62 and 39-09. Trends and correlation values similar to the ones exemplified in Figs. 6-8 are observed for all instrumented tie-rods, whose long-tem behavior is significantly affected by the indoor temperature. Furthermore, the strain-temperature plots (Figs. 6b, 7b and 8b) highlight a fairly regular trend with slight deviation of the regression line from linearity. Concerning this aspect, it is worth mentioning that the outdoor temperature also affects the strain variation, whereas almost negligible effects are due to the (average) relative humidity. In addition, the observed non-linear correlations might depend on delayed temperature-induced effects, caused by thermal inertia of the massive masonry church.

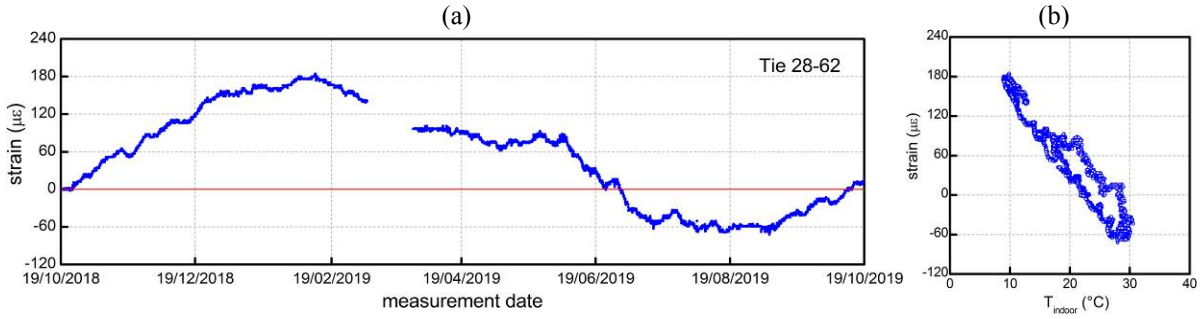


Figure 6: Tie-rod 28-62: (a) Evolution in time of measured strain; (b) Strain vs. indoor temperature.

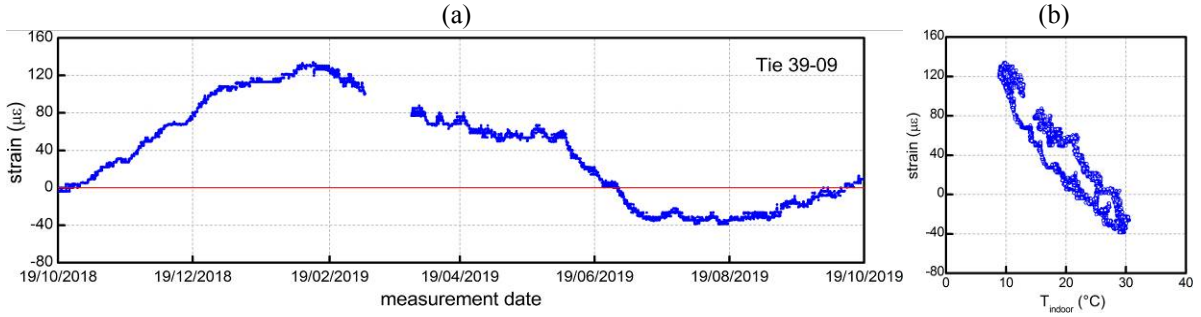


Figure 7: Tie-rod 39-09: (a) Evolution in time of measured strain; (b) Strain vs. indoor temperature.

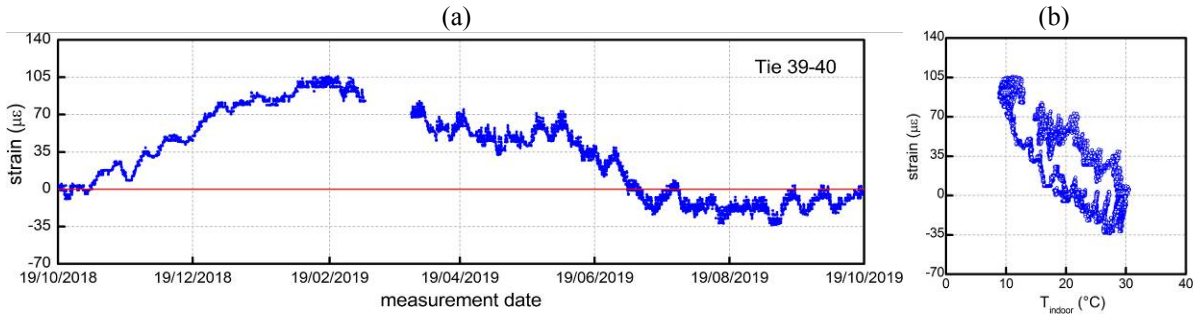


Figure 8: Tie-rod 39-40: (a) Evolution in time of measured strain; (b) Strain vs. indoor temperature.

Deeper investigation of the correlation between indoor/outdoor temperature and strain variations reveals that the currently measured strains exhibit: (a) high correlation coefficients with the indoor temperature measured in the preceding days (until 2-3 weeks before); (b) a remarkable dependence on the outdoor temperature measured in the preceding 12-24 hours.

The effects of environmental changes can be removed from measured strains (or from any other measured quantity) using statistical techniques [9-11]. Among these techniques, multiple linear regressive (MLR) models are often adopted, where linear correlations between a dependent variable (i.e., the strain) and a set of p independent variables (i.e, the indoor and outdoor temperatures) are exploited. The above observation on the effects of delayed temperature suggests the use of a "dynamic" model [10-11], involving the use of past observations to re-construct the independent variables (rather than a "static" model, where dependent and independent quantities are sampled at current time).

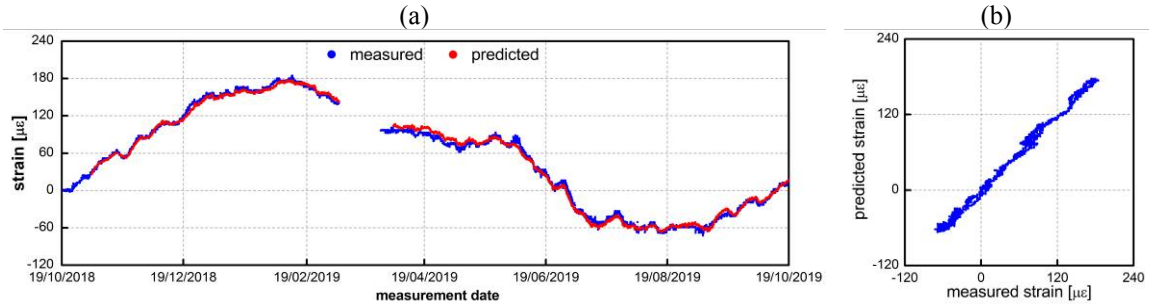


Figure 9: Tie-rod 28-62: (a) Statistical reconstruction of the measured strain; (b) Correlation between measured and predicted strain.

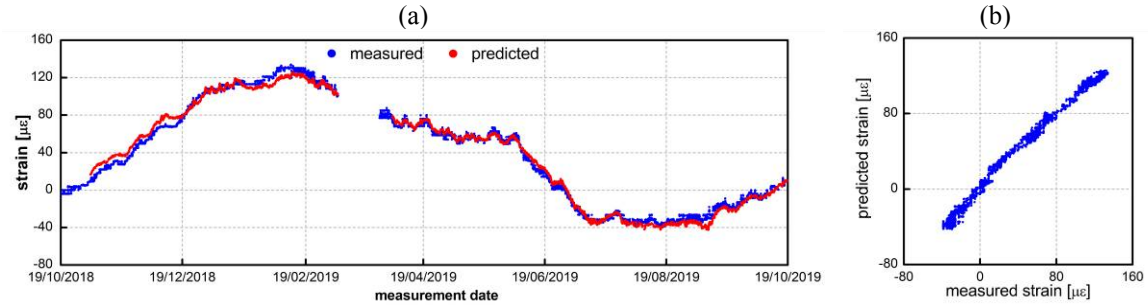


Figure 10: Tie-rod 39-09: (a) Statistical reconstruction of the measured strain; (b) Correlation between measured and predicted strain.

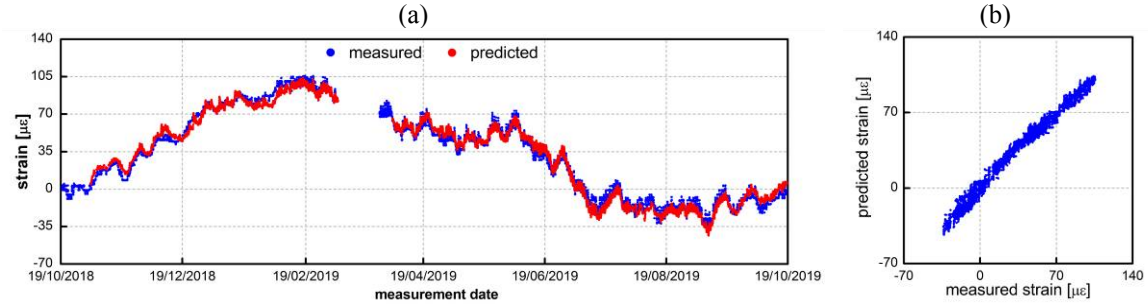


Figure 11: Tie-rod 39-40: (a) Statistical reconstruction of the measured strain; (b) Correlation between measured and predicted strain.

In the present case, a satisfactory statistical reconstruction of the measured strains (Figs. 9-11) was obtained by using: (a) the current indoor temperature and observations of the preceding 2 weeks, sampled at 36 hours; (b) the current outdoor temperature and a varying number (12-24) of past observations sampled at 1 hours; (c) the current relative humidity.

To exemplify the quality of the dynamic regression predictive models, Figs. 9a, 10a and 11a shows the time series of measured and predicted strains, considering the entire period of monitoring as training period. Furthermore, Figs. 9b, 10b and 11b show the correlation between measured identified and predicted observations. It is worth noting that Figs. 9-11 clearly demonstrate that the adopted statistical technique is capable of re-constructing both daily and long-term variations and, hence, to remove the environmental effects from monitoring data so that damage sensitive features are defined.

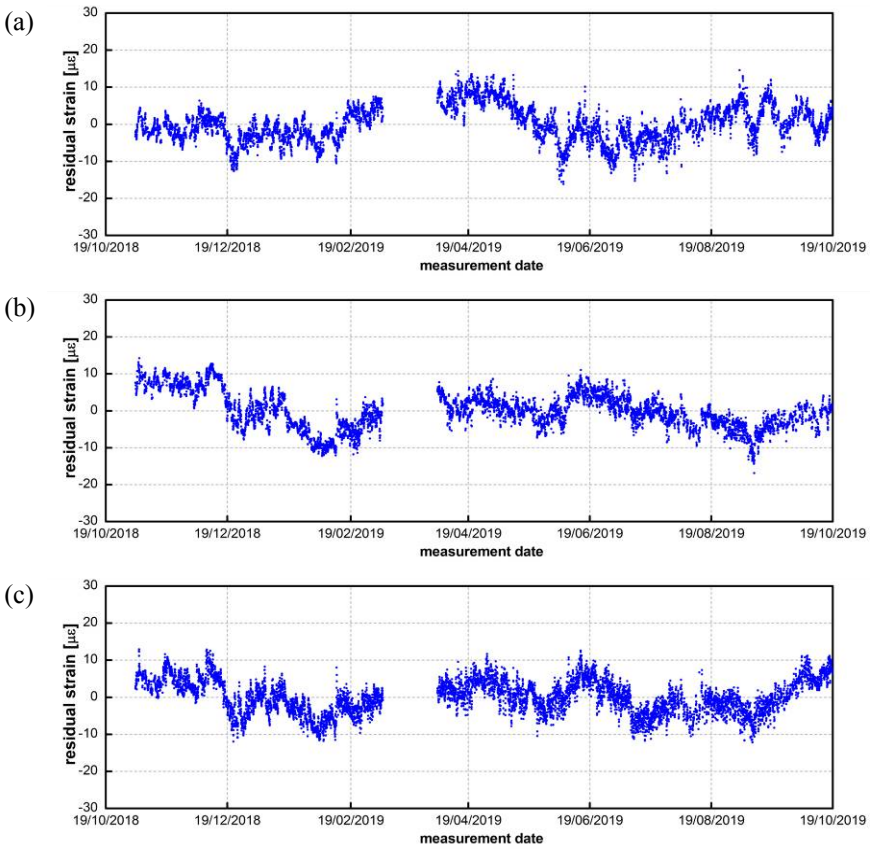


Figure 12: Evolution in time of residual strain in tie-rods: (a) 28-62; (b) 39-09; (c) 39-40.

Figure 12 shows the temporal evolution of the (residual) strains in tie-rods 28-62, 39-09 and 39-40 after the elimination of the environmental effects performed by using the dynamic regression. It can be observed that the variation of the residuals is reduced to a small range: any residual variation exceeding the range established in the training period could imply the occurrence of a potential damage (see e.g. [10]).

The indoor temperature turns out to be the main driver of the changes observed in the piers rotation as well. Fig. 13 shows the evolution of the E-W rotation of selected piers: inspecting the tilt data shows that pier 64 (façade) tends to lean towards east (positive direction) from October to June, whereas all other piers are leaning towards west in the same period, with pier 85 (*tiburio*) exhibiting the maximum tilt. As previously observed for the strain variation in the tie-rods, the rotation cumulated during Winter and Springs tend to be recovered (zero crossing) after mid June.

The correlation between E-W tilt and indoor (average) temperature for piers 64 (façade), 74 (*tiburio*) and 47 (apse) is shown in Figs. 14a-c. The correlation is approximately linear for most piers (Figs. 14a and 14c) but a non-linear correlation between E-W rotation and indoor temperature is observed for pier 74.

Also in the case of strain in tie-rods, the dynamic MLR technique might be adopted for removing the temperature effects from tilt data. It is further noticed that the availability of dynamic data (natural frequencies and mode shapes are automatically identified every hour

[8]) should conceivably be exploited in a data fusion framework for an enhanced program of condition-based structural maintenance.

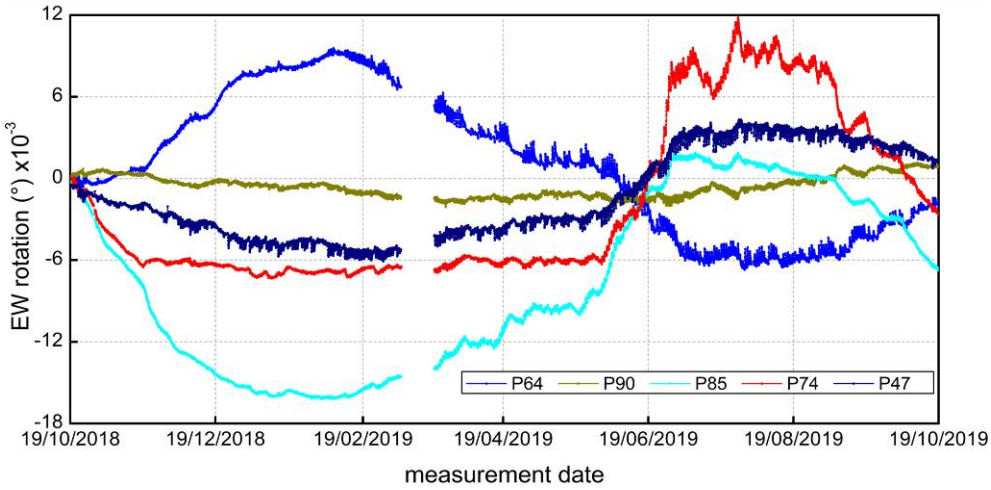


Figure 13: (a) Variation of E-W rotation of selected piers from 19/10/2018 to 18/10/2019.

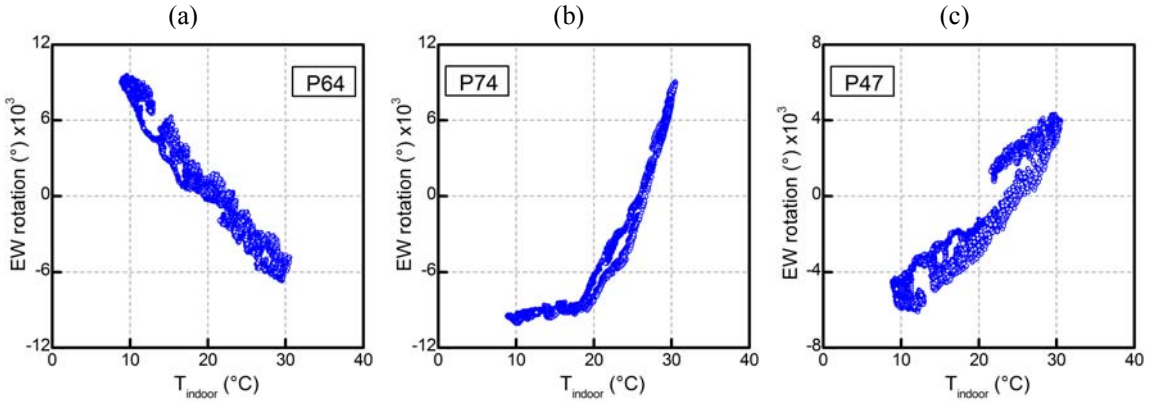


Figure 14: Rotation-temperature correlation for: (a) pier 64 (façade); (b) pier 74 (*tiburio*); (c) pier 47 (apse).

5 CONCLUSIONS

The paper focuses on the description of the monitoring system recently designed and installed in the Milan Cathedral. The monitoring system [6], aimed at enhancing the knowledge and assisting the condition-based structural maintenance of the historic building, includes more than 120 sensors belonging to different classes (i.e., a network of 12 extensometers, 15 bi-axial tilt-meters, 36 seismometers, 30 temperature sensors, 12 hygrometers and 1 weather station) and is fully computer based and characterized by distributed architecture.

Selected results are presented from the first year of the static measurements. Based on those results, the following main conclusions can be drawn:

- The (outdoor and indoor) temperature turned out to be a dominant driver of the variations observed in the quasi-static measurements (strain of the tie-rods and tilt of the columns). The relative humidity seems to slightly affects only the strain variation

in the tie-rods;
- The temporal evolution of measured strains and the strain-temperature correlations highlight a fairly regular behavior of the instrumented tie-rods;
- The dynamic multiple linear regression turns out to be an effective tool to remove the environmental effects from measured data and to derive damage sensitive features.

As a final remark, the simultaneous availability of several quasi-static measurements and of the automatically identified modal parameters (resonant frequencies, mode shapes and modal damping ratios) should conceivably provide a data fusion framework for an enhanced SHM program.

Acknowledgements. The support of *Veneranda Fabbrica del Duomo di Milano* and the co-operation of Francesco Canali in the design of the monitoring system is gratefully acknowledged. The authors would like to thank the technical staff of AgisCo and *Veneranda Fabbrica del Duomo di Milano* for the installation of all static monitoring devices.

REFERENCES

[1] *Annali della Fabbrica del Duomo di Milano. Dall'origine fino al presente* (in Italian). Veneranda Fabbrica del Duomo di Milano (1885).
[2] Ferrari da Passano, C. *Storia della Veneranda Fabbrica* (in Italian). Cassa di Risparmio delle Province Lombarde (1973).
[3] Ferrari da Passano, C. *Il Duomo rinato* (in Italian). Veneranda Fabbrica del Duomo di Milano (Diakronia) (1988).
[4] Vicentini, G. *Il pendolo registratore dei movimenti dell'aguglia maggiore del Duomo di Milano* (in Italian). Hoepli (1906).
[5] Gentile, C., Poggi, C., Ruccolo, A. and Vasic, M. Vibration-based assessment of the tensile force in the tie-rods of the Milan Cathedral. *Int. J. Archit. Herit.* (2019) 13(3): 402-415.
[6] Gentile, C., Ruccolo, A. and Canali, F. Long-term monitoring for the condition-based structural maintenance of the Milan Cathedral. *Constr. Build. Mater.* (2019) **228**:117101.
[7] Zacchi, A. *Private communication* (in Italian). Archives of Veneranda Fabbrica del Duomo di Milano (1941).
[8] Aste, N., Adhikari, R.S., Buzzetti, M., Della Torre, S., Del Pero, C., Huerto, H.E. and Leonforte, C.F. Microclimatic monitoring of the Duomo (Milan Cathedral): risks-based analysis for the conservation of its cultural heritage. *Build. Environ.* (2019) **148**: 240-257.
[9] Mason, R.L., Gunst, R.F. and Hess, J.L. Statistical design and analysis of experiments with applications to engineering and science. John Wiley & Sons (2003).
[10] Gentile, C., Guidobaldi, M. and Saisi, A. One-year dynamic monitoring of a historic tower: damage detection under changing environment. *Meccanica* (2016) **51**: 2873-89.
[11] Kita, A., Cavalagli, N. and Ubertini F. Temperature effects on static and dynamic behavior of Consoli Palace in Gubbio, Italy. *Mech. Syst. Signal Pr.* (2019) 120: 180-202.

12th International Conference on Structural Analysis of Historical Constructions
SAHC 2020
P. Roca, L. Pelà and C. Molins (Eds.)

PROPOSAL FOR A TIME-DEPENDENT DYNAMIC IDENTIFICATION ALGORITHM FOR STRUCTURAL HEALTH MONITORING

MANUEL F. HORMAZÁBAL[1]*, MARIA GIOVANNA MASCIOTTA[2], DANIEL V. OLIVEIRA[1]

[1] Institute for Sustainability and Innovation in Structural Engineering (ISISE)
Institute of Science and Innovation for Bio-Sustainability (IB-S)
Department of Civil Engineering
University of Minho
Campus de Azurém, 4800-058 Guimarães, Portugal
E-mails: m.hormazabal@gmail.com*, danvco@civil.uminho.pt - Web page: http://www.isise.net

[2] Department of Engineering and Geology (InGeo)
G. d'Annunzio University of Chieti–Pescara
Viale Pindaro 42, 65127, Pescara, Italy
E-mail: g.masciotta@unich.it - Web page: http://www.ingeo.unich.it

Keywords: Structural Health Monitoring, Non-Destructive Inspection, Operational Modal Analysis, Time-dependent, Structural Dynamic Identification.

Abstract. *This paper describes the design, test and validation processes of a dynamic identification algorithm aimed at the time-dependent assessment of modern structures and heritage buildings for civil and seismic engineering purposes. Full validation of the algorithm is performed through analysis of numerically simulated data from an idealized masonry tower. Making use of output-only vibration measurements, the non-parametric algorithm can generate dynamic features results as time-dependent functions for the complete observation period. The algorithm can work in the presence of different dynamic loads and non-linear structural behaviours, close spectral frequency components and noise-contaminated data. Time-dependent structural dynamic parameters that can be computed are modal frequencies, modal displacements, modal curvatures, and higher derivatives of mode shapes. The proposed algorithm aims to be used as the core estimator of time-dependent identification methods devoted to the health monitoring of structures and infrastructures, being suitable for a multitude of tasks ranging from the simple operational modal analysis (in pre and post-event condition) to the complex online assessment of the structural response during seismic events for rapid damage identification.*

1 INTRODUCTION

In order to appropriately plan maintenance and conservation actions in existing structures and heritage buildings, the execution of field dynamic testing under operational conditions supported by periodic Structural Health Monitoring (SHM) campaigns has become imperative

[1,2,3]. Traditional dynamic identification methods used in Operational Modal Analysis (OMA) can accurately estimate parameters like modal frequencies, damping ratios and mode shapes [4,5,6], but some methods present problems related to the difficulties in identifying close-spaced modes or uncertainties when working with noise-contaminated measurements [7,8,9]. On the other hand, most methods based on output-only data work with parametric eigenvalue decompositions of a weighted data matrix, like the Singular Value Decomposition (SVD) of the Power Spectral Density matrix (PSD) – as far as the Frequency Domain Decomposition (FDD) methods are concerned [10,11,12] – or the SVD of Hankel matrixes in case of Stochastic System Identification methods (SSI) [13,14,15]. Thus, they are restricted to the linear-elastic range (no-damage, no-yielding) and are not suitable to identify dynamic features in the presence of nonlinearities. Moreover, these methods cannot generate results as time-dependent functions since they are limited to the comparative assessment between different structural conditions (usually before and after a particular event), thereby being unable to provide any information about the actual temporal evolution of dynamic parameters like natural frequencies and mode shapes during the damage progress. To effectively upgrade state-of-the-art dynamic identification techniques for SHM intents, performing dynamic identification in the presence of nonlinearities and tracking relevant time-dependent modal parameters are essential tasks to accomplish [16,17,18,19]. The development, testing and preliminary validation of a non-parametric algorithm suitable for this purpose are hereby presented. The proposed algorithm is capable of processing linear (no damage) and nonlinear (with damage) data and can properly conduct dynamic identification either with forced accelerations measured during seismic events or with random data coming from ambient vibration tests. Results are generated as time-dependent functions, allowing to follow the evolution of dynamic parameters before, during and after the occurrence of damage. The algorithm aims to be used as the core estimator of vibration-based structural health monitoring tools in tasks ranging from the simple OMA for pre- and post-event analysis to the complex online assessment of the structural response during seismic events for rapid damage identification of ordinary as well as strategic structures and infrastructures, including heritage buildings.

2 BRIEF THEORETICAL FRAMEWORK

2.1 Wavelet Transform

Mathematically, the Wavelet Transform (WT) or wavelet Time-Frequency Analysis (TFA) is an integral transform that represents a signal $x(t)$ in terms of a series of coefficients related to convolutions of the signal data with dilated and translated versions of a compactly supported wavelet function $\psi(\cdot)$ [20]. The Continuous Wavelet Transform (CWT) is one of the most widely high-resolution TFA, and it has been extensively exploited for a variety of purposes [21]–[24]. The CWT of a signal $x(t)$ is mathematically defined as:

$$CWT\{x(t)\} = |a|^{-1/2} \int_{-\infty}^{\infty} x(t)\, \psi\left(\frac{t-b}{a}\right) dt \tag{1}$$

where a indicates the dilatation factor, b the translation factor , and $\psi(\cdot)$ is the wavelet function.

In the discrete version of the WT, namely the Discrete Wavelet Transform (DWT), the wavelet function and the dilatation and translation factors are discretized in order to compute the wavelet coefficients only on specific time instants and at specific frequency scales. A discrete wavelet $\psi_{n,m}(s)$ is defined as:

$$\psi_{n,m}(s) = {a_0}^{m/2}\,\tilde{\psi}({a_0}^{-m}s - nb_0) \tag{2}$$

in which $\{s: \psi_{n,m}(s) \neq 0\}$ is the set that supports the wavelet function, whereas $a = a_0^m$ $\{\forall\, a \in \mathbb{R}_+ : a \neq 0\}$ is the discrete dilatation coefficient, and $b = nb_0a_0^m$ $\{\forall\, b \in \mathbb{R}\}$ is the discrete translation coefficient. If required, the original sequence $x[n]$ can be fully reconstructed through the following equations:

$$x[n] = \sum_{n,m} \langle x, \psi_{n,m} \rangle\, \hat{\psi}_{n,m} \tag{3}$$

$$\hat{\psi}_{n,m}(s) = {a_0}^{-m/2}\,\psi^*({a_0}^{-m}s - n) \tag{4}$$

2.2 Discrete Wavelet Transform Decompositions

Equations (3) and (4) shed light on the idea that DWT represents the discrete signal $x[n]$ through sets of coefficients computed through convolutions of $x[n]$ with a set of properly selected filters. According to the previous, on a discrete wavelet decomposition algorithm a new subsequence of data is produced by the convolution of signal $x[n]$ with a linear low-pass filter $g_m[n]$ as the scale function and a linear high-pass filter $h_m[n]$ as the wavelet function, where m is the number of the decomposition levels. After convoluting the signal $x[n]$ with the corresponding pair of filters, two subsequences of coefficients are obtained from every convolution: the *Approximation Coefficients* sequence $A_{n,1}$, generated from the convolution with low-pass filter $g_{n,1}[n]$, and the *Details coefficients* sequence $D_{n,1}$, generated from the convolution with the high-pass filter $h_{n,1}[n]$. For every new level of decomposition, the high half of the frequency spectrum is discarded, so according to Nyquist-Shannon criteria [25,26] the original number of samples will be redundant. Due to this, a decimation of $A_{n,1}$ and $D_{n,1}$ is performed in each level of decomposition, so every subsequence will have half the samples of his immediate superior parent sequence. The convolution of the filters impulse responses with the signal will apply repeatedly until reaching maximum level, decomposing the signal in the form of a cascade serial processing algorithm, where every new $D_{n,m}[n]$ sequence obtained is decomposed into a pair of new $A_{n,m+1}[n]$ and $D_{n,m+1}[n]$ subsequences. If an orthogonal mother wavelet function is selected, all the generated sub-sequences will be also orthogonal, thus, they will keep the energy distribution according to the original data.

2.3 Maximum Overlap Discrete Wavelet Packet Transform

In the Maximum Overlap Discrete Wavelet Packet Transform (MODWPT) [27], there is no decimation applied to the original data nor any $W_{n,m}$ subsequence, thus all $W_{n,m}$ sub-sequences will maintain the same number of samples than the original stream of data and there will be no

loss of resolution on low frequencies. The original spectrum is sliced into 2^m discrete frequency bands, each one corresponding to a family of packets of mother wavelets and scale functions.

2.4 Instantaneous frequency through Hilbert transform

The Hilbert Transform (HT) is defined as the convolution of $x(t)$ with the function $g(t) = 1/\pi t$ and it is essential for constructing analytic signals. The *Analytic Signal* (AS) is the representation of any signal or data stream as a complex pair where the imaginary part is the Hilbert transform of the real-valued signal $x(t)$. By the modulus operation, the *Instantaneous Amplitude* is calculated, and by the time derivative of the analytic signal´s complex angle, the *Instantaneous Frequency* is obtained. The Hilbert spectrum is a graphical representation of the instantaneous frequency, the instantaneous amplitude and the time evolution of the signal, usually, in the form of a spectrograph of instantaneous frequency vs time with the instantaneous amplitude in the colour scale. The Hilbert transform of a discrete Gaussian white noise will produce as many different instantaneous frequency values as the number of samples of the signal. Due to the previous, broadband signals are not good candidates for Hilbert spectrum analysis and it is better to decompose or band filter the raw data before any further analysis or process with HT.

3 METHODS AND MATERIALS

3.1 Algorithm description

The Enhanced Modal Identification for Long-Term Integrity Assessment algorithm (EMILIA) proposed in this work was designed in two main stages. The first stage relies on the MODWPT decomposition to compute Single Degree of Freedom (SDOF) or pseudo-SDOF sub sequences from raw Multi Degrees of Freedom (MDOF) structural ambient vibration measurements. MODWPT was selected due to the capabilities of the transform to deal with highly noise-contaminated data and to properly work in the low-frequency range without losing resolution. Mode shapes are computed from direct integration of the SDOF accelerations computed by the wavelet decomposition (this step is not necessary if displacement measurements are analysed). In the second stage, the Hilbert Transform is applied to each pseudo-SDOF to compute the analytical signals and subsequently obtain the instantaneous frequency and instantaneous amplitude functions. As the instantaneous frequency is computed through the time derivative of the oscillatory phase, it follows that the instantaneous frequency is a time-dependent parameter. Ambient structural vibration measurements have deterministic data well-hidden between stochastic data. Due to this, the initial Wavelet decomposition is of critical importance to analyse ambient vibrations with Hilbert transform. The capability of this integral transform to compute a frequency value for each sample of the analysed signal is used as an intent to reduce the influence of uncertainties. A deep analysis of these aspects can be found in [28]. Final computations involve statistical analyses. Probability Density Functions (PDFs) with a Kernel distribution are computed for each instantaneous frequency function to identify the values with higher probabilities and their corresponding damping factors. PDF resorts to a supposed probability data distribution to fit the data, where the most commonly

used is the parametric Gaussian normal distribution. Such a distribution can be found in most measured data with a universe bigger than thirty samples, nevertheless, the previous does not apply to the frequency data distribution of an undamped structural mode featuring a resonant peak that goes over the maximum value given by a normal distribution, thus the frequency peak bandwidth is also narrower. This could lead to overestimations on damping factor values for each modal component. To overcome this issue, Kernel distribution was chosen due to the well-fitting capabilities of assessing data which is highly contaminated with aleatory variables. Further information about Kernel distribution can be found in [29]. The schematics for the complete algorithm are presented in Figure 1.

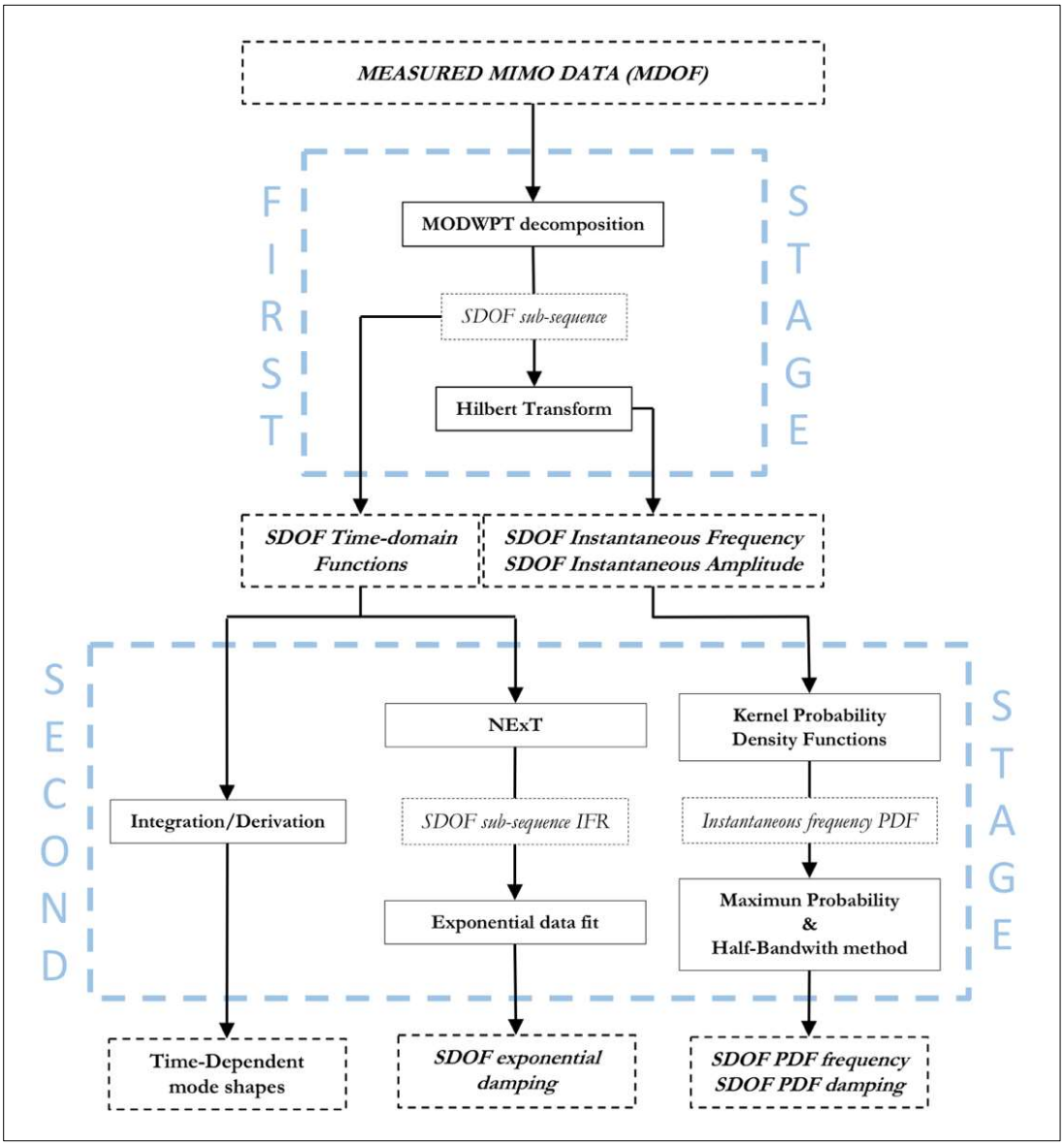


Figure 1: Proposed algorithm schematic.

3.2 FEM-based validation

A Finite Element Model (FEM) of an idealized masonry tower was developed in Diana FEA® software in order to numerically validate the proposed algorithm. The model was built resorting exclusively to volumetric elements. Concerning the morphological aspects, the tower features a square plan of 6 m side, with double-leaf masonry walls of 0.6 m thickness, two timber floors 10 m and 20 m high, respectively, and a total height of 28 m. Floor slabs are directly connected to the timber beams inserted in the masonry wall thickness. The material properties adopted for the numerical model are reported in . It is noted that a linear behaviour was assumed for all timber elements, whereas nonlinear properties were assigned to the masonry material. Particularly, the latter were set based on values retrieved from the literature [30].

Table 1: Material properties adopted for the numerical model.

Timber Properties		
Linear Properties		
Young´s modulus	10000	[N/mm^2]
Poisson's ratio	0.35	
Mass density	428.28	[kg/m^3]
Masonry Properties		
Linear Properties		
Young´s modulus	2200	[N/mm^2]
Poisson's ratio	0.2	
Mass density	1400	[kg/m^3]
Tensile behaviour		
Tensile curve	Exponential	
Tensile strength	0.18	[N/mm^2]
Mode-I tensile fracture energy	10	[N/m]
Crack bandwidth specification	Rots	
Residual tensile strength	0.12	[N/m^2]
Poisson's ratio reduction	Damage based	
Compressive behaviour		
Compression curve	Parabolic	
Compressive strength	3.7	[N/mm^2]
Compressive fracture energy	5900	[N/m]

Interaction between tower foundations and soil was modelled as a boundary interface connection with Coulomb friction with cohesion of 100 kN/m, that was used between the model base elements and the ground fixed supports. The FE model counted a total of 8467 quadratic/hexagonal elements with quadratic mesh order and linear mid-side point interpolation. Elements maximum side length was 0.5 m. A Total-Lagrange geometrical formulation and crack-model based on total strain were used. For an initial understanding of the tower's dynamic behaviour, a free vibration eigenvalue analysis was conducted first. This

allowed to properly define the acquisition parameters necessary for the subsequent Time-History Non-Linear analyses (THNL) as well as the number and position of measurement points to guarantee a sufficient spatial density of the system's vibration response under simulated ambient noise and real seismic inputs. THNL analyses were performed using the Hilbert-Hughes-Taylor (HHT) transient time integration with α = -0,1 through the Secant iteration method, setting Δt = 0.01 s (see also section 4.1). Requested data outputs were the accelerations in X, Y and Z directions. The first THNL analysis was conducted by randomly applying Gaussian white noise excitations to different points of the structure. The second THNL analysis was performed using the same white noise excitations from first analysis in combination with a real earthquake signal applied as base excitation in all three directions. The ground motion selected for this purpose was the *Loma Prieta* earthquake of magnitude M_w = 7.0 that occurred on October 18th, 1989 and was recorded at the *CGS-CSMIP Station 47381*, located on a sewer farm around 31.1 km far from the epicentre. Data were sampled at 0.01 s for a total duration of 39.9 seconds, resulting into 3991 data points. The earthquake featured a PGA equal to 0.5 g and a maximum displacement of 0.1 m (Y-axis). From each corner of the tower 15 nodes equally spaced in height each 2 m were selected along the four edges of the tower to acquire its nodal response in terms of accelerations. All nodal processes collected in X and Y directions were then loaded into the core algorithm coded in MATLAB® as well as into ARTeMIS® software for output-only modal analysis with traditional estimators.

4 DISCUSSION OF THE RESULTS

4.1 Eigenvalue Analysis

A structural free vibration eigenvalue analysis was initially performed to estimate the modal frequencies of the masonry tower in sound condition and to properly identify the modes with the highest effective mass participation per axis as well as the nodes with the largest displacement per mode. The modal periods, frequencies and deformed shapes of the first six vibration modes of the tower are presented in Figure 2 along with the relevant mass participation. From the results, it was concluded that the dynamic response of the tower could be adequately described by the first six vibration modes since the accumulated participating mass in the frequency range 1-12 Hz was about 85% in all three directions (Figure 2). Thus, T = 0.09 s and f = 11.14 Hz were considered as the lowest period and as the highest frequency of interest for the structure, respectively. Though, as the sixth mode mainly presented vertical displacements along the Z direction, only the first five modes were considered for dynamic benchmarking between the traditional estimators and the proposed algorithm. Based on the highest period of interest estimated from the eigenvalue analysis, a time step of 0.01 seconds was considered enough to ensure a good resolution for the subsequent THNL analyses. As expected, due to the symmetry of the FE model, the first two vibration modes of the tower are very close-spaced, reading frequency values of 1.79 Hz and 1.82 Hz, respectively. Both modes present essentially translation components, the first one along the x direction and the second one along the y direction, and features more than 60% of effective mass participation each. Thus, they were chosen as representative modes for conducting a point-wise assessment of the

frequency temporal evolution through time-dependent functions computed via the proposed algorithm, using as input data the numerical accelerations of the nodes featuring the highest displacements for the modes of interest.

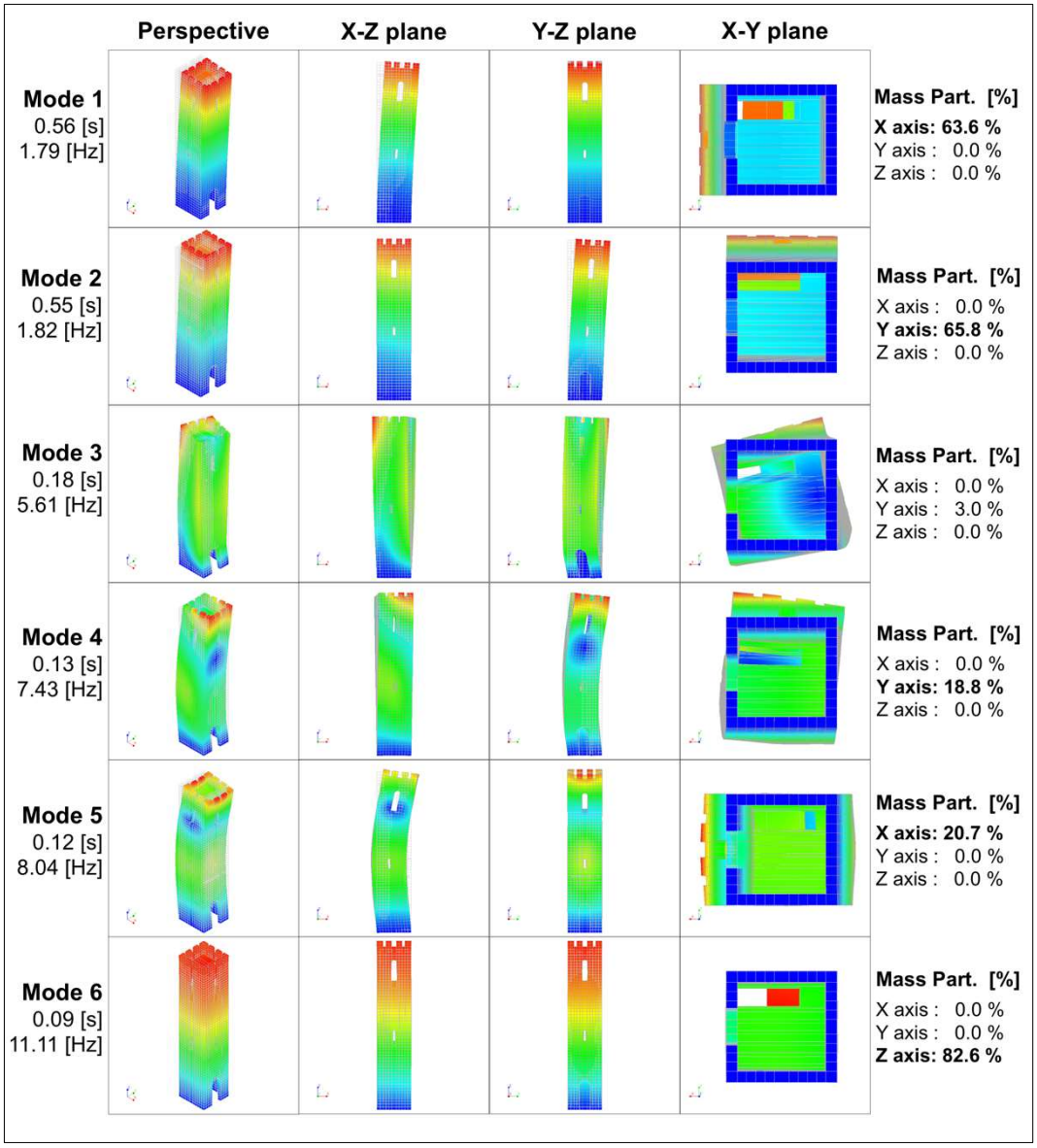


Figure 2: Vibration modes of the tower estimated through the eigenvalue analysis.

4.2 Time-history analysis with simulated ambient excitations

Six output-only identification methods available in the commercial software ARTeMIS® were selected as traditional estimators for the feature extraction process, three based on the FDD algorithm and three on the SSI algorithm. In parallel, EMILIA algorithm was run as a Matlab@ application. Seventy-one modes with a modal frequency value below the Nyquist frequency

were found through the FE eigenvalue analysis, thus a six-level MODWPT decomposition was selected for applying the EMILIA algorithm in order to obtain 64 sub-sequences. The results obtained from the different estimators are summarized in Table 2 in terms of modal frequencies of the first ten vibration modes of the tower. By comparing these results against those computed through the eigenvalue analysis, it is observed that SSI-UPC, SSI-UPCX and EMILIA algorithms provide the best results. In particular, EMILIA was capable of identifying most of the searched modes with high accuracy, especially as far as the higher modes are concerned, which results to be a clear advantage for structural health assessment considering that damage is a localized phenomenon that mainly affects high-frequency modes. It is also important to highlight that the frequency values extracted from the EMILIA algorithm are just a statistical approximation, since the main characteristic of the algorithm lies in its capability of computing the dynamic parameters as time-dependent functions.

Table 2: Results for the modal frequency of the first ten modes computed by all estimators.

Nº	T[s]	Frequency [Hz]								Type
		Eigen	FDD	EFDD	CFDD	SSI			EMILIA	
						UPC	PC	UPCX		
1	0.56	1.79	---	---	---	1.78	1.77	1.78	1.81	Trans.
2	0.55	1.82	2.30	2.26	2.25	1.83	1.83	1.82	1.83	Trans.
3	0.18	5.61	---	---	---	5.51	5.52	5.51	5.73	Tors.
4	0.13	7.43	---	---	---	7.25	7.25	7.25	7.48	Trans.
5	0.12	8.04	8.30	8.30	8.30	7.84	7.84	7.84	8.03	Trans.
6	0.09	11.11	---	---	---	10.68	---	10.68	11.09	Norm.
7	0.071	13.97	---	---	---	---	---	---	13.50	Tors.
8	0.069	14.45	14.20	14.22	14.22	14.41	14.40	14.41	14.55	Tors.
9	0.066	15.08	---	---	---	---	---	---	14.80	Trans.
10	0.063	15.70	---	---	---	15.30	15.32	15.30	---	Trans.

4.3 Time-history analysis with simulated ambient and real earthquake excitations

(left) shows the Hilbert spectra of the first and second modes of the masonry tower plotted as time-dependent functions, allowing to track the evolution of the instantaneous frequency through a 21 minutes THNL analysis, comprising ten minutes of initial ambient excitations randomly applied to different points of the tower, one minute of earthquake excitation applied to the base of the model, and finally ten minutes of additional ambient excitations. Since the analysed data presents non-linearities and high transients, a Daubechies 2 wavelet was selected for conducting the MODWPT decomposition in other to properly identify the abrupt changes in the simulated accelerations. The spectrum corresponding to the first mode (, top-left) clearly shows how the content of the time-dependent frequency function suddenly drops down after 600 seconds (blue continuous line) with the beginning of the earthquake excitation. Further analysis, according to the slope of the first-order polynomial data fits (white-striped lines), also showed a subtle drop down of the global frequency, allowing to infer the occurrence of structural damage in the tower.

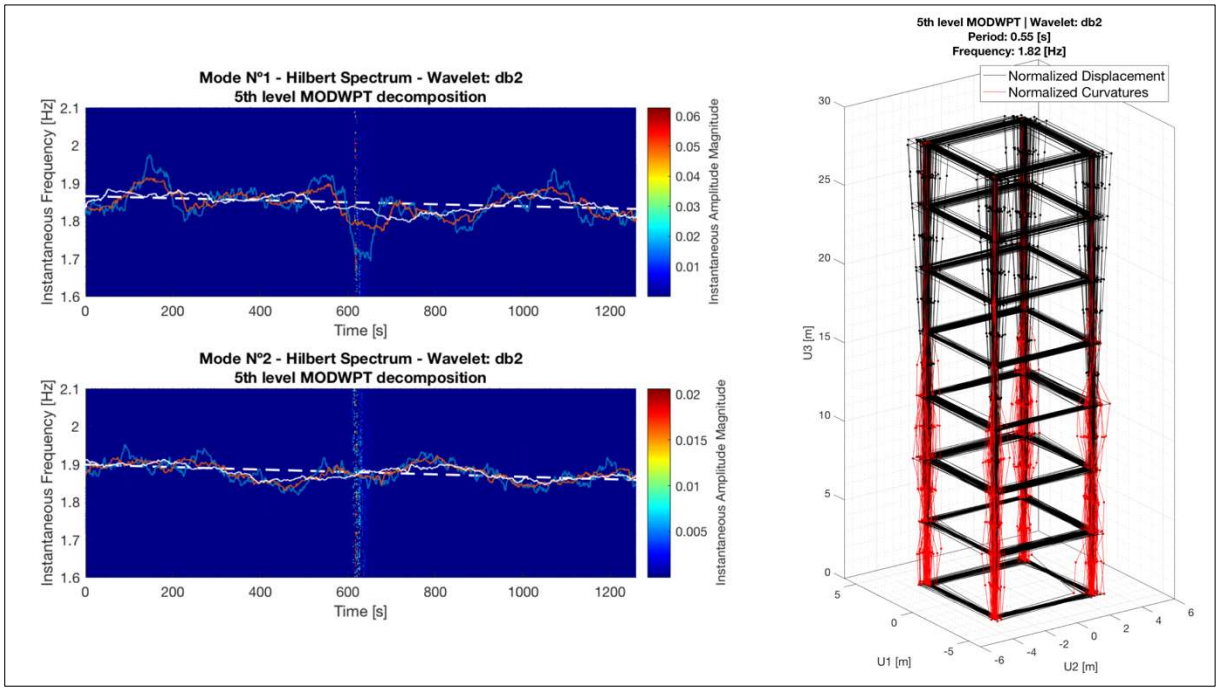


Figure 3: Hilbert spectrum of first (top-left) and second (bottom-left) modes from the idealized masonry tower excited with the 1989 "Loma Prieta" earthquake (all values normalized). White-striped lines show a first-order polynomial fit, continuous blue, red, and white lines show 60s, 120s and 280s moving averages respectively. On the right, a 3D overlapped plot of several mode shapes computed with the EMILIA algorithm.

A three-dimensional overlapped plot of several mode shapes computed at different time-steps during the seismic event is also presented in Figure 3, where the black shapes show the modal displacements and the red shapes the modal curvatures (other higher derivatives of mode shapes can also be assessed as time-dependant functions). The visual comparison of these coordinate-dependent parameters at different temporal instants highlights clear changes in terms of modal curvatures in the lower half of the tower. Such changes are due to the structural damage induced in the tower by the earthquake and provide indications not only about its approximate location of the damage, but also about the time of occurrence of the damage.

5 CONCLUSIONS

The results obtained from the current research allow to draw the following conclusions:

- Wavelet data analysis and Hilbert TFA analysis are rock-solid tools for assessing, decomposing and processing non-linear structural data;
- Wavelet discrete decompositions can appropriately separate MIMO vibration measurements into time-dependent orthogonal functions;
- Hilbert transform instantaneous frequency data can be used to assess temporal changes on structural modal frequencies;
- Displacement mode shape time-dependent functions, and their higher derivatives, are useful tools for the assessment of the structural modal response evolution for health monitoring and damage identification purposes.

Acknowledgements.
This work was funded by the National Agency for Research and Development (ANID), through the programme "Doctorado en el Extranjero Becas Chile, Convocatoria 2020" [PhD abroad grants programme, Becas Chile, call 2020], Folio – 72210443 [Sheet number – 72210443].
This work was partially funded by FEDER funds through the Competitiveness Factors Operational Programme (COMPETE) and by national funds through the Foundation for Science and Technology (FCT) within the scope of project POCI-01–0145-FEDER-007633.

REFERENCES

[1] D. V. Oliveira, L. F. F. Ramos, P. B. B. Lourenço, and J. Roque, "Structural Monitoring of the Monastery of Jerónimos," in *250th Anniversary of the 1755 Lisbon Earthquake International Conference*, 2005.

[2] M. J. Morais *et al.*, "A proactive approach to the conservation of historic and cultural Heritage: The HeritageCare methodology," in *IABSE Symposium*, 2019, pp. 64–71.

[3] M. G. Masciotta, M. J. Morais, L. F. Ramos, D. V. Oliveira, L. J. Sánchez-Aparicio, and D. González-Aguilera, "A Digital-based Integrated Methodology for the Preventive Conservation of Cultural Heritage: The Experience of HeritageCare Project," *Int. J. Archit. Herit.*, 2019.

[4] R. Brincker, "Some Elements of Operational Modal Analysis," *Shock Vib.*, vol. 2014, p. 11, 2014.

[5] N. M. M. Maia, "Extraction of Valid Modal Properties from Measured Data in Structural Vibrations," University of London, 1988.

[6] C. Rainieri and G. Fabbrocino, *Operational Modal Analysis of Civil Engineering Structures: An Introduction and Guide for Applications*. 2014.

[7] R. Pintelon, P. Guillaume, and J. Schoukens, "Uncertainty calculation in (operational) modal analysis," *Mech. Syst. Signal Process.*, vol. 21, no. 6, pp. 2359–2373, 2007.

[8] X. X. Bao, C. L. Li, and C. B. Xiong, "Noise elimination algorithm for modal analysis," *Appl. Phys. Lett.*, vol. 107, no. 4, Jul. 2015.

[9] S. K. Au, J. M. W. Brownjohn, and J. E. Mottershead, "Quantifying and managing uncertainty in operational modal analysis," *Mech. Syst. Signal Process.*, vol. 102, pp. 139–157, 2018.

[10] R. Brincker, L. Zhang, and P. Andersen, "Modal identification of output-only systems using frequency domain decomposition.," *Smart Mater. Struct.*, vol. 10, no. 3, pp. 441–445, 2001.

[11] R. Brincker, C. E. . Ventura, and P. Andersen, "Damping Estimation by Frequency Domain Decomposition," in *Proceedings of IMAC XIX*, 2001, pp. 698–703.

[12] J. Rodrigues, R. Brincker, and P. Andersen, "Improvement of frequency domain output-only modal identification from the application of the random decrement technique," in *Proceedings of IMAC XXII*, 2004, pp. 92–100.

[13] R. Brincker and P. Andersen, "Understanding Stochastic Subspace Identification," in *Proceedings of IMAC XXIV*, 2006, pp. 461–466.

[14] P. Van Overschee and B. De Moor, *Subspace Identification For Linear Systems*. Kluwer

Academic Publishers, 1996.
[15] B. Peeters and G. De Roeck, "Reference-based stochastic subspace identification for output-only modal analysis," *Mech. Syst. Signal Process.*, vol. 13, no. 6, pp. 855–878, 1999.
[16] F. Ubertini, C. Gentile, and A. L. Materazzi, "Automated modal identification in operational conditions and its application to bridges," *Eng. Struct.*, vol. 46, pp. 264–278, 2013.
[17] M. G. Masciotta, "Damage Identification of Structures based on Spectral Output Signals," University of Minho, 2015.
[18] M. G. Masciotta, L. F. Ramos, P. B. Lourenço, and M. Vasta, "Spectral algorithm for non-destructive damage localisation: Application to an ancient masonry arch model," *Mech. Syst. Signal Process.*, vol. 84, pp. 286–307, 2017.
[19] M. G. Masciotta, L. F. Ramos, P. B. Lourenço, M. Vasta, and G. De Roeck, "A spectrum-driven damage identification technique: Application and validation through the numerical simulation of the Z24 Bridge," *Mech. Syst. Signal Process.*, vol. 70–71, pp. 578–600, 2016.
[20] I. Daubechies, *Ten Lectures of Wavelets*. Springer-Verlag, 1992.
[21] Y. Wang, Z. He, and Y. Zi, "A demodulation method based on improved local mean decomposition and its application in rub-impact fault diagnosis," *Meas. Sci. Technol.*, vol. 20, no. 2, p. 025704, Feb. 2009.
[22] I. Provaznik and J. Kozumplik, "lnformatics Wavelet transform in electrocardiography-data," *Int. J. Med. Inform.*, vol. 45, no. 1–2, pp. 111–128, 1997.
[23] A. Grossmann and J. Morlet, "Decomposition of hardy functions into square integrable Wavelets of constant shape.," *SIAM J. Math. Anal.*, vol. 15, no. 4, pp. 723–736, 1984.
[24] B. Adhikari *et al.*, "Application of wavelet for seismic wave analysis in Kathmandu Valley after the 2015 Gorkha earthquake, Nepal," *Geoenvironmental Disasters*, vol. 7, no. 1, 2020.
[25] H. Nyquist, "Certain Topics in Telegraph Transmission Theory," *Trans. Am. Inst. Electr. Eng.*, vol. 47, no. 2, pp. 617–644, 1928.
[26] C. E. Shannon, "Communication in the Presence of Noise," *Proc. IRE*, vol. 37, no. 1, pp. 10–21, 1949.
[27] A. T. Walden and A. Contreras Cristan, "The phase-corrected undecimated discrete wavelet packet transform and its application to interpreting the timing of events," *Proc. R. Soc. London A Math. Phys. Eng. Sci.*, vol. 454, no. 1976, pp. 2243–2266, 1998.
[28] M. Feldman, *Hilbert Transform Applications in Mechanical Vibration*, First Edit. Chichester: John Wiley & Sons, 2011.
[29] A. W. Bowman and A. Azzalini, *Applied Smoothing Techniques for Data Analysis: The Kernel Approach with S-PLUS Illustrations*, vol. 18. UK, 1997.
[30] E. Ramírez, P. B. Lourenço, and M. D'Amato, "Seismic Assessment of the Matera Cathedral," in *11th International Conference on Structural Analysis of Historical Constructions (SAHC)*, 2019, vol. 18, pp. 1346–1354.

12th International Conference on Structural Analysis of Historical Constructions
SAHC 2020
P. Roca, L. Pelà and C. Molins (Eds.)

QUANTIFICATION OF THE STRUCTURAL RESPONSE OF HISTORICAL CONSTRUCTIONS: INVESTIGATION OF THE STRAIN VARIATION AT THE ACROPOLIS CIRCUIT WALL

ELENA KAPOGIANNI*, PRODROMOS PSARROPOULOS AND MICHAEL SAKELLARIOU

National Technical University of Athens 9 Heroon Polytechniou str.
Zografou, 15780 Athens, Greece
email* : elkapogianni@mail.ntua.gr
email: mgsakel@mail.ntua.gr, email : prod@central.ntua.gr

Keywords: Historical Complex Sites, Acropolis, Strain Recordings, Masonry Wall, Structural Monitoring, Optical Fibre Sensors

Abstract. *The current study aims to assist the preservation of the structural integrity of historical complex sites, utilizing smart instrumental monitoring / remote sensing. The main idea is that smart instrumental monitoring can provide important real-time information (records) of both the actual natural hazard(s) and the corresponding vulnerability, in terms of structural response and distress of structures and monuments of historically complex sites. The study focuses on the Acropolis Circuit Wall, where strain recordings via Smart Rod optical fibre sensors have been made possible. More specifically, wavelength recordings have been obtained and then converted into strain recordings, while the temperature influence has been taken into consideration. Furthermore, reference measurements have been defined during the initial system operation and then they are used for deduction of subsequent recordings. Strains recorded 2 and 1/2years after the initial system installation are shown, after the deduction of the reference measurements. Finally, strain variation between sensors located at the inner and outer side of the same optical fibre Smart Rod are shown.*

1 INTRODUCTION

Constructions of high and of national importance are often threatened by a variety of natural hazards, which may lead to damages and / or extended failures, resulting in some cases to injuries, fatalities, or even natural disasters. These constructions can be referred also as critical structures and have high socio-economic interest. Given their significance, it is essential to identify, manage and mitigate their structural risk, which is directly related, not only to the natural hazards, but also to the structural vulnerability. Regarding the natural hazards, they can be classified into two board categories: geological and climatological / meteorological (Figure 1). Furthermore, certain geographical regions are characterized by moderate or high seismicity which leads to various earthquake-related geohazards, such as earthquake-triggered landslides, fault rapture and soil liquefaction phenomena. On the other hand, structural vulnerability depends on the design, construction and operational conditions, while the age of the

construction plays also an important role. Structural risk assessment requires the quantification of the loading conditions (including the hazards), and the realistic assessment of structural vulnerability in terms of structural response. Furthermore, climate change phenomena are related to the increase of the structural risk [1].

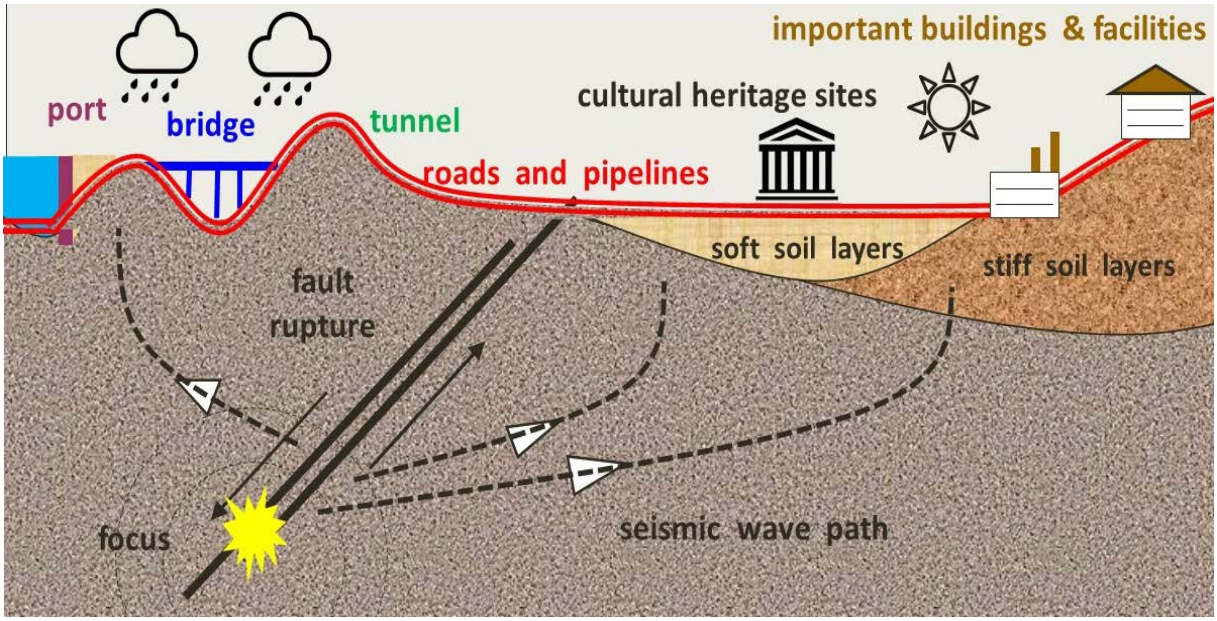


Figure 1: Critical structures and infrastructures

Historical complex sites fall into the category of the critical structures, since they usually include sensitive engineering structures and monuments, such as temples, buildings and masonry retaining walls, exposed to a range of natural hazards, eventually leading to structural failures [2], [3]. They comprise fundamental elements of the national and international cultural heritage, with limitless lifetime, featuring an elevated risk level, since a serious damage and especially a total failure of a structure and/or monument is practically irreversible. In addition, historical complex sites attract high numbers of visitors / tourists, and a potential structural failure due to insufficient risk management could have a direct impact on their safety, while potential intervention options are rather limited. Due to these reasons, the cost-efficient assessment and management of their structural risk forms a demanding task in comparison to a similar analysis applied to modern structures.

For the evaluation of the structural risk, quantitative hazard assessment and realistic evaluation of the structural vulnerability are indispensable. The risk assessment can be performed utilizing advanced computational simulations, smart instrumental monitoring. The advanced computational simulations (such as numerical modelling utilizing finite element software) can predict the expected response and distress of the structure(s) under examination when subjected to the anticipated natural hazard(s), being thus essential for the vulnerability assessment. On the other hand, smart instrumental monitoring can provide real-time information (i.e., records) of both the actual natural hazard(s) and in parallel the corresponding vulnerability, in terms of

structural response and distress, leading to a dynamic (i.e., time-dependent) structural risk assessment.
In the current study the historical complex site of the Athenian Acropolis is examined in the above framework. In Figure 2 the Acropolis Hill, the Parthenon, and the masonry Circuit Wall are shown.



Figure 2. The historical complex site of the Athenian Acropolis, including the Parthenon and the masonry Circuit Wall

2 METHODS REVIEW AND APPLICATION AT THE ACROPOLIS OF ATHENS

Smart structural monitoring/ remote sensing is a rapidly growing scientific area, traditionally applied to critical structures and infrastructures of national and economic importance comprising a high failure risk, aiming to their "smart" transformation [4], [5]. Apart from remote hazard assessment (i.e. assessment of the loading conditions), monitoring instruments can provide useful real-time information on specific location(s), necessary for the early detection of probable damage or failure during their lifetime, contributing thus to optimal risk management and overall safety. Furthermore, in an environment where various networks of sensors have been deployed, the need for intelligent management and processing of the recorded and transmitted data has emerged. Integral part of the data processing is the combination (i.e.,

data fusion between heterogeneous networks), [6] and the support of additional meta-data in order to efficiently handle the available measurements [7].

Regarding the computational modelling, numerical methods such as the finite-element method [8] can be applied to provide useful information regarding structural response and distress of any structure or monument. Usually, a computational simulation requires the geometrical and mechanical properties of the structure(s) and the anticipated static and dynamic loading, either external or internal. In order to achieve a more realistic simulation of the response / distress of a structure or a monument, the local site conditions (i.e., soil, geomorphology, and topography) and the corresponding potential soil-structure interaction should be taken into consideration.

Over the last twenty-five (25) centuries, numerous structural damages have been observed at the historical complex site of the Athenian Acropolis, which are attributed to various natural hazards (either geological or meteorological) and to the human interference (such as war invasions, air pollution, etc.), increasing in parallel the risk of local or extensive structural failures in the future. Given the potential natural hazards of Athens (mainly seismicity and meteorological conditions) and the great vulnerability of the structures / monuments on the site, the structural risk is considered to be very high [9], [10]. Furthermore, apart from the structural risk, the significance of the monuments and the safety of the visitors / tourists and employees make the assessment and management of the overall risk of the Acropolis of Athens issues of paramount importance.

In this framework, an optical-fibre-sensor array has been installed on the Circuit Wall of the Acropolis Hill, consisting of eight (8) active strain sensors, two (2) temperature sensors and one (1) acceleration sensor, continuously transmitting real-time data since June 2016 to date [11], [12]. In addition, finite-element modelling of the Circuit Wall has provided useful information concerning its structural response due to various types of loading [13]. Furthermore, ground response analyses have been performed in order to investigate the impact of local site conditions (i.e., topography) on the seismic motion at the ground surface of the Acropolis Hill, as well as to verify the available records and comprehend the amplification. The seismic motions applied during the numerical analyses have been recorded by 10 high-quality broadband accelerographs installed at various locations at the Acropolis Hill, recording in continuous mode [14].

In Figure 3 part of the structural monitoring scheme of the Acropolis of Athens with optical fibre sensors [15, 16] can be seen and in Figure 4, part of the 2D numerical modelling of the Acropolis Circuit Wall and part of the 2D numerical modelling for the evaluation of the seismic response of Acropolis Hill.

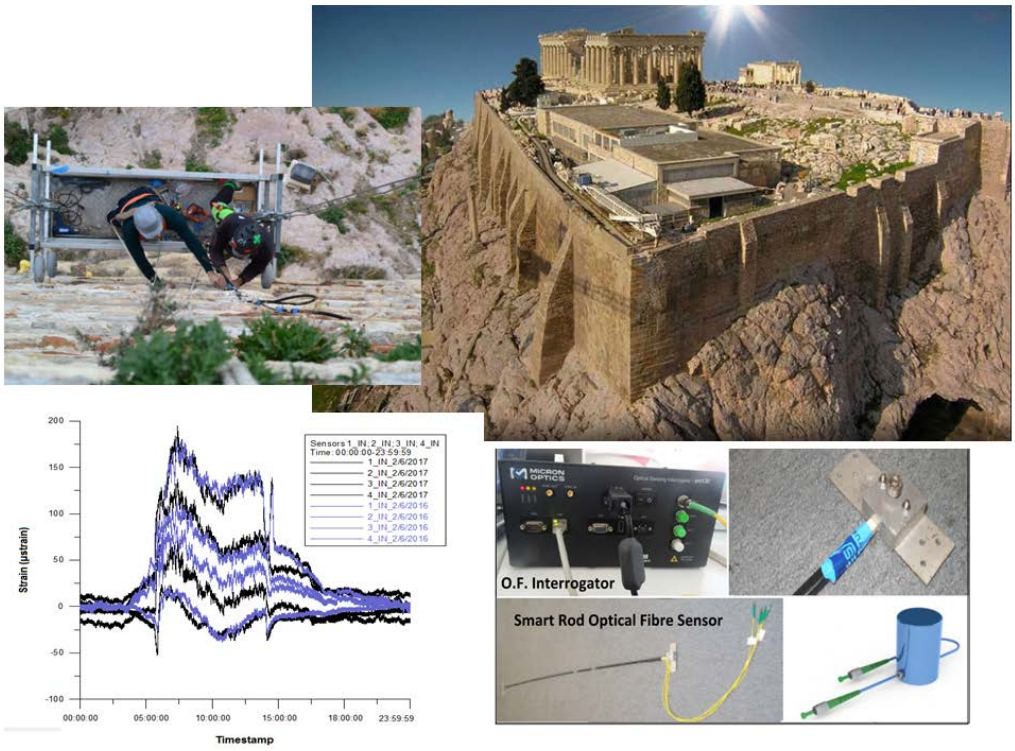
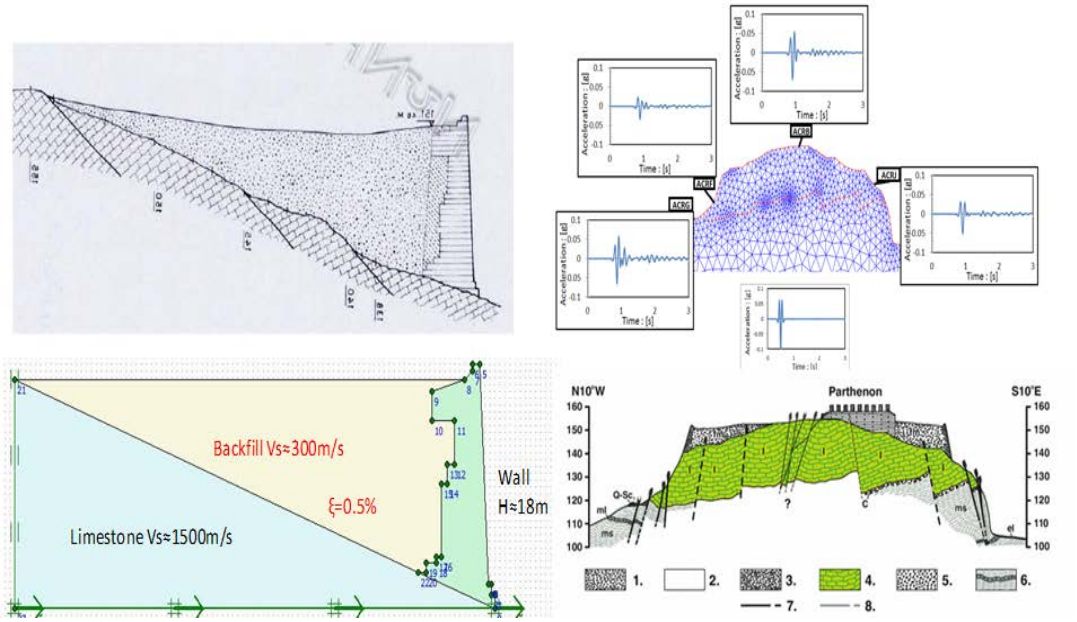


Figure 3. The South-East view of the Acropolis Hill, typical equipment of the optical-fibre array, the installation procedure on the Circuit Wall and indicative recordings after processing.



(a) (b)

Figure 4. (a) Cross section sketch of the south Wall, and 2D numerical model, and (b) 2D numerical model for the evaluation of the seismic response of Acropolis Hill and geological cross section.

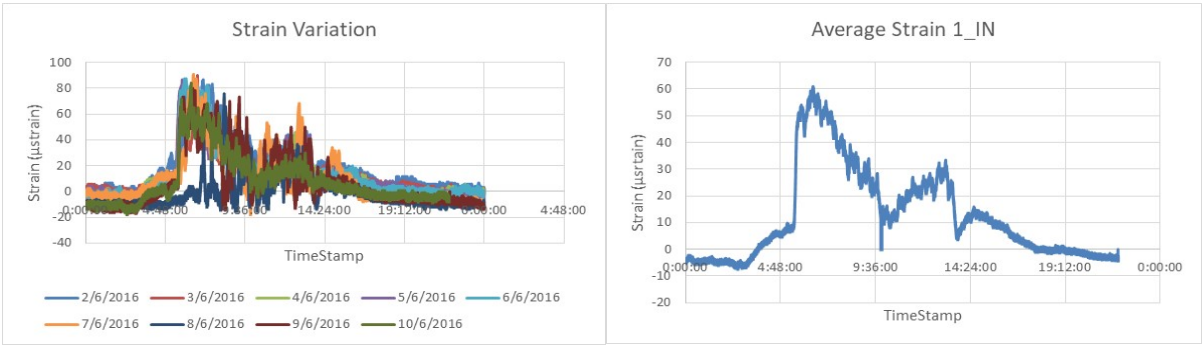
3 STRAIN VARIATION AT THE ACROPOLIS CIRCUIT WALL

In this section recordings of the strain variation at the Acropolis Circuit Wall, with the use of optical fibre sensors are presented and discussed. As mentioned in the previous section, the optical fibre array consists of: (a) eight active strain sensors fixed every two, one on the inner side and one on the outer side of four Smart Rods, (noted as IN and OUT, respectively), and (b) two temperature sensors, fixed on one Smart Rod. The Smart Rods are attached on the Circuit Wall, transmitting time-stamped data since June 2016 to date. The influence of the temperature on the recordings is considered via thermal compensation. The wavelength changes were transformed into strains with the use of Equation 1.

$$\Delta\varepsilon=(\Delta\lambda-K\tau*\Delta\tau)/K\varepsilon \quad (1)$$

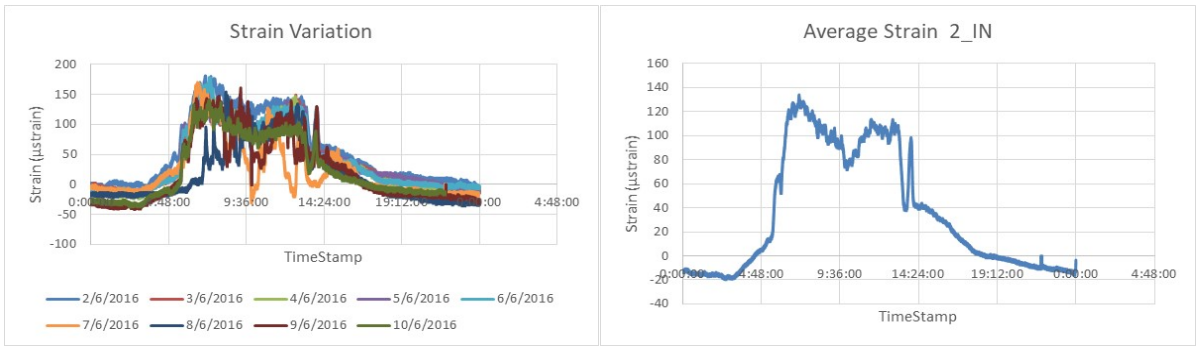
where $\Delta\varepsilon$ is the strain change, $\Delta\lambda$ the wavelength change, $K\varepsilon$ is a ratio expressing the strain-wavelength relation and is equal to 1.2 picometer (pm)/μstrain for the type of sensors that was used in the current study, $K\tau$. $\Delta\tau$ incorporates the wavelength changes due to the temperature variations. $K\tau$ is equal to 11.2 pm/C^0 for the sensors used in the current study, and $\Delta\tau$ is the temperature variation, measured during the tests (starting value and actual-final value).

In Figure 5a, the 9-day period of initial strain recordings on the Circuit Wall, via sensor 1_IN, are shown, and in Figure 5b, the average of these recordings. In Figure 6a, the 9-day period of initial strain recordings on the Circuit Wall, via sensor 2_IN are shown, and in Figure 6b the average of these recordings. The average of the recordings obtained during the first 9 days of the monitoring system operation (2nd of June 2016), are considered as reference measurement and is deducted from subsequent recordings.



(a) (b)

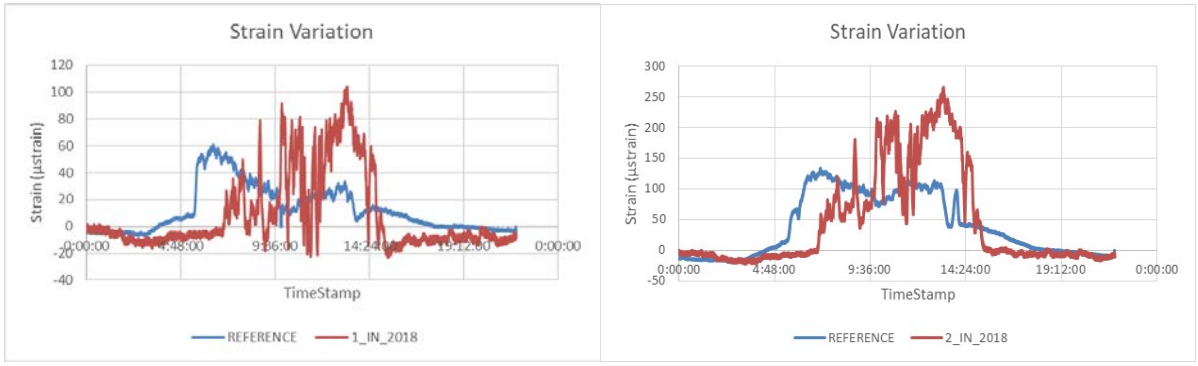
Figure 5. (a) Strain recordings via sensor 1_IN during a 9-day period, (b) average (reference) strain recordings via sensor 1_IN.



(a) (b)

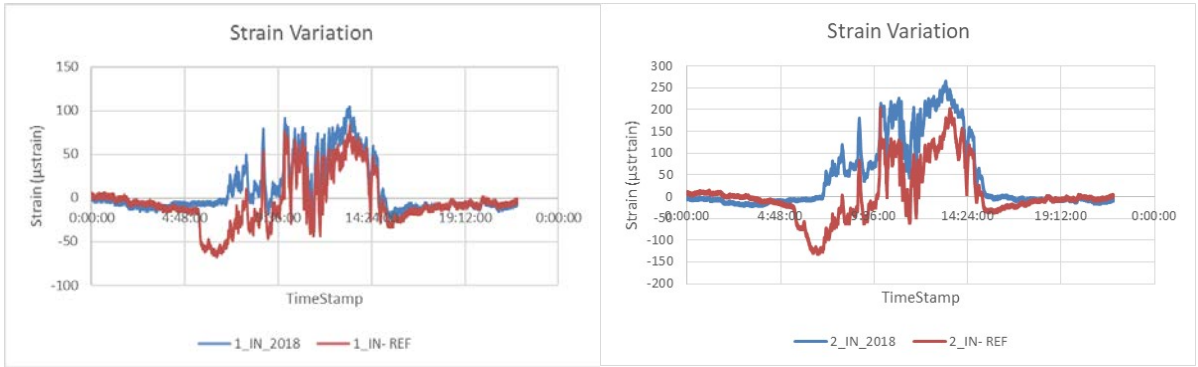
Figure 6. (a) Strain recordings via sensor 2_IN during a 9-day period, (b) average (reference) strain recordings via sensor 2_IN.

In Figures 7a and 7b, recordings during January 2018 for sensors 1_IN and 2_IN respectively, in comparison to the reference measurements of 2016 are shown. Furthermore, in Figures 8a and 8b, recordings before and after the deduction of the reference measurements are noted, for sensors 1_IN and 2_IN respectively.



(a) (b)

Figure 7. Recordings during January 2018 via sensors 1_IN (a) and 2_IN (b), in comparison to the reference measurements of 2016.



(a) (b)

Figure 8. Recordings before and after the deduction of the reference measurements, via sensors 1_IN (a) and 2_IN (b).

Finally, in Figures 9a, b, c and d, the strain variation between sensors located at the inner and outer side of the same Smart Rods, i.e. 1_IN and 1_OUT, 2_IN and 2_OUT, 3_IN and 3_OUT, 4_IN and 4_OUT, respectively are shown.

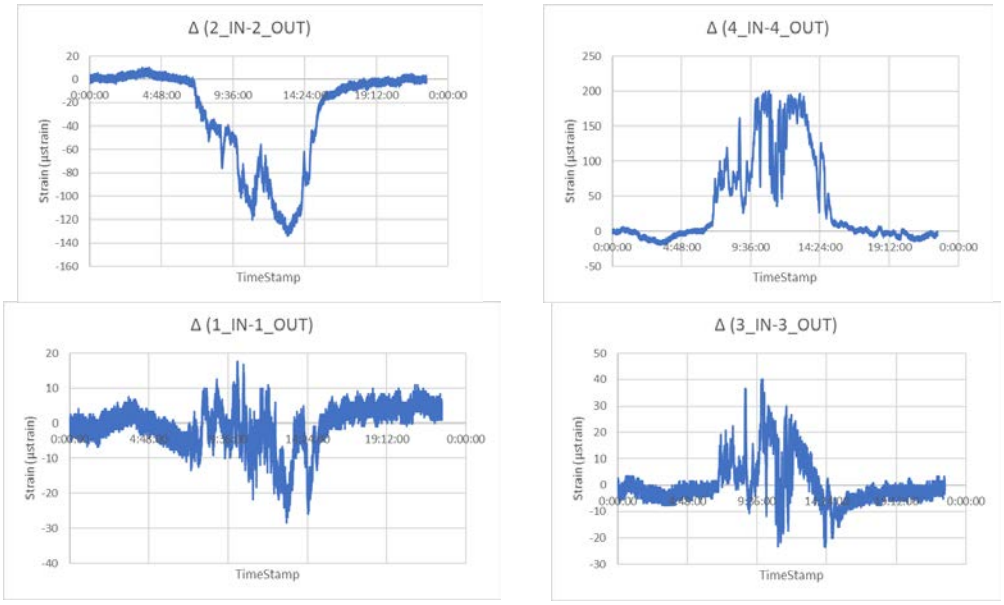


Figure 9. (a) Strain recordings via sensor 2_IN during a 9-day period, (b) average (reference) strain recordings via sensor 2_IN.

4 CONCLUSIONS

In the current study, the strain variation at the Acropolis Circuit Wall was investigated, with the use of a real-time structural monitoring scheme of Smart Rod optical fibre sensors. The wavelength measurements obtained by the optical fibre sensors where converted into strain measurements, while the temperature influence was taken into consideration via thermal compensation. At first, the period of strain recordings during the initial system operation in June 2016 was examined and the reference measurements were defined, as the average of the first days of the system operation recordings. Results of two of the eight sensors recording strain have been presented (i.e. sensors 1_IN and 2_IN). The reference measurements were used for the deduction of future strain recordings, always including thermal compensation.

In the above framework, recordings during January 2018 were compared to the reference measurements of June 2016, for sensors 1_IN and 2_IN, showing increased strains at the Circuit Wall, as expected. Furthermore, the initial strain recordings during January 2018 were compared to strains at the same locations on the Circuit Wall, after the deduction of the reference measurements, which were smaller as expected, and especially for sensor 2_IN.

Finally, strain variation between sensors located at the inner and outer side of the same optical fibre Smart Rod was presented, showing that for Smart Rods 1, 3 and 4, higher strains were recorded by the sensors located at the inner side (i.e. closer to the Wall), and especially for Smart Rod 4, while for Smart Rod 2, higher strains were recorded by the sensor located at the outer side of the Smart Rod.

The current study and the conclusions can be used for future investigation and interpretation of the strain recordings at the Acropolis Circuit Wall. In addition, the method utilized, and the results can be potentially used for the structural monitoring of other critical structures of high importance, in order to define their structural response due to various types of loading. Finally, the current study aims to assist the transformation of historical complex sites / cultural heritage sites into "smart" which is expected to have a multiplier effect on the applied scientific knowledge enhancing the diffusion of new technologies and methods.

ACKNOWLEDGMENTS

The author is grateful for financial support provided by the State Scholarships Foundation of Greece (IKY). This research is co-financed by Greece and the European Union (European Social Fund- ESF) through the Operational Programme «Human Resources Development, Education and Lifelong Learning» in the context of the project "Reinforcement of Postdoctoral Researchers - 2nd Cycle" (MIS-5033021), implemented by the State Scholarships Foundation (IKY).

REFERENCES

[1] HERACLES Consortium. Heritage Resilience Against Climate Events on Site. EU-funded Research Programme (2019).

[2] UNESCO Amman Office. *Risk Management at Heritage Sites: A case study of the Petra World Heritage Site*. Project Report, Paris; Aman, (2012) p 128.

[3] ICOMOS, 1965. *International Charter for the Conservation and Restoration of Monuments and Sites*. 2nd International Congress of Architects and Technicians of Historic Monuments, Venice, Italy.

[4] Kapogianni, E., Psarropoulos, P., Sakellariou, M. *Securing the Future of Cultural Heritage Sites, Utilizing Smart Monitoring Technologies: From the Laboratory Applications to the Acropolis of Athens* (2020) In: Correia A., Tinoco J., Cortez P., Lamas L. (eds) Information Technology in Geo-Engineering. ICITG 2019. Springer Series in Geomechanics and Geoengineering. Springer, pp 750-762.

[5] Chatzi, E. A *Monitoring Approach to Smart Infrastructure Management*. Journal: Proceedings (2017), 1(8), 755.

[6] Sun, D., Lee, V., Lu, Y. *An intelligent data fusion framework for structural health monitoring.* IEEE 11th Conference on Industrial Electronics and Applications (2016).

[7] Vilbrandt, C., G. Pasko, A. Pasko, P-A. Fayolle, T. Vilbrandt, J. R. Goodwin, J. M. Goodwin, & T. L. Kunii. *Cultural Heritage preservation using constructive shape modeling*, Computer Graphics Forum (2004) V23(1), pp. 25-41.

[8] Kapogianni, E., Sakellariou, M.G., Laue, J., Springman, S.M., *Investigation of the mechanical behavior of the interface between soil and reinforcement, via experimental and numerical modeling*. Advances in Transportation Geotechnics 3. Procedia Engineering, Elsevier (2016) V143, 419–426.

[9] Ambraseys N. *Material for the investigation of the seismicity of Central Greece, in Historical Investigation of the Seismicity of European Earthquakes*. Albinii, P. and Moroni (eds.), (1994) V2: pp 1-10.

[10] Zambas C., Ambraseys N., Boletis C., Zampa I. *The two Choragic Columns of the south slope of the Acropolis, as witnesses of the seismic history of the centre of Athens*. Scientific Project Report, John Latsis Public Benefit Foundation (2011)

[11] Kapogianni, E., Kalogeras, I., Psarropoulos, P., Michalopoulou D., Eleftheriou, V., Sakellariou, M. *Suitability of Optical Fibre Sensors and Accelerographs for the Multi-disciplinary Monitoring of a Historically Complex Site: The Case of the Acropolis Circuit Wall and Hill*. Journal: Geotechnical and Geological Engineering, Springer International Publishing (2019). Volume 37, Number 5, p 4405

[12] Kapogianni E., Kalogeras I., Psarropoulos P.N., Giokaris S., Sakellariou M.G., 2016. *Structural health monitoring of the Athenian Acropolis' Walls via optical fibre sensors, accelerographs and numerical simulations*. Structural Analysis of Historical Constructions: Anamnesis, diagnosis, therapy, controls. Van Balen, K.,Verstrynge, E. (eds), Taylor & Francis Group, CRC Press (2016) 701–707.

[13] Psarropoulos P., Kapogianni E., Kalogeras I., Michalopoulou D., Eleftheriou V., Dimopoulos G., Sakellariou M. *Seismic response of the Circuit Wall of the Acropolis of Athens: Recordings versus numerical simulations*. Soil Dynamics & Earthquake Engineering (2018) pp. 309-316.

[14] Kalogeras I., Evangelidis C., Melis N., Boukouras K. *The Athens' Acropolis Strong Motion Array*, EGU General Assembly, Geophysical Research Abstracts, vol. 12.EGU 1012-9523, Vienna, Austria (2012).

[15] Kapogianni, E., Sakellariou, M.G., Laue, J. *Experimental investigation of reinforced soil slopes in a geotechnical centrifuge, with the use of optical fibre sensors*. Geotechnical and Geological Engineering, Springer International Publishing, (2017) V35(2), pp. 585-605.

[16] Kapogianni E., Psarropoulos P.N., Kokoris, D., Kalogeras I., Michalopoulou, D., Eleftheriou, V., Sakellariou M.G. 2020. *Impact of Local Site Conditions on the Seismic Response of the Athenian Acropolis Hill*. Geotechnical and Geological Engineering, Springer International Publishing. https://doi.org/10.1007/s10706-020-01589-8

12th International Conference on Structural Analysis of Historical Constructions
SAHC 2020
P. Roca, L. Pelà and C. Molins (Eds.)

REAL-TIME STRUCTURAL MONITORING OF BIBI-KHANUM IN SAMARKAND (UZBEKISTAN) COMBINED WITH SUBSEQUENT LASER SCANS

SHAKHZOD M. TAKHIROV[1*], ILYAS ARIPOV[2] AND DAVRON MATRASULOV[2]

[1] Structures Laboratory, Civil and Environmental Engineering Department, University of California, Berkeley; 337 Davis Hall, Berkeley, CA 94720; email: takhirov@berkeley.edu; https://ce.berkeley.edu (*corresponding author)

[2] Turin Polytechnic University in Tashkent, 100095, Tashkent, Uzbekistan email: iljasar@mail.ru, dmatrasulov@gmail.com; https://polito.uz/en/

Keywords: Structural Health Monitoring, Seismic Assessment, Laser Scanning, Seismometers, Real-time monitoring, Bibi-Khanum, Samarkand, Great Silk Road.

Abstract. *The Bibi-Khanum Mosque was originally built in 1399-1405 and was one of the largest and most magnificent mosques in the Islamic world during the 15th century. In recent years, the monument underwent several complex reconstructions. Among many other major restoration activities, the inner arch of the portal that collapsed in the 1897 earthquake was restored. The monument has been restored to be one of the best shapes in its history, thus it has become essential to conduct continuous structural health monitoring (SHM) of it to ensure its preservation for humanity. The SHM became the main objective of an ongoing extensive project, some results of which are presented herein. The structural health monitoring consisted of three major phases. The first phase includes a real-time monitoring of the monument by seismometers, which are permanently installed throughout the monument. They are used to monitor the effects of large and small earthquakes and ambient vibrations on the resonant frequencies of all major structures of the monument. By utilizing a system identification approach, the possibility of a structural anomaly development can be detected from the change in its resonance frequency. The second phase consists of subsequent laser scanning that is deployed to monitor anomalies of the monument's geometry in 3D. The monument's geometry is captured as a collection of points, which is called a "point cloud". Laser scanning is planned to be conducted several times a year to capture global movements of the monument due to changes in the elevation of the underground water table in rainy and dry seasons. The third phase focuses on a development of a finite-element (FE) model based on the as-found geometry of the point clouds. It is calibrated based on the collected data to ensure acceptable correlations with the results of the measurements. The FE model is generated for use in future restoration efforts to evaluate the performance and efficiency (if any) of the proposed restoration measures. Based on the results of numerical simulations and structural health monitoring, preventive measures will be developed. In addition, recommendations for further preservation of the historic monument will be developed. This paper describes the preliminary results of the first phase and current results of the second phase of this multiphase project.*

1 INTRODUCTION

The Bibi-Khanum Mosque was originally built in 1399-1405 and was one of the largest and most magnificent mosques in the Islamic world during the 15th century. The heritage structure was studied by Ratiia in the 1940s. Based on these studies, Rattia developed the first restoration plan drawings in his book published in 1950 [1]. One of these drawings is reproduced in Figure 1. As shown in the plan drawing, the Bibi-Khanum Mosque was built as a courtyard ensemble with three domed masonry structures (mosques) along the walls. The main mosque is located on the west side, and two smaller mosques are located along the north and the south walls. The Bibi-Khanum Mosque was also studied in [2].

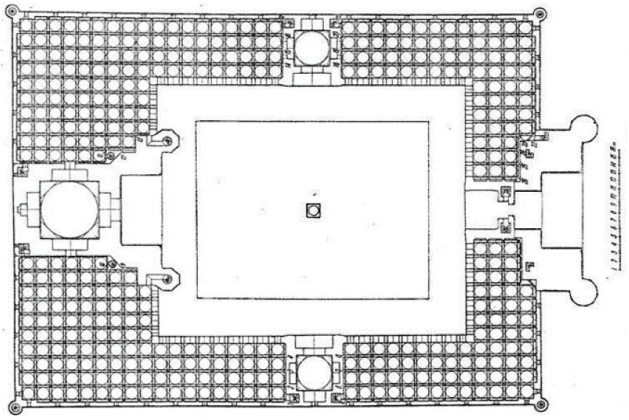
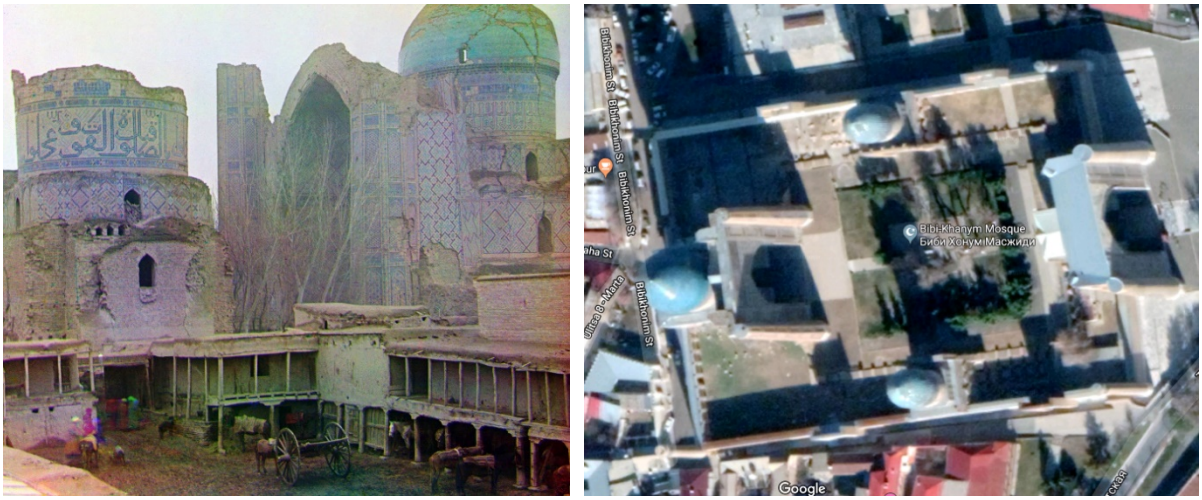


Figure 1: Plan view of Bibi-Khanum Mosque (after [1])

One of the most recent studies on its history and architecture is published in [3]. In recent years, the monument underwent several complex reconstructions and some of them are mentioned in [4]. Among many other major restoration activities, the inner arch of the portal that collapsed in the 1897 earthquake was restored. The view of the monument at the beginning of the twentieth century is presented in Figure 2a.



a) Photo dated by 1905-1915 b) Aerial view (Google maps)

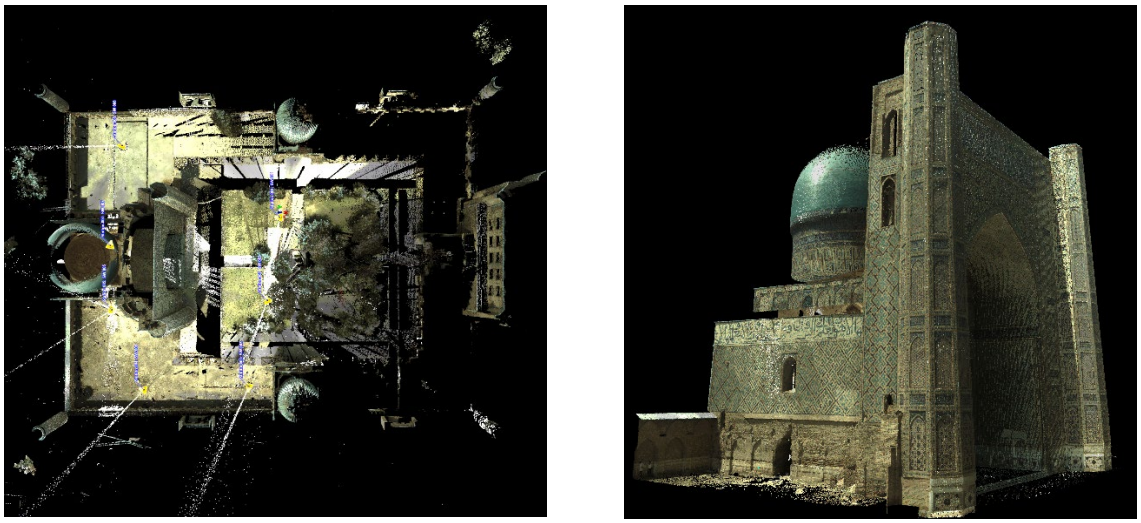
Figure 2: The Bibi-Khanum Mosque

The photograph presented in Figure 2a was taken between 1905 and 1915 by color photography pioneer Sergei Mikhailovich Prokudin-Gorskii. It shows the mosque's appearance after its collapse in the 1897 earthquake. Figure 2b shows its aerial view taken from Google maps.

2 LASER SCANNING

The Bibi-Khanum Mosque was scanned in July 2019. Observations indicated that the mosque had undergone a recent reinforcement and some of the work was ongoing. To capture the current geometry of the monument, a terrestrial scanner was deployed. A laser scanner from Leica Geosystems, Scan Station C10 [5], was utilized for the project.

The scanning was conducted from seven stations to capture the exterior and interior walls of the monument. No reference targets were used in the laser scanning process. To stitch the point clouds collected from each station, a point cloud to point cloud matching was utilized. A complete registration of the point clouds collected from these seven stations is presented in Figure 3a and the registration was conducted in Cyclone [6]. Figure 3a also shows the locations of the stations (yellow triangular icons) on the fully registered point cloud of the monument. The point cloud was colored based on the photos obtained from the scanner's built-in camera. Figure 3b shows a typical point cloud of the mosque with its natural colors. A view from the ground level is shown here.



a) TruView with stations b) Ground view of point cloud: main mosque

Figure 3: Fully registered point cloud combining seven stations

The remaining analysis of the point cloud was conducted in a Matlab environment [7]. For the convenience of presentation and clarity of discussion, several local coordinate systems were introduced. It is worth noting that all these coordinate systems can be correlated to a single global coordinate system (GCS). The latter GCS can be geo-referenced if needed.

2.1 Analysis of main mosque's entrance (portal)

The portal of the main mosque is presented in Figure 4. A new coordinate system with the

origin at ground level and coinciding with the middle of the portal's arch was introduced.

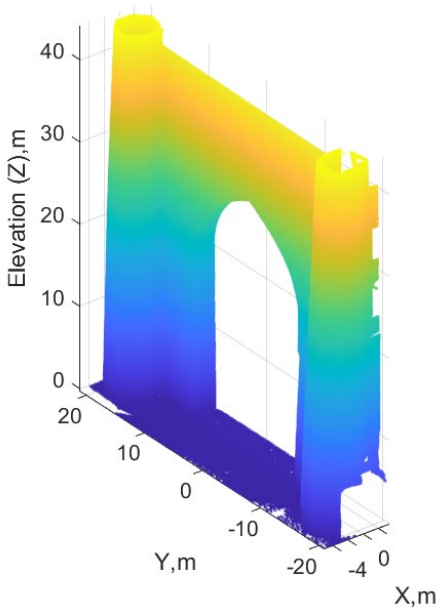
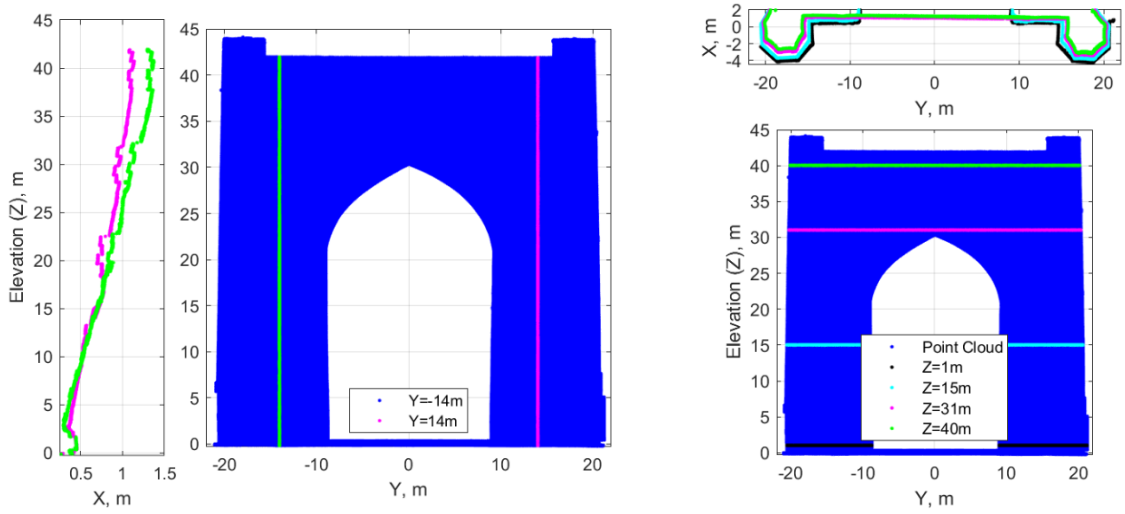


Figure 4: Main mosque's portal

Figure 5a shows cross sections of the portal's front surface. The images quantify the inclination of the surface that can be also related to the wall's taper. Figure 5a shows vertical cross sections, whereas Figure 5b presents horizontal cross sections. The largest difference of inclination on the top of the portal is about 0.25 m between the sections at Y=-14 m and Y=14 m. Most likely this difference in inclination is related to the age of construction and does not represent any structural concern as it did in the case of the Kuk-Gumboz monument in Shakhrisyabz (Uzbekistan) [8]. Nevertheless, subsequent laser scanning expeditions are planned to ensure that this difference in the inclination does not progress.



a) Vertical b) Horizontal

Figure 5: Cross sections of the frontal surface of the portal

Figure 6 shows a contour map of the inclinations of the portal. The points are colored based on the distance from the vertical plane. This color map clearly shows the difference in the inclinations on the left and right sides of the portal as was mentioned earlier in the example of the two vertical sections. As shown in the image, the inclination of the portal is gradually increasing towards the top left side. Since the region of interest is relatively narrow, the minarets on both sides of the portal are not presented in Figure 6.

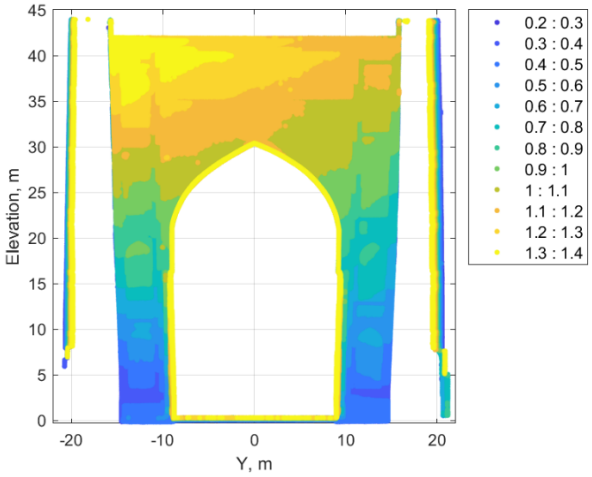
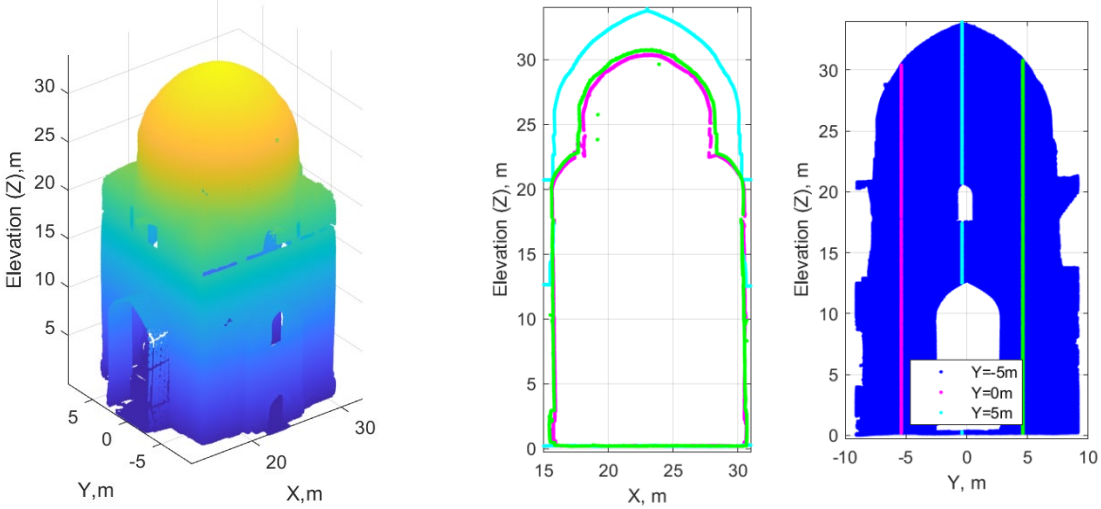


Figure 6: Color map of portal's inclinations (legend's units are meters)

2.2 Analysis of main mosque

The inner surface of the main mosque is presented in Figure 7. The image on the left shows a 3D view of the point cloud, whereas the image on the right presents its horizontal sections with *Y=const* planes. The local coordinate system is aligned with the highest peak in the dome. There is a relatively small difference between the *Y=5m* and *Y=-5m* sections, and this can be related to imperfections in the construction. To ensure that the imperfection is not progressing or creating structural deficiencies, a follow-up laser scan is planned in several months.



a) 3D view b) Cross sections with vertical plane *Y=const.*

Figure 7: Inner surface of main mosque

2.3 Analysis of main mosque's walls

Analysis of the walls' point cloud is discussed herein. Due to the size limitations of this paper, only two walls of the main mosque are discussed below. The inner surface of the east wall is presented in Figure 8a. It shows a sagging in its top middle portion right under the dome. Several cracks serve as evidence that the structural integrity of this wall needs to be investigated and addressed. In the case of the south wall shown in Figure 8b, there is no sagging, this most likely relates to a concrete retrofit that is incorporated into the wall.



a) East wall (sagging under dome) b) South wall (a portion of arch is missing)

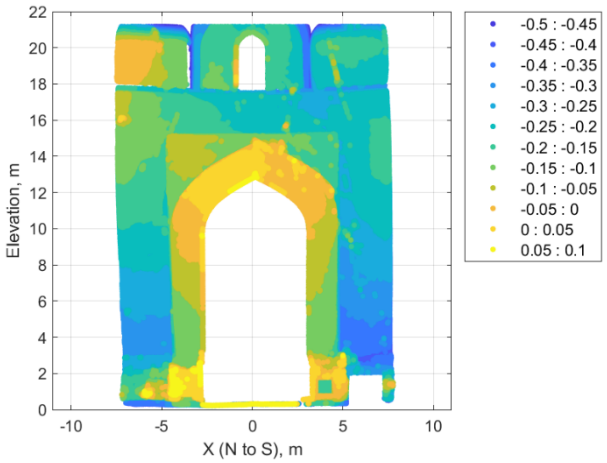
Figure 8: Analysis of point clouds (main mosque's inner walls)

As can be seen from the right image, a large volume of reinforced concrete was introduced above the arch. The arch is missing a piece at its tip. The reinforced concrete is most likely very beneficial for holding together the failing parts of the wall; however, it may result in an introduction of a large weight at higher elevation of the building due to the large difference in density of concrete and masonry. The latter can result in significant changes in the dynamics of the whole structure. In the earlier studies [9, 10] an experimental investigation of a typical brick material was conducted. The test results show that the density of the bricks is about 1,600 kg/m^3. The latter test results are consistent with the results obtained for the bricks recovered from heritage buildings in Europe [11]. Hence, the bricks are about 1.5 lighter than the reinforced concrete, the density of the latter is typically assumed as 2,400 kg/m^3.

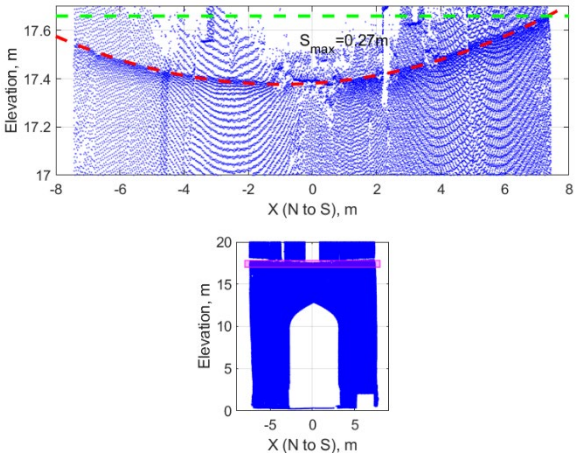
The following conclusions can be drawn from the analysis of the walls' point clouds. There is a large difference between the east and south walls that will result in a difference in their structural performance under static loads. In addition, a large mass of reinforcement in the south wall can result in large differences in structural performance during seismic events.

To assess the performance of the building with such large irregularities, extensive monitoring is required. The latter is addressed by utilizing seismometers at critical locations throughout the monument.

The out-of-plane inclinations of the east wall is presented in Figure 9a. An estimate of the sagging at the lowest point of the east wall in respect to its highest point (green line) is presented in Figure 9b. The sagging can be closely approximated by a parabolic line as indicated by a red dashed line in the top image of Figure 8b. Based on the availability of future funding, the east wall will be instrumented by position sensors to monitor sagging and crack development.



a) Out-of-plane inclinations (the top leans toward the portal, which is behind)



b) Parabolic approximation of sagging and maximum sag (top image shows close-up version of region shown in magenta box of lower image)

Figure 9: Analysis of east wall's point cloud

3 REAL-TIME MONITORING

To study the structural performance of the monument subjected to ambient and seismic excitations, an array of tri-axial seismometers is installed. The seismometers are used to estimate resonant frequencies and damping of the monument, and to monitor their changes due to structural anomalies, if any. The process of installing seismometers is completed. In addition, a power supply and reliable internet connections are established.

The seismometer based SHM will register not only ambient vibrations, but also the frequent local earthquakes in Uzbekistan and Tajikistan. Monitoring the modal parameters (resonant frequencies and critical damping values) of the monument in real-time is the main objective of SHM and will also serve for rapid-response actions in case of significant changes of modal parameters.

3.1 Preliminary instrumentation layout

A layout of the instrumentation is presented in Figure 10. As seen in the image, fifteen tri-axial seismometers are installed at strategic locations throughout the monument. The main entrance portal to the whole ensemble is instrumented by four seismometers. Smaller structures on the north and south sides of the ensemble are instrumented by three seismometers. The mosque is instrumented by eight seismometers, from which four seismometers monitor the vibrations of the mosque's portal and the other four seismometers are installed on the main structure of the mosque. The latter set includes one seismometer to monitor the dome's

vibrations. A summary of the accelerations' locations is presented in Table 1.

It is worth noting that the outer surface of the monument is protected by decorative tiles and as such, the deformations measured on the outer surface may not reflect inner deformations. In this case, other measuring techniques need to be implemented. For example, a penetrating georadar can be utilized.

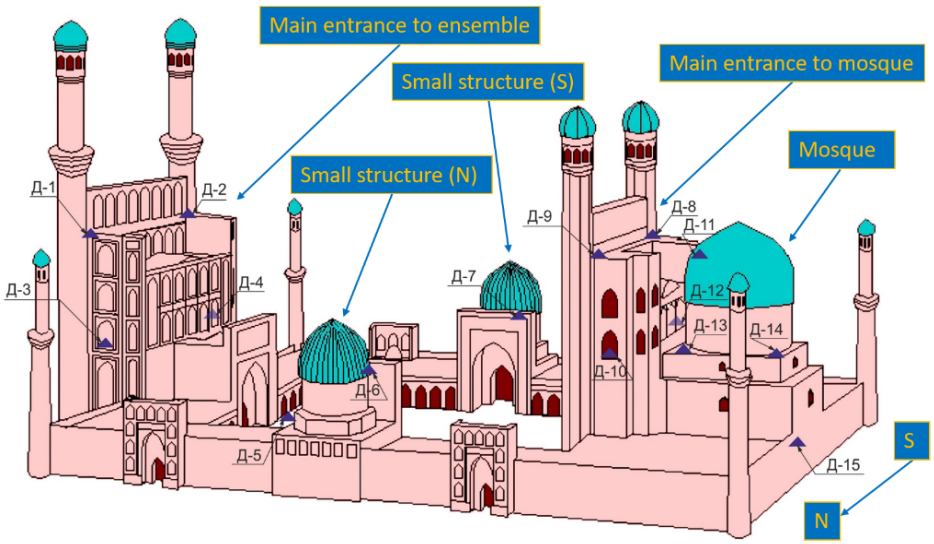


Figure 10: Preliminary layout of seismometers

Table 1: Summary of seismometer locations

Russian notation	English notation	Part of ensemble	Location
Д1	A01	Main Entrance	Top elevation (north)
Д2	A02	Main Entrance	Top elevation (south)
Д3	A03	Main Entrance	Mid-elevation (north)
Д4	A04	Main Entrance	Mid-elevation (sourth)
Д5	A05	Small structure (north)	Top of structure
Д6	A06	Small structure (north)	Dome
Д7	A07	Small structure (sourth)	Top of portal
Д8	A08	Entrance to mosque	Top elevation (south)
Д9	A09	Entrance to mosque	Top elevation (north)
Д10	A10	Entrance to mosque	Mid-elevation (north)
Д11	A11	Main structure of mosque	Dome
Д12	A12	Entrance to mosque	Mid-elevation (sourth)
Д13	A13	Main structure of mosque	Top elevation (west)
Д14	A14	Main structure of mosque	Top elevation (east)
Д15	A15	Main structure of mosque	Mid-elevation (east)

3.2 Finite element modeling and optimization of seismometer layout

The instrumentation layout shown in Figure 10 was considered to be the first step in determining of the best possible location for the seismometers. In the next step of the study, a finite element model of the monument will be developed which will reflect all anomalies captured by the laser scanner. The finite element model will be calibrated by utilizing the ambient test data collected from the instruments at the locations presented in Figure 10. As a result, a finite element model closely replicating the actual monument will be developed. The model will be used in the optimization process to identify the best locations for the seismometers. Depending on the results of this optimization study, the seismometers will be rearranged at the newly identified locations. Based on the results of ambient vibration tests from the new locations, the finite element model will be updated. This part of the project is ongoing.

4 CONCLUSIONS

- The Bibi-Khanum monument is a historic monument, which was repaired and/or reinforced several times throughout its long history. The materials and methods used in these efforts vary widely. As a result, the monument represents a building, of which its structural performance is difficult to assess by conventional means. To address the issue, this paper highlights the usage of modern technologies to monitor the monument and predict its structural performance.
- The results of this study show that the current anomalies of the monument can be captured with high accuracy by a terrestrial laser scanner deployed in the project. These structural anomalies need to be monitored over time to evaluate their progression, if any. Future restoration strategies will be based on the comparative analysis of subsequential laser scanning data.
- The next steps regarding instrumentation installation, finite element modeling and optimization of the seismometers locations are ongoing and will be reported in future publications.

5 ACKNOWLEDGEMENTS

A photograph presented in Figure 2a was taken between 1905 and 1915 by color photography pioneer Sergei Mikhailovich Prokudin-Gorskii and it shows the mosque's appearance after its collapse in the 1897 earthquake. This work is partially supported by the Ambassador’s Fund for Cultural Preservation of the Embassy of USA in Tashkent (Ref. Nr. S-UZ800-17-GR-0043). The expenses associated with renting a terrestrial laser scanner was covered by the Turin Polytechnic University in Tashkent (Uzbekistan), and is greatly appreciated. Special thanks are due to Dr. Sultan Kudratov of the Tashkent University of Information Technologies, Tashkent (Uzbekistan) for his help during the laser scanning in Samarkand. The deployment of the laser scanner and the data reduction of the point clouds was provided by Sensor Fusion and Monitoring Technologies, LLC (USA), and is greatly appreciated. Special thanks are due to Holly Halligan of UC Berkeley for editing the paper. The paper’s registration fee required for the participation in the 12th International Conference on Structural Analysis of Historical Constructions, SAHC 2020, was sponsored by University of California, Berkeley, and is greatly appreciated.

REFERENCES

[1] Ratiia, Sh. E. (1950) Mechet Bibi-Khanym. Moscow: Gosudarstvennoe izdatelstvo arkhitektury i gradostroitelstva.

[2] Zakhidov, Pulat (1996) Architectural glories of Temur's era. Tashkent: Sharq.

[3] Paskaleva, Elena (2012) The Bibi Khanum Mosque in Samarqand: Its Mongol and Timurid Architecture. The Silk Road 10: 81–98.

[4] Paskaleva, Elena (2013) Epigraphic restorations of Timurid architectural heritage. https://www.academia.edu/3703325/Epigraphic_restorations_of_Timurid_architectural_heritage. International Institute for Asian Studies. Retrieved 22 January 2021.

[5] Leica Geosystems AG (2011) Leica ScanStation C10: Product Specifications. https://w3.leica-geosystems.com/downloads123/hds/hds/ScanStation%20C10/brochures-datasheet/Leica_ScanStation_C10_DS_en.pdf. Accessed January 3 2020.

[6] Leica Geosystems AG (2015) Cyclone Version 9.1.

[7] The MathWorks Inc (2019) Matlab Version R2019b.

[8] Takhirov, Shakhzod & Gilani, Amir & Quigley, Brian & Myagkova, Liliya. (2018). Assessment of Seismic Vulnerability and Retrofit Strategies of a Historic Building on the Great Silk Road Based on its Current Condition Captured by Laser Scans. *International Journal of Architectural Heritage*. 1-13. 10.1080/15583058.2018.1497231.

[9] Shakhzod Takhirov, Khalid M. Mosalam, Mohamed A. Moustafa, Liliya Myagkova, and Brian Quigley (2015) LASER SCANNING, MODELING, AND ANALYSIS FOR DAMAGE ASSESSMENT AND RESTORATION OF HISTORICAL STRUCTURES. COMPDYN 2015. 5th ECCOMAS Thematic Conference on Computational Methods in Structural Dynamics and Earthquake Engineering. M. Papadrakakis, V. Papadopoulos, V. Plevris (eds.). Crete Island, Greece, 25–27 May 2015.

[10] Shakhzod Takhirov, Amir Gilani, Brian Quigley, Liliya Myagkova (2017) Assessment of Seismic Vulnerability of Historic Buildings Based on their Current Condition Captured by Laser Scans and Retrofit Strategies. The 16th World Conference on Earthquake Engineering. January 7-13, 2017 Santiago, Chile.

[11] Francisco M. Fernandes, Paulo B. Lourenço and Fernando CastroChapter. Ancient Clay Bricks: Manufacture and Properties. Chapter 3 in M. Bostenaru Dan et al. (eds.), Materials, Technologies and Practice in Historic Heritage Structures, DOI 10.1007/978-90-481-2684-2_3 , © Springer Science+Business Media B.V. 2009.

12th International Conference on Structural Analysis of Historical Constructions
SAHC 2020
P. Roca, L. Pelà and C. Molins (Eds.)

STRUCTURAL HEALTH MONITORING OF A HISTORIC CHURCH: THEORY AND PRACTICE OF DIAGNOSTIC APPROACHES USED TO CONTROL RISKS AND COSTS

DR. THOMAS MORRISON, PENG, ISCARSAH[1*] AND SONYA BURRILL, MSC[1]

[1]Heritage Standing Inc. (HSI)

PO Box 66, Stn A, Fredericton, NB, E3B 4Y2, Canada
e-mail: tmorrison@heritagestanding.ca, www.heritagestanding.ca (*corresponding author)

Keywords: Structural Health Monitoring, Masonry, Case Study, Damage Detection, Risk Mitigation

Abstract. *Structural Health Monitoring is an exciting opportunity to use real time quantitative data of a structure's response in analysis and evaluation. However, this technology has yet to achieve common use in practice and remains linked to research of iconic buildings. This paper discusses the challenges and opportunities for use of SHM for widespread projects with damaged buildings and limited budgets. The SHM approach used was long term low frequency (static) data collection of both environmental inputs and structural responses. This data was used to develop relationships between loads and responses that could be effectively used to determine safety of the building and where in the structure deterioration continues.*

1 INTRODUCTION

Structural health monitoring (SHM) provides an option for historic buildings with multiple limitations. For some historic buildings' owners must balance maintenance demands, constrained budgets, remote sites, and limited access to heritage professionals to avoid demolition. SHM can be used to objectively analyze safety and risk, allowing the professional to phase construction safely over longer periods of time, in alignment with the client's budget. Structural health monitoring provides data that is accessible through standard cellular service, reducing the need for frequent and costly remote site visits.

Stone Church, an unreinforced masonry structure built in 1826 in rural Eastern Canada, had significant structural deterioration issues due to a recent incompatible intervention. A full repair was not immediately possible, and closure for several months would likely have resulted in the closure of the parish and loss of the building. SHM was selected as the best option to meet these challenges by demonstrating building performance and safety. The system selected provided solutions for:

- monitoring damage from past incompatible repairs
- managing potential risk while building remains in use
- monitoring the success of phased construction

- the distance of heritage professionals from the site
- a limited budget

2 BACKGROUND

Structural health monitoring is used extensively in industry for civic infrastructure, such as bridges and damns.[1] Many of these approaches rely on data analytics and are often prohibitively expensive to apply to smaller and less well funded historic building.[2] In the heritage community SHM systems have been applied to some iconic historic structures.[3] The structures are typically culturally and financially well supported. They also benefit from long term study and monitoring by experienced heritage professionals. The use of vibrational analysis-based software for SHM alongside dynamic systems has become increasingly common, which allow the removal of environmental effects in evaluation to identify deficiencies occurring over time.[4]

Our approach applies SHM to control risk in lesser known, remote, and financially constrained sites where initial stability is unclear. By combining information from both structural and environmental inputs, this approach allows a more intuitive interpretation, and allows for understanding changes in structural stability due to climate-change induced weather pattern shifts.

3 METHODOLOGY

The conceptual structural health monitoring approach as applied to these constrained sites, including Stone Church, was:

- Extensively pre-study the building to understand critical areas for monitoring.
- Design and set-up structural and environmental sensors, with the goal to minimize the hardware required while obtaining enough information to maintain safety.
- Acquire static data (more than one minute between data points) from the sensors and transmit to remote professionals
- Use the in-house software MIROVY[5] to analyze data. This software is based on static and dynamic statistical analysis approaches.[6,7]
- Combine numerical results with knowledge of the building to come to conclusions of safety and next steps.

The MIROVY software was benchmarked against two historic sites. Portugal's Oporto Cathedral and Monastery of Jerónimos had extensive ongoing structural monitoring and evaluation that provided base data sets for comparison.

4 APPLICATION TO STONE CHURCH

4.1 Structural health monitoring system design

The SHM system was designed in response to structural stability concerns in the Church. Past incompatible repairs, completed in 2007, were done on the front façade half of the building (including around the bell tower). An attached hall, which acted as a buttress for the western side of the building, was removed in 2015.

The condition assessment noted the most urgent areas of concern:

- An archway, previously buttressed by the hall, was splaying.

- Extensive deterioration of the masonry was found in the areas of the 2007 repairs. Deterioration included failure of the wall core, delamination of masonry wythes, and cracking indicative of the wall no longer functioning as a unified structural system.
- Significant new cracking was observed by the owners a few weeks prior to the first site visit.

The structural health monitoring system was designed to be as minimal as possible while monitoring the above structural vulnerabilities to allow for safe continued use. Environmental sensors were chosen to monitor conditions most likely to impact the chosen structural sensors. Figure 1 and figure 2 show the final placement of structural and environmental sensors for Stone Church.

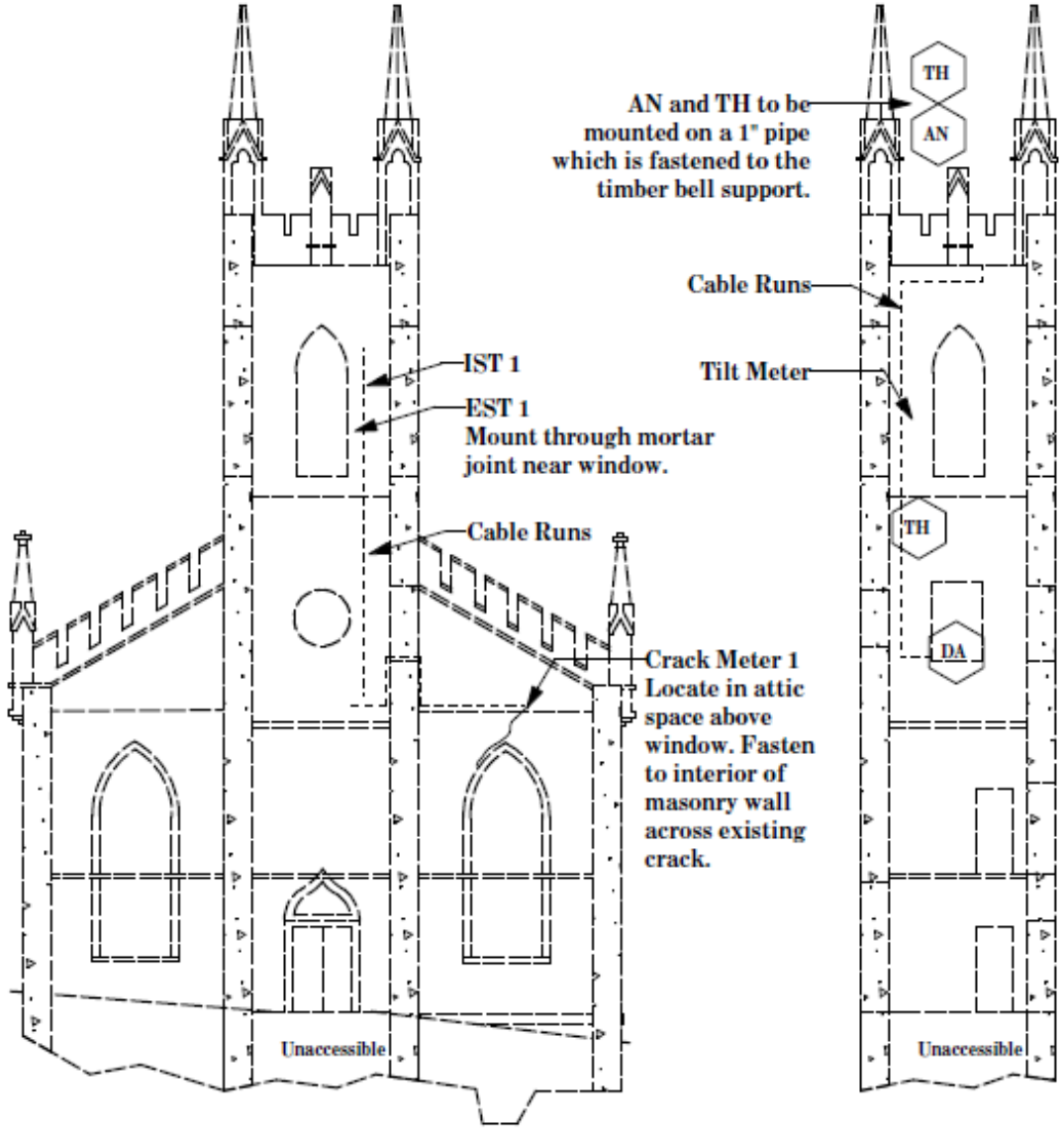
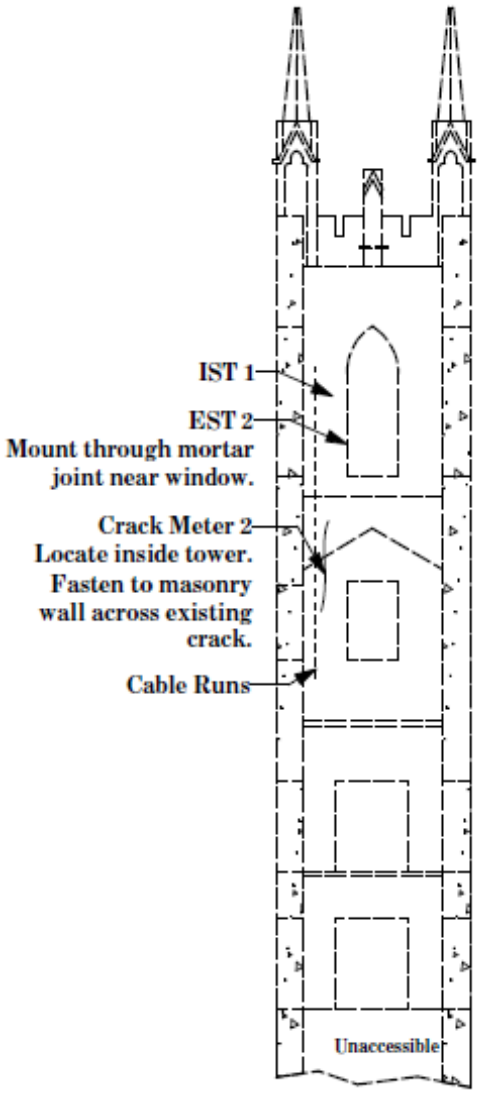


Figure 1. Sensor locations looking South and West.



Legend:
AN Anemometer (wind meter)
TH Temperature and humidity sensor
DA Data acquisition system
IST Interior surface temperature
EST Exterior surface temperature
Note: **Crack meter 3**, not shown, measured the splaying of an arch at the rear of the church.

Figure 2. Sensor positions looking North.

4.2 Short-term results

Initial data was analyzed with direct results analysis, plotting sensor values over time. These plots confirmed the integrity of the data and became a baseline for future measurements.[5,8] They also allowed the professional to identify significant changes, such as the continual expansion of crack meter 3 (Figure 3). In other cases, the direct results analysis quickly informed users of problems; this plot of crack meter 2 showed that a sensor was knocked from its mount (Figure 4).

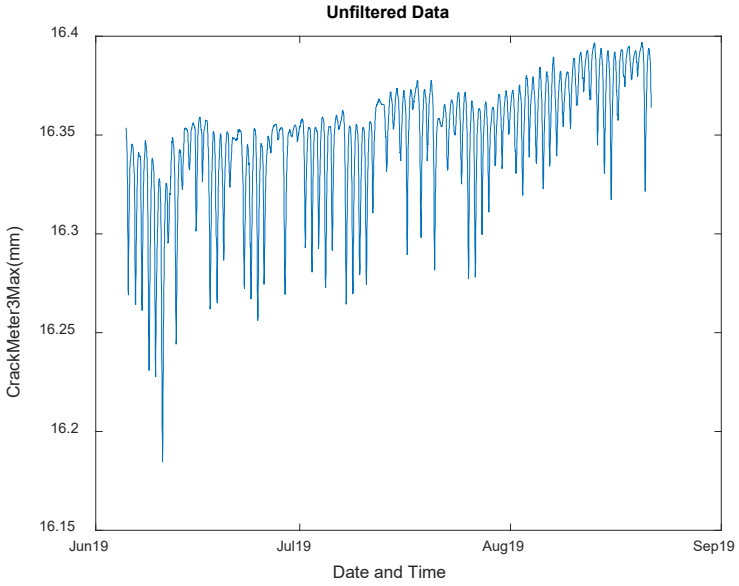


Figure 3. Continual expansion of Crack 3

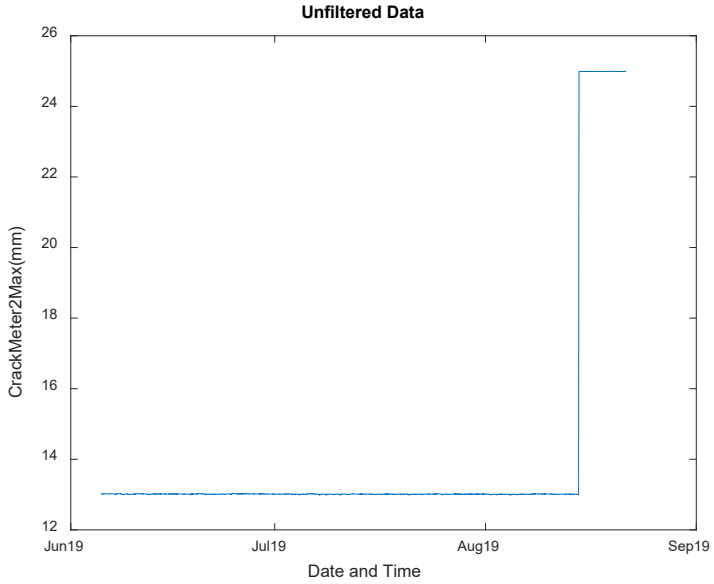


Figure 4. Crack Meter 2 knocked from its mount.

As the structural stability was a concern it was important to identify changes at as small a movement level as possible, focusing monitoring on trends and relationships so that problems could be addressed early.

The direct analysis plots also allowed the professional to quickly compare structural trends and environmental trends. Structural trends that showed no relation to environmental or use factors suggested gradual failure of a component. This did depend upon the correct environmental factors being included in the monitoring program.

Early results provided simple statistical information: histograms were plotted to visualize the frequency of sensor measurements. Known statistical distributions should result, but when they did not, further investigation was undertaken (Figure 5). A coefficient of determination table was also developed for all signals, measuring the extent to which changes in a structural sensor were dependent on the changes in an environmental sensor.[9]

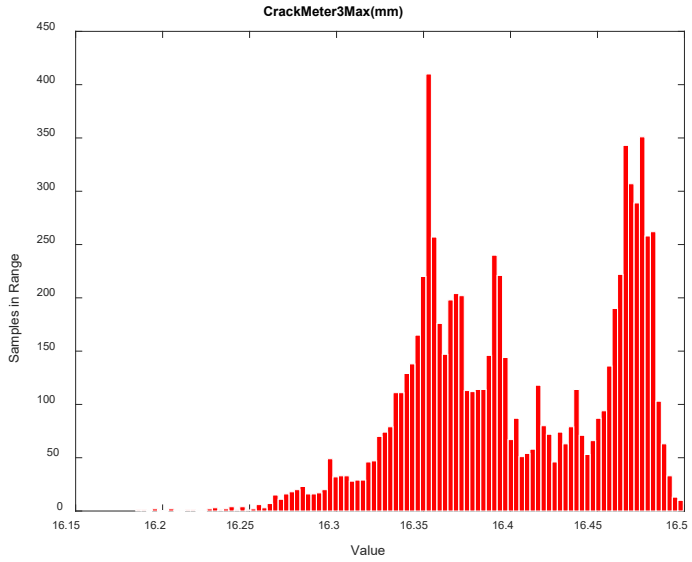


Figure 5. Irregular statistical distribution for crack meter 3.

4.3 Data surrounding emergency stabilization – the first 6 to 9 months

Emergency stabilization work was started late August 2019. Figure 6 shows crack meter 1, where following the intervention the amplitude of short-term movements noticeably decreased.

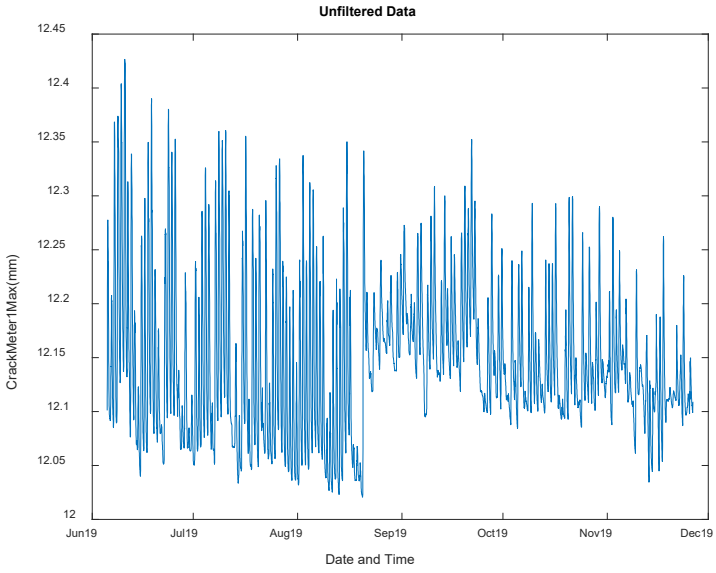


Figure 6. Before and after August 2019 construction work.

The emergency stabilization work had a limited budget and focused on providing additional confinement for the masonry. Stainless steel rods and exterior mounted face plates were used in multiple locations, alongside mortar repairs in as many critical locations as possible. Changes in structural responses were seen immediately.

Along with direct results analysis and simple statistical evaluation, an algorithm for damage detection also provided evidence for improvement. Damage detection algorithms in the MIROVY program rely on two different statistical methods: standard deviation comparison and ARMA (auto-regressive moving average) dynamic regression.[9,10] User selects the section of data from which the relationships are established, then projects this relationship for the entire signal. While these algorithms are more reliable for multi-year data sets, they were still beneficial for analyzing damage and improvement on shorter data sets. For example, after construction crack meter 3 showed more predictable behaviour (Figure 7).

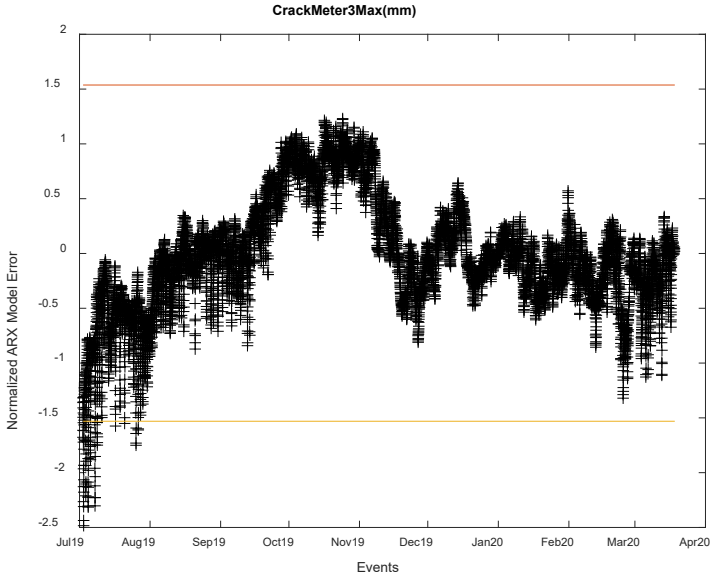


Figure 7. Reduced error in crack meter 3 after construction.

These initial results were beneficial in helping provide a means to establish temporary safety limits with the monitoring data as well as underlining that further intervention was necessary. With continued monitoring it was decided that the building could remain in use while the owners raised money in the coming years.

4.4 Data from one to one and a half years

With data covering more than one year of seasonal variations, baselines were better established and structural movements outside of the expected were easier to evaluate. Collecting environmental data allowed us to compare newly observed structural minimums and maximums with temperatures, opposing surface temperatures, humidity, or wind. For example, if newly observed tilt meter maximums corresponded to new maximums of wind speed, that would contribute to a possible explanation of the tilt meter's unexpected movement.

Longer term data allowed for the set-up of defined limits on sensors, which when exceeded

would trigger an alarm that notified the owner and professional that unexpected behaviour was occurring. This would ensure that if unexpected changes occurred between pre-set evaluation times, those changes would be noticed and immediately addressed. The notification was to trigger a full data analysis to understand potential causes.

Data sets of longer than one year could benefit more from static regression analysis[11,12] and dynamic regression analysis. For example, Figure 8 shows the multiple static regression analysis for comparing crack meter 3 with outside temperature, relative humidity, and surface temperature 2 difference. There is fair agreement between actual and modeled behaviour.

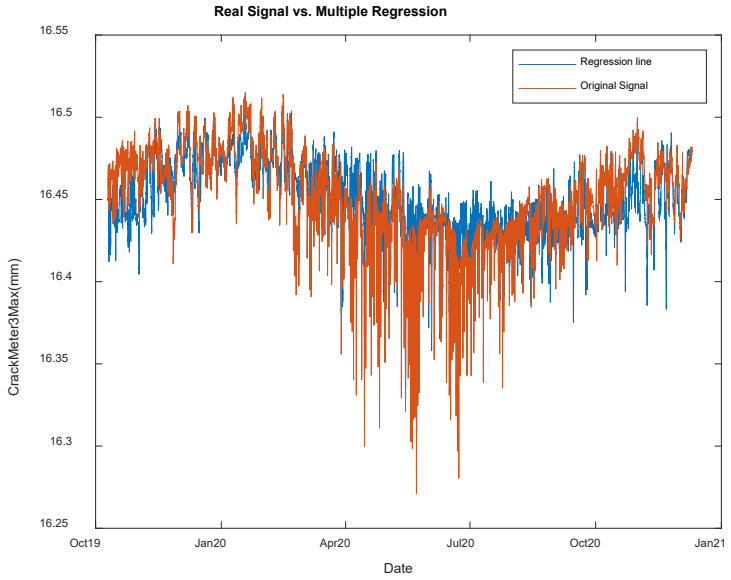


Figure 8. Fair agreement between multiple regression prediction and actual for crack meter 3.

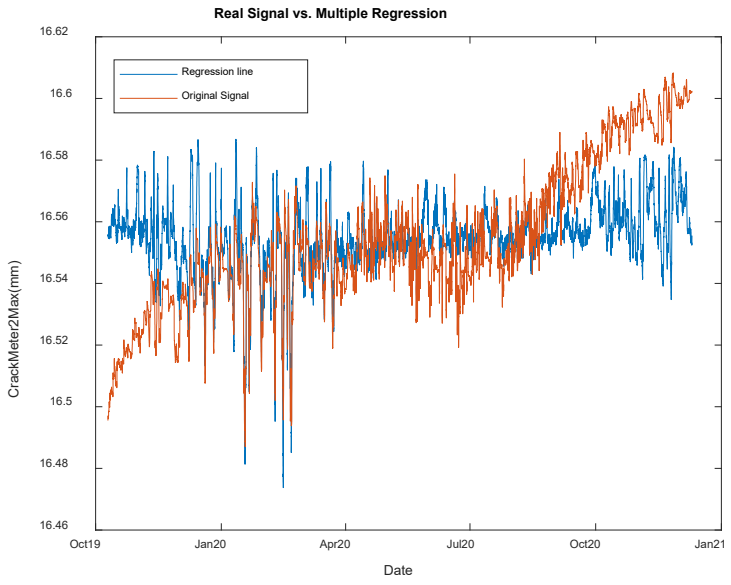


Figure 9. Poor agreement between multiple regression prediction and actual for crack meter 2.

The same analysis for crack meter 2 (Figure 9) shows disagreement between actual and modeled behaviour, indicating that the continual expansion is not well modelled by changes in environmental effects and may require further investigation. Likewise, tilt meter B, North-South movement, is not well modelled by environmental variables (Figure 10). Inclusion of max wind speed in the multiple regression modelling also showed that max wind speed was more relevant for tilt meter B than for any other structural sensor.

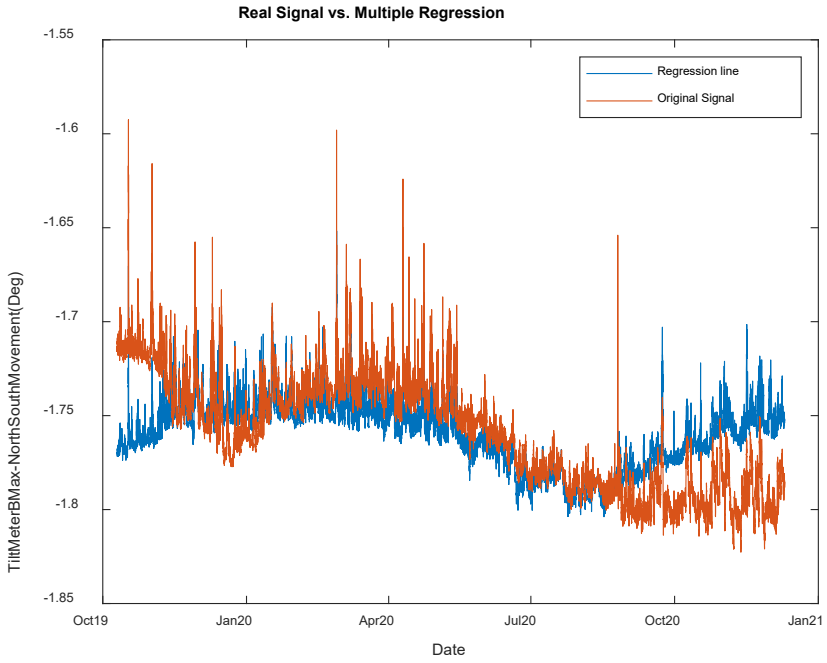


Figure 10. Multiple regression for tilt meter B

The damage detection algorithms, based on dynamic regression algorithms and produced from normalized values, considered results that included delayed factors, such a thermal inertia.[9, 10] The data set was divided into two sections. The first section was used to develop the model relationship between the structural sensor in question and relevant environmental variables. The second section provided structural predictions from the model, based on actual environmental measurements. The division between data used for the regression analysis and the predictions made was dependent upon building history and available data. For easier comparison one plot could be produced to show upper and lower bounds (set at a preferred standard deviation) and the difference between actual and predicted results. A second plot that showed the relationship as normalized model error provided easier visualization of trends in the predicted versus the actual value. If the structure were in good condition the error would remain within bounds with minor variation from start to end. If damage occurred after the control data, early in the signal, then the error would trend upwards or downwards late in the signal, extending beyond the bounds. Using dynamic regression-based damage detection analysis, figure 11 and figure 12 show a change in trends for tilt meter A, East-West movement.

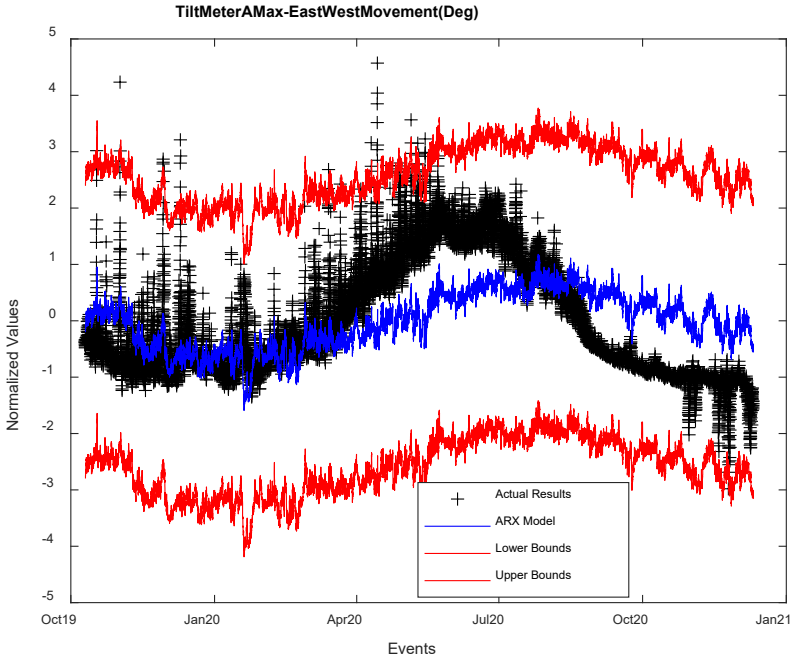


Figure 11. Tilt meter A dynamic regression damage detection.

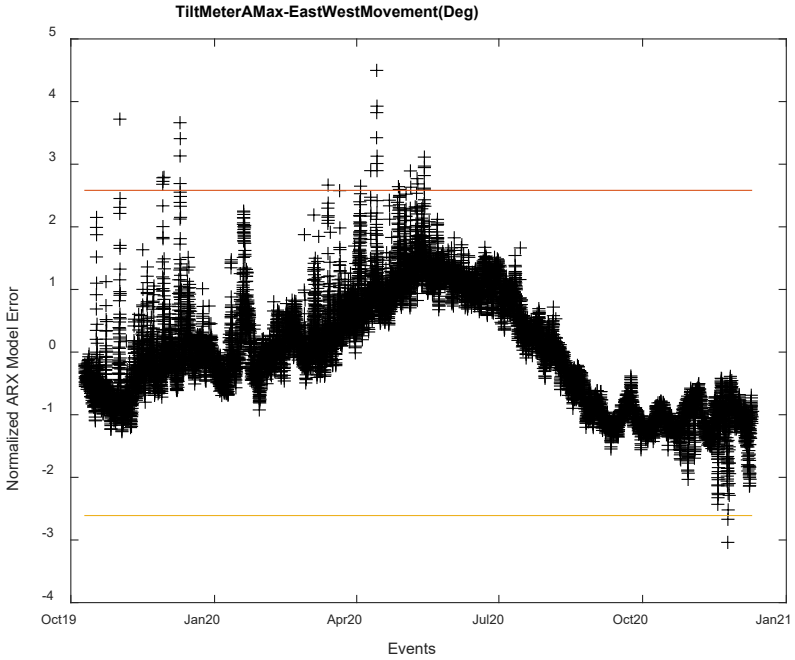


Figure 12. Tilt meter A dynamic regression model error

The most recent interpretation of data, which combined direct results analysis, simple statistical analysis, multiple static regression analysis, dynamic regression analysis and damage detection, found the following:

- Interventions have provided benefit.
- Instabilities remain in the tower, and monitoring should continue.
- Crack meter 2 and tilt B, North-South movement, are still being closely monitored.
- The North wall and tower concerns remain, however the decision regarding which is the highest priority can be delayed for additional data.
- The difference in exterior and interior surface temperature on masonry response did not relate well to movements initially, but after two small sets of repairs the relationship has become important – as had been anticipated.
- Crack meter 3 has been stabilized.

This interpretation led to recommendations for the owner of continued monitoring, immediate reporting of new changes, a visual inspection in summer of 2021 and making plans to undertake additional building conservation projects (which could be linked to an upcoming major anniversary of the building).

6 DISCUSSION AND CONCLUSION

Our case studies confirmed that structural health monitoring could be successfully used to demonstrate building performance and safety for widespread application. Our base concept to use the relationship between the environmental causes and the structural responses to understand the building and meet client needs was successful. Additional advantages are provided with real time alarm for defined safety limits and regular professional monitoring of building performance without the necessity of site inspection.

Our SHM applications have also provided additional considerations. As we continue to collect data and analysis experience lessons include:

a) Only a small number of sensors are required, but what sensors and where must be carefully considered. Some redundancy is important as some sensors will likely be damaged during use.
b) Ensure the objectives and data analysis plans are prepared before implementation. Changes to data collection after starting monitoring create challenges for data processing.
c) Improved dynamic regression models would be valuable, particularly for wind data which may only have impact above specific thresholds.
d) Essential data will depend upon the site and the nature of the structural vulnerability being monitored. For the case study capturing wind gust data as well as interior and exterior surface temperatures was important to establishing expected performance.
e) A thorough understanding of the likely structural deficiencies and dynamics is necessary to determine and justify the monitoring required, and to interpret its meaning. This type of data would have limited value without this understanding.
f) Having a small number of likely theories to explain impacts to each structural sensor should guide identification of environmental data to be collected.

There remain many aspects of this SHM approach where further research would be beneficial. Finding ways to setup and run a system for low a budget situation requires considerable planning and knowledge. Determining how to make these processes accessible to a less specialized engineer would improve the ability for industry to take up the technology. Our ability to effectively use these tools for this type of project continues to rely on a small

number of highly specialized engineers who have an intuitive understanding of structural dynamics and data. Our internal training has struggled, and we have lacked the resources to undertake some of the larger innovation necessary.

7 REFERENCES

[1] Pines, D. and Aktan, A.E. Status of structural health monitoring of long-span bridges in the United States. *Prog. Struct. Engng. Mater.* (2002), **4**: 372-380.
[2] Gulgec N.S., Shahidi G.S., Matarazzo T.J., and Pakzad S.N. Current Challenges with BIGDATA Analytics in Structural Health Monitoring. In: Niezrecki C. (Eds.): *Structural Health Monitoring & Damage Detection, Volume 7*. Conference Proceedings of the Society for Experimental Mechanics Series. Springer, Cham (2017).
[3] Oliveira, D., Ramos, L., Lourenco, P., and Roque, J. Structural Monitoring of the monastery of Jeronimos. Proceeding of the *international conference on the 250th Anniversary of the 1755 Lisbon Earthquake* (2005), pp.466-473.
[4] Ramos, L.F. *Damage Identification on Masonry Structures Based on Vibration Signatures*. PhD Thesis: Universidad do Minho – Escola de Engenharia (2007).
[5] Morrison, T.E. *Advanced Numerical Tool to Analyze Monitoring Data*, Master's Thesis: University of Minho (2008).
[6] Peng, C., & Zhang, B. A note on goodness-of-fit test of continuation ratio logistic regression models under case-control data. *Journal of Statistical Planning and Inference* (2008) pp. 2355-2365.
[7] Oliveira, D.V. *Experimental and Numerical Analysis of Blocky Masonry Structures Under Cyclic Loading*. Universidade do Minho (2003).
[8] Soong, T. T. *Fundamentals of Probability and Statistics for Engineers*. Chichester, West Sussex, England: Wiley-Interscience (2004).
[9] Smith, S.W. Digital Signal Processing*: A practical Guide for Engineers and Scientists*. London: Newnes – An Imprint of Elsevier Science (2003).
[10] Peeters, B. *System Identification and Damage Detection in Civil Engineering*. PhD Thesis: Catholic University of Leuven, Belgium (2000).
[11] Green, P., & Silverman, B. *Non-parametric Regression and Generalized Linear Models: A roughness penalty approach*. London: Chapman & Hall / CRC (2005)
[12] Hosmer, D. W., & Lemeshow, S. *Applied Logistic Regression: Second Edition*. Chichester: Wiley-Interscience (2000).

12th International Conference on Structural Analysis of Historical Constructions
SAHC 2020
P. Roca, L. Pelà and C. Molins (Eds.)

STRUCTURAL HEALTH MONITORING OF THE JUMA MOSQUE IN ITCHAN KALA IN KHIVA (UZBEKISTAN): LASER SCANNING COMBINED WITH NUMERICAL MODELLING

SHAKHZOD M. TAKHIROV[1*] AND BAKHODIR S. RAKHMONOV[2]

[1] Structures Laboratory, Civil and Environmental Engineering Department, University of California, Berkeley; 337 Davis Hall, Berkeley 94720; email: takhirov@berkeley.edu; https://ce.berkeley.edu
(*corresponding author)

[2] Construction and Architecture Department, Urgench State University, 14, Khamid Olimjon Str., Urgench, 220100
email: rah-bahodir@yandex.com; https://urdu.uz/en

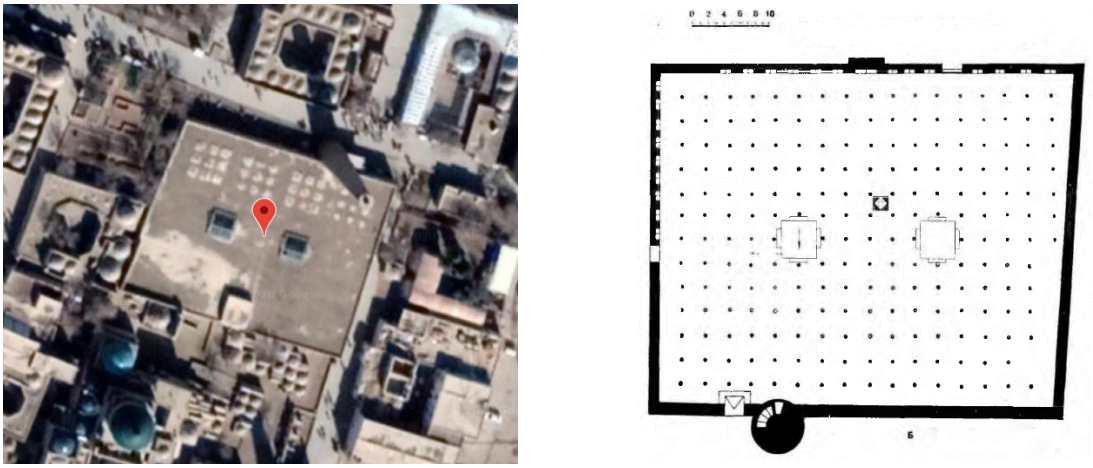
Keywords: Heritage Structure, Brick Masonry, On-demand Monitoring, Noncontact Inspection, Laser Scanning, Point Clouds, Finite Element Modelling, Ambient Vibration Study, Material Testing, Structural Health Monitoring.

Abstract. *This paper highlights the main objectives and some of the results of an extensive structural health monitoring (SHM) project begun in Khiva, Uzbekistan. The research team consists of experts from the University of California, Berkeley (Berkeley, USA) and Urgench State University (Urgench, Uzbekistan). According to archaeological data, the city of Khiva was established approximately 1500 years ago. The project started from Itchan Kala, the walled inner town of the city of Khiva. This paper describes results obtained for the Juma Mosque located inside of Itchan Kala. A continuous SHM became essential to ensure its preservation for humanity because a few structural anomalies were reported in the past. The ongoing project consists of three major phases. First, a terrestrial laser scanning (TLS) was deployed to capture and monitor anomalies of the monument's geometry in 3D. A laser scanner was used, and the monument's geometry was captured as a collection of points, which is called a "point cloud". Second, there is a plan to monitor the monument by in-situ measurements conducted by accelerometers, position transducers and thermocouples in the next phase. The high-sensitivity accelerometers will be used to study the resonant frequencies due to the ambient vibrations. The position transducers and thermocouples will be used for measuring the thermal expansion and retraction of the monument's minaret. They will also be used for monitoring the crack openings. Third, a finite-element (FE) model based on the as-found geometry of the point cloud will be generated. Its calibration will be based on the collected data to ensure acceptable correlations with the results of the conventional measurements. The FE model will be used for future restoration efforts to evaluate the performance and efficiency (if any) of the proposed restoration measures. This paper focuses on the results obtained for the Juma Mosque's minaret. It discusses the major findings of the laser scanning project and estimates the minaret's residual inclination and its taper. The paper shows that the minaret can be approximated by a truncated cone. A preliminary FE model of the minaret was developed, which will be updated based on the results of the upcoming ambient vibration study.*

1 INTRODUCTION

The paper discusses results of the ongoing educational and research program in Uzbekistan. The main objective of the program is to train local engineers on the utilization of the modern tools of structural health monitoring. It consists of an extensive theoretical course and two hands-on projects. The projects to be conducted at a historic site in the ancient city of Khiva. The first project was focused on the utilization of a terrestrial laser scanner for capturing the as-found geometry of a heritage building. The second hands-on project was aimed at the utilization of conventional instruments typically used for in-situ measurements. The theoretical course and the first hands-on project have been completed. The hands-on training on the practical application of conventional instruments is scheduled for Spring 2021. This educational and research program was conducted in collaboration with the faculty and students of Urgench State University in Uzbekistan. The results of the laser scanning project and the preparatory activities for the second hands-on project are discussed herein.

Juma Mosque, a heritage structure in the inner city of Itchan Kala (Khiva, Uzbekistan), was selected for both practical projects. It was studied by many authors (see [1,2, and 3] as representative examples), but there is the first time laser scanning was used. Figure 1a shows a top view of the monument taken from Google maps and Figure 1b shows a plan view of the historic monument reproduced from [1].



a) Image from Google maps b) Plan view after [1]

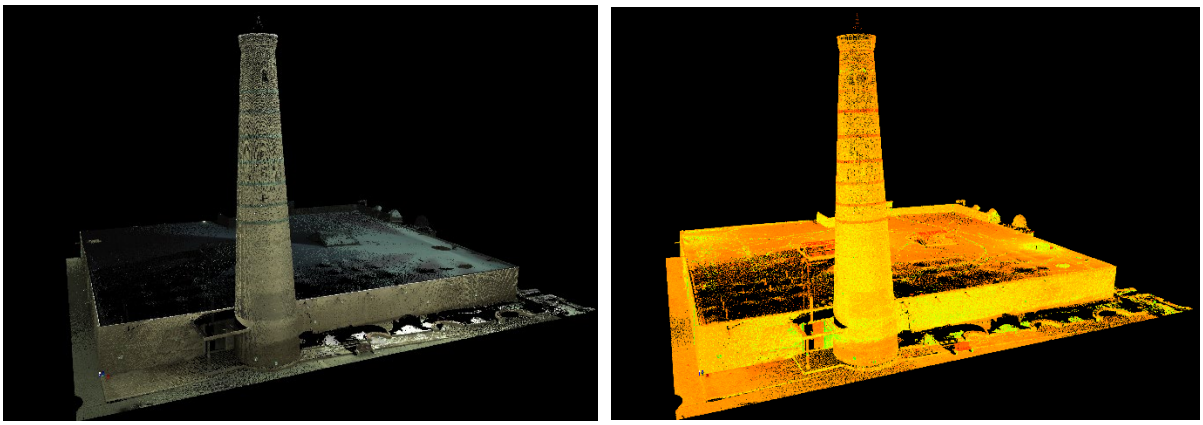
Figure 1: Juma Mosque

As can be seen from the images, Juma Mosque is comprised of a courtyard surrounded by four walls and a minaret integrated in its north wall. The courtyard's wooden roof is supported by numerous columns.

2 LASER SCANNING

A terrestrial laser scanner C10 from Leica Geosystems [4] was used to collect the point clouds of the heritage structure. The point clouds were collected from eleven positions of the laser scanner, the so-called stations. Eight stations were set at ground level around the walls and three stations were set on the roof. The point clouds collected from all the stations were

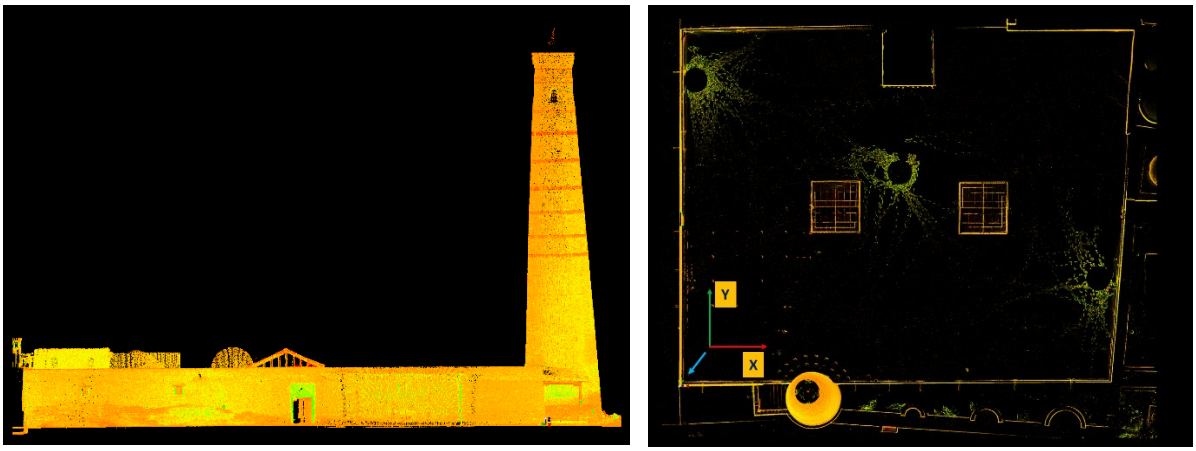
stitched together into one point cloud, the so-called registration. The manipulation of the point clouds including their registration was conducted in Cyclone from Leica Geosystems [5]. The point clouds were exported in an ASCII format for further analysis in Matlab [6]. The final registration of all stations is presented in Figure 2. It shows the monument in its natural colors and in the intensity of the returned laser beam shown in the left and right images, respectively. In addition to the laser scans, C10 takes images with a built-in still imaging camera. The colors captured by the camera are used for coloring the point clouds collected by the laser scanner. The natural coloring of the point cloud is quite dark because the scans were conducted on a cloudy day with very limited sunlight and, because a few scans were done right before, during and right after sunset.



c) Natural colors d) Intensity colors

Figure 2: Point cloud of Juma Mosque

Figure 3a shows the elevation view from the side of the east wall. As shown in Figure 3b, a local Cartesian coordinate system was selected in such a way that the Y axis is located in the plane of the east wall and the vertical axis is the true gravitational axis. The origin was selected at the lowest point of the intersection of the east and north walls.

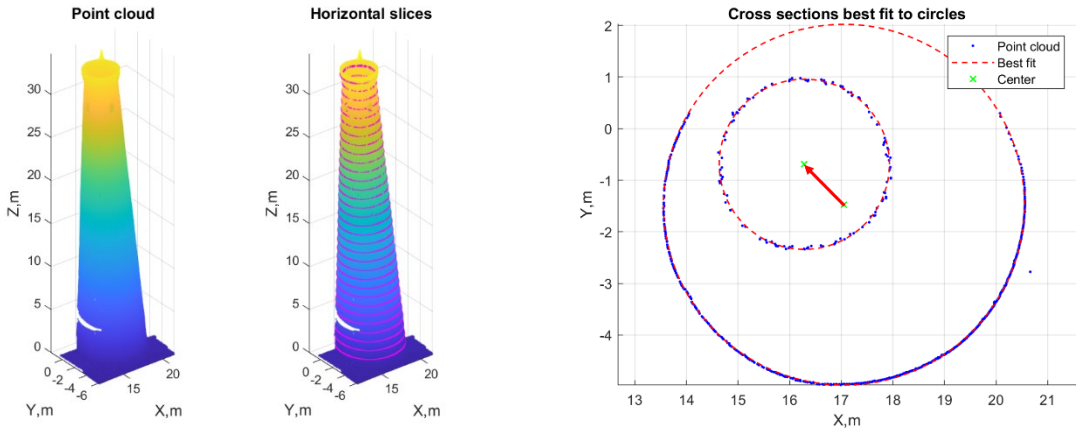


a) Elevation view: east wall side b) Local coordinate system

Figure 3: Elevation view and local coordinate system of Juma Mosque

3 ANALYSIS OF MINARET'S POINT CLOUD

The details on how the laser scanning was conducted and some of the results of the preliminary analysis of the point cloud are discussed in [7]. This paper focuses on the minaret in greater detail. The minaret was studied in the following way. A number of horizontal sections were introduced which were incrementally increased from the bottom of the minaret to its top as presented in Figure 4a. The point clouds of the sections were best fit to circles. The application of the best fitting procedure resulted in two major parameters. First, a radius of the circle was estimated as the minaret's radius at each elevation. Second, a center of the circle representing a location of the minaret's axis at each elevation was calculated. Two examples of the sections' point clouds and their respective best fit circles are presented in Figure 4b. They show the section of the minaret at the bottom and the smallest section on the top. The blue dots correspond to the point clouds and the red dashed circles are the corresponding best fit circles. The green crosses show the centers of the sections. The red arrow shows the direction and the value of the minaret's drift measured between these two sections.



a) Horizontal sections b) Example of two sections

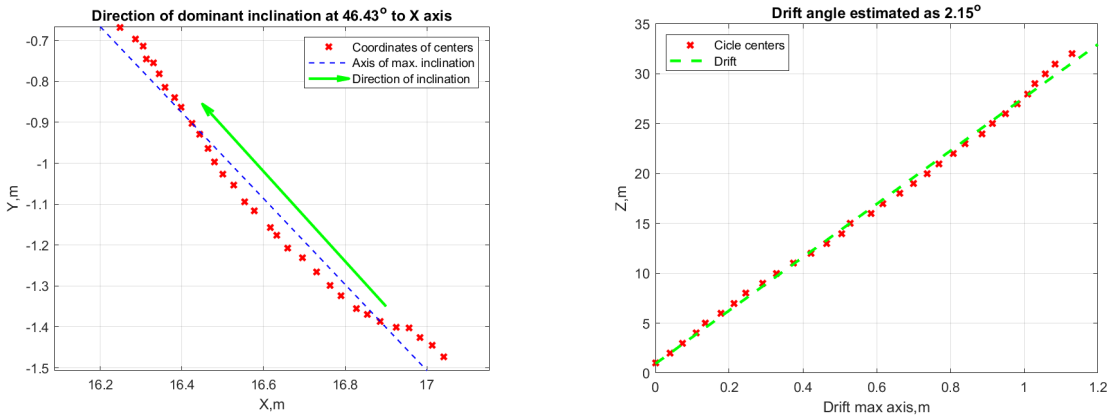
Figure 4: Global inclination of the Juma Mosque based on horizontal sections

A plot showing center point locations of all sections in presented in Figure 5a. The red crosses correspond to the centers and the blue dashed line is the least square approximation of the center points. The green arrow shows the overall direction of the inclination. As presented in this image, it is estimated to be about 46.4 degrees to the negative branch of the X axis. A plot showing the location of the centers in the plane of the maximum inclination in respect to the cross-section's elevation is presented in Figure 5b. The centers are shown as red crosses and the green dashed line is the least square approximation of these center points. Based on the plot, the following can be concluded. First, the center points are very close to an inclined straight line, which means that the inclination of the minaret is most likely related to the rigid body rotation of the minaret's whole structure. Second, the overall inclination is estimated as 2.15 degree including the 2 m deep foundation. Third, the maximum inclination from the true gravitational vertical axis is estimated as a 1.378 m inclination at the very top of the minaret.

Figure 6a shows the variation of the section's radius over the elevation of the minaret. Based on this plot, the original taper of the minaret was estimated. It is based on the best square

approximation of the radii with respect to the elevations.

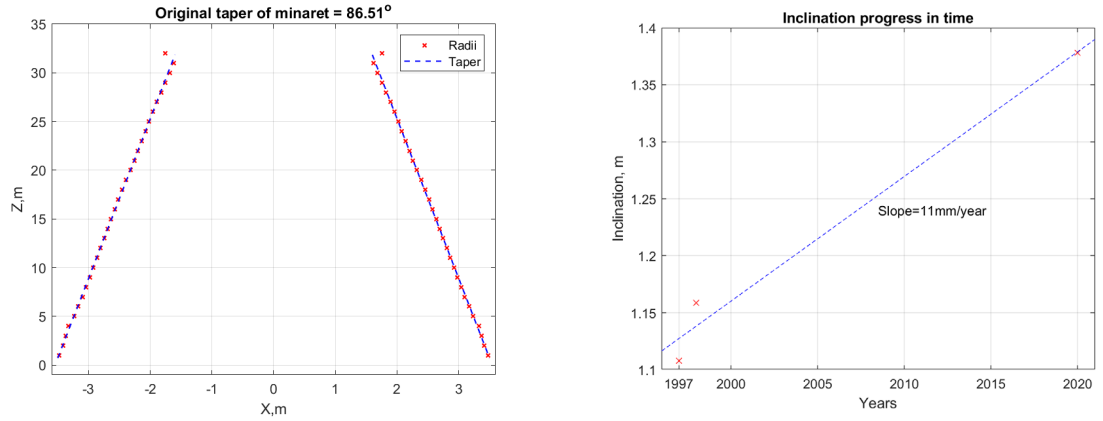
The inclination measured in this project was compared to that conducted by other means in 1997 and 1998 [3]. The difference between the 1997 and 1998 measurements was close to 0.05m [3], which corresponds to 50 mm/year. Based on the measurements of this project, the inclination slowed down but remains at about 11 mm/year on average for 23 years as presented in Figure 6b. A subsequential laser scanning project is needed to monitor a progression of the minaret's inclination.



a) Drift based on all horizontal sections in XY plane

b) Center locations in the plane of maximum inclination

Figure 5: Analysis of center locations



a) Radius versus elevation: taper estimate

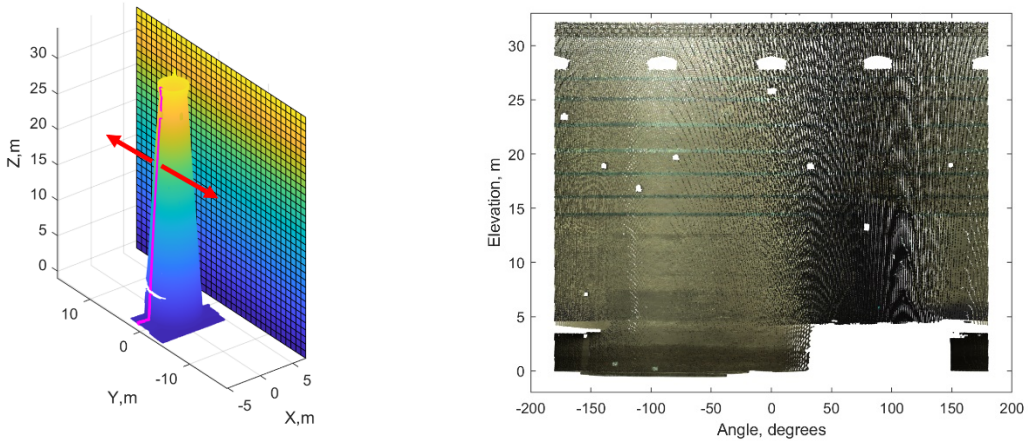
b) Inclination monitoring in time

Figure 6: Taper estimate and inclination monitoring in time

3.1 Minaret's Exterior Surface

Since the point clouds were collected from many stations including both on the ground and on the roof positions, the minaret's external surface was almost completely covered. The outer surface of the minaret was unwrapped in order to study the locations of the openings and the elevation and width of strips made of blue colored tiles as presented in Figure 7a. To achieve that for each point, an angle of a polar coordinate system based on X and Y coordinates was

calculated in order to estimate a correlation between the Z coordinate of each point and its polar angle. The surface was unwrapped along the line where the polar angle is equal to 180 degrees (shown by the magenta line in Figure 7a). The red arrows show the unwrapping direction and the plane right next to the minaret shows the plane on which the unwrapped surface is projected. The resultant relationship between the polar angle and the elevation is shown in Figure 7b. It is worth noting, that prior to these calculations the minaret's inclined axis was assigned to the vertical Z axis. In other words, the inclination of the minaret was removed to come up with this unwrapped image of the minaret's surface. It shows four large openings on the minaret's top and a number of smaller openings at other elevations. It also shows seven blue colored strips assembled from blue tiles, which start from an elevation of about 14 meters. The elevation of each strip is summarized in Table 1. They were estimated based on the changes in the Red-Green-Blue (RGB) coloring of the surface at a narrow strip around -140 degrees. Because of the size limitations of this paper, only the final result is presented herein without a detailed discussion on how it was conducted.



a) Details of unwrapping b) Unwrapped surface

Figure 7: Outer surface of minaret

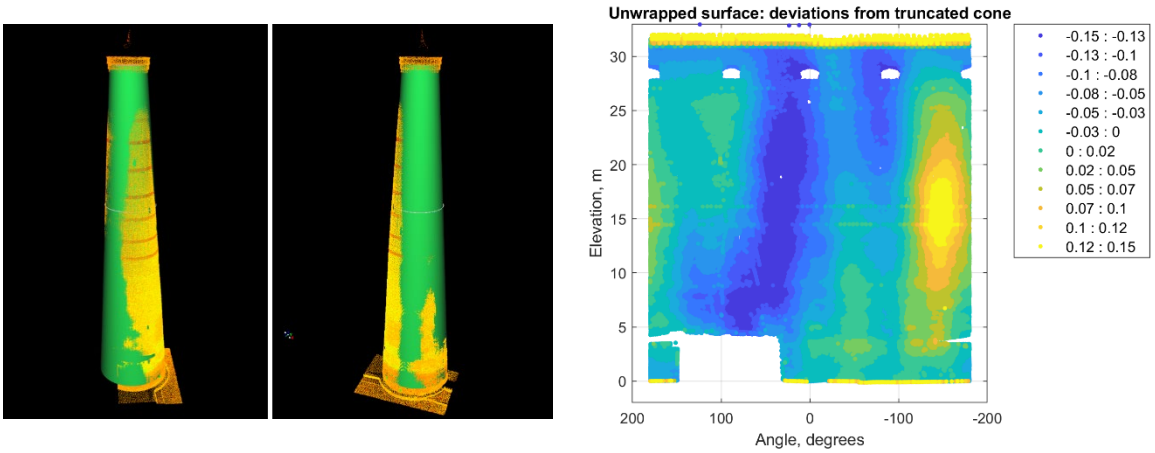
Table 1: Elevation of each blue colored strip

Strip numbering	Elevation, m
Strip 1	13.87
Strip 2	15.86
Strip 3	17.93
Strip 4	20.09
Strip 5	22.46
Strip 6	24.85
Strip 7	26.72

3.2 Approximation by Truncated Cone

The minaret was approximated by a truncated cone. It was conducted for the minaret, in which the inclined axis was forced to coincide with the vertical axis. The cone was based on the diameters of the best fit circles at the bottom of the minaret and its narrowest cross section

on top. The 3D representation is presented Figure 8a. This image shows two views of the point clouds and the truncated cone. The left 3D image shows a view toward the positive direction of the X axis and the right 3D image shows a view toward the positive direction of the Y axis. The deviations of the minaret from the truncated cone are presented in Figure 8b. They show the deviations on the unwrapped exterior surface of the minaret. As presented in the latter image the deviations from the truncated cone remain within ±0.15 m and as such it was utilized in the finite element modelling discussed below.



c) Approximation by cone (green): two views

d) Deviations from cone

Figure 8: Minaret's approximation by truncated cone

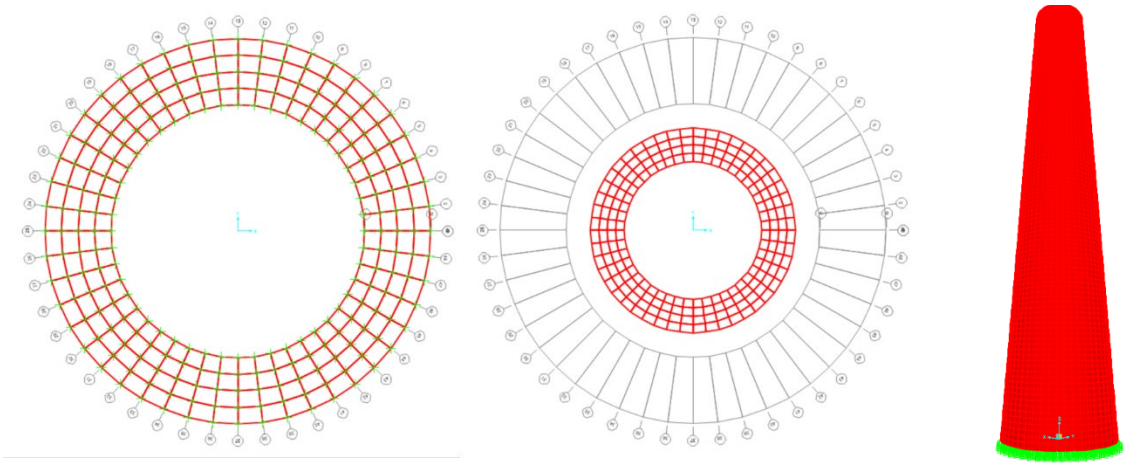
3.3 Minaret's Finite Element Model

A finite element model of the minaret was developed in the following way. Based on the design of typical minarets in Uzbekistan, the minaret was assumed to consist of a brick masonry core and a brick masonry conical shell. A spiral staircase is located between the core and the shell. Material properties were based on tests of a sample brick [8,9]. The truncated cone discussed above was selected as an outer surface of the minaret. The radius of the core and the thickness of the wall at each elevation was obtained in the following way. It was assumed that the ratios of the minaret's radius to the radius of the core and the thickness of the wall remain the same as those measured in the Islom Khodja minaret which was studied in [10]. It was also assumed that the core's participation can be neglected, especially in the case of very small amplitude vibrations which typically occur in an ambient vibration study. In addition, the participation of the staircase is also assumed to be negligible. These assumptions are acceptable for a preliminary estimate of the resonant frequency of the minaret, which will be evaluated in the ambient vibration studies scheduled for Spring 2021.

The minaret was modelled in SAP2000 [11] by utilizing solid elements as presented in Figure 9. The meshes at the bottom and top cross sections are shown in Figure 9a. A complete model of the tapered minaret with the wall thickness changing over the elevation is presented in Figure 9b.

Although the brick material was tested in the past, the effective Young modulus of the minaret will be much lower than that [12]. This is related to the fact that the brick masonry wall consists of the bricks and the mortar between the bricks and, the Young modulus of the mortar

is much lower than that of the brick. To address this, the effective Young modulus was taken as 3.0 GPa. The density of the brick masonry was assumed to be 1,600 kg/m3. The Poisson's ratio was assumed as 0.2. Based on these assumptions, the first resonant frequency was estimated at 2.1 Hz. It is much greater than the resonant frequency of a minaret in Turkey built of stone masonry [13]. The first resonant frequency of the latter minaret of about the same height was estimated as 0.71 Hz. This can be related to the fact that the minaret in Juma Mosque is tapered and the thickness of the wall is much greater than that of the stone masonry minaret in Turkey. In the Juma Mosque's minaret the wall thickness at the bottom and the top were assumed as 1.2 m and 0.64 m, respectively. The stone masonry minaret had almost no taper and the wall thickness varied from 0.36 m to 0.18 m.



a) Bottom (left) and top (right) sections b) 3D mesh

Figure 9: Finite element model of Juma Mosque minaret

The estimated resonant frequency of the Juma Mosque minaret will be re-evaluated in the upcoming ambient vibration studies. Based on the field measurements the model will be updated.

4 CONCLUSIONS

- A large residual inclination of a minaret in the Juma Mosque monument was measured by the terrestrial laser scanner. This inclination is evenly distributed over the elevation of the monument which is evidence that it is related to a rigid body rotation of the minaret's body.
- Based on a comparison of the recently obtained measurements to those reported earlier, it is concluded that the inclination is progressing, and it has increased by 270 mm since 1997. A continuous monitoring of this inclination is crucial for the structural integrity of the minaret and for finding a mitigation measure to slow its increase.
- Resonant frequency of the minaret's preliminary finite element model is greater than that of a stone masonry minaret with a much smaller wall thickness. The model will be updated after the ambient vibration study to be conducted in 2021.

Acknowledgements. The project would not be possible without funding provided by the

Central Asia University Partnerships Program (UniCEN). UniCEN is sponsored by the U.S. Embassy in Tashkent, Uzbekistan and administered by American Councils for International Education. The registration fee of the paper was sponsored by University of California, Berkeley (UC Berkeley), which is greatly appreciated. Special thanks are due to Mr. Brian Quigley of BNZ, Uzbekistan for providing access to a terrestrial laser scanner. The authors would like to acknowledge the Delta Group Max, Uzbekistan for logistical and technical support provided for the laser scanning project. Special thanks are due to Holly Halligan of UC Berkeley for editing the paper.

REFERENCES

[1] Mankovskaya, L., Bulatova, V. Monuments of the architecture of Khorezm. Uzbekistan: Gafur Gulyam Publishing House. 162 p. 1978 (in Russian).

[2] Durdieva, G., Davletov, B. Results of Technical Condition's Monitoring Conducted in Itchan Kala: Juma Mosque. 2008 (in Uzbek).

[3] Abdurashidov, K., Kabulov, F., Rakhmanov, B. Engineering Problems of Architectural Monuments. "Fan" publishing house of Academy of Sciences of Republic of Uzbekistan, Tashkent, 2011 (in Russian).

[4] Leica Geosystems AG (2011). Leica ScanStation C10. https://w3.leica-geosystems.com/downloads123/hds/hds/ScanStation%20C10/brochures-datasheet/Leica_ScanStation_C10_DS_en.pdf.

[5] Leica Geosystems (2018). Cyclone Version 9.2.1.

[6] MathWorks (2016). Matlab Version R2016b.

[7] Takhirov, S., Rakhmonov, B., Nafasov, R., Samandarov, A., Sultanova, S., Musurmanov, J. and Takhirov, B. Structural Health Monitoring of Juma Mosque in Itchan Kala, Uzbekistan by Laser Scanning. Submitted for publication in proceedings of the 10th International Conference on Structural Health Monitoring of Intelligent Infrastructure. 30 June - 2 July, 2021, Porto, Portugal.

[8] Takhirov, S., Mosalam, K., Moustafa, M., Myagkova, L., and Quigley, B. (2015). LASER SCANNING, MODELING, AND ANALYSIS FOR DAMAGE ASSESSMENT AND RESTORATION OF HISTORICAL STRUCTURES. COMPDYN 2015. 5th ECCOMAS Thematic Conference on Computational Methods in Structural Dynamics and Earthquake Engineering. M. Papadrakakis, V. Papadopoulos, V. Plevris (eds.). Crete Island, Greece, 25–27 May 2015.

[9] Takhirov, S., Gilani, A., Quigley, B., and Myagkova, L. (2018). Structural Health Monitoring and Assessment of Seismic Vulnerability of Historic Monuments on the Great Silk Road Based on Laser Scanning. The International Conference on Structural Analysis of Historical Constructions (SAHC 2018). 2254-2263. September 11-13, 2018, Cusco, Perú.

[10] Rakhmanov, B. Engineering analysis of the design features of the Islom Khoja minaret. A paper in preparation for publication.

[11] Computers and Structures, Inc. (CSI), 2014. SAP2000. Ultimate Version 16.1.1. Structural Analysis Program.

[12] Sayari Arash. MECHANICAL PROPERTIES OF MASONRY SAMPLES FOR THEORETICAL MODELING. 15th International Brick and Block Masonry Conference

Florianópolis , Brazil, 2012.
[13] Dogangun, A, Acar, R, Sezen, H, Livaoglu R. Investigation of dynamic response of masonry minaret structure. Bulletin of Earthquake Engineering, August 2008, DOI 10.1007/s10518-008-9066-5.

12th International Conference on Structural Analysis of Historical Constructions
SAHC 2020
P. Roca, L. Pelà and C. Molins (Eds.)

STRUCTURAL MONITORING IN THE "SANTA MARIA DE LA ASUNCIÓN" CATHEDRAL OF CHILPANCINGO, GUERRERO, MEXICO; THROUGH TOPOGEODESIC-PHOTOGRAMMETRIC SURVEYING AND AMBIENT VIBRATION. A METHODOLOGICAL PROPOSAL

SULPICIO SÁNCHEZ TIZAPA[1*], RODOLFO AURELIO FELICITO[1], RENÉ VÁZQUEZ JIMÉNEZ[1], JOSÉ LUIS CARRANZA BELLO[2] AND ROBERTO ARROYO MATUS[1]

[1]Facultad de Ingeniería
Universidad Autónoma de Guerrero (UAGro)
Av. Lázaro Cárdenas s/n, Ciudad Universitaria, 39070 Chilpancingo, Guerrero
e-mail: sstizapa@uagro.mx, www.posgradoingenieria.uagro.mx (*corresponding author)
rodolfofelicito@uagro.mx, rvazquez@uagro.mx, arroyomatus@hotmail.com

[2]Instituto Nacional de Estadística y Geografía (INEGI)
Av. Prolongación Baltazar R. Leyva Mancilla, Manzana 3, Lote 9, Primer Piso
Colonia Universal, 39080 Chilpancingo, Guerrero
luis.carranza61@yahoo.es, www.inegi.org.mx

Keywords: Historical Structure, Structural Health Monitoring, UAV, GPS.

Abstract. *This paper presents a review of the state of the art of structural health monitoring using three inspection techniques and their application in the proposed methodology for the study of a historic structure located in a high seismic hazard area. The proposed approaches are a) use of an unmanned aerial vehicle (UAV), a reliable platform for data acquisition in photogrammetric inspection and surveillance work due to its simple handling and accessibility to human risk zones; b) Global Positioning System (GPS), which offers the capability of static or dynamic monitoring, using kinetic navigation (RTK), precise point positioning (PPP) or combination of both methods; c) ambient vibration (AV), an accelerometer test that determines the dynamic properties of a structure, of which values indicate the structural safety status. The building to be studied is the "Santa María de la Asunción" Cathedral of Chilpancingo in Mexico, which represents a great historical value because it hosted the First "Anahuac" Congress in 1813. The structure covers an area of 1056 sqm and has a height of 33.31 m. The construction began after 1902 and has been affected by several seismic events. Because of the earthquake of December 2011, cracks occurred in the basements and keystones of the arches of the two bell towers, severe damage to the right tower, and moderate to the left one. In the frontispiece, top of the arches, and in front of the central nave vault also appeared cracks. The reinforcement process is currently complete. The expected results are a matrix of distances among control points in the building, high-resolution ortho-images, and values of the dynamic structural properties. According to the architectural and structural characteristics, location, importance, and use of the structure, it is proposed to perform a monitoring every six months*

or after an earthquake with a seismic magnitude greater than six and epicenter less than 60 km. The comparison of the measurement parameters will indicate the structural health of the building.

1 INTRODUCTION

The damage reduces the mechanical properties of the structural elements, which adversely affect their current state. The implementation of a strategy for the identification of structural damage is known as structural health monitoring (SHM). It can be established in the short, medium, long term, or after extreme events occur. The goal of the evaluation is to provide, almost all in real-time, reliable data about the structural system conditions [1]. Currently, there are various inspection and structural monitoring techniques, among which stand out a) UAV [2], b) GPS [3], c) AV [4], d) laser scanning [5], among others.

1.1 Unmanned aerial vehicles

Historically, the development of unmanned aerial vehicle systems and platforms were generated for military applications (inspection, surveillance, reconnaissance, and mapping of hostile areas). The early geomatics applications started about 35 years ago. UAVs are a valuable platform for data acquisition in inspection, surveillance, mapping, and 3D modeling. UAVs are considered a low-cost alternative compared to conventional manned aerial photogrammetry [6]. Figure 1 shows the acquisition and processing of UAV images.

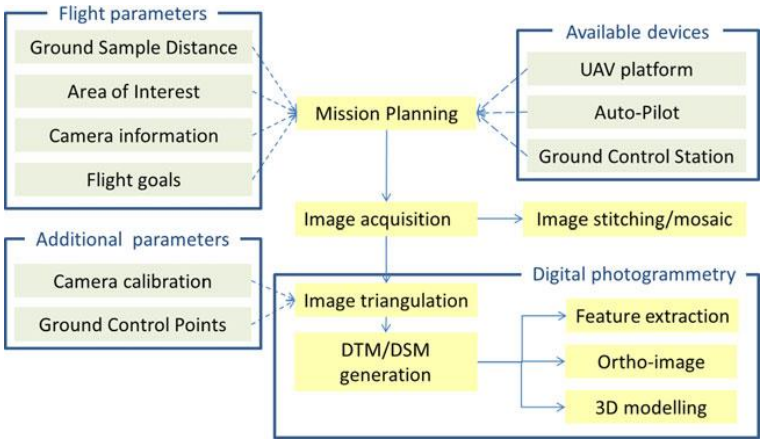


Figure 1: Typical acquisition and processing pipeline for UAV images [6]

Various researchers have made significant contributions to damage detection by using UAVs, i.e., the aim of a work conducted in South Dakota (USA) was to evaluate its effectiveness as a complementary tool for bridge damage quantification. In the study, a covered wooden arch bridge (88 m length and 7.9 m lane width) was selected. The protocol consisted of four stages: a) inspection, b) image assessment, c) damage quantification, d) damage classification according to the AASHTO standard. On inspection, the lengths and widths of cracks, thicknesses, and areas of rust spots were measured. Image quality parameters, including sharpness and entropy, were used to determine the quality of the obtained images. Then, pixel-based measurements and photogrammetry were obtained to quantify bridge damage and

compared it with the field measurements. Next, the damage level classification was established based on current standards. The measurement difference shows a suitable accuracy with results within 3.5%, 7.9%, and 14.9% for the length of the crack, the thickness, and the area of rust spots, respectively [7].

Another research conducted in Alaska (USA) on the Placer River Trail Bridge served as the evidence base for an inspection method with UAVs. The goal was to produce a three-dimensional (3D) model using the captured images and a densely structured hierarchical algorithm based on motion. This aim guided the choice and equipment of the UAV as well as the planning of the flight mission. The resulting inspection integrates the technical characteristics of the UAV, the capture and analysis of data to supply a 3D model, which gives the inspection information allowing for defect monitoring. Results compared to models generated by laser scanning show that this method supplied more accurate information to identify defects or damages. Thus, data were obtained for decision-making by infrastructure managers [8].

For a long time, three-dimensional models of heritage buildings have employed image-based techniques. The technological development of optical sensors and dense matching algorithms complement the existing photogrammetric procedures in the study of historical buildings. An example is the studies of Rohan's palace and St-Pierre-le-Jeune Catholic Church (Strasbourg, France), where using aerial triangulation and a dense coincidence of UAVs Sensefly Albris and Phantom 3, the quality of the model was determined. Among the several used software (PhotoScan, Pix4D, MicMac, and PhotoModeler), MicMac obtained greater accuracy in both cases, it is a handy open-source alternative to existing commercial solutions [9].

More recent research describes the use of UAVs in the long-term monitoring of crack patterns for the conservation of architectural heritage. In a preliminary study of the Old Fortress "Livorno" (Italy), a 3D indicator was developed for monitoring cracks. Using ArUco markers and rotation/translation matrix arrays, distances, and orientation of marker the barycenters were evaluated, obtaining a 5 mm projection error. The second method of simultaneous location and mapping based on ChArUco markers determined the coordinates of the corners and their distance between the barycenters, results show an accuracy of 1 mm [10]. As can be seen, this second type of markers had greater accuracy.

1.2 Ambient vibration test

The need for maintenance of structures has led to the development of experimental tests capable of determining the static and dynamic properties. In large structures, the most used structural health monitoring dynamic method is the Ambient Vibration (AV) test [11], which is measured by accelerometers. The human movement, traffic, building use, and machine vibrations excited the structures; its response can be measure by the Operational Modal Analysis.

Extensive research had been developed to obtain the dynamic properties and dynamic monitoring of the Mallorca cathedral [12], to know the global dynamic behavior of the structure and update the structural models. In the first case, modal parameters as natural frequencies, mode shapes, and damping ratios were obtained. Then, the mid-span points of the central and lateral arches of the structure were chosen to adapt the sensors to measure the ambient vibrations. The measure times for each setup test was greater or equal to 1000 times the

fundamental period of the cathedral, around 15 minutes with a sampling frequency of 100 Hz. Three tri-axial forced balanced accelerometers were used to carry out the tests. Four methods allowed to identify the dynamic properties: a) frequency domain decomposition, b) reference-based covariance-driven stochastic subspace identification, c) reference-based data-driven stochastic subspace identification, and d) poly-reference least-squares complex frequency domain identification. Eight natural frequencies were possible identified, the first was 1.15 Hz, and the last was 2.6 Hz. Respect to the damping ratios, the lowest was 0.44% (Mode 7), and the highest was 2.6% (Mode 1); however, there were vast variations of different methods values. About the modes shape, the first mode has a predominant longitudinal over the transverse movement, the second and third modes show longitudinal movement, and the fourth showed transversal displacement, the torsion movement appeared in the eight mode shape. The wind blowing caused a transversal mode shape.

The dynamic monitoring system of Mallorca cathedral was developed with the tri-axial accelerometers above defined. Devices were exposed to the sunlight, rains, and out of the reach of anthropogenic action. The system worked for two periods: a) from December 17, 2010, to September 13, 2011, b) from May 18; 2012 to December 29, 2012, with an interruption from July 20 to September 4. The data were used to calculate the powers spectral density (PSD) for a signal length of half an hour with windows overlapped 33%. The natural frequencies were determined using the picking method. The PSD calculation was carried out four times per day during the monitored period. The frequencies calculated every 6 hours is a detailed image of the daily change under different environmental conditions. In this case, the eight modes shape recorded during the AVT were confirmed in the vicinity of high-speed winds and some captured seismic events. Besides, the global modes were more detectable than the local ones because of their higher mass participation. The temperature and wind were the most influential environmental parameters on the dynamic behavior. The authors concluded that the usage of a higher cost dynamic monitoring system was useful to evaluate the behavior of structures subject to low ground seismic accelerations. [12].

Another structure with a static and dynamic monitoring system is the Milan Cathedral [13]. The structure was built from 1386 to 1765, and it is a mix of Gothic style and regional Lombardy style, where also neo-classic, neo-gothic. Even renaissance influences are present due to the prolonged period of construction. A distinctive characteristic is the connection of all adjacent piers using metallic elements to reduce the thrust on the slender lateral buttresses. The two-monitoring system measure different physical quantities, i. e.: a) quasi-static strains of selected tie-rods, b) indoor-outdoor environmental temperature, and relative humidity. Of the static monitoring system, eight modes were obtained by using referenced-based data-driven stochastic subspace identification (SSI-Cov). The first and second ones correspond to the sway motion of all instrumented columns in the North-South (f_1=1.58 Hz) and the Est-West (f_2=1.69 Hz), respectively. The third and fourth modes recorded values of f_3=1.98 Hz and f_4=1.98 Hz. Damping of the North-South modes had values from 1.79 to 4.14%, and damping of the Est-West modes varies between 2.21 and 5.04%. Almost all identified modes in the first hours of monitoring were detected in the subsequent months.

Dynamic monitoring results of Milan cathedral show that the outdoor temperature recorded variations from -2 to +28 °C and indoor relative humidity from 38 to 64%. About the modal frequencies, the lower five ones were greater than 98% of static monitoring values, while the coefficient of variation ranges between 0.34 and 1.10 %. All resonant frequencies increase

linearly with decreased temperature. However, the relative humidity slightly affects only the first mode frequency. Finally, the mode shapes do not show visible fluctuations associated with the environmental effects, so that a suitable strategy of SHM should be based on the time invariance of those parameters. The period for two kinds of monitoring systems was from October 16, 2018, to February 13, 2019 [13].

1.3 Precise positioning of points and ground control points with GPS

The development of low-cost systems to collect spatial information near real-time eases the detection of the environment or the monitoring of disasters. At Cheng-Kung National University, Taiwan, a platform for obtaining spatial information based on fixed-wing unmanned aerial vehicles (UAVs) that works without Ground Control Points (GCP) is evaluated. The platform has a Direct Georeferencing (DG) module that includes a low-cost Global Positioning System (GPS). A flight test was performed to verify positioning accuracy in DG mode without using GCP. Preliminary results of a 300 m high flight show accuracy of 5 m in the horizontal direction, and 10 m vertically. It is concluded that the proposed platform is safe and economical to collect critical spatial information in case of urgent response for relief applications, and disaster assessment, where GCPs are not available [14].

The photogrammetric mapping work with a fixed-wing Q200 UAV, through the use of Precise Positioning of Points established with Global Positioning System (GPS-PPP), is a solution to space operation restrictions such as a) installation and use of terrestrial control points, b) use of local terrestrial GPS reference station, c) operation within a permanent network of referenced stations. This activity began with the planning of two 25-minute and 29-minute flight missions, respectively, at the height of 120 m. The results determined accuracies of one to three centimeters in plan and ten centimeters in height, simplifying operational logistics and allowing large-scale photogrammetric mapping from UAVs, even in the most remote and challenging geographical locations [15].

2 OBJECTIVE

Establish a long-term structural health monitoring methodology for the historic building “Santa María de la Asunción” Cathedral using unmanned aerial vehicles, Global Position System, and ambient vibration tests.

3 DESCRIPTION OF THE STRUCTURE UNDERSTUDY

The “Santa María de la Asunción” Cathedral, located in the city of Chilpancingo; Guerrero, Mexico (coordinates 17 ° 33'09.4 "N 99 ° 30'04.6" W), (Figure 2) was built in the mid-16th century in a neoclassical style, on an area of 1056 sqm and 33.31 m of height. It has great historical value since it was the place where the First Anahuac Congress was held headed by General José María Morelos y Pavón, a patriot from New Spain and the architect of the Mexican independence movement. Figure 2 shows the current state of this historic building.



a) b)

Figure 2: "Santa María de la Asunción" Cathedral, a) Main façade, b) Top view

The original adobe-based structure partially collapsed and was demolished after the 1902 earthquake. Some years later, the construction began in the same place as the original temple. The left tower partially collapsed with the earthquake of 1957, and with the earthquake of 1985, the right tower suffered severe damage, so they were repaired after those events. Earthquake of December 2011 (Mw = 6.5) caused cracks at the bases and the keystones of the arches of the two bell towers, severe ones in the right tower, and moderate ones in the left tower. Large cracks also appeared in the frontispiece, in the upper part of the arches, and the front of the central nave vault [16].

4 METHODOLOGY

According to the technical resources available: a) DJI UAV equipment, Mavic Pro model, b) Leica-Viva GPS receivers and Sokkia Set 330R Total Station, c) Sequoia-GEA II accelerometer (Figure 3); and based on the monitoring techniques referenced in the literature, the methodology described below has been defined (Figure 4).



Figure 3: Scheme of integration for structural health monitoring

a) Establishment of azimuthal geodetic control line (ACL)

The establishment of precise points (PPs) will be done with the GPS receivers and will be linked to the National Active Geodetic Network (NAGN). The geodetic survey will be carried out by the static method, following the Methodological guide established by the National Institute of Statistics and Geography of Mexico (INEGI), the minimum two-point junction defines the ACL.

b) Establishment of the topographic support polygonal

To set up the points of the polygonal from the PPs of the ACL, a Sokkia total station will be used, and the topographic survey will be performed by the point trilateration method. After, the coordinates must be adjusted by the method of least-squares to improve the accuracy.

c) Establishment of Ground Control Points (GCPs)

GCPs will be placed 50m from the cathedral and will be measured the same way as PPs. GCPs will be used for horizontal adjustment of images taken by the UAV during the photogrammetric process.

d) Propagation of coordinates to the structure

The coordinates of the points of the topographic polygonal will be propagated to characteristic points or control points (SCPs) in the construction, using the method of propagation of points. These must be adjusted to fix the accuracy obtained with the geodetic survey.

e) Data processing

Once the topo-geodetic study has been carried out, the coordinates of the structure control points (SCPs) will be obtained, the distance between each couple of these values is an entry of a matrix; it will be useful for monitoring the structural health.

f) Flight plan

Revision of the UAV, batteries, drivers, control, calibration of the camera, and compass are necessary before the flight. It is planned to use the DJI GS Pro software, compatible with the UAV, where the parameters (area, height, speed, camera angle) will be defined.

g) Image acquisition

The acquisition of images in the field will be realized according to data of the flight plan. For greater accuracy, the take-off site of the UAV will be at one of the PP.

h) Digital image processing

Image processing will be achieved using Agisoft PhotoScan, photogrammetry software that allows image inspection to filter out those that do not fulfill the quality needed for processing. After filtering, if images are not enough for the processing, image acquisition will be repeated.

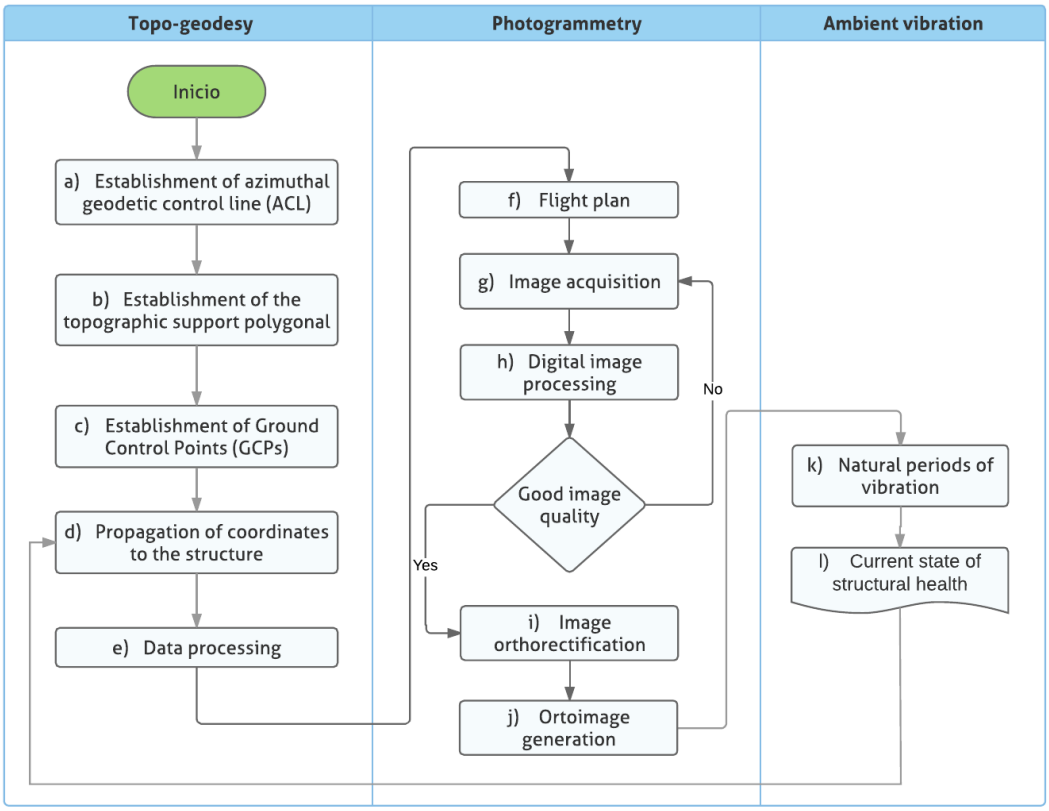


Figure 4: Methodological proposal for structural health monitoring (SHM) in the "Santa María de la Asunción" Cathedral

i) Image orthorectification

It will do in PhotoScan using data from GCPs. The goal is removing the effects of image perspective and relief effects to create a planimetrically correct image.

j) Orthoimage generation:

After the image orthorectification, a georeferenced orthoimage will be generated to identify the SCPs. The distance among the SCPs and the characteristic points of the construction in orthoimages will measure at different moments. Additionally, structural damage caused by cracks could be detected

k) Natural periods of vibration

A Sequoia-GEA II accelerometer will be used to measure the AV effect on the ground and structure. The obtained data will be processed by using two different identification methods: the Enhanced Frequency Domain Decomposition (EFDD) technique and the Stochastic Subspace Identification (SSI) method. EFDD is a frequency domain technique instead of SSI method, which is developed in the time domain. Modal Assurance Criterion between the EFDD and SSI results will be obtained for confirming the process [17].

l) The current state of structural health

At the end of the first cycle, an evaluation report of the existing structural health conditions of the "Santa María de la Asunción" Cathedral will be obtained. The comparison of measurement parameters of two consecutive cycles will define the change of structural level safety.

5 CONCLUSIONS

It is expected that the methodological proposal assesses the current state of the physical and dynamic conditions of the "Santa María de la Asunción" Cathedral. These data can help the authorities in making maintenance decisions and future monitoring of the structure. At the end of the project, the methodology can be qualified by making the necessary modifications. According to the architectural, structural characteristics, and use of the building, it is proposed to perform a monitoring every six months or after an earthquake with a seismic magnitude greater than six and epicenter less than 60 km.

The combination of the three techniques (topo-geodesy, photogrammetry, and ambient vibration) was based on two reasons: a) the problems in historical constructions by repetitive seismic action, b) human and material resources. It would help if we remembered that in 2019, Mexico was affected by two major earthquakes, of which the effects were devastating on historical buildings near the epicenter.

Acknowledgments. The authors gratefully acknowledge the support of the National Council for Science and Technology (CONACYT), with reference number 918449.

REFERENCES

[1] K. Worden and J. M. Dulieu-Barton, "An Overview of Intelligent Fault Detection in Systems and Structures," Struct. Heal. Monit. An Int. J., vol. 3, no. 1, pp. 85–98, Mar. 2004.

[2] B. Lei, N. Wang, P. Xu, and G. Song, "New Crack Detection Method for Bridge Inspection Using UAV Incorporating Image Processing," J. Aerosp. Eng., vol. 31, no. 5, p. 04018058, Sep. 2018.

[3] S. B. Im, S. Hurlebaus, and Y. J. Kang, "Summary Review of GPS Technology for Structural Health Monitoring," J. Struct. Eng., vol. 139, no. 10, pp. 1653–1664, Oct. 2013.

[4] V. Gattulli, M. Lepidi, and F. Potenza, "Dynamic testing and health monitoring of historic and modern civil structures in Italy," Struct. Monit. Maint., vol. 3, no. 1, pp. 71–90, Mar. 2016.

[5] A. Guarnieri, N. Milan, and A. Vettore, "Monitoring of Complex Structure For Structural Control Using Terrestrial Laser Scanning (Tls) And Photogrammetry," Int. J. Archit. Herit., vol. 7, no. 1, pp. 54–67, Jan. 2013.

[6] F. Nex and F. Remondino, "UAV for 3D mapping applications: a review," Appl. Geomatics, vol. 6, no. 1, pp. 1–15, Mar. 2014.

[7] L. Duque, J. Seo, and J. Wacker, "Bridge Deterioration Quantification Protocol Using UAV," J. Bridg. Eng., vol. 23, no. 10, p. 04018080, Oct. 2018.

[8] A. Khaloo, D. Lattanzi, K. Cunningham, R. Dell'Andrea, and M. Riley, "Unmanned aerial

vehicle inspection of the Placer River Trail Bridge through image-based 3D modeling," Struct. Infrastructure. Eng., vol. 14, no. 1, pp. 124–136, Jan. 2018.

[9] A. Murtiyoso and P. Grussenmeyer, "Documentation of heritage buildings using close-range UAV images: dense matching issues, comparison and case studies," Photogramm. Rec., vol. 32, no. 159, pp. 206–229, Sep. 2017.

[10] D. Germanese, G. Leone, D. Moroni, M. Pascali, and M. Tampucci, "Long-Term Monitoring of Crack Patterns in Historic Structures Using UAVs and Planar Markers: A Preliminary Study," J. Imaging, vol. 4, no. 8, p. 99, Aug. 2018.

[11] M. Gul and F. N. Catbas, "Ambient Vibration Data Analysis for Structural Identification and Global Condition Assessment," J. Eng. Mech., vol. 134, no. 8, pp. 650–662, Aug. 2008.

[12] A. Elyamani, O. Caselles, P. Roca, and F. Clapes, "Dynamic investigation of a large historical cathedral," Struct. Control Health Monit., vol 24, no. 3, pp. 1-25, May. 2016.

[13] C. Gentile, A. Ruccolo, and F. Canali, "Continuous Monitoring of the Milan Cathedral: dynamic characteristics and vibration-based SHM," Journal of Civil Structural Health Monitoring, vol. 9, pp. 671-688, Oct. 2019.

[14] K.-W. Chiang, M.-L. Tsai, and C.-H. Chu, "The Development of an UAV Borne Direct Georeferenced Photogrammetric Platform for Ground Control Point Free Applications," Sensors, vol. 12, no. 7, pp. 9161–9180, Jul. 2012.

[15] B. Grayson, N. T. Penna, J. P. Mills, and D. S. Grant, "GPS precise point positioning for UAV photogrammetry," Photogramm. Rec., vol. 33, no. 164, pp. 427–447, Dec. 2018.

[16] R. Arroyo Matus, S. Sanchez Tizapa, T. Tapia, and E. Herrera, "Diagnosis of the behavior observed during the earthquake of Zumpango, Guerrero, (Mw-6.5) of December 11, 2011 and proposals to reduce structural vulnerability" Tlamati, vol 5, no. 2, 2014.

[17] M. Romero, P. Pachón, V. Compán, M. Cámara, and F. Pinto, " Operational Modal Analysis: A tool for assessing changes os structural health of historical constructions after consolidation and reinforcement works-Jura Chapel (Jerez de la Frontera, Spain)," Shock and Vibration, vol. 2018, pp. 1-12, Aug. 2018.

12th International Conference on Structural Analysis of Historical Constructions
SAHC 2020 P. Roca, L. Pelà and C. Molins (Eds.)

THE INFLUENCE OF EXTERNAL CLIMATE ON CHURCH INTERNAL MICROCLIMATE

L.BALIK[1*], L. KUDRNACOVA[1] AND K. NEDVEDOVA[1]

Klokner institute
Czech Technical University Solinova 7,
16608 Praha 6, Czech Republic
e-mail: lukas.balik@cvut.cz, web page: http://www.klok.cvut.cz

Keywords: Monument Maintenance, Long-term Microclimate Monitoring, Moisture Regulation

Abstract. *This paper deals with monitoring microclimate in the area of church and describes influence of exterior microclimate to interior microclimate, changes during one year. The basic parameters of the interior space (temperature, relative humidity, dew point and specific air humidity) were monitored in the long-term in the selected sacral building. These parameters were monitored at the same time as monitoring the surroundings in the exterior. The long-term monitoring of the internal microclimate of ossuary showed significant instability of the interior environment during the annual cycle, where the appropriate limits of humidity of the environment (excessive moisture in the spring and over-drying in the winter) are significantly exceeded. The microclimate behavior of ossuary is also different in different height levels, where the lower space acts as a pool with heavy cold air and vice versa, the space under the vault is moistened with vapor. The fact that under no circumstances of the exterior climate in winter is the temperature of the interior below freezing point is specific. The negative phenomenon of the internal environment of ossuary is the fact that in certain periods optimal conditions are created for condensation of water on the surfaces of walls and interior equipment of ossuary and also for the creation of ideal conditions for the formation and development of mold. Monitoring of the internal microclimate of ossuary during everyday operation has become the basis for the subsequent design of the reconstruction of the building. The remediation proposal must address several issues at once. It has to solve the issue of reducing moisture in the peripheral and inner walls of the building, restoring original materials while maximizing their preservation, stabilizing the internal microclimate in terms of humidity, creating optimum conditions for the natural drying of residual structural moisture and, last but not least, ensuring the mode of future operation with minimal effect on changes in the internal microclimate. Due to the historical value of the building and its layout, it is possible to use forced air treatment only to a limited extent, and great emphasis must be placed on addressing this issue by using the natural physical properties of air and phenomena involving its natural flow and controlled temperature exchange between spaces.*

L. Balik, L. Kudrnacova1 and K. Nedvedova1

1 INTRODUCTION

The article deals with the results of measurements of the internal microclimate of the ossuary sacral building (church) in Central Bohemia, which serves as a necessary basis for the correct design of a complete reconstruction. The specificity of the ossuary space lies both in the design arrangement and in its operation. From a structural point of view, it is a basement partially recessed below the level of the surrounding terrain, whose perimeter walls are affected by high humidity and there is a high representation of salts. Moisture material degradation can be seen both on plaster walls, as well as on paving and vaults. The internal climate of this space is diverse at individual heights and is very strongly influenced by the way of operation i.e. by the way of ventilation and the presence and movement of excessive amounts of people producing water vapour. Also specific is the internal exhibited inventory, which dominantly forms human historical bones arranged into various clusters and ornaments, and which are distributed practically throughout the whole ossuary space. It is clear that the life span of these bones is fundamentally affected by the environment in which they are found. In the case of ossuary they are currently stored in different environments within one space, and in addition, each environment lives by its specific mode with a different period of change. The remediation designer faces a complex issue that must address the reduction of masonry moisture and related structures, minimizing condensation on indoor surfaces (plaster, paving, stone and wooden elements) while ensuring maximum optimization of the internal microclimate for long-term bone exposure. Optimization of the indoor microclimate consists in unifying the parameters of the indoor microclimate in individual height areas and also minimizing its fundamental changes in connection with demanding operation. Aim of the presented long-term measurement was to create an idea of the behavior of the ossuary space during its operation and to create thematic circuits necessary for the solution in the reconstruction design [1].

2 MONITORING DESCRIPTION

The church itself consists of two chapels. The lower one, which serves as an ossuary, is partially embedded in the ground and carries the upper single nave chapel with presbytery. Several probes were placed in the area of the church in order to monitor the microclimate. The probes were in different height level in order to cover each area of the space.

Long-term measurement of indoor microclimate parameters took place from March 2013 to early April 2017 when the control panel was disconnected. This report processes data obtained from March 2016 to March 2017. The data from the beginning of measurement were described in another paper [2]. Due to unscheduled inputs to measurements caused by various technical interventions carried out in the building, it was not possible to obtain data from all the measured places during the whole measured period but only from shorter (but sufficient for analysis) sections. Data loggers and data logger with probes measuring internal space parameters (temperature, relative humidity and surface temperature) were placed inside of the building [3]. The basic measurements were carried out in the ossuary area and additional measurements were performed in the entrance hall above the staircase (1st floor window), in the chapel (church) above the ossuary and in the roof truss. To make the analysis more precise, the measurements were supplemented by scanning the parameters of the external microclimate (exterior) in the tower area by means of a mounted weather station. For the main measurement of the ossuary

space was used measuring center collecting data from three probes connected at different height levels. The location of the probes in the area of the object is shown in Fig. 1.

3 RESULTS OF MEASUREMENT

The microclimate of the space of the ossuary of the Church of All Saints during the current operation has been showing very high values of internal relative humidity in the long term. The lower parts of the space (the area below the stairs entry landing level) show worse conditions (higher values of relative humidity), as evidenced by the theory of the lower space, which acts as a "closed trap of humid air", which currently has little possibility to escape or circulate. The consequence of this condition causes relatively frequent and long periods of surface condensation of water on cold surfaces (walls, tiles and vaults). This condensation worsens the overall moisture state of the building and radically increases the risk of vegetation of fungi, molds and algae and accelerates the process of natural mechanical degradation of materials (plasters, mortars, stones, bricks, etc.). Based on the results of measurements of indoor microclimate in the premises of ossuary from March 2016 to March 2017, the following basic points can be stated:

- the indoor microclimate of ossuary is highly unstable, which may affect the durability of its structures and movable equipment,
- the temperature of the ossuary did not drop below 0 ° C during the frost period,
- the average value of the relative humidity in the room in the annual period of 2016 was within 68.6% rel. up to 75.1% rel.
- up to 26% of the data measured on the sensors below (up to 3.25 m above the floor) reported values exceeding 80% rel.
- in terms of water vapor condensation on the walls and equipment of ossuary, the most risky period in the annual cycle was found between February and July,
- in terms of optimal environment defined by a temperature between 18 to 20 ° C and rel. humidity between 50 and 60% rel. Excessive humidity in the ossuary air was found to be between mid-May and mid-September and, on the contrary, the specific humidity was excessive between November and April.

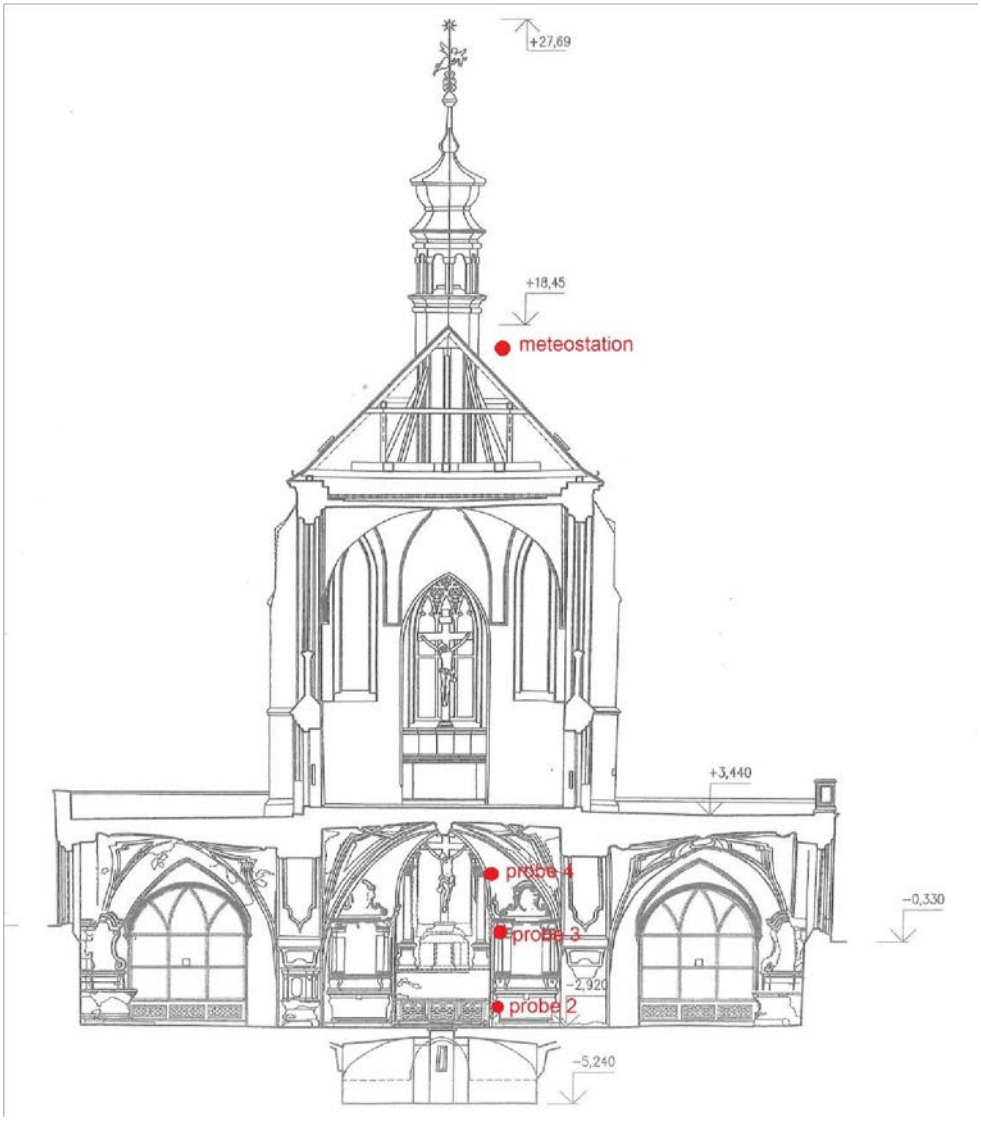


Figure 1: Drawing of sensor placement in building section.

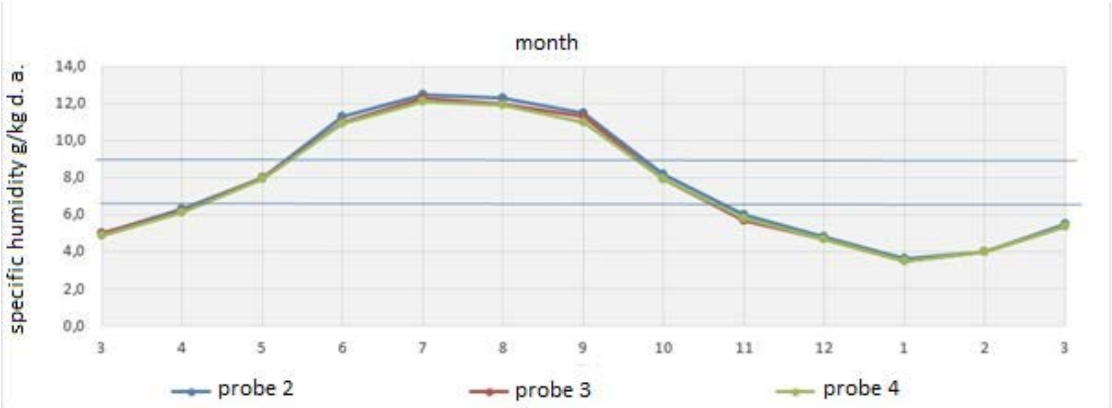


Figure 2: Specific air humidity between March 2016 and March 2017, indicating the boundary areas for 20˚C and 60% rel. (8.9 g / kg b.w.) and 18 ° C and 50% rel. (6.5 g / kg b.w.)

Year	Point of measurig	January	February	March	April	May	June	July	August	Septemberer	October	November	December
Interior temperature close to the dew point (difference < 3^{O}C)													
2016	Probe 2	-	-										
	Probe 3	-	-										
	Probe 4	-	-										
2017	Probe 2				-	-	-	-	-	-	-	-	-
	Probe 3				-	-	-	-	-	-	-	-	-
	Probe 4				-	-	-	-	-	-	-	-	-
Relative humidity above 80%													
2016	Probe 2	-	-										
	Probe 3	-	-										
	Probe 4	-	-										
2017	Probe 2				-	-	-	-	-	-	-	-	-
	Probe 3				-	-	-	-	-	-	-	-	-
	Probe 4				-	-	-	-	-	-	-	-	-
Dew point above 19^{O}C													
2016	Probe 2	-	-										
	Probe 3	-	-										
	Probe 4	-	-										
2017	Probe 2				-	-	-	-	-	-	-	-	-
	Probe 3				-	-	-	-	-	-	-	-	-

	Probe 4				-	-	-	-	-	-	-	-	-

Legend:	
	up to 10 days during the month
	from 10 to 20 days durimg the month
	more than 20 days during the month

Figure 3: Critical temperature, relative humidity and dew point above 19˚C in March 2016 to March 2017

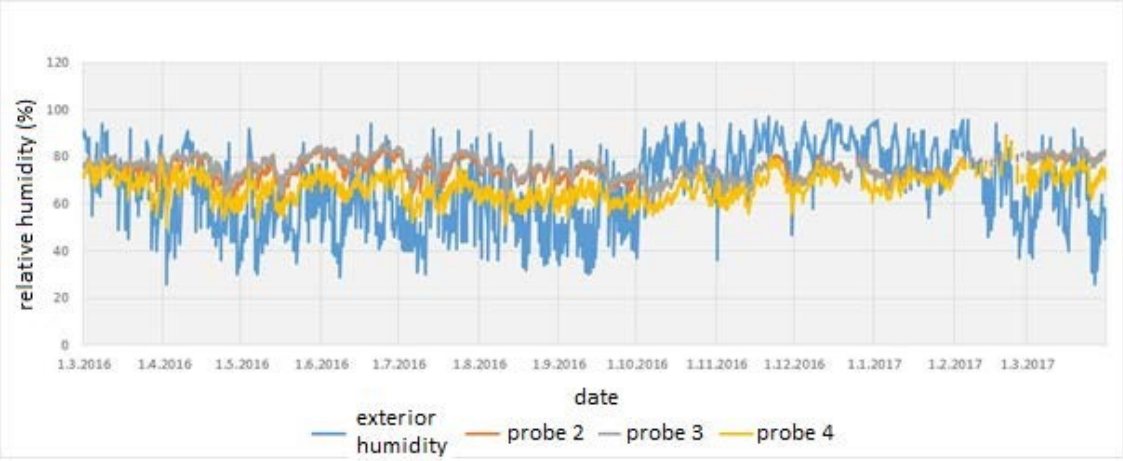


Figure 3: Relative humidity (%) in exterior (from weather station) compared to relative humidity in interior

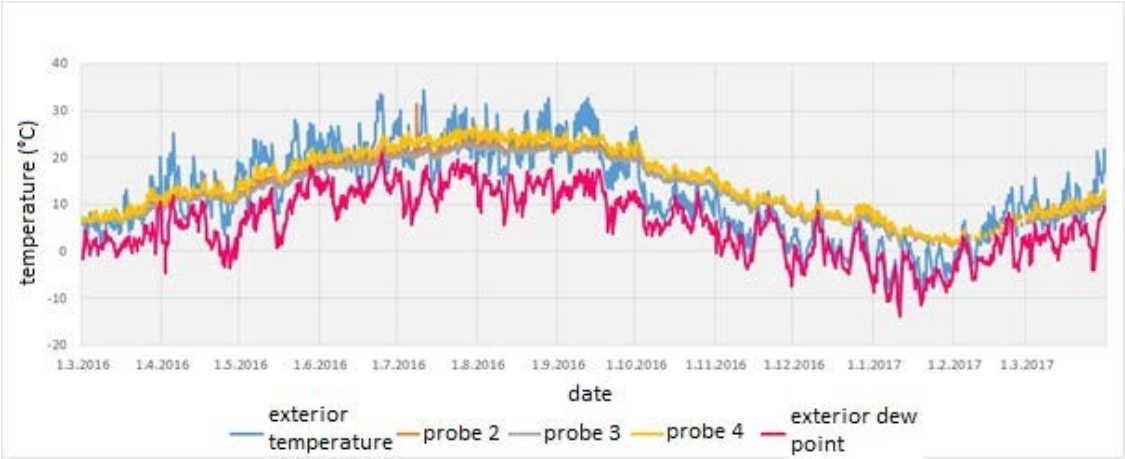


Figure 3: Temperatures (° C) and dew point (° C) of outdoor temperatures (from the weather station) compared to indoor temperatures from March 2016 to March 2017

The causes of the high relative humidity in the ossuary are:

- penetration and long-term retention of humid air from the exterior into the lower situated area of the ossuary without the possibility of proper circulation,
- supplying moisture to the ossuary space from damp walls and floors,
- increase of the relative humidity of the ossuary space caused by the repeated presence of a high number of people.

3 CONCLUSIONS

Based on the findings, it is clear that the internal microclimate of ossuary is at some risk when using the space for the purpose it is used today (exposing or storing human bones). The most risky is the instability of the environment, where the specific air humidity changes during the annual cycle and therefore changes in the environmental conditions (temperature, relative humidity and specific humidity) in which the bones are stored. The indoor microclimate varies not only with changes in weather during the year, but also shows different values at different height levels of the space. The bones placed in the lower part are in more humid environment than the bones suspended under the ceiling. The solution of indoor microclimate should follow three main points:

- stabilization of the internal microclimate of the ossuary space in time and space,
- ensuring an optimal bone storage environment;
- elimination of the reasons that may cause undesirable fluctuation of indoor microclimate parameters.

Fulfillment of the above points is possible only to a certain “reasonable” level in mater of improving the conditions of the indoor microclimate. By stabilizing the environment and eliminating the effects it is meant to influence the sources of humidity, which increase the relative humidity in the environment. Therefore it was recommended:

- remediation of peripheral masonry in terms of moisture,
- creation of an interruption zone (eg by the construction of a partition or enclosure) in the area of the cash register which interrupts the direct external influence on the internal microclimate of the ossuary,
- creation of the possibility of extracting humid air from the ossuary area (e.g. controlled "discharge" of humid ground air through the crypt to the exterior and controlled removal of water vapor from the vault areas through the upper suction).

Optimal bone storage environment is desirable to be assessed by a specialist in the field of ventilation and consultation with anthropology experts who can recommend optimal parameters for storage and display, also with regard to the presence of visitors (optimal stabilization of the environment in terms of temperature and humidity). Subsequently, we recommend securing and installing ventilation (or air-conditioning) units in the ossuary area, in order to ensure the removal of humid air and to improve the parameters of the largest part of the ossuary area. The air conditioner parameters will be:

- setting of switching conditions,
- ensuring its establishment and solving the issue of connection to the air inlet and outlet,
- ensuring its adequate capacity, ie the capability of exchanging a specified volume of air over time.

The optimal solution would be adjustable switching of the unit when the defined specific humidity (between 6.5 and 9.8 g / kg dry air) is exceeded [4]. Unfortunately, this criterion cannot be evaluated by conventional devices and it is therefore possible to rely at least on a relative humidity sensor. We suggested a value of 60% rel. If only the use of fans were considered, then the solution would be to reduce rel. humidity in the lower part of the ossuary and its removal e.g. through the floor into the crypt and from there further out. Even in the case of air-conditioning units, the microclimate of the lower part of the ossuary should be addressed, preferably by controlling the microclimate in both directions, too humid and too dry air.

All measures considered must take into account the area from which the air will be pumped and the area (e.g. exterior) where the air will be vented. It is also possible to consider a variant where the air extraction units would be supplemented by a separate fan with a sensor and a MaR system, which would supply air from the exterior at a time when the optimum climate in terms of specific humidity will be present. Capacity must be decided by a specialized designer. The basic question is the speed of air exchange throughout the ossuary space and the frequency of switching depending on the space operation.

4 RESULTS

The whole measurement led to the finding that there is a different behavior of the microclimate in the individual levels of the ossuary. It was found that there are a number of moments when surface condensation occurs on both plasters and inventory. There is a periodic change in specific humidity in the area, so that in winter low specific humidity prevails, which damages the inventory, and in summer there is excessive specific humidity, which causes the absorption of water vapor into the material and its subsequent degradation. There are sharp changes in the microclimate in the given area, which are harmful in themselves. This worsens already high humidity of the plinth part of the perimeter and internal walls. This resulted in two basic remediation measures for the area:

- material dehumidification of masonry,
- modification of the internal microclimate.

It is necessary to reduce sudden changes in specific humidity and to unify the differences of the microclimate in individual parts of the given space as much as possible. Eliminate condensation to the maximum extent available. As the use of space will remain the same, a large number of visitors will alternate with empty space it is also necessary to deal with this somehow.

All these requirements were included in the remediation project. Heavy humid air will be extracted to the outside. The air is treated by air conditioning units. An artificial barrier has been created which separates the entrance space from the ossuary space by means of an air curtain to prevent unstable outdoor air from being poured in. The visitor circulation mode has changed by directing the movement of visitors in one direction. They enter through the air curtain into the ossuary in one end and exit elsewhere through the newly built space. That reduced the source of moisture by reducing large concentration of people during ascent and descent into the space.

Acknowledgements. The activity presented in the paper is part of the research grant NAKI II DG18P02OVV012 project of the Ministry of Culture of the Czech Republic.

REFERENCES

[1] Dorokhov, V. Pintelin, N. *Control of Temperature and Humidity Conditions of Church Buildings-Architectural Monuments as a Method of Preservation*, 2018 IOP Conf. Ser.: Mater. Sci. Eng. 463 032076

[2] Pavlík, Z., Balík, L. Kudrnáčová, L., Maděra, J. and Černý, R. Chapel of Cemetry Church of All Saints in Sedlec – Long-Term Analysis of hygrothermal Conditions. *Thermophysics* 2017, AIP, Santa Fe, 2017

[3] Kudrnáčová, L. Balík, L. Sledování mikroklimatu v prostorách kostela. In: *Sanace a rekonstrukce 2017*, WTA Praha, 2017, p. 71-77. ISBN 978-80-01-06347-7

[4] Černý, M. Němeček, M. *Mikroklima v historických interiérech*. NPÚ Praha, 2011, ISBN 97880-87104-82-8

12th International Conference on Structural Analysis of Historical Constructions
SAHC 2020
P. Roca, L. Pelà and C. Molins (Eds.)

A COMPARISON BETWEEN EMPIRICAL PROCEDURES FOR THE DEFINITION OF VULNERABILITY CLASSES OF MASONRY BUILDINGS: APPLICATION TO FIVE HISTORICAL CENTRES STRUCK BY 2016 CENTRAL ITALY EARTHQUAKE

YLENIA SARETTA[1*], LUCA SBROGIÓ[1] AND MARIA R. VALLUZZI[1]

[1]Department of Cultural Heritage (dBC)
Università degli Studi di Padova
Piazza Capitaniato 7, 35139 Padova, Italy
e-mail: ylenia.saretta@unipd.it (*corresponding author), luca.sbrogio@phd.unipd.it, mariarosa.valluzzi@unipd.it

Keywords: Masonry, Vulnerability Classes, Damage Analysis, Strengthened Interventions

Abstract. *The definition of seismic risk scenarios necessarily depends on the attribution of a vulnerability class to each building of a stock. In the macroseismic scale (EMS-98) the vulnerability class – from A to F – results from the combination between horizontal and vertical structures. On the basis of post-event surveys carried out in Italy after the earthquakes occurred in the last 50 years, many rules for converting the masonry quality and the stiffness of horizontal diaphragms into a vulnerability class have been proposed. However, despite the now high number of retrofitted or strengthened buildings in Italy, structural interventions are not mentioned in these procedures, except for metal tie rods and r.c. tie beams.*

The paper proposes a critical approach to the definition of vulnerability classes, by the means of applying the conversion rules to the same sample of 525 masonry buildings located in five historical centres struck by 2016 Central Italy earthquake: Acquasanta Terme, Campi Alto di Norcia, Castelsantangelo sul Nera, Muccia and Vezzano. They have been chosen due to the extensive strengthening campaigns that had been carried out after earlier seismic events. The preliminary recognition of the structural features of each building happens at the terms of the MUSE-DV Masonry, a rapid visual screening procedure recently proposed by the authors.

The damage probability matrices (DPMs), obtained from each conversion, are compared to those from a theoretical model proposed for the EMS-98. Given the same poor masonry quality, the existing rules classify buildings in class A or B depending only on floors' stiffness and horizontal connections. As a result, both low and high damage may appear in the same vulnerability class causing a bimodal trend in the damage distributions. Conversely, the MUSE-DV procedure allows to reduce these two frequency peaks by considering interventions. In fact, overall interventions, even on very poor masonry structures, may lead to a very low damage and, consequently, to low vulnerability classes (even C or D), while uncontrolled interventions could obtain a high damage and a high vulnerability. The twofold consequence is that a) structural interventions have a 'relative', i.e. positive or negative, contribution; b) the usual limitation to A and B vulnerability classes for random masonry buildings needs to be widened to better explain the damage observed in the 2016 Central Italy earthquake.

1 INTRODUCTION

A vulnerability class is an essential factor in the definition of damage scenarios at urban scale and, consequently, in the calibration of prevention strategies and vulnerability models for the reduction of seismic risk. Such class, which is an empirical evaluation of a building's aptitude to suffer a certain damage grade, is rapidly attributed through the observation of a building's structural features. The European Macroseismic Scale (EMS-98, [1]) proposes six classes, from A to F, at decreasing vulnerability; the scale identifies a most likely vulnerability class and a range of probable behaviour for each structural type. Typically, masonry buildings may belong to classes A, B and C; D is only referred to seismically designed buildings. Classes D, E and F are attributed to r.c. or steel structures.

However, the earlier macroseismic scales (MCS, [2]; MSK-76 [3]) were limited to just three classes (i.e. A, B and C), related both to masonry and r.c. structures, which may be compared to the first three EMS-98 classes [4].

Damage Probability Matrices (DPMs), which define the observed or expected damage grade (from 0, negligible damage, to 5, collapse, according to EMS-98) depending on vulnerability class and macroseismic intensity, are widely used to sum up empirical damage analysis. Theoretical DPMs have been derived from those implicitly described in the EMS-98 by [5] and, in this paper, are compared to those obtained from the empirical sample.

The paper deals with a critical approach in the definition of vulnerability classes starting from the observation of structural elements, by the means of applying some of the rules proposed in the scientific literature (§1.1). These rules have been defined in the hindsight of the data coming from surveys begun after the Irpinia earthquake in 1980. They allowed to derive the empirical DPMs for a sample of 525 masonry buildings located in five historic centres struck by the Central Italy earthquake in 2016 and characterized by different level of macroseismic intensity [6]: Acquasanta Terme, Campi Alto di Norcia, Castelsantangelo sul Nera, Muccia e Vezzano di Arquata del Tronto. The evaluation of each building happened at the terms of the *MUSE-DV Masonry (MUltilivel assessment of SEismic Damage and Vulnerability of masonry buildings*), a rapid visual screening procedure proposed by the authors to evaluate the specific structural features of the buildings in the involved area (§1.2). The results are compared both to the theoretical model (§2.2) and to the real observed behaviour (§3), in order to underline the contribution of strengthening interventions on buildings.

1.1 Literature procedures for the attribution of the vulnerability class

The seismicity of Italy is remarkable [7]. Most effort of researchers aims at developing and improving rapid visual screening procedures to estimate seismic damage and vulnerability [8]. The amount of data collected in the last 50 years represents an inestimable scientific heritage for prevention purposes [9]. DPMs have been used in Italy since 1980 (Irpinia earthquake) referring to MSK-76 scale [10]. This scale has been commonly employed also for later empirical elaborations. In that occasion, the data collection happened by the means of a standardized rapid visual screening (RVS) procedure called *GNDT I level* [11], whose heir is the *AeDES* RVS, the present standard procedure to define a building's usability and damage grade [12]. In both procedures, the combination of masonry quality and horizontal structures' stiffness yields the estimated vulnerability class of a building.

In the *GNDT I level* RVS, surveyors are asked to recognize the vertical structures among

eleven categories, according to masonry units and their texture, and the horizontal ones among nine categories, according to the bearing elements' material and the presence of connections to the walls. Aiming at defining the vulnerability classes from the mutual combination of vertical and horizontal elements, [13] developed a conversion rule based on *GNDT I level* RVS, while [14] simplified the vertical types distinguishing only among *bad*, *medium,* and *good* quality. [15] used a more descriptive approach referring to *field stone* as a bad quality, *hewn stone* as a medium quality and *bricks* as the good one.

Table 1: Comparison among different interpretations of conversion of Section 3 of AeDES RVS according to MSK-76. Grey background highlights different attribution of vulnerability class

Horizontal str.	Vertical structures																	
	Bad quality						Medium quality						Good quality					
	Without ties/tie rods			With ties/tie rods			Without ties/tie rods			With ties/tie rods			Without ties/tie rods			With ties/tie rods		
Conversion rule	Zuccaro et al. 2000	Dolce et al. 2003	Dolce et al. 2019	Zuccaro et al. 2000	Dolce et al. 2003	Dolce et al. 2019	Zuccaro et al. 2000	Dolce et al. 2003	Dolce et al. 2019	Zuccaro et al. 2000	Dolce et al. 2003	Dolce et al. 2019	Zuccaro et al. 2000	Dolce et al. 2003	Dolce et al. 2019	Zuccaro et al. 2000	Dolce et al. 2003	Dolce et al. 2019
Vaults without ties	A	A	A	/	/	A	A	A	/	/	/	/	A	A	A	/	/	B
Vaults with ties	A	A	A	/	/	B	B	A	/	/	/	/	B	A	A	/	/	B
Vaults and floors	A	A	/	A	/	/	A	A	/	B	/	/	B	A	/	B	/	/
Flexible floors	A	A	A	A	A	B	A	A	/	B	A	/	B	B	A	B	B	B
Semi-rigid floors	A	B	A	A	B	B	B	B	/	B	B	/	B	C	B	C	C	C
Rigid floors	A	B	B	/	/	B	B	C	/	/	/	/	C	C	C	/	/	C

For masonry buildings, the *AeDES* RVS requires i) to distinguish only between *random layout and bad quality (stones, pebbles)* and *coursed layout and good quality (hewn stones, bricks)*, ii) to define the presence of tie rods and/or tie beams and iii) to recognize vaults and floors' stiffness (*flexible, semirigid* or *rigid* floors). Comparing to the previous RVS procedure, this empirical evaluation represents an important simplification in the surveyors' work. At the beginning [14,15], surveyors were asked to recognize masonry features (units, texture, and layout) and floors elements in a very detailed way; conversely, in [9]'s opinion surveyors should have a different role, in which they may be identified as "evaluators" instead of "observers". That is why in the *AeDES* RVS they are asked to identify masonry's good or bad *behaviour* and floors' capability to redistribute seismic loads rather than their structural features.

Strengthening interventions may be characterized but they are not included in any of the procedures for the identification of the vulnerability classes [16].

After the L'Aquila earthquake (2009), [17] proposed another rule, while [9] widened it starting from a complete review of post-earthquake data collected since 1980. In this case, D class identifies seismically resistant dwellings built after 1974 (first seismic Italian code).

Table 1 proposes a comparison among three different procedures [9,13,14] to determine the vulnerability class. For the sake of comparability, the eleven vertical structures in [13] are grouped in *bad, medium,* or *good* quality, although they were all used for the identification of

the class. [13] propose the only procedure which considers the differences between masonry block structures (tuff, full bricks, lightweight hollow bricks, no load-bearing lightweight hollow bricks used as load-bearing structure, concrete blocks).

As one may observe in Table 1, in the behavioural approach by [9], medium quality masonry is not included, while the presence of tie rods or tie beams definitely improves a building's estimated seismic response (from class A to B), regardless of its masonry quality. The presence of rigid floors leads to class C. The comparison between [13] and [14] highlights that the latter proposes less vulnerable classes, excepted for vaults.

2 THE ATTRIBUTION OF THE VULNERABILITY CLASSES TO ORDINARY BUILDINGS IN FIVE HISTORICAL CENTRES STRUCK BY 2016 CENTRAL ITALY EARTHQUAKE

2.1 The case studies

Starting from August 24th, 2016, 140 municipalities located in Central Italy had been struck by a strong seismic swarm [18,19]. Devastating effects on civil and monumental heritage have been observed, especially on buildings located near the epicentres or where site effects exist [20]. Poor quality of masonry structures caused the crumbling of the stones rather than the activation of rigid macro-blocks and the identification of damage mechanisms. As matter of a fact, Central Italy dwellings' masonries are characterized by uncoursed or brought to courses rubble or hewn stones with poor clay-lime mortar, lacking in binding capacity. Moreover, the 'relative' effects, i.e. positive or negative, of structural interventions applied after 1979, when an earthquake hit the same area, may be nowadays identified.

Horizontal timber structures were generally replaced by precast r.c. joists or cast-in-place ribbed slabs with tie beams chased into the walls or they were reinforced with thin r.c. overlays [21,22]. If vertical structures were not reinforced and therefore, they could not stand the increase of seismic loads, *partial* interventions are obtained. Conversely, *holistic* interventions result from their application on horizontal and vertical structures (by the means of injections, r.c. jacketing, deep repointing of mortar, internal bricks wythes) and on the mutual connection, ensuring a favourable effect and, thus, decreasing the damage grade [19,23].

The recognition of the type and the effectiveness of the structural interventions of each building happened at the terms of the *MUSE-DV Masonry* RVS, a rapid visual screening procedure recently developed by the authors [8]. The RVS procedure is divided into four sections; *sections 0, 1* and *2* evaluate a building's seismic damage and vulnerability, with increasing level of accuracy. Finally, *section 3* analyses masonry quality, horizontal and roofing structures and strengthening interventions.

In this paper, the application of the RVS to 525 masonry buildings located in five case studies is presented. In order to define the damage grade and the structural features of each building, *Section 0* (Building identification, overall vulnerability and damage) and *Section 3* (Building features) were compiled. The application of the conversion rules to this sample of masonry buildings allowed to define the vulnerability classes.

Five historical centres have been chosen according to different macroseismic intensities [6] and, hence, damage situations (Table 2): they are Acquasanta Terme (ACQ) and Vezzano di Arquata del Tronto (VZZ) in the district of Ascoli Piceno, Campi Alto di Norcia (CMP) in the district of Perugia, Castelsantangelo sul Nera (CSN) and Muccia (MCC) in the district of

Macerata. They are characterized by quite homogeneous structural features; a more detailed analysis about buildings' seismic behaviour, historical and structural features is developed in [19,23]. According to empirical damage grades, CSN suffered the most severe damage (mean value=3,08, using [24]). A medium level of mean damage was registered in VZZ (2,24) and in CMP (2,39), even though 37% of buildings suffered of low damage thanks to favourable structural interventions applied after past seismic events. No collapses were recognized in MCC and in ACQ, where a relatively low mean damage was registered, respectively of 1,51 and 0,98.

Table 2: Distance from epicentre (Oct 30, 2016), EMS-98 intensities registred by [6], total number of analyzed structural units, damage grades and mean damage calculated according to [24]

Settlement	Epic. Dist. [km]	I_{EMS-98}	Nr of inspected buildings	Damage grades						μ_D
				D0 %	D1 %	D2 %	D3 %	D4 %	D5 %	
CMP	2,1	VIII	57	5	37	19	10	11	18	2,39
CSN	8,1	IX	129	4	16	13	22	25	20	3,08
VZZ	16,3	VIII	79	4	31	29	15	15	6	2,24
ACQ	25,8	VII	129	36	41	15	6	2	0	0,98
MCC	28,5	VIII	133	7	47	33	11	2	0	1,51

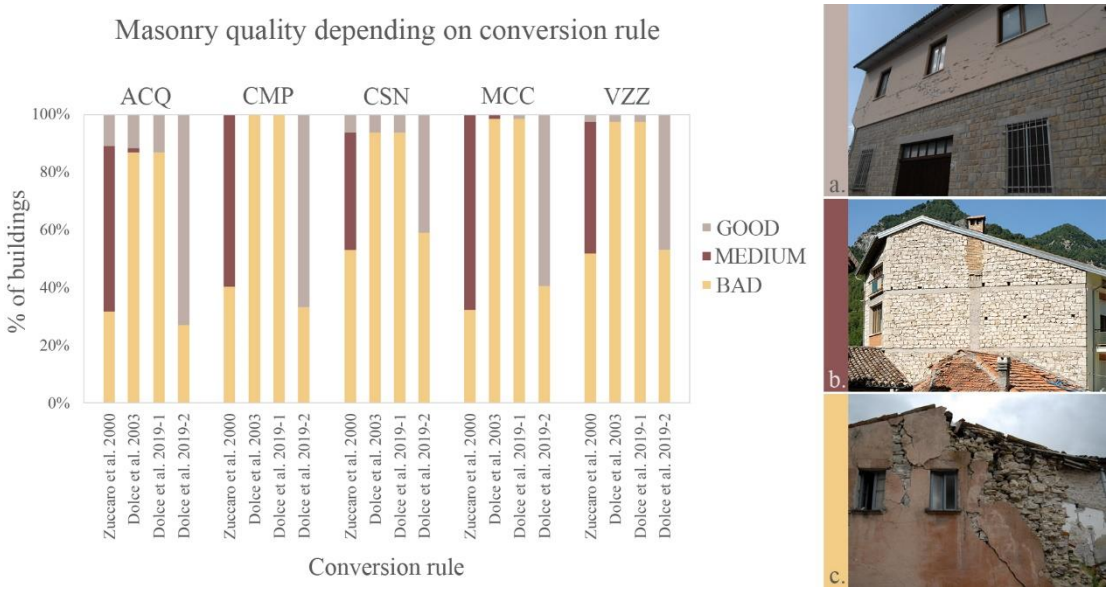


Figure 1: Masonry quality depending on conversion rule. On the right, some examples of masonry quality: a) good, CSN; b) medium, ACQ; c) bad, CSN

2.2 The attribution of the vulnerability classes using literature procedures

Structural features recognized by *MUSE-DV Masonry* RVS were adapted to the conversion rules (Table 1) as a function of i) masonry units and mortars or the overall quality of bearing walls and ii) floors' types and stiffness.

Two approaches were followed in applying the rule proposed by [9]: i) in the first one (in the following defined as [9]–*1*), the mere observation of masonry texture and mortar consistency yielded *random/bad quality* o *coursed/good quality*; ii) in the second one ([9]–*2*), strengthening interventions' influence participated in the classification as well, changing the

final result. In other words, in the latter case the surveyor was asked to be an *evaluator* more than an observer. Such information is collected by the *AeDES* RVS, but it is not considered in the vulnerability class definition.

Figure 1 shows masonry quality as a function of the conversion rule. In the case of compresence of different masonry textures, the worst were considered. As one may see, *medium quality* results only from the application of [13], characterized by more possibilities in the structural combination, at the expense of the rapidity of the whole procedure. Results from the application of [14] and [9]–*1* are similar, while a more precise interpretation of a building's behaviour comes from [9]–*2*.

The evaluation of horizontal structures' stiffness is the same in each procedure; sometimes the floors' identification was prevented by exterior surveys only, hence roofs' stiffness becomes relevant. Semirigid diaphragms are the most recurrent (35%), followed by flexible (32%) and rigid ones (25%); the remaining cases are vaults with or without tie rods (typically in CMP) and not evaluated structures (N.E.). Almost a half of the surveyed buildings (52%) shows tie rods and tie beams, partially evaluated by [9] and [13].

The empirical DPMs of the sample were defined according to the three chosen conversion rules (Table 1) and considering also the two approaches for [9] (Figure 2). It is worth noting that class D is totally absent and only a few buildings belong to class C (Table 3). Class A is typical of most cases, especially with [13]'s rule, except for MCC, where the widespread rigid diaphragms cause a half of the buildings to belong to class B. According to [9]–*1* rule, most buildings are classified as B, but in the case of ACQ the 12% of the surveyed dwellings are in class C, thanks to a better masonry quality (coursed layout). The application of [9]–*2* allows to observe an increase of buildings in class C and a decrease in class A, except for VZZ where masonry's original features are more preserved.

Table 3: Relative distribution of the estimated vulnerability class according to conversion rules

Settlement	Zuccaro et al. (2000)			Dolce et al. (2003)			Dolce et al. (2019) - 1			Dolce et al. (2019) - 2		
	A %	B %	C %	A %	B %	C %	A %	B %	C %	A %	B %	C %
ACQ (I=VII)	60	29	12	57	31	12	45	43	12	20	39	41
CMP (I=VIII)	82	18	0	63	37	0	39	61	0	9	72	19
CSN (I=IX)	65	3	5	53	42	5	25	71	4	22	53	25
MCC (I=VIII)	54	45	1	41	58	1	35	64	1	26	44	30
VZZ (I=VIII)	84	13	3	75	22	3	65	32	3	57	23	20

The obtained DPMs were compared to the theoretical ones, defined starting from the EMS-98 [5], with poor results. The recurring presence of peaks in low damage grades (D0 and D1) and an overlapping of damage grades for the three classes happen at low macroseismic intensity (ACQ, I=VII), differently from [5]. Similarly happens for I=VIII:

- in MCC, A and B classes overlap, D1 and D2 are the most recurrent damage grades, even though D3 and D4 should be the peaks according to [5];
- in VZZ a bimodal trend characterizes the damage grades of the two most vulnerable classes, with two frequency peaks in D2 and D4 for class A and in D1 and D3 for class B: as a consequence, B appears more vulnerable than A for [9]–*1*. One may suppose that the D2 peak for class A should describe buildings that actually belong to B or lower classes and that the D3 peak for class B could gather higher vulnerable dwellings;

- in CMP different results come out from each procedure.

In the case of CSN (I=IX), the first two procedures seem to be comparable to the theoretical model, although low damage for class A exceeds the expected, while [9]–*1*'s procedure provides unfavourable results which could describe a I=X situation. More coherent results come from [9]–*2*'s procedure, even though they cannot solve the contrast between the other procedures and the theoretical model. Therefore, the theoretical model derived from the EMS-98 is not coherent with the DPMs obtained from the conversion rules, although specifically adapted to the sample. Class A sometimes appears to be less vulnerable than B or they show the same damage grades. This fact may be explained with the compresence of buildings belonging to different vulnerability classes in the same group.



Figure 2: DPMs for surveyed centres. Application of conversion rules to the sample of buildings (from second to fifth column) and comparison with theoretical model [5] (first column, dashed lines)

3 SOME OBSERVATIONS IN THE HINDSIGHT OF 2016 SEISMIC SWARM: THE ROLE OF INTERVENTIONS IN BUILDINGS' SEISMIC BEHAVIOUR

The application of the literature conversion rules to the data set (Figure 2) has highlighted their limits in the vulnerability classification. In fact, these procedures do not take into account the influence of structural strengthening interventions applied on buildings in a recent past, observing only the presence of tie rods or tie beams. The effectiveness of these connection systems on seismic behaviour is taken for granted, especially if they are associated to rigid diaphragms (cfr. Table 1 and 3). However, observations demonstrated that the effectiveness of tie rods is limited by masonry quality at the anchoring (Figure 3a, see also [25]), while r.c. curbs on weak masonries cause crumbling, overturning and sliding of the walls (Figure 3b, c) [21].

Interventions revealed a 'relative', i.e. favourable or unfavourable, contribution to a building's seismic behaviour [8,16,20,21,23]. Table 4 sums up the typical structural interventions observed in the five centres. This information cannot be ignored anymore: a great amount of strengthened buildings were recognized in CSN (85%), MCC (94%) and CMP (98%). In the last case, structural interventions applied after the 1979 earthquake [26] caused a dichotomy in buildings' behaviour (see Table 2): buildings with holistic interventions suffered of minor damage, while on the other hand buildings with partial interventions (see §2.1) caused severe damage and buildings' collapses. The miss use of this data in conversion rules does not allow to attribute the correct vulnerability class to strengthened buildings.

Moreover, according to the conversion rules, the unconditional favourable effect of rigid slabs on a building's seismic behaviour yields to classes B or C. In the authors' opinion, on the basis of the empirical evidence, that could be true only in case of low levels of seismic input (Figure 4a), while near the epicentre rigid diaphragms on poor masonries induce crumbling phenomena and a building's collapse (Figures 4b and 4c). Therefore, the vulnerability increases, and the building is prone to suffer of a higher damage, as already appeared after the 1997 Umbria-Marche earthquake [27].

Another problem of the literature rules is the limitation to the first three classes, among which class C generally defines buildings with artificial blocks or dressed stone masonries; this classification needs to be widened to better explain the real seismic behaviour. The issue has been recently discussed by the authors [21,23], underlining that buildings with holistic interventions could be actually described by class D, typical of new buildings (§1.1), while partial interventions yield class A. Original buildings without strengthening interventions (stone masonries and timber floors) belong to class A, such as buildings with original unreinforced stone masonries and replaced diaphragms with rigid or semirigid ones (Figure 5a). As well as recent buildings (Table 5), deep repointing and thick cementitious plasters on bearing walls allow to reach class C (Figure 5b), while core interventions, such as grout injections and r.c. jacketing, could lead to class D, regardless floors' stiffness (Figure 5c). Class B is not explicitly defined, but it expresses the possible range of vulnerability thanks to the structural details and the masonry quality.

Figure 6 shows the new DPMs derived from the proposed classification for the five case studies: the widened classification (from class A to D) better describes the observed buildings' seismic behaviour and the comparison with the theoretical model (Figure 2), with more coherent results. Bimodal trends have been removed, the use of class D and the spreading of class C for each centre lead to a better distribution of the six damage peaks.

a.  b.  c. 

Figure 3: Examples of poor seismic behaviour in a strengthened masonry building, CSN: a) Not effective tie rods on bad quality masonry; b) overturning of last storey and c) of internal bearing walls due to r.c. curbs and to excess of stiffness and weight of reinforced timber roof

a.  b.  c. 

Figure 4: Examples of damage due to rigid roofs: a) Slip of the roof and horizontal arch (VZZ); b) Masonry leaves separation and local overturning (CSN); c) Total collapse due to crumbling of masonry (CMP)

a.  b.  c. 

Figure 5: a) Class A building: poor masonry quality and floors replaced with rigid ones (MCC); b) C class building: random layout limestone masonry reinforced by deep repointing with cementitious mortar (CSN); c) D class building: random layout limestone masonry reinforced by grout injections and r.c. jacketing (internal side) (CMP)

Table 4: Relative presence of interventions on walls and horizontal structures in the sample

Settlements	No. of inspected buildings	No structural interventions	Built starting from the 80' s	With structural interventions	Replacing or strengthening of floors, no strengthening interventions on walls	Superficial interventions on walls (repointing, thick cementitious plaster)	Core interventions on walls (injections, r.c. jacketing, internal wythes)
ACQ	129	12%	11%	78%	8%	45%	5%
CMP	57	2%	0%	98%	32%	63%	47%
CSN	128	10%	5%	85%	32%	20%	9%
MCC	133	6%	0%	94%	24%	44%	13%
VZZ	79	18%	1%	81%	10%	20%	5%

Table 5: Vulnerability class according to empirical observations of the authors

No structural interventions	Built starting from the 80's	Replacing or strengthening of floors, no strengthening interventions on walls	Superficial interventions on walls (repointing, thick cementitious plaster)	Core interventions on walls (injections, r.c. jacketing, internal wythes)
A	D	A	C	D

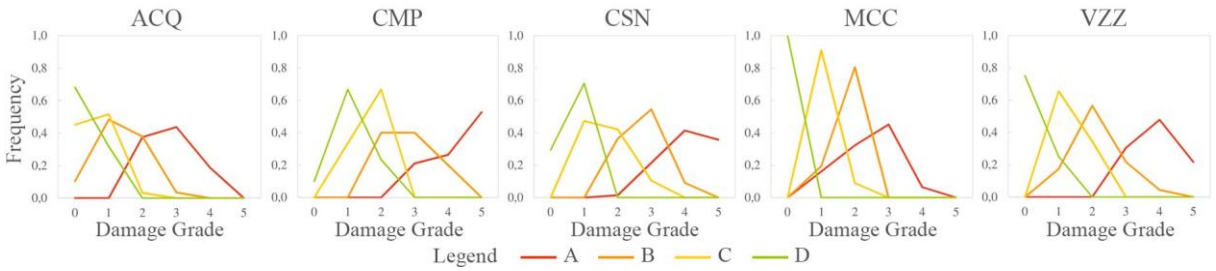


Figure 6: Empirical DPMs according to Table 5

4 CONCLUSIONS

The definition of a building's vulnerability class is a staple in the proposal of risk reduction strategies. Using post-earthquake survey data, some procedures have been developed in order to identify the vulnerability class considering the interaction among bearing walls, horizontal structures and connections. The application of these procedures to 525 buildings inside five centres struck by the 2016 Central Italy earthquake underlined a conceptual lack in those rules for the specific context. In fact, the empirical DPMs highlighted i) an overlapping of damage distributions of different classes and ii) a bimodal trend in the damage grades.

In field surveys, the effects of strengthening or retrofit interventions applied to buildings after past seismic events are evident. The authors observed substantially different seismic behaviours within the same centre between unreinforced and strengthened buildings, and between partially or completely strengthened ones. Holistic interventions on the ensemble of a building's structural elements lead to negligible seismic damage, while partial and local ones cause severe damage. Consequently, some discrepancies between the observed damage (hence the explicated vulnerability) and the vulnerability estimate (hence the expected damage grade) through literature rules have been remarked. In particular:

i) according to those rules, rigid slabs always improve the seismic behaviour, regardless of the masonry quality; the same happens for r.c. tie beams;

ii) those rules consider only the first three vulnerability classes (A to C), but class C (buildings with coursed layout and good masonry quality) is uncommon in the sample, where random stone masonries prevail. Classes A or B only, defined according to the floors' stiffness, are not able to completely describe the observed buildings' behaviour;

iii) the lack in those rules of the observation of strengthening interventions cannot lead to the correct vulnerability class. Actually, flexible diaphragms replaced with rigid ones caused such severe damage phenomena (e.g. masonry crumbling) that classes B or C do not express these situations. On the other hand, holistic interventions both on vertical and horizontal structures cannot be described by classes A or B, as the random layout of stone masonries would classify them.

Trying to reduce these limitations, the authors have revised the attribution of the EMS-98

vulnerability class to strengthened buildings [21,23]. As a rule:

i) unfavourable interventions allow to attribute class A, regardless of floors' stiffness;
ii) favourable interventions could lead to class C (superficial interventions on the walls) or D (core interventions). B is a 'possible' class, resulting from the evaluation of structural details and materials.

These statements allowed to propose more coherent *DPMs* if compared to the empirical observations, thanks to a wider range of vulnerability classes.

The procedure needs to be developed through the validation on other case studies and the evaluation of other parameters, in order to better describe the empirical data according to the EMS-98 model, preserving the rapidity that large scale vulnerability assessment needs.

Acknowledgements. This research is framed within the 2016-2018/2019-2021 Reluis Projects. The authors wish to thank eng. F. Molinari and eng. M. Vettore for their help during the surveys.

REFERENCES

[1] Grünthal, G. European Macroseismic Scale 1998. *Cahiers du Centre Européen de Géodynamique et de Séismologie*, Vol. XV, Luxembourg, (1998).
[2] Sieberg, A. Geologie der Erdbeben. *Handbuch der Geophysik* (1930) **2**(4):552-555.
[3] Medvedev, S.V. Seismic Intensity Scale MSK-76. *Publications of the Institute of Geophysics, Polish Academy of Sciences* (1977) **A-6**(117):95-102.
[4] Molin, D. Considerazioni sull'eventuale adozione in Italia della scala macrosismica europea (EMS-1998). *XXII GNGTS "Gruppo Nazionale di Geofisica della Terra Solida", Rome, 18-20 November* (2003).
[5] Bernardini, A., Giovinazzi, S., Lagomarsino, S. and Parodi, S. The vulnerability assessment of current buildings by a macroseismic approach derived from the EMS-98 scale, *Asociaciòn Espanola de Ingenierìa Sismica. Girona, 8-11 May* (2007).
[6] Locati, M., Camassi, R., Rovida, A., Ercolani, E., Bernardini, et al. *Database macrosismico italiano (DBMI15), version 2.0,* INGV (2019).
[7] Rovida, A., Locati, M., Camassi, R., Lolli, B. and Gasperini, P. *Catalogo Parametrico dei Terremoti Italiani (CPTI15), version 2.0,* INGV (2019).
[8] Saretta, Y., Sbrogiò, L., Molinari, F., Vettore, M. and Valluzzi M.R. Proposta di un nuovo strumento multilivello per la valutazione del danno e della vulnerabilità a scala urbana: la procedura MUSE-DV Masonry per la valutazione empirica del comportamento di edifici consolidati. *Progettazione sismica* (2020) no.1, Quaderno 1.
[9] Dolce, M., Speranza, E., Giordano, F., Borzi, B., Bocchi, F., et al. Observed damage database of past Italian earthquakes: the Da.D.O. WebGIS. *Bollettino di Geofisica Teorica ed Applicata* (2019) **60**(2):141-164.
[10] Braga, F., Dolce, M. and Liberatore, D. A statistical study on damaged buildings and an ensuing review of the MSK-76 scale. *Proceedings of the 7th ECEE, Athens* (1982).
[11] Gruppo Nazionale per la Difesa dai Terremoti & Consiglio Nazionale delle Ricerche. *Scheda di esposizione e vulnerabilità di primo livello e di rilevamento danni*, GNDT (1994).
[12] Baggio, C., Bernardini, A., Colozza, R., Corazza, L., Della Bella, M. et al. *Manuale per la compilazione della scheda di 1° livello di rilevamento danno, pronto intervento e agibilità per edifici ordinari nell'emergenza post-sismica (AeDES).* PCM-DPC, (2014).
[13] Zuccaro, G., Papa, F. and Baratta, A. Aggiornamento delle mappe a scala nazionale di

vulnerabilità sismica delle strutture edilizie. In: Bernardini A. (Ed.): *La vulnerabilità degli edifici: valutazione a scala nazionale della vulnerabilità sismica degli edifici ordinari.* Roma, CNR-GNDT, (2000), pp. 133-166.

[14] Dolce, M., Masi, A., Marino, M. and Vona, M. Earthquake damage scenarios of the building stock of Potenza (Southern Italy) including site effects. *Bull. Earthquake Engineering* (2003) **1**(1):115-140.

[15] Di Pasquale G., Orsini G. and Romeo R.W. New Developments in Seismic Risk Assessment in Italy. *Bull. Earthquake Engineering* (2005) **3**(1):101-128.

[16] Sisti, R., Di Ludovico, M., Borri, A. and Prota, A. Damage assessment and the effectiveness of prevention: the response of ordinary unreinforced masonry buildings in Norcia during the Central Italy 2016-2017 seismic sequence. *Bull. Earthquake Engineering* (2019) **17**:5609-5629.

[17] Dolce M. and Goretti A. Building damage assessment after the 2009 Abruzzi earthquake. *Bull. Earthquake Engineering* (2015) **13**(8):2241-2264.

[18] Valensise, G., Tarabusi, G., Guidoboni, E. and Ferrari, G. The forgotten vulnerability: A geology-and history-based approach for ranking the seismic risk of earthquake-prone communities of the Italian Apennines. *Int. J. Disaster Risk Reduction* (2017) **25**:289-300.

[19] Valluzzi, M.R., Sbrogiò, L., Saretta, Y. and Wenliuhan, H. Seismic response of masonry buildings in historical centres struck by the 2016 Central Italy earthquake. Part 1-feature recognition and damage evaluation. *International Journal of Architectural Heritage* (n.d.) Submitted.

[20] Fiorentino, G., Forte, A., Pagano, E., Sabetta, F., Baggio, C., et al. Damage patterns in the town of Amatrice after August 24th 2016 Central Italy earthquakes. *Bull. Earthquake Engineering* (2018) **16**:1399-1423.

[21] Vettore, M., Saretta, Y., Sbrogiò, L. and Valluzzi, M.R. (2020). A New Methodology for the Survey and Evaluation of Seismic Damage and Vulnerability Entailed by Structural Interventions on Masonry Buildings: Validation on the Town of Castelsantangelo sul Nera (MC), Italy. *Int. J. Architectural Heritage* (2020) Published Online.

[22] Gavarini, C. (ed.) *Costruzioni e terremoto*. Roma, Nisa, (1983).

[23] Sbrogiò, L., Saretta, Y. and Valluzzi, M.R. Seismic response of masonry buildings in historical centres struck by the 2016 Central Italy earthquake. Part 2-calibration of a vulnerability model for strengthened conditions. *Construction and Building Materials* (n.d.) Submitted.

[24] Giovinazzi, S. The vulnerability assessment and the damage scenario in seismic risk analysis. PhD Thesis, University Carolo-Wilhelmina and University of Florence, (2005).

[25] D'Ayala, D. F. and Paganoni, S. Assessment and analysis of damage in L'Aquila historic city centre after 6th April 2009. *Bull. Earthquake Engineering* (2011) **9**(1):81-104.

[26] Sbrogiò, L., Valluzzi, M. R. and Cardani G. Recenti sviluppi sulle previsioni di vulnerabilità sismica di Campi Alto di Norcia alla luce degli interventi di riparazione e/o consolidamento e del sisma Centro Italia 2016, *XVIII Congresso Nazionale ANIDIS "L'ingegneria Sismica in Italia", Ascoli Piceno, 15-19 settembre* (2019).

[27] Borri, A. and De Maria, A. Alcune considerazioni in materia di analisi e di interventi sugli edifici in muratura in zona sismica. *XI Convegno Nazionale ANIDIS "L'ingegneria sismica in Italia", Genova, 25-29 gennaio* (2004).

12th International Conference on Structural Analysis of Historical Constructions
SAHC 2020
P. Roca, L. Pelà and C. Molins (Eds.)

A QGIS PLUGIN FOR THE SEISMIC VULNERABILITY ASSESSMENT OF URBAN CENTERS: APPLICATION TO THE CITY OF POPOLI IN ABRUZZO (ITALY)

A. GONZALEZ[1], A. BASAGLIA[1], E. SPACONE[1] AND G. BRANDO[1*]

[1]Department of Engineering and Geology
University "G. D'Annunzio" Chieti-Pescara
Viale Pindaro 42, 65127 Pescara, Italy
email: giuseppe.brando@unich.it (*corresponding author)

Keywords: Seismic vulnerability assessment, Seismic Maps, GIS

Abstract. *Seismic vulnerability assessment of buildings is a process of paramount importance for identifying those areas in a city demanding higher attention with respect to potential earthquake attacks. Methods for evaluating seismic vulnerability require a more or less accurate survey of the buildings geometrical and mechanical features, as well as of the structural systems, in order to identify the vulnerability classes to which they belong. However, even for relatively small-sized cities, the task of deriving vulnerability maps may be truly time consuming. Therefore, the development of automatic tools for mapping vulnerabilities of urban areas is necessary to reduce this effort significantly.*
QGIS (www.qgis.org) is a free open source software which includes a large number of peculiar packages, that make it a powerful tool and that can be well integrated or adapted with new components or plugins. In this paper, a plugin for assisting in the generation of vulnerability maps of an urban area is shown. The presented QGIS tool is applied to a case study, the historic city centre of Popoli, in the Abruzzi region (Central Italy), which belongs to a relevant earthquake-prone area and that was affected by two major seismic sequences in 2009 and in 2016-2017. Potential damage scenarios are presented and discussed, deriving useful information that could be applied in risk mitigation strategies.

1 INTRODUCTION

The evaluation of seismic risk at the urban scale, as well as its visualization on maps, is a theme of crucial interest for public stakeholders and private entities, such as insurance or reinsurance companies. Seismic risk, R, includes the potential physical, economic, social and environmental losses due to the earthquake hazard that may occur in a specified region, given the vulnerability of its built environment, and within a defined period of time. A commonly used definition of the seismic risk is the convolution of hazard (H), exposure (E), and vulnerability (V), as symbolically expressed by Eq. 1 [1]:

$$R = H \otimes E \otimes V \tag{1}$$

Seismic hazard is the "*potentially damaging effects of earthquake at a particular location*".

These effects are related to the surface rupture or induced ground shaking.
Exposure is related to the socio-economic value of the built environment in the area under assessment. It includes the buildings occupants, the replacement costs (repair or reconstruction), the turnover of commercial and industrial facilities, and other aspects.
Vulnerability is related to the quality of the built environment and can be defined as "*the degree of damage that is expected under a specified level of seismic demand*" [2].

The seismic vulnerability of a building is usually evaluated through finite-element (FEM) analyses, which allow to accurately model the structure and its response under different ground shakings. However, when the evaluation moves to the urban scale and several constructions are considered, the use of more rapid approaches is preferable. Among rapid approaches, those based on the evaluation of vulnerability indices or based on the adoption of fragility curves, after the reconnaissance of few structural features, found a large consensus in the last years [3,4,5]. These studies often represent scenarios on geo-referenced maps, to make easier to communicate risk to Stakeholders and the population.

In the light of this premise, this paper presents a tool implementing different vulnerability models to be applied at the urban scale, as well as their outcomes through maps. The tool is implemented in a QGIS environment (www.qgis.org) and applied to a case study, the city centre of Popoli, Abruzzi Region, Italy. In order to prove the versatility of the tool, two types of predictive model are used: a vulnerability index-based method for old masonry buildings, that represent a specific vulnerability class, and fragility curves retrieved by literature for other types of buildings.

2. THE PREDICTIVE MODELS USED FOR THE SEISMIC VULNERABILITY PLUGIN

2.1 The vulnerability index-based method for masonry buildings in historic centers

In recent years, a predictive model for the seismic vulnerability assessment of historic centres has been proposed and validated by the Authors [6]. This method considers, for masonry buildings, a vulnerability index i_v, resulting from a weighted sum of 14 vulnerability parameters, P_k, assigned downstream of an accurate geometrical and structural survey carried out on all the buildings -or on a statistically representative stock- that form the centre. Given the average value of all the vulnerability indices, i_v^*, this is used in order to assess the mean damage grade μ_D expected for the whole historic centre under a specific earthquake intensity, I (MKS scale), according to the formulation given by Sandi and Floricel [7]. The damage grade μ_D is therefore used for applying the binomial distribution reported in Eq. (2) in order to assess the probability p_k of attaining one of the six damage grades k -expressed by integers ranging between 0 (no damage) and 5 (full collapse)- according to the classification proposed for the European Macroseismic Scale, EMS-98 [8].

$$p_k = \frac{5!}{k!(5-k)!} \cdot \left(\frac{\mu_D}{5}\right)^k \cdot \left(1-\frac{\mu_D}{5}\right)^{5-k} \qquad (2)$$

2.2 The fragility curves dataset-based method for RC buildings outside of the historic centre

Fragility curves relates the probability of a building to reach or exceed a certain level of damage, $P(Dk)$, for increasing earthquake intensities [9], see Figure 1 [10]. Fragility curves are derived through non-linear static or dynamic analyses of structures. Levels of damage are defined by fixing thresholds or Engineering-Demand Parameters (EDP), such as the inter-storey drift. Different earthquake intensity measures (IMs) can be used to quantify the level of shaking. The peak ground acceleration (PGA) is commonly used in Europe, while the pseudospectral acceleration (PSA) is commonly used in the United States.

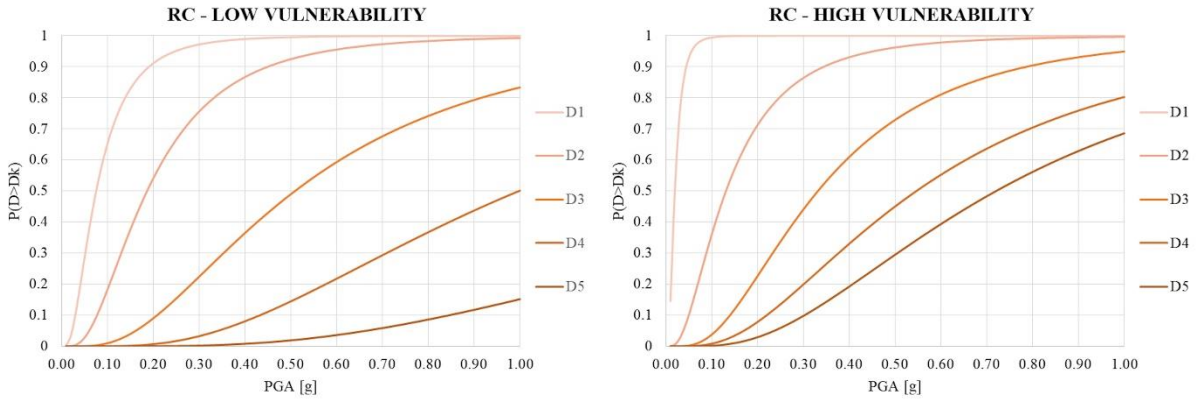


Figure 1. Examples of fragility curves for RC buildings [10].

The biggest available database of fragility curves, which has been considered for the case study dealt with in this paper, are provided by the Syner-G project in Europe [10] and by the Federal Emergency Management Agency (FEMA) in the United States [11]. Databases usually present fragility curves as cumulative lognormal distribution along with their two parameters, that are the median and standard deviation.

3. DECRIPTION OF THE SEISMIC VULNERABILITY PLUGIN

3.1 General description

Quantum GIS or QGIS (www.qgis.org) is a free open source Geographical Information System (GIS) software that includes particular packages that make it a powerful tool. QGIS is currently used by a wide and international community and is constantly updated [12]. The User interacts with the software via a Graphical User Interface (GUI), which contains an integrated set of menus, toolbars and other options. The GUI gives access to the GIS tools, while the toolset defines the capabilities or function of the GIS for processing geographic data.

The inclusion of the plugin function to the interface QGIS is shown in

Figure **2**. It adds a seismic risk calculator to the QGIS environment and supports the User with new integrated functionalities related to the automated application of adopted vulnerability models.

Once that a shapefile (.shp) that holds the geometry and attribute information (identification, address, description, etc.) of all the buildings under assessment is uploaded, so

that a geographical database is generated into the GIS environment, the functionalities, whose development is described in the following paragraphs, have to be implemented. For a better comprehension, the map referred to the studied urban centre of Popoli is shown.

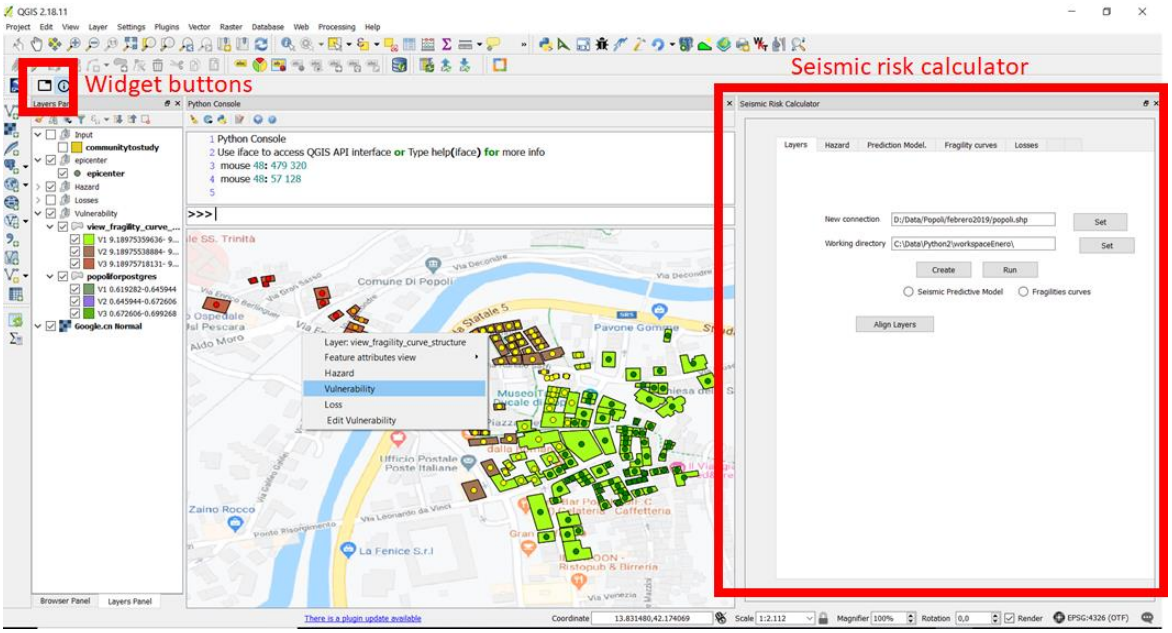


Figure 2. Seismic risk plugin interface

3.2 The hazard assessment

At first, the seismic hazard has to be defined, according to the flowchart of Figure 3.

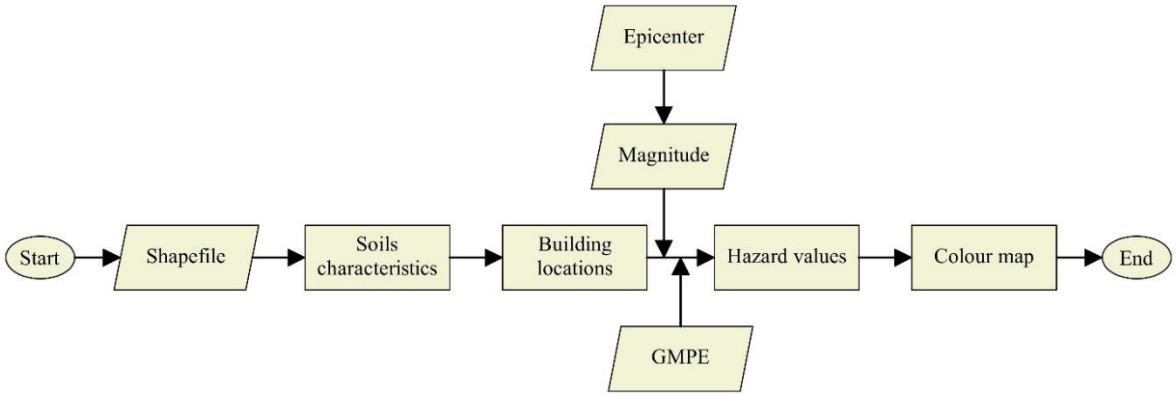


Figure 3. Seismic hazard analysis with the proposed QGIS tool.

The tool gives an estimation of the hazard values, taking in consideration Ground Motion Prediction Equations (GMPEs) [13] or attenuation laws. These equations return the level of ground shaking at any given location, considering the possible amplification phenomena due to the soil characteristics and the attenuation due to the distance. In particular, the general form of the equation Eq.3 used for regression analysis [14] is implemented

$$\log(PSA) = a + bM + cR + dS \quad (3)$$

where, PSA is the geometric mean of two horizontal spectral accelerations at various periods; M [15] is moment magnitude, R is hypocentral distance in km, S is a site factor (0 for rock sites and 1 for soil sites) and a, b, c and d are constants to be determined from regression analysis.

Having defined all inputs, the tool is able to calculate the ground acceleration corresponding to the site of each all building, as reported in Figure 4.

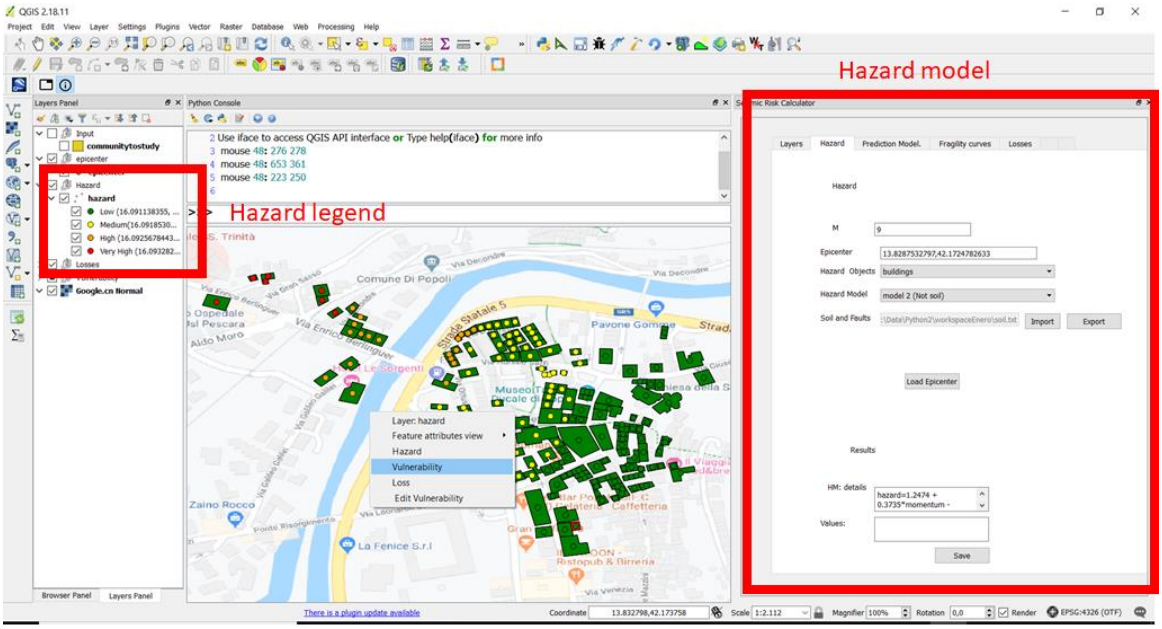


Figure 4. Calculated hazard for a community of study (shapefile).

3.3 Vulnerability evaluation

As stated before, two methods for the vulnerability evaluation have been considered: a method based on the definition of a vulnerability index, reliable for masonry buildings belonging to historic centres, and the other based on the application of fragility curves, for the other building types (Fig. 5). Obviously, the methods cannot be applied simultaneously, thus a preliminary step consists in dividing the urban centre in homogeneous compound, where most of the building present the same features, and to merge at the end the obtained maps, such as the one shown in Figure 6.

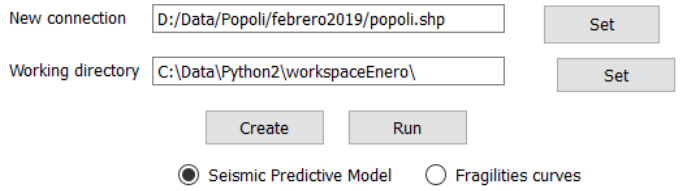


Figure 5. Selection of the method to apply in the seismc vulnerabilty evaluation.

With reference only to the masonry building of the historic centre, after a structural and geometrical survey of all examined buildings, the vulnerability parameters, P_k, have been assigned so that the vulnerability index, i_v, has been evaluated and mapped, see Figure 6.

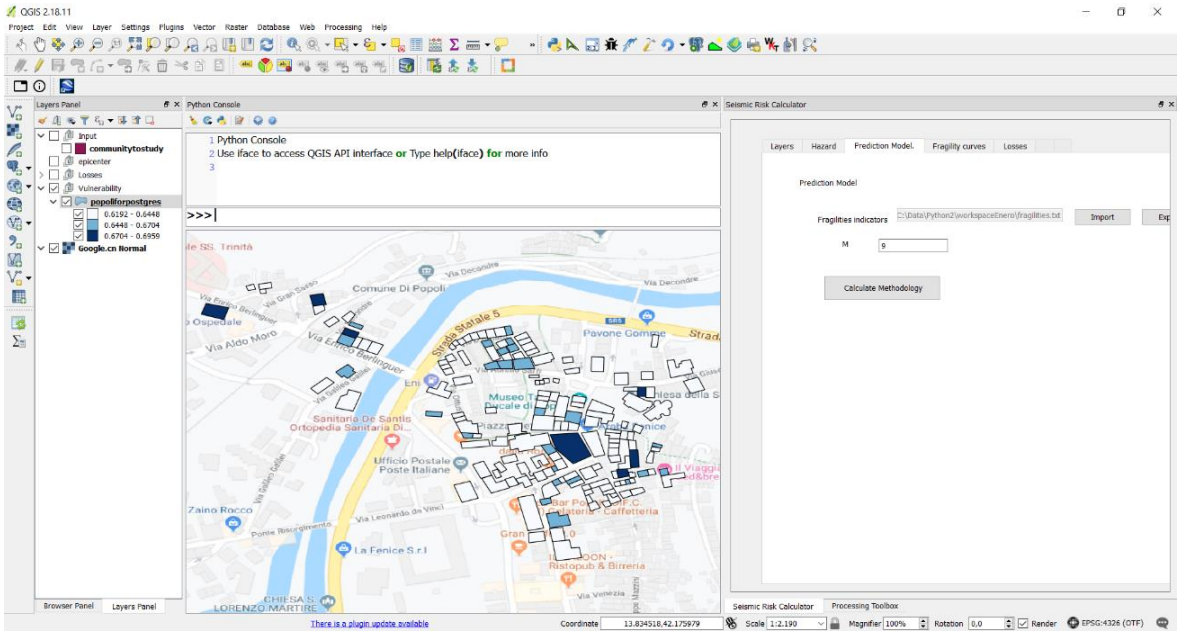


Figure 6. Vulnerability map for the masonry buildings' portfolio

The obtained thematic map allows to immediately observe which areas of the city present the higher vulnerability, thus allowing prioritizing any future risk-mitigation interventions. The coloured map is realized based on the shapefile loaded by the User at the beginning of the analysis. The user can update any of the vulnerability parameters in one Excel file and automatically generate a new vulnerability map. Once that all the buildings i_v have been determined, the mean damage grade, μ_D, is evaluated according to the chosen methodology [6].

The evaluation and mapping of the vulnerability and damage is shown in the flow diagram of Figure 7.

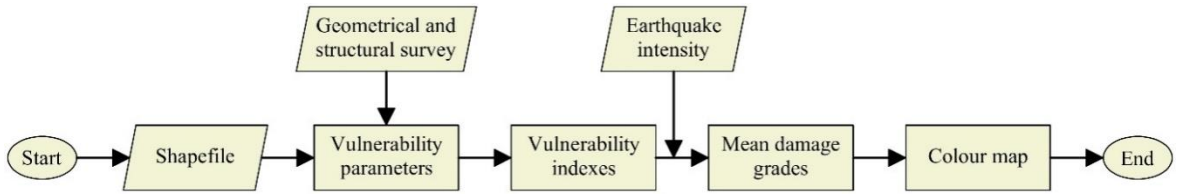


Figure 7 . Calculation and mapping of the vulnerability index and mean damage grade using a predictive model.

Then, RC buildings outside the historical centre are divided into topological classes after a visual structural and geometrical inspection. Each class represents all buildings whose response towards a seismic event is deemed comparable. Usually, similarities in terms of construction material, construction period, number of floor and irregularities in plan and in height are considered in the class definition. Subsequently, a set of fragility curves is assigned to each class [10], and are uploaded in the tool. In this way, given an earthquakes of defined intensity,

the fragility curves will return the expected damage probabilities, $P(Dk)$. The process is shown in the flow diagram of Figure 8.

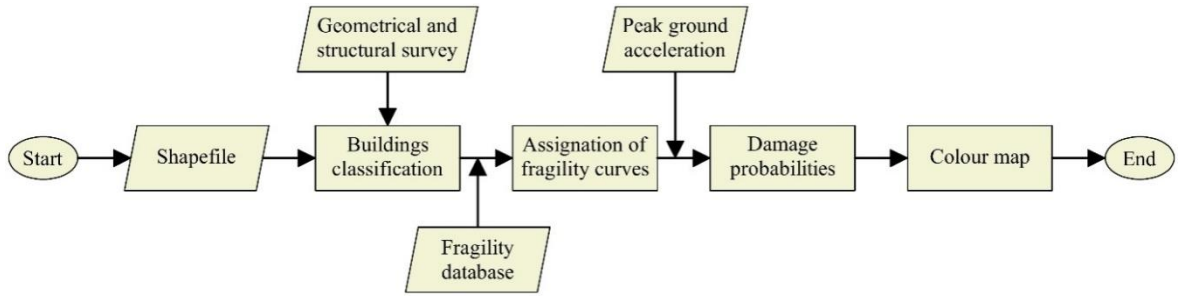


Figure 8. Calculation and mapping of the damage probabilities using fragility curves.

3.4 Exposure definition for loss assessments

In seismic risk assessments, losses are usually considered in terms of expected fatalities, injuries, and repair/replacement costs. In order to include the losses in the proposed tool, the building repair/replacement cost per square meter has to be assigned. The repair/replacement cost is defined as the required monetary value to construct a building with the same characteristics according to the current costs [16]. In case this information is not available, average values may be used. For example, average values of repair/replacement costs for residential buildings in Central Italy are available thanks to an extensive survey of the reconstruction after the 2009 L'Aquila earthquake [17,18,19,20].

Moreover, building occupants can be included in the analysis. Also this data can be inputted in the tool by filling a worksheet that has been arranged to this purpose.

Once the hazard is defined -for example through the macro-seismic intensity I or the PGA- and once that the vulnerability model is defined, based on the obtained damage scenario, the expected number of casualties and repair/replacement costs can be evaluated. Loss estimations are automatically provided by the proposed tool, and the process is shown in Figure 9. At the current stage, the casualty estimation is performed using the approach proposed by Zuccaro and Cacace (2011) [20] that can be applied with both the Vulnerability Index method and the fragility curves.

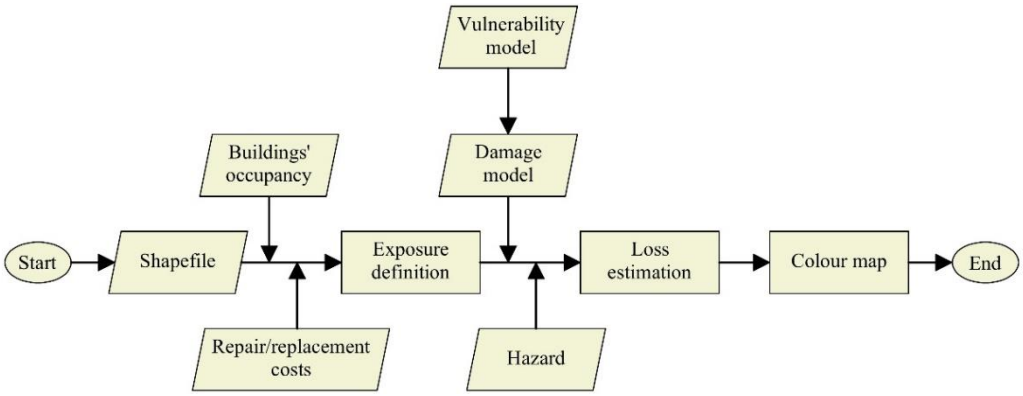


Figure 9. Calculation of socio-economic losses.

3.5 Visualization of results

Once that the necessary data are loaded and once that the different kind of analysis are performed, the User can query the outcomes of the evaluation in an interactive way, as it is shown in Figure 10. It is possible to click on one of the buildings and the tool will show the detail of both the input and the output data used of the analysis. For doing this, the "Inspect data button" has to be activated.

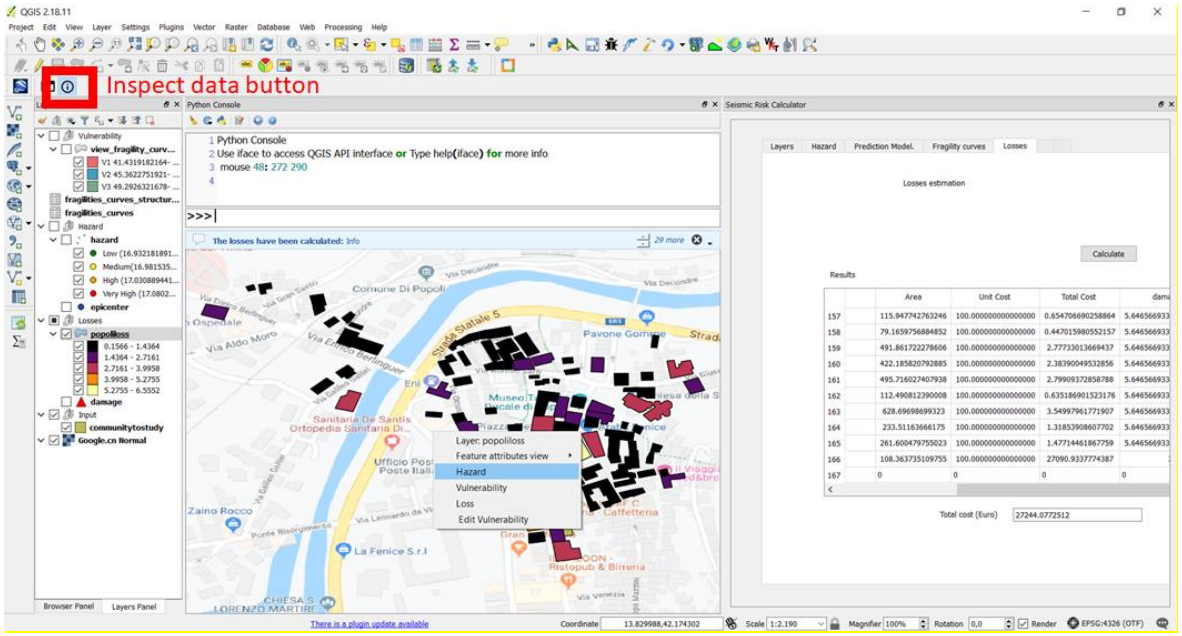


Figure 10. Querying the result of the runned seismic risk assessment.

4. APPLICATION TO A CASE STUDY: THE HISTORIC CITY-CENTER OF POPOLI

Popoli is a small town of approximately 5000 people in the Abruzzi Region, Central Italy, see Figure 11.



Figure 11. Popoli aerial view.

The area has been affected by two major seismic sequences in 2009 [22] and in 2016-2017 [23]. The city has been selected as a case study because, despite its small size, it has a public hospital, a K-12 school system, two major industrial areas, two electric power network (EPN) substations and a train station. Moreover, the city is crossed longitudinally by a river and the two parts are connected by a series of bridges.

165 buildings of Popoli have been modelled in a shapefile and loaded into QGIS. The map uses the WGS84 coordinated system [24]. Figure 11 shows the hazard map of a hypotetical earthquake scenario, with the earthquake epicentre in the coordinates (13.47; 42.37). In this example, local soil effects are neglected. With the support of the tool, it has been possible to immediately visualize the effects on the city.

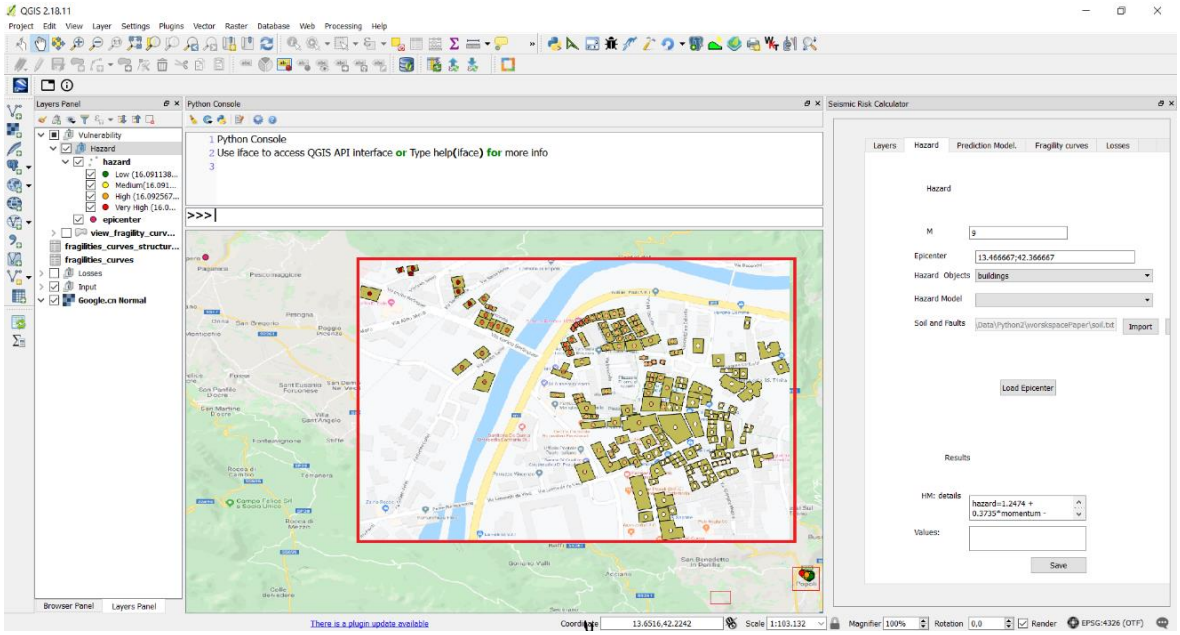


Figure 11: Hazard map of Popoli for a defined earthquake location.

Vulnerability parameters, for the masonry buildings of the historic center, and the fragilities curves, for the other buildings, have been loaded, producing the damage scenarios shown in Figure 12. The colored map clearly identifies the most affected buildings.

The loss estimation is shown in Figure 13 and Figure 14. The total number of casualties and injured as well as the sum of direct economic losses is displayed and, like the damage scenario, a colour map is used to clearly identify the most affected buildings.

5. CONCLUSIONS

In this paper, a semi-automated tool to produce seismic risk maps has been presented. This tool includes risk evaluation routines into a GIS platform and it is able to calculate the expected damage or losses, given that information on vulnerability and hazard are provided. The adopted GIS platform is open source. Therefore it can be used by communities free of charge. Future studies will aim to apply this tool to additional case studies in order to improve the method and help cities to achieve a better knowledge of their seismic risk. The proposed tool is a combined effort between civil engineers and computer scientist.

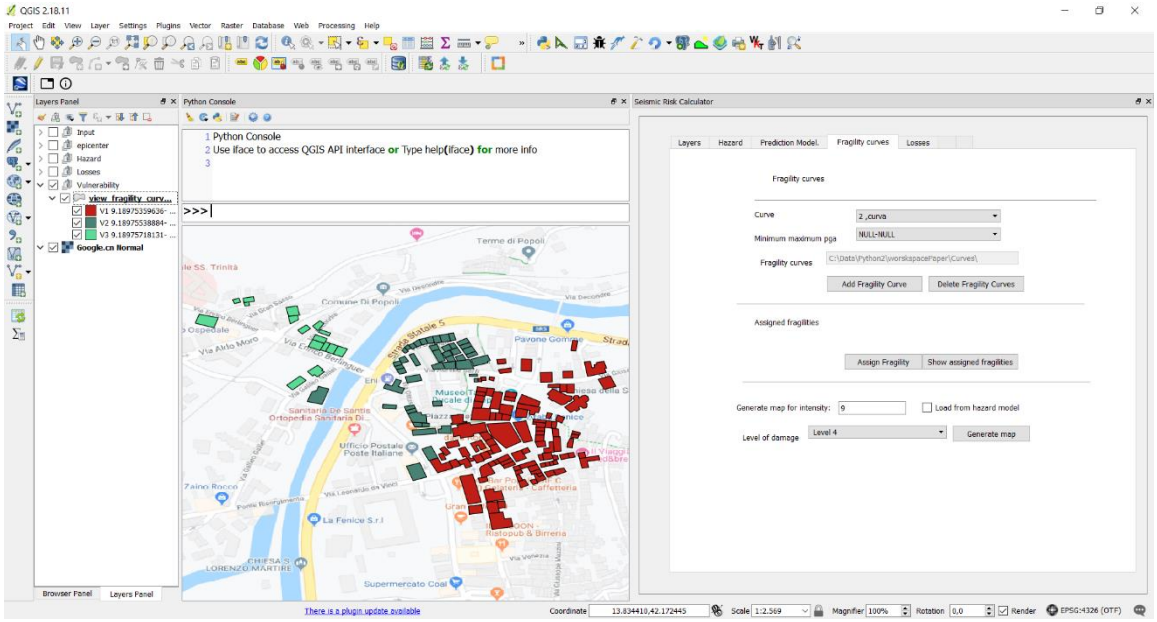


Figure 12. Damage scenarios of Popoli for a hypothetical earthquake location.

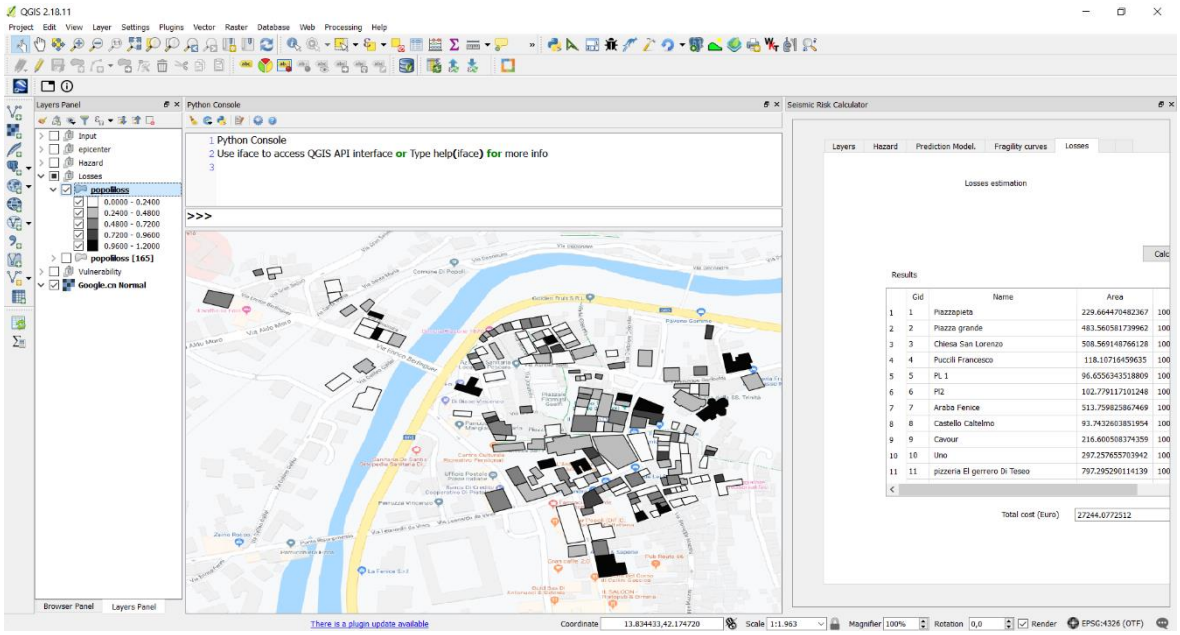


Figure 13: Casualty estimation of Popoli for a defined earthquake location.

Additional developments or inclusion of routines will need not only a proper knowledge of seismic risk but also the technical expertise to implement the desired functionalities. For this reason, it is important to continuously encourage the bridging and cooperation between the two areas of research.

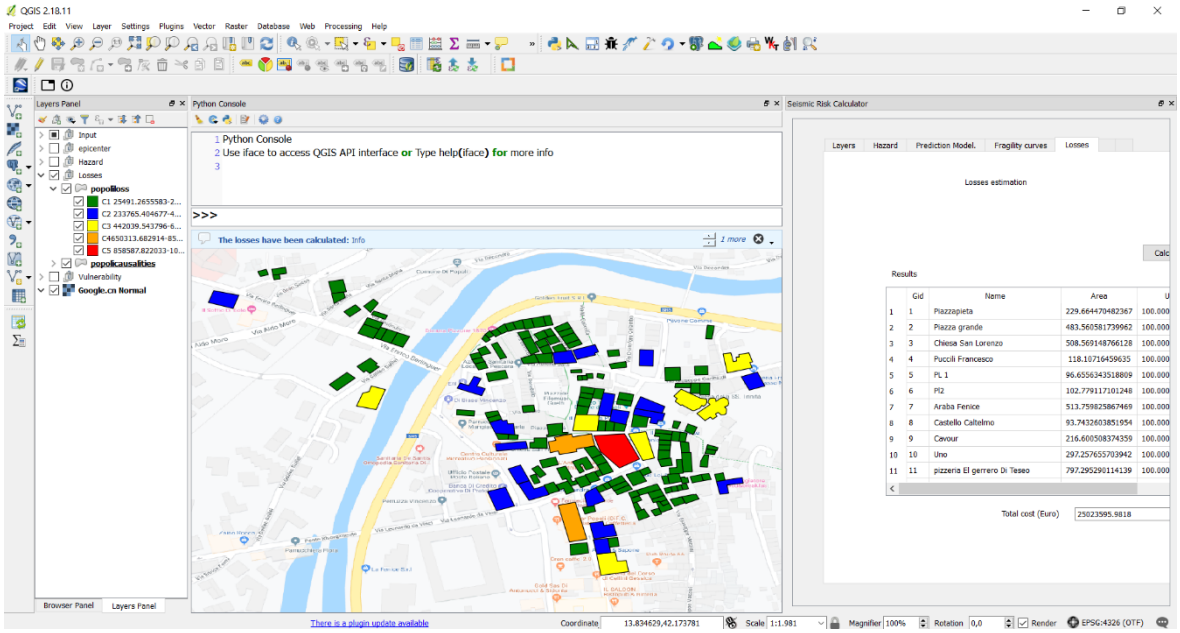


Figure 14. Economic loss estimation of Popoli for a defined earthquake location.

REFERENCES

[1] Bommer, J.J., Crowley, H., and Pinho, R. A risk-mitigation approach to the management of induced seismicity, *Journal of Seismology* (2015) **19**: 623-646.

[2] Environmental Hazards Methodologies for Risk Assessment and Management (2017) Dalezios N.R. (Ed.) *IWA Publishing*.

[3] Rapone, D., Brando, G., Spacone, E. and De Matteis G. Seismic vulnerability assessment of historic centers: description of a predictive method and application to the case study of scanno (Abruzzi, Italy) *International Journal of Architectural Heritage* (2018) **12**: 1171-1195.

[4] Basaglia A., Aprile, A., Spacone, E. and Pilla, F. Performance-based Seismic Risk Assessment of Urban Systems. *International Journal of Architectural Heritage* (2018) **12**: 1131-1149.

[5] De Matteis, G., Brando, G. and Corlito, V. Predictive model the seismic vulnerability assessment of churches based on the 2009 L'Aquila earthquake. *Bulletin of Earthquake Engineering* (2019) **17**: 4909-4936.

[6] Brando, G., De Matteis, G. and Spacone, E. Predictive model for the seismic vulnerability assessment of small historic centres: Application to the inner Abruzzi Region in Italy. *Engineering Structures* (2017) **153**: 81-96.

[7] Sandi, H., Floricel, I. Analysis of seismic risk affecting the existing building stock. In: *Proceedings of the 10th European conference on earthquake engineering* (1994) Vienna, 2, pp. 1105-1110.

[8] Grünthal, G. European Macroseismic Scale 1998. *Cahiers du Centre Europeen de Geodynamique et de Seismologie* (1998) **15**: 1-99.

[9] Porter, K. Beginner's guide to fragility, vulnerability, and risk. *Encyclopedia of earthquake engineering* (2015): 235-260.
[10] Pitilakis, K., Crowley, H., and Kaynia, A.M. (Eds) SYNER-G: Typology definition and fragility functions for physical elements at seismic risk: buildings, lifelines, transportation networks and critical facilities. *Springer Science and Business Media* (2014) **27**
[11] Federal Emergency Management Agency (2003) Hazus®–MH 2.1Technical Manual. Available at: https://www.fema.gov/media-library/assets/documents/24609.
[12] Longley P. Geographic information systems and science 4thedition. (2015) John Wiley & Sons.
[13] Bindi, D., Pacor, F., Luzi, L., Puglia, R., Massa, M., Ameri G. and Paolucci R. Ground motion prediction equations derived from the Italian strong motion database. *Bulletin of Earthquake Engineering*, **9**(6): 1899-1920.
[14] Chopra S., Choudhury P. A study of response spectra for different geological conditions in Gujarat, India. *Soil Dynamics and Earthquake Engineering*,(2011) 31(11):1551-1564, DOI: 10.1016/j.soildyn.2011.06.+007
[15] Kircher, C. A., Reitherman, R. K., Whitman, R. V. and Arnold, C. Estimation of earthquake losses to buildings. *Earthquake spectra* (1997) **13**: 703-720.
[16] Dolce, M. and Manfredi, G. Libro bianco sulla ricostruzione privata fuori dai centri storici nei comuni colpiti dal sisma dell'Abruzzo del 6 aprile 2009. *Doppiavoce Edizioni* (2015). Italian.
[17] Di Ludovico, M., Prota, A., Moroni, C., Manfredi, G., and Dolce, M. Reconstruction process of damaged residential buildings outside historical centres after the L'Aquila earthquake: part I- "light damage" reconstruction. *Bulletin of Earthquake Engineering* (2017) **15**: 667-692.
[18] Di Ludovico, M., Prota, A., Moroni, C., Manfredi, G., and Dolce, M. Reconstruction process of damaged residential buildings outside historical centres after the L'Aquila earthquake: part II- "heavy damage" reconstruction. *Bulletin of Earthquake Engineering* (2017) **15**: 693-729.
[19] De Martino, G., Di Ludovico, M., Prota, A., Moroni, C., Manfredi, G. and Dolce M. Estimation of repair costs for RC and masonry residential buildings based on damage data collected by post-earthquake visual inspection. *Bulletin of Earthquake Engineering* (2017) **15:** 1681–1706.
[20] Zuccaro, G. and Cacace, F. Seismic casualty evaluation: The Italian model, an application to the L'Aquila 2009 event. In: R. Spence et al. (Eds): *Human casualties in earthquakes*, Springer, Dordrecht (2011), pp. 171-184.
[21] Chiarabba, C., Amato, A., Anselmi, M., et al. The 2009 L'Aquila (central Italy) MW6. 3 earthquake: Main shock and aftershocks. *Geophysical Research Letters* (2009) **36**:L18308.
[22] Livio, F.A., Michetti, A.M, Vittori E., et al. (2016) Surface faulting during the August 24, 2016, Central Italy earthquake (Mw 6.0): preliminary results. *Annals of geophysics* (2016) **59**(5).
[23] Smith, R.W. (1987). Department of Defense World Geodetic System 1984: its definition and relationships with local geodetic systems. *Defense Mapping Agency*.

12th International Conference on Structural Analysis of Historical Constructions
SAHC 2020
P. Roca, L. Pelà and C. Molins (Eds.)

ASSESSMENT OF SEISMIC FRAGILITY OF HISTORICAL BUILDINGS AT THE URBAN SCALE BY TYPOLOGICAL-MECHANICAL APPROACHES: THE CASE STUDY OF FOGGIA

VALERIA LEGGIERI[1], SERGIO RUGGIERI[1], GIUSEPPINA UVA[1*]

[1] Department DICATECh, Polytechnic University of Bari, Via Orabona, 4 – 70126, Italy
e-mail: g.uva@poliba.it (*corresponding author)
{valeria.leggieri; sergio.ruggieri}@poliba.it

Keywords: Masonry buildings, Urban aggregate, Fragility analysis, regional vulnerability analysis

Abstract. *The study of the seismic vulnerability of historical centres, especially in the Mediterranean zone, is one of the main issues in ongoing scientific research. This is due, on the one hand, to the continuous evolution of the seismic demand and, on the other hand, to the high vulnerability of the masonry existing building stock.*
The seismic events of the last few years highlighted the necessity to perform a large-scale survey of the huge amount of masonry buildings in historical centres, in order to provide prioritization scales for planning mitigation strategies. With this regard, the scientific literature provides several methodologies that allow a rapid assessment based on pre-defined survey forms. The data obtained from the surveys are usually used as the input for algorithms aimed at estimating the vulnerability level of the building investigated.
The aim of the present work is to propose a general framework for analysing seismic vulnerability of masonry historical centres and deriving fragility curves basing on multiple data sources. In particular, using data collected through existing territorial databases, supplemented by a set of vulnerability forms available for the city centre of the Municipality of Foggia, Southern Italy, some vulnerability classes are defined. Based on the mechanical and geometrical features identified for each class, several ideal and representative buildings are generated, and their seismic behaviour is investigated through the variation of significant parameters.
At the end, the capacity of the buildings is evaluated by performing simplified nonlinear analyses and, subsequently, by estimating the damage level of the sample through the definition of regional fragility curves.

1 INTRODUCTION

In the last few decades, the interest in the seismic behaviour of existing buildings has continuously grown, considering the high vulnerability to earthquakes exhibited by the existing building stock. In particular, the cities in the seismic-prone areas present a variegated portfolio of buildings, mainly including Reinforced Concrete (RC) and masonry ones.

To quantify the capacity of the existing building stock to cope seismic events, the first approach usually adopted is the sweep assessment of the structural health of all buildings

through fast methods, based on the compilation of survey forms and retrieval of few observational parameters, which allow to provide a first prioritization useful for optimizing the funds destination to mitigate the seismic risk.

The scientific literature provides several examples of this approach [1], both for RC [2-5] and masonry [6-8] buildings. For example, the CARTIS form [9], developed by the Italian Civil Protection Department (DPC), within the ReLUIS project, allows to define homogenous urban sectors, which are composed by same typologies of RC and masonry buildings. The form is composed by 4 survey sections for collecting information about the building typologies, structural and constructive features in each urban sector of the Municipality investigated.

Another example is provided by the GNDT form [10], which allows to collect relevant information about some observational parameters (e.g. configuration in plan and elevation, structural and non-structural elements,…) on the basis of which an indirect methodology for calculating a seismic vulnerability index for each building investigate is implemented.

In [11], a methodology for the study of seismic vulnerability of historical centres at the regional scale was developed, based on the collection of data for 4519 housing units in the municipality of Foggia, through an ad-hoc electronic survey sheet.

Usually, the data collected with survey form methods are useful for providing results about regional seismic vulnerability and, in particular, can be used for computing regional fragility and losses curves through probabilistic analysis based on mechanical models. Also in this case, the scientific literature provides a lot of methodologies for achieving this goal both for RC [12-17] and masonry [18-19] buildings.

In this framework, the Geographic Information System (GIS) represents an important informatic tool useful for managing the big data generated by rapid assessments methods, and it allows to extract, integrate and elaborate information from different sources developing a geo-referenced database. In a GIS environment, all kinds of information are organized and structured through the assignment of features and attributes to specific points, or in this case, buildings. [20-24].

One of the main limits of this kind of fast procedures is represented by the nature of the form survey. In fact, all the above-mentioned methods provide the survey of the individual building units, both for RC and types. For RC buildings, this does not represent a big limitation but, for masonry buildings, the consideration of individual units does not allow to consider the typical structure of historical urban centres, which usually are rather urban aggregates.

The scope of this paper is the study of the urban masonry aggregates at regional scale, by matching the information provided by rapid visual survey methods and the data visualization provided in GIS environment. The proposed methodology, tested on a pilot example -the Municipality of Foggia- consists in the identification of the typical configuration of masonry buildings in a specified urban sector, that becomes an “index building” and the base for a mechanical model. According with the available information, some characteristic geometric and mechanical parameters are varied within predefined ranges, generating several numerical models of the same aggregate. Nonlinear analyses are performed according to the pushover approach, and regional fragility curves for serviceability and ultimate limit states are derived.

2 SEISMIC VULNERABILITY OF MASONRY AGGREGATES: STATE OF ART

The historical centres of the Mediterranean cities are prevalently constituted by masonry

buildings, which usually were built chaotically, covering the greater part of the urban territory. In addition, the urban fabric was continually modified with the addition of masonry units in elevation or in plan to existing ones.

Because of this complex aggregation of masonry buildings, it is difficult to investigate the structural and seismic behaviour of the single units (due to the interaction among adjacent units), and of the entire aggregate (since it is difficult to investigate in detail all the geometrical and mechanical features of all interacting units, especially in a large-scale analysis).
Recent technical codes do not provide methodologies for tackling this issue and, in fact, they provide only methods to investigate the seismic behaviour of individual, independent masonry buildings. On the other hand, the scientific literature provides some studies that analyse the seismic vulnerability of masonry building compounds, considering both large scale and single scale analyses.

In [25], the building aggregates of the historical centre of Coimbra at regional scale was investigated, looking for the variation of some generic parameters, such as geometrical and mechanical features and seismic demand. In [26], an easy method for large scale analysis of seismic behaviour of masonry aggregates was proposed, consisting in a new form for defining the key features to use in numerical models. After the calibration of the methodology, it was tested on an historical centre, damaged from the Aquila Earthquake. The same author [27], developed a simple methodology to forecast the seismic behaviour of masonry aggregate, providing a design scheme for predicting the force distribution of each building unit.

With regard to the single building aggregate, in [28], the aggregation of masonry units is investigated from the global point of view, reporting that the aggregate effect allows to have greater safety factors than the single units, with change of every single building stiffness. In [29] some parameters influencing the aggregates behaviour were investigated, as length of row conglomerations and of flexible floors. The study was aimed to extract the single unit from the compound and to analyse the single unit as representative of the entire aggregate.

In [30], a study on the urban aggregates of Azores Islands was presented, wherein a numerical model was developed and investigated through nonlinear pushover analyses. The results showed the global seismic response of the compound, highlighting the effects due to the different heights of each adjacent unit.

In [31], a computational model was performed for the case study representative of Foggia and Sant'Agata di Puglia historical centres. The numerical model was investigated with nonlinear dynamic analyses, showing the differences, in terms of stress and strain distribution, obtained among each part of the compound. Other studies investigated also the interaction of both RC and masonry single units, as shown in [32].

The complexity of all the aspects involved in the seismic vulnerability of masonry urban aggregates, as reported by the scientific literature, has motivated the authors of this paper to propose a methodology for full investigating the effects of some geometrical and mechanical parameters in a large scale analysis. In particular, the procedure has been applied to a urban district of the Municipality of Foggia, generating a set of numerical models so that they can represent the typical configuration of the local building aggregates and computing the vulnerability curves.

3 SEISMIC VULNERABILITY OF URBAN MASONRY AGGREGATES AT THE REGIONAL SCALE: PROPOSAL OF A METHODOLOGY

The proposed methodology allows to compute vulnerability curves to regional scale of masonry urban aggregates, following the steps shown in Figure 1.

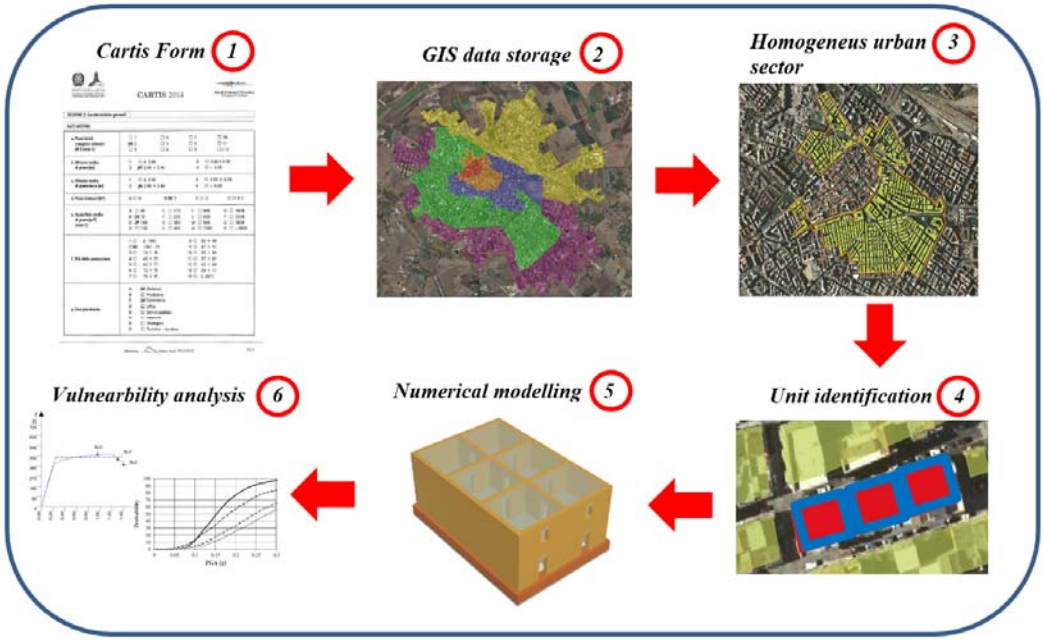


Figure 1: Conceptual steps of the proposed methodology

The first step consists in the collection of the information provided by rapid surveys, as the ones provided by CARTIS form. Generally, for masonry buildings, the reliefs are performed for single units and then, it is necessary to collect all data in a unique database, made through GIS layers, in order to have a general view about each urban sector.

The second step consists in the generation of the GIS database, which allows to identify different urban sectors in the Municipality.

Once that the urban sectors are identified, it is possible to select the one to be investigated. In particular, we have chosen the one constituted mainly by aggregate masonry buildings, which coincides with a part of the historical centre. In the selected urban sector, a set of recurring building compound typologies has been identified.

By matching data and features collected for all surveyed units with those derived from Cartis forms, it has been possible to define a variation range for the properties of the reference building unit. In particular, using the GIS tools, the features and attributes of each record (e.g., height of the storeys, dimensions in plan, of the building units, percentage of openings in masonry panels, the masonry type, …) can be extracted and processed in order to identify the input data for generating a representative FE numerical model of the entire compound. This model is then the starting basis for a sensitivity analysis for the study of the seismic vulnerability at large scale. Basing on the information collected through the above-mentioned methodology, a set of

characteristic geometrical and mechanical parameters is selected for the single unit typology and a corresponding plausible range of variation is identified. Starting from this reference "index" model, a series of parametrical variation is performed on the geometrical and mechanical features by adopting the following procedure. According to [2], given n parameters (n_{par}) and a range subdivided into m steps (m_{steps}), the total number of FE models (N_{models}) to be generated is calculated as:

$$N_{models} = \prod_{i=1}^{n_{par}} m_{steps,i} \quad (1)$$

In order to define the numerical model of the entire aggregate, an elementary Reference Building Cell shall be repeated in-plan and in height, with the aim to cover the entire area of the compound displayed in the GIS map and reproduce the target aggregate.

Generally, according to the parameters chosen, it will be possible to define different reference units, which will be the basis for generating a series of building aggregates. In this work, for brevity sake, only one of the many possible type of building cells will be considered, in order to the number of possible combinations in the sensitivity analysis.

For each FE model (i.e. one random realization of the target aggregate, obtained by repeating a single cell on a 3D grid), nonlinear pushover analyses are performed and the vulnerability index is computed in terms of capacity/demand (C/D) ratio for the different limit states, .In order to compute the vulnerability curves, the values of C/D are evaluated for increasing levels of the seismic demand (this is achieved by progressively increasing the return periods that define the design spectrum, correspondingly evaluating the capacity ratios and extracting the regional vulnerability curve for that building aggregate typology .

More in detail, each regional vulnerability curve is expressed as the probability to have FE models with a capacity-demand ratio of the entire aggregate C/D<1, calculated for increasing values of the Intensity Measure (IM) (that is assumed to be the peak ground acceleration - PGA), conditioned by each limit state assumed.

4 APPLICATION OF THE METHODOLOGY: THE CASE STUDY OF THE URBAN CENTRE OF FOGGIA

By following the framework described in Figure 1, the proposed methodology has been applied to the municipality of Foggia, Southern Italy. Within the activities of the ReLUIS project, the Cartis forms have been compiled for the city and the data have been collected into a GIS database. Based on the investigations about building typologies, both for RC [33] and masonry buildings, six urban sectors have been identified, as shown in Figure 2.

The 6 urban sectors listed in the legend of Figure 2 have been sorted according to the more frequent building structural typology, basing on the attributes provided by the Cartis form (e.g., construction year, materials, shape,…). In this case, as it often happens in Southern Italy, the main part of the historical building stock is located in the city centre, covering the urban sectors named C01-C02-C03. We focused on the urban sector C02, as shown in Figure 3, dating back to 1700. The entire urban sector is composed mainly by masonry buildings (about the 60% of all buildings) classified, in the framework of CARTIS data collection, in 2 different structural-typological classes, surveyed using CARTIS form which contain general data, geometrical features and the information for identifying the mechanical parameters.

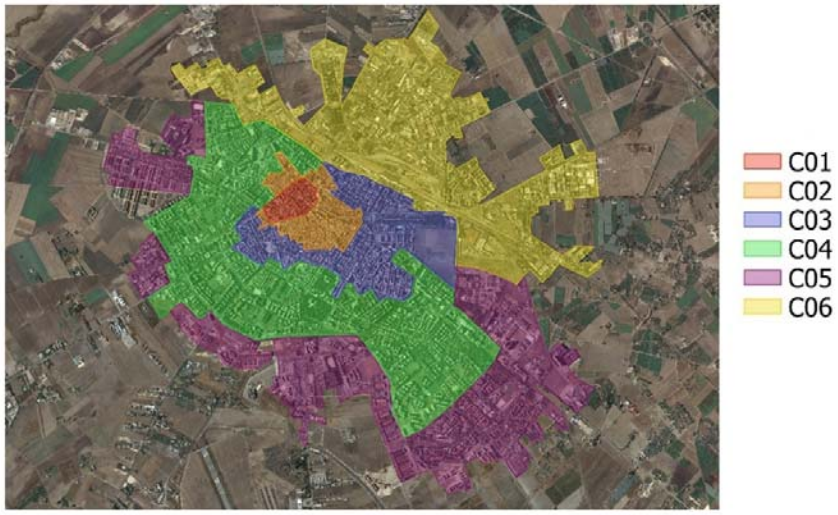


Figure 2: Urban sectors of Foggia Municipality, through GIS elaboration

From Figure 3 it can be observed that in the considered sector urban aggregates of different shapes are present. Anyway, they are mostly rectangular, and the typology of the basic building unit is a duplex terrace configuration. By analysing the information of the Cartis form and taking an average of the values detected, we have defined the reference building cell that represents the more frequent structural typology in that urban sector and that is repeated in the urban compounds

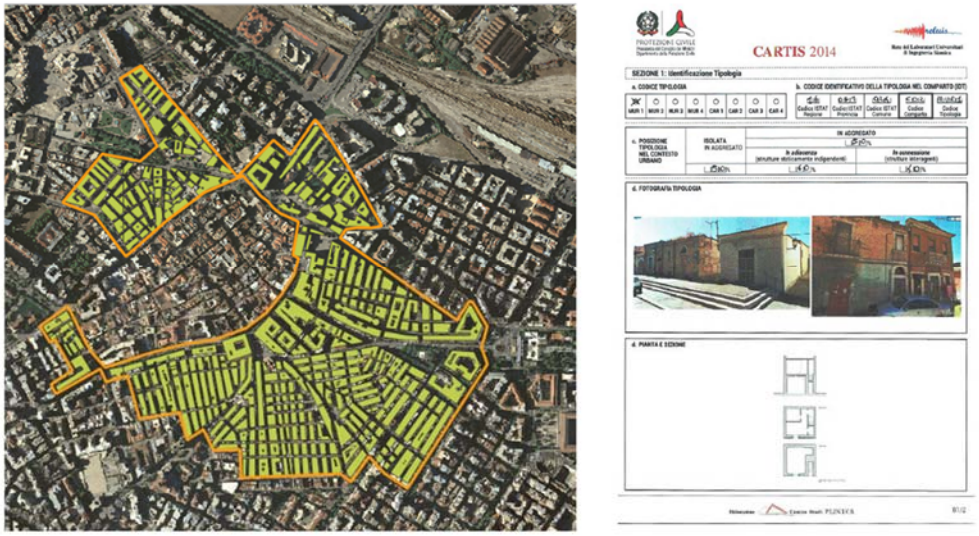


Figure 3: View of the historical centre of Foggia and structural typology identification through CARTIS form.

This reference unit is a rectangular masonry building of in-plan dimension of 10m x 15m and interstorey height of 3.5m. All the perimetral walls and the central wall in the longitudinal direction are load-bearing walls, with a width of 40cm. The central walls have a width of 20cm and are partitions. On the shorter side some openings are present and, in particular, it is assumed, that each wall presents 2 windows of dimensions 80cm x 120cm and 2 doors of

dimensions 90cm x 220cm. The floor is a ribbed slab with RC joists and hollow clay blocks 16cm high, covered completed by a RC plate 5cm thick. Regarding materials, according to the reports made by surveyors, the masonry panels are made by regular limestone blocks, similar to those provided in the Italian Building Code.

4.1 Numerical modelling and sensitivity analysis

The numerical modelling of the reference cell and of the overall aggregate has been carried out through the software POR2000 [34], which use the methodology proposed by Tomaževic [35]. In particular, masonry walls are modelled as shell elements with fixed restraints at the base; horizontal slabs are considered as rigid diaphragms through the application of internal constraints. The applied loads are permanent and live loads, partially computed by the software, according to the geometrical and mechanical features of the masonry, and partially implemented by the user, according to the specific destination use (in this case, residential).

With regard to the nonlinear behaviour, as suggested by POR methodology, each masonry wall is assumed to have a shear-type behaviour, with the limit displacement, for each limit state, defined according to Section 4.2.

The procedure, at this point, provides firstly the choice of a specific Reference Building Cell, with a defined geometry, and subsequently the sensitivity analysis. With regard to the dimension of the urban aggregate, the first parameter varied is the clustering pattern of the cells in order to fill the in-plan footprint shown in the GIS map. As shown in Figure 4, in the urban sector analysed, 4 typologies of building aggregates, with rectangular shape, have been identified.

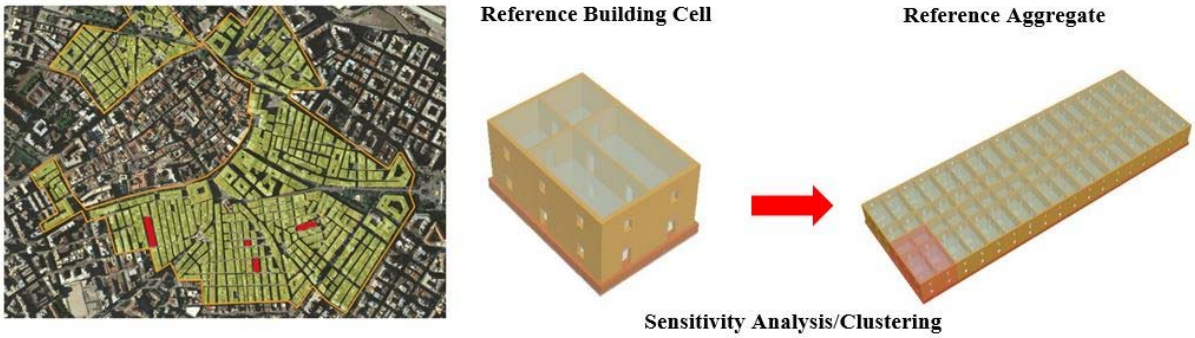


Figure 4: Left: identification of the recurrent building blocks in the Sector C02. Right: an example of random clustering of the building cells.

Table 1 reports the ratio between the sides of the rectangular building block, which will be reproduced by clustering the single cells according to the pattern of a duplex terraced buildings. In addition, Table 1 reports the geometrical and mechanical parameters varied in the sensitivity analysis, which are the height of masonry aggregate (a maximum of 2 storeys is assigned, with the second storey that can recess by ½ and ¼ from the ground floor -) and the mechanical parameter of the limestone, defined according to the range provided by the annex of the Italian Building Code [36], and indicated in the table with the symbol σ_m, which is the compression strength of the masonry.

Table 1: List of the parameters varied in the sensitivity analysis and variation range adopted.

Ratio between aggregate sides	Number of storeys	σ_m (N/mm^2)	
		min	max
1:1	1	2,00	3,20
	2		
	1+1/2		
	1+1/4		
1:2	1	2,00	3,20
	2		
	1+1/2		
	1+1/4		
1:3	1	2,00	3,20
	2		
	1+1/2		
	1+1/4		
1:4	1	2,00	3,20
	2		
	1+1/2		
	1+1/4		

The other relevant mechanical parameters of the masonry are associated to the value of σ_m: shear strength of the masonry τ_0, (which varies between 0,04 and 0,08 N/mm^2), the elastic modulus E, which varies between 1200 and 1800 N/mm^2), the shear modulus G which varies between 400 and 500 N/mm^2), the Poisson's ratio ν= 0,05 and the specific weight w= 16000 N/m^3.

According to the Eq. 1, 32 FE models have been generated and each of them has been investigated in nonlinear field through pushover analysis.

4.2 Pushover results and regional vulnerability curves

It is worth highlighting that in the analyses only in-plane failure mechanisms have been considered, i.e., only global response has been taken into account. Assuming the centre of the mass of the last storey as the control node, for each capacity curve the software provides the different performance points (V_b – roof displacement δ_R) corresponding to the attainment of the limit states. In particular, according to the Italian Building Code, the limit state thresholds considered are defined as follows:

- for immediate occupancy (IO), the limit state threshold is defined as the value of the horizontal displacement equal to 0.3% of the generic masonry panel height;
- for life safety (LS), the limit state threshold is defined as the value of the horizontal displacement obtained to a reduction of 10% of the maximum V_b in the pushover curve;
- for near collapse (NC) limit state, the limit state threshold is defined as the value of the horizontal displacement corresponding to a reduction of 15% of the maximum V_b in the pushover curve.

According to the N2 method, the Capacity/Demand ratios are computed for all the models and limit states. The seismic demand has been assumed as the one provided by a code spectrum

computed for the average coordinates of the sector C02, for the return periods: T_R= 50 years for IO, T_R=475 years for LS, T_R= 975 years for NC. In order to compute the vulnerability curves for all the considered limit states, the C/D values have been recomputed by changing the T_R of the spectrum and increasing the seismic demand. In particular, the computations have been performed for other values of T_r. The results in terms of C/D obtained for all the models, which are 96 values for each limit state, have been processed for the computation of urban vulnerability curves for the urban sector considered, assuming as IM the a_g parameter. These curves express the probability of exceeding the IM corresponding to a safety level greater than 1 (C/D>1) for the Building aggregates in the urban sector investigated, conditioned by the above-defined limit state's threshold.

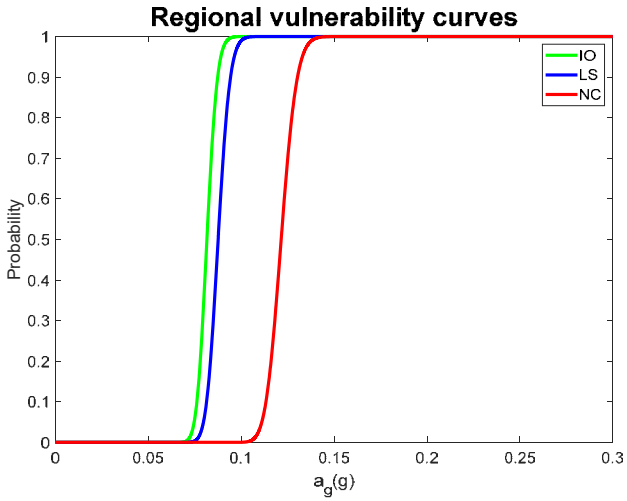


Figure 5: Regional vulnerability curves obtained for the urban sector C02, for LS: IO, LS, NC

The results obtained in terms of vulnerability curves are shown in Figure 5, while the parameters that identify the curves: median (μ_{reg}) and dispersion (β_{reg}), are reported in Table 2.

Table 2: Median and dispersion of regional vulnerability curves

Vulnerability curves	μ_{reg}	β_{reg}
IO	0.082	0.053
LS	0.088	0.057
NC	0.122	0.058

5 CONCLUSION AND FUTURE DEVELOPMENTS

In this work, a mechanical-based procedure is developed for computing the vulnerability curves of masonry building aggregates at the large scale. In particular, input data are obtained by combining information extrapolated from Cartis forms and data stored in a GIS platform.

By using data about the recurrent structural typologies defined within each of the

homogeneous urban sectors detected in the municipality, it has been possible to identify the sector constituted mainly by masonry buildings, located in the historical centre. Moreover, a Reference Building Cell has been defined, which can be spatially repeated in order to cover the aggregates' shape as seen in the GIS map.

By numerically modelling the Building aggregate and varying the geometrical and mechanical features within plausible variation ranges, different numerical configurations have been generated and investigated by nonlinear pushover analysis. The values of the vulnerability indexes, expressed in terms of C/D, have been computed for increasing seismic demands. and vulnerability curves for three limit states have been derived.

This procedure has been applied to the case study of Foggia, Southern Italy, where an extensive survey campaign has been performed. After storing and organizing data storage in the GIS environment, attention has been focused on the masonry buildings of a specific urban sector, conceiving a proper Reference Building Cell. Varying some characteristic parameters, according to the information derived from CARTIS form, a sensitivity analysis has been performed and vulnerability curves for 3 limit states have been plotted.

The future developments will provide the extension of the analyses on the same urban sector, by increasing the number of reference cells. Furthermore, additional numerical combinations will be proposed, accounting for more information and more variables, in order to compute full vulnerability curves for the urban sector investigated.

Acknowledgements. The research presented in this article was partially funded by the Italian Department of Civil Protection in the framework of the national project DPC-ReLUIS 2019-2021.

REFERENCES

[1] Calvi G.M., Pinho R., Magenes G., Bommer J.J., Restrepo-Veléz L.F., Crowley H., (2006) The development of seismic vulnerability assessment methodologies for variable geographical scales over the past 30 years. ISET Journal of Earthquake Technology, 43(3), 75-104.

[2] G. Uva, P. L. Ciampoli, V. Leggieri, A. Nettis, and S. Ruggieri, A mechanical approach for estimating regional fragility curves of existing RC buildings stock in Puglia, in COMPDYN 2019 7th ECCOMAS Thematic Conference on Computational Methods in Structural Dynamics and Earthquake Engineering (2019).

[3] Uva G, Sangiorgio V., Ciampoli P.L., Leggieri V, Ruggieri S., A novel rapid survey form for the vulnerability assessment of existing building stock based on the "Index Building" approach, Conference Proceedings - IEEE International Conference on Systems, Man and Cybernetics (2019), Bari 6-9 Oct. DOI:10.1109/SMC.2019.8914063

[4] Perrone D, et al, Rapid visual screening for seismic evaluation of RC hospital buildings, Structures (2015), http://dx.doi.org/10.1016/j.istruc.2015.03.002

[5] Porco F., Ruggieri S., Uva G., (2018) Seismic assessment of irregular existing building: appraisal of the influence of compressive strength variation by means of nonlinear conventional and multimodal static analysis, Ingegneria Sismica, 35(3), pp. 64-86

[6] Lagomarsino S., Podesta S. (2004). Seismic vulnerability of ancient churches: I. Damage assessment and emergency planning. Earthquake Spectra, 20(2), pp. 377–394.

[7] Uva G, Sangiorgio V., Ruggieri S., Fatiguso F., Structural vulnerability assessment of

masonry churches supported by user-reported data and modern Internet of Things (IoT), Measurement (2019), https://doi.org/10.1016/j.measurement.2018.08.014;
[8] De Matteis, G., Brando, G. & Corlito, V. Predictive model for seismic vulnerability assessment of churches based on the 2009 L'Aquila earthquake. Bull Earthquake Eng 17, 4909–4936 (2019). https://doi.org/10.1007/s10518-019-00656-7.
[9] G. Zuccaro, M. Dolce, D. De Gregorio, E. Speranza, and C. Moroni, La Scheda Cartis Per La Caratterizzazione Tipologico-Strutturale Dei Comparti Urbani Costituiti Da Edifici Ordinari. Valutazione dell'esposizione in analisi di rischio sismico 34° Convegno Nazionale GNGTS, Trieste, 17-19 novembre 2015.
[10] A. Bernardini (A cura di), La vulnerabilità degli edifici: valutazione a scala nazionale della vulnerabilità sismica degli edifici ordinari, CNR-Gruppo Nazionale per la Difesa dai Terremoti - Roma, 2000, 175 pp. + CD-ROM allegato
[11] G. Uva, C.A. Sanjust, S. Casolo, M. Mezzina, ANTAEUS project for the regional vulnerability assessment of the current building stock in historical centers International Journal of Architectural Heritage, 10(1), pp. 20-43, 2016. http://dx.doi.org/10.1080/15583058.2014.935983
[12] FEMA (2001) HAZUS99 Technical Manual. Service Release 2. Federal Emergency Management Agency, Washington, D.C., USA.
[13] Cosenza E., Manfredi G., Polese M., Verderame G.M., (2005) A multi-level approach to the capacity assessment of existing RC buildings. J. of Earthq. Eng., 9(1), 1-22.
[14] Borzi B., Pinho, R. Crowley H. (2008). Simplified pushover-based vulnerability analysis for large-scale assessment of RC buildings. Engineering Structures 30(3), 804-820.
[15] Del Vecchio C., Gentile R., Di Ludovico M., Uva G., Pampanin S. (2018). Implementation and Validation of the Simple Lateral Mechanism Analysis (SLaMA) for the Seismic Performance Assessment of a Damaged Case Study Building, Journal of Earthquake Engineering, https://doi.org/10.1080/13632469.2018.1483278
[16] Gentile R., del Vecchio C., Pampanin S., Raffaele D., Uva G. (2019). Refinement and Validation of the Simple Lateral Mechanism Analysis (SLaMA): Procedure for RC Frames. Journal of Earthquake Engineering. doi:10.1080/13632469.2018.1560377
[17] Ruggieri, S., Porco, F. & Uva, G. A practical approach for estimating the floor deformability in existing RC buildings: evaluation of the effects in the structural response and seismic fragility. Bull. Earthq. Eng. (2019).
[18] Lagomarsino S. and Giovinazzi S., Macroseismic and mechanical models for the vulnerability and damage assessment of current buildings, Bull. Earthq. Eng. 4, 415–443, (2006).
[19] Borzi B., Crowley H., Pinho R. Simplified Pushover-Based Earthquake Loss Assessment (SP-BELA) Method for Masonry Buildings, International Journal of Architectural Heritage, (2008) 2:4, 353-376, DOI: 10.1080/15583050701828178A
[20] Y. Liu, Z. Li, B. Wei, X. Li and B. Fu, Seismic vulnerability assessment at urban scale using data mining and GIScience technology: application to Urumqi (China), Geomatics, Nat. Hazards Risk 10, 958–985 (2019).
[21] L. Matassoni, S. Giovinazzi, M. Pollino, A. Fiaschi, L. La Porta and V. Rosato, A Geospatial Decision Support Tool for Seismic Risk Management: Florence (Italy) Case Study, Computational Science and Its Applications – ICCSA 2013, 7974, 278–293 (2013).
[22] G. Uva, M. Dassisti, F. Iannone, G. Florio, F. Maddalena, M. Ruta, A. Grieco, I.

Giannoccaro, V. Albino, M. Lezoche, A. Aubry, A. Giovannini, A. Buscicchio, Y. Eslami, V. Leggieri, Modelling Framework for Sustainable Co-management of Multi-purpose Exhibition Systems: The 'Fiera del Levante' Case, Procedia Engineering 180, 812-821, (2017).

[23] Uva G., Leggieri V., Morrone M., USE of data derived by different sources for the seismic vulnerability assessment of current building stock in GIS environment: an application to the municipality of Bisceglie, Italy. 3rd International Conference on International Conference on Recent Advances in Nonlinear Design, Resilience and Rehabilitation of Structures, CoRASS 2019 H. Barros, C. Ferreira, José M. Adam and Norb Delatte (Eds)

[24] Uva G., Leggieri V., Mastrodonato G., Proposal of a procedure for gathering data for the structural and energy classification of residential building stock: a case study in Puglia. 3rd International Conference on International Conference on Recent Advances in Nonlinear Design, Resilience and Rehabilitation of Structures, CoRASS 2019 H. Barros, C. Ferreira, José M. Adam and Norb Delatte (Eds)

[25] Pagnini LC, Vicente R, Lagomarsino S, Varum H. A mechanical model for the seismic vulnerability assessment of old masonry buildings. Earthq Struct 2011;2(1)

[26] Formisano A., Florio G., Landolfo R., Mazzolani F. Numerical calibration of an easy method for seismic behaviour assessment on large scale of masonry building aggregates. Advances in Engineering Software 80 (2015) 116–138

[27] Formisano A. Theoretical and Numerical Seismic Analysis of Masonry Building Aggregates: Case Studies in San Pio Delle Camere (L'Aquila, Italy). Journal of Earthquake Engineering, 00:1–19, 2016

[28] Ramos LF, Lourenço PB. Modeling and vulnerability of historical city centers in seismic areas: a case study in Lisbon. Eng Struct 2004;26(9):1295–310.

[29] Senaldi I, Magenes G, Penna A. Numerical investigations on the seismic response of masonry building aggregates. Adv Mater Res 2010;133– 134:715–20.

[30] Casolo S., Sanjust C. A., Uva G., Diana V., Seismic modelling and analysis of masonry building in aggregate: a case study. Compdyn 2017 6th ECCOMAS Thematic Conference on Computational Methods in Structural Dynamics and Earthquake Engineering M. Papadrakakis, M. Fragiadakis (eds.) Rhodes Island, Greece, 15–17 June 2017

[31] Fagundes C., Bento R., Cattari S., On the seismic response of buildings in aggregate: Analysis of a typical masonry building from Azores, Structures (2016).

[32] Ferrito T, Milosevic J, Bento R, Seismic vulnerability assessment of a mixed masonry–RC building aggregate by linear and nonlinear analyses. Bull Earthquake Eng. (2016).

[33] Aiello, M.A., Ciampoli, P.L., Fiore, A., Perrone, D., Uva, G. (2017a) Influence of infilled frames on seismic vulnerability assessment of recurrent building typologies, Ingegneria Sismica, 34(4), pp. 58-80

[34] Tomazevic, M., "The computer program POR", Report ZRMK, 1978 (in Slovenian)

[35] https://www.newsoft-eng.it/software/por-2000/

[36] Circolare 21 gennaio 2019, n.7 C.S.LL.PP. Istruzioni per l'applicazione dell'Aggiornamento delle "Norme tecniche per le costruzioni" di cui al DM 17/01/2018.

12th International Conference on Structural Analysis of Historical Constructions
SAHC 2020
P. Roca, L. Pelà and C. Molins (Eds.)

CRITERIA FOR THE VULNERABILITY ANALYSIS OF STRUCTURAL AGGREGATES IN HISTORICAL CENTERS

S. TONNA[1], M. BORIANI[2], M. C. GIAMBRUNO[3], C. CHESI[4]

[1] Politecnico di Milano – DAStU Department
Piazza Leonardo da Vinci, 32 – 20133 Milano, Italy
e-mail: sandra.tonna@polimi.it (*corresponding author)

[2] Politecnico di Milano – DAStU Department
Piazza Leonardo da Vinci, 32 – 20133 Milano, Italy
e-mail: maurizio.boriani@polimi.it

[3] Politecnico di Milano – DAStU Department
Piazza Leonardo da Vinci, 32 – 20133 Milano, Italy
e-mail: mariacristina.giambruno@polimi.it

[4] Politecnico di Milano– A.B.C. Department
Piazza Leonardo da Vinci, 32 – 20133 Milano, Italy
e-mail: claudio.chesi@polimi.it

Keywords: Aggregate, historical center, seismic vulnerability, on-site survey

Abstract. *The need to define earthquake prevention and intervention strategies, in order to limit dramatic consequences for the society, has acquired a high priority in countries where, like in Italy, a large number of historic masonry buildings (listed or not) are located in areas with medium to high seismic hazard. From the point of view of the level of safety to be reached through interventions, the concept of improvement, as opposed to that of full strengthening, is nowadays widely accepted in the case of monumental heritage; what is still lacking, in many cases, is a procedure for the vulnerability analysis, as a synthetic evaluation tool for the definition of intervention priorities. In a modern perspective, where territorial planning is conceived as a safety project for the territory, the seismic vulnerability analysis should not be confined to specific technical documents, but should rather be considered at a general level; in this way only, indeed, the issue of seismic risk could acquire widespread knowledge and awareness in the population, also pushing urban planning in the direction of general programs for the increase of seismic safety. In the above perspective, revised criteria have to be developed for a global vulnerability assessment, to be introduced at a general level in territorial planning. Considering that seismic vulnerability analyses are strictly dependent on specific building typologies, attention has been focused, in the present study, on to the case of structural aggregates in historical centers, thus following the needs of the Italian Civil Protection Agency in relation to seismic prevention activities in historical towns. The research, which is still in progress, takes advantage from the application to a few study cases, suitable for the experimental testing of procedures.*

1 INTRODUCTION

The frequent recurrence of seismic events in Italy in recent times has stressed the need, for the society, to develop effective levels of preparedness, in order to reduce the negative impact on the safety of people, the conservation of the built environment, and the continuity of normal life. To this purpose, the seismic vulnerability analysis of buildings and public works in general is a fundamental prevention tool; within this context, vulnerability has to be intended in its original meaning, i.e., a fast qualitative evaluation of the inclination, for the structure, to suffer damage from an earthquake. Based on meaningful indicators, not necessarily of a structural nature, the vulnerability analysis is therefore suitable for being applied to large groups of buildings with a statistical purpose.

Originally, vulnerability analyses were conceived in view of risk reduction strategies with the purpose of highlighting the possible lack of seismic resistance, thus suggesting consolidation interventions and favouring seismic damage prevention. In recent times, as a consequence of the development of effective and well organized Civil Protection Services for natural disasters and, in particular, earthquakes, vulnerability analyses have also been recognized as the necessary tool for a positive management of emergency situations, in the sense of supporting preparedness to damage scenarios.

Starting from the traditional approach to vulnerability evaluations, based on the analysis of single structural units, new procedures have now to be formulated, extending consideration to entire structural aggregates, in view of the development of wide damage scenarios at the urban scale. Recently, this specific need has been formulated by the Italian Civil Protection Agency as a support to the development of Civil Protection plans; specifically, in accordance with the typical nature of the Italian built environment, the study is focused on the vulnerability analysis of historical aggregates of ancient urban centers (Fig. 1).



Figure1: Typical views of historical aggregates.

The paper presents the criteria adopted for the re-formulation of traditional vulnerability analyses at the scale of aggregates of structural units, in the spirit of a qualitative analysis for

a fast application at a wide scale, taking advantage of the numerous studies on seismic vulnerability procedures which have been developed through time.

2 THEMATIC FRAMEWORK

The vulnerability analysis, as originally conceived [1], clearly showed the possibility of developing the formal implementation of a qualitative approach to the analysis of the seismic capacity of masonry buildings. This was supported by the high degree of knowledge which had been reached in relation to the seismic performance of masonry buildings, as a result of the repeated post earthquake field surveys documenting typical damage modalities, followed by analytical interpretations. Specifically, vulnerability analyses focused on the occurrence of the structural details which have been generally recognized in favour of the positive performance of a masonry building under the effect of seismic actions; typically, wall-to-wall connections, diaphragmatic behaviour of floor slabs, shear resistance of masonry piers, etc [1, 2, 3].

At present, in consideration of the remarkable growth of experience in this field in recent times, qualitative approaches to the evaluation of masonry structures are even more justified [4, 5, 6, 7]. In addition to vulnerability analyses, indeed, similar procedures have been developed in relation to other needs. Meaningful examples are given by the special form which is normally used in Italy for the evaluation of buildings after a seismic event in terms of the possibility of safe access and usage, and by the procedure for the definition of seismic risk classes for residential buildings.

It is also of interest to recall that the application of the above qualitative procedures for the assessment of seismic safety, not requiring analytical computations, is not for civil engineers only, but can be extended to all those who have a professional activity related to buildings and, through an experience based knowledge, have developed sensitivity on construction details and structural behaviour.

Vulnerability analyses were originally based on the field inspection of single structural units; a fast survey was normally performed by a specially trained team, and completed within a few hours, filling in a form and evaluating, as a final result, the vulnerability index.

Extending such procedure to the case of aggregates, still preserving the nature of a fast qualitative evaluation, new meaningful parameters have to be identified for a correct interpretation of the structural behaviour. Also, it has to be considered that the vulnerability analysis, in this case, is mainly addressed to the needs of Civil Protection plans and, therefore, the identification of situations involving high danger levels.

Looking at typical aspects characterizing the seismic response, attention has to be focused primarily onto structural regularity, degree of connection of the different units, and possible transformations occurred through time, which may have altered the original structural layout. All this has to be recognized through a simple visual inspection of the different fronts of the aggregate.

More in detail, the issue of plan and elevation irregularities now corresponds to a generally acquired concept, normally addressed also by building codes. It has to be considered that both irregularity forms may be enhanced in the case of an aggregate, thus assuming a special relevance in terms of potential damage. Similarly, the degree of connection of different parts, which has normally to do with the connection of wall panels and floor slabs within a single

building, has to be extended to the scale of the aggregate in terms of interaction of the different structural units.

Finally, having to do with historical aggregates, modifications of the original resisting system may have been introduced due to changes in the usage conditions of the building; in some cases such modifications may have seriously compromised the lateral strength of the building.

The above considerations clearly show that a qualitative approach to the evaluation of the seismic vulnerability of an aggregate is meaningful and, probably, should be always considered before developing accurate models for the analysis of single structural units. The original concept of a vulnerability analysis, therefore, is totally justified also in the case of aggregates in relation to the present needs of analysing seismic safety.

3 URBAN-LEVEL VULNERABILITY ANALYSIS

Several research works [3, 8, 9, 10] have been addressed to the analysis of seismic vulnerability in historical centers, showing a wide variety in the methodological trends. All the analyzed methods can be classified on the basis of a single criterion according to the assumptions done for the investigation scale and the analytical approach. Following the classification proposed by [10, 11], the various methodologies can be organized, from the point of view of the analysis scale, into three macro-groups (*urban, district, building*) and each of these can be further organized into sub-categories, in relation to the method of analysis (*direct, indirect, conventional and hybrid*) [12, 13, 14, 15, 16].

For the research in progress, the most appropriate reference key is the urban one, as it provides a methodology for a global view of a stratified *urban* fabric constituted of more or less connected structural aggregates. Among the different proposals, attention has been addressed to the methodologies defined as "indirect" and "hybrid". These make reference to a homogeneous group of buildings, which is globally assigned the vulnerability index of a model case, which was analyzed through an in-depth study. Such methods are both derived from the criterion proposed by Benedetti & Petrini in 1984 [1], which was the base for the formulation of the first and second level vulnerability analyses. It is still in use at the international level and has inspired all the other methodologies for vulnerability analysis which were introduced subsequently.

In the various alternatives, modifications to the original method concerned both the scale (from building to aggregate), and the methodology for the choice of the pilot case. Recently, indeed, an opposite approach has been introduced: following a general investigation of the whole urban center, the most representative case studies are selected for a second phase in-depth research [5, 6, 12].

Finally, to the purpose of a really effective vulnerability analysis, a critical issue is given by the choice of the evaluation parameters and the definition of the relative weighting coefficients. In the original formulation by Benedetti & Petrini [1] eleven parameters were defined; among these, only one was based on a numerical evaluation (item 3 in Table 1), two accounted for general aspects (items 10 and 11 in Table 1), while the remaining eight parameters were based on a qualitative evaluation of structural aspects. In recent works [8, 11] the number of the parameters has increased to 14 [8] or 15 [11], in order to take into

account stratifications occurred with time and interactions among structural units within the aggregate.

Tables 1, 2, and 3 show details about the different procedures developed by Benedetti & Petrini in 1984 [1], Vincente in 2011 [8], and Ferreira in 2017 [11], respectively.

Methodologies present differences in the selection and ordering of the vulnerability parameters and in the relative weighting coefficients, whereas all of them make reference to four vulnerability classes (A-B-C-D) for the evaluation of each single parameter.

Table 1: Items considered in the Benedetti & Petrini, vulnerability index method [1]

Item n.	Parameters	Class				Weight
		A	B	C	D	
1.	Type and organization of the lateral force resisting system	0	5	20	45	1.00
2.	Quality of the resisting system	0	5	25	45	0.25
3.	Conventional strength	0	5	25	45	1.50
4.	Position of building and foundations	0	5	15	45	0.75
5.	Floor systems	0	5	25	45	variable
6.	Horizontal layout regularity	0	5	25	45	0.50
7.	Regularity in elevation	0	5	25	45	variable
8.	Maximum distance between parallel walls	0	5	25	45	0.25
9.	Roof system	0	15	25	45	variable
10	Non-structural elements	0	0	25	45	0.25
11.	Present state of the building	0	5	25	45	1.00

In the approach developed by Vincente vulnerability parameters are grouped into four categories. In comparison to the approach by Benedetti & Petrini, one parameter is modified, shifting the attention from the structural unit to the aggregate (P7) and 2 more are introduced: opening alignment on the facade (P10) and aggregate fragilities (P13).

As far as vulnerability classes (A-B-C-D) are concerned, they are associated to similar scores, with the only differences in class C, where the value is decreased to 20, and class D, where it is increased to 50. Weighting coefficients also present differences, being always associated to fixed values.

Ferreira, like Benedetti & Petrini, makes reference to individual parameters, without grouping them into categories. The vulnerability analysis of the aggregate is based on fifteen parameters, considering also structural stratifications and the presence of typological or structural heterogeneities between adjacent buildings (item n. 14). Modifications in the vulnerability classes are also present, due to the introduction of negative values for parameters 11, 12, 14, and 15; fixed values are used for weighting coefficients.

Through a quick comparison of the above procedures, differences can be easily identified: vulnerability analysis, initially addressed to a single structural unit, is then extended to a structural aggregate and, consequently, the choice of parameters is different. Moreover, while the original method was based on a field survey of the building to be performed from both

outside and inside, the other two are more concentrated on the external survey of the building; in addition, they are structured in order to allow for an easier final calculation.

Table 2: Items considered in the Vincente, vulnerability index method [8]

Item n.	Categories and Parameters	Class				Weight
		A	B	C	D	
1.	Structural building system					
	P1. Type of the resisting system	0	5	20	50	0.75
	P2. Quality of the resisting system	0	5	20	50	1
	P3. Conventional strength	0	5	20	50	1.50
	P4. Maximum distance between walls	0	5	20	50	0.50
	P5. Number of floors	0	5	20	50	1.50
	P6. Location and soil conditions	0	5	20	50	0.75
2.	Irregularities and interactions					
	P7. Aggregate position and interactions	0	5	20	50	1.50
	P8. Plan configuration	0	5	20	50	0.75
	P.9 Regularity in height	0	5	20	50	0.75
	P10. Wall facade openings and allignments	0	5	20	50	0.50
3.	Floor slabs and roof					
	P11. Horizontal diaphgrams	0	5	20	50	1.00
	P12. Roofing systems	0	5	20	50	1.00
4.	Conservation status and other elements					
	P13. Fragilities and conservation state	0	5	20	50	1.00
	P14. Non-structural elements	0	5	20	50	0.50

Table 3: Items considered in the Formisano et al.,vulnerability index method [11]

Item n.	Parameters	Class				Weight
		A	B	C	D	
1.	Organization of the vertical resisting system	0	5	20	45	1.00
2.	Type of the vertical resisting system	0	5	25	45	0.25
3.	Position of building and foundations	0	5	25	45	0.75
4.	Resistant elements distribution in plan	0	5	25	45	1.50
5.	Regularity in plan	0	5	25	45	0.50
6.	Regularity in elevation	0	5	20	45	1.00
7.	Floor systems	0	5	25	45	0.75
8.	Roof system	0	15	25	45	0.75
9.	Details	0	0	25	45	0.25
10.	Present state of the building	0	5	20	45	1.00
11.	Altimetric interaction	-20	0	15	45	1.00
12.	Planimetric interaction	- 45	-25	-15	0	1.50
13.	Horizontal layout regularity	0	15	25	45	0.50
14.	Typological and structural discontinuities	-15	-10	0	45	1.20
15.	Percentage difference between full and openings in the facade	-20	0	25	45	1.00

In the present research, the proposal of a new method for vulnerability analyses has benefited from all the previous works; in particular, in line with the approach by Vincente [8], the grouping of vulnerability parameters into macro-classes has been adopted, as it allows for a more effective management of on-site surveys, a better organization of data and, globally, a faster procedure. Criteria for the development of the new procedure are illustrated in the following, together with implementation details.

4 A PROPOSAL FOR A METHODOLOGY BASED ON KNOWLEDGE LEVELS

Procedures for the evaluation of seismic vulnerability are based on the definition of a set of meaningful parameters, from which a realistic view of the seismic capacity of the structure can be obtained. This is not a purely theoretical process, as the effectiveness of the selected parameters has to be verified on the field through the analysis of selected case studies. Specifically, an iterative multi-step procedure has to be undertaken, with continuous testing and updating of the evaluation process, until a fast, clear and stable procedure is defined, providing as much as possible user independent results.

Such a process has been started within the current research work and is still in progress; it is believed, however, that the implementation of the final version of a data sheet to be systematically used for on-site applications should come soon to an end. The final product, resulting from the iterative process, will reflect the original idea of a two-step procedure, consisting in a first phase dedicated to the collection of meaningful documents, followed by the field inspection of the buildings, as it is detailed in the following. Also, the original criterion for the field analysis has been confirmed, based on the following sequence:

- select a front of the structural aggregate,
- recognize all structural units,
- evaluate each of them in relation to six categories of parameters,
- define, for each parameter, the vulnerability level as: *low* (A), *medium-low* (B), *medium-high* (C), *high* (D).

Details about the two-step procedure are discussed in the following. As previously mentioned, this vulnerability analysis is intended for use in the specific case of structural aggregates in historical centers; masonry, therefore, is the main reference material.

4.1 Investigation method

As known, it has become a common practice, well reflected also in building codes, to base the analysis of existing buildings on the acquisition of all the available information, coming to the definition of a specific knowledge level. Normally, information is collected with reference to the building historical analysis, the characterization of structural properties (typology, material, geometry), and action definition.

In the present research it was believed of interest to organize the vulnerability analysis from the point of view of two different knowledge levels: a first one (KL0), consisting in the collection of meaningful documentation from historical archives, municipality offices, and web data (typically, Google Maps), and a second one (KL1), consisting in the field inspection of the aggregate under study. This should be limited, in general, to the external survey of the aggregate fronts but might require, in some cases, a more detailed one to be performed at a

second time (KL2), based on the internal inspection of buildings and a deeper analysis of the archival documentation.

Clearly, the original formulation of the vulnerability analysis [1] simply consisted in the field survey, while the recognition of different knowledge levels belongs to recent studies and is still under testing [17]. In any case, the added value coming from the analysis of documents marks a meaningful increase in the relevance of vulnerability analysis, also allowing for a lower accuracy level in the field inspection.

Details about the two phases in the knowledge acquisition process are given in the following.

4.2 Analysis of documents

The phase defined as KL0 is aimed at providing the vulnerability analysis with a minimum knowledge of the building under consideration in view of the on-site survey and the consequent qualitative assessment and classification within vulnerability categories. The parameters to be considered in this phase can all be analyzed in the office through the inspection of several documents, as listed in the following; a major outcome of this analysis would be in the possibility of highlighting the transformations occurred over time through the comparison of the intended use, as noticed in the historical registers, with the current one. Structural transformations may have a remarkable effect on seismic vulnerability; a typical case, frequently occurring, is given by the presence of large openings at the ground floor, which were not present in the original building configuration (Fig. 2). Normally, this kind of intervention is done providing a suitable propagation path to the vertical loads, with no consideration of horizontal actions; the soft-story configuration is therefore automatically generated.

During this phase, the historical center and its aggregates will be investigated through the analysis of the following data and parameters:

1. Archival data, with the main purpose of comparing the intended building use and quality, as described in the historical land registers, with the current classifications.
2. Where available, the damage evaluation forms which are normally filled after an earthquake for a first assessment of the building conditions in terms of possible use and restoration needs. In Italy, the "AeDES" form has been developed to this purpose and is normally available in the municipality offices [18].
3. General information at the territorial level, as the urban morphology, its historical development and the topographic profile of the historical center.
4. Ratios between building height and road width and structural connections with neighboring aggregates (Fig. 1).
5. In the presence of a ground slope, the aggregate orientation with respect to the contour lines.
6. The aggregate morphology, namely, regularity in plan, any front offset, or the presence of internal courtyards.
7. The general aggregate conservation status.

a)



b)



Figure 2: Transformations: a) XX century image of a traditional Italian historical center with the detail of a three storey building, b) widening of the original openings, compromising resistance to horizontal actions.

4.3 On-site survey

The next phase, KL1, is based on the analysis of the actual state of the structural aggregate through the qualitative survey of each external front. The main purpose is identifying both structural and architectural characteristics, the current usage conditions and the maintenance state for each facade of the aggregate. This on-site investigation will lead to the achievement of a vulnerability classification for the entire front on the basis of the evaluation of each single structural unit and of its possible interaction with the adjacent ones.
This phase is organized so that the six categories of parameters, as detailed in the following, can be assessed simultaneously for each structural unit of the front under examination:

1. The vertical resisiting system, through the relationship between full and empty spaces and openings alignments. In addition, the presence of openings wider than 2 m in order to recognize the possible presence of a soft story condition.
2. Fragilities and interactions, through the survey of material inhomogeneity, added portions in elevation, filling of separation joints.

3. Fragilities in structural units, i.e., the presence of porches, covered walkways, slender elements, large and empty structural units within the aggregate (churches and theatres), chimneys and elements protruding on the road (Figs. 3, 4).
4. The conservation status through all its variants, such as surface degradation, presence of superficial or deep cracks, local collapses.
5. Protruding roof structure, as detectable from the street. The materials and the state of conservation will be indicated.
6. Seismic protection elements belonging to local building techniques, such as buttresses, contrast arches, chains and tie rods, blind arches in the masonry, cantonal, structural joints.

As previously commented, the recourse to a KL2 phase might also be required, in case a deeper knowledge of the building structural conditions is required. This, however, is believed to be a special case,

4.4 A vulnerability index

As a result of the two-level evaluation procedure, a number of parameters are assigned to one of the vulnerability classes, A, B, C, or D. In traditional vulnerability analyses, as previously recalled, each vulnerability class is associated to a score to the purpose of performing an easy combination of all the values and coming to the definition of a vulnerability index, expressed as a numeric value within a pre-defined range. This procedure allows for the possibility of specifying weighting coefficients for the different categories of parameters, thus accounting for the different relevance of the vulnerability categories onto the global vulnerability evaluation.

Scores and weighting coefficients will be defined for the illustrated procedure also. In the beginning, the choice will be in line with the existing vulnerability procedures, considering that such values should be based on the results of a wide statistical investigation.

However, it is believed that, mainly in the case of an aggregate resulting from the assemblage of several structural units, a single numerical value might not be representative of the real vulnerability conditions, or even misleading in the case of local critical conditions within a generally sound context. For this reason it has been planned to provide, as the main result of this vulnerability analysis, plant views of the aggregate showing, through colored maps, the distribution of the most critical vulnerability parameters. In this way, local critical situations will be easily recognizable.

CONCLUSIONS

A renovated interest is present in the research community for seismic vulnerability analyses of buildings, in line with the original meaning of fast qualitative evaluations of the susceptibility to suffer damage from earthquakes. This is due, on the one side, to the need of Civil Protection Services to develop damage scenarios and emergency plans; on the other side, the qualitative approach to the analysis of the seismic performance of masonry buildings has widely improved in recent times.

The continuous progress in earthquake engineering studies, with special reference to the case of existing buildings, is also reflected in the new approach to vulnerability analyses

through the introduction of different knowledge levels, taking advantage of preliminary information coming from the analysis of archival documentation.

The development of a new procedure for vulnerability analyses, as it has been presented in this work with reference to the special case of structural aggregates in historical centers, has to face still now the problem of defining meaningful numerical values for the different evaluation parameters. The solution to this problem necessarily requires the recourse to a wide statistical campaign. In general, the formulation of a meaningful procedure for seismic vulnerability analyses still remains a complex problem, also in consideration of the need to develop an fast, clear, and stable procedure, suitable for the use by a wide community of technicians.

a)  b) 

Figure 3: Fragilities in the structural units: a) porch and b) covered walkways.

a)  b) 

Figure 4: Fragilities in the structural units: a) slender elements; b) elements protruding on the road.

REFERENCES

[1] Benedetti, D., Petrini, V., *Sulla vulnerabilità sismica di edifici in muratura: Proposta su un metodo di valutazione*. *L'industria delle Costr.* (1984) **149**, 66–74.

[2] Giuffrè, A. *Sicurezza e conservazione dei centri storici: il caso Ortigia*. Laterza, (1993).

[3] Aguado, J.L.P., Ferreira, T.M., Lourenço, P.B., The Use of a Large-Scale Seismic Vulnerability Assessment Approach for Masonry FaçadeWalls as an Effective Tool for Evaluating, Managing and Mitigating Seismic Risk in Historical Centers. *Int. J. Archit. Herit.* (2018) **12**, 1259–1275.

[4] Petrini , V., Sede indagine: regione Lombardia, provincia Brescia (1995).

[5] Carocci C. et al, *Il caso di Faenza (RA)- Identificazione preliminare delle caratteristiche degli aggregati del centro storico e delle vulnerabilità osservate,* (2011).

[6] Carocci C. et al, *Piano di Ricostruzione del centro storico di Fossa (AQ)* (2012).

[7] Rondelet, J. Traité théorique et pratique de l'art de bâtir. Parigi, Francia, 1802-1817, *in :* Tocci, C., Masiani, R., Lagomarsino, S., Cocina, S., Carocci, C. F., *Sicurezza e conservazione degli edifici storici monumentali*, pag. 78, ed.Gangemi Editore (2016).

[8] Vicente, R., Parodi , S., Lagomarsino, S., Varum, H., Mendes Silva, J. A. R., Seismic vulnerability and risk assessment: case study of the historic city centre of Coimbra, Portugal, *Bull Earthquake Eng* - © Springer Science+Business Media (2011).

[9] Ferreira, T.M., Maio, R., Vicente, R., Analysis of the impact of large scale seismic retrofitting strategies through the application of a vulnerability-based approach on traditional masonry buildings. *Earthq. Eng. Eng*. Vib. (2017) **16**, 329–348.

[10] Ferreira T.M., Mendes N., Silva R., Multiscale Seismic Vulnerability Assessment and Retrofit of Existing Masonry Buildings, *MDPI Journal* (2019).

[11] Formisano, A., Florio, G., R. Landolfo, Mazzolani, F. M., *Un metodo per la valutazione su larga scala della vulnerabilità sismica degli aggregati storici,* ANIDIS. Bari, (2011).

[12] Bernardini, A., Giovinazzi S., Lagomarsino S., Parodi S. *Vulnerabilità e previsione di danno a scala territoriale secondo una metodologia macrosismica coerente con la scala EMS-98.* Convegno A.N.I.D.I.S. Pisa, Italia, (2007).

[13] Dolce, M., Masi, A., Marino, M., Vona, M., Earthquake damage scenarios of the building stock of Potenza (Southern Italy) including site effects. *Bull. Earthq. Eng*. (2003) **1**, 115–140.

[14] Braga, F., Dolce, M., Liberatore, D. *A statistical study on damaged buildings and an ensuing review of the MSK-76 scale.* In Proceedings of the 7th European Conference on Earthquake Engineering, Athens, Greece, 20–25 September (1982) pp. 431–450.

[15] ATC-13. Earthquake Damage Estimation Data for California; Report ATC-13; Applied Technology Council: Redwood City, CA, USA, (1985).

[16] Faccioli, E., Pessina, V., Calvi G. M. and Borzi, B., A study on damage scenarios for residential buildings in Catania city, *Article in Journal of Seismology* (1999) **3**, 327–343.

[17] L. Berto, P. Faccio, A. Saetta, D. Talledo, I. Zamboni, 2017, *Valutazione di vulnerabilità sismica di edifici complessi/in aggregato: metodi di primo livello*, in : Atti del XVII Convegno Nazionale ANIDIS, L'ingegneria sismica in Italia (Pistoia, 17-21 settembre 2017), Pisa University press, Pisa.

[18] PCM-DPC. Manuale compilazione scheda di 1° livello di rilevamento danno, pronto intervento e agibilità per edifici ordinari nell'emergenza post-sismica (AeDES) (2014).

12th International Conference on Structural Analysis of Historical Constructions
SAHC 2020
P. Roca, L. Pelà and C. Molins (Eds.)

DECISION SUPPORT SYSTEM FOR VULNERABILITY ASSESSMENT OF MASONRY CHURCHES INCLUDING ARCHITECTURAL AND ARTISTIC ASSETS

V. SANGIORGIO[1*], G. UVA[2] and J. M. ADAM[3]
[1] DICATECh, Polytechnic of Bari, Via Edoardo Orabona, 4, 70126 Bari BA
E-mail: valentino.sangiorgio@poliba.it, webpage:
https://www.researchgate.net/profile/Valentino_Sangiorgio

[2] DICATECh, Polytechnic of Bari, Via Edoardo Orabona, 4, 70126 Bari BA
E-mail: giuseppina.uva@poliba.it,

[3] ICITECH Universitat Politècnica de València, Camí de Vera, s/n, 46022 València, Spagna
E-mail: joadmar@upv.es, webpage: http://www.upv.es/ficha-personal/joadmar

Keywords: Historical Structure, Masonry Churches, Non-Destructive Inspection, Failure Mechanisms, Macro-elements approach, Vulnerability Index, Architectural and Artistic Assets.

ABSTRACT

The heritage building stock represents a significant element at risk from earthquakes, as recent seismic events have shown, especially in the Mediterranean area. In fact, in the last few years, the issue of assessing its seismic vulnerability has been widely discussed by the scientific community. The vulnerability assessment procedures involve many critical points related to the complexity and uncertainty of the parameters involved. If a detailed analysis of the individual buildings is to be performed this of course requires a great effort in both the data retrieval, modelling and analysis phases.
In particular, historical masonry churches have been studied in detail in Italy and empirical approaches have been proposed in which a vulnerability index based on the classification of recurrent failure mechanisms is defined, exploiting a macro-elements approach to identify the parameters that influence the index. On the other hand, intangible aspects related to the architectural, historical and artistic value are not included in the Index, either in the structural parts themselves or in additional non-structural elements or contents.
This paper proposes a procedure that combines the well-known vulnerability analysis based on the macro-elements approach and classification of recurrent failure mechanisms with an evaluation of the church's architectural and artistic assets, such as frescoes, statues and paintings, by applying the Analytic Hierarchy Process. The novel procedure is integrated in a useful Decision Support System to provide a complete overview of a church's structural condition, including its artworks, in order to create a priority scale for the assessment, retrofitting and protection of existing masonry churches.

1 INTRODUCTION

The masonry churches represent a significant building typology at risk from earthquakes, as recent seismic events have shown, especially in the Mediterranean area [1]. In fact, in the last few years, the issue of assessing its seismic vulnerability has been widely discussed by the scientific community. In the related literature, several multi-level procedures for the regional scale analysis of existing churches have been proposed [2,3]. In particular, historical masonry churches have been studied in detail in Italy and several empirical approaches have been developed to define a vulnerability index based on a macro-elements approach and exploiting the classification of recurrent failure mechanisms [4,5]. Such procedures involve a suitable on-site examination to identify damage, anti-seismic devices and vulnerability indicators. On the other hand, intangible aspects related to the architectural, historical and artistic value are not included in these approaches, either in the structural parts themselves or in additional non-structural elements or contents.

This paper proposes a procedure to incorporate the potential losses (related to the artistic and architectural value of structural parts and additional artworks such as frescoes, statues and paintings) in the well-known vulnerability evaluation process of existing masonry churches. This methodology will provide a new "Index of artistic and architectural assets" through the application of the Analytic Hierarchy Process (AHP) [6]. Such multicriteria approach is particularly effective for the considered problem because it considers both quantitative and qualitative data in the analysis [7,8,9]. In addition, the resulting methodology can be implemented in a Decision Support System for a fast data acquisition. The resulting tool provide a complete overview of a church's structural condition, including its artworks, in order to create a priority scale for the assessment, retrofitting and protection of existing masonry churches.

2 OVERVIEW OF MACRO-ELEMENT APPROACH FOR ASSESSING CHURCH VULNERABILITY

The Macro-Element analysed is based on the decomposition of a church in macro-elements in which the seismic behaviour is almost independent from the rest of the structure (facade, apse, dome, bell tower) [4].

For each macro-element, the related collapse mechanism is evaluated through an on-site survey by considering the construction characteristics and quality (to provide an example the collapse mechanism "Façade Overturning" and "In Plane Mechanisms Of Façade" are belonging of macro-element of "Façade") [5].

In particular, a *Vulnerability Index* i_v , ranging between 0 and 1 [10,11], is defined as a weighted average of the vulnerability of each macro-element ad it is defined as follows:

$$i_v = \frac{1}{6}\frac{\sum_{k=1}^{28}\rho_k(v_{ki}-v_{kp})}{\sum_{k=1}^{28}\rho_k}+\frac{1}{2} \tag{1}$$

Where ρ_k is assigned to the generic mechanism k ($1 \leq k \leq 28$) that represents the influence of each mechanism on the overall behaviour of the structure (variable from 0.5 to 1). Moreover, v_{ki} and v_{kp} are respectively the vulnerability score and the anti-seismic score of the macro-element and are variable from 1 to 3 (during the survey the presence and of vulnerability elements such as thrusts of vaults, heavy elements, etc. or earthquake resistant elements such as tie rods and chains, buttresses, etc. is considered).

In the present work, in order to consider intangible aspects of the architectural, historical and artistic value, an i_a, novel index, is defined by following in the footsteps of the simplified macro-element approach.
The *Analytic Hierarchy Process* [6] is applied to structure the problem and obtain tabulated values to determine i_a. This approach is able to take the artistic and architectural weighting of every church macro-element into account [5].

3 AHP TO ANALYSE THE ARCHITECTURAL AND ARTISTIC ASSETS

3.1 First step of AHP: Definition of macro-criteria, criteria and alternatives

The first step of the AHP consists in the decomposition of the problem structure in a flowchart. The purpose is to determine the tabulated weights useful for quantifying the potential losses in terms of artistic and architectural value. In particular the the goal of the flowchart is defined as the *Artistic and architectural value* quantification. Nine *criteria* i (with i=1,…,9) are defined and grouped into three *macro-criteria*. For each *criterion* a set of *alternatives* j (with j=1,…, n_i) is defined to characterize the church, the macro elements and the related artistic asset. The nine *criteria* and related *alternatives* are structured in a hierarchical flowchart (see Figure 1) described below.

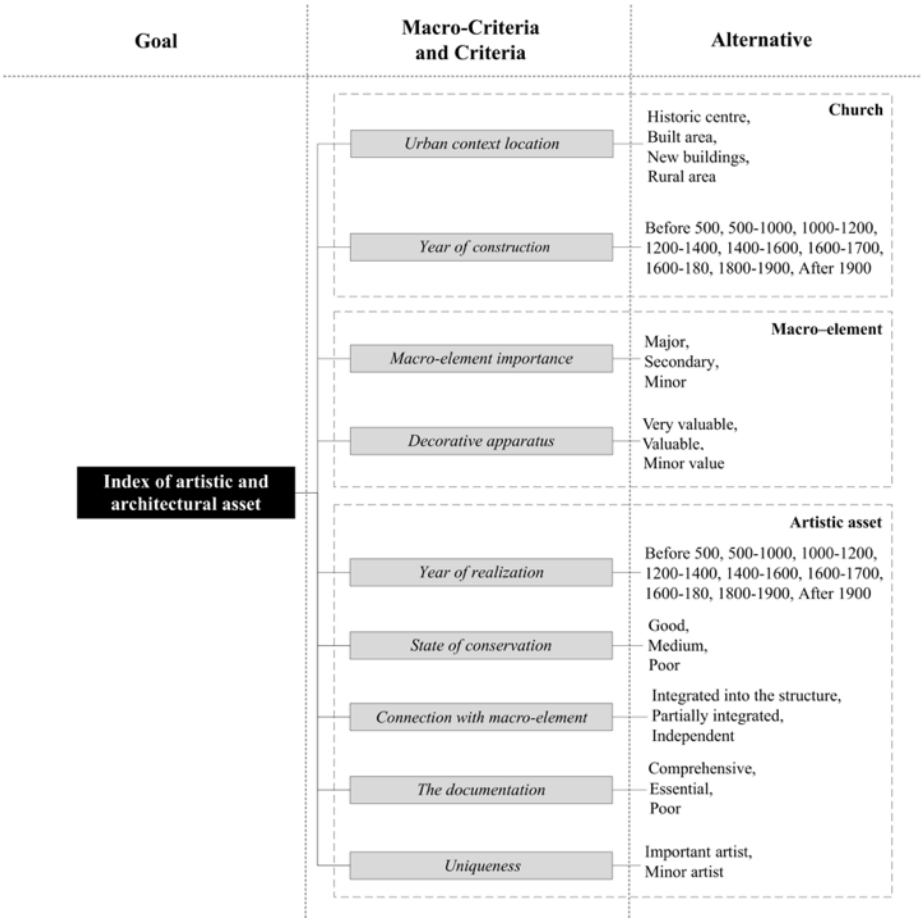


Figure 1: Structure of the problem in a flowchart: criteria and alternatives to determine an Index of artistic and architectural asset vulnerability.

The First *macro-criterion* refers to the *Church* artistic and architectural value, in which the first two criteria are grouped together: 1) *Urban context location* to evaluate the importance of a structure in relation to their urban context [12]; 2) *Year of construction* to include value increasing connected to the antiquity [13].
The Second *macro-criterion* takes the characteristics of the church into account and contemplates two criteria: 3) *Macro-element importance* to consider the architectural value of the component and takes into account the contextualization of the asset [14]; 4) *Decorative apparatus* to evaluate the quantity and quality of the decoration of the macro-element, such as stuccos, pilasters, capitals, etc.
The Third *macro-criterion* considers the *Artistic asset* of every macro element, including any external and internal artistic heritage. This macro criterion includes the value of additional artwork such as frescoes, statues and paintings by five other criteria: 5) *Year of creation* because it influences the *artistic asset,* as in the case of architectural value [13]; 6) *State of conservation* that is directly connected with artistic value; 7) *Likelihood of damage* to contemplate the connection between the artistic asset and the *Macro*-element (some artistic assets such as frescos are closely connected to structural damage, while statues on the façade may be partially related to it, and some, such as an organ, can be completely independent of it); 8) *Documentation* to include the progress of studies that may have attributed different values to the asset over time [14]; 9) *Uniqueness* that is a fundamental qualitative parameter to take the existence of a masterpiece or a rare or invaluable art object into account[14].

3.2 Second step of AHP: weights evaluation

The second step (weight evaluation) is the core of the method and provides tabulated weights useful to generate the ranking. Considering n ordered criteria of comparison (criteria or alternatives) a $n \times n$ *judgments matrix A* is defined. Each upper diagonal element a_{ij}>0 is obtained by comparing the i^{th} with the j^{th} element through the fundamental scale of absolute numbers [6]. This semantic scale correlates verbal judgement and numerical values (1=Equal importance; 3=Moderate importance of one over another; 5=Strong importance; 7=Very strong importance; 9=Extreme importance). The AHP uses the principal eigenvalue method to derive ratio scale priority vectors from *judgments matrix A*. In particular, weights are obtained by solving the following eigenvector problem:

$$A\,w = \lambda_{max}\,w \tag{2}$$

where *w* is the eigenvector and λ_{max} is the principal eigenvalue.
In particular, the *criteria* and *alternative* weights are defined as follows:

- v_i is the weight associated with each i^{th} *criterion*
- w_{ij} is the weight associated with each j^{th} *alternative* related to the i^{th} *criterion*

This Section shows an example of how the literature on artistic and architectural assets can be exploited in order to obtain the *judgment matrices A* and identify the weights v_i and w_{ij}.
For the sake of brevity, the weight calculations of the *alternative* related to *Urban context location* in the *Church* macro-criterion is shown. A qualitative analysis is carried out to obtain pairwise comparisons of the alternatives based on [12] and achieve the *judgment matrix* A_1. The weights are obtained by solving the eigenvector problem, as shown in Eq. (2) for matrix A_1.

Table 1: Judgment Matrix A_1, weights, and CR obtained for the alternatives related to Urban context location.

A_1	(a)	(b)	(c)	(d)	*CR*	$w_{1,j}$
Historic centre (a)	1.0	5.0	8.0	3.0	0.002	1.00
Built-up area (b)	0.2	1.0	2.0	0.7		0.22
New buildings (c)	0.1	0.5	1.0	0.5		0.13
Agricultural area (d)	0.3	1.5	2.0	1.0		0.30

In the classical AHP approach [6] a suitable Consistency Ratio test (*CR*<0.1) is used to verify the coherence of the resulting weights. In this example the *CR* is equal to 0.002 and therefore the weights w_{1j} can be considered consistent (see Table 1).
After obtaining the weights of the *intensity ranges* related to each criterion, the second AHP step obtained the tabulated weights [5] related to the *Structure of the Problem*.

3.3 Third step of AHP: global weight evaluation

In the third and final step of the 'summary of priority' the global weights associated with each alternative are obtained by multiplying the criteria weight by the alternative weight, as in the classical AHP procedure:

$$w'_{ij} = v_i \times w_{ij} \tag{3}$$

These weights can be used obtain a synthetic index.

4 INDEX OF ARTISTIC AND ARCHITECTURAL ASSET VULNERABILITY

After weighting, the Index of artistic and architectural assets (i_a) can be defined.
i_a is assessed in relation to the 28 possible damage mechanisms of specific macro-elements.
Index i_a is defined as a weighted average of each macro-element's artistic and architectural vulnerability:

$$i_a = \frac{1}{6}\frac{\sum_{k=1}^{28} \alpha_k (v_{ki} - v_{kp})}{\sum_{k=1}^{28} \alpha_k} + \frac{1}{2} \tag{4}$$

Where, as in the classical procedure, v_{ki} and v_{kp} are respectively the seismic score and the anti-seismic score of the macro-element (variable from 1 to 3) [4] and α_k is the artistic and architectural importance of the macro-element in relation to the damage mechanisms. This parameter is evaluated by using the obtained global weights as follows.

4.1 The Artistic asset survey and α_k evaluation.

α_k can be evaluated by means of a specific survey using the obtained AHP global weights. A suitable *Survey form* is proposed in order to identify and classify all the information and the alternatives associated with the church under study. An example of a *Survey form* is shown in Figure 2. The form is used to store information regarding the criteria of artistic and architectural importance and starts with information on its location. During the on-site survey, the Church,

every macro element and the related architectural and artistic assets are evaluated by assigning an alternative in accordance with the AHP structuring of the problem.
The survey finishes after all the 28 damage mechanisms of the Macro-elements have been classified.
All the j alternatives of the architectural and artistic asset are identified and stored for all the macro elements in a church. The weight w'_{ij} associated with every alternative can be obtained using the Tabulated weights [5] and Eq. (3), while α_k can be evaluated by the following equation:

$$\alpha_k = \sum_{i=1}^{9} w'_{ij} \tag{5}$$

where k is the considered mechanism and w'_{ij} is the global weight associated with the artistic assets of the macro element related to it.

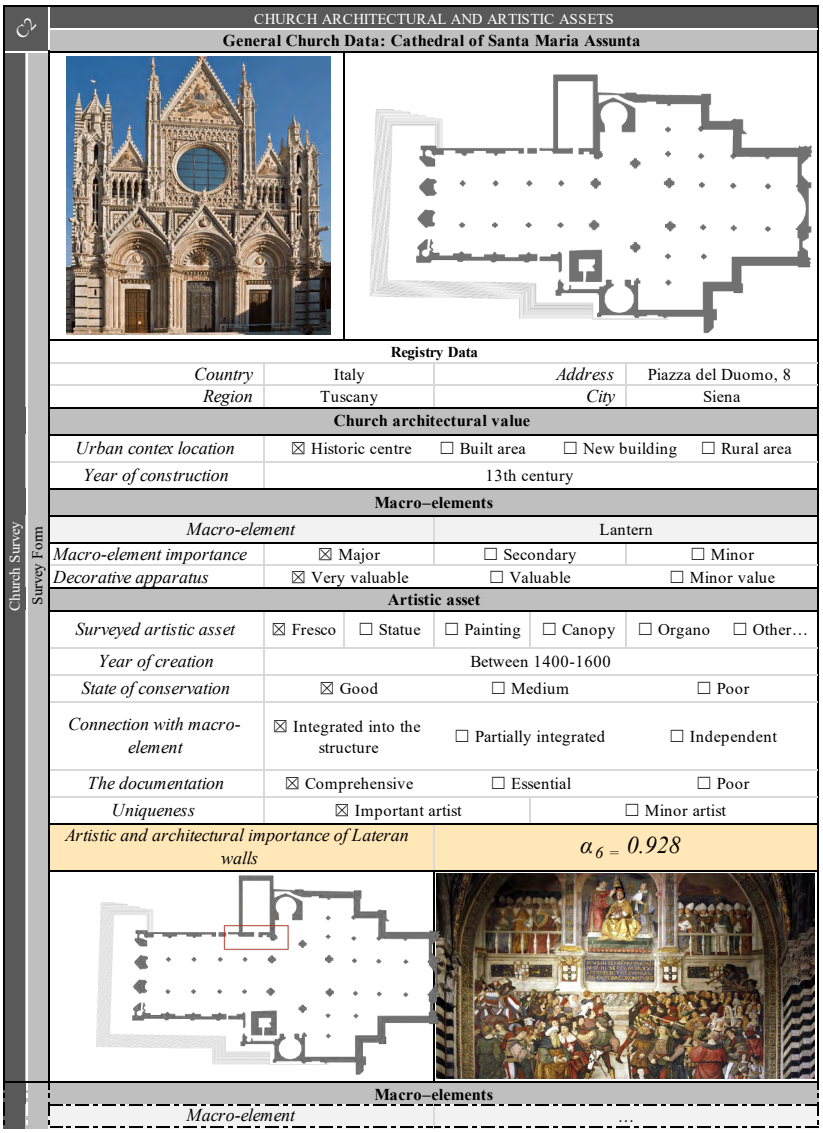


Figure 2: Extract from the *Survey form* of the *Cathedral of Santa Maria Assunta*: The "*Libreria Silvio Picclomini*" decorated by *Pinturicchio*.

Note that α_k range between 0.25 and 1 and it can be useful to numerically evaluate the *local artistic asset* of every macro-element and also provides useful information on the church's *global artistic and architectural assets*. Indeed, its average value α_{med} (medium) can be evaluated by the following equation:

$$\alpha_{med} = \sum_{k=1}^{28} \frac{\alpha_k}{k} \tag{6}$$

Conclusively, α_k, α_{med} and i_a allow to evaluate numerically the local *artistic asset* of the single macro-element, the global *artistic asset* of the church and the global Vulnerability of the church respectively.

5 THE INTEGRATION OF THE AHP-BASED APPROACH IN DSS

The proposed approach can be easily exploited to set a spreadsheet useful to a rapid survey of an historical church [15]. In particular a suitable *Survey form* for a fast survey is developed and a suitable flowchart is realized to better explain the DSS process.

A. DSS Architecture

The architecture of the proposed DSS is constituted by five components (Figure 3): i) A Data Management System (DMS) which collects the information provided by the users by the *Survey form*; ii) A Web-Based Platform, that represents the intelligence of the system. This platform processes the *Survey form* data, classifies the churches components and calculate the α_k, α_{med} and finally the vulnerability index i_a; iii) The *Survey form* consisting of a suitable spreadsheet implementable in a APP for smart devices; iv) Web Application used by technicians to display the reported *Survey form* history, the register information about the church; v) finally an Application Programming Interface (API) connecting the *Survey form* (APP) and the Web Application with the Web-Based Platform and the DMS.

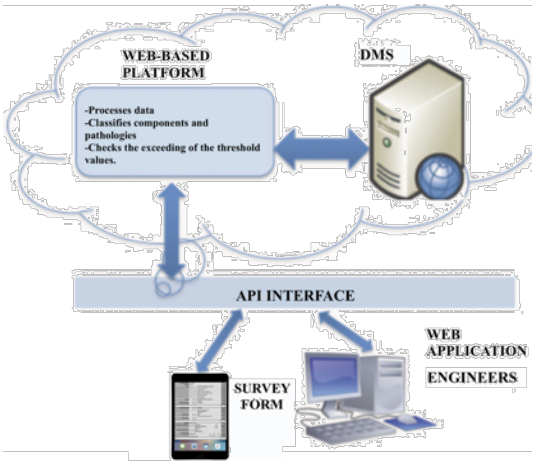


Figure 3: The generic matrix of judgments A

5.1 Survey form

The core of the proposed approach is the definition of the *Survey form* implementable in an APP for smart devices. Such spreadsheet allows the user (technicians) to acquire data during a

fast-visual inspection. The proposed APP can be used to perform the fast on-site survey by taking into account all the criteria and alternatives of the considered AHP problem.

5.2 The DSS procedure

In order to better specify the DSS procedure and the use of the *Survey forms* a suitable flowchart is realized in accordance with the UML framework (Figure 4). The rules and tasks of the actors involved in the process are pointed out.

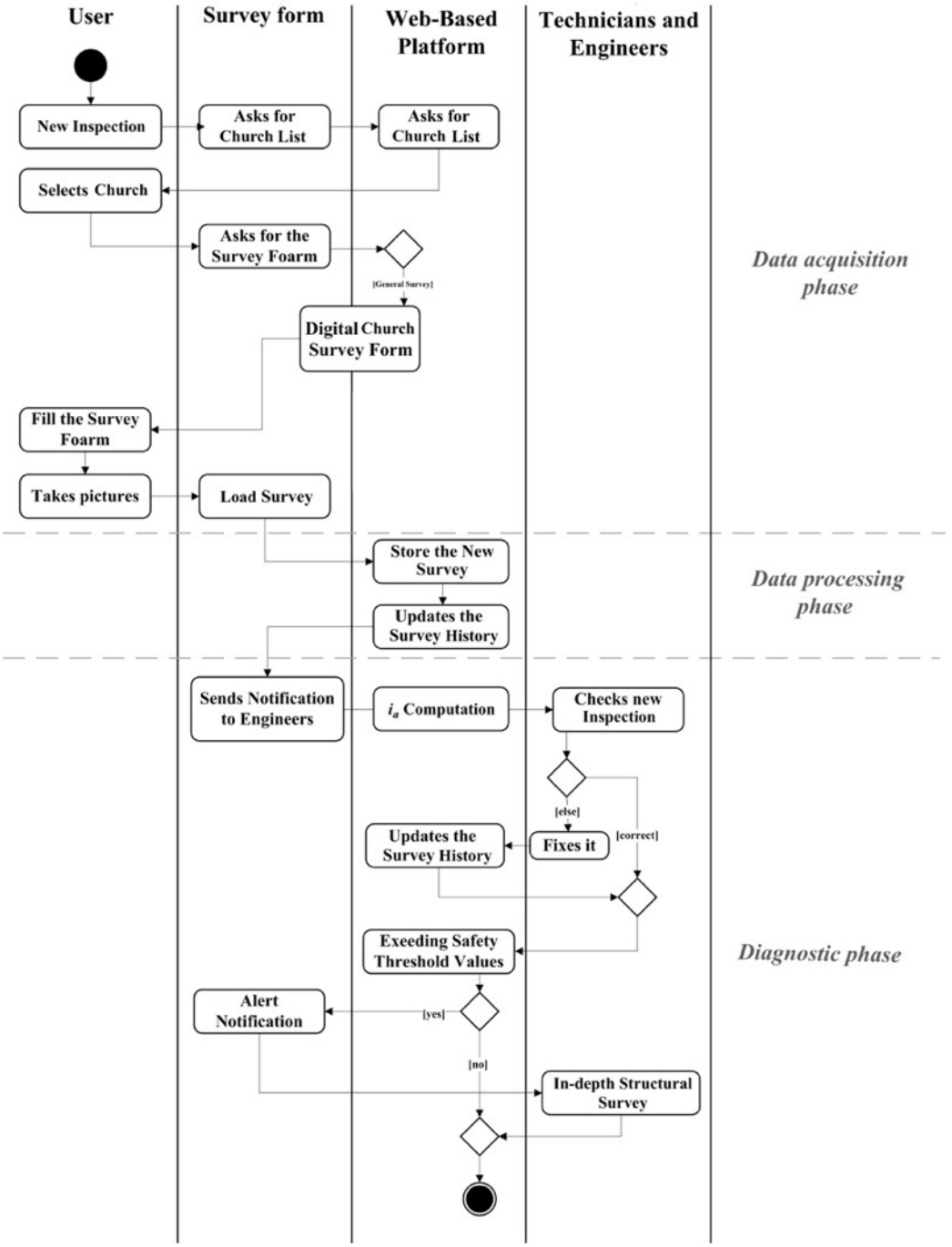


Figure 4: Flowchart to explain the procedure of the use of the System

The flowchart procedure explains all the interactions between the two main components of the DSS, (i.e. *Survey form* implemented in smart devices and Web Application), and the actors involved in the process (i.e. Users of the *Survey form* and bridge technicians and engineers). The flow is described by defining three phases of the process: Data Acquisition Phase, Data Processing Phase and Diagnostic Phase.

i) During the Data Acquisition Phase, firstly, the user access to the churches list of the web-based platform to select the churches to survey. Secondly the user can ask to use the *Survey form* for the inspection. Thirdly the user can complete the inspection by taking photographs of vulnerability and earthquake resistant elements and sending the complete inspection to the Platform;

ii) in the Data Processing Phase, the Web Based Platform exploits the received surveys to store the new data and update the surveys history;

iii) finally, during Diagnostic Phase, the Web-Based Platform send new damages notification to the building staff that can read, change or validate the inspection. At this point, the System is able to automatically evaluate the vulnerability index, exploiting equation (3-4-5) and the tabulated weights obtained by the AHP. Finally, if the condition rating overcome some defined threshold values, a suitable the alarm protocol is triggered. An alert notification is sent to all users of the DSS to set up an emergency intervention.

6 SITE TEST

In order to test the proposed method, eight case studies were carried out in four cities in two European countries, Valencia (Spain) and Tuscany (Italy): i) the churches of San Agustín (13th century), St. John (13th century) and San Juan del Hospital (13th century) in Valencia, ii) the church of Santa Justa & Rufina (14th century) and the Cathedral of Salvador (13th century) in Orihuela; iii) the Basilica of Santa María (17th century) in Elche; iv) and the Cathedral of Santa Maria Assunta (13th century) and the Basilica of San Francesco (15th century) in Siena. These churches are of different architectural styles, types of construction and different artistic importance. Both Italy and Spain are excellent site test due to their high seismic hazard.

6.1 Church vulnerability analysis.

In the preliminary phase the existing information and documentation on the church design, modifications after construction and seismic history are collected. This information can be useful to identify some artistic and architectural assets or to verify the effectiveness of any vulnerability or earthquake-resistant elements.

After the preliminary phase, the on-site survey can be performed with the support of the *Survey forms.* For each church, every k mechanism is analysed by assigning v_{ki} and v_{kp} in accordance with the classical method [4]. The *Survey forms* can then be filled in and the values of α_k can be identified by means of Eq. (5).

To provide an example, the 13th century Cathedral of Santa Maria Assunta is considered a masterpiece of Italian Gothic architecture. Both the exterior and the interior are built with white marble and green-and-black-striped marble, with the addition of red marble in the façade. The Cathedral is one of Italy's and the world's most valuable architectural assets, both for the materials used and the importance of the artists who decorated it. For example, Giovanni Pisano worked on the façade, Gian Lorenzo Bernini designed the lantern on the dome, Nicola Pisano created the pulpit of Carrara marble, many of the frescoes, paintings and stained glass were the work of Michelangelo, Donatello, Duccio di Buoninsegna and Cimabue. Another important

macro-element is the chapel known as Libreria Piccolomini, with frescoes made by Pinturicchio on the drawings of Michelangelo (Figure 2). After the survey, the overall artistic value of the church was the highest of all those in the site test, with α_{med} =0.922. However, except for some vulnerable elements such as the upper façade (due to the presence of a large rose window in addition to a high slenderness of the spire) and the many external statues, the quality of the masonry and some effective anti-seismic components (tie rods and buttresses) ensure a limited global vulnerability value of i_a =0.599.

6.2 Site test results.

The results showed that the most vulnerable churches are the Basilica of Santa María in Elche and the church of Santa Justa & Rufina in Orihuela, due to their critical structural conditions in terms of seismic resistance and the importance of their artistic and architectural heritage. Anti-seismic devices should be installed to improve their anti-seismic behaviour and avoid major damage. Figure 5 shows the façades of the churches and *site test output*.



Figure 5: Façades of the churches and site test output.

7 CONCLUSIONS

This paper proposes a novel procedure implementable in a Decision Support System to quantify masonry church vulnerability, including architectural and artistic assets in the analysis. This ambitious research has been carried out in four phases: i) the study of the existing macro-element approach and the related literature to identify the parameters that influence the architectural and artistic asses; ii) the application of the Analytic Hierarchy Process to quantify architectural and artistic assets and redefine the evaluation of the Index i_a; iii) the realization of *Survey forms* implemented in a DSS to support the data acquisition, and iv) the application of the method to a set of churches located in Valencia (Spain) and Tuscany (Italy) regions to prove potential of the novel approach.
The project involved a combination of interdisciplinary skills, including: structural engineering, forensic engineering, statistics, multi-criteria analysis and the evaluation of artistic assets. The results show the importance of providing a complete overview of a church's structural condition and its artistic assets in order to create a priority scale for the assessment, retrofitting and protection of existing masonry churches. The DSS is a powerful and easy-to-apply tool and includes important information on potential artistic losses during a seismic event.
Further research will be carried out to apply the novel Decision Support Systems at a large-scale.

REFERENCES

[1] Canuti, C., S. Carbonari, A. Dall'Asta, L. Dezi, F. Gara, G. Leoni, M. Morici, E. Petrucci, A. Prota, and A. Zona. 2019. Post- earthquake damage and vulnerability assessment of churches in the Marche Region struck by the 2016 central Italy seismic sequence. *International Journal of Architectural Heritage* 1–22. doi:10.1080/15583058.2019.1653403.

[2] Sangiorgio, V., G. Uva, and F. Fatiguso. 2018. User-reporting based semeiotic assessment of existing building stock at the regional scale. *Journal of Performance of Constructed Facilities* 32 (6):04018079. doi:10.1061/(ASCE)CF.1943- 5509.0001227.

[3] Sangiorgio, V., G. Uva, F. Fatiguso, and J. M. Adam. 2019. A new index to evaluate exposure and potential damage to RC building structures in coastal areas. *Engineering Failure Analysis* 100:439–55. doi:10.1016/j.engfailanal.2019.02.052.

[4] Lagomarsino, S., S. Podestà, G. Cifani, and A. Lemme. 2004. The 31st October 2002 earthquake in Molise (Italy): A new methodology for the damage and seismic vulnerability survey of churches. *Proceeding of the 13th World Conference on Earthquake Engineering* Vancouver, B.C., Canada, August 1–6.

[5] Sangiorgio, V., Uva, G., and Adam, J. M. 2020. Integrated Seismic Vulnerability Assessment of Historical Masonry Churches Including Architectural and Artistic Assets Based on Macro-element Approach. *International Journal of Architectural Heritage*, 1-14. doi: 10.1080/15583058.2019.1709916.

[6] Saaty, T. L. (2008). Decision making with the analytic hierarchy process. *International journal of services sciences*, 1(1), 83-98.

[7] Sangiorgio, V., G. Uva, and F. Fatiguso. 2017. Optimized AHP to overcome limits in weight calculation: A building perfor- mance application. *Journal of Construction Engineering and Management*. doi:10.1061/(ASCE)CO.1943-7862.0001418.

[8] Uva, G., Sangiorgio, V., Ruggieri, S., & Fatiguso, F. (2019). Structural vulnerability assessment of masonry churches supported by user-reported data and modern Internet of Things (IoT). *Measurement*, 131, 183-192.
[9] Sangiorgio, V., Uva, G., & Fatiguso, F. (2016). A procedure to assess the criticalities of structures built in absence of earthquake resistant criteria. REHABEND, 2016, 631-639.
[10] De Matteis, G., E. Criber, and G. Brando. 2016. Damage probability matrices for three-nave masonry churches in Abruzzi after the 2009 L'Aquila earthquake. International Journal of Architectural Heritage 10 (2–3):120–45.
[11] De Matteis, G., G. Brando, and V. Corlito. 2019a. Predictive model for seismic vulnerability assessment of churches based on the 2009 L'Aquila earthquake. Bulletin of Earthquake Engineering 17 (9):4909–36. doi:10.1007/s10518-019-00656-7.
[12] Jokilehto, J. 2006. World heritage: Defining the outstanding universal value. City and Time 2 (2):1.
[13] İpekoğlu, B. 2006. An architectural evaluation method for con- servation of traditional dwellings. *Building and Environment* 41 (3):386–94. doi:10.1016/j.buildenv.2005.02.009.
[14] Ghizzi, S. 1994. Aspetti economici del restauro archeolgoico, in Note di Economia dei Beni Culturali ed Ambientali. *Rivista di Analisi dei Problemi di Finanziamento, Valutazione e Gestione dei Progetti di Investimento per il Restauro e la Valorizzazione dei Beni Culturali*, Anno II, Numero 1, Roma. doi:10.3168/jds.S0022-0302(94)77044-2.
[15] Sangiorgio, V., Martiradonna, S., Uva, G., & Fatiguso, F. (2017, September). An information system for masonry building monitoring. In 2017 IEEE International Conference on Service Operations and Logistics, and Informatics (SOLI) (pp. 230-235). IEEE.

12th International Conference on Structural Analysis of Historical Constructions
SAHC 2020
P. Roca, L. Pelà and C. Molins (Eds.)

DEVELOPMENT OF A FIRE DAMAGE INDEX FOR IMMOVABLE CULTURAL HERITAGE

L. GERARDO F. SALAZAR[1*], ESMERALDA PAUPÉRIO[2] AND XAVIER ROMÃO[3]

[1] CONSTRUCT-LESE, Faculty of Engineering - University of Porto (FEUP)
Rua Dr. Roberto Frias, 4200-465Porto, Portugal
Email: gsalazar@fe.up.pt

[2] Construction Institute, CONSTRUCT-LESE, Faculty of Engineering - University of Porto (FEUP)
Rua Dr. Roberto Frias, 4200-465 Porto, Portugal
Email: pauperio@fe.up.pt

[3] CONSTRUCT-LESE, Faculty of Engineering - University of Porto (FEUP)
Rua Dr. Roberto Frias, 4200-465 Porto, Portugal
Email: xnr@fe.up.pt

Keywords: Fire Damage Impact Index, Immovable Cultural Heritage, Vulnerability Assessment

Abstract. *Available fire risk assessment approaches are mostly developed for new buildings. These approaches encompass minimum provisions defined by standards that are valid in certain countries, and few of these methods were thought exclusively for assessing the fire safety of cultural heritage. Given the diversity and specificity of cultural heritage assets, simple approaches are thus required to analyse their fire safety and establish their risk mitigation needs. In this context, a simplified fire damage index dedicated to assessing the fire vulnerability of immovable cultural heritage assets is proposed. The proposed index is the result of a weighted multi-parameter evaluation that can be correlated with the level of damage that the cultural heritage asset (including its contents) is expected to suffer under a fire. The proposed index involves twenty-one indicators divided into four categories and offers a flexible approach for universal applicability. The performance of the proposed approach is illustrated for two case studies in Portugal. The results highlight the advantages of having a simple methodology that can be used for the preliminary risk analysis of a large number of assets to identify those requiring risk mitigation measures or detailed and resource-demanding analyses.*

1 INTRODUCTION

Fires that affected cultural heritage assets in recent years (e.g. the National Museum of Rio de Janeiro (Brazil) in 2018, and of the Cathedral of Notre Dame (France) in 2019) emphasise the need for more studies related to their fire safety. The occurrence of these fires can be connected to various factors ranging from a general lack of maintenance, to a lack of adequate safety measures during restoration works. Moreover, historic constructions exhibit a higher fire vulnerability since they were constructed without considering fire preparedness measures, namely aspects commonly considered in current construction standards such as adequate evacuation routes or emergency exits. The combustible nature of many cultural heritage elements often forces stakeholders to address these issues by integrating modern fire protection

systems in historic constructions. However, the integration of such systems needs careful consideration to avoid the loss of cultural heritage values due to their installation, as well as the occurrence of further damage during their use (e.g. water sprinkler systems in scenarios involving cultural heritage assets sensitive to water damage).

Several methods have been developed to assess fire risk in buildings, but most of the robust approaches were developed for new buildings and involve formulations that are not compatible with cultural heritage values or are exclusively for one type of heritage. The development of a robust fire safety assessment method for multiple cultural heritage assets is thus needed, namely one that accounts for both the building and its cultural contents, and that can be implemented in any country. To address this need, a fire damage impact index of vulnerability is proposed herein. The index is presented in the following and some of its components are detailed for the case of single cultural heritage assets (i.e. assets physically separated from other assets or constructions) that can host movable heritage or have heritage elements attached to the main asset. Typical examples of such heritage assets are historic houses, religious buildings or museums. Following the description of the proposed index, an application to two real cases with different expected damage impacts if case of fire is also presented.

2 FIRE DAMAGE INDEX METHODOLOGY

The proposed index was developed following a thorough literature review focusing, in particular, methods that gave more emphasis to historical constructions. The indicators selected for the fire index were determined by examining international statistics concerning the causes of multiple fires, existing fire risk assessment methods, as well as checklists and standards providing guidance on fire prevention. The general type of indicators that were selected can be seen to generally be in agreement with those considered by other fire risk assessment methods for historical constructions [1-7]. This fire index assesses the expected Level of Damage (D_V) in case of fire, ranked in three levels (i.e. light ($0 \leq D_V \leq 35$), medium ($35 \leq D_V \leq 70$), and heavy ($70 \leq D_V \leq 100$)). Light damage refers to cases where the cultural asset is expected to sustain negligible damage and safety is ensured, but a regular monitoring of the situation is recommended. Medium damage refers to situations where the cultural asset can suffer damage that may be partially recovered in case of fire. Heavy damage refers to cases that may involve irreparable damage or the total loss of the cultural asset. The proposed index is compatible with the Level of Vulnerability (V_L) assessment proposed by [8] that integrates a factor of easiness of reparation and restoration (R_f) and a heritage value factor (BV_f) and can be defined as:

$$V_L = D_V \times R_f \times BV_f \tag{1}$$

The fire index establishes the relevance of all the twenty-one indicators divided into four groups (G_i) (building properties (BP); utilities: electric power, gas and telecommunications (UEPGT); firefighting measures (FM); emergency preparedness planning (EPP)). Each indicator is assigned to one of five damage impact classes (very low (A), low (B), moderate (C), high (D), and very high (E)). The classification of a group corresponds to that of the indicator that exhibits the worst performance. This assumes that the bad performance of one indicator within a group is enough to intensify the susceptibility of having an ignition, the fire propagation or the difficulty to fight fire. The classes (C_i) are then scored with values of 0 (A), 25 (B), 50 (C), 75 (D), 100 (E). The final index is then obtained by a weighted combination of

the classification of each group. Based on the literature review, weights of 35 %, 20 %, 30 % and 15 % were defined for BP, UEPGT, FM and EEP, respectively.

2.1 Building Properties (BP)

Indicators of this group refer to different aspects related to the physical properties of the building (material properties, geometrical properties, spaces and their separation, the existence of combustible materials), except installations considered in the UEPGT, and to its immediate surrounding area. Physical properties are relevant for fire risk assessment in terms of their fire resistance, combustibility and the amount of fire load that they represent (considering movable contents and building materials). Moreover, spaces (corridors, halls, rooms, etc.) and their separation provide information related to fire propagation. Indicators in this group are the fire load density (P_1), the fire resistance (P_2), the compartmentalisation (P_3), the type of adjacent buildings (P_4), the possibility of vertical fire propagation (P_5), the building conservation status (P_6), the existence of fire breaks/buffer zones (P_7) according to:

$$G_1 = BP = [Max\left(P_{i,i=1:7}\right)] \times 0.35 \quad (2)$$

For this simplified assessment, P_1 is defined using values from the literature for historical constructions as the sum of two components: the immovable load density I_q and the movable contents M_q related to the building use. Parameter I_q is defined by the combustibility of constructive materials. Combustible materials are, for example, timber, textile, organic materials, plastics, resins, while non-combustible materials are clay, soil, concrete, gypsum, steel or stucco. Based on the literature review [9, 10], I_q was defined according to the predominant combustible or non-combustible material of the historical construction under assessment (Table 1). Parameter M_q is determined by the current use of the historical building (Table 2). These and other values can be found in [11, 12].

Table 1: Values proposed for parameter I_q.

Type of structure (Finishes and Supports)	Fire Load
Structure made with a least 80% of combustible materials, e.g. floors and walls made of timber.	3,000 MJ/m^2
Structure made with a balance of non-combustible and combustible materials, e.g. masonry walls and timber floors or thatch roofs.	1,100 MJ/m^2
Structure made with at least 80% of non-combustible materials, e.g. masonry walls and reinforced concrete slabs.	200 MJ/m^2

Table 2: Values proposed for parameter M_q according to the building activity.

Type of Use (Current activity)	Fire Load	Type of Use (Current activity)	Fire Load
Housing/Apartment/Dwelling	780 MJ/m^2	Officine	1,200 MJ/m^2
Museum/Art galleries	300 MJ/m^2	Hotels, Hospitals	300 MJ/m^2
Churches (furniture and candles)	1,300 MJ/m^2	School	300 MJ/m^2
Libraries/Archives	1,500 MJ/m^2	Shopping/Cinema/Theatre	800 MJ/m^2

Parameter P_2 is defined based on [13, 14] to be consistent with the European Reaction to

Fire classification system. The classification is based on the predominant material as for I_q, and its susceptibility to produce flashover according to seven types (A1, A2, B, C, D, E and F). From A1 to F, materials have a decreasing fire resistance, thus a higher likelihood of producing a flashover. Parameter P_3 is related to the possibility of containing the occurrence of a fire within certain areas of the building to avoid its propagation, and reflects the size of the largest fire compartment with combustible or flammable materials. The lack of containment elements between compartments (i.e. doors) can lead to an increase of the class of P_3 by one level. The classification of this parameter is based on criteria defined in [7, 14] but accounts for other features such as the existence of self-closing doors or windows. When there are self-closing systems, the classification of P_3 can be reduced by one level (e.g. if the compartmentalisation classification leads to Class B, it can be upgraded to Class A if there are self-closing systems).

Parameter P_4 reflects the influence of adjacent buildings according to their location and type of construction (i.e. in terms of combustible materials). Following the distance criteria in [15], P_4 is classified as type IS if the construction under assessment has no surrounding constructions with exposed combustible materials closer than 12m, made of timber closer than 6m, or made of quasi-fire resistant materials closer than 3m. Otherwise, P_4 is classified as type IC. P_4 can also be classified as AC if there are adjacent constructions made mostly with combustible materials, as ACN if there are adjacent constructions made with a balance of combustible and non-combustible materials, or as AN if there are adjacent constructions made with non-combustible materials. When the adjacent constructions are abandoned, P_4 is increased by one level. The classification of parameter P_5 reflects the likelihood of vertical fire propagation within the construction under assessment, depending on the geometric proportion and number of vertical aligned openings. This parameter is graded by the ratio $r = l/h$ and the number of levels between openings (nl), where l is the vertical distance between openings and h is the height of the opening of the lower level [14] (see Table 3). The same ratio r is also used to analyse the relation between openings of the top building level and a roof structure made of combustible material. The classification of P_5 can be reduced by one level if the construction material is combustible but was upgraded to have a reasonable fire resistance. When a construction presents situations with both $r \geq 1$ and $r < 1$, P_5 can be graded as C, regardless of the number of levels. In case there are no aligned openings and roofs have non-combustible materials (NAI), P_5 can be graded as A. Parameter P_6 reflects the level of conservation and cleanliness of the construction's combustible materials (e.g. timber, thatch, or bamboo). This parameter is graded according to five levels ranging from Very Good (when there are no combustible materials in the building), Good (when the combustible materials are in good condition and have a fire-resistance finishing), Medium (when the combustible materials appear to be in good condition, without any type of biological colonisation (i.e. termites) and high porosity), Bad (when the materials exhibit high porosity produced by biological colonisation), and Very Bad (when the combustible materials exhibit high concentration of humidity, biological colonisation, porosity, and vegetation growth; a common situation in abandoned historical constructions). Parameter P_7 reflects the horizontal propagation of fire from exterior combustible materials through the distance between the construction under assessment and the surrounding vegetation, rubbish or other elements that may exist. In the case of surrounding vegetation, based on criteria from the United States National Fire Protection Association and recommendations from the Portuguese Civil Protection, P_7 was graded from A to E when the

referred distance is more than 50m, between 50m and 30m, between 30m and 5m, from 5m to 1.5m, and less than 1.5m, respectively. P_7 is also associated with the criteria used by [15] which involve the critical distance between constructions made of combustible materials defined by types I to IV. In this case the critical distance is defined with respect to other possible exterior combustible materials, namely street furniture, rubbish or other elements that are not vegetation or other constructions. Types I to IV correspond to cases where the distance from ignition sources is more than 12m, between 12m and 6m, between 6m and 3m, and less than 3m, respectively. The classification of P_7 can be reduced by one level if the heritage asset near combustible or flammable materials is made of non-combustible materials. Table 3 summarizes the classifications of indicators P_1 to P_7.

Table 3: Classification of parameters P_1 to P_7.

Indicator	Class					Units
	A	**B**	**C**	**D**	**E**	
	0	**25**	**50**	**75**	**100**	
P_1	<500	500-750	750-1500	1500-3000	>3000	MJ/m^2
P_2	A1	B2	B	C, D	E, F	-
P_3	<50	50-100	100-200	200-400	>400	m^2
P_4	IS or AN	IC	ACN	AC	ACA	-
P_5	NAI	$r \geq 1$	$r \geq 1$ and $r < 1$	$r < 1$ and $nl \leq 2$	$r \leq 1$ and $nl > 2$	-
P_6	Very Good	Good	Medium	Bad	Very Bad	-
P_7	>50 and I	50-30 or II	30-5 or III	5-1.5 or IV	<1.5 and IV	m

2.2 Utilities: Electric Power, Gas and Telecommunications (UEPGT)

The second group of parameters is related to the characteristics and components of the existing utilities that can facilitate the occurrence or propagation of a fire due to their maintenance conditions or contribute to increase the overall fire safety. It must be noted that some of these utilities that were not part of the original cultural heritage asset are often found to be operating under inadequate safety conditions (e.g. unprotected electrical wiring or electrical overload of power outlets). These unsafe conditions increase the vulnerability of the construction and its contents. The UEPGT group considers five indicators related to the electrical (P_8), gas (P_9), HVAC (P_{10}), telecommunications and CCTV systems (P_{11}), to the technical control room (P_{12}), and that are combined according to:

$$G_2 = UEGPT = [Max\left(P_{i,i=8:12}\right)] \times 0.20 \quad (3)$$

The classification of parameter P_8 follows principles referred in [6, 16] to reflect the level of maintenance of the electrical installation. The grading levels (see Table 5) are Excellent (EX) (adequate isolation of electrical components and combustible materials installed by professionals), Good (G) (refers to installations similar to EX but not installed by professionals), Medium (M) (installation with both new and older electrical components), Bad (BA) (installation with older electrical components only), and Very Bad (VB) (installation similar to BA but with known electrical deficiencies). The deficient implementation of a lightning rod in buildings with tall vertical elements (e.g. a bell tower, pinnacle or cupola) can also be considered to increase the classification of P_8 by one level [17]. Parameter P_9 is graded

in Table 4 according to the type of gas supply [6], which can be piped (P), a gas reservoir (GR), an external gas container (EGC), an internal gas container in a well-ventilated area (IGCV), or an internal gas container in a poorly-ventilated area or close to heat sources (IGCNV). The absence of gas installations is graded as A. The classification of P_9 is increased one level when gas installations or gas heaters are near flammable materials. Parameter P_{10} reflects the existence of an HVAC system, that could be decentralized (D) or centralized (C). If the system exhibits a good working condition P_{10} is graded as B (see Table 4). If the system's level of maintenance is inadequate, the classification increases to C for a decentralized system (DCF) and to D for a centralized system (CCF). These classifications increase one more level if the system is near combustible or flammable materials (to LMD and LMC for decentralized and centralized systems, respectively). The absence of HVAC (NH) is equivalent to Class A. Parameter P_{11} combines information related to the likely level of criminality of the area of the construction under assessment and to the availability of systems with automatic communication with the fire brigade services and video surveillance (CCTV). Parameter P_{11} is thus graded in Table 4 as TT1 when there is a good CCTV system in low criminality zones, TT2 when there is a good CCTV system in moderate or high criminality zones, TT3 when there is an incomplete CCTV system (i.e. cameras are not available in all the relevant spaces), and TT4 when there is no adequate CCTV system. The TT1-TT4 grading assume there is an efficient communication system with the fire brigade. If this condition is not met, the classification can increase one level. A grading TT5 is assigned when there is no CCTV system and no automatic communication system with the fire brigade.

Table 4: Classification of parameters P_8 to P_{12}.

Indicator	**Class**				
	A	**B**	**C**	**D**	**E**
	0	**25**	**50**	**75**	**100**
P_8	EX	G	M	BA	VB
P_9	P	GR	EGC	IGCV	IGCNV
P_{10}	NH	D or C	DCF	CCF or LMD	LMC
P_{11}	TT1	TT2	TT3	TT4	TT5
P_{12}	Out≥5	Out<5	IMC	IMM	IB

Due to the flammability of components that a technical control room can have, its contribution to the impacts is assessed independently by P_{12} (Table 5). This parameter reflects the location of the technical control room within the construction under assessment, its degree of maintenance, and the fire-resistant nature of the surface materials. When the technical control room is located outside the main construction at a distance more than 5m, P_{12} is assigned to Class A, whereas when the engine room is located at a distance equal or less than 5m, P_{12} is assigned to Class B. Assigning P_{12} to Class C (IMC) corresponds to cases where the technical control room is inside the construction and exhibits a good condition and there are some fire control systems in place (e.g. an active suppression system, fire-retardant materials, or self-closing doors). If the technical control room is located inside the construction and exhibits a good condition but there are no active or passive fire suppression systems, class D (IMM) is assigned. If the technical control room does not exhibit a good condition or there are no fire suppression systems, P_{12} is assigned to class E (IB). If there are flammable elements or

combustible materials that are not associated to the functionality of the technical control room (e.g. textiles, mattresses, candles, ropes), the classification of P_{12} is increased one level.

2.3 Firefighting measures (FM)

The firefighting measures involves five parameters graded according to Table 5 and combined according to Equation 4. This group addresses the existence of alarm and detection systems (P_{13}), of smoke control systems (P_{14}), of active suppression systems (P_{15}), of water supply systems (P_{16}), and the site accessibility by and its proximity to fire rescue services (P_{17}).

$$G_3 = FM = [Max\left(P_{i,i=13:17}\right)] \times 0.30 \quad (4)$$

Parameter P_{13} reflects the existence of an efficient alarm and fire detection system where all components are in good working condition (except when stated otherwise). The grading of P_{13} involves the classes AM (when there is a dual (automatic and manual) system in all the relevant zones of the construction under assessment), AA (when there is only an automatic system), AMN (when there is a dual system with deficiencies in the automatic component), AAN (when there is only an automatic system that is not in perfect working conditions), and NAD (when there is no system). The classification of P_{13} can increase one level when there is a significant likelihood of false alarms. Parameter P_{14} refers to the existence of smoke control systems in enclosed compartments (automatic systems, through the spatial arrangement of the building, or both) that can facilitate evacuation or firefighting actions [18]. Parameter P_{14} is graded as SC1 (when there are active and passive systems in good working conditions), SC2 (when there is only a functional active system in corridors, stairs, or elevator shafts), SC3 (when there is only passive extraction systems), SC4 (when there is a partially working SC2 or SC3 system) and SC5 (when there are no smoke control systems). Parameter P_{15} reflects the existence of active fire suppression systems that have any of the following components: sprinklers, extinguishers, hydrants, hose reels, wet and dry rising mains, drencher systems, sparge pipes, water curtains, or foam systems. Parameter P_{15} is graded as AS1 (when there are firefighting systems in evacuation routes and inner compartments that will not affect water-sensitive movable assets in case of a fire), AS2 (when there are firefighting systems in locations that can affect water-sensitive movable assets in case of a fire), AS3 (when there are only fire suppression systems in evacuation zones), AS4 (when there are suppression systems that have faulty or unreliable components), and AS5 (when there is no firefighting equipment). Parameter P16 addresses the water supply systems that include interior (e.g. water tanks) or exterior (e.g. fire hydrants, rivers, lakes, etc.) water sources. Parameter P_{16} is graded as W1 (when the supply can be either from the interior of the construction under assessment with a well-designed water tank or from its exterior by a source with enough capacity (e.g. at least 20 m^3), that is closer than 20m), W2 (when the source is from an interior water tank with insufficient capacity, and exterior sources closer than 10m), W3 (when all the possible exterior sources are between 10m and 20m away), W4 (the possible exterior sources are between 20 and 40m away), and W5 (when there are no interior or exterior sources for water supply). In situations where the exterior water sources are fundamental, and if their availability is known to be scarce or water is frozen in specific times of the year, the classification of P_{16} should increase by two levels. When the fire suppression system presents an adequate automatic non-water-based alternative, P_{16} can be graded as W1. With respect to parameter P_{17}, the selected criteria are based on the firefighters' expected time

of arrival at the construction under assessment, partially based on [19] (see Table 5). When P_{17} is graded as E or D, this construction can be reduced two levels if P_{13}, P_{15} or P_{16} are of Class A (e.g. if the construction has AM, AS1, W1 and $P_{17} > 40\ min$, P_{17} should be graded as C). The grade of P_{17} increases one level if the access to the façade of the construction has physical obstacles, if there is a unique or no road access, or if the access routes have heavy traffic.

Table 5: Classification of parameters P_{13} to P_{17}.

Indicator	Class					Unit
	A	**B**	**C**	**D**	**E**	
	0	**25**	**50**	**75**	**100**	
P_{13}	AM	AA	AMN	AAN	NAD	-
P_{14}	SC1	SC2	SC3	SC4	SC5	-
P_{15}	AS1	AS2	AS3	AS4	AS5	-
P_{16}	W1	W2	W3	W4	W5	-
P_{17}	0-10	10-20	20-30	30-40	>40	min

2.4 Emergency Preparedness Planning (EPP)

This group reflects the availability of measures and strategies implemented to safeguard the construction and its movable assets given their cultural value. This group integrates parameters addressing the existence of emergency planning (P_{18}), the elevation of relevant compartments of the construction (P_{19}), evacuation routes (P_{20}), and emergency signage (P_{21}) according to:

$$G_4 = EPP = [Max\ (P_{i,i=18:21})] \times 0.15 \quad (5)$$

Parameter P_{18} is graded as EA when the staff is trained to handle emergency situations and there is an emergency response plan with measures for the evacuation or protection of cultural assets in case of fire and specific procedures for the fire brigade that will deal with the fire [16]. This emergency response plan needs to involve guidance for staff training, information about the governance hierarchy and the control of access to the construction during emergencies, guidance for the evacuation of cultural assets during emergencies and procedures to carry out regular safety/risk assessments. The emergency plan, must have strategies to address scenarios where rehabilitation or refurbishment operations that may involve hot works are carried out [18]. If the emergency plan only accounts for the safety of people, P_{18} is graded as EB. P_{18} is graded as EC when the staff is trained to handle emergency situations, but there is no emergency plan. P18 is graded as ED when there is an emergency plan but the staff is not trained to handle emergencies. If there is no emergency plan and if the staff is not trained to handle emergencies, P_{18} is graded as EE. Parameter P_{19} is linked to the elevation of the habitable space (HS) or the compartments with cultural assets (CUA), considering the most disadvantageous case (see Table 6). The classification of P_{19} can be modified when CUA and/or HS are located at a height over 9 m but there are active suppression systems (AS1 or AS2) and when efficient strategies of staff training are also integrated into the emergency plan (EA) [18]. Parameter P_{20} combines multiple factors (i.e. travel distance to safety points (d), the width of corridors (w) and their slope (s)) based on [5, 16], to reflect the characteristics of the evacuation routes relevant for the evacuation of movable assets (from A to E), or for people (from B to E). If P_{20} is classified as D or E, it can be improved by one level (up to three) each time one of the following are

available: efficient active suppression systems (AS3), smoke control systems (SC1, SC2 or SC3) and EA in evacuation zones or specific meeting points. On the other hand, P_{20} is increased by one level when there are combustible materials obstructing evacuation routes. Parameter P_{21} considers the contribution of signage and emergency lights to the safeguard of movable assets and the safety of people during an emergency. When there are emergency lights in the evacuation routes (EL) and the signage provides instructions for both the safeguard of movable assets (SM) and the safety of people (SP) during an emergency, P_{21} is of class A. When there are emergency lights in the evacuation routes (EL) but the signage only addresses the safety of people (SP), P_{21} is of class B. When there is only one element (i.e. emergency lights or signage) that provides the safeguard of movable assets (SM) and the safety of people (SP) during an emergency, P_{21} is of class C. When there is only signage addressing the safety of people (SP), P_{21} is of class D. When there are no emergency lights and signage (N), P_{21} is of class E. If the emergency lights are not in good working condition, P_{21}increases by one level.

Table 6: Classification of parameters P_{18} to P_{22}.

Indicator	Class				
	A	**B**	**C**	**D**	**E**
	0	**25**	**50**	**75**	**100**
P_{18}	EA	EB	EC	ED	EE
P_{19}	CUA ≤ 7 m and HS ≤ 9 m	HS and CUA ≤9 m, or CUA and HS >9 m and AS1 and EA	HS or CUA>9 m and AS1/AS2 and EA	HS or CUA>9 m and EA	HS and/or CUA >9 m
P_{20}	*s*=0-5º	*s*=0-5º	*s*=0-5º	*s*>15º	*s*>15º
	d≤15 m and *w*>3 m	*d*≤20 m or *w*>3 m	*d*>20 m and *w*>3 m	*d*>20 m or *w*<3 m	*d*>20 m and *w*<3m
P_{21}	SM and SP and EL	SP and EL	SP/SM or EL	SP	N

3 APLICATION OF THE PROPOSED METHODOLOGY

3.1 Description of the case studies

The first case study is the 16th century Church of Misericordia in Esposende, Portugal, (41°31'51.85"N, 8°46'50.18"W). Based on data available from an in-situ survey, the BP group was classified as D. The church exhibits a balance between combustible (i.e. main and secondary altars, roof, mezzanine and stairs made of timber (see Figure 1a)) and non-combustible materials (i.e. stone walls), and its current use is religious with an archive, thus leading to an estimated fire load for P_1 of 2600 MJ/m^2 (Class D). P_2 was graded as C, considering since the unprotected timber, namely, in the altars and the furniture, is a fire susceptible material. P_3 is graded as C since the largest compartment size is approximately 103 m^2, whereas P_4 is equal to A since the church is an isolated construction. The ratios r that were evaluated lead to a P_5 of Class C. Due to the level of degradation exhibited by some combustible materials and the lack of intumescent materials, P_6 is graded as C. For P_7, E was assigned due to a tree located approximately 4.48 m from one of the entrances (see Figure 1b). UEGPT was assigned to Class E due to P_8, and P_{12}. The former is graded as E because there are extension cords close to the combustible materials behind the main altar (see Figure 1c), and there are

frequent power surges when many electric components are turned on. The existence of gas containers stored in a poorly-ventilated area inside the building (see Figure 1d) and the use of gas heaters during ceremonies leads to a class D for P_9. The building does not have a HVAC system, leading to P_{10} of Class A. Since the building has a few cameras in the interior, P_{11}, is graded as C. P_{12} was graded as E due to a lack of fire suppression systems and the fact there is a mattress located in the compartment of the electrical control panel. FM was assessed as E due to a lack of fire detection (P_{13}), smoke control (P_{14}) and fire suppression systems (P_{15}). Still, P_{16} is graded as C (there is an exterior fountain 10m away and a public hydrant at approximately 20m), and P_{17} is graded as B (the firefighter services are nearby). Even though the height of the upper level is lower than 7m (P_{19} is A), EPP was graded as E due to a lack of emergency planning (Class E), the travel distance being more than 20m (Class E), and the door widths being lower than 3m (Class E). The absence of signage and the presence of emergency lights that are not in good working conditions lead to P_{21} of Class D. Table 7 and Figure 3a summarize the assessed parameters and present a final damage level D_V of 91.25 (heavy damage).

Table 7: Fire Risk Assessment Church of Misericordia in Esposende, Portugal.

	BP							**UEGPT**					**FM**					**EPP**			
P_i	P_1	P_2	P_3	P_4	P_5	P_6	P_7	P_8	P_9	P_{10}	P_{11}	P_{12}	P_{13}	P_{14}	P_{15}	P_{16}	P_{17}	P_{18}	P_{19}	P_{20}	P_{21}
C_i	**D**	**C**	**C**	**A**	**C**	**C**	**D**	**E**	**D**	**A**	**C**	**E**	**E**	**E**	**E**	**C**	**B**	**E**	**A**	**E**	**D**
G_i	$G_1 = 75 * 0.35 = 26.25$							$G_2 = 100 * 0.2 = 20$					$G_3 = 100 * 0.3 = 30$					$G_4 = 100 * 0.15 = 15$			
D_V	$26.25 + 20 + 30 + 15 = 91.25 \ \therefore Heavy\ Level\ of\ Damage$																				



(a) (b) (c) (d)

Figure 1: (a) Main Altar; (b) Exterior View; (c) Extension cords behind the main altar; (d) Storage room.

The second case is the 14th century Museum of Carmo in Lisbon, Portugal (38°42'43.5"N 9°08'25.4"W). The BP group was ranked as D, given that, in P_5, $r < 1$ and $nl \leq 2$. P_3 was graded as C since the largest compartment has approximately 190 m^2. P_1 and P_7 were graded as B due to the current use of the building (being a museum 80% with non-combustible material leads to a fire load of 500 MJ/m^2) and the existence of vegetation 5-30m away from non-combustible materials, respectively. The other parameters of BP were graded as A, due to the non-combustible materials of the walls and the type of adjacent buildings (P_2 and P_4), and the good level of conservation of the few combustible materials in the structure (P_6). In terms of UEGPT, the building was graded as B, given that utilities are in good condition, the technical room is in the exterior but near the administrative zones, there is a CCTV system (Figure 2b) and the building is in a moderate criminal area. FM is graded as C since there is a fire suppression system (Figure 2a), an alarm and detection system (Figure 2b), a passive smoke control system (atrium), water supply and the firefighters are less than 10min away. Even though P_{20} leads to

a Class D (travel d <20 m and w<3), it is upgraded to B due to the integration of AS1 and SC3. EPP is graded as C since there are some measures of emergency preparedness but no emergency plan, given that the elevation is lower than 7 m and that there are signage and emergency lights, (see Figures 2c and 2d). The summary of the parameters is shown in Table 8 and Figure 3b, leading to a final damage level of 53.75 (medium damage).

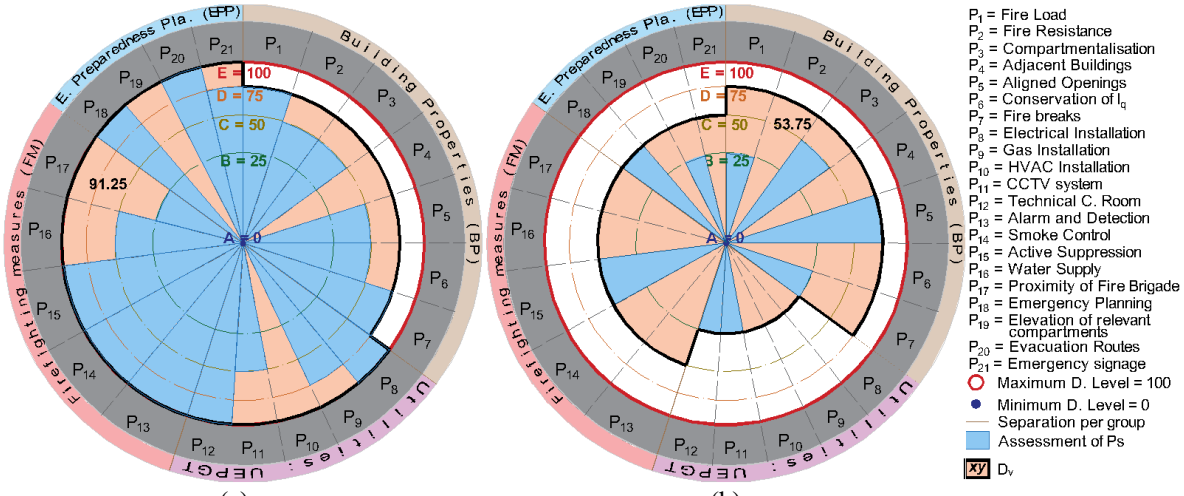
Table 8: Fire Risk Assessment of Museum of Carmo Convent in Lisbon, Portugal.

	BP							**UEGPT**					**FM**					**EPP**			
P_i	P_1	P_2	P_3	P_4	P_5	P_6	P_7	P_8	P_9	P_{10}	P_{11}	P_{12}	P_{13}	P_{14}	P_{15}	P_{16}	P_{17}	P_{18}	P_{19}	P_{20}	P_{21}
C_i	**B**	**A**	**C**	**A**	**D**	**A**	**B**	**A**	**A**	**A**	**B**	**B**	**A**	**A**	**C**	**A**	**A**	**C**	**A**	**B**	**A**
G_i	$G_1 = 75 * 0.35 = 26.25$							$G_2 = 25 * 0.2 = 5$					$G_3 = 50 * 0.3 = 15$					$G_4 = 50 * 0.15 = 7.5$			
D_V	$26.25 + 5 + 15 + 7.5 = 53.75 \ \therefore \ Medium\ Level\ of\ Damage$																				



(a) (b) (c) (d)

Figure 2: (a) Suppression System; (b) CCTV; (c) Alarms system; (d) Signage.



(a) (b)

Figure 3: Fire index assessment (a) 16th Church of Misericordia; (b) 14th century Museum of Carmo.

4 CONCLUSIONS

Given the diversity and specificity of cultural heritage assets, simple approaches are required to analyse their fire safety and establish their risk mitigation needs. In this context, a simplified fire damage index dedicated to assessing the expected damage impact due to fires in immovable cultural heritage assets is proposed. The proposed index involves a weighted multi-parameter

evaluation that can be correlated with the level of damage that the cultural heritage asset (including its contents) is expected to suffer under a fire. The fire index was applied to two case studies in Portugal to illustrate the flexibility of its applicability.

Acknowledgements. The authors acknowledge the support of the BD scholarship funded by FCT (Fundação para a Ciência e a Tecnologia) with reference PD/BD/150405/2019, the project POCI-01-0145-FEDER-030469 - RIACT - Risk Indicators for the Analysis of Cultural heritage under Threat, funded by FEDER funds through COMPETE2020 - POCI and by national funds through FCT, and the Base Funding UIDB/04708/2020 of CONSTRUCT - Instituto de I&D em Estruturas e Construções, funded by national funds through FCT/MCTES (PIDDAC).

5 REFERENCES

[1] Wen, I., Lee M. and Wu, S. Factors Affecting Fire Risk Assessment of Historic Buildings in Taiwan, *J. Applied Fire Science,* 4 (2013) **22**:447-460
[2] NFPA, *Code for the Protection of Cultural Resource Properties — Museums, Libraries, and Places of Worship* (2013).
[3] Watts, J. and Kaplan, M. Fire Risk Index for Historic Build., *F. Tech.* (2001)**37**:167-180.
[4] Chichorro, M., Ferreira, R. and Correia, A. Risk Assessment of Urban Fire – Proposal of a Model for Analysis and Management of Existing Building. (2016).
[5] Lopes, J. P., Coelho, A. L. and Rodrigues J. P. C. Urban Fire Risk Evaluation and the Municipal Emergency Plans. (2012).
[6] Granda, S. and Ferreira , T. M. Assessing Vulnerability and Fire Risk in Old Urban Areas: Application to the Historical Centre of Guimarães. *Fire Technology* (2019) **55**:105-127.
[7] Arborea, A., Mossa, G. and Cucurachi. Preventive fire risk assessment of Italian architectural heritage: An index-based approach. *Key Eng. Mat.* (2015) **628**:27-33.
[8] Romão, X., Paupério, E. and Pereira, N. A framework for the simplified risk analysis of cultural heritage assets. *Journal of Cultural Heritage.* (2016) **20**:696–708.
[9] Claret, M. and Andrade, A. Fire Load Survey of Historic Buildings: A Case Study. *Journal of Fire Protection Engineering.* (2007) **17**:103-112.
[10] Li, J., Li, H., Zhou, B., Wang, X. and Zhang, H. Investigation and Statistical Analysis of Fire Loads of 83 Historic Buildings in Beijing. *Int. J. of Architectural Her.* (2018) 1-12.
[11] Coelho, A.L. *Incêndios em edifícios*, Orion (2010).
[12] EN1991-1-2. *Eurocode 1: Actions on structures - Part 1-2: General actions - Actions on structures exposed to fire*. (2002).
[13] Hakkarainen,H and Y. Hayashi, Comparison of Japanese and European Fire Classification Systems for Surface Linings *Fire Sci. & Technology ,* 1 (2001) **21**:19-42.
[14] Karlsson, B. *Fire Risk Index Method - Multistorey Apart. Build. FRIM-MAB*, V.1.2, (2000).
[15] Matsumiya and Oikawa. Quantitative Analysis of Fire Spreading Potential for Surrounding Areas of Cultural Properties in Kyoto City. *J. of Asian A. and B. Eng.* (2013) **12**:269-276.
[16] CFPA-E, *Managing fire safety in historical buildings*, (2013).
[17] Rager, G. *La conservation des objets mobiliers dans les églises La conservation des objets mobiliers dans les églises*, Optimisa, (2004).
[18] Kidd, S. *Fire Safety Management in Traditional Buildings. Technical applications and management solutions*, Technical Conservation Group Historic Scotland, (2010).
[19] NFPA, *Code for Fire Protection of Historic Structures*, USA: NFPA Association, (2015).

12th International Conference on Structural Analysis of Historical Constructions
SAHC 2020
P. Roca, L. Pelà and C. Molins (Eds.)

EVALUATION OF INVASIVE RETROFITTING INTERVENTIONS ON AN UNREINFORCED MASONRY HERIRAGE BUILDING

A.SCUPIN[1*], R.VĂCĂREANU[1] AND F.PAVEL[1]

[1]Seismic Risk Assessment Research Center (CCERS)
Technical University of Civil Engineering Bucharest
Bd. Lacul Tei no. 122-124, Bucharest 020396, Romania
e-mail: anda.scupin@yahoo.com, www.ccerc.utcb.ro

Keywords: Historical Structure, Geology Museum, Unreinforced Masonry, Invasive retrofitting

Abstract. *The present study case highlights the importance of considering local failures for irregular unreinforced masonry buildings, by means of nonlinear seismic analyses. Simplified seismic assessments based on equivalent frame method were used in order to capture the structural behavior of the National Geological Museum from Bucharest in its initial form and also the current structural layout.*

The retrofitting works realized in the 1982 were focused on strengthening the transversal masonry walls and on creating horizontal diaphragms to improve the "box behavior" of the building subjected to lateral forces. Retrofitting of unreinforced masonry walls by reinforced concrete jacketing and the replacement of flexible floors by reinforced concrete slabs were previously considered to be effective only though post-earthquake visual inspections of the strengthened elements. The efficiency of past interventions is studied in the present paper through comparisons between the two models in terms of damage patterns, global behavior and also performance levels established function of maximum relative displacements.

1 INTRODUCTION

1.1 Brief history

The building hosting nowadays the National Geological Museum was built at the beginning of the 20th century, in between 1904-1906 by architect Ion Ștefănescu. Located in Bucharest, it was initially designed as headquarters of the National Geological Institute and transformed in museum in 1975. The building is listed on the cultural heritage list as having significant importance in the local context.

1.2 Structural layout

The museum's complex is formed by two wings with different heights and layouts, even

though not separated through seismic joints. The main wing has a U-shape layout composed of a semi-basement of 4.40 m height, a ground floor of 6.80 m and a first floor of 5.60 m. The secondary wing is located on the backside of the building and hosts the main staircase shown in Figure 1, as well as the exhibition hall with more than 12 m clear height. The connection between the two wings is done only through the circular walls of the hallway and though the stair landings. The lack of appropriate separation joints between the two wings with different stiffnesses represents one of the major structural deficiencies.



Figure 1: Main stairway linking the principal wing and the exhibition hall

Both exterior and interior walls are made of clay brick masonry and lime mortar with variable thicknesses along the height of the building. Reductions of the walls' thickness range from 25% up to 55%, thus creating major differences of wall's areas for each floor. In most of the cases, the masonry walls are continuous along the entire height, following the proportions of structural elements specific for the time of construction. Even though increased story height favors the creation of high horizontal coupling elements above openings of about 2 m, the openings of the main facades do not follow this layout. The uneven placement of windows on the principal façade, as well as the reduced height of the spandrels from the first floor creates considerable stiffness differences in between exterior and interior walls. Similarly, the openings on the walls of the back façade present an irregular alignment. These deficiencies led most probably to the creation of buttresses to support the walls of the secondary wing, as it can be observed in Figure 2Figure ~~2~~



Figure 2: View of the back facade of the National Geological Museum (secondary wing)

Apart from uneven placement of openings, the front façade also has an important discontinuity at the upper level of the balcony. The area situated above the main entrance is composed of columns and arches that support the upper level of the attic, as pictured in Figure 3.

Initially, the building had flexible floors made of metallic profiles and vaults for the partial basement and made of metallic profiles or wooden beams for the upper floors. The roof structure is made of wooden frames, having a particularly increased height reaching about 10 m. Hence, several high walls from the attic level present inappropriate anchorages in order to support horizontal actions. The vault covering the exhibition hall is made of reinforced concrete, while the vault of the stairways is made of a light weight material, namely reinforced mortar. The vaulted structure of the secondary wing marks one of the first practices for using reinforced concrete in Romania.



Figure 3: Main facade of the National Geological Museum

2 POST EARTHQUAKE STRUCTURAL BEHAVIOUR

Some of the main structural deficiencies noted in previous seismic assessments refer to the aspects previously presented with respect to the openings positioning and proportions, masonry walls' thickness reduction along height, lack of separation joints between the two wings and also improper connections of the structural walls at the attic level.

The museum was strongly affected by strong earthquakes which happened during the 20th century in Romania (1940, 1977, 1986 and 1990) and also by the World War II bombing in Bucharest (1944). Severe local damages were caused in the 1944, as it can be seen in Figure 4. According to past damage assessments [1], the earthquake from 1940 caused "significant degradations of the structural walls" that were not repaired not strengthened. Therefore, the strong ground motion from 1977 acted on a structure already damaged. Some of the damages observed after this seismic event range from cracking and debonding up to local collapse of nonstructural parts. The failure mechanisms consisted mainly in diagonal cracking (step-wise) and bending failure in the case of slender piers, such as the ones from the main façade of the building. The global behavior was governed by "walls with small openings" due to the increased width of spandrels, which remained undamaged. The most affected area was the portico of the front façade, due to uneven layout of transversal walls from the interior, with respect to the marginal walls of the balcony. This led to partial detachments of the portico from the main façade. Moreover, the asynchronous movement of the two wings caused significant damages to the curves walls that link the exhibition hall to the main building. At the last level, nonstructural walls improperly linked collapsed on top of the vault above the stairway and caused its destruction.



Figure 4: The National Geological Institute after the bombing from 1944, 23rd August (Agerpres Archive – foto no. 7646690)

In order to repair and strengthen the building, retrofitting works started in 1982. The main goals were to replace the flexible flooring with reinforced concrete slabs, to repair cracks by means of grout injections and also strengthen masonry walls using reinforcement bars or welded meshes. Metallic tie-rods were added in the most vulnerable parts, namely the portico and other partially collapsed parts. Apart from these local interventions, several transversal interior walls of the main wing were jacketed with reinforced concrete (10 cm thick layers) or reinforced mortar (4 cm thick layers).

The following seismic events from 1986 and 1990 did not cause any damages in the retrofitted areas and even improved the "box behavior" of the building subjected to lateral forces. Even though the global behavior was observed to be improved, supplementary retrofitting works were recommended to be undertaken in order to reach the safety standards for existing buildings, according to current regulations.

3 NUMERICAL MODELS

Starting from the damage assessment previously presented and also based on previous research related to material behavior of clay bricks used in the beginning of the 20th century, a numerical model of the buildings was calibrated. The software used was Tremuri [2] due to its ability to model masonry walls as assemblages of deformable macro-elements (piers and spandrels) linked by rigid nodes. The layout of the structure was slightly simplified in order to adapt to the modeling strategy of the software. Accordingly, the curved walls were approximated by orthogonal walls and the roof structures was not modeled explicitly. The final layout of the building modelled in Tremuri is shown in Figure 5.

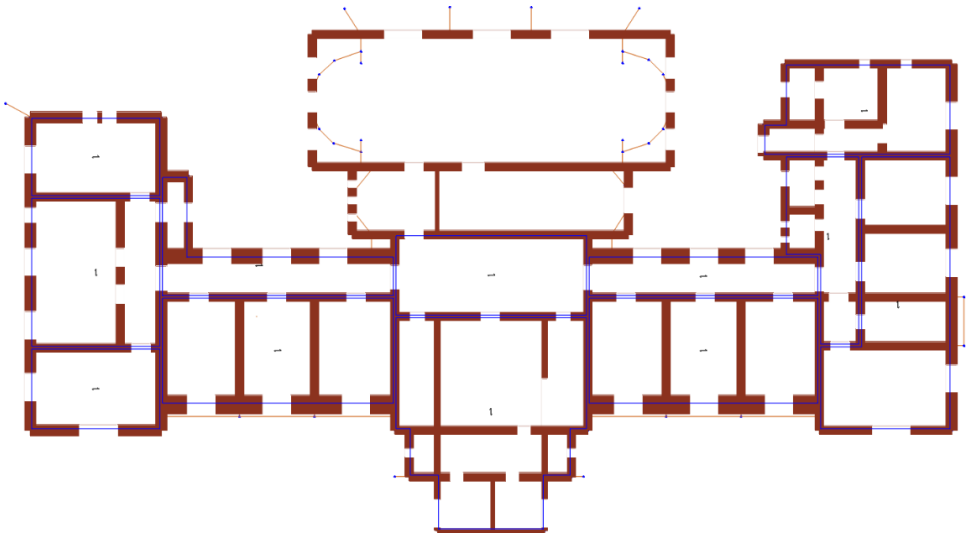


Figure 5: Structural layout of the building (Tremuri)

4 COMPARATIVE RESULTS OF THE STATIC NONLINEAR ANALYSES

In order to analyze the change in behavior generated by the retrofitting interventions done in the 80s', two numerical models were compared (initial structure and retrofitted structure) through Pushover analyses, damage patters and maximum displacements. The changes

implemented for the retrofitted model consist in improved material characteristics for the masonry walls retrofitted by RC jacketing, according to the sketch presented in Figure 6 and also modelling the slabs as rigid diaphragms.

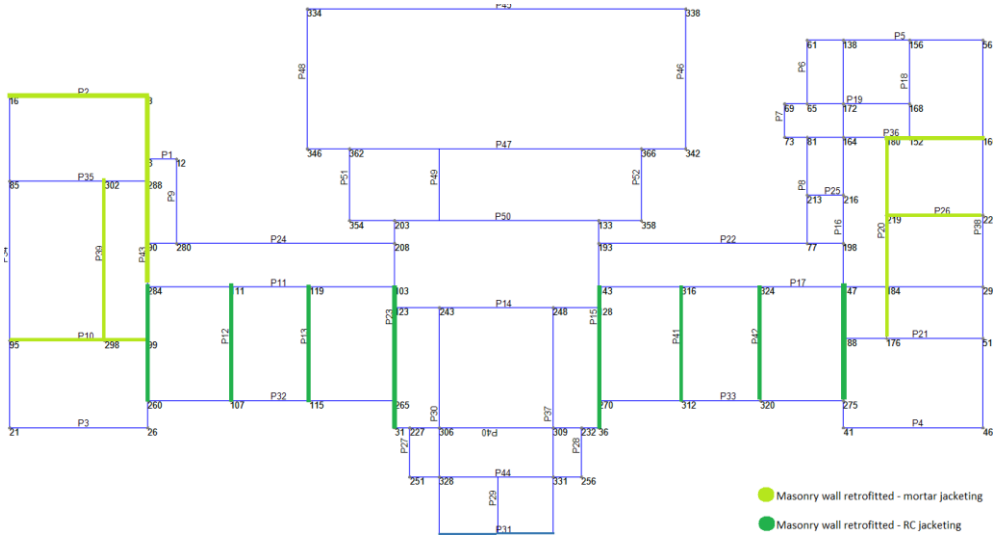


Figure 6: Masonry walls retrofitted by jacketing

4.1 Damage pattern

The pushover analyses were performed considering both positive directions of actions (along longitudinal and transversal directions) and a proportional application of horizontal forces along the height of the building.

Figure 7 illustrates the elements' damage state recorded at the last step of the Pushover analysis on X direction of loading. The most affected elements are found on the front façade of the building due to shear damage (light yellow) in case of spandrels from the first floor and bending damage of the slender piers from the upper floors. The piers facing shear failure are colored in orange and they correspond to the level where changes in openings position appear (ground floor – first floor). Comparing these damages stages with the ones recorded on the retrofitted model on the left, it can be observed that bending failure (red colored elements) appear on top of the back-façade walls. The lack of proper separation between the two wings was not solved through the retrofitting interventions carried out in 1982-1984. Moreover, since jacketing measures were taken for walls of the main wing, even greater difference in terms of stiffness tend to appear in between the two building parts.

4.2 Pushover curves

Pushover curves were obtained for both static and uniform loading patterns are presented in Figure 8 in order to highlight the differences between the initial and the retrofitted models. From the point of view of stiffness of the models, it can be observed that the initial model with flexible floors has different results for both loading directions. In the case of the retrofitted model, there are no longer present such variations in terms of stiffness, due to a more unitary behavior along the orthogonal directions, as desired for the structures with rigid diaphragms.

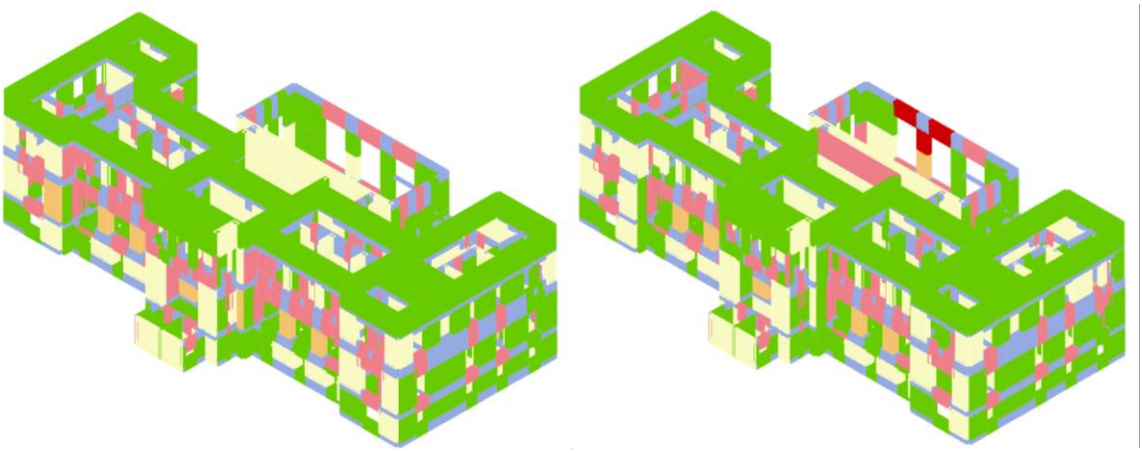


Figure 7: Comparative results for the Static Pushover: initial structure (left) and retrofitted structure (right) – longitudinal loading direction (X)

The improvements observed in terms of maximum horizonal force are significant on Y direction, where both Pushover loading patterns reach about 80% increase in strength. Taking into account that most of the interventions were concentrated on transversal walls, almost no changes are recorded on the results from longitudinal loading direction, when comparing the initial structure with the retrofitted one.

Since the retrofitting works were designed to increase the strength, no improvements are observed in terms of increased displacement capacity. The maximum global displacements from the nonlinear static analyses of the retrofitted models reach lower values then the initial model, especially in the case of the transversal loading direction, along which improvement works on masonry walls were concentrated.

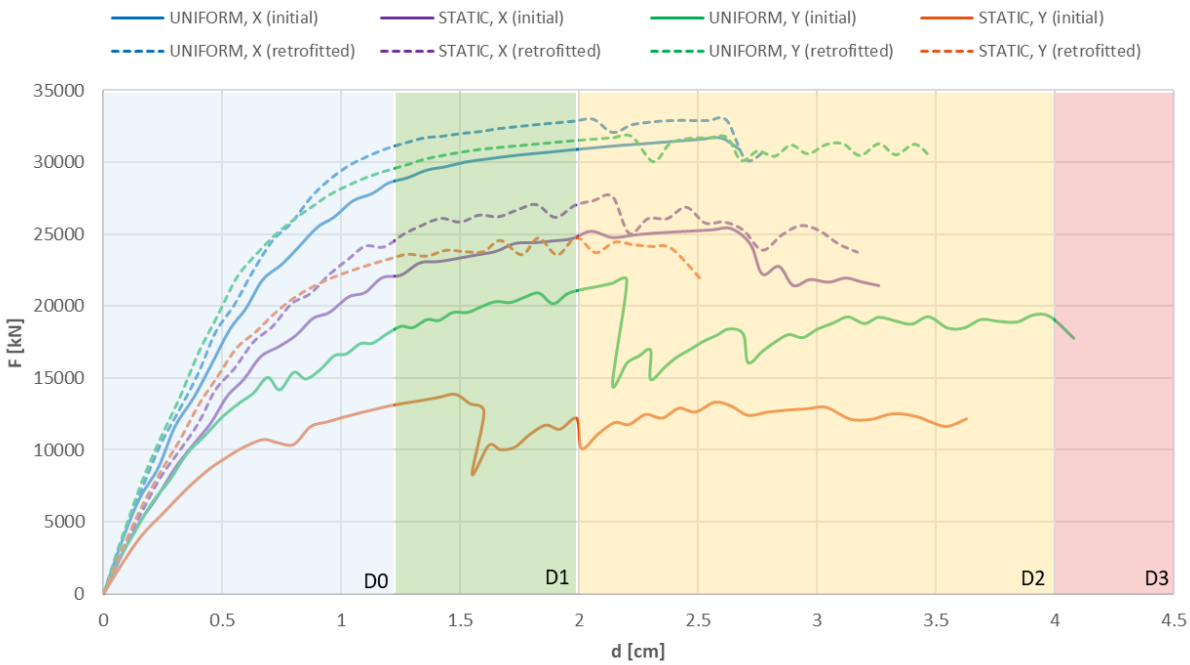


Figure 8: Pushover curves comparison

4.3 Global and relative displacements

In case of unreinforced masonry buildings with variable wall thicknesses, irregular damage distribution is frequently observed in post-damage seismic assessments [3]. As in the case herein presented, severe damages tend to concentrated at floors where changes of layout or wall thickness appear. Since global values of ultimate displacements may not reflect the maximum displacement values reached in areas with local failures, an additional analysis was done in order to evaluate relative displacements at the floor and at the wall level.

Previous literature studies highlight the significant differences between global and local ultimate displacements in case of masonry structures, proposing also threshold limits for each of these [3]. Typical drift values for unreinforced masonry walls presented in ASCE [4], as well as global drift limits proposed in literature [5] were summarized in Table 1 and further compared with the relative displacements obtained for the National Geological Museum. The global drift limits expressed function of the height of the building (19.85 m) are overlapped with the global Pushover curves in Figure 8. It can be observed that only for one of the analyses the collapse prevention limit is reached, namely for the initial model, uniform loading pattern in transversal direction, while all the other ultimate displacements indicate the life safety performance level.

Table 1: Relative displacement values for URM walls and URM structures

Structural performance levels		Drift values for URM walls	Drift values for URM buildings
D0	Immediate Occupancy (IO)	0 – 0.3%	0 – 0.06%
D1	Damage Control (DC)	0.3% - 0.6%	0.06% - 0.1%
D2	Life safety (LS)	0.6% - 1%	0.1% - 0.2%
D3	Collapse Prevention (CP)	≥ 1%	≥ 0,2 %

Taking into account that the global nonlinear analyses do not reach target displacements estimated based on equivalent single degree of freedom systems, it can be concluded that local failures occur before the global collapse of the structure. In order to check if the numerical models were able to capture the damage areas noted in the post-earthquake assessments, the relative floor and walls displacements, as well as the damage state of the elements was analyzed.

The highest relative displacements resulted from the Static Pushover case on the initial model appear at the walls from the ground floor level in case of longitudinal loading direction and on the first level for the transversal loading direction. For X direction, almost 30% of the masonry walls form the ground floor overpass the drift limit corresponding to damage control, with 2- 3 cm displacement. In case of Y loading direction, more than 20% of the walls reach the life safety stage with relative displacements higher than 3.6 cm. The highest relative displacements are recorded on one of the portico's sides (wall 28) and also the adjacent interior wall no. 15, marked with red on Figure 9. Their displacements correspond to the collapse prevention performance limit, according to the drift proposed as reference by ASCE [4]. The highest relative displacement recorded for the longitudinal direction is also highlighted in green for the wall no. 44 in Figure 9.

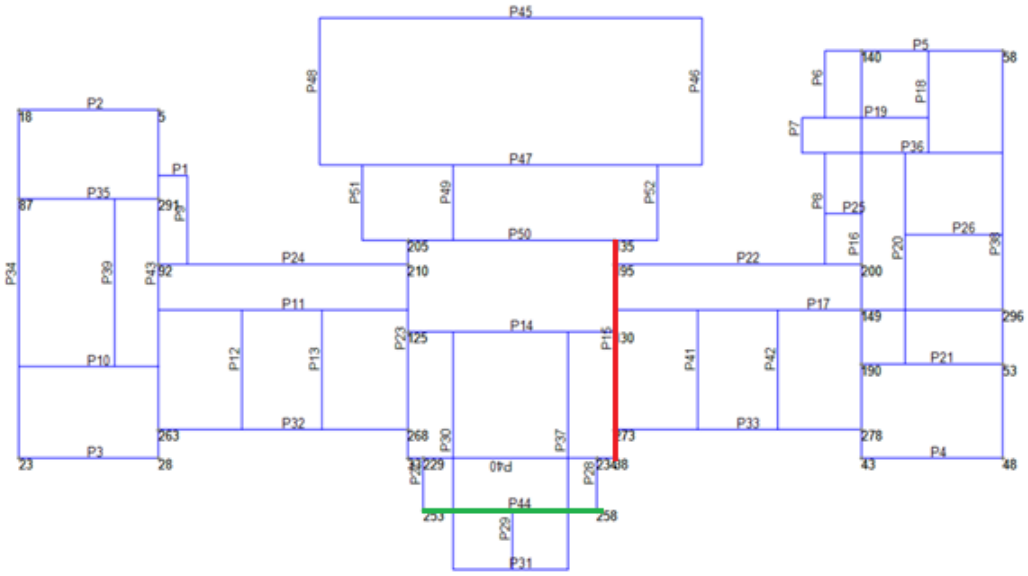


Figure 9: Damage stage color code for all the walls with highest relative displacements

These results are in good accordance with the information regarding the damage assessment, showcasing once again the local vulnerabilities caused by the portico, the openings layout of the main façade as well as the misalignment of transversal interior walls. For wall no. 44 and no. 15, detailed results are presented in Table 2 and Table 3 with respect to the ultimate displacements recorded in nodes along the height and also the damage stage of the macro elements. Since wall no. 15 was retrofitted by jacketing, unlike wall no. 44, a comparison between results of the initial model and of the retrofitted model is also shown.

For wall no. 44, placed on the longitudinal direction of the building, the slender piers of the portico are placed on top of the main entrance, so that the entire layout is highly irregular. Moreover, transversal connections with the rest of the building are not continuous, therefore favorizing local detachments. Considering there were no strengthening works performed on this façade wall, nor other significant works on the longitudinal direction, there are no major changes observed for the retrofitted model.

In case of wall no.15, the highest drift appears at the first level, where important stiffness differences appear along the height of the wall due to placement of openings. After the jacketing of the wall with 20 cm of RC on both sides, the damage distribution along the macro-elements is completely changed, as it can be observed in the retrofitted model from Table 3. Bending of the pier from the first floor is avoided and the relative displacements decrease below the Damage Control drift limit.

When comparing the initial model with the retrofitted one, significant improvements are observed for the transversal direction. Considering the numerous constrained specific for heritage buildings, jacketing works were only possible in few places, mostly on the transversal direction. These types of traditional reinforcements applied for unreinforced masonry are considered to be similar to the addition of new reinforced concrete walls [6] and were extensively used at the end of the 20th century and combined with less invasive interventions [7]. Adding layers of reinforced concrete on masonry walls increases strength, anyhow restraining the deformation capacity of the structural element. Lateral cyclic laboratory tests

performed in Skopje [8] concluded that jacketing of URM walls subjected to high compressive forces decreases their displacement capacity. Therefore, the efficiency of this retrofitting method depends on their proportions, being more adequate for walls with an aspect ratio between height and length of about 0.7, rather than slender walls.

Table 2: Relative displacements of wall no. 44 (longitudinal loading direction)

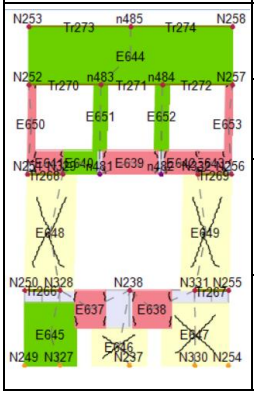
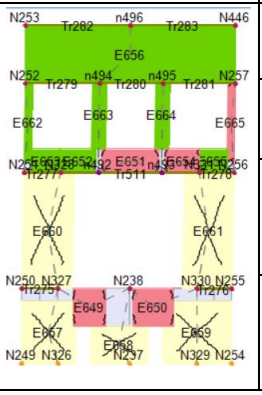
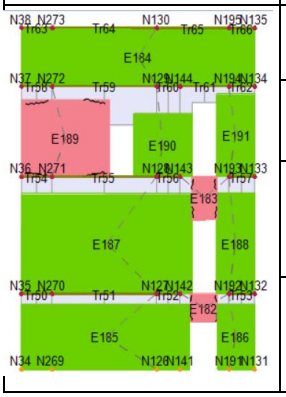
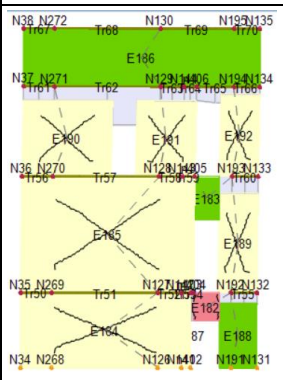
Initial model			Retrofitted model		
Damage stage of macro-elements	Ultimate displacement per floor [cm]	Ultimate drift per floor [%]	Damage stage of macro-elements	Ultimate displacement per floor [cm]	Ultimate drift per floor [%]
	3.69	0.01		3.31	0.01
	3.68	0.18		3.28	0.16
	2.76	0.39		2.42	0.33
	0.08			0.15	

Table 3: Relative displacements of wall no. 15 (transversal loading direction)

Initial model			Retrofitted model		
Damage stage of macro-elements	Ultimate displacement per floor [cm]	Ultimate drift per floor [%]	Damage stage of macro-elements	Ultimate displacement per floor [cm]	Ultimate drift per floor [%]
	5.57	0.01		2.62	0.02
	5.55	1.01		2.54	0.27
	0.24	0.03		1.13	0.15
	0.11			0.14	

5 CONCLUSIONS

The numerical models proposed for the National Geological Museum were validated by comparison with the post-earthquake damage assessments presented in technical documents. The macro-element method implemented in Tremuri was able to capture the structural behavior of the building, where slender piers suffer from bending damage and diagonal cracking appears for elements subjected to shear forces. Significant damages recorded for the masonry walls were also captured in the model by means of high damage percentages for macro-elements. The damages from the portico area observed after the 1977 earthquake were also present in the numerical model through large relative displacements of the structural elements.

The layout of openings on the façade, as well as the transition area between the two wings of the building favorized the accumulation of damage on certain areas and levels. Therefore, distinct analyses were done to evaluate the performance level function of relative displacements at global level and also at the wall's level. The ultimate drift recorded for the entire building indicated the exceedance of life safety performance level, while the relative damages from the portico overpass the collapse prevention drift limits.

A distinct model was done for the retrofitted version of the museum, based on the interventions performed in 1982. When comparing the results of the initial model with the retrofitted one, the lateral capacity increased up to 80% along the transversal direction, where most of the works were carried out, while the ultimate displacement was slightly reduced. Therefore, the overall seismic energy dissipation capacity reaches a 25% increase for the retrofitted model. On the other hand, significant reductions of relative displacements appear in case of the most vulnerable parts of the buildings, namely the portico and the façade walls, thus leading to a more uniform load distribution along structural walls on both directions. Taking into account that these types of invasive interventions are difficult to apply on heritage buildings due to architectural constraints, alternative retrofitting solutions should be considered for future interventions.

Acknowledgements. The authors would like to acknowledge the help of STAdata for providing an academic license of the Tremuri software.

REFERENCES

[1] Gospodinov, N. and Lozincă, E. *Raport de expertiză tehnică privind starea structurii ansamblului imobiliar Muzeul Național de Geologie Sector 1, București* (2011).

[2] Lagomarsino, S., Penna, A., Galasco, A. and Cattari, S. TREMURI program: An equivalent frame model for the nonlinear seismic analysis of masonry buildings. *Eng.Struct.* (2013) **56**:1787-1799.

[3] Derakhshan, H. and Griffith, M. *Final report on Pushover analysis of classes of URM building to characterize drift ratios for different damage levels.* (2018).

[4] ASCE *Prestandard and commentary for the seismic rehabilitation of buildings.* FEMA 356 (2000).

[5] Cattari, S., Giongo, I., Marino, S. and Lin, Y. Numerical simulation of the seismic response of an earthquake damaged URM building. In: *New Zeeland Society for Earthquake*

Engineering Technical Conference 2015 (2015).
[6] Fulop, L. and Sippola, M. *Constructive and performance analysis of the retrofit systems for vertical masonry elements. Research report* (2011).
[7] Hancilar, U., Durukal, E. and Erdik, M. Seismic assessment and rehabilitation of historical unreinforced masonry (URM) buildings in Istanbul. In*: Improving the Seismic Performance of Existing Buildings and Other Structures* (2009), pp. 1305-1316.
[8] Churilov, S. and Dumova-Javanoska, E. Analysis of masonry walls strengthened with RC jackets. In: *15 World Conference on Earthquake Engineering* (2012)

12th International Conference on Structural Analysis of Historical Constructions
SAHC 2020
P. Roca, L. Pelà and C. Molins (Eds.)

KINEMATIC APPROACH FOR SEISMIC VULNERABILITY ASSESSMENT OF MASONRY CHURCHES

V.CORLITO[1], G. DE MATTEIS[1*] AND P. ROCA[2]

[1] Department of Architecture and Industrial Design (DADI)
University of Campania "Luigi Vanvitelli"
San Lorenzo Abbey, 81030 Aversa, Italy
e-mails: gianfranco.dematteis@unicampania.it (*corresponding author)
valentina.corlito@unicampania.it

[2] Department of Civil and Environmental Engineering
Universitat Politècnica de Catalunya
(UPC - Barcelona Tech), 08034 Barcelona, Spain
e-mail: pere.roca.fabregat@upc.edu

Keywords: Vulnerability Assessment; Kinematic Analysis; Masonry Churches; L'Aquila Earthquake

Abstract. *The application of reliable predictive methods for the seismic vulnerability assessment of historical buildings represents a challenging issue in the process of risk mitigation at regional/national scale, in order to undertake appropriate strategies aimed at achieving acceptable safety levels. For the application of such policies, the availability of adequate procedures for the correct evaluation of the seismic risk of specific assets, like churches, is a fundamental topic of investigation. In this paper, a simple procedure based on the linear and non-linear kinematic approach is applied to evaluate the seismic capacity of masonry churches, both in terms of spectral acceleration and spectral displacement. To check the reliability of such a procedure, the obtained results have been compared with the damage scenario observed on a population of churches analysed by the research group in the aftermath of the 2009 L'Aquila earthquake.*

1 INTRODUCTION

Recent seismic events produced extraordinary costs for reconstruction of damaged buildings, showing also a considerable impact on social and cultural factors of the affected territories. In particular, the earthquakes occurred in Italy in the last decades evidenced severe states of damage and significant losses of important historical and architectural assets, emphasising the great fragility of the existing building heritage and stressing the necessity to prevent losses through the definition of reliable preventive protection strategies.

As far as masonry churches are concerned, different methodologies of assessment have been developed, considering various approaches with different levels of investigation [1-4]. The damage probability matrix (DPM) method and the vulnerability index method (VIM) are among the most common vulnerability assessment approaches found in literature [5, 6].

Such methods are mainly based on the observational analyses carried out at territorial scale on churches in the aftermath of significant seismic events (such as Friuli [7], Umbria and Marche [8], Molise [9], L'Aquila [10, 11] and Central Italy [12, 13] earthquakes) which allowed to learn more about the most recurrent damage mechanisms and seismic fragilities of existing churches. Alternative methodologies were also developed on the basis of analytical evaluations, mainly based on the study of macro-element behaviour through linear and non-linear analyses. Different simplified methodologies to derive fragility curves can be found in literature [14, 15]. With general reference to the approaches used for existing masonry buildings, many studies are definitely worth of being mentioned [16-19].

In this paper a predictive methodology for the seismic vulnerability assessment of masonry churches in large territorial areas is presented, focusing the attention on the three-nave churches of the Abruzzi Region. A simplified procedure, based on the kinematic limit approach, is proposed with the aim to identify the structural capacity of the main detectable macro-elements and to provide predictive tools useful for the development of suitable risk mitigation strategies.

2 LOCAL RIGID-BLOCK ANALYSIS

2.1 Introduction

A masonry building can be considered as an assembly of statically determined elements connected to each other in a unilateral restraint condition. The possible lack of effectiveness (or maybe the absence) of the connections between these elements can compromise the behaviour of the whole structure, making it particularly vulnerable to the stresses induced by a seismic event. This statement assumes a particular value for the masonry churches, in which the typological configuration of the buildings and also the possible historical stratifications may imply the presence of remarkable internal disconnections. The seismic action stresses these disconnections, favouring different behaviours for the several structural components: in case of good quality masonry, the damage can occur with the loss of equilibrium of rigid blocks that can sustain relevant displacements before collapsing. This hypothesis is confirmed by the partial collapses observed in the damaged masonry churches after the recent seismic events (Figure 1).

The above observation allows to state that the study of the global seismic response may be less appropriate for many types of historical buildings, for which the use of local models may be more suitable. The analysis of local rigid-body mechanisms [20] considers each structural element composed of a certain number of non-deformable wall blocks, connected to each other and to the rest of construction through internal and external constraints. The set of these constrained rigid blocks must be such as to constitute a kinematic chain with a single degree of freedom (SDOF).

The study of a local mechanism is conducted through the method of limit analysis, following a kinematic approach, according to the following steps: *(i)* identification of possible collapse mechanisms; *(ii)* definition of the value of the horizontal load multiplier α involving the activation of the relevant mechanism; *(iii)* safety check, through the comparison between seismic demand and structural capacity.

More specifically, the structural capacity is evaluated through the linear and non-linear approach, to evaluate the acceleration of the kinematic activation and its ultimate displacement capacity, respectively [14, 21, 22].

These criteria can be extended to monumental buildings by recognizing SDOF elements that identify the typical kinematic configurations of macro-elements.



Figure 1: Partial collapses observed in the Italian churches of Sant'Eusanio Martire in Sant'Eusanio Forconese (a), Santa Maria degli Angeli in Paganica (b) and Santa Gemma in Goriano Sicoli (c) (L'Aquila district, Abruzzi).

2.2 Simplified kinematic procedure

In this paper, a simplified method for a large-scale vulnerability assessment of churches is considered. The procedure is aimed at identifying the kinematically admissible mechanisms for a population of 64 three-nave churches located in the territory of L'Aquila [AQ] and Sulmona-Valva [SU-VA] Dioceses (in Abruzzi, Italy), verifying their capacity in terms of possible accelerations (linear kinematic analysis) and ultimate displacements (non-linear kinematic analysis). The analysis regards the macro-element "Façade".

The analysis of the local mechanisms for masonry churches has been conducted assuming the macro-elements approach identified by the Italian Cultural Heritage Guidelines [22], based on the statistical studies carried out in the aftermath of the last Italian seismic events. In particular, a number of I MODE kinematically admissible collapse mechanisms, defined by different positions of the cylindrical hinges, has been identified for the analysed macro-element. Then, the analyses have been performed considering the detected constraint conditions, the presence/absence of possible retaining or thrusting elements and the influence of the typological features of the macro-element (Figure 2) on the activation of each possible mechanism, as schematically shown in Figure 3 and in Table 1.

Namely, the identified kinematic motions are:

- global façade monolithic overturning [K1];
- double-skin façade monolithic overturning [K2];
- global façade composed overturning [K3];
- top of the façade monolithic overturning [K4, K5, K6];
- top of the façade composed overturning [K7];
- monolithic vertical bending [K8];
- monolithic vertical bending (external skin) [K9];
- horizontal bending [K10];
- double-skin façade horizontal bending [K11];
- double-skin façade horizontal bending (external skin) [K12].

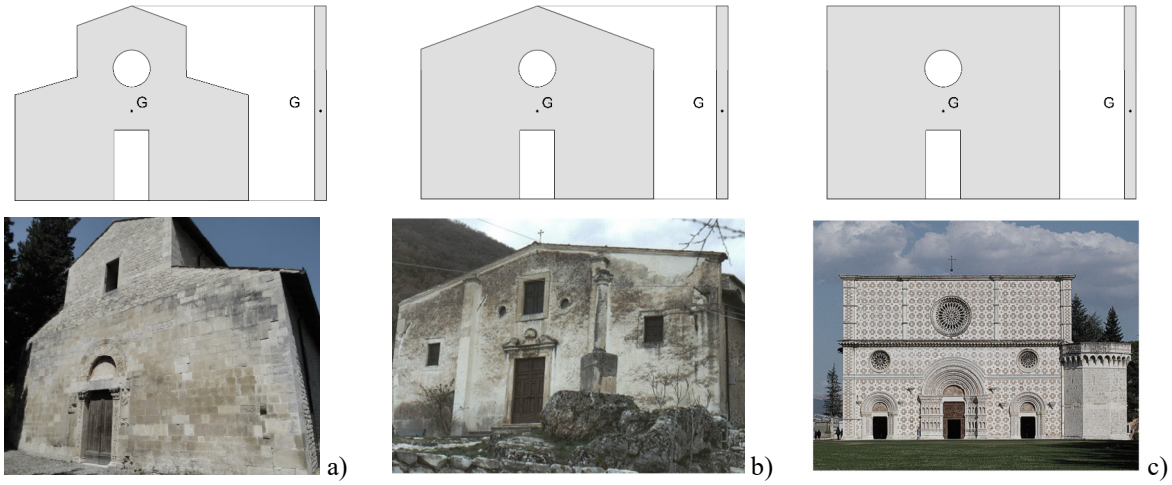


Figure 2: Common type of façades observed in L'Aquila district: salient façade_ church of San Pietro ad Oratorium in Capestrano (Aq)[SU-VA] (a); gabled façade _church of Sant'Agata in Tussillo (Aq) [AQ] (b); flat façade_ church Santa Maria di Collemaggio in L'Aquila [AQ] (c).

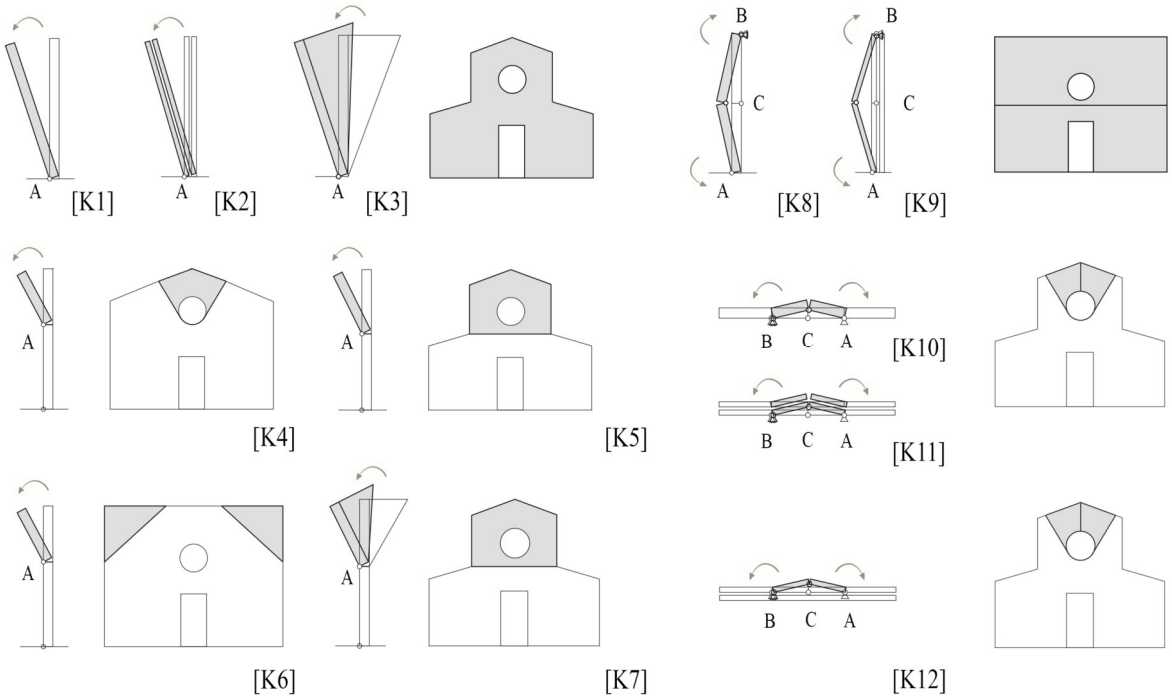


Figure 3: Possible kinematic motions for the macro-element "Façade".

3 LINEAR KINEMATIC ANALYSIS

3.1 General

A linear kinematic analysis has been performed for the façades of the considered stock of churches. For each analysed façade and for each identified mechanism, the horizontal load

Table 1: Influence of typological characteristics and constraint conditions on the identified mechanisms.

Kinematic motion	Façade typology	Constraint conditions
[K1]	Salient façade	No retaining elements
[K2]	Flat façade	No connections on the top
	Gable façade	No connection between transversal walls
[K3]	Salient façade	No retaining elements
	Flat façade	No constraints on the top
	Gable façade	Connection between transversal walls
[K4]	Salient façade	No constraints on the top
	Flat façade	
	Gable façade	
[K5]	Salient façade	No constraints on the top
[K6]	Flat façade	No constraints on the top
[K7]	Salient façade	No constraints on the top
		Connection between transversal walls
[K8]	Salient façade	Connections on the top
[K9]	Flat façade	No connection between transversal walls
	Gable façade	
[K10]	Salient façade	No connections on the top
[K11]	Flat façade	Connection between transversal walls
[K12]	Gable façade	

multiplier α has been defined, according to the static theorem of limit analysis. The spectral acceleration a^*_0 that activates the identified collapse mechanisms, related to the specific values of α, has been calculated according to equation (1) [20]:

$$a^*_0 = \frac{\alpha \cdot g}{FC \cdot e^*} \tag{1}$$

where g is the gravity acceleration, FC is the confidence factor related to the level of knowledge (LC) of the investigated structures (geometry, material, etc.), and e^* is the portion of mass participating in the considered mechanism. For the cases being, given the limited knowledge of the characteristics of the structures, FC = 1.35 for LC1 has been assumed.

For the generic mechanism, the safety check for SLV (Life-saving Limit State) is assumed to be satisfied when the spectral acceleration a^*_0 activating the mechanism complies with the structural capacity of the considered macro-element. The evaluation has been based on the definition of the safety index $I_{S,\,SLV}$, which, for the reference limit state, is obtained as a ratio between the seismic capacity of the structure $Cap_{,\,SLV}$ [g] and the seismic demand $Dem_{,\,SLV}$ [g], according to the standards requirements [20].

The limit value for $I_{S,\,SLV}$ has been determined according to the Italian Guidelines [22], defining a ratio between the T_{SLV} return period of the seismic action corresponding to the attainment of the SLV Limit state and the corresponding return period $T_{R,\,SLV}$ computed with the equation (2), in relation to the reference period V_R and to the probability of exceeding in the reference period P_{VR}.

The limit value for the safety index estimated for the considered structures is $I_{S,\,SLV} = 0.614$.

$$T_R = -\frac{V_R}{\ln(1 - P_{V_R})} \tag{2}$$

3.2 Application to the investigated churches

The above linear kinematic analysis with reference to the macro-element "Façade" has been applied to the 64 investigated churches. The relevant results together with a statistical elaboration are given in Table 2, where the following main outcomes are provided:

- the frequency of the collapse mechanisms that the constraint conditions of the structure make kinematically possible (*Possible [K]; α>0*);
- the frequency of the mechanisms for which the $I_{S,\,SLV}$ safety index is lower than 1 (*Possible [K];* $I_{S,\,SLV} < 1$);
- the frequency of the mechanisms for which the safety verification in terms of $Cap_{,\,SLV}/Dem_{,\,SLV}$ ratio is not satisfied and for which the $I_{S,\,SLV}$ safety index is lower than 0.614 (*Possible [K];* $I_{S,\,SLV} < 0.614$).

By the obtained results, it is possible to determine the kinematic motions that cannot be activated (namely [K2], [K9] and [K11]) as well as to identify the probability of activation of the possible kinematics.

The results show that generally there is a high vulnerability of the façades with respect to the kinematic motion [K1] (global façade monolithic overturning), [K4] (top of the façade monolithic overturning) and [K10] (horizontal bending), for which the values of the $I_{S,\,SLV}$ safety indexes are less than the unit for the 48%, 25% and 22% of the analysed cases. For the same mechanisms the values of the $I_{S,\,SLV}$ safety do not respect the limit condition ($I_{S,\,SLV}$ <0.614) for the 13%, 7% and 22% of the analysed cases.

The performed linear kinematic analysis also revealed the frequency of the mechanisms that could be potentially activated by the PGA values associated with the 2009 seismic event (*Possible Activation* $PGA_{[INGV]}$), in accordance with the INGV Shake Map based on the Faenza and Michelini assumption [23].

In Table 3, the above results have been also compared with the frequencies of the damage level d_k (with $0 \leq d_k \leq 5$) registered for the analysed churches in the aftermath of the seismic event [24], with refence to the out-of-plane mechanisms of the façade (mechanism [M1]) and of the top of it (mechanism [M2]). In order to check the reliability of the analytical results, the damage level d_k corresponding to the activation of the damage mechanism has been considered separately for both values d_k=1 and d_k=2, accounting for possible evaluation errors connected to the ambiguous classification of damage.

The comparison shows that for all the kinematic mechanisms related to the whole façade [K1, K3, K8] (to be compared with [M1]) and for all those related to the top of the façade [K4, K5, K6, K7, K10, K12] (to be compared with [M2]), the frequency of *Possible Activation* $PGA_{[INGV]}$ is lower than the activation frequency actually recorded following the seismic event (*Observed Activation*). Indeed, a better comparison has been obtained with reference to the damage levels d_k>2, for which more objective criteria in the classification of the damage can be hypothesised.

The correlations between the values of the collapse multiplier α calculated for the *Possible [K] (α>0)* and the damage levels observed for each church for the mechanism [M1] and [M2]

are shown in Figure 4 and in Figure 5, respectively. As it could be expected, higher values of the collapse multiplier α have been generally obtained for the *Possible [K]* detected in churches which suffered a lower level of damage d_k for the collapse mechanisms [M1] and [M2], stating that the analysed mechanisms has been mainly observed for those churches characterized by lower value of the factor α, confirming the validity of the applied analytical procedure.

Table 2: Frequencies of possible kinematic motions for the façades for the 64 analysed churches.

	Possible [K] (α>0)	**α** (average value)	**a^*_0 [g]** (average value)	**Cap, SLV [g]** (average value)	**Dem, SLV [g]** (average value)	**Possible [K] IS, SLV< 1**	**Possible [K] IS, SLV<0.614**
[K1]	67%	0.126	0.172	0.344	0.369	48%	13%
[K3]	13%	0.261	0.354	0.708	0.369	10%	0%
[K4]	63%	0.232	0.313	0.625	0.521	25%	7%
[K5]	30%	0.589	0.796	1.592	0.535	0%	0%
[K6]	10%	0.437	0.591	1.183	0.519	5%	0%
[K7]	5%	0.557	0.760	1.519	0.523	0%	0%
[K8]	5%	0.405	0.558	1.116	0.369	0%	0%
[K10]	22%	0.047	0.064	0.127	0.521	22%	22%
[K12]	2%	0.009	0.012	0.024	0.521	2%	2%

Table 3: Comparison between the results of the linear kinematic analysis and the frequencies of the d_k damage levels registered in the aftermath of the 6th April 2009 earthquake for [M1] and [M2] mechanisms.

	$I_{S,SLV}$ < 1	**$I_{S,SLV}$ < 0.614**	**Possible Activation** $PGA_{[INGV]}$			**Observed Activation** [d_k>1]	[d_k>2]
[K1]	58%	13%	15%	18%	[M1]	37%	24%
[K3]			3%				
[K8]			0%				
[K4]	53%	30%	3%	18%	[M2]	35%	28%
[K5]			0%				
[K6]			2%				
[K7]			0%				
[K10]			12%				
[K12]			2%				

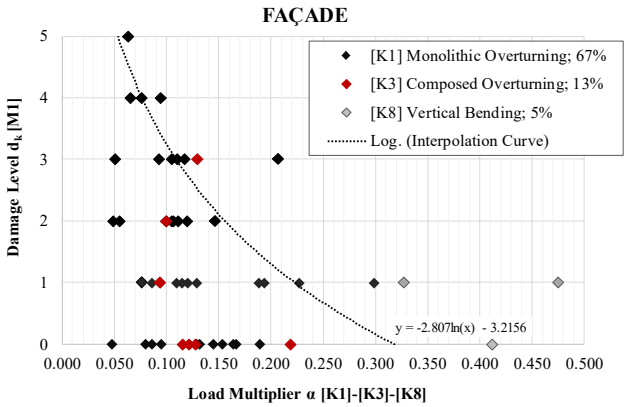


Figure 4: Correlations between the values of the collapse multiplier α calculated for the [K1] [K3] [K8] (with *α>0*) and the registered damage levels d_k for mechanism [M1].

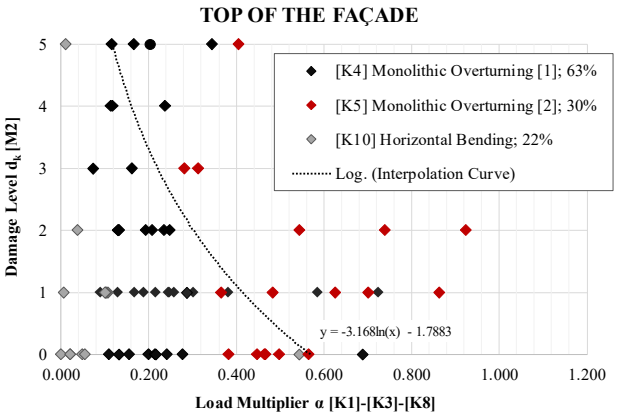


Figure 5: Correlations between the values of the collapse multiplier α calculated for the [K4] [K5] [K10] (with $\alpha>0$) and the observed damage levels d_k for mechanism [M2].

4 NON-LINEAR KINEMATIC ANALYSIS

4.1 General

The non-linear kinematic analysis is devoted to investigate the displacement capacity of the structure when the collapse of the considered mechanism occurs. To this aim, the horizontal load multiplier α can be calculated on the deformed configuration, following the evolution of the mechanism, which can be exhaustively defined by a relationship $\alpha= \alpha(d_k)$, relating the load multiplier α with the displacement d_k of a pivot point (the centre of masses) of the façade [20]. The analysis finishes when the load multiplier equals zero: the corresponding displacement of the pivot point $d_{k,0}$ is representative of a collapse situation.

From the relationship $\alpha= \alpha(d_k)$, the capacity curve of the equivalent SDOF system, in terms of spectral acceleration a^* and spectral displacement d^*, can be derived. The value a^*_0 is the maximum acceleration to which the macro-element can resist before the kinematic motion activation; d^*_0 is the spectral displacement corresponding to $d_{k,0}$. Since the displacement d^*_0 is not trustworthy in describing the real behaviour of the macro-element, the actual ultimate displacement of the SDOF system is evaluated as $d^*_u = 0.4\, d^*_0$.

The safety check of the local mechanism in the SLV limit state consists in comparing the ultimate spectral displacement d^*_u with the displacement demand $\Delta T(Ts)$ obtained from the displacement spectrum defined according to the Italian Code OPCM 3431 [25]. The check is satisfied when $d^*_u > \Delta T(Ts)$.

4.2 Application to the investigated churches

The non-linear kinematic analysis has been performed for the façade of the 64 analysed churches with reference to the mechanisms for which the safety check in terms of $Cap_{,SLV}/Dem_{,SLV}$ ratio is not satisfied. The check has been carried out considering the displacement demand $\Delta T(Ts)$ related to the seismic hazard of the inspected sites.

The results and the corresponding statistical elaboration are given in Table 4 and Table 5; the outcomes reveal a high percentage of *Possible Collapse* [$d^*_u > \Delta d\,(Ts)_{,SLV}$] for the kinematic motions [K4] (top of the façade monolithic overturning).

The non-linear kinematic analysis also reveals the frequency of the possible collapses occurred through the analysed mechanisms by considering the displacement demand $\Delta T(Ts)_{,E}$ induced by the PGA values associated with the 2009 L'Aquila seismic event [INGV] [23].

In Table 6, the results have been compared with the frequencies of the effective collapses (with d_k =5) observed for the out-of-plane mechanisms [M1] and [M2] for the 64 churches following the seismic event [24]. The comparisons shows that, for the kinematic mechanism related to the whole façade [K1] (to be compared with [M1]) and for all those related to the top of the same [K4, K6, K10, K12] (to be compared with [M2]), the frequencies of the possible collapses induced by the PGA values of the seismic event (with $d^*_u < \Delta d\ (Ts),\ _E$) are similar to the percentages of the observed collapses, in particular when the condition *Not Verified [K]*-($I_{S,\ SLV}<1$) is considered.

Table 4: Results of the non-linear kinematic analysis. Not Verified [K]-($I_{S,\ SLV}$ <1).

	Not Verified [K] ($I_{S,\ SLV}$<1)	d^*_0 **[mm]** (average value)	d^*_u **[mm]** (average value)	**Δd (Ts), SLV [mm]** (average value)	**Possible Collapse** d*u > Δd (Ts), SLV
[K1]	48%	544.63	217.85	141.25	2%
[K4]	25%	556.24	222.49	198.64	12%
[K6]	5%	584.45	233.78	246.11	3%
[K10]	22%	601.49	240.60	239.42	2%
[K12]	2%	290.90	116.36	203.44	2%

Table 5: Results of the non-linear kinematic analysis. Not Verified [K]-($I_{S,\ SLV}$ <0.614).

	Not Verified [K] ($I_{S,\ SLV}$<0.614)	d^*_0 **[mm]** (average value)	d^*_u **[mm]** (average value)	**Δd (Ts), SLV [mm]** (average value)	**Possible Collapse** d*u > Δd (Ts), SLV
[K1]	13%	556.50	222.60	187.56	2%
[K4]	7%	495.00	198.00	220.07	5%
[K10]	22%	610.68	244.27	172.14	2%
[K12]	2%	290.90	116.36	203.44	2%

The correlations between the values of the ultimate displacement d^*_u calculated for the *Not Verified [K]s* and the damage levels observed in each church for the mechanism [M2] (characterized by a higher percentage of possible activation and collapse compared to [M1]) are shown in Figure 6a and Figure 6b for ($I_{S,\ SLV}$<1) and ($I_{S,\ SLV}$ <0.614), respectively.

The obtained output shows that a lower level of damage d_k has generally been observed in the cases characterized by a higher structural capacity (in terms of ultimate displacement d^*_u); on the contrary, lower value of d^*_u can be found in churches which experienced partial or total collapses during the 2009 seismic event.

5 CONCLUSIONS

In this paper a study related to seismic vulnerability of the facades of existing churches has been carried out. In particular, a kinematic analysis, based on the macro-element approach proposed by the Italian Guidelines, has been applied in order to assess the structural capacity

Table 6: Comparison between the results of the non-linear kinematic analysis and collapse frequencies (d_k=5) observed after the 6th April 2009 earthquake for [M1] and [M2] mechanisms.

	Possible Collapse $d^*_u < \Delta d$ (Ts), E ($I_{S, SLV}$ <1)		**Possible Collapse** $d^*_u < \Delta d$ (Ts), E ($I_{S, SLV}$ <0.614)		**Observed Collapses** [d_k=5]	
[K1]	5%	5%	5%	5%	[M1]	2%
[K4]	3%	8%	2%	5%	[M2]	10%
[K6]	2%		-			
[K10]	3%		3%			
[K12]	0%		0%			

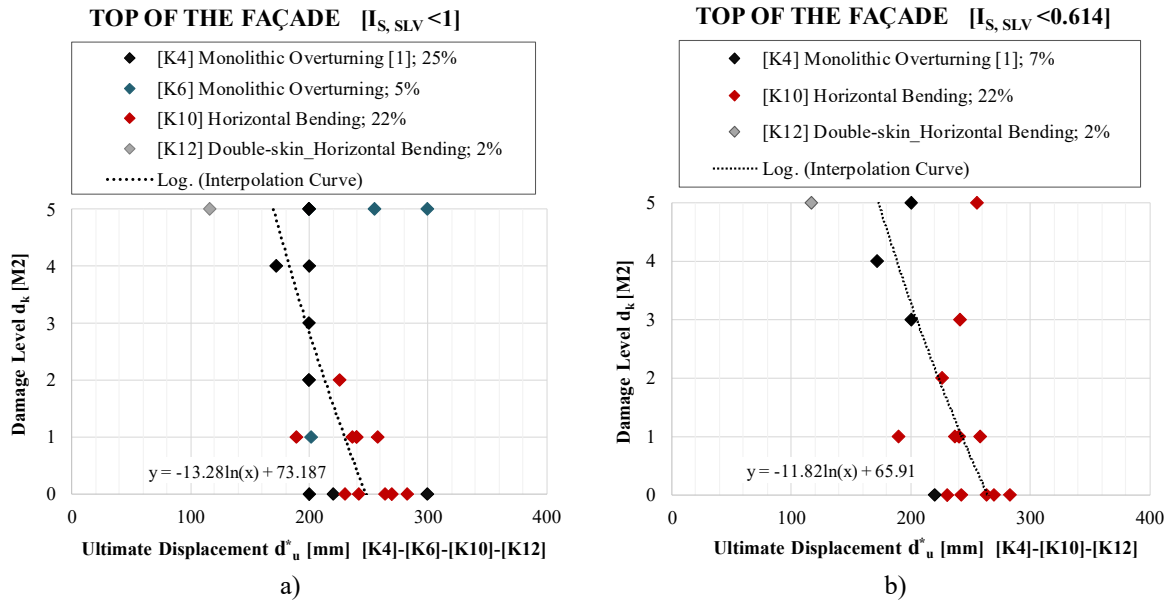


Figure 6: Correlation between ultimate displacement d^*_u obtained for the *Not Verified [K]s* (linear analysis) and the damage levels observed in each church for the mechanism [M2].

of 64 churches that experienced the 2009 L'Aquila earthquake. The analysis and the comparison of the damage levels experienced by the investigated churches allowed the following main outcomes to be outlined:

- the data collected in a territorial scale analysis can be profitably used for the implementation of simplified analytical procedures to be applied on a large-scale approach on homogeneous populations of churches;
- the kinematic approach, based on the identification of the mechanisms kinematically admissible for the analysed churches and the verification of their capacity in terms of resisting accelerations and ultimate displacements, allows to perform an immediate analysis of the structural deficiencies of the examined buildings;
- the applied procedure could allow to avoid, when not necessary, the development of more rigorous and time-consuming analyses, constituting a valid support in the simulation of possible post-earthquake damage scenarios and, consequently, in the definition of adequate preventive strategies for seismic risk mitigation.

REFERENCES

[1] Roca, P., Cervera, M., Gariup, G., Pelà, L. Structural Analysis of Masonry Historical Constructions. Classical and Advanced Approaches. *Archives of Computational Methods in Engineering* (2010). **17**: 299-325.

[2] Valente, M., Milani, G. Damage survey, simplified assessment, and advanced seismic analyses of two masonry churches after the 2012 Emilia earthquake. *International Journal of Architectural Heritage*, (2018), pp 1-24.

[3] Brando, G., Criber, E., De Matteis, G. The effects of L'Aquila earthquake on the St. Gemma church in Goriano Sicoli: part II-fem analysis. *Bulletin of earthquake engineering* (2015). **13(12)**: 3733–3748.

[4] Endo, Y., Pelà, L., Roca, P., Da Porto, F., Modena, C. Comparison of seismic analysis methods applied to a historical church struck by 2009 L'Aquila earthquake. Bulletin of Earthquake Engineering (2015). **13**: 3749-3778.

[5] Braga, F., Dolce, M., Liberatore, D. A statistical study on damaged buildings and an ensuing review of the MSK-76 scale. *Proceedings of the 7th European Conference on Earthquake Engineering* (1982). Athens, Greece.

[6] Di Pasquale, G., Orsini, G., Romeo, R.W. New developments in seismic risk assessment in Italy, *Bulletin of Earthquake Engineering* (2005). **3(1)**.

[7] Doglioni, F., Moretti, A., Petrini, V. *Le chiese e il terremoto - Dalla vulnerabilità constatata nel terremoto del Friuli al miglioramento antisismico nel restauro, verso una politica di prevenzione*. Edizioni Lint., Trieste, Italy (1994). (In Italian).

[8] Lagomarsino, S., Podestà, S. Seismic Vulnerability of Ancient Churches: II. Statistical Analysis of Surveyed Data and Methods for Risk Analysis. *Earthquake Spectra* (2004). **20(2)**: 395–412.

[9] Lagomarsino, S., Podestà, S. Damage and vulnerability assessment of churches after the 2002 Molise, Italy, earthquake. *Earthquake Spectra* (2004). **20**, Special Issue I, pp. S271-S283.

[10] Lagomarsino, S. Damage assessment of churches after L'Aquila earthquake (2009). *Bulletin of Earthquake Engineering* (2012). **10(1)**: 73-92.

[11] De Matteis, G, Brando, G, Corlito, V. Predictive model for seismic vulnerability assessment of churches based on the 2009 L'Aquila earthquake. *Bulletin of Earthquake Engineering* (2019). **17(9)**: 4909-4936.

[12] Hofer, L., Zampieri, P., Zanini, M. A., Faleschini, F., Pellegrino, C. Seismic damage survey and empirical fragility curves for churches after the August 24, 2016 Central Italy earthquake. *Soil Dynamics and Earthquake Engineering*, (2018). **111**: 98-109.

[13] De Matteis, G, Zizi, M. Seismic Damage Prediction of Masonry Churches by a PGA-Based Approach. *International Journal of Architectural Heritage*, (2019). **13(7)**: 1165–1179.

[14] D'Ayala, D. Force and displacement based vulnerability assessment for traditional buildings. *Bulletin of Earthquake Engineering* (2005). **3(3)**: 235-265.

[15] Bernardini, A., Gori, R., Modena, C. Application of Coupled Analytical Models and Experiental Knowledge to Seismic Vulnerability Analyses of Masonry Buildings. *Earthquake Damage Evaluation and Vulnerability Analysis of Buildings Structures.* (1990). **3**:161-180. Koridze A (ed), Omega Scientific.

[16] De Matteis, G., Mazzolani, F.M. The Fossanova church: seismic vulnerability assessment

by numerical and physical testing. *International Journal of Architectural Heritage* (2010). **4 (3)**: 222-245.

[17] Milani, G., Lourenco, P. CFE homogenised limit analysis model for masonry structures. *Engineering and Computational Mechanics* (2011). **164(2)**: 65-78.

[18] Elyamani, A., Roca, P., Caselles, O., Clapes, J. Seismic safety assessment of historical structures using updated numerical models: The case of Mallorca cathedral in Spain. *Engineering Failure Analysis* (2017). **74**: 54-79.

[19] Roca, P. Studies on the structure of Gothic Cathedrals. *Structural Analysis of Historical Constructions* (2001), pp.71-90.

[20] Circolare del Ministero delle infrastrutture e dei trasporti 21 gennaio 2019, n. 7 del Consiglio superiore del Lavori Pubblici recante "Istruzioni per l'applicazione dell'*Aggiornamento delle "Norme tecniche per le costruzioni"* di cui al decreto ministeriale 17 gennaio 2018". (In Italian).

[21] Doherty, K., Griffith, M.C., Lam, N., Wilson, J. Displacement-based seismic analysis for out-of-plane bending of unreinforced masonry walls. *Earthquake Engineering & Structural Dynamics* (2002). **31**: 833 - 850.

[22] Minister of Heritage and Cultural Activities, Circular n.26, Italian Code for protection of cultural heritage. "*Linee Guida per la valutazione e la riduzione del rischio Sismico del patrimonio culturale con riferimento alle norme tecniche per le costruzioni*". Prot 10953 of 02/12/2010 (updated to 2011). (In Italian).

Faenza, L., Michelini, A. Regression analysis of MCS intensity and ground motion spectral accelerations (SAs) in Italy, *Geophysical Journal International* (2011). **186(3)**: 1415-1430.

[23] Grunthal, G. *European Macroseismic Scale*. Vol. 15 (1998). Centre Européen de Géodynamique et de Séismologie, Luxembourg.

[24] O.P.C.M. 3 maggio 2005, n. 3431 (1). Ulteriori modifiche ed integrazioni all'O.P.C.M. 20 marzo 2003 n. 3274, recante «*Primi elementi in materia di criteri generali per la classificazione sismica del territorio nazionale e di normative tecniche per le costruzioni in zona sismica*». Gazz. Uff. 10 maggio 2005, n. 107, S.O (In Italian).

12th International Conference on Structural Analysis of Historical Constructions
SAHC 2020
P. Roca, L. Pelà and C. Molins (Eds.)

MANAGING NATURAL DISASTERS IN HISTORIC AREAS: A NOVEL HOLISTIC SEISMIC RISK ASSESSMENT METHOD APPLIED TO A RELEVANT CASE STUDY

M. LUCESOLI[1], G. BERNARDINI[1] AND E. QUAGLIARINI[1*]

[1]Department of Construction, Civil Engineering and Architecture (DICEA)
Università Politecnica delle Marche
via di Brecce Bianche 60131 Ancona, Italy
e-mail: e.quagliarini@staff.univpm.it (*corresponding author)

Keywords: Historic Urban Centre, Urban Paths Network, Seismic Risk Index, Emergency Planning, Risk-Mitigating Solution, Evacuation Strategies

Abstract. *The resilience of historic areas is highly threatened by natural sudden onset events such as earthquakes. Major weak points of an urban environment, widely debated in the past literature, concern mainly masonry buildings. However, also the complex urban paths system could be prone to lose its functionality in the aftermath of a seismic event. Urban paths alterations due to earthquake effects can be attributed to extrinsic (i.e.: ruins formation from buildings) and intrinsic (e.g.: ground instability due to landslide or underground cavities) vulnerability; these factors jointly combined with exposure condition of hosted population in urban areas and with the local seismic hazard represent a possible impediment to evacuation process and at the same time, an obstacle to rescuers' teams occupied in offering a first aid response. Therefore, the work aim is to apply a tool for preliminary evaluation of risk, strictly related to urban paths system considering all abovementioned aspects from a holistic point of view. This goal is achieved by a simplified methodology applicable to a wide-scale on a whole historic centre that takes advantages from a series of easy-to-detect parameters influencing the risk with limited availability of resources. Parameters grouped by topics (i.e.: path use and exposure; geometric features; physical-structural features; extrinsic vulnerability; seismic hazard) are assigned to scores and weights according to a multi-criteria decision-making process generating a numerical index. A typical Italian urban centre made by historical masonry constructions is assumed as a case study to implement the existing method. The detected risk indexes are then graphically provided through risk maps, a chromatic scale indicates which areas are more prone to possible unavailability of paths rather than others. Evacuation planners and emergency managers could embody this tool in their studies to prevent the high number of losses by guiding evacuees toward assembly points through the risk lower paths and to direct risk-reduction interventions punctually where critical condition emerges with different priority levels. Paths accessibility evaluation through a risk characterization could also result useful as a tool for rescuers' activities optimization and for inhabitant disaster preparedness in terms of being familiar with safest and alternatives paths in emergency conditions.*

1 INTRODUCTION

Historical urban centres in earthquake-prone regions are exposed to severe threats not only referred to the stability of the constructions but principally related to their trapped inhabitants and victims. Preventive measures and actions should be planned to avoid or limit losses especially in these complicated scenarios. Current literature had focused insistently on buildings vulnerability by developed novel interventions techniques or adopting innovative survey tools. The historic built environment cannot be intended as limited to constructions, but it could be a blend of further composing elements [1], two at least: open spaces (e.g.: squares), defined as urban voids where people can gather for everyday life activities in ordinary conditions, but these could become extremely important in an emergency too; moreover, between buildings and open spaces, an interconnection exists embodied by the urban streets defined as an intricate network of paths. The present contribution is mainly centred to the urban paths network without never leave the holistic perspective just introduced above.

Catastrophic effects of an earthquake on populations could be reduced through consciously evacuation procedures that should be preventively planned. Emergency planners necessitate of reliable tools supporting their choices [2], with this aim factors influencing the seismic risk related to the built environment have to be rapidly collected at the wide urban scale to evaluate all the possible scenarios. Focusing on evacuation paths in urban fabrics the risk can be influenced by three main aspects [3]. The first is embodied by the hazard, connected to soil category, morphology and topography, local amplification phenomena [4]. A key role is played by vulnerability subdivided in intrinsic vulnerability, which relates to the elements composing the street itself (i.e.: street pavements, foundations, embankment, and lifelines) [5] and extrinsic vulnerability, which refers to the elements that do not directly belong to the path itself but can compromise or block it (i.e.: buildings collapse into narrow streets). Finally, the human presence and their use of spaces have to be evaluated constituting the exposure conditions (i.e.: high density of citizen, tourists' presence, mass-gathering events) [6].

The present work takes advantage of the application of the seismic risk assessment method developed by [7] to a significant case study Sulmona (Italy) representative of the central regions of Italy frequently exposed to earthquakes. The work aim is to indicate ad hoc emergency solutions measured on the inquired scenarios for the studied historic centre starting from specific indication provided by the employed method. The multiple capabilities of the method are tested promoting it as a functional supporting tool for emergency management, especially for indicate to rescuers which are the possible higher populated safe areas where to direct their first aid actions and at the same time how they could reach them through the safer and without damages urban paths. This method could be proper to promoting sustainable evacuation strategies or to guide punctual interventions, in case of limited resources, directed to mitigate the seismic risk in historic areas.

2 MATERIALS AND METHODS

2.1 Historic urban area characterization

Historic parts of urban centres are generally characterized by a complex system made by irregular buildings aggregates that not always follow a specific expansion plan, especially if they are belonging to the mediaeval period (European regions). The most ancient buildings are

principally made by masonry and they could be affected by serious lacks in their maintenance or could be not well-made, constituting a weak point in case of a seismic event. For these reasons, their vulnerability has to be assessed by taking advantages from the Macroseismic method [8] selected for its rapid application.

Other key components of the historic urban layout are the open spaces that could be privates (e.g.: courtyards, private parking areas, gardens) that are generally fenced and not accessible by pedestrians or public (e.g.: urban squares, widenings street area, parking areas, public parks); these lasts could be assumed as fundamental elements in the emergency planning process. In fact, wide areas dislocated within the built environment must be individuated to host pedestrians during a sudden onset emergency and constitute a safe area where wait for rescuers' arrival and first aids in case of necessity.

Interconnection among buildings stocks and public open spaces are made by streets, in other words, the infrastructure systems play the role of the emergency paths network that should be guaranteed the accessibility to the historic part of the city (to rescuers) and the reachability of safe areas to hosted populations.

The described paths network constituting the urban layout merged among buildings is now categorized in three basic elements: Nodes, Squares, and Links. Nodes are placed at crossroads, at significant plano-alti-metric variation or at the start and endpoint of a specific road structure. Squares are wider nodes that can be considered as assembly points or rescuers' first-aid areas. Finally, a Link is a connection between two consecutive nodes.

2.2 Risk influencing factors for emergency paths: a holistic methodology

Risks that influence the availability of an urban paths network in emergency condition have to be inquired. The adopted methodology [7] in this work could be defined as semeiotic, for its rapid application thanks to easy to detect data about the built environment, and holistic because it jointly combine several aspects that have different influence on paths safety. Thanks to a series of alternatives differently weighted related to a list of parameters the method is able to quantify numerically (0-100%) the seismic risk of each element (introduced in Section 2.1) composing the urban layout. For this purpose, a multi-criteria decision-making process is established by grouping parameters in six main topics. The final risk index calculation is achieved by the weighted sum of the Analytical Hierarchy Process [9].

Each risk influencing factors are discussed below following the subdivision in topics:

- The first condition to be established is necessary to guarantee the total accessibility of the link width, however sometimes urban street could be partially obstructed by temporary maintenance interventions on pavements or on facing buildings, in other cases, vehicles access could be impeded by traffic bollards; all these situations that could reduce the ordinary use must be reported;
- Exposure conditions represent a key aspect in emergency conditions to be evaluated under a different point of view. Firstly, in terms of path role and importance that it assumes within the urban fabric during the emergency through a functional analysis. Indeed, certain paths can represent an access route to the urban environment, strategic in emergency phases, or can constitute simply an interconnection among safe areas and strategic buildings defined in the emergency plan. Moreover, links are preferred without barriers, traffic lane dividers or further obstacles that entirely limit the width of lanes.

A semi-quantitative assessment of the average flow of vehicles and pedestrians highly influence the importance of an urban street, while for squares is involved their intended use (e.g.: wide crossroad characterized by multi-directional movement of both vehicles and pedestrians, pedestrian zone, parking area characterized by possible available areas limitations due to parked vehicles). In addition, other square-specific parameters refer to the presence of architectural elements like street furniture, fences, low walls, trees which could be widespread in the square area and could interfere with pedestrians' motion/rescuers' access or emergency operations;

- Length of the street could affect the travel time required to reach a safe area, while its width can influence the evacuation flows because of interfering obstacles that could also limit the effective width of the path (i.e.: urban furniture; debris presence due to damaged buildings). Longer and narrower paths in the sample are considered more hazardous in respect to the others. For squares, the considered geometrical parameter concerns the area extension;
- Street surface conditions (i.e.: asphalted, paved or rough) could influence the streets' accessibility also related to its conservation state causing pedestrians accidents or injuries during the escape. Potential slide down of soil and rocks on both sides of the path and the preventing measures (e.g.: retaining walls) are identified so as to include the linked risks. A specific parameter is also added in this work to include the existence of caves, cisterns and natural or artificial underground structures that are typical of the historical urban environment. These subsoil vulnerable elements could provoke instability leading to local collapses of streets. Furthermore, the study also assumes as weak points the risk connected to pipelines of gas or water supply system that could lead to cascade effects (i.e.: dangerous gas leaks, fires, local soil destabilization).
- Extrinsic vulnerability (of buildings) constitutes one of the major parameters to take into account for paths accessibility. The adopted method evaluates the risk connected to the buildings' presence along street sides as a function of their vulnerability index V_b (obtained through a macroseismic method to ensure quick application [8]) and the single building incidence I_b on the studied link, defined as the ratio between building L_b and link L lengths ($I_b = L_b/L$). For each link j the formulation proposed by [1] permit to quantify this parameter calculating the $V_{link,j}$ index as shown in Equation (1):

$$V_{link,j} = \sum_{b \in j} V_b * I_b \tag{1}$$

  However, in the same scenario, $V_{link,j}$ values must be normalized by the maximum obtainable and divided into four alternatives according to [10].
- Real cases highlights how both base and local features of soil can be relevant for the paths' damaging, because of cracks or damages occurring on the ground and directly affecting the carriageway state [4]. Proposed methodology, taking advantages from Eurocode 8, evaluates the seismic hazard basing on the design ground acceleration (a_g) [g] related to each seismic zone, to the ground types.

Applying this method, a percentual risk index is associated to each network element (i.e.: nodes, links and squares), for a more comprehensive visualization indexes are graphically returned on risk maps by choosing at least four different colours to diversify values within their variation interval.

2.3 Case study individuation: a relevant historic city centre highly prone to earthquakes

The method is applied to a significant case study from the central region of Italy, the city of Sulmona (AQ) is located in a valley along the Apennine's ridge interested by conspicuous seismic hazard. Within the city centre of about 25.000 inhabitants is possible recognise three main urban areas: the historic centre (of Roman origin) enclosed by two expansion areas one mediaeval and the other erected in the second half of last century. In the 1706 Sulmona know the most violent seismic event (9-10 MCS intensity) that produced over a thousand human life losses and lead to a massive reconstruction of the city. For this reason, the constructive typologies of the historic centre are almost homogeneous, buildings belonging to this area are generally made by massive thickness walls in rough stone punctually improved with regular brick inserts but the masonry quality is very low.

Sulmona is erected in one of the worst zones according to the Italian seismic hazard map [11], its territory is interested by an expected peak ground acceleration (PGA) equal to 0.256g and maximum expected magnitude equal to 7.06Mw. The municipal territory extends on seismogenic sources and it is characterized by faults systems in direction NW-SE as it is visible in ***Errore. L'origine riferimento non è stata trovata.***. Additionally, the bedrock under the city is located to a depth that varies between 200 and 400 meters left the built areas within the valley exposed to further amplification phenomena due to an alluvial layer of clays. The right side of ***Errore. L'origine riferimento non è stata trovata.*** shows a database reporting the main historic seismic events (64 since the IV century) and their intensity during the time.

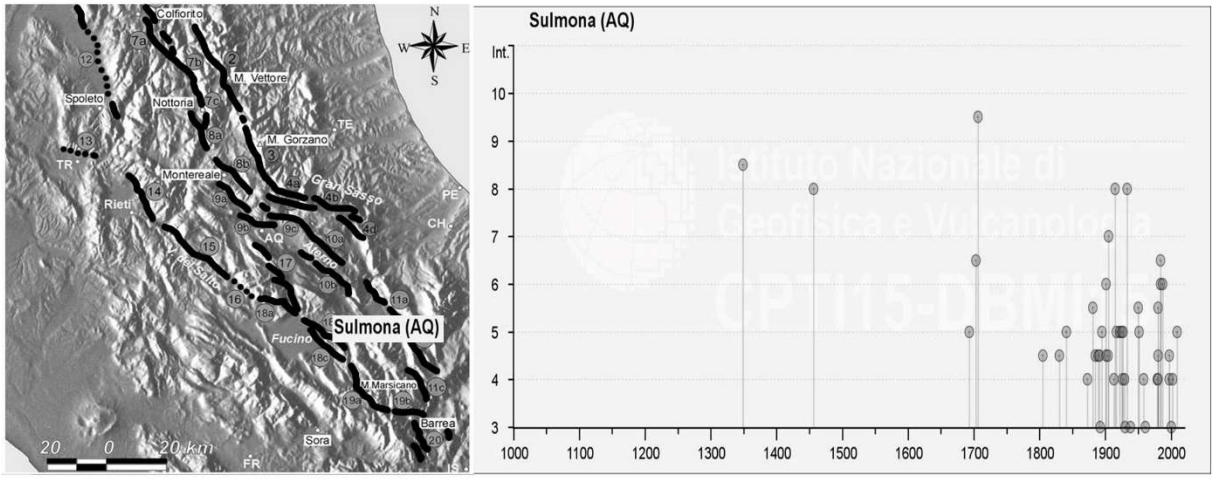


Figure 1: Central Italy faults systems on the left and the seismic history of Sulmona in the right respective sources: *https://emidius.mi.ingv.it/GNDT/P512/pictures/lavecchia.jpg* and *https://emidius.mi.ingv.it/CPTI15-DBMI15/query_place/* (last access: 03/12/19)

The sample choice is relapsed to this urban centre not only because of it has been prone to relevant seismic events but also for the large availability of collected data. In fact, about urban geometry (e.g.: streets width and squares extension) and structural-physical aspects (e.g.: conservation state, streets typologies, morphologic information related to soil, possible landslides) data are obtained through remote data collection technologies (e.g. desktop web mapping services, photographs, aerial maps); more detailed data for instance related to the

seismic hazard and soil category have obtained by asking directly municipal offices. A different process is followed for data and information related to features and vulnerability values of buildings, these data are collected from [12] where are obtained through the GNDT methodology, however according to Section 2.2 extrinsic vulnerability have to be inquired by employing vulnerability values of [8]. Hence, the translation from one to the other vulnerability index is achieved by establishing a linear correlation on maximum increasing values of a known sample, a similar process has been already experimented also in [13].

3 RESULTS

3.1 Scenario characterization: urban paths network elements

Errore. L'origine riferimento non è stata trovata. gives a graphical representation of the elements composing the urban paths network (defined in Section 2.1) individuated for the assumed case study. Particular attention is paid for the main urban streets of Sulmona connecting the principal square "Giuseppe Garibaldi" (letter D in the ***Errore. L'origine riferimento non è stata trovata.***) to widening areas immediately out of the historic perimeter of the urban centre that can be considered as safe places ("Access", green arrows in the ***Errore. L'origine riferimento non è stata trovata.***) where waiting for rescuers' arrival (*Evacuation Scenario*). At the same time, the central square (D) is also able to host thousands of people considering a density of 2 pp/m^2 (according to Italian regulations [14]) thank to its considerable dimension of 13.000 m^2; additionally, in two periods of the year the same square is the location of religious events and historical commemorations bringing in a massive flow of citizen, visitors and tourist for a capacity that must be limited to 10.000 people. Hence, it is thus desirable to inquire the risk of paths, in a rescuers' accessibility perspective toward this hot spot, also in case of a seismic emergency during these drastic circumstances (*Rescue Scenario*). Other small squares along main streets could constitute a possible assembly points within the historic centre (A, B, C, E, F, and G in ***Errore. L'origine riferimento non è stata trovata.***) where trapped people could safely stop their evacuation; thus specific risk evaluation is also necessary here.

Available data according to Section 2.3 related to the vulnerability of built areas are graphically reported in the ***Errore. L'origine riferimento non è stata trovata.*** through the assumption of a chromatic scale, just to give an idea of the location of highly vulnerable masonry structures along urban streets. It is easy to comprehend how the most vulnerable buildings are unfortunately placed on each side of the evacuation paths embodied a serious problem for their availability in the aftermath of a considerable earthquake. These values combined with geometrical features of buildings and street are employed to esteem the extrinsic vulnerability component in the paths risk index assessment methodology (Section 2.2).

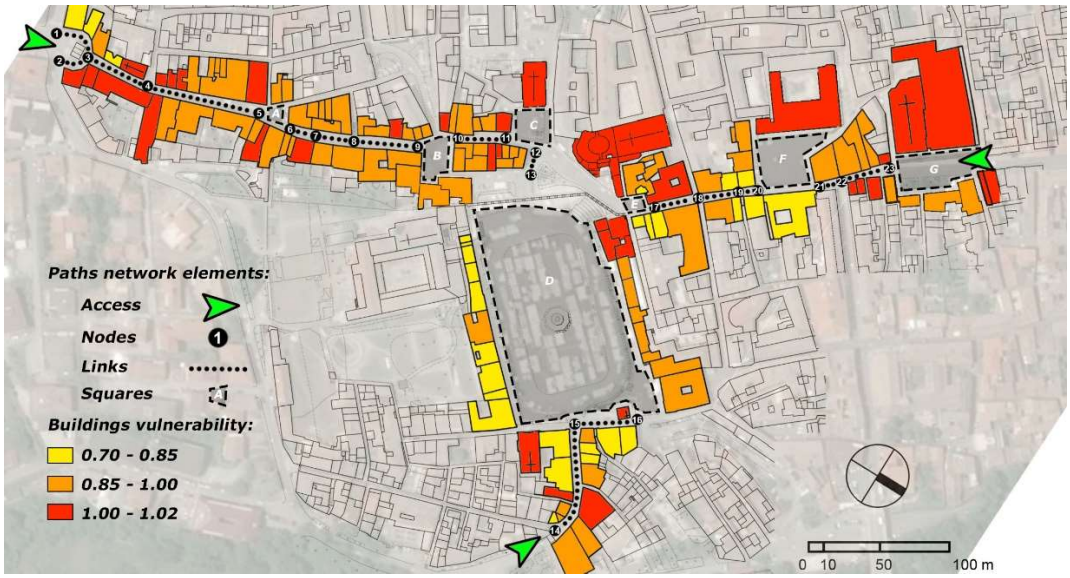


Figure 2: Case study map with the individuation of urban paths network elements and buildings vulnerability.

3.2 Seismic risk entity and mapping, weak points of the emergency paths network

The methodology [7] application highlights from one side, a certain homogeneity in the outcoming risk indexes due to the similar features of inquired links but, from the other side, the complex situation of the Sulmona's historic centre especially for those streets that could be considered as the main connections for the central square of the city. In *Figure 3* different colours are associated to four risk levels individuated between the maximum and minimum risk index by dividing into equal parts this interval and rounding the obtained indexes reported in *Table 1* for each inquired links and squares.

Table 1: Obtained risk indexes for case study links and squares [7]

Link	Risk index	Square	Risk index
1-3	0.418	A	0.489
2-3	0.402	B	0.482
3-4	0.443	C	0.482
4-5	0.489	D	0.470
6-7	0.459	E	0.482
7-8	0.474	F	0.419
8-9	0.474	G	0.482
11-10	0.482		
12-13	0.402		
14-15	0.484		
15-16	0.419		
17-18	0.482		
18-19	0.482		
19-20	0.435		
21-22	0.404		
22-23	0.482		

From the point of view of the *Evacuation Scenario*, concerning the necessity for pedestrians to leave the historic centre perimeter, from the obtained indexes it emerges that the southern escape route from the "Giuseppe Garibaldi" square is constituted by high-risk links (i.d.:4-5, 6-7, 7-8 and 8-9 in *Figure 3*); at the same time also the squares displaced along this path are not able to guarantee low levels of risk where evacuees can seek refuge. Additionally, crossing information with the ***Errore. L'origine riferimento non è stata trovata.***, the same street arch is very long and faced by interminable buildings aggregates with relevant values of vulnerability. Links 17-18 and 18-19 in *Figure 3* show a high-risk level but the presence of the F square reveals the possibility for evacuees to reach it and wait for rescuers' arrival in this safe assembly point, also people coming from the link 22-23 should be conducted to this area instead of the more risky square G. Further consideration could be made by combining also data related to the number of evacuees and the capacity of the single safe areas.

The shortest way to reach a wide and safe area out of the built environment from the "Giuseppe Garibaldi" square could be given by travelling the link 14-15 although it is interested by a high level of risk. The main square D, because of its extension, in case of earthquake occurrence in ordinary conditions (i.e.: without particular events that gather a large mass of people) is able to host a large number of evacuating inhabitants, thus it can be reached by rescuers through the link 14-15 only if no obstruction deriving from the buildings collapse would impede the passage of vehicles (*Rescue Scenario*).

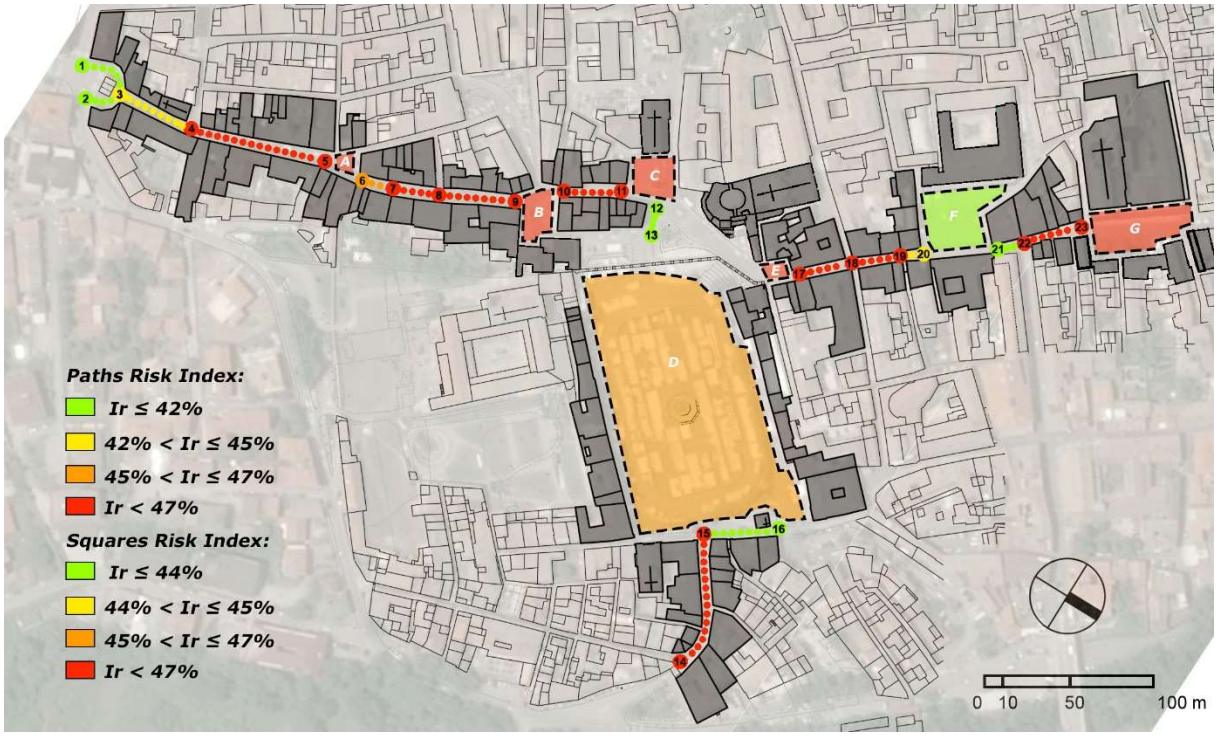


Figure 3: Case study map with the evaluation of the risk indexes for emergency paths and squares along Sulmona's main streets according to the adopted method [7].

3.3 Proposing risk reduction strategies from risk indexes analysis

From the results of the previous Section 3.2, three interesting situations emerge and can be

deeply analysed by proposing evacuation strategies and rescuers' action strictly related to the outcoming data from the applied methodology. Hence, the evaluated risk index for each paths network element is not limited to embody a unique and overall value to quantify the risk but for its structure, it can be decomposed in values referred to each single risk topics (i.e. accessibility, exposure, geometrical features, physical and structural features, extrinsic vulnerability and hazard). Taking advantage of this subdivision the method is capable to justify and determine causes of a high-risk level rather than a low one, in this sense emergency planners can inquire punctually which factor leads to a specific risky situation and they can promote ad hoc interventions.

- The square F in *Figure 4-A* shows a low level of risk index in contrast with the other squares along considered paths, from an accurate analysis of single values composing the index it emerges that this urban area is wider than the others (it is detectable making comparisons among geometrical parameters), it is also surrounded by low height building suffered by moderate vulnerability (extrinsic vulnerability parameter) and finally it is can be considered as a pedestrian areas, easily accessible with generally few obstacles and parked vehicles. During a seismic event, trapped people along adjacent riskier links (18-19 and 22-23) have to be guided by placing wayfinding signs (green arrow in *Figure 4-A*) towards this area, thanks also to the low risk registered for the contiguous links 18-20 and 21-22 (*Evacuation Scenario*). These last-mentioned links are considered safer than others, in fact, their evaluation reveals a low risk in: geometrical parameters due to their shortness, exposure conditions for the one-way travel direction and their low extrinsic vulnerability.
- A worst condition is represented by all those evacuees that in case of high magnitude event are trapped in the proximity of the square A and along links 4-5, 6-7, 7-8 and 8-9 in *Figure 4-B*. Analysing single risk components in relation to the whole sample average values, two are the factors that characterise these risk indexes: the street narrowness (geometrical features) and the presence of high vulnerable buildings homogeneously distributed along paths (extrinsic vulnerability). Guiding evacuees towards less risky links (1-3, 2-3 and 3-4) through an urban wayfinding signs system is probably not sufficient to guarantee a safe evacuation of this street (*Figure 4-B*). Further vulnerability analysis should guide planners to indicate precise retrofitting interventions on such buildings to mitigate the risk level (*Evacuating Scenario*).
- The last issue concerns the *Rescue Scenario* considering the entrance of rescuers' teams and vehicles within the major square D capable to gather a large mass crowd of people during an emergency and characterised by a medium risk level. The link 14-15 is the shortest path to reach the gathering area from the road system out of the urban centre (*Figure 4-C*). For this reason, the exposure parameter is higher rather than other links because it can be considered as a strategic direct access to the historic centre. Extrinsic vulnerability value is high too, but through the investigation on the single buildings vulnerability indexes in *Figure 2* is demonstrable how the main problem is represented by the two more vulnerable buildings of the link that are placed on opposite sides in front of each other. In case of a disruptive earthquake, there could be the possibility that buildings collapse could cause an impediment to the vehicles passages due to debris presence. In this case, retrofitting interventions are directed on these single buildings reducing costs related to large scale vulnerability reduction measures, and the final aim

to obtain a safe access path to the main assembly point is pursued.

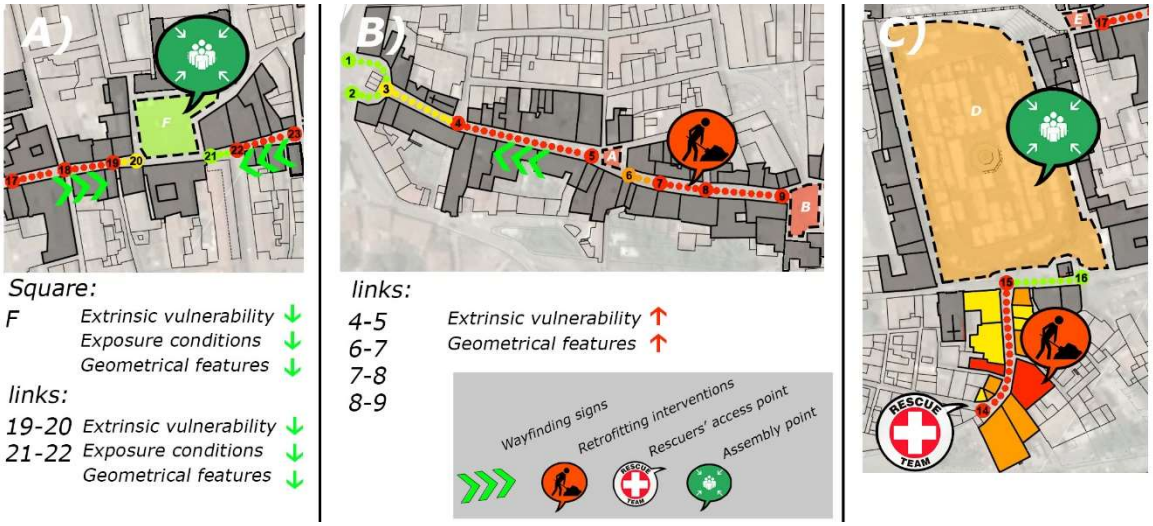


Figure 4: Specific analysis of risk components and mitigating strategies for the three situations (A, B and C).

4 CONCLUSIONS

Seismic events could modify the current scenarios in historic urban areas where high density of people and vulnerable buildings coexist in combination with intricated paths networks usually made by narrow streets. The exposed population could also be trapped in these scenarios during their escape or they could not be reached to rescuers' teams for first aid. Damages affecting streets integrity or make them inaccessible (e.g.: buildings collapse blocking the streets, ground failures or links interruptions due to their damage) can compromise the emergency phases with adverse effects.

Emergency actions (i.e.: risk-mitigating solutions and alternative evacuation strategies) should be planned by considering all the possible aspects that could affect the inhabitants' safety. This contribution takes advantage of a holistic methodology able to assess the seismic risk principally of an urban paths network but also considering other risk influencing factors specifically for the historic urban centre in the post-earthquake scenario (i.e.: vulnerability, hazard, and exposure conditions). Each factor and related parameters are specifically evaluated and assigned to weights and values in order to obtain a numerical risk index. The application of a representative case study in this paper permits to test how it is possible to represent urban fabric criticalities into thematic maps graphically through a discrete risk scale. Moreover, it is possible to realize a deeper analysis of single factors that modify the risk index, promoting specific and punctual intervention with certain priority to allocate the available resources. Making comparison among risk indexes of different strategic paths it is possible to adopt some evacuation strategies rather than the other to better manage the emergency phases. This adopted method ensures the rapidity and easy application that could be preferred instead of models that require onerous and detailed surveys, this advantage can allow to employ it at a wide-scale application that concerns the urban fabric, in the same context, graphical outputs permit to have under control the situation of the overall scenario.

The case study implementation demonstrates the functionality and the reliability of the entire

process suggesting which links of Sulmona should be excluded from safer paths selection because of their high-risk level, and which could be considered as possible escape routes. As it is demonstrated, results can also be employed to guide rescuers' actions by considering the method as a supporting tool to paths availability assessment and as a standalone procedure to verify or justify adopted approaches within emergency plans.
The work limits are related to the availability of information, especially for data concerning the buildings' vulnerability that are adjusted through a linear regression from other vulnerability indexes based on a limited sample, at the same time these data are not recently updated, the same buildings may have been recently refurbished. In addition, the adopted methodologies to collect the other information (about exposure conditions rather than geometrical features for instance) could be not sufficiently accurate and could be substituted by others more proper.

Future activities may focus on the necessity to esteem (in terms of damages quantity) the built environment alterations related to debris formation and losses of street integrity and availability provoked by earthquakes of different and settable severities. This kind of tool could be combined with the evaluation of criteria related to pedestrians' safer path choice, behavioural aspects and human motion speed which could be integrated into pedestrians' evacuation simulation models.

Acknowledgements. The authors would like to thank Dr. Valeria Neigre for the support in the case study application activities.

REFERENCES

[1] S. Santarelli, G. Bernardini, E. Quagliarini, M. D'Orazio, New Indices for the Existing City-Centers Streets Network Reliability and Availability Assessment in Earthquake Emergency, Int. J. Archit. Herit. december (2017) 1–16. doi:10.1080/15583058.2017.1328543.

[2] A. Zlateski, M. Lucesoli, G. Bernardini, T.M. Ferreira, Integrating human behaviour and building vulnerability for the assessment and mitigation of seismic risk in historic centres: Proposal of a holistic human-centred simulation-based approach, Int. J. Disaster Risk Reduct. 43 (2019) 101392. doi:10.1016/j.ijdrr.2019.101392.

[3] P. Mouroux, B. Le Brun, Presentation of RISK-UE project, Bull. Earthq. Eng. 4 (2006). doi:10.1007/s10518-006-9020-3.

[4] L. Xinpo, H. Siming, Seismically induced slope instabilities and the corresponding treatments: The case of a road in the Wenchuan earthquake hit region, J. Mt. Sci. 6 (2009) 96–100. doi:10.1007/s11629-009-0197-1.

[5] G. Tesoriere, G. Marinella, M. Russello, Analisi della Vulnerabilità delle Reti Stradali in Aree Soggette a Rischio Sismico, in: XI S.I.I.V, 2001: p. 12.

[6] A. Cherubini, Progetto: SAVE - Strumenti Aggiornati per la Vulnerabilità sismica del patrimonio Edilizio e dei sistemi urbani, TASK 4 - Cap 2. (2003).

[7] E. Quagliarini, G. Bernardini, S. Santarelli, M. Lucesoli, Evacuation paths in historic city centres: A holistic methodology for assessing their seismic risk, Int. J. Disaster Risk Reduct. 31 (2018) 698–710. doi:10.1016/j.ijdrr.2018.07.010.

[8] S. Lagomarsino, S. Giovinazzi, Macroseismic and mechanical models for the vulnerability and damage assessment of current buildings, Bull. Earthq. Eng. 4 (2006) 415–443. doi:10.1007/s10518-006-9024-z.

[9] T.L. Saaty, The Analytic Hierarchy Process: Planning, Priority Setting, Resource Allocation, McGraw-Hill, 1980. https://books.google.it/books?id=Xxi7AAAAIAAJ.
[10] R. Ferlito, A.G. Pizza, A seismic vulnerability model for urban scenarios. Quick method for evaluation of roads vulnerability in emergency (Modello di vulnerabilità di un centro urbano. Metodologia per la valutazione speditiva della vulnerabilità della viabilità d'emergenza), Ing. Sismica. 4 (2011) 31–43.
[11] Ordinanza Presidente del Consiglio dei Ministri, Opcm 3519 28/04/2006, (2006).
[12] A. Martinelli, L. Corazza, Censimento di vulnerabilita degli edifici pubblici, strategici e speciali nelle regioni Abruzzo, Basilicata, Calabria, Campania, Molise, Puglia e Sicilia: valutazione della vulnerabilità degli edifici pubblici rilevati in 1510 comuni nelle regioni: Abruzz, Dipartimento della protezione civile, 1999.
[13] E. Quagliarini, M. Lucesoli, G. Bernardini, Rapid tools for assessing building heritage's seismic vulnerability: a preliminary reliability analysis, J. Cult. Herit. (2019). doi:10.1016/j.culher.2019.03.008.
[14] Piantedosi Matteo, Circolare del 18 luglio 2018 - N. 11001/1/110/(10) Modelli organizzativi e procedurali per garantire alti livelli di sicurezza in occasione di manifestazioni pubbliche, (2018).

12th International Conference on Structural Analysis of Historical Constructions
SAHC 2020
P. Roca, L. Pelà and C. Molins (Eds.)

RISK ASSESSMENT METHODOLOGIES TO SAFEGUARD HISTORIC URBAN AREAS FROM THE EFFECTS OF CLIMATE CHANGE

LAURA QUESADA-GANUZA[1*], LEIRE GARMENDIA[1], EDUARDO ROJÍ[1], IRANTZU ÁLVAREZ[2], ESTIBALIZ BRIZ[1], MARTA OLAZABAL[3]

[1] University of the Basque Country UPV/EHU, School of Engineering in Bilbao, Mechanical Engineering Department,
Plaza Ingeniero Torres Quevedo s/n (48013) Bilbao. Spain.
e-mail: {laura.quesada*, leire.garmendia, eduardo.roji, estibaliz.briz}@ehu.eus, (*corresponding author)

[2] University of the Basque Country UPV/EHU, School of Engineering in Bilbao, Department of Graphic Design and Engineering Projects, Rafael Moreno "Pitxitxi", (48013) Bilbao. Spain
email: Irantzu.alvarez@ehu.eus

[3] Basque Centre for Climate Change (BC3), Sede Building 1, 1st floor
Scientific Campus of the University of the Basque Country,
(48940) Leioa. Spain
email: marta.olazabal@bc3research.org

Keywords: Historic Urban Areas; Climate Change; Risk Assessment; Vulnerability Assessment; Key Performance Indicators

Abstract. *A systematic and critical review of the existing literature on climate-change risk-assessment methodologies for historic urban areas is presented, in view of the increasing likelihood of extreme weather events. Key performance indicators are identified for use in future risk assessment methodologies that address both the elements of historic urban areas as a system and the potential impact of prolonged heat waves. To do so, a systematic search of the existing literature on Web of Science and Scopus was conducted, with the aim of identifying and characterizing existing methodologies on vulnerability and risk assessment for cultural heritage exposed to the effects of a changing climate. The main characteristics of the methodologies that need to be addressed in the near future and key knowledge gaps were identified, among them, the lack of holistic heat-wave risk-assessment methodologies for historic urban areas.*

1 INTRODUCTION

Given the increasing number of extreme weather events over recent decades, the debate over climate change in the scientific community has intensified. Global warming has increased over the past four decades, so much so that the 21st century is now the warmest on record according to the reports from the World Meteorological Organization (WMO)[1]. This increase in global

mean temperatures mainly due to anthropogenic activity adds to the risk of extreme events, such as heavy rains, heat waves and floods [2].

Over half of the global population now resides in urban areas [3] and maximum temperature rises are recorded within urban centers and their areas of influence [2], as the global population is inexorably drawn towards cities. The most recent special report from the Intergovernmental Panel on Climate Change (IPCC) highlighted urban areas and infrastructure as a system that is among others in major need of transformation, in order to ensure a resilient future. The negative effects of unrelenting global warming and the consequences of extreme weather events are significantly affecting the health of urban residents, and their assets, wellbeing and livelihoods [2,4].

Even if cities suffer the same climatic conditions as the surroundings countryside, specific events within urban settings result in microclimates and heat-island effects. Low permeability of the soil, higher population densities, higher concentrations of productive activities, and urban planning define urban areas and differentiate their relationship with and response to the changing climate. Urban areas are therefore complex systems formed of several interrelated layers that require specific approaches for assessing their exposure to climate change. Even though it is not frequently considered in their assessment, cultural heritage represents an intrinsic layer within a city. The specific characteristics of a historic city center or historic urban area are of special relevance as they are the source of urban identity and an important asset for the economic sector. The specific vulnerabilities of historic areas to changes in weather patterns [5] are not only because of physical impacts on the built structures, but also other consequences that are very relevant for the cultural landscape, such as changes to population patterns, changes to tourism, and the disruption of socio-economic activities.

Over the past decade, climate change has become a central focus for relevant heritage organizations such as ICOMOS and UNESCO [6,7] . Likewise, the European Union maintains cultural heritage risk assessment and prevention firmly on its agenda, mainly through the EU Work Plan for Culture 2019-2022 including a topic on adaptation to climate change [8,9]. The Office of the United Nations Disaster Relief Coordinator defined risk as the probability of loss of value that defined a vulnerability index (0 no damage to 1 total loss) [10]. Assessing the risk that historic urban areas face with regard to climate change is therefore at the heart of the policy discussion and a very important research area, if we are to understand how the future resilience of cities may be increased. It means adding the layer of cultural heritage, and the specific characteristics of the historic urban grid to the assessment of urban areas.

The objective of this paper is twofold. The first objective is to perform a critical review of the current state of the art of climate-change risk-assessment methodologies for historic areas. The second objective is to respond to the research gap that has been identified in this field, by proposing key performance indicators that should be included in risk assessment methodologies to develop a holistic approach for the risk assessment of historic urban areas that are exposed to heat waves.

2 CRITICAL REVIEW ON CLIMATE CHANGE RISK ASSESMENT METHODOLOGIES

In this section, the results are presented of a systematic search of the literature, in order to conduct a critical review of climate-change risk-assessment methodologies for historic areas

[11], as well as to determine any relevant knowledge gaps. The research question [12] is therefore as follows. Which risk or vulnerability assessment methodologies are related to the effects of climate change on historic areas? A critical review of those methodologies [13] will then assess the main characteristics of the methodologies, mainly the hazards that are addressed and the risk elements (hazard, exposure, vulnerability) under consideration, including which aspect of the urban system they assess, with the understanding that an urban system is for our purposes an historic urban area.

The risk elements under analysis were derived from the IPCC approach that is the most widely used framework [2]. Risk was defined as a "*probability or likelihood of occurrence of hazardous events or trends multiplied by the impacts if these events or trends occur*" Moreover, the term impact is defined in relation to "*the effects on natural and human systems of extreme weather and climate events and of climate change. Impacts generally refer to effects on lives, livelihoods, health, ecosystems, economies, societies, cultures, services, and infrastructure due to the interaction of climate changes or hazardous climate events occurring within a specific time period and the vulnerability of an exposed society or system*" [2]. We can therefore conclude from these definitions that risk is characterized as an outcome of the interaction between hazard, vulnerability (the combination of an assets sensitivity to the hazard and its lack of capacity to cope with its adverse effects) and exposure (related to the location of the asset). It is therefore essential to note that an asset may be exposed but not vulnerable, although there must be a likelihood of its exposure to the event for it to be vulnerable.

Based on the Fifth Assessment Report (AR5) of the IPCC [2], the following events are likely to affect urban areas: extreme temperature events, cold and heat waves, including wildfires derived from heat waves; flooding events derived from extreme precipitation, storms and sea level rise; and climate change as a whole, which is the overall rise of temperature and consequential change in climatic conditions. These hazards were therefore addressed in the review.

The keywords for the search were selected with reference to the research question and the main hazards that the IPCC have identified. The keywords combined "vulnerability/risk assessment" with the individual hazards and different synonyms for "historic area", specifying the root word of each keyword with its possible variations. The Web of Science and Scopus database search settings included title, keywords and abstract. A total of 616 results were returned on both platforms with all of the different combinations of keywords. A first filtration consisted of reading the title, and selecting papers related with the subject. This step was repeated for every search and on both platforms. Many of the search results from both databases were duplicated in the different searches, so the papers were screened and then unified to determine their eligibility in the next step. To do so, the abstract of each paper was individually reviewed to determine whether a risk assessment methodology or a climate change related hazard and its impact on each historic urban area was actually defined in the paper. Subsequently, a final full text analysis of the thirty-four articles remaining after the initial screening was conducted, in which some were excluded after a thorough final re-reading. In all, twenty-nine methodologies were identified and then studied (Figure 1). The selected papers were fully reviewed and classified depending on the hazard addressed and its associated aspects of risk (hazard, exposure, vulnerability).

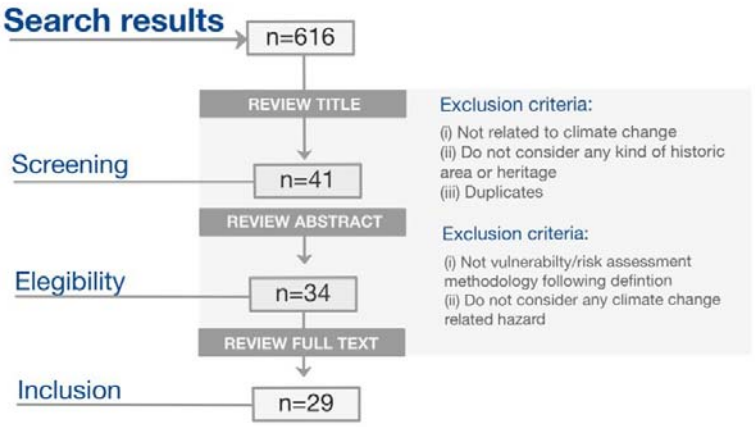


Figure 1: Literature search and evaluation for inclusion in the critical review (adapted from [12]).

2.1 Risk aspects and dimensions within the methodologies

The review of the twenty-nine methodologies served to determine the aspects of risk (hazard, exposure, vulnerability) that they were designed to consider and distinguishing between social, economic, cultural, governance (services and resources) and physical dimensions (gathering tangible characteristics of all infrastructure, elements and buildings). It should be noted that risk assessment is evaluated in phases, that hazard should be characterized to analyze exposure, and that both hazard and exposure should be evaluated to assess the vulnerability of a system. Hence, the results may be classified as: (i) methodologies that only characterize hazard likelihood and severity; (ii) methodologies that also consider exposure; and (iii) methodologies that continue to assess vulnerability, distinguishing between sensitivity and coping capacity [2].

As figure 2 shows, hazard likelihood and severity were only considered in seven of the twenty-nine methodologies and the exposure of the elements was only also assessed in one.

Vulnerability was mentioned in twenty-one methodologies which were reviewed to determine whether sensitivity indicators and/or coping capacity indicators were also mentioned in them. Sensitivity was considered in almost half of the methodologies, though it was only acknowledged as such in a few studies and was referred to as vulnerability in the others. Taking into consideration the aforementioned categories and with regard to the vulnerability aspects, nineteen studies were focused on physical sensitivity, only eight of which included other aspects. Among the methodologies with a focus on physical vulnerability, the vulnerability of buildings to flooding was considered in eight and the physical vulnerability of assets to general climatic change was considered in four of them. The remaining two methodologies assessed vulnerability without contemplating physical vulnerability, placing their focus on governance vulnerability and the adaptive capacity [14] and their social coping capacity [15]. Socioeconomic vulnerability was also considered in some methodologies that addressed the coping capacity of inhabitants facing the hazard. Cultural value was only considered in several studies by A. Gandini [16,17,18] and in one methodology [19], all addressing flooding.

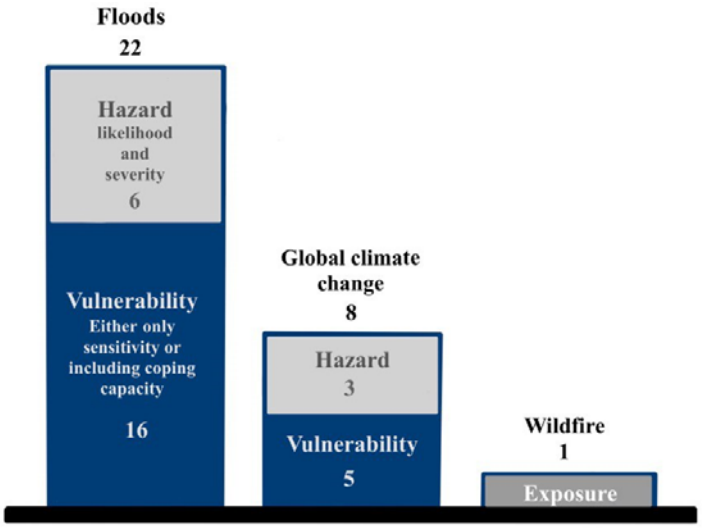


Figure 2: Overview of the results of the review.

2.2 Hazards

Figure 3 presents the results of the critical review classified by the hazard that is addressed. In the literature, flooding that is either due to extreme precipitation or to sea-level rise is one of the most frequently analyzed hazards. It was considered in twenty-two out of the twenty-nine methodologies. Flooding together with other hazards was considered in three multi-hazard methodologies [20,21,22] and nineteen methodologies focused solely on this hazard. General climatic change caused by climate change was considered as a hazard in seven out of the twenty-nine methodologies in the review. Wildfires were only considered as a hazard in one methodology [23]. Cold and heat waves were therefore not considered as hazards in any of the single or multi-hazard methodologies.

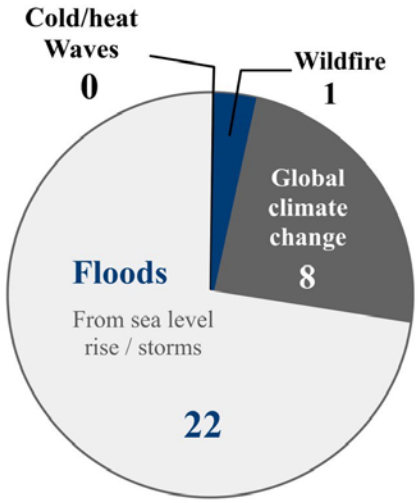


Figure 3: Number of risk assessment methodologies classified by type of hazard.

2.3 Outcomes of the critical review

Starting with the hazards and the extreme events related to climate change events, the conclusions were clear, in so far as they determined that a large body of the literature addressed flooding, from either sea-level rise or storms, and a considerable number of studies addressed the general change in climatic conditions. In contrast, such hazards as cold and heat waves were not present in the methodologies found in the review.

As explained in the introduction, the vulnerability of urban environments is frequently linked in the literature to their socio-economic and physical conditions, such as geographical position, materials, urban plot, and morphology, wealth and governance system *etc*. [24]. These characteristics will determine the severity of the resulting impacts when considering climate change and consequent extreme events. In the case of historic urban areas, the review revealed a sharp focus on the physical vulnerability of the built environment while the vulnerabilities of other aspects of the system were overlooked. The effects of climate change on cultural diversity and socio-cultural interactions; and impacts such as the loss of the sense of community, traditional knowledge, cultural identity and natural and socio-economic systems have previously been documented elsewhere [2,6,25], but few studies have considered climate impacts on cultural heritage through a holistic approach [26].

A higher frequency of heat waves of lengthier duration and higher intensity will occur according to current predictions at least once a year towards the end of the present century [27]. The high temperatures reached during heat waves are often exacerbated due to Urban Heat Island (UHI) effects [28] found in urban and suburban areas rather than in outlying rural surroundings. The ongoing effects of heat waves include consequences for human health and mortality and significant environmental and economic impacts [29]. These impacts are even more pronounced in urban areas with high population densities such as historic centers, which will therefore be very vulnerable to extreme temperature events. Thus, assessing this type of event is crucial, and, as seen in this review, there is a relevant need for risk-assessment methodologies for historic areas that address heat waves.

3 PRELIMINARY PROPOSAL FOR KEY PERFORMANCE INDICATORS

As demonstrated, holistic risk assessment methodologies to safeguard historic urban areas from heat waves are needed. In a holistic framework, social, economic, cultural, governance and physical dimensions should be considered and specific parameters or indicators that support the assessment of their individual risk should be determined. Individual and composite indicators are the foundation for vulnerability and risk assessment and are among the most common tools used to generate information on non-measurable conditions and to compare differently measured data, by synthesizing complex measurements into a single number [30].

Even if heat waves are characterized differently depending on the climate of the region, the WMO guidance on heat-health warning (WMO-No.1142) defined heatwaves as periods of unusually hot and dry or hot and humid weather that can extend over at least two to three days and can have a discernible impact on human activities [31]. The main indicators for the characterization of heat waves are therefore temperature and relative humidity; with levels of relative humidity defining whether it is a dry or a humid heat wave [32]. Consequently, exposure and vulnerability indicators must be derived from the cause-effect relationship between high heat, and low or high humidity and the elements that comprise the system of an

historic urban area; including additional exposure variables.

Studies on UHI effects have shown that the morphological layout of an urban area that affects shading and ventilation, combined with the technical characteristics of urban elements and both the type and the distribution of green spaces are the main factors influencing its intensity [33]. Urban geometry and materials influence the wind flow, energy absorption, and surface reflectance properties that emit long wave radiation back into the atmosphere [28], which in turn condition the UHI effect.



Figure 4. Development of indicators (Adapted from [34])

If we are to define the elements that comprise historic urban areas, the system needs to be addressed from two perspectives: as an urban system, and as an historic area. The indicators have been gathered revising key documents that, either from an urban perspective, wellness of the population or the weathering of historic materials, address evaluative aspects. For the identification of the indicators, we have conceptually followed the approach in Figure 4. The historic urban area is considered as a combination of an urban system [35] with the addition of carriers of significance in historic urban landscapes [36], equating each carrier to the element of the urban system. So as to provide a holistic approach, each dimension of the system needs to be assessed, as seen in the literature review, by distinguishing between social and economic, cultural, governance (services and resources) and physical (gathering tangible characteristics of all infrastructures, elements and buildings) dimensions.

The indicators are therefore a result of the potential impacts of heat waves and the UHI that have been characterized on the elements of the historic urban area and their different aspects. The indicators can be developed through this approach in combination with the AR5 framework from the IPCC. Therefore, the indicators proposed follow this order; hazard characterization, exposure, and vulnerability, divided between sensitivity and coping capacity.

With regard to the hazard indicators, the above-mentioned characterization of heat waves is based on the main factors: temperature, humidity, sun exposure and wind. The different ways that humidity variations can affect traditional materials means that additional indicators are humidity cycles and shocks [37].

The exposure is divided into the two main physical components of urban areas, buildings and open spaces. The exposure of a building is mainly defined by its exposure to sunlight, calculated in terms of hourly exposure of the envelope to solar radiation, depending on the orientation of the building and considering the different angles of façade exposure and the possible shading from the surrounding buildings. Meanwhile open spaces require the addition of UHI indicators, such as the Sky View Factor that determines the proportion of an urban space with heat-storage capabilities [38] that can contribute to the 'urban canyon' effect [28]. Another relevant indicator for open spaces is related to the presence of green elements that can be assessed using the Normalized Difference Vegetation Index (NDVI), which is based on the quantification of vegetation through the analysis of satellite imagery. Other location-dependent

urban characteristics that have been linked to interactions with heat in the literature are tropospheric Ozone (O3) levels and acoustic pollution. There is abundant research to show that ozone levels can increase under specific meteorological conditions such as high temperature, intense solar radiations, and long sunshine hours, all characteristics of heatwaves [39], which can have consequences for the health of urban populations [40]. With regard to acoustic pollution, studies have shown that people living in areas with high noise levels tend to ventilate their homes less, which increases heat storage within the building [41].

The sensitivity indicators are divided into three components: social sensitivity, buildings, and open spaces; with the last two considering physical, economic, and cultural dimensions. Social sensitivity is dependent on the characteristics of the population, both because of age groups and socioeconomic data, as well as population density. The sensitivity indicators of the buildings are in turn divided into three main dimensions: physical, economic, and cultural. Physical sensitivity is mainly based on the possible weathering of sensitive traditional materials under heat-wave conditions [37] and the thermal characteristics of the materials, such as their albedo and thermal diffusivity rates. Economic aspects are based on the use of a building, either because of its use for production, or as housing, or because of its touristic value. The main indicators of cultural sensitivity are the symbolism of the building either for collective memories, or rituals or traditions. With regard to the sensitivity of public spaces, the indicators are divided into the same three main categories mentioned above in relation to the buildings, as well as the solar reflectance of the materials in terms of their physical sensitivity.

As with the sensitivity indicators, the three coping capacity dimensions are again social, and physical, considering buildings, and open spaces. When assessing social coping capacity, the two main indicators are healthcare access (distance to hospital and availability of hospital beds), and awareness of the hazard among the population, such as the existence of emergency plans. In the case of buildings and open spaces, both elements rely on similar indicators: accessibility and building elevators and accessibility for ambulances and firefighters, respectively.

4 CONCLUSIONS

The risk assessment indicators in the second part of this paper have been proposed to address the knowledge gap that has been identified in the first part; namely, the scarcity of heat-wave risk-assessment methodologies for historic urban areas. The analysis of the urban system or urban area with an historic layer is flexible and could be adapted to any other urban area or district. The indicators have been developed with data availability in mind, ensuring repeatability and easy comparison of results.

A future goal following this study will be to produce a complete risk assessment methodology for historic urban areas, with an output based on an accessible and easily replicated Geographical Information System (GIS) model.

Acknowledgements. The authors wish to acknowledge the funding from the European Commission through the SHELTER project (GA 821282) and the University of the Basque Country UPV/EHU (PPGA20_26) as well as the support of research groups IT1314-19 of the Basque Government and GIU19/029 of the University of the Basque Country UPV/EHU. MO would like to acknowledge the funding received by BC3 under the Spanish State Research Agency through Maria de Maeztu program (MDM-2017-0714) and under the Basque

Government BERC 2018-2021 program.

REFERENCES

[1.] WMO. WMO Statement on the Status of the Global Climate in 2012 (2013). http://www.wmo.int/pages/mediacentre/press_releases/documents/WMO_1108_EN_web_000.pdf.

[2.] IPCC. Climate Change 2014: Synthesis Report. Contribution of Working Groups I, II and III to the Fifth Assessment Report of the Intergovernmental Panel on Climate Change [Core Writing Team, R.K. Pachauri and L.A. Meyer (eds.)]. IPCC, Geneva, Switzerland, 151 pp. (2014)

[3.] UN-Habitat. World Cities Report 2016: Urbanization and Development - Emerging Futures, (2016). https://unhabitat.org/world-cities-report.

[4.] EEA. Climate Change, Impacts and Vulnerability in Europe 2016: An Indicator-Based Report, (2017). https://doi.org/10.2800/534806.

[5.] Sabbioni, C., Brimblecombe, P., Cassar, M., and Noah's Ark (Project). The atlas of climate change impact on European cultural heritage: scientific analysis and management strategies. EC cultural heritage research series ; n. 19. London; SE.: Anthem, (2010).

[6.] Cassar, M., Young, C., Weighell, T., ICCROM, ICOMOS, Sheppard, D., Bomhard, B., Rosabal, P., and UNESCO. Climate Change and World Heritage. Report on Predicting and Managing the Impacts of Climate Change on World Heritage and Strategy to Assist States Parties to Implement Appropriate Management Responses. Edited by Augustin Colette, (2007).

[7.] Markham, A., Brabec, E., Burke, S., Cox, P., Daly, C., Diop, A., Downes, J., et al. The Future of Our Pasts: Engaging Cultural Heritage in Climate Action - Outline of Climate Change and Cultural Heritage, (2019).

[8.] Bonazza, A., Maxwell, I., Drdácký, M., Vintzileou, E., and Hanus, C.. Safeguarding Cultural Heritage from Natural and Man-Made Disasters: A Comparative Analysis of Risk Management in the EU. Luxembourg: Publications Office of the European Union, (2018).

[9.] Council of Europe. Recommendation CM/Rec(2018)3 of the Committee of Ministers to Member States on Cultural Heritage Facing Climate Change: Increasing Resilience and Promoting Adaptation, (2018).

[10.] UNDRO. *Natural Disasters and Vulnerability Analysis : Report of Expert Group Meeting, 9-12 July 1979*. Geneva: Office of the United Nations Disaster Relief Coordinator, (1980).

[11.] Berrang-Ford, L., Pearce, T., and Ford, J.D.. *Systematic Review Approaches for Climate Change Adaptation Research*. Regional Environmental Change 15, no. 5 (2015): 755–69. https://doi.org/10.1007/s10113-014-0708-7.

[12.] Xiao, Y., and Watson, M. Guidance on Conducting a Systematic Literature Review. Journal of Planning Education and Research 39, no. 1 (2017): 93–112. https://doi.org/10.1177/0739456X17723971.

[13.] Grant, M. J., and Booth, A. A Typology of Reviews: An Analysis of 14 Review Types

and Associated Methodologies. Health Information and Libraries Journal 26, no. 2 (2009): 91–108. https://doi.org/10.1111/j.1471-1842.2009.00848.x.

[14.] Sesana, E., Gagnon, A. S., Bertolin, C., and Hughes, J. Adapting Cultural Heritage to Climate Change Risks: Perspectives of Cultural Heritage Experts in Europe. Geosciences (Switzerland) 8, no. 8 (2018): 1–23. https://doi.org/10.3390/geosciences8080305.

[15.] Bernardini, G., Postacchini, M., Quagliarini, E., D'Orazio, M., and Brocchini, M. Flooding Pedestrians' Evacuation in Historical Urban Scenario: A Tool for Risk Assessment Including Human Behaviors. RILEM Bookseries 18 (2019): 1152–61. https://doi.org/10.1007/978-3-319-99441-3_124

[16.] Gandini, A., Garmendia, L., Prieto, I., Álvarez, I., and San-José, J.-T. A Holistic and Multi-Stakeholder Methodology for Vulnerability Assessment of Cities to Flooding and Extreme Precipitation Events. Sustainable Cities and Society 63 (2020). https://doi.org/10.1016/j.scs.2020.102437

[17.] Gandini, A., Prieto, I., Garmendia, L., San-José, J.-T., and Egusquiza, A.. Adaptation to Flooding Events through Vulnerability Mapping in Historic Urban Areas. In International Archives of the Photogrammetry, Remote Sensing and Spatial Information Sciences - ISPRS Archives, 42:221–26, (2018). https://doi.org/10.5194/isprs-archives-XLII-3-W4-221-2018

[18.] Gandini, A., Garmendia, L., and San Mateos, R.. Towards Sustainable Historic Cities: Adaptation to Climate Change Risks. Entrepreneurship and Sustainability Issues 4, no. 3 (2017): 319–27. https://doi.org/10.9770/jesi.2017.4.3S(7).

[19.] Vojinovic, Z., Hammond, M., Golub, D., Hirunsalee, S., Weesakul, S., Vorawit Meesuk, Medina, N., Sanchez, A., Kumara, S., and Abbott, M. Holistic Approach to Flood Risk Assessment in Areas with Cultural Heritage: A Practical Application in Ayutthaya, Thailand. Natural Hazards 81, no. 1 (2016): 589–616. https://doi.org/10.1007/s11069-015-2098-7.

[20.] Forino, G., MacKee, J., and von Meding, J. A Proposed Assessment Index for Climate Change-Related Risk for Cultural Heritage Protection in Newcastle (Australia). International Journal of Disaster Risk Reduction 19 (2016): 235–48. https://doi.org/10.1016/j.ijdrr.2016.09.003.

[21.] Kotova, L., Jacob, D., Leissner, J., Mathis, M., and Mikolajewicz, U. Climate Information for the Preservation of Cultural Heritage: Needs and Challenges. Communications in Computer and Information Science 961 (2019): 353–59. https://doi.org/10.1007/978-3-030-12957-6_25

[22.] Ravankhah, M., Chmutina, K., Schmidt, M., and Bosher, L. Integration of Cultural Heritage into Disaster Risk Management: Challenges and Opportunities for Increased Disaster Resilience. In Going Beyond. Heritage Studies No. 2, edited by M.-T. Albert et al. (eds.), 307–21. Springer International Publishing AG, (2017). https://doi.org/10.1007/978-3-319-57165-2.

[23.] Mallinis, G., Mitsopoulos, I., Beltran, E., and Goldammer, J. G.. Assessing Wildfire Risk in Cultural Heritage Properties Using High Spatial and Temporal Resolution Satellite Imagery and Spatially Explicit Fire Simulations: The Case of Holy Mount Athos, Greece. FORESTS 7, no. 2 (2016). https://doi.org/10.3390/f7020046.

[24.] Georgi, B., Swart, R., Marinova, N., Hove, B., Jacobs, C., Klostermann, J., et al. Urban

Adaptation to Climate Change in Europe Challenges and Opportunities for Cities Together with Supportive National and European Policies, Rep. No. 2/2012, (2012). https://doi.org/10.2800/41895.

[25.] Adger, W. N., Barnett, J., Brown, K., Marshall, N., and O'Brien, K. Cultural Dimensions of Climate Change Impacts and Adaptation. Nature Climate Change 3, no. 2 (2013): 112–17. https://doi.org/10.1038/nclimate1666.

[26.] Gandini, A., Egusquiza, A., Garmendia, L., and San-Jose, J.-T. Vulnerability Assessment of Cultural Heritage Sites towards Flooding Events. In Florence Heri-Tech - The Future Of Heritage Science And Technologies, Vol. 364. IOP Conference Series-Materials Science and Engineering. Dirac House, Temple Back, Bristol Bs1 6be, England: Iop Publishing Ltd, (2018). https://doi.org/10.1088/1757-899X/364/1/012028

[27.] Lemonsu, A., Viguié V., Daniel M., and Masson V. Vulnerability to Heat Waves: Impact of Urban Expansion Scenarios on Urban Heat Island and Heat Stress in Paris (France). Urban Climate 14 (2015): 586–605. https://doi.org/10.1016/j.uclim.2015.10.007.

[28.] Gartland, L. Heat islands : understanding and mitigating heat in urban areas. London SE - xiii, 192 p. : il.: Earthscan, (2010).

[29.] Zuo, J., Pullen S., Palmer, J., Bennetts, H., Chileshe, N., and Ma, T. Impacts of Heat Waves and Corresponding Measures: A Review. Journal of Cleaner Production 92 (2015): 1–12. https://doi.org/10.1016/j.jclepro.2014.12.078.

[30.] Kalisch, A., y Satapath S., Porsché I., r Rolke D., Bhatt S., Tomar S., and Nair S. A Framework for Climate Change Vulnerability Assessments | CCARDESA, (2014).

[31.] World Meteorological Organization. Guidelines on the Defintion and Monitoring of Extreme Weather and Climate Events, (2018). https://doi.org/10.1109/CSCI.2015.171.

[32.] Chen, X., Li, N., Liu J., Zhang Z., and Liu Y. Global Heat Wave Hazard Considering Humidity Effects during the 21st Century. International Journal of Environmental Research and Public Health 16, no. 9 (2019). https://doi.org/10.3390/ijerph16091513.

[33.] Li, D., and Bou-Zeid, E. Synergistic Interactions between Urban Heat Islands and Heat Waves: The Impact in Cities Is Larger than the Sum of Its Parts. Journal of Applied Meteorology and Climatology 52, no. 9 (2013): 2051–64. https://doi.org/10.1175/JAMC-D-13-02.1.

[34.] UNESCO. Managing Disaster Risks for World Heritage. Paris: UNESCO World Heritage Center, (2010). https://whc.unesco.org/en/managing-disaster-risks/.

[35.] Rus, K., Kilar V., and Koren, D. Resilience Assessment of Complex Urban Systems to Natural Disasters: A New Literature Review. International Journal of Disaster Risk Reduction 31, no. March (2018): 311–30. https://doi.org/10.1016/j.ijdrr.2018.05.015.

[36.] Araoz, G. F. World-Heritage and Defining Historic Protecting Urban Landscapes : Authenticity. APT Bulletin: Journal of Preservation Technology 2–3, no. 39 (2008): 33–37.

[37.] Brimblecombe, P., Grossi C. M., and Harris I. Climate Change Critical to Cultural Heritage. Survival and Sustainability, (2011), 195–205. https://doi.org/10.1007/978-3-540-95991-5.

[38.] Dirksen, M., Ronda R. J., Theeuwes N. E., and Pagani G. A. Sky View Factor Calculations and Its Application in Urban Heat Island Studies. Urban Climate 30 (2019): 100498. https://doi.org/10.1016/j.uclim.2019.100498.

[39.] Pyrgou, A., Hadjinicolaou P., and Santamouris M. Enhanced Near-Surface Ozone under Heatwave Conditions in a Mediterranean Island. Scientific Reports 8, no. 1 (2018): 9191. https://doi.org/10.1038/s41598-018-27590-z.

[40.] Stedman, J. R. The Predicted Number of Air Pollution Related Deaths in the UK during the August 2003 Heatwave. Atmospheric Environment 38, no. 8 (2004): 1087–90. https://doi.org/10.1016/j.atmosenv.2003.11.011.

[41.] Núñez Peiró, M., Sánchez, C., Sanz-Fernández, A., Heredia, M., López-Bueno, J., Neila, J., C. Linares, Díaz, J., and Muñoz, G. Exposure and Vulnerability towards Sum*mer Energy Poverty in the City of Madrid: A Gender Perspective*, In Press, (2020).

12th International Conference on Structural Analysis of Historical Constructions
SAHC 2020
P. Roca, L. Pelà and C. Molins (Eds.)

RISK MANAGEMENT AND BUILT HERITAGE: TOWARDS A SYSTEMATIC APPROACH

ANTHOULA KONSTA[1*] AND STEFANO DELLA TORRE[1]

[1]Department of Architecture, Building environment and Construction engineering (ABC)
Politecnico di Milano
31 Ponzio St., 20133 Milan, Italy
e-mail: anthoula.konsta@polimi.it, stefano.dellatorre@polimi.it; www.abc.polimi.it
(*corresponding author)

Keywords: Risk Classification, Risk Assessment, Risk Management, Built Heritage Management

Abstract. *This paper discusses the classification of risks as a tool for the identification, the assessment and the management of risks for the built heritage. Existing typologies of risk vary according to the selected criteria on which they are based and their utility within the risk management process. Indicative examples of risk classifications proposed and used in the field of cultural heritage management, as well as in other fields, are examined. The comparison of the selected criteria for analysing risks and the reflection upon their relevant aspects to the built heritage conservation provide a frame for a systematic approach to the built heritage management.*

1 INTRODUCTION

During the last thirty years, the risk management methodology has been recognised as an effective approach to the conservation decision-making process. Among the various efforts that have been made to develop coherent and clear procedures for the risk management in the field of cultural heritage, the experience carried out in museums preventive conservation practices stands out.

With respect to the field of built heritage, we can notice the prevalence of a fragmentary vision of the problems and their solution. Indeed, many methods have been elaborated for the analysis of the different risks to which built heritage is exposed. From air pollution and acid rain to natural hazards, and from inappropriate intervention and use to mass tourism, we can find a relevant number of studies and practice involving respectively numerous specialists and skills from a variety of fields. Naturally, this kind of "separation" arises from the necessity to deepen the knowledge of the different problems and their solution and it cannot be undoubtedly considered as a stumbling block. The problem emerges from the difficulty to coordinate interdisciplinarity, to understand multifaceted problems, and to put together all the findings.

With the aim to frame a more methodical and holistic approach to the built heritage risk management, firstly, the different parts of a risk management process are examined, and their main characteristics, as well as their relationship are underlined. Secondly, different risk classification schemes are discussed with regard to their usefulness and practicality to respond to the diverse needs of the process.

2 RISK ASSESSMENT IN RELATION TO RISK MANAGEMENT

2.1 The importance of meaningful measurements for a successful risk management

David J. Ball [1] in his article about the evolution of risk-based thinking describes the contribution of the studies of mathematicians and scientists during the 17th and 18th centuries to the development of risk based approaches to the first insurance companies. The mathematical calculation of the probability of future adverse events in a defined period and the wide range of its application has given rise, in the 20th century, to the extension of risk management approaches from the financial and insurance sectors to the industrial and public health sectors

Similarly, Douglas W. Hubbard in his brief history of risk management highlights the determinant role of probability theory and statistics in assessing risks: "[…] throughout most of human history, we were dealing with only half of the risk management problem, at most. From Babylon through the Middle Ages, risk management was an unguided mitigation of risks. Choosing what risks to prepare for was always a matter of gut feel. What differentiates risk management since the start of the Age of Enlightenment is in part a more systematic approach to assessing the risk. The development of probability theory and statistics in the 17th century allowed for risk to be quantified in a meaningful way" [2, p. 22].

However, Hubbard warns that the predominant approach to risk management is not based on actual measurements of risks. Indeed, the probabilistic models will be adopted only in select industries for select applications, such as the quantitative methods used in insurance and financial industry, as well as the "probabilistic risk analysis" used in engineering. In contrast, many of the risk analysis techniques adopted and widely used by consultants and standards are based on arbitrary and ineffectual scoring approaches that are not supported by any theoretical or empirical analysis. In addition, he concludes, "if the initial assessment of risk is not based on meaningful measures, the risk mitigation methods, even if they could have worked, are bound to address the wrong problems. If risk assessment is a failure, then the best case is that risk management effort is simply a waste of time and money because decisions are ultimately unimproved. In the worst case, the erroneous conclusions lead the organization down a more dangerous path that it would be probably not have otherwise taken" [2, p. 6].

2.2 Risk analysis for better decisions

The big influence of risk-based approaches over all the agencies has been determined not because of the willingness to reduce all risks (Ball considers three factors, firstly the lack of resources, secondly the non-exclusive interest for risks, and thirdly the positive aspects of risky activities), but as a consequence of the capacity to prioritise the activities when managing a great number of risks, and above all to reach efficient decisions [1].

In this perspective, the definition of acceptable-risk problems and the critical analysis of the viability of various approaches to decision making offered by Fischhoff et al [3] is very relevant. As stated in their report, "risk acceptable problems are decision problems, i.e. they require a choice between alternatives. That choice depends upon the alternatives, values, and beliefs that are considered" [3, pp. ii, 4-6]. As for the decision making methods, three categories have been identified and analysed: professional judgment, bootstrapping techniques and formal analysis, such as the cost/benefit analysis or the multi-criteria analysis.

Similarly, Kaplan and Garrick [4] in the light of two quantitative definitions of risk they

discussed the notion of risk acceptability and argued that "[…] the purpose of risk analysis and risk quantification is always to provide input to an underlying decision problem which involves not just risks but also other forms of costs and benefits. Risk must thus be considered always within a decision theory context. Within this context, that risk is acceptable, which comes along with the optimum decision option, all other risks are unacceptable, even if smaller".

Thus, risk assessment is only one phase in the process of risk management. It is the technical estimation of risks or else the "tool of gaining knowledge about the risks" and consists in identifying hazards, assessing their probabilities and measuring their consequences [5]. The other phase regards the decision process and includes further considerations, incorporating social and economic concerns as well as legal requirements and policy issues [1,6]. In other words, "risk analysis is only part of decision analysis and analysis is only part of any kind of management – risk management or otherwise" [2, p. 242].

2.3 Parts and content of the risk management process

The review of the main current approaches to risk in a wide set of environments, provided by the International Risk Governance Council IRGC [5, pp. 86-156], comes to the conclusion that although there is a lack of consistency in the use of terms, as well as different emphases placed on the parts of the risk management process, the basic processes involved in assessing and managing risks are to a great extent the same.

Thus, without dwelling on the terminology differences between the wide range of organisations and publications concerning risk management, the intention is to understand the logic and the function of the common process phases or else, as Hubbard proposed, a simplified risk management cycle. Necessary conditions of an informed risk mitigation is first to identify and then to assess risks. Although there are cases of easily understood risks that can be addressed apparently without great assessment efforts, in most situations there is a large number of risks, with different potential risk mitigation strategies but only a restricted availability of resources. For this reason, it is necessary to assess not only the initial risks but also the expected risk reduction if various measures were taken against their costs. In this way, as Hubbard underlines, "risk assessment appears prior to and as part of the selection of risk mitigation methods". Once the mitigation options have been selected and implemented, they have to be monitored with the same manner and the risk management cycle is about to begin again [2, pp. 30-31].

3 RISK CLASSIFICATION SYSTEMS IN THE FIELD OF MUSEUMS

The publication of *The ABC Method: a risk management approach to the preservation of cultural heritage* in 2016 represents the updated version of the risk management practices developed by the Canadian Conservation Institute, the ICCROM, and the Netherlands Cultural Heritage Agency [7]. The manual, based on the experiences carried out in the field of museums since 1980 [8,9,10], is built around the five principal steps of a risk management process [11,12], and provides detailed explanations about tasks and activities for the implementation of each step.

Two aspects are of particular interest for the purpose of this study. The first one regards the use of frameworks "for thinking about risks in the identify, analyse and treat steps" [7, p. 69]. Five classification schemes are proposed based on "agents", "types", "stages", "layers", and

"sources of knowledge".

The ten agents of deterioration are used to identify risks and serve as channels to organise all the scenario paths from hazards to adverse effects [7, pp. 70-72].

In terms of occurrence, risks can be classified in three practical types, i.e. rare events, common events, and cumulative processes, with the aim to "guide the risk discovery process, to guide the location of information during the analyse step, and to guide thinking during the treat step" [7, p. 73].

The analysis of risks according to the five stages of control – corresponding to preventive conservation (1. avoid sources of the agent, 2. detect the agent, 3. block the agent, 4. respond to the agent), disaster planning (5a. recover from the fast agent), and remedial conservation/restoration (5b. recover from the slow agent) [8] – ascertains the feasibility and the effectiveness of the risk treat options [7, pp. 75-76].

As for the six layers – region, site, building, room, fittings, packaging/support, and items – besides being useful for the analysis of the block stage of control, they organize possible sources of hazards and agents of deterioration, as well as they structure the knowledge and expertise needed for the analysis [7, pp. 77-78].

The last framework of the three sources of knowledge is closely related to the three types of occurrence. Regional statistics is the source of knowledge about the frequency/intensity of rare events; local knowledge (surveys) is the source for common events, the intensity of cumulative hazards, the five stages of control and the local layers; scientific and technical knowledge is the source for the sensitivity to cumulative processes and for most theories that can analyse risks [7, p. 79].

The second aspect concerns the quantification of risks. The two basic criteria, probability and consequences, have been formulated in order to place events and cumulative processes side by side and to include the relative importance/significance of the various items of the collection [7, p. 17]. The former becomes Frequency (for events) or Rate (for cumulative processes) and the latter is called Loss of value and is divided into two parts, the fractional loss of value to each affected item, and the items affected expressed as a percentage of the total value of the asset [7, p. 93]. The estimation of these three factors constitutes the basis for the comparison of risks.

Following the common practice in risk assessment of distinguishing between the technical components of risk analysis and the subjective components, i.e. the value judgements, the manual affirms the necessity to provide a clear description of the two stages in derivation of the loss of value to each affected item: the expected damage in technical terms and the impacts on value [7, p. 129]. As stated in the manual "comparing risks with different kinds of deterioration requires the adoption of a common scale to convert the predicted deterioration into predicted loss of value. This is the hard part of comparative risk assessment and the essential part. It links material science to cultural values" [7, p. 23]. In addition to the loss of value, criteria such as uncertainty, constraints, opportunities, or the cost-effectiveness of options and the cost of options can be assessed and used during the risk evaluation phase [7, pp. 134-138, 142].

4 RISK CLASSIFICATIONS SYSTEMS IN THE FIELD OF BUILT HERITAGE

4.1 Classifications based on "hazard" and "vulnerability" categories and levels

The first example taken into consideration is the Risk Map of Cultural Heritage developed

by the Italian Central Restoration Institute (ICR) [13]. The division in three groups made by Risk Map attempts to the characterisation of the risks according to three hazard categories and the corresponding vulnerability aspects of the building elements that have to be considered. In detail, the three clusters defined, the environmental-air domain, the static-structural domain, and the anthropic domain, connect the three diverse nature of risk factors – i.e. the climatic/microclimatic and air pollutants risk factors, the geomorphological characteristics of the ground and of the subsurface, and the demographic/socio-economic dynamics – to the three different aspects of vulnerability defined by the material surface characteristics, the structural characteristics and the use/safety aspects of the building.

Even if the taxonomy is referred to the nature (climatological, geophysical, and anthropic) of risk factors and the building vulnerability aspects, we can notice that the two of the three types defined are equal to the types defined by Waller. Indeed, in the first category of rare/catastrophic risks we can link the static-structural domain, where the hazards considered are: seismic, landslides, floods, coastal dynamics, avalanches and volcanic, i.e. with low probability but severe effects, involving the structure of the building. In the third category of constant/mild-gradual risks we can associate the environmental-air domain characterised by threats, such as temperature, precipitation, wind, air humidity, pollution etc., that have cumulative effects on the surfaces of the building materials.

Another project that follows the same groups of risks with Risk Map is the European CHIC protocol [14]. In this case, the distinction between certain/long term and uncertain/rapid onset effects for the natural risks is clarified.

Similarly to the three types of risks defined in museum collections, they contribute to the identification of risks, they organise the knowledge and the expertise necessary for the analysis and finally guide thinking in the treat step. Moreover, this sort of classification, as Baer [15] explains, is significant in the risk management process. A rapid onset event with low probability may not justify preventive actions, whereas a slow acting agent that it is expected to affect with certainty the elements exposed may is a reason to take immediate action. On the other hand, the risk of a catastrophic event, characterised by a worrying rate of occurrence may necessitates a significant allocation of resources.

As for the measurement of risks, Risk Map considers three different detail levels according to the scale considered: territorial, individual, and local risk. The territorial risk is based on the hazard and exposure indicators related to the municipal area; the individual risk concerns the hazard indicator of the municipal area combined with the vulnerability of a single building; and lastly the local risk that relates the indicator of local hazard with the building vulnerability.

Recent developments of Risk Map tool concern the elaboration of a new evaluation model of seismic risk by updating the indicators of seismic hazard and vulnerability according to the new recommendations for the assessment and mitigation of seismic risk to cultural heritage approved in 2011 [16], as well as a proposal to adapt the tool to the characteristics of the buildings in historical centres [17].

4.2 Classification schemes based on “nature”, “temporality”, “scale” and “probability” of risk factors.

Another example of risk classification schemes for the built heritage is Dario Camuffo’s work “Perspectives on risk to architectural heritage” [18], in which the author compiles a list

of the major risk factors. He focuses on the problems related to the physicochemical decay of the buildings and discusses the gaps in our scientific and technological knowledge, the controversies over the interpretation of results, and the latest trends. At the end of the chapter proposes a classification of selected risk factors to cultural heritage. The risk factors are divided in two large groups, natural and anthropogenic and qualitative indications of "nature", "temporality", "scale", and "probability" are given.

With regard to the nature, risk factors are characterised mainly by a physical, chemical, or biological action. Concerning the temporality, they are separated in long term, medium term and rapid onset, while in respect of the scale, they can be local, regional, and global. As for the probability, risk factors vary from rare, infrequent and frequent events, to continuous cycles and continuous. Although the criteria and the various categories proposed in this table by Camuffo are not new, on the contrary they are commonly used in the conservation field, this work gains importance because of its holistic and systematic approach. Indeed, the organisation of the major threats to which is exposed built heritage and their qualitative characteristics contributes to their understanding and their management.

4.3 Classification schemes based on "cause-effect" relationships, "building materials", "building elements", and "building typologies"

Another common risk classification scheme in the field of build heritage is the consequence-based approach. In fact, thanks to several efforts matured in architectural preservation field, guided procedures for the analysis of the decay/damage have been introduced in national and international recommendations. The data collected from different sources, such as literature, in situ investigations, and laboratory simulation tests has improved our knowledge on the possible decay/damage causes and their consequences.

Indicative examples are the *Damage Atlas* published in 1998 [19] and the subsequent development of a *Structural Damage Atlas* in recent years [20]. The first gathers and schematize into relations between damage types, causes and deterioration processes the current knowledge of the environmental effects on brick masonry deterioration by drawing attention on the complex interaction of different materials and different boundary conditions [21]. The second focuses on the mechanical behaviour of brick- and stonework masonry under different actions, caused by sudden events such as earthquakes, floods etc. or by long term phenomena such as soil settlement, heavy loads and lack of maintenance, and forms a basis for the definition of typical structural damage patterns.

Without going into details, the damage classification concerning the structural behaviour and the failure mechanisms of the building elements takes into account not only the construction materials, but also the different building typologies and the role of the various structural elements and their connections.

4.4 Classification schemes based on the "combination of risk factors" and the "risk level change" in the course of time

During the last years, the studies on the effects of the environmental factors on the cultural heritage have drawn attention to the issues related to climate change and the new pressures that will be caused by variations in temperature and precipitation, changes in soil conditions, groundwater and sea level, and extreme climatic events.

The Noah's Ark project has developed quantitative models for the global climate change impacts on the deterioration of different heritage materials on European geographical scale [22]. The results of the research project, gathered in different types of maps, correspond to the methodological approach adopted. Firstly, "climate maps" were elaborated by selecting the traditional climate parameters, both meteorological and pollution, relevant to cultural heritage. Estimations were carried out by taking into account different future scenarios and three periods, recent past, near future and far future. In order to obtain the most critical synergetic effects for the historic building materials, the previous climate maps were combined and specific "heritage climate maps" were produced, representing the advancement of the conservation science to adapt the classic meteorology to the needs of conservation [18]. The next step regarded the quantitative expression of damages or else the development of damage functions for the different building materials, based on different information sources, such as field data, literature survey, and laboratory investigations. The results were translated into "damage maps" which in their turn were summarized in "risk maps", showing the type of risks that are likely to increase or decrease in the different regions of Europe.

Among the various classification schemes used in this example, two of them stand out. On the one hand, the examination of synergetic effects based on the combination of different risk factors is necessary for the identification and the assessment of risks for different materials .On the other, the reflection on the risk level change in the course of time becomes useful for the understanding of the priorities and the need of measures.

4.5 Classification schemes based on the "building elements relationships" and the "dependency of risks"

The need for improving management tools has given rise to regular inspection surveys, to systematic monitoring, to periodic maintenance and risk assessment practices as the most proper preventive strategies, e.g. Monumentenwacht organisations in different European countries, Maintain our Heritage in UK, Preventive and Planned Conservation in Italy, the Heritage Care project in South-West Europe, etc. [23,24,25,26,27]. Indeed, the European standard *Conservation of cultural property – Condition survey of immovable heritage* [28] integrates the risk assessment with the condition assessment and represents an attempt to implement preventive strategies.

In the first draft of the standard, despite the consideration of relevant aspects related to the analysis of risks during the phase of assessment, the identification of the related measures was not based on the previous analysis or rather it was not based in an explicit way. Indeed, the activities of condition and risk assessment were not separated and the classification of measures was linked directly to the condition classes. The final version of the standard, approved in 2012, has resolved the previous ambiguities firstly by pointing out the difference between condition and risk assessment, and secondly by setting up a classification of urgency categories, i.e. urgent and immediate, short term, intermediate term, and finally long term, connected to the risk analysis. This sort of classification, based not only on the level of risk but also on the risk level change in the course of time (or the velocity of damage progression), as it has already been mentioned in the previous paragraph, is essential for the planning of the necessary measures.

Another important aspect of the risk analysis that the document proposes is the relationships between the building components. In fact, the description of the elements interactions is

fundamental for the understanding of the unity and the complexity of the building system. For instance, the four basic interaction modalities between the various building technological elements suggested by the Italian guidelines for the conservation plan contribute to the better understanding of the effects that could be caused by the changes of the conditions of the elements in the course of time and in relation with the use of the building [26, pp.41-42]. Another example is the classification of typical seismic damage of the immovable artistic assets according to their connection with the structural elements proposed by the PERPETUATE project [29].

4.6 Classification based on "risk reduction measures", their "control level" and the "time of action"

The most important international organizations, such as UNESCO, ICOMOS, ICCROM, Council of Europe, etc., have strengthened their activities to develop operative methods for an overall prevention and mitigation strategy for the protection of cultural heritage against disasters. For example, the *Risk-Preparedness Manual for World Cultural Heritage* in 1998 [30] and *Between Two Earthquakes* in 1987 [31] are two of the first publications in a series of handbooks that is still being added to and updated in view of current concerns related mainly to the risks of climate change faced by cultural heritage.

The planning framework proposed in these manuals usually takes into account three elements: the action time, i.e. the preparedness (before), the response (during), and the recovery (after) phases; the typology of risk reduction measure; and the control level or else the different role of public institutions and private owners.

Apart from a guide to the identification and organisation of the measures that can be taken against disasters, this scheme could be also used to classify the risks to which built heritage is exposed according to the feasibility/effectiveness of implementing the various typologies of measures [32,33]. What is more, this classification not only indicates the prevalent strategies for the prevention/mitigation of risks but defines also the priorities for their assessment.

5 RISK CLASSIFICATION SCHEMES PROPOSED IN OTHER FIELDS

The most common approaches to the classification of risks employed in other fields, e.g. in insurance and financial industry, in the safety engineering field, or in health and environmental sector, are based on causal agents, risk events, and their potential consequences.

A different approach was developed by WBGU [34], and reviewed later by IRGC [5]. It is based on the concept of systemic risk, i.e. draws attention to the interdependencies and interactions between environmental, social, financial, and economic risks and opportunities. As Klinke and Renn [35] argue there are two key elements that characterise this approach, firstly the extension of factors that should be taken into consideration when managing systemic risks and secondly, the inclusion of analytic-deliberative processes in the regulatory framework.

In detail, the analysis increases the number of criteria, from two– the two classic components of risk, probability and magnitude of damage– to eight, by adding other physical and social impact categories, i.e. the incertitude, the ubiquity, the persistency, the reversibility, the delay effects, and the potential of mobilization.

Considering these criteria, four risk clusters have been identified, according to the different states of knowledge for each risk, distinguishing between 'simple', 'complex', 'uncertain' and

'ambiguous' risk problems. "The characterisation of a particular risk depends on the degree of difficulty of establishing the cause-effect relationship between a risk agent and its potential consequences, the reliability of this relationship and the degree of controversy with regard to both what a risk actually means for those affected and the values to be applied when judging whether or not something needs to be done about it" [5, p. 12]. Based on these risk categories different strategies have been defined for both risk assessment and risk management, as well as about the level and the form of stakeholder participation, supported by suitable methods and tools.

The importance of this classification lies, on the one hand, in the acknowledgement of social, political and cultural contexts, as well as of individual and cultural value judgments, beyond the level of risk, that influence the acceptability/tolerability evaluation of risks (34, p. 29; 5, p. 37]. On the other hand, it allows flexibility in regard to the appropriate position of decision-making concerning the acceptability/tolerability of a risk by assisting assessors and managers in assigning, or dividing this judgement task through the consideration of its two distinct components, the evidence-based and the value-based component [5, pp. 37, 40].

These two factors become relevant to the management of built heritage. The concern about the broader context of the built heritage and their coevolutive relationship, as well as the maturing of sustainable principles, and the necessity of a long term perspective [36] can be reflected by the above systemic approach.

6 CONCLUSIONS

The study of various examples of risk classification schemes draws attention to the different criteria on which they are based and the variety of the risk aspects analysed, useful in diverse ways in the risk management process.

Specifically, the analysis indicates that two main groups can be distinguished according to their utility within the risk management process. The first one contributes mostly to the identification and the assessment of risks, and the second one is associated mainly with the management phase. If in the first group, criteria such as nature, scale, timing, probability/frequency, severity, relations and consequences of risk factors play a part in establishing and/or estimating cause-effect relationships, in the second group, the criteria suggest priorities, strategies, and their efficiency.

In fact, these sorts of classifications have been already applied in an organised manner to the risk management methodology elaborated by the museum sector as it is shown in the example taken into consideration here. Concerning the built heritage conservation, it can be noticed that the various classification schemes proposed and analysed have not been incorporated into a systematic risk management methodology.

In this perspective, the overview provided in this paper represents an attempt to frame a more methodical and holistic approach to the built heritage risk management. In other words, the combination of different classification schemes could be integrated with the various phases of risk management in order to respond adequately to the diverse needs of the process.

However, the different classification schemes analysed in this study cannot be considered exhaustive. The examples that are presented here cover basic and generic classes of risk and they are indicative. According to the particularities of each case, the classifying criteria can be adapted to the specific needs and more precise categories can be formed. Thus, the

methodological approach suggested depends not only on the different needs of the process but also on the needs of the specific built heritage case.

Table 1: Different risk classification schemes according to the selected criteria on which they are based and their utility/scope within the risk management process

Selected criteria	Risk classes	Utility
Risk factors nature	Cause based or mechanism based classes	Risk identification, risk assessment, risk management
Scale	Local, regional, global	
Temporality	Long term, rapid onset	
Probability/Frequency	Rare events, common events, cumulative processes	
Hazard and vulnerability categories	Environmental-air, static-structural, and anthropic domain	
Damage mechanism, building elements characteristics, building typologies	Consequence based classes (decay/damage types)	
Combination of risk factors	Synergetic effects-based classes	
Building elements interactions Relationships of risks	Dependency based classes	
Probability, consequences (direct and indirect, tangible and intangible) Hazard level, exposure level, vulnerability level	Risk level based classes	Risk assessment
Risk level Risk level, constraints, opportunities Risk level, risk level change in the course of time	Priority based or urgency based classes	Risk management
Reduction measure, response level, action time Feasibility/effectiveness/cost-effectiveness of measures Knowledge characterisation	Management strategy based classes or management strategy efficiency based classes	

REFERENCES

[1] Ball, D.J. The evolution of risk assessment and risk management: a background to the development of risk philosophy, *Arboricultural Journal* (2007) **30**(2): 105-112.

[2] Hubbard, D.W. *The failure of risk management: why it's broken and how to fix it*. New Jersey: John Wiley & Sons (2009).

[3] Fischhoff, B., Lichtenstein, S., Slovic, P., Derby, S.L. and Keeney, R.L. *Approaches to Acceptable Risk: A Critical Guide.* Work Performed for U.S. Nuclear Regulatory Commission under NRC Interagency Agreement 40-550-75. Oak Ridge National Laboratory, operated by Union Carbide Corporation for the Department of Energy (1980).

[4] Kaplan, S. and Garrick, B.J. On the quantitative definition of risk. *Risk Analysis* (1981) **1**(1).
[5] Renn, O. (ed.), *White Paper on Risk Governance: Towards an Integrative Approach*. Geneva: International Risk Governance Council (2005).
[6] Watt, J.M. The management of risk with respect to cultural heritage – a case study, *Arboricultural Journal* (2007) **30**(2): 175-185.
[7] Michalski, S. and Pedersoli J.L. (eds), *The ABC Method: a risk management approach to the preservation of cultural heritage*. Ottawa: CCI, ICCROM (2016).
[8] Michalski, S. An overall framework for preventive conservation and remedial conservation. In: *ICOM Committee for Conservation, 9th triennial meeting, Dresden, German Democratic Republic, 26-31 August 1990, preprints*, ICOM Committee for Conservation (1990), pp. 589-591.
[9] Waller, R. Conservation risk assessment: a strategy for managing resources for preventive conservation. *Studies in Conservation* (1994) **39**(sup2): 12-16.
[10] Waller, R. Risk management applied to preventive conservation. In: C.L. Rose, C.A. Hawks, H.H. Genoways (eds), *Storage of natural history collections: A preventive conservation approach*, New York: Society for the preservation (1995), pp. 21-27.
[11] Joint Standards Australia / Standards New Zealand Committee OB-007, *Risk Management*, AS/NZS 4360 (2004).
[12] ISO International Organization for Standardization, *Risk Management*, ISO 31000 (2018).
[13] Accardo, G., Giani, E. and Giovagnoli ,A. The Risk Map of Italian Cultural Heritage, *Journal of Architectural Conservation* (2003) **9**(2): 41-57.
[14] eu-chic.eu. Eu-CHIC project official website. [online] Available at: http://www.eu-chic.eu/ [Accessed Oct. 2019].
[15] Baer, N.S. Assessment and management of risks to cultural property. In N.S. Baer, C. Sabbioni, A.I. Sors (eds), *Science, Technology and European cultural heritage, proceedings of the European Symposium, Bologna, Italy 13-16 June 1989*, Luxembourg: ECSC-EEC-EAEC (1991), pp.27-36.
[16] Cacace, C. and Donatelli, A. Carta del Rischio del patrimonio culturale: studio sulla vulnerablità e pericolosità sismica del patrimonio culturale in Sicilia e Calabria. In S. Della Torre and M.P. Borgarino (eds), *Proceedings of the International Conference Preventive and Planned Conservation, Monza, Mantova - 5-9 May 2014, Protezione dal rischio sismico*, Milano: Nardini editore (2014), pp.107-118.
[17] Cacace, C. and Fiorani, D. Centri storici, vulnerabilità, rischio e gestione della conservazione. Una proposta d'implementazione dello strumento Carta del Rischio. In S. Della Torre and M.P. Borgarino (eds), *Proceedings of the International Conference Preventive and Planned Conservation Monza, Mantova - 5-9 May 2014, Protezione dal rischio sismico*, Milano: Nardini editore (2014), pp. 119-128.
[18] Camuffo, D. Perspectives on risks to architectural heritage. In: N. S. Baer and R. Snethlage (eds), *Saving our architectural heritage: the conservation of historic stone structures*, New York: John Willey &Sons Ltd. (1997), pp. 63-92.
[19] Franke, L., Schumann, I., van Hees, R., van der Klugt L, Naldini. S., Binda, L., Baronio, G., Van Balen, K. and Mateus, J. *Damage Atlas - Classification and Analyses of Damage Patterns found in Brick Masonry*. Project EV5V-CT92-0108, Research report No 8, Volume 2, Stuttgart: Fraunhofer IRB Verlag (1998).

[20] Binda L., Saisi A., de Vent, I.A.E., Van Hees, R.P.J. and Naldini, S. Structural Damage in Masonry: Description and interpretation of crack patterns as basis for finding the damage causes. *Restoration of buildings and monuments, Bauinstandsetzen und Bauenkmalpflege* (2010) **16**(2), pp. 1-22.
[21] Van Hees, R., Binda, L., Van Balen, K. and Naldini, S. Expert system for evaluation of deterioration of ancient brick masonry structures. *The science of the Total Environment* (1996) **189/190**, pp. 247-254.
[22] Sabbioni, C., Brimblecombe, P. & Cassar, M. (eds), *The atlas of climate change impact on European cultural heritage: scientific analysis and management strategies*. London, New York: Anthem Press (2012).
[23] Van Balen, K. and Vandesande, A. (eds), *Innovative built heritage models.* London: Taylor and Francis Group (2018).
[24] *Journal of Cultural Heritage Management and Sustainable Development* (2018) **8**(2), Special Issue: Preventive and planned conservation approaches for built heritage management.
[25] Dann, N. Planned and preventative conservation and England: experiences, opportunities and requirements. In: *Preventive and planned conservation: proceedings of the international conference. Vol 4: Metodi e strumenti per la prevenzione e la manutenzione, Monza - Mantova, 5-9 May 2014*, Firenze: Nardini (2014), pp. 1-10.
[26] Della Torre, S. (ed.), *La conservazione programmata del patrimonio storico architettonico. Linee guida per il piano di manutenzione e consuntivo scientifico*. Milano: Guerini & associati (2003).
[27] Moioli, R. and Baldioli, A. *Conoscere per conservare. Dieci anni per la conservazione programmata*. Quaderni dell'Osservatorio, 29. Milano: Fondazione Cariplo (2018).
[28] CEN/TC 346 – Conservation of Cultural Heritage. *Conservation of cultural property – Condition survey of immovable heritage*, EN 16096 (2012).
[29] Abbas, N., Calderini, C., Cattari, S., Ginanni Corradini, R., Lagomarsino, S., Marghella, G., Piovanello, V., and Rossi, M. PERPETUATE FP7 - Theme ENV.2009.3.2.1.1 – ENVIRONMENT Grant agreement n°: 244229, Deliverable D4 (2010), pp. 78-94.
[30] Stovel, H. *Risk preparedness: a management manual for world cultural heritage*. Rome: ICCROM (1998).
[31] Feilden, B. *Between two earthquakes: Cultural property in seismic zones*. Rome, California: ICCROM, Getty Conservation Institute (1987)
[32] Della Torre, S. The management process for built cultural heritage: preventive systems and decision making. In: K. Van Balen, A Vandesande,. (eds), *Innovative Built Heritage Models*. London: Taylor and Francis Group (2018), pp. 13-20.
[33] Presidenza del Consiglio dei Ministri (PCM), Struttura di Missione Casa Italia. *Rapporto sulla Promozione della sicurezza dai Rischi naturali del Patrimonio abitativo* (2017).
[34] WBGU, German Advisory Council on Global Change, *World in transition. Strategies for managing Global Envirinmental Risks. Annual Report 1998*. Berlin: Springer (2000).
[35] Renn, O., and Klinke, A. Systemic risks: a new challenge for risk management, *EMPO reports* (2004).
[36] Della Torre, S. A coevolutionary approach to the reuse of built cultural heritage. In: G. Biscontin, G. Driussi, (eds), *Il patrimonio culturale in mutamento. Le sfide dell'uso*. Venezia: Arcadia Ricerche (2019), pp. 25-34.

12th International Conference on Structural Analysis of Historical Constructions
SAHC 2020
P. Roca, L. Pelà and C. Molins (Eds.)

SEISMIC DAMAGE SCENARIOS INDUCED BY SITE EFFECTS OF MASONRY CLUSTERED BUILDINGS: A SOUTH ITALY CASE STUDY

A. FORMISANO[1*], N. CHIEFFO[2]

[1]Department of Structures for Engineering and Architecture
School of Polytechnic and Basic Sciences, University of Naples "Federico II"
P.le V. Tecchio, 80125 Naples, Italy
e-mail: antoform@unina.it (*corresponding author)

[2] Faculty of Architecture and Urbanism
Politehnica University of Timişoara
Traian Lalescu Street 2/A, 300223 Timişoara, Romania
email: nicola.chieffo@student.upt.ro

Keywords: Site-Effects, Vulnerability Assessment, Masonry Aggregates, Damage Scenarios, Vulnerability Curves

Abstract. *The present research aims to investigate the influence of site amplification on the seismic vulnerability of the historical centre of the municipality of Baranello in the Molise Region of Italy. Structural and typological characterization of the investigated area has been done according to the EMS-98 scale. The vulnerability assessment of the historical buildings located there has been carried out through an appropriate survey form in order to identify the buildings most susceptible at seismic damage. Furthermore, according to the AeDES form implemented by the Italian Civil Protection Department, the calibration of the typological vulnerability curves of the built-up area has been done based on the seismic motions recorded after the 2002 Molise earthquake. Finally, the local amplification factor, which negatively influences the severity of the seismic damage on the structures, has been taken into account according to the time-domain method. To this purpose, a refined and simplified approach to foresee the expected damage of the inspected urban sector has been proposed, so to use more appropriately the achieved results for reliable seismic risk mitigation plans.*

1 INTRODUCTION

The seismic vulnerability of a given built area indicates the expected amount of damage triggered by an earthquake of a specific magnitude. The recent tragic earthquakes occurred in Italy during the last decades are a living testimony of the bad seismic behaviour of the historical centres of many municipalities [1]. Generally, the occurrence of near-field earthquakes has required to adopt methods of predicting the expected damage taking into account the influence of the local seismic response on inhabited areas. This is due to a series of hazardous factors, such as the age of buildings, the poor quality of materials and the insufficient maintenance of constructions, which lead towards the high seismic vulnerability of several built-up areas.

Focusing on the urban scale, rapid urbanization has dramatically increased the vulnerability and risk of urban dwellers in densely populated areas. The available strategies for seismic vulnerability assessment usually have as starting point the compilation appropriate survey forms, based on several parameters, i.e. the seismic-resistant system type to lateral loading, the structural regularity and maintenance conditions and the presence of existing damages, to collect information on historical centre buildings. The application of these survey forms allows to fully understand the various structural types located within heterogeneous urban centres [2, 3].

Nowadays, the evaluation of geological effects has been taken into consideration in the framework of risk assessment in order to have a better and correct forecast of the expected damage. In this framework, it is recognised that soil layers amplify or reduce the seismic waves on the crustal surface. Site effects are, thus, dangerous when the amplification of seismic waves in surface geological layers occurs.

Based on these considerations, the municipality of Baranello, in the province of Campobasso, has been selected as a case study to evaluate the possible damages under seismic events considering site effects. The proposed work aims to evaluate the local amplification effects considering the time domain of a 1D half-space ground model. The main goal of this work is to investigate the influence of soil amplification on the seismic behaviour of typical masonry aggregates with the final target to plot the damage scenarios expected under different earthquake moment magnitudes and site–source distances.

2 THE MUNICIPALITY OF BARANELLO

2.1 Historical background

Baranello (Figure 1) is a small town located in the province of Campobasso in the Molise Region of Italy. The municipality has 2759 inhabitants and rises at 610 m above sea level with an extended area of 25 km^2. The town has medieval origins and it is bordered by the towns of Busso, Colle d'Anchise, Spinete and Vinchiaturo.

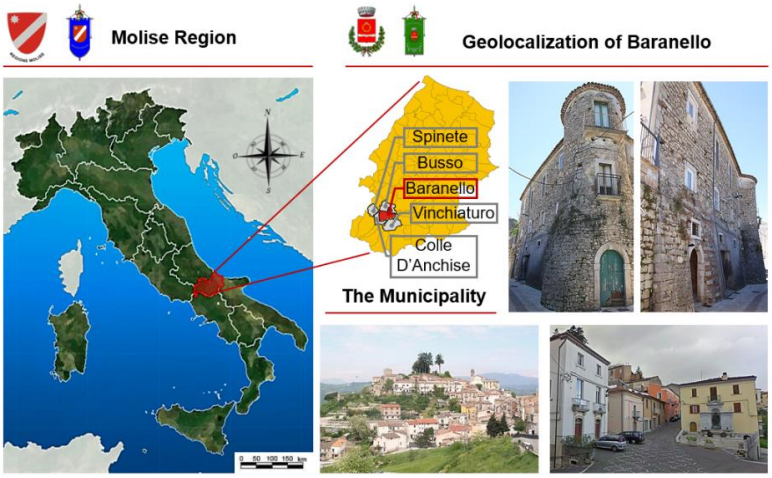


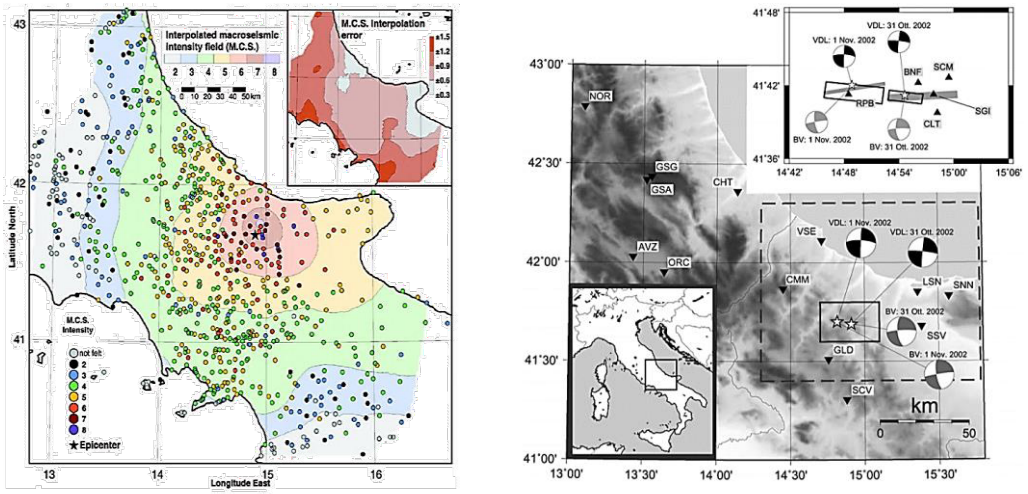
Figure 1: Geographical localization of the municipality of Baranello.

There are limited historical news about the evolution of the centre during time. The village was mentioned for the first time in the fourteenth century as a possession of Capece Galeota's family dating back to Norman ages. Only in 1591 the feud was sold by the Carafa family, from which the Pope Paul IV descended, to the Marquis one and then to Angelo Barone. Nowadays, the territory has the characteristics of a mountain centre: narrow and steep streets that enlarge towards the area of new settlements. The urban centre is characterized by both houses preserving their original appearance, which are located around the church and along the main streets, and more modern buildings, that are placed in other districts belonging to the municipal territory.

2.2 The 2002 Molise seismic event

The Molise earthquake was a significant event, occurred on 2002 October 31st, having the epicentre localized in the province of Campobasso among the municipalities of San Giuliano di Puglia, Colletorto, Santa Croce di Magliano, Bonefro, Castellino del Biferno and Provvidenti. This seismic event, having magnitude M_w= 5.7, was perceived in a large area of Central-Southern Italy, causing significant damage in a restricted area between Frentani, Sannio and Foggia (Figure 2).

The aftershocks (more than 1900 seismic events) showed a predominantly vertical seismogenic structure, having a depth between 10 and 25 km, which was oriented in an east–west direction and consisted of two main segments, each with a length of about 15 km. Also, a 10.5×8.0 km^2 fault plan, that extended between 12 and 19.9 km in depth, was associated to the October 31st event [4].



(a) (b)

Figure 2: Distribution of earthquakes in the Molise Region area: (a) macroseismic intensities; (b) focal mechanisms of the fault model.

Figure 2a shows the macroseismic intensities occurred after the events previously mentioned. In the area near the epicentre, the maximum intensity recorded was VI according to the MCS scale. Moreover, Figure 2b describes the surface projections and focal mechanisms of the fault model for the Molise earthquake. In particular, in the central panel the accelerometric

stations, that recorded the mainshocks of the seismic sequence, have been marked with triangles, while dashed rectangle denotes the recording stations and the upper solid rectangle points out the seismogenic sources which generated the seismic event.

3 TYPOLOGICAL AND STRUCTURAL DESCRIPTION OF THE BUILT-UP AREA

3.1 The CARTIS survey form

The structural and typological characterization of the built-up is considered indispensable for the census of the buildings exposed at risk, which is a preliminary phase for their classification into typological classes.

The CARTIS form has been conceived by both the PLINIVS research centre of the University of Naples "Federico II" and the Italian Civil Protection Department in the framework of the ReLUIS 2014–2016 project "Development of a systematic methodology for the territorial scale exposure assessment based on the typological/structural characteristics of buildings" [5]. The CARTIS form has been herein used in order to detect the prevalent ordinary building typologies in municipal or sub-municipal territorial parts, called urban sectors, characterized by typological and structural homogeneity. In the historical centre of Baranello one unique compartment, labelled as C01 and composed of 300 buildings, has been considered (Figure 3).

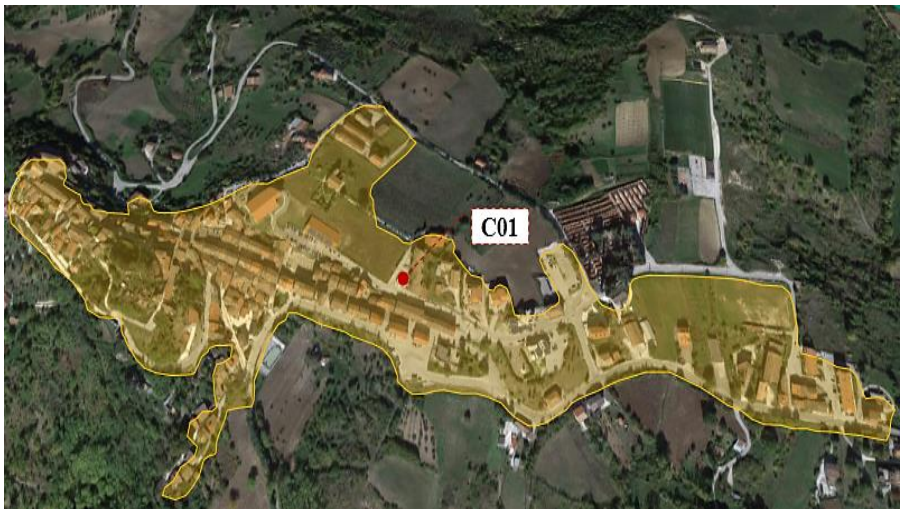


Figure 3: The C01 urban sector detected in the municipality of Baranello.

Most of the buildings have been built using rough-hewn stones assembled according to the technique of either sack or mixed walls, which in some cases do not respect the “rules of art” indispensable to guarantee a satisfactory behaviour of the masonry apparatus against seismic actions.

The houses characterising the historical centre are composed of walls with an average thickness of 0.65 m and an average inter-storey height of 3.50 m.

Other than masonry vaults, horizontal structures are represented by timber or steel floors, which are also the main structure of coverages (Figure 4).

The data collected through the CARTIS form has allowed, through statistical elaborations, to provide indications on the constructive age, number of storeys, average surface and wall type

of the sample of buildings surveyed within the municipality examined. The results obtained are summarized in the cumulative distributions reported in Figure 5.



Figure 4: Street views of the prevalent building typologies inside the inspected area.

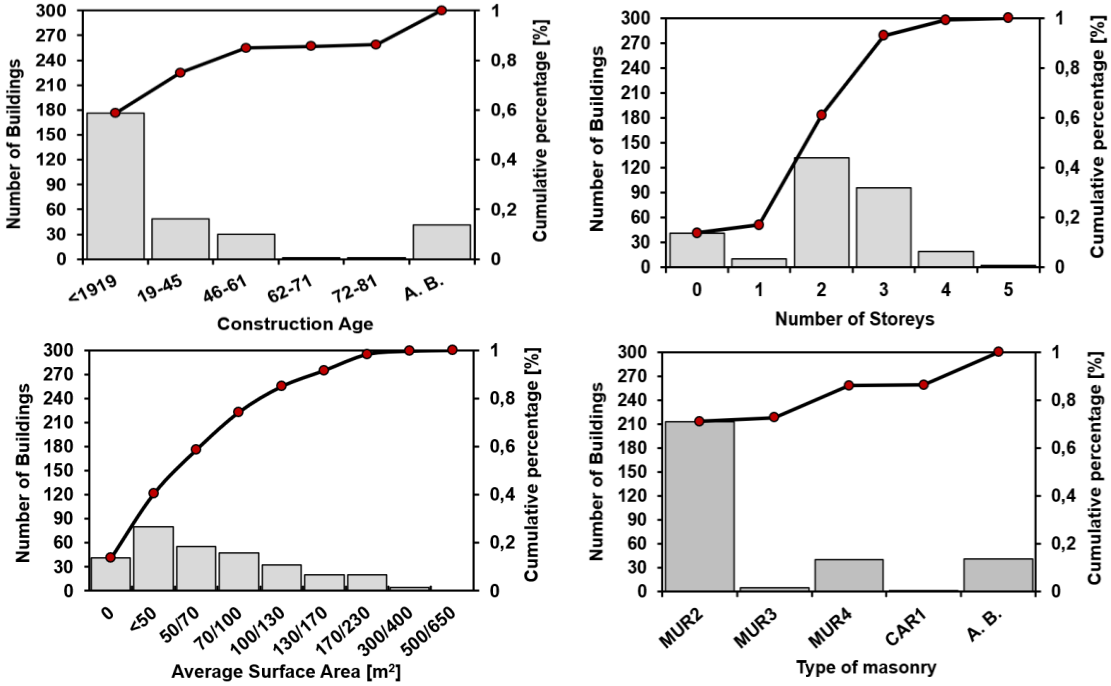


Figure 5: Preliminary characteristics of buildings surveyed in the municipality of Baranello.

From the data surveyed on the inspected buildings, the prevailing typological class is the MUR2 (rough-hewn stones) one, which has been detected in 73% of the cases (220 buildings). The other classes detected in the study area are the MUR3 (rough-hewn masonry stones or pseudo-regular stones, 2% of the building sample) and MUR4 (regular masonry with squared or brick stones, 13% of the building sample) ones, whereas 12% of the building sample are represented by unused constructions.

3.2 Large scale seismic vulnerability assessment

A seismic vulnerability assessment at urban scale has been herein implemented in order to evaluate the propensity at damage of buildings placed in the municipality of Baranello. In this context, a vulnerability index-based method has been adopted. The proposed method has the peculiarity of investigating the seismic vulnerability of buildings grouped in compounds through a specific vulnerability form [6-9].

The used survey form, composed of 15 parameters, is appropriate for masonry building aggregates, since it takes into account the effects of mutual interaction among aggregated Structural Units (S.Us) under earthquakes.

Methodologically, the vulnerability index, I_V, for each S.U., is intended as the weighted sum of the class selected for each of the 15 parameters multiplied by the respective weight. Each of the estimated parameters are grouped into four vulnerability classes (A, B, C and D, from the best to the worst), characterised by a specific score (also with a negative sign in case of a vulnerability reduction), to which a correspondent weight, W_i, is assigned. The weight of parameters is variable from a minimum of 0.25 for the less important factors up to a maximum of 1.50 for the most important ones.

The compilation of the survey forms for the aggregated S.Us of Baranello has provided the distribution of the vulnerability indexes reported in Figure 6.

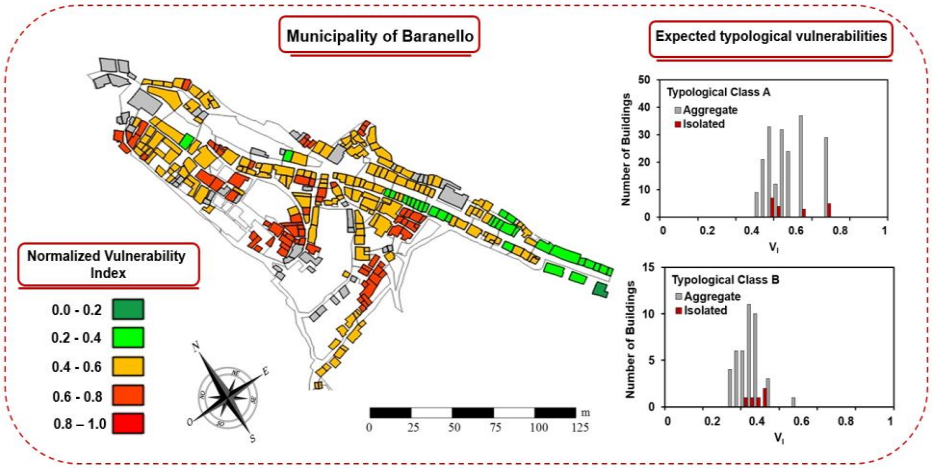


Figure 6: Seismic vulnerability distribution in the examined area.

3.2 Seismic impact scenarios

The prediction of the seismicity of a specific site can be evaluated by adopting appropriate seismic attenuation laws, which are empirical formulations calibrated on the statistical data (instrumental or macroseismic) derived from earthquakes occurred. Generally, these laws are based on simplified models in order to represent seismic propagation. In practice, an empirical relationship is established between the parameter representative of the motion, which can be given by the macroseismic intensity, and other factors, like the energy released at the source in terms of magnitude (M_w) and the epicentre distance (R). In the current research, the severity of the seismic effects has been analysed by predictive analyses using the Esteva and Harris' seismic attenuation law [10].

In detail, a deterministic approach has been used by selecting as reference earthquakes, according to the Parametric Catalogue of Italian Earthquakes (CPTI15) [11], three events of increasing moment magnitudes (4, 5 and 6) occurred in the past in the Molise region of Italy.

After these magnitudes have been selected, the selection of different epicentre distances, namely 5, 17 and 35 Km, has allowed to plot the expected damage scenarios.

Based on the attenuation law above mentioned, the macroseismic intensities have been correlated to the earthquake magnitudes and epicentre distances, leading towards the nine damage scenarios reported in Table 1.

Table 1: Correlation between moment magnitude, M_w, and macroseismic intensity, I_{EMS-98}.

Magnitude M_w	**Macroseismic Intensity I_{EMS-98}**		
	R = 5 km	R = 17 km	R = 35 km
4	X	VII	V
5	XI	VIII	VII
6	XII	X	VIII

Therefore, the damage scenarios achieved according to the Esteva and Harris' attenuation law considering R= 5 Km have been plotted in Figure 7 to show the most dangerous seismic analysis case.

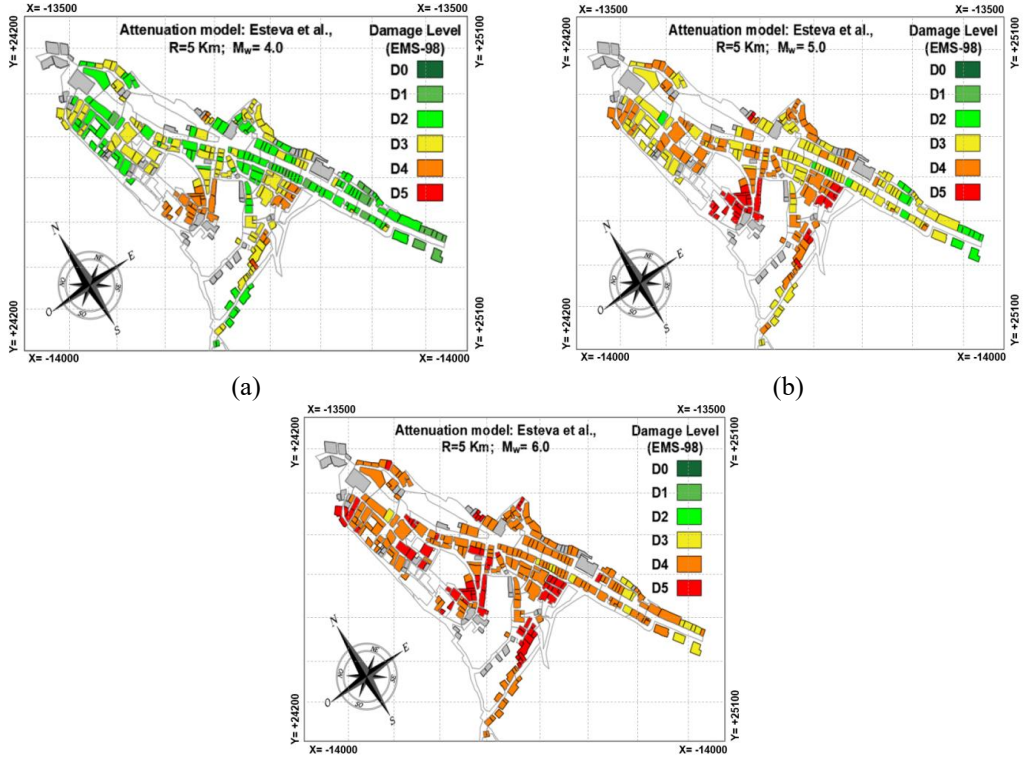


Figure 7: The impact damage scenarios for variable magnitudes and epicentre distance of 5 Km in the investigated urban area.

Then, the correlation between the mean damage grade, μ_D, and the damage thresholds, D_K,

have been developed according to the EMS-98 scale (Figure 8).

From the analysis results, it appears that for M_w= 4 about 61% of the buildings suffer damage D2, while for M_w= 6, damage thresholds D4 (near-collapse) and D5 (collapse) are attained in 68% and 25% of the cases, respectively. Contrary, when M_w= 5, a more variable damage distribution is achieved.

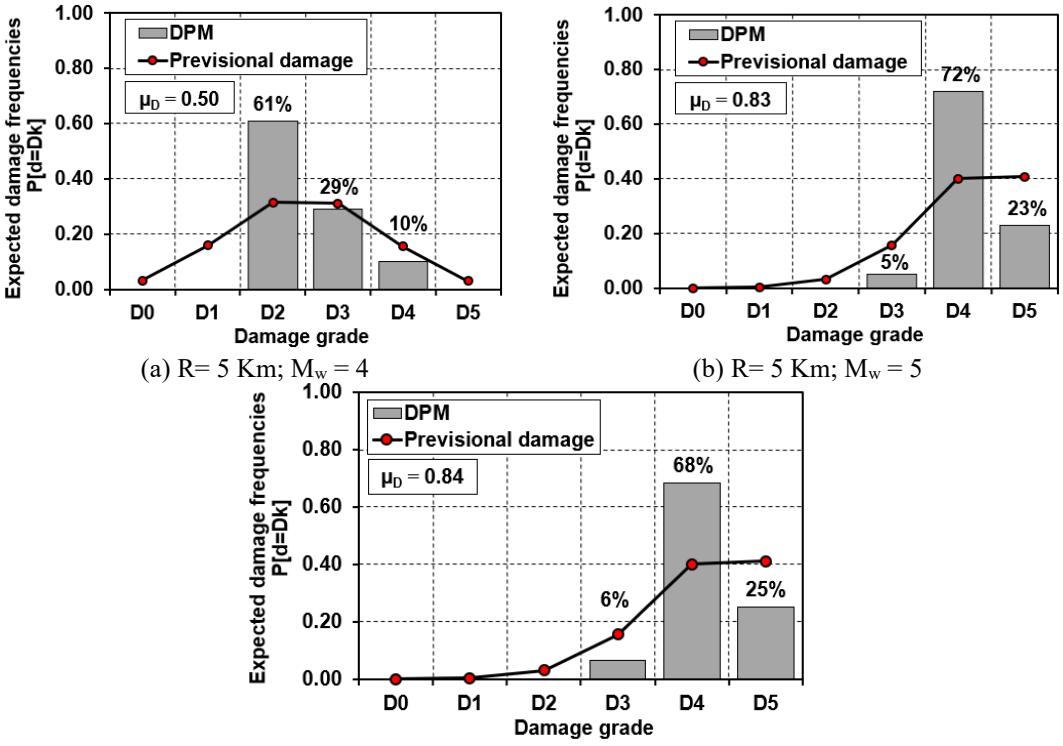


Figure 8: Damage probability matrix (DPM) derived from the considered impact scenarios.

4 INFLUENCE OF LOCAL SITE EFFECTS ON THE VULNERABILITY ASSESSMENT

From the physical point of view, the local seismic response can be intended as a set of changes in amplitude, duration and frequency content that the seismic motion undergoes through the overlying layers of soil up to the surface. In other words, the ground layers can increase the amplitude of the seismic motion at some frequencies and reduce it for other ones.

The schematization of seismic motion can be represented in the domain of either time or frequencies. In particular, considering the time domain, the parameters most frequently used to describe the earthquake characteristics are the peak value of the acceleration, of the velocity, of the displacement, and the duration. Contrary, in the frequency domain, the seismic motion parameters are characterized by either the Fourier spectrum or the response spectrum.

The problem of geo-hazard effects has been already contemplated in [12] where, under a macroseismic approach and on the basis of macroelement numerical analysis on clustered buildings, the site effects were taken into account through a local amplification coefficient, f_{PGA}, defined as the ratio between the maximum recorded acceleration at the ground surface ($a_{max,\,s}$)

and that at the bedrock ($a_{max, r}$).

Focusing on the case study, the historic centre area of Baranello is characterized by a geological structure mainly derived from covering tectonics related to the formation of the Apennine chain and sub-Apennine reliefs.

The sedimentary series, variously displaced and dismembered, were poured into the Molise basin causing anomalous overlaps and outcropping of very different units both for facies and for age and paleogeographic genesis.

For the seismic microzonation of this historic centre, data from in-situ surveys were made available by the Municipal Administration of Baranello. Furthermore, in-situ tests were carried out to identify the stratigraphy. Figure 9 shows the areas where the Down-Hole geological characterization tests were carried out. These tests provided the velocity of the propagation of seismic compression and shear waves at different depths.

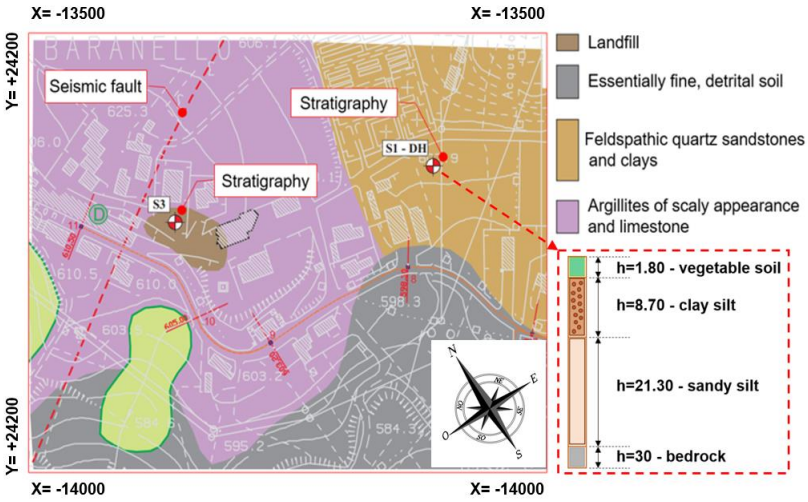


Figure 9: In situ geological tests in the area of Baranello.

The evaluation of the local amplification coefficient due to soil conditions has been estimated according to a time domain approach, since the main purpose of the work is to characterize the maximum ground amplification deriving from local site effects to correctly predict damage scenarios. Therefore, the accelerogram of the event occurred in Molise in 2002 with epicentre located in Bonefro has been used. The event was characterized by a magnitude, M_w, equal to 6 and a maximum PGA of 0.55 g.

To this purpose, STRATA 1.0 software, developed at the University of Texas, was used for simplified 1D numerical modelling of the geological conditions of seismic motion at bedrock [13].

Thus, based on these considerations, starting from the accelerogram recorded after the Molise earthquake, the accelerogram at the bedrock and the corresponding one amplified on the crustal-surface have been derived (Fig. 10).

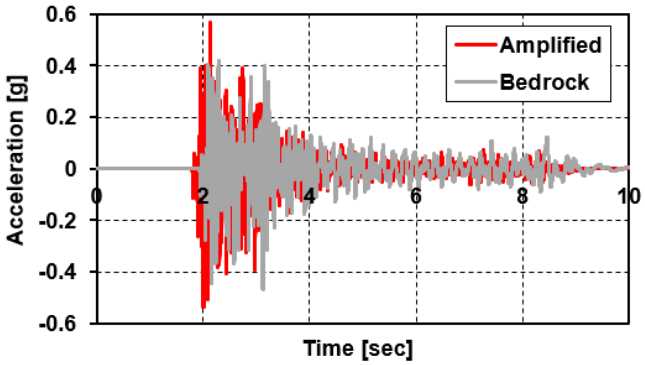


Figure 10: The elaborated accelerograms.

In Table 3, the amplification coefficient f_{PGA} derived from local site effects connected to the examined ground layers has been proposed.

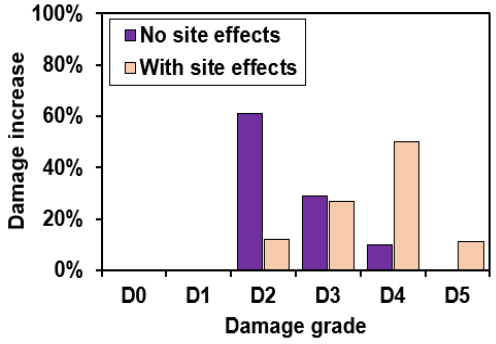
Table 2: Site amplification factor based on time domain.

Time history	Acceleration [g]		
	Amplified	Bedrock	f_{PGA} =
	$a_{max,s}$	$a_{max,r}$	$a_{max,s}/ a_{max,r}$
10 s	0.56	0.42	1.33

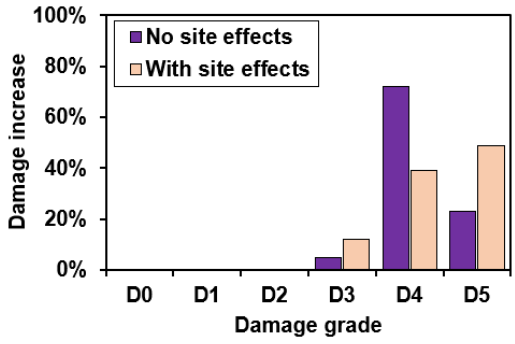
From the achieved result, the increment of the seismic motion from the bedrock basement to the crustal surface is equal to 33%. Therefore, depending on the geologic conditions detected for the case study area, the mean damage degree, μ_D, of the investigated structural units determined in Section 3.2 can be amplified by the above f_{PGA} factor, leading to a more correct expected damage grade $\mu_{D,s}$ according to the Equation (1).

$$\mu_{D,s}=\mu_D \times f_{PGA} \quad (1)$$

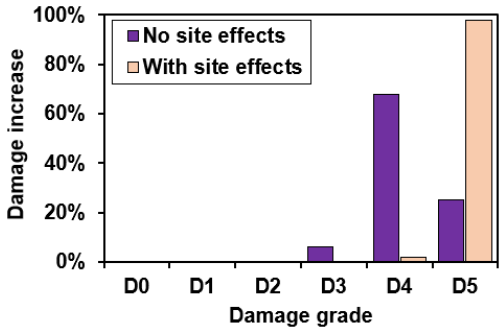
Finally, comparing the new damage scenario to that reported in Section 3.2 (Figure 8), it is possible to estimate the damage increase due to site effects, as reported in Figure 11.



(a) R= 5 Km; M_w = 4



(b) R= 5 Km; M_w = 5



(c) R= 5 Km; M_w = 6

Figure 11: The influence of local site conditions on the damage scenarios.

5 CONCLUSIONS

This study has proposed a simplified methodology to analyse the seismic vulnerability of masonry building aggregates located in historic centres considering the influence of geo-hazard conditions. An urban sector of 300 buildings in the historical centre of Baranello, in the district of Campobasso (Italy), has been identified as study area for the application of the proposed analysis method.

Firstly, the characterisation of the typological classes of the urban sector examined has been done by means of the CARTIS form. From on-site recognition, it has been detected that the prevailing typological class of masonry buildings is the MUR2 (rough-stone) one, which represents 73% of the building stock examined.

The seismic vulnerability of the inspected urban sector has been estimated through a vulnerability index method conceived for building aggregates. In the urban area, two distinct typological classes, namely A and B, have been identified according to the EMS-98 scale with an expected medium-high vulnerability enclosed in the range [0.4–0.6], while only 30% of the building sample has a vulnerability index equal to 0.76. Contrary, for the analysed typological class B, the expected frequency is in the range [0.2–0.4].

Finally, a local seismic amplification factor to consider local site effects has been defined according to the time domain method. Looking at the analysis results, the esteemed amplification factor has been found as equal to 1.33, which means that the seismic motion increment from the bedrock basement to the crustal surface is equal to 33%. From the new damage scenarios considering local effects, it has been detected a considerable damage increment. In particular, it has been noted that for the epicentre distance of 5 km and moment magnitude of 4, damage thresholds D2 and D3 have been attained with a damage occurrence probability less than that of the basic case, in which the soil influence has been neglected. Contrary, the D4 and D5 damage levels significantly increase due to the site effects. Instead, considering the worst scenario (R= 5 km and M_w= 6), the site effects have reduced drastically the damage levels D3 and D4, but they have increased the D5 threshold with the collapse of 98% of the buildings in the analysed area.

In conclusion, the proposed work has represented an important starting point for large-scale vulnerability and risk analysis considering site effects, so providing a comprehensive method to predict more precisely damage scenarios into historical centres.

ACKNOWLEDGEMENTS

The Authors would like to acknowledge the DPC-ReLUIS 2019-2021 research project for the financial support to the development of the research activity presented in the current paper.

REFERENCES

[1] Ferreira, T.M., Maio, R.,Vicente, R. Seismic vulnerability assessment of the old city centre of Horta, Azores: calibration and application of a seismic vulnerability index method. *Bull. Earthquake Eng.* (2017), **15**:2879–2899.

[2] Chieffo, N., Formisano, A., Ferreira, T.M. Damage scenario-based approach and retrofitting strategies for seismic risk mitigation: an application to the historical Centre of Sant'Antimo (Italy). *Eur. J. Environ. Civ. Eng*. (2019).

[3] Chieffo, N., Formisano, A. Geo-hazard-based approach for the estimation of seismic vulnerability and damage scenarios of the old city of senerchia (Avellino, Italy). Geosciences (Switzerland) (2019), **9**:1-21.

[4] Morasca, P., Zolezzi, F., Spallarossa, D., Luzi, L. Ground motion models for the Molise region (Southern Italy). *Soil Dyn. Earthq. Eng*. (2008), **28**:198–211.

[5] Cacace, F., Zuccaro, G., De Gregorio, D., Perelli, F.L. Building Inventory at National scale by evaluation of seismic vulnerability classes distribution based on Census data analysis: BINC procedure. *Int. J. Disaster Risk Reduct*. (2018), **28**:384–393.

[6] Formisano, A., Florio, G., Landolfo, R., Mazzolani, F.M. Numerical calibration of an easy method for seismic behaviour assessment on large scale of masonry building aggregates. *Adv. Eng. Softw*. (2015), **80**:116–138.

[7] Formisano, A., Chieffo, N., Mosoarca, M. Seismic Vulnerability and Damage Speedy Estimation of an Urban Sector within the Municipality of San Potito Sannitico (Caserta, Italy). *Open Civ. Eng. J*. (2018), **11**:1106–1121.

[8] Mosoarca M., Onescu I., Azap B.; Onescu E., Chieffo N. Szitar-Sirbu M.; Seismic vulnerability assessment for the historical areas of the Timisoara city, Romania. *Eng. Fail. Anal*. (2019), **101**:86–112.

[9] Onescu I., Mosoarca M., Azap B., Onescu E. Seismic Losses Scenario for Cultural Promenade in Timisoara Capital of Culture 2021, Romania. *IOP Conf. Ser.: Mater. Sci. Eng*. (2019), 471.

[10] Esteva, D., Harris, D.L. Comparison of pressure and staff wave gage records. *Coast. Eng. Proc*. (1970), 1, 7.

[11] Locati, M. DBMI15, the 2015 Version of the Italian Macroseismic Database, 2016. Available online: https://emidius.mi.ingv.it (accessed on 02 January 2020) (in Italian).

[12] Chieffo, N., Formisano, A. The influence of geo-hazard effects on the physical vulnerability assessment of the built heritage: An application in a district of Naples. *Buildings*. (2019), 9.

[13] Flemings, P.B., Grotzinger, J.P., Morris, J.E. Strata: A Stratigraphic Modeling Package, (n.d.). Available online: http://www.jsg.utexas.edu/flemings/intranet/software/strata/strata-download-the-code-manual-and-tutorial/(accessed on 02 January 2020).

12th International Conference on Structural Analysis of Historical Constructions
SAHC 2020
P. Roca, L. Pelà and C. Molins (Eds.)

SEISMIC VULNERABILITY ASSESSMENT METHOD FOR VERNACULAR ARCHITECTURE CONSIDERING UNCERTAINTY

JAVIER ORTEGA[1*], SAVVAS SALOUSTROS[2], PERE ROCA[2]

[1] ISISE Department of Civil Engineering, University of Minho
Campus de Azurém, 4800-058 Guimarães, Portugal
e-mail: javier.ortega@civil.uminho.pt (*corresponding author)

[2] Department of Civil and Environmental Engineering
Universitat Politècnica de Catalunya (UPC-BarcelonaTech)
Jordi Girona 1-3, 08034 Barcelona, Spain
email: {savvas.saloustros;pere.roca.fabregat}@upc.edu

Keywords: Seismic vulnerability, Vernacular heritage, Masonry, Uncertainty, Probabilistic analysis, Pushover analysis

Abstract. *Built vernacular heritage embraces buildings that are not designed by specialists, but are part of a process that involves many people over many generations and relies on empirical knowledge. Its value as a key-element for cultural identity is unquestionable. However, precisely due to its empirical and traditional nature, it is often seen as an obsolete and unsafe way of construction, which leads to its progressive abandonment. This lack of proper construction details and poor maintenance increases the seismic vulnerability of the vernacular heritage. There is an evident need for simplified easy-to-use seismic vulnerability assessment methods for vernacular architecture, given the generalized lack of resources that can be normally assigned to its study and preservation. Most of the times, visual inspection will be the only tool available to carry out the assessment.*

Nevertheless, simplified methods demand a deep understanding of the seismic behavior of vernacular architecture. This is a complex task given the great heterogeneity in the geometrical, structural, construction and material characteristics of vernacular buildings. The present works explores the development of a probabilistic method for the analytical derivation of seismic fragility functions of vernacular buildings considering uncertainty in material parameters and structural characteristics. The procedure followed to investigate the effect of uncertainty and to evaluate the influence of a set of key parameters on the seismic response of vernacular buildings is based on stochastic analysis. In the end, a simplified numerical tool is proposed which can be applied based on visual inspection. The process applied and shown here is considered as an example of application and can be replicated in other contexts. It ultimately intends to extend the applicability and reliability of current seismic vulnerability assessment methods.

1 INTRODUCTION

Seismic vulnerability assessment methods for the built environment play an important role on risk mitigation, as they are the main components of models capable of predicting damage to buildings and estimating losses in future earthquakes. That is why they have become a valuable tool for the preservation of the built heritage, allowing to identify the most vulnerable elements at risk. As a result, structural retrofitting strategies at an urban or regional level can be defined and optimized. This has a particular importance when dealing with the preservation of the built vernacular heritage, which is rarely represented by single structures, but usually involves a group of buildings and settlements within a region or historical city center.

Because of its empirical and traditional nature, vernacular architecture is considered in many places as an obsolete way of building and only valued as part of the region's identity [1]. Typically, people tend to see vernacular construction technologies as unsafe and eventually abandon and substitute them with modern ones. The risk of vernacular heritage to disappear due to a global economic, cultural, and architectural homogenization was already highlighted by ICOMOS [1]. As a result of this progressive abandonment, there is also an increasing vulnerability of vernacular architecture facing natural hazards, including earthquakes.

There is also a typical lack of resources assigned to the study and preservation of the vernacular heritage. When dealing with monumental architecture, many sophisticated tools are available, such as non-destructive evaluation techniques and advanced structural analysis methods. Moreover, monuments are typically well documented and historical research can provide a significant amount of information of the structure. Nevertheless, when assessing the seismic safety of vernacular architecture, visual inspection will most likely be the only tool available. Thus, seismic vulnerability assessment methods targeting vernacular architecture should be easy-to-use and make use of qualitative or simple quantitative data that can be rapidly obtained from simple visual inspections.

Additionally, being vernacular architecture deeply rooted to a place, as well as local traditional construction techniques and materials, it typically shows great heterogeneity in terms of geometry, materials, or construction techniques. Therefore, there is a high amount of uncertainty in the characterization of the geometry and morphology of the structural elements, as well as the mechanical parameters of the constituent materials. Unknown parameters showing a high variability include masonry material properties, diaphragm type and quality of wall-to-floor connections, or quality of wall-to-wall connections.

Given the preceding challenges (i.e. lack of resources and the structural heterogeneity), the present work intends to explore the development of a seismic vulnerability assessment method adequate for vernacular constructions. Previous works by the authors have proposed to use finite element modeling and pushover analysis to evaluate the influence of a set of key parameters on the seismic response of vernacular buildings. As a result, a simplified numerical tool was developed particularly intended to assess the seismic vulnerability of vernacular buildings [3]. However, the final developed tool did not consider the high amount of uncertainty in the definition of geometrical, structural and material parameters of vernacular architecture. The present work explores a probabilistic methodology for the analytical derivation of seismic fragility functions of vernacular buildings including uncertainty in materials and construction characteristics. The procedure followed to investigate the effect of uncertainty in the proposed method is based on stochastic analysis previously applied for the assessment of masonry

structures [4][5]. This approach is meant to extend the applicability and reliability of the seismic vulnerability assessment method previously developed by considering uncertainty in structural characteristics and material properties.

2 PROBABILISTIC ASSESSMENT

The present work shows an example of the procedure proposed to perform the seismic vulnerability assessment for vernacular constructions. The city of Vila Real de Santo António (VRSA) is used as a case study. VRSA is located in Algarve, the southernmost area of Portugal. This region was considerably affected by the 1755 Lisbon earthquake and was practically abandoned at the time. As an attempt to boost the Algarve local economy through industrial development, the Marquis of Pombal enacted an official recovery program during the 1760s and 1770s that included the construction from scratch of the city of VRSA. Despite the important transformation process in the city since its construction, the Pombaline city center still show a certain degree of homogeneity.

The proposed procedure to develop the seismic vulnerability assessment method consists of the following seven steps: (1) definition of a reference representative example of the vernacular typology under study in terms of geometry and construction, selection of the uncertain parameters and definition of ranges of variation for each parameter; (2) preparation of numerical finite element models according to the reference example and parameters under study; (3) definition of probabilistic distribution for each selected parameter; (4) stochastic analysis to create a representative sample; (5) seismic analysis, based on the finite element method and nonlinear static (pushover) analysis, of the whole sample; (6) construction of fragility curves based on the numerical analysis performed; and (7) regression analysis on the results database to obtain analytical expressions that allow deriving fragility curves without the need of performing numerical analysis.

Once the regression expressions are formulated for the studied typology, they can be used for several purposes, such as: (a) to perform a new seismic vulnerability assessment on an increased sample that includes new buildings belonging to the same or similar typology; (b) to perform a new assessment of the same sample with reduced uncertainty after performing a more detailed inspection or non-destructive evaluation of some buildings; or (c) to study the effect of different retrofitting strategies on the seismic vulnerability of the sample. Moreover, the procedure proposed and shown in the present work allows its replication to other contexts. Indeed, the application of the same procedure to other contexts and typology can enlarge and make a more comprehensive database allowing the update of the regression expressions.

2.1 Case study and unknown variables

The structural system of the original built-up environment of VRSA mainly consisted of load-bearing stone masonry walls as the main vertical resisting elements, coupled with horizontal timber diaphragms (floors and roofs). Nowadays, the great majority of the original buildings have been replaced by new ones or are highly altered at a formal and structural level. The original single-story dwellings were the main target of the demolitions, substitutions and large modifications. The most common modifications included the addition of new floors, the enlargement or addition of new openings or the substitution of the timber floors and roofs. The deep mischaracterization of the built-up environment is not only detrimental in terms of loss of

authenticity of an important architectural and urban heritage, but also reflects the loss of seismic awareness, having an important impact on the seismic vulnerability of the buildings [6].

There are currently 284 stone masonry buildings in VRSA city center (7 of them original unaltered buildings) [6]. Figure 1 shows two original single-story dwellings that were altered with the addition of a second floor. Detailed reports on the construction characteristics and state of conservation of most of the buildings [7] are available, which allowed to define a representative reference model, using average dimensions and following the typical construction characteristics.

The present work shows a first example of the application of the proposed methodology for estimating the seismic vulnerability of vernacular buildings at urban scale. In this case, six uncertain parameters were considered as random variables. Four of them are related to the material mechanical parameters of the masonry walls (Figure 2 – left). These are the tensile and compressive strength, the Young's modulus, and the tensile fracture energy of the masonry walls. The other two are related with structural characteristics of the buildings: the type of diaphragm and quality of floor-to-wall connection (Figure 2 – middle); and the quality of wall-to-wall connections (Figure 2 – right).



Figure 1: Two vernacular buildings in the historical city center of Vila Real de Santo António.



Figure 2: Typical constructive details observed in Vila Real de Santo António: (left) masonry morphology; (middle) diaphragm type; (right) wall-to-wall connections.

2.2 Numerical model

After the definition of a reference representative example of the vernacular typology, numerical finite element models were prepared. The reference models were prepared in a generic way to easily accommodate the variations required to assess the influence of the different parameters. The software selected to perform the numerical parametric analysis was

DIANA [8]. Three models were created assuming different types of diaphragm and floor-to-wall connection (Figure 3) with general dimensions of 8 m x 5.5 m x 5.2. m (length x width x height). All elements are simulated with ten-node isoparametric 3D solid tetrahedron elements (CTE30), with four-point integration scheme over the volume.

Masonry with varying material properties is considered for the walls. The properties of the masonry at the corners (in red in Figure 3) is also varied, assuming different levels of quality of wall-to-wall connections. Timber is used for the lintels and floor construction elements. Only the materials used for the walls are considered to present nonlinear behavior, adopting standard isotropic Total Strain Rotating Crack Model (TSRCM) [8].

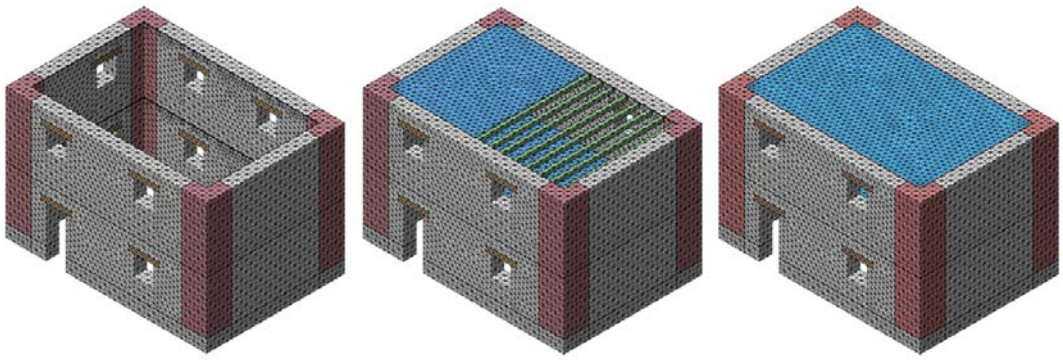


Figure 3: Three reference numerical models with different diaphragm type and floor-to-wall connection: (left) flexible diaphragm poorly connected; (middle) flexible diaphragm with beams properly connected to the walls; (right) flexible diaphragm properly connected to the walls.

2.3 Uncertainty analysis of the random variables

The effect of the six uncertain parameters, modelled as random variables, on the seismic response of the studied structure was evaluated through stochastic simulation. Probability density functions (PDF) represent the range of values (or structural configurations) and their probability of occurrence for each of these parameters. A Monte Carlo simulation created 200 random combinations of these random variables, which correspond to the same number of numerical models. The sample number is based on previous experience [4,5]. Additionally, a Latin Hypercube sampling approach was employed to improve the efficiency of the sampling process. Figure 4 presents the results of the sampling procedure for the six random variables.

The variation of Young's modulus (E), compressive strength (fc) and tensile strength (ft) was defined using lognormal distributions, in line with the recommendations of CNR-DT 212/2013 [9][1]. The values of the mean (μ) and the standard deviation of the logarithm (σ_{ln}) for the Young's modulus ($\mu=1740$ MPa, $\sigma_{ln}=0.14$) and the compressive strength ($\mu=3.2$ MPa, $\sigma_{ln}=0.19$) correspond to the values for an "uncut stone masonry with good texture" typology in [9], which is considered adequate for the current case study [6]. The tensile strength is a more difficult parameter to obtain experimentally and is usually defined as a fraction of the compressive strength. A mean value of $\mu=0.06$ MPa and a standard deviation equal to the one used for the compressive strength ($\sigma_{ln}=0.19$) were assumed. The resulting ratio between tensile and compressive strength for all the cases varies between 0.01 and 0.04. Concerning the tensile fracture energy, there is limited experimental information. Only rough assessments about its

variation intervals can be provided. Thus, the variation was defined using a uniform distribution with the upper and lower limits being 10 and 100 N/mm, respectively.

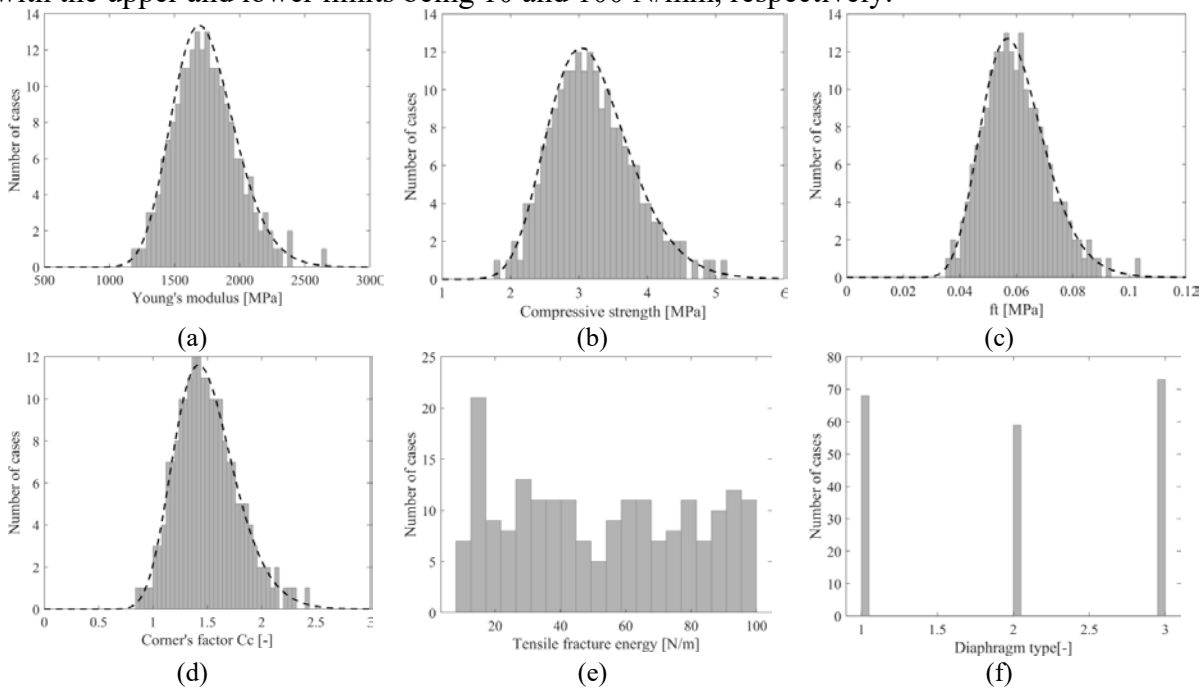


Figure 4: Histograms with the distributions of the sampled values of: (a) Young's modulus *E*, (b) Compressive strength *fc*, (c) Tensile/compressive strength ratio *ft/fc*, (d) Corner's coefficient *C*c, (e) Fracture Energy and (f) Type of diaphragm (1: Embedded beams and wooden planks, 2: Embedded beams, 3: No-diaphragm).

The other two random variables are associated with structural details; the quality of the wall-to-wall connections and the quality of the floor-to-wall connection. Regarding the former, a good interlocking between transverse walls is possible when special care is given in the connections, such as regular stonework and big stone blocks (see Figure 2-right). On the contrary, when no special care is given to provide sufficient interlocking between transversal walls, these connections become one of the most vulnerable parts of the structure and their capacity compromises the structural behavior. To account for this important structural characteristic, the mechanical properties of the masonry at the corners of the building were considered as proportional to the chosen values for the masonry walls through a proportionality factor *Cc.* In this way, the mechanical properties of the corners were defined with a single variable, instead of one for each mechanical property. For the particular case study, the large stone blocks seen in the corners of many buildings indicate overall good wall-to-wall connections. Accordingly, it can be assumed that the masonry quality of the corners will be in average better than that of the rest of the walls. This feature was considered in the assessment by using a mean value $\mu=1.5$ for the proportionality coefficient *Cc*, indicating a 50% higher properties in the masonry at the corners as an average. The standard deviation of the proportionality factor Cc was defined equal to that used for the compressive strength ($\sigma_{ln}=0.19$).

The last random variable concerns the diaphragmatic action of the floors and three scenarios were considered. In the worst-case scenario, there is no diaphragmatic action due to the poor connection between the floors and the walls. The second scenario considers an improved diaphragmatic action of the floor due to the proper embedment of the beams within the façade

walls. Finally, in the best-case scenario, the floor beams are properly embedded in the façade walls and the floor wooden planks contribute to the stiffness of the floor. These three cases were simulated by adopting three modelling strategies for the floor (Figure 3). For the first scenario, the structural model does not include the floors. For the second scenario, the floor beams are embedded up to the half of the wall's length. The same assumption holds for the last scenario including also the modelling of the wooden planks. As a first attempt, considering a scenario without a proper inspection of the interior of the buildings, a uniform distribution was used to represent the equal possibility of having any of the above cases in a vernacular building in VRSA.

Regarding the rest of the material parameters, the compressive fracture energy of masonry was defined as $Gfc = 1.6fc$ according to [10]. The timber beams and floors were modelled as linear elastic with Young's modulus equal to 10 GPa and Poisson's ratio of 0.3. Poisson's ratio of 0.20 was used for the masonry walls.

2.4 Seismic analysis

Figure 5 presents the capacity curves (horizontal acceleration vs displacement) for the 200 numerical models analyzed with different combinations of the random variables. The analyses show a large range of the maximum acceleration, varying approximately between 0.25g and 1.3g. It is easy to observe two families of capacity curves, one with notably higher strength capacity and stiffness than the second. The use of three line types and colors, corresponding to the floor-to-wall connection used in each case, highlights the importance of the diaphragm effect on the seismic response. All the cases with no connection between floor and walls (shown with a grey continuous line) present a much lower stiffness and capacity compared to the rest of the cases.

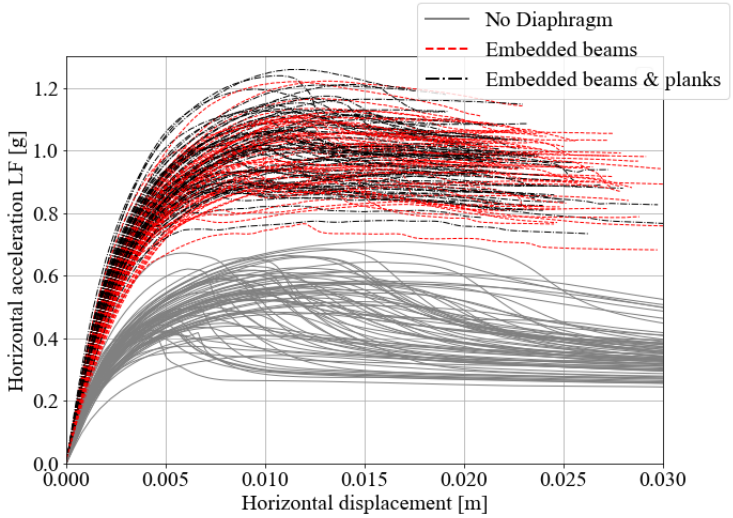
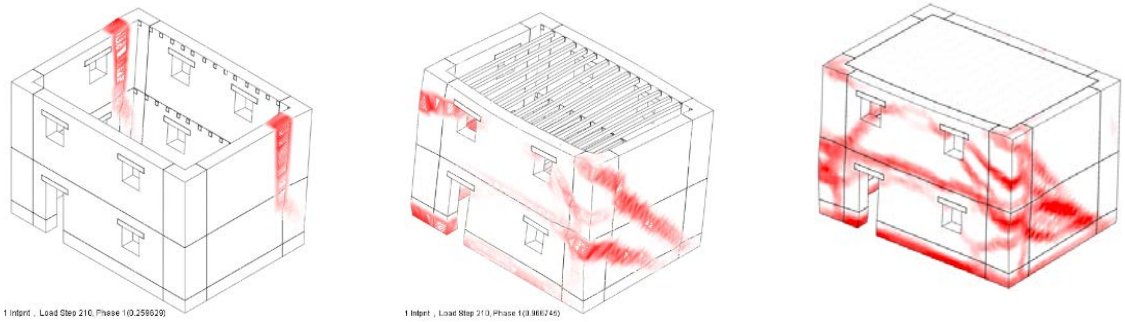


Figure 5: Pushover capacity curves obtained corresponding to the 200 analysis with different combinations of six random variables (colors according to diaphragm type considered in the analysis).

The change in the type of diaphragm results in a different failure mechanism, as shown in Figure 6, presenting three representative cases for each of the defined wall-to-diaphragm types. The lack of any diaphragmatic action provokes local mechanisms characterized mainly by the

out-of-plane failure of the façade. This failure mechanism is not observed when the diaphragm is assumed to be well connected with the two facades. For these cases, the structure presents a more global response against the seismic action.



(a) (b) (c)

Figure 6: Principal crack strains for different types of diaphragm: (a) no diaphragmatic action, (b) embedded beams, (c) embedded beams and wooden planks

2.5. Fragility curves

The seismic vulnerability of the studied vernacular buildings can be expressed through the following fragility function [11]:

$$P[LS_i|IM] = \Phi\left[\frac{1}{\beta_{LS_i}} ln\left(\frac{IM}{\theta_{LS_i}}\right)\right] \quad (1)$$

which represents the probability that a generic Limit State *LSi* be reached given a value *IM* of the intensity measure. In the above equation, θ_{LS_i} is the median value of the lognormal distribution of the *IM* at which the analyzed structure reaches the limit state *LSi*, β_{LS_i} is the standard deviation of the natural logarithm of the *IM* for limit state *LSi* and Φ is the standard normal cumulative distribution function. Finally, N=200 is the total number of structural analysis carried out.

In this work, the fragility curves are obtained for the Limit State *LS3*, as defined in [3,6], corresponding to a life safety limit state. *LS3* is defined in [3,6] in terms of the horizontal acceleration and displacement obtained from a pushover analysis that correspond to the maximum strength of the building. As a first step in the proposed methodology, the maximum horizontal acceleration computed by each pushover analysis was considered as the intensity measure. The use of this measure instead of other common intensity measures (e.g. macroseismic intensity, Peak Ground Acceleration, spectral acceleration Sa, etc.) aims to serve as a simple indicator that facilitates the comparative assessment of the capacity of the individual buildings, as will be shown in Section 3.

Figure 7 presents the fragility curves corresponding to *LS3* obtained by considering all the 200 analyzed cases, as well as three more curves that were obtained considering: i) only the cases without a floor-to-wall connection; ii) only the cases with embedded beams; and iii) only the cases with embedded beams and wood planks. It can be again seen how the absence of a diaphragm drops the strength capacity of the structure, affecting the estimations of the fragility of all the population. These graphs clearly indicate that the implementation of wooden planks would be beneficial for the capacity of the investigated buildings, which was not so easily distinguishable in Figure 5.

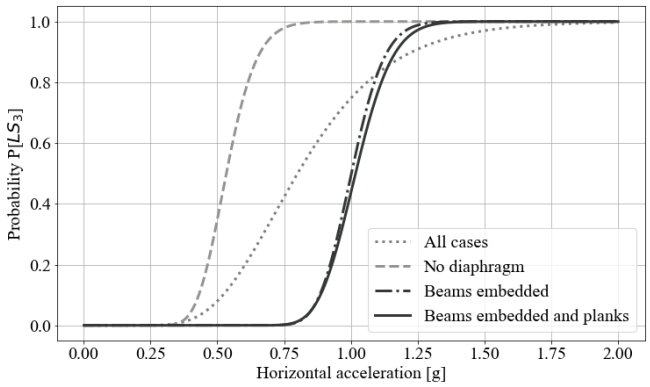


Figure 7: Fragility curves corresponding to Limit State 3 (maximum strength capacity) against horizontal acceleration obtained from the pushover analyses. The different lines correspond to different populations related with the floor-to-wall connection assumption.

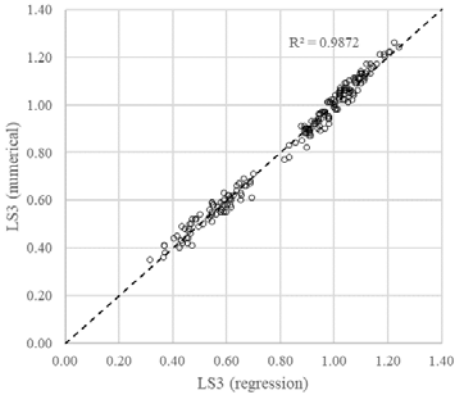


Figure 8: *LS3* predicted (regression) vs observed (numerical).

2.6. Regression analysis and empirical Expressions

The statistical analysis and the definition of the regression models are carried out by using R open source software [12]. Multiple linear regression (MR) was applied, intended to investigate the dependence of the maximum seismic capacity of the building (*LS3*) on the six parameter variables selected: (1) four material parameters (*E*, *ft*, *fc*, *Gft*); (2) type of diaphragm (*Dia*); and (3) quality of wall-to-wall connection (*Cc*). As a result, a mathematical model is obtained to define and quantify the relationship among them through. The relationship between variables is often very complex and the simplest approach consists of fitting a multilinear equation to the data:

$$Y = \beta_0 + \beta_1 x_1 + \beta_2 x_2 + \ldots + \beta_k x_k + \varepsilon \tag{2}$$

where Y is the output variable and k is the number of input explanatory variables (x_k). The parameters β_k are called the regression coefficients and ε is the error. The line defined by Eq. (2) describes how the response changes according to the explanatory variables.

Before carrying out the analysis, all the parameter values were normalized by dividing every value of each parameter by the maximum value among the N=200 values from the sampling. It should be noted that the regression model constructed excluded the intercept and after some trials also excluded the parameter *fc*, which was shown to have no statistical influence. The remaining five variables were found to be statistically significant in the prediction of the maximum capacity of the building, i.e. the maximum load factor obtained in the pushover analysis. The final regression resulted in the following regression equation:

$$LS3 = 0.099E + 0.391ft + 0.262Gf + 0.3101c + 1.907Dia - 1.988Dia^2 \tag{3}$$

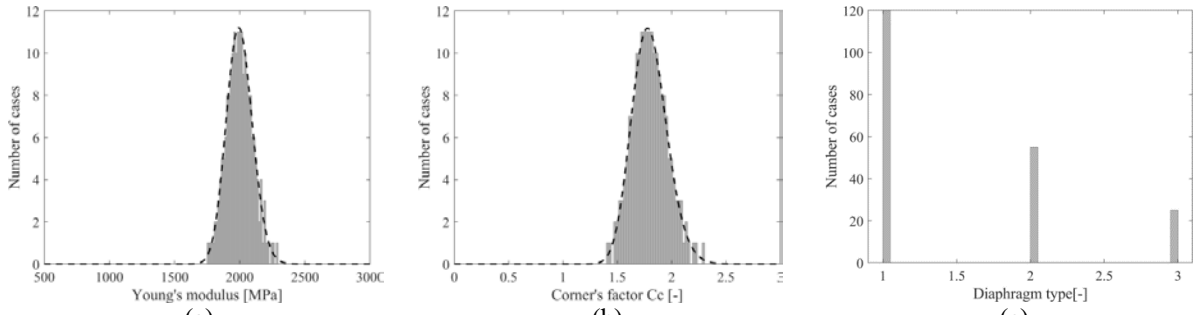
Note that the regression equation includes a quadratic term for the parameter *Dia* because the relationship between *LS3* and *Dia* was observed to be nonlinear. The mean absolute error (MAE) of the model is 0.023g and the maximum absolute error is 0.085g. The coefficient of determination or adjusted R-squared is 0.9872, which illustrates that the regression equation is able to match very well the numerical data, see Figure 8.

3 APPLICATION AND VALIDATION

The present section shows an example on how the regression expression from Eq. (3) could be used after it has been defined for the estimation of the seismic vulnerability of the selected case study. Previously, the probabilistic distributions were defined assuming that there was a lack specific information about the buildings. All the information was assumed to be based on simple exterior visual inspection. This section investigates the use of the expression from Eq. (3) after a second assessment has been performed on the buildings, including a more detailed visual inspection (including the interior) and non-destructive testing. The new information allows the definition of new probabilistic distributions of the random variables. In this case, the fragility function of *LS3* will be defined using the expression from Eq. (3). The validity of these blind predictions will be assessed afterwards through a comparison with the results of a new set of numerical analysis corresponding to the updated set of random variables.

3.1 Updated PDFs

Concerning the six uncertain parameter variables selected, the following hypotheses were considered to allow a better characterization and new updated probabilistic distributions. Three possible scenarios are investigated that would reduce the uncertainty of some of the selected parameters. In the case of the material properties, non-destructive evaluation techniques, namely sonic tests, can be performed on buildings to obtain a more representative distribution. Here, it is assumed that the use of sonic tests on the masonry walls allowed a better accuracy in the estimation of the mean value and the variation of the Young's modulus of the masonry walls (μ*=2000 MPa,* σ_{ln}*=0.05*) (Figure 9a). The same tests on the masonry at corners, along with a more detailed inspection, allowed the estimation of an overall better quality of the wall-to-wall connections and define a more representative PDF for the proportionality factor *Cc* (Figure 9b), with μ*=1.8* and σ_{ln}*=0.09*. In the case of the diaphragm type, interior visual inspection of some buildings can allow obtaining a more representative distribution compared to the assumed one. In this case, it is assumed that a more detailed inspection revealed a good connection between the floor and the walls for the majority of the inspected buildings (Figure 9c).

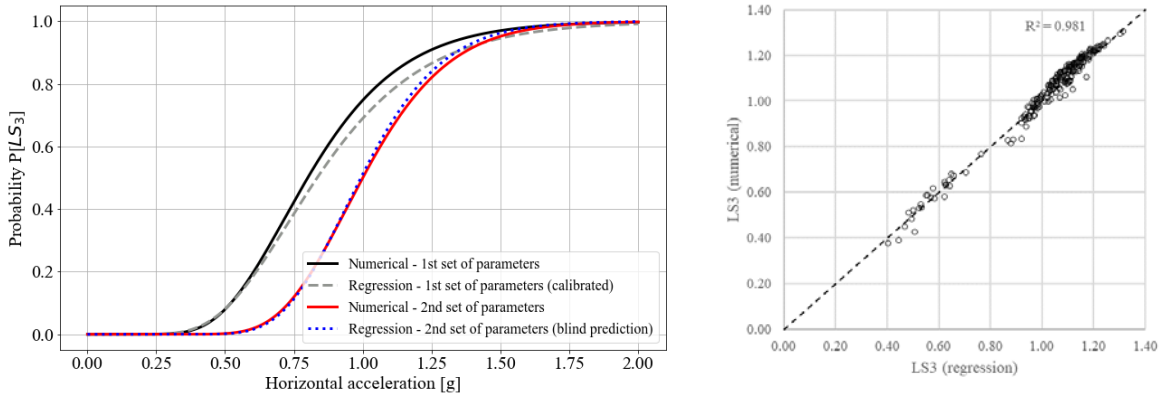


(a) (b) (c)

Figure 9: Updated probabilistic distributions of: (a) Young's modulus; (b) Corner's coefficient Cc, and (c) Diaphragm type (1: Embedded beams and wooden planks, 2: Embedded beams, 3: No-diaphragm).

3.1 Estimation of fragility and validation

Figure 10a presents a comparison of the fragility curve corresponding to *LS3* before and after the update of the probability density functions (PDFs), following the scenarios of an improved in-situ inspection. The improvement of the mechanical properties of the masonry at walls and corners and the increase of the number of cases with a good floor-to-wall connection decreases notably the vulnerability of the buildings. The comparison of the fragility curve obtained using the *LS3* from Eq. (3) and the *LS3* from the new set of the pushover analyses corresponding to the updated PDFs shows a good correlation between numerical and empirical results. This is further demonstrated in Figure 10b, presenting a direct comparison of the *LS3* obtained with the two methods. The regression expression fits well the numerical results with a mean absolute error of 0.025g and a maximum absolute error of 0.088g. The coefficient of determination or adjusted R-squared is 0.981 (Figure 10b), validating the procedure and the expression obtained.



(a) (b)

Figure 10: (a) Comparison of the fragility curves corresponding to *LS3* before and after updating the PDFs of the random variables. (b) *LS3* predicted vs observed for the new sample of analysis (blind prediction).

4 CONCLUSIONS

This paper has presented the development and application of a probabilistic method for the seismic vulnerability assessment of vernacular architecture. The method aims to confront some major challenges that arise when dealing with vernacular heritage, such as the lack of resources and the structural heterogeneity. With that purpose, the method aims first to develop a simple numerical tool that provides an estimation of the seismic vulnerability of a building based on qualitative and simple quantitative data that can be obtained through visual inspection. Secondly, the proposed method explores the inclusion of uncertainty in materials and construction variables, aiming to reflect the characteristic heterogeneity of the vernacular heritage.

The method proposed has been described showing the step-by-step procedure used to carry out the seismic vulnerability assessment. The historical city center of Vila Real de Santo António (Portugal) has been considered as a case study. The proposed methodology has been validated by comparing the results obtained using the resulting regression expression with numerical results. The good correlation between numerical and empirical results illustrates the applicability of the method.

Acknowledgements. The authors gratefully acknowledge the financial support from the Ministry of Science, Innovation and Universities (MCIU) of the Spanish Government, the State Agency of Research (AEI) and the European Regional Development Fund (ERDF) through the SEVERUS project (Multilevel evaluation of seismic vulnerability and risk mitigation of masonry buildings in resilient historical urban centres, ref. num. RTI2018-099589-B-I00).

REFERENCES

[1] Correia M. Experiences from past for today's challenges. In: *The road to sustainable development. Chapter 6 – Traditional and generational change*, La Fábrica, Fundación Contemporánea (2017), pp. 128–133.

[2] ICOMOS. *Charter on the built vernacular heritage*. International Council of Monuments and Sites (ICOMOS), ICOMOS 12th General Assembly, Mexico (1999).

[3] Ortega, J., Vasconcelos, G., Rodrigues, H., Correia, M. and Miranda, T. Development of a Numerical Tool for the Seismic Vulnerability Assessment of Vernacular Architecture. *Journal of Earthquake Engineering* (2019).

[4] Saloustros, S., Pelà, F.L., Contrafatto, P., Roca, P. and Petromichelakis, I. Analytical derivation of seismic fragility curves for historical masonry structures based on stochastic analysis of uncertain material parameters. *International Journal of Architectural Heritage* (2019).

[5] Petromichelakis, I. and Saloustros, S. Seismic assessment of historical masonry construction including uncertainty. In: Cunha Á, Caetano E, Ribeiro P, Müller G (eds) *9th Int. Conf. Struct. Dyn. EURODYN 2014, Porto (Portugal)* (2014), pp. 297-304.

[6] Ortega, J., Vasconcelos, G., Rodrigues, H. and Correia, M. Seismic Vulnerability and Loss Assessment of Vila Real de Santo António, Portugal: Application of a Novel Method. *International Journal of Architectural Heritage* (2020).

[7] SGU. *Plano de Pormenor de Salvaguarda do Núcleo Pombalino de Vila Real de Santo António, Sociedade de Gestão Urbana (SGU) de Vila Real de Santo António*. Vila Real de Santo António, Portugal (2008).

[8] TNO. *Displacement method analyser. User's manual, release 9.4.4*. TNO DIANA BV, Delft, Netherlands (2011).

[9] CNR-DT 212/2013. Guide for the Probabilistic Assessment of the Seismic Safety of Existing Buildings. Rome, Italy: 2014.

[10] Angelillo M, Lourenço PB, Milani G. Masonry behaviour and modelling. Mech. Mason. Struct., vol. 551, 2014. doi:10.1007/978-3-7091-1774-3.

[11] Federal Emergency Management Agency. HAZUS-MH MR4: Technical Manual, Vol. Earthquake Model. Washington DC: 2010.

[12] R Development Core Team. *R: A language and environment for statistical computing.* R Foundation for Statistical Computing, Vienna, Austria (2008).

12th International Conference on Structural Analysis of Historical Constructions
SAHC 2020
P. Roca, L. Pelà and C. Molins (Eds.)

SEISMIC VULNERABILITY ASSESSMENT METHODOLOGY FOR HISTORICAL BUILDINGS WITH CULTURAL VALUE

E. ONESCU[1*], I. ONESCU[2] AND M. MOSOARCA[2]

[1] Faculty of Architecture and Urban Planning, Politehnica University of Timisoara, Romania
e-mail: eugen.eugen@student.upt.ro (*corresponding author)

[2] Urban Planning and Architecture Research Center, Politehnica University of Timisoara, Romania
e-mail: iasmina.onescu@upt.ro, marius.mosoarca@upt.ro

Keywords: Historical Structure, Masonry, Cultural value, Vulnerability assessment

Abstract. *Banat seismic region represents the second most important seismic area of Romania. The area is characterized by shallow earthquakes, with a peak ground acceleration ag=0,20g [1]. The city was influenced by several architectural styles, keeping until nowadays many valuable masonry historical buildings.*
Most of the historical buildings present severe decay due to the lack of proper maintenance over time. Timisoara was selected to be European Capital of Culture 2021, so the buildings in the historical districts are expected to be visited by a large amount of tourists.

This paper presents the seismic vulnerability assessment of two of the most important historical urban districts of Timisoara. The evaluation is based on existing Italian vulnerability assessment methodology [2], following on-site investigation. Moreover, there is considered also the influence of the cultural value of the historical buildings. Following a set of new proposed architectural-artistic, urbanistic and social-economic factors, there was developed a new investigation form, presented and explained in the paper [1].

In the end, the authors present a detailed empirical seismic vulnerability assessment influenced by the cultural value for historical masonry buildings in Timisoara city, Romania.

This study could help the local authorities to realize prioritization lists for rehabilitation work, considering first the historical buildings that are the most important for the local community identity. The cultural value and the history of a city must be well known and promoted.

1 INTRODUCTION

Living in cities in seismic areas represent an important aspect of everyday life for many people. Natural disasters are unpredictable, but cities vulnerability and level of exposure can be reduced through prevention policies. Effective protection policies must be strategically planned to be implemented before an earthquake occurs, so the necessity of assessing the vulnerability of a city to know what measures to implement in underlined.

Protection of historical urban areas represent a subject of high interest and actuality, as many cities with historical value are located in seismic areas. Through seismic scenarios and seismic

vulnerability assessment it is possible to appreciate the possible losses in case of an earthquake and to propose preliminary protection measures.

Nowadays, there are several vulnerability assessment methodologies, but they focus mainly on the structural component and not on the cultural one. To prevent the irrecoverable loss of cultural value, it is important to develop the existing methodologies to they consider also the architectural-artistic values, cultural and socio-economical components. Special attention must be given to the protection of historical cities, as history shown us that many historical cities were changed completely by earthquakes, such as Messina [3], Cusco [4], Lisbon [5], Christchurch [6] and others.

Historical buildings being the most likely to be destroyed in case of an earthquake, is highlighted the opportunity of preparing quick and simplified assessment procedures to help local authorities to obtain prioritization list for rehabilitation work.

The present research paper presents such a methodology that aims to assess the seismic vulnerability of historical buildings in Timisoara, by considering also their cultural value. The entire procedure with detailed analysis was published by I. Onescu in the Ph.D. thesis entitled "Seismic vulnerability assessment of historical centers" [7].

2 CASE STUDY AREA

Romania is a country with moderate seismicity, with two important seismic zones. The highest seismicity is registered in Vrancea seismic area, which is located in the center part of the country, while the second most important seismicity is observed in Banat seismic area, in the western part of the country, where Timisoara city is also located [8].

The seismicity of Timisoara is characterized by a peak ground acceleration a_g= 0.20g and the existence of two seismic faults in the western part of the city. The earthquakes in the area are shallow earthquakes of crustal type, with maximum magnitudes of 5.6 M_w [9]. To determine the most probable seismic scenario for the city, there was applied the relation between peak ground acceleration and macroseismic intensity (Eq.1), illustrating that the expected macroseismic intensity for the area is IX EMS-98 [10].

$$ln(PGA) = 0.24 \times IEMS\text{-}98 - 3.9 \quad (1)$$

Timisoara city is recognized from 1177, but there are signs that the city existed even before XIIth Century. The city was influenced by several cultures, such as the Ottoman and Habsburgic [11]. The nowadays shape of the city is the results of past influences and more recent interventions, resulting in three historical districts that merged together, forming a cultural promenade that was proposed in the context of Timisoara European Capital of Culture 2023 [7], as shown in Figure 1.

The buildings that represent the case study area are located along the cultural promenade, in a total number of 105, from which 68 are located in Iosefin district and 37 in Fabric historical area, as illustrated in Figure 2 [7].

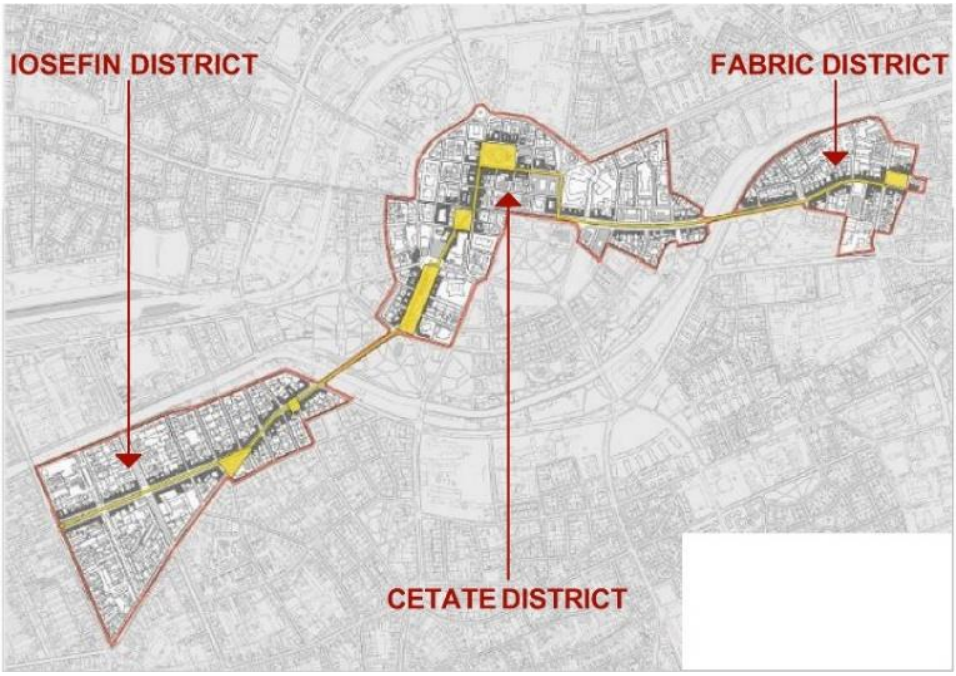


Figure 1. Proposed cultural promenade for Timisoara European Capital of Culture 2021 [7]



Figure 2. Selected historical buildings for investigation: a) Iosefin district; b) Fabric district; [7]

All the investigated buildings present brick masonry structure of burnt clay brick and lime. Their perimetral walls have 40-80 cm thicknesses, as well as the medial longitudinal wall, which is also parallel with the main façade. Transversal walls have 10-15 cm thicknesses, with the only role of ensuring the rigidity of the buildings. The aren't usually connected with the façade wall, increasing the risk of activating the out-of-plane failure mechanism in case of an earthquake. At the basement and sometimes at the ground floor, the horizontal structural elements are represented by 15-20 centimeters brick vaults, while at the upper floors there can be found wooden floors. The rigid framework of the roof is usually complex, made after German influences and very high [12]. The main characteristics of the investigated building

structures are illustrated in Figure 3 [7]. Regarding the height regime, there can be find buildings with basement and ground floor, buildings with basement, ground floor and one top level, respectively buildings with basement, ground floor and two levels above. The total height of the buildings can reach up to 15 meters, as illustrated in Figure 4 [7].

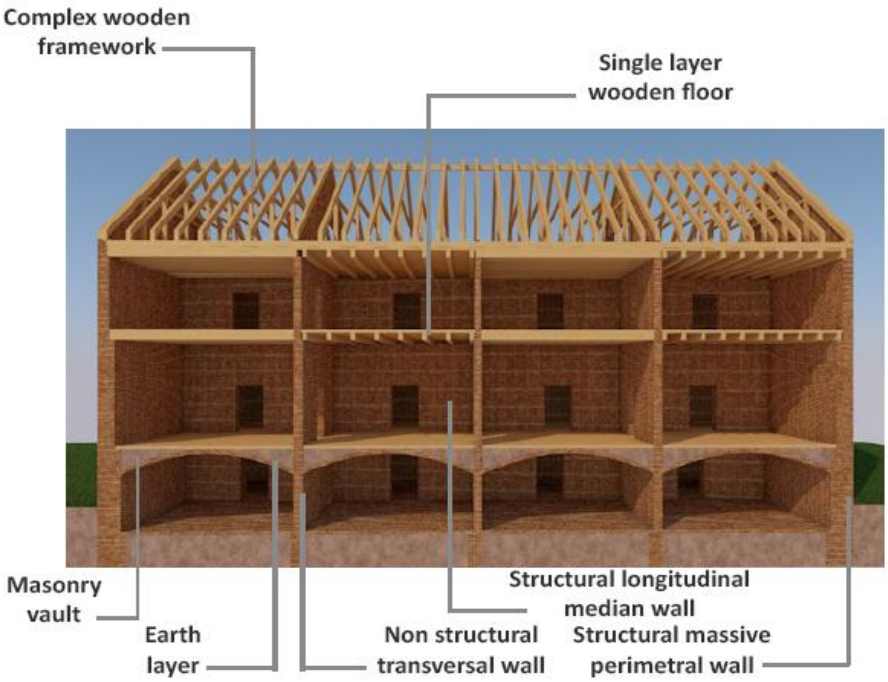


Figure 3. Main structural characteristics of the investigated historical buildings [7]

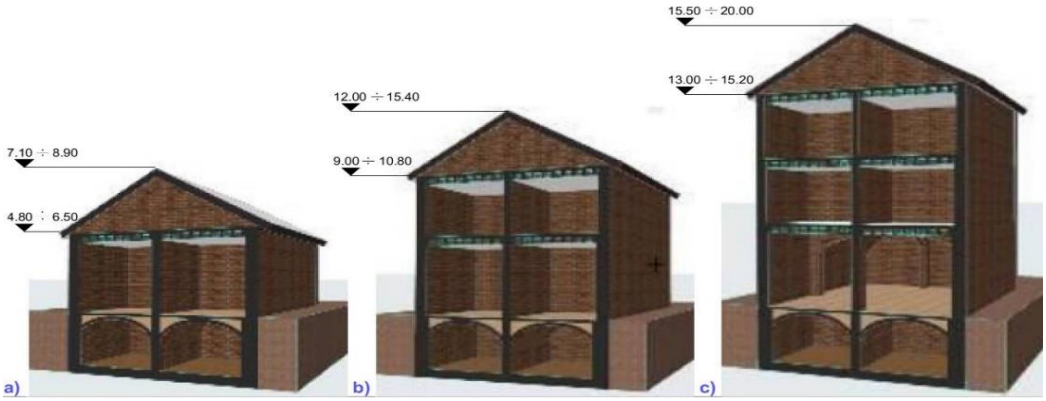


Figure 4. Height of the investigated buildings in dependence of the story number [7]

Buildings in the area are in Eclectic, Art Nouveau and Seccession architectural style. Usually, for the buildings with only ground floor, there can be seen very few architectural-artistic components (Fig. 5a). For buildings with one top level, the decoration level is moderate one, with bosses, decorated balusters and commercial spaces at the ground floor (Fig. 5b). The tallest buildings present also the highest level of architectural-artistic decorative elements, such as frontons, moldings, sculptures with different organic and complex themes (Fig. 5c) [7].



Figure 5. Selected historical buildings for investigation: a) Iosefin district; b) Fabric district; [7]

3 METHODOLOGY

Several seismic vulnerability assessment methodologies are widely used or developed, some of them with a general character and some of them calibrated to the particularities of a specific area. Three types of simplified methodologies can be considered, such as empirical, numerical and hybrid ones. To apply a methodology at large scale, it is recommended to use an empirical procedure that was previously calibrated to each urban area by numerical analysis [7].

This is also the case of Timisoara, for which was used the original Vulnerability index method that was proposed at first by Benedetti and Petrini [13] and later on by Formisano and Mazzolani [14]. This original methodology was calibrated for Banat seismic region by Mosoarca and Onescu [15] and was developed even more by Onescu [7] to consider also the cultural value of the buildings.

The final seismic vulnerability assessment methodology is based on a vulnerability form with 42 parameters, for each of them being assigned a score (s). Each parameter can be associated with one vulnerability class, from A (the most favorable) to D (the most dangerous), while the importance of each parameter is underlined by its weight (w).

The 42 parameters are divided into four main categories, such as structural, architectural-artistic, urbanistic and social-economic category. The structural parameters represent the 15 parameters from the original vulnerability form in the original assessment methodology [14]. The architectural-artistic parameters are proposed by Onescu [7] and they refer to the importance and originality of elements such as architectural style, originality, coherency, plastics, artistic assets, decay level, the statute of national monument, existing intervention

works and others (Fig. 6a). For the urbanistic category, there were considered the context, the importance of the location, the street profile and city silhouette, the presence of the roof and others (Fig. 6b). For the social-economic category, the proposed parameters refer to the importance of the building for the local community, the existence of important social or cultural functions, the representative past events for the building and also the actual economic value [7].

The final proposed vulnerability form is presented in Table 1, while the vulnerability index is represented by the sum of each individual score of the associated vulnerability class multiplied the associated weight (Eq. 2) [7].

a)



b)

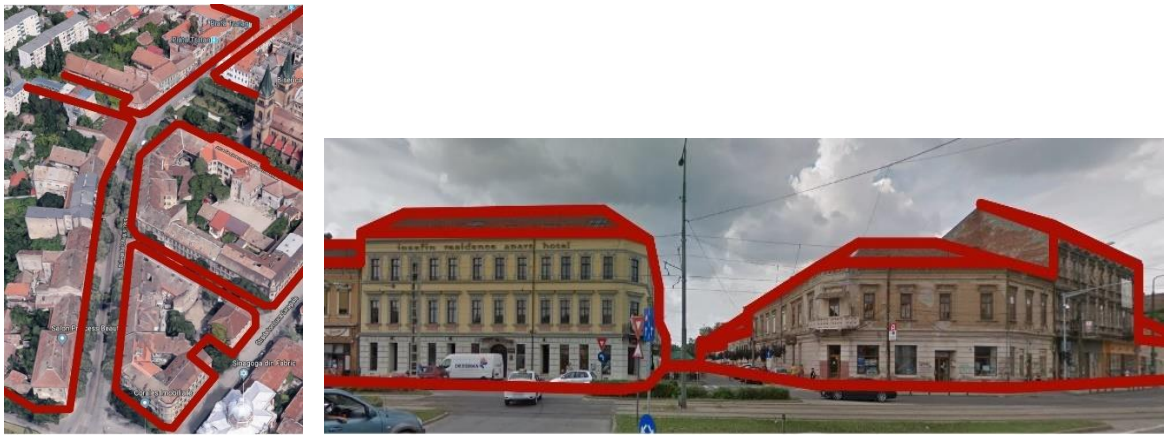


Figure 6. Exemplification of proposed parameters: a) architectural-artistic category; b) urbanistic category; [7]

Table 1. Proposed vulnerability form that considers also the cultural value [7]

%	Criteria	No.	Element	Class				Weight
				A	B	C	D	
70 %	STRUCTURAL	1	Vertical structure organisation	0	5	20	45	1.00
		2	Vertical structure nature	0	5	25	45	0.25
		3	Type of foundation and location/soil	0	5	25	45	0.75
		4	Distribution of structural elements in plan	0	5	25	45	1.50
		5	Regularity in plan	0	5	25	45	0.50
		6	Regularity in elevation	0	5	25	45	1.00
		7	Floor type	0	5	15	45	0.75

		8	Roofing	0	15	25	45	0.75
		9	Other details	0	0	25	45	0.25
		10	Conservation state	0	5	25	45	1.00
		11	Different height between current and adjacent buildings	-20	0	15	45	1.00
		12	Location of the building into the aggregate	-45	-25	-15	0	1.50
		13	Staggered floors	0	15	25	45	0.50
		14	Structural or typological heterogeneity	-15	-10	0	45	1.20
		15	Opening area percentage difference	-20	0	25	45	1.00
						$I_{V\ STRUCT}$		
15 %	ARCHITECTURAL ARTISTIC	16	Representative architectural style for the area	0	10	15	25	1.50
		17	Age, importance of the build époque	0	10	15	25	1.20
		18	Original woodwork/joinery	0	10	15	25	1.00
		19	Original stucco, brick, floors or ceilings	0	10	15	25	1.00
		20	Original statues or bass-reliefs	0	10	15	25	1.00
		21	Original gable/fronton	0	10	15	25	1.00
		22	Original balconies and railings	0	10	15	25	1.00
		23	Original mosaics or stone work	0	10	15	25	1.00
		24	Original paintings or frescoes	0	10	15	25	1.00
		25	Conservation state of artistic assets	-5	10	15	25	1.00
		26	Authenticity/ originality (global, elements)	0	10	15	25	1.00
		27	Official monument (national, regional, local, protected area) status	0	10	15	25	1.50
		28	Particular construction techniques/materials	0	10	15	25	0.50
		29	Conservation state of original materials	-5	10	15	25	0.50
		30	Representative historical events	0	10	15	25	0.50
		31	Archaeological site	0	10	15	25	1.50
		32	Representative/ original wooden framework	0	10	15	25	1.00
		33	Past restoration work	-5	10	15	25	1.00
						$I_{V\ ARCH\text{-}ART}$		
10 %	URBANISTIC	34	Importance in contouring the street profile	-5	10	15	25	1.50
		35	Importance in contouring the urban silhouette	-5	10	15	25	1.50
		36	Annexes, relation with the urban pattern	0	10	15	25	1.00
		37	Location (central area, touristic area)	0	10	15	25	1.50
		38	Representative/particular shape of the roof	0	10	15	25	1.00
						$I_{V\ URB}$		
5 %	SOCIAL ECONOMIC	39	Public/social functions	0	10	15	25	1.50
		40	Importance for the local community memory	-5	10	15	25	1.00
		41	Economic value	0	10	15	25	1.50
		42	Cultural functions	0	10	15	25	1.50
						$I_{V\ SOC\text{-}EC}$		
						$I_{V\ CULT}$		

$$I_{V\ CULT} = 0.70 \times \sum_{i=1}^{15} s_i \times w_i + 0.15 \times \sum_{i=16}^{33} s_i \times w_i + 0.10 \times \sum_{i=34}^{38} s_i \times w_i + 0.05 \times \sum_{i=39}^{42} s_i \times w_i \quad (2)$$

Moreover, the proposed methdology considers also the importance of the investigated site, by itnroducing an attenuation factor that can increase the considered cultural vulnerability with up to 50% for the most important historical sites. The parameters that are considered for the attenuation factor are illustrated in Table 2, while the formula for calculating the actual factor is presented in Equation 3. In the end, the normalized vulnerability index influenced by the cultural value is determined following Equation 4 [7].

Table 2. Parameters considered for the attenuation factor [7]

Parameter		Options	Points (p_i)
1	Age of the urban area	Ancient period (before year 500)	0.30
		Classical period (500 – 1500)	0.25
		Modern period (1500 - 1945)	0.22
		Contemporary period (1945- present)	0.20
2	Population	Very high populated (> 1 million inhabitants)	0.30
		High populated (< 1 million inhabitants)	0.25
		Moderate populated (< 300000 inhabitants)	0.22
		Low populated (< 100000 inhabitants)	0.20
3	Tourism	Very touristic city	0.25
		Touristic city	0.23
		Little touristic city	0.22
		Not a touristic city	0.20
4	Worldly recognition	UNESCO site	0.35
		Continental importance	0.30
		National importance	0.25
		Regional importance	0.20
5	Conservation state	Poor	0.30
		Moderate	0.25
		Good	0.23
		Very good	0.20
		A_F	

$$A_F = \sum_{i=1}^{5} p_i \quad (3)$$

$$V_{CULT} = \frac{I_{V\,CULT} - I_{V\,CULT\,MIN}}{I_{V\,CULT\,MAX} - I_{V\,CULT\,MIN}} \times A_F \quad (4)$$

After the determination of the normalized vulnerability index influenced by the cultural value, there can be determined the most probable damage state by applying Equation 5, where Φ represents a factor that induces the curve slope and is considered to be 2.3 for residential buildings [16] and I representes the most expected macroseismic intensity for the investigated área, which was previously determined to be IX EMS-98 for Timisoara [7].

$$\mu_D = 2.5\left[1 + \tanh\left(\frac{I + 12.50 \times V_{CULT} - 13.1}{\Phi}\right)\right] \quad (5)$$

The proposed methodoloy has the main advantage of introducing the cultural component, while being based on a well-known european original empirical procedure.

4 RESULTS

The proposed methodology was applied to all 105 historical buildings from the investigated districts in Timisoara, to determine the seismic vulnerability influenced by the cultural value. There were determined the mean vulnerability curves following the standard deviation for the 37 buildings in Fabric area (Fig. 7), for the 68 historical buildings in Iosefin district (Fig. 8), respectively the mean vulnerability for all 105 buildings (Figure 9) [7].

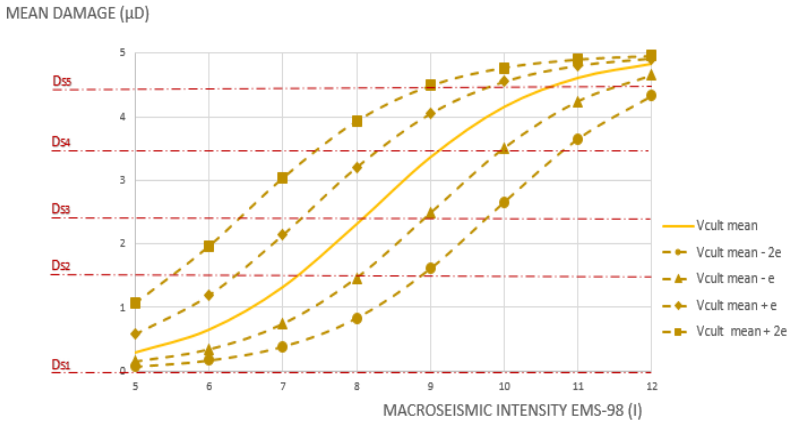


Figure 7. Mean vulnerability curves influenced by the cultural value for buildings in Fabric district; [7]

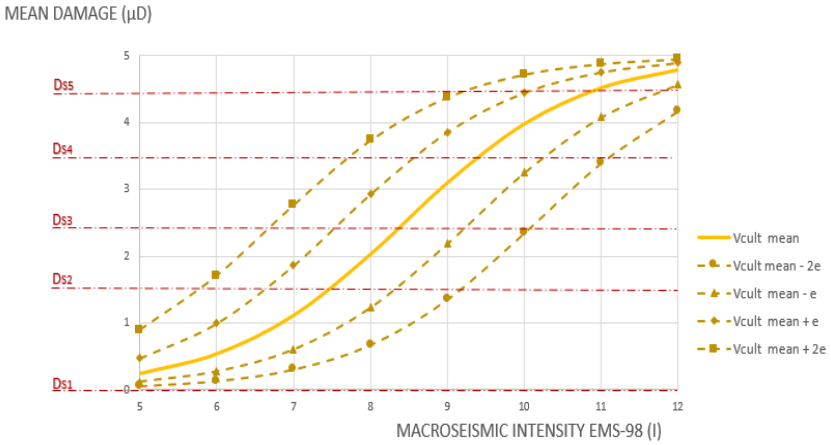


Figure 8. Mean vulnerability curves influenced by the cultural value for buildings in Iosefin historical area [7]

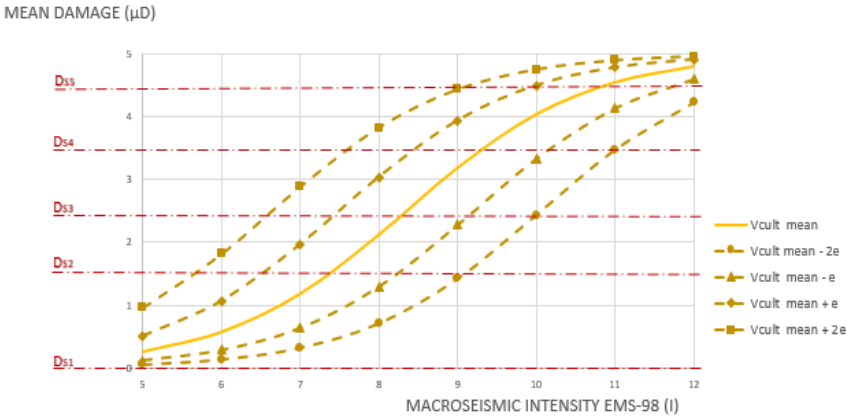


Figure 9. Mean vulnerability curves influenced by the cultural value for all 105 investigated historical buildings [7]

The results obtained for the investigated historical buildings in Timisoara, for the considered seismic scenario, highlight a medium seismic-cultural vulnerability for the expected macroseismic intensity IX EMS-98. Both Fabric and Iosefin expect a general D3 damage state, with a total range of D1-D4 damage states (Table 3) [7]. Despite the fact that there isn't expected the loss of the bearing capacity of the investigated buildings, the moderate vulnerability is still meaning damages to both structural and non structural elements, leading to the decay of many important artistic assets.

Table 3. Expected damage states for the investigated districts [7]

Historical district	Damage state D1	Damage state D2	Damage state D3	Damage state D4	Damage state D5
Iosefin	3.00%	25.00%	42.50%	28.00%	1.50%
Fabric	0.00%	16.00%	43.50%	38.00%	2.50%

Following the empirical results, there was designed also the vulnerability maps influenced by the cultural value for both Fabric and Iosefin historical districts, for all the investigated buildings [7], as presented in Figures 10-11.

The seismic vulnerability maps influenced by the cultural value illustrates a 5% higher level of decay in Fabric area, aspect which is caused by the lack of proper maintenance of historical buildings in the area on one hand and by the increased height of the same building on the other hands.

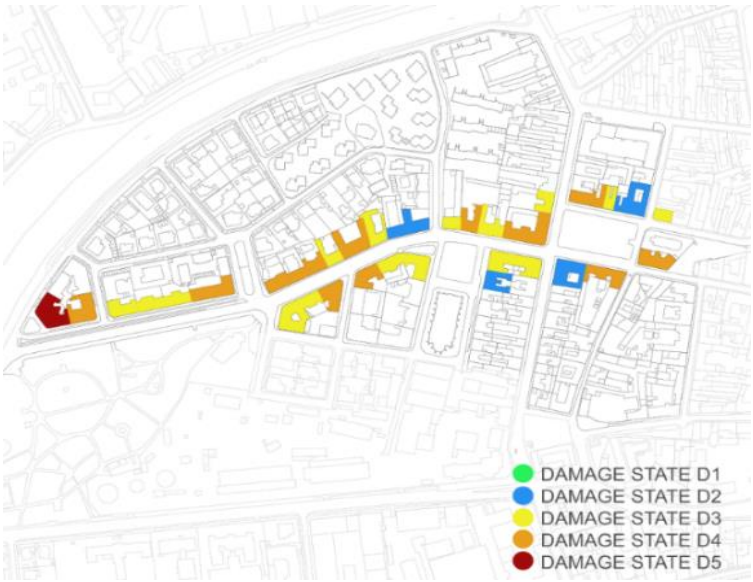


Figure 10. Seismic vulnerability map influenced by the cultural value for Fabric district [7]



Figure 11. Seismic vulnerability map influenced by the cultural value for Iosefin area [7]

In conclusion, only one building in each district was determined to be in danger of losing its bearing capacity in case of an earthquake with IX EMS-98 macroseismic intensity. In general, the most vulnerable buildings are the one located on corner position within the aggregate.

5 CONCLUSIONS

The proposed seismic vulnerability assessment influenced by the cultural value represent a useful tool for the local authorities to obtain in a quick and simplified way a prioritization list for rehabilitation work in the historical districts of the city.

The main advantage of the proposed procedure is the fact that is suitable for territorial scale application, with minimum resources in terms of time, human resources and finances.

The presented multidisciplinary methodology can be easily applied to any other historical city in similar seismic area with Banat one, while it can also be easily adapted for any other site.

It brings a plus of knowledge in the field of seismic vulnerability assessment, while harmoniously intertwining the field of civil engineering with that of architecture.

Least but not last, the proposed procedure aims to protect historical cities against earthquakes, by allowing a simplified assessment of their vulnerabilities, while considering also the cultural values of the area.

The results presented in this paper indicate the fact that the city of Timisoasa, which was elected European Capital of Culture 2023, has a moderate seismic vulnerability influenced by the cultural value, with more buildings that will need rehabilitation work in Fabric historical district.

REFERENCES

[1] M. Mosoarca, I. Onescu, E. Onescu, B. Azap, N. Chieffo, M. Szitar-Sirbu, Seismic vulnerability assessment for the historical areas of the Timisoara city, Romania, *Eng. Fail. Anal. 101* (2019) 86–112. doi:10.1016/J.ENGFAILANAL.2019.03.013.

[2] A. Formisano, F. Mazzolani, G. Florio, R. Landolfo, A quick methodology for seismic vulnerability assessement of historical masonry aggregates, *COST Action C26 Urban Habitat Constr. under Catastrophic Events*. (2010). doi:10.13140/2.1.1706.3686.

[3] S. Chen, Hazard Mitigation for Earthquake and Subsequent Fire, *ANCER Annual Meeting: Networking of Young Earthquake Engineering Researchers and Professionals* (2004).

[4] G. E. Ericksen, J. F. Concha, and E. Silgado, The Cusco, Peru, Earthquake of May 21, 1950, *Bulletin of the Seismological Society of America* (1954), vol. 44, no. 2A, pp. 97–112.

[5] A. S. Pereira, The opportunity of a disaster: The economic impact of the 1755 Lisbon earthquake, *Journal of Economic History* (2009), vol. 69, no. 2, pp. 466–499.

[6] A. Kaiser et al., The Mw 6.2 Christchurch earthquake of February 2011: Preliminary report, *New Zealand Journal of Geology and Geophysics* (2012), vol. 55, no. 1, pp. 67–90.

[7] I. Onescu, Seismic vulnerability assessment of historical urban centers, *Ph.D. thesis* (2020).

[8] A. Bala and V. Raileanu, Crustal seismicity and active fault systems in Romania, *International Multidisciplinary Scientific GeoConference Surveying Geology and Mining Ecology Management* (2015), SGEM, vol. 3, no. 1, pp. 799–806.

[9] E. Oros, Macroseismic and instrumental seismicity of the Banat Region and its significance on the local seismic hazard and risk, in *Proc. and CD-Rom of the "Thirty Years from the Romania Earthquake of March 4, 1977" Symposium* (2007).

[10] M. Kostov, Site specific estimation of cumulative absolute velocity, in *18th International Conference on Structural Mechanics in Reactor Technology* (SMiRT 18) (2005) , Beijing, China.

[11] M. Opris, Timisoara - small urbanistic monography, In Romanian. Bucuresti: Editura Tehnica (1987).

[12] M. Mosoarca, I. Onescu, E. Onescu, B. Azap, N. Chieffo, and M. Szitar-Sirbu, Seismic vulnerability assessment for the historical areas of the Timisoara city, Romania, *Engineering Failure Analysis* (2019), vol. 101, pp. 86–112.

[13] D. Benedetti and V. Petrini, On the seismic vulnerability of masonry buildings: an evaluation method (in Italian), *L'Industria delle Costruzioni* (1984), vol. 149, pp. 66–74.

[14] A. Formisano, R. Landolfo, F. Mazzolani, and G. Florio, A quick methodology for seismic vulnerability assessement of historical masonry aggregates, *COST Action C26: Urban Habitat Constructions under Catastrophic Events* (2010), no. September.

[15] Mosoarca M., Onescu I., Onescu E., Anastasiadis A., Seismic vulnerability assessment methodology for historical masonry buildings in the near-field areas, *Engineering Failure Analysis* (2020), Vol. 115.

[16] R. Vicente, S. Parodi, S. Lagomarsino, H. Varum, J. A. R. Mendes, and D. Silva, Seismic vulnerability assessment, damage scenarios and loss estimation. Case study of the old city centre of Coimbra, Portugal, in *Proceedings of the 14th World Conference on Earthquake Engineering* (2008).

12th International Conference on Structural Analysis of Historical Constructions
SAHC 2020
P. Roca, L. Pelà and C. Molins (Eds.)

SEISMIC VULNERABILITY ASSESSMENT OF A HISTORIC BRICK MASONRY BUILDING BY FRAGILITY FUNCTIONS

KULTIGIN DEMIRLIOGLU[1*] AND SERDAR SOYOZ[2]

[1]Department of Civil Engineering and Energy Technology
Oslo Metropolitan University
Pilestredet 35, 0166 Oslo, Norway
e-mail: kultigin@oslomet.no, (*corresponding author)

[2] Civil Engineering Department
Boğaziçi University
South Campus/ Bebek, 34342 İstanbul, Turkey
email: serdar.soyoz@boun.edu.tr, www.shm.ce.boun.edu.tr/

Keywords: Seismic Fragility Curve, Incremental Dynamic analysis, Vulnerability Assessment

Abstract. *This paper aims at contributing to the seismic vulnerability assessment of a historic brick masonry building constructed in Istanbul by comparison of the derived analytical and empirical fragility functions. For this purpose, Incremental Dynamic Analysis for each ground motion record was initially performed by series of Nonlinear Time History Analyses on the most vulnerable façade of the case study building modelled using Equivalent Frame Method. By scaling the PGA values of the fifteen earthquake records selected from PEER NGA West2 Data Base, it was aimed to observe the structural response corresponding the all limit states from yield point to collapse and identify each PGA causing the structure to reach these limit states. Herein, PGA and Spectral Displacements were considered as the seismic intensity parameters, and the ultimate storey drifts were referred as Engineering Demand Parameter. Both analytical and empirical seismic fragility functions were derived using lognormal probability distribution. Consequently, the obtained analytical fragility curves for vulnerability assessment of the building were compared with the fragility curves derived according to European (RISK-UE), HAZUS and Istanbul Building Taxonomies for the same building classification with the case study building in attempt to investigate the concordance of the results.*

1 INTRODUCTION

The recent studies regarding seismic risk analysis have revealed that unreinforced masonry buildings are the most seismically vulnerable building type, which constitutes a significant percentage of the existing building stock all over the world. Their high vulnerability to seismic events and aggressive environmental conditions arises a substantial need for improving the knowledge of their seismic behaviour, and developing analytical and numerical models for their risk assessment. Seismic vulnerability refers to the structural susceptibility to damage or loss due to a seismic activity. It can be identified by means of fragility functions, giving the likelihood of reaching or exceeding a certain limit state as a function of the Intensity Measure (IM) such as Peak Ground Acceleration (PGA), Peak Ground Velocity (PGV), Spectral displacement (S_d), etc. or using vulnerability functions, providing the expected value of loss. [1].

In literature, there have been a wide range of studies carried out on vulnerability assessment and derivation of fragility functions since the existence of complex structural typologies leads to a very demanding task including a high amount of uncertainty in the characterization of the structural members, as well as the mechanical properties of the constituent materials particularly for masonry structures [2]. Some researchers have made substantial contributions to the inherent probabilistic nature of the seismic risk assessment, developing distinctive methodologies such as RISK-UE, SYNER-G and PERPETUATE to derive seismic fragility functions for common and cultural heritage masonry buildings in consideration of load bearing wall material, the number of stories, different building taxonomies, etc. [3-7]. In addition to these, empirical, analytical, expert judgement and hybrid-based methods for derivation of fragility functions were developed [8-10].

This paper presents the vulnerability evaluation of a historical brick masonry building dating back to the 1920s. The probability distribution of the seismic demand for each limit state (limited damage, significant damage and near collapse) is obtained performing Incremental Dynamic Analyses (IDA) under 15 different earthquake records. By using PGA and S_d as intensity measure, and using ultimate storey drift as Engineering Demand Parameter (EDP), both empirical and analytical seismic fragility curves are derived, employing the lognormal probability distribution. Therefore, the obtained fragility curves provide information regarding the likelihood of occurrence and exceeding of each damage level that the building may experience under the seismic actions induced. Via the comparison of the results obtained from the empirical fragility curves when the analytical fragility curve is taken as a reference , this study finally points out which fragility curve parameters proposed by RISK-UE, HAZUS, and ISTANBUL can be more convenient to be used for vulnerability assessment of the taxonomy of old-brick masonry buildings representing the case study building.

2 CASE STUDY BUILDING

A historic building built in 1925 in Istanbul is registered in the cultural heritage list by Turkish Republic Ministry of Culture and Tourism. In the scope of this study, seismic vulnerability assessment was carried out to determine the current health condition of this building [11]. The building symbolizes a specific typology of the traditional Turkish historical building architecture in the early 20th century. It consists of three storeys with different heights 3.45 m, 4.84 m and 4.45 m belonging to basement, ground and first storeys, respectively. With

respect to the load-bearing system, the walls are made of solid bricks and Khorasan mortar which is a widely used local mortar in the construction of historical masonry structures in Turkey and commonly includes hydraulic lime, kaolin, calcite, refined Khorasan clay, etc. The slabs of ground floor and first floor consist of brick arch floor systems, where the steel beams of INP180 are installed with an interval of 60 cm, and the roof slab is made of oak timber elements. The wall thicknesses vary between 68–88 cm in the basement, 45–76 cm in the ground floor, and 32–65 cm in the first floor. More detail about the building geometry and the mechanical property of the material used can be found in [12].

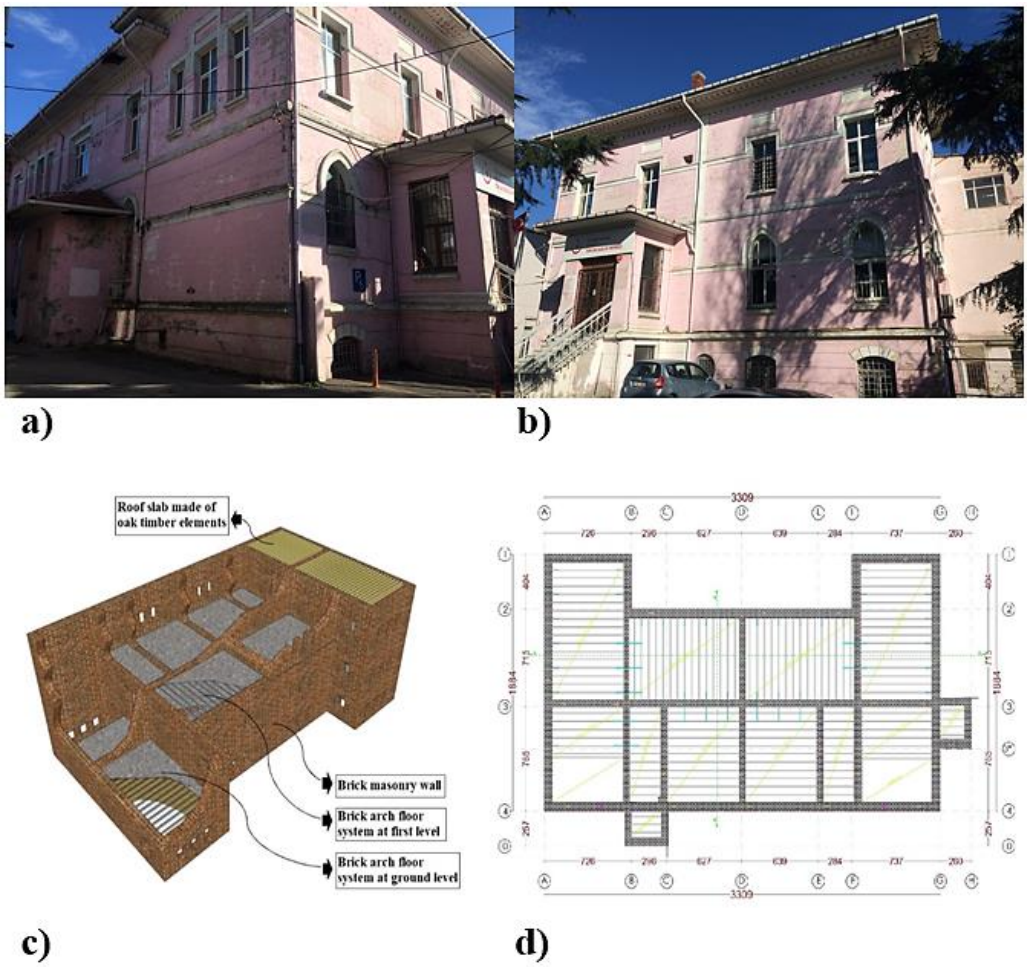


Figure 1: (a) Corner view (b) front view (c) illustration of the load-bearing system of the URM building and (d) plan of the ground floor.

In-situ investigation showed that the connection of intersecting walls and clamping between bearing walls and floor systems were in good condition. No local damages and cracking between bearing wall and the floor system have been detected. The presence of proper connections in the existing property made us consider that the connections would prevent out-of-plane behaviour; therefore, only in-plane behaviour was considered in this study.

3 NUMERICAL MODELING OF THE HISTORICAL BUILDING

In the literature, for masonry walls, there have been a various type of modelling techniques such as Rigid Body and Spring Model, Fibber Contact Element Method, Applied Element Method etc. However, in this study, the 3D Finite Element Model (FEM), the most frequently used method, was adopted for generation of the numerical model of the building. Initially, the linear dynamic analysis was performed using FEM so as to carry out a general assessment procedure in terms of the stress and displacement demands occurring under the design earthquake. As a result of the linear dynamic analysis, it was detected that both right and front façades governed the collapse state of the URM structure in terms of the limit states. However, the front façade was the most vulnerable one in terms of principal and shear stresses exceeding their threshold values due to having more openings, compared to the right façade. Therefore, 2D Equivalent Frame (EF) model of the front façade was generated by adopting the criterion proposed by Dolce (1991). In the light of in-situ observations, which provide a basis for the assumption of the bearing walls properly connected to the floor, only in-plane behaviour was deemed in analyses to accurately simulate the global response of the structure. The EF method simplifies modelling masonry walls with frame elements via consideration of the homogeneous and isotropic material idealization and defining the nonlinear behaviour of structural masonry. For generating seismic fragility curves that will be used in vulnerability assessment procedure of the building, as a nonlinear dynamic method, a set of Nonlinear Time History analyses (NLTHA) was employed to perform series of simulations. In an attempt to diminish dissipation of time and computational burden due to NLTH, the nonlinear behaviour was only represented by the definition of shear hinges assigned to the mid-heights of the piers. Since Magenes, G., and G. M. Calvi (1997) highlighted that the failure in masonry is generally characterized by shear either in diagonal tension mode or by sliding on the predefined planes of mortar rather than other in-plane failure mechanisms such as rocking, toe crushing, only shear hinge assignment was considered adequate for nonlinear simulation [13]. Therefore, the ultimate resistance was controlled by the shear failure and the shear failure was controlled by the shear displacement capacity of the piers. According to NTC (2008), the shear collapse corresponds to the achievement of the ultimate drift δu which is assumed to be 0.4% of the effective height of the pier [14]. Please note that the effective height of the pier was changed to 0.5% in 2018 with the new version of the standard (NTC, 2018) [15].

According to Eurocode 8 Part 3 (EN 1998-3 2005), the limit states of URM walls were determined, which correspond to the attainment of the global displacement capacity on the pushover curve [16]. The ultimate displacement capacity is described as the top displacement, and three limit states exist on the pushover curve in terms of top displacement, as follows.

- Limit state of Limited Damage (LD) is where the structure yields on the curve of idealized elasto-perfectly plastic force/displacement relationship.
- Limit state of Significant Damage (SD) is equal to 3/4 of the top displacement capacity corresponding the total base shear.
- Limit state of Near Collapse (NC) is equal to below 80 percent of the peak resistance of the structure.

Structural collapse was assumed once the in-plane deformation capacity of piers was firstly reached due to the ultimate shear displacement controlled by shear hinges.

4 VULNERABILITY ASSESSMENT

4.1 Incremental Dynamic Analysis

Incremental dynamic analysis (IDA) is a computational analysis method for performing a comprehensive assessment of the behaviour of structures under seismic loads, which reveals the structural response from linear range to nonlinear range leading to collapse. It has been utilized to rely on the results of probabilistic seismic hazard analysis in attempt to evaluate the seismic risk confronted by a given structure [17]. IDA comprises performing numerous nonlinear dynamic analyses of a structural model under a set of ground motion records. Each record should be properly scaled to several levels of seismic intensity to enable structures to cover the entire range of structural response from elastic to inelastic and ultimately to global dynamic instability where the structures no longer resist. Moreover, the selection of earthquake inputs is a momentous phase to acquire reliable results regarding vulnerability assessment, since a seismic action can alter with regards to the frequency content, the energy content and duration, which lead to different effects on the same structure. For this purpose, 15 earthquake records were advertently selected from PEER NGA West2 Data Base in accordance with the design response spectrum generated as shown in Figure 2.

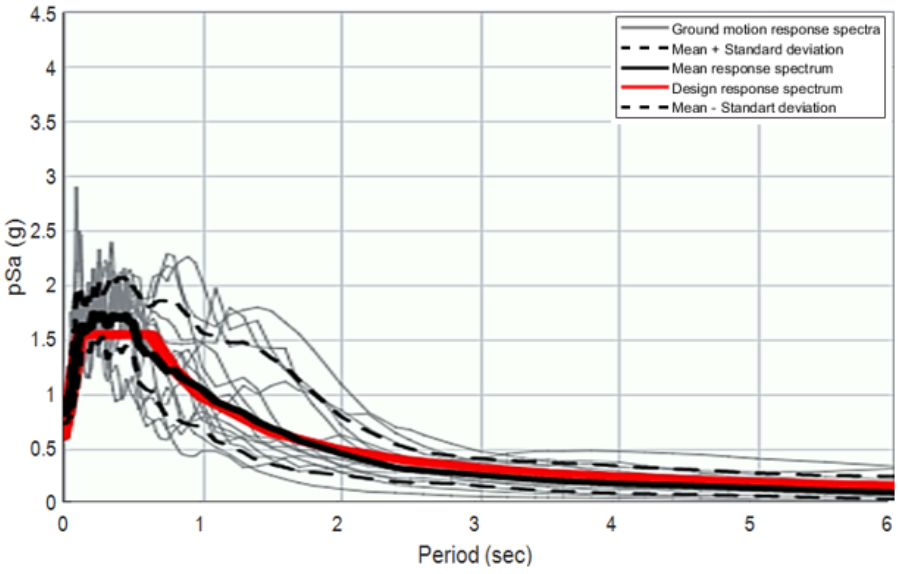


Figure 2: Spectra of selected ground motions.

In this study, PGA values were used as an Intensity Measure (IM) that characterizes the conditional probability of attaining a given damage state for a given hazard level. By scaling the PGA values, it is aimed at leading the structure to reach all limit states from yield point to collapse. As a result of scaling procedures, each PGA value being a component of the total 15 scenario earthquakes, which caused the building to reach the limit states of limited damage, significant damage and near collapse were identified (Figure 3). Engineering Demand Parameters (EDP), which are measures of the structural response were represented by the ultimate drift.

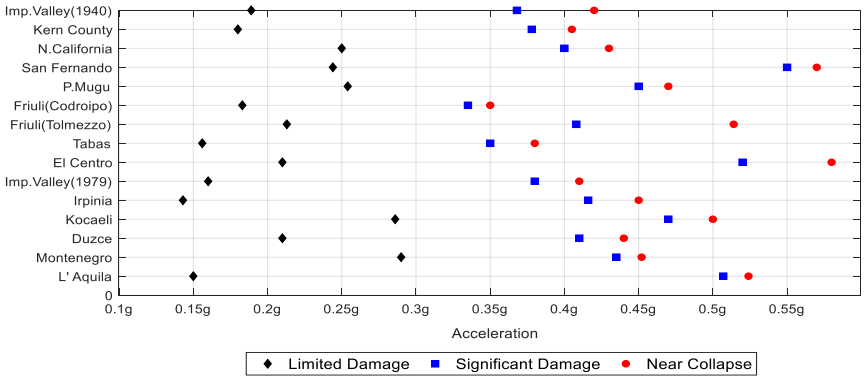


Figure 3: Summary of PGA values leading the structure to reach LD, SD and NC limit states.

4.2 Seismic Fragility Curve

In seismic risk assessment, vulnerability curves are frequently used to identify the probability that structures at risk will withstand different levels of loss under a series of earthquake ground motion intensities. These vulnerability curves can be generated using the empirical approaches based on statistical analysis of loss values observed in past earthquakes, analytical or numerical approaches, and hybrid approaches that are combination of these methodologies and expert opinion [18]. For the purposes of vulnerability assessment, fragility curves are gaining more importance as a statistical tool which establishes the relationship between the likelihood of reaching or exceeding a specified level of damage and the effects of the projected ground motions on the built environment. In this study, the generation of fragility curves will cover analytical and empirical approaches by use of lognormal distribution for the vulnerability assessment of the case study building. The resulting data sets, used in lognormal distribution for constructing the analytical fragility curves, were obtained considering only the uncertainty in the strong ground motion records while the FEM model of the structure was fully deterministic.

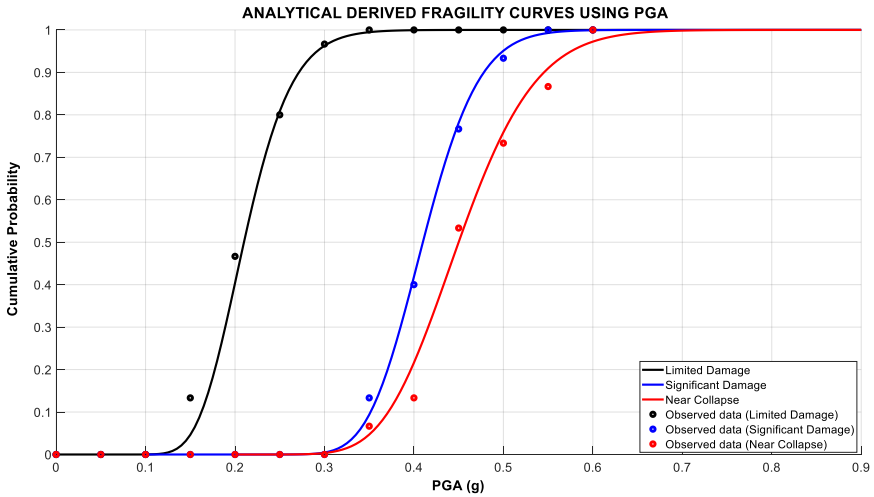


Figure 4: Analytical derived fragility curves based on the PGAs leading the structure to reach LD, SD and NC.

Using the PGA values leading the structure to reach LD, SD and NC limit states presented in Figure 3, the analytical fragility curves were derived as shown in Figure 4. By employing lognormal distributions in calculations, the obtained fragility curves properly fitted the observed data. Therefore, they provided an opportunity to assess the seismic vulnerability by direct comparison with the subjected PGA values. It showed that when the case study building is subjected to the strong ground motions with the PGA values slightly more than 0.2 g and 0.4 g, it will experience limited and significant damages, respectively, with an exceedance probability of 50% while a PGA of 0.45 g will be a sufficient intensity to reach the limit state of near collapse for the same exceedance probability. Regarding empirically derived fragility curves, they were generally represented through spectral displacements as IM. Moreover, herein, the fragility curves obtained from empirical approaches will be compared to each other and interrogated to clarify whether they can be addressed to the vulnerability assessment of a single case study building in a specific taxonomy even though in practice they are to be used in the seismic risk assessment of a specific building stock at a certain location.

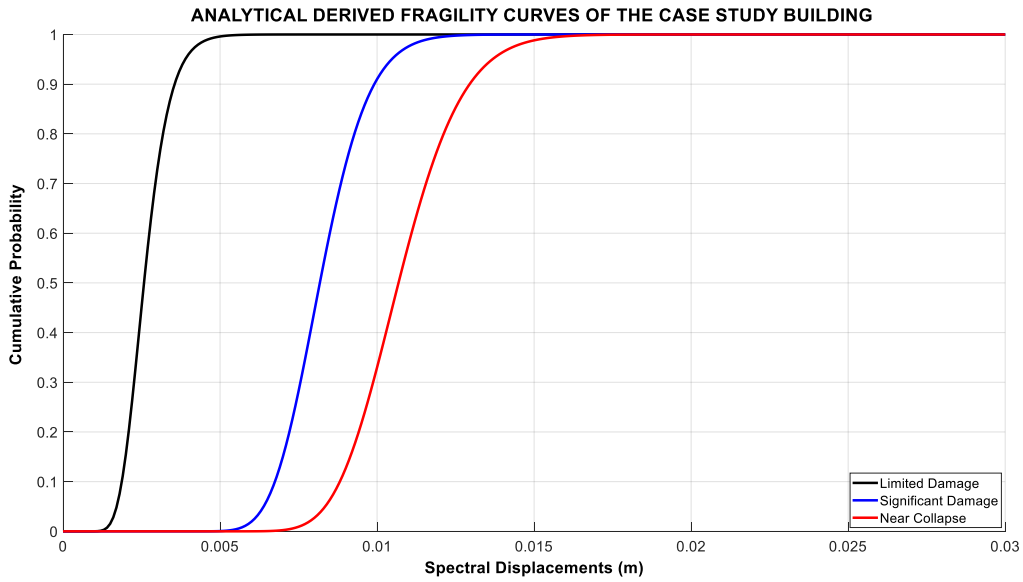


Figure 5: Analytical derived fragility curves of the case study building using Spectral Displacements.

Thorough the IDAs, each spectral displacement was identified for a certain damage level. The analytical fragility curves were generated on the basis of spectral displacements (Figure 5). Since the case study building is a type of 2-storey brick masonry building constructed in 1925, in literature its taxonomy is equivalent to **M5- L** according to European Building Taxonomy [19] representing Unreinforced Masonry (old bricks), **URML** according to pre-code buildings of HAZUS 99 Building Taxonomy [20-21] representing Unreinforced Masonry Bearing Walls, and **B211** according to Istanbul Building Taxonomy [22] representing 1-4 storey masonry buildings (built in pre 1979). The fragility curve parameters of the empirical approaches mentioned were presented in Table 1 where S_d is the median value of the lognormal distribution of the intensity measure (spectral displacement) and β is the dispersion related to the uncertainties in the seismic demand.

Table 1: Fragility curve parameters.

Building Taxonomy	Limited Damage (Slight)		Significant Damage (Moderate)		Near Collapse (Extensive)	
	$S_{d,\,s}$ (m)	β_s	$S_{d,\,m}$ (m)	β_m	$S_{d,\,e}$ (m)	β_e
EUROPE (M5-L)	0.0013	1.07	0.0029	1.07	0.006	1.07
HAZUS (URML)	0.0081	1.15	0.0165	1.19	0.0411	1.2
ISTANBUL (B211)	0.0135	0.99	0.0315	1.05	0.072	1.1

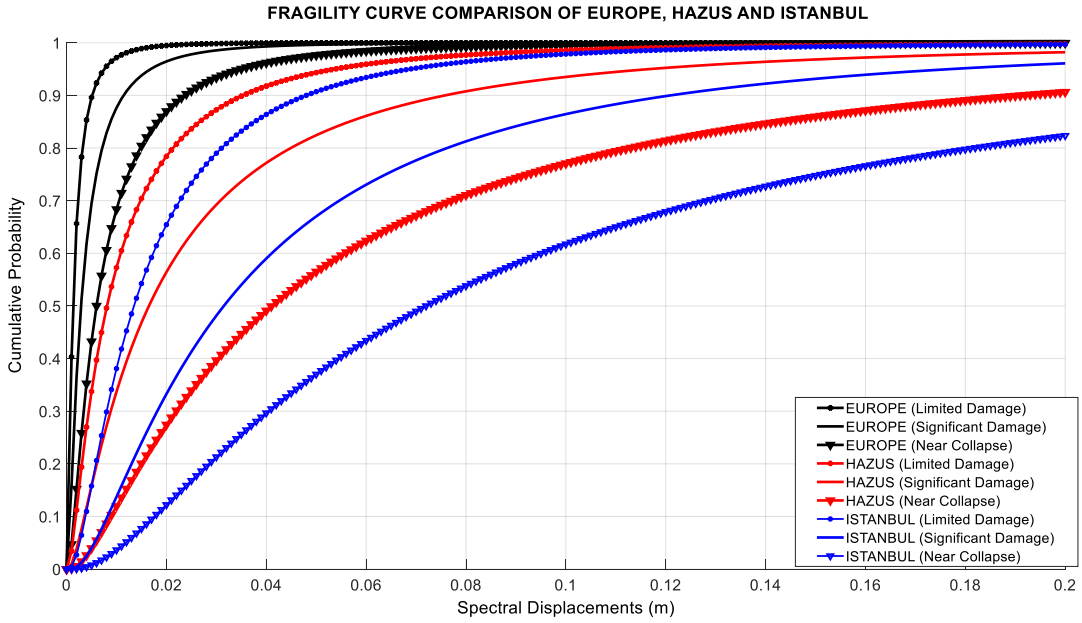


Figure 6: Comparison of the empirical derived fragility curves.

In Figure 6, the obtained empirical fragility curves for the same taxonomy with the case study building were compared. As it can be seen from the figure, fragility curves derived from HAZUS and Istanbul building taxonomy demonstrate relatively close behaviour and their spectral displacement demands anticipated for the limited damage underestimate the spectral displacement demands corresponding to the limit state of near collapse by European building taxonomy (RISK-UE). In other words, if the building is subjected to a spectral displacement demand of 20 mm, it will experience the limit state of the near collapse with a probability of approximately 90 % according to RISK UE, whereas it is expected to reach the collapse probabilities of 15% and 25 % for the same level of the IM according to ISTANBUL and HAZUS, respectively. When considering the structural response of the case study building based on the results obtained from the analytical fragility curves in Figure 5, the building reaches a complete collapse under earthquake-shaking intensity of a 20 mm-spectral displacement. As a result of the vulnerability assessment via the fragility functions derived from the analytical and RISK UE based empirical approaches, it can be concluded that they are more coherent in terms of the anticipated cumulative probabilities corresponding to IM for the given damage levels (Figure 7).

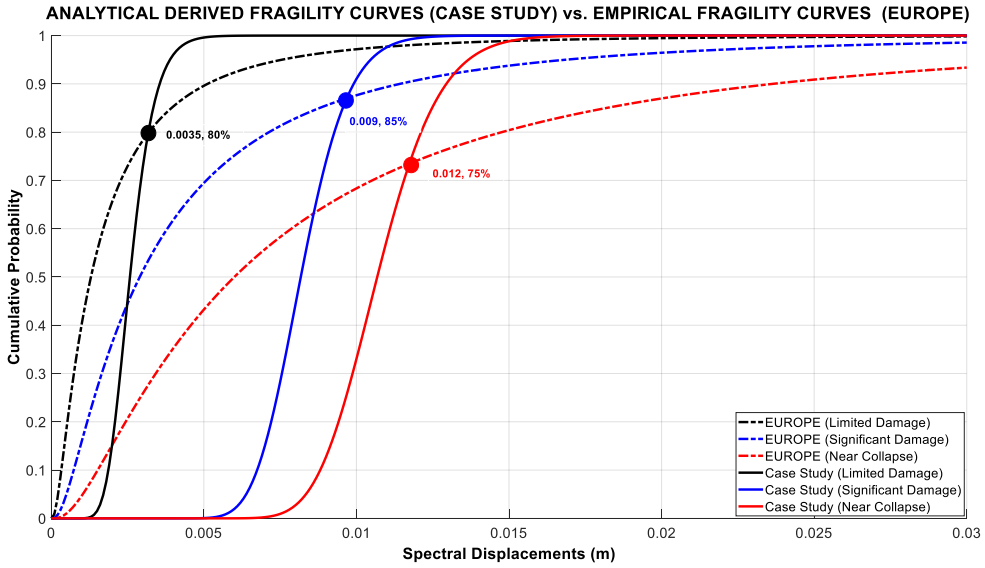


Figure 7: Comparison of the analytical derived fragility curves of the case study building and the empirical derived fragility curves (Europe).

5 CONCLUSION

The article has presented the seismic vulnerability assessment of a historic brick masonry building through the empirically and analytically derived fragility curves. Derivation of analytical fragility curves requires rigorous and demanding work, which encompasses the implementation of IDAs to determine the IM levels causing the occurrence and non-occurrence of the damage states. However, the analytical approaches can yield more accurate results in the estimation of vulnerability since they are directly derived from the structural analysis of the objective buildings. As an alternative to use of this computationally expensive procedure, the effectiveness of the empirically derived fragility curves has been questioned so as to see the possibility of their application in the vulnerability assessment of a single building, whereas in practice they are utilized for the seismic risk assessment of a certain building inventory in a specific location. By means of the comparison of the results obtained from the empirical fragility curves when the analytical fragility curve is taken as a reference, it has been observed that RISK-EU produces the closest result in terms of the anticipated cumulative probabilities for the given damage levels. Moreover, the spectral displacement demands, causing the limited damage, proposed by HAZUS and ISTANBUL strikingly exceed the required spectral intensity for near collapse by RISK-EU. For the masonry taxonomy, RISK-EU proposes well-defined fragility curve parameters since they are individually categorized into each masonry material in detail, while the other empirical approaches consider a larger range of masonry classification in general. Consequently, this study also has pointed out that the fragility curve parameters proposed by RISK-UE compared to the others can be more convenient to be used for vulnerability assessment of the taxonomy of old-brick masonry buildings representing the case study building.

REFERENCES

[1] Simões, A.G., Bento, R., Lagomarsino, S., Cattari, S. and Lourenço, P.B. Fragility Functions for Tall URM Buildings around Early 20th Century in Lisbon. Part 1: Methodology and Application at Building Level. *International Journal of Architectural Heritage* (2019), pp.1-24.

[2] Saloustros, S., Pelà, L., Contrafatto, F.R., Roca, P. and Petromichelakis, I. Analytical derivation of seismic fragility curves for historical masonry structures based on stochastic analysis of uncertain material parameters. *International Journal of Architectural Heritage* (2019), **13**(7), pp.1142-1164.

[3] Lagomarsino, S., and Cattari, S. Fragility functions of masonry buildings. *SYNER-G: Typology definition and fragility functions for physical elements at seismic risk*. Springer, Dordrecht, (2014), pp.111-156.

[4] Lagomarsino, S. and Cattari, S. PERPETUATE guidelines for seismic performance-based assessment of cultural heritage masonry structures. *Bulletin of Earthquake Engineering* (2015), **13**(1), pp.13-47.

[5] Mouroux, P. and Le Brun, B. Presentation of RISK-UE project. *Bulletin of Earthquake Engineering* (2006), **4**(4), pp.323-339.

[6] Hancilar, U., F. Taucer, and G. Tsionis. Guidelines for typology definition of European physical assets for earthquake risk assessment. *SYNER-G Reference Report* 2 (2013).

[7] Erberik, M.A. Generation of fragility curves for Turkish masonry buildings considering in-plane failure modes. *Earthquake Engineering & Structural* Dynamics (2008), **37**(3), pp.387-405.

[8] Porter, K., Kennedy, R. and Bachman, R. Creating fragility functions for performance-based earthquake engineering. *Earthquake* Spectra (2007), **23**(2), pp.471-489.

[9] Jaiswal, K., Wald, D. and D'Ayala, D. Developing empirical collapse fragility functions for global building types. *Earthquake Spectra* (2011), **27**(3), pp.775-795.

[10] Sarabandi, P., Pachakis, D., King, S. and Kiremidjian, A. Empirical fragility functions from recent earthquakes. *In Proceedings of the 13th World Conference on Earthquake Engineering, Vancouver, BC, Canada. Paper* (2004) (No. 1211).

[11] Demirlioglu, K., Gonen, S. and, Soyoz, S. Performance Evaluation of a Historical Brick Masonry Building Using Linear and Nonlinear Analyses. *13th International Congress on Advances in Civil Engineering September 12-14* (2018).

[12] Demirlioglu, K., Gonen, S., Soyoz, S. and Limongelli, M.P. In-Plane seismic response analyses of a historical brick masonry building using equivalent frame and 3D FEM modeling approaches. *International Journal of Architectural* Heritage (2020),**14**(2), pp.238-256.

[13] Magenes, G., and G. M. Calvi. In-plane seismic response of brick masonry walls. *Earthquake Engineering &Structural Dynamics* (1997), **26** (11):1091–1112.

[14] Norme Tecniche per le Costruzioni (NTC 2008). 2008. *Technical standards for Buildings D.M. Suppl. ord. n° 30 alla G.U. n.29.* Roma, Italy: Gazzetta Ufficiale (2008).

[15] Norme Tecniche per le Costruzioni (NTC 2018). 2018. *Technical standards for Buildings D.M. Suppl. ord. n° 42 alla G.U. n. 8*. Roma, Italy: Gazzetta Ufficiale (2018).

[16] EN 1998-3. 2005. *Eurocode 8: Design of structures for earthquake resistance Part 3: Assessment and retrofitting of buildings*. European Committee for Standardization (2005).

[17] Vamvatsikos, D. and Cornell, C.A. Incremental dynamic analysis. *Earthquake engineering & structural dynamics* (2002), **31**(3), pp.491-514.
[18] Maio, R. and Tsionis, G. Seismic fragility curves for the European building stock. Brussels: *JRC Technical Report, European Commission* (2015).
[19] RISK-UE. *The European Risk-UE Project: An Advanced Approach to Earthquake Risk Scenarios.* (2001-2004) www.risk-ue.net
[20] FEMA, (1999). *HAZUS99 user and technical manuals*. Federal Emergency Management Agency Report: HAZUS 1999, Washington D.C., USA. (1999).
[21] FEMA (2003). "HAZUS-MH Technical Manual", Federal Emergency Management Agency,Washington, DC, U.S.A
[22] Risk yönetimi ve kentsel iyileştirme daire başkanliği deprem ve zemin inceleme müdürlüğü, *İstanbul Olasi Deprem Kayip Tahminleri* Deprem, (2009).

12th International Conference on Structural Analysis of Historical Constructions
SAHC 2020
P. Roca, L. Pelà and C. Molins (Eds.)

SEISMIC VULNERABILITY ASSESSMENT OF REPRESENTATIVE BUILDING TYPOLOGIES FROM BARCELONA'S EIXAMPLE DISTRICT

SARA DIMOVSKA[1*], SAVVAS SALOUSTROS[1], LUCA PELÀ[1] AND PERE ROCA[1]

[1]Universitat Politècnica de Catalunya (UPC-BarcelonaTech)
Jordi Girona 1-3, 08034 Barcelona, Spain
e-mails: sara.dimovska@upc.edu*, savvas.saloustros@upc.edu, luca.pela@upc.edu, pere.roca.fabregat@upc.edu

Keywords: Seismic Vulnerability, Masonry, Building Taxonomy, Pushover analysis

Abstract. *Unreinforced masonry buildings prevail in many old historical centres and urban areas worldwide. These structures may present inadequate seismic performance because they were often designed without considering any seismic resistance requirements. Therefore, they may be highly vulnerable and susceptible to damage caused by earthquakes, even of low intensity.*

This work investigates the seismic vulnerability of typical unreinforced masonry buildings situated in the Eixample district of Barcelona, Spain. Most of the buildings of the district were designed only for vertical static loads with slender load-bearing masonry walls and flexible diaphragms. A typical characteristic is the presence of openings with considerable size on the facades. The identification of the main parameters affecting the structural behaviour under lateral loading is necessary to evaluate the seismic vulnerability.

As a first step, a building taxonomy for the Eixample district has been prepared in order to classify the different building typologies by taking into account the influence of the structural features in the overall response. This typology classification serves two aims. The first aim is to empirically evaluate the vulnerability of each category. The second one is to provide the basis for creating a numerical model of a representative building and analyse its seismic performance.

The main objective of this paper is to assess the seismic behaviour of a typical unreinforced masonry structure by means of nonlinear static analysis. For this purpose, a three-dimensional Finite Element model of a representative building has been prepared. Pushover analyses have been performed in two directions (parallel and perpendicular to the façades) aiming to identify the typical failure mechanisms and the seismic capacity.

The performance of the representative building typology, with its typical heterogeneities and irregularities, is compared with that of a reference regular unreinforced masonry structure. Additionally, a parametric analysis is carried out to evaluate the different seismic response by adding more storeys in height. This work is the basis for future analyses devoted to large scale seismic vulnerability assessment of the most representative building typologies of the Eixample district.

1 INTRODUCTION

Unreinforced masonry buildings prevail in many old historical centres and urban areas worldwide. A large number of these buildings present an unquestionable cultural and architectural value due to their significant contribution to the urban landscape [1]. In several cases, these structures mainly consist of load-bearing walls made of brick or stone masonry. Often, masonry buildings were designed without considering seismic requirements and may be highly vulnerable against seismic actions even in a region with moderate seismic hazard.

In the last years, there has been an increasing interest in the study of seismic risk in urban areas, which has resulted in various seismic risk assessment methodologies. The choice of the appropriate approach depends on several factors, including the nature of the problem and the purpose of the study. Different methods of assessment are currently available in the scientific literature based on empirical, analytical or hybrid procedures. Empirical methods, also known as indirect methods, are less accurate but more affordable for large scale assessments [2]. On the contrary, analytical (direct) methods require sophisticated structural analyses, based for instance in the Finite Element Method. The hybrid procedure is a combination of both indirect and direct methods.

In this work, the analytical method is used to analyse and understand the seismic performance of a typical unreinforced masonry building. By doing so, this study aims to identify the critical features of their seismic performance and to estimate the likely damage that may be produced due to the seismic action.

As a first step, a building taxonomy has been elaborated in order to assist in the selection of a representative structure. This taxonomy has facilitated the categorization of different types of structures according to their structural features, singularities and sources of vulnerability. The taxonomy has assisted as well in the selection of the variables related to the buildings' geometry and structure to be considered in an extended parametric study.

2 CASE STUDY – EIXAMPLE DISTRICT OF BARCELONA

The focus of the present study is the evaluation of the seismic vulnerability of a typical building typology located in the Eixample district of Barcelona.

The urban area of Eixample is characterized by its straight avenues, laid out in a grid in the central part of the city (Figure 1). Built during the 19th and the beginning of the 20th century, this district stands out for its architectural and cultural heritage. Most of the buildings were constructed as unreinforced masonry ones, forming aggregates that comprise typical building blocks, so-called "manzanas" in Spanish [3]. Each block is composed of rectangular buildings along the streets and pentagonal building at the chamfered corners. The structures that typify the district remain in use today, mainly unaltered since their construction. The peculiar structural systems of unreinforced masonry bearing walls were designed for gravitational loads only, without considering any seismic design criteria. Therefore, these typologies may be highly vulnerable under horizontal actions, even though the seismic hazard in this region is low to moderate.



Figure 1: View of Eixample district

Recent studies [5] [6] have confirmed the high seismic vulnerability of the unreinforced masonry buildings of Barcelona and highlighted the need for the assessment of each building's seismic demand and performance. The current study uses a different analysis tool to that of the previous ones, i.e. a 3D finite element analysis. This approach considers the global response of the structure, helping to obtain a better understanding of the seismic capacity and vulnerability of the unreinforced masonry buildings.
The first step has been to build a proper building taxonomy for the definition and classification of the building typologies according to their characteristics, heterogeneities and sources of seismic vulnerability.

3 BUILDING TAXONOMY

The building taxonomy describes the characteristics of an individual building or a class of similar structures, generally referred to as a building typology. The development of a building taxonomy of existing buildings is essential to understand their structural and architectural configuration relevant to their seismic behaviour. This typology classification has assisted to empirically evaluate the buildings' vulnerability and also to provide the basis for creating a numerical model of a representative building for analysing its seismic performance.

The division of the building stock in a city or a region is among the main challenges for carrying out a seismic risk assessment at urban scale. The primary purpose of a building taxonomy is to classify and group building typologies that show comparable overall performance during a seismic action. Therefore, it is necessary to classify buildings by referring to some parameters that describe a specific characteristic, affecting the seismic behaviour of an individual building or a group of buildings. Geometry, material properties, lateral load resisting system, construction date, seismic design level, structural irregularities, foundation details are among the usual typology parameters that are considered for a building taxonomy. The main features influencing the structural vulnerability are the building's load resisting system and the used construction materials. Secondary classification parameters may be the overall building height, period of construction, shape of the building plan, foundation, irregularities, etc. The

flow chart of Figure 2 presents all the parameters considered in the building taxonomy of the Eixample district.

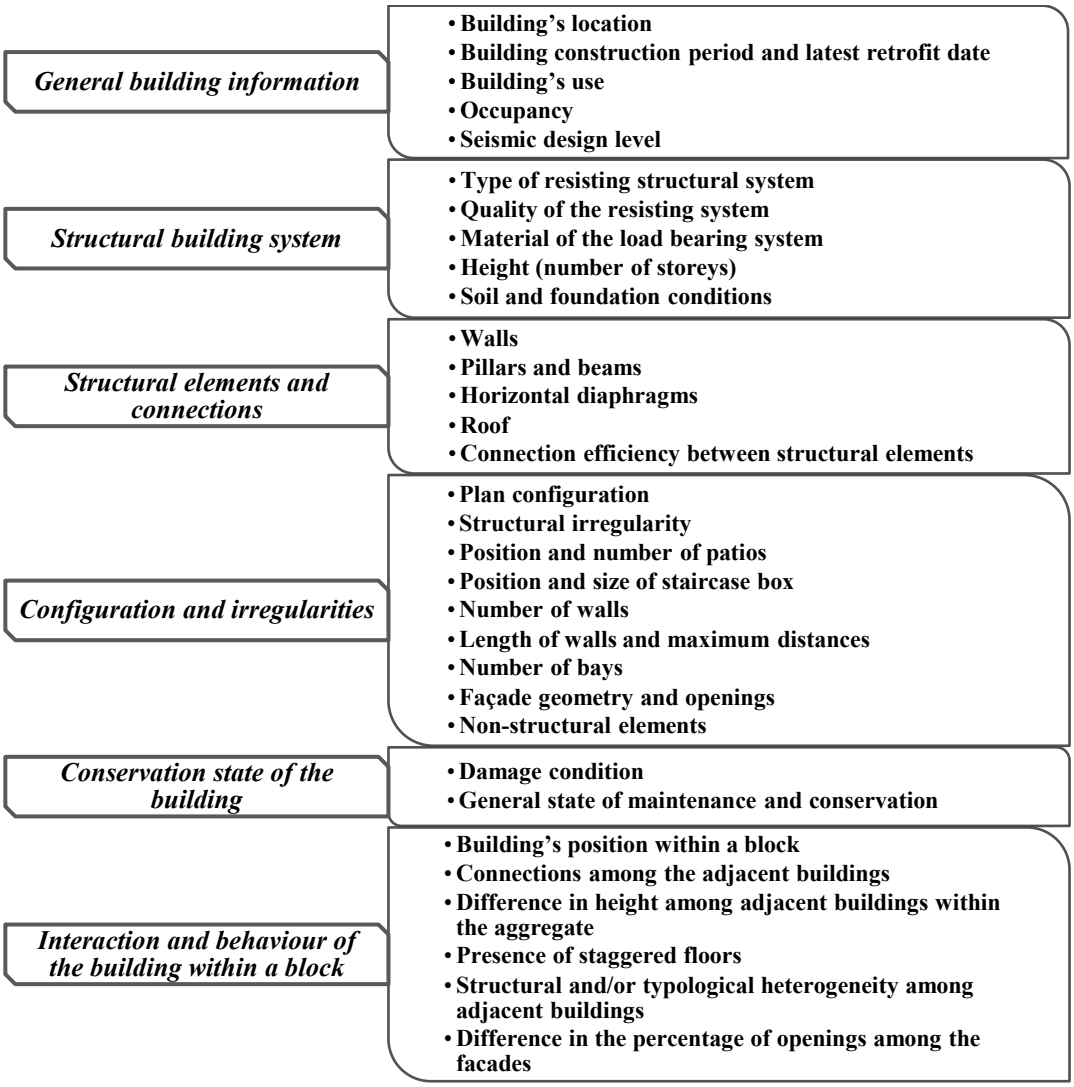


Figure 2: Parameters for a specified building taxonomy

The building taxonomy has been prepared for the purpose of classifying the different structural typologies and selecting some representative buildings for the seismic vulnerability assessment by means of numerical methods. Accordingly, the building classification has been done by taking into account the influence of the most important characteristics in the buildings' seismic performance.

The construction of the buildings was carried out between 1860 and 1940, with an average of 25 buildings per block (Figure 3). Nearly 70% of the buildings of Eixample are unreinforced masonry ones, designed without considering any seismic requirements [5]. From the '60s, reinforced concrete structures were built, leading to the beginning of contemporary architecture [3].

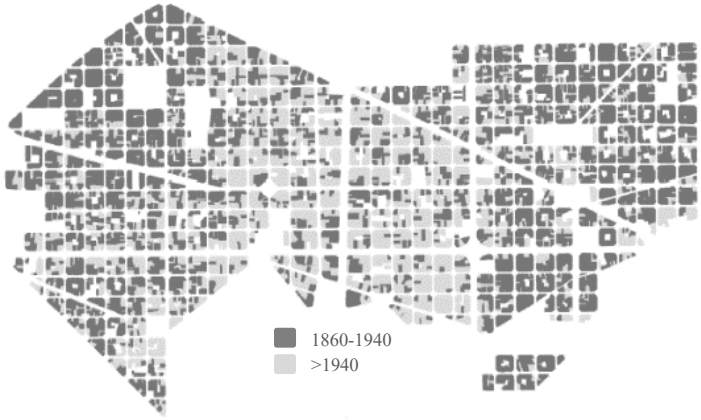


Figure 3: Construction period of Eixample district [6]

Eixample buildings can be categorised in the following typologies (Figure 4): one with load-bearing masonry walls throughout the full height and a second one with a hybrid structural system of steel/concrete columns on the ground floor and unreinforced masonry walls on the upper ones. The floor system is mostly flexible, made of timber or steel beams connected with tile barrel vaults. However, due to some rehabilitations, rigid reinforced concrete slabs can be found in some structures.

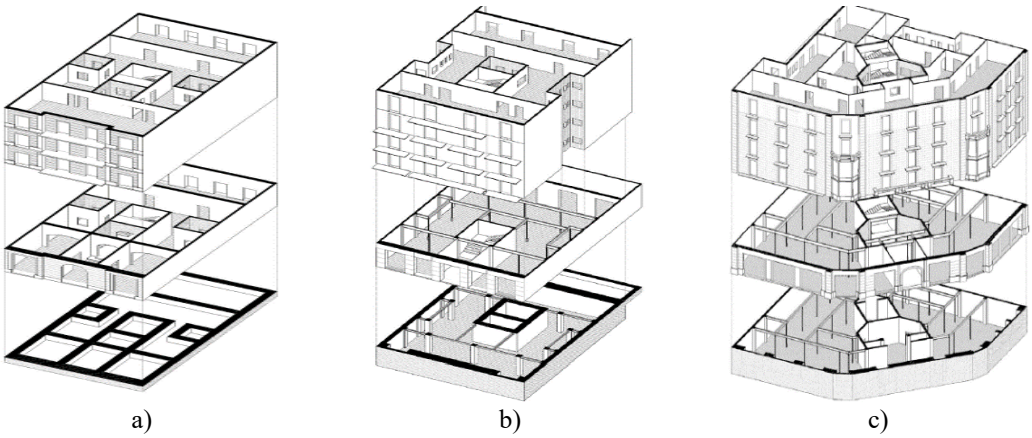


Figure 4: Different structural systems [3]: a) homogenous system of slender walls; b) hybrid system – concrete columns and masonry walls; c) hybrid system – steel columns and masonry walls

The number of floors of the buildings varies between four and seven. Due to the changes in the regulations, the height limit was modified during the years, and so additional storeys at the upper levels were constructed. Regarding the position of the buildings, two groups can be distinguished: buildings in the middle of the block (rectangular shape) and chamfer buildings in the corner of the urban block (pentagonal shape). The ground floor of these buildings has a higher height than any other level since it was intended for commercial use and required a more versatile space.

The configuration of Eixample's buildings can be described by some typical characteristics such as the position and number of patios (central and lateral, see in Figure 5), the position and size of the staircase box, the number of walls (parallel to the facades and parallel to the lateral walls), the distance between walls, etc. The size and position of the openings is another important parameter being a source of seismic vulnerability.

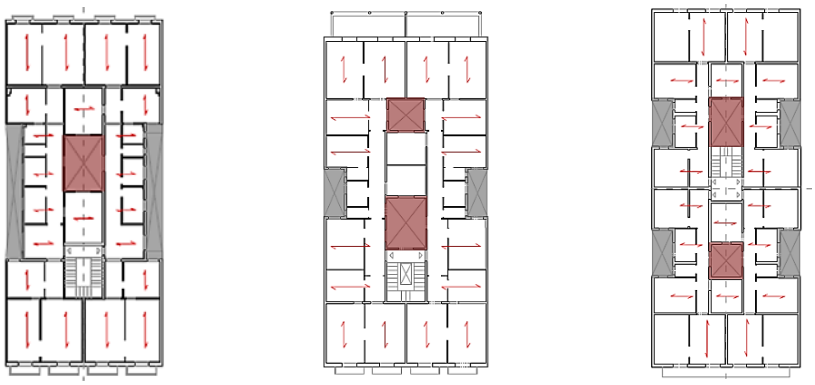


Figure 5: Position and number of central and lateral patios in plan

This building taxonomy has allowed us to define the most frequent building typology classes in order to evaluate their expected vulnerability during an occurrence of an earthquake. Furthermore, representative buildings have been chosen for the numerical simulation. For the preparation of the building taxonomy, an extensive database of Eixample's building available in [6] was used, as well with some building plans obtained from the public archives of Barcelona City municipality [2].

4 NUMERICAL MODELS

4.1 Description of a representative model

This section investigates the seismic performance of a representative building typology from Eixample district. Focus is given on a selection of structural characteristics identified by the building taxonomy. The performance of the representative building typology has been compared with that of a reference regular unreinforced masonry structure. This comparison aims to provide insight into the influence of the structural features of the building typology on its seismic performance.

Eixample blocks are formed by a series of individual buildings, having their lateral walls in contact with each other (see Figure 1). The representative building of the studied structural typology is composed of 5 floors and has an internal patio at its middle and two semi-patios at the two lateral sides (Figure 6). In this work, the building has been studied as isolated without considering any interaction with neighbouring structures, which will be the focus of future work. The load-bearing system consists of two main parallel façade walls with two perpendicular lateral walls. The thickness of the facade walls is 0.30 m, and that of the lateral ones is 0.15 m. Also, the representative model has interior walls parallel to the façade with a thickness of 0.15 m. The dimensions of the representative model are 14×22 m^2 in plan. The total height of the building is 16 m. A common feature of Eixample buildings is that the height

of the ground floor is higher than the rest of them. Therefore, the ground floor is 4 m high while the rest of the storeys are 3 m high. The load capacity of the load-bearing walls is very much affected by the presence of several openings. The façade has 19 openings with considerable size, which results in an area of approximately 32% of the façade. The ground floor is used for commercial activities, and thus the configuration of the openings at this part of the façade walls is different, as shown in Figure 6. Due to the presence of larger openings, steel beams have been used to model the lintels above all the doors and windows.

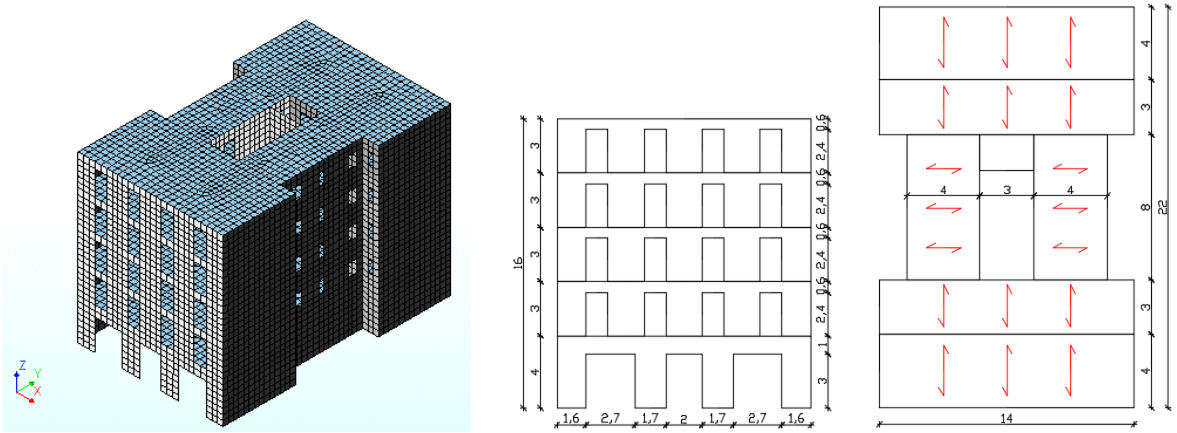


Figure 6: The representative model: a) finite element mesh; b) façade geometry (in metres); c) floor plan section

The reference model is an idealised regular unreinforced masonry structure with plan dimensions of 8.9 × 22 m^2 and a total height of 13 m. For comparison purposes, a regular pattern of the façade openings has been assumed, as well as a central staircase box with an interior patio. Figure 7 illustrates a general view of the model with the dimensions of the plan and façade in metres.

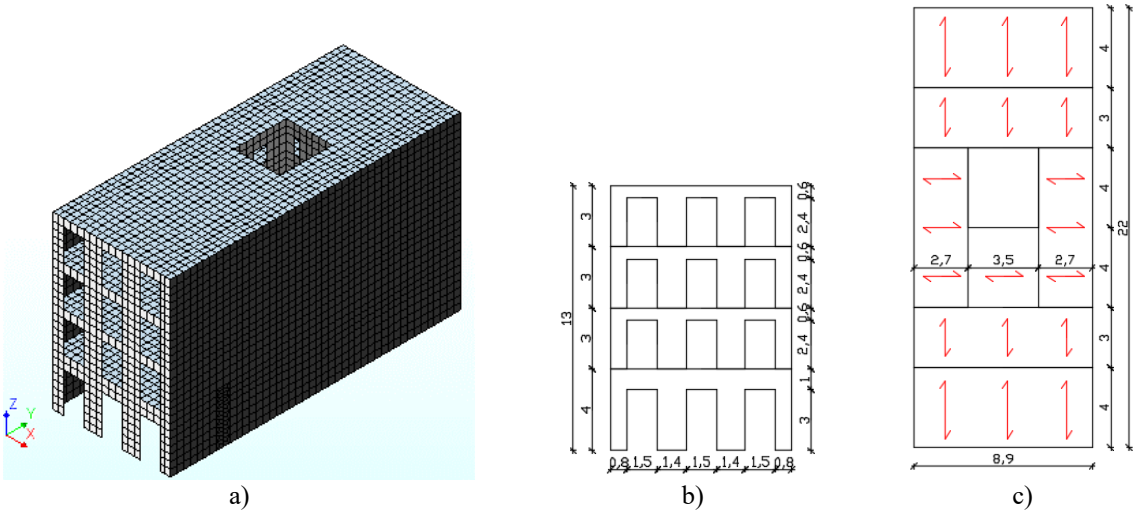


Figure 7: The reference model: a) finite element mesh; b) façade geometry (in metres); c) floor plan section

The finite element models have been prepared and analysed using the software DIANA-FEA 10.3 [7]. Curved shell (quadrilateral CQ40S type) elements have been used for the walls and floors of the buildings. This element is defined by eight nodes and five degrees of freedom for each node. An in-plane Gauss integration scheme has been chosen with 3×3 integration points on the faces, and a Simpson integration scheme with seven points through the thickness of the elements. The beam element CL18B has been used for the steel lintels, composed of three nodes and six degrees of freedom at each of them.

The total number of nodes and elements of the idealised model is 26545 and 8927, respectively. The representative model is composed of 13646 quadrilateral curved shell elements, 664 beam elements and 2390 one-node translational mass elements to provide the load over the unidirectional flexible diaphragms. The final mesh has been selected after performing a series of sensitivity analyses on mesh sizes. The average element size is 0.5 m. The base of the building has been considered fixed to the ground by restricting both translational and rotational movements. All the analyses have considered mechanical and geometrical nonlinear behaviour.

4.2 Material properties

Table 1 and Table 2 summarize the mechanical parameters and gravity loads adopted in the numerical model.

Table 1: Material properties used in all the numerical models

Masonry walls		
Young's modulus	1800	MPa
Poison's ratio	0.2	
Mass density	1800	kg/m^3
Compressive strength	4	MPa
Compressive fracture energy	6400	N/m
Tensile strength	0.08	MPa
Tensile fracture energy	50	N/m
Flexible floors		
Young's modulus E_x	1100	MPa
Young's modulus E_y	7000	MPa
Young's modulus E_z	1100	MPa
Poison's ratio	0.06	
Poison's ratio	0.38	
Poison's ratio	0.15	
Shear modulus G_{xy}	450	MPa
Shear modulus G_{yz}	450	MPa
Shear modulus G_{xz}	450	MPa
Steel beams		
Young's modulus	210000	MPa
Poison's ratio	0.3	
Mass density	7850	kg/m^3

Table 2: Loads used in all the numerical models

	Load (kN/m^2)
Steel beams + tile vaults	1.8
Pavement	1
Division walls	1
Live load	2

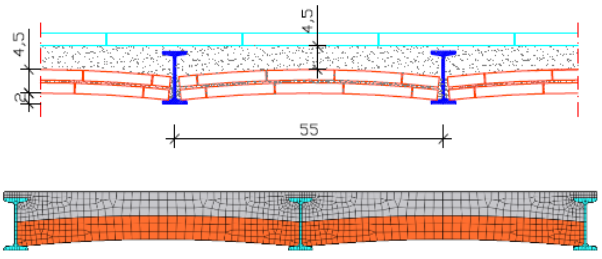


Figure 8 - Flexible diaphragm system of tile vaults with steel beams

The mechanical masonry properties as the compressive strength and Young's modulus are based on some experimental tests done on specimens extracted from some buildings in Barcelona [8]. The values are within the range of the proposed ones for solid brick masonry in the Italian code [9]. The nonlinear physical behaviour of the masonry walls has been defined through the total strain fixed crack model detailed in DIANA-FEA [7]. This constitutive model considers a parabolic softening curve under compression and an exponential one under tension.

The floors have been modelled as unidirectional flexible diaphragms assuming a linear orthotropic material. The elastic properties for the floors were obtained from a 3D numerical model with steel beams and tile vaults (Figure 8). The Young's modulus in both X and Y directions (perpendicular and parallel to the beams), as well as the shear modulus, have been calculated through in-plane nonlinear analysis of the floor system. The connections between the different materials in the floor system has been assumed perfect, without including any interfaces. Table 2 shows the loads considered that have been applied as mass to the nodes of the floors (considering the distribution for one-way slab diaphragms).

5 PUSHOVER ANALYSIS

The pushover analysis is a nonlinear static analysis that aims at simulating the structural response of the investigated building during a seismic action with the application of a monotonically increasing lateral load pattern [10]. The response of the structure is given by the capacity curve, which represents the building's lateral load resistance versus its characteristic lateral displacement. Despite its limitations, pushover analysis can give an insight into the seismic capacity and the expected damage, as well as identifying the most vulnerable parts of the structure [11].

The horizontal loads have been applied by adopting a mass equivalent distribution. For each analysed case, pushover analyses in both +X direction (parallel to the façade) and +Y direction (perpendicular to the façade) have been performed for both models. Self-weight has been applied in the first stage of the analysis, and then horizontal seismic forces proportional to the mass of the structure have been applied incrementally until the analysis stops due to non-convergence. A Newton-Raphson regular procedure has been used along considering an arc-length for solving the nonlinear system of algebraic equations. The convergence has been checked using energy criteria with a convergence tolerance of 0.001.

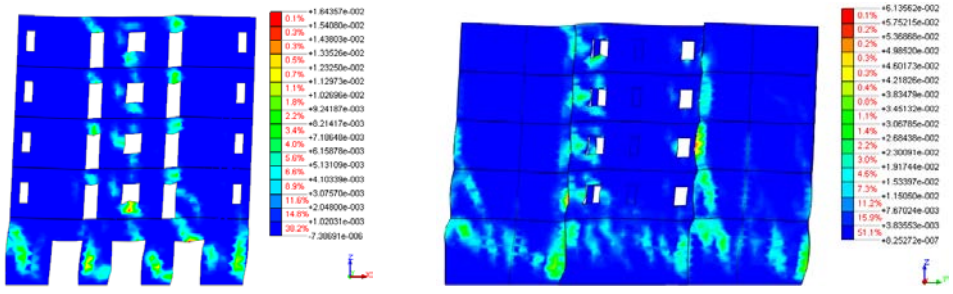


Figure 9: Contour of principal tensile strains: interior wall parallel to the facade for a pushover in +X direction (left) and the lateral walls for a pushover in +Y direction (right)

As can be seen from Figure 9, the formation of the cracks (identified using a contour of the maximum principal strains) is located at the load-bearing walls (parallel to the action of the force). The first cracks are formed around the openings on the façade and the interior walls, as the seismic action is applied in the +X direction. Diagonal shear cracks appear on the interior walls parallel to the facade in the direction of the seismic action, while vertical cracks develop above the openings due to bending of the spandrels. For the pushover analysis in +Y direction, the lateral walls start to present damage with shear cracks starting from the lower floor level and progressing throughout the walls.

Regarding the pushover analysis in the direction parallel to the façade (+X), first, the shear cracks appear on the walls of the ground floor, causing a local out-of-plane mechanism of the perpendicular lateral wall. After the continued opening of these cracks, the collapse of the structure happens as a result of the shear failure of the interior walls on the ground floor. This mechanism is caused by the presence of bigger openings in these walls. In the other direction (+Y), the collapse mechanism is due to the shear failure of the lateral load-bearing walls. The lateral patios present discontinuity of the lateral walls and thus decreases the capacity of the structure.

Figure 10 presents pushover capacity curves in terms of horizontal acceleration against horizontal displacement at the roof level. The difference in the seismic capacity of the buildings is 5% and 40% for the pushover analyses in +X and +Y directions, respectively. The response of the building in the +X direction (parallel to the façade) differs significantly from the response in the +Y direction (perpendicular to the façade). In particular, the structure in X direction is more flexible due to the presence of more openings on the façades and the interior walls.

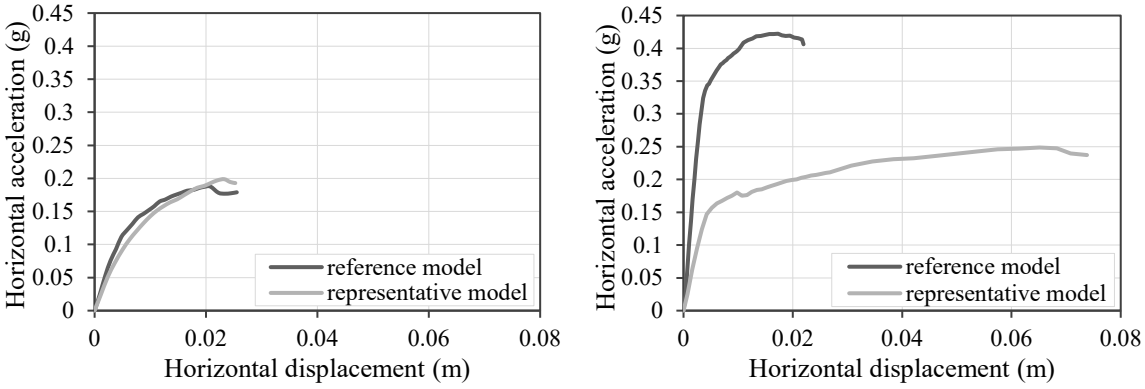


Figure 10: Capacity curves of the representative and the reference model: pushover +X direction (left) and pushover +Y direction (right)

As it was mentioned previously, the representative model considers some typical characteristics and heterogeneities of the presented building taxonomy. Thus, it presents a distinctive seismic behaviour than the one of the reference model. This is due to the differences in the width and height of the buildings, and the changes in the size of the openings on the ground floor. As a comparison with the reference model, the seismic capacity of the representative building is much different in the +Y direction as a result of the presence of the lateral patios. This building typology shows lower capacity in the +Y direction, but it presents higher displacements in the direction perpendicular to the façade.

Parametric analysis has been carried out to evaluate the different seismic response of the representative building by adding more storeys in height (changing the total height of the building). Figure 11 illustrates the capacity curves from the parametric analysis.

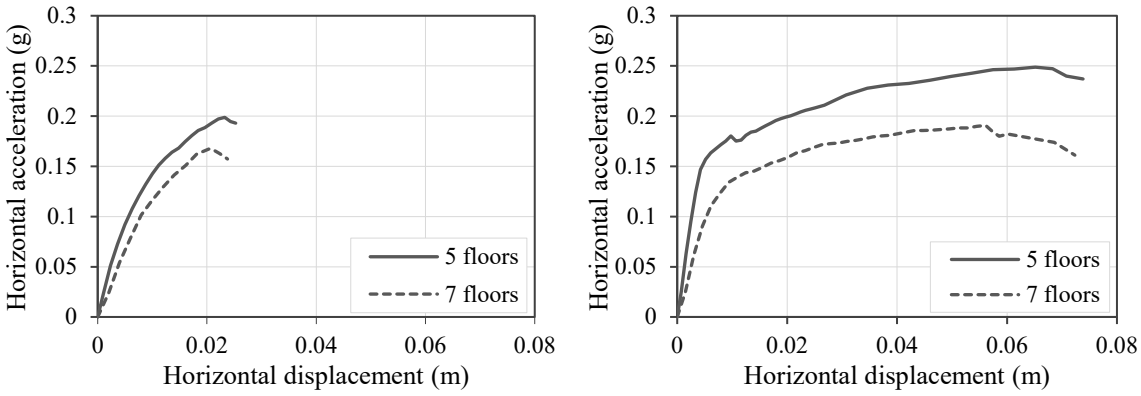


Figure 11: Parametric analysis - addition of floors in the representative building: pushover in +X direction (left) and +Y direction (right)

The results of the parametric analysis related to the addition of floors to the representative building demonstrate the influence of the total height in the seismic response of this typology. As anticipated, the seismic capacity of the higher buildings is decreased and they are more vulnerable. It can be observed a difference of 20% between the capacity of the models of 5 and 7 floors in the direction perpendicular to the façade (+Y). The height is one of the many parameters mentioned in the building taxonomy that are an apparent source of vulnerability regarding these typical unreinforced masonry buildings.

12 CONCLUSIONS

The results of this preliminary study can be summarized in the following:

- A detailed building taxonomy, considering all the parameters that may influence on the seismic vulnerability, is a necessary step for the purpose of selecting representative buildings and variants to be analysed into more detail by means of numerical methods.
- The numerical models can aid to a better understanding of the seismic performance of representative buildings. Certain structural irregularities may produce a significant increase of the seismic vulnerability. Among these are the presence of big openings on the ground floor, central and lateral patios and different height levels.
- The analysed cases showed a typical shear failure with diagonal cracking in walls parallel to the action of the earthquake equivalent loads. Comparisons were made among different models by varying some structural parameters. The numerical results afforded satisfactory predictions of seismic response and the influence of the building's structural characteristics.
- Future works will focus on the investigation of the influence on the seismic performance of other heterogeneities or irregularities not yet considered in the analyses but identified as relevant in the building taxonomy.

Acknowledgements. The authors gratefully acknowledge the financial support from the Ministry of Science, Innovation and Universities (MCIU) of the Spanish Government, the State Agency of Research (AEI) and the European Regional Development Fund (ERDF) through the SEVERUS project (Multilevel evaluation of seismic vulnerability and risk mitigation of masonry buildings in resilient historical urban centres, ref. num. RTI2018-099589-B-I00). The support from Secretaria d'Universitats i Investigació de la Generalitat de Catalunya through a pre-doctoral grant awarded to the first author is also gratefully acknowledged.

REFERENCES

[1] Pelà, L. New Trends and Challenges in Large-Scale and Urban Assessment of Seismic Risk in Historical Centres. *Int. J. Archit. Herit.* (2018) **12**:1051-1054.

[2] Cara, S., Aprile, A., Pelà, L. and Roca, P. Seismic Risk Assessment and Mitigation at Emergency Limit Condition of Historical Buildings along Strategic Urban Roadways. Application to the "Antiga Esquerra de L'Eixample" Neighborhood of Barcelona. *Int. J. Archit. Herit.* (2018) **12**: 1055-1075.

[3] Paricio Casademunt, A. Secrets d'un sistema constructiu: l'Eixample. Barcelona: Edicions UPC (2001) [in Catalan].

[4] Lantada, N., Pujades, L.G. and Barbat, A.H. Vulnerability index and capacity spectrum based methods for urban seismic risk evaluation. A comparison. *Natural Hazards* (2009) **51**:501-524.

[5] Pujades, L.G., Barbat, A.H., González-Drigo, J.R., Avila, J. and Lagomarsino, S. Seismic performance of a block of buildings representative of the typical construction in the Eixample district in Barcelona (Spain). *Bull. Earthq. Eng.* (2012) **10**:331–349.

[6] Cornadó Bardón, C. Comportament mecánic-estructural dels edificis històrics de murs d'obra de fàbrica de maó de l'Eixample de Barcelona. Tesis doctoral UPC, Barcelona, (2015) [in Catalan].

[7] TNO DIsplacement method ANAlyser (DIANA FEA), release 10.3, Delft, Netherlands (2019).

[8] Segura, J., Pelà, L., Roca, P. and Cabané, A. Experimental analysis of the size effect on the compressive behaviour of cylindrical samples core-drilled from existing brick masonry. *Construction and building materials* (2018) **228**:116759.

[9] Italian code - Italian Ministry of Infrastructure and Transport. Circolare 21 Gennaio 2019. Istruzioni per l'applicazione delle nuove norme tecniche per le costruzioni, (2019) [in Italian].

[10] Endo, Y., Pelà, L. and Roca, P. Review of Different Pushover Analysis Methods Applied to Masonry Buildings and Comparison with Nonlinear Dynamic Analysis. *Earthq. Eng.* (2017a) **21**:1234–1255.

[11] Saloustros, S., Pelà, L., Contrafatto, F.R., Roca, P. and Petromichelakis, I. Analytical Derivation of Seismic Fragility Curves for Historical Masonry Structures Based on Stochastic Analysis of Uncertain Material Parameters. *Int. J. Archit. Herit.* (2019) **13** (7):1142–64.

12th International Conference on Structural Analysis of Historical Constructions
SAHC 2020
P. Roca, L. Pelà and C. Molins (Eds.)

SEISMIC VULNERABILITY ASSESSMENT OF A ROMANIAN HISTORICAL BUILDING UNDER NEAR-SOURCE EARTHQUAKE

N. CHIEFFO[1*], M. MOSOARCA[1], A. FORMISANO[2], P.B. LOURENÇO[3]

[1]Faculty of Architecture and Urbanism
Politehnica University of Timişoara
Traian Lalescu Street 2/A, 300223 Timişoara, Romania
email: nicola.chieffo@student.upt.ro (*corresponding author), marius.mosoarca@utp.ro

[2]Department of Structures for Engineering and Architecture
School of Polytechnic and Basic Sciences, University of Naples "Federico II"
P.le V. Tecchio, 80125 Naples, Italy
e-mail: antoform@unina.it

[3]Department of Civil Engineering
ISISE, Institute of Science and Innovation for Bio-Sustainability (IB-S), University of Minho
Azurém Campus, Guimaraes, Portugal
e-mail: pbl@civil.uminho.pt

Keywords: Vertical Ground Motion, Seismic Vulnerability Assessment, Non-Linear Dynamic Analysis, Damage Analysis

Abstract. *The ground motion vertical component is generally ignored in the analysis of ordinary building structures, even though observed damages after last earthquakes highlighted its marked influence especially on the response of masonry structures. In the present research work, the effect of ground motion vertical components in case of near-source excitations has been analysed. The investigation has been made on the Banloc Castle, a historical masonry building damaged by the Banat-Voiteg earthquake occurred on December 1991 in the Region of Banloc in Romania. A FEM model of the building, setup with the DIANA FEA analysis software, has been investigated in the non-linear dynamic field. In particular, the records have been referred to the Banloc site, located 7.01 km far from the epicentre with a moment magnitude M_w=5.5 and a focal depth of 9 km. The behaviour of the ground motion components has been characterised by the V/H peak ground acceleration ratio. In order to estimate the influence of the vertical seismic motion in terms of both displacements and stress regime, two different scenarios have been analysed. The first scenario has taken into account the horizontal component only, whereas the second one has analysed the simultaneous effects of three components of the seismic action. Finally, numerical damage patterns have been plotted aiming to simulate the real cracks detected in the case study after the considered seismic event.*

1 INTRODUCTION

The existing unreinforced masonry (URM) buildings are typically identified as "potentially at risk" structures since, during an earthquake, they are not able to resist the simultaneous actions due to horizontal and vertical inertia forces. In general, the seismic design codes dealing with masonry structures take into account the effects of horizontal actions only, completely neglecting the vertical component of the design ground motion [1-5]. This circumstance is particularly relevant in case of near-field events, where the vertical actions are much more influential than the horizontal ones. In this framework, the studies proposed in [6] showed the relevance of the vertical component for seismic events, called near-field or near-source earthquakes, which are characterized by small site-source distances.

Generally, the vertical component of ground motion is mainly associated to the arrival of vertically propagating compressive P-waves and secondary shear S-waves. However, the propagation direction of volume waves (P and S) is not influenced by the site geology, but by the site distance, the fault type and the magnitude. In these circumstances, it is evident that the effects induced by the ground motion vertical component are prominent in areas characterized by high hazard level. Therefore, they should be appropriately considered in the seismic behaviour analysis of existing masonry buildings.

Other studies [7, 8] have analyzed the behaviour of masonry buildings subjected to vertical seismic actions, asserting that the vertical component of the ground motion in epicentre areas characterized by a *Joyner and Boore* distance (R_{jb} <30 km) causes a variation of the axial stress regime in the walls. Consecutively, the dynamic amplification due to soil stratigraphy leads to a reduction in terms of the shear capacity of structural resistant elements, which show a deficit in terms of resistance, stability and ductility.

In this framework, focusing on the Banat-Voiteg seismic event occurred on December 1991, the Castle of Banloc has been selected as a case study. In order to take into account the influence of vertical accelerations on the seismic capacity of the examined building, non-linear dynamic analysis have been carried out considering the ground motion records representative of the earthquake occurred in that region. The displacements and stress regime have been analysed in order to point out the influence of vertical component. Finally, the damages achieved from analytical modelling have been presented, discussed and compared to the really detected ones.

2 SEISMICITY OF THE BANAT REGION

The Banat region is characterized by an important seismic activity observed in the years from 1991 to 2014. The main records have been obtained by the INCERC seismic network (Banloc Town-Hall and Timisoara stations) during the 1991 Banat earthquakes. In particular, the accelerometer records taken by INCERC for the cities of Timişoara and Banloc provided earthquakes with the following characteristics: (i) relatively short duration of 9-24 s and (ii) significant spectral values in the range 0.1-0.3 s, which extends up to 0.7 s for the Timişoara record and up to 1.2 s for the Banloc one.

Focusing on the event recorded in the city of Banloc, it is characterized by a reduced site-source distance (7.01 km far from the epicentre), which makes it as a near-source event. This event has showed an impulsive and high vertical peak acceleration of 1.2863 ms^{-2}, a focal depth of 9 km, a moment magnitude, M_w, of 5.5 and an intensity, I, of VIII according to Mercalli

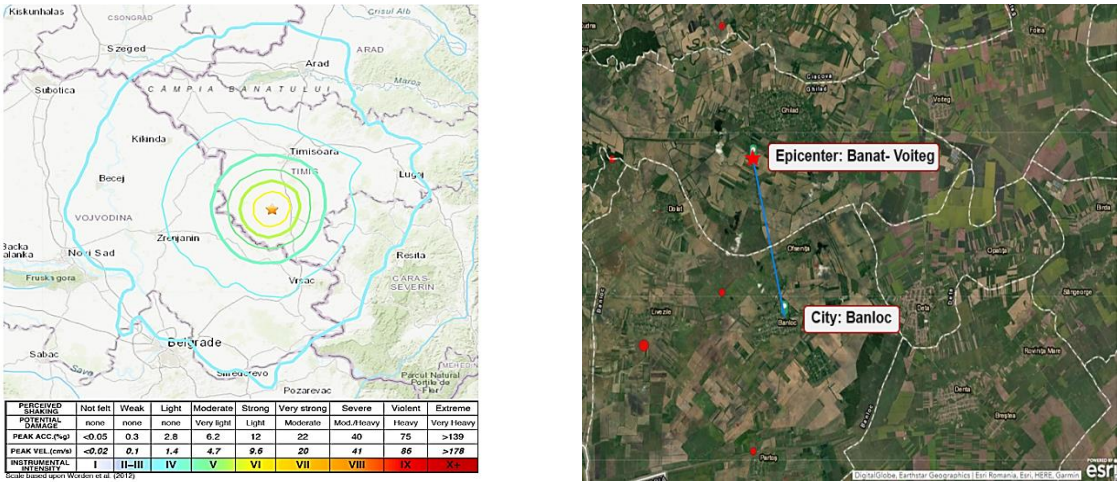
Intensity Scale (MCS).

The data provided by the SM-ROM-GL Earthquakes DB [9] related to the 1991 event occurred in the Banat Region are shown in Table 1

Table 1: Reference event occurred in the Banat seismogenic zone in December 1991.

Earthquake	Date	LatN	LongE	Depth - *h* (km)	M_w	Station
Banat-Voiteg	1991/12/02	45.45	21.12	9	5.5	BNL1

Furthermore, the ShakeMap of the event occurred and the geolocation of the city of Banloc are shown in Figure 1.



(a) (b)

Figure 1: ShakeMap of the Banat-Voiteg event (a) and geolocation of the city of Banloc.

3 CASE STUDY STRUCTURE

3.1 History of the Banloc Castle

The Banat Region was released in 1716, when it was under Turkish rule, by the Marshal-Austrian-Prince Eugene of Savoy Feld and was incorporated into the Habsburg Empire as a military province. Turkish domination destroyed the last vestiges of Western civilization and Austrian rulers had no concerns other than military ones. This is why Banat is poor in historic buildings, both in villages and in cities. In 1759 the construction of the castle of Banloc was completed.

The Castle of Banloc (Figure 2) is the most important monument of the municipality. It is a massive building with a "U" plan built in the early nineteenth century. The main façade faces south, while on the opposite side the two wings border a terraced courtyard. The castle is a massive historical masonry building with very heavy perimeter brick walls, having generally thickness of 0.90 m, while the internal walls, made of the same material, have thickness of 0.80 m.

On the top, vaulted ceilings with thickness of 0.25 m are present. The inter-storey heights of first and second floors are 4.00 m and 5.70 m, respectively. The roof is solid and robust, with

a timber supporting structure, whose construction technique was frequently used in the Banat region.

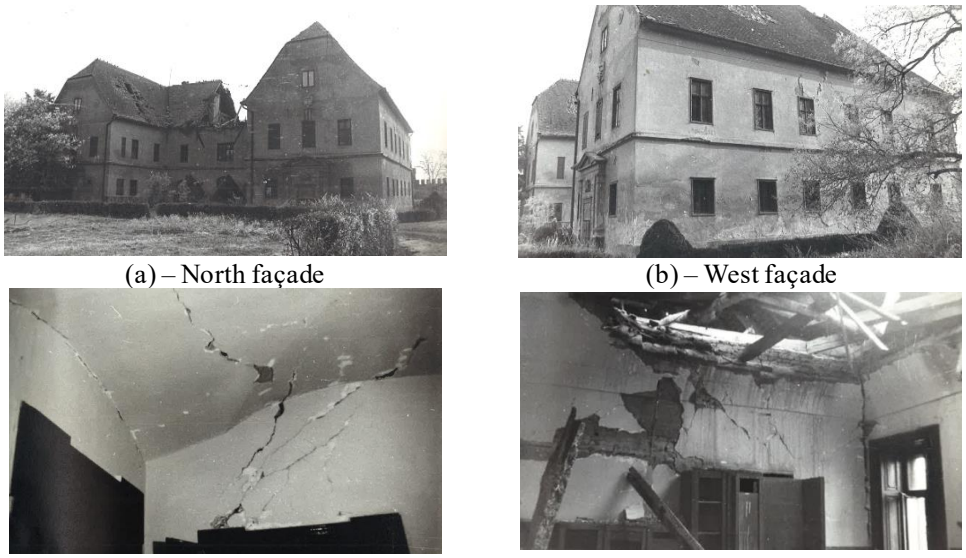


(a) (b)

Figure 2: Castle of Banloc: (a) external view and (b) architectural plan layout.

3.2 Damage recognition after 1991 Banloc earthquake

The Banloc earthquake, occurred on 1991 December 2nd, was a very significant event in the seismic historicity of the Banat region. It is characterized by a focal depth of 9 km. The released seismic energy produced a magnitude (M_w) of 5.5 on the Richter scale. This earthquake can be classified as a medium-deep geological event. It caused slight damages to new designed structures, but several masonry buildings in the area were characterized by very serious damages, also with partial collapses. Referring to the case study building, the damage was detected through on-site inspections after the earthquake occurred. The achieved post-earthquake damages are presented in Figure 3.



(a) – North façade (b) – West façade

(c) (d)

Figure 3: Damage reconnaissance on the study Castle after 1991 Banloc earthquake: (a, b) external façade; (c) first floor room; (d) second floor room [19].

As it is seen from the previous figures, the higher damage has been localized in the vaults, which are elements characterized by large spans and resistance lower than that of vertical structures (Figures 3c and 3d). In particular, the cracks in the vaults are attributable to the impulsive vertical component, which produced very extensive damages. Contrary, vertical structures were affected by shear (sliding or diagonal) mechanisms induced by horizontal seismic components with widespread cracks.

4 NON-LINEAR DYNAMIC ANALYSIS

4.1 Ground motion characterization

The accelerograms adopted are representative of the event occurred in Banloc in December 1991 considering the BNL1 seismometric station [9]. The accelerations are characterized by maximum components in X direction of 0,08g, in Y direction of 0,13g and in Z direction of 0,13g (Figures 4a and 4c). The seismic phenomenon can be defined of near-source type, since the city of Banloc is located approximately at 7 km from the epicentre.

Furthermore, in order to contextualize the induced effects of the vertical component on the global vulnerability of the building, a 6 seconds time history has been considered. This choice is supported from the fact that, on one hand, in the first 6 seconds all the seismic energy input is concentrated, and, on the other hand, the analysis elaboration time is short [10].

In addition, the elastic spectra have been derived from the recorded accelerograms and have been processed with the Seismosignal software [11]. Consecutively, the spectral ratios between vertical accelerations, V, and the corresponding horizontal ones, H, in case of near-source ground motions recorded on soil type C, have been depicted in Figure 4d. These results have shown how the vertical component effects are more evident for earthquakes, characterized by small site-source distances, exceeding the V/H limit of 2/3 proposed by [12]. This condition shows that for short periods (around 0,2 seconds), the V/H ratio is greater than 1 [6].

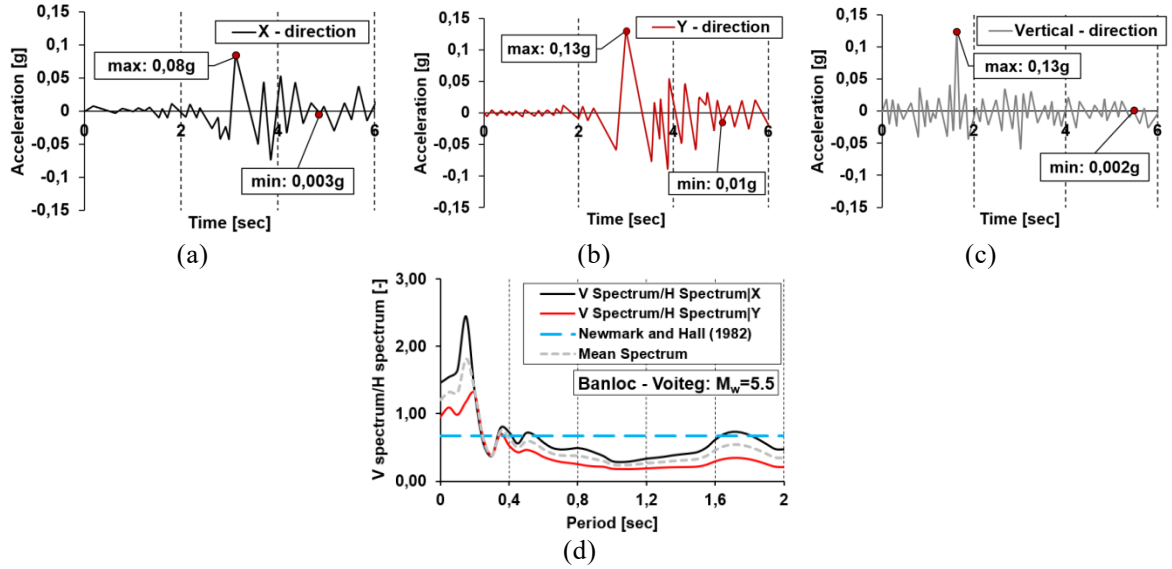
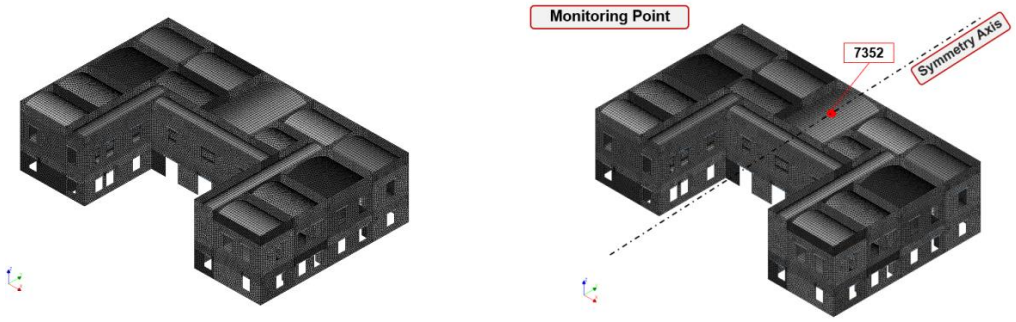


Figure 4: Accelerograms of the Banat-Voiteg seismic event in all directions (a-c) and V/H spectral ratios for near-source records.

4.2 Time-history analysis

Time-history analysis provides a global assessment of the castle dynamic structural response varying specified ground motion accelerograms. The implementation of the model was set-up using the DIANA FEA software [13], where the structure has been modelled as set of interconnected shell elements (Figure 5).



(a) (b)

Figure 5: 3D-shell element model (a) and selected monitoring points (b).

Masonry has a non-linear response and manifests a nonductile post-peak softening behaviour; to this purpose, tensile stresses are assumed to diminish exponentially, while compression combines hardening and softening parabolic phases according to [14, 15]. Based on this assumption, in Table 2 the mechanical properties adopted in the analysis for the case study building have been shown.

Table 2: Mechanical properties of masonry.

Mechanical Properties		
Modulus of elasticity	E [N/mm^2]	1500
Shear modulus	G [N/mm^2]	500
Compressive strength	f_m [N/mm^2]	2.40
Tensile strength	τ_0 [N/mm^2]	0.24
Specific weight	w [KN/m^3]	18
Poisson ratio	ν [-]	0.20
Fracture energy (compression)	G_{fc} [N/mm]	4.64
Fracture energy – Mode I (tensile)	G_{ft} [N/mm]	0.012

The results obtained have been represented, for the two scenarios considered, namely (H) and (H+V), in terms of dispersion of both displacements and resistances. They are referred to the centroid of the second floor as monitoring point and are summarized in Figure 6. Concerning displacements and strengths regime, positive and negative values of the points cloud denote the change of direction induced by the seismic input with respect to the straight line with equation x=y (bisector). Furthermore, in order to better highlight the influence of the vertical component, the upper (y=0,5x) and lower (y=2x) bounds of the dispersion range have been considered. In this way, the greater scatter with respect to the bisector, the larger effect of the ground motion vertical component [6].

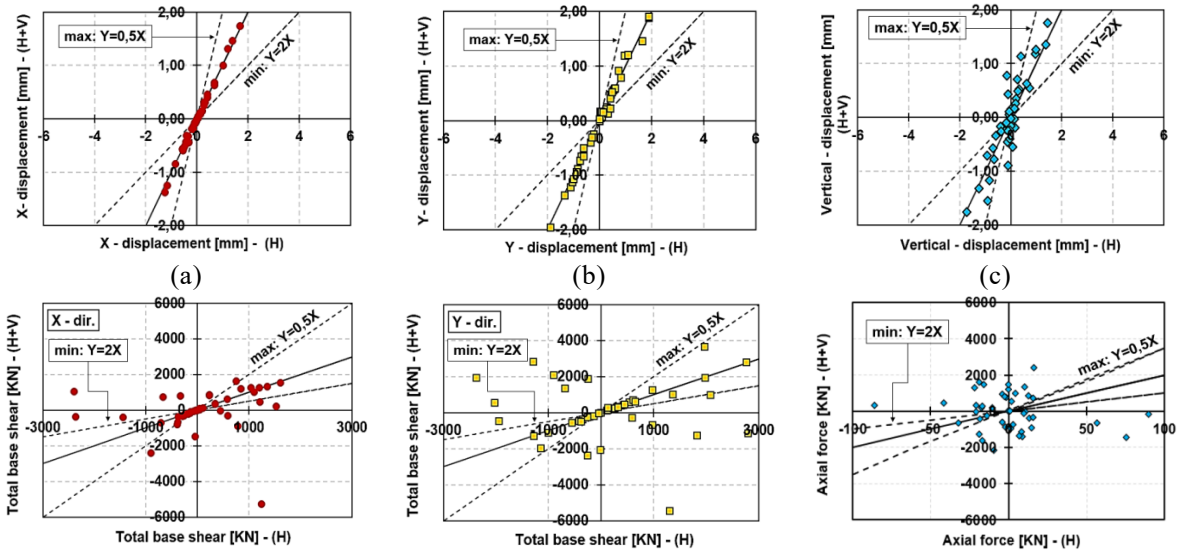


Figure 6: Scatter results in terms of displacements (a-c) and base shear (d-f).

From results obtained, it is possible to notice how the vertical component provides a variation of the displacements regime in vertical direction. Furthermore, regarding the strength regime, the effect of ground motion in vertical direction is more considerable and, therefore, the scatter associated is more marked. Consequently, in order to better contextualize the impulsive effect of the vertical seismic action, a time step of 2 seconds has been considered. This choice has been done since in the first two seconds the vertical component effect, which releases all its energy input, is maximized. So, for the sake of representation, considering (H) and (H+V) scenarios, the differences detected in terms of both shear [16] and axial demands for one of the most stressed pier of the West façade have been assessed. The achieved results, plotted according to the recommendations provided by EC8 [17], are shown in Figure 7.

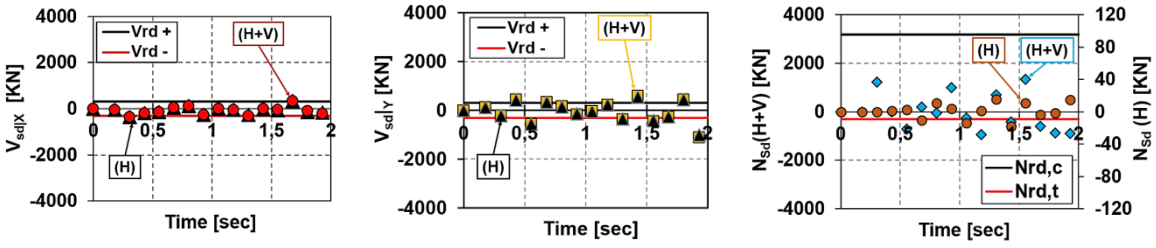


Figure 7: Safety checks for shear stresses (a-b) and axial loads (c) in case of (H) and (H+V) scenarios.

Firstly, in Figures 7a and 7b, it is possible to notice how the seismic vertical component in the two main directions, X and Y, does not produce any significant stress variation for both considered scenarios. Secondly, in Figure 7c, it is shown how the vertical component produces a significant increase in terms of axial load. In fact, at time step of 1.55 seconds (which corresponds to the maximum peak vertical acceleration), the difference between (H) and (H+V) is very high (more than two times). Moreover, it is detected that the axial load demands exceed averagely the corresponding tensile capacities ($N_{rd,t}$) of 2 times.

4.3 Experimental-numerical damage comparison

The reliability of the implemented numerical model is strictly based on the reproduction of the damages really achieved [18]. The damages detected by means of in-situ inspections after the Banloc earthquake are characterised by a widespread distribution of cracks, that affect the vertical and horizontal structures and produce globally the structure deterioration.

In particular, several failure mechanisms closely related to the seismic event were identified. More specifically, in the first two seconds of the time-history, the maximum vertical peak acceleration produced an extensive damage in the vaults, characterized by a brittle behaviour (Figure 8) [19].

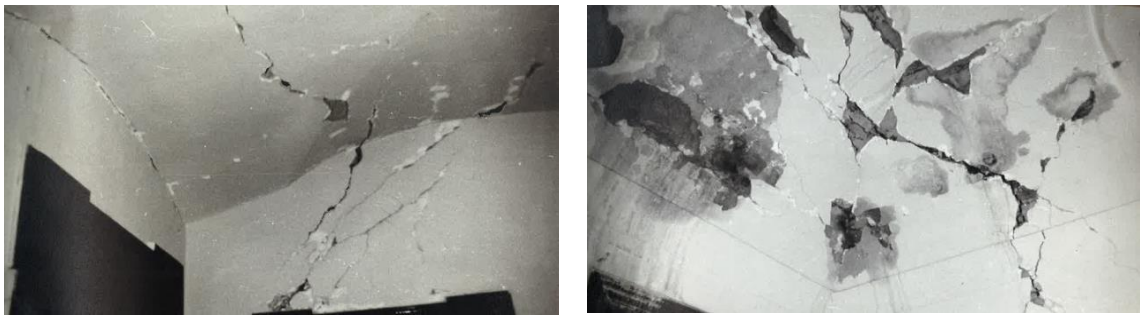


Figure 8: Damages detected in the second-floor vaults mainly due to ground motion vertical component [19].

Consecutively, following the impulsive action, the arrival of the horizontal components produced damage to the vertical structures, mainly in the spandrel beams due to the formation of shear failures, as shown in Figure 9 [19].



Figure 9: Vertical and diagonal shear cracks detected in the South façade of the case study building [19].

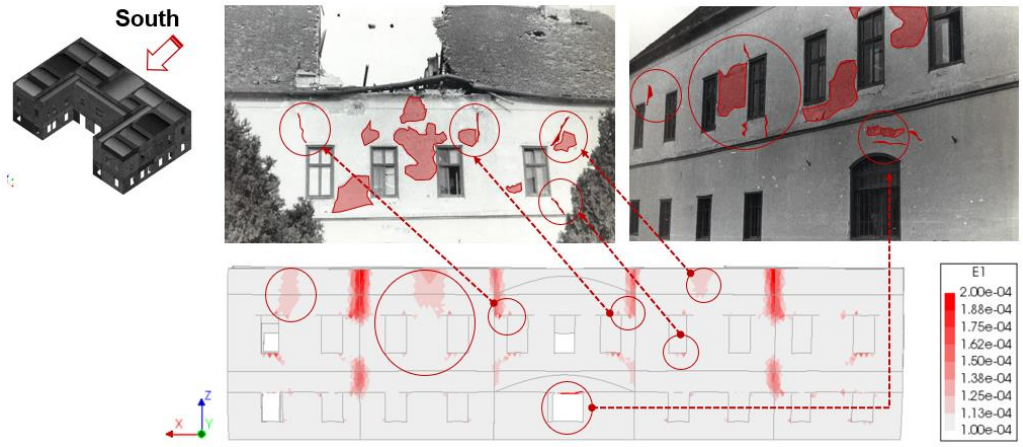
Finally, in the internal court of the building, a partial collapse of the roofing structure was observed. This collapse mechanism was triggered by the impulsive seismic action, as depicted in Figure 10 [19].



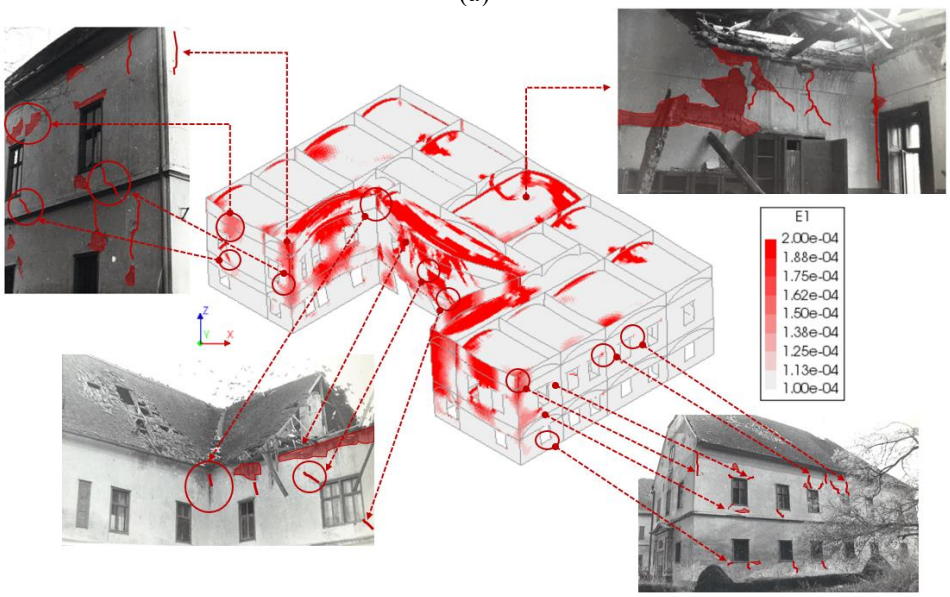
(a) – left view (b) – right view

Figure 10: Failure mechanisms observed in the internal court of the case study building [19].

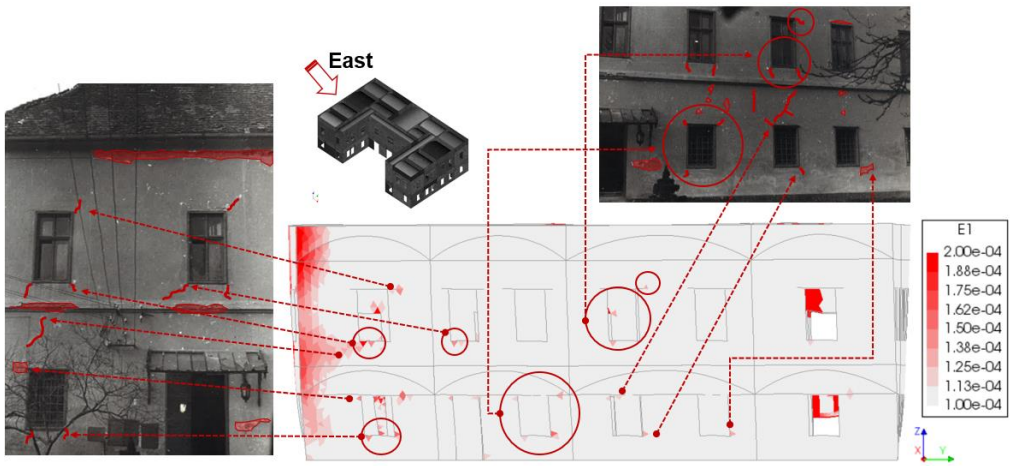
The damages achieved from numerical analyses have been presented and compared to experimental ones in Figure 11.



(a)



(b)



(c)

Figure 11: Numerical damages obtained simulating the Banloc-Voiteg event and comparison with experimental evidences.

From the above comparison, it appears that the non-linear analysis identified local damages very similar to those produced by the earthquake. The identification parameter used to evaluate the damage state in the numerical analysis is the *tensile fracture energy* (G_f), according to which, when the maximum principal stress reaches the defined cracking criterion, the fracture begins to distribute in the structural element. In particular, the numerical model catches in a satisfactory way the detected local damages and failure mechanisms, providing, as depicted in Figure 11, the right distribution of *Principal Total Strain* (E1).

5 CONCLUSIONS

The proposed work has analysed the effects induced by the vertical earthquake component on a historic masonry building located in the Romanian region of Banloc. The seismic event, occurred in December 1991 with a moment magnitude of 5.5, was characterised by a small (about of 7 km) site-source distance. This impulsive event was identified by a seismic directivity, low frequency content and maximum PGAs comparable in vertical and horizontal directions. The accelerometric records were used to perform non-linear dynamic analyses on the case study building modelled with the DIANA FEA software using shell elements.

The effects of the ground motion vertical component were evaluated considering the comparison between two different scenarios: the first, named H, where only horizontal acceleration components were considered, and the second, called H+V, where also the vertical components were taken into account. The main results are summarized as follows:

- The considered record, due to the combination of high magnitude and short site-to-source distance, had high energy in terms of vertical component.
- There was a dispersion of the displacements induced by the vertical component in the first two seconds of the time-history, since the impulsive action releases a high input energy in that time period.
- In the first two seconds of time history, where the maximum vertical energy content of the seismic motion occurred, the comparison of the two scenarios (H and H+V) in

terms of stress regime was done. In particular, in terms of shear strength the vertical component does not produce any significant variation of results in the two-analysis directions. Conversely, referring to the axial stress regime, the vertical component induces a considerable increase of axial tensile loads, which exceeded averagely the corresponding tensile capacities of about 2 times.

– The numerical damage assessment was carried out considering the *Principal Total Strains* (E1), which take into account the overcoming of the tensile fracture energy in the structural elements. The numerical analysis results provided with satisfactory accuracy the same damage mechanisms really detected in the castle, namely cracks in the vaults (produced by vertical components) and vertical structures (mainly caused by horizontal components), as well as the out-of-plane horizontal bending mechanism in the façade facing the courtyard, which was produced by the partial collapse of the roofing structures.

Acknowledgements. The Authors would like to acknowledge Dr. Eng. Joao Pereira and Dr. Eng. Nuno Mendes from University of Minho for the interest demonstrated towards the present study and the suggestions provided on the use of the DIANA FEA software. Also, the contribution of Prof. Gian Piero Lignola from University of Naples Federico II, who provided very useful suggestions on the performed analyses, is gratefully acknowledged.

REFERENCES

[1] Mosoarca, M., Onescu I., Azap, B.; Onescu, E., Chieffo, N. Szitar-Sirbu, M. Seismic vulnerability assessment for the historical areas of the Timisoara city, Romania. Eng. Fail. Anal. (2019), **101**:86–112.

[2] Chieffo, N., Clementi, F., Formisano, A., Lenci, S. Comparative fragility methods for seismic assessment of masonry buildings located in Muccia (Italy). *Journal of Building Engineering*, (2019), **25**, 100813.

[3] Formisano, A. Theoretical and Numerical Seismic Analysis of Masonry Building Aggregates: Case Studies in San Pio Delle Camere (L'Aquila, Italy). *Journal of Earthquake Engineering*, (2017), **21**:227-245.

[4] Onescu, I., Mosoarca, M., Azap, B., Onescu, E. Seismic Losses Scenario for Cultural Promenade in Timisoara Capital of Culture 2021, Romania. *IOP Conf. Ser. Mater. Sci. Eng.* (2019), 471, 102041.

[5] Chieffo, N., Formisano, A., Ferreira, T.M. Damage scenario-based approach and retrofitting strategies for seismic risk mitigation: an application to the historical Centre of Sant'Antimo (Italy). *Eur. J. Environ. Civ. Eng*. (2019).

[6] Di Michele, F., Cantagallo, C., Spacone, E. Effects of the vertical seismic component on seismic performance of an unreinforced masonry structures. *Bull. Earthquake Eng.* (2019), https://doi.org/10.1007/s10518-019-00765-3.

[7] Diotallevi, P.P., Landi, L. Effect of the axial force and of the vertical ground motion component on the seismic response of R/C frames. *In: 12th World conference on earthquake engineering*, (2000), Auckland.

[8] Di Sarno, L., Elnashai, A.S., Manfredi, G. Assessment of RC columns subjected to horizontal and vertical ground motions recorded during the 2009 L'Aquila (Italy) earthquake. *Eng. Struct*. (2011), **33**:1514–1535.
[9] Borcia, I.S., Craifaleanu, I.G., Calarasu, E.A. Examples of use of the SM-ROM-GL Database. *In 5th National Conference on Earthquake Engineering and 1st National Conference on Earthquake Engineering and Seismology–5CNIS & 1CNISS*, Bucharest, Romania, (2014), **1:**165-172.
[10] Panza, G., Romanelli, F., Vaccari, F. Realistic modelling of waveforms in laterally heterogeneous anelastic media by modal summation. *Geophysical Journal International*, (2000), **143**:340-352.
[11] Seismosoft. SeismoSignal, User's Manual. 2018.
[12] Newmark, N.M., Hall, W.J. Earthquake spectra and design. *EERI monograph series*, (1982), Oakland.
[13] DIANA, Displacement methods ANAlyser, release 10.2, User's Manual. n.d.
[14] Lourenço, P.B., Pereira, J.M. Seismic Retrofitting Project, recommendations for advanced modeling of historic earthen site. *The Getty Conservation Institute, LA* (2018), ISBN: 978-1-937433-53-6.
[15] Mendes, N., Lourenço, P.B., Campos-Costa, A. Shaking table testing of an existing masonry building: Assessment and improvement of the seismic performance. *Earthquake Engineering and Structural Dynamics,* (2014), **43**:247-266.
[16] Turnšek, V., Čačovič, F. Some experimental results on the strength of brick masonry walls. *In Proceedings of the 2nd international brick masonry conference*, (1971), 149–156.
[17] EN 1998-1:2004 (2004) Eurocode 8-Design of structures for earthquake resistance. Part 1: general rules, seismic actions and rules for buildings. European Committee for Standardization, Brussels.
[18] Mosoarca, M., Gioncu, V. Seismic management and damage prevention of religious buildings situated in seismic areas. *Journal of Cultural Heritage,* (2013) **14**:e65-e72.
[19] IPROTIM TIMISOARA. Expertiza cu principii de consolidare (In Romanian). Pr. Nr. 35353/330, (1990).

12th International Conference on Structural Analysis of Historical Constructions
SAHC 2020
P. Roca, L. Pelà and C. Molins (Eds.)

SEISMIC VULNERABILITY OF HERITAGE CHURCHES IN QUÉBEC: THE NÉO-ROMAN TYPOLOGY

G. SFERRAZZA PAPA[1*], M-J. NOLLET[2] AND M.A. PARISI[3]

[1] Politecnico di Milano, Dept. Architecture, Built Environment and Construction Engineering
piazza Leonardo Da Vinci, 32, 20133 Milano, Italy
e-mail: gessica.sferrazza@polimi.it (*corresponding author)

[2] École de Technologie Supérieure, Department of Construction Engineering,
1100 Notre-Dame St W, Montréal, QC H3C 1K3, Canada
e-mail: Marie-Jose.Nollet@etsmtl.ca
[3] Politecnico di Milano, Dept. Architecture, Built Environment and Construction Engineering
piazza Leonardo Da Vinci, 32, 20133 Milano, Italy
e-mail: maria.parisi@polimi.it

Keywords: seismic vulnerability assessment, masonry churches, Néo-Roman typology, Québec

Abstract. *Several seismic events have demonstrated the vulnerability of masonry churches. The long seismic history of the Italian territory has provided materials to observe and to study the structural performance of churches. Since the 1976 Friuli earthquake many studies have contributed to the definition of specific damage and vulnerability assessment methods for churches, based on the identification of macro-elements and kinematic mechanisms. In this context, the paper presents the application of a vulnerability assessment methodology developed and currently applied in Italy to a case study representative of the néo-roman church typology in Montreal, Québec. The study is part of a collaborative project between Politecnico di Milano and École de Technologie Supérieure of Montreal. The relevance of such a study derives from the moderate seismicity of Montreal associated to a high density of churches. Starting from a previous inventory of 108 churches in Montreal Island, the Néo-roman church typology was selected to be investigated. Specificities of this typology are the position of the bell tower in the middle of the façade and the interaction between the timber structure and masonry walls. This combination between the façade and bell tower macro-elements requires to reconsider the mechanisms associated to these elements in the original reference method. A detailed survey of the roof and bell tower timber structures of a néo-roman church was done, and a three-dimensional numerical model was developed for a better understanding of this type of structure. Modal analysis of a global model was then carried out and the first results of the modal shapes discussed.*

1 INTRODUCTION

Churches are distinctive features of the urban and landscape scenarios. In seismic prone areas, their existence is frequently put at risk: unreinforced masonry churches have shown worldwide their seismic vulnerability [e.g. 1-4], due to their proper characteristics such as the presence of tall and little restrained walls of the nave, arches and vaults, large openings, and overhanging elements (e.g. gables, bell towers, pinnacles, statues…). Damage mainly occurs with recurring patterns in the different elements that compose the church, or macro-elements. Crack lines separate masonry blocks that eventually may develop a kinematic chain bringing to local collapse. Several decades of earthquakes and damage observations have brought to define for churches the most frequent damage -or limit- mechanisms [e.g. 5]. At the actual state of knowledge, an abacus of 28 such mechanisms has been developed in Italy, where it constitutes a reference for damage recognition and seismic vulnerability assessment campaigns [6,7]. The literature provides several examples of applications of this methodology, especially in damage surveys in the major earthquakes that arrived in the last decades, as L'Aquila (2009) [8,9], Emilia-Lombardy (2012) [10], and Central Italy (2016) [11,12].

In 2018-2019, a collaborative research project between Politecnico di Milano and École de Technologie Supérieure in Montreal started, in order to test the applicability of the Italian seismic vulnerability assessment methodology to the churches of Québec. The basic question was to detect possible local construction characteristics that could require modifications of the original procedure or its extension for this new territory. An inventory of 108 churches for the island of Montreal had been prepared in 2009 [13]. The seismic risk level of the area concerned is high even though the seismicity is moderate. This is justified by the high density of buildings and the presence of several unreinforced masonry churches. Starting from the inventory of 108 churches, for a selected subset, a detailed survey was carried out also to sort out possible *territorial specificities,* intended as the typical characteristics which are subjected to significant changes from one territory to another [14]. Four principal typologies were identified, and some initial considerations were formulated [15]. Here, the objective is to present results from a case study for the Néo-roman typology, also pointing out some difficulties in applying the Italian methodology to churches from this territory and the need for its updating with local characteristics.

2 SEISMIC VULNERABILITY OF CHURCHES

In Italy, the long seismic history and the collection of damage data after each earthquake since the Friuli earthquake of 1976 have provided a large amount of material for the study of the seismic damage and vulnerability assessment. Since the first steps moved in 1994 by Doglioni et al. [5], 28 possible failure mechanisms have been identified as the most recurrent in the Italian churches. This set is today a reference for two principal actions of assessment, that is:

- *Damage assessment after an earthquake*. In Italy such procedure was made official in 2006 and a specific form for damage survey of churches was issued [6].
- *Rapid vulnerability assessment, in a prevention perspective.* Possible initial damage, presence or absence of seismic protection devices, unfavorable conditions are pointed out and an evaluation of the vulnerability level of the asset is expressed. A detailed

procedure is recommended by the Ministry of Cultural Heritage (MiBACT) [7].
In both cases, the assessment procedure is qualitative, and the result based on suitable reference scales. The basic assumption is that the masonry quality is sufficiently high to form monolithic blocks defined by fracture lines, acting as rotation hinges [16, 17]. When structural verification is required, limit equilibrium analysis may be performed for out-of-plane mechanisms, yielding the corresponding lateral force level.
The method of damage mechanisms is supported by extensive observational data, but it has been verified as well by more sophisticated models and analyses. Finite element models, usually requiring significant computational effort, may be adopted to follow the global behavior and the evolution of damage, often pointing out local damage situations that may be amenable to mechanisms. [i.e.18]. Where the global model evidences a local damage concentration, detailed local models may be performed defining suitable boundary conditions. This is often the case of the façade macro-element, highly subjected to damage and extensively investigated [i.e. 19].

3 SEISMICITY OF QUÉBEC AND HISTORICAL DAMAGE TO CHURCHES

The province of Québec, in the Eastern part of Canada, is characterized by a moderate seismic hazard, except for the Charlevoix area, considered the most seismically active region [20]. Among the three seismic zones of Québec, Montreal is located in the so-called Western Québec Seismic Zone (figure 1).

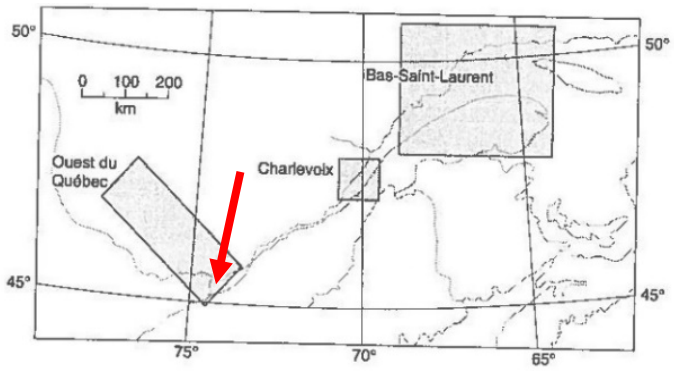


Figure 1 Principal seismic areas of east Canada: the west Québec (in the map 'Ouest du Québec'), Charlevoix, and Bas Saint Laurent. Montreal is in the west Québec zone (red arrow) [20].

The seismic hazard combined with the vulnerability of the churches evidences a considerable damage risk and points to the importance of a preventive action, including a seismic vulnerability analysis of this building typology. Indeed, just in the island of Montreal a total of 108 catholic churches have been inventoried in 2009 [13].
Table 1 provides an overview of the historical seismicity of the province. Major earthquakes, which struck Québec from the 17th to the 21st century, are listed in the table together with the damage suffered by churches and other unreinforced masonry structures. A territorial aspect to be considered in reading this table is the fact that before the end of the 17th century most of the buildings were realized in timber. It is in consequence of the major fires occurred in 1682

(Québec) and 1720 (Montreal) that masonry construction was enforced inside the fortification walls of the cities by Intendant Dupuy of Nouvelle France. Little photographic documentation is available on recent church damage compared to the extensive documentation collected in Italy after the systematic studies performed on the topic.

Table 1 Historical church damage in Québec [21]

Year	Magnitude Mw (*Estimate)	Region	Reported damage to churches and unreinforced masonry elements
1663	7*	Charlevoix-Kamouraska	Nonstructural damage to churches / Collapse of chimneys
1732	5.8*	Montréal	Bending of bell towers / Light damage to houses / Failure of chimneys
1791	6*	Charlevoix-Kamouraska	Damage to 3 churches
1860	6*	Charlevoix-Kamouraska	Failure of one bell tower and wall cracking
1870	6.5*	Charlevoix-Kamouraska	Severe damage to 2 churches: Collapse of the portal and part of the vault, cracking of walls
1925	6.2	Charlevoix-Kamouraska	Collapse of one church (out of plane failure of lateral walls and roof collapse) / Severe damage to 2 churches: Falling of blocks of bell tower, out of plane failure of unreinforced walls, shear cracking, / Collapse of chimneys / Severe damage to masonry houses
1935	6.1	Témiscamingue	Damage to 80% of chimneys and masonry walls
1988	5.9	Saguenay	In-plane shear failure of unreinforced masonry walls and infill, and cracking at opening corners / Out of plane failure of unattached partition walls and masonry claddings / Damage to churches (out of plane failure of façade) / Cracking of foundation masonry blocks / Damage to chimneys
2010	5.0	Val des Bois	Damage to chimneys and out of plane failure of a church gable

4 CONSIDERATIONS ON THE IDENTIFIED TYPOLOGIES

During a collaborative project between Politecnico di Milano and École de Technologie Superieure of Montreal some churches from the sample of 108 have been surveyed in detail, identifying among them four main typologies: the Baillargé (1790-1820), the Conefroy (from 1800), the Néo-roman (1880-1930), and the Italian baroque (second half of 1800) (figure 2).
Some initial considerations on the seismic vulnerability related to these typologies were expressed and detailed in [15] and are summarized here.
From a first screening of the visited churches it was possible to observe that among the inspected cases there is no use of seismic protection provisions and devices, such as tie rods. Only one case, the church of Notre Dame de Bon Secours, shows these elements. The church is classified as 'A', according to the regional scale of value of protection and conservation elaborated by the Council of the Religious building stock of Québec [22]. A seismic vulnerability assessment of these churches was performed recurring to the rapid procedure based on the abacus of 28-mechanism outlined in section 2 [7]. It was observed that the direct applicability of the Italian methodology to the Québec churches is impractical, due to the

territorial specificities of the churches. With respect to this condition, the category that showed to be more easily interpretable recurring to the Italian methodology is the so-called Italian baroque, for which the major vulnerability is associated to the gable macro-element. This portion of the façade, indeed, appears highly soaring and without any devices retaining it from overturning. For what concerns the other three identified typologies, the common aspect that stands out is the combined use of masonry and timber. The first is employed for the box structure of the church composed by the main walls and the second is used for the nave columns system, where a colonnade is present, the bell tower, and the roof structure. In all cases, the macro-elements supposedly most involved in case of earthquake are the façade, the bell tower and the lateral walls of the nave.

In the Baillargé typology, the façade interacts with two bell towers without being directly connected with the lateral walls of the nave, and at the same time creating a massive portion of structure with an atrium area. This configuration requires a deeper and specific investigation for a thorough understanding of the seismic response.

In the Conefroy typology, the façade is characterized by a hut shape with a series of openings. The bell tower does not interact with the roof structure, but it occupies an unusual position compared to the common Italian cases. It is located a step back from the façade plane. Understanding its structural behavior together with the transversal response of the nave requires a deeper analysis. These two aspects could lead to reconsider and possibly increment the 28 Italian mechanisms tailoring the set for Québec on the ground of these territorial specificities.

In the Néo-roman typology, the façade is discontinuous, with the bell tower at the center. This is a determinant aspect in the structural response, influenced by the tower position and height. Moreover, in the visited churches, recurring crack patterns were observed in the lateral walls of the nave and in the façade plane in proximity of the bell tower, as well as near openings, suggesting the development of specific damage mechanisms.

This typology was, thus, chosen as the first to be investigated in more detail.



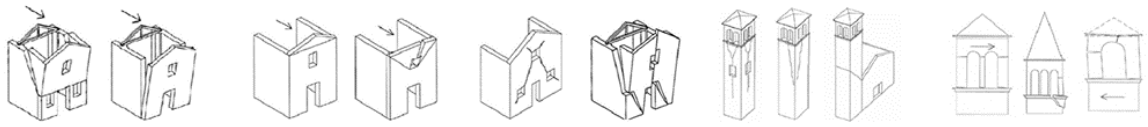
a. **b.** **c.** **d.**

Figure 2 Main typologies identified in the island of Montreal: **a.** the Baillargé; **b.** the Conefroy; **c.** the Néo-roman; **d.** the Italian baroque.

5 THE NÉO-ROMAN TYPOLOGY: A CASE STUDY

Direct application of the above-mentioned assessment procedure to the Néo-roman church typology appeared problematic because of the position of the bell tower, which is considered as a separate body in the original reference mechanisms. The mechanisms proposed for these two macro-elements by the abacus, reported in the following list and in fig.3, do not consider their interaction:

- Mechanism 1: overturning of the façade (figure 3a);
- Mechanism 2: overturning of the upper part of the façade (figure 3b);
- Mechanism 3: in-plane failure of the façade (figure 3c);
- Mechanism 27: failure of the bell tower along the height (figure 3d);
- Mechanism 28: failure of the upper portion of the bell tower (figure 3e).



a. **b.** **c.** **d.** **e.**

Figure 3 Mechanisms associated to the façade and bell tower macro-elements: **a.** Mechanism 1; **b.** Mechanism 2; **c.** Mechanism 3; **d.** Mechanism 27; **e.** Mechanism 28.

The Néo-Roman church of St. Joseph des-Prairies in Montreal was chosen for a case study. The church dates back to 1875-1876. Its tall bell tower constitutes a reference point for the neighborhood in the north of Montreal island. Visible from far away in the natural landscape (figure 4), it confirms the importance of the preservation of such elements for the urban scenario. Indeed, Montreal was defined the city of the 100 bell towers [23].



Figure 4 Bell tower of St. Joseph visible from far away in the landscape.

The main body of the church is isolated from the presbytery and it is composed of the nave and the apse, and in the back side, of the sacristy (figure 5).

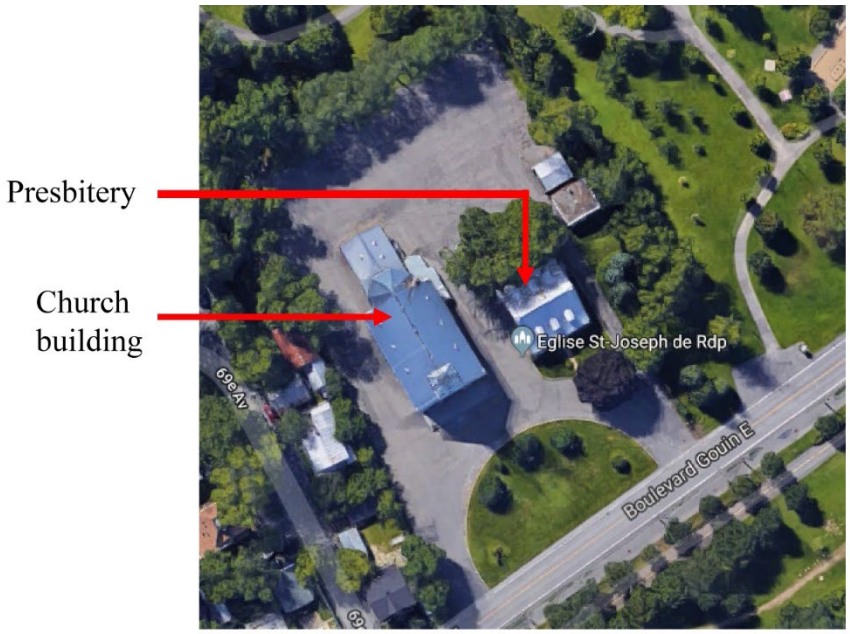
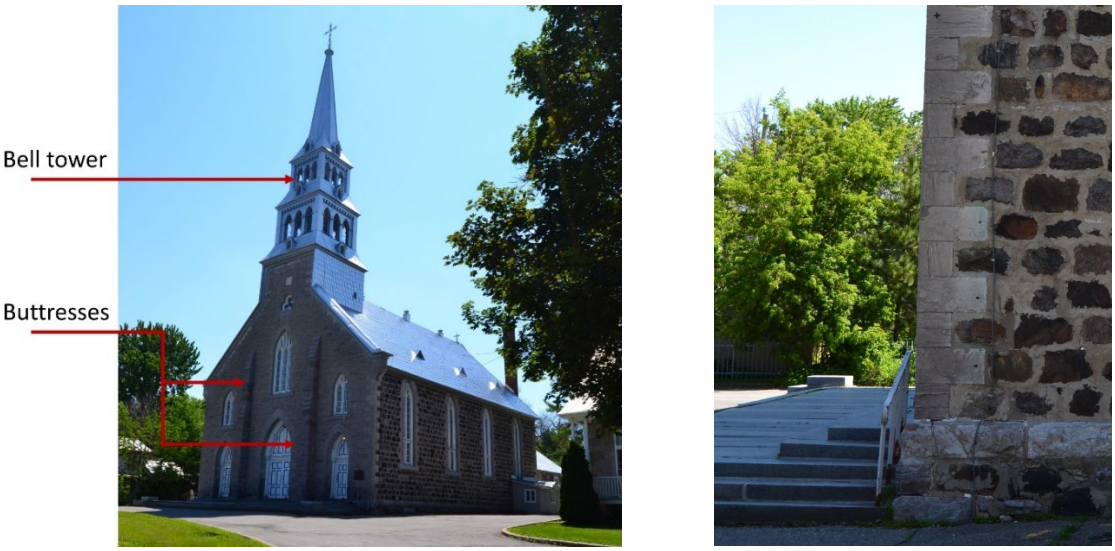


Figure 5 St. Joseph: the church and the presbitery

The façade of this church has a distinguishing aspect. The bell tower, which interrupts the hut shape of the façade at the middle, is flanked by a pair of buttresses (figure 6a). The curtain walls of the church are made of stone masonry. Multi-leaf walls are connected one to the other through well-defined stone blocks (Figure 6b). This solution was frequently observed in the inspected churches and, therefore, it has been identified as a territorial specificity.



a. **b.**

Figure 6 The exterior of the church: **a.** The principal elevation; **b**. The detail of interconnection between walls.

The church has three naves with a timber colonnade that, giving rhythm to the space of the

nave, supports the roof structure together with the lateral walls of the nave (figure 7). An overhanging deck, called “jubé”, hosting the choir and, as in most of the churches, the organ, characterizes the space of the church entrance.

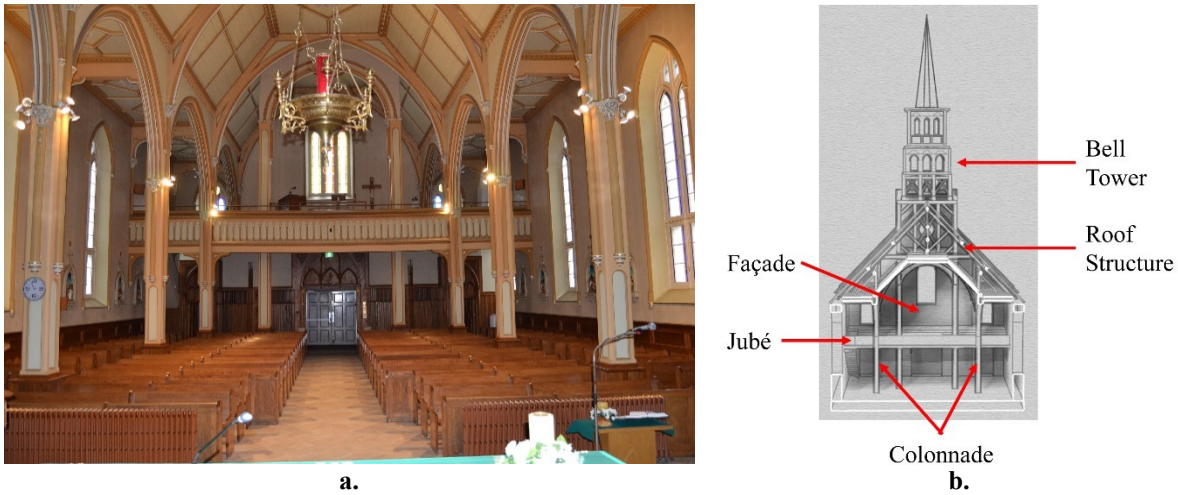


Figure 7 The configuration of the structure of the church: **a.** Colonnade of the nave and jubé; **b.** Transversal section of the church.

In order to interpret the structural behavior, also a detailed inspection of the roof and bell tower area was performed. This action was a fundamental step to understand the complexity of the structure of roof and bell tower and the interrelation with the masonry box, which brought to elaborate a complete three-dimensional model (figure 8) [24-26]. This has constituted the basis for a finite element model. During the survey, it was possible to observe the state of conservation of the timber roof structure, the connection between timber elements and between timber elements and masonry, and to detect the presence of existing cracks that, in case of earthquake, could be the starting point of damage and mechanism development.

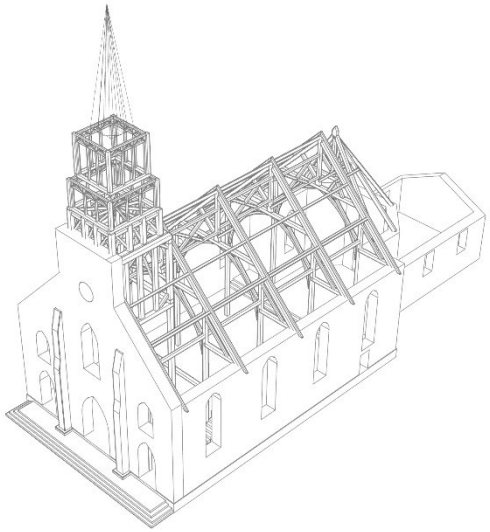


Figure 8 Three-dimensional geometrical model of St. Joseph.

5.1 Structural analysis

A finite element model was elaborated in Abaqus [27] to investigate the global structural behavior of the church. A first stage of the study concerned the masonry structure, with the aim at understanding the role of the main structural elements on the response. At this step, linear analyses were implemented, while non-linear analyses were not performed due to the lack of extensive damage data, as it occurs in the Italian territory. Indeed, such comparison would allow the calibration of the results, considering them reliable. A mesh of over 36000 tetrahedral elements was developed, with two elements in the thickness of the walls (figure 9).

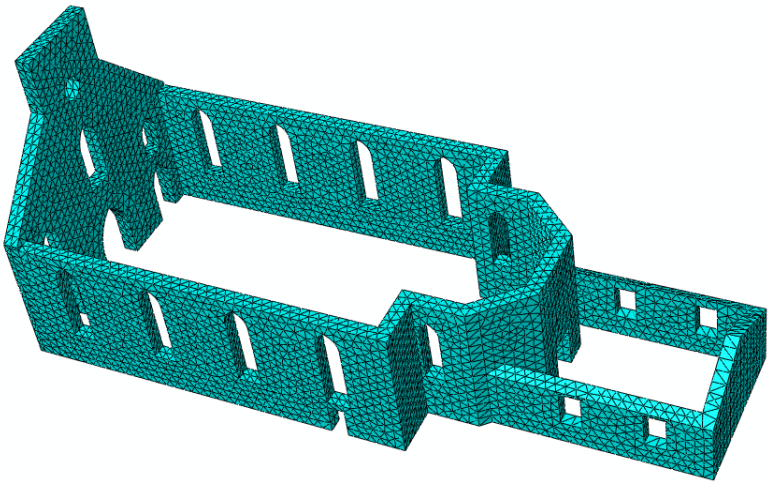


Figure 9 Tetrahedral mesh of the global model of St. Joseph.

The heterogeneity of the masonry was neglected in the model and an equivalent homogeneous isotropic material was defined, with the following properties: Young's modulus E= 2200 MPa, and weight density w = 20 kN/m^3. The contributions of the roof and the bell tower were included in the model considering the mass of the wood structure, with weight density w = 4.5 kN/m^3.

Figure 10 shows the first most significant modal shapes and the relevant natural periods for the longitudinal and transversal directions of St Joseph.

The first and the fourth mode involve mainly the façade in its upper portion, which, in the Néo-roman church, is also part of the bell tower. The second and third mode, on the contrary, develop mainly in the lateral nave walls. The out-of-plane mechanism of the nave wall top seen here corresponds to a very frequent situation in the Italian multi-nave churches and as such it is represented in the abacus of typical mechanisms. It may be applied here as well. In this case, however, it would be worth investigating further the role of the roof structure. In the Italian case its interaction is often considered as a cause of failure. In this case, the roof structure is important, as seen in fig. 8. The lateral stiffness it offers to the nave walls may produce a retaining effect limiting the development of such mechanism and in general may foster a collaborative behavior among walls in the nave and in the apse area. This effect must rely on efficient connections between timber elements and walls. The quality of construction and conservation observed for the timber structure during the survey seem to confirm this assumption. Numerical evaluation of complete models is in progress.

The main characteristics of this Néo-Roman church reside in the bell tower and the façade. Contrary to the assumption of interaction of the roof structure with the façade that is made very frequently in the Italian cases, often ascribing to roof pounding the damage produced at the tympanum top, the Canadian case has no connection between the two. The fundamental modal shape, as well as the third mode, recall what is probably the most frequent mechanism listed in the abacus, i.e. the bending failure of the façade top. The assumption of full connection of the façade with the nave walls in the numerical model is confirmed by the careful execution of the masonry at the corner as in fig. 6.b, which inhibits a full rotation of the façade limiting the mechanism to the upper part. The presence of the timber structure of the bell tower, which in this first phase has been considered only as applied mass, is under investigation to detail better the façade top mechanism, which appears as the dominating one for this church typology.

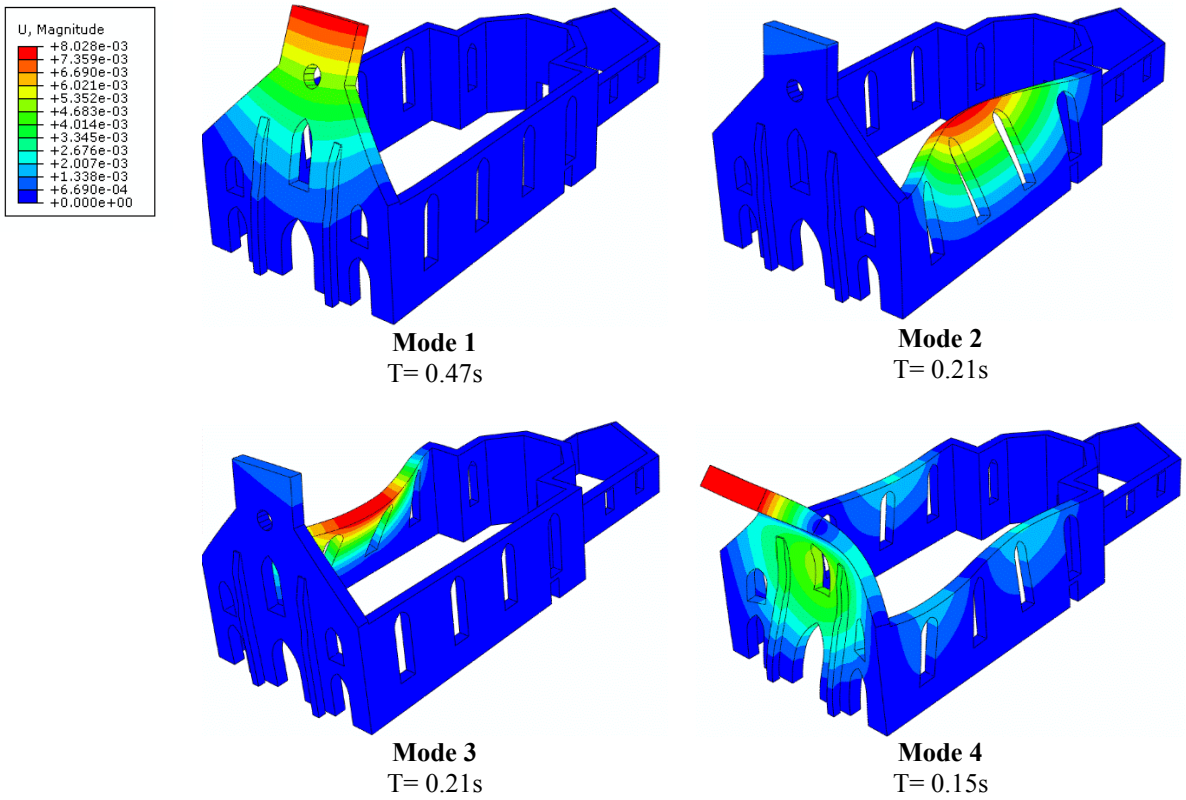


Figure 10 First modal shapes with the corresponding period .

6 CONCLUSIONS

The seismic vulnerability of churches is a well-known problem in the preservation of cultural heritage. The seismic damage documented for the churches in Québec and their numerousness elicited studying the seismic behavior of one of the identified church

typologies, the Néo-roman.
Starting from an assessment procedure developed for churches in Italy, a case study has given indication of local construction characteristics that influence the seismic behavior; this information may be used to increment the original reference damage mechanisms extending the procedure in order to its application in a different territory.
Additional analyses concerning the timber elements and their interaction with masonry as well as more advanced material behavior are in progress.

Acknowledgements.

The financial support provided to the first author by the Fonds de recherche du Québec – Nature et technologies (FRQNT) for an International internship is gratefully acknowledged. The third author acknowledges partial support from the Reluis-DPC 2019-21 project. The authors also wish to thank all the persons in the Diocèse de Montréal and the parishes of the visited churches for their indefectible collaboration and their generosity in sharing their time and knowledge. The participation of Roxanne Carrier to this project as a visiting student in Politecnico di Milano from ETS is also greatly acknowledged.

REFERENCES

[1] D'Ayala, D. and Benzoni, G. (2012) Historic and traditional structures during the 2010 chile earthquake: Observations, codes, and conservation strategies. *Earth Spectr* 28 (S1): S425-51.
[2] Cancino, C. (2011) *Damage assessment of historic earthen buildings after the August 15, 2007, Pisco, Peru earthquake.* Getty Conservation Institute, Los Angeles.
[3] D'Ayala, D., C. Galasso, V. Putrino, D. Fanciullacci, P. Barucco, V. Fanciullacci, C. Bronzino, et al. (2016) Assessment of the multi-hazard vulnerability of priority cultural heritage structures in the Philippines. Proceedings of the *1st International Conference on Natural Hazards and Infrastructure*, Chania, Greece.
[4] Marotta A., Sorrentino L., Liberatore D., Ingham J. (2017) Vulnerability assessment of unreinforced masonry churches following the 2010–2011 Canterbury earthquake sequence. *J Earthq Eng* 21(6):912–934.
[5] Doglioni, F., Moretti, A., Petrini, V. (1994) *Le chiese e il terremoto.* Trieste, Lint.
[6] DC PCM-DPC MIBAC. 2006. Form of damage for churches. Form A. Available from http://www.beniculturali.it/mibac/multimedia/MiBAC/documents/1338454237471_allegato4.pdf (Accessed January 31, 2020).
[7] MiBACT (2011). *Linee Guida per la Valutazione e Riduzione del Rischio Sismico del Patrimonio Culturale Allineate alle Nuove Norme Tecniche per le Costruzioni* (D.M. 14 Gennaio 2008). Attachment C.
[8] Da Porto, F., Silva, B., Costa, C., and Modena, C. (2012) Macro-scale analysis of damage to churches after earthquake in Abruzzo (Italy) on April 6, 2009, *J. Earth. Eng.*, 16, 739–758.
[9] Brandonisio, G., Lucibello, G., Mele, E., and De Luca, A. (2013) Damage and performance evaluation of masonry churches in the 2009 L'Aquila earthquake, *Engineering Failure Analysis*, 34, 693–714.

[10] Sorrentino, L., Liberatore,L. Decanini, L. D., Liberatore, D. (2014) The performance of churches in the 2012 Emilia earthquakes, *Bull Earthquake Eng* **12**: 2299–2331
[11] De Matteis, G., Zizi, M., and Corlito, V. (2017) Analisi preliminare degli effetti del terremoto del Centro Italia del 2016 sulle chiese a una navata. In *ANIDIS XVII Convegno L'Ingegneria sismica in Italia*, Pistoia, Italy, 17–21 September.
[12] Cescatti, E., Taffarel, S., Leggio, A., da Porto, F., and Modena, C. (2017) Macroscale damage assessment of URM churches after the 2016 earthquake sequence in Centre of Italy In: *ANIDIS XVII Convegno L'Ingegneria sismica in Italia*, Pistoia, Italy, 17–21 September.
[13] Youance, S. (2009) *Évaluation de la vulnérabilité sismique des églises du Québec*, ETS, Montreal.
[14] Sferrazza Papa, G. (2020) *Seismic vulnerability of churches: a territorial knowledge approach*, PhD Thesis, Politecnico di Milano, Milano.
[15] Sferrazza Papa, G., Parisi, M.A., Nollet, M-J. (2019) Seismic vulnerability of churches: the effect of context-related characteristics. In: *ANIDIS XVIII L'Ingegneria sismica in Italia*, Ascoli Piceno, Italy, 17–21 September.
[16] Lagomarsino, S. and Podestà, S. (2004a) Damage and vulnerability assessment of churches after the 2002 Molise, Iitaly, earthquake. *Earth Spect* 20 (S1): S271-83.
[17] Lagomarsino, S. and Podestà, S. (2004b) Seismic vulnerability of ancient churches: I. damage assessment and emergency planning. *Earth Spect* 20 (2): 377-94.
[18] Valente, M. and Milani, G. (2018) Seismic response and damage patterns of masonry churches: Seven case studies in Ferrara, Italy. *Eng. Struct.* 177 : 809-35.
[19] Casolo, S., S. Neumair, M. A. Parisi, and V. Petrini. 2000. Analysis of seismic damage patterns in old masonry church façades. *Earth Spect* 16 (4): 757-73.
[20] Adams, J. and Basham, P. (1989) The seismicity and seismotectonics of Canada East of the Cordillera. *Geoscience Canada*, Vol.16 (1).
[21] Nollet, M.-J., Abo El Ezz, A., and Nastev, M. (2013). Seismic risk assessment of unreinforced masonry buildings in Québec, In: *12th Canadian Masonry Symposium* Vancouver, Bristish Columbia, June 2-5, 2013.
[22] Le Patrimoine religieux du Québec. Les églises de la deuxième moitié du XIXe siècle. Available from http://www.gdcr.umontreal.ca/patrimoine/connaissance/catholicisme/dossier4.html (Accessed January 31 2020).
[23] Québec's National Shrines. *Montreal: The city of a hundred bell towers*. Available from http://www.sanctuairesquebec.com/en/ (Accessed December, 28 2018).
[24] Parisi M A, Chesi C, Tardini C, Piazza M, (2008). Seismic vulnerability and preservation of timber roof structures. In: Proceedings SAHC08, Bath,UK, pp. 1253-1260.
[25] Chesi C, Parisi MA and Tardini C (2012) Inferring seismic behavior from morphohology in timber roofs, *International Journal of Architectural Heritage*, 6:100-116.
[26] Parisi MA and Chesi C (2014) Seismic vulnerability of traditional buildings: the effect of roof-masonry walls interaction. In: *10th U.S. National Conference on Earthquake Engineering*. Anchorage, Alaska, 21-25 July.
[27] Abaqus (2016) Theory manual, version 2016.

12th International Conference on Structural Analysis of Historical Constructions
SAHC 2020
P. Roca, L. Pelà and C. Molins (Eds.)

SIMPLIFIED SEISMIC VULNERABILITY ASSESSMENT OF MEDIEVAL MASONRY CHURCHES

V. CORLITO[1], M. ZIZI[1] AND G. DE MATTEIS[2*]

[1] Department of Architecture and Industrial Design (DADI)
University of Campania "Luigi Vanvitelli"
San Lorenzo Abbey, 81030 Aversa, Italy
email: {valentina.corlito, mattia.zizi}@unicampania.it

[2] Department of Architecture and Industrial Design (DADI)
University of Campania "Luigi Vanvitelli"
San Lorenzo Abbey, 81030 Aversa, Italy
e-mail: gianfranco.dematteis@unicampania.it, (*corresponding author)

Keywords: Masonry Churches, Typological Characterization, Seismic Vulnerability Assessment, FEM Model, Seismic damage

Abstract. *The meaningful seismic events occurred in Italy in the last decades showed the high vulnerability of monumental buildings and in particular of churches. In order to preserve such a precious heritage, operations aimed at the seismic risk mitigation based on the definition of suitable vulnerability assessment procedure are necessary. The high hazard of the Italian Peninsula and the huge amount of ecclesiastic buildings located in the exposed territories, stress the need to face the problem with innovative large-scale approaches. In this study, an architectural-engineering integrated procedure for the seismic assessment of existing masonry churches at a regional scale is proposed. Based on accurate historical investigation of typical Abruzzi churches, a typological characterization has been established, aimed at recognizing the common geometrical and constructive features of two types of medieval churches widespread in this area. Then, a numerical analysis has been carried out. In particular, by assuming simplified modelling hypotheses, two FE models representative of significant real cases have been implemented in Abaqus. By the elastic analyses, the main collapse mechanisms and the corresponding activation seismic accelerations have been determined. The obtained outcomes show an acceptable correspondence with the actual seismic damage revealed on similar churches in the aftermath of last seismic events, corroborating the reliability of the adopted integrated approach.*

1 INTRODUCTION

Due to the geographical location and the complex tectonic system, the Abruzzi is one of the most earthquake-prone area in Italy. The dramatic impact of the last seismic events (i.e. L'Aquila 2009 and Central Italy 2016-17) highlighted the strong exposure of such area and the high fragility of the relevant architectural heritage, with particular reference to the historical masonry churches.

The above remarks emphasise the necessity to plan effective strategies at territorial scale

for a preventive framework, based on the definition of suitable large-scale vulnerability assessment methodologies, aimed at estimating the hypothetical consequences of a seismic event [1-4]. In this perspective, a seismic risk assessment should require a multidisciplinary approach taking into consideration not only the immediate structural issue, but also the influence of the architectural and geometrical features of the investigated constructions on their seismic behaviour [5, 6].

In this paper, a brief overview of the historical and typological characterization of the Abruzzi ecclesiastic architecture is presented, focusing on two of the most common types of medieval churches, namely the Benedictine and the Franciscan typologies. Then, a numerical investigation is carried out by assuming simplified modelling hypotheses concerning the thickness of the structural elements, the roofing systems and the mechanical properties of the materials. Finally, a comparison between the outcomes of the simplified elastic analyses and the actual damage scenarios observed in the aftermath of the L'Aquila (2009) and the Central Italy (2016-17) earthquakes is presented, allowing to prove the reliability of the proposed approach.

2 RELIGIOUS ARCHITECTURE IN ABRUZZI

2.1 Historical basis

The historical investigation of the religious architecture of Abruzzi starts from the Middle Ages, with the construction of some important Benedictine monasteries at the beginning of the 11th century [7]. Among others, the Benedictine church of San Liberatore alla Majella erected in 1080 in Serramonacesca (Pe) still preserves its original Romanesque layout (Figure 1). Different Benedictine churches built in Abruzzi between the 11th and 12th centuries can be typologically linked to the abbey of Serramonacesca, so that it is possible to assume the existence of a Benedictine school, characterized by the use of common architectural and structural elements. Among these, the following elements are recognizable: *i)* the use of a three-nave basilica layout; *ii)* the general use of round arches; *iii)* the presence of one or (more frequently) three external semi-circular apses; *iv)* the absence of vaults, except for the presbytery; *v)* the use of a simple salient shape for the façade.

The Benedictine abbeys almost never received the stylistic and structural innovations proposed by the French Gothic architecture, which were instead introduced in Abruzzi by the Cistercian Order. Few examples of Cistercian churches can be found in the region, which appear significantly modified or in ruins; nonetheless, the influence of such an Order on the religious architecture of the area was certainly decisive from a structural point of view, since it involved the widespread use of pointed arches, cross vaults and external buttresses in the churches.

The Middle Ages were also very important for the typological definition of the Franciscan Architecture. The churches built in Abruzzi between the 13th and 14th centuries according to this Order were generally composed of a single nave covered with wooden trusses and with a single vaulted apse (Figure 2a). Less commonly, and in particular in the area of Avezzano (Aq), the single nave was defined by the juxtaposition of three squared cells, covered by cross vaults. In all cases, the façades were typically characterized by a simple flat shape.

The Franciscan type experienced a wide diffusion in Abruzzi, so extensively to represent a valid alternative to the prevalent Benedictine model. Most of the Franciscan buildings were



(a) (b) (c)

Figure 1: S. Liberatore alla Majella church in Serramonacesca (Pe): (a) model; (b) external and (c) internal photographic survey.



(a) (b) (c)

Figure 2: Franciscan church: (a) model of typical medieval type; (b) external and (c) internal photographic survey of S. Francesco church in Campli (Te).

subjected to significant variations over the centuries. In many churches, the original type is still clearly visible in the external layout, despite the complete Baroque reinterpretation of the interiors in the 17th and 18th centuries. The solutions are in these cases very heterogeneous. In some modified Franciscan churches, the reinterpretation of the internal space was carried out simply by proposing a succession of vaulted cells. The church of San Francesco in Campli (Te) is the only case of not-modified Franciscan structure in the Abruzzi territory (Figure 2c). In this specific case, the gabled facade represents a variation from the more common flat shape (Figure 2b).

The foundation of the city of L'Aquila in the 13th century represents another fundamental step in the study of the medieval religious architecture of Abruzzi, given its influence in defining the main features of the religious architecture of the whole region [8]. Even if none of the original churches preserved its first structure, the presence of common features allows to identify basic medieval types, mainly characterized by a one-nave or basilica layout and by the common use of structural elements typical of the Cistercian-Franciscan Gothic and Romanesque style.

In Figure 3 the distribution of the most common types of medieval churches, namely the Benedictine [BN] and the Franciscan [FR] ones, in the Dioceses of Abruzzi is shown.

2.2 Geometric characterization

It is well known that the architecture of specific religious Orders is generally characterized by precise design rules and geometric proportions related to functional, cultural and symbolic

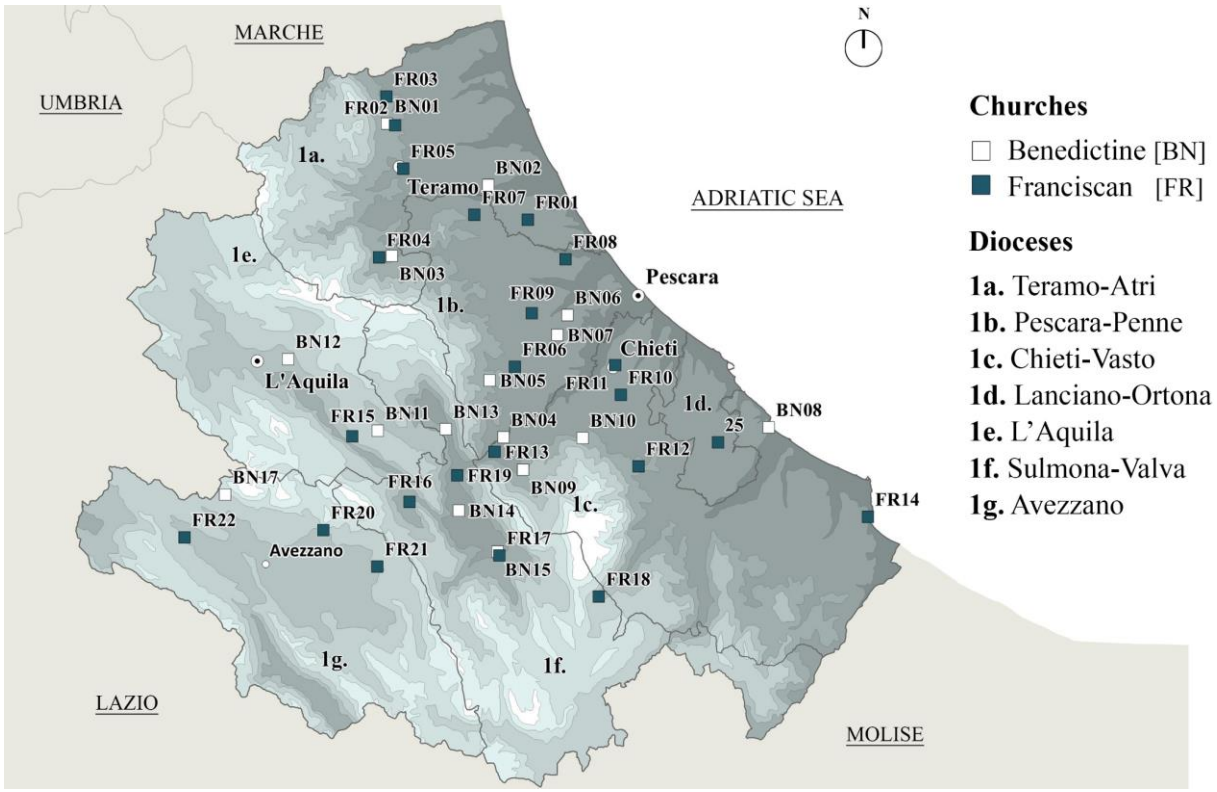


Figure 3: Territorial distribution of the Benedictine [BN] and Franciscan [FR] churches in the Dioceses of Abruzzi**.**

requirements. The geometric analysis of the religious architecture of Abruzzi evidences the presence of recurrent proportions connected to both specific constructive techniques and design rules. These proportional devices are fundamental in defining the aesthetics of buildings but may also significantly influence their structural behaviour. Therefore, in the field of seismic vulnerability assessment of churches, the reduction to specific recurrent geometric models may provide a valid simplified tool for the large-scale study of these historical buildings.

In the Benedictine monastic churches of Abruzzi different common elements related to the Benedictine school of San Liberatore can be recognized [7]. The used unit of measurement is the cubit of Roman derivation. The basilica layout is defined by the combination of *ad quadratum* (i.e. squared) modules, which can also be recognized in the development of the façade and in the definition of the interiors. The plan is characterized by the juxtaposition of four large squares for the central nave and eight smaller ones for each aisle. The central nave width-total width ratio is equal to 0.43, meaning that the span of the central nave is almost twice the width of the aisles. The design rules used in the church of San Liberatore were also transposed in all the Benedictine churches built in Abruzzi in the successive years. Despite the clear reference to the San Liberatore model, in these buildings tangible dimensional and proportional differences can be identified (Figure 4).

As far as the Franciscan architecture is concerned, relevant churches reached generally a maximum length of about 60 meters, including the apse. The churches built according to this model were characterized by a one-nave layout defined by the combination of three *ad*

quadratum modules, completed by an external quadrangular apse. The width-length ratio of the nave was generally 1:3 (0.33). The church of San Francesco in Campli (Te) is one of the few examples of Franciscan churches of Abruzzi; it is very close to the typical features and proportions of the architecture of this Order. In Figure 5 the plan-height variations of some Franciscan buildings identified in the Abruzzi territory are shown.

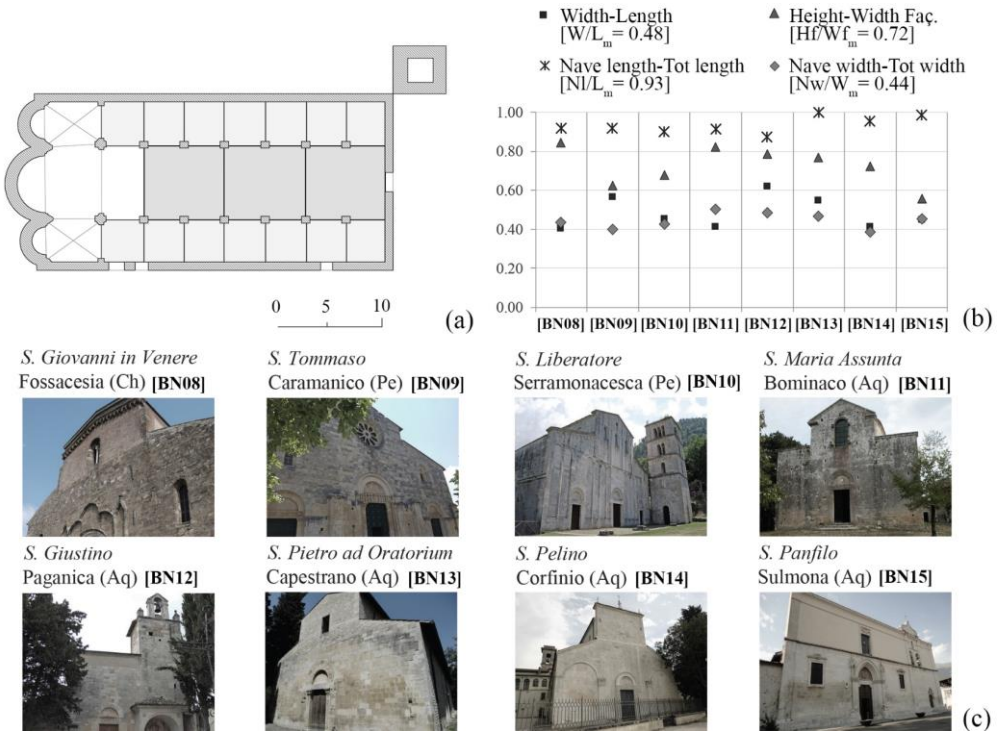


Figure 4: Benedictine churches [BN]: (a) geometric proportions of the San Liberatore church; (b) plan-height ratios; (c) examples of typical churches in Abruzzi.

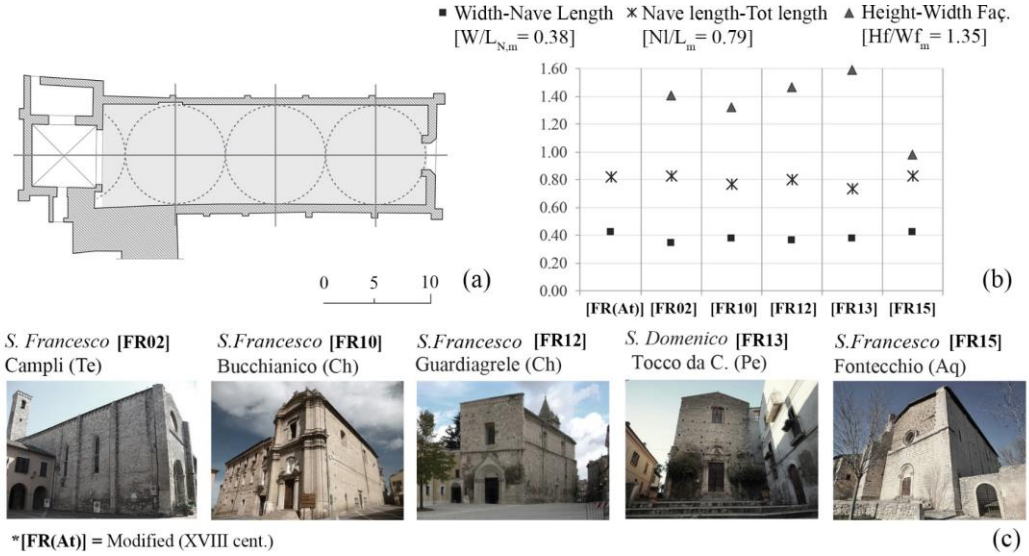


Figure 5: Franciscan churches [FR]: (a) geometric proportions of the San Francesco church in Campli (Te); (b) plan-height ratios; (c) examples of typical churches in Abruzzi.

It is worth noting that the proportions led by the religious Orders for ecclesiastic buildings are not recognizable when larger populations of churches are examined; in fact, the historical events and the possible marginality of some cultural contexts generally implied the absence of specific typological references, favouring the use of varying geometrical rules.

2.3 Material and construction techniques

The widespread presence of stones in the inner part of Abruzzi justifies the large use of this material for historical masonry constructions [9, 10]. In the Medieval churches, namely Romanesque and Gothic churches or, more generally, religious structures built by the Orders from the 11th to the 14th century, the quality of masonry is typically good, because of a well refined arrangement characterised by a regular pattern of stones.

A significant example of the typical constructional features of Benedictine churches is represented by the masonry pattern detected in the church of S. Pietro ad Oratorium in Capestrano (Figure 6).

In some cases, and in particular for the Franciscan churches, the lateral walls are made up of poorer materials arranged with a less regular pattern. This solution was linked to different factors, including the need to use in-situ materials and the frequent post-seismic reconstructions.

In the Adriatic part of Abruzzi, a wider variation of the building materials connected to the various local outcrops can be identified. Differently from the inner part of the Region, the predominance of clays in the coastal soils led to a frequent use of fire clay bricks in every parts of the ecclesiastical buildings.

Such aspects put into clear evidence how the use of materials in historical constructions can be influenced by the nature of the lithological outcrops of the sites, so that it is possible to identify variations in the used raw materials, although obvious difference in the adopted construction techniques are not always recognizable.

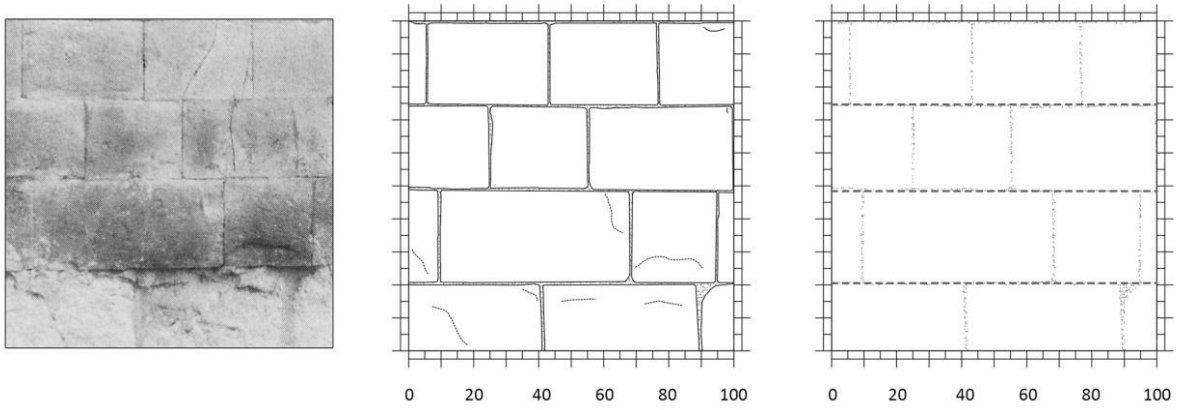


Figure 6: Masonry pattern observed in the church of S. Pietro ad Oratorium church in Capestrano (Aq).

3 SEISMIC VULNERABILITY ANALYSIS

3.1 General

Based on the typological characterization proposed in the previous section, a numerical

study has been carried out. In particular, the seismic response of the two typical examples of Benedictine and Franciscan churches have been investigated by means of simplified FEM Models. The adopted models and the assumptions underlying their implementations, as well as the obtained outcomes, are provided in the following.

3.2 Implemented numerical model and performed analysis

The seismic response assessment of a masonry church by means of FEM Model is generally a complex issue, which is highly affected by the global and local behaviour of the structural elements [11-13]. Since the present study aims at determining the main structural vulnerabilities of the detected architectural types, simplified and common assumptions have been made in the implemented numerical models. In particular, the linear analyses have been carried out by modelling the masonry material as a continuum, adopting a macro-modelling technique [14] and assuming a conventional engineering level of the material strength (referable to a limestone masonry) equal to 0.3 MPa and 5 MPa in tension and compression, respectively [15]. A material density ρ=2000 Kg/m^3, an Elastic Modulus E=2100 MPa and a Poisson's coefficient υ=0.35 have been adopted. Hence, by assuming seismic forces proportional to the mass distribution, the first collapse mechanisms and the corresponding horizontal acceleration levels have been determined by using simple models implemented in Abaqus, considering solid elements with 8 and 6 nodes (i.e. C3D8R and C3D6, respectively) for masonry walls.

To this purpose, reference to San Liberatore a Majella church (Serramonacesca, Pe) [BN10] and San Francesco in Campli church (Te) [FR02] has been made, although a typical flat shape has been considered for the façade of the Franciscan typology. The thickness of all masonry walls has been considered constant and equal to 1 meter. For the apse vault of the Franciscan church a conventional thickness of 20 centimetres has been assumed. In such a way, the study has been unified, as the obtained outcomes only depend on the geometrical configurations typical of each religious Order.

Analogously, the roofing elements has been simplified in the model. Hence, the presence of typical timber trusses or simple beams with regular spans of 4 meters and a uniform weight of 2 kN/m^2 has been assumed. The roof loads have been distributed on the lateral (80%) and transversal (20%) walls, while the stiffening contribution has been accounted for by means of axial springs. In particular, based on a preliminary analytical evaluation, axial springs placed in the central nave between the node on the top of lateral walls with a stiffness of 1kN/mm have been hypothesized. Similarly, the stiffening contribution of the roofing system of the lateral naves of the Benedictine church has been simulated by using springs with an axial stiffness of 0.1 kN/m.

Since the medieval typologies are commonly characterized by good constructional quality, a perfect continuity between adjacent masonry walls has been considered in the adopted meshes to define the connection between orthogonal elements.

Hence, the analyses have been developed in two steps: in the first one, vertical loads have been applied (roofing loads and gravity loads), while in the second one, a uniform horizontal acceleration have been introduced. Since the geometric models are characterized by symmetry about the longitudinal axis, three analyses for each model have been carried out, one for the transversal direction (+x) and two for the longitudinal directions (±y).

Some pictures of the implemented FEM models for both [BN] and [FR] church types are provided in Figure 7.

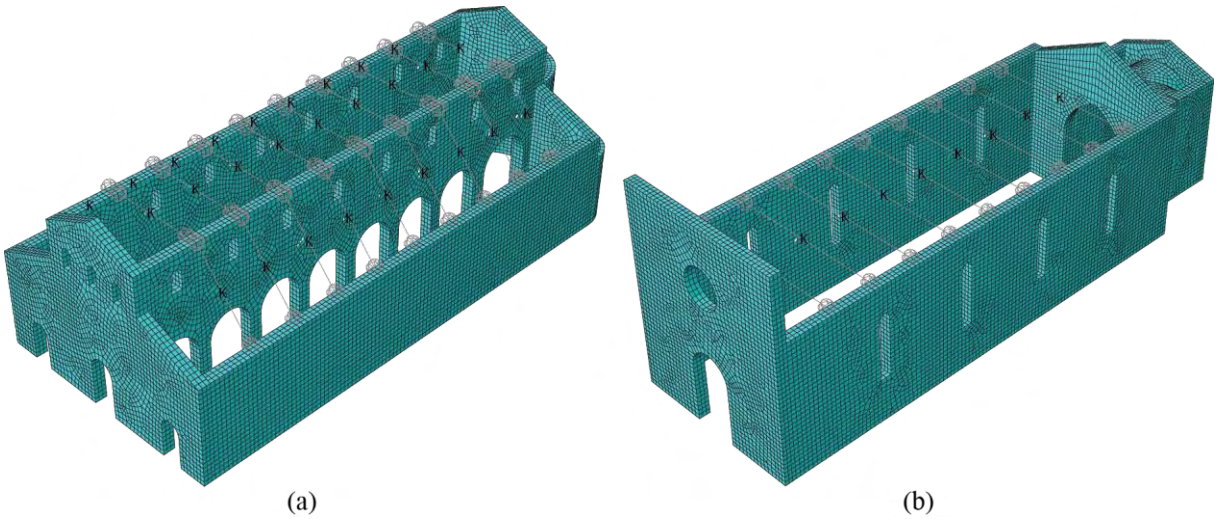


Figure 7: Implemented FEM Models: (a) [BN] and (b) [FR] church types.

3.3 The obtained results

The main outputs of the performed analyses are the first activated collapse mechanism and the corresponding acceleration. It should be observed that, since significant factors (e.g. soil quality and topography type, position in the urban context, presence of bell tower, etc.) have been disregarded in these analyses, the obtained acceleration values should be not considered in absolute terms, but they must be taken as a basis for comparison between the seismic behaviour of the two analysed typologies. The main outcomes are summarized in Table 1, where the collapse mechanisms and the corresponding accelerations of activation are provided. For convenience of the reader, it is worth mentioning that the positive y-direction corresponds to accelerations applied in the frontal direction of the façades. In Figure 8 and Figure 9, the stress pattern obtained in each analysis at the acceleration corresponding to the mechanism activation are provided for [BN] and [FR] types, respectively.

Table 1: Main outcomes of the numerical study.

Church typology	Seismic direction	Collapse mechanism	Activation acceleration
Benedictine [BN10]	+x	- In-plane cracking of the façade - Detachment of the connection between longitudinal walls and façade	0.06 g
	+y	- Failure of the colonnades (apse side)	0.16 g
	-y	- In-plane failure of the longitudinal arch (apse side)	0.10 g
Franciscan [FR02]	+x	- Cracking of the apse vault	0.24 g
	+y	- Overturning of the top of the façade	0.14 g
	-y	- Overturning of the top of the façade	0.06 g

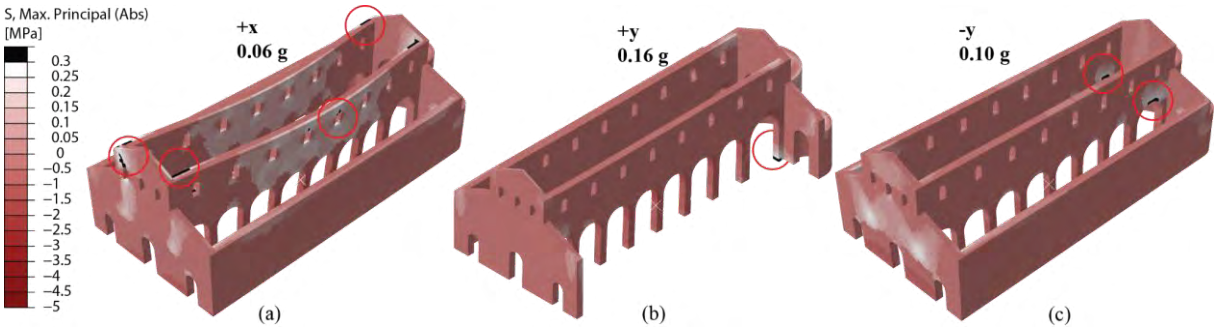


Figure 8: Results of the FEM Model for [BN] church: stress pattern at the failure points for +x (a), +y (b) and –y (c) directions

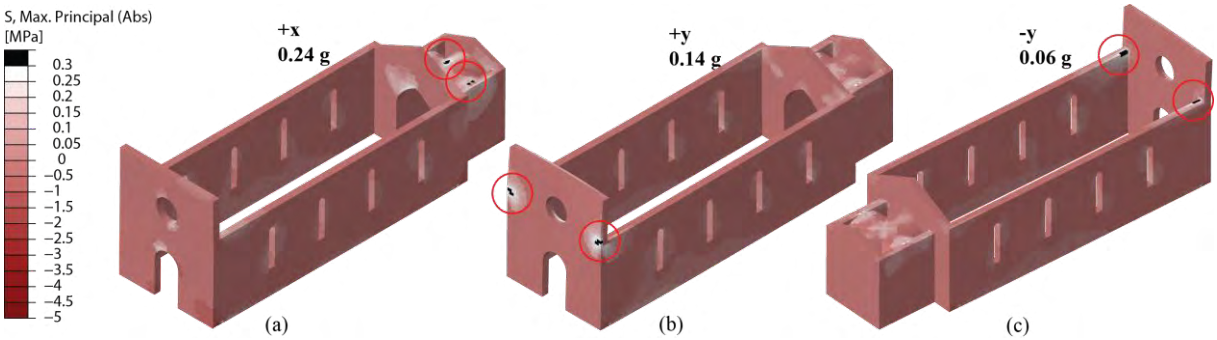


Figure 9: Results of the FEM Model for [FR] church: stress pattern at the failure points for +x (a), +y (b) and –y (c) directions

The obtained results reveal that the [FR] typology provides a good response in the transversal direction, whereas the façade configuration of such a typology represents a clear fragility indicator when the church is subjected to longitudinal actions. In fact, the cantilever behaviour assumed by the top of the façade in case of acceleration acting on its orthogonal direction may lead to a premature collapse.

As far as the [BN] typology is concerned, the longitudinal colonnades represent the weakest elements of this three-nave layout. In fact, in case of transversal actions, they may exhibit a response similar to a double fixed beam with a uniformly distributed vertical loads, with stress concentrations in the extremities and in the mid-span. On the contrary, the longitudinal response is highly affected by the presence of the apses, where there is a concentration of the mass and consequently of the internal forces.

3.4 Comparison with the observed damage

In order to corroborate the evidences obtained by the above numerical analyses, a comparison with the damage scenario induced by the last seismic events has been carried out. To this purpose, two examples of the damage undergone by Benedictine churches, namely the S. Pietro ad Oratorium church in Capestrano (Aq) and the S. Giustino church in Paganica (Aq), which experienced the L'Aquila 2009 seismic event, are provided in Figure 10.

In both these cases, the seismic damage was mostly concentred in the longitudinal colonnade, confirming the results arisen from the numerical analyses. In particular, in the church of Capestrano a diffused damage in the piers was surveyed, such as to lead the

National



(a) (b) (c)

Figure 10: Seismic damage observed in the colonnades of the churches of (a, b) S Pietro ad Oratorium in Capestrano (Aq) and (c) S. Giustino in Paganica (Aq).

Fire Brigades to operate a diffused provisional intervention in order to avoid a possible collapse (Figure 10a, 10b). Moreover, it is interesting to note in Figure 10c that the revealed damage exactly corresponded to the one predicted by the numerical analysis in the negative and positive y direction: a failure of the arch in proximity of the apse with a collapse mechanism involving also the piers was exhibited, although in this example lateral apses are missing.

As far as the Franciscan type churches are concerned, some significant information on the seismic behaviour of such a typology can be obtained by considering the historical evolution of the S. Francesco church in Atri (TE) [FR(At)] (Figure 11a), which was deeply modified after the strong earthquake that struck the region in 1703 [16]. After that seismic event, the Franciscan church resulted hugely damaged; the collapses interested the cross vault of the apse, the timber roofing system, the bell tower and the façade, which in particular revealed the activation of an out-of-plane mechanism. Such a damage description faithfully confirms the outcomes of the numerical analyses.

Moreover, some evidences of the seismic behaviour of such a typology can be found also considering the churches of S. Francesco in Amatrice (RI) and Norcia (PG), which were both dramatically damaged after the swarm occurred in the Central Italy in 2016-17. Despite both churches exhibited an almost total collapse due to the strong earthquake occurred on the 30th October 2016 (epicentre in Norcia), they resulted seriously damaged also after the first seismic event of August 2016, as shown in Fig. 11b and 11c. Therefore, as predicted by the numerical investigation, the flat termination of the façade represents a significant vulnerability indicator in the Franciscan type.

It is worth noting that, since many churches can reveal similar common geometrical dimensions and constructional features, although they are related to few analysed cases, the above outcomes can have a larger impact and could be extended to the whole category of the examined churches.



(a) (b) (c)

Figure 11: (a) S. Francesco church in Atri (TE) and significant seismic damage after the first seismic event of the Central-Italy 2016-17 earthquake: S. Francesco churches in (b) Amatrice and (c) Norcia.

4 CONCLUSIONS

The present study deals with the seismic vulnerability assessment of monumental buildings. Simplified numerical analyses based on a preventive in-depth historical investigation of medieval Benedictine and Franciscan churches present in Abruzzi have been carried out.

Based on a suitable typological characterization, simplified numerical analyses have been implemented on two churches representative of the investigated typologies. The obtained outcomes showed a good correspondence in terms of collapse mechanisms with the real damage observed in examples of churches that experienced the L'Aquila (2009) and the Central Italy (2016-17) earthquakes.

In the whole, the obtained results demonstrate the reliability of the adopted integrated approach, which appears to be useful to perform large-scale studies and to provide suitable preventive strategies for the protection of the architectural assets in the most earthquake-prone areas.

REFERENCES

[1] Lagomarsino, S., Podestà, S. Seismic Vulnerability of Ancient Churches: II. Statistical Analysis of Surveyed Data and Methods for Risk Analysis. *Earthquake Spectra* (2004) **20**(2):395–412.

[2] D'Ayala, D. Force and displacement-based vulnerability assessment for traditional buildings. *Bulletin of Earthquake Engineering* (2005) **3**(3):235-265.

[3] De Matteis, G, Brando, G, Corlito, V. Predictive model for seismic vulnerability assessment of churches based on the 2009 L'Aquila earthquake. *Bulletin of Earthquake Engineering* (2019) **17**(9):4909–4936.

[4] De Matteis, G, Zizi, M. Seismic Damage Prediction of Masonry Churches by a PGA-Based Approach. *International Journal of Architectural Heritage* (2019) **13** (7):1165–1179.

[5] Lourenco, P., Roque, J. Simplified indexes for the seismic vulnerability of ancient masonry buildings. *Construction and Building Materials* (2006) **20**:200-208.

[6] Palazzi, N. C., Rovero, L., Llera, J., Sandoval, C. Preliminary Assessment on Seismic Vulnerability of Masonry Churches in Central Chile. *International Journal of*

Architectural Heritage (2019). doi:10.1080/15583058.2019.1570388.
[7] Bartolini, S. L. Delle tipologie religiose nell'architettura abruzzese fra 11. e 19. secolo, Pescara: Tipolitografia SIGRAF. (2015). *(In Italian).*
[8] Gavini I. C. Storia dell'architettura in Abruzzo. Milano; Roma: Casa editrice d'arte Bestetti e Tumminelli. *(In Italian).*
[9] Di Nucci, A. L'arte di costruire in Abruzzo. Tecniche murarie nel territorio della diocesi di Valva e Sulmona Gange. (2011) *(In Italian).*
[10] Mancini, R. Le pietre aquilane: processi di approvvigionamento della pietra e sue forme di lavorazione nell'architettura storica. Roma: G.B.E. (2012) *(In Italian).*
[11] Lourenço, P. B. Computations on historic masonry structures. *Progress in Structural Engineering and Materials* (2002) **4**:301-319.
[12] Brando, G., Criber, E. and De Matteis, G. The effects of L'aquila earthquake on the St. Gemma church in Goriano Sicoli: part II—fem analysis. *Bulletin of Earthquake Engineering* **13**:3733–3748 (2015).
[13] Kujawa, M., Lubowiecka, I. and Szymczak, C. Finite element modelling of a historic church structure in the context of a masonry damage analysis. *Engineering Failure Analysis* (2020) doi: 10.1016/j.engfailanal.2019.104233.
[14] Lourenço, P.B., Rots, J. and Blaauwendraad, J. Two approaches for the analysis of masonry structures: Micro and macro-modeling. *HERON* (1995), **40**(4):313-340.
[15] De Matteis, G. and Mazzolani, F.M. The Fossanova church: seismic vulnerability assessment by numerical and physical testing. *International Journal of Architectural Heritage* (2010) **4**(3):222-245.
[16] Bartolini Salimbeni, L. Architettura francescana in Abruzzo dal XIII al XVIII secolo. Edigrafica. (1993) *(In Italian).*

THE ASSESSMENT AND REDUCTION OF SEISMIC RISK: TOWARDS A SYSTEM OF KNOWLEDGE FOR ARCHAEOLOGICAL PRE-EXISTENCES

E. MONTENEGRO*

* Department of History, Design and Restoration of Architecture
Sapienza University of Rome
Piazza Borghese 9, 00186 Rome, Italy
e-mail: elisabetta.montenegro@uniroma1.it

Keywords: Archaeology, Seismic Vulnerability, Risk Assessment, Territorial Scale Analysis

Abstract: *The earthquake is a serious risk factor for archaeological heritage and, especially in this thematic area, the preventive protection assumes a strategic importance due to the lack of purpose that a reconstructive intervention would produce. However, the multiple problems of conservation and enhancement of the archeological heritage make the planning of damage mitigation complex, according to the criteria adopted for historical architecture.*
From the evolutionary framework of the sectoral regulations in Italy emerges a generic extension of the provisions for specific architectural monuments to the archaeological ones, in which the absence of connections or their intrinsic weakness, if any, increases their vulnerability.
Currently, it is clear that the absence of a specific "functional connotation" of ruins, apart from the visit one, places these contexts on the margin of the most recent regulations reconsiderations. Indeed, the current Linee Guida Mibact 2011 (Mibact Guidelines 2011) introduce a rapid evaluation methodology on a territorial scale (L_{V1}) which does not consider the archaeological structures.
The paper proposes a rapid assessment method for the archaeological seismic vulnerability, which tries to connect the knowledge system with the analytical result on a territorial scale. This approach, based on a hierarchical system identification of structural 'morphos-types', is developed with applications conducted on the Roman Forum structures. Specifically, the attention is focused on the ruins constituted by walls without connections, whose structural behaviour, far from the global one, can be assimilated to a 'macro-element'. The seismic risk assessment is set according to the Carta del Rischio (the Risk Map) system methodology. This method introduces an algorithm for calculating structural vulnerability able to grasp the constructive and conservative specificities that influence the structural behaviour of the archaeological pre-existences.

1 THE SEISMIC RISK PROBLEM FOR THE ARCHAEOLOGICAL HERITAGE

The seismic risk and the archaeological heritage have always lapped. On the one hand, the weak prevention, which often transforms the natural event into a catastrophic moment, inevitably focuses the attention on the historical architecture still in use. On the other hand, the complexities related to the conservation and enhancement of these pre-existences overshadow the reflections on exceptional events like the earthquake and, consequently, the *planning of damage mitigation* according to the criteria adopted for historical architecture. However, the earthquake preventive protection assumes strategic importance due to the loss of meaning that a reconstructive intervention would produce.

When we talk about archaeological ruins, we usually refer to structures whose height does not exceed four meters, in which the instabilities caused by the earthquake rarely damage visitors. However, the large monumental complexes (temples, amphitheaters, baths) are an exception. The morphological complexity and the geometric relationships of their structures amplify their vulnerability. In these cases, the potential risk has been managed for a long time by implementing provisions such as the limitation of using and approaching the monument.

However, an exceptional event such as the earthquake, which is intrinsic with the geological nature of the Italian territory, represents a risk not only for the public safety of the users but also for the material conservation of the monument itself. Nevertheless, with the exception of singular structures, for a long time the archaeological heritage seismic risk has been managed as a secondary problem with respect to the more general conservative needs and the first attention to the topic has been developed only in recent times.

2 THE EVOLUTIONARY PATH OF ANTI-SEISMIC LEGISLATION

In the last years of the previous century in Italy, there has been an evolution of the technical legislation on the prevention of seismic risk, which has had a significant impact on the planning of historical building interventions. There are several contributions in the literature on the subjects. As an example, some of them are given below.

In the past, the preservation of the historical architectures had been entrusted for centuries to continuous control, through the introduction of corrections suggested by the periodic observation of the structural behaviour, or through the experimentation of reinforcement techniques when a new instability arose. Starting from the end of the XVIII century and throughout the XIX century, this tradition was implemented in the first anti-seismic regulations [1]. With the advent of new construction technologies, the first seismological researches and the first studies on the dynamic behaviour of buildings, the need to conduct safety checks arose, giving a scientific aspect to the legislation [2]; but the attention to the historical and monumental heritage is the result of a gradual process of awareness-raising on the theme, which became explicit only in the early 1980s.

Indeed, the first seismic regulation of 1909 [3], provided for the adoption of the new building rules in case of repair of masonry constructions, with the only possibility for protected buildings to apply the "case by case" criterion. Although the historic building was formally excluded from specific obligations, in many cases the need for a discreet structural safety led to the adoption of technologically invasive solutions, regardless of the competences attributed to the Superintendencies by the Law 1089 of 1939 [4] or by the contents of the Restoration Papers of those years (Athens 1931, Venice 1964). The heavy impacts, produced both on the minor

building and on the monumental heritage, immediately demonstrate the limits of the 1981 regulation, which establishes 'seismic adjustment' [5] in repairing post-earthquake damage. With the *Raccomandazioni* of 1986 (*Recommendations)* [6], a technical-cultural reflection on the conservation of historical and monumental heritage is articulated for the first time, introducing the concept of 'improvement', conveyed through alternative and less invasive interventions, acquired by reflection from the seismic regulation of 1986 [7]. It is in this context that starts a different and more effective attention to the archaeological pre-existences theme, with the idea of excluding them from the application of the rules valid for ordinary buildings. This attention is explicit in the document drawn up during the National Seismic Engineering Conference of 1991, which took place in Palermo [8]. However, the non-approval of the document causes the marginalization of this issue in the following rules, as evidenced by the Ministerial Decree of 1996 [9], with the result that the practice has recklessly continued to extend the current architecture provisions to the archaeological heritage. If, with the redefinition of the entire national territory seismic risk of 2003 [10] were introduced more stringent structural checks even for protected buildings, the *Norme Tecniche per le Costruzioni* of 2008 *(Technical Regulations for Constructions)* [11] clarify the difference between 'improvement' and 'adjustment' in the possibility of 'improving' a historic building by seeking a balance between conservation and structural safety. The *Linee Guida per la valutazione e riduzione del rischio sismico del patrimonio culturale* (Mibact 2011) [12] translate this concept by outlining a methodological tool for the knowledge, the diagnosis and the project of conservation. The choice of an appropriate level of safety to be achieved by controlling the nominal life of the building also expresses a renewed approach to the seismic 'improvement', in which historical - constructive knowledge, seismic risk and structural behaviour converge [13]. Once again, the document, designed for the historical architecture in use, does not include specific indications for archaeological artefacts. From the new technical standards' orientations of *Norme Tecniche per le Costruzioni* of 2018 [14], which in case of 'improvement' interventions introduce a minimum safety value to be reached according to the building class of use, it emerges that the absence of a specific functional connotation of the archaeological heritage, apart from the visit, continues to place these contexts at the edge of regulatory reconsiderations.
From the evolutionary scheme outlined, alongside the significant progress made towards the conservation of cultural heritage, emerge the open problems and possible lines of development. Undoubtedly, archaeological pre-existences take on a priority place, whose conservation does not depend only on a methodologically correct project approach, but on the territorial vulnerability knowledge towards the seismic risk, to which this paper is dedicated.

2.1 The *Linee Guida Mibact 2011* and the three risk assessment levels

The *Linee Guida Mibact 2011* articulate the assessment of seismic risk on three distinct levels. Starting from some analysis which govern the territorial scale ('L_{V1}' type), we move on to more detailed assessments conducted on the architectural scale ('L_{V2}' and 'L_{V3}' type).
The simplified evaluation system 'L_{V1}', suitable for a large area rapid control, estimates the structural collapse acceleration through limited geometric and mechanical parameters and using qualitative tools like the visual interrogation and the critical survey. Given the limited level of knowledge, are adopted low 'Fc' confidence factors. The evaluation systems referring to the 'L_{V2}' and 'L_{V3}' levels, suitable for more complex analyses, requires the identification of the

historical and construction specificities of the construction, an accurate characterization of the mechanical properties of the materials, and greater precision of geometric relief.
The 'L_{V1}' analysis models, based on the qualitative interpretation of seismic behaviour by macroelements (architectural portions characterized by an autonomous behaviour with respect to the rest of the building [15]), are introduced for three architectural typologies like *palaces*, *churches* and *towers*, not contemplating archaeological structures.

2.2 The *Linee Guida per la conservazione di architetture di interesse archeologico (Guidelines for the conservation of architectures of archaeological interest)*

To deal with the emergency that hit the archaeological area of Rome and Ostia Antica in 2008, with widespread conservation problems due to the rapid progression of the risk of collapse, a working group was set up and coordinated by Roberto Cecchi, who drafted the *Schema di Linee Guida per la conservazione di architetture di interesse archeologico* [16]. This document represents the most up-to-date status of studies on the assessment and reduction of seismic risk relating to archaeological sites, because it complements the *Linee Guida Mibact 2011* contents for a possible application to archaeological pre-existences. The methodological peculiarity consists in combining the *knowledge path proper to the stratigraphic analysis* of the elevated with the *structural analysis*. Given the number of archaeological artefacts at risk, 'L_{V1}-type' assessments are used to define a preliminary ranking of territorial vulnerability.
Specifically for the archaeological artefacts *made in itself*, characterized by a behaviour similar to that of historical architecture, the analysis models of the *Linee Guida Mibact 2011* are extended, defining seismic vulnerability indices for each construction phase identified with the stratigraphic analysis. Whereas, *f*or *ruderal artefacts* are proposed simplified models which express the collapse mechanisms that can potentially be activated for construction components which, although coming from different architectural types, are attributable to the same behavioural scheme. This defines the 'domains' which, given the site's danger, indicate the geometric and proportional characteristics of the archeological artefact beyond which the verification is not satisfied. These include *isolated blocks* originating from vertical structures (columns and wall fragments), *single arch structures* (triliths or triumphal arches) and *linear systems* (bridges, aqueducts). The applications carried out on some monuments demonstrate the strengths and limitations of this methodology. For the analysis of the *Oratorio dei Quaranta Martiri*, taken as artefact made in itself, the 'palaces' model is adopted, verifying the second-way mechanisms that engage the shear wall resistance. However, in a stratigraphically complex building with not always effective connections, collapse is more likely to occur due to off-plan mechanisms. The inspection activities carried out in 2011 on some Pompeii Domus [17] further develop the method, using the 'isolated blocks' domain of the ruined artefacts. This approach, methodologically opposite to the previous one, assesses the safety of the entire complex by verifying that the slenderness of each wall does not exceed that limit, ignoring the contribution offered by the connections. While recognizing the difficulty in simulating the real behaviour of the architectural complex, even in this case modelling involves significant approximations.
In general, it is clear that the path of knowledge proposed by the *Schema di Linee Guida* at the territorial scale, strongly anchored to the tools of stratigraphic analysis, is weakly connected to the analytical dimension, renouncing the control of material and conservative aspects in favour of primarily geometric factors. If what has been illustrated so far represents a step forward

towards the characterization of rapid analysis tools specific to archaeology, below it is an attempt to implement the state of the art which tries to best combine the knowledge system with the analytical dimension.

3 A METHODOLOGY FOR SPEDITIVE READING OF VULNERABILITY

The proposed methodological approach aims to a speedy assessment of the seismic vulnerability of archaeological pre-existences [18]. To define a reading methodology based on a knowledge system calibrated according to archaeological specificities, this study presents some results obtained with applications conducted on structures and architectural components of the Roman Forum. Leaving aside the ruins *made in itself*, which show an overall structural behaviour attributable to that of historic buildings still in use, and for which the *Linee Guida Mibact 2011* indications are generally considered valid, attention has been focused on ruins made up of walls without connections, whose structural behaviour, far from the global one, is in itself comparable to that of a 'macroelement'. It should be remembered that in the architectural context some experiences, such as the 1976 Friuli earthquake, promoted an important analysis of the effects generated by the earthquake, allowing the identification of precise breakdown mechanisms and recurring behavioural patterns for some building types. On the contrary, in an archaeological context, there is no real systematization of the structural behaviour of the ruins in the event of an earthquake. For this reason, direct observation conducted in a sample site such as the Roman Forum represented an essential step for identifying the main structural types. Believing that the stratigraphic reading involves a significant difficulty in relating a large amount of data to be acquired and that clashes with the need to carry out a speedy evaluation, a hierarchical identification system of *structural 'morphologies-types'* is used. These are in turn broken down in constructive elements, in order to facilitate the identification of the main damage mechanisms that can be activated in an archaeological pre-existence. The abacus of the *morpho-typologies* identified considers simple typologies, such as *vertical structures* (columns, pillars and masonry fragments), and the more complex systems according to the trilithic or triumphal arch, to *single span* or to *multiple spans*, called *linear systems*. For the ruderal structures originated from the masonry buildings, depending on the different level of conservation it is possible to identify *incomplete*, *complete* or *aggregate masonry cells*. For the ruins originated from the remains of masonry buildings, depending on the different level of conservation observed, it is possible to identify *incomplete wall cells* (which at least preserve the angular connections between the walls); *complete masonry cells* (in which the walls bordering the base cell and possible horizontal connections are preserved); *aggregate wall cells* (with reciprocal connections between buildings).

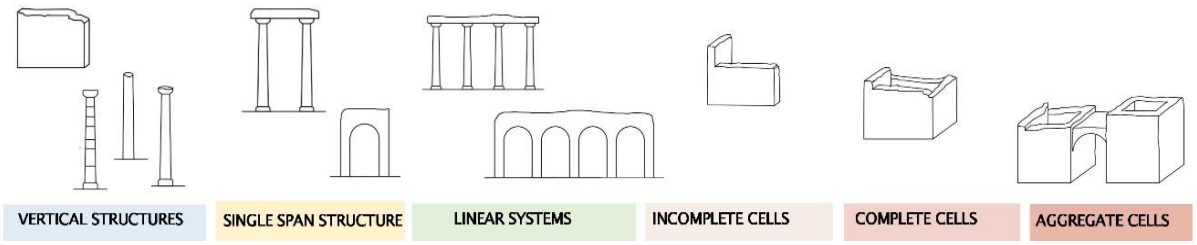


Figure 1: Diagram of the morpho-typologies identifiable in an archaeological site

In the north-western and central quadrant of the Roman Forum, components and buildings sample were identified, as representative as possible of each morphology-type.
The structures analysed include nine isolated columns (the *Colonna di Foca*, the two *Colonne Onorarie*, the columns facing the Via Sacra, the columns in front of the *Tempio di Romolo* and two columns of the Basilica Emilia), four linear structures (*Tempio di Vespasiano*, *Tempio di Saturno*, *Tempio dei Castori*, *Portico degli Dei Consenti*), and various wall cells with different levels of articulation and complexity belonging to the complex of the *Casa delle Vestali*. The direct reading conducted on the site was supported by the use of appropriate speedy and flexible scheduling traces (the main section of which are declinable according to the specific features of each structural *'morpho-typology'*) and, at the same time, homogeneous in the basic structure, making it possible to compare heterogeneous structures. Therefore, starting from models already tested by *Mibact*, the sections necessary for the structural aspects have been developed. To the specifically registry section, follows the one that registers the presence of provisional coverings, the conditions of access and approach to the monument and the presence of valuable elements. Two sections describe the site's morphology and its seismic chronology respectively. A subsequent part is dedicated to the geometric identification of the *macroelements*, indicating the main geometric parameters and the external constraint conditions. Following are the materials, the state of conservation and the dimensions of each construction element making up the '*morpho-typology'* examined. For each of these are also investigated the effectiveness and state of conservation of the consolidations resulting from previous interventions (metal clamps, pins, chains, circles, material additions etc.); mutual connections between the parties; deterioration signs and structural discontinuity (flaking, potential breaking planes, integrity of the elements etc.); the overhang conditions of coatings and the finishes. The last two sections are dedicated respectively to the description of the state of damage (injuries, collapses, expulsions, gaps, crushing, overhanging, differential settlements etc.) and to the interpretation of the results.

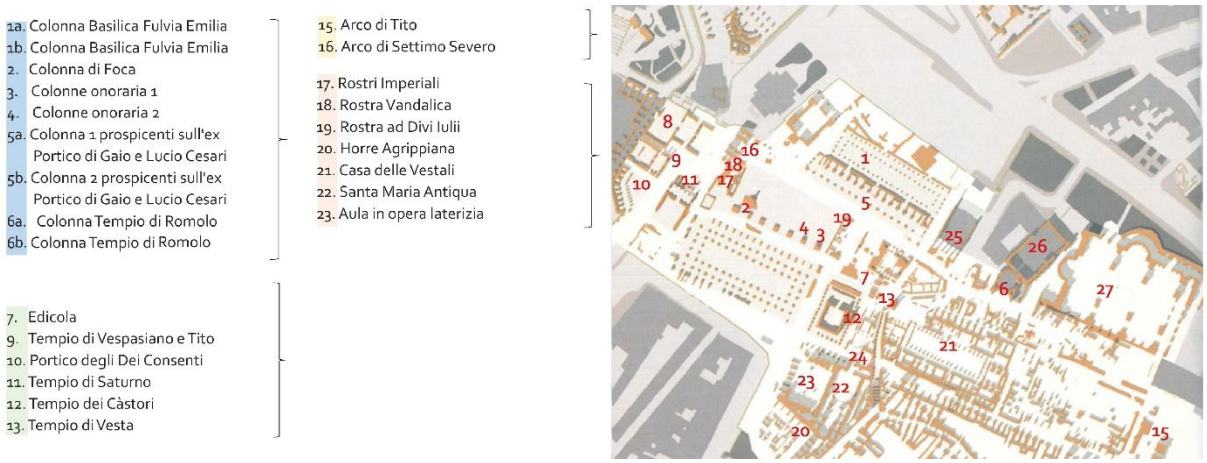


Figure 2: *Localization of the monuments analysed in the Roman Forum*

Through the reorganization of the data collected with the scheduling activity, concerning the isolated columns, the recurring aspects that prefigure conditions of vulnerability have been highlighted, diversified according to the characterization of the shaft (monolithic or articulated

in drums). These include the reduction of the resistant section caused by the gaps in the shaft, the presence of reintegration sections and the bad contact between the drums.
Geometric features such as slenderness and top projections that influence global vulnerability are associated with the material - construction evidence. Specifically, the presence of various sections fractured and reintegrated with mortar was found for some of the highest columns of the *Basilica Emilia* with monolithic shafts; a misalignment, albeit slight, of the drums of the *Colonna di Foca* and the first *Colonna Onoraria* (for which the presence of pivots is ignored) and various fractures and partitions in correspondence with the second *Colonna Onoraria*.



Figure 3: The isolated columns analysed in the Roman Forum

3.1 The *Carta del Rischio* system and the proposal of a calculation algorithm

The direct reading was followed by the vulnerability calculation phase of the structures analysed. In this regard, a critical comparison between the different models of safety and structural vulnerability assessment has been adopted by the *Linee Guida Mibact 2011* and by the system of *Carta del Rischio del Patrimonio Culturale* made by Mibact [19].
The *Carta del Rischio* system, drawn up in the nineties by the *Istituto Centrale per il Restauro*, has made the concept of "preventive restoration" formulated by Cesare Brandi, intending to define a rapid identification system for the most exposed monuments and the ones at risk of loss, to plan intervention priorities objectively. If the *Linee Guida Mibact 2011* set the structural verification on the calculation of the safety index (concerning the acceleration that leads to the collapse of the structure and the peak acceleration characteristic of the site), the *Carta del Rischio* system expresses this according to the architectural vulnerability and the territorial danger. For archaeological constructions, the vulnerability is estimated with the support of the *'Scheda Manufatto Archeologico'*, which observes for each construction element of the pre-existence six different forms of material and surface degradation, contemplating, only in general, the specific structural problems [20]. From the comparative framework conducted, it was decided to set the seismic risk assessment according to a coherent methodology with the operative model of the *Carta del Rischio* system and, at the same time, calibrated according to the setting already illustrated for an 'L_{V1}' analysis regulated by the *Linee Guida Mibact 2011.*

The development of a spreadsheet, connected to the previously illustrated scheduling layouts, has allowed the calculation of the vulnerability index for each structure investigated through an algorithmic formulation that is exemplified here for the *isolated column morpho-typology.*
The structure of the algorithm takes up the approach adopted in the *Carta del Rischio* system and in previous experiences in managing the cultural heritage [21, 22]. The vulnerability is calculated as a weighted average of 5 sub-indices, each of which depends on variables depicted with the scheduling made on the site. The value of each variable is included in a range of six intervals. The sub-inches are calculated as the arithmetic average of the variables on which they depend. The arithmetic average represents an initial setting, which is subject to changes downstream of the appropriate validation of the schedules. The direct on-site study highlighted the main critical issues that affect the vulnerability of an archaeological artefact, such as the geometric relationships between the overhangning parts; the quality of the connections; the state of damage of the construction elements; etc. To each of these parameters, has been assigned a sub-index.
The first sub-index registers the geometric parameters that have a moderate incidence in the activation of a rigid body mechanism such as slenderness; the second evaluates the connection and reinforcement elements present and the basic constraint conditions; the third records the structural discontinuities through variables such as the integrity of the sections, the deterioration of the materials and the presence of breakage planes; the fourth takes into account the presence of protrusions and overhangs that can influence the activation of the mechanism; the fifth registers, for each construction element, the variables that express the state of damage. Each sub-index is currently set as the arithmetic mean of the values attributed to the variables on which it depends, which are measured according to a maximum number of six intervals.

$$Iv = (p1 * Igm + p2 * Icn + p3 * Ids + p4 * Ia + p5 * Isd) / (p1 + p2 + p3 + p4 + p5) \quad (1)$$

The direct study, for example, facilitated the identification of the collapse mechanisms potentially activated for the *isolated column morpho-typology*, useful for calibrating the formulation of the algorithm. The weight system, indeed, is determined according to the incidence that each sub-index is believed to assume in activating the most plausible and heavy damage mechanisms, as will be seen with an example. Through iterative corrections, an attempt was made to improve the architecture of the algorithm, to make it more able to grasp the constructive and conservative specificities that influence the structural behaviour of each column. A further revision and calibration level are currently in progress, entrusted to the comparison of the results from the 'L_{V1}' type analysis conducted, with those of a more accurate 'L_{V2}' analysis, which governs the architectural scale, performed on some sample structures. The first index is based on a limited number of qualitative and quantitative parameters taken from direct reading; the second index, instead, requires the identification of the historical and constructive specificities, a more careful characterization of the materials mechanical properties, and a more accurate relief.

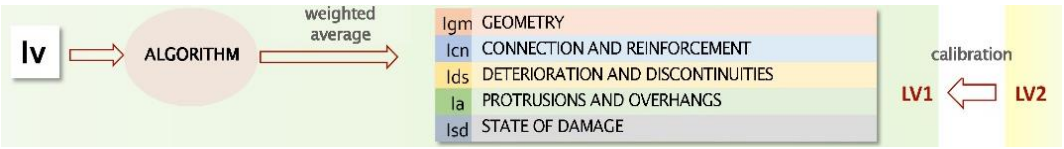


Figure 4: *Architecture of the calculation algorithm*

3.2 Example for the *Colonna di Foca*

The marble column of the Corinthian order, erected in the central sector of the Forum in 608 AD. in honour of Emperor Phocas, through the assembly of recovery elements from a third-century monument, represents the last monument erected in the Roman Forum [23]. It consists of seven grooved drums and stands 13.60 meters high on a marble-covered plinth placed on a brick-lined cement base, once hidden by a wide staircase leading up to the podium, currently poorly preserved. From the compilation of the schedule, more critical elements emerged such as the misalignments of the drums (which could prefigure preferential planes of rotation or sliding between the elements) and the significant inclination of the shaft. Doubts remain about the presence of pivots between the elements, not directly deducible with the visual investigation. The historiographic and technical documentation available has confirmed that the inclination of the column was caused by a serious alteration of the support surfaces. As is known, the column, which remained buried for a long time up to the base of the shaft, was completely brought to light during the nineteenth-century excavations [24, 25]. Probably, during the long burial period, the bedding layers of the marble slab placed as an elevation of the podium must have suffered disruptions, causing the fracture of the slab itself, the reduction of the support areas with the podium below and the consequent rotation of the shaft. The archival documentation indicates that in 1980 the continuity of support was restored with mortar additions, without, however, restoring the axiality of the shaft.

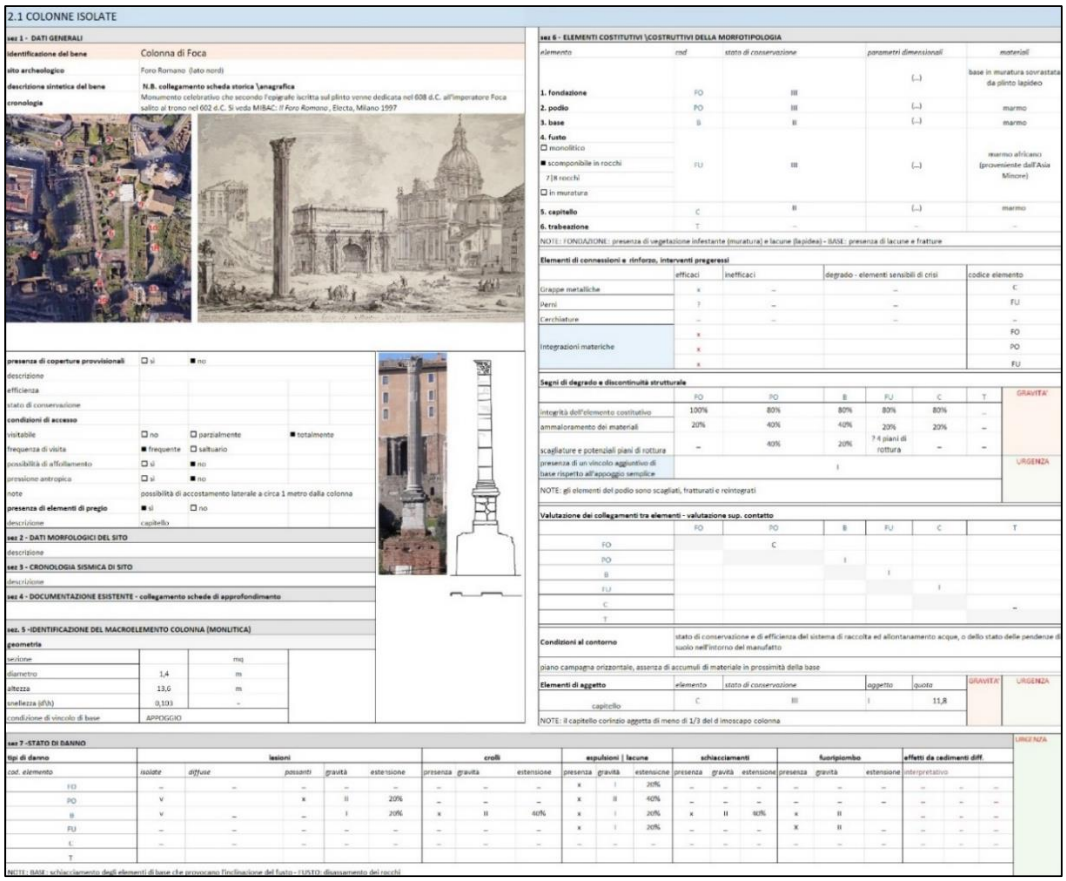


Figure 1: Scheduling traces Colonna di Foca

For the construction of the algorithm, it is observed that the first sub-index ('Igm'), linked to the geometry, assumes a rather high value, equal to 0.6, due to the slenderness of the column greater than 1\10. The second sub-index ('Icn'), however, given the uncertain presence of pivots between the stem's drums and on the nature constraint with the base and the upper capital, assumes a lower value, equal to 0.3. Even lower is the third sub-index ('Ids'), linked to the degradation and structural discontinuities of the elements, recently integrated, as it has been ascertained. The projection of the capital with respect to the shaft and the related out of plumb determine a value for the fourth sub-index ('Ia') equal to 0.4. The last sub-index ('Isd'), which records the damage status for each element, is approximately equal to 0.3. Based on appropriate reflections on the collapse mechanisms of a column divided into drums, the weights to be attributed to each sub-index were set. If the horizontal sliding is subordinate to the nature of the connections between the drums (in this case unknown), the overturning of the entire shaft or parts of it can be influenced by misalignments, overhangs and slenderness. Based on the evidence found, weights have been assumed that are useful for conducting a weighted average between sub-index, determining, as follows, the final vulnerability index.

$$Iv = (0,4*0,6 + 0,1*0,317 + 0,1*0,213 + 0,2*0,4 + 0,2*0,313) / (0,4 + 0,1 + 0,1 + 0,2 + 0,2) = 0,438 \quad (1)$$

In general, the vulnerability obtained for the columns is consistent with what emerged from the direct knowledge gained during the first data collection. The most vulnerable structures include the *Colonna di Foca* and the first *Colonna Onoraria* which, although different in slenderness and state of damage, exhibit vulnerability indices between 0.3 and 0.5. The column in front of the *Tempio di Romolo*, instead, due to its slenderness, the substantial flakes of the shaft, and the considerable overhang of the top entablature, assumes a vulnerability index close to 0.6. The remaining columns, although different in geometric and conservative characteristics, do not present particularly compromised conditions, as well as indicating a lower vulnerability index.

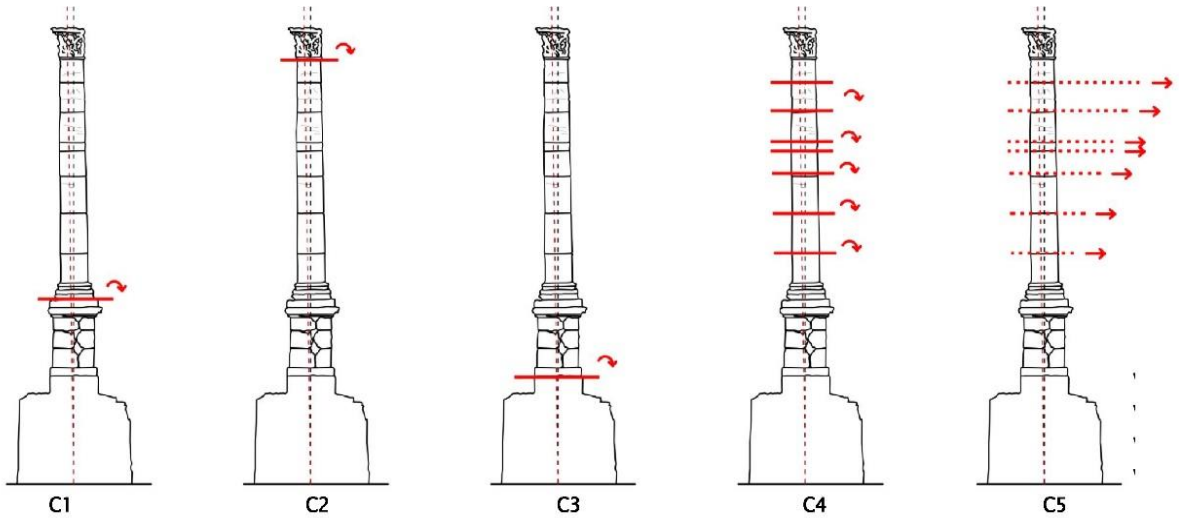


Figure 6: Schematization of possible collapse mechanisms for the Colonna di Foca

4 CONCLUSIONS

The illustrated methodology finds space in the complex relationship between conservation and structural safety that the regulatory excursus reflects. Although in development, it offers the possibility of integrating existing tools for the rapid assessment of the seismic risk of archaeological pre-existences, combining the deck of the *Linee Guida Mibact* with the *Carta del Rischio*. The set of knowledge, articulated around specific scheduling layouts, appropriately relates to the analytical dimension, through algorithmic formulations with the high management capacity of input data, as tested in initial and more recent experiences [26]. It should be remembered that the formulations exemplified for the isolated columns analysed are based on first working hypotheses and require appropriate checks and validations [27]. Lastly, it is believed that the evaluation of particularly vulnerable structures such as archaeological pre-existences represents a complex problem that cannot be trivialized with extremely simplistic solutions. Therefore, through the use of confidence factors, in full consistency with the *Linee Guida Mibact 2011*, the system designed for an 'L_{VI}' level of analysis, is suitable for managing a more complex knowledge coming from the *Mibact* databases available and the historiographic study, which importance in structural safety assessments must not be overlooked.

REFERENCES

[1] A. De Ioanna, F. Picarreta: *Il consolidamento antisismico nell'edilizia del XVIII e XIX secolo: regole dell'arte e processo evolutivo della normativa antisismica: le fonti storiche d'archivio a riscontro con l'osservazione in situ* in "Palladio", n.s., XIII, 26 (2000), pp. 93 – 124;

[2] S. Lagomarsino: *La nuova normativa sismica è buona per il resturo?* in "Responsabilità della conservazione del costruito storico – Atti del convegno per il ventennale dell'Arco", Gangemi, Roma (2011), pp. 95 – 106;

[3] R. D. 18.04.1909 n.193, *Norme tecniche ed igieniche obbligatorie per le riparazioni, ricostruzioni e nuove costruzioni degli edifici pubblici e privati nei luoghi colpiti dal terremoto del 28.12.1908 e da altri precedenti elencati nel R.D. 15.04.1909* (G.U. 22.04.1909, n.95);

[4] Legge 1.06.1939, n.1089, *Tutela delle cose d'interesse Artistico o Storico,* (G.U. 8.10.1939 n.184);

[5] D.M.LL. PP. 2.07.1981 *Normativa per le riparazioni ed il rafforzamento degli edifici danneggiati dal sisma nelle regioni Basilicata, Campania e Puglia* (G.U. 21.07.1981 n. 198 suppl.);

[6] Circolare M.BB.CC.A. 18 luglio 1986, n. 1032, Comitato nazionale per la prevenzione del patrimonio culturale dal rischio sismico, *Interventi sul patrimonio monumentale a tipologia specialistica in zone sismiche: raccomandazioni;*

[7] D.M.LL.PP. 24.01.1986, *Norme tecniche relative alle costruzioni antisismiche*, (G.U. 12.05.1986 n. 108);

[8] R. Argalia, G. Augusti (a cura di): *L'ingegneria sismica in Italia, 1991: atti del 5° Convegno Nazionale: 29 settembre-2 ottobre 1991*, Facoltà di Ingegneria, Università degli studi di Palermo, Esagrafica, Roma (1991);

[9] D.M.LL.PP. 16.01.1996, *Norme tecniche per le costruzioni in zone sismiche*, (G.U. 05.02.1996 n. 29);

[10] O. P. C. M. 20.03.2003 n. 3274, *Primi elementi in materia di criteri generali per la classificazione sismica del territorio nazionale e normative tecniche per le costruzioni in zona sismica;*

[11] D. M. I. T. 14.01. 2008, *Norme Tecniche per le Costruzioni*, (G.U. 04.02.2008 n. 29);
[12] D. P. C. M. 9.02. 2011, *Valutazione e Riduzione del rischio sismico del patrimonio culturale con riferimento alle Norme Tecniche per le Costruzioni di cui al D. M. Infrastrutture e Trasporti del 14 gennaio 2008*, (G.U. 26.02.2011 n.47 – suppl. ord. n. 54);
[13] S. Lagomarsino: *Linee Guida per la protezione del patrimonio culturale dal rischio sismico* in "Quale sicurezza per il patrimonio architettonico? - atti del VI Convegno Nazionale Arco (Mantova 30/11 – 2/12 2006), Nuova Argos, Roma (2007), pp. 70 – 89;
[14] D. M. I. T. 17.01.2018, Aggiornamento delle "*Norme Tecniche per le Costruzioni"*, (G.U. 20.02.2018 n.42 – suppl. ord. n. 8);
[15] F. Doglioni, A. Moretti, V. Petrini: *Le chiese e il terremoto - Dalla vulnerabilità constatata nel terremoto del Friuli al miglioramento antisismico nel restauro, verso una politica di prevenzione*, Edizioni LINT, Trieste (1994);
[16] R. Cecchi: *Schema di Linee Guida per la conservazione di architetture di interesse archeologico* in "Roma Archaeologia: interventi per la tutela e la fruizione del patrimonio archeologico: terzo rapporto", vol. 1 – 2, Electa, Milano (2011);
[17] R. Cecchi: *Pompei Archaeologia*, *progetto di conservazione e fruizione del patrimonio archeologico,* Electa, Milano (2011);
[18] This study is the result of a PhD research in progress in History, Design and Restoration of Architecture - XXXIII cycle (cv restoration) - Department of History, Design and Restoration of Architecture of the Sapienza University of Rome (Italy); supervisor: Prof.ssa D. Fiorani, co-supervisors: Prof.ssa A. Donatelli, Prof. F. De Cesaris;
[19] ICR: *La Carta del Rischio del Patrimonio Culturale*, Bonifica s.p.a. (1997);
[20] C. Cacace, A. Ferroni: *Carta del Rischio: La vulnerabilità Archeologica* in "Apparati Musivi Antichi nell'area del Mediterraneo", Atti del Convegno Internazionale di Studi (Piazza Armerina 9-13 aprile 2003), Quaderni di Palazzo Montalbo n°4, Dario Flaccovio, Palermo (2004), pp 466–472;
[21] R. Coppi: *Metodologia per la costruzione dei modelli di rischio del Patrimonio Culturale* in "La Carta del Rischio del Patrimonio Culturale", Bonifica s.p.a.,(1997);
[22] A. Donatelli: *Addenda: Considerazioni per la definizione degli algoritmi per le schede di Unità Urbana* in "Il futuro dei centri storici. Digitalizzazione e strategia conservativa" (di D. Fiorani), Quasar, Roma (2019);
[23] MIBAC: *Il Foro Romano*, Electa, Milano (1997), pp. 33 – 34;
[24] *Archivio del Parco Archeologico del Colosseo* and *Archivio Storico di Palazzo Altemps* in Rome.
[25] Soprintendenza archeologica d Roma: *Forma. La città antica e il suo avvenire*, De Luca Editori d'Arte, Roma (1985), pp. 83 – 86;
[26] D. Fiorani: *Il futuro dei centri storici. Digitalizzazione e strategia conservativa*, Quasar, Roma (2019);
[27] P. Angeletti, A. Bianchi, C. Cacace, A. Donatelli, O. Ceistllini, E. Rasimelli: *Un metodo speditivo di valutazione della vulnerabilità e del rischio sismico di beni culturali. Caso di studio: Sicilia e Calabria* in "Atti del XIII convegno ANIDIS" (Bologna, 28 giugno-2 luglio), (2009), sessione 4.1, cdrom.

12th International Conference on Structural Analysis of Historical Constructions
SAHC 2020
P. Roca, L. Pelà and C. Molins (Eds.)

THE DAMAGE SURVEY OF CULTURAL BUILT HERITAGE BETWEEN SIMPLIFIED PROCEDURES AND NEEDS FOR IMPLEMENTATION: THE CASE STUDY OF EMILIA-ROMAGNA CEMETERIES

VERONICA VONA[1*], MARCO ZUPPIROLI[2]

[1]Department of Architecture, Laboratory of Architectural Restoration (LABORA)
University of Ferrara
Via Quartieri 8, 44121 Ferrara, Italy
e-mail: vnovnc@unife.it, www.architettura.unife.it (*corresponding author)

[2] Department of Architecture, Laboratory of Architectural Restoration (LABORA)
University of Ferrara
Via Quartieri 8, 44121 Ferrara, Italy
email: zppmrc@unife.it, www.architettura.unife.it

Keywords: "Emilia 2012" earthquake, Specialised type, Morpho-typological characters, Recurring Collapse Mechanisms

Abstract. *Seven years after the earthquake occurred in Emilia-Romagna, the planning phases related to the cultural heritage reconstruction are coming to a conclusion. At this point, the Agency for reconstruction - earthquake 2012 has launched an unprecedented process aimed at verifying, also through the recognition of the main critical issues, the simplified damage assessment procedures whose application has allowed an aware and sustainable management of the emergency. The Guidelines for the evaluation and reduction of seismic risk on Cultural Heritage, and the Directive 12/12/2013 "Procedures for management of activities for cultural heritage securing and safeguarding in the event of emergencies caused by natural disasters" of MiBAC identify as first cognitive procedure the compilation of sheet to provide vulnerabilities and damage level representation on movable and immovable assets. In particular, they establish two important survey instruments: the A-Church and the B-Palaces sheets.*

These are the only two instruments used between 2012 and 2013 for the damage level characterization of the cultural heritage caused by the "Emilia 2012" earthquake. The widespread use of these sheets has brought to light several problems that have negatively affected the successive economic assessment of the intervention. In fact, if these sheets well describe the vulnerabilities of the specialized types Churches or Palaces, they are ill suited to types with different features, which, in the Emilia-Romagna case, represent about 30% of damage cultural heritage numerically and economically. In particular, the most relevant sample in this set are the cemeteries.

After the analysis of sheets produced for the cemetery type, the need to implementation for the already consolidated procedures has become clear, in order to be able to manage the post-emergency phases on those types that, as cemeteries, represent an important part of the local cultural identity, but that are not addressed in existing tools.

1 INTRODUCTION

Seven years after the earthquake in Emilia in 2012, we have been witnessing an extraordinary response capacity and transformation of the socio-economic system [1]. Now that even the Architectural heritage - the last priority identified - are entering the construction process [2], the key point in the reconstruction phase has been played by the "*invariant factors*" [3], which can be adjusted to other similar disaster areas. The ambitious project promoted by the Emilia-Romagna region, aiming at the capitalization of experiences, is the analysis of what has been achieved so far and the identification of both strong and weak points of the reconstruction process in order to implement the best policies. The project led to the activation of specific research projects [4]. In the field of Cultural Heritage the earthquake made us more aware of the building evolution [5] but at the same time it puts to a test both its structures and its conservative principles [6]. The damage survey is among the first operations to carry out in an emergency phase with the hard task of identifying all buildings requirements (structural, conservative and economic).

In Emilia-Romagna 80% of the damaged public buildings is under protection and the survey campaign has showed some peculiarities in the damage survey report. The significant change in the grants provided for the reconstruction represents a first evidence of this criticality nonetheless it shows the great potentialities in the evolution of the damage survey research started in the Seventies.

One of the most challenging type of buildings is the cemetery, especially from an economic point of view and for a lack of efficacy in the survey tools (Figure 1).

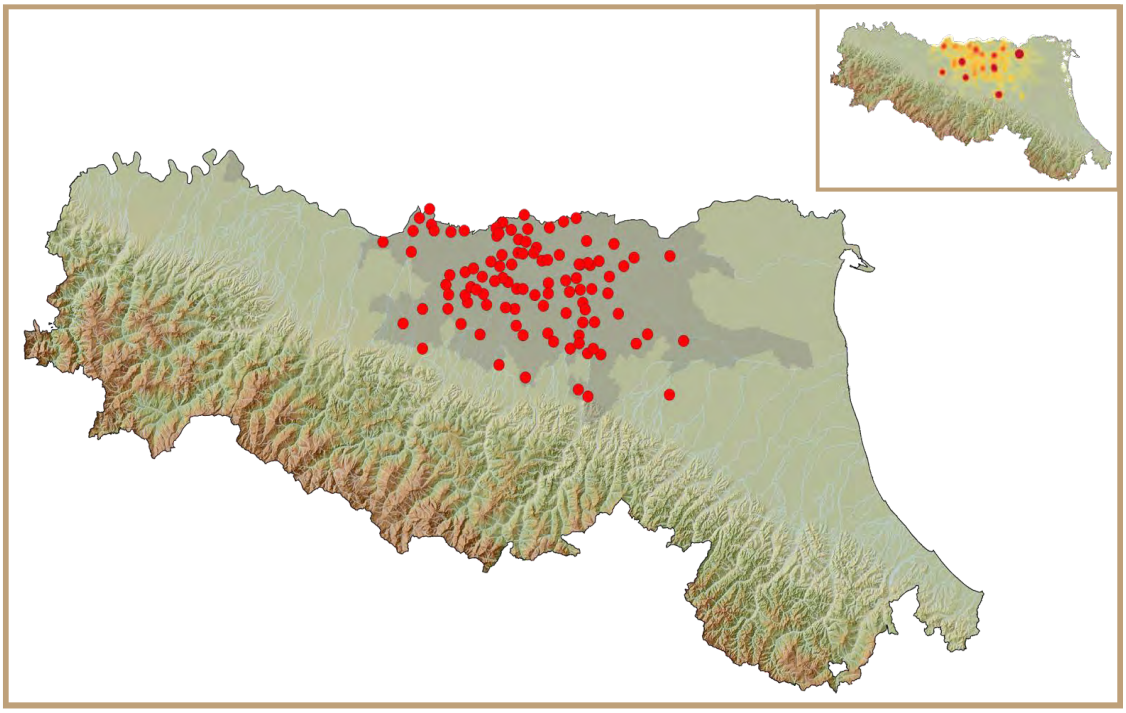


Figure 1: Heatmap of the all Architectural Heritage damaged by the earthquake (top right image) and distribution of the damaged cemetery in the *"crater"* area of Emilia-Romagna.

2 SHEETS TO MEASURE THE DAMAGE SURVEY ON THE ARCHITECTURAL HERITAGE

The earthquakes occurred in the last 30 years have revealed the significant vulnerabilities of architectural heritage. These are strictly related to the building construction quality, the form and dimension of architectural components and anti-seismic devices which are connected to the seismic activity of the area and to the time distance between construction/renovation and the earthquake [7]. A proper identification both of the historic buildings' vulnerabilities and the related activation level of the collapse is a useful tool for prevention and for managing the after-earthquake reconstruction phase. With the aim of providing a support in the complex and delicate emergency management phase, in Italy a series of sheets of different levels have been studied, that through a guided procedure should eventually assess vulnerability, damage [8], practicability and lastly the intervention costs.

The sheets currently in use are the result of several studies and experiences. These range from studies of the research unit coordinated by Doglioni on all churches in the Friuli region damaged by the 1976 earthquake [9] - to whom we owe the decomposition of buildings in macro-elements - to researches carried out by GNDT, INGV and the Department of Engineering of Genova coordinated by Lagomarsino [10,11,12], regarding religious buildings only.

The fact that churches are more vulnerable compared to other historical buildings led in 1987 to a practical application of the first damage survey sheet, the GNDT-S3, which later would become the well-known "FORM A-DC church". This sheet was officially adopted for all religious buildings in 2001 [13], later modified and re-approved in 2006 [14] with a change in the section regarding the collapse mechanisms. More sheets have been added over the years, related both to movable assets and to other *buildings types*. Indeed the protocols for unmovable assets are based on the tendency of *same-type buildings* of being damaged in a similar way regardless of construction age, place, and materials used. Therefore, it was created the "FORM B –DP palaces" [14] for the most relevant historical buildings, which is quite recent and for this reason it is still object of discussion, improvement and optimization. All these sheets were then incorporated by the Italian Ministry of Cultural Heritage in the "*Guidelines for the evaluation and reduction of seismic risk on Cultural Heritage*" [15] and in the Directive 12/12/2013 "*Procedures for management of activities for cultural heritage securing and safeguarding in the event of emergencies caused by natural disasters* which, together with the NTC2018, represent the most relevant legal texts for any intervention on the architectural heritage damaged by earthquakes.

3 THE EMILIA-ROMAGNA CEMETERIES CASE

3.1 Morpho-typological observation on the Emilia-Romagna cemeteries

Modern cemeteries were born in 1804 with the Saint-Cloud edict through which Napoleon Bonaparte regulated the cemeteries construction and definitely demanding to build them far from urban areas. Through the edict, changes already taking place in burial areas were normalised. As a matter of fact, in the 17th century, cemeteries finally gained a topographic autonomy from the church's holy area, opening a debate whether burials should take place inside the church.

Between the second half of the 17th century and the first half of 18th century, public health debates and historical events affected the way people conceive death and especially the concept of "individual" burial (before it was a prerogative of illustrious figures only or for those who could afford it). Indeed through the Saint Cloud edict the individual burial became a "universal" right and since then it has been considered the founding event of the "culte des morts" (cult of the dead) in the modern western culture [16]. Subsequently practices as the "perpetual use" (i.e. the hereditary property of the land) and the funerary monuments became of common use. The modern cemetery, also called by some scholar "cimitero borghese" (bourgeois cemetery) [17], was then defined and seen as a mirror of the society and of a new hierarchical organization.

Furthermore, the decree of 12th June 1804 designated the garden-cemetery as a role model for the cemetery, like for example the Paris Père Lachaise cemetery (France, 1803).

Contrary to basic building, which are strictly connected to the settlement area [18], the *specialised building* such as cemetery does not undergo relevant changes in a *diatopic* sense [19]. Once its features have become solid, they tend to duplicate irrespective of territorial borders. The Père Lachaise model is the first example of the garden-cemetery *typological series* and spread throughout most of Europe and America (e.g. Mount Auburn Cemetery in Boston (USA, 1831).

In Southern Europe, the Saint Cloud edict collided with a still strong medieval tradition: the "*camposanto*" (literally holy field). The pre-existent burial ground integrated new norms and defined a second *typological series*, called by Donghi [20] "*a pianta architettonica*" (architectural drawing series) and by Vovelle "*paysage lapidaire*" (lapidary landscape) [21], in opposition to the garden-cemetery. This is a high architectural value solution, characterized by quadrangular areas fenced by walls, with porticoes of different sizes, which would have later become the most used solution in all small-and-medium-size cemeteries in Italy, especially in the area that we are examining: the Emilia-Romagna Region.

Based on this model, we can identify three different *variants*: a cemetery delimited by porticoes and with a central chapel, a cemetery delimited by porticoes without a central chapel and the reuse and/or renovation of huge buildings outside the city (Figure 2).

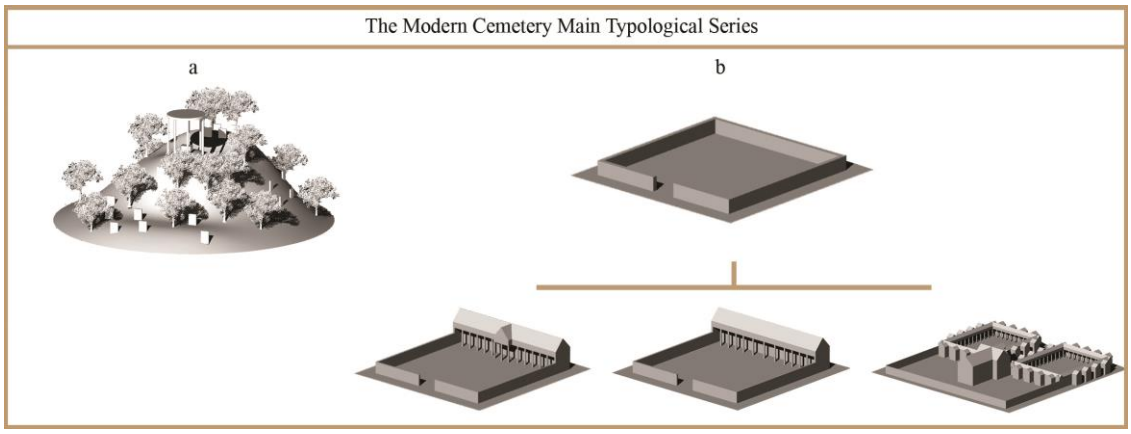


Figure 2: The main *typological series* of modern cemetery. The garden cemetery (a) and the architectural cemetery (b) with its three *variants* presented in Emilia-Romagna

The third group includes two buildings which historically arose on the border of the city: the chartreuses of the cities of Bologna and Ferrara which represent the only cases in Italy of conversion from chartreuse to cemetery [22]. The other *cemetery types* are the most common *variants* in the region, instead. They later have developed in different manners.

The requirements of the enlargement have led to a process that we can find in cities as well. A first growth was made possible through an *infill process* of the enclosure, through the porticoes extension (cemetery of Dosso (FE)), or the combination of family vaults next to each other (cemetery of Vigarano Mainarda (FE)). Alternatively, the cemetery has doubled in the area behind in the cases where an enlargement occurred within a large time distance to last developing phase (cemetery of Finale Emilia (MO)).

Once the space of first enclosure was full, the enlargement has followed the *successive doubling law* [18]. Cemeteries extended more and more and the whole area doubled in volume. Depending on the morphology and on soil availability, the enlargement took place in the area below (cemetery of Bondeno (FE)), or on one side (cemetery of Cento (FE) or Monumental cemetery of Concordia sulla Secchia (MO)). It is worth mentioning also the chartreuses of Ferrara where in the first half of the 19th century the renovation project provided for the creation of a new cloister standing alongside the existent one.

Further observations on cemeteries in Emilia-Romagna can also be made from a constructive point of view. The huge time windows of building development (from the second half of the 19th century – ongoing) coincides in the initial phases with a great transformation of the building process as a result of the introduction of new industrial materials and techniques: reinforced concrete and steel. A first analysis reveals how cemeteries were initially made of long porticoes, often in masonry, that enlarged over time and showed a more frequent use of reinforced concrete. Due to this progressive add-ons and juxtapositions cemeteries are an extremely complicated *building type*, also because traditional technologies exist alongside with new materials like reinforced concrete and steel. At the beginning porticoes are almost always covered by a non-structural bricks vault, usually a barrel vault but still we find several examples of cross vaults as well. The arch then progressively became a depressed-arch and finally turning into a false flat ceiling. Another relevant typological-constructive feature is the presence of columbaria introduced in the Italian cemeteries after the half of the 19th century in order to rationalise space. Indeed it is still possible to find cemeteries (cemetery of Bondeno(FE)) where the "camposanto" model is still a strong reference point. In this case columbaria are absent and the cemetery is a closed arcaded enclosure with headstone set in the floors.

Finally, we should consider the roofing structures. In the first phase they were generally made of wood and they show under two possible aspects: gable roof or single pitch roof reclined outwards. It is interesting to note that the geographical distribution of the two solutions has revealed a tendency in the Ferrara, Reggio Emilia and Bologna's territories to apply the first solution while in the Modena's area they preferred the second one. They both include elements as attics and/or decorations aimed at hiding pitches and crowning the entablature above the portico arcade.

In conclusion cemetery is a complex *building type*, where *morphological variants* are combined with a variety of building techniques and materials came up in the next enlargement processes (Figure 3). Both of these aspects are essential features to better understand the structure and the seismic response of an area.

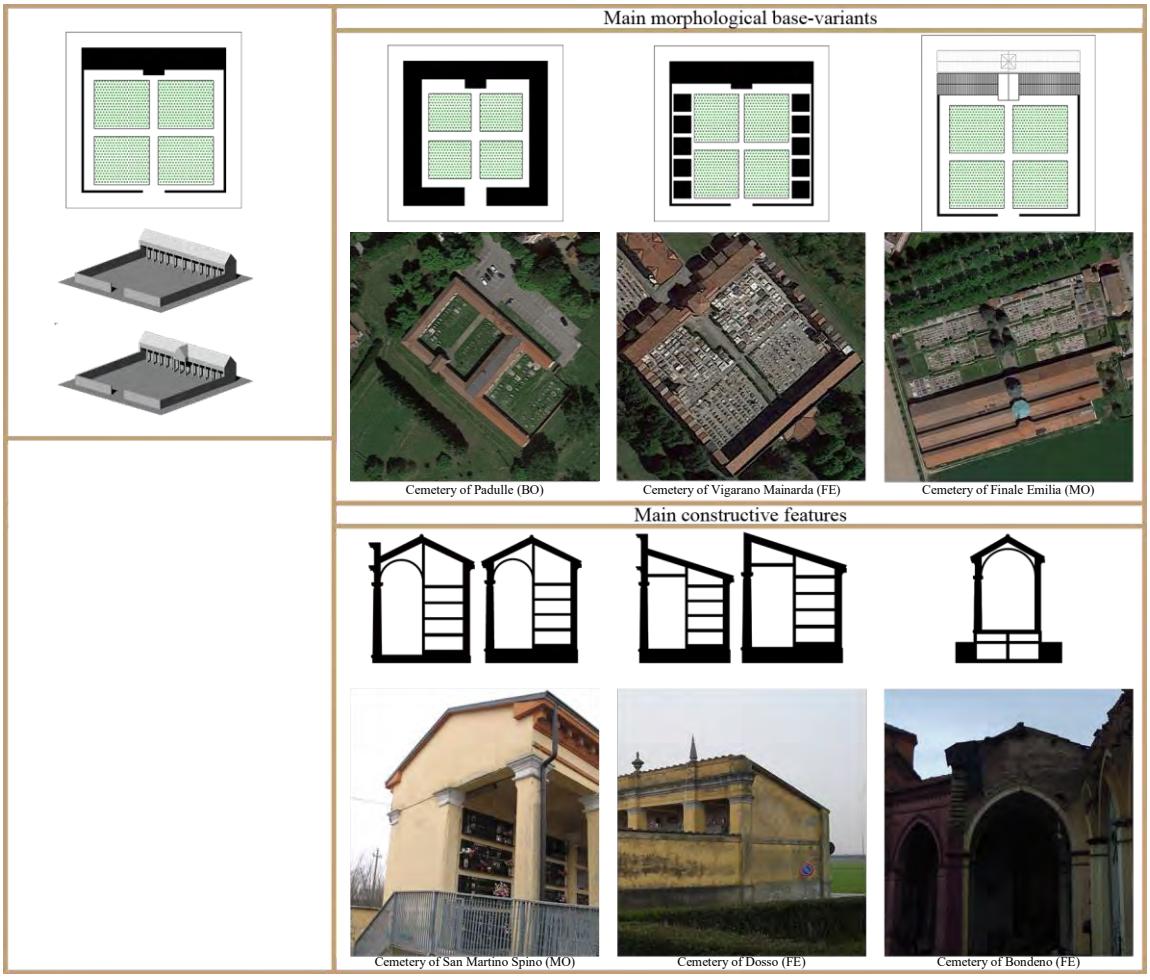


Figure 3: Main morphological and constructive features of the cemeteries in Emilia-Romagna

3.2 Recurring mechanisms of damage shown by cemeteries in Emilia-Romagna

The earthquake in Emilia-Romagna shed light on the vulnerability of historical cemeteries. Out of 300 protected cemeteries in the Region, over 100 were damaged following aftershocks, some of which were affected by major collapses. On average, there are two damaged cemeteries for each municipality in the area hit by the earthquake. Although this is a small percentage when compared to the total architectural heritage affected by the earthquake (more than 1800), issues of a hygienic-sanitary nature, but above all of a socio-cultural nature, require a targeted analysis. As a matter of fact, cemeteries are a place of memories and are an important component in the identity of places that must be safeguarded, especially in earthquake centers.

The analysis of the damage status of cemeteries in Emilia-Romagna allows an initial reflection, which can then be extended on a national scale, concerning the most recurrent collapse mechanisms.

The first evident, typological characteristic that generates an intrinsic vulnerability in the structure is, definitely, the presence of the portico. In this case, it is not a matter of a limited

extension within a larger volume, but of a macro-element which, when it is present, covers large areas, often on all sides, extending in length even for several tens of meters. In most cases, moreover, the portico is characterised by arches and vaults that add an additional element of weakness to the structure.

Covering structures are another element of great vulnerability. In both *typological variants*, these are thrust structures which generally have no seismic protection. In this regard, the case of the monumental cemetery of Finale Emilia is relevant. The first core area of the cemetery was built by two porticoed wings, with a single pitch, initially not connected to one another. The project was not brought to immediate completion and it was only from the 1930s onwards that the construction works of the monumental central atrium began. The project for the first expansion dates back from 1945 and the significant modification of the roof, changing it from a single pitch to a double pitch, occurred between 1930 and 1945. From the analysis of the 1945 project, it can be seen that the new roof had tie rods for reducing thrust. Following a survey of the attic of the cemetery, it can be observed that there is no trace of these tie rods and, perhaps, there never was.

It should also be emphasised that, during the expansion phases of the cemeteries, the roofing structure is the element that has undergone the greatest transformation with a marked tendency to replace the wooden structure with a brick-cement structure that is more rigid and heavier, which has entailed an additional burden on the wall structures subjected to seismic action.

The considerations mentioned above are even more evident in light of the collapse mechanisms activated most following the 2012 earthquake:

- Tipping over away from the colonnade floor (Figure 4). It represents the main collapse mechanism of the porticoed wings of the cemeteries, activated for most of the damaged units. This is a result of the summation of the seismic action to that of the thrust roof on the point feature of the portico. Furthermore, the presence of large replaced parts has almost always aggravated the situation, which in some cases led to collapse.



Figure 4: Cemetery of Mirandola - Tipping over away from the colonnade floor. It is worth mentioning the use of reinforced concrete beams and elements in steel in the structures.

- Collapse and/or damage to the vaults and suspended ceilings (Figure 5). Secondary mechanism with respect to that of the portico generally activated for the rotation of the plinths due to the tipping over of the colonnade.



Figure 5: Cemetery of Bondeno (a) and cemetery of Mirabello - damage to the vaults

- Damage by interaction of the structures. The heterogeneous set of buildings that develop by successive additions (see the arms of the columbaria which are completed in the extensions with the preparation of the walls for a new construction) is conducive to triggering interaction mechanisms among the structures (see, for example the interaction between the columbaria and the single central compartment, or when they are inserted in the same building).
- Tipping over of the projecting elements away from the floors (Figure 6). Although it does not trigger a structural collapse mechanism, the presence of attic solutions, point and/or linear architectural elements aimed at hiding the pitches of the roof constitutes a serious vulnerability in the structure. The tipping over of these elements can take place externally or inwards.



Figure 6: Monumental cemetery of Concordia Sulla Secchia -Tipping over of the projecting elements away. In this case the projecting elements are collapsed inside the structures

- Mechanisms of the surrounding wall. The relationship between a modern cemetery and sacred ground is substantiated with the presence of the wall that surrounds the consecrated area. If the saturation of the perimeter has not been completed or if it was carried out for subsequent doubling of the buildings or, also, if the cemetery is saturated by burial in the ground (a typical feature of Israelite cemeteries), the surrounding wall can only represent one of the first vulnerabilities. This manifests itself through the activation of mechanisms of bottom subsidence or tipping over away from the floors.

Finally, the records described here do not deliberately take into account the presence of the single central room, atrium or often chapel, present in almost all the cemeteries. In general, part of the collapse mechanisms reported in "FORM A-DC church" describe the various vulnerabilities that occur under seismic action for these elements.

3.3 The application of existing tools to cemeteries

"FORM A-DC church" and "FORM B –DP palaces" are, therefore, the models applied in the 2012 earthquake in Emilia-Romagna. The use of these tools, strictly connected to the *type* they describe, even if they are the only ones currently available, has highlighted the need to intervene with appropriate adjustments, in particular with reference to *types* of a different nature such as cemetery units. In this case, numerous problems have affected the damage detection process.

First of all, the operators chose the most suitable form to use. The answer to this question in 2012 was ambiguous and followed three different approaches. In some cases, the choice fell on the use of only "FORM A-DC church". This preference, which has the certain advantage of embracing all the aspects borrowed from ecclesiastical buildings (chapels with apses, domes, pediments, etc.), probably arises from the willingness to identify the element of greatest vulnerability in the portico. When filling in the form of the cemetery of Sant'Agostino, both mechanism 5 and 7 are identified as a vulnerability, i.e. 'transversal response of the hall' and 'longitudinal response of the colonnade', so as to be able to insert collapse mechanisms for both actions of the forces acting on the porch. In contrast, the "FORM A-DC church" does not face a problem such as the large spatial articulation of cemeteries, the wings of which can be damaged in different ways.

This is probably the motivation that led most compilers to use "FORM B –DP palaces", a model that, since it is studied for buildings, by means of dividing it into areas it allows greater articulation in the description of the damage, considering the responses of the structure and different mechanisms of collapse for the different parts examined. Although from a first analysis, the form seems to allow greater descriptive freedom, it however lacks the description of the typical mechanisms of large halls of an ecclesiastical nature. The impossibility of indicating the mechanism in the section dedicated to the calculation of the damage index (although it is often correctly reported in the note) prevents the correct calculation of the index itself. Furthermore, it is the same freedom and at the same time the descriptive rigidity of the form that causes excessive simplifications in relation to the extension of the cemetery unit. In the monumental cemetery of Mirandola, with reference to the precise cataloguing of the walls, we finally come to describe the state of collapse of a portion of them but not the initial collapse of the surrounding areas, therefore indicating only one part of the damage.

The inadequacy is even more evident if it is reflected in the damage indices associated with the two cemeteries mentioned above: 0.17 for the Sant'Agostino cemetery and 0.12 for the Mirandola cemetery on a scale from 0 to 1. The first is severely damaged due to the relative movement between the parts generated by the liquefaction of the soil. In addition to collapsed areas, the second cemetery has large portions that are close to collapse. In both cases, the damage index should have been greater than was actually calculated.

Probably, the need to interpolate both characteristics present in the two forms has led to a percentage of compilers for the choice of breaking down the cemetery according to the two models using "FORM A-DC church" for the mortuary chapel and "FORM B –DP palaces" for the remaining areas. Although the choice seems to be the natural solution to the problem of the inadequacy of the single instrument, in reality it does not provide a uniform indication of the damage to the building.

Furthermore, the breakdown of the cemetery into multiple micro-units is an additional problem. The use of multiple forms is in fact allowed in relation to the identification of a structurally separate unit. Although this criterion seems to have been respected for some cemeteries, where the subdivision follows the scan in separate blocks of the columbarium, in other cases the unit is considered as unified giving up the compilation of separate forms for each block and, in others, it is still divided into several parts (for example by construction period), without which they can necessarily be considered structurally independent. In the first case, there is a summary description of the damage. In the second case, there is also a detailed description for each unit that does not necessarily take into account the probable interaction between the different parts.

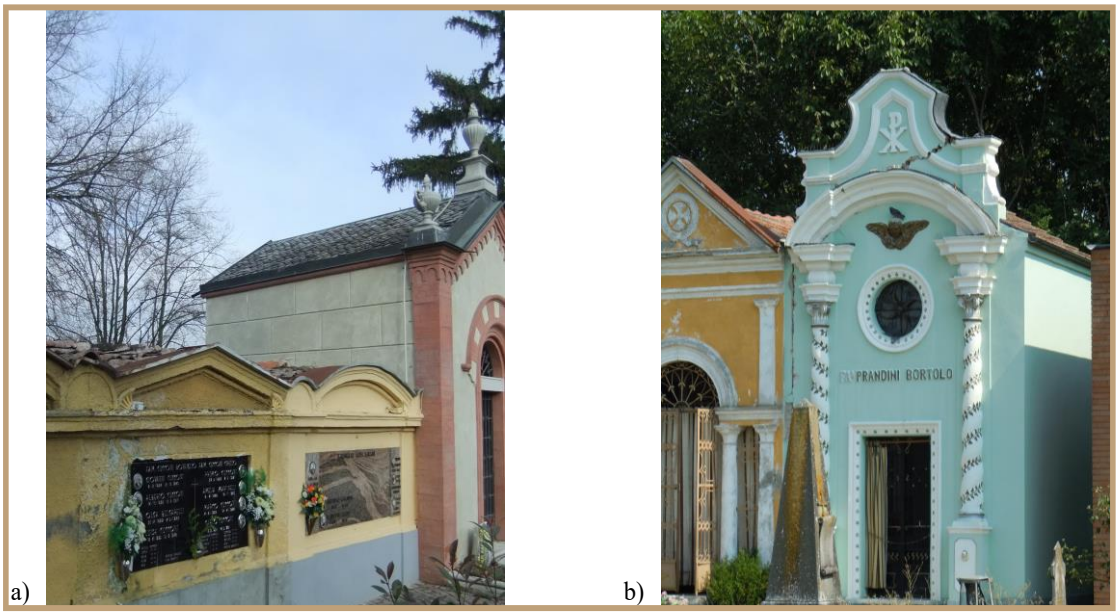


Figure 7: Different types of family chapels: a) chapels connected at columbaria and at the structures of the cemetery; b) chapels as separated units.

Finally, a further issue found in the damage characterisation process is linked to the experimentation, during 2013, of a "FORM B –DP palaces" aimed at facilitating the

compilation of the one adopted to date, which is considered too complex and not very expeditious. The attempt to simplify the new form - which no longer required a detailed description of all the walls, but a twofold rating of the level of damage and on the level of vulnerability - has proved to be particularly complex for compilers as evidenced by a significant amount of forms where the only damage correctly reported is the one related to the roof covering.

In the margin, a necessary reflection is added on whether family chapels are to be considered as annexed bodies (on the same form) or else should they be considered as structurally separate units (a new form)(Figure 7) ? On wall and/or statuary headstones, and on other characteristics related to the *cemeterial type*. It is easy to understand how the tools existing today are insufficient in damage detection operations.

4 CONCLUSIONS

The "2012 Emilia" earthquake has enabled us to identify both the strengths and the weaknesses in the procedures of emergency management useful for the reconstruction.

The damage survey aims at giving a first description useful to understand the damage level of the Architectural Heritage and at improving the safety measures. It also aims at making a first economic assessment of the reconstruction costs, that is why if the evaluation is as close as possible to the real needs we are more aware of the resource management and easily identify priority actions.

Economically, in Emilia-Romagna the *specialised types* not including Churches and Palazzos cost more than 300 million of euros, 59 of which are used for cemeteries. Through a deeper analysis we can see that the costs - intervention by intervention - sometimes end up totally different from what has been previously estimated in the sheets.

The analysis of the buildings damaged by "2012 Emilia" earthquake, belonging to different *specialised types*, currently represents a great opportunity to implement the existent instruments. Such as for previous earthquakes [9,10,11,12], the typological analysis, the vulnerability evaluation, and the observation deriving from the same sheets compiled after the "2012 Emilia" earthquake, would give us new tools to use together with the existent ones.

Acknowledgements. The authors would like to acknowledge the Emila-Romagna Region for funding the research. Funding provided by European Social Fundings of the Operational Programme 2014/2020 Regione Emilia-Romagna: High Competences for Research, for Technology Transfer and Business.

REFERENCES

[1] Zuppiroli, M. La regione Emilia-Romagna a sette anni dal sisma 2012. *Ananke* (2019) **87**: 84-87.

[2] Regione Emilia-Romagna. *2012-2019 L'Emilia dopo il sisma. Report su sette anni di ricostruzione*. Centro stampa Regione Emilia-Romagna, (2019).

[3] Capriotti, P. (edited by) *Ricostruire l'emergenza - Cronologia della gestione istituzionale del sisma e sintesi tematica.* (2014). [online] Available at: http://territorio.regione.emilia-

romagna.it/paesaggio/pubblicazioni/Dossiersisma.pdf.
[4] Zuppiroli, M., Vona, V. Dall'analisi del costruito storico danneggiato dal sisma alla definizione di nuove procedure per l'analisi del danno. *Paesaggio Urbano* (2019) **1**: 170-179.
[5] C. Bartolomucci et alii. Dopo la catastrofe: una casistica rappresentativa dello stato dei monumenti danneggiati dai terremoti aquilano ed emiliano. *Materiali e strutture. Problemi di conservazione, n.s., a. I* (2012) **1- 2**: 45-80.
[6] Dalla Negra, R. Eventi eccezionali e principi conservativi: il terremoto emiliano. *Materiali e strutture. Problemi di conservazione*, *n.s., a. I* (2012) **1-2**: 32-34.
[7] Lagomarsino, S., Podestà, S. (edited by) *Inventario e vulnerabilità del patrimonio monumentale dei parchi dell'Italia centro-meridionale e meridionale, Vol. III - Analisi di vulnerabilità e rischio sismico degli edifici monumentali*. I.N.G.V.-G.N.D.T (2005).
[8] Papa, S., Di Pasquale, G. (edited by) *Manuale per la compilazione della scheda per il rilievo del danno ai beni culturali, Chiese MODELLO A – DC*. Presidenza del Consiglio dei Ministri, Dipartimento di Protezione Civile (2013).
[9] Doglioni, F., Moretti, A., Petrini, V. (edited by) *Le chiese e il terremoto - Dalla vulnerabilità constatata nel terremoto del Friuli al miglioramento antisismico nel restauro, verso una politica di prevenzione*. LINT (1994).
[10] Lagomarsino, S., Podestà, S. Seismic vulnerability of ancient churches. Part 1: damage assessment and emergency planning. *Earthquake Spectra* (2004) **20(2)**: 377-394.
[11] Lagomarsino, S., Podestà, Seismic vulnerability of ancient churches. Part 2: statistical analysis of surveyed data and methods for risk analysis. *Earthquake Spectra* (2004) **20(2)**: 395-412.
[12] Lagomarsino, S., Podestà, S. Damage and vulnerability assessment of churches after the 2002 Molise, Italy, earthquake. *Earthquake Spectra* (2004) **20(S1)**: S271-S283.
[13] Presidenza del Consiglio dei Ministri. Decreto del 3 maggio 2001. *GU Serie Generale* (2001) **116**: 17-30.
[14] Presidenza del Consiglio dei Ministri. Decreto del 23 febbraio 2006. *GU Serie Generale* (2006) **55**: 26-51.
[15] Ministero per i Beni e le Attività Culturali, *Linee guida per la valutazione e riduzione del rischio sismico del patrimonio culturale*. Gangemi (2006).
[16] Aries P. *L'homme devant la mort*, Éditions du seuil (1977).
[17] AA VV. *La città dei morti: breve storia del cimitero*. M&B (2000).
[18] Caniggia, G., Maffei, G. L. *Lettura dell'edilizia di base*. Marsilio Editori (1987).
[19] Maffei, M., Maffei, G. L. *Lettura dell'edilizia speciale*. Alinea editrice (2011).
[20] Donghi, D. *Manuale dell'architetto*. UTET (1935).
[21] Vovelle, M. A la croisée des mémoires. In Bowie, K., Healey, C., Bos, A. (edited by) *Le Père-Lachaise*. Action Artistique de la Ville de Paris (1998).
[22] Guerzoni, G. *Le pietre, gli orti, l'arte, la morte: san Cristoforo di Ferrara da Certosa a cimitero*. Interbooks (1992).

12th International Conference on Structural Analysis of Historical Constructions
SAHC 2020
P. Roca, L. Pelà and C. Molins (Eds.)

TYPOLOGICAL CLASSIFICATION AND OBSERVED DAMAGE PATTERNS OF MASONRY CHURCHES AFTER THE 2016 CENTRAL ITALY EARTHQUAKE

G. CIANCHINO[1], G. DE MATTEIS[2] AND G. BRANDO[1*]

[1]Department of Engineering and Geology,
University ''G. d'Annunzio'' of Chieti Pescara, Pescara, Italy
e-mail: giorgia.cianchino@unich.it,
gbrando@unich.it (*corresponding author)

[2]Department of Architecture and Industrial Design,
University of Campania "Luigi Vanvitelli", Aversa, Italy
email: gianfranco.dematteis@unicampania.it

Keywords: Historical Structures, Masonry Churches, Cultural Heritage, Damage Probability Matrices, Damage Scenarios, 2016 Central Italy Earthquake.

Abstract. *The seismic protection of cultural heritage is an important topic that has been faced by several researchers in the last decades. Seismic events of the past have highlighted the need of achieving a proper knowledge of the vulnerability of cultural heritage, in particular of churches, in order to put in the field proper mitigation measures at the large scale. According to this premise, this paper deals with the damage scenario observed on eighty seven churches hit by the 2016 Central Italy earthquake. In a first stage, the most important structural features of the studied churches are discussed and threated by the statistical standpoint. The reported information have been collected through the A-DC form, adopted by the Civil Protection Department and by the Ministry of Heritage and Cultural Activity and Tourism (MiBACT), which was used in the framing of the damage reconnaissance activity carried out by the ReLUIS Italian consortium in the aftermath of the earthquake. Also, the form has been used in order assess the damage of each macro-element and, then, to assign a damage index to each church. The presented work is framed in a wider research activity that aims at providing a predictive methodology for the vulnerability assessment of churches at the regional scale. This methodology was already calibrated on the basis of the 2009 L'Aquila seismic event. The outcomes presented in this paper will serve to further prove the reliability of the proposed model.*

1 INTRODUCTION

The last seismic sequence that hit the central regions of Italy began the 24th August 2016, with an event of magnitude 6.0 MW occurred in Amatrice and Accumuli (in the district of Rieti). Then, it had its peak the 30th October, with epicenter in Norcia, in the district of Perugia, when a magnitude of 6.5 MW was reached. The whole seismic sequence affected 1200 square kilometers in the central Apennines and included the Regions of Abruzzi, Lazio, Marche and Umbria, as it is shown in Figure 1 when the affected areas and the epicenters are shown.

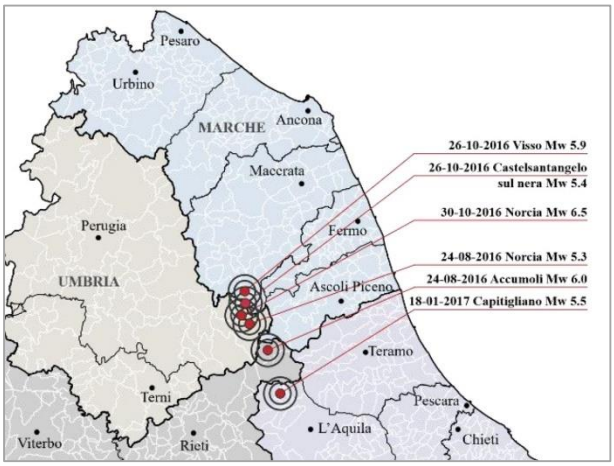


Figure 1: Seismic sequence of Central Italy earthquake

Since the first shock it was immediately clear that the earthquake was capable to produce devastating scenarios. In fact, 299 deaths and more than 300 injuries were registered, with the destruction of entire municipalities such as Accumuli, Amatrice and Arquata del Tronto. Fortunately, the following earthquakes did not provoke analogous quantities of deaths and injuries, as people were properly dislocated, but several buildings in the affected urban centers collapsed.

Churches undertook an outstanding damage: they showed, again, a high fragility following a seismic event because of the high number of sources of fragility. An important example is the cathedral of Norcia, where the central part of the church collapsed following the shock of the 30th October. Only the façade remained standing, becoming one of the saddest symbol of the 2016 Central Italy earthquake.

The work presented in this paper offers the possibility of outlining the damage suffered by a group of 87 churches affected by the 2016 earthquake. This damage was analyzed following the post-earthquake inspections conducted by the authors with the technicians of the Civil Protection and of the Ministry of Cultural Heritage, through the application of the " A-DC" form. The latter was used for emergency management purpose after the earthquake, with the aim of evaluating the accessibility of Cultural Heritage.

The paper is articulated as follows. In Section 2, the seismicity of the area is briefly shown; next the group of churches dealt with in the paper, as well as their characteristics, are described. Then (Section 3) the damage scenario is analyzed by comparing the formulation of the A-DC forms and the methodology proposed by the Cultural Heritage Guidelines. Finally, a statistical analysis of the damage undertook by both the whole churches and the single macro-elements is presented.

2 HISTORICAL SEISMICITY OF THE ANALYZED AREA

The 2016 Central Italy earthquake hit an area characterized by a relevant historic seismicity [1][2][3]. In the core of the “seismic crater” (the area hit by the earthquake appointed by the Italian government for economical support) the strongest event occurred in the 18th century, during the 1703 earthquakes in Valnerina and L'Aquila (Magnitude 6.7 Mw). These earthquakes were really devastating and caused tens of thousands of victims overall [4]. The

Amatrice area suffered 4 strong historical earthquakes: those are the earthquake of 1627, with the epicenter in Accumuli (5.3 MW), the earthquake of 1639 with epicenter in Amatrice (6.2 MW), the earthquake of 1646 with epicenter in Monti della Laga (5.9 MW) and the earthquake occurred in 1672 with the epicenter in Amatrice (5.3 MW). In the southern area of the crater, affected by the seismic event of the 18th January, the most historically important events are those deriving from the Abruzzo area: in 1619 in the L'Aquila area, magnitude 5.3 MW, in 1950 in the Teramo area, magnitudo 5.7 MW and in the 2009, again in the L'Aquila area.

3 THE STUDIED CHURCHES

87 churches located in the area affected by the earthquake have been inspected by the authors. For this analysis, the "A-DC" form, proposed by the Ministry of Cultural Heritage, was used. This form allows to evaluate the state of usability of the churches according to the severity of the collapse mechanisms activated by the earthquake on the single macro elements.

The considered churches were built at very different times, with a minimal prevalence of 17th century buildings (18%). They are distributed in the three regions of Abruzzi (70%), Lazio (15%) and Marche (15%), with a larger distribution in the provinces of Teramo (Abruzzi) and Ascoli Piceno (Marche). Overall the churches present features that are typical of the Apennine areas.

The analyzed churches are often characterized by very regular plants. As shown in Figure 2a, 79% has a single rectangular nave, 5% has two naves and the remaining 16% is made of a three naves plant.

Most of the churches are very small, often belonging to small municipalities and characterized by a single nave, with a gabled facade and light coverage. A representative example of the typology is the church of Madonna delle Grazie in Isola Del Gran Sasso (TE), shown in Figure 2b.

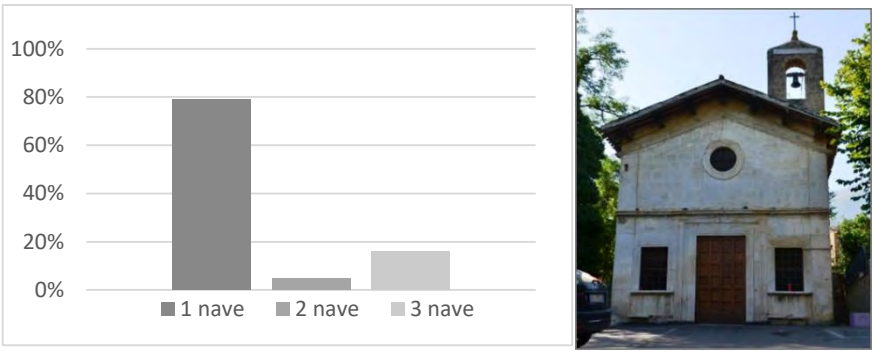


Figure 2: a) Typological distribution of churches; b) Madonna delle Grazie church in Isola del Gran Sasso (TE).

The analysis highlighted the different types of facades, with a predominance of gable façades (51%) and a minority made of façades enclosed within two towers (1%), as shown in figure 3.

In figure 4a the frequencies of the observed types of bell tower is shown. A prevalence of bell gables and tower bells (almost 40% each) has been revealed; cell bell tower have been observed for the 10% of the cases, whereas, for the remaining 10 % no bell towers have been observed.

The presence of the other architectural elements that generally characterize churches with huge dimensions, such as transepts, domes and chapels, have been found seldom. In particular,

the transept is present only in 2% of cases, the dome in 6%, the chapels in 21%. The results are summarized in Figure 4b.

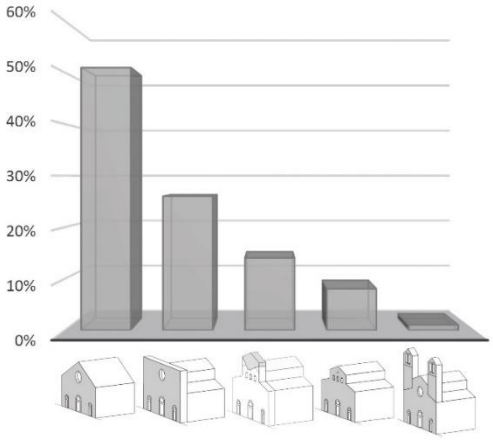


Figure 3: Different types of facades

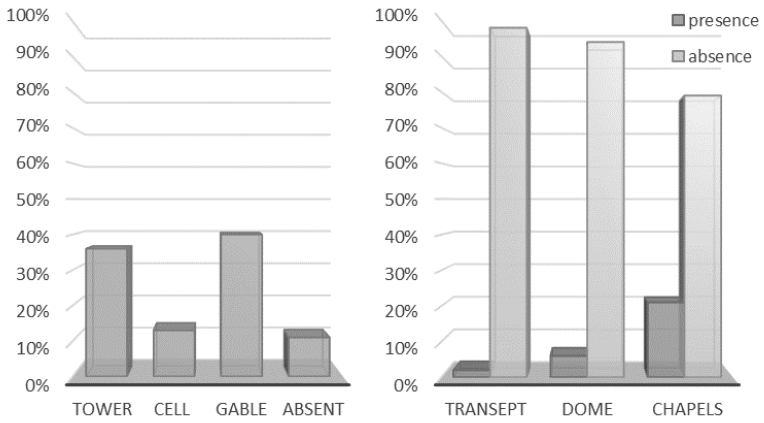


Figure 4: a) Type of bell tower b) Presence/absence of the macroelements transept, dome and chapels

The 39% of churches present vaulted roofs. However, it should be considered that a substantial number of churches (36%), have wooden cover. The remaining churches (24%) have flat roof, and the 1% have present steel roofs that, evidently, were added recently.

4 DAMAGE ANALYSIS

4.1 Damage analysis according to the A-DC form

The damage analysis was carried out by collecting the information given by the A-DC form. The form defines 28 potential collapse mechanisms, according to the Cultural Heritage Guidelines (2010) [5]. These are listed in table 1.

or each mechanism, a judgment on the severity of the damage provoked by the earthquake was given. This judgment consisted in a score d_k ranging from k=0 to k=5 and increasing with the severity of damage (d_0=0 in case of absent mechanism, d_5=5 for mechanisms associated to collapse of the macroelement) .

Table 1. The 28 mechanisms considered by the A-DC form

m	mechanism	ρ_m
1.	Façade overturning;	1
2.	Mechanism at the top façade	1
3.	Mechanism in plane of façade	0.5
4.	Narthex	0.25
5.	Transversal response	1
6.	Shear mechanism lateral walls	1
7.	Longitudinal response	1
8.	Central nave vaults	1
9.	Aisles vaults	0.75
10.	Transept façade overturning	0.75
11.	Shear mechanism in transept	0.5
12.	Transept vaults	0.75
13.	Triumphal arches	1
14.	Dome	0.75
15.	Lantern	0.25
16.	Apse overturning	0.75
17.	Shear mechanism in apse	0.5
18.	Apse vaults	1
19.	Mechanism in roof of the nave	0.5
20.	Mechanism in roof of transept	0.5
21.	Mechanism in roof of apse	0.5
22.	Chapel overturning	0.25
23.	Shear mechanism in chapels	0.25
24.	Chapel vaults	0,5
25.	Plan-height irregularity	1
26.	Architectural details	0.25
27.	Bell tower	1
28.	Bell cell	0.5

Then a damage index $i_{dA\text{-}DC}$, for each church, has been defined, according to the expression eq(1).

$$i_{dA-DC} = \frac{\sum_{m=1}^{n} d_{k,m}}{5 \cdot n} \tag{1}$$

where m is a generic mechanism to which the score $d_{k,m}$ is associated and n is the number of possible mechanisms that are present in the analysed church.

4.2 Damage analysis according to Cultural Heritage Guidelines

The procedure described in Section 4.1, used for the purpose of defining an immediate judgment for accessibility on the churches during the reconnaissance activity, does not actually take into due account that the different collapse mechanisms may have a different importance to the for the purpose of global stability. To take this into account, a second analysis was conducted using the indications of the Guidelines on Cultural Heritage (2010) that associate to the generic mechanism m a weight factors ρ_m to be introduced in the formulation of the damage index i_d expressed in eq. (1), which is modified as reported in eq. (2).

$$i_{dGuid} = \frac{1}{5} \cdot \frac{\sum_{m=1}^{n} \rho_m \cdot d_{k,m}}{\sum_{m=1}^{n} \rho_m} \tag{2}$$

The ρ_m factor is 0 when the mechanisms that cannot be activated in the church due to the absence of the macroelement, while it ranges between 0.5 and 1 in the other cases [6]. The considered values of ρ_m, as indicated in [7], are given in Table 1.

4.3 Damage levels for the whole churches

The damage indices, obtained for each church by applying both the two procedures described above, were used to define a global damage level D_k, variable from 0 to 5 ($D_0 = 0$, $D_1 = 1$ ... $D_5 = 5$) according to criteria defined in the literature by Lagomasino and Podestà (2004) [8].The criteria are summarized in table 2.

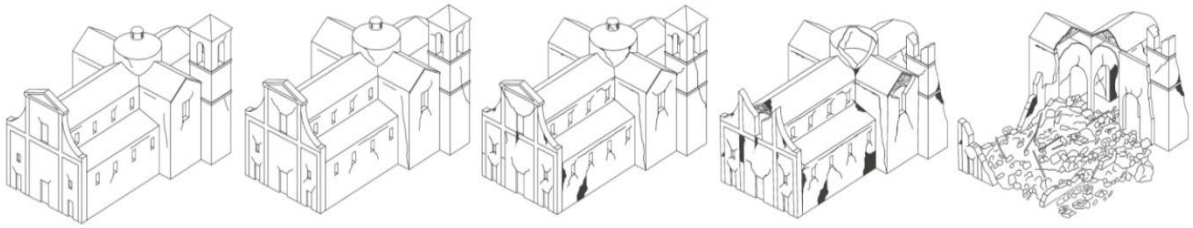
Table 2: Relation between the damage index i_d and the global damage level D_k, according to [8]

D_k	i_d
D_0	$i_d \leq 0.05$
D_1	$0.05 < i_d \leq 0.25$
D_2	$0.25 < i_d \leq 0.4$
D_3	$0.4 < i_d \leq 0.6$
D_4	$0.6 < i_d \leq 0.8$
D_5	$i_d > 0.8$

The damage level D_k can be related to the limit states listed below [9]:

- D_0: no damage
- D_1: light damage
- D_2: moderate damage
- D_3: serious damage
- D_4: very serious damage (partial collapses)
- D_5: collapse

They are schematically represented in Figure 5.



$D_k=1$ $D_k=2$ $D_k=3$ $D_k=4$ $D_k=5$

Figure 5: Limit states corresponding to the five damage levels D_k

The obtained D_k, obtained according to the two procedures discussed in Section 4.1 and 4.2, are reported in Figure 6 (organized in two graphs arranged on two rows). As it is possible to observe, the two procedures give almost the same results except for six cases.

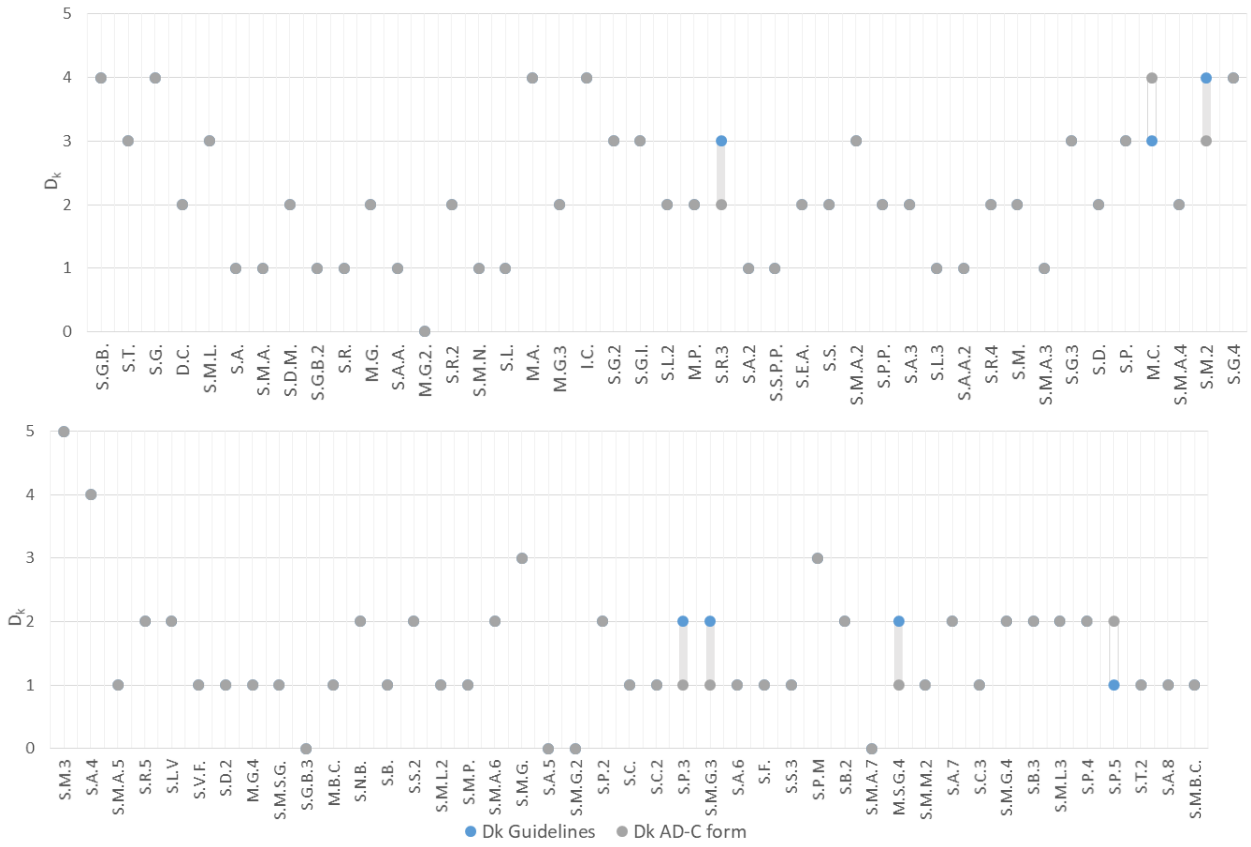


Figure 6: Damage levels (D_k) for churches

4.3 Observed and predicted damage

The elaboration of the frequencies of the obtained D_k evaluated for the studied 87 churches has allowed the definition of the so called Damage Probability Matrix (DPM), shown in Figure 7, which is as a useful tool for representing the occurred damage scenario.

It must be pointed out that the conducted analysis concerns a very large territory, with macroseismic intensity varying between IV and VII measured in the MCS scale. For this reason, the proposed DPM can be intended, in a predictive key, as a tool for the evaluation of the vulnerability of the churches at regional scale. This evaluation can be generally applied also to other territories presenting churches with the same features of the here analysed ones.

Always in Figure 7, it is possible to observe that the gathered frequencies could have been predicted by applying the binomial probability distribution (DPF) provided in eq. (3), once that the mean damage μ_D had been assessed.

$$p_k = \frac{5!}{k!\cdot(5-k)!}\cdot\left(\frac{\mu_D}{5}\right)^k\cdot\left(1-\frac{\mu_D}{5}\right)^{5-} \tag{3}$$

where

$$\mu_D = \frac{\sum_{i=1}^{\kappa} D_\kappa}{\kappa} \tag{4}$$

Being κ the number of analyzed churches.

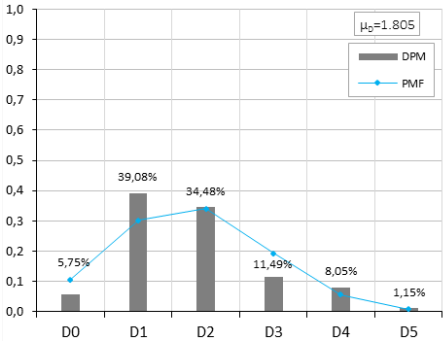


Figure 7: Damage Probability Matrix (DPM) of the analyzed churches

This result confirms what has been found by other studied related to Italian churches hit by earthquakes of the past (see, for example, [10]).

4.4 Macroelement analysis

The most important damages observed during the inspection in the churches were mostly related to mechanisms involving the facades and roofing system in the central nave. Significant damage levels were also found on the bell towers and gables.

With reference to failure mechanisms of the facade macro-element [11], the 26% of the churches presented damage D_0, the 17% damage D_1, the 28% damage D_2, the 14% damage D_3, the 7% damage D_4 and the remaining 3% damage D_5. An example of this type of mechanism was found in the Church of Santa Giusta in Cortino (TE), which has very serious cracks in the facade plan to which damage D4 has been attributed (Figure 8a).

Many of the out-of-plane mechanisms occurred in the presence of poor masonry. This is the case of the church of San Michele in Valle Castellana (TE), which showed a collapse of a portion of the facade. The poor wall quality and the absence of transverse connections contributed to the delamination of the external material (Figure 8b).



Figure 8: a) Santa Giusta church in Cortino (TE); b) San Michele church in Valle Castellana (TE)

It is important to note that more than half of the bell towers or gables resulted seriously damaged. These are slender elements, which often do not present any type of anti-seismic devices. Therefore important damages and, in some cases, collapses have been observed. An example is the bell gable of the church of San Paolo in Cortino (TE), where a partial collapse

was found (Figure 9).



Figure 9: The damaged bell gable of San Paolo a Cortino (TE)

The damage analysis was also carried out for all the other macroelements. The data have been gathered according to the observed mechanisms listed in Table 1 and organized as listed below:

- Out of plane (mechanisms number 1-10-16)
- Facade (mechanisms number 2-3-4)
- Lateral walls (mechanisms number 6-11-17-25)
- Chapels (mechanisms number 22-23)
- Columns (mechanism number 7)
- Dome (mechanisms number 14-15)
- Roofing system (mechanisms number 19-20-21)
- Bell tower/gable (mechanisms number 27-28)
- Arches and vaults (mechanisms number 5-8-9-12-13-18-24)
- Decorations (mechanism number 26)

The frequencies of the reported damage are shown in Figure 10. It is interesting to note that, also in this case, the associated damage levels can be well interpreted through the application of the binomial probability distribution that, therefore, can be intended as a predictive tool also when the prevision is carried out on the single mechanisms involving the single macroelements. This result confirm what was found in [12] by the Authors with reference to the churches in Abruzzi hit by the 2009 L'Aquila earthquake.

4 CONCLUSIONS

In this paper an extensive analyses of the damage observed on 87 churches hit by the 2016 Central Italy earthquake has been proposed. The main results can be summarized as follows:

- In the analyzed stock, mainly composed by small churches with a single nave and a rectangular plan, the higher damage was observed on the façade and on the bell towers/gables;
- The observed damage scenario has been represented in terms of Damage Probability Matrix (DPM) and the gathered frequencies have been interpreted by means of the binomial probability distribution that proved to be reliable in reproducing the observed scenario once that the mean damage is known;

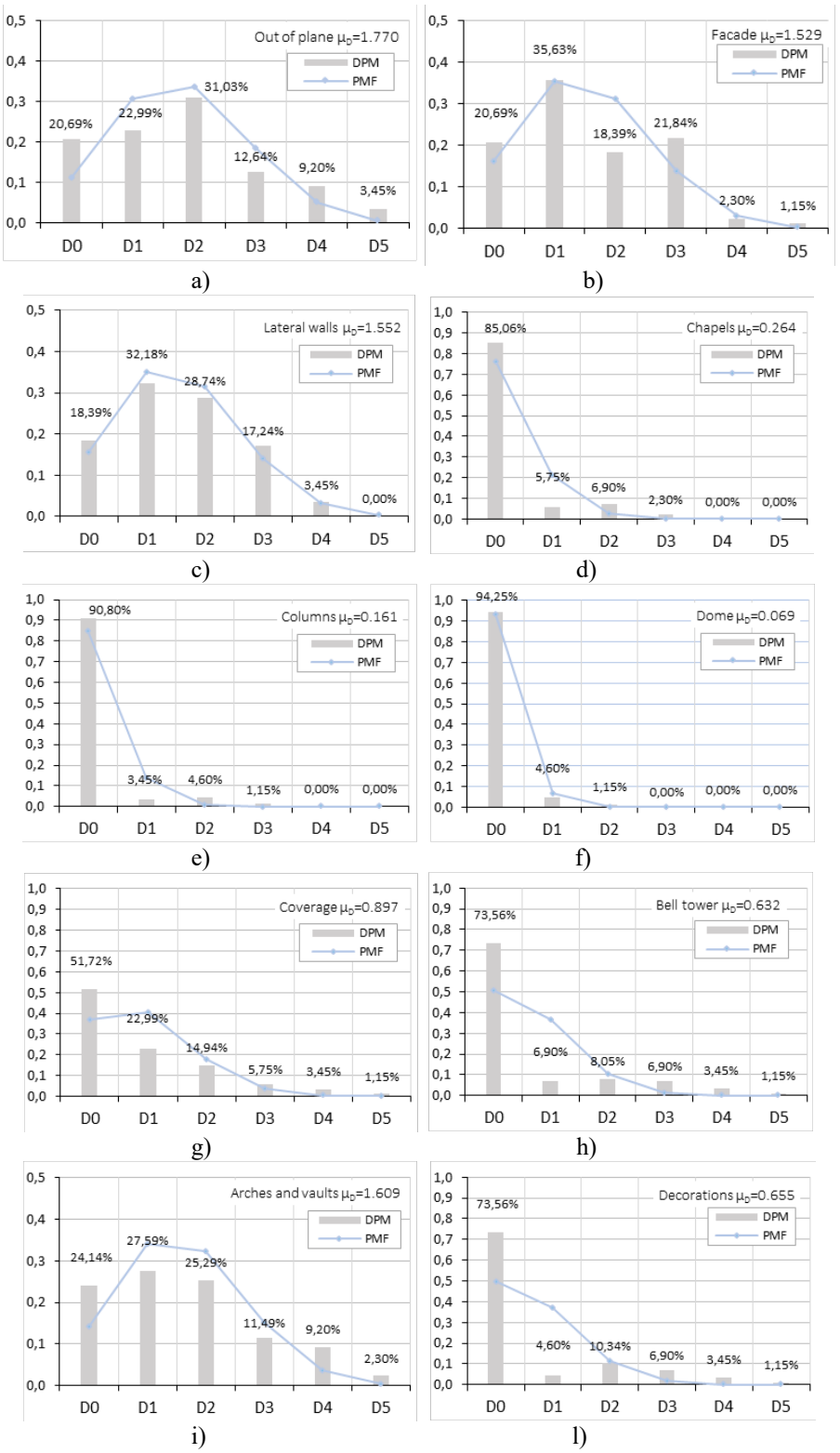


Figure 11: Statistical analysis of damage by macroelements with probabilistic interpretation according to binomial distribution (a) Out of plane, (b) Facade, (c) Lateral wall, (d) Chapels, (e) Column, (f) Dome, (g) Coverage, (h) Bell tower, (i) Arches and vaults, (l) Decorations.

- As already discussed in previous studies carried out by the authors, DPMs are an effective tool also to interpret the damage provoked by mechanisms involving single macroelements.

Acknowledgements. This study has been developed within the Italian research Project ReLuis. The reconnaissance activities have been carried out by the authors with the technicians of the Ministry of Cultural Heritage (MIBACT). A part of the presented study has been extracted from the graduation thesis of Dr. Cristina Schiavi.

REFERENCES

[1] Gruppo di Lavoro INGV sul terremoto in centro Italia, 2016. Rapporto di sintesi sul Terremoto in centro Italia Mw 6.5 del 30 ottobre 2016, [DOI: 10.5281/zenodo.166019].

[2] Gruppo di lavoro INGV 2017. "Relazione sullo stato delle conoscenze sulla sequenza sismica in centro italia 2016-2017 (Aggiornamento Al 2 Febbraio 2017)." 2017.

[3] Gruppo di lavoro INGV. 2016. "Second Summary Report of the Ml 6.0 Amatrice Earthquake of August 24, 2016 (Central Italy)." 2016.

[4] Tashkov, L., Krstevska, L., Naumovski, N., De Matteis, G., Brando, G. 2010. Ambient vibration tests on three religious buildings in Goriano Sicoli damaged during the 2009 L'Aquila earthquake COST ACTION C26: Urban Habitat Constructions under Catastrophic Events - Proceedings of the Final Conference, pp. 433-438.

[5] Linee Guida per la valutazione e riduzione del rischio sismico del patrimonio culturale allineate alle nuove Norme tecniche per le costruzioni (d.m. 14 gennaio 2008). Normativa Italiana per la protezione dei beni culturali. Ministero per i Beni e le Attività Culturali, 2010. Circolare n.26.

[6] Criber, E., Brando, G., De Matteis, G., 2015. The effects of L'Aquila earthquake on the St. Gemma church in Goriano Sicoli: part I—damage survey and kinematic analysis. Bulletin of Earthquake Engineering, 13 (12), pp. 3713-3732.

[7] De Matteis, G., Criber, E., Brando, G. 2016. Damage Probability Matrices for Three-Nave Masonry Churches in Abruzzi After the 2009 L'Aquila Earthquake. International Journal of Architectural Heritage, 10 (2-3), pp. 120-145

[8] Lagomarsino, S., Podestà, S., 2004. Seismic Vulnerability of Ancient Churches: II. Statistical Analysis of Surveyed Data and Methods for Risk Analysis. Earthquake Spectra, Volume 20, No. 2, pages 395–412, May 2004.

[9] Grunthal, G., 1998. European Macroseismic Scale. Centre Européen de Géodynamique et de Séismologie, Luxembourg; Vol. 15.

[10] De Matteis, G., Brando, G., Corlito, V., 2019. Predictive model for seismic vulnerability assessment of churches based on the 2009 L'Aquila earthquake. Bulletin of Earthquake Engineering. In press

[11] Brando, G., Criber, E., De Matteis, G. 2015.The effects of L'aquila earthquake on the St. Gemma church in Goriano Sicoli: part II—fem analysis. Bulletin of Earthquake Engineering, 13 (12), pp. 3733-3748.

[12] De Matteis, G., Criber, E., Brando, G. Damage Probability Matrices for Three-Nave Masonry Churches in Abruzzi after the 2009 LAquila Earthquake (2016) International Journal of Architectural Heritage, 10 (2-3), pp. 120-145.

12th International Conference on Structural Analysis of Historical Constructions
SAHC 2020
P. Roca, L. Pelà and C. Molins (Eds.)

VULNERABILITY ASSESSMENT OF DWELLINGS IN THE HISTORIC CENTER OF CUSCO (PERU)

G. BRANDO[1*], G. COCCO[1], C. MAZZANTI[1], M. PERUCH[1], E. SPACONE[1], C. ALFARO[2], K. SOVERO[2] AND N. TARQUE[3]

[1]Department of Engineering and Geology,
University ''G. d'Annunzio'' of Chieti Pescara, Pescara, Italy
email: gbrando@unich.it (*corresponding author)

[2]Department of Engineering, Urb. Ingegneria Larapa Grande A-5
Universidad Andina del Cusco
San jeronimo, Cusco 08006, Peru

[3]Department of Engineering
Pontifical Catholic University of Peru (PUCP)
San Miguel 15088, Peru

Keywords: Seismic Vulnerability, Historic center, Cusco, Adobe, UNESCO sites

Abstract. *The seismic vulnerability assessment of the historic center of Cusco (Peru), an important UNESCO world heritage site, is dealt with in this paper. First, historical development of the city is presented through an in-depth historical analysis of its transformation over time, from the Inca empire to modern days. Then, an extensive in-situ survey activity, that allowed to collect several information about the main structural features concerning ordinary residential buildings, is shown.*

Based on the collected data, an empirical method calibrated on Italian historic centers from the authors is applied. It allowed to obtain Damage Probability Matrices and Fragility Curves for different earthquake intensities, as well as to assess the probability of exceeding certain levels of damage when seismic events of different intensities occur.

Based on these predicted damage frequencies, it is possible to prevent irremediable losses and to propose retrofitting interventions which can lead to the seismic vulnerability mitigation for the whole historic center.

1 INTRODUCTION

Seismic vulnerability of buildings is defined as their aptitude to present damages or collapses due to seismic events. Considering the frequent occurrence of earthquakes, seismic vulnerability assessment is an essential process for building heritage preservation, especially when it is applied to UNESCO word heritage sites such as Cusco, which is dealt with in this paper.

The Seismic Vulnerability Assessment is an issue that can be managed in different ways, to be selected based on the problem size and the resources available. When the stock of buildings to analyze is quite large, empirical methods represent an expeditious way for an assessment at

the urban scale, based on engineering judgments and statistical data elaboration [1],[2]. Conversely, numerical methods, based on FEM (Finite Element Method) models characterized by a high computational effort and time-consuming, allow to focus the attention on the seismic response of a single building [3],[4], [5]. This kind of methodology is mainly used in case of structures with an important historical/cultural/architectonical value. However, analyses with a medium complexity can be applied by means analytical methods that, focusing the attention on a stock of buildings considered representative of the whole historic center, allow to perform analyses that are more feasible with respect to numerical analyses but more detailed in comparison to the empirical methods [6],[7], [8] .

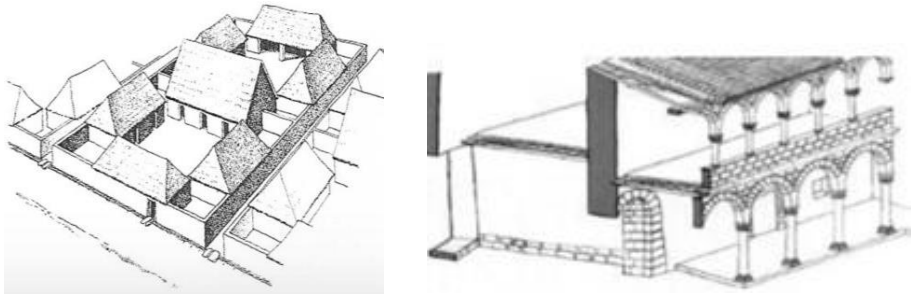
The methodology applied to the historic center of Cusco, presented in this paper, is an empirical vulnerability index-based method, in which Vulnerability Indices were obtained through observation procedures that have involved many residential adobe structures. The application of this procedure allowed to evaluate the main vulnerability sources and, therefore, to propose possible interventions aimed at mitigating the seismic risk of the whole historic center.

To estimate the Vulnerability Indices, it was necessary to carry out a preliminary study concerning the historical evolution of the historic center and an in-situ investigation in order to collect all useful information, presented in Section 2 and 3. The applied Vulnerability Index-based Method is explained in Section 4. Finally, Damage Probability Matrices, provided by the method, and the related Empirical Fragility Curves are shown in Section 5.

2 THE CITY OF CUSCO AND ITS HISTORICAL EVOLUTION

The current urban configuration of Cusco is the result of several changes that took place over a long time [9], going from the Inca period to the Spanish colonies, up to the Republican period [10].

The different historical phases also had repercussions on the built heritage of the city. In fact, the urban configuration of Cusco passed from the presence of common squares surrounded by rectangular-shaped aggregate buildings with internal courtyards of the Inca period (Figure 1a), to the reduction of the common squares extensions, during the Spanish domination, with the construction of adobe buildings atop the ancient walls of the Inca period that worked as foundations (Figure 1b), [11].



a) b)

Figure 1: Evolution of structural typologies in Cusco: from the "kancha" of the Inca period (a) to the colonial houses of the Spanish domination (b).

Despite the succession of building types characterizing each historical phase, one of the main factors that influenced the built heritage evolution of Cusco was the relevant seismic activity in the area. Several seismic events led to continuous processes of reconstruction, shaping and reshaping the configuration of the city, such as the one implemented after the destructive 1950 earthquake, which led to the collapse of several structures including adobe buildings, colonial churches, but also new structures [12].

In addition, the large flow of tourists that every year involve the historic center of Cusco has been the cause of the growing demand for hotels and shops located in the heart of the historic center. For this reason, most of the adobe houses located close to the hugest squares experienced changes of use and deep structural modifications, which led to the loss of the original vernacular structure's identity.

3 THE STRUCTURAL SURVEY OF ADOBE DWELLINGS

In order to assess the seismic vulnerability of dwellings in the historic center of Cusco, a reconnaissance activity characterized by rapid surveys was necessary. A special form to collect all necessary data was used for the purpose [13]. Each survey form served to identify the main features of each structural unit belonging to a building aggregate: type of material, number of floors, structural system typology, foundation system, roof characteristics, façade thickness and site topographical features.

However, it has not been possible always to inspect all buildings from inside and, in some cases, the survey was integrated with historical documents, books and aerial views. The survey activity allowed to ascertain that, approximately 78% of residential buildings are built in adobe, while the remaining 22% presents a reinforced concrete main structure (Figure 2).

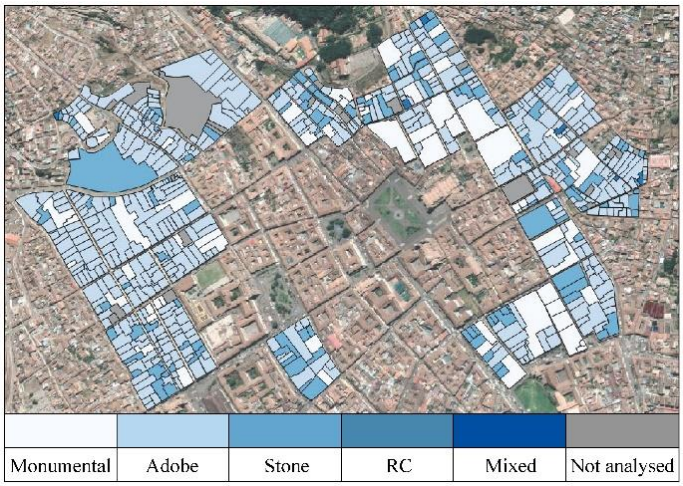


Figure 2: Map of Cusco and territorial distribution of the main structural typologies.

Focusing the attention on adobe structural units, they are mostly organized on two or three floors, with a height of about 2.5m. The adobe walls thickness ranges from 80cm to 100cm. The foundation system extends above the street level, to isolate the adobe walls from the humidity rising from the ground: stone foundations have been identified in about 77% of the

analyzed buildings (Figure 3a), however, in 2% of the structures the ancient Inca foundations are still recognizable (Figure 3b). These are made of very large granite blocks dry assembled. Floors and roofs are made of wooden structures which, due to the poor connections with the vertical walls, do not guarantee any type of restrain. Furthermore, sporadically, steel ties or ring beams that act as anti-seismic devices have been identified.



a) b)

Figure 3: Main foundation typologies: the most recent stone foundations (a) and the ancient Inca foundations (b).

Single structural units identified during the survey activity belong to large building clusters called "cuadra", which have large internal courtyards typical of Spanish colonial houses and which are surrounded by roads, as shown in Figure 4. For this reason, an entry concerning the possible evacuation routes in case of a seismic event occurrence, has been also included in the survey form. This represents an important factor, since the escape route can be blocked by the collapse of a façade overlooking that street.

The collection of all these data and their statistical re-elaboration, allowed to ascertain that a high percentage of the analyzed structures presents irregularities in plan (65%) and in elevation (96%), poor quality connections and total absence of seismic protection (80%) [14].



Figure 4: Graphic representation of a typical block in the historic center of Cusco.

4 THE VULNERABILITY INDEX-BASED METHOD

An empirical methodology has been applied. In detail, the data collected during the in-situ investigations through observational procedures were used to evaluate vulnerability indices for adobe dwellings.

A Vulnerability-index for each adobe dwelling presents in the historic center of Cusco has been defined, considering the seven vulnerability parameters reported in Table 1. These parameters come from a Vulnerability-Index Based Method calibrated through the damage observation of masonry buildings belonging to the Italian historic centers [15], which led to the definition of fourteen Vulnerability Parameters. However, considering the different structural typologies present in Cusco and their main vulnerability sources, only seven of them have been considered.

Table 1: Vulnerability parameters Pj considered for the proposed VI Method.

Vulnerability Parameters	Vulnerability type	ρk
P1	Position (in the cluster)	1.5
P2	Number of stories	1.5
P3	1st mode mechanisms	1.5
P4	2nd mode mechanisms	1.0
P5	Slabs	1.0
P6	Irregularities	0.8
P7	Site effects	1.5

Through a critical observation of each structural unit, engineering judgments have been expressed based on these seven vulnerability parameters, so to compute the Vulnerability Indices for about 340 structural units according to eq. (1):

$$i_v = \frac{1}{6} \cdot \frac{\sum_{j=1}^{m} \rho_j \cdot (v_{j,f} - v_{j,p})}{\sum_{j=1}^{m} \rho_j} \quad (1)$$

Where:

- ρ is a factor that weight the influence of the general parameter on the whole stability of the building. It was calibrated based on damage reconnaissance activities carried out on masonry buildings and its value can range from 0 to 1.5 [15];
- $v_{j,f}$ is the fragility score that is higher as the structural feature makes the vulnerability sources more severe;
- $v_{j,p}$ is defined as the protection score which consider the effectiveness of the applied anti-seismic device in order to contrast the development of undesired mechanisms related to the vulnerability source P_k.

Once the vulnerability indices for the considered structural units have been defined, their average value i_v^* has been computed. This allows the definition of the so-called vulnerability factor V, suitably calibrated in [15] and defined by eq. (2):

$$V = 0.53 + 1.16 \cdot i_v^* - 4.00 \cdot i_v^{*2} + 4.21 \cdot i_v^{*3} \quad (2)$$

This factor allowed the definition of an expected mean damage value μ_D by means of eq. (3). It has been computed for different seismic intensities I_{MCS}(expressed in the Mercalli – Cancani - Sieberg Scale-MCS) and considering the ductility of analyzed buildings through the factor Q, set equal to 2.3.

$$\mu_D = 2.5 \cdot \left[1 + tanh\left(\frac{I_{MCS} + 6.25 \cdot V - 13.1}{Q}\right)\right] \quad (3)$$

Then, the mean damage μ_D has been used to evaluate the probability $p[k|I]$ of achievement of a certain damage level k for each seismic intensity I_{MCS}, through a binomial probability distribution expressed by eq. (4):

$$p[k|I_{MCS}] = \frac{5!}{k! \cdot (5-k)!} \cdot \left(\frac{\mu_D}{5}\right)^k \cdot \left(1 - \frac{\mu_D}{5}\right)^{5-k} \quad (4)$$

The coefficient k represents the damage level according to Grünthal [16]. It can vary from 0 to 5 based on the damage extension:

- k = 0 No structural damage;
- k = 1 Negligible to slight damage. No structural damage, slight non-structural damage. Hair-line cracks in very few walls; fall of small pieces of plaster; fall of loose stones from upper parts of buildings in very few cases;
- k = 2 Moderate damage. Slight structural damage, moderate non-structural damage. Cracks in many walls; fall of large pieces of plaster; partial collapse of chimneys;
- k = 3 Substantial to heavy damage. Moderate structural damage, heavy non-structural damage. Large and extensive cracks in most walls; roof tiles detach; chimneys fracture at the roof line; failure of individual non-structural elements;
- k = 4 Very heavy damage. Heavy structural damage, very heavy non-structural damage. Serious failure of walls; partial structural failure of roofs and floors.
- k = 5 Destruction. Very heavy structural damage. Total or near total collapse.

5 FINAL RESULTS

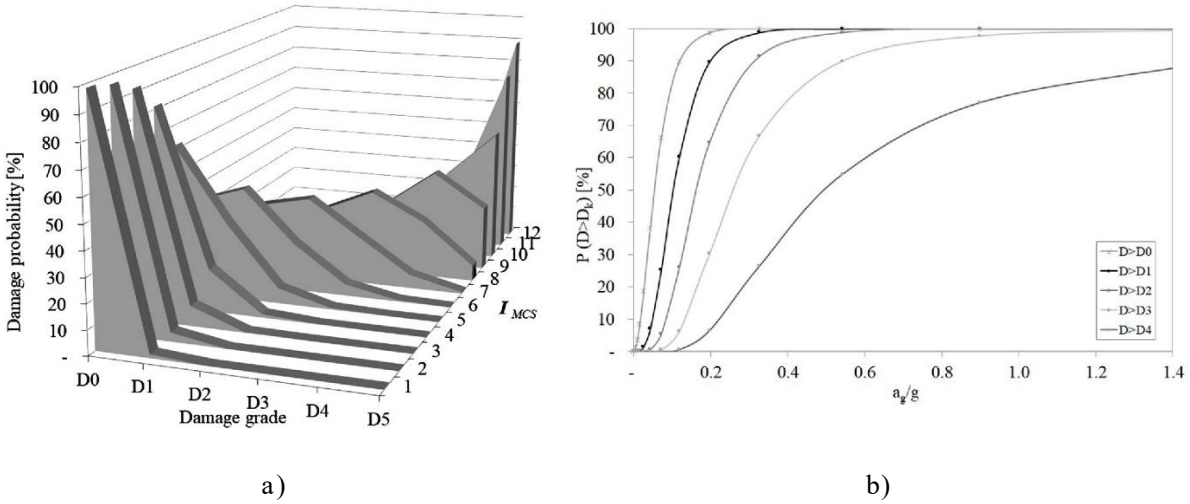
The empirical methodology implemented in this study allowed to assess the expected damage scenarios through the Damage Probability Matrices (DPMs) for different seismic intensities I_{MCS}. These are shown in Figure 5a and allow to assess how the damage scenarios evolve when the seismic intensity increases. Moreover, by summing the estimations coming from the DPMs, it was possible to define the Fragility Curves, shown in Figure 5b. They represent the probability of exceeding a certain damage level $P\ [D > Dk]$, in relation to a given Peak Ground Acceleration (PGA). To move from the Macroseismic Intensity I_{MCS}, in which the Damage Probability Matrices are expressed, to the PGA, the relation proposed by Margottini in 1992 was used [17].

Information that can be derived from these Fragility Curves are of considerable importance. For instance, if Cusco is hit by an earthquake characterized by a PGA/g equal to 0.6, the fragility

curves allow to predict the following damage scenario: about 60% of the buildings will have total collapses or collapses affecting more than 50% of the structure (D > D4); serious damage (D > D3) recognizable by large cracks and activation of overturning mechanisms, will affect 30% of the analyzed buildings; while, the remaining 10% of the examined stock will suffer damages that go from negligible to moderate (D0 < D < D3).

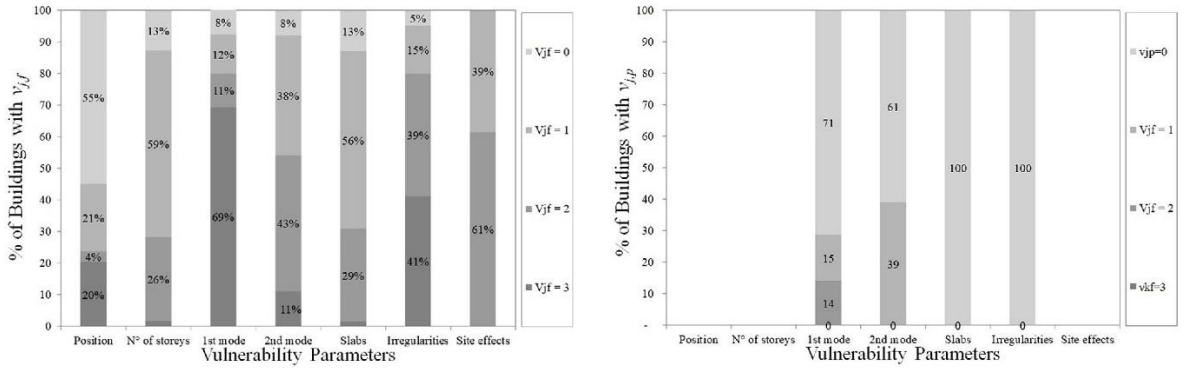
The vulnerability index-based method not only allows a prediction of the expected damage scenarios, but also a critical assessment of the structural deficiencies found, as well as possible proposal of interventions, through the analysis of fragilities ($v_{j,f}$) and protections ($v_{j,p}$)(Figure 6a and 6b), computed according to the procedures previously presented.

From their analysis it was possible to notice that, most of the buildings belonging to the analyzed stock, have a high vulnerability with respect to overturning mechanisms and site effects. Although the latter cannot be avoided in any way, the undesired kinematic mechanisms can be limited through the insertion of anti-seismic devices, like iron ties or buttresses, able to restrain more effectively vertical walls. These interventions, if implemented on an urban scale, would lead to a lowering of the average vulnerability index i_v^* from 0.72 to 0.65 [12]. If further interventions are added, so to also improve the slab performance and to enhance the wall textures, a remarkable seismic vulnerability mitigation of the whole historic center of Cusco would be achieved.



a) b)

Figure 5: Expected Damage Scenarios represented by means of Damage Probability Matrices (a) and Fragility Curves in terms of Peak Ground Acceleration (b).



a) b)

Figure 6: Statistical distribution of the scores (a) v_{mf} and (b) v_{mp}.

6 CONCLUSIONS

This paper dealt with the seismic vulnerability assessment, carried out on the urban scale of a large area of the historic center of Cusco, in Peru, focusing the attention on adobe dwellings. This analysis was carried out through the application of an empirical methodology calibrated on masonry buildings belonging to several Italian historic centers and adapted to the building types observed after a careful reconnaissance activity.

The first phase of analysis was historical-critical and was devoted to the knowledge of the evolution processes of the historic center. After that, investigations that allowed the collection of all needful data for the seismic vulnerability assessment were performed. The consequent Vulnerability Indices computation allowed to elaborate the expected damage scenarios for different seismic intensities, by means Damage Probability Matrices and Fragility Curves.

The main conclusions that can be defined are the following:

- the current configuration of the historic center of Cusco and its buildings are the result of several transformation processes, mostly related to the seismic history of the area;
- the analyzed buildings are characterized by a structural organization on two or three floors with stone foundations, wooden horizontal slabs and poor connections;
- the most common vulnerability sources are related to the lack or ineffectiveness of seismic prevention devices able to guarantee an effective connection of the orthogonal walls and between vertical and horizontal elements;
- since the implemented method represents a procedure calibrated on Italian masonry buildings, with characteristics that are different from the Peruvian adobe dwellings, the results will have to be confirmed by means of more detailed analysis.

Acknowledgements. The study presented in this paper was carried out within the framework of an ongoing cooperation agreement signed in 2017 between the University of Chieti-Pescara (Italy), the Andina University del Cusco (Peru) and the Pontifical Catholic University of Peru (Peru).

REFERENCES

[1] Rapone, D., Brando,G. Spacone, E. and De Matteis, G. "Seismic vulnerability assessment of historic centers: description of a predictive method and application to the case study of Scanno (Abruzzi, Italy)," Int. J. Archit. Herit., vol. 12, no. 7–8, pp. 1171–1195, 2018.

[2] Ferreira, T. M., Vicente, R., Silva, J. A. R. M., Varum, H. and Costa, A. "Seismic vulnerability assessment of historical urban centres: case study of the old city centre in Seixal, Portugal," Bull. Earthq. Eng., vol. 11, no. 5, pp. 1753–1773, 2013.

[3] Tarque, N., Crowley, H., Pinho, R. and Varum, H. "Seismic capacity of adobe dwellings," Proc. 14th Eur. Conf. Earthq. Eng., no. September 2014, 2010.

[4] Illampas, R., Charmpis, D. C. and Ioannou, I. "Non-linear Dynamic Finite Element Analysis of Adobe Masonry Structures with Various Roof Diaphragm Configurations," pp. 475–487, 2015.

[5] Brando, G., Criber, E., De Matteis, G. The effects of L'aquila earthquake on the St. Gemma church in Goriano Sicoli: part II—fem analysis (2015) Bulletin of Earthquake Engineering, 13 (12), pp. 3733-3748.

[6] Allahvirdizadeh, R., Oliveira, D. V. and Silva, R. A. "Modelling the seismic out - of - plane behaviour of rammed earth components modelling," no. September, pp. 19–21, 2018.

[7] Cocco, G., D'Aloisio, A., Spacone, E. and Brando, G. "Seismic Vulnerability of Buildings in Historic Centers: From the 'Urban' to the 'Aggregate' Scale," Front. Built Environ., vol. 5, no. June, pp. 1–14, 2019.

[8] Criber, E., Brando, G., De Matteis, G. The effects of L'Aquila earthquake on the St. Gemma church in Goriano Sicoli: part I—damage survey and kinematic analysis (2015) Bulletin of Earthquake Engineering, 13 (12), pp. 3713-3732.

[9] Angles, V. Historia del Cusco, book II. Lima, 1983.

[10] Mazzanti, C. "Between natural disasters and social exclusion. The development of the historic center of Cusco (Peru)," in VIIIth CIRICE International Conference, 2018, pp. 483–490.

[11] Vinuales, G. El espacio urbano en el Cusco colonial: uso y organizaciòn de las estructuras sim bòlicas. Lima, 2004.

[12] Samanez, R. "El terremoto que afectò a Cusco en 1950 y los aportes de George A. Kubler," Arkinka, vol. 16, no. 204, pp. 91–95, 2012.

[13] Spacone, E., Brando, G., Peruch, M., Mazzanti, C., Sovero, K. and Tarque, N. "An extensive survey of the Historic Center of Cusco for its seismic vulnerability assessment," RILEM Bookseries, vol. 18, 2019.

[14] Brando, G., Cocco, G., Mazzanti, C., Peruch, M., Spacone, E., Alfaro, C., Sovero, K. and Tarque, N. "Structural Survey and Empirical Seismic Vulnerability Assessment of Dwellings in the Historical Centre of Cusco, Peru," Int. J. Archit. Herit., pp. 1–29, 2019.

[15] Brando, G., De Matteis, G. and Spacone, E. "Predictive model for the seismic vulnerability assessment of small historic centres: Application to the inner Abruzzi Region in Italy," Eng. Struct., vol. 153, no. December 2016, pp. 81–96, 2017.

[16] Grünthal, G. European Macroseismic Scale, vol. 15. Luxembourg, 1998.

[17] Margottini, C., Molin, D., Narcisi, B. and Serva, L. "Intensity vs acceleration: Italian data," Proc. Work. Hist. Seism. Cent. Mediterr. Reg., pp. 213–226, 1987.

12th International Conference on Structural Analysis of Historical Constructions
SAHC 2020
P. Roca, L. Pelà and C. Molins (Eds.)

VULNERABILITY ASSESSMENT OF ITALIAN UNREINFORCED MASONRY CHURCHES USING MULTI-LINEAR REGRESSION MODELS

A. MAROTTA[1*], D. LIBERATORE[1] AND L. SORRENTINO[1]

[1] Department of Structural and Geotechnical Engineering
Sapienza University of Rome
Via Antonio Gramsci 53, 00197 Rome, Italy
e-mail: alessandra.marotta@uniroma1.it (*corresponding author) –
domenico.liberatore@uniroma1.it – luigi.sorrentino@uniroma1.it

Keywords: Local Collapse Mechanisms, Macroseismic Intensity, Global Damage Index

Abstract. *The extensive damage occurred to the Italian historical and architectural heritage during the 2016-2017 earthquake sequence, and particularly to unreinforced masonry churches, highlights the need to better recognize the vulnerability of religious buildings. A sample of 158 churches belonging to the four stricken regions is studied and their performance analysed statistically. Structural behaviour of these churches is described in terms of mechanisms affecting the so-called macroelements, being portions of the building behaving more or less independently. In order to define fragility curves correlating the damage related to each collapse mechanism against ground motion intensity and churches' specific characteristics, the observed behaviour of the sample is herein analysed by means of statistical procedures accounting for possible local collapse mechanisms. Several regressions strategies are considered, accounting for vulnerability modifiers increasing/reducing the vulnerability of each macroelement, since the severity of shaking alone is not capable to fully explain the observed damage, strongly influenced by structural details that can worsen the seismic performance or improve it through earthquake-resistant elements. A synthetic damage index, purely based on observed data, is used to summarise the overall severity of damage related to relevant mechanisms, highlighting the contributions of ground shaking and building vulnerability. Results show the relevance of the proposed multi-linear regression models for the national heritage of churches and the advisability of extending mechanism-based regressions to other countries besides Italy. The proposed global damage index can be used as predictive tool to support seismic vulnerability mitigation at a territorial scale.*

1 INTRODUCTION

In 2016-2017 a strong seismic sequence struck a wide area of Central Italy within the boundaries of Latium, Abruzzi, Umbria and Marche regions (Figure 1), causing severe damage and hundreds of casualties. The first two events, occurred on August 24 (M_w 6.0 and 5.4) caused 299 fatalities and several hundreds of injuries, mostly affecting the municipalities of Amatrice, Arquata del Tronto, and Accumoli. The strongest event took place on October 30, 2016 (M_w 6.5) and caused extensive damage to the municipalities of Norcia and Castelsantangelo sul Nera, with no further fatalities.

The building portfolio of the affected area is characterised by numerous historical constructions, which were strongly damaged by the seismic swarm. The October event was particularly destructive for the religious buildings in the city of Norcia, where almost all churches suffered extensive damage and collapses [1]. In fact, it is widely known that churches frequently exhibit a seismic vulnerability higher than ordinary buildings [2], because of their architectural and structural characteristics such as open plan, large wall height-to-thickness and length-to-thickness ratios, and the use of thrusting horizontal structural elements for vaults and roofs [3]. As known, historical unreinforced masonry (URM) buildings, and particularly churches, tend to respond to earthquakes with local mechanisms rather than with a global behaviour, with a set of different architectural components, commonly called macro-elements, behaving more or less independently one from the adjacent [4–7]. According to such observation, the behaviour of a sample of 158 URM churches is herein analysed accounting for 28 possible local collapse mechanisms (Table 1), as currently adopted in Italy for post-earthquake assessment of churches [8]. In order to correlate the observed damage related to each collapse mechanism against ground motion intensity and churches' specific characteristics, several statistical procedures are used.

Table 1: List of the possible 28 collapse mechanisms

Ref. no.	Description	Ref. no.	
1	Overturning of the façade	**15**	Roof lantern
2	Gable mechanisms	**16**	Overturning of the apse
3	Shear in the façade	**17**	Shear in the apse
4	Damage in the porch	**18**	Vaults in the apse
5	Transversal response of the nave	**19**	Interactions between the nave and its roof
6	Shear in longitudinal walls	**20**	Interactions between the transept and its roof
7	Longitudinal response of the columns	**21**	Interactions between the apse and its roof
8	Vaults in the main nave	**22**	Overturning of the chapels
9	Vaults in the aisles	**23**	Shear in the chapels
10	Overturning of the transept	**24**	Vaults in the chapels
11	Shear in the transept	**25**	Interactions next to irregularities
12	Vaults in the transept	**26**	Projections
13	Triumphal arch	**27**	Bell tower
14	Dome	**28**	Belfry

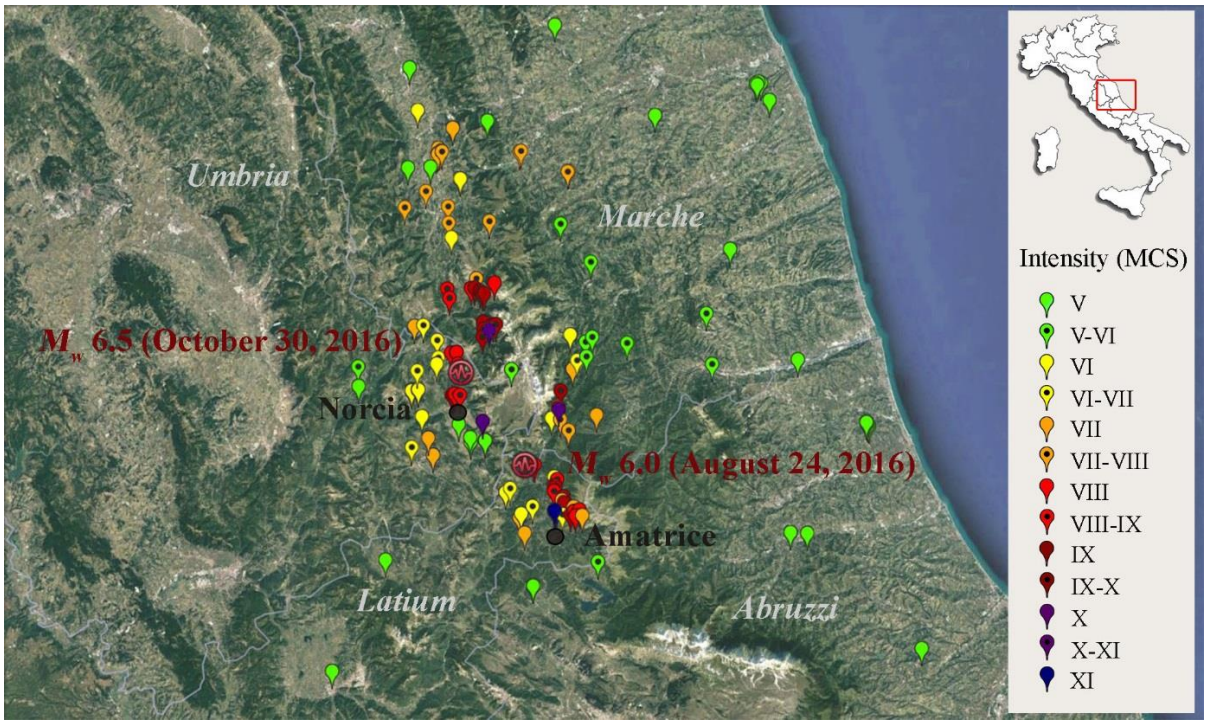


Figure 1: Locations of the 158 URM churches pertaining to the four regional boundaries, along with the epicentres of the main seismic events

Generally, when the interpretation of observed damage is of interest, a macroseismic intensity is used [9,10] because it is directly assigned to stricken locations on the basis of the occurred effects on the built and natural environment. Consequently, Mercalli-Cancani-Sieberg (MCS) macroseismic intensity (Figure 1) is considered as intensity measure in this study. Local values of MCS intensity [11,12] are attributed to each church location using a triangulation-based linear 2-D interpolation when macroseismic intensity was not available for the settlement of interest. Either one of the two main earthquakes of the sequence, the August 24, 2016 (M_w 6.0) or the October 30, 2016 (M_w 6.5) shock is used as reference event, depending on the location of the church and the following date of survey. Therefore, the damage of 49 churches out of 158 is referred to the August 24 shock, and that of 109 churches to the October 30 shock. The majority of churches experienced a macroseismic intensity equal to V (20%), VII-VIII (15%) and VIII-IX (13%). The remaining churches' distribution decreases with MCS intensities, ranging between V-VI (10%), and XI (2%).

2 LOCAL DAMAGE ASSESSMENT

The assessment of the damage occurred to the Central Italy churches was carried out by assigning six levels of damage, ranging between 0 (no damage) and 5 (total collapse), to each possible collapse mechanism in Table 1 following the qualitative expert judgment approach of the European Macroseismic Scale [13]. The percentage of mechanisms whose activation was identified is presented in Figure 2, in conjunction with the percentage of the possible mechanisms. Some of the 28 mechanisms in Table 1 were rarely observed in the analysed stock because they are related to macro-elements that were seldom present. Nevertheless, some of

them (#9, #11) showed systematic activation (above 80% in the buildings where possible) although their macro-elements (vaults in the aisles, transept) were present in few buildings. Because of their rather poor sample size, these mechanisms, together with #10, 12, 15, 20, 24, are not further discussed in the following, reducing the number of accounted mechanisms to twenty-one.

As already pointed out in Marotta et al. 2017 [14], the seismic vulnerability of URM churches is strongly modified by structural details that can improve the seismic performance, (such as connections between walls and to horizontal structures, buttresses, tie rods, top beams, lateral restraint, lintels, braced roof pitch), or worsen the seismic performance (such as poor masonry quality, asymmetry conditions, thrusting elements, large slenderness, large openings, heterogeneous materials, vertical-stacked-bond vaults, lunettes). For this reason, the presence and effectiveness of the aforementioned fifteen vulnerability modifiers (Table 2) were also recorded during the investigation, and the influence of each of them on the damage of single mechanism was addressed in a disaggregated fashion, following the approach in Marotta et al. 2018 [15] originally proposed for URM churches damaged by the 2010-2011 Canterbury, New Zealand, seismic sequence.

The vulnerability of each analysed mechanism is evaluated by using multi-linear regressions, in which the response, d, representing the observed damage, and the considered explanatory variables are fitted by a linear formulation, according to:

$$d = m_0 I + m_1 x_1 + m_2 x_2 ... + m_v x_v + b + \varepsilon \quad (1)$$

where I represents the MCS intensity measure univocally assigned to each church location and referred to one of the two main shocks; x_1, x_2, … x_v are the vulnerability modifiers considered for each mechanism; m_0, m_1, m_2, … m_v are the obtained regression coefficients; b is the intercept and ε is the error term.

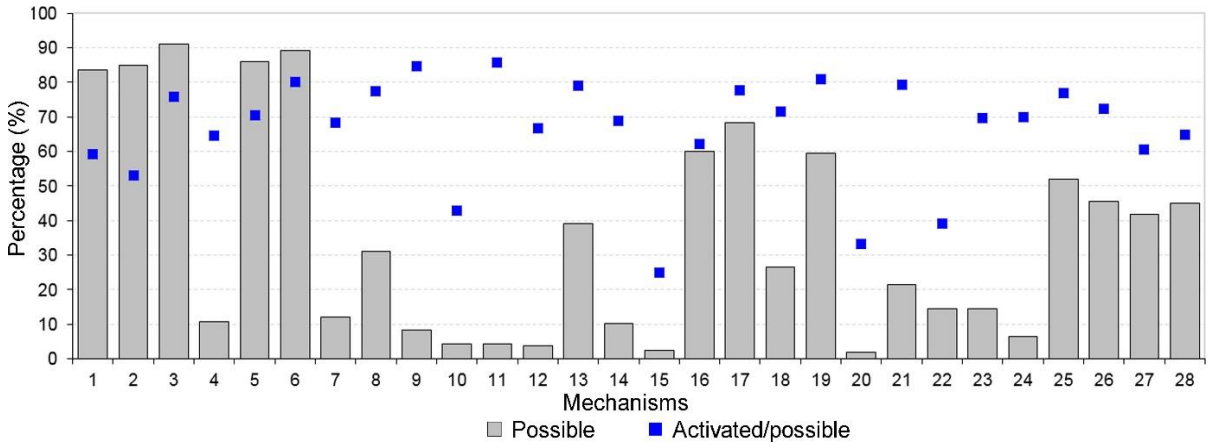


Figure 2: Percentages of possible (over the sample of 158 churches) and activated (over the sample of possible) mechanisms mentioned in Table 1

Table 2: List of the vulnerability modifiers, x_v, used in the multi-linear regression models

Ref. no.	Description
x_1	Tie rods
x_2	Lateral restraint
x_3	Buttresses
x_4	Lintels
x_5	Thrusting elements
x_6	Large openings
x_7	Top beam
x_8	Heterogeneous materials
x_9	Connections
x_{10}	Braced roof pitch
x_{11}	Slenderness
x_{12}	Asymmetry conditions
x_{13}	Poor masonry quality
x_{14}	Vertical-stacked-bond vaults
x_{15}	Lunettes

The influence of each vulnerability modifier is considered assigning it a score as indicator of either the absence or presence of a characteristic and its effectiveness. The scores range between −1 and 0 as for the structural details that are expected to improve the seismic performance, or between 0 and 1 as for the structural details that are expected to aggravate the seismic performance. Consequently, a modifier reducing the vulnerability, such as an earthquake-resistant element, will score close to −1 if effective and 0 if ineffective or absent. On the contrary, a modifier increasing the vulnerability will score close to 1 if present and 0 if absent or negligible. The effectiveness of an earthquake-resistant element and the incidence of a vulnerability increaser are entrusted to an expert judgment.

Two statistical procedures, namely Stepwise and Best Subsets [16], were used to determine the variables that generate the most efficient predictive model: the Stepwise selection method, which consists in inserting variables in turn until the regression equation involves a *p*-value below a selected threshold, and the Best Subsets procedure, which selects the subset of parameters that optimises an objective criterion, such as having the largest coefficient of determination. Since the coefficient of determination, R^2, automatically increases when numerous variables are considered, for multiple-linear regressions the best regression model is identified by means of the adjusted coefficient of determination, R^2_{adj}:

$$R^2_{adj} = 1 - \left[\left(1 - R^2\right) \frac{n-1}{n-(v+1)} \right] \tag{2}$$

where n is the sample size of churches and $v + 1$ is the number of considered explanatory variables , including the MCS intensity measure.

Differently from a generic multi-linear regression model, the two procedures used allow to identify those parameters that can be neglected, while providing both a better damage prediction and the possibility of a faster territorial-scale vulnerability assessment [17].

For the twenty-one mechanisms considered, the coefficients defining the selected multiple-linear regressions of Eq. (1) are presented in Table 3.

Table 3: Computed coefficients of the selected regression models according to Eq. (1) for MCS as intensity measure

		Variable								
		I	x_1	x_2	x_3	x_4	x_5	x_6	x_7	x_8
Mech. No.	**1**	0.203								
	2	0.392	0.384				0.958	0.757	-1.023	
	3	0.193								1.172
	4	0.788					0.731	2.245		
	5	0.395			0.590					1.163
	6	0.240							0.487	1.485
	7	0.228					0.513			1.600
	8	0.136						1.843	0.837	2.724
	13	0.239	0.323							0.730
	14	0.325								
	16	0.175	0.482	0.540	1.136					
	17	0.268								
	18	0.142								2.156
	19	0.429	0.610				0.738			1.280
	21	0.509								
	22	0.191	0.575	0.847				1.554		
	23	0.342					0.708			
	25	0.424		0.851		1.015			1.250	1.001
	26	0.219						0.820		
	27	0.197	0.314	0.487	1.184	0.565				
	28	0.545	0.552							1.983

		Variable							
		x_9	x_{10}	x_{11}	x_{12}	x_{13}	x_{14}	x_{15}	b
Mech. No.	**1**	2.211		0.577		1.877			1.213
	2	1.987		0.638		2.314			-2.610
	3	1.306				2.039			0.931
	4					2.941			-5.974
	5	0.681		0.577		1.085	1.801		-1.037
	6	0.714		0.334		1.333	1.952		0.052
	7			0.732		2.226			-3.074
	8			0.936		2.349		-0.435	0.194
	13	1.357			1.605	1.450			1.010
	14			2.388					-0.880
	16	1.636		1.456		1.416			0.998
	17	1.316				1.409			0.822
	18					1.784		1.481	-0.008
	19	1.484	0.786			1.423			-0.292
	21	1.180				1.341			-1.581
	22					1.828			-0.444
	23				1.236	1.649			-1.387
	25	1.123		1.154		0.887			-0.412
	26			1.048	0.898	2.447			-0.731
	27	1.976		0.792	1.045	2.275			1.932
	28			1.885	3.425	1.606			-2.293

Although not included in the current Italian form, poor masonry quality was found to be crucial for at least twenty mechanisms. It is also important to highlight that the presence of poor masonry can lead to wall fragmentation (example in Figure 3a), before a rigid-body mechanism can be triggered. In the case at hand, this phenomenon was observed in 21% of the activated mechanisms. Therefore, masonry performance is confirmed to be crucial and the investigation of its mortar is highly recommended [18]. Other very relevant modifiers are connections, between intersecting walls (example in Figure 3b) or between walls and horizontal structures, which influence twelve mechanisms. On the contrary, despite it is widely known that tie rods help to reduce wall overturning [19,20], they seem to play a negligible role, probably due to the predominance of other modifiers such as connections. Similarly, buttresses only slightly influenced the predicted damage, but their presence was detected only in about 15% of the investigated churches. Large slenderness noticeably influenced the two mechanisms associated with the presence of dome and belfry (#14 and #28).

a)  b)

Figure 3: a) Example of poor quality masonry causing wall disintegration: Santa Maria Assunta (Torrita, Amatrice); b) Example of the relevance of connections: San Lorenzo (San Lorenzo e Flaviano, Amatrice)

a)  b)

Figure 4: Examples of reed-mat vaults: a) Santa Chiara (Camerino); b) Santa Maria in Via (Camerino), released from the Corps of Firefighters (www.vigilifuoco.it)

Other parameters, such as large openings (whose combined length exceeds 1/3 of the wall length), heterogeneous materials (assigned in case of reed-mat vaults, Figure 4, for mechanism #8 and when two adjacent structural elements are made of different masonry types), asymmetry conditions (e.g., due to eccentricity of a projection with respect to the underlying masonry, or due to juxtaposition of a new extension) and the presence of vertical-stacked-bond vaults, are relevant for specific mechanisms. Negative values of the coefficients are obtained in two cases, since related to vulnerability modifiers rarely present in the relative mechanisms and will require further investigation.

3 GLOBAL DAMAGE INDEX

In buildings where multiple local collapse mechanisms take place, it is important to define a synthetic index expressing the overall severity of damage. Commonly, a normalized average, i_d, proposed by Lagomarsino et al. [6], and computed as the mean of the damage scores, d_k, assigned to each of the N mechanisms that might have been activated in the church (twenty-one at most in the present case), weighted by the coefficients ρ_k, is used:

$$i_d = \frac{1}{5} \frac{\sum_{k=1}^{N} \rho_k \, d_k}{\sum_{k=1}^{N} \rho_k} \tag{3}$$

where the factor 1/5 normalizes i_d in the range [0,1].

The normalized average, i_d, can be transformed into a discrete variable, varying from 0 to 5, using the correlation suggested by Lagomarsino and Podestà [21]. In order to overcome a conventional estimation of the ρ_k weights, an alternative synthetic damage index has been proposed in Marotta et al. [15]. Re-expressing in vector form Eq. (1), it follows:

$$\mathbf{d} = \mathbf{m}_0 I + \mathbf{c} + \mathbf{b} + \boldsymbol{\varepsilon} \tag{4}$$

where $\mathbf{d}$ represents the vector of observed damage, $\mathbf{m}_0$ is the vector of the regression coefficients of the intensity measure I, vector $\mathbf{c}$ groups the regression modifiers associated with the twenty-one mechanisms (e.g., for the j-th mechanism: $c_j = m_{j1}x_{j1} + m_{j2}x_{j2} \ldots + m_{jv}x_{jv}$), $\mathbf{b}$ is the vector of intercepts and $\boldsymbol{\varepsilon}$ is the vector of error terms. The ground motion parameter I that best fits the observed damage can be obtained by minimizing the sum of squares of the error terms:

$$I = \frac{\mathbf{m}_0^T(\mathbf{d} - \mathbf{b} - \mathbf{c})}{\mathbf{m}_0^T \mathbf{m}_0} = \frac{\mathbf{m}_0^T(\mathbf{d} - \mathbf{b})}{\mathbf{m}_0^T \mathbf{m}_0} - \frac{\mathbf{m}_0^T \mathbf{c}}{\mathbf{m}_0^T \mathbf{m}_0} \tag{5}$$

The ground motion parameter x_1 is equal to the difference of two terms, where the first depends on observed damage (including intercepts) and can be considered as a damage index, D_s:

$$D_s = \frac{\mathbf{m}_0^T(\mathbf{d} - \mathbf{b})}{\mathbf{m}_0^T \mathbf{m}_0} \tag{6}$$

The second term depends on the vulnerability modifiers alone, and can be considered as a vulnerability index, V:

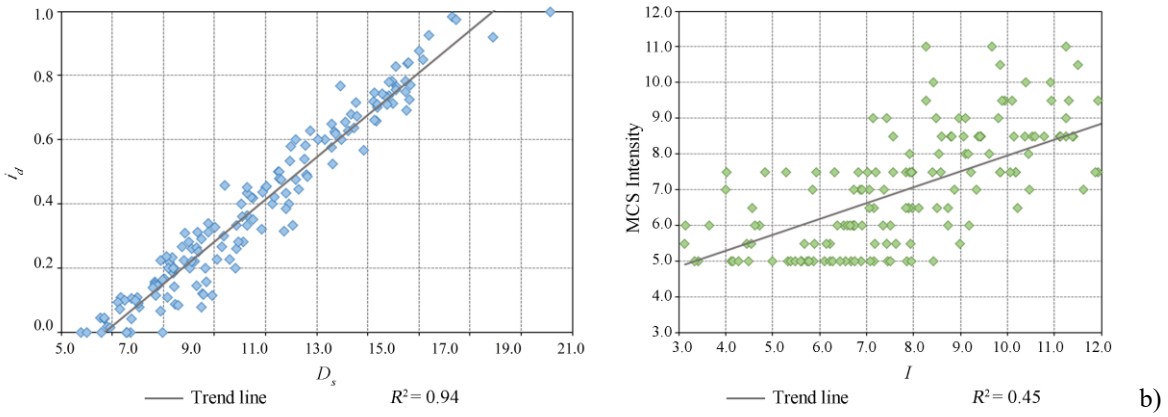
$$V = \frac{\mathbf{m}_0^T \mathbf{c}}{\mathbf{m}_0^T \mathbf{m}_0} \tag{7}$$

Accordingly, Eq. (5) can be rewritten as:

$$I = D_s - V \tag{8}$$

A simple additive model is therefore established, where the ground motion parameter, I, is computed as the difference between the synthetic damage index, D_s, and the vulnerability index, V, and all quantities share the same unit of measure. The synthetic damage index of Eq. (6) is an *observed* damage, which can be used for comparisons and model validation. A comparison of the *observed* synthetic damage index with the normalised average i_d, computed for Central Italy churches according to Eq. (3) assuming ρ_k = 1, is provided in Figure 5a, and a good correlation is achieved, confirming the efficacy of the proposed index.

As Eq. (8) establishes a relationship between three quantities, once damage and vulnerability are known (e.g. after an earthquake) it is possible to estimate the ground motion severity, gaining a quantitative alternative to the conventional macroseismic intensity, which enables an estimate of ground motion severity on a specific class of buildings accounting for their vulnerability. The limited correlation (Figure 5b) between the MCS intensity assigned after the seismic sequence and the ground motion parameter, I, obtained with Eq. (8) depends on the different stock of buildings considered for their computation, in the case of x_1 solely churches, whereas all constructions for the attribution of MCS intensity (in the case at hand mostly ordinary unreinforced masonry buildings).



a) b)

Figure 5: a) Correlation between normalised average, i_d, computed for Central Italy churches following Eq. (3) and *observed* synthetic damage index, D_s, obtained with Eq. (6); b) Comparison between assigned MCS intensities and ground motion parameter, I, computed following Eq. (8)

On the other hand, when the expected ground motion and vulnerability are provided (e.g. in a risk analysis), the expected damage can be forecasted as follows:

$$D_s = I + V \tag{9}$$

Considering the long timespan covered by Italian macroseismic catalogues [22], law of occurrence and expected intensities can be estimated for most places. Therefore, the coefficients in Table 3 can be used in future preventive assessments, as done by Marotta et al. [15], wherein a worked out example is shown.

4 CONCLUSIONS

The 2016–2017 Central Italy earthquake sequence caused extensive damage to the national architectural heritage, especially to unreinforced masonry churches. The damage data collected in the aftermath of the main events for a sample of 158 religious buildings in the affected area highlighted once again the intrinsic structural vulnerability of this architectural type.

Because unreinforced masonry churches respond to earthquakes as a composition of macro-elements, observed damage was interpreted mechanism by mechanism, also accounting for differences in vulnerability besides the severity of shaking alone. Such investigation was conducted by using multiple-linear regressions, according to statistical procedures, in order to obtain the model having the largest coefficient of determination together with the smallest number of relevant modifiers for a faster territorial scale application. Accordingly, the coefficients defining the regression models of twenty-one mechanisms were computed.

Commonly, damage occurred to churches is analysed by computing a global damage index, based upon summing up and weighting separate mechanism damage levels. Herein, an alternative synthetic damage index has been identified, by minimizing the sum of squares of the difference between expected and observed damage. The proposed index has the advantage of not requiring a conventional estimation of the weights used in previous definitions of a global damage index and is exclusively based on observed data. The applied method, already calibrated on observed damage from other earthquakes affecting unreinforced masonry buildings, and herein recalibrated for the assessment of the global response of the Central Italy unreinforced masonry churches, provides good results and a good correlation when compared to a mean damage. An innovative advantage of the proposed damage index, which is a combination of a ground motion intensity measure and building vulnerability, is the possibility to highlight the specific influence to damage of each component, separating the role of ground motion severity from that of building vulnerability.

Acknowledgements. This work has been partially carried out under the program “Dipartimento di Protezione Civile – Consorzio RELUIS”. The opinions expressed in this publication are those of the authors and are not necessarily endorsed by the Dipartimento di Protezione Civile.

REFERENCES

[1] Penna, A., Calderini, C., Sorrentino, L., Carocci, C.F., Cescatti, E., Sisti, R. et al. Damage to churches in the 2016 Central Italy earthquakes. *Bulletin of Earthquake Engineering* (2019) **17**: 5763–5790. https://doi.org/10.1007/s10518-019-00594-4

[2] D'Ayala, D. Establishing Correlation Between Vulnerability and Damage Survey for Churches. *Proc 12th World Conference on Earthquake Engineering, Auckland, New Zealand* (2000) **Paper No.**: 1–8.

[3] Sorrentino, L., Bruccoleri, D. and Antonini, M. Structural interpretation of post-earthquake (19th century) retrofitting on the Santa Maria degli Angeli Basilica, Assisi, Italy. *Structural Analysis of Historic Construction: Preserving Safety and Significance* (2008) 217–25. https://doi.org/10.1201/9781439828229.ch23

[4] Giuffré, A. Restoration and safety in sismic areas. The Cathedral of S. Angelo dei Lombardi (in Italian). *Palladio1* (1988) 95–120.

[5] Doglioni, F., Moretti, A., Petrini, V. and By), (Ed. (1994) Le chiese e il terremoto. Dalla vulnerabilità constatata nel terremoto del Friuli al miglioramento antisismico nel restauro. Verso una politica di prevenzione. (1994) Lint Editoriale Associati, Trieste.

[6] Lagomarsino, S., Podestà, S., Cifani, G. and Lemme, A. The 31st October 2002 earthquake in Molise (Italy): a new methodology for the damage and seismic vulnerability survey of churches. *13th World Conference on Earthquake Engineering* (2004) 1–11.

[7] Borri, A., Corradi, M., Castori, G., Sisti, R. and De Maria, A. Analysis of the collapse mechanisms of medieval churches struck by the 2016 Umbrian earthquake. *International Journal of Architectural Heritage* (2019) **13**: 215–28.

[8] DPCM. (2011) Direttiva del Presidente del Consiglio dei Ministri "Valutazione e riduzione del rischio sismico del patrimonio culturale con riferimento alle Norme tecniche per le costruzioni di cui al DM 14 gennaio 2008. (2011).

[9] Dolce, M., Kappos, A., Masi, A., Penelis, G. and Vona, M. Vulnerability assessment and earthquake damage scenarios of the building stock of Potenza (Southern Italy) using Italian and Greek methodologies. *Engineering Structures* (2006) **28**: 357–71. https://doi.org/10.1016/j.engstruct.2005.08.009

[10] Vicente, R., Ferreira, T. and Maio, R. Seismic Risk at the Urban Scale: Assessment, Mapping and Planning. *Procedia Economics and Finance* (2014) **18**: 71–80. https://doi.org/10.1016/S2212-5671(14)00915-0

[11] Azzaro, R., Tertulliani, A., Bernardini, F., Camassi, R., Del Mese, S., Ercolani, E. et al. The 24 august 2016 amatrice earthquake: Macroseismic survey in the damage area and EMS intensity assessment. *Annals of Geophysics* (2016) **59**: 1–8. https://doi.org/10.4401/ag-7203

[12] Galli, P., Peronace, E., Bramerini, F., Castenetto, S., Naso, G., Cassone, F. et al. The MCS intensity distribution of the devastating 24 august 2016 earthquake in central Italy (Mw6.2). *Annals of Geophysics* (2016) **59**. https://doi.org/10.4401/ag-7287

[13] Grünthal, G. (1998) European Macroseismic Scale. Eur. Cent. Geodyn. Seismol. (1998).

[14] Marotta, A., Sorrentino, L., Liberatore, D. and Ingham, J.M. Vulnerability Assessment of Unreinforced Masonry Churches Following the 2010–2011 Canterbury Earthquake

Sequence. *Journal of Earthquake Engineering* (2017) Taylor & Francis. **21**: 912–34. https://doi.org/10.1080/13632469.2016.1206761

[15] Marotta, A., Sorrentino, L., Liberatore, D. and Ingham, J.M. Seismic Risk Assessment of New Zealand Unreinforced Masonry Churches using Statistical Procedures. *International Journal of Architectural Heritage* (2018) Taylor & Francis. **12**: 448–64. https://doi.org/10.1080/15583058.2017.1323242

[16] Draper, N.R. and Smith, H. (1998) Applied regression analysis, Volume 1. 3rd ed. (1998) Wiley.

[17] Marotta, A., Goded, T., Giovinazzi, S., Lagomarsino, S., Liberatore, D., Sorrentino, L. et al. An inventory of unreinforced masonry churches in New Zealand. *Bulletin of the New Zealand Society for Earthquake Engineering* (2015) **48**: 171–90.

[18] Roselli, G., AlShawa, O., Liberatore, D., Sorrentino, L., Di Girolami, G., Cinaglia, P. et al. Mortar analysis of historic buildings damaged by recent earthquakes in Italy. *The European Physical Journal Plus* (2019) **134**.

[19] Giresini, L., Casapulla, C., Denysiuk, R., Matos, J. and Sassu, M. Fragility curves for free and restrained rocking masonry façades in one-sided motion. *Engineering Structures* (2018) Elsevier. **164**: 195–213. https://doi.org/10.1016/j.engstruct.2018.03.003

[20] AlShawa, O., Liberatore, D. and Sorrentino, L. Dynamic one-sided out-of-plane behaviour of unreinforced-masonry wall restrained by elasto-plastic tie-rods. *International Journal of Architectural Heritage* (2019) **13**: 340–57. https://doi.org/10.1080/15583058.2018.1563226

[21] Lagomarsino, S. and Podestà, S. Seismic vulnerability of ancient churches: II. Statistical analysis of surveyed data and methods for risk analysis. *Earthquake Spectra* (2004) **20**: 395–412. https://doi.org/10.1193/1.1737736

[22] Rovida, A., Locati, M., Camassi, R., Lolli, B. and Gasperini, P. CPTI15, the 2015 Version of the Parametric Catalogue of Italian Earthquakes. *Istituto Nazionale Di Geofisica e Vulcanologia* (2016).

AUTHORS INDEX

Aşikoğlu, A. 2858
Abdalla, S.B. 1641
Abelezele, S.A. 1170
Abuhatsira, D. 1478
Achig, M.C 1393
Adam, J.M. 626, 2737, 3438
Adamek, J. 2306
Addessi, D. 1893, 2217
Adell, J.M. 279
Aguilar, R. 504, 1618, 3145, 3218
Aita, D. 433, 1338
Al Shawa, O. 651, 2894
Alaboz, M. 3005
Alfaro, C. 302, 3652
Alonso , E. M. 769
Alonso-Martinez, M. 1145
Alvarez-Rabanal, F.P. 1145
Alykow, K. 1206
Amano, Y. 3240
Amato, G. 2642
Amorosi, A. 933, 2780
Andic, D. 2708
Angelillo, M. 445, 2066
Angjeliu, G. 1834
Antuna, J. 2240
Anzilotti, Y. 3065
Aoki, T. 2696
Apak, K. 2600
Aprile, A. 2757
Argiento, L. 2007
Argiento, L.U. 614
Aripov, I. 3339
Arleo, L. 3193
Arroyo Matus, R. 3371
Artioli, G. 2564
Asad, M. 537
Askouni, P.D. 2528
Auletta, G. 2586
Aurelio Felicito, R. 3371
Autiero, F. 492
Avşar, O. 2858
Aznar, A. 2240
Álvarez, I. 3498
Badillo-Almaraz, H. 2354
Baez, J. 257
Baeza, F.J. 559
Baggio, C. 943, 2282, 3252
Bai, W. 2993, 3077
Bajramovic, A. 2768
Baldantoni, F. 2586
Balik, L. 3381
Baraldi, D. 1755
Barbo, S. 3065
Barchetta, L. 2824
Barou, L. 1571
Barroso, C.E. 809
Barsallo, G. 1393
Barsi, F. 1338
Barsotti, R. 1338
Basaglia, A. 2757, 3402
Basirico, T. 1133
Basso, A. 1547
Bayer, J. 802
Bedolla , J. A. 769
Bedoya, C. 279
Belleri, A. 2926
Bellin, S. 3181
Bellini, A. 2620
Benedetti, A. 1871
Benedetti, L. 1871
Bennati, S. 1338
Bento, R. 1457, 2870
Berardi, R. 1074
Berkowski, P. 144, 897
Berlucchi, N. 3169
Bernardi, P. 1502
Bernardini, G. 3486
Bernat-Maso, E. 746
Berto, L. 3181
Bertolesi, E. 626, 2737
Bertolin, C. 791, 3284
Betti, M. 1109
Biagini, C. 421
Bianchini, N. 3098
Biggs, D. 1222
Bisegna, P. 2088, 2425
Bishara, S. 1559
Blank, M. 1303
Block, P. 1736, 1882, 2019, 2124, 2846
Blondet, M. 3133
Bocan, C. 1535
Boem, I. 2470
Boggian, F. 2958
Boothby, T. 2318

Bordo, D. 1490
Boriani, M. 3426
Borin, P. 1547
Borlenghi, P. 697
Boroschek, R. 3218
Bourgeois, E. 2400
Bozza, E. 821
Bracchi, S. 2946, 3028
Bragadin, M.A. 2790
Braglia, V. 267
Brando, G. 302, 3402, 3641, 3652
Brencich, A. 59
Bristogianni, T. 1571
Briz, E. 117, 3498
Brookes, S. 1409
Brožovský, J. 2687
Bru, D. 559
Brugnera, P. 47
Bucur-Horváth, I. 94
Buitrago, M. 626, 2737
Burrill, S. 3349
Bustamanta-Altamirano, J. 1663
Cabané, A. 662
Cabezas, K. 325
Cacace, D. 2262
Cacciotti, R. 2836
Caddemi, S. 2612
Calì, A. 1158
Calderón, P.A. 626, 2737
Calderini, C. 569, 1074, 1256, 3098
Cali, A. 1315
Caliò, I. 909, 2007, 2294, 2612
Camassa, D. 559
Camata, G. 1789, 1928, 2516
Cambiaggi, L. 1074, 1256
Campione, S. 1133
Campos Costa, A. 3098
Candeias, P. 3098
Candela, M. 1050
Cannizzaro, F. 909, 1002, 2294, 2612
Cantini, L. 469
Caprili, S. 2076
Cardani, G. 1834
Cardona, O. D. 885
Cardoso, F. 1393
Carloni, C. 2451
Carranza Bello, J. L. 3371
Carvalho, J. 852
Casapulla, C. 614, 1822, 1846, 2007
Casarin, F. 639, 821, 1369, 1421
Cascini, L. 1014
Castañeda, B. 504, 1618
Castellano, A. 722, 1959, 2504
Cattari, S. 3016
Cavalagli, N. 2100, 2552
Cazzani, A. 2342
Cecil, R.T. 1170
Čejka, T. 2687
Celano, T. 1846, 2007
Celik, O. C. 1675
Cennamo, C. 445
Ceraldi, C. 614
Ceravolo, R. 71, 1996
Cerioni, R. 1502
Ceroni, F. 2007
Charmpis, D.C. 200
Chaves Moreno, E.A. 2054
Chácara, C. 2294
Chávez, M. 757, 2882, 2938
Chen, J.F. 2642
Chenyi, L. 2378
Chesi , C. 3426
Chieffo, N. 3522, 3581
Chiorino, C. 71
Chiozzi, A. 1971
Chisari, C. 1724
Chounta, A. 3109
Chun, Q. 1214
Chunxia, Y. 2378
Cianchetti, R. 1421
Cianchino, G. 3641
Cianci, E. 2802
Ciocci, M.P. 1811, 1846
Clark, K. 1409
Cluni, F. 1651
Coïsson, E. 267, 1687
Coccia, S. 397
Cocco, G. 3652
Cocking, S.H. 2066
Cocuzza Avellino, G. 909
Coisson, E. 1502
Coll Pla, S. 1086
Colucci, A. 3252
Comert, M. 3169
Cominelli, S. 2926
Condoleo, P. 3156
Cooke, J. 978
Cordero Espinosa, L. 734
Corlito, V. 2262, 3474, 3605
Coronelli, D. 1834

Costa, M.G. 47
Costa-Jover, A. 1086
Cottone, A. 1133
Coz-Diaz, J.J. 1145
Crété, E. 3193
Crespi, P.G. 1699
Croonenborghs, T. 1268
Cucchi, M. 830
Cusano, C. 445
Cusmano, V. 1002
D'Angelo, F. 2718
D'Anna, J. 2642
Da Gai, E. 943
Dahabreh, P. 1369
Dai, J. 2993, 3077
Daigo, T. 3296
Dalla Via, T. 1421
Damiani, N. 2946
Dauda, J. A. 2206, 2576
De Angelis, A. 1097
De Bellis, M.L. 2043
De Canio, G. 651, 2894
De Cesaris, F. 966
De Falco, A. 1490
De Felice, G. 651, 933, 1917,
....2632, 2780, 2894
De Ferri, L. 791, 3284
De Filippis, L. 1097
De La Llera, J.C. 1244, 2439
De La Rosa, S.G. 2354
De Lucia, G. 71, 1996
De Martino, G. 492
De Matteis, C. 3641
De Matteis, G. 2262, 3474, 3605
De Santis, S. 651, 2632, 2894
Declercq, P. Y. 1268
Degli Abbati, S. 3016
DeJong, M.J. 2066, 2846
Delagrammatikas, M. 2480
Dell'Endice, A. 1882, 2019
Della Torre, S. 469, 674, 3510
Demir, C. 3169
Demirlioglu, K. 3558
Desbordes, A. 2400
Di Biase, C. 385
Di Carlo, F. 397
Di Gennaro , L. 2718
Di Ludovico, M. 492
Di Marco, L. 1369
Di Marco, S. 2790
Di Martino, A. 909
Di Napoli, B. 1846
Di Sivo, M. 1490
Dias De Moraes, P. 1158
Dimovska, S. 3569
Dinç-Şengönül, B. 2136
Dmochowski, G. 144, 897
Do Valle, A. 1158
Dobon, J. 2664, 2729
Dogu, D.. 1291
Dongmo, B.F. 3181
Doran, B. 2136
Dos Santos, M.N. 1170
Douroux, J. F. 2400
Drdácký, M. 2836
Drdácký, T. 2836
Drdácky, M. 639
Drougkas, A. 1268
Drygiannakis, M. 3272
Durán, D. 2882
Dutu, A. 2181
Džombić, N.M. 1026
Edmisten, J. 2330
Egiluz, Z. 117
Eichberg, M. 1050
Enciso, R. 3145
Endo, Y. 1778, 3264
Esparza-Carrillo, A. 1663
Esponda, M. 734, 978
Esposito, R. 2652
Facchi, E. 373
Falcão, A. P. 1457
Farahza, N. 3193
Fenialdi, A. 1256
Fernández, J. 3121
Ferrari, L. 267
Ferrández, A. 3121
Ferrero, C. 569, 1074, 1256
Ferretti, D. 1687
Ferretti, F. 525, 2540
Figueiredo, R. 2746
Fioriti, V. 3252
Florea, M. 1183
Flores-Sasso, V. 921, 1470
Fontana, C. 2802
Foppoli, D. 674
Forliti, S. 651, 2894, 3252
Formigoni, F. 1971
Formisano, A. 3522, 3581
Fraddosio, A. 722, 1959, 2504

Franchi, A. 1699
Franzoni, E. 2451
Friedman, D. 1947
Frostick, R. 1409
Frunzio, G. 2718
Fuentes Rivera, G.I. 3065
Fuertes, P. 361
Fugger, R. 1917
Funari, M.F. 211
Fusco, D. 2217
Gaglio, F. 1490
Galassi, S. 2413
Gandini, A. 117
Garbin, E. 2564
García, J. 3121
García, N. 2882
García-Alvarez, J. 1559
García-Baltodano, K. 1326
García-Muñoz, J. 2112
Garcia-Cuetos, M.P. 1145
Garcia-Ramonda, L. 2516
Gard , W. 709
Garmendia, L. 117, 3498
Garnier, P. 3193
Gattesco, N. 2470
Gáspár, O. 1984, 2229
Gendelman, P. 1478
Gentile, C. 697, 1315, 1346, 3305
Gentilini, C. 2451
Georgiou, A.V. 82
Gharib, M. 1766
Giambruno, M.C. 3426
Gianfriddo, G. 909
Giannetti, I. 397
Giardina, G. 1905
Gil, L. 746
Giordano, A. 1547
Girardi, M. 2031
Giresini, L. 2168
Gisbert, I. 559
Giuliani, F. 1490
Giuliano, A.A. 1433
Giuriani, E. 2926
Gobbin, F. 1917
Godinho, M. 1457
Gonçalves, A. B. 1457
Gonzalez, A. 3402
Gonzalez-Libreros, J. 2612
González, G.A. 2354
González, J. A. 2318
González-Aguilera, D. 1559
Grandic, D. 245
Grandits, D. 1038
Graziotti, F. 2946, 3028
Greppi, A. 385
Grillanda, N. 1971, 2342
Grimes, M. 593
Grimoldi, A. 373
Grottesi, G. 791
Guerrini, G. 2946
Guntur, M. 954
Gusella, V. 1651, 2100, 2552
Hadid, S. 1478
Hadjimichael, M.M. 82
Hajmirbaba, M. 3193
Haldenwang, R. 515
Halici, O.F. 3169
Hamamoto, T. 3296
Hassanieh, A. 1766
Hatletveit, M. 2958
Hayen, R. 1268
Höst, F. 1799
Herbig, U. 1038
Hernando, J.I. 2240
Hernández-Salazar, I. 1326
Hettinga, J. 1232
Hicks, N.A. 2914
Higashizawa, B. 1859
Hola, A. 842
Hola, J. 842
Holowaty, J. 781
Hormazábal, M.F. 3317
Horvat, M. 2708
Hosamo, H. 873
Hothot, Y.M. 2136
Hrivnák, J. 639
Huaranga, S. 1618
Huizinga, W. 1905
Hurata, A. 3169
Iannuzzo, A. 1882, 2019, 2124
Ilić, I.D. 1026
Ilki, A. 3169
Illampas, R. 1062
Impollonia, N. 909
Incerti, A. 525, 2540, 2620
Intrigila, C. 2425
Ioannou, I. 82, 1062
Ion, A.C. 1594
Ireland, R. 1409
Isopescu, B. 1122

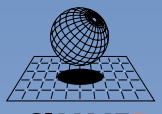
Iuorio, O. 2206, 2576
Ivorra, S. 559, 626
Iwanami, G. 1778
Iwicki, P. 409
Izzuddin, B.A. 1724
Jaeger-Klein, C. 2768
Jara, J.M. 3052
Jasieńko, C. 602
Jiménez Rios, A. 593
Jimenez, B. 2194
Kabele, P. 2306
Kalagri, A. 2480
Kalkbrenner, P. 1712
Kaminsky, J. 547
Kao, G.T.C. 1882
Kapogianni, E. 291, 3329
Karolak, A. 602
Kaymak Heinz, G. 233
Keller, A. 1122, 1535
Keller, A.I. 2902
Key, E.T. 2054
Kido, T. 3240
King, M. 1766
Kioumarsi, M. 873
Kloiber, M. 639
Kněž, P. 2156
Koch, M. 325
Kodzoman, E. 1038
Koh, B. 2330
Kolísko, J. 2156
Kondo, Y. 1778
Konsta, A. 3510
Korslund, K.A. 1170
Kosciuk, J. 481
Kruithof, M. 1905
Kubát, J. 2687
Kudrnacova, L. 3381
Kumar, A. 1279
Kundu, T. 722
Kuran, F. 3169
Kurata, N. 3296
Kurniawan, K. R. 954
La Mendola, L. 2642
Ladiana, D. 1490
Lagomarsino, S. 3016
Landi, A. G. 373
Landolfo, R. 1014
Lapucci, D. 2824
López López, D. 1736
Leggieri, V. 3414
Lembo, F. 2586
Lenticchia, E. 71
Li, X. 2673
Liberatore, D. 651, 2894, 3661
Liberotti, R. 1651, 2100, 2552
Licciardello, L. 2652
Liew, A. 1736, 2846
Lin, Y. 1214
Lindenbergh, R. 709
Liu, C. 990
Lluis i Ginovart, J. 685, 1086
Lluis-Teruel, C. 685
Lo Faro, A. 1002
Loke, M. E. 515
Lopez-Piquer, M. 685
Lorenzoni, F. 2251
Lourenço, P.B. 211, 1746, 1811, 1846, 1893, 2007, 2206, 2294, 2576, 2858, 3098, 3218, 3581
Lozano Martinez-Luengas, A. 1145
Lubelli, B. 105
Lubowiecka, I. 2274
Lucesoli, M. 3486
Lysandrou, V. 1062
Macaya, F. 757
Machete , R. 1457
Macorini, L. 1724
Maddaloni, G. 1097
Maeda, T. 1859
Magdalena, F. 2240
Magdalena-Layos, F. 2112
Maia Avelino, R. 1882, 2124
Maino, S. 325
Maklada, N. 1478
Makoond, N. 1291, 3228
Malakoudi, C. 3109
Malcata, M. 2870
Marano, C. 1789, 1928
Marcos, I. 117
Margani, G. 2958
Mariano, F. 1433
Marini, A. 2926
Marino, E. 2958
Marino, F.P.R. 2586
Marotta, A. 3661
Marques, R. 1811
Martinez, G. 3052
Martini, R. 852
Martins, T. 3121
Masciotta, M.G. 1559, 3317

Massaro, L. 2718
Matracchi, P. 421
Matrasulov, D. 3339
Matta, E. 71
Mazzanti, C. 302, 3652
Mazzotti, C. 525, 2540, 2620
Mària, M. 1445
Meade, E.P. 2914
Meggiato, M. 1421
Mehrotra, A. 2330, 2846
Mejia, L. 3052
Mencías-Carrizosa, D. 2112
Mendes, N. 3098
Mentese, V. G. 1675
Mercedes, L. 746
Meriggi, P. 2632, 2894
Messali, F. 2217, 3028
Michelini, E. 1502
Miglietta, M. 2946
Milani, G. 1746, 1755, 1971, 2342, 2492, 2504, 2981
Mileto, C. 2814
Miltiadou-Fezans, A. 2480
Minafò, G. 2642
Minch, M. 144, 897
Mirabella Roberti, G. 47
Mirabile Gattia, D. 651
Miraglia, G. 71
Misseri, G. 1244, 2439
Miyamoto, M. 2366, 2390, 2696, 3240
Mocellini, M. 1369, 1421
Molins, C. 1291, 3228
Montenegro, E. 3617
Monteys, X. 1445
Moragues, J.J. 626, 2737
Moreno Garcia, D. 1086
Moreno Regan, O. 2400
Mornati, S. 397
Morrison, T. 3349
Mosoarca, M. 1122, 1183, 1594, 2902, 3546, 3581
Mosseri, A. 337
Mourek, J. 1303
Mousavian, E. 614, 1822
Murai, S. 2366
Myrianthefs, D. 1062
Naldini, S. 105, 1583
Nan, Z. 2378
Nanni, A. 2620
Napiórkowska-Alykow, M. 1206
Natali, M. 2564
Nebiacolombo, M. 59
Nedvedova, K. 3381
Nicol, L.M. 156
Nicolaou, D. 1062
Niculescu, M. 1183
Niitsu, Y. 3264
Nijsse, R. 1571
Nocera, M. 1893
Nodargi, N.A. 2088, 2425
Noel, M. 3145
Nollet, M-J. 3593
Nuñez, E. 757
O'Dwyer, D. 593
Occhipinti, G. 2802
Ohashi, Y. 3087
Oikonomopoulou, F. 1571
Okada, M. 3240
Oktay, D. 2136
Olagoke, O.A. 1514
Olazabal, M. 3498
Oliveira, B. 1523
Oliveira, D.V. 211, 809, 1559, 2168, 3317
Olivieri, C. 2066
Olivito, R.S. 2492
Olmos, B. 3052
Olstad, T.M. 3284
Onescu, E. 3546
Onescu, I. 3546
Oprita, R. 127
Orduña, A. 2354
Ortega, J. 2054, 3534
Ota, K. 3240
Ottonelli, D. 3016
Ottoni, F. 267
Oyarzo, C. 757
Oz, Y. 1478
Pașcu, G. 1535
Pachta, V. 581
Padovani, C. 2031
Pagliari, F. 1687
Pakowska, M. 481
Palade, M. 1183
Palazzi, N.C. 1244, 2439
Palinic, N. 245
Pallav, K. 515, 1279
Pampanin, S. 2217
Panizza, M. 2564
Pantò, B. 1002, 1724, 2007, 2294
Papanicolaou, C.G. 2528

Papasavvas, G. 1062
Pardo Redondo, G. 105
Paret, T.F. 2458
Parisi, M.A. 3065, 3593
Parisse, F. 2181
Passoni, C. 2926
Pasterkamp, S. 192
Paterno, E. 909
Paupério, E. 2746, 3450
Pavel, F. 3462
Pérez-Cuevas, J. 921
Pórcel, P. 1618
Peña, F. 2882, 2938
Pecce, M.R. 1097
Pejatovic, M. 2981
Pelà, L. 662, 1712, 1789, 2194,
..... 2516, 2757, 3228, 3569
Pellegrini, D. 2031
Pellegrino, C. 2612
Pema, P. 2696
Penna, A. 2946, 3028
Perobelli, S. 651
Perria, E. 2673
Persia, F. 651
Perucchio, R. 457, 1170
Peruch, M. 3652
Petetta, L. 1433
Petracca, M. 1789, 1928
Petridis, C. 3109
Petrou, M.L. 200
Petrović, M. 1026
Petrucci, E. 2824
Philokyprou, M. 1062
Piñero, I. 117
Piccinini, F. 1433
Piccioni, M.D. 722, 1959, 2504
Pino, O. 2054
Pintus, V. 2342
Pisarra, W. 2814
Pitilakis, D. 3109
Plevris, V. 873
Pojatina, J. 2708
Poletti , E. 2054
Poletti, E. 2181
Ponte, M. 1457, 2870
Ponzo, F.C. 2586
Porcel, P. 504
Porras-Alfaro, D. 1326
Portioli, F. 1014
Porzio, S. 2492
Prieto, S. D. 885
Prieto-Vicioso, E. 921, 1470
Prota, A. 492
Przewlocki, J. 409
Psarropoulos, P. 3329
Puncello, I. 2076
Quagliarini, E. 3486
Quattrone, A. 71
Quesada-Ganuza, L. 3498
Ragueneau, M. 1940
Rajabzadeh, S. 734
Rakhmanov, B. 3361
Ramos, L.F. 809
Rampello, S. 933
Randall , L. 1409
Rapicavoli, D. 2294, 2612
Rashid, M. 1641
Rautenberg, J.M. 2458
Rózsás, A. 1905
Reccia, E. 2342
Ricci, E. 1959
Riggio, M. 3206
Rihal, S. 2330
Rinaldi, Z. 397
Rjolli, L. 1490
Roca, P. 569, 662, 1256, 1629,
..... 1736, 2076, 2262, 2516,
..... 3228, 3474, 3534, 3569
Rocca, I. 3181
Rodas, T. 1393
Rodrigues, H. 2181
Rodriguez-Mariscal, J.D. 852
Roeder, G.M. 2354
Rojí, E. 3498
Romagnoli, G. 2802
Romão, X. 2746, 3450
Roscini, F. 2632
Roselli, I. 2894, 3252
Rossi, M. 569, 3098
Rossi, R. 1712
Rots, J.G. 2217, 2652
Rouhi, A. 168, 180
Rovero, L. 1244, 2439
Ruccolo, A. 3305
Rucka, M. 863
Ruggieri, S. 3414
Ruiz-Valero, L. 921, 1470
Sabbatini, V. 943, 2251, 3252
Sabri, R. 1514, 1641
Sacco, E. 1959

Sadocchi, A. 421
Sadowski, L. 842
Saetta, A. 3181
Saisi, A. 697, 1315, 3305
Saitta, F. 3252
Sajtos, I. 1984, 2229
Sakellariou, M. 3329
Sala, M. 674
Salas, C. 279
Salazar, L.G. 3450
Saloustros, S. 3534, 3569
Salvadó, N. 361
Salvalaggio, M. 2251
Sammartano, G. 71
Samol, P. 409
Sampaio, M.S. 221
Sandoval, C. 2439
Sandoval, S. 921
Sangiorgio, V. 3438
Sangirardi, M. 933, 2780
Santa Ana, L. 257
Santa Ana, P. 257
Santa Cruz, S. 3133
Santamato, F. 1097
Santini, S. 943, 2282, 3252
Santoro, R. 2451
Sanver, A.N. 3169
Saracco, M. 1433
Saretta, Y. 3390
Sarhosis, V. 1755, 2981
Saruwatari, S. 3296
Sauquet, R. 361
Sánchez, A. 769
Sánchez Tizapa, S. 3371
Sánchez-Aparicio, L.J. 1559
Sbrogiò, L. 1547, 3390
Scacco, J. 1746, 2504
Scamardo, M. 1699
Scancelli, L. 639, 821
Schaaf, U. 1381
Šculac, P. 245
Scupin, A. 3462
Scuro, C. 2492
Sebastiani, C. 943, 3252
Šekularac, N.D. 1026
Sepe, V. 2043
Sesigur, H. 3005
Setyastuti, A. 1038
Sferrazza Papa, G. 3065, 3593
Shabani, A. 873
Shehu, R. 2970
Shimoni, M. 1268
Shin, S. 2696
Shirahashi, M. 1859
Shrestha, K.C. 2696
Shrive, N. 168
Shrive, N.G. 180
Shu, C. 2378
Siani, A. M 791
Siboni, D. 1478
Sidawi, R. 1369
Sieder, M. 2673
Siedler, G. 547
Sieffert, Y. 3193
Siegert, S. 2673
Sielicki, P.W. 137
Silva, L.C. 211, 1893, 2206, 2858
Simoncello, N. 2612
Šimunić Buršić, M.I. 349
Sinchi, E. 1393
Sinopoli, A. 433
Sipos, A. 1984
Sipos, A. A. 2229
Sire, S. 1940
Slobbe, A. 1905
Solarino, F. 2168
Solís, M. 852
Soria, M.A. 2664, 2729
Sorrentino, L. 651, 2894, 3661
Sovero, K. 302, 3652
Soyoz, S. 3558
Spacone, E. 302, 1789, 1928,
..... 2757, 3402, 3652
Spano, A. 71
Spinelli, P. 1109
Stabrauskaite, D. 1606
Stampfer, L. 1038, 2768
Stefanidou, M. 581
Stoian, V. 1122, 1183
Strojecki, M. 791
Stumpf, W. 1194
Suárez, J. 2318
Sumali, A. 1358
Sun, J. 457
Szepietowska, K. 2274
Szolomicki, J. 144, 897
Szymanowski, J. 842
Takahashi, N. 2696
Takai, K. 3296
Takhirov, S. 3361

Takhirov, S.M. 3339
Taliercio, A. 3156
Tamburini, S. 2564
Tanaka, H. 1859
Tarantino, C. 1014, 1050
Tardo, C. 2958
Tarozzi, M. 1871
Tarque, N. 302, 3121, 3652
Taweel, A.K. 1369
Tedeschi, C. 830
Tej, P. 1303, 2156
Tempesta, G. 2413
Teneva, E. 746
Tenzin, K. 2696
Tezcan, S. 457, 1170
Thamboo, J. 537
Thelin, C. 1799
Theodossopoulos, D. 990
Tiberti, S. 2492
Tisserand, P.-J. 1940
Tomasi, R. 2958
Tomioka, A. 3296
Tondolo, F. 71
Tonietti, U. 2439
Tonna, S. 830, 3426
Torres, A. 3133
Torres, B. 559, 626
Torres-Acosta, A. 1663
Tralli, A. 1971
Traykov, A.V. 3040
Traykova, M.D. 3040
Trizio, F. 2814
Truong-Hong, L. 709
Tzigounaki, A. 3272
Ulivieri, D. 1338
Ulukaya, S. 2136
Uplekar , A. 2054
Urushadze, S. 802
Uva, G. 3414, 3438
Vacareanu, R. 3462
Valente, M. 1971
Valenti, R. 909
Valieri, M. 421
Valluzzi, M.R. 639, 821, 1547, 2251, 3390
Van Balen, K. 1268
Van de Kuilen, J.-W. 709
Van der Grijp, E. 1583
Van Hees, R. 1583
Van Mele, T. 1736, 1882, 2019, 2124
Varum, H. 852
Vasconcelos, G. 2054
Vassiliou, P. 2480
Vasta, M. 2043
Vázquez Jiménez, R. 3371
Vecchiattini, R. 1074, 1256
Veer, F.A. 1571
Vegas López-Manzanares, F. 2814
Vera, E. 1402
Verstrynge, E. 1268
Vetter, S. 547
Virág, J. 94
Vitaliani, R. 3181
Vlachakis, G. 3272
Vona, V. 3629
Walstra, J. 1268
Wangmo, P. 2696
Wasilewski, K. 2146
Wenliuhan, H. 2251
Wibaut, R. 313
Wichtowski, B. 781
Witzany, J. 802, 2687
Woudenberg, P. 709
Wouters, I. 313
Wu, B. 2993
Yadav, S. 3193
Yamasaki, T. 3240
Yang, Y. 3077
Yaya, C. 1618
Yüzer, N. 2136
Yokouchi, H. 3087
Yuasa, N. 2696
Zahra, T. 537
Zamperini, E. 373
Zampieri, P. 2612
Zbiciak, A. 2146
Zhang, C. 1214
Zhang, J. 2696
Zielińska, M. 863
Zigler, R. 2687
Zizi, M. 2262, 3605
Zonno, G. 1346, 3218
Zuppiroli, M. 3629



CIMNE

International Center
for Numerical Methods in Engineering

3682